Biosynthesis of mollisin by *Mollisia caesia*[1]

A. GAVIN MCINNES, JOHN A. WALTER, AND JEFFREY L. C. WRIGHT
Atlantic Research Laboratory, National Research Council of Canada, Halifax, N.S., Canada B3H 3Z1
LEO C. VINING AND NEELIMA RANADE
Biology Department, Dalhousie University, Halifax, N.S., Canada B3H 4J1
AND
RONALD BENTLEY AND EDWARD P. MCGOVERN
Department of Life Sciences, University of Pittsburgh, Pittsburgh, PA 15260, U.S.A.

Received May 2, 1989

A. GAVIN MCINNES, JOHN A. WALTER, JEFFREY L. C. WRIGHT, LEO C. VINING, NEELING RANADE, RONALD BENTLEY, and EDWARD P. MCGOVERN. Can. J. Chem. **68**, 1 (1990).

The ^2H nuclear magnetic resonance spectrum of mollisin from cultures of the fungus *Mollisia caesia* supplemented with [2-$^2H_3$]acetate was consistent with biosynthesis of the metabolite via a single-chain polyketide. The presumption that chain scission accompanies dichlorination of a reactive methylene group in such a polyketide was supported by the detection of chloroperoxidase activity with monochlorodimedone as a substrate, and failure to detect chlorinating activity when the substrate was acetoacetyl coenzyme A. However, a decisive choice between single-chain and two-chain polyketide intermediates cannot be made with information provided by the techniques used so far.

Key words: biosynthesis, mollisin, deuterium labelling and NMR; deuterium labelling and NMR, mollisin biosynthesis; labeling of mollisin by deuterium, NMR analysis; mollisin biosynthesis, deuterium, labeling and NMR; NMR deuterium, mollisin biosynthesis.

A. GAVIN MCINNES, JOHN A. WALTER, JEFFREY L. C. WRIGHT, LEO C. VINING, NEELING RANADE, RONALD BENTLEY et EDWARD P. MCGOVERN. Can. J. Chem. **68**, 1 (1990).

Les spectres en résonance magnétique nucléaire du ^2H de la mollisine provenant de milieux de cultures du champignon *Mollisia caesia* auxquels on a ajouté du [2-$^2H_3$]acetate sont en accord avec ceux auxquels on pourrait s'attendre sur la base d'un mécanisme de biosynthèse du métabolite impliquant une chaîne unique de polycétide. L'hypothèse d'après laquelle une scission de la chaîne accompagne la dichloration d'un groupement méthylène réactif d'un polycétide est en accord avec la détection d'une activité de la choroperoxydase sur la monochlorodimédone comme substrat et le fait que l'on ne peut dètecter de chloration lorsque le substrat est l'acétoacétyl coenzyme A. Toutefois, sur la base des résultats obtenus avec les techniques utilisées jusqu'à maintenant, on ne peut choisir entre les mécanismes impliquant des intermédiaires polycétides à chaînes uniques ou doubles.

Mots Clés: biosynthèse, mollisine, marquage au deutérium et RMN; marquage au deutérium et RMN, biosynthèse de la mollisine; marquage de la mollisine par du deutérium, analyse par RMN; biosynthèse de la mollisine, marquage au deutérium et RMN; RMN, deutérium, biosynthèse de la mollisine.

[Traduit par la revue]

Early experiments with ^{14}C-labeled acetate and malonate indicated that mollisin (**1**, Fig. 1) was formed in the fungus *Mollisia caesia* by condensation of acetate and malonate (1). Subsequently it was shown (2) by measuring the increase in intensity of ^{13}C-H satellite resonances in the proton magnetic resonance spectrum of mollisin that [2-^{13}C]acetate enriched C-3, C-6, C-11, C-12, and C-14 to equal extents with ^{13}C. When cultures were supplemented with [1,2-$^{13}C_2$]acetate and the metabolite was examined by ^{13}C nmr spectrometry, the labelling pattern obtained was consistent with biosynthetic pathways (a) or (b) in Fig. 1, and excluded several other possibilities (3–5).

In an attempt to distinguish between the one-chain (a) and two-chain (b) polyketide pathways, we have grown *M. caesia* in cultures containing [2-$^2H_3$]acetate and determined the isotopic enrichment in mollisin by using ^2H nmr spectrometry. Figure 2 shows the ^1H and ^2H nmr spectra of the product displayed on the same ppm scale by assuming that the chemical shift for natural abundance C^2HCl_3 (relative to TMS-$^2H_{12}$) in the ^2H spectrum corresponds to that for $CHCl_3$ (referred to TMS) in the ^1H spectrum (6). The ^2H spectrum contains resonances only for C^2HCl_3 and ^2H-12; from the relative intensities of the two signals and the weight of chloroform used as solvent, the ^2H-enrichment at C-12 was estimated to be 0.27 ± 0.05% (cf. 0.015% natural abundance).

The integral of the ^2H-12 resonance was more than 12 times that of the ^2H-11 region, confirming that the two methyl groups, although both ultimately derivable from the methyl group of acetate, have different biosynthetic histories. The integral of the ^2H-12 resonance was at least 25 times greater than the noise level of the integrals over the regions corresponding to ^2H-3 and ^2H-14. After correction for the number of hydrogens at each position, the ^2H-enrichment at C-12 was, therefore, at least eight times that at C-14. The results are consistent with the single-chain pathway (a) for mollisin biosynthesis.

Within the single envelope for ^2H-12, isotopically shifted peaks corresponding to the species $C^1H_2{}^2H$, $C^1H^2H_2$, and C^2H_3 were resolved ($\Delta\delta(^2H)$ 0, 0.048 ± 0.010, and 0.093 ± 0.010, respectively). The resonance displacements indicated that the three species were present in the proportions 2.5:2.7:1.0 (error ±0.3). A mixture of partially and fully deuterated methyl groups has also been found in other fungal metabolites biosynthesized in the presence of [$^2H_3$]acetate (10–12). Activation of [2-$^2H_3$]-acetate to acetyl coenzyme A is not accompanied by exchange of deuterium with water, or with hydrogens at enzyme reaction centres (7). However, acetyl coenzyme A is reversibly converted to malonyl coenzyme A by the action of acetyl coenzyme A carboxylase, and the methylene hydrogens of malonyl coen-

[1]NRCC No. 30826.

Printed in Canada / Imprimé au Canada

Can. J. Chem. Downloaded from www.nrcresearchpress.com by 186.148.149.217 on 09/07/12
For personal use only.

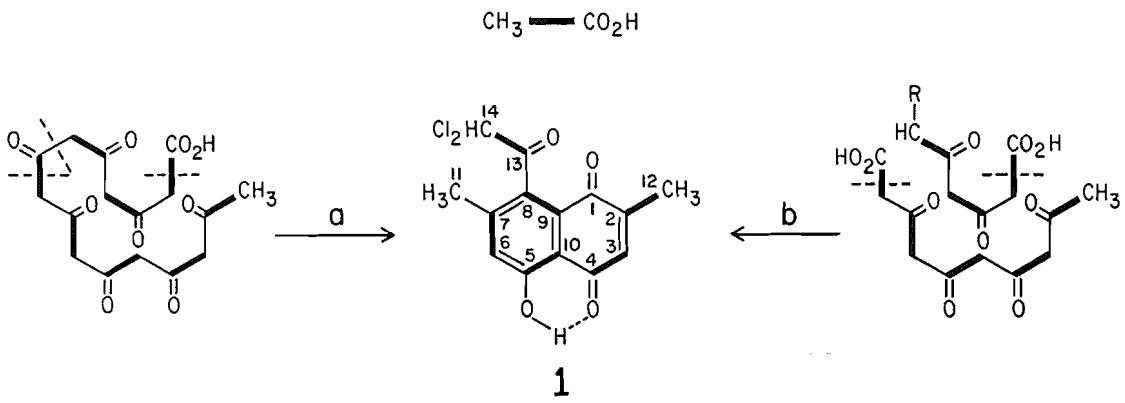

FIG. 1. Potential routes for the biosynthesis of mollisin.

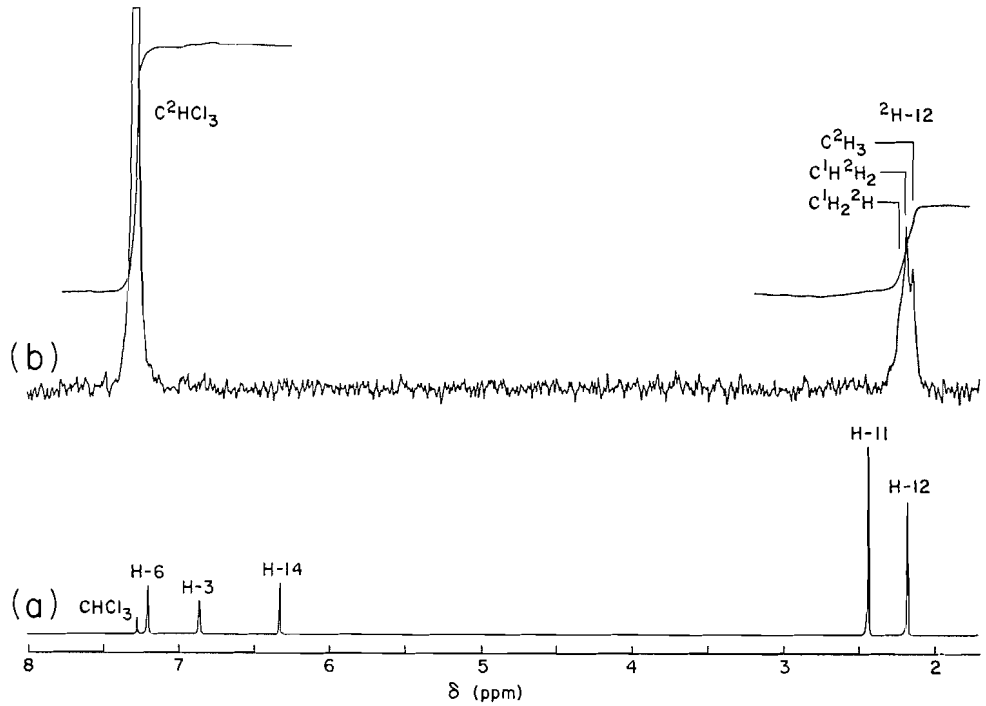

FIG. 2. (a) Portion of the ^1H spectrum of mollisin biosynthesized in the presence of [2-$^2H_3$]acetate (99%; ^2H); (b) ^2H spectrum and integral.

zyme A are known to undergo stereospecific exchange (8, 9). This could account for the observed distribution of isotopic species at C-12 of mollisin. Since some exchange of deuterium in methyl groups derived from [2-$^2H_3$]acetate can be anticipated, survival of the C^2H_3 species along with partially exchanged forms of the precursor is considered to be useful evidence in locating the starter unit of a polyketide chain (13, 14).

If the labelling at H-12 is accounted for by interconversion of acetyl coenzyme A and malonyl coenzyme A, mono- and dideuteromalonate must have been present in the malonate pool drawn upon for polyketide chain extension during mollisin biosynthesis. However, no peaks could be detected at positions expected for ^2H-3, ^2H-6, ^2H-11, or ^2H-14 in the ^2H nmr spectrum. The absence of deuterium at sites other than C-12 in the labeled metabolite implies that further exchange of deuterium occurred during or after the biosynthesis of mollisin. To determine whether hydrogens in mollisin could have exchanged after formation of the metabolite, an unlabeled sample recrystallized from benzene–isooctane was spread in agar containing ^2H_2O. After 3 weeks the mollisin was recovered and its ^1H nmr spectrum was compared with that of the original sample. No change in peak integration values was detected, indicating that the absence of label at methylene-derived carbons is more likely due to exchange at activated positions of enzyme-bound polyketide intermediates during mollisin biosynthesis. Similar examples of deuterium loss during the biosynthesis of other polyketide-pathway aromatic compounds from ^2H-labeled acetate have been reported, and have been attributed to exchange of labile hydrogens in biosynthetic intermediates or in the product (10, 11, 15). The degree of ^2H retention at positions derived from the malonate methylene group appears to be quite unpredictable (14), and can vary from complete loss to almost complete retention (16).

Since the introduction of chlorine into metabolites such as mollisin is catalyzed by chloroperoxidases that require a strongly nucleophilic target site (17, 18), a two-chain pathway in which both chains have acetate starter units (Fig. 1; path b; R = H_2) can be discounted on the grounds that the methyl of a chain-initiating acetate group is not sufficiently acidic to have furnished the nucleophilic enol required as the substrate for a

Can. J. Chem. Downloaded from www.nrcresearchpress.com by 186.148.149.217 on 09/07/12
For personal use only.

Can. J. Chem. Downloaded from www.nrcresearchpress.com by 186.148.149.217 on 09/07/12
For personal use only.

chlorination reaction. However, a two-chain pathway remains feasible if the chlorinated chain-initiating unit were to be generated from a more appropriate precursor. One possibility is for the dichloroacetyl unit to be synthesized from a suitable acetate-derived substrate before being used to initiate a polyketide chain (Fig. 1; path b; R = Cl_2). Such a starter unit might exchange deuterium with its environment during formation or after serving as a chain initiator.

To ascertain whether dichloroacetic acid itself might function as a precursor of mollisin, the deuterated compound was included in a medium used to grow *M. caesia*. At the concentration used, the supplement did not inhibit mollisin production, and ^2H nmr examintaion of broth extracts verified that excess [2-^2H]dichloroacetic acid was present throughout metabolite biosynthesis. Neither in the ^2H nmr spectrum nor in the gas chromatography – mass spectrum of mollisin extracted from the cultures was any evidence of ^2H enrichment detected. The upper limits for detection of the isotope, estimated to be approximately 1% and 0.6%, respectively, were higher than those for the experiment with [2-$^2H_3$]acetate because of the smaller sample size. Because of the more limited opportunities for metabolism of the chlorinated substrate, however, higher specific incorporations might also have been expected if it were a precursor of mollisin.

While the foregoing result suggests that free dichloroacetic acid is not incorporated, it is not conclusive. The absence of isotopic enrichment might have been due to cellular impermeability or to the inability of thiokinase to activate this substrate. Endogenous synthesis from an acetate-derived progenitor metabolite would likely furnish the chain-initiating precursor in an activated form. By analogy with biosynthesis of the dichloroacetyl moiety of chloramphenicol in *Streptomyces venezeulae* (Ranade and Vining, unpublished), a plausible precursor candidate would be acetoacetyl coenzyme A. To ascertain whether a chloroperoxidase that catalyzes formation of dichloroacetyl coenzyme A from acetoacetyl coenzyme A was present in *M. caesia*, extracts of the mycelium from cultures producing mollisin were assayed for this enzyme. No activity could be detected. In contrast, chloroperoxidase activity could be demonstrated when the assay was carried out with monoclorodimedone as the substrate. Since this compound is widely accepted as an analogue of the natural substrate by chloroperoxidases that introduce chlorine at the methylene group of β-diketones (18), activity under these conditions suggests that the natural substrate is an extended polyketide, perhaps constrained in a cyclic conformation.

A second way in which a dichloroacetyl chain-initiating group might be formed is through generation *in situ* from a longer polyketide (Fig. 1; path b, R = CH_3CO- or multiples). This could serve as a chloroperoxidase substrate by providing the necessary β-diketone grouping in a manner similar to that postulated for the single-chain polyketide precursor. Thus although the enzyme assay results are consistent with the single-chain polyketide pathway of biosynthesis, they do not exclude the possibility of two chains if the second chain were processed in this way. Clearly it is difficult to decide between such alternatives by the type of isotopic labeling and enzyme experiments described above, since both involve similar chain scission reactions that remove the distinguishing features of the progenitor polyketide (or polyketides). Answers to questions of this kind will probably require enzyme isolation and characterization of substrate specificities.

Experimental

Cultures and labeled substrates

"[1,2-$^2H_4$]Acetic acid" (99 at.% ^2H) and "[1,2-$^2H_2$]dichloroacetic acid" (98 at.% ^2H) were from MSD Isotopes, Pointe Claire, Que. Aqueous solutions were neutralized before filter sterilization.

In labeling experiments with deuterated acetate, ten 25 × 150 mm culture tubes, each containing 10 mL of malt extract agar plus NaCl (1), were inoculated with *M. caesia* and incubated at 22°C. To each tube, 100 μL of a 0.3 M sterile aqueous solution of sodium [2-$^2H_3$]acetate was added on the fifth day; a further 50 μL was added on the eleventh day. After 26 days mollisin was extracted as described (1) and purified by recrystallization.

When deuterated dichloroacetic was used, cultures of *M. caesia* were grown in five 100 × 15 mm Petri plates, each containing 20 mL of potato dextrose agar (BBL) supplemented with a sterile solution of sodium [2-^2H]dichloroacetate (0.1 mmol). After 16 days incubation at 22°C, mollisin was extracted with chloroform and purified by preparative thin-layer chromatography (silicia gel Sil 60, Merck; chloroform as solvent). Mollisin (bright-yellow zone, R_f 0.56) was the main component in the extract. It was eluted with acetone as a yellow solid (4.8 mg), mp 203°C, with an absorption maximum at 420 nm, as reported (1). Unused [2-^2H]dichloroacetate was transferred from the chloroform culture extract into bicarbonate solution and recovered as the free acid with chloroform. Its presence in the extract was established by ^2H nmr.

For enzyme assays, an inoculum was first prepared by transferring mycelium from 8-day-old slant cultures on 2% malt agar to Sabouraud's broth (50 mL/250-mL Erlenmeyer flask) and incubating the culture without agitation at 22°C for 10 days. The mycelium was washed, resuspended in 0.1 M phosphate buffer, pH 7.0, homogenized, and added (10 mL/200 mL) to 2% malt extract (200 mL/l-L Erlenmeyer flask). These cultures were grown in the same way as the inoculum for 19 days.

Enzyme assays

Mycelium from the 19-day cultures was collected and washed with 0.1 M phosphate buffer, pH 7.0, by centrifugation. It was resuspended in twice its volume of buffer and disrupted with a sonic oscillator (8 × 30 s). After clarification (10 000 × *g*, 30 min), the cell homogenate was assayed for chloroperoxidase activity and its protein content was measured.

Chloroperoxidase activity was determined by two procedures: the first used monochlorodimedone as the substrate and was based on the increase in absorbance at 278 nm accompanying formation of dichlorodimedone (17). The second depended upon the formation of a ^{36}Cl-labeled organic product from $^{36}Cl^-$ and acetoacetyl coenzyme A; it was performed by incubating 10 μL of 0.5 M K^{36}Cl (0.8 μCi/mmol), 0.5 μmol of acetoacetyl coenzyme A, 2 μL of 30% (v/v) aqueous H_2O_2, 84 μL of 0.1 M acetate buffer, pH 4.5, and 100 μL of cell extract. After agitation for 1 h at 22°C, the reaction was stopped and coenzyme A esters were hydrolyzed by adding 1 M NaOH. The mixture was acidified, and the radioactivity in an ethyl acetate extract was measured.

Nuclear magnetic resonance spectra

The ^2H nmr spectra were recorded at 46.075 MHz without lock or ^1H decoupling on a Bruker MSL-300 spectrometer. The experimental parameters were as follows: 10 mg of mollisin enriched from [2-$^2H_3$]-acetate in 0.40 mL of chloroform; 5-mm sample tube; spectral width 2000 Hz; one pulse sequence with flip angle ca. 40° (6 μs); repetition time 2.5 s; data size 8 K. Spectra were collected in six lots of 12 000 transients, each lot being zero-filled to 32 K and Fourier transformed before addition to allow for small field drifts, which were correctable from the position of the natural abundance C^2HCl_3 peak. The ^1H spectrum (300.13 MHz) was recorded after the sample was dried and redissolved in C^2HCl_3; the spectral width was 4505 Hz; data size 16 K zero-filled to 32 K; flip angle 45° (6 μs); repetition time 6.8 s.

Similar conditions were adopted to record the ^2H and ^1H nmr spectra

of mollisin from cultures supplemented with [2-^{2}H]dichloroacetate; for the ^{2}H spectrum, a 0.5 mg sample in 0.5 mL of C^2HCl_3 was used and approximately 80 000 transients were accumulated. Chemical shifts in the spectrum for mollisin have been assigned (2).

Mass spectra

A Finnigan model 4500 gc/ms was used with a DB5 chromatographic column. The sample was examined by chemical ionization with isobutane at 0.7 Torr (1 Torr = 133.3 Pa); ion source at 230°C.

Acknowledgements

The mass spectra were obtained by Dr. R.K. Boyd and Mr. D.J. Embree, and technical assistance was provided by Mr. J. Van Ingen, Atlantic Research Laboratory. The research was supported by a grant to L.C.V. from the Natural Sciences and Engineering Research Council of Canada.

1. R. BENTLEY and S. GATENBECK. Biochemistry, **4**, 1150 (1965).
2. M. TANABE and H. SETO. Biochemistry, **9**, 4851 (1970).
3. H. SETO, L. W. CARY, and M. TANABE. J. Chem. Soc. Chem. Commun. 867 (1973).
4. M. L. CASEY, R. C. PAULICK, and H. W. WHITLOCK, JR. J. Am. Chem. Soc. **98**, 2636 (1976).
5. A. G. MCINNES, J. A. WALTER, J. L. C. WRIGHT, and L. C. VINING. Topics in carbon-13 nmr spectroscopy. Vol. 2. *Edited by* G. C. Levy. John Wiley and Sons, New York. 1976. Chap. 3, p. 163.
6. H. H. MANTSCH, H. SAITO, and I. C. P. SMITH. Deuterium magnetic resonance, applications in chemistry, physics and biology. Progress in NMR spectroscopy. Vol. 11. *Edited by* J. W. Emsley, J. Feeney, and L. H. Sutcliffe. Pergamon Press, London. 1974. p. 211.
7. D. M. WILSON, A. L. BURLINGAME, T. CRONHOLM, and J. SJOVALL. Biochem. Biophys. Res. Commun. **56**, 828 (1974).
8. B. SEDGEWICK, J. C. CORNFORTH, S. J. FRENCH, R. T. GRAY, E. KELSTRUP, and P. WILLADSEN. Eur. J. Biochem. **75**, 481 (1977).
9. A. G. MCINNES, J. A. WALTER, and J. L. C. WRIGHT. Tetrahedron, **34**, 3515 (1983).
10. I. KUROBANE, L. C. VINING, A. G. MCINNES, and J. A. WALTER. Can. J. Chem. **58**, 1380 (1980).
11. I. KUROBANE, L. C. VINING, A. G. MCINNES, D. G. SMITH, and J. A. WALTER. Can. J. Chem. **59**, 422 (1981).
12. J. BARBER, A. C. CHAPMAN, and T. D. HOWARD. J. Antibiot. **40**, 245 (1987).
13. M. J. GARSON and J. STAUNTON. Chem. Soc. Rev. **8**, 539 (1979).
14. J. C. VEDERAS. Nat. Prod. Rep. **4**, 277 (1987).
15. V. SANKAWA, H. SHIMADA, and K. YAMASAKI. Chem. Pharm. Bull. **29**, 3601 (1981).
16. F. J. LEEPER and J. STAUNTON. J. Chem. Soc. Perkin Trans. **1**, 2919 (1984).
17. D. R. MORRIS and L. P. HAGER. J. Biol. Chem. **241**, 1763 (1966).
18. L. P. HAGER, D. R. MORRIS, F. S. BROWN, and H. EBERWEIN. J. Biol. Chem. **241**, 1769 (1966).

Can. J. Chem. Downloaded from www.nrcresearchpress.com by 186.148.149.217 on 09/07/12
For personal use only.

Solvatation et complexation des métaux dans les mélanges eau – fluorure d'hydrogène. Sn, Cd, Pb et Tl

RÉJEAN BEAUDOIN ET HUGUES MÉNARD

Département de chimie, Faculté des sciences, Université de Sherbrooke, Sherbrooke (Québec), Canada J1K 2R1

Reçu le 17 mai 1989

RÉJEAN BEAUDOIN et HUGUES MÉNARD. Can. J. Chem. **68**, 5 (1990).

Le comportement électrochimique de l'étain et du thallium dans les mélanges eau–HF a été étudié sur toute la gamme de concentration. Le thallium ne forme pas de complexes fluorés. L'étain Sn^{2+} forme deux complexes fluorés, SnF_2 et SnF^+, dans les mélanges contenant moins de 60% en HF. Le complexe SnF_2 est suffisamment fort pour empêcher la formation de complexes chlorés. La formation de SnF_6^{2-} et SnF_5^- a aussi été démontrée pour l'étain Sn^{4+}. La force relativement grande des complexes fluorés de l'étain se réflète bien sur la fonction R_0 (M). Tous les métaux étudiés, Sn, Cd, Pb et Tl, sont soins solvatés dans les mélanges eau–HF que dans l'eau, sauf là où la complexation par l'ion fluorure est importante, c.-à-d. l'étain. Aux hautes concentrations en HF, l'espèce HF_2^- semble devenir l'expèce complexante.

Mots clés : polarographie, thallium, étain, cadmium, plomb, fluorure d'hydrogène.

RÉJEAN BEAUDOIN and HUGUES MÉNARD. Can. J. Chem. **68**, 5 (1990).

The behavior of tin and thallium has been studied in water–HF mixtures. The formation of thallium fluoride complexes was not observed. Tin Sn^{2+} forms two complexes, SnF_2 and SnF^+, in mixtures containing less than 60% in HF. SnF_2 is strong enough to prevent the formation of chloride complexes. SnF_6^{2-} and SnF_5^- have been determined for Sn^{4+} in the same solutions. The relatively high strength of the tin fluoride complexes is reflected in the R_0 (M) function. In fact, all the metals studied, Sn, Cd, Pb, and Tl, are less solvated in water–HF mixtures than in water, except for the case where the fluoride complex is strong, i.e., tin. HF_2^- seems to be the complexing species at high HF concentrations.

Key words: polarography, thallium, tin, cadmium, lead, hydrogen fluoride.

[Journal translation]

Introduction

Les mélanges eau – fluorure d'hydrogène ont été largement utilisé pour la solubilisation de divers matériaux et pour le décapage de semi-conducteurs. Le comportement électrochimique des ions métalliques dans ces mélanges a été étudié surtout pour des applications analytiques. Les variations des propriétés d'oxydoréduction en fonction de la composition en HF méritent néanmoins d'être mieux définies.

Le comportement du mélange eau–HF lui-même est relativement bien défini, soit au niveau de l'acidité avec les fonctions H_0 (1, 2) et R_0(H) (3, 4), au niveau de l'activité en ions fluorure libres R_0(F) (4, 5) de même qu'au niveau de l'association moléculaire grâce aux études par spectroscopie infrarouge (6–9).

La fonction R_0(M) a été utilisé de façon à obtenir les variations d'activité des ions métalliques en fonction de la composition du mélange eau–HF (10). Il a cependant été démontré que la solvatation de l'ion F^- est beaucoup plus importante dans les mélanges eau–HF que dans l'eau (5), principalement dû à la formation de la paire d'ions ($H_3O^+ \ldots F^-$) (6–8). Il est donc évident que les ions métalliques seront moins solvaté dans les mélanges eau–HF que dans l'eau. De récentes études ont montrées que le cadmium et le plomb sont complexés par l'ion fluorure aux basses concentrations en HF mais que cette complexation diminue avec la concentration en HF (11, 12).

Le comportement de l'étain et du thallium sera discuté et des conclusions générales pourront étre tirées sur la solvatation sur tout le domaine de concentration en HF.

Partie expérimentale

Le potentiel de réduction du métal a été mesuré par polarographie. Un capillaire recouvert de polyéthylène (13) résistant au HF a été utilisé comme électrode de mercure. Aux concentrations de HF inférieures à 60%, une électrode de référence au calomel a été utilisée alors qu'aux hautes concentrations en HF, le système Cu/CuF_2 (14) offre une meilleure stabilité. Les mesures ont été effectuées à 25 ± 1°C pour les concentrations en HF inférieures à 60% et à 0°C pour les concentrations supérieores à 60%.

Les polarogrammes ont été enregistrés à une concentration de 10^{-3} M pour l'espèce ionique considérée. Pour l'étude des complexes fluorés, le potentiel de réduction du système de référence indépendant du solvant (4, 10, 15) Fc^+/Fc est mesuré dans la même solution que celle du métal étudié. La précision sur le potentiel de demi-vague est de ±5 mV. Pour les mesures de complexes chlorés, la concentration du métal est de 10^{-3} M, auquel du KCl est ajouté en quantité voulue. Une description complète du système de mesure de la cellule et les données expérimentales sont présentées aux références 16 et 17.

Résultats

L'étain dans les mélanges eau–HF

L'évolution des complexes fluorés en fonction de la concentration en HF dépend de l'activité en ions fluorure libres. Un déplacement du potentiel de demi-vague ($E_{1/2}$) mesuré par rapport au potentiel d'une électrode réversible aux ions fluorure est donc indicatif du type de complexe fluoré en solution. Il faut noter ici que la réduction des complexes étudiés présentent des vagues polarographiques réversibles. Il est donc possible de calculer, à partir de l'équation de Nernst, les pentes du déplacement de $E_{1/2}$ en fonction de l'activité en ions fluorure libres que l'on devrait mesurer pour des complexes fluorés d'ordre croissant (11, 12). Les pentes théoriques calculées en fonction de l'activité en ions fluorure libres sont les suivantes : SnF^+, +0,029; SnF_2, 0; SnF_3^-, −0,029 volt. La figure 1 illustre l'évolution du $E_{1/2}$ de réduction de l'étain et la figure 2 illustre le comportement du $E_{1/2}$ de l'oxydation de même métal en fonction de l'activité en ions fluorure libres R_0 (F). Les pentes mesurées sur ces graphiques, et présentées aux tableaux 1 et 2, permettent de déterminer l'ordre des complexes fluorés en solution. Les complexes déterminés pour la réduction de l'étain, soit le SnF_3^-, le SnF_2 et le SnF^+, sont utilisés comme complexe de départ pour déterminer les complexes de l'étain oxydés vers l'état Sn^{4+}.

Can. J. Chem. Downloaded from www.nrcresearchpress.com by 91.144.44.67 on 09/07/12
For personal use only.

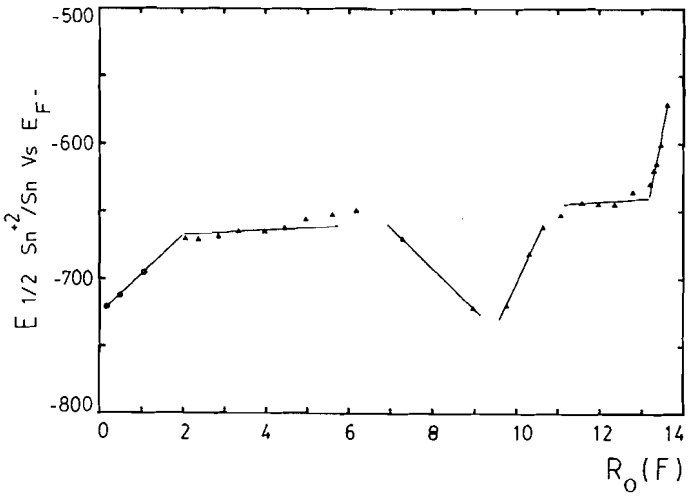

FIG. 1. Potentiel de réduction de l'étain vs. E_{F^-} en fonction de R_0(F). (Chaque point sur les figures représente la moyenne de 5–10 mesures.) Les pentes ont été calculées par régression linéaire.

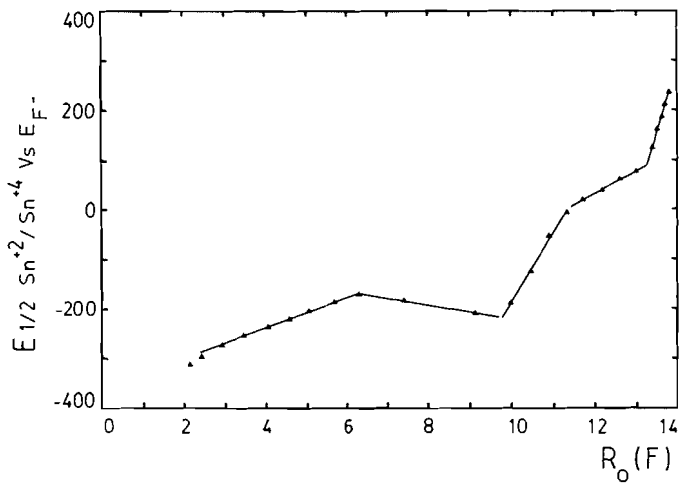

FIG. 2. Potentiel d'oxydation de l'étain vs. E_{F^-} en fonction de R_0(F).

L'étain en présence d'ions chlorure

La présence d'ions chlorure dans une solution eau–HF contenant de l'étain (Sn^{2+}) cause un déplacement du $E_{1/2}$ de réduction à partir d'une concentration en HF supérieure à 30% et ce pour des concentrations en ions chlorure de l'ordre d'un molaire. La figure 3 montre le déplacement du potentiel de demi-vague pour quelques concentrations en HF en fonction de la concentration en ions chlorure. Le tableau 3 donne les constantes de formation successives des complexes chlorés de l'étain calculées selon la théorie de DeFord et Hume (19).

Le thallium dans les mélanges eau–HF

L'étude de la réduction du thallium dans les mélanges eau–HF nous donne une pente de $E_{1/2}$ vs. E_{F^-} en fonction de R_0 (F) (fig. 4) près de 0,059 V, ce qui indique que le thallium n'est pas complexé par l'ion fluorure dans les mélanges eau–HF. Aux très hautes concentrations en HF, c.'à'd. plus de 80%, la vague de réduction du thallium se confond avec la réduction de l'hydrogène, mais la tendance semble toujours être la même au niveau de la pente.

Le thallium en présence d'ions chlorure

La figure 5 montre le déplacement de $E_{1/2}$ en présence d'ions

TABLEAU 1. Pentes expérimentales et calculées pour Sn^{2+}/Sn

Domaine de % en HF (poids)	Pente (V)	Complexe	Pente calculée (V)
0–2[a]	−0,034	SnF_3^-	−0,029
2–45	−0,002	SnF_2	0
45–55	+0,031	SnF^+	+0,029
55–70	+0,065		
70–90	−0,010		
90–100	Négative		

[a]Références 17, 18.

TABLEAU 2. Pentes expérimentales et calculées pour Sn^{2+}/Sn^{4+}

Domaine de % en HF (poids)	Pente (V)	Complexe	Pente calculée (V)
0–2[a]	−0,034	SnF_6^{2-}	−0,029
2–40	−0,030	SnF_5^{-}[b]	−0,029
40–50	+0,013	SnF_3^+	+0,029
50–70	−0,130		
70–95	−0,031		
95–100	Négative		

[a]Référence 18.
[b]Le complexe de départ n'est pas le même qu'en solution aqueuse.

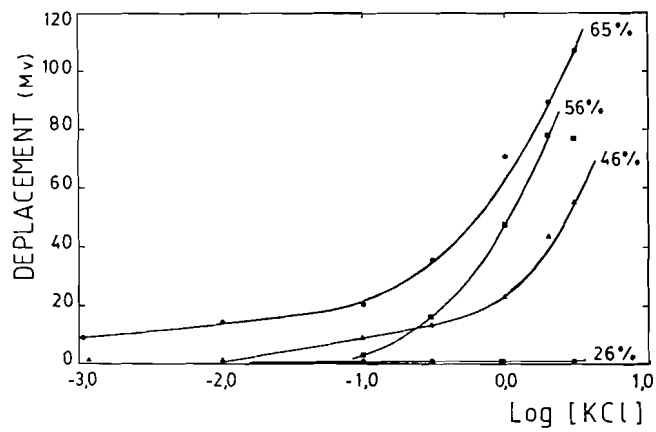

FIG. 3. Déplacement du potentiel de demi-vague de réduction de l'étain en fonction de la concentration en KCl, à différentes concentrations en HF.

TABLEAU 3. Constantes de formation successives des complexes chlorés de l'étain

%HF (poids)	β_1	β_2	β_3
65	13 ± 1	52 ± 5	30 ± 5
56	4,5 ± 0,5	24 ± 4	12 ± 2
47	4,6 ± 0,2	2,1 ± 0,2	1,0 ± 0,5
26	0	0	0
	$SnCl^+$	$SnCl_2$	$SnCl_3^-$

Can. J. Chem. Downloaded from www.nrcresearchpress.com by 91.144.44.67 on 09/07/12
For personal use only.

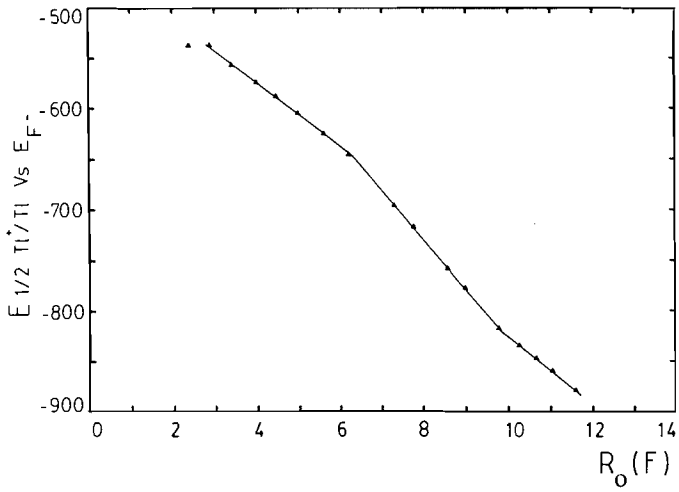

FIG. 4. Potentiel de réduction du thallium vs. E_{F^-} en fonction de R_0(F).

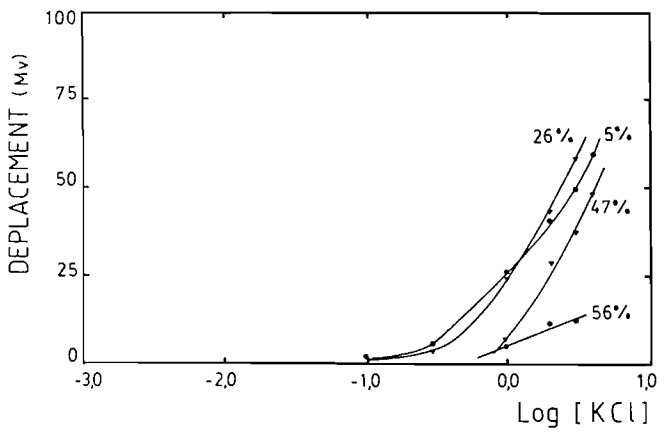

FIG. 5. Déplacement du potentiel de demi-vague de réduction du thallium en fonction de la concentration en KCl, à différentes concentrations en HF.

TABLEAU 4. Constantes de formation successives des complexes chlorés du thallium

% HF (Poids)	β_1	β_2
56	0,22 ± 0,2	
47	0,6 ± 0,1	~0,12
26	1,4 ± 0,4	0,20 ± 0,05
5	1,5 ± 0,1	0,20 ± 0,02
	TlCl	$TlCl_2^-$

chlorure à plusieurs concentrations en HF. Le déplacement de $E_{1/2}$ est relié à la formation de complexes chlorés en solution mais la faible amplitude du déplacement montre une complexation relativement faible. Le tableau 4 donne les constantes de formation successives pour les complexes chlorés du thallium.

Le cadmium et le plomb dans les mélanges eau–HF

Les vagues de réduction du cadmium et du plomb ont été mesurées à haute concentration en HF de façon à compléter les résultats déjà publiés (11, 12).

Discussion

L'étain

L'étain en solution aqueuse contenant l'ion fluorure a été étudié par plusieurs auteurs. Schaap *et al.* (18) puis Bond et Taylor (20) ont déterminé les constantes de formation des complexes fluorés en milieu acide et neutre. Le pourcentage de distribution montre que le complexe SnF_3^- est prédominant jusqu'à 10^{-7} M en ions fluorure libres. Hall et Slater (21) ont calculé les relations thermodynamiques ΔG, ΔH et ΔS pour la réaction [1] et ils concluent que le complexe fluoré est plus stable, en solution aqueuse, que les complexes avec le chlore et le brome.

[1] $Sn^{2+} + 3F^- \rightleftarrows SnF_3^-$

Donc on considère que le complexe d'étain formé à faible concentration en HF sera le SnF_3^-. Le tableau 1 montre une pente de −0,034 volt pour des concentrations en HF jusqu'à 2%, ce qui confirme que le complexe en solution est le SnF_3^-.

Dans le domaine de 2 à 60% en HF, il y a formation de deux complexes fluorés différents de celui qui prédomaine dans les solutions inférieures à 2% en HF. Les pentes mesurées sur la figure 1 permettent de dire qu'on a le complexe SnF_2 dans le domaine de 2 à 45% en HF et le complexe SnF^+ dans la région de 45 à 55% en HF. L'évolution des complexes dans les mélanges eau–HF s'explique bien puisque l'activité en ions fluorure libres diminue lorsque la proportion de HF augmente dans la solution.

Schaap *et al.* (18) ont proposé l'équilibre suivant pour l'oxydation de l'étain dans les solutions aqueuses d'ions fluorure :

[2] $SnF_3^- + 3F^- \rightleftarrows SnF_6^{2-} + 2é$

Leblond-Routhier (17) a démontré que la vague d'oxydation due à la réaction [3] est réversible (pente de 29 mV) dans les solutions aqueuses

[3] $Sn^{2+} \rightleftarrows Sn^{4+} + 2é$

de HF, quoiqu'aucune vague n'apparaît pour la réduction de l'étain au degré d'oxydation plus quatre vers plus deux. Même en voltamétrie à balayage rapide, on n'observe pas la réduction de Sn(IV). On peut donc exprimer l'équation de Nernst sous la forme suivante :

$$[4] \quad (E_{Sn}) = (E^0_{Sn}) + \frac{0{,}059}{2} \log \frac{[SnF_6^{2-}]}{[SnF_3^-][F^-]^3}$$

Au potentiel de demi-vague $[SnF_3^-] = [SnF_6^{2-}]$ et l'équation [4] devient

$$[5] \quad (E_{Sn}) = (E^0_{Sn}) - \frac{0{,}059}{2} \log [F^-]^3$$

$$[6] \quad E_{F^-} = E^0_{F^-} - 0{,}059 \log [F^-]$$

$$[7] \quad \Delta E_{1/2} = (E_{Sn}) - (E_{F^-}) = \text{cte} + 0{,}059 \log [F^-] - \frac{3 \times 0{,}059}{2} \log [F^-]$$

$$[8] \quad \Delta E_{1/2} = \text{cte} - 0{,}029 \log [F^-]$$

La pente du potentiel versus le logarithme de l'activité en ions fluorure devrait donc être de −0,029 volt pour l'équilibre [2]. La pente mesurée à moins de 2% en HF est de −0,034 volt, ce qui permet donc de considérer le complexe SnF_6^{2-} en solution. L'écart mesuré entre la valeur théorique et les valeurs mesurées pour les concentrations inférieures à 2% est dû à la vague

Can. J. Chem. Downloaded from www.nrcresearchpress.com by 91.144.44.67 on 09/07/12
For personal use only.

TABLEAU 5. Constantes d'equilibre et de formation successives des complexes fluorés de l'étain dans les mélanges eau–HF

	log K	log β
SnF_2	9.5	16.0
SnF^+	6.5	9.5

d'oxydation qui n'est pas totalement réversible pour ce domaine de concentration par rapport aux hautes concentrations en HF où la vague d'oxydation est réversible (17).

En solution aqueuse, on peut considérer le complexe SnF_3^- pour Sn(II) et SnF_6^{2-} pour Sn(IV) comme exprimé aux équations [1] et [2].

Les résultats obtenus pour l'oxydation de Sn(II) à Sn(IV) dans les mélanges eau–HF de 2 à 55% en HF montrent la présence de deux complexes selon la concentration en HF. Si on applique le même raissonnement que dans les solutions diluées de HF et la même façon de calculer la pente, on peut établir l'équilibre suivant:

[9] $SnF_2 + 3F^- \rightleftarrows SnF_5^- + 2é$

pour les mélanges de 2 à 45% en HF. La pente est de −0,030 volt, ce qui correspond au complexe SnF_5^-.

Dans les mélanges de 45 à 55% en HF, la pente est plus difficile à mesurer avec précision. On peut seulement proposer le complexe SnF_3^+. Les complexes de coordination 5 et 6 sont relativement commun pour les éléments du groupe IV. La possibilité d'utiliser les orbitales d pour la complexation rend difficile la prédiction du nombre de coordination à cause de la faible différence d'énergie entre les deux états (22). Un complexe chargé comme le SnF_3^+ a cependant peu de chance d'exister à moins d'être largement stabilisé par une autre espèce en solution.

Aux concentrations en HF de plus de 60%, l'évolution des $E_{1/2}$ de réduction et d'oxydation permet de conclure que l'espèce complexante en solution n'est plus l'ion fluorure.

Il est possible d'évaleur les constantes de formation à partir du changement de pente du potentiel de demi-vague réversible aux ions fluorure en fonction de l'activité en ions fluorure R_0(F) (10, 11). Aux points d'inflection à la figure 1, le logarithme des constantes de formation peut être considéré égal à R_0(F). Le tableau 5 montre les valeurs ainsi obtenues et la figure 6 présente la distribution des divers complexes fluorés en fonction de l'activité en ions fluorure dans le mélange eau–HF. Le complexe SnF_3^- se retrouve seulement en solution où la concentration en HF est moins de 2%.

En solution aqueuse, l'étain donne trois complexes chlorés. D'autre part, dans les mélanges eau–HF sans chlorure, l'étain donne deux complexes fluorés. Le complexe SnF_2 existe de façon majoritaire dans les mélanges jusqu'à 30% en HF. En présence de KCl à la figure 3, on constate qu'il n'y a pas de déplacement du potentiel de demi-vague de l'étain aux concentrations inférieures à 30% en HF. On peut donc supposer que le complexe fluoré est suffisamment fort pour empêcher la formation de complexes chlorés. Dans HF 47% on observe un déplacement rapide du potentiel de demi-vague avec la concentration en KCl. L'espèce fluorée en solution eau–HF est le SnF^+. Il semble qu'il soit possible dans ce mélange d'ajouter des ligands sur l'étain. L'espèce en solution est probablement

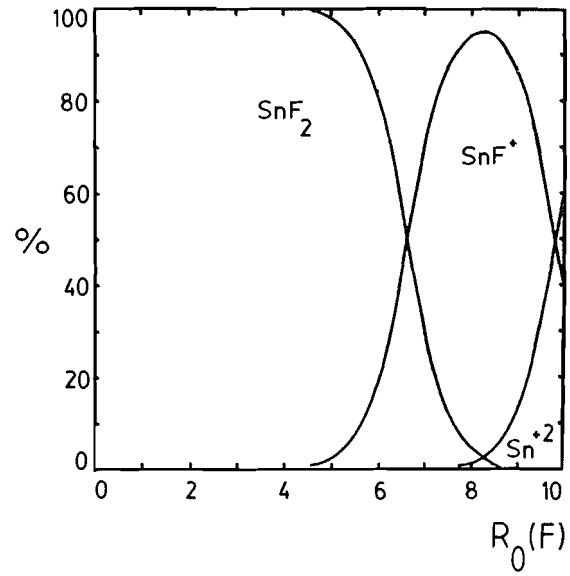

FIG. 6. Distribution des complexes fluorés de l'étain en fonction de R_0(F).

SnClF, un complexe mixte qui n'implique pas le remplacement d'un ion fluorure sur le métal. Le complexe $SnCl_2$ n'apparaît qu'à très grande concentration en ions chlorure. Le tableau 3 montre que les constantes de formation des complexes chlorés de l'étain augmentent avec la concentration en HF. Dans HF 56 et 65%, la diminution de la force des complexes fluorés permet la formation de complexes chlorés de degré supérieur.

Le thallium

Les solutions aqueuses de thallium contenant l'ion fluorure ont été étudié par plusieurs auteurs. Bond (23) a étudié le thallium en présence d'ions fluorure par polargraphie et par potentiométrie. Les complexes du thallium sont en général très faibles. À partir de résultats potentiométriques, il apparaît concevable que l'ion perchlorate soit plus complexant pour le thallium que l'ion fluorure. La constante de stabilité pour le complexe TlF est très faible, de l'ordre de 0,4 ou moins. Les complexes chlorés sont relativement faibles avec β_1 et β_2 de 1,00 et 0,36 respectivement. $TlCl_2^-$ est d'ailleurs observé seulement à force ionique élevée. Notre graphique du potentiel de demi-vague en fonction de l'activité en ions fluorure donne une pente de −0,056 V. Cette valeur est près de la valeur théorique de −0,059 V et indique donc que le thallium n'est pas complexé par l'ion fluorure dans les mélanges eau–HF.

En solution aqueuse contenant des ions Cl^-, le thallium n'est que faiblement complexé par ces ions. Selon la force ionique, Bond (23) a observé soit un complexe ou deux complexes chlorés. Dans les mélanges eau–HF, la force ionique est élevée et en présence d'ions Cl^- on devrait donc s'attendre à obtenir deux complexes chlorés comme c'est le cas en solution aqueuse à force ionique élevée. Dans HF 5%, nous observons deux complexes chlorés, une diminution du courant de diffusion a été relié à la précipitation du chlorure de thallium. Le précipité a été identifié par diffraction des rayons-X. Dans HF 26 et 47%, nous observons aussi deux complexes chlorés. L'évolution du courant de diffusion montre bien qu'il y a précipitation du chlorure de thallium suivi d'une resolubilisation à plus haute concentration en ions chlorure.

Le thallium ne forme pas de complexes fluorés dans les mélanges eau–HF. Par contre, en présence des ions Cl^-, on

Can. J. Chem. Downloaded from www.nrcresearchpress.com by 91.144.44.67 on 09/07/12
For personal use only.

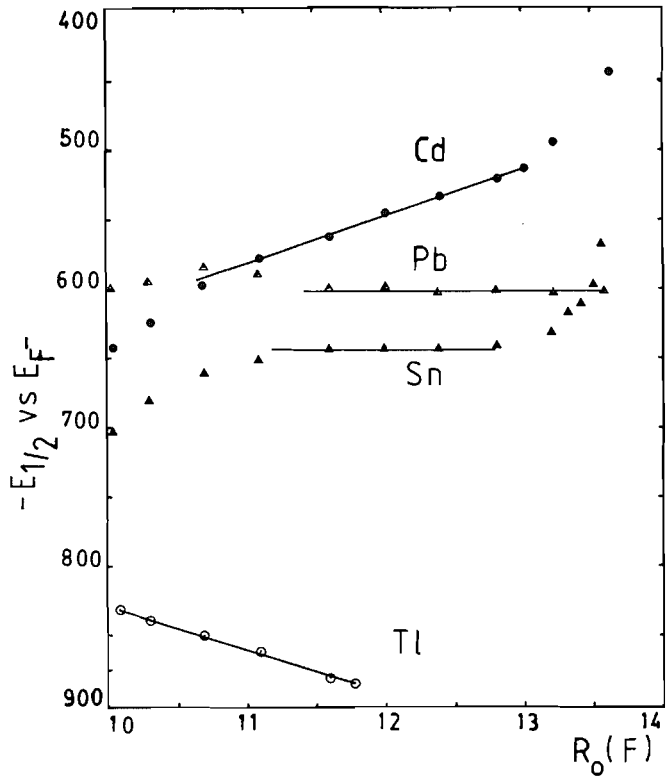

FIG. 7. Potentiel de réduction des métaux vs. E_{F^-} dans la région des hautes concentrations en HF.

forme des complexes chlorés faibles dans les mêmes mélanges. Il est donc raisonnable, en présence d'ions Cl^- de supposer la présence des complexes chlorés faibles dans les mélanges eau–HF et une distribution de la même façon que dans l'eau. La principale distinction entre les deux milieux, c'est la force ionique élevée pour les mélanges eau–HF.

Les hautes concentrations en HF

L'état d'ionisation dans les mélanges eau–HF a été établi par voie électrochimique (3–5) et spectroscopique (6, 7, 9). Les équations suivantes résument les équilibres en solution :

[10] $H_2O + HF \rightleftarrows [H_3O^+ \cdot F^-]$

[11] $[H_3O^+ \cdot F^-] \rightleftarrows H_3O^+ + F^-$

Les mesures de $R_0(F)$ montrent que l'équilibre [13] est largement porté vers la gauche.

[12] $[H_3O^+ \cdot F^-] + HF \rightleftarrows H_3O^+ + HF_2^-$

[13] $HF + F^- \rightleftarrows HF_2^-$

Des mesures spectroscopiques ont mis en évidence la présence de HF_2^- à haute concentration en HF et la formation de polymères de HF (9).

Pour les faibles concentrations en HF, nous avons établi la présence de complexes fluorés. À des concentrations en HF supérieures à 60%, l'évolution du potentiel de demi-vague, tel que présenté à la figure 7, ne peut pas être expliqué en terme de complexes fluorés.

L'apparition de l'espèce HF_2^- en solution peut venir expliquer le déplacement important du potentiel de réduction du Cd^{2+}/Cd et de Sn^{2+}/Sn. Il n'y a pas de techniques électrochimiques qui permettent de mesurer l'activité ou la concentration de l'espèce HF_2^- mais, sur une base purement qualitative, on peut estimer que la concentration en HF_2^- suit la concentration en H_3O^+ dans le domaine de 70 à 80% en HF. Si on calcule la molarité de H_3O^+ à 70% et à 80% en poids de HF, on obtient respectivement 21 et 14 molaires. La variation est de 7 moles et la variation de $R_0(F)$ est de 0,9 dans ce domaine. La variation est donc comparable, log 7 = 0,85.

La pente du potentiel de réduction réversible aux ions fluorure des quatre métaux étudiés est linéaire dans le domaine de 70 à 80% en HF. On peut donc considérer que la pente mesurée en fonction de $R_0(F)$ ($-\log a_{F^-}$) est comparable à celle qu'on pourrait tracer en fonction de $-\log [HF_2^-]$, les deux fonctions ayant une variation parallèle.

Dans la région de 70 à 80% en HF nous mesurons les pentes suivantes : thallium, +0,040 V; plomb, +0,010 V; étain, −0,010 V; cadmium, −0,027 V. Si on introduit la concentration de HF_2^- à la place de a_{F^-} dans les équations de Nernst, il est possible de définir les complexes présents dans les mélanges eau–HF concentrés.

Le thallium ne forme pas de complexes fluorés. Il est donc raisonnable que celui-ci ne forme pas de complexe avec HF_2^-. La pente mesurée est la même que pour les solutions peu concentrées en HF. Le comportement particulier du thallium est très bien illustré à la figure 4. Il n'y a pas de changement notable en passant du système eau plus ions complexants aux mélanges de solvants eau–HF plus ions complexants, contrairement aux autres métaux qui eux forment des complexes fluorés à divers degrés.

Le plomb et l'étain forment des complexes contenant deux ions fluorure à faible concentration en HF. Il apparaît raisonnable que ces métaux forment des complexes avec HF_2^- du même ordre qu'avec l'ion fluorure. Les pentes mesurées sont près de zéro. Si on considère les approximations faites précédemment on peut conclure à la formation de complexes selon les équilibres suivants :

[14] $Pb^{2+} + 2HF_2^- \rightleftarrows Pb(HF_2)_2$

[15] $Sn^{2+} + 2HF_2^- \rightleftarrows Sn(HF_2)_2$

Le cadmium forme un complexe contenant trois ions fluorure à faible concentration en HF. Comme pour le plomb et l'étain, on peut considérer la formation d'un complexe contenant trois ions HF_2^- à haute concentration en HF. La pente de −0,027 V nous permet de déduire le complexe $Cd(HF_2)_3^-$.

[16] $Cd^{2+} + 3HF_2^- \rightleftarrows Cd(HF_2)_3^-$

Conclusion

L'analyse du comportement électrochimique des ions métalliques en milieu eau–HF montre que l'énergie de solvatation y est plus faible qu'en solution aqueuse, c'est-à-dire que le potentiel de réduction mesuré par rapport à une référence independante (Fc^+/Fc) du solvant y est moins négatif qu'en milieu aqueux. L'ion thallium qui ne forme que de très faibles complexes avec l'ion fluorure illustre bien ce comportement. Dans certains cas, comme pour l'étain, la formation d'un complexe fluoré fort compense la perte de solvatation dans le domaine des faibles concentrations en HF. Le fait qu'il n'y ait pas de complexes chlorés formés en présence du complexe SnF_2 démontre bien la force de ce dernier.

Le déplacement important du potentiel de réduction de certain ions métalliques aux hautes concentrations en HF a été relié à la présence de l'ion HF_2^- qui devient l'espèce complexante. L'ordre de ces complexes ne peut cependent qu'être proposé car l'activité de l'espèce HF_2^- n'est pas mesurable.

Can. J. Chem. Downloaded from www.nrcresearchpress.com by 91.144.44.67 on 09/07/12
For personal use only.

Remerciements

Les auteurs sont reconnaissants des octrois de recherche du Conseil de recherches en sciences naturelles et en génie du Canada et du Ministère de l'Éducation du Québec qui ont rendu ce travail possible.

1. H. H. HYMAN, M. KILPATRICK et J. J. KATZ. J. Am. Chem. Soc. **79**, 3668 (1957).
2. G. DALLINGA, J. GRAAF and E. L. MARKOR. Recl. Trav. Chim. Pays-Bas, **89**, 1068 (1970).
3. A. VALLIANT, J. DEVYNCK et B. TREMILLON. Anal. Lett. **6**, 1095 (1973).
4. H. MÉNARD, J. P. MASSON, J. DEVYNCK et B. TREMILLON. J. Electroanal. Chem. **63**, 163 (1975).
5. A. VAILLANT, J. DEVYNCK et B. TREMILLON. J. Electroanal. Chem. **57**, 219 (1974).
6. P. A. GIGUÈRE. Chem. Phys. Lett. **41**, 598 (1976).
7. P. A. GIGUÈRE, C. MARTEL et S. TURRELL. Chem. Phys. Lett. **56**, 231 (1978).
8. P. A. GIGUÈRE et S. TURRELL. J. Am. Chem. Soc. **102**, 5473 (1980).
9. R. BEAUDOIN, J. KHORAMI et H. MÉNARD. Can. J. Chem. **65**, 817 (1987).
10. J. DEVYNCK, A. VAILLANT, B. TREMILLON, F. LEBLOND-ROUTHIER et H. MÉNARD. J. Electroanal. Chem. **100**, 885 (1979).
11. R. BEAUDOIN et H. MÉNARD. Can. J. Chem. **65**, 528 (1987).
12. R. BEAUDOIN et H. MÉNARD. Can. J. Chem. **66**, 236 (1988).
13. H. MÉNARD et F. LEBLOND-ROUTHIER. Anal. Chem. **50**, 687 (1978).
14. B. BURROWS et R. JASINSKI. J. Electrochem. Soc. **115**, 348 (1968).
15. G. GRITZNER et J. KUTA. Pure J. Appl. Chem. **56**, 461 (1984).
16. R. BEAUDOIN. Thèse de doctorat, Université de Sherbrooke, Canada (1985).
17. F. LEBLOND-ROUTHIER. Mémoire de maîtrise, Université de Sherbrooke, Sherbrooke, Canada (1978).
18. W. B. SCHAAP, J. A. DAVIS et W. H. NEBERGALL. J. Am. Chem. Soc. **76**, 5226 (1954).
19. D. D. DEFORD et D. N. HUME. J. Am. Chem. Soc. **73**, 5321 (1951).
20. A. M. BOND et R. J. TAYLOR. J. Electroanal. Chem. **28**, 207 (1970).
21. F. M. HALL et S. J. SLATER. AUST. J. CHEM. **21**, 2663 (1968).
22. F. A. COTTON et G. WILKINSON. *Dans* Advanced inorganic chemistry. Interscience Publishers, John Wiley and Sons, New York, NY. 1972.
23. A. M. BOND. J. Phys. Chem. **74**, 331 (1970).

Can. J. Chem. Downloaded from www.nrcresearchpress.com by 91.144.44.67 on 09/07/12
For personal use only.

Frondoside A. A novel triterpene glycoside from the holothurian *Cucumaria frondosa*[1]

MICHEL GIRARD,[2,3] JACQUELINE BÉLANGER,[4] AND JOHN W. APSIMON[2]
Ottawa–Carleton Chemistry Institute, Carleton Campus, Carleton University, Ottawa, Ont., Canada K1S 5B6

FRANÇOIS-XAVIER GARNEAU[2] AND CHRISTIAN HARVEY
Département des sciences fondamentales, Université du Québec à Chicoutimi, Chicoutimi (Québec), Canada G7H 2B1

AND

JEAN-ROBERT BRISSON
Division of Biological Sciences, National Research Council, Sussex Drive, Ottawa, Ont., Canada K1A 0R6

Received April 27, 1989

MICHEL GIRARD, JACQUELINE BÉLANGER, JOHN W. APSIMON, FRANÇOIS-XAVIER GARNEAU, CHRISTIAN HARVEY, and JEAN-ROBERT BRISSON. Can. J. Chem. **68**, 11 (1990).

The isolation and characterization of a novel triterpene glycoside from the sea cucumber *Cucumaria frondosa*, collected from the Gulf of St. Lawrence, are described. Physico-chemical data obtained on the underivatized saponin are presented in support of structure **1** for frondoside A. The structure is characterized by the presence of a branched oligosaccharidic chain composed of five units. The holostane-type aglycone features an endocyclic double bond at position C-7,8 and a β-acetoxy group at C-16.

Key words: triterpene glycoside; *Cucumaria frondosa* saponins; saponins, triterpene from holothurians; holothurian saponins; echinoderm triterpene saponins.

MICHEL GIRARD, JACQUELINE BÉLANGER, JOHN W. APSIMON, FRANÇOIS-XAVIER GARNEAU, CHRISTIAN HARVEY et JEAN-ROBERT BRISSON. Can. J. Chem. **68**, 11 (1990).

On décrit l'isolation et l'élucidation structurale d'un nouveau triterpène-glycoside, obtenu de l'holothurie *Cucumaria frondosa* provenant du golfe du St-Laurent. En se basant sur les données physico-chimiques du produit intact, on propose la structure **1** pour le frondoside A. Le composé est caractérisé par la présence d'une chaîne oligosaccharidique branchée, de cinq unités. L'aglycone de type holostane possède une insaturation en position C-7,8 et un groupement acétoxy-β en C-16.

Mots clés : triterpènes, glycosides; *Cucumaria frondosa*, saponines; saponines triterpénique des holothuries; saponines des holothuries; saponines des échinodermes.

[Traduit par la revue]

Can. J. Chem. Downloaded from www.nrcresearchpress.com by 91.144.44.67 on 09/07/12
For personal use only.

Introduction

Sea cucumber saponins, commonly referred to as holothurins, are triterpene glycosides of the lanosterol type, with a distinctive D-ring fused γ-lactone (1). Traditionally, structural studies of these saponins have involved degradation into the various components and formation of derivatives, hence requiring large amounts of material and, in many cases, leading to the formation of artifacts. The development in the last two decades of high resolution NMR techniques, and more specifically ^{13}C NMR spectroscopy, alleviates the need for large quantities of material, and also permits the first studies of intact saponins. The advent of modern high-field two-dimensional (2D) NMR techniques now provides an extremely useful tool for the characterization of complex molecules since these techniques allow for the unambiguous assignment of most signals observed in conventional unidimensional ^{1}H and ^{13}C NMR spectra. Findlay *et al.* (2, 3) have recently demonstrated the usefulness of these techniques by deducing the complete structure of several starfish saponins. In our continuing investigation of marine species of the Atlantic Coast of Canada, we have isolated a novel triterpene glycoside from the holothurian *Cucumaria frondosa* that we have successfully characterized using several of these NMR techniques, and without the need to derivatize the product.

[1]Taken in part from the M.Sc. Thesis of M. Girard (1981) and from the Ph.D. Thesis of J. Bélanger (1984), Carleton University.

[2]Authors to whom correspondence may be addressed.

[3]Present address: Bureau of Drug Research, Health and Welfare Canada, Tunney's Pasture, Ottawa, Ont., K1A 0L2.

[4]Present address: Centre de recherches alimentaires de St-Hyacinthe (CRASH), St-Hyacinthe, Québec.

Results and discussion

The brown-colored sea cucumbers were collected off the north coast of the Gulf of St. Lawrence (near Sept-Isles and Port-Cartier, Québec). Frondoside A (**1**) was one of the major constituents separated from the 70% aqueous ethanol extract, and purified by the previously described chromatographic methods (4).

Frondoside A was obtained as a colorless crystalline solid, mp 234–236°C (dec.), $[\alpha]_D$ −13° (H_2O), with no UV absorption maximum above 210 nm. The infrared spectrum (KBr) showed strong hydroxyl absorption at 3400 cm^{-1} (broad) as well as a carbonyl absorption band at 1750 cm^{-1} (broad) indicating the presence of the characteristic γ-lactone and an acetate group. The two bands at 1230 and 825 cm^{-1} suggested the presence of a sulfate moiety; this observation was substantiated by a positive rhodizonate test (5). The location of the sulfate group on C-4 of the xylose unit directly attached to the aglycone was determined by spectroscopic methods (*vide infra*).

Aglycone portion

The assignments for the NMR signals associated with the aglycone moiety (Table 1) showed a close similarity to those reported for cucumariogenin acetate (**2**) (6). The ^{13}C NMR spectrum (Fig. 1) featured signals at 120.41 and 145.80 ppm in the downfield region, indicative of the presence of an endocyclic double bond at the 7,8 position, and two low-field

Can. J. Chem. Downloaded from www.nrcresearchpress.com by 91.144.44.67 on 09/07/12
For personal use only.

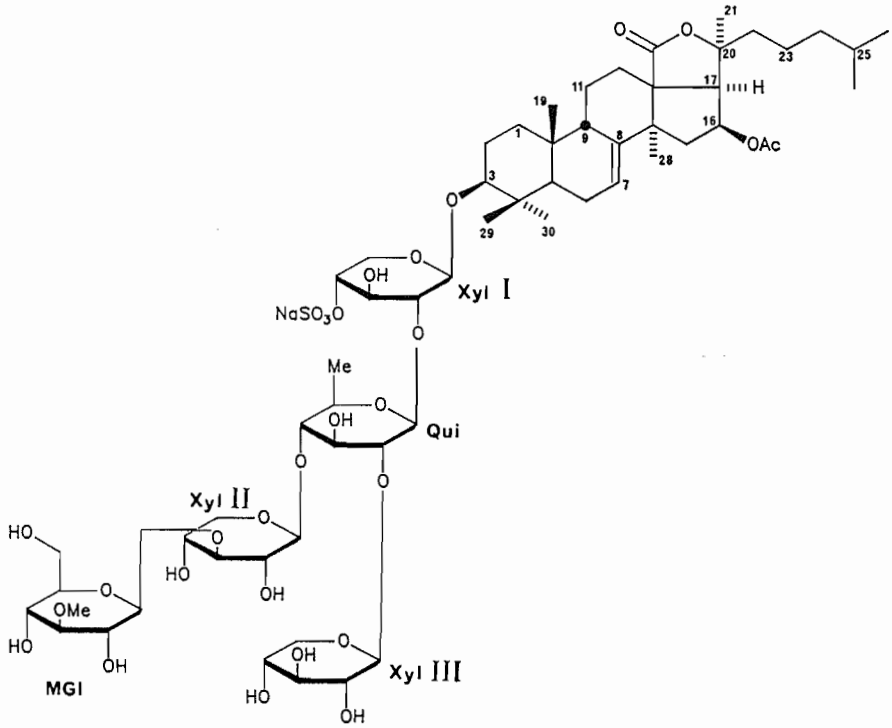

1 (FRONDOSIDE A)

TABLE 1. NMR data for the aglycone of frondoside A in C_5D_5N:D_2O/5:1

Carbon	^{13}C NMR (ppm)	Proton	^1H NMR (ppm)
1	36.00	1α, 1β	1.42 m; 1.42 m
2	26.87	2α, 2β	2.05 m; 1.89 m
3	89.15	3α	3.327 dd, J = 4.0 and 11.4 Hz
4	39.50		
5	47.96	5α	1.02 m
6	23.28	6α, 6β	2.05 m; 2.05 m
7	120.41	7	5.736 m
8	145.80		
9	47.21	9β	3.423 bd, J = 14 Hz
10	35.50		
11	22.60	11α, 11β	1.84 m; 1.60 m
12	31.40	12α, 12β	2.23 m; 2.23 m
13	59.48		
14	47.47		
15	43.63	15α	2.672 dd, J = 7.4 and −12.2 Hz
		15β	1.731 dd, J = 8.6 and −12.2 Hz
16	75.38	16α	5.963 m, J = 7.4, 8.6, 9.0 Hz
17	54.51	17α	2.792 d, J = 9.0 Hz
18	180.58		
19	24.00	19	1.206 s, 3H
20	85.90		
21	28.36	21	1.659 s, 3H
22	39.13	22, 22′	2.370 m; 1.85 m
23	22.76	23, 23′	1.37 m; 1.26 m
24	39.63	24, 24′	1.20 m; 1.06 m
25	28.12	25	1.513 m
26	22.42	26	0.912 d, 3H, J = 6.5 Hz
27	22.92	27	0.905 d, 3H, J = 6.5 Hz
28	32.36	28	1.282 s, 3H
29	17.47	29	1.128 s, 3H
30	28.77	30	1.290 s, 3H
31	171.00		
32	21.46	32	2.129 s, 3H

resonances at 180.58 and 171.00 ppm, assigned to the γ-lactone carbonyl and acetoxy carbonyl carbons respectively. The 500-MHz ^1H NMR spectrum (pyridine-d_5:D_2O/5:1) showed a pattern characteristic of most holothurins in the high-field region, and which featured many overlapping signals. In this instance, the use of the COSY experiment allowed the establishment of the connectivities within the framework and thus permitted the assignments of the chemical shifts for the overlapping proton signals.

Assignments were completed using two-dimensional nuclear Overhauser effect (2D-NOE) (Fig. 2a–i). Such an effect only occurs between resonances whose protons are in close proximity to each other and is dependent on interproton distance to the inverse sixth power. Then, the ^{13}C resonances were assigned by a ^{13}C–^1H correlation analysis. Using this information it was possible to complete the elucidation of the aglycone structure.

Of particular interest, the C-9Hβ configuration was confirmed by (a) the presence of a broad doublet at 3.423 ppm, the downfield shift of which had been previously attributed to the anisotropic effect of the γ-lactone carbonyl (7), and (b) a strong NOE between C-9Hβ and C-19H_3 (Fig. 2e), due to the close proximity of these protons.

The presence of an acetoxy group at C-16 was deduced from

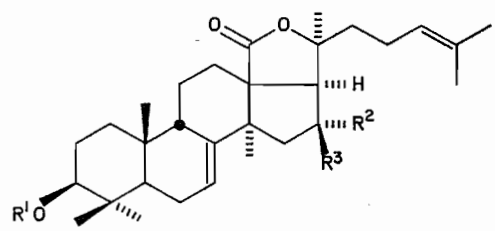

2 R^1 = Ac; R^2 = H; R^3 = OAc

3 R^1, R^3 = H; R^2 = OAc

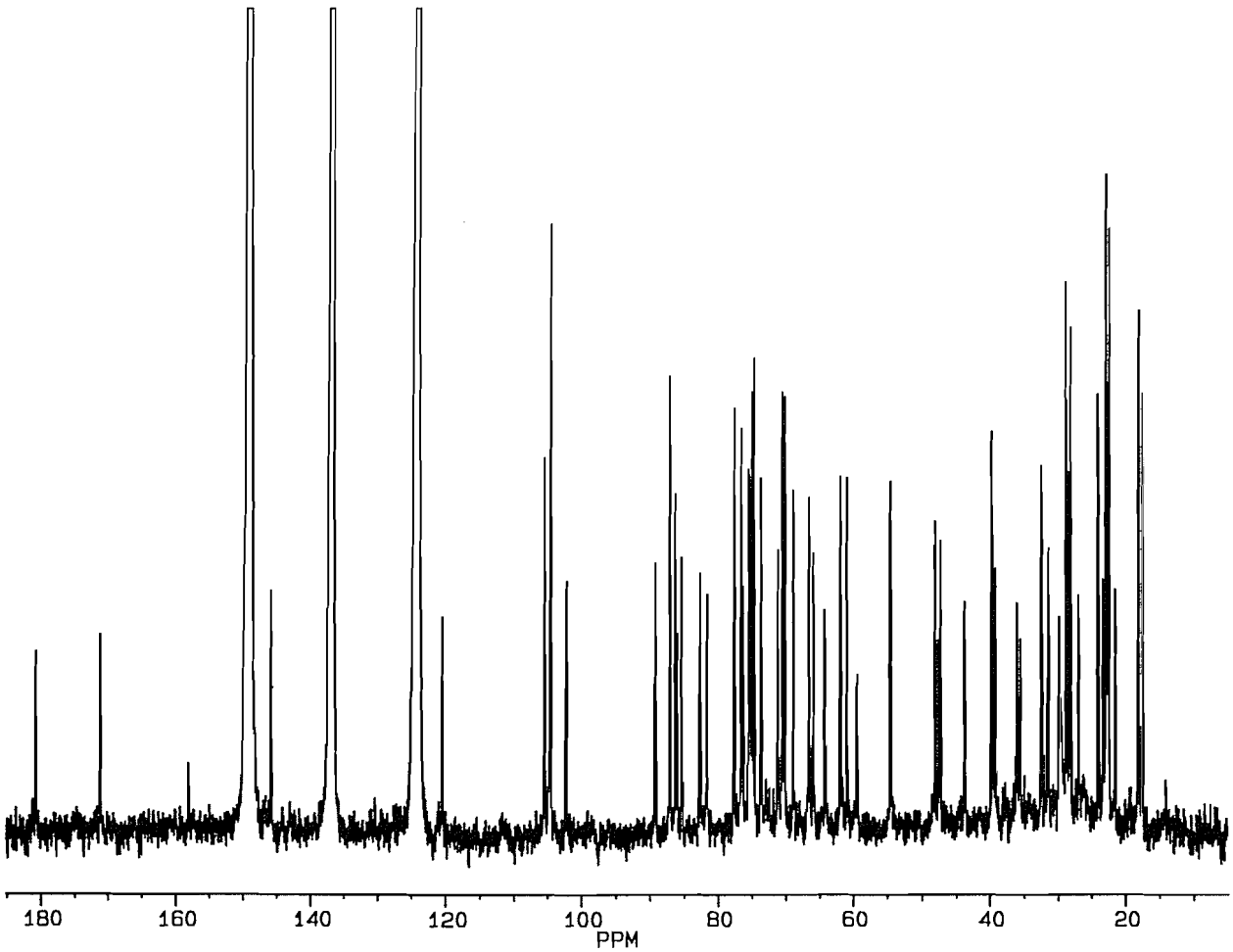

FIG. 1. ^{13}C NMR spectrum of frondoside A in C_5D_5N:D_2O/5:1.

the chemical shift of the C-16H signal (5.963 ppm) (6, 8), which showed coupling to signals at 2.792 (C-17H), 2.672 (C-15Hα), and 1.731 (C-15Hβ) ppm in the 2D-COSY spectrum. The assignments for the two C-15 protons were made here based on a clearly visible long-range coupling (W-coupling) of the C-28H_3 resonance to the C-15Hβ resonance, and its absence at C-15Hα since only the C-15β proton is geometrically well positioned for the known W coupling path (9, 10).

The β configuration of the C-16 acetoxy group was deduced primarily from the 2D-NOE trace of the C-16H signal (Fig. 2f) and the C-17H signal (Fig. 2g). Enhancements were detected between the C-16H resonance (5.963 ppm) and the C-17Hα, the C-15Hα, and the C-28H_3 resonances. An NOE between the C-17Hα and the C-28H_3 resonances was also observed, indicating that the latter group is on the α face of the molecule. Thus, since all the enhancements for C-16H arose for protons that are α, C-16H must also be assigned as α. Coupling constant calculations (11) for the C-16 proton with C-17Hα and the C-15 protons, based on a distorted envelope conformation for the D-ring, again supported the β configuration for the C-16 acetoxy group (Table 2). Therefore, it appears that the presence of the pseudo-equatorial (β) C-16 substituent induces larger downfield shifts on the pseudo-equatorial C-15α and C-17α vicinal protons, a situation analogous to the reported effect of substituents in cyclohexanoid systems (9).

In a recent report on the hydrolysis products from *C. frondosa*, Findlay and Daljeet (8) proposed the epimeric C-16α acetoxy structure for frondogenin (**3**) while reporting spectroscopic data similar to ours. Their assignment of the C-16 OAc configuration was based solely on a presumed, and as yet unconfirmed, deshielding effect on C-17Hα and C-15Hβ, due to the presence of a *syn* substituent, in contrast to our observations supported by the NOE results.

The α configuration of the C-21H_3 group was also confirmed by the presence of an NOE between the C-21H_3 singlet and the C-12 proton resonances (Fig. 2i) and an NOE between the C-21H_3 and C-17Hα resonances (Fig. 2g), indicating the close proximity of C-21H_3 to the C-12 and C-17Hα protons.

Oligosaccharide chain

The constitution of the oligosaccharide chain was studied by gas-chromatographic (GC) analysis of the trimethylsilylated methyl glycosides obtained from mild anhydrous acid methanolysis. Three units of xylose and one unit each of 3-*O*-methyl glucose and quinovose (6-deoxyglucose) were detected while glucose, a sugar usually present in holothurins containing more than two sugar units, was not found. This unusual situation has also been observed in neothyonidioside, the major holothurin from *Neothyonidium magnum* (12).

The sugar sequence and the position of the interglycosidic linkages were determined mainly using a combination of COSY, relay COSY, ^{13}C–^{1}H correlation, and 2D-NOE experiments, and confirmed by fast-atom bombardment (FAB) mass spectrometry. The chemical shift assignments for the proton

Can. J. Chem. Downloaded from www.nrcresearchpress.com by 91.144.44.67 on 09/07/12
For personal use only.

Can. J. Chem. Downloaded from www.nrcresearchpress.com by 91.144.44.67 on 09/07/12
For personal use only.

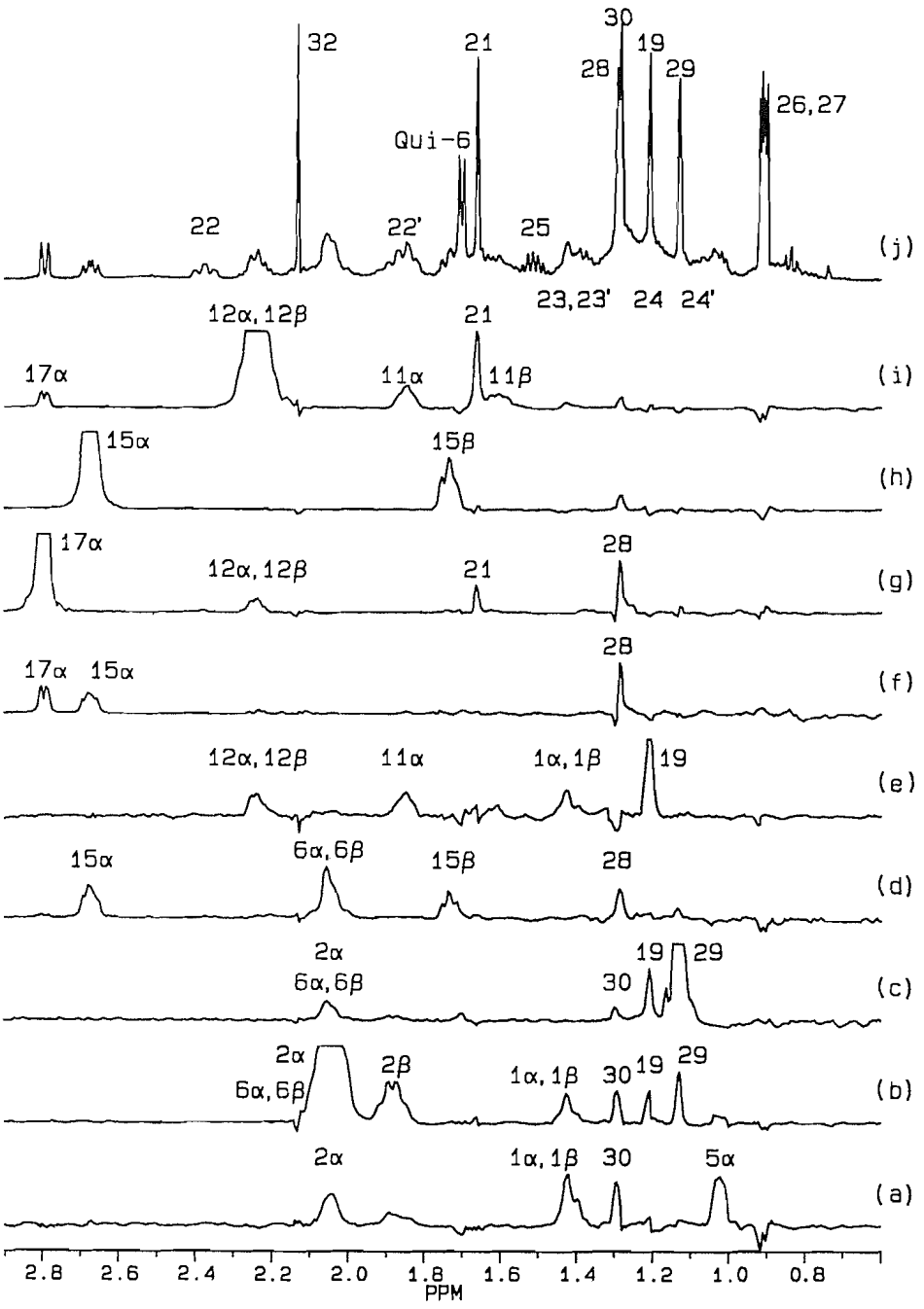

FIG. 2. High-field region of the ^{1}H NMR spectrum and cross sections of the 2D-NOE contour map for frondoside A in C_5D_5N:D_2O/5:1. Cross sections through (a) 3Hα; (b) 2Hα, 6Hα, 6Hβ; (c) 29-CH_3; (d) 7H; (e) 9Hβ; (f) 16Hα; (g) 17Hα; (h) 15Hα; (i) 12Hα, 12Hβ; and (j) normal spectrum.

TABLE 2. Experimental and calculated[a] vicinal proton coupling constants for the four-proton system 15H_2-16H-17H of the D ring of frondoside A

H–H	J_{exp}	J_{calc}	Dihedral angle (deg)
15α, 16α	7.4	8.0	32
15β, 16α	8.6	9.0	155
16α, 17α	9.0	9.2	345
16β, 17α		1.5	110
15β, 16β		6.0	32
15α, 16β		1.2	270

[a]Based on a distorted envelope conformation. For calculations see ref. 8.

and carbon signals are summarized in Table 3 and the spin simulation of the sugar chain is shown in Fig. 3. Using the data from the ^{13}C–^{1}H correlation experiment, it was possible to determine the position of the interglycosidic linkages by comparison of the carbon chemical shifts observed with those of the corresponding methyl glycopyranoside (13) and taking into account the downfield shift resulting from glycosidation (Table 3).

The presence of five sugar units was confirmed in the ^{1}H NMR spectrum where the signals for the five anomeric protons appeared as doublets in the 4.8–5.4 ppm region. The large coupling constants observed for these signals and the intra-residue NOE between their respective C-1H, C-3H, and C-5H resonances (Fig. 4) confirmed the β configuration.

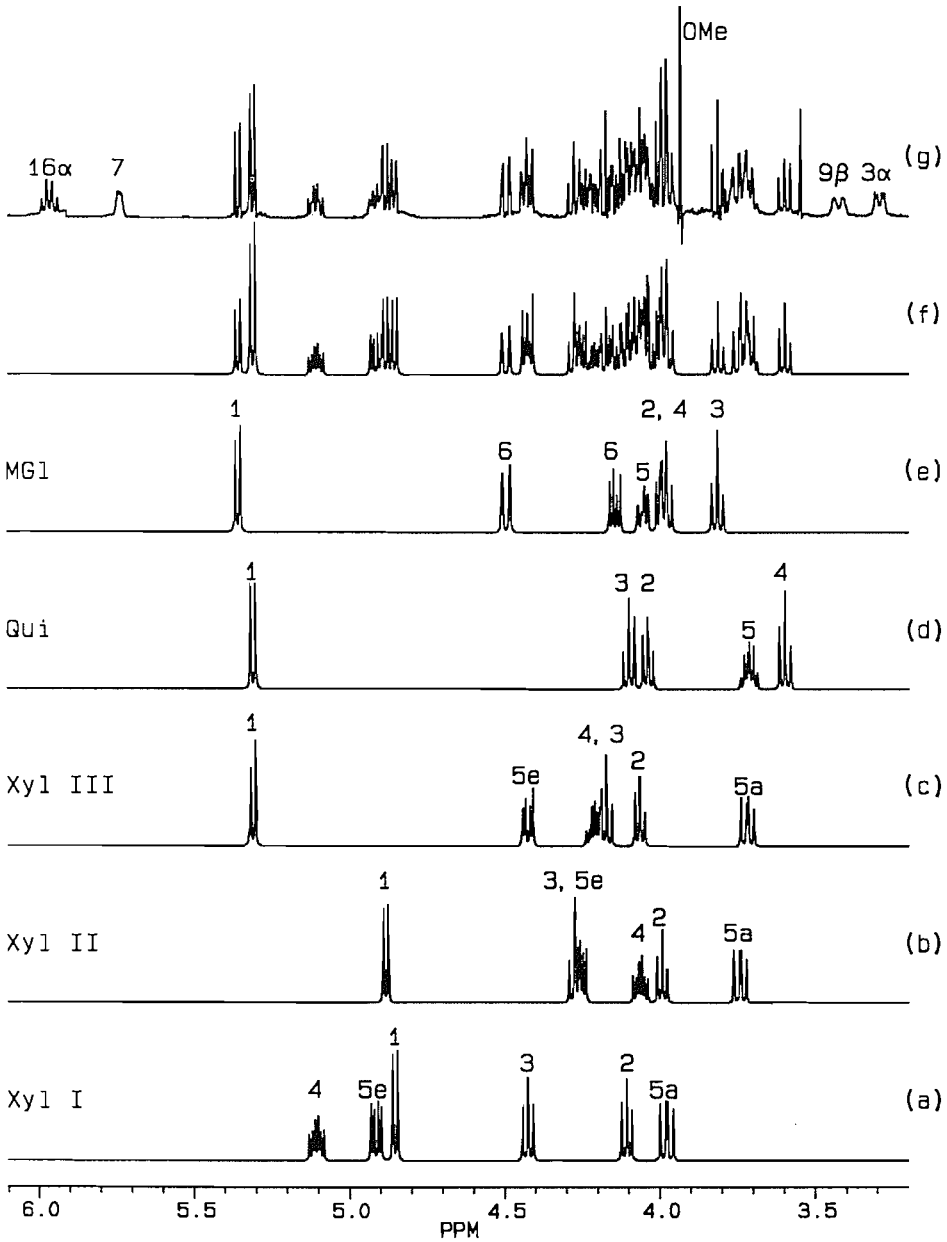

FIG. 3. Downfield region of the ^{1}H NMR spectrum with HOD peak removed, and spin simulation of the pentasaccharide moiety of frondoside A in C_5D_5N:D_2O/5:1.

Xylose I must be linked to the aglycone C-3 due to the strong NOE observed between C-1H of xylose I and the C-3α proton of the aglycone (Fig. 4a). The interglycosidic position of attachment of Xyl I was assigned at C-2 based on the significant downfield shift (7.0 ppm) observed for this carbon resonance. Another important downfield shift (5.4 ppm) was observed at C-4 and was attributed to the presence of a sulfate group at that position. This shift could not be the consequence of a glycosidic linkage since no inter-residue NOE involving C-4H of Xyl I was observed. The FAB mass spectrum also showed evidence of the presence of the sulfate group in the xylose unit directly attached to the aglycone (*vide infra*).

The 3-*O*-methyl glucose (MG1) and one xylose (Xyl III) were terminal units as suggested by the absence of any ^{13}C glycosidation shifts for these sugars. An enhancement between C-1H of MG1 and C-3H of Xyl II (Fig. 4b), as well as a large glycosidation shift on C-3 of Xyl II (8.2 ppm), confirmed that MG1 was β1–3 linked to Xyl II. Similarly, the presence of an inter-residue NOE between C-1H of Xyl II and C-4H of Qui (Fig. 4c), the NOE between the C-6H$_3$ resonance of Qui and C-1H of Xyl II (Fig. 4d), and the downfield shift of C-4 of Qui (8.0 ppm), were indicative that Xyl II was β1–4 linked to Qui. Hence, by deduction, the downfield shift of the C-2 of Qui (6.0 ppm) further suggested that the terminal xylose unit must be attached at this position, and therefore that the quinovose unit is linked at C-2 on the xylose (Xyl I) attached to the aglycone. The 2D-NOE trace for the coincidental doublets (5.308 ppm), corresponding to the anomeric proton signals of Xyl III and Qui (Fig. 4e), showed enhancements on C-2H of Xyl I and C-2H of Qui consistent with the above deductions. Hence, the oligosaccharide moiety of frondoside A consists of a pentasaccharide having the following structure:

Can. J. Chem. Downloaded from www.nrcresearchpress.com by 91.144.44.67 on 09/07/12
For personal use only.

Can. J. Chem. Downloaded from www.nrcresearchpress.com by 91.144.44.67 on 09/07/12
For personal use only.

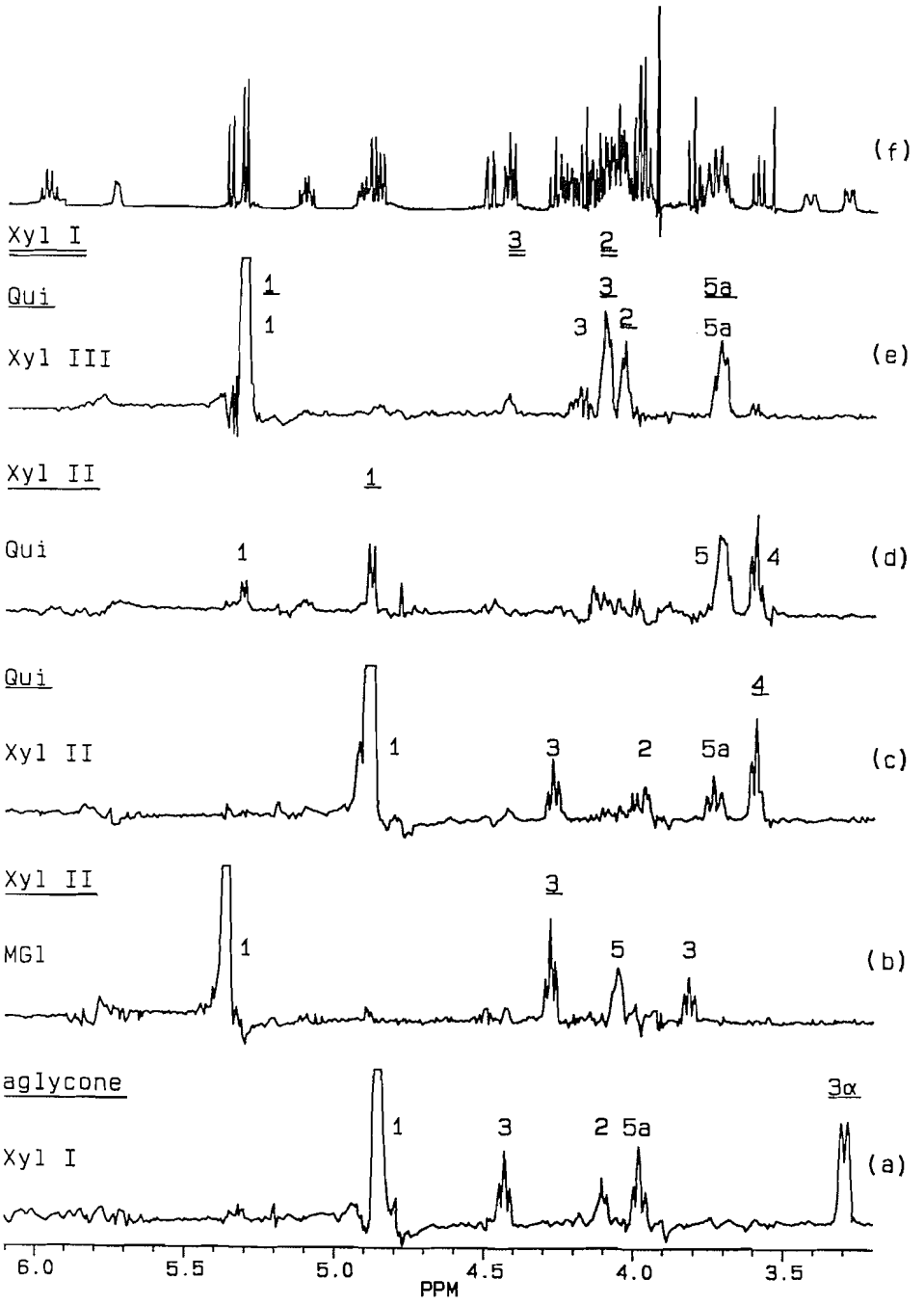

FIG. 4. Downfield region of the ^{1}H NMR spectrum and cross sections of the 2D-NOE contour map for frondoside A in C_5D_5N:D_2O/5:1. Cross section through (a) H-1 of xylose I; (b) H-1 of 3-*O*-methyl glucose; (c) H-1 of xylose II; (d) H-6 of quinovose; (e) H-1 of xylose III and H-1 of quinovose; and (f) normal spectrum with the HOD peak removed.

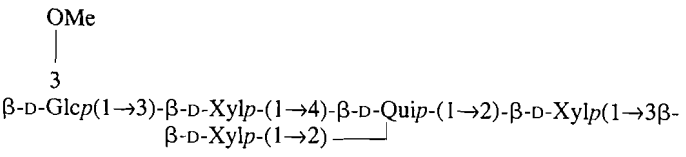

The FAB mass spectra, obtained in the positive and negative ion modes (Fig. 5), are in good agreement with the assigned structure. Molecular weight information was obtained from peaks at *m/z* 1351 $[M_K + H]^+$ and *m/z* 1311 $[A]^-$ in the positive and negative modes respectively.

Therefore, based on the above results, frondoside A possesses structure **1**, that is, 3β-*O*-{3-*O*-methyl-β-D-glucopyranosyl (1→3)-*O*-β-D-xylopyranosyl (1→4)-*O*-[β-D-xylopyranosyl (1→2)]-*O*-β-D-quinovopyranosyl (1→2)-*O*-β-D-4-sulfonato-xylopyranosyl}-16β-acetoxy-holost-7-ene, sodium (or potassium) salt. This is the first example of a naturally occurring holothurin containing an odd number of sugar units (five), and it is the first complete structure reported for a holothurin from the Cucumaridae family.

Experimental

All NMR measurements were performed on a Bruker AM500 spectrometer at ambient temperature with 50 mg of frondoside A dissolved in 0.5 mL of pyridine-d_5/D_2O (5:1) and tetramethylsilane

TABLE 3. NMR data for the oligosaccharide moiety of frondoside A in C_5D_5N:D_2O/5:1

Unit	Atom no.	^1H NMR, δ_H (ppm)	$J_{H,H}$ (Hz)	^{13}C NMR, δ_C (ppm)	$(\delta\delta_C)^a$ (ppm)
Xyl I	1	4.853	7.6	104.48	
	2	4.107	7.6, 8.6	81.58	7.0
	3	4.425	8.6, 8.9	75.31	−2.8
	4	5.106	8.9, 9.4, 4.9	76.30	5.4
	5	3.978	−11.7, 9.4	64.24	−2.8
		4.914	−11.7, 4.9		
Qui	1	5.309	7.9	102.17	
	2	4.038	7.9, 9.0	82.62	6.0
	3	4.096	9.0, 9.0	75.16	−2.8
	4	3.597	9.0, 9.0	85.30	8.0
	5	3.711	9.0, 6.1	71.18	−2.6
	6	1.701	6.1	18.00	−0.5
Xyl II	1	4.881	7.6	104.71	
	2	3.992	7.6, 8.6	73.59	−1.0
	3	4.272	8.6, 8.9	86.22	8.2
	4	4.062	8.9, 9.4, 4.9	68.92	−2.0
	5	3.741	−11.7, 9.4	65.97	−0.5
		4.252	−11.7, 4.9		
MGl	1	5.356	8.0	104.48	
	2	3.990	8.0, 9.0	74.67	0.1
	3	3.812	9.0, 9.5	87.04	−1.1
	4	3.978	9.5, 10.0	70.57	−0.1
	5	4.051	10.0, 6.0, 1.6	77.57	−0.4
	6	4.142	−12.3, 6.0	61.90	−0.5
		4.493	−12.3, 1.6		
	OMe	3.931		60.94	1.0
Xyl III	1	5.308	7.6	105.36	
	2	4.064	7.6, 8.6	74.92	0.3
	3	4.171	8.6, 8.9	76.56	−1.6
	4	4.211	8.9, 9.4, 4.9	70.15	−0.7
	5	3.717	−11.7, 9.4	66.56	−0.4
		4.423	−11.7, 4.9		

[a]Difference from corresponding methyl glycopyranoside (12).

as the internal reference. Proton assignments were made using homonuclear shift correlation (COSY) and relay COSY as previously described (2, 3). The two-dimensional nuclear Overhauser experiment (2D-NOE) was done according to Bodenhausen *et al.* (14). The ^{13}C–^1H correlation was performed using a least-squares analysis of the ^{13}C intensity as a function of four proton evolution times of 0.16, 1.0, 2.4, and 3.2 ms (15). Spectral simulations with a linewidth of 1 Hz were done using Bruker's program PANIC.

Melting points were determined on a Fisher–Johns hot stage melting point apparatus or on a Buchi SMP-20 using capillary tubes, and are uncorrected.

Infrared spectra were recorded on a Perkin–Elmer 237-B grating spectrophotometer. Ultraviolet spectra were recorded on a Perkin–Elmer Coleman 124 "double beam" UV–visible spectrophotometer in ethanol solutions. Optical rotations were measured on a Perkin–Elmer 141 polarimeter using a sodium lamp operating at 589 nm. Fast atom bombardment mass spectra (FAB-MS) were recorded on a glycerol support in the positive ion mode on a VG Analytical 7070E instrument.

Gas–liquid chromatography experiments were performed on a Hewlett–Packard 5730-A gas chromatograph equipped with a flame ionization detector. Stainless steel columns (1.8 m long) packed with 3% OV-17 support were used. Thin-layer chromatographic analyses were carried out on precoated silica gel GF-254 (Merck) and reverse-phase KC-18 (Whatman) glass plates. Glycoside fractions were developed in the solvent mixtures $CHCl_3$–MeOH–H_2O: 60-15-2, 60-20-2.5, and 60-25-4. Detection was accomplished by spraying a

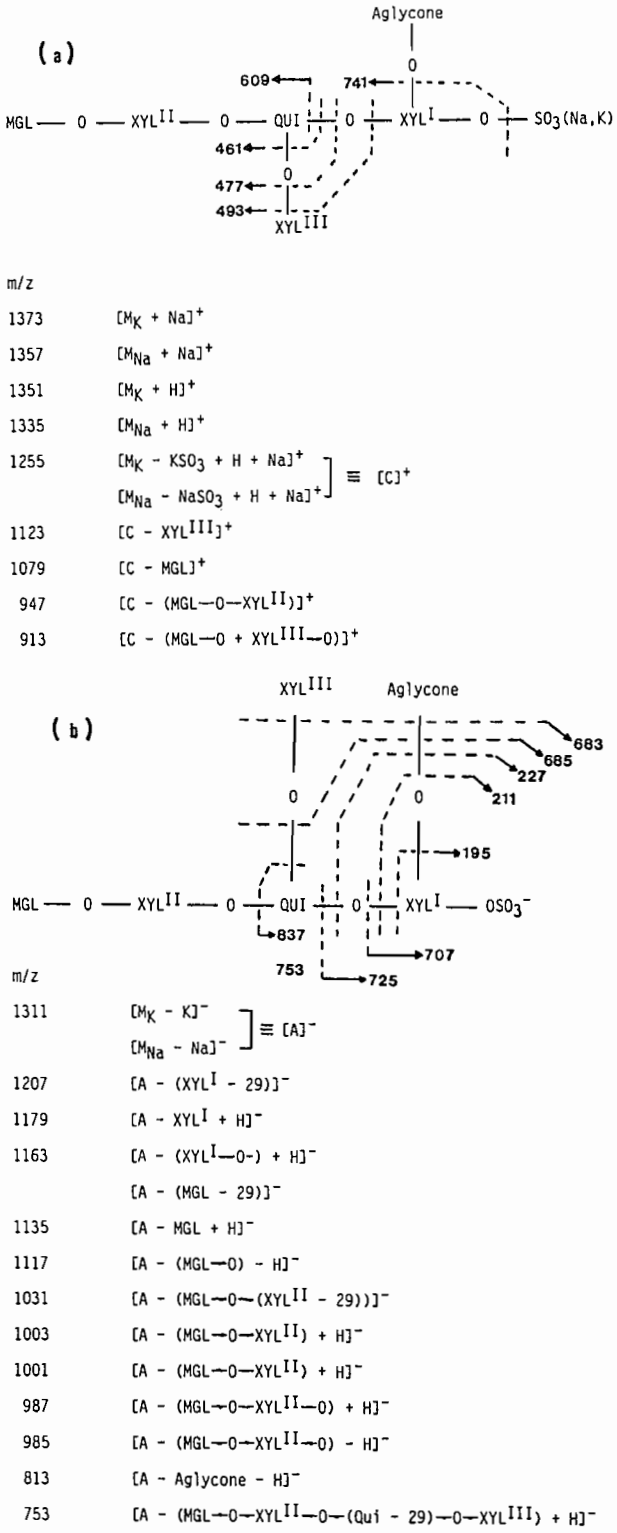

FIG. 5. (a) FAB^+ fragmentation and (b) FAB^- fragmentation of frondoside A.

1% ceric ammonium nitrate in 50% sulfuric acid solution followed by heating at 100–120°C. Low pressure column chromatography separations were carried out on silica gel 60H (Merck), or Whatman silica gel LPS-1 (13–24 μm) and LPS-2 (37–53 μm). Columns were prepared as a slurry in $CHCl_3$. HPLC separations were performed on a column (1 × 25 cm) of Spherisorb ODS, 10 μm (C18), using a Waters-244 chromatograph linked to a Kratos SF-770 UV detector.

All solvents were glass-distilled before use.

Can. J. Chem. Downloaded from www.nrcresearchpress.com by 91.144.44.67 on 09/07/12
For personal use only.

Can. J. Chem. Downloaded from www.nrcresearchpress.com by 91.144.44.67 on 09/07/12
For personal use only.

Extraction and purification of frondoside A (1)

Fifty-one specimens of the sea cucumber *Cucumaria frondosa* were collected at the Iles de Mai, Port-Cartier, Québec, Canada and at the Matamek Research Station of the Woods Hole Oceanographic Institution, Québec, Canada.

The body walls were treated with 1.5 L of acetone (residue after evaporation: 21 g) and ground to a fine powder (0.78 kg; 15.3 g/specimen). The powder was successively extracted several times with benzene and methanol to remove the residual pigments and lipids. The 70% ethanol extracts were combined and evaporated under reduced pressure to give the crude frondosides (19.3 g). Part of this extract (4.6 g) was then subjected to an Amberlite XAD-2 resin (Mallinckrodt, 20–50 mesh) column chromatography. This gave a salt-free, partially purified, glycoside mixture (350 mg). Low pressure column chromatography (silica gel LPS-2, 199 g; 4 × 30 cm; bed volume: 390 mL; elution at 12 psi (1 psi = 6.9 kPa); flow rate 6 mL/min; eluting solvents: $CHCl_3$–MeOH–H_2O, 60-15-2, 60-20-2.5, and 60-25-4) of the mixture furnished **1** (32 mg) along with other constituents.

Frondoside A (**1**) ($C_{60}H_{95}O_{29}SNa$), mp 234–236°C; $[\alpha]_D$ −13° (*c* 26, H_2O); UV λ_{max} (H_2O): transparent above 210 nm; IR ν_{max} (KBr): 3400 (OH, br), 1750 (γ-lactone), 1230 (S=O), 825 (C—O—S); FAB-MS: see Fig. 5; ^1H and ^{13}C NMR (pyridine-d_5:D_2O/5:1): see Tables 1 and 3; potassium rhodizonate test: positive (yellow coloration); CD (*c* = 0.18, H_2O): $[\Theta]_{303}$ 0, $[\Theta]_{247}$ −4293 (neg. max.), $[\Theta]_{238}$ 0, $[\Theta]_{224}$ +5075 (pos. max.), $[\Theta]_{213}$ 0, $[\Theta]_{211}$ −1168!

Methanolysis of frondoside A (1)

Carbohydrate constituents

A solution of frondoside A in anhydrous 1% HCl–MeOH was refluxed for 5 h. After cooling, the solution was evaporated to dryness under reduced pressure to afford a mixture of methyl glycosides quantitatively analysed by GC of the TMS derivatives.

The retention times were identical to those of the authentic methyl-D-glycosides of the following sugars: xylose (14.5), quinovose (16.5), and 3-*O*-methyl glucose (18.3, 19.5). The relative quantities were determined to be 3:1:1 respectively (peak area/mass of TMS derivatives).

Desulfatation of frondoside A

A solution of frondoside A (2 mg in 1 mL of 0.04 M anhydrous HCl in methanol) was stirred at room temperature for 20 min. The solution was then neutralized with silver carbonate, filtered on a small pad of Celite, and evaporated under reduced pressure. The desulfated glycoside was separated from the accompanying salts on a reverse-phase Sep-Pak (Waters) by elution with water (1 mL), 50% aqueous methanol (2 mL), and methanol (2 mL). The FAB-MS of the mixture showed fragments corresponding to the desulfated glycoside at *m/z* 1255 $[M + Na]^+$ and the deacetylated analogue at *m/z* 1213 $[M + Na]^+$.

Acknowledgements

We wish to acknowledge the financial help of the Natural Sciences and Engineering Research Council of Canada (J.W.A.), the Gouvernement du Québec via the F.C.A.C. program (F.X.G.), the Québec–Ontario exchange projects (J.W.A., F.X.G.), and the Fondation de l'Université du Québec à Chicoutimi (F.X.G.).

We are grateful to C. Kazakoff, University of Ottawa, and B. Lau, Health and Welfare Canada, for the FAB-MS spectra.

One of us (J.B.) wishes to thank Prof. L. J. Goad, University of Liverpool, for his kind hospitality during a sojourn in his laboratory in September 1982, at which time FAB-MS experiments were done.

We would like to thank the Woods Hole Oceanographic Institution for the use of their facilities at Matamek, Sept-Isles, Québec.

1. D. J. Burnell and J. W. ApSimon. *In* Marine natural products. Chemical and biological perspectives. Vol. V. *Edited by* P. J. Scheuer. Academic Press, New York, NY. 1983. Chap. VI. pp. 287–389.
2. J. A. Findlay, M. Jaseja, D. J. Burnell, and J. R. Brisson. Can. J. Chem. **65**, 1384 (1987).
3. J. A. Findlay, M. Jaseja, and J. R. Brisson. Can. J. Chem. **65**, 2605 (1987).
4. F.-X. Garneau, J.-L. Simard, O. Harvey, J. W. ApSimon, and M. Girard. Can. J. Chem. **61**, 1465 (1983).
5. I. Kitagawa, M. Kobayashi, and T. Sugarawa. Chem. Pharm. Bull. **26**, 1852 (1978).
6. S. S. Afiyatullov, V. A. Stonik, A. I. Kalinovski, and G. B. Elyakov. Khim. Prir. Soedin. (1), 59 (1983).
7. I. Kitagawa, M. Kobayashi, T. Inamoto, T. Yasuzawa, Y. Kyogoku, and M. Kido. Chem. Pharm. Bull. **29**, 1189 (1981).
8. J. A. Findlay and A. Daljeet. J. Nat. Prod. **47**, 320 (1984).
9. H.-J. Schneider, U. Buchheit, N. Becker, G. Schmidt, and U. Siehl. J. Am. Chem. Soc. **107**, 7027 (1985).
10. N. S. Bhacca and D. H. Williams. Applications of NMR spectroscopy in organic chemistry. Holden-Day, San Francisco, CA. 1964. p. 108ff.
11. C. A. G. Haasnoot, F. A. A. M. de Leeuw, and C. Altona. Tetrahedron, **36**, 2783 (1980).
12. M. BedoyaZurita, A. Ahond, C. Poupat, P. Potier, and J. L. Menou. J. Nat. Prod. **49**, 809 (1986).
13. I. Kitagawa, T. Nishino, M. Kobayoshi, and Y. Kyogoku. Chem. Pharm. Bull. **29**, 1951 (1981).
14. G. Bodenhausen, H. Kogler, and R. R. Ernst. J. Magn. Reson. **58**, 370 (1984).
15. G. A. Pearson. J. Magn. Reson. **64**, 487 (1985).

Isolation and structure of sporidesmolide V from cultures of *Pithomyces chartarum*[1]

H. A. GILLIS,[2] D. W. RUSSELL,[3] A. TAYLOR,[4] AND J. A. WALTER

National Research Council of Canada, Atlantic Research Laboratory, Halifax, N.S., Canada B3H 3Z1

Received June 16, 1989

H. A. GILLIS, D. W. RUSSELL, A. TAYLOR, and J. A. WALTER. Can. J. Chem. **68**, 19 (1990).

The total sporidesmolide fraction from cultures of *Pithomyces chartarum* contains at least five cyclodepsipeptides. Four of these are known compounds but the fifth, cyclo-2-oxyisovaleryl-D-alloisoleucyl-D-leucyl-2-oxyisocaproyl-L-valyl-L-*N*-methylleucyl, appears to be new. Its isolation, physical properties, and structure determination are reported.

Key words: *Pithomyces chartarum*, sporidesmolide II, sporidesmolide V, sporidesmolic acid D.

H. A. GILLIS, D. W. RUSSELL, A. TAYLOR et J. A. WALTER. Can. J. Chem. **68**, 19 (1990).

La fraction totale de sporidesmolide provenant de cultures de *Pithomyces chartarum* contient au moins cinq cyclodepsipeptides. Quatre d'entre eux sont des composés connus; toutefois, le cinquième, le cyclo-2-oxyisovaléryl-D-alloisoleucyl-D-leucyl-2-oxyisocaproyl-L-valyl-L-*N*-méthyl-leucyl, semble être nouveau. On rapporte son isolement, ses propriétés physiques ainsi que la détermination de sa structure.

Mots clés : *Pithomyces chartarum*, sporidesmolide II, sporidesmolide V, acide sporidesmolic D.

[Traduit par la revue]

Can. J. Chem. Downloaded from www.nrcresearchpress.com by 186.148.149.217 on 09/07/12
For personal use only.

The production of sporidesmolides I (1), II (2), and III (1) by *Pithomyces chartarum* has been reported. Examination of the total sporidesmolide fraction (3) of isolates of this fungus from Brazil, Colombia, Texas, and Nova Scotia has revealed the presence of two more congeners. One of these proved to be the known sporidesmolide IV (4), while the other, named sporidesmolide V, appears to be new.

Sporidesmolide V was purified by repetitive reversed phase partition chromatography and finally by vacuum sublimation. Elemental analysis and high resolution mass spectroscopy indicated that its molecular formula was $C_{35}H_{62}N_4O_8$, confirmed by ^1H and ^{13}C NMR data. The compound is therefore a higher homologue of sporidesmolide II (ref. 2, $C_{34}H_{60}N_4O_8$), here isolated for the first time from cultures of *Pithomyces chartarum* unenriched with isoleucine. It was possible to separate the synthetic sporidesmolides II (5) with residues of D-alloisoleucine and D-isoleucine and thus show that this residue in the natural product was D-alloisoleucine. Acid hydrolysis of sporidesmolide V gave one mole each of L-valine, D-leucine, D-alloisoleucine, and L-*N*-methylleucine. Mild alkaline hydrolysis gave two sporidesmolic acids (1), *m/z* 344 and *m/z* 358. Dakin–West degradation showed that leucine and *N*-methylleucine were, respectively, the C-terminal amino acids of these two sporidesmolic acids, and chromatography of their hydrazides in solvent *a* (see experimental) showed that one had R_f identical to the hydrazide of sporidesmolic acid C (4) and the other to either sporidesmolic acid B (1) or D (one of the two alkaline hydrolysis products of sporidesmolide II). In solvent *b*, sporidesmolic acids B and D were resolved and it was shown that one of the acids from the new metabolite had the same R_f as the latter. Thus the structure of one of these degradation products was 2-hydroxyisovalerylisoleucylleucine and the other was probably 2-hydroxyisocaproylvalyl-*N*-methylleucine. This conclusion was confirmed by mass spectroscopic analysis of individual molecular ions of the two acids, the fast-atom bombardment fragments corresponding to the suggested sequences. It was also confirmed by comparative analysis of the ^1H and ^{13}C NMR spectra of sporidesmolides II, IV, and V. In the case of

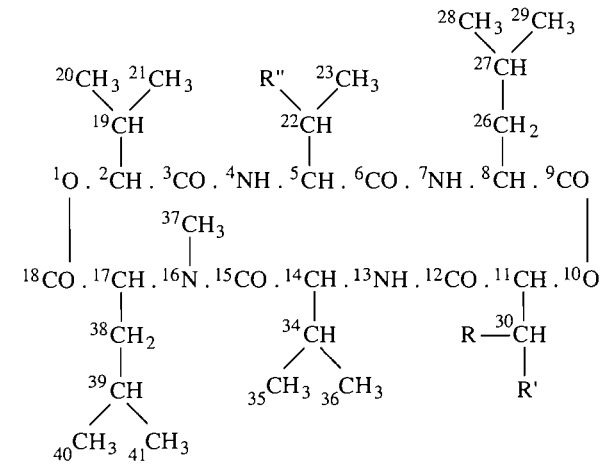

Sporidesmolide II, R'' = $^{24}CH_2\,^{25}CH_3$; R = R' = $^{31(32)}CH_3$

Sporidesmolide IV, R'' = $^{24}CH_3$; R = H, R' = $^{31}CH(^{32}CH_3)(^{33}CH_3)$

Sporidesmolide V, R'' = $^{24}CH_2\,^{25}CH_3$; R = H, R' = $^{31}CH(^{33}CH_3)(^{32}CH_3)$

sporidesmolide IV, most of the ^{13}C signals and many of the ^1H signals could be assigned by heteronuclear correlation, DEPT, and COSY experiments. In particular there were three CH_2 groups in the spectrum of sporidesmolide IV at δ_C 37.81, 39.28, and 40.75, but the three CH_2 groups in sporidesmolide II had δ_C 26.47, 37.79, and 39.38. A COSY experiment showed that the CH_2 group at 40.75 ppm was coupled to two CH groups, the chemical shift of one (δ_C 79.66) indicating it to have an oxygen substituent. It follows that this methylene group is part of a 2-oxyisocaproyl residue. In the ^{13}C spectrum of sporidesmolide V, resonances at δ_C 26.43, 37.43, 39.72, and 40.68 were shown by a DEPT experiment to be CH_2 groups. Thus, by analogy with the spectra of sporidesmolides II and IV, the resonance at 40.68 ppm can be assigned to an isocaproyl CH_2 group and that at 26.43 ppm to an isoleucyl CH_2 group.

The mass spectrum of sporidesmolide V was closely similar

[1]NRCC No. 30829.

[2]Present address: St. Francis Xavier University, Antigonish, N.S.

[3]Biochemistry Department, Dalhousie University, Halifax, N.S.

[4]Author to whom correspondence may be addressed.

Can. J. Chem. Downloaded from www.nrcresearchpress.com by 186.148.149.217 on 09/07/12
For personal use only.

to those of all other sporidesmolides from the genus *Pithomyces*, i.e., the main ion reactions in the electron impact source involved loss of butene or propene from the amino/hydroxy acid side chains, and three protons were exchanged with ^2H_2O in the source of the mass spectrometer (6). However, there were also ions of low abundance that indicated the sequence of residues in the macro-ring. Thus the ion *m/z* 227 contained no exchangeable protons and corresponded to $C_{12}H_{21}NO_3$ = MeN.CH(C_4H_9)CO_2.CH(C_3H_7)CO (because of relative abundances the protonated ion at *m/z* 228 was mass measured), establishing that the *N*-methylleucine residue was esterified to the 2-hydroxy-3-methylvaleric acid moiety and hence the sequence of the residues in the depsipeptide. From the close similarity of the ^{13}C NMR spectra of sporidesmolides II, IV, and V it may be inferred that the stereochemistries of the three depsipeptides are the same. Hence, the structure of the new metabolite is established.

Experimental

Melting points are not corrected. Specific optical rotations were measured on a Perkin–Elmer 141 polarimeter. Mass spectra were obtained on a VG Analytical ZAB-EQ mass spectrometer with a VG 11-250 data system. Accurate mass measurements were made by the peak-matching method using an appropriate ion in the spectrum of perfluorokerosene as a reference. NMR spectra at 20°C were obtained in chloroform (C^2HCl_3) and were recorded on a Bruker MSL-300 instrument at 300 MHz for proton spectra and at 75.5 MHz for ^{13}C spectra. All chemical shifts are given in ppm downfield from the signal of tetramethylsilane. Coupling connectivity was determined by ^1H COSY and $^{13}C/^1H$ heterocorrelation experiments. Assignments were based on this coupling information, DEPT experiments, known chemical shifts of amino acid nuclei (7), and comparison of spectra of compounds of known structure. Chemical shifts and coupling constants are presented with reference to the arbitrarily numbered formula given in the text. Depsipeptides (1 mg) were hydrolysed in a solution (0.2 mL) of hydrochloric acid (*d* = 1.2) and acetic acid (0.2 mL) in an atmosphere (0.1 Torr; 1 Torr = 133.3 Pa) of nitrogen at 120°C. Analysis of amino acids was performed on a Beckman amino-acid analyser model no. 6300, and of *N*-methylleucine by paper chromatography (8). Analytical reversed phase partition chromatography was done using the equipment described (9). Elution volumes were (sporidesmolide, volume in mL): I, 12.2; II (natural and synthetic), 13.5; II (synthetic, D-isoleu), 14.8; III, 10.2; IV, 14.0; V, 15.5. Thin-layer chromatograms were run on silica gel plates (0.25 mm, Macherey–Nagel, Doren, FGR) using acetonitrile–triethylamine (500:1, *a*) or ethyl acetate – ethyl alcohol – triethylamine (1000:250:1, *b*) as the developing solvents. Sporidesmolides or methyl sporidesmolates were treated with a solution (10 mL) of hydrazine (1 g) in ethyl alcohol (0.1 mL per mg of sample) for 30 min at 75°C. The reaction mixtures were evaporated, the residues dissolved in ethyl alcohol at the same concentration, and portions applied as spots to the tlc plates. The plates were thoroughly dried in air and were developed 3 times with solvent *a*, or once with solvent *b*. The hydrazides were detected by spraying the plates with ethanolic picryl chloride (0.5%).

Isolation of sporidesmolides II, IV, and V from spores of Pithomyces chartarum

Spores (460 g) from rye-grain cultures of *P. chartarum* (3) were dried for 48 h at 20°C/0.2 Torr and then stirred with chloroform (1 L) for 40 min. The mixture was filtered through an alumina pad (5 mm) and the spores washed with three portions of chloroform (1 L). The filtrate and washings were combined and evaporated. The residue (28.7 g) was dissolved in dichloromethane (28 mL), carbon tetrachloride (560 mL) added, and the solution concentrated to 50 mL. The mixture was kept at 4°C for 18 h and the resulting gel broken up under carbon tetrachloride (100 mL) and filtered. The filtrate was evaporated, the residue (5.5 g) was digested with diethyl ether (110 mL), and the insoluble material (4 g) was applied to a radially packed reversed phase (C_{18}) column (4 × 25 cm). The column was developed with methyl alcohol – water (17:3) and the first 4.5 L of eluate were discarded. The following 3 L were collected and evaporated. The material soluble in carbon tetrachloride and insoluble in ether (1.05 g; sporidesmolides I:II:IV:V = 43:32:18:7) was dissolved in ethyl alcohol (5 mL) and dichloromethane (15 mL) was added. The filtered solution (2 mL) was evaporated, the residue taken up in dichloromethane (2.5 mL), ethyl alcohol (0.2 mL) added, and the solution (50 μL) chromatographed as before (10). The column was eluted with methyl alcohol – water (41:9) and the sporidesmolides were collected separately as they eluted from the column in the following order: sporidesmolide II (72 mL), sporidesmolide IV (75 mL), and sporidesmolide V (82 mL). Like fractions from about 40 chromatograms were combined. Analysis of the material (16 mg) from the sporidesmolide II band indicated that it contained about 4% of sporidesmolide I (1), which was removed by recrystallization from 70% acetic acid, 95% ethyl alcohol, and finally from 70% aqueous acetic acid, as needles, mp 233–234°C, $[\alpha]_D^{24}$ −216° (*c* 0.268, $CHCl_3$); δ_C: 173.97, 171.79 (3C), 169.43, 169.27, 79.50, 78.36, 65.72, 63.97, 54.40, 51.44, 40.08, 39.28, 37.79, 34.21, 30.09, 29.94, 29.36, 26.47, 25.34, 24.90, 23.05, 22.40, 22.24, 22.19, 19.54, 19.43, 18.97, 18.85, 17.06, 16.59, 16.10, 11.05; *m/z*: 652.4411 ($C_{34}H_{60}N_4O_8$ requires 652.4411). The combined sporidesmolide IV fractions contained ca. 5% sporidesmolide I and 34% sporidesmolide II. A solution (30 μL) of this material (3 mg) in methyl alcohol – water (41:19) was applied to the reversed phase column (10), and the fraction eluting at 75 mL was collected. These fractions from 17 runs were combined and evaporated. The residue (30.2 mg), which still contained 6% of sporidesmolide I, was rechromatographed in the same way and fractions from the apex of the elution profile were collected. The residue (20 mg) from the combined (evaporated) fractions was triturated with ether (0.2 mL) and the insoluble material (18.8 mg) sublimed to give sporidesmolide IV, R_v 75 mL, mp 227–229°C; $[\alpha]_D^{24}$ −207° (*c* 0.1, $CHCl_3$); δ_H: 7.91 (e, $J_{H_4H_5}$ 6.5 Hz), 7.83 (e, $J_{H_7H_8}$ 6.6 Hz), 7.14 (e, $J_{H_{13}H_{14}}$ 9.8 Hz), 5.12 ($J_{H_{11}H_{30}}$ 9.9 Hz), 4.86 ($J_{H_2H_{19}}$ 3.7 Hz), 4.56 ($J_{H_{14}H_{34}}$ 10.2 Hz), 4.35 (m, H8), 3.57 ($J_{H_{17}H_{38}}$ 5.8 Hz), 3.40 (3H37), 3.27 ($J_{H_5H_{22}}$ 11.45 Hz), 2.92 (m, H22), 2.3 (m, H2 and H34), 2.0 (m, H38), 1.9 (m, H31), 1.6 (m, H27, 2H26), 1.05–0.8 (m, 36H); δ_C: 173.97, 171.81 (2C), 171.6, 170.3, 169.43, 79.66 (C_{11}), 73.24 (C_2), 67.18 (C_5), 64.04 (C_{17}), 54.27 (C_{14}), 51.54 (C_8), 40.74 (C_{30}), 40.20 (C_{37}), 39.30 (C_{26}), 37.82 (C_{38}), 29.97 (C_{19}), 29.65 (C_{34}), 27.93 (C_{22}), 25.38 (C_{39}), 24.99 (C_{27}), 24.73 (C_{31}), 23.28, 23.05, 22.40, 22.27, 22.23, 21.17, 20.21, 19.97, 19.45, 19.41, 18.57, 19.07 (12 Me groups). The material (23 mg, sporidesmolides I:II:IV:V = 7:10:8:72) from the combined fractions eluting at 82 mL was rechromatographed using the same solvent and column, and the sporidesmolide V band (11.4 mg) was collected from about 10 chromatograms. This fraction was washed with diethyl ether and sublimed at 185–190°C/0.01 Torr, and the sublimate resublimed under the same conditions gave *sporidesmolide V*, 5.27 mg, mp 215–216°C; $[\alpha]_D^{24}$ −198° (*c* 0.26, $CHCl_3$); δ_C: 174.09, 171.83, 171.73, 171.64, 170.3, 169.52 (6 *C*O), 79.64 (C_{11}), 73.19 (C_2), 65.55 (C_5), 63.93 (C_{17}), 54.23 (C_{14}), 51.57 (C_8), 40.68 (C_{30}), 40.19 (C_{37}), 39.17 (C_{26}), 37.72 (C_{38}), 29.95 (C_{19}), 29.59 (C_{34}), 26.43 (C_{24}), 25.33 (C_{27}), 24.96 (C_{39}), 24.73 (C_{31}), 23.32, 23.11, 22.23 (2C), 21.08, 19.47, 18.56, 17.12, 16.17 (C_{23}), 10.98 (C_{25}); *m/z*: 666.4577 ($C_{35}H_{62}N_4O_8$ requires 666.4567); 228.1599 ($C_{12}H_{22}NO_3$ requires 228.1600). *Anal.* calcd. for $C_{35}H_{62}N_4O_8 \cdot 0.5H_2O$: C 62.2, H 9.4, N 8.3; found: C 62.1, H 8.9, N 8.4%.

Sporidesmolic acid D

Sporidesmolide II (84 mg) in boiling ethyl alcohol (95%, 10 mL) was treated with sodium hydroxide solution (2 N, 2 mL) and the solution concentrated to 3 mL. Hydrochloric acid (6 N, 1 mL) was added, the solution evaporated, and the residue digested with chloroform (10 mL) and water (10 mL). The insoluble material was collected and was recrystallized from dilute acetic acid as needles, 16 mg, mp 199–200°C. *Anal.* calcd. for $C_{17}H_{32}N_2O_5$: C 59.3, H 9.4, N 8.1%; found: C 59.1, H 9.4, N 8.4%.

Dakin–West reaction on sporidesmolic acids from sporidesmolide V

Sporidesmolide V (1.8 mg) was dissolved in methyl alcohol (0.25 mL) and sodium hydroxide solution (2 N, 70 μL) added. After 1 h at room temperature the solution was treated with hydrochloric acid (6 N, 35 μL) and then was evaporated to dryness. The residue after mass spectroscopic analysis was extracted with ethyl alcohol (3 × 0.25 mL), the combined extracts (= A, 0.38 mL) were evaporated, and the residue was treated with pyridine (0.2 mL) and acetic anhydride (0.3 mL). The reaction mixture was heated in a sealed tube at 110°C for 2.5 h after which time it was evaporated and the residue treated with hydrochloric acid (6 N, 0.5 mL) at 110°C for 24 h. The hydrolysis mixture was cooled and evaporated. The residue was dissolved in water (0.1 mL) and 10 μL was chromatographed on Whatman 3MM paper, with marker chromatograms (of val, leu, allo-isoleu, and N-Meleu) to its left and right. The chromatograms were developed with *tert*-butyl alcohol – ammonium hydroxide (4.25 N, 4:1). The marker strips showed the presence of valine and isoleucine, which were recovered from the paper by the method described in the next paragraph.

Determination of chirality of amino acids in acid hydrolysates of sporidesmolic acids

The remaining ethanolic extract (= A, see above, 0.37 mL) was evaporated and the residue treated with hydrochloric acid (6 N, 0.5 mL). The mixture was heated at 110°C for 24 h, evaporated to dryness, and the residue dissolved in water (0.1 mL) and chromatographed on Whatman 3MM paper as described for the hydrolysis products of the Dakin–West reaction. The bands of amino acids were cut out, rolled longitudinally, saturated with water, and centrifuged. The amino acid solutions obtained were concentrated to 0.1 mL and were applied to silica gel plates containing a chiral Cu^{2+} reagent (Macherey–Nagel, "Chiralplate"). The plates were developed with methyl alcohol – water–acetonitrile (1:1:4). In all cases the L isomers had the greatest R_f (L in the range 0.53–0.57; D, 0.45–0.50). The R_f values for the four amino acids were as follows: valine, 0.53 (L); isoleucine, 0.45 (D); leucine, 0.45 (D); and *N*-methylleucine, 0.56 (L).

Acknowledgements

We thank the late Professor M. M. Shemyakin for samples of his synthetic depsipeptides, Dr. K. Dooley for amino acid analyses, and D. Embree for mass spectroscopy.

1. D. W. Russell. J. Chem. Soc. 753 (1962).
2. W. S. Bertaud, M. C. Probine, J. S. Shannon, and A. Taylor. Tetrahedron, **21**, 677 (1965).
3. J. Done, P. H. Mortimer, A. Taylor, and D. W. Russell. J. Gen. Microbiol. **26**, 207 (1961).
4. E. Bishop and D. W. Russell. J. Chem. Soc. (C), 634 (1967).
5. M. M. Shemyakin, Yu. A. Ovchinnikov, V. T. Ivanov, and A. A. Kiryushkin. Tetrahedron Lett. 1927 (1963).
6. C. G. Macdonald, J. S. Shannon, and A. Taylor. Tetrahedron Lett. 2087 (1964).
7. K. Wuthrich. NMR in biological research; peptides and proteins. North Holland, Amsterdam. 1987.
8. T. K. Audhya and D. W. Russell. J. Chromatogr. **84**, 361 (1973).
9. D. W. Russell. Can. J. Bot. **66**, 1474 (1988).
10. D. W. Russell and H. A. Gillis. Proc. N.S. Inst. Sci. **37**, 13 (1987).

Can. J. Chem. Downloaded from www.nrcresearchpress.com by 186.148.149.217 on 09/07/12
For personal use only.

Identification of isodomoic acid D and two new geometrical isomers of domoic acid in toxic mussels[1]

JEFFREY L. C. WRIGHT,[2] MICHAEL FALK, A. GAVIN MCINNES, AND JOHN A. WALTER
National Research Council, Atlantic Research Laboratory, 1411 Oxford Street, Halifax, N.S., Canada B3H 3Z1

Received April 28, 1989

JEFFREY L. C. WRIGHT, MICHAEL FALK, A. GAVIN MCINNES, and JOHN A. WALTER. Can. J. Chem. **68**, 22 (1990).

Isodomoic acids E and F, two new geometrical isomers of the neurotoxin domoic acid, have been found to occur with domoic acid and isodomoic acid D in extracts of toxic mussels. The entire set of geometrical isomers can be prepared in the laboratory by photolysis.

Key words: amnesic shellfish toxin, domoic acid, isodomoic acid, neurotoxin.

JEFFREY L. C. WRIGHT, MICHAEL FALK, A. GAVIN MCINNES et JOHN A. WALTER. Can. J. Chem. **68**, 22 (1990).

Dans les extraits de moules toxiques, on a trouvé que les acides neurotoxiques, domoïque et isodomoïque D, sont accompagnés des acides isodomoïques E et F, deux nouveaux isomères géométriques de l'acide domoïque. Faisant appel à la photolyse, il est possible de préparer au laboratoire l'ensemble des isomères géométriques.

Mots clés : toxine amnésique du testacé, acide domoïque, acide isodomoïque, neurotoxine.

[Traduit par la revue]

Introduction

We recently isolated and identified the neurotoxin domoic acid **1** as the toxic agent in an outbreak of shellfish poisoning traced to cultured mussels *Mytilus edulis* L. from a localized area of eastern Prince Edward Island, Canada (1). This compound was originally isolated from the red macroalga *Chondria armata* Okamura some 30 years ago (2, 3). Based on its toxic properties and its discovery in shellfish, it has been proposed[3] that **1** be termed an amnesic shellfish poison (ASP). As **1** is the most potent known activator of the kainate receptors in the central nervous system[4] it is of interest from a chemical and neurophysiological standpoint that domoic acid isomers or derivatives be characterized as fully as possible. We report here the isolation of isodomoic acid D **2** (4) and two new geometrical isomers, isodomoic acids E **3** and F **4**, obtained in small quantities during further studies of these toxic mussels.[5]

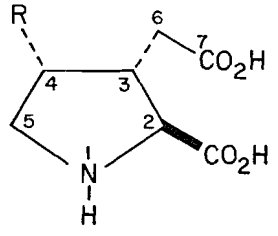

1 R = 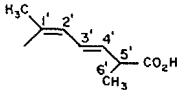

2 R = 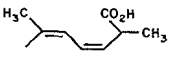

3 R = 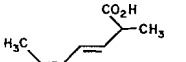

4 R = 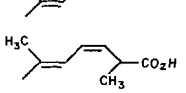

5 R =

Results and Discussion

In the original identification of **1** in toxic mussels (1) the chemical and physical properties were identical with published data (5) and the optical rotation of an anhydrous sample of **1** (α_D^{24} −120°) showed that the enantiomeric form was the same as that previously reported from *Chondria armata*. Our NMR experiments (1) confirmed the ^1H assignments and spin–spin coupling constants of ref. 5 and led to minor reassignment of ^{13}C resonances compared to those of ref. 4. Additional homonuclear NOE experiments confirmed the (*Z*, *E*) configuration of double bonds in the side chain and the conformation of the prolyl ring (1).

During subsequent large-scale extraction and purification of domoic acid, additional peaks displaying essentially the same ultraviolet spectra as the toxin were observed. These compounds were obtained pure by repeated reversed-phase chromatography.

The UV spectrum (λ_{max} 244 nm) of the major isomer **2** (MH^+ 312.1448, $C_{15}H_{22}NO_6$, α_D^{25} −72°) indicated the presence of conjugated double bonds, although the IR spectrum showed no absorption in the region 955–980 cm^{-1} characteristic of a *trans*-disubstituted double bond. The NMR data (Tables 1 and 2) show this compound to be isodomoic acid D **2**, previously isolated as a minor component of extracts of *C. armata* (4). Values of δ(H) and *J*(H, H) (Tables 1 and 2) from our spectra are close to the published values, recorded at unspecified pH (4). They indicate that the conformation of the prolyl ring is virtually identical with **1**. Our NOE measurements, showing the proximity of H-2′ and 1′-CH_3, H-2′ and H-5′, H-3′ and H-4′, H-4′ and H_3-6′, confirm the (*Z*, *Z*) configuration of the two conjugated double bonds.

The (*E*, *E*) isomer structure was consistent with the UV absorption (241 nm) and IR spectrum (960 cm^{-1}) of isodomoic acid E **3** (MH^+ 312.1430, $C_{15}H_{22}NO_6$, α_D^{25} −19.5°), which eluted after **2**, and was confirmed by the NOE data showing the proximity of H-3′ to H-5′, H_3-6′ and 1′-CH_3, and of H-4′ to H-5′, H_3-6′ and H-2′. The values of δ(H) and *J*(H, H) (Tables 1 and 2) show similarity of the prolyl ring protons to **1** and **2**, except that a reduction in *J*(2, 3) indicates that the average conformation of the ring reduces the (H-2)—C—C—(H-3) angle, from ca. 143° to ca. 120°, if Karplus-type parameters for proline (6) are applied to this case. Closer proximity of these protons seems to be indicated by NOE between H-2 and H-3, which is not observed in **1** and **2**. Similarly, *J*(4, 5α) shows an increase in the relative angle of the 4-H and 5-αH bonds, also reflected in the occurrence of NOE between H-4 and H-5β.

The last compound to elute (MH^+ 312.1444, $C_{15}H_{22}NO_6$,

[1]NRCC No. 30838.

[2]Author to whom correspondence may be addressed.

[3]T. M. Perl, L. Bedard, T. Kosatsky, R. S. Remis, E. C. D. Todd, and J. C. Hockin. Submitted for publication.

[4]G. Dobennel, L. Beauchesne, and C. De Montigny. Submitted for publication.

[5]Aspects of this work were reported at a Symposium on Domoic Acid Toxicity in Ottawa, April 10–11, 1989.

Can. J. Chem. Downloaded from www.nrcresearchpress.com by 186.148.149.217 on 09/07/12
For personal use only.

TABLE 1. ^{1}H and ^{13}C chemical shifts[a] and nuclear Overhauser enhancements[b] for domoic acid and isodomoic acids from toxic mussels

			Position								
	Isomer	pH	2	3	4	5α	5β	6a	6b	7	2-CO_2H
δ(H) (ppm) and multiplicity	**1**	3.4	3.98d	3.05dddd	3.84ddd	3.49dd	3.71dd	2.76dd	2.50dd		
	2	1.9	4.15d	3.10dddd	3.87ddd	3.52dd	3.72dd	2.75dd	2.53dd		
	3	1.8	4.36d	3.26dddd	3.23ddd	3.58dd	3.72dd	2.57dd	2.53dd		
	4	1.6	4.39d	3.27dddd	3.32ddd	3.63dd	3.77dd	2.63dd	2.53dd		
NOE (%) when H at head of column is irradiated	**1**	3.4	None	H4 4.7	H3 6.4 H3′ 14.9 H5β[e]	H5β 12.5 1′Me 1.0	H5α 11.2 H4[e]	H6b 5.8	H6a 9.0		
	2	1.9	None	H4 2.5	H3 2.3 H3′ 6.3	H5β 4.7 1′Me 0.4	H5α 1.6[c]	H6b 4.4	H6a 1.8		
	3	1.8	H3 1.1 H6a 1.2 H6b 0.9	H2 2.9 H4[c,e] H6a 3.2 H6b 1.5 H2′ 3.6 1′Me 1.9	H3[c,e] H5β 4.3	H5β 8.1 H6a 1.0 H6b 1.0 H2′ 7.4	H5α 5.0	H6b[d,f] H2 2.9 H2′ 0.8 H3 3.0 1′Me 0.3	H6a[d,f]		
	4	1.6	H6a 1.4 H6b 0.8 1′Me 0.4	H2 2.2[c] H6a 4.7 H6b 4.1	H5β 3.5[c] H2′ 3.9 1′Me 1.8	H5β 3.0 H2′ 5.9	H4 2.8[d]	H2 1.1 H3 2.3	H2 1.1 H3 2.9 1′Me 0.7		
δ(C) (ppm)	**1**	3.4	67.1	44.6	42.7	49.1		35.4		177.5	174.9
	1	0.6	65.4	43.9	42.7	49.7		35.1		177.6	172.9
	2	0.3	65.6	43.9	42.8	49.8		35.1		177.6	172.9
	3	0.7	66.1	43.3[h]	49.6[h]	49.2		35.3		177.7	173.3
	4	0.6	66.0	43.3[h]	50.0[h]	49.3		35.3		177.6	173.1

			Position							
	Isomer	pH	1′	2′	3′	4′	5′	6′	1′-Me	5′-CO_2H
δ(H) (ppm) and multiplicity	**1**	3.4		6.13d	6.35dd	5.78dd	3.30dq	1.27d	1.81s	
	2	1.9		6.43d	6.28dd	5.49dd	3.69dq	1.25d	1.85s	
	3	1.8		5.95d	6.55dd	5.87dd	3.38dq	1.33d	1.85s	
	4	1.6		6.19d	6.47dd	5.60dd	3.73dq	1.33d	1.87s	
NOE (%) when H at head of column is irradiated	**1**	3.4		H4′ 13.0 1′Me 1.5	H4 8.5 H5′ 4.5	H2′ 8.0 H5′ 4.7	H3′ 3.5 H4′ 3.0	H4′ 5.2 H5′ 10.7	H5α 4.5 H6b 2.4 H2′ 13.3	
	2	1.9		H5′ 6.2 1′Me 0.6	H4 5.3 H4′ 3.2	H3′ 2.8 H_36' 0.7	H2′ 6.1[c] H_36' 1.2	H4′ 2.8 H5′ 3.6	H5α 3.3 H2′ 3.3	
	3	1.8		H5α 3.6 H3 0.8 H4 0.8 H4′[g]	H5′ 6.0 H_36' 0.3 1′Me 2.0	H5′ 3.4 H_36' 0.5 H2′ 1.6[g]	H3′ 5.4 H4′ 2.8 H_36' 3.0	H3′ 2.2 H4′ 3.1 H5′ 6.5	H3 1.0 H4 1.5 H3′ 8.7	
	4	1.6		H4 3.5 H5α 5.1 H6b 1.3 H5′ 6.3	H4′ 8.5 1′Me 1.9	H3′ 6.7 5′Me 0.5	H2′ 8.2[d] H4′ 1.4 H_36' 1.1	H4′ 4.1 H5′ 6.6	H2 1.1 H3 1.8 H4 1.9 H3′ 7.6	
δ(C) (ppm)	**1**	3.4	133.8	132.8	128.6	135.2	44.9	18.6	23.5	181.9
	1	0.6	133.7	133.5	128.9	135.5	45.0	18.8	23.7	181.9
	2	0.3	136.1	128.5	127.2	133.2	40.7	19.8	24.2	181.9
	3	0.7	134.2	130.0	129.5	135.6	45.0	18.9	18.7	181.9
	4	0.6	136.7	125.2	127.8	133.1	40.7	19.7	18.6	181.8

[a]Reference TSP in concentric tube, temperature 20°C, s = singlet, d = doublet, q = quartet. Data previously reported (1) for domoic acid are included for comparison. Solvent: D_2O.

[b]Error ca ±0.5% for single protons, ca ±0.2% for methyl protons.

[c,d]Resonances too close for separate irradiation.

[e,f,g]Resonances too close for observation of full NOE between them.

[h]Assignments by heterocorrelation might be reversed; ^{1}H peaks nearly overlap.

Can. J. Chem. Downloaded from www.nrcresearchpress.com by 186.148.149.217 on 09/07/12
For personal use only.

TABLE 2. ^1H—^1H scalar coupling constants for domoic and isodomoic acids from toxic mussels

		Coupled pair											
	Isomer	2,3	3,4	3,6a	3,6b	4,5α	4,5β	5α,5β	6a,6b	2′,3′	3′,4′	4′,5′	5′,6′
J(H,H)	**1**	8.1	8.4	5.8	9.1	7.3	7.9	−12.2	−16.7	11.1	14.9	7.8	7.1
(Hz)[a]	**2**	8.1	7.9±0.5	6.3	8.3	7.9±0.4	7.7	−12.4	−17.1	11.6	10.0	10.0	7.0
	3	4.0	7.4	6.4	6.4	10.0	7.3	−11.9	−16.9	10.5	15.2	7.9	7.0
	4	4.6	7.2	7.2	7.1	9.5	7.3	−11.9	−17.1	11.0	11.1	10.0	7.0

[a]Error ca. ±0.2 Hz unless stated. Coupling connectivity confirmed by ^1H COSY spectra. Some couplings determined by simulation using Bruker PANIC program. Data previously reported (1) for domoic acid are included for comparison. pH as for ^1H data in Table 1.

α_D^{25} −85°) was identified as isodomoic acid F **4**. The UV (243 nm) spectrum confirms the presence of two conjugated double bonds. The IR spectrum (no band in the region 955–980 cm^{-1}) shows there is no *trans*-disubstituted double bond. Occurrence of NOE between H-3′ and H-4′, as well as between H-2′ and H-5′, and H-3′ and 1′-CH_3, confirms the (*E*, *Z*) configuration of the double bonds. The reduction in *J*(2, 3) and increase in *J*(4, 5α) compared to **1** and **2**, and the occurrence of NOEs between H-2 and H-3, and H-4 and H-5β, indicate that the ring conformation is more similar to **3**. In this regard it is noteworthy that **3** and **4** both possess a (1′*E*) configuration. In all the isomers, the coupling constants (Table 2) and ^{13}C chemical shifts (Table 1) were consistent with the proposed structures. The chirality at C-5′ and the enantiomeric form of each isomer remain to be established.

The isomers are only available in small amounts following tedious and repetitive chromatography. However, more material was required for toxicological studies so alternative methods for their production were investigated. Exposure of dilute aqueous solutions of domoic acid to ultraviolet light (250 nm) resulted in the rapid conversion to the geometrical isomers. Maximum yield of the isomers **2**–**4** was reached after 9–12 min, at which time the proportions of **1**–**4** were respectively 0.28:0.12:0.27:0.13 relative to an initial unit amount of **1**.

It is now well established that domoic acid is produced by the diatom *Nitzschia pungens* (7, 8). Traces of the isomers **2**, **3**, and **4** have been observed in laboratory cultures of *N. pungens* using sensitive analytical techniques (M. Quilliam, personal communication), but these isomers are much more obvious in extracts of various shellfish, suggesting that further conversion of domoic acid occurs within the digestive system of the mollusc. Optical rotations for the isomers produced by photolysis were identical within error (±2°) to those for the corresponding isomers from mussels.

As the isomers have been observed in essentially the same proportions in both steamed and uncooked mussels, it appears that the steaming process does not contribute significantly to isomer production. Another popular recipe is to heat mussels in a solution of vinegar and white wine for several minutes. When domoic acid was warmed (80°C) in aqueous solutions containing acetic acid (3%; 15%; 60%) or trifluoracetic acid (10%) no trace of the isomers was observed by HPLC–DAD analysis, even after prolonged periods (up to 3 h).

Domoic acid is the most potent member of a family of glutamate agonists that includes kainic acid **5**. A portion of these molecules (C2-CO_2H, C-2, C-3, C-6, and C-7) can mimic glutamic acid and bind to glutamate receptors in the brain (9–14). The nature of the side chain has obvious implications with respect to the efficacy of binding to these receptors located in the membrane, and to the potency of the compound as a neuro-excitatory amino acid. Work on the relationship between biological activity and chemical structure of the four geometrical isomers is in progress.

Experimental

HPLC–DAD analysis and all NMR, MS, IR, and UV spectra were obtained with the instruments and conditions previously described (1).

Isolation of isomers

The aqueous methanol extract of blended steamed mussel tissue was concentrated and partially purified by flash chromatography using a C_{18} reversed-phase support (55–105 μm; Waters Prep Pak) and elution with acetonitrile–water mixtures containing 1% acetic acid. The fraction (20% acetonitrile/water) containing domoic acid and the isomers was further purified by Lobar chromatography (C_8 reversed-phase support) and elution with the same mixtures. Finally, fractions enriched in domoic acid and the isomers were separated into various components by repeated reversed-phase HPLC (10 μm; Vydac 201TP 1010; 8% acetonitrile–water containing 0.1% trifluoracetic acid) runs using diode-array detection. Domoic acid **1** was the major component (>90% of the mixture) and the isomers eluted at relative retention times (RRT) **2** (0.84), **3**(0.90), and **4**(1.34) (Vydac 201TP52, 250 mm × 2 mm). The isomers were obtained as oils in the proportions indicated: **2** (ca. 5%), **3** (ca. 2%), **4** (ca. 1%).

The physical and spectroscopic properties of the isomers are described in Results and discussion and in Tables 1 and 2.

Photolysis of domoic acid

Photochemical reactions were carried out at 30°C in a quartz tube (35 × 5 cm diameter) using an ultraviolet photoreactor (Southern New England Ultraviolet Company, Middletown, Conn.) equipped with eight ultraviolet tubes (253.7 nm Rayonet photochemical reactor lamp). Dilute aqueous solutions (500 mL) of domoic acid (100 μg/mL) were degassed by filtration followed by purging with argon. Initially, to set up optimum reaction conditions, the isomerisation was followed by HPLC–DAD analysis. In a typical production run the photolysis reaction was halted after 15 min, the solution concentrated *in vacuo*, and the isomers collected by repeated reversed-phase HPLC runs as described above. The ratio of isomers **1**–**4** was 1:0.42:0.96:0.46. Isomers prepared in this way had identical spectroscopic properties (UV, IR, NMR, $[\alpha_D]$) to those obtained from cooked mussels.

Acknowledgements

The authors are grateful to Cheryl Craft, Pat LeBlanc, Colleen O'Connell, and Don Leek for technical assistance, to Dr. Robert Boyd for high resolution mass spectrometry, and to Dr. Michael Quilliam for helpful discussions.

1. J. L. C. WRIGHT, R. K. BOYD, A. S. W. DE FREITAS, M. FALK, R. A. FOXALL, W. D. JAMIESON, M. V. LAYCOCK, A. W. MCCULLOCH, A. G. MCINNES, P. ODENSE, V. V. PATHAK, M. A. QUILLIAM, M. A. RAGAN, P. G. SIM, P. THIBAULT, J. A. WALTER, M. GILGAN, D. J. A. RICHARD, and D. DEWAR. Can. J. Chem. **67**, 481 (1989).
2. T. TAKEMOTO and K. DAIGO. Chem. Pharm. Bull. **6**, 578 (1958).

Can. J. Chem. Downloaded from www.nrcresearchpress.com by 186.148.149.217 on 09/07/12
For personal use only.

3. T. TAKEMOTO and K. DAIGO. Arch. Pharm. (Weinheim), **293**, 627 (1960).
4. M. MAEDA, T. KODAMA, T. TANAKA, H. YOSHIZUMI, K. NOMOTO, T. TAKEMOTO, and T. FUGITA. Tennen Yuki Kagobutsu Toronkai Koen Yoshishu, **27th**, 616, (1985).
5. Y. OFUNE and M. TOMITA. J. Am. Chem. Soc. **104**, 3511 (1982).
6. L. POGLIANI, M. ELLENBERGER, and J. VALAT. Org. Magn. Reson. **7**, 61 (1975).
7. S. S. BATES, C. J. BIRD, R. K. BOYD, A. S. W. DEFREITAS, M. FALK, R. A. FOXALL, L. A. HANIC, W. D. JAMIESON, A. W. MCCULLOCH, P. ODENSE, M. A. QUILLIAM, P. G. SIM, P. THIBAULT, J. A. WALTER, and J. L. C. WRIGHT. Atlantic Research Laboratory, Technical Report Number 57, 1988.
8. S. S. BATES, C. J. BIRD, A. S. W. DE FREITAS, R. FOXALL, M. W. GILGAN, L. A. HANIC, G. E. JOHNSON, A. W. MCCULLOCH, P. ODENSE, R. POCKLINGTON, M. A. QUILLIAM, P. G. SIM, J. C. SMITH, D. V. SUBBA RAO, E. C. D. TODD, J. A. WALTER, and J. L. C. WRIGHT. Can. J. Fish. Aquat. Sci. **46**, 1203 (1989).
9. R. ZACZEK and J. T. COYLE. Neuropharmacology, **21**, 15 (1982).
10. J. S. KIZER, C. B. NEMEROFF, and W. W. YOUNGBLOOD. Pharmacol. Rev. **29**, 301 (1978).
11. J. T. COYLE. J. Neurochem. **41**, 1 (1983).
12. R. ASCHWARTZ and Y. BEN-ARI (*Editors*). Excitatory amino acids and epilepsy. *In* Adv. Exp. Med. Biol. **203** (1986).
13. J. C. WATKINS and H. J. OLVERMAN. Trends Neurosci. **10**, 265 (1987).
14. C. ANGST and M. WILLIAMS. Transmissions, **3**, 1 (1987).

Can. J. Chem. Downloaded from www.nrcresearchpress.com by 186.148.149.217 on 09/07/12
For personal use only.

Determination of the charge density of acrylamide/acrylate copolymers by tensammetry

TRUIS SMITH-PALMER AND BYRON R. WENTZELL
Chemistry Department, St. Francis Xavier University, Antigonish, N.S., Canada B2G 2E2

Received January 23, 1989

TRUIS SMITH-PALMER and BYRON R. WENTZELL. Can. J. Chem. **68**, 26 (1990).

The charge densities of acrylamide/acrylate copolymers can be determined using tensammetry. The tensammograms were run using 20 ppm solutions of polymer in 0.1 *M* tetraethylammonium chloride. A standard curve of desorption peak height versus mol% anionicity was useful in the range 10–50%. A second standard curve of the potential at which the capacitive current measured 1 μA versus mol% anionicity allowed the determination of charge density in the range 0–15%.

Key words: tensammetry, polyacrylamide, charge density, tetraethylammonium, desortion peaks.

TRUIS SMITH-PALMER et BYRON R. WENTZELL. Can. J. Chem. **68**, 26 (1990).

On peut déterminer la densité de charge du copolymère acrylamide/acrylate par tensammétrie. On a obtenu les tensammogrammes à partir de solutions de chlorure de tétraéthylammonium 0.1 *M* contenant 20 ppm de polymère. Une courbe standard de la hauteur du pic de désorption en fonction du % molaire d'anionicité s'est avérée utile dans l'intervalle allant de 10 à 50%. Une deuxième courbe standard d potentiel auquel le courant capacitif mesure 1 μA en fonction du % molaire d'anionicité permet de déterminer la densité de charge dans l'intervalle allant de 0 à 15%.

Mots clés : tensammétrie, polyacrylamide, densité de charge tétraéthylammonium, pic de désorption.

[Traduit par la revue]

Introduction

Acrylamide/acrylate copolymers (pams) have many industrial applications, particularly in coal and oil processing. Their usefulness is often a function of their charge density. Charge density refers to the percentage of the monomers which contain charged functional groups, i.e., acrylate rather than acrylamide. For example, in pure polyacrylamide, all the monomers contain the amide functional group and it is considered to be non-ionic. However, as more of the monomers are acrylic acid, the charge density increases. Charge density affects things such as solubility, conformation, and electrostatic interaction, and itself is sensitive to pH.

A number of methods have been used to determine charge density, including conductimetric and potentiometric titrations (1), nmr (1), ir (2), differential scanning calorimetry (1), and thermogravimetric methods (3). The titrations are tedious and time-consuming (1), while the latter three methods require preparation of a pure sample in the solid state. The nmr method is absolute, but not all labs are equipped with a suitable instrument. We have previously shown that the concentrations of solutions of pams can be determined by tensammetry (4) and by the suppression of polarographic maxima (5), and when using either of these methods, it would be convenient if one could further use the same apparatus to determine the charge density of pams of interest.

We had observed that the shapes of tensammograms changed as the charge density of the pams changed and this suggested a means by which the charge density of pams might easily be determined. In this study we choose to use a set of pams of the same molecular weight but varying charge density to see if we could establish a relationship between capacitive current and charge density at one or more potentials.

Experimental

Tensammograms were recorded, as described previously (4), using a Princeton Applied Research (PAR) Model 174A Polarographic Analyzer and a Model 303 static mercury drop electrode (SMDE) in conjunction with a PAR Model 174A/50 AC Polarographic Analyzer Interface and a PAR Model 122 Lock-In Amplifier. The analog output of the polarograph was digitized using an Apple IIe microcomputer with Interactive Microware software (Lab Data Manager, Scientific Plotter) and hardware (ADALAB Interface card, ADA-AMP Instrumentation Amplifier). A modulation amplitude of 10 mV (p-p) at 200 Hz was used. The phase was adjusted to be 135 degrees away from the phase of the reference modulation to minimize faradaic currents. The HMDE (small) and a scan rate of 5 mV/s were used. Scans in the positive and negative direction were started at −600 mV after a 2 min hold time. All potentials reported are relative to a silver – silver chloride reference electrode containing KCl (saturated).

Infrared spectra were run on an FT IR microscope (A.R.L., Halifax, N.S.) on thin films obtained by evaporation of solutions at room temperature.

The Magnifloc pams (Table 1) used as standards were obtained from the American Cyanamid Corp. Other pams (Table 1) were obtained from Energy, Mines and Resources, Edmonton. Alkylammonium salts were obtained from Aldrich. Standard deviations were determined using 12 measurements.

TABLE 1. Properties of pams used in this paper

Polymer	Anionicity (mol%)	Molecular weight
Magnifloc 905N	<1	$14–17\times10^6$
Magnifloc 837A	6–9	$14–17\times10^6$
Magnifloc 836A	12–16	$14–17\times10^6$
Magnifloc 835A	30–34	$14–17\times10^6$
Magnifloc 833A	40–43	$14–17\times10^6$
Magnifloc 832A	~50	$14–17\times10^6$
Percol E10	5	—
Praestol 2830	12.5	—
Praestol 2900	25	$5–10\times10^6$
Praestol 2935	37	—

Results and discussion

As a check on the charge densities of the standard samples supplied by Cyanamid, their ir spectra were run and ratios of the peaks at 1569 and 1670 cm^{-1} (COO^- and $CONH_2$, respectively) were plotted versus charge density (2). A straight line was obtained with a correlation of 0.991 (Fig. 1).

Tensammograms of the Magnifloc standards in 0.25 *M* KCl (as used previously for the determination of concentration) were

Can. J. Chem. Downloaded from www.nrcresearchpress.com by 186.148.149.217 on 09/07/12
For personal use only.

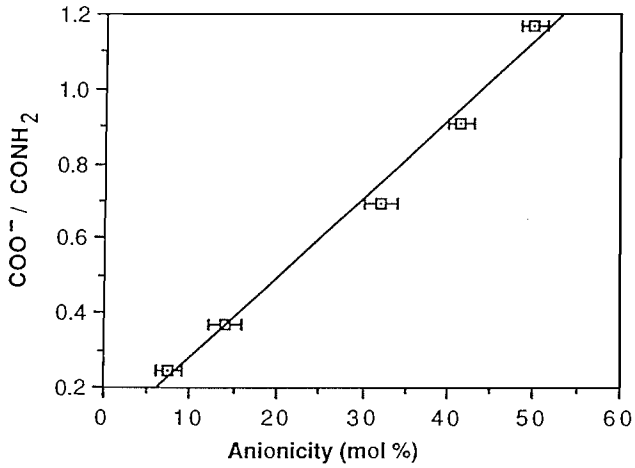

FIG. 1. Standard curve of the ratio of the IR absorbances at 1569 and 1670 cm^{-1} (COO^- and $CONH_2$, respectively) versus the charge density, for a series of films of known Magnifloc polymers of the same molecular weight.

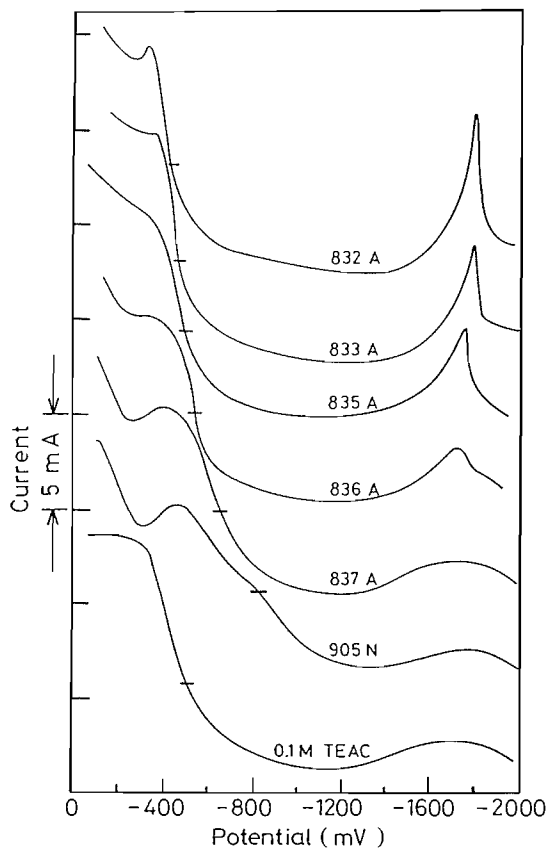

FIG. 2. Tensammograms of 0.1 *M* tetraethylammonium chloride (TEAC) and 20 ppm solutions of various Magnifloc pams in 0.1 *M* TEAC. Each tensammogram is composed of a negative and a positive scan, each beginning at −600 mV. A dash (—) is drawn through each tensammogram at the potential at which the capacitive current is 1 μA.

then run. The shape of the tensammograms obtained differed with charge density, but there was no potential at which the capacitive current was a simple function of the charge density. However, when tensammograms of the standard polymers in 0.1 *M* tetraethyl ammonium chloride (TEAC) were run, desorption peaks appeared at potentials around −1750 mV (Fig. 2). The exact peak potential became more negative as the charge density of the polymer increased. Previously such desorption peaks have been used to determine the concentration of various small surface-active species (6). The heights of the desorption peaks on our tensammograms were a function of the charge density of the pam used. The best (most reproducible) results were obtained when pam concentrations of 20 ppm were used. At lower concentrations, the tensammetric curves are affected by concentration (4). Higher concentrations can be used and give similar results, but are slightly less reproducible, perhaps because of the greater viscosities of the pam solutions involved. Figure 2 also shows the tensammograms for 0.1 *M* TEAC and for the non-ionic pam 905N in 0.1 *M* TEAC. They are very similar in the region where the desorption peaks occur and results were compared using each as the baseline for peak height. The standard curve plotted using the peak heights read with respect to the capacitive current for a nonionic pam in 0.1 *M* TEAC (Fig. 3) gave a slightly better correlation coefficient than the curve plotted using peak heights read with respect to the capacitive current for TEAC alone (0.992 compared to 0.988). In other respects the curves were not very different. The maximum charge density of a polymer used was 50%, reflecting the fact that acrylamide/acrylate copolymers of 0–50% charge density are the most widely used industrially — Magnifloc pams of higher charge density were not available.

The potential was held at −600 mV for 2 min before a scan in either the positive or negative direction. The hold time allowed the capacitive current to stabilize. If the potential was held at −600 mV (close to the potential of zero charge (7)), the current dropped in the first 20–30 s during which the voltage was applied and then increased again. This occurred with or without the pam present. After 2 min the drift in each was steady and would cancel out.

No desorption peaks were found for pams in 0.1 *M* tetramethylammonium chloride, and 0.1 *M* tetrabutylammonium chloride gave a desorption peak at −1990 mV which was not affected by the addition of pams. The latter suggests that the tetrabutylammonium ion adsorbs more strongly than do pams (8). Tetraalkylammonium ions are known to be strongly adsorbed at a mercury surface, with the tetramethylammonium ion being less strongly adsorbed than the tetraethylammonium (9). Normally, anionic pams are not adsorbed on a negatively charged mercury surface (10), as is evidenced by their tensammograms being identical to those of the electrolytes at negative potentials (4). Thus the tetraethylammonium ion presumably complexes with the pams. Desorption peaks for other complexes with tetraethylammonium ion have previously been reported (11). The complex may hold together by both electrostatic and dispersion type bonds. Thus the greater charge density of the tetraethylammonium ion in comparison with tetrabutylammonium, and its greater organic character in comparison with tetraethylammonium, may be important deciding factors in the stability of the complex. As the height of the desorption peak is usually a function of concentration (6), we suggest that the more highly charged pams are able to complex with more tetramethylammonium ions and thus produce higher desorption peaks. Desorption peaks have previously been found in differential capacity – voltage curves of copolymers of methacrylic and methylmethacrylic acid at ~ −0.3 V in 0.1 *N* NaF, with the copolymers of higher charge density giving higher peaks (12), and differential capacity – voltage curves are the same shape as corresponding tensammograms (13). Our pams showed no peaks when run under these conditions, presumably because of the much higher molecular weights involved.

The charge densities of some other pams of nominal charge

Can. J. Chem. Downloaded from www.nrcresearchpress.com by 186.148.149.217 on 09/07/12
For personal use only.

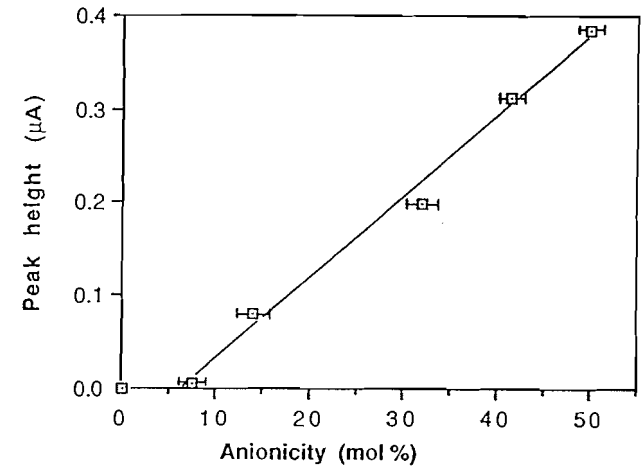

FIG. 3. Standard curve of height of desorption peak (with respect to the capacitive current of a nonionic pam in 0.1 *M* TEAC at the same potential) versus the charge density for a series of 20 ppm solutions of known Magnifloc pams of the same molecular weight.

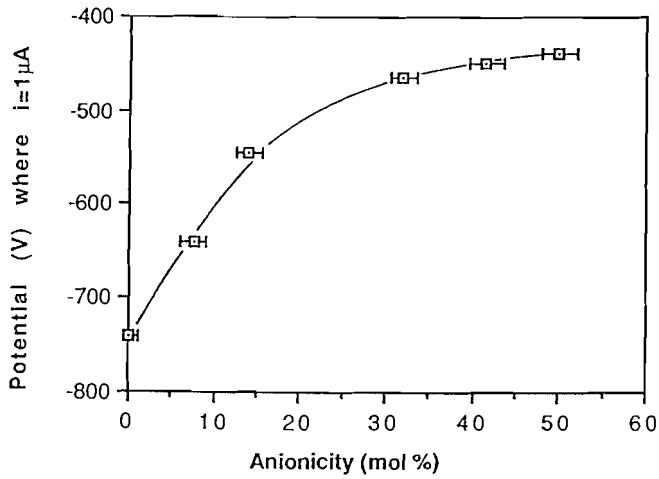

FIG. 4. Standard curve of potential at which the capacitive current is 1 μAmp versus the charge density for a series of 20 ppm solutions of known Magnifloc polymers of the same molecular weight.

densities 5, 12.5, 25, and 37.5% (Table 1) were read from the standard curve (Fig. 3) to demonstrate its general applicability. Values of 10, 12, 26, and 34%, respectively, were found using non-ionic pam in TEAC as blank. This standard curve is obviously not useful for determining low charge densities, as it is flat until just under 10% charge density. However, using the same tensammograms (Fig. 2) we found that we could construct another standard curve which was most sensitive in the region of low charge density. To do this, we plotted the potential at which the capacitive current read 1 μA versus the charge density (Fig. 4). Non-ionic pams and those of low negative charge density stay adsorbed on the mercury surface at potentials where pams of higher charge density have little affect and the capacitive current in this region is sensitive to the charge density up to a limiting value which would cause all pam to be desorbed. Thus the curve was not reliable at charge densities above ~15% (pams of nominal charge density 5, 12.5, and 25% were analyzed as having values of 5, 13, and 18.5%, respectively) and is complementary to our other standard curve. Charge densities of 10–15% should give the same answer on either curve. Standard deviations of 1.3% and 0.33% were found for repeat analyses of Magnifloc 832A (50%) and Magnifloc 837A (7.5%), respectively.

In determining such as this, it is very likely that clean samples would be used, but if this is not the case some interferences may be present. Other surface active substances, especially if negatively charged, can interfere with the peak height, and also some salts. For example, 10 ppm humic acid decreases the peak height for 832A by over 60%. However, most interferences, including humic acid, can be removed by the various chromatographic processes we developed for cleaning up pam solutions prior to determining concentrations. The procedures are fairly quick and typical interferences and appropriate removal procedures have been described in detail in previous papers (4, 5).

Conclusions

The charge density of pams can be determined by means of standard curves using parameters obtained from tensammograms of the pams in TEAC. The method uses solutions and is not critically dependent on pam concentration. Thus pure, dry samples are not strictly necessary.

Acknowledgement

This work was supported in part by a grant from the U.C.R., St. Francis Xavier University.

1. W. M. LEUNG, D. E. AXELSON, and D. SYNE. Colloid Polymer Sci. **263** 812 (1985).
2. D. W. ROGERS and G. W. POLING. CIM Bull. (793) 152 (1978).
3. N. L. DASSANAYAKE and R. W. PHILLIPS. Anal. Chem. **56**, 1753 (1984).
4. T. SMITH-PALMER, B. R. WENTZELL, J. C. DONINI, and R. J. JERRARD. Can. J. Chem. **66**, 2658 (1988).
5. B. R. WENTZELL, T. SMITH-PALMER, and J. C. DONINI. Can. J. Chem. **65**, 557 (1987).
6. B. BREYER and H. H. BRAUER. Alternating current polarography and tensammetry. Interscience, New York. 1963.
7. E. BEDNARKIEWICZ, M. DONTEN, and Z. KUBLIK. J. Electroanal. Chem. **127**, 241 (1981).
8. N. ITOH. Bull. Soc. Sci. Photo. Jpn. **16**, 24 (1966).
9. M. A. LANGHORST, T. BIEGLER, and H. H. BAUER. Electrochim. Acta, **24**, 1137 (1979).
10. I. R. MILLER and D. C. GRAHAME. J. Coll. Sci. **16**, 23 (1961).
11. W. J. M. VAN TILBORG. Recueil, **96**, 213 (1977).
12. I. R. MILLER and D. C. GRAHAME. J. Am. Chem. Soc. **79**, 3006 (1957).
13. A. N. FRUMKIN and B. B. DAMASKIN. J. Electroanal. Chem. **3**, 36 (1962).

Can. J. Chem. Downloaded from www.nrcresearchpress.com by 186.148.149.217 on 09/07/12
For personal use only.

Chromic oxidation of lactic acid in very strong acid media

MARÍA PIEDAD ALVAREZ-MACHO AND MARÍA ISABEL MONTEQUI-MARTIN
Departamento de Química-Física, Facultad de Ciencias, Universidad de Valladolid, 47005 -Valladolid, Spain

Received April 5, 1989

MARÍA PIEDAD ALVAREZ-MACHO and MARÍA ISABEL MONTEQUI-MARTIN. Can. J. Chem. **68**, 29 (1990).

The oxidation of lactic acid by chromic acid was studied at high concentrations of $HClO_4$, HNO_3, and H_2SO_4. It was observed that the reaction rate depends not only on the acidity of the medium, but also on the nature of the mineral acid. The use of the Bunnett and Bunnett–Olsen criteria and the excess acidity concept allows us to propose a reaction mechanism of the A-2 type, the rate-determining step being a bimolecular process in which water participates as a nucleophile. The enthalpy and entropy of activation were determined; the decrease of the magnitude of these parameters when the acidity of the medium was increased suggests the existence of a compensation effect.

Key words: chromic acid, oxidation, lactic acid, acidic media.

MARÍA PIEDAD ALVAREZ-MACHO et MARÍA ISABEL MONTEQUI-MARTIN. Can. J. Chem. **68**, 29 (1990).

Opérant à des concentrations de $HClO_4$, HNO_3 et H_2SO_4 élevées, on a étudié l'oxydation de l'acide lactique par l'acide chromique. On a observé que la vitesse de la réaction ne dépend pas seulement de l'acidité du milieu mais aussi de la nature de l'acide minéral. L'utilisation des critères de Bunnett et de Bunnett–Olsen ainsi que du concept d'acidité en excès nous permet de proposer un méchanisme réactionnel de type A-2 dans lequel l'étape déterminante de la vitesse de la réaction est un processus bimoléculaire où l'eau agit comme nucléophile. On a détermine l'enthalpie et l'entropie d'activation de la réaction; le fait que l'amplitude de ces paramètres diminue avec une augmentation de l'acidité du milieu suggère qu'il existe un effet de compensation.

Mots clés : acide chromique, oxydation, acide lactique, milieu acidique.

[Traduit par la revue]

Introduction

The functional group of the lactic acid molecule that is attacked by Cr(VI) species depends upon both the acidity and the temperature used (1). If the oxidant attacks the alcohol group, a reaction mechanism of the Westheimer type (2) is suggested, with the modification given by Kwart and Francis (3). In this case, the rate-determining step is the intermolecular decomposition of a cyclic ester, giving the corresponding ketoacid (pyruvic acid) due to the breaking of the C—H bond in the α position (4–7).

On the other hand, when the oxidant attacks the carboxyl group it breaks the C—C bond, giving aldehyde and CO_2 as a result of this decarboxylation (8, 9).

In this work, the chromic oxidation of lactic acid in very strong acid media has been studied, and a reaction mechanism is proposed, in agreement with the results obtained when different correlations of rate constant with acidity of the medium were analyzed.

Experimental

Materials

Lactic acid (Merck) and potassium dichromate (Merck) were used without further purification. The acid solutions were prepared from perchloric, nitric, and sulfuric acids (Panreac) in bidistilled water.

Kinetic measurements

The oxidation of lactic acid by chromic acid was followed at 350 nm with a Perkin–Elmer spectrophotometer, model Coleman 55, equipped with a thermostatted cell holder. All oxidation experiments in these studies were carried out with a large excess of substrate over oxidant concentration ($\sim 10^{-4}$ M). Thus, pseudo-first-order rate constants for the disappearance of chromium(VI), k_{exp}, could be determined by plotting log absorbance vs. time.

Results and discussion

The influence of the concentration of lactic acid on the reaction rate at different concentrations of perchloric acid was studied (Table 1). Linear variations of log k_{exp} vs. log [lactic acid] were found, with slope values of 0.98 ($r_{xy} = 0.9996$), 0.94 ($r_{xy} = 0.9992$), and 0.99 ($r_{xy} = 0.9961$) respectively for the three acidities studied, which indicates that the kinetic order for the lactic acid was one.

TABLE 1. Rate constants at several lactic acid concentrations

	$10^4\ k_{exp}$ (s^{-1})		
	$[HClO_4]$ (M)		
10^2 [Lactic acid] (M)	1.5	2.5	3.5
7.0	25.82	57.12	151.80
6.0	21.77	50.23	132.98
5.0	18.65	42.83	110.08
4.0	15.35	36.63	78.25
3.0	11.53	26.43	72.00
2.0	7.62	18.05	42.83
1.0	3.77	9.37	21.97

$[K_2Cr_2O_7] = 4.6 \times 10^{-4}$ M; $T = 25$°C.

Studies on the variation of rate constant with acidity (Table 2) show that the reaction rate is influenced not only by the acidity of the medium but also by the nature of the mineral acid used as solvent.

To establish a relationship between k_{exp} and the acidity of the medium, the criterion proposed by Zucker and Hammett (10) was first taken into consideration. Good linear correlations were found between log k_{exp} and $-H_0$. However, it was necessary to consider treatments given by other authors (11) because the slope was not one.

Bunnett (12) considered that the water activity had a very important role in acid-catalysed processes and he proposed the following correlation:

$$[1] \quad \log k + H_0 = w \log a_{H_2O} + \text{const.}$$

In which the w parameter is much more sensitive to changes of

Can. J. Chem. Downloaded from www.nrcresearchpress.com by 186.148.149.217 on 09/07/12
For personal use only.

Can. J. Chem. Downloaded from www.nrcresearchpress.com by 186.148.149.217 on 09/07/12
For personal use only.

TABLE 2. Influence of the solvent acidity upon the rate constant

	$10^4 k_{exp}$ (s^{-1})		
	$HClO_4$	HNO_3	H_2SO_4
$[H^+]$ (M)	1.5	2.5	3.5
0.5	4.17	3.98	—
1.0	8.55	8.82	—
1.5	15.35	15.07	—
2.0	24.82	22.90	—
2.5	36.63	32.18	4.47
3.0	53.83	44.45	7.32
3.5	78.25	59.13	11.35
4.0	109.60	75.48	17.45
4.5	—	—	25.93
5.0	—	—	37.75
5.5	—	—	56.72
6.5	—	—	87.10

$[K_2Cr_2O_7] = 4.6 \times 10^{-4}$ M; [Lactic acid] $= 4.0 \times 10^{-2}$ M; $T = 25°C$.

reacting substrate than the slopes of the conventional Zucker–Hammett plots.

Later Bunnett and Olsen (13) obtained very satisfactory results by using linear free energy relationships:

[2] $$\log k + H_0 = \Phi (H_0 + \log[H^+]) + \text{const.}$$

The parameters defining the slopes of these criteria (eqs. [1] and [2]) can be associated for substrates protonated on the oxygen atom as follows:

Water role	w	Φ
Not involved	$-2.5 < w < 0.0$	$\Phi < 0.0$
Nucleophile	$1.2 < w < 3.3$	$0.22 < \Phi < 0.56$
Proton transfer agent	$w > 3.3$	$\Phi > 0.58$

Our findings (Table 3) show that the water participates in the rate-determining step as a nucleophile, allowing us to propose a reaction scheme of the A-2 type, as follows:

[3] $S + H \rightleftharpoons SH^+$ (fast)

[4] $SH^+ + H_2O \rightarrow$ Prod. (slow)

in which "S" represents a 1:1 complex between lactic acid and Cr(VI) species.

Recently Cox and Yates (14) have recommended the use of the excess acidity function X instead of the traditional acidity functions, because it gives important mechanistic information (15). The corresponding correlation equation for an A-2 scheme is

[5] $$\log k - \log[H^+] - n \log a_{H_2O} = m^* m^{\neq} X + \text{const.}$$

In practice, it is necessary to test different values for the factor n ($n = 1,2,...$) until a linear fit of the left side of eq. [5] vs. X is obtained. Our findings indicate that, in a perchloric medium (Fig. 1), two water molecules in the transition state will participate, while in a sulfuric medium (Fig. 2) only one participates. It was not possible to consider the case of nitric acid, because the values of X are not available for this solvent.

The slope of these plots correspond to $m^* m^{\neq}$, where m^* is a parameter that depends only upon the medium (~0.7 in perchloric and ~1.0 in sulfuric) while the value of the $m^{\neq}$ parameter depends upon the mechanism through which the reaction takes

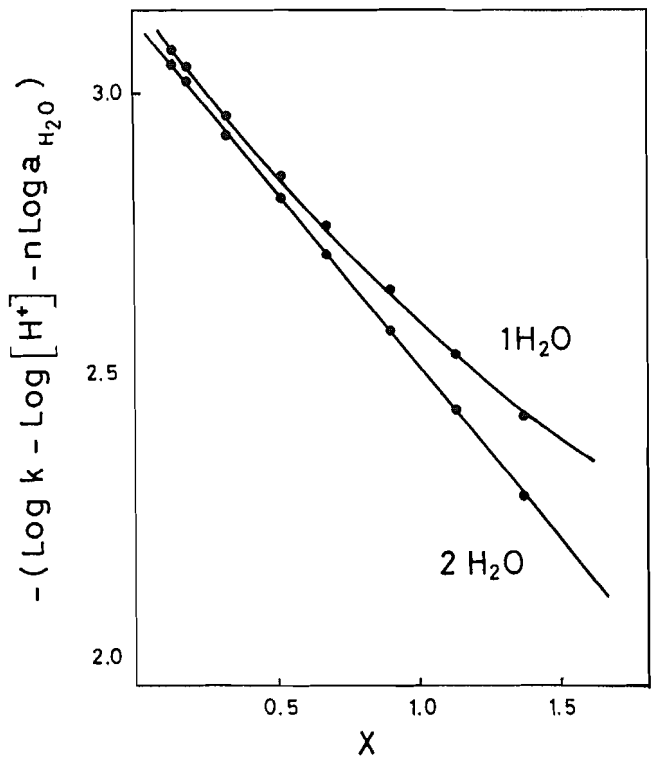

FIG. 1. Plot according to eq. [5] for the chromic oxidation of lactic acid in perchloric acid medium, assuming the involvement of one or two water molecules.

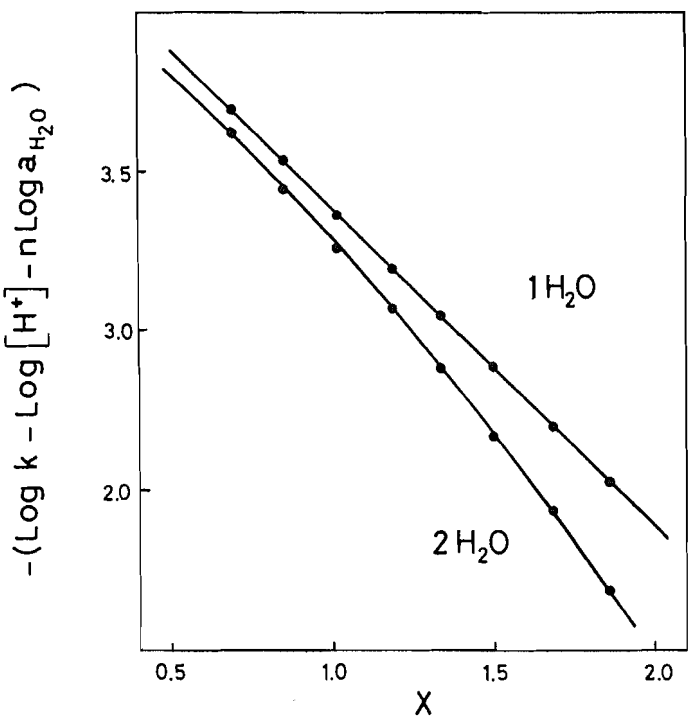

FIG. 2. Plot according to eq. [5] for the chromic oxidation of lactic acid in sulfuric acid medium, assuming the involvement of one or two water molecules.

place. The values obtained for $m^* m^{\neq}$: 0.63 ($r_{xy} = 0.9993$) in perchloric acid and 1.00 ($r_{xy} = 0.9994$) in sulfuric acid, give a value $m^{\neq} \simeq 1$, characteristic of an A-2 type mechanism (15, 16).

The influence of the temperature on the reaction rate at different acidities of the medium was studied and the activation parameters determined (Table 4). The decrease in the magni-

Can. J. Chem. Downloaded from www.nrcresearchpress.com by 186.148.149.217 on 09/07/12
For personal use only.

TABLE 3. Correlation of rate constants with the acidity of the medium

Criterion	Slope $HClO_4$	Slope HNO_3	Slope H_2SO_4	Role of water
Zucker–Hammett $\log k_{exp} = -H_0 + \text{const.}$	0.79 ± 0.02 (r_{xy} = 0.9980)	0.86 ± 0.01 (r_{xy} = 0.9993)	0.79 ± 0.02 (r_{xy} = 0.9998)	—
Bunnett (Equation [1])	2.93 ± 0.06 (r_{xy} = 0.9985)	3.02 ± 0.08 (r_{xy} = 0.9981)	1.32 ± 0.05 (r_{xy} = 0.9959)	Nucleophile
Bunnett–Olsen (Equation [2])	0.41 ± 0.01 (r_{xy} = 0.9988)	0.35 ± 0.01 (r_{xy} = 0.9993)	0.28 ± 0.01 (r_{xy} = 0.9992)	Nucleophile

$[K_2Cr_2O_7] = 4.6 \times 10^{-4}$ M; [Lactic acid] = 4.0×10^{-2} M; T = 25°C.

TABLE 4. Variation of rate constant with temperature. Experimental activation parameters

	$10^2 k_{exp}$ ($M^{-1} s^{-1}$)				
	[$HClO_4$] (M)				
T (°C)	1.0	1.5	2.0	2.5	3.0
25.0	2.14	3.84	6.20	9.16	13.46
27.5	2.82	4.66	6.73	10.96	17.35
30.0	3.35	5.55	8.18	12.50	20.36
32.5	3.98	6.45	9.30	15.02	23.45
35.0	4.74	7.76	11.23	17.64	27.88
$\Delta H^{\neq}$ (kJ mol^{-1})	52.23	50.42	49.03	47.16	45.47
$-\Delta S^{\neq}$ (J mol^{-1} K^{-1})	101.0	102.9	104.3	106.6	108.3

$[K_2Cr_2O_7] = 4.6 \times 10^{-4}$ M; [Lactic acid] = 4.0×10^{-2} M.

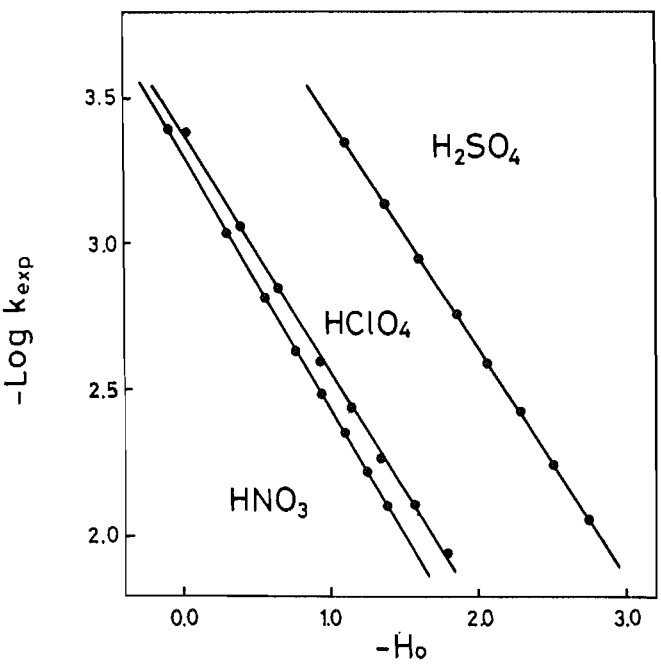

FIG. 3. Variation of rate constant with H_0 for the chromic oxidation of lactic acid.

tude of these parameters, as a consequence of the nucleophilic attack of water, suggests the existence of a compensation effect.

An isokinetic relationship between the activation parameters was found ($\Delta H^{\neq} = \Delta H_0^{\neq} + \beta \Delta S^{\neq}$), the isokinetic temperature being β = 915 K. However, the verification of this isokinetic relationship and the estimation of β involved difficult statistical problems, since $\Delta H^{\neq}$ and $\Delta S^{\neq}$ were determined simultaneously from the same set of experimental data and hence are mutually dependent (17, 18). This problem was avoided by a statistical method (19, 20), which on the one hand permits a reliable estimation of the isokinetic temperature (β = 909 K) and on the other hand vouches for the validity of the isokinetic relationship.

In this work, it was found (Table 2) that the reaction rate depends on the nature of the mineral acid used as solvent. Therefore, in agreement with other authors (19–22), it is possible that the protonation of the acid chromate ion will be accompanied by the incorporation of the anion form of the mineral acid used as solvent, which will considerably affect the subsequent oxidant capability of the new species of Cr(VI), according to the following equilibrium:

$$HCrO_4^- + A^- + 2H^+ \rightleftharpoons HCrO_3A + H_2O$$

From the pK_a values (22), the oxidant ability of these species (for a given value of the Hammett function, H_0) varies in the order:

$$HCrNO_6 > HCrClO_7 > H_2CrSO_7$$

This sequence coincides with that experimentally observed for the values of k_{exp} in different media (Fig. 3). Therefore it is likely that the Cr(VI) will mainly act as $HCrO_3A$, although it is not possible to completely discard the participation of the $HCrO_4^-$ species, especially for low values of the acidity (23).

All the results mentioned above, together with the isotopic effect (7) that indicates the breaking of the α C—H bond in the

rate-determining step, allow us to propose the following mechanism:

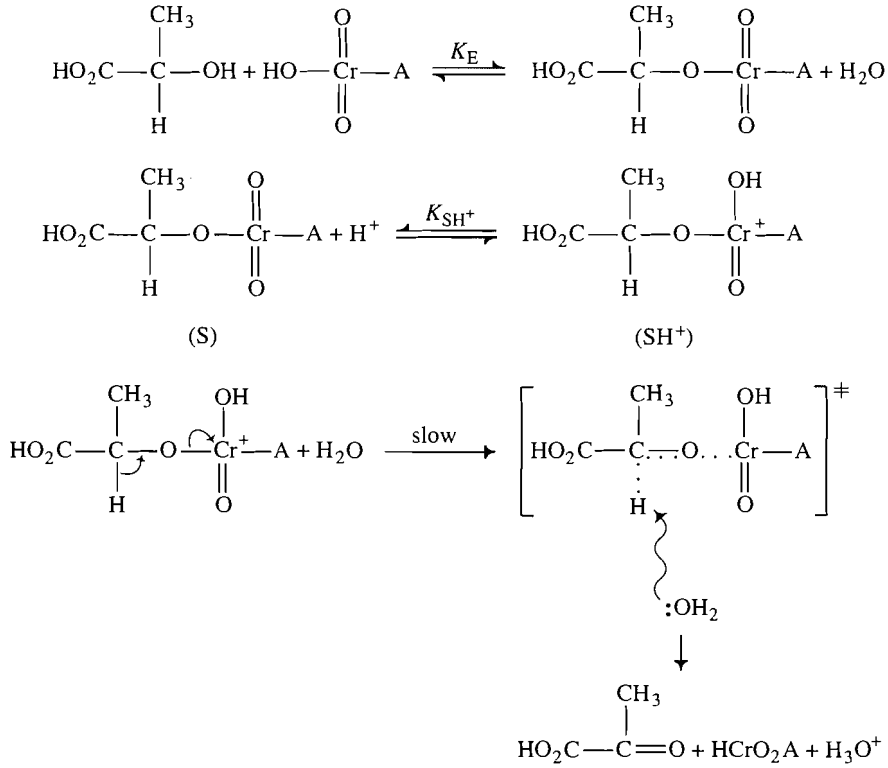

in which "S" represents a chromic ester similar to that proposed by other workers (5–7) for this type of oxidation. The subsequent protonation of the ester will probably take place in the chromate part, which increases the capability of the chromium to accept electrons (22). The results obtained using different criteria of acidity allow us to propose, as the rate-determining step, a bimolecular process in which water acts as a nucleophile and, therefore, represents our formulation of the mechanism for the chromic oxidation of lactic acid at high values of the solvent acidity of the Westheimer type.

1. K. S. Srivastava. Proc. Natl. Acad. Sci. India, Sect. A, **39**, 273 (1969).
2. F. H. Westheimer. Chem. Rev. **45**, 419 (1949).
3. H. Kwart and P. S. Francis. J. Am. Chem. Soc. **77**, 4907 (1955).
4. G. V. Bakore and S. Narain. J. Chem. Soc. 3419 (1963).
5. P. S. Radhakrishnamurti and T. Ch. Behera. Tetrahedron Lett. **53**, 4619 (1970).
6. P. C. Samal, B. B. Pattanaik, S. Ch. Dharma Rao, and S. N. Mahapatro. Tetrahedron, **39**, 143 (1983).
7. G. P. Haight, G. M. Jursich, M. T. Kelso, and P. I. Merrill. Inorg. Chem. **24**, 2740 (1985).
8. S. Sundaran and N. Venkatasubramanian. Proc. Indian Acad. Sci. Sect A, **70**, 157 (1969).
9. N. K. Saran, R. C. Acharya, and S. A. Rao. J. Indian Chem. Soc. **62**, 747 (1985).
10. L. Zucker and L. P. Hammett. J. Am. Chem. Soc. **61**, 2791 (1939). M. A. Paul 1and F. A. Long. Chem. Rev. **57**, 935 (1957).
11. F. Coussemant, M. Hellin, and B. Torck. Les fonctions d,acidité et leurs utilisations en catalyse acido-basique. Gordon and Breach, Paris, 1969; C. H. Rochester. Acidity functions. Academic Press, New York. 1970.
12. J. F. Bunnett. J. Am. Chem. Soc. **83**, 4956 (1961); **83**, 4968 (1961); **83** 4973 (1961); **83**, 4978 (1961).
13. J. F. Bunnett and F. P. Olsen. Chem. Commun. **23**, 601 (1965); Can. J. Chem. **44**, 1899 (1966); **44**, 1917 (1966).
14. R. A. Cox and K. Yates. J. Am. Chem. Soc. **100**, 3861 (1978).
15. R. A. Cox and K. Yates. Can. J. Chem. **57**, 2944 (1979).
16. R. A. Cox and K. Yates. Can. J. Chem. **60**, 3061 (1982).
17. O. Exner. Collect. Czech. Chem. Commun. **29**, 1094 (1964); **37**, 1425 (1972).
18. O. Exner. Nature, **201**, 488 (1964); **227**, 366 (1970).
19. M. Cohen and F. H. Westheimer. J. Am. Chem. Soc. **74**, 4387 (1952).
20. F. Holloway. J. Am. Chem. Soc. **74**, 224 (1952).
21. A. Carrington and M. C. R. Symons. Chem. Rev. **63**, 443 (1963).
22. D. G. Lee and R. Stewart. J. Am. Chem. Soc. **86**, 3051 (1964).
23. F. Westheimer and A. Novick. J. Chem. Phys. **11**, 506 (1943).

Can. J. Chem. Downloaded from www.nrcresearchpress.com by 186.148.149.217 on 09/07/12
For personal use only.

Coupled diffusion of butanol solubilized in aqueous sodium dodecylsulfate micelles

DEREK G. LEAIST
Department of Chemistry, University of Western Ontario, London, Ont., Canada N6A 5B7

Received May 11, 1989

DEREK G. LEAIST. Can. J. Chem. **68**, 33 (1990).

Ternary interdiffusion coefficients have been measured for ten compositions of the system sodium dodecylsulfate (NaDS) + 1-butanol (BuOH) + water at 25°C. The diffusivity of BuOH in this system is lower than in pure water because about one half of the alcohol is solubilized in the slowly-diffusing NaDS micelles. Yet, surprisingly, diffusion of the NaDS component transports only minor amounts of BuOH. Diffusion of the BuOH component, however, produces a substantial coupled flow of NaDS. Although added BuOH increases the solution viscosity and the size of the micelles, the diffusivity of the NaDS component does not change significantly. The Harned restricted diffusion method for the determination of electrolyte diffusivities is extended to electrolyte + nonelectrolyte solutes.

Key words: micelles, ionic; solubilization; diffusion, coupled.

DEREK G. LEAIST. Can. J. Chem. **68**, 33 (1990).

On a mesuré les coefficients d'interdiffusion ternaire pour dix compositions du système dodécylsulfate de sodium (DSna) + 1-butanol (BuOH) + eau, à 25°C. La diffusivité du BuOH dans ce système est plus faible que dans l'eau pure parce qu'environ la moitié de l'alcool est solubilisé dans des micelles de DSNa qui diffusent lentement. Malgré tout et d'une façon surprenante, la diffusion de la composante DSNa ne transporte que de faibles quantités de BuOH. La diffusion de la composante BuOH provoque un flux couplé important du DSNa. Même si l'addition de BuOH provoque une augmentation de la viscosité de la solution et de la grosseur des micelles, la diffusivité de la composante DSNa ne change pas beaucoup. On a étendu la méthode de la diffusion restreinte, développée par Harned pour la détermination des diffusivités électrolytiques, à des solutions du type électrolyte + non-électrolyte.

Mots clés : micelles, ionic; solubilization, diffusion, couplée.

[Traduit par la revue]

Can. J. Chem. Downloaded from www.nrcresearchpress.com by 186.148.149.217 on 09/07/12
For personal use only.

1. Introduction

Organic molecules that do not dissolve appreciably in pure water can often be solubilized by aqueous micelles (1, 2). The research reported here was undertaken to study the coupled diffusion of ionic micelles + solubilizate. To supplement the analysis, ternary interdiffusion coefficients are reported for aqueous sodium dodecylsulfate (NaDS) + 1-butanol (BuOH). Since about one half of the total alcohol is solubilized (3–5) and therefore transported in the NaDS micelles, this system should provide an interesting exception to the rule that diffusion of electrolytes and nonelectrolytes is weakly coupled (6–8). Aqueous NaDS and BuOH were chosen because accurate binary interdiffusion data (9–12) are available for comparison with the ternary results, and because the distribution of BuOH between micellar and aqueous environments has been reported (3, 4).

There have been a number of studies of intradiffusion in micelle + solubilizate solutions (1, 3, 13–15). This type of diffusion refers to the interchange of magnetically- or isotopically-tagged species with untagged species in chemically uniform solutions (6). The interdiffusion coefficients (also known as mutual diffusion coefficients) reported here, by contrast, describe mass transport during the interchange of solute and solvent driven by gradients in chemical composition. Interdiffusion of micelles + solubilizate finds important applications in detergency, tertiary oil recovery and the controlled release of drugs and pesticides. Ternary interdiffusion coefficients are required, for example, to describe the rate of diffusion of aqueous micelles to an oil/water interface, and the subsequent diffusion of the oil-laden micelles back into the aqueous phase. No interdiffusion coefficients for micelles + solubilizate have been reported previously.

2. Experimental

NaDS (BDH specially pure grade) was dried in a vacuum oven at 60°C. 1-Butanol (Fisher reagent grade) was used as received. Solutions were prepared with distilled deionized water in calibrated volumetric flasks.

A simplified version of Harned's restricted diffusion technique (16, 17) was used to measure diffusion of the solutes. The initial concentration gradients were prepared by injecting solutions into the lower end of a short (3.05 cm) column of less dense solution. At each mean cell composition, three runs were performed with the initial gradient in NaDS, and another three with an initial BuOH gradient. The rate of decay of the concentration gradients was followed by measuring changes in electrical conductance across pairs of small platinum electrodes located at 1/6 and 5/6 of height of the solution column. Each run lasted about one week. Ternary interdiffusion coefficients were computed by moments analysis of the conductance versus time data (16). Details of the equipment and procedure have been reported (16, 17).

It might seem inappropriate to use a conductimetric procedure to monitor diffusion of a nonelectrolyte, such as BuOH. But in aqueous NaDS solutions, provided the concentration of NaDS is above the critical micelle concentration, added BuOH increases the conductance (18, 19) by displacing bound Na^+ counterions from the micelles. This gives BuOH a partial molar conductance about one tenth as large as that of the NaDS component, which is sufficiently large for the successful employment of Harned's method.

3. Results

Interdiffusion of aqueous NaDS + BuOH is a complicated process involving the coupled flow of several rapidly-equilibrating solute species: charged micelles (composed of aggregated DS^- ions together with bound Na^+ counterions and solubilized BuOH), free BuOH molecules, and monomeric Na^+ and DS^- ions. A detailed treatment of the diffusion behavior

would have to include interactions between the species (such as electrophoresis), nonideal solute activities, polydispersity of the micelles, and possible changes in micelle shape or structure with composition. These and other complications are included implicitly in the multicomponent diffusion equations (6–8)

$$[1] \quad -J_i = \sum_{k=1}^{2} D_{ik} \nabla C_k \qquad i = 1, 2$$

$$[2] \quad \partial C_i/\partial t = \sum_{k=1}^{2} \nabla (D_{ik} \nabla C_k)$$

J_1 and J_2 denote the molar flux densities of the neutral solute components: 1. total NaDS (micellar + nonassociated electrolyte); 2. total BuOH (solubilized + free alcohol). C_i denotes the total concentration of component i, and coefficient D_{ik} gives the flux of component i produced by the gradient in the concentration of component k. Cross-coefficients D_{12} and D_{21} are included to allow for interactions between the diffusing solutes.

Although multicomponent diffusion equations have not been used in previous studies of micelle + solubilizate transport, they provide a concise but accurate description of the diffusion. No assumptions are made concerning the number or the composition of the various diffusing species. Since the transport equations are written in terms of known total solute concentrations, the D_{ik} values can be determined by experiment (6), using optical or diaphragm–cell methods, or the conductimetric method used here.

Interdiffusion coefficients of aqueous NaDS(1) + BuOH(2) were measured at 25.00 ± 0.05°C and concentrations of each solute from 0.05 to 0.3 M. The results are given in Table 1. D_{11} and D_{12} which describe transport of the NaDS component were reproducible within $\pm 0.01 \times 10^{-9}$ m^2 s^{-1}. The reproducibility of D_{21} and D_{22}, $\pm 0.03 \times 10^{-9}$ m^2 s^{-1}, was poorer due to the lower partial molar conductance of BuOH which meant that its diffusion could not be followed as precisely.

Table 1 includes values of D_{11}, the interdiffusion coefficient of aqueous NaDS, interpolated from an earlier binary conductimetric study on aqueous NaDS in BuOH-free solutions (11). D_{11} might reasonably be expected to decrease with C_2 due to the viscosity increase and the increase in effective micelle diameter with the solubilization. Comparison of the binary data with the present results, however, indicates that added BuOH appears to have little effect on D_{11}, the diffusivity of NaDS. In the most concentrated solution that was studied ($C_1 = 0.3\,M$, $C_2 = 0.3\,M$), however, a drop in D_{11} is noted. This behavior may reflect a breakdown of the micelles structure in favor of a microemulsion (19, 20).

Lyons and Sandquist (12) have used Gouy interferometry to measure accurate binary interdiffusion coefficients for aqueous BuOH. As the concentration of the alcohol increased from 0 to 0.3 M, D_{22} dropped from 0.97×10^{-9} to 0.88×10^{-9} m^2 s^{-1}. The values of the diffusivity of BuOH in NaDS solutions listed in Table 1 are 20–30% lower, no doubt because of the portion of the alcohol that is solubilized is transported in the slowly-diffusing micelles. As the ratio of BuOH to NaDS increases, the solubilized fraction of the total alcohol drops and D_{22} increases.

The ratio D_{12}/D_{22} takes values as large as 1/4, indicating that each mole of diffusing BuOH cotransports up to 1/4 mole NaDS. On the other hand, the relatively small values of D_{21} suggests that NaDS does not co-transport significant amounts of BuOH. This is surprising since the diffusing NaDS micelles carry up to about one-half of the total alcohol (3–5). Consider

TABLE 1.[a] Ternary interdiffusion coefficients of aqueous sodium dodecylsulfate(1) + 1-butanol(2) at 25°C

C_1	C_2	D_{11}	D_{12}	D_{21}	D_{22}
0.05	0.00	(0.38)			
0.05	0.10	0.43	0.04	0.05	0.67
0.10	0.00	(0.47)			
0.10	0.05	0.47	0.09	0.02	0.63
0.10	0.10	0.48	0.12	0.01	0.62
0.10	0.20	0.46	0.08	0.01	0.68
0.10	0.30	0.45	0.07	0.03	0.73
0.20	0.00	(0.51)			
0.20	0.10	0.51	0.12	0.09	0.59
0.30	0.00	(0.49)			
0.30	0.05	0.48	0.12	0.02	0.54
0.30	0.10	0.49	0.17	0.03	0.57
0.30	0.20	0.49	0.13	0.07	0.58
0.30	0.30	0.40	0.12	0.07	0.58

[a] C_i in units of mol dm^{-3} (M), D_{ik} in units of 10^{-9} m^2 s^{-1}.

the solutions containing equimolar amounts of total NaDS and BuOH, for example. It would seem that each mole of the total NaDS should cotransport on the order of 1/2 mole BuOH, and hence the value of D_{21} should equal approximately $D_{11}/2$, about 0.25×10^{-5} m^2 s^{-1}, which is considerably larger than the measured D_{21} values.

4. Discussion

The experimental results suggests that NaDS micelles do not co-transport large amounts of BuOH. This puzzling behavior can be understood by noting that the solubilized fraction of BuOH increases with the concentration of NaDS. Once a gradient in the concentration of NaDS is formed, the region with excess NaDS becomes deficient in free BuOH molecules. Free BuOH molecules then diffuse "up" the NaDS gradient, countercurrent to the solubilized BuOH carried "down" the NaDS gradient by the micelles. Since the diffusivity of free BuOH is about one order of magnitude larger than the diffusivity of the micelles, the rapidly-diffusing free alcohol effectively "levels" the total concentration of BuOH before significant cotransport of micellar alcohol can occur.

By what mechanism does BuOH cotransport relatively large amounts of NaDS? As mentioned earlier, added BuOH releases bound Na^+ counterions from the NaDS micelles. As a result, a gradient in the concentration of total BuOH produces a gradient in the same direction in the concentration of free Na^+ ions. The Na^+ ions, the most mobile solute species, diffuse rapidly down the BuOH gradient. To maintain electroneutrality, negatively-charged micelles are dragged along by the diffusion-induced electric field. The freed Na^+ ions have the additional effect of increasing the diffusivity of the NaDS component, D_{11}. The flow of NaDS is more strongly coupled to the flow of NaDS than expected for typical electrolyte–nonelectrolyte pairs because transport of BuOH produces both an electric field and ionic gradients in the present system.

In the present work, diffusion with solubilization is described by using coupled diffusion equations for the total solute components. However, the diffusion of associating solutes is more frequently described by using pseudobinary transport equations (8, 21–29)

$$[3] \quad j_i = -D_i \nabla c_i$$

$$[4] \quad \partial c_i/\partial t = D_i \nabla c_i^2 + r_i$$

Can. J. Chem. Downloaded from www.nrcresearchpress.com by 186.148.149.217 on 09/07/12
For personal use only.

for each solute species. Since the individual species that constitute the total solute components are not conserved, eqs. [4] include the reaction rate of species i per unit volume, r_i. It is often overlooked that unlike the multicomponent diffusion equations [1] and [2], eqs. [3] and [4] are accurate only for dilute solutions in which solute–solute interactions are negligible. Moreover, for many systems, including the one under discussion, the identity of the various species and their concentrations (c_i), diffusion coefficients (D_i), and reaction rates are not known accurately, nor are they easily measured. For charged solute species, there is the additional complication that eqs. [3] and [4] should include terms for the transport driven by the electric field that is generated whenever the diffusing ions have different mobilities (30, 31).

Despite their limitations, the pseudobinary transport equations can be used to help interpret multicomponent diffusion (32). With this goal in mind, attempts were made to predict the multicomponent diffusion coefficients using estimates of the concentrations and the diffusion coefficients of the various transported solute species. As a first approximation, three major solute species were assumed: mixed micelles (DS_nNa_q-$BuOH_s)^{q-n}$; free alcohol molecules, BuOH; and free counterions, Na^+. (The concentration of free dodecylsulfate ions is negligible provided the concentration of total NaDS is well above the critical micelle concentration (0.008 M at 25°C (33)). Unfortunately, it was not possible to obtain estimates of the D_{ik} coefficients in reasonable agreement with experiment. A more successful treatment of the problem could be formulated by using the stepwise aggregation model.

$$nDS^- + qNa^+ + sBuOH = (DS_nNa_qBuOH_s)^{q-n} \qquad K_{nqs}$$

It would be necessary, however, to determine the values of a large number of association constants K_{nqs}. The stepwise aggregation models that have been reported for ionic micelles + solubilizate (34–37) do not include variable degrees of counterion binding, an important feature for diffusion. Even with a better description of the speciation, the problem of evaluating the diffusivities of the various species remains. In view of these difficulties, it is likely that multicomponent diffusion experiments will be required for a quantitative description of micelle + solubilizate transport for some time to come.

Acknowledgments

The author thanks D. Valic for technical assistance. This research was supported by the Natural Sciences and Engineering Research Council of Canada.

1. H. Wennerstrom and B. Lindman. Phys. Rep. **52**, 1 (1979).
2. P. A. Winsor. Chem. Rev. **68**, 1 (1968).
3. P. Stilbs. J. Colloid Interface Sci. **87**, 385 (1982).
4. G. A. Smith, S. D. Christian, and E. E. Tucker. Langmuir. **3**, 598 (1987).
5. J. A. Butler, C. N. Ramchandani, and D. W. Thomson. J. Chem. Soc. 280 (1935).
6. H. J. V. Tyrrell and K. R. Harris. Diffusion in liquids. Butterworths, London. 1984.
7. E. L. Cussler. Multicomponent diffusion. Elsevier, Amsterdam. 1976.
8. E. L. Cussler. Diffusion. Cambridge University Press, Cambridge. 1974.
9. D. F. Evans, S. Mukherjee, D. J. Mitchell, and B. W. Ninham. J. Colloid Interface Sci. **93**, 184 (1983).
10. R. M. Weinheimer, D. F. Evans, and E. L. Cussler. J. Colloid Interface Sci. **80**, 357 (1981).
11. D. G. Leaist. J. Colloid Interface Sci. **111**, 230 (1986).
12. P. A. Lyons and C. L. Sandquist. J. Am. Chem. Soc. **75**, 3896 (1953).
13. B. Lindman, M. C. Puyal, N. Kamenka, B. Brun, and G. Gunnarsson. J. Phys. Chem. **86**, 1702 (1982).
14. P. Stilbs. J. Colloid Interface Sci. **89**, 547 (1982).
15. J. B. Rosenholm and B. Lindman. J. Colloid Interface Sci. **57**, 362 (1976).
16. D. G. Leaist. Can. J. Chem. **63**, 2933 (1985).
17. D. G. Leaist and P. A. Lyons. J. Solution Chem. **13**, 77 (1984).
18. A. S. C. Lawrence and J. T. Pearson. Trans. Faraday Soc. **62**, 495 (1966).
19. I. Vikholm, G. Douheret, S. Backlund, and H. Høiland. J. Colloid Interface Sci. **116**, 582 (1987).
20. G. Roux-Desgranges, A. H. Roux, J. P. E. Grolier, and A. Viallard. J. Solution Chem. **11**, 357 (1982).
21. W. J. Ward. A.I.Ch.E. J. **16**, 405 (1970).
22. J. S. Schultz, J. D. Goddard, and S. R. Suchdeo. A.I.Ch.E. J. **20**, 417 (1974); **20**, 625 (1974).
24. D. G. Leaist. Can. J. Chem. **66**, 1129 (1988).
25. R. H. Stokes. J. Phys. Chem. **69**, 4012 (1965).
26. H. Schönert. Z. Phys. Chem. N. F. **119**, 53 (1980).
27. K. R. Krovvidi and P. Stroeve. J. Colloid Interface. Sci. **110**, 437 (1986).
28. A. C. Lam and R. S. Schecter. J. Colloid Interface Sci. **120**, 43, 57 (1987).
29. A. Ekman, S. Liukkonen, and K. Kontturi. Electrochim. Acta, **23**, 243 (1978).
30. F. M. Choy, D. F. Evans, and E. L. Cussler. J. Am. Chem. Soc. **96**, 7085 (1974).
31. D. G. Leaist. Can. J. Chem. **65**, 2489 (1987).
32. D. G. Leaist. J. Chem. Soc. Trans. Faraday Soc. 1, **78**, 3069 (1982).
33. P. Mukerjee and K. J. Mysels. Critical micelle concentrations of aqueous surfactant solutions. Nat. Stand. Ref. Data Ser. Nat. Bur. Stand. (U.S.) 1971.
34. D. Hetu, A. H. Roux, and J. E. Desnoyers. J. Solution Chem. **16**, 529 (1987).
35. R. de Lisi, V. T. Liveri, M. Castagnolo, and A. Inglese. J. Solution Chem. **15**, 23 (1986).
36. R. de Lisi, C. Genova, R. Testa, and V. T. Liveri. J. Solution Chem. **13**, 121 (1984).
37. S. D. Christian, E. E. Tucker, G. A. Smith, and D. S. Bushong. J. Colloid Interface Sci. **113**, 439 (1986).

Can. J. Chem. Downloaded from www.nrcresearchpress.com by 186.148.149.217 on 09/07/12
For personal use only.

Enhanced polymerization of molybdate ions in the presence of antimonic acid

M. KONE, P. COURTIN, AND J. LEMERLE

Laboratoire de chimie des polymères inorganiques, Unviersité Pierre et Marie Curie, 75252 Paris Cedex 05, France

Received July 31, 1989

M. KONE, P. COURTIN and J. LEMERLE. Can. J. Chem. **68**, 36 (1990).

Polymer compounds including both antimony and molybdenum were formed by mixing freshly prepared solutions of antimonic and molybdic acid. These acids were formed through an ion exchange process. When antimony is in excess, molybdenum is included in the high polymers having the ccp structure of β antimonic acid. When molybdic acid is in excess in the starting mixture, molybdenum-rich polymers with a larger molecular weight than molybdic acid were formed. In GPC experiments the behaviour of the compounds is related to their Mo and Sb content. The elution volume is only related to the molecular weight of the compound when Sb is the main component and imposes its structure.

Key words: molybdoantimonic acids, inorganic polymers, ultracentrifugation, GPC.

M. KONE, P. COURTIN et J. LEMERLE. Can. J. Chem. **68**, 36 (1990).

Des polymères composés d'antimoine V et de molybdène VI sont élaborés par mélange d'acides molybdiques et antimoniques fraîchement préparés. Ceux-ci sont eux-mêmes préparés par échange d'ions. La nature des composés obtenus dépend de l'élément en excès dans le milieu. Quand l'antimoine est en excès, le molybdène est inclus dans des hauts polymères ayant la structure pyrochlore de l'acide antimonique β. Quand le molybdène est en excès, des polymères riches en molybdène incluent de l'antimoine. Leur nombre d'atomes de molybdène est nettement supérieur à celui de l'acide molybdique. Quand les polymères sont riches en molybdène le fractionnement par GPC est fortement perturbé par l'adsorption sur le gel. Cet artéfact peut être utilisé pour caractériser la nature des polymères formés.

Mots clès : acides molybdoantimoniques, polymères inorganiques, ultracentrifugation, GPC.

[Traduit par la revue]

Introduction

Polymerization of some transition or post-transition metals occurs spontaneously upon acidification. For example, acidification results in the formation of polymer built up from MO_6 octahedra (M = W, V, Mo, Sb...) (1). The nature of the polymers depends not only on the experimental conditions (e.g. pH) but also on the history of the sample since some of the conversions are slow (2).

If the protonation goes through an ion exchange process, tungstate solutions lead to α tungstic acid (polymerization degree $n = 24$) which spontaneously polymerizes to form a gel and then WO_3 (3). Molybdate solutions lead to molybdic acid ($n = 48$) but this acid does not age to form polymers with a higher molecular weight (4). Nevertheless, polymerization of molybdic acid can be enhanced by mixing with polytungstic acids even with the less reactive ones (5). Antimonic acid spontaneously ages to form high polymers which sedimentate (6). Before its polymerization it reacts with α tungstic acid to form suluble mixed compounds (7). In this paper we study the formation of polymerized anions, including both molybdic and antimonic acids.

Experimental

The solutions were prepared by mixing solutions of antimonic and molybdic acids. The antimonic acid was prepared by ion exchange in a resin (DOWEX 50 WX2 100–200 mesh) from potassium hexahydroxoantimonate solutions (Merck, analytical grade). Just after the exchange, turbid solutions were obtained. They became clear after aging (1 h) and α antimonic acid was formed (6). The molybdic acid was also prepared by ion exchange in a resin (DOWEX 50 WX8 100–200 mesh) from sodium molybdate solutions (Prolabo analytical grade). In this paper we use x_i for the initial molar fraction of molybdenum in the mixtures of the two acids. To prepare mixtures whose x_i lies from 0 to 1, two series of samples were prepared: Samples A with a constant antimony concentration (6×10^{-2} mol L^{-1}) and a variable molydbenum concentration ($0 \leq x_i \leq 0.64$); samples B with a constant molybdenum concentration (8×10^{-2} mol L^{-1}) and a variable antimony concentration ($0.65 \leq x_i \leq 1$).

To study the influence of the total concentration of the reactants, samples with the same x_i as samples A but with lower antimony concentration (3.45×10^{-2} mol L^{-1}) were prepared (samples C).

All mixtures were allowed to age. Measurements were carried out after 2 and 15 months.

The concentrations of antimony and molybdenum were measured after alkaline degradation of the compounds. The samples were heated for 1 day in an excess of potassium hydroxide. The resulting solution was adjusted to pH 8 in a volumetric flask and aliquot reactions were used for titrations. Antimony was titrated by atomic absorption with an air–acetylene flame with a Perkin-Elmer 373 spectrophotometer. Molybdenum was colorimetrically titrated using the molybdenum–pyrocatechol complex formed at pH 7 (8). Measurements were carried out at $\lambda = 400$ nm with a Beckman spectrophotometer.

Analytical ultracentrifuge experiments were carried out with a Beckman model E ultracentrifuge equipped with schlieren and absorption optics. Double sector cells manufactured in Kel F were used. The rotation speed ranges from 8000 to 56000 rpm depending on the sample. To avoid the effects of electric charges, an electrolyte (LiCl 5×10^{-2} mol L^{-1}) was added to the sample just before the run. Specific volumes were measured from density measurements carried out with a PAAR automatic densimeter.

Preparative ultracentrifugations were carried out with a Beckman microfuge at 10000 rpm for 1 h. In this centrifuge the tube axis is colinear with the centrifugal field.

The ultrafiltration of the sample was carried out in a Millipore assembly using Pellicon PTGC membranes under a nitrogen flow (NMWL tested for similar compounds 15000 daltons (9)). Polyacrylamide gel manufactured by Bio-Rad was used for gel permeation chromatography (GPC). This gel has been standardized with known antimonic polymers and has an exclusion limit corresponding to 16000 daltons (10).

Results

The aged samples corresponding to small x_i (low molybdenum content) were turbid, but they do not precipitate even after several months at rest. When x_i increases, the turbidity decreases and a yellow colour appears. For x_i values higher than 0.3 the samples were limpid and yellow colored.

The ultracentrifugation measurements exhibit three types of

Printed in Canada / Imprimé au Canada

Can. J. Chem. Downloaded from www.nrcresearchpress.com by 186.148.149.217 on 09/07/12
For personal use only.

TABLE 1. Ultracentrifugation results for samples A and B

x_i	Sample	Free sedimentation S^*		Without free sediment, molecular weight		Amount of small polymer†
		$v < 8000$	$v = 56000$	Small polymer	Oligomer	
0.17	A	7303				
0.23	A	6476			2050	
0.28	A	6250				
0.38	A	3510	17.3		1500	
0.43	A	3180	16.2		850	
0.47	A	3055	16.6		915	
0.50	A		15.8		1300	
0.52	A		17.5; 6.9			
0.56	A		6.9			
0.60	A		7.6			
0.64	A		6.9			
0.65	B			10950	1090	58
0.70	B			7340	950	70
0.75	B			5540	1210	49
0.80	B			5700	1170	43
0.85	B			7500	920	16
0.94	B				1680	

*Expressed in Svedberg.
†Expressed in g/100.

TABLE 2. Ultracentrifugation results for samples C

x_i	Age (months)	Free sedimentation		Without free sediment		Amount of small polymer†
		S_1*	S_2	M small polymer	M_2 oligomer	
0.09	2	3785	2696			
0.14	2	3872	2743			
0.30	2	3085	2190		1870	
0.40	2			13800	1300	18
0.49	2			8300	840	45
0.56	2			6400	1060	62
0.64	2			12500	1500	72
0.14	15	5181	3560			
0.30	15	4137			1890	
0.40	15	3529	2710		2250	
0.49	15	2681	1878		1915	
0.56	15			16200	1018	45
0.64	15			12450	990	64

*Expressed in Svedberg.
†Expressed in g/100.

compounds according to their behaviour in the centrifugal field. The low speed experiments ($\leq$ 8000 rpm) exhibit free sedimenting species when $x_i < 0.50$ (samples A and C). Their sedimentation coefficients S range from 2000 to 8000 Svedberg (Tables 1 and 2). In these experimental conditions, only one sedimentation peak was observed for samples A and two for samples C. The S value decreases with decreasing antimony concentration (x_i constant) or increasing x_i. Moreover, the S values are enhanced when the samples age (Table 2). All sedimenting species having an S value greater than 2000 are labelled "high polymers."

The high speed experiments (56000 rpm) exhibit free sedimenting species when $0.38 < x_i < 0.64$ (samples A only). Their sedimentation coefficient range from 6.9 to 17.3 (Table 1). At the same speed non-sedimenting species were observed for most samples. Their molecular weight is calculated by the Archibald's method (11, 12) assuming the compounds to be in equilibrium at the meniscus of the cell (Tables 1 and 2). According to the x_i value, two types of patterns were observed on the photographic plates and one of them ($x_i > 0.65$) corresponds to a mixture of two species. The heavier species has a molecular weight near 7000 and would freely sedimentate if it was alone in the medium. These compounds (M = 7000) and the free sedimenting species ($6.9 < S < 17.3$) are considered to have the same range of molecular weight; and are labelled "small polymers." Nevertheless, we will distinguish the small polymers obtained from samples A (small polymers A) and those from samples B (small polymers B). The compounds

Can. J. Chem. Downloaded from www.nrcresearchpress.com by 186.148.149.217 on 09/07/12
For personal use only.

Can. J. Chem. Downloaded from www.nrcresearchpress.com by 186.148.149.217 on 09/07/12
For personal use only.

TABLE 3. Relative abundance and composition of high polymers

x_i	Sample	Mo/Sb*	%†
0.17	A	0.085	90
0.23	A	0.11	79
0.38	A	0.32	22
0.43	A	0.47	10
0.47	A	0.60	6

*Mo/Sb: composition of high polymers.
†%: ratio of antimony concentration in the high polymers to the whole antimony concentration (expressed in %).

TABLE 4. Composition and abundance of high polymers, samples C

x_i	Age (month)	Mo/Sb*	%†
0.09	2	0.045	0.84
0.14	2	0.08	0.64
0.30	2	0.20	0.26
0.40	2	0.37	0.03
0.09	15	0.045	0.85
0.14	15	0.08	0.76
0.30	15	0.19	0.46
0.40	15	0.35	0.28

*Mo/Sb: composition of high polymers.
†%: ratio of antimony concentration in the high polymers to the whole antimony concentration (expressed in %).

having the smaller molecular weight ($M < 2000$) are labelled "oligomers." Each type of polymer (high polymers, small polymers, and oligomers) was isolated using a technique which splits the samples according to their molecular weight: preparative ultracentrifugation, ultrafiltration, and GPC.

In preparative ultracentrifugation the high polymers were packed down to the bottom of the centrifugation tube and the small polymers and oligomers remain in the supernatant solution. Mo and Sb were titrated in the supernatant solution and by difference with the initial concentrations, we obtain the high polymers composition. This composition was also obtained by direct titration. The two values are in good agreement. When x_i increases, the amount of high polymer decreases and the Mo content increases (Table 3). The composition of high polymers is only dependant on x_i. Their abundance increases when the sols age (Table 4).

Powder patterns of solid high polymers exhibit the same cubic close packing (ccp) structure (pyrochlore type) as the β antimonic acid (6). The length of the unit cell decreased slightly as in other mixed compounds with antimonic acid (7, 9) (a = 10.35 Å). The diffraction patterns obtained with a sol containing high polymers and those obtained with solid high polymers isolated from this sol were the same. Thus we can expect that the crystals exist in the aqueous phase with the same size as in the solid state.

The supernatant solutions and the samples which do not contain high polymers were splitted by ultrafiltration ($x_i < 0.52$) and high speed ultracentrifugation ($x_i > 0.52$). When $0.30 < x_i < 0.52$, one compound does not pass through the membrane. These samples correspond to those which exhibit free sedimenting species ($S \simeq 17$ Svedberg). The compounds which were stopped by the membrane were dissolved in water. This solution was analysed with the ultracentrifugation technique and Mo and Sb were titrated. The ultracentrifugation exhibits a free sedimenting compound ($S \simeq 17$ Svedberg). Therefore these compounds were the small polymers A. Their composition is reported in Table 5. The high speed ultracentrifugation experiments lead to the composition of small polymers B (Table 5).

TABLE 5. Composition and relative abundance of small polymers

x_i	Name of small polymers	Mo/Sb	%*
0.23	A		0
0.30	A	0.65	11.5
0.41	A	0.60	33.5
0.47	A	0.69	51.7
0.52	A	0.76	15
0.56	B	1.38	81
0.60	B	1.56	85
0.64	B	1.76	89

*%: ratio of antimony concentration in the small polymers to the antimony concentration (expressed in %).

All samples were studied by GPC. If they contain high polymers, a preparative centrifugation was done before chromatography to remove the high polymers. Some compounds containing Mo and Sb in a constant ratio Mo/Sb = 2/3 were excluded when $0.30 < x_i < 0.52$ (samples A). All samples exhibit one or several elution peaks for the following volumes:

$1.5v_m$, $x_i > 0.65$

$2.25v_m$, $x_i < 0.52$

$3.75v_m$, $x_i > 0.4$ (these fractions were yellow coloured)

$5.25v_m$, $x_i > 0.8$

where v_m = the outer volume of the gel.

The composition of the various fractions corresponding to these peaks are reported in Table 6. Pure molybdic acid was eluated for a volume corresponding to $5.25v_m$. Molybdenum-rich samples (samples B) were also passed through a column containing an ion exchange resin (Amberlite CG 400 100–200 mesh Cl^- form). Molybdic acid was fixed. The remaining solution was studied with GPC technique in the same conditions as previously. The elution peak located at $5.25v_m$ does not exist.

Discussion

Upon aging α antimonic acid transforms into insoluble β antimonic acid (6). In previous works (7, 9) it has been seen that mixed polymers can be formed with antimonic acid by substitution of a SbO_6 octahedron by another octahedral group MO_6 if the size substituting atoms are close to that of antimony atoms. The amount of mixed compound formed decreases when the ratio of substituting atoms increases. These MO_6 groups limit the extent of the β antimonic structure formed by polymerization (9). The aged samples A, B, or C never exhibit any precipitate. Thus in each sample all the antimony combines with the molybdenum to form new mixed compounds, thus preventing antimony precipitation. From the experimental

TABLE 6. Composition of GPC fraction*

	Elution volume							
	v_m		$1.5v_m$	$1.25v_m$		$3.75v_m$		$5.25v_m$
x_i	Mo/Sb	%a	%a	Mo/Sb	%a	Mo/Sb	%a	%b
0.23				0.68	25			
0.38	0.67	18		0.68	40			
0.43	0.70	33		0.70	35			
0.47	0.68	45		0.74	25			
0.52				0.70	ϵ			
0.65			76			3.75	24	
0.70			69			4.68	31	
0.75			60			6.60	40	
0.80			41			6.17	59	ϵ
0.85			31			6.37	69	43
0.89			50			5.50	50	67
0.94			51			6.22	49	89

*%a: ratio of the antimony concentration in the fraction to the whole antimony concentration expressed in %; %b: ratio of the molybdenum concentration in the fraction to the whole molybdenum concentration expressed in %.

TABLE 7. Composition and abundance of oligomers*

x_i	Mo/Sb	%†
0.23	1	20
0.30	0.65	47
0.38	0.65	52
0.41	0.89	55
0.47	1.12	35
0.56	1.12	20
0.60	1.12	15
0.65	3	10
0.70	4.53	15
0.75	6.20	25

*The composition of the oligomers was obtained from the concentrations of molybdenum and antimony obtained after deduction of molybdenum and antimony contained in high and small polymers.

†%: ratio of antimony concentration in the oligomers to the whole antimony concentration (expressed in %).

results the composition and the relative abundance of different compounds can be calculated (Tables 5 to 7).

When x_i reaches to 0.5, high polymers including molybdenum in the ccp structure of antimonic acid are formed. The other compounds formed are oligomers ($x_i < 0.28$) or oligomers and small polymers A ($0.28 < x_i < 0.5$).

The compositions (Mo/Sb) of the small polymers A and the oligomers are in the same range. Therefore small polymers can be formed from oligomers through a condensation process.

In a previous work (9) the formation process of mixed polymers has been described. In such a process the chemical element in excess impose its "structure." The formation of high polymers with a ccp structure ($x_i < 0.5$) agrees with this rule. When $x_i < 0.5$, the GPC experiments give fraction whose composition agrees with that of small polymers A and oligomers. The molecular weight of these compounds are in good agreement with the volume of eluent used for these fractions. Thus in the GPC experiments, the antimony-rich compounds have the same behaviour as the α antimonic acid or its derivatives (10, 13, 14). When $x_i > 0.5$ the compounds eluted for $v = 1.5v_m$ and $3.75v_m$ have the same composition as small polymers B and oligomers, respectively. Molybdic acid is eluted for $5.75v_m$. All these elution volumes are abnormal: elution occurs for larger volumes than the volume of the gel and molybdic acid whose molecular weight is greater than oligomers (4) is eluted for these largest elution volumes. One factor to be considered is the adsorption of molybdenum-rich compounds onto the gel. For antimony-rich compounds the splitting of the sols by gel chromatography is based upon the difference in molecular weight and for molybdenum-rich compounds, the splitting is based upon the difference in chemical reactivity between gel and molybdic compounds. This reactivity can be related to the structure of the compounds due to the excess of molybdenum in these mixed compounds.

For a given x_i only the molecular weight and the amount of high polymer depend on the sol concentration, but the samples do not have the same behaviour in a centrifugal field. With samples C, two peaks are observed and for a given aging time the sedimentation coefficients are smaller than the corresponding ones for samples A and B. We can therefore assume that the particles can associate or dissociate into large units without change in chemical composition if the molecular weight of high polymer is large enough. When the concentration of the sols increases an association equilibrium between high polymers particles is displaced towards the formation of associated particles, and only one sedimentation peak is seen. When the sols age, the high polymer particles grow through a water elimination process involving particles having the same composition.

In mixtures of α tungstic acid and α antimonic acid only two types of mixed compounds are formed for a given initial ratio of W/Sb (7). In their formation process, the first step is the depolymerization of both α antimonic and α tungstic acids. The second step is the polymerization of the monomer units of each element including monomer units of the other element. With molybdenum, the starting material (molybdic acid) can not be considered a monomer unit to stop the polymerization of antimony. However, it does not polymerize enough to form particles with more than 48 atoms per molecule (4). Moreover, molybdic acid exists in two forms according to the concentration and the pH of the solution (4). In the concentration range used in this paper the molybdic acid always exists under its two forms. As a result the number of mixed compounds is enhanced.

Conclusion

Stable aqueous sols of mixed compounds including both antimony and molybdenum can be made by mixing freshly prepared solutions of antimonic and molybdic acids. Depending on the composition of the inital mixture, different types of polymers can be formed. The element (Mo or Sb) in excess imposes its structure and the properties of the compounds. Gel chromatography can be used to split the sols. The elution volume is related to the molecular weight of the species if antimony is the main constituent. On the other hand, if molybdenum is the main constituent the chemical reactions between the gel and the mixed compounds control the splitting.

1. M. T. POPE. Heteropoly and isopoly oxometalates. Springer Verlag. 1983.
2. P. SOUCHAY. Ions minéraux condensés. Masson Paris. 1969.
3. J. LEMERLE and J. LEFEBVRE. Can. J. Chem. **55**, 3758 (1977).

Can. J. Chem. Downloaded from www.nrcresearchpress.com by 186.148.149.217 on 09/07/12
For personal use only.

4. P. COURTIN and J. LEMERLE. To be published.
5. P. COURTIN and J. LEFEBVRE. Can. J. Chem. **64**, 220 (1986).
6. J. LEMERLE. Rev. Chim. Min. **9**, 863 (1972).
7. J. LEMERLE and J. LEFEBVRE. Bull. Soc. Chim. **3.4**, 409 (1976).
8. S. SEIFTER and B. NOVIC. Anal. Chem. **23**, 188 (1951).
9. J. MANDAVO and J. LEMERLE. Nouv. J. Chim. **11**, 3 (1987).
10. J. P. JOLIVET and J. LEFEBVRE. Bull. Soc. Chim. **11–12**, 2420 (1975).
11. W. J. ARCHIBALD. J. Phys. Colloïd Chem. **51**, 1204 (1947).
12. P. TRAUTMAN. J. Phys. Chem. **60**, 1211 (1956).
13. J. LEMERLE and J. LEFEBVRE. C.R. Acad. Sci. Ser. C, **268**, 1125 (1969).
14. J. LEMERLE. Rev. Chim. Min. **10**, 431 (1973).

Can. J. Chem. Downloaded from www.nrcresearchpress.com by 186.148.149.217 on 09/07/12
For personal use only.

Arene σ,π complexes: synthesis and electrochemistry of $(\eta^6\text{-}1,4\text{-}C_6H_4XFp)Cr(CO)_3$ (where X = H, Me, Cl, or OMe; Fp = $(\eta^5\text{-}C_5H_5)Fe(CO)_2$)[1]

GEORGE B. RICHTER-ADDO, ALLEN D. HUNTER,[2] AND NADIA WICHROWSKA
Department of Chemistry, University of Alberta, Edmonton, Alta., Canada T6G 2G2

Received April 11, 1989

GEORGE B. RICHTER-ADDO, ALLEN D. HUNTER, and NADIA WICHROWSKA. Can. J. Chem. **68**, 41 (1990).

The bimetallic complexes $(\eta^6\text{-}1,4\text{-}C_6H_4XFp)Cr(CO)_3$ (where X = H, Me, Cl, or OMe; Fp = $(\eta^5\text{-}C_5H_5)Fe(CO)_2$) were synthesized in 32–80% yields by the reaction of NaFp with $(\eta^6\text{-}1,4\text{-}C_6H_4XF)Cr(CO)_3$ (where X = H, Me, or OMe) or $(\eta^6\text{-}1,4\text{-}C_6H_4Cl_2)Cr(CO)_3$. They were fully characterized by conventional spectroscopic techniques. In these complexes, the arenes are σ bound to the Fp group and π bound to the $Cr(CO)_3$ group. The ^{13}C NMR data suggest that a synergic substituent–arene–Fp π interaction is occurring. Cyclic voltammetric studies of these complexes in CH_2Cl_2 show that they are oxidized reversibly to give stable radical cations, and confirm that the Fp substituents are strong net electron donors to the $Cr(CO)_3$ fragments.

Key words: bimetallic, iron, chromium, arene, oxidation.

GEORGE B. RICHTER-ADDO, ALLEN D. HUNTER et NADIA WICHROWSKA. Can. J. Chem. **68**, 41 (1990).

Faisant appel à la réaction du NaFp avec le $(\eta^6\text{-}1,4\text{-}C_6H_4XF)Cr(CO)_3$ (dans lesquels X = H, Me ou OMe) ou $(\eta^6\text{-}1,4\text{-}C_6H_4Cl_2)Cr(CO)_3$, on a réalisé la synthèse des complexes bimétalliques $(\eta^6\text{-}1,4\text{-}C_6H_4XFp)Cr(CO)_3$ (dans lesquels X = H, Me, Cl ou OMe et Fp = $(\eta^5\text{-}C_5H_5Fe(CO)_3)$ avec des rendements allant de 32 à 80%. On les a pleinement caractérisés grâce aux techniques spectroscopiques conventionnelles. Dans ces complexes, les arènes sont liés au groupement Fp par une liaison σ et au groupement $Cr(CO)_3$ par une liaison π. Les données de la RMN du ^{13}C suggèrent qu'il existe une interaction π substituant–arène–Fp. Des études de voltamétrie cyclique réalisées sur ces complexes en solution dans le CH_2Cl_2 montrent qu'ils s'oxydent d'une façon réversible pour donner des cations radicaux stables et elles confirment que les substituants Fp sont de forts donneurs nets d'électrons aux fragments $Cr(CO)_3$.

Mots clés : bimétallique, fer, chrome, arène, oxydation.

[Traduit par la revue]

Introduction

Organic ligands having delocalized π systems can act as electronic bridges between adjacent metal centers. This property should allow the synthesis of linear-chain organometallic polymers exhibiting one-dimensional electronic conductivity, i.e.,

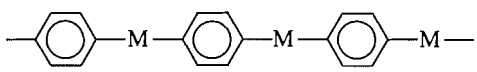

Our initial studies in this area have focussed on the synthesis of model complexes containing arenes as the bridging ligands (e.g., $C_6H_{6-n}(ML_m)_n$, where ML_m = Fp, $Mn(CO)_5$, etc., and Fp = $(\eta^5\text{-}C_5H_5)Fe(CO)_2$) (1). Particular emphasis has been placed on the elucidation of the factors controlling the degree and nature of electronic linkage in such species. During the course of these studies, we have shown that the strongest electronic interactions occur when the organometallic groups are arranged *para* to one another. A consequence of this 1,4 interaction is that the bonding in such complexes develops significant dimetalloquinone character (1*b*), i.e.,

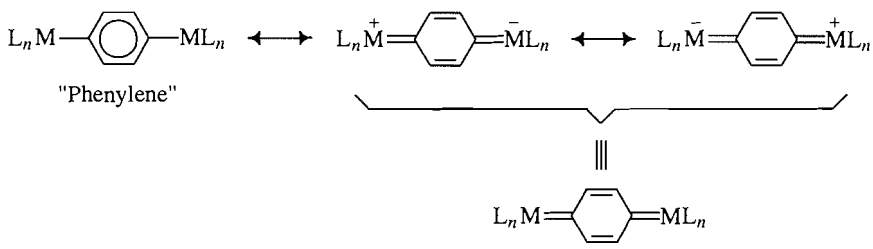

which may be related to the mode of electrical transmission in any phenylene-bridged polymers to be synthesized in the future. An additional effect of polymetallic substitution is that the arene bridges in these species are likely to be very electron rich (due to σ and π donation from the organometallic fragments) and should thus form π complexes with 12-electron fragments such as $Cr(CO)_3$. Such species would be expected to exhibit significantly different electronic properties than do their uncomplexed precursors (e.g., giving better conductors or photoconductors). We are therefore interested in elucidating the nature of any such perturbations of the σ,σ metal–arene–metal interaction. To this end, we have prepared a series of σ,π model complexes $((\eta^6\text{-}C_6H_{6-n}Fp_n)Cr(CO)_3$, n = 2 or 3) and have investigated their various metal–arene–metal interactions. We have found that their Cr centers are very electron rich and that substantial transfer of electron density from Fe to Cr is observed (1). In addition, our studies have shown that the nature of the Fe–

[1]Organometallic Complexes with Electronic Bridges: Part V; for part IV see G. B. Richter-Addo and A. D. Hunter. Inorg. Chem. In press.

[2]Author to whom correspondence may be addressed.

Can. J. Chem. Downloaded from www.nrcresearchpress.com by 91.144.44.67 on 09/07/12
For personal use only.

Can. J. Chem. Downloaded from www.nrcresearchpress.com by 91.144.44.67 on 09/07/12
For personal use only.

arene–Fe π-bonding interactions are not dramatically altered upon η^6 complexation (1*c*). However, the separation of the σ,σ and σ,π components of the bonding interactions in these species is difficult due to the complexities inherent when dealing with complexes containing three or four metal centers.

To overcome these difficulties and to help in the elucidation of the nature of this σ,π interaction, we decided to synthesize a series of simpler complexes containing only a single σ-bound Fp group. At the time of this study,[3] only a single member of this class of complexes had been reported (i.e., $(\eta^6\text{-}C_6H_5Fp)Cr(CO)_3$) and it was prepared by the reaction of the parent Fp–phenyl complex with $Cr(CO)_6$ (2), i.e., eq. [1].

[1] $C_6H_5Fp + Cr(CO)_6 \xrightarrow{\Delta} (\eta^6\text{-}C_6H_5Fp)Cr(CO)_3$

Given the high nucleophilicity of the Fp^- anion (3) and facility with which strong organic nucleophiles substitute for halides in $(\eta^6\text{-}C_6H_{6-n}Y_n)Cr(CO)_3$ complexes (where Y = F, Cl, etc.) (4), we felt a more promising and interesting route to such species would be nucleophilic displacement of halide by the Fp^- anion, e.g., eq. [2].

[2] $(\eta^6\text{-}C_6H_5Y)Cr(CO)_3 + Fp^- \rightarrow (\eta^6\text{-}C_6H_5Fp)Cr(CO)_3$

This approach proved successful and produces the desired complexes in high yields. In this paper, we would like to report the complete results of our studies of these complexes including syntheses and spectroscopic and electrochemical characterization of the resultant σ,π products. These data will be compared to the analogous polysubstituted complexes (1) and, in particular, our ^{13}C NMR and cyclic voltammetric data will be discussed with reference to the nature of the Fe–arene–Cr interaction in these complexes.

Experimental

Unless otherwise noted, all reactions and subsequent manipulations were performed under anaerobic and anhydrous conditions using conventional techniques for the manipulation of air-sensitive compounds as described in detail previously (1*b*). The chemicals used were of reagent grade or comparable purity and where necessary were purified before use and had their purity ascertained by elemental analyses and (or) other suitable methods (6). Solvents used were dried and deaerated by standard procedures and stored under N_2 or Ar (6). The (arene)$Cr(CO)_3$ and Fp_2 reagents were prepared and purified by the standard procedures (7, 8). Unless specified otherwise, the chemical reactions described below were effected at ambient temperatures (≈25°C).

Infrared spectra were recorded on a Pye Unicam PU9522 infrared spectrophotometer calibrated with the 1601 cm^{-1} band of polystyrene. Nuclear magnetic resonance spectra were recorded on a Bruker WH-300 spectrometer with reference to the deuterium signal of the solvent employed. The ^1H and ^{13}C chemical shifts are reported in parts per million downfield from external Me_4Si and were obtained with the assistance of the departmental NMR staff. The low- and high-resolution and the fast atom bombardment (FAB) mass spectra were recorded as previously described (1*b*).

The analytical, mass-spectral, IR, and NMR data for the complexes synthesized during this work are collected in Tables 1 and 2. Synthetic procedures and yields are recorded below.

Preparation of $(\eta^6\text{-}1,4\text{-}C_6H_4XFp)Cr(CO)_3$ (where X = H, Me, OMe, or Cl; Fp = $(\eta^5\text{-}C_5H_5)Fe(CO)_2$)

All these complexes were synthesized in a similar fashion. The procedure for $(\eta^6\text{-}1,4\text{-}C_6H_4MeFp)Cr(CO)_3$ is described in detail as a representative example.

An excess of solid sodium amalgam (1*b*) (18.0 g, 18.0 mmol Na) was liquified by the addition of mercury (≈3 mL), and then THF (60 mL) and Fp_2 (1.45 g, 4.10 mmol) were added. The resultant dark red solution was vigorously stirred for 1 h to produce a solution of NaFp (8). Excess amalgam was drained from the reaction through a sidearm of the reaction flask and the solution was then filtered through Celite (2 × 3 cm) supported on a medium porosity frit (2 × 10 mL THF wash) and the resulting orange-red solution was cooled to −78°C (Dry Ice/acetone). To this stirred solution was added $(\eta^6\text{-}1,4\text{-}C_6H_4MeF)Cr(CO)_3$ (1.08 g, 4.39 mmol) and the resultant mixture was held at −78°C for 4 h and then allowed to warm to ambient temperature overnight. The solution was taken to dryness *in vacuo* and the resultant red solid was washed with hexane (7 × 15 mL). The hexane wash contained Fp_2 and unreacted $(\eta^6\text{-}1,4\text{-}C_6H_4MeF)Cr(CO)_3$ (by IR) and was discarded. Crystallization of the residue from CH_2Cl_2 (100 mL) and hexanes (15 mL) at −30°C resulted in the formation of a yellow precipitate. This crystalline material was collected by filtration and washed with hexanes (30 mL) to give the desired product, $(\eta^6\text{-}1,4\text{-}C_6H_4MeFp)Cr(CO)_3$, in good yield (1.77 g, 62%).

The other products (where X = H, OMe, and Cl) were produced in a similar manner from $(\eta^6\text{-}C_6H_5F)Cr(CO)_3$, $(\eta^6\text{-}1,4\text{-}C_6H_4(OMe)F)Cr(CO)_3$, and $(\eta^6\text{-}1,4\text{-}C_6H_4Cl_2)Cr(CO)_3$ in 52, 32, and 80% yields, respectively.

The related reaction of NaFp with $(\eta^6\text{-}1,4\text{-}C_6H_4FNH_2)Cr(CO)_3$ did not proceed as cleanly as those described above; however, the presence of traces of $(\eta^6\text{-}1,4\text{-}C_6H_4(NH_2)Fp)Cr(CO)_3$ was confirmed by mass-spectral analysis. Attempts to react NaFp with $(\eta^6\text{-}C_6H_6)Cr(CO)_3$ or $(\eta^6\text{-}C_6H_5OMe)Cr(CO)_3$, even at ambient temperature, gave no new products on work-up, *vide supra*. Instead, the (arene)$Cr(CO)_3$ starting materials were recovered unchanged.

Electrochemical analysis of the products

A standard three-electrode cell (9) of approximately 40 mL volume was used for the cyclic voltammetry experiments. The working electrode was a small (≈1 mm diameter) Pt bead sealed in soft glass. A coiled Pt wire (≈15 cm in length) was used as the auxiliary electrode. The aqueous SCE reference electrode was separated from the working electrode compartment by a fine frit and a Luggin probe. The $[n\text{-}Bu_4N]PF_6$ support electrolyte (10) and the cell parts were dried in an oven at 130°C overnight just prior to use. The working electrode was cleaned by placing the electrode tip over boiling HNO_3 (reagent grade) for 0.5 h, rinsing with distilled water (2 L), and then soaking it in a saturated ferrous ammonium sulphate solution (made up in 1 M H_2SO_4) for 0.5 h. Finally, it was rinsed with distilled water (2 L) and reagent acetone (1 L) and then was dried with a hot air gun just prior to use. Dichloromethane (Spectrograde, BDH) was stirred over alumina (5 g, Woelm neutral, W200 Super 1) while simultaneously being purged with prepurified nitrogen for 20 min. The solvent with some entrained alumina (≈0.5 g) was then transferred by cannula to the electrochemical cell, which had been previously set up on a vacuum line under dinitrogen.

The potentials were supplied by a BAS CV27 voltammograph, and the resulting cyclic voltammograms were recorded on a Hewlett–Packard 7090A X–Y recorder. The formal oxidation potential ($E^{0\prime}$) for reversible couples is defined as the average of the anodic ($E_{p,a}$) and cathodic ($E_{p,c}$) peak potentials. ΔE is defined by $|E_{p,c} - E_{p,a}|$, and the cathodic to anodic peak current ratio is defined by $i_{p,c}/i_{p,a}$ (11). Diffusion control was established for the redox processes by the observation of a linear plot of i_p versus the square root of scan rate ($v^{1/2}$) over at least one order of magnitude of scan rate. The oxidation of ferrocene is reported to be highly reversible in many solvents (10). After each experiment, ferrocene was added as an internal reference (12). Under our experimental conditions, ferrocene is reversibly oxidized ($E^{0\prime}$ = +0.47 V vs. SCE; $i_{p,c}/i_{p,a}$ = 1.0; ΔE = 60 mV at 0.1 V s^{-1}). Occasionally the ferrocene/ferricinium redox couple was obscured by the redox couple of the analyte, and in these cases cobaltocene was used as the internal reference ($E^{0\prime}$ = −0.86 V vs.

[3]After the completion of our synthetic and spectroscopic studies, a related report was published (5). A complete comparison of the two sets of independent results will be presented in the results and discussion section.

Can. J. Chem. Downloaded from www.nrcresearchpress.com by 91.144.44.67 on 09/07/12
For personal use only.

SCE; $i_{p,a}/i_{p,c} = 1$; $\Delta E = 74$ mV at 0.10 V s^{-1}). In general, reversible oxidations were exhaustively studied before irreversible waves, since the irreversible oxidations lead to extensive coating of the electrode surface. However, when electrode coating was observed, cleaning of the working electrode with facial tissues and its replacement into the cell often appeared to remedy the problem (although no quantitative data for publication were used after such operations).

Electrochemical data for the complexes synthesized during this work are collected in Table 4.

Results and discussion

Synthesis of the complexes

The reaction of NaFp (where Fp = $(\eta^5\text{-}C_5H_5)Fe(CO)_2$) with (haloarene)$Cr(CO)_3$ complexes produces the desired bimetallic products, i.e.,

[3] NaFp + $(\eta^6\text{-}1,4\text{-}C_6H_4XY)Cr(CO)_3$ $\xrightarrow[-78°C]{THF}$ $(\eta^6\text{-}1,4\text{-}C_6H_4XFp)Cr(CO)_3$

(where X = H, Me, or OMe, Y = F; X = Y = Cl). The use of a small excess of Fp^- anion (10–20%) ensures complete consumption of the starting material; however, a larger excess should be avoided since it will simply be converted to Fp_2 in the work-up. In addition, this reaction should be carried out at low temperature to minimize the formation of the Fp_2 dimer, *vide infra*. Using this method, the yields (nonoptimized) of these products vary from 32 to 80%, which is two to four times higher than those reported earlier from an analogous reaction using $[Et_4N]Fp$ at ambient temperatures (5), i.e., eq. [4]

[4] $[Et_4N]Fp + (\eta^6\text{-}1,4\text{-}C_6H_4XY)Cr(CO)_3 \xrightarrow[RT]{THF}$

$(\eta^6\text{-}1,4\text{-}C_6H_4XFp)Cr(CO)_3 + (\eta^6\text{-}C_6H_5X)Cr(CO)_3 + Fp_2$

This increased yield is probably due to the suppression of an ambient temperature side reaction, which has been ascribed to single electron transfer reactions, SET (5), and which produces $(\eta^6\text{-}C_6H_5X)Cr(CO)_3$ as a major product. In our low temperature syntheses, no evidence for such SET-derived products was observed.

The IR spectra of the reaction solutions after 3 h at −78°C indicate that the desired bimetallic species are formed cleanly and in very high yield under these conditions even in the presence of excess NaFp. However, when the solution is allowed to warm to room temperature, a number of new IR bands between 1840 and 1960 cm^{-1} are observed. The new species responsible for these bands have not been isolated but it is tempting to speculate that they may be due to a reversible addition (4) of Fp^- to the complexes.

The detailed mechanism of these syntheses is not known but, by analogy with the related reactions with organic nucleophiles (4), they probably proceed through an S_NAr nucleophilic displacement reaction involving a $Cr(CO)_3$ stabilized Meisenheimer intermediate, i.e.,

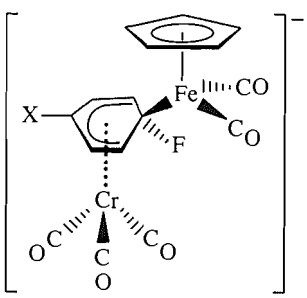

Interestingly, when an excess of NaFp is added to solutions of $(\eta^6\text{-}1,4\text{-}C_6H_4ClFp)Cr(CO)_3$, even at ambient temperatures, we see no evidence for the formation of the expected product $(\eta^6\text{-}1,4\text{-}C_6H_4Fp_2)Cr(CO)_3$, **2***a*, i.e., eq. [5]

[5] xsNaFp + $(\eta^6\text{-}1,4\text{-}C_6H_4ClFp)Cr(CO)_3$ $\xrightarrow{\cancel{THF}}$ $(\eta^6\text{-}1,4\text{-}C_6H_4Fp_2)Cr(CO)_3$

This is in accord with previous reports (5) but is somewhat surprising given the stability of the desired products (1) and the fact that weaker organic nucleophiles (3) readily give disubstituted products in high yields under these conditions (4*a*), i.e.,

[6] 2NaSR + $(\eta^6\text{-}1,4\text{-}C_6H_4Cl_2)Cr(CO)_3$ $\xrightarrow{THF}$ $(\eta^6\text{-}1,4\text{-}C_6H_4(SR)_2)Cr(CO)_3$ $\xrightarrow{I_2}$ 60–90% $C_6H_4(SR)_2$

(where R = Me, *n*-Bu, and *t*-Bu, for 1,2-, 1,3-, and 1,4-$C_6H_4Cl_2$ complexes). This difference is probably due to a combination of the greater electron-donating ability and steric bulk of the Fp groups. The more strongly electron-donating Fp group (1*b*, *c*) would make the monosubstituted complex, $(\eta^6\text{-}1,4\text{-}C_6H_4ClFp)Cr(CO)_3$, less prone to nucleophilic attack (and would perhaps destabilize the transition state). This monosubstituted complex is also much more sterically crowded and thus the formation of the Meisenheimer intermediate would probably be inhibited, i.e.,

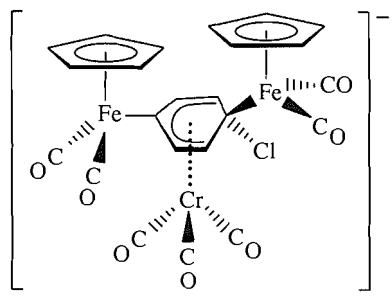

These new 18-electron complexes, $(\eta^6\text{-}1,4\text{-}C_6H_4XFp)Cr(CO)_3$ (where X = H, Me, OMe, or Cl), i.e.,

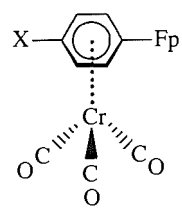

X = H (**1***a*), Me (**1***b*), OMe (**1***c*), or Cl (**1***d*)

are yellow crystalline solids that are sufficiently air stable to be handled in air as solutions, for short periods of time, without the occurrence of noticeable decomposition. In fact, these complexes are sufficiently air stable that we have been able to store them as solids in air for up to a year without noticeable decomposition occurring. They are more soluble in common organic solvents than are the complexes $(\eta^6\text{-}C_6H_{6-n}Fp_n)Cr(CO)_3$, (where n = 2 or 3 (1)), i.e.,

TABLE 1. Analytical, mass-spectral, and infrared data for the complexes

Complex[a]	Analytical data C Calcd.	C Found	H Calcd.	H Found	Low resolution mass-spectral data P^+, m/z[b]	Infrared data ν_{CO} (CH_2Cl_2, cm^{-1})[c]
$(C_6H_5Fp)Cr(CO)_3$, **1***a*	49.26	49.06	2.58	2.69	390	2030 (s), 1980 (s), 1951 (s), 1868 (s, br)
$(1,4\text{-}C_6H_4MeFp)Cr(CO)_3$, **1***b*	50.53	50.22	2.99	2.98	404[d]	2029 (s), 1977 (s), 1947 (s), 1865 (s, br)
$(1,4\text{-}C_6H_4(OMe)Fp)Cr(CO)_3$, **1***c*	48.60	48.10	2.88	3.00	420	2030 (s), 1979 (s), 1948 (s), 1865 (s, br)
$(1,4\text{-}C_6H_4ClFp)Cr(CO)_3$, **1***d*[e]	49.27	49.18	2.14	2.34	424	2032 (s), 1984 (s), 1960 (s), 1883 (s, br)

[a]Where Fp = $(\eta^5\text{-}C_5H_5)Fe(CO)_2$.
[b]Probe temperature 150–280°C. Assignments involve the naturally occurring isotopes ^{56}Fe and ^{52}Cr.
[c]Abbreviations w (weak), m (medium), s (strong), sh (shoulder), v (very), br (broad).
[d]Peak assignments confirmed by high resolution mass spectra.
[e]Chlorine analysis calcd.: 8.35; found: 8.50.

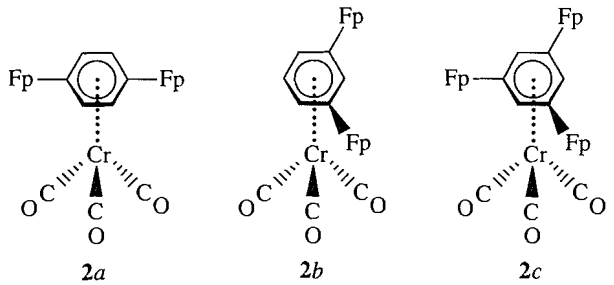

but are less soluble than are their halo-arene precursors and are almost totally insoluble in nondonor solvents such as hexanes at ambient temperature. The analytical and spectral data for these complexes (Tables 1 and 2) confirm the proposed formulations as σ,π clusters with three-legged piano-stool geometries, as do the X-ray crystal structures, previously reported, of the CH_2Cl_2 solvate of **2***c* (1*a*, *c*) and of **1***d* (5).

Spectroscopic characterization of the complexes and the nature of the σ,π metal–arene–metal interactions

It is well established that many substituents (e.g., OMe, NMe_2, Fp, etc.) act as π donors in both uncomplexed and $Cr(CO)_3$ complexed arenes (1*b*,*c*, 13–17). In addition, the Fp group also acts as a σ donor (1*b*,*c*, 13). When two Fp groups are bonded to the same arene in a 1,4 fashion, we have shown that for both $1,4\text{-}C_6H_4Fp_2$ and $(\eta^6\text{-}1,4\text{-}C_6H_4Fp_2)Cr(CO)_3$ a synergic metal–arene–metal interaction occurs giving these complexes significant dimetalloquinone resonance character (1*b*,*c*). In $(arene)Cr(CO)_3$ complexes, the substituents may interact with one another through both the σ- and π-bonding frameworks. In comparison to noncomplexed arenes, the σ interactions are sharply attenuated but the π interactions remain largely unchanged (1, 14*d*,*e*, 15*a*,*c*). Thus, our observation that the magnitude of the 1,4-dimetalloquinone interactions is not changed significantly upon complexation by $Cr(CO)_3$ indicates that this interaction occurs through the arene's π system (1*c*). Of particular relevance to the present study, the IR spectra of the Fp complexes, $(\eta^6\text{-}C_6H_{6-n}Fp_n)Cr(CO)_3$, clearly indicated that substantial transfer of electron density from Fe to Cr is occurring in these species (1); however, elucidating the exact nature of this Fe–arene–Cr interaction is difficult for these species because of the presence of the Fe–arene–Fe interactions.

Four IR bands are observed in solution that may be attributed to the carbonyl ligands of our σ,π complexes (Table 1, Fig. 1). These complexes all exhibit two bands below 1960 cm^{-1}, the lower energy band being broader. The positions of these bands are all lower than those of the parent $(\eta^6\text{-}C_6H_6)Cr(CO)_3$ complex (i.e., ν_{CO} (CH_2Cl_2) 1973 (s), 1893 (s, br) cm^{-1}) but are higher than those of the polysubstituted species (i.e., $(\eta^6\text{-}C_6H_{6-n}Fp_n)Cr(CO)_3$, **2***a*–*c*, ν_{CO} (CH_2Cl_2) 1937, 1854 and 1919, 1835 cm^{-1} for n = 2 and 3, respectively (1*a*,*c*)). They are also quite dependent on the identity of the organic substituents, X (varying by 10–15 cm^{-1} between **1***b* and **1***d*). In addition, their relative intensities are somewhat greater than those of the higher energy bands but lower than those found in the corresponding bands of polysubstituted complexes. Those bands above 1970 cm^{-1} have positions that show only a weak dependence (3–7 cm^{-1}), as expected (13*a*), on the arene

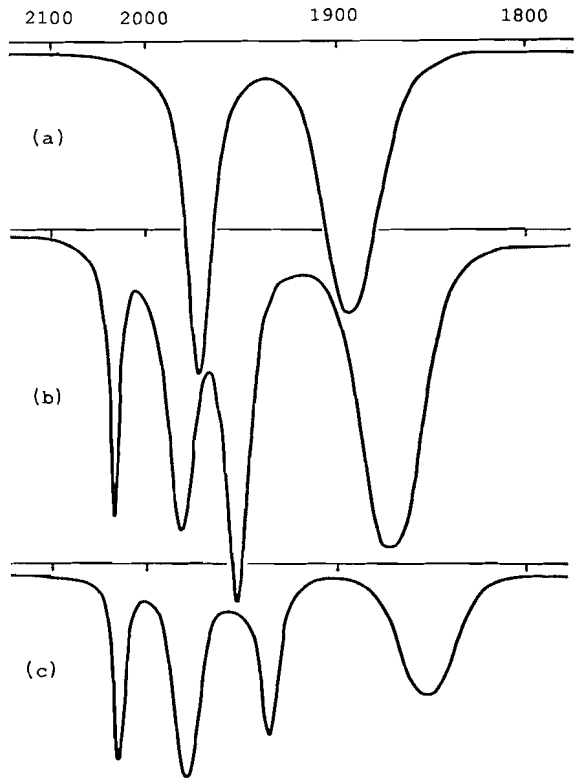

FIG. 1. The IR spectra in the carbonyl region of the complexes (a) $(\eta^6\text{-}C_6H_6)Cr(CO)_3$, (b) $(\eta^6\text{-}C_6H_5Fp)Cr(CO)_3$, and (c) $(\eta^6\text{-}1,4\text{-}C_6H_4Fp_2)Cr(CO)_3$ in CH_2Cl_2 are shown. Note the shifts in the low-frequency bands due to the $Cr(CO)_3$ group, the invariance in the Fp bands, and the changes in relative intensities.

Can. J. Chem. Downloaded from www.nrcresearchpress.com by 91.144.44.67 on 09/07/12
For personal use only.

Can. J. Chem. Downloaded from www.nrcresearchpress.com by 91.144.44.67 on 09/07/12
For personal use only.

substituents. They are also similar in position to those in **2***a–c* (i.e., ν_{CO} (CH_2Cl_2) 2030, 1980 cm^{-1} (1*a*,*c*)). These facts conclusively indicate that the lower energy pair of bands are due to the $Cr(CO)_3$ fragment and that the higher energy pair are due to the Fp fragments. Thus, these data can be entirely explained without having to invoke vibrational mixing[4] and the assignments are most consistent with those of related species (1) and other Fp and $Cr(CO)_3$ complexes (13–16). We therefore believe that each set of carbonyl bands can be uniquely assigned to either the Fe or the Cr fragments and that any vibrational mixing between these fragments is negligible in solution.

The trends in IR stretching frequencies as a function of the organic substituents, X, are as expected for the Fe (13*a*,*b*) and Cr (14*f*) carbonyls. The decrease observed in the Cr-carbonyl stretching frequencies upon the replacement of the halogens of the starting materials by the Fp group confirms that this substituent is a net electron donor to the $Cr(CO)_3$ center. This suggestion of substantial electron transfer is confirmed by the electrochemical data, *vide infra*, and by the ^{13}C NMR data of these complexes (Table 2). Thus, the Fp carbonyls are shielded by about 2 ppm compared to uncomplexed Fp-phenyls (i.e., δ_{CO} of 1,4-$C_6H_4Fp_2$, **3***a*, at 217.47 ppm in $(CD_3)_2SO$ (1*b*)) while the Cr carbonyls are deshielded by 1–2 ppm compared to those in (η^6-C_6H_6)$Cr(CO)_3$ (i.e., δ_{CO} at 234.00 in $(CD_3)_2SO$). These changes are in the direction that would be predicted (on the basis of the expected changes in the paramagnetic screening of the carbonyls) and confirm that electron density is transferred from Fe to Cr (1*c*, 13*b*, 15*b*). The ^1H and ^{13}C NMR signals attributable to the cyclopentadienyl rings of our complexes are also as expected (1, 13) and confirm that the Fp groups in these complexes retain their three-legged pianostool geometries in solution.

The NMR spectral data for the phenyl groups in these complexes are listed in Table 2 and may be compared with those of the related uncomplexed and $Cr(CO)_3$ complexed Fp-phenylenes (1*b*,*c*). The ^1H and ^{13}C NMR spectra of the phenyl groups are relatively simple due to the high symmetry of these molecules and were assigned using the peak multiplicities, chemical shifts, and homo- and heteronuclear coupling constants of the signals. In addition, the ^{13}C assignments were confirmed by consideration of the characteristic substituent effects of the pendant metal fragment, *vide infra*, and by heteronuclear decoupling and NOE difference experiments on **1***c*. As expected, the ^1H NMR signals of the Fp-phenyl groups are shielded by about 2 ppm compared to the uncomplexed Fp-phenyls (i.e., for **3***a* in $(CD_3)_2SO$, $\delta(C_6H_4)$ is 6.95 ppm (1*c*, 14, 15)) and exhibit the expected AB quartet structures for **1***b–d*. The J_{CH} and the J_{HH} coupling constants are also as expected (13–15).

The ^{13}C NMR chemical shifts of arene carbons are particularly useful since they are related to the arene-carbon electron density. For this reason, they have been used to elucidate the nature of arene–substituent bonding interactions of both complexed and uncomplexed arenes (1*b*,*c*, 15, 17). They are best understood in terms of the substituent constants, Δ (which measure the effect that a particular substituent will have on the chemical shift of each arene carbon), which are generally linearly additive (15, 17). The Δ_π values are the most useful and may be interpreted in terms of the π-donor and π-acceptor properties of the substituents (1*b*,*c*, 15*a*, 17). Using the

[4]The solid state IR spectra (KBr) of some of these complexes were assigned differently (5) and vibrational mixing was invoked to explain the observed trends in stretching frequencies.

TABLE 2. ^1H and ^{13}C NMR data for the complexes (1,4-C_6H_4XFp)$Cr(CO)_3$ (δ in ppm; $(CD_3)_2SO$)[a]

	^1H NMR[b]		^{13}C NMR[b] ($^1J_{CH}$ in Hz)					
				Arene				
X =	Cp	C_6H_{6-n}	Cp	Fe-*C*	H-*C*[c]	X-*C*	Fe-CO	Cr-CO
H, **1***a*	5.17 (s, 5H)	5.59 (d, 2H, *J* = 5.5 Hz) 5.45 (m, 3H)	86.86 (181.8)	125.22	110.20 (172.8) 96.36 (173.3)	92.20 (174.8)	215.07	235.86
Me, **1***b*	5.15 (s, 10H)	5.65 (d, 2H, J_{AB} = 6.4 Hz) 5.34 (d, 2H) 2.03 (s, 3H, CH_3)	86.29 (181.8)	118.19	111.32 (171) 96.46 (170)	108.38 19.50 (CH_3, 128.1)	215.00	236.36
OMe, **1***c*[d]	5.17 (s, 5H)	5.70 (d, 2H, J_{AB} = 6.9 Hz)[e] 5.39 (d, 2H) 3.60 (s, 3H, OCH_3)	86.72 (181.9)	109.38	110.92 (171.4) 82.07 (71.3)	142.58 (*C*OMe) 55.34 (OCH_3, 145.7)	214.87	236.37
Cl, **1***d*	5.24 (s, 5H)	5.82 (d, 2H, J_{AB} = 6.5 Hz) 5.77 (d, 2H)	86.90 (182.5)	119.11	109.98 (175.2) 94.76 (179.4)	111.60	214.77	235.01

[a]Where Fp = (η^5-C_5H_5)$Fe(CO)_2$; Cp = η^5-C_5H_5.
[b]^1H NMR were measured at 300.135 MHz and ^{13}C NMR were measured at 75.469 MHz unless otherwise specified.
[c]Carbons C2/C6 (where C1 is the carbon attached to Fp) occur downfield of carbons C3/C5, see text for the basis of the assignments.
[d]^1H and ^{13}C assignments confirmed by ^1H NOE difference spectra and by heteronuclear decoupling experiments.
[e]The *ortho* hydrogens are the downfield members of the pair, see text for the basis of the assignments.

TABLE 3. ^{13}C substituent effects for $(\eta^6\text{-}C_6H_5X)Cr(CO)_3$[a]

X	Substituent constants[b] Δ_{ipso}	Δ_{ortho}	Δ_{meta}	Δ_{para}	Δ_{π}[b]	Reference
OMe	49.1	−14.8	2.4	−7.7	−10.1	c
Cl	18.3	−1.5	0.9	−3.8	−4.7	c
Me	16.6	1.5	−0.3	−3.3	−3.6	c
Fp	30.0	16.0	2.0	−3.0	−5.0	d

[a]Where the values for the substituent constants, Δ, are quoted in ppm relative to (benzene)$Cr(CO)_3$ (at 95.1 ppm in $(CD_3)_2SO$) and positive shifts indicate deshielding.

[b]The Δ_{π} values are the substituent chemical shifts, $\Delta_{\pi} = \delta_{\text{arene carbon}} - \delta_{(C_6H_6)Cr(CO)_3}$ and $\Delta_{\pi} = \Delta_{para} - \Delta_{meta}$.

[c]This work ($(CD_3)_2SO$).

[d]This work and reference 1*c*, derived to give the most consistent set of values from the data for all the Fp–phenylene π complexes ($(CD_3)_2SO$).

substituent constants of Fp, Me, OMe, and Cl (Table 3), the ^{13}C spectra of the complexes (Table 2) can be assigned with an average error of less than 1 ppm (with the exception of the *ipso* carbons of **1***b–d*, *vide infra*).

The carbon atom *ipso* to Fp in $(\eta^6\text{-}1,4\text{-}C_6H_4(OMe)Fp)Cr(CO)_3$ is shielded by about 8.1 ppm *more* than would be predicted on the basis of linear additivity. This implies that when these substituents are arranged 1,4 to each other on the benzene ring the OMe group (which is the stronger π donor substituent, i.e., $\Delta_{\pi} = -10.1$ vs. -5.0 for Fp) experiences an increase in its *para* substituent constant, Δ_{para}, from its usual value of −7.7 to −15.8 ppm. Similar, although less pronounced, effects are observed for the Me and Cl substituted complexes. These apparent increases in Δ_{para} are probably (15*a*, 17*a–c*) due to an increase in the π donor ability of the "organic" substituents, X. This suggests that a synergic interaction is occurring between the Fp and X substituents. We have observed similar synergic interactions for $(\eta^6\text{-}1,4\text{-}C_6H_4Fp_2)Cr(CO)_3$ (1*c*) and they are well established for uncomplexed 1,4-disubstituted arenes (1*b*, 17*b*). It seems tempting to speculate that (in valence bond terms and by analogy with these systems) such synergic interactions are due to a quinoidal contribution to the resonance structure of the complexes, e.g., for **1***c*,

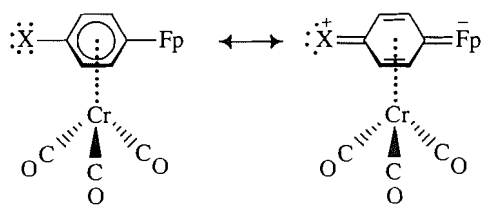

(where X = OMe). However, with the data at hand we cannot entirely rule out the possibility that these unexpected chemical shift changes are due to an anomalous *ipso* sensitization (17*b*) by Fp. Experiments to eliminate this and related difficulties are currently in progress and preliminary results (using the methods of Bromilow, Brownlee, *et al.* (17*b*)) indicate that an anomalous sensitization is not involved and that such a synergic interaction is occurring.[5] Indeed, such a resonance effect is somewhat analogous to the conjugation observed in complexes such as $(\eta^6\text{-}1,4\text{-}C_6H_4(CHO)(NMe_2))Cr(CO)_3$ (in which one substituent acts as a π donor and the other as a π acceptor (18)). However, confirmation of this proposal must await the crystallographic characterization of a number of such species and a detailed molecular orbital analysis of the bonding in these unusual complexes.

[5]V. Mozol, A. D. Hunter, and L. Shilliday, unpublished observations.

TABLE 4. Cyclic voltammetry data for the oxidation of $(\eta^6$-arene)$Cr(CO)_3$ derivatives in CH_2Cl_2[a]

Compound[b] (arene)	Scan rate v, V s^{-1}	$E^{0\prime}$, V	ΔE, mV	$i_{p,c}/i_{p,a}$
C_6H_6	0.05	+0.87	74	0.99
	0.10	+0.87	80	0.99
FpC_6H_5, **1***a*	0.05	+0.64	75	0.96
	0.10	+0.64	75	0.96
1,4-C_6H_4MeFp, **1***b*	0.10	+0.60	72	0.89
	0.20	+0.60	73	1.00
1,4-C_6H_4(OMe)Fp, **1***c*	0.05	+0.56	67	0.96
	0.20	+0.56	70	1.00
1,4-C_6H_4ClFp, **1***d*	0.04	+0.73	64	0.98
	0.10	+0.73	66	1.00

[a]In 0.1 M $[n\text{-}Bu_4N]PF_6$ at a Pt-bead electrode. Potentials are measured vs. SCE for which the ferrocene couple is observed at +0.47 V in CH_2Cl_2.

[b]Where Fp = $(\eta^5\text{-}C_5H_5)Fe(CO)_2$.

Electrochemical characterization of the complexes

To the best of our knowledge, the electrochemistry of complexes containing σ-bound transition-metal substituents on (arene)$Cr(CO)_3$ complexes has not been reported (19*b*). We therefore decided to investigate the electrochemical behavior of our σ,π complexes since such studies should provide evidence for the nature of the metal–metal interactions in these species.[6]

The complexes **1***a–d* undergo diffusion-controlled, reversible one-electron oxidations in CH_2Cl_2 (0.1 M $[n\text{-}Bu_4N]PF_6$) to give the corresponding radical cations. In general, these oxidations may be represented as

[7] $(\eta^6\text{-}1,4\text{-}C_6H_4XFp)Cr(CO)_3 \underset{+e^-}{\overset{-e^-}{\rightleftharpoons}} [(\eta^6\text{-}1,4\text{-}C_6H_4XFp)Cr(CO)_3]^{\cdot+}$

(where X = H, Me, Cl, or OMe) and the electrogenerated radical cations persist in dichloromethane solution, as judged by the high $i_{p,c}/i_{p,a}$ values. The electrochemical data for the oxidations of the complexes are summarized in Table 4. As can be seen from the table, all these complexes exhibit similar electrochemical behavior. Diffusion control in these oxidations was established by obtaining linear plots of $i_{p,a}$ vs. (scan rate)$^{1/2}$ over at least one order of magnitude of scan rate. Cyclic voltammograms of a representative example (i.e., $(\eta^6\text{-}C_6H_5Fp)Cr(CO)_3$) are shown in Fig. 2. As may be noted in Fig. 2a, this compound undergoes a reversible oxidation at $E^{0\prime} = +0.64$ V. Comparison of CV peak separations and anodic peak current heights with those of ferrocene established this process as involving one electron. As is observed in Fig. 2b, when the anodic scan is taken out to the solvent limit (≈2 V), a second oxidation is observed at +1.38 V. The magnitude of the current in this process is similar to that of the first, and indicates the transfer of one electron. This second oxidation peak occurs in the range for the irreversible oxidations of many Fp–alkyl (or –aryl) complexes (20), as well as the range for the second oxidation

[6]Some of these results have been communicated previously, see: G. B. Richter-Addo and A. D. Hunter. Inorg. Chem. In press.

Can. J. Chem. Downloaded from www.nrcresearchpress.com by 91.144.44.67 on 09/07/12
For personal use only.

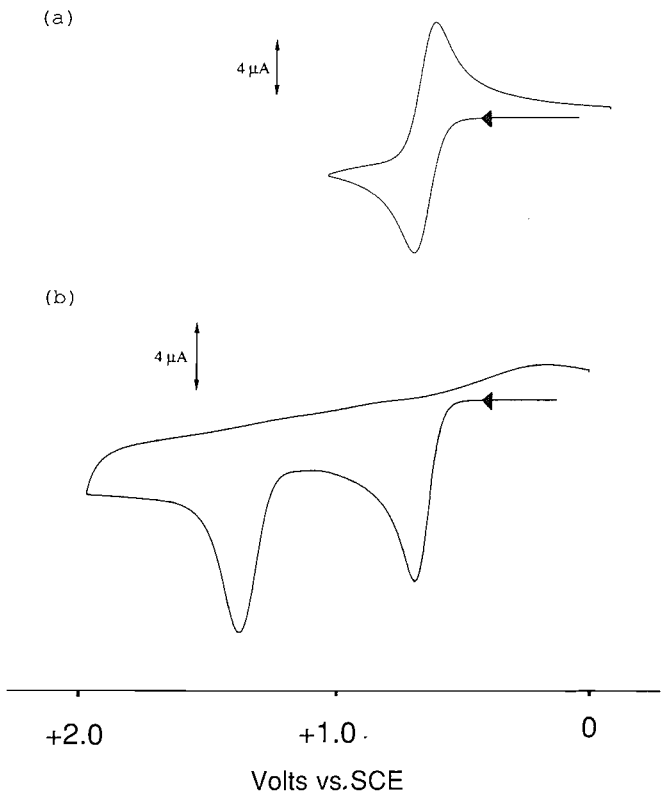

FIG. 2. The cyclic voltammograms of $(\eta^6\text{-}C_6H_5Fp)Cr(CO)_3$ in CH_2Cl_2 at a Pt-bead electrode (0.1 M $[n\text{-}Bu_4N]PF_6$, scan rate of 0.1 V s^{-1}).

of (arene)$Cr(CO)_3$ species (21). Therefore, it cannot be conclusively assigned to either metal center. Unlike the first oxidation process, which is reversible, this second oxidation is irreversible, indicating a very rapid decomposition of the electrogenerated dication. In addition, extensive electrode coating occurs after this second oxidation wave is passed, and subsequent waves become ill-defined. Indeed, all of the title complexes exhibit second (irreversible) waves (at $\geq$1.37 V) which lead to a similar degradation of the electrode surface. As such, these secondary oxidations were not investigated further. Moreover, the observation of somewhat lower $i_{p,c}/i_{p,a}$ values for the first redox couple at lower scan rates indicates that secondary chemical reactions (leading to decomposition of the radical cations) are occurring.

The formal potentials ($E^{0\prime}$) for these oxidations show a marked dependence on the arene substituents. As expected on the basis of the trends in the IR and ^{13}C NMR data for the carbonyl ligands in these complexes, *vide supra*, the $E^{0\prime}$ values are more cathodic (by about -0.22 to -0.24 V) than those found in the analogous complexes without Fp substituents (i.e., $E^{0\prime}$ in dichloromethane for the complexes $(\eta^6\text{-}C_6H_5X)Cr(CO)_3$ is observed at +0.97, +0.87, +0.84, +0.78 V for X = Cl, H, Me, and OMe, respectively). This is consistent with our hypothesis that the Fp groups in these complexes are transferring substantial electron density to the Cr center since the magnitude of these shifts is similar to that caused by six methyl groups (-0.26 V) or an NH_2 group (-0.27 V).

Conclusions

The IR, NMR, and electrochemical data obtained in this study confirm the substantial transfer of electron density from Fe to Cr in these complexes. The observed trends are in accord with what one might expect if this electron-density transfer were proceeding through the σ and π frameworks of the arene bridge. We therefore find no evidence to support any direct Cr–Fe interaction. However, some evidence for a synergic Fp–arene–substituent interaction is observed. We are currently extending our investigations of related complexes to confirm or deny the existence of such interactions. Finally, the derivative chemistry of these unusual complexes (especially as applied to organic synthesis) is also being explored.

Acknowledgments

The authors are grateful to the Natural Sciences and Engineering Research Council of Canada and the University of Alberta for support of this work.

1. (*a*) A. D. HUNTER. Organometallics, **8**, 1118 (1989); (*b*) A. D. HUNTER and A. SZIGETY. Organometallics. In press; (*c*) A. D. HUNTER and J. L. MCLERNON. Organometallics. In press; (*d*) A. D. HUNTER. Third Chemical Congress of North America, Toronto. June 1988, INOR 87.
2. A. N. NESMEYANOV, I. V. POLOVYANYUK, and L. G. MAKAROVA. Dokl. Akad. Nauk SSSR, **230**, 1351 (1976) (English transl. 650).
3. R. G. PEARSON and P. E. FIGDORE. J. Am. Chem. Soc. **102**, 1541 (1980), and references cited therein.
4. (*a*) A. ALEMAGNA, P. CREMONESI, P. D. BUTTERO, E. LICANDRO, and S. MAIORANA. J. Org. Chem. **48**, 3114 (1983); (*b*) F. HOSSNER and M. VOYLE. J. Organomet. Chem. **347**, 365 (1988); (*c*) B. NICHOLLS and M. C. WHITING. J. Chem. Soc. 551 (1959); (*d*) M. F. SEMMELHACK and H. T. HALL. J. Am. Chem. Soc. **96**, 7091 (1974); (*e*) J. Am. Chem. Soc. **96**, 7092 (1974); (*f*) J. F. BUNNETT and H. HERMANN. J. Org. Chem. **36**, 4081 (1971); (*g*) D. A. BROWN and J. R. RAJU. J. Chem. Soc. (A), 40 (1966); (*h*) J. HAMILTON and C. A. L. MAHAFFY. Synth. React. Inorg. Met.-Org. Chem. **16**, 61 (1986); (*i*) Synth. React. Inorg. Met.-Org. Chem. **16**, 1363 (1986); (*j*) A. C. KNIPE, S. J. MCGUINNESS, and W. E. WATTS. J. Chem. Soc. Perkin Trans. 2, 193 (1981).
5. J. A. HEPPERT, M. A. MORGENSTERN, D. M. SCHERUBEL, F. TAKUSAGAWA, and M. R. SHAKER. Organometallics, **7**, 1715 (1988).
6. (*a*) D. F. SHRIVER and M. A. DREZDZON. *In* The manipulation of air-sensitive compounds. 2nd ed. John Wiley and Sons, New York, NY. 1986; (*b*) D. D. PERRIN, W. L. F. ARMAREGO, and D. R. PERRIN. *In* Purification of laboratory chemicals. 2nd ed. Pergamon Press, New York, NY. 1980.
7. C. A. L. MAHAFFY and P. L. PAUSON. Inorg. Synth. **19**, 154 (1979).
8. R. B. KING and J. J. EISCH. Organomet. Synth. **1**, 114 (1965); **1**, 151 (1965).
9. P. LEGZDINS and B. WASSINK. Organometallics, **3**, 1811 (1984).
10. J. D. L. HOLLOWAY and W. E. GEIGER. J. Am. Chem. Soc. **101**, 2038 (1979).
11. R. S. NICHOLSON. Anal. Chem. **38**, 1406 (1966).
12. R. R. GAGNE, C. A. KOVAL, and G. C. LISENSKY. Inorg. Chem. **19**, 2854 (1980).
13. (*a*) O. A. GANSOW, D. A. SCHEXNAYDER, and B. Y. KIMURA. J. Am. Chem. Soc. **94**, 3406 (1972); (*b*) I. R. BUTLER, W. E. LINDSELL, and M. J. K. THOMAS. J. Organomet. Chem. **262**, 59 (1984); (*c*) B. E. R. SCHILLING, R. HOFFMANN, and D. L. LICHTENBERGER. J. Am. Chem. Soc. **101**, 585 (1979); (*d*) R. P. STEWART and P. M. TREICHEL. J. Am. Chem. Soc. **92**, 2710 (1970); (*e*) E. S. BOLTON, G. R. KNOX, and C. G. ROBERTSON. J. Chem. Soc. Chem. Commun. 664 (1969); (*f*) C. P. CASEY, M. S. KONINGS, M. A. GOHDES, and M. W. MESZAROS. Organometallics, **7**, 2103 (1988); (*g*) R. P. STEWART, JR., L. R. ISBRANDT, J. L. BENEDICT, and J. G. PALMER. J. Am. Chem. Soc. **98**, 3215 (1976), and refs. cited therein.

Can. J. Chem. Downloaded from www.nrcresearchpress.com by 91.144.44.67 on 09/07/12
For personal use only.

14. (*a*) R. P. A. SNEEDEN. *In* Organochromium compounds. Academic Press, New York, NY. 1975; (*b*) R. DAVIS and L. A. P. KANE-MAGUIRE. *In* Comprehensive organometallic chemistry. *Edited by* G. Wilkinson. Pergamon Press, Oxford, England. 1982. p. 975; (*c*) W. E. SILVERTHORN. Adv. Organomet. Chem. **13**, 47 (1975); (*d*) C. V. SENOFF. Coord. Chem. Rev. **32**, 111 (1980); (*e*) T. A. ALBRIGHT, P. HOFMANN, and R. HOFFMANN. J. Am. Chem. Soc. **99**, 7546 (1977); (*f*) E. W. NEUSE. J. Organomet. Chem. **99**, 287 (1975), and refs. cited therein.
15. (*a*) G. M. BODNER and L. J. TODD. Inorg. Chem. **13**, 360 (1974); (*b*) D. A. BROWN, J. P. CHESTER, N. J. FITZPATRIC, and I. J. KING. Inorg. Chem. **16**, 2497 (1977); (*c*) L. A. FEDOROV, P. V. PETROVSKII, E. I. FEDIN, G. A. PANOSYAN, A. A. TSOI, N. K. BARANETSKAYA, and V. N. SETKINA. J. Organomet. Chem. **182**, 499 (1979); (*d*) D. COZAK, I. S. BUTLER, J. P. HICKEY, and L. J. TODD. J. Magn. Reson. **33**, 149 (1979), and references cited therein.
16. (*a*) K. SCHOLLKOPF, J. J. STEZOWSKI, and F. EFFENBERGER. Organometallics, **4**, 922 (1985); (*b*) J. Y. SAILLARD, D. GRANDJEAN, P. LE MAUX, and G. JAOUEN. Nouv. J. Chim. **5**, 153 (1981).
17. (*a*) G. C. LEVY, R. L. LICHTER, and G. L. NELSON. *In* Carbon-13 nuclear magnetic resonance spectroscopy. John Wiley and Sons, New York, NY. 1980; (*b*) J. BROMILOW, R. T. C. BROWNLEE, D. J. CRAIK, M. SADEK, and R. W. TAFT. J. Org. Chem. **45**, 2429 (1980); (*c*) D. F. EWING. Org. Magn. Reson. **12**, 499 (1979); (*d*) B. E. MANN. Adv. Organomet. Chem. **12**, 135 (1974), and references cited therein.
18. B. P. ROQUES. J. Organomet. Chem. **136**, 33 (1977).
19. (*a*) N. G. CONNELLY and W. E. GEIGER. Adv. Organomet. Chem. **23**, 1 (1984); (*b*) W. E. GEIGER and N. G. CONNELLY. Adv. Organomet. Chem. **24**, 87 (1985).
20. (*a*) P. LEGZDINS, B. WASSINK, F. W. B. EINSTEIN, and R. H. JONES. Organometallics, **7**, 477 (1988); (*b*) P. LEGZDINS and B. WASSINK. Organometallics, **7**, 482 (1988); (*c*) R. E. DESSY, F. E. STARY, R. B. KING, and M. WALDROP. J. Am. Chem. Soc. **88**, 471 (1966); (*d*) R. E. DESSY, R. B. KING, and M. WALDROP. J. Am. Chem. Soc. **88**, 5112 (1966); (*e*) S. N. ANDERSON, C. W. FONG, and M. D. JOHNSON. J. Chem. Soc. Chem. Commun. 163 (1973); (*f*) R. H. MAGNUSON, S. ZULU, W.-M. T'SAI, and W. P. GIERING. J. Am. Chem. Soc. **102**, 6887 (1980); (*g*) W. ROGERS, J. A. PAGE, and M. C. BAIRD. J. Organomet. Chem. **156**, C37 (1978); (*h*) D. A. SLACK and M. C. BAIRD. J. Am. Chem. Soc. **98**, 5539 (1976); (*i*) L. I. DENISOVICH, A. A. IOGANSON, S. P. GUBIN, N. E. KOLOBOVA, and K. N. ANISIMOV. Izv. Akad. Nauk SSSR, Ser. Khim. 258 (1969), (English transl. 218); (*j*) C. J. PICKETT and D. PLETCHER. J. Chem. Soc. Dalton Trans. 879 (1975); (*k*) L. I. DENISOVICH and S. P. GUBIN. J. Organomet. Chem. **57**, 109 (1973).
21. (*a*) M. K. LLOYD, J. A. MCCLEVERTY, J. A. CONNOR, and E. M. JONES. J. Chem. Soc. Dalton Trans. 1768 (1973); (*b*) N. J. STONE, D. A. SWEIGART, and A. M. BOND. Organometallics, **5**, 2553 (1986); (*c*) J. P. BULLOCK, D. C. BOYD, and K. R. MANN. Inorg. Chem. **26**, 3084 (1987); (*d*) C. G. ZOSKI, D. A. SWEIGART, N. J. STONE, P. H. RIEGER, E. MOCELLIN, T. F. MANN, D. R. MANN, D. K. GOSSER, M. M. DOEFF, and A. M. BOND. J. Am. Chem. Soc. **110**, 2109 (1988); (*e*) S. N. MILLIGAN, I. TUCKER, and R. D. RIEKE. Inorg. Chem. **22**, 987 (1983); (*f*) T. IKESHOJI and V. D. PARKER. Bull. Chem. Soc. Jpn. **57**, 1112 (1984); (*g*) K. M. DOXSEE, R. H. GRUBBS, and F. C. ANSON. J. Am. Chem. Soc. **106**, 7819 (1984); (*h*) C. DEGRAND, A. RADECKI-SUDRE, and J. BESANCON. Organometallics, **1**, 1311 (1982); (*i*) T. IKESHOJI and V. D. PARKER. Acta Chem. Scand. B, **37**, 715 (1983).

Can. J. Chem. Downloaded from www.nrcresearchpress.com by 91.144.44.67 on 09/07/12
For personal use only.

An example of conformational disorder in solids: X-ray crystallographic and ^{13}C CPMAS NMR studies of dibenzo and dicyclohexano-13-crown-4 ethers and some lithium complexes

G. W. BUCHANAN[1] AND R. A. KIRBY

Ottawa–Carleton Chemistry Institute, Department of Chemistry, Carleton University, Ottawa, Ont., Canada K1S 5B6

AND

J. P. CHARLAND

Division of Chemistry, National Research Council of Canada, Ottawa, Ont., Canada K1A 0R9

Received May 23, 1989

G. W. BUCHANAN, R. A. KIRBY, and J. P. CHARLAND. Can. J. Chem. **68**, 49 (1990).

For the *cis–anti–cis* isomer of dicyclohexano-13-crown-4 ether, disorder has been detected in the crystal structure, with two conformations being present in the ratio of ca. 3:2. Crystal structures for two Li^+ complexes of the *cis–syn–cis* isomer have also been determined. Representative ^{13}C solid phase NMR spectra are presented and discussed for these systems and the related dibenzo substituted compounds.

Key words: crown ethers, solids, NMR, conformation.

G. W. BUCHANAN, R. A. KIRBY et J. P. CHARLAND. Can. J. Chem. **68**, 49 (1990).

Dans la structure cristalline de l'isomère *cis–anti–trans* de l'éther dicyclohexano-13-couronne-4, on a détecté du désordre; deux conformations sont présentes dans un rapport d'environ 3:2. On a aussi déterminé les structures cristallines de deux complexes du Li^+ de l'isomère *cis–syn–cis*. On présente et on discute des spectres RMN du ^{13}C en phase solide qui sont représentatifs de ces systèmes et de composés apparentés substitués par deux groupements benzo.

Mots clés : éthers couronne, solides, RMN, conformation.

[Traduit par la revue]

Introduction

Recent publications from these laboratories have reported the use of X-ray crystallography and ^{13}C NMR (solution and solid phase) to describe the stereochemical features of substituted 14-crown-4 (1–3) and 12-crown-4 ethers (4, 5) and their complexes with Li^+. In contrast to the now well-documented behaviour of these molecules and 12-crown-4 itself (6), rather little is known regarding the analogous 13-crown-4 systems. The only 13-crown-4 that has been studied in any detail is the benzo derivative (7, 8), for which results indicate effective and selective Li^+ complexation.

Herein we present results for two dicyclohexano-13-crown-4 ethers, specifically the *cis–anti–cis* (**1**) and *cis–syn–cis* derivatives. In the structures depicted below for **1** and the LiNCS (**2**) and $LiClO_4$ (**3**) complexes of the *cis–syn–cis* isomer, the dispositions of the cyclohexane rings are consistent with the X-ray crystallographic data (*vide infra*).

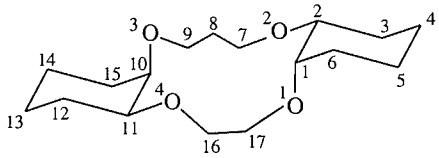

1

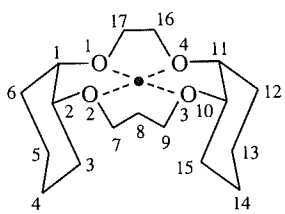

• ≡ Li

2, 3

An interesting feature of these compounds is that **1** lacks any element of symmetry and thus is potentially resolvable into the structure as depicted and as its nonsuperimposable mirror image.

In addition, ^{13}C CPMAS spectra are presented for two materials where X-ray data are not available, these being dibenzo-13-crown-4 ether **4** (below) and its LiNCS complex **5**. Stereochemical influences on ^{13}C chemical shifts are examined along with the utility of these techniques for the detection of conformational disorder in solids.

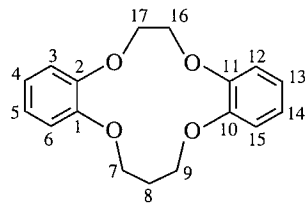

4

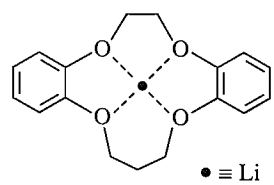

• ≡ Li

5

Results and discussion

The ORTEP drawings of the *cis–anti–cis* isomer **1** are presented in Fig. 1 while those for the LiNCS complex (**2**) of the *cis–syn–cis* isomer and the $LiClO_4$ complex (**3**) of the *cis–syn–cis* isomer are depicted in Figs. 2 and 3 respectively. The ^{13}C CPMAS NMR spectra are illustrated in Fig. 4. In Table 1 are listed refinement details for structures **1**, **2**, and **3** while the refined coordinates of the non-H atoms for all materials are presented in Table 2. Bond lengths and angles involving all non-H atoms are collected in Table 3 while torsional angles involving only C and O atoms are given in Table 4. Table 5 contains the ^{13}C NMR chemical shifts. Lists of anisotropic temperature factors, hydrogen atomic parameters, all torsional angles, and calculated, observed, and unobserved structural factors are available as Supplementary Material.[2]

[1]Author to whom correspondence may be addressed.

[2]These data may be purchased from the Depository of Unpublished Data, CISTI, National Research Council of Canada, Ottawa, Ont., Canada K1A 0S2.

Can. J. Chem. Downloaded from www.nrcresearchpress.com by 186.148.149.217 on 09/07/12
For personal use only.

Can. J. Chem. Downloaded from www.nrcresearchpress.com by 186.148.149.217 on 09/07/12
For personal use only.

TABLE 1. Crystal data for **1**, **2**, and **3**

Parameter	**1**	**2**	**3**
Empirical formula	$C_{17}H_{30}O_4$	$C_{18}H_{30}LiNO_4S$	$C_{17}H_{30}LiO_8Cl$
Formula weight	298.42	363.44	404.81
Isomer	*cis–anti–cis*	← *cis–syn–cis* →	
Crystal dimensions, mm	0.3 × 0.4 × 0.4	0.15 × 0.25 × 0.25	0.15 × 0.2 × 0.35
Crystal system	Orthorhombic	← Monoclinic →	
Space group	*Pbc*2	← $P2_1/a$ →	
a, Å	8.1263(4)	9.252(5)	8.586(3)
b, Å	10.117(1)	18.523(3)	18.413(7)
c, Å	20.438(1)	11.800(2)	12.917(4)
β, deg		94.05(2)	97.70(2)
Z (molecules/cell)	← 4 →		
Cell volume, Å^3	1680.3	2017.2	2023.7
Accurate cell parameters from:			
No. of reflections	68	28	30
2θ range	100–116	90–100	90–103
D_{calc}, g cm^{-3}	1.180	1.197	1.329
μ, mm^{-1}	0.63	1.55	2.02
λ (CuKα$_1$), Å	← 1.54056 →		
Octants measured	*hkl*, $\bar{h}k\bar{l}$	← ±*h*, *k*, *l* →	
$2\theta_{max}$, degrees	← 120 →		
h range	0–9	−10–10	−9–9
k range	0–11	0–20	0–20
l range	0–22	0–13	0–14
Reflections measured	2617	3574	3173
Unique reflections	1294	2997	2917
Observed reflections	1124	2195	2317
$I_{net}/\sigma(I_{net})$ ratio	3.0	2.5	2.5
R_f (sign. reflns)	0.052	0.042	0.043
R_w sign. reflns)	0.038	0.054	0.056
Goodness-of-fit	1.9	1.9	2.1
Weighting scheme	$w = 1$	← $w^{-1} = \sigma^2(F_o) + 0.0003F_o^2$ →	
No. of parameters	298	347	365
Maximum δ/σ (last cycle)	0.4	0.1	0.1
Final *D*-map background, e/Å^3	≤0.16	≤0.32	≤0.33

X-ray crystallographic structures

The crystal structure of **1** is disordered. The disordered positions are carbons 8, 9, and 17, which show occupancy factors in a 60:40 ratio. The conformation with the 60% occupancy is depicted in Fig. 1a while that occupied to the extent of 40% is illustrated in Fig. 1b. The disordered positions are centrosymmetrically related from a positional but not an occupancy standpoint and represent nonsuperimposable mirror image sites.

The presence of the ethylene and propylene chains induces asymmetry in the structure of **1**. However, since the material was prepared and recrystallized as a racemic mixture, there will be equal amounts of each enantiomer present. The unit cell composition is consistent with this expectation despite the 60:40 conformer ratio present, since mirror related sites in the crystal contain these same forms in a 40:60 ratio.

In the cases of **2** and **3**, the Li^+ is pentacoordinated to the four ethereal oxygens of the crown ether and to the anions (SCN^- in **2** and ClO_4^- in **3** respectively). The four oxygens are not coplanar; the mean deviations from the least-squares plane connecting them are 0.20 and 0.24 Å in **2** and **3** respectively.

The macrocyclic ring conformation of **1** is almost identical with that found for the *cis–anti–cis* isomer of dicyclohexano-14-crown-4 (2). The only differences are found in the torsional networks involving C17′ and C17″ of **1**, which are anticipated since one of the propano bridges of the 14-crown-4 system has been replaced by an ethano bridge in the 13-crown-4 cases.

The more abundant conformer of **1** has a fairly regular geometry while the minor form shows some geometrical distortions centered at the disordered positions C9″ and C17″ (Table 3). The O–O diagonal distances in **1** are 4.2 and 4.3 Å for the O1–O3 and O2–O4 diagonals respectively. These, as expected, are somewhat smaller than in the corresponding 14-crown-4 molecule (2), where these distances are 4.4 and 4.7 Å. The O–O distances between equatorial oxygens are more affected than those involving axial oxygens when the macrocyclic ring size is decreased.

Comparison of bond lengths, angles, and torsional angles in the Li^+ complexes **2** and **3** shows that they are basically the same except for a small variation in the torsional angle about the O2—C2 bond. This difference is one of steric hindrance related to the different nature and orientation of the coordinating anion. In **3**, the ClO_3 base of the bonded anion is located over the six-membered O1—C7—C8—C9—O2—Li portion of the molecule. O7, one of the noncoordinating ClO_4^- oxygens, is 3.8 Å away from C8, a distance that is slightly longer than the sum of the van der Waals radii of CH_2 and O, ~3.6 Å (9).

Can. J. Chem. Downloaded from www.nrcresearchpress.com by 186.148.149.217 on 09/07/12
For personal use only.

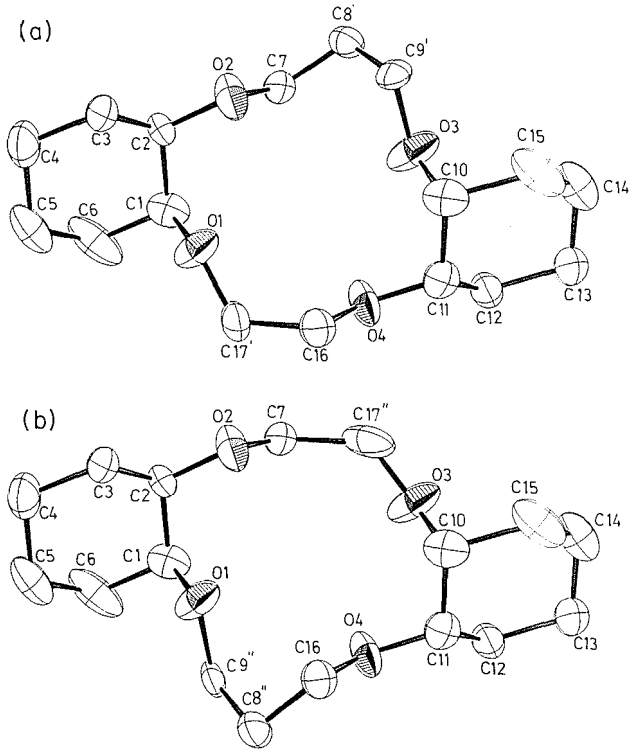

FIG. 1. (a) ORTEP diagram of **1** (60% isomer), (b) ORTEP diagram of **1** (40% isomer).

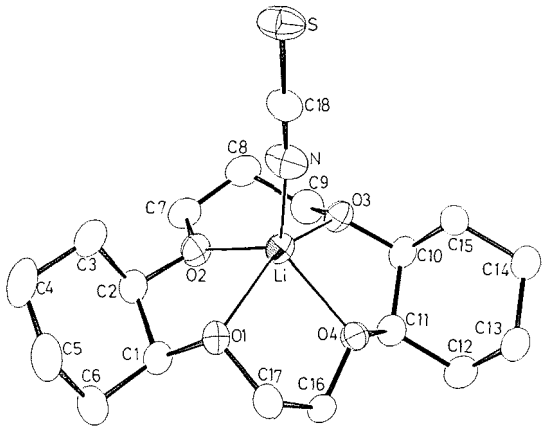

FIG. 2. ORTEP diagram of **2**.

To minimize possible repulsive interactions, a rotation of ca. 12° about the C2—O2 bond in **3** has the effect of pushing the whole propano chain away from O7. The overall orientation of the anion relative to Li^+ and the macrocyclic crown is subsequently different in **2** and **3**. The differences are most evident from comparison of the two pairs of corresponding angles O2—Li—N (116°) and O4—Li—N (125°) in **2** with O2—Li—O4 (123°) and O4—Li—O5 (112°) in **3**. Thus in **2**, the binding of the N atom of the linear NCS^- is located on the propano side of the crown while in **3**, for the steric reasons mentioned above, the binding O atom of the tetrahedral ClO_4^- is located on the ethano side but the ClO_3 moiety is bent towards the propano bridge of the 13-membered ring.

In the $O_{eq}—(CH_2)_3—O_{eq}$ portions of **2** and **3**, there are substantial conformational differences relative to the corresponding LiNCS complex of dicyclohexano-14-crown-4 (2), most

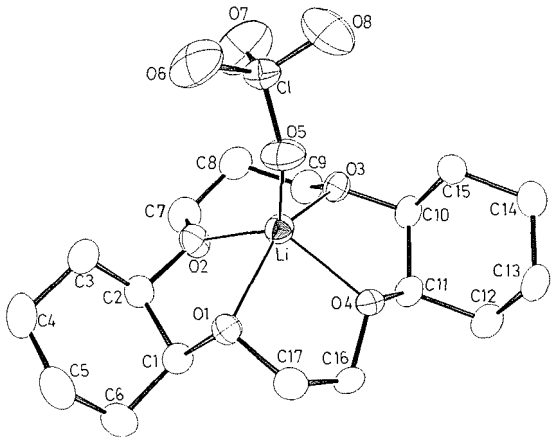

FIG. 3. ORTEP diagram of **3**.

notably in the C9—O3—C10—C11 and C7—O2—C2—C1 networks. In the 14-crown-4 system (2), these angles are near 180°, which is the common "relaxed" conformation in larger ring crown systems (10, 11). By contrast, in **2** and **3**, the C9—O3—C10—C11 angles are 95.0 and 93.6° respectively while the C7—O2—C2—C1 networks have torsion angles of 146.9 and 134.6° respectively.

In the $O_{ax}—(CH_2)_2—O_{ax}$ portions of **2** and **3** additional torsional strain is evident, especially in the C1—O1—C17—C16 network where the angles are 80.6 and 77.9° respectively. Hence the O1 and O3 regions appear to account for most of the strain present in **2** and **3**.

An additional interesting feature of **2** and **3** relative to the corresponding 14-crown-4 system (2) is the overall geometry of complexation. In the present cases, the four ethereal oxygens are directed towards the "concave" side of the molecule, with Li^+ and the anion coming in from this side. In the 14-membered system, the four oxygens are directed towards the "convex" side of the crown and hence the Li^+ complexes preferentially from the convex direction.

With respect to the lithium environment, some comparison with the known (8) X-ray structure of the LiNCS complex of benzo-13-crown-4 can be made. In **2** and **3**, the diagonal distances, O1–O3 and O2–O4, are 4.05 and 3.54 Å respectively, which result in an adjusted cavity diameter of 0.74–1.25 Å, a value nearly identical to that present in the benzo-13-crown-4 system. This diameter is small compared to the effective diameter of the Li^+ ion (1.18–1.52 Å) (12), and thus favours, as expected, five-coordinate lithium complexation. In **2** and **3**, the Li is lying 0.75 Å out of the least-squares plane going through the four binding oxygen atoms. For the related benzo system (8), the Li^+ lies slightly farther (distance ~0.80 Å) out of the plane of the four complexing oxygens, a result consistent with the anticipated increase in flexibility of the dicyclohexano substituted molecules relative to benz-annelated crowns.

It appears that the 13-crown-4 cavity size is less ideal for Li^+ complexation than was the case in the related 14-crown-4 molecules (2). For the LiNCS complex of *cis–syn–cis*-dicyclohexano-14-crown-4, the Li^+ lies less far (0.55 Å) out of the plane of the four coplanar oxygens. This distance is still sufficient, however, to leave the other side of the lithium ion open for anion coordination (2).

The $Li—O_{crown}$ distances listed in Table 3 are shorter for equatorial than for axial oxygens, a trend similar to that noted in the related 14-crown-4 case (2). On the average, these bond lengths are 2.07 Å, which is nearly identical to those in the

TABLE 2. Atomic parameters x, y, z, and B_{iso}; esd's refer to the last digit printed

Atom	x	y	z	B_{iso}
		1		
O1	0.1298(5)	0.1792(4)	0.8335 (4)	7.2(3)
O2	−0.0079(6)	0.0402(6)	0.74946(19)	7.0(3)
O3	0.2890(5)	0.0751(5)	0.6379 (5)	8.3(3)
O4	0.4863(6)	0.1909(6)	0.73486	6.7(3)
C1	0.1433(9)	0.0494(7)	0.8504 (4)	6.0(3)
C2	−0.0164(8)	0.0235(8)	0.8182 (4)	4.7(3)
C3	−0.1478(10)	0.1179(11)	0.8432 (5)	6.7(5)
C4	−0.1691(14)	0.1031(10)	0.9165 (5)	7.8(5)
C5	−0.0064(16)	0.1261(11)	0.9517 (6)	8.8(7)
C6	0.1275(19)	0.0392(12)	0.9236 (5)	10.1(7)
C7	0.0687(8)	−0.0604(8)	0.7155 (5)	6.4(4)
C8′	0.0500(15)	−0.0523(11)	0.6440 (6)	5.0(5)
C8″	0.456 (3)	0.2955(18)	0.8408 (9)	6.0(9)
C9′	0.1116(16)	0.0802(14)	0.6200 (7)	4.6(5)
C9″	0.381 (3)	0.1668(20)	0.8628 (8)	5.1(9)
C10	0.3498(9)	0.2026(7)	0.6304 (5)	6.0(3)
C11	0.5059(8)	0.2157(8)	0.6673 (5)	5.2(3)
C12	0.6396(9)	0.1283(8)	0.6409 (4)	5.7(4)
C13	0.6671(11)	0.1480(10)	0.5679 (5)	7.7(5)
C14	0.5092(14)	0.1359(10)	0.5313 (6)	7.7(6)
C15	0.3818(15)	0.2288(11)	0.5556 (5)	8.8(6)
C16	0.4182(8)	0.2980(8)	0.7713 (4)	6.6(4)
C17′	0.3582(17)	0.2289(19)	0.8341 (7)	6.3(8)
C17″	0.141 (4)	0.019 (4)	0.6470 (15)	9.6(19)
		2		
S	0.62798(9)	0.09134(6)	0.75490(7)	6.41(5)
O1	1.17794(19)	0.04791(9)	0.55874(14)	3.75(8)
O2	1.24492(22)	0.13808(10)	0.72467(16)	4.76(9)
O3	1.20515(21)	0.03261(9)	0.90052(14)	4.32(8)
O4	1.24153(19)	−0.05196(9)	0.72361(13)	3.71(8)
N	0.9206 (3)	0.05927(17)	0.74422(21)	5.92(15)
C1	1.2871 (3)	0.10111(15)	0.53832(24)	4.07(13)
C2	1.2541 (3)	0.16481(16)	0.6107 (3)	4.62(15)
C3	1.1151 (5)	0.20304(21)	0.5681 (4)	6.32(21)
C4	1.1185 (6)	0.2223 (3)	0.4437 (4)	8.0 (3)
C5	1.1440 (5)	0.15701(23)	0.3716 (3)	6.62(21)
C6	1.2845 (4)	0.12046(20)	0.4126 (3)	5.24(16)
C7	1.2932 (5)	0.18710(18)	0.8127 (3)	5.43(17)
C8	1.2479 (5)	0.15874(19)	0.9239 (3)	6.15(19)
C9	1.3001 (5)	0.08424(19)	0.9568 (3)	5.78(18)
C10	1.2426 (4)	−0.04160(15)	0.92070(24)	4.42(14)
C11	1.3310 (4)	−0.06849(16)	0.82589(23)	4.27(13)
C12	1.3602 (4)	−0.14869(18)	0.8363 (3)	5.29(16)
C13	1.2212 (5)	−0.19088(17)	0.8428 (3)	5.37(18)
C14	1.1355 (6)	−0.16477(18)	0.9395 (3)	6.02(20)
C15	1.1042 (4)	−0.08397(16)	0.9296 (3)	4.79(16)
C16	1.3141 (4)	−0.05721(17)	0.62163(24)	4.61(15)
C17	1.2169 (4)	−0.02415(15)	0.53006(24)	4.58(15)
C18	0.7993 (3)	0.07277(17)	0.74990(22)	4.36(14)
Li	1.1325 (5)	0.04750(23)	0.7349 (4)	4.00(19)
		3		
Cl	0.23389(8)	0.07916(4)	0.75129(6)	4.45(3)
O1	−0.17642(21)	0.04435(10)	0.92419(14)	3.81(8)
O2	−0.2407 (3)	0.13560(11)	0.76665(16)	4.95(10)
O3	−0.19131(22)	0.02812(9)	0.60905(15)	3.93(8)
O4	−0.22295(21)	−0.05766(10)	0.77072(14)	3.64(7)
O5	0.10732(25)	0.04108(14)	0.78885(20)	5.99(12)
O6	0.3163 (4)	0.11882(18)	0.83415(23)	9.10(17)
O7	0.1745 (5)	0.12504(19)	0.6698 (3)	11.11(21)
O8	0.3337 (4)	0.02823(22)	0.7163 (4)	12.8 (3)

Can. J. Chem. Downloaded from www.nrcresearchpress.com by 186.148.149.217 on 09/07/12
For personal use only.

TABLE 2. (*Concluded*)

Atom	x	y	z	B_{iso}
C1	−0.3054 (3)	0.09328(16)	0.9289 (3)	4.21(15)
C2	−0.2682 (4)	0.15960(17)	0.8687 (3)	4.49(15)
C3	−0.1294 (5)	0.20049(21)	0.9238 (3)	5.73(19)
C4	−0.1567 (7)	0.22049(25)	1.0336 (4)	6.88(23)
C5	−0.1901 (6)	0.15507(24)	1.0955 (3)	6.53(21)
C6	−0.3251 (5)	0.1127 (3)	1.0412 (4)	5.94(20)
C7	−0.3166 (6)	0.17806(22)	0.6817 (3)	5.94(19)
C8	−0.2641 (5)	0.15246(19)	0.5821 (3)	5.37(18)
C9	−0.3045) 5)	0.07528(19)	0.5525 (3)	5.07(16)
C10	−0.2197 (4)	−0.04821(15)	0.59034(24)	4.00)13)
C11	−0.3129 (3)	−0.07721(16)	0.67304(24)	3.98(13)
C12	−0.3336 (4)	−0.15939(18)	0.6625 (3)	5.22(17)
C13	−0.1774 (5)	−0.19740(18)	0.6665 (3)	4.89(17)
C14	−0.0858 (6)	−0.16805(18)	0.5832 (3)	5.31(18)
C15	−0.0648 (4)	−0.08601(16)	0.5918 (3)	4.41(15)
C16	−0.3035 (4)	−0.06665(18)	0.8598 (3)	4.53(14)
C17	−0.2091 (5)	−0.03011(17)	0.9488 (3)	4.75(16)
Li	−0.1225 (5)	0.04493(25)	0.7648 (4)	3.85(21)

′ occupancy factor = 0.60; ″ occupancy factor = 0.40.
B_{iso} is the mean of the principal axes of the thermal ellipsoid.

Can. J. Chem. Downloaded from www.nrcresearchpress.com by 186.148.149.217 on 09/07/12
For personal use only.

benzo-13-crown-4 complex (8), but substantially longer than those in the 14-crown-4 analog (2.02 Å). Notably, the Li—O1 bonds in both **2** (2.149 Å) and **3** (2.170 Å) are significantly longer than the others.

In summary, the coordination geometry around the lithium in both **2** and **3** is a distorted intermediate between square pyramid and trigonal bipyramid, in contrast to the related 14-crown-4 case where an essentially square pyramid exists (2). Also it is evident that no major conformational changes are induced in the 13-membered ring in the presence of differing anions.

Solid phase ^{13}C NMR spectra

The ^{13}C NMR spectrum of solid **1** (Fig. 4) reflects the disorder present in the crystal. Although the spectrum is rather complex, there are ten resolved resonances in the range of 60–80 ppm indicative of oxygenated carbons. If an ordered racemic mixture were present, only eight resonances would be observed in this region. Regarding detailed peak assignments, a number of these can be made based on analogy with earlier work (2) and are indicated in Table 5. The effects are in accord with the well-established steric shifts in ^{13}C NMR spectra of molecules in which cyclohexane functions are present bearing axial and equatorial oxygenated functions (13, 14).

In contrast to the situation in solution ^{13}C NMR, methods of unambiguous signal attribution in solid state spectra are relatively few. The most common technique is interrupted decoupling, alternatively known as dipolar dephasing (15, 16), a method that allows discrimination between immobile protonated carbons and nonprotonated or very mobile protonated carbon sites. Unfortunately this method does not effectively discriminate between methine and methylene carbons, which is the major problem in the ^{13}C CPMAS spectrum of **1**, especially in the 68–80 ppm range. Consequently, many of the assignments in Table 5 must be regarded as being interchangeable as indicated.

One method was, however, of some utility. It was observed that the low temperature (173 K) solution ^{13}C spectrum of **1** (major conformer) is remarkably similar to that of the solid in the 68–80 ppm range.[3] The APT test (17) was subsequently performed on the low temperature sample to identify the CH vs. CH_2 resonances in this region and the results were utilized to aid in partial assignment of the solid state spectrum. Hopefully, recent advances in assignment methods, such as that based on separated local field methods (18), will become applicable to the solution of such problems.

No isolable Li^+ complexes of **1** could be prepared. This observation is consistent with that found in related 12-crown-4 and 14-crown-4 ethers (2, 3, 5), where stable complexes of the *cis–syn–cis* dicyclohexano system could be prepared, but not for the configurationally isomeric *cis–anti–cis* cases. Presumably the conformational distortions required to allow the four oxygen atoms to become coplanar (as is preferred for complexation) are too extreme in the *cis–anti–cis* isomers.

The LiNCS and $LiClO_4$ complexes of the *cis–syn–cis* isomer (an oil in the uncomplexed form) gave essentially identical ^{13}C CPMAS spectra and thus only that for the LiNCS case is shown in Fig. 4. In contrast to the spectrum of **1**, the relatively sharp resonances for **2** indicate an ordered situation in the crystal. In fact seven out of eight possible oxygenated carbon resonances in the range of 64–80 ppm are resolved.

With the X-ray data in hand, some interesting stereochemical aspects of the ^{13}C chemical shifts can be explored. The cyclohexyl carbons, which are γ–gauche to the axial oxygens (i.e., C5 and C13), will resonate at highest field (1–5, 13, 14). Since the X-ray structure of **2** indicates no symmetry, separate resonances are anticipated and, indeed, observed for these carbons (at 18.6 and 20.3 ppm). An examination of the torsional environments for C5 and C13 in **2** reveals one significant difference as delineated below.

Ignoring hydrogens, C5 and C13 are each involved in five torsional networks. With respect to their environments relative to the other cyclohexyl carbons, there is little difference between these two sites. For C5, the average of four torsional

[3]G. W. Buchanan, R. A. Kirby, and K. Bourque. Unpublished observations.

TABLE 3. Bond lengths (A) and angles (deg) (non-H atoms only)

Bond	Length	Bond	Length	Bonds	Angle	Bonds	Angle
				1			
O1—C1	1.416(9)	C4—C5	1.523(17)	C2—O2—C7	115.7(6)	O3—C10—C11	109.3(7)
O2—C2	1.416(9)	C5—C6	1.512(18)	C11—O4—C16	114.8(6)	O3—C10—C15	108.8(8)
O2—C7	1.380(9)	C10—C11	1.482(11)	O1—C1—C2	107.8(6)	C11—C10—C15	109.8(8)
O3—C10	1.390(9)	C10—C15	1.573(15)	O1—C1—C6	109.3(8)	O4—C11—C10	112.7(6)
O4—C11	1.413(10)	C11—C12	1.501(10)	C2—C1—C6	110.8(9)	O4—C11—C12	109.2(6)
O4—C16	1.426(9)	C12—C13	1.520(13)	O2—C2—C1	112.2(6)	C10—C11—C12	112.6(7)
C1—C2	1.479(10)	C13—C14	1.491(15)	O2—C2—C3	107.0(6)	C11—C12—C13	112.5(7)
C1—C6	1.505(15)	C14—C15	1.483(15)	C1—C2—C3	110.8(7)	C12—C13—C14	110.9(8)
C2—C3	1.521(11)	C3—C4	1.516(14)	C2—C3—C4	110.5(9)	C13—C14—C15	112.4(9)
O1—C17′	1.435(16)	C16—C17′	1.542(10)	C3—C4—C5	110.6(8)	C10—C15—C14	109.5(8)
O3—C9′	1.489(14)	C8′—C9′	1.513(18)	C4—C5—C6	110.9(9)	C1—C6—C5	113.5(8)
C7—C8′	1.470(16)			C1—O1—C17′	126.0(9)	C7—C8′—C9′	109.8(10)
O1—C9″	1.649(22)	C8″—C9″	1.51(3)	O4—C16—C17′	102.3(8)	O1—C17′—C16	116.6(11)
C7—C17″	1.72(4)	O3—C17″	1.34(4)	O2—C7—C8′	114.3(7)	O3—C9′—C8′	102.1(9)
C8″—C16	1.454(22)			C9′—O3—C10	106.5(7)		
				C1—O1—C9″	96.0(8)	C9″—C8″—C16	102.8(14)
				O1—C9″—C8″	101.6(15)	O4—C16—C8″	114.5(10)
				C10—O3—C17″	136.4(15)	O3—C17″—C7	128.0(20)
				O2—C7—C17″	102.5(11)		
				2			
S—C18	1.627(3)	C2—C3	1.522(5)	C1—O1—C17	114.00(23)	C1—O1—Li	110.54(19)
O1—C1	1.443(3)	C1—C2	1.501(4)	C17—O1—Li	107.18(19)	O1—C17—C16	111.22(23)
O1—C17	1.430(3)	C3—C4	1.513(6)	C2—O2—C7	115.10(23)	C2—O2—Li	114.41(20)
O1—Li	2.149(5)	C4—C5	1.506(7)	C7—O2—Li	129.27(23)	S—C18—N	178.7(3)
O2—C2	1.441(4)	C5—C6	1.514(5)	C9—O3—C10	115.51(24)	O1—Li—O2	78.40(18)
O2—C7	1.428(4)	C7—C8	1.500(5)	C9—O3—Li	120.30(23)	O1—Li—O3	148.5(3)
O2—Li	1.982(5)	C8—C9	1.504(6)	C10—O3—Li	110.38(19)	O1—Li—O4	79.34(17)
O3—C9	1.430(4)	C10—C11	1.516(4)	C11—O4—C16	114.53(23)	O1—Li—N	108.37(21)
O3—C10	1.433(3)	C10—C15	1.512(5)	C11—O4—Li	112.35(19)	C16—O4—Li	111.69(19)
O3—Li	2.040(5)	O4—Li	2.109(5)	C18—N—Li	173.8(3)	O1—C1—C2	105.59(23)
O4—C11	1.447(3)	C11—C12	1.513(4)	O1—C1—C6	111.08(24)	O2—Li—O3	91.93(20)
O4—C16	1.422(3)	C12—C13	1.511(6)	C2—C1—C6	112.3(3)	O2—Li—O4	118.69(24)
C13—C14	1.514(5)	C14—C15	1.527(4)	O2—C2—C1	106.79(22)	O2—Li—N	115.81(24)
N—C18	1.157(4)	N—Li	1.983(6)	O2—C2—C3	111.4(3)	C1—C2—C3	112.3(3)
C16—C17	1.488(4)			O3—Li—O4	79.37(16)	C2—C3—C4	110.8(3)
C1—C6	1.524(4)			O3—Li—N	102.80(23)	C3—C4—C5	111.9(3)
				C4—C5—C6	110.1(4)	C1—C6—C5	111.7(3)
				O2—C7—C8	108.7(3)	C7—C8—C9	116.3(3)
				O4—Li—N	125.36(25)	O3—C9—C8	108.5(3)
				O3—C10—C11	109.22(23)	O3—C10—C15	108.3(3)
				C11—C10—C15	112.6(3)	O4—C11—C10	103.87(23)
				O4—C11—C12	111.35(24)	C10—C11—C12	111.4(3)
				C11—C12—C13	111.3(3)	C12—C13—C14	111.4(3)
				C13—C14—C15	111.2(3)	C10—C15—C14	110.9(3)
				O4—C16—C17	106.8(3)		
				3			
Cl—O5	1.4316(22)	Cl—O6	1.406(3)	O5—Cl—O6	108.90(17)	O5—Cl—O7	109.63(19)
Cl—O7	1.392(3)	C1—O8	1.386(3)	O5—C1—O8	108.03(21)	O6—C1—O7	110.89(21)
C2—C3	1.506(5)	C3—C4	1.514(6)	O6—C1—O8	109.2(3)	O7—C1—O8	110.1(3)
C4—C5	1.495(7)	O1—C1	1.435(3)	C1—O1—C1	114.39(23)	O1—Li—O2	79.38(18)
C5—C6	1.492(7)	O1—C17	1.443(4)	C1—O1—Li	107.53(21)	O1—Li—O3	149.68(25)
C7—C8	1.495(6)	O2—Li	1.955(5)	C17—O1—Li	106.62(20)	O1—Li—O4	79.56(17)
O1—Li	2.170(5)	C8—C9	1.500(5)	C2—O2—C7	114.87(25)	O1—Li—O5	100.85(22)
O2—C2	1.439(4)	C10—C11	1.515(4)	C2—O2—Li	114.99(22)	C7—O2—Li	129.8(3)
O2—C7	1.431(4)	C10—C15	1.499(5)	C9—O3—C10	114.74(23)	C9—O3—Li	119.91(24)
O3—C9	1.429(4)	C11—C12	1.528(4)	C10—O3—Li	109.45(20)	C11—O4—C16	114.68(22)
O3—C10	1.441(3)	C1—C6	1.525(5)	C11—O4—Li	111.86(20)	O2—Li—O3	93.39(21)
O3—Li	2.043(5)	C12—C13	1.507(5)	C16—O4—Li	112.45(21)	O2—Li—O4	123.77(24)
O4—C11	1.434(3)	C13—C15	1.524(5)	Cl—O5—Li	136.34(21)	O2—Li—O5	122.9(3)
O4—C16	1.430(3)	C14—C15	1.524(5)	O1—C1—C2	105.61(23)	O1—C1—C6	111.8(3)
O4—Li	2.082(5)	C16—C17	1.476(5)	C2—C1—C6	111.1(3)	O2—C2—C1	107.23(24)
O5—Li	1.957(5)	C1—C2	1.505(4)	O3—Li—O4	80.33(18)	O2—C2—C3	111.7(3)
				O3—Li—O5	107.64(24)	C1—C2—C3	111.8(3)
				C2—C3—C4	110.6(3)	C3—C4—C5	111.7(3)
				C4—C5—C6	111.3(4)	O4—Li—O5	112.03(23)
				C1—C6—C5	113.1(3)	O2—C7—C8	109.2(3)
				C7—C8—C9	115.6(3)	O3—C9—C8	109.1(3)
				O3—C10—C11	108.60(23)	O3—C10—C15	108.71(24)
				C11—C10—C15	112.3(3)	O4—C11—C10	105.00(22)
				O4—C11—C12	111.7(3)	C10—C11—C12	110.6(3)
				C11—C12—C13	111.4(3)	C12—C13—C14	110.7(3)
				C13—C14—C15	111.7(3)	C10—C15—C14	111.3(3)
				O4—C16—C17	107.4(3)	O1—C17—C16	111.4(3)

Can. J. Chem. Downloaded from www.nrcresearchpress.com by 186.148.149.217 on 09/07/12
For personal use only.

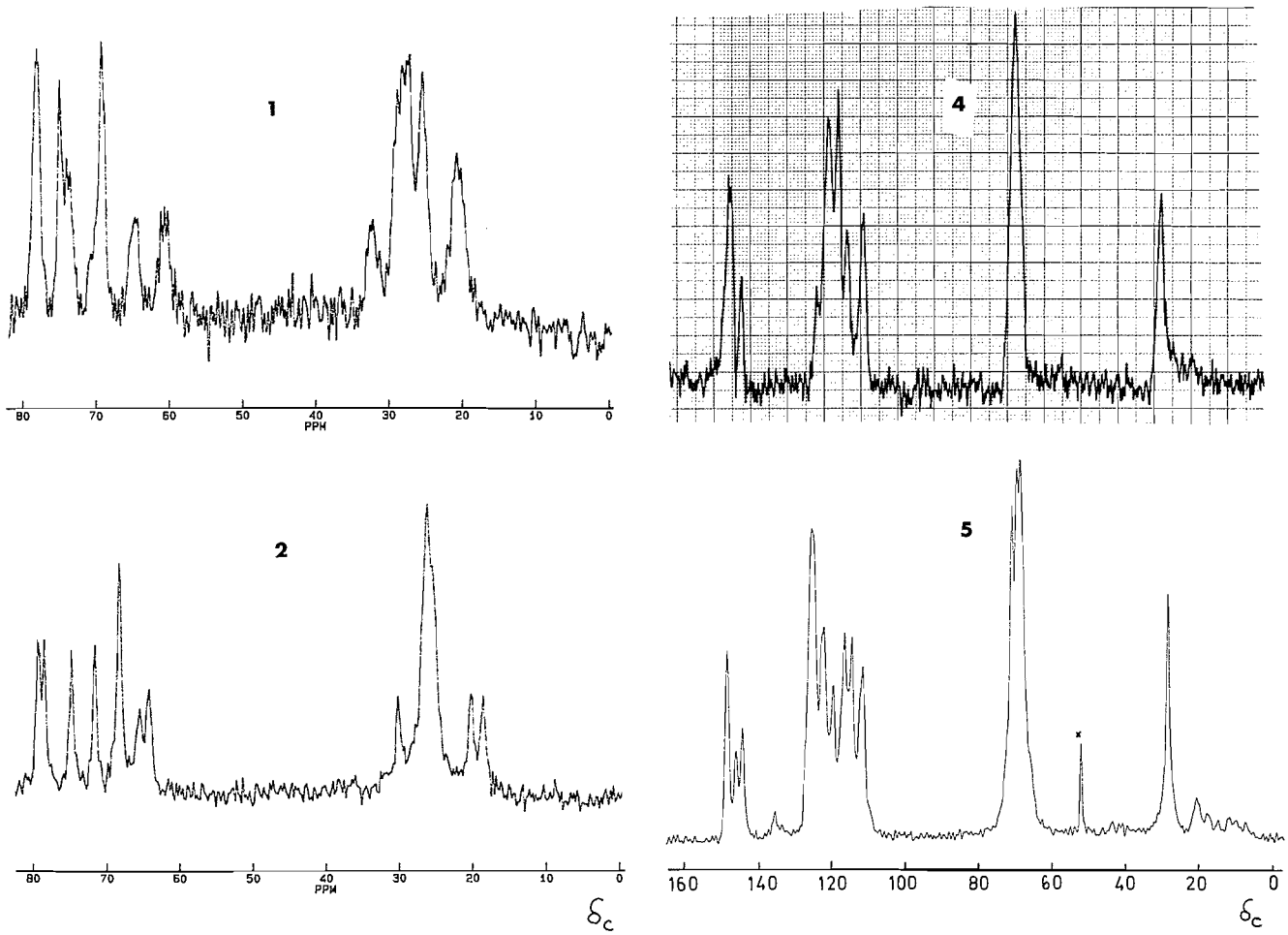

FIG. 4. 45.3 MHz ^{13}C CPMAS NMR spectra.

angles is 55.7° while for C13, the value is 56.1°. The most significant difference in their environments occurs in the networks O1—C1—C6—C5 vs. O4—C11—C12—C13. Whereas the former has a dihedral angle of 60.6°, this expands to 64.6° in the latter. Although no theoretical ^{13}C chemical shift calculations have appeared for the O—C—C—C network, results for the geometrically similar C—C—C—C network (19) indicate that expansion of a torsional angle above that of a pure *gauche* interaction would be expected to lead to a deshielding of the terminal carbon atom. On this basis, we assign the resonance at 20.3 ppm to C13 and that at 18.6 ppm to C5.

In the methine carbon region of the spectrum (72–80 ppm), the resonances for the carbons bearing equatorial oxygen (C2 and C10) are separated by less than 1 ppm and hence no attempt will be made to provide separate assignments. On the other hand, there is a 3.2 ppm difference between the resonances for C1 and C11, the carbons bearing axial oxygen, (appearing at 74.7 and 71.5 ppm). Each of these carbons is involved in twelve torsional networks if one ignores the hydrogen atoms. Examination of the data in Table 4 reveals that two torsional networks show large differences in dihedral angles involving these two sites in the crystal as depicted below.

C16—C17—O1—*C1* θ = 168.1° vs. C17—C16—O4—*C11* θ = 81.0°

C1—C2—O2—C7 θ = 95.1° vs. *C11*—C10—O3—C9 θ = 147.0°

Unfortunately no experimental ^{13}C chemical shift data exist for these particular torsional networks in either solution or the solid phase. One can, however, theoretically model these networks using the simple aliphatic ether CH_3—O—CH_2—CH_3 and employing INDO MO calculations of the ^{13}C chemical shifts.[4] In the case of a C—C—O—*C* network, the results indicate that the designated carbon in the situation in which θ = 81.0° will be more shielded (i.e., lower δ_C), by ca. 4 ppm, than that for θ = 168.1°. For the *C*—C—O—C situation, the calculations[4] indicate nearly identical chemical shifts for the torsion angles of 95.1° and 147.0°. On the basis of these considerations, we assign the 71.5 ppm resonance to C11 and the line at 74.7 to C1.

The final points of interest in the ^{13}C CPMAS spectrum of **2** concern the CH_2-O resonances at 68.2 ppm (intensity two) and the single intensity resonances at 65.4 and 64.2 respectively. In view of the discussion of the chemical shifts of C1, 5, 11, and 13 in terms of their torsional environments, it is instructive to carry out the same type of analysis for C7, 9, 16, and 17 of **2**. The results, however, do not lead to any clear arguments for one set of assignments being more valid than any other. Part of the problem with these carbons is the present lack of theoretical shift calculations for the C—C—C—O network. An additional complicating factor is the unknown influence of the spatially proximate lithium ion on the ^{13}C shieldings.

For dibenzo-13-crown-4, **4**, and its LiNCS complex, **5**, no

[4]G. W. Buchanan, R. A. Kirby, and J. S. Tse. Unpublished observations.

Can. J. Chem. Downloaded from www.nrcresearchpress.com by 186.148.149.217 on 09/07/12
For personal use only.

TABLE 4. Torsion angles (deg) (C and O atoms only)

Atoms				Angle	Atoms				Angle
				1 (occupancy factor = 60%)					
C17′	O1	C1	C2	−157.0(10)	C17′	O1	C1	C6	82.5(9)
C1	O1	C17′	C16	128.5(13)	C7	O2	C2	C1	75.8(6)
C7	O2	C2	C3	−162.4(9)	C2	O2	C7	C8′	169.7(9)
C10	O3	C9′	C8′	−167.8(13)	C9′	O3	C10	C11	161.4(10)
C9′	O3	C10	C15	−78.7(8)	C16	O4	C11	C10	−79.0(6)
C16	O4	C11	C12	155.1(8)	C11	O4	C16	C17′	161.6(10)
O1	C1	C2	O2	56.9(5)	O1	C1	C2	C3	−62.7(6)
C6	C1	C2	O2	176.5(10)	C6	C1	C2	C3	56.9(7)
O1	C1	C6	C5	64.4(8)	C2	C1	C6	C5	−54.3(8)
O2	C2	C3	C4	178.1(11)	C1	C2	C3	C4	−59.3(7)
C2	C3	C4	C5	56.9(7)	C3	C4	C5	C6	−53.1(8)
C4	C5	C6	C1	52.1(8)	O2	C7	C8′	C9′	56.0(8)
C7	C8′	C9′	O3	63.0(8)	O3	C10	C11	O4	−59.6(6)
O3	C10	C11	C12	64.5(6)	C15	C10	C11	O4	−178.9(10)
C15	C10	C11	C12	−54.9(7)	O3	C10	C15	C14	−62.6(8)
C11	C10	C15	C14	57.0(7)	O4	C11	C12	C13	179.4(10)
C10	C11	C12	C13	53.4(6)	C11	C12	C13	C14	−52.2(7)
C12	C13	C14	C15	56.0(8)	C13	C14	C15	C10	−58.2(8)
O4	C16	C17′	O1	−89.8(10)					
				1 (occupancy factor = 40%)					
C9″	O1	C1	C2	−169.5(10)	C9″	O1	C1	C6	70.0(9)
C1	O1	C9″	C8″	173.7(18)	C7	O2	C2	C1	75.8(6)
C7	O2	C2	C3	−162.4(9)	C2	O2	C7	C17″	−153.3(13)
C17″	O3	C10	C11	139.6(16)	C17″	O3	C10	C15	−100.5(16)
C10	O3	C17″	C7	−111.9(21)	C16	O4	C11	C10	−79.0(6)
C16	O4	C11	C12	155.1(8)	C11	O4	C16	C8″	−157.0(11)
O1	C1	C2	O2	56.9(5)	O1	C1	C2	C3	−62.7(6)
C6	C1	C2	O2	176.5(10)	C6	C1	C2	C3	56.9(7)
O1	C1	C6	C5	64.4(8)	C2	C1	C6	C5	−54.3(8)
O2	C2	C3	C4	178.1(11)	C1	C2	C3	C4	−59.3(7)
C2	C3	C4	C5	56.9(7)	C3	C4	C5	C6	−53.1(8)
C4	C5	C6	C1	52.1(8)	O2	C7	C17″	O3	92.3(21)
C16	C8″	C9″	O1	−51.3(10)	C9″	C8″	C16	O4	−60.6(11)
O3	C10	C11	O4	−59.6(6)	O3	C10	C11	C12	64.5(6)
C15	C10	C11	O4	−178.9(10)	C15	C10	C11	C12	−54.9(7)
O3	C10	C15	C14	−62.6(8)	C11	C10	C15	C14	57.0(7)
O4	C11	C12	C13	179.4(10)	C10	C11	C12	C13	53.4(6)
C11	C12	C13	C14	−52.2(7)	C12	C13	C14	C15	56.0(8)
C13	C14	C15	C10	−58.2(8)					
				2					
C17	O1	C1	C2	−159.5(3)	C17	O1	C1	C6	78.5(2)
C1	O1	C17	C16	80.6(2)	C7	O2	C2	C1	146.9(3)
C7	O2	C2	C3	−90.3(3)	C2	O2	C7	C8	167.9(4)
C10	O3	C9	C8	178.4(4)	C9	O3	C10	C11	−95.0(3)
C9	O3	C10	C15	142.0(3)	C16	O4	C11	C10	166.6(3)
C16	O4	C11	C12	−73.4(2)	C11	O4	C16	C17	−168.5(3)
O1	C1	C2	O2	52.9(2)	O1	C1	C2	C3	−69.4(2)
C6	C1	C2	O2	174.1(4)	C6	C1	C2	C3	51.8(2)
O1	C1	C6	C5	64.8(3)	C2	C1	C6	C5	−53.2(2)
O2	C2	C3	C4	−172.6(4)	C1	C2	C3	C4	−53.0(3)
C2	C3	C4	C5	56.2(3)	C3	C4	C5	C6	−57.5(3)
C4	C5	C6	C1	55.4(3)	O2	C7	C8	C9	57.2(3)
C7	C8	C9	O3	−82.4(3)	O3	C10	C11	O4	−54.1(2)
O3	C10	C11	C12	−174.1(4)	C15	C10	C11	O4	66.2(2)
C15	C10	C11	C12	−53.8(2)	O3	C10	C15	C14	174.4(4)
C11	C10	C15	C14	53.6(2)	O4	C11	C12	C13	−61.1(2)
C10	C11	C12	C13	54.4(2)	C11	C12	C13	C14	−56.0(3)
C12	C13	C14	C15	56.0(3)	C13	C14	C15	C10	−54.4(2)
O4	C16	C17	O1	55.1(2)					

Can. J. Chem. Downloaded from www.nrcresearchpress.com by 186.148.149.217 on 09/07/12
For personal use only.

TABLE 4. (*concluded*)

Atoms				Angle	Atoms				Angle
				3					
C17	O1	C1	C2	−162.0(3)	C17	O1	C1	C6	77.0(3)
C1	O1	C17	C16	77.9(3)	C7	O2	C2	C1	134.6(3)
C7	O2	C2	C3	−102.6(3)	C2	O2	C7	C8	173.8(4)
C10	O3	C9	C8	178.0(4)	C9	O3	C10	C11	−93.6(3)
C9	O3	C10	C15	144.0(3)	C16	O4	C11	C10	168.0(3)
C16	O4	C11	C12	−72.1(2)	C11	O4	C16	C17	−168.2(3)
O1	C1	C2	O2	54.5(2)	O1	C1	C2	C3	−68.2(3)
C6	C1	C2	O2	176.0(4)	C6	C1	C2	C3	53.3(3)
O1	C1	C6	C5	65.6(3)	C2	C1	C6	C5	−52.1(3)
O2	C2	C3	C4	−176.0(4)	C1	C2	C3	C4	−55.9(3)
C2	C3	C4	C5	56.7(3)	C3	C4	C5	C6	−55.2(3)
C4	C5	C6	C1	53.0(3)	O2	C7	C8	C9	62.1(3)
C7	C8	C9	O3	−81.4(3)	O3	C10	C11	O4	−54.3(2)
O3	C10	C11	C12	−175.0(3)	C15	C10	C11	O4	65.9(2)
C15	C10	C11	C12	−54.7(2)	O3	C10	C15	C14	174.3(4)
C11	C10	C15	C14	54.2(2)	O4	C11	C12	C13	−60.9(2)
C10	C11	C12	C13	55.6(2)	C11	C12	C13	C14	−56.2(3)
C12	C13	C14	C15	55.4(3)	C13	C14	C15	C10	−54.4(2)
O4	C16	C17	O1	53.8(2)					

TABLE 5. Solid phase ^{13}C chemical shifts (δ_C from TMS ± 0.1)

Carbon	**1**	**2**	**3**	**4**
C1	(74.9)[a]	74.7	(146.2)[h]	(148.2)[k]
C2	78.0	(79.2)[f]	(146.2)[h]	(146.1)[k]
C3	(28.2)[b]	26.2	(111.0)[i]	(114.0)[l]
C4	25.3	26.2	(120.0)[j]	(121.5)[m]
C5	(20.7)[c]	18.6	(120.0)[j]	(125.0)[m]
C6	(27.1)[d]	26.2	(111.0)[i]	(111.5)[l]
C7	(64.7)[e]	(64.2)[g]	67.9	(68.6)[n]
C8	32.1	30.3	28.0	27.0
C9	(60.6)[e]	(65.4)[g]	67.9	(68.6)[n]
C10	(73.8)[a]	(78.4)[f]	(146.0)[h]	(148.2)[k]
C11	78.0	71.5	(143.0)[h]	(144.0)[k]
C12	(28.7)[b]	26.2	(115.2)[i]	(115.8)[l]
C13	25.3	20.3	(117.2)[j]	(125.0)[m]
C14	(20.9)[c]	26.2	(117.2)[i]	(125.0)[m]
C15	(27.3)[d]	26.2	(115.2)[i]	(119.8)[l]
C16	69.2	68.2	67.9	(69.6)[n]
C17	69.2	68.2	67.9	(70.9)[n]

[a–n]Indicate possible interchange of resonance assignments.

X-ray crystallographic data are available. In the case of **4**, a single broad resonance for the oxygenated carbons is observed at 67.9 ppm, whereas in **5**, there are three resolved resonances in this region of the spectrum. This suggests that there may be less mobility in the LiNCS complex than in the free crown ether, which is intuitively reasonable. In view of the number of observed aromatic carbon resonances, it appears that neither **4** nor **5** possesses any elements of symmetry. Of course in the absence of X-ray data, one cannot rule out crystal packing phenomena or the existence of different molecules in the crystal as the cause of spectral multiplicity (20), but the occurrence of such phenomena is relatively rare.

To conclude, attempts are presently underway to resolve the enantiomeric forms of **1** via complexation with optically pure α-methylbenzylammonium salts. Results of these investigations, as well as the detailed low temperature solution NMR behaviour of these materials, will be the subject of a future report.

Experimental

Spectra

The ^{13}C CPMAS NMR spectra were recorded at 45.3 MHz on a Bruker CXP-180 spectrometer using techniques described previously (2). Chemical shifts were measured relative to external solid hexamethylbenzene (HMB) and converted to the TMS scale via the factor of 16.9 ppm, which is the chemical shift of the CH_3 group of HMB.

Crystallographic measurements and structure solution and refinement

Single crystals of **1**, **2**, and **3** were mounted on glass fibres and transferred and studied on a Picker 4-circle diffractometer. Accurate cell parameters and intensity data were obtained at room temperature using graphite-monochromatized CuKα radiation. Crystal data are provided in Table 1.

The space group $P2_1/a$ was uniquely defined from the systematic absences noted in the data sets of **2** and **3**. The intensity data for **1** showed systematic absences consistent with the space groups *Pbcm* and $Pbc2_1$. The space group $Pbc2_1$ was selected for **1** based on the Z value of four molecules per unit cell (Table 1) and the lack of symmetry in the expected structure of **1**. **1** was solved and refined successfully in this space group and inspection of the structure rules out any possibility of describing it in the centrosymmetric space group *Pbcm*. The data were corrected in the standard fashion for Lorentz and polarization ratio factors but not for absorption. Other details pertaining to the data reduction step are listed in Table 1.

The structure of **1** is disordered and will be discussed in the following paragraph. The positions of the non-hydrogen atoms of the three structures were determined by direct methods with MULTAN (21). At this stage, isotropic refinement of all non-hydrogen atoms was carried out by full-matrix least squares. Subsequent difference maps revealed the positions of the H atoms of **2** and **3**. They were included and refined isotropically while non-H atoms were refined anisotropically. The three structures were refined to convergence by full-matrix least squares; $\Sigma w(|F_o|-|F_c|)^2$ was minimized with $w = 1$ for **1** and $w^{-1} = {}^2(F_o) + 0.0003F_o{}^2$ for **2** and **3**. Details related to the structure refinements and final D-maps are given in Table 1.

After isotropic refinement of all non-H atoms of **1** and close inspection of the refined positions, some carbon atoms of the ethano and propano bridges had large isotropic thermal parameters and dis-

Can. J. Chem. Downloaded from www.nrcresearchpress.com by 186.148.149.217 on 09/07/12
For personal use only.

Can. J. Chem. Downloaded from www.nrcresearchpress.com by 186.148.149.217 on 09/07/12
For personal use only.

torted geometries, suggesting possible disorder and (or) the presence of highly mobile bridging units. Refinement was resumed with the ethano and propano C atoms having U_{iso} values fixed at 0.07 Å^2 (based on the average U_{iso} value from a Wilson plot) and varying occupancies. A subsequent *D*-map gave split peaks for three of the ethano and propano carbon atoms. These were included and refined also on occupancy with fixed thermal parameters. At convergence, the disordered positions showed occupancy factors in a 60:40 ratio.

Despite the 60:40 conformer ratio (*vide supra*), the unit cell of **1** contains equal amounts of each enantiomer. Refinement was pursued and H atoms of the two cyclohexyl rings were located on the next *D*-map. Non-H atoms were refined anistropically and H atoms of the rings isotropically. H atoms of the ethano and propano bridges were introduced at calculated positions (sp^3 hybridized; C—H distances of 1.08 Å) and taking into account the two disordered orientations. They were included in the next least-squares cycles but not refined. Refinement details for **1** are listed in Table 1. All computations were performed with the NRCVAX crystal structure package (22). The scattering curves were from standard sources (23).

Materials

Dibenzo-13-crown-4 (**4**) was prepared from the previously described (5) 1,2-bis(*o*-hydroxyphenoxy)ethane via the following procedure. In 1.5 L 1-butanol were dissolved 50.0 g (0.20 mol) of 1,2-bis(*o*-hydroxyphenoxy)ethane and 19.0 g (0.44 mol) $LiOH \cdot H_2O$. This solution was refluxed for 1 h. To this dark solution was added slowly 40.0 g (0.20 mol) of 1,3-dibromopropane, with agitation and reflux being continued for 27 h. After removal of the butanol by rotary evaporation, a solid residue remained, which was dissolved in methylene chloride and washed with water. Subsequent to drying, evaporation of the organic phase yielded 27.1 g of crude product. Recrystallization from methylene chloride – hexanes mixture gave 19.3 g (33% yield) of pure **4**, mp 134–136°C; *ms* (CI) *m*/e 287 (M + 1), base peak *m*/e 121.

Hydrogenation of **4** to a mixture of **1** and the *cis–syn–cis* isomer was accomplished using an American Instrument Co. 50 000 psi (1 psi = 6.9 kPa) maximum pressure high pressure apparatus. In 60 mL of 1-butanol were dissolved 2.0 g (0.007 mol) of **4** and 0.40 g of 5% ruthenium on alumina catalyst. A pressure of 1200 psi was used and the reaction was continued for 12 h at a temperature of 120°C. The catalyst was removed via filtration and the butanol by rotary evaporation at 70°C, to yield 1.9 g of a clear yellow oil. From ^{13}C NMR, there appeared to be two configurational isomers present in the ratio of ca. 2:1. Separation of these isomers was accomplished via column chromatography on activated silica gel of mesh size 100–200. Initially the mixture (1.9 g) was applied to the column (30 g of solid phase) in 50:50 methylene chloride – hexanes. Subsequent to the collection of 100 mL of eleunt, 100-mL aliquots were employed containing 3, 5, 10, 15. and 20% of diethyl ether respectively. Initial fractions contained pure **1** only, while the latter fractions were essentially pure *cis–syn–cis* isomer, the major isomer formed in the hydrogenation (as later determined via X-ray of its complexes). Recrystallization from hexanes yielded crystalline **1**, mp 78–80°C, while the other isomer remained an oil. The complexes **2** and **3** were prepared according to the following procedures. Equimolar amounts of the oil from the chromatographic column and LiNCS or $LiClO_4$ were mixed and dissolved in a minimum quantity of dry methanol. After allowing these mixtures to stand for 2–3 h, the solvent was removed by rotary evaporation. Following recrystallization from a hexane – methylene chloride solvent pair, **2**, mp 210–212°C, and **3**, mp 225–228°C, were obtained. For the preparation of **5**, solid **4** was dissolved in a minimum volume of methanol, to which an equimolar quantity of LiNCS was added. After 3 h, the methanol was removed. Recrystallization from hexane – methylene chloride yielded **5**, mp 239–241°C.

Acknowledgements

G.W.B. thanks the Natural Sciences and Engineering Research Council of Canada for continuing financial support via operating grants, and postgraduate scholarships to R.A.K.. Also we thank Drs. J.A. Ripmeester and C.I. Ratcliffe for their hospitality and access to the solid phase NMR facilities.

1. G. W. Buchanan and R. A. Kirby. Tetrahedron Lett. **28**, 1507 (1987).
2. G. W. Buchanan, R. A. Kirby, and J. P. Charland. J. Am. Chem. Soc. **110**, 2477 (1988).
3. G. W. Buchanan, R. A. Kirby, K. Bourque, and C. Morat. Can. J. Chem. **66**, 2204 (1988).
4. J. P. Charland, G. W. Buchanan, and R. A. Kirby. Acta Crystallogr. Sect. C: Cryst. Struct. Commun. **C45**, 165 (1989).
5. G. W. Buchanan, R. A. Kirby, and K. Bourque. Can. J. Chem. **67**, 449 (1989).
6. P. P. Power. Acc. Chem. Res. **21**, 147 (1988).
7. U. Olsher and J. Jagur-Grodzinski. J. Chem. Soc. Dalton Trans. 501 (1981).
8. G. Shohan, W. N. Lipscomb, and U. Olsher. J. Am. Chem. Soc. **105**, 1247 (1983).
9. J. E. Huheey. Inorganic chemistry: principles of structure and reactivity. 2nd ed. Harper and Row, New York. 1978. pp. 232–233.
10. M. R. Truter. Structure Bonding (Berlin), **16**, 71 (1973).
11. M. D. Dalley. *In* Synthetic multidentate macrocyclic compounds. *Edited by* R. M. Izatt and J. J. Christensen. Academic Press, New York. 1978. pp. 207–243.
12. R. D. Shannon. Acta Crystalogr. Sect. A: Cryst. Phys. Diffr. Theor. Gen. Crystallogr. **A32**, 751 (1976).
13. N. K. Wilson and J. B. Stothers. Top. Stereochem. **8**, 1 (1973).
14. H.-J. Schneider and V. Hoppen. Tetrahedron Lett. 579 (1974).
15. S. J. Opella and M. H. Frey. J. Am. Chem. Soc. **101**, 5854 (1979).
16. M. G. Munowitz, R. G. Griffin, G. Bodenhausen, and T. H. Huang. J. Am. Chem. Soc. **103**, 2529 (1981).
17. S. L. Patt and J. N. Shoolery. J. Magn. Reson. **46**, 535 (1982).
18. G. G. Webb and K. W. Zilm. J. Am. Chem. Soc. **111**, 2455 (1989).
19. G. E. Maciel and K. Seidman. J. Am. Chem. Soc. **99**, 659 (1977).
20. P. S. Belton, S. F. Tanner, K. M. Wright, M. P. Payne, M. R. Truter, and J. N. Wingfield. J. Chem. Soc. Perkin Trans. 2, 1307 (1985).
21. G. Germain, P. Main, and M. M. Woolfson. Acta Crystallogr. Sect. A: Cryst. Phys. Diffr. Theor. Gen. Crystallogr. **A27**, 368 (1971).
22. E. J. Gabe, F. L. Lee, and Y. LePage. *In* Crystallographic computing 3. *Edited by* C. Sheldrick, C. Krueger, and R. Goddard. Clarendon Press, Oxford. 1985. p. 167.
23. International tables for X-ray crystallography. Vol. 4. 2nd ed. Kynoch Press, Birmingham. 1974.

Pyrazagaboles, pyrazolyl-bridged heterocycles containing boron and gallium

STEVEN J. RETTIG, MARK SANDERCOCK, ALAN STORR, and JAMES TROTTER
Department of Chemistry, University of British Columbia, 2036 Main Mall, Vancouver, B.C., Canada V6T 1Y6

Received June 7, 1989

STEVEN J. RETTIG, MARK SANDERCOCK, ALAN STORR, and JAMES TROTTER. Can. J. Chem. **68**, 59 (1990).

The synthesis and structural characterization of representative and novel pyrazagaboles, boron- and gallium-containing compounds with a central six-membered heterocyclic B—(N—N)$_2$—Ga ring feature, are detailed. Crystals of dimethylgalliumbis(μ-pyrazolyl)dimethylboron are orthorhombic, a = 7.6135(5), b = 16.2917(5), c = 22.331(1) Å, Z = 8, space group *Pbca*, and those of hydroxy(methyl)galliumbis(μ-pyrazolyl)dimethylboron are orthorhombic, a = 7.6197(3), b = 16.2184(7), c = 22.190(1) Å, Z = 8, space group *Pbca*. Both structures were solved by conventional heavy atom methods and were refined by full-matrix least-squares procedures to R = 0.054 and 0.040 for 1243 and 1272 reflections with $I \geq 1.5$ and $3\sigma(I)$, respectively. The crystal structures are isomorphous and both feature six-membered B—(N—N)$_2$—Ga rings having highly asymmetric boat conformations, unlike those observed for the majority of the homobinuclear analogs previously reported. The mean Ga—N and B—N distances in the two compounds are 1.977 and 1.61 Å.

Key words: pyrazagaboles, pyrazolyl-bridged heterocycles, crystal structures, synthesis of pyrazagaboles.

STEVEN J. RETTIG, MARK SANDERCOCK, ALAN STORR et JAMES TROTTER. Can. J. Chem. **68**, 59 (1990).

On rapporte les détails relatifs à la préparation et à la caractérisation de la structure de nouveaux pyrazagaboles représentatifs, des composés contenant du bore et du gallium dans un hétérocycle central à six chaînons B—(N—N)$_2$—Ga. Les cristaux du diméthylgalliumbis(μ-pyrazolyl)diméthylbore sont orthorhombiques avec a = 7,6135(5), b = 16,2917(5) et c = 22,331(1) Å, Z = 8 et groupe d'espace *Pbca* alors que ceux de l'hydroxy(méthyl)galliumbis(μ-pyrazolyl)diméthylbore sont orthorhombiques avec a = 7,6197(3), b = 16,2184(7) et c = 22,190(1) Å, Z = 8 et groupe d'espace *Pbca*. On a résolu les deux structures par les méthodes usuelles aux atomes lourds et on les a affinées par la méthode les moindres carrés jusqu'à des valeurs de R de 0,054 et 0,040 pour 1243 et 1272 réflexions avec respectivement $I \geq 1{,}5$ et $3\sigma(I)$. Les structures cristallines sont isomorphes et chacune présente des cycles à six chaînons B—(N—N)$_2$—Ga possédant des conformations bateaux hautement asymétriques; ces conformations sont très différentes de celles observées; pour la majorité des analogues homobinucléaires rapportés antérieurement. Les distances Ga—N et B—N moyennes dans les deux composés sont 1,977 et 1,61 Å.

Mots clés : pyrazagaboles; hétérocycles pyrazolyles pontés; structures cristallines; synthèses de pyrazagaboles.

[Traduit par la revue]

Introduction

Pyrazaboles, $R_2B(pz)_2BR_2$ (where R = H, alkyl, Cl, or aryl and pz = pyrazolyl, $N_2C_3H_3$) were first described some time ago by Trofimenko (1) and consist of two "R_2B" moieties bridged by pyrazolyl groups to give heterocyclic six-membered B—(N—N)$_2$—B ring systems. The first structural characterization of this class of compound came with the introduction of the pyrazolylgallane analogs, namely the structure of $D_2Ga(pz)_2GaD_2$ (2). Since these early reports numerous other derivatives of these symmetrical six-membered ring systems involving B, Al, or Ga have been detailed (3). The present account describes the synthesis and characterization of the first examples of pyrazagaboles, six-membered heterocycles containing both B and Ga moieties bridged by two exobidentate pyrazolyl ligands. The crystal structures of two of these compounds are described.

Experimental

Air-sensitive materials were handled in a glove box under oxygen-free dry nitrogen or on a high-vacuum line. Diethyl ether was dried by refluxing over Na/benzophenone and benzene by refluxing over molten potassium. Both solvents were distilled under N_2 before use. Trimethylgallium (4), $Na^+Me_2Bpz_2^-$ (5), and $K^+H_2Bpz_2^-$ (6) were prepared as described previously.

Preparation of $Me_2GaCl.OEt_2$ (7)

Trimethylgallium (2.828 g, 24.66 mmol) was transferred into a vessel containing diethyl ether (~30 mL). The mixture was cooled to −196°C and the vessel evacuated. Hydrogen chloride gas (24.65 mmol) was condensed into the reaction vessel which was then flame sealed and allowed to warm to room temperature. After ~24 h, the reaction mixture was again cooled to −196°C and the methane evolved was measured (24.65 mmol). The product solution was then transferred to a 250 mL volumetric flask to give a standard solution (0.0986 mmol/mL) for subsequent reactions.

*Preparation of $Me_2Gapz_2BMe_2$, **1***

$Na^+Me_2Bpz_2^-$ (0.780 g, 3.94 mmol) was reacted in Et_2O with an aliquot of the above standard solution of $Me_2GaCl.OEt_2$ (40.0 mL, 3.94 mmol). The reaction mixture was stirred for 2 days after which time the precipitated NaCl was removed by filtration. The solvent was then removed from the filtrate under vacuum and the solid product recrystallized from benzene in ~80% yield. *Anal.* calcd. for $Me_2Gapz_2BMe_2$: C 43.71, H 6.60, N 20.39; found: C 43.43, H 6.54, N 20.32. ^{1}H nmr (C_6D_6; 80, 270 MHz; $\delta(C_6H_6)$ = 7.16 ppm): δ = 0.10 (s, $GaMe_2$), 0.51 (s, BMe_2), 5.88 (t, pzH^4, J = 2.2 Hz), 7.15 (d, pzH^5, J = 2.2 Hz), 7.45 (dd, pzH^3, J = 2.2 and 0.75 Hz). The mass spectrum of the compound displayed a strong signal due to the parent − methyl ion, P − Me^+, in addition to the expected fragment ion signals.

A single crystal of the compound $Me(OH)Gapz_2BMe_2$, **2**, was isolated as a by-product of the above reaction and was characterized by a crystal structure analysis (see below). The formation of **2** probably resulted from an accidental use of wet solvent on the first attempt to prepare compound **1**. In all subsequent preparations, no trace of **2** could be detected.

Preparation of $Me_2Gapz_2BH_2$

This compound was prepared by reacting $K^+H_2Bpz_2^-$ (0.732 g, 3.94 mmol) in Et_2O with an aliquot of the standard solution of $Me_2GaCl.OEt_2$ (40.0 mL, 3.94 mmol). Recrystallization of the product from benzene afforded white crystals of the desired compound in ~75% yield. *Anal.* calcd. for $Me_2Gapz_2BH_2$: C 38.94, H 5.72, N 22.71; found: C 39.12, H 5.42, N 22.71. ^{1}H nmr (C_6D_6; 80, 270 MHz; $\delta(C_6H_6)$ = 7.16 ppm): δ = 0.53 (s, $GaMe_2$), 5.77 (t, pzH^4, J = 2.2 Hz), 7.07 (d, pzH^5, J = 2.2 Hz), 7.41 (dd, pzH^3, J = 2.2 and 0.75 Hz). The mass spectrum again displayed a strong signal due to the P − Me^+ ion and the ir spectra (Nujol, KBr disk) showed ν_{BH_2} vibrations at ~2430 cm^{-1}.

Can. J. Chem. Downloaded from www.nrcresearchpress.com by 186.148.149.217 on 09/07/12
For personal use only.

Can. J. Chem. Downloaded from www.nrcresearchpress.com by 186.148.149.217 on 09/07/12
For personal use only.

TABLE 1. Crystallographic data[a]

Compound	**1**	**2**
Formula	$C_{10}H_{18}BGaN_4$	$C_9H_{16}BGaN_4O$
fw	274.81	276.78
Crystal system	Orthorhombic	Orthorhombic
Space group	*Pbca*	*Pbca*
a (Å)	7.6135(5)	7.6197(3)
b (Å)	16.2917(5)	16.2184(7)
c (Å)	22.331(1)	22.190(1)
V (Å^3)	2769.9(3)	2742.2(2)
Z	8	8
ρ_c (g/cm^3)	1.318	1.341
F (000)	1136	1136
μ (Cu-K_α) (cm^{-1})	25.3	26.1
Crystal dimensions (mm)	0.06 × 0.27 × 0.50	0.17 × 0.28 × 0.48
Transmission factors	0.488–0.863	0.447–0.702
Scan type	ω–2θ	ω–2θ
Scan range (deg in ω)	0.90 + 0.14 tan θ	0.75 + 0.14 tan θ
Scan speed (deg/min)	1.3–10.0	1.0–10.0
Data collected	$+h, +k, +l$	$+h, +k, +l$
$2\theta_{max}$ (deg)	150	150
Crystal decay	Negligible	Negligible
Unique reflections	2847	2816
Reflections with $I \geq n\sigma(I)$	1243 (n = 1.5)	1272 (n = 3)
Number of variables	145	146
R	0.054	0.040
R_w	0.050	0.046
S	0.794	0.848
Mean Δ/σ (final cycle)	0.004	0.0004
Max Δ/σ (final cycle)	0.05	0.005
Residual density (e/Å^3)	0.58	0.40

[a]Temperature 294 K, Enraf-Nonius CAD4-F diffractometer, Cu-K_α radiation ($\lambda_{K\alpha_1}$ = 1.540562, $\lambda_{K\alpha_2}$ = 1.544390 Å), nickel filter, takeoff angle 2.7°, aperture (2.0 + tan θ) × 4.0 mm at a distance of 173 mm from the crystal, scan range extended by 25% on both sides for background measurement, $\sigma^2(I) = C + 2B + [0.04(C - B)]^2$ (C = scan count, B = normalized background count), function minimized: $\sum w(|F_o| - |F_c|)^2$ where $w = 1/\sigma^2(F)$, $R = \sum||F_o| - |F_c||/\sum|F_o|$, $R_w = (\sum w(|F_o| - |F_c|)^2/\sum w|F_o|^2)^{1/2}$, $S = (\sum w(|F_o| - |F_c|)^2/(m - n))^{1/2}$. Values given for R, R_w, and S are based on those reflections with $I \geq 3\sigma(I)$.

*X-ray crystallographic analyses of dimethylgalliumbis(μ-pyrazolyl)dimethylboron, **1**, and hydroxy(methyl)galliumbis(μ-pyrazolyl)dimethylboron, **2***

Crystallographic data for the two compounds are presented in Table 1. Unit-cell parameters were refined by least-squares on 2 sin θ/λ values for 25 reflections (2θ = 45–70° for **1**, 60–80° for **2**) measured with Cu-$K\alpha_1$ radiation. Data were corrected[1] for Lp and absorption. The structure of **2** was solved by conventional heavy atom methods. The coordinates of the gallium atom being determined from the Patterson function and those of the remaining non-hydrogen atoms from a subsequent difference Fourier synthesis. Compound **1** is isomorphous with **2**, the analysis of **1** being initiated with the coordinates of the non-hydrogen atoms of **2**.

The hydroxy compound **2** was initially believed to be compound **1**, thus the oxygen atom was refined as a carbon atom. The anomalously small equivalent isotropic thermal parameter which resulted from this atom prompted us to refine this atom as an oxygen (the only reasonable alternative). The agreement factors improved by about 0.5% and the thermal parameter for the oxygen atom was consistent with those of the methyl carbon atoms. The subsequent structure analysis of a genuine sample of **1** provided additional evidence for the formulation of **2**. The lattice constants, unit-cell volumes, and calculated densities (Table 1) for the isoelectronic species **1** and **2** are significantly different. The crystal of **2** chosen for data collection from the first batch of compound **1** was selected simply because it was of higher quality than the crystals of **1** which formed the bulk of the sample.

For both structures, **1** and **2**, the non-hydrogen atoms were refined with anisotropic thermal parameters and hydrogen atoms were fixed in idealized positions (staggered methyl groups, OH based on observed position, O—H = 0.874 Å, C—H = 0.98 Å, $U_H \propto U_{bonded\ atom}$). Neutral atom scattering factors and anomalous dispersion corrections were taken from ref. 8. An isotropic Type I extinction correction (Thornley–Nelmes definition of mosaic anisotropy with a Lorentzian distribution) was applied for **2** (9–11), the final value of g being 0.45(6) × 10^4. Final positional and anisotropic thermal parameters are given in Tables 2 and 7,[2] respectively. Measured and calculated structure factors have been placed in the Depository of Unpublished Data.[2] Bond lengths, bond angles, and intra-annular torsion angles appear in Tables 3–5, respectively. Hydrogen atom parameters and a complete listing of torsion angles (Tables 6 and 8) have been deposited.[2]

Results and discussion

The pyrazagaboles, $Me_2Gapz_2BMe_2$ and $Me_2Gapz_2BH_2$ (Fig. 1), have been synthesized from $Me_2GaCl.OEt_2$ and the bispyrazolyl borate anions $Me_2Bpz_2^-$ and $H_2Bpz_2^-$, respectively. Crystalline samples were obtained from benzene solution.

[1]The computer programs used include locally written programs for data processing and locally modified versions of the following: AGNOST, absorption corrections, by J. A. Ibers; ORFLS, full-matrix least-squares, and ORFFE, function and errors, by W. R. Busing, K. O. Martin and H. A. Levy; FORDAP, Patterson and Fourier syntheses, by A. Zalkin; ORTEP II, illustrations, by C. K. Johnson.

[2]Supplementary material mentioned in the text may be purchased from the Depository of Unpublished Data, CISTI, National Research Council of Canada, Ottawa, Ont., Canada K1A 0S2.

Can. J. Chem. Downloaded from www.nrcresearchpress.com by 186.148.149.217 on 09/07/12
For personal use only.

TABLE 2. Final positional (fractional × 10^4, Ga × 10^5) and isotropic thermal parameters ($U \times 10^3$ Å^2) with estimated standard deviations in parentheses

Atom	x	y	z	U_{eq}
		1		
Ga	40053(12)	43434(5)	39463(4)	63
N(1)	3736(7)	3927(3)	3122(2)	58
N(2)	4013(8)	3127(3)	2947(2)	60
N(3)	5508(8)	3399(3)	4177(2)	52
N(4)	5614(7)	2668(3)	3879(3)	56
C(1)	5589(10)	5292(4)	3912(4)	89
C(2)	1769(11)	4392(5)	4389(3)	90
C(3)	4885(13)	1591(5)	3057(4)	101
C(4)	2349(13)	2243(4)	3734(3)	92
C(5)	3491(10)	4362(5)	2624(4)	78
C(6)	3609(11)	3872(6)	2126(4)	87
C(7)	3942(11)	3101(5)	2349(3)	75
C(8)	6854(12)	3411(5)	4568(3)	68
C(9)	7785(12)	2695(6)	4546(4)	78
C(10)	6988(11)	2253(5)	4111(3)	69
B	4123(10)	2367(4)	3399(2)	28
		2		
Ga	39595(11)	43255(5)	39539(4)	64
O	5584(7)	5320(3)	3958(3)	91
N(1)	3695(7)	3922(3)	3119(2)	58
N(2)	4012(8)	3136(3)	2939(3)	56
N(3)	5501(7)	3398(3)	4184(3)	53
N(4)	5619(7)	2668(3)	3880(3)	56
C(1)	1744(10)	4400(5)	4396(4)	89
C(2)	4915(14)	1589(4)	3043(4)	95
C(3)	2355(12)	2235(5)	3736(3)	80
C(4)	3456(10)	4377(5)	2626(4)	75
C(5)	3581(11)	3887(6)	2125(4)	86
C(6)	3931(11)	3116(5)	2339(3)	74
C(7)	6819(12)	3409(5)	4576(3)	69
C(8)	7781(11)	2702(5)	4545(4)	75
C(9)	6992(11)	2253(5)	4095(4)	71
B	4204(12)	2380(4)	3403(4)	55

The ^{1}H nmr spectra of the two compounds can be rationalized on the basis of either planar six-membered Ga—(N—N)$_2$—B heterocycles or rapidly inverting boat conformations for these ring systems. Thus the spectrum of $Me_2Gapz_2BMe_2$ consists of singlets for both the —$GaMe_2$ and —BMe_2 groups and a doublet–doublet–triplet pattern for the three different C—H protons of the pyrzolyl rings. Similarly the $Me_2Gapz_2BH_2$ complex gave a singlet for the —$GaMe_2$ protons and the expected doublet–doublet–triplet pattern for the pyrazolyl ring protons in its ^{1}H nmr spectrum.

Previous X-ray crystallographic studies on pyrazagallole derivatives containing the central six-membered Ga—(N—N)$_2$—Ga heterocycle, have shown that all of the complexes possess a central boat conformation for the Ga—(N—N)$_2$—Ga ring in the solid state with the one exception of $Me_2Ga(3,5\text{-}Me_2pz)_2GaMe_2$ where steric requirements force a planar arrangement on the central ring (2, 12, 13). Similarly, extensive structural studies on pyrazabole compounds, with the central B—(N—N)$_2$—B feature, reveal that the large majority of the solid state structures exhibit a boat conformation for this heterocyclic ring (14–16). However, steric effects can again dictate alternate structural arrangements in some complexes and indeed the first structure of this class of compound reported, the bis-3,5-dimethyl-

TABLE 3. Bond lengths (Å) with estimated standard deviations in parentheses

Bond	Length (Å)	Bond	Length (Å)
	1		
Ga—N(1)	1.971(6)	N(3)—C(8)	1.346(9)
Ga—N(3)	1.986(5)	N(4)—C(10)	1.349(8)
Ga—C(1)	1.962(7)	N(4)—B	1.636(8)
Ga—C(2)	1.971(8)	C(3)—B	1.587(9)
N(1)—N(2)	1.378(7)	C(4)—B	1.557(11)
N(1)—C(5)	1.332(8)	C(5)—C(6)	1.371(10)
N(2)—C(7)	1.337(8)	C(6)—C(7)	1.374(10)
N(2)—B	1.600(7)	C(8)—C(9)	1.366(9)
N(3)—N(4)	1.366(6)	C(9)—C(10)	1.354(9)
	2		
Ga—O	2.033(5)	N(3)—C(7)	1.328(9)
Ga—N(1)	1.976(6)	N(4)—C(9)	1.332(9)
Ga—N(3)	1.976(5)	N(4)—B	1.581(9)
Ga—C(1)	1.957(8)	C(2)—B	1.605(10)
N(1)—N(2)	1.357(7)	C(3)—B	1.608(11)
N(1)—C(4)	1.332(8)	C(4)—C(5)	1.370(11)
N(2)—C(6)	1.335(8)	C(5)—C(6)	1.364(11)
N(2)—B	1.607(9)	C(7)—C(8)	1.363(9)
N(3)—N(4)	1.366(6)	C(8)—C(9)	1.374(10)

TABLE 4. Bond angles (deg) with estimated standard deviations in parentheses

Bonds	Angle (deg)	Bonds	Angle (deg)
	1		
N(1)—Ga—N(3)	92.0(2)	N(3)—N(4)—C(10)	107.2(6)
N(1)—Ga—C(1)	107.3(3)	N(3)—N(4)—B	122.6(5)
N(1)—Ga—C(2)	113.1(3)	C(10)—N(4)—B	129.7(6)
N(3)—Ga—C(1)	105.5(3)	N(1)—C(5)—C(6)	111.1(7)
N(3)—Ga—C(2)	113.5(3)	C(5)—C(6)—C(7)	104.5(7)
C(1)—Ga—C(2)	121.3(3)	N(2)—C(7)—C(6)	109.9(7)
Ga—N(1)—N(2)	125.1(4)	N(3)—C(8)—C(9)	111.1(7)
Ga—N(1)—C(5)	127.7(5)	C(8)—C(9)—C(10)	104.3(7)
N(2)—N(1)—C(5)	106.6(6)	N(4)—C(10)—C(9)	110.9(7)
N(1)—N(2)—C(7)	107.9(6)	N(2)—B—N(4)	102.6(5)
N(1)—N(2)—B	124.1(5)	N(2)—B—C(3)	109.4(5)
C(7)—N(2)—B	127.5(6)	N(2)—B—C(4)	111.0(6)
Ga—N(3)—N(4)	125.6(5)	N(4)—B—C(3)	107.4(6)
Ga—N(3)—C(8)	126.5(5)	N(4)—B—C(4)	109.1(5)
N(4)—N(3)—C(8)	106.5(6)	C(3)—B—C(4)	116.4(6)
	2		
O—Ga—N(1)	109.2(2)	N(3)—N(4)—C(9)	108.2(6)
O—Ga—N(3)	103.9(2)	N(3)—N(4)—B	122.8(5)
O—Ga—C(1)	118.3(3)	C(9)—N(4)—B	128.8(6)
N(1)—Ga—N(3)	92.9(2)	N(1)—C(4)—C(5)	109.6(7)
N(1)—Ga—C(1)	113.8(3)	C(4)—C(5)—C(6)	105.3(7)
N(3)—Ga—C(1)	115.5(3)	N(2)—C(6)—C(5)	109.5(7)
Ga—N(1)—N(2)	124.6(4)	N(3)—C(7)—C(8)	111.3(7)
Ga—N(1)—C(4)	126.9(5)	C(7)—C(8)—C(9)	104.3(7)
N(2)—N(1)—C(4)	107.7(6)	N(4)—C(9)—C(8)	109.7(7)
N(1)—N(2)—C(6)	107.9(6)	N(2)—B—N(4)	105.4(5)
N(1)—N(2)—B	123.0(5)	N(2)—B—C(2)	108.7(6)
C(6)—N(2)—B	128.7(6)	N(2)—B—C(3)	109.0(6)
Ga—N(3)—N(4)	124.8(5)	N(4)—B—C(2)	109.8(6)
Ga—N(3)—C(7)	127.5(5)	N(4)—B—C(3)	109.5(6)
N(4)—N(3)—C(7)	106.6(6)	C(2)—B—C(3)	114.1(6)

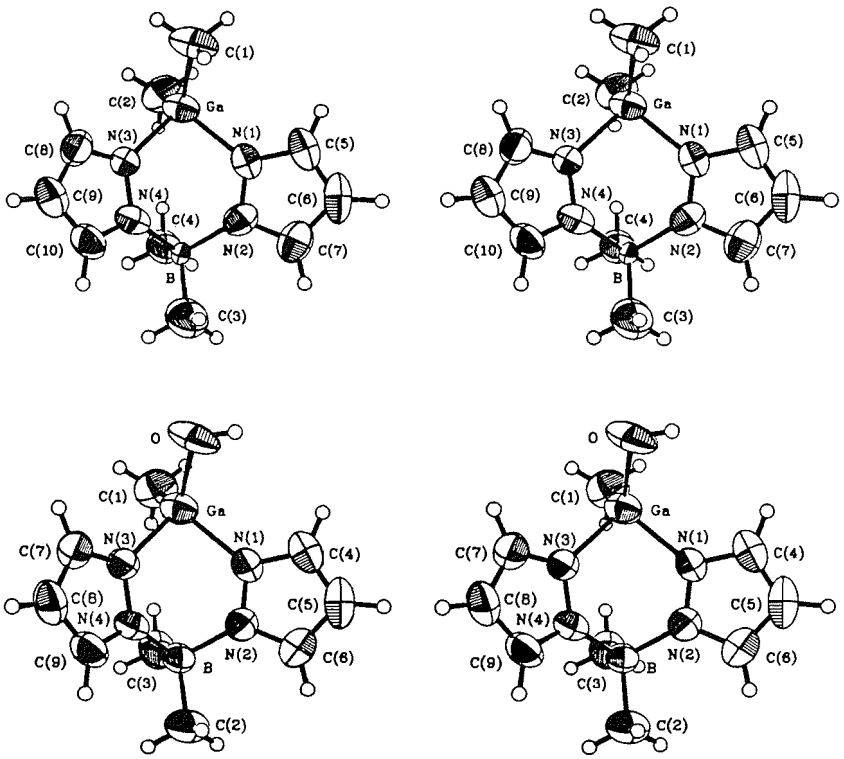

FIG. 1 Stereoscopic views of dimethylgalliumbis(μ-pyrazolyl)dimethylboron (**1**, top) and hydroxy(methyl)galliumbis(μ-pyrazolyl)dimethylboron (**2**, bottom); 50% probability thermal ellipsoids are shown for the non-hydrogen atoms.

TABLE 5. Intra-annular torsion angles (deg) standard deviations in parentheses

Atoms	Torsion angle (deg)
1	
N(3)—Ga—N(1)—N(2)	20.0(6)
Ga—N(1)—N(2)—B	16.1(9)
N(1)—N(2)—B—N(4)	−53.1(8)
N(3)—N(4)—B—N(2)	53.7(7)
Ga—N(3)—N(4)—B	−17.8(8)
N(1)—Ga—N(3)—N(4)	−18.8(5)
2	
N(3)—Ga—N(1)—N(2)	19.6(6)
Ga—N(1)—N(2)—B	15.0(9)
N(1)—N(2)—B—N(4)	−52.1(8)
N(3)—N(4)—B—N(2)	52.5(8)
Ga—N(3)—N(4)—B	−16.1(8)
N(1)—Ga—N(3)—N(4)	−19.4(5)

pyrazolyl borane dimer, exhibited a slightly chair-shaped B—(N—N)$_2$—B ring (17), whilst others have displayed a planar B—(N—N)$_2$—B ring system (18, 19). The present study reports the first hybrid compounds of the pyrazaboles and pyrazagalloles with both a B and a Ga atom incorporated into the six-membered heterocyclic ring system, B—(N—N)$_2$—Ga. It was of obvious interest to determine the solid state structure of this type of compound for comparison with the wealth of structural data available on the parent species. Interestingly, whilst this work was in progress two reports on related structures have appeared. Cowley et al. have reported the structure of a cation containing a central gallium atom octahedrally coordinated by two tridentate pyrazolyl borate ligands, [HB(3,5-Me$_2$pz)$_3$]$_2$Ga$^+$ (20), and also that of the neutral three-coordinate complex [HB(3,*t*-Bupz)$_3$]Tl(I) (21).

The present structures, **1** and **2**, both display the B—(N—N)$_2$—Ga rings in asymmetric boat conformations. The four nitrogen atoms are planar within 0.008 Å in **1** and 0.002 Å in **2**. The angles θ_1 and θ_2 are defined (14) as the dihedral angles between the N_4 and NNE (E = B or Ga), and the N_4 and pyrazolyl mean planes respectively. The θ_1(Ga) angles of 15.8 and 16.0° in **1** and **2** lie within the range observed for pyrazagalloles (2, 12, 13) while the θ_1(B) values of 42.5 and 42.0° in **1** and **2** are larger than any yet reported for pyrazaboles (14, and references therein). The large difference between the θ_1(Ga) and θ_1(B) values highlights the asymmetry of the present B—(N—N)$_2$—Ga rings, a feature not observed in any of the homobinuclear analogs. The θ_2 values (22.3 and 23.9° in **1**, 22.3 and 24.0° in **2**, mean 23.1°) are consistent with the average θ_1 value of 29.1° in **1** and **2** (from a plot of θ_1 vs. θ_2 for pyrazabole structures (14)).

The Ga—N distances in **1** and **2** average 1.977 Å, shorter than the average Ga—N bond length of 1.993 Å for the four pyrazagallole molecules having Me$_2$Ga— groups (12, 13) but similar to the mean Ga—N distance of 1.974 Å in D$_2$Gapz$_2$GaD$_2$ (2). The short Ga—N distances in **1** and **2** are balanced by a lengthening of the B—N distances to an average of 1.61 Å compared to average B—N distances of 1.521–1.567 Å reported for all pyrazabole structures (14–19) except that of Et$_2$B(4-Brpz)$_2$BEt$_2$ (22) which has an unusually long average B—N distance of 1.69 Å. The long B—N distances in **1** and **2** may be a result of the large deviations of the boron atoms from the N_4 mean planes (0.68 and 0.65 Å in **1** and **2**). Remaining features of the molecular geometries are as expected (Tables 3–5). Both crystal structures consist of well-separated molecules, all intermolecular

Can. J. Chem. Downloaded from www.nrcresearchpress.com by 186.148.149.217 on 09/07/12
For personal use only.

distances corresponding to van der Waals interactions. The O—H group in **2** is not hydrogen-bonded. The shortest intermolecular contact involving the O atom in **2** is O···C(9) = 3.652(8) Å and, as expected, the corresponding C(1)···C(10) distance in **1** is longer at 3.72(1) Å. Since the structures of **1** and **2** are isomorphous, it is likely that the potential H-bonding in compound **2** is precluded by other aspects of the molecular packing.

Acknowledgments

We thank the Natural Sciences and Engineering Research Council of Canada for financial support and the University of British Columbia Computing Centre for assistance.

1. S. TROFIMENKO. J. Am. Chem. Soc. **88**, 1842 (1966).
2. D. F. RENDLE, A. STORR, and J. TROTTER. J. Chem. Soc. Chem. Commun. 189 (1973).
3. S. TROFIMENKO. Prog. Inorg. Chem. **34**, 116 (1986).
4. A. STORR and B. S. THOMAS. Can. J. Chem. **48**, 3667 (1970).
5. K. R. BREAKELL, D. J. PATMORE, and A. STORR. J. Chem. Soc. Dalton Trans. 749 (1975).
6. S. TROFIMENKO. Inorg. Synth. **12**, 99 (1970).
7. B. ARMOR and H. SCHMIDBAUR. Chem. Ber. **100**, 1521 (1967).
8. International tables for X-ray crystallography. Vol. IV. Kynoch press, Birmingham. 1974. pp. 99–102 and 149.
9. P. J. BECKER and P. COPPENS. Acta Crystallogr. Sect. A, **30**, 129 (1974); **30**, 148 (1974); **31**, 417 (1975).
10. P. COPPENS and W. C. HAMILTON. Acta Crystallogr. Sect. A, **26**, 71 (1970).
11. F. R. THORNLEY and R. J. NELMES. Acta Crystallogr. Sect. A, **30**, 748 (1974).
12. D. F. RENDLE, A. STORR, and J. TROTTER. Can. J. Chem. **53**, 2930 (1975).
13. D. F. RENDLE, A. STORR, and J. TROTTER. Can. J. Chem. **53**, 2944 (1975).
14. C. P. BROCK, K. NIEDENZU, E. HANECKER, and H. NOTH. Acta Crystallogr. Sect. C, **41**, 1458 (1985).
15. J. BIELAWSKI, M. K. DAS, E. HANECKER, K. NIEDENZU, and H. NOTH. Inorg. Chem. **25**, 4623 (1986).
16. C. M. CLARK, M. K. DAS, E. HANECKER, J. F. MARITEGUI, K. NIEDENZU, P. M. NIEDENZU, H. NOTH, and K. R. WARNER. Inorg. Chem. **26**, 2310 (1987).
17. N. W. ALCOCK and J. F. SAWYER. Acta Crystallogr. Sect. B, **30**, 2899 (1974).
18. K. NIEDENZU and H. NOTH. Chem. Ber. **116**, 1132 (1983).
19. E. HANECKER, T. G. HODGKINS, K. NIEDENZU, and H. NOTH. Inorg. Chem. **24**, 459 (1985).
20. A. H. COWLEY, C. J. CARRANO, R. L. GEERTS, R. A. JONES, and C. M. MUNN. Angew. Chem. Int. Ed. Engl. **27**, 277 (1988).
21. A. H. COWLEY, R. L. GEERTS, C. M. NUNN, and S. TROFIMENKO. J. Organomet. Chem. **365**, 19 (1989).
22. E. M. HOLT, S. L. TEBBEN, and S. L. HOLT. Acta Crystallogr. Sect. B, **33**, 1986 (1977).

Can. J. Chem. Downloaded from www.nrcresearchpress.com by 186.148.149.217 on 09/07/12
For personal use only.

Structural studies of organoboron compounds. XXXVII.[1] 8,8-Pentamethylene-6-phenyl-6,9-epoxy-5,7-dioxa-8-azonia-6-borata-6,7,8,9-tetrahydro-5*H*-benzocycloheptene

WOLFGANG KLIEGEL, HANS-WALTER MOTZKUS, AND KLAUS DRÜCKLER

Institut für Pharmazeutische Chemie, der Technischen Universität Braunschweig, Beethovenstraße 55, 3300 Braunschweig, Bundesrepublik Deutschland

AND

STEVEN J. RETTIG AND JAMES TROTTER

Department of Chemistry, University of British Columbia, 2036 Main Mall, Vancouver, B.C., Canada V6T 1Y6

Received March 1, 1989

WOLFGANG KLIEGEL, HANS-WALTER MOTZKUS, KLAUS DRÜCKLER, STEVEN J. RETTIG, and JAMES TROTTER. Can. J. Chem. **68**, 64 (1990).

Condensation of equimolar amounts of salicylaldehyde, *N*-hydroxypiperidine, and phenylboronic acid yields the title compound. Crystals of 8,8-pentamethylene-6-phenyl-6,9-epoxy-5,7-dioxa-8-azonia-6-borata-6,7,8,9-tetrahydro-5*H*-benzocycloheptene are monoclinic, $a = 12.773(1)$, $b = 11.9600(7)$, $c = 10.6411(6)$ Å, $\beta = 103.786(7)°$, $Z = 4$, space group $P2_1/c$. The structure was solved by direct methods and was refined by full-matrix least-squares procedures to $R = 0.039$ and $R_w = 0.047$ for 2420 reflections with $I \geq 3\sigma(I)$. The compound has a bridged heterocyclic *B,N*-betaine structure with a $PhB(OR)_3$ anionic centre. Bond lengths (corrected for libration) include: B—O(aryl C) = 1.481(2), B—O(alkyl C) = 1.488(2), B—O(N) = 1.539(2), and B—C = 1.591(2) Å.

Key words: organoboron, boron compounds, crystal structure.

WOLFGANG KLIEGEL, HANS-WALTER MOTZKUS, KLAUS DRÜCKLER, STEVEN J. RETTIG et JAMES TROTTER. Can. J. Chem. **68**, 64 (1990).

La condensation de quantités équimoléculaires de salicylaldéhyde, de *N*-hydroxypipéridine et d'acide phénylboronique fournit le composé mentionné dans le titre. Les cristaux du 8,8-pentaméthylène-6-phényl-6,9-époxy-5,7-dioxa-8-azonia-6-borata-6,7,8,9-tétrahydro-5*H*-benzocycloheptène sont monocliniques, groupe d'espace $P2_1/c$, avec $a = 12,773(1)$, $b = 11,9600(7)$ et $c = 10,6411(6)$ Å, $\beta = 103,786(7)°$ et $Z = 4$. On a résolu la structure par des méthodes directes et on l'a affinée par la méthode des moindres carrés (matrice entière) jusqu'à des valeurs de $R = 0,039$ et $R_w = 0,047$ pour 2420 réflexions avec $I \geq 3\sigma(I)$. La molécule possède une structure *B,N*-bétaïne hétérocyclique pontée comportant un centre anionique $PhB(OR)_3$. Les longueurs des liaisons (corrigées pour la libration) incluent : B—O(C aryle) = 1,481(2), B—O(C alkyle) = 1,488(2), B—O(N) = 1,539(2) et B—C = 1,591(2) Å.

Mots clés : organobor, composés du bor, structure cristalline.

[Traduit par la revue]

Introduction

The reaction of equimolar amounts of salicylaldehyde, *N*-hydroxypiperidine, and phenylboronic acid leads to a 1:1:1 condensation product, the elemental analysis of which shows that 2 mole equivalents of water have been eliminated. This is consistent with the fact that the infrared and ^1H nmr spectra show no evidence of free hydroxyl groups. On the basis of the elemental analysis and spectroscopic data several structures are possible for this compound. The absence of a C=O absorption in the infrared spectrum (solid state, KBr pellets) implies that the aldehyde function is involved in an intra- or intermolecular addition reaction resulting in the loss of the C=O double bond. The result could be a zwitterionic condensate **1** with a five-membered cyclophenylboronate structure, or a six-membered phenylboronate ring system such as that in the *N*-oxide **2** or its rearrangement product **3** (which could also be formed directly by condensation of the three reactants).

Both isomers, **1** and **2**, could also be transformed by intramolecular O → B coordination into the bridged heterocyclic *B,N*-betaine **4**, whereas **3** would give the isomeric bridged heterocycle **5** by intramolecular N → B coordination. All of the structures **1**–**5** are consistent with the appearance of a singlet in the ^1H nmr spectrum of the compound at $\delta = 6$ ppm, a typical shift value for the resonance of methine protons of *O,O*- or *N,O*-acetals. This signal, however, only accounts for about 90% of the expected peak area for the methine proton. The remaining 10% appears as a singlet at about $\delta = 10$ ppm which can be ascribed to the methine proton of a free aldehyde group in the open-chain isomers **4′** and **5′**. The appearance of this downfield signal, the peak area of which varies only slightly upon changing the solvent, demonstrates the existence of **4′** or **5′**, at least in solution, and is also consistent with the formation of the bridged ring forms **4** or **5** containing tetracoordinated boron via the open chain forms **4′** and **5′**, respectively. An X-ray crystallographic analysis was undertaken in order to establish unambiguously which of the most probable structures, **4** or **5**, is correct.

Experimental

*8,8-Pentamethylene-6-phenyl-6,9-epoxy-5,7-dioxa-8-azonia-6-borata-6,7,8,9-tetrahydro-5*H*-benzocycloheptene*

Five millimoles each of salicylaldehyde, *N*-hydroxypiperidine, and phenylboronic acid were dissolved in 10 mL ethanol and refluxed for 15 min. Colorless crystals are obtained upon cooling of the solution. Yield: 80%. Melting point 161°C (recrystallized from ethanol). *Anal.* calcd. for $C_{18}H_{20}BNO_3$: C 69.93, H 6.52, B 3.50, N 4.53; found: C 69.93, H 6.53, B 3.46, N 4.53. Infrared (KBr): 1580, 1610 cm^{-1}

[1]Previous paper in this series: ref. 19.

Printed in Canada / Imprimé au Canada

Can. J. Chem. Downloaded from www.nrcresearchpress.com by 186.148.149.217 on 09/07/12
For personal use only.

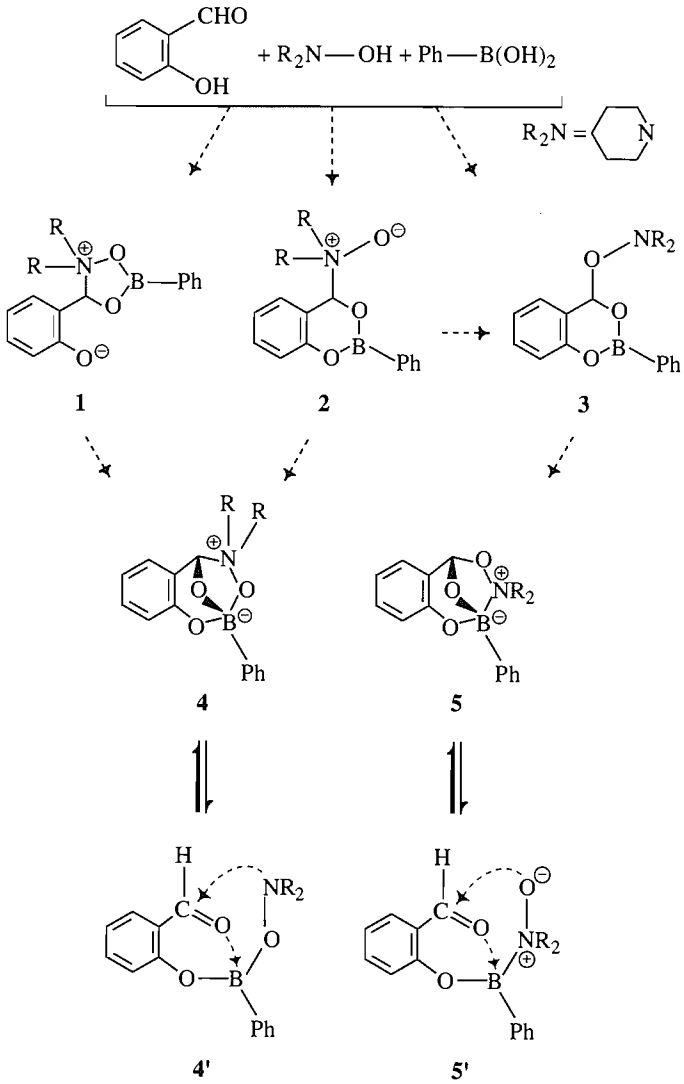

(aromatic C=C). ^{1}H nmr ($CDCl_3$/TMS): δ (ppm) = 1.4–3.9 (m, $(CH_2)_5$), 5.69 (s, N—CH—O [86%]), 6.6–7.8 (m, C_6H_4 and C_6H_5), 9.79 (s, CH=O [14%]); (d_6-DMSO/TMS): δ (ppm) = 6.07 (s, N—CH—O [94%]), 10.17 (s, CH=O [6%]). Crystals suitable for X-ray analysis were obtained by very slow recrystallization from ethanol at room temperature.

X-ray crystallographic analysis

A crystal bounded by the six faces (followed by the distances in mm between parallel faces): {0 1 1}, 0.46, and {1 0 0}, 0.32 was mounted in a general orientation. Unit-cell parameters were refined by least-squares on 2 sin θ/λ values for 25 reflections (2θ = 37–44°) measured on a diffractometer with Mo-$K\alpha$ radiation ($\lambda(K\alpha_1)$ = 0.70930, $\lambda(K\alpha_2)$ = 0.71359 Å). Crystal data at 22°C are:

$C_{18}H_{20}BNO_3$ f.w. = 309.17

Monoclinic, a = 12.773(1), b = 11.9600(7), c = 10.6411(6) Å, β = 103.786(7)°, V = 1578.8(2) Å^3, Z = 4, ρ_c = 1.301 Mg m^{-3}, $F(000)$ = 656, μ(Mo-$K\alpha$) = 0.81 cm^{-1}. Absent reflections: $0k0$, k odd, and $h0l$, l odd, uniquely indicate the space group $P2_1/c$ (C_{2h}^5, No. 14).

Intensities were measured with graphite-monochromated Mo-$K\alpha$ radiation on an Enraf-Nonius CAD4-F diffractometer. An ω-2θ scan at 1.1–10.0° min^{-1} over a range of (0.95 + 0.35 tan θ) degrees in ω (extended by 25% on both sides for background measurement) was employed. Data were measured to 2θ = 55°. The intensities of three check reflections, measured every 4000 s throughout the data collection, remained constant to within 3.5%. Of the 3615 independent reflections measured and processed,[2] 2420 (67.0%) had intensities greater than or equal to $3\sigma(I)$ above background where $\sigma^2(I) = S + 2B + (0.04(S - B))^2$ with S = scan count and B = normalized background count.

TABLE 1. Final positional (fractional × 10^5) and isotropic thermal parameters (U × 10^3 Å^2) with estimated standard deviations in parentheses

Atom	x	y	z	U_{eq}
O(1)	77209(8)	101(8)	61482(9)	36
O(2)	85464(8)	5033(8)	83926(9)	38
O(3)	70499(8)	15306(8)	70765(9)	40
N	76668(10)	9640(10)	53460(10)	35
C(1)	92087(12)	13139(13)	81439(13)	37
C(2)	102500(13)	14096(15)	89087(16)	47
C(3)	109152(16)	22467(18)	86488(19)	61
C(4)	105677(19)	29880(18)	76465(19)	67
C(5)	95407(17)	28995(15)	68886(17)	55
C(6)	88508(13)	20672(12)	71189(14)	41
C(7)	77216(13)	19363(13)	63433(14)	40
C(8)	85819(14)	9210(15)	46917(15)	43
C(9)	84780(15)	−824(16)	37964(16)	51
C(10)	73945(16)	−1070(19)	28200(17)	59
C(11)	64892(15)	−401(16)	35050(17)	52
C(12)	66013(14)	9694(15)	43669(15)	46
C(13)	67346(11)	−4528(13)	79256(13)	37
C(14)	62751(13)	−13740(14)	72053(16)	44
C(15)	56107(14)	−21091(15)	76516(18)	52
C(16)	53890(15)	−19474(17)	88314(18)	57
C(17)	58308(17)	−10552(20)	95696(18)	69
C(18)	65000(16)	−3160(18)	91234(16)	57
B	75021(13)	4017(14)	74353(15)	34

The structure was solved by direct methods. The non-hydrogen atoms were positioned from an E-map and the hydrogen atoms from a subsequent difference Fourier synthesis. The non-hydrogen atoms were refined with anisotropic thermal parameters and the hydrogen atoms with isotropic thermal parameters. Scattering factors for all atoms were taken from ref. 1. The weighting scheme $w = 1/\sigma^2(F)$, where $\sigma^2(F)$ is derived from the previously defined $\sigma^2(I)$, gave uniform average values of $w(|F_o| - |F_c|)^2$ over ranges of both $|F_o|$ and sin θ/λ and was employed in the final stages of full-matrix refinement of 288 variables. Reflections with $I < 3\sigma(I)$ were not included in the refinement. Convergence was reached at R = 0.039 and R_w = 0.047 for 2420 reflections with $I \geq 3\sigma(I)$. For all 3615 reflections R = 0.070. The function minimized was $\Sigma w(|F_o| - |F_c|)^2$, $R = \Sigma||F_o| - |F_c||/\Sigma|F_o|$ and $R_w = (\Sigma w(|F_o| - |F_c|)^2/\Sigma w|F_o|^2)^{1/2}$.

On the final cycle of refinement the mean and maximum parameter shifts corresponded to 0.001 and 0.009σ, respectively. The mean error in an observation of unit weight was 2.081. The largest peak on the final difference map was 0.24 e Å^{-3}. The final positional and thermal parameters appear in Tables 1 and 6,[3] respectively. Measured and

[2]The computer programs used include locally written programs for data processing and locally modified versions of the following: MULTAN 80, multisolution program by P. Main, S. J. Fiske, S. E. Hull, L. Lessinger, G. Germain, J. P. Declercq, and M. M. Woolfson; ORFLS, full-matrix least-squares, and ORFFE, function and errors, by W. R. Busing, K. O. Martin, and H. A. Levy; FORDAP, Patterson and Fourier syntheses, by A. Zalkin; ORTEP II, illustrations, by C. K. Johnson.

[3]The structure factor table, Table 6 (anisotropic thermal parameters) and other material mentioned in the text may be purchased from the Depository of Unpublished Data, CISTI, National Research Council of Canada, Ottawa, Ont., Canada K1A 0S2.

Can. J. Chem. Downloaded from www.nrcresearchpress.com by 186.148.149.217 on 09/07/12
For personal use only.

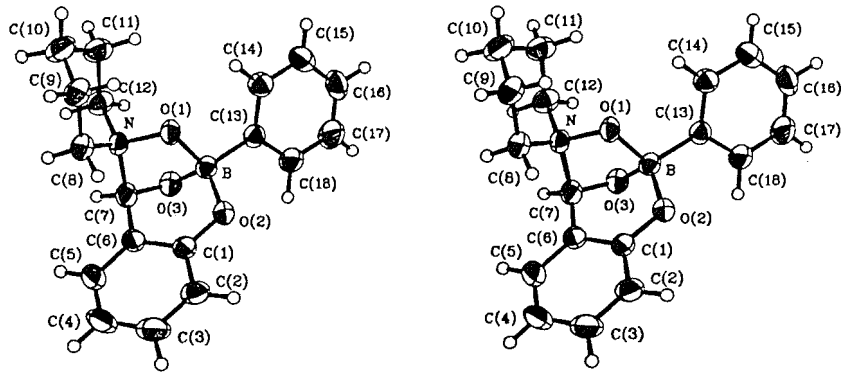

FIG. 1. Stereoscopic view of 8,8-pentamethylene-6-phenyl-6,9-epoxy-5,7-dioxa-8-azonia-6-borata-6,7,8,9-tetrahydro-5*H*-benzocycloheptene; 50% probability thermal ellipsoids are shown for the non-hydrogen atoms.

TABLE 2. Bond lengths (Å) with estimated standard deviations in parentheses

	Length			Length	
Bond	Uncorr.	Corr.	Bond	Uncorr.	Corr.
O(1)—N	1.417(1)	1.424	C(5)—C(6)	1.389(2)	1.395
O(1)—B	1.535(2)	1.539	C(6)—C(7)	1.489(2)	1.494
O(2)—C(1)	1.354(2)	1.358	C(8)—C(9)	1.518(2)	1.523
O(2)—B	1.478(2)	1.481	C(9)—C(10)	1.520(3)	1.527
O(3)—C(7)	1.378(2)	1.382	C(10)—C(11)	1.509(3)	1.516
O(3)—B	1.482(2)	1.488	C(11)—C(12)	1.502(2)	1.507
N—C(7)	1.565(2)	1.569	C(13)—C(14)	1.390(2)	1.400
N—C(8)	1.497(2)	1.505	C(13)—C(18)	1.387(2)	1.398
N—C(12)	1.504(2)	1.512	C(13)—B	1.588(2)	1.591
C(1)—C(2)	1.389(2)	1.393	C(14)—C(15)	1.382(2)	1.385
C(1)—C(6)	1.405(2)	1.410	C(15)—C(16)	1.365(3)	1.377
C(2)—C(3)	1.383(3)	1.389	C(16)—C(17)	1.365(3)	1.375
C(3)—C(4)	1.377(3)	1.381	C(17)—C(18)	1.390(3)	1.393
C(4)—C(5)	1.370(3)	1.374			

calculated structure factors have been placed in the Depository of Unpublished Data.[3]

The ellipsoids of thermal motion for the non-hydrogen atoms are shown in Fig. 1. The thermal motion has been analysed in terms of the rigid-body modes of translation, libration, and screw motion (2). The rms standard error in the temperature factors σU_{ij} (derived from the least-squares analysis) is 0.0008 Å^2. Four structural subunits were separately analysed: the two aromatic rings, the piperidine ring, and the bicyclo[3.2.1]octane system, plus non-hydrogen atoms directly bonded to these moieties (rms ΔU_{ij} = 0.0013–0.0021, mean 0.0016 Å^2). The appropriate bond distances have been corrected for libration (2, 3), using shape parameters q^2 of 0.08 for all atoms involved. Corrected bond lengths appear in Table 2 along with the uncorrected values; bond angles appear in Table 3 and intra-annular torsion angles in Table 4. Hydrogen atom parameters (Table 5), bond lengths and angles involving hydrogen and a complete listing of torsion angles (Tables 7–9) have been deposited.[3]

Results and discussion

The X-ray analysis shows that the molecule (Fig. 1) adopts the bridged heterocyclic *B*,*N*-betaine structure **4** in the solid state. The polycyclic chelate system with a tridentate ligand and a tetrahedrally coordinated boron atom within an arylboronate function is composed of a bicyclo[3.2.1]octane skeleton with a fused benzene component and a spiro piperidine ring. Similar bridged heterocyclic arylboronates with an $ArB(OR)_3$ anionic centre in a *B*,*N*-betaine structure containing bicyclo[3.3.1]-octane (4), tricyclo[3.3.1.1^{3,7}]decane (5), and bicyclo[2.2.2]-octane (6) ring skeletons have been reported. A crystal structure has been reported for an example of the latter, namely compound **6** (7). In this series, compound **4** represents a new ring system.

The sum of B—O distances[4] in **4** (4.508 Å) is essentially equal to the corresponding sum for **6** (4.510 Å) (7) and the B—C(phenyl) bond lengths in **4** and **6** are both 1.591 Å. The B(sp^3)—C bond, as expected, is longer than in trigonal planar phenylboronates where the B(sp^2)—C distances range from 1.548 Å (8, 9) to 1.566 Å (10), consistent with at least partial loss of π-interaction between the boron atom and the aromatic system.

Compound **4** contains a five-membered ring system which can be synthesized from an *N*-hydroxydialkylamine, a carbonyl compound, and a chelate-forming boron reagent such as phenylboronic acid (and derivatives thereof). Crystal structures have been reported for two examples of the BONCO ring system **7**: **7***a*, R = Me, R^1 = R^2 = H (11); and **7***b*, R = R^1 = R^2 = Me (12). The BONCO ring in **4** has a distorted half-chair conformation (see Table 4), similar to those observed in **7***a* and **7***b*. The N—O, (N)O—B, B—O(C), and O—C bond lengths

[4]Libration corrected bond lengths (esd's assumed equal to those of the uncorrected values) are employed in the discussion and are compared with similarly treated (2) distances unless otherwise stated.

Can. J. Chem. Downloaded from www.nrcresearchpress.com by 186.148.149.217 on 09/07/12
For personal use only.

TABLE 3. Bond angles (deg) with estimated standard deviations in parentheses

Bonds	Angle (deg)	Bonds	Angle (deg)
N—O(1)—B	107.4(1)	N—C(7)—C(6)	109.6(1)
C(1)—O(2)—B	115.3(1)	N—C(8)—C(9)	111.0(1)
C(7)—O(3)—B	102.1(1)	C(8)—C(9)—C(10)	111.9(2)
O(1)—N—C(7)	101.65(9)	C(9)—C(10)—C(11)	110.3(1)
O(1)—N—C(8)	108.7(1)	C(10)—C(11)—C(12)	111.4(2)
O(1)—N—C(12)	109.1(1)	N—C(12)—C(11)	111.0(1)
C(7)—N—C(8)	115.3(1)	C(14)—C(13)—C(18)	116.4(1)
C(7)—N—C(12)	110.7(1)	C(14)—C(13)—B	122.8(1)
C(8)—N—C(12)	110.8(1)	C(18)—C(13)—B	120.8(1)
O(2)—C(1)—C(2)	120.0(1)	C(13)—C(14)—C(15)	121.9(2)
O(2)—C(1)—C(6)	120.6(1)	C(14)—C(15)—C(16)	120.3(2)
C(2)—C(1)—C(6)	119.4(1)	C(15)—C(16)—C(17)	119.5(2)
C(1)—C(2)—C(3)	119.4(2)	C(16)—C(17)—C(18)	120.3(2)
C(2)—C(3)—C(4)	121.4(2)	C(13)—C(18)—C(17)	121.6(2)
C(3)—C(4)—C(5)	119.5(2)	O(1)—B—O(2)	108.3(1)
C(4)—C(5)—C(6)	120.7(2)	O(1)—B—O(3)	101.0(1)
C(1)—C(6)—C(5)	119.6(2)	O(1)—B—C(13)	110.8(1)
C(1)—C(6)—C(7)	117.1(1)	O(2)—B—O(3)	109.6(1)
C(5)—C(6)—C(7)	123.3(2)	O(2)—B—C(13)	110.7(1)
O(3)—C(7)—N	100.9(1)	O(3)—B—C(13)	116.0(1)
O(3)—C(7)—C(6)	112.0(1)		

TABLE 4. Intra-annular torsion angles (deg) standard deviations in parentheses

Atoms	Torsion angle (deg)
C(12)—N—C(8)—C(9)	−56.0(2)
N—C(8)—C(9)—C(10)	54.8(2)
C(8)—C(9)—C(10)—C(11)	−54.0(2)
C(9)—C(10)—C(11)—C(12)	55.2(2)
C(10)—C(11)—C(12)—N	−57.5(2)
C(8)—N—C(12)—C(11)	57.6(2)
B—O(1)—N—C(7)	14.7(1)
O(1)—N—C(7)—C(6)	76.3(1)
C(1)—C(6)—C(7)—N	−79.8(2)
O(2)—C(1)—C(6)—C(7)	0.6(2)
B—O(2)—C(1)—C(6)	6.7(2)
C(1)—O(2)—B—O(1)	66.3(1)
N—O(1)—B—O(2)	−100.3(1)
B—O(2)—C(1)—C(6)	6.7(2)
O(2)—C(1)—C(6)—C(7)	0.6(2)
C(1)—C(6)—C(7)—O(3)	31.3(2)
B—O(3)—C(7)—C(6)	−64.4(1)
C(7)—O(3)—B—O(2)	71.6(1)
C(1)—O(2)—B—O(3)	−43.0(2)
B—O(1)—N—C(7)	14.7(1)
O(1)—N—C(7)—O(3)	−41.9(1)
B—O(3)—C(7)—N	52.1(1)
C(7)—O(3)—B—O(1)	−42.5(1)
N—O(1)—B—O(3)	14.8(1)

of 1.424, 1.539, 1.488, and 1.382 Å in the BONCO ring of **4** are similar to the corresponding values of 1.409, 1.556, 1.506, and 1.378 Å in **7***a* (11) and 1.410, 1.534, 1.507, and 1.387 Å in **7***b* (12). The acetal carbon – nitrogen distance in **4** (C(7)—N = 1.569 Å) lies between the corresponding distances of 1.505 Å in **7***a* and 1.591 Å in **7***b*, the latter bond being an extremely long (sp^3)N—C bond resulting from steric interactions (12). The long N—C(7) bond in **4** is consistent with evidence of dissociation (ring-chain isomerism) in solution indicated by nmr studies.

The six-membered BOCCCO ring in **4** originates from the salicylaldehyde. Comparison with the structure of the diphenylboron chelate of salicylaldehyde, **8** (13), shows, of course, the dramatic change in the carbonyl C=O bond length from 1.263 Å in **8** to 1.382 Å in **4** associated with the sp^3 hybridization of C(7) in **4**. The bond between C(7) and the aromatic ring also lengthens considerably with the change in hybridization at C(7): from 1.413 Å in **8** to 1.494 Å in **4**. Both B—O bonds are shorter in **4** than in **8**, the most notable difference involving the dative interaction between the carbonyl oxygen atom and boron in **8** (1.574 Å) and the corresponding single bond in **4** (1.488 Å). The O(2)—C(1)—C(6)—C(7) ring fragment in **4** is planar to within experimental error. The six-membered BOCCCO ring has a distorted semi-planar (O(3)-envelope) conformation.

The seven-membered BONCCCO ring in **4** may be compared with those observed in diphenylboron chelates of salicylaldehyde nitrones (14, 15) and certain salicylohydroxamic acid derivatives (16) having the general structure **9**. The main

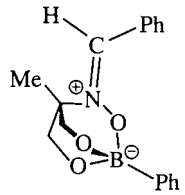

6

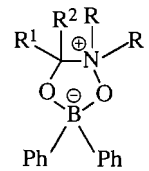

7

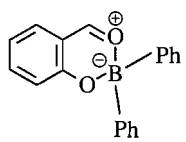

8

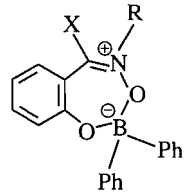

9

Can. J. Chem. Downloaded from www.nrcresearchpress.com by 186.148.149.217 on 09/07/12
For personal use only.

difference between these seven-membered rings in **9** and **4**, apart from substantial conformational differences, is the longer C(7)—N distance in **4** (1.569 Å) relative to the corresponding C=N double bond in **9** (1.291 Å for the salicylaldonitrone with X = H and R = Me) (15). The N—O and C(6)—C(7) bonds are also longer in **4**. The sum of bond lengths in the BONCCCO ring of **4** (10.275 Å), when compared with the corresponding value of 9.907 Å for **9** (X = H, R = Me), is consistent with the higher degree of saturation in the seven-membered ring of **4**.

The piperidine ring in **4** has an essentially undistorted chair conformation (see Table 4). The oxygen substituent at the nitrogen atom occupies an axial position, and the carbon substituent is equatorial. The same positioning of substituents has been observed for other cyclic *N*-oxide derivatives such as ethylenebis(piperidine *N*-oxide) salts (17) and hydrates (18). The N—O distance in **4** (1.424 Å) is similar to those in *N*-alkylpiperidine *N*-oxide perchlorates (1.411–1.412 Å) (17).

The crystal structure of **4** consists of well-separated molecules, the most significant intermolecular contact (O(1)···C(4) ($2 - x$, $y - \frac{1}{2}$, $\frac{3}{2} - z$) = 3.307(2) Å and O(1)···H(4) = 2.57(2) Å) corresponding to a normal van der Waals interaction. Features of the molecular geometry (Tables 2–4) not discussed above are normal.

Acknowledgments

We thank the Natural Sciences and Engineering Research Council of Canada and the Fonds der Chemischen Industrie, Frankfurt am Main, for financial support and the University of British Columbia Computing Centre for assistance.

1. International tables for X-ray crystallography. Vol. IV. Kynoch Press, Birmingham. 1974. pp. 99–102 and 149.
2. V. SCHOMAKER and K. N. TRUEBLOOD. Acta Crystallogr. Sect. B, **24**, 63 (1968).
3. D. W. J. CRUICKSHANK. Acta Crystallogr. **9**, 747 (1956); **9**, 754 (1956); **14**, 896 (1961).
4. W. KLIEGEL. Z. Chem. **10**, 437 (1970).
5. W. KLIEGEL and E. AHLENSTIEL. Chem. Ber. **109**, 3547 (1976).
6. W. KLIEGEL and E. AHLENSTIEL. Chem. Ber. **110**, 1623 (1977).
7. W. KLIEGEL, L. PREU, S. J. RETTIG, and J. TROTTER. Can. J. Chem. **63**, 509 (1985).
8. W. KLIEGEL, D. NANNINGA, S. J. RETTIG, and J. TROTTER. Can. J. Chem. **61**, 2329 (1983).
9. W. KLIEGEL, S. J. RETTIG, and J. TROTTER. Can. J. Chem. **62**, 515 (1984).
10. W. KLIEGEL, H.-W. MOTZKUS, S. J. RETTIG, and J. TROTTER. Can. J. Chem. **63**, 3516 (1985).
11. S. J. RETTIG, J. TROTTER, and W. KLIEGEL. Can. J. Chem. **52**, 2531 (1974).
12. W. KLIEGEL, H.-W. MOTZKUS, S. J. RETTIG, and J. TROTTER. Can. J. Chem. **62**, 838 (1984).
13. S. J. RETTIG and J. TROTTER. Can. J. Chem. **54**, 1168 (1976).
14. W. KLIEGEL and D. NANNINGA. J. Organometal. Chem. **243**, 373 (1983).
15. W. KLIEGEL, U. LAUTERBACH, S. J. RETTIG, and J. TROTTER. Can. J. Chem. **65**, 1457 (1987).
16. W. KLIEGEL, M. TAJERBASHI, S. J. RETTIG, and J. TROTTER. Can. J. Chem. **66**, 2621 (1988).
17. M. JASKOLSKI, I. OLOVSSON, R. TELLGREN, and D. MICKIEWICZ-WICHLACZ. Acta Crystallogr. Sect. B, **38**, 291 (1982); M. JASKOLSKI, M. GDANIEC, and Z. KOSTURKIEWICZ. Pol. J. Chem. **56**, 297 (1982).
18. M. JASKOLSKI. Acta Crystallogr. Sect. C, **43**, 2391 (1987).
19. K. DRÜCKLER, W. KLIEGEL, S. J. RETTIG, and J. TROTTER. Can. J. Chem. **67**, 2218 (1989).

Can. J. Chem. Downloaded from www.nrcresearchpress.com by 186.148.149.217 on 09/07/12
For personal use only.

Structural studies of organoboron compounds. XXXVIII.[1] 2,2-Diphenyl-4,4-tetramethylene-1,3,5-trioxa-3*a*-azonia-2-borata-2,3,4,5-tetrahydro-1*H*-cyclopenta[*a*]naphthalene

WOLFGANG KLIEGEL and MAHMOOD TAJERBASHI

Institut für Pharmazeutische Chemie, der Technischen Universität Braunschweig, Beethovenstraße 55, 3300 Braunschweig, Bundesrepublik Deutschland

AND

STEVEN J. RETTIG and JAMES TROTTER

Department of Chemistry, University of British Columbia, 2036 Main Mall, Vancouver, B.C., Canada V6T 1Y6

Received April 21, 1989

WOLFGANG KLIEGEL, MAHMOOD TAJERBASHI, STEVEN J. RETTIG, and JAMES TROTTER. Can. J. Chem. **68**, 69 (1990).

Reaction of oxybis(diphenylborane) with the condensation product of salicylohydroxamic acid and cyclopentanone gives the title compound in good yield. Crystals of 2,2-diphenyl-4,4-tetramethylene-1,3,5-trioxa-3*a*-azonia-2-borata-2,3,4,5-tetrahydro-1*H*-cyclopenta[*a*]naphthalene are monoclinic, $a = 12.521(1)$, $b = 12.409(1)$, $c = 12.975(1)$ Å, $\beta = 93.784(8)°$, $Z = 4$, space group $P2_1/n$. The structure was solved by direct methods and was refined by full-matrix least-squares procedures to $R = 0.043$ and $R_w = 0.044$ for 1502 reflections with $I \geq 2\sigma(I)$. The molecule has a typical diphenylboron hydroxamate structure featuring a five-membered COBON chelate ring. The *O*,*O*-chelating ligand is weakly bound to the diphenylboron moiety. Bond lengths (corrected for libration) include: (N)O—B = 1.558(4), (C=)O—B = 1.578(4), and C—B = 1.589(5) and 1.603(5) Å.

Key words: crystal structure, boron compound, organoboron compound.

WOLFGANG KLIEGEL, MAHMOOD TAJERBASHI, STEVEN J. RETTIG et JAMES TROTTER. Can. J. Chem. **68**, 69 (1990).

La réaction de l'oxybis(diphénylborane) avec le produit de condensation de l'acide salicylehydroxamique et la cyclopentanone conduit au composé mentionné dans le titre, avec un bon rendement. Les cristaux du 2,2-diphényl-4,4-tétraméthylène-1,3,5-trioxa-3a-azonia-2-borata-2,3,4,5-tétrahydro-1*H*-cyclopenta[*a*]naphtalène sont monocliniques, groupe d'espace $P2_1/n$, avec $a = 12{,}521(1)$, $b = 12{,}409(1)$ et $c = 12{,}975(1)$ Å, $\beta = 93{,}784(8)°$ et $Z = 4$. On a résolu la structure par des méthodes directes et on l'a affinés par la méthode des moindres carrés (matrice entière) jusqu'à des valeurs de $R = 0{,}043$ et $R_w = 0{,}044$ pour 1502 réflexions avec $I \geq 2\sigma(I)$. La molécule possède une structure hydroxamate de diphénylbore typique comportant un cycle chélate COBON à cinq chaînons. Le ligand chélatant-*O*,*O* est faiblement lié à la portion diphénylbore. Les longueurs des liaisons (corrigées pour la libration) incluent: (N)O—B = 1,558(4), (C=)O—B = 1,578(4) et C—B = 1,589(5) et 1,603(5) Å.

Mots clés : structure cristalline, composé du bore, composé du organobore.

[Traduit par la revue]

Introduction

The condensation of salicylohydroxamic acid and aldehydes (1, 2) or ketones (2) gives crystalline compounds which were formulated as cyclic *N*,*O*-acetals **1**. Structure **1** is a cyclic *N*-(α-phenoxyalkyl)hydroxamic acid and, as such, is of interest to us as a ligand for boron chelation in the course of our investigation of *N*-substituted hydroxamic acids (3–8). Compound **1** ($R^1 + R^2 = -(CH_2)_4-$) was synthesized from salicylohydroxamic acid and cyclopentanone and was reacted with oxybis(diphenylborane).

The resulting diphenylboron chelate was expected to possess the molecular structure **2** by analogy with the general structure **3** found for other boron chelates of *N*-substituted hydroxamic acids (3–7). If there had been another mode of reaction between salicylohydroxamic acid and the carbonyl compound, the five-membered *O*,*O*-acetal **4** could have been formed as in the acid-catalysed cyclization of 3-hydroxycarbohydroxamic acids with cyclohexanone (9). The 1,4,2-dioxazole partial structure of **4** is well documented in the literature (10). Compound **4** would lead to a diphenylboron chelate of structure **5** with a six-membered chelate ring, the formation of which is demonstrated by the known diphenylboron chelate **6** (11). Infrared and ^{1}H nmr data do not allow an unambiguous choice between the structures **2** and **5**. This also applies for the less probable structure **7** which contains a seven-membered chelate ring iden-

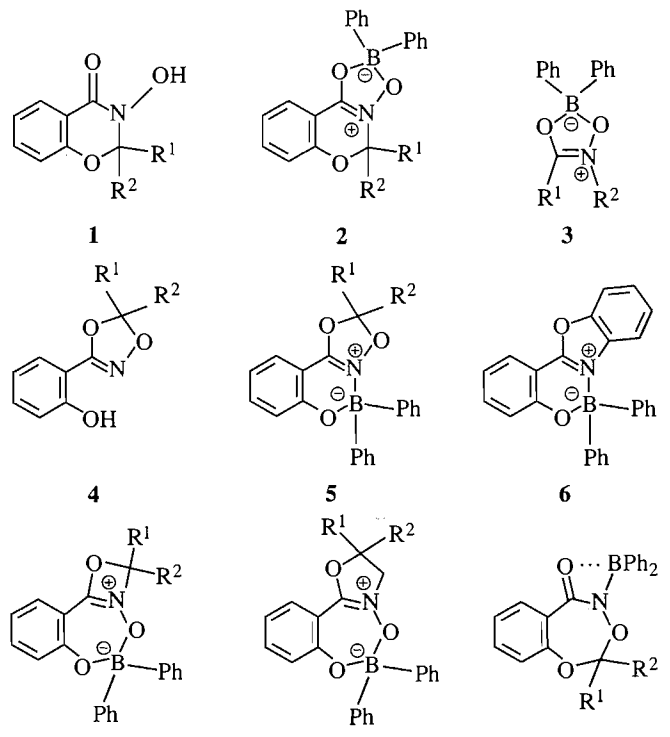

[1]For Part XXXVII, see ref. 27.

Printed in Canada / Imprimé au Canada

Can. J. Chem. Downloaded from www.nrcresearchpress.com by 91.144.44.67 on 09/07/12
For personal use only.

Can. J. Chem. Downloaded from www.nrcresearchpress.com by 91.144.44.67 on 09/07/12
For personal use only.

tical to that observed for compound **8** (12). The formation and stability of the 1,3-oxazetine ring system in **7**, however, seems unlikely.[2] An additional structural isomer that has to be considered would have a seven-membered cyclic *O,O*-acetal structure with *N*-diphenylboryl substitution, **9**. Simple amidoboranes are reported to exist as monomers or cyclic dimers (16). To decide definitively between the structures **2**, **5**, **7**, and **9** an X-ray crystallographic analysis was undertaken.

Experimental

2,3-Dihydro-3-hydroxy-2,2-tetramethylene-4H-1,3-benzoxazin-4-one, 1 ($R^1 + R^2 = -(CH_2)_4-$)

Salicylohydroxamic acid (1.22 g, 8 mmol) and cyclopentanone (0.67 g, 8 mmol) are dissolved in benzene (100 mL) and, after addition of *p*-toluenesulfonic acid (0.15 g), refluxed for 80 min using a Dean–Stark trap for the continuous removal of water. After partial evaporation of the solvent and addition of petroleum ether, colorless needles were obtained upon cooling. Yield: 1.51 g (86%). Melting point: 114°C (benzene/petroleum ether). *Anal.* calcd. for $C_{12}H_{13}NO_3$: C 65.74, H 5.97, N 6.39; found: C 65.87, H 5.99, N 6.35. The substance gives a red-to-violet solution upon reaction with $FeCl_3$ in ethanol. Infrared (KBr): 1650 (C=O / C=N), 2200–3600 cm^{-1} (broad, OH). ^1H nmr (90 MHz, $CDCl_3$/TMS): δ(ppm) = 1.70–2.73 (m, $(CH_2)_4$), 6.75–7.90 (m, C_6H_4), 9.55 (s, exchangeable, OH).

2,2-Diphenyl-4,4-tetramethylene-1,3,5-trioxa-3a-azonia-2-borata-2,3,4,5-tetrahydro-1H-cyclopenta[a]naphthalene, 2 ($R^1 + R^2 = -(CH_2)_4-$)

A solution of **1** (1.10 g, 5 mmol) and oxybis(diphenylborane) (0.87 g, 2.5 mmol) in 20–30 mL ethanol is refluxed for 15 min. After partial evaporation of the solvent, colorless needles crystallize upon cooling. Yield: 1.63 g, (85%). Melting point: 163°C (absolute ethanol). *Anal.* calcd. for $C_{24}H_{22}BNO_3$: C 75.22, H 5.78, N 3.65; found: C 75.24, H 5.95, N 3.72. Mass spectrum (70 eV, 120°C): m/z = 306 (100%, $M^+ - C_6H_5$), 121 (14%). Infrared (KBr): 1615 cm^{-1} (C=O / C=N). ^1H nmr (90 MHz, $CDCl_3$/TMS): δ(ppm) = 1.69–2.78 (m, $(CH_2)_4$), 6.85–7.80 (m, C_6H_4 and BPh_2). ^{13}C nmr (400 MHz, $CDCl_3$): δ(ppm)[3] = 23.57 (C(10),C(11), 34.93 (C(9),C(12)), 104.17 (C(7)), 110.06 (C(1)), 117.53–136.03 (C(3)—C(6), C(13)—C(18), C(19)—C(24)). The substance gives a blue-colored solution upon addition of diphenylcarbazone in ethanol, indicating the chelated diphenylborenium ion in **2** (17).

X-ray crystallographic analysis

A crystal bounded by the six faces (followed by the distances in mm between parallel faces): ±(−1 0 1), 0.22, ±(1 0 1), 0.48, {0 1 0}, 0.54, was mounted in a general orientation. Unit-cell parameters were refined by least-squares on 2 sin θ/λ values for 25 reflections (2θ = 20–31°) measured on a diffractometer with Mo-Kα radiation (λ($K\alpha_1$) = 0.70930, λ($K\alpha_2$) = 0.71359 Å). Crystal data at 22°C are as follows:

$C_{24}H_{22}BNO_3$ fw = 383.25

Monoclinic, a = 12.521(1), b = 12.409(1), c = 12.975(1) Å, β = 93.784(8)°, V = 2011.5(3) Å^3, Z = 4, ρ_c = 1.265 Mg m^{-3}, F(000) = 808, μ(Mo-Kα) = 0.77 cm^{-1}. Absent reflections: 0k0, k odd, and h0l, $h + l$ odd, uniquely indicate the space group $P2_1/n$ (C_{2h}^5, No. 14).

Intensities were measured with graphite-monochromated Mo-Kα radiation on an Enraf-Nonius CAD4-F diffractometer. An ω-2θ scan at 0.7–6.7° min^{-1} over a range of (0.65 + 0.35 tan θ) degrees in ω (extended by 25% on both sides for background measurement) was employed. Data were measured to 2θ = 50°. The intensities of three check reflections, measured every 4000 s throughout the data collection, showed only small random fluctuations. Of the 3525 independent reflections measured and processed,[4] 1502(42.6%) had intensities greater than or equal to 2σ(I) above background where $\sigma^2(I) = S + 2B + (0.04(S - B))^2$ with S = scan count and B = normalized background count.

The structure was solved by direct methods, the coordinates of the non-hydrogen atoms being determined from an *E*-map. The non-hydrogen atoms were refined with anisotropic thermal parameters and the hydrogen atoms were fixed in idealized positions (C(sp^2)—H = 0.97, C(sp^3)—H = 0.98 Å, and $U_H \propto U_{\text{bonded atom}}$). Scattering factors for all atoms were taken from ref. 18. The weighting scheme $w = 1/\sigma^2(F)$, where $\sigma^2(F)$ is derived from the previously defined $\sigma^2(I)$, gave uniform average values of $w(|F_o| - |F_c|)^2$ over ranges of both $|F_o|$ and sin θ/λ and was employed in the final stages of full-matrix refinement of 262 variables. Reflections with $I < 2\sigma(I)$ were not included in the refinement. Convergence was reached at R = 0.043 and R_w = 0.044 for 1502 reflections with $I \geq 2\sigma(I)$. The function minimized was $\Sigma w(|F_o| - |F_c|)^2$, $R = \Sigma||F_o| - |F_c||/\Sigma|F_o|$ and $R_w = (\Sigma w(|F_o| - |F_c|)^2/\Sigma w|F_o|^2)^{1/2}$.

On the final cycle of refinement the mean and maximum parameter shifts corresponded to 0.001 and 0.006σ, respectively. The mean error in an observation of unit weight was 1.598. The largest peak on the final difference map was 0.19 e Å^{-3}. The final positional and thermal

TABLE 1. Final positional (fractional × 10^4) and isotropic thermal parameters (U × 10^3 Å^2) with estimated standard deviations in parentheses

Atom	x	y	z	U_{eq}
O(1)	6775(2)	793(2)	4875(2)	67
O(2)	5295(2)	3260(2)	4577(2)	64
O(3)	4072(2)	2111(2)	3619(2)	62
N	5608(2)	2204(2)	4507(2)	50
C(1)	6736(2)	1935(3)	4768(2)	52
C(2)	6197(3)	168(3)	4157(3)	58
C(3)	6557(3)	−859(3)	3965(3)	77
C(4)	5943(4)	−1507(3)	3295(3)	83
C(5)	4995(4)	−1152(3)	2810(3)	74
C(6)	4637(3)	−128(3)	3011(3)	61
C(7)	5235(3)	543(3)	3684(2)	50
C(8)	4936(3)	1622(3)	3932(2)	48
C(9)	7174(3)	2430(3)	5792(2)	66
C(10)	8158(3)	3041(4)	5557(3)	93
C(11)	8503(3)	2581(3)	4556(3)	84
C(12)	7450(3)	2345(3)	3954(2)	64
C(13)	3276(3)	3563(3)	4787(3)	52
C(14)	3490(3)	4167(3)	5685(3)	64
C(15)	2713(4)	4418(3)	6342(3)	80
C(16)	1691(4)	4068(4)	6135(4)	94
C(17)	1450(3)	3472(4)	5265(4)	104
C(18)	2236(3)	3228(3)	4610(3)	77
C(19)	4195(3)	4099(3)	3033(3)	56
C(20)	4978(3)	4025(4)	2334(3)	90
C(21)	5024(4)	4736(5)	1505(3)	103
C(22)	4264(4)	5518(4)	1350(3)	95
C(23)	3476(3)	5606(3)	2008(3)	89
C(24)	3456(3)	4908(3)	2842(3)	73
B	4164(3)	3312(3)	4007(3)	55

[2]The 2*H*-1,3-oxazet-1-ine ring system is reported sporadically in the literature: as an intermediate salt (13), SO_3-adduct (14), or mass spectral fragment (15).

[3]Shifts relative to TMS; numbering of the C atoms is as shown in Fig. 1.

[4]The computer programs used include locally written programs for data processing and locally modified versions of the following: MULTAN 80, multisolution program by P. Main, S. J. Fiske, S. E. Hull, L. Lessinger, G. Germain, J. P. Declercq, and M. M. Woolfson; ORFLS, full-matrix least-squares, and ORFFE, function and errors, by W. R. Busing, K. O. Martin and H. A. Levy; FORDAP, Patterson and Fourier syntheses, by A. Zalkin; ORTEP II, illustrations, by C. K. Johnson.

TABLE 2. Bond lengths (Å) with estimated standard deviations in parentheses

Bond	Length		Bond	Length	
	Uncorr.	Corr.		Uncorr.	Corr.
O(1)—C(1)	1.425(4)	1.432	C(9)—C(10)	1.495(5)	1.504
O(1)—C(2)	1.380(4)	1.386	C(10)—C(11)	1.508(5)	1.515
O(2)—N	1.373(3)	1.376	C(11)—C(12)	1.516(4)	1.524
O(2)—B	1.554(4)	1.558	C(13)—C(14)	1.397(4)	1.408
O(3)—C(8)	1.283(3)	1.288	C(13)—C(18)	1.372(4)	1.389
O(3)—B	1.576(4)	1.578	C(13)—B	1.582(5)	1.589
N—C(1)	1.468(4)	1.475	C(14)—C(15)	1.371(5)	1.378
N—C(8)	1.305(3)	1.309	C(15)—C(16)	1.360(5)	1.378
C(1)—C(9)	1.532(4)	1.539	C(16)—C(17)	1.367(5)	1.377
C(1)—C(12)	1.516(4)	1.525	C(17)—C(18)	1.376(5)	1.383
C(2)—C(3)	1.380(5)	1.386	C(19)—C(20)	1.383(5)	1.398
C(2)—C(7)	1.395(4)	1.405	C(19)—C(24)	1.376(4)	1.391
C(3)—C(4)	1.380(5)	1.386	C(19)—B	1.599(5)	1.603
C(4)—C(5)	1.378(5)	1.387	C(20)—C(21)	1.395(6)	1.400
C(5)—C(6)	1.378(5)	1.384	C(21)—C(22)	1.365(5)	1.381
C(6)—C(7)	1.389(4)	1.395	C(22)—C(23)	1.351(5)	1.366
C(7)—C(8)	1.432(4)	1.438	C(23)—C(24)	1.387(5)	1.392

TABLE 3. Bond angles (deg) with estimated standard deviations in parentheses

Bonds	Angle (deg)	Bonds	Angle (deg)
C(1)—O(1)—C(2)	118.7(3)	C(9)—C(10)—C(11)	105.7(3)
N—O(2)—B	105.3(2)	C(10)—C(11)—C(12)	103.1(3)
C(8)—O(3)—B	107.7(2)	C(1)—C(12)—C(11)	103.8(3)
O(2)—N—C(1)	118.4(3)	C(14)—C(13)—C(18)	115.4(3)
O(2)—N—C(8)	112.9(2)	C(14)—C(13)—B	122.3(3)
C(1)—N—C(8)	125.4(3)	C(18)—C(13)—B	122.2(3)
O(1)—C(1)—N	106.0(3)	C(13)—C(14)—C(15)	122.4(3)
O(1)—C(1)—C(9)	107.8(3)	C(14)—C(15)—C(16)	120.2(4)
O(1)—C(1)—C(12)	112.5(3)	C(15)—C(16)—C(17)	119.2(4)
N—C(1)—C(9)	113.1(3)	C(16)—C(17)—C(18)	120.1(4)
N—C(1)—C(12)	111.5(3)	C(13)—C(18)—C(17)	122.7(3)
C(9)—C(1)—C(12)	106.0(3)	C(20)—C(19)—C(24)	115.3(4)
O(1)—C(2)—C(3)	118.6(4)	C(20)—C(19)—B	122.2(4)
O(1)—C(2)—C(7)	120.6(3)	C(24)—C(19)—B	122.5(3)
C(3)—C(2)—C(7)	120.7(4)	C(19)—C(20)—C(21)	122.1(4)
C(2)—C(3)—C(4)	118.5(4)	C(20)—C(21)—C(22)	120.0(4)
C(3)—C(4)—C(5)	121.9(4)	C(21)—C(22)—C(23)	119.7(4)
C(4)—C(5)—C(6)	119.3(4)	C(22)—C(23)—C(24)	119.6(4)
C(5)—C(6)—C(7)	120.2(3)	C(19)—C(24)—C(23)	123.4(3)
C(2)—C(7)—C(6)	119.4(3)	O(2)—B—O(3)	99.1(2)
C(2)—C(7)—C(8)	116.3(3)	O(2)—B—C(13)	111.1(3)
C(6)—C(7)—C(8)	124.3(3)	O(2)—B—C(19)	109.4(3)
O(3)—C(8)—N	114.7(3)	O(3)—B—C(13)	110.5(3)
O(3)—C(8)—C(7)	126.7(3)	O(3)—B—C(19)	109.3(3)
N—C(8)—C(7)	118.5(3)	C(13)—B—C(19)	116.1(3)
C(1)—C(9)—C(10)	106.2(3)		

parameters appear in Tables 1 and 6,[5] respectively. Measured and calculated structure factors have been placed in the Depository of Unpublished Data.[5]

The ellipsoids of thermal motion for the non-hydrogen atoms are shown in Fig. 1. The thermal motion has been analysed in terms of the rigid-body modes of translation, libration, and screw motion (19). The rms standard error in the temperature factors σU_{ij} (derived from the least-squares analysis) is 0.0025 Å^2. Five structural subunits were separately analysed: 2 PhB, O(1)C(2–7), O(1)NC(1)C(9–12), and the central fused-ring system (rms ΔU_{ij} = 0.0029–0.0051, mean 0.0036 Å^2). The appropriate bond distances have been corrected for libration (19, 20), using shape parameters q^2 of 0.08 for all atoms involved. Corrected bond lengths appear in Table 2 along with the uncorrected values; bond angles appear in Table 3 and intra-annular torsion angles in Table 4. Hydrogen atom parameters (Table 5) and a complete listing of torsion angles (Table 7) have been deposited.[5]

[5]The structure factor table, Table 6 (anisotropic thermal parameters) and other material mentioned in the text may be purchased from the Depository of Unpublished Data, CISTI, National Research Council of Canada, Ottawa, Ont., Canada K1A 0S2.

Can. J. Chem. Downloaded from www.nrcresearchpress.com by 91.144.44.67 on 09/07/12
For personal use only.

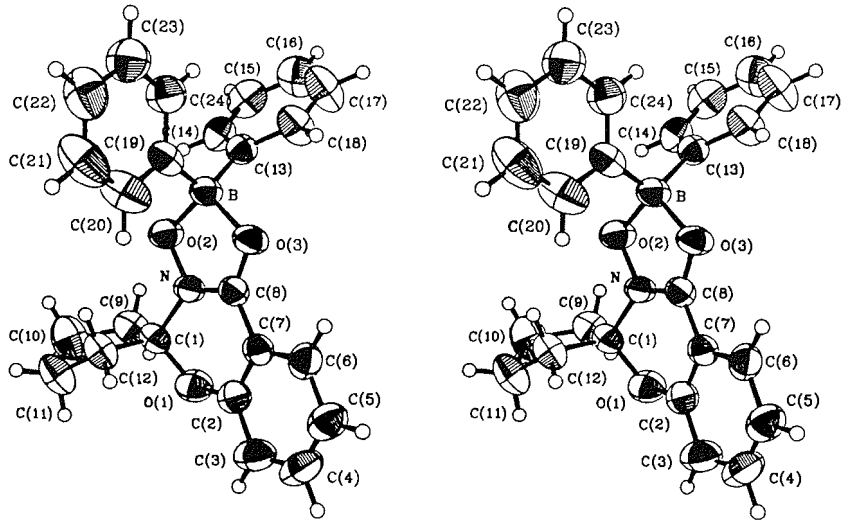

FIG. 1. Stereoscopic view of 2,2-diphenyl-4,4-tetramethylene-1,3,5-trioxa-3a-azonia-2-borata-2,3,4,5-tetrahydro-1*H*-cyclopenta[*a*]naphthalene; 50% probability thermal ellipsoids are shown for the non-hydrogen atoms.

TABLE 4. Intra-annular torsion angles (deg) standard deviations in parentheses

Atoms	Torsion angle (deg)
C(2)—O(1)—C(1)—N	43.3(3)
C(8)—N—C(1)—O(1)	−35.6(4)
C(1)—N—C(8)—C(7)	12.5(4)
C(2)—C(7)—C(8)—N	5.3(4)
O(1)—C(2)—C(7)—C(8)	4.2(4)
C(1)—O(1)—C(2)—C(7)	−31.7(4)
B—O(2)—N—C(8)	5.7(3)
O(2)—N—C(8)—O(3)	−6.0(4)
B—O(3)—C(8)—N	3.3(4)
C(8)—O(3)—B—O(2)	0.3(3)
N—O(2)—B—O(3)	−3.4(3)
C(12)—C(1)—C(9)—C(10)	−3.7(4)
C(1)—C(9)—C(10)—C(11)	−20.2(4)
C(9)—C(10)—C(11)—C(12)	36.4(4)
C(10)—C(11)—C(12)—C(1)	−38.2(4)
C(9)—C(1)—C(12)—C(11)	25.9(4)

Results and discussion

The structure of **2**, deriving from the cyclic *N*-alkyl hydroxamic acid **1**, is verified by the X-ray analysis (Fig. 1). The molecule has a typical diphenylboron hydroxamate structure featuring a five-membered COBON chelate system, also realized in similar hydroxamates of the general type **3** (3, 4) and in the diphenylboron chelates of *N*-hydroxy-2-pyridinones (7). The six-membered *N*,*O*-acetal ring system of **1** is retained in the chelate **2**.

The C=O bond of the hydroxamate group (1.288(3) Å) has lost some of its double bond character compared to that in free salicylohydroxamic acid (1.258(3) Å, uncorrected[6]) (21), but a π-bond order of 0.53 can be estimated from a plot of bond length versus π-bond order (22). The C—N bond of salicylohydroxamic acid (1.316(4) Å, uncorrected) (21), which already exhibits considerable double bond character, gains even more in the chelate **2** (1.309(3) Å). The latter C—N distance corresponds to an estimated π-bond order of 0.70 (22). The formulation of the chelate ring in **2** as a cyclic *B*,*N*-betaine is thus justified, this being reflected by the nomenclature employed to describe the chelate **2** (which is similar to boron chelates of the type **3**).

Compared to the boron chelates of *N*-methylacethydroxamic acid (3, 4) and *N*-hydroxy-2-pyridinone (7), which have C=O bond lengths of about 1.34 Å, the hydroxamate C=O bond in **2** is shorter (1.309(3) Å). More double bond character is retained upon chelate formation in the present structure than in the above mentioned hydroxamate complexes. This could be attributed to the influence of the (conjugated) aryl substituent at the hydroxamate function. Similar dimensions within the hydroxamate group are found in a MoO_2 complex of salicylohydroxamic acid (23): C=O = 1.288 and 1.265, C=N = 1.304 and 1.317, N—O = 1.374 and 1.380 Å (uncorrected).

Enhanced π-interaction between the hydroxamate system and the adjacent aryl group is also manifested by shortening of the C(7)—C(8) bond (1.438(4) Å) in **2** relative to that in free salicylohydroxamic acid (1.489(5) Å, uncorrected) (21). This effect is more pronounced in **2** than in the MoO_2 complex (23), so the alkylation of the phenol group in **2** by cycloacetal formation may contribute to the shorter C(7)—C(8) bond. The angle between the normals to the C(2)—C(7) and hydroxamate group mean planes is 8.8°.

The phenolic C(2)—O(1) bond in **2** (1.386(4) Å) is 0.03 Å longer than the corresponding C(ar)—O bond in salicylohydroxamic acid (1.355(4) Å, uncorrected) (21). Lengthening of C(ar)—O bonds by alkylation is well known: aryl alkyl ethers show an average uncorrected C(ar)—O distance of 1.370 Å (24). The somewhat longer bond in **2** could reflect an influence of the α-iminoalkyl substituent at the phenolic oxygen atom and/or the cyclic alkylation mode.

The average O—B and C—B distances in **2** are 1.568 and 1.596 Å, respectively. The mean C—B/mean O—B ratio, which is a good indicator of the overall binding strength of the *O*,*O*-chelating ligand with respect to the diphenylboron moiety (25), of 1.018 for compound **2** lies at the low end of the range 1.017–1.066 (mean 1.035) observed for Ph_2BO_2 compounds

[6]Libration corrected bond lengths (esd's assumed equal to those of the uncorrected values) are employed in the discussion and are compared with similarly treated (19) distances unless otherwise stated.

Can. J. Chem. Downloaded from www.nrcresearchpress.com by 91.144.44.67 on 09/07/12
For personal use only.

having five-membered chelate rings (ref. 26 and references therein). Only the diphenylboron chelates of *N*-hydroxy-2-pyridinone (7) and 3-hydroxy-2-methyl-4-pyridinone (26), which both have C—B / O—B ratios of 1.017, have average O—B distances longer than compound **2**.

The cyclopentane ring in **2** has a distorted C(11)-envelope comformation (see Table 4) with the phenol ether group in a pseudo-axial and the chelate ring in a pseudo-equatorial position. The 1,3-oxazine ring (cyclic *N,O*-acetal) has a "semi-planar" (envelope-like) conformation with O(1)—C(2)—C(7)—C(8)—N qualitatively planar. The five-membered COBON ring has a flattened N-envelope conformation, the ring being planar to within ±0.032(3) Å. The hydroxamate group itself is non-planar, the angle between normals to the N and C(8) coordination planes being 19.7°. The crystal structure consists of molecules separated by normal van der Waals distances, the shortest intermolecular contact between non-hydrogen atoms being O(1)···C(6) = 3.461(4) Å.

Acknowledgments

We thank the Natural Sciences and Engineering Research Council of Canada and the Fonds der Chemischen Industrie, Frankfurt am Main, for financial support and the University of British Columbia Computing Centre for assistance.

1. D. B. Reisner and B. J. Ludwig. J. Heterocycl. Chem. **6**, 953 (1970).
2. S. Inamasu and M. Tsuruta (Yoshitomi Pharmaceutical Industries, Ltd.). Japan. Pat. 69 12,420 (June 5, 1969): Chem. Abstr. **71**, 101869m (1969).
3. S. J. Rettig, J. Trotter, W. Kliegel, and D. Nanninga. Can. J. Chem. **55**, 1 (1977).
4. S. J. Rettig, J. Trotter, W. Kliegel, and D. Nanninga. Can. J. Chem. **56**, 1675 (1978).
5. W. Kliegel and D. Nanninga. Pharmazie, **38**, 131 (1983).
6. W. Kliegel and D. Nanninga. Chem. Ber. **116**, 2616 (1983).
7. W. Kliegel, D. Nanninga, S. J. Rettig, and J. Trotter. Can. J. Chem. **61**, 2493 (1983).
8. W. Kliegel, M. Tajerbashi, S. J. Rettig, and J. Trotter. Can. J. Chem. **67**, 2218 (1989).
9. D. Geffken. Arch. Pharm. (Weinheim) **318**, 895 (1985).
10. (*a*) O. Exner. Coll. Czech. Chem. Commun. **21**, 1500 (1956); (*b*) H. Nohira, K. Inoue, H. Hattori, T. Okawa, and T. Mukayama. Bull. Chem. Soc. Jpn. **40**, 664 (1967); (*c*) S. Morrocchi, A. Quilico, A. Ricca, and A. Selva. Gazz. Chim. Ital. **98**, 891 (1968); (*d*) R. Huisgen and W. Mack. Chem. Ber. **105**, 2805 (1972); (*e*) N. V. Vasil'ev, S. A. Khokhlova, A. F. Kolomiets, and G. Sokol'skii. Zh. Org. Khim. **20**, 1983 (1984); J. Org. Chem. USSR **20**, 1364 (1984); (*f*) E. J. Breaux. J. Heterocycl. Chem. **23**, 463 (1986); (*g*) D. Mackay, E. G. Neeland, and N. J. Taylor. J. Org. Chem. **51**, 2351 (1986).
11. F. Umland and E. Hohaus. Angew. Chem. **79**, 1072 (1967).
12. W. Kliegel, M. Tajerbashi, S. J. Rettig, and J. Trotter. Can. J. Chem. **66**, 2621 (1988).
13. H. Iwamura, M. Tsuchimoto, and S. Nishimura. Tetrahedron Lett. 1405 (1975).
14. V. L. Vershinin, N. V. Asil'ev, A. F. Kolomiets, and G. A. Sokol'skii. Zh. Org. Khim. **20**, 1333 (1984); J. Org. Chem. USSR **20**, 1213 (1984).
15. A. G. Giumanini, G. Verardo, and S. Cauci. J. Prakt. Chem. **329**, 417 (1987).
16. W. Maringgele and A. Meller. Monatsh. Chem. **110**, 473 (1979).
17. (*a*) R. Neu. Z. Anal. Chem. **176**, 334 (1960); (*b*) B. Friese and F. Umland. Anal. Chim. Acta, **96**, 303 (1978).
18. International tables for X-ray crystallography. Vol. IV. Kynoch press, Birmingham. 1974. pp. 99–102.
19. V. Schomaker and K. N. Trueblood. Acta Crystallogr. Sect. B, **24**, 63 (1968).
20. D. W. J. Cruickshank. Acta Crystallogr. **9**, 747 (1956); **9**, 754 (1956); **14**, 896 (1961).
21. I. K. Larsen. Acta Crystallogr. Sect. B. **34**, 962 (1978).
22. G. Häfelinger. Chem. Ber. **103**, 2941 (1970).
23. Kh. Shapirov, N. K. Makhmudova, T. S. Khodashova, N. A. Parpiev, and M. A. Porai-Koshits. Koord. Khim. **9**, 266 (1983).
24. F. H. Allen, O. Kennard, D. G. Watson, L. Brammer, A. G. Orpen, and R. Taylor. J. Chem. Soc. Perkin Trans. II, S1 (1987).
25. W. R. Cullen, S. J. Rettig, J. Trotter, and E. B. Wickenheiser. Can. J. Chem. **66**, 2007 (1988).
26. W. O. Nelson, C. Orvig, S. J. Rettig, and J. Trotter. Can. J. Chem. **66**, 132 (1988).
27. W. Kliegel, H.-W. Motzkus, K. Drückler, S. J. Rettig, and J. Trotter. Can. J. Chem. **68**, 64 (1990).

Can. J. Chem. Downloaded from www.nrcresearchpress.com by 91.144.44.67 on 09/07/12
For personal use only.

Topological investigations of the volumetric and enthalpic effects in some binary mixtures of non-electrolytes

PREM P. SINGH AND MEENU BHATIA
Department of Chemistry, Maharshi Dayanand University, Rohtak-124001, India

Received January 30, 1989[1]

PREM P. SINGH and MEENU BHATIA. Can. J. Chem. **68**, 74 (1990).

Volumetric and enthalpic effects have been measured at 308.15 K for pyridine (A) + aniline, *o*-toluidine, formamide, or *N*,*N*-dimethylformamide (B) mixtures and the same have been rationalized by graph–theoretical arguments to suggest that while aniline in the pure state exists as an equilibrium mixture of monomers and dimers, *o*-toluidine exists mainly as dimers. This analysis has further yielded information about the state of association in formamide and *N*,*N*-dimethylformamide that is consistent with the existing views on their nature of association. This analysis has further yielded information about the molecular entities in these mixtures that has been supported by their infrared spectral studies. The energetics of the various interactions that result in the formation of these A + B mixtures have also been investigated and the results have been rationalized by graph–theoretical arguments.

Key words: topological, association, solvation, energetics, volumetric, enthalpic effects.

PREM P. SINGH et MEENU BHATIA. Can. J. Chem. **68**, 74 (1990).

Opérant à 308,15 K, on a mesuré les effets volumétriques et enthalpiques de mélanges de pyridine (A) avec les composés suivants (B) : l'aniline, l'*o*-toluidine, la formamide et la *N*,*N*-diméthylformamide; en se basant sur la théorie des graphes, on suggère que l'aniline à l'état pur existe sous la forme d'un équilibre entre des monomères et des dimères alors que l'*o*-toluidine existe principalement sous la forme de dimères. Cette analyse a aussi fourni des informations concernant l'état d'association dans la formamide et la *N*,*N*-diméthylformamide et ces informations sont en accord avec les vues généralement acceptées concernant la nature de l'association qui existe dans ces composés. Cette analyse a aussi fourni de l'information concernant les entités moléculaires présentes dans ces mélanges; ces informations sont en accord avec les données obtenues en se basant sur les spectres infrarouges de ces mélanges. On a aussi examiné les énergies impliquées dans les diverses interactions qui conduisent à la formation de ces A + B mélanges et on a rationalisé les résultats à l'aide d'arguments basés sur la théorie des graphes.

Mots clés : topologie, association, solvatation, énergies, effets enthalpiques, effets volumétriques.

[Traduit par la revue]

Introduction

In view of the two well known resonance structures of the amide group (1), it is reasonable to assume that like alkanols (2–5), the lower amides in the pure state exist as dimers, trimers, or higher *r*-mers. Davies (6), however, maintains that the association of amides in solution is limited to dimer formation. On the other hand, while Bellamy and Williams (7) maintain that aniline in the pure state exists as monomers, Wolff and Mathias (8) and Kreglewski and Wilhoit (9) favour the associated structure of aniline and suggest that only one of the hydrogen of its NH_2 group is free to form hydrogen bond and the other hydrogen atom is involved in weak interactions with the π-electron cloud of another aniline molecule. Further *ab initio* molecular orbital calculations on the structural, energetic, and electronic properties of substituted pyridine have suggested (10) that the π-electron density at the C_2, C_4, and C_6 positions in pyridine is less than that in benzene so that even pyridine, in the pure state, may be characterized (11) by pyridine–pyridine interactions. The addition of aniline, *o*-toluidine (OT), formamide (FD) or *N*,*N*-dimethylformamide (NND) (B) to pyridine (A) may then bring changes in the topology (12) of A and or B components of these A + B mixtures. Consequently, graph–theoretical concepts that have been successfully utilized to explain a number of physical and chemical properties of non-electrolytes (13–17) could be helpful in understanding the nature of A and or B in binary mixtures of non-electrolytes. Following Kier and Hall (18), Singh *et al.* (11, 19) have recently employed the graph–theoretical approach to investigate the association and solvation of components of binary mixtures. It was felt that volumetric and enthalpic effects in A + B mixtures where A is pyridine and B is aniline, OT, FD, or NND may yield valuable information about the association and solvation of A and/or B in these A + B mixtures.

Experimental

Materials and methods

Aniline (E. Merck, Analytical grade 99.5%) was refluxed (20) with 10% acetone for 10 h, the mixture was acidified with hydrochloric acid to Congo red, and extracted with ethyl ether until it no longer showed any color. The hydrochloride was purified by crystallizations, the aniline freed, dried with potassium hydroxide pellets (AR grade), and distilled under nitrogen at reduced pressure. The middle fraction was stored in amber-coloured bottles in a nitrogen chamber.

o-Toluidine (Merck, Pro. Analysis 99.5%) was distilled (21) and then dissolved in four times its volume of ethyl ether. An etheral solution of an equivalent amount of oxalic acid (AR grade) was next added and the crystals of *o*-toluidine dioxalate were removed by filtration. These were then recrystallized from water containing some amount of oxalic acid (to prevent hydrolysis), treated with dilute sodium carbonate solution, dried with anhydrous calcium chloride, and distilled under nitrogen under reduced pressure. The middle fraction was collected and stored in amber-coloured bottles in a nitrogen chamber.

Formamide (BDH, Analytical reagent 98%) was purified by passing (22*a*) ammonia gas into it until a slight alkaline reaction was obtained. The reaction mixture was then treated with acetone to precipitate the ammonium formate. The filtered solution was dried over magnesium sulphate, fractionally distilled under nitrogen at reduced pressure, and the middle fraction was collected and stored in small bottles over anhydrous calcium chloride in a desiccator.

N,*N*-Dimethylformamide (LOBA, analytical reagent 99%) was shaken (22*b*) with powdered barium oxide, filtered, and the filtrate distilled under nitrogen at reduced pressure. The middle fraction was collected and stored in small bottles over anhydrous calcium chloride in a desiccator.

[1]Revision received August 10, 1989.

Can. J. Chem. Downloaded from www.nrcresearchpress.com by 186.148.149.217 on 09/07/12
For personal use only.

Can. J. Chem. Downloaded from www.nrcresearchpress.com by 186.148.149.217 on 09/07/12
For personal use only.

TABLE 1. Comparison of the measured densities at 298.15 ± 0.01 K of the various compounds with their corresponding literature values

Compound	Density (g cm^{-3}) This work	Literature value
Aniline	1.01745	1.01750 (23)
o-Toluidine	0.99435	0.99430 (22)
Formamide	1.12922	1.12918 (25)
N,*N*-Dimethylformamide	0.9440	0.94397 (25)
Pyridine	0.97756	0.9776 (26)

Pyridine (Merck, 99.5%, analytical reagents) was refluxed (22*c*) over KOH (AR) pellets and then distilled. The middle fraction was collected and stored over solid KOH pellets. All the compounds were used within 10 days of their purification.

The purities of the purified samples were checked by measuring their densities at 298.15 + 0.01 K and these agreed to within 5 × 10^{-5} g cm^{-3} with their corresponding available literature values (23–26) as is evident from Table 1.

Molar excess volumes, V^E, at 308.15 K for the various A + B mixtures were determined in a V-shaped dilatometer (27). A column of pure and distilled mercury was placed in the dilatometer and the dilatometer was weighed. One of the degassed component was then placed in one bulb of the dilatometer and the bulb was then closed with a vacuum tested B-7 standard cone in such a way that no air bubbles were entrapped in it. It was weighed again. The second component was similarly introduced in the other bulb and its stopper replaced in such a way that the liquid stood to a certain height in the dilatometer capillary. The entire assembly was then placed in a water bath controlled to ±0.01 K by a mercury-in-toluene regulator. The position of the liquid in the dilatometer capillary, relative to the reference mark, R, on it was then noted, at equilibrium by a cathetometer (M/S OSAW, India) within an accuracy of ±0.001 cm. The contents of the dilatometer were mixed, after equilibrium, by tilting it gently sideways several times. In order that the liquid in the capillary had the same composition as that of the bulk solution, the dilatometer was placed in a cold bath so that a minimum liquid was present in the capillary. The dilatometer was again placed in the thermostat maintained at the desired temperature and this process was repeated three or four times. The position of the liquid in the dilatometer capillary relative to the reference mark R on it was again noted. The dilatometer was taken out, dried completely, and weighed to determine the weight of the second liquid. Molar excess volume, V^E, for the A + B mixture at that composition was then calculated (27) from the expression,

$$V^E(T,x_A) = \pi r^2 \Delta h/(n_A + n_B)$$

where r is the radius of the dilatometer capillary, Δh is the change in the liquid level in the capillary after mixing, and $(n_A + n_B)$ are the total number of moles of A and B in the A + B mixture.

The radius of the dilatometer capillary was measured from the weight, w, of an average length, l, of mercury column in it (the length of the mercury column of density ρ at the room temperature at various positions in the capillary was measured by a travelling microscope that could read to ±0.001 cm) utilizing the relation $r^2 = w/\pi\rho l$.

Our measured V^E values are subjected to uncertainties in w, ρ, l, Δh, and $n_A + n_B$. The uncertainty in the measured V^E values is ca. 0.5%. The performance of the dilatometer was checked by determining V^E values at 298.15 K for benzene + cyclohexane mixtures and these agreed well within the experimental uncertainties with the values reported elsewhere (28).

Molar excess enthalpies, H^E, for the various mixtures were measured at 308.15 K in a flow microcalorimeter (LKB, Broma, Sweden) in the manner described by Monk and Wadso (29). According to the specification of the instrument, the temperature can be set with a precision of 0.1 K and its stability is 0.02 K/24 h. Two identical Braun Perfusor Pumps (B. Braun, Melsungen AG. W. Germany) and gas-tight Hamilton syringes were employed to pump liquids through the calorimeter. By using 10 and 20 cm^3 syringes and 10 speed gear boxes of the perfusor pumps different mixing ratios were achieved. The flow rates were determined by pumping distilled water through the calorimeter and weighing the amount collected in a specific time interval. For each typical H^E measurement, different calibration constants were determined according to the flow rates, amplification needed, and the composition of the mixture. Molar excess enthalpies were then evaluated from the relation.

$$H^E(T,x_A) = C^2R\left(\frac{\Delta h_1}{\Delta h_2}\right)\Big/(n_A + n_B)$$

where C is the current in amperes, R is the resistance (in ohms) of the calorimeter heater, $\Delta h_1/\Delta h_2$ is the factor used to determine the amount of heat during compensation, Δh_1, and Δh_2 have the same significance as described by Adcock and McGlashan (30). The performance of the calorimeter was checked by measuring the H^E values (31) for benzene + carbon tetrachloride mixtures at 298.15 K and these agreed to within the experimental limits with the corresponding literature values (32). The uncertainty in the measured H^E values is ca. 1%.

Results

The measured V^E and H^E data at 308.15 K (recorded in Tables 2 and 3) for the various binary mixtures were fitted to eq. [1]

$$[1]\quad X^E(X = V \text{ or } H) = x_A x_B \sum_n X^{(n)}(2x_A - 1)^n$$

where $X^{(n)}$ (n = 0–2 or 3) are adjustable parameters and x_A is the mole fraction of A in the A + B mixture. These parameters were evaluated by fitting X^E/x_Ax_B to eq. [1] by the least-squares method and are recorded together with the standard deviation of X^E, $\sigma(X^E)$, in Table 4. The choice of n to have 0–2 values was dictated by the consideration that the maximum deviation $\sigma_m(X^E)$ of X^E (as calculated from [1] from the corresponding experimental X^E values) satisfied the relation $\sigma_m(X^E) \leq 2\sigma(X^E)$.

Discussion

We are unaware of any V^E or H^E data at 308.15 K of the present A + B mixtures with which to compare our results.

V^E for pyridine (A) + FD or NND (B) mixtures are negative and while the V^E data for A + FD mixtures exhibit a maxima ($V^E_{max} = -0.2$ cm^3 mol^{-1}) at $x_A = 0.55$, V^E data for A + NND mixtures are highly unsymmetrical about x_A, and exhibit a maxima (V^E_{max} = 0.04 cm^3 mol^{-1} at x_A = 0.7). Further although V^E values for both pyridine + aniline or OT (B) mixtures are negative, yet while the V^E data for pyridine (A) + aniline (B) exhibit a maximum ($V^E_{max} = -0.42$ cm^3 mol^{-1}) at $x_A = 0.6$, the V^E values for pyridine (A) + OT (B) mixtures are unsymmetrical about x_A and exhibit a maxima (V^E_{max} = -0.440 cm^3 mol^{-1}) at $x_A = 0.58$. On the other hand, the H^E data for pyridine (A) + aniline, OT, FD, or NND (B) mixtures are negative and for equimolar mixtures, vary as FD > NND > aniline > OT.

As the addition of A influences the topology of B in the present A + B mixtures, their V^E data should be expressible (32) by [2]

$$[2]\quad V^E = \alpha_{AB}\left[\frac{1}{\sum_{i=A,B} x_i({}^3\xi_i)_m} - \sum \frac{x_i}{{}^3\xi_i}\right]$$

Can. J. Chem. Downloaded from www.nrcresearchpress.com by 186.148.149.217 on 09/07/12
For personal use only.

TABLE 2. Measured V^E values at 308.15 K for the various A + B mixtures as functions of the mole fraction x_A of component A

x_A	V^E / $cm^3\ mol^{-1}$	x_A	V^E / $cm^3\ mol^{-1}$
Pyridine (A) + aniline (B)			
0.0548	−0.056	0.6217	−0.422
0.1162	−0.118	0.6940	−0.400
0.2426	−0.236	0.7243	−0.388
0.2648	−0.258	0.8004	−0.330
0.3312	−0.309	0.8465	−0.280
0.4451	−0.380	0.9217	−0.164
0.5591	−0.419	0.9591	−0.090
Pyridine (A) + *o*-toluidine (B)			
0.0816	−0.099	0.6084	−0.433
0.1160	−0.140	0.6543	−0.421
0.1600	−0.188	0.7189	−0.389
0.2269	−0.257	0.7644	−0.353
0.2726	−0.300	0.8125	−0.305
0.3581	−0.363	0.8461	−0.262
0.4232	−0.399	0.9328	−0.130
0.5202	−0.436		
Pyridine (A) + formamide (B)			
0.0701	−0.037	0.5756	−0.198
0.1125	−0.058	0.6019	−0.197
0.1951	−0.098	0.6511	−0.190
0.2541	−0.126	0.7119	−0.178
0.3212	−0.151	0.7315	−0.169
0.3644	−0.167	0.8145	−0.134
0.4019	−0.179	0.8564	−0.110
0.4356	−0.185	0.9021	−0.079
0.5224	−0.199		
Pyridine (A) + *N*,*N*-dimethylformamide (B)			
0.0851	−0.008	0.5561	−0.038
0.1234	−0.009	0.6019	−0.037
0.1298	−0.011	0.7012	−0.035
0.2341	−0.018	0.7892	−0.030
0.2764	−0.021	0.8119	−0.028
0.3245	−0.026	0.8789	−0.021
0.3781	−0.029	0.9212	−0.013
0.4224	−0.032	0.9687	−0.007
0.4981	−0.034		

TABLE 3. Measured H^E values at 308.15 K for the various A + B mixtures as functions of x_A, the mole fraction of component A

x_A	H^E / $J\ mol^{-1}$	x_A	H^E / $J\ mol^{-1}$
Pyridine (A) + aniline (B)			
0.0815	−442	0.4969	−1652
0.1544	−778	0.6113	−1634
0.1647	−823	0.6428	−1600
0.2345	−1099	0.6870	−1528
0.2887	−1266	0.7310	−1421
0.3097	−1325	0.8445	−998
0.3495	−1426	0.9012	−694
Pyridine (A) + *o*-toluidine (B)			
0.0913	−538	0.5561	−1971
0.1714	−954	0.6318	−1918
0.1826	−1008	0.7131	−1742
0.3149	−1550	0.7548	−1604
0.3370	−1623	0.7823	−1488
0.3784	−1739	0.8602	−1087
0.4267	−1849	0.8715	−1014
0.5281	−1965		
Pyridine (A) + formamide (B)			
0.1214	−282	0.6413	−738.9
0.1561	−352	0.6991	−690.3
0.2245	−478	0.7342	−648.6
0.2891	−576	0.7886	−563.4
0.3234	−622	0.8421	−460.0
0.3789	−684	0.8691	−398.2
0.4122	−714	0.9481	−177.6
0.4694	−746	0.9878	−42.8
0.5118	−763		
Pyridine (A) + *N*,*N*-dimethylformamide (B)			
0.0785	−35.3	0.5289	−123.6
0.1091	−44.8	0.5981	−121.2
0.1543	−63.2	0.6432	−151.1
0.2019	−77.8	0.6781	−109.5
0.2785	−99.0	0.7222	−103.0
0.3124	−105.4	0.7999	−80.1
0.3689	−114.5	0.8243	−74.0
0.4215	−121.4	0.9001	−46.1
0.4910	−125.0	0.9456	−25.2

where $({}^3\xi_i)_m$ and ${}^3\xi_i$ denote respectively the connectivity parameters of the third degree of i (defined (18) by [3])

$$[3]\quad {}^3\xi_i = \sum_{m<n<o<p} (\delta_m^v \delta_n^v \delta_o^v \delta_p^v)^{-0.5}$$

in the mixture and in the pure state, x_A is the mole fraction of A, α_{AB} is a characteristic constant, and all other terms have their usual significance (33, 34). For this purpose we regarded $({}^3\xi_i)_m$ and $({}^3\xi_i)$ (i = A, B) as adjustable parameters (due to the complex nature of A and B in the present A + B mixtures), evaluated them by fitting the V^E data and V_I^E data (read at round mole fractions from V^E vs. x_A plot) to [2] by trial and error method and retained only those ${}^3\xi$ values for which the variance of fit, ρ (defined (11) by $|\Sigma(V^E(\text{calcd}) - V_I^E)^2/(Q - P)|$ was minimum. Such ${}^3\xi$ values (along with the range in their values to reproduce the V_I^E data points to $\pm 0.001\ cm^3\ mol^{-1}$) recorded in Table 4, when used to investigate the molecular state of B and A through [3] as explained elsewhere (11, 19), suggest that while FD exists mainly as cyclic dimer (${}^3\xi$ = 0.855) and open chain trimer (${}^3\xi'$ = 0.856), NND exists as open chain dimer (${}^3\xi'$ = 0.974) or dipolar dimer (${}^3\xi'$ = 0.794) or as an equilibrium mixture of open chain or dipolar dimer with the monomer (${}^3\xi$ = 0.210). Similarly while aniline (B_n) exists as an equilibrium mixture of B(${}^3\xi'$ = 1.37) and B_2(${}^3\xi'$ = 0.75), OT(B_n) exists as B(${}^3\xi'$ = 0.974), and pyridine A exists as A_2 (through weak N....π interaction) (10, 11) (${}^3\xi'$ = 0.706). This is consistent with the available information (1, 6–11) about them. Further, if changes in the topology of B and A is due probably to the formation of AB_n etc. species, then the $({}^3\xi)_m$ values (Table 4) for B in the present A + B mixtures answers specifically to the presence of the following species in these mixtures.

Can. J. Chem. Downloaded from www.nrcresearchpress.com by 186.148.149.217 on 09/07/12
For personal use only.

TABLE 4. Comparison of V^E (V) and H^E (H) values (calculated from the appropriate equations (see text)) with their corresponding experimental values at 308.15 K for the various A + B mixtures as functions of x_A, mole fraction of A; also included are the various interaction energies χ, χ' etc., and the parameters X^n ($X = V$ or H, $n = 0$–2) of eq. [1] together with the standard deviation $\sigma(X^E)$

Property	Value for x_A = 0.1	0.2	0.3	0.7	0.8	0.9
Pyridine (A) + aniline (B)						
V(calcd.)	−0.117	−0.217	−0.300	−0.407	−0.365	−0.288
V(exptl.)[a]	−0.099	−0.192	−0.280	−0.400	−0.335	−0.210
H(calcd.)	−464.2	−953.6	−1305.6	−1488.6	−1161.2	−668.4
H(exptl.)[b]	−460	−950	−1300	−1500	−1150	−700
$V^{(0)} = -1.61$, $V^{(1)} = -0.680$, $V^{(2)} = -0.1126$, $\sigma(V^E) = 0.002$ cm^3 mol^{-1}, $\alpha_{AB} = 8.3563$ cm^3 mol^{-1}						
$H^{(0)} = -6600.0$, $H^{(1)} = -1191.1$, $H^{(2)} = -415.3$, $\sigma(H^E) = 1.9$ J mol^{-1}; $({}^3\xi_A)_m = 0.70 \pm 0.1$, ${}^3\xi_A = 0.69 \pm 0.1$						
$({}^3\xi_B)_m = 1.0 \pm 0.1$, ${}^3\xi_B = 1.0 \pm 0.1$; $\chi = -5616.0$ J mol^{-1}, $\chi' = -2686.3$ J mol^{-1}						
Pyridine (A) + *o*-toluidine (B)						
V(calcd.)	−0.114	−0.213	−0.293	−0.365	−0.296	−0.178
V(exptl.)[a]	−0.115	−0.220	−0.319	−0.400	−0.210	−0.190
H(calcd.)	−582.0	−1103.2	−1526.9	−1765.0	−1379.5	−793.3
H(exptl.)[b]	−600	−1150	−1500	−1760	−1390	−800
$V^{(0)} = -1.72$, $V^{(1)} = -0.460$, $V^{(2)} = 0.035$, $\sigma(V^E) = 0.002$ cm^3 mol^{-1}; $\alpha_{AB} = 5.928$ cm^3 mol^{-1}						
$H^{(0)} = -7800$, $H^{(1)} = -1666.65$, $H^{(2)} = -59.53$, $\sigma(H^E) = 1.7$ J mol^{-1}; $({}^3\xi_A)_m = 0.8 \pm 0.02$, ${}^3\xi_A = 0.8 \pm 0.02$						
$({}^3\xi_B)_m = 1.4 \pm 0.02$, ${}^3\xi_B = 1.4 \pm 0.02$; $\chi = -9773.0$ J mol^{-1}, $\chi' = -2988.3$ J mol^{-1}						
Pyridine (A) + formamide (B)						
V(calcd.)	−0.075	−0.131	−0.169	−0.160	−0.121	−0.067
V(exptl.)[a]	−0.065	−0.105	−0.145	−0.182	−0.140	−0.080
H(calcd.)	−252.3	−466.2	−635.0	−733.7	−580.3	−333.7
H(exptl.)[b]	−250	−480	−605	−700	−580	−330
$V^{(0)} = -0.784$, $V^{(1)} = -0.2082$, $V^{(2)} = 0.0636$, $\sigma(V^E) = 0.001$ cm^3 mol^{-1}, $\alpha_{AB} = 32.928$ cm^3 mol^{-1}						
$H^{(0)} = -3040.0$, $H^{(1)} = -571.38$, $H^{(2)} = -583.44$, $\sigma(H^E) = 1.11$ J mol^{-1}; $({}^3\xi_A)_m = 0.8 \pm 0.1$, ${}^3\xi_A = 0.8 \pm 0.1$						
$({}^3\xi_B)_m = 0.8 \pm 0.1$, ${}^3\xi_B = 0.7 \pm 0.1$; $\chi = -700.0$ J mol^{-1}, $\chi^{(a)} = -2000.0$ J mol^{-1}						
Pyridine (A) + *N*,*N*-dimethylformamide (B)						
V(calcd.)	−0.009	−0.017	−0.024	−0.043	−0.046	−0.029
V(exptl.)[a]	−0.001	−0.017	−0.025	−0.038	−0.032	−0.020
H(calcd.)	−41.4	−75.7	−101.7	−112.8	−88.2	−50.9
H(exptl.)[b]	−35	−65	−100	−120	−80	−42
$V^{(0)} = -0.140$, $V^{(1)} = -0.0675$, $V^{(2)} = 0.000$, $\sigma(V^E) = 0.001$ cm^3 mol^{-1}, $\alpha_{AB} = 0.5292$ cm^3 mol^{-1}						
$H^{(0)} = -500.0$, $H^{(1)} = -119.0$, $H^{(2)} = -148.75$, $\sigma(H^E) = 0.9$ J mol^{-1}, $({}^3\xi_A)_m = 0.75 \pm 0.1$, ${}^3\xi_A = 0.7 \pm 0.1$						
$({}^3\xi_B)_m = 0.6 \pm 0.1$, ${}^3\xi_B = 0.6 \pm 0.1$; $\chi = -49.0$ J mol^{-1}, $\chi^{(a)} = -400.0$ J mol^{-1}						

V^n ($n = 0$–2) are in cm^3 mol^{-1}
H^n ($n = 0$–2) are in J mol^{-1}

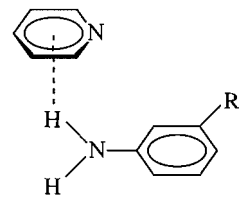

R = H, $({}^3\xi_B)_m = 1.035$ (**I**)
R = CH_3, $({}^3\xi'_B)_m = 1.355$ (**II**)

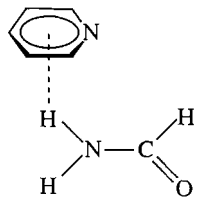

$({}^3\xi'_B)_m = 0.853$ (**III**)

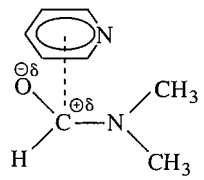

$({}^3\xi'_B)_m = 0.726$ (**IV**)

In evaluating these $({}^3\xi'_B)_m$ values we have considered contributions from the π-cloud of A and valencies of all (*i*) the vertices of aniline for **I** and **II**, (*ii*) but the one hydrogen atom of the NH_2 group of FD for **III**, and (*iii*) but the aldehyde proton of NND for **IV**. This would then require that in the appropriate A + B mixture, in addition to the ring vibrations in A, the C—N, —NH_2 vibrations of aniline, =C=O, —C—N, and N—H bending vibrations of FD, and =C=O, C—N, and N—(CH_3), vibrations of NND should have been influenced. The infrared spectral data of pure A, B, and the 1:1 (V/V) appropriate A + B mixture do in fact support this.

Again if the A + B mixture formation involves (*a*) the establishment of A.....B contacts (with molar interaction energy X_{AB}) that cause (*b*) (*i*) rupture of self-association in B (molar interaction energy X_{BB}) to yield monomer and (*ii*) changes of intramolecular interactions in A (molar interaction energy X_{AA}) to yield free A entities, and (*c*) interaction of

Can. J. Chem. Downloaded from www.nrcresearchpress.com by 186.148.149.217 on 09/07/12
For personal use only.

monomers of B with free "A" to yield AB species (molar interaction energy X_{12}), then the enthalpy changes due to (*a*), *b*(*i*), *b*(*ii*), and *c* would be given (10, 11) by

$$\Delta H_1 = x_A X_{AB} V_B / P$$

$$\Delta H_2 = K(x_A)^2 x_B X_{BB} V_B / P$$

$$\Delta H_3 = K(x_A)^2 x_B X_{AA} V_B / P$$

and

$$\Delta H_4 = K' x_A (x_B)^2 X_{12} V_B / P$$

where $P = \sum_{i=A,B} (x_i V_i)$ and V_i is the molar volume of i. The net enthalpy change, H^E, would then be given (10, 11) by [4]

$$[4] \quad H^E = \sum_{j=1}^{4} \Delta H_j = \frac{x_A x_B Y}{x_A + x_B Y}(X_{AB} + K x_A X_{BB} + K x_A X_{AA} + K' x_B X_{12})$$

where $Y = ({}^3\xi_A / {}^3\xi_B)$. For pyridine (A) + aniline/OT (B) mixtures it would be reasonable to assume that $X_{AA} \ll X_{AB}$, X_{BB}, or X_{12}, and if $X_{AB} = KX_{AA} = K'X_{12} = X$ and $KX_{BB} = X'$, then [4] reduces to [5]

$$[5] \quad H^E(T, x_A) = \frac{x_A x_B Y}{x_A + x_B Y}|2X + x_A X'|$$

However, for pyridine (A) + FD/NND (B), it would be more reasonable to assume that $X_{AB} = KX_{AA} = X^*$ and $X_{BB} = K'X_{12} = X^{(a)}$ so that in this case [4] yields [6]

$$[6] \quad H^E(T, x_A) = \frac{x_A x_B Y}{x_A + x_B Y}[(1 + x_A)X^* + X^{(a)}]$$

The parameters X and X' etc. of [5] and [6] were evaluated from the H^E (T, $x_A = 0.4$ and 0.5) data (read from H^E vs. x_A plot) of the appropriate A + B mixture and were re-employed to calculate the H^E data for the same mixture at other rounded-off mole fractions. Such the H^E data (recorded in Table 4) evidently compare well with the corresponding values read from H^E vs. x_A plot). Again for pyridine + aniline/OT mixtures, the X values in Table 4 suggest that compared to aniline, OT should not only boil at higher temperature (which is true), it should also interact strongly (as expected) with pyridine. However, no such conclusions could be deduced for FD and NND in their mixtures with pyridine. This is understandable as $H^E = H^E(\text{chem}) + H^E(\text{phys})$ and $H^E(\text{chem}) > H^E(\text{phys})$ only if H^E is large and negative. This is more true of pyridine aniline/OT mixtures than of pyridine + FD/NND mixtures.

The present study, therefore, reveals that volumetric and enthalpic effects in binary mixtures of non-electrolytes can be rationalized by graph–theoretical arguments to yield meaningful insight into the states of the components and the energetics of the formation of binary solution from the pure components.

Acknowledgements

Authors express their thanks to the Head of the Chemistry Department, and the authorities of Maharshi Dayanand University, Rohtak, for providing the necessary research facilities. Authors also greatly appreciate the help from Mr. Satyamanyu Yadav with the experimental work.

1. L. PAULING. The nature of chemical bond. 3rd ed. Cornell University Press. 1960. p. 281.
2. F. FRANKS and D. J. G. IVES. Q. Rev. Chem. Soc. **20**, 1 (1966).
3. E. M. WOOLLEY, J. G. TRAVERS, B. P. ERNO, and L. G. HEPLER. J. Phys. Chem. **25**, 3591 (1971).
4. K. B. WHETSEL and J. H. LADY. Spectroscopy of fuels. Plenum, New York. 1970. pp. 259–279.
5. J. R. JOHNSON, S. D. CHRISTIAN, and H. E. AFFSPRUNG. J. Chem. Soc. 764 (1967).
6. M. DAVIES. *In* Hydrogen bonding. *Edited by* D. Hadzi and H. W. Thompson. Pergamon, New York. 1956. p. 271.
7. L. J. BELLAMY and R. L. WILLIAMS. Spectrochim. Acta, **9**, 341 (1957).
8. H. WOLFF and D. MATHIAS. J. Phys. Chem. **77**, 2081 (1973).
9. A. KREGLEWSKI and R. C. WILHOIT. J. Phys. Chem. **7**, 144 (1975).
10. J. E. DELBENE. J. Am. Chem. Soc. **101**, 6184 (1978).
11. P. P. SINGH. J. Chem. Soc. Faraday Trans. I, **84**, 1807 (1988).
12. A. GRAOVAC, I. GUTMAN, and N. TRINJSTIC. *In* Topological approach to the chemistry of conjugated molecules. Lecture notes in chemistry, No. 4. Springer Verlag, Berlin. 1977.
13. D. H. RAUVRAY. RIC Rev. **4**, 173 (1971).
14. A. CAYLEY. Phil. Mag. **67**, 444 (1974).
15. M. RANDIC. J. Am. Chem. Soc. **97**, 660 (1975).
16. M. GORDON and J. W. KENNEDY. J. Chem. Soc. Faraday Trans. II, **69**, 484 (1973).
17. A. T. BALABAN (*Editor*). Chemical applications of graph theory. Academic Press, London. 1976.
18. L. B. KIER and L. H. HALL. *In* Molecular connectivity in chemistry and drug research. Academic Press, New York. 1976.
19. P. P. SINGH, V. K. SHARMA, and S. P. SHARMA. Thermochim. Acta, **106**, 293 (1986).
20. A. HANTZSCH and H. FREESE. Ber. Deut. Chem. Gesell. **27**, 2529 (1984); **27**, 2966 (1984).
21. J. F. T. BERLINER and O. E. MAY. J. Am. Chem. Soc. **49**, 1007 (1927).
22. A. VOGEL. Practical organic chemistry. 4th ed. English Language Book Society, London. 1978. (*a*) p. 276, (*b*) p. 277, (*c*) p. 659.
23. P. WALDEN. Z. Phys. Chem. Leipzig, **65**, 129 (1909).
24. E. C. BINGHAM, H. VAN KLOOSTER, and W. G. KLEINSPEHN. J. Phys. Chem. **24**, 1 (1920).
25. J. C. SMITH. J. Chem. Soc. 802 (1931).
26. T. J. V. FINDLEY, J. S. KENIERY, A. D. KIDMAN, and V. A. PICKLES. Trans. Faraday Soc. **63**, 846 (1967).
27. P. P. SINGH and S. P. SHARMA. J. Chem. Eng. Data, **30**, 477 (1985).
28. G. SCATCHARD and L. B. TICKNOR. J. Am. Chem. Soc. **74**, 3722 (1952).
29. P. MONK and I. WADSO. Acta Chem. Scand. **22**, 1842 (1968).
30. D. S. ADCOCK and M. L. MCGLASHAN. Proc. R. Soc. A**226**, 226 (1954).
31. H. P. DAHIYA, P. P. SINGH, and S. DAGAR. Fluid Phase Equilibr. **33**, 191 (1987).
32. R. H. STOKES, K. N. MARSH, and R. P. TOMLINS. J. Chem. Thermodyn. **1**, 211 (1969).
33. P. P. SINGH. Thermochim. Acta, **66**, 37 (1983).
34. L. B. KIER. *In* Physical chemical properties of drugs. *Edited by* S. H. Yalkowski, A. A. Sinkula, and S. C. Valvani. Marcel Dekker, New York. 1980. Chap. 9, (*a*) p. 295, (*b*) p. 297.

Iodimetric determinations in organic solvents: Determination of manganese oxidation states in methylene chloride solutions

JOAQUIN F. PEREZ-BENITO, ENRIQUE BRILLAS, AND CONCHITA ARIAS
Departamento de Quimica Fisica, Facultad de Quimica, Universidad de Barcelona, Marti i Franques, 1, 08028-Barcelona, Spain

Received March 16, 1989

JOAQUIN F. PEREZ-BENITO, ENRIQUE BRILLAS, and CONCHITA ARIAS. Can. J. Chem. **68**, 79 (1990).

An iodimetric technique has been developed to quantitatively analyze the oxidants present in organic solutions. Addition of excess tetrabutylammonium iodide and excess glacial acetic acid results in the formation of tetrabutylammonium triiodide, whose concentration can be measured spectrophotometrically at 295 or 365 nm. Application of this technique to the determination of the final oxidation state of manganese in permanganate reactions in methylene chloride solutions is described. The equilibrium constant for formation of tetrabutylammonium triiodide in methylene chloride has been measured: $K = (3.48 \pm 0.12) \times 10^4$ at 25.0°C.

Key words: iodimetric determinations, manganese oxidation states, methylene chloride, quaternary ammonium permanganate, quaternary ammonium triiodide.

JOAQUIN F. PEREZ-BENITO, ENRIQUE BRILLAS et CONCHITA ARIAS. Can. J. Chem. **68**, 79 (1990).

On a mis au point une technique iodométrique permettant d'analyser d'une façon quantitative les produits oxydants qui sont présents dans des solutions organiques. L'addition d'un excès d'iodure de tétrabutylammonium et d'un excès d'acide acétique glacial provoque la formation de triiodure de tétrabutylammonium dont la concentration peut être déterminée d'une façon spectrophotométrique à 295 ou à 365 nm. On décrit l'application de cette technique à la détermination de l'état final d'oxydation du manganèse dans des réactions du permanganate dans des solutions de chlorure de méthylène. A 25°C, on a déterminé que la constante d'équilibre pour la formation du triiodure de tétrabutylammonium dans le chlorure de méthylène est $K = (3,48 \pm 0,12) \times 10^4$.

Mots clés : déterminations iodométriques; états d'oxydation du manganèse; chlorure de méthylène; permanganate d'un sel d'ammonium quaternaire; triiodure d'un sel d'ammonium quaternaire.

[Traduit par la revue]

Can. J. Chem. Downloaded from www.nrcresearchpress.com by 186.148.149.217 on 09/07/12
For personal use only.

Introduction

Potassium permanganate is one of the most useful oxidants in the laboratory. However, its insolubility in most organic solvents prevents this substance from being more widely used in organic synthesis. Different ways of solubilizing $KMnO_4$ in low-polarity organic solvents have been reported. Among them, the use of phase-transfer agents (1) is notable: in particular, crown ethers (2) and quaternary ammonium or phosphonium salts (3) have been used. Quaternary ammonium additives are appealing because of the possibility of preparing economical, relatively stable quaternary ammonium permanganates. Many studies of permanganate reactions in non-aqueous media concerning the identification of products (4–16) and a few concerning the kinetic and mechanistic aspects of those reactions (17–19) have been undertaken. Although the application of standard techniques allowed the identification of organic reaction products, a method to determine the oxidation state of product manganese has so far been lacking.

In this paper, we report a new iodimetric technique which allows the final oxidation state of manganese in methylene chloride solutions to be measured. The general applicability of this technique is demonstrated with several organic functional groups as reductants of permanganate.

Experimental

Reagents and instrumentation

Anhydrous methylene chloride was purified by double distillation over 4 Å molecule sieves in an all-glass apparatus. Methyltributylammonium permanganate ($QMnO_4$) was obtained by precipitation from a concentrated aqueous mixture of potassium permanganate and methyltributylammonium bromide. The precipitate was separated by filtration, washed with distilled water, and dried overnight under vacuum. Purple $QMnO_4$ degenerates into brown manganese dioxide at room temperature. However, when stored in the dark and at low temperature, its decomposition can be avoided for several months.

The compounds used to reduce permanganate in methylene chloride solutions were tributylamine, methyl cinnamate, 1-decyne, 1-tridecanol, perfluorocyclohexene, formic acid, and cinnamic acid. These commercial organic substances were purified when necessary by recrystallization from a methylene chloride solution (for solids) or by simple distillation (for liquids). The reagent grade substances for the iodimetric determinations, tetrabutylammonium iodide (Q'I) and glacial acetic acid, were used without further purification.

Absorbance measurements were made with a Hewlett-Packard 8450A and a Varian Cary 219 UV-vis spectrophotometers, both provided with a thermostated cuvette holder.

Procedure

Freshly made $QMnO_4$ was dissolved in 50 mL of a methylene chloride solution containing a reducing organic compound. The permanganate concentration was 3×10^{-4} mol dm^{-3} and the reductant was in five- to ten-fold excess of the oxidant. A 3 mL aliquot was extracted and transferred to a quartz cuvette (pathlength = 1 cm), and the disappearance of permanganate was monitored at its 526 nm peak ($\epsilon = 2.63 \times 10^3$ dm^3 mol^{-1} cm^{-1}). The remaining solution was kept in a thermostated bath whose temperature was the same as that of the thermostated cuvette holder in the spectrophotometer (25.0°C). When the spectrum indicated that all the permanganate had been reduced, a 5 mL aliquot was extracted from the solution kept in the thermostated bath and transferred to a 50 mL volumetric flask. Excess tetrabutylammonium iodide (0.02 g) and glacial acetic acid (5 mL) were added, followed by dilution with methylene chloride up to 50 mL. The solution was stirred and its absorbance was measured.

Some precautions have to be taken when using this iodimetric technique: (*1*) The solvent must be perfectly anhydrous to avoid precipitation of manganese dioxide during the reduction of permanganate; (*2*) a large excess of acetic acid (which acts as a catalyst) must be used to accelerate the iodimetric reaction; (*3*) the iodimetric absorbance measurement must be made as soon as the corresponding solution is

Printed in Canada / Imprimé au Canada

prepared because quaternary ammonium iodide in methylene chloride solutions tends to spontaneously liberate iodine in the presence of light.

Results and discussion

Iodimetric determinations

A red solution was expected to be obtained from the oxidation of Q'I, its spectrum being that of iodine in methylene chloride solutions (broad peak at 504 nm). However, a yellow solution was obtained instead, its spectrum showing two definite peaks at 295 and 365 nm. The same spectrum was recorded when excess quaternary ammonium iodide was added to a solution of iodine in methylene chloride, the colour changing from red to yellow. Moreover, the spectrum of the yellow species in methylene chloride very much resembled that of triiodide ion in water (peaks at 287 and 351 nm). Therefore, the product obtained from the iodimetric technique can be identified as $Q'I_3$, formed by addition of a molecule of Q'I to the iodine liberated by the oxidant contained in the methylene chloride solution.

Excess Q'I was added to several solutions of iodine in methylene chloride to prepare $Q'I_3$ solutions of different concentrations. Their respective absorbances at 295 and 365 nm were measured in the spectrophotometer. Fulfillment of the Beer's law at those wavelengths was excellent, the results being:

$$[1] \quad A(295) = (0.003 \pm 0.004) + (4.511 \pm 0.015) \times 10^4 [Q'I_3]$$

$$[2] \quad A(365) = (-0.005 \pm 0.003) + (2.577 \pm 0.013) \times 10^4 [Q'I_3]$$

The linear correlation coefficients in eqs. [1] and [2] are 0.99998 and 0.99995, respectively (six points per equation). Hence the concentration of $Q'I_3$ in a methylene chloride solution can be determined with accuracy by means of its absorbance at either of those two wavelengths.

The final oxidation state of manganese in the iodimetric experiments was obtained by reducing several methylene chloride solutions of $QMnO_4$ with excess Q'I in the presence of acetic acid. The results from different determinations indicated that the triiodide liberated and the permanganate consumed were in the following ratio:

$$[3] \quad [Q'I_3]/[QMnO_4] = 5/2\ (\pm 2\%)$$

which corresponds to the following stoichiometry:

$$[4] \quad 2QMnO_4 + 15Q'I + 16HAc \rightarrow 2MnAc_2 + 5Q'I_3 + 10Q'Ac + 2QAc + 8H_2O$$

Thus, the final oxidation state of the manganese atom in the iodimetries is II.

Therefore, if a solution containing manganese with an oxidation state equal to s (its value being between VII and II) is subjected to the iodimetric technique described above, the stoichiometric ratio expected for the reaction is:

$$[5] \quad [Q'I_3]/[Mn^s] = (s - 2)/2$$

It is clear that the value of s can be obtained by means of eq. [5]. However, more accurate values of the oxidation state can be determined if two identical aliquots of two solutions with the same concentration of oxidizing agent ($QMnO_4$ one of them, and Mn^s the other) are subjected to iodimetric titration. Then, s, can be obtained as:

$$[6] \quad s = 2 + 5\,[Q'I_3]_P/[Q'I_3]_R$$

where $[Q'I_3]_P$ and $[Q'I_3]_R$ are the concentrations of $Q'I_3$ liberated by the product (Mn^s) and the reactant ($QMnO_4$) solution, respectively. The higher reliability of eq. [6] (cf. eq. [5]) is based upon the fact that when eq. [6] is used the systematic errors made in the determination of $[Q'I_3]_P$ and $[Q'I_3]_R$ are partially compensated.

TABLE 1. Final oxidation states of manganese for the reduction of methyltributylammonium permanganate by several organic compounds in methylene chloride solutions[a]

Organic compound	Oxidation state
Tributylamine	4.04
Methyl cinnamate	4.01
1-Decyne	3.97
1-Tridecanol	3.97
Perfluorocyclohexene	3.25
Formic acid	3.25
Cinnamic acid	2.99

[a]The average standard deviation for each oxidation state was ±0.05.

The results obtained when this iodimetric technique was applied to the product solutions from the reduction of $QMnO_4$ by several organic compounds in methylene chloride are summarized in Table 1. These results were confirmed from the spectra of the corresponding solutions, since a broad band with the absorbance uniformly decreasing as the wavelength increases was recorded when the iodimetric technique showed that the oxidation state was ca. IV (tributylamine, methyl cinnamate, 1-decyne, and 1-tridecanol as reductants), that band being typical of colloidal MnO_2 (20–26), which may be stabilized in methylene chloride by adsorption of the substance used to reduce permanganate on the surface of its colloidal particles. However, when the iodimetric technique led to a value of ca. III (cinnamic acid as reductant) the spectra exhibited a peak at 470 nm typical of Mn (III) (27–29), the nature of the Mn(III) species being still unknown. On the other hand, the non-integral value s = 3.25 obtained when the reductants were perfluorocyclohexene and formic acid indicates the existence of either Mn(IV)–Mn(III) or Mn(IV)–Mn(II) mixtures.

Although the iodimetric technique described in this paper has been developed for the determination of manganese oxidation states in methylene chloride solutions, we believe that it might also be used to determine the presence of different kinds of oxidants in other low-polarity organic solvents.

Equilibrium constant

The equilibrium constant for the formation of $Q'I_3$ in methylene chloride has been determined. The method was tested first for the equilibrium corresponding to the formation of triiodide ion in water solutions. This reaction can be written as:

$$[7] \quad I_2 + I^- \rightleftharpoons I_3^-$$

Since I_2 is a non-charged species, its activity coefficient is near unity; since both I^- and I_3^- are monovalent ions, the ratio between their respective activity coefficients is (according to the Debye-Hückel theory) also near unity. Therefore, the equilibrium constant associated with eq. [7] can be approximately written as:

$$[8] \quad K = c_3/c_2c_1$$

where c_1, c_2, and c_3 are the molar concentrations of I^-, I_2, and

Can. J. Chem. Downloaded from www.nrcresearchpress.com by 186.148.149.217 on 09/07/12
For personal use only.

I_3^-, respectively (the subscript indicates the number of iodine atoms in the corresponding species). If I_3^- is formed from a mixture of I_2 and a great excess of I^-, then:

[9] $$K = c_3/(c_2^0 - c_3)\,c_1^0$$

where the concentration of iodine in the equilibrium mixture is given by the difference between the initial concentration of iodine (c_2^0) and the concentration of triiodide ion (c_3). The decrease in the concentration of iodide ion has been taken as negligible against its initial concentration (c_1^0): the condition $c_1^0 \gg c_2^0$ implies also that $c_1^0 \gg c_3$. From eq. [9] it can be inferred that

[10] $$c_1^0\,c_2^0/c_3 = 1/K + c_1^0$$

The following equation was obtained at 25.0°C for several solutions of iodine (ranging from 0.8 to 4.0×10^{-5} mol dm^{-3}) and potassium iodide (from 1.2 to 5.9×10^{-3} mol dm^{-3}) in water:

[11] $$c_1^0\,c_2^0/c_3 = (1.50 \pm 0.06) \times 10^{-3} + (0.985 \pm 0.014)\,c_1^0$$

The corresponding plot is linear (correlation coefficient = 0.9997, number of points = 5); furthermore, we can see that the slope is in good agreement with the value expected (unity, see eq. [10]). From the intercept, the equilibrium constant $K = (6.67 \pm 0.25) \times 10^2$ is obtained for the formation of triiodide ion in aqueous solutions at 25.0°C. This result agrees with the value reported in the literature (30).

The same procedure was repeated with several solutions of iodine (ranging from 0.2 to 1.1×10^{-5} mol dm^{-3}) and Q'I (from 0.5 to 2.6×10^{-4} mol dm^{-3}) in methylene chloride. The resulting equation is

[12] $$c_1^0\,c_2^0/c_3 = (2.87 \pm 0.10) \times 10^{-5} + (0.976 \pm 0.006)\,c_1^0$$

The corresponding plot was also linear (correlation coefficient = 0.99994, number of points = 5), and the slope was also near unity (see eq. [10]). From the intercept, the equilibrium constant for the formation of tetrabutylammonium triiodide in methylene chloride solutions is $K = (3.48 \pm 0.12) \times 10^4$ at 25.0°C. The availability of the latter equilibrium constant is important to the iodimetric technique described in this paper, since the spectrophotometric measurements require that the excess of Q'I with respect to I_2 be large enough to ensure that almost all the iodine liberated is present as $Q'I_3$. Since the ratio of equilibrium constants is $K(CH_2Cl_2)/K(H_2O) = 52$, the required excess of Q'I in methylene chloride solutions is lower than that of potassium iodide in aqueous media.

Acknowledgments

Thanks are given to Professor Donald G. Lee for helpful discussions, to the Department of Chemistry, University of Regina (Canada), for experimental facilities, and to the Spanish Ministry of Education and Science for financial assistance to J.F.P.B.

1. D. G. LEE. *In* Oxidation in organic chemistry. Part D. *Edited by* W. S. Trahanovsky. Academic Press, New York. 1982. p. 147.
2. F. FREEMAN. Rev. React. Species Chem. React. **1**, 179 (1976).
3. H. KARAMAN, R. J. BARTON, B. E. ROBERTSON, and D. G. LEE. J. Org. Chem. **49**, 4509 (1984).
4. A. W. HERRIOTT and D. PICKER. Tetrahedron Lett. 1511 (1974).
5. T. A. FOGLIA, P. A. BARR, and A. J. MALLEY. J. Am. Oil Chem. Soc. **54**, 858A (1977).
6. A. P. KRAPCHO, J. R. LARSON, and J. M. ELDRIDGE. J. Org. Chem. **42**, 3749 (1977).
7. T. OKIMOTO and D. SWERN. J. Am. Oil Chem. Soc. **54**, 867A (1977).
8. T. SALA and M. V. SARGENT. J. Chem. Soc., Chem. Commun. 253 (1978).
9. T. OGINO and K. MOCHIZUKI. Chem. Lett. 443 (1979).
10. H. J. SCHMIDT and H. J. SCHÄFER. Angew. Chem. Int. Ed. Engl. **20**, 104 (1981).
11. B. P. LEDDY, M. A. MCKERVEY, and P. MCSWEENEY. Tetrahedron Lett. **21**, 2261 (1980).
12. T. OGINO. Tetrahedron Lett. **21**, 177 (1980).
13. R. SANGAIAH and G. S. KRISHNA RAO. Synthesis, 1018 (1980).
14. K. C. BROWN, V. S. CHANG, F. H. DAR, S. E. LAMB, and D. G. LEE. J. Chem. Educ. **59**, 696 (1982).
15. D. G. LEE and N. S. SRINIVASAN. Sulfur. Lett. **1**, 1 (1982).
16. V. BHUSHAN, R. RATHORE, and S. CHANDRASEKARAN. Synthesis, 431 (1984).
17. D. G. LEE and K. C. BROWN. J. Am. Chem. Soc. **104**, 5076 (1982).
18. D. G. LEE and J. F. PEREZ-BENITO. Can. J. Chem. **63**, 1275 (1985).
19. D. G. LEE, K. C. BROWN, and H. KARAMAN. Can. J. Chem. **64**, 1054 (1986).
20. F. MATA and J. F. PEREZ-BENITO. Can. J. Chem. **63**, 988 (1985).
21. J. F. PEREZ-BENITO and D. G. LEE. Can. J. Chem. **63**, 3545 (1985).
22. F. FREEMAN and J. C. KAPPOS. J. Am. Chem. Soc. **107**, 6628 (1985).
23. F. MATA and J. F. PEREZ-BENITO. Z. Phys. Chem. (Leipzig), **267**, 120 (1986).
24. F. FREEMAN and L. Y. CHANG. J. Am. Chem. Soc. **108**, 4504 (1986).
25. F. FREEMAN and J. C. KAPPOS. J. Org. Chem. **51**, 1654 (1986).
26. F. FREEMAN, L. Y. CHANG, J. C. KAPPOS, and L. SUMARTA. J. Org. Chem. **52**, 1460 (1987).
27. C. F. WELLS and G. DAVIES. J. Chem. Soc. A 1858 (1967).
28. J. F. PEREZ-BENITO. Chem. Scr. **27**, 433 (1987).
29. J. F. PEREZ-BENITO and D. G. LEE. J. Org. Chem. **52**, 3239 (1987).
30. H. M. DAWSON and E. SPIVEY. J. Chem. Soc. 1838 (1932).

Can. J. Chem. Downloaded from www.nrcresearchpress.com by 186.148.149.217 on 09/07/12
For personal use only.

Characterization of lignin residues derived from the alkaline hydrolysis of glycol lignin

RONALD W. THRING, ESTEBAN CHORNET,[1] JEAN BOUCHARD, AND PIERRE F. VIDAL
Department of Chemical Engineering, University of Sherbrooke, Sherbrooke, Que., Canada J1K 2R1
AND
RALPH P. OVEREND
National Research Council of Canada, Ottawa, Ont., Canada K1A 0R6

Received April 12, 1989

RONALD W. THRING, ESTEBAN CHORNET, JEAN BOUCHARD, PIERRE F. VIDAL, and RALPH P. OVEREND. Can. J. Chem. **68**, 82 (1990).

Lignin residues from the alkaline hydrolysis of solvolytic lignin have been characterized by elemental analysis, size exclusion chromatography, Fourier transform infrared spectroscopy, ^{13}C NMR, and for methoxyl content. All lignin residues were found to have higher carbon and lower oxygen contents than the original glycol lignin. Methoxyl contents decreased with increasing severity of treatment. All treated lignins have lower molecular weights than the original, which is indicative of the extensive depolymerization of glycol lignin by alkaline hydrolysis. The appearance of new bands in the 3050–2800 cm^{-1} and 900–800 cm^{-1} regions in the infrared spectra along with increasing absorption intensity under more severe conditions demonstrates that, despite the tendency to depolymerization, new carbon–carbon bonds are formed due to repolymerization reactions. ^{13}C NMR revealed that extensive cleavage of the side chains and β-O-4 interunit linkages had occurred during alkaline hydrolysis and that the new bonds formed due to condensation reactions at higher severities are of the methine, methylene, methyl and carboxyl types.

Key words: residual lignins, alkaline hydrolysis, characterization.

RONALD W. THRING, ESTEBAN CHORNET, JEAN BOUCHARD, PIERRE F. VIDAL et RALPH P. OVEREND. Can. J. Chem. **68**, 82 (1990).

Des lignines solvolytiques obtenus par un traitement solvolytique avec l'éthylène glycol ont été dépolymérisées hydrolytiquement en milieu aqueux alcalin à haute temperature. Une partie de la lignine est solubilisée en forme des monomères et d'oligomères. La fraction non-solubilisée constitue la lignine résiduelle que nous avons caractérisée par analyse élémentaire, teneur en groupements méthoxy, chromatographie d'exclusion par la taille, spectroscopie infrarouge à transformée de Fourier, et spectroscopie de RMN ^{13}C. Les lignines résiduelles issues de la dépolymérisation à différents niveaux de sévérité ont une teneur en carbone plus élevée que la lignine solvolytique initiale. La teneur en groupements méthoxy diminue avec la sévérité du traitement. Toutes les lignines résiduelles ont des poids moléculaires infrérieurs à ceux de la lignine initiale : effet de la dépolymérisation hydrolytique. La présence de pics, dans le spectre infrarouge dans les régions 3050–2800 cm^{-1} et l'augmentation de leur intensité avec la sévérité du traitement, suggère que de nouveaux liens C—C dus à des recondensations sont formés. Des analyses RMN au ^{13}C ont montré que le clivage des chaines alkyles et des liens β-O-4 a eu lieu pendant l'hydrolyse en milieu alcalin. Aussi de nouveaux liens ont été crées par des réactions de condensation induites à haute sévérité. Ces nouveaux liens sont du type méthine, méthylène et méthyle ainsi que carboxyle.

Mots clés : lignines résiduelles, hydrolyse alcaline, caractérisation.

Can. J. Chem. Downloaded from www.nrcresearchpress.com by 91.144.44.67 on 09/07/12
For personal use only.

Introduction

A large number of publications have dealt with the depolymerization of lignin to obtain monomeric compounds, and have been comprehensively reviewed by Goheen (1), Goldstein (2), and more recently by Chum *et al.* (3).

One method commonly employed to separate the reaction products derived from lignin depolymerization into liquid and solid phases uses acid to precipitate the unreacted (unconverted) lignin as well as to convert the phenate salts in solution to phenols. These phenolic compounds are then isolated from the liquid phase by extraction with a selective solvent (4–6). Such "residual lignins" recovered from the established degradation techniques have not been extensively studied or characterized. Connors *et al.* (7), for example, hydrocracked kraft lignin in a hydrogen-donor solvent (tetralin). The unconverted lignin, isolated as an "acetone soluble" solid, was examined by GPC, IR, and NMR, and it was concluded that extensive side-chain cleavage had occurred, as well as a reduction in molecular weight.

Much of the interest in lignin degradation has been focussed upon the production of low molecular weight chemicals, especially monomeric compounds. The work conducted in this area by many workers has confirmed the production of numerous compounds whose individual yields have so far been too low to warrant commercialization.

The aim of the present work was to characterize the lignin remaining after depolymerizing glycol lignin in alkaline media at conditions of different severities. Such a study would possibly elucidate new uses of isolated glycol lignin, which has been found to be a potential source of phenolic compounds by Thring *et al.* (8). This paper then deals with a comparative characterization of these lignin residues under conditions of increasing reaction severity.

Experimental

Preparation of residual lignins

Glycol lignin was isolated from the hardwood *Populus deltoides* by the method described previously (8).

The alkaline hydrolysis was carried out in a 500-mL stainless steel autoclave equipped with a magnetic stirrer. The procedure adopted was to load the reactor with 5 g of dried (50°C in a forced-air oven for 14 h) lignin and 100 mL of a 2% (w/w) aqueous sodium hydroxide solution. The glycol lignin dissolved completely upon agitation in this medium. After pressure testing for leaks, the batch autoclave was flushed twice with nitogen. The stirrer was then set to 500 rpm and switched on.

To start a run, the reactor was immersed in a preheated salt bath whose initial temperature was at a value such that the reaction temperature of the mixture reached the desired value (±2°C) within 10 min. The reaction temperature – time history was continuously

[1]Author to whom correspondence may be addressed.

TABLE 1. Reaction conditions used for obtaining residual lignins

Expt. no.	Temp. (°C)	Time (h)	$\log_{10}R_0$
1 (RL-1)	180	1	3.6
2 (RL-2)	235	1	5.8
3 (RL-3)	300	1	7.7
4 (RL-4)	340	1	8.5

Heat-up rate, 30°C/min; cool down rate, 44°C/min. Rate of agitation, 500 rpm; substrate/solvent ratio, 5 g dry lignin/100 mL (2% wt. NaOH).

recorded for subsequent calculation of a reaction ordinate, to be defined later. These reaction conditions were as follows: temperatures of 180, 235, 300 and 340°C, for 1 hour (Table 1). Maximum reaction pressures did not exceed 3.8 MPa even for the most severe conditions (340°C, 1 h) employed.

To end the reaction, the reactor was quenched in a cold water bath. The stirrer and data acquisition system were stopped when the reactor temperature reached ambient. The reactor was depressurized, removed from its frame, opened, and its contents recovered.

The product slurry was filtered and the remaining residue rinsed with water. The residual lignin (RL) was precipitated from the filtrate by acidification to a pH of 1–2 with addition of a 10%(v/v) solution of aqueous HCl, filtered, and then dried in a vacuum desiccator for 2 days. The analysis carried out on the liquid phase and the results have been discussed (8).

Elemental analysis

The samples were analysed for C, H, and N using a Perkin–Elmer model 240 C elemental analyzer in our laboratories. Oxygen was determined by difference.

Methoxyl content

Determinations of methoxyl content were made according to the method initially proposed by Zeisel (9) and later modified by Haluk and Metche (10).

High performance size exclusion chromatography (HPSEC)

Analysis by HSPEC was performed with a Varian 5000 liquid chromatograph connected to an on-line computer (NEC APCIV) via a Waters Maxima 820 data system. Two stainless steel columns connected in series were used (length 30 cm; i.d. 7.5 mm) packed with PLgel spherical particles (Polymer Laboratories) of particle size 5–10 μm, and pore sizes 50 Å (column 1) and 500 Å (column 2). Detection was made with a UV monitor at 254 nm. A constant flow rate through the system was maintained by a single-piston reciprocating pump. The following operating conditions were utilized: eluent, tetrahydrofuran (continuously bubbled with N_2 to prevent the formation of peroxides); flow rate, 1 mL/min; pressure, 7.0 MPa; temperature, 20–25°C; injection volume, 10 μL; sample concentration, 1 mg/mL.

The calibration curve was obtained using monodisperse polystyrene compounds of known molecular weight as reference substances. A third-order polynomial of the form $y = ax^3 + bx^2 + cx + d$ best describes the relation between the log of the actual molecular weights of polystyrene standards (y) and their retention volumes (x). The following coefficients were calculated: $a = -0.00714$, $b = 0.3253$, $c = -5.149$, and $d = 30.69$. These gave a fit with a multiple regression coefficient of $r^2 = 0.998$.

Infrared spectra

Lignin samples were prepared in a KBr matrix at a concentration of 1–2% (w/w) by grinding in a stainless steel ball mill for 30 s at room temperature. Spectra were obtained from a 5DXB Nicolet FTIR spectrometer in diffuse reflectance mode using the collector cell (Spectra-Tech). Conditions of analysis were as follows: resolution 4 cm^{-1}; coadding 400 scans; frequency range of 400–4600 cm^{-1} (DTGS detector); Happ–Genzel apodization.

^{13}C NMR

^{13}C NMR spectra of the acetylated lignin samples were obtained with a Bruker 250 WM Fourier transform spectrometer. Deuterated dimethyl sulfoxide (DMSO-d_6) was used as solvent. Sample concentrations of ca. 800 mg in 2 mL of DMSO-d_6 were placed in 10 mm i.d. glass tubes and run at a temperature of 50°C. The instrument was set in proton inverse gated decoupled mode and the delay between scans was 2 s.

Acetylation of lignins

The criteria used for a successful acetylation method were the complete solubility in tetrahydrofuran and the absence of the OH absorption band in the IR spectrum of the acetylated product. An effective method for our samples consisted of adding 5 mL of pyridine to about 0.5 g of sample (dried at 60°C overnight *in vacuo*) with stirring. Acetic anhydride (5 mL) was then added, the mixture flask flushed with nitrogen and sealed, and stirring continued for 2 days at room temperature. The product was recovered by precipitation in an ice–water mixture, filtered, and dried at room temperature under vacuum overnight.

Results and discussion

The yields of lignin residue are shown in Fig. 1 as a function of severity of treatment R_0 whose significance and utility have been discussed elsewhere (11). The reaction ordinate, R_0, is defined as $R_0 = t \times \exp((T-100)/14.75)$; t = time (min), and T = temperature (°C). As seen, R_0 varies exponentially with temperature and linearly with time. In our case, R_0 was varied by increasing T, keeping t constant. A reduction in the yields with increasing severity may then be attributed primarily to the increasing importance of pyrolytic reactions. These reactions give rise to extensive C—C and C—O—C bond cleavage in the lignin and its primary decomposition fractions to produce volatile products and char.

Elemental composition of residual lignins

The results shown in Table 2 are average values from duplicate analyses of the samples. Using the original lignin as reference, a number of trends are observed.

The C content of all the residual lignins is higher than that of the original lignin and increases linearly with treatment severity when the latter is expressed as $\log_{10}R_0$, as shown in Fig. 2. The O content is observed to decrease with increasing severity. Chua and Wayman (12) observed a similar trend for autohydrolysis lignins of aspen (*Populus tremuloides*) at 195°C with increasing reaction time, and attributed these changes to (a) condensation reactions which involve the elimination of water, and (or) (b) incorporation into the lignin of entities derived from carbohydrates having higher C to H/O ratios formed during autohydrolysis, and (or) (c) the initial preferential removal of syringyl rather than guaiacyl units at the shorter hydrolysis times.

The higher heating values of the lignins, shown in Table 2, were determined using Dulong's formula (13). This formula is claimed to usually give heating values within 5% error. It is evident that the alkaline hydrolysis of glycol lignin with increasing severity of treatment produces residual lignins of higher heating values than the original lignin. It is noteworthy to point out that residual lignin RL-3 (C.V. = 28.5 MJ/kg) was obtained under the same reaction conditions that gave the highest amount (11%) of identifiable monomeric compounds, based on the original lignin, of which 9%, also based on the original lignin, were catechols (8). Thus, at these optimum reaction conditions, we not only obtain monomeric degradation products that can be used as chemical feedstocks, but also produce a residual lignin that can be utilized as a fuel source of higher heating value than the original glycol lignin.

Can. J. Chem. Downloaded from www.nrcresearchpress.com by 91.144.44.67 on 09/07/12
For personal use only.

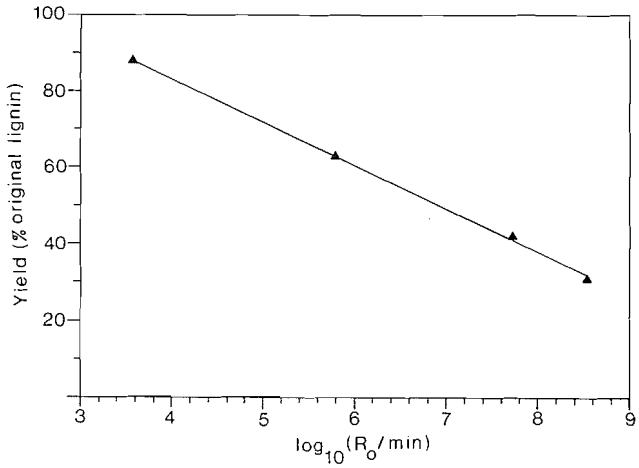

FIG. 1. Yields of residual lignins as a function of the severity of treatment, $R_0 = t \times \exp((T-100)/14.75)$, where t = time(min) and T = temperature(°C).

TABLE 2. Elemental composition, methoxyl content, and C.V. (calorific value) of glycol lignin and residual lignins

Sample no.	%C	%H	%O*	%OCH_3	$\log_{10}R_0$	C.V. (MJ/kg)
Lignin	61.8	6.0	31.9	20.3	—	23.8
RL-1	62.9	5.9	30.9	19.6	3.6	24.3
RL-2	67.8	5.9	26.0	16.3	5.8	26.7
RL-3	72.5	5.5	21.7	0.7	7.7	28.5
RL-4	74.4	5.6	19.8	0.4	8.5	29.6

*Calculated by difference.

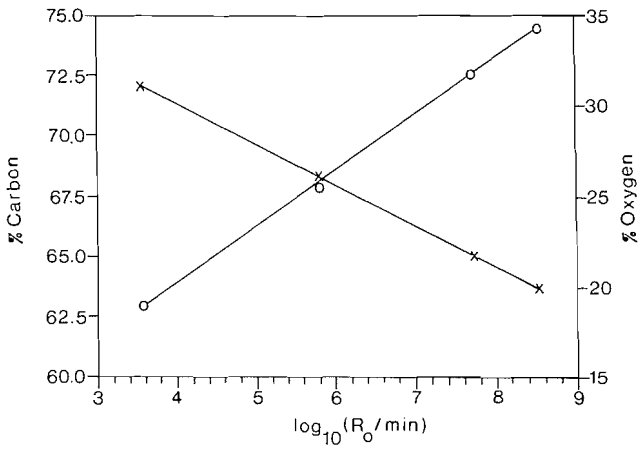

FIG. 2. Carbon (O) and oxygen (X) content of residual lignins versus severity of treatment.

Another trend is the steady decrease in the methoxyl content with increasing severity of reaction. This may be attributed to the increase in pyrolytic/hydrolytic reactions, giving rise to demethylation and demethoxylation of the lignin to produce gaseous and liquid products. Evidence of demethylation is found in the occurrence of catechol and its derivatives in the ether-soluble fraction containing low molecular weight products (8). These products occurred only under conditions of medium to high severity. The presence of methanol in the hydrolysate liquids, especially at higher R_0, provided direct evidence of demethoxylation of the lignin during alkaline

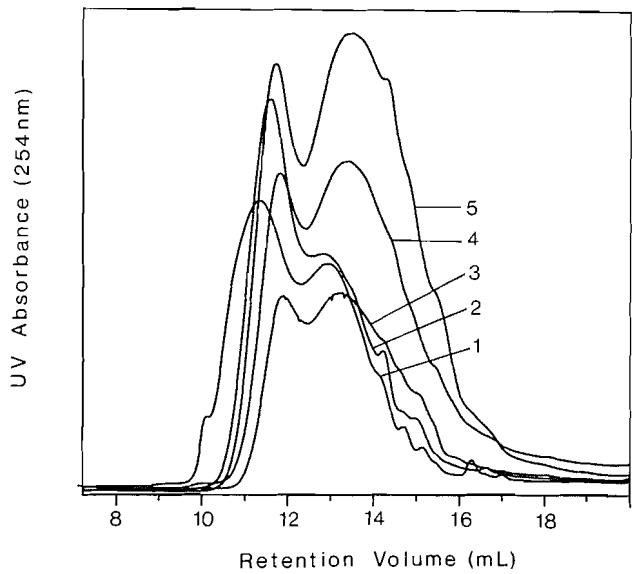

FIG. 3. Molecular weight distribution (polystyrene equivalents) of (1) glycol lignin, (2) RL-1, (3) RL-2, (4) RL-3, and (5) RL-4.

hydrolysis. Pepper and Siddiquellah (14), in their lignin acidolysis work, also encountered similar changes in the content of C, H, and O and a lowering in the methoxyl content with increasing time of acidolysis. Furthermore, it was previously seen (8) that the mass yields of syringol and guaiacol increased and then, under more severe reaction conditions, decreased. Since these contain most of the methoxyl groups in the lignin macromolecule, a variation in the proportion of these units would also account for the observed trend in methoxyl content in the residue.

High performance size exclusion chromatography (HPSEC)

In the last decade HPSEC, using polystyrene beads and organic solvents such as THF, has become a widely used method to study the molecular weight distribution (MWD) of isolated, modified lignin samples.

Although it is generally agreed that this technique allows the fractionation of a polydisperse polymer into fractions of difference molecular size, the quantification of each fraction into terms of molecules N_i (or weight fraction W_i) as well as the correlation between the elution volume and corresponding molecular weight M_i is still a matter of argument. The use of UV detection for lignins is very common. Since this detection method is governed at low substrate concentrations by the Beer–Lambert law, a usual assumption is that the molar extinction coefficients are proportional to the molecular weights, that is, the weight absorption coefficients are constant throughout the MWD. According to Lange *et al.* (15), non-homogeneity in such coefficients for organosolv lignins leads to an error of not more than 5% in the molecular weight determination by HPSEC. Moreover, when considering the method of calibration employed, the molecular weight values presented herein should be taken as polystyrene-standard equivalent molecular weights.

As shown in Fig. 3, a common and prominent feature of all the molecular weight distribution patterns is the occurrence of two absorption maxima. Table 3 presents the molecular weight values MW_{p1} and MW_{p2} at the two absorption maxima associated with the low and high MW fractions, their corresponding degree of depolymerization DP_1 and DP_2 calculated on the

Can. J. Chem. Downloaded from www.nrcresearchpress.com by 91.144.44.67 on 09/07/12
For personal use only.

TABLE 3. Peak molecular weight values MW_{p1} and MW_{p2}, corresponding degree of polymerization DP_1 and DP_2, and H_2/H_1 ratios of glycol lignin and residual lignins

Sample no.	MW_{p1}	DP_1	MW_{p2}	DP_2	H_2/H_1
Lignin	1200	6	5400	26	1.40
RL-1	1250	6	4000	20	1.60
RL-2	1000	5	3000	15	0.96
RL-3	900	4	3000	15	0.97
RL-4	900	4	3600	18	0.93

basis of a monomer having a molecular weight of 205 daltons, as well as the H_2/H_1 ratio, which represents the height of the high-MW maximum over the height of the low-MW maximum derived from Fig. 3. The most important effects of the severity of the alkaline treatment on the glycol lignin are (a) a slow decrease of MW_{p1}, (b) a rapid decrease of MW_{p2} for reaction conditions having $\log_{10}R_0$ values in the range 3.6–5.8, followed by an increase under more severe conditions, and (c) a variation of the ratio H_2/H_1 from an initial value of 1.4 to a value of 1.6 at $\log_{10}R_0 = 3.6$ and to a plateau value close to unity for conditions having $\log_{10}R_0$ values in the range of 5.8–8.5.

When interpreting the results derived from Fig. 3, it may be concluded that the variation of the H_2/H_1 ratio reflects the depolymerization of high molecular weight material (MW_{p2}), which transforms significantly into low molecular weight material (MW_{p1}) under the three most severe conditions, while

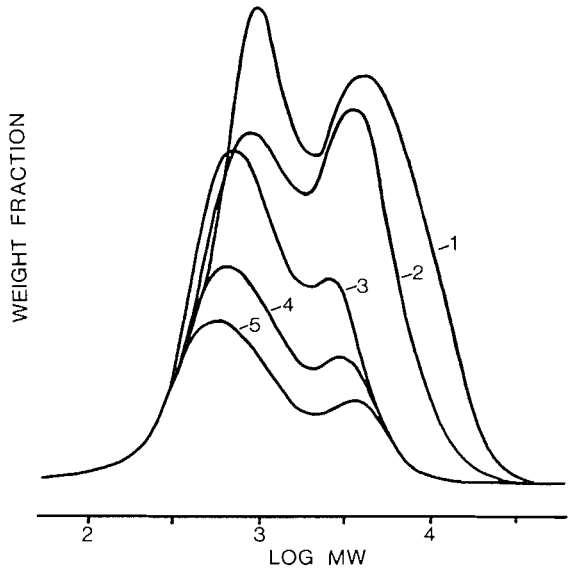

FIG. 4. Molecular weight distribution (polystyrene equivalents) by weight of (1) glycol lignin, (2) RL-1, (3) RL-2, (4) RL-3, and (5) RL-4.

at $\log_{10}R_0 = 3.6$, the depolymerization of the low molecular weight material is predominant over the depolymerization of MW_{p2} into MW_{p1}.

This interpretation does not take into account the fact that the analysed residual lignin samples represent only a fraction of the starting glycol lignin, which depolymerizes and solubilizes in basic media according to the following process scheme:

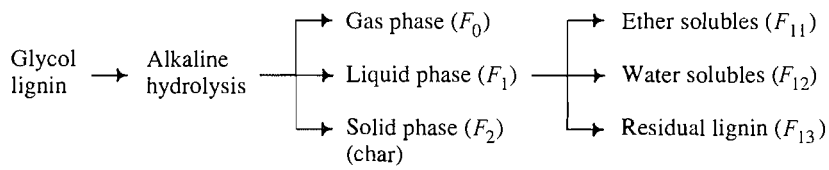

SCHEME 1

In Fig. 4 we have plotted the molecular weight distributions of each sample so that the area under the curve is proportional to the reaction yield of the given residual lignin (shown in Table 4). The trend with increasing severity is now clear: while the yield of the residual lignin (F_{13}) decreases along with its molecular weight (Fig. 4), there is also an increase of the yield of the char fraction (F_2) as shown in Table 4. This char must be a result of extensive cross-linking of the residual lignin. It is clear that at the severity corresponding to the RL-3 experiment recondensation reactions begin to be significant and at the highest severity (RL-4) they predominate over the depolymerization reactions.

The picture that emerges is then rather straightforward. In the alkaline hydrolysis of glycol lignin, depolymerization is the predominant mechanism at low severities with recondensation dominating with increasing severities. The optimum reaction conditions, defined as those at which the maximum yield of monomer fraction is obtained concomitant with a decrease in the MW of the lignin without char formation, should lie at $\log_{10}R_0$ values in the range of 5.8–7.7. At optimum, the yield of ether solubles (F_{11}) attains a value of about 25% of the mass of initial glycol lignin used and the residual lignin (RL) still has molecular properties similar to those of the initial material.

From the MWD patterns in Figs. 3 and 4 it is clear that a bimodal MW distribution is present in glycol lignin, which is composed principally of a low molecular weight subunit (DP = 5–6) and a high molecular weight macrostructure (DP = 26). Wayman and Obiaga (16) proposed the concept of a "modular structure" of lignin and they provided experimental evidence by means of which a molecular weight of 5400 (DP = 26) was derived. This value coincides with our high molecular weight macrostructure. The presence of a low molecular weight subunit is consistent with the cleavage of specific bonds in the high molecular weight macrostructure. This cleavage is accomplished by the action of the OH^-ion in our experiments. Since the initial glycol lignin also shows a low molecular weight fraction, one must conclude that our ethylene glycol treatment either isolates a lignin fraction that has already been cleaved at specific linkages via an unknown mechanism in which the glycol must play a "solvolytic effect" or helps to disaggregate specific complexes that already have a low molecular weight material. The alkali treatment leads to the depolymerization of both the high and low molecular weight fractions. The preferred route is probably the cleavage of ether bonds (see below). At higher severities the loss of the alkyl groups (see also sections on FTIR and ^{13}C NMR) could explain why the DP of the low molecular

Can. J. Chem. Downloaded from www.nrcresearchpress.com by 91.144.44.67 on 09/07/12
For personal use only.

TABLE 4. Mass balances in the alkaline depolymerization of glycol lignin

Experiment no.	$\log_{10}R_0$	F_{11}	$(F_0 + F_{12})$*	F_{13}(RL)	F_2(char)
1 (RL-1)	3.6	4.25	7.26	87.90	0.59
2 (RL-2)	5.8	21.00	16.05	62.00	0.95
3 (RL-3)	7.7	24.90	25.89	42.00	7.21
4 (RL-4)	8.5	18.30	22.00	30.80	28.90

*Calculated by difference; F = product fractions (% of starting lignin).

weight unit is reduced to a value of 4. In fact, if the loss of alkyl groups is accounted for in the evaluation of the molecular weight of a monomer, then the DP would stay at 5–6 regardless of the treatment severity.

A mechanistic view of the alkaline depolymerization of glycol lignin consistent with our results can thus be presented as follows:

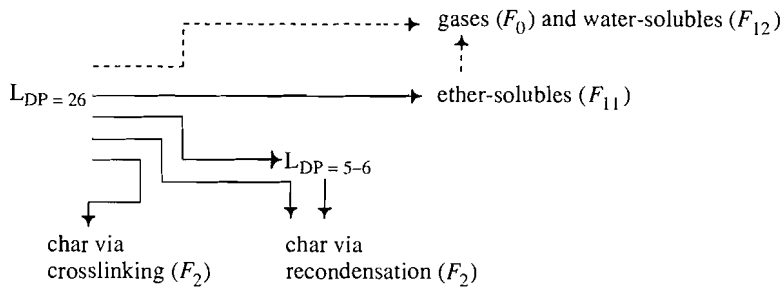

SCHEME 2

At low severities, the depolymerization of the higher molecular weight macrostructure (DP = 26), either through the intermediate (DP = 5–6) or directly through specific cleavages, liberates low molecular weight compounds that in the final separation appear predominantly as ether-solubles and some water-solubles. At high severities, extensive cross-linking of the macrostructure and recondensation of the DP = 5–6 subunit leads to char and gas formation with a decrease in the yield of liquid products.

FTIR spectra

In the present investigation, comparisons are made between the spectra of the residual lignins obtained from the alkaline hydrolysis of glycol lignin at different conditions of severity. Assignments for the absorption bands are based on the information given by Sarkanen *et al.* (17), Herget (18), and Winston (19).

The following comments may be made by comparing the spectra shown in Fig 5:

1. The spectra of RL-1 and RL-2 are essentially similar to that of the original lignin except for a general decrease in the relative band intensity in the 1600–1100 cm^{-1} region and a small broadening of the bands.

2. Increasing the severity of treatment to obtain the RL-3 and RL-4 fractions significantly modifies the residual lignin. Major absorption bands have disappeared and these spectra are now almost unrelated to that of the original lignin. However, the increase in the reaction severity between the RL-3 and RL-4 experiments does not significantly modify the residual lignins isolated, since the spectra are identical.

As the severity of the treatment increases, the hydroxyl absorption band spreads out and its maximum of absorbance shifts from 3460 cm^{-1} for glycol lignin to 3320 cm^{-1} for the RL-4 sample. This may be interpreted as a decrease in the aliphatic/phenolic hydroxyl group ratio with an increase in the carboxylic acid groups (also suggested by the increase in the relative intensity of the 1710 cm^{-1} band) with increasing severity.

Bands in the 1330–1035 cm^{-1} region, due to aromatic ether ring breathing and aromatic C–H deformation of the syringyl and guaiacyl units, decrease in relative intensity with increasing severity and have almost completely disappeared in the RL-3 and RL-4 samples. This indicates cleavage of the ether linkages and the liberation of methylene and methoxyl groups.

The spectra of RL-3 and RL-4 indicate that the glycol lignin has been extensively degraded and modified by the hydrolytic treatment, as seen by their characteristically less defined absorption bands. The similarity in band intensity of these residual lignins, even though the severities are substantially different, provides further evidence that glycol lignin degrades to products and a remaining core structure, which is relatively stable even at high severities of treatment. The position of the peaks indicates that these residual lignins are still aromatic in character, even though restructuring by degradation and recondensation has occurred as shown by the appearance of new bands in the 3050–2800 cm^{-1} and 900–800 cm^{-1} regions.

^{13}C NMR spectra

The ^{13}C NMR spectra of the acetylated samples of glycol lignin and residual lignins are given in Figs. 6(a) and (b). Table 5 presents assignments of the important signals as proposed by Lapierre *et al.* (20), Mörck and Kringstad (21, 22), Kanazawa *et al.* (23), and Robert (24). Comparison between the spectra reveals a number of important features.

Signals 1 and 2 (assigned to aliphatic carboxyl groups) are absent in glycol lignin but increase considerably in intensity for the series RL-1, RL-2 to RL-3, RL-4.

The intensities of signals 3 and 4 (primary and secondary aliphatic hydroxyl groups respectively) are highest in the glycol

Can. J. Chem. Downloaded from www.nrcresearchpress.com by 91.144.44.67 on 09/07/12
For personal use only.

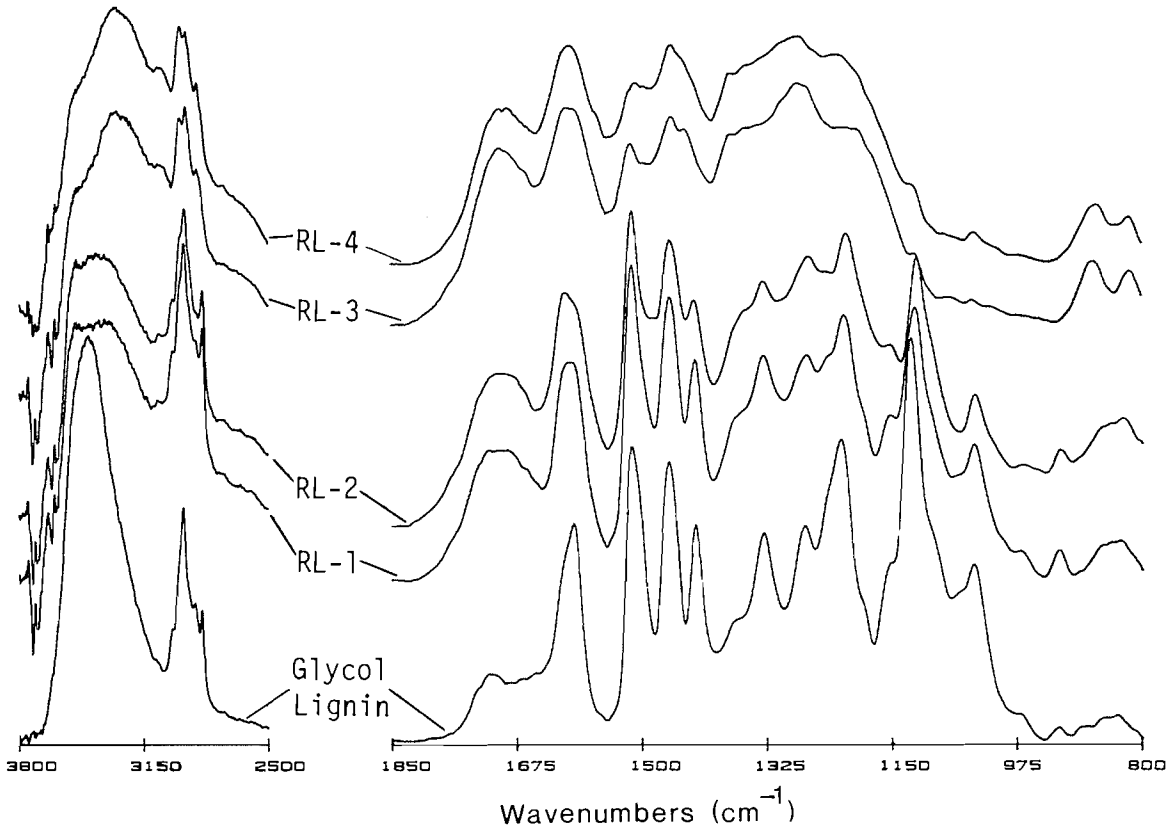

FIG. 5. Infrared spectra of glycol lignin and residual lignins.

lignin but are much lower in RL-1 and RL-2, and absent in RL-3 and RL-4. This indicates extensive cleavage of the alcohol-containing side chains of glycol lignin during alkaline hydrolysis. The intensity of signal 5 (phenolic hydroxyl), on the other hand, increases significantly in intensity from the initial lignin to RL-4. This is to be expected since it is known that hydrolysis of lignin with sodium hydroxide increases the phenolic hydroxyl groups in lignin (22).

The decrease in intensity of signals 6 and 8 (syringyl) and the corresponding increase in the intensity of signal 7 (guaiacyl) indicate that one of the important reactions occurring during the alkali treatment of glycol lignin with increasing severity of reaction conditions is demethoxylation/demethylation of syringyl-type groups to more stable guaiacyl-type structures within the lignin macromolecule.

The 110–148 ppm region (aromatic carbons) is difficult to interpret in detail. The broad signal at 137–148 ppm, particularly in RL-3 and RL-4, may originate from phenolic carbons in catchol units (23). The presence of well-defined signals in RL-4 in this region suggests that new C–C bonds are formed in the residual lignin due to condensation reactions.

The low intensity of signal 10 (carbohydrates) in glycol lignin and its absence in all the residual lignins indicate that this signal is probably from a lignin–carbohydrate complex (LCC). Analysis for sugars (monosaccharides) by acid hydrolysis in glycol lignin revealed that these were present in low quantities (<1%) (8). Since the lignin was thoroughly washed with distilled water during its preparation, these sugars are most likely from a LCC whose carbohydrate component is easily cleaved upon alkaline hydrolysis.

The presence and intensities of signals in the 64–85 ppm region (aliphatic carbons) in the spectrum of glycol lignin suggest that cleavage of interunit linkages (-C—C- and -C—O—C-) as well as those of side chains is insignificant during the lignin recovery step. This reaffirms the previous conclusion (8) on the high amount of oxygenated interlinkages of the β-O-4 type from observation of the spectrum of unacetylated glycol lignin. The noticeable reduction in intensity of the signals in this region

TABLE 5. Assignments of important signals in the ^{13}C NMR spectra of acetylated glycol lignin and residual lignins

Signal no.	Chemical shift (ppm)	Assignments
1	174.2	Aliphatic carboxyl(-COOH)
2	171.6	Aliphatic carboxyl(-COOH)
3	169.7	Primary alcoholic acetate(-CO)
4	169.1	Secondary alcoholic acetate(-CO)
5	167.8	Phenolic acetate(-CO)
6	151.7	Syringyl (C-3/C-5)
7	149.2	Guaiacyl (C-3), etherified
	110–148	Aromatic carbons
8	104.3	Syringyl (C-2/C-6)
9	79.9	Cβ in β-O-4 linkage
10	74.1	Carbohydrates (C-3 in xylan)
	64–85	Aliphatic carbons
11	63.0	Cγ in β-O-4 linkage
12	55.8	Methoxyl
13	28.8	-CH_2 and (or) -CH_3
14	22.5	
15	20.7	-CH_3 (acetyl)
	20.1	
	15.5	β- and (or) γ-methyl
	13.6	

Can. J. Chem. Downloaded from www.nrcresearchpress.com by 91.144.44.67 on 09/07/12
For personal use only.

Can. J. Chem. Downloaded from www.nrcresearchpress.com by 91.144.44.67 on 09/07/12
For personal use only.

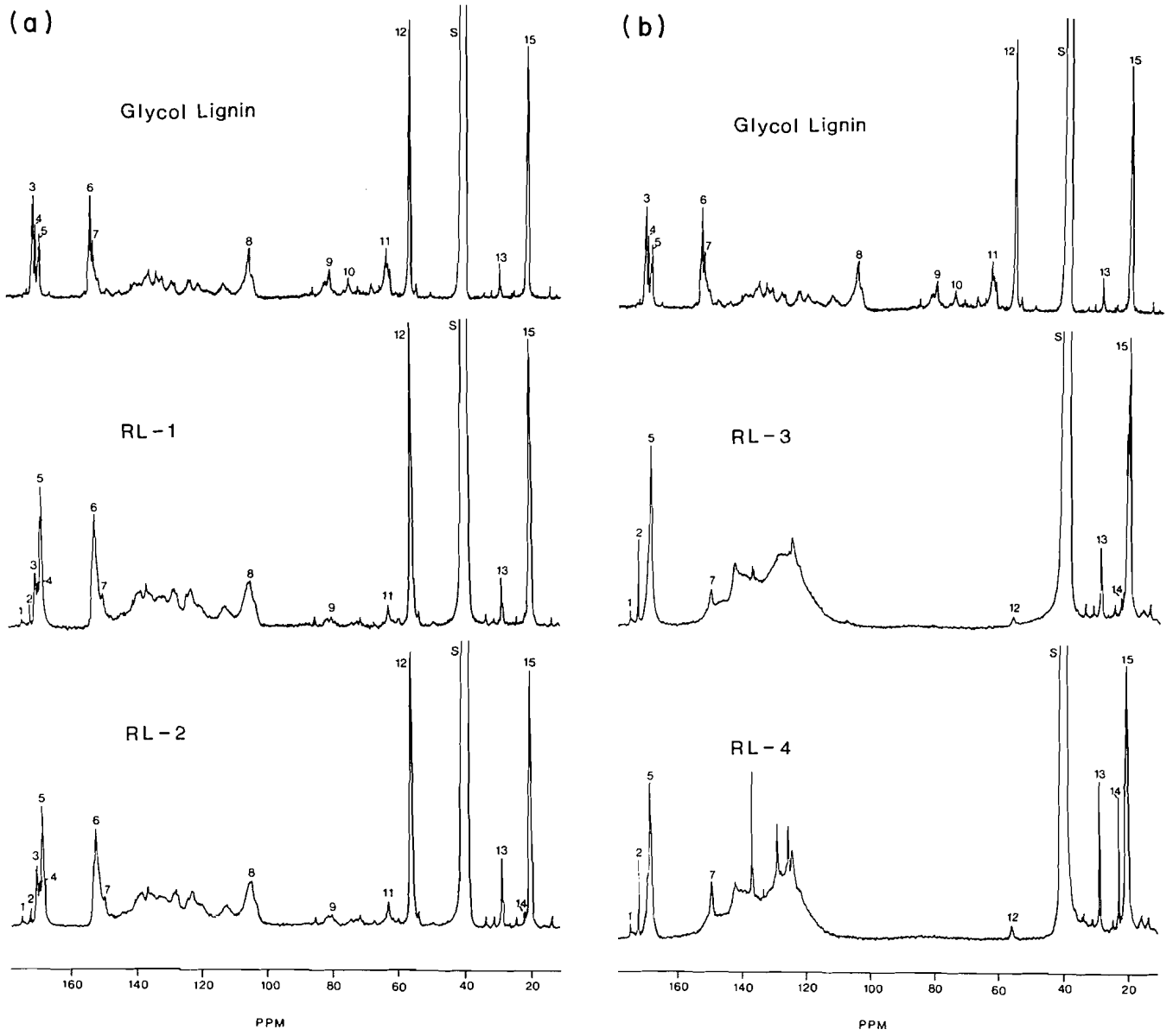

FIG. 6. ^{13}C NMR spectra of glycol lignin and residual lignins.

(RL-1 and RL-2) and their subsequent disappearance (RL-3 and RL-4) with increasing severity of reaction conditions, particularly signals 9 and 11 (β-O-4 carbons), demonstrate the facile rupture of these bonds in glycol lignin during alkaline hydrolysis.

The dramatic decrease in intensity of signal 12 (methoxyl carbons) from RL-2 to RL-3 is further evidence of the extensive demethoxylation of glycol lignin at higher reaction severities. This result confirms the analytically determined values of the methoxyl group content of the residual lignins shown in Table 2.

The appearance of new signals in the 10–34 ppm region (methine, methylene, and methyl carbons) and the increase in intensity of signals 13 and 14 at higher reaction severities suggest the formation of new bonds due to condensation reactions. As suggested by Gierer *et al.* (25), these reactions involve intermediary coniferyl alcohol structures generated after initial cleavage of phenolic β-aryl ether bonds, and may introduce conjugated double bonds as well as saturated hydrocarbon structures to the side chains in lignin. However, signals in the 25–34 ppm region, particularly signal 13, may include contributions from other types of condensation reactions (21).

Conclusions

The results of this study demonstrate how severity of treatment influences the structure and chemical composition of glycol lignin during depolymerization by alkaline hydrolysis. Complementary information on these chemical changes was obtained from elemental analysis, methoxyl determination, GPC, FTIR, and ^{13}C NMR methods.

It is apparent that as the severity is increased, the residual lignin becomes more highly condensed and even carbonized. The molecular weight distribution patterns show that the residual lignins largely consist of a high molecular weight fraction and a lower molecular weight one, with the latter increasing relative to the former with severity of treatment. Infrared spectroscopy and ^{13}C NMR have, in particular, demonstrated that during the alkaline hydrolysis of glycol lignin, depolymeriza-

tion/repolymerization reactions are competing, with the repolymerization reactions becoming more evident at higher severity conditions, as shown by the appearance of new bands and signals of increasing relative intensity in the spectra of the residual lignins. The lignin is extensively demethylated and demethoxylated at higher severity conditions during alkaline hydrolysis.

The evidence presented shows that the residual lignins obtained from the alkaline hydrolysis of glycol lignin, although drastically modified from the original lignin, still remain aromatic in character. Also, since the calorific value of these residual lignins is increased with treatment severity, they could be utilized as a fuel source of higher heating value than the original lignin, in a depolymerization process of glycol lignin by alkaline hydrolysis targeting monomeric compounds (i.e., catechol) and residual fuel to run the process.

Acknowledgements

The authors are indebted to T.S. Nguyen, M. Trottier, and J.P. Lemmonier for their technical support. We would like to thank Dr. John Ripmeester (National Research Council, Ottawa) for obtaining the NMR spectra of the lignin samples. Financial assistance by FCAR and NSERC is deeply appreciated.

1. D. W. GOHEEN. Low molecular weight chemicals. *In* Lignins, occurrence, formation, structure, and reactions. *Edited by* K. V. Sarkanen and C. H. Ludwig. Wiley–Interscience, New York. 1971. pp. 797–831 Chap. 19.
2. I. S. GOLDSTEIN. J. Appl. Polym. Sci. (Appl. Polym. Symp.), No. 28, 259 (1975).
3. H. L. CHUM, D. K. JOHNSON, S. BLACK, M. RATCLIFF, and D. W. GOHEEN. Lignin hydrotreatment to low-molecular-weight compounds. *In* Advances in solar energy: annual review of research and development. Vol. 4. *Edited by* K. W. Boer. American Chemical Society, Boulder, CO. 1987. pp. 92–171.
4. J. M. PEPPER and D. C. HAGERMAN. Can. J. Chem. **32**, 614 (1954).
5. I. T. CLARK and J. GREEN. TAPPI, **51**(1), 44 (1968).
6. J. M. PEPPER and R. W. FLEMING. Can. J. Chem. **56**, 896 (1978).
7. W. J. CONNORS, L. N. JOHANSON, K. V. SARKANEN, and P. WINSLOW. Holzforschung, **34**, 29 (1980).
8. R. W. THRING, E. CHORNET, R. P. OVEREND, and M. HEITZ. Production and hydrolytic depolymerization of ethylene glycol lignin. *In* Lignin: properties and materials. *Edited by* W. G. Glasser and S. Sarkanen. ACS Symp. Ser. No. 397, pp. 228–244 (1989).
9. S. ZEISEL. Monatsh. Chem. **6**, 989 (1885).
10. J. P. HALUK and M. METCHE. Cellul. Chem. Technol. **20**, 31 (1986).
11. R. P. OVEREND and E. CHORNET. A Unified Treatment for Liquefaction. *In* Research in thermochemical biomass conversion. *Edited by* A. V. Bridgewater and J. L. Kuester. Elsevier Applied Science, New York. 1988. pp. 411–428.
12. M. G. S. CHUA and M. WAYMAN. Can. J. Chem. **57**, 1141 (1979).
13. D. G. B. BOOCOCK and D. MACKAY. The production of liquid hydrocarbons by wood hydrogenation. IGT (Chicago) Symp. Papers, Energy from Biomass and Wastes IV, pp. 765–777 (1980).
14. J. M. PEPPER and M. SIDDIQUELLAH. Can. J. Chem. **39**, 1454 (1961).
15. W. LANGE, O. FAIX, and O. REINHOFF. Holzforschung, **37**, 63 (1983).
16. M. WAYMAN and T. I. OBIAGA. Can. J. Chem. **52**, 2102 (1974).
17. K. SARKANEN, H. M. CHANG, and G. ALLAN. TAPPI, **50**(12), 587 (1967).
18. H. L. HERGET. Infrared spectra. *In* Lignins, occurrence, formation, structure, and reactions. *Edited by* K. V. Sarkanen and C. H. Ludwig. Wiley–Interscience, New York. 1971. pp. 267–293.
19. M. H. WINSTON. Ph.D. thesis, North Carolina State University, Raleigh, NC. (1987).
20. C. LAPIERRE, J. Y. LALLEMAND, and B. MONTIES. Holzforschung, **36**, 275 (1982).
21. K. P. KRINGSTAD and R. MÖRCK. Holzforschung, **37**, 237 (1983).
22. R. MÖRCK and K. P. KRINGSTAD. Holzforschung, **39**, 109 (1985).
23. K. KANAZAWA, R. MÖRCK, M. KOYAMA, and K. P. KRINGSTAD. Holzforchung, **41**, 299 (1987).
24. D. ROBERT. Quantitative structural analysis of lignins by ^{13}C NMR analysis. Proc., Canadian Wood Chemistry Symp. CIC, Niagara Falls, Ont. 1982. pp. 63–66.
25. J. GIERER, F. IMSGARD, and AND I. PETTERSON. Possible condensation and polymerization reactions of lignin fragments during alkaline pulping processes. Appl. Polym. Symp. No. 28. John Wiley & Sons, New York. 1976. pp. 1195–1211.

Can. J. Chem. Downloaded from www.nrcresearchpress.com by 91.144.44.67 on 09/07/12
For personal use only.

Scaled *ab initio* force field and vibrational spectra of 2-methylthietane

R. A. SHAW, N. IBRAHIM, AND H. WIESER[1]

Department of Chemistry, University of Calgary, Calgary, Alta., Canada T2N 1N4

Received July 18, 1989

R. A. SHAW, N. IBRAHIM, and H. WIESER. Can. J. Chem. **68**, 90 (1990).

The vibrational spectra have been measured for 2-methylthietane over the range 100–1600 cm^{-1} (Raman) and 400–3200 cm^{-1} (solution and vapour phase infrared). *Ab initio* calculations at the 3-21G and 6-31G* levels indicate that both the axial and equatorial conformers represent minima on the ring inversion potential surface, the latter suggesting the equatorial species to be more stable by 191 cm^{-1}. Vibrational force fields were evaluated for each of the two conformers and scaled using factors previously optimized for thietane and 2-methyloxetane. All of the major experimental features were readily assigned to the equatorial species, and most transitions expected for the axial species were also located. Calculated absorption intensities, although not accurate in an absolute sense, proved useful in predicting the relative intensities for corresponding axial and equatorial transitions.

Key words: 2-methylthietane, vibrational spectra, *ab initio* force fields, vibrational assignment, conformations.

R. A. SHAW, N. IBRAHIM et H. WIESER. Can. J. Chem. **68**, 90 (1990).

On a mesuré les spectres de vibration du 2-méthylthiétane de 100 à 1600 cm^{-1} (Raman) et de 400 à 3200 cm^{-1} (infrarouge en solution et en phase gazeuse). Des calculs *ab initio* aux niveau 3-21G et 6-31G* indiquent que les conformères tant axial qu'équatorial représentent des minima sur la surface de potentiel d'inversion du cycle; la dernière base suggère que l'espèce équatoriale est plus stable par 191 cm^{-1}. On a calculé les champs de force vibrationnels de chacun des deux conformères et on en a fixé l'échelle en utilisant des fracteurs qui ont été optimisés antérieurement pour le thiétane et le 2-méthyloxéthane. On a attribué pratiquement l'ensemble des caractéristiques expérimentales importantes aux espèces équatoriales; de plus, la plupart des transitions attendues pour les espèces axiales ont aussi été localisées. Même si les intensités d'absorption calculées ne sont pas nécessairement exactes en termes absolus, elles se sont avérées utiles pour prédire les intensités relatives des transitions axiale et équatoriales correspondantes.

Mots clés : 2-méthylthiétane, spectres de vibration, champs de force *ab initio*, assignation vibrationelle, conformations.

[Traduit par la revue]

Introduction

Small chiral ring molecules play an important role in both experimental and theoretical studies of vibrational circular dichroism (VCD) (for reviews, see ref. 1). An accurate force field is an essential prerequisite to such an investigation, both as a means of assigning the vibrational spectrum and in providing the eigenvectors required for model calculations of the VCD (and infrared) intensities.

In this paper we report the vibrational spectra and *ab initio* MO structural calculations for 2-methylthietane (2MT, see Fig. 1). The vapour phase infrared absorption spectrum has been reported previously over the range 50–500 cm^{-1}, with the observed sequence of low frequency ring puckering transitions interpreted to suggest an inversion barrier of 341 cm^{-1} and an energy difference of 118 cm^{-1} separating the two conformers (2). The more stable conformer could not be inferred from the far-infrared study. We have evaluated the force constants and vibrational frequencies for each conformer using the 3-21G and 6-31G* basis sets, and adopted the scaling procedure of Pulay *et al.* (3) to correct for systematic deficiencies in the calculated force constants. The success of this approach in the accurate *prediction* of vibrational spectra rests upon the availability of scaling factors suitable for correcting the calculated force constants. Although different types of force constant may require quite different correction factors, it has been shown that for a particular coordinate type the scaling factor is transferable over a range of molecules (3–6).

We have previously reported scaled 3-21G force fields for 2-methyloxetane (4) and thietane (5), each of which incorporates structural features (and hence also vibrational coordinates) common to those of 2MT. In each case the spectra of several deuteriated isotopomers were recorded and assigned, providing sufficient experimental data that a relatively large number of scaling factors could be defined and optimized independently. The decision to permit such flexibility in the scaling procedure was motivated partially as a means of resolving certain ambiguities in the assignments. More importantly in the present context, we have suggested previously that such an approach should also optimize the predictive power of the scaling factors (4–6).

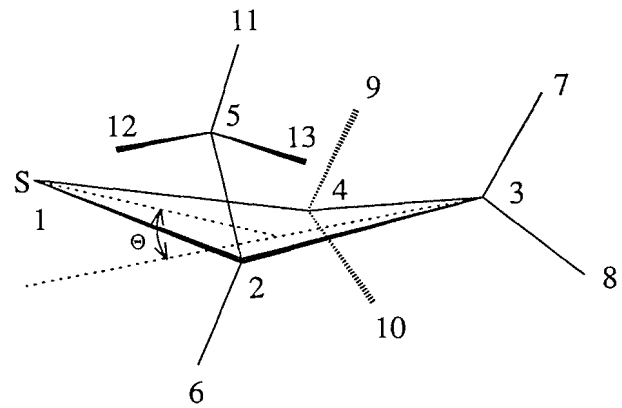

FIG. 1. Atom numbering for 2-methylthietane, used for defining structural parameters and local symmetry coordinates of Tables 2 and 3.

The spectra of 2MT offer an opportunity to test the reliability of this approach. Both the axial and equatorial 3-21G force fields are scaled using factors determined for thietane and 2-methyloxetane, and the spectra assigned on the basis of the predicted frequencies. Recognizing that this basis set has certain deficiencies, particularly in the C—S bond length, we have also reevaluated both the thietane and 2-methyloxetane force fields using the 6-31G* basis set and calculated both axial and

[1]Author to whom correspondence may be addressed.

Can. J. Chem. Downloaded from www.nrcresearchpress.com by 91.144.44.67 on 09/07/12
For personal use only.

Can. J. Chem. Downloaded from www.nrcresearchpress.com by 91.144.44.67 on 09/07/12
For personal use only.

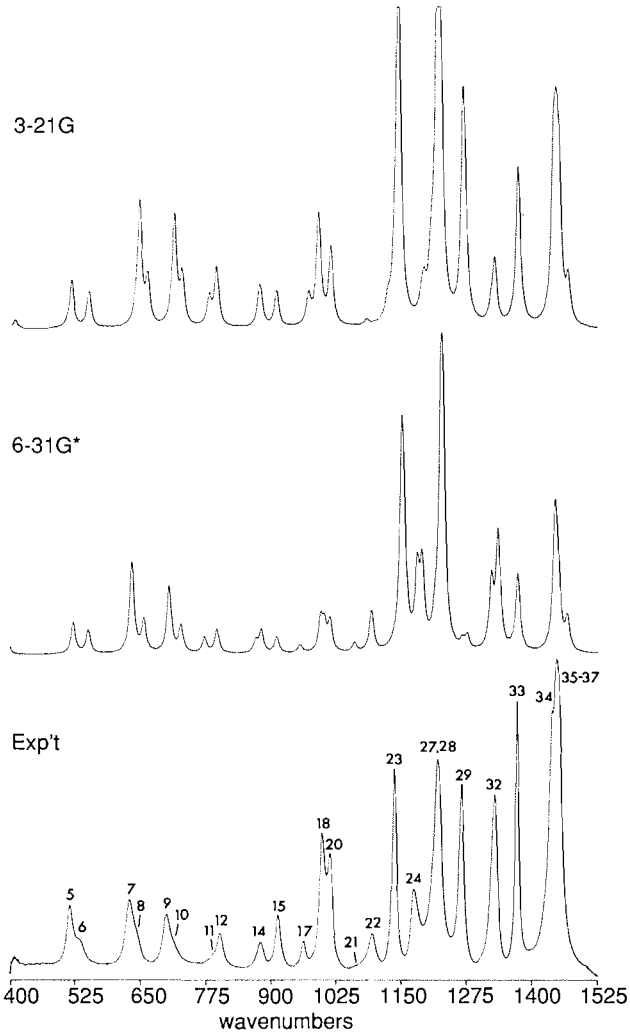

FIG. 2. Mid-infrared absorption spectrum of 2-methylthietane. Lower: experimental, vapour phase. Center: calculated using 6-31G* force field and atomic polar tensors. Upper: calculated using scaled 3-21G force field and atomic polar tensors. All calculated spectra are plotted on the same intensity scale, using an assumed bandwidth (full width at half height) of 10 cm^{-1}. Peaks numbered as in Tables 1 and 6.

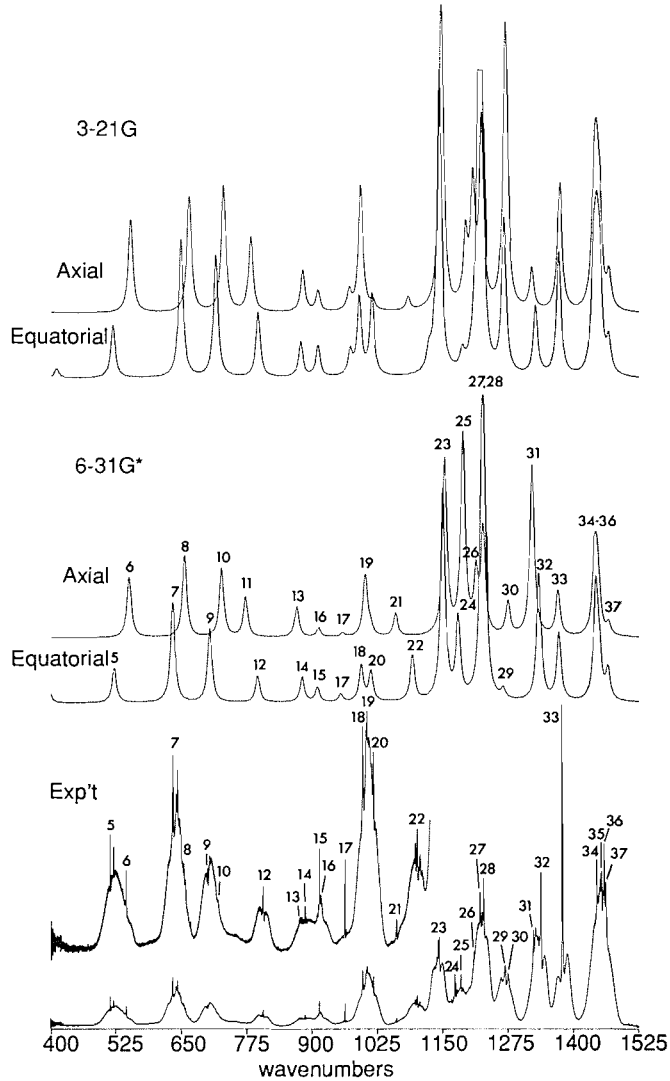

FIG. 3. Lower: infrared absorption spectrum of 2-methylthietane (neat liquid). Center: calculated spectrum for the 6-31G* force field, assuming a mixture of 70% equatorial and 30% axial, see text. Upper: calculated with the 3-21G basis set, assuming the same mixture.

equatorial structures and force fields using the same basis set. The 3-21G and 6-31G* force fields are thus developed in exactly analogous fashion, which then permits assessment of the relative accuracy of the two basis sets in this application.

The calculated absorption intensities are examined both as a means of verifying the proposed assignments and in assessing the relative populations of the two conformers. The evidence derived through this study is then discussed in the context of both the experimental and calculated inversion potential surfaces. Finally, the normal coordinates and force constants are compared for the different conformers and force fields.

Experimental and computational details

2-Methylthietane was synthesized following the method outlined by Etienne and Soulas (7), with a purity of at least 98% as determined by gas chromatography.

Infrared spectra were run using a Nicolet 8000 FT-IR spectrometer at a pathlength of about 1.5 m (Wilkes cell) for the vapour, 0.1 mm for the solutions, and 0.015 mm for the neat liquid. The spectra are displayed in Figs. 2–5, and the measured positions listed in Table 1. Absorption intensities for the solution spectra were measured using the band fitting program CAPR supplied by Nicolet. The Fourier self-deconvolution (8) software, used for resolution enhancement of the solution spectra, was also supplied by Nicolet.

The Raman spectrum was recorded with a Jarell–Ash 25-100 double grating spectrometer, using the 5145 Å argon ion line of a Coherent Radiation laser, with the slitwidth set for 7 cm^{-1} resolution at 1000 cm^{-1}. The spectrometer is interfaced to an IBM PC and Tektronix digitizer. The plotted spectrum (Fig. 6) represents the average of 2 scans, with data points collected every 2 cm^{-1} and a dwell time of 1 s at each point.

Optimized structures were determined for 2-methylthietane (6-31G*), thietane (6-31G*), and both stable conformers of 2-methylthietane (3-21G and 6-31G*) using the Gaussian 82 program (9) modified by Rauk and Dutler (10) to run on the Cyber 205 supercomputer at the University of Calgary. The optimized structural parameters are listed in Table 2 (see refs. 4 and 5 for optimized 3-21G structures of 2-methyloxetane and thietane, respectively). The harmonic force constants were evaluated at the respective optimized structures using the same basis set(s), and transformed to local symmetry coordinates. The coordinates for thietane are given in ref. 5. For 2-methylthietane the coordinates used (Table 3) are identical to those for 2-methyloxetane. The atomic polar tensors (APT) were evaluated using a separate program that makes use of the analytical derivatives of the density

Can. J. Chem. Downloaded from www.nrcresearchpress.com by 91.144.44.67 on 09/07/12
For personal use only.

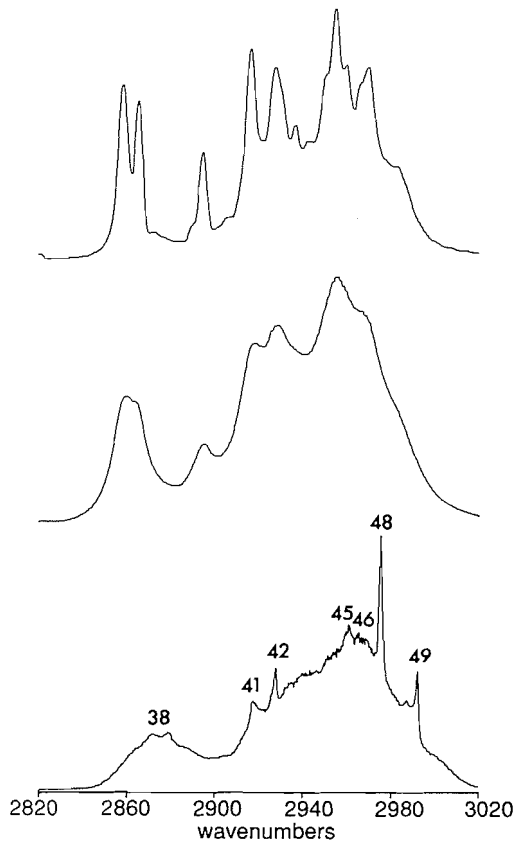

FIG. 4. CH stretching region of the infrared absorption spectrum of 2-methylthietane. Lower: vapour phase. Center: CCl_4 solution. Upper: Fourier self-deconvolution (8) of solution spectrum, see text.

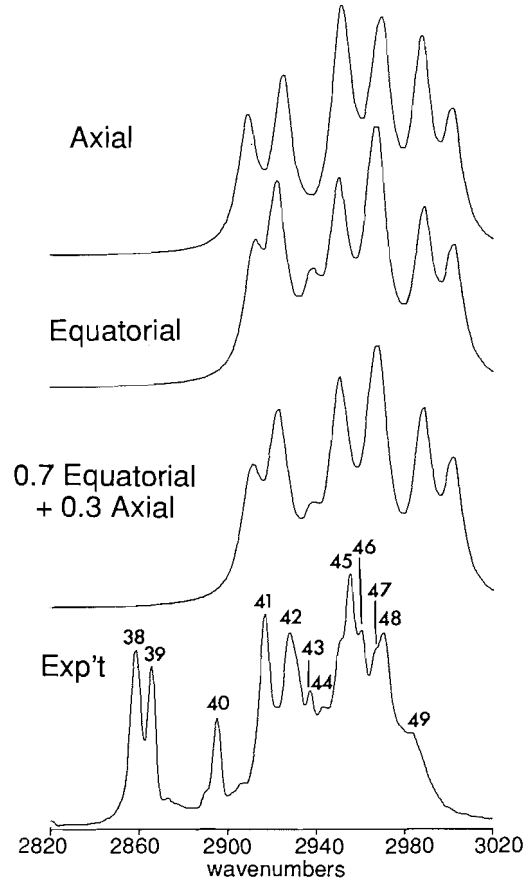

FIG. 5. CH stretching region of the infrared absorption spectrum of 2-methylthietane. Lower: deconvolved solution spectrum (see Fig. 4). Upper: calculated (6-31G*) spectra for the individual conformers. Center: weighted average (70% equatorial and 30% axial) spectra calculated for the two separate conformers.

matrix provided by Gaussian 82. A list of the APTs is available from the authors upon request.

All force fields were scaled according to $F_{ij} = (C_iC_j)^{1/2}K_{ij}$, where C_i and C_j denote the scaling factors for modes "i" and "j", and K_{ij} and F_{ij} the unscaled and scaled *ab initio* force constants, respectively (3). For 2-methyloxetane and thietane the 6-31G* scaling factors were refined to fit the observed transitions reported in refs. 4 and 5. These optimized scaling factors were thus derived following a procedure exactly analogous to that used for the 3-21G basis set.

The absorption spectra for both conformers of 2-methylthietane were predicted by transferring the appropriate optimized scaling factors from thietane and 2-methyloxetane (see Table 4). Table 5 summarizes the calculated positions and infrared absorption intensities for each conformer. For the 3-21G and axial 6-31G* calculations the frequencies are listed such that the associated normal coordinates are matched with the corresponding modes of the equatorial conformer (6-31G* calculation), according to criteria outlined below.

Results and discussion

The *ab initio* calculations agree qualitatively with the experimental inversion potential, with both axial and equatorial structures predicted to be stable and similar in energy. The two basis sets differ somewhat with respect to the dihedral angles, 3-21G predicting the two conformers to be folded by equal and opposite amounts and 6-31G* indicating the axial to be slightly less puckered than the equatorial.

With respect to the structure calculations, the major advantage of 6-31G* lies in the improved C—S bond lengths and in the predicted relative energies for the two conformers. For thietane the C—S distance of 1.834 Å is within 0.013 Å of experimental (11), and the corresponding 2MT parameters are presumably equally accurate. The difference of 191 cm^{-1} calculated with 6-31G* is in good agreement with the experimental value of 124 cm^{-1}, while the 3-21G basis predicts the two conformers to be essentially equal (within 5 cm^{-1}) in energy. The 6-31G* basis set further suggests that the equatorial species is the more stable of the two.

Vibrational assignments

The mid-infrared assignments were initially approached following the guidance of the 3-21G calculated positions for the equatorial conformer (Table 5). All of the dominant features in the mid-infrared solution spectra were readily assigned on this basis, with the only ambiguity occurring in the 1220 cm^{-1} region. Two fundamental transitions are predicted here where only a single absorption is evident in the condensed phase spectra. Subsequent Fourier self-deconvolution (FSD) over this region revealed two closely spaced absorptions of nearly equal intensity, which are clearly resolved in the vapour phase absorption spectrum. The assignments for the equatorial species were thus completed with no apparent ambiguities. They are listed in Tables 1 and 6.

The vibrational spectrum was then predicted for the axial species, placing several transitions well separated from the corresponding equatorial modes (see Table 5). The search for these features in the experimental spectra was initially confined to the lower frequency modes, in particular ν_{26}–ν_{31}, each of which is suggested to shift by at least 14 cm^{-1}. Among these the

TABLE 1. Observed infrared and Raman bands (cm^{-1}) and vibrational assignments for 2-methylthietane

Peak no[a]	Solution[b] CCl_4	Solution[b] CS_2	Liquid	Vapour	Raman liquid	Assignment[c]
1				280.8[d]		ν_{31} (eq)
2				301.1[d]	289	ν_{31} (ax)
3				370.0[d]	379	ν_{30} (ax)
4				403.3[d]	405	ν_{30} (eq)
5	516.1 m	517.3	516.2	514.4	518	ν_{29} (eq)
6	536.9 w,sh	535.8	536.9	545.2	533	ν_{29} (ax)
7	630.0 m	630.5	630.2	633.7	631	ν_{28} (eq)
8	643.7 w,sh	640		655.0		ν_{28} (ax)
9	701.1 m	700.2	700.2	700.4	700	ν_{27} (eq)
10		714.4 w,sh	714.0	718.4		ν_{27} (ax)
11			790.0 w,sh,dcn	790		ν_{26} (ax)
12		801.3 w	802.7	806.8	802	ν_{26} (eq)
13				876.4		ν_{25} (ax)
14	880.3 w	880.2	881.1	887.1	878	ν_{25} (eq)
15	914.0 m	912.7	913.9	914.2	914	ν_{24} (eq)
16				916.8		ν_{24} (ax)
17	963.2 w	962.5	963.1	963.1	962	ν_{23}
18	998.7 s	997.0	998.4	997.1	998	ν_{22} (eq)
19				1005.9		ν_{22} (ax)
20	1014.5 s	1012.4	1013.4	1017.4	1012 sh	ν_{21}
21	1078 w,sh	1078	(1078.9 w,sh)	1061.5	1062 sh	ν_{20} (ax)
22	1096.6 w	1094.0	1095.6	1101.4	1092	ν_{20} (eq)
23	1137.3 s	1135.7	1136.8	1142.8	1136	ν_{19}
24	1175.2 m	1171.6	1174.9	1172.7	1173	ν_{18} (eq)
25	1179 sh	1179		1184.3		ν_{18} (ax)
26				1208.8		ν_{17} (ax)
27	1218. s,dcn	1218	1218.9	1220.6	1216	ν_{17} (eq)
28	1222.2 s,dcn	1220.4	1222.4	1227.8		ν_{16}
29	1266.2 s	1264.5	1265.6	1269.5	1265	ν_{15} (eq)
30				1274.5		ν_{15} (ax)
31	1323 w,sh	1323	1323	1323.8		ν_{14} (ax)
32	1330.7 s	1328.9	1330.0	1338.3	1329	ν_{14} (eq)
33	1373.2 s	1370.6	1371.8	1378.5	1372	ν_{13}
34	1439.1 s,dcn			1445.2		ν_{12} (eq), ν_{11} (ax)
35	1446.5 s,dcn			1454.1	1442	ν_{11} (eq), ν_{10} (ax)
36	1450.0 s,dcn			1459.0		ν_{10} (eq), ν_{12} (ax)
37	1454.3 s,dcn			1461.3	1449	ν_9
38	2858.6 s	2858.7		2875.2		
39	2865.7 s	2865.7		2889.5		
40	2895.1 m	2895.0		2894.5		
41	2917.0 s	2916.9		2918.2		ν_8
42	2928.0 s	2929.0		2928.8		ν_7
43	2937.0 m	2935.4				ν_6 (eq)
44	2942.7 m	2943				ν_5
45	2955.5 s	2953.8		2962.0		ν_4, ν_6 (ax)
46	2960.3 s	2958.7		2965.9		ν_3
47	2967 sh	2967.3				
48	2970.2 s	2969.8		2976.6		ν_2
49	2983.0 m	2980.9		2992.7		ν_1

[a]Corresponding peaks labelled in Figs. 2–6.
[b]Abbreviations: s = strong; m = medium; w = weak; dcn denotes transitions resolved by Fourier self-deconvolution (5); eq = equatorial; ax = axial.
[c]Band assigned to both axial (ax) and equatorial (eq) species unless otherwise indicated.
[d]From ref. 2.

ring deformation, ν_{29}, provided the clearest experimental evidence that the axial species is both stable and present in appreciable concentration at room temperature. The condensed phase spectra (Figs. 3 and 6) show a clear high frequency shoulder (peak no. 6) on the absorption at 516 cm^{-1} (peak no. 5). In CCl_4 solution the two transitions are clearly resolved upon Fourier self-deconvolution at 516.1 and 536.9 cm^{-1}. The corresponding vapour phase transitions at 514.4 and 545.2 cm^{-1} match very well the positions calculated for the equatorial and axial species, respectively. The excellent agreement between the calculated (33.7 cm^{-1}) and observed (30.8 cm^{-1}) frequency shifts further supports these assignments, and also suggests that the shifts calculated for other modes may be taken as a reliable guide in searching for other transitions of the axial conformer.

Can. J. Chem. Downloaded from www.nrcresearchpress.com by 91.144.44.67 on 09/07/12
For personal use only.

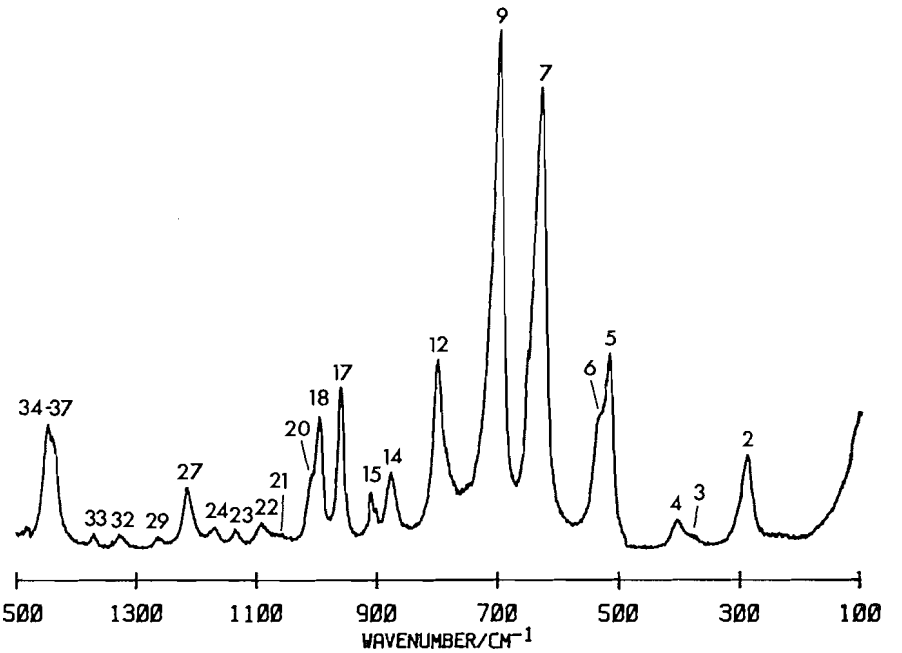

FIG. 6. Raman spectrum of 2-methylthietane (neat liquid). Peaks numbered as in Tables 1 and 6.

The two methyl bending modes ν_{30} and ν_{31} both occur below 450 cm^{-1} and appear in the absorption spectra reported in ref. 2 for the region 100–500 cm^{-1}. The predicted frequencies suggest that the two absorptions reported at 403.3 and 370 cm^{-1} correspond to equatorial and axial transitions in the CH_3 out-of-plane bending mode, ν_{30}, calculated at 411.3 and 380.7 cm^{-1}, respectively. These two bands are also clearly present in the Raman spectrum (Fig. 6). The two in-plane bends, ν_{31}, calculated at 280.3 cm^{-1} (equatorial) and 295.8 cm^{-1} (axial) are observed at 280.8 and 301.1 cm^{-1} in the vapour phase spectrum. In each case the lower intensity transition of the pair arises from the axial species.

The two C–S stretches for the equatorial conformer occur at 700.4 cm^{-1} (ν_{27}, H_2C–S stretch) and 633.7 cm^{-1} (ν_{28}, CH_3C–S stretch). The corresponding axial transitions are predicted about 15 cm^{-1} higher in frequency. Close examination of the solution spectrum reveals shoulders to high frequency (peaks no. 10 and 8, Fig. 3). Although FSD does resolve these axial transitions, albeit with a noise level nearly as intense as the resolved bands, they are clear enough to confirm the corresponding vapour phase transitions as fundamentals of the axial conformer.

The mode predicted with the largest shift is ν_{20}, the 3-21G calculation placing the fundamentals at 1125 cm^{-1} (equatorial) and 1085 cm^{-1} (axial). The 6-31G* calculation is more accurate, both in reproducing the position observed for the equatorial mode (obsd. 1101 cm^{-1}, calcd. 1093 cm^{-1}) and in confirming the weak band observed at 1061.5 cm^{-1} (peak no. 21, Figs. 2 and 6) as the corresponding axial fundamental (calcd. 1061 cm^{-1}). This example illustrates that where the two basis sets differ, the 6-31G* positions are probably the better guide in searching for the more elusive transitions of the axial conformer. This preference is important only for one other mode, ν_{25}, which is the only case in the 100–1600 cm^{-1} region where a shift predicted to exceed 5 cm^{-1} by 6-31G* is opposite in sign to that of 3-21G. Again, the former suggests a plausible assignment for the axial transition whereas the latter does not. For ν_{20} the equatorial fundamental is split into three separate features in the vapour phase spectrum (peak no. 22 of Fig. 2), which we suspect to represent the same fundamental occurring in the three different puckering levels within the equatorial well. Analogous transitions are evident also for ν_{28} and ν_{29} (peaks no. 7 and 5), corresponding to distinct Q-branches evident at slightly higher frequency in each case. The band splitting then confirms the sensitivity of these modes to subtle structural changes.

With these examples confirming that the axial species is present and that the calculated positions faithfully reproduce the observed frequency shifts, several of the remaining mid-infrared axial transitions were identified readily in the vapour phase spectrum. With the exception of the CH stretching and the CH_2 scissoring/CH_3 asymmetric deformation regions, both of which are too congested to permit positive identification of the axial transitions, all but four of the axial fundamentals in the region 250–1500 cm^{-1} have been located and are listed in Table 5.

The CH stretching region was assigned for the most part by considering the deconvolved (FSD) solution spectrum, which clearly displays a number of transitions that are not resolved in either the vapour phase or solution spectra. The transitions at 2858.6, 2865.7, and 2895.1 cm^{-1} (peaks no. 38, 39, and 40 in Fig. 5) are ascribed to Fermi resonances involving combinations and (or) overtones of the scissoring modes (at least one such resonance enhanced overtone has also been identified for the parent thietane molecule (5)) and the CH_3 asymmetric deformations. With the CH stretching region complicated by these resonances the calculated shifts become less dependable in attempting to assign the weaker transitions, which may or may not correspond to transitions of the axial conformer. The shifts are generally small in any case, and the calculated absorption profile (6-31G*, see Fig. 5) matches the observed very well for each of the conformers. The only qualitative difference occurs over the region 2935–2945 cm^{-1}, where only the equatorial conformer is predicted to display any absorption. Our assignment (peak no. 42) matches the equatorial prediction well, with the axial transition then assigned either as coincident with ν_4 (peak no. 45) or to the shoulder apparent to slightly lower frequency in the deconvolved spectrum (see Figs. 4 and 5). For all

Can. J. Chem. Downloaded from www.nrcresearchpress.com by 91.144.44.67 on 09/07/12
For personal use only.

TABLE 2. Optimized structural parameters for 2-methylthietane, thietane, and 2-methyloxetane

Parameter[a]	2-Methylthietane[b] Axial 3-21G	Axial 6-31G*	Equatorial 3-21G	Equatorial 6-31G*	Thietane[c] 6-31G*	2-Methyloxetane[d] 6-31G*
CS(1–4)	1.918	1.832	1.918	1.833	1.834	1.418
CS(1–2)	1.923	1.844	1.923	1.844		1.425
CC(3–4)	1.553	1.541	1.553	1.539	1.541	1.535
CC(2–3)	1.556	1.546	1.556	1.542		1.539
CC(CH)(2–5)	1.521	1.521	1.518	1.517	(1.081)	1.513
CH(2–6)	1.077	1.082	1.078	1.083	1.082	1.086
CH(4–9)	1.077	1.081	1.076	1.081		1.084
CH(4–10)	1.076	1.081	1.077	1.082		1.085
CH(3–7)	1.082	1.085	1.081	1.084	1.083	1.083
CH(3–8)	1.081	1.083	1.081	1.085	1.084	1.082
CH(5–11)	1.083	1.085	1.083	1.084		1.085
CH(5–12)	1.083	1.085	1.084	1.085		1.085
CH(5–13)	1.087	1.088	1.087	1.087		1.087
CSC	75.3	78.1	75.3	77.3	77.5	92.8
S—C4—C3	91.9	91.7	91.9	91.4	91.4	91.6
S—C2—C3	91.6	91.1	91.7	90.9		91.2
C2—C3—C4	98.0	97.2	97.9	96.4	96.3	84.1
S—C4—H9	110.0	112.0	112.7	114.2		112.0
S—C4—H10	112.5	113.7	109.8	111.4		111.7
C3—C4—H9	114.0	114.2	115.9	116.1		116.7
C3—C4—H10	115.8	115.5	113.8	113.6		115.1
H9—C4—H10	111.2	109.1	111.3	109.3		109.0
C4—C3—H7	114.3	114.6	110.3	110.6		114.8
C4—C3—H8	110.4	111.3	114.4	115.4		116.3
C2—C3—H7	113.5	114.1	110.0	110.4	110.9	114.4
C2—C3—H8	110.8	111.4	114.3	115.2	115.0	116.3
H7—C3—H8	109.4	108.1	109.5	108.3	108.3	109.3
C3—C2—C5(H5)	114.2	115.6	116.7	117.8	(116.0)	118.4
C3—C2—H6	114.4	113.3	111.9	110.1	113.6	113.1
S—C2—C5(H5)	111.9	114.6	114.8	117.0	(114.2)	112.5
S—C2—H6	111.2	111.4	108.3	108.9	111.5	110.2
C5(H5)—C2—H6	111.9	109.8	111.8	109.9	(109.2)	110.2
C2—C5—H11	110.8	111.3	110.6	111.1		110.6
C2—C5—H12	110.8	111.1	110.8	111.1		110.3
C2—C5—H13	110.0	110.0	110.1	110.0		110.5
H11—C5—H12	108.1	108.1	108.3	108.2		108.3
H11—C5—H13	108.8	108.3	109.0	108.5		108.6
H12—C5—H13	108.3	108.0	108.1	107.8		108.4
H11—C5—C2—H6	179.0	179.6	177.6	178.8		
Dihedral θ	19.1	14.6	18.8	21.1	19.2	6.3
Energy (hartrees)						
3-21G	−550.807148090		−550.807123950			
6-31G*		−553.619733658		−553.618865072		

[a]Bond distances in Å, angles in degrees.
[b]See Fig. 1 for atom numbering.
[c]Atoms numbered as for 2-methylthietane, but with C5 replaced by H5. See ref. 5 for 3-21G structure.
[d]Atoms numbered as for 2-methylthietane, but with sulfur replaced by oxygen. See ref. 4 for 3-21G structure.

other modes the equatorial and axial transitions are assumed to coincide. With three strong bands ascribed to combinations and (or) overtones it is likely that several of the lower frequency CH stretching fundamentals are perturbed and shifted to higher frequency as a result of the Fermi resonance interactions. This then accounts for the appearance of the experimental spectrum as being compressed along the frequency axis relative to the calculated spectrum, while qualitatively the two compare quite well in overall appearance.

The assignments are reproduced with an average error of 5.1 (equatorial) and 5.9 cm^{-1} (axial) for the 6-31G*, and 7.6 and 7.9 cm^{-1}, respectively, for the 3-21G force field. The calculated intensities for the two conformers must be weighted to reflect their relative populations in order to compare quantitatively the theoretical and experimental spectra. This is discussed in the following section.

Inversion potential and relative abundance of conformers

The relative populations of the two conformers may be estimated either through the relative intensities for corresponding axial and equatorial transitions or through consideration of the energy difference implied by the inversion potential func-

Can. J. Chem. Downloaded from www.nrcresearchpress.com by 91.144.44.67 on 09/07/12
For personal use only.

TABLE 3. 2-Methylthietane local symmetry coordinates[a]

1. C_2–S stretch	6. C_2–H_6 stretch
2. C_4–S stretch	7. C_4–H_9 stretch
3. C_2–C_3 stretch	8. C_4–H_{10} stretch
4. C_3–C_4 stretch	9. C_3–H_7 stretch
5. C_2–C_5 stretch	10. C_3–H_8 stretch
11. Ring deformation	$\gamma(C_4\text{-}S\text{-}C_2) - \gamma(S\text{-}C_2\text{-}C_3) + \gamma(C_2\text{-}C_3\text{-}C_4) - \gamma(C_3\text{-}C_4\text{-}S)$
12. α-CH_2 scissor	$5\alpha(H_9\text{-}C_4\text{-}H_{10}) + \gamma(C_3\text{-}C_4\text{-}S)$
13. α-CH_2 rock	$\beta(S\text{-}C_4\text{-}H_9) - \beta(S\text{-}C_4\text{-}H_{10}) + \beta(C_3\text{-}C_4\text{-}H_9) - \beta(C_3\text{-}H_4\text{-}H_{10})$
14. α-CH_2 wag	$\beta(S\text{-}C_4\text{-}H_9) + \beta(S\text{-}C_4\text{-}H_{10}) - \beta(C_3\text{-}C_4\text{-}H_9) - \beta(C_3\text{-}C_4\text{-}H_{10})$
15. α-CH_2 twist	$\beta(S\text{-}C_4\text{-}H_9) - \beta(S\text{-}C_4\text{-}H_{10}) - \beta(C_3\text{-}C_4\text{-}H_9) + \beta(C_3\text{-}C_4\text{-}H_{10})$
16. β-CH_2 scissor	$5\alpha(H_7\text{-}C_3\text{-}H_8) + \gamma(C_2\text{-}C_3\text{-}C_4)$
17. β-CH_2 rock	$\beta(C_2\text{-}C_3\text{-}H_7) - \beta(C_2\text{-}C_3\text{-}H_8) + \beta(C_4\text{-}C_3\text{-}H_7) - \beta(C_4\text{-}C_3\text{-}H_8)$
18. β-CH_2 wag	$\beta(C_2\text{-}C_3\text{-}H_7) + \beta(C_2\text{-}C_3\text{-}H_8) - \beta(C_4\text{-}C_3\text{-}H_7) - \beta(C_4\text{-}C_3\text{-}H_8)$
19. β-CH_2 twist	$\beta(C_2\text{-}C_3\text{-}H_7) - \beta(C_4\text{-}C_3\text{-}H_8) - \beta(C_2\text{-}C_3\text{-}H_7) + \beta(C_4\text{-}C_3\text{-}H_8)$
20. CH_3 sym. def.	$\beta(C_2\text{-}C_5\text{-}H_{11}) + \beta(C_2\text{-}C_5\text{-}H_{12}) + \beta(C_2\text{-}C_5\text{-}H_{13}) - \alpha(H_{11}\text{-}C_5\text{-}H_{12}) - \alpha(H_{11}\text{-}C_5\text{-}H_{13}) - \alpha(H_{12}\text{-}C_5\text{-}H_{13})$
21. CH_3 rock	$2\beta(C_2\text{-}C_5\text{-}H_{11}) - \beta(C_2\text{-}C_5\text{-}H_{13}) - \beta(C_2\text{-}C_5\text{-}H_{12})$
22. CH_3 rock	$\beta(C_2\text{-}C_5\text{-}H_{13}) - \beta(C_2\text{-}C_5\text{-}H_{12})$
23. CH_3 asym. def.	$2\alpha(H_{12}\text{-}C_5\text{-}H_{13}) - \alpha(H_{11}\text{-}C_5\text{-}H_{12}) - \alpha(H_{11}\text{-}C_5\text{-}H_{13})$
24. CH_3 asym. def.	$\alpha(H_{11}\text{-}C_5\text{-}H_{12}) - \alpha(H_{11}\text{-}C_5\text{-}H_{13})$
25. C*–H bend (i/p)	$\beta(S\text{-}C_2\text{-}H_6) - \beta(C_3\text{-}C_2\text{-}H_6)$
26. C*–H bend (o/p)	$2\beta(C_5\text{-}C_2\text{-}H_6) - \beta(S\text{-}C_2\text{-}H_6) - \beta(C_3\text{-}C_2\text{-}H_6)$
27. CH_3 bend (i/p)	$\gamma(S\text{-}C_2\text{-}C_5) - \gamma(C_3\text{-}C_2\text{-}C_5)$
28. CH_3 bend (o/p)	$\gamma(S\text{-}C_2\text{-}C_5) + \gamma(C_3\text{-}C_2\text{-}C_5)$
29. Ring pucker	$\tau(S\text{-}C_2\text{-}C_3\text{-}C_4) - \tau(C_2\text{-}C_3\text{-}C_4\text{-}S) + \tau(C_3\text{-}C_4\text{-}S\text{-}C_2) - \tau(C_4\text{-}S\text{-}C_2\text{-}C_3)$
30. CH_3 torsion	$\tau(H_{12}\text{-}C_5\text{-}C_2\text{-}S) + \tau(H_{13}\text{-}C_5\text{-}C_2\text{-}H_6) + \tau(H_{11}\text{-}C_5\text{-}C_2\text{-}C_3)$
31. C_5–H_{11} stretch	
32. C_5–H_{12} stretch	
33. C_5–H_{13} stretch	

[a]All coordinates were normalized. Normalization constants not shown. See Fig. 1 for atom numbering.

Can. J. Chem. Downloaded from www.nrcresearchpress.com by 91.144.44.67 on 09/07/12
For personal use only.

tion. In practice the first approach is limited to only one pair of transitions, namely peaks no. 5 and 6, corresponding to the ring deformation mode ν_{29}. Although both ν_{27} and ν_{28} also exhibit shoulders corresponding to the axial conformer, the bands are not sufficiently resolved for this purpose. For ν_{29} the measured absorption intensity for the equatorial transition is greater by a factor of 1.55, with the axial band being appreciably broader (23 vs. 13 cm^{-1} FWHH). The calculated molar absorptivities are in the opposite order, both basis sets predicting an intensity ratio of 1 to 1.77 equatorial to axial, thus suggesting an excess of the former by about 2.7 (1.55 × 1.77) or 73%.

One way of estimating the relative abundance of the two conformers from the inversion potential is to assume only two possible ring orientations, each of which corresponds to a local (axial or equatorial) energy minimum. The 6-31G* (191 cm^{-1}) and experimental (118 cm^{-1}) (2) energy differences separating these minima then indicate that, respectively, 73 or 64% of the molecules adopt the equatorial conformation. Probably the soundest method for evaluating the relative abundance in the vapour phase is to determine the population, at room temperature, of each energy level of the ring inversion mode. Among the levels below the barrier, three correspond to the equatorial conformer and two to the axial, with the Boltzmann distribution indicating overall populations of 52 and 24% respectively. The remaining 24%, which occupy the levels above the barrier, may either be designated as "equatorial" or "axial" in the same ratio, or divided equally between the two. These two alternatives indicate a range of 64–68% equatorial conformation.

Adopting the mean of 66% as a fair reflection of the experimental inversion potential, and with the solution infrared absorption intensities for ν_{29} suggesting that 73% of molecules occupy the equatorial conformation, we have taken the average of these two as our best estimate of the true value. The theoretical spectra plotted in Figs. 3 and 5 thus represent a sum of the spectra calculated for the equatorial and axial species, weighted by 70 and 30%, respectively.

Infrared intensities, force constants, and normal mode descriptions

The two weighted calculated spectra (3-21G and 6-31G*) are both in reasonably good qualitative agreement with the observed (see Figs. 3 and 5). Perhaps most surprising is that the mid-infrared 6-31G* spectrum is not clearly more accurate than the 3-21G. Most striking is the discrepancy for the β-CH_2 wag (ν_{15}, peak no. 29), for which the 6-31G* band is substantially weaker than either the experimental or 3-21G transition. A number of other apparent discrepancies between the 6-31G* and experimental spectra may be attributed to differences between the experimental bandwidths and the assumed value of 10 cm^{-1} used for the calculated spectrum.

The calculated infrared absorption intensities are useful in confirming many of the assignments for the axial conformer, particularly for cases where the calculated molar absorptivity differs for the two conformers. For example the relative prominence of ν_{29}^{ax} at 545.2 cm^{-1} (peak no. 6, Figs. 2 and 3) is rationalized by noting that the calculated intensity of 3.9 km mol^{-1} is nearly twice that predicted for the equatorial mode. Other cases where the axial transition is conspicuous include ν_{14} (peaks no. 32 and 31 equatorial and axial, respectively), ν_{25} (no. 29 and 30), ν_{18} (no. 24 and 25), and ν_{22} (no. 18 and 19). In each of these cases the molar absorptivity is calculated to be higher for the axial conformer than for the equatorial (see 6-31G* calculation, Table 5 and Fig. 2).

The normal modes of the equatorial conformer are described in terms of the potential energy distribution in local symmetry

TABLE 4. Scaling factors for thietane, 2-methyloxetane, and 2-methylthietane

	Thietane[b]		2-Methyloxetane[c]		2-Methylthietane[d]	
Coordinate[a]	3-21G	6-31G*	3-21G	6-31G*	3-21G	6-31G*
CS stretch	1.048	0.809	0.851	0.710	1.048	0.809
CC stretch (ring)	0.960	0.852	1.013	0.872	0.960	0.852
CC stretch (methyl)	—	—	0.988	0.823	0.988	0.852
α-CH stretch	0.804	0.818	0.790	0.810	0.804	0.818
β-CH stretch	0.815	0.820	0.818	0.824	0.815	0.820
CH_3 stretch	—	—	0.832	0.829	0.832	0.829
Ring deformation	0.743	0.812	[0.706]	0.832	0.743	0.812
Ring pucker	[0.970]	[0.80]	[0.80]	[0.80]	[0.970]	[0.80]
α-CH_2 scissor	0.802	0.782	0.764	0.767	0.802	0.782
α-CH_2 rock	0.957	0.799	0.849	0.808	0.957	0.799
α-CH_2 wag	0.799	0.753	0.802	0.757	0.799	0.753
α-CH_2 twist	0.795	0.792	0.797	0.768	0.795	0.792
β-CH_2 scissor	0.786	0.789	0.780	0.774	0.786	0.789
β-CH_2 rock	0.772	0.829	0.843	0.849	0.772	0.829
β-CH_2 wag	0.762	0.772	0.744	0.751	0.762	0.772
β-CH_2 twist	0.757	0.804	0.743	0.792	0.757	0.804
CH_3 sym. def.	—	—	0.761	0.764	0.761	0.764
CH_3 asym. def.	—	—	0.758	0.781	0.758	0.781
CH_3 rock	—	—	0.749	0.806	0.749	0.806
CH_3 torsion	—	—	[0.865]	[0.80]	[0.865]	[0.80]
CH_3 bend (i/p)	—	—	0.830	0.835	0.830	0.835
CH_3 bend (o/p)	—	—	1.016	0.874	1.016	0.874
C2-H bend (i/p)	—	—	0.822	0.757	0.822	0.757
C2-H bend (o/p)	—	—	0.788	0.776	0.788	0.776

[a]Coordinate definitions for thietane are given in ref. 5. Designations α and β refer to the 4- and 3-positions respectively for both 2-methylthietane and 2-methyloxetane. The α-CH stretch factor also scales the C2–H stretching coordinate.
[b]Thietane 3-21G scaling factors from ref. 5.
[c]2-Methyloxetane 3-21G scaling factors from ref. 4.
[d]Scaling factors transferred from 2-methyloxetane and thietane, used for predicting the frequencies listed in Table 5.

Can. J. Chem. Downloaded from www.nrcresearchpress.com by 91.144.44.67 on 09/07/12
For personal use only.

coordinates. To demonstrate the correspondence between the normal modes of the two conformers we use a method analogous to "normal mode scrambling", which relates the normal coordinates of a deuterated species to those of the parent compound. We begin using the standard relationships,

$$[1] \quad Q_{eq} = L_{eq}^{-1} R_{eq}$$

$$[2] \quad Q_{ax} = L_{ax}^{-1} R_{ax}$$

where R denotes the local symmetry coordinates of Table 3, and Q and L the normal coordinates and eigenvectors in terms of displacements of R. We now define a new set of displacement coordinates for the axial conformer,

$$[3] \quad S_{ax} = L_{eq}^{-1} R_{ax}$$

whereby each coordinate S_{ax}^{i} corresponds to the normal coordinate Q_{eq}^{i} of the equatorial conformer. Combining [2] and [3] gives

$$[4] \quad S_{ax} = L_{eq}^{-1} L_{ax} Q_{ax}$$

where the eigenvectors of the matrix $L_{eq}^{-1}L_{ax}$ then express the normal coordinates Q_{ax} in terms of displacements of S_{ax}. Table 6 describes the normal coordinates of the axial conformer in terms of the potential energy distribution among diagonal elements of the matrix $L_{eq}' F_{ax}^{R} L_{eq}$ (F_{ax}^{R} being the scaled local symmetry force constants) whose elements are the force constants in the S_{ax} coordinate system,

$$[5] \quad PED_{ax}^{i} = \sum_{j} (L^{-1}{}_{eq} L_{ax})_{ji} (L_{eq}' F_{ax} L_{eq})_{jj} / \lambda_i$$

For clarity the S_{ax}^{i} have been identified with Q_{eq}^{i} in Table 6.

The correct correspondence among the CH_2 scissor/CH_3 asymmetric deformation modes is shown clearly by this analysis, with those calculated at 1448.9, 1447.7, and 1442.9 cm^{-1} for the axial conformer corresponding to ν_{12}, ν_{10}, and ν_{11} of the equatorial structure. The frequency ordering for ν_5 and ν_6 is similarly reversed when the ring is inverted, although in this case the two normal coordinates for the equatorial conformer essentially mix to form in-phase and out-of-phase combinations. The calculated intensities support interchanging the order for the axial conformer, with ν_5^{eq} (calcd. 2950.2 cm^{-1}, 44.8 km mol^{-1}) then matched with the axial transition calculated at 2950.9 cm^{-1} (52.0 km mol^{-1}), and ν_6^{eq} (2937.7 cm^{-1}, 17.8 km mol^{-1}) with the axial mode at 2955.0 cm^{-1} (10.8 km mol^{-1}). For the two bending modes ν_{21} and ν_{22} the normal coordinates of the axial conformer consist of in-phase and out-of-phase combinations of Q_{21}^{eq} and Q_{22}^{eq}. Here we have labelled the two modes ν_{21}^{ax} and ν_{22}^{ax} in order of descending frequency in Table 5, although in such a case the alternative designation is equally valid.

The apparent interchange in the ordering of ν_{26} and ν_{27} is very surprising. The transitions calculated at 796.8 and 704.9 cm^{-1} for the equatorial conformer are suggested to correspond to those predicted at 727.6 and 773.1 cm^{-1} for the axial, implying

TABLE 5. Observed and calculated transitions for 2-methylthietane[a]

	Equatorial				Axial				Difference (Ax−Eq)		
	Calcd. ν (cm^{-1}), A ($km\,mol^{-1}$)				Calcd. ν (cm^{-1}), A ($km\,mol^{-1}$)				Calcd. (cm^{-1})		
ν	3-21G	6-31G*	Obsd. (cm^{-1})	Peak no.[b]	3-21G	6-31G*	Obsd. (cm^{-1})	Peak no.[b]	3-21G	6-31G*	Obsd. (cm^{-1})
1	3011.9 (12.2)	3002.3 (31.3)	2992.7	49	3012.9 (11.3)	3001.8 (31.6)	2992.7	49	1.0	−0.5	
2	2989.9 (26.6)	2988.7 (39.9)	2976.6	48	2989.8 (30.9)	2987.8 (49.4)	2976.6	48	−0.1	−0.9	
3	2962.1 (15.6)	2967.9 (44.2)	2965.9	46	2968.0 (18.3)	2970.0 (41.6)	2965.9	46	5.9	2.1	
4	2972.9 (11.3)	2964.8 (23.7)	2962.0	45	2974.7 (10.1)	2966.2 (17.9)	2962.0	45	1.8	1.4	
5	2949.2 (29.3)	2950.2 (44.8)	2942.7	44	2950.1 (29.3)	2950.9 (52.0)	2942.7	44	0.9	0.7	
6	2950.7 (5.2)	2937.7 (17.8)	2937.0	43	2960.9 (2.0)	2955.0 (10.8)	(2962.0)	45	10.2	27.3	(24.3)
7	2926.2 (25.2)	2922.2 (45.5)	2928.8	42	2926.3 (25.5)	2924.9 (42.1)	2928.8	42	0.1	2.7	
8	2909.3 (22.4)	2911.4 (28.8)	2918.2	41	2908.9 (23.9)	2908.5 (32.5)	2918.2	41	−0.4	−2.9	
9	1470.2 (2.1)	1468.0 (1.9)	1461.3	37	1470.6 (2.2)	1469.5 (0.7)	1461.3	37	0.4	1.5	
10	1452.6 (5.9)	1450.6 (2.7)	1459.0	36	1452.6 (5.2)	1447.7 (1.7)	1459.0	36	0.0	−2.9	
11	1447.7 (6.0)	1445.3 (6.3)	1454.1	35	1447.2 (6.0)	1442.9 (4.5)	1454.1	35	−0.5	−2.4	
12	1442.0 (6.5)	1444.3 (0.5)	1445.2	34	1442.5 (7.0)	1448.9 (2.6)	1445.3	34	0.5	4.6	
13	1374.5 (7.9)	1373.8 (4.3)	1378.5	33	1376.1 (8.3)	1372.2 (2.9)	1378.5	33	1.6	−1.6	
14	1330.2 (4.4)	1335.8 (8.2)	1338.3	32	1323.0 (2.7)	1323.0 (10.9)	1323.8	31	−7.2	−12.8	−14.5
15	1269.0 (9.8)	1267.3 (0.6)	1269.5	29	1271.5 (18.4)	1276.7 (2.1)	1274.5	30	2.5	9.4	5.0
16	1220.3 (22.8)	1229.2 (12.2)	1227.8	28	1224.5 (11.8)	1228.0 (6.6)	1227.8	28	4.1	−1.2	
17	1224.7 (13.0)	1225.6 (10.1)	1220.6	27	1207.9 (7.6)	1214.2 (3.6)	1208.8	26	−16.8	−11.4	−11.8
18	1188.7 (1.1)	1180.2 (5.1)	1172.7	24	1194.1 (4.4)	1189.6 (12.7)	1184.3	25	5.3	9.4	11.4
19	1143.5 (19.2)	1151.1 (13.4)	1142.8	23	1147.6 (20.6)	1155.0 (11.2)	1142.8	23	4.1	3.9	
20	1124.7 (1.2)	1093.2 (2.9)	1101.4	22	1084.6 (0.9)	1060.9 (1.5)	1061.5	21	−40.1	−32.3	−39.9
21	1015.5 (5.2)	1014.0 (1.9)	1017.4	20	1017.0 (0.6)	1013.1 (0.6)	1017.4	20	1.5	−0.9	
22	991.3 (5.0)	995.8 (2.3)	997.1	18	993.9 (8.1)	1003.0 (3.9)	1005.2	19	2.6	7.2	8.1
23	973.9 (1.6)	956.2 (0.5)	963.1	17	972.0 (1.2)	959.7 (0.2)	963.1	17	−1.9	3.5	
24	911.8 (2.0)	911.2 (0.9)	914.2	15	911.8 (1.3)	913.6 (0.6)	916.8	16	0.0	2.4	2.4
25	878.8 (2.3)	882.3 (1.6)	887.1	14	882.5 (2.7)	871.5 (2.0)	876.4	13	3.7	−10.8	−10.7
26	796.8 (4.2)	796.8 (1.7)	806.8	12	782.6 (4.8)	773.1 (2.6)	(790)	11	−14.2	−23.7	(−6.8)
27	715.7 (7.8)	704.9 (4.7)	700.4	9	730.6 (8.1)	727.6 (4.4)	718.4	10	14.9	22.7	18.4
28	649.0 (8.9)	634.0 (6.4)	633.7	7	664.9 (7.4)	656.8 (5.3)	655.0	8	15.9	22.8	21.3
29	519.4 (3.4)	522.7 (2.2)	514.4	5	553.1 (5.9)	551.2 (3.9)	545.2	6	33.7	28.5	30.8
30	411.3 (0.6)	399.3 (0.6)	403.3	4	380.7 (0.5)	365.6 (0.4)	370.0	3	−30.6	−33.7	−33.3
31	285.2 (1.7)	280.3 (1.2)	280.8	1	303.8 (1.3)	295.8 (1.1)	301.1	2	18.6	15.5	20.3
32	234.5 (0.2)	225.4 (0.2)			257.0 (0.1)	248.3 (0.1)			22.5	22.9	
33	94.6 (1.0)	105.2 (0.9)			95.1 (1.2)	56.7 (1.0)			0.5	−48.5	
Average error	7.6	5.1			7.9	5.9					

[a]Force fields scaled using factors listed in Table 4. Absorption intensities (A_i) in parentheses are calculated for the scaled force field.
[b]Peak nos. correspond to bands labeled in Figs. 2–6, and listed in Table 1. All frequencies except those for certain C–H stretches (see Table 1) and ν_{26}^{ax} are from the vapour phase spectrum.

shifts of −69.2 and 68.2 cm^{-1} respectively. We have labelled these two modes for the axial conformer in Table 5 as ν_{26} and ν_{27} in order of descending frequency. The large changes in the nature of these normal coordinates does provide a rationalization of certain features in the vapour phase infrared spectrum. One would anticipate on this basis that the band contour for ν_{27}^{ax} would resemble closely that observed for ν_{26}^{eq}, and vice versa. Indeed, the transition assigned as ν_{27}^{ax} (peak no. 10, Fig. 2) shows a distinct Q-branch in the vapour phase spectrum, and in this respect is more similar in shape to ν_{26}^{eq} (peak no. 12) than to ν_{27}^{eq} (peak no. 9). The absence of any distinct vapour phase transition for ν_{26}^{ax} is then explained by the possibility that it adopts the same band contour as observed for ν_{27}^{eq} (peak no. 9), and is hence indistinguishable from the P-branch of ν_{26}^{eq} (peak no. 12).

We have compared the scaled 3-21G and 6-31G* force fields for the equatorial conformer in the same fashion, expressing the 3-21G normal coordinates as combinations of those predicted for the 6-31G* calculation (details not shown). The two force fields are very similar, with the leading term in the potential energy distribution exceeding 0.9 in all but 7 cases. Three of these are the very closely spaced modes ν_{10}–ν_{12}, where the normal coordinates are very sensitive to small changes in the relevant diagonal force constants. For similar reasons, $Q_{16}^{6\text{-}31G*}$ and $Q_{17}^{6\text{-}31G*}$ are mixed to some extent for 3-21G, with the two frequencies calculated at 1220.3 and 1224.3 cm^{-1} corresponding most closely to ν_{16}^{eq} and ν_{17}^{eq}, respectively. The frequency ordering is also interchanged for the two CH stretches ν_5 and ν_6, calculated for the 3-21G force field at 2949.2 and 2950.7 cm^{-1}, respectively, although in this case the normal modes match the 6-31G* coordinates very closely. Finally, the coordinates $Q_{13}^{6\text{-}31G*}$ and $Q_{14}^{6\text{-}31G*}$ are mixed for the 3-21G force field, with the normal coordinates $Q_{13}^{3\text{-}21G} = 0.9\ Q_{13}^{6\text{-}31G*} - 0.4\ Q_{14}^{6\text{-}31G*}$ and $Q_{14}^{3\text{-}21G} = 0.9\ Q_{14}^{6\text{-}31G*} + 0.4\ Q_{13}^{6\text{-}31G*}$. This reflects a relatively strong coupling of the CH_3 symmetric deformation and C*–H bending (out-of-plane) coordinates for the 6-31G* force field, which is almost entirely absent for 3-21G.

The 6-31G* force fields optimized for 2-methyloxetane and

Can. J. Chem. Downloaded from www.nrcresearchpress.com by 91.144.44.67 on 09/07/12
For personal use only.

TABLE 6. Vibrational assignments for 2-methylthietane

	Equatorial		Axial	
ν	Calcd.	Assignment[a]	Calcd.	Assignment[b]
1	3002.3	α-CH_2 asym str	3001.8	Q_1^{eq}
2	2988.7	CH_3 asym str	2987.8	Q_2^{eq}
3	2967.9	CH_3 asym str	2970.0	0.6 Q_3^{eq} + 0.3 Q_4^{eq}
4	2964.8	β-CH_2 asym str	2966.2	0.6 Q_4^{eq} + 0.3 Q_3^{eq}
5	2950.2	α-CH_2 sym str	2955.0	0.6 Q_6^{eq} + 0.4 Q_5^{eq}
6	2937.7	C*–H str	2950.9	0.5 Q_5^{eq} + 0.4 Q_6^{eq}
7	2922.2	β-CH_2 sym str	2924.9	Q_7^{eq}
8	2911.4	CH_3 sym str	2908.5	Q_8^{eq}
9	1468.0	0.5 α-CH_2 sc + 0.5 β-CH_2 sc	1469.5	Q_9^{eq}
10	1450.6	0.6 CH_3 asym def (24) + 0.3 CH_3 asym def (23)	1448.9	Q_{12}^{eq}
11	1445.3	0.3 CH_3 asym def (24) + 0.3 CH_3 asym def (23)	1447.7	Q_{10}^{eq}
12	1444.3	0.4 CH_3 asym def (23) + 0.3 β-CH_2 sc	1442.9	Q_{11}^{eq}
13	1373.8	CH_3 sym def	1372.2	Q_{13}^{eq}
14	1335.8	0.5 C*–H bend (o/p) + 0.2 CH_3 sym def	1323.0	Q_{14}^{eq}
15	1267.3	β-CH_2 wa	1276.9	0.6 Q_{15}^{eq} + 0.2 Q_{17}^{eq}
16	1229.2	0.4 C*–H bend (i/p) + 0.2 α-CH_2 wa	1228.0	0.6 Q_{16}^{eq} + 0.2 Q_{18}^{eq}
17	1225.6	0.5 β-CH_2 tw + 0.3 α-CH_2 wa	1214.2	0.5 Q_{17}^{eq} + 0.2 Q_{16}^{eq}
18	1180.2	0.3 α-CH_2 wa + 0.2 α-CH_2 tw	1189.6	0.6 Q_{18}^{eq} + 0.2 Q_{17}^{eq}
19	1151.1	0.3 CH_3 ro (22) + 0.2 α-CH_2 wa + 0.1 CH_3*C*–*C*str	1155.0	Q_{19}^{eq}
20	1093.2	0.4 H_3*C*–*C* str + 0.1 C*–H bend (i/p)	1060.9	Q_{20}^{eq}
21	1014.0	0.3 CH_3 ro (22) + 0.3 α-CH_2 tw + 0.2 C*–H bend (i/p)	1013.1	0.5 Q_{22}^{eq} + 0.4 Q_{21}^{eq}
22	995.8	0.3 α-CH_2 tw + 0.2 CH_3 ro (21)	1003.0	0.5 Q_{21}^{eq} + 0.4 Q_{22}^{eq}
23	956.2	H_2*C*–*C* str	959.7	0.6 Q_{23}^{eq} + 0.3 Q_{24}^{eq}
24	911.2	0.3 CH_3 ro (21) + 0.2 β-CH_2 ro + 0.2 α-CH_2 ro	913.6	0.6 Q_{24}^{eq} + 0.3 Q_{23}^{eq}
25	882.3	0.4 CH_3*C*–*C* str + 0.2 CH_3 ro (22)	871.5	0.5 Q_{25}^{eq} + 0.3 Q_{26}^{eq}
26	796.8	0.4 α-CH_2 ro + 0.2 β-CH_2 ro	773.1	0.7 Q_{27}^{eq} + 0.2 Q_{25}^{eq}
27	704.7	H_2*C*–*S* str	727.6	0.6 Q_{26}^{eq} + 0.2 Q_{25}^{eq}
28	634.0	CH_3*C*–*S* str	656.8	Q_{28}^{eq}
29	522.7	Ring deformation	551.2	Q_{29}^{eq}
30	399.3	CH_3 bend (o/p)	365.6	Q_{30}^{eq}
31	280.3	CH_3 bend (i/p)	295.8	Q_{31}^{eq}
32	225.4	CH_3 torsion	248.3	Q_{32}^{eq}
33	105.2	Ring pucker	56.7	Q_{33}^{eq}

[a]As inferred from potential energy distribution (PED) for the scaled 6-31G* force field. Coordinates with coefficients less than 0.1 are omitted. Abbreviations: sc, ro, wa, tw = scissor, rock, wag, twist; str = stretch; i/p, o/p = in-plane, out-of-plane. Designations α and β distinguish the CH_2 groups at the 4- and 3-positions, respectively. The CH_2 and CH_3 stretching coordinates are combined as in-phase/out-of-phase (CH_2) or C_{3v} symmetry coordinates for determining the potential energy distribution. Italics (e.g., CH_3*C*–*C*) indicate the bond involved for skeletal stretch.

[b]Potential energy distribution in group coordinates S_{ax} which are defined by the eigenvectors for the normal coordinates Q_i^{eq} of the equatorial compound. See text.

thietane have also been compared to the scaled 3-21G force fields reported previously (4, 5) with equally good correspondence among the normal modes. In addition, the infrared absorption intensities calculated for thietane in conjunction with the 6-31G* force field are invariably compatible with the published assignments (5). These comparisons thus support the accuracy of the scaled force constants in each case, which in turn reinforces the accuracy of the 2-methylthietane force fields scaled using the same factors.

For 2-methylthietane the scaled 3-21G force constants agree well with the corresponding 6-31G* values (see Table 7), with the changes that result upon inversion of the ring also reproduced. Such differences as do arise between corresponding 3-21G and 6-31G* values may be ascribed in general to differences in the optimized structures (G-matrices). This is confirmed by scaling the 3-21G force constants using factors that give diagonal force constants equal to the 6-31G* values. The frequencies calculated for this force field do not agree well either with the 6-31G* calculations or with the experimental positions. For the methyl C–C stretch (coordinate no. 5) the discrepancy between the 6-31G* and 3-21G force constants is very large. In this case we believe the 3-21G value to be high, which then explains the anomalously large discrepancy between the 3-21G and 6-31G* calculated positions for ν_{20}. The 3-21G scaling factor optimized for the methyl C–C stretch of 2-methyloxetane is evidently not suitable for transfer to 2-methylthietane, which is not surprising given the influence of the C—O bond upon the scaling factors for CH_2 and CH_3 deformations involving the -CH_2—O and CH_3—O units (5, 6).

Some of the larger frequency shifts that occur upon immersion of the ring may be explained by changes in the diagonal force constants. Such is the case for the two methyl bends ν_{30} and ν_{31}, which are, respectively, lowered and raised in frequency for the axial conformer in accordance with changes in the diagonal force constants for coordinates no. 28 and 27 of Tables 3 and 7. The C*–H stretching force constant increases

Can. J. Chem. Downloaded from www.nrcresearchpress.com by 91.144.44.67 on 09/07/12
For personal use only.

TABLE 7. Scaled diagonal force constants for 2-methylthietane[a]

Coord. no.	Type[b]	Conformer[c]	3-21G	6-31G*	Coord. no.	Type	3-21G	6-31G*
1	C–S str	eq	2.868	2.675	18	β-CH_2 wa	0.668	0.659
		ax	2.879	2.689			0.668	0.659
2	C–S str	eq	2.942	2.858	19	β-CH_2 tw	0.652	0.670
		ax	2.939	2.880			0.652	0.667
3	C–C str	eq	3.991	3.965	20	CH_3 sym def	0.561	0.526
		ax	4.030	3.973			0.553	0.527
4	C–C str	eq	4.058	4.067	21	CH_3 asym def	0.643	0.643
		ax	4.054	4.064			0.645	0.643
5	C–C str	eq	4.678	4.319	22	CH_3 asym def	0.606	0.618
		ax	4.656	4.265			0.611	0.626
6	C*–H str	eq	4.798	4.752	23	CH_3 ro	0.529	0.536
		ax	4.839	4.809			0.531	0.538
7	β-CH str	eq	4.890	4.890	24	CH_3 ro	0.533	0.539
		ax	4.864	4.845			0.531	0.538
8	β-CH str	eq	4.862	4.839	25	C*–H bend (i/p)	0.737	0.716
		ax	4.895	4.883			0.675	0.665
9	α-CH str	eq	4.804	4.777	26	C*–H bend (o/p)	0.522	0.532
		ax	4.774	4.757			0.532	0.546
10	α-CH str	eq	4.782	4.760	27	CH_3 bend (i/p)	0.883	0.840
		ax	4.818	4.802			1.021	0.943
11	Ring def	eq	1.275	1.305	28	CH_3 bend (o/p)	1.300	1.225
		ax	1.299	1.329			1.241	1.132
12	α-CH_2 sc	eq	0.713	0.715	29	Ring pucker	0.069	0.076
		ax	0.714	0.718			0.068	0.034
13	α-CH_2 ro	eq	0.515	0.487	30	CH_3 torsion	0.034	0.032
		ax	0.513	0.489			0.040	0.037
14	α-CH_2 wa	eq	0.688	0.656	31	Methyl C–H str	4.876	4.860
		ax	0.687	0.657			4.860	4.840
15	α-CH_2 tw	eq	0.622	0.625	32	Methyl C–H str	4.827	4.831
		ax	0.619	0.622			4.854	4.848
16	β-CH_2 sc	eq	0.719	0.717	33	Methyl C–H str	4.743	4.760
		ax	0.719	0.718			4.738	4.743
17	β-CH_2 ro	eq	0.498	0.534				
		ax	0.497	0.523				

[a]Units of mdyn $Å^{-1}$ (stretches) or mdyn rad^{-1} (bends). See Table 3 for coordinate definitions.
[b]Abbreviations sc, ro, wa, tw, str = scissor, rock, wag, twist, stretch.
[c]Refers to orientation of the methyl group, as throughout this paper, and *not* to the orientation of the coordinates listed under "Type".

for the axial conformer (the C*–H bond assuming the *equatorial* orientation), with analogous changes occurring also for the α-CH stretching force constants. In the latter case the α-CH_2 symmetric and asymmetric stretching frequencies ν_1 and ν_5 are unaffected, as the roles simply interchange for the CH displacements comprising Q_1 and Q_5. For the C*–H stretch the increased diagonal force constant shifts the calculated position for ν_6 by over 17 cm^{-1}, in exact agreement with the shift expected for a CH bond undergoing the shift (0.057 mdyn/Å) calculated for the 6-31G* force field.

Conclusion

The vibrational spectra have been measured for 2-methylthietane from 400–3200 cm^{-1} (infrared) and 100–1600 cm^{-1} (Raman), and assigned through systematic scaling of harmonic force fields calculated at the 3-21G and 6-31G* levels. Each basis set gives two stable conformers (axial and equatorial) as energy minima. The spectra were assigned through prediction of the vibrational spectrum, by scaling the *ab initio* force fields using factors derived solely through optimization to other molecules. The accuracy of the frequencies calculated in each case results from the availability of a large pool of experimental data for the related molecules thietane and 2-methyloxetane, permitting in each case statistically meaningful refinement of a sufficiently flexible set of scaling factors. Both the axial and equatorial structures have been shown to contribute to the observed spectra of 2-methylthietane, with the latter confirmed as the more stable both by the 6-31G* *ab initio* results and by the intensity of the infrared spectrum as compared to that of the axial. All transitions of the equatorial and nearly all those of the axial conformer have been assigned, and the two are suggested to coexist in the ratio 70% equatorial to 30% axial as inferred from measurement of the solution infrared intensity measurements and consideration of the published inversion potential.

A method is outlined for comparing the normal coordinates as calculated for different basis sets or conformers. This procedure establishes the correspondence between the normal modes of the equatorial and axial conformers, and demonstrates clearly those instances where appreciable changes do occur. By the same criterion the scaled 3-21G and 6-31G* force fields are shown to provide very similar descriptions of the normal modes in general, with the only discrepancies occurring for very closely spaced transitions. Frequency shifts that occur upon ring inversion may in some cases be traced to alterations in the relevant diagonal force constants, with 3-21G invariably reproducing 6-31G* in this regard. We have thus found the 6-31G*

Can. J. Chem. Downloaded from www.nrcresearchpress.com by 91.144.44.67 on 09/07/12
For personal use only.

calculation to have only marginal advantages over 3-21G in the prediction of frequencies and, perhaps more surprising, the absorption intensities. Both basis sets clearly provide structures and force constants of sufficient accuracy to confirm the axial species as stable, with success of the vibrational analysis resting primarily upon the accuracy of scaling factors transferred to scale the force constants and, less critically, upon the choice of basis set. The evaluation of vibrational circular dichroism (VCD) intensities is certainly more sensitive to details of the force fields. This will be discussed in a forthcoming publication concerning the VCD spectrum of 2-methylthietane.[2]

1. (*a*) T. B. FREEDMAN and L. A. NAFIE. Top. Stereochem. **17**, 213 (1987); (*b*) P. J. STEPHENS and M. A. LOWE. Annu. Rev. Phys. Chem. **36**, 213 (1985).
2. J. A. DUCKETT, T. L. SMITHSON, and H. WIESER. J. Mol. Struct. **56**, 157 (1979).
3. P. PULAY, G. FOGARASI, and J. E. BOGGS. J. Am. Chem. Soc. **101**, 2550 (1979).
4. R. A. SHAW, N. IBRAHIM, and H. WIESER. J. Phys. Chem. In press.
5. R. A. SHAW, C. CASTRO, A. RAUK, and H. WIESER. J. Phys. Chem. **92**, 6528 (1988).
6. R. A. SHAW, C. P. URSENBACH, A. RAUK, and H. WIESER. Can. J. Chem. **66**, 1318 (1988).
7. Y. ETIENNE and R. SOULAS. *In* Heterocyclic compounds. Vol. 19 (2). *Edited by* A. Weissburger. Wiley–Interscience, New York. 1964. p. 725.
8. (*a*) J. K. KAUPPINEN, D. J. MOFFATT, H. H. MANTSCH, and D. G. CAMERON. Appl. Spectrosc. **35**, 271 (1981); (*b*) J. K. KAUPPINEN, D. J. MOFFATT, D. G. CAMERON, and H. H. MANTSCH. Appl. Opt. **20**, 1866 (1981).
9. J. S. BINKLEY, M. J. FRISCH, D. J. DEFREES, K. RAGHAVACHARI, R. A. WHITESIDE, H. B. SCHLEGEL, L. M. FLUDER, and J. A. POPLE. Department of Chemistry, Carnegie–Mellon University, Pittsburgh, Pennsylvania.
10. A. RAUK and R. DUTLER. J. Comput. Chem. **8**, 324 (1987).
11. K. KARAKIDA and K. KUCHITSU. Bull. Chem. Soc. Jpn. **48**, 1961 (1975).

[2]R. A. Shaw, N. Ibrahim, and H. Wieser. Manuscript in preparation.

Can. J. Chem. Downloaded from www.nrcresearchpress.com by 91.144.44.67 on 09/07/12
For personal use only.

The system fluorosulfuric acid (HSO_3F) and bis(fluorosulfuryl)peroxide ($S_2O_6F_2$) — a solution study[1]

W. V. CICHA, F. G. HERRING, AND F. AUBKE[2]

Department of Chemistry, The University of British Columbia, Vancouver, B.C., Canada V6T 1Y6

Received June 13, 1989

W. V. CICHA, F. G. HERRING, and F. AUBKE. Can. J. Chem. **68**, 102 (1990).

Solutions of bis(fluorosulfuryl)peroxides, $S_2O_6F_2$, in fluorosulfuric acid, HSO_3F, are synthetically very useful. The nature of the solvent (HSO_3F)–solute ($S_2O_6F_2$ or $SO_3F^{\bullet}$) interaction is probed by Raman, ^1H and ^{19}F NMR, and ESR spectroscopy, the latter focussing on the radical $SO_3F^{\bullet}$ formed by the dissociation of $S_2O_6F_2$. Both $S_2O_6F_2$ and $SO_3F^{\bullet}$ behave as very weak bases in HSO_3F. Proton transfer between solvent and solute and SO_3F exchanges are suggested on the basis of NMR and ESR measurements. The symmetry and electronic structure of the $SO_3F^{\bullet}$ radical are altered in HSO_3F solution. A g_{iso} value of 1.97267 is obtained. The radical appears to be formed on dissolution of $S_2O_6F_2$ at room temperature and persists down to 183 K. The solvent–solute interaction depends on the acid strength of the protonic solvent and addition of the base KSO_3F to HSO_3F leads to a loss of solubility and the separation of $S_2O_6F_2$ as a second phase.

Key words: solution study in HSO_3F of weak bases, Raman spectrum, ESR study in HSO_3F.

W. V. CICHA, F. G. HERRING et F. AUBKE. Can. J. Chem. **68**, 102 (1990).

Des solutions de peroxyde de bis(fluorosulfuryle), $S_2O_6F_2$, dans de l'acide fluorosulfurique, HSO_3F, sont très utiles en synthèse. On a étudié la nature de l'interaction solvant (HSO_3F)–soluté ($S_2O_6F_2$ ou $SO_3F^{\bullet}$) en faisant appel aux spectroscopies Raman, rmn du ^1H et ^{19}F ainsi que rpe; cette dernière méthode est orientée vers le radical $SO_3F^{\bullet}$ qui se forme par la dissociation du $S_2O_6F_2$. Le $S_2O_6F_2$ ainsi que le $SO_3F^{\bullet}$ se comportent comme des bases faibles dans le HSO_3F. Sur la base des mesures effectuées à l'aide de la rmn et de la rpe, on suggère qu'il existe un transfert de proton entre le solvant et le soluté ainsi qu'un échange avec le SO_3F. En solution dans le HSO_3F, la symétrie et la structure électronique du radical $SO_3F^{\bullet}$ sont modifiées. On a obtenu une valeur de g_{iso} de 1,97267. Le radical semble se former lors de la dissolution du $S_2O_6F_2$ à la température ambiante et sa présence persiste jusqu'à 183 K. L'interaction solvant–soluté dépend de la force de l'acide du solvant protonique; l'addition de la base KSO_3F à l'acide HSO_3F provoque une diminution de la solubilité et la séparation du $S_2O_6F_2$ dans une deuxième phase.

Mots clés : étude du solution des bases faibles dans HSO_3F, spectre Raman, étude RPE dans HSO_3F.

[Traduit par la revue]

Introduction

In the past, we have employed solutions of bis(fluorosulfuryl)peroxide, $S_2O_6F_2$ (1), in fluorosulfuric acid, HSO_3F (2), for the synthesis of a wide range of binary and ternary fluorosulfates by either one of the two general routes:

$$[1]\quad E + (n/2)S_2O_6F_2 \xrightarrow[HSO_3F]{25\text{–}135^\circ C} E(SO_3F)_n$$

or

$$[2]\quad mM^ISO_3F + E + (n/2)S_2O_6F_2 \xrightarrow[HSO_3F]{25\text{–}135^\circ C} M^I_m[E(SO_3F)_{n+m}]$$

where E = main group or transition metal, n = 2, 3, 4, or 5; M^ISO_3F = alkali metal fluorosulfate, prepared in situ from M^ICl and HSO_3F, and m = 1, 2, or 3. Recent representative examples with E = Au (3), Ta (3), Nb (3), Rh (4), Mn (5), Ru (6), Pt (7), Sn (8), Ge (8), Br or I (9), illustrate the wide range of this method. While $S_2O_6F_2$ is the principal oxidizing agent in this reagent combination, the role of HSO_3F is three-fold: (*a*) to allow an expansion of the temperature range well beyond the boiling point of $S_2O_6F_2$, 67.1°C (10), (*b*) to maintain in solution and hence at the reactive site a high concentration of $SO_3F^{\bullet}$ radicals formed by the reversible dissociation of $S_2O_6F_2$ (11), and (*c*) to dissolve reaction product from the metal surface during reaction. All three factors contribute to fast, complete oxidation reactions, where $S_2O_6F_2$ alone often gives only incompletely reacted products or requires excessively long reaction times.

Both $S_2O_6F_2$ and HSO_3F are miscible at 25°C in any proportion to give stable, clear, colorless solutions. On the other hand, $S_2O_6F_2$ is virtually insoluble at 25°C in the related protonic acid H_2SO_4. This observation is found useful when crude $S_2O_6F_2$, formed in the catalytic fluorination of SO_3 (12), is purified by extracting SO_3 with concentrated H_2SO_4. We became interested in investigating the HSO_3F–$S_2O_6F_2$ system to find an answer to this rather puzzling behaviour.

Previous studies of this system by cryoscopy and conductometry (13) allow preliminary conclusions. In HSO_3F solution, $S_2O_6F_2$ is said to be a non-electrolyte at 25°C (13). It is reportedly present in its molecular form and has been used to determine the cryoscopic constant of HSO_3F (13). However, the second observation based on cryoscopy is strictly valid only for temperatures at or around the melting point of HSO_3F at −88.98°C.

These observations by Gillespie *et al.* (13) appear to argue against two possible interaction modes between HSO_3F and $S_2O_6F_2$: (*i*) extensive ionizing solvation of $S_2O_6F_2$ in HSO_3F, with protonation the most probable initial process:

$$[3]\quad HSO_3F + S_2O_6F_2 \overset{HSO_3F}{\rightleftharpoons} HS_2O_6F_2^{+}{}_{(solv)} + SO_3F^{-}{}_{(solv)}$$

and (*ii*) electron transfer between the $SO_3F^{\bullet}$ radical and the self-ionization ion SO_3F^-, according to

$$[4]\quad SO_3F^{\bullet}{}_{(solv)} \overset{+e^-}{\underset{-e^-}{\rightleftharpoons}} SO_3F^{-}{}_{(solv)}$$

However, caution is indicated for two reasons: (*i*) the absence

[1]This paper is dedicated to Professor Ronald J. Gillespie on the occasion of his 65th birthday.

[2]Author to whom correspondence should be addressed.

Can. J. Chem. Downloaded from www.nrcresearchpress.com by 186.148.149.217 on 09/07/12
For personal use only.

Can. J. Chem. Downloaded from www.nrcresearchpress.com by 186.148.149.217 on 09/07/12
For personal use only.

of appreciable dissociation of $S_2O_6F_2$ into radicals at room temperature in HSO_3F–$S_2O_6F_2$ solutions needs to be demonstrated. An ESR study (14) on pure $S_2O_6F_2$ has concluded that $SO_3F^\bullet$ radicals are present at ambient temperature and may persist to 4°C. (*ii*) The conductivities measured on solutions of $S_2O_6F_2$ in HSO_3F are small but increase linearly with increasing $S_2O_6F_2$ concentrations (13). In a strongly acidic, protonic solvent like HSO_3F, a true non-electrolyte is expected to reduce proton mobility, and hence electrical conductance in these media, due to a structure breaking effect on the hydrogen bonded system. Based on the reported electrical conductivity alone, it appears more appropriate to view $S_2O_6F_2$ as a weak electrolyte in HSO_3F.

To address these points, three methods are employed in this study: (*i*) Raman spectroscopy on solutions of $S_2O_6F_2$ in HSO_3F. The vibrational spectra of the individual compounds are well known (15–17); (*ii*) NMR spectroscopy of both ^1H and ^{19}F nuclei; (*iii*) ESR spectroscopy of the system, to detect the onset of the formation of $SO_3F^\bullet$ radicals and their persistence in HSO_3F. Again, the ESR spectrum of the SO_3F radical has been reported (14).

Two variations are promising: (*a*) temperature variation of both the NMR and ESR spectra, the former between −75 and +45°C, the latter between −90 and +50°C; and (*b*) a variation of the acidity of HSO_3F. The autoprotolysis equilibrium:

$$[5] \quad 2HSO_3F \rightleftharpoons H_2SO_3F^+ + SO_3F^-$$

may be shifted to the basic side by addition of SO_3F^- in form of the standard base KSO_3F (18), while removal of the base ion results in an increase in overall acidity.

Experimental

Chemicals

Fluorosulfuric acid (Allied Chemical) was purified by double distillation at atmospheric pressure (18). Bis(fluorosulfuryl)peroxide, $S_2O_6F_2$ (12) and KSO_3F (18), were prepared by published methods. Anhydrous hydrogen fluoride was obtained from Matheson of Canada. The solutions studied were prepared by distilling weighed amounts of volatile compounds ($S_2O_6F_2$, HSO_3F) into reactor flasks equipped with Teflon coated stir bars, used for effective mixing. KSO_3F was added initially before distilling $S_2O_6F_2$ and HSO_3F onto the solid. Additions were carefully weighed. All solutions were vigorously stirred before use. Samples for Raman, ESR, or NMR studies were prepared inside an inert atmosphere box (3) from stock solutions previously prepared as described above. Solutions in anhydrous HF were obtained in Kel-F [poly(chlorotrifluoroethylene)] reaction vials fitted with Monel metal tops. A metal vacuum line was used for the HF transfer. All solutions in HSO_3F were made up in 25 or 50 mL Pyrex vessels fitted with Kontes Teflon stem valves.

Instrumentation

All NMR spectra were obtained on a Varian XL-300 FT spectrometer, operating at 282.231 MHz for the ^{19}F experiments. The Raman spectrometer has been described previously (8). Electron spin resonance measurements were made using an X-band (9.0 GHz) homodyne spectrometer employing a Varian 12 in. magnet equipped with a MK II Fieldial control. Phase-sensitive detection at 100 kHz was achieved with an Ithaco Dynatrac 391 A lock-in amplifier. The temperature was controlled to within ±0.1°C using a Varian E-257 temperature controller. The ESR samples were loaded via a Teflon-tipped syringe into 100 μL glass tubes under inert atmosphere and sealed with Teflon plugs. No signals were observed for background runs at room temperature with HSO_3F or N_2 gas.

^{19}F NMR chemical shifts are all relative to $CFCl_3$, while ^1H NMR chemical shifts are relative to TMS, with both utilizing $CDCl_3$ as the external locking agent.

Results and discussion

(a) Raman spectroscopy

The Raman spectrum recorded on a 1:2 (by volume) solution of $S_2O_6F_2$ in HSO_3F is shown in Fig. 1. A comparison with the previously reported Raman spectra for HSO_3F (15) and $S_2O_6F_2$ (16) as well as with a re-recorded spectrum on freshly distilled $S_2O_6F_2$ allows the following conclusions: (*i*) The solution spectrum is in first approximation a composite spectrum of the two major components. (*ii*) The relatively strong, polarized vibrational bands of $S_2O_6F_2$ are unperturbed and are clearly recognizable, while some of the weaker bands are not observed. It is clear that the bulk of bis(fluorosulfuryl)peroxide is present as such in solution of HSO_3F. (*iii*) The O—O stretching band at 801 cm^{-1} is unchanged in both position and relative intensity. It appears that the O—O bond strength is not altered in HSO_3F solution. This may be viewed as evidence that at room temperature no change in reactivity of $S_2O_6F_2$ in solution has occurred. (*iv*) The OH stretching mode is observed as a broad band centered at 3096 ± 10 cm^{-1}, a position comparable to the reported IR band at 3125 cm^{-1} in liquid HSO_3F (17). This implies that intermolecular interaction between HSO_3F and $S_2O_6F_2$ effects νOH in a very similar way as intermolecular association does in liquid HSO_3F. (*v*) Besides bands due to $S_2O_5F_2$ (19), the only other new, weak bands found at 1281, ~1100 and 774 cm^{-1} are attributed to the presence of SO_3F^- in solution, based on a precedent (15) and the fact that addition of KSO_3F results in an increase in intensity for all three bands. Weakly basic behavior of $S_2O_6F_2$, suggested previously from electrical conductivity data (13), is seen as the reason for the formation of SO_3F^- according to eq. [3].

If hydrogen bonding or even proton transfer plays a role in the solution process, it is valid to ask why HSO_3F is capable of interacting with $S_2O_6F_2$ in this manner while H_2SO_4 is seemingly not. There are two plausible, interrelated explanations: (*i*) HSO_3F is a better proton donor than H_2SO_4, as reflected in their respective $-H_0$ values of 15.07 and 11.93 (21, 22) or 10.09 for 96.5% H_2SO_4 (22*a*), and (*ii*) tight intermolecular hydrogen bonding in H_2SO_4, causing its high viscosity (22*b*), is not effectively broken up by the insufficiently basic $S_2O_6F_2$ molecule.

It should hence be possible to (*a*) dissolve $S_2O_6F_2$ in acids stronger than H_2SO_4 using the $-H_0$ values as a guide and (*b*) diminish the solubility of $S_2O_6F_2$ in HSO_3F by reducing its acidity through addition of KSO_3F.

(b) Solubility studies of $S_2O_6F_2$ in strong protonic acids

There are, in addition to HSO_3F, two simple protonic acids which are of higher acidity than H_2SO_4, are available in anhydrous form and will not dissociate or decompose at room temperature as, for example, HSO_3Cl or $HClO_4$: anhydrous HF, $-H_0$ = 15.1 (23) and HSO_3CF_3, $-H_0$ = 14.1 (24). The latter, trifluoromethylsulfuric acid is similar in acidity to a number of additional sulfonic acids with various other fluorocarbon substituents on sulfur (24).

As we reported some time ago (25), $S_2O_6F_2$ is extremely soluble in HSO_3CF_3. However, these solutions are unstable and slowly give rise to the evolution of heat and volatile products, among them CF_3OSO_2F. There is sufficient evidence from the reported interaction of the two acids HSO_3F and HSO_3CF_3 (26, 27) and from the thermal instability of the peroxide $(CF_3)_2S_2O_6$ (28) to conclude that oxidative cleavage of the S—C bond occurs (29). It appears then that HSO_3CF_3 is not a good solvent for $S_2O_6F_2$ in spite of high solubility of the latter, and synthetic

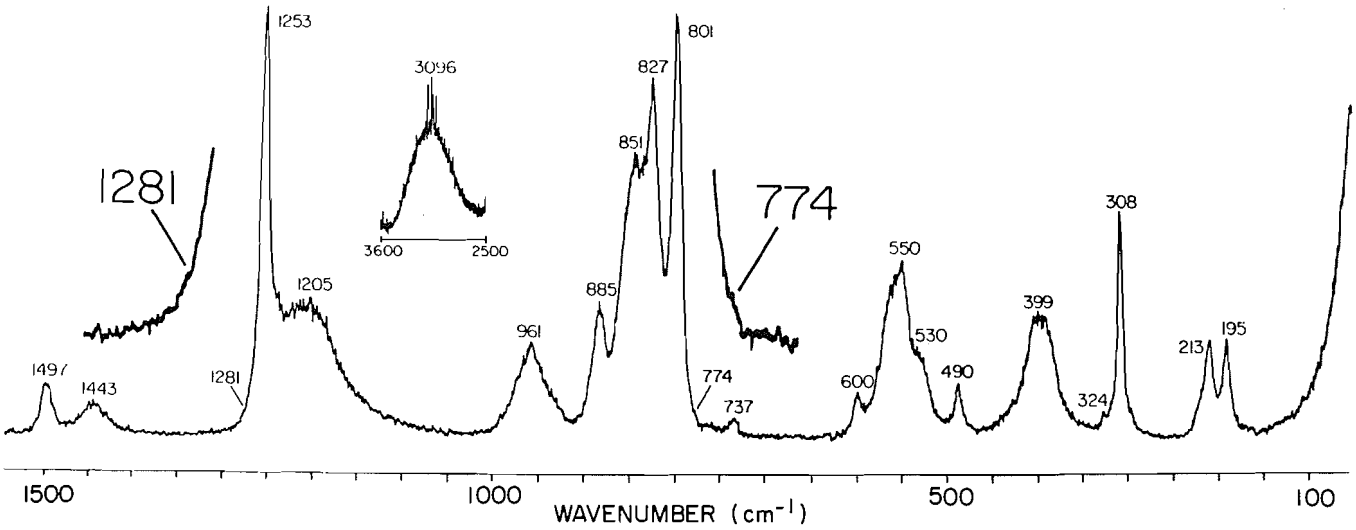

FIG. 1. Raman spectrum of $S_2O_6F_2$ in HSO_3F (1:2 solution by volume) at 20°C.

use of the mixture is only indicated where oxidation reactions proceed rapidly (25).

In anhydrous HF, the solubility of $S_2O_6F_2$ is lower than in either HSO_3F or HSO_3CF_3 but is still appreciable. The $-H_0$ value of 15.1 would suggest a higher solubility than is actually observed. This value, however, has been obtained by extrapolation during a study of the HF–SbF_5 system (23). On account of small amounts of H_2O acting as a base in "anhydrous" HF, measured $-H_0$ values have ranged as low as ~11 (24). Difficulties encountered in removing the last traces of water from HF (30), the low boiling point, and the possibility of F^- vs. SO_3F^- exchange during synthesis argue against extensive synthetic use of HF–$S_2O_6F_2$ solutions.

Addition of the base KSO_3F (13, 18) to a solution of $S_2O_6F_2$ in HSO_3F (molar ratio acid to peroxide = 1.72) at room temperature results in a separation into two phases once the concentration of KSO_3F exceeds 1.8 *M*. Assuming that KSO_3F is the only base in the system, its concentration would correspond to a $-H_0$ value of 11.8 (20).

As expected from the reported densities at 25°C of 1.726 g cm^{-3} (26) for HSO_3F and 1.645 g cm^{-3} for $S_2O_6F_2$ (31), the latter is the principle constituent of the upper layer. The volume of this upper layer increases steadily with increasing KSO_3F concentration or decreasing temperature and contains at 25°C the bulk of the $S_2O_6F_2$ for a 3.1 *M* KSO_3F solutions. The physical separation of both phases by pipetting inside the inert atmosphere box is now possible.

The observed solubility loss of $S_2O_6F_2$ can be explained by the lowered acidity as argued above. Alternatively, one may view the strongly basic SO_3F^- as competing effectively with $S_2O_6F_2$ for HSO_3F to form solvates. The strength of the SO_3F^-–HSO_3F interaction is evident from the isolation and structural characterization of solid monosolvates of the type $M^1[H(SO_3F)_2]$ with M^1 = Na or Cs (32, 33). It does seem that the acid strength of a protonic acid or superacid is instrumental in forming stable solutions of $S_2O_6F_2$. When the acid strength of HSO_3F is increased by addition of $Ta(SO_3F)_{5(solv)}$ (3*b*), complete miscibility with $S_2O_6F_2$ is noted over the whole temperature range (318–198 K).

The solubility loss found has some implications regarding the synthetic use of $S_2O_6F_2$ solutions in HSO_3F. Metal oxidation in the presence of alkali metal fluorosulfates, aimed at forming ternary fluorosulfato complexes according to eq. [2], may show (at least initially) the same phase separation. It becomes important to choose reaction conditions and reactant concentrations where sufficient $S_2O_6F_2$ remains in the acid phase to effect oxidation.

The qualitative solubility study described here has pointed to conditions where $S_2O_6F_2$ ceases to be soluble in HSO_3F and to the role acidity or protonating ability plays in the system. The subsequent section will probe into the nature of the interaction using NMR. There are now two sides to the problem: (*a*) the acid phase where $S_2O_6F_2$ is the solute and HSO_3F the solvent, and (*b*) the upper phase formed under basic conditions, where the roles may be reversed.

(c) ^{19}F and ^1H NMR spectroscopy studies

Both $S_2O_6F_2$ and HSO_3F give rise to sharp, single line resonances in the ^{19}F NMR spectrum, which at 298 K occur at 39.03 and 40.74 ppm relative to $CFCl_3$, respectively. Both resonances show only a small temperature dependence over the temperature range studied. The $S_2O_6F_2$ line gradually shifts from 39.04 ppm at 318 K to 38.83 ppm at 198 K, while the ^{19}F resonance line of HSO_3F shifts from 40.77 to 40.61 ppm in the same temperature range. The expected peak separation between both lines remains reasonably constant at 1.72 ± 0.04 ppm over the whole range.

The ^1H resonance of HSO_3F also shifts very gradually from 10.47 ppm relative to TMS at 298 K to 10.67 ppm at 198 K. Weak ^{19}F resonances due to coupling of ^{33}S or ^{34}S isotopes have previously been observed for both HSO_3F and $S_2O_6F_2$ (34, 35). The low natural abundance (0.76% for ^{33}S and 4.22% for ^{34}S) and ^{33}S–^{19}F coupling result in very weak signals.

It hence appears that in the anticipated absence of spin–spin interactions (^{19}F–^1H), only single lines are expected and any evidence for solvent–solute interaction will have to come from two sources: (*a*) ^{19}F and ^1H chemical shifts relative to their positions in pure HSO_3F and $S_2O_6F_2$ and (*b*) the integration of peak areas of the ^{19}F resonances obtained on mixtures of known composition. Of these two, chemical shift information obtained on a 300 MHz instrument should be more accurate and reliable than peak area integration, due to the ~10% systematic error

Can. J. Chem. Downloaded from www.nrcresearchpress.com by 186.148.149.217 on 09/07/12
For personal use only.

TABLE 1. Summary of ^{19}F and ^{1}H NMR data for $S_2O_6F_2$–HSO_3F solutions

Temperature (K)	Molar ratio (H/OX)[a]	I/S[b]	Δ $^{19}FS_2O_6F_2$ (ppm) A[c]	Δ $^{19}FHSO_3F$ (ppm) B[c]	$B - A$ (ppm)	Δ ^{1}H HSO_3F (ppm)[c]
318	4.44	1.33	+0.31	−0.20	−0.51	—
298		1.34	+0.24	−0.16	−0.40	0
253		1.32	+0.19	+0.05	−0.14	+0.01
218		1.34	+0.18	+0.12	−0.06	−0.52
198		1.30	+0.18	+0.12	−0.06	−0.41
318	1.86	1.40	+0.32	−0.15	−0.47	—
298		—	—	—	—	−0.09
253		—	—	—	—	−0.09
218		—	—	—	—	−0.61
198		1.26	+0.10	+0.06	−0.04	−0.57
318	0.96	1.44	+0.31	−0.12	−0.43	—
298		1.39	+0.13	−0.14	−0.27	—
253		1.46	+0.05	0	−0.05	—
198		1.28	+0.11	+0.12	+0.01	—
298	0.078	0.95	−0.06	−0.07	−0.01	−0.65
198		0.89	0	+0.06	+0.06	−0.09

[a] H = HSO_3F; OX = $S_2O_6F_2$.
[b] I = integration peak area H/OX ratio, S = H/OX fluorine content ratio from stoichiometry.
[c] Difference between signal position of pure species and that found in solution.

associated with the latter. However, peak integration is useful in the detection of SO_3F^- group exchange between solvent and solute.

From previous studies on the KSO_3F–HSO_3F system (36), it is expected that increased SO_3F^- concentration will cause a small, concentration dependent upfield shift of the ^{19}F solvent resonance line. Such a shift is indeed noticed at 298 and 318 K for mixtures of HSO_3F and $S_2O_6F_2$ of various molar ratios, as seen in Table 1. The solute resonance, on the other hand, shifts gradually downfield, but the magnitude of this shift decreases with decreasing temperature. Below 298 K, the ^{19}F resonance due to HSO_3F begins to move downfield as well, and at 198 K the initial peak separation is nearly restored. A downfield shift of the ^{19}F resonances, indicative of reduced shielding of the F-nucleus, is expected for protonated bis(fluorosulfuryl)peroxide, $HS_2O_6F_2^+$, as well as for its hydrogen bridged solvate, formulated tentatively as $S_2O_6F_2 \cdot HSO_3F$.

The observations made for various mole ratios and temperatures, summarized in Table 1, may be expressed in terms of two simple processes, *solvate formation* and *ionic dissociation of the solvate* according to the overall reaction scheme:

$$[6] \quad S_2O_6F_2 + HSO_3F \rightleftarrows S_2O_6F \cdot HSO_3F \rightleftarrows S_2O_6F_2H^+_{(solv)} + SO_3F^-_{(solv)}$$

It appears that ionic dissociation is slowed down at lower temperatures while solvate formation is now favoured. Consistent with this view is a noticeable upfield shift of the ^{1}H resonance by about 0.5 to 0.6 ppm which is best observed at 218 and 198 K for solutions with HSO_3F in excess.

The overall process [6] involving proton bridging and proton transfer from HSO_3F to $S_2O_6F_2$ is, however, not the only exchange process in the system. As peak area integrations (also summarized in Table 1) indicate, the "acid" ^{19}F resonance is increased at the expense of the signal attributed to $S_2O_6F_2$ over the whole temperature range (318 to 198 K), with no pronounced temperature dependency recognizable. It must be concluded that fluorosulfate exchange involving the acid, its self-ionization ions $H_2SO_3F^+$ and more so SO_3F^-, the solute ion $S_2O_6F_2H^+$ and the solvate, formulated as $S_2O_6F_2 \cdot HSO_3F$, occurs in addition to proton exchange. As seen from the tabulated integration ratios, SO_3F exchange is consistently observed, apparently independent of temperature and molar ratio of solute and solvent. This exchange involves about 10 to 20% of the $S_2O_6F_2$ present in the mixture, increasing slightly with temperature and acid/peroxide molar ratio.

Addition of KSO_3F to the HSO_3F–$S_2O_6F_2$ mixture initially has no significant effect on either proton or SO_3F-exchange, as long as the concentration of KSO_3F in HSO_3F remains below 1.8 M. This is apparent from the trends in the observed chemical shifts and measured integrated peak areas seen in Figs. 2 and 3, respectively. When the concentration of KSO_3F is raised above 1.8 M, a two-phase system results, and the ^{19}F NMR spectrum becomes more complicated.

Figure 4 shows the ^{19}F NMR spectrum of a typical two-phase system, with a KSO_3F concentration of 3.14 M, and a molar $HSO_3F/S_2O_6F_2$ ratio of 1.72. As the temperature is lowered from 298 to 198 K, peak A gets less intense and eventually completely vanishes, while peak B increases in intensity. The intense, unlabelled peak at ~40 ppm is due to HSO_3F while the two resonances labelled A′ and B′ are assigned to $S_2O_5F_2$ present as an impurity in both phases. Resonances A and A′ are attributed to $S_2O_6F_2$ and $S_2O_5F_2$, respectively, dissolved in HSO_3F, while B and B′ resonances are due to the same respective species found in the upper phase. As the temperature is lowered, the solubility of both $S_2O_6F_2$ and $S_2O_5F_2$ in HSO_3F decreases while the upper layer consequently increases in volume.

Peak B and the downfield B′ resonance are both distorted triplets, indicative of a comparable perturbation effecting both the $S_2O_6F_2$ and $S_2O_5F_2$ resonances. Similar triplets are observed in all solutions studied with the KSO_3F concentrations greater than 3 M. Unequal spacings, relative intensities and difference

Can. J. Chem. Downloaded from www.nrcresearchpress.com by 186.148.149.217 on 09/07/12
For personal use only.

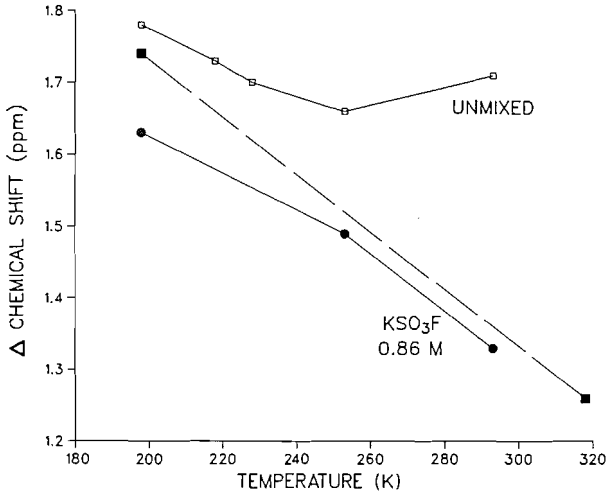

FIG. 2. Temperature dependence of the separation between HSO_3F and $S_2O_6F_2$ ^{19}F NMR signals (■: "neutral", H/OX molar ratio = 1.86; ●: "basic", H/OX molar ratio = 1.68; □: H and OX measured separately (unmixed)).

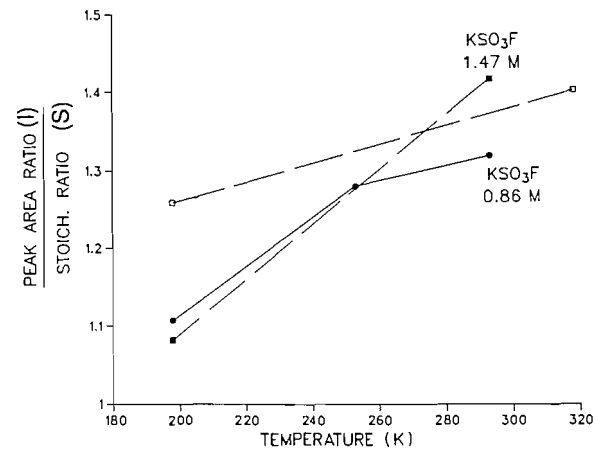

FIG. 3. Temperature dependence of $HSO_3F/S_2O_6F_2$ ^{19}F NMR integration peak area ratio relative to the stoichiometric fluorine content ratio (□: "neutral", H/OX molar ratio = 1.86; ■: "basic", H/OX molar ratio = 2.22; ●: "basic", H/OX molar ratio = 1.68).

in temperature dependency of the resonances within the triplet pattern argue against any spin-spin coupling as the cause. The most likely explanation of the triplet patterns is hence hydrogen bridging from the HSO_3F dissolved in the upper phase to both $S_2O_6F_2$ and $S_2O_5F_2$. A possible bridging conformation is shown in the Fig. 4-inset for $HSO_3F \cdot S_2O_6F_2$, where the acid proton is involved in a hydrogen bridge to one of the S—O bonds of $S_2O_6F_2$, creating different environments for each of the three fluorine atoms present. The intense middle peak of the triplet is assigned to F_2 in Fig. 4-inset, since its chemical shift is within ±0.05 ppm of the free $S_2O_6F_2$ resonance. Accordingly, the presence of free, unsolvated $S_2O_6F_2$ in the upper phase would contribute to this peak as well, accounting for its greater relative intensity, seen especially at 198 K. A similar interpretation applies to the $S_2O_5F_2$ resonance B′.

The structure observed for both $S_2O_6F_2$ and $S_2O_5F_2$ resonances in the upper phase also suggests the absence of exchange or ionization processes and the presence of well defined solvates at low temperatures with both sulfur(VI) oxyfluorides acting as proton acceptors. In the acid phase, with solvent and solute roles

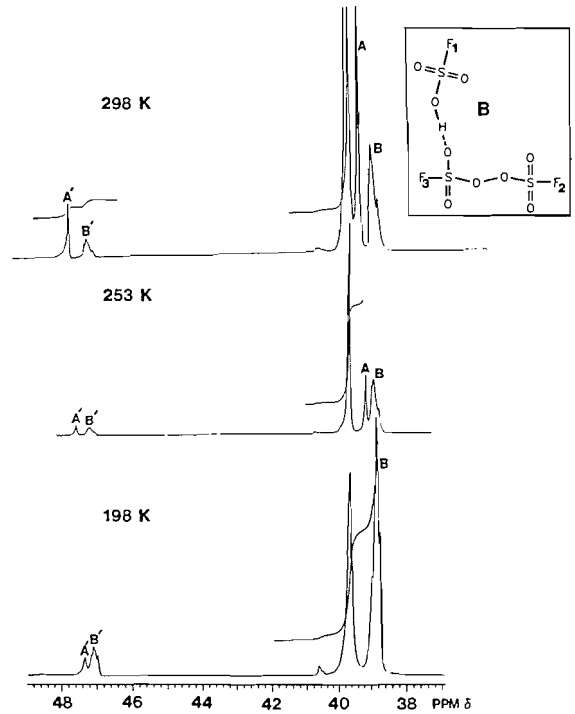

FIG. 4. ^{19}F NMR spectra of two-phase KSO_3F–$S_2O_6F_2$–HSO_3F solution ([KSO_3F] = 3.14 *M*, H/OX molar ratio = 1.72).

reversed, only single, reasonably sharp signals A and A′ (see Fig. 4) are present. Hence, no inferences can be made regarding the structure of the solvates in the strongly ionizing medium. The mechanism of SO_3F exchange between HSO_3F and $S_2O_6F_2$, reflected in the peak area integration for both, remains unclear. The question arises whether cleavage of the O—O bond resulting in the formation of radicals like $SO_3F^{\bullet}_{(solv)}$ and their subsequent recombination may occur differently in HSO_3F solution. The NMR spectra provide no indication for the presence of radicals in concentrations large enough to effect peak positions, in respect to previous reports (37), or to cause line broadening, which has been observed in liquid $S_2O_6F_2$ at elevated temperature (38). The possibility of finding radicals in HSO_3F solution at lower concentrations is therefore better probed by ESR.

(d) Electron spin resonance study of the solvated fluorosulfate radical

The reversible dissociation of bis(fluorosulfuryl)peroxide into radicals according to:

[7] $S_2O_6F_2 \rightleftarrows 2SO_3F^{\bullet}$

has been studied previously by ESR with the radical $SO_3F^{\bullet}$ observed in the liquid (14), gaseous (39), and solid phase (38, 40). In addition, the radical has been generated by photolysis of fluorine fluorosulfate, $FOSO_2F$ and studied in a solid $CFCl_3$ matrix at 77 K (40). All reports agree on a *g*-value of close to 2.011, with hyperfine splitting observed in the solid state (39). In the liquid phase a single, structureless component with a temperature dependent linewidth of ~25 G at 290 K is observed (14). A similar band shape is reported for the gas phase spectrum of the radical (39).

Our own observations for liquid $S_2O_6F_2$ at 293 K differ slightly and probably not significantly from the previous reports, considering differences in computational analysis and magnetic field calibration of the spectra (41). A slightly higher

Can. J. Chem. Downloaded from www.nrcresearchpress.com by 186.148.149.217 on 09/07/12
For personal use only.

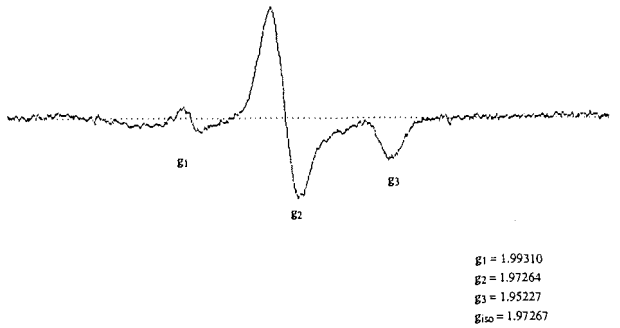

FIG. 5. Electron spin resonance spectrum of $S_2O_6F_2$ in HSO_3F (1:2.12 solution by volume) at 183 K.

g value of 2.0207 ± 0.0005 is obtained, but the linewidth of $\Delta H_{pp} \sim 26$ G is similar to previous reports (14).

When $S_2O_6F_2$ is dissolved in HSO_3F, a single, inhomogeneously broadened line is observed, which shows very little change in linewidth and g value between 283 and 323 K, with a g_0 value at 322 K of 1.9693. This signal persists when the temperature is gradually lowered and the spectrum obtained at 183 K is shown in Fig. 5. As can be seen, g is clearly anisotropic with g_{iso} found to be 1.97267. Hyperfine splitting is not observed.

The radical observed in solution is clearly not identical with $SO_3F^\bullet$ as reported previously (14, 38–40) or observed by us in liquid $S_2O_6F_2$. Consistent with the observation of three g-values (see Fig. 5), it can be concluded that the symmetry of the radical in HSO_3F solution is reduced below C_{2v}. On the other hand, $SO_3F^\bullet$ according to the vibrational analysis of the electronic spectrum (42) or to its vibrational spectrum studied in an inert gas matrix (43) has C_{3v} symmetry for both the electronic ground state ($^2A_2$) and the nearest excited state (^2E). Conversion of $SO_3F^\bullet$ to other radicals, such as $FSO_2^\bullet$ in solution (via a reduction), is rather unlikely because this species is short-lived and highly reactive, while the radical encountered here is persistent. Furthermore, $FSO_2^\bullet$ reportedly has a g value of 2.005 (40). It is more likely that the fluorosulfate radical, just like SO_3F^- (33) and to a lesser extent its dimer $S_2O_6F_2$, will form a solvate with HSO_3F which may subsequently (depending on the temperature) undergo ionic dissociation in an analogous manner as suggested for $S_2O_6F_2$ above:

[8] $$SO_3F^\bullet + HSO_3F \rightleftharpoons [FSO_3 \cdot HSO_3F]^\bullet \rightleftharpoons [HSO_3F^+]^\bullet + SO_3F^-$$

For both the mono-solvated or protonated radical, the overall symmetry would be at best C_s, assuming that protonation and hydrogen bridging involve oxygen, the more basic site, rather than fluorine on the $SO_3F^\bullet$ radical. Hence, three g values are expected and observed. In addition to the previously postulated radical displacement reaction in liquid $S_2O_6F_2$ (14) according to:

[9] $$SO_3F^\bullet + S_2O_6F_2 \rightleftarrows S_2O_6F_2 + SO_3F^\bullet$$

a similar displacement with HSO_3F:

[10] $$SO_3F^\bullet + HSO_3F \rightleftharpoons [FSO_3 \cdot HSO_3F]^\bullet \rightleftharpoons HSO_3F + SO_3F^\bullet$$

could compete effectively with the recombination reaction [7] and hence account for its persistence down to 183 K, close to the melting point of HSO_3F. Furthermore, a radical mediated SO_3F group exchange involving $S_2O_6F_2$ and HSO_3F could well explain observations made in the NMR section concerning peak area integrations. In view of the anticipated low radical concentration, alternate exchange pathways may, however, also be involved.

Finally, SO_3F radical migration via reactions [9] and [10] together with SO_3F^- migration involving a proton jump mechanism are seen to account for the fast and efficient metal oxidations performed in $HSO_3F/S_2O_6F_2$ (3–9). Hence, postulated hydrogen bridging to, and protonation of the $SO_3F^\bullet$ radical by HSO_3F not only explains the observed ESR spectrum, but also the radical's persistence in HSO_3F and its reactivity in this medium.

The proposed interaction of the $SO_3F^\bullet$ radical with HSO_3F is reversible, which accounts for the fact that both the solvent, HSO_3F, and the solute, $S_2O_6F_2$, can be separated quantitatively by distillation on account of differences in vapor pressures and boiling points (31). Hence, irreversible degradation of the $SO_3F^\bullet$ radical to, for example, $FSO_2^\bullet$ or other radical fragments is rather unlikely.

Summary and conclusions

The principle solute $S_2O_6F_2$ and its monomeric radical $SO_3F^\bullet$ behave as very weak bases in HSO_3F. All manifestations of the acid–base interaction are rather subtle with the possible exception of the ESR spectrum of solvated $SO_3F^\bullet$, where a change in symmetry and electronic structure seems to be apparent. Ironically, two principle conclusions reached in an earlier study of the HSO_3F–$S_2O_6F_2$ system (13), that $S_2O_6F_2$ is a non-electrolyte and present in undissociated form in HSO_3F are found to be not entirely valid. However, the solvated radical which is detectable at the freezing point of HSO_3F appears to be present in an extremely low concentration, and will not restrict the value of $S_2O_6F_2$ for cryoscopy in HSO_3F (13).

The techniques used in this study, Raman, ^1H, and ^{19}F NMR, and finally ESR spectroscopy show increasing usefulness (in the listed order) in studying the very weak bases. The solubility loss found for $S_2O_6F_2$ in HSO_3F–KSO_3F is very helpful in two respects: (*i*) it allows us to demonstrate that acidity or proton donor strength plays a key role in the weak acid–base interaction, and (*ii*) it permits the study of $S_2O_6F_2$ and HSO_3F in reversed roles, with $S_2O_6F_2$ now the solvent, using ^{19}F and ^1H NMR spectroscopy.

The formulation of monosolvated $S_2O_6F_2$ and $SO_3F^\bullet$ is chosen because for the related SO_3F^- ion such hydrogen bridged solvates are known (32), and in the case of $Cs[SO_3F \cdot HSO_3F]$ structurally characterized (33). Solvation of the $SO_3F^\bullet$ radical is seen to increase the lifetime and mobility of this species in HSO_3F. Both persistence and mobility of the radical contribute to the synthetic usefulness of the HSO_3F–$S_2O_6F_2$ system, demonstrated by us previously (3–9). While, consistent with the Raman spectra, there is no evidence for a weakening of the O—O bond in $S_2O_6F_2$ and hence a more facile formation of radicals in HSO_3F, there is evidence for a longer lifetime of the radical at low temperatures due to solvate formation.

Acknowledgement

Financial support of the Natural Sciences and Engineering Research Council of Canada is gratefully acknowledged.

1. R. A. DE MARCO and J. M. SHREEVE. Adv. Inorg. Radiochem. **16**, 109 (1974).
2. A. W. JACHE. Adv. Inorg. Radiochem. **16**, 177 (1974); (*b*) R. C. THOMPSON. *In* Inorganic sulphur chemistry. *Edited by* G. Nickless. Elsevier, Amsterdam. 1968. p. 587.
3. (*a*) K. C. LEE and F. AUBKE. Inorg. Chem. **18**, 389 (1979); **19**,

Can. J. Chem. Downloaded from www.nrcresearchpress.com by 186.148.149.217 on 09/07/12
For personal use only.

119 (1980); (*b*) W. V. CICHA and F. AUBKE. J. Am. Chem. Soc. **111**, 4328 (1989).
4. P. C. LEUNG, G. B. WONG, and F. AUBKE. J. Fluorine Chem. **35**, 607 (1987).
5. S. P. MALLELA and F. AUBKE. Inorg. Chem. **24**, 2969 (1985).
6. P. C. LEUNG and F. AUBKE. Can. J. Chem. **62**, 2892 (1984).
7. K. C. LEE and F. AUBKE. Inorg. Chem. **23**, 2124 (1984).
8. S. P. MALLELA, K. C. LEE, and F. AUBKE. Inorg. Chem. **23**, 653 (1984).
9. M. S. R. CADER, S. KARUNANITHY, and F. AUBKE. Synth. Metals, **30**, 9 (1989).
10. F. B. DUDLEY and G. M. CADY. J. Am. Chem. Soc. **78**, 290 (1956).
11. F. B. DUDLEY and G. H. CADY. J. Am. Chem. Soc. **85**, 3375 (1963).
12. G. H. CADY and J. M. SHREEVE. Inorg. Synth. **7**, 124 (1963).
13. R. J. GILLESPIE, J. B. MILNE, and R. C. THOMPSON. Inorg. Chem. **5**, 468 (1966).
14. P. M. NUTKOWITZ and G. VINCOW. J. Am. Chem. Soc. **91**, 5936 (1969); J. Phys. Chem. **75**, 245 (1975).
15. R. J. GILLESPIE and E. A. ROBINSON. Can. J. Chem. **40**, 644 (1962); **40**, 675 (1962).
16. A. M. QURESHI, L. E. LEVCHUK, and F. AUBKE. Can. J. Chem. **49**, 2544 (1971).
17. R. SAVOIE and P. A. GIGUÈRE. Can. J. Chem. **42**, 277 (1964).
18. J. BARR, R. J. GILLESPIE, and R. C. THOMPSON. Inorg. Chem. **3**, 1149 (1964).
19. R. J. GILLESPIE and E. A. ROBINSON. Can. J. Chem. **39**, 2179 (1961).
20. R. J. GILLESPIE and T. PEEL. J. Am. Chem. Soc. **95**, 5173 (1973).
21. R. J. GILLESPIE, T. PEEL, and E. A. ROBINSON. J. Am. Chem. Soc. **93**, 5083 (1971).
22. (*a*) C. R. JOHNSON, A. R. KATRITZKI, and S. A. SHAPIRO. J. Am. Chem. Soc. **91**, 6654 (1969); (*b*) T. C. WADDINGTON. Non-aqueous solvents. Appleton-Century-Crofts, New York, 1969.
23. (*a*) R. J. GILLESPIE and J. LIANG. J. Am. Chem. Soc. **110**, 6053 (1988); (*b*) T. A. O'DONELL. J. Fluor. Chem. **25**, 75 (1984).
24. G. A. OLAH, G. K. S. PRAKASH, and J. SOMMER. Superacids. John Wiley and Sons, New York. 1985.
25. J. R. DALZIEL and F. AUBKE. Inorg. Chem. **12**, 2707 (1973).
26. G. A. OLAH and T. OYAMA. Synthesis, **5**, 319 (1976).
27. R. E. NOFTLE. Inorg. Nucl. Chem. Lett. **16**, 195 (1980).
28. R. E. NOFTLE and G. H. CADY. Inorg. Chem. **4**, 1010 (1965).
29. S. P. MALLELA, J. R. SAMS, and F. AUBKE. Can. J. Chem. **63**, 3305 (1985).
30. M. F. A. DOVE and A. F. CLIFFORD. *In* Chemistry in non-aqueous ionizing solvents. Vol. 2.1. *Edited by* J. Jander, H. Spandau, and C. C. Addison. Viehweg, Braunschweig. 1971.
31. G. H. CADY. Adv. Inorg. Radiochem. **2**, 105 (1960).
32. C. JOSSON, M. DEPORCQ-STRATMAINS, and P. VAST. Bull. Soc. Chim. Fr. (9-10), 820 (1977).
33. C. BELIN, M. CHARBONNEL, and J. POTIER. J. Chem. Soc. Chem. Commun. 1036 (1981).
34. R. J. GILLESPIE and J. W. QUAIL. J. Chem. Phys. **39**, 2555 (1963).
35. R. A. STEWART, S. FUJIWARA, and F. AUBKE. J. Chem. Phys. **49**, 965 (1966).
36. A. M. QURESHI, H. A. CARTER, and F. AUBKE. Can. J. Chem. **49**, 35 (1971).
37. F. A. HOHORST and J. M. SHREEVE. Inorg. Chem. **5**, 2069 (1964).
38. R. A. STEWART. J. Chem. Phys. **51**, 3406 (1969).
39. R. A. STEWART, S. FUJIWARA, and F. AUBKE. J. Chem. Phys. **48**, 5524 (1968).
40. F. NEUMAYR and N. VANDERKOOI. J. Inorg. Chem. **4**, 1234 (1965).
41. P. S. PHILLIPS and F. G. HERRING. J. Magn. Reson. **57**, 43 (1984).
42. G. W. KING and C. H. WARREN. J. Mol. Spectrosc. **32**, 121 (1969).
43. E. M. SUZUKI, J. W. NIBLER, K. A. OAKES, and D. EGGERS, JR. J. Mol. Spectrosc. **58**, 201 (1975).

Can. J. Chem. Downloaded from www.nrcresearchpress.com by 186.148.149.217 on 09/07/12
For personal use only.

Synthesis, characterization, and fluxional behavior in solution of the salts $Et_4N^+[Me_2Ga(N_2C_5H_7)(OCH_2CH_2X)]M(CO)_3^-$ (where $N_2C_5H_7$ = 3,5-dimethylpyrazolyl, X = NMe_2 or SEt, and M = Cr, Mo, or W). X-Ray crystal structure of the W complex with X = NMe_2

KENNETH S. CHONG, STEVEN J. RETTIG, ALAN STORR, AND JAMES TROTTER

Department of Chemistry, University of British Columbia, 2036 Main Mall, Vancouver, B.C., Canada V6T 1Y6

Received May 8, 1989

KENNETH S. CHONG, STEVEN J. RETTIG, ALAN STORR, and JAMES TROTTER. Can. J. Chem. **68**, 109 (1990).

The tricarbonyl anions of Cr, Mo, and W incorporating unsymmetrical tridentate chelating pyrazolyl gallate ligands, $[Me_2Ga(N_2C_5H_7)(OCH_2CH_2X)]M(CO)_3^-$, have been isolated as their crystalline Et_4N^+ salts. ^1H nmr and solution infrared studies indicate that the octahedral anions display a facial arrangement of the gallate ligand and the three carbonyl groups. This stereochemistry has been proven definitively for the tungsten complex with X = NMe_2 by an X-ray structure determination (see below). Fluxional behavior for the anions in d_6-acetone solution has been demonstrated by variable temperature ^1H nmr studies and is compared to similar behavior displayed by the neutral molybdenum "allyl" complex, $[Me_2Ga(N_2C_3H_3)(OCH_2CH_2NMe_2)]Mo(CO)_2(\eta^3\text{-}C_4H_7)$. Crystals of tetraethylammonium [dimethyl(3,5-dimethylpyrazol-1-yl)(2-*N*,*N*-dimethylaminoethoxy)gallato-N^2,N^3,*O*]tricarbonyltungstate are orthorhombic, a = 11.312(9), b = 33.111(9), c = 7.445(6) Å, Z = 4, space group $P2_12_12_1$. The structure was solved by conventional heavy atom methods and was refined by full-matrix least-squares procedures to R = 0.033 and R_w = 0.034 for 2508 reflections with $I \geq 3\sigma(I)$. The $[Me_2Ga(N_2C_5H_7)(OCH_2CH_2NMe_2)]W(CO)_3^-$ anion has *fac*-octahedral coordination geometry with W—O = 2.228(7), W—N(pyrazolyl) = 2.299(8), W—N(amine) = 2.37(1), and W—CO = 1.91(1)–1.92(1) Å.

Key words: pyrazolyl-gallate complexes, fluxional behavior of Ga–W complexes, crystal structure of Ga–W complex, gallate–tungsten complexes.

KENNETH S. CHONG, STEVEN J. RETTIG, ALAN STORR et JAMES TROTTER. Can. J. Chem. **68**, 109 (1990).

On a isolé les anions tricarbonyl du Cr, du Mo et du W incorporant les ligands chélatants tridentates non-symétriques gallate de pyrazolyle, $[Me_2Ga(N_2C_5H_7)(OCH_2CH_2X)]M(CO)_3^-$, sous la forme de sels cristallins de tétraéthylammonium. Les études rmn du ^1H et infrarouge en solution indiquent que les anions octaédriques présentent un arrangement facial du ligand gallate et des trois groupements carbonyles. On a démontré cette stéréochimie sans ambiguïté en déterminant la structure de la complexe de tungstène, avec X = NMe_2, par diffraction des rayons-X (voir plus bas). Faisant appel à la rmn du ^1H à température variable, on a démontré le comportement fluxionnel des anions en solution dans la d_6-acétone et on l'a comparé au comportement semblable que présente la complexe neutre de l'«allyl» molybdène, $[Me_2Ga(N_2C_3H_3)(OCH_2CH_2NMe_2)]Mo(CO)_2(\eta^3\text{-}C_4H_7)$. Les cristaux du [diméthyl(3,5-diméthylpyrazol-1-yl) (2-*N*,*N*-diméthylaminoéthoxy) (gallato-N^2,N^3,*O*] tricarbonyltungstate de tétraéthylammonium sont orthorhombiques, avec a = 11,312(9), b = 33,111(9) et c = 7,445(6) Å, Z = 4 et groupe d'espace $P2_12_12_1$. On a résolu la structure par les méthodes conventionnelles aux atomes lourds et on l'a affinée par la méthode des moindres carrés (matrice entière) jusqu'à des valeurs de R = 0,033 et R_w = 0,034 pour 2508 réflexions avec $I \geq 3\sigma(I)$. L'anion $[Me_2Ga(N_2C_5H_7)(OCH_2CH_2NMe_2)]W(CO)_3^-$ possède une géométrie de coordination *fac*-octaédrique avec W—O = 2,228(7), W—N(pyrazolyl) = 2,299(8), W—N(amine) = 2,37(1) et W—(CO) = 1,91(1)–1,92(2) Å.

Mots clés : complexes gallate de pyrazole, comportement fluxionnel des complexes Ga–W, structure cristalline d'une complexe Ga–W, complexes Ga–W.

[Traduit par la revue]

Introduction

The preparation of THF solutions of the salts $Na^+[Me_2Ga(N_2C_3HR_2)(OCH_2CH_2X)]M(CO)_3^-$, (where R = H or Me, X = NH_2, NMe_2, or SEt, M = Cr, Mo, or W), has been reported previously (1, 2). At that time the salts were not isolated but, rather, their THF solutions were used directly in decarbonylation reactions to produce various neutral complexes of the type $[Me_2Ga(N_2C_3HR_2)(OCH_2CH_2X)]M(CO)_2L$, (where L = NO, N_2Ph, η^3-allyl, η^3-C_7H_7, or η^2-CH_2SMe) (1–5). The present account details the synthesis and characterization of representative tetraethylammonium salts of the above carbonyl anions where R = Me, X = NMe_2 or SEt, and M = Cr, Mo, or W, and describes the X-ray crystal structure determination of the $Et_4N^+[Me_2Ga(N_2C_5H_7)(OCH_2CH_2NMe_2)]W(CO)_3^-$ complex. The fluxional behavior of the anions in d_6-acetone solution has been studied using variable temperature ^1H nmr techniques and a rationale for the observed behavior is proposed.

Experimental

Air-sensitive materials were handled in a glove box under an atmosphere of oxygen-free dry nitrogen, or in a nitrogen-blanketed apparatus. Tetrahydrofuran (THF) was dried by refluxing over sodium/benzophenone and used immediately following distillation. The sodium salts $Na^+[Me_2Ga(N_2C_3HR_2)(OCH_2CH_2X)]M(CO)_3^-$ were prepared in THF solution as described previously (1, 2).

Preparation of $Et_4N^+[Me_2Ga(N_2C_3HR_2)(OCH_2CH_2X)]M(CO)_3^-$

To the sodium salt, $Na^+[Me_2Ga(N_2C_3HR_2)(OCH_2CH_2X)]M(CO)_3^-$, in THF solution was added an equimolar amount of Et_4NCl dissolved in a minimum amount of MeOH. Formation of a precipitate (NaCl) was immediate. After 5–10 min, the mixture was filtered and the solvent removed from the filtrate *in vacuo* to leave a yellowish solid. This was recrystallized from THF to give yellow crystals of the product in approximately 50–60% yield. Physical data for the six salts prepared are presented in Table 1.

X-Ray crystallographic analysis of $Et_4N^+[Me_2Ga(N_2C_5H_7)(OCH_2CH_2NMe_2)]W(CO)_3^-$

A crystal *ca.* 0.25 × 0.25 × 0.40 mm in size was mounted in a general orientation. Unit-cell parameters were refined by least-squares on setting angles for 25 reflections (2θ = 20–30°) measured on a diffractometer with Mo-$K\alpha$ radiation (λ = 0.71069 Å). Crystal data at 21°C are

$C_{23}H_{43}GaN_4O_4W$ f.w. = 598.04

Orthorhombic, a = 11.312(9), b = 33.111(9), c = 7.445(6) Å, V =

Can. J. Chem. Downloaded from www.nrcresearchpress.com by 91.144.44.67 on 09/07/12
For personal use only.

TABLE 1. Physical data for Et_4N^+

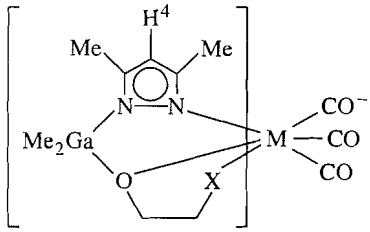

X	M	Found (%)/Calcd. (%) C	H	N	^{1}H nmr τ (ppm)* Ga—Me	N—Me	pz—Me	H^4	Et_4N	Coalescence temperature† (°C)	IR (cm^{-1}) ν_{CO}
NMe_2	Cr	48.11	7.84	10.21	10.37s	7.20s	7.44s	4.24s	8.66 br	6	1800, 1720‡
		48.01	7.71	10.19	10.48s	7.90s	7.88s		6.37 br		1881, 1729§
NMe_2	Mo	44.54	7.25	9.45	10.37s	7.10s	7.49s	4.27s	8.59 br	30	1878, 1705‡
		44.33	7.15	9.32	10.40s	7.79s	7.84s		6.40 br		1879, 1730§
NMe_2	W	38.79	6.32	8.23	10.32s	7.04s	7.45s	4.23s	8.57 tt‖	40	1870, 1700‡
		38.65	6.21	8.21	10.35s	7.74s	7.81s		6.45 q		1873, 1725§
SEt	Cr	46.67	7.42	7.42	10.60s	—	7.87s	4.29s	8.54 br	−18	1875, 1715‡
		46.62	7.38	7.41	10.29s	—	7.53s		6.52 br		1876, 1724§
SEt	Mo	43.30	6.89	6.89	10.48s	—	7.90s	4.26s	8.64 br	12	1871, 1700‡
		42.97	6.76	6.81	10.30s	—	7.58s		6.50 br		1870, 1725§
SEt	W	37.85	6.02	6.02	10.47s	—	7.90s	4.21s	8.65 br	29	1863, 1695‡
		37.78	6.05	5.98	10.28s	—	7.59s		6.52 br		1865, 1720§

*Low temperature limiting spectrum in d_6-acetone, br = broad, s = singlet, t = triplet, q = quartet.
†Coalescence temperature of $GaMe_2$ signals. All τ values relative to τ_{d_6}-acetone = 7.89 ppm.
‡Measured as Nujol mulls.
§Measured as CH_2Cl_2 solutions.
‖J_{N-CH_3} = 1 Hz, J_{CH-CH} = 7 Hz.

2788(3) Å^3, Z = 4, ρ_c = 1.42 Mg m^{-3}, F(000) = 1176, μ(Mo-Kα) = 51.9 cm^{-1}. Absent reflections: *h*00, *h* odd, 0*k*0, *k* odd, and 00*l*, *l* odd, uniquely indicate the space group $P2_12_12_1$ (No. 19).

Intensities were measured with graphite-monochromated Mo-Kα radiation on a Rigaku AFC6S diffractometer. An ω scan at 16° min^{-1} over a range of (0.88 + 0.35 tan θ) degrees in ω (with up to nine rescans, background/scan time ratio = 0.5) was employed. Data were measured to 2θ = 60°. The intensities of three check reflections, measured every 150 reflections throughout the data collection, showed only small random fluctuations (<3%). After data reduction,[1] an empirical absorption correction, based on azimuthal scans for three reflections, was applied which resulted in transmission factors ranging from 0.843 to 1.000. Of the 4593 independent reflections measured, 2508 (54.6%) of these had intensities greater than or equal to $3\sigma(F^2)$ above background where $\sigma^2(F^2) = (S^2(C + 4B) + (0.35(F_o^2))^2)/Lp^2$ with *S* = scan rate, *C* = scan count, *B* = total background count, and Lp = Lorentz-polarization factor.

The structure was solved by conventional heavy atom methods, the W and Ga coordinates being determined from the Patterson function and those of the remaining non-hydrogen atoms from subsequent difference Fourier syntheses. The non-hydrogen atoms were refined with anisotropic thermal parameters and the hydrogen atoms were fixed in idealized positions (methyl orientations from difference Fourier, C—H = 0.98 Å, $U_H \propto U_{bonded\ atom}$). Scattering factors for all atoms and anomalous dispersion corrections for non-hydrogen atoms were taken from ref. 6. The weighting scheme $w = 4F_o^2/\sigma^2(F_o^2)$ gave uniform average values of $w(|F_o| - |F_c|)^2$ over ranges of both $|F_o|$ and sin θ/λ and was employed in the final stages of full-matrix refinement of 289 variables. Reflections with $I < 3\sigma(I)$ were not included in the refinement. Convergence was reached at $R = 0.033$ and $R_w = 0.034$ for 2508 reflections with $I \geq 3\sigma(I)$. Parallel refinement of the opposite enantiomer (for the particular crystal used for data collection) resulted in substantially higher residuals (R_w and *R* factor ratios of 1.16 and 1.15, respectively). The anisotropic thermal parameters of C(13) indicate a probable minor conformational disordering of the chelate ring that would also involve the *N*-methyl carbon atoms C(14) and C(15). The inconsistency of the thermal parameters of C(15) with those of C(13) and C(14) suggest that little is to be gained by the refinement of a disordered model. The function minimized was $\Sigma w(|F_o| - |F_c|)^2$, $R = \Sigma||F_o| - |F_c||/\Sigma|F_o|$ and $R_w = (\Sigma w(|F_o| - |F_c|)^2/\Sigma w|F_o|^2)^{1/2}$.

On the final cycle of refinement the maximum parameter shift corresponded to 0.07σ. The mean error in an observation of unit weight was 1.13. The final difference map showed maximum fluctuations of −0.73 to 0.90 e Å^{-3}, both near W. The final positional and equivalent isotropic thermal parameters for the non-hydrogen atoms appear in Table 2. Bond lengths and angles for the anion are listed in Tables 3–4. Hydrogen parameters, anisotropic thermal parameters, bond lengths and angles for the cation, torsion angles, intermolecular contacts, least-squares planes, and structure factors have been deposited.[2]

Spectra

Infrared spectra were recorded on a Perkin-Elmer 457 spectrophotometer and ^{1}H nmr on a Varian XL 100 spectrometer using FT techniques.

[1]All computations performed using the TEXSAN–TEXRAY Structure Analysis Package which includes versions of the following: AGNOST, absorption corrections, by J. A. Ibers; ORFLS, full-matrix least-squares, and ORFFE, function and errors, by W. R. Busing, K. O. Martin, and H. A. Levy; DIRDIF, phase extension and refinement of difference structures, by P. T. Beurskens; ORTEP II, illustrations, by C. K. Johnson.

[2]Supplementary material mentioned in the text may be purchased from the Depository of Unpublished Data, CISTI, National Research Council of Canada, Ottawa, Ont., Canada K1A 0S2.

Can. J. Chem. Downloaded from www.nrcresearchpress.com by 91.144.44.67 on 09/07/12
For personal use only.

Can. J. Chem. Downloaded from www.nrcresearchpress.com by 91.144.44.67 on 09/07/12
For personal use only.

TABLE 2. Final atomic coordinates (fractional) and B(eq)

Atom	x	y	z	B(eq)
W(1)	0.11151(3)	0.14488(1)	0.47872(4)	2.95(1)
Ga(1)	−0.1048(1)	0.07148(3)	0.5631(2)	4.37(5)
O(1)	−0.0473(6)	0.1100(2)	0.3937(9)	4.0(3)
O(2)	0.3523(7)	0.1867(2)	0.550(1)	6.4(5)
O(3)	0.0521(7)	0.2257(2)	0.289(1)	4.5(4)
O(4)	0.0051(8)	0.1909(2)	0.804(1)	5.0(4)
N(1)	0.0574(8)	0.0579(2)	0.646(1)	3.9(4)
N(2)	0.1470(7)	0.0837(2)	0.614(1)	3.3(4)
N(3)	0.1705(8)	0.1128(2)	0.209(1)	3.7(4)
N(4)	0.6737(8)	0.1951(2)	0.218(1)	3.7(4)
C(1)	0.259(1)	0.1706(3)	0.528(2)	4.3(5)
C(2)	0.0736(8)	0.1940(3)	0.359(1)	3.3(5)
C(3)	0.046(1)	0.1720(3)	0.684(1)	3.5(5)
C(4)	0.096(1)	0.0259(3)	0.740(1)	4.3(5)
C(5)	0.215(1)	0.0297(3)	0.769(1)	4.1(5)
C(6)	0.245(1)	0.0662(3)	0.686(1)	3.8(5)
C(7)	0.014(1)	−0.0065(4)	0.802(2)	7.5(9)
C(8)	0.366(1)	0.0850(3)	0.683(1)	4.8(6)
C(10)	−0.193(1)	0.0981(4)	0.755(2)	6.5(8)
C(11)	−0.172(1)	0.0240(4)	0.437(2)	10(1)
C(12)	−0.043(1)	0.0986(5)	0.211(2)	7.0(8)
C(13)	0.070(1)	0.0895(7)	0.147(2)	11(1)
C(14)	0.208(2)	0.1434(4)	0.078(2)	8.1(8)
C(15)	0.268(1)	0.0844(4)	0.222(2)	6.1(8)
C(16)	0.779(1)	0.2081(3)	0.106(2)	4.5(5)
C(17)	0.778(1)	0.2514(4)	0.045(2)	6.3(7)
C(18)	0.691(1)	0.1511(3)	0.260(1)	4.4(5)
C(19)	0.592(1)	0.1309(4)	0.365(2)	7.7(8)
C(20)	0.662(1)	0.2197(3)	0.389(1)	4.2(5)
C(21)	0.767(1)	0.2169(3)	0.512(2)	5.0(5)
C(22)	0.557(1)	0.2015(3)	0.116(2)	4.6(6)
C(23)	0.550(1)	0.1788(4)	−0.064(2)	5.8(6)

TABLE 3. Selected bond lengths (Å) with estimated standard deviations in parentheses

Atom	Atom	Distance	Atom	Atom	Distance
W(1)	C(2)	1.91(1)	O(4)	C(3)	1.18(1)
W(1)	C(1)	1.91(1)	N(1)	C(4)	1.34(1)
W(1)	C(3)	1.92(1)	N(1)	N(2)	1.35(1)
W(1)	O(1)	2.228(7)	N(2)	C(6)	1.36(1)
W(1)	N(2)	2.299(8)	N(3)	C(13)	1.45(2)
W(1)	N(3)	2.37(1)	N(3)	C(15)	1.45(1)
Ga(1)	O(1)	1.908(7)	N(3)	C(14)	1.47(1)
Ga(1)	C(10)	1.95(1)	C(4)	C(5)	1.37(2)
Ga(1)	C(11)	1.98(1)	C(4)	C(7)	1.49(2)
Ga(1)	N(1)	1.988(9)	C(5)	C(6)	1.40(1)
O(1)	C(12)	1.42(1)	C(6)	C(8)	1.50(2)
O(2)	C(1)	1.20(1)	C(12)	C(13)	1.39(2)
O(3)	C(2)	1.19(1)			

Results and discussion

The sodium salts, $Na^+[Me_2Ga(N_2C_3HR_2)(OCH_2CH_2X)]M(CO)_3^-$, are extremely sensitive to both oxygen and water (especially in solution), darkening visibly on exposure to air after several minutes. Qualitatively it was found that air-stability was in the order W > Mo > Cr and salts where R = Me were observed to be more stable than those with R = H. Representative anions for each metal (M = Cr, Mo, or W) and the ligands where R = Me; X = NMe_2 or SEt have been isolated as their crystalline tetraethylammonium salts. These salts, although considerably less air sensitive than the corresponding sodium salts, decomposed slowly over a period of days when exposed to the laboratory atmosphere. They are stable indefinitely under a nitrogen atmosphere.

The ir spectra of the anions, in both CH_2Cl_2 and as Nujol

TABLE 4. Selected bond angles (deg) with estimated standard deviations in parentheses

Atom	Atom	Atom	Angle	Atom	Atom	Atom	Angle
C(2)	W(1)	C(1)	84.5(4)	C(4)	N(1)	N(2)	110.2(8)
C(2)	W(1)	C(3)	83.6(4)	C(4)	N(1)	Ga(1)	130.1(8)
C(2)	W(1)	O(1)	97.4(3)	N(2)	N(1)	Ga(1)	119.7(6)
C(2)	W(1)	N(2)	176.3(4)	N(1)	N(2)	C(6)	106.0(8)
C(2)	W(1)	N(3)	92.8(3)	N(1)	N(2)	W(1)	120.4(6)
C(1)	W(1)	C(3)	88.6(5)	C(6)	N(2)	W(1)	133.5(7)
C(1)	W(1)	O(1)	172.2(4)	C(13)	N(3)	C(15)	106(1)
C(1)	W(1)	N(2)	99.0(4)	C(13)	N(3)	C(14)	112(1)
C(1)	W(1)	N(3)	96.7(4)	C(13)	N(3)	W(1)	106.6(7)
C(3)	W(1)	O(1)	99.1(4)	C(15)	N(3)	C(14)	106(1)
C(3)	W(1)	N(2)	97.4(4)	C(15)	N(3)	W(1)	116.6(7)
C(3)	W(1)	N(3)	173.3(4)	C(14)	N(3)	W(1)	109.6(6)
O(1)	W(1)	N(2)	79.0(3)	O(2)	C(1)	W(1)	177(1)
O(1)	W(1)	N(3)	75.7(3)	O(3)	C(2)	W(1)	177.3(8)
N(2)	W(1)	N(3)	85.8(3)	O(4)	C(3)	W(1)	175.6(9)
O(1)	Ga(1)	C(10)	110.8(5)	N(1)	C(4)	C(5)	109(1)
O(1)	Ga(1)	C(11)	110.3(6)	N(1)	C(4)	C(7)	121(1)
O(1)	Ga(1)	N(1)	92.5(3)	C(5)	C(4)	C(7)	129(1)
C(10)	Ga(1)	C(11)	120.5(7)	C(4)	C(5)	C(6)	105(1)
C(10)	Ga(1)	N(1)	110.4(5)	N(2)	C(6)	C(5)	110(1)
C(11)	Ga(1)	N(1)	108.8(5)	N(2)	C(6)	C(8)	124(1)
C(12)	O(1)	Ga(1)	118.0(9)	C(5)	C(6)	C(8)	126(1)
C(12)	O(1)	W(1)	112.6(8)	C(13)	C(12)	O(1)	115(1)
Ga(1)	O(1)	W(1)	115.7(3)	C(12)	C(13)	N(3)	120(1)

Can. J. Chem. Downloaded from www.nrcresearchpress.com by 91.144.44.67 on 09/07/12
For personal use only.

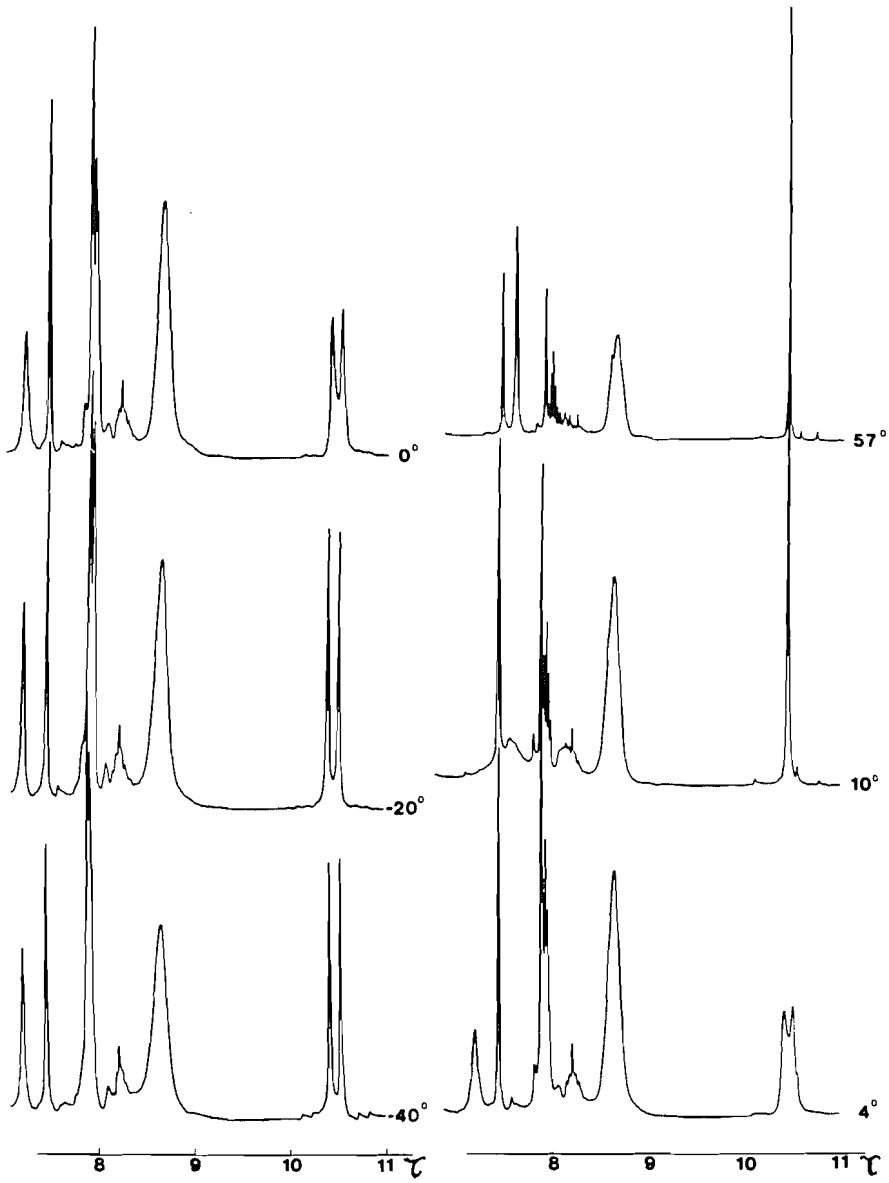

FIG. 1. Temperature-dependent 100 MHz ^{1}H nmr spectrum of $Et_4N^+[Me_2Ga(N_2C_5H_7)(OCH_2CH_2NMe_2)]Cr(CO)_3^-$ in d_6-acetone solution.

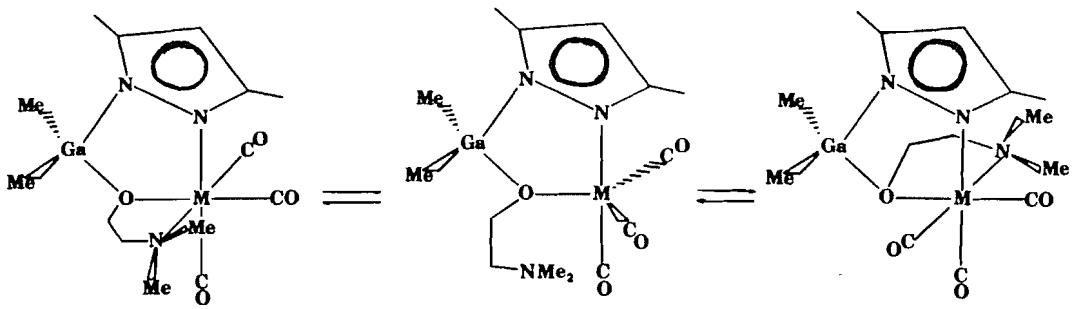

FIG. 2. Suggested fluxional behavior for the $[Me_2Ga(N_2C_5H_7)(OCH_2CH_2NMe_2)]M(CO)_3^-$ anions in d_6-acetone solution.

mulls (see Table 1) show two bands in the ν_{CO} region, bands of approximately equal intensity with the lower frequency band (*e* mode) being quite broad. This pattern is indicative of a facial arrangement for the three CO groups in the anions (7) although the lack of resolution of the broad band into two components, a splitting observed for the neutral, valence isoelectronic, manganese tricarbonyl compounds (1), is puzzling. The low temperature limiting ^{1}H nmr spectra obtained for the complexes (see Table 1) are in agreement with this assignment since the tridentate gallate ligands give ^{1}H nmr patterns consistent with a *facial* coordination geometry. Thus two signals are observed for the —$GaMe_2$ moiety, and, in the cases where X = NMe_2, two

Can. J. Chem. Downloaded from www.nrcresearchpress.com by 91.144.44.67 on 09/07/12
For personal use only.

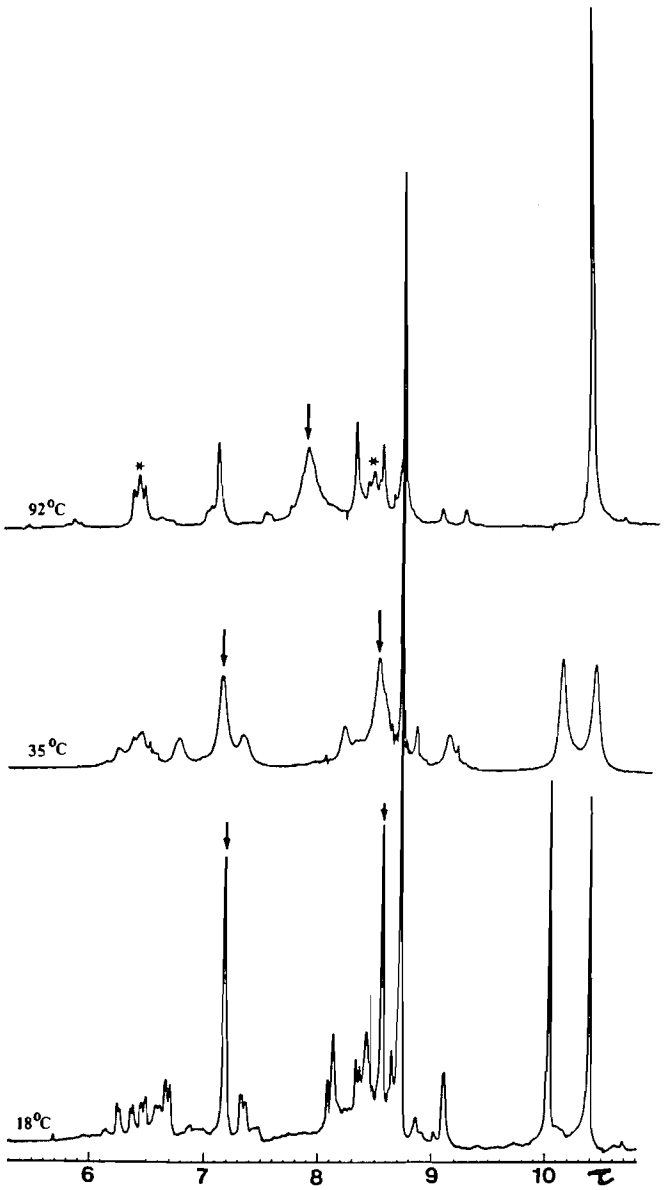

FIG. 3. Temperature dependent 100 MHz ^{1}H nmr spectrum of $[Me_2Ga(N_2C_3H_3)(OCH_2CH_2NMe_2)]Mo(CO)_2(\eta^3\text{-}C_4H_7)$ in C_6D_6 solution. (*): $—CH_2CH_2—$ protons (↓): $—NMe_2$ protons.

signals are observed for the $—NMe_2$ moiety. A *meridional* arrangement of the gallate ligands would lead to one signal for each of these groupings if the inversion from the λ to δ conformation of the $(OCH_2CH_2NMe_2)M$ five-membered ring were facile. Such facile inversions have been well documented in our earlier studies (8–12) and of necessity involve pyramidal inversion at the three-coordinate oxygen atom in the *mer* structures. However, the ^{1}H nmr spectra of five of the six complexes studied show, even at room temperature, only one signal for the $—GaMe_2$ group, and one signal for the $—NMe_2$ group, where applicable. A fluxional process, rather than a *meridional* coordination for the tridentate ligand, was immediately suspected to give rise to these observations and this was confirmed by variable temperature ^{1}H nmr studies. The temperature-dependent ^{1}H nmr spectrum of a representative sample, $Et_4N^+[Me_2Ga(N_2C_5H_7)(OCH_2CH_2NMe_2)]Cr(CO)_3^-$, in d_6-acetone solution is shown in Fig. 1. At −40°C, two signals are observed for each of the $—GaMe_2$ and $—NMe_2$ moieties. On warming the solution these signals broaden, collapse, and then at higher temperatures appear as one strong singlet for each of these groupings. Similar temperature-dependent spectra were observed for the remaining five compounds listed in Table 1. The coalescence temperatures (see Table 1) depend on both the transition metal, being lowest for Cr and highest for W, and also on the nature of the X group, being lower for a particular transition metal when X = SEt rather than NMe_2. The lower the coalescence temperature the more facile the fluxional process, and steric factors may play an important role with the variation of X and also with the change in transition metal M, but with the latter electronic factors may be of greater importance.

A suggested mechanism for the fluxional process is illustrated in Fig. 2. It is assumed that at low temperatures in solution the *facial* arrangement, as observed in the solid state, exists. The proposed mechanism requires the breaking of the $M—NMe_2$ bond, rearrangement to a five-coordinate intermediate having a plane of symmetry, and reforming of the $M—NMe_2$ bond (pyramidal inversion at oxygen in the *facial* arrangement without concomitant M—N bond breaking cannot be invoked to explain the observed spectra). A fast equilibrium, via inversion at the oxygen atom between the two limiting structures would result in the observation of one signal for each of the $—NMe_2$ and $—GaMe_2$ groups as seen in the higher temperature spectra. Bond length data would support the breaking of the weaker $W—NMe_2$ bond (2.37 Å) rather than the shorter, stronger, W—N(pz) bond (2.299 Å).

Interestingly the related neutral complex, $[Me_2Ga(N_2C_3H_3)(OCH_2CH_2NMe_2)]Mo(CO)_2(\eta^3\text{-}C_4H_7)$, which was suspected earlier (1) to exhibit fluxional behavior in solution because of the broad signals observed in the ^{1}H nmr spectrum at room temperature for the $—NMe_2$ and $—GaMe_2$ protons, has now been shown to display a temperature dependent ^{1}H nmr spectrum. Representative spectra are given in Fig. 3. The $—NMe_2$ and $—GaMe_2$ signals, broad at room temperature, are observed to sharpen at lower temperatures and collapse at higher temperatures. A fluxional process similar to that proposed above for the tricarbonyl anions but with the $\eta^3\text{-}C_4H_7$ group occupying the position opposite the pyrazolyl nitrogen in the five-coordinate intermediate could again rationalize the observed spectra. The much higher coalescence temperature observed for the allyl complex is expected considering the steric requirements of the methallyl vis-a-vis the carbonyl ligand. Supportive of this proposal is the positioning of the $\eta^3\text{-}C_4H_7$ group in the related complex $[Me_2Ga(N_2C_5H_7)(OCH_2CH_2NH_2)]Mo(CO)_2(\eta^3\text{-}C_4H_7)$. An X-ray crystallographic analysis has revealed the allyl ligand to be positioned *trans* to pyrazolyl nitrogen in this pseudo octahedral complex (13).

The structure of the $[Me_2Ga(N_2C_5H_7)(OCH_2CH_2NMe_2)]W(CO)_3^-$ anion (Fig. 4) shows the expected facial coordination by the unsymmetrical tridentate ligand. This is the first structure of a tricarbonyl anion incorporating a pyrazolyl gallate ligand. Crystal structures have been reported for neutral Mn and Re tricarbonyl species $[Me_2Ga(N_2C_5H_7)(OCH_2CH_2X)]M(CO)_3$: X = SPh and M = Mn (14); X = SPh and NMe_2, M = Re (15); as well as the related molecules $[Me_2Ga(N_2C_5H_7)(OCH_2(C_5H_4N))]Re(CO)_3$ (9) and $[Me_2Ga(N_2C_5H_7)(OCH_2CH_2NMe_2)]Mo(CO)_2(\eta^2\text{-}CH_2SMe)$ (4). The W—O, W—N(2), and W—N(3) bond lengths in the $[Me_2Ga(N_2C_5H_7)(OCH_2CH_2NMe_2)]W(CO)_3^-$ anion (2.228(7), 2.299(8), and 2.37(1) Å) are longer by an average of 0.085 Å than the corresponding distances in the isoelectronic neutral Re tricar-

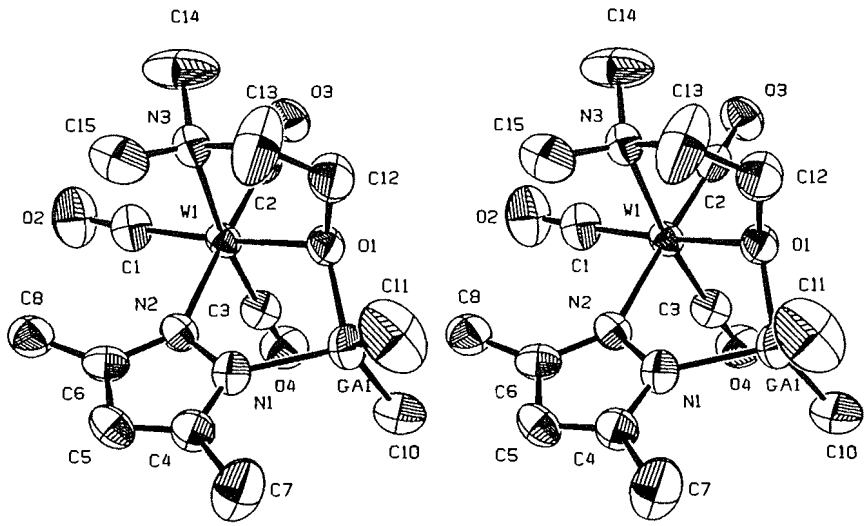

FIG. 4. Stereoscopic view of the $[Me_2Ga(N_2C_5H_7)(OCH_2CH_2NMe_2)]W(CO)_3^-$ anion; 50% probability thermal ellipsoids are shown for the non-hydrogen atoms.

bonyl complex (15) (2.153(6), 2.189(7), and 2.300(7) Å) while the metal–carbonyl distances in these two species are equal within experimental error with W—CO = Re—CO = 1.91 Å. The W—O and W—N(3) distances are very similar to the Mo—O and Mo—N distances of 2.245(2) and 2.396(3) Å in $[Me_2Ga(N_2C_5H_7)(OCH_2CH_2NMe_2)]Mo(CO)_2(\eta^2\text{-}CH_2SMe)$ (4), while the Mo—N(pyrazolyl) bond (trans to the η^2-CH_2SMe ligand) is shorter at 2.199(2) Å. The relatively long W—N(3) distance is consistent with the mechanism suggested above for the fluxional process in solution.

Other bond lengths and angles (Tables 3 and 4) are normal. The crystal structure of $Et_4N^+[Me_2Ga(N_2C_5H_7)(OCH_2CH_2NMe_2)]W(CO)_3^-$ consists of discrete cations and anions, the most significant interspecies contacts being a pair of cation–anion C—H···O interactions. These interactions [C(16)—H(24)···O(3)(1 + x, y, z) and C(18)—H(30)···O(1)(1 + x, y, z), C···O = 3.41(1) and 3.43(1) Å, H···O = 2.53 and 2.53 Å, C—H···O = 152 and 149°] both involve hydrogen atoms associated with α-carbon atoms of the Et_4N^+ cation. Stereoviews of the cation and the packing arrangement have been deposited.[2]

Acknowledgments

We thank the Natural Sciences and Engineering Research Council of Canada for financial support and the University of British Columbia Computing Centre for assistance. We are indebted to Mr. P. Borda for the C, H, N analyses.

1. K. S. CHONG and A. STORR. Can. J. Chem. **57**, 167 (1979).
2. K. S. CHONG and A. STORR. Can. J. Chem. **59**, 1331 (1981).
3. K. S. CHONG and A. STORR. Can. J. Chem. **58**, 2278 (1980).
4. K. S. CHONG, S. RETTIG, A. STORR, and J. TROTTER. Can. J. Chem. **58**, 1080 (1980).
5. K. S. CHONG. Ph.D. Thesis, 1980. University of British Columbia.
6. International tables for X-ray crystallography. Vol. IV. Kynoch Press, Birmingham. 1974. pp. 99–102 and 149.
7. D. M. ADAMS. Metal–ligand and related vibrations. Edward Arnold, London. 1967.
8. K. S. CHONG, S. RETTIG, A. STORR, and J. TROTTER. Can. J. Chem. **57**, 3113 (1979).
9. S. RETTIG, A. STORR, J. TROTTER, and K. UHRICH. Can. J. Chem. **62**, 2783 (1984).
10. B. LOUIE, S. RETTIG, A. STORR, and J. TROTTER. Can. J. Chem. **63**, 3019 (1985).
11. D. COOPER, S. RETTIG, and A. STORR. Can. J. Chem. **64**, 566 (1986).
12. E. ONYIRIUKA and A. STORR. Can. J. Chem. **65**, 1367 (1987).
13. K. S. CHONG, S. RETTIG, A. STORR, and J. TROTTER. Can. J. Chem. **57**, 1335 (1979).
14. S. RETTIG, A. STORR, and J. TROTTER. Can. J. Chem. **59**, 2391 (1981).
15. B. LOUIE, S. RETTIG, A. STORR, and J. TROTTER. Can. J. Chem. **63**, 2261 (1985).

Can. J. Chem. Downloaded from www.nrcresearchpress.com by 91.144.44.67 on 09/07/12
For personal use only.

The total synthesis of (+)-ryanodol. Part I. General strategy and search for a convenient diene for the construction of a key tricyclic intermediate

PIERRE DESLONGCHAMPS,[1] ANDRÉ BÉLANGER, DANIEL J. F. BERNEY, HANS-JUERG BORSCHBERG, ROBERT BROUSSEAU, ALAIN DOUTHEAU, ROBERT DURAND, HAJIME KATAYAMA, RICHARD LAPALME, DOMINIQUE M. LETURC, CHUN-CHEN LIAO, FREDERICK N. MACLACHLAN, JEAN-PIERRE MAFFRAND, FABRIZIO MARAZZA, ROBERT MARTINO, CLAUDE MOREAU, LUC RUEST, LOUISELLE SAINT-LAURENT, ROGER SAINTONGE, and PIERRE SOUCY

Laboratoire de synthèse organique, Département de chimie, Faculté des sciences, Université de Sherbrooke, Sherbrooke (Québec), Canada J1K 2R1

Received April 14, 1989

This paper is dedicated to the memory of Professor Karel Wiesner

PIERRE DESLONGCHAMPS, ANDRÉ BÉLANGER, DANIEL J. F. BERNEY, HANS-JUERG BORSCHBERG, ROBERT BROUSSEAU, ALAIN DOUTHEAU, ROBERT DURAND, HAJIME KATAYAMA, RICHARD LAPALME, DOMINIQUE M. LETURC, CHUN-CHEN LIAO, FREDERICK N. MACLACHLAN, JEAN-PIERRE MAFFRAND, FABRIZIO MARAZZA, ROBERT MARTINO, CLAUDE MOREAU, LUC RUEST, LOUISELLE SAINT-LAURENT, ROGER SAINTONGE, and PIERRE SOUCY. Can. J. Chem. **68**, 115 (1990).

This paper reports a retrosynthetic analysis that led to the conception of a synthetic strategy for the construction of ryanodol (**2**). The preparation of a key diene, i.e., spirolactone dienone **47** (**19** → **31** → **33** → **48** → **49** → **52** → **47**), and its Diels–Alder reaction with methyl vinyl ketone are reported.

Key words: strategy, synthesis, ryanodol, diterpene.

PIERRE DESLONGCHAMPS, ANDRÉ BÉLANGER, DANIEL J. F. BERNEY, HANS-JUERG BORSCHBERG, ROBERT BROUSSEAU, ALAIN DOUTHEAU, ROBERT DURAND, HAJIME KATAYAMA, RICHARD LAPALME, DOMINIQUE M. LETURC, CHUN-CHEN LIAO, FREDERICK N. MACLACHLAN, JEAN-PIERRE MAFFRAND, FABRIZIO MARAZZA, ROBERT MARTINO, CLAUDE MOREAU, LUC RUEST, LOUISELLE SAINT-LAURENT, ROGER SAINTONGE et PIERRE SOUCY Can. J. Chem. **68**, 115 (1990).

On rapporte l'analyse rétrosynthétique qui a conduit à la conception d'une stratégie menant à la synthèse du ryanodol (**2**). On décrit la synthèse du diène-clé, la spirolactone diénone **47** (**19** → **31** → **33** → **48** → **49** → **52** → **47**), et sa réaction de Diels–Alder avec la méthylvinylcétone.

Mots clés : stratégie, synthèse, ryanodol, diterpène.

Ryanodine (**1**), a natural product isolated from *Ryania speciosa Vahl*, is the ester of pyrrole α-carboxylic acid and the complex diterpene (+)-ryanodol (**2**) (1) (Scheme 1). The structure of ryanodine including its absolute configuration was elucidated by Wiesner *et al.* at the University of New Brunswick (2). This work constitutes one of the most brilliant accomplishments in structure elucidation using chemical degradation, and remains a classic piece. The X-ray analysis of the *p*-bromobenzyl ether **3** of ryanodol was carried out by Srivastava and Przybylska (3). The original assignment of Wiesner was confirmed except for a minor point; the X-ray analysis revealed that the configuration of the isopropyl and tertiary hydroxyl groups at C_2 had to be reversed and is as indicated in structures **1**–**3**.[2]

We completed a total synthesis of (+)-ryanodol in 1979. This work was published in a preliminary form (4) and we now wish to report our investigation in detail. In Part I (this paper), we explain our general synthetic strategy (5, 6) and describe the preliminary experiments leading to the discovery of a very convenient unsymmetrical diene, which was needed for the construction of a key tricyclic intermediate via a Diels–Alder cycloaddition. Parts II–IV describe the remaining work (see accompanying papers).

General strategy

Ryanodol, a $C_{20}H_{32}O_8$ compound, is a pentacyclic diterpene, which has a ring skeleton consisting of 14 carbons and one oxygen atom. Thus, four rings (A, B, C, and E) are carbocyclic whereas the fifth one (ring D) contains an oxygen atom. There is an isopropyl group as well as a tertiary methyl group in ring A, a tertiary methyl group in ring B, and an equatorially oriented secondary methyl group in ring C. In addition, there are five tertiary hydroxyl groups, one of which is part of a hemi-ketal function at one of the junctions of ring D and ring E (cf. C_{15}), and two secondary hydroxyl groups, one in ring A (α-oriented) and one in ring C (α-oriented and equatorial).

Ryanodol also has 11 contiguous asymmetric carbons (C_{1-6}, C_{9-12}, and C_{15}). Due to the bridged nature of the skeleton, five chiral centers (C_1, C_5, C_{11-12}, and C_{15}) are geometrically related and can only take the relative configuration shown. However, the other six chiral centers could, in principle, have a configuration opposite to that shown. It can be concluded from this analysis that ryanodol is indeed a very complex diterpene in which only three carbons of the skeleton (C_{7-8} and C_{14}) are left unfunctionalized as methylene groups.

With a complex target such as ryanodol, there are a rather large variety of synthetic strategies that can be devised theoretically. Our synthetic plan did not, however, originate directly from an analysis of the skeleton of ryanodol; it was based rather

[1]Author to whom correspondence may be addressed.

[2]The chemical abstract name for ryanodol: [3*S*-(3α,4β,4a*S*, 6α,6aα,7α,8β,8aα,8bβ,9β,9aα)]-hexahydro-3,6a,9-trimethyl-7-(1-methylethyl) - 6,9 - methanobenzo[1,2]pentaleno[1,6 - *be*[furan - 4,6, 7,8a, 8b,9a(6a*H*,9*H*)-heptol) (Chem. Abstr. **101**, 6830CS (1984)). To facilitate the discussion on the synthetic strategy, the numbering system of ryanodol is used throughout, regardless of the skeleton considered.

Can. J. Chem. Downloaded from www.nrcresearchpress.com by 186.148.149.217 on 09/07/12
For personal use only.

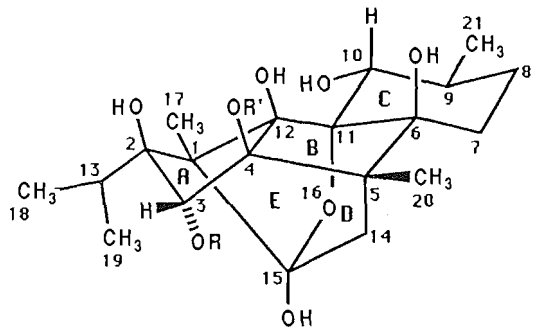

1 R = -OC- (pyrrole) , R' = H

2 R = R' = H

3 R = H, R' = p-$BrC_6H_4CH_2$-

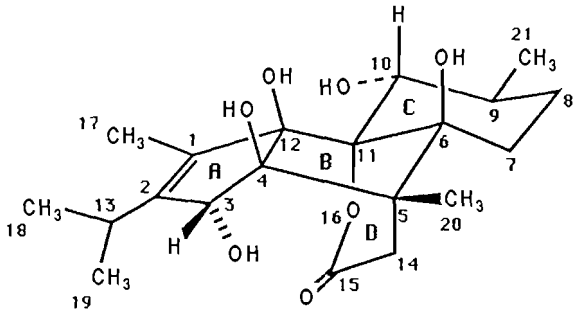

4

SCHEME 1

on the structure of a degradation product, namely anhydroryanodol (**4**), and on the conviction that there must be a way to reconstruct ryanodol from this degradation product.[3]

In the course of the structure elucidation, it was observed that, under acidic conditions, ryanodol loses one molecule of water to produce anhydroryanodol (**4**). It turned out also that anhydroryanodol (**4**) became the principal degradation product; its structure was determined first (7) and that of ryanodol and ryanodine were deduced later on that basis.

Anhydroryanodol (**4**) contains three carbocyclic rings and a six-membered lactone. Rings A and B are five-membered while ring C is six-membered. Each carbocyclic ring possesses a methyl group, and ring A has in addition an isopropyl group. Four tertiary hydroxyl groups are attached to ring B, and one of them is part of the lactone ring. In addition, there is a tetrasubstituted double bond and an allylic secondary alcohol, which is also α-oriented in ring A, as well as a secondary equatorial alcohol in ring C. Thus, by comparison, the double bond and the lactone function of anhydroryanodol are replaced in ryanodol by one additional carbocyclic ring, two tertiary alcohols (one being part of a hemi-ketal), and three chiral centers (C_{1-2} and C_{15}). Thus anhydroryanodol (**4**) with its eight contiguous chiral centers is much less complex than ryanodol. Further comparison of the structure of anhydroryanodol with that of ryanodol indicates that the reconversion of the former into the latter involves essentially a reconnection of C_1 and C_{15} and the introduction of a β-oriented hydroxyl group at C_2.

The basic plan for the synthesis of anhydroryanodol is outlined in Scheme 2. We were very much interested in the rather simple tricyclic system **5**, which is a bicyclo[2.2.2.]octane derivative containing an extra five-membered ring, a tertiary methyl group at C_5, and a tetrasubstituted double bond. This interest was created by the fact that the oxidation of the double bond in **5** should yield the macrobicyclic diketone **6**, which is ideally built to undergo a transannular aldol condensation[4] yielding the tricyclic hydroxy-ketone **7**.

Some common features between **7** and anhydroryanodol can be foreseen already. Indeed, in compound **7** we can recognize the carbon atoms of the B, C, D rings of anhydroryanodol as well as the tertiary methyl group at C_5 and the tertiary alcohol at C_6. Furthermore, the carbonyl group at C_{10} can be used to introduce and control the stereochemistry of the methyl group at C_9. Also, reduction of this carbonyl group could yield the desired equatorial alcohol at C_{10}, and this would complete ring C.

In principle, what is required to complete the synthesis of anhydroryanodol from **7** is a functional group at C_{15} to induce the formation of the lactone ring, and functional groups at C_5 and C_{12}, which are necessary to incorporate ring A and to introduce the two hydroxyl groups at these positions. Thus, what is really needed initially is a compound such as **8** that incorporates all the prerequisite functional groups to build anhydroryanodol. Indeed, with its three additional functional groups, X, Y and Z, compound **8** can in principle yield compound **10** via intermediate **9**. The formation of **11** from **10**, which completes rings C and D, has already been discussed and would thus be straightforward. The next task would be the stereocontrolled introduction of ring A and the two hydroxyl groups at C_4 and C_{12} using the functional groups X and Y at C_4 and C_{12} of intermediate **11**. For this, it was necessary to envisage that an appropriate synthon such as **12**, which is a three-carbon fragment containing two functional groups (V and W) and an isopropyl group, could be discovered and would be capable of reacting with **11** to produce the tetracyclic intermediate **13**. The final conversion of intermediate **13** into anhydroryanodol would then involve a series of appropriate functional group modifications in ring A.

The above general scheme deserves further comment. For instance, in contrast to diketone **6**, the diketone **9** is no longer symmetrical, and the consequence of this is that **9** can now yield two different aldol products, compounds **10** or **14**. Also, we did not know what synthon **12** would be, or its regio- and stereoselectivity on reaction with an intermediate such as **11** or an equivalent thereof. It was therefore clear that it was impossible to circumvent all the difficulties beforehand, that we had to take several risks. However, we felt confident in finding adequate solutions to these problems by undertaking a meticulous study of the reactivity of the key intermediates that would become available in the course of this investigation.

We also believed that this synthetic plan had a great potential for an easy control of the stereochemistry of all the chiral centers of anhydroryanodol. This was based on our conviction that there are only three chiral centers in anhydroryanodol that need to be carefully controlled. These crucial centers are C_6, C_{11}, and C_{12}.

[3]This synthetic plan was in fact conceived in 1965, prior to the discovery of the real structure of ryanodol, which was found in 1967 (7).

[4]In **6**, alternative internal aldol condensations are disfavored because they would produce strained four-membered ring aldol products.

Can. J. Chem. Downloaded from www.nrcresearchpress.com by 186.148.149.217 on 09/07/12
For personal use only.

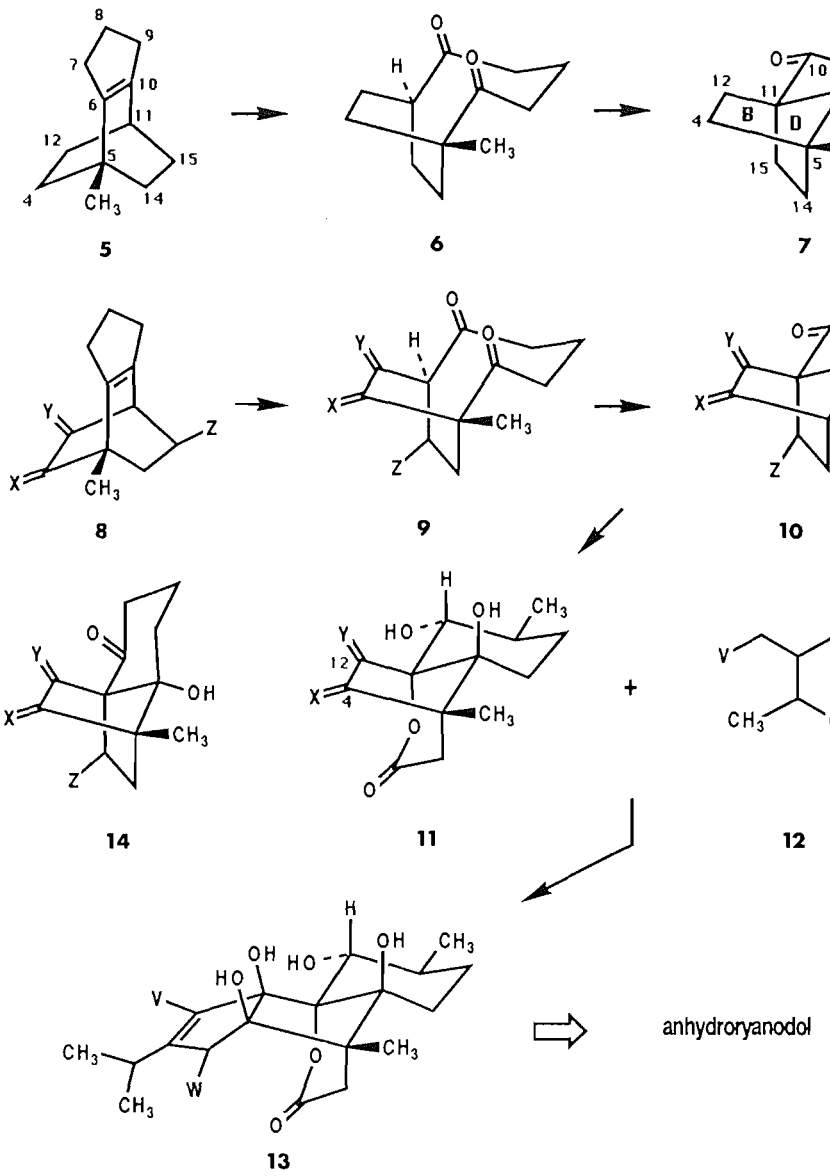

SCHEME 2

Indeed, chiral center C_5 is geometrically related to C_{11} and the relative stereochemistry of these two centers is automatically solved by the strategy used. Since rings A and B are both five-membered, it can be anticipated that production of a *cis* junction between these two rings could be a preferred pathway in our bond-forming process to produce ring A. Thus, C_4 is in principle also geometrically related to C_{12}. Similarly, the relative stereochemistry of rings C and B depends on the relative configuration at C_6 and C_{11}. Thus it follows that the relative stereochemistry of rings A, B, C, and D of anhydroryanodol depends on the relative configuration at C_6, C_{11}, and C_{12}. A solution for the control of these chiral centers will be presented later in this article. We have already discussed how to control the stereochemistry at C_9 and C_{10} and we did not anticipate any difficulty with the last chiral center of anhydroryanodol. Indeed, it is safe to expect that the hydride reduction of a carbonyl group at C_3 would occur from the least hindered face, producing the desired α secondary alcohol at that position.

When the structure of ryanodol was finally determined unambiguously (2, 3), it appeared clear to us that the reconversion of anhydroryanodol into ryanodol might be feasible in a relatively simple manner. An additional advantage of our strategy was that anhydroryanodol was readily available from the natural product and could be used to learn how to carry out the desired transformations concurrently with the synthetic work towards anhydroryanodol. Eventually, it turned out that a very simple reconversion of anhydroryanodol into ryanodol was discovered and is reported in detail in Part IV.

To begin our investigation, it was necessary to find an acceptable method for the preparation of tricyclic compounds of type **8**. The remaining part of this paper describes our work, which led to a very convenient synthesis of this type of compound.

Synthesis of compounds of type 8

Our approach to the synthesis of compounds of type **8** was influenced by the fact these compounds can be considered as bicyclo[2.2.2.]octene systems, which are in principle readily available by employing the Diels–Alder reaction.[5] It is conceivable on that basis that the simple dienophile **16** could react with

[5]We have also considered another approach, which is described in ref. 8.

Can. J. Chem. Downloaded from www.nrcresearchpress.com by 186.148.149.217 on 09/07/12
For personal use only.

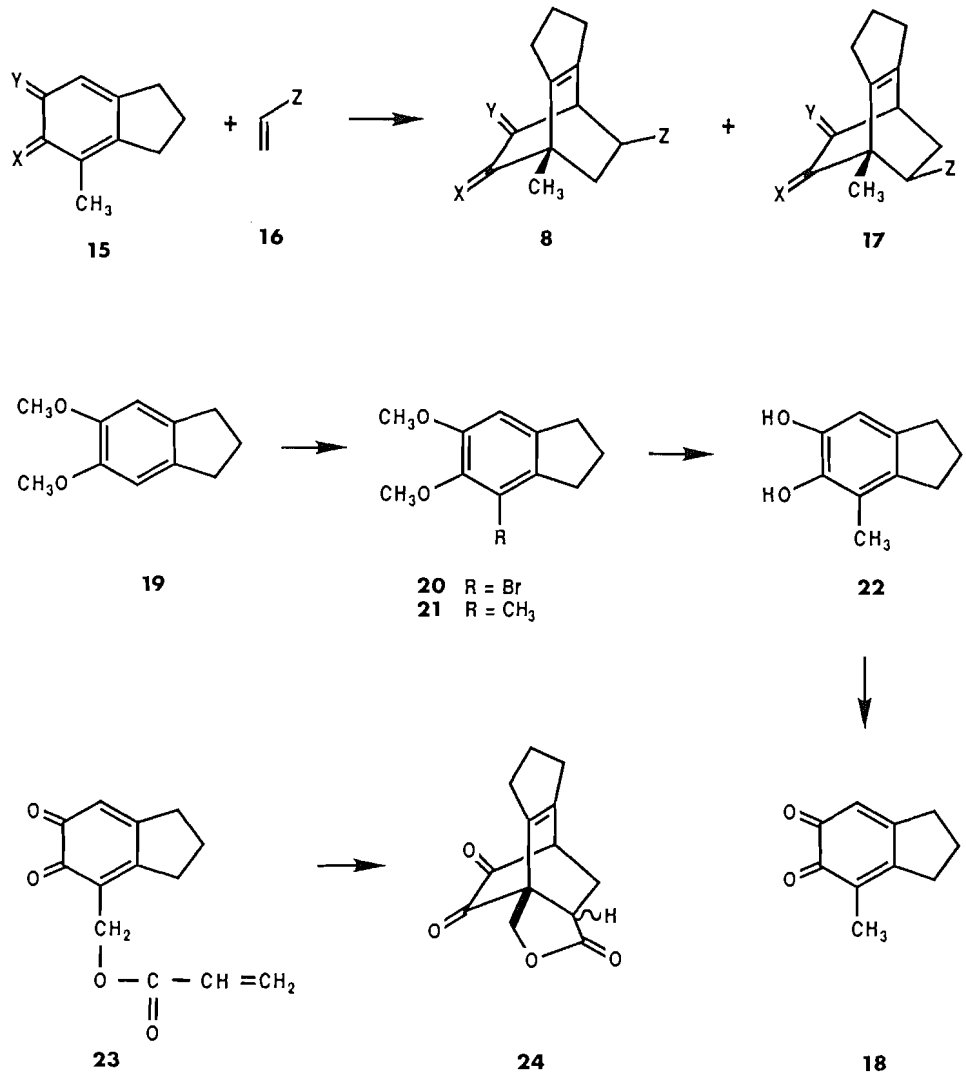

SCHEME 3

the diene **15** to yield the desired product **8** (Scheme 3). There was, however, a difficulty in this approach because the diene and the dienophile are both unsymmetrical and could give either the desired adduct **8** or its regioisomer **17**. First, we decided to find out if this type of Diels–Alder reaction would work, and then to try to solve the problem of regioselectivity later if the reaction occurred.

In this approach, the functional group Z, which is needed in **8**, can also serve to activate the dienophile **16**, and we concluded that the choice of Z can only be made experimentally. Ideally X and Y of the diene **15** should be oxygen atoms because these atoms will be needed to introduce ring A and to eventually form the hydroxyl groups at C_4 and C_{12} of anhydroryanodol (cf. **11** + **12** → **13**). On that basis, diene **15** should be the *o*-quinone **18**. We had some hope that *o*-quinone **18** could be used as a diene because *o*-quinones are reactive compounds that dimerize via the Diels–Alder reaction (9). Consequently they are good dienes and dienophiles. The next step was to find a dienophile of type **16** that would react with the diene of *o*-quinone **18**. We were encouraged by the fact that substituted *o*-benzoquinones were reported to react as dienes with styrene (10) or cyclopentadiene (11), yielding the corresponding Diels–Alder products.

5,6-Dimethoxyindane (**19**) was chosen as starting material. This compound can be easily obtained in large quantity from veratraldehyde (12). It can also be prepared in one step from 5,6-dimethoxy-1-indanone, which is commercially available. 5,6-Dimethoxyindane (**19**) was first treated with bromine to give the bromide **20**. Reaction of **20** with magnesium gave the corresponding Grignard reagent, which was reacted with dimethyl sulfate to yield methylindane **21**. Cleavage of the two methoxy groups in **21** was carried out with hydrobromic acid in acetic acid and the resulting phenol **22** was obtained pure by crystallization. The phenol **22** was then oxidized with silver oxide in ether (13) to yield the desired *o*-quinone **18**.

The *o*-quinone **18** was found to be quite unstable due to either dimerization or polymerization (14) and all attempts to trap **18** with dienophiles such as acrolein, methyl acrylate, or vinyl acetate failed. Before discontinuing this approach, we were interested in verifying whether a better result would be obtained by attaching the diene and the dienophile together. Therefore, the next goal was to prepare the *o*-quinone acrylate **23** in the hope that it would be converted into the intramolecular Diels–Alder adduct **24** (14).

The Grignard reagent **25** derived from 4-bromo-5,6-dimethoxyindane (**20**) was reacted with triethylorthoformate, heated a short time at 75°C, then hydrolyzed to give methoxyphenol aldehyde **26** (Scheme 4). When the final heating of the residue, before acid hydrolysis (see Experimental), was omit-

Can. J. Chem. Downloaded from www.nrcresearchpress.com by 186.148.149.217 on 09/07/12
For personal use only.

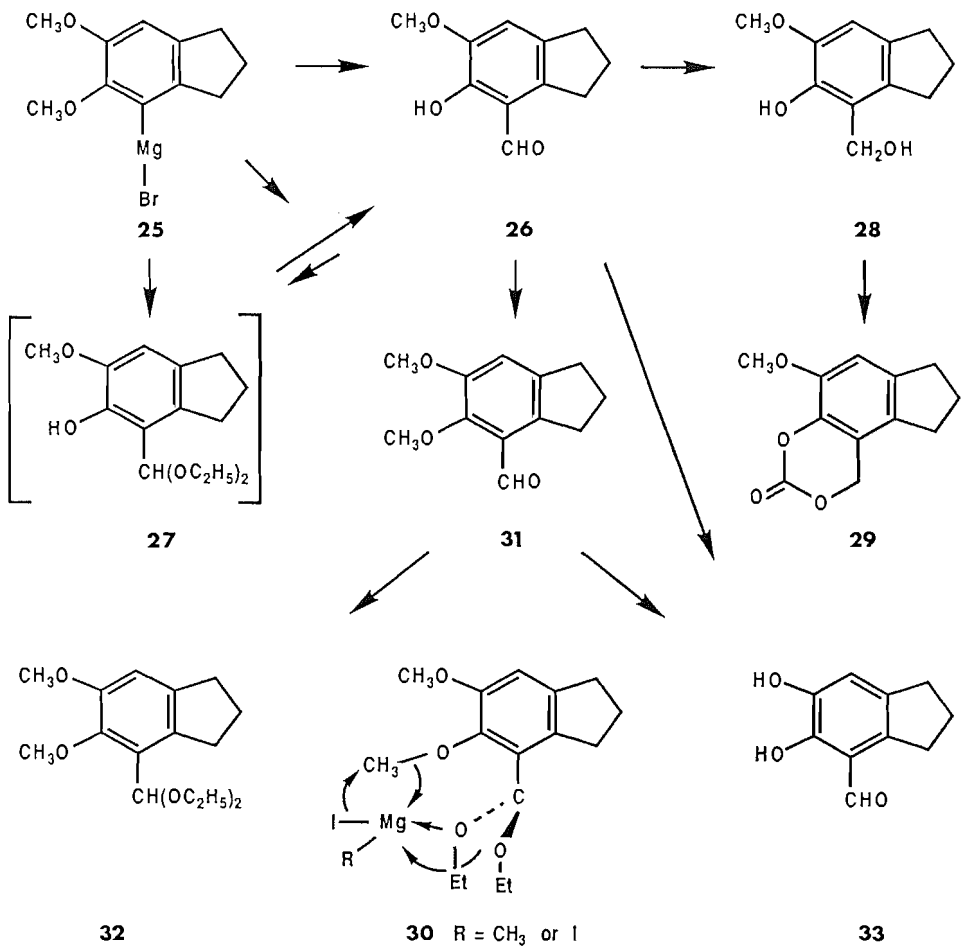

SCHEME 4

ted, dimethoxyaldehyde **31** was isolated. The position of the methoxy group in **26** was established by transforming compound **26** into compound **28** ($LiAlH_4$, ether), which was then converted into the carbonate **29** by reaction with phosgene.

The unexpected cleavage of one methoxy group can be explained in the following manner: methylmagnesium iodide (15*a*) and (or) magnesium iodide (15*b*), which are present in the Grignard reaction, can act as a demethylating agent. The specificity of the process can be explained by invoking the chelation of the reagents by the two oxygen atoms of the acetal function (cf. **30**).[6]

Alkylation of methoxyphenol aldehyde **26** with dimethylsulfate gave dimethoxyaldehyde **31**, which was then converted into dimethoxyacetal **32** by acetalization.

Treatment of methoxyphenol aldehyde **26** with boron tribromide in dichloromethane (16) afforded the desired 4-formyl-5,6-dihydroxyindane (**33**). Compound **33** became an important key product in our synthesis and a more convenient method for its preparation was developed later on. Dimethoxyindane **19** was first directly converted into dimethoxyaldehyde **31** with α,α-dichloromethyl methyl ether in the presence of titanium tetrachloride in dichloromethane (17), which was then transformed (BBr_3, CH_2Cl_2) into *o*-diphenol aldehyde **33** (80% yield for the two steps).

The *o*-diphenol aldehyde **33** was converted into the carbonate aldehyde **34** by reaction with phosgene (Scheme 5). Compound **34** was then reduced (H_2, PtO_2, THF) to the corresponding carbonate alcohol **35**, which was esterified (acryloyl chloride, pyridine, benzene) to carbonate acrylate **36**. The next operation was the removal of the carbonate protecting group to obtain **37**, which would then be oxidized to the desired *o*-quinone acrylate **23**. However, the conversion of **36** into **37** was not successful. All attempts to selectively remove the carbonate group by mild hydrolysis (18) or mild reduction failed. We then tried a more direct approach that avoids the removal of the carbonate protecting group. *o*-Diphenol aldehyde **33** was reduced ($LiAlH_4$, ether) to *o*-diphenol benzyl alcohol **38**. Compound **38** was then oxidized to the unstable *o*-quinone alcohol **39**, which was characterized spectroscopically. All attempts to esterify compound **39** to give *o*-quinone acrylate **23** failed. This result indicated again that *o*-quinones are quite unstable and that it is difficult to work with them. An important modification in our synthetic approach was therefore necessary.

[6]This interesting hypothesis was confirmed by the treatment of dimethoxyacetal **32** with methylmagnesium iodide in ether, which gave after a short heating period at 75°C and acid hydrolysis the anticipated major product **26** along with other minor products: (a) 5,6-dimethoxy-4-(ethoxy-1)ethylindane; (b) 4-(ethoxy-1)ethyl 5-hydroxy-6-methoxyindane, and (c) 5-hydroxy-4-isopropyl 6-methoxyindane. Treatment of dimethoxyacetal **32** with freshly prepared magnesium iodide in ether gave compound **26** almost quantitatively after a 10-min heating period at 75°C followed by acid hydrolysis. Without the heating period, dimethoxyaldehyde **31** was obtained. We have further verified that dimethoxyaldehyde **31** does not yield methoxyphenol aldehyde **26** under the acidic conditions employed and that phenolacetal **27** is very easily hydrolyzed under those conditions.

Can. J. Chem. Downloaded from www.nrcresearchpress.com by 186.148.149.217 on 09/07/12
For personal use only.

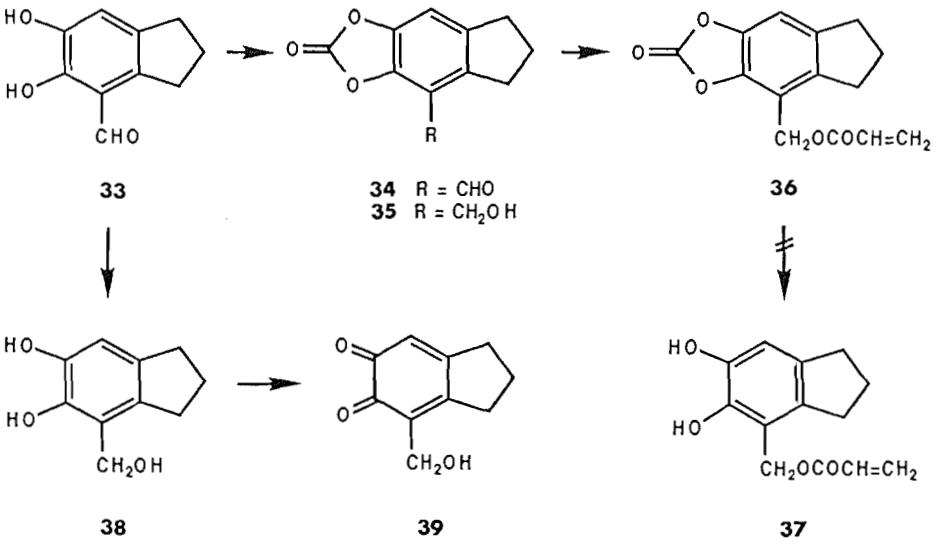

SCHEME 5

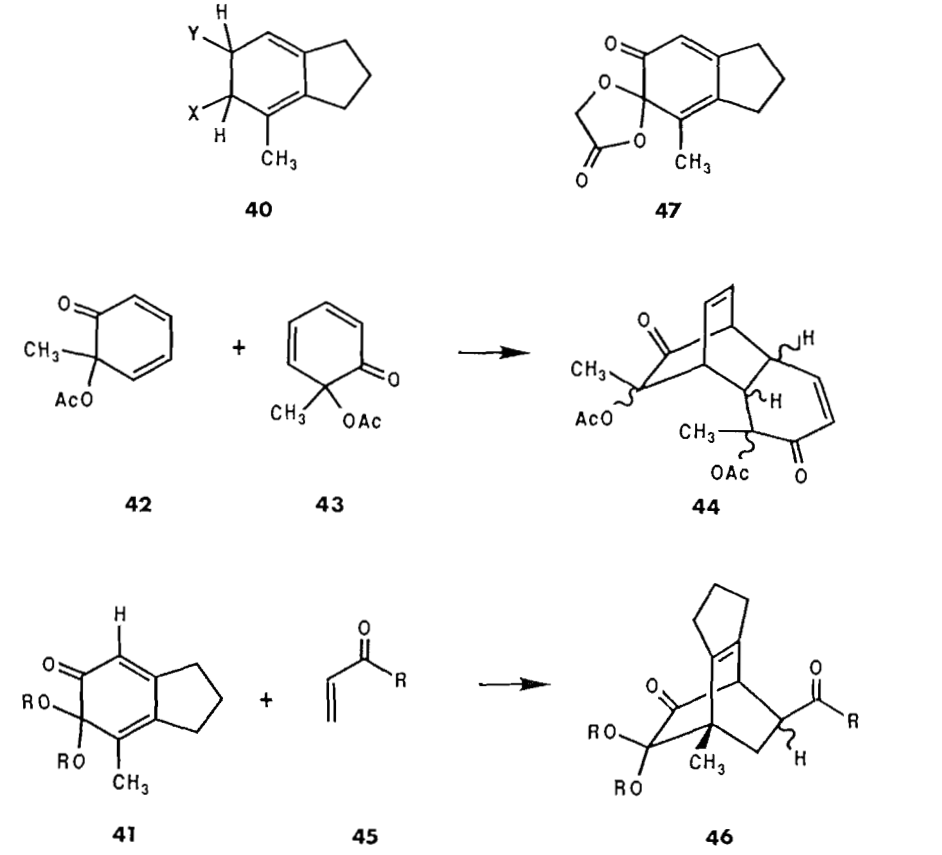

SCHEME 6

The difficulty in obtaining a convenient diene for our synthetic plan resides in the fact that the diene must also contain two extra functional groups X and Y. We could conceive dienes that would have a different level of oxidation than that of an *o*-quinone. For instance, we could envisage dienes of type **40** (Scheme 6), but we felt that such an approach was not very promising and it was not considered further because such dienes might not have the stability required to withstand the thermal conditions of an anticipated Diels–Alder reaction. Theoretically, the *o*-quinone was the ideal diene. It had just the right oxidation level to lead to a Diels–Alder adduct having the correct oxidation level, a 1,2-diketone, permitting the attachment of ring A directly. In practice, this approach did not work because *o*-quinones are unstable. Consequently, the only possibility that remained was to modify the *o*-quinone in such a way that the resulting derivative would be more stable, that it would not dimerize (or at least dimerize more slowly), and yet it would still be capable of reacting as a diene. The only modification that appeared attractive seemed to be at the carbonyl groups of the *o*-quinone, and on that basis we considered dienes of type **41**.

Can. J. Chem. Downloaded from www.nrcresearchpress.com by 186.148.149.217 on 09/07/12
For personal use only.

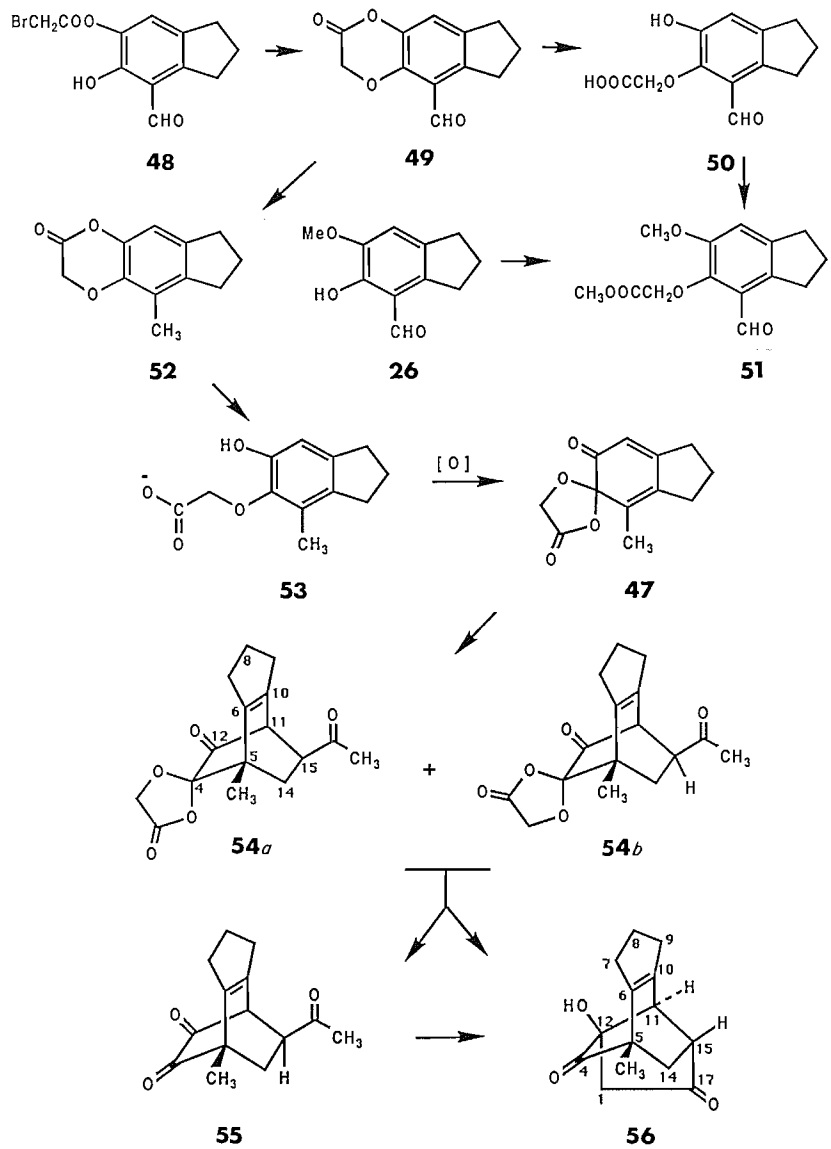

SCHEME 7

We had great hope with diene **41** because we thought that the ketal protecting group would not only make **41** a good diene, but it would render its reaction with an unsymmetrical dienophile completely regiospecific in the desired sense. This belief was based on the chemistry of quinol acetate.

It is known that quinol acetate (19) (or 6,6-disubstituted cyclohexadienone (20)) can act as a diene and as a dienophile (cf. **42** and **43**) to very readily give dimer **44** regiospecifically. Since diene **41** is more substituted than quinol acetate, we expected that **41** would dimerize slowly and it would prefer to react with a small active dienophile. There was one literature example of a substituted quinol acetate that underwent a Diels–Alder condensation with maleic anhydride as a dienophile (21). Furthermore, by analogy with the dimerization of quinol acetate, we could also expect that the reaction of diene **41** with an unsymmetrical dienophile such as vinyl ketone **45** should be completely stereo- and regiospecific. Indeed quinol acetate can be considered as a vinyl homolog (cf. **43**) of vinyl ketone **45**; thus both compounds should exhibit similar dienophilic behavior. Consequently, it was possible to predict that if vinyl ketone **45** reacted with diene **41**, it should give specifically the desired adduct **46**. We also decided that the most convenient diene of type **41** was the *o*-spirolactone dienone **47**. This decision was made on the basis that this type of compound should be easily prepared by oxidation of the corresponding *o*-hydroxyindanoxyacetic acid (*vide infra*). Indeed, there was literature precedent for such a transformation (22). We will now describe its preparation.

o-Diphenol aldehyde **33** was selectively esterified with α-bromoacetyl bromide in benzene containing pyridine to yield the monobromoacetate derivative **48** (Scheme 7). This crude product **48** was then heated to reflux in tetrahydrofuran in the presence of anhydrous sodium carbonate to furnish the crystalline lactone aldehyde **49** in 80% yield from **33**. A rigorous chemical proof for the position of the lactone ring in aldehyde **49** was obtained in the following way: alkylation of the known methoxyphenol aldehyde **26** with ethyl bromoacetate (K_2CO_3, THF) followed by basic hydrolysis and diazomethane esterification gave the methoxy aldehyde methyl ester **51**. Basic hydrolysis of **49** gave the corresponding phenol carboxylic acid **50**, which was successively esterified with diazomethane and alkylated with dimethyl sulfate (K_2CO_3, THF) to yield a product identical with compound **51**.

Wolff–Kishner reduction of lactone aldehyde **49** gave the

Can. J. Chem. Downloaded from www.nrcresearchpress.com by 186.148.149.217 on 09/07/12
For personal use only.

Can. J. Chem. Downloaded from www.nrcresearchpress.com by 186.148.149.217 on 09/07/12
For personal use only.

crystalline lactone **52** in 80% yield. The lactone **52** was then hydrolyzed with sodium hydroxide and the crude salt **53** was oxidized with *N*-bromosuccinimide in aqueous acetonitrile (22*b*, *c*) to give the desired crystalline *o*-spirolactone dienone **47** (≈90% yield). Interestingly, the *o*-spirolactone dienone **47** was found to be a stable crystalline compound. It did not dimerize even in refluxing benzene. The next task was to verify its reactivity as a diene with an active dienophile.

We discovered that *o*-spirolactone dienone **47** was an exceptionally good diene. With excess methyl vinyl ketone, it reacted in less than 1 h at room temperature to provide an almost 1:1 mixture of two isomers (**54***a* and **54***b*), which were separated. Brief treatment of either isomer (**54***a* or **54***b*) with aqueous base followed by acidification gave the same tricyclic ketone (**55**). This result showed that the two isomers differ by the configuration of the spirolactone ring only. This is not unexpected, as the attack of the dienophile can be just as facile from above or below the plane of structure **47**. Consequently, the Diels–Alder condensation between diene **47** and methyl vinyl ketone was essentially completely regio- and stereoselective.

The position of the methyl ketone side chain in compounds **54***a*, **54***b*, and **55** was easily established by ^{1}H nuclear magnetic resonance spectroscopy (H_{11} and H_{15} appear respectively as a doublet (J = 2 Hz) and an octuplet (J = 2, 6, and 9 Hz)). The configuration of the methyl ketone side chain was assigned *syn* to the double bond on the basis of the Alder *endo* rule (23), which predicts that the activating group of the dienophile must become *syn* to the double bond in the resulting adduct.

In the process of trying to obtain chemical evidence for the orientation of the methyl ketone side chain, we obtained a most interesting result. Treatment of tricyclic ketone **55** with aqueous tetrahydrofuran containing sodium hydroxide gave the tetracyclic hydroxydiketone **56**. We then found out that compound **56** was best prepared by directly treating the crude mixture **54***a* and **54***b* under the same basic conditions (75% yield). The direct conversion of **54***a* and **54***b* into **56** combines several steps in a single operation: (a) opening of the spirolactone to give a hemiketal, (b) breakdown of the hemi-ketal to give a carbonyl group, (c) epimerization of the methyl ketone side chain, and (d) aldol condensation of the methyl ketone group with one of the carbonyls of the α-diketone system.

The structure of **56** follows from the spectral data; for example, the ir shows a five-membered ring ketone. The formation of **56** was further confirmed by carrying out a series of deuterium experiments, and these results gave added support to the structures of **54***a* and **54***b*. When compound **56** was added to a deuterated basic medium (NaOD, D_2O–THF), it incorporated two deuterium atoms to give **56** deuterated at C_1. Since H_{15} was not exchanged, this result showed that the aldol condensation is an irreversible process. When **54***a* and **54***b* were placed in a deuterated basic medium, a trideuterated hydroxydiketone **56** (two D at C_1 and one D at C_{15}) was isolated in which H_{15} was totally exchanged for deuterium. These results were further confirmed by the treatment of trideuterated **56** with unlabelled aqueous sodium hydroxide, which gave monodeuterated hydroxydiketone **56** (D at C_{15}) exclusively.[7]

The above results show that the two primary objectives of our synthetic strategy were successfully reached. A good synthesis of spirolactone dienone **47** was achieved in six steps (**19** → **31** → **33** → **48** → **49** → **52** → **47**) from 5,6-dimethoxyindane (**19**) in an overall yield of ≈50%. It was also shown that spirolactone dienone **47** undergoes a selective Diels–Alder reaction with methyl vinyl ketone yielding the desired tricyclic structure **8**, i.e., compounds **54***a* and **54***b*. Furthermore, with the formation of the tetracyclic hydroxydiketone **56** in a single operation from **54**, we realized that we had made a greater advance than anticipated. Indeed, in compound **56**, one of the carbon–carbon bonds (C_1—C_{12}) of ring A of anhydroryanodol is generated and it is formed with the correct stereochemistry relative to ring A and ring B. Thus, two (C_{11}(or C_5) and C_{12}) of the three crucial asymmetric centers (C_6, C_{11}, and C_{12}) of ryanodol can be controlled.

The next objective was to show that the main basic idea of our strategy, i.e., the conversion **5** → **6** → **7**, can be realized. This work is reported in the following article.

Experimental

Apparatus, materials, and methods

Melting points were determined on a Büchi M-50 apparatus and are uncorrected. Ether, tetrahydrofuran, and 1,2-dimethoxyethane were dried by distilling over sodium benzophenone ketyl. Benzene, dichloromethane, dimethyl sulfoxide, and amines were distilled over calcium hydride. All reactions were performed under nitrogen or argon atmosphere. Analytical and preparative thin-layer chromotography (tlc) were carried out on glass plates precoated (0.25, 0.5, 1.0, 2.0 mm) with silica gel 60 F-250 (Merck). Materials were detected by visualization under an ultraviolet lamp (254 or 350 nm) and (or) by spraying with sulfuric acid (50%) or a solution of phosphomolybdic acid or vanillin followed by heating on a hot plate. Column chromatography was performed with silica gel (Baker (60–200 mesh) or Merck 60 (200–400 mesh)).

The infrared spectra (ir) were taken on a Perkin–Elmer 257 or 681 spectrophotometer. Proton nuclear magnetic resonance (^{1}H nmr) spectra were recorded (with chloroform or tetramethylsilane as internal standard) on a Varian A-60, a Bruker WP-60, a Bruker HX-90, or a Bruker WM-250 instrument. Carbon nuclear magnetic resonance (^{13}C nmr) spectra were measured on a Bruker HX-90 or WM-250 instrument. The following abbreviations have been used: s, singlet; d, doublet; dd, doublet of doublets; t, triplet; q, quartet; qn, quintet; m, multiplet; br, broad. For most of the hydroxylated compounds, the multiplicity of the hydrogens attached to a carbinol was analyzed after D_2O exchange. The mass spectra were recorded on a Hitachi–Perkin–Elmer RMU-6 mass spectrometer and peak matching (hrms) on a VG Micromass ZAB-2F spectrometer. The ultraviolet spectra (uv) were recorded on a Varian Techtron 635 spectrophotometer. Microanalyses were carried out by Mr J. Tamas, Laboratoire de microanalyses, Université de Sherbrooke; Schwarzkopf Microanalytical Laboratories, New York; and by Dr C. Daesslé, Organic Microanalyses, Montreal.

4-Bromo-5,6-dimethoxyindane (20)

A solution of bromine (46.0 g, 0.287 mol) in carbon tetrachloride (200 mL) was added dropwise, at room temperature, to a solution of 5,6-dimethoxyindane (**19**) (50.0 g, 0.284 mol) in carbon tetrachloride (200 mL). A strong flow of nitrogen was bubbled into the reaction mixture throughout the addition to remove hydrogen bromide formed during the reaction. After the addition, nitrogen bubbling was continued for an additional 30 min. The mixture was then washed with aqueous sodium thiosulfate (0.1 N) to remove traces of bromine. The organic phase was dried over anhydrous sodium sulfate, filtered, and evaporated to dryness. The yellow oil obtained (68 g, 93%) was kept in the cold (where it crystallized) and in the dark to avoid its rapid darkening by light; ^{1}H nmr ($CDCl_3$, δ ppm): 6.65 (s, 1H, Ar-H), 3.68 (s, 3H, O-CH_3), 3.55 (s, 3H, O-CH_3), 2.85 (m, 4H, 2 Ar-CH_2-), 2.08 (m, 2H, ArCH_2CH_2); ms *m/e*: 256 (M^+).

[7]The fact that there is a complete deuterium incorporation at C_{15} in the transformation **54**a + **54**b → **56** is a strong indication that the orientation of the methyl ketone side chain must be *syn* to the double bond as shown in structures **54**a and **54**b.

Can. J. Chem. Downloaded from www.nrcresearchpress.com by 186.148.149.217 on 09/07/12
For personal use only.

5,6-Dimethoxy-4-indanyl magnesium bromide (25)

A solution of 4-bromo-5,6-dimethoxyindane (**20**) (26.1 g, 0.101 mol) in anhydrous ether (250 mL) was added to magnesium turnings (12 g, 0.49 mol) in a three-neck, 1-L flask equipped with a mechanical stirrer and an efficient condenser. At the bottom of this mixture, methyl iodide (8 g, 0.057 mol) was slowly added with a pipet, care being taken not to disturb the phases of different density. After a few minutes, the reaction started and then methyl iodide (40 g, 0.28 mol) was slowly dropped into the mixture to maintain a strong reflux. The separation of an oily phase was reduced by strong mechanical stirring. When all the methyl iodide was added, the heating was stopped and this preparation was immediately used for the next step.

The formation of the Grignard reagent can be checked by hydrolysis of an aliquot (formation of 5,6-dimethoxyindane (**19**), R_f 0.47) and comparison on tlc (solvent: benzene – petroleum ether, 1:1) with the starting bromide **20** (R_f 0.67).

5,6-Dimethoxy-4-methyl indane (21)

To the Grignard reagent **25** prepared from bromide **20** (26 g, 0.10 mol) was added dropwise, with vigorous stirring, freshly distilled dimethyl sulfate (64 g, 0.51 mol). After the addition, the mixture was gently refluxed for 36 h (oil bath), then cooled, hydrolyzed (HCl, 1 M), and extracted with ether. The combined organic layers were evaporated to dryness and the residue was heated under reflux with aqueous sodium hydroxide (1 M, 10 mL) to remove the excess of dimethyl sulfate. Then the mixture was dissolved in ether, washed thoroughly with water, dried over anhydrous sodium sulfate, filtered, and the solvent removed under reduced pressure. Chromatography of the crude product (alumina, petroleum ether) gave 5,6-dimethoxy-4-methyl indane (**21**) (32%, 5.2 g of purity 85%) contaminated by 15% of a side product, 5,6-dimethoxyindane (**19**); ir ($CHCl_3$, ν cm^{-1}): 1660, 1330, 1105; ^1H nmr ($CDCl_3$, δ ppm): 6.68 (s, 1H, Ar-H), 3.83 (s, 3H), and 3.76 (s, 3H, OCH_3), 2.88 (t, 7.4 Hz, 2H), and 2.78 (t, 7.4 Hz, 2H) (2 ArCH_2), 2.18 (s, 3H, $ArCH_3$) 2.06 (quintet, 7.3 Hz, $ArCH_2CH_2$); ms *m/e*: 192 (M^+).

5,6-Dihydroxy-4-methyl indane (22)

A solution of 5,6-dimethoxy-4-methyl indane (**20**) (1.5 g, 9.1 mmol) in a mixture of glacial acetic acid (15 mL) and hydrobromic acid 47% (15 mL) was refluxed under nitrogen for 3 h. To that mixture was then added water (20 mL) and the reflux was pursued for an additional 10 min. The mixture was then cooled and extracted with ether. The combined extracts were washed with saturated aqueous sodium bicarbonate, dried over anhydrous sodium sulfate, filtered, and the solvent evaporated under reduced pressure. The residue was triturated with petroleum ether to dissolve the diphenol and the solution was filtered and the solvent evaporated. The colourless solid residue was recrystallized from petroleum ether to give 5,6-dihydroxy-4-methyl indane (**22**) (650 mg, 49%, mp 124°C); ir ($CHCl_3$, ν cm^{-1}): 3600, 3550, 1615, 1280; ^1H nmr ($CDCl_3$, δ ppm): 6.61 (s, 1H, Ar-H), 4.93 (s, 1H) and 4.88 (s, 1H) (2 OH), 2.82 (t, 7.4 Hz, 2H) and 2.77 (t, 7.4 Hz, 2H) (2 ArCH_2), 2.17 (s, 3H, $ArCH_3$), 2.04 (quintet, 7.3 Hz, $ArCH_2CH_2$); ms *m/e*: 164.

Oxidation of diphenol 22

To a solution of 5,6-dihydroxy-4-methyl indane (**22**) (1.00 g, 6.08 mmol) in anhydrous ether (100 mL) was added sodium sulfate (2 g) and freshly prepared silver oxide (3 g). The mixture was stirred at room temperature for 10 min, then filtered and the clear red solution evaporated to dryness to give a dark red residue; 0.95 g, 96%; ir (CH_2Cl_2): 1660 cm^{-1}.

4-Formyl-5-hydroxy 6-methoxyindane (26)

To the Grignard reagent **25** prepared from bromide **20** (26 g, 0.10 mol), under vigorous stirring, was slowly added ethyl orthoformate (83 g, 0.56 mol). The mixture was refluxed for 15 h (oil bath, 50°C), then ether was distilled out and the residue kept at 75°C (water bath) for 10 min under vacuum. The residue was then cooled (ice bath), cautiously hydrolyzed by slow addition of hydrochloric acid (300 mL, 3 M), and extracted with ether (3 × 300 mL). The combined extracts were dried over sodium sulfate, filtered, and concentrated to a volume of ~200 mL under reduced pressure. Then petroleum ether (600 mL) was added to precipitate the impurities. After filtration, the solution was cooled and 4-formyl-5-hydroxy-6-methoxyindane crystallized (13.5 g, 68%, mp 118–119°C); ir (CH_2Cl_2, ν cm^{-1}): 3525 (OH), 2780 (CHO), 1665 (C=O), 1610 (arom); uv (EtOH, λ_{max}): 273 mμ (ε 1620); ^1H nmr ($CDCl_3$, δ ppm): 11.37 (s, 1H, OH), 10.10 (s, 1H, CHO), 7.01 (s, 1H, ArH), 3.88 (s, 3H, OCH_3), 3.14 (t, 7.5 Hz, 2H) and 2.86 (t, 7.5 Hz, 2H) (2 ArCH_2), 2.16 (quintet), $ArCH_2CH_2$); ms *m/e*: 192 (M^+). *Anal.* calcd. for $C_{11}H_{12}O_3$: C68.74. H 6.29; found: C 68.67, H 6.05.

4-Diethoxymethyl-5-hydroxy 6-methoxyindane (27)

Triethylorthoformate (1 mL, large excess) was added at 25°C to a yellow solution of 4-formyl-5-hydroxy-6-methoxyindane (55 mg, 0.29 mmol) in dry ethanol (5 mL). To that mixture was added a crystal (≈1 mg) of *p*-toluenesulfonic acid. After 3 min the color was completely discharged. Potassium carbonate (≈3 mg) was then added and the volatile materials were removed under vacuum. The partly solid residue was triturated with dry ether and the ethereal fraction was filtered and evaporated. The almost colorless oil residue (75 mg, quant.) was kept in the cold and under argon. When exposed to moist air, it rapidly became yellow and crystallized (formation of compound **26**); ^1H nmr ($CDCl_3$, δ ppm): 8.42 (s, 1H, OH), 6.75 (s, 1H, Ar-H), 5.74 (s, 1H, *H*-$C(OEt)_2$), 3.84 (s, 3H, OCH_3), 3.65 (m, 4H, 2 CH_3CH_2O), 2.84 (t, 2H, 7.3 Hz) and 2.82 (t, 2H, 7.3 Hz) (2 ArCH_2), 2.04 (quintet, 2H, 7.3 Hz, $Ar(CH_2CH_2)$, 1.23 (t, 6H, 7.1 Hz) (2 CH_3CH_2O).

Carbonate 29

To a solution of 4-formyl-5-hydroxy-6-methoxyindane (**26**) (1.0 g, 5.2 mmol) in anhydrous ether (100 mL) was added portionwise lithium aluminium hydride (0.5 g). The mixture was stirred until decoloration occurred, then it was poured in small portions onto cold hydrochloric acid (100 mL, 0.2 M) and extracted with ether. The combined organic layers were washed with water, dried over magnesium sulfate, filtered, and evaporated under reduced pressure to give crystalline diol **28** (0.97 g, 96%, mp 99–100°C; ir 3650 cm^{-1}). To a solution of 4-hydroxymethyl-5-hydroxy-6-methoxyindane (**28**) (500 mg, 2.57 mmol) in benzene (50 mL) containing pyridine (960 mg) was slowly added a saturated benzenic phosgene solution (10 mL). The mixture was stirred for 15 min, then filtered. The filtrate was kept to dryness and the crude residue was recrystallized from petroleum ether to give pure white needles (420 mg, 74%, mp 146°C); ir (CH_2Cl_2, ν cm^{-1}): 1770; uv (EtOH, λ_{max}): 287 mμ (ε 350); ^1H nmr ($CDCl_3$, δ ppm): 6.83 (s, 1H, Ar-H), 4.50 (s, 2H, Ar-CH_2-O), 3.79 (s, 3H, -OCH_3), 2.90 (m, 4H, 2 Ar-CH_2-CH_2), 2.12 (quintet, 7 Hz, 2H, Ar-CH_2-CH_2); ms *m/e*: 220 (M^+). *Anal.* calcd. for $C_{12}H_{12}O_4$: C 65.45, H 5.49; found: C 65.65, H 5.48.

5,6-Dimethoxy-4-formylindane (31)

(*a*) *From 4-formyl-5-hydroxy-6-methoxyindane (26)*

To a solution of 4-formyl-5-hydroxy-6-methoxyindane (**26**) (500 mg, 2.60 mmol) in tetrahydrofuran (50 mL) was added finely powdered potassium carbonate (1.4 g) and dimethyl sulfate (480 mg, 3.8 mmol). The mixture was refluxed for 15 h with good stirring, then cooled and filtered. The filtrate was evaporated to dryness and the solid residue recrystallized from petroleum ether at −20°C to give cristalline aldehyde **31** (420 mg, 78%, mp 52°C); ir (CH_2Cl_2, ν cm^{-1}): 1685; uv (EtOH, λ_{max}): 263 mμ (ε 1050); ^1H nmr ($CDCl_3$, δ ppm): 10.42 (s, 1H, *CH*O), 7.05 (s, 1H, Ar-H), 3.89 (s, 3H, OCH_3), 3.85 (s, 3H, OCH_3), 2.98 (m, 4H, Ar-CH_2-), 2.08 (q, 7 Hz, $ArCH_2CH_2$); ms *me*: 206 (M^+). *Anal.* calcd. for $C_{12}H_{14}O_3$: C 69.89, H 6.84; found: C 69.91, H 7.06.

(*b*) *From 5,6-dimethoxyindane (19)*

In a 2-L three-necked flask equipped with a condenser, a mechanical stirrer, and a dropping funnel was dissolved 5,6-dimethoxyindane (**19**) (74.0 g, 0.416 mol) in dry dichloromethane (900 mL). To the cooled solution (0°C) was then added, at a good rate, titanium tetrachloride (96 mL). The solution became deep red-violet. Then dichloromethyl methyl ether (100 g, 0.97 mol) was added dropwise at the same temperature. The reaction mixture was stirred at 0°C for 15 min, at room temperature for 2 h, and refluxed for 2 h. The mixture was cooled, poured onto ice cold water (1 L), and stirred for 48 h. The two layers were separated and the aqueous phase extracted with dichloromethane

Can. J. Chem. Downloaded from www.nrcresearchpress.com by 186.148.149.217 on 09/07/12
For personal use only.

(3 × 200 mL). The combined organic layers were washed with water (2 × 100 mL), dried ($MgSO_4$), filtered, and the solvent evaporated. The viscous residue was crystallized from petroleum ether to give crystalline aldehyde **31** (pale yellow crystals, 68 g, 80%, mp 52°C).

4-Diethoxymethyl-5,6-dimethoxyindane (*32*)

To a solution of aldehyde **31** (200 mg, 0.97 mmol) in anhydrous ethanol (10 mL) was added triethyl orthoformate (177 mg, 1.19 mmol) and *p*-toluenesulfonic acid (4 mg). The mixture was stirred at room temperature for 17 h, then reacted with saturated aqueous sodium carbonate, and extracted with ether. The organic layer was washed with water, dried over magnesium sulfate, and evaporated to dryness. The oily residue was purified by column chromatography on silica gel to give pure acetal **32** (170 mg, 62%); ir (CH_2Cl_2, ν cm^{-1}): 1605, 1480, 1330, 1100; ^1H nmr ($CDCl_3$, δ ppm): 6.78 (s, 1H, Ar-H), 5.79 (s, 1H, *H*-C(OEt)$_2$), 3.83 (s, 3H, OCH_3), 3.80 (s, 3H, OCH_3), 3.70 (m, 2H, OCH_2CH_3), 3.50 (m, 2H, OCH_2CH_3), 3.08 (t, 7.4 Hz, 2H) and 2.81 (t, 7.4 Hz, 2H) (2 $ArCH_2$-), 2.03 (quintet, 7.4 Hz, 2H, $ArCH_2CH_2$-), 1.22 (t, 7.4 Hz, 6H, OCH_2CH_3).

5,6-Dihydroxy-4-formylindane (*33*)

(*a*) *From 4-formyl-5-hydroxy-6-methoxyindane* (*26*)

To a solution of 4-formyl-5-hydroxy-6-methoxyindane (**26**) (18.0 g, 93.7 mmol) in dry methylene chloride (200 mL) was slowly added a solution of boron tribromide (25.0 g, 100 mmol) in dry methylene chloride (100 mL) (formation of a red complex). The reaction mixture was stirred at room temperature for 45 min, then reacted with aqueous methanol (20 mL, 90%). The volume was then reduced to ~50 mL under reduced pressure, water (50 mL) was added, and the resulting mixture extracted (3 × 300 mL) with the mixed solvent ether – petroleum ether (2:3). The combined extracts were dried ($MgSO_4$) and treated with silica gel (10 g) to adsorb acid impurities. After filtration, the solvent was evaporated under reduced pressure and the crude material crystallized from ether–pentane to give compound **33** (14 g of bright yellow crystals that darken in moist air, 84%, mp 130–131°C); ir CH_2Cl_2, ν cm^{-1}): 3550, 1650; uv (EtOH, λ_{max}): 278 mμ (ε 710); ^1H nmr ($CDCl_3$, δ ppm): 10.05 (s, 1H, CHO), 7.21 (s, 1H, Ar-H), 3.02 (m, 4H, 2 Ar-CH_2), 2.21 (quintet, 7 Hz, 2H, $ArCH_2CH_2$); ms *me*: 178 (M^+). *Anal.* calcd. for $C_{10}H_{10}O_3$: C 67.41, H 5.66; found: C 67.47, H 5.48.

(*b*) *From 5,6-dimethoxy-4-formylindane* (*31*)

Boron tribromide (81 mL, 0.854 mol) was slowly added to a cooled solution (−70°C) of 5,6-dimethoxy-4-formylindane (**31**) (80.0 g, 0.388 mol) in dichloromethane (1.5 L) under good mechanical stirring. When the addition was complete, the cold bath was removed and the mixture was allowed to warm to room temperature. The reaction was monitored by thin-layer chromatography. When the reaction was complete the mixture was cooled to −70°C and reacted successively with methanol (400 mL), aqueous methanol (1:1, 200 mL), and water (500 mL). The hydrolysis was then pursued for 15 h at room temperature. The two layers were separated and the aqueous phase was extracted with dichloromethane (4 × 250 mL). The combined organic layers were washed with water (2 × 250 mL), dried ($MgSO_4$), filtered, and the solvent evaporated under reduced pressure. The crude product was recrystallized (ether–pentane 1:1) to give an almost quantitative yield of the known (*vide supra*) 5,6-dihydroxy-4-formylindane (**33**) (68 g, 98%, mp 129–131°C).

5,6-Carbonyldioxy-4-formylindane (*34*)

To a yellow solution of 5,6-dihydroxy-4-formylindane (**33**) (5.50 g, 30.9 mmol) in dry benzene were added pyridine (8 g) and a benzenic saturated solution of phosgene until complete decoloration. The mixture was filtered, washed with dilute hydrochloric acid (0.1 M) and water, dried over magnesium sulfate, and the solvent evaporated. The crude product was recrystallized from ether–pentane to give carbonate **34** (5.9 g, 93%, mp 104°C); ir (CH_2Cl_2, ν cm^{-1}): 1835, 1780; ^1H nmr ($CDCl_3$, δ ppm): 10.35 (s, 1H, *CH*O), 7.41 (s, 1H, Ar-H), 3.13 (m, 4H, 2 Ar-CH_2), 2.20 (quintet, 7 Hz, $ArCH_2$-CH_2); ms *me*: 204 (M^+).

5,6-Carbonyldioxy-4-hydroxymethylindane (*35*)

A solution of 5,6-carboxyldioxy-4-formylindane (**34**) (2.0 g, 9.8 mmol) in tetrahydrofuran (100 mL), containing previously reduced platinum oxide (150 mg), was shaken in a hydrogen atmosphere for 24 h (atmospheric pressure, room temperature). The solution was then filtered and the solvent was evaporated under reduced pressure. The crude crystalline product was recrystallized from petroleum ether to give alcohol **35** (1.7 g, 84%, mp 107–109°C); ir (CH_2Cl_2, ν cm^{-1}): 3620, 1830; ^1H nmr ($CDCl_3$, δ ppm): 7.04 (s, 1H, Ar-H), 4.80 (s, 2H, -CH_2OH), 3.00 (m, 4H, 2 Ar-CH_2-CH_2), 2.16 (quintet, 7 Hz, 2H, Ar-CH_2-CH_2-); ms *me*: 206 (M^+). *Anal.* calcd. for $C_{11}H_{10}O_4$: C 64.08, H 4.89; found: C 64.16, H 4.73.

Ester 36

To a benzenic solution (250 mL) of 5,6-carbonyldioxy-4-hydroxymethylindane (**35**) (1.2 g, 5.8 mmol) containing pyridine (1.8 g) was added dropwise a solution of acryloyl chloride (0.9 g, 10 mmol) in benzene (50 mL). After 30 min at room temperature, the mixture was filtered, washed with dilute hydrochloric acid (0.1 M), water, then dried over magnesium sulfate, filtered, and the solvent evaporated. The solid residue was recrystallized from petroleum ether to give ester **35** (1.32 g, 87%, mp 60–61°C); ir (CH_2Cl_2, ν cm^{-1}): 1835, 1720; uv (EtOH, λ_{max}): 283 mμ (ε 320); ^1H nmr ($CDCl_3$, δ ppm): 7.15 (s, 1H, Ar-H), 6.13 (m, 3H, olefinic), 5.30 (s, 2H, $ArCH_2$-O-), 2.95 (m, 4H, 2 $ArCH_2$-CH_2), 2.16 (quintet, 7 Hz, 2H, $ArCH_2CH_2$-); ms *me*: 260 (M^+). *Anal.* calcd. for $C_{14}H_{12}O_5$: C 64.61, H 4.65; found: C 64.39, H 4.51.

o-*Quinone alcohol 39*

To a solution of 5,6-dihydroxy-4-formylindane (**33**) (1.00 g, 5.6 mmol) in anhydrous ether (100 mL) was added portionwise lithium aluminum hydride (0.5 g). The mixture was stirred until decoloration occurred, then it was poured in small portions over cold hydrochloric acid (100 mL, 0.2 M) and extracted with ether. The combined organic layers were washed with water, dried over magnesium sulfate, filtered, and evaporated under reduced pressure to give crystalline triol **38** (0.95 g, 94%, mp 118°C; ir (CH_2Cl_2, ν cm^{-1}): 3550). The oxidation was done following the procedure given for compound **22** (*vide supra*) using the following quantities: triol **38** (500 mg, 2.7 mmol) in ether (50 mL), sodium sulfate (1 g), and silver oxide (1.5 g). Quinone alcohol **39** was obtained (450 mg, 92%); ir (CH_2Cl_2, ν cm^{-1}): 3610, 1660; ^1H nmr ($CDCl_3$, δ ppm): 6.35 (s, 1H, Ar-H), 4.45 (s, 2H, -CH_2OH), 2.82 (m, 4H, 2 allylic CH_2), 2.06 (quintet, 7 Hz, 2H, CH_2-CH_2-CH_2).

6-Bromoacetoxy-4-formyl-5-hydroxyindane (*48*)

A solution of bromoacetylbromide (6.20 g, 30.6 mmol) in anhydrous benzene (50 mL) was added slowly (25 min) to a well-stirred solution of 5,6-dihydroxy-4-formylindane (**33**) (5.14 g, 28.7 mmol) in dry benzene and pyridine (8 mL). The mixture was washed with 3 M hydrochloric acid (2 × 100 mL) and water (2 × 100 mL). The organic layer was dried over magnesium sulfate, filtered, then evaporated. The solid residue was recrystallized from ether–pentane to give bromoacetate **48** (6.3 g, 73%); mp 109–110°C; ir: (CH_2Cl_2, ν cm^{-1}): 3300, 1750, 1660; ^1H nmr ($CDCl_3$, δ ppm): 9.94 (s, 1H, *CH*O), 7.15 (s, 1H, Ar-H), 4.05 (s, 2H, Br-CH_2-), 3.15 (t, J = 7 Hz, 2H), and 2.82 (t, J = 7 Hz, 2H) (benzylic hydrogens), 2.15 (quintet, 7 Hz, 2H, $ArCH_2$-CH_2); ms *me*: 298, 300 (M^+). *Anal.* calcd. for $C_{12}H_{11}O_4Br$: C 48.20, H 3.70; found: C 48.28; H 3.76.

4-Formyl-6-hydroxy-5-indanoxyacetic acid (*50*)

Anhydrous potassium carbonate (115 g, 0.835 mmol) was added to a solution of bromoacetate **48** (50 g, 0.167 mol) in freshly distilled tetrahydrofuran (800 mL). The mixture was stirred mechanically, refluxed for 48–50 h, then cooled, filtered, and the solid dissolved in water (1 L). This aqueous phase was acidified (pH 1, HCl 2 M) and extracted continuously with ether. The extract was dried ($MgSO_4$), filtered, and the solvent evaporated to give light yellow crystals: 4-formyl-6-hydroxy-5-indanoxyacetic acid (37.7 g, 96%). This product was shown to be a mixture of lactone **49** and acid **50** and was characterized in the form of lactone **49**.

Lactone aldehyde 49

A suspension of crude acid **50** (36.32 g, 0.154 mol) in benzene (750 mL) was refluxed in the presence of *p*-toluenesulfonic acid (100 mg) in

Can. J. Chem. Downloaded from www.nrcresearchpress.com by 186.148.149.217 on 09/07/12
For personal use only.

a flask (1 L) equipped with a water trap (Dean–Stark) and a condenser. After 3 h, the solution was cooled and a small quantity of silica gel (~1 g) was added to the mixture. After filtration, evaporation of the benzene under reduced pressure afforded a residue that was crystallized from ether–pentane to give lactone aldehyde **49** (30.2 g, 92%); mp 131–132°C; ir (CH_2Cl_2, ν cm^{-1}): 1780, 1680, 1580; ^1H nmr ($CDCl_3$, δ ppm): 9.90 (s, 1H, CHO), 7.15 (s, 1H, Ar-H), 4.75 (s, 2H, O-CH_2-CO_2), 3.20 (t, J = 7 Hz, 2H) and 2.85 (t, J = 7 Hz, 2H) (benzylic hydrogens), 2.15 (quintet, 7 Hz, 2H, $ArCH_2CH_2$-). *Anal.* calcd. for $C_{12}H_{10}O_4$: C 66.22, H 4.78; found: C 66.05, H 4.62.

Methyl 4-formyl-6-methoxy-5-indanoxyacetate (***51***)

(*a*) *From 4-formyl-5-hydroxy-6-methoxyindane* (***26***)

To a solution of 4-formyl-5-hydroxy-6-methoxyindane (**26**) (1.5 g, 7.8 mmol) in anhydrous tetrahydrofuran (150 mL) was added finely powdered anhydrous potassium carbonate (6.0 g, 43 mmol) and ethyl bromoacetate (1.67 g, 10.0 mmol). The mixture was refluxed for 24 h, then cooled, filtered, and the volatiles removed under reduced pressure. The residue was crystallized from hexane in the cold to give ethyl 4-formyl-6-methoxy-5-indanoxyacetate (1.8 g, 83%, mp 83–84°C); ir (CH_2Cl_2, ν cm^{-1}): 1750, 1690, 1460, 1325, 1220; ^1H nmr ($CDCl_3$, δ ppm): 9.73 (s, 1H, -CHO), 7.10 (s, 1H, Ar-H), 4.78 (s, 2H, -OCH_2CO_2-), 4.28 (q, J = 7 Hz, 2H, -OCH_2CH_3), 3.92 (s, 3H, OCH_3), 3.25 (t, J = 7 Hz, 2H), and 2.90 (t, J = 7 Hz, 2H) (benzylic hydrogens), 2.10 (m, 2H, Ar-CH_2-CH_2), 1.30 (t, J = 7 Hz, 3H, -OCH_2CH_3). *Anal.* calcd. for $C_{15}H_{18}O_5$: C 64.73, H 6.52; found: C 64.43, H 6.63. That ethyl ester (1.0 g, 3.6 mmol) was dissolved in 5% methanolic potassium hydroxide (100 mL) and the mixture was refluxed for 1 h, cooled, acidified (HCl, 1 M), and extracted with ether (3 × 100 mL). The combined organic layers were dried ($MgSO_4$), filtered, and the solvent removed under reduced pressure. The residue (0.9 g) was dissolved in ether (50 mL) and reacted (0°C) with an ethereal solution of diazomethane. After removal of the volatiles *in vacuo*, the residue was crystallized from ether – petroleum ether to give crystalline methyl ester **51** (0.68 g, 72% from the ethyl ester; mp 99–100°C); ir (CH_2Cl_2, ν cm^{-1}): 1740, 1670, 1460, 1320, 1205; ^1H nmr $CDCl_3$, δ ppm): 10.48 (s, 1H, *CHO*), 7.00 (s, 1H, Ar-H), 4.75 (s, 2H, -OCH_2CO_2-), 3.85 (s, 3H, -CO_2CH_3), 3.75 (s, 3H, -Ar-OCH_3), 3.13 (t, J = 7 Hz, 2H), and 2.80 (t, J = 7 Hz, 2H) (2 Ar-CH_2-), 2.05 (quintet, 7 Hz, 2H, $ArCH_2CH_2$). *Anal.* calcd. for $C_{14}H_{16}O_5$: C 63.62, H 6.10; found: C 63.89, H 6.29.

(*b*) *From phenol carboxylic acid* ***50***

To a solution of phenol carboxylic acid **50** (2.0 g, 8.4 mmol) in ether (250 mL), at 0°C, was added dropwise an ethereal diazomethane solution until a yellow coloration persisted. The solution was evaporated and the residue was crystallized from ether to give methyl 4-formyl-6-hydroxy-5-indanoxyacetate (2.0 g, 97%, mp 110–111°C); ir (CH_2Cl_2, ν cm^{-1}): 3300, 2720, 1740, 1680, 1452; ^1H nmr ($CDCl_3$, δ ppm): 10.32 (s, 1H, -*CHO*), 6.92 (s, 1H, Ar-H), 4.52 (s, 2H, -OCH_2CO_2-), 3.76 (s, 3H, -CO_2CH_3), 3.06 (t, J = 7 Hz, 2H), and 2.76 (t, J = 7 Hz, 2H) (2 Ar-CH_2-), 2.08 (quintet, 7 Hz, $ArCH_2CH_2$). *Anal.* calcd. for $C_{13}H_{14}O_5$: C 62.39, H 5.64; found: C 62.22, H 5.77.

This phenol methyl ester (0.20 g, 0.80 mmol) in anhydrous tetrahydrofuran (30 mL) were reacted with anhydrous potassium carbonate (0.55 g, 3.9 mmol) and dimethyl sulfate (0.5 g, 2.4 mmol). The mixture was refluxed under good stirring for 36 h, then cooled, filtered, and the resulting solution evaporated *in vacuo* and using a water bath. The solid residue was recrystallized from ether–pentane and was shown to be identical with the compound **51** obtained in part (*a*).

Lactone ***52***

To a solution of the crude acid **50** (2.0 g, ~8.4 mmol) (*vide supra*) in ethylene glycol (50 mL) containing potassium hydroxide (2 g) was added hydrazine hydrate (3 mL, 85%) and the mixture was gradually heated to reflux temperature (195°C, oil bath). After 3 h, the brown mixture was cooled, poured onto iced water (300 mL), and acidified (pH 1, HCl 2 M). The aqueous phase was saturated with sodium chloride and extracted with ether (5 × 100 mL). The combined extracts were dried ($MgSO_4$), filtered, and the solvent evaporated under reduced pressure. The yellow-red partly crystalline residue (1.8 g) was dissolved in hot benzene (100 mL) and the solution was refluxed (Dean–Stark trap) for 2 h in the presence of *p*-toluenesulfonic acid (50 mg). It was then cooled, stirred some minutes with silica gel (~1 g), filtered, and the solvent evaporated to give crude lactone **52**, which was recrystallized from ether – petroleum ether (1.4 g, 81%, mp 75–76°C); ir (CH_2Cl_2, ν cm^{-1}): 1775, 1620, 1335, 1305; ^1H nmr ($CDCl_3$, δ ppm): 6.75 (s, 1H, Ar-H), 4.55 (s, 2H, O-CH_2-CO_2-), 2.80 (m, 4H, 2 $ArCH_2$-), 2.13 (s, 3H, Ar-CH_3), 2.08 (m, 2H, $ArCH_2CH_2$); ms *m/e*: 204 (M^+). *Anal.* calcd. for $C_{12}H_{12}O_3$: C 70.57, H 5.92; found: C 70.99, H 5.81.

o-*Spirolactone dienone* ***47***

To a solution of lactone **52** (2.41 g, 11.8 mmol) in acetonitrile (30 mL) containing aqueous sodium hydroxide (120 mL, 0.1 M) was added rapidly a solution of *N*-bromosuccinimide (2.10 g, 11.8 mmol) in water (100 mL) and acetonitrile (100 mL). After 3 min, water (200 mL) was added and the mixture was extracted with dichloromethane (3 × 100 mL). The combined extracts were dried over magnesium sulfate, filtered, and the solvent evaporated. The solid residue was crystallized from ether – petroleum ether to give *o*-spirolactone dienone **47** (2.3 g, 89%, mp 98–98°C); ir (CH_2Cl_2, ν cm^{-1}): 1790, 1665, 1640, 1600; uv (EtOH, λ_{max}): 355 mμ (ε 3100); ^1H nmr ($CDCl_3$, δ ppm): 6.03 (br s, 1H, olefinic proton), 4.75 (d, J = 15 Hz, 1H), and 4.40 (d, J = 15 Hz, 1H) (AB pattern) (O-CH_2-CO_2), 2.74 (m, 4H, two allylic CH_2), 2.05 (m, 2H, homoallylic CH_2), 1.90 (s, 3H, -CH_3); ms *m/e*: 220 (M^+). *Anal.* calcd. for $C_{12}H_{12}O_4$: C 65.44, H 5.49; found: C 65.48, H 5.54.

Isomers ***54***a *and* ***54***b (Diels–Alder reaction)

Dienone **47** (4.00 g, 18.2 mmol) was dissolved in methyl vinyl ketone (6 mL) and the mixture was refluxed for 20 min; then the volatiles were removed under reduced pressure (water bath) to give a 1:1 mixture of isomers **54***a* and **54***b*. These isomers were separated on a small scale by preparative thin-layer chromatography (benzene – petroleum ether 1:1).

Isomer ***54***a (mp 113–115°C, R_f 0.68); ir (CH_2Cl_2, ν cm^{-1}): 1810, 1740, 1720; ^1H nmr ($CDCl_3$, δ ppm): 4.64 (d, J = 14 Hz, 1H), and 4.32 (d, J = 14 Hz, 1H) (AB pattern, -OCH_2CO_2), 3.64 (d, J = 2 Hz, 1H, bridgehead), 3.17 (ddd, J = 2, 6, and 9.8 Hz, *CH*$COCH_3$), 2.46 (m, 4H, two allylic CH_2), 2.17 (s, 3H, CH_3CO), 2.16 (dd, 1H J_{AM} = 13 Hz, J_{AX} = 9.8 Hz, H_{endo}C14), 1.97 (m, 2H, H_2C8), 1.67 (dd, 1H, J_{AM} = 13 Hz, J_{MX} = 6 Hz, H_{exo}C14), 1.26 (s, 3H, CH_3-); ^{13}C nmr ($CDCl_3$, δ ppm): 204.8, 199.4, 170.5, 145.6, 133.7, 103.4, 65.2, 48.8, 46.9, 42.8, 33.4, 31.1, 28.0, 22.5, 13.5; ms *m/e*: 290 (M^+).

Isomer ***54***b (83–84°C, R_f 0.74); ir (CH_2Cl_2, ν cm^{-1}): 1810, 1740, 1720; ^1H nmr ($CDCl_3$, δ ppm): 4.66 (d, J = 14 Hz, 1H), and 4.26 (d, J = 14 Hz, 1H) (AB pattern, -O-CH_2-CO_2), 3.56 (d, J = 2 Hz, 1H, bridgehead), 3.07 (ddd, J = 2, 6, and 9 Hz, *CH*$COCH_3$), 2.48 (m, 4H, two allylic CH_2), 2.13 (s, 3H, CH_3CO), 2.12 (dd, 1H, J_{AM} = 13 Hz, J_{AX} = 9.8 Hz, H_{endo} C14), 1.97 (m, 2H, H_2C8), 1.73 (dd, 1H, J_{AM} = 13 Hz, J_{MX} = 6 Hz, H_{exo}C14), 1.25 (s, 3H, CH_3-); ^{13}C nmr ($CDCl_3$, δ ppm): 204.9, 197.3, 170.5, 146.7, 133.9, 102.9, 64.3, 46.6, 42.2, 33.9, 30.8, 30.7, 28.0, 22.4, 13.5. ms *m/e*: 290 (M^+). *Anal.* calcd. for $C_{16}H_{18}O_5$: C 66.18, H 6.24; found: C 66.13, H 6.10.

Tricyclic ketone ***55***

A mixture (~1:1) of isomers **54***a* and *b* (0.54 g, 1.86 mmol) in ether (50 mL) was vigorously shaken in a separatory funnel with aqueous sodium hydroxide (1 M, 50 mL) for 5 min. The mixture was then shaken with aqueous hydrochloric acid (1 M, 70 mL) during 3 min and the layers were separated. The aqueous phase was extracted with ether (3 × 50 mL) and the combined extracts washed with water (2 × 50 mL), brine, dried over magnesium sulfate, filtered, and the solvent evaporated under reduced pressure to give a single product, tricyclic ketone **55** (0.41 g, 95%); ir (CH_2Cl_2, ν cm^{-1}): 1725 br; ^1H nmr ($CDCl_3$, δ ppm): 3.76 (d, J = 2 Hz, 1H, bridgehead), 3.25 (ddd, J = 2, 6, and 9 Hz, 1H, *H*$CCOCH_3$), 2.21 (s, 3H, CH_3-CO), 1.36 (s, 3H, CH_3-); ms *m/e*: 232 (M^+).

Tetracyclic ketone ***56***

The crude mixture **54***a* + *b* (Diels–Alder adduct) (5.4 g) was dissolved in THF (250 mL) and treated with aqueous sodium hydroxide

(1 M, 50 mL) during 2 h. The main part of the tetrahydrofuran was evaporated under reduced pressure and the aqueous phase was saturated with sodium chloride and extracted with ether (3 × 100 mL). The combined extracts were dried over magnesium sulfate, filtered, and solvent evaporated. The residue was crystallized from ether – petroleum ether to give tetracyclic hydroxydiketone **56** (3.31 g, 76.6%, mp 69–70°C); ir (CH_2Cl_2, ν cm^{-1}): 3520, 1745, 1720; ^1H nmr ($CDCl_3$, δ ppm): 3.55 (br s, 1H, hydroxyl), 3.30 (d, $J = 4$ Hz, 1H, HC11), 2.42 (s, 2H, H_2Cl), 1.22 (s, 3H, $-CH_3$); ms *m/e*: 232 (M^+). *Anal.* calcd. for $C_{14}H_{16}O_3$: C 72.39, H 6.94; found: C 72.40, H 7.14.

Dideuterated tetracyclic ketone ***56***-d_2

To a stirred solution of tetracyclic ketone **56** (30 mg, 0.13 mmol) in tetrahydrofuran (5 mL) was added a solution of sodium hydroxide (1 M, 5 mL) in deuterium oxide (D_2O). After 2 h at room temperature the organic solvent was evaporated and the mixture was extracted with ether (3 × 10 mL). The combined extracts were washed with water (2 × 10 mL, exchange of hydroxyl), dried over magnesium sulfate, filtered, and the solvent evaporated to give **56**-d_2 (23 mg); nmr: same as **56** except that the singlet (2H) at δ 2.42 has disappeared; ms *m/e*: 234 (M^+).

Trideuterated tetracyclic ketone ***56***-d_3

To the crude mixture of isomers **54***a* and *b* (52 mg, 0.18 mmol) dissolved in tetrahydrofuran (5 mL) was added under good stirring a solution (5 mL) of sodium hydroxide (1 M) in deuterium oxide. After 2 h at room temperature the compound **56**-d_3 (41 mg) was obtained by an extraction similar to that described in the preceding experiment (*vide supra*); nmr: same as **54** except that the doublet (4 Hz) at δ 3.30 has become a singlet and the singlet (2H) at δ 2.42 has disappeared; ms *m/e*: 235 (M^+).

Monodeuterated tricyclic ketone ***56***-d_1

To a stirred solution of **56**-d_3 (21 mg, 0.09 mmol) in tetrahydrofuran (5 mL) was added aqueous sodium hydroxide (1 M, 5 mL). After 2 h at room temperature, the product **56**-d_1 (17 mg) was extracted following the preceding procedure (*vide supra*); nmr: same as **56**-d_3 except that the singlet (2H) at δ 2.42 has appeared, the singlet at δ 3.30 is still present; ms *m/e*: 233 ($^M+$).

Acknowledgements

A generous gift of 5,6-dimethoxyindane from Ayerst Laboratories (Montreal) is deeply appreciated. We also wish to thank Mr. Denis Viens for the large-scale preparation of spirolactone dienone **47**. This work was financially supported by the National Research Council of Canada (NRC) and by the "Ministère de l'Éducation du Québec (FCAC)"; this support is gratefully acknowledged.

1. E. F. Rogers, F. R. Koniuszy, J. Shavel, Jr., and K. Folkers. J. Am. Chem. Soc. **70**, 3086 (1948).
2. (*a*) K. Wiesner, Z. Valenta, and J. Findlay. Tetrahedron Lett. 221 (1967); (*b*) K. Wiesner. Adv. Org. Chem. **8**, 295 (1972).
3. S. N. Srivastava and M. Przybylska. Can. J. Chem. **50**, 1882 (1972).
4. A. Bélanger, D. J. F. Berney, H.-J. Borschberg, R. Brousseau, A. Doutheau, R. Durand, H. Katayama, R. Lapalme, D. M. Leturc, C.-C. Liao, F. N. MacLachlan, J.-P. Maffrand, F. Marazza, R. Martino, C. Moreau, L. Saint-Laurent, R. Saintonge, P. Soucy, L. Ruest, and P. Deslongchamps. Can. J. Chem. **57**, 3348 (1979).
5. D. Berney and P. Deslongchamps. Can. J. Chem. **47**, 515 (1969); D. J. F. Berney. Ph.D. Thesis, Université de Sherbrooke, 1969.
6. P. Deslongchamps. Pure Appl. Chem. **49**, 1329 (1977).
7. K. Wiesner. Pure Appl. Chem. **7**, 285 (1963).
8. C. Mercier, A. R. Addas, and P. Deslongchamps. Can. J. Chem. **50**, 1882 (1972).
9. (*a*) L. Horner and K. Sturm. Liebigs Ann. Chem. **597**, 1 (1955); (*b*) J. Harley-Mason and A. H. Laird. J. Chem. Soc. 1718 (1958).
10. L. Horner and H. Mertz. Liebigs Ann. Chem. **570**, 89 (1950).
11. L. Horner and D. W. Baston. Chem. Ber. **98**, 1252 (1965).
12. R. Granger, P. F. G. Nau, J. Nau, and C. François. Bull. Soc. Chim. Fr. 496 (1948).
13. R. Willstätter and F. Müller. Chem. Ber. **44**, 2171 (1911).
14. D. J. F. Berney. M.Sc. Thesis, Université de Montréal, 1967.
15. (*a*) P. Rayet, M. Prost, and M. Urbain. Helv. Chim. Acta, **39**, 87 (1956); (*b*) S. Yamaguchi, K. Sugiura, R. Fukuoka, K. Okazaki, M. Takeuchi, and Y. Kawase. Bull. Chem. Soc. Jpn. **57**, 3607 (1984).
16. F. L. Benton and T. E. Dillon. J. Am. Chem. Chem. **64**, 1128 (1942).
17. A. Rieche, H. Gross, and E. Höft. Org. Synth. **47**, 1 (1967).
18. G. Barger. J. Chem. Soc. 563 (1908).
19. (*a*) W. Metlesics and F. Wessely. Monatsh. Chem. **88**, 108 (1957); (*b*) A. Siegel, F. Wesseley, P. Stockhammer, and P. Klezl. Tetrahedron, **4**, 49 (1958).
20. (*e*) K. Alder, F. H. Floch, and H. Lessenich. Chem. Ber. **90**, 1709 (1957); (*b*) T. L. Brown, D. Y. Curtin, and R. R. Fraser. J. Am. Chem. Soc. **90**, 4339 (1958); (*c*) A. S. Kende and P. MacGregor. J. Am. Chem. Soc. **83**, 4197 (1961).
21. W. Metlesics, F. Wessely, and H. Budzikiewicz. Monatsh. Chem. **88**, 102 (1957).
22. (*a*) A. Patchornik, W. B. Lawson, and B. Witkop. J. Am. Chem. Soc. **80**, 4747 (1958); **80**, 4748 (1958); (*b*) E. J. Corey and L. F. Haefele. J. Am. Chem. soc. **81**, 2225 (1959); (*c*) G. L. Schmir, L. A. Cohen, and B. Witkop. J. Am. Chem. Soc. **81**, 2228 (1959); (*d*) H. Iwasaki, L. A. Cohen, and B. Witkop. J. Am. Chem. Soc. **85**, 3701 (1963); (*e*) A. I. Scott, P. A. Dodson, F. McCapra, and M. B. Meyers. J. Am. Chem. Soc. **85**, 3702 (1963); (*f*) G. G. Gallo, C. R. Pasqualucci, and A. Diena. J. Org. Chem. **30**, 1657 (1965).
23. K. Alder and G. Stein. Angew. Chem. Int. Ed. Engl. **50**, 510 (1937).

Can. J. Chem. Downloaded from www.nrcresearchpress.com by 186.148.149.217 on 09/07/12
For personal use only.

The total synthesis of (+)-ryanodol. Part II. Model studies for rings B and C of (+)-anhydroryanodol. Preparation of a key pentacyclic intermediate

PIERRE DESLONGCHAMPS,[1] ANDRÉ BÉLANGER, DANIEL J. F. BERNEY, HANS-JUERG BORSCHBERG, ROBERT BROUSSEAU, ALAIN DOUTHEAU, ROBERT DURAND, HAJIME KATAYAMA, RICHARD LAPALME, DOMINIQUE M. LETURC, CHUN-CHEN LIAO, FREDERICK N. MACLACHLAN, JEAN-PIERRE MAFFRAND, FABRIZIO MARAZZA, ROBERT MARTINO, CLAUDE MOREAU, LUC RUEST, LOUISELLE SAINT-LAURENT, ROGER SAINTONGE, AND PIERRE SOUCY

Laboratoire de synthèse organique, Département de chimie, Faculté des sciences, Université de Sherbrooke, Sherbrooke (Québec), Canada J1K 2R1

Received April 24, 1989

This paper is dedicated to the memory of Professor Karel Wiesner

PIERRE DESLONGCHAMPS, ANDRÉ BÉLANGER, DANIEL J. F. BERNEY, HANS-JUERG BORSCHBERG, ROBERT BROUSSEAU, ALAIN DOUTHEAU, ROBERT DURAND, HAJIME KATAYAMA, RICHARD LAPALME, DOMINIQUE M. LETURC, CHUN-CHEN LIAO, FREDERICK N. MACLACHLAN, JEAN-PIERRE MAFFRAND, FABRIZIO MARAZZA, ROBERT MARTINO, CLAUDE MOREAU, LUC RUEST, LOUISELLE SAINT-LAURENT, ROGER SAINTONGE, and PIERRE SOUCY. Can. J. Chem. **68**, 127 (1990).

This paper reports several model studies that were necessary for the rational conception of a simple four-step synthesis (**6** + (*S*)-**74** → **81***a*–*b* → **83** ↠ **87** → **89**) (Scheme 11) of the carbonate derivative **89** of the optically active pentacyclic dihydroxy ketoaldehyde **87**, an important key intermediate for the synthesis of (+)-ryanodol (**5**). The optically active vinyl ketone (*S*)-**74** that was used as starting material was prepared in four steps from *d*-carvone ((*S*)-**94**) (Scheme 13). The preparation of the other starting material, the *o*-spirolactone dienone **6**, was reported in Part I.

Key words: strategy, synthesis, ryanodol, key intermediate, diterpene.

PIERRE DESLONGCHAMPS, ANDRÉ BÉLANGER, DANIEL J. F. BERNEY, HANS-JUERG BORSCHBERG, ROBERT BROUSSEAU, ALAIN DOUTHEAU, ROBERT DURAND, HAJIME KATAYAMA, RICHARD LAPALME, DOMINIQUE M. LETURC, CHUN-CHEN LIAO, FREDERICK N. MACLACHLAN, JEAN-PIERRE MAFFRAND, FABRIZIO MARAZZA, ROBERT MARTINO, CLAUDE MOREAU, LUC RUEST, LOUISELLE SAINT-LAURENT, ROGER SAINTONGE et PIERRE SOUCY. Can. J. Chem. **68**, 127 (1990).

On rapporte plusieurs études modèles qui ont été nécessaires à la conception rationnelle d'une synthèse simple en quatre étapes (**6** + (*S*)-**74** → **81***a*–*b* → **83** ↠ **87** → **89**) (Schéma 11) d'un intermédiaire-clé important dans la synthèse du (+)-ryanodol (**5**) : le dérivé carbonate **89** du dihydroxy cétoaldéhyde pentacyclique **87** optiquement actif. La vinylcétone (*S*)-**74** optiquement active fut synthétisée à partir de la *d*-carvone ((*S*)-**94**) (Schéma 13). La synthèse de l'autre produit de départ, l'*o*-spirolactone diénone **6**, est rapportée dans la Partie I.

Mots clés : stratégie, synthèse, ryanodol, intermédiaire-clé, diterpène.

Can. J. Chem. Downloaded from www.nrcresearchpress.com by 91.144.44.67 on 09/07/12
For personal use only.

Our general strategy (1–3) for the construction of ryanodol (**5**) via anhydroryanodol (**4**) is summarized in Scheme 1. In this approach, the macrobicyclic diketone **2**, which can be obtained by oxidation of an appropriate precursor such as **1**, would undergo a transannular aldol condensation to produce the tricyclic hydroxyketone **3**. This compound would then be converted into ryanodol **5** via anhydroryanodol **4**.

This general strategy for the synthesis of ryanodol, which is based on an analysis of the skeleton of anhydroryanodol, is explained in detail in Part I (4). Our method for the preparation of a tricyclic compound such as **1**, which contains a bicyclo[2.2.2]octene unit, was also reported in that paper. More specifically, we have shown that the Diels–Alder reaction of methyl vinyl ketone with *o*-spirolactone dienone **6** gives a ≃1:1 mixture of adducts **7***a* and **7***b*, which are then converted under basic conditions into a single product, the tetracyclic hydroxydiketone **8**.

In this paper, we wish to report our studies demonstrating that the key transformation **1** → **2** → **3** can be realized in the laboratory. This work was carried out (1, 5) using the tricyclic hydroxydiketone **8** as a starting point. We also wish to report our detailed analysis and experimental studies (6–8), which led to the development of a very convenient strategy for the synthesis of a pentacyclic key intermediate that contains ring A of anhydroryanodol.

[1]Author to whom correspondence may be addressed.

In the key transformation **1** → **2** → **3**, the oxidative cleavage of the tetrasubstituted double bond should produce two carbonyl groups that are expected to undergo a transannular aldol condensation; it was therefore desirable to avoid the presence of other carbonyl groups in the same molecule (*vide infra*). Consequently, the two carbonyl groups in the tetracyclic hydroxydiketone **8** were first modified before attempting the desired key transformation. Compound **8** was converted (Ac_2O, pyridine) into the diketoacetate **9** (Scheme 2), which was then selectively ketalized under standard conditions to give monoketal acetate **10**. It was then found that the reduction of **10** with lithium borohydride gave mainly the *trans* diol **11** together with a very small quantity of the *cis* diol **12**. When the reduction was carried out with lithium in liquid ammonia, the *cis* diol **12** was obtained as the major isomer. The configuration of the *cis* ketal diol **12** was rigorously established by its transformation into the five-membered carbonate **13** upon reaction with phosgene.

The *trans* ketal diol **11**, which was easily purified by crystallization, was selected for the cleavage study and it was first converted into ketal monoacetate **14** by acetylation (Ac_2O, pyridine). The diketone resulting from ozonolysis of ketal monoacetate **14** can exist in two different conformations, **15** and **16** (Scheme 3), which can each undergo a transannular aldol condensation yielding, respectively, the aldol diastereoisomers **17** and **18**. The ozonolysis of **14** was carried out in methanol; it was followed by a catalytic reduction with palladium-on-charcoal and by a short reflux in pyridine. This series of

Can. J. Chem. Downloaded from www.nrcresearchpress.com by 91.144.44.67 on 09/07/12
For personal use only.

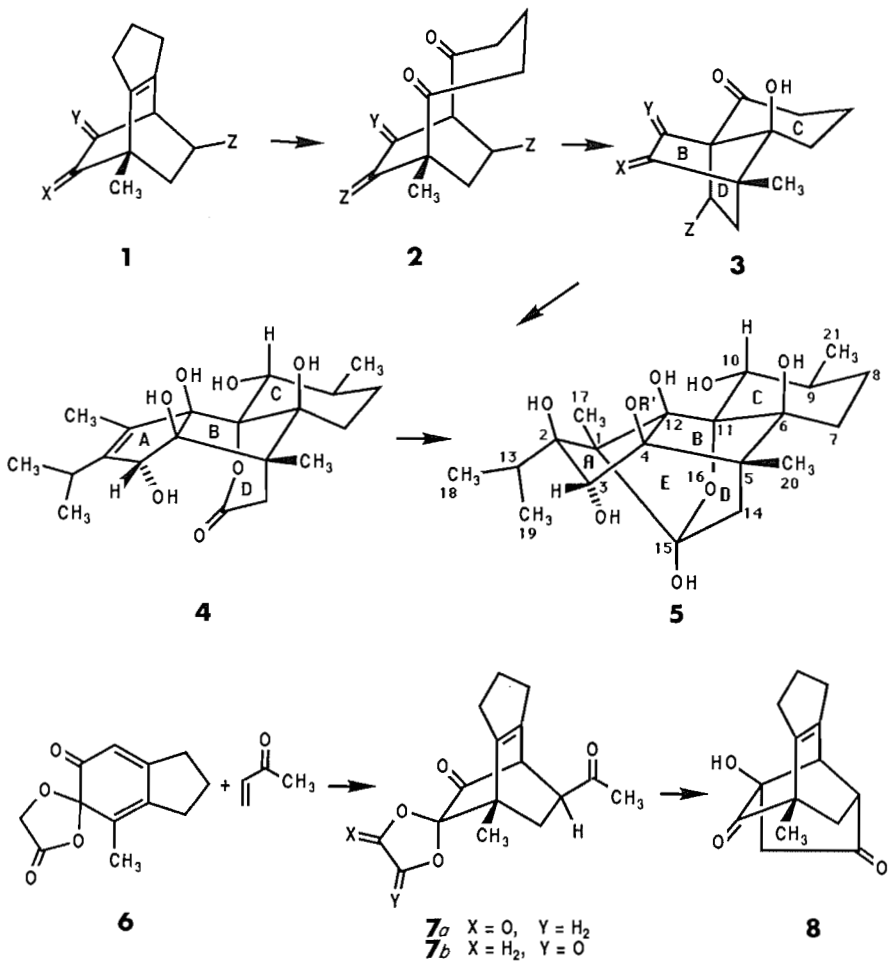

SCHEME 1

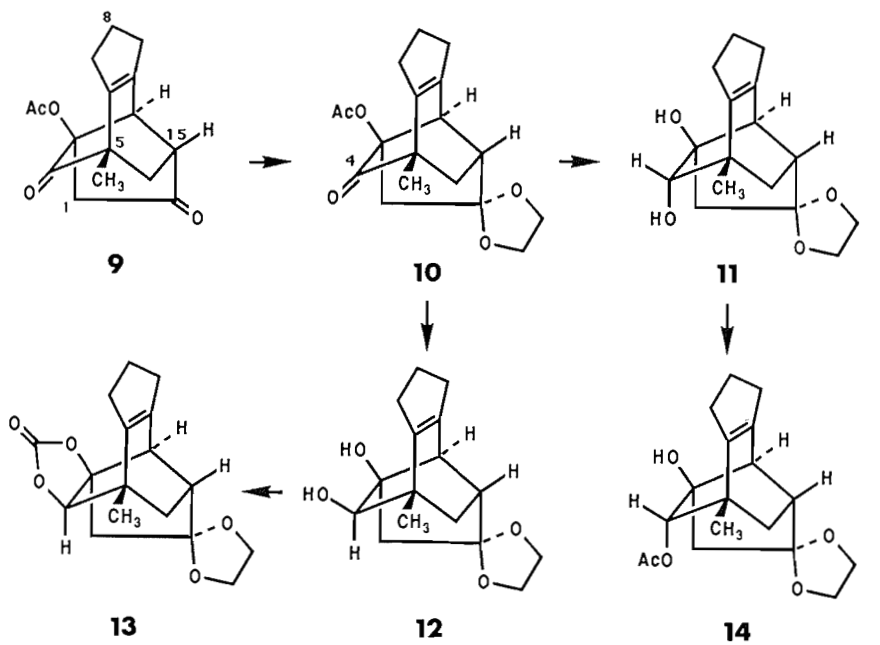

SCHEME 2

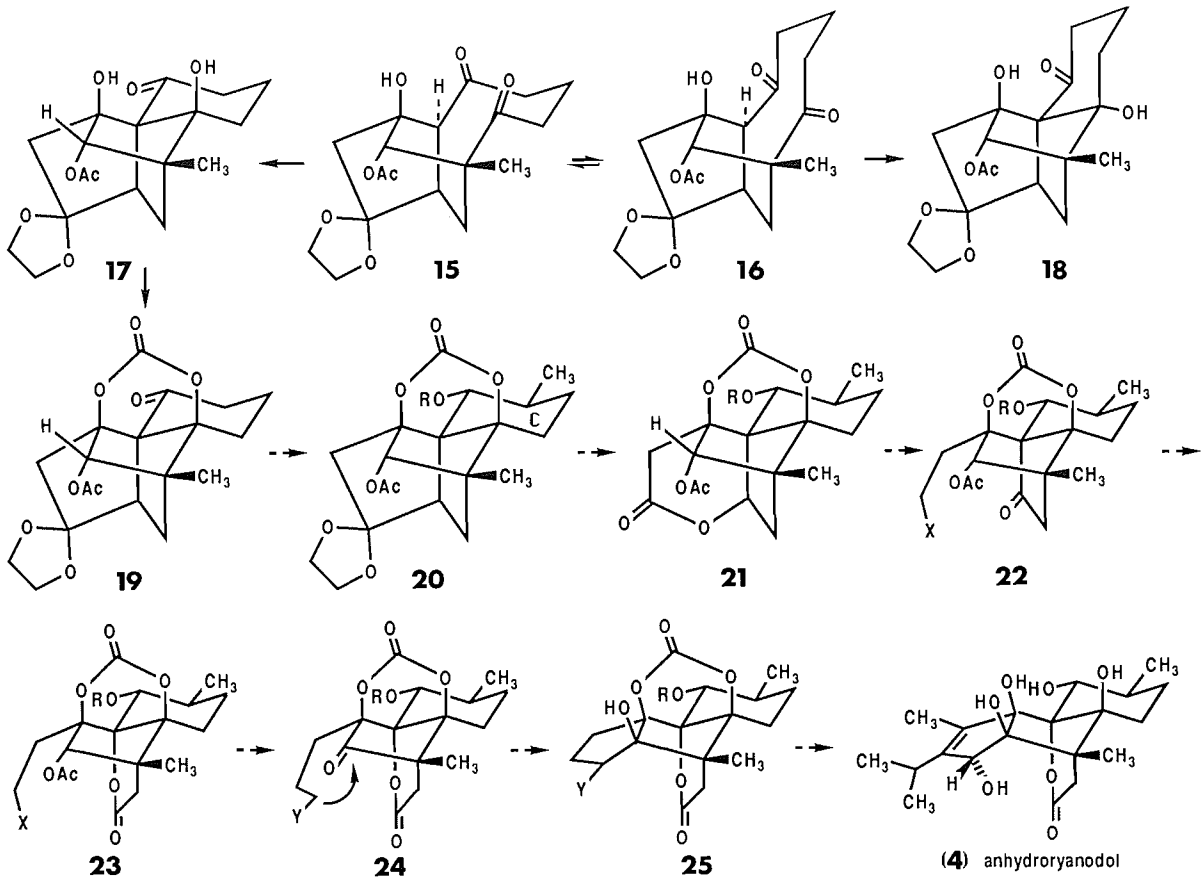

SCHEME 3

operations gave the dihydroxy ketoacetate **17** as the major product along with the isomer **18** (ratio 7:3), which were separated. The structure of **17** was firmly established by its reaction with phosgene, which afforded the crystalline six-membered carbonate derivative **19**.

The successful transformation of **14** into **17** proved that our basic synthetic strategy to build rings B and C of anhydroryanodol from the oxidative cleavage and the subsequent transannular aldol condensation of a tricyclic precursor containing a bicyclo[2.2.2]octene precursor was valid (1).

At this stage, we had to make a choice between two completely opposite directions for our future work. Either we accept compound **17** as a valuable key intermediate, or we consider the transformation **15** → **17** as a model experiment.

For instance, in the first case, one can imagine that after completing ring C, i.e., **19** → **20**, the removal of the ketal protecting group followed by Baeyer–Villiger oxidation would produce lactone **21**. This product could then be converted into ketone **22** (X to be determined), which in principle can also be oxidized via Baeyer–Villiger reaction to lactone **23**. Appropriate homologation of the side chain CH_2CH_2X and conversion of the secondary acetate at C_4[2] into a carbonyl group would then give an intermediate **24**, which would allow the formation of ring A, i.e., **25**. Anhydroryanodol would then be obtained from the tetracyclic intermediate **25**.

The proposed conversion **19** → **25** → anhydroryanodol, although certainly not easy to accomplish, is essentially a series of functional group transformations, which is quite attractive for producing a relatively simple synthesis of racemic anhydroryanodol. However, we deliberately refused to consider this route further because we felt that we would be missing a great opportunity to make a contribution to the development of knowledge in synthetic strategy.

One of the first priorities in doing organic synthesis is to discover simple schemes that avoid unnecessary steps. The preceding route already involves four extra steps, reduction of the carbonyl group at C_4, protection of the resulting secondary alcohol as an acetate (**10** → **11** → **14**), and, later on, removal of the acetate protecting group followed by reoxidation to a carbonyl group (**23** → **24**). These operations can in principle be eliminated by following one of the two alternative routes: (a) to simply carry out the ozonolysis and the transannular aldol condensation on a compound bearing a carbonyl group at C_4, i.e., **9** or **10**; (b) to transform the carbonyl group at C_4 into a hydroxyl group while forming the desired C_3—C_4 bond prior to the oxidative cleavage of the tetrasubstituted olefin. The second alternative meant that ring A would be constructed first. Both approaches were attractive because advantage was taken of the fact that our synthetic scheme generates intermediates that have the right level of oxidation at C_4 to produce ring A directly.

The first alternative route was tested with monoketal ketoacetate **10**. The ozonolysis of **10** was carried out and the expected

[2]The chemical abstract name for ryanodol: [3*S*-(3α,4β,4a*S*,6α,6aα,7α,8β,8aα,8bβ,9β,9aα] - hexahydro - 3,6a,9 - trimethyl - 7 - (1 - methyl-ethyl)-6,9-methanobenzo[1,2]pentaleno[1,6-*be*]furan-4,6,-7,8a,8b,9a(6a*H*,9*H*)-heptol) (Chem. Abstr. **101**, 6830CS (1984)). To facilitate the discussion on the synthetic strategy, the numbering system of ryanodol is used throughout, regardless of the skeleton considered.

Can. J. Chem. Downloaded from www.nrcresearchpress.com by 91.144.44.67 on 09/07/12
For personal use only.

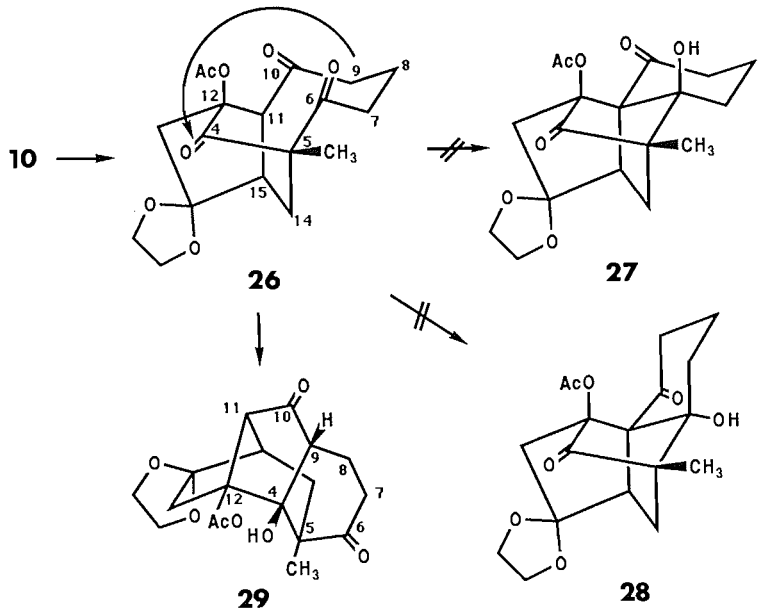

SCHEME 4

triketone **26** (Scheme 4) was isolated in good yield as crystals. Heating triketone **26** in pyridine produced a tetracyclic transannular aldol product that, on the basis of its nmr spectra, was found to have the undesired structure **29**. A close examination of a molecular model of triketone **26** revealed that in addition to the two aldol condensations that we have previously discussed, and which lead to **27** and **28**, a third aldol condensation is possible between C_4 and C_9, yielding the isomeric aldol product **29**. Compound **29** is presumably produced preferentially because enolization at C_9 might be favored over that at C_{11}. Since **29** appears less strained than the bridged isomers **27** and **28**, which each contain a bicyclo[2.2.1]heptane unit, the former might also be preferentially formed because of a thermodynamically controlled aldol process. This result meant that the oxidative cleavage of the olefin cannot be performed in the presence of a carbonyl group at C_4, and the first alternative pathway was thus eliminated from further considerations.

The second alternative route, which invokes the possibility of synthesizing ring A prior to the oxidative cleavage of the olefin, was then analysed in detail.

There are in principle two different approaches to building ring A from hydroxydiketone **8**. The first one is described by the route **8** → **32** → **33** → **4** (Scheme 5) and the second one by the route **8** → **31** → **34** → **4**. The first approach is interesting because there was a good possibility of generating the desired chirality at C_1 in **32** in a relatively simple manner. Indeed, with a dissymmetrical molecule like **8**, it is logical to expect a high degree of stereochemical control in the alkylation at C_1 and, depending on the course of this process, intermediate **32** would be produced from **8** from either of the monoalkylated products **30** or **31**. Once intermediate **32** is obtained, its conversion to pentacyclic intermediate **33** should be straightforward. The attractiveness of this route is the apparently facile construction of **33**. However, there might be a serious difficulty in this route because this compound has an extra carbon atom. By comparing the numbering system of anhydroryanodol (**4**) with that of **33**, it becomes clear that the carbonyl group (C*=O) in **33** is extra and will have to be removed eventually to produce anhydroryanodol. This means that some degradation chemistry will have to take place at a later stage. This appeared neither easy nor elegant; this route was not considered further on this basis, and also because the second approach appeared more promising.

The second approach, **8** → **31** → **34** → **4**, is interesting because the tetracyclic intermediate **34** does not have an extra carbon atom; the carbonyl group that corresponds to C_{17} can be eventually transformed into the methyl group of ring A of anhydroryanodol. The success of this route depends on the ease of controlling the configuration of the side chain at C_1 in **31**, which must be inside to produce ring A (cf. **31** → **34**). This approach was also quite interesting because there was a possibility of eliminating the alkylation step **8** → **31**. For instance, there was the possibility of producing intermediate **31** in two operations from the *o*-spirolactone dienone **6** and a methyl vinyl ketone derivative where the methyl group was replaced by a CH_2—CH_2—CH_2—Y group.

The next step was therefore to verify if substituted vinyl ketone could be used successfully in the Diels–Alder reaction and if the stereochemistry of the side chain at C_1 could be controlled.

The first study was carried out using ethyl vinyl ketone. The reaction of *o*-spirolactone dienone **6** with ethyl vinyl ketone proceeded as expected, producing a ≃1:1 mixture of adducts **35***a* and **35***b* isomeric at the spirolactone ring (Scheme 6). Treatment of crude **35***a* and **35***b* with sodium hydroxide in aqueous tetrahydrofuran gave a good yield (>60%) of two isomeric products in a 2:1 ratio; these were separated and identified as the *endo* and the *exo* epimers **36** and **37**. The assignment of configuration was carried out by ^1H nmr spectroscopy on their corresponding acetate derivatives **38** and **39**. In the major epimer **38**, H_1 appears as an octuplet (J = 2.3 and 7.2 Hz), whereas in the minor isomer **39**, H_1 appears as a quadruplet (J = 7.6 Hz). The additional coupling found in the major isomer **38** is the result of a W coupling between H_1 and H_{15}; such a coupling is not possible for the *exo* isomer **39**. This assignment was made unambiguous by observing the loss of W coupling in **38** on replacing the hydrogen at C_{15} by a deuterium atom. Monodeuterated **38** at C_{15} was obtained by repeating the epimerization – aldol condensation sequence **35***a*–*b* → **36** + **37**

Can. J. Chem. Downloaded from www.nrcresearchpress.com by 91.144.44.67 on 09/07/12
For personal use only.

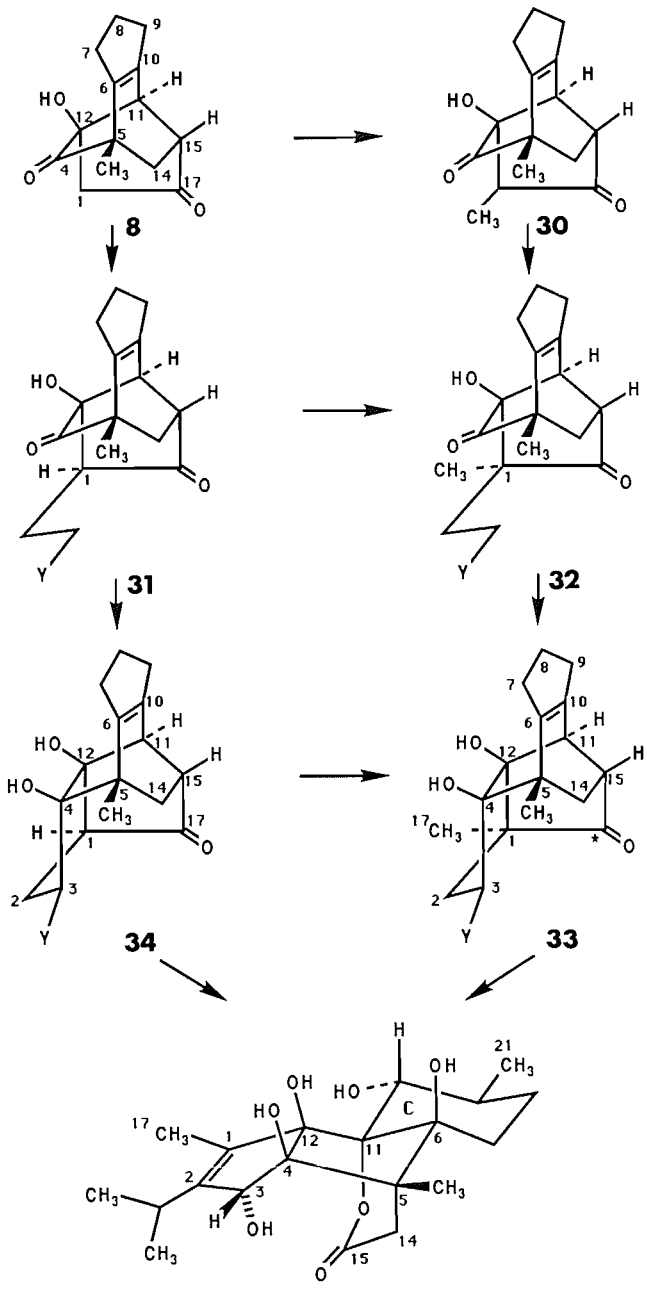

SCHEME 5

using deuterated water as solvent. This produced **36** and **37** having two deuterium atoms (at C_1 and C_{15}). Treatment of dideuterated **36** and **37** under basic conditions with H_2O gave **36** and **37** monodeuterated at C_{15} only, which upon acetylation and chromatography yielded the corresponding C_{15} monodeuterated acetates **38** and **39**.

This study demonstrated that substituted vinyl ketones could be used with success. More importantly, it also showed that the most stable epimer at C_1 had the *endo* configuration. This last result was not expected and came as a surprise.[3] It had, however, a very favorable consequence. It meant that there was no need to imagine a special device or strategy for the control of the *endo* stereochemistry at C_1, and a synthesis of a pentacyclic intermediate such as **34** via an intermediate like **31** could be readily envisaged.

The ketal vinyl ketone **44** (Scheme 7) was studied next (7). It was prepared from ethyl acetoacetate by a standard route via the intermediates **40–43**. The reaction of dienophile **44** with *o*-spirolactone dienone **6** proceeded well to give a ≃1:1 mixture of **45***a* and **45***b* that, after treatment with aqueous base followed by acidification, gave the tetracyclic triketone **46** in an impressive yield of over 95%. Acetylation of **46** with acetic anhydride and pyridine gave a diacetate, which on treatment with aqueous sodium carbonate produced the acetate derivative **47**.

We were hoping that the methyl ketone side chain in **46** could be used to induce the formation of ring A through an internal aldol condensation. However, all our attempts in this direction were unsuccessful. This is presumably due to the fact that compound **47** is too reactive and easily undergoes other reactions. For instance, treatment of **47** with anhydrous methanol containing *p*-toluenesulfonic acid provided mainly the *cis* enedione methyl ester **49**. This transformation can be explained by the addition of methanol to the five-membered ketone group, producing intermediate **48**, which undergoes on acid-catalyzed Grob type fragmentation (9). The *endo* methyl ketone side chain in **46** is responsible for the formation of the *cis* geometry of the enedione **49**. On heating at 150°C, *cis* enedione **49** was quantitatively converted into the more stable *trans* enedione **50**. When triketone alcohol **46** was treated with water under acidic conditions, the five-membered lactone **51** was isolated. Treatment of **51** with potassium *tert*-butoxide in *tert*-butanol furnished the *trans* enedione carboxylic acid **52**, which was transformed into the corresponding *trans* enedione methyl ester **50** by reaction with diazomethane. The formation of **51** must first take place via the addition of water at C_{17} followed by a fragmentation similar to that described by **47** → **48** → **49**, producing *in situ* the *cis* enedione carboxylic acid **53**, which underwent an intramolecular Michael addition to yield the five-membered lactone **51**. In the following step, it is anticipated that the basic elimination would produce directly the more stable *trans* enedione carboxylic acid **52**.

In conclusion, this study did not prove to be successful in providing a synthetic route for the construction of ring A, but it provided a rigorous chemical proof that compounds of type **31** are definitely more stable in the *endo* configuration.

We also learned from this study that the functional group of the side chain should be at a more remote position than C_2 in order to induce the formation of ring A while preventing fragmentation as previously observed. This left two possibilities, a functional group either at C_3 or linked to C_3.

An example of the second possibility is the vinyl ketone **58** (Scheme 8), which possesses a masked aldehyde linked to C_3. Compound **58** was prepared in three steps (6). Reaction of dihydropyran with 2,2-dimethylpropanediol gave the acetal alcohol **54**, which upon oxidation with Jones reagent gave the crystalline carboxylic acid acetal **55**. Treatment of the lithium salt of **55** with vinyllithium gave the vinyl ketone acetal **58**. In large-scale preparation, it was found more convenient to prepare vinyl ketone **58** via the intermediates **56** and **57**.

Diels–Alder reaction of **58** with *o*-spirolactone dienone **6** gave a quantitative yield of adducts **59***a* and **59***b* in a ≃1:1 ratio. This mixture was then treated under the now "usual" basic conditions to furnish the crystalline tetracyclic *endo* epimer **60** in 70% yield. The next step for the construction of ring A

[3]After the facts, it is, however, relatively easy to rationalize this result by an examination of molecular models of **38** and **39**: the methyl group appears to be more severely crowded in **39** (cf. steric interaction between CH_3 and H_{11}) than in **38**.

Can. J. Chem. Downloaded from www.nrcresearchpress.com by 91.144.44.67 on 09/07/12
For personal use only.

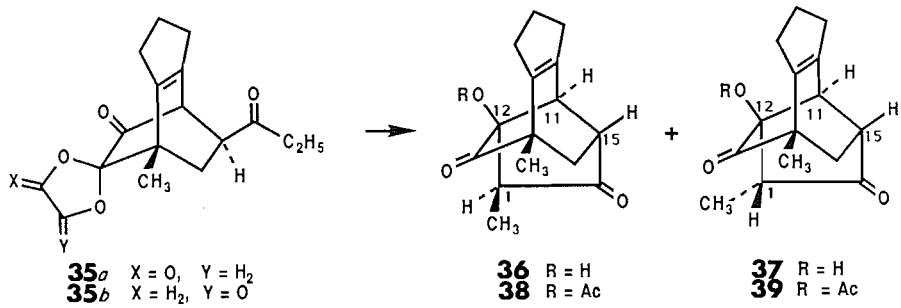

SCHEME 6

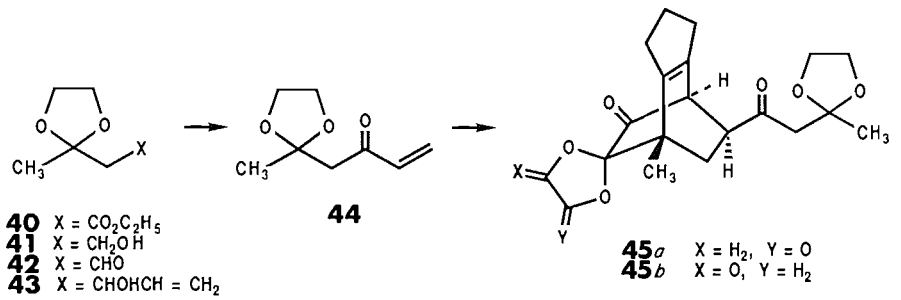

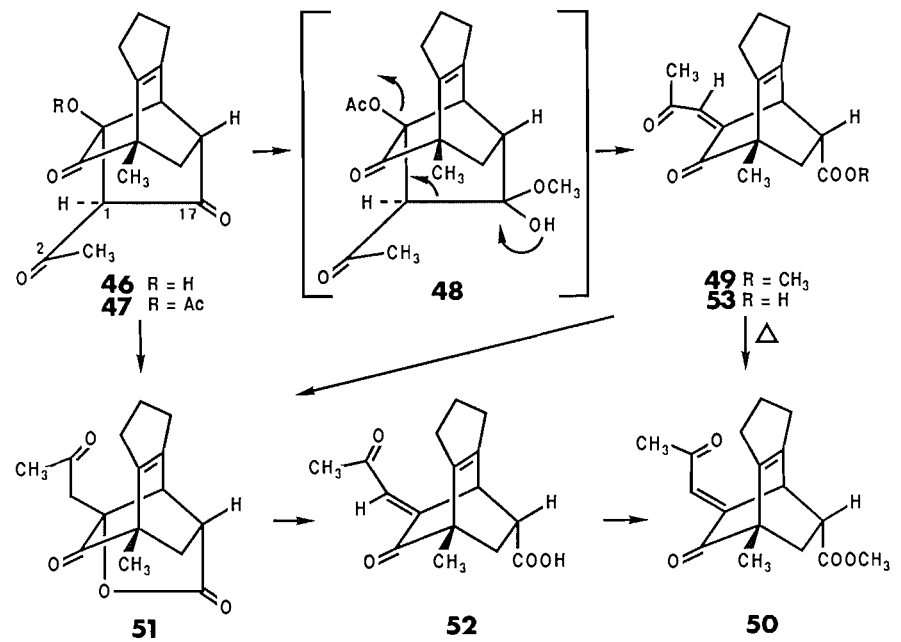

SCHEME 7

consisted of the deprotection of the aldehyde function to verify if the anticipated intramolecular aldol condensation would take place. When compound **60** was heated to reflux in a mixture of acetone and 3 M hydrochloric acid, hydrolysis and aldol condensation took place in a single operation, yielding directly the crystalline pentacyclic dihydroxyketone aldehyde **61**. However, the yield was only 25% and this was attributed mainly to the vigorous acidic conditions needed for the acetal hydrolysis.[4] Nevertheless, we had in hand an exceptionally short and simple synthesis of a pentacyclic intermediate containing ring A of anhydroryanodol. Indeed, the three steps, **58** + **6** → **59***a*–*b* → **60** → **61**, required very simple experimental conditions.

It was decided to regard this work as a model study essentially for two reasons. First, the acetal function of the dienophile had to be modified in order to be hydrolyzed under milder conditions. Second, there was also the possibility of taking further advantage of the dienophile. If a compound like **61** were accepted as an intermediate, the subsequent introduction of the isopropyl group had to be considered at a later stage. However, our strategy provided us with the opportunity of simplifying this task by pre-introducing this isopropyl group in the dienophile. We also retained the possibility of having a functional group

[4]A model study indicated that 2-alkyl-5,5-dimethyl-1,3-dioxanes require strong acidic conditions (>3 M HCl) for hydrolysis, and under such conditions compound **61** is not very stable.

Can. J. Chem. Downloaded from www.nrcresearchpress.com by 91.144.44.67 on 09/07/12
For personal use only.

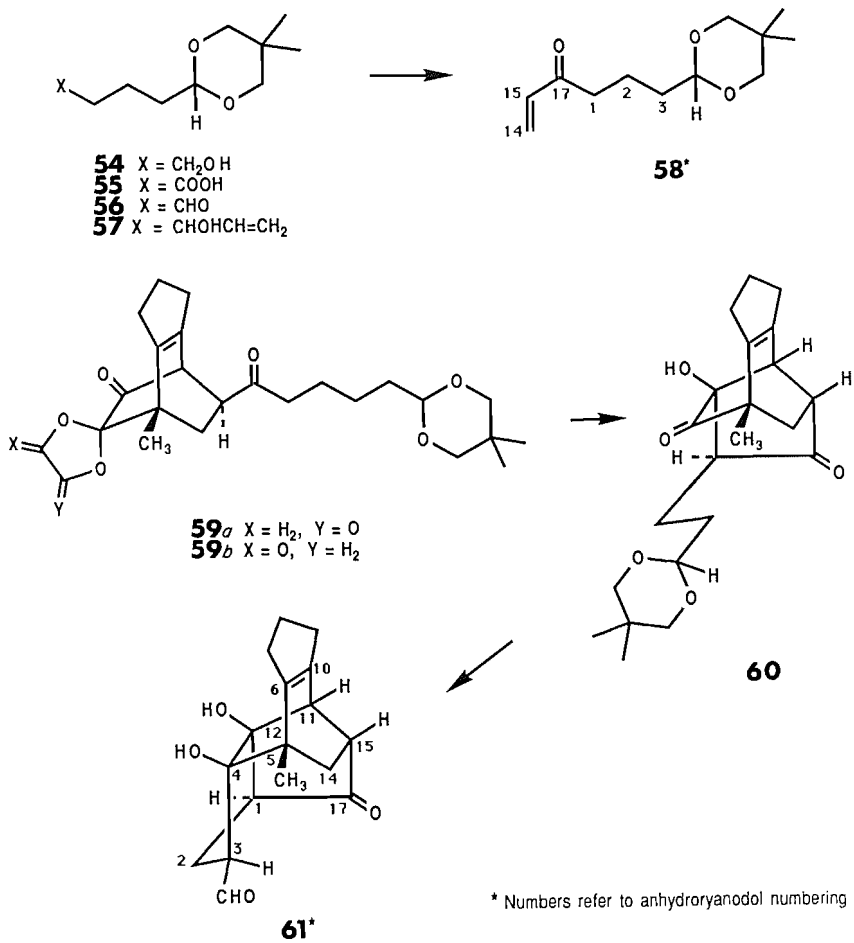

SCHEME 8

directly at C_3 or attached to C_3, and on that basis it was decided to study the dienophiles **67** and **74** (Scheme 9).

The racemic dienophiles **67** and **74** were (6) prepared from the same intermediate, the aldehyde ester **62**. Compound **62** was obtained from the condensation of the eneamine derived from diisobutylamine and isovaleraldehyde (10) with ethyl bromoacetate. Acetalization of **62** with ethylene glycol gave the acetal ester **63**, which was converted into the dienophile **67** via the intermediates **64–66** using standard conditions. Using methoxymethyl triphenylphosphorane as a reagent, the aldehyde **62** underwent a Wittig reaction to give a mixture of the *trans* and the *cis* (ratio 70:30) enol ether **68**, which can be separated by chromatography. Treatment of the isomeric mixture of enol ether **68** with ethylene glycol (PTSA, benzene) gave the homologated acetal ester **69** (R = CH_2CH_3). Basic hydrolysis of ester **69** gave the corresponding carboxylic acid **70**, which on reaction with 2 moles of vinyllithium furnished the vinyl ketone dienophile **74** having an isopropyl group at C_2 and an acetal group attached to C_3. Dienophile **74** was more conveniently prepared in large scale via the alternative route **69** → **71** → **72** → **73** → **74**.

The Diels–Alder reactions of **67** and **74** were next investigated. In both dienophiles, there is a chiral center and this will lead to the formation of diastereoisomers isomeric at C_2 and at the spirolactone moiety. For instance, the condensation of racemic dienophile **67** with *o*-spirolactone dienone **6** is expected to produce a mixture of four racemic diastereoisomers, i.e., 50% of **75***a* and **75***b* in a ≃1:1 ratio and 50% of **76***a* and **76***b* also in a ≃1:1 ratio (Scheme 10). These relative proportions are due to the fact that the chiral center at C_2, which carries the isopropyl group, is far from the vinyl ketone and it should not influence the ratio of isomers **75** and **76**. Also, our previous Diels–Alder studies have shown that the *o*-spirolactone moiety of the dienophile **6** has essentially no influence on the relative formation of the *a* and *b* spirolactone isomers in the Diels–Alder adducts. This mixture of four adducts should be convertible into a mixture of four racemic aldol condensation products **77–80**, which are diastereoisomeric at C_1 and C_2. Indeed, isomers **75***a* and **75***b* can each give a mixture of **77** and **78** whereas isomers **76***a* and **76***b* can each give a mixture of **79** and **80**. However, since the *endo* epimers are expected to predominate over the *exo* epimers, it is expected that the *endo* epimers **77** and **79** should be formed predominantly and with approximately equal ease.

The Diels–Alder reaction of vinyl ketone **67** with *o*-spirolactone dienone **6** was carried out and gave the expected mixture of **75***a–b* and **76***a–b* as indicated by ^{1}H nmr spectroscopy. Treatment of this mixture under basic conditions gave the expected mixture of aldol products **77–80** from which one isomer was obtained pure, by a simple crystallization, in 35% yield. This crystalline product has either the *endo* structure **77** or **79**. The next step in this investigation was the determination of the orientation of the isopropyl group in the crystalline product. This would then be followed by the hydrolysis of the acetal functions at C_3 and attempts to induce the formation of the desired C_3—C_4 bond via a reductive cyclization process involving the C_3-aldehyde function and the C_4-carbonyl group.

There was no doubt a greater chance of success in pursuing

Can. J. Chem. Downloaded from www.nrcresearchpress.com by 91.144.44.67 on 09/07/12
For personal use only.

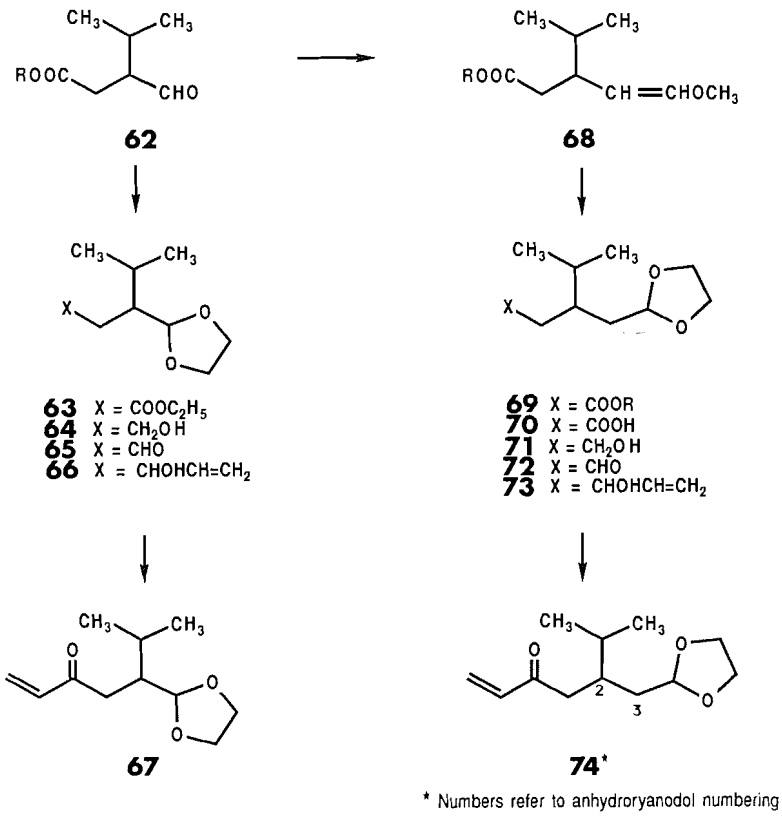

SCHEME 9

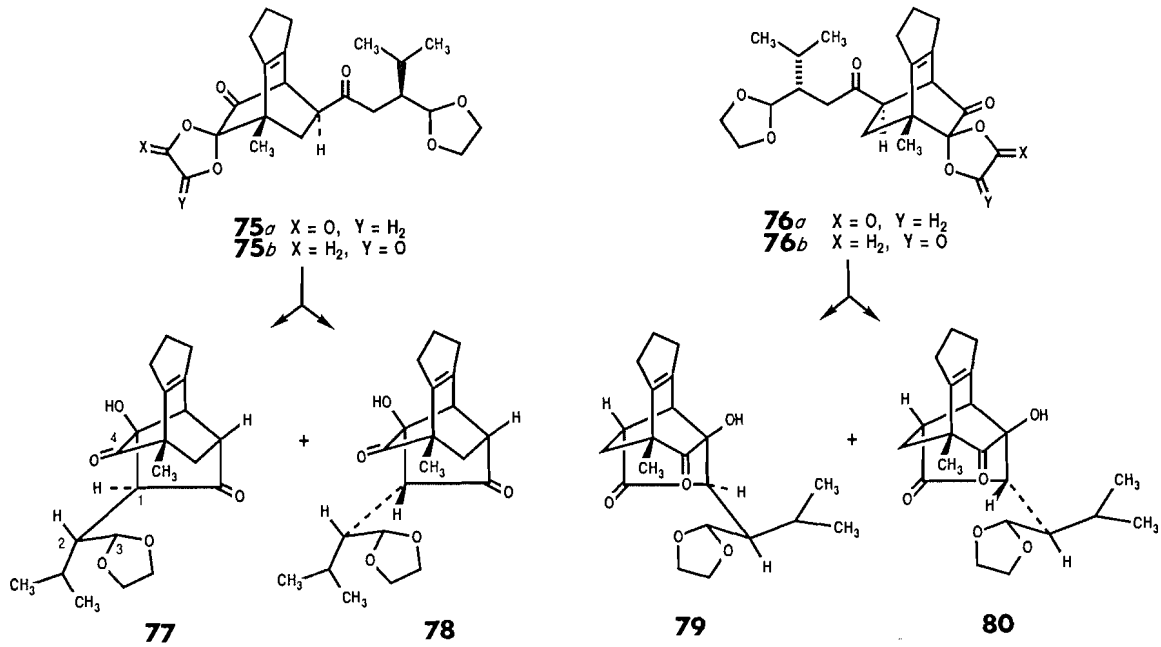

SCHEME 10

this route, but it was not investigated further because a concurrent study with the homologated dienophile **74** provided a very simple access to a pentacyclic system containing ring A. The strategy followed was essentially the same as that previously described in Scheme 8, except for the fact that the new dienophile i.e., **74**, had an isopropyl group, and a dioxolane rather than a dioxane acetal.

o-Spirolactone dienone **6** was reacted with racemic dienophile **74** to produce a quantitative yield of racemic adducts **81***a–b* and **82***a–b* (Scheme 11). Treatment of this crude mixture with sodium hydroxide in aqueous tetrahydrofuran gave a mixture of the four racemic diastereoisomers **83–86**. This mixture was heated in aqueous acetic acid and then treated with sodium hydroxide in aqueous tetrahydrofuran. This gave the racemic

Can. J. Chem. Downloaded from www.nrcresearchpress.com by 91.144.44.67 on 09/07/12
For personal use only.

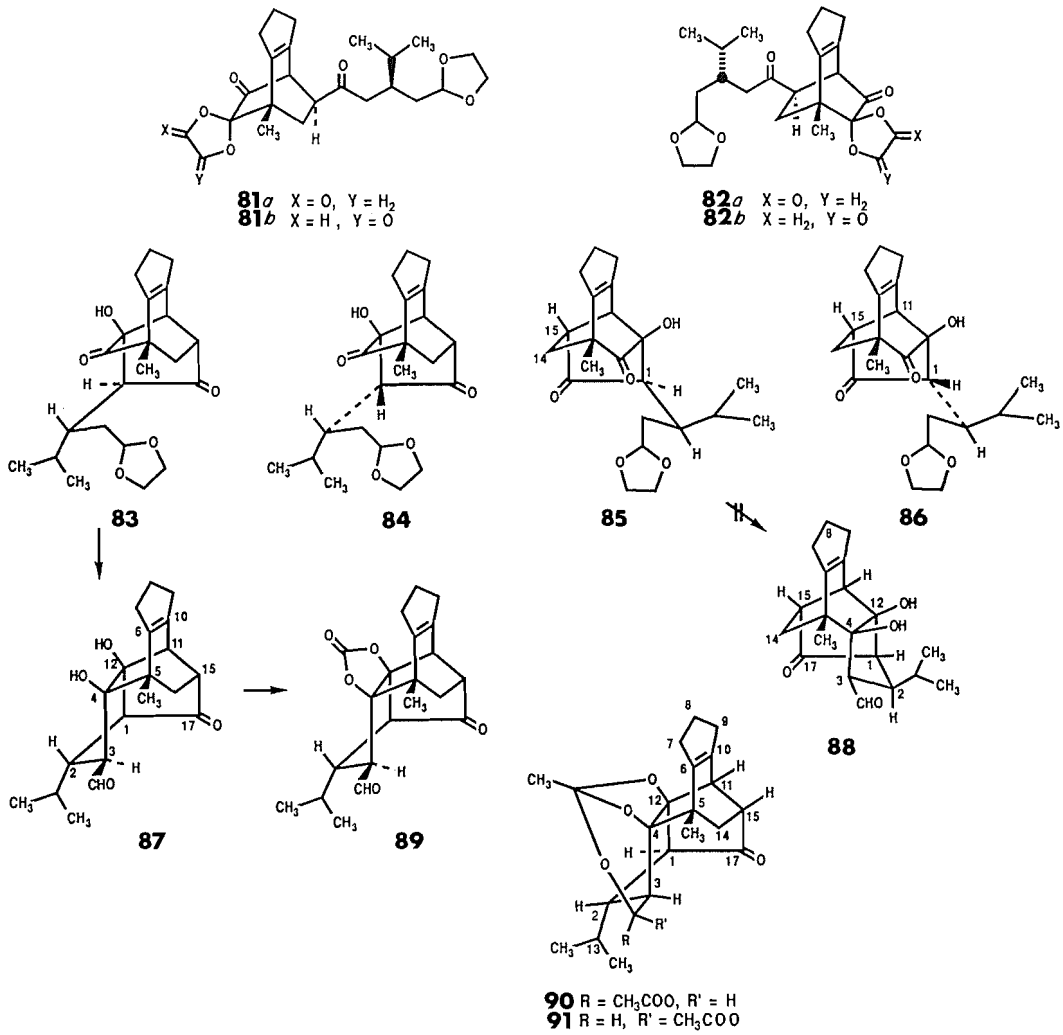

SCHEME 11

pentacyclic dihydroxyketone aldehyde **87**, which was isolated by crystallization in 23% yield from *o*-spirolactone dienone **6**. On reaction with phosgene, compound **87** gave the corresponding five-membered carbonate derivative **89**. On reaction with acetic anhydride and *p*-toluenesulfonic acid, compound **87** gave the two epimeric orthoester derivatives **90** and **91**, which could be separated by chromatography.

The relative orientation of the isopropyl group was determined by examining the ^{1}H nmr spectra of orthoester derivatives **90** and **91**, which have an almost completely rigid conformation (7). This assignment is due to the fact that in both compounds, H_1 appears as a doublet of doublets (J = 6 and 2 Hz). Molecular models show that the dihedral angle between H_1 and H_2 is near 30° in derivatives **90** and **91** and this explains the J value of 6 Hz. If these derivatives had a configuration for the isopropyl group opposite to that shown in structures **90** and **91** (cf. **88**), the dihedral angle between H_1 and H_2 would be near 90°, and the J value would have been much smaller than 6 Hz. The additional coupling of 2 Hz is due to the occurrence of W coupling H_1 and H_{15}. This overall assignment was confirmed by the synthesis of derivatives **90** and **91** having a deuterium atom at C_{15}. In those monodeuterated compounds, H_{11} and H_1 appear as a singlet and a doublet (J = 6 Hz) respectively.

The preparation of **90** and **91** monodeuterated at C_{15} was carried out by the technique previously described for deuterium incorporation in compounds **8** (4), **36**, and **37**. Starting with the mixture **81–82**, the aldol condensation was repeated using deuterated water; this produced a mixture of **83–86** bis-deuterated at C_1 and C_{15}. This mixture was then treated under basic conditions using unlabelled water to produce a mixture of **83–86** monodeuterated at C_{15}. This mixture was resubmitted under the acidic and basic conditions previously described to produce monodeuterated **87**, which was then converted into **90** and **91** having each one deuterium at C_{15}.

An extremely simple, four-step synthesis (**74** + **6** → **81–82** → **83–86** ↠ **87**) of a pentacyclic intermediate containing the isopropyl side chain of ring A was in hand. This intermediate, **87**, also had the required hydroxyl groups at C_4 and C_{12}, the tertiary methyl group at C_5, and the tetrasubstituted olefin between C_6 and C_{10}. It had two additional functional groups, the aldehyde at C_3 and the carbonyl at C_{17}, both of which are essential for the completion of rings A and D of anhydroryanodol.

Thus we had arrived at a very interesting point in our investigation. We decided that the pentacyclic compound **87** should be considered seriously as a real intermediate for our synthesis. Yet, further analysis revealed that we could take additional advantage of our dienophile **74**! This analysis started by examining in more detail the chemistry that is taking place in the course of the formation of the pentacyclic intermediate **87**. We

Can. J. Chem. Downloaded from www.nrcresearchpress.com by 91.144.44.67 on 09/07/12
For personal use only.

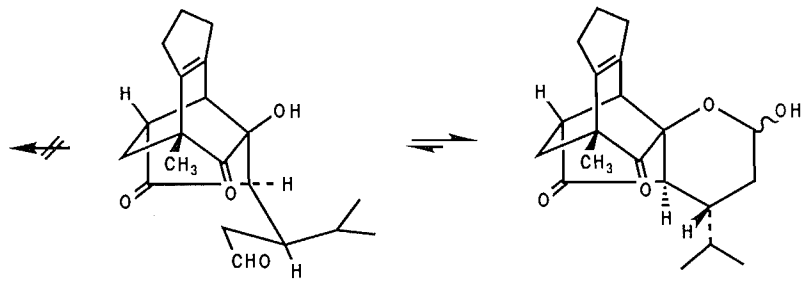

SCHEME 12

were interested in understanding why the other isomer **88** was not isolated. For instance, was it due to the fact that **87** crystallizes more readily than **88** or because only the former is being formed in the second aldol condensation process?

The tetracyclic diastereoisomeric mixture **83**–**86** was purified by chromatography (7). Isomers **83** and **85** were isolated pure and isomers **84** and **86** were obtained as a mixture from which isomer **86** could be isolated pure by crystallization. The relative configuration of the four isomers could be established by ^{1}H nmr spectroscopy and by the following reactions and chemical correlations. Equilibration[5] under basic conditions indicated that **83** and **84** are epimeric at C_1 and, since the former is the most stable epimer, **83** and **84** must have, respectively, the *endo* and the *exo* configuration. Similarly, equilibration showed that **85** and **86** are epimeric at C_1 and, since the former isomer is more stable, it has the *endo* orientation. Interestingly, when isomer **83** was submitted to the acidic and basic conditions necessary for the formation of the pentacyclic system, compound **87** was isolated in essentially quantitative yield. On the other hand, when compound **85** (or **86**) was submitted to the same reaction conditions, a complex mixture of products was formed, from which we did not succeed in isolating the anticipated pentacyclic isomer **88**. These experiments determined the relative configuration of the isopropyl group in isomers **83** and **85** since the configuration of this group has been established in compound **87** (*vide supra*). They also demonstrated that the specific formation of **87** is due to the fact that the aldehyde intermediate derived from **83** undergoes a quantitative internal aldol condensation, whereas that from **85**, under the same conditions, does not.

It is sometimes difficult to speculate on why a reaction takes place and more difficult on why a reaction does not take place. However, examination of molecular models suggests the following two alternative explanations. The isopropyl group is much more sterically hindered in isomer **88** than in **87**. On that basis, it is possible that in the case of **88** the equilibrium of the reaction is towards the retroaldol rather than the aldol product. It is also possible that the aldehyde **92** (Scheme 12) derived from **88** would prefer to exist in the form of the cyclic hemiacetal **93**, which has an isopropyl group in the equatorial orientation.[6] This would slow the rate of enolate formation from the aldehyde **92**, which is necessary for the aldol condensation, and, as a result, other competing reactions would take place and predominate. In the case of the aldehyde derived from **87**, formation of a cyclic hemiacetal would not occur because the isopropyl group would have to take an axial orientation. Thus enolization of the aldehyde would take place readily, followed by the internal aldol condensation.

The fact that the pentacyclic compound **88** is not formed and that the process leads to the specific formation of the pentacyclic isomers **87** has the disadvantage that the yield of the reaction cannot be higher than 50%. On the other hand, this approach has the advantage that if an optically active dienophile is used, the optically active enantiomer of pentacyclic **87** should be produced. To illustrate this point, let us assume that the dienophile would be optically active and would have the absolute configuration described by formula **74** (Scheme 13), i.e., having the *S* configuration. Optically active dienophile (*S*)-**74** has no preference for a particular face of the racemic diene **6**; the reaction will therefore take place with equal ease from the α and the β faces the racemic diene **6**, producing a 50:50 mixture of optically active **81***a*–*b* and **82***a*–*b* having the absolute configuration shown and where the *a*/*b* ratio due to the spirolactone isomerism will also be near 1:1. On treatment with base, optically active **81***a*–*b* will produce optically active *endo* and *exo* epimers having the absolute configuration described by structures **83** and **84**. Similarly, **82***a*–*b* will produce a mixture of optically active *endo* and *exo* epimers **85** and **86**. In the next step, **83** will be transformed into optically active **87** having the absolute configuration shown, whereas **85** cannot be converted into **88**. As a result, starting with dienophile **74** with the *S* absolute configuration leads to the optically active pentacyclic **87** having the absolute configuration shown. This also means that if one starts with dienophile **74** having the opposite *R* absolute configuration, the mirror image enantiomer of **87** would be produced. However, the absolute configuration of ryanodol is known and corresponds to formula **5**; consequently, we need the pentacyclic compound having the absolute configuration described by **87**. Thus we must synthesize an optically active dienophile **74** having the *S* absolute configuration.

The next step in our work was to find a method of obtaining an optically active dienophile of known absolute configuration in order to produce an optically active pentacyclic product. The monoterpene carvone was selected as starting material because

[5]More specifically, on treatment of **83** under basic equilibrating conditions for 18 h, **84** is not isolated but **83** was reisolated in only 85% yield. This indicates that **84** is much less stable than **83** and that **83** decomposed slightly under these conditions. Basic equilibration of **86** gave a mixture of **85** and **86** in 43% yield, where **85** predominates. Similar treatment of a mixture of **84** and **86** gave a mixture of **85** and **86**. This result confirms that isomer **84**, which can be characterized by nmr, is, however, unstable under basic conditions. It may also explain the unstability of isomer **83** because it is slowly converted into **84**, which is not stable under these conditions.

[6]These explanations were confirmed much later with the evidence of hemiketal formation (see **93**): nmr observation of anomeric proton signals at 5.38 (dd, J = 6 and 3 Hz) and 6.18 (dd, J = 12 and 3 Hz).

Can. J. Chem. Downloaded from www.nrcresearchpress.com by 91.144.44.67 on 09/07/12
For personal use only.

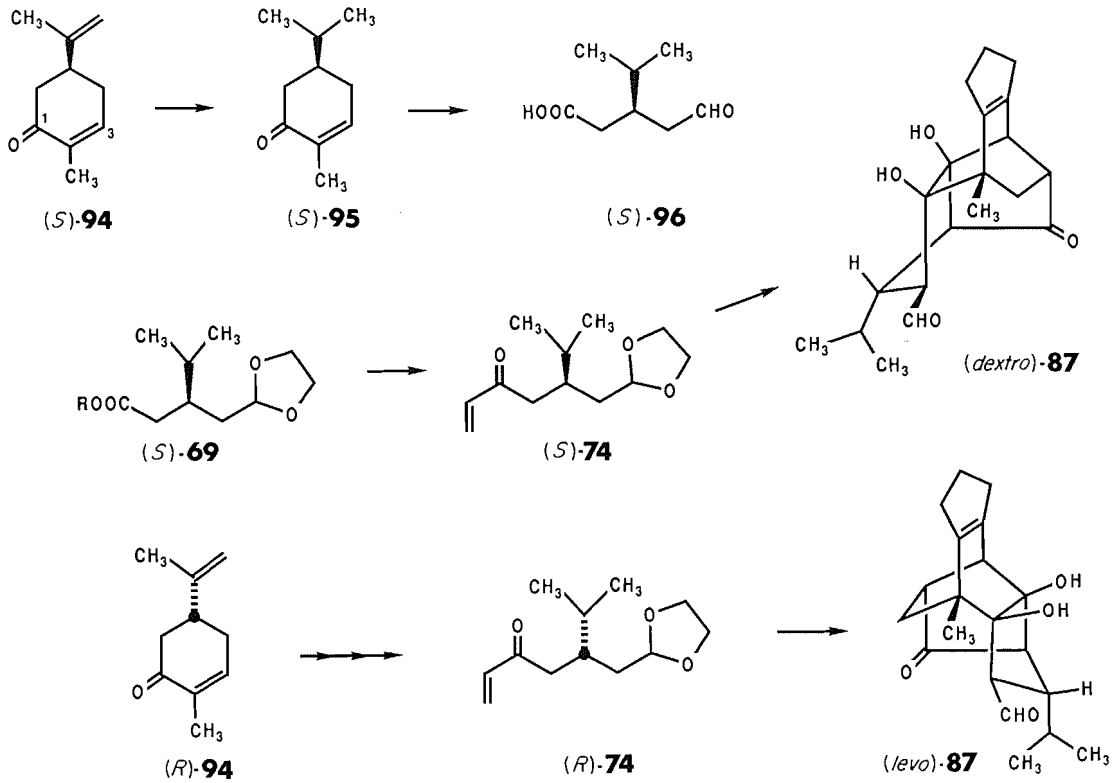

SCHEME 13

it presented several advantages. Both optically active forms *d* and *ℓ* are commercially available and their absolute configuration is well established as being *S* and *R* respectively (11). Also we were able to conceive and realize a very simple synthesis of the dienophile starting from carvone.

Scheme 13 describes the preparation of the optically active dienophile (*S*)-**74**. *d*-Carvone ((*S*)-**94**) was reduced catalytically (12) over platinum with hydrogen to give the dihydro derivative (*S*)-**95**. Ozonolysis of (*S*)-**95** (O_3 in CH_3COOEt; H_2–Pd/C) gave the aldehyde carboxylic acid (*S*)-**96**, which was transformed into the optically active acetal methyl ester (*S*)-**69** (R = CH_3) by successive acetalization (ethylene glycol, cat. PTSA in benzene; NaOH in CH_3OH) and esterification (CH_2N_2 or CH_3I, K_2CO_3 in acetone (13)). Using the methods previously described for the preparation of racemic material, acetal ester (*S*)-**69** was converted into optically active dienophile (*S*)-**74**, which was found to be dextrorotatory ($[\alpha]_{578}$ +0.6°). *o*-Spirolactone diene **6** was then heated with a slight excess of (*S*)-**74** in benzene. The crude Diels–Alder adduct was treated with an aqueous solution of sodium hydroxide in tetrahydrofuran to effect the first aldol condensation. It was then treated with aqueous acetic acid at 70°C followed by a treatment of the resulting crude material with aqueous sodium hydroxide in tetrahydrofuran. This produced, after chromatography, the crystalline pentacyclic dihydroxyketone aldehyde, which is dextrorotatory, i.e., (*dextro*)-**87** ($[\alpha]_{578}$ +142.2°). Starting with *ℓ*-carvone, i.e., (*R*)-**94**, a small quantity of the levorotatory dienophile (*R*)-**74** was also prepared and, following a sequence similar to that described above, (*R*)-**74** was converted into the crystalline levorotatory pentacyclic dihydroxyketone aldehyde, which is the mirror image of (*dextro*)-**87**, i.e., (*levo*)-**87** ($[\alpha]_{578}$ −137.5°). The pentacyclic key intermediate was thus available in both optically active forms. However, as previously mentioned, we needed (*dextro*)-**87** since its absolute configuration corresponds to that of ryanodol. In practice, it was easier to isolate the pentacyclic intermediate as the five-membered carbonate derivative **89** ($[\alpha]_D$ +121.3°) (Scheme 11). However, the overall yield of this product (**89**) from diene **6** was 27%. This 27% yields represents 54% of the theoretical yield. Our synthetic scheme being convergent, it meant that using ≈50 g of diene **6** with 50 g of dienophile (*S*)-**74** leads to approximately 25 g of (*dextro*)-**89**. It was thus relatively easy to obtain a large quantity of (*dextro*)-**89**, and we prepared approximately 100 g of it.[7]

Before preparing a large quantity of the optically active pentacyclic intermediate (*dextro*)-**89**, we carried out one additional study. So far, our investigation has led to improvement of the dienophile, but further analysis of our synthetic route revealed that there was also the possibility of improving the diene. This could be done by introducing, in the diene, the secondary methyl group that is found in ring C of ryanodol. This meant that the Diels–Alder reaction would take place with an *o*-spirolactone diene having a secondary methyl group at C_9. Since this diene would have a chiral center,[8] it could be optically active, having either the absolute configuration (*S*)-**97** or the opposite (*R*)-**97** (Scheme 14). This is theoretically interesting because each, the diene and the dienophile, have one chiral center.

This new situation can be analyzed by considering the combination of optically active dienophile (*S*)-**74** with the two

[7]When this material was prepared, Fourier transform nmr was not yet available. So, a large quantity of material was required for further investigation.

[8]*o*-Spirolactone diene **6** has one chiral center due to the spirolactone ring. However, as previously discussed, this chiral center is not important because it does not influence the Diels–Alder reaction and it is destroyed in the following step.

Can. J. Chem. Downloaded from www.nrcresearchpress.com by 91.144.44.67 on 09/07/12
For personal use only.

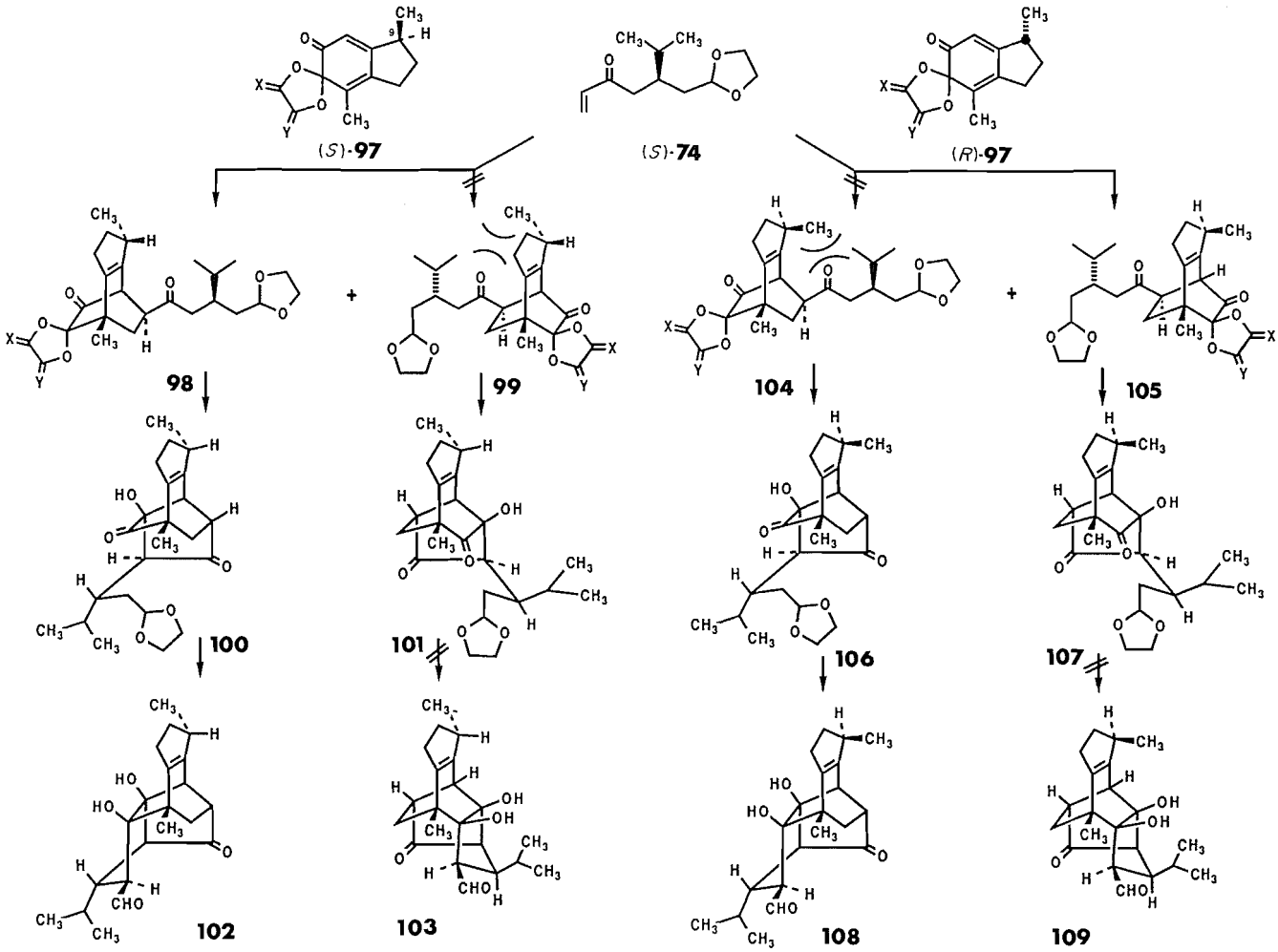

SCHEME 14

enantiomeric dienes (*S*)-**97** and (*R*)-**97**. The combination of (*S*)-**74** with (*S*)-**97** can theoretically produce **98** and **99**, which can lead to the formation of the tetracyclic intermediates **100** and **101** respectively. Then, due to the chirality of the isopropyl group, **101** would not be converted into **103** whereas **100** would lead to the formation of the pentacyclic intermediate **102**. Furthermore, it is also possible that **98** would be produced but not **99**, and this would be due to the fact that, in the transition state leading to **99**, the secondary methyl group of the diene comes close to the carbonyl group of the dienophile (cf. **99**). This is not the case during the formation of **98**, and it is possible that this steric interaction might be large enough to completely prohibit the formation of **99**. If this is true, it means that not only **103** but also **99** would not be formed and the net result would be that the theoretical yield for the production of **102** would be 100% rather than 50%.

Further advantage could also be drawn from this situation by examining the combination of optically active dienophile (*S*)-**74** with the other enantiomeric diene, i.e., (*R*)-**97**. This combination can theoretically lead to **104** and **105**, which can then yield **108** and **109** via **106** and **107** respectively. However, because of the additional steric hindrance caused by the secondary methyl group in the Diels–Alder reaction, **104** would not be produced, and only **105** would be observed. Then, **105** would be converted into **107**. However, due to the relative chirality of the isopropyl group, **107** would not yield **109**. The net result would be that the combination of (*S*)-**74** with (*R*)-**97** would not be productive. The interesting conclusion of this analysis is that it would not be necessary to resolve the diene, this resolution would be achieved by the dienophile (*S*)-**74**! Indeed, (*S*)-**74** would react with a racemic mixture of (*S*)-**97** and (*R*)-**97** producing a mixture of optically active Diels–Alder adducts **98** and **105** only, of which only the former (i.e., **98**) can lead to a pentacyclic optically active intermediate (i.e., **102**).

This interesting conclusion is valid only if the steric hindrance caused by the secondary methyl group is large enough to completely inhibit the formation of **99** and **104**. If not, it is expected that a mixture of the four Diels–Alder adducts would be produced where **98** and **105** should predominate. Since **99** and **105** cannot produce a pentacyclic product, a mixture of **102** (from **98**) and **108** (from **104**) would be produced, both optically active and where the former would predominate.

The preparation (8) of racemic *o*-spirolactone diene **97** is shown in Scheme 15. The reaction of 5,6-dimethoxyindanone (**110**) with methyllithium gave a crude mixture of **111** and **112**. Dehydration of **111** took place in the work-up and, upon purification by chromatography, crystalline methylindene **112** was isolated. Catalytic hydrogenation of **112** (PtO_2/H_2, CH_3COOH) gave methylindane **113**, which was converted into the racemic *o*-spirolactone dienone **97** by a route essentially identical to that

Can. J. Chem. Downloaded from www.nrcresearchpress.com by 91.144.44.67 on 09/07/12
For personal use only.

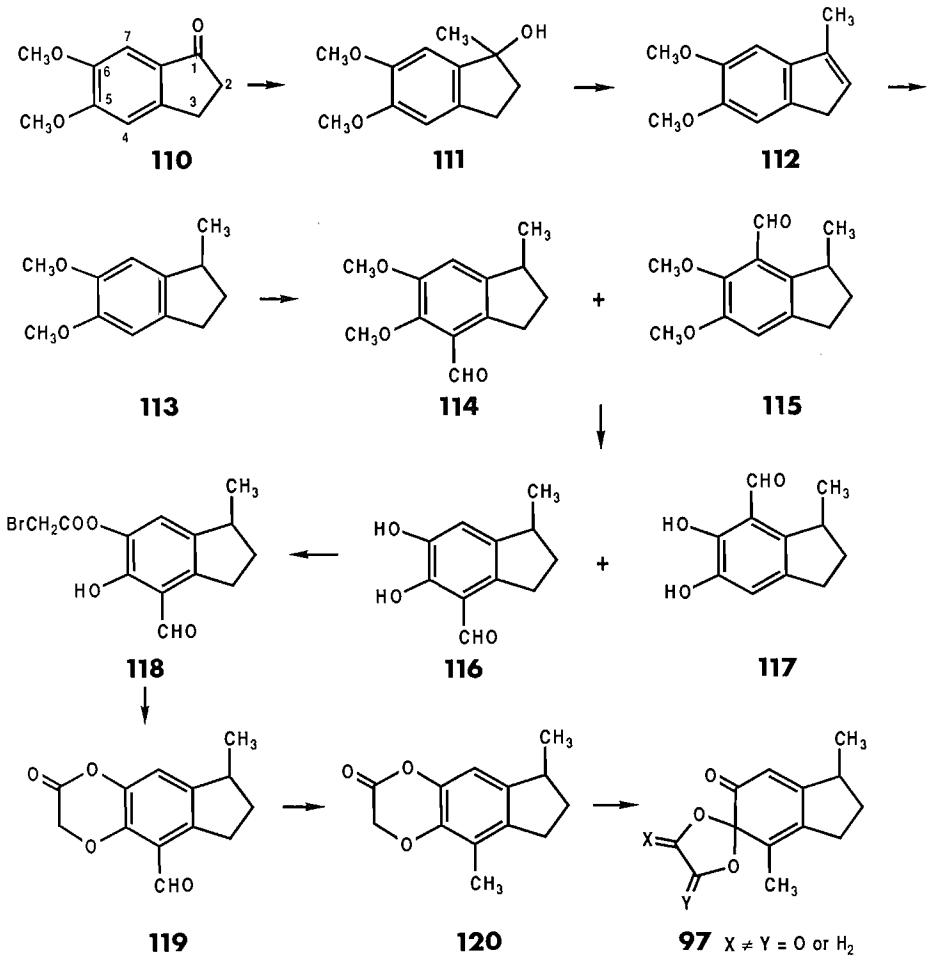

SCHEME 15

previously developed for the preparation of *o*-spirolactone dienone **6** (4). In this series, however, the chemistry was somewhat more complicated because the methylindane **113** is dissymmetric.

Reaction of methylindane **113** with dichloromethyl methyl ether and titanium tetrachloride in benzene (14) gave a 2:1 mixture of isomeric dimethoxyindane aldehydes **114** and **115**. Treatment of this mixture with boron tribromide (15) gave a 2:1 mixture of dihydroxyindane aldehydes **116** and **117**. Using the technique of fractional crystallization, **116** and **117** were obtained pure in low yield of 12 and 1% respectively. Nevertheless, this provided **116** in sufficient quantity to test our hypothesis. Reaction of **116** with bromoacetyl bromide in pyridine gave the bromoacetate **118**, which was then converted using potassium carbonate into the lactone aldehyde **119**. Catalytic reduction and hydrogenolysis of **119** with hydrogen in the presence of palladium-on-charcoal in acetic acid yielded the lactone indane **120**. Finally, treatment of lactone **120** with sodium hydroxyde followed by oxidation with *N*-bromosuccinimide (16) provided the racemic *o*-spirolactone dienone **97** ($X \neq Y = O$ or H_2).

The selectivity of diene **97** was first examined by studying its reactivity with methyl vinyl ketone (Scheme 16). This cycloaddition provided a mixture of the four isomers **121***a–b* and **122***a–b*, which were separated by chromatography. The relative stereochemistries of these compounds were not firmly established. This mixture was also treated with sodium hydroxide in water and tetrahydrofuran to produce a 55:45 mixture of isomers **123** and **124**, which were obtained pure by chromatography. The ratio obtained clearly demonstrated that the secondary methyl group in **97** does not create sufficient steric interaction to prevent the formation of **122***a–b* over that of **121***a–b*. It was therefore clear that the reaction of optically active dienophile (*S*)-**74** with racemic diene **97** would not lead to the exclusive formation of **102** as anticipated. Nevertheless, since we had both components in our hand, the Diels–Alder reaction of racemic diene **97** and optically active dienophile (*S*)-**74** was carried out, and the resulting product was treated successively with base (NaOH, THF–H_2O), acid (CH_3COOH–H_2O), and base (NaOH, THF–H_2O) to produce a crude material that was reacted with phosgene in the presence of pyridine in benzene. Preparative thin-layer chromatography provided a ≃55:45 mixture of isomers **125** and **126** in a low yield of 10%. Each isomer was then obtained pure by fractional crystallization.

This approach was abandoned because it was difficult to produce a large quantity of racemic diene **97**, and a low yield of an isomeric mixture of pentacyclic material was isolated. This approach is, however, theoretically interesting because it corresponds to a new strategy in synthesis, where the novel aspect comes from the fact that the resolving agent remains part of the target molecule afterward. It is likely that such a procedure will eventually be used with complete success in another synthesis.

Before ending Part II, we wish to add that we also considered to some extent another type of dienophile. The strategy previously described using vinyl ketone dienophiles requires a

Can. J. Chem. Downloaded from www.nrcresearchpress.com by 91.144.44.67 on 09/07/12
For personal use only.

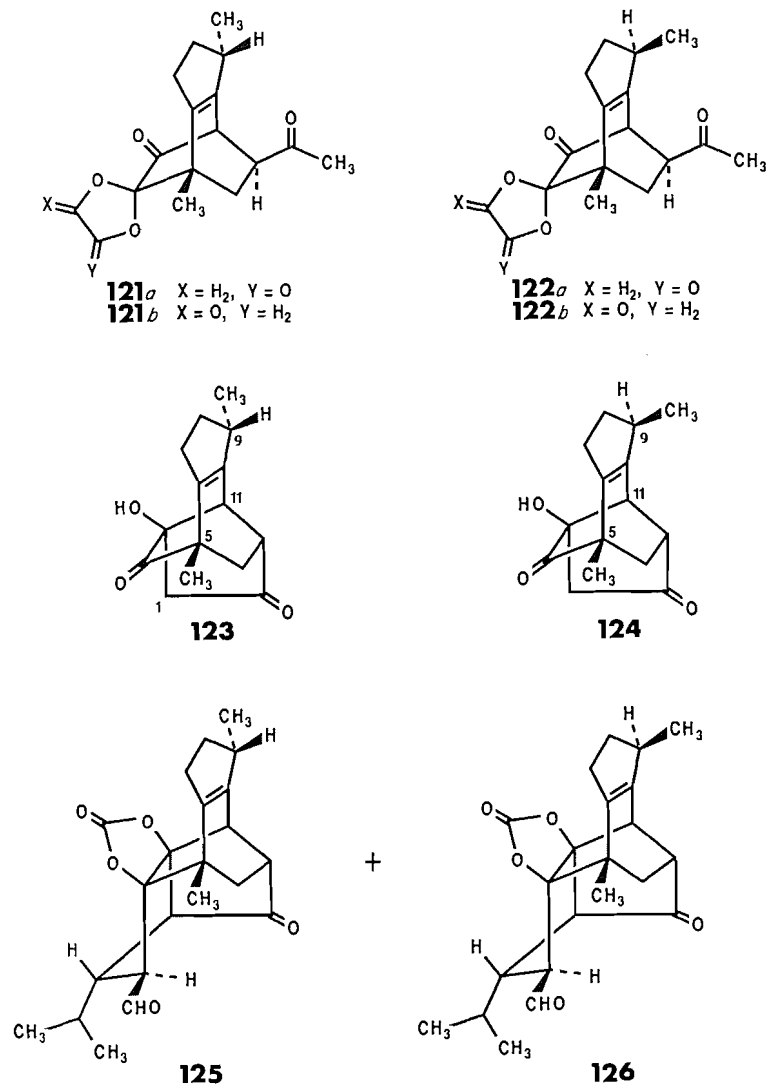

SCHEME 16

cleavage of a carbon–carbon bond between C_{15} and C_{17} (cf. Scheme 5) at a later stage, and we have considered ways either to prevent or at least to ease this task. For this reason, we considered, as dienophile, acrylonitrile having an ester group at carbon-2 (8*a*).

The first dienophile investigated was the known (17) 2-acetoxy-acrylonitrile (**127**) (Scheme 17). The Diels–Alder reaction of **127** with *o*-spirolactone dienone went smoothly, but without following the *endo* rule, yielding a mixture of four stereoisomers **128***a–b* and **129***a–b* that could, however, be separated by chromatography. The most polar of these Diels–Alder adducts (mp 191–192°C) was shown to have structure **128***b* by single crystal X-ray diffraction analysis (8*b*). It was then hoped that the two isomers that correspond to **128***a–b* would undergo an intramolecular aldol condensation to produce the cyanohydrin lactone **130**. However, in our hands, all attempts to produce **130** under either basic or acidic conditions failed. In acidic conditions, isomers **129***a–b* showed their interrelation, giving the same cyanohydrin diketone, which therefore had structure **132** and not **131**. The cyanohydrin diketone **132** was further characterized by acetylation (Ac_2O, pyridine) to an acetate derivative, which should have structure **134** and not **133**. The failure of these aldol condensation experiments might be due to the fact that the acetate group requires strong conditions to enolize. To facilitate the aldol condensation, the more complex acrylonitrile **139** was synthesized (8) (Scheme 18). Thus using a strategy similar to that described for the β-diketone **46** (Scheme 7), it was hoped that **139** would react with *o*-spirodienone lactone **6** to produce **140***a–b*, which would undergo, after acetal hydrolysis, an internal aldol condensation. This would produce **142**, which might thus undergo a second aldol condensation yielding ring A (i.e., **143**).

The synthesis of **139** was started with the dioxolane acetal **40** of ethyl acetoacetate. Basic hydrolysis of **40** gave the corresponding carboxylic acid **135**, which was then converted ($(COCl)_2$, pyridine, benzene) into the acid chloride **136**. Reaction of **136** with the cyanohydrin of chloroacetaldehyde (**137**) gave the corresponding ester **138**. Treatment of ester **138** with triethylamine gave the desired substituted acrylonitrile **139**. The Diels–Alder reaction of **139** with *o*-spirolactone dienone **6** gave a mixture of isomers **140***a–b and* **141***a–b* from which two isomers were isolated pure by fractional crystallization. The most polar (mp 189–190°C) of these adducts was shown to have structure **140***b* (X = O, Y = H_2) by single crystal X-ray diffraction analysis (8*b*). Again, it was hoped that the isomers that correspond to **140***a–b* would have produced the aldol product **142**. However, all attempts were unsuccessful and this approach was abandoned.

Can. J. Chem. Downloaded from www.nrcresearchpress.com by 91.144.44.67 on 09/07/12
For personal use only.

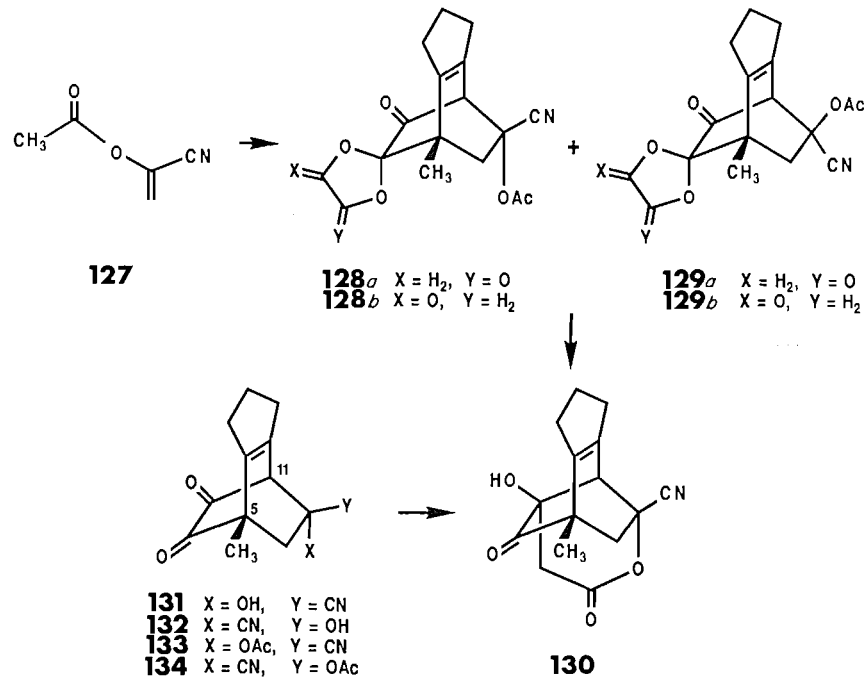

SCHEME 17

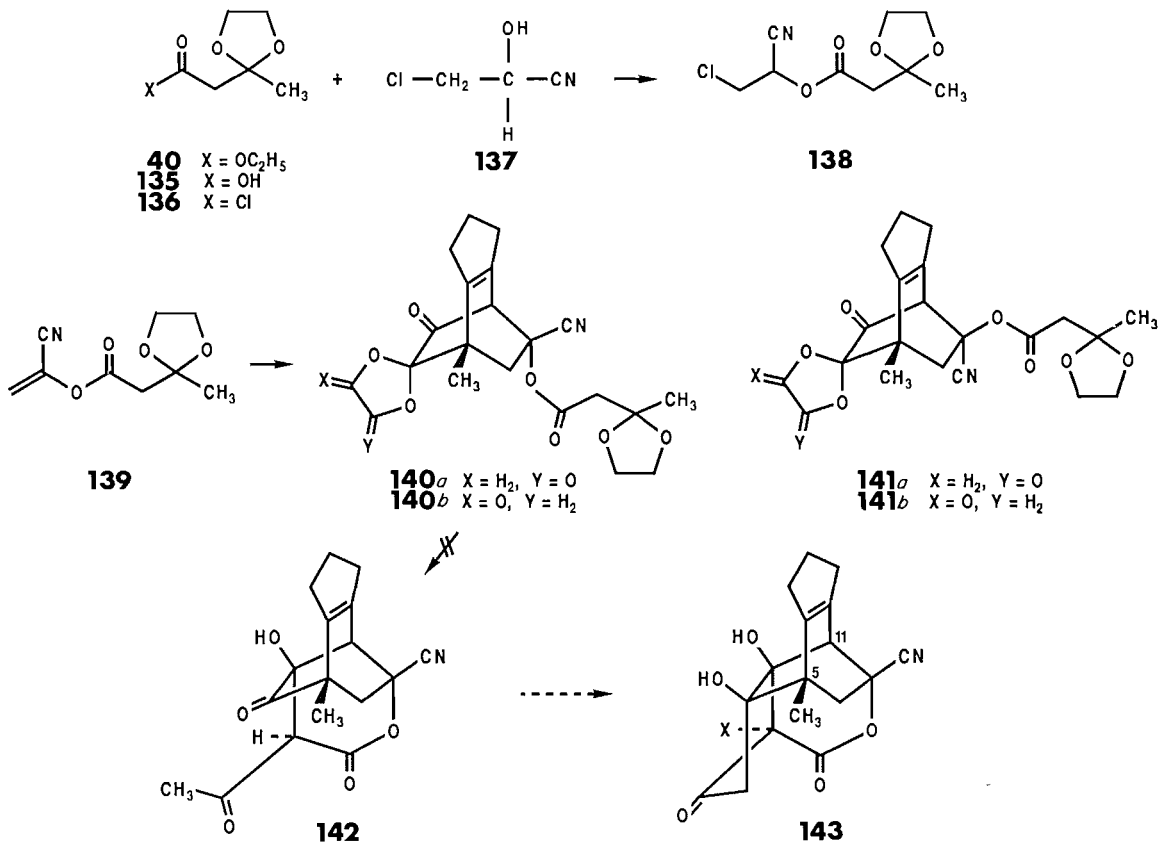

SCHEME 18

In conclusion, the chemistry described in Part II that is relevant to our total synthesis can be summarized in the following way. We have developed a simple synthesis of optically active dienophile (*S*)-**74** starting from carvone (*S*)-**94** (Scheme 13). Using this dienophile and racemic *o*-spirolactone dienone **6**, we have obtained, in four steps, the five-membered carbonate derivative **89** (Scheme 11) of the optically active pentacyclic dihydroxy ketoaldehyde **87**, having the desired absolute configuration, in 54% of a 50% theoretical yield, i.e., 27% overall yield.

Can. J. Chem. Downloaded from www.nrcresearchpress.com by 91.144.44.67 on 09/07/12
For personal use only.

Can. J. Chem. Downloaded from www.nrcresearchpress.com by 91.144.44.67 on 09/07/12
For personal use only.

Experimental

Apparatus, materials, and methods

Melting points were determined on a Büchi M-50 apparatus and are uncorrected. Ether, tetrahydrofuran, and 1,2-dimethoxyethane were dried by distilling over sodium benzophenone ketyl. Benzene, dichoromethane, dimethyl sulfoxide, and amines were distilled over calcium hydride. All reactions were performed under nitrogen or argon atmosphere. Analytical and preparative thin-layer chromatography (tlc) were carried out on glass plates precoated (0.25, 0.5, 1.0, and 2.0 mm) with silica gel 60 F-250 (Merck). Materials were detected by visualization under an ultraviolet lamp (254 or 350 nm) and (or) by spraying with sulfuric acid (50%) or a solution of phosphomolybdic acid or vanillin followed by heating on a hot plate. Column chromatography was performed with silica gel (Baker 60–200 Mesh) or Merck 60 (200–400 mesh)).

The infrared spectra (ir) were taken on a Perkin–Elmer 257 or 681 spectrophotometer. Proton nuclear magnetic resonance (^{1}H nmr) spectra were recorded (with chloroform or tetramethylsilane as internal standard) on a Varian A-60, a Bruker WP-60, a Bruker HX-90, or a Bruker WM-250 instrument. Carbon nuclear magnetic resonance (^{13}C nmr) spectra were measured on a Bruker HX-90 or WM-250 instrument. The following abbreviations have been used: s, singlet; d, doublet; dd, doublet of doublets; t, triplet; q, quartet; qn, quintet; m, multiplet; br, broad. For most of the hydroxylated compounds, the multiplicity of the hydrogens attached to a carbinol was analyzed after D_2O exchange. The mass spectra were recorded on a Hitachi–Perkin–Elmer RMU-6 mass spectrometer and peak matching (hrms) on a VG Micromass ZAB-2F spectrometer. The ultraviolet spectra (uv) were recorded on a Varian Techtron 635 spectrophotometer. Microanalyses were carried out by Mr. J. Tamas, Laboratoire de Microanalyses, Université de Sherbrooke; Schwarzkopf Microanalytical Laboratories, New York; and by Dr. C. Daesslé, Organic Microanalyses, Montreal.

Diketoacetate ***9***

A solution of diketoalcohol **8** (2.5 g, 10.4 mmol) in a mixture of pyridine (3 mL) and acetic anhydride (4 mL) was heated for 0.5 h at 100°C. The volatile materials were removed under vacuum and the residue was crystallized from ether–pentane to give pure acetate **9** (2.6 g, 91%); mp 128–130°C; ir (CH_2Cl_2, ν cm^{-1}): 1745, 1720, and 1230; ^{1}H nmr ($CDCl_3$, δ ppm): 3.75 (d, 1H, J = 5 Hz, HC11), 3.07 (dd, 1H, J_{AB} = 19.4 Hz, J_W = 2.3 Hz, H_{exo}-C1), 2.66 (d, 1H, J_{AB} = 19.4 Hz, H_{endo}-C1), 2.68 (m, 1H, H-C15), 2.45 (m, 4H, allylic protons), 2.05 (s, 3H, CH_3CO_2), 2.00 (m, 2H), 1.82 (dd, 1H, J_{AB} = 13.8 Hz, J_{AX} = 11.6 Hz, H_{exo}-C14), 1.52 (dd, 1H, J_{AB} = 13.8 Hz, J_{BX} = 1.6 Hz, H_{endo}-C14), 1.27 (3H, s, CH_3-C5); ms *m/e*: 274 (M^+). *Anal.* calcd. for $C_{16}H_{18}O_4$: C 70.05, H 6.61; found: C 69.97, H 6.52.

Monoketal acetate ***10***

A mixture of diketoacetate **9** (2.4 g, 8.8 mmol), ethylene glycol (2 mL), and *p*-toluenesulfonic acid (20 mg) in benzene (50 mL) was refluxed for 4 h (Dean–Stark water separator). The cooled reaction mixture was then washed with aqueous sodium carbonate solution (1 M) and brine. Evaporation of the solvent gave a solid residue, which was crystallized from ether (2.55 g, 91%); mp 149–152°C; ir (CH_2Cl_2, ν cm^{-1}): 1745, 1730, 1230; ^{1}H nmr ($CDCl_3$, δ ppm): 3.88 (m, 4H), 3.52 (d, 1H, 4 Hz, H-C11), 2.8–1.4 (m, 11H), 1.98 (s, 3H, CH_3CO_2), 1.25 (s, 3H, CH_3-C5); ms *m/e*: 318 (M^+). *Anal.* calcd. for $C_{18}H_{22}O_5$: C 67.91, H 6.97; found: C 68.22, H 6.96.

Reduction of ketoacetate ***10***

(a) With lithium borohydride

To a cooled (0°C) solution of monoketal acetate **10** (2.4 g, 7.6 mmol) in tetrahydrofuran (120 mL) was added lithium borohydride (0.42 g, 20 mmol). The mixture was stirred for 2 h at 0°C, 1 h at 25°C, and 1 h at reflux temperature. Then was added lithium aluminum hydride (0.80 g, 20 mmol) and the reflux was pursued for 1 h. The cooled mixture was then cautiously reacted with moist ether, then water. The mixture was extracted with ether. The organic phase was dried ($MgSO_4$) and evaporated to give a mixture (≈95:5) of *trans* diol **11** and *cis* diol **12** respectively. The crude mixture was crystallized from ether to give pure *trans* ketal diol **11** (1.6 g, 76%); mp 145–147°C; ir (CH_2Cl_2, ν cm^{-1}): 3580, 3400, 1030; ^{1}H nmr ($CDCl_3$, δ ppm): 4.00 (m, 4H), 3.16 (d, 1H, J_W = 2 Hz, H-C4), 3.03 (d, 1H, J = 4 Hz, HC11), 2.8–1.6 (m, 11H), 1.13 (s, 3H, CH_3-C5); ms *m/e*: 278 (M^+). *Anal.* calcd. for $C_{16}H_{22}O_4$: C 69.04, H 7.97; found: C 68.90, H 8.15.

(b) With lithium in ammonia

To a solution of monoketal acetate **10** (2.0 g, 6.3 mmol) in tetrahydrofuran (15 mL) and dry ethanol (5 mL), at −78°C, was added liquid ammonia (freshly distilled, ~50 mL). Small pieces of lithium (total 1.0 g) were added to that mixture over a period of 1 h. The cold bath was then removed, the ammonia was evaporated, and the residue was reacted with ethanol (2 mL), then diluted with water and extracted with ether (3 × 50 mL). The combined organic layer were dried over magnesium sulfate, filtered, and the solvents evaporated to give a mixture (31:58) of *trans* ketal diol **11** and *cis* ketal diol **12** respectively. The two isomers were separated by crystallization or by chromatography (silica, Et_2O). *trans* Ketal diol **11** (0.53 g, 31%) (*vide supra*); *cis* ketal diol **12** (1.0 g, 58%); mp 115–117°C; ir (CH_2Cl_2, ν cm^{-1}): 3400, 1180, 1060, 1030; ^{1}H nmr ($CDCl_3$, δ ppm): 3.90 (m, 4H), 3.35 (s, 1H, H-C4), 2.95 (d, 1H, J = 4 Hz, HC11), 2.6–1.3 (m, 1H), 1.24 (s, 3H, CH_3-C5); ms *m/e*: 278 (M^+). *Anal.* calcd. for $C_{16}H_{22}O_4$: C 69.04, H 7.97; found: C 68.83, H 7.78.

Carbonate ***13***

To a solution of *cis* ketal diol **12** (0.5 g, 1.8 mmol) in a mixture of benzene (30 mL) and pyridine (0.5 mL) was added, at 25°C, a saturated benzene solution of phosgene (20 mL). After 15 min the mixture was filtered and evaporated. The oily residue was crystallized from ether–hexane to give carbonate **13** (0.45 g, 82%); mp 102–103°C; ir (CH_2Cl_2, ν cm^{-1}): 1795, 1210, 1190, 1065; ^{1}H nmr ($CDCl_3$, δ ppm): 4.15 (s, 1H, H-C4), 3.95 (m, 4H), 3.20 (d, 1H, J = 4 Hz, H-C11), 2.7–1.4 (m, 11H), 1.30 (s, 3H, CH_3-C5); ms *m/e*: 304 (M+). *Anal.* calcd. for $C_{17}H_{20}O_5$: C 67.10, H 6.75; found: C 66.68, H 6.48.

Ketal monoacetate ***14***

A solution of *trans* ketal diol **11** (4.3 g, 14.2 mmol) in pyridine (10 mL) was reacted overnight with acetic anhydride (12 mL) at room temperature. Evaporation of volatile materials under vacuum afforded monoacetate **14** as an oil (5.0 g, quant.); ir (CH_2Cl_2, ν cm^{-1}): 3420, 1720, 1030; ^{1}H nmr ($CDCl_3$, δ ppm): 3.92 (d, 1H, J_W = 2 Hz, H-C4), 3.90 (m, 4H), 3.07 (d, 1H, J = 4 Hz, H-C11), 2.6–1.7 (m, 11H), 2.17 (s, 3H, CH_3CO_2), 1.09 (s, 3H, CH_3-C5); ms *m/e*: 320 (M^+).

Dihydroxy ketoacetates ***17*** *and* ***18***

A solution of ketal monoacetate **14** (4.90 g, 15.3 mmol) in methanol (100 mL) was reacted, at −78°C, with a stream of ozone for 25 min. The mixture was then shaken for 3 h in an atmosphere of hydrogen in the presence of 10% palladium-on-carbon catalyst (50 mg). After filtration, the solvent was evaporated and the residue dissolved in pyridine (5 mL), refluxed for 20 min, and kept to dryness. The residue was purified by column chromatography on silica gel (ether) to give dihydroxy ketoacetates **17** and **18**.

Dihydroxyacetate ***17*** (3.10 g, 57%); mp 176–177°C; ir (CH_2Cl_2, ν cm^{-1}): 3450, 1735, 1690; ^{1}H nmr ($CDCl_3$, δ ppm): 5.24 (d, 1H J_W = 2 Hz, H-C4), 4.3 (br s, 1H, -OH), 3.90 (m, 4H), 3.35 (br signal, 1H, -OH), 2.8–1.2 (m, 11H), 2.21 (s, 3H, CH_3CO_2), 1.02 (s, 3H, CH_3-C5). *Anal.* calcd. for $C_{18}H_{24}O_7$: C 61.35, H 6.86; found: C 61.03, H 6.72.

Dihydroxyacetate ***18*** (1.10 g, 20%); mp 99–101°C; ir (CH_2Cl_2, ν cm^{-1}): 3450, 1715; ^{1}H nmr ($CDCl_3$, δ ppm): 4.70 (d, 1H, J_W = 2 Hz, H-C4), 3.85 (m, 4H), 3.50 (br signal, 1H, -OH), 2.4–1.1 (m, 11H), 2.12 (s, 3H, CH_3CO_2), 0.80 (s, 3H, CH_3-C5).

Carbonate derivative ***19***

To a solution of dihydroxyacetate **17** (0.50 g, 1.42 mmol) in a mixture of benzene (30 mL) and pyridine (0.5 mL) was added, at 25°C, a saturated benzene solution of phosgene (30 mL). After 4 h, the mixture was filtered and evaporated. Crystallization of the crude product (CH_2Cl_2–Et_2O) yielded carbonate **19** (0.46 g, 86%); mp 204–205°C; ir (CH_2Cl_2, ν cm^{-1}): 1760, 1740, 1715, 1230, 1060; ^{1}H nmr ($CDCl_3$, δ ppm): 4.90 (d, 1H, J_W = 2 Hz, H-C4), 3.88 (m, 4H), 3.50 (br signal, 1H, -OH), 2.45–1.1 (m, 11H), 2.12 (s, 3H, CH_3CO_2), 0.80 (s, 3H,

Can. J. Chem. Downloaded from www.nrcresearchpress.com by 91.144.44.67 on 09/07/12
For personal use only.

CH_3-C5); ms *m/e*: 378 (M^+). *Anal.* calcd. for $C_{19}H_{22}O_8$: C 60.31, H 5.86; found: C 60.12, H 6.07.

Triketone **26**

A solution of monoketal ketoacetate **10** (0.80 g, 2.5 mmol) in ethyl acetate (50 mL) was reacted with a stream of ozone during 15 min. Then the mixture was shaken for 2 h in an atmosphere of hydrogen in the presence of 10% palladium-on-carbon catalyst (20 mg). After filtration, the solvent was evaporated and the solid residue was crystallized from ether to give triketone **26** (0.72 g, 82%); mp 212–218°C (dec.); ir (CH_2Cl_2, ν cm^{-1}): 1750, 1720, 1710, 1235; ^1H nmr ($CDCl_3$, δ ppm): 4.00 (m, 4H), 3.50 (m, 1H), 3.4–1.8 (m, 11H), 2.22 (s, 3H, CH_3CO_2), 1.32 (s, 3H, CH_3-C5). *Anal.* calcd. for $C_{18}H_{22}O_7$: C 61.70, H 6.33; found C 61.42, H 6.41.

Tetracyclic aldol product **29**

Triketone **26** (0.50 g, 1.43 mmol) was refluxed in pyridine (2 mL) for 1 h. Evaporation of pyridine yielded a solid residue, which was crystallized from dichloromethane–ether mixture to give compound **29** (0.43 g, 86%); mp 240–243°C; ir (CH_2Cl_2, ν cm^{-1}): 3450, 1760, 1720; ^1H nmr ($CDCl_3$, δ ppm): 3.80 (m, 4H), 3.6–1.6 (m, 12H), 2.01 (s, 3H, CH_3CO_2), 1.18 (s, 3H, CH_3-C5). *Anal.* calcd. for $C_{18}H_{22}O_7$: C 61.70, H 6.33; found: C 61.45, H 6.26.

Diels–Alder adducts **35***a and* **35***b*

A solution of spirolactone dienone **6** (500 mg, 2.27 mmol) and ethyl vinyl ketone (267 mg, 3.18 mmol) in benzene (3 mL) was refluxed for 4 h under nitrogen. Removal of the volatile substances under vacuum and a rapid filtration on silica gel (hexane–EtOAc, 20%) furnished a 1:1 mixture (680 mg, quant.) of isomers **35***a* and **35***b*; ^1H nmr ($CDCl_3$, δ ppm): ~4.5 (two embodied AB patterns, 2H, J_{AB} = 14 Hz, -OCH_2CO_2), 3.63 (two d, 1H, J = 2 Hz, H-C11), 3.4–1.5 (m, 9H), 2.5 (q, J = 6 Hz, CH_3CH_2CO), 1.28 (s, 3H, CH_3-C5), 1.08 (t, 3H, CH_3CH_2CO). This mixture was used without any further purification for the next step.

Tetracyclic ketones **36** *and* **37**

To a solution of the Diels–Alder adducts **35***a* and *b* (652 mg, 2.14 mmol) in tetrahydrofuran (25 mL) was added aqueous sodium hydroxide (1 M, 6 mL) and the mixture was stirred at room temperature for 20 h. The main part of the tetrahydrofuran was removed under reduced pressure and the residue was extracted with ether. Chromatography of the crude extract (540 mg, silica gel, benzene–ether 10%) furnished minor isomer *exo* **37** (110 mg, 20%) and major isomer *endo* **36** (more polar, 230 mg, 45%).

Major isomer endo **36**: mp: 135–136°C; ir (CH_2Cl_2, ν cm^{-1}): 3510, 1742, 1715; ^1H nmr ($CDCl_3$, δ ppm): 3.30 (d, 1H, J = 5.0 Hz, H-C11), 3.21 (br s, 1H, -OH), 2.73 (dddd, 1H, J = 11.6, 5.0, 2.4, 1.7 Hz, H-C15), 2.53 (qd, 1H, J = 7.5, 2.4 Hz, H_{exo}-C1), 2.55 (m, 2H), and 2.42 (m, 2H) (allylic protons), 2.04 (m, 2H, H_2-C8), 1.86 (dd, 1H, J_{AB} = 14.0 Hz, J_{AX} = 11.6 Hz, H_A-C14), 1.57 (dd, 1H, J_{AB} = 14.0 Hz, J_{BX} = 1.7 Hz, H_B-C14), 1.24 (s, 3H, CH_3-C5), 1.00 (d, 3H, J = 7.5 Hz, CH_3-C1); ms *m/e*: 246 (M^+).

Minor isomer exo **37**: mp: 110–111°C; ir (CH_2Cl_2, ν cm^{-1}): 3510, 1742, 1718; ^1H nmr ($CDCl_3$, δ ppm): 3.30 (d, 1H, J = 5.0 Hz, H-C11), 2.83 (br s, 1H, OH), 2.65 (ddd, 1H, J = 11.5, 5.0, 1.7 Hz, H-C15), 2.55 (m, 2H) and 2.44 (m, 2H) (allylic protons), 2.02 (m, 2H, H_2-C8), 1.85 (dd, 1H, J_{AB} = 14 Hz, J_{AX} = 11.5, H_A-C14), 1.57 (dd, 1H, J_{AB} = 14 Hz, J_{BX} = 1.7 Hz, H_B-C14), 1.28 (s, 3H, CH_3-C5), 1.18 (d, 3H, J = 7.7 Hz, CH_3-C1); ms *m/e*: 246 (M^+).

Diketoacetate endo **38**

A solution of diketoalcohol *endo* **36** (100 mg, 0.41 mmol) and *p*-toluenesulfonic acid (7 mg) in acetic anhydride was heated at 70°C for 2 h. After evaporation of acetic anhydride, the residue was extracted with ether, washed with dilute sodium bicarbonate, and the extract was dried ($MgSO_4$) and filtered. Evaporation of ether left a solid residue, which was recrystallized from ether–hexane (112 mg, 95%); mp 102–103°C; ir (CH_2Cl_2, ν cm^{-1}): 1745, 1725, 1235; ^1H nmr ($CDCl_3$, δ ppm): 3.79 (d, 1H, J = 5.1 Hz, H-C11), 3.23 (qd, 1H, J = 7.3, 2.3 Hz, H_{exo}-C1), 2.75 (dddd, 1H, J = 11.7, 5.1, 2.3, 1.7 Hz, H-C15), 2.45 (m, 4H, allylic protons), 2.06 (s, 3H, CH_3CO_2), 1.98 (m, 2H, H_2-C8), 1.84 (dd, 1H, J_{AB} = 13.9 Hz, J_{AX} = 11.7 Hz, H_A-C14), 1.49 (dd, 1H, J_{AB} = 13.9 Hz, J_{BX} = 1.7 Hz, H_B-C14), 1.23 (s, 3H, CH_3-C5), 1.06 (d, 3H, J = 7.3 Hz, CH_3-C1); ms *m/e*: 288 (M^+). *Anal.* calcd. for $C_{17}H_{20}O_4$: C 70.81, H 6.99; found: C 70.66, H 6.94.

Diketoacetate exo **39**

Acetylation of diketoalcohol *exo* **37** (40 mg, 0.16 mmol) was done as for compound **36** (*vide supra*). Filtration on silica gel (hexane–EtOAc, 20%) gave pure acetate **39** (44 mg, 94%); ir (CH_2Cl_2, ν cm^{-1}): 1745, 1725, 1230; ^1H nmr ($CDCl_3$, δ ppm): 3.42 (d, 1H, J = 5.0 Hz, H-C11), 2.66 (ddd, 1H, J = 11.8, 5.0, 1.5 Hz, H-C11), 2.61 (q, 1H, J = 7.6 Hz, H_{endo}-C1), 2.44 (m, 4H, allylic protons), 2.04 (s, 3H, CH_3CO_2), 1.93 (m, 2H, H_2-C8), 1.84 (dd, 1H, J_{AB} = 13.8 Hz, J_{AX} = 11.8 Hz, H_A-C14), 1.46 (dd, 1H, J_{AB} = 13.8 Hz, J_{BX} = 1.5 Hz, H_B-C14), 1.28 (s, 3H, CH_3-C5), 1.25 (d, 3H, J = 7.6 Hz, CH_3-C1); ms *m/e*: 288 (M^+).

Monodeuterated diketoacetates 15-d-endo **38** *and* exo **39**

To a stirred solution of compounds **35***a* and *b* (crude Diels–Alder adducts) (860 mg, 2.98 mmol) in tetrahydrofuran (50 mL) was added a solution of sodium hydroxide (1 M in D_2O, 14 mL). After 2 h at room temperature, the organic solvent was evaporated and the mixture was extracted with ether (3 × 20 mL). The combined organic layers were washed with water (2 × 10 mL), brine, and dried over magnesium sulfate. After evaporation of ether the crude dideuterated isomers **36** and **37** (485 mg, *m/e*: 248 (M^+)) were dissolved in THF (15 mL) and stirred with a solution of potassium hydroxide (1 M in H_2O, 5 mL) for 2 h at room temperature. After the usual ether extraction, the mixture was purified by chromatography (*vide supra*) to give monodeuterated (15-*d*) *endo* **36** (242 mg, 34% from **35**) and monodeuterated (15-*d*) *exo* **37** (17 mg, 11% from **35**). These compounds were acetylated separately (*vide supra*) to produce monodeuterated acetates **38** and **39**.

Monodeuterated diketoacetate 15-d endo **38**: ^1H nmr: identical with the unlabelled **38** (*vide supra*) except for the following: 3.79 (s, 1H, H-C11), 3.23 (q, 1H, J = 7.2 Hz, H-C1); ms *m/e*: 289 (M^+).

Monodeuterated diketoacetate 15-d exo **39**: ^1H nmr: identical with the unlabelled **39** (*vide supra*) except for the following: 3.42 (s, 1H, H-C11); ms *m/e*: 289 (M^+).

*Ethyl 3,3-ethylenedioxy-butanoate (***40***)*

A mixture of ethyl acetoacetate (200 g, 1.54 mol), ethylene glycol (150 mL, 2.68 mol), and *p*-toluenesulfonic acid (250 mg) in benzene (2.5 L) was refluxed for 24 h (Dean–Stark water separator), then cooled and washed with aqueous sodium bicarbonate (5%) and water. The organic layer was dried ($MgSO_4$), filtered, and solvent removed under reduced pressure. The crude product (255 g, 93%) did not need purification; ir ($CHCl_3$, ν cm^{-1}): 1724, 1180, 1042; ^1H nmr ($CDCl_3$, δ ppm): 4.10 (q, 2H, J = 7.2 Hz, -OCH_2CH_3), 3.89 (s, 4H, 2 × -OCH_2-), 2.50 (s, 2H, -CH_2CO_2-), 1.40 (s, 3H, CH_3-), 1.23 (t, 3H, J = 7.2 Hz, -OCH_2CH_3); ms *m/e*: 159 ($M^+ - CH_3$).

*3,3-Ethylenedioxy-1-butanol (***41***)*

A solution of ethyl acetoacetate ketal (**40**) (50.0 g, 0.287 mol) in dry ether (200 mL) was slowly added to a suspension of lithium aluminum hydride (12 g, 0.31 mol) in ether (1 L) (smooth reflux). The mixture was refluxed for 1 h, then cooled (0°C) and reacted with a slow addition of moist ether (350 mL), then water, (350 mL) until the formation of a white precipitate. The organic layer was decanted, dried ($MgSO_4$), filtered, and the solvent evaporated. The oily residue was distilled under reduced pressure (28 g, 75%); ir ($CHCl_3$, ν cm^{-1}): 3420, 1380, 1050; ^1H nmr ($CDCl_3$, δ ppm): 3.96 (s, 4H, OCH_2CH_2O), 3.72 (t, 2H, J = 6.0 Hz, CH_2OH), 3.35 (s, 1H, -OH), 1.92 (t, 2H, J = 6.0 Hz, -CH_2CH_2OH), 1.32 (s, 3H, CH_3-); ms *m/e*: 117 ($M^+ - 15$).

*3,3-Ethylenedioxy-butanal (***42***)*

A solution of 3,3-(ethylenedioxy)butanol (**41**) (13.2 g, 0.10 mol) in dimethyl sulfoxide (60 mL) was reacted with *N,N'*-dicyclohexylcarbodiimide (41.2 g, 0.20 mol) in the presence of pyridinium trifluoroacetate (10.0 g, 0.05 mol). After a few minutes of efficient mechanical stirring, an exothermic reaction took place together with orange coloration. After 1 h, benzene was added to precipitate di-

Can. J. Chem. Downloaded from www.nrcresearchpress.com by 91.144.44.67 on 09/07/12
For personal use only.

cyclohexyl urea, which was separated by filtration. The solvents were evaporated under reduced pressure and the liquid residue was distilled under vacuum to give 3,3-ethylenedioxy-butanal (**42**), (10.3 g, 78%), bp 42°C/0.5 Torr; 1 Torr = 133.3 Pa); ir ($CHCl_3$, ν cm^{-1}): 2720, 1720, 1055; ^1H nmr ($CDCl_3$, δ ppm): 9.73 (t, 1H, J = 3 Hz, CHO), 4.01 (s, 4H, OCH_2CH_2O), 2.70 (d, 2H, J = 3 Hz, CH_2CHO), 1.42 (s, 3H, CH_3-); ms *m/e*: 115 ($M^+ - 15$).

*5,5-Ethylenedioxy-1-hexen-3-ol (**43**)*

Magnesium turnings (8.0 g, 0.32 mol) and one crystal of iodine were covered with dry tetrahydrofuran (40 mL). Vinyl bromide (50.0 g, 0.46 mol) was then added dropwise until an exothermic reaction took place (~3 mL). The addition was continued in order to maintain a good reflux. After the addition was completed, the mixture was refluxed for 45 min. A solution of ketal aldehyde **42** (37.2 g, 0.28 mol) in THF (70 mL) was then added dropwise to the mixture and the reflux was continued for 45 min. The reaction mixture was poured onto ice and brine (1.5 L), neutralized to pH 7 (2 M HCl), and extracted with dichloromethane (4 × 200 mL). Evaporation of the solvents yielded pure alcohol **43** (42 g, 92%) as an oil; ir ($CHCl_3$, ν cm^{-1}): 3500, 1650, 1380, 1060; ^1H nmr ($CDCl_3$, δ ppm): 6.2–4.9 (m, 3H, olefinic), 4.42 (m, 1H, *H*-C-OH), 4.00 (s, 4H, OCH_2CH_2O), 3.50 (br s, -OH), 2.00 (br s, 1H) and 1.80 (br s, 1H) (CH_2CHOH), 1.39 (s, 3H, CH_3-); ms *m/e*: 143 ($M^+ - 15$).

*5,5-Ethylenedioxy-1-hexen-3-one (**44**)*

A solution of allylic alcohol **43** (10.0 g, 63.4 mmol) in acetone (150 mL) was reacted at −30°C under good stirring with Jones reagent (dropwise, 23.7 mL, 63.5 mmol). After the addition, the mixture was warmed to room temperature and decanted. After evaporation of the acetone, the residue was dissolved in ether (300 mL), then washed with aqueous sodium bicarbonate solution and brine. The organic layer was dried ($MgSO_4$), filtered, and the ether evaporated. The oily residue was chromatographed on silica gel (benzene–ether, 98:2) to give vinyl ketone **44** (4.4 g, 44%) as an oil; ir ($CHCl_3$, ν cm^{-1}): 1680, 1610, 1050; ^1H nmr ($CDCl_3$, δ ppm): 6.52–5.70 (m, 3H, olefinic), 3.98 (s, 4H, $-OCH_2CH_2O-$), 2.95 (s, 2H, CH_2-CO), 1.44 (s, 3H, CH_3-); ms *m/e*: 141 ($M^+ - 15$).

*Isomers **45**a and **45**b*

Spirolactone dienone **6** (2.59 g, 11.8 mmol) was dissolved in benzene (4 mL) and reacted with ketal vinyl ketone **44** (2.20 g, 14.1 mmol) at reflux temperature for 45 min. Evaporation of benzene and removal of the excess of dienophile **44** under vacuum left an oily residue (4.4 g, ~quant.) containing two products (~1:1), isomers **45***a* and *b*, which were not separated; ir ($CHCl_3$, ν cm^{-1}): 1820, 1740, 1715; ^1H nmr ($CDCl_3$, δ ppm): 4.70 (d, 0.5H) and 4.35 (d, 0.5H), 4.65 (d, 0.5H) and 4.34 (d, 0.5H) (two embodied AB patterns), (J_{AB} = 14.5 Hz) (spirolactonic methylene), 3.94 (s, 4H, OCH_2CH_2O), 3.5–1.6 (m, 10H), 2.82 (s, 2H, CH_2-CO-), 1.38 (s, 3H, CH_3-COO-), 1.26 (s, 3H, CH_3-C5); ms *m/e*: 376 (M^+).

*Tetracyclic triketone **46***

A crude mixture of isomers **45***a* and *b* (4.44 g, 11.8 mmol) in tetrahydrofuran (16 mL) was stirred at 25°C with aqueous sodium hydroxide (1 M, 240 mL) for 24 h. The basic aqueous mixture was successively extracted with ether (2 × 75 mL), acidified with aqueous hydrochloric acid (2 M, 130 mL), then extracted with ether (4 × 100 mL). This acidic extract was dried ($MgSO_4$) and filtered, and solvents were evaporated under reduced pressure to give pure tetracyclic hydroxytriketone **46** (3.147 g, 97%); ir ($CHCl_3$, ν cm^{-1}): 3520, 1710, 1655, 1610; ^1H nmr ($CDCl_3$, δ ppm): 3.93 (br s, 1H, OH), 3.32 (d, 1H, J = 4 Hz, H-C11), 2.9–1.6 (m, 10H), 2.15 (s, 3H, CH_3-CO), 1.26 (s, 3H, CH_3-C5); ms *m/e*: 246 ($M^+ - CO$). *Exact Mass* (hrms) calcd. for $C_{16}H_{18}O_4 - CO$: 246.121; found: 246.125.

*Monoacetate derivative **47***

A solution of tetracyclic ketone **46** (3.25 g, 11.8 mmol) in pyridine (40 mL) and acetic anhydride (45 mL) was stirred in the absence of light for 24 h. The volatile substances were then evaporated under vacuum and the solid residue purified by crystallization and chromatography (3.1 g, 73%); mp 185–189°C (chloroform–hexane); ir ($CHCl_3$, ν cm^{-1}): 1760, 1725, 1645; ^1H nmr ($CDCl_3$, δ ppm): 3.93 (d, 1H, J = 5 Hz, H-C11), 2.9–1.7 (m, 10H), 2.41 (s, 3H, CH_3CO_2), 2.22 (s, 3H, CH_3CO), 2.10 (s, 3H, CH_3—C=), 1.27 (s, 3H, CH_3-C5).

A solution of that crystalline diacetate (0.619 g, 1.72 mmol) in tetrahydrofuran (13 mL) was reacted with aqueous sodium carbonate (5%, 30 mL) at room temperature for 6 h. The aqueous mixture was first washed with ether (3 × 15 mL), acidified with hydrochloric acid (2 M, 18 mL), and extracted again with ether to give monoacetate **47** (0.491 g, 90%) as a mixture of epimers in position 1; ir ($CHCl_3$, ν cm^{-1}): 1760, 1730, 1660, 1615; ^1H nmr ($CDCl_3$, δ ppm): 3.79 (d, 1H, H-C11), 2.9–1.6 (m, 10H), 2.12 (s, 3H, CH_3CO-), 2.08 (s, 3H, CH_3CO_2), 1.26 (s, 3H, CH_3-C5); ms *m/e*: 288 ($M^+ - 28$). *Exact Mass* (hrms) calcd. for $C_{18}H_{20}O_5 - CO$: 288.136; found: 288.131.

cis- *and* trans-*Enedione methyl esters **49** and **50***

A solution of crude monoacetate **47** (0.258 g, 0.817 mmol) and *p*-toluenesulfonic acid (5 mg) in dry methanol (6 mL) was stirred at 55–60°C for 6 h. The mixture was then poured into aqueous sodium bicarbonate (5%, 25 mL) and extracted with ether. The organic layer was dried and evaporated. By nmr, the crude residue (181 mg) showed a proportion of 86:14 for the *cis*/*trans* isomers **49** and **50**. Chromatography (benzene–ether 2:1) of this mixture on silica gave pure isomers **49** (more polar) and **50** (less polar).

*cis Enedione **49*** (102 mg, 43%); ir ($CHCl_3$, ν cm^{-1}): 1730, 1700, 1635; ^1H nmr ($CDCl_3$, δ ppm): 5.72 (s, 1H, olefinic), 3.67 (s, 3H, CO_2CH_3), 3.55 (d, 1H, J = 3 Hz, H-C11), 2.9–1.5 (m, 9H), 2.18 (s, 3H, CH_3CO), 1.24 (s, 3H, CH_3-C5); ms *m/e*: 288 (M^+).

*trans Enedione **50*** (43 mg, 20%); uv (λ max, ethanol): 251 nm (ε 8200); ir ($CHCl_3$, ν cm^{-1}): 1730, 1680, 1620; ^1H nmr ($CDCl_3$, δ ppm): 6.80 (s, 1H, olefinic), 4.91 (d, 1H, J = 3 Hz, H-C11), 3.67 (s, 3H, CO_2CH_3), 3.0–1.6 (m, 9H), 2.28 (s, 3H, CH_3CO), 1.32 (s, 3H, CH_3-C5); ms *m/e*: 288 (M^+). *Anal.* calcd. for $C_{17}H_{20}O_4$: C 70.80, H 6.99; found: C 70.65, H 7.05.

trans *Enedione methyl ester **50** by isomerization of* cis *isomer **49***

Pure *cis*-enedione methyl ester **49** (150 mg, 0.52 mmol, neat) was heated at 150°C in a sealed tube for 1.5 h. Chromatography (benzene–ether 2:1) of the crude product on silica gel furnished *trans* enedione methyl ester **50** (105 mg, 70%) and unreacted starting material (30 mg, 20%).

*Tetracyclic lactone **51***

A solution of tetracyclic triketone **46** (196 mg, 0.72 mmol) in methanol (5 mL) was poured into an aqueous solution of sulfuric acid (8 M, 40 mL) in a separatory funnel. The mixture was shaken for 2 min, then rapidly extracted with ether (4 × 50 mL). The combined organic layers were dried ($MgSO_4$), filtered, and the solvent evaporated. The solid residue was crystallized (ether–hexane) to give tetracyclic lactone **51** (100 mg, 49%); mp 95–96°C; ir ($CHCl_3$, ν cm^{-1}): 1785, 1730, 1710 (sh); ^1H nmr ($CDCl_3$, δ ppm): 3.95 (d, 1H, J = 4 Hz, H-C11), 3.25 (d, 1H, J_{AB} = 15 Hz) and 2.38 (d, 1H, J_{AB} = 15 Hz), 2.9–1.6 (m, 9H), 2.19 (s, 3H, CH_3CO), 1.29 (s, 3H, CH_3-C5); ms *m/e*: 274 (M^+). *Anal.* calcd. for $C_{16}H_{18}O_4$: C 70.05, H 6.62; found: C 69.74, H 6.49.

trans *Enedione carboxylic acid **52***

Lactone **51** (51 mg, 0.186 mmol) was dissolved in a solution of potassium (16 mg) in *tert*-butanol (10 mL) and stirred under nitrogen for 23 h at room temperature. The mixture was then poured onto water (20 mL) and extracted with ether (2 × 10 mL) to remove a neutral fraction (16 mg). The aqueous basic layer was acidified (HCl, 1 M, pH 4) and extracted with ether (3 × 25 mL). Evaporation of the solvent furnished crude acid **52** (36 mg, 70%); ir ($CHCl_3$, ν cm^{-1}): 3500–2500 (br), 1710, 1680, 1620; ^1H nmr ($CDCl_3$, δ ppm): 11.6 (br s, $-CO_2H$), 6.82 (s, 1H, olefinic), 5.00 (d, 1H, J = 3 Hz, H-C11), 2.9–1.5 (m, 9H), 2.28 (s, 3H, CH_3CO), 1.31 (s, 3H, CH_3-C5).

trans *Enedione methyl ester **50** by esterification of acid **52***

A solution of acid **52** (60 mg, 0.22 mmol) in ether at 0°C was reacted with a slight excess of diazomethane in ether (~2 mL). After 2 min of stirring, the volatile substances were evaporated and the crude product

Can. J. Chem. Downloaded from www.nrcresearchpress.com by 91.144.44.67 on 09/07/12
For personal use only.

was purified by thin-layer chromatography on silica gel (benzene–ether 2:1) to yield the known *trans* methyl ester **50** (30 mg, 48%) (*vide supra*).

*Alcohol **54** and acid **55***

Dihydropyran (88 g, 1.0 mol) and 2,2-dimethylpropanediol (125 g, 1.20 mol) were refluxed in toluene (500 mL) in the presence of *p*-toluenesulfonic acid (20 mg). After 24 h, the mixture was cooled and washed with water (3 × 50 mL). Evaporation of toluene left an oil (188 g) containing acetal alcohol **54** and the mono THP derivative of 2,2-dimethylpropanediol in a proportion of 4:1. Separation of these isomers is delicate and was performed at a later stage (*vide infra*). The analytical data for the major desired alcohol **54** come from reduction of acid **55** (*vide infra*). The crude product (1.88 g, 10.0 mmol) in dry acetone (60 mL) was cooled at −20°C and reacted with Jones reagent (3.75 mL, 10.0 mmol) over a period of 30–40 min. Isopropanol (1 mL) was added to the mixture and the organic layer was decanted, diluted with water (20 mL), and extracted with ether. The combined organic layers were washed with water, dried ($MgSO_4$), and solvents evaporated to leave an oil that was crystallized to give ketal acid **55** (1.60 g, 80%); mp 92–93°C; ir ($CHCl_3$, ν cm^{-1}): 3500–2500 (br), 1720; ^1H nmr ($CDCl_3$, δ ppm): 11.2 (s, 1H, CO_2H), 4.45 (br t, 1H, J = 5 Hz, HCO_2-), 3.5 (m, 4H, $(CH_2O)_2$), 2.42 (m, 2H, CH_2CO_2H), 1.7 (m, 4H), 1.16 (s, 3H, -CH_3), 0.70 (s, 3H, -CH_3). *Anal.* calcd. for $C_{10}H_{18}O_4$: C 59.39, H 8.97; found: C 59.35, H 9.16.

*Alcohol **54** from acid **55***

A solution of ketal acid **55** (2.02 g, 10.0 mmol) in dry ether (50 mL) was added to a mixture of lithium aluminum hydride (700 mg) in ether (25 mL) and refluxed for 12 h. The excess hydride was destroyed by slow addition, at 0°C, of moist ether and water and the mixture was extracted with ether to give pure alcohol **54** as an oil (1.69 g, 90%); ir ($CHCl_3$, ν cm^{-1}): 3590, 3450, 1140, 1030; ^1H nmr ($CDCl_3$, δ ppm): 4.45 (br t, 1H, J = 5 Hz, H-CO_2), 3.5 (m, 6H, 3 × CH_2O-), 1.6 (m, 6H), 1.18 (s, 3H, CH_3), 0.73 (s, 3H, CH_3). *Anal.* calcd. for $C_{10}H_{20}O_3$: C 63.79, H 10.71; found: C 63.70, H 10.69.

*Vinylketone **58** (via acid **55**)*

To a solution of acid **55** (2.02 g, 10.0 mmol) in dry ether (150 mL) was added, under nitrogen, a solution of vinyllithium (~2 M in THF, 10 mL, 20 mmol). After 40 min at 25°C, the mixture was hydrolyzed (pH ≃ 6, 2 M H_2SO_4) and extracted with ether. The purity of the crude oily product was largely related to the quality of the lithium reagent. Flash chromatography of the crude product (silica gel, benzene) furnished fragile enone **58** (1.1 g, 52%); ir ($CHCl_3$, ν cm^{-1}): 1700, 1620; ^1H nmr ($CDCl_3$, δ ppm): 6.5–5.7 (m, 3H, olefinic), 4.45 (br t, 1H, J = 5 Hz, HCO_2), 3.50 (m, 4H, $(CH_2O)_2$), 2.65 (m, 2H, CH_2CO), 1.75 (m, 4H), 1.20 (s, 3H, CH_3), 0.70 (s, 3H, CH_3).

*Aldehyde **56***

A solution of acetal alcohol **54** (1.88 g, 10.0 mmol) in dichloromethane (4 mL) was added at 15°C to a mixture of Collins reagent prepared from chromic oxide (8 g, 80 mmol) and pyridine (13 mL) in dichloromethane (350 mL). After 20 min, the mixture was poured onto ice-water and extracted with dichloromethane. The organic layer was washed several times with water, dried, and the solvents were evaporated. The residual colored oil was purified by chromatography on Florisil (benzene) to give pure aldehyde **56** (1.1 g, 60%); ir ($CHCl_3$, ν cm^{-1}): 2820, 2720, 1730; ^1H nmr ($CDCl_3$, δ ppm): 9.84 (t, 1H, J = 2 Hz, -CHO), 4.48 (br t, 1H, J = 5 Hz, HCO_2), 3.52 (m, 4H, $(CH_2O)_2$), 2.50 (m, 2H, CH_2CHO), 1.70 (m, 4H), 1.18 (s, 3H, CH_3), 0.71 (s, 3H, CH_3).

*Allylic alcohol **57***

To magnesium turnings (2.45 g, 0.10 mol) in dry tetrahydrofuran (30 mL) were added successively a crystal of iodine and a solution of vinyl bromide (10.5 g, 0.10 mol) in tetrahydrofuran. When the magnesium had almost disappeared, ketal aldehyde **56** (14.9 g, 80.0 mmol) in tetrahydrofuran (20 mL) was added dropwise. After 12 h at room temperature the mixture was poured onto ice-water, neutralized (pH 7) with hydrochloric acid (1 M), and extracted with dichloromethane. Chromatography of the crude extract (Florisil, benzene) furnished allylic alcohol **57** (15.9 g, 93%) as a colorless oil; ir ($CHCl_3$, ν cm^{-1}): 3600, 3450, 1650; ^1H nmr ($CDCl_3$, δ ppm): 6.1–4.9 (m, 3H, olefinic), 4.45 (br t, 1H, HCO_2), 4.1 (br m, 1H, OH), 3.80 (m, *H*-COH), 3.50 (m, 4H, $(CH_2O)_2$), 2.0–1.3 (m, 6H), 1.18 (s, 3H, CH_3), 0.70 (s, 3H, CH_3).

*Enone **58***

To a cooled (−20°C) and well-stirred solution of allylic alcohol **57** (2.14 g, 10.0 mmol) in dry acetone (60 mL) was added, dropwise, Jones reagent (3.75 mL, 10 mmol). After 2 h and addition of isopropanol (1 mL) the mixture was warmed to room temperature, diluted with water, and extracted with ether. The combined organic layers were washed with aqueous sodium bicarbonate, dried ($MgSO_4$), and evaporated under reduced pressure. The colorless oily residue (1.95 g, 91%) was stored in the cold. The ir and nmr data have been given (*vide supra*).

*Diels–Alder adducts **59a** and **59b***

Spirolactone dienone **6** (1.00 g, 4.54 mmol) was dissolved in benzene (5 mL) and reacted with vinyl ketone acetal **58** (975 mg, 4.60 mmol) at reflux temperature for 15 h. Evaporation of benzene left an oily residue (1.9 g, ~98%) containing two products (~1:1), isomers **59***a* and *b*, which were not separated ir (CH_2Cl_2, ν cm^{-1}): 1820, 1740, 1710; ^1H nmr ($CDCl_3$, δ ppm): 4.70 (d, 0.5H) and 4.32 (d, 0.5H), 4.65 (d, 0.5H) and 4.30 (d, 0.5H) (two embodied AB patterns, J_{AB} = 14.5 Hz) (spirolactonic methylene), 4.45 (br t, 1H, J = 5 Hz, HCO_2), 3.7–3.2 (m, 5H, $(CH_2O)_2$ and H-C11), 3.2–1.4 (m, 15H), 1.23 (s, 3H, CH_3-C5), 1.18 (s, 3H), and 0.70 (s, 3H) (two methyl groups of acetal moiety).

Tetracyclic endo *epimer **60***

To a crude mixture of Diels–Alder adducts **59***a* and *b* (982 mg, 2.27 mmol) in tetrahydrofuran (150 mL) was added aqueous sodium hydroxide (1 M, 9.1 mL). After 4 h of vigorous stirring at room temperature, the solvent was evaporated and the aqueous residue was extracted with ether. Evaporation of the ether furnished a solid residue, which was recrystallized from ether–hexane to give pure *endo* isomer **60** (606 mg, 71%); mp 142–143°C; ir (CH_2Cl_2, ν cm^{-1}): 3500, 1745, 1720; ^1H nmr ($CDCl_3$, δ ppm): 4.50 (br t, 1H, J = 5 Hz, HCO_2), 3.55 (m, 4H, $(CH_2O)_2$), 3.26 (d, 1H, J = 5 Hz, H-C11), 3.0–1.4 (m, 14H), 1.26 (s, 3H, CH_3-C5), 1.20 (s, 3H) and 0.70 (s, 3H) (two methyl groups of acetal moiety); ms *m/e*: 374 (M^+). *Anal.* calcd. for $C_{22}H_{30}O_5$: C 70.52, H 8.07; found: C 70.19, H 8.22.

*Pentacyclic aldehyde **61***

To a solution of tetracyclic diketoacetal **60** (174 mg, 0.46 mmol) in acetone (25 mL) was added hydrochloric acid (3 M, 12 mL) and the mixture was refluxed for 3 h. Acetone was then partly evaporated and the residue was extracted with ether. Chromatography (benzene–ether 1:1) of the crude product on silica gel furnished crystalline pentacyclic aldehyde **61** (33 mg, 25%); mp 147–149°C; ir (CH_2Cl_2, ν cm^{-1}): 3500, 2720, 1740, 1720; ^1H nmr ($CDCl_3$, δ ppm): 9.64 (d, 1H J = 1 Hz, CHO), 3.22 (d, 1H, J = 5 Hz, H-C11), 3.0–1.4 (m, 15H), 1.29 (s, 3H, CH_3); ms *m/e*: 288 (M^+). *Anal.* calcd. for $C_{17}H_{20}O_4$: C 70.81, H 6.99; found: C 70.96, H 6.91.

*Ethyl 3-formyl-4-methylpentanoate (**62**, R = C_2H_5)*

A mixture of diisobutylamine (103 g, 0.79 mol) and isovaleraldehyde (43 g, 0.5 mol) in benzene (250 mL) was refluxed for 12 h (Dean–Stark water separator). Benzene was evaporated and the residue distilled under reduced pressure to give the corresponding enamine (91.6 g, 93%); bp 82°C/1 Torr; ir ($CHCl_3$, ν cm^{-1}): 1650, 1465, 1120, 945; ^1H nmr ($CDCl_3$, δ ppm): 5.80 (br d, 1H, J = 15 Hz, N—C*H*=), 3.95 (dd, 1H, J = 15 and 8 Hz, N—CH=C*H*—), 2.70 (br s, 2H, CH_2), 2.58 (br s, 2H, CH_2), 2.40–1.40 (m, 3H, 3 × -CH-), 0.82 (apparent t, 18H, J = 7.5 Hz, 6 × CH_3-CH). The purified enamine (91.6 g) in acetonitrile (300 mL) was refluxed with ethyl bromoacetate (98 g, 0.55 mol) for 15 h. Water (50 mL) was then added to the mixture and the reflux was continued for 5 h. The cooled reaction mixture was then poured onto cold brine (800 mL) and extracted with ether.

Can. J. Chem. Downloaded from www.nrcresearchpress.com by 91.144.44.67 on 09/07/12
For personal use only.

Evaporation of the dried extract left an oil that was distilled under reduced pressure to give ethyl 3-formyl-4-methylpentanoate (**62**, R = C_2H_5) (68 g, 79%); bp 92°C/3 Torr; ir (CH_2Cl_2, ν cm^{-1}): 2720, 1730, 1200; ^1H nmr ($CDCl_3$, δ ppm): 9.96 (br s, 1H, CHO), 4.15 (q, 2H, J = 7 Hz, OCH_2CH_3), 3.0–2.0 (m, 4H), 1.22 (t, 3H, J = 7 Hz, OCH_2CH_3), 1.05 (d, 3H, J = 6 Hz, CH_3CH), 0.95 (d, 3H, J = 6 Hz, CH_3CH); derivative: 2,4-dinitrophenylhydrazone: mp 96.5°C. *Anal.* calcd. for $C_{15}H_{20}O_6N_4$: C 51.13, H 5.59, N 15.90; found: C 51.39, H 5.47, N 15.70.

*Ethyl 3-(1,3-dioxolan-2-yl)-4-methylpentanoate (**63**)*

A mixture of aldehyde ester **62** (R = C_2H_5) (51.5 g, 0.33 mol), ethylene glycol (74 g, 1.2 mol), and *p*-toluenesulfonic acid (20 mg) was refluxed (Dean–Stark water separator) for 24 h. The cooled mixture was then washed with sodium bicarbonate and water and the solvent was evaporated. Distillation of the residue furnished pure acetal **63** (56 g, 91%); bp 96°C/1.5 Torr; ir (CH_2Cl_2, ν cm^{-1}): 1730, 1180, 1170; ^1H nmr ($CDCl_3$, δ ppm): 4.85 (br d, 1H, J = 3 Hz, H-CO_2), 4.09 (q, 2H, J = 7 Hz, -OCH_2CH_3), 3.83 (m, $(CH_2O)_2$), 2.25 (br s, 2H, CH_2CO_2), 2.5–1.6 (m, 2H), 1.21 (t, 3H, J = 7 Hz, OCH_2CH_3), 0.90 (br d, 6H, J = 6 Hz, 2 × CH_3CH). *Anal.* calcd. for $C_{11}H_{20}O_4$: C 61.08, H 9.32; found: C 60.99, H 9.39.

*3-(1,3-Dioxolan-2-yl)-4-methylpentanol (**64**)*

To a mixture of lithium aluminum hydride (9.5 g, 0.25 mol) in dry ether (600 mL) was added dropwise a solution of acetal ester **63** (54 g, 0.25 mol) in dry ether (500 mL). After a stirring period of 14 h at 25°C, the mixture was refluxed for 1 h, then cooled (0°C), and moist ether was added slowly to the mixture. After addition of water, the mixture was extracted with ether. Evaporation of the solvent left pure alcohol **64** (38.2 g, 88%); ir (CH_2Cl_2, ν cm^{-1}): 3600, 3450, 1050; ^1H nmr ($CDCl_3$, δ ppm): 4.82 (br d, 1H, J = 4 Hz, H-CO_2), 3.92 (m, 4H, $(CH_2O)_2$), 3.68 (br t, 2H, J = 7 Hz, CH_2OH), 2.98 (s, 1H, OH), 2.2–1.5 (m, 2H), 1.63 (t, 2H, J = 7 Hz, CH_2CH_2OH), 0.92 and 0.86 (two d, J = 6.5 Hz, $(CH_3)_2CH$). *Anal.* calcd. for $C_9H_{18}O_3$: C 62.04, H 10.41; found: C 61.75, H 10.48.

*3-(1,3-Dioxolan-2-yl)-4-methyl pentanal (**65**)*

Following exactly the same procedure as previously described for oxidation of alcohol **54** (*vide supra*, aldehyde **56**), alcohol **64** (1.74 g, 10.0 mmol) was oxidized to aldehyde **65**. The crude product was chromatographed (silica gel, benzene) to give pure aldehyde **65** (1.07 g, 62%) together with starting material (3.40 mg, 19%) (eluted with benzene–ether 2:1); ir (CH_2Cl_2, ν cm^{-1}): 2720, 1720, 1120, 1050; ^1H nmr ($CDCl_3$, δ ppm): 9.65 (t, 1H, J = 2.5 Hz, CHO), 4.96 (d, 1H, J = 4 Hz, H-CO_2), 3.86 (m, 4H, $(CH_2O)_2$), 2.33 (br s, CH_2CHO), 2.5–1.5 (m, 2H), 1.02 and 0.95 (two d, J = 6.5 Hz, $(CH_3)_2CH$).

*Allylic alcohol **66***

Following exactly the same procedure previously described for allylic alcohol **57** (*vide supra*), allylic alcohol **66** was obtained from aldehyde **65** (13.6 g, 80.0 mmol) in a pure form after chromatography on Florisil (hexane–ether 9:1) (14.9 g, 94%); ir (CH_2Cl_2, ν cm^{-1}): 3600, 3450, 1125; ^1H nmr ($CDCl_3$, δ ppm): 6.1–5.5 (m, 1H) and 5.4–4.8 (m, 2H) (olefinic), 4.78 (d, 1H, J = 4 Hz, HCO_2), 4.3–3.5 (m, 2H, CH-OH), 3.80 (m, 4H, $(CH_2O)_2$), 2.1–1.3 (m, 4H), 0.88 (d, 6H, J = 6.5 Hz, $(CH_3)_2CH$). *Anal.* calcd. for $C_{11}H_{20}O_3$: C 65.97, H 10.07; found: C 65.70, H 10.28.

*Enone **67***

Following exactly the same procedure previously described for enone **58** (*vide supra*), enone **67** was obtained from allylic alcohol **66** (2.0 g, 10 mmol) as a sensitive colorless oil. An analytical sample was prepared by thin-layer chromatography (benzene) (1.81 g, 90%); ir (CH_2Cl_2, ν cm^{-1}): 1720, 1620; ^1H nmr ($CDCl_3$, δ ppm): 6.4–5.5 (m, 3H, olefinic), 4.82 (d, 1H, J = 3 Hz, HCO_2), 3.80 (m, 4H, $(CH_2O)_2$), 2.8–2.1 (m, 2H, (CH_2CO), 2.0–1.4 (m, 2H), 0.88 (d, 3H, J = 6 Hz) and 0.82 (d, 3H, J = 6 Hz) ($(CH_3)_2CH$). *Anal.* calcd. for $C_{11}H_{20}O_3$: C 66.70, H 9.15; found: C 66.70, H 9.08.

*Ethyl 3-isopropyl-5-methoxy-4-pentenoate (**68**, R = C_2H_5)*

Sodium hydride (~50% oil, 3.12 g, 65 mmol) was washed with dry hexane (3 × 50 mL), then dissolved in dry dimethyl sulfoxide (33 mL). After stirring for 45 min at 60°C the mixture was cooled at ~15°C and reacted with a solution of (methoxymethyl)triphenylphosphonium chloride (22.3 g, 65 mmol) in dry dimethyl sulfoxide (70 mL). After 15 min at 25°C, the deep red mixture was treated with a solution of ester aldehyde **62** (R = C_2H_5) (8.6 g, 50 mmol) in dimethyl sulfoxide (25 mL), and stirring was continued for 17 h. The mixture was then poured onto ice-water (200 mL) and extracted several times with pentane. Solvent was evaporated from the dried extract and a rapid filtration (silica gel, hexane) of the crude product removed the residual triphenylphosphine oxide. A mixture of isomers, *cis* and *trans* (*30:70*) enol ethers **68** (R = C_2H_5), (6.79 g, 68%) was obtained pure after distillation under reduced pressure; bp 85°C/2 Torr; ir (CH_2Cl_2, ν cm^{-1}): 1730, 1675, 1660, 950; ^1H nmr ($CDCl_3$, δ ppm): 6.25 (d, 0.7H, J = 12 Hz, *trans*-CH_3O-CH=CH), 5.92 (d, 0.3H, J = 6 Hz, *cis*-CH_3OCH=CH), 4.7–4.2 (m, 1H, CH_3OCH=CH-), 4.10 (q, 2H, J = 7 Hz, OCH_2CH_3), 3.53 (s, 0.9H, *cis*-OCH_3), 3.48 (s, 2.1H, *trans*-OCH_3), 2.30 (m, 3H, -CH_2CO_2- and -$CHCH_2CO_2$), 1.66 (m, 1H, $CH(CH_3)_2$), 1.20 (t, 3H, J = 7.5 Hz, OCH_2CH_3, 0.85 (d, 3H, J = 6 Hz) and 0.81 (d, 3H, J = 6 Hz) ($(CH_3)_2CH$). *Anal.* calcd. for $C_{11}H_{20}O_3$: C 65.97, H 10.07; found: C 65.75, H 10.07.

*Ketal ester **69** (R = CH_2CH_3)*

A mixture of isomers **68** (R = CH_2CH_3) (10.0 g, 50 mmol), ethylene glycol (6.2 g, 100 mmol), and *p*-toluenesulfonic acid (10 mg) was refluxed in benzene (100 mL) for 24 h (Dean–Stark). The cooled mixture was then washed with aqueous sodium bicarbonate and water. Evaporation of the solvent from the dried extract furnished crude ketal ester **69** (R = CH_2CH_3), which was purified by distillation under reduced pressure (10.8 g, 94%); bp 96°C/1.5 Torr; ir (CH_2Cl_2, ν cm^{-1}): 1730, 1180, 1040; ^1H nmr ($CDCl_3$, δ ppm): 4.88 (t, 1H, J = 5 Hz, HCO_2), 4.10 (q, 2H, J = 7 Hz, -OCH_2CH_3), 3.85 (m, 4H, $(CH_2O)_2$), 2.4–1.5 (m, 6H), 1.25 (t, 3H, -OCH_2CH_3), 0.85 (d, 6H, J = 6 Hz, $(CH_3)_2CH$). *Anal.* calcd. for $C_{12}H_{22}O_4$: C 62.24, H 9.56; found: C 62.83, H 9.34.

*Ketal acid **70***

To a solution of acetal ester **69** (4.6 g, 20 mmol) in ethanol (100 mL) was added, at 25°C, aqueous sodium hydroxide (50 mL, 1 M). After 2 h of stirring, the main part of the ethanol was evaporated and the aqueous basic layer was first washed with ether (2 × 50 mL), then acidified (pH ~5) with hydrochloric acid (55 mL, 1 M) and extracted with ether (4 × 50 mL). Evaporation of the solvent furnished pure acid **70** (3.98 g, 98%); ir (CH_2Cl_2, ν cm^{-1}): 3500–2400 (br), 1710, 1150; ^1H nmr ($CDCl_3$, δ ppm): 11.18 (s, 1H, CO_2H), 4.90 (t, 1H, H-CO_2), 3.90 (m, 4H, $(CH_2O)_2$), 2.5–1.5 (m, 6H), 0.88 (d, 6H, J = 6 Hz, $(CH_3)_2CH$). *Anal.* calcd. for $C_{10}H_{18}O_4$: C 59.42, H 8.95; found: C 59.55, H 9.13.

*Alcohol **71***

This reduction was done as for ester **63** (*vide supra*, compound **64**). Thus, ester **69** (7.45 g, 32.4 mmol) furnished ketal alcohol **71** (6.0 g, 98%); ir ($CHCl_3$, ν cm^{-1}): 3600, 3450, 1050; ^1H nmr ($CDCl_3$, δ ppm): 4.91 (br t, 1H, J = 5 Hz, HCO_2), 4.05–3.5 (m, 6H, $(CH_2O)_2$ and CH_2OH), 2.77 (br s, 1H, OH), 1.8–1.3 (m, 6H), 0.80 (d, 6H, J = 6 Hz, $(CH_3)_2CH$).

*Aldehyde **72***

To a solution of chromic oxide – pyridine complex (25.0 g, 95 mmol) in dry dichloromethane (250 mL) was added rapidly a solution of alcohol **71** (3.05 g, 16 mmol) in dichloromethane (50 mL). After 30 min of vigorous stirring at 25°C, the mixture was poured onto ice-water and extracted with dichloromethane. The organic layer was dried over magnesium sulfate and the solvent was evaporated. The crude colored residue was filtered through a short pad of silica gel to give pure aldehyde **72** as a colorless oil (2.77 g, 95%); ir (CH_2Cl_2, ν cm^{-1}): 2720, 1720, 1122; ^1H nmr ($CDCl_3$, δ ppm): 9.79 (t, 1H, J = 3 Hz, CHO), 4.90 (t, 1H, J = 5 Hz, HCO_2), 3.90 (m, 4H, $(CH_2O)_2$), 2.6–1.2 (m, 6H), 0.90 (d, 6H, J = 6.5 Hz, $(CH_3)_2CH$).

*Allylic alcohol **73***

Following exactly the same procedure previously described for the

Can. J. Chem. Downloaded from www.nrcresearchpress.com by 91.144.44.67 on 09/07/12
For personal use only.

formation of allylic alcohol **57** (*vide supra*), allylic alcohol **73** was obtained from aldehyde **72** (4.13 g, 23 mmol) as a colorless oil (4.9 g, 98%); ir (CH_2Cl_2, ν cm^{-1}): 3600, 3450, 1650; ^1H nmr ($CDCl_3$, δ ppm): 6.1–4.8 (m, 3H, olefinic), 4.91 (br t, 1H, J = 5 Hz, H-CO_2), 3.90 (m, 4H, $(CH_2O)_2$), 3.81 (m, 1H, *H*COH), 2.1–1.1 (m, 6H), 0.86 (d, 6H, J = 6 Hz, $(CH_3)_2CH$).

Dienophile 74

(a) From ketal acid 70

To a stirred suspension of lithium hydride (680 mg, 0.085 mol) in tetrahydrofuran (200 mL) was added dropwise a solution of ketal acid **70** (15.15 g, 0.075 mol) in tetrahydrofuran (40 mL). After 2 h at 75–80°C, the mixture was cooled at 0°C, treated with vinyllithium (2.9 M in THF, 36 mL, 0.10 mol), then warmed (50–55°C) for 1 h. It was then poured onto an ice – hydrochloric acid mixture (200 mL, 1 M), and extracted with ether. The organic layers were combined, washed with aqueous sodium carbonate solution (5%) and brine, dried, and the solvents evaporated to give a crude neutral extract. Acidification (pH 6) of basic aqueous washings and extraction (ether) gave unreacted starting ketal acid **70** (6.1 g, 40%). Chromatographic purification (silica gel, hexane, benzene–ether mixtures) of the crude neutral extract furnished enone **74** as a sensitive colorless oil (7.37 g, 78% based on reacted acid **70**); ir (CH_2Cl_2, ν cm^{-1}): 1690, 1615, 1410, 1140; ^1H nmr ($CDCl_3$, δ ppm): 6.4–5.6 (m, 3H, olefinic), 4.85 (t, 1H, J = 5 Hz, HCO_2), 3.85 (m, 4H, $(CH_2O)_2$), 2.7–2.4 (m, 2H, CH_2CO), 2.3–1.4 (m, 4H), 0.86 (br d, 6H, J = 6 Hz, $(CH_3)_2CH$).

(b) From alcohol 73

Following exactly the same procedure previously described for the formation of enone **58** (*vide supra*), oxidation of alcohol **73** (4.91 g, 22 mmol) by Jones reagent (8.6 mL, 23 mmol) gave enone **74** (3.77 g, 81%) as a pure colorless oil; ir and nmr data have been given (*vide supra*).

Diels–Alder adducts 75a + b and 76a + b

A solution of spirolactone dienone **6** (4.30 g, 19.5 mmol) and enone **67** (4.64 g, 23.4 mmol) in benzene (60 mL) was refluxed for 9 h. Evaporation of benzene left an oily residue containing compounds **75***a* and *b*, **76***a* and *b*, which were not separated; ^1H nmr ($CDCl_3$, δ ppm): 4.85 (br d, 1H, J = 3.5 Hz, H-CO_2), 4.70 (d, 0.5H) and 4.32 (d, 0.5H), 4.65 (d, 0.5H) and 4.30 (d, 0.5H) (two embodied AB patterns, J_{AB} = 14 Hz) (spirolactonic methylene), 3.82 (br s, 4H, $CH_2O)_2$), 3.60 (m, 1H, H-C11 for 4 isomers), 3.2 (m, 1H, H-CCO), 3.0–1.3 (m, 12H), 1.25 (br s, 3H, CH_3-C5), 0.93 (d, 3H, J = 7 Hz) and 0.88 (d, 3H, J = 7 Hz) $(CH_3)_2CH$).

Tetracyclic ketal diketones 77–80

To a crude mixture of Diels–Alder adducts **75***a* + *b* and **76***a* + *b* (3.00 g, 7.2 mmol) in tetrahydrofuran (200 mL) was added an aqueous solution of potassium hydroxide (1 M, 28.7 mL). After 20 h of stirring at 25°C, tetrahydrofuran was evaporated and the aqueous residue was extracted with ether. The crude extract (1.83 g) showed three acetalic protons as doublets at δ 5.25 (J = 9 Hz) (major one), 5.08 (J = 6 Hz), and 4.75 (J = 7 Hz). Crystallization of the crude mixture (ether) furnished ketal diketone **77** (or **79**) (750 mg, 29%) plus a mixture of **77** and *exo* epimer **78** (or **80**). This mixture was submitted to the same basic treatment and gave an additional crop of crystalline *endo* **77** (or **79**) (153 mg, 6%) (total 35% yield in isomer *endo* **77** (or **79**); mp 204–206°C; ir ($CHCl_3$, ν cm^{-1}): 3500, 1735, 1710, 1210 cm^{-1}; ^1H nmr ($CDCl_3$, δ ppm): 5.25 (d, 1H, J = 9 Hz, HCO_2), 4.0–3.6 (m, 4H, $(CH_2O)_2$), 3.26 (d, 1H, J = 5 Hz, H-C11), 3.01–1.6 (m), 1.25 (s, 3H, CH_3-C5), 0.90 (d, 6H, J = 6.5 Hz, $(CH_3)_2CH$); ms *m/e*: 360 (M^+). *Anal.* calcd. for $C_{21}H_{28}O_5$: C 69.98, H 7.83; found: C 69.88, H 7.76.

Diels–Alder racemic adducts 81a + b and 82a + b

A solution of spirolactone dienone **6** (0.935 g, 4.22 mmol) and racemic dienophile **74** (1.117 g, 5.26 mmol) in benzene (6 mL) was refluxed for 16 h under nitrogen. Benzene was then evaporated to leave a mixture containing essentially 4 components (hardly separated on tlc after multiple elutions). Rapid filtration on silica gel (hexane–Et_2O 30%) removed the unreacted dienophile to give a pure mixture of adducts **81** and **82** (1.84 g, 99%); ir ($CHCl_3$, ν cm^{-1}): 1815, 1735, 1710 cm^{-1}; ^1H nmr ($CDCl_3$, δ ppm): 4.80 (m, 1H, HCO_2), ~4.5 (two embodied AB patterns, J = 14 Hz, OCH_2CO_2), 3.85 (m, 4H, $(CH_2O)_2$), 3.60 (m, 1H, H-C11), 3.4–1.4 (m, 15H), 1.27 (s, 3H, CH_3C5), 0.85 (br d, 6H, J = 7 Hz, $(CH_3)_2CH$). This mixture was used for the next step without any further purification.

Racemic tetracyclic ketones 83–86

To a stirred solution of Diels–Alder racemic adducts **81***a* + *b* and **82***a* + *b* (1.840 g, 4.22 mmol) in tetrahydrofuran (75 mL) was added aqueous sodium hydroxide solution (1 M, 14 mL). After 15 h at room temperature, the main part of THF was evaporated and the residue was extracted with ether (4 × 75 mL). Evaporation of the solvent gave an oily residue containing four compounds: **83**:**84**:**85**:**86** in the relative proportions (37:19:16:28) as given by the integration of the bridgehead proton (H-C11) of each component of the mixture. These compounds showed the following relative R_f values (benzene–ether 15%, solutions): **85** < **83** < **84** < **86**. By preparative thin-layer chromatography (benzene–ether 10%, 4 elutions) and crystallization, it was possible to obtain pure compounds **83**, **85**, and **86**.

Isomer 83: mp 57°C, ir ($CHCl_3$, ν cm^{-1}): 3530, 1745, 1715 cm^{-1}; ^1H nmr ($CDCl_3$, δ ppm): 4.84 (t, 1H, J = 4.5 Hz, HCO_2), 3.87 (m, 4H, $(CH_2O)_2$), 3.28 (d, 1H, J = 5.0 Hz, H-C11), 2.68 (m, 1H, H-C14), 2.6–1.6 (m, 13H), 1.27 (s, 3H, CH_3-C5), 0.88 (d, 6H, J = 7.3 Hz, $(CH_3)_2CH$); ms *m/e*: 374 (M^+). *Anal.* calcd. for $C_{22}H_{30}O_5$: C 70.55, H 8.07; found: C 69.50, H 8.36.

Isomer 84: obtained as a mixture (~1:1) with **86**: ^1H nmr ($CDCl_3$, δ ppm): 4.90 (t, 1H, J = 4.6 Hz, HCO_2), 3.90 (m, 4H, $(CH_2O)_2$), 3.48 (d, 1H, J = 5.2 Hz, H-C11), 2.7–1.6 (m, 14H), 1.25 (s, 3H, CH_3-C5); 0.93 (d, 3H, J = 6.7 Hz, CH_3CH), 0.84 (d, 3H, J = 6.7 Hz, CH_3CH).

Isomer 85: mp 78–80°C; ir ($CHCl_3$, ν cm^{-1}): 3500, 1740, 1715 cm^{-1}; ^1H nmr ($CDCl_3$, δ ppm): 4.88 (t, 1H, J = 4.4 Hz, HCO_2), 3.90 (m, 4H, $(CH_2O)_2$), 3.54 (s, 1H, OH), 3.17 (d, 1H, J = 4.9 Hz, HC15), 3.01 (dd, 1H, J_{vic} = J_W = 2.3 Hz, H_{exo}-C1), 2.70 (dddd, 1H, HC15), 2.50 (m, 2H) and 2.40 (m, 2H) (allylic protons), 2.00 (m, 2H, H_2C8), 1.80 (m, 6H), 1.27 (s, 3H, CH_3-C5), 0.88 (d, 3H, J = 7 Hz) and 0.85 (d, 3H, J = 7 Hz) $(CH_3)_2CH$); ms *m/e*: 374. *Anal.* calcd. for $C_{22}H_{30}O_5$: C 70.55, H 8.07; found C 69.53, H 8.38.

Isomer 86: mp 120–122°C; ir ($CHCl_3$, ν cm^{-1}): 3530, 3400, 1740, 1715; ^1H nmr ($CDCl_3$, δ ppm): 4.86 (t, 1H, J = 4.8 Hz, HCO_2), 3.90 (m, 4H, $(CH_2O)_2$), 3.43 (d, 1H, J = 5.3 Hz, HC11), 3.14 (s, 1H, -OH), 2.57 (ddd, 1H, HC15), 2.52 (m, 2H), and 2.41 (m, 2H) (allylic protons), 2.29 (m, 1H, $CH(CH_3)_2$), 2.14 (d, 1H, J = 3.9 Hz, H_{endo}-C1), 2.02 (m, 2H, H_2C8), 1.95–1.50 (m, 5H), 1.25 (s, 3H, CH_3-C5), 0.93 (d, 3H, J = 6.7 Hz) and 0.87 (d, 3H, J = 6.7 Hz) $(CH(CH_3)_2)$; ms *m/e*: 374 (M^+).

Racemic pentacyclic diol aldehyde 87

A solution of the preceding crude mixture of compounds **83–86** (1.975 g, 5.28 mmol) in aqueous acetic acid (70%, 50 mL) was heated at 70°C for 1 h. The solvents and volatile substances were removed by evaporation under reduced pressure, then the oily residue was dissolved in tetrahydrofuran (150 mL) and stirred (25°C, 15 h) in the presence of aqueous sodium hydroxide (1 M, 40 mL). After removal of the organic solvent, the aqueous residue was extracted with ether (5 × 100 mL). The organic layers were combined, dried, filtered, and evaporated. The residue was crystallized from chloroform – petroleum ether to give racemic pentacyclic diol aldehyde **87** (400 mg, 23% from dienone **6**); mp 198–199°C; ir ($CHCl_3$, ν cm^{-1}): 3500, 2710, 1725; ^1H nmr ($CDCl_3$, δ ppm): 9.57 (d, 1H, J = 3.1 Hz, -CHO), 3.14 (d, 1H, J = 5.1 Hz, H-C11), 2.75 (dd, 1H, J = 5.1, 3.0 Hz, H-C1), 2.65 (dd, 1H, J = 11.0, 3.1 Hz, H-C3), 2.70–2.38 (m, 5H, H-C2, allylic protons, $HC(CH_3)_2$), 1.44 (m, 2H, H_2C14), 1.28 (s, 3H, CH_3C5), 1.11 (d, 3H, J = 6.4 Hz) and 0.77 (d, 3H, J = 6.7 Hz) $(CH(CH_3)_2)$; ms *m/e*: 330 (M^+). *Anal.* calcd. for $C_{20}H_{26}O_4$: C 72.70, H 7.93; found: C 72.63, H 8.06.

Pentacyclic carbonate aldehyde 89

To a solution of diol aldehyde **87** (120 mg, 0.36 mmol) in benzene (10 mL) was added pyridine (4 mL) and a saturated benzenic solution of

Can. J. Chem. Downloaded from www.nrcresearchpress.com by 91.144.44.67 on 09/07/12
For personal use only.

phosgene (10 mL). After 15 min at room temperature the mixture was poured onto ice-water and extracted with ether. The crude product was crystallized from chloroform – petroleum ether to give carbonate aldehyde **89** (88 mg, 68%); mp 186–188°C; ir ($CHCl_3$, ν cm^{-1}): 1805, 1740, 1725; ^1H nmr ($CDCl_3$, δ ppm): 9.57 (d, 1H, J = 3.0 Hz, -CHO), 3.40 (d, 1H, J = 5.3 Hz, H-C11), 3.03 (dd, 1H, J = 6.7 Hz, 2.2 Hz, H-C1), 2.87 (m, 1H, H-C2), 2.74 (dd, 1H, J = 11.4, 3.0 Hz, H-C3), 2.50 (m, 5H, H-C15 and allylic protons), 2.1–1.8 (m, 3H, H_2C8 and $CH(CH_3)_2$), 1.56 (m, 2H, H_2C14), 1.36 (s, 3H, CH_3C5), 1.14 (d, 3H, J = 6.5 Hz) and 0.81 (d, 3H, J = 6.8 Hz) ($(CH_3)_2CH$); ms m/e: 356 (M^+).

*Orthoacetates **90** and **91***

A solution of diol aldehyde **87** (525 mg, 1.59 mmol) and *p*-toluenesulfonic acid (6 mg) in acetic anhydride (60 mL) was heated at 70°C for 3 h. Acetic anhydride was then evaporated and the oily residue was purified by preparative thin-layer chromatography (benzene–ether 9:1, three elutions) to give orthoacetates **90** (120 mg, 18%), and **91** (108 mg, 16%).

*Orthoacetate **90***: mp 157–158°C; ir ($CHCl_3$, ν cm^{-1}): 1735, 1370, 1230, 1040; ^1H nmr ($CDCl_3$, δ ppm): 6.06 (d, 1H, J = 2 Hz, *H*COAc), 4.09 (d, 1H, J = 5 Hz, H-C11), 3.68 (dd, 1H, J = 6.5, 2.0 Hz, H-C1), 2.7–1.5 (m, 13H), 2.15 (s, 3H) and 2.12 (s, 3H) (acetate and orthoacetate), 1.39 (s, 3H, CH_3-C5), 1.20 (d, 3H, J = 5.5 Hz) and 0.87 (d, 3H, J = 5.5 Hz) ($(CH_3)_2CH$); ms m/e: 414 (M^+). *Anal.* calcd. for $C_{26}H_{32}O_7$: C 68.40, H 7.06; found: C 68.50, H 7.20.

*Orthoacetate **91***: ir ($CHCl_3$, ν cm^{-1}): 1735, 1370, 1230, 1070, 1040; ^1H nmr ($CDCl_3$, δ ppm): 6.41 (d, 1H, J = 5.5 Hz, *H*COAc), 4.15 (d, 1H, J = 5 Hz, HC11), 3.65 (dd, 1H, J = 6.5, 2.0 Hz, H-C1), 2.8–1.2 (m, 13H), 2.15 (s, 3H) and 2.12 (s, 3H) (acetate and orthoacetate), 1.39 (s, 3H, CH_3C5), 1.26 (d, 3H, J = 6 Hz) and 0.78 (d, 3H, J = 6 Hz) ($(CH_3)_2CH$); ms m/e: 414 (M^+).

*Monodeuterated diol aldehyde **87**-d_1*

A crude mixture of tricyclic Diels–Alder adducts **81***a* + *b* and **82***a* + *b* (3.93 g, 9.1 mmol) in tetrahydrofuran (100 mL) was reacted with a solution of sodium hydroxide (1.22 g) in deuterium oxide (30.5 mL) at room temperature for 16 h. The main part of the tetrahydrofuran was evaporated and the aqueous residue extracted with ether. The crude extract (3.3 g, 96%) was dissolved in tetrahydrofuran (100 mL) and reacted with aqueous sodium hydroxide (1 M, 30 mL) for 6 h at room temperature. Evaporation of tetrahydrofuran and ether extraction of the aqueous residue gave crude monodeuterated (position 15) mixture **77–80** (2.5 g, 76%), which was dissolved in aqueous acetic acid (70%, 80 mL) and heated at 70°C for 45 min. Evaporation of the volatile substances left a residue that was dissolved in tetrahydrofuran (100 mL) and reacted with aqueous sodium hydroxide (1 M, 60 mL). After 16 h at room temperature the aqueous residue was extracted with ether to give an oily mixture, which was purified by chromatography and crystallization as previously described (*vide supra*, compound **87**) to give diol aldehyde **87**-d_1 (320 mg, 15%); ^1H nmr ($CDCl_3$) identical to nmr spectrum of **87** except for the following: 3.14 (s, 1H, H-C11), 2.75 (d, J = 5.1 Hz, HC1) and 2.33 (no multiplet).

*Monodeuterated orthoacetates **90**-d_1 and **91**-d_1*

A solution of monodeuterated diol aldehyde **87**-d_1 (280 mg, 0.85 mmol) was reacted with acetic anhydride and *p*-toluenesulfonic acid as previously described (see the preceding preparation) to give monodeuterated **90**-d_1 (82 mg, 21%, mp 156–157°C) and **91**-d_1 (90 mg, 23%).

*Orthoacetate **90**-d_1*: ^1H nmr ($CDCl_3$, δ ppm) same as for **90** except for the following: 4.09 (s, 1H, H-C11), 3.68 (d, 1H, J = 6.5 Hz, H-C1).

*Orthoacetate **91**-d_1*: ^1H nmr ($CDCl_3$, δ ppm) same as for **91** except for the following: 4.15 (s, 1H, H-C11), 3.65 (d, 1H, J = 6.5 Hz, H-C1).

*Basic treatment performed on isomers **83–86***

*On isomer **83***: To a stirred solution of isomer **83** (30 mg, 0.080 mmol) in tetrahydrofuran (3 mL) was added aqueous sodium hydroxide (0.75 mL, 1 M). After 18 h at 25°C, extraction of the reaction mixture with ether furnished unchanged starting material (26 mg, 86%) as shown by nmr and tlc analysis.

*On isomer **84***: same as for **83** with the following quantities: 14 mg of a mixture ~2:1 of **84** and **86**; NaOH, 1 M, 0.4 mL. Crude product (4 mg, 28%) showed the presence of **83**, **85**, and **86** by nmr.

*On isomer **85***: same as for **83** with the following quantities: isomer **85** (33 mg, 0.088 mmol), sodium hydroxide (0.8 mL, 1 M), tetrahydrofuran (3 mL). Crude product (10 mg, 30%) showed the presence of **85** and **86** (respectively ~2:1, by nmr).

*On isomer **86***: same as for **83**: isomer **86** (28 mg, 0.075 mmol), sodium hydroxide (0.8 mL, 1 M), tetrahydrofuran (3 mL). Crude product (12 mg, 43%) showed the presence of isomers **85** and **86** (respectively ~2:1, by nmr).

*Cyclization of isomer **83***

A solution of pure isomer **83** (30 mg, 0.080 mmol) in aqueous acetic acid (70%, 5 mL) was heated at 70°C for 45 min. Evaporation of the volatile substances left a residue that was dissolved in tetrahydrofuran (3 mL) and reacted with aqueous sodium hydroxide (1 mL, 1 M). After 16 h at room temperature, the mixture was extracted with ether to give pure diol aldehyde **87** (26 mg, 98%).

*(+)-Dihydrocarvone ((S)-**95**)*

A mixture of (+)-carvone ((*S*)-**94**) (50.0 g, 0.33 mol) and platinum oxide (0.10 g) was stirred under hydrogen at 25°C for 7 h. The catalyst was then removed by filtration through a short column of silica gel (ether). Evaporation of the solvent left colorless pure (+)-dihydrocarvone ((*S*)-**94**) (50 g, 99%); ir (neat, ν cm^{-1}): 1680, 1200; ^1H nmr ($CDCl_3$, δ ppm): 6.78 (m, 1H, H-C3), 2.7–1.3 (m, 6H), 1.77 (m, 3H, CH_3-C2), 0.88 (d, 6H, J = 5.5 Hz, $(CH_3)_2CH$). *(−)-Dihydrocarvone* ((*R*)-**95**): hydrogenation of (−)-carvone ((*R*)-**94**) (33.0 g, 0.217 mol) was done in the same way to furnish (−)-dihydrocarvone ((*R*)-**95**) (33 g, 99%).

*(3S)-3-Isopropyl-5-oxopentanoic acid ((S)-**96**)*

A solution of (+)-dihydrocarvone ((*S*)-**95**, 20.06 g, 131.5 mmol) in ethyl acetate (150 mL) was treated by a stream of ozone at −78°C until a blue color persisted (50 min approximately). The mixture was warmed at room temperature while a stream of nitrogen was bubbled through the yellowish solution. The reaction mixture was then cooled (ice water) and stirred in a hydrogen atmosphere in the presence of 10% palladium-on-charcoal (200 mg) catalyst. After 5 h, removal of the catalyst by filtration on Celite left the crude aldehyde acid (*S*)-**96** (20.5 g); ir (CCl_4, ν cm^{-1}): 3500–2800 br, 1770–1715 br; ^1H nmr ($CDCl_3$, δ ppm): 9.6 (m, 1H, CHO), 9.1 (br m, 1H, CO_2H), 2.8–1.2 (m, 6H), 0.90 (d, 6H, J = 6 Hz, $CH(CH_3)_2$).

*(3S)-5,5-Ethylenedioxy-3-isopropylpentanoic acid ((S)-**70**)*

To a solution of the crude aldehyde acid (*S*)-**96** (20.5 g, 130 mmol) in benzene (250 mL) were added ethylene glycol (25.2 g, 0.41 mol) and *p*-toluenesulfonic acid (0.50 g). The mixture was refluxed (Dean–Stark) for 16 h, then cooled, diluted with ether (200 mL), and washed with water (2 × 50 mL) and brine. Evaporation of the solvents left a crude mixture that was dissolved in methanol (150 mL) and reacted with aqueous sodium hydroxide (1 M, 150 mL) at 65°C for 4 h. Methanol was then evaporated under reduced pressure and the aqueous layer was washed with ether to remove neutral impurities. Acidification (pH 5, 0°C, 1 M HCl) of the basic aqueous layer and extraction with ether (4 × 100 mL) furnished ketal acid (*S*)-**70** (22.2 g, 99%): *vide supra* for spectroscopic data.

*(3R)-5,5-Ethylenedioxy-3-isopropylpentanoic acid ((R)-**70**)*

Same procedure as for (*S*)-**70** from aldehyde acid (*R*)-**96**.

*Methyl (3S) and (3R)-5,5-ethylenedioxy-3-isopropyl pentanoate ((S)-**69**, R = CH_3)*

(a) By esterification with diazomethane

A solution of ketal acid (*S*)-**70** (5.6 g, 27 mmol) or (*R*)-**70** (5.15 g, 25 mmol) in dry ether (100 mL) was reacted at −78°C with a slight excess of diazomethane in ether (~20 mg/mL, 100 mL). Evaporation of the solvent left ester (*S*)-**69** (R = CH_3, 5.3 g, 95%) or ester (*R*)-**69** (R

Can. J. Chem. Downloaded from www.nrcresearchpress.com by 91.144.44.67 on 09/07/12
For personal use only.

= CH_3, 5.18 g, 96%): ir (neat, ν cm^{-1}): 1740; ^1H nmr ($CDCl_3$, δ ppm): 4.93 (t, 1H, J = 5 Hz, HCO_2), 3.92 (m, 4H, $(CH_2O)_2$), 3.69 (s, 3H, OCH_3), 2.5–1.4 (m, 6H), 0.88 (d, 6H, $(CH_3)_2CH$); ms *m/e*: 216 (M^+). *Anal.* calcd. for $C_{11}H_{20}O_4$: (*S*)-**69** (R = CH_3): C 61.08, H 9.32; found: C 60.95, H 9.44; for (*R*)-**69** (R = CH_3): found: C 60.84, H 9.20; $[\alpha]_{578}^{25}$ for (*S*)-**69** (R = CH_3): +0.6°, neat, and for (*R*)-**69** (R = CH_3): −0.6°, neat.

(b) By esterification with methyl iodide

A mixture of the crude acetal acid (*S*)-**70** (142 g, 0.7 mol), anhydrous potassium carbonate (146 g), and methyl iodide (300 mL, 4.8 mol) in acetone (2 L) was refluxed for 25 h under nitrogen. The cooled mixture was then filtered and the solvent evaporated. The oily residue was dissolved in ether (1.4 L), washed twice with aqueous potassium carbonate (10%), twice with brine, and dried ($MgSO_4$). Evaporation of the solvent left an oil, which was distilled under reduced pressure (bp 84–86°C, 0.2 Torr, ~136 g, 90%) to give pure ketal ester (*S*)-**69** (R = CH_3).

Dienophile (S)-74

From ketal acid (*S*)-**70**. This reaction was done as for racemic dienophile **74** (*vide supra*). Dienophile **74** ($[\alpha]_{578}^{25}$ +0.7°, neat) was obtained in 75% yield based on reacted acid.

From ketal ester (*S*)-**69** (R = CH_3). This sequence was done exactly as for racemic material (*vide supra*, **69** → **74**) in an overall yield of ~80%.

Dienophile (R)-74

This material was obtained from ketal ester (*R*)-**69** (R = CH_3) as just described for dienophile (*S*)-**74** in the same overall yield of ~80% ($[\alpha]_{578}^{25}$ −0.6°, neat).

Pentacyclic diol aldehyde (dextro)-87

Starting from *o*-spirolactone dienone **6** (6.75 g, 30.6 mmol) and dienophile (*S*)-**74** (7.4 g, 34.8 mmol), the synthesis of (*dextro*)-**87** was done in the same way as described for racemic aldehyde **87** (*vide supra*); mp 165–165.5°C; $[\alpha]_{578}^{25}$ +142.2°.

Pentacyclic diol aldehyde (levo)-87

Starting from *o*-spirolactone dienone **6** (2.00 g, 9.13 mmol) and dienophile (*R*)-**74** (2.13 g, 10.04 mmol), aldehyde (*levo*)-**87** was obtained (0.52 g, 17%); mp 161–162°C; $[\alpha]_{578}^{25}$ −137.5°. *Anal.* calcd. for $C_{20}H_{26}O_4$: C 72.70, H 7.93; found: C 72.63, H 8.06.

Pentacyclic carbonate aldehyde (dextro)-89

This compound was synthesized from diol aldehyde (*dextro*)-**87** as for racemic **89** (*vide supra*); mp 186–188°C, $[\alpha]_D^{25}$ +121.3°.

5,6-Dimethoxy-1-methylindene (112)

To a solution of 5,6-dimethoxy-1-indanone (**110**) (100 g, 0.52 mol) in tetrahydrofuran (3.2 L) was added, at −55°C and under nitrogen, a solution of methyllithium in ether (1 mol, 500 mL). The mixture was then warmed to room temperature and stirred for 16 h. Water (100 mL) and hydrochloric acid (1 mol) were added to the cooled mixture and the organic layer was separated. The aqueous layer was then extracted (4 × 250 mL) with ether. The usual evaporation of the dried ($MgSO_4$) organic extract afforded a crude material, which was chromatographed on Florisil (benzene) to give pure compound **112** (96.4 g, 97%); mp 91–92°C (ether–hexane); ir ($CHCl_3$, ν cm^{-1}): 1610, 1580, 1490, 1340, 1270, 1220, 1130, 1060; ^1H nmr (CCl_4, δ ppm): 6.88 (br s, 1H, H-C7), 6.75 (s, 1H, H-C4), 5.99 (m, 1H, H-C2), 3.79 (s, 3H, OCH_3), 3.76 (s, 3H, OCH_3), 3.14 (m, 2H, H_2C3), 2.08 (m, 3H, CH_3-C1); ms *m/e*: 190 (M^+). *Anal.* calcd. for $C_{12}H_{14}O_2$: C 75.76, H 7.42; found: C 75.84, H 7.24.

5,6-Dimethoxy-1-methylindane (113)

A mixture of methylindene **112** (40 g, 0.21 mol) and platinum oxide (320 mg) in acetic acid (800 mL) was shaken in an hydrogen atmosphere for 48 h. The catalyst was removed by filtration and the acetic acid was evaporated under reduced pressure to leave an oil, which was filtered on Florisil (benzene as eluent) to give oily methylindane **113** (33.27 g, 83%): ir ($CHCl_3$, ν cm^{-1}): 1610; ^1H nmr (CCl_4, δ ppm): 6.17 (br s, 2H, aromatic), 3.72 (s, 3H, OCH_3), 3.69 (s, 3H, OCH_3), 3.2–1.5 (m, 5H), 1.22 (d, 3H, J = 7 Hz, CH_3-C1); ms *m/e*: 192 (M^+). *Anal.* calcd. for $C_{12}H_{16}O_2$: C 74.97, H 8.39; found: C 74.94, H 8.24.

Isomeric dimethoxyindane aldehydes 114 and 115

To a solution of methylindane **113** (7.50 g, 39 mmol) in dry dichloromethane (125 mL) was added, at 0°C, titanium tetrachloride (10.5 mL, 18.16 g, 95.7 mmol). To the red-violet mixture was then added a solution of dichloromethyl methyl ether (9.0 mL, 11.4 g, 100 mmol) in dichloromethane (25 mL). After stirring at 0°C for 15 min, at room temperature for 1 h, and at reflux for 4 h, the mixture was cooled and poured onto an ice–water mixture and stirred for 3 h. Separation of the organic layer and extraction of the aqueous phase with dichloromethane furnished an organic extract, which was dried (Na_2SO_4), filtered, and evaporated. The crude extract contained isomers **114** and **115** (respectively 2:1) together with unreacted starting material (~20%) as shown by nmr. As these aldehydes do not support chromatography, removal of the starting material was done by transforming these aldehydes to their corresponding Girard's T derivatives: a solution of the crude reaction mixture (4.58 g, ~20 mmol) in ethanol (35 mL) and acetic acid (3.5 mL) was reacted with Girard's T reagent (3.5 g, 20.8 mmol). After 1 h at reflux, the reaction mixture was cooled and diluted with brine (200 mL), and washed with ether (3 × 100 mL) to remove methylindane **113** and other impurities. Addition of hydrochloric acid (2 M, 20 mL) to the aqueous layer followed by ether extraction (5 × 100 mL) and a rapid filtration of the colored extract through a short path of silica gel (CH_2Cl_2) gave a pure mixture of aldehydes **114** and **115** (3.1 g, 68%).

Dihydroxyaldehydes 116 and 117

To a cooled (−70°C) solution of the purified mixture of compounds **114** and **115** (6.00 g, 27.3 mmol) in dry dichloromethane (250 mL) was added dropwise boron tribromide (6.0 mL, 62 mmol) over a period of 15 min. The mixture was then stirred at room temperature for 2 h, cooled again at −70°C, treated with methanol (10 mL), aqueous methanol (50%), and water (100 mL). After 4 h at room temperature, the organic layer was separated and the aqueous layer extracted with dichloromethane (4 × 100 mL). The combined extracts were washed with water, dried, and the solvent was evaporated. The crude extract (3.8 g) was filtered through a short path of Florisil (CH_2Cl_2). Fractional crystallization of the semicrystalline extract (3.0 g) (CH_2Cl_2 – Et_2O – hexane) furnished pure aldehydes **116** (630 mg, 12%) and **117** (49 mg, 1%).

Aldehyde 116: mp 91.5–92.5°C; ir ($CHCl_3$, ν cm^{-1}): 3500, 3460, 2760, 1660, 1605; ^1H nmr (CCl_4, δ ppm): 11.28 (s, 1H, HO-C5), 10.0 (s, 1H, CHO), 6.94 (1H, s, H-C7), 5.73 (s, 1H, HO-C6), 3.2–1.5 (m, 5H), 1.22 (d, 3H, J = 7 Hz, CH_3Cl); ms *m/e*: 192 (M^+). *Anal.* calcd. for $C_{11}H_{12}O_3$: C 68.74, H 6.29; found: C 68.75, H 6.15. Irradiation of methyl signal (δ 1.22) resulted in an increase (15%) of aromatic signal at δ 7.01.

Aldehyde 117: mp 81–82.5°C; ir ($CHCl_3$, ν cm^{-1}): 3560, 2760, 1660, 1605; ^1H nmr (δ ppm): 11.41 (s, 1H, HO-C6), 10.10 (s, 1H, CHO), 7.01 (s, 1H, H-C4), 6.04 (s, 1H, HO-C5), 3.8–1.6 (m, 5H), 1.24 (d, 3H, J = 7 Hz, CH_3-C1); ms *m/e*: 192 (M^+). Irradiation of the methyl signal (δ 1.24) had no apparent effect on the intensity of the aromatic proton signal.

Bromoacetate 118

To a solution of 4-formyl-5,6-dihydroxy-1-methylindane (**116**) (1.42 g, 7.4 mmol) in dry benzene (30 mL) and pyridine (0.6 mL, 7.4 mmol) was added dropwise at 25°C a solution of bromoacetyl bromide (1.63 g, 8.1 mmol) in benzene (10 mL). After 3 h, the mixture was washed with water and the solvent was evaporated to leave a yellow oil sufficiently pure for the next step (2.35 g, crude 98%); ir ($CHCl_3$, ν cm^{-1}): 3600–3000 (br), 1760, 1660; ^1H nmr ($CDCl_3$, δ ppm): 11.39 (s, 1H, OH), 10.04 (s, 1H, CHO), 7.19 (s, 1H, H-C7), 4.10 (s, 2H, $BrCH_2$-), 3.3–1.4 (m, 5H), 1.22 (d, 3H, J = 7 Hz, CH_3-); ms *m/e*: 312 and 314 (M^+).

Lactone aldehyde 119

To a solution of bromoacetate **118** (2.51 g, 8.0 mmol) in tetrahydrofuran (60 mL) was added powdered potassium carbonate (10.0 g,

Can. J. Chem. Downloaded from www.nrcresearchpress.com by 91.144.44.67 on 09/07/12
For personal use only.

2.5 mmol). The mixture was refluxed for 48 h. After cooling, the mixture was centrifuged and decanted. The solid material was dissolved in water (100 mL), and the aqueous solution was acidified to pH 1 (2 M HCl) and extracted with ether (3 × 70 mL). The crude acid (2.0 g) was dissolved in benzene (50 mL) and refluxed (Dean–Stark, 4 h) in the presence of *p*-toluenesulfonic acid (25 mg). The cooled mixture was filtered through a short pad of silica gel. Evaporation of benzene left pure lactone **119** (1.69 g, 91%), which was crystallized from ether–hexane; mp 111.5–112°C; ir ($CHCl_3$, ν cm^{-1}): 2770, 1800, 1698, 1605, 1325, 1300, 1270, 1200; ^1H nmr ($CDCl_3$, δ ppm): 10.35 (s, 1H, CHO), 7.07 (br s, 1H, H-C7), 4.75 (s, 2H, $-OCH_2CO_2-$), 3.4–1.4 (m, 5H), 1.22 (d, 3H, J = 7 Hz, CH_3-); ms *m/e*: 232 (M^+). *Anal.* calcd. for $C_{13}H_{12}O_4$: C 67.23, H 5.21; found: C 67.13, H 5.15.

Lactone ***120***

A mixture of lactone aldehyde **119** (1.66 g, 7.1 mmol) and palladium-on-charcoal catalyst (10%, 440 mg) in acetic acid was shaken under hydrogen at 25°C for 24 h. Filtration of the catalyst and evaporation of the solvent left pure crystalline lactone indane **120** (1.55 g, 99%), which was recrystallized from hexane; mp 68–70°C; ir ($CHCl_3$, ν cm^{-1}): 1785, 1610; ^1H nmr (CCl_4, δ ppm): 6.70 (br s, 1H, H-C7), 4.49 (s, 2H, OCH_2CO_2), 3.3–1.4 (m, 5H), 2.11 (s, 3H, CH_3-C4), 1.22 (d, 3H, J = 7 Hz, CH_3Cl); ms *m/e*: 218 (M^+). *Anal.* calcd. for $C_{13}H_{14}O_3$: C 71.54, H 6.47; found: C 71.65, H 6.45.

Spirolactones ***97***

To a solution of lactone indane **120** (502 mg, 2.30 mmol) in acetonitrile (10 mL) was added aqueous sodium hydroxide (1 M, 2.7 mL). After 45 min of stirring at room temperature, a solution of *N*-bromosuccinimide (430 mg, 2.41 mmol) in aqueous acetonitrile (16 mL, 1:1) was rapidly added to the mixture. After 2.5 min, addition of brine and extraction with ether furnished a colored crude product, which was rapidly filtered on silica gel (benzene) to give a sensitive mixture of racemic lactones **97** (515 mg, ~95%); ir ($CHCl_3$, ν cm^{-1}): 1820, 1685, 1665, 1602; ^1H nmr ($CDCl_3$, δ ppm): 5.87 (br s, 1H, H-C7), 4.66 (br d, 1H, J = 14 Hz) and 4.39 (d, 1H, J = 14 Hz) (two embodied AB patterns, O-CH_2CO_2), 3.1–1.4 (m, 5H), 1.92 (br s, 3H, CH_3-C4), 1.22 (d, 3H, J = 7 Hz, CH_3Cl); ms *m/e*: 234 (M^+).

Adducts ***121****(a–b) and* ***122****(a–b)*

A solution of mixed dienones **97** (160 mg, 0.68 mmol) in excess methylvinylketone (0.3 mL) was refluxed for 20 min under nitrogen. Removal of the volatile substances under vacuum and careful chromatography of the oily residue (215 mg) on a thick layer of silica gel (carbon tetrachloride, ethyl acetate, benzene, hexane 1:1:5:3, two elutions) furnished four adducts (total yield ~65%). These compounds showed the following R_f values, 0.75, 0.70, 0.61, 0.56, and relative proportions 2:2:1:2.

Least polar isomer: mp 124–126°C; ir ($CHCl_3$, ν cm^{-1}): 1820, 1740, 1715; ^1H nmr (C_6H_6, δ ppm): 4.38 (d, 1H, J_{AB} = 14 Hz) and 3.77 (d, 1H, J_{AB} = 14 Hz) (AB pattern, OCH_2CO_2), 3.35 (d, 1H, J = 2 Hz, H-C11), 2.6–1.2 (m, 8H), 1.57 (s, 3H, CH_3CO), 1.00 (s, 3H, CH_3-C5), 0.77 (d, 3H, J = 7 Hz, CH_3-C9); ms *m/e*: 304 (M^+).

Second least polar isomer: mp 149–151°C; ir ($CHCl_3$, ν cm^{-1}): 1820, 1740, 1715; ^1H nmr (C_6H_6, δ ppm): 4.39 (d, 1H, J_{AB} = 14 Hz) and 3.77 (d, 1H, J_{AB} = 14 Hz) (AB pattern, OCH_2CO_2), 3.45 (d, 1H, J = 2 Hz, H-C11), 2.6–1.1 (m), 1.55 (s, 3H, CH_3CO), 1.15 (s, 3H, CH_3C5), 0.90 (d, 3H, J = 7 Hz, CH_3C9); ms *m/e*: 304 (M^+).

Third least polar isomer: mp 160–161°C; ir ($CHCl_3$, ν cm^{-1}): 1820, 1735, 1715; ^1H nmr (C_6H_6, δ ppm): 4.32 (d, 1H, J_{AB} = 14 Hz) and 3.76 (d, 1H, J_{AB} = 14 Hz) (AB pattern, OCH_2CO_2), 3.37 (d, 1H, J = 2 Hz, H-C11), 2.8–1.1 (m, 8H), 1.55 (s, 3H, CH_3CO), 1.01 (s, 3H, CH_3-C5), 0.77 (d, 3H, J = 7 Hz, CH_3C9); ms *m/e*: 304 (M^+).

Most polar isomer: ir ($CHCl_3$, ν cm^{-1}): 1820, 1745, 1715; ^1H nmr (C_6H_6, δ ppm): 4.34 (d, 1H, J_{AB} = 14 Hz) and 3.78 (d, 1H, J_{AB} = 14 Hz) (AB pattern, OCH_2CO_2), 3.48 (d, 1H, J = 2 Hz, H-C11), 2.8–1.1 (m, 8H), 1.55 (s, 3H, CH_3CO), 1.00 (s, 3H, CH_3-C5), 0.83 (d, 3H, J = 7 Hz, CH_3-C9); ms *m/e*: 304 (M^+).

Isomers ***123*** *and* ***124***

To a solution of the preceding Diels–Alder adduct mixtures (**121***a–b* and **122***a–b*) (200 mg, 0.66 mmol) in tetrahydrofuran (3 mL) was added aqueous sodium hydroxide (2.0 mL, 1 M). After 16 h of stirring at room temperature, the mixture was extracted with ether (5 × 20 mL). After evaporation of the solvents, the crude oily residue was chromatographed (preparative thick layer of silica gel, carbon tetrachloride, ether, benzene, 2:1:2) to give two products (55:45 of R_f values 0.30:0.25 respectively).

Less polar compound (**123** or **124**): R_f 0.30; mp 132–132.5°C; ir ($CHCl_3$, ν cm^{-1}): 3520, 1752, 1722; ^1H nmr ($CDCl_3$, δ ppm): 3.32 (d, 1H, J = 4.5 Hz, H-C11), 3.18 (br s, 1H, OH), 2.6–1.3 (m, 8H), 2.50 (br s, 2H, H_2Cl), 1.28 (s, 3H, CH_3-C5), 1.06 (d, 3H, J = 7 Hz, CH_3C9); ms *m/e*: 246 (M^+). *Anal.* calcd. for $C_{15}H_{18}O_3$: C 73.14, H 7.36; found: C 72.82, H 7.49.

More polar compound (**124** or **123**): R_f 0.25; mp 160–161°C; ir ($CHCl_3$, ν cm^{-1}): 3515, 1752, 1722; ^1H nmr ($CDCl_3$, δ ppm): 3.29 (d, 1H, J = 4.5 Hz, H-C11), 3.21 (br s, 1H, OH), 1.28 (s, 3H, CH_3-C5), 1.09 (d, 3H, J = 7 Hz, CH_3C9); ms *m/e*: 246 (M^+).

Diels–Alder adducts ***125*** *and* ***126***

A mixture of diene **97** (505 mg, 2.16 mmol) and optically active dienophile (*S*)-**74** (515 mg, 2.42 mmol) in benzene (4 mL) was refluxed for 12 h; then benzene was removed by evaporation to give an oily residue (1.0 g), which was dissolved in tetrahydrofuran (14 mL) and reacted with aqueous sodium hydroxide (5 mL, 1 M) for 24 h at 25°C. The mixture was then extracted with ether, washed with water, and ether was removed under reduced pressure to give a crude mixture (580 mg) that was dissolved in aqueous acetic acid (70%, 25 mL) and heated at 70°C for 1.5 h. Removal of acetic acid and ether extraction of the residue furnished a mixture of compounds (490 mg), which was dissolved in tetrahydrofuran (10 mL) and reacted with aqueous sodium hydroxide (1 M, 1.45 mL) for 16 h at 25°C. Extraction of the reaction medium with ether gave a crude mixture (400 mg) containing several compounds. This last mixture was dissolved in benzene (15 mL) and pyridine (0.25 mL) and reacted with an excess of phosgene in benzene during 1 h at room temperature. The mixture was then washed with water and extracted with ether. Chromatography of the crude extract on preparative thin layer (benzene–ether, 4:1) furnished a mixture (46 mg, 10%) of two compounds, isomers **125** and **126**, which were separated by fractional crystallization.

Isomer (***125*** or ***126***): mp 162–163°C; ir ($CHCl_3$, ν cm^{-1}): 2720, 1812, 1750, 1732; ^1H nmr ($CDCl_3$, δ ppm): 9.65 (d, 1H, J = 3 Hz, CHO), 3.40 (d, 1H, J = 5.5 Hz, H-C11), 3.2–1.5 (m), 1.35 (s, 3H, CH_3-C5), 1.14 (d, 3H, J = 7 Hz) and 0.80 (d, 3H, J = 7 Hz) ($CH(CH_3)_2$), 1.08 (d, 3H, J = 7 Hz, CH_3-C9). *Mol. Wt.* (ms) calcd. for $C_{21}H_{26}O_5$: 370.178; found 370.173.

Isomer (***126*** or ***125***): ir ($CHCl_3$, ν cm^{-1}): 2720, 1812, 1750, 1732; ^1H nmr ($CDCl_3$, δ ppm): 9.48 (d, 1H, J = 3 Hz, CHO), 3.38 (d, 1H, J = 5.5 Hz, H-C11), 3.2–1.5 (m), 1.35 (s, 3H, CH_3-C5), 1.14 (d, 3H, J = 7 Hz) and 0.80 (d, 3H, J = 7 Hz) ($CH(CH_3)_2$), 1.02 (d, 3H, J = 7 Hz, CH_3-C9); ms *m/e*: 370 (M^+).

Diels–Alder adducts ***128****a–b and* ***129****a–b*

A mixture of diene **6** (834 mg, 3.8 mmol) and acetoxy-2-acrylonitrile (1.0 g, 9.0 mmol) was heated at 127°C for 5 h. Removal of the dienophile under vacuum afforded a mixture of four compounds in the following proportion: 39:17:20:24, as determined by gas chromatography and increasing polarity. These were separated on a small scale by preparative thin-layer chromatography (carbon tetrachloride, ethyl acetate, benzene, 2:3:15).

Least polar compound (39%, R_f 0.70): mp 131–132°C; ir ($CHCl_3$, ν cm^{-1}): 1822, 1752; ^1H nmr ($CDCl_3$, δ ppm): 4.65 (d, 1H, J_{AB} = 15 Hz) and 4.38 (d, 1H, J_{AB} = 15 Hz) (AB pattern, OCH_2CO_2), 3.97 (s, 1H, H-C11), 2.7–2.0 (m, 8H), 2.12 (s, 3H, CH_3CO_2), 1.25 (s, 3H, CH_3C5); ms *m/e*: 331 (M^+). *Anal.* calcd. for $C_{17}H_{17}NO_6$: C 61.62, H 5.17, N 4.23; found: C 60.49, H 5.17, N 4.37.

Second least polar compound (17%, R_f 0.62): mp 182–182.5°C; ir ($CHCl_3$, ν cm^{-1}): 1822, 1752; ^1H nmr ($CDCl_3$, δ ppm): 4.70 (d, 1H, J_{AB} = 15 Hz) and 4.38 (d, 1H, J_{AB} = 15 Hz) (AB pattern, OCH_2CO_2), 3.99 (s, 1H, H-C11), 2.8–2.0 (m, 8H), 2.12 (s, 3H, CH_3CO_2), 1.25 (s, 3H, CH_3C5); ms *m/e*: 331 (M^+). *Anal.* calcd. for $C_{17}H_{17}NO_6$: C 61.62, H 5.17; found: C 62.17, H 5.16.

Third least polar compound (20%, R_f 0.55): ir ($CHCl_3$, ν cm^{-1}):

Can. J. Chem. Downloaded from www.nrcresearchpress.com by 91.144.44.67 on 09/07/12
For personal use only.

1822, 1752; ^{1}H nmr ($CDCl_3$, δ ppm): 4.65 (d, 1H, J_{AB} = 15 Hz) and 4.41 (d, 1H, J_{AB} = 15 Hz) (AB pattern, OCH_2CO_2), 4.14 (s, 1H, H-C11), 3.2–1.6 (m, 8H), 2.08 (s, 3H, CH_3CO_2), 1.25 (s, 3H, CH_3C5); ms *m/e*: 331 (M^+).

Most polar compound (24%, R_f 0.46): mp 191–192°C; ir ($CHCl_3$, ν cm^{-1}): 1822, 1752; ^{1}H nmr ($CDCl_3$, δ ppm): 4.70 (d, 1H, J_{AB} = 15 Hz) and 4.37 (d, 1H, J_{AB} = 15 Hz) (AB pattern, OCH_2CO_2), 4.16 (s, 1H, H-C11), 3.2–1.6 (m, 8H), 2.10 (s, 3H, CH_3CO_2), 1.25 (s, 3H, CH_3C5); ms *m/e*: 331 (M^+). *Anal.* calcd. for $C_{17}H_{17}NO_6$: C 61.62, H 5.17; found: C 60.99, H 5.25. Monocrystal X-ray diffraction analysis of this compound revealed that it had the structure shown by the formula **128***b* (Scheme 17). Complete X-ray data will be published elsewhere (8*b*).

Cyanohydrin diketone ***132***

(*a*) To Diels–Alder adduct **129***a* (or *b*) (least polar isomer, R_f 0.70, 18 mg, 0.054 mmol) in dimethoxyethane (1.5 mL) was added aqueous hydrochloric acid (0.2 mL, 1 M). After 12 h at 80°C, the mixture was extracted with ether to give a crude colored residue, cyanohydrin diketone **132** (17 mg); ir ($CHCl_3$, ν cm^{-1}): 3400, 1740; ^{1}H nmr ($CDCl_3$, δ ppm): 4.82 (br s, 1H, OH), 4.66 (s, 1H, HC11), 2.9–1.9 (m, 8H), 1.35 (s, 3H, CH_3-C5).

(*b*) With Diels–Alder adduct **129***b* (or *a*) (third least polar, R_f 0.55, 13 mg, 0.039 mmol), the same treatment gave the same cyanohydrin diketone **132** (9 mg).

Cyanohydrin diketone acetate ***134***

The preceding crude cyanohydrin diketone **132** (17 mg) was dissolved in pyridine (0.4 mL) and acetic anhydride (0.4 mL). After 20 h at room temperature, evaporation of the volatile materials left a residue that was dissolved in benzene, washed with water, and discolored with Norit. Removal of the solvent left a semicrystalline residue (18 mg). Crystallization from dichloromethane–ether gave an analytical sample of cyanohydrin acetate **134**; mp 210–210.5°C; ir ($CHCl_3$, ν cm^{-1}): 1752, 1740; ^{1}H nmr ($CDCl_3$, δ ppm): 4.24 (s, 1H, H-C11), 2.9–1.9 (m, 8H), 2.10 (s, 3H, CH_3CO_2), 1.37 (s, 3H, CH_3-C5); ms *m/e*: 273 (M^+). *Anal.* calcd. for $C_{15}H_{15}NO_4$: C 65.93, H 5.53; found: C 65.15, H 5.43.

*3,3-Ethylenedioxy-butanoic acid (****135****)*

A mixture of ketal ester **40** (*vide supra*) (15.0 g, 86 mmol) and aqueous potassium hydroxide (100 mL, 1.1 M) was refluxed for 5 h. The cooled mixture was then extracted with ether and the aqueous layer was acidified (pH 5) at 0°C with hydrochloric acid (1 M) and extracted with ether (3 × 50 mL). Evaporation of the solvent furnished pure acid **135** (7.02 g, 56%) as a white solid; mp 48–50°C; ir ($CHCl_3$, ν cm^{-1}): 3600–2900 (br), 1710; ^{1}H nmr (CCl_4, δ ppm): 11.45 (s, 1H, CO_2H), 3.92 (s, 4H, OCH_2CH_2O), 2.60 (s, 2H, CH_2CO_2), 1.47 (s, 3H, CH_3); ms *m/e*: 131 ($M^+ - CH_3$). *Anal.* calcd. for $C_6H_{10}O_4$: C 49.31, H 6.90; found: C 48.89, H 7.00.

*3,3-Ethylenedioxy-butanoyl chloride (****136****)*

To a cooled solution (6°C) of ketal acid **135** (17.5 g, 0.12 mol) in dry benzene (200 mL) and pyridine (10.7 mL, 0.132 mol) was added oxalyl chloride (16.8 g, 0.132 mol) in benzene (200 mL). After 3 h at room temperature the mixture was filtered and the solvent removed by evaporation. The residue was distilled under reduced pressure to furnish pure acid chloride **136** (18 g, 92%); bp 120°C (0.1 Torr); ir (CCl_4, ν cm^{-1}): 1811, 1100; ^{1}H nmr ($CDCl_3$, δ ppm): 3.96 (s, 4H, OCH_2CH_2O), 3.21 (s, 2H, CH_2CO_2), 1.43 (s, 3H, CH_3); ms *m/e*: 149 and 151 ($M^+ - 15$).

Ester ***138***

To a cooled (5°C) solution of acid chloride **136** (20.00 g, 120 mmol) in dry benzene (200 mL) and dry pyridine (9.50 g, 120 mmol) was added dropwise (10 min) a solution of 3-chloro-2-hydroxy propanenitrile (**137**) (12.65 g, 120 mmol) in benzene (200 mL). The mixture was warmed to room temperature, stirred for 12 h, and then decanted from the solid residue. The benzenic solution was washed with water and brine and the solvent evaporated. The oily residue was crystallized in the cold from ether–hexane to give pure ester **138** (22 g, 80%); mp 54–56°C; ir ($CHCl_3$, ν cm^{-1}): 1757, 1160, 1040; ^{1}H nmr ($CDCl_3$, δ ppm): 5.60 (t, 1H, *J* = 6 Hz, H-CCN), 4.00 (s, 4H, OCH_2CH_2O), 3.82 (d, 2H, H_2CCl), 2.74 (s, 2H, CH_2CO_2), 1.45 (s, 3H, $-CH_3$); ms *m/e*: 218 and 220 ($M^+ - 15$). *Anal.* calcd. for $C_9H_{12}NO_4Cl$: C 46.27, H 5.18, Cl 15.17; found: C 46.36, H 5.33, Cl 15.09.

*2-(3,3-Ethylenedioxy-butanoyloxy)acrylonitrile (****139****)*

To a solution of chloronitrile **138** (20.70 g, 89 mmol) in dry ether (200 mL) was added a solution of triethylamine (10.50 g, 98 mmol) in ether (200 mL). After 72 h of stirring at room temperature the mixture was decanted from the solid residue, which was washed with ether and the combined etheral fractions were evaporated. The residual liquid was distilled under vacuum to give pure nitrile **139** (13.34 g, 76%); bp 100°C, 0.03 Torr; mp 31°C; ir ($CHCl_3$, ν cm^{-1}): 2225, 1770, 1635; ^{1}H nmr ($CDCl_3$, δ ppm): 5.80 (d, 1H, J_{AB} = 3 Hz) and 5.74 (d, 1H, J_{AB} = 3 Hz) (AB pattern, H_2C=), 4.00 (s, 4H, OCH_2CH_2O), 2.84 (s, 2H, CH_2CO_2), 1.50 (s, 3H, CH_3); ms *m/e*: 182 ($M^+ - 15$). *Anal.* calcd. for $C_9H_{11}NO_4$: C 54.82, H 5.62; found: C 54.47, H 5.48.

Diels–Alder adducts ***140***a–b *and* ***141***a–b

A mixture of diene **6** (834 mg, 3.78 mmol) and dienophile **139** (1.020 g, 5.18 mmol) was heated at 120°C under nitrogen for 40 h. Crystallization of the crude mixture containing four main compounds of very similar polarity gave a low yield (30%) of a crystalline mixture of two compounds (470 mg), which were separated by thin-layer chromatography (silica gel, carbon tetrachloride – ethyl acetate – benzene, 2:3:15) to give two pure adducts.

Least polar compound (R_f 0.64): mp 151–152°C; ir ($CHCl_3$, ν cm^{-1}): 1820, 1750; ^{1}H nmr ($CDCl_3$, δ ppm): 4.60 (d, 1H, J_{AB} = 14 Hz) and 4.33 (d, 1H, J_{AB} = 14 Hz) (AB pattern, OCH_2CO_2), 3.96 (s, 4H, OCH_2CH_2O), 3.92 (s, 1H, H-C11), 2.70 (s, 2H, CH_2CO_2), 2.7–1.8 (m, 10H), 1.49 (s, 3H, CH_3-), 1.24 (s, 3H, CH_3-C5); ms *m/e*: 417 (M^+). *Anal.* calcd. for $C_{21}H_{23}NO_8$: C 60.42, H 5.55; found: C 60.46, H 5.67.

More polar compound **140***b* (R_f 0.56): mp 189–190°C; ir ($CHCl_3$, ν cm^{-1}): 1820, 1750; ^{1}H nmr ($CDCl_3$, δ ppm): 4.58 (d, 1H, J_{AB} = 15 Hz) and 4.34 (d, 1H, J_{AB} = 15 Hz) (AB pattern, OCH_2CO_2), 3.96 (s, 5H, OCH_2CH_2O and H-C11), 2.73 (s, 2H, CH_2CO_2), 2.42 (s, 2H, H_2C14), 2.8–1.8 (m, 6H), 1.47 (s, 3H, CH_3-), 1.24 (s, 3H, CH_3C5); ms *m/e*: 417 (M^+). *Anal.* calcd. for $C_{21}H_{23}NO_8$: C 60.42, H 5.55; found: C 60.10, H 5.32. Monocrystal X-ray diffraction analysis of this compound revealed that it had the structure shown by **140***b* (X = O, Y = H_2). Complete X-ray data will be published elsewhere (8*b*).

Acknowledgements

This work was financially supported by the Natural Sciences and Engineering Research Council of Canada (NSERCC) and by the "Gouvernement du Québec : Science et Technologie" (FCAR).

1. D. J. F. Berney and P. Deslongchamps. Can. J. Chem. **47**, 515 (1969).
2. A. Bélanger, D. J. F. Berney, H.-J. Borschberg, R. Brousseau, A. Doutheau, R. Durand, H. Katayama, R. Lapalme, D. M. Leturc, C.-C. Liao, F. N. MacLachlan, J.-P. Maffranc, F. Marazza, R. Martino, C. Moreau, L. St-Laurent, R. Saintonge, P. Soucy, L. Ruest, and P. Deslongchamps. Can. J. Chem. **57**, 3348 (1979).
3. P. Deslongchamps. Pure Appl. Chem. **49**, 1329 (1977).
4. P. Deslongchamps, A. Bélanger, D. J. F. Berney, H.-J. Borschberg, R. Brousseau, A. Doutheau, R. Durand, H. Katayama, R. Lapalme, D. M. Leturc, C.-C. Liao, F. N. MacLachlan, J.-P. Maffrand, F. Marazza, R. Martino, C. Moreau, L. Ruest, L. St-Laurent, R. Saintonge, and P. Soucy. Can. J. Chem. **68**, 115 (1990).
5. D. J. F. Berney. Ph.D. Thesis, Université de Sherbrooke. 1969.
6. D. Leturc. M.Sc. Thesis, Université de Sherbrooke. 1972.
7. R. Brousseau. Ph.D. Thesis, Université de Sherbrooke. 1972.
8. (*a*) A. Bélanger. Ph.D. Thesis, Université de Sherbrooke. 1974; (*b*) A. Michel, N. Michel-Dewez, and L. Ruest.

Laboratoire de chimie structurale, Université de Sherbrooke, Qué., Canada. To be published.
9. C. A. GROB. Angew. Chem. Int. Ed. Engl. **8**, 535 (1969).
10. (*a*) G. STORK, A. BRIZZOLARA, H. LANDESMAN, J. SZMUSKOVICZ, and R. TERRELL. J. Am. Chem. Soc. **85**, 207 (1963); (*b*) T. J. CURPHEY and JENNIE CHAO-YU HUNG. Chem. Commun. 510 (1967).
11. E. E. ROYALS and S. E. HORNE, JR. J. Am. Chem. Soc. **73**, 5856 (1951), and references therein.
12. A. S. HALLSWORTH, H. B. HENBEST, and T. I. WRIGLEY. J. Chem. Soc. 1969 (1957).
13. R. E. IRELAND, D. A. EVANS, D. CLOVER, G. M. RUBOTTOM, and H. YOUNG. J. Org. Chem. **34,** 3717 (1969).
14. A. RITCHIE, H. GROSS, and E. HÖFT. Org. Synth. **47**, 1 (1967).
15. F. L. BENTON and T. E. DILLON. J. Am. Chem. Soc. **64**, 1128 (1942).
16. S. N. SRIVASTAVA and M. PRZYBYLSKA. Can. J. Chem. **50**, 1882 (1972).
17. R. M. NOWAK. J. Org. Chem. **28**, 1182 (1963).

Can. J. Chem. Downloaded from www.nrcresearchpress.com by 91.144.44.67 on 09/07/12
For personal use only.

The total synthesis of (+)-ryanodol. Part III. Preparation of (+)-anhydroryanodol from a key pentacyclic intermediate

PIERRE DESLONGCHAMPS,[1] ANDRÉ BÉLANGER, DANIEL J. F. BERNEY, HANS-JUERG BORSCHBERG, ROBERT BROUSSEAU, ALAIN DOUTHEAU, ROBERT DURAND, HAJIME KATAYAMA, RICHARD LAPALME, DOMINIQUE M. LETURC, CHUN-CHEN LIAO, FREDERICK N. MACLACHLAN, JEAN-PIERRE MAFFRAND, FABRIZIO MARAZZA, ROBERT MARTINO, CLAUDE MOREAU, LUC RUEST, LOUISELLE SAINT-LAURENT, ROGER SAINTONGE, AND PIERRE SOUCY

Laboratoire de synthèse organique, Département de chimie, Faculté des sciences, Université de Sherbrooke, Sherbrooke (Québec), Canada J1K 2R1

Received May 8, 1989

This paper is dedicated to the memory of Professor Karel Wiesner

PIERRE DESLONGCHAMPS, ANDRÉ BÉLANGER, DANIEL J. F. BERNEY, HANS-JUERG BORSCHBERG, ROBERT BROUSSEAU, ALAIN DOUTHEAU, ROBERT DURAND, HAJIME KATAYAMA, RICHARD LAPALME, DOMINIQUE M. LETURC, CHUN-CHEN LIAO, FREDERICK N. MACLACHLAN, JEAN-PIERRE MAFFRAND, FABRIZIO MARAZZA, ROBERT MARTINO, CLAUDE MOREAU, LUC RUEST, LOUISELLE SAINT-LAURENT, ROGER SAINTONGE, and PIERRE SOUCY. Can. J. Chem. **68**, 153 (1990).

This paper reports several studies that were carried out to learn how to transform the dextrorotatory pentacyclic key intermediate **5** into (+)-anhydroryanodol (**6**). This transformation requires 24 steps, and takes place via the following intermediates: **5** → **11** → **19** → **34** → **36** → **39** → **144** → **150** → **6**. The preparation of the key pentacyclic intermediate **5** is reported in Parts I and II of this series.

Key words: anhydroryanodol, ryanodol, diterpene, organic synthesis, strategy.

PIERRE DESLONGCHAMPS, ANDRÉ BÉLANGER, DANIEL J. F. BERNEY, HANS-JUERG BORSCHBERG, ROBERT BROUSSEAU, ALAIN DOUTHEAU, ROBERT DURAND, HAJIME KATAYAMA, RICHARD LAPALME, DOMINIQUE M. LETURC, CHUN-CHEN LIAO, FREDERICK N. MACLACHLAN, JEAN-PIERRE MAFFRAND, FABRIZIO MARAZZA, ROBERT MARTINO, CLAUDE MOREAU, LUC RUEST, LOUISELLE SAINT-LAURENT, ROGER SAINTONGE et PIERRE SOUCY. Can. J. Chem. **68**, 153 (1990).

On rapporte plusieurs études qui ont conduit à la transformation de l'intermédiaire-clé pentacyclique optiquement actif **5** en (+)-anhydroryanodol (**6**). Cette transformation de 24 étapes fait intervenir les intermédiaires suivants : **5** → **11** → **19** → **34** → **36** → **39** → **144** → **150** → **6**. La préparation de l'intermédiaire-clé pentacyclique **5** est rapportée dans les Parties I et II de la présente série.

Mots clés : anhydroryanodol, ryanodol, diterpène, synthèse organique, stratégie.

Can. J. Chem. Downloaded from www.nrcresearchpress.com by 186.148.149.217 on 09/07/12
For personal use only.

Introduction

Part I (1) of this series of papers describes the general strategy that we have developed for the synthesis of (+)-ryanodol (**7**) (Scheme 1) via (+)-anhydroryanodol (**6**), and the finding that *o*-spirolactone dienone **1** is an excellent dissymmetrical diene, which undergoes a completely regiocontrolled Diels–Alder reaction with methyl vinyl ketone as a dienophile. Part II (2) describes our detailed investigations, which led to the discovery of a four-step synthesis (**1** + **2** → **3** → **4** →→ **5**) of the optically active dextrorotatory pentacyclic intermediate **5** starting from *o*-spirolactone dienone **1** and optically active vinyl ketone **2** (prepared from *d*-carvone). In this paper, we wish to report our studies leading to the transformation of the key pentacyclic intermediate **5** into (+)-anhydroryanodol (**6**).

The transformation of pentacyclic intermediate **5** into (+)-anhydroryanodol (**6**) requires several operations, which need to be examined in detail. First, comparison of the carbon structure of pentacyclic intermediate **5** with that of anhydroryanodol (**6**) revealed that the former contains all but one carbon atom to construct the latter, since it will be necessary to introduce one methyl group at C_9. There is, however, one extra carbon atom in intermediate **5**, i.e., that of the aldehyde functional group linked at C_3, which must be degraded into a C_3 *endo* alcohol. In addition to the methylation step at C_9 and the aldehyde degradation step at C_3, it is necessary to carry out a series of functional group transformations to produce anhydroryanodol (**6**) from intermediate **5**. These transformations are discussed next.

Using the carbonyl group at C_{17}, it will be necessary to discover a fragmentation process for the C_{15}—C_{17} bond that will leave functional groups at C_{15} and C_{17} respectively. The functional group left at C_{17} can then either be simply reduced to give a methyl group or can be used to produce the tetrasubstituted olefin at C_1—C_2 while generating the C_{17} methyl group by using a functional group transfer methodology. This second proposal is of course more profitable than the first one and it will be shown that we could very efficiently reduce this strategy to practice. Indeed, by utilizing a functional group at C_{17} it was possible to produce an *exo* olefin, between C_1 and C_{17}, which was then isomerized to simultaneously generate the endocyclic olefin between C_1 and C_2 and the C_{17} methyl group. Thus, alternative approaches to use a functional group at C_3 to introduce a degree of unsaturation between C_1 and C_2 were not seriously considered. It will, however, be shown that the functional group at C_3 was used to facilitate the formation of the exocyclic C_1—C_{17} olefin and its concomitant isomerization to the endocyclic position.

The functional group left at C_{15} from the C_{15}—C_{17} fragmentation process must be used to induce the formation of the lactone ring of anhydroryanodol (**6**). Originally, it was anticipated that the desired oxygen insertion between C_{11} and C_{15} would be carried out by a Baeyer–Villiger oxidation of a ketone function at C_{15}. It will, however, be shown that the oxidation of

[1]Author to whom correspondence may be addressed.

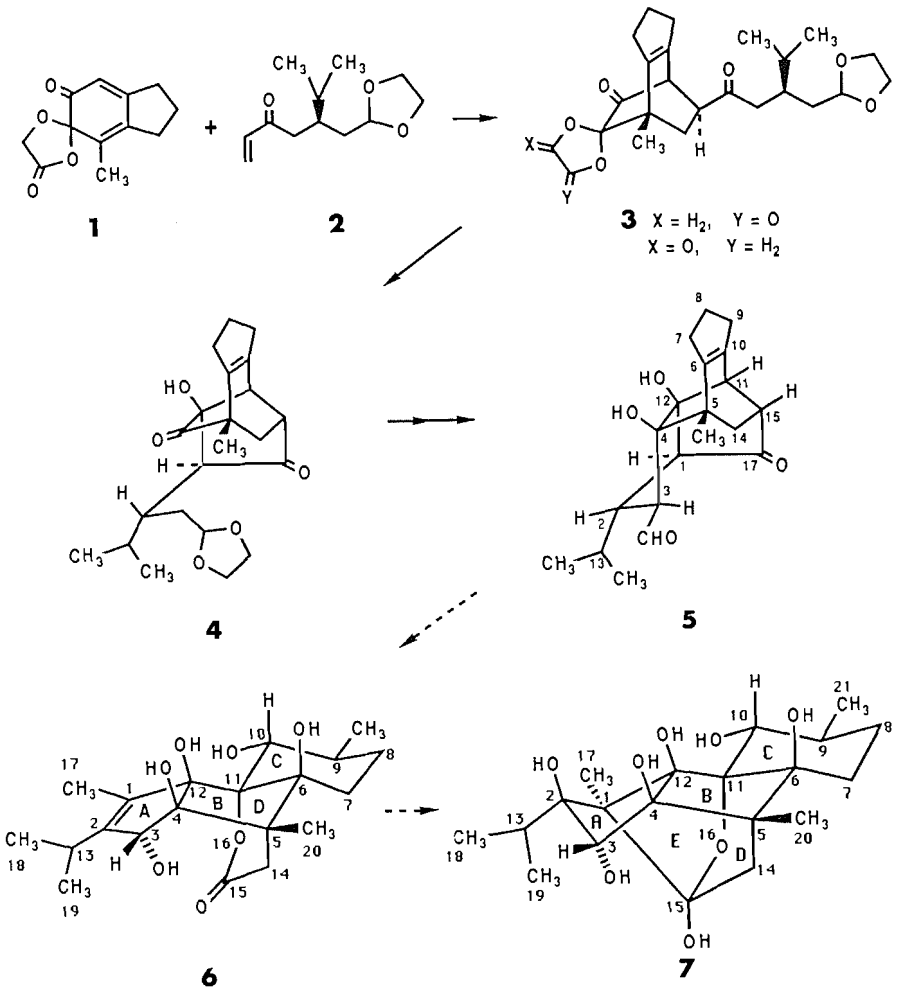

SCHEME 1

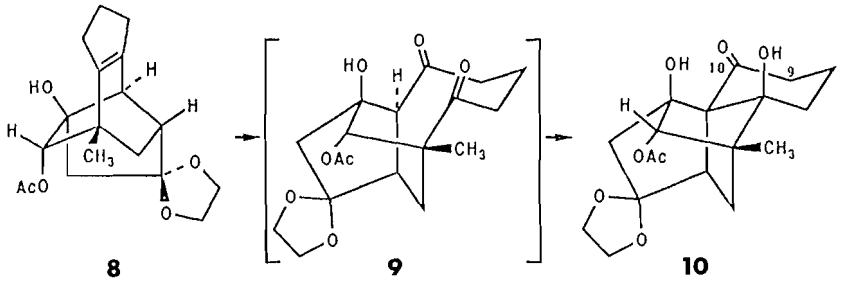

SCHEME 2

the C_{15} ketone function was attempted on several occasions, but was found to be completely unsuccessful. Consequently, a more lengthy procedure had to be conceived, which involves, first, a cleavage of the C_{11}—C_{15} bond, followed by lactone formation as a second step at a later stage.

To complete the synthesis, it was also necessary to oxidatively cleave the C_6—C_{10} tetrasubstituted olefin to generate *in situ* a macrocyclic diketone that would undergo a transannular aldol condensation producing simultaneously rings B and C as well as the hydroxyl group at C_6 and a carbonyl group at C_{10}. The feasibility of this important key transformation, which gives an entry into the anhydroryanodol skeleton from the oxidative cleavage of a tricyclic precursor containing a bicyclo[2.2.2]octene unit, had previously been verified using the model compound **8** (Scheme 2). Indeed, this compound was successively transformed into **10** via the intermediate formation of macrocyclic diketone **9** as described in Part II. The completion of the synthesis of anhydroryanodol would then be carried out by using the carbonyl group at C_{10} to introduce the methyl group at C_9 and to generate the secondary equatorial alcohol at C_{10} by reduction.

It can therefore be seen from the above analysis that several operations had to be performed to transform the key pentacyclic intermediate **5** into anhydroryanodol (**6**). In summary, these operations were (a) cleavage of the C_{15}—C_{17} bond, (b) introduction of a tetrasubstituted olefin between C_1 and C_2, (c) modification at C_{17} to yield a methyl group, (d) insertion of an oxygen atom between C_{11} and C_{15} to produce the lactone ring,

Can. J. Chem. Downloaded from www.nrcresearchpress.com by 186.148.149.217 on 09/07/12
For personal use only.

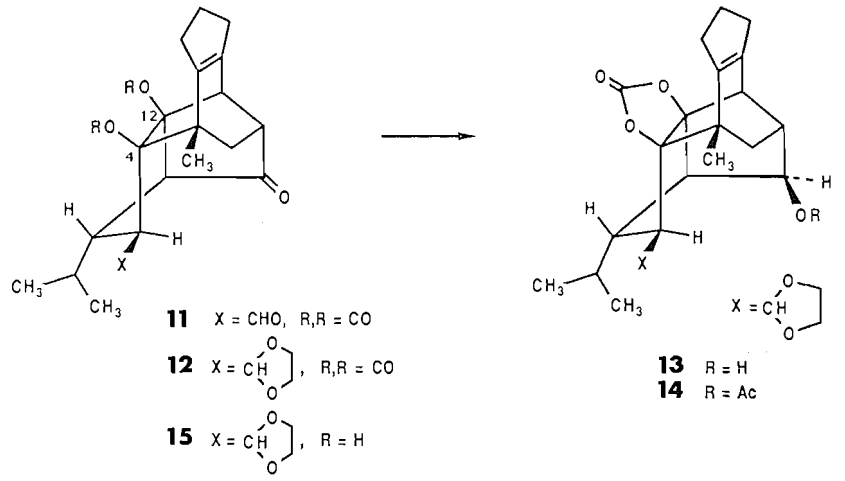

SCHEME 3

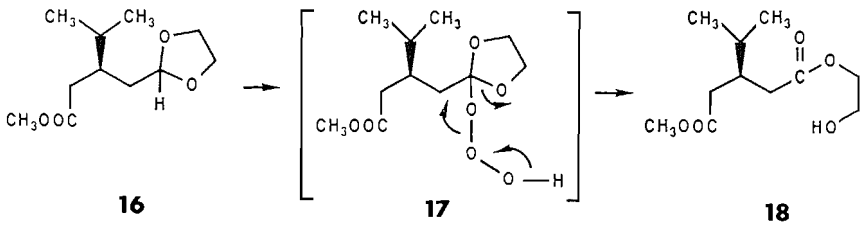

SCHEME 4

(e) oxidative cleavage of the double bond between C_6 and C_{10} and transannular aldol condensation, (f) introduction of a methyl group at C_9, (g) reduction of the newly generated ketone function at C_{10} into an equatorial alcohol, and (h) conversion of the aldehyde group at C_3 into an *endo* hydroxyl group.

Appropriate reagents and reaction conditions had to be found to carry out these various operations. Also, *it was important to discover the most convenient order* in which these transformations should be carried out from intermediate **5**, starting either from the aldehyde at C_3, the C_6—C_{10} olefin, or the ketone function at C_{17}. Among the above operations, some were considered more important than others, either because we were not completely sure how to realize them or because we had almost one unique way of achieving them. Operations (a) (cleavage of the C_{15}—C_{17} bond) and (d) (lactone formation) were classified in the former category whereas operation (e) (oxidative cleavage of olefin and transannular aldol condensation) was in the latter. We were convinced that there were several alternative solutions for solving the remaining chemical operations. Studies were therefore initiated to find acceptable pathways to solve operations (a), (d), and (e) first.

Oxidative cleavage and transannular aldol condensation (step (e))

Operation (e) was a great success in our model studies using compound **8** and we were confident that it would work equally well in the real series. However, we were most interested in verifying this and studies with the pentacyclic intermediate **5** were first started in this direction. The intermediate **5** was converted into the five-membered carbonate derivative **11** (cf. Part II) to prevent oxidative cleavage of the C_4—C_{12} *gem*-diol function. It was also decided that the aliphatic aldehyde function needs to be protected before attempting the oxidative cleavage of the tetrasubstituted olefin. The aldehyde **11** was therefore transformed into the dioxolane acetal **12** (Scheme 3) with ethylene glycol under standard acidic conditions (benzene, PTSOH).

The ozonolysis of **12** using a reductive work-up was carried out under conditions similar to those previously used in the model experiments. The starting material **12** was consumed rapidly but it gave a complex mixture of various products, as judged by thin-layer chromatography, from which no specific compound could be isolated. Furthermore, and to our complete dismay, various attempts at modification of the experimental conditions did not lead to further improvement. Being ignorant of the cause of this unpleasant and unexpected result, and being convinced that the dioxolane acetal was completely inert toward ozone, other derivatives of **12** were prepared by modification either of the C_{17} carbonyl group or of the 5-membered carbonate ring. Reduction ($NaBH_4$) of **12** gave the corresponding *endo* alcohol **13**, which was also converted to the acetate **14** (Ac_2O, Et_3N, DMAP). Also, basic hydrolysis of **12** gave the corresponding diol acetal **15**.

The oxidative cleavage of compounds **13**–**15** with ozone was also unsuccessful, yielding again an ill-defined mixture of products. Examination of the various reaction mixtures by ^1H nmr spectroscopy revealed that the characteristic doublet for the methine hydrogen of the dioxolane acetal had disappeared, and this suggested that, contrary to our expectation, this protecting group might not have survived the ozonolysis reaction. We therefore had to verify this assertion and submitted to ozonolysis the readily available acetal **16** (Scheme 4), an intermediate used in the preparation of optically active dienophile **2**. To our great surprise, compound **16** reacted with one equivalent of ozone, even at −78°C, producing the diester **18** quantitatively!

Thus, completely unexpectedly, we had discovered (3) a new reaction, which we decided to investigate in detail. Evidence was provided (4, 5) that this reaction proceeds via the insertion of ozone in the C—H bond of the acetal function, producing a hydrotrioxide tetrahedral intermediate (cf. **17**), which decom-

Can. J. Chem. Downloaded from www.nrcresearchpress.com by 186.148.149.217 on 09/07/12
For personal use only.

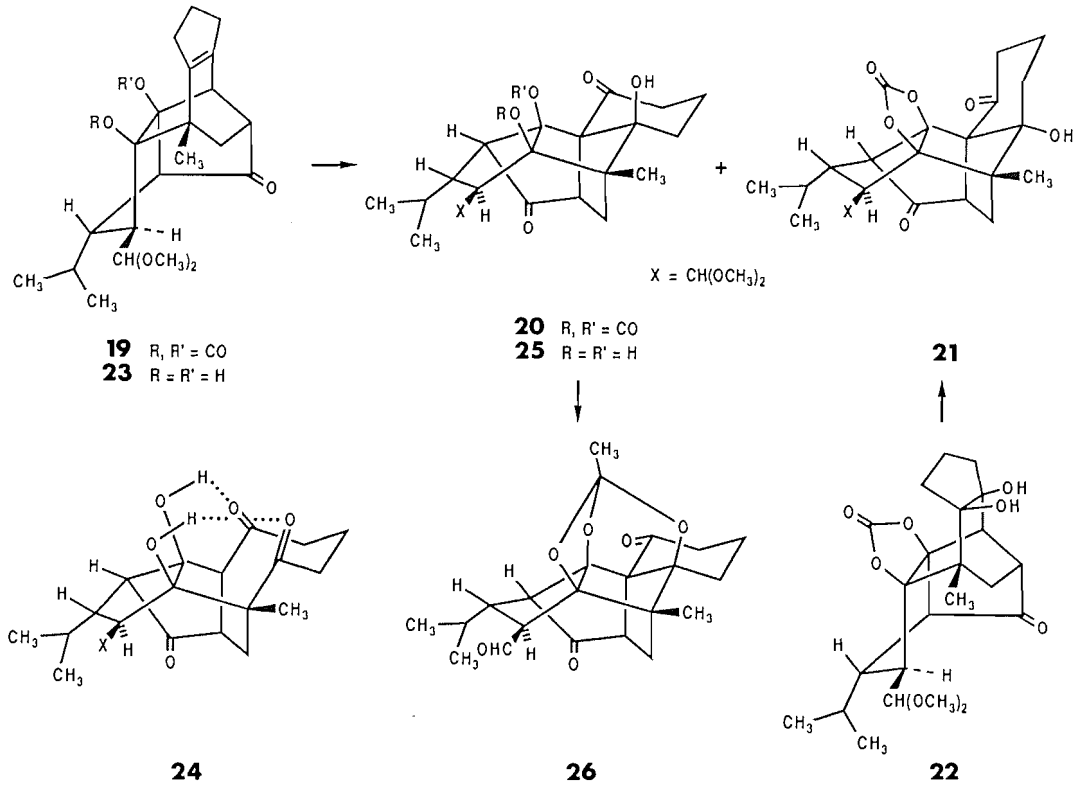

SCHEME 5

poses to yield the corresponding hydroxyester and molecular oxygen. We are now convinced that the ill-defined mixtures of products were obtained from compounds **13–15** because ozone reacted first with the dioxolane acetal, generating singlet oxygen (6) that must have been trapped by the tetrasubstituted olefin, producing unstable peroxide-containing compounds that underwent various decompositions.

Further studies (7, 8) of the ozonolysis reaction led us to discover that the ozone insertion is conformation dependent and is governed by stereoelectronic effects that come from the orientation of the nonbonded electron pairs of the oxygen atoms of the acetal function. It was also observed that the fragmentation of the resulting tetrahedral hydrotrioxide intermediates is also conformation dependent and the results could also be rationalized on the basis of stereoelectronic effects. Further studies (9, 10) on the stereocontrolled fragmentation of various tetrahedral intermediates were carried out in our laboratory and this work led us to propose a new general theory for the understanding of hydrolytic processes, which is primarily based on stereoelectronic principles (11–13). Consequently, this completely unexpected annoying result led to the discovery of a rather fruitful event!

In the course of the study on the ozonolysis of acetals, we had also found that by comparison with cyclic dioxolane acetals, dialkoxy acetals were oxidized at a much slower rate, and on that basis, a dimethoxy acetal could likely be used as a protecting group for the aldehyde function. The dimethoxyacetal **19** (Scheme 5) was therefore prepared from the pentacyclic aldehyde **11** under standard conditions (CH_3OH, $HC(OCH_3)_3$, PTSOH), and submitted to the ozonolysis reaction (O_3, CH_3OH, $(CH_3)_2S$). Contrary to the previous ozonolysis experiments, a very clean reaction took place, producing 95% yield of a mixture of the isomeric aldol products **20** and **21** in a 1:2 ratio. It was also observed that if the same ozonolysis reaction was carried out in the presence of an equivalent of *p*-toluenesulfonic acid, the proportion of the desired isomer **20** was raised (7:3 ratio). Since isomers **20** and **21** did not equilibrate under these conditions, the presence of acid must favor kinetically the formation of the desired isomer **20**. Interestingly, hydroxylation of olefin **19** with osmium tetroxide gave a *cis* diol assigned structure **22**, which upon cleavage with periodic acid gave exclusively the undesired aldol isomer **21**.

The ozonolysis of the diol olefin **23**, which was obtained from the basic hydrolysis of **19**, was also investigated. It was hoped that the presence of the diol function would create internal hydrogen bonding with the carbonyl groups in the diketone intermediate, favoring conformation **24**, which should lead to the desired aldol product **25**. The reaction was carried out and produced only the desired product **25** as anticipated, but the yield was only 28%. This low yield was explained by the presence of the vicinal diol, a grouping known to be sensitive to oxidative reagents. The structure of **25** was rigorously established by its conversion into the orthoacetate aldehyde **26** upon treatment with acetic anhydride containing perchloric acid followed by mild basic hydrolysis (Na_2CO_3, H_2O).[2]

In another series of experiments, mild acetylation (Ac_2O, AcONa) of pentacyclic diol aldehyde **5** gave a monoacetate assigned structure **27** (Scheme 6), which was also investigated. This compound was interesting because the aldehyde was left unprotected; also, one of the tertiary hydroxyl groups was available to direct the transannular aldol condensation (via intramolecular hydrogen bonding), and the presence of the acetate

[2]In acidic medium, **25** is first converted into the enol acetate (of the aldehyde at C_3) of compound **26**, which is then transformed under basic conditions into the orthoacetate aldehyde product **26**.

Can. J. Chem. Downloaded from www.nrcresearchpress.com by 186.148.149.217 on 09/07/12
For personal use only.

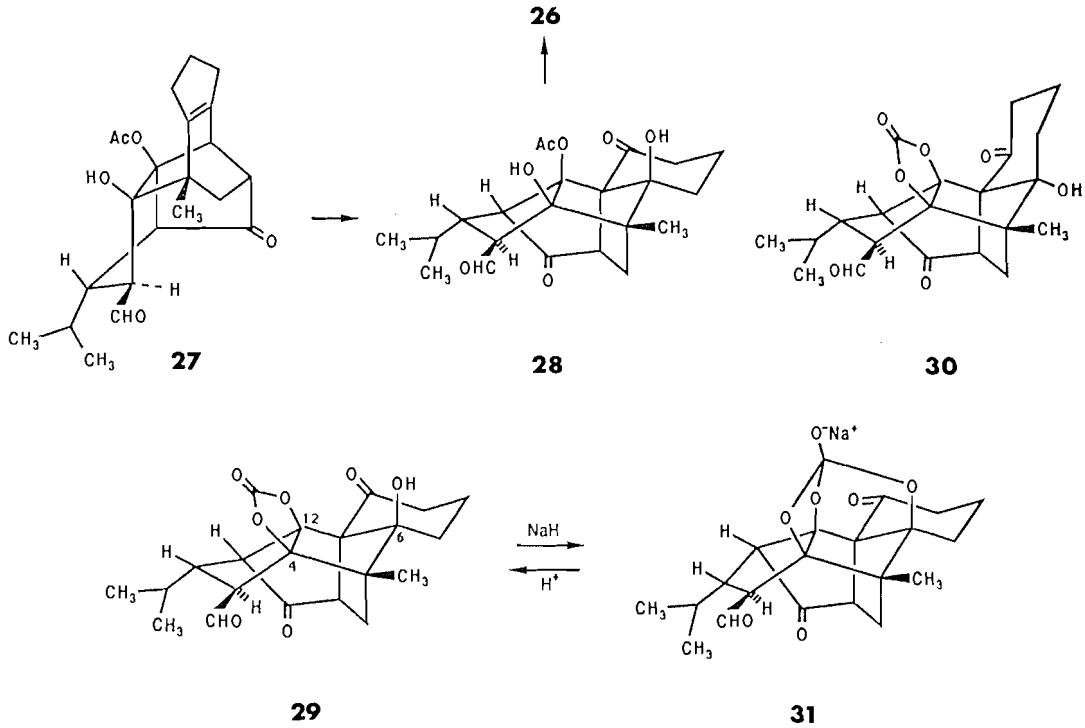

SCHEME 6

group was protecting the diol function from further oxidation. Ozonolysis of **27** gave a moderate 50% yield of monoacetate **28**, which on simple heating in benzene afforded the previously described orthoacetate **26** in 80% yield.

Formation of orthoacetate derivatives had previously been used in the chemical elucidation of anhydroryanodol (14) to establish the relative configuration for the tertiary alcohols at C_4, C_6, and C_{12}. In our work, the formation of orthoacetate derivative **26** rigorously established the stereochemistry of the desired aldol condensation products (i.e., **25** and **28**). There was also the possibility of using the orthoester as a protecting group. We found, however, that this group was extremely resistant to hydrolysis. For instance, on attempted acid hydrolysis with 50% sulfuric acid, compound **26** was completely recovered. So we learned that if the triol needs protection, an orthoacetate cannot be used.

We also learned from the oxidation of compound **27** that the aliphatic aldehyde does not need protection during the course of the oxidative cleavage of the tetrasubstituted olefin. This was further verified by treating the pentacyclic olefin **11** with ozone. Under neutral conditions, a 70% yield of **29** and **30** was obtained in a 1:2 ratio; under acidic conditions, the yield was the same but the ratio changed to 5:2. We thus realized that it is not absolutely necessary to protect the aldehyde function. On the other hand, had we not carried out the above investigation, we would not have discovered the ozonolysis reaction of acetals that led to the stereoelectronic theory!

Another interesting observation was made while trying to prove the relative stereochemistry of the isomeric aldol products **29** and **30**. Using isomer **29**, it was found that upon addition of sodium hydride in anhydrous tetrahydrofuran, the infrared bands at 3540 and 1825 cm^{-1} responsible for the tertiary alcohol and the five-membered ring carbonate disappeared. On addition of acid, these absorptions reappeared on the spectrum. This was explained by the formation of the hemi-orthocarbonate sodium salt **31**. This experiment thus provided a rigorous proof of stereochemistry for the aldol product **29** and gave us an indication on how to develop reversible protecting groups for the triol grouping at C_4, C_6, and C_{12} (*vide infra*).

We were also satisfied with the above results that demonstrated that the oxidative cleavage and transannular aldol condensation could easily take place on the pentacyclic system, and our attention was turned to the cleavage of the C_{15}—C_{17} bond followed by the insertion of an oxygen atom between C_{11} and C_{15} to produce the lactone of anhydroryanodol, i.e., operations (a) and (d) as previously classified.

Cleavage of the C_{15}—C_{17} bond (step (a)) and synthesis of intermediates 37, 38, and 39

The cleavage of the C_{15}—C_{17} bond was studied using two different reactions, the Beckmann rearrangement and the Baeyer–Villiger oxidation. In the first study, the ketone **19** was converted into the oxime derivative **32** (Scheme 7), which was mesylated and subjected to rearrangement by refluxing in dioxane–water. This provided one major product isolated in 70% yield, the structure of which corresponds to pentacyclic lactam **33**. By nmr spectroscopy, after deuterium exchange, the methine-bearing nitrogen atom appears at δ 3.93 as a doublet (J = 3.5 Hz). This multiplicity is possible for structure **33**. Thus, the undesired C_1—C_{17} cleavage had taken place and this approach was not continued further.

The second study, using the Baeyer–Villiger rearrangement, proved to be more successful. Oxidation of compound **19** with 40% peracetic acid gave a good yield of isomeric epoxylactones **34** and **35** in a 85:15 ratio. These compounds were easily distinguished by the multiplicity of their lactonic proton in nmr. Lactone **34** shows a doublet of doublets of doublets (J = 4.5, 2.5, and 9.8 Hz) at δ 4.60 for H-C_{15} and lactone **35** shows a doublet (J = 3.3 Hz) at δ 4.89 for H-C_1. Use of other peracids like *m*-chloroperbenzoic or trifluoroperacetic led to lower yields and a ratio less in favor of the desired epoxylactone **34**. The mixture of **34** and **35** was submitted to retroepoxidation condi-

Can. J. Chem. Downloaded from www.nrcresearchpress.com by 186.148.149.217 on 09/07/12
For personal use only.

Can. J. Chem. Downloaded from www.nrcresearchpress.com by 186.148.149.217 on 09/07/12
For personal use only.

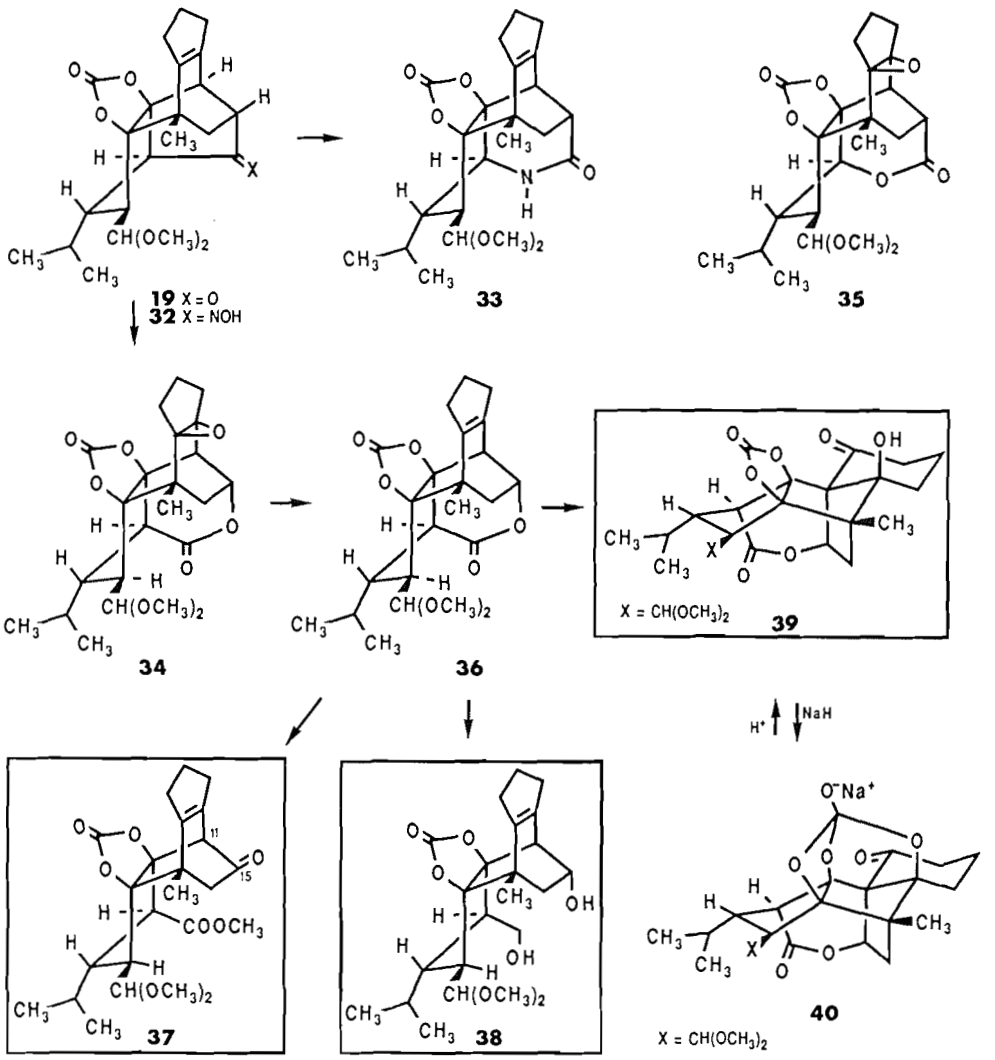

SCHEME 7

tions (WCl_6, 3BuLi in THF) (15), and the desired pentacyclic olefinic lactone **36** was obtained pure (chromatography followed by crystallization) with an overall yield of 75% from **19**.

The desired C_{15}—C_{17} cleavage had taken place with the formation of lactone **36**. The remaining chemical investigations were all carried out starting from this key intermediate from which three different type of products were obtained, the ketoester **37**, the diol **38**, and the transannular aldol product **39**. The chemical reactivity of each of these products was then studied in some detail to find the most appropriate method of elaborating the correct functionalities of ring A, and to learn when it would be most convenient to carry out step (e) (oxidative cleavage and transannular aldol condensation). These studies were also essential to discover a method for step (d) (oxygen insertion between C_{11} and C_{15}) to produce the lactone ring of anhydroryanodol.

The ketoester **37** was obtained in 74% yield from pentacyclic lactone **36** using the following three-step procedure: (a) selective hydrolysis of the lactone ring of **36** using lithium hydroxide in a mixture of dimethoxyethane and water, (b) esterification of the resulting hydroxycarboxylic acid salt with trimethyloxonium tetrafluoroborate (16) in the same aqueous medium (17, 18), and (c) oxidation of the secondary alcohol at C_{15} with Collins reagent (19). On the other hand, the diol **38** was conveniently obtained in a single operation by selective reduction of lactone **36** with lithium borohydride in tetrahydrofuran. Finally and most interestingly, the ozonolysis (O_3, PTSOH, CH_3OH; $(CH_3)_2S$) of pentacyclic olefin lactone **36** gave the desired transannular aldol isomer **39** in an impressive yield (>95%). The stereochemistry of aldol product **39** was again established by observing the formation of the hemi-orthocarbonate sodium salt **40** with sodium hydride in anhydrous tetrahydrofuran. It was also observed that, upon acidification, salt **40** gave back compound **39** as expected.

Studies with ketoester 37

The successful formation of ketoester **37** gave us our first opportunity to try the oxygen insertion between C_{11} and C_{15}. However, all attempts to carry out the Baeyer–Villiger reaction (step (d)) on ketoester **37** failed. The epoxyketoester **41** (Scheme 8) could be easily prepared from **37** under the Baeyer–Villiger reaction conditions, but it could not not be further transformed into the desired lactone. The poor reactivity of compound **41** towards the Baeyer–Villiger reaction is presumably due, at least in part, to the steric hindrance caused on one side of the carbonyl group by the oxirane ring, and by the carbomethoxy group on the other. Attempts were then made to epimerize the *endo* carbomethoxy group at C_1 in order to reduce

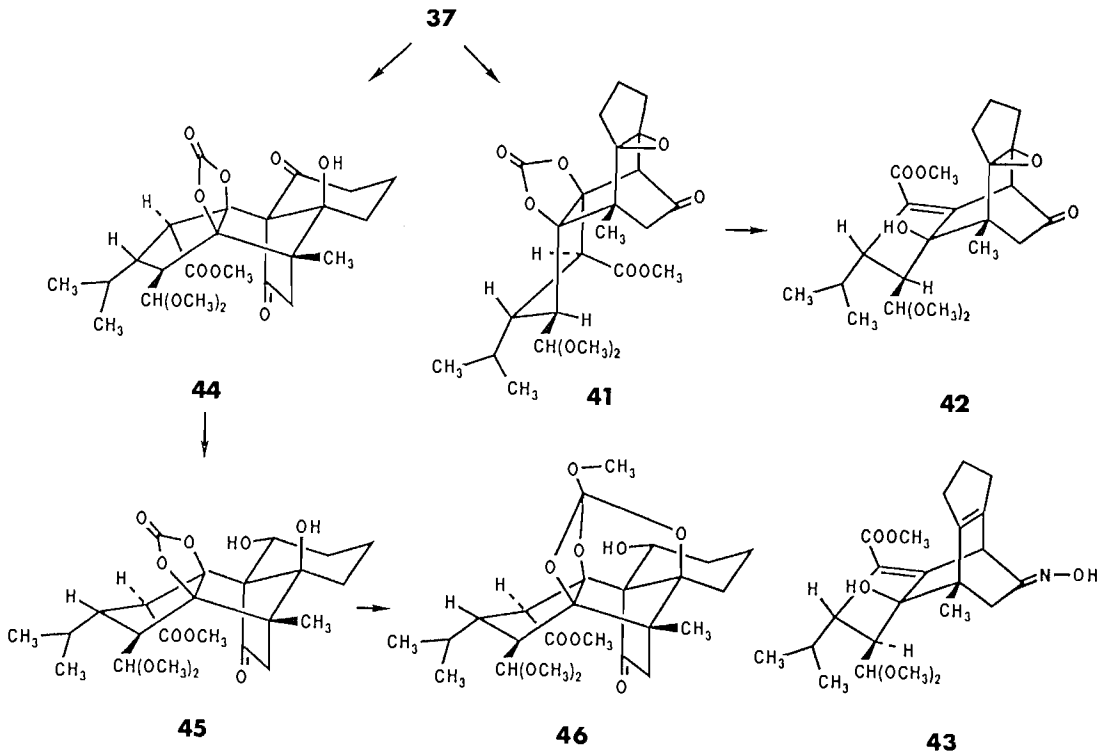

SCHEME 8

the steric hindrance of the C_{15} carbonyl group. However, no isomerization was observed with potassium *tert*-butoxide in *tert*-butanol and treatment of ketoester **37** with 1,5-diazabicyclo[4.3.0]non-5-ene (DBN) in dimethoxyethane led to the undesired elimination product, epoxyester **42**. Even the formation of the oxime derivative of **37** was not successful under mild conditions: the oxime isolated was that of the conjugated ester, i.e., compound **43**, indicating that the elimination of the carbonate was a rather facile process under those conditions.

Ketoester **37** was then submitted to the ozonolysis reaction (O_3, CH_2Cl_2–CH_3OH, PTSOH (cat); $(Me)_2S$) and it produced the desired aldol product **44** in 80% yield. Selective reduction of **44** with sodium borohydride gave dihydroxyketone **45** having an equatorial alcohol in ring C. Upon basic treatment (NaH, THF) compound **45** formed the corresponding hemi-orthocarbonic acid sodium salt, which gave back **45** by the addition of acid. Moreover, it was discovered that compound **45** reacts smoothly with diazomethane in chloroform–ether to provide the stable methyl orthocarbonate **46** in good yield. The formation of **46** suggested that alkyl orthocarbonate could be used to protect the triol grouping if that becomes necessary later on. Again, the Baeyer–Villiger oxidation was attempted with compounds **45** and **46**, but no reaction was observed. The poor reactivity of **45** and **46** towards the Baeyer–Villiger reaction is not surprising since molecular models clearly showed that the C_{15} carbonyl group is even more hindered in these two compounds than in epoxyketoester **41**. This is confirmed by the fact that under the conditions used to form the oxime derivative **43** from ketoester **37**, no reaction was observed with **45** and **46**, starting material being recovered in both cases. No further experiment was then carried out starting from ketoester **37**.

Studies with pentacyclic carbonate diol 38

One of the first experiments carried out with diol **38** was the Jones oxidation, which led to the isolation of hemi-ketal **47** in 80% yield (Scheme 9). This result is readily explained because (a) a secondary alcohol is usually oxidized faster than a primary one (28) and (b) as soon as the ketone is produced at C_{15}, the remaining primary alcohol forms the hemi-ketal and is thus protected from oxidation.

Further oxidation of hemi-ketal **47** was next investigated, and it was found that oxidation of **47** with ceric ammonium nitrate (20, 21) yielded the interesting bridged eight-membered lactone **48**. This compound was very interesting because the desired C_{11}—C_{15} bond cleavage, half of step (d), was being achieved by using this new oxidative cleavage reaction. The next step was to find a method to form the lactone ring that corresponds to that found in anhydroryanodol (cf. → **52**). Basic hydrolysis (LiOH in DME–H_2O) of **48** gave the corresponding hydroxycarboxylic acid **49**. This compound was further characterized by forming the acetate carboxylic acid **50** with acetic anhydride and pyridine, and the hydroxy methyl ester **51** with diazomethane. It was hoped that a treatment of the acetate carboxylic acid **50** with a strong proton source, such as *p*-toluenesulfonic acid in benzene, would result in the formation of the desired lactone **52**. However, the product formed under these conditions was the methoxylactone **53**. This result showed that, under these conditions, the lactonization of the carboxylic acid chain with the enol ether at C_3 (presumably formed *in situ* by the elimination of methanol from the dimethoxyacetal grouping) was more facile. It is in principle possible to avoid this undesired lactonization process either by changing the reaction conditions or by modification of the dimethoxyacetal into a more appropriate protecting group. This type of investigation was not continued further. However, it will be seen that an analogous C_{11}—C_{15} fragmentation involving the formation of a bridged eight-membered lactone was eventually used in the final sequence.

Two additional experiments within this particular series are worth reporting, both involving the oxidative cleavage – transannular aldol condensation process. Ozonolysis (O_3, CH_2Cl_2–

Can. J. Chem. Downloaded from www.nrcresearchpress.com by 186.148.149.217 on 09/07/12
For personal use only.

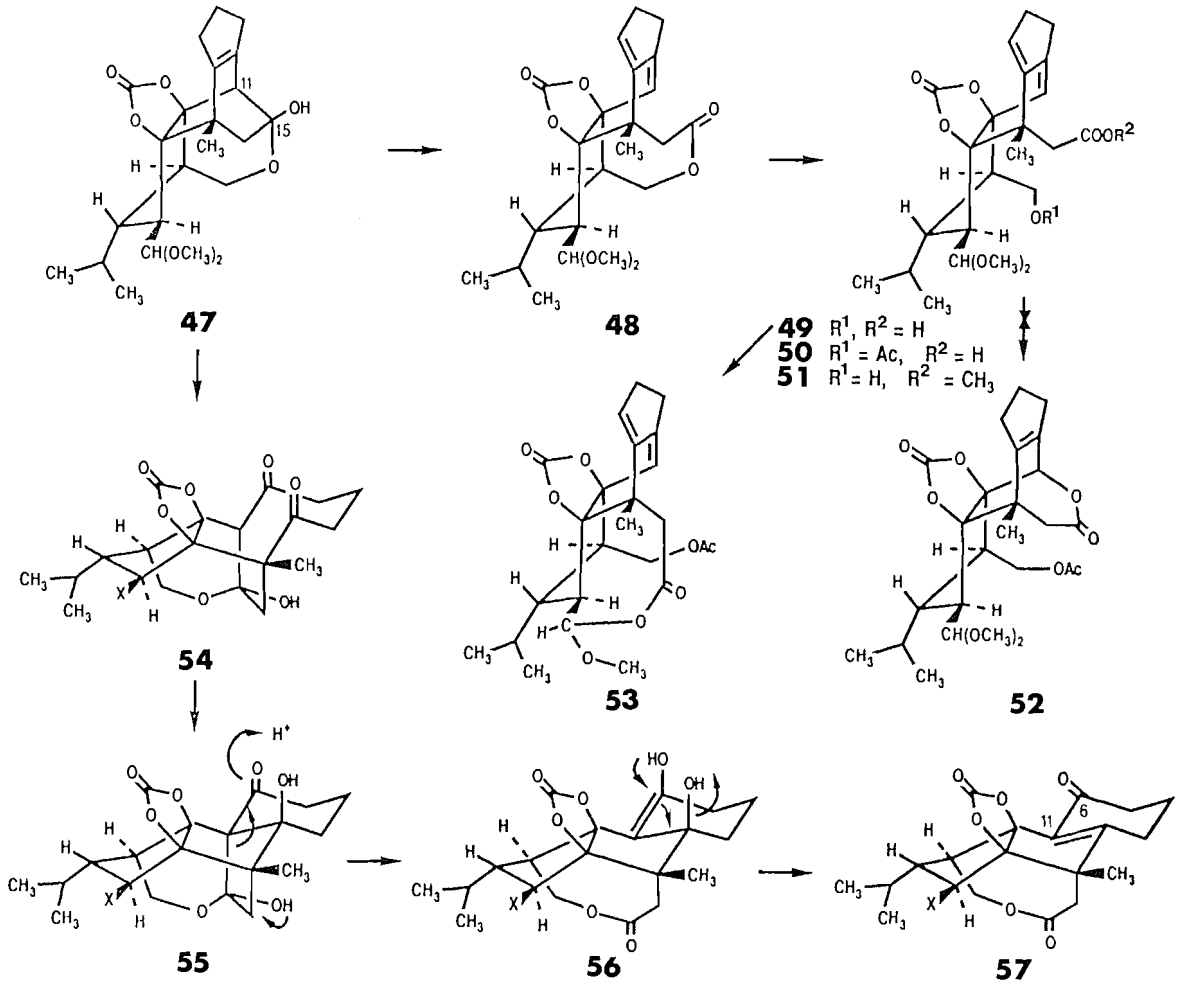

SCHEME 9

CH_3OH, PTSOH; $(CH_3)_2S$) of hemi-ketal **47** provided directly the lactone product **57** (75% yield) having a general skeleton corresponding to that of anhydroryanodol (**6**). This remarkable transformation can be explained via the intermediate formation of aldol product **55** via diketone **54**, which must have gone through a retro-Claisen fragmentation followed by the elimination of the OH group at C_6 (cf. **47** → **54** →→→ **57**) to produce conjugated enone **57**. In principle, *trans* hydroxylation at C_6 and C_{11} on **57** should yield a useful synthetic intermediate for the synthesis of anhydroryanodol; however, all attempts to realize such conversion were unsuccessful.

Olefin diol **38** was also treated with ozone under the above conditions and the tricyclic enone aldehyde **60** (Scheme 10) was isolated in moderate yield. The expected product should have had structure **58**; however, the formation of aldehyde **60** can be readily explained by a retro-aldol condensation of **58** followed by carbonate elimination as shown. Thus, contrary to the previous fragmentation process **47** → **57**, the carbonate group at C_{12} rather than the hydroxyl group at C_6 was eliminated. This result is easily understood because a carbonate oxygen is a much better leaving group than a hydroxyl group and step **59** → **60** is then not surprising. In the previous fragmentation **47** → **57**, the hydroxyl group at C_6 was preferably eliminated (**56** → **57**) because the ejection of the carbonate oxygen would have generated a highly strained C_{11}—C_{12} olefin (cf. **61**). Indeed, molecular models clearly indicate that this olefin is quite strained when the bridged eight-membered lactone ring is present as in **61**.

In another investigation (Scheme 11), diol **38** was selectively converted into a mono-*p*-nitrobenzoate, which was oxidized with Collins reagent (19) to yield keto-*p*-nitrobenzoate **62** (>95% yield) from which several important studies were undertaken. The *p*-nitrobenzoate ester was chosen in preference to an acetate, a benzoate, a methyl carbonate, or a mesylate (all of these have been prepared) protecting group for the following reasons: The selective esterification of the primary alcohol with *p*-nitrobenzoyl chloride in pyridine took place in high yield. Also, the various *p*-nitrobenzoate intermediates were stable compounds, and yet this group became a relatively good leaving group when it became necessary to generate the *exo* olefin (*vide infra*).

One of the main studies with *p*-nitrobenzoate **62** was the development of an appropriate sequence for the elaboration of the correct functionalization of ring A of anhydroryanodol (**6**). This is discussed next.

Functionalization of ring A (steps (b), (c), and (h))

Keto-*p*-nitrobenzoate **62** was converted into the epoxide **63** by treatment with *m*-chloroperbenzoic acid. As in the previous cases, epoxide **63** did not undergo the Baeyer–Villiger rearrangement, but it turned out to be a useful compound to elaborate ring A because the oxirane ring served to prevent the oxidative cleavage of the tetrasubstituted olefin in the course of the degradation of the dimethylacetal at C_3.

When compound **63** was heated to reflux in benzene contain-

Can. J. Chem. Downloaded from www.nrcresearchpress.com by 186.148.149.217 on 09/07/12
For personal use only.

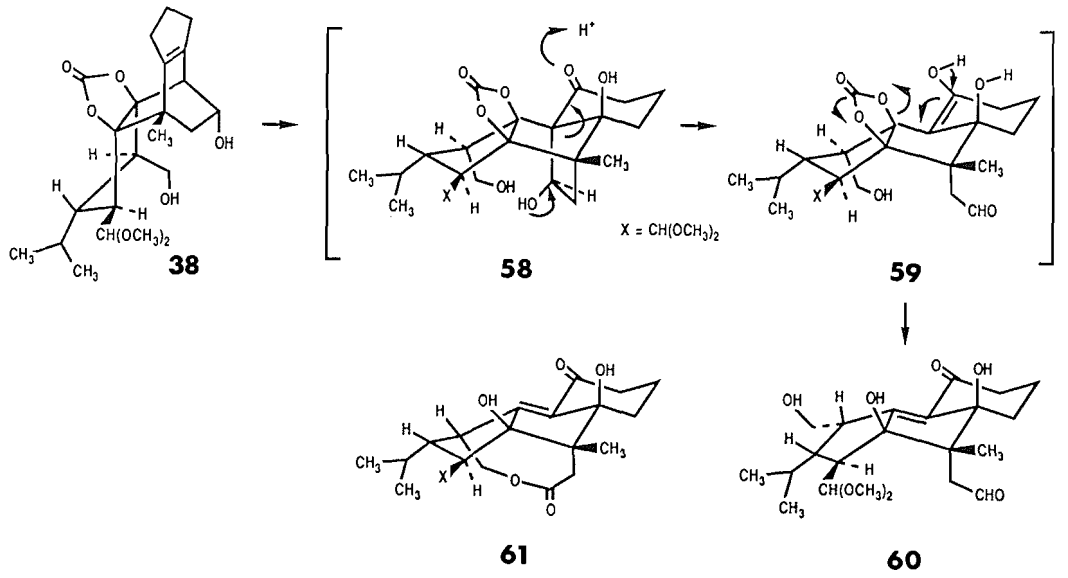

SCHEME 10

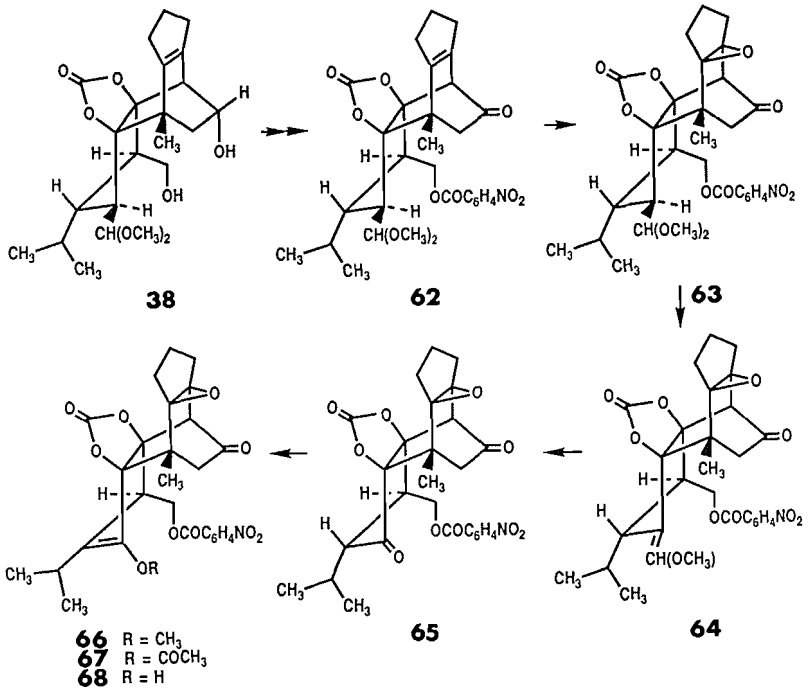

SCHEME 11

ing a catalytic amount of *p*-toluenesulfonic acid, there was obtained a mixture of isomeric enol ethers **64**, which were converted into norketone **65** (90% yield from **63**) by reaction with ozone. It was then discovered that norketone **65** reacted smoothly with diazomethane in ether at room temperature within a few hours, producing the endocyclic enol ether **66**. This smooth and unexpected reaction indicates that the unactivated five-membered ketone **65** must undergo enolization very readily. The easy formation of enol acetate derivative **67** from ketone **65** under mild conditions (CH_3COONa, $(CH_3CO)_2O$, 90°C, 1 h) further illustrates this facile enolization, and we suggest that steric strain might be responsible for this unusual reactivity. Indeed, molecular models show that the isopropyl group in **65** is quite severely hindered (raising the energy level of **65**) and that this steric repulsion is completely released in the corresponding enol **68**.

Reaction of enol ether **66** with 1,5-diazabicyclo[4.3.0]non-5-ene (DBN) in refluxing benzene afforded dienol ether **69** (76% yield from **65** (Scheme 12)). Under similar conditions, enol acetate **67** gave directly the enone **71** (65% yield from **65**). The absence of the expected dienol acetate **70** from **67** was explained by proposing that DBN should be basic enough to generate the enolate anion of the acetate grouping, which could then cleave to form ketene and the enolate anion of enone **71**. The facile elimination of the *p*-nitrobenzoate ester, which is a relatively poor leaving group, is likely due to the fact that the hydrogen at C_1 is allylic in compounds **66** and **67**.

The retroepoxidation step (WCl_6, 3BuLi in THF) (15) was carried out on epoxide **69** to give the corresponding olefin **72**, which was then converted into the desired enone **73** with boron trifluoride etherate, completing the appropriate functionalization of ring A of anhydroryanodol (**6**). Once the pentacyclic

Can. J. Chem. Downloaded from www.nrcresearchpress.com by 186.148.149.217 on 09/07/12
For personal use only.

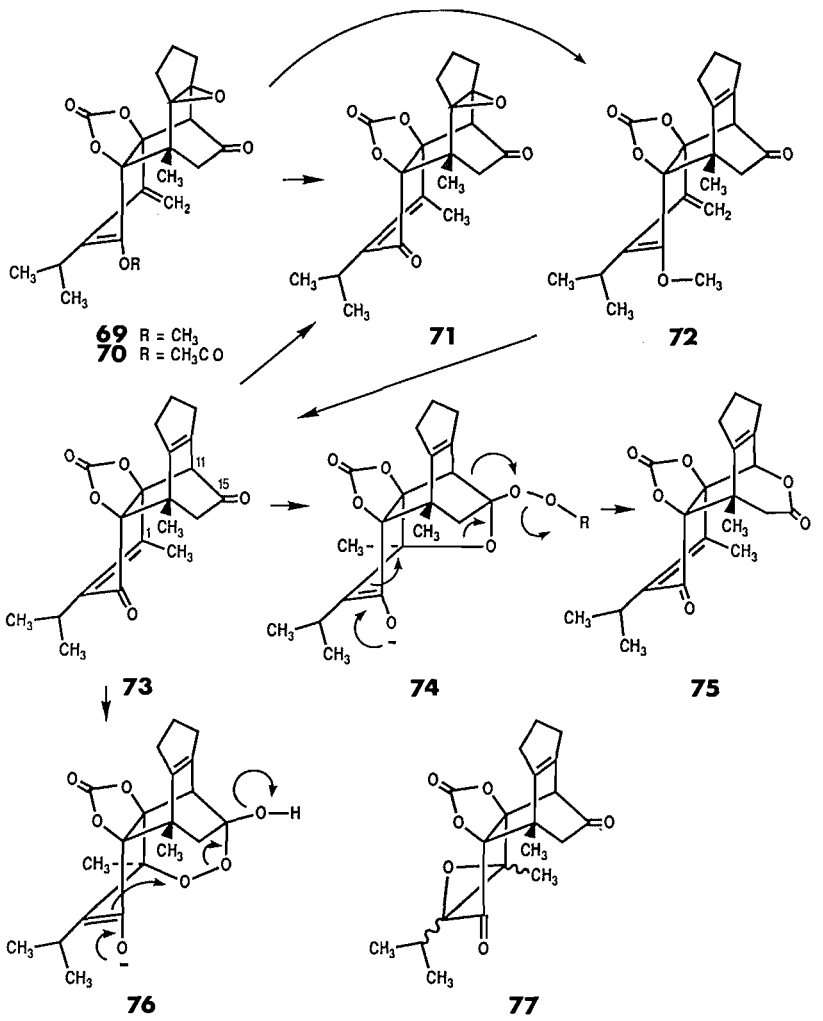

SCHEME 12

enone olefin **73** was secured, we had great hope that we could successfully accomplish step (d), i.e., the insertion of an oxygen atom between C_{11} and C_{15}. This was based on the fact that the carbonyl group at C_{15} is now much less hindered than in previous examples because C_1 is sp^2 hybridized. It could also be anticipated that the presence of an enone in ring A might activate the carbonyl group at C_{15} towards nucleophilic reagents. Indeed, it was plausible that the required intermediate for the Baeyer–Villiger oxidation **73** → **75** would form easily because it would exist in the trapped form **74**.

Treatment of enone **73** with trifluoroperacetic acid gave epoxyenone **71**, previously obtained from enol acetate **70**. Epoxyenone **71** proved to be completely inert toward various peracids and the desired Baeyer–Villiger oxidation could not be realized. Also, attempts to effect the Baeyer–Villiger rearrangement under basic conditions failed. For instance, enone **73** reacted under basic conditions with hydrogen peroxide to give α,β-epoxyketone **77** of undetermined configuration. It is possible that the epoxide has the α-configuration, which would be the result of the preferred formation of peroxide intermediate **76**. There are precedents in the literature for similar epoxidation being directed by a neighboring carbonyl group (22). However, the exact stereochemistry of the epoxide **77** was not established.

The oxidative cleavage of the olefin at C_6 and C_{10} followed by the transannular aldol condensation (step (e)) was also investigated with enone **73**. It led to the formation of interesting compounds that were, however, completely useless for the synthesis of anhydroryanodol. For instance, when the ozonolysis was carried out in dichloromethane–methanol, the bicyclic product **81** (Scheme 13) was isolated in excellent yield. This rather interesting transformation is easily understood: tetraketone **78** must first be formed and must react with methanol to undergo a Claisen rearrangement (**78** → **79** → **80**), producing *in situ* enol **80**, which then undergoes the elimination of the carbonate group. When methanol was omitted, the ozonolysis reaction took a completely different course, producing an unstable transannular aldol product that was identified spectroscopically. The undesired transannular aldol structure **82** was assigned to this product on the basis that it was found to be unreactive with diazomethane. Indeed, if this compound had the isomeric aldol structure at C_6, the corresponding methoxyorthocarbonate should have been observed.

No further work was carried out from enone **73**. We had learned how to functionalize ring A, and it was also concluded that the oxidative cleavage – transannular aldol condensation process had to be carried out first. With this in mind, we returned to keto-*p*-nitrobenzoate **62**.

Studies with p-*nitrobenzoate* ***62***

Ozonolysis (O_3, EtOAc, PTSOH; $(CH_3)_2S$) of keto-*p*-nitrobenzoate **62** gave the desired transannular aldol product **83** (Scheme 14), which was converted with diazomethane into the

Can. J. Chem. Downloaded from www.nrcresearchpress.com by 186.148.149.217 on 09/07/12
For personal use only.

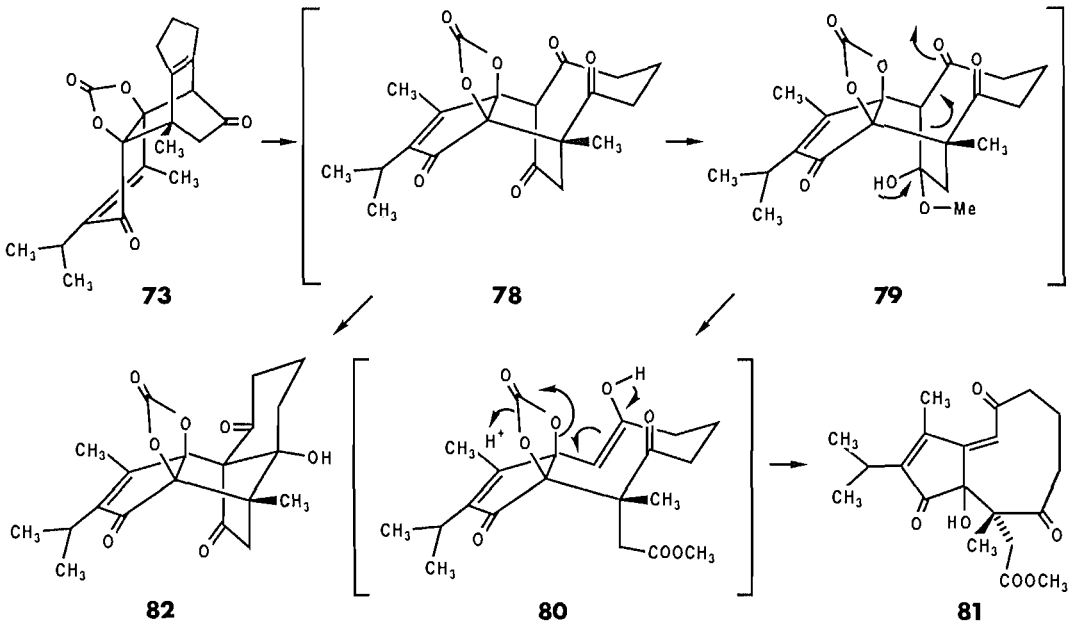

SCHEME 13

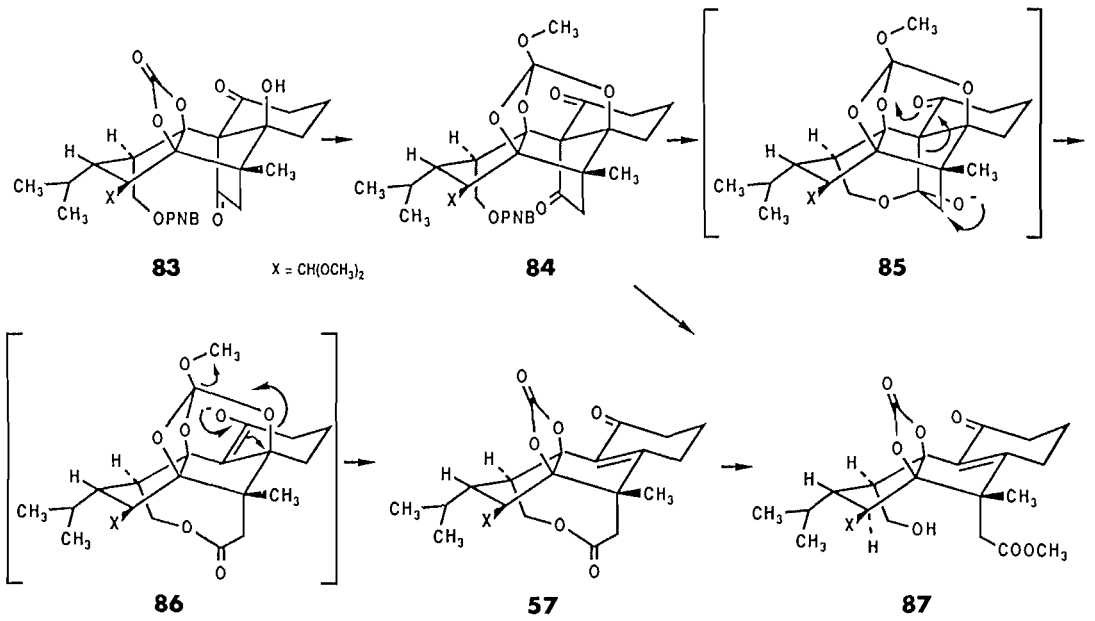

SCHEME 14

corresponding methoxyorthocarbonate diketone **84** (75% yield from **62**).

In an attempt to selectively reduce one of the carbonyl groups, compound **84** was treated with lithium tri-*sec*-butylborohydride (L-Selectride) at low temperature, and quite surprisingly the compound isolated was found to correspond to the known bridged eight-membered lactone **57**, which was previously described. This result could, however, be readily explained if the *p*-nitrobenzoate primary ester of compound **84** is preferably reduced, because this allows the formation of hemi-ketal oxyanion **85**, which can undergo a retro-Claisen reaction followed by the loss of methoxide ion from the fragmentation of the methoxyorthocarbonate moiety as indicated (**86** → **57**). It was also found that the bridged eight-membered lactone **57** was easily transesterified by reaction of lithium methoxide at 0°C, yielding the corresponding methyl ester **87**. If the above mechanistic interpretation is correct, it suggests that methoxyorthocarbonate **84** could be directly transformed into the methyl ester **87** by reaction with methoxide ion. Indeed, upon reaction of **84** with methoxide ion, transesterification of the primary *p*-nitrobenzoate ester should take place yielding *in situ* intermediate **85**, which should then give **87** via **57** and **86**. This proved to be the case experimentally; treatment of **84** with lithium methoxide (MeOH–THF) provided methyl ester **87** in 60% yield.

Having a good method for the preparation of methoxyorthocarbonate diketone **84**, the next step was its transformation into an intermediate having ring A correctly functionalized, i.e., diketone enone **91** (Scheme 15). This conversion was accomplished with an excellent overall yield of 70% following essentially our previous procedure: compound **84** was first transformed into the isomeric enol ethers **88**, which upon ozonolysis gave norketone **89**. Reaction of **89** with acetic anhydride and

Can. J. Chem. Downloaded from www.nrcresearchpress.com by 186.148.149.217 on 09/07/12
For personal use only.

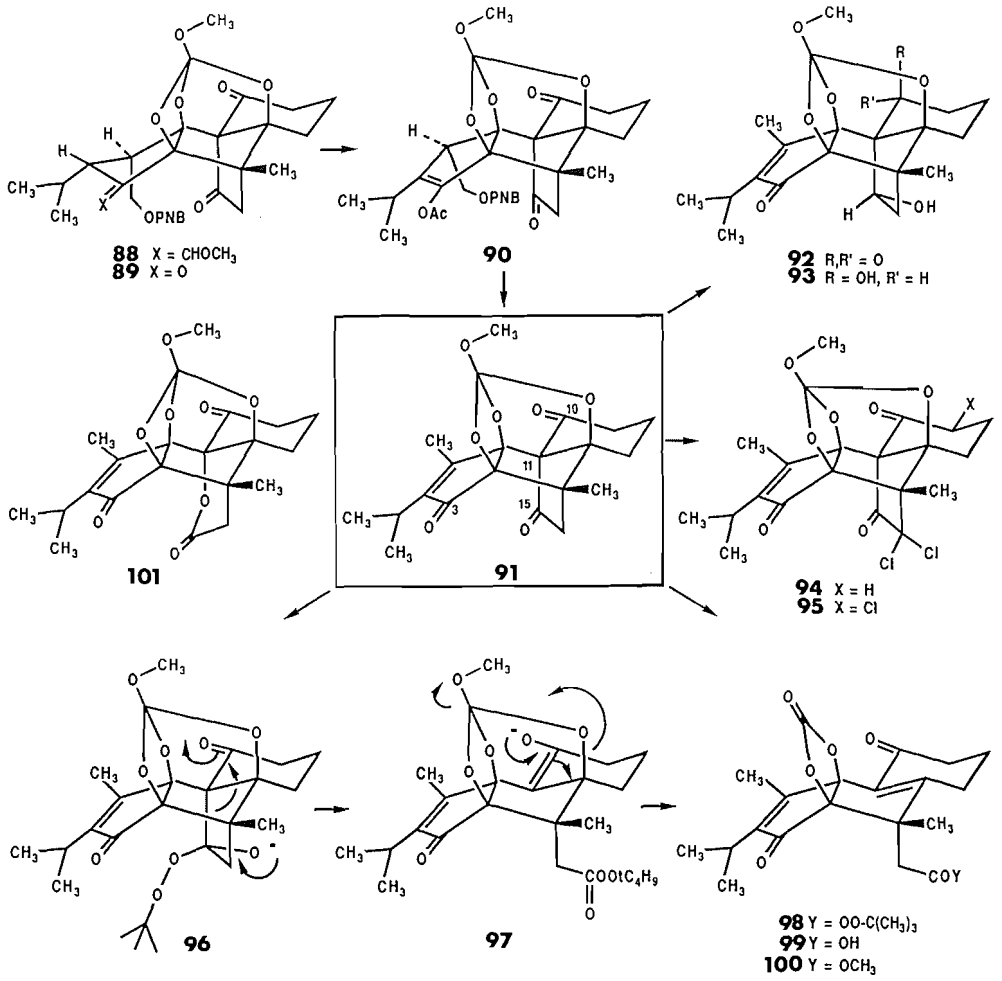

SCHEME 15

sodium acetate provided enol acetate **90**, which upon treatment with DBN in benzene gave the desired diketone enone **91**.

We had great hope with compound **91**, since we were very close to the anhydroryanodol structure **6**. Indeed, oxygen insertion between C_{15} and C_{11} would give the desired lactone ring. This, followed by methylation at C_9 and reduction of the carbonyl groups at C_3 and C_{10}, would complete the synthesis of anhydroryanodol (**6**). The reactivity of diketone enone **91** was therefore carefully examined.

Examination of a molecular model indicates that the C_{15} carbonyl group of diketone enone **91** is the most hindered of the three carbonyl groups; yet it was found to be the most reactive, and this gave us hope that we could accomplish the Baeyer–Villiger oxidation.

Reduction of diketone enone **91** with sodium borohydride at −78°C (THF–MeOH) gave a mixture of ketoalcohol **92** and diol **93**. On further reduction, **92** was converted into diol **93**. These results indicate that the C_{15} carbonyl group is the more easily reduced. However, diketone enone **91** was found to be inert in the presence of various peracids (*m*-chloroperbenzoic, peracetic, trifluoroacetic acid, H_2O_2) and we did not succeed with the desired Baeyer–Villiger oxidation. The next step was to try oxidation under basic conditions. Several experiments were carried out, none again were successful; however, some interesting results were observed. Upon treatment with an aqueous solution of sodium hypochlorite, diketone enone **91** gave two new products having infrared frequencies near 1780–1790 cm^{-1}. They were shown, however, not to have the desired lactone structure. Rather, their spectra (nmr and ms) showed that they had structures **94** and **95** respectively, which are the results of α-chlorination of the two saturated ketone functions.

Treatment of diketone enone **91** with lithium *tert*-butyl hydroperoxide (*t*-BuO_2Li) in tetrahydrofuran at −78°C gave a new compound identified as the *tert*-butyl perester **98**. Reduction of this perester with zinc gave the corresponding carboxylic acid **99**, which was then converted into the methyl ester **100**. This methyl ester **100** was also obtained directly from the reaction of diketone enone **91** with lithium methoxide.

In the above experiment with lithium *tert*-butyl hydroperoxide, we had gone as far as generating the required intermediate for the Baeyer–Villiger reaction: i.e., peroxide hemi-ketal **96**. However, this intermediate underwent a Claisen fragmentation to produce perester **98** via enolate **97** rather than the desired rearrangement, which would have produced lactone **101**.

Clearly, one way to prevent the undesired Claisen rearrangement is to transform the carbonyl group at C_{10} into an alcohol. However, we were also afraid that the removal of the C_{10} carbonyl group might considerably reduce the electrophilicity of the C_{15} carbonyl group and the desired Baeyer–Villiger oxidation would not take place. In diketone enone **91**, the π orbital of the C_{10} carbonyl group is parallel to the axially oriented C_{11}—C_{15} σ bond. As a result, the C_{15} carbonyl group must be less electron rich and more reactive towards nucleophilic reagents. This stereoelectronic effect, by which one carbonyl

Can. J. Chem. Downloaded from www.nrcresearchpress.com by 186.148.149.217 on 09/07/12
For personal use only.

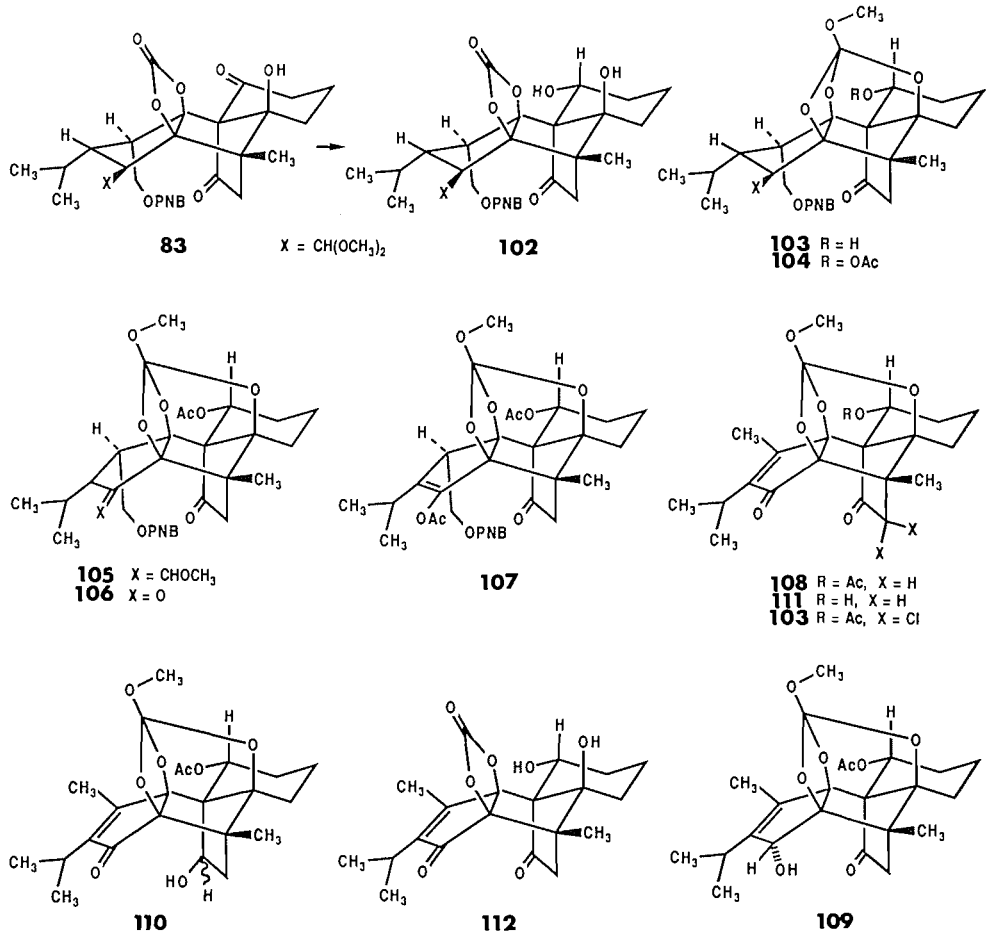

SCHEME 16

group of a β-diketone activates the other, can be best represented by the two resonance structures **i** and **ii**. We think that it does explain the observed reactivity of diketone enone **91**.

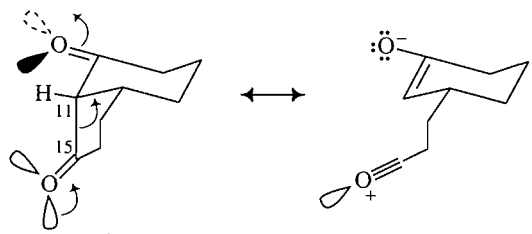

i ii

Returning to the synthetic discussion, our next task was clear; we had to prepare an intermediate without a carbonyl group at C_{10}, and then test the carbonyl reactivity at C_{15}. We have already described that the reduction of diketone enone **91** yields diol **93** having an axial alcohol at C_{10}. This result is probably due to an approach of the reducing agent from the less hindered face of the carbonyl group, because two oxygens (at C_6 and C_{12}) of the methoxyorthocarbonate severely hinder the axial approach of the reducing agent. The stereochemical course of this reduction can, however, be reversed by replacing the methoxyorthocarbonate by the hydroxycarbonate grouping. For instance, selective reduction of *p*-nitrobenzoate hydroxycarbonate diketone **83** with sodium borohydride gave a high yield of the equatorial alcohol **102** (Scheme 16). We presume that the free hydroxyl group at C_6 directs the axial approach of the hydride reagent. Reaction of compound **102** with diazomethane gave methoxyorthocarbonate **103** with an equatorial alcohol, which was further converted into the acetate derivative **104** upon reaction with acetic anhydride and pyridine.

Appropriate functionalization of ring A was then undertaken using our previously described method and the desired acetate derivative **108** was thus obtained from **104** via the formation of intermediates **105–107**. Reduction of **108** with sodium borohydride gave a mixture of the *endo*-allylic alcohol **109** and the alcohols **110**, indicating that by comparison with compound **91**, the electrophilicity of the C_{15} carbonyl group is reduced when the C_{10} carbonyl group is removed. Basic hydrolysis of **108** provided the corresponding alcohol **111**, which on mild acid hydrolysis was converted into dihydroxycarbonate **112**. The reactivity of the C_{10} carbonyl group with various oxidizing reagents was then tested experimentally.

First, compound **108** was found to be unreactive with a variety of reagents normally used for the Baeyer–Villiger reaction in acid and basic media. It reacted only with sodium hypochlorite to produce the α-dichlorinated product **113**. The monoketone **109** was used to verify whether a photochemical cleavage of the C_{11}—C_{15} bond could be realized (23). This was, however, not successful. Further, a rather interesting transformation was observed when dihydroxydiketone **112** was treated with lithium *tert*-butyl peroxide. Rather than producing the desired Baeyer–Villiger product, it gave the tricyclic ketodiol **116** (Scheme 17), which was further characterized as its diacetate **117**, in 75% yield. This interesting degradation is presumably the result of hemi-orthocarbonate salt formation, followed

Can. J. Chem. Downloaded from www.nrcresearchpress.com by 186.148.149.217 on 09/07/12
For personal use only.

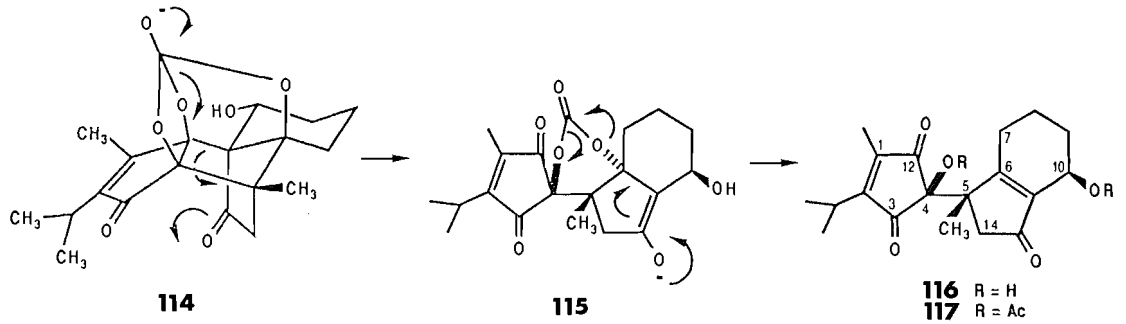

114 **115** **116** R = H **117** R = Ac

SCHEME 17

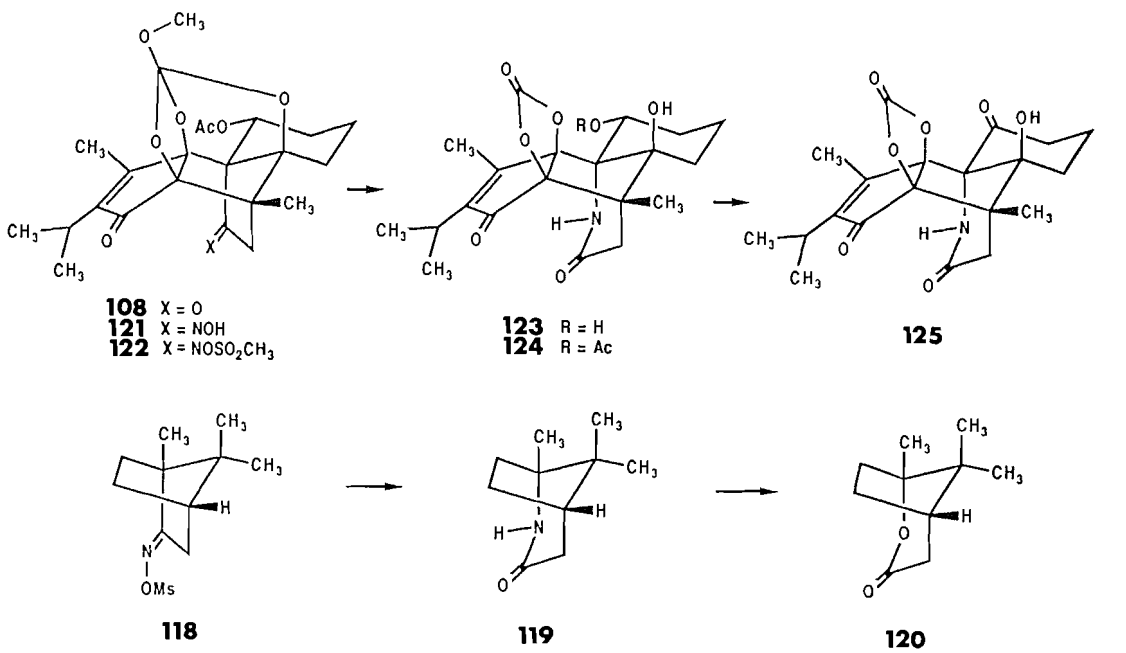

108 X = O **121** X = NOH **122** X = $NOSO_2CH_3$ **123** R = H **124** R = Ac **125**

118 **119** **120**

SCHEME 18

by retro-aldol reaction and loss of carbon dioxide as shown by **114** → **115** → **116**.

The possibility that the lactone ring of anhydroryanodol could be obtained via the intermediate formation of a lactam was also investigated (24). We were confident that this approach could work because we successfully carried out this transformation using camphor lactam **119** as a model (Scheme 18). First, camphor lactam **119** was produced, albeit in a low yield, from the Beckmann rearrangement[3] of the unisolated oxime mesylate **118** of camphor. Then reaction of nitrosyl hexafluorophosphate (24, 26) with **119** gave the desired lactone **120**. Oximation of **108** gave the desired oxime **121**, which was successfully transformed into the lactam **123** via the oxime mesylate **122**. In the course of the Beckmann rearrangement, the methoxyorthocarbonate and the secondary acetate were both hydrolyzed under the reaction conditions (water–dioxane, 135°C, 17 h).

The lactam alcohol **123** was also converted into the acetate **124** by acetylation and into the ketolactam **125** by oxidation. The lactam–lactone transformation with compounds **124** and **125** was then attempted under the usual conditions, but it was not successful. This failure might be due to the fact that although camphor lactam **119** is a relatively close model to lactams **124** and **125**, the nitrogen in the latter compounds is more hindered than in the former. As a result, electrophilic species such as the nitrosonium ion could react on the oxygen rather than the nitrogen of the amide function, and that could of course inhibit the desired rearrangement!

A solution for the lactone ring of anhydroryanodol

Analysis of the above results led us to the conclusion that a major change in our strategy was necessary in order to effect the formation of the desired lactone ring. We started to think in terms of a two-stage process where the C_{11}—C_{15} bond would be cleaved first, and the lactone ring would then be formed later on. One conceivable approach was the cleavage of the C_{11}—C_{15} bond with concomitant formation of an unsaturation between C_{10} and C_{11}. Such an operation was in principle possible via a 1,4 "Grob" fragmentation process (27), which can be triggered by the functional groups at C_{10} and C_{15}. With that in mind, we started investigating with methoxyorthocarbonate alcohol **103**.

The equatorial alcohol **103** was converted into the corresponding mesylate **126** (Scheme 19), which on treatment with lithium methoxide yielded the corresponding cyclic hemi-ketal **127**. When compound **127** was submitted to dimsyllithium ($LiCH_2SOCH_3$) in dimethylsulfoxide, a smooth fragmentation took place, yielding the medium ring lactone **128**. This compound was found to be unstable under acidic conditions.

[3]Thus contrary to literature (25), Beckmann rearrangement of camphor oxime gives some of the expected lactam product **119**.

Can. J. Chem. Downloaded from www.nrcresearchpress.com by 186.148.149.217 on 09/07/12
For personal use only.

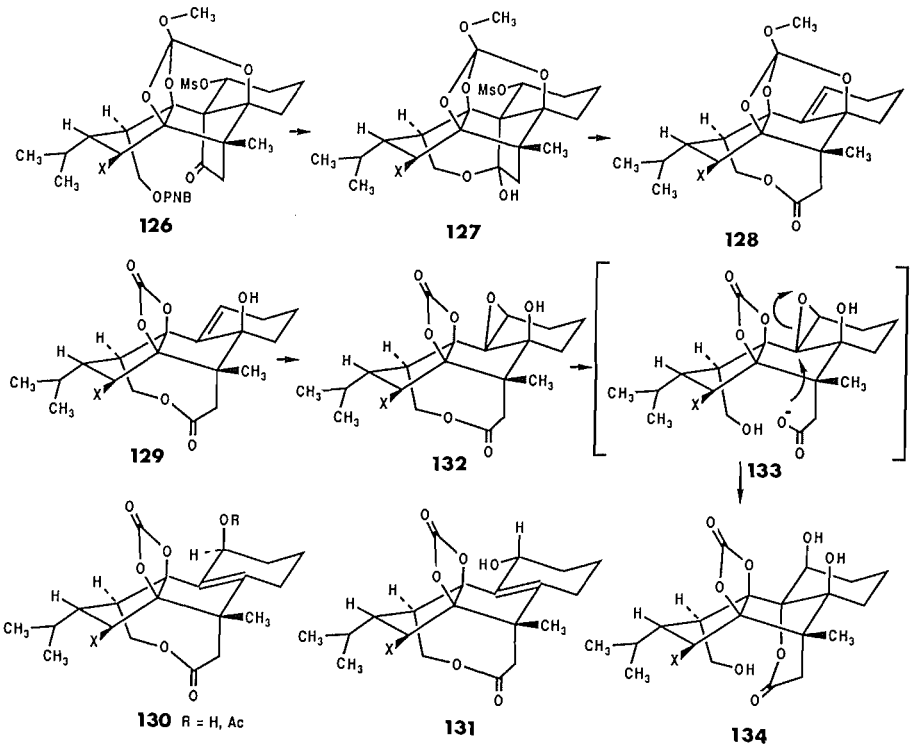

SCHEME 19 (X = $CH(OCH_3)_2$)

Mild acid hydrolysis of **128** gave a mixture of the desired hydroxycarbonate **129** and isomeric allylic axial alcohol **130** (R = H). The best conditions were found using fluoroboric acid (HBF_4) in water, giving a 3:1 ratio in favor of **129**. The structure of the minor product, i.e., axial allylic alcohol **130** (R = H), was further established by acetylation to acetate **130** (R = Ac) and by oxidation into the previously described lactone enone **57**. Furthermore, on reduction with sodium borohydride, enone **57** gave the corresponding equatorial allylic alcohol **131**, which was different from the axial isomer **130** (R = H).

Molecular models indicate that structure **128** is quite strained, and this tension is removed when the methoxyorthocarbonate is replaced by the hydroxycarbonate moiety (cf. **129**). The release of strain might be the main driving force for the relatively facile hydrolysis of **128**. Now, returning to the Grob fragmentation **127** → **128**, it is interesting to point out that this process can only work if ring C adopts a twist-boat conformation so that the leaving mesylate group becomes antiperiplanar to the C_{11}—C_{15} bond. Indeed, according to Grob (27), this stereoelectronic condition must be fulfilled in order to observe a given cleavage. Interestingly, the Grob fragmentation **127** → **128** is essentially the same reaction that transforms ryanodol into anhydroryanodol (see ref. 11, p. 264).

Compound **129** was treated with trifluoroperacetic acid to yield an epoxide that was assigned the β configuration on the basis that the medium lactone ring completely blocks the approach of a reagent on the α face of the C_{10}—C_{11} unsaturation. When epoxide **132** was treated with sodium hydroxide, it was smoothly converted into the desired lactone **134**. Thus, the anticipated intramolecular opening at the most substituted end of the oxirane ring by the carboxylic ion (cf. **133**) occurred with ease.

At last we had found a solution for the introduction of the lactone ring of anhydroryanodol. We had hope for a one-step conversion, but this stepwise method was of course quite an acceptable strategy. It led us to the axial rather than the desired equatorial alcohol at C_{10}, so an appropriate correction had to be made later on.

Synthesis of anhydroryanodol from lactone 39

Consideration of when the secondary methyl group at C_9 should be introduced led us to modify and, at the same time, simplify our method for the construction of the desired hemiketal mesylate that is necessary for carrying out the Grob fragmentation. For that matter, we decided to go back to a very early key intermediate, i.e., pentacyclic lactone carbonate **39**. Indeed this compound, which is easily prepared in four steps from the pentacyclic carbonate aldehyde **11** (**11** → **19** → **34** → **36** → **39**; cf. Scheme 7), possesses the correct functionality for the introduction of the methyl group at C_9 (*vide infra*). However, the new route was first explored using **39** without carrying out the methylation step at C_9.

Borohydride reduction of compound **39** gave the expected equatorial alcohol **135** (R′ = H) (Scheme 20). At this stage, we decided to modify the methoxyorthocarbonate protecting group[4] to avoid the formation of the secondary alcohol product **130** (R = H) (Scheme 19) during the acid hydrolysis. Treatment of **135** with sodium hydride in tetrahydrofuran and methoxymethyl chloride gave the corresponding methoxymethyl orthocarbonate **136**. We could easily envisage this reaction since we had already demonstrated the formation of the orthocarbonate sodium salt **40** from **39** (Scheme 7) under basic conditions. Now

[4]An additional reason to effect this modification was the fact that the formation of the corresponding methoxyorthocarbonate did not take place under our previously successful reaction conditions, i.e., there was no reaction between diazomethane and dihydroxycarbonate **135**. We also observed that the methoxyorthocarbonate derivative could be isolated by reacting **39** with diazomethane, but the reaction was slow and gave several products.

Can. J. Chem. Downloaded from www.nrcresearchpress.com by 186.148.149.217 on 09/07/12
For personal use only.

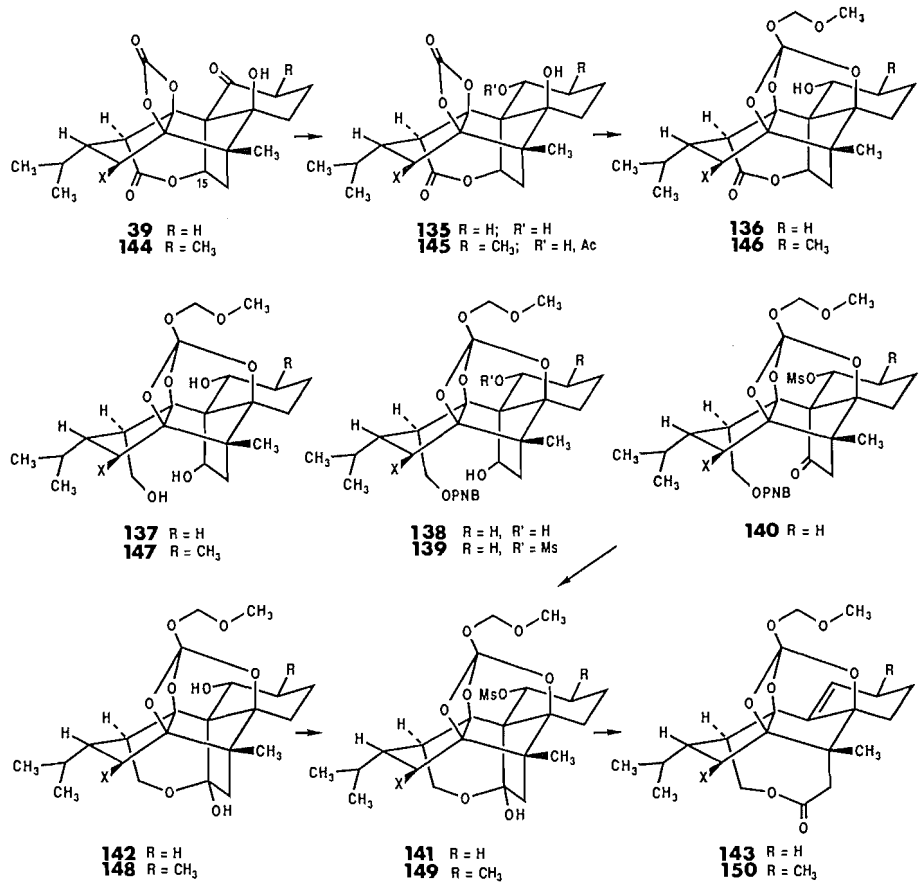

SCHEME 20 (X = $CH(OCH_3)_2$)

that the acid hydrolysis of the methoxymethyl orthocarbonate can be triggered by the hydrolysis of the methoxymethyl first, we could anticipate that the formation of the secondary product **130** (R = H) could be avoided (*vide infra*).

Reduction of **136** with lithium aluminium hydride provided the triol **137**, which was selectively esterified with *p*-nitrobenzoyl chloride to yield the corresponding primary *p*-nitrobenzoate **138**. Selective mesylation of **138** gave the secondary mesylate **139**, still having the most hindered secondary hydroxyl group free. Oxidation of **139** gave the corresponding ketone **140**, which on treatment with lithium methoxide gave the hemi-ketal mesylate **141** having a methoxymethyl orthocarbonate protecting group. This compound could also be prepared from a more simple two-step procedure starting from triol **137**. It was shown later that carefully controlled oxidation ($CrO_3 \cdot 2C_5H_5N$) of **147** provided the hemi-ketal alcohol **148**, which was then mesylated to give **149** (*vide infra*). The successful conversion **147** → **148** (or **137** → **142**) is due to the fact that hindered secondary alcohols are usually oxidized at a faster rate (28).

The previously described Grob fragmentation **127** → **128** was attempted under the same conditions with compound **141** and it gave the expected olefin lactone **143**, which was also found to be unstable. However, acid hydrolysis (HBF_4, H_2O) of crude product **143** provided the desired hydroxycarbonate **129** without any trace of the isomeric allylic alcohol **130**. Thus, the use of the methoxymethyl orthocarbonate was successful, as anticipated.

Having lactone **129** in hand, it remained, as previously mentioned, to introduce a secondary methyl group at C_9, to invert the alcohol configuration at C_{10}, and to complete ring A formation using the method previously described.

The last two operations were first carried out as a model series that provided 9-normethyl anhydroryanodol. This series of experiments will, however, not be reported, as it is essentially identical to the final route with the exception that the C_9 methyl group was missing.

Selective monomethylation was realized by the procedure of Rathke and co-workers (29), which uses triethylborane to form trialkylborane enolate intermediate, which then undergoes a single methylation. Thus reaction of ketone **39** with lithium diisopropyl amide in tetrahydrofuran followed by the successive addition of triethylborane ($(C_2H_5)_3B$) and iodomethane provided, after a brief treatment under basic conditions, the equatorial monomethylated derivative **144** in 70% yield (Scheme 20).[5]

The ketone function in **144** was selectively reduced with sodium borohydride to give the equatorial alcohol **145** (R′ = H) (95% yield), which was further characterized as its acetate derivative **145** (R′ = Ac). Compound **145** (R′ = H) was then transformed into the methoxymethyl orthocarbonate **146** (94% yield) using the previously described conditions. Reduction of **146** with lithium aluminium hydride produced the triol **147** (95% yield). Selective oxidation of **147** ($CrO_3 \cdot 2C_5H_5N$) gave hemi-ketal **148** (76% yield), which was converted into the mesylate **149** (89% yield). Then, the Grob fragmentation **149** →

[5]Careful examination of the crude product prior to the work-up under basic conditions indicated that the first product formed was the axial monomethylated isomer.

Can. J. Chem. Downloaded from www.nrcresearchpress.com by 186.148.149.217 on 09/07/12
For personal use only.

Can. J. Chem. Downloaded from www.nrcresearchpress.com by 186.148.149.217 on 09/07/12
For personal use only.

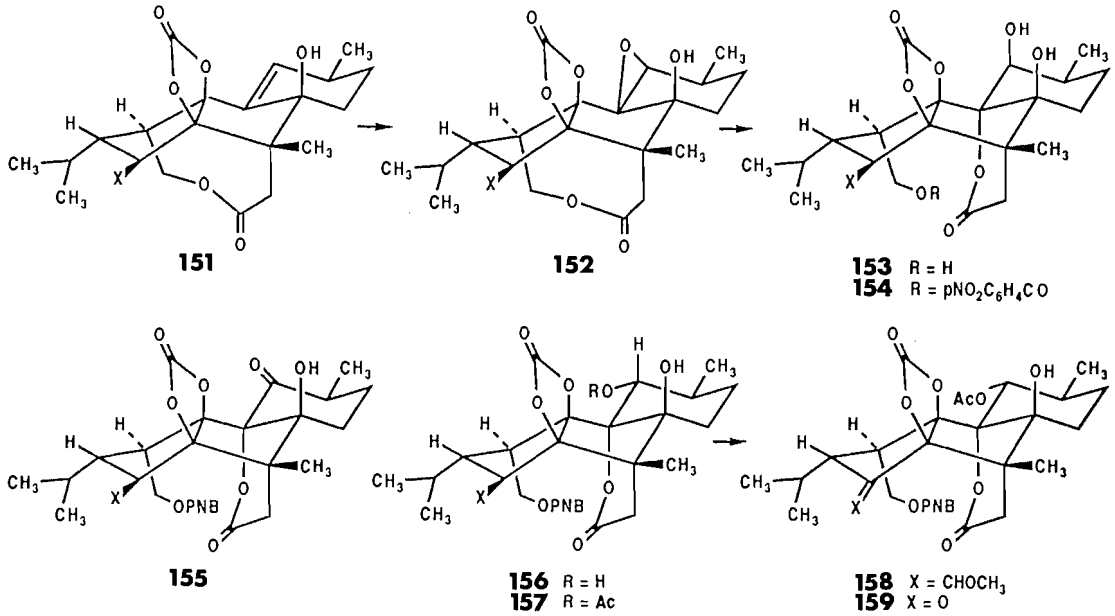

SCHEME 21 (X = $CH(OCH_3)_2$)

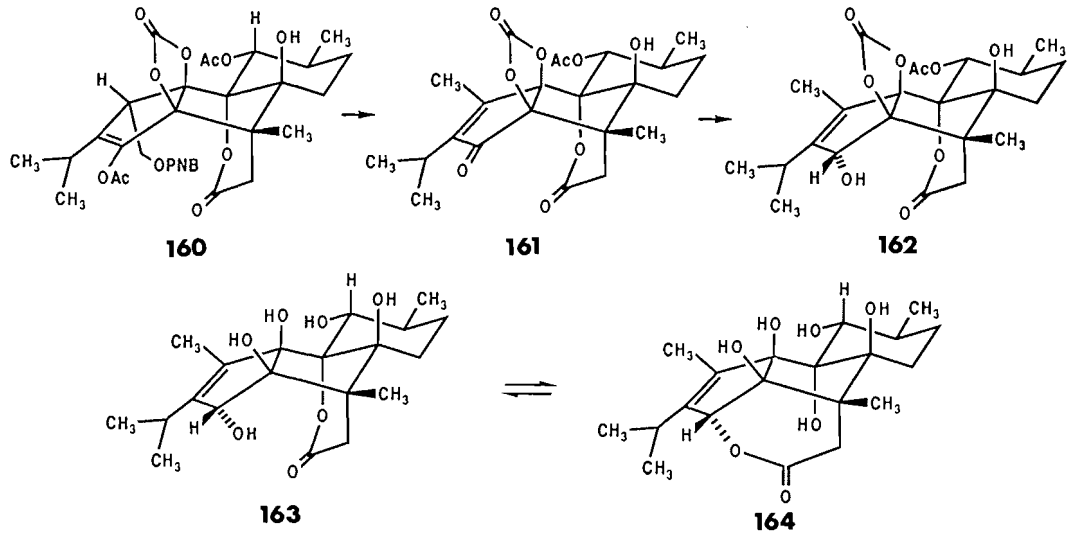

SCHEME 22

150 followed by mild acid hydrolysis (0.3 M HBF_4, THF, 0°C, 3 h) provided the desired hydroxycarbonate **151** in 97% yield (Scheme 21). Epoxidation of **151** afforded the β-epoxide **152** (98% yield), which upon aqueous basic treatment gave triol lactone **153** (77% yield).

Compound **153** was converted into the *p*-nitrobenzoate **154** (95% yield), which was oxidized (CrO_3·$2C_5H_5N$) to yield ketone **155** (78% yield). Reduction of ketone **155** with lithium borohydride in tetrahydrofuran (−30 to −20°C) gave the desired equatorial alcohol **156** in 73% yield after chromatographic separation from a small quantity of the axial isomer **154**. Acetylation (Ac_2O, C_5H_5N) of **156** gave the acetate **157** in good yield.

Modification of ring A in acetate **157** to produce enone **161** was then carried out by following the method previously described. Compound **157** was converted (PTSA, benzene, reflux) to a mixture of enol ethers **158**, which was oxidized (O_3, CH_2Cl_2; $(CH_3)_2S$) to cyclopentanone **159**. Compound **159** was transformed (Ac_2O, AcONa, 100°C) into the corresponding enol acetate **160** (Scheme 22), which under basic conditions (DBN, benzene, 75°C) gave the carbonate-acetate derivative **161** of 3-oxo-anhydroryanodol, the overall yield of **161** from acetate **157** being 50%.

Compound **161** was then reduced in good yield with sodium borohydride to give the *endo* allylic alcohol **162**, completing the synthesis of ring A. Finally, removal of the carbonate and the acetate groups in **162** under basic aqueous conditions gave a 3:1 mixture of anhydroryanodol **163** and epianhydroryanodol **164**, which were separated by chromatography. We had previously observed that under basic aqueous conditions anhydroryanodol **163** exists as a 3:1 equilibrium mixture with epianhydroryanodol **164**. Crystalline samples of synthetic anhydro- and epianhydroryanodol were found to be completely identical with authentic samples derived from natural ryanodine. The above comparison showed also that the synthetic and the naturally

derived material had essentially identical optical rotations, confirming that we had obtained optically active material with the correct absolute configuration.

Conclusion

In conclusion, the total synthesis of optically active (+)-anhydroryanodol **163** having the correct absolute configuration was completed via the following series of intermediates: **11** → **19** → **34** → **36** → **39** → **144** → **145** → **146** → **147** → **148** → **149** → **150** → **151** → **152** → **153** → **154** – **155** → **156** → **157** → **158** → **159** → **160** → **161** → **162** → **163**. This amounts to 24 different steps starting from optically active dextrorotatory pentacyclic carbonate aldehyde **11**. We consider this as a very acceptable solution within our synthetic strategy, although it could of course be improved on further work.

The next operation is the reconversion of (+)-anhydroryanodol into (+)-ryanodol and this is reported in the next article.

Experimental

Apparatus, materials, and methods

Melting points were determined on a Büchi M-50 apparatus and are uncorrected. Ether, tetrahydrofuran, and 1,2-dimethoxyethane were dried by distilling over sodium benzophenone ketyl. Benzene, dichloromethane, dimethyl sulfoxide, and amines were distilled over calcium hydride. All reactions were performed under nitrogen or argon atmosphere. Analytical and preparative thin-layer chromatography (tlc) were carried out on glass plates precoated (0.25, 0.5, 1.0, and 2.0 mm) with silica gel 60 F-250 (Merck). Materials were detected by visualization under an ultraviolet lamp (254 or 350 nm) and (or) by spraying with sulfuric acid (50%) or a solution of phosphomolybdic acid or vanillin followed by heating on a hot plate. Column chromatography was performed with silica gel (Baker (60–200 mesh) or Merck 60 (200–400 mesh)).

The infrared spectra (ir) were taken on a Perkin–Elmer 257 or 681 spectrophotometer. Proton nuclear magnetic resonance (^{1}H nmr) spectra were recorded (with chloroform or tetramethylsilane as internal standard) on a Varian A-60, a Bruker WP-60, a Bruker HX-90, or a Bruker WM-250 instrument. Carbon nuclear magnetic resonance (^{13}C nmr) spectra were measured on a Bruker HX-90 or WM-250 instrument. The following abbreviations have been used: s, singlet; d, doublet, dd, doublet of doublets; t, triplet, q, quartet; qn, quintet; m, multiplet; br, broad. For most of the hydroxylated compounds, the multiplicity of the hydrogens attached to a carbinol was analyzed after D_2O exchange. The mass spectra were recorded on a Hitachi–Perkin–Elmer RMU-6 mass spectrometer and peak matching (hrms) on a VG Micromass ZAB-2F spectrometer. The ultraviolet spectra (uv) were recorded on a Varian Techtron 635 spectrophotometer. Specific rotations were determined on a Perkin–Elmer polarimeter at 25°C. Microanalyses were carried out by Mr. J. Tamas, Laboratoire de Microanalyses, Université de Sherbrooke; Schwarzkopf Microanalytical Laboratories, New York; and by Dr. C. Daesslé, Organic Microanalyses, Montreal.

*Dioxolane acetal **12***

A mixture of aldehyde **11** (900 mg, 2.27 mmol), ethylene glycol (1.00 g, 16.1 mmol), and *p*-toluenesulfonic acid (10 mg) in benzene (80 mL) was refluxed (Dean–Stark) for 88 h. Ether was then added to the cooled mixture and the organic layer was washed with aqueous sodium bicarbonate and water. Evaporation of the dried (Na_2SO_4) extract furnished crystalline acetal **12** (877 mg, 87%); mp 143–144°C (chloroform–hexane); ir ($CHCl_3$, ν cm^{-1}): 1810, 1745; ^{1}H nmr ($CDCl_3$, δ ppm): 5.10 (d, 1H, J = 2 Hz, HCO_2), 3.95 (m, 4H, OCH_2CH_2O), 3.33 (d, 1H, J = 5 Hz, HC11), 3.1–1.4 (m, 13H), 1.31 (s, 3H, CH_3C5), 1.15 (d, 3H, J = 6.5 Hz), and 1.05 (d, 3H, J = 6.5 Hz) ($(CH_3)_2CH$); ms m/e: 400 (M^+). *Anal.* calcd. for $C_{23}H_{28}O_6$: C 68.98, H 7.04; found: C 69.18, H 7.34.

endo *Alcohol **13***

To a solution of ketone **12** (308 mg, 0.77 mmol) in dry methanol (40 mL) was added, at 0°C, sodium borohydride (35 mg, 0.92 mmol). After 45 min, ether (50 mL) was added and the mixture was washed with a mixture of brine (30 mL) and hydrochloric acid (2 M, 5 mL), then with brine. Evaporation of the dried extract furnished crystalline alcohol **13** (300 mg, 97%); mp 168–169°C (chloroform–hexane); ir ($CHCl_3$, ν cm^{-1}): 3620, 3500, 1800; ^{1}H nmr ($CDCl_3$, δ ppm): 5.12 (br s, 1H, HCO_2), 4.67 (m, 1H, HC17), 3.95 (m, 4H, OCH_2CH_2O), 2.98 (d, 1H, J = 5 Hz, HC11), 2.8–1.5 (m, 14H), 1.27 (s, 3H, CH_3C5), 1.00 (br t, 6H, $HC(CH_3)_2$); ms m/e: 402 (M^+). *Anal.* calcd. for $C_{23}H_{30}O_6$: C 68.64, H 7.51; found: H 68.70, H 7.62.

endo *Acetate **14***

To a solution of *endo* alcohol **13** (56 mg, 0.14 mmol) in triethylamine (2 mL) was added acetic anhydride (0.5 mL) and 4-dimethylaminopyridine (DMAP, 2 mg). After 4 h at 25°C, the volatile substances were evaporated and the residue was filtered on silica gel to give *endo* acetate **14** (61 mg, 98%); ir ($CHCl_3$, ν cm^{-1}): 1800, 1740; ^{1}H nmr ($CDCl_3$, δ ppm): 5.47 (dd, 1H, J = 11.0 and 6.8 Hz, HC17), 5.03 (s, 1H, HCO_2), 3.95 (m, 4H, OCH_2CH_2O), 2.99 (d, 1H, J = 5 Hz, HC11), 2.79 (dd, 1H, J = 11.0 and 5.1 Hz, HCl), 2.57 (m, 2H, HC2 and HC3), 2.43 (m, 5H, HC15, H_2C7, H_2C9), 2.10 (s, 3H, CH_3CO_2), 2.01 (m, 3H, H_2C8, HC13), 1.64 (d, 1H, J_{AB} = 14.2 Hz, *endo* HC14), 1.27 (s, 3H, CH_3C5), 1.02 (dd, 1H, J_{AB} = 14.2 Hz, J_{AX} = 10.2 Hz, *exo* HC14), 0.97 (d, 3H, J = 6.5 Hz) and 0.91 (d, J = 6.8 Hz) ($(CH_3)_2CH$); ms m/e: 444 (M^+).

*Diol acetal **15***

To a solution of carbonate **12** (21 mg, 0.052 mmol) in tetrahydrofuran (2 mL) was added aqueous sodium hydroxide (1 M, 0.5 mL, 0.5 mmol). The mixture was stirred under argon at room temperature for 15 h, then extracted with dichloromethane to give pure diol **15** (19 mg, 96%); ir ($CHCl_3$, ν cm^{-1}): 3500, 1735; ^{1}H nmr ($CDCl_3$, δ ppm): 4.92 (d, 1H, J = 3.3 Hz, HCO_2), 3.95 (m, 4H, -OCH_2CH_2O-), 3.88 (s, 1H, OH), 3.46 (s, 1H, OH), 2.99 (d, 1H, J = 4.8 Hz, HC11), 2.5 (m, 7H), 2.27 (m, 1H, HC15), 2.01 (m, 3H, H_2C8 and HC13), 1.44 (dd, 1H, J_{AB} = 14.5 Hz, J_{AX} = 1.6 Hz, *endo* HC14), 1.28 (dd, 1H, J_{AB} = 14.5 Hz, J_{BX} = 11 Hz, *exo* HC14), 1.20 (s, 3H, CH_3C5), 1.10 (d, 3H, J = 6.8 Hz) and 0.96 (d, 3H, J = 6.9 Hz) ($CH(CH_3)_2$); ms m/e: 374 (M^+).

*Ozonolysis of acetal **16***

A cooled (−78°C) solution of ketal **16** (310 mg, 1.43 mmol) in ethyl acetate (25 mL) was reacted with a stream of ozone for 10 min. To the blue reaction mixture was then added dimethyl sulfide (1 mL) and the mixture was allowed to warm to room temperature (25 min). After evaporation of the volatile substances the crude product was chromatographed on silica gel (hexane – ethyl acetate, 1:2) to give pure hydroxy diester **18** (316 mg, 95%); ir ($CHCl_3$, ν cm^{-1}): 3620, 3500, 1730; ^{1}H nmr ($CDCl_3$, δ ppm): 4.20 (t, 2H, J = 6 Hz, CO_2CH_2), 3.80 (m, 2H, CH_2OH), 3.66 (s, 3H, OCH_3), 2.4 (m, 1H, OH), 2.34 (s, 4H, CH_2CO_2), 1.75 (m, 2H), 0.90 (d, 6H, J = 7 Hz, $(CH_3)_2$); ms m/e: 232 (M^+).

*Dimethyl acetal **19***

To a solution of aldehyde **11** (500 mg, 1.41 mmol) in methanol (10 mL) was added *p*-toluenesulfonic acid (7 mg) and methyl orthoformate (165 mg, 1.55 mmol). The mixture was refluxed for 17 h under argon, then cooled, diluted with ether (100 mL), washed with aqueous sodium bicarbonate, and dried over magnesium sulfate. Evaporation of the solvents left pure dimethyl acetal **19** (550 mg, 98%); mp 114–115°C; $[\alpha]_D$ +106.4° (*c* 1.00, $CHCl_3$); ir ($CHCl_3$, ν cm^{-1}): 1805, 1745; ^{1}H nmr ($CDCl_3$, δ ppm): 4.31 (d, 1H, J = 1.5 Hz, *H*$C(OCH_3)_2$), 3.51 and 3.44 (2s, 6H, 2 × OCH_3), 3.27 (d, 1H, J = 5.1 Hz, HC11), 2.90 (m, 2H, HCl, HC2), 2.45 (m, 7H), 2.05 (m, 3H, H_2C8, HC13), 1.60 (dd, 1H, J_{AB} = 14.5 Hz, J_{AX} = 1.5 Hz, *endo* HC14), 1.46 (dd, 1H, J_{AB} = 14.5 Hz, J_{AX} = 11 Hz, *exo* HC14), 1.31 (s, 3H, CH_3C5), 1.10 (d, 3H, J = 6.9 Hz) and 0.97 (d, 3H, J = 6.9 Hz) ($CH(CH_3)_2$); ms m/e: 402 (M^+). *Anal.* calcd. for $C_{23}H_{30}O_6$: C 68.64, H 7.51; found: C 68.94, H 7.51.

Can. J. Chem. Downloaded from www.nrcresearchpress.com by 186.148.149.217 on 09/07/12
For personal use only.

Can. J. Chem. Downloaded from www.nrcresearchpress.com by 186.148.149.217 on 09/07/12
For personal use only.

*Ozonolysis of ketal olefin **19***

(*a*) A stream of ozone was bubbled through a solution of dimethoxyacetal **19** (200 mg, 0.497 mmol) in methanol (20 mL) at −78°C until a blue color persisted (~2 min); then dimethyl sulfide (1 mL) was added and the mixture was allowed to warm to room temperature (1.5 h). Evaporation of the volatile substances left a residue containing two components **20** and **21** in the relative proportion of 1:2 (nmr integration of acetal protons at ~4.29 ppm), which were separated by column chromatography on silica gel (dichloromethane–acetone 85:15).

*Compound **21*** (less polar, 130 mg, 60%): mp 196–197°C; ir ($CHCl_3$, ν cm^{-1}): 3600, 3400, 1815, 1750, 1705; ^1H nmr ($CDCl_3$, δ ppm): 4.31 (d, 1H, J = 3.9 Hz, $HC(OCH_3)_2$), 3.50 and 3.49 (2s, 6H, 2 × OCH_3), 3.01 (m, $H_{eq}C9$), 2.93 (dd, 1H, J = 10.4 and 2.8 Hz, HCl), 2.8–1.7 (m), 2.57 (dd, J = 3.9 Hz and 9 Hz, HC3), 2.45 (dd, 1H, J_{AB} = 14.1, J_{AX} = 11.5 Hz, $H_{exo}C14$), 1.45 (dd, 1H, J_{AB} = 14.1, J_{BX} = 2.0 Hz, $H_{endo}C14$), 1.18 (s, 3H, CH_3C5), 1.08 and 0.97 (2d, 6H, J = 6.9 Hz, $CH(CH_3)_2$); ms *m/e*: 434 (M^+). *Anal.* calcd. for $C_{23}H_{30}O_8$: C 63.57, H 6.96; found: C 63.31, H 6.73.

*Compound **20*** (more polar, 75 mg, 35%); mp 194–195°C; ir ($CHCl_3$, ν cm^{-1}): 3600, 3400, 1820, 1752, 1705; ^1H nmr ($CDCl_3$, δ ppm): 4.28 (d, 1H, J = 5.2 Hz, $HC(OCH_3)_2$), 3.51 and 3.48 (2s, 6H, 2 × OCH_3), 3.18 (dd, 1H, J = 6.8 and 2.5 Hz, HCl), 2.80 (m, 2H, HC2 and $H_{eq}C9$), 2.5–1.7 (m), 2.20 (dd, 1H, J_{AB} = 14.9, J_{AX} = 11.3 Hz, $H_{exo}C14$), 1.75 (dd, 1H, J_{AB} = 14.9, J_{BX} = 2 Hz, $H_{endo}C14$), 1.21 (s, 3H, CH_3C5), 1.10 and 0.91 (2d, 6H, J = 7.0 Hz, $CH(CH_3)_2$); ms *m/e*: 402 (M^+). *Anal.* calcd. for $C_{23}H_{30}O_8$: C 63.31, H 6.73; found: C 63.19, H 6.98.

(*b*) The same reaction was performed in the presence of *p*-toluenesulfonic acid (95 mg, 0.5 mmol). The crude product, after removal of the acid, left a residue containing compounds **20** and **21** in the relative proportion of 7:3 as shown by nmr.

cis-*Diol **22***

To a solution of pentacyclic olefin **19** (106 mg, 0.264 mmol) in ether (10 mL) was added osmium tetroxide (81 mg, 0.32 mmol) and the mixture was stirred at room temperature for 16 h. Evaporation left a brown residue, which was dissolved in ethanol (95%, 20 mL) and reacted with sodium sulfite (266 mg, 2.11 mmol) in water (2 mL) at reflux temperature for 1 h. The reaction mixture was filtered, ethanol was evaporated, and the reside was extracted with ether, washed with brine, and dried over sodium sulfate. Evaporation of ether left a solid residue, which was crystallized from chloroform – hexane (72 mg, 63%); mp 211–212°C; ir ($CHCl_3$, ν cm^{-1}): 3600–3420, 1810, 1750, 1075; ^1H nmr ($CDCl_3$, δ ppm): 4.36 (s, 1H, $HC(OCH_3)_2$, 3.53 and 3.45 (7H, 2s, 2 × OCH_3 and HC11), 3.0–1.0 (m, 13H), 1.21 (s, 3H, CH_3C5), 1.10 (d, 3H, J = 6.5 Hz), 0.96 (d, 3H, J = 6.5 Hz) ($CH(CH_3)_2$); ms *m/e*: 434 (M^+). *Anal.* calcd. for $C_{23}H_{32}O_8$: C 63.28, H 7.39; found: C 63.12, H 7.22.

Periodic cleavage of cis-*diol **22***

To a stirred solution of glycol **22** (50 mg, 0.12 mmol) in ether (20 mL) was added a solution of periodic acid in ether (3.5 mL, 16 mg/mL). After 5 h at room temperature the mixture was washed with aqueous sodium bicarbonate and brine. Evaporation of the dried extract gave pure compound **21** (40 mg, 80%).

*Diol **23***

To a solution of carbonate acetal **19** (300 mg, 0.746 mmol) in tetrahydrofuran (10 mL) was added aqueous sodium hydroxide (1 M, 11 mL) and the mixture was stirred at 65°C for 1.5 h, then poured onto brine and extracted with ether. Evaporation of the dried (Na_2SO_4) extract gave pure diol **23** (275 mg, 98%); ir ($CHCl_3$, ν cm^{-1}): 3450, 1745, 1080; ^1H nmr ($CDCl_3$, δ ppm): 4.44 (d, 1H, J = 2 Hz, $HC(OCH_3)_2$), 4.31 (s, 1H, OH), 3.47 (s, 6H, 2 × OCH_3), 2.97 (d, 1H, J = 5 Hz, HC11), 2.7–1.5 (m, 14H), 1.21 (s, 3H, CH_3C5), 1.10 (d, 3H, J = 6.5 Hz), 1.00 (d, 3H, J = 6.5 Hz) ($HC(CH_3)_2$); ms *m/e*: 376 (M^+).

*Ozonolysis of diol olefin **23***

A cooled (−78°C) solution of olefin **23** (194 mg, 0.517 mmol) in methanol (50 mL) was reacted with a stream of ozone for 10 min. The blue reaction mixture was reacted with dimethyl sulfide (10 mL) and allowed to warm to room temperature during 1.5 h. Evaporation of the volatile substances gave a residue that was dissolved in ether, then washed with water and brine. The dried extract was evaporated and the residue was chromatographed on thin layer (ether–methanol, 99:1) to give pure triol **25** (60 mg, 28%); mp 157–158°C; ir ($CHCl_3$, ν cm^{-1}): 3440, 1735, 1695, ^1H nmr ($CDCl_3$, δ ppm): 5.72 (s, 1H, OH), 4.67 (s, 1H, OH), 4.49 (s, 1H, OH), 4.44 (d, 1H, J = 2.5 Hz, $HC(OCH_3)_2$), 3.51 (s, 6H, 2 × OCH_3), 2.8–1.2 (m, 13H), 1.11 (s, 3H, CH_3C5), 1.10 (d, 3H, J = 6.5 Hz), 1.05 (d, 3H, J = 6.5 Hz) ($HC(CH_3)_2$); ms *m/e*: 376 (M^+–32). *Anal.* calcd. for $C_{22}H_{32}O_7$: C 64.69, H 7.89; found: C 64.56, H 7.63.

*Orthoacetate **26***

A cooled (−10°C) solution of triol **25** (148 mg, 0.363 mmol) in acetic anhydride (21 mL) was reacted with perchloric acid (70%, 3 drops). After 10 min, methanol (15 mL) was slowly added and the volatile substances were then removed under reduced pressure. The oily residue was extracted with ether, washed once with brine, and reacted with aqueous sodium hydroxide for 0.5 h at room temperature under good stirring. The aqueous layer was separated and extracted with ether. The combined organic layer extracts were dried and evaporated to yield a residue that was purified by crystallization in chloroform–hexane (59 mg, 42%); mp 263–267°C; ir ($CHCl_3$, ν cm^{-1}): 1745, 1725, 1710; ^1H nmr ($CDCl_3$, δ ppm): 9.48 (d, 1H, J = 3 Hz, CHO), 3.2–1.5 (m), 1.63 (s, 3H, CH_3CO_3), 1.16 (s, 3H, CH_3C5), 1.12 (d, 3H, J = 6.5 Hz), 0.80 (d, 3H, J = 6.5 Hz) $CH(CH_3)_2$); ms *m/e*: 386 (M^+). *Anal.* calcd. for $C_{22}H_{26}O_6$: C 68.38, H 6.78; found: C 68.52, H 7.03.

*Monoacetate **27***

A mixture of aldehyde **5** (59 mg, 0.18 mmol), acetic anhydride (5 mL), and anhydrous sodium acetate (50 mg, 0.61 mmol) was heated under nitrogen (70°C) for 37 h. The cooled reaction mixture was then filtered and the volatile substances were evaporated. The crude product was chromatographed (thin layer) (silica gel, benzene–ether, 7:3) to give monoacetate **27** (39 mg, 59%); mp 142–144°C; ir ($CHCl_3$, ν cm^{-1}): 3570, 2730, 1735, 1730, 1220; ^1H nmr ($CDCl_3$, δ ppm): 9.53 (d, 1H, J = 2.4 Hz, CHO), 3.96 (d, 1H, J = 5.5 Hz, HC11), 3.58 (dd, 1H, $J_{1,2}$ = 6.5 Hz, J_W = 2.5 Hz, HCl), 2.9–1.1 (m), 2.13 (s, 3H, CH_3CO_2), 1.32 (s, 3H, CH_3C5), 1.10 and 0.93 (2d, 6H, J = 6.5 Hz, $CH(CH_3)_2$); ms *m/e*: 372 (M^+).

*Ozonolysis of olefin **27***

A cold (−78°C) solution of olefin **27** (30 mg, 0.08 mmol) in methanol (20 mL) was reacted with a stream of ozone for 4 min, then methyl sulfide (5 mL) was added and the mixture was warmed to room temperature for 1 h. Evaporation of volatile substances left a residue that was dissolved in chloroform and washed with water. The dried extract was evaporated. The solid residue was recrystallized from chloroform–ether mixture to give monoacetate **28** (16 mg, 49%); mp 182–182.5°C; ir ($CHCl_3$, ν cm^{-1}): 3400, 2740, 1740, 1725, 1700; ^1H nmr ($CDCl_3$, δ ppm): 9.60 (d, 1H, J = 3.6 Hz, -CHO), 6.20 (s, 1H, OH), 4.38 (m, 1H, OH), 3.80 (dd, 1H, $J_{1,2}$ = 5 Hz, J_W = 1.5 Hz, HCl), 2.30 (s, 3H, CH_3CO_2), 3.4–1.5 (m), 1.28 (s, 3H, CH_3C5), 1.06 and 0.96 (2d, 6H, J = 6.5 Hz, $CH(CH_3)_2$); ms *m/e*: 404 (M^+). *Anal.* calcd. for $C_{22}H_{28}O_7$: C 65.33, H 6.97; found: C 65.36, H 6.99.

*Orthoacetate **26** from monoacetate **28***

A solution of monoacetate **28** (18 mg, 0.041 mmol) and *p*-toluenesulfonic acid (10 mg) in benzene (5 mL) was heated at 75°C for 2 h, then cooled, diluted with ether (30 mL), and washed with aqueous sodium carbonate and brine. The dried extract was evaporated and the residue was crystallized from chloroform–hexane to give orthoacetate **26** (14 mg, 82%, mp 265–266°C) (*vide supra*).

*Ozonolysis of aldehyde olefin **11***

(*a*) Ozonolysis was performed as for ketal olefin **19** on the following quantities: **11** (50 mg, 0.14 mmol) in methanol (50 mL) during 8 min. After the usual work-up the crude product was purified by thin-layer chromatography to give aldol isomers **29** and **30** (chloroform–acetone, 9:1).

Can. J. Chem. Downloaded from www.nrcresearchpress.com by 186.148.149.217 on 09/07/12
For personal use only.

Aldol isomer ***29*** (more polar) (12 mg, 21%): mp 261–264°C; ir ($CHCl_3$, ν cm^{-1}): 3400, 2720, 1798, 1745, 1725, 1700; ^1H nmr (acetone-d_6, δ ppm): 9.66 (br s, 1H, CHO), 3.3–1.6 (m), 1.26 (s, 3H, CH_3C5), 1.13 and 0.79 (2d, 6H, J = 6.5 Hz, $CH(CH_3)_2$); ms *m/e*: 388 (M^+). *Anal.* calcd. for $C_{21}H_{24}O_7$: C 64.94, H 6.23; found: C 64.97, H 6.25.

Aldol isomer ***30*** (less polar) (27 mg, 50%); mp 227–228°C; ir ($CHCl_3$, ν cm^{-1}): 3590, 3400, 2720, 1820, 1750, 1735, 1710, ^1H nmr (acetone-d_6, δ ppm): 9.71 (d, 1H, J = 2 Hz, CHO), 3.5–1.5 (m), 1.30 (s, 3H, CH_3C5), 1.12 and 0.77 (2d, 6H, J = 6.5 Hz, $CH(CH_3)_2$); ms *m/e*: 388 (M^+). *Anal.* calcd. for $C_{21}H_{24}O_7$: C 64.94, H 6.23; found: C 64.76, H 6.47.

(*b*) The same reaction was performed in the presence of *p*-toluenesulfonic acid (20 mg). The crude product was shown to be a 5:2 mixture of compounds **29**:**30** respectively (nmr integration of aldehydic proton).

Hemi-orthocarbonate sodium salt ***31***

To a solution of aldol product **29** (34 mg, 0.088 mmol) in dry tetrahydrofuran (680 μL) was added excess sodium hydride (10 mg, 57% oil dispersion) and the mixture was stirred under nitrogen for 1.5 h; stirring was then stopped and a part of the clear supernatant solution was injected into an ir cell (IRTRAN II): ir (THF, ν cm^{-1}): 1740, 1715. Acidification of the reaction mixture (1 M HCl, 2 mL) was followed by ether extraction and evaporation of the solvents, which gave back pure aldol product **29** (33 mg). A similar procedure performed on compound **30** did not result in the disappearance of the carbonate absorption at ~1820 cm^{-1}.

Oxime ***32***

To a solution of ketone **19** (105 mg, 0.273 mmol) in anhydrous methanol (10 mL) was added hydroxylamine hydrochloride (385 mg, 5.53 mmol) and anhydrous sodium acetate (450 mg, 5.48 mmol). After 19 h at reflux temperature, the mixture was cooled, extracted with chloroform, and washed with water and brine. Evaporation of the dried extract left a residue that was chromatographed on silica gel (benzene – ethyl acetate, 3:1) to give oxime **32** (99 mg, 91%); mp 186–187°C ($CHCl_3$–hexane); ir ($CHCl_3$, ν cm^{-1}): 3580, 3320, 1810; ^1H nmr ($CDCl_3$, δ ppm): 8.80 (br s, 1H, NOH), 4.33 (br s, 1H, $HC(OCH_3)_2$), 3.52 and 3.44 (2s, 6H, 2 × OCH_3), 3.5–1.4 (m), 1.29 (s, 3H, CH_3C5), 1.06 and 1.02 (2d, 6H, J = 6.5 Hz, $CH(CH_3)_2$); ms *m/e*: 417 (M^+). *Anal.* calcd. for $C_{23}H_{31}NO_6$: C 66.17, H 7.49; found: C 65.89, H 7.42.

Lactam ***33***

To a cooled solution (0°C) of oxime **32** (33 mg, 0.079 mmol) in dichloromethane (6 mL) was added an excess of triethylamine (200 μL) and methanesulfonyl chloride (100 μL). After 40 min, the mixture was extracted with methylene chloride, then washed with sodium bicarbonate solution and brine. Evaporation of the solvent left a residue, which was chromatographed on silica gel (benzene – ethyl acetate, 85:15) to give intermediate mesylate (38 mg, 97%): ir ($CHCl_3$, ν cm^{-1}): 1805, 1705, 1360, 1165; ^1H nmr ($CDCl_3$, δ ppm): 4.34 (s, 1H, $CH(OCH_3)_2$), 3.52 and 3.45 (2s, 6H, 2 × OCH_3), 3.15 (s, 3H, SO_2CH_3), 3.5–1.4 (m), 1.31 (s, 3H, CH_3C5), 1.10 and 1.06 (2d, 6H, J = 6.6 Hz, $CH(CH_3)_2$); ms *m/e*: 495 (M^+). This mesylate (38 mg, 0.077 mmol) was refluxed in a mixture of dioxane (4 mL), water (1 mL), and pyridine (25 μL) for 1.2 h. Evaporation of the solvents and chromatography of the residue (silica plate, chloroform:acetone, 9:1) furnished lactam **33** (22 mg, 69%); ir ($CHCl_3$, ν cm^{-1}): 3400, 1810, 1670; ^1H nmr ($CDCl_3$, δ ppm): 5.48 (br s, 1H, NH), 4.41 (s, 1H, $CH(OCH_3)_2$), 3.93 (d (after D_2O exchange), 1H, J = 3.5 Hz, HCl), 3.54 and 3.40 (2s, 6H, 2 × OCH_3), 3.15 (d, 1H, J = 3.7 Hz, HC11), 2.6–1.5 (m), 1.31 (s, 3H, CH_3C5), 1.07 and 1.02 (2d, 6H, J = 6.8 Hz, $CH(CH_3)_2$); ms *m/e*: 417 (M^+).

Isomeric epoxylactones ***34*** *and* ***35***

A mixture of ketone **19** (1.088 g, 2.71 mmol) and anhydrous sodium acetate (2.00 g, 24.4 mmol) in 40% peracetic acid in acetic acid (20 mL) was stirred at room temperature for 20 h, then at 85°C for 1 h. The mixture was cooled at 0°C, reacted slowly with aqueous sodium bisulfite (4 M, 50 mL), and extracted with chloroform. Evaporation of the solvents and remaining acetic acid left a residue (1.136 g, 95%) that contained two main compounds **34** and **35** (85:15 respectively, integration of lactonic proton at C15 for **34** and Cl for **35**); ir ($CHCl_3$, ν cm^{-1}): 1820, 1749; ^1H nmr ($CDCl_3$, δ ppm): 4.89 (d, ~0.15 H, J = 3.3 Hz, HCl in **35**), 4.60 (ddd, 1H, J = 4.5, 2.5, and 9.8 Hz, HC15 in **34**), 4.41 (s, 1H, $CH(OCH_3)_2$), 3.58 and 3.44 (2s, 6H, $CH(OCH_3)_2$), 3.03 (d, 1H, J = 4.5 Hz, HC11), 3.3–1.2 (m), 1.35 (s, 3H, CH_3C5), 1.10 and 0.96 (2d, 6H, J = 7 Hz, $CH(CH_3)_2$). Several recrystallizations of this mixture from methylene chloride – methanol furnished a pure sample of **34** for analysis: mp 268–269°C; ms *m/e*: 434 (M^+). *Anal.* calcd. for $C_{23}H_{30}O_8$: C 63.58, H 6.96; found: C 63.56, H 6.82.

Olefinic lactones ***36*** *and* ***36a***

To cold (−78°C) tetrahydrofuran (180 mL) under argon was added all at once tungsten hexachloride (metallic black, 6.9 g, 17.4 mmol). Five minutes later, under good stirring, butyllithium (2.4 M in hexane, 21.7 mL, 52.2 mmol) was added dropwise over 20 min. After 10 min at −78°C, the mixture was warmed slowly (~1 h) to room temperature. After several gradual changes in the color of the reaction mixture (successively greenish brown, light yellow, dark brown), lithium iodide (60 mg, 0.45 mmol) was added and 5 min later a dry solid mixture of epoxy lactones (85:15) **34** and **35** (2.80 g, 6.45 mmol). After 6 h at room temperature, the reaction mixture was poured into a cold solution of basic sodium tartrate (200 mL, 1.5 M in sodium tartrate and 2 M in sodium hydroxide) and extracted several times with ether. The combined organic layers were washed with brine, dried, and evaporated. The crude product (2.8 g) was chromatographed on silica gel to furnish olefinic lactones **36** (less polar) and **36***a* (from **35**) (chloroform–acetone, 98:2).

Olefinic lactone ***36*** (2.15 g, 80%, colorless tetrahedrons from ether); mp 179–181°C; $[\alpha]_D$ −10.5° (*c* 1.0, $CHCl_3$); ir ($CHCl_3$, ν cm^{-1}): 1812, 1745; ^1H nmr ($CDCl_3$, δ ppm): 4.56 (ddd, 1H, J = 4.5, 4.5, and 8.5 Hz, HC15), 4.42 (s, 1H, $CH(OCH_3)_2$), 3.56 and 3.43 (2s, 6H, 2 × OCH_3), 3.16 (d, 1H, J = 4.5 Hz, HC11), 3.2–1.5 (m), 1.33 (s, 3H, CH_3C5), 1.29 and 0.98 (2d, 6H, J = 7 Hz, $CH(CH_3)_2$); ms *m/e*: (M^+). *Anal.* calcd. for $C_{23}H_{30}O_7$: C 66.01, H 7.23; found: C 65.95, H 7.29.

Olefinic lactone ***36a*** (400 mg, 14%, needles); mp 168–169°C; ir ($CHCl_3$, ν cm^{-1}): 1810, 1740; ^1H nmr ($CHCl_3$, δ ppm): 4.90 (d, 1H, J = 4.5 Hz, HCl), 4.46 (s, 1H, $HC(OCH_3)_2$), 3.57 and 3.47 (2s, 6H, 2 × OCH_3), 3.28 (d, 1H, J = 4.5 Hz, HC11), 2.9–1.4 (m), 1.33 (s, 3H, CH_3C5), 1.15 and 1.05 (2d, 6H, J = 7 Hz, $CH(CH_3)_2$); ms *m/e*: 418 (M^+).

Ketoester ***37***

To a solution of lactone **36** (150 mg, 0.359 mmol) in 1,2-dimethoxyethane (6 mL) was added a solution of lithium hydroxide (50 mg, 2.1 mmol) in water (2 mL). After 18 h at room temperature, the mixture was partly evaporated, neutralized with a stream of carbon dioxide (phenolphthalein), and reacted during 15 min alternatively, by small portions, with an excess of sodium bicarbonate (560 mg) and trimethyloxonium tetrafluoroborate (1.0 g). Dilution with water (~10 mL) and extraction with dichloromethane afforded a crude product (155 mg) that was dissolved in dry dichloromethane (2 mL) and added to chromium trioxide – pyridine complex (215 mg CrO_3, 356 μL pyridine) in dichloromethane (8 mL) at 0°C. After 10 min, isopropanol (1 mL) was added and the mixture was diluted with ether. The organic layer was washed with water, dried, and evaporated. Chromatography of the crude product on silica gel (hexane – ethyl acetate, 4:1) gave ketoester **37** (119 mg, 74%); mp 143–144°C; ir ($CHCl_3$, ν cm^{-1}): 1798, 1735, ^1H nmr ($CDCl_3$, δ ppm): 4.54 (s, 1H, $CH(OCH_3)_2$), 3.61 (s, 3H, CO_2CH_3), 3.56 (s, 1H, HC11), 3.55 and 3.30 (2s, 6H, $CH(OCH_3)_2$), 3.22 (d, 1H, J = 7 Hz, HCl), 3.10 (d, 1H, J_{AB} = 12 Hz) and 2.55 (d, 1H, J_{AB} = 12 Hz) (H_2C14); 2.8–1.4 (m), 1.41 (s, 3H, CH_3C5), 1.02 and 0.82 (2d, 6H, J = 7 Hz, $CH(CH_3)_2$); ms *m/e*: 448 (M^+).

Carbonate diol ***38***

A mixture of olefinic lactone **36** (52.0 mg, 0.124 mmol) and lithium borohydride (50 mg, 2.5 mmol) in dry tetrahydrofuran (8 mL) was refluxed for 30 h, then cooled at −78°C and reacted with ammonium chloride aqueous solution. The mixture was warmed to room tempera-

Can. J. Chem. Downloaded from www.nrcresearchpress.com by 186.148.149.217 on 09/07/12
For personal use only.

ture, extracted with dichloromethane, washed with brine, and the solvent was evaporated. Chromatography (chloroform–acetone, 4:1) of the crude product gave a small quantity of starting material and its hemi-ketal (2 mg, 4%) and carbonate diol **38** (48 mg, 95%); mp 213–214°C; ir ($CHCl_3$, ν cm^{-1}): 3600, 3350, 1790; ^1H nmr ($CDCl_3$, δ ppm): 4.37 (s, 1H, $CH(OCH_3)_2$), 3.9 (m, 3H, CH_2OH and HC15), 3.89 and 3.49 (2s, 6H, 2 × OCH_3), 3.48 (d, 1H, J = 4.5 Hz, HC11), 3.0–1.4 (m), 1.26 (s, 3H, CH_3C5), 0.98 and 0.96 (2d, 6H, $CH(CH_3)_2$); ms *m/e*: 422 (M^+). *Exact Mass* calcd. for $C_{23}H_{34}O_7-CH_3OH$: 390.2042; found: 390.2052.

Ozonolysis of olefin lactone 36

A stream of ozone was bubbled through a cold (−78°C) solution of olefin lactone (740 mg, 1.77 mmol) in dry methanol–dichloromethane (1:1, 25 mL) in the presence of *p*-toluenesulfonic acid (155 mg, 0.81 mmol) during 10 min. To the blue solution was then added dimethyl sulfide and the mixture was warmed to room temperature, extracted with chloroform, and washed with aqueous potassium carbonate and brine. Removal of the solvent left a residue that was purified by crystallization (acetone–hexane) and chromatography on silica gel ($CHCl_3$–acetone, 9:1) to give compound **39** (757 mg, 95%); mp 238–238.5°C; ir ($CHCl_3$, ν cm^{-1}): 3380, 1780, 1755, 1710; ^1H nmr (acetone-d_6, δ ppm): 5.38 (dd, 1H, J = 10.5 and 3.0 Hz, HC15), 4.42 (d, 1H, J = 3.6 Hz, $HC(OCH_3)_2$), 3.48 and 3.46 (2s, 6H, 2 × OCH_3), 3.22 (d, 1H, J = 4 Hz, HCl), 3.1–1.6 (m), 1.21 (s, 3H, CH_3C5), 1.16 and 0.93 (2d, 6H, J = 7.1 Hz, $CH(CH_3)_2$); ms *m/e*: 450 (M^+). *Anal.* calcd. for $C_{23}H_{30}O_9$: C 61.32, H 6.71; found: C 61.63, H 6.51.

Hemi-orthocarbonate sodium salt 40

Formation of orthocarbonate anion **40** from **39** was carried out as for compound **31** (*vide supra*). Analysis of its ir spectrum showed the disappearance of the carbonate absorption at 1780 cm^{-1} and the presence of the other two carbonyl absorptions at 1755 and 1710 cm^{-1}.

Epoxyketoester 41

A mixture of ketoester **37** (15 mg, 0.034 mmol) and anhydrous sodium acetate (25 mg, 0.30 mmol) in 40% peracetic acid in acetic acid (1 mL) was stirred at 25°C for 20 h, then at 85°C for 1 h. The mixture was cooled to 0°C, reacted with cold aqueous sodium bisulfite (4 M, 1.5 mL), and extracted with chloroform. The organic layer was washed with aqueous sodium bicarbonate, then brine, and evaporated. Chromatography of the crude product (silica gel, benzene – ethyl acetate, 4:1) gave pure epoxyketoester **41** (13 mg, 85%); mp 183–184°C; ir ($CHCl_3$, ν cm^{-1}): 1804, 1750, 1740; ^1H nmr ($CDCl_3$, δ ppm): 4.63 (s, 1H, $CH(OCH_3)_2$), 3.65 (br s, 7H, CO_2CH_3, CH-OCH_3 and HC11), 3.49 (s, 3H, CH-OCH_3), 3.27 (d, 1H, J = 7 Hz, HCl), 3.12 (d, 1H, J = 12 Hz, HC3), 2.9–1.2 (m), 1.48 (s, 3H, CH_3C5), 1.03 and 0.81 (2d, 6H, J = 7 Hz, $CH(CH_3)_2$); ms *m/e*: 464 (M^+).

Basic treatment of ester 37

To a solution of ester **37** (50 mg, 0.11 mmol) in 1,2-dimethoxyethane (3 mL) was added 1,5-diazabicyclo[4.3.0]non-5-ene (DBN) (40 μL, 0.32 mmol) and the mixture was stirred for 4 h at 25°C. Evaporation of the volatile materials left a residue, which was filtered through silica gel (benzene – ethyl acetate, 9:1) to give unsaturated ketoester **42** (45 mg, 98%); λ_{max} (ethanol): 227 nm (ε 45 000); ir ($CHCl_3$, ν cm^{-1}): 3430, 1730, 1680, 1650; ^1H nmr ($CDCl_3$, δ ppm): 4.65 (d, 1H, J = 2.5 Hz, $CH(OCH_3)_2$), 4.58 (s, 1H, HC11), 3.83 (s, 3H, CO_2CH_3), 3.53 and 3.51 (2s, 6H, 2 × OCH_3), 2.8–1.5 (m), 1.32 (s, 3H, CH_3C5), 0.85 and 0.81 (2d, 6H, J = 7 Hz, $CH(CH_3)_2$); ms *m/e*: 404 (M^+).

Oxime *43*

(a) From ketoester 37

A mixture of unsaturated ketoester **37** (21 mg, 0.047 mmol), hydroxylamine hydrochloride (65 mg, 0.70 mmol), and anhydrous sodium acetate (81 mg, 0.82 mmol) in dry methanol was refluxed for 20 h, then cooled and diluted with ether. The organic layer was washed with water, brine, then evaporated to give a residue, which was chromatographed on thin layer (silica gel, hexane–ether, 1:1) to give starting material **37** (11 mg, 52%) and oxime **43** (2 mg, 5%) (*vide infra*).

(b) From unsaturated ketoester 42

A mixture of unsaturated ketoester **42** (12 mg, 0.049 mmol), hydroxylamine hydrochloride (33 mg, 0.30 mmol), and anhydrous sodium acetate (41 mg, 0.41 mmol) in anhydrous methanol (1 mL) was refluxed for 1 h, then cooled and diluted with ether. After the usual extraction, the crude product was chromatographed to give oxime **43** (10 mg, 83%); mp 182–182.5°C; ir ($CHCl_3$, ν cm^{-1}): 3630, 3300, 1705, 1650; ^1H nmr ($CDCl_3$, δ ppm): 4.68 (s, 1H, HC11), 4.65 (d, 1H, J = 3 Hz, $CH(OCH_3)_2$), 3.82 (s, 3H, CO_2CH_3), 3.54 and 3.49 (2s, 6H, $CH(OCH_3)_2$), 2.90 (br s, 1H, OH), 2.8–1.1 (m), 1.37 (s, 3H, CH_3C5), 0.85 and 0.80 (2d, 6H, J = 7 Hz, $CH(CH_3)_2$); ms *m/e*: 419 (M^+).

Ozonolysis of ketoester 37

Ozone was bubbled through a cold (−78°C) solution of ketoester **37** (25 mg, 0.056 mmol) and *p*-toluenesulfonic acid (5 mg) in a mixture of methanol–dichloromethane (2:1, 3 mL) during 2 min (blue color). Dimethyl sulfide (1 mL) was added, the mixture was warmed to room temperature, and the volatile substances were evaporated. The crude residue was dissolved in dichloromethane, washed with sodium bicarbonate solution and brine, and the solvent was evaporated to leave a residue that was chromatographed on silica gel (benzene – ethyl acetate, 3:2) to give aldol product **44** (20 mg, 80%), an amorphous solid: ir ($CHCl_3$, ν cm^{-1}): 3565, 3400, 1795, 1755, 1730, 1715; ^1H nmr ($CDCl_3$, δ ppm): 4.45 (d, 1H, J = 6 Hz, $CH(OCH_3)_2$), 3.57 (s, 3H, CO_2CH_3), 3.54 and 3.47 (2s, 6H, $CH(OCH_3)_2$), 3.40 (d, 1H, J = 4 Hz, HCl), 3.1–1.6 (m), 1.42 (s, 3H, CH_3C5), 1.00 and 0.76 (2d, 6H, J = 7 Hz, $CH(CH_3)_2$); ms *m/e*: 480 (M^+).

Dihydroxyketone 45

To a cooled (0°C) solution of diketone ester **44** (20 mg, 0.042 mmol) in tetrahydrofuran (2 mL) and methanol (2 mL) was added sodium borohydride (40 mg, large excess). After 15 min, saturated aqueous ammonium chloride was added and the mixture was extracted with chloroform, washed with water and brine, and the solvent was evaporated. Chromatography of the residue (dichloromethane – acetone, 4:1) (thin layer) furnished diol **45** (18 mg, 90%): amorphous solid; ir ($CHCl_3$, ν cm^{-1}): 3530, 3420, 1795, 1740, 1730; ^1H nmr ($CDCl_3$, δ ppm): 4.39 (d, 1H, J = 5.8 Hz, $CH(OCH_3)_2$), 4.05 (after D_2O exchange, dd, 1H, J = 11 and 5 Hz, $H_{ax}C10$), 3.60 (s, 3H, CO_2CH_3), 3.50 (s, 3H) and 3.44 (s, 3H) (2 × OCH_3), 3.35 (dd, 1H, J = 14.4 and 5.9 Hz, HC3), 3.27 (d, 1H, J = 6.2 Hz, HCl), 2.78 (d, 1H, J_{AB} = 19.9 Hz) and 2.22 (d, 1H, J_{AB} = 19.9 Hz) (H_2C14), 2.51 (ddd, 1H, J = 14, 6.2, and 6.1 Hz, HC2), 2.03 (m, 1H, HC13), 1.75–1.2 (m), 1.31 (s, 3H, CH_3C5), 1.00 and 0.76 (2d, 6H, J = 6.8 Hz, $CH(CH_3)_2$); ms *m/e*: 482 (M^+).

Methyl orthocarbonate 46

To a cold (0°C) solution of carbonate **45** (25 mg, 0.051 mmol) in chloroform was added ethereal diazomethane (excess) and the mixture was warmed to room temperature for 1.5 h. Evaporation of volatile materials and chromatography (silica plate, ether – ethyl acetate, 4:1) gave orthocarbonate **46** (20 mg, 80%); ir ($CHCl_3$, ν cm^{-1}): 3515, 1735, 1730, 1430, 1320; ^1H nmr ($CDCl_3$, δ ppm): 4.43 (d, 1H, J = 6 Hz, $CH(OCH_3)_2$), 4.4–3.8 (br m, 1H, $H_{ax}C10$), 3.72 (s, 3H, O_3COCH_3), 3.60 (s, 3H, CO_2CH_3), 3.51 and 3.46 (2s, 6H, $CH(OCH_3)_2$), 3.3–2.7 (m, 2H, HCl and HC3), 2.88 and 2.12 (2d, 2H, J_{AB} = 20 Hz, H_2C14), 1.9–1.2 (m), 1.30 (s, 3H, CH_3C5), 1.05 and 0.75 (2d, 6H, J = 7.0 Hz, $CH(CH_3)_2$); ms *m/e*: 496, weak (M^+).

Hemi-ketal 47

To a cooled (0°C) solution of diol **38** (110 mg, 0.259 mmol) in acetone was added dropwise Jones reagent (0.29 mL, 0.29 mmol). After 2 min, the mixture was poured onto iced water and extracted with ether. The extract was washed with water and brine, and the solvent was evaporated. The crude product was chromatographed on silica plate (benzene – ethyl acetate, 4;1) to give pure hemi-ketal **47** (89 mg, 80%); mp 158–160°C; ir ($CHCl_3$, ν cm^{-1}): 3600, 3460, 1795; ^1H nmr ($CDCl_3$, δ ppm): 4.56 (s, 1H, $CH(OCH_3)_2$), 4.28–4.04 (m, 2H, CH_2O), 3.64 and 3.53 (2s, 6H, $CH(OCH_3)_2$), 3.20 (s, 1H, HC11), 1.33 (s, 3H, CH_3C5), 1.09 and 0.98 (2d, 6H, J = 7 Hz, $CH(CH_3)_2$); ms *m/e*: 420 (M^+).

Can. J. Chem. Downloaded from www.nrcresearchpress.com by 186.148.149.217 on 09/07/12
For personal use only.

*Lactone **48***

To a solution of hemi-ketal **47** (30 mg, 0.071 mmol) in acetonitrile was added a solution of ceric ammonium nitrate (330 mg, 0.54 mmol) in water (3 mL). After 0.5 h at 0°C, the mixture was extracted with dichloromethane. Evaporation of the solvents left a residue, which was purified by chromatography on silica plate (benzene – ethyl acetate, 4:1) to give compound **48** (16.8 mg, 56%); mp 168–170°C; ir $CHCl_3$, ν cm^{-1}): 1800, 1765, 1660; ^1H nmr ($CDCl_3$, δ ppm): 6.35 and 5.48 (2m, 2H, olefinic protons), 4.75 (dd, 1H, J_{AB} = 12 Hz, J_{AX} = 2 Hz) and 4.30 (dd, 1H, J_{AB} = 12 Hz, J_{BX} = 3 Hz) (CH_2O), 4.60 (s, 1H, $CH(CH_3)_2$), 3.60 (s, 6H, $CH(OCH_3)_2$), 3.00 and 2.15 (2d, 2H, J_{AB} = 12 Hz, H_2C14), 3.3–2.5 (m), 1.60 (s, 3H, CH_3C5), 1.15 and 1.05 (2d, 6H, J = 7 Hz, $CH(CH_3)_2$); ms *m/e*: 418 (M^+).

*Hydroxyacid **49***

To a solution of lactone **48** (2.0 mg, 0.0047 mmol) in 1,2-dimethoxyethane (DME) (1 mL) was added aqueous lithium hydroxide (0.72 mg, 0.0052 mmol). After 20 min at 25°C the mixture was poured onto water, acidified (pH 6.5, 0.1 M HCl), and extracted with dichloromethane to give crude acid **49** (2.0 mg, 95%); ir ($CHCl_3$, ν cm^{-1}): 3600–2700 (br), 1795, 1740, 1660; ^1H nmr ($CDCl_3$, δ ppm): 6.48 and 5.67 (2m, 2H, olefinic protons), 5.10 (very br, 1H, CO_2H), 4.61 (br s, 1H, $CH(OCH_3)_2$), 3.64 and 3.54 (2s, 6H, 2 × OCH_3), 3.2–1.3 (m), 1.50 (s, 3H, CH_3C5), 0.88 and 0.77 (2d, 6H, J = 7 Hz, $CH(CH_3)_2$); ms *m/e*: 436 (M^+).

*Acetate acid **50***

To a solution of hydroxyacid **49** (7.4 mg, 0.015 mmol) in pyridine (0.7 mL) was added acetic anhydride (0.7 mL). After 3 h at room temperature, water (0.8 mL) was added and the mixture was stirred at 0°C for 30 min. Evaporation of the volatile materials left a residue, which was dissolved in dichloromethane, and washed with water and brine. Evaporation of the extract furnished pure acid **50** (7 mg, 86%); ir ($CHCl_3$, ν cm^{-1}): 3600–2400 (br), 1800, 1740, 1660; ^1H nmr ($CDCl_3$, δ ppm): 8.00 (br m, CO_2H), 6.48 and 5.62 (2m, 2H, olefinic protons), 4.50 (m, 2H, -CH_2O-), 4.30 (br s, 1H, $CH(OCH_3)_2$), 3.61 and 3.52 (2s, 6H, 2 × OCH_3), 3.0–1.1 (m), 2.11 (s, 3H, O_2CCH_3), 1.28 (s, 3H, CH_3C5), 0.85 and 0.75 (2d, 6H, J = 7 Hz, $CH(CH_3)_2$); ms *m/e*: 478 (M^+).

*Hydroxyester **51***

To a solution of hydroxyacid **49** (2 mg, crude) in dichloromethane at 0°C was added ethereal diazomethane (0.5 mL). After 10 min, evaporation of the volatile substances left a residue, which was chromatographed on silica plate (benzene – ethyl acetate, 4:1) to give hydroxyester **51** (1.5 mg, 75%); ir ($CHCl_3$, ν cm^{-1}): 3500 (weak), 1800, 1740, 1650, 1600; ms *m/e*: 450 (M^+).

*Methoxylactone **53***

To a solution of acid **50** (6 mg, 0.013 mmol) in dry benzene was added *p*-toluenesulfonic acid (0.7 mg). The mixture was refluxed for 25 h, then cooled, poured onto water, extracted with dichloromethane, washed with water, and the solvent evaporated. The crude product was chromatographed on silica plate (benzene – ethyl acetate, 4:1) to give methoxylactone **53** (3.2 mg, 57%); ir ($CHCl_3$, ν cm^{-1}): 1810, 1745, 1665, 1600; ^1H nmr ($CDCl_3$, δ ppm): 6.10 and 5.52 (2m, 2H, olefinic protons), 5.03 (d, 1H, J = 6 Hz, $CH_3OCHOCO_2$), 4.01 (m, 2H, $CH_2OCO_2CH_3$), 3.50 (s, 3H, OCH_3), 3.2–1.8 (m), 2.00 (s, 3H, CH_3CO_2), 1.54 (s, 3H, CH_3C5), 1.30 and 0.97 (2d, 6H, J = 7 Hz, $CH(CH_3)_2$); ms *m/e*: 446 (M^+).

*Lactone **57***

A solution of hemi-ketal **47** (110 mg, 0.26 mmol) and *p*-toluenesulfonic acid (60 mg) in dry dichloromethane (25 mL) was cooled to −78°C and reacted with a stream of ozone (~4 min). Then dimethyl sulfide (2 mL) was added to the mixture and after 5 min the excess of the sulfide was evaporated, and the reaction mixture was washed with aqueous sodium bicarbonate and brine. Evaporation of the solvent left a crude product, which was chromatographed to give crystalline enone lactone **57** (85 mg, 75%); mp 215–216°C (dec.); uv (λ_{max}, EtOH): 238 nm (ε 15 000); ir ($CHCl_3$, ν cm^{-1}): 1810, 1760, 1680, 1630; ^1H nmr ($CDCl_3$, δ ppm): 4.36 (d, 1H, J = 5.6 Hz, $CH(OCH_3)_2$), 4.23 (d, 2H, J = 1.5 Hz, H_2C17), 3.56 and 3.52 (2s, 3H each, 2 × OCH_3), 3.30 (dd, 1H, J = 11.1 and 5.6 Hz, HC3), 3.08 (d, 1H) and 2.42 (d, 1H) (J_{AB} = 12.6 Hz, H_2C14), 2.88 (m, 2H, HC2 and HC1), 2.4 and 2.13 (2m), 1.39 (s, 3H, CH_3C5), 1.07 and 1.03 (2d, 3H each, $CH(CH_3)_2$); ms *m/e*: 434 (M^+, weak).

*Tricyclic enone aldehyde **60***

A cold saturated solution of ozone in dichloromethane was added dropwise to a cold (−78°C) solution of olefin diol **38** (17 mg, 0.04 mmol) and *p*-toluenesulfonic acid (10 mg) in anhydrous methanol (7 mL) until the disappearance of the starting material. Dimethyl sulfide (1 mL) was added and the mixture was warmed to room temperature, then washed with aqueous sodium bicarbonate and brine. Evaporation of the solvent left a residue, which was chromatographed on silica gel to give enone aldehyde **60** (9.2 mg, 56%); ir ($CHCl_3$, ν cm^{-1}): 3450, 1720, 1658, 1570; ^1H nmr ($CDCl_3$, δ ppm): 9.71 (t, 1H, J = 3 Hz, OHC15), 4.60 (d, 1H, J = 5 Hz, $CH(OCH_3)_2$), 4.5 (m, 3H, OH and CH_2OH), 3.56 and 3.51 (2s, 6H, 2 × OCH_3), 2.5–1.5 (m), 1.43 (s, 3H, CH_3C5), 0.95 (d, 6H, J = 7 Hz, $CH(CH_3)_2$); ms *m/e*: 392 (M^+-H_2O).

*Keto p-nitrobenzoate **62***

To a cold (0°C) solution of diol **38** (200 mg, 0.474 mmol) in pyridine (4 mL) was added freshly recrystallized (petroleum ether) p-nitrobenzoyl chloride (105 mg, 0.566 mmol). After 1 h at 0°C the mixture was diluted with chloroform (100 mL), then washed with cold aqueous sodium carbonate and brine. Evaporation of the solvent left a solid residue (260 mg, 96%) that was used directly for the next step; mp 181–182°C (benzene); ir ($CHCl_3$, ν cm^{-1}): 3610, 3490, 1790, 1728, 1605, 1537, 1270; ^1H nmr ($CDCl_3$, δ ppm): 8.27 (s, 4H, aromatic), 5.10 (dd, 1H, J_{AB} = 11 Hz, J_{AX} = 10 Hz, H_AC17), 4.80 (dd, 1H, J_{AB} = 11 Hz, J_{BX} = 6 Hz, H_BC17), 4.28 (d, 1H, J = 1.9 Hz, $CH(OCH_3)_2$), 3.88 (m, 1H, HC15), 3.48 and 3.45 (2s, 6H, 2 × OCH_3), 3.21 (d, 1H, J = 2.5 Hz, HC11), 2.8–1.4 (m), 1.27 (s, 3H, CH_3C5), 0.95 (br d, 6H, J = 6.5 Hz, $CH(CH_3)_2$); ms *m/e*: 539 (M^+-CH_3OH). Collins reagent was prepared by the addition of anhydrous pyridine (1.47 mL) to a suspension of chromium trioxide (920 mg, 0.92 mmol) in dry dichloromethane (30 mL). After 15 min at 25°C, this reagent was cooled at 0°C and a solution of the preceding hydroxyester (260 mg, 0.455 mmol) in dichloromethane (2 mL) was added. Five minutes later, isopropanol (2 mL) was added and the mixture was poured onto cold aqueous sodium carbonate and extracted with dichloromethane. The extract was dried and the solvent was evaporated. The crude residue was purified by chromatography on silica gel (benzene – ethyl acetate, 9:1) to give pure ketone **62** (255 mg, 98%); ir ($CHCl_3$, ν cm^{-1}): 1794, 1737, 1600, 1524, 1265; ^1H nmr ($CDCl_3$, δ ppm): 8.29 (s, 4H, aromatic), 4.82 (dd, 1H, J_{AB} = 12 Hz, J_{AX} = 4 Hz, H_AC17), 3.90 (dd, J_{AB} = 12 Hz, J_{BX} = 11 Hz, H_BC17), 4.50 (br s, 1H, $CH(OCH_3)_2$), 3.85 (s, 1H, HC11), 3.58 and 3.46 (2s, 6H, 2 × OCH_3), 2.4–1.5 (m), 1.45 (s, 3H, CH_3C5), 1.09 and 1.03 (2d, 6H, J = 6.7 Hz, $CH(CH_3)_2$); ms *m/e*: 569 (M^+). *Exact Mass* calcd. for $C_{30}H_{35}O_{10}N$ (M^+): 569.2261; found: 569.2256.

*Epoxide **63***

To a solution of keto *p*-nitrobenzoate **62** (560 mg, 0.984 mmol) in dichloromethane (50 mL) was added solid *m*-chloroperbenzoic acid (1.7 g, 98% 9.8 mmol). The mixture was stirred in the dark (aluminium foil) for 18 h at room temperature, then cooled (0°C) and slowly added to cold aqueous sodium bisulfite (~4%, 100 mL). The organic layer was separated and washed with aqueous sodium bicarbonate. The aqueous layer was extracted with dichloromethane and the combined organic layers were dried and the solvent evaporated. The crude product was filtered through silica gel (benzene – ethyl acetate, 95:5) to give epoxide **63** (570 mg, 99%); ir ($CHCl_3$, ν cm^{-1}): 1815, 1755, 1737, 1605, 1526, 1260; ^1H nmr ($CDCl_3$, δ ppm): 8.30 (s, 4H, aromatic), 4.76 (dd, 1H, J_{AB} = 12 Hz, J_{AX} = 4 Hz, H_AC17), 3.81 (dd, 1H, J_{AB} = 12 Hz, J_{BX} = 11.5 Hz, H_BC17), 4.47 (br s, 1H, $CH(OCH_3)_2$), 3.68 (s, 1H, HC11), 3.2–1.2 (m), 1.48 (s, 3H, CH_3C5), 1.03 and 0.97 (2d, 6H, J = 6.5 Hz, $CH(CH_3)_2$). *Exact Mass* calcd. for $C_{30}H_{35}O_{11}N-CH_3O$ (M^+-CH_3O): 554.2026; found: 554.2038.

Can. J. Chem. Downloaded from www.nrcresearchpress.com by 186.148.149.217 on 09/07/12
For personal use only.

Enol ethers ***64***

From a solution of epoxide **63** (910 mg, 1.55 mmol) in benzene (350 mL), in a 3-neck 500-mL flask, was distilled a small quantity of benzene (~25 mL, Dean–Stark head filled with molecular sieve 4Å); then *p*-toluenesulfonic acid (~3 mg) was added on the inner side of the flask. The reflux was continued for 15 h and the reaction mixture was concentrated by distillation of benzene to a small volume (~10 mL), cooled to room temperature, and rapidly filtered through a small column of silica gel (benzene – ethyl acetate, 2:1). The crude product (850 mg, 99%) was used directly for the next step. The isomeric enol ethers **64** (~1:1) were separated by thin-layer chromatography (benzene – ethyl acetate, 20:1, two elutions).

Enol ether ***64***a (less polar): mp 258–259°C; ir ($CHCl_3$, ν cm^{-1}): 1808, 1750, 1740, 1668, 1608, 1527, 1256; ^1H nmr ($CDCl_3$, δ ppm): 8.30 (m, 4H, aromatic), 6.44 (br s 1H, =C*H*OCH_3), 4.95 (m, 1H) and 5.25 (m, 1H) (H_2C17), 3.75 (s, 4H, OCH_3 and HC11), 3.03 (m, 2H, HC1 and HC2), 2.5–1.5 (m), 1.43 (s, 3H, CH_3C5), 0.96 (m, 6H, $CH(CH_3)_2$); ms *m/e*: 553 (M^+).

Enol ether ***64***b (more polar): mp 127–128°C; ir ($CHCl_3$, ν cm^{-1}): 1808, 1748, 1740, 1667, 1610, 1528, 1255; ^1H nmr ($CDCl_3$, δ ppm): 8.28 (m, 4H, aromatic), 6.15 (d, 1H, J = 1.2 Hz, =C*H*OCH_3), 4.86 (dd, 1H, J_{AB} = 12 Hz, J_{AX} = 5 Hz, H_AC17), 4.20 (dd, 1H, J_{AB} = 12 Hz, J_{BX} = 11 Hz, H_BC17), 3.73 (s, 4H, OCH_3 and HC11), 3.3–1.3 (m), 1.51 (s, 3H, CH_3C5), 0.95 (d, 6H, J = 7 Hz, $CH(CH_3)_2$); ms *m/e*: 553 (M^+). *Anal.* calcd. for $C_{29}H_{31}O_{10}N$: C 62.92, H 5.64; found: C 62.88, H 5.78.

Norketone ***65***

To a cold (−78°C) solution of enol ethers **64** (35 mg, 0.063 mmol) in dichloromethane (10 mL) was added a cold (−78°C) saturated ozone solution in dichloromethane until the starting enol ethers disappeared (tlc monitoring). Then dimethyl sulfide (1.5 mL) was added and the mixture was warmed to room temperature. Evaporation of the volatile substances left a residue that was rapidly filtered on silica gel (benzene – ethyl acetate, 10%) to give pure slightly unstable norketone **65** (31 mg, 94%); mp 188–189°C; ir ($CHCl_3$, ν cm^{-1}): 1830, 1755, 1740, 1610, 1530; ^1H nmr ($CDCl_3$, δ ppm): 8.29 (m, 4H, aromatic), 4.84 (dd, 1H, J_{AB} = 12 Hz, J_{AX} = 4.4 Hz, H_AC17), 4.33 (dd, 1H, J_{AB} = 12 Hz, J_{BX} = 10.5 Hz, H_BC17), 3.93 (s, 1H, HC11), 2.88 (m, 1H, HC1), 2.45 (d, 1H, J_{AB} = 19 Hz, H_AC14), 1.60 (d, 1H, J_{AB} = 19 Hz, H_BC14), 2.5–1.2 (m), 1.51 (s, 3H, CH_3C5), 1.06 and 1.03 (2d, 6H, J = 7 Hz, $CH(CH_3)_2$); ms *m/e*: 525 (M^+). *Anal.* calcd. for $C_{27}H_{27}O_{10}N$: C 61.71, H 5.17; found: C 61.53, H 4.91.

Endocyclic enol ether ***66***

To a cold (0°C) solution of norketone **65** (183 mg, 0.34 mmol) in tetrahydrofuran (4 mL) and ethanol (1 mL) was added a freshly prepared solution of diazomethane (~10 mL in ether, excess). After 18 h at 0°C, the volatile substances were evaporated to leave pure enol ether **66** (188 mg, 99%); ir ($CHCl_3$, ν cm^{-1}): 1815, 1750, 1735, 1665, 1605, 1525, 1255; ^1H nmr ($CDCl_3$, δ ppm): 8.28 (m, 4H, aromatic), 4.83 (dd, 1H, J_{AB} = 12 Hz, J_{AX} = 4 Hz, H_AC17), 4.03 (dd, 1H, J_{AB} = 12 Hz, J_{BX} = 11 Hz, H_BC17), 3.81 (s, 1H, HC11), 3.70 (s, 3H, OCH_3), 3.45 (dd, 1H, J = 4 and 11 Hz, HC1), 2.73 (m, 1H, *H*$C(CH_3)_2$), 2.35 (d, 1H, J_{AB} = 18.5 Hz) and 1.80 (d, 1H, J_{AB} = 18.5 Hz) (H_2C14), 2.1–1.3 (m), 1.61 (s, 3H, OCH_3), 1.16 and 1.08 (2d, 6H, J = 7 Hz, $CH(CH_3)_2$).

Enol acetate ***67***

To a solution of norketone **65** (64 mg, 0.12 mmol) in acetic anhydride (3 mL) was added anhydrous sodium acetate (120 mg) and the mixture was heated to 95°C for 1 h. The cooled mixture was then filtered through cotton and the solvent was evaporated. Rapid filtration of the crude product through silica gel (benzene – ethyl acetate, 85:15) furnished pure enol acetate **67** (64 mg, 93%); ir ($CHCl_3$, ν cm^{-1}): 1822, 1780, 1755, 1740, 1670, 1610, 1530; ^1H nmr ($CDCl_3$, δ ppm): 8.28 (m, 4H, aromatic), 4.92 (dd, 1H, J_{AB} = 12 Hz, J_{AX} = 4 Hz, H_AC17), 4.25 (dd, 1H, J_{AB} = 12 Hz, J_{BX} = 10 Hz, H_BC17), 3.90 (s, 1H, HC11), 3.68 (dd, 1H, J = 10 and 4 Hz, HC1), 2.60 (qn, 1H, J = 7 Hz, *H*$C(CH_3)_2$), 2.45 (d, 1H J_{AB} = 20 Hz) and 2.05 (d, 1H, J_{AB} = 20 Hz, H_2C14), 2.33 (s, 3H, CH_3CO_2), 1.50 (s, 3H, CH_3C5), 1.08 and 0.93 (2d, 6H, $CH(CH_3)_2$).

Dienol ether ***69***

From a solution of enol ether **66** (390 mg, 0.723 mmol) in benzene (150 mL) was distilled some benzene (~20 mL). A quantity of 1,5-diazabicyclo[4.3.0]non-5-ene (DBN) (1.2 mL, freshly distilled, excess) was then added and the mixture was refluxed for 10 h. The cooled mixture was then poured onto ice-cold hydrochloric solution (0.5 M, 50 mL) and extracted with dichloromethane. The combined organic layers were washed with aqueous sodium bicarbonate and brine. Evaporation of the solvent left a colored residue, which was chromatographed (silica gel, benzene – ethyl acetate, 96:4) to give pure colorless dienol ether **69** (207 mg, 77%); mp 203–204°C; ir ($CHCl_3$, ν cm^{-1}): 1810, 1755, 1635, 1620; ^1H nmr ($CDCl_3$, δ ppm): 5.34 and 5.26 (2d, 2H, J = 1.4 Hz, H_2C17), 3.78 (s, 3H, OCH_3), 3.59 (s, 1H, HC11), 2.68 (qn, 1H, J = 7 Hz, *H*$C(CH_3)_2$), 2.20 (d, 1H, J_{AB} = 18 Hz) and 1.78 (d, 1H, J_{AB} = 18 Hz) (H_2C14), 1.58 (s, 3H, CH_3C5), 1.17 and 1.14 (2d, 6H, J = 7 Hz, $CH(CH_3)_2$); ms *m/e*: 372 (M^+). *Anal.* calcd. for $C_{21}H_{24}O_6$: C 67.73, H 6.50; found: C 67.90, H 6.62. *Exact Mass* calcd. for $C_{21}H_{24}O_6$: 373.1573; found: 372.1569.

Enone ***71***

A solution of enol acetate **67** (40 mg, 0.073 mmol) in dry benzene (8 mL) was refluxed in the presence of freshly distilled DBN (2.2 equiv., 34 μL). After 20 h, the cooled mixture was diluted with dichloromethane, washed with water, and the extract was dried. Evaporation of the solvent left a residue that was purified by silica gel chromatography (benzene – ethyl acetate, 9:1) to give crystalline enone **71** (18 mg, 69%); mp 129–130°C; ir ($CHCl_3$, ν cm^{-1}): 1820, 1750, 1725, 1630; ^1H nmr ($CDCl_3$, δ ppm): 3.58 (s, 1H, HC11), 2.72 (qn, 1H, J = 7 Hz, *H*$C(CH_3)_2$), 2.13 (d, 1H, J_{AB} = 18 Hz) and 1.47 (d, 1H, J_{AB} = 18 Hz) (H_2C14), 2.08 (s, 3H, H_3C17), 1.50 (s, 3H, CH_3C5), 1.14 and 1.08 (2d, 6H, J = 7 Hz, $CH(CH_3)_2$); ms *m/e*: 358 (M^+).

Olefin ***72*** (*vide supra*, preparation of compound ***36***)

To cold THF (8 mL, −78°C) under argon was added tungsten hexachloride (black, 80 mg, 0.20 mmol) and, 5 min later, *n*-butyllithium in hexane (dropwise, 266 μL, 2.2 M, 0.586 mmol, time of the addition ~20 min). The mixture was allowed to warm to room temperature and was stirred for 1 h. About half (~4 mL, ~3 equiv.) of the dark brown solution obtained was transferred, under argon, to crystalline epoxide **69** (25 mg, 0.067 mmol). The mixture was stirred for 3 h, then filtered through silica gel (~20 g) and eluted with ether. Evaporation of the solvents left a mixture of olefin **72** and starting material **69**, which were separated by chromatography (chloroform) to give starting material **69** (12 mg) and olefin **72** (10 mg, 80% based on recovered starting material). In our hands, modification of these conditions resulted in lower yield of the desired product; mp 181–181.5°C; ir ($CHCl_3$, ν cm^{-1}): 1810, 1745, 1640, 1620; uv (EtOH, λ_{max}): 240 nm (ε 17 320); ^1H nmr ($CDCl_3$, δ ppm): 5.34 and 5.27 (2d, 2H, J = 1.2 Hz, H_2C17), 3.76 (s, 3H, OCH_3), 3.74 (s, 1H, HC11), 2.70 (qn, 1H, J = 7.1 Hz, *H*$C(CH_3)_2$), 1.56 (s, 3H, CH_3C5), 1.20 and 1.15 (2d, 6H, J = 7.1 Hz, $CH(CH_3)_2$); ms *m/e*: 356 (M^+). *Exact Mass* calcd. for $C_{21}H_{24}O_5$: 356.1624; found: 356.1634.

Enone ***73***

To a solution of dienol ether **72** (90 mg, 0.253 mmol) in benzene (20 mL) was added boron trifluoride etherate (0.8 mL) and the mixture was stirred at room temperature for 18 h. The mixture was then washed with aqueous sodium bicarbonate, the aqueous phase was extracted with dichloromethane, and the combined organic layers were dried and evaporated. The residue was filtered through silica gel (hexane –ether, 4:1) to give pure enone **73** (80 mg, 93%); mp 135–136°C; ir ($CHCl_3$, ν cm^{-1}): 1825, 1740, 1725, 1630; uv (EtOH, λ_{max}): 233 nm (ε 7749); ^1H nmr ($CDCl_3$, δ ppm): 3.84 (s, 1H, HC11), 2.78 (qn, 1H, J = 7 Hz, *H*$C(CH_3)_2$), 2.15 (d) and 1.75 (d) (J_{AB} = 19 Hz, H_2C14), 2.15 (s, 3H, H_3C17), 1.56 (s, 3H, CH_3C5), 1.19 and 1.15 (2d, 6H, J = 7 Hz, $CH(CH_3)_2$); ms *m/e*: 342 (M^+). *Exact Mass* calcd. for $C_{20}H_{22}O_5$: 342.1465; found: 342.1465.

Can. J. Chem. Downloaded from www.nrcresearchpress.com by 186.148.149.217 on 09/07/12
For personal use only.

Reaction of compound 73 with trifluoroperacetic acid

The reagent was prepared by mixing, at 0°C, 90% hydrogen peroxide (0.41 mL, 15 mmol) in dry dichloromethane (10 mL) and adding, with good stirring, trifluoroacetic anhydride (2.54 mL, 12 mmol). After 10 min of stirring at 0°C the reagent (which can be stored for weeks at −20°C) was ready for use. To a solution of enone **73** (3.0 mg, 0.0087 mmol) in dichloromethane (2 mL) was added powdered dibasic sodium phosphate (20 mg) and trifluoroperacetic acid solution prepared as above (1.0 mL, ~1.0 mmol). After 20 h in the dark, the solution was washed with aqueous sodium bicarbonate and dried over sodium sulfate. The crude product was shown to be pure enone epoxide **71** (3 mg, ~quant).

Epoxyketone 77

To a solution of enone **73** (6.0 mg, 0.017 mmol) in ether (5 mL) was added aqueous basic hydrogen peroxide (0.05 M in H_2O_2, 0.05 M in NaOH) (1 mL) and the mixture was vigorously stirred at 25°C for 40 h. The mixture was then poured into aqueous diluted sodium bisulfite and extracted with ether at pH 6. The organic layer was washed with brine and the solvent was evaporated. Chromatography (benzene – ethyl acetate, 9:1) on silica gel furnished epoxide **77** (3.2 mg, 50%); ir ($CHCl_3$, ν cm^{-1}): 1830, 1765, 1742; ^1H nmr ($CDCl_3$, δ ppm): 3.79 (s, 1H, HC11), 2.7–1.7 (m), 1.67 (s, 3H, H_3C17), 1.48 (s, 3H, CH_3C5), 1.25 and 1.11 (2d, 6H, J = 6.6 Hz, $CH(CH_3)_2$); ms *m/e*: 358 (M^+).

Bicyclic triketone 81

A solution of enone **73** (70 mg, 0.20 mmol) in dichloromethane (8 mL) containing methanol (3 mL) and *p*-toluenesulfonic acid (3 mg) was reacted at −78°C with a cold saturated solution of ozone in dichloromethane until the starting material disappeared (tlc monitoring). After the addition of dimethyl sulfide (1 mL) the mixture was warmed to 0°C, poured onto cold aqueous sodium bicarbonate, and extracted with dichloromethane. The crude product was purified by chromatography on silica gel (ether) to give light yellow crystalline bicyclic triketone **81** (60 mg, 81%); mp 99–100°C; uv (EtOH, λ_{max} nm): 296 (ε 21 000), 224 (ε 7000); ir ($CHCl_3$, ν cm^{-1}): 3350, 1724, 1680 (sh), 1662, 1631, 1588; ^1H nmr ($CDCl_3$, δ ppm): 5.96 (s, OH), 5.95 (s, 1H, HC11), 3.68 (s, 3H, OCH_3), 3.12 and 2.33 (2d, 2H, J_{AB} = 17.1 Hz, H_2C14), 2.94 (qn, 1H, J = 6.5 Hz, $CH(CH_3)_2$), 2.88 (dt, 1H, J_{AB} = 18.9 Hz, J = 6.7 Hz) and 2.66 (dt, 1H, J_{AB} = 18.9 Hz, J = 6.7 Hz) (H_2C9), 2.43 (br t, 2H, J = 7.3 Hz, H_2C7), 2.17 (s, 3H, H_3C17), 1.98 (qn, 2H, J = 6.9 Hz, H_2C8), 1.25 and 1.22 (2d, 6H, J = 6.5 Hz, $CH(CH_3)_2$), 1.15 (s, 3H, CH_3C5); ^{13}C nmr ($CDCl_3$, δ ppm): 216.1, 201.8, 196.6, 174.4, 158.8, 157.8, 152.7, 116.7, 78.5, 51.6, 48.9, 44.2, 38.9, 32.7, 26.2, 20.1, 19.8, 18.5, 17.7, 11.9; ms *m/e*: 362 (M^+). *Exact Mass* calcd. for $C_{20}H_{26}O_6-OCH_3$: 331.1545; found: 331.1538.

Ozonolysis of enone 73

To a cold (78°C) solution of enone **73** (4.0 mg, 0.011 mmol) in dry dichloromethane (2 mL) containing *p*-toluenesulfonic acid (1 mg) was added dropwise a cold solution of ozone in dichloromethane until the starting material disappeared (tlc monitoring). After addition of dimethyl sulfide (0.5 mL) the mixture was warmed to ~0°C, poured into cold aqueous bicarbonate solution, and extracted with dichloromethane. The extract was washed with water and brine, dried, and the solvent was evaporated to give a single, but unstable, compound, which could not withstand chromatography and to which was assigned structure **82** (crude, 4 mg, 95%); ir ($CHCl_3$, ν cm^{-1}): 3450, 1828, 1770, 1725, 1620; ^1H nmr ($CDCl_3$, δ ppm): 3.18 (br s, 1H, OH), 2.75 (qn, 1H, J = 7 Hz, $HC(CH_3)_2$), 2.60 and 2.00 (2d, 2H, J_{AB} = 18 Hz, H_2C14), 2.19 (s, 3H, H_3C17), 1.53 (s, 3H, CH_3C5), 1.18 and 1.12 (2d, 6H, J = 7 Hz, $CH(CH_3)_2$; ms *m/e*: 374 (M^+).

Ozonolysis of keto p*-nitrobenzoate 62*

Ozone was added to a cold (−78°C) solution of keto *p*-nitrobenzoate **62** (774 mg, 1.36 mmol) and *p*-toluenesulfonic acid (228 mg) in ethyl acetate until the blue color persisted. After the addition of dimethyl sulfide (4 mL), the mixture was warmed to room temperature, poured onto an iced solution of sodium bicarbonate (~2%), and extracted with dichloromethane. Evaporation of the solvents left a residue that was shown to be the sensitive hydroxydiketone **83**; ir ($CHCl_3$, ν cm^{-1}): 3540, 3400, 1808, 1763, 1730, 1610, 1527, 1371, 1340, 1311, and 1265. The crude product was then dissolved in ethyl acetate (20 mL) and reacted with an excess of ethereal diazomethane for 2 h at 25°C. Evaporation of the volatile substances left a residue that was purified by chromatography on silica gel (hexane – ether, 2:3) to give diketone **84** (630 mg, 75%); ir $CHCl_3$, ν cm^{-1}): 1751, 1729, 1610, 1528, 1455, 1341, 1264; ^1H nmr ($CDCl_3$, δ ppm): 8.22 (m, 4H, aromatic), 4.6–3.5 (m, 2H, H_2C17), 4.32 (d, 1H, J = 5.1 Hz, $HC(OCH_3)_2$), 3.64 (s, 3H, CH_3OCO_3), 3.53 and 3.49 (2s, 6H, 2 × OCH_3), 2.9–1.3 (m), 1.35 (s, 3H, CH_3C5), 1.10 and 0.98 (2d, 6H, J = 7.4 Hz, $CH(CH_3)_2$); ms *m/e*: 585 (M^+-30).

Lactone 57

To a cold (−70°C) solution of diketone **84** (10.8 mg, 0.0175 mmol) in tetrahydrofuran (5 mL) was added a solution of lithium tri-*sec*-butylborohydride (1 M in THF, 70 μL, 0.070 mmol). After 1 h, additional reducing agent (30 μL) was added and, again, 1 h later (20 μL) for a total of ~7 equivalent. Acetone (3 mL) was added to the mixture 30 min after the last addition, followed by saturated aqueous ammonium chloride. Extraction with dichloromethane led to a residue that was chromatographed to give the known crystalline lactone **57** (*vide supra*, 5.0 mg, 64%).

Methyl ester 87

From lactone 57

A solution of lactone **57** (5.0 mg, 0.011 mmol) in dry methanol (5 mL) containing lithium methoxide solution in methanol (0.3 mL of a 0.2 M solution) was stirred at room temprature for 20 h. The mixture was then poured into aqueous ammonium chloride and extracted with dichloromethane to leave a residue that was chromatographed (ether) to give enone ester **87** (4 mg, 75%); ir ($CHCl_3$, ν cm^{-1}): 3500, 1800, 1740, 1680, 1633, 1390, 1220; ^1H nmr ($CDCl_3$, δ ppm): 4.30 (d, 1H, J = 6.5 Hz, $CH(OCH_3)_2$), 3.65 (s, 3H, OCH_3), 3.56 and 3.45 (2s, 6H, 2 × OCH_3), 3.7–3.3 (masked m, 2H, CH_2OH), 3.3–1.5 (m), 1.42 (s, 3H, CH_3C5), 1.05 and 1.00 (2d, 6H, J = 7 Hz, $CH(CH_3)_2$; ms *m/e*: 464 (M^+).

From diketone 84

To a cold (0°C) solution of diketone **84** (25 mg, 0.040 mmol) in tetrahydrofuran (8 mL) was added a solution of lithium methoxide in methanol (0.2 M, 200 μL). After 5 h, the mixture was poured into aqueous ammonium chloride and extracted with dichloromethane. The residue was purified by chromatography on silica gel (ether) to give hydroxyester **87** (11.5 mg, 61%).

Enol ether 88

This elimination was carried out as for enol ether **64** (*vide supra*). From compound **84** (230 mg, 0.374 mmol) was thus obtained, after a rapid filtration through silica gel, a purified mixture of enol ether **88** (216 mg, 99%), which was used directly for the next reaction. Spectroscopic data for the more abundant, less polar isomer: ir ($CHCl_3$, ν cm^{-1}): 1751, 1730, 1698, 1611, 1528, 1455, 1341, 1316, 1266; ^1H nmr ($CDCl_3$, δ ppm): 8.26 (s, 4H, aromatic), 5.98 (d, 1H, J = 1.9 Hz, $=CHOCH_3$), 4.42 (dd, 1H, J_{AB} = 12 Hz, J_{AX} = 2 Hz, H_AC17), 3.72 (s, 3H, OCH_3), 3.67 (s, 3H, OCH_3), 3.55 (dd, 1H, J_{AB} = J_{BX} = 12 Hz, H_BC17), 3.1–1.4 (m), 1.52 (s, 3H, CH_3C5), 1.20 and 1.10 (2d, 6H, J = 6 Hz, $CH(CH_3)_2$); ms *m/e*: 553 (M^+-30).

Norketone 89

To a cold (−78°C) solution of enol ether mixture **88** (100 mg, 0.171 mmol) in dry dichloromethane (20 mL) was added a cold dark-blue solution of ozone in dichloromethane until both isomers of **88** had disappeared (tlc monitoring). Then dimethyl sulfide (1 mL) was added, the mixture was warmed to room temperature, and the volatile substances were evaporated. This crude product (yellowish foam) was used directly for the next reaction. A small quantity was chromatographed on silica plate (benzene – ethyl acetate, 3:1) to give sensitive norketone **89**; ir ($CHCl_3$, ν cm^{-1}): 1760, 1733, 1610, 1529, 1456, 1348, 1320, 1258; ^1H nmr ($CDCl_3$, δ ppm): 8.2 (m, 4H, aromatic), 4.40 (m, 2H, H_2C17), 3.73 (s, 3H, OCH_3), 3.4–1.5 (m), 1.26 (s, 3H, CH_3C5), 1.10 and 1.00 (2d, 6H, J = 6 Hz, $CH(CH_3)_2$).

Can. J. Chem. Downloaded from www.nrcresearchpress.com by 186.148.149.217 on 09/07/12
For personal use only.

Enol acetylation

This reaction was carried out as for enol acetate **67** (*vide supra*). Thus norketone **89** (crude, 102 mg) furnished crude enol acetate **90** (102 mg, crude). A small quantity was purified on silica plate (benzene – ethyl acetate, 2:1) for spectroscopic data: ir ($CHCl_3$, ν cm^{-1}): 1770, 1760, 1735, 1610, 1529, 1458, 1350, 1310, 1264; ^1H nmr ($CDCl_3$, δ ppm): 8.28 (s, 4H, aromatic), 4.75 (dd, 1H, J_{AB} = 13 Hz, J_{AX} = 2.5 Hz, H_AC17), 4.50 (dd, 1H, J_{AB} = 13 Hz, J_{BX} = 5 Hz, H_BC17), 3.65 (s, 3H, OCH_3), 3.50 (d, 1H, J = 15 Hz) and 2.90 (d, 1H, J = 15 Hz) (H_AH_BC14), 3.37 (dd, 1H, J = 5 and 2.5 Hz, H_XC1), 2.44 (qn, 1H, J = 7 Hz, $CH(CH_3)_2$), 2.32 (s, 3H, CH_3CO_2), 2.4–1.5 (m), 1.29 (s, 3H, CH_3C5), 1.13 and 1.06 (2d, 6H, J = 7 Hz, $CH(CH_3)_2$.

*Diketone enone **91***

Following the procedure described for enone epoxide **71** (*vide supra*), crude enol acetate **90** (102 mg), after 3 h of reflux, led to enone **91** (52 mg, 78% from dimethyl acetal **84**); ir ($CHCl_3$, ν cm^{-1}): 1765, 1720, 1614, 1460, 1382, 1355, 1318; ^1H nmr ($CDCl_3$, δ ppm): 3.66 (s, 3H, OCH_3), 2.68 (qn, 1H, J = 6.9 Hz, $CH(CH_3)_2$), 2.50 and 1.99 (2d, 1H each, J_{AB} = 20 Hz, H_2C14), 2.25 (s, 3H, CH_3C1), 2.5–1.5 (m), 1.52 (s, 3H, CH_3C5), 1.16 and 1.13 (2d, 6H, J = 6.9 Hz, $CH(CH_3)_2$); ms m/e: 388 (M^+).

*Reduction of diketone enone **91***

To a cold (−78°C) solution of diketone enone **91** (27 mg, 0.069 mmol) in mixture of tetrahydrofuran (5 mL) and methanol (5 mL) was added a large excess of solid sodium borohydride (~10 mg) in small portions, until the starting material had just disappeared (tlc monitoring, benzene – ethyl acetate, 3:1). The mixture was then poured into saturated aqueous ammonium chloride and extracted with dichloromethane. The crude product was chromatographed on silica plate (benzene – ethyl acetate, 3:1) to give ketoalcohol **92** (6 mg, 22%) and diol **93** (15.6 mg, 57%).

*Ketoalcohol **92***: ir ($CHCl_3$, ν cm^{-1}): 3610, 3500, 1730, 1711, 1615, 1457, 1321, 1309; ^1H nmr ($CDCl_3$, δ ppm): 4.64 (dd, 1H, J = 10.7 and 4.6 Hz, HC15), 3.60 (s, 3H, OCH_3), 2.80 (qn, 1H, J = 7 Hz, $CH(CH_3)_2$), 2.6–1.15 (m), 2.33 (s, 3H, CH_3C1), 1.33 (s, 3H, CH_3C5), 1.19 and 1.16 (2d, 6H, J = 7 Hz, $CH(CH_3)_2$; ms m/e: 390 (M^+).

*Diol **93***: mp 225–226°C; ir ($CHCl_3$, ν cm^{-1}): 3620, 3500, 1711, 1620, 1459, 1308; ^1H nmr ($CDCl_3$, δ ppm): 4.57 (m, 1H, $W_{\frac{1}{2}}$ = 6 Hz, $H_{eq}C10$), 4.30 (dd, 1H, J = 10.8 and 4.2 Hz, HC15), 3.65 (s, 3H, OCH_3), 2.79 (qn, 1H, J = 7 Hz, $CH(CH_3)_2$), 2.20 (s, 3H, CH_3C1), 1.25 (s, 3H, CH_3C5), 1.20 and 1.17 (2d, 6H, J = 7 Hz, $CH(CH_3)_2$); ms m/e: 392 (M^+).

*Reduction of ketoalcohol **92***

Ketoalcohol **92** (5.0 mg, 0.013 mmol) was submitted to the same reaction conditions as above and furnished, after purification, diol **93** (3.8 mg, 76%).

*Dichloro and trichloroketones **94** and **95***

To a cold (−20°C) solution of enone **91** (6.3 mg, 0.016 mmol) in a mixture of tetrahydrofuran (1 mL) and dioxan (1 mL) was added an aqueous solution of sodium hypochlorite (0.92 M, 50 μL, 0.046 mmol) and the mixture was stirred at 0°C for 15 h. More reagent (25 μL, 0.023 mmol) was then added and after 9 h the mixture was poured into an aqueous solution of ammonium chloride and extracted with dichloromethane. The crude extract (7.4 mg) was chromatographed (hexane–ether, 1:2) on silica plate to give dichlorodiketone **94** (3.0 mg, 40%) and trichlorodiketone **94** (1.5 mg, 19%).

*Dichlorodiketone **94***: ir ($CHCl_3$, ν cm^{-1}): 1780, 1730, 1615, 1458, 1346, 1327, 1312, 810; ^1H nmr ($CDCl_3$, δ ppm): 3.64 (s, 3H, OCH_3), 2.70 (qn, 1H, J = 7 Hz, $CH(CH_3)_2$), 2.20 (s, 3H, CH_3C1), 2.5–1.7 (m), 1.83 (s, 3H, CH_3C5), 1.15 and 1.13 (2d, 6H, J = 7 Hz, $CH(CH_3)_2$); ms m/e: 458 and 456 (M^+, weak).

*Trichlorodiketone **95***: ir ($CHCl_3$, ν cm^{-1}) 1790, 1751, 1730, 1610, 1458, 1348, 1325, 1312, 810; ^1H nmr ($CDCl_3$, δ ppm): 3.63 (s, 3H OCH_3), 2.95 (dd, 1H, J = 12 and 6 Hz, $H_{ax}C9$), 2.75 (qn, 1H, J = 7 Hz, $CH(CH_3)_2$), 2.29 (s, 3H, CH_3C1), 2.3–1.6 (m), 1.82 (s, 3H, CH_3C5), 1.15 and 1.14 (2d, 6H, J = 7 Hz, $CH(CH_3)_2$); ms m/e: 493, 491, 489 (M^+).

tert-*Butyl perester **98***

To a solution of *tert*-butylhydroperoxide (80.5 mg, 0.89 mmol) in tetrahydrofuran (3 mL) was added at −70°C a solution of *n*-butyllithium (1.6 M in hexane, 0.53 mL, 0.85 mmol). After 15 min of stirring at this temperature, the reagent was used for the following reaction. To a cold (−78°C) solution of diketone enone **91** (50 mg, 0.13 mmol) in tetrahydrofuran (5 mL) were added quantities of the above solution of reagent (initially: 600 μL; 1 h later: 600 μL; 2 h later: 600 μL). After a total of 5 h of stirring, aqueous saturated ammonium chloride (2 mL) was added, and the mixture was warmed to room temperature and extracted with dichloromethane. The crude product was purified on silica plate to give unreacted starting material (10.5 mg, 21%) and perester **98** (35 mg, 61%): ir ($CHCl_3$, ν cm^{-1}): 1820, 1772, 1720, 1685, 1618; ^1H nmr ($CDCl_3$, δ ppm): 3.41 (d, 1H) and 2.53 (d, 1H) (J_{AB} = 18.5 Hz) (H_2C14), 2.75 (qn, 1H, J = 7 Hz, $CH(CH_3)_2$), 2.25 (s, 3H, CH_3C1), 1.26 (s, 3H, CH_3C5), 1.19 (s, 9H, $C(CH_3)_3$), 1.05 (d, 6H, J = 7 Hz, $CH(CH_3)_2$); ms m/e: 373 ($M^+ - t\text{-}C_4H_9O$).

*Acid **99***

To a solution of perester **98** (30 mg, 0.074 mmol) in glacial acetic acid (5 mL) stirred at 14–15°C was added zinc powder (200 mg). The mixture was warmed to room temperature and after 50 min was poured onto iced aqueous solution of potassium bicarbonate (1 M, 150 mL) and extracted with dichloromethane. The aqueous layer was acidified (1 M HCl, pH 5) and extracted with dichloromethane. The two extracts, identical by tlc (ethyl acetate – acetic acid, 98:2), were combined to give a crude product (33 mg) that after crystallization (dichloromethane – hexane) furnished pure acid **99** (17.5 mg, 63%); mp 144–145°C; ir ($CHCl_3$, ν cm^{-1}): 3600–2700 (br), 1825, 1730, 1687, 1620; ^1H nmr ($CDCl_3$, δ ppm): 3.44 (d, 1H) and 2.58 (d, 1H) (J_{AB} = 18 Hz) (H_2C14), 2.72 (qn, 1H, J = 7 Hz, $CH(CH_3)_2$), 2.29 (s, 3H, CH_3Cl), 2.5–1.6 (m), 1.26 (s, 3H, CH_3C5), 1.09 and 1.03 (2d, 6H, J = 7 Hz, $CH(CH_3)_2$); ms m/e: 329 ($M^+ - 45$).

*Methyl ester **100***

*(a) From acid **99***

To a solution of acid **82** (30 mg, 0.080 mmol) in freshly distilled chloroform (10 mL) was added at 0°C an excess of ethereal diazomethane solution. After 10 min, the solvents were removed under vacuum and the solid residue was crystallized (dichloromethane – hexane) to give methyl ester **100** (22 mg, 76%); mp 188–188.5°C; ir ($CHCl_3$, ν cm^{-1}): 1826, 1745, 1730, 1687, 1621; ^1H nmr ($CDCl_3$, δ ppm): 3.50 (s, 3H, OCH_3), 3.39 (d, 1H) and 2.55 (d, 1H) (J_{AB} = 18.5 Hz) (H_2C14), 2.70 (qn, 1H, J = 7 Hz, $CH(CH_3)_2$), 2.30 (s, 3H, CH_3C1), 2.5–1.6 (m), 1.20 (s, 3H, CH_3C5), 1.09 and 1.06 (2d, 6H, J = 7 Hz, $CH(CH_3)_2$); ms m/e: 388 (M^+). *Anal.* calcd. for $C_{21}H_{24}O_7$: C 64.94, H 6.23; found: C 65.19, H 6.42.

*(b) From diketone enone **91***

A solution of lithium methoxide (0.079 M, 88 μL, 0.0069 mmol) in dry methanol–tetrahydrofuran mixture (1:3) was added to a cold (0°C) solution of diketone enone **91** (2.7 mg, 0.0069 mmol) in tetrahydrofuran (1 mL). After 2.5 h, the mixture was poured into aqueous sodium bicarbonate and extracted with dichloromethane. The crude product was chromatographed on silica plate to give a small quantity of unreacted starting material and methyl ester **100** (0.7 mg, 26%), together with other products.

*Reduction of diketone **83***

To a cold (−22°C) solution of diketone **83** (168 mg, 0.28 mmol) in a mixture of tetrahydrofuran (15 mL) and methanol (5 mL) was added sodium borohydride (80 mg). After 1 h of stirring at the same temperature, saturated aqueous ammonium chloride and ice cold water were added. The mixture was extracted (pH ~6.0, 1 M HC1) with dichloromethane and the crude extract was used directly for the next step (crude 165 mg, compound **102**).

*Orthocarbonate **103***

To a cold (0°C) solution of diol **102** (195 mg, 0.323 mmol) in

Can. J. Chem. Downloaded from www.nrcresearchpress.com by 186.148.149.217 on 09/07/12
For personal use only.

chloroform (30 mL) and methanol (1 mL) was added an ethereal solution of diazomethane (excess). After 1 h, the volatile substances were evaporated and the crude product was chromatographed on silica gel (benzene – ethyl acetate, 4:1) to give pure orthocarbonate alcohol **103** (170 mg, 85%); ir ($CHCl_3$, ν cm^{-1}): 3550, 1740, 1610, 1530, 1450, 1340, 1315, 1260; ^1H nmr ($CDCl_3$, δ ppm): 8.20 (m, 4H, aromatic), 4.83 (dd, 1H, J_{AB} = 15 Hz, J_{AX} = 2.5 Hz, H_AC17), 4.26 (dd, 1H, J_{AB} = 15 Hz, J_{BX} = 3.6 Hz, H_BC17), 4.30 (d, 1H, J = 4 Hz, $HC(OCH_3)_2$), 4.05 (m, 1H, HC10), 3.67 (s, 3H, OCH_3), 3.53 (s, 3H, OCH_3), 3.50 (s, 3H, OCH_3), 2.6–1.4 (m), 2.25 (d, 1H) and 1.80 (d, 1H) (J_{AB} = 20 Hz) (H_2C14), 1.24 (s, 3H, CH_3C5), 1.06 and 0.96 (2d, 6H, J = 7 Hz, $CH(CH_3)_2$); ms *m/e*: 617 (M^+, weak).

*Acetate **104***

A solution of alcohol **103** (95 mg, 0.154 mmol) in pyridine (5 mL) and acetic anhydride (3 mL) was heated at 80°C for 4 h. Evaporation of the volatile substances left a residue that was filtered through silica gel (benzene – ethyl acetate, 3:1) to give pure acetate **104** (94 mg, 93%); ir ($CHCl_3$, ν cm^{-1}): 1760, 1740, 1610, 1530, 1455, 1350, 1320; ^1H nmr ($CDCl_3$, δ ppm): 8.20 (m, 4H, aromatic), 5.40 (dd, 1H, J = 11 and 4 Hz, $H_{ax}C10$), 4.68 (dd, 1H, J_{AB} = 14 Hz, J_{AX} = 3 Hz, H_AC17), 4.31 (dd, 1H, J_{AB} = 14 Hz, J_{BX} = 4 Hz, H_BC17), 4.28 (d, 1H, J = 5.5 Hz, $HC(OCH_3)$, 3.65 (s, 3H, OCH_3), 3.50 and 3.46 (2s, 6H, 2 × OCH_3), 2.8–1.3 (m), 2.30 (d, 1H) and 1.80 (d, 1H) (J_{AB} = 20 Hz) (H_2C14), 2.08 (s, 3H, CH_3CO_2), 1.20 (s, 3H, CH_3C5), 1.00 (apparent t, 6H, J = 6.5 Hz, $CH(CH_3)_2$; ms *m/e*: 659 (M^+, weak).

*Enol ether **105***

Elimination of methanol was effected as for compound **64** (*vide supra*). Thus, after only 2 h, compound **104** (48.0 mg, 0.073 mmol) furnished a mixture of enol ethers **105** (47 mg, ~quant); ir ($CHCl_3$, ν cm^{-1}): 1755, 1735, 1695, 1605, 1530, 1450, 1330, 1315, 1260; ^1H nmr ($CDCl_3$, δ ppm, major isomer, less polar): 8.22 (m, 4H, aromatic), 6.27 (d, 1H, =$CHOCH_3$), 5.40 (br dd, 1H, J = ~12 and 5 Hz, HC10), 4.65 (dd, 1H, J_{AB} = 13 Hz, J_{AX} = 3 Hz, H_AC17), 4.25 (dd, 1H, J_{AB} = 3 Hz, J_{BX} = 6 Hz, H_BC17), 3.70 and 3.68 (2s, 3H each, 2 × OCH_3), 2.70 (m, 1H, $HC(CH_3)_2$), 2.5–1.4 (m), 2.10 (s, 3H, CH_3CO_2), 1.40 (s, 3H, CH_3C5), 1.05 (apparent t, 3H, J = 6 Hz, $CH(CH_3)_2$).

*Norketone **106***

Ozonolysis of enol ether **105** was carried out as for enol ether **88** (*vide supra*). Thus crude enol ether **105** (47 mg) furnished crude sensitive norketone **106** (43 mg, 94%); ir ($CHCl_3$, ν cm^{-1}): 1760, 1740, 1610, 1530, 1455, 1350, 1320, 1260. This compound was used directly in the next step.

*Enol acetate **107***

Enol acetylation of norketone **106** was effected as for ketone **65** (*vide supra*). Thus norketone **106** (43 mg, crude) furnished enol acetate **107** (44 mg, 95%); ir ($CHCl_3$, ν cm^{-1}): 1760, 1740, 1610, 1530, 1452, 1260; ^1H nmr ($CDCl_3$, δ ppm): 8.45 (s, 4H, aromatic), 5.40 (dd, 1H, J = 14 and ~5Hz, $H_{ax}C10$), 5.15 (dd, 1H, J_{AB} = 13 Hz, J_{AX} = 2 Hz, H_AC17), 4.40 (dd, 1H, J_{AB} = 13 Hz, J_{BX} = 5 Hz, H_BC17), 3.65 (s, 3H, OCH_3), 3.10 (dd, 1H, J = 5 and 2 Hz, HCl), 2.55 (qn, 1H, J = 7 Hz, $CH(CH_3)_2$), 2.29 (s, 3H, CH_3CO_2), 2.21 (s, 3H, CH_3CO_2), 1.25 (s, 3H, CH_3C5), 1.15 and 1.05 (2d, 3H each, J = 7 Hz, $CH(CH_3)_2$).

*Enone **108***

Elimination reaction on compound **107** was carried out as for enol acetate **67**. Thus from enol acetate **107** (40 mg, 0.062 mmol) was obtained enone **108** (17 mg, 63%) after a 4 h reflux period and purification by chromatography on silica gel (hexane–ether, 1:1); mp 155–156°C; ir ($CHCl_3$, ν cm^{-1}): 1755, 1740, 1720, 1620, 1455, 1230; ^1H nmr ($CDCl_3$, δ ppm): 5.31 (dd, 1H, J = 11 and 4.5 Hz, HC10), 3.69 (s, 3H, OCH_3), 2.72 (qn, 1H, J = 7 Hz, $HC(CH_3)_2$), 2.28 (d, 1H) and 1.88 (d, 1H) (J_{AB} = 20 Hz) (H_2C14), 2.15 (s, 3H, CH_3CO_2), 2.03 (s, 3H, CH_3C1), 1.43 (s, 3H, CH_3C5), 1.18 and 1.17 (2d, 3H each, J = 7 Hz) ($CH(CH_3)_2$); ms *m/e*: 432 (M^+).

*Reduction of enone **108***

To a cold (0°C) solution of ketoenone **108** (25 mg, 0.058 mmol) in a mixture of tetrahydrofuran (1 mL) and methanol (1 mL) was added sodium borohydride (~8 mg, excess). After the disappearance of the starting material (~1.5 h), aqueous saturated ammonium chloride was added and the mixture was extracted with dichloromethane. The crude product, containing three main products, each more polar than the starting material, was chromatographed on silica plate (benzene – ethyl acetate, 3:1) to give *endo* allylic alcohol **109** (6 mg, 24%, invisible under uv, R_f 0.4) and the alcohols **110** as a mixture that was rechromatographed (hexane – ether, 1:1, two elutions) to give alcohol **110**a (less polar, 8 mg, 32%) and alcohol **110**b (more polar, 10 mg, 40%).

*Allylic alcohol **109***: mp 228–230°C; ir ($CHCl_3$, ν cm^{-1}): 3600, 3450, 1755, 1740, 1640, 1450, 1300, 1230; ^1H nmr ($CDCl_3$, δ ppm): 5.26 (dd, 1H, J = 12 and 5 Hz, HC10), 4.88 (m, 1H, J = ~2 Hz, HC3), 3.66 (s, 3H, OCH_3), 3.14 (d, 1H) and 2.12 (d, 1H), (J_{AB} = 20 Hz) (H_2C14), 2.66 (qn, 1H, J = 7 Hz, $CH(CH_3)_2$), 2.13 (s, 3H, CH_3CO_2), 1.68 (d, 3H, J = 2 Hz, CH_3C1), 1.37 (s, 3H, CH_3C5), 1.13 and 1.08 (2d, 3H each, J = 7 Hz, $CH(CH_3)_2$); ms *m/e*: 434 (M^+).

*Alcohol **110***a (less polar): ir ($CHCl_3$, ν cm^{-1}): 3600, 3500, 1745, 1620, 1455, 1310, 1220; ^1H nmr ($CDCl_3$, δ ppm): 5.75 (dd, 1H, J = 12 and 6 Hz, HC10), 3.75 (dd, 1H, J = 10 and 5 Hz, HC15), 3.64 (s, 3H, OCH_3), 2.78 (qn, 1H, J = 7 Hz, $CH(CH_3)_2$), 2.14 (s, 3H, CH_3CO_2), 1.99 (s, 3H, CH_3C1), 1.31 (s, 3H, CH_3C5), 1.20 (d, 6H, J = 7 Hz, $CH(CH_3)_2$); ms *m/e*: 434 (M^+).

*Alcohol **110***b (more polar): ir ($CHCl_3$, ν cm^{-1}): 3600, 3450, 1750, 1715, 1620, 1455, 1320, 1220; ^1H nmr ($CDCl_3$, δ ppm): 5.70 (dd, 1H, J = 12 and 5 Hz, HC10), 4.72 (dd, 1H, J = 11 and 4.5 Hz, HC15), 3.63 (s, 3H, OCH_3), 2.75 (qn, 1H, J = 7 Hz, $CH(CH_3)_2$, 2.11 (s, 3H, CH_3CO_2), 1.99 (s, 3H, CH_3C1), 1.26 (s, 3H, CH_3C5), 1.19 and 1.18 (2d, 3H each, J = 7 Hz, $CH(CH_3)_2$); ms *m/e*: 434 (M^+).

*Alcohol **111***

To a solution of acetate **108** (10.5 mg, 0.024 mmol) in methanol (2 mL) was added aqueous sodium hydroxide (0.5 mL). After 3 h at room temperature, the mixture was poured into ammonium chloride solution and extracted with dichloromethane to give pure alcohol **111** (9.4 mg, quant): ir ($CHCl_3$, ν cm^{-1}): 3540, 1745, 1720, 1610, 1455; ^1H nmr ($CDCl_3$, δ ppm): 4.20 (dd, 1H, J = 12 and 5 Hz, HC10), 3.69 (s, 3H, OCH_3), 2.76 (qn, 1H, J = 7 Hz, $CH(CH_3)_2$), 2.27 (d, 1H) and 1.96 (d, 1H) (J_{AB} = 20 Hz) (H_2C14), 2.24 (s, 3H, CH_3C1), 2.2–1.1 (m), 1.43 (s, 3H, CH_3C5), 1.17 and 1.14 (2d, 3H each, J = 7 Hz) ($CH(CH_3)_2$); ms *m/e*: (M^+).

*Dihydroxycarbonate **112***

To a solution of orthocarbonate **111** (6.0 mg, 0.0154 mmol) in acetone (1 mL) was added hydrochloric acid (1 M, 0.5 mL) and the mixture was stirred at room temperature for 24 h. The mixture was then poured into cold water, extracted with dichloromethane, washed with brine, and the solvent was evaporated. The crude product was chromatographed on silica plate (ether) to give pure dihydroxycarbonate **112** (5.7 mg, 95%); ir ($CHCl_3$, ν cm^{-1}): 1815, 1752, 1725, 1618; ^1H nmr ($CDCl_3$, δ ppm): 4.50 (dd, 1H, J = 11 and 5 Hz, HC10), 3.01 (qn, 1H, J = 7 Hz, $CH(CH_3)_2$), 2.90 (d, 1H) and 1.95 (d, 1H) (J_{AB} = 19 Hz) (H_2C14), 2.4–1.3 (m), 2.03 (s, 3H, CH_3C1), 1.37 (s, 3H, CH_3C5), 1.25 and 1.22 (2d, 3H each, J = 7 Hz) ($CH(CH_3)_2$); ms *m/e*: 376 (M^+).

*Dichloroketone **113***

A solution of ketoenone acetate **108** (5.0 mg, 0.0115 mmol) in a mixture of tetrahydrofuran (0.3 mL), dioxan (0.3 mL), and water (0.1 mL) was reacted with aqueous hypochlorite (0.92 M, 24 μL) at 0°C for 2 h. The reaction mixture was then poured into water and extracted with dichloromethane. The crude product was chromatographed on silica plate to give less polar dichloroketone **113** (4.4 mg, 76%) together with some starting material (0.5 mg, 10%); mp 160–161°C; ir $CHCl_3$, ν cm^{-1}): 1780, 1740 (sh), 1730, 1620, 1460, 1350, 1310, 1220, 905, 820; ^1H nmr ($CDCl_3$, δ ppm): 5.46 (dd, 1H, J = 12 and 4.5 Hz, HC10), 3.66 (s, 3H, OCH_3), 2.72 (qn, 1H, J = 7 Hz, $CH(CH_3)_2$), 2.17 (s, 3H, CH_3C1), 1.99 (s, 3H, CH_3CO_2), 1.76 (s, 3H, CH_3C5), 1.14 and 1.11 (2d, 3H each, J = 7 Hz, $CH(CH_3)_2$); ms *m/e*: 500 (M^+, absent), 465 M^+-35).

*Tricyclic ketodiol **116***

To a solution of diol **112** (2.5 mg, 0.0064 mmol) in dry tetrahydrofuran (0.3 mL) at −78°C was added a solution of lithium *tert*-

Can. J. Chem. Downloaded from www.nrcresearchpress.com by 186.148.149.217 on 09/07/12
For personal use only.

butylperoxide in tetrahydrofuran (0.099 M, 135 μL, ~2 equiv.). After 1 h, the same quantity of reagent was added and the temperature was raised to −22°C for 1 h. The mixture was then poured into water and extracted with dichloromethane. The crude product was chromatographed on silica plate (ether) to give tricyclic ketodiol **116** (1.7 mg, 75%); ir ($CHCl_3$, ν cm^{-1}): 3550, 1705, 1630; ^1H nmr ($CDCl_3$, δ ppm): 4.50 (dd, 1H, J = 11 and 5 Hz, HC10),[6] 3.04 (qn, 1H, J = 7 Hz, C*H*$(CH_3)_2$), 2.90 (d, 1H) and 1.95 (d, 1H) (J_{AB} = 19 Hz, H_2C14), 2.07 (s, 3H, CH_3C1), 1.37 (s, 3H, CH_3C5), 1.26 and 1.25 (2d, 3H each, J = 7 Hz, $CH(CH_3)_2$); ms *m/e*: 332 (M^+).

*Diacetate **117***

A solution of tricyclic ketodiol **116** (2 mg, 0.006 mmol) in pyridine (0.2 mL) and acetic anhydride (0.2 mL) was stirred 20 h at room temperature. Evaporation of volatile substances left a residue, which was chromatographed on silica plate (hexane – ether) to give diacetate **117** (2.3 mg, 90%); ir ($CHCl_3$, ν cm^{-1}): 1745, 1710, 1640, 1620, 1220; ^1H nmr ($CDCl_3$, δ ppm): 5.60 (dd, 1H, J = 9 and 4 Hz, HC10),[6] 3.00 (qn, 1H, J = 7 Hz, $CH(CH_3)_2$, 2.92 (d, 1H) and 1.92 (d, 1H) (J_{AB} = 18.5 Hz) (H_2C14), 2.07 (s, 3H, CH_3-C1), 2.04 and 2.02 (2s, 3H each, 2 × CH_3CO_2), 1.26 and 1.24 (2d, 3H each, J = 7 Hz, $CH(CH_3)_2$).

Camphor oxime

A solution of camphor (5.00 g, 0.0329 mol) and hydroxylamine hydrochloride (7.00 g, 0.10 mol) in pyridine (30 mL) was heated at 75°C for 2 h. The mixture was poured into cold water and extracted with dichloromethane to give a crude product that was recrystallized from ether – hexane to give pure camphor oxime (5.39 g, 98%, mp 116–117°C (lit. (26*c*, *d*) mp 116°C)).

*Lactam **119** and α-camphidone*

To a cold (−22°C) solution of camphor oxime (5.38 g, 0.0322 mol) in pyridine (25 mL) was added methanesulfonyl chloride (5.0 mL, 0.065 mmol) and the mixture was stirred 3 h. Then the temperature was raised. At ~10°C a strong exothermic reaction took place and the mixture became dark yellow. After 2 h of additional stirring at 25°C, the mixture was poured onto iced water and extracted with dichloromethane. The organic layer was washed with sodium bicarbonate and brine. The crude product was first filtered on silica gel to remove the major products of low polarity (mixture of nitriles, 4.03 g, ~84%, chloroform – acetone, 4:1). The polar compounds (450 mg) were eluted with acetone and chromatographed on silica gel (chloroform – acetone, 3:1) to give pure lactam α-camphidone (35 mg, 0.7%, mp 234–235°C (lit. (25*a*, *e*) mp 234–236°C), less polar) and "normal" camphor lactam **119** (390 mg, 7.2%); mp 196–197°C; ir ($CHCl_3$, ν cm^{-1}): 3400, 3200, 1680, 1420, 1400, 1385; ^1H nmr ($CDCl_3$, δ ppm): 5.91 (br, 1H, NH), 2.58 (ddd, 1H, J_{AB} = 18 Hz, J_{AX} = 4.7 Hz, J_W = 2.5 Hz, $H_{exo}CCO$), 2.16 (dd, 1H, J_{AB} = 18 Hz, J_{BX} = 1.6 Hz, $H_{endo}CCO$), 2.1–1.4 (m), 1.10 (s, 3H, CH_3), 1.00 (s, 3H, CH_3), 0.96 (s, 3H, CH_3); ^{13}C nmr ($CDCl_3$, δ ppm): 172.6, 63.4, 43.2, 42.8, 40.0, 39.3, 27.7, 23.3, 18.1, 17.8; ms *m/e*: 167 (M^+).

*Lactone **120***

To a solution of camphor lactam **119** (25 mg, 0.15 mmol) in dry pyridine (1.5 mL) was added, at room temperature, nitrosyl hexafluorophosphate (52 mg, 0.29 mmol). The coloured mixture was refluxed for 3 h, then cooled, poured onto cold water, and extracted with dichloromethane to give a neutral extract (21 mg, 83%) containing a mixture (~3:1) of lactone **120** and another unidentified lactonic compound together with a trace of starting lactam. The aqueous layer was acidified (1 M HCl, pH 5) and extracted with dichloromethane to give a mixture of two unsaturated carboxylic acids (2 mg, 8%) that was not examined further. The neutral extract was chromatographed on silica gel (benzene – ethyl acetate, 4:1) (14 mg, 66%) to yield pure lactone **120**, identical in all respects with authentic material obtained from the Baeyer–Villiger oxidation of camphor; ir ($CHCl_3$, ν cm^{-1}): 1730, 1340, 1260, 1140; ^1H nmr ($CDCl_3$, δ ppm): 2.85 (ddd, 1H, J_{AB} = 19, 4.0 and 2 Hz, $H_{exo}CCO_2$), 2.35 (dd, 1H, J_{AB} = 19 and 1.8 Hz, $H_{endo}CCO_2$), 2.2–1.4 (m), 1.29 (s, 3H, $OCCH_3$), 1.06 (s, 3H, CH_3), 1.00 (s, 3H, CH_3); ms *m/e*: 168 (M^+).[7]

*Oxime **121***

A solution of ketone **108** (54.0 mg, 0.125 mmol) and hydroxylamine hydrochloride (400 mg, large excess) in pyridine (8 mL) was refluxed for 15 h, then cooled, poured onto cold water, and extracted with dichloromethane. The crude product was chromatographed on silica gel (benzene – ethyl acetate, 4:1) to give pure oxime **121** (42 mg, 75%); ir ($CHCl_3$, ν cm^{-1}): 3575, 3360, 1740, 1715, 1620, 1455, 1350, 1255; ^1H nmr ($CDCl_3$, δ ppm): 10.22 (s, 1H, OH), 5.55 (dd, 1H, J = 12 and 5 Hz, HC10), 3.67 (s, 3H, OCH_3), 2.70 (qn, 1H, J = 7 Hz, C*H*$(CH_3)_2$, 2.41 (d, 1H) and 2.06 (d, 1H) (J_{AB} = 19 Hz) (H_2C14), 2.04 (s, 3H, CH_3Cl), 1.97 (s, 3H, CH_3CO_2), 1.37 (s, 3H, CH_3C5), 1.19 and 1.14 (2d, 3H each, J = 7 Hz, $CH(CH_3)_2$); ms *m/e*: 447 (M^+).

*Oxime mesylate **122***

To a solution of oxime **121** (40 mg, 0.089 mmol) in pyridine (1.5 mL) was added methanesulfonyl chloride (150 μL) and the mixture was stirred at 25°C for 3.5 h after which it was poured into cold dilute aqueous sodium bicarbonate and extracted with dichloromethane. Chromatography of the crude extract on silica plate (benzene – ethyl acetate, 5:1) gave pure oxime mesylate **122** (40 mg, 85%); ir ($CHCl_3$, ν cm^{-1}): 1740, 1720, 1615, 1455, 1360, 1315, 1230, 1170, 945; ^1H nmr ($CDCl_3$, δ ppm): 5.55 (d, 1H, J = 12 and 4 Hz, HC10), 3.67 (s, 3H, OCH_3), 3.13 (s, 3H, CH_3SO_2), 2.72 (qn, 1H, J = 7 Hz, C*H*$(CH_3)_2$), 2.60 (d, 1H) and 2.20 (d, 1H) (J_{AB} = 20 Hz) (H_2C14), 2.10 (s, 3H, CH_3C1), 2.06 (s, 3H, CH_3CO_2), 1.34 (s, 3H, CH_3C5), 1.17 and 1.15 (2d, 3H each, J = 7 Hz, $CH(CH_3)_2$).

*Lactam alcohol **123** and acetate **124***

A solution of oxime mesylate (13 mg, 0.025 mmol) in dioxane (1 mL) and water (0.5 mL) was heated in a sealed (vacuum) tube at 135°C for 17 h. The crude product was then poured into cold dilute aqueous sodium bicarbonate solution and extracted with dichloromethane to give a crude product, which was chromatographed on silica plate (ethyl acetate) to give pure lactam alcohol **123** (more polar, 5.5 mg, 57%) and lactam acetate **124** (less polar, 3.5 mg, 33%). *Lactam alcohol **123***: mp 240°C (dec.); ir ($CHCl_3$, ν cm^{-1}): 3600, 3480, 3360, 1825, 1720, 1670, 1620, 1230, 1050; ^1H nmr ($CDCl_3$, δ ppm): 6.27 (br s, 1H, NH), 4.60 (m, 1H, HC10), 2.75 (qn, 1H, J = 7 Hz, C*H*$(CH_3)_2$), 2.82 (s, 2H, H_2C14), 2.22 (s, 3H, CH_3C1), 2.2–1.4 (m), 1.23 (s, 3H, CH_3C5), 1.16 (d, 6H, J = 7 Hz, $CH(CH_3)2$); ms *m/e*: 391 (M^+). *Lactam acetate **124***: ir ($CHCl_3$, ν cm^{-1}): 3600, 3380, 1825, 1745 (sh), 1720, 1680, 1620, 1220, 1050; ^1H nmr ($CDCl_3$, δ ppm): 5.97 (br s, 1 H, NH), 5.65 (dd, 1H, J = 12 and 5 Hz, HC10), 2.78 (qn, 1H, J = 7 Hz, C*H*$(CH_3)_2$), 2.37 (s, 2H, H_2C14), 2.18 (s, 1H, OH), 2.14 and 2.13 (2s, 3H each, CH_3Cl and CH_3CO_2), 2.3–1.3 (m), 1.31 (s, 3H, CH_3C5), 1.18 (d, 6H, J = 7 Hz, $CH(CH_3)_2$); ms *m/e*: 433 (M^+).

*Acetylation of lactam alcohol **123***

A solution of alcohol **123** (15 mg, 0.038 mmol) in pyridine (0.5 mL) and acetic anhydride (0.5 mL) was stirred at 25°C overnight. Evaporation of volatile materials and rapid filtration on silica gel (ethyl acetate) furnished a quantitative yield of acetate **124** (16.5 mg).

*Oxidation of alcohol **123***

To a solution of alcohol **123** (12 mg, 0.031 mmol) in acetone (1.5 mL) was added freshly prepared Jones reagent (3 drops) at 25°C and the

[6]Ryanodol numbering.

[7]The other lactone (less polar, 6 mg, 27%) probably has the structure shown below according to its spectroscopic data: ir ($CHCl_3$, ν cm^{-1}): 1765, 1370, 1310, 1230; ^1H nmr ($CDCl_3$, δ ppm): 2.86 (dd, 1H, J_{AB} = 15 and 11.5 Hz, $HCCO_2$), 2.60 (dd, 1H, J_{AB} = 15 and 0.5 Hz, $HCCO_2$), 1.30 (s, 3H, CH_3CO), 1.09 (s, 3H, CH_3), 0.90 (s, 3H, CH_3); ms *m/e*: 168 (M^+).

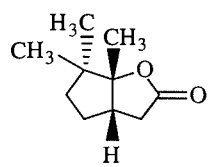

Can. J. Chem. Downloaded from www.nrcresearchpress.com by 186.148.149.217 on 09/07/12
For personal use only.

mixture was stirred for 45 min, poured into cold water, and extracted with dichloromethane. The crude product was chromatographed on silica plate (ethyl acetate) to give ketolactam **125** (12 mg, quant); mp 205–207°C; ir ($CHCl_3$, ν cm^{-1}): 3600, 3300, 1810, 1725, 1680, 1620, 1230, 1050; ^1H nmr ($CDCl_3$, δ ppm): 6.26 (br s, 1H, NH), 3.40 (br s, OH), 2.70 (qn, 1H, J = 7 Hz, C*H*$(CH_3)_2$), 2.35 (s, 2H, H_2C14), 2.18 (s, 3H, CH_3C1), 2.6–1.5 (m), 1.32 (s, 3H, CH_3C5), 1.16 and 1.14 (2d, 3H each, J = 7 Hz, CH(C*H*$_3)_2$); ms m/e: 389 (M^+).

Mesylate ***126***

Methanesulfonyl chloride (0.50 mL, 6.4 mmol) was added to a cold (0°C) solution of alcohol **103** (95 mg, 0.154 mmol) in pyridine (5 mL). The mixture was stirred for 30 min, then poured into cold aqueous sodium bicarbonate and extracted with dichloromethane. The crude product was chromatographed (hexane – ethyl acetate, 1:1) on silica plate to give pure mesylate **126** (102 mg, 95%); ir ($CHCl_3$, ν cm^{-1}): 1755, 1735, 1610, 1530, 1450, 1340, 1315, 1260, 1160; ^1H nmr ($CDCl_3$, δ ppm): 8.25 (m, 4H, aromatic), 5.50 (dd, 1H, J = 11 and 5 Hz, HC10), 4.40 (m, 3H, H_2C17 and C*H*$(OCH_3)_2$), 3.72 (s, 3H, OCH_3), 3.56 and 3.52 (2s, 3H each, 2 × OCH_3), 3.08 (s, 3H, CH_3SO_2), 2.70 (m, 3H), 2.35 (d, 1H) and 1.82 (d, 1H) (J = 20 Hz) (H_2C14), 2.3–1.4 (m), 1.27 (s, 3H, CH_3C5), 1.03 (apparent t, J = 7 Hz, CH(C*H*$_3)_2$).

Hemi-ketal ***127***

A solution of lithium methoxide (0.21 M in methanol, 0.58 mL, 1.1 equiv.) was added to a cold (0°C) solution of compound **126** (82 mg, 0.12 mmol) in tetrahydrofuran (10 mL). After 3 h the mixture was poured into aqueous ammonium chloride and extracted with dichloromethane. Chromatography (benzene – ethyl acetate, 1:1) of the crude extract on silica plate furnished pure hemi-ketal **127** (56 mg, 87%); ir ($CHCl_3$, ν cm^{-1}): 3580, 1450, 1350, 1315, 1160; ^1H nmr ($CDCl_3$, δ ppm): 5.35 (dd, 1H, J = 11 and 6 Hz, HC10), 4.37 (dd, 1H, J_{AB} = 13 Hz, J_{AX} = 4.5 Hz, H_AC17), 4.24 (d, 1H, J = 5.6 Hz, C*H*$(OCH_3)_2$), 4.01 (dd, 1H, J_{AB} = 13 Hz, J_{BX} = 12 Hz, H_BC17), 3.67 (s, 3H, CH_3O), 3.46 and 3.44 (2s, 3H each, 2 × OCH_3), 3.07 (s, 3H, CH_3SO_2), 2.62 (m, 3H), 2.4–1.3 (m), 1.13 (s, 3H, CH_3C5), 1.05 and 0.98 (2d, 3H each, J = 7 Hz, CH(C*H*$_3)_2$); ms m/e: 546 (M^+).

Lactone ***128***

A solution of *n*-butyllithium (1.6 M in hexane, 427 μL, 0.683 mmol) was added to dry, freshly distilled dimethyl sulfoxide (20 mL) at room temperature. After 1 h this reagent was transferred to hemi-ketal **127** (187 mg, 0.342 mmol) and the reaction mixture was stirred at room temperature for 3.5 h, then poured into cold water and extracted with dichloromethane. The organic layers were washed with water, dried, and evaporated. The sensitive lactone **128** (155 mg, crude quantitative) was used directly for the next step; ir ($CHCl_3$, ν cm^{-1}): 1750, 1600, 1450, 1310; ^1H nmr ($CDCl_3$, δ ppm): 6.02 (dd, 1H, J = 5 and 3 Hz, HC10), 4.81 (ddd, 1H, J_{AB} = 12 Hz, J_{AX} = 2 Hz, J_W = 1 Hz, $H_{exo}C17$), 4.40 (dd, 1H, J_{AB} = 12 Hz, J_{BX} = 2 Hz, $H_{endo}C17$), 4.22 (d, 1H, J = 6.7 Hz, C*H*$(OCH_3)_2$), 3.63, 3.55, and 3.47 (3s, 3H each, 3 × OCH_3), 3.32 (dd, 1H, J = 11 and 6.7 Hz, HC3), 2.67 (d, 1H) and 2.22 (d, 1H) (J_{AB} = 13.8 Hz) (H_2C14), 2.8–1.6 (m), 1.27 (s, 3H, CH_3C5), 1.10 and 1.06 (2d, 3H, each, J = 7 Hz, CH(C*H*$_3)_2$).

Hydrolysis of ***128***

The crude product **128** from the preceding reaction (155 mg) was dissolved in tetrahydrofuran (20 mL) containing water (6 mL) and reacted at 0°C with an aqueous solution of tetrafluoroboric acid (0.3 M, 80 μL). After 3 h, the mixture was poured into dilute aqueous sodium bicarbonate and extracted with dichloromethane. Evaporation of the solvents left a residue that was chromatographed on silica gel (hexane – ethyl acetate, 25%) to give hydroxycarbonate **129** (less polar, 107 mg, 72% for 2 steps) and allylic alcohol **130** (R = H) (more polar, 28 mg, 19%). *Compound* ***129***: mp 169–170°C; ir ($CHCl_3$, ν cm^{-1}): 3600, 1805, 1750, 1255; ^1H nmr ($CDCl_3$, δ ppm): 6.14 (dd, 1H, J = 5 and 3 Hz, HC10), 4.60 (ddd, 1H, J_{AB} = 12 Hz, J_{AX} = 2 Hz, J_W = 0.5 Hz, $H_{exo}C17$), 4.25 (d, 1H, J = 5 Hz, C*H*$(OCH_3)_2$), 4.24 (dd, 1H, J_{AB} = 12 Hz, J_{BX} = 2 Hz, $H_{endo}C17$), 3.53 and 3.50 (2s, 3H each, 2 × OCH_3), 3.46 (dd, 1H, J = 12 and 5 Hz, HC3), 2.85 (qn, 1H, J = 7 Hz, C*H*$(CH_3)_2$), 2.75 (d, 1H) and 2.28 (d, 1H) (J_{AB} = 13 Hz) (H_2C14), 2.6–1.4 (m), 1.30 (s, 3H, CH_3C5), 1.05 (d, 6H, J = 7 Hz, CH(C*H*$_3)_2$); ms m/e: 436 (M^+). *Compound* ***130*** (R = H): ir ($CHCl_3$, ν cm^{-1}): 3600, 1810, 1760, 1265; ^1H nmr ($CDCl_3$, δ ppm): 4.33 (d, 1H, J = 5.4 Hz, C*H*$(OCH_3)_2$), 4.32 (ddd, 1H, J_{AB} = 12.2 Hz, J_{AX} = 1.5 Hz, J_W = 0.5 Hz, $H_{exo}C17$), 4.26 (m, 1H, $W_{\frac{1}{2}} \simeq 5$ Hz, $H_{eq}C10$), 4.20 (dd, 1H, J_{AB} = 12.2 Hz, J_{BX} = 2.2 Hz, $H_{endo}C17$), 3.53 and 3.50 (2s, 3H each, 2 × OCH_3), 3.33 (dd, 1H, J = 11.6 and 5.4 Hz, HC3), 2.95 (d, 1H) and 2.35 (d, 1H) (J_{AB} = 12.7 Hz) (H_2C14), 2.89 (ddd, 1H, $J \simeq 12$, 6 and 4 Hz, HC2), 2.63 (br d, 1H, J = 6.2 Hz, HC1), 2.11 (qn, 1H, J = 7 Hz, C*H*$(CH_3)_2$), 2.1–1.6 (m), 1.27 (s, 3H, CH_3C5), 1.06 and 1.01 (2d, 3H each, J = 7 Hz, CH(C*H*$_3)_2$); ms m/e: 436 (M^+).

Acetylation of alcohol ***130*** (R = H)

Acetic anhydride (100 μL, excess) was added to a stirred (25°C) solution of alcohol **130** (22 mg, 0.050 mmol), triethylamine (100 μL), and *p*-dimethylaminopyridine (DMAP, ~1 mg) in dichloromethane (2 mL). After 1 h the mixture was poured into dilute aqueous sodium bicarbonate and extracted with dichloromethane to give a residue that was filtered through silica gel (hexane – ethyl acetate, 4:1) to give pure axial acetate **130** (R = Ac) (24 mg, quantitative); mp 137–138°C; ir ($CHCl_3$, ν cm^{-1}): 1800, 1750, 1730, 1650, 1370, 1270, 1250, 1045; ^1H nmr ($CDCl_3$, δ ppm): 5.51 (narrow m, 1H, $W_{\frac{1}{2}}$ = 5 Hz, $H_{eq}C10$), 4.37 (dd, 1H, J_{AB} = 12.3 Hz, J_{AX} = 0.5 Hz, H_AC17), 4.34 (d, 1H, J = 5.2 Hz, C*H*$(OCH_3)_2$, 4.23 (dd, 1H, J_{AB} = 12.3 Hz, J_{BX} = 2.3 Hz, H_BC17), 3.54 and 3.52 (2s, 3H each, 2 × OCH_3), 3.28 (dd, 1H, J = 11.6 and 5.2 Hz, HC3), 2.96 (d, 1H) and 2.24 (d, 1H) (J_{AB} = 12.5 Hz) (H_2C14), 2.86 (ddd, 1H, J = 11.6, 6.6, and 5.0 Hz, HC2), 2.50 (br d, 1H, J = 6.6 Hz, HC1), 2.13 (qn, 1H, J = 7 Hz, C*H*$(CH_3)_2$, 2.06 (s, 3H, CH_3CO_2), 2.1–1.7 (m), 1.30 (s, 3H, CH_3C5), 1.06 and 1.01 (2d, 3H each, J = 7 Hz, CH(C*H*$_3)_2$).

Oxidation of alcohol ***130*** (R = H)

To a stirred suspension of chromic anhydride (100 mg) in dry dichloromethane (5 mL) was added anhydrous pyridine (170 μL). After 15 min at 25°C, the mixture was cooled to 0°C and treated with a solution of alcohol **130** (R = H) (5.0 mg, 0.011 mmol) in dichloromethane (0.5 mL). After 5 min, isopropanol (1 mL) was added to the mixture, which was poured into aqueous sodium bicarbonate and extracted with dichloromethane. Chromatography of the crude product (benzene – ethyl acetate, 4:1) furnished the known enone **57** (4.5 mg, 92%, mp 214–216°C (dec.)).

Equatorial allylic alcohol ***131***

Sodium borohydride (5 mg, excess) was added to a cold (0°C) solution of enone **57** (20 mg, 0.046 mmol) in dry tetrahydrofuran. After 30 min, saturated aqueous ammonium chloride was added and the mixture was extracted with dichloromethane to give alcohol **131** (17 mg, 85%); ir ($CHCl_3$, ν cm^{-1}): 3500, 1800, 1750, 1650, 1050, 1030; ^1H nmr ($CDCl_3$, δ ppm): 4.85 (dd, 1H, J_{AB} = 12 Hz, J_{AX} = 1 Hz, H_AC17), 4.36 (d, 1H, J = 5 Hz, C*H*$(OCH_3)_2$), 4.4–4.2 (m, 1H, $W_{\frac{1}{2}}$ = 12 Hz, $H_{ax}C10$), 4.19 (dd, 1H, J_{AB} = 12 Hz, J_{BX} = 2.5 Hz, H_BC17), 3.55 and 3.53 (2s, 3H each, 2 × OCH_3), 3.30 (dd, 1H, J = 12 and 5 Hz, HC3), 2.98 (d, 1H) and 2.35 (d, 1H) (J_{AB} = 13 Hz) (H_2C14), 2.9–1.3 (m), 1.26 (s, 3H, CH_3C5), 1.08 and 1.04 (2d, 3H each, J = 7 Hz, CH(C*H*$_3)_2$); ms m/e: 436 (M^+).

Epoxide ***132***

To a mixture of olefin lactone **129** (28.6 mg, 0.0656 mmol) and sodium bicarbonate (350 mg, large excess) in 1,2-dichloroethane (5 mL) was added, at room temperature, freshly prepared trifluoroperacetic acid (130 μL, 1.1 M in dichloromethane). After 2 h at room temperature the volatile substances were carefully evaporated and the residue was washed with dichloromethane, filtered, and evaporated. The residue (26 mg) was submitted to the same reaction conditions for 3 h, then the volatile materials were evaporated, the residue was triturated with dichloromethane, and the extract was filtered. Evaporation of the solvent gave a crude product (54 mg), which was purified by crystallization (ether) and chromatography on silica plates (hexane – ethyl acetate, 1:1, two elutions) to give pure epoxide **132** (27 mg, 92%), slightly less polar than olefin **129**: mp 200–205°C (dec.); ir

Can. J. Chem. Downloaded from www.nrcresearchpress.com by 186.148.149.217 on 09/07/12
For personal use only.

($CHCl_3$, ν cm^{-1}): 3550, 1812, 1754, ^1H nmr ($CDCl_3$, δ ppm): 4.50 (d, 2H, J = 2.4 Hz, H_2C17), 4.33 (d, 1H, J = 4.0 Hz, $CH(OCH_3)_2$), 3.86 (dd, 1H, J = 2.0 and 1.2 Hz, HC10), 3.54 and 3.53 (2s, 3H each, 2 × OCH_3), 3.2–1.5 (m), 1.37 (s, 3H, CH_3C5), 1.05 and 1.01 (2s, 3H each, J = 7 Hz, $CH(CH_3)_2$); ms m/e: 452 (M^+, weak).

*Triol lactone **134***

To a solution of epoxylactone **132** (40 mg, 0.088 mmol) in a mixture of 1,2-dimethoxyethane (10 mL, freshly distilled) and water (1 mL) was added at 25°C aqueous sodium hydroxide (0.1 M, 350 μL, 0.4 equiv.). After 2 h and 4 h of reaction, the same quantity of reagent was added for a total of 1.2 equivalents. After a total of 6 h of reaction time, the mixture was poured into water, acidified to pH 6.5 (0.5 M, HC1), and extracted with dichloromethane to give a crude product that was chromatographed on silica plate (ether – ethyl acetate, 4:1) to give pure lactone **134** (34 mg, 82%); mp 194–195°C; ir ($CHCl_3$, ν cm^{-1}): 3600, 3450, 1810, 1750, 1250, 1015; ^1H nmr ($CDCl_3$, δ ppm): 4.86 (narrow m, 1H, $W_{\frac{1}{2}} \simeq 6$ Hz, $H_{eq}C10$), 4.31 (d, 1H, J = 5.3 Hz, $CH(OCH_3)_2$), 3.86 (dd, 1H, J_{AB} = 12 Hz, J_{AX} = 5 Hz, H_AC17), 3.58 (dd, 1H, J_{AB} = J_{BX} = 12 Hz, H_BC17), 3.47 and 3.45 (2s, 3H each, 2 × OCH_3), 2.95 (d, 1H) and 2.63 (d, 1H) (J_{AB} = 20 Hz) (H_2C14), 2.79 (m, 1H, HC1), 2.48 (m, 1H, HC2), 2.33 (dd, 1H, J = 12 and 5.3 Hz, HC3), 2.15–1.5 (m), 1.21 (s, 3H, CH_3C5), 1.04 and 0.91 (2d, 3H each, J = 7 Hz, ($CH(CH_3)_2$); ms m/e: 470 (M^+). *Exact Mass* calcd. for $C_{23}H_{34}O_{10}$–CH_3OH: 438.1889; found: 438.1890.

*Equatorial alcohol **135***

Sodium borohydride (43 mg, 1.1 mmol) was added to a cold (0°C) solution of ketone **39** (400 mg, 0.888 mmol) in a mixture of methanol (10 mL) and tetrahydrofuran (10 mL). After 30 min, the mixture was poured into dilute aqueous ammonium chloride, brought to pH 6 (1 M, HC1), and extracted with dichloromethane. Evaporation of the solvent gave a solid residue that was purified by crystallization (acetone–hexane) and chromatography on silica gel (benzene – ethyl acetate, 1:1) to yield diol **135** (381 mg, 95%); mp 281–282°C; ir ($CHCl_3$, ν cm^{-1}): 3580, 3420, 1802, 1745, 1070; ^1H nmr (acetone-d_6, δ ppm): 5.20 (dd, 1H, J = 10.5 and 3 Hz, HC15), 4.45 (d, 1H, J = 3 Hz, $CH(OCH_3)_2$), 4.28 (br m, $W_{\frac{1}{2}} \cong 12$ Hz, $H_{ax}C10$), 3.50 and 3.47 (2s, 3H each, 2 × OCH_3), 3.2–1.6 (m), 1.23 (s, 3H, CH_3C5), 1.35 and 0.96 (2d, 3H each, J = 7 Hz, $CH(CH_3)_2$); ms m/e: 452 (M^+). *Anal.* calcd. for $C_{23}H_{32}O_9$: C 61.05, H 7.13; found: C 61.11, H 6.99.

*Methoxymethyl orthocarbonate **136***

Sodium hydride (dry, washed with THF from commercial 60%in oil, 40 mg large excess), was added to a solution of diol **135** (75.0 mg, 0.166 mmol) in tetrahydrofuran (10 mL). After 30 min at 25°C, chloromethyl methyl ether (100 μL, freshly distilled from calcium hydride) was added and the mixture was stirred for 18 h at 28°C, then cooled to −78°C, and treated with aqueous ammonium chloride. The mixture was warmed to room temperature and extracted with dichloromethane to give a residue that was chromatographed on silica gel (chloroform – acetone, 4:1) to give a small quantity of starting material (4 mg, 5%) and compound **136** (70 mg, 85%); mp 147–151°C; ir ($CHCl_3$, ν cm^{-1}): 3600, 3450, 1735, 1200; ^1H nmr ($CDCl_3$, δ ppm): 5.15 (s, 2H, OCH_2O), 5.08 (dd, 1H, J = 8.7 and 3.5 Hz, HC15), 4.50 (br m, 1H, HC10), 4.36 (d, 1H, J = 5.5 Hz, $CH(OCH_3)_2$), 3.55, 3.51, and 3.48 (3s, 3H each, 3 × OCH_3), 3.00 (dd, 1H, J = 5.5 and 3 Hz, HC3), 3.2–1.5 (m), 1.15 (s, 3H, CH_3C5), 1.21 and 0.96 (2d, 3H each, J = 7 Hz, $CH(CH_3)_2$); ms m/e: 496 (M^+). *Anal.* calcd. for $C_{25}H_{36}O_{10}$: C 60.47, H 7.31; found: C 60.76, H 7.30.

*Reduction of lactone **136***

To a solution of lactone **136** (49 mg, 0.10 mmol) in tetrahydrofuran (6 mL) was added lithium aluminium hydride (30 mg, large excess) and the mixture was stirred for 4 h at room temperature. The mixture was cooled (−78°C) and reacted with ammonium chloride solution, warmed to 25°C, and extracted with dichloromethane. Chromatography of the crude extract on silica column (chloroform – acetone, 5:1, containing ~0.01% of pyridine) furnished triol **137** (45 mg, 91%); ir ($CHCl_3$, ν cm^{-1}): 3600–3200, 1445, 1285, 1050; ^1H nmr ($CDCl_3$, δ ppm): 5.04 (s, 2H, OCH_2O), 4.70 (dd, 1H, J_{AB} = 11 Hz, J_{AX} = 4 Hz, H_AC17), 4.60 (d, 1H, J_{AB} = 11 Hz, J_{BX} = 1.5 Hz, H_BC17), 4.24 (d, 1H, J = 4.5 Hz, $CH(OCH_3)_2$), 4.00 (br m, 2H, HC10 and HC15), 3.49, 3.47, and 3.43 (3s, 3H each, 3 × OCH_3), 2.6–1.2 (m), 1.07 (s, 3H, CH_3C5), 0.94 and 0.85 (2d, 3H each, J = 7 Hz, $CH(CH_3)_2$; ms m/e: 500 (M^+).

Primary p*-nitrobenzoate **138***

Freshly recrystallized (hot hexane) *p*-nitrobenzoyl chloride (8 mg, 0.04 mmol) was added to a solution of triol **137** (18 mg, 0.036 mmol) in pyridine (1.5 mL). After 1 h at room temperature the mixture was poured into dilute aqueous sodium bicarbonate and extracted with dichloromethane. Chromatography (chloroform – acetone, 3:1) of the crude product on silica gel furnished pure compound **138** (21.6 mg, 92%); ir ($CHCl_3$, ν cm^{-1}): 3600–3400, 1725, 1605, 1528; ^1H nmr ($CDCl_3$, δ ppm): 8.25 (s, 4H, aromatic), 5.05 (s, 2H, OCH_2O), 5.0–4.3 (m, 4H, H_2C17, HC15, and HC10), 4.30 (d, 1H, J = 4 Hz, $CH(OCH_3)_2$), 3.48, 3.46, and 3.45 (3s, 3H each, 3 × OCH_3), 2.9–1.2 (m), 1.06 (s, 3H, CH_3C5), 0.95 (d, 6H, J = 7 Hz, $CH(CH_3)_2$).

*Mesylate **139***

Methanesulfonyl chloride (100 μL, excess) was added to a cold (0°C) solution of diol **138** (6.8 mg, 0.010 mmol) in pyridine (1.0 mL). After 45 min, the mixture was poured into aqueous sodium bicarbonate (1 M) and extracted with dichloromethane. Chromatography of the crude product (chloroform – acetone, 4:1) on silica plate gave pure monomesylate **139** (6 mg, 79%); ir ($CHCl_3$, ν cm^{-1}): 3550, 1728, 1605, 1528, 1350–1310, 1160; ^1H nmr ($CDCl_3$, δ ppm): 8.25 (s, 4H, aromatic), 5.60 (br m, 1H, HC10), 5.06 (s, 2H, OCH_2O), 4.76 (br d, 3H, J = 6 Hz, H_2C17 and HC15), 4.32 (d, 1H, J = 4 Hz, $CH(OCH_3)_2$, 3.50, 3.49, and 3.47 (3s, 3H each, 3 × OCH_3), 3.14 (s, 3H, CH_3SO_2), 2.9–1.4 (m), 1.12 (s, 3H, CH_3C5), 1.04 and 0.93 (2d, 3H each, J = 7 Hz, $CH(CH_3)_2$).

*Ketone **140***

To a stirred suspension of chromic anhydride (100 mg) in dry dichloromethane (5 mL) was added anhydrous pyridine (170 μL). After 15 min at 25°C, the mixture was cooled (0°C) and treated with a solution of alcohol **139** (5 mg, 0.007 mmol) in dichloromethane (0.5 mL). After 5 min, isopropanol (0.5 mL) was added and the mixture was poured into aqueous sodium bicarbonate and extracted with dichloromethane. The crude extract was chromatographed on silica plate (hexane – ethyl acetate, 1:1) to give ketone **140** (4.3 mg, 88%); ir ($CHCl_3$, ν cm^{-1}): 1758, 1737, 1605, 1527, 1342, 1262, 1163; ^1H nmr ($CDCl_3$, δ ppm): 8.23 (m, 4H, aromatic), 5.33 (br m, 1H, HC10), 5.17 (d, 1H) and 5.05 (d, 1H) (J_{AB} = 6 Hz, OCH_2O), 4.40 (m, 3H, H_2C17 and $CH(OCH_3)_2$), 3.56, 3.54, and 3.51 (3s, 3H each, 3 × OCH_3), 3.11 (s, 3H, CH_3SO_2), 2.8–1.3 (m), 2.40 (d, 1H), and 1.90 (d, 1H) (J = 20 Hz) (H_2C14), 1.28 (s, 3H, CH_3C5), 1.11 and 0.98 (2d, 3H each, J = 7 Hz) ($CH(CH_3)_2$).

*Hemi-ketal **141***

This reaction was carried out as for hemi-ketal **127** (*vide supra*). In the same conditions compound **140** (3.1 mg, 4.3 μmol) furnished pure hemi-ketal **141** (2.2 mg, 90%); ir ($CHCl_3$, ν cm^{-1}): 3600, 1440, 1350, 1320, 1160; ^1H nmr ($CDCl_3$, δ ppm): 5.42 (dd, 1H, J = 11 and 6 Hz, HC10), 5.07 (br s, 2H, OCH_2O), 4.38 (dd, 1H, J_{AB} = 13 Hz, J_{AX} = 4 Hz, H_AC17), 4.23 (d, 1H, J = 5.5 Hz, $CH(OCH_3)_2$), 4.05 (dd, 1H, J_{AB} = 13 Hz, J_{BX} = 12 Hz, H_BC17), 3.52, 3.46, and 3.43 (3s, 3H each, 3 × OCH_3), 3.06 (s, 3H, CH_3SO_2), 2.65 (m, 3H), 2.5–1.3 (m), 1.14 (s, 3H, CH_3C5), 1.06 and 0.96 (2d, 3H each, J = 7 Hz, $CH(CH_3)_2$); ms m/e: 576 (M^+).

*Fragmentation and hydrolysis of hemi-ketal **141***

Following exactly the same experimental conditons used for fragmentation of compound **127** (*vide supra*), hemi-ketal **141** (2.0 mg, 0.0035 mmol) furnished very sensitive lactone **143** (1.8 mg), which was submitted to acid hydrolysis in the same conditions as for lactone **128** (THF, HBF_4, 0.3 M) (*vide supra*) to furnish a single compound, crystalline lactone **129** (1.4 mg, >90%) already described (*vide supra*).

Can. J. Chem. Downloaded from www.nrcresearchpress.com by 186.148.149.217 on 09/07/12
For personal use only.

Monomethylation of ketone ***39***

To a cold (−78°C) solution of ketone **39** (1.002 g, 2.23 mmol) in dry tetrahydrofuran (100 mL) was added dropwise, over 16 min, a cold (0°C) solution of lithium diisopropylamide (0.487 M in THF, 10.0 mL, 4.87 mmol, 2.19 molar equivalents) in tetrahydrofuran. The mixture was kept at −78°C for 1 h, warmed to −25°C for 3 h, then treated with a cold (0°C) solution of triethylborane in tetrahydrofuran (1.278 M, 3.6 mL, 4.6 mmol, 2.06 molar equivalents). After 0.5 h at −25°C a clear solution resulted and dry iodomethane (2.28 g, 7.2 molar equivalent) was added. The temperature was maintained at −22°C for 16 h before the addition of saturated ammonium chloride (100 mL) and water (50 mL) to the red solution. Extraction with dichloromethane furnished a crude product that was chromatographed on silica gel (chloroform – acetone, 20:1) to separate the less polar dimethylated derivative (105 mg, ~10%) and the more polar starting material (196 mg, 19%) from a mixture (719 mg, 69.8%) of monomethylated compounds (~3:1, nmr integration of the C15 protons). This mixture in methanol (20 mL) was submitted to aqueous sodium carbonate (0.1 N, 5 mL) for 2 h, then extracted with dichloromethane to give pure crystalline equatorial monomethylated compound **144** (disappearance of the dd at δ 5.17 and the d at δ 1.15); mp 245.5–254°C (dec.); $[\alpha_D$ −56.6° (*c* 1.00, THF); ir ($CHCl_3$, ν cm^{-1}): 3500, 1820, 1760, 1720; ^1H nmr (acetone-d_6, δ ppm): 5.40 (dd, 1H, *J* = 10.3 and 2.9 Hz, HC15), 4.38 (d, 1H, *J* = 4.5 Hz, C*H*(OCH_3)$_2$), 3.48 and 3.46 (2s, 3H each, 2 × OCH_3), 3.2–1.7 (m), 1.23 (s, 3H, CH_3C5), 1.08 (d, 3H, *J* = 7 Hz, CH_3C9), 1.05 and 0.95 (2d, 3H each, *J* = 7 Hz, CH(C*H*$_3$)$_2$), ms *m/e*: 464 (M^+). *Anal.* calcd. for $C_{24}H_{32}O_9$: C 62.06, H 6.95; found: C 62.33, H 7.08.

Equatorial alcohol ***145*** (R′ = H)

This reduction was carried out under the same conditions as for the formation of alcohol **135** (*vide supra*). Thus ketone **144** (1.024 g, 2.207 mmol) furnished crude diol **145** (995 mg, 97%); mp 257–267°C (dec.); ir ($CHCl_3$, ν cm^{-1}): 3600–3450, 1810, 1740, 1060; ^1H nmr ($CDCl_3$, δ ppm): 5.08 (dd, 1H, *J* = 9 and 3.5 Hz, HC15), 4.29 (d, 1H, *J* = 4 Hz, C*H*(OCH_3)$_2$), 3.88 (br d, 1H, *J* ≃ 11 Hz, HC10), 3.50 and 3.49 (2s, 3H each, 2 × OCH_3), 3.2–1.5 (m), 1.15 (s, 3H, CH_3C5), 1.18 and 1.06 (2d, 3H each, CH(C*H*$_3$)$_2$); ms *m/e*: 466 (M^+). This product was analyzed as its acetate **145** (R′ = Ac).

Acetate ***145*** (R′ = Ac)

A solution of diol **145** (R′ = H) (59 mg, 0.13 mmol) in pyridine (2 mL) and acetic anhydride (1 mL) was stirred at 25°C for 18 h. The volatile substances were evaporated and the crude product was chromatographed (silica plates, chloroform – acetone, 4:1) to give pure crystalline (dichloromethane – hexane) acetate **145** (R′ = Ac) (55 mg, 78%) and unchanged starting material (4.7 mg, 8%); mp 244–246°C; $[\alpha]_D$ −34.7° (*c* 1.00, $CHCl_3$); ir ($CHCl_3$, ν cm^{-1}): 3600, 3460, 1815, 1750, 1370, 1230, 1065; ^1H nmr ($CDCl_3$, δ ppm): 5.47 (d, 1H, *J* = 10 Hz, HC10), 5.10 (dd, 1H, *J* = 10 and 3.5 Hz, HC15), 4.30 (d, 1H, *J* = 4 Hz, C*H*(OCH_3)$_2$), 3.49 and 3.48 (2s, 3H each, 2 × OCH_3), 2.95 (m, 2H, HC2 and C*H*(CH_3)$_2$), 2.88 (d, 1H, *J* = 8 Hz, HC1), 2.74 (dd, 1H, *J* = 10 and 4 Hz, HC3), 2.26 (m, 1H, HC9), 2.18 (dd, 1H, J_{AB} = 14 Hz, J_{AX} = 10 Hz, H_{exo}C14), 2.03 (s, 3H, CH_3CO_2), 1.93 (dd, J_{AB} = 14 Hz, J_{BX} = 3 Hz, H_{endo}C14), 1.8–1.3 (m, 3H), 1.16 (s, 3H, CH_3C5), 1.15 (d, 3H, *J* = 7 Hz, CH_3C9), 0.98 and 0.93 (2d, 3H each, *J* = 7 Hz, CH(C*H*$_3$)$_2$); ms *m/e*: 508 (M^+). *Anal.* calcd. for $C_{26}H_{36}O_{10}$: C 61.40, H 7.13; found: C 61.60, H 7.37.

Methoxymethyl orthocarbonate ***146***

To a suspension of freshly washed (THF) sodium hydride (400 mg, of 50% in oil, ~8.3 mmol) in tetrahydrofuran (40 mL) was added a solution of hydroxycarbonate **145** (R′ = H) (341 mg, 0.732 mmol) in tetrahydrofuran. After 30 min at 25°C, methoxymethyl chloride (freshly distilled from CaH_2, 440 μL, 5.78 mmol) was added to the mixture and the temperature of the oil bath was raised to ~33°C. After 6 h, the mixture was concentrated to one third of the initial volume, then cooled (−75°C) and treated with pyridine (~0.8 mL) and a saturated solution of sodium carbonate in methanol (6 mL, foam!). The mixture was then warmed to room temperature (~20 min), poured into cold water, and extracted with dichloromethane to give a crude product that was chromatographed on silica gel (chloroform – acetone, 5:1, trace of pyridine) to give methoxymethyl orthocarbonate **146** (350 mg, 94%); mp 169–170°C; $[\alpha]_D$ −12.1° (*c* 1.00, $CHCl_3$); ir ($CHCl_3$, ν cm^{-1}): 3610, 3450, 1745, 1450, 1050; ^1H nmr ($CDCl_3$, δ ppm): 5.06 (s, 2H, OCH_2O), 5.00 (dd, 1H, *J* = 9 and 3.5 Hz, HC15), 4.28 (d, 1H, *J* = 5 Hz, C*H*(OCH_3)$_2$), 3.90 (m, 1H, HC10), 3.52, 3.47, and 3.43 (3s, 3H each, 3 × OCH_3), 3.02 (d, 1H, *J* = 5 Hz, HC1), 3.1–1.4 (m), 1.20 (d, 3H, *J* = 7 Hz, CH_3C9), 1.13 (s, 3H, CH_3C5), 1.06 and 0.95 (2d, 3H each, *J* = 7 Hz, CH(C*H*$_3$)$_2$); ms *m/e*: 510 (M^+). *Anal.* calcd. for $C_{26}H_{38}O_{10}$: C 61.16, H 7.50: C 61.33, H 7.49.

Triol ***147***

To a solution of lactone **146** (137 mg, 0.269 mmol) in tetrahydrofuran (15 mL) was added lithium aluminium hydride (70 mg); the mixture was stirred at 25°C overnight, then cooled (−78°C). An aqueous saturated solution of sodium sulfate (1 mL) was added and the mixture was allowed to warm to room temperature, poured into cold water, and extracted with dichloromethane. Filtration of the crude product through silica gel (chloroform – acetone, 5:1) gave pure triol **147** as a foam (131 mg, 95%); $[\alpha]_D$ −40.1° (*c* 1.00, $CHCl_3$); ir ($CHCl_3$, ν cm^{-1}): 3350 (br), 1450, 1290, 1050; ^1H nmr ($CDCl_3$, δ ppm): 5.03 (s, 2H, OCH_2O), 4.80 (dd, 1H, *J* = 11 and 5.5 Hz, HC15), 4.25 (d, 1H, *J* = 4 Hz, C*H*(OCH_3)$_2$), 4.14 (dd, 1H, J_{AB} = J_{AX} = 11.1 Hz, H_AC17), 4.06 (d, 1H, *J* = 10 Hz, HC10), 4.01 (dd, 1H, J_{AB} = 11.1 Hz, J_{BX} = 6.2 Hz, H_BC17), 3.48, 3.45, and 3.41 (3s, 3H each, 3 × OCH_3), 3.43 (dd, 1H, *J* = 12 and 4 Hz, HC3), 2.8–2.4 (m), 2.0–1.4 (m), 1.10 (d, 3H, *J* = 6.2 Hz, CH_3C9), 1.05 (s, 3H, CH_3C5), 0.95 and 0.88 (2d, 3H each, *J* = 6.8 Hz, CH(C*H*$_3$)$_2$); ms *m/e*: 514 (M^+). *Anal.* calcd. for $C_{26}H_{42}O_{10}$: C 60.68, H 8.23; found: C 60.44, H 7.98.

Hemi-ketal ***148*** *by selective oxidation of triol* **147**

Chromium trioxide (770 mg) was added to a cold (0°C) solution of pyridine (1.4 mL) in dichloromethane (70 mL). After 15 min, this stock solution of reagent was used in small portions (~4–5 mL portions) for the selective oxidation of triol **147** (500 mg, 0.972 mmol) in dichloromethane (125 mL) maintained below −22°C. The reaction was monitored by thin-layer chromotography and was complete after a total addition of about 40 mL of the stock solution. Then isopropanol (~2 mL) was added and the mixture was warmed to 0°C, poured into aqueous sodium bicarbonate, and extracted with dichloromethane. The crude product was chromatographed on silica gel (chloroform – acetone, 93:7) containing traces of pyridine ~0.1%) to give pure hemiketal **148** (380 mg, 76%); mp 123–123.5°C; $[\alpha]_D$ −39.2° (*c* 1.00, $CHCl_3$); ir ($CHCl_3$, ν cm^{-1}): 3550 (br), 1740,[8] 1455, 1318, 1290, 1050; ^1H nmr ($CDCl_3$, δ ppm):[8] 5.06 (s, 2H, OCH_2O), 4.78 (dd, 1H, J_{AB} = 12 Hz, J_{AX} = 4 Hz, H_AC17), 4.23 (d, 1H, *J* = 5.5 Hz, C*H*(OCH_3)$_2$), 4.05 (d, 1H, *J* = 12 Hz, HC10), 3.77 (dd, 1H, J_{AB} = 12 Hz, J_{BX} < 0.5 Hz, H_BC17), 3.51, 3.45, and 3.43 (3s, 3H each, 3 × OCH_3), 2.8–1.3 (m), 1.11 (s, 3H, CH_3C5), 1.07, 1.05, and 0.93 (3d, 3H each, *J* = 7 Hz, CH_3C9 and CH(C*H*$_3$)$_2$); ms *m/e*: 512 (M^+). *Anal.* calcd. for $C_{26}O_{40}O_{10}$: C 60.92, H 7.88; found: C 60.96, H 8.11.

Hemi-ketal mesylate ***149***

To a cold (0°C) solution of hemi-ketal **148** (380 mg, 0.742 mmol) in pyridine (16 mL) was added methanesulfonyl chloride (378 μL, 4.89 mmol). After 1 h the mixture was concentrated under vacuum (<30°C), then poured into aqueous sodium bicarbonate and extracted with dichloromethane. The crude mesylate was chromatographed on silica gel (hexane – ethyl acetate, 1:1, traces of pyridine) to give mesylate **149** (391 mg, 89%); ^1H nmr ($CDCl_3$, δ ppm); 5.27 (d, 1H, *J* = 11 Hz, HC10), 5.15 (d, 1H) and 5.01 (d, 1H) (J_{AB} = 6 Hz, OCH_2O), 4.33 (dd, 1H, J_{AB} = 12 Hz, J_{AX} = 4 Hz, H_AC17), 4.23 (d, 1H, *J* = 5 Hz, C*H*(OCH_3)$_2$), 3.88 (dd, 1H, J_{AB} = 12 Hz, J_{BX} = 2 Hz, H_BC17), 3.52, 3.47, and 3.43 (3s, 3H each, 3 × OCH_3), 3.11 (s, 3H, CH_3SO_2),

[8]The open form hydroxyketone of **148** is present in solution ($CHCl_3$, ~15%).

Can. J. Chem. Downloaded from www.nrcresearchpress.com by 186.148.149.217 on 09/07/12
For personal use only.

2.7–1.4 (m), 1.10 (d, 3H, J = 7 Hz, CH_3C9), 1.01 and 0.98 (2d, 3H each, J = 7 Hz, $CH(CH_3)_2$); ms m/e: 448 ($M^+ - CH_3SO_3H - CH_3OCH_2$).

*Hydroxycarbonate lactone **151***

This reaction was carried out exactly as for compounds **141** and **127** (*vide supra*). Thus mesylate **149** (255 mg, 0.43 mmol) furnished very sensitive lactone **150**, which was hydrolyzed as for lactone **128** (*vide supra*) to yield hydroxycarbonate lactone **151**. This sequence was repeated on two quantities of hemi-ketal **149** (300 and 323 mg) for a total yield of compound **151** (650 mg, 97% from **149**); mp 229.5–231°C; $[\alpha]_D$ −126° (*c* 0.98, $CHCl_3$); ir ($CHCl_3$, ν cm^{-1}): 3600, 1800, 1754, 1680, 1450, 1353, 1045, 1025; ^1H nmr ($CDCl_3$, δ ppm): 5.93 (br d, 1H, $J \simeq 2$ Hz, HC10), 4.62 (ddd, 1H, J_{AB} = 12.5 Hz, J_{AX} = 2 Hz, $J_W \cong 0.5$ Hz, $H_{exo}C17$), 4.28 (d, 1H, J = 5 Hz, $CH(OCH_3)_2$), 4.25 (dd, 1H, J_{AB} = 12.5 Hz, J_{BX} = 2 Hz, $H_{endo}C17$), 3.56 and 3.53 (2s, 3H each, 2 × OCH_3), 3.45 (dd, 1H, J = 12 and 5 Hz, HC3), 2.76 (d, 1H) and 2.23 (d, 1H) (J_{AB} = 13 Hz, H_2C14), 3.1–1.4 (m), 1.30 (s, 3H, CH_3C5), 1.07 (d, 9H, J = 7 Hz, CH_3C9 and $CH(CH_3)_2$); ms m/e: 450 (M^+). *Anal.* calcd. for $C_{24}H_{34}O_8$: C 63.98, H 7.61; found: C 64.40, H 7.24.

*Epoxide **152***

A solution of freshly prepared trifluoroperacetic acid (1.125 M; 720 μL, 0.81 mmol) in 1,2-dichloroethane was added dropwise (over 2 min) to a cold (0°C) mixture of anhydrous disodium hydrogen phosphate (3.46 g, 24.4 mmol) and olefin **151** (163 mg, 0.362 mmol) in dry 1,2-dichloroethane (35 mL). After 2 h the same quantity of peracid was added; after an additional 3.5 h, the mixture was cooled to −24°C for 15.5 h, then poured into aqueous sodium bicarbonate and extracted with dichloromethane. Evaporation of the solvents gave a pure crystalline (dichloromethane – ether – hexane) compound, epoxy lactone **152** (165 mg, 98%); mp 173–175°C; ir ($CHCl_3$, ν cm^{-1}): 3550, 1810, 1755, 1250, 1050; ^1H nmr ($CDCl_3$, δ ppm): 4.51 (br d, 2H, J = 2.5 Hz, H_2C17), 4.11 (d, 1H, J = 4 Hz, $CH(OCH_3)_2$), 3.67 (br s, 1H, HC10), 3.54 and 3.53 (2s, 3H each, 2 × OCH_3), 3.2–1.7 (m), 1.36 (s, 3H, CH_3C5), 1.15 (d, 3H, J = 7 Hz, CH_3C9), 1.08 and 1.04 (2d, 3H each, $CH(CH_3)_2$); ms m/e: 466 (M^+).

*Triol lactone **153***

This translactonisation was accomplished exactly as for lactone **132** (*vide supra*). Thus lactone epoxide **152** (341 mg, 0.732 mmol) furnished triol lactone **153** (273 mg, 77%) after crystallization and chromatography on silica gel (ether – ethyl acetate, 4:1); mp 246–248°C; $[\alpha]_D$ −32.9° (*c* 1.00, $CHCl_3$); ir ($CHCl_3$, ν cm^{-1}): 3600, 3450, 1810, 1760, 1440, 1020; ^1H nmr ($CDCl_3$, δ ppm): 4.58 (dd, 1H, J = 3.0 and ~0.5 Hz, $H_{eq}C10$), 4.30 (d, 1H, J = 5.4 Hz, $CH(OCH_3)_2$), 3.86 (dd, 1H, J_{AB} = 12 Hz, J_{AX} = 5 Hz, H_AC17), 3.58 (dd, 1H, $J_{AB} = J_{BX}$ = 12 Hz, H_BC17), 3.47 and 3.45 (2s, 3H each, 2 × OCH_3), 2.95 (d, 1H) and 2.60 (d, 1H) (J_{AB} = 20 Hz, H_2C14), 2.78 (m, 1H, HCl), 2.47 (m, 1H, HC2), 2.32 (dd, 1H, J = 12 and 5.4 Hz, HC3), 2.04 (m, 2H, HC9 and $CH(CH_3)_2$), 1.8–1.4 (m), 1.21 (s, 3H, CH_3C5), 1.05, 1.02, and 0.92 (3d, 3H each, J = 7 Hz, CH_3C9 and $CH(CH_3)_2$); ms m/e: 484 (M^+). *Anal.* calcd. for $C_{24}H_{36}O_{10}$: C 59.49, H 7.48; found: C 59.67, H 7.55.

p-*Nitrobenzoate **154***

Freshly recrystallized (hot hexane) *p*-nitrobenzoyl chloride (444 mg, 2.39 mmol) was added to a cold (4°C) solution of triol lactone **153** (480 mg, 0.991 mmol) in dry pyridine (15 mL). After 25 min, the mixture was poured into saturated aqueous sodium bicarbonate (20 mL) and extracted with dichloromethane. The crude product was filtered through silica gel (hexane – ethyl acetate, 1:1 containing a trace of pyridine) to give pure ester lactone **154** (552 mg, 95%); mp 130–131°C (benzene); $[\alpha]_D$ −33.0° (*c* 1.0, $CHCl_3$); ir ($CHCl_3$, ν cm^{-1}): 3600, 3480, 1820, 1765, 1730, 1610, 1530, 1260, 1080, 1030; ^1H nmr ($CDCl_3$, δ ppm): 8.26 (m, 4H, aromatic), 4.63 (dd, 1H, J_{AB} = 12 Hz, J_{AX} = 6 Hz, H_AC17), 4.48 (dd, 1H, J_{AB} = 12 Hz, J_{BX} = 10 Hz, H_BC17), 4.37 (d, 1H, J = 2 Hz, $H_{eq}C10$), 4.35 (d, 1H, J = 5.4 Hz, $CH(OCH_3)_2$), 3.50 and 3.48 (2s, 3H each, 2 × OCH_3), 3.02 (m, 1H, HC1), 2.96 (d, 1H) and 2.64 (d, 1H) (J_{AB} = 20 Hz, H_2C14), 2.63 (m, 1H, HC2), 2.39 (dd, 1H, J = 12 and 5.4 Hz, HC3), 2.16 (m, 1H, HC9), 1.97 (m, 1H, $CH(CH_3)_2$), 1.8–1.4 (m), 1.23 (s, 3H, CH_3C5), 1.14 (d, 3H, J = 7 Hz, CH_3C9), 1.04 and 0.82 (2d, 3H each, J = 7 Hz, $CH(CH_3)_2$); ms m/e: 633 (M^+). *Anal.* calcd. for $C_{31}H_{39}O_{13}N$: C 58.78, H 6.21; found: C 59.05, H 6.36.

*Ketone **155***

Chromium trioxide (400 mg, 4.0 mmol) was added to a cold (0°C) solution of pyridine (680 μL, 8.4 mmol) in dichloromethane (30 mL). After 15 min, a solution of diol **154** (100 mg, 0.158 mmol) in dichloromethane (~1 mL) was added to the mixture and the temperature was raised to 25°C. After 45 min, isopropanol (1 mL) was added and the mixture was poured onto aqueous sodium bicarbonate and extracted with dichloromethane. The same reaction was performed on another quantity of diol **154** (200 mg, 0.316 mmol) and the combined crude extracts were chromatographed on silica gel (chloroform, acetone, 4:1) to give pure *more* polar ketone **155** (233 mg, 78%); $[\alpha]_D$ −30.3° (*c* 1.00, $CHCl_3$); ir ($CHCl_3$, ν cm^{-1}): 3600, 3450, 1820, 1775, 1740, 1610, 1530, 1260; ^1H nmr ($CHCl_3$, δ ppm): 8.20 (m, 4H, aromatic), 4.68 (dd, 1H, J_{AB} = 12 Hz, J_{AX} = 6 Hz, H_AC17), 4.38 (d, 1H, J = 5 Hz, $CH(OCH_3)_2$), 4.21 (dd, 1H, $J_{AB} = J_{BX}$ = 12 Hz, H_BC17), 3.50 and 3.48 (2s, 3H each, 2 × OCH_3), 3.22 (d, 1H) and 2.78 (d, 1H) (J_{AB} = 18 Hz, H_2C14), 3.0–1.6 (m), 1.25 (s, 3H, CH_3C5), 1.25 (d, 3H, J = 7.5 Hz, CH_3C9), 1.10 and 0.90 (2d, 3H each, J = 7 Hz, $CH(CH_3)_2$); ms m/e: 631 (M^+). *Exact Mass* calcd. for $C_{31}H_{37}O_{13}N$: 631.2274; found: 631.2263. *Anal.* calcd. for $C_{31}H_{37}O_{13}N$: C 58.97, H 5.89; found: C 59.37, H 6.34.

*Equatorial alcohol **156***

To a cold (−30°C) solution of ketone **155** (200 mg, 0.317 mmol) in tetrahydrofuran (45 mL) was added lithium borohydride (15 mg, 0.69 mmol). Four hours later another quantity (5 mg, 0.23 mmol) of reagent was added, and after 1 h the mixture was cooled (−70°C), quenched with saturated ammonium chloride, and warmed to room temperature. The mixture was poured into dilute aqueous ammonium chloride and extracted with dichloromethane. Chromatography of the crude product (hexane – ethyl acetate, 1:1) furnished the already known axial alcohol **154** (30 mg, 15%) and equatorial alcohol **156** (150 mg, 75%), less polar than starting ketone **155**; $[\alpha]_D$ −15.3° (*c* 1.00, $CHCl_3$); ir ($CHCl_3$, ν cm^{-1}): 3600, 3470, 1810, 1765, 1735, 1610, 1530, 1270; ^1H nmr ($CDCl_3$, δ ppm): 8.20 (m, 4H, aromatic), 4.78 (m, 2H, H_2C17), 4.38 (d, 1H, J = 5 Hz, $CH(OCH_3)_2$), 4.12 (d, 1H, J = 10 Hz, $H_{ax}C10$), 3.53 and 3.51 (2s, 3H each, 2 × OCH_3), 3.00 (d, 1H) and 2.50 (d, 1H) (J_{AB} = 20 Hz, H_2C14), 2.9–1.5 (m), 1.23 (s, 3H, CH_3C5), 1.20, 1.12, and 1.05 (3d, 3H each, CH_3C9 and $CH(CH_3)_2$); ms m/e: 633 (M^+). *Anal.* calcd. for $C_{31}H_{39}O_{13}N$: C 58.78, H 6.21; found: C 58.71, H 6.41.

*Acetate **157***

Acetic anhydride (5 mL) was added to a solution of alcohol **156** (252 mg, 0.398 mmol) in pyridine (5 mL) at 25°C. After 20 h, the volatile substances were evaporated and the crude product was filtered through a small silica column (benzene – ethyl acetate, 4:1) to give pure acetate **157** (258 mg, 96%); mp 318–319°C (dec.); $[\alpha]_D$ +20.6° (*c* 1.00, $CHCl_3$); ir ($CHCl_3$, ν cm^{-1}): 3600, 3445, 1820, 1770, 1740, 1610, 1530, 1260; ^1H nmr ($CDCl_3$, δ ppm): 8.24 (m, 4H, aromatic), 5.57 (d, 1H, J = 11 Hz, HC10), 4.80 (dd, 1H, J_{AB} = 12 Hz, J_{AX} = 4 Hz, H_AC17), 4.72 (dd, 1H, J_{AB} = 12 Hz, J_{BX} = 6 Hz, H_BC17), 4.36 (d, 1H, J = 5.6 Hz, $CH(OCH_3)_2$), 3.54 and 3.50 (2s, 3H each, 2 × OCH_3), 2.94 (d, 1H) and 2.54 (d, 1H) (J_{AB} = 20 Hz, H_2C14), 2.78 (dd, 1H, J = 13.0 and 5.6 Hz, HC3), 2.69 (m, 1H, HC1), 2.53 (m, 1H, HC2), 2.14 (m, 2H, HC9 and $CH(CH_3)_2$), 2.07 (s, 3H, CH_3CO_2), 1.78–1.54 (m), 1.23 (s, 3H, CH_3C5), 1.10 (d, 3H) and 0.93 (d, 6H) (J = 7 Hz, CH_3C9 and $CH(CH_3)_2$); ms m/e: 675 (M^+). *Anal.* calcd. for $C_{33}H_{41}O_{14}N$: C 58.68, H 6.12; found: C 58.61, H 6.16.

*Enol ethers **158***

Elimination of methanol from dimethylacetal **157** (385 mg, 0.570 mmol) was accomplished in the same way as already described for compound **64** (*vide supra*). Thus after 5 h in refluxing benzene, acid

Can. J. Chem. Downloaded from www.nrcresearchpress.com by 186.148.149.217 on 09/07/12
For personal use only.

treatment furnished a mixture (~5:1) of isomeric enol ethers **158**, which were not separated (368 mg, crude 100%); mp 298–300°C (dec.)); ir ($CHCl_3$, ν cm^{-1}): 3600, 3450, 1815, 1765, 1740, 1690, 1610, 1530, 1260.

*Norketone **159** and enol acetate **160***

Crude enol ethers **158** (368 mg, 0.570 mmol) were ozonized in the same way as previosuly described for enol ethers **88** (*vide supra*). Thus was obtained crude norketone **159**, which was immediately acetylated in acetic anhydride (15 mL), at 95°C for 12 h, in the presence of dry sodium acetate (1.6 g). After evaporation of the volatile substances, filtration, and chromatography of the crude product (benzene – ethyl acetate, 1:1) on silica gel, enol acetate **160** (224 mg, 65% from **157**) was isolated; mp 316–318°C (dec.); ir ($CHCl_3$, ν cm^{-1}): 3450, 1825, 1770, 1735, 1680, 1610, 1530, 1265, 1170, 1035; ^1H nmr ($CDCl_3$, δ ppm): 8.25 (m, 4H, aromatic), 5.69 (d, 1H, J = 11 Hz, HC10), 5.66 (dd, 1H, J_{AM} = 12.5 Hz, J_{AX} = 2.0 Hz, H_AC17), 4.48 (dd, 1H, J_{AM} = 12.5 Hz, J_{MX} = 8.4 Hz, H_MC17), 3.62 (dd, 1H, J = 8.4 and 2.0 Hz, HCl), 2.89 (d, 1H) and 2.62 (d, 1H) (J_{AB} = 19.4 Hz, H_2C14), 2.56 (qn, 1H, J = 7 Hz, $CH(CH_3)_2$), 2.23 (s, 3H, CH_3CO_2-C3), 2.20 (m, 1H, HC9), 2.10 (s, 3H, CH_3CO_2), 1.85–1.60 (m), 1.12 (s, 3H, CH_3C5), 1.13 and 1.01 (2d, 3H each J = 7.0 Hz, $CH(CH_3)_2$), 0.95 (d, 3H, J = 6.5 Hz, CH_3C9); ms m/e: 657 (M^+).

*Enone **161***

Benzene (~30 mL) was distilled from a solution of enol acetate **160** (124 mg, 0.188 mmol) in benzene (100 mL), then freshly distilled (CaH_2) 1,5-diazabicyclo[4.3.0]non-5-ene (DBN) (0.8 mL) was added and the mixture was refluxed for 2.5 h. The reaction was followed by extraction and analysis (tlc) of aliquots. The mixture was then cooled, poured into cold hydrochloric acid (150 mL, 0.2 M), and extracted with dichloromethane to give a crude product that was chromatographed on silica gel (benzene – ethyl acetate, 3:1) to give enone **161** (70 mg, 83%); mp 301–302°C; $[\alpha]_D$ +150.6° (*c* 1.00, $CHCl_3$); uv λ_{max} (MeOH): 238 nm (ε 8775); ir ($CHCl_3$, ν cm^{-1}): 3600, 3470, 1835, 1770, 1730, 1620, 1025; ^1H nmr ($CDCl_3$, δ ppm): 5.72 (d, 1H, J = 10 Hz, HC10), 2.70 (qn, 1H, J = 7 Hz, $CH(CH_3)_2$), 2.71 (s, 1H, OH), 2.57 (s, 2H, H_2C14), 2.21 (s, 3H, H_3C17), 2.19 (s, 3H, CH_3CO_2), 1.9–1.5 (m), 1.34 (s, 3H, CH_3C5), 1.19 and 1.17 (2d, 3H each, J = 7 Hz, $CH(CH_3)_2$), 0.97 (d, 3H, J = 6.8 Hz, CH_3C9); ms m/e: 448 (M^+). *Exact Mass* calcd. for $C_{23}H_{28}O_9$: 448.1733; found: 448.1743.

*Allylic alcohol **162***

To a cold (0°C) solution of enone **161** (6.1 mg, 0.014 mmol) in tetrahydrofuran (2 mL) containing methanol (1 mL) was added sodium borohydride (~2 mg). After 2 h, the mixture was poured into cold aqueous ammonium chloride and extracted with dichloromethane. Chromatography of the crude product (benzene – ethyl acetate, 1:1) on silica plate furnished pure anhydroryanodol carbonate-acetate derivative **162** (5.8 mg, 95%); mp 300–301°C (dec.); $[\alpha]_D$ +89.6° (*c* 1.00, CH_3OH); ir ($CHCl_3$, ν cm^{-1}): 3600, 3470, 1810, 1770–1745, 1230, 1030; ^1H nmr ($CDCl_3$, δ ppm): 5.56 (d, 1H, J = 10 Hz, HC10), 5.09 (m, 1H, HC3), 3.95 (d, 1H) and 2.35 (d, 1H) (J_{AB} = 20 Hz, H_2C14), 2.70 (m, 1H, $CH(CH_3)_2$), 2.20 (m, 1H, HC9), 2.14 (s, 3H, CH_3CO_2), 1.83 (d, 3H, J = 2 Hz, H_3C17), 2.0–1.5 (m), 1.29 (s, 3H, CH_3C5), 1.15 and 1.12 (2d, 3H each, J = 7 Hz, $CH(CH_3)_2$), 0.92 (d, 3H, J = 6 Hz, CH_3C9); ms m/e: 450 (M^+).

*Anhydroryanodol **163*** and epianhydroryanodol ***164***

To a solution of carbonate acetate **162** (38 mg, 0.084 mmol) in tetrahydrofuran (6 mL) was added aqueous sodium hydroxide (0.1 M, 2.5 mL, 0.25 mmol). After 20 h at 0°C, the mixture was poured into saturated aqueous ammonium chloride and thoroughly extracted with dichloromethane (8 times). The crude product was chromatographed on silica gel (chloroform – methanol, 9:1) to give less polar epianhydroryanodol (**164**, 6 mg, 20%) and anhydroryanodol **163** (19 mg, 62%): *Epianhydroryanodol* (***164***): mp 227–228°C, $[\alpha]_D$ −97.8° (*c* 0.41, CH_3OH); ir ($CHCl_3$, ν cm^{-1}): 3500, 1750; ^1H nmr (CD_3OD, δ ppm): 5.05 (q, 1H, J = 2.0 Hz, HC3), 4.05 (d, 1H, J = 9.7 Hz, HC10), 3.57 (dd, 1H, J_{AB} = 15.8 Hz, J_W = 1.0 Hz, H_AC14), 2.81 (qn, 1H, J = 7 Hz, $CH(CH_3)_2$), 2.02 (d, 1H, J_{AB} = 15.8 Hz, H_BC14), 1.84 (d, 3H, J = 2.0 Hz, H_3C17), 1.83–1.20 (m), 1.65 (m, 1H, HC9), 1.25 (d, 3H, J = 7 Hz, $CH(CH_3)$), 1.03 (d, 3H, J = 1.0 Hz, CH_3C5), 1.02 (d, 3H, J = 6.3 Hz, CH_3C9), 0.97 (d, 3H, J = 7 Hz, $CH(CH_3)$); ms m/e: 382 (M^+). *Anhydroryanodol* (***163***): mp 148–150°C (from dichloromethane); $[\alpha]_D$ +54.3° (*c* 1.00, CH_3OH); ir (KBr, ν cm^{-1}): 3480 (br), 1750, 1240, 1010; ^1H nmr (CD_3OD, δ ppm): 4.70 (q, 1H, J = 2.4 Hz, HC3), 3.98 (d, 1H, J = 10.2 Hz, HC10), 3.61 (d, 1H) and 2.28 (d, 1H) (J_{AB} = 20 Hz, H_2C14), 2.74 (qn, 1H, J = 7 Hz, $CH(CH_3)_2$), 1.79 (m, 1H, HC9), 1.76 (d, 3H, J = 2.4 Hz, H_3C17), 1.62–1.40 (m), 1.16 (s, 3H, CH_3C5), 1.14 (d, 3H, J = 7 Hz) and 1.10 (d, 3H, J = 7 Hz) ($CH(CH_3)_2$), 1.07 (d, 3H, J = 6.3 Hz, CH_3C9); ms m/e: 382 (M^+).

Acknowledgements

This work was financially supported by the Natural Sciences and Engineering Research Council of Canada (NSERCC) and by the "Gouvernement du Québec : Science et Technologie" (FCAR).

1. P. Deslongchamps, A. Bélanger, D. J. F. Berney, H.-J. Borschberg, R. Brousseau, A. Doutheau, R. Durand, H. Katayama, R. Lapalme, D. M. Leturc, C.-C. Liao, F. N. MacLachlan, J.-P. Maffrand, F. Marazza, R. Martino, C. Moreau, L. Ruest, L. St-Laurent, R. Saintonge, and P. Soucy. Can. J. Chem. **68**, 115 (1990).
2. P. Deslongchamps, A. Bélanger, D. J. F. Berney, H.-J. Borschberg, R. Brousseau, A. Doutheau, R. Durand, H. Katayama, R. Lapalme, D. M. Leturc, C.-C. Liao, F. N. MacLachlan, J.-P. Maffrand, F. Marazza, R. Martino, C. Moreau, L. Ruest, L. St-Laurent, R. Saintonge, and P. Soucy. Can. J. Chem. **68**, 127 (1990).
3. P. Deslongchamps and C. Moreau. Can. J. Chem. **49**, 2465 (1971).
4. F. Kovac and B. Plesniscar. J. Chem. Soc. Chem. Commun. 122 (1978); J. Am. Chem. Soc. **101**, 2677 (1979).
5. R. J. Taillefer, S. E. Thomas, S. E. Nadeau, S. Fliszar, and H. Henry. Can. J. Chem. **58**, 1138 (1980).
6. P. D. Bartlett. Chem. Rev. **5**, 149 (1976).
7. P. Deslongchamps, C. Moreau, D. Fréhel, and P. Atlani. Can. J. Chem. **50**, 3402 (1972).
8. P. Deslongchamps, P. Atlani, D. Fréhel, A. Malaval, and C. Moreau. Can. J. Chem. **52**, 3651 (1974).
9. P. Deslongchamps, P. Atlani, D. Fréhel, and A. Malaval. Can. J. Chem. **50**, 3405 (1972).
10. P. Deslongchamps, C. Lebreux, and R. Taillefer. Can. J. Chem. **51**, 1665 (1973).
11. P. Deslongchamps. Stereoelectronic effects in organic chemistry. Organic Chemistry Series. Vol. 1. *Edited by* J. E. Baldwin. Pergamon Press, Oxford. 1983.
12. P. Deslongchamps, J. Lessard, and Y. Nadeau. Can. J. Chem. **63**, 2485 (1985).
13. P. Deslongchamps, D. Guay, and R. Chênevert. Can. J. Chem. **63**, 2493 (1985).
14. K. Wiesner. Adv. Org. Chem. **8**, 295 (1972).
15. K. B. Scharpless, M. A. Umbreit, M. T. Nieh, and T. C. Flood. J. Am. Chem. Soc. **94**, 6538 (1972).
16. H. Meerwein. Org. Synth. **46**, 120 (1966).
17. H. Meerwein, G. Hinz, P. Hoffmann, E. Kroning, and E. Pfeil. J. Prakt. Chem. **147**, 257 (1937).
18. O. Yonemitsu, T. Hamada, and Y. Kanaoka. Tetrahedron Lett. **10**, 1819 (1969).
19. J. C. Collins, W. W. Hess, and F. J. Frank. Tetrahedron Lett. **9**, 3363 (1968).
20. W. S. Trahanovsky, P. J. Flash, and L. M. Smith. J. Am. Chem. Soc. **91**, 5068 (1969).
21. P. Soucy, T.-L. Ho, and P. Deslongchamps. Can. J. Chem. **50**, 2047 (1972).

22. B. M. TROST and T. N. SALTZMANN. J. Chem. Soc. Chem. Commun. 571 (1975).
23. P. YATES and J. C. L. TAM. J. Chem. Soc. Chem. Commun. 737 (1975).
24. E. H. WHITE. J. Am. Chem. Soc. **77**, 6014 (1955).
25. (*a*) G. R. KROW and S. SZCZEPANSKI. Tetrahedron Lett. **21**, 4593 (1980), and references therein; (*b*) G. R. KROW. Tetrahedron, **37**, 1283 (1981), and references therein; (*c*) G. G. LYLE and R. M. BARRERA. J. Org. Chem. **29**, 3311 (1964); (*d*) E. BECKMANN. Ann. **250**, 322 (1888); (*e*) H. RUPE and I. SPLITTBERGER. Chem. Ber. **40**, 4311 (1907).
26. (*a*) G. A. OLAH, N. A. OVERCHUCK, and J. C. LAPIERRE. J. Am. Chem. Soc. **87**, 5785 (1965); (*b*) M. S. NEWMAN and A. KUTNER. J. Am. Chem. Soc. **73**, 4199 (1951).
27. C. A. GROB. Angew. Chem. Int. Ed. Engl. **8**, 535 (1969), and references therein.
28. (*a*) J. SCHREIBER and A. ESCHENMOSER. Helv. Chim. Acta, **38**, 1529 (1955); (*b*) J. C. RICHER, L. A. PILATO, and E. L. ELIEL. Chem. Ind. 2007 (1961).
29. M. W. RATHKE and A. LINDERT. Synth. Commun. **8**, 9 (1978); E. NEGISHI and M. J. IDACAVAGE. Tetrahedron Lett. 845 (1979).

Can. J. Chem. Downloaded from www.nrcresearchpress.com by 186.148.149.217 on 09/07/12
For personal use only.

The total synthesis of (+)-ryanodol. Part IV. Preparation of (+)-ryanodol from (+)-anhydroryanodol

PIERRE DESLONGCHAMPS,[1] ANDRÉ BÉLANGER, DANIEL J. F. BERNEY, HANS-JÜRG BORSCHBERG, ROBERT BROUSSEAU, ALAIN DOUTHEAU, ROBERT DURAND, HAJIME KATAYAMA, RICHARD LAPALME, DOMINIQUE M. LETURC, CHUN-CHEN LIAO, FREDERICK N. MACLACHLAN, JEAN-PIERRE MAFFRAND, FABRIZIO MARAZZA, ROBERT MARTINO, CLAUDE MOREAU, LUC RUEST, LOUISELLE SAINT-LAURENT, ROGER SAINTONGE, AND PIERRE SOUCY

Laboratoire de synthèse organique, Département de chimie, Faculté des sciences, Université de Sherbrooke, Sherbrooke (Québec), Canada J1K 2R1

Received July 4, 1989

This paper is dedicated to the memory of Professor Karel Wiesner

PIERRE DESLONGCHAMPS, ANDRÉ BÉLANGER, DANIEL J. F. BERNEY, HANS-JÜRG BORSCHBERG, ROBERT BROUSSEAU, ALAIN DOUTHEAU, ROBERT DURAND, HAJIME KATAYAMA, RICHARD LAPALME, DOMINIQUE M. LETURC, CHUN-CHEN LIAO, FREDERICK N. MACLACHLAN, JEAN-PIERRE MAFFRAND, FABRIZIO MARAZZA, ROBERT MARTINO, CLAUDE MOREAU, LUC RUEST, LOUISELLE SAINT-LAURENT, ROGER SAINTONGE, and PIERRE SOUCY. Can. J. Chem. **68**, 186 (1990).

This paper reports the transformation of (+)-anhydroryanodol (**6**) to (+)-ryanodol (**7**) by reductive cyclization of lactone epoxide derivatives **9** and **20** (Scheme 4).

Key words: anhydroryanodol, ryanodol, diterpene, synthesis, reductive cyclization.

PIERRE DESLONGCHAMPS, ANDRÉ BÉLANGER, DANIEL J. F. BERNEY, HANS-JÜRG BORSCHBERG, ROBERT BROUSSEAU, ALAIN DOUTHEAU, ROBERT DURAND, HAJIME KATAYAMA, RICHARD LAPALME, DOMINIQUE M. LETURC, CHUN-CHEN LIAO, FREDERICK N. MACLACHLAN, JEAN-PIERRE MAFFRAND, FABRIZIO MARAZZA, ROBERT MARTINO, CLAUDE MOREAU, LUC RUEST, LOUISELLE SAINT-LAURENT, ROGER SAINTONGE et PIERRE SOUCY. Can. J. Chem. **68**, 186 (1990).

On rapporte la transformation du (+)-anhydroryanodol (**6**) en (+)-ryanodol (**7**) par cyclisation réductrice des lactones époxydes intermédiaires **9** et **20** (Schéma 4).

Mots clés : anhydroryanodol, ryanodol, diterpène, synthèse, cyclisation réductrice.

Introduction

Part I (1) of this series of papers discloses the general plan that we have elaborated for the construction of (+)-ryanodol (**7**) via the key intermediate (+)-anhydroryanodol (**6**) (Scheme 1). It also describes the preparation of *o*-spirolactone dienone **1** and its reactivity as a diene in the Diels–Alder reaction. Part II (2) reports the four-step synthesis of the optically active key pentacyclic intermediate **5** starting from *o*-spirolactone dienone **1** and optically active vinyl ketone **2** prepared from *d*-carvone. Part III (3) describes the transformation in 24 steps of pentacyclic intermediate **5** into (+)-anhydroryanodol (**6**). There remains only a description of the conversion of (+)-anhydroryanodol (**6**) into (+)-ryanodol (**7**) to have a total synthesis of this compound. This conversion is the object of this paper.[2]

Discussion

The conversion of (+)-anhydroryanodol (**6**) into (+)-ryanodol (**7**) consists essentially of the formation of a bond between C_1 and C_{15} and the introduction of a hydroxyl group in the β configuration at C_2. It is thus necessary to discover a reductive cyclization process that will generate a C—C bond between the lactone carbonyl group and the tetrasubstituted olefin at C_1, and an oxidation process that will introduce the required β-hydroxyl group at C_2.

Before starting our investigation, we considered two different routes to achieve the above transformations. In the first one, it was hoped that the epoxidation of the olefin of (+)-anhydroryanodol (**6**) would take place from its less hindered face to yield the β-epoxide **9**, which would then be directly converted into (+)-ryanodol (**7**) under reductive conditions (Scheme 2). For instance, it was conceivable that under treatment with lithium in liquid ammonia, the lactone carbonyl group of **9** would be reduced to the dianion **10** (or a radical anion), making C_{15} nucleophilic enough to undergo a transannular displacement of the epoxide function at C_1, and generating at the same time the C_2 tertiary hydroxyl group of (+)-ryanodol (**7**). Examination of molecular models further suggested that competitive opening of the oxirane ring at C_2 would be less probable due to severe steric hindrance from the *endo* alcohol at C_3.

In the second route, we considered that the cyclopentenone **11** (Scheme 2), which can be obtained by oxidation of (+)-anhydroryanodol (**6**), could undergo a cyclization to produce the enolate-hemiacetal **13** under reductive conditions such as lithium in liquid ammonia. In this step, the enone **11** would first be reduced into the anticipated dianion (or radical-anion) **12** (5), which would then undergo a transannular nucleophilic addition to the lactone carbonyl group.[3] This step would then be followed by an oxidation of the resulting enolate **13** from its less hindered face, using a peroxide to yield the β-hydroxyketone hemiacetal **14**. This compound would then be converted into (+)-ryanodol (**7**) using a hydride reducing agent.

Both routes were mechanistically highly attractive and most probably feasible. The first approach was investigated because

[1]Author to whom correspondence may be addressed.

[2]For a preliminary report on the total synthesis of (+)-ryanodol, see ref. 4.

[3]The enolate-hemiacetal **13** can also be obtained by reducing first the lactone carbonyl of **11**, producing a dianion (similar to that described in **10**) that can undergo a transannular 1,4-addition on the cyclopentenone moiety.

Can. J. Chem. Downloaded from www.nrcresearchpress.com by 186.148.149.217 on 09/07/12
For personal use only.

Can. J. Chem. Downloaded from www.nrcresearchpress.com by 186.148.149.217 on 09/07/12
For personal use only.

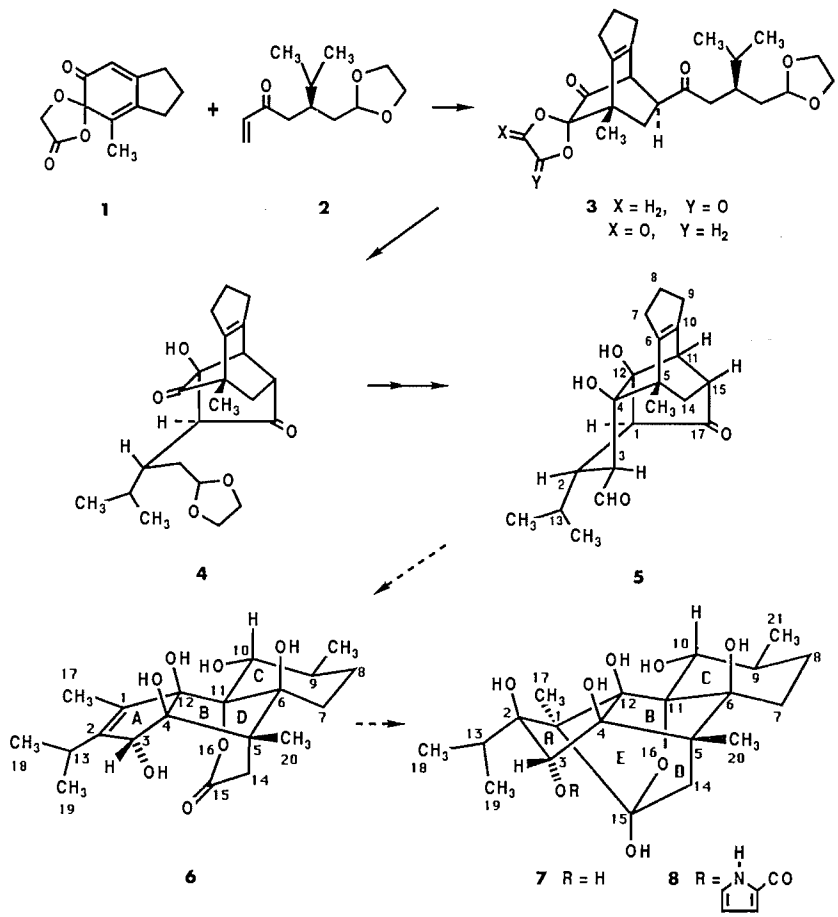

SCHEME 1

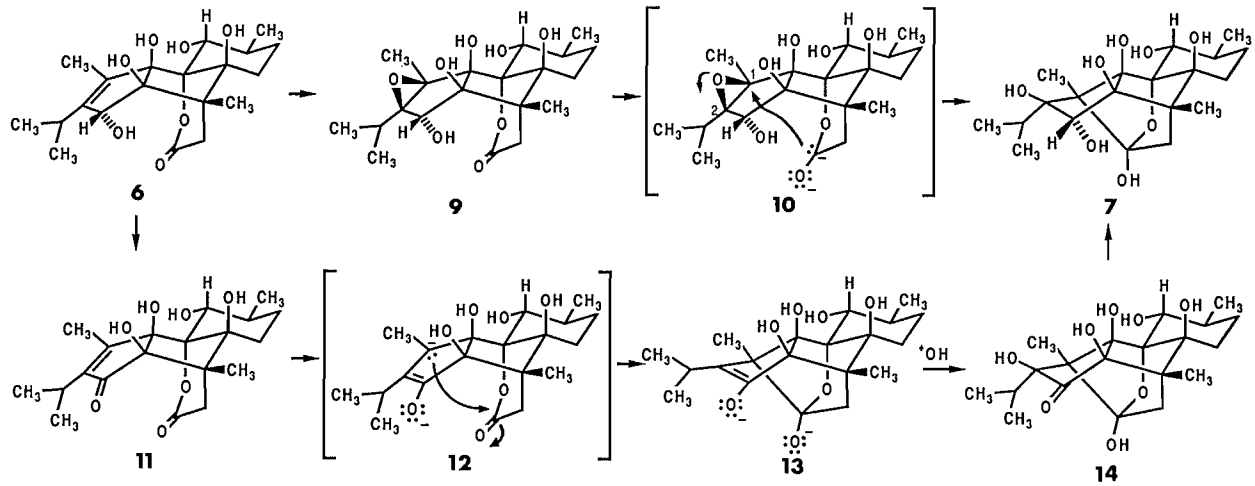

SCHEME 2

it appeared simpler and more readily realizable. Indeed, we did not anticipate difficulties in the epoxidation step and there were relatively close precedents in the literature (6) for the remaining reductive transannular cyclization step. It turned out that this approach was successful and the second one was therefore not investigated.

Results

As (+)-anhydroryanodol (**6**) can be easily obtained from (+)-ryanodine (**8**) (7), the desired transformation of (+)-anhydroryanodol (**6**) to (+)-ryanodol (**7**) was first carried out with material derived from the natural source. This transformation was then repeated with synthetic (+)-anhydroryanodol (**6**) obtained as described in the preceding paper (Part III).

Ryanodine (**8**) was isolated (7, 8)[4] and converted by basic hydrolysis to (+)-ryanodol (**7**), which was transformed under acidic conditions into (+)-anhydroryanodol (**6**) following the procedure described by Wiesner and his collaborators (7).

Direct epoxidation of (+)-anhydroryanodol (**6**) with *m*-

[4]A generous gift of powdered Ryania wood from Professor K. Wiesner was greatly appreciated.

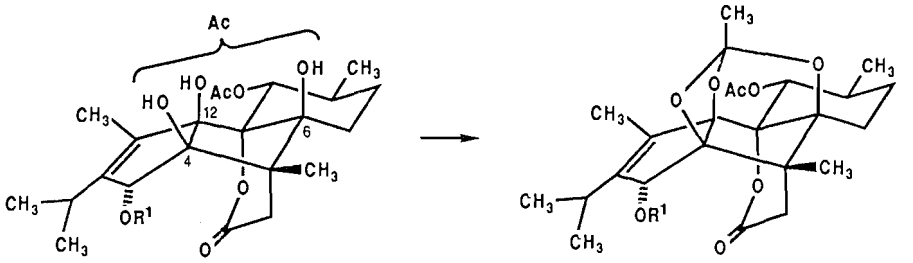

15 $R^1 = H$
16 $R^1 = Ac$
17 $R^1 = H$
18 $R^1 = Ac$

SCHEME 3

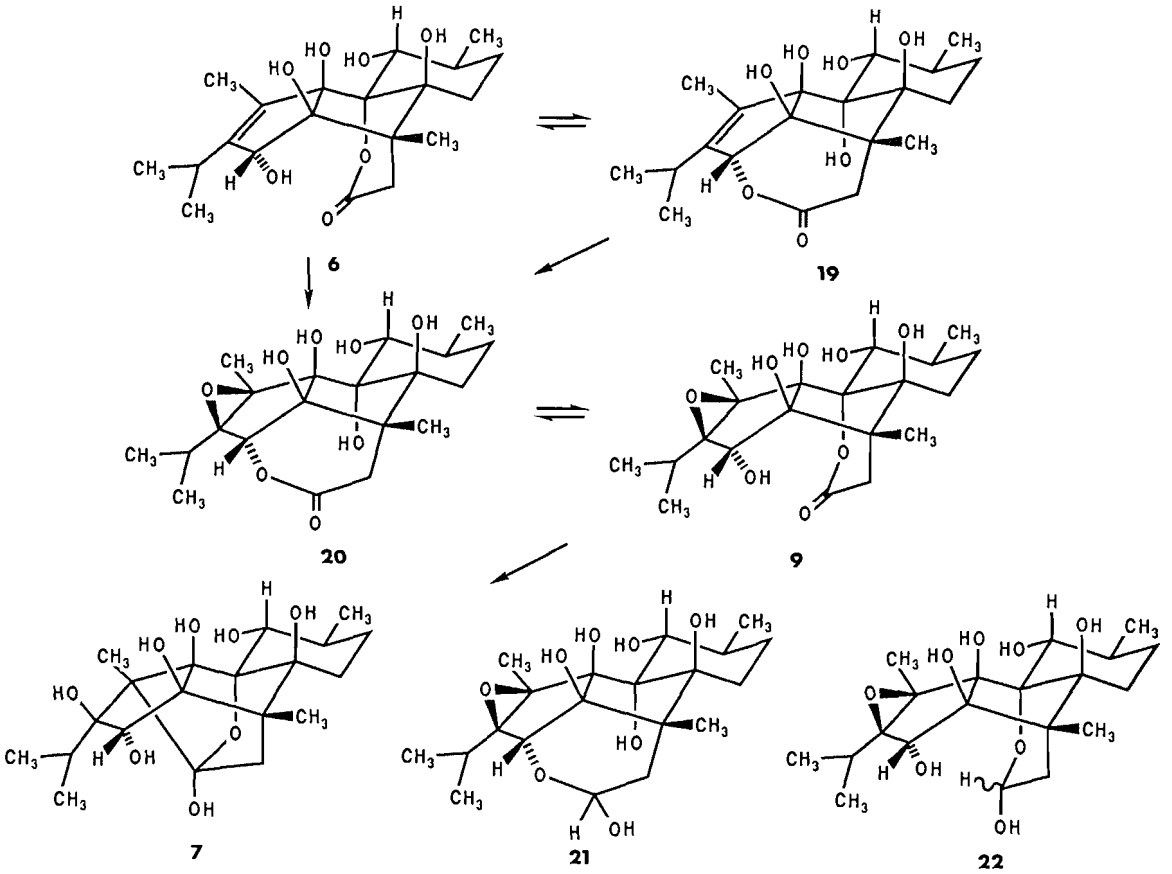

SCHEME 4

chloroperbenzoic acid was shown to be very slow and gave, instead of the desired epoxide **9** (Scheme 2), a small amount of cyclopentenone **11** along with a complex mixture of unidentified products. Cyclopentenone **11** could also be obtained by oxidation of **6** with manganese dioxide in chloroform. This result indicated that the allylic alcohol must be protected before carrying out the epoxidation reaction, and several experiments were undertaken on (+)-anhydroryanodol (**6**) with that in mind.

It soon became apparent that the selective protection of the C_3 hydroxyl group would not be a simple task. For example, simple acetylation (Ac_2O, pyridine or Ac_2O, NaOAc) led to a complex mixture that contained di- and triacetates with one of the hydroxyl groups, at either C_4, C_6, or C_{12}, being acetylated. These compounds were relatively fragile as they were readily transformed into their corresponding orthoacetate derivatives, even on silica gel during their purification. From this mixture, the diacetate **15** and triacetate **16**, having one of the tertiary OH groups at C_4, C_6, or C_{12} acetylated (Scheme 3), were isolated. On heating in benzene in the presence of *p*-toluenesulfonic acid (PTSA), compounds **15** and **16** were converted into the corresponding orthoacetates **17** and **18** respectively. These compounds had previously been isolated by Babin and are reported in his thesis (9). He also showed that orthoacetate **18** could be obtained directly from anhydroryanodol (**6**) using another method ($HClO_4$, Ac_2O).

The orthoacetate moiety appeared at first to be a very effective protecting group, which could in principle be used in the course of the synthesis of (+)-ryanodol. It was, however, shown (cf. Part III of this series) that the orthoacetate moiety was very stable (10) even under very strong acidic conditions (50% H_2SO_4). Since it was clear that (+)-ryanodol (**7**) would not survive under such strong acidic conditions, this idea was

Can. J. Chem. Downloaded from www.nrcresearchpress.com by 186.148.149.217 on 09/07/12
For personal use only.

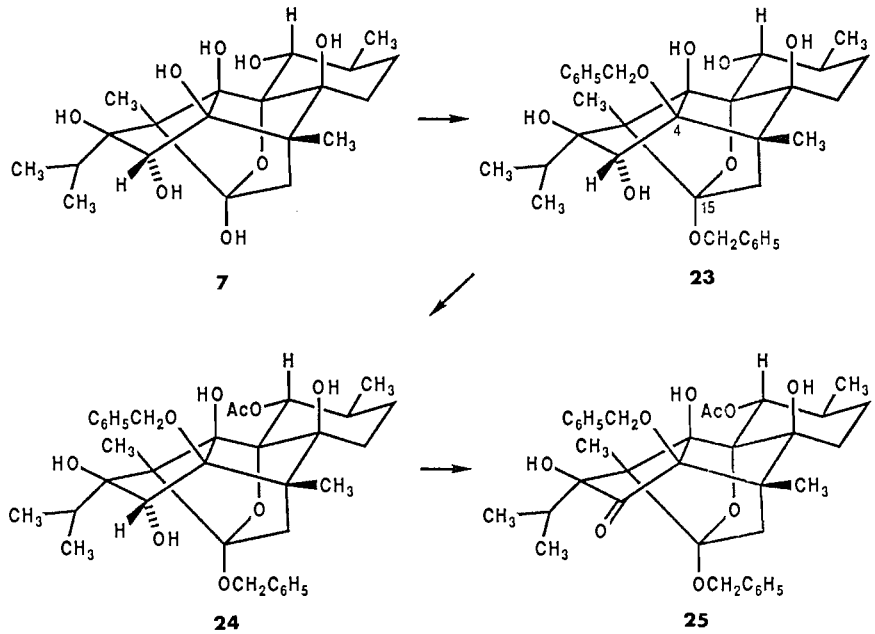

SCHEME 5

rapidly abandoned. Meanwhile, it was observed that under basic (1 M NaOH, THF) or acidic (dioxan, PTSA) conditions, (+)-anhydroryanodol (**6**) forms (Scheme 4) an equilibrium mixture (~3:1) with (−)-epianhydroryanodol (**19**) that can be separated by chromatography. The formation of (−)-epianhydroryanodol (**19**) is the result of a translactonization process with the allylic alcohol function at C_3. Once this compound was characterized,[5] it appeared clear that the problems encountered in the course of the epoxidation of (+)-anhydroryanodol (**6**) could be avoided since the allylic alcohol is now protected.

(−)-Epianhydroryanodol (**19**) was submitted to *m*-chloroperbenzoic acid (11) ($CHCl_3$, K_2CO_3) to give the β-epoxide **20** of epianhydroryanodol in 55% yield. This yield was increased to 85% using trifluoroperacetic acid in 1,2-dichloroethane in the presence of disodium hydrogen phosphate (12). It was also found that when (+)-anhydroryanodol (**6**) is submitted to these later conditions, it also yields directly, in 85% yield, the epoxide **20** of epianhydroryanodol. Thus, under those buffered acidic conditions, (+)-anhydroryanodol (**6**) must first isomerize into **19** before undergoing the epoxidation reaction. Finally, basic treatment (1 M NaOH, THF) of epianhydroryanodol epoxide **20**, followed by neutralization with acetic acid, afforded a mixture of epoxides **20** and **9**, which were separated for the characterization of epoxy-anhydroryanodol **9**. Having prepared the desired epoxide **9**, the reductive cyclization step was next attempted. It was found that treatment of epoxide **9** with lithium in liquid ammonia and tetrahydrofuran afforded, as anticipated, a satisfactory 60% yield of (+)-ryanodol (**7**) along with the minor formation of two dihydro compounds, the more polar of which was isolated in 20%, and the other in 10%, yield. These compounds were separated by chromatography and (+)-ryanodol (**7**), isolated, was found to be identical in all respects with an authentic sample.[6]

On oxidation (Br_2, CH_3OH–H_2O, $NaHCO_3$, 6 h, 25°C), the more polar dihydro derivative was transformed into epianhydroryanodol epoxide **20**. As anhydroryanodol epoxide **9** does not isomerize to **20** under the same conditions, this compound must have structure **21**. The stereochemistry at C_{15} was not defined since both epimers at that position (in two different twist conformations) can account for the observed coupling constants (10 and 1.7 Hz) for the hydrogens at C_{14} and C_{15}.

Although the ^1H nmr spectrum of the less polar dihydro compound is consistent with structure **22**, we found that this compound was not oxidized under the above conditions. Also, it did not isomerize to **21** in basic (CH_3OH, K_2CO_3) or acidic (PTSA, THF or CH_3OH) medium at room temperature. On that basis, the structure of the minor dihydro compound cannot be **22**, but no attempts were made to characterize its structure further.

The minor formation of hemiacetal epoxide **21**, which must come from the reduction of the lactone carbonyl group of epianhydroryanodol epoxide **20** followed by protonation of the resulting dianion, is an indication that the proposed mechanistic pathway (cf. Scheme 2) for the production of (+)-ryanodol (**7**) from anhydroryanodol epoxide **9** is probably correct.

The formation of (+)-ryanodol (**7**) was also observed starting directly either from the epi-epoxide **20** or from a mixture of **9** and **20**, indicating that prior to the reductive cyclization process, epi-epoxide **20** must first be isomerized into epoxide **9** in the reaction mixture. This sequence was then applied to synthetic (+)-anhydroryanodol (**6**) (see Part III) and furnished totally synthetic (+)-ryanodol (**7**) as expected.

The reconversion of (+)-ryanodol (**7**) into (+)-ryanodine (**8**) was also considered but only briefly investigated. Analysis of molecular models shows that the hydroxyl group at C_3 is

[5]To our knowledge the presence of the lactone isomer **19** of anhydroryanodol (**6**) was already observed by Babin (ref. 9, p. 109 ("isoanhydroryanodol"), pp. 143–144 and 155) but at that time its structure was not completely clarified. We called that compound **19** "epianhydroryanodol" to avoid confusion with the "iso-series," so called by Wiesner (7) to describe a different isomeric series.

[6]Synthetic (+)-ryanodol (**7**) was further identified by its reconversion into (+)-anhydroryanodol (**6**) and (−)-epianhydroryanodol (**19**) under acidic conditions.

Can. J. Chem. Downloaded from www.nrcresearchpress.com by 186.148.149.217 on 09/07/12
For personal use only.

Can. J. Chem. Downloaded from www.nrcresearchpress.com by 186.148.149.217 on 09/07/12
For personal use only.

severely hindered, and presumably impossible to esterify in a selective manner. To protect the most reactive hydroxyl groups, (+)-ryanodol (**7**) was benzylated (Scheme 5) under standard conditions ($C_6H_5CH_2Br$, NaH, THF) to provide a mixture from which dibenzyl ether derivative **23** was isolated as the major product of the reaction. Acetylation of compound **23** gave monoacetate **24**, which can be oxidized to cyclopentanone **25**.[7] However, several attempts to esterify the C_3-hydroxyl group of compound **24** with α-pyrrole carboxylic acid or its derivatives were not successful. The conversion of (+)-ryanodol (**7**) into (+)-ryanodine (**8**) was not investigated further.

Conclusion

The successful conversion of (+)-anhydroryanodol (**6**) into (+)-ryanodol (**7**) has been accomplished in two steps (**6** → **9** → **7**). The total synthesis of optically active (+)-ryanodol (**7**) is thus completed. There remains the task of converting (+)-ryanodol (**7**) into (+)-ryanodine (**8**).

Experimental

Apparatus, materials, and methods

Melting points were determined on a Büchi M-50 apparatus and are uncorrected. Ether, tetrahydrofuran, and 1,2-dimethoxyethane were dried by distilling over sodium benzophenone ketyl. Benzene, dichloromethane, dimethyl sulfoxide, and amines were distilled over calcium hydride. All reactions were performed under nitrogen or argon atmosphere. Analytical and preparative thin-layer chromatography (tlc) were carried out on glass plates precoated (0.25, 0.5, 1.0, and 2.0 mm) with silica gel 60 F-250 (Merck). Materials were detected by visualization under an ultraviolet lamp (254 or 350 nm) and (or) by spraying with sulfuric acid (50%) or a solution of phosphomolybdic acid or vanillin followed by heating on a hot plate. Column chromatography was performed with silica gel (Baker (60–200 mesh) or Merck 60 (200–400 mesh)).

The infrared spectra (ir) were taken on a Perkin–Elmer 257 or 681 spectrophotometer. Proton nuclear magnetic resonance (^{1}H nmr) spectra were recorded (with chloroform or tetramethylsilane as internal standard) on a Varian A-60, a Bruker WP-60, a Bruker HX-90, or a Bruker WM-250 instrument. Carbon nuclear magnetic resonance (^{13}C nmr) spectra were measured on a Bruker HX-90 or WM-250 instrument. The following abbreviations have been used: s, singlet; d, doublet, dd, doublet or doublets; t, triplet, q, quartet, qn, quintet; m, multiplet; br, broad. For most of the hydroxylated compounds, the multiplicity of the hydrogens attached to a carbinol was analyzed after D_2O exchange. The mass spectra were recorded on a Hitachi–Perkin–Elmer RMU-6 mass spectrometer and peak matching (hrms) on a VG Micromass ZAB-2F spectrometer. The ultraviolet spectra (uv) were recorded on a Varian Techtron 635 spectrophotometer. Specific rotation data were determined on a Perkin–Elmer polarimeter at 25°C. Microanalyses were carried out by Mr. J. Tamas, Laboratoire de Microanalyses, Université de Sherbrooke; Schwarzkopf Microanalytical Laboratories, New York; and by Dr. C. Daesslé, Organic Microanalyses, Montreal.

(+)-Ryanodol (7) from ryanodine (8)

Ryanodol was obtained as described in the literature (7) by basic hydrolysis of ryanodine **8** with potassium hydroxide in ethanol; mp 266–267°C; $[\alpha]_D$ +40.0° (CH_3OH); ^{1}H nmr (CD_3OD, δ ppm): 4.11 (s, 1H, HC3), 3.76 (d, 1H, J = 10.1 Hz, HC10), 2.49 (d, 1H, J = 13.4 Hz, H_AC14), 2.16 (qn, 1H, J = 6.8 Hz, HC13), 2.05 (m, 1H), 1.82 (m, 1H, HC9), 1.73 (d, 1H, J = 13.4 Hz, H_BC14), 1.55–1.19 (m), 1.32 (s, 3H, CH_3C5), 1.10 (s, 3H, CH_3C1), 1.07 (d, 3H, J = 6.4 Hz), 0.99 (d, 3H, J = 6.4 Hz), 0.98 (d, 3H, J = 6.4 Hz); ms m/e: 400 (M^+). *Exact Mass* calcd. for $C_{20}H_{32}O_8$: 400.2097; found: 400.2099.

Dehydration of ryanodol (7): anhydroryanodol (6) and epianhydroryanodol (19)

With aqueous sulfuric acid 20%

Following literature procedure (7), ryanodol (**7**) was dehydrated to give a mixture (~1:2) of epianhydroryanodol (**19**, less polar) and anhydroryanodol (**6**, more polar) in a total yield of ~90%. The mixture was separated by chromatography on silica gel (chloroform–methanol: 9:1). Epianhydroryanodol (**19**): mp 225–226°C; $[\alpha]_D$ −103.2° (CH_3OH); ir ($CHCl_3$, ν cm^{-1}): 3500, 1750; ^{1}H nmr (CD_3OD, δ ppm): 5.05 (q, 1H, J = 2.0 Hz, HC3), 4.05 (d, 1H, J = 9.7 Hz, HC10), 3.57 (dd, 1H, J_{AB} = 15.8 Hz, J_W = 1.0 Hz, H_AC14), 2.81 (qn, 1H, J = 7 Hz, $CH(CH_3)_2$), 2.02 (d, 1H, J_{AB} = 15.8 Hz, H_BC14), 1.84 (d, 3H, J = 2.0 Hz, H_3C17), 1.83–1.20 (m), 1.65 (m, 1H, HC9), 1.25 (d, 3H, J = 7 Hz, $CH(CH_3)$), 1.03 (d, 3H, J = 1.0 Hz, CH_3C5), 1.02 (d, 3H, J = 6.3 Hz, CH_3C9), 0.97 (d, 3H, J = 7 Hz, $CH(CH_3)$); ms m/e: 382 (M^+).

Anhydroryanodol (**6**): mp 150–151°C (CH_2Cl_2); $[\alpha]_D$ +53.3° (*c* 1.00, CH_3OH); ir (KBr, ν cm^{-1}): 3480 (br), 1750, 1240, 1010; ^{1}H nmr (CD_3OD, δ ppm): 4.70 (q, 1H, J = 2.4 Hz, HC3), 3.98 (d, 1H, J = 10.2 Hz, HC10), 3.61 (d, 1H) and 2.28 (d, 1H) (J_{AB} = 20 Hz, H_2C14), 2.74 (qn, 1H, J = 7 Hz, $CH(CH_3)_2$), 1.79 (m, 1H, HC9), 1.76 (d, 3H, J = 2.4 Hz, H_3C17), 1.62–1.40 (m), 1.16 (s, 3H, CH_3C5), 1.14 (d, 3H, J = 7 Hz) and 1.10 (d, 3H, J = 7 Hz) ($CH(CH_3)_2$), 1.07 (d, 3H, J = 6.3 Hz, CH_3C9); ms m/e: 382 (M^+).

With p-toluenesulfonic acid in dioxane

To a solution of ryanodol (**7**) (17 mg, 0.042 mmol) in pure dioxane (3 mL) was added *p*-toluenesulfonic acid (15 mg, 0.079 mmol). After 18 h at 25°C, the mixture was poured onto saturated aqueous sodium bicarbonate and extracted 10 times with chloroform to give a mixture (~1:2) of compounds **19** and **6**.

Enone 11 from anhydroryanodol 6

By treatment with m-chloroperbenzoic acid

To a solution of anhydroryanodol **6** (20 mg, 0.052 mmol) in chloroform (10 mL) was added *m*-chloroperbenzoic acid (12 mg, 82%, 0.059 mmol) dissolved in chloroform (2 mL). After 24 h, the same quantity of reagent was added and 10 h later the mixture was poured onto a diluted aqueous solution of sodium carbonate and extracted with chloroform. Chromatography of the crude product furnished starting material (8 mg, 40%) together with enone **11** (5 mg, 20%) and a complex mixture of less polar unidentified products. Enone **11**: ir (KBr, ν cm^{-1}): 3450 (br), 1750, 1720, 1625; uv (λ_{max}, EtOH): 234 nm (ε 8500); ^{1}H nmr ($CDCl_3$, δ ppm): 4.04 (d, 1H, J = 10.3 Hz, HC10), 2.74 (qn, 1H, J = 7.0 Hz, $CH(CH_3)_2$), 2.59 (d, 1H, J_{AB} = 19.8 Hz, H_AC14), 2.24 (d, 1H, J_{AB} = 19.8 Hz, H_BC14), 2.21 (s, 3H, H_3C17), 2.21 (m, 1H), 1.75 (m, 1H, HC9), 1.64–1.45 (m), 1.17, 1.14, and 1.11 (3d, 3H each, J = 7 Hz, 3 × $CH(CH_3)$); 1.10 (s, 3H, CH_3C5); ms m/e: 380 (M^+). *Exact Mass* calcd. for $C_{20}H_{28}O_7$: 380.1835; found: 380.1845.

By oxydation with manganese dioxide

A solution of anhydroryanodol (**6**) (50 mg, 0.13 mmol) in chloroform (35 mL) was refluxed with manganese dioxide (500 mg) during 42 h. The mixture was then filtered (Celite) and the solvent evaporated. The residue was chromatographed on silica plate ($CHCl_3$–CH_3OH, 9:1) to give enone **11** (22 mg, 44%).

Acetylation of anhydroryanodol (6)

Following literature procedure (9), anhydroryanodol (**6**) (75 mg, 0.20 mmol) in a mixture of pyridine (2 mL) and acetic anhydride (2 mL) was stirred at 25°C for 4 days. Evaporation of volatile

[7]The assignment of the position of the *O*-benzyl ether groups in compound **23** has not been rigorously established. This assignment is based on the following facts: (a) successful conversion of **23** into **24** and **25**; (b) the major mono-*p*-bromobenzyl ether derivative of (+)-ryanodol is known by X-ray diffraction, and the *p*-bromobenzyl ether group is located at C_4 (ref. 13); (c) compound **23** was shown to be stable under acidic conditions that transform (+)-ryanodol into (+)-anhydroryanodol, suggesting that the hemiketal OH group at C_{15} has been protected, and (d) compound **23** does not react under the *cis*-glycol cleavage conditions ($NaIO_4$, CH_3OH), which readily cleave the C_4—C_{12} bond in ryanoids (7).

Can. J. Chem. Downloaded from www.nrcresearchpress.com by 186.148.149.217 on 09/07/12
For personal use only.

substances left a residue that was chromatographed (chloroform–methanol 2%) to give two major products: diacetate **15** (more polar, 26 mg, 28%) and triacetate **16** (less polar, 35 mg, 35%), together with several other minor products. Diacetate **15**: mp 230–231°C (dec.); ir (KBr, ν cm^{-1}): 3450 (br), 1740 (br), 1230; ^1H nmr ($CDCl_3$, δ ppm): 5.66 (d, 1H, J = 10.7 Hz, HC10), 5.04 (q, 1H, J = 2.3 Hz, HC3), 3.55 (d, 1H, J = 20 Hz, H_AC14), 2.79 (qn, 1H, J = 7.2 Hz, $CH(CH_3)_2$), 2.55–1.3 (m), 2.35 (d, 1H, J = 20 Hz, H_BC14), 2.11 (s, 3H, CH_3CO_2), 2.05 (s, 3H, CH_3CO_2), 1.67 (d, 3H, J = 2.3 Hz, H_3C17), 1.19 (s, 3H, CH_3C5), 1.14 (d, 6H, J = 7.0 Hz, $CH(CH_3)_2$), 0.92 (d, 3H, J = 6.5 Hz, $CHCH_3$); ms m/e: 466 (M^+, weak). *Exact mass* calcd. for $C_{24}H_{34}O_9$: 466.2203; found: 466.2195. Triacetate **16**: mp 204–206°C (dec.); ir (KBr, ν cm^{-1}): 3450, 3250 (br, 1750 (br), 1230; ^1H nmr ($CDCl_3$, δ ppm): 5.90 (q, 1H, J = 2.3 Hz, HC3), 5.69 (d, 1H, J = 10.7 Hz, HC10), 3.05 (d, 1H, J = 19.7 Hz, H_AC14), 2.80 (qn, 1H, 7.0 Hz, $CH(CH_3)_2$), 2.39 (d, 1H, J = 19.7 Hz, H_BC14), 2.21, 2.10, and 2.04 (3s, 3H each, 3 × CH_3CO_2), 2.08 (m, 1H), 1.72 (d, 3H, J = 2.3 Hz, H_3C17), 1.8–1.4 (m), 1.12 and 1.03 (2d, 3H each, J = 7.0 Hz, 2 × $CH(CH_3)$), 0.96 (s, 3H, CH_3C5), 0.92 (d, 3H, J = 6.6 Hz, $CH(CH_3)$); ms m/e: 508 (M^+, weak), 491 (M^+ − OH). *Exact Mass* calcd. for $C_{26}H_{36}O_{10}$ − OH: 491.2281; found: 491.2268.

*Acid treatment of diacetate **15***

To a solution of diacetate **15** (10 mg, 0.021 mmol) in benzene (3 mL) was added *p*-toluenesulfonic acid (6 mg) and the mixture was stirred for 3 h at 25°C, then poured onto aqueous sodium bicarbonate and extracted with dichloromethane. The crude product was purified on silica plate to give orthoacetate monoacetate **17** (9.5 mg, 98%), also described by Wiesner (7) and Babin (9); mp 271–272°C; ir (KBr, ν cm^{-1}): 3550 (br), 1750 (br), 1650, 1230; ^1H nmr ($CDCl_3$, δ ppm): 5.78 (d, 1H, J = 10 Hz, HC10), 4.90 (q, 1H, J = 2 Hz, HC3), 3.95 (d, 1H, J = 20 Hz, H_AC14), 2.60 (qn, 1H, J = 7 Hz, $CH(CH_3)_2$), 2.26 (d, 1H, J = 20 Hz, H_BC14), 2.12 (s, 3H, CH_3CO_2), 1.73 (d, 3H, J = 2 Hz, H_3C17), 1.62 (s, 3H, CH_3CO_3), 1.20 (s, 3H, CH_3C5), 1.10, 1.00, and 0.90 (3d, 3H each, $J \approx$ 7 Hz, 3 × $CH(CH_3)$); ms m/e: 449 (MH^+). *Exact Mass* calcd. for $C_{24}H_{32}O_8$: 449.2175 (MH^+); found: 449.2149.

*Acid treatment of triacetate **16***

A mixture of triacetate **16** (17 mg, 0.033 mmol) and *p*-toluenesulfonic acid (10 mg) in benzene (2 mL) was stirred at 25°C for 24 h, then poured onto aqueous sodium bicarbonate and extracted with dichloromethane. The crude product was purified on silica plate to give orthoacetate diacetate **18** (13 mg, 80%) (also described by Babin (9)), and starting triacetate **16** (3 mg, 18%): mp 224–225°C; ir ($CHCl_3$, ν cm^{-1}): 1750, 1730, 1650, 1220; ^1H nmr ($CDCl_3$, δ ppm): 6.01 (q, 1H, J = 2 Hz, HC3), 5.80 (d, 1H, J = 10 Hz, HC10), 3.40 (d, 1H, J = 20 Hz, H_AC14), 2.75 (qn, 1H, J = 7 Hz, $CH(CH_3)_2$), 2.50 (d, 1H, J = 20 Hz, H_BC14), 2.18 and 2.13 (2s, 3H each, 2 × CH_3CO_2), 2.2–0.9 (m), 1.78 (d, 3H, J = 2 Hz, H_3C17), 1.68 (s, 3H, CH_3CO_3), 1.08 (s, 3H, CH_3C5), 1.04, 0.96, and 0.90 (3d, 3H each, $J \approx$ 7 Hz, 3 × $CHCH_3$); ms m/e: 491 (MH^+). *Exact Mass* calcd. for $C_{26}H_{34}O_9H^+$: 491.2281; found: 491.2272.

*Basic equilibration of anhydroryanodol (**6**): epianhydroryanodol (**19**)*

To a solution of epianhydroryanodol (**19**) (1.93 g, 5.05 mmol) in tetrahydrofuran (30 mL) was added aqueous sodium hydroxide (8 mL, 1 M) and the mixture was stirred vigorously for 30 min at room temperature. The mixture was then poured onto water, neutralized with 1 M acetic acid, and the aqueous phase was saturated with sodium chloride and extracted with dichloromethane to give a mixture (~3:1) of anhydroryanodol (**6**) and epianhydroryanodol (**19**) (1.88 g).

*Epianhydroryanodol epoxide (**20**)*

*From anhydroryanodol (**6**)*

To a solution of anhydroryanodol (**6**) (19.6 mg, 0.051 mmol) in 1.2-dichloroethane (8 mL) was added, at 25°C, disodium hydrogen phosphate (40 mg) followed by a freshly prepared trifluoroperacetic acid (96 μL, 1.08 M) solution in 1,2-dichloroethane (12). After 2 h, the mixture was filtered, the volatile substances were evaporated, and the residue was chromatographed on silica plate (chloroform–methanol 10%) to give epianhydroryanodol epoxide (**20**) (17.5 mg, 85%); $[\alpha]_D$ (from natural source) −43.2° (*c* 1.00, $CHCl_3$); (from synthetic anhydroryanodol): −41.7° (*c* 1.00, $CHCl_3$); ir ($CHCl_3$, ν cm^{-1}): 3550, 1750; ^1H nmr (CD_3OD, δ ppm): 4.57 (s, 1H, HC3), 4.06 (d, 1H, J = 9.9 Hz, HC10), 3.64 (d, br, 1H, J = 16 Hz, H_AC14), 2.16 (d, 1H, J = 16 Hz, H_BC14), 1.8 (m, 3H), 1.65 (m, 1H), 1.62 (s, 3H, H_3C17), 1.55–1.12 (m), 1.22, 1.07, and 1.06 (3d, 3H each, 3 × $CH(CH_3)$), 1.00 (s, 3H, CH_3C5); ms m/e: 398 (M^+, weak), 380 ($M^+ - H_2O$). *Exact Mass* calcd. for $C_{20}H_{30}O_8$: 398:1943; found: 398.1931.

*From epianhydroryanodol (**19**)*

To a solution of epianhydroryanodol (**19**) (5.6 mg, 0.014 mmol) in 1,2-dichloroethane (4 mL) was added at 25°C dihydrogen phosphate (12 mg) and freshly prepared trifluoroperacetic acid solution in 1,2-dichloroethane (27 μL, 1.08 M). After 2 h, the mixture was filtered, and evaporation of the volatile substances left a residue that was chromatographed on silica plate to give epoxide **20** (5 mg, 86%).

*Anhydroryanodol epoxide (**9**)*

To a solution of epianhydroryanodol epoxide (**20**) (32 mg, 0.080 mmol) in tetrahydrofuran (2 mL) was added aqueous sodium hydroxide (0.6 mL, 1 M). The mixture was stirred at 25°C for 30 min, then poured onto brine containing acetic acid (0.6 mL, 1 M), and extracted with chloroform. Evaporation of the solvent left a residue that was chromatographed on silica plate to give starting epoxide **20** (19 mg, 59%) and anhydroryanodol epoxide **9** (12 mg, 37%); mp 232–234°C (dec.); $[\alpha]_D$ +29.9° (*c* 1.00, CH_3OH); ir (KBr, ν cm^{-1}): 3450 (br), 1750; ^1H nmr (CD_3OD, δ ppm): 4.18 (d, 1H, J = 20.6 Hz, H_AC14), 4.13 (s, 1H, HC3), 4.03 (d, 1H, J = 10.4 Hz, HC10), 2.43 (d, 1H, J = 20.6 Hz, H_BC14), 1.80 (m, 2H), 1.68 (qn, 1H, J = 7.1 Hz, $CH(CH_3)_2$), 1.57 (s, 3H, H_3C17), 1.65–1.4 (m), 1.19 and 1.15 (2d, 3H each, J = 7.1 Hz, 2 × $CH(CH_3)$), 1.12 (s, 3H, CH_3C5), 1.06 (d, 3H, J = 6.2 Hz, $CH(CH_3)$); ms m/e: 398 (M^+). *Exact Mass* calcd. for $C_{20}H_{30}O_8$: 398.1943; found: 398.1939.

*Totally synthetic ryanodol (**7**)*

*From totally synthetic epianhydroryanodol epoxide (**20**)*

A solution of synthetic epianhydroryanodol epoxide (**20**) (20 mg, 0.050 mmol) in tetrahydrofuran (5 mL) was added to liquid ammonia (20 mL) maintained at −78°C. Then small pieces of freshly cut lithium wire (~20 mg) were added until a blue color persisted. After 1 h, solid ammonium chloride (~500 mg) was added and the mixture was warmed to room temperature (evaporation of ammonia), dissolved in a minimum volume of water, and extracted four times with dichloromethane. This first extract (7 mg) furnished a mixture of two products, less polar than ryanodol, which were chromatographed on silica plate (chloroform–methanol, 9:1).

Less polar dihydro compound (2 mg, 10%); mp 170–171°C; ir (KBr, ν cm^{-1}): 3600–3350 (br), 1470, 1110; ^1H nmr (CD_3OD, δ ppm): 5.55 (d, 1H, J = 3.4 Hz, HC15), 4.54 (s, 1H, HC3), 3.90 (d, 1H, J = 10.2 Hz, HC10), 2.53 (d, 1H, J = 15.2 Hz, H_AC14), 2.43 (qn, 1H, J = 7.0 Hz, $CH(CH_3)_2$), 1.95 (m, 1H, $H_{ax}C7$), 1.75 (m, 1H, HC9), 1.56 (s, 3H, H_3C17), 1.53 (dd, 1H, J = 15.3 and 3.4 Hz, H_BC14), 1.55–1.15 (m, 3H, H_2C8 and $H_{eq}C7$), 1.06 (s, 3H, CH_3C5), 1.02 and 0.94 (2d, 3H each, J = 7.0 Hz, $CH(CH_3)_2$), 1.00 (d, 3H, J = 6.4 Hz, H_3C21); ms m/e: 400 (M^+). *Exact Mass* calcd. for $C_{20}H_{32}O_8$: 400.2097; found: 400.2093.

More polar dihydro compound (**21**) (4 mg, ~20%); mp 143–145°C; ir ($CHCl_3$, ν cm^{-1}): 3600, 3470 (br), 1460, 1100; ^1H nmr (CD_3OD, δ ppm): 4.73 (dd, 1H, J = 10.0 Hz, HC15), 4.00 (s, 1H, HC3), 3.88 (d, 1H, J = 10.1 Hz, HC10), 2.41 (dd, 1H, J_{AB} = 12 Hz, J_{AX} = 10 Hz, H_AC14), 2.0–1.7 (m), 1.74 (dd, 1H, J_{AB} = 12 Hz, J_{BX} = 1.6 Hz, H_BC14), 1.55 (s, 3H, H_3C17), 1.54–1.08 (m), 1.20 (d, 3H, J = 6.9 Hz), 1.18 (d, 3H, J = 7.3 Hz), and 1.04 (d, 3H, J = 6.4 Hz) (3 × $CH(CH_3)$), 0.99 (s, 3H, CH_3C5); ms m/e: 400 (M^+). *Exact Mass* calcd. for $C_{20}H_{30}O_8$: 400.2097; found: 400.2100.

The aqueous layer was then saturated with carbon dioxide (9) and sodium chloride and extracted continuously with chloroform (40 h) to give almost pure totally synthetic ryanodol (**7**) (12 mg, 60%), which was recrystallized from dichloromethane and a trace of methanol; mp 267–268°C; $[\alpha]_D$ +38.5° (CH_3OH). *Exact Mass* calcd. for $C_{20}H_{32}O_8$:

Can. J. Chem. Downloaded from www.nrcresearchpress.com by 186.148.149.217 on 09/07/12
For personal use only.

400.2097; found: 400.2090. This material was found to be totally identical (^{1}H nmr, tlc, mass spectrum, mixture mp, rotation) with authentic ryanodol (*vide supra*) obtained from ryanodine (**8**). It was also dehydrated in acidic medium (dioxan; PTSA, *vide supra*) to give compounds **6** and **19**.

*From equilibrium mixture of epoxylactones **9** and **20***

The same reductive cyclization was performed on a mixture (~3:2) of epoxides **9** and **20** (natural source, 125 mg, 0.314 mmol) to give ryanodol (**7**) as well as the two dihydro compounds (**21** and unknown) in approximately the same yields and proportions.

*Ryanodol dibenzylether **23***

To a solution of ryanodol (**7**) (470 mg, 1.18 mmol) in a mixture of tetrahydrofuran (10 mL) and benzene (10 mL) was added sodium hydride (~99%, 85 mg, 3.5 mmol). After 25 min of stirring at room temperature, benzyl bromide (343 μL, 493 mg, 2.88 mmol) was added and the mixture was stirred for 54 h at the same temperature, then poured onto cold brine, and extracted ten times with chlorofom. The crude product was chromatographed on silica gel (chloroform–methanol, 97:3) to give ryanodol dibenzyl ether **23**[7] (472 mg, 69%); mp 183–184°C; ir (KBr, ν cm^{-1}): 3400 (br), 1600, 1130, 890; ^{1}H nmr (CD_3OD, δ ppm): 7.36 (m, 10 H, Ar-H), 5.13 and 4.91 (2d, 1H each, J_{AB} = 10.8 Hz, $ArCH_2O$), 4.82 (s, 1H, HC3), 4.75 and 4.68 (2d, 1H each, J_{AB} = 10 Hz, $ArCH_2O$), 3.84 (d, 1H, J = 10.1 Hz, HC10), 2.46 and 2.17 (2d, 1H each, J_{AB} = 13.5 Hz, H_2C14), 2.21 (qn, 1H, J = 7 Hz, $CH(CH_3)_2$), 2.05–1.80 (2m), 1.50 (m), 1.38 and 1.27 (2s, 3H each, CH_3C5 and CH_3C1), 1.06, 1.02, and 0.99 (3d, 3H each, J = 6.9 Hz, 3 × $CHCH_3$); ms m/e: 580 (M^+). *Exact Mass* calcd. for $C_{34}H_{44}O_8$: 580.3036; found: 580.3089.

*Ryanodol dibenzylether acetate **24***

To a solution of ryanodol dibenzyl ether **23** (150 mg, 0.241 mmol) in pyridine (2 mL) was added acetic anhydride (1.5 mL) and the mixture was stirred at 25°C for 30 h. Evaporation of the volatile substances left a residue that was filtered on silica gel (chloroform–methanol, 98:2) to give pure acetate **24** (155 mg, 97%); ir (KBr, ν cm^{-1}): 3500, 3400, 1720, 1600, 1250; ^{1}H nmr ($CDCl_3$, δ ppm): 7.36 (m, 10H, Ar-H), 5.27 (d, 1H, J = 10.5 Hz, HC10), 5.06 (d, 1H) and 5.00 (d, 1H) (J_{AB} = 11.2 Hz, $ArCH_2O$), 4.82 (s, 1H, HC3), 4.83 (d, 1H) and 4.71 (d, 1H) (J_{AB} = 11.7 Hz, $ArCH_2O$), 2.41 (d, 1H) and 2.18 (d, 1H) (J_{AB} = 13.7 Hz, H_2C14), 2.17 (qn, 1H, $CH(CH_3)_2$), 2.09 (s, 3H, CH_3CO_2), 2.00 (m), 1.65 (m), 1.42 (s, 3H) and 1.41 (s, 3H) (CH_3C5 and CH_3C1), 1.13, 1.02, and 0.87 (3d, 3H each, 3 × $CH(CH_3)$); ms m/e: 622 (M^+, weak), 605 (M^+ − OH). *Exact Mass* calcd. for $C_{36}H_{46}O_9$ − OH: 605.3114; found: 605.3100.

*Ryanodol dibenzyl ether ketone **25***

Chromic trioxide (32 mg, 0.32 mmol) was added to a solution of pyridine (55 μL, 0.64 mmol) in dichloromethane (3 mL) and the mixture was stirred 15 min at room temperature. To this preparation was added ryanodol dibenzyl ether acetate **24** (20 mg, 0.032 mmol); the mixture was stirred for 10 min at 25°C, then poured onto aqueous sodium bicarbonate and extracted with dichloromethane. The crude product was chromatographed on silica plate (chloroform–methanol, 98:2) to give starting material (3 mg, 15%) and ketone **25** (12 mg, 60%); ir ($CHCl_3$, ν cm^{-1}): 3500, 3420, 1750, 1720, 1450, 1230; ^{1}H nmr ($CDCl_3$, δ ppm): 7.35 (m, 10H, Ar-H), 5.34 (d, 1H, J = 10.4 Hz, HC10), 4.96 and 4.69 (2d, 1H each, J_{AB} = 10.9 Hz, $ArCH_2O$), 4.83 and 4.65 (2d, 1H each, J_{AB} = 11.6 Hz, $ArCH_2O$), 2.31 and 1.48 (2d, 1H each, J_{AB} = 14.3 Hz, H_2C14), 2.25–1.90 (m), 2.17 (s, 3H, CH_3CO_2), 1.75–1.2 (m), 1.42 (s, 3H, CH_3C5), 1.25, 1.13, and 0.93 (3d, 3H each, J = 6.7 Hz, 3 × $CH(CH_3)$), 1.05 (s, 3H, CH_3C1); ms m/e: 620 (M^+, weak). *Exact Mass* calcd. for $C_{36}H_{44}O_9$: 620.2985; found: 620.2971.

Acknowledgements

This research was supported by the Natural Sciences and Engineering Research Council of Canada (NSERCC) and by the "Ministère de l'Education (FCAR)" of Québec.

1. P. Deslongchamps, A. Bélanger, D. J. F. Berney, H.-J. Borschberg, R. Brousseau, A. Doutheau, R. Durand, H. Katayama, R. Lapalme, D. M. Leturc, C.-C. Liao, F. N. MacLachlan, J.-P. Maffrand, F. Marazza, R. Martino, C. Moreau, L. Ruest, L. St-Laurent, R. Saintonge, and P. Soucy. Can. J. Chem. **68**, 115 (1990).
2. P. Deslongchamps, A. Bélanger, D. J. F. Berney, H.-J. Borschberg, R. Brousseau, A. Doutheau, R. Durand, H. Katayama, R. Lapalme, D. M. Leturc, C.-C. Liao, F. N. MacLachlan, J.-P. Maffrand, F. Marazza, R. Martino, C. Moreau, L. Ruest, L. St-Laurent, R. Saintonge, and P. Soucy. Can. J. Chem. **68**, 127 (1990).
3. P. Deslongchamps, A. Bélanger, D. J. F. Berney, H.-J. Borschberg, R. Brousseau, A. Doutheau, R. Durand, H. Katayama, R. Lapalme, D. M. Leturc, C.-C. Liao, F. N. MacLachlan, J.-P. Maffrand, F. Marazza, R. Martino, C. Moreau, L. Ruest, L. St-Laurent, R. Saintonge, and P. Soucy. Can. J. Chem. **68**, 153 (1990).
4. A. Bélanger, D. J. F. Berney, H.-J. Borschberg, R. Brousseau, A. Doutheau, R. Durand, H. Katayama, R. Lapalme, D. M. Leturc, C.-C. Liao, F. N. MacLachlan, J.-P. Maffrand, F. Marazza, R. Martino, C. Moreau, L. St-Laurent, R. Saintonge, P. Soucy, L. Ruest, and P. Deslongchamps. Can. J. Chem. **57**, 3348 (1979).
5. D. Caine. Org. React. **23**. 1 (1976).
6. G. Stork, P. Rosen, N. Goldman, R. V. Coombs, and J. Tsuji. J. Am. Chem. Soc. **87**, 275 (1965); M. Tanabe, J. W. Chamberlin, and P. Y. Nishiura. Tetrahedron Lett. 601 (1961); B. G. Magerlein and J. A. Hoog. J. Am. Chem. Soc. **80**, 2223 (1958); G. Stork and J. Tsuji. J. Am. Chem. Soc. **83**, 2783 (1961); R. R. Sauers, R. M. Hawthorne, and B. I. Dentz. J. Org. Chem. **32**, 4071 (1967); R. S. Venkataramani and W. Reusch. Tetrahedron Lett. 5283 (1968); C. D. Gutsche, I. Y. C. Tao, and J. Kozma. J. Org. Chem. **32**, 1782 (1967); R. G. Carlson and R. G. Blecke. Chem. Commun. **93** (1969).
7. K. Wiesner, Z. Valenta, and J Findlay. Tetrahedron Lett. 221 (1967); K. Wiesner. Adv. Org. Chem. **8**, 295 (1972); R. B. Kelly, D. J. Whittingham, and K. Wiesner. Can. J. Chem. **29**, 905 (1951); E. F. Rogers, F. R. Koniuszi, J. Shavel, and F. Folkers. J. Am. Chem. Soc. **70**, 3086 (1948).
8. L. Ruest, D. R. Taylor, and P. Deslongchamps. Can. J. Chem. **63**, 2840 (1985).
9. D. R. Babin. Ph.D. Thesis, University of New Brunswick, Fredericton, N.B., Canada, 1962.
10. O. Bouab, G. Lamaty, C. Moreau, O. Pomares, L. Ruest, and P. Deslongchamps. Can. J. Chem. **58**, 567 (1980).
11. N. N. Schwartz and J. H. Blumbergs. J. Org. Chem. **29**, 1976 (1964).
12. W. D. Emmons and A. S. Pagano. J. Am. Chem. Soc. **77**, 4557 (1955).
13. S. N. Srivastava and M. Przybylska. Can. J. Chem. **46**, 795 (1968).

Crystal structures of 7-azaindole, an unusual hydrogen-bonded tetramer, and of two of its methylmercury(II) complexes

PASCAL DUFOUR, YVES DARTIGUENAVE, AND MICHÈLE DARTIGUENAVE
Laboratoire de chimie de coordination du Centre national de la recherche scientifique, 31077-Toulouse CEDEX, France

AND

NATHALIE DUFOUR, ANNE-MARIE LEBUIS, FRANCINE BÉLANGER-GARIÉPY, AND ANDRÉ L. BEAUCHAMP[1]
Département de chimie, Université de Montréal, C.P. 6128, Succ. A, Montréal (Québec), Canada H3C 3J7

Received August 1, 1989

PASCAL DUFOUR, YVES DARTIGUENAVE, MICHÈLE DARTIGUENAVE, NATHALIE DUFOUR, ANNE-MARIE LEBUIS, FRANCINE BÉLANGER-GARIÉPY, and ANDRÉ L. BEAUCHAMP. Can. J. Chem. **68**, 193 (1990).

Crystals of 7-azaindole ($P\bar{1}$, a = 11.312(4), b = 14.960(6), c = 15.509(5) Å, α = 102.86(3), β = 108.78(3), γ = 90.71(3)°, Z = 16, R = 0.052) contain tetrameric units of approximate S_4 symmetry, in which the molecules are associated by means of four complementary N—H...N hydrogen bonds. [CH_3Hg(7-azaindole)]NO_3 ($P\bar{1}$, a = 7.818(3), b = 7.884(3), c = 9.135(4) Å, α = 97.89(3), β = 109.13(3), γ = 103.28(3)°, Z = 2, R = 0.039) contains well-separated nitrate ions and complex cations in which the methylmercury group is linearly bonded to the pyridine nitrogen atom, whereas the five-membered ring remains protonated. In the neutral [CH_3Hg(azaindolate)] complex ($P\bar{1}$, a = 10.926(10), b = 11.333(8), c = 11.647(10) Å, α = 92.13(8), β = 104.83(9), γ = 111.86(7)°, Z = 6, R = 0.048), methylmercury groups have substituted the N—H proton in the five-membered ring for the three symmetry-independent molecules. Intermolecular secondary Hg...N bonds are found with pyridine nitrogens.

Key words: azaindole, methylmercury, crystal structure.

PASCAL DUFOUR, YVES DARTIGUENAVE, MICHÈLE DARTIGUENAVE, NATHALIE DUFOUR, ANNE-MARIE LEBUIS, FRANCINE BÉLANGER-GARIÉPY et ANDRÉ L. BEAUCHAMP. Can. J. Chem. **68**, 193 (1990).

Les cristaux de l'aza-7 indole ($P\bar{1}$, a = 11,312(4), b = 14,960(6), c = 15,509(5) Å, α = 102,86(3), β = 108,78(3), γ = 90,71(3)°, Z = 16, R = 0,052) contiennent des motifs tétramères de symétrie voisine de S_4, dans lesquels l'association se fait au moyen de quatre liaisons hydrogène N—H...N complémentaires. [CH_3Hg(7-azaindole)]NO_3 ($P\bar{1}$, a = 7,818(3), b = 7,884(3), c = 9,135(4) Å, α = 97,89(3), β = 109,13(3), γ = 103,28(3)°, Z = 2, R = 0,039) contient des ions nitrate et des cations complexes où le groupe méthylmercure est lié linéairement à l'atome d'azote pyridinique, tandis que le cycle à cinq chaînons demeure protoné. Dans le complexe neutre [CH_3Hg(azaindolate)] ($P\bar{1}$, a = 10,926(10), b = 11,333(8), c = 11,647(10) Å, α = 92,13(8), β = 104,83(9), γ = 111,86(7)°, Z = 6, R = 0,048), un groupe méthylmercure a substitué le proton du cycle à cinq chaînons dans les trois molécules symétriquement indépendantes. Il existe des liaisons secondaires Hg...N intermoléculaires avec l'azote pyridinique.

Mots clés : azaindole, méthylmercure, structure du cristal.

[Traduit par la revue]

Introduction

Purines and related rigid N-donor ligands have attracted our attention as potential binucleating agents for stabilizing pairs of bonded metal atoms via extended aromatic systems. 7-Azaindole[2] (Scheme 1) can be regarded as a simplified purine, retaining only a pair of nitrogen atoms properly arranged for bridging. We are currently examining its reactions with various dimetal units like Mo_2^{4+}, Rh_2^{4+}, Ru_2^{5+}, Re_2^{6+}, etc. In a previous paper (1), we reported the structure of a dinuclear molybdenum system in which half of the carboxylates in Mo_2(acetate)$_4$ had been replaced by bridging azaindole anions. We were able to interpret the X-ray data in terms of azaindole units disordered over two orientations, the positions of the five- and six-membered rings being interchanged. Disorder probably resulted from the very similar van der Waals envelopes in these two orientations. The same situation has been noted for complexes of Co, Ni, and Cu (2, 3), so that disorder in complexes of the azaindole anion is likely to be the rule rather than the exception.

The present study was undertaken to help solve some of the problems encountered with our dinuclear systems. The structure determination of azaindole was intended to provide an accurate reference geometry that could be imposed when describing overlapping ligands in disordered crystalline complexes. However, when preliminary work revealed that the triclinic cell contained 16 independent molecules, it became obvious that the structure would be unusual and interesting in its own right. On the other hand, probably because of the disorder, dinuclear metal complexes generally fail to grow into crystals large enough for X-ray diffraction to be used. Hence, elucidation of the structures has to depend solely on spectroscopic data. However, no reliable diagnostic tools are available at the moment. We felt that the CH_3Hg^+ ion could yield compounds corresponding to the different possible coordination patterns. The present paper also includes structure determinations on two types of 1:1 methylmercury complexes with 7-azaindole. The

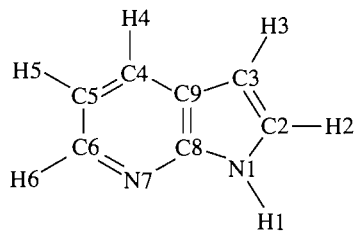

SCHEME 1

[1]Author to whom correspondence may be addressed.
[2]Abbreviations: neutral azaindole, Haza; monoanion, aza$^-$.

Printed in Canada / Imprimé au Canada

Can. J. Chem. Downloaded from www.nrcresearchpress.com by 186.148.149.217 on 09/07/12
For personal use only.

Can. J. Chem. Downloaded from www.nrcresearchpress.com by 186.148.149.217 on 09/07/12
For personal use only.

TABLE 1. Crystal data and conditions for data collection

	7-Azaindole	$[CH_3Hg(Haza)]NO_3$	$[CH_3Hg(aza)]$
Formula	$C_7H_6N_2$	$C_8H_9HgN_3O_3$	$C_8H_8HgN_2$
Formula weight	118.14	395.77	332.75
Crystal system	Triclinic	Triclinic	Triclinic
Space group	$P\bar{1}$	$P\bar{1}$	$P\bar{1}$
a, Å	11.312(4)	7.818(3)	10.926(10)
b, Å	14.960(6)	7.884(3)	11.333(8)
c, Å	15.509(5)	9.135(4)	11.647(10)
α, deg	102.86(3)	97.89(3)	92.13(8)
β, deg	108.78(3)	109.13(3)	104.83(9)
γ, deg	90.71(3)	103.28(3)	111.86(7)
V, Å^3	2412.4	503.7	1279.7
D_{calc}, g cm^{-3}	1.301	2.609	2.591
Z	16	2	6
Radiation, λ, (Å)	CuKα, 1.54178	MoKα, 0.71069	MoKα, 0.71069
$F(000)$	992	364	900
μ, cm^{-1}	6.2	152.7	179.8
Crystal size, mm (faces)	0.21	0.074(010–0$\bar{1}$0)	0.076(1$\bar{1}$0–$\bar{1}$10)
	0.24	0.096(1$\bar{1}$0–$\bar{1}$10)	0.323(001–00$\bar{1}$)
	0.41	0.176(001–00$\bar{1}$)	0.341(010–0$\bar{1}$0)
Transmission range	—	0.061–0.182	0.017–0.266
2θ max, deg	120.0	50.0	45.0
No. unique reflections	7176	1789	3347
No. observed reflections	4329	1554	2169
Rejection criterion, $I/\sigma(I) <$	2.0	3.0	3.0
T, K	293	293	293
R factor[a]	0.052	0.039	0.048
R_w factor[a]	0.055	0.048	0.052
Goodness-of-fit, S[a]	1.53	2.58	2.22
Residual in ΔF map, e/Å^3:			
general background	<±0.14	<±0.8	<±0.9
particular positions	0.23, C(9)	<±1.8, Hg	<±1.9, Hg
Standards, number	7	3	3
fluctuations	3.1%	2.1%	3.7%

[a] $R = \Sigma \| Fo \| - | Fc \| / \Sigma | Fo |$; $R_w = [\Sigma w(| Fo | - | Fc |)^2 / \Sigma w | Fo |^2]^{1/2}$; $S = [\Sigma w(| Fo | - | Fc |)^2 / \Sigma (m-n)]^{1/2}$.

preparation and spectroscopic work in the methylmercury complexes will be discussed elsewhere.[3]

Experimental

Single crystals of 7-azaindole were obtained by slow evaporation of a benzene solution of the commercial compound (Aldrich). The methylmercury complexes were prepared as described elsewhere.[3] Crystals were obtained directly from the reaction mixtures.

The crystallographic work was done with an Enraf–Nonius CAD-4 diffractometer, following similar procedures for the three compounds. The reduced cell was determined from a set of 25 randomly distributed reflections generated by the automatic search routine of the CAD-4 software and centered in the counter aperture of the diffractometer. The cell was checked by means of long-exposure oscillation photographs taken along each of the cell axes. In the case of free azaindole and $[CH_3Hg(aza)]$, where the asymmetric unit contains more than one formula, cell dimensions and space group were checked by repeating the above procedure on a different crystal mounted differently. In all cases, the Niggli coefficients unambiguously ruled out all lattices of higher symmetry. Thus, the possible space groups were $P1$ or $P\bar{1}$. The structures solved and refined normally in the centric $P\bar{1}$ space group.

The intensity data were measured as described earlier (5). For the methylmercury compounds, they were collected on crystals glued to the tip of a glass fiber. The crystal of azaindole had to be sealed in a Lindermann capillary, because it sublimed. The crystal data are given in Table 1. Standard reflections were monitored for crystal decay every hour and for misorientation every 200 reflections. The four octants defining the half-sphere data set were collected for each compound. These data were corrected for the effects of Lorentz and polarization. An absorption correction based on crystal geometry was applied for the Hg compounds (Gaussian integration, grid 10 × 10 × 10).

The structures were refined on $| F |$. Individual weights based on counting statistics were applied. The coordinates and isotropic temperature factors of all non-hydrogen atoms were first refined by full-matrix least-squares procedures. The block-diagonal approximation was used in the final steps of the anisotropic refinement. The scattering curves were from standard sources (6). The anomalous dispersion components for Hg (7) were included in structure factor calculations. The computer programs used are listed elsewhere (8).

$[CH_3Hg(Haza)]NO_3$

The asymmetric unit corresponds to one formula. The Hg atom was located from a Patterson map. The remaining non-hydrogen atoms were then positioned from a difference Fourier (ΔF) map. Hydrogens on the ring were fixed at idealized positions (B = 6 Å^2). The methyl hydrogens were visible in the ΔF map; an idealized methyl group was defined to give optimum fit with these positions. The coordinates of the hydrogens were recalculated after each cycle. All non-hydrogen atoms were refined anisotropically.

$[CH_3Hg(aza)]$

There are three molecules per asymmetric unit. The three Hg atoms

[3] N. Dufour, A. M. Lebuis, and A. L. Beauchamp. Manuscript in preparation.

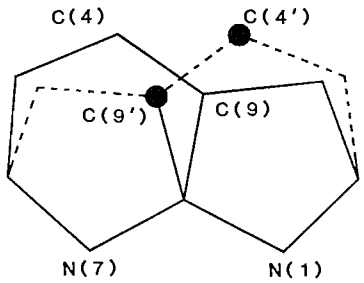

FIG. 1. Disorder found in the crystal of 7-azaindole (molecules A–D). Full bonds represent one of the components, the dashed ones correspond to the same molecule after inversion. Residual electron densities corresponding to ca. 1/8 C atom are found in the ΔF map at positions marked by black circles.

were located by the direct methods of the SHELX package (9). The remaining non-hydrogen atoms were then found from a ΔF map. The ring hydrogens were treated as above. The methyl hydrogens were neglected. All non-hydrogen atoms were refined anisotropically.

7-Azaindole

Solving this structure was not straightforward, because the asymmetric unit contained 8 independent molecules. After a series of attempts using different starting reflections in the phasing procedure of MULTAN (10), four consistent azaindole molecules could be recognized. Subsequent ΔF maps revealed the remaining four molecules in the unit cell. Isotropic refinement of the non-hydrogen atoms by full-matrix least squares converged to $R = 0.117$ and $R_w = 0.124$. Refinement was continued with the block-diagonal approximation, anisotropically for the non-hydrogen atoms, isotropically for the hydrogens.

After the known model had been refined to convergence, it was noticed that molecules A–D had some of their distances and angles systematically different from those of E–H (see next section and Table A-2, supplementary material[4]). The eight strongest peaks in the ΔF map occurred in pairs, which were located as shown in Fig. 1 with respect to azaindole molecules A–D. A similar situation had been encountered with $Mo_2(acetate)_2(azaindolate)_2.2DMF$ (1), where the disorder depicted in the figure is also present. Starting with occupancy factors of 0.1 deduced from peak height (0.35 e/Å^3), four C(4′) atoms were introduced in the structure and independently refined. The second peak in each pair corresponded to an alternate position C(9′) for the inverted individual. However, these fractional carbons were too close to the main C(9) components to be refined independently. The other atomic positions were not resolved.

The fractional carbons C(4′A–D) were first assigned an isotropic temperature factor B of 5.4 Å^2, the mean refined value for the C(4) atoms in the E–H tetramer. Their coordinates and occupancy factors were refined, together with the positions and anisotropic temperature factors of the remaining non-hydrogen atoms. Occupancies converged to 0.12 ± 0.01 ($\sigma = 0.01$). For the rest of the refinement, fixed values of 0.12 were used for C(4′A–D) and 0.88 for C(4A–D). Interpretation was completed by refining the non-hydrogen atoms anisotropically, the hydrogens and the C(4′A–D) atoms isotropically.

The refined coordinates for the three compounds are listed in Tables 2–4.[4]

Results and discussion

7-Azaindole

The unit cell contains eight independent 7-azaindole molecules associated into two tetramers via hydrogen bonding (Fig. 2). Individual distances and angles are available in the supplementary material (Table A-2). Mean values for each tetramer are listed in Table 5. Since the geometry can be artificially distorted by disorder for the tetramer that contains molecules A–D (see below), the results obtained for the E–H unit will be used in the discussion.

The molecules are planar as expected (Table A-4, supplementary material). The mean and maximum deviations from the least-squares planes through the nine non-hydrogen atoms are 0.006(4) and 0.014(4) Å, respectively. This is within the range reasonably ascribed to normal packing forces. The distances in the six-membered ring are similar to those of pyridine (C—C = 1.380(4), C—N = 1.336(4) Å) (11), except for the C(8)—C(9) bond shared by the two rings, which is longer (1.398(5) Å). The common C—C bonds are also long for 1-azacarbazole (12) and indole derivatives (13, 14). Deviations from 120° in the ring follow a pattern well documented for purines (15): the nitrogen lone pair decreases the angle at N(7) by 6.1(3)°, whereas the adjacent angles at C(6) and C(8) react in the opposite direction by 4.8(3)° and 6.3(3)°, respectively. The remaining angles undergo small changes, keeping the ring planar. The geometry of the five-membered ring follows the pattern noted for indole compounds (13, 14, 16) and it is consistent with greater bond localization. Bond order is clearly lower for C(9)—C(3) (1.419(5) Å) than for C(3)—C(2) (1.342(5) Å). Also, the C—N bonds (mean 1.366(5) Å) are loser to single bonds that in the six-membered ring (mean 1.339(5) Å).

Four molecules form tetrameric units (Fig. 2) of approximately 4 (S_4) symmetry in the crystal. The nitrogens occupy the central region, where they all participate in complementary hydrogen bonding. This pocket is shielded from the surrounding molecules by the rings directed outward and providing a hydrophobic surface. The hydrogen bonds are all very strong: the N(1)—N(7) separations (Table 6) are at the lower limit of the range (2.88—3.88 Å) proposed by Stout and Jensen (17), and departure from linearity is within 15°.

7-Azaindole can be compared with 1-azacarbazole, which contains an extra benzene ring (Fig. 3). This molecule crystallizes as flat cyclic dimers associated via a pair of complementary N—H...N bonds (N...N = 2.946(2) Å, N—H...N = 172°) (12). A similar arrangement has been proposed for a 7-azaindole dimer detected in nonpolar solution (18, 19). A tetrameric arrangement had also been considered as possible on the basis of model building, but no evidence for its formation had been obtained.

Assuming that the hydrogen-bonding framework in a cyclic azaindole dimer would have the geometry observed in 1-azacarbazole, several factors can be put forward to explain that a tetrameric structure is preferred for 7-azaindole in the solid state:

(*i*) The N...N separation (mean 2.917 Å) is shorter than in the dimer.

(*ii*) Hydrogen lies closer to the expected lone-pair direction: the difference between the C(6)—N(7)...H and C(8) — N(7)...H angles, which should ideally be 0°, is only 6° on average here, but it is 12° in the dimer.

(*iii*) The van der Waals interactions between the π systems of the roughly parallel rings are retained within the tetramer, although they could be somewhat less efficient than between strictly parallel molecules.

(*iv*) The van der Waals envelope of the tetramer corresponds roughly to a box, favoring efficient packing and some intertetramer "stacking" interactions between the ring π systems

[4]The supplementary material includes tables of refined temperature factors, fixed hydrogen coordinates (Hg compounds), distances and angles involving the light atoms and the hydrogens, least-squares plane calculations, and structure factor amplitudes. Complete set of data may be purchased from the Depository of Unpublished Data, CISTI, National Research Council of Canada, Ottawa, Ont., Canada K1A 0S2.

Can. J. Chem. Downloaded from www.nrcresearchpress.com by 186.148.149.217 on 09/07/12
For personal use only.

TABLE 2. Fractional coordinates ($\times 10^4$, H $\times 10^3$) and equivalent isotropic temperature factors ($\times 10^3$) for 7-azaindole[c]

Atom	x	y	z	U_{eq}
N(1A)	7807(2)	5907(2)	9170(2)	71
C(2A)	6760(3)	5481(2)	8452(2)	78
C(3A)	5715(3)	5530(2)	8684(2)	77
C(4A)[a]	5604(3)	6370(3)	10317(3)	75
C(5A)	6376(3)	6865(2)	11185(2)	83
C(6A)	7636(3)	7044(2)	11389(2)	82
N(7A)	8250(2)	6757(2)	10766(2)	75
C(8A)	7461(3)	6274(2)	9941(2)	61
C(9A)	6171(3)	6064(2)	9682(3)	79
N(1B)	10918(2)	7267(2)	11117(2)	73
C(2B)	11690(3)	6580(2)	11156(3)	84
C(3B)	12854(3)	6862(2)	11236(3)	83
C(4B)[a]	13624(3)	8531(3)	11290(3)	73
C(5B)	13179(3)	9387(2)	11270(3)	85
C(6B)	11964(3)	9538(2)	11189(3)	83
N(7B)	11110(2)	8874(2)	11129(2)	72
C(8B)	11581(3)	8055(2)	11163(2)	62
C(9B)	12815(3)	7848(3)	11248(2)	79
N(1C)	8520(2)	9072(2)	10839(2)	73
C(2C)	8051(3)	9532(2)	11511(2)	79
C(3C)	6805(3)	9502(2)	11212(2)	76
C(4C)[a]	5328(3)	8677(3)	9546(3)	73
C(5C)	5349(3)	8164(3)	8682(3)	86
C(6C)	6510(3)	7953(2)	8579(2)	79
N(7C)	7646(2)	8221(2)	9240(2)	73
C(8C)	7536(3)	8719(2)	10047(2)	62
C(9C)	6429(3)	8967(2)	10232(3)	81
N(1D)	9956(2)	7668(2)	8828(2)	73
C(2D)	10647(3)	8350(3)	8706(3)	88
C(3D)	11698(3)	8063(2)	8545(3)	88
C(4D)[a]	12378(3)	6398(3)	8468(3)	78
C(5D)	12001(3)	5550(2)	8549(3)	83
C(6D)	10909(3)	5411(2)	8716(3)	80
N(7D)	10136(2)	6075(2)	8824(2)	70
C(8D)	10553(3)	6882(2)	8750(2)	61
C(9D)	11640(3)	7082(3)	8563(2)	82
N(1E)	10157(2)	3272(2)	6247(2)	72
C(2E)	9453(3)	4005(2)	6369(3)	80
C(3E)	8399(3)	3723(2)	6487(3)	78
C(4E)	7629(3)	2079(2)	6486(2)	71
C(5E)	8001(3)	1192(2)	6390(2)	77
C(6E)	9135(3)	1025(2)	6253(3)	77
N(7E)	9920(2)	1663(2)	6197(2)	72
C(8E)	9531(3)	2511(2)	6282(2)	59
C(9E)	8409(3)	2765(2)	6434(2)	59
N(1F)	9193(2)	1814(2)	3914(2)	71
C(2F)	8394(3)	1084(2)	3823(2)	78
C(3F)	7229(3)	1334(2)	3734(3)	76
C(4F)	6458(3)	2973(2)	3760(2)	72
C(5F)	6917(3)	3861(2)	3834(2)	75
C(6F)	8151(3)	4045(2)	3936(2)	75
N(7F)	8985(2)	3417(2)	3961(2)	68
C(8F)	8522(3)	2564(2)	3891(2)	60
C(9F)	7292(3)	2297(2)	3778(2)	57
N(1G)	11594(2)	3709(2)	4167(2)	67
C(2G)	12092(3)	3830(2)	3493(2)	69
C(3G)	13348(3)	3892(2)	3838(2)	68
C(4G)	14783(3)	3801(2)	5494(2)	70
C(5G)	14695(3)	3694(2)	6333(2)	76
C(6G)	13546(3)	3603(2)	6428(2)	75
N(7G)	12446(2)	3594(2)	5762(2)	68
C(8G)	12566(3)	3700(2)	4954(2)	56
C(9G)	13690(2)	3807(2)	4781(2)	55

TABLE 2 (*Concluded*)

Atom	x	y	z	U_{eq}
N(1H)	12235(2)	1301(2)	5823(2)	69
C(2H)	13269(3)	1178(2)	6519(2)	73
C(3H)	14268(3)	1077(2)	6230(2)	70
C(4H)	14388(3)	1122(2)	4588(2)	70
C(5H)	13648(3)	1227(2)	3744(2)	75
C(6H)	12400(3)	1376(2)	3591(2)	77
N(7H)	11827(2)	1410(2)	4233(2)	71
C(8H)	12584(3)	1294(2)	5054(2)	59
C(9H)	13861(3)	1149(2)	5291(2)	58
C(4A')[b]	5334(19)	5980(15)	9576(15)	40(6)
C(4B')[b]	13698(22)	7734(18)	11281(18)	58(7)
C(4C')[b]	5650(21)	9047(16)	10257(16)	48(6)
C(4D')[b]	12424(21)	7163(16)	8457(17)	50(6)
H(1A)	879(3)	598(2)	916(2)	113(12)
H(2A)	683(3)	525(2)	776(2)	113(12)
H(3A)	479(2)	529(2)	828(2)	83(9)
H(4A)[a]	462(3)	621(2)	1007(2)	72(10)
H(5A)	601(3)	710(2)	1173(2)	121(12)
H(6A)	824(3)	735(2)	1197(2)	98(10)
H(1B)	993(3)	715(2)	1099(2)	103(11)
H(2B)	1130(3)	594(2)	1109(2)	132(13)
H(3B)	1352(2)	651(2)	1128(2)	73(9)
H(4B)[a]	1456(3)	838(2)	1137(2)	79(10)
H(5B)	1370(3)	987(2)	1128(2)	112(12)
H(6B)	1159(3)	1012(2)	1110(2)	109(11)
H(1C)	952(2)	903(2)	1091(2)	95(10)
H(2C)	866(2)	978(2)	1214(2)	83(9)
H(3C)	625(2)	976(2)	1154(2)	78(9)
H(4C)[a]	446(3)	886(2)	965(2)	86(11)
H(5C)	455(3)	795(2)	814(2)	116(12)
H(6C)	659(2)	763(2)	802(2)	94(10)
H(1D)	910(3)	776(2)	899(2)	101(11)
H(2D)	1029(3)	894(2)	875(2)	152(15)
H(3D)	1234(3)	837(2)	844(2)	104(11)
H(4D)[a]	1309(3)	657(2)	824(2)	97(12)
H(5D)	1260(3)	500(2)	848(2)	114(12)
H(6D)	1062(2)	485(2)	877(2)	67(8)
H(1E)	1090(2)	332(2)	611(2)	86(10)
H(2E)	979(2)	463(2)	635(2)	102(11)
H(3E)	771(3)	409(2)	656(2)	98(11)
H(4E)	681(2)	215(2)	659(2)	66(8)
H(5E)	748(2)	69(2)	642(2)	90(10)
H(6E)	935(2)	38(2)	621(2)	95(10)
H(1F)	1006(2)	180(2)	406(2)	92(10)
H(2F)	867(3)	46(2)	384(2)	103(11)
H(3F)	651(2)	98(2)	370(2)	82(9)
H(4F)	550(2)	282(2)	366(2)	78(9)
H(5F)	637(2)	439(2)	383(2)	83(9)
H(6F)	844(2)	468(2)	394(2)	91(10)
H(1G)	1070(3)	367(2)	410(2)	119(12)
H(2G)	1156(2)	387(2)	290(2)	83(9)
H(3G)	1391(2)	397(2)	354(2)	71(9)
H(4G)	1554(2)	385(2)	543(2)	67(8)
H(5G)	1542(2)	371(2)	683(2)	75(9)
H(6G)	1350(2)	357(2)	702(2)	87(10)
H(1H)	1147(3)	134(2)	591(2)	98(10)
H(2H)	1322(2)	114(2)	713(2)	85(10)
H(3H)	1510(2)	99(2)	659(2)	78(9)
H(4H)	1532(2)	103(2)	477(2)	76(9)
H(5H)	1394(3)	122(2)	325(2)	96(10)
H(6H)	1183(2)	142(2)	299(2)	74(9)

Occupancy factors: [a]0.88, [b]0.12.
[c]Isotropic temperature factor for hydrogens and C(4'A–D) atoms.

Can. J. Chem. Downloaded from www.nrcresearchpress.com by 186.148.149.217 on 09/07/12
For personal use only.

Can. J. Chem. Downloaded from www.nrcresearchpress.com by 186.148.149.217 on 09/07/12
For personal use only.

TABLE 3. Fractional coordinates ($\times 10^4$, Hg $\times 10^5$) and equivalent isotropic temperature factors ($\times 10^3$) for $[CH_3Hg(Haza)]NO_3$

Atom	x	y	z	U_{eq}
Hg(7)	6013(6)	25291(7)	38224(5)	36
O(10)	618(15)	−3724(13)	2960(13)	67
O(11)	1269(14)	−964(13)	4101(11)	59
O(12)	−1(17)	−1812(17)	1584(12)	71
N(1)	3761(14)	6540(14)	5782(12)	40
N(7)	3008(13)	3486(13)	5989(11)	38
N(10)	632(14)	−2159(14)	2842(11)	39
C(2)	5223(21)	8114(19)	6666(19)	52
C(3)	6465(18)	7751(18)	7917(15)	47
C(4)	6363(18)	4724(19)	8742(15)	49
C(5)	5223(19)	2919(19)	8226(16)	50
C(6)	3616(18)	2385(16)	6923(15)	42
C(7)	−1662(18)	1852(19)	1743(16)	55
C(8)	4066(15)	5193(15)	6485(12)	31
C(9)	5770(17)	5852(17)	7875(14)	41

TABLE 4. Fractional coordinates ($\times 10^3$, Hg $\times 10^5$) and equivalent isotropic temperature factors ($\times 10^3$) for $[CH_3Hg(aza)]$

Atom	x	y	z	U_{eq}
Hg(1A)	24304(12)	46406(10)	3147(8)	56
Hg(1B)	22910(12)	13797(10)	12370(8)	52
Hg(1C)	19464(12)	15412(11)	41473(8)	60
N(1A)	349(2)	446(2)	−92(2)	82
N(7A)	328(2)	226(2)	−77(1)	58
N(1B)	56(2)	157(2)	49(2)	44
N(7B)	−15(2)	169(2)	223(1)	71
N(1C)	89(2)	−41(2)	396(1)	60
N(7C)	309(2)	−81(2)	460(2)	87
C(1A)	133(3)	498(3)	145(2)	121
C(2A)	398(3)	538(2)	−162(2)	71
C(3A)	452(3)	489(3)	−234(2)	65
C(4A)	460(3)	255(3)	−254(2)	86
C(5A)	418(3)	145(3)	−211(2)	71
C(6A)	360(3)	135(2)	−123(2)	58
C(8A)	362(2)	333(2)	−126(2)	40
C(9A)	439(2)	359(2)	−212(2)	48
C(1B)	409(3)	117(3)	211(2)	68
C(2B)	0(3)	167(2)	−71(2)	60
C(3B)	−118(3)	187(2)	−89(2)	69
C(4B)	−256(3)	218(3)	69(2)	97
C(5B)	−231(4)	210(3)	193(2)	97
C(6B)	−120(3)	189(3)	263(2)	74
C(8B)	−43(2)	173(2)	105(2)	41
C(9B)	−146(3)	191(2)	26(2)	46
C(1C)	313(3)	351(2)	443(2)	70
C(2C)	−47(2)	−119(2)	359(2)	49
C(3C)	−46(2)	−246(3)	372(2)	73
C(4C)	143(4)	−336(2)	432(2)	86
C(5C)	287(3)	−286(3)	469(2)	87
C(6C)	352(3)	−169(3)	480(3)	90
C(8C)	167(3)	−117(2)	424(2)	59
C(9C)	76(3)	−256(2)	407(2)	60

(Fig. 4). For a compound with bulky substituents pointing outward and producing a less regular volume, packing of such a tetramer could be less efficient, and a flat cyclic dimer might be preferred.

Disorder is often observed in crystals of compounds containing fused five- and six-membered rings, unless large substituents destroy the near equivalence of the van der Waals envelopes of the two halves of the molecule. Indole (20) and its trinitrobenzene adduct (21) are disordered, as are all the known metal complexes with the azaindole anion playing a bridging role (1–3, 22). Until a very late stage in structure resolution, 7-azaindole seemed not to follow this rule. However, careful inspection of the refined results for an ordered model showed unexplained differences in the C(3)—C(9)—C(4) region between the two tetramers. Mean values for each tetramer are given in Table 5. Details are available in the supplementary material. Corresponding distances or angles within a given tetramer were usually equal within experimental errors, but some large discrepancies between the tetramers were identified. For instance, tetramers A–D and E–H showed differences of +0.059 and −0.042 Å for the C(3)—C(9) and C(4)—C(9) bond lengths, respectively. Angles were also affected, e.g., C(2)—C(3)—C(9), +3.0°. A Fourier map showed residual

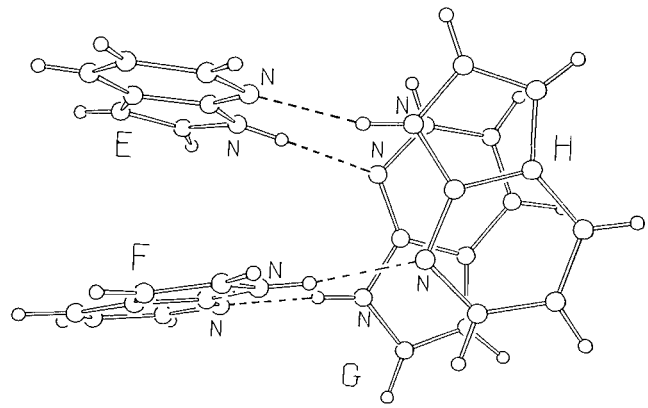

FIG. 2. 7-Azaindole molecules E–H defining a hydrogen-bonded tetramer in the crystal. The atoms are represented by spheres of arbitrary size and can be identified by reference to Scheme 1. Dashed lines correspond to hydrogen bonds. The same tetramer is formed by molecules A–D.

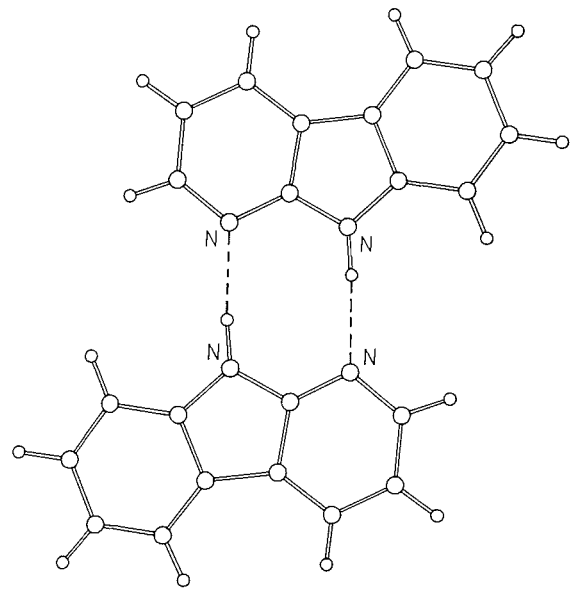

FIG. 3. Planar hydrogen-bonded cyclic dimer observed in the crystal structure of 1-azacarbazole (ref. 12).

Can. J. Chem. Downloaded from www.nrcresearchpress.com by 186.148.149.217 on 09/07/12
For personal use only.

TABLE 5. Geometry of the azaindole rings

	7-Azaindole[a]			
	A–D	E–H	$[CH_3Hg(Haza)]NO_3$	$[CH_3Hg(aza)]^b$
Distances (Å)				
N(1)—C(2)	1.364(5)	1.370(5)	1.40(2)	1.38(4)
N(1)—C(8)	1.366(4)	1.361(4)	1.34(2)	1.42(4)
C(2)—C(3)	1.339(5)	1.342(5)	1.35(2)	1.39(4)
C(3)—C(9)	1.478(5)	1.419(5)	1.46(2)	1.42(4)
C(4)—C(5)	1.390(5)	1.377(6)	1.41(2)	1.38(4)
C(4)—C(9)	1.341(5)	1.383(6)	1.33(2)	1.43(4)
C(5)—C(6)	1.363(6)	1.375(5)	1.35(2)	1.31(4)
C(6)—N(7)	1.351(5)	1.337(5)	1.35(2)	1.34(4)
N(7)—C(8)	1.342(4)	1.341(4)	1.33(2)	1.35(4)
C(8)—C(9)	1.400(5)	1.398(5)	1.43(2)	1.43(4)
Angles (deg)				
C(2)—N(1)—C(8)	108.4(3)	107.6(3)	109(1)	107(2)
N(1)—C(2)—C(3)	112.9(3)	110.6(3)	109(1)	108(2)
C(2)—C(3)—C(9)	103.9(3)	106.9(3)	108(1)	112(2)
C(5)—C(4)—C(9)	116.7(4)	117.9(4)	117(1)	117(2)
C(4)—C(5)—C(6)	121.7(4)	119.9(4)	121(1)	121(2)
C(5)—C(6)—N(7)	124.0(3)	124.8(3)	124(1)	127(2)
C(6)—N(7)—C(8)	112.0(3)	113.9(3)	115(1)	113(2)
N(1)—C(8)—N(7)	124.7(3)	125.2(3)	127(1)	124(2)
N(1)—C(8)—C(9)	107.6(3)	108.5(3)	109(1)	110(2)
N(7)—C(8)—C(9)	127.7(3)	126.3(3)	124(1)	125(2)
C(3)—C(9)—C(4)	134.9(4)	136.5(4)	136(1)	141(2)
C(3)—C(9)—C(8)	107.2(3)	106.4(3)	104(1)	102(2)
C(4)—C(9)—C(8)	117.8(3)	117.1(3)	119(1)	116(2)

[a]Mean values for rings A–D and E–H, respectively. Individual values given in Table A-2 (supplementary material).

[b]Mean values for three independent molecules. Individual values given in Table C-4 (supplementary material).

TABLE 6. Distances (Å) and angles (deg) for the hydrogen bonds in 7-Azaindole

	N(1)—N(7)	N(1)—H—N(7)	C(6)—N(7)—H	C(8)—N(7)—H
N(1A)—H(1A)...N(7D)	2.872(4)	165(3)	126(1)	121(1)
N(1B)—H(1B)...N(7A)	2.947(4)	171(3)	123(1)	125(1)
N(1C)—H(1C)...N(7B)	2.847(4)	172(2)	123(1)	123(1)
N(1D)—H(1D)...N(7C)	2.969(4)	166(3)	119(1)	129(1)
N(1E)—H(1E)...N(7G)	2.981(4)	172(3)	115(1)	132(1)
N(1F)—H(1F)...N(7H)	2.952(4)	165(3)	124(1)	122(1)
N(1G)—H(1G)...N(7F)	2.881(4)	172(3)	125(1)	121(1)
N(1H)—H(1H)...N(7E)	2.891(4)	170(3)	122(1)	124(1)

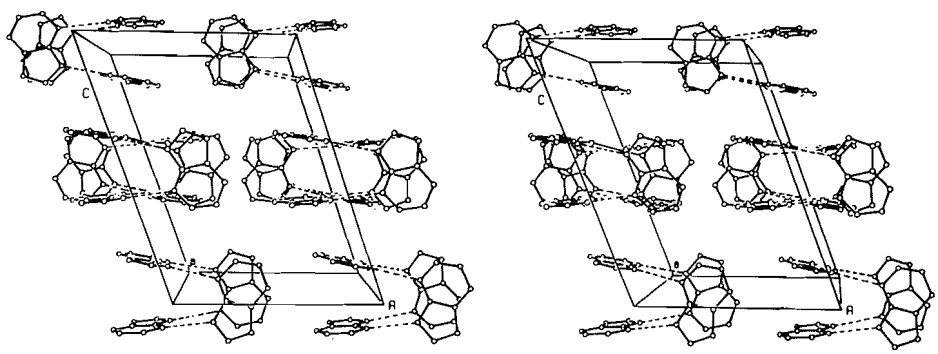

FIG. 4. Stereoview of the unit cell of 7-azaindole. Hydrogens are omitted for simplicity. Dashed lines represent hydrogen bonds. Tetramers A–D are centered at $z \sim 0$, tetramers E–H at $z \sim 1/2$.

TABLE 7. Selected interatomic distances (Å) and bond angles (deg) for the methylmercury compounds

	$[CH_3Hg(Haza)]NO_3$		
Distances (Å)			
Hg(7)—N(7)	2.13(1)	O(10)—N(10)	1.25(2)
Hg(7)—C(7)	2.03(1)	O(11)—N(10)	1.25(1)
Hg(7)—O(11)	2.95(1)	O(12)—N(10)	1.19(1)
Hg(7)—O(11)[a]	2.98(1)	N(1)—O(10)[b]	2.86(2)
Angles (deg)			
N(7)—Hg(7)—C(7)	174.8(5)	O(10)—N(10)—O(11)	118(1)
Hg(7)—N(7)—C(6)	122.2(9)	O(10)—N(10)—O(12)	122(1)
Hg(7)—N(7)—C(8)	122.3(8)	O(11)—N(10)—O(12)	120(1)
C(7)—Hg(7)—O(11)	101.8(5)	C(2)—N(1)—O(10)[b]	125.2(9)
N(7)—Hg(7)—O(11)	83.3(3)	C(8)—N(1)—O(10)[b]	125.8(8)
C(7)—Hg(7)—O(11)[a]	99.8(5)	N(7)—Hg(7)—O(11)[a]	83.0(3)
	$[CH_3Hg(aza)]$		
Distances (Å)			
Hg(1A)—N(1A)	2.11(2)	Hg(1B)—N(7A)	2.88(2)
Hg(1A)—C(1A)	2.11(3)	Hg(1C)—N(1C)	2.05(2)
Hg(1B)—N(1B)	1.96(2)	Hg(1C)—C(1C)	2.08(3)
Hg(1B)—C(1B)	2.07(3)	Hg(1C)—N(7B)	2.82(2)
Angles (deg)			
N(1A)—Hg(1A)—C(1A)	173.8(11)	Hg(1B)—N(7A)—C(6A)	107.7(15)
N(7A)—Hg(1B)—N(1B)	90.2(7)	Hg(1B)—N(7A)—C(8A)	137.7(16)
N(7A)—Hg(1B)—C(1B)	92.8(9)	Hg(1B)—N(1B)—C(2B)	128.9(16)
N(1B)—Hg(1B)—C(1B)	177.0(9)	Hg(1B)—N(1B)—C(8B)	129.1(14)
N(7B)—Hg(1C)—N(1C)	90.2(7)	Hg(1C)—N(7B)—C(6B)	112.2(16)
N(7B)—Hg(1C)—C(1C)	93.7(9)	Hg(1C)—N(7B)—C(8B)	139.5(16)
N(1C)—Hg(1C)—C(1C)	176.0(10)	Hg(1C)—N(1C)—C(2C)	133.3(17)
Hg(1A)—N(1A)—C(2A)	124.6(18)	Hg(1C)—N(1C)—C(8C)	117.6(16)
Hg(1A)—N(1A)—C(8A)	124.3(17)		

[a] $-x, -y, 1-z$.
[b] $x, 1+y, z$.

Can. J. Chem. Downloaded from www.nrcresearchpress.com by 186.148.149.217 on 09/07/12
For personal use only.

electron density near molecules A–D. The eight highest peaks in the map, corresponding to ca. 1/8 C atom, were located in pairs at corresponding positions about each of the four azaindole molecules. The two positions (black atoms, Fig. 1) could correspond to alternate positions for C(4) and C(9) of an inverted molecule. The remaining atoms were too close to those of the other unit to be detected as resolved contributions in the electron density map. Refinement of occupancy factors (see experimental section) led to a 88%–12% distribution of the two orientations in tetramer A–D. There was no evidence of disorder for tetramer E–H.

Although the X-ray results cannot determine how the inverted molecules are locally distributed, it can safely be argued that inversion must take place simultaneously for the four molecules in a given tetrameric unit. Partial inversion would destroy the pattern of complementary hydrogen bonds. The resulting repulsions between N—H bonds should force severe molecular reorientations, which are not observed here.

Methylmercury complexes

The methylmercury cation has been found to be a convenient probe to study the relative affinity of the various sites in multidentate ligands like purines (4). This same cation was used to prepare complexes that could exemplify the different possible coordination patterns for 7-azaindole. Once unambiguously characterized by X-ray diffraction, these complexes could be used to calibrate routine spectroscopic methods and identify diagnostic features to be applied to our dinuclear compounds.

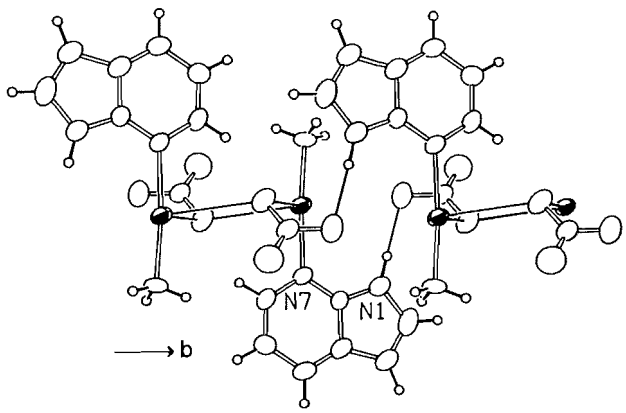

FIG. 5. Ribbons of molecules along the *b* axis showing the interactions between the nitrate ions and the complex cations in $[CH_3Hg(Haza)]NO_3$. Ellipsoids correspond to 50% probability, hydrogens are shown as small spheres of arbitrary size. Thin lines represent Hg...O contacts and dashed lines, hydrogen bonds.

In the compound obtained by reacting CH_3HgNO_3 with azaindole, the CH_3Hg^+ and H^+ ions are in competition for the two nonequivalent nitrogens. In the free ligand, the proton is bound to N(1), as confirmed by the above X-ray work. The structure of $[(CH_3Hg)(Haza)]NO_3$ (Fig. 5) is found to contain N(7)-coordinated $[CH_3Hg(Haza)]^+$ cations, without displacement of the proton from N(1).

Can. J. Chem. Downloaded from www.nrcresearchpress.com by 186.148.149.217 on 09/07/12
For personal use only.

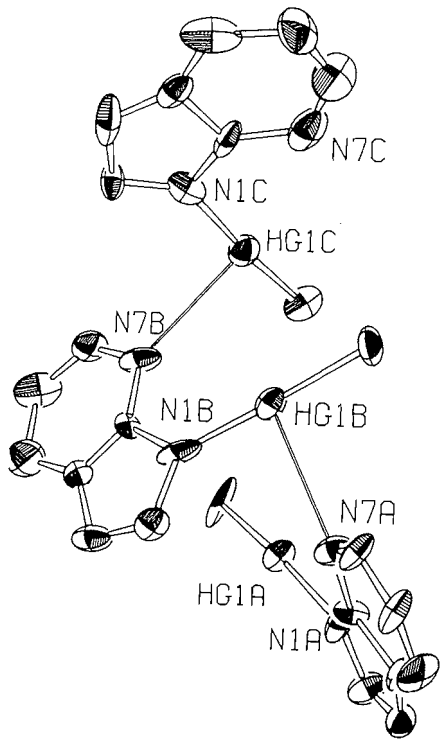

FIG. 6. Asymmetric unit containing three [CH_3Hg(aza)] molecules. Ellipsoids correspond to 50% probability. Thin lines correspond to secondary Hg...N bonds. Hydrogens are omitted for simplicity.

Selected distances and angles are listed in Table 7. The metal shows a roughly liner coordination (N—Hg—C = 174.8(5)°), and it lies along the expected direction of the N(7) lone pair, making equal C—N(7)—Hg angles. A portion of the ribbon resulting from anion–cation interactions is shown in Fig. 5. Nitrate oxygen O(10) forms a hydrogen bond of 2.86(2) Å with N(1)—H, whereas O(11) is bridging two consecutive Hg atoms by means of secondary Hg—O bonds (2.95(1), 2.98(1) Å) near the plane perpendicular to the N(7)—Hg—CH_3 direction.

When 7-azaindole is reacted with CH_3HgOH, the 1:1 compound obtained is neutral and contains azaindole in the deprotonated form. The asymmetric unit consists of three unequivalent [CH_3Hg(aza)] molecules, in which the CH_3Hg^+ ion is bound to the N(1) site formerly occupied by the proton (Fig. 6). The coordination of mercury is roughly linear (Table 7).

The presence of three independent molecules is apparently needed to produce secondary Hg—N(7) bonding interactions. Generally speaking, azaindole is not a good chelating ligand, as the resulting ring would be four-membered and the lone pairs are divergent (1). As for the CH_3Hg^+ compound, the definite preference of Hg for linear two-coordination makes the N(1)-bound Hg atom unsuitable for coordination to N(7) via intramolecular chelating interactions. The structure is a compromise between packing efficiency and intermolecular Hg...N(7) secondary bonding. As shown in Fig. 6, the N(7) atoms of molecules A and B form secondary intermolecular Hg...N bonds of 2.88(2) and 2.82(2) Å, respectively. Mercury makes no contact shorter than 3.3 Å with N(7C), which is less accessible than N(7A) and N(7B) because the N(1)-bonded methylmercury group is displaced in its direction (Hg(1C)—N(1C)—C(2C) = 133.3(17), Hg(1C)—N(1C)—C(8C) = 117.6(16)°).

Distances and angles in the ligand for both complexes are compared with those of uncoordinated azaindole in Table 5. Large esd's on light-atom distances and angles cannot be avoided in these structures, because mercury has a high atomic number. Any coordination-induced structural changes in the ligand remain within the limits of error of the present study.

Conclusion

The structure of 7-azaindole has revealed that the molecule does not form the hydrogen-bonded flat dimer often encountered for similar systems and proposed to exist in 7-azaindole solution. Instead, the crystal contains unusual tetrameric units, with a central region containing four complementary N—H...N interactions and a hydrophobic surface. These tetramers interact by van der Waals forces.

The coordination sites for the methylmercury cation have been determined for two types of 1:1 complexes. In the neutral [CH_3Hg(aza)] compound, the N(1)-H proton has been displaced by mercury, and the N(7) lone pair participates only in secondary Hg...N intermolecular contacts. In [CH_3Hg(Haza)]NO_3, however, the metal is bound to N(7) and the N(1)-H proton is retained. [$(CH_3Hg)_2$(aza)]X complexes have also been prepared[3], but they have not been studied by X-ray diffraction. They obviously contain CH_3Hg^+ groups coordinated to both nitrogens of azaindole according to a pattern observed with purines (4). These structural results will be used to interpret the vibrational spectra and NMR data on these complexes and those obtained with the dinuclear systems.

Acknowledgments

We wish to thank M. Simard for assistance in solving the structure of azaindole and collecting the X-ray data. The financial support of the Natural Sciences and Engineering Research Council of Canada, and the Programme d'Échanges Interuniversitaires Franco-Québecois is gratefully acknowledged.

1. F. ALLAIRE and A. L. BEAUCHAMP. Inorg. Chim. Acta, **156**, 241 (1989).
2. S. M. PENG and Y. N. LIN. Acta Crystallogr. Sect. C: Cryst. Struct. Commun. **C42**, 1725 (1986).
3. S. M. PENG and C. H. LAI. J. Chin. Chem. Soc. (Taipei), **35**, 325 (1988).
4. L. GRENIER, J. P. CHARLAND, and A. L. BEAUCHAMP. Can. J. Chem. **66**, 1663 (1988).
5. F. BÉLANGER-GARIÉPY and A. L. BEAUCHAMP. J. Am. Chem. Soc. **102**, 3461 (1980).
6. D. T. CROMER and J. T. WABER. Acta Crystallogr. **18**, 104 (1965); R. F. STEWART, E. R. DAVIDSON, and W. T. SIMPSON. J. Chem. Phys. **42**, 3175 (1965).
7. D. T. CROMER. Acta Crystallogr. **18**, 17 (1965).
8. M. AUTHIER-MARTIN and A. L. Beauchamp. Can. J. Chem. **55**, 1213 (1977).
9. G. SHELDRICK. SHELX-76, crystallographic program system. Cambridge University, U.K. 1976.
10. P. MAIN, S. J. FISKE, S. E. HULL, L. LESSINGER, G. GERMAIN, J. DECLERCQ, and M. M. WOOLFSON. MULTAN80, a system of computer programs for the automatic solution of crystal structure from X-ray diffraction data. Univ. of York, U.K., and Louvain, Belgium. 1980.
11. D. MOOTZ and H. G. WUSSOW. J. Chem. Phys. **75**, 1517 (1981).
12. K. SUWINSKA. Acta Crystallogr. Sect. C: Cryst. Struct. Commun. **C41**, 973 (1985).
13. D. K. CHAKRABORTY and S. K. TALAPATRA. Acta Crystallogr. Sect. C: Cryst. Struct. Commun **C42**, 1435 (1986).

14. B. SCHMELTER, H. BRADACZEK, and P. LUGER. Acta Crystallogr. Sect. B: Struct. Crystallogr. Cryst. Chem. **B29**, 971 (1973).
15. R. TAYLOR and O. KENNARD. J. Mol. Struct. **78**, 1 (1982).
16. A. G. M. BARRETT, D. DAUZONNE, and D. J. WILLIAMS. J. Chem. Soc. Chem. Commun. 636 (1982).
17. G. H. STOUT and L. H. JENSEN. X-ray structure determination, a practical guide. Macmillan, London. 1968. p. 303.
18. J. A. WALMSLEY. J. PHYS. CHEM. **85**, 3181 (1981).
19. P. STAGLICH and M. ZANDER. Z. Naturforsch. **31A**, 1391 (1976).
20. P. ROYCHOWDHURY and B. S. BASAK. Acta Crystallogr. Sect. B: Struct. Crystallogr. Cryst. Chem. **B31**, 1559 (1975).
21. A. W. HANSON. Acta Crystallogr. **17**, 559 (1964).
22. F. A. COTTON, D. G. LAY, and M. MILLAR. Inorg. Chem. **17**, 186 (1978).

Can. J. Chem. Downloaded from www.nrcresearchpress.com by 186.148.149.217 on 09/07/12
For personal use only.

CdS/chloroaluminum phthalocyanine heterojunctions: effect of CdS preparation method on the efficiency of photovoltaic cells

L. GASTONGUAY AND J. P. DODELET
INRS-Energie, 1650, montée Ste-Julie, C.P. 1020, Varennes (Québec), Canada J3X 1S2

R. CÔTÉ AND M. F. LAWRENCE
Chemistry Department, Concordia University, Montreal, Que., Canada H3G 1M8

AND

D. GRAVEL
Département de chimie, Université de Montréal, Montréal (Québec), Canada H3C 3J7

Received November 23, 1988[1]

L. GASTONGUAY, J. P. DODELET, R. CÔTÉ, M. F. LAWRENCE, and D. GRAVEL. Can. J. Chem. **68**, 202 (1990).

Heterojunctions of the type CdS/chloroaluminum phthalocyanine have been obtained by using the following methods to prepare the CdS layer: electrochemical deposition in dimethylsulfoxide (I); electrochemical aqueous deposition at constant reduction potential (II), or cyclic potential (III), or constant oxidation current (IV); and chemical aqueous deposition (V). The CdS films were characterized by SEM, EDAX, optical microscopy with Nomarski interference, X-ray diffraction, and photoelectrochemistry in polysulfide solution. The best cells show a conversion efficiency of about 0.2% under white light illumination of 90 mW cm^{-2}. They were obtained with a 1.0 μm thick layer of the organic semiconductor and a 0.4 μm thick CdS film prepared by method I. This method yields a polycrystalline electrode characterized by large plates (1–3 μm) of tightly packed single oriented (111) cubic CdS crystallites showing low sub-bandgap absorption. The better performances of the CdS/ClAlPc heterojunctions obtained by method I can be understood in terms of absorbance of the CdS layer of optimum thickness, hole diffusion length in the CdS and electron–hole recombination efficiency at the CdS/ClAlPc interface.

Key words: CdS, phthalocyanine, heterojunction, organic semiconductor, photovoltaic cell.

L. GASTONGUAY, J. P. DODELET, R. CÔTÉ, M. F. LAWRENCE et D. GRAVEL. Can. J. Chem. **68**, 202 (1990).

Des hétérojonctions du type CdS/phtalocyanine de chloroaluminium ont été obtenues en utilisant les méthodes de préparation suivantes pour la couche de CdS : dépôt électrochimique dans le diméthylesulfoxyde (I); dépôt électrochimique en phase aqueuse à potentiel de réduction constant (II), ou potentiel cyclique (III), ou courant d'oxydation constant (IV); et dépôt par bain chimique (V). Les films de CdS ont été caractérisés par MEB, EDAX, microscopie optique avec interférence Nomarski, diffraction des rayons X et photoélectrochimie en solution de polysulfure. Les meilleures cellules ont une efficacité de conversion de 0,2% environ, sous lumière blanche à 90 mW cm^{-2}. Elles ont été obtenues avec une couche de semiconducteur organique de 1,0 μm d'épaisseur et un film de CdS de 0,4 μm préparé par la méthode (I). Cette méthode produit une électrode polycristalline caractérisée par une mosaïque de larges plaques (1–3 μm) contenant un ensemble très serré de petits cristaux de CdS cubique ayant une orientation cristallographique unique (111) et une faible absorption pour des photons dont l'énergie est inférieure à la bande interdite. Les meilleures performances des hétérojonctions du type CdS/ClAlPc obtenues par la méthode I peuvent s'expliquer en termes d'absorbance de la couche de CdS ayant l'épaisseur optimum, de longueur de diffusion des trous dans le CdS et de l'efficacité de recombinaison des charges à l'interface CdS/ClAlPc.

Mots clés : CdS, phtalocyanine, hétérojonctions, semiconducteurs organiques, cellules photovoltaïques.

Introduction

In recent years, phthalocyanines (Pcs) have generated interest as inexpensive organic semiconductors for use in solar energy conversion. Since most of the Pcs investigated are characterized by a p-type behavior, the photovoltaic effects were first observed with Schottky barriers obtained by contacting the dyes with metals like Al or In (1–4). Besides showing stability problems, these metallic electrodes also absorb a large fraction of the light in the Q band absorption region of the organic semiconductor.

Later on, following the example of inorganic cells like n-CdS/p-Cu_2S, photovoltaic devices of the type n-CdS/p-Pc were developed (5–9). Under an AM2 illumination of 75 mW cm^{-2}, conversion efficiencies of 0.22% were measured for the most performing Pcs: ClAlPc and ClAlClPc (7). Unlike the case of n-CdS/p-Cu_2S, where the space charge region is situated in the CdS layer, it has been demonstrated that for an heterojunction with a phthalocyanine (5, 8), the space charge region is located exclusively in the organic semiconductor film. Using CdS instead of a metal allows an increase in the amount of light reaching the active region of the cell because CdS absorbs mainly in the visible below 500 nm, while Pcs absorb above that wavelength. Using CdS also increases the open circuit photopotential of the cell due to its smaller electroaffinity compared to the affinity of metals used previously to produce the Schottky barriers.

In previous studies, the CdS electrode used with the Pcs was always prepared by cathodic electrodeposition of Cd^{2+} in the presence of sulfur in non-aqueous solution (5–9). The purpose of this work is to investigate other electrochemical techniques to prepare CdS. These electrodes, after characterization by SEM, EDAX, optical microscopy using Nomarski interference, X-ray diffraction, and photoelectrochemistry in polysulfide solution have been tested in heterojunction with chloroaluminum phthalocyanine. Chemical bath deposition of CdS is also included in this investigation to compare between electrochemical and a non-electrochemical CdS preparation technique.

Experimental

CdS and CdS/ClAlPc preparation

CdS was electrochemically and chemically deposited on various substrates: indium – tin oxide (PPG Industries) and SnO_2 coatings

[1]Revision received July 28, 1989.

Can. J. Chem. Downloaded from www.nrcresearchpress.com by 186.148.149.217 on 09/07/12
For personal use only.

Can. J. Chem. Downloaded from www.nrcresearchpress.com by 186.148.149.217 on 09/07/12
For personal use only.

(Pyrex infrared reflecting glass, Swift glass Co), 99.999% Cd foil (Alfa Products), Puratronic Pt foil (Johnson Matthey), and graphite electrodes (Fisher).

CdS was electrochemically deposited in non-aqueous solution according to the method described by Baranski and Fawcett (10). The cadmium chloride, elemental sulfur, and dimethylsulfoxide were reagent grade. In aqueous solution, CdS films were prepared by three different methods: (*i*) at constant reduction potential (−1 V vs. SCE) according to Power *et al.* (11). For this deposition, $Na_2S_2O_3$, $CdSO_4$, and HCl were all reagent grade; (*ii*) at cyclic potential (−1.3 to 0 V vs. SCE and 5 mV s^{-1} sweep rate) according to Fatas *et al.* (12). For this deposition, two solutions A and B were mixed together: solution A contained $CdSO_4$, $(NH_4)_2SO_4$, and glycerol; solution B contained $Na_2S_2O_3$ and NaCl. HCl was used to induce the sulfur generation by decomposition of $Na_2S_2O_3$. All chemicals were reagent grade; (*iii*) at constant oxidation current (50 mA cm^{-2}) following the method of Miller and Heller (13). A 1 *M* reagent grade sulfide solution was used for this anodization.

CdS was chemically deposited in aqueous solution according to Mondal and Chaudhuri (14). The chemicals used for this deposition were reagent grade cadmium acetate, triethanolamine, ammonium hydroxide, and thiourea.

Chloroaluminum phthalocyanine was synthetized by a modified Owen procedure (15). The solvents for the reaction were nitrobenzene and quinoline (dried over CaH_2). The crude ClAlPc was purified by two subsequent sublimations. The elemental analysis of the pigment shows good agreement between the expected C (66.84%), H (2.81%), N (19.49%), and Cl (6.17%) contents and the measured ones: C (66.79%), H (2.72%), N (19.50%), and Cl (6.06%). The Al content was measured by neutron activation analysis: expected value (4.7%), measured value (4.8%). To form the heterojunctions, films of ClAlPc were sublimed onto the CdS film previously deposited on ITO or SnO_2 substrates by the methods mentioned above. The sublimation of the organic material was done at a temperature between 350 and 375°C and under a pressure of about 1×10^{-5} Torr. The deposition rate was about 0.2 μm min^{-1}.

The heterojunction cell was completed by evaporating, under vacuum ($\leq 5 \times 10^{-6}$ Torr), a gold collecting (0.5 cm^2) and guard electrodes (99.9% pure from Alfa).

Characterization

CdS

CdS electrodes (between 1 and 2 cm^2) were characterized by (*i*) scanning electrode microscopy (Hitachi, SEM Model S570); (*ii*) electron dispersive analysis; (*iii*) X-ray diffraction (Philips PW 1849) using CuKα; (*iv*) visible absorption spectroscopy (Hitachi Model 100-60), and (*v*) photoelectrochemistry in a three-electrode single compartment cell. A saturated calomel electrode (SCE) served as the reference and Pt foil (15 cm^2) served as a counterelectrode. The redox solution was S^{2-}/S_x^{2-} 1 *M*/1 *M* in 1 *M* NaOH. The working electrode was placed as close as possible to the cell window to minimize the amount of light absorbed by the solution. The white light illumination source was a 300 W Xe lamp equipped with a 10 cm water filter and a 385 nm cut-off UV filter (Oriel corp.). The light intensity was measured with a United Detector Technology 21A power meter equipped with a radiometric filter. Neutral density filters (Oriel corp.) were used to vary the light intensity.

All electrochemical measurements were performed in a Faraday cage. When working in the photogalvanic mode, the measurements were taken with a Keithley 614 electrometer. *J–V* curves were obtained with a Model 173 potentiostat and a Model 175 programmer from Princeton Applied Research. Mott–Schottky plots for the CdS electrodes were done in polysulfide solution using a Model 273 potentiostat and a Model 5206 two phase Lock-in analyser from Princeton Applied Research driven by an Apple IIe computer.

Heterojunctions

The cells were installed in a Faraday cage where they could be irradiated through the ITO or SnO_2 electrode with monochromatic light from a 650 W tungsten–halogen lamp (Schoeffel) passing through a Kratos monochromator (Schoeffel) and/or with white light from a Kodak Ektagraphic slide projector (300 W tungsten–halogen lamp). The reported intensities correspond to light incident on the cell. *J–V* curves measured for the cells were obtained with a Model 175 programmer and a Keithley 616 electrometer.

Results

CdS characterization

To obtain meaningful results, it is important to characterize CdS films of about the same thickness as those used in making heterojunctions with the phthalocyanine. In the latter case, photogenerated holes in the CdS diffuse to the interface where they react with electrons photogenerated in the organic semiconductor. As light penetrates the cell on the CdS side, the optimum CdS thickness corresponds to the hole diffusion length in the CdS film. This was found to be about 0.4 μm in CdS prepared electrochemically in DMSO (8). Larger CdS thicknesses cause a filtering effect resulting in decrease of number of holes reaching the interface and therefore smaller short circuit photocurrents. The following characterizations, unless mentioned otherwise, were performed on CdS films of about 0.4 μm thick.

SEM and EDAX

Figures 1 and 2 depict the scanning electron microscope (SEM) photographs of all the CdS electrodes used in this study. In Fig. 1: electrochemical non-aqueous (DMSO) deposition on ITO at three magnifications: ×10K, ×25K, ×50K; in Fig. 2: electrochemical aqueous deposition at constant reduction potential on SnO_2 (A), cyclic potential on SnO_2 (B), constant oxidation current on Cd foil (C), and chemical aqueous deposition on ITO (D), respectively. All films are shown at the same magnification (×10K). For CdS electrochemically deposited in aqueous solution (Fig. 2A, B, and C), individual crystallites are visible. In Fig. 2A and B, all crystallites have about the same size (0.3 μm) while for Fig. 2C, the size of the crystallites varies between 0.3 to 2 μm.

Individual crystallites are not easily distinguished in Fig. 1 and in Fig. 2D. Both films seem to be made of a homogeneous CdS layer with an intricate pattern of crevices attributed to solvent loss. The crevices, however, are more numerous in Fig. 2D compared to Fig. 1. The surface of CdS obtained by electroreduction of Cd^{2+} in the presence of sulfur in DMSO looks very flat when it is observed by SEM. Under optical microscopy with Nomarski interference (Fig. 3), the same electrode shows a surface morphology completely different from the other CdS films studied. It is composed of a mosaic of tightly packed elements of various shapes having sizes estimated between 1 and 3 μm. Nomarski interference yields an image with high contrast and enables the observation of fine scale surface roughness. Looking at Fig. 3, one might think that each element of the mosaic is a CdS crystallite but this does not agree with Fig. 1. In fact, irregularities in the film flatness revealed by Nomarski interference seem to follow a pattern corresponding mainly to the largest crevices, assuming that these were extended and joined to define the complete perimeter of each element in the mosaic. At a magnification greater than ×10K, the film surface begins to show some structure which resembles a very dense aggregation of small crystallites. The crystallinity of CdS obtained by the non-aqueous method is confirmed by the X-ray diffraction study. Chemically deposited CdS films seem rather amorphous even at magnifications up to 50K. This is also confirmed by X-ray diffraction. The white

Can. J. Chem. Downloaded from www.nrcresearchpress.com by 186.148.149.217 on 09/07/12
For personal use only.

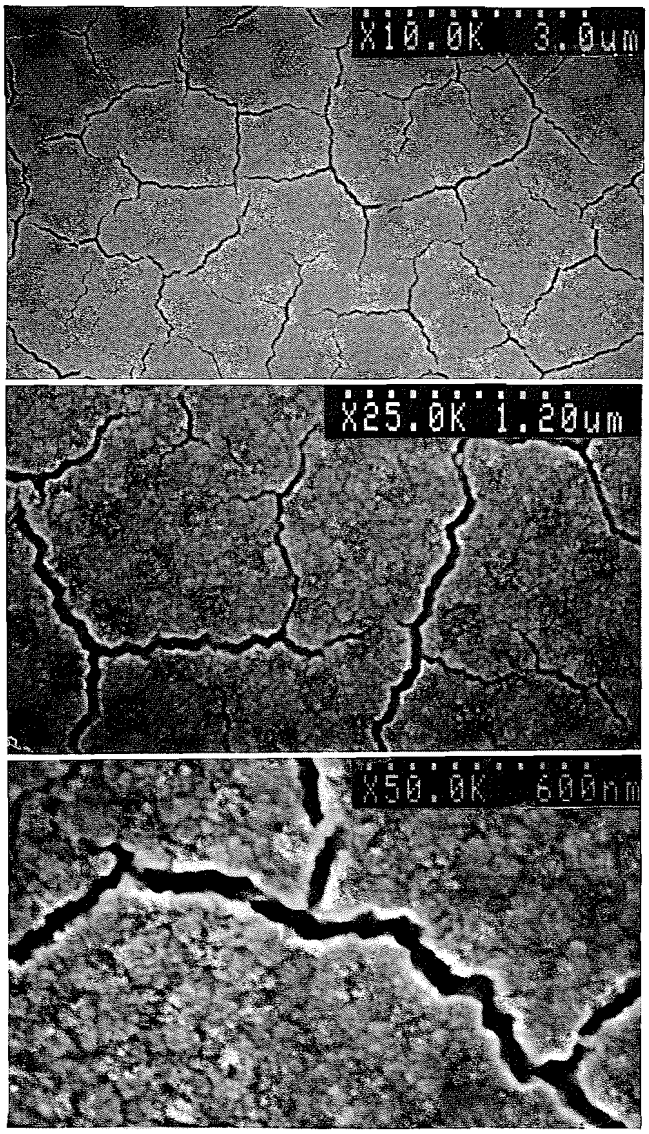

FIG. 1. SEM pictures of a 0.4 μm thick CdS film prepared electrochemically in non aqueous solution (DMSO).

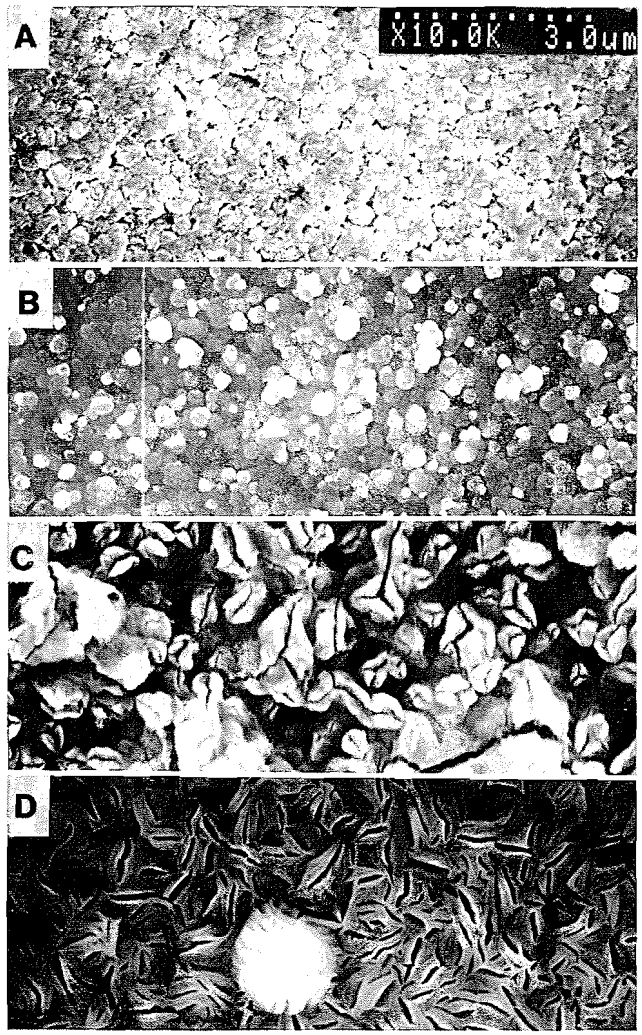

FIG. 2. SEM pictures of a 0.4 μm thick CdS film prepared electrochemically in aqueous solution at constant reduction potential (A), at cyclic potential (B), at constant oxidation current (C) and prepared by chemical bath (D).

spot seen in the picture is probably due to the presence of elemental sulfur.

Table 1 presents the Cd and S weight percentage obtained by EDAX for each CdS deposition method. For the EDAX measurements, the CdS films were prepared on graphite electrodes except for the anodization. Stoichiometric CdS is characterized by 77.8% of Cd and 22.2% of S. Therefore, from the results presented in Table 1, it can be concluded that all the preparation methods show about the same excess of S incorporated either by the solvent (DMSO), or as elemental S for the aqueous depositions. These results agree with the EDAX results already published for deposition method III (12, 16).

X-ray

X-ray diffraction spectra have been obtained for the CdS films prepared by all the deposition methods used in this work. CdS obtained electrochemically in DMSO and obtained chemically in aqueous solution, could be prepared on ITO. This substrate shows no specific diffraction peaks. Therefore, the only peak seen for method I at $2\theta = 26.8°$, which corresponds to an interplanal distance of 3.33 Å, can be attributed to the (111)

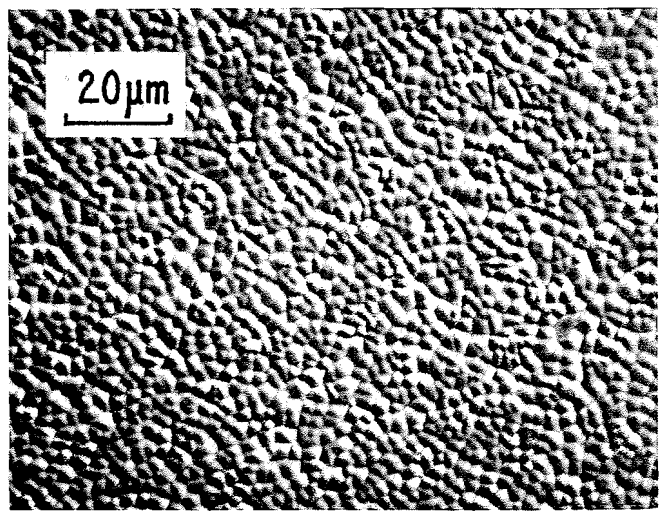

FIG. 3. Optical microscope picture using Nomarski interference of a 0.4 μm thick CdS film prepared electrochemically in non-aqueous solution (DMSO) on ITO.

TABLE 1. Cd and S weight percentage obtained by EDAX for the same deposition methods as in Figs. 1 and 2

Deposition methods[a]	% Cd	% S
I	68.4	31.6
II	71.0	29.0
III	69.1	30.9
IV	—	—
V	73.0	27.0

[a]Electrochemical deposition in DMSO, I; electrochemical aqueous deposition at constant reduction potential, II; cyclic potential, III; constant oxidation current, IV; and chemical aqueous deposition, V.

planes of cubic CdS. This result agrees with the previous report (17). For method V, the X-ray diffraction pattern shows no specific peak that could be attributed to the CdS layer. For the other deposition methods where acidic solutions had to be used for the preparation of the CdS layer, ITO substrates had to be substituted by SnO_2 electrodes or Cd foils. The contribution to the diffraction pattern by the CdS layer is so small that no difference is observed for the diffraction pattern of the SnO_2 and Cd foil substrates before and after CdS deposition. It seems, therefore, that the crystallinity of the ~0.4 μm thick films obtained by all the CdS deposition methods, except for the non-aqueous one (I), is quite poor.

Photoelectrochemistry

The photoelectrochemicals properties of the CdS layers deposited on metallic substrates by the five methods used in this work, have been measured. Our results (short-circuit photocurrents, J_{sc}, and open-circuit photovoltages, V_{oc}) are reported in Table 2 along with literature values. CdS layers of thickness ranging from 1 to 2 μm had to be used to yield results comparable with those previously reported under comparable light intensities. This is easily deduced from the data of Table 2, since it was found that J_{sc} varies quite linearly with the light intensity for all the CdS preparation methods. Changing the substrate on which the deposition was done, from Cd foil to SnO_2, only affects the reverse dark J–V characteristics. Indeed, leakage currents are already observed for CdS deposited on SnO_2 at −0.5 V as compared to 0 V for equivalent currents in the case of CdS depositions on Cd foil. The equilibrium potential of the electrolyte is −0.74 V. Leakage currents are also observed at −0.5 V in the reverse dark J–V characteristics of the bare SnO_2. For this reason, C–V Mott–Schottky plots were measured for CdS deposited on Cd. Table 3 reports the flatband potential, V_{fb}, and the charge carrier density, N_D, for the CdS electrodes used in this work. The $1/C^2$ vs. V curves are almost the same when the applied modulated voltage is varied from 1 to 15 kHz. They always display two regions with different slopes. The V_{fb} is obtained by extrapolation of the straight line occurring in the voltage region spanning from −0.7 to −1.1 V. It is to be noticed that the V_{fb} obtained by Mott–Schottky curves are always lower than the photocurrent onset potential (−1.1 to −1.2 V). This discrepancy is probably due to the fact that the V_{fb} values are obtained by extrapolation of $1/C^2$ vs. V data over only a small range of voltage. A value of $V_{fb} = -1.05$ V has already been published (21) for polycrystalline CdS in polysulfide redox using Mott–Schottky curves.

Charge carrier densities reported in Table 3 are high and cover practically three orders of magnitude. However, the measurements are sensitive to the actual area of the electrode which could be quite different from the geometrical one as it can be seen from the SEM pictures (Figs. 1 and 2). Therefore, the reported values in Table 3 correspond to the upper limit of N_D. Hall measurements have been performed on CdS electrodeposited from aqueous diethylene glycol solutions. In that case, values of N_D ranging from 8.3×10^{16} to $\geq 2 \times 10^{18}$ cm^{-3} have been reported (22). They are of the same order of magnitude as the N_D values obtained in this work.

CdS/ClAlPc heterojunctions

Heterojunctions have been produced using sublimation of ClAlPc onto previously characterized CdS. All CdS preparation methods have been used except for anodization (IV). In the case of anodization, small currents yielded uniform CdS films, but showed bad adhesion to SnO_2. The CdS layers obtained by applying large anodization currents were found to have pinholes.

Table 4 presents the J_{sc}, V_{oc}, fill factor (ff), and conversion efficiency (η) measured in this work for the various hetero-

TABLE 2. Short circuit photocurrents, J_{sc}, open circuit photovoltages, V_{oc}, and power conversion efficiencies, η, of electrochemical cells with CdS electrodes prepared in this work and reported in the literature; the redox is polysulfide

Deposition methods[a]	Substrates	Light intensity (mW cm^{-2})	J_{sc} (μA cm^{-2})	V_{oc} (V)	η (%) (×10^{-2})	Heat treatment	Reference
I	Cd foil	35	59	0.26	1.3	—	This work
	SnO_2	75	120	0.32	—	—	18
	Ti	70	220	0.41	—	500°C in air	19
II	Cd foil	35	74	0.27	1.9	—	This work
III	Pt foil	35	56	0.27	1.6	—	This work
IV	Cd foil	35	180	0.31	6.4	—	This work
	Cd on Pt foil	92	~120	~0.20	—	—	20
V	Cd foil	35	62	0.30	1.8	—	This work
	SnO_2	75	140	0.59	—	—	18
	Ti	70	190	0.58	—	500°C in air	19

[a]See footnote of Table 1.

Can. J. Chem. Downloaded from www.nrcresearchpress.com by 186.148.149.217 on 09/07/12
For personal use only.

TABLE 3. Flatband potential, V_{fb}, and charge carrier density, N_D, obtained from Mott–Schottky plots measured for CdS electrodes prepared in this work

Deposition methods[a]	V_{fb} (V)	N_D (cm^{-3})
I	−0.91	6.4×10^{18}
II	−0.89	6.7×10^{20}
III	[b]	[b]
IV	−1.03	1.2×10^{19}
V	−1.01	9.5×10^{17}

[a]See footnote of Table 1.
[b]Results not reproducible.

TABLE 4. Short circuit photocurrents, J_{sc}, open circuit photovoltages, V_{oc}, fill factor, ff, conversion efficiency, η, for CdS/ClAlPc heterojunctions measured under white light illumination of 90 mW cm^{-2}

Deposition methods[a]	J_{sc} ($\mu A\ cm^{-2}$)	V_{oc} (V)	ff	η (%)
I	1 080	0.64	0.26	0.193
II	57	0.59	0.26	0.009
III	8	0.53	0.26	0.001
IV	—	—	—	—
V	150	0.65	0.26	0.027
	220[b]	0.63	0.26	0.039

[a]See footnote of Table 1.
[b]When the CdS thickness is decreased from 0.4 to 0.15 μm.

FIG. 4. SEM picture of a 1 μm thick ClAlPc film sublimed onto CdS.

junctions under white light illumination at 90 mW cm^{-2}. The CdS and ClAlPc thicknesses used in Table 4 are 0.4 and 1 μm, respectively. The ClAlPc film with an optimum thickness of about 1 μm is not compact as illustrated by the SEM picture (×50K) in Fig. 4. The organic semiconductor is made of crystallites having a length of 1 μm and a cross section of about 50 to 100 nm. From Table 4 it can be seen that the best heterojunction is obtained with CdS prepared by electrodeposition in DMSO. Lowering the light intensity to 30 mW cm^{-2} increases the conversion efficiency to a maximum of 0.25%. These values of η correspond to the ones already published for a similar cell (7).

The CdS thickness used in Table 4 is, however, optimum for the CdS preparation method in DMSO. The optimum thickness of CdS prepared by chemical bath is about 0.15 μm. A CdS/ClAlPc heterojunction obtained with this thickness yields J_{sc} = 220 $\mu A\ cm^{-2}$, V_{oc} = 0.63 V, ff = 0.26, and η = 0.039%. The other CdS preparation methods have not been optimized. The optimum thicknesses obtained for both methods allow the ClAlPc film, which absorbs above 500 nm, to receive the same amount of light as shown in Fig. 5. The stability of the heterojunction formed with the CdS obtained by electrodeposition in DMSO has been checked. It was found that over a period of 5 h, the photocurrent decreases by about 10%. Only 60% of the initial J_{sc} value remains after 30 h.

Discussion

Table 4 shows that the best performing heterojunctions are obtained with CdS electrodeposited in DMSO. Furthermore, there is a factor of about five between the optimum efficiency of that cell and the next best one which uses CdS obtained by chemical bath. As the fill factors and open circuit voltages for all cells are quite similar, the difference in power conversion of these cells is essentially related to large variations in their short circuit photocurrents.

It is not possible to explain differences for J_{sc} given in Table 4 on the basis of either differences in the CdS film composition (Table 1) or in their photoelectrochemical properties (Table 2 shows that $\eta = 1.6 \pm 0.3 \times 10^{-2}$%), or in the charge carrier densities of the CdS (Table 3 indicates that $N_D \geq 10^{18}\ cm^{-3}$). The only major difference observed between all the CdS films used in this work is the peculiar crystallinity of CdS grown by method I. Indeed, it is the only method that not only gives a distinct diffraction pattern for layers as thin as 0.4 μm, but the X-ray diffractogram also shows that these films are characterized by only one crystallographic orientation (111).

The mechanism for photocurrent collection in CdS/Pc junctions is illustrated in Fig. 5. It has previously been observed (8) that when such junctions are illuminated with red light only (600 nm) in the absorption region of the Pc, the cell photocurrent decreases rapidly and continues to do so unless a certain amount of blue light (430 nm) is added. Under white light illumination, electron–hole pairs are formed simultaneously in both semiconductors. The major mechanism at work for current production involves the recombination, at the junction, of electrons from the Pc conduction band (minority carriers) with holes from the CdS valence band (minority carriers), leaving extra electrons in CdS and extra holes in Pc to be recuperated. Another mechanism of current production, however secondary, involves a direct injection of holes from the CdS valence band

Can. J. Chem. Downloaded from www.nrcresearchpress.com by 186.148.149.217 on 09/07/12
For personal use only.

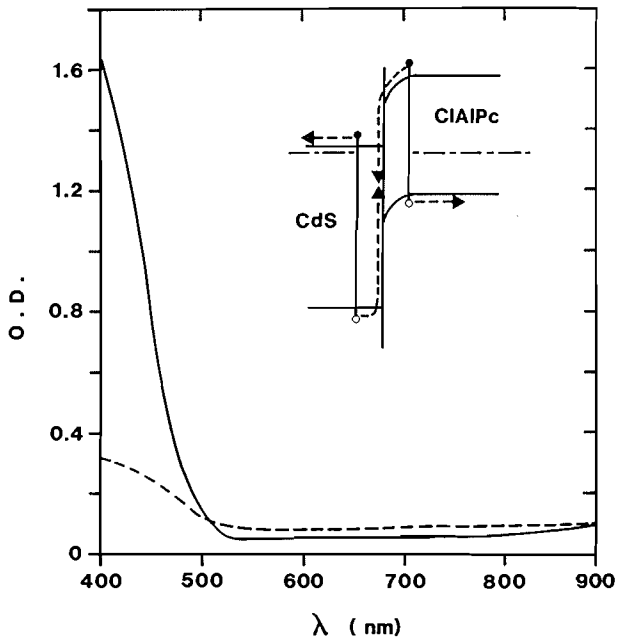

FIG. 5. Optical densities for the optimum CdS film thicknesses prepared electrochemically in DMSO (—) and by chemical bath (- - -). The insert describes the major mechanism for current production.

into the Pc valence band (8). The short circuit photocurrent measured in CdS/Pc junctions is then essentially a function of three factors: (*i*) the collection efficiency of the holes photogenerated in the ClAlPc layer, (*ii*) the collection efficiency of the electrons photogenerated in the CdS layer, and (*iii*) the photogenerated electron–hole recombination efficiency at the CdS/ClAlPc interface. Let us see how it is possible to rationalize a ratio of about five between J_{sc} (method I) and J_{sc} (method V).

Figure 5 shows the optical density of the CdS layers obtained in DMSO and by chemical bath, after optimization of their thicknesses to yield the maximum power efficiency in heterojunction with ClAlPc. This optimum thickness is 0.4 and 0.15 μm for CdS prepared by methods I and V, respectively. In the wavelength region between 500 and 900 nm, it is clear from Fig. 5 that about the same light intensity reaches the ClAlPc layer after passing through the CdS prepared by method I or V. This wavelength range covers the Q band absorption region of Pc. Excitation of the Soret band of the pigment can be disregarded because only a small intensity of light with $\lambda <$ 400 nm is emitted by tungsten–halogen lamp and these photons are mainly absorbed by CdS. It seems therefore that the amount of electrons and holes generated in the 1 μm thick ClAlPc layer and the hole collection from that layer will be independent of the CdS preparation method.

On the other hand, Fig. 5 shows that the absorbance of the CdS layer below 500 nm is drastically different for both optimum thicknesses. The amount of electrons collected from the CdS layer is a function of the photo-generated charge density. It also depends on the hole diffusion length in CdS. Between 400 and 500 nm, there is about 1.7 times more photons absorbed in the optimum CdS layer obtained by method I compared to the optimum film produced by method V. The same ratio is expected between the densities of photogenerated charges in these films. As far as the hole diffusion length is concerned, a value of 0.4 μm was determined (8) for CdS obtained in DMSO on the basis of a drastic decrease of the photocurrent for cells with CdS layers thicker than 0.4 μm. On the same basis, the hole diffusion length for CdS obtained by chemical bath would only be 0.15 μm. However, it is possible that the value of 0.15 μm, deduced for the hole diffusion length of CdS obtained by method V, is only a lower limit estimate. Indeed, part of the photocurrent decrease observed for CdS layers thicker than 0.15 μm could be attributable to the decrease of the Pc illumination since, for those films, the absorbance of CdS above 500 nm is not negligible anymore compared to their absorbance below the same wavelength. If the optimum thickness of CdS prepared by method V is smaller than the hole diffusion length in that material, a lowering of the short circuit photocurrent is then expected. By comparison, for CdS prepared by method I, there is a 1.3 times reduction in the cell photocurrent when the CdS layer is reduced from 0.4 to 0.15 μm (8).

The third factor to take into account is the electron–hole recombination efficiency at the CdS/Pc interface. As it was already mentioned, the CdS/ClAlPc needs to be illuminated at the same time by blue and red light to reach a steady-state photocurrent. Blue light is essential because the holes it generates in CdS are needed to balance the electrons generated by red light in ClAlPc. When the photocurrent produced with red light only (600 nm) is balanced with just the right amount of added blue light (430 nm), it is found that $N(e)/N(ph) = 0.7 \pm 0.1$ for CdS obtained in DMSO, but only 0.5 ± 0.02 for CdS prepared by chemical bath, where $N(e)$ is the total number of electrons collected per second and $N(ph)$ is the total number of blue photons absorbed in the CdS within a distance from the phthalocyanine not exceeding the diffusion length of holes in CdS.

By combining the CdS absorbance effect, the electron–hole recombination efficiency at the CdS/Pc interface, and the possibility of using a CdS layer with an optimum thickness smaller than the hole diffusion length for CdS obtained by chemical bath, it is therefore possible to rationalize J_{sc} (method I:method V) ratios ranging from 2.6 to 3.8. The experimental value obtained from Table 4 is 4.9.

Conclusion

In the framework of our investigation, the best performing CdS/ClAlPc heterojunctions are obtained when the organic semiconductor is sublimed on a 0.4 μm thick CdS film prepared by cathodic electrodeposition in DMSO. This method yields a polycrystalline electrode characterized by large plates (1–3 μm) of tightly packed single oriented (111) cubic CdS crystallites showing low sub-bandgap absorption. The better performances of the CdS/ClAlPc heterojunctions obtained by that method can be understood in terms of absorbance of the CdS layer, of optimum thickness vs. hole diffusion length in the CdS, and electron–hole recombination efficiency at the CdS/ClAlPc interface.

This work demonstrates that the current density in these organic–inorganic heterojunctions could be limited by the inorganic layer which has to play an active role in the photogeneration and transport of the charges. It seems that future developments in this particular area of solar collectors will favor the use of an all organic heterojunction since power efficiencies of about 1% have already been obtained for these junctions under 75 mW cm^{-2} AM2 irradiation (23).

1. A. K. GHOSH, D. L. MOREL, J. FENG, R. F. SHOW, and C. A. ROWE, JR. J. Appl. Phys. **45**, 230 (1974).

Can. J. Chem. Downloaded from www.nrcresearchpress.com by 186.148.149.217 on 09/07/12
For personal use only.

2. R. O. LOUTFY and J. H. SHARP. J. Chem. Phys. **71**, 1211 (1979).
3. R. O. LOUTFY, J. H. SHARP, C. K. HSIAO, and R. HO. J. Appl. Phys. **52**, 5218 (1981).
4. J. P. DODELET, H. P. POMMIER, and M. RINGUET. J. Appl. Phys. **53**, 4270 (1982).
5. H. J. WAGNER and R. O. LOUTFY. J. Vac. Sci. Technol. **20**, 300 (1982).
6. A. M. HOR and R. O. LOUTFY. Can. J. Chem. **61**, 901 (1983).
7. A. M. HOR, R. O. LOUTFY, and C. K. HSIAO. Appl. Phys. Lett. **42**, 165 (1983).
8. M. F. LAWRENCE, J. P. DODELET, and L. H. DAO. J. Electrochem. Soc. **131**, 2977 (1984).
9. M. F. LAWRENCE and J. P. DODELET. J. Phys. Chem. **89**, 1395 (1985).
10. A. S. BARANSKI and W. R. FAWCETT. J. Electrochem. Soc. **127**, 766 (1980).
11. G. P. POWER, D. R. PEGGS, and J. A. PARKER. J. Electrochim. Acta, **26**, 681 (1981).
12. E. FATAS, P. HERRASTI, F. ARJONA, and G. CAMARERO. J. Electrochem. Soc. **134**, 2799 (1987).
13. B. MILLER and A. HELLER. Nature, **262**, 680 (1976).
14. A. MONDAL and T. K. CHAUDHURI. Sol. Energy Mat. **7**, 431 (1983).
15. J. E. OWEN and M. E. KENNEY. Inorg. Chem. **1**, 331 (1962).
16. E. FATAS, R. DUO, P. HERRASTI, F. ARJONA, and E. GARCIA CAMARERO. J. Electrochem. Soc. **131**, 2243 (1984).
17. A. S. BARANSKI, W. R. FAWCETT, A. C. MCDONALD, and R. M. DENOBRIGA. J. Electrochem. Soc. **128**, 963 (1982).
18. R. O. LOUTFY, L. F. MCINTYRE, D. K. MURTI, and C. K. HSIAO. Sol. Energy Mat. **5**, 221 (1981).
19. R. C. BHARDWAJ, C. M. JADHAV, and M. M. TAQUIKHAN. Solar Cells, **12**, 371 (1984).
20. P. K. MAHAPATRA and C. B. ROY. Electrochim. Acta, **29**, 1435 (1984).
21. A. S. N. MURTHY and K. S. REDDY. J. Power Sources, **13**, 159 (1984).
22. A. S. BARANSKI, M. S. BENNETT, and W. R. FAWCETT. J. Appl. Phys. **54**, 6390 (1983).
23. C. W. TANG. Appl. Phys. Lett. **48**, 183 (1986).

Can. J. Chem. Downloaded from www.nrcresearchpress.com by 186.148.149.217 on 09/07/12
For personal use only.

The voltammetric determination of cobalt(II) in seawater — adsorptive preconcentration of the dimethylglyoxime complex

W. W. WESTENBRINK, J. A. PAGE, AND G. W. VANLOON[1]

Department of Chemistry, Queen's University, Kingston, Ont., Canada K7L 3N6

Received June 9, 1989

W. W. WESTENBRINK, J. A. PAGE, and G. W. VANLOON. Can. J. Chem. **68**, 209 (1990).

Conditions for the determination of trace Co in seawater are described. The method involves formation of the dimethylglyoxime complex and adsorptive accumulation onto a hanging mercury drop electrode at an applied potential of −0.70 or −0.96 V vs. SCE. The adsorbed complex is then reduced by scanning the electrode potential to −1.20 V; the reduction peak potential (E_p) is −1.12 V. Nickel behaves in a similar manner with E_p of −0.99 V but the Co complex appears to be preferentially adsorbed, making analysis for Co possible even in the presence of a large excess of Ni. Adsorption of organic matter also occurs; this does not affect analytical sensitivity but limits the maximum deposition time allowed in the analysis.

Determination of Co in six seawater samples yielded results ranging from 4 to 114 ng L^{-1}. Good agreement was obtained with the one reference sample (NASS-1) for which there was a certificate value.

Key words: cobalt, dimethylglyoxime, stripping voltammetry, adsorption, seawater.

W. W. WESTENBRINK, J. A. PAGE et G. W. VANLOON. Can. J. Chem. **68**, 209 (1990).

On décrit des conditions permettant de déterminer des traces de Co dans l'eaud e mer. La méthode implique la formation du complexe avec la diméthylglyoxime et une accumulation par adsorption sur une électrode à goutte de mercure pendante, à un potentiel appliqué de −0,70 ou−0,96 V vs. SCE. Le complexe adsorbé est alors réduit en balayant le potentiel de l'électrode jusqu'à −1,20 V; le potentiel maximal de la réduction (E_p) se situe à −1,12 V. Le nickel se comporte d'une manière semblable avec un E_p de −0,99 V; toutefois, le complexe de Co semble être adsorbé d'une façon préférentielle et cette propriété permet d'analyser le Co même en présence d'un large excès de Ni. Il se produit aussi une adsorption des composés organiques; cette propriété n'affecte pas la sensibilité analytique mais elle limite le temps maximal de déposition permis par l'analyse.

La détermination du Co dans six échantillons d'eau de mer a fourni des résultats allant de 4 à 114 ng L^{-1}. On a obtenu une bonne corrélation avec le seul échantillon de référence (NASS-1) pour lequel il existe une valeur certifiée.

Mots clés : cobalt, diméthylglyoxime, voltamétrie, adsorption, eau de mer.

[Traduit par la revue]

Introduction

Anodic stripping voltammetry (ASV) is an appropriate technique for the determination of metal ions in aqueous solutions and seawater at sub-ppb levels. The method is highly sensitive and, in the case of seawater the dissolved salts do not constitute an interference but rather serve as the supporting electrolyte for the voltammetry. Applications of the technique are limited by the requirement that the metal be readily deposited at the electrode and then stripped within a potential window appropriate to the aqueous solution. Methods, usually employing a Hg drop or thin film electrode, exist for about 10 elements in seawater (1). In some cases, the technique can distingush amongst the oxidation states and forms of a metal on the basis of differences in electroactivity of the analyte species (2).

Recently, a technique derived from ASV but involving the collection of the metal species at an electrode surface by adsorptive accumulation (AdAc) has widened the scope of voltammetric analysis (3). There are variants, but the method usually involves complexation of the metal ion followed by adsorption of the complex on the electrode surface. The amount or surface concentration of the adsorbed species is then determined by scanning the electrode potential through a range of values. If the species is electroactive and the charge transfer process relatively rapid, a current–potential response in the form of a peak at a characteristic potential is obtained. The peak height (current) or peak area (quantity of electricity) is the analytical signal. Variables include the choice of complexing agent, electrolyte composition and pH, electrode material and adsorption potential, adsorption time and mass transfer parameters; appropriate choices enable a selective determination of a number of elements. Calibration of the method is usually by standard addition of the analyte ion.

One widely used AdAc method is the determination of Ni(II) after complexation with excess dimethylglyoxime (DMG, butane-2,3-dione dioxime). The method is attributable to Nurnberg (4) and involves adsorption of the metal complex ($Ni(DMG)_2$) onto a Hg drop electrode from a slightly basic, buffered medium. The electrode potential is then scanned to reduce the adsorbed complex. Using the method, good results have been obtained in intercalibration studies on reference seawater samples. Since Co(II) forms a $Co(DMG)_2$ complex similar to that of Ni(II), a related method is to be expected. The possibility has been recognized and it has been indicated that trace Co(II) in seawater can be determined although details, procedure or results were not given (3). Methods for trace Co(II) in biological materials (6–9), sediments (8), reactor water coolant (10), rain water (11), and estuarine and fresh water samples containing elevated Co levels (12) have been described. Each of the methods involves the accumulation of the $Ni(DMG)_2$ and $Co(DMG)_2$ complexes at a Hg electrode followed by a voltammetric determination of the adsorbed species.

Recently, a determination of Co in seawater samples based on AdAc of the related Nioxime (cyclohexane-1,2-dione dioxime) complex at a Hg drop electrode has been reported (13). The sensitivity of the method was highly dependent upon the pH of the electrolyte and the buffer used, but with a HEPES (*N*-(2-hydroxyethyl)piperazine-*N*′-2-ethanesulfonic acid) buffer at pH 7.6, a detection limit of 0.35 ng L^{-1} Co was achieved

[1]To whom correspondence should be addressed.

Can. J. Chem. Downloaded from www.nrcresearchpress.com by 91.144.44.67 on 09/07/12
For personal use only.

using a 15 min adsorption and differential pulse voltammetry. The method was successfully applied to seawater samples after uv irradiation to destroy organic surfactants.

In the present work, the adsorption of $Co(DMG)_2$ at a Hg drop electrode is used for the determination of Co(II) in seawater. Since Ni(II) is usually present in seawater at much higher concentrations than Co(II), a particular concern was the effect of this element in the determination. Surface active materials are also known to interfere in adsorption processes (12) and a study of the effect of organic material in the analyte on the determination was also undertaken.

Experimental

The voltammograms were recorded using an EG & G Princeton Applied Research Model 384 Polarographic Analyzer and a Model 303 Static Hg Drop Electrode with a Model 305 Stirrer. The cell and electrodes were identical to those in a previous study (5). A Ag/AgCl/seawater reference electrode and a Pt counter electrode were used with the counter electrode isolated from the analyte by a bridge tube. Stirring in the adsorption stage was by a magnetically driven stirring bar. Sample handling and cell manipulation were done in a laminar flow clean hood. The seawater (SW) analyzed in the study included a NASS-1 reference water (14) and samples taken from Sandy Cove (SC) and Bedford Basin (BB), Nova Scotia, and Passamaquoddy Bay (PB), New Brunswick. Samples of ICES-5 seawater used in a previous study (15) were also analyzed. The Co(II) and Ni(II) standard stock solutions were prepared determinately from pure metal dissolved in excess reagent grade HNO_3. Dilute standard solutions were prepared from the stock solution as needed.

For analysis, the cell was rinsed and filled with a 8.0 mL sample and 200 μL of a 4.0 *M* NH_3/NH_4Cl aqueous buffer and 20 μL of a 0.010 *M* ethanolic dimethylglyoxime reagent added. This gave a pH of 9.2 and a reagent concentration $C_{DMG} = 2.5 \times 10^{-4}$ *M*. The final seawater analyte had ionic strength $I = 0.70$ *M* and chloride concentration $C_{Cl^-} = 0.55$ *M*. The electrolyte was dearated and blanketed with purified N_2 gas for analysis. The buffer and reagent concentrations are identical to those which may be used for the determination of Ni(II) in seawater.

The adsorptive accumulation of the $Co(DMG)_2$ was carried out at −0.70 V or −0.96 V under controlled mass transfer conditions with accumulation times of 100 to 360 s. Stirring during this stage was at "slow" (500 Hz). A fresh Hg drop (Size "M") was used for each run. Since adsorption of the complex begins on formation of the drop, the drop was dispensed immediately at the start of the accumulation stage. At the end of the first stage there was a further 20 s rest stage without stirring; then the electrode potential was scanned to −1.30 V at 0.020 V s^{-1} and the voltammogram recorded. The peak for the reduction of the adsorbed complex was well defined, even with trace amounts of $Co(DMG)_2$, as shown in Fig. 1. For analysis, peak heights were measured with respect to a tangent fit baseline and calibration was by the method of standard additions. An analysis normally involved repeated additions of Co(II). Up to 12 measurements were thus made on each sample with an accompanying accumulation of Hg in the cell. A fresh sample was taken for each replicate analysis. The standard addition plots were highly linear indicating that the Hg drops were reproducibly dispensed during the analysis and calibration.

Results and discussion

In developing the method, the type and strength of the buffer, the pH and DMG concentration were set at values used for the determination of Ni(II) so that a simultaneous determination of the two elements could be considered. The effect of variation of the other operational parameters was systematically studied.

Using an adsorption potential of −0.70 V, the voltammetry gave a Co reduction peak at −1.12 V with the Ni peak at −0.99 V. Since Co(II) concentrations in seawater are generally much less than those of Ni(II) (e.g. 1:64 in NASS-1 seawater) simultaneous analysis is difficult as the Co peak tends to be

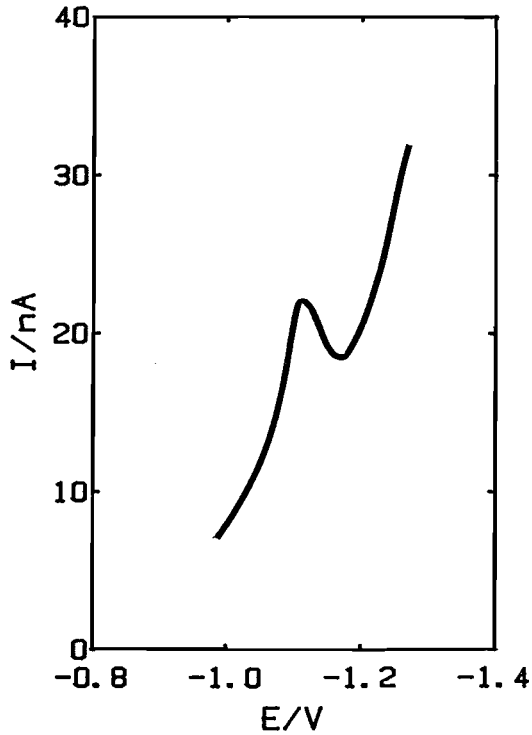

Fig. 1. Typical voltammogram for adsorbed $Co(DMG)_2$. NASS-1 seawater spiked with 0.11 μg L^{-1} Co. $E_{ads} = -0.96$ V, $t_{ads} = 120$ s, scan rate = 0.020 V s^{-1}.

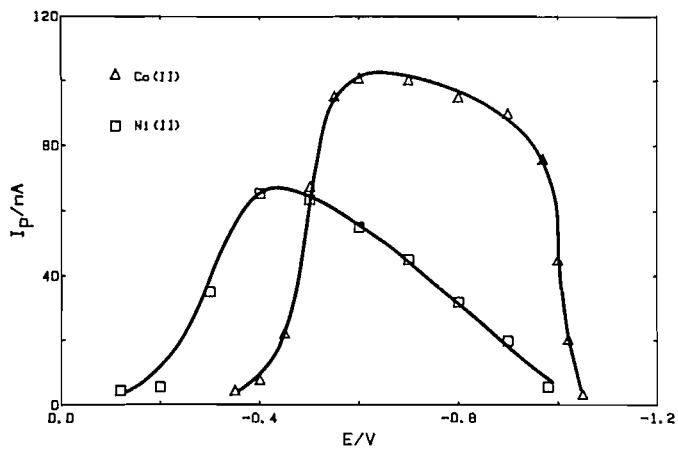

FIG. 2. The effect of E_{ads} on Co and Ni response. Sandy Cove seawater, spiked with 0.91 μg L^{-1} Co. $t_{ads} = 120$ s, scan rate = 0.020 V s^{-1}.

obscured by the preceding Ni peak. An attempt was made to identify an electrode potential which would permit the determination of Co with a minimal Ni interference and Fig. 2 shows the peak currents obtained for reduction of the complexes after adsorption for a fixed time at differing potentials from a seawater containing added Co(II) and Ni(II). For $Co(DMG)_2$, potentials more negative than −0.60 V were required for significant adsorption, but $Ni(DMG)_2$ was adsorbed at less negative potentials. At potentials that resulted in adsorption of both species, there was evidently preferential adsorption of the $Co(DMG)_2$ as shown by the decrease in the Ni peak signal at increasingly negative adsorption potentials. In the absence of added Co(II), the Ni peak signal obtained was constant over a wide range of adsorption potentials. At adsorption potentials

Can. J. Chem. Downloaded from www.nrcresearchpress.com by 91.144.44.67 on 09/07/12
For personal use only.

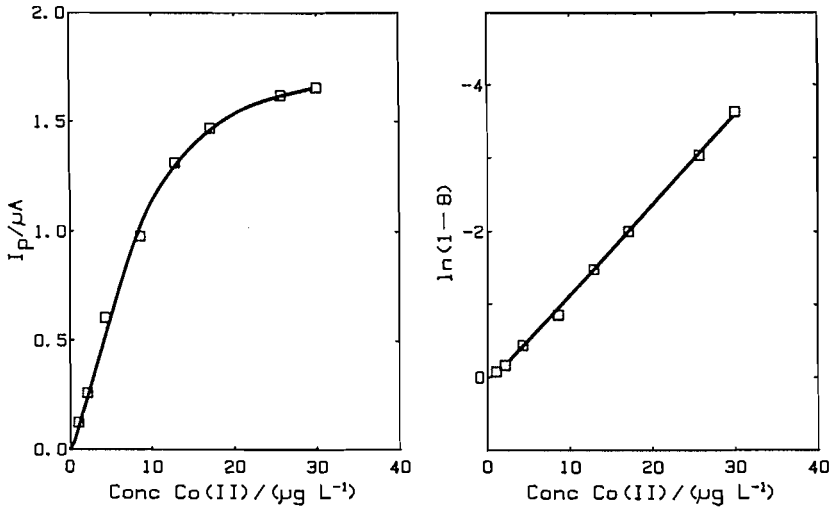

FIG. 3. (*a*) Calibration curve for Co analysis by adsorption stripping voltammetry. NASS-1 seawater with added Co(II). t_{ads} = 300 s, scan rate = 0.050 V s^{-1}. (*b*) Plot of data from (*a*) exhibiting Langmuir adsorption behaviour.

approaching −0.96 V the Ni peak disappeared, probably because of simultaneous adsorption and reduction of the $Ni(DMG)_2$. For the analysis of seawater where Co(II) is at a lower concentration than the Ni(II) an adsorption potential of −0.96 V appears appropriate. For cases where the simultaneous determination of Co(II) and Ni(II) is feasible, an adsorption potential of −0.70 V is recommended.

Using adsorption potentials of −0.70 V and −0.96 V, calibration curves for Co(II) exhibited the behaviour in Fig. 3. With Co(II) concentrations higher than 1 μg L^{-1}, there was an asymptotic approach to a limiting value of peak current and peak area. The behaviour is similar to that previously observed with $Ni(DMG)_2$ and the limit probably corresponds to saturation of the electrode surface with adsorbed $Co(DMG)_2$. For Fig. 3, the limiting values were I_p = 1.7 μA and Q_p = 2.3 μC. If the reduction process involves 2 Faradays per mol, the 2.3 μC corresponds to 1.4 × 10^{-11} mol of adsorbed $Co(DMG)_2$. Assuming monolayer coverage of the electrode surface (A = 0.014 cm^2) each adsorbed $Co(DMG)_2$ molecule then occupies 0.18 nm^2. The crystal structure of $Co(DMG)_2$ has evidently not been determined; however the 0.87 nm^2 for $Ni(DMG)_2$ in the 001 plane should be a reasonable approximation to the area of a planar $Co(DMG)_2$ molecule (16). An explanation for the large discrepancy could be that saturation of the electrode surface does not correspond to a simple monolayer but rather to a multilayer or compact layer (where the $Co(DMG)_2$ is not planar to the electrode surface). An alternative argument is that the adsorbed complex forms a simple monolayer but reduction of the $Co(DMG)_2$ is not a simple 2 electron process. Recent work (unpublished) with the $Ni(DMG)_2$ system lends support to the latter hypothesis. Catalytic mechanisms have been postulated to explain the enhanced currents observed in the polarographic reduction of both $Ni(DMG)_2$ and $Co(DMG)_2$ (17).

There is also a simple time-dependent relation between the concentration of $Co(DMG)_2$ in the analyte and the coverage of the electrode by adsorbed complex. The data of Fig. 3 were obtained using a fixed adsorption time, but the ratio of peak current to the limiting value representing surface saturation is a measure of the fractional coverage of the electrode with adsorbed complex ($\theta = i_p/1.7\ \mu A$). Figure 3 also shows a plot of ln (1 − θ) vs. $Co(DMG)_2$ concentration. If it is presumed that adsorption results in no significant decrease in the concentration of $Co(DMG)_2$ in the electrolyte, the linear plot is characteristic of a Langmuir isotherm and indicates that the rate of adsorption is proportional to both the concentration of $Co(DMG)_2$ and to (1 − θ), the fraction of the electrode surface not covered by adsorbed complex. Linear analytical calibration curves should result when coverage of the electrode with adsorbed complex is restricted to small fractional values of the electrode area. In the absence of other effects, adsorption times of 300 s are appropriate for concentrations of Co(II) up to a few μg L^{-1}, but for larger concentrations the adsorption time should be proportionately less.

Interferences

Seawater spiked with Cd(II), Cr(III), Cu(II), Fe(II), Mn(II), Pb(II), and Zn(II) at concentrations up to 10 mg L^{-1} produced no new peak, nor did the additions have any effect on the Co response. As noted before, Ni(II) gives a preceding reduction peak at −0.99 V. The effect of added Ni on the Co peak was investigated by adding increasing amounts of Ni(II), to solutions containing between 1 and 18 μg L^{-1} added Co(II). The analyses were carried out using a 300 s adsorption at both −0.70 V and −0.96 V. The Ni(II), up to at least 30 μg L^{-1}, affected neither the sensitivity of the Co determination nor the blank signal value. However, Co(II) did interfere in the Ni(II) response as shown in Fig. 4. The significant decrease in the Ni peak can be explained by a preferential adsorption of $Co(DMG)_2$ and displacement of adsorbed $Ni(DMG)_2$. Similar conclusions have been stated elsewhere (10), although a small enhancement of the Co signal by Ni was reported in that work.

In the analysis for Ni(II), a decrease in sensitivity in the presence of surface-active organic materials has been observed (3, 12) and similar effects are to be expected in the Co(II) determination. Figure 5 shows the effect of added humic material (HM) on the Co peak. In the presence of added HM, the Co peak current shows an initial increase with adsorption time but at increasingly longer adsorption times reaches a maximum value and then decreases. The adsorption time required to reach the maximum is dependent upon the concentration of added HM. The slope of the initial linear region is however independent of the concentration and indicates that organic material does not affect the sensitivity of the analysis at short adsorption times. The behaviour suggests that there is a preferential slow

Can. J. Chem. Downloaded from www.nrcresearchpress.com by 91.144.44.67 on 09/07/12
For personal use only.

TABLE 1. Analysis of seawater samples for Co(II)

Sample	AdAc	C_{Co} (CI)[a] /ng L^{-1}	Mean C_{Co} (SD)[b] /ng L^{-1}	Sensitivity[c] /nA (ng L^{-1})$^{-1}$
NASS-1	360 s	4.0 (0.3), 5.2 (1.4), 3.8 (2.0), 4.4 (1.5), 4.0 (1.0)	4.28 (0.56)[d]	0.27 (0.09)
ICES-5	360 s	5.3 (1.0), 4.4 (2.2), 4.5 (1.4), 3.5 (1.1), 5.3 (1.9), 6.1 (1.2), 5.4 (2.1), 4.2 (1.2)	4.83 (0.83)	0.18 (0.03)
SC	360 s	5.1 (1.9), 3.2 (1.3), 3.3 (1.6)	3.87 (1.07)	0.33 (0.06)
PB	360 s	9.9 (4.0), 8.1 (1.3)	9.0 (1.3)	
BB	120 s	119 (19), 109 (10)	114	0.061, 0.085

[a]Individual samples with standard addition calibration (95% confidence interval associated with calibration line).
[b]Mean of individual values (standard deviation of the mean).
[c]Mean slope of individual calibration lines (standard deviation).
[d]NASS-1 certificate value: 4.0 (1.0) ng L^{-1} Co. (14).

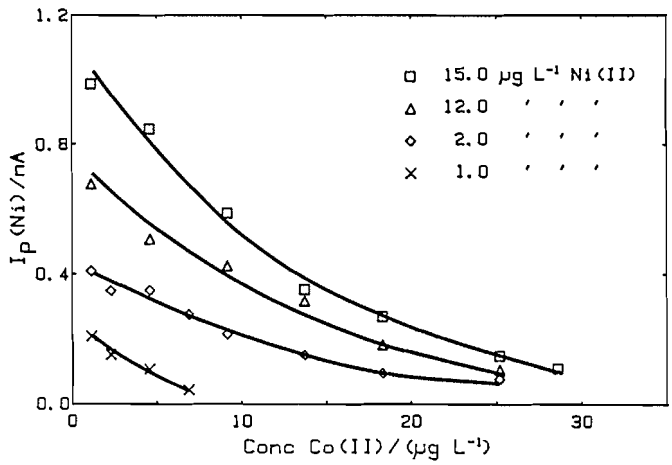

FIG. 4. Ni response in the presence of added Co. NASS-1 seawater with added Co and Ni t_{ads} = 300 s, scan rate = 0.050 V s^{-1}.

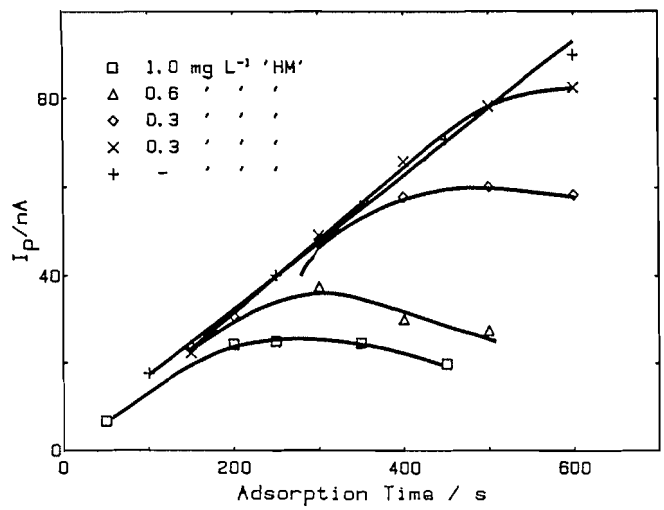

FIG. 5. The effect of added humic acid on Co response. NASS-1 seawater spiked with 0.30 μg L^{-1} Co. E_{ads} = −0.96 V, scan rate = 0.020 V s^{-1}.

adsorption of HM on the Hg drop and this can interfere with the adsorption and reduction of $Co(DMG)_2$.

The effect is a limitation in the analysis of real samples. For very low concentrations of Co(II) the sensitivity of the method can, in theory, be increased by increasing the adsorption time. However, the presence of HM or other surface-active materials in the analyte will restrict the analysis to short adsorption times and limit the sensitivity obtainable. Fulvic acid and Triton X-100 were also found to produce effects similar to that of the added humic material. The interference from Triton X-100 was substantially greater than from HM on a mass concentration basis. Added albumin and linoleic acid produced no significant change in the Co response.

A claim has been made that the DMG complexes compete effectively with the dissolved organic material in the adsorption processes and there is no interference in analyses for Co(II) and Ni(II) (12). The adsorption times reported were short and if mass transfer conditions are comparable the claim is within the limits where an interference was not apparent in Fig. 5.

Figure 6 shows response curves obtained with three seawater samples containing added Co(II). The slopes at short adsorption times are proportional to the concentration of Co(II) in the samples. Each curve shows a broad maximum, with that for the NASS-1 seawater at the longest time. This can be explained if the NASS-1 water is regarded as 'clean' while the Passamaqu-

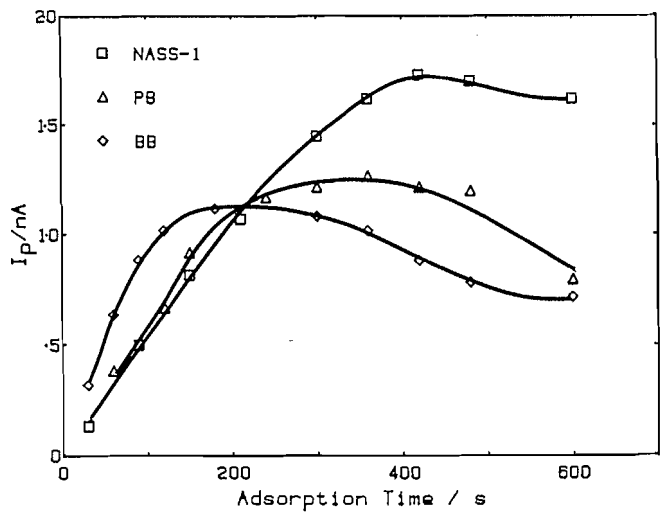

FIG. 6. Effect of adsorption time on Co response. NASS-1, Passamaquoddy Bay (PB) and Bedford Basin (BB) seawater. Scan rate = 0.050 V s^{-1}.

Can. J. Chem. Downloaded from www.nrcresearchpress.com by 91.144.44.67 on 09/07/12
For personal use only.

oddy Bay and Bedford Basin waters contain significantly greater concentrations of dissolved organic material.

Analytical results

Analyses were performed on a variety of seawater samples and the results are reported in Table 1. The uncertainty in each of the individual values reported was derived from the intercepts of the confidence band associated with the standard addition calibration curve. Considering the trace levels of Co(II) reported, the replicate analyses exhibited good reproducibility, indicating that sample handling did not contribute significantly to the overall error.

The adsorption times used in the analyses were chosen as the longest time possible without significant interference from surface active materials in the analyte. The Bedford Basin seawater appeared to contain a level of surface-active material higher than that of the other samples and with this sample an adsorption time of much over 120 s produced a dramatic decrease in the (normalized) sensitivity of the analytical system. Variations in the sensitivities between samples can be attributed at least partly to the use of a number of different electrode capillaries and other electrodes as well as cells with different mass transfer parameters over the period of time involved in this work. The results for the NASS-1, ICES-5, Sandy Cove, and Passamaquoddy Bay Basin, surrounded by a major urban centre, are significantly higher. The ratio of Co to Ni in the latter sample is near 1:8 compared to a ratio of 1:64 in the NASS-1 seawater. The analyses of the NASS-1 water were carried out blind as a part of the interlaboratory analysis program of the Marine Analytical Chemistry Standards Program of the National Research Council of Canada (14). The voltammetric results coincide with the certificate value of 0.004 $\mu g\ L^{-1}$ derived from values obtained by a number of techniques. The main attribute of the present procedure is that the determination of Co(II) is direct and requires only a minimal sample pretreatment.

Due to the lack of a sample with a negligible Co(II) concentration, estimation of a detection limit based on repeated measurements of a blank signal was not possible. Instead, a detection limit was estimated from the peak current values obtained in the repeated measurements on 'clean' seawater samples. In each standard addition analysis, the measurements of the unspiked sample were made in triplicate and for the NASS-1 seawater, the sample standard deviation was ± 0.154 nA (3×5 values) corresponding to ± 0.58 ng L^{-1} and for the ICES-5 sample it was ± 0.90 nA (3×8 values) or ± 0.51 ng L^{-1}. The pooled sample standard deviation was ± 0.54 ng L^{-1}. Therefore, the detection limit for the analytical system ($3 \times$ SD) would be 1.6 ng L^{-1}. The Co(II) concentrations of the NASS-1, ICES-5, and Sandy Cove seawater samples were thus about twice the system detection limit value.

Acknowledgements

Support from the Marine Analytical Chemistry Standards Program of the National Research Council of Canada in the way of a contract and support from the Natural Sciences and Engineering Research Council of Canada in the way of an operating grant is gratefully acknowledged. Scholarship support from Queen's University for W. Westenbrink is also gratefully acknowledged.

1. T. M. FLORENCE. Analyst, **111**, 489 (1986).
2. J. WANG. Stripping analysis. VCH Publishers, Inc., Deerfield Beach. 1985.
3. B. PIGLAR, P. VALENTA, and H. W. NURNBERG. FRESENIUS Z. ANAL. CHEM. **307**, 337 (1981).
4. H. W. NURNBERG. Pure Appl. Chem. **54**, 853 (1982).
5. J. ELWERFALLI, J. A. PAGE, AND G. W. VANLOON. Can. J. Chem. **65**, 1139 (1986).
6. A. MEYER and R. NEEB. Fresenius Z. Anal. Chem. **315**, 118 (1983).
7. S. B. ADELOJU, A. M. BOND, and M. H. BRIGGS. Anal. Chim. Acta, **164**, 181 (1984).
8. H. ESKILSSON, C. HARALDSSON, and D. JAGNER. Anal. Chim. Acta, **175**, 79 (1985).
9. V. GEMMER-COLES and R. NEEB. Fresenius Z. Anal. Chem. **327**, 547 (1987).
10. K. TORRANCE and C. GATFORD. TALANTA, **32**, 273 (1985).
11. L. VOS, Z. KOMY, G. REGGERS, E. ROEKENS, and R. VAN GRIEKEN. Anal. Chim. Acta, **184**, 271 (1986).
12. A. M. BOND and K. L. LUSCOMBE. J. Electroanal. Chem. **214**, 21 (1986).
13. J. R. DONAT and K. W. BRULAND. Anal. Chem. **60**, 240 (1988).
14. S. S. BERMAN, R. E. STURGEON, J. A. H. DESAULNIERS, and A. P. MYKYTIUK. Marine Poll. Bull. **14**, 69 (1983).
15. J. M. BEWERS, J. DALZIEL, P. A. YEATS, and J. L. BARRON. International Council for the Exploration of the Sea. Report of the ICES Fourth Round Intercalibration for Trace Metals in Seawater, CM 1979/E:37.
16. L. E. GODYKI and R. E. RUNDLE. Acta Crystallogr. **6**, 487 (1953).
17. J. WEINZIERL and F. UMLAND. Fresenius Z. Anal. Chem. **312**, 608 (1982).

Can. J. Chem. Downloaded from www.nrcresearchpress.com by 91.144.44.67 on 09/07/12
For personal use only.

A multinuclear (^{13}C, ^{31}P, ^{77}Se, ^{125}Te, ^{199}Hg) magnetic resonance study of the adamantane-like clusters $[(\mu\text{-}ER)_6(HgE'PR'_3)_4]^{2+}$ (E = S, Se, Te; E′ = S, Se; R′ = Ph, c-C_6H_{11}) and the precursors $[Hg(E'PR'_3)_n]^{2+}$ [1-3]

PHILIP A. W. DEAN[4] AND VEERAGATHY MANIVANNAN
Department of Chemistry, University of Western Ontario, London, Ont., Canada N6A 5B7

Received June 30, 1989

PHILIP A. W. DEAN and VEERAGATHY MANIVANNAN. Can. J. Chem. **68**, 214 (1990).

The cations $[Hg(E'PR'_3)_n]^{2+}$ (E′ = S or Se; R′ = c-C_6H_{11}, n = 2–4; R′ = Ph, n = 3 or 4) are obtained in solution from the new salts $[Hg(E'PR'_3)_n](ClO_4)_2$ (E′ = S or Se; n = 2, R′ = c-C_6H_{11}; n = 3, R′ = Ph) and their stoichiometric mixtures with $E'PR'_3$. They have been characterized at reduced temperature using multinuclear (^{13}C, ^{31}P, ^{77}Se (where appropriate), and ^{199}Hg) NMR. Cations of the type $[(\mu\text{-}ER)_6(HgE'PR'_3)_4]^{2+}$ (ER = S alkyl, SePh, or TePh, but not SPh), prepared cleanly in solution from $Hg(ER)_2$, $[Hg(E'PR'_3)_n](ClO_4)_2$, and $E'PR'_3$ in the correct stoichiometric ratio, have been characterized in the same manner, and shown to possess an adamantanoid structure. The product with ER = TePh, $E'PR'_3$ = $SPPh_3$ has been isolated analytically pure. These tetranuclear cations are the first discrete species containing the adamantanoid skeleton $(\mu\text{-}ER)_6(HgE')_4$ (E, E′ = chalcogen). At reduced temperature, inversion at E is slow on the NMR time scale for ER = TePh. Under these conditions, the TePh-bridged cations occur predominantly as an isomer of C_1 symmetry for $E'PR'_3$ = $SPPh_3$, $SPCy_3$, $SePPh_3$. However, the $SePCy_3$ analogue appears to exist as an equilibrium mixture of an isomer of C_1 symmetry and an isomer of C_3 symmetry. Ligand redistribution occurs in the binary system $[(\mu\text{-}SePh)_6(HgE'P(C_6H_{11})_3)_4]^{2+}$ (E′ = S or Se):$[(\mu\text{-}SePh)_6(HgPPh_3)_4]^{2+}$, giving equilibrium mixtures of $[(\mu\text{-}SePh)_6(HgPPh_3)_{4-n}(HgE'P(C_6H_{11})_3)_n]^{2+}$ for which the individual components have been fully characterized using NMR.

Key words: adamantanoid clusters, benzene chalcogenate, mercury(II), NMR, phosphine chalcogenide.

PHILIP A. W. DEAN et VEERAGATHY MANIVANNAN. Can. J. Chem. **68**, 214 (1990).

On a obtenu les cations $[Hg(E'PR'_3)_n]^{2+}$ (E′ = S ou Se; R′ = c-C_6H_{11}, n = 2–4; R′ = Ph, n = 3 ou 4) en solution en faisant réagir les nouveaux sels $[Hg(E'PR'_3)_n](ClO_4)_2$ (E′ = S ou Se; n = 2, R′ = c-C_6H_{11}; n = 3, R′ = Ph) ainsi que leurs mélanges stoechiométriques avec du $E'PR'_3$. On les a caractérisés à basse température en faisant appel à la RMN multinucléaire (^{13}C, ^{31}P, ^{77}Se (lorsqu'approprié) et ^{199}Hg). On peut préparer très proprement des solutions des cations du type $[(\mu\text{-}ER)_6[Hg(E'PR'_3)_4]^{2+}$ (ER = S-alkyle, SePh ou TePh, mais pas SPh) en faisant réagir des quantités stoechiométriques de $Hg(ER)_2$, de $[(Hg(E'PR'_3)_n](ClO_4)_2$ et de $E'PR'_3$, on les a caractérisés de la même manière et on a démontré qu'ils possèdent une structure adamantanoïde. On a isolé à l'état pur le composé dans lequel ER = TePh et $E'PR'_3$ = $SPPh_3$. Ces cations tétranucléaires constituent les premières espèces définies contenant le squelette adamantanoïde $(\mu\text{-}ER)_6(HgE')_4$(E, E′ = chalcogène). À basse température, lorsque ER = TePh, l'inversion au niveau de E est lente par rapport à l'échelle de temps de la RMN. Dans ces conditions, les cations dans lesquels $E'PR'_3$ = $SPPh_3$, SPCy, et SePPh, et qui comportent un pont TePh se présentent principalement sous la forme d'un isomère de symétrie C_1. Toutefois, l'analogue $SePCy_3$ semble exister sous la forme d'un équilibre entre deux isomères de symétrie respectives C_1 et C_3. Il se produit une redistribution de ligand dans les systèmes binaires $[(\mu\text{-}SePh)_6(HgE'P(C_6H_{11})_3)_4]^{2+}$ (E′ = S ou Se) : $[(\mu\text{-}SePh)_6(HgPPh_3)_4]^{2+}$, et elle conduit à des mélanges en équilibre des ions $[(\mu\text{-}SePh)_6(HgPPh_3)_{4-n}(HgE'P(C_6H_{11})_3)_n]^{2+}$ dont les composants individuels ont été complètement caractérisés par la RMN.

Mots clés : groupes adamantanoïde, benzene chalcogénate, mercure(II), RMN, phosphine chalcogénide.

[Traduit par la revue]

Introduction

In the zinc family, adamantanoid anions of the type $[(\mu\text{-}ER)_6(MER)_4]^{2-}$ are firmly established for M = Zn or Cd, E = S or Se (refs. 1–3, and unpublished work by P. A. W. Dean, J. J. Vittal, and N. C. Payne).[5] They have the skeleton **I**. Previous studies from this laboratory have dealt with the terminal substitution of these Zn_4 and Cd_4 species by halogens (3*b*, *c*, 4)[6] and pseudohalogens (3*c*) to give $[(\mu\text{-}ER)_6(MX)_4]^{2-}$. Attempts to synthesize analogous Hg(II) anions containing the $(\mu\text{-}ER)_6Hg_4$ core have so far been unfruitful (8). However, this

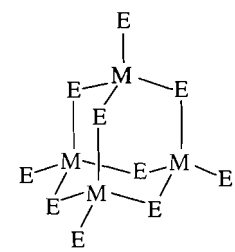

I

core has been shown to exist in the adamantanoid *cations* $[(\mu\text{-}ER)_6(HgL)_4]^{2+}$ (E = S or Se; L = tertiary phosphine or $AsPh_3$) (9), and very recently we have extended the series to include $[(\mu\text{-}TeR)_6(HgL)_4]^{2+}$ and $[(\mu\text{-}TePh)_6(Hg)(HgL)_3]^{2+}$ (L = PR'_3) (10). It seemed to us that, in the absence of $[(\mu\text{-}ER)_6(HgER)_4]^{2-}$, cationic species might provide an alternative way of investigating the properties of the $(\mu\text{-}ER)_6(HgE')_4$ skeleton (E, E′ = chalcogen). Accordingly we report here the results of a study of cations of the general type $[(\mu\text{-}ER)_6(HgE'PR'_3)_4]^{2+}$ (E′ = S or Se). These cations may possess a variety of spin-1/2

[1]Presented in part at the 72nd Canadian Chemical Conference, Victoria, B.C., June 1989.

[2]No reprints available.

[3]Abbreviations used: Cy = c-C_6H_{11}; $dppmSe_2$ = $Ph_2P(Se)CH_2P(Se)Ph_2$; Ar = aryl.

[4]Author to whom correspondence may be addressed.

[5]Thiolate-bridged adamanatanoid clusters are known for a wide range of divalent metal ions (see, for example, ref. 5).

[6]Substituted anions of the type $[(\mu\text{-}SR)_6(MX)_4]^{2-}$ are also known for Fe(II) (6) and Co(II) (3*c*, 7).

Can. J. Chem. Downloaded from www.nrcresearchpress.com by 91.144.44.67 on 09/07/12
For personal use only.

Can. J. Chem. Downloaded from www.nrcresearchpress.com by 91.144.44.67 on 09/07/12
For personal use only.

probe nuclei, making them favorable candidates for study by NMR: ^{13}C, ^{31}P, and ^{199}Hg are always present, and also the bridging E atoms may be ^{77}Se or ^{125}Te, while E′ may be ^{77}Se.[7]

Though many complexes of Hg(II) with phosphine chalcogenides are known (12), the compounds $[Hg(E'PR'_3)_n](ClO_4)_2$, containing monodentate $E'PR'_3$,[8] do not seem to have been described earlier. These salts are required in the synthesis of the title adamantanoid cations. Their synthesis and characterization in solution by the NMR method are included here.

In principle, four configurational isomers of $(\mu\text{-}ER)_6M_4$ are possible as a result of inversion at the pyramidal E atoms of the six μ-ER groups, two of C_3 symmetry and two of C_1 symmetry (4, 5). Examples of each of the possible isomers are known in the solid state (4, 5), but the cations containing the $(\mu\text{-}TeR)_4Hg_4$ cage (10) are the first species of this type for which it has been possible to detect preferential isomer formation in solution using NMR. The TeR-bridged cations included in the present work provide several further examples of this phenomenon.

Experimental

Materials

The ligands Ph_3PE and Cy_3PE (E = S or Se) were prepared as in earlier studies (14), as were $Hg(SR)_2$ (R = Et, *n*-Pr or Ph) and $Hg(SePh)_2$ (9) and $Hg(TePh)_2$ (10). Dimethyl diselenide (Strem) showed no significant impurities by NMR and was used as received, as were $Hg(ClO_4)_2\cdot 3H_2O$ and $AgClO_4$ (both from Strem). Following ref. 15, an attempt was made to synthesize $Hg(SeMe)_2$ by stirring Me_2Se_2 and Hg in benzene at room temperature. It was anticipated that pure $Hg(SeMe)_2$ would be yellow, like $Hg(SePh)_2$. However, the product was always dull green and apparently contaminated with finely dispersed Hg, and no satisfactory method of separation was found. Accordingly, the $Hg(SeMe)_2$ was used in its crude form.

For synthesis or preparation of NMR samples of the chalcogenate-bridged clusters, all solvents were dried over 3Å molecular sieves and thoroughly deoxygenated with Ar before use.

Carbon and hydrogen microanalyses were performed by Analytische Laboratorien, Gummersbach, West Germany and Guelph Chemical Laboratories, Guelph, Ontario.

Synthesis

CAUTION! While no problems have been experienced in the synthesis or handling of the perchlorate salts used in this work, such salts are known to represent an explosion hazard.

$[Hg(SPCy_3)_2](ClO_4)_2$

Initially $HgCl_2(SPCy_3)_2$ was prepared following the procedure described for $HgCl_2(PR_3)_2$ (16*a*). To a solution of $HgCl_2$ (0.669 g, 2.46 mmol) in 20 mL of Me_2CO was added a solution of $SPCy_3$ (1.55 g, 4.95 mmol) in 80 mL of Me_2CO. The mixture was reduced in volume and on cooling gave a white solid, which was separated by filtration and dried *in vacuo*, to give a yield of 1.6 g (72%). The chloride complex was converted to the ClO_4^- salt using $AgClO_4$ in exactly the same way used for various $Hg(PR_3)_2(ClO_4)_2$ (16*b*). After recrystallization from CH_2Cl_2/hexane, the yield of the white crystalline ClO_4^- complex (after recrystallization from CH_2Cl_2/hexane) was 1.1 g (66%). *Anal.* calcd. for $C_{36}H_{66}Cl_2HgO_8P_2S_2$ (*Mol.Wt.* 1024.49): C 42.21, H 6.49; found: C 42.40, H 6.43.

$[Hg(SePCy_3)_2](ClO_4)_2$

This compound was prepared in the same manner as the Cy_3PS analogue. $HgCl_2(SePCy_3)_2$ was isolated in 63% yield, then converted to the ClO_4^- salt in 86% yield. *Anal.* calcd. for $C_{36}H_{66}Cl_2HgO_8P_2Se_2$ (*Mol.Wt.* 1118.27): C 38.67, H 5.95; found: C 37.99, H 5.78.

$[Hg(SPPh_3)_3](ClO_4)_2$

Following the method used for $[Hg(dppmSe_2)_2](ClO_4)_2$ (13), this complex was synthesized by direct reaction of $Hg(ClO_4)_2$ and Ph_3PS. A mixture of $Hg(ClO_4)_2\cdot 3H_2O$ (0.54 g, 1.2 mmol) and Ph_3PS (1.1 g, 3.6 mmol)[9] in CH_2Cl_2 (60 mL) was stirred at room temperature, then warmed carefully on a steam bath until dissolution of the ClO_4^- salt was complete. The solution was filtered, then concentrated, at which point addition of hexane gave the crude material. The yield of the white crystalline product (after recrystallization from CH_2Cl_2/hexane) was 1.2 g (78%). *Anal.* calcd. for $C_{54}H_{45}Cl_2HgO_8P_3S_3$ (*Mol.Wt.* 1282.55): C 50.57, H 3.54; found: C 50.07, H 3.45.

$[Hg(SePPh_3)_3](ClO_4)_2$

The procedure was the same as that used for the sulfur analogue. The yield of the pale yellow crystalline product was 88%. *Anal.* calcd. for $C_{54}H_{45}Cl_2HgO_8P_3Se_3$ (*Mol.Wt.* 1423.25): C 45.57, H 3.19; found: C 44.61, H 3.43.

$[\mu\text{-}TePh)_6(HgSPPh_3)_4](ClO_4)_2$

Into a solution of $Hg(SPPh_3)_3(ClO_4)_2$ (0.19 g, 0.15 mmol) in 3 mL of CH_2Cl_2 at room temperature was stirred first solid $SPPh_3$ (0.045 g, 0.15 mmol), then solid $Hg(TePh)_2$ (0.27 g, 0.45 mmol). The mixture was stirred for 5 min, then filtered to remove traces of mercury. Onto the yellow filtrate was layered Et_2O (4 mL). Crystallization occurred on cooling to 5°C in the refrigerator. The yellow crystalline product was separated by decantation of the mother liquor, washed with Et_2O, and dried *in vacuo* to yield 0.30 g (58%). *Anal.* calcd. for $C_{108}H_{90}Cl_2Hg_4O_8P_4S_4Te_6$ (*Mol.Wt.* 3406.58): C 38.08, H 2.66; found: C 37.70, H 2.77.

Attempts to synthesize $[(\mu\text{-}SePh)_6(HgSPCy_3)_4](ClO_4)_2$ and $[(\mu\text{-}TePh)_6(HgSePCy_3)_4](ClO_4)_2$ in an essentially identical manner gave yellow and orange crystals, respectively. These products gave elemental analyses consistent with the formulation $[Hg_4(EPh)_6(E'PR'_3)_3](ClO_4)_2$. *Anal.* calcd. for $C_{90}H_{129}Cl_2Hg_4O_8P_3S_3Se_6$ (*Mol.Wt.* 2875.04): C 37.59, H 4.52; found: C 37.20, H 4.33. *Anal.* calcd. for $C_{90}H_{129}Cl_2Hg_4O_8P_3Se_3Te_6$ (*Mol.Wt.* 3307.58): C 32.68, H 3.93; found: C 32.72, H 3.70. In the absence of additional supporting evidence (see below) we regard these formulations as tentative.

Nuclear magnetic resonance spectra

All samples were prepared on the basis of (mass of solute/volume of solvent).

NMR spectra were measured and referenced as reported in earlier papers from this laboratory (3*c*, 10). For ^{13}C, ^{31}P, ^{77}Se, ^{125}Te, and ^{199}Hg NMR spectra, chemical shifts are quoted relative to internal TMS, external 85% H_3PO_4, external pure Me_2Se, external pure Me_2Te, and external pure Me_2Hg, respectively.

Results and discussion

The complexes $[Hg(E'PR'_3)_n]^{2+}$

Treatment of $HgCl_2(E'PCy_3)_2$ (E = S or Se) with $AgClO_4$ gave $[Hg(E'PCy_3)_2]^{2+}$ as the ClO_4^- salt. We were unable to synthesize the $E'PPh_3$ analogues by this route, but $[Hg(E'PPh_3)_3](ClO_4)_2$ results from the direct stoichiometric reaction of $E'PPh_3$ and $Hg(ClO_4)_2\cdot 3H_2O$.

The new cations were characterized in solution by ^{13}C, ^{31}P, ^{199}Hg, and (where appropriate) ^{77}Se NMR (Table 1). Stepwise addition of further $E'PR'_3$ causes formation of more highly ligated complexes up to $[Hg(E'PR'_3)_4]^{2+}$, and NMR data for these species are included in Table 1 also. For each of the complexes at reduced temperature, the ^{31}P NMR spectrum shows a singlet centreband with ^{199}Hg satellites due to $^2J(PHg)$. Under these conditions, the ^{31}P NMR spectra of the phosphine selenide complexes show the expected ^{77}Se satellites in addition

[7]The natural abundances of ^{13}C, ^{31}P, ^{77}Se, ^{125}Te, and ^{199}Hg are 1.108, 100, 7.58, 6.99, and 16.84% respectively; their relative receptivities, D^C, are 1, 3.77×10^2, 3.01, 12.7, and 5.57, respectively (11).

[8]The synthesis and ^{31}P, ^{77}Se, and ^{199}Hg NMR spectra of $[Hg(dppmSe_2)_2](ClO_4)_2$ have been given recently (13); the $dppmSe_2$ behaves in a bidentate manner.

[9]Use of $SPPh_3/Hg(ClO_4)_2 < 3$ also yields $[Hg(SPPh_3)_3](ClO_4)_2$ as the soluble product.

TABLE 1. Selected NMR parameters for $Hg(E'PR'_3)_n(ClO_4)_2$ in CH_2Cl_2[a,b]

E'PR'$_3$	n	T (K)	$\delta_P(\Delta\delta_P)$	$\delta_{Se}(\Delta\delta_{Se})$	δ_{Hg}	^2J(PHg) (Hz)[c]	^1J(PSe)(Δ^1J) (Hz)[d]	$\delta_C(C_1)(\Delta\delta_C)$[e]	^1J(PC)(Δ^1J) (Hz)[e,f]
$SPPh_3$	3	213	47.4 (4.2)		−673	155[g]		126.0 (−7.2)	85 (0)
	4	178	44.2 (1.1)		−565	127		127.4 (−5.8)	86 (1)
$SePPh_3$	3	213	36.5 (0.7)	−72.0[h] (206.2)	−1012	176	544 (−181)	125.2 (−6.5)	78 (1)
	4	178	34.4 (−1.4)	−149.0[i] (131.4)	−971	150[g]	589 (−125)	126.4 (−5.3)	78 (1)
$SPCy_3$	2	213	70.6 (8.0)		−1125	193[g]		37.12 (−0.04)	34 (−11)
	3		68.6 (6.0)		−645	180		36.95 (−0.21)	37 (−8)
	4		67.8 (5.2)		−589	175		37.02 (−0.16)	38[j] (−7)
$SePCy_3$	2	213	67.5 (8.4)	−176.4[k] (292.7)	−1639	206[l]	456 (−208)	36.79 (+0.15)	28 (−12)
	3		66.1 (7.0)	−242.3[m] (226.8)	−1036	188	514 (−150)	36.58 (−0.06)	29 (−11)
	4		63.7 (4.6)	−319.8[n] (149.3)	−1111	185	560 (−104)	36.60 (−0.04)	32 (−8)

[a]Concentration is 0.05 moles per litre of CH_2Cl_2 at room temperature.
[b]^{31}P, ^{77}Se, and ^{199}Hg NMR chemical shifts are quoted relative to 85% H_3PO_4, pure Me_2Se, and pure Me_2Hg at 295 K as external references (see experimental section), with estimated errors of ±0.1, ±0.5, and ±1 ppm or less. ^{13}C NMR chemical shifts are relative to internal TMS with estimated errors of ±0.02 ppm or less. Complexation changes, $\Delta X(X = \delta$ or $J)$, are relative to the free ligand property at the temperature of interest; $\Delta X = X_{complex} - X_{free\ ligand}$.
[c]Estimated error ±2 Hz, except as noted.
[d]Estimated error in ^1J is ±3 Hz.
[e]At 295 K.
[f]Estimated error in ^1J is ±1 Hz, except as noted.
[g]Estimated error ±3 Hz.
[h]^1J(HgSe) = 1270 ± 3 Hz.
[i]^1J(HgSe) = 1130 ± 3 Hz.
[j]Estimated error ±2 Hz.
[k]^1J(HgSe) = 1645 ± 5 Hz.
[l]Estimated error ±5 Hz.
[m]^1J(HgSe) = 1502 ± 4 Hz.
[n]^1J(HgSe) = 1308 ± 3 Hz.

to ^{199}Hg satellites, and the corresponding ^{77}Se NMR spectra are doublets (from ^1J(PSe)) with ^{199}Hg satellites (from ^1J(HgSe)). As a result of ^2J(PHg), the centrebands in the corresponding ^{199}Hg NMR spectra are triplets, quartets, and quintets for two, three, and four E'PR'$_3$ coordinated, respectively, with the SePR'$_3$ complexes showing ^{77}Se satellites from ^1J(HgSe). When the temperature is raised, the ^{199}Hg satellites collapse in the ^{31}P and ^{77}Se NMR spectra, as do the ^2J(HgP) coupling and ^{77}Se satellites in the ^{199}Hg NMR spectra, showing that intermolecular ligand exchange is occurring.

Full ^{13}C NMR data have been deposited.[10] Here we point out only those changes in the free ligand ^{13}C NMR spectra that indicate coordination, as these may be of general utility. As can be seen from the data in Table 1, complexation of $SPPh_3$ or $SePPh_3$ is associated with a marked deshielding of C_1 but negligible change in ^1J(PC), while complexation of $SPCy_3$ or $SePCy_3$ causes a negligible change in $\delta(C_1)$ but a marked reduction in ^1J(PC). For the phosphine selenides, coordination is at least as easily detected by the larger changes observed in ^1J(PSe) and δ_{Se} (see below). However, for the phosphine sulfides only a small change in δ_P may otherwise be available to show coordination. In this case the ^{13}C NMR spectral changes could provide the major evidence for ligation, though in the complexes of interest here the ^{199}Hg NMR spectra provide clear evidence for coordination.

Complexation of Ph_3PSe or Cy_3PSe causes a reduction in the magnitude of ^1J(PSe). At the same time, extensive deshielding of the ^{77}Se resonance occurs. Both of these effects have been observed in earlier NMR studies of phosphine selenide complexes (e.g., refs. 13, 14, 17–19 and references therein). In the series $[Hg(SePCy_3)_n]^{2+}$ (n = 2–4) it is worth noting that both $\Delta\delta_{Se}$ and Δ^1J(PSe) change close to linearly with n. A further point of interest is the remarkable similarity between the values of ^1J(PSe) in the various Hg(II) complexes and those in the analogous complexes of divalent Zn (19) and Cd (14*b*, *c*).

For analogous complexes, $[M(E'PR'_3)_n]^{2+}$, the range of the ^{199}Hg NMR chemical shifts is close to four times that of the ^{113}Cd NMR chemical shifts found (20) for the Cd(II) analogues. More normally this ratio is smaller (21). Particularly unusual is the reversal of chemical shifts found for the complexes $[M(SePCy_3)_n]^{2+}$ (n = 3 or 4). Whereas the ^{113}Cd chemical shifts are $\delta_{4:1} > \delta_{3:1}$, the ^{199}Hg NMR shifts are in the reverse order.[11]

The values of ^2J(PHg) given in Table 1 are ca. 3.5 times larger than the values of ^2J(PCd) found (14*b*, *c*) for the Cd(II) analogues. Grim *et al.* (17) observed a similar ratio for $(n\text{-}Bu_3PSe)_2MBr_2$ (M = Cd or Hg). The ratio seems to indicate a substantial Fermi Contact component for ^2J: we note that for the ground state atoms $|\Psi_{ns}(0)Hg|^2/|\Psi_{ns}(0)Cd|^2$ is ca. 3.3 after relativistic correction (22).

The complexes $[(\mu)\text{-}ER)_3(HgE'PR'_3)_4]^{2+}$

These complexes can be prepared in solution in CH_2Cl_2 according to eq. [1]. This reaction is the exact analogue of that used earlier to prepare $[(\mu\text{-}ER)_6(HgL)_4]^{2+}$ (E = S or Se, L = PR'$_3$ or $AsPh_3$; E = Te, L = PR'$_3$) (9, 10). In the case of ER = SeMe, SePh, and TePh, reaction was indicated by dissolution of the poorly soluble $Hg(ER)_2$. With the four ligands used here (E' = S or Se, R' = Ph or Cy) no dissolution was observed for ER =

[10]Copies may be purchased from the Depository of Unpublished Data, CISTI, National Research Council of Canada, Ottawa, Ont., Canada K1A 0S2.

[11]Both the previous ^{113}Cd data and the current ^{199}Hg NMR data have been double checked.

Can. J. Chem. Downloaded from www.nrcresearchpress.com by 91.144.44.67 on 09/07/12
For personal use only.

TABLE 2. Selected NMR parameters for the cations $[(\mu\text{-ER})_6(HgE'PR'_3)_4]^{2+}$ (E = S or Se) in CH_2Cl_2[a,b]

ER	E'PR'$_3$	T (K)	δ_P	δ_{Hg}	^1J(HgP) (Hz)[c,d]	δ_{Se} ($\Delta\delta_{Se}$)	^1J(PSe)[c,e] (Δ^1J) (Hz)	^1J(HgSe) (Hz)[f]
SPr	$SPPh_3$	213	44.1	−400	[g]			
	$SPCy_3$	178	64.5	−417	112			
	$SePPh_3$	178	34.7	−457	103	−193.3 (86.8)[h]	620 (−93)	1070 ± 1[h]
	$SePCy_3$	178	60.7	−508	128	−381.0 (83.8)[h]	574 (−83)	1080 ± 20[h]
SEt	$SPCy_3$	178	64.4	−411	114			
	$SePCy_3$	178	62.5	−501	128	−379.1 (85.7)[h]	572 (−85)	1080 ± 20[h]
SeMe	$SPCy_3$	213	64.5	−835	108[i]	−209.7[j]		875 ± 20[j]
SePh	$SPPh_3$	213	44.2	−878	[g]	48.5[j]		955 ± 8[j]
	$SePPh_3$	178	35.0	−931	108	−195.0 (88.5)[h]	608 (−105)	[g,h]
						49.9[j]		927 ± 10[j]
	$SPCy_3$	213	65.0	−890	121	53.8[j]		900 ± 10[j]
	$SePCy_3$	213	61.8	−1003	140	−349.0 (120.1)[h]	563 (−101)	1164 ± 25[h]
						62.9[j]		980 ± 8[j]

[a]Concentration 0.05 moles of Hg_4 per litre of CH_2Cl_2 at room temperature.
[b]^{31}P, ^{77}Se, and ^{199}Hg NMR chemical shifts are quoted relative to 85% H_3PO_4, pure Me_2Se, and pure Me_2Hg at 295 K as external references (see experimental section), with estimated errors of ±0.1, ±0.5, and ±1.5 ppm or less. Complexation changes, ΔX ($X = \delta$ or J), are relative to the free ligand properties at the temperature of interest; $\Delta X = X_{complex} - X_{free\ ligand}$.
[c]Measured in the ^{31}P NMR spectrum.
[d]Estimated error ±2 Hz or less, unless noted otherwise.
[e]Estimated error ±3 Hz or less.
[f]Measured in the ^{77}Se NMR spectrum.
[g]Not observed.
[h]For *Se*PR'$_3$.
[i]At 178 K; not observed at 213 K; estimated error ±3 Hz.
[j]For bridging *Se*R.

SPh. The solubility of $Hg(SPh)_2$ is not significantly increased in the 3:1:(4 − n) mixture required for eq. [1], and we could obtain no evidence for $[(\mu\text{-SPh})_6(HgE'PR'_3)_4]^{2+}$. The thiolates $Hg(SR)_2$(R = Et or *n*-Pr) are quite soluble in CH_2Cl_2 at room temperature, but not at reduced temperature. In these two cases, reaction is shown by enhanced solubility of $Hg(SR)_2$ at reduced temperatures. At the concentration used for NMR (0.05 mol/L of CH_2Cl_2) the colours of the solutions are colourless (with SPR'$_3$) to pale yellow (with SePR'$_3$) for the μ-SEt and μ-SPr^n complexes. For both SPR'$_3$ and SePR'$_3$ as terminal ligands, the solutions are yellow for the μ-SeMe and μ-SePh complexes, and yellowish orange for the μ-TePh complexes.

[1] $3Hg(ER)_2 + [Hg(E'PR'_3)_n](ClO_4)_2 + (4 - n)\ E'PR'_3 \rightarrow [(\mu\text{-ER})_6(HgE'PR'_3)_4](ClO_4)_2$

Using multinuclear NMR, a total of 15 new adamantanoid complexes were characterized in solution (ER = SPr^n, SePh, or TePh, E' = S or Se, R' = Ph or Cy; ER = SEt, E' = S or Se, R' = Cy; ER = SeMe, E' = S, R' = Cy). All of these complexes except $[(\mu\text{-SeMe})_6(HgSPCy_3)_4]^{2+}$ were formed cleanly (≥95%) in solution. The ^{31}P spectrum of the μ-SeMe complex contained broad unidentified resonances, but the ^{77}Se and ^{199}Hg NMR spectra showed no extra resonances. We attribute this problem to the absence of pure $Hg(SeMe)_2$ (see Experimental). Selected NMR data for RS- and RSe-bridged clusters are given in Table 2. Table 3 contains data for PhTe-bridged species. The various NMR data are discussed below.

The μ-SePh complexes with SePR'$_3$ showed significant decomposition on standing at or around room temperature, with the formation of red selenium. Most of the SPR'$_3$ complexes seem to be fragile also, but we were able to isolate the salt $[(\mu\text{-TePh})_6(HgSPPh_3)_4](ClO_4)_2$ analytically pure. To our surprise, attempts to isolate $[(\mu\text{-ER})_6(HgE'PR'_3)_4](ClO_4)_2$ with ER = SePh, E'PR'$_3$ = $SPCy_3$ and ER = TePh, E'PR'$_3$ = $SePCy_3$ gave compounds analyzing for $[(\mu\text{-ER})_6(HgE'PR'_3)_3Hg](ClO_4)_2$, for which there is precedent in $[(\mu\text{-TePh})_6(HgPAr_3)_3Hg](ClO_4)_2$ (10). NMR studies of these compounds in solution gave no evidence for $[(\mu\text{-ER})_6(HgE'PR'_3)_3(Hg)]^{2+}$, however; the major component of these solutions was $[(\mu\text{-ER})_6(HgE'PR'_3)_4]^{2+}$. Accordingly we regard their formulations as tentative.

(i) E = Se

The existence of $[(\mu\text{-SePh})_6(HgSePCy_3)_4]^{2+}$ in solution at reduced temperature is evident from a combination of ^{31}P, ^{77}Se, and ^{199}Hg NMR (see Fig. 1 and Table 2). In the ^{31}P NMR spectrum (Fig. 1a) the magnitude of ^1J(PSe) is reduced from the free ligand value, as normally found for coordinated SePR'$_3$ (see above), and in addition a two-bond coupling to ^{199}Hg is observed. The ^{77}Se NMR spectrum contains signals in two regions (Fig. 1b). The singlet from *Se*Ph is in the same general region as for SePh in $[(SePh)_6(HgPR'_3)_4]^{2+}$ (9, 10), and has ^{199}Hg satellites with ^1J(HgSe) comparable to the PR'$_3$ clusters (9, 10). The signal from *Se*PCy$_3$ is a doublet, from ^1J(PSe), less shielded than that of free $SePCy_3$, as expected (see above). A one-bound coupling to ^{199}Hg is observed, which is larger than the coupling to SePh but smaller than the values found for $[Hg(SePCy_3)_4]^{2+}$ (Table 1). The ^{199}Hg NMR spectrum is a doublet, from ^2J(PHg), showing the presence of one $SePCy_3$ per mercury (Fig. 1c). The ^{199}Hg NMR signal is more shielded than those of $[(\mu\text{-SePh})_6(HgPAr_3)_4]^{2+}$ (9, 10) but less shielded than $Hg(SePh)_2$ itself (9). An increase in σ_{Hg} relative to $[(\mu\text{-SePh})_6(HgPAr_3)_4]^{2+}$ is expected from the ^{199}Hg NMR chemical shifts of, say, $[Hg(SePCy_3)_4]^{2+}$ vs. $[Hg(PAr_3)_4]^{2+}$ ($\delta_{Hg}([Hg(SePCy_3)_4]^{2+}) < \delta_{Hg}([Hg(PAr_3)_4]^{2+})$ (Table 1 and ref. 16*b*)), if substituent effects on the $(\mu\text{-SePh})_3HgL$ kernel of the clusters are approximately additive. Selenium-77 satellites

Can. J. Chem. Downloaded from www.nrcresearchpress.com by 91.144.44.67 on 09/07/12
For personal use only.

TABLE 3. Selected NMR parameters for the cations $[(\mu\text{-TePh})_6(HgE'PR'_3)_4]^{2+}$ in CH_2Cl_2[a–c]

E'PR'$_3$	T (K)	δ_P[b]	^1J(PHg) (Hz)[d]	^1J(PSe) (Hz)[d]	δ_{Hg}[b]	δ_{Se}[b]	δ_{Te}[b]	^1J(HgTe) (Hz)[e]
$SPPh_3$	178[f,g]	42.0[h]	70		−1243[h]		−264[h]	3040
		42.4[h]	72		−1228[h]		−175[h]	3240
		45.4[h]	[i]		−1114[h]		−169[h]	3025
		45.6[h]	[i]		−1110[h]		−152[j]	3120
	295	43.8	[i]		[k]		−108	3340
$SePPh_3$	178[f]	34.5[h]	≈85	642	−1307[h]	−225[l]	−254[h]	3530[m]
		≈35.0[h]	[i]	655[n]	−1302[h]	−217[l]	−180[h]	≈3130
		36.4[h]	85	636	−1190[o]	−214[l]	−162[h]	≈3100
		36.7[h]	82	630			≈−143[j,p]	≈3300
	233[q]	35.4	[i]	647	[k]	−216	−127	≈3300
$SPCy_3$	178[f]	63.2[h,r]	108		−1308[h]		−269[h]	3300
		64.3[h,r]	≈96		−1285[h]		−162[h]	3300
		64.5[h,r]	132		−1179[h]		−155[h]	3150
		64.9[h,r]	105		−1127[h]		−148[o,p]	≈3000
							−76[h]	2450
	295	64.2	[i]		[k]		−112	3250
$SePCy_3$	178[s]	59.6[t]	[i]	[y]	−1368[u]	−381[h,v]	−244[w]	[y]
		60.4[t]	[i]	[y]	−1322[t]	−365[h,x]	−181[w]	[y]
		≈61[w]	[i]	[y]	−1281[v]		−159[w]	[y]
		61.7[w]	[i]	[y]	−1252[t,w]		−153[w]	[y]
		62.3[w]	[i]	[y]	−1214[v]		−138[w]	[y]
		63.4[w]	[i]	[y]			−115[t]	[y]
							−82[t]	[y]
							−57[w]	3180[m]
	273[q]	61.3[t]	[i]	603	−1330	−362	−119	3100

[a]Concentration 0.05 moles of Hg_4 per litre of CH_2Cl_2 at room temperature; ^{31}P, ^{77}Se, ^{199}Hg, and ^{125}Te NMR chemical shifts are quoted relative to 85% H_3PO_4, pure Me_2Se, pure Me_2Hg, and pure Me_2Te at 295 K as external references (see experimental section) with estimated errors of ±0.1, ±0.5, ±1.5, and ±2 ppm or less, except as noted.

[b]Where multiple resonances are observed, the correlation between ^{31}P, ^{77}Se, ^{125}Te, and ^{199}Hg resonances is not known.

[c]See text.

[d]Measured in the ^{31}P NMR spectrum, except as noted; estimated errors ±3 Hz or less, except as noted.

[e]As measured in the ^{125}Te NMR spectrum; estimated errors ±50 Hz or less, except as noted.

[f]Probably a C_1 isomer (see text).

[g]At 193 K six approximately equally intense ^{125}Te NMR signals are observed: $\delta_{Te}(^1J(HgTe))$ = −252(3560 ± 75), −166(3180 ± 75), −161(3050 ± 75), −147(3160 ± 75), −145(3200 ± 75), −141(3150 ± 100). At this temperature two ^{31}P NMR signals (δ_P = 42.4, 45.4) and three ^{199}Hg signals (δ_{Hg} = −1248, −1240, −1120, approximate relative intensities 1,1, and 2) are seen.

[h]Relative intensity ≈1.

[i]Not observed.

[j]Relative intensity ≈3.

[k]Too broad to be observed.

[l]In order of decreasing ^{77}Se shielding, ^1J(PSe) and approximate relative intensity = 644 ± 15 and 2, 624 ± 10 and 1, 644 ± 10 Hz and 2.

[m]Estimated error ±100 Hz.

[n]Estimated error ±6 Hz.

[o]Relative intensity ≈2.

[p]Broad resonance: probable signal overlap.

[q]This sample decomposes at 295 K.

[r]At 173 K.

[s]Possibly a mixture of a C_1 isomer and a C_3 isomer (see text).

[t]Tentatively assigned to a C_3 isomer.

[u]Estimated error ±2 ppm.

[v]^1J(PSe) ≈600 Hz.

[w]Tentatively assigned to a C_1 isomer.

[x]^1J(PSe) ≈640 Hz.

[y]Could not be measured with certainty.

are expected in the ^{199}Hg NMR spectrum, with coupling to both *Se*PCy$_3$ and *Se*Ph, but these are weak and somewhat broad and consequently it is easier to measure the values of ^1J(HgSe) in the ^{77}Se NMR spectrum.

The NMR data for $[(\mu\text{-SePh})_6(HgSePCy_3)_4]^{2+}$ at reduced temperature show that the cation has the adamantane-like structure. The NMR spectra are simpler than expected for the static C_1 or C_3 symmetries that are possible for $(\mu\text{-ER})_6M_4$ (see Introduction) showing that inversion at the bridging selenium atom is rapid on the NMR time scale. Further confirmation of the proposed formulation was obtained by observing the number of species in $[(\mu\text{-SePh})_6(HgSePCy_3)_4]^{2+}$:$[(\mu\text{-SePh})_6(HgPPh_3)_4]^{2+}$ mixtures. The PPh_3 complex has been characterized unambiguously by NMR in earlier work (9). In the mixtures a total of five species occur. This is just as expected for redistribution of terminal ligands between the two tetranuclear clusters, thereby confirming the formulation of the $SePCy_3$ species. The ^{31}P, ^{77}Se, and ^{199}Hg NMR spectra of

Can. J. Chem. Downloaded from www.nrcresearchpress.com by 91.144.44.67 on 09/07/12
For personal use only.

Can. J. Chem. Downloaded from www.nrcresearchpress.com by 91.144.44.67 on 09/07/12
For personal use only.

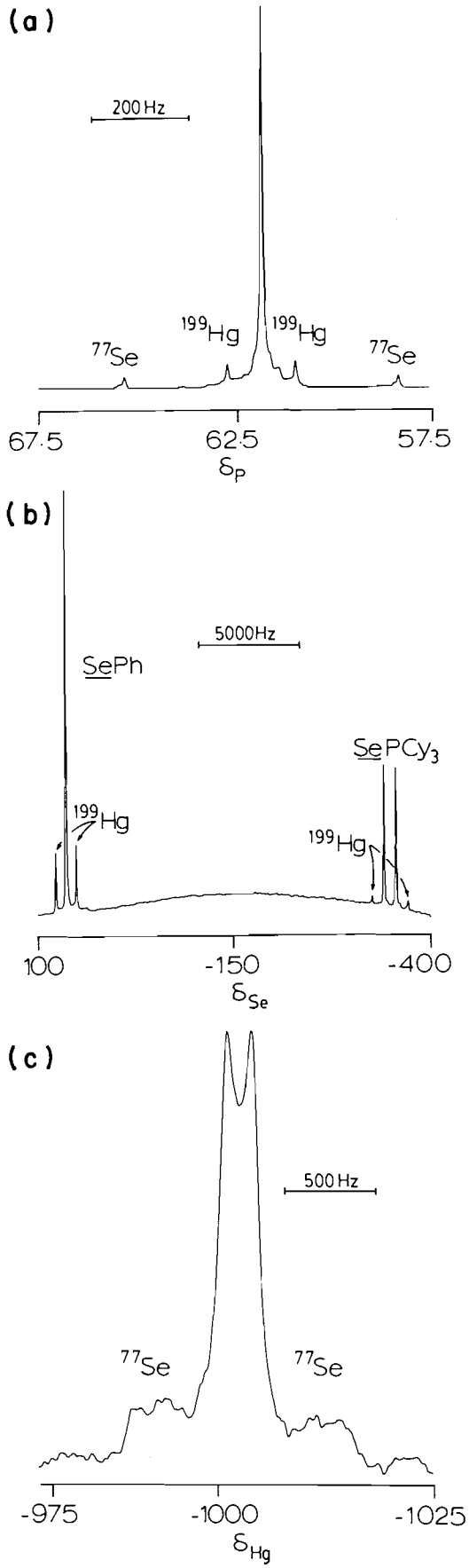

FIG. 1. NMR spectra of $[(\mu\text{-SePh})_6(HgSePCy_3)_4]^{2+}$ in CH_2Cl_2 at 213 K: (a) 80.98 MHz ^{31}P; (b) 38.15 MHz ^{77}Se; (c) 35.75 MHz ^{199}Hg.

$[(SePh)_6(HgPPh_3)_{4-n}(SePCy_3)_n]^{2+}$ can be analyzed straightforwardly and the results are included in Table 4. The ^{31}P and ^{77}Se NMR spectra of a mixture with n = 2(ave) have been deposited.[10]

When the temperature of $[(\mu\text{-SePh})_6(HgSePCy_3)_4]^{2+}$ is raised from 213 K, the two-bond P–Hg coupling collapses by ca. 238 K and both one-bond Hg–Se couplings collapse by ca. 243 K. Cleavage of both types of Hg–Se bonds must be rapid on the ^2J and ^1J time scales by 243 K. We note that both ^{77}Se resonances become less shielded as the temperature is raised. Decomposition to red Se starts to occur at ca. 273 K.

The various NMR spectra of $[(\mu\text{-SePh})_6(HgSePPh_3)_4]^{2+}$ at 178 K resemble closely those of the $SePCy_3$ cluster at 213 K. They can be analyzed similarly in terms of an adamantanoid skeleton with rapid inversion at μ-Se, and the results are given in Table 2. In the $SePPh_3$ complex ^2J(PHg) is collapsed by ca. 213 K, showing that the intermolecular ligand exchange is faster than for the $SePCy_3$ analogue. By 233 K, the *Se*PPh_3 doublet in the ^{77}Se NMR spectrum is broad. The *Se*Ph signal still shows ^{199}Hg satellites, but these too are collapsed by ca. 253 K.

The reduced temperature ^{31}P, ^{77}Se, and ^{199}Hg NMR spectra of $[(SePh)_6(HgSPR'_3)_4]^{2+}$ (R′ = Ph or Cy) show sufficient features in common with their $SePR'_3$ analogues that they can also be assigned the same (time-averaged) structure. Details of the spectra are included in Table 2. In the SPR'_3 complexes σ_{Hg} is less than in the corresponding $SePR'_3$ complexes, as it is in mononuclear $[Hg(E'PR'_3)_n]^{2+}$ also (Table 1). The coupling ^2J(PHg) could not be observed for $[(\mu\text{-SePh})_6(HgSPPh_3)_4]^{2+}$ at any temperature. In the $SPCy_3$ analogue this coupling is observed but it has collapsed by ca. 253. In both cases ^1J(HgSe) is observed up to ca. 273 K. For $[(\mu\text{-SePh})_6(HgSPCy_3)_4]^{2+}$, tetranuclearity is confirmed by the occurrence of a total of five species in $[(\mu\text{-SePh})_6(HgSPCy_3)_4]^{2+}$:$[(\mu\text{-SePh})_6(HgPPh_3)_4]^{2+}$ mixtures. The NMR spectra of $[(\mu\text{-SePh})_6(HgPPh_3)_{4-n}(HgSPCy_3)_n]^{2+}$ are summarized in Table 4.

The ^{31}P NMR spectrum of $[(\mu\text{-SeMe})_6(HgSPCy_3)_4]^{2+}$ at 213 K is a singlet with ^{199}Hg satellites from ^2J(PHg). The ^{199}Hg NMR spectrum shows the doublet splitting expected for one terminal ligand. In the ^{77}Se NMR spectrum, the signal from μ-SeMe is less shielded than found for the μ-SePh clusters described above, occurring close to the region ascribed to μ-SeMe in $[(\mu\text{-SePh})_{6-x}(\mu\text{-SeMe})_x(ZnI)_4]^{2-}$ (3*b*). The μ-SeMe signal shows ^{199}Hg satellites, with ^1J(HgSe) comparable to that of the μ-SePh complexes. Clearly the μ-SeMe species has the adamantane-like structure, and again the comparative simplicity of the NMR spectra are explicable in terms of rapid inversion at μ-SeMe.

(ii) E = S

A complete series of complexes $[(\mu\text{-SR})_6(HgE'PR'_3)_4]^{2+}$ was characterized with the stereotypical alkanethiolate PrS^-, and in addition the complexes $[(\mu\text{-SEt})_6(HgE'PCy_3)_4]^{2+}$ (E′ = S or Se) were examined. Details of the various NMR spectra are given in Table 2.

Except for the absence of a signal from the bridging group in their ^{77}Se NMR spectra, the various low temperature NMR spectra of $[(\mu\text{-SPr})_6(HgSePR'_3)_4]^{2+}$ (R′ = Ph or Cy) show the same features as do the RSe-bridged analogues (Table 2 and discussion above). Evidently the cations have the same (time-averaged) structure. This conclusion can be drawn for $[(\mu\text{-SEt})_6(HgSePCy_3)_4]^{2+}$ also. Mercury-199 is less shielded in the μ-SPr complexes than in the corresponding μ-SePh species, as expected from earlier results for $[(\mu\text{-ER})_6(PR'_3)_4]^{2+}$ (9).

TABLE 4. NMR spectra of the complexes $[(\mu\text{-SePh})_6(HgPPh_3)_{4-n}(HgL)_n]^{2+}$ (L = $SPCy_3$ or $SePCy_3$) in CH_2Cl_2 at 213 K[a]

n	$\delta_P(PPh_3)$[b]	δ_{Se}[c]			δ_{Hg}[d]		$^1J(HgP)$[e] (Hz)	$^1J(HgSe)$[f] (Hz)	$^3J(HgP)$[g,h] (Hz)	$^4J(PP)$[g] (Hz)
0	32.5	6.5[i,j]			−693		2963	940 ± 30	50	16
(a) L = $SPCy_3$										
1[k]	34.8	−8.2[i,l]	27.6[l,m]		−632[n]	≈−900[o]	2952	900 ± 30, 940 ± 30	61[p]	17
2[k]	36.0	−20.3[i,l]	23.5[m,q]	58.7[l,r]	−618[n]	≈−899[o]	2992	≈900, 910 ± 20, 950 ± 30	(92)	20
3[k]	37.2		9.8[l,m]	60.3[l,r]	−572[n]	−891[o]	3025	910 ± 50, 943 ± 15	(108)	
4[k]				53.9[r]		−890				
(b) L = $SePCy_3$										
1[s]	33.7	−7.4[i,l,t]	31.6[l,m]		−661[n]	≈−1000[o]	2880	≈900, ≈900	58, (54)	16
		(−345)[u]						(570 ± 15)[u]		
2[s]	34.7	−18.6[i,l,v]	24.6[m,q]	69.1[l,r]	−640[n]	≈−1000[o]	2810	≈900, 950 ± 25, 1025 ± 250	59, (74)	18
		(−340)[u]						(565 ± 15)[u]		
3[s]	37.1		8.2[l,m,w]	72.9[l,r]	−602[n]	≈−1000[o]	2761	925 ± 25, 1000 ± 15	(87)	
		(−341)[u]						(560 ± 15)[u]		
4[s]				63.5[r]				975 ± 15		
		(−349)[u]				≈−1000[o]		(565 ± 15)[u]		

[a]Concentration 0.05 moles per litre of CH_2Cl_2 at room temperature.
[b]Relative to external 85% H_3PO_4 at 295 K; estimated error of ±0.1 ppm.
[c]Relative to external pure Me_2Se at 295 K; estimated error ±0.2 ppm.
[d]Quoted relative to external pure Me_2Hg at 295 K (see experimental section); estimated error ±1 ppm.
[e]Estimated error ±2 Hz.
[f]Given in the same order as δ_{Se}.
[g]Estimated error ±1 Hz.
[h]Values in parentheses are for coupling to $HgEPCy_3$.
[i]For Se with two geminal PPh_3 ligands, $Ph_3PHgSeHgPPh_3$.
[j]$^2J(PSe) + {}^4J(PSe) \approx {}^2J(PSe) \approx 29$ Hz.
[k]In all the complexes $\delta_P(SPCy_3) = 65.1$, $^2J(PSHg) = 129 \pm 2$ Hz.
[l]Relative intensity ≈1.
[m]For Se with one geminal PPh_3 and one geminal $EPCy_3$ ligand, $Ph_3PHgSeHgEPCy_3$.
[n]Assigned to the grouping $(Se)_3HgPPh_3$.
[o]Assigned to the grouping $(Se)_3HgEPCy_3$.
[p]Average of couplings to $HgEPCy_3$ and $HgPPh_3$.
[q]Relative intensity ≈4.
[r]For Se with two geminal $EPCy_3$ ligands, $Cy_3PEHgSeHgEPCy_3$
[s]In all the complexes $\delta_P(SePCy_3) = 61.9$, $^2J(PSeHg) = 148 \pm 2$ Hz, $^1J(PSe) = 562 \pm 2$ Hz.
[t]$2(^2J(PSe)) + {}^4J(PSe) \approx 2(^2J(PSe)) \approx 56$ Hz.
[u]Values given in parentheses are for $SePCy_3$.
[v]$^2J(PSe) = 33 \pm 3$ Hz.
[w]$^2J(PSe) = 23 \pm 3$ Hz.

The $^2J(PHg)$ coupling found in the NMR spectra of $[(\mu\text{-SPr})_6(HgSePR'_3)_4]^{2+}$ at 178 K has collapsed by ca. 213 K showing the occurrence of intermolecular exchange of $SePR'_3$. The ^{77}Se resonances broaden and become less shielded as the temperature is raised. This change is particularly large for the $SePCy_3$ complex for which δ_{Se} changes from −381 to −329 as the temperature is changed from 178 K to 298 K. A chemical shift of −329 ppm is close to that of $Hg(SePCy_3)_4]^{2+}$ (−320 ppm (Table 1)). This might be taken to indicate dissociation of $[(\mu\text{-SPr})_6(HgSePCy_3)_4]^{2+}$ to $Hg(SPr)_2$ and $[Hg(SePCy_3)_4]^{2+}$ at 298 K. However, on the basis of ^{13}C NMR spectra in the aliphatic region (Table 5) the extent of dissociation to give free $Hg(SPr)_2$ appears to be slight for any of the μ-SPr species. The ^{13}C NMR spectra of the complexes do not change a great deal from low to ambient probe temperature and are at all times quite distinct from the spectrum of $Hg(SPr)_2$. For comparison, Table 5 includes data for $[(\mu\text{-SPr})_6(HgPPh_3)_4](ClO_4)_2$ and $[(\mu\text{-SPr})_6(HgPPh_3)_4](O_2CCF_3)_2$. Both these salts contain undissociated $[(\mu\text{-SPr})_6(HgPPh_3)_4]^{2+}$ at 213 K. At ambient probe temperature this cation persists as the ClO_4^- salt, but as the $CF_3CO_2^-$ salt is extensively dissociated to $Hg(SPr)_2$ and $[Hg(PPh_3)_4]^{2+}$ (9).

Less NMR information is available for $[(\mu\text{-SPr})_6(HgSPR'_3)_4]^{2+}$ than for other complexes included in this study. Nevertheless, the similarity between the ^{13}C NMR spectra of $[(\mu\text{-SPr})_6(HgSPR'_3)_4]^{2+}$ and $[(\mu\text{-SPr})_6(HgSePR'_3)_4]^{2+}$ (Table 5), and a comparison of the pattern of ^{199}Hg chemical shifts for the series $[(\mu\text{-SPr})_6(HgE'PR'_3)_4]^{2+}$ and $[(\mu\text{-SePh})_6(HgE'PR'_3)_4]^{2+}$ (Table 2), leave little doubt that $[(\mu\text{-SPr})_6(HgSPR'_3)_4]^{2+}$ is the correct formulation.

(iii) E = Te

The complexes $[(\mu\text{-TePh})_6(HgE'PR'_3)_4]^{2+}$ show much more complicated NMR spectral behaviour at reduced temperature than do their S- and Se-bridged analogues. This additional complexity can be accounted for in terms of slow inversion at the bridging tellurium, a phenomenon we have demonstrated recently for $[(\mu\text{-TeR})_6(HgPR'_3)_4]^{2+}$ and $[(\mu\text{-TePh})_6(HgPAr_3)_3(Hg)]^{2+}$ (10). When inversion at Te is slow on the NMR time scale, separate NMR spectra can be observed for

Can. J. Chem. Downloaded from www.nrcresearchpress.com by 91.144.44.67 on 09/07/12
For personal use only.

TABLE 5. Carbon-13 NMR spectra of *n*-propylthiolate in some Hg(II) species[a,b]

Compound	T (K)	δ_C[c] C_1	C_2	C_3
$Hg(SPr)_2$	295[d,e]	31.0_8	31.0_0	13.5
	298[e,f]	31.6	30.7	13.6
$[(\mu\text{-}SPr)_6(HgSPPh_3)_4](ClO_4)_2$[d]	178	34.6[g]	28.9	13.9
	295	34.8	29.5	13.5
$[(\mu\text{-}SPr)_6(HgSePPh_3)_4](ClO_4)_2$[d]	178	34.6[g]	28.9	13.5
	273[h]	35.0	29.3	13.5
$[(\mu\text{-}SPr)_6(HgSPCy_3)_4](ClO_4)_2$[d]	295	34.2	29.9	13.5
	178	34.8	29.8	13.9
$[(\mu\text{-}SPr)_6(HgSePCy_3)_4](ClO_4)_2$[d]	295	33.5	30.2	13.5
	178	34.8	29.9	14.1
$[(\mu\text{-}SPr)_6(HgPPh_3)_4](ClO_4)_2$[f]	298	34.0	30.0	13.4
	213	34.9	29.8	13.5
$[(\mu\text{-}SPr)_6(HgPPh_3)_4](O_2CCF_3)_2$[f,i]	298	31.3	30.5	13.5
	213	34.9	29.8	13.5

[a]In CH_2Cl_2 as solvent, except as noted.
[b]Concentration 0.05 moles of compound per litre of solvent at room temperature.
[c]Estimated error ±0.1 ppm or less, except as noted.
[d]This work.
[e]$Hg(SPr)_2$ is insufficiently soluble in CH_2Cl_2 or $CDCl_3$ for reduced temperature spectra to be obtained.
[f]In $CDCl_3$ as solvent; previously unpublished data of P. A. W. Dean, J. J. Vittal, and M. H. Trattner.
[g]Estimated error ±0.2 ppm.
[h]This complex decomposes at 295 K.
[i]In a mixture where $Hg(SPr)_2$:$Hg(O_2CCF_3)_2$:PPh_3 = 3:1:4.

the isomer(s) (see Introduction) occurring in the equilibrium mixture. In the slow exchange limit, each of the two isomers of C_1 symmetry should give rise to four ^{31}P NMR signals, four ^{199}Hg NMR signals, and six ^{125}Te NMR signals, while the corresponding numbers for each of the isomers of C_3 symmetry are two (relative intensities 3 and 1), two (relative intensities 3 and 1), and two (relative intensities 3 and 3) (10). It is possible for the spectra of any of these isomers to be simplified by intra- and (or) inter-molecular exchange, e.g., ref. 10.

Figures 2a and b show that ^{31}P and ^{199}Hg NMR spectra of $[(\mu\text{-}TePh)_6(HgSPCy_3)_4]^{2+}$ at 173 and 178 K (the temperatures of best resolution), respectively. The ^{31}P spectrum shows four major centreband signals, with ^{199}Hg satellites.[12] Four major signals are seen in the ^{199}Hg NMR spectrum also, three of them with clear $^2J(PHg)$ coupling. Evidently the cation exists predominantly as one C_1 isomer under these conditions. In the ^{125}Te NMR spectrum at 178 K (Fig. 2c) there are five signals covering the range δ_{Te} −76 to −269, with ^{199}Hg satellites. Six ^{125}Te NMR signals are expected for a C_1 isomer, but one of the observed resonances (δ_{Te} −148) is comparatively broad, indicating probable partial overlap of two signals. The ^{125}Te NMR spectrum collapses as the temperature is raised until, at temperatures above 253 K, only a single ^{125}Te resonance with one pair of ^{199}Hg satellites is found. Above 253 K, inversion at Te must be rapid on the time scale of δ_{Te}. The ^{199}Hg NMR spectrum broadens also as the temperature is raised. In this case site exchange must still be occurring at an intermediate rate at 295 K, since the ^{199}Hg resonance is unobservably broad at this

[12]The small signal at δ_P = 62.8 may indicate the presence of a minor isomer.

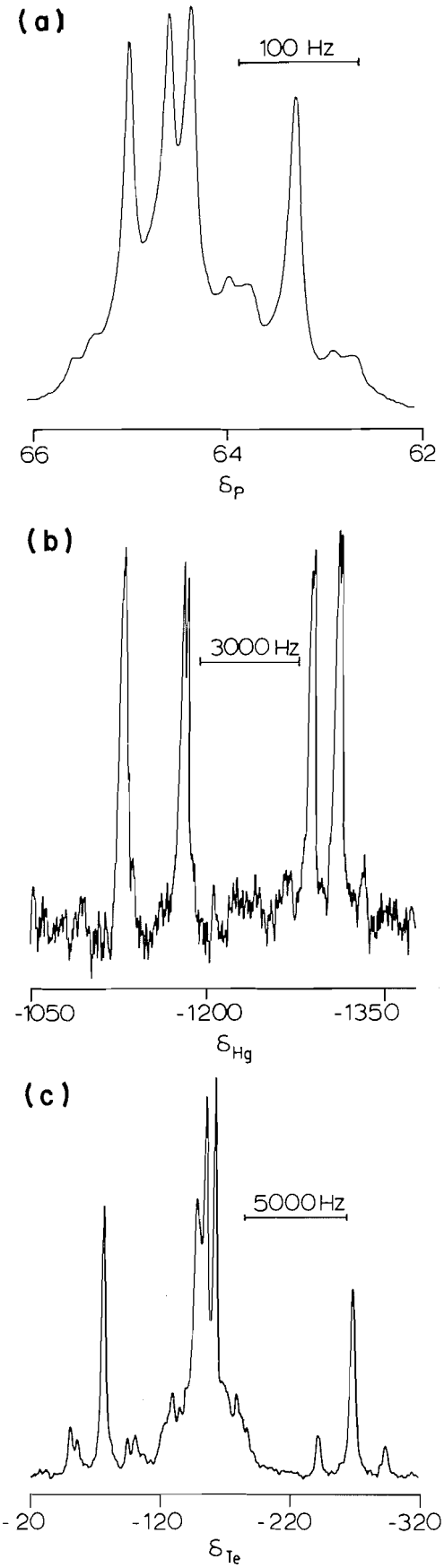

FIG. 2. NMR spectra of $[(\mu\text{-}TePh)_6(HgSPCy_3)_4]^{2+}$ in CH_2Cl_2: (a) 80.98 MHz ^{31}P at 173 K; (b) 35.75 MHz ^{199}Hg at 178 K; (c) 63.14 MHz ^{125}Te at 178 K.

Can. J. Chem. Downloaded from www.nrcresearchpress.com by 91.144.44.67 on 09/07/12
For personal use only.

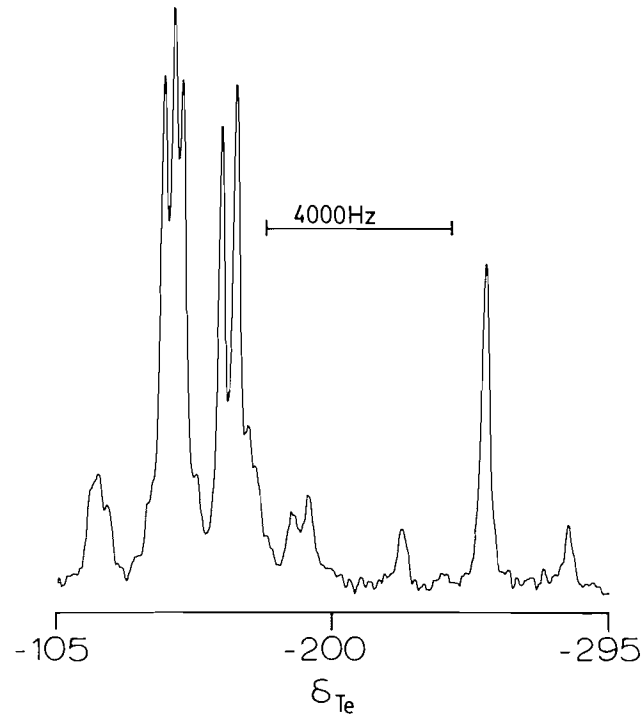

FIG. 3. 63.14 MHz ^{125}Te NMR spectrum of $[(\mu\text{-TePh})_6(HgSPPh_3)_4]^{2+}$ in CH_2Cl_2 at 193 K.

temperature. The ^{31}P NMR spectrum collapses to a singlet with no ^{199}Hg satellites around 213 K, indicating the occurrence of rapid intermolecular exchange of $SPCy_3$. The NMR spectra of $[(\mu\text{-TePh})_6(HgSPCy_3)_4]^{2+}$ are summarized in Table 3.

The NMR spectroscopic behaviour of $[(\mu\text{-TePh})_6(HgSPPh_3)_4]^{2+}$ is generally very similar to that of the $SPCy_3$ analogue, and the analysis is identical. An important difference is the observation of six clear resonances in the ^{125}Te NMR spectrum at 193 K, as shown in Fig. 3. This spectrum provides strong evidence for an adamantanoid cation of C_1 symmetry. At 178 K, the three highest frequency ^{125}Te NMR signals overlap. However, the ^{31}P and ^{199}Hg NMR spectra at 178 K are consistent with C_1 symmetry: both show four major resonances. As the temperature is raised, the spectra of the $SPPh_3$ cluster collapse in essentially the same manner described for the SPCy complex. Representative NMR data for the $SPPh_3$ cation are included in Table 3.

The ^{31}P NMR spectrum of $[(\mu\text{-TePh})_6(HgSePPh_3)_4]^{2+}$ at 178 K shows four resonances, as expected for a species of C_1 symmetry. The corresponding ^{125}Te and ^{199}Hg NMR spectra of $[(\mu\text{-TePh})_6(HgSePPh_3)_4]^{2+}$ are also consistent with this symmetry, though three of the expected six ^{125}Te resonances overlap (cf. for the $SPPh_3$ complex at 178 K), as do two of the expected four ^{199}Hg signals. For C_1 symmetry, four different doublets (from ^1J(PSe)) are expected in the ^{77}Se NMR spectrum also. In fact, three are found, one approximately twice as intense as the other two. Clearly two of the expected resonances are isochronous. Table 3 shows NMR data for this complex. As can be seen from the data given, the multiple ^{31}P and ^{125}Te signals collapse to singlets, with and without ^{199}Hg satellites, respectively, as the temperature is raised. Similarly, the three doublets of the low temperature ^{77}Se NMR spectrum are reduced to a single doublet. The ^{199}Hg NMR spectrum is unobservably broad at 233 K (above which decomposition becomes apparent). Once more, fast Te inversion and intermolecular exchange of the terminal ligands must be occurring.

The NMR spectra of $[(\mu\text{-TePh})_6(HgSePCy_3)_4]^{2+}$ are more complicated than those of the μ-TePh complexes already discussed. Typical NMR results are given in Table 3. At 178 K, the ^{77}Se NMR spectrum contains only two doublets (from ^1J(PSe)). These are broad, almost certainly as a result of signal overlap. The corresponding ^{31}P, ^{125}Te, and ^{199}Hg NMR spectra contain six, eight, and five resonances, respectively. Such results are inconsistent with the presence of any single isomer (see above) or with a mixture of the two C_3 isomers. The spectra are consistent with a mixture of a C_1 isomer and a C_3 isomer, and we have made tentative assignments on this basis, primarily from approximate relative intensities. Independent of the exact assignments, the ^{125}Te NMR spectrum shows that the population ratio C_1/C_3 is ca. 3. By 273 K, complete time-averaging occurs for all of the various nuclei. Above ca. 273 K, the complex is thermally unstable.

1. K. S. HAGEN and R. H. HOLM. Inorg. Chem. **22**, 3171 (1983); K. S. HAGEN, D. W. STEPHAN, and R. H. HOLM. Inorg. Chem. **21**, 3928 (1982).
2. J. L. HENCHER, M. KHAN, F. F. SAID, and D. G. TUCK. Polyhedron, **4**, 1261 (1985).
3. P. A. W. DEAN and J. J. VITTAL. (*a*) Inorg. Chem. **25**, 514 (1986); (*b*) Inorg. Chem. **26**, 278 (1987); (*c*) Can. J. Chem. **66**, 2443 (1988).
4. P. A. W. DEAN, J. J. VITTAL, and N. C. PAYNE. Inorg. Chem. **26**, 1683 (1987).
5. I. G. DANCE. Polyhedron, **5**, 1037 (1986), and references therein.
6. D. COUCOUVANIS, M. KANATZIDIS, E. SIMHON, and N. C. BAENZIGER. J. Am. Chem. Soc. **104**, 1874 (1982).
7. D. FENSKE, J. MEYER, and K. MERZWEILER. Z. Naturforsch. **42**(B), 1207 (1987).
8. G. CHRISTOU, K. FOLTING, and J. C. HUFFMAN. Polyhedron, **3**, 1247 (1984).
9. P. A. W. DEAN, J. J. VITTAL, and M. H. TRATTNER. Inorg. Chem. **26**, 4245 (1987).
10. P. A. W. DEAN, V. MANIVANNAN, and J. J. VITTAL. Inorg. Chem. **28**, 2360 (1989).
11. R. K. HARRIS. Nuclear magnetic resonance spectroscopy. Pitman, London. 1983. p. 230.
12. K. BRODERSEN and H.-U. HUMMEL. *In* Comprehensive coordination chemistry. Vol. 5. *Edited by* G. Wilkinson, R. D. Gillard, and J. A. McCleverty. Pergamon, Oxford. 1987. Chap. 56.2, and references therein.
13. A. M. BOND, R. COLTON, and J. EBNER. Inorg. Chem. **27**, 1697 (1988).
14. (*a*) P. A. W. DEAN. Can. J. Chem. **57**, 754 (1979); (*b*) P. A. W. DEAN and M. K. HUGHES. Can. J. Chem. **58**, 180 (1980); (*c*) P. A. W. DEAN and L. POLENSEK. Can. J. Chem. **58**, 1627 (1980).
15. Y. OKAMOTO and T. YANO. J. Organometal. Chem. **29**, 99 (1971).
16. T. ALLMAN and R. G. GOEL. (*a*) Can. J. Chem. **62**, 615 (1984); (*b*) Can. J. Chem. **62**, 621 (1984).
17. S. O. GRIM, E. D. WALTON, and L. C. SATEK. Can. J. Chem. **58**, 1476 (1980).
18. I. J. COLQUHOUN and W. MCFARLANE. J. Chem. Soc. Dalton Trans. 658 (1981).
19. P. A. W. DEAN and G. K. CARSON. Can. J. Chem. **61**, 1800 (1982).
20. P. A. W. DEAN. Can. J. Chem. **59**, 3221 (1981).
21. R. J. GOODFELLOW. *In* Multinuclear NMR. *Edited by* J. Mason. Plenum, New York. 1987. Chap. 21.
22. C. J. JAMESON. *In* Multinuclear NMR. *Edited by* J. Mason. Plenum, New York. 1987. Chap. 4. Fig. 3.

Can. J. Chem. Downloaded from www.nrcresearchpress.com by 91.144.44.67 on 09/07/12
For personal use only.

Characterization and spectroelectrochemical properties of a binuclear *trans,trans*-bis(ferrocenylidene)acetone $[(C_5H_5)Fe(C_5H_4CHCH)]_2CO$

PIERRE D. HARVEY[1] AND JEFF G. SHARMAN

Département de chimie, Université de Sherbrooke, Sherbrooke (Québec), Canada J1K 2R1

Received March 28, 1989

PIERRE D. HARVEY and JEFF G. SHARMAN. Can. J. Chem. **68**, 223 (1990).

The binuclear compound *trans,trans*-bis(ferrocenylidene)acetone $[(C_5H_5)Fe(C_5H_4CHCH)]_2CO$ (dFca) has been synthesized in quantitative yield and characterized by FT-IR, ^1H and ^{13}C NMR, and mass spectroscopy. Cyclic voltammetry and coulometry measurements suggest that a reversible two-electron oxidative process takes place at 0.68 V vs. SSCE. FT-IR and UV–VIS spectroelectrochemical analyses show that this oxidative process occurs at the ferrocenyl centers. The compound is also found to be emissive in the solid state (λ_{max} = 780 nm), and charge transfer assignments for the lowest singlet and triplet excited states are made.

Key words: ferrocenyl, spectroelectrochemistry, electronic charge transfer, emission spectroscopy.

PIERRE D. HARVEY et JEFF G. SHARMAN. Can. J. Chem. **68**, 223 (1990).

Le complexe binucléaire *trans,trans*-bis(ferrocenylidène)acétone $[(C_5H_5)Fe(C_5H_4CHCH)]_2CO$ (dFca) a été synthétisé avec un rendement quantitatif et a été caractérisé par FT-IR, ^1H et ^{13}C RMN et spectroscopie de masse. Les mesures de voltamétrie cyclique et de coulométrie suggèrent qu'un processus oxydatif réversible de deux électrons survient à 0,68 V vs. SSCE. Les analyses spectroélectrochimiques FT-IR et UV–VIS montrent que ces processus surviennent aux centres ferrocènyliques. Une émission (λ_{max} = 780 nm) pour le composé à l'état solide est montrée, et des attributions de type de transfert de charge sont données pour les états singulet et triplet de plus basse énergie.

Mots clés : ferrocenyl, spectroélectrochimie, transfert de charge électronique, spectroscopie d'émission.

Can. J. Chem. Downloaded from www.nrcresearchpress.com by 91.144.44.67 on 09/07/12
For personal use only.

Introduction

The cross-conjugated diarylideneacetone ligands (Ar—CH=CH—(CO)—CH=CH—Ar) are capable of forming a few stable organometallic compounds both in the solid state and in solutions (1–9). In the non-complexed state, they generally exhibit rich photochemical (9–12), electrochemical (12–14), and photoluminescent properties (12).[2] Recent resonance Raman, UV–VIS, and emission spectroscopic investigations of the binuclear Pd(O)– and Pt(O)–dibenzylideneacetone complexes reveal the metal-to-ligand charge transfer (MLCT) character of the lowest singlet and triplet excited states (15). Further studies have shown that these binuclear compounds appear photochemically inert (12). We have undertaken the synthesis and study of a series of new diarylideneacetone ligands where the aryl groups are either photo- or electroactive in order to tune photoreactivity in organo-transition binuclear Pd(O) and Pt(O) complexes (12).

We wish to report our recent results on the newly synthesized electroactive *trans,trans*-bis(ferrocenylidene)acetone $[(C_5H_5)Fe(C_5H_4CHCH)]_2CO$ (dFca) (see structure in Scheme 1). We chose the ferrocene-based substituent (Fc), because ferrocene-centered oxidations should be reversible (16). There are many examples of spectroscopic property and reactivity changes induced in a metal center by reduction of a pendant redox-active substituent (17–19). In this paper, it is shown that inductive perturbation is indeed felt along the dienylketone moiety upon change of state of charge of the ferrocenes. The dFca compound also exhibits low-energy emission in the solid state, and appears to be reasonably photochemically stable.

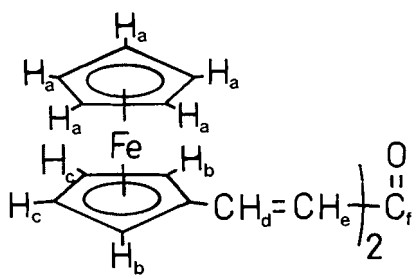

SCHEME 1. Structure of dFca.

Experimental

Chemicals

Ferrocenealdehyde ($[(C_5H_5)Fe(C_5H_4CHO)]$) (Aldrich Chem. Co.) was used as received. Acetone, ethanol, methylene chloride, carbon tetrachloride (Anachemia), tetrahydrofuran (THF), and 2-methyltetrahydrofuran (2MeTHF; Aldrich Chem. Co.) were purified according to standard procedures (20, 21). The spectrograde solvents benzene, ethyl acetate, acetone, ethyl ether, and chloroform (Fisher) were used as received; purity was checked by UV–VIS spectroscopy. Chloroform-*d* and benzene-d_6 (Aldrich Chem. Co.) were also used as received. Tetra-*n*-butylammonium hexafluorophosphate (TBA(PF_6); Aldrich Chem. Co.) was recrystallized three times from ethanol, and tetraethylammonium perchlorate (TEAP) was prepared according to literature procedures (22).

Instruments

The ^1H and ^{13}C NMR spectra were obtained on a Bruker WM 250 spectrometer at room temperature; they were recorded with reference to the deuterium signal of $CDCl_3$ and they are reported with reference to TMS (see Table 1). The mass spectra were collected on a VG ZAB-1F spectrometer in EI mode at 70 eV. The FT-IR spectra were measured on a BOMEM DA 3.002 spectrometer. The UV–VIS data were acquired on a Perkin–Elmer Lambda 3B spectrophotometer. The emission spectra measurements were made on an Instruments SA Raman spectrometer equipped with a U-1000 Jobin–Yvon 1.0 m double monochromator using the 647.088 nm red line of a Spectra Physics krypton ion laser for excitation. A 200 W Rayonet photochemical reactor was used for the photolysis.

Electrochemistry

Electrochemical measurements were made with a PAR model 173 potentiostat, a model 175 voltage programmer, and a current follower model 176 and were recorded on a EG & G Princeton Research model RE 0089 X–Y recorder. Cyclic voltammograms were measured

[1]Author to whom correspondence should be addressed.

[2]Also, P. D. Harvey, C. Aubry, and G. Goffoy, unpublished results.

Can. J. Chem. Downloaded from www.nrcresearchpress.com by 91.144.44.67 on 09/07/12
For personal use only.

in CH_2Cl_2/0.1 M TBA(PF_6) and in CH_3CN/0.1 M TEAP. Typically cyclic voltammograms were obtained at concentrations less than 1.5 mM. The Pt disk electrodes (0.5 mm diameter) were polished with alumina (0.3 μm size) for 15 min in distilled water before use. The experiments were done under an atmosphere of N_2(g) or Ar(g) and carried out using a Pt disk as working electrode, a tungsten wire as the reference electrode, and a mercury pool as the counter electrode. The three-electrode cell was equipped with a luggin capillary (in which the reference electrode was inserted) and IR compensation was applied. Coulometry measurements were performed in an H-cell with Pt gauze (1 cm × 1 cm) working and auxiliary electrodes under an atmosphere of Ar(g). The SSCE reference electrode in the bulk electrolysis experiments was filled with a 3% agar-agar solution (~0.5 m thickness) at the fritted junction to minimize solvent and water diffusion, and was inserted in the auxiliary electrode compartment. The coulometry setup was checked by measuring the number of electrons transferred during oxidation of ferrocene (1.0 e). The spectroelectrochemical IR cell was built from a conventional IR cell in which the Pt gauze working and auxiliary electrodes were in the same compartment, and an Ag wire was used as quasi-reference electrode in these experiments. The solution concentrations were typically 5 mM in the IR and UV–VIS experiments. In a typical experiment, the cell was purged with Ar(g), filled with solution, and the initial IR and UV–VIS spectra were measured. A cyclic voltammogram was recorded (100 mV/s) and the potential was held fixed at the potential at which the current was about one-half the peak current in the cyclic voltammogram. At the end of the electrolysis (~10 min) no further spectroscopic changes in the IR and UV–VIS spectra were observed. The IR and UV–VIS spectra were obtained and stored electronically. The difference spectra were obtained by subtracting the final spectrum from the initial one, and produce positive and negative components. The positive components correspond to the neutral species that disappear upon oxidation and the negative ones to the oxidized species appearing. Then the potential was moved ~0.6 V negative to regenerate the original species and the final IR and UV–VIS spectra were obtained. The difference spectrum is obtained by taking the last spectrum from the oxidation experiment as initial spectrum and the last spectrum from the subsequent reduction experiment, and by again making the mathematical subtraction. This time the positive components are the regenerated species (neutral) and the negative ones are oxidized species disappearing upon reduction.

Synthesis of [(C_5H_5)Fe(C_5H_4CHCH)]$_2$CO

To a cooled solution of 50 mL 1:1 ethanol/10% aqueous NaOH, a saturated ethanol solution containing 5 g (23.4 mmol) of [(C_5H_5)Fe(C_5H_4CHO)] and 0.87 mL of acetone (11.7 mmol) was added dropwise. After stirring the solution for 1 h, a red oil appeared, and was decanted. The oily residue was dissolved in a minimal amount of acetone and precipitated by adding water dropwise (precipitation occurred at a 1:1 addition ratio). The deep red solid was filtered and dried *in vacuo* (10^{-6} Torr; 1 Torr = 133.3 Pa). No trace of the sublimable [(C_5H_5)Fe(C_5H_4CHO)] was observed. The dried product provided 4.9 g (93% yield); mp >250°C. *Anal.* calcd. for $C_{25}H_{22}Fe_2O$: C 66.71, H 4.93, Fe 24.81%; found: C 66.35, H 4.85, Fe 25.27%. On some occasions, residual impurities were identified as the monocondensed ferrocenylideneacetone compound (Fc—CH=CH—$COCH_3$) (23) by comparison with ^{1}H NMR, IR, and UV–VIS data.

Results and discussion

Spectroscopic characterization

The synthesis proceeds via a double aldehyde–acetone condensation in the presence of a strong base such as the hydroxy anion. In stoichiometric amount, the reaction is conveniently quantitative, as shown in reaction [1]:

[1] $2FcCHO + CH_3COCH_3 \xrightarrow[H_2O/EtOH]{OH^-} \underset{(dFca)}{Fc—CH=CH—(CO)—CH=CH—Fc} + 2H_2O$

where Fc = (C_5H_5)Fe(C_5H_4). The deep red product is appreciably stable up to 250°C in the solid state. This new molecule contains three active parts: two electroactive groups (Fc), one spectroscopic IR probe (C=O), and two conjugated groups (CH=CH) providing the possibility of electronic density transfer via resonance structures between the Fc and CO groups.

TABLE 1. Selected spectroscopic data for dFca

(a) NMR data[a]

Chemical shifts (^{1}H)/ppm	$^3J_{HH}$/Hz	Chemical shifts (^{13}C)/ppm	Assignments
		187.2	f
7.63	15.7	144.4	d
6.61	15.5	123.7	e
4.57		70.9	c
4.46		69.5	b
4.18		78.6	a

(b) Selected IR data[b]

ν(IR)/cm^{-1}	Assignments
1649 s	ν(C=O)
1613 vs	vinylic ν(C=C)
1589 s	vinylic ν(C=C)
1467 w	
1412 w	Fc ν(C=C)
1396 m	Fc ν(C=C)

(c) Selected MS data[c]

m/e	Assignments
450	(dFca)$^+$
385	(dFca − Cp)$^+$
261	
254	
214	(FcCH=CH)$^+$
189	
185	(Fc)$^+$
121	(CpFe)$^+$

[a]In $CDCl_3$ at 293 K, the chemical shifts are reported with reference to TMS (see Scheme 1 for nuclei labelling).

[b]In CCl_4 at 293 K, s = strong, m = medium, w = weak, v = very. The vibrational assignments are based upon reports in the literature (see, for example, ref. 25).

[c]The reported peaks are the eight dominating peaks of the spectra; Cp = C_5H_5.

The dFca complex was characterized by a combination of IR, UV–VIS, ^{1}H and ^{13}C NMR, and mass spectroscopies. Some relevant spectroscopic data are reported in Table 1. From the NMR data, the $^3J_{HH}$ values averaging 15.6 Hz clearly establish the *trans* geometry of the olefinic groups. Furthermore, the large ^{1}H and ^{13}C NMR chemical shifts associated with these vinylic groups and the unusually low ν(CO) suggest that large e$^-$-delocalization occurs along the Fc—CH=CH—C=O moieties. The FT-IR spectrum of dFca in CCl_4 is shown in Fig. 1. The 800–1500 cm^{-1} region is characteristic of an Fc group absorption (25), while the IR bands located in the 1500–1700 cm^{-1} region arise from the presence of the CH=C—(CO)—CH=CH moiety. The particularly intense IR band associated with the vinylic ν(C=C)'s implies that there is a significant dipole moment located at the vinylic centers, and is consistent with the large differences in chemical shifts

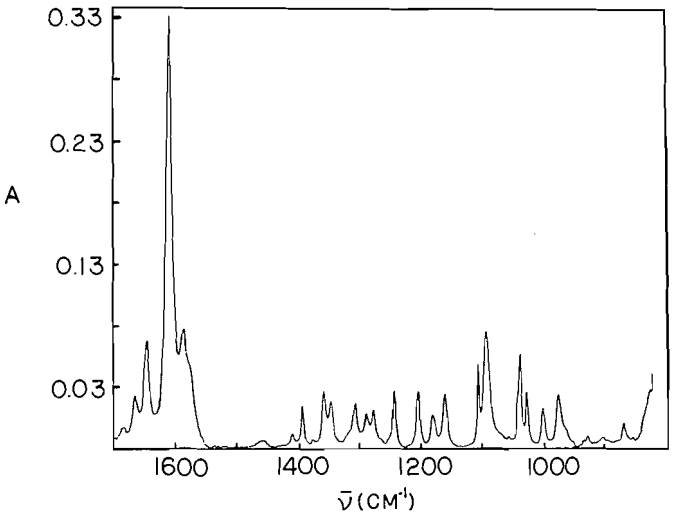

FIG. 1. FT-IR spectrum in the 800–1700 range of dFca in saturated CCl_4 solution at 293 K. Experimental conditions: 32 scans; 2 cm^{-1} resolution.

between the two C's (see details in Table 1). These spectroscopic observations show that the resonance structures play an important role in the postulated planarity of the biferrocenyl complex (see Scheme 2). There is no indication whether the Fc groups adopt the *cis* or *trans* geometry relative to each other.

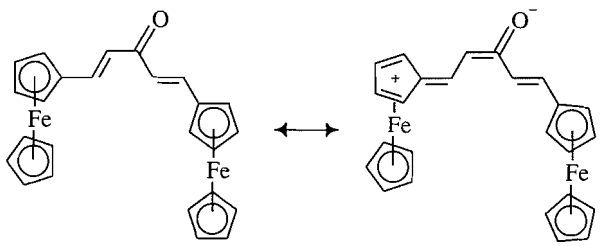

SCHEME 2. Two possible resonance structures of dFca.

The mass spectra of dFca have been obtained and the data are reported in Table 1. Eight peaks dominate the spectra, from which five are assigned. Attempts to obtain Raman data failed uniformly.

Spectroelectrochemistry

The cyclic voltammogram (cv) of 1.3 mmol dFca in CH_3CN containing 0.1 M TEAP is shown in Fig. 2. There is a quasi-reversible electrochemical oxidation process at 0.53 V vs. tungsten wire (ip, c/ip, a = 1.0). In a CH_2Cl_2 solution containing 0.1 M TBA(PF_6) this oxidation process occurs at 0.68 V vs. SSCE. No other redox process takes place between 0.68 and 2.00 V vs. SSCE. The key feature of the CV results is that with sweep rate of 100 mV/s, the ΔEp is 96 mV. At 20 and 50 mV/s, ΔEp is still 96 mV. This ΔEp independence with the scan rate is unusual and two hypotheses are given: first, dFca adsorption at the surface of the electrode can produce such behavior; second, the possibility that two one-electron processes (see the coulometry results below) occurring at very close potentials is also considered. No further experiment was attempted to elucidate the exact nature of this phenomenon. Nevertheless, from a plot of the peak current vs. the square of the scan rate, the linearity of the slope suggests that the redox processes are diffusion controlled. Coulometric measurements suggest that a 1.9-e^- oxidation process takes place at 0.68 V vs. SSCE. Typically, when ferrocene is oxidized to ferrocenium, a

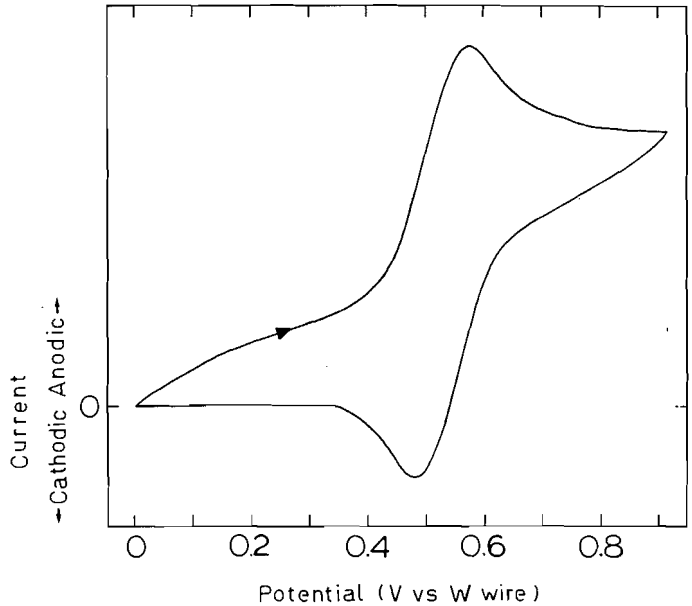

FIG. 2. Cyclic voltammograms for dFca measured at 100 mV/s in CH_3CN/0.1 M TEAP at a Pt electrode at 293 K.

new UV band located at 617 nm, with ε being 450 M^{-1} cm^{-1}, appears (24). Complete electrooxidation of a dFca solution in CH_2Cl_2 produces a color change from red to violet (λ_{max} = 750 nm, ε ~ 1000 M^{-1} cm^{-1}), which is indeed characteristic of the presence of ferrocenium centers and the larger value for ε is consistent with the coulometry results. This double oxidation process seems to occur almost simultaneously within the time frame of the experiment (see reaction [2]).

[2] Fc—CH=CH—(CO)—CH=CH—Fc

$$\xrightarrow{-2e^-} Fc^+—CH=CH—(CO)—CH=CH—Fc^+$$

There is no reduction process in the −2.0–0.0 V vs. SSCE region, contrary to the dba analogues (12–14).

The FT-IR spectra of the dFca compound in CH_2Cl_2 solutions containing 0.1 M of TBA(PF_6) have been monitored as a function of potential. Figure 3 shows the *difference* FT-IR spectra of dFca upon oxidation and reduction of the oxidized species. The IR bands associated with the Fc groups (which appear in the 800–1500 cm^{-1} region) are minimally affected as expected, while the strong vinylic ν(C=C) and ν(C=O) bands vanish (they appear as the strong negative components in the difference IR spectra) and a new weaker feature at 1675 cm^{-1} (attributable to ν(C=O)) appears upon oxidation (positive component). This result shows that the oxidation of the Fc groups is felt along the cross-conjugated system where the increase in ν(CO) is believed to be related to a less extended set of resonance structures in the oxidized species as shown in Scheme 3. Features attributable to new vinylic ν(C=C) are not observed in the spectra, presumably due to weak intensity. This redox experiment is perfectly reproducible upon multiple cycling.

Electronic spectra

The lowest electronic excited states for dFca are expected to be centered at the Fc groups. The electronic absorption spectrum of ferrocene is well known and consists of ligand field (LF), ligand-to-metal charge transfer (LMCT), and MLCT bands. The two low-energy singlets (at 22 700 cm^{-1}, ε =

Can. J. Chem. Downloaded from www.nrcresearchpress.com by 91.144.44.67 on 09/07/12
For personal use only.

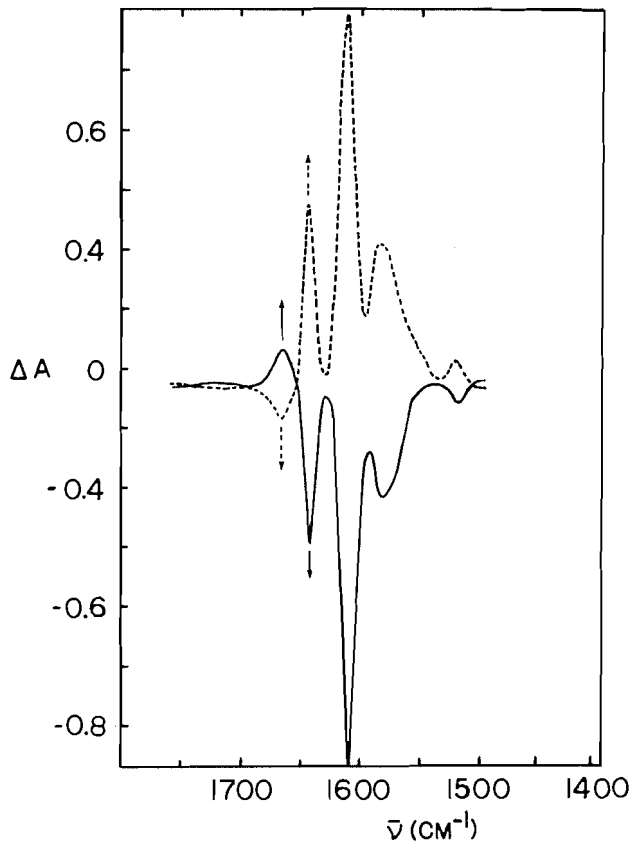

FIG. 3. Difference FT-IR spectra in the 1500–1800 cm^{-1} range of dFca in CH_2Cl_2 solution containing 0.1 M TBA(PF_6) at 293 K after complete oxidation (—) and after reduction of the oxidized species (---). Experimental conditions: 300 scans, 2 cm^{-1} resolution.

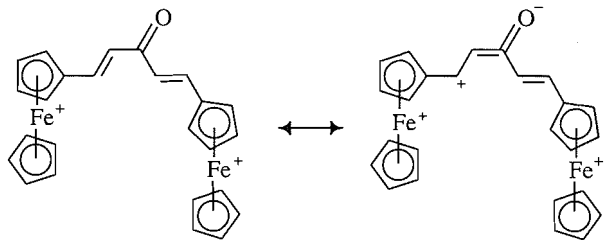

SCHEME 3. Two possible resonance structures of $(dFca)^{2+}$.

TABLE 2. UV–VIS data for dFca and FcCHO[a]

dFca		FcCHO	
ν_{max}/cm^{-1} ($\varepsilon/M^{-1}\,cm^{-1}$)	Assignments	ν_{max}/cm^{-1} ($\varepsilon/M^{-1}\,cm^{-1}$)	Assignments
29 900 (22 000)	LMCT	30 200 (1190)	LMCT
25 400 (5380)	LF-CT	27 100 (590)	LF
19 600 (5450)	LF-CT	22 000 (412)	LF

[a]In THF solution at 293 K.

TABLE 3. Solvent dependencies of the electronic bands

Solvent	$\lambda_{max}^{\#1}/nm^a$	$\lambda_{max}^{\#2}/nm^a$	$\lambda_{max}^{\#3}/nm^a$
Benzene	503	391	329
Toluene	500	391	329
Ethyl acetate	497	390	328
Acetone	503	390	328
Chloroform	515	390	331

[a]±1 nm.

91 $M^{-1}\,cm^{-1}$, and at 30 800 cm^{-1}; ε = 49 $M^{-1}\,cm^{-1}$) are LF bands (24, 26). Substitution of ferrocene by conjugated groups such as olefins, ketones, and aromatics produces an increase in absorptivity ($400 < \varepsilon < 1000\,M^{-1}\,cm^{-1}$) and a small red shift of the low-energy LF band (<1000 cm^{-1}; see Table 2 and ref. 27). The 77 K absorption spectrum of dFca in 2MeTHF is shown in Fig. 3 and the 293 K spectroscopic data are reported in Table 2. The low-energy band is now located at 19 100 cm^{-1} (ε = 5450 $M^{-1}\,cm^{-1}$ at 293 K) in dFca and the presence of two Fc groups together with the substituent effect does not account for the large intensity and transition energy changes with respect to ferrocene. Table 3 shows the solvent dependence on the electronic band position of dFca. There is a variation in λ_{max} for the lowest energy band, while the second appears to remain unaffected. Similar solvent dependencies have been reported for dba (28), for which a CT electronic transition has been attributed to the low-energy band. The spectroscopic data on dFca and literature observation strongly suggest that the lowest energy excited state in dFca possess a significant CT character.

Solid dFca is also found to be luminescent (see Fig. 4). The emission band (ν_{max} = 12 800 cm^{-1}) lies at ~6300 cm^{-1} from the lowest energy absorption band and this energy gap (Δ) is longer than the one for ferrocene (ν(singlet) − ν(triplet) ~ 4000 cm^{-1} where ν(triplet) = 18 600 cm^{-1}; see refs. 24, 29–32). The Δ value (5000 cm^{-1}) for $Ru(bpy)_3^{2+}$ (which possesses a low-energy MLCT absorption system) compares better with the Δ value observed for dFca (33). These spectroscopic data suggest that both low-energy singlet and triplet excited states possess significant CT character.

Long-term (48 h) broad band irradiation (λ_{max} = 350 nm) of both degassed and oxygenated dFca-containing solutions (C_6D_6 and $CDCl_3$) have produced only small photodegradation (less than 3% from the NMR measurements). The photoproducts have not been isolated.

Conclusion

The synthesis of this diarylideneacetone compound has provided an example of an easy preparation of a compound containing electroactive centers, a spectroscopic probe, and a conjugated system linking these groups. The presence of the olefins makes this type of compound attractive as they provide at least two binding sites for one or two extra metallic centers to enter the conjugated system. Such a concept introduces the idea of tuning thermo- and photochemical reactivity of the *added* metallic centers to the dFca-type compounds by changing the state of charge of the electroactive groups. This work has demonstrated that such a compound exhibits the required chemical and physical properties necessary to achieve the targeted goals. The electrochemistry findings show the essential chemical reversibility, where the CO group acts as a sensitive spectroscopic IR probe, and the compound is definitely thermally stable and reasonably photochemically stable.

The binding of transition metals (particularly of Pd and Pt) with dFca and other related ligands as well as their characterization and reactivity studies will be published in due course.

Can. J. Chem. Downloaded from www.nrcresearchpress.com by 91.144.44.67 on 09/07/12
For personal use only.

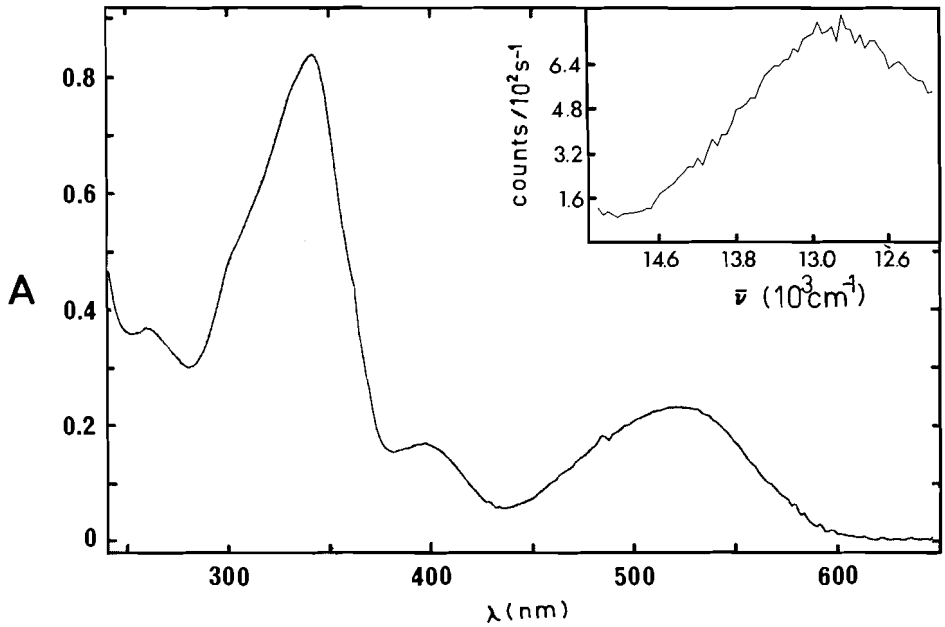

FIG. 4. UV–VIS spectrum of dFca in 2MeTHF solution at 77 K. Inset: solid state emission spectrum at 293 K. Experimental conditions: 647 nm excitation, 25 mW laser power at the sample, 50 cm^{-1}/pt, 2 s/pt, 300 μm slits.

Can. J. Chem. Downloaded from www.nrcresearchpress.com by 91.144.44.67 on 09/07/12
For personal use only.

Acknowledgments

This research was generously supported by grants from NSERC (Canada), FCAR (Quebec), and the University of Sherbrooke. P.D.H. thanks Mr. Serge Bérubé and Mr. G. Boulay for acquiring the NMR and mass spectra, respectively. The assistance of Professor I. S. Butler (McGill University) is acknowledged, for providing access to the Raman spectrometer. P.D.H. is also indebted to Professor A. Lasia and G. Brisard (Université de Sherbrooke) for helpful discussion and technical assistance in the cyclic voltammetry measurements.

1. N. W. ALCOCK and P. DEMEESTER. Acta Crystallogr. Sect. B: Struct. Crystallogr. Cryst. Chem. **B35**, 609 (1979).
2. N. W. ALCOCK, N. HERRON, T. J. KEMP, and C. W. SHOPPEE. J. Chem. Soc. Chem. Commun. 785 (1975).
3. C. G. PIERPONT, R. M. BUCHANAN, and H. H. DOWNS. J. Organomet. Chem. **124**, 103 (1977).
4. J. A. IBERS. J. Organomet. Chem. **73**, 389 (1974).
5. C. G. PIERPONT and M. C. MAZZA. Inorg. Chem. **13**, 1891 (1974).
6. T. UKAI, H. KAWAZURA, Y. ISHII, J.-J. BONNET, and J. A. IBERS. J. Organomet. Chem. **65**, 253 (1974).
7. M. C. MAZZA and C. G. PIERPONT. Inorg. Chem. **12**, 2955 (1973).
8. M. C. MAZZA and C. G. PIERPONT. J. Chem. Soc. Chem. Commun. 207 (1973).
9. N. W. ALCOCK, P. DEMEESTER, and T. J. KEMP. J. Chem. Soc. Perkin Trans. 2, 921 (1979).
10. H.-D. BECKER, B. W. SKETON, and A. H. WHITE. Aust. J. Chem. **38**, 1471 (1985).
11. H.-D. BECKER and K. ANDERSON. J. Org. Chem. **48**, 4542 (1983).
12. P. D. HARVEY and C. AUBRY. J. Phys. Chem. Submitted for publication.
13. N. ITO, T. SAJI, and S. AOYAGUI. J. Electroanal. Chem. Interfacial Electrochem. **144**, 153 (1983).
14. N. ITO, S. AOYAGUI, and T. SAJI. J. Electroanal. Chem. Interfacial Electrochem. **130**, 357 (1981).
15. P. D. HARVEY, F. ADAR, and H. B. GRAY. J. Am. Chem. Soc. **111**, 1312 (1989).
16. N. G. CONNELY and W. E. GEIGER. Adv. Organomet. Chem. **23**, 1 (1984), and references therein.
17. S. E. CREAGER and R. W. MURRY. Inorg. Chem. **26**, 2612 (1987).
18. R. D. RIEKE, W. P. HENRY, and J. S. ARNEY. Inorg. Chem. **26**, 420 (1987).
19. K. M. KADISH, A. TABARD, A. ZRINEH, M. FERHAT, and R. GUILAND. Inorg. Chem. **26**, 2459 (1987).
20. D. D. PERRIN, W. L. F. ARMAREGO, and D. R. PERRIN. Purifications of laboratory chemicals. Pergamon, Oxford. 1966.
21. A. J. GORDON and R. A. FORD. The chemist's companion. A handbook of practical data, techniques, and references. Wiley, New York. 1972. p. 436.
22. W. R. FAWCETT and A. LASIA. J. Phys. Chem. **89**, 5695 (1985).
23. M. ROSENBLUM. Chemistry of iron group metallocenes: ferrocene, ruthenocene, osmocene. John Wiley, New York. 1965. p. 162.
24. Y. S. SOHN, D. N. HENDRICKSON, and H. B. GRAY. J. Am. Chem. Soc. **93**, 3603 (1971).
25. I. S. BUTLER, P. D. HARVEY, and G. C. ALLEN. J. Raman Spectrosc. **130**, 1 (1987).
26. N. ROSCH and K. H. JOHNSON. Chem. Phys. Lett. **24**, 179 (1974).
27. K. SCHLOGL and A. MOHAR. Monastsh. Chem. **93**, 861 (1962).
28. A. A. KHALAF, S. H. ETAIW, R. M. ISSA, and A. K. EL-SHALEI. Rev. Roum. Chim. **22**, 1251 (1977).
29. D. R. SCOTT and R. S. BECKER. J. Chem. Phys. **35**, 516 (1961).
30. V. BALZANI, F. BOLLETTA, and F. SCANDOLLA. J. Am. Chem. Soc. **102**, 2152 (1980).
31. W. G. HERKSTROETER. J. Am. Chem. Soc. **96**, 4161 (1975).
32. M. S. WRIGHTON, L. PDUNGSAP, and D. L. MORSE. J. Phys. Chem. **79**, 66 (1975).
33. G. D. HAGER and G. A. CROSBY. J. Am. Chem. Soc. **97**, 7031 (1975).

Acid–base behaviour of the ferricyanide ion in perchloric acid media. Spectrophotometric and kinetic study

PEDRO L. DOMINGO, BEGOÑA GARCÍA, AND JOSÉ M. LEAL[1]

Universidad de Valladolid, Departamento de Química Física, Colegio Universitario Integrado, 09001 Burgos, Spain

Received May 19, 1989

PEDRO L. DOMINGO, BEGOÑA GARCÍA, and JOSÉ M. LEAL. Can. J. Chem. **68**, 228 (1990).

A wide study was carried out of the acid–base behaviour of ferricyanide ions in aqueous perchloric acid media in the range 0.1–11.5 M. This study shows that protonation and decomposition of the ferricyanide ions occur simultaneously. The three successive protonation equilibria were found in the acidity ranges 0.1–4.0, 3.5–8.5, and 7.0–11.5 M $HClO_4$, respectively. A kinetic study was also made of the decomposition reaction at 60°C. The kinetic data are explained by considering a reaction mechanism involving homolytic and heterolytic dissociation steps. The homolytic and heterolytic rate constants corresponding to each of the four protonated species were determined, along with the acid–base protonation constants, $pK_1 = -6.25 \pm 0.10$; $pK_2 = -3.23 \pm 0.03$; and $pK_3 = -0.60 \pm 0.02$.

Key words: acid–base behaviour, protonated species, decomposition, homolytic dissociation, heterolytic dissociation.

PEDRO L. DOMINGO, BEGOÑA GARCÍA et JOSÉ M. LEAL. Can. J. Chem. **68**, 228 (1990).

On a réalisé une étude importante du comportement acide–base des ions ferricyanures en solution dans de l'acide perchlorique aqueux, à des concentrations allant de 0,1 à 11,5 M. Cette étude a permis de démontrer que la protonation et la décomposition des ions ferricyanures se produisent simultanément. On a observé trois équilibres de protonations à des plages d'acidités respectives de 0,1 à 4,0, 3,5 à 8,5 et 7,0 à 11,5 M de $HClO_4$. On a aussi réalisé une étude cinétique de la décomposition, à 60°C. On explique les données cinétiques à l'aide d'un mécanisme réactionnel impliquant des étapes de dissociation homolytique ainsi qu'hétérolytique. On a déterminé les constantes de vitesse des étapes homolytique et hétérolytique de chacune des quatre espèces protonées ainsi que les constantes de protonation acide–base, $pK_1 = -6{,}25 \pm 0{,}10$; $pK_2 = -3{,}23 \pm 0{,}03$ et $pK_3 = -0{,}60 \pm 0{,}02$.

Mots clés : comportement acide–base, espèces protonées, décomposition, dissociation homolytique, dissociation hétérolytique.

[Traduit par la revue]

Introduction

In a previous paper, the acid–base behaviour of the ferrocyanide ion in perchloric acid media was studied by potentiometry and spectrophotometry (1). In this paper, the corresponding acid–base investigation of the ferricyanide ion is undertaken; this study, however, involves also kinetic measurements, since ferricyanide ions decompose at high acid concentrations.

The potentiometric titration of a sample of 0.01 N $K_3Fe(CN)_6$ with aqueous HCl shows no evidence of protonation; the curve coincides with that obtained in the titration of a blank solution containing pure water, this fact indicating that the three ionization constants of ferricyanic acid, $H_3Fe(CN)_6$, are higher than 0.1 (2, 3). On the other hand, the titration curves of a sample of 0.01 M $H_3Fe(CN)_6$ with NaOH, obtained by potentiometric and conductimetric techniques, are identical to those achieved titrating 0.03 M HCl. Thus the three constants must be quite high (4). None of the three pK values was found in the literature; however, to be able to explain the effect of acidity on the rate constant, several contributions on the oxidation of organic substrates by ferricyanide in acid media (5–11) suggest that the first protonation occurs in the range 0.1–3.8 M $HClO_4$.

Results and discussion

The effect of acidity on the absorption UV–VIS spectra of ferricyanide shows no noticeable change in the range 0–3.5 M $HClO_4$; however, the appearance of isosbestic points in the range 3.5–8.0 M indicates the existence of an acid–base equilibrium. Above 7.0 M, the UV–VIS spectral curves of ferricyanide change with time and a characteristic smell of HCN is observed, which evidences the decomposition of ferricyanide. This phenomenon constitutes a major difficulty in studying the influence of acidity on the spectra (Fig. 1).

The appearance of a brown suspension is observed in freshly prepared solutions of ferricyanide above 5×10^{-4} M, using aqueous $HClO_4$ 7 M and above; the higher the acid concentration, the more abundant the suspension becomes. This suspension was isolated and identified as $H_3Fe(CN)_6$; identification was made by comparison with a sample of this acid prepared according to Brauer's method (12). Figure 2 shows the most characteristic IR peaks, which are coincident for both samples.

The successive protonation equilibria may be expressed in the following simplified notation:

$$[1] \quad H_3Fe(CN)_6 \overset{K_1}{\rightleftharpoons} [H_2Fe(CN)_6]^- + H^+$$

$$[2] \quad [H_2Fe(CN)_6]^- \overset{K_2}{\rightleftharpoons} [HFe(CN)_6]^{2-} + H^+$$

$$[3] \quad [HFe(CN)_6]^{2-} \overset{K_3}{\rightleftharpoons} [Fe(CN)_6]^{3-} + H^+$$

K_1, K_2, and K_3 being the thermodynamic ionization constants of the tri-, bi-, and mono-protonated species, which will be designated BH_3, BH_2^-, and BH^{2-}; B^{3-} refers to the non-protonated species.

Equilibrium [3] should occur in the range 0.1–3.8 M $HClO_4$, since the species BH^{2-} exist mainly within this range (5–11); no appreciable change was observed in the spectral curves, but this fact should not be sufficient to discard equilibrium [3], given that the UV–VIS spectra of ferrocyanide change by addition of different cations due to ion-pair formation, but no change is observed in the case of ferricyanide (13–15) in spite of the conductimetric evidence supporting such association. As an example, $pK_{ass} = 1.3$ for the association $Fe(CN)_6^{3-} - K^+$ (16). The formation of ferricyanic acid as a brown suspension indicates that equilibrium [1] occurs above 7.0 M $HClO_4$; the spectral changes observed in the range 3.5–8.0 M $HClO_4$ should be attributed to equilibrium [2].

[1]Author to whom correspondence may be addressed.

Can. J. Chem. Downloaded from www.nrcresearchpress.com by 91.144.44.67 on 09/07/12
For personal use only.

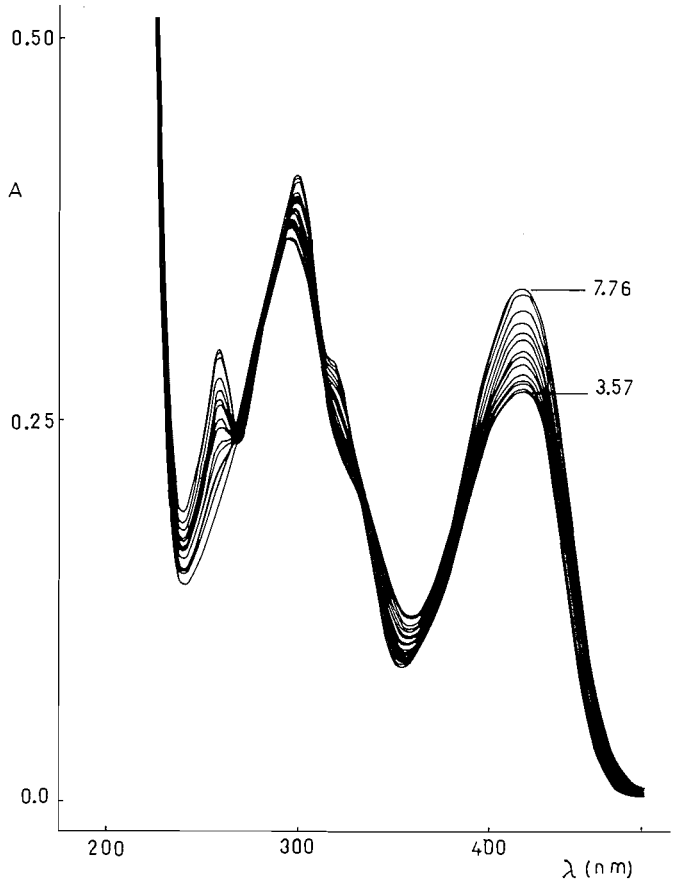

FIG. 1. Absorption UV–VIS spectra of 2.5×10^{-4} M potassium ferricyanide in aqueous perchloric acid solutions of concentration 3.57, 3.96, 4.19, 4.52, 4.73, 5.04, 5.35, 5.66, 5.90, 6.20, 6.52, 6.83, 7.14, 7.45, and 7.76 M.

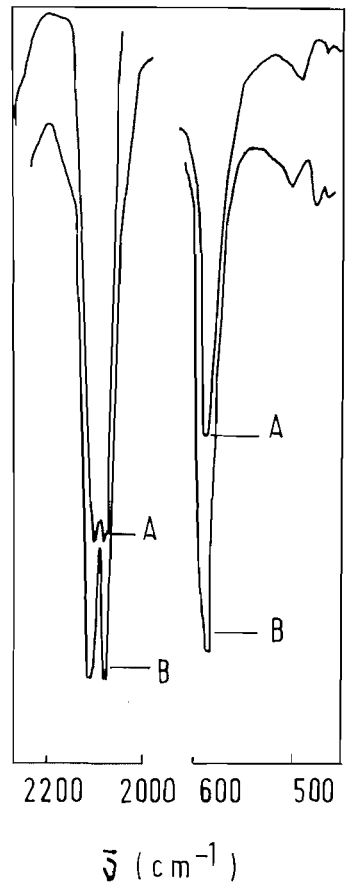

FIG. 2. Characteristic IR bands of (A) ferricyanic acid prepared according to ref. 12, and (B) the brown solid obtained from concentrated potassium ferricyanide solutions (perchloric acid 7 M and above).

To explore the acid–base behaviour of the ferricyanide ion, it was necessary to make a kinetic study of the decomposition process by studying the influence of acidity on the rate constant.

Decomposition of the ferricyanide ion in high acidity media

Several authors (17–19) have studied the formation of pentacyanoferrate(III), $[Fe(CN)_5H_2O]^{2-}$, from ferricyanide solutions in the pH range 0–14. In this work, the decomposition of ferricyanide is investigated at acidity levels of 0.1 M $HClO_4$ and above, where protonation equilibria are evidenced to start, and the analysis of reaction products confirms that decomposition does not stop in pentacyanoferrate. Some authors describe the reaction only qualitatively; the effect of mineral acids above 2 M on the ferricyanide ion is not noticeable in cold media, but at high temperature HCN is produced, along with a Prussian Blue precipitate. Ferricyanic acid is still more unstable than ferrocyanic acid, so the physical properties are not well known; it generates Prussian Blue when exposed to light and produces HCN under air atmosphere (20).

A very small decomposition is observed after 2 h in a sample of 10^{-4} M ferricyanide in the acidity range 0.1–7.0 M $HClO_4$ at 25°C; the UV–VIS spectra remain unchanged. This is not the case above 7.0 M: the absorption maxima at 420 and 300 nm decrease, and the first of these disappears with the result of a final spectral curve identical to that of ferrocyanide. The decomposition was investigated at 60°C over the whole acidity range above 0.1 M $HClO_4$.

A quantitative analysis of the reaction products reveals that about 80% ferricyanide decomposes, producing HCN and ferric ion, and 20% reduces, generating ferrocyanide. An independent test showed that 8×10^{-5} M $K_4Fe(CN)_6$ in 8.7 M $HClO_4$ did not exhibit any change in the UV–VIS absorption spectra after 3 h; Fig. 3 shows the spectral changes recorded during the decomposition of ferricyanide, with the isosbestic point at 280 nm characteristic of the ferricyanide–ferrocyanide system. The kinetics was monitored following the changes in absorbance with time; the A/t data fitted fairly well the first-order rate equation:

$$[4] \quad \ln (A - A_\infty) = \ln (A_0 - A_\infty) - kt$$

The data processing was carried out using the program RLP (weighting linear regression) with weighting $W_i \sim A^2$; Fig. 4 shows a typical straight line obtained. The variation in the initial concentration of ferricyanide did not affect the observed rate constant. Figure 5 shows the influence of acidity on the pseudo-first-order rate constant; three different regions can be distinguished: 0.1–3.5, 3.5–7.5, and 7.5–11.5 M $HClO_4$, corresponding to the first, second, and third protonation, respectively. On the other hand, the use of H_2SO_4 instead of $HClO_4$ leads to the same results for the rate constant: $k_{obs} = 3.21 \times 10^{-3}$ min^{-1} in 2 M H_2SO_4 ($[H^+] = 2.6$ M), and $k_{obs} = 4.03 \times 10^{-3}$ min^{-1} in 4.4 M H_2SO_4 ($[H^+] = 5$ M) (Table 1).

The variation of the ionic strength did not affect the reaction rate (see Table 2). Above 1.2 M $NaClO_4$ a Prussian Blue suspension appeared, $Fe^{III}NaFe^{II}(CN)_6$, which shortened the

Can. J. Chem. Downloaded from www.nrcresearchpress.com by 91.144.44.67 on 09/07/12
For personal use only.

Can. J. Chem. Downloaded from www.nrcresearchpress.com by 91.144.44.67 on 09/07/12
For personal use only.

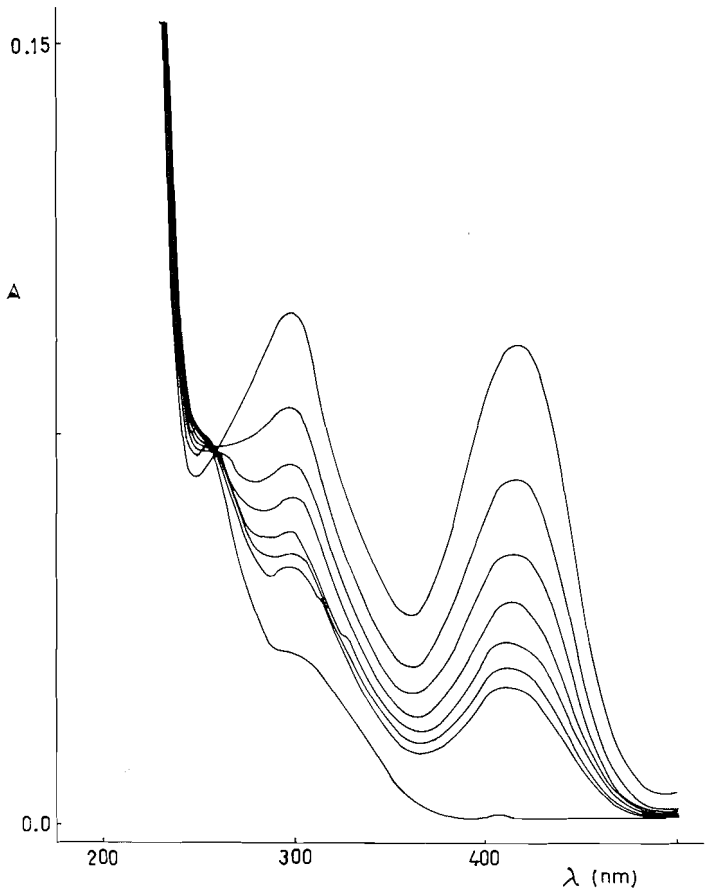

FIG. 3. UV–VIS spectral changes with time of a sample of 10^{-4} M potassium ferricyanide in aqueous 8.73 M $HClO_4$ at 60°C.

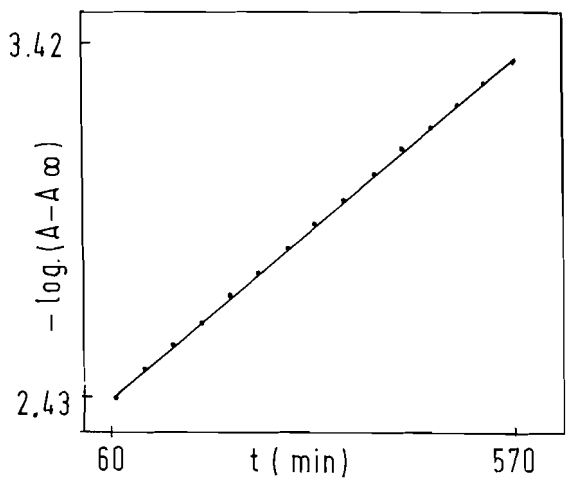

FIG. 4. Typical straight line log $(A - A_\infty)/t$ obtained by linear regression, corresponding to the decomposition reaction; T = 60°C, $K_3Fe(CN)_6 = 10^{-4}$ M, and $HClO_4$ = 1.98 M.

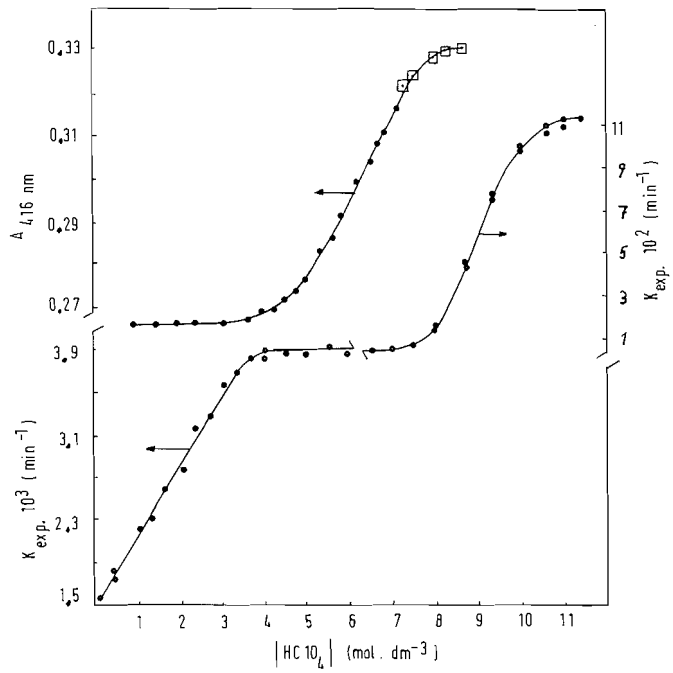

FIG. 5. Variation of k_{obs} (60°C) and $A_{416\ nm}$ (25°C) with perchloric acid concentration (the square points were corrected taking into account the decomposition reaction).

TABLE 1. Variation of k_{obs} with the initial concentration of ferricyanide: $[HClO_4]$ = 4 M, T = 60°C (θ = degrees of freedom)

$K_3Fe(CN)_6$ (10^{-4} M)	$k_{obs}(min^{-1})$	r_{xy}	θ
0.5	0.00384 ± 0.00032	−0.9937	11
1.0	0.00381 ± 0.00007	−0.9979	13
1.0	0.00390 ± 0.00008	−0.9986	20
1.5	0.00391 ± 0.00006	−0.9988	15
2.0	0.00357 ± 0.00005	−0.9992	13
2.0	0.00384 ± 0.00004	−0.9997	9
2.5	0.00375 ± 0.00005	−0.9993	17

TABLE 2. Variation of k_{obs} with the ionic strength: T = 60°C, $[HClO_4]$ = 1.01 M, $[K_3Fe(CN)_6] = 10^{-4}$ M (θ = degrees of freedom)

I (M)	$k_{obs}(min^{-1})$	r_{xy}	θ
1.01	0.00224 ± 0.00006	−0.9982	28
1.41	0.00223 ± 0.00004	−0.9987	10
1.81	0.00234 ± 0.00005	−0.9989	12
2.21	0.00224 ± 0.00004	−0.9992	10
2.21	0.00243 ± 0.00004	−0.9990	9

limit in the ionic strength to be used. This observation leads to the conclusion that noncharged species participate in the rate-determining step.

The addition of cyanide ions did not affect the rate constant, which indicates that the decomposition is not reversible and also that HCN does not react in the rate-determining step (Table 3), and may be excluded as reductant of the ferricyanide ions.

The addition of potassium ferrocyanide also has no effect on the reaction rate (Table 4), which indicates that the decomposition is not reversible; neither does the addition of Fe^{3+} ions change the rate constant, which denotes a nonreversible decomposition and excludes the Fe^{3+} ions as reactant in the rate-determining step (Table 5).

The variation of the dielectric constant of the medium displays no noticeable influence on the decomposition rate (Table 6). However, in a kinetic run using aqueous 1–4 dioxane

Can. J. Chem. Downloaded from www.nrcresearchpress.com by 91.144.44.67 on 09/07/12
For personal use only.

TABLE 3. Variation of k_{obs} with the initial concentration of cyanide: $[K_3Fe(CN)_6] = 10^{-4}$ M, T = 60°C (θ = degrees of freedom)

$[HClO_4]$ (M)	$[CN^-]$ (M)	$k_{obs}(min^{-1})$	r_{xy}	θ
8.73	0.008	0.0421 ± 0.0017	−0.9939	11
	0.010	0.0485 ± 0.0017	−0.9956	10
	0.012	0.0448 ± 0.0018	−0.9942	10
	0.016	0.0472 ± 0.0016	−0.9959	10
	0.016	0.0444 ± 0.0016	−0.9953	11
	0.020	0.0426 ± 0.0017	−0.9946	10
	0.024	0.0462 ± 0.0020	−0.9934	10
1.01	0.004	0.00232 ± 0.00005	−0.9989	16
	0.008	0.00212 ± 0.00004	−0.9992	11
	0.012	0.00251 ± 0.00003	−0.9993	17
	0.016	0.00220 ± 0.00006	−0.9988	10
	0.020	0.00243 ± 0.00007	−0.9979	11
	0.024	0.00218 ± 0.00003	−0.9995	17

TABLE 4. Variation of k_{obs} with the initial concentration of ferrocyanide: $[K_3Fe(CN)_6] = 10^{-4}$, $[HClO_4] = 8.73$, T = 60°C (θ = degrees of freedom)

$K_4Fe(CN)_6$ (10^{-5} M)	$k_{obs}(min^{-1})$	r_{xy}	θ
2	0.0479 ± 0.0018	−0.9940	10
4	0.0462 ± 0.0017	−0.9933	10
6	0.0436 ± 0.0015	−0.9939	10
8	0.0430 ± 0.0017	−0.9922	10
10	0.0459 ± 0.0017	−0.9934	10
50	0.0447 ± 0.0017	−0.9936	11

TABLE 5. Variation of k_{obs} with the initial concentration of Fe^{3+}: $[K_3Fe(CN)_6] = 10^{-4}$ M, $[HClO_4] = 8.73$ M, T = 60°C (θ = degrees of freedom)

$[Fe^{3+}]$ (10^{-4} M)	$k_{obs}(min^{-1})$	r_{xy}	θ
0.25	0.0444 ± 0.0016	−0.9937	12
0.50	0.0465 ± 0.0017	−0.9933	10
0.75	0.0436 ± 0.0016	−0.9934	10
1.00	0.0450 ± 0.0016	−0.9935	10

TABLE 6. Variation of k_{obs} with the dielectric constant of the medium: $[K_3Fe(CN)_6] = 10^{-4}$ M, $[HClO_4] = 0.99$ M, T = 60°C (θ = degrees of freedom)

Dioxane % v/v	ε	$k_{obs}(min^{-1})$	r_{xy}	θ
7	28.66	0.00227 ± 0.00005	−0.9985	11
14	27.54	0.00242 ± 0.00005	−0.9982	13
21	26.46	0.00226 ± 0.00006	−0.9982	11
28	25.42	0.00208 ± 0.00006	−0.9979	10
35	24.41	0.00213 ± 0.00007	−0.9970	10

TABLE 7. Variation of k_{obs} with temperature: $[K_3Fe(CN)_6] = 10^{-4}$ M

$[HClO_4]$ (M)	T (°C)	$k_{obs}(min^{-1})$	r_{xy}	θ
0.10	60	0.00156 ± 0.00004	−0.9982	18
	55	0.00122 ± 0.00001	−0.9998	13
	50	0.00025 ± 0.000006	−0.9995	17
	45	0.00014 ± 0.000003	−0.9986	15
	40	0.00005 ± 0.000002	−0.9980	10
4.00	60	0.00390 ± 0.00008	−0.9986	20
	60	0.00381 ± 0.00007	−0.9979	13
	55	0.00165 ± 0.00005	−0.9991	13
	50	0.00088 ± 0.00006	−0.9996	11
	45	0.00048 ± 0.00004	−0.9980	11
7.50	60	0.00780 ± 0.00023	−0.9962	10
	55	0.00510 ± 0.00021	−0.9911	10
	50	0.00286 ± 0.00016	−0.9962	12
	45	0.00216 ± 0.00021	−0.9979	15
	40	0.00164 ± 0.00015	−0.9972	12
8.73	60	0.0457 ± 0.0017	−0.9911	12
	55	0.0361 ± 0.0016	−0.9908	11
	50	0.0277 ± 0.0011	−0.9940	10
	45	0.0191 ± 0.0007	−0.9942	11
	40	0.0151 ± 0.0006	−0.9941	9
	35	0.0113 ± 0.0005	−0.9961	10
10.60	60	0.1069 ± 0.0027	−0.9960	12
	55	0.0844 ± 0.0027	−0.9965	11
	50	0.0630 ± 0.0017	−0.9974	11
	45	0.0485 ± 0.0023	−0.9934	10
	40	0.0413 ± 0.0015	−0.9952	11

35% v/v, a Prussian Blue suspension appeared after the first 30% of the reaction, due to the low dielectric constant of the medium.

Table 7 exhibits the variation of the observed pseudo-first-order rate constant with temperature at five acidity levels, and Table 8 collects the activation parameters. The activation energy decreases as the acidity increases, indicating an easier decomposition.

According to these features, the following possibilities may be discussed with respect to the reductant of the ferricyanide ions:

1. HCN is to be excluded, since the external addition of cyanide does not change the decomposition rate. Two contributions were found in the literature on the reduction of ferricyanide by cyanide (21, 22). In basic medium, cyanide reduces ferricyanide to ferrocyanide in 48 h; this reduction is pH dependent. Below pH 9 the reaction rate decreases greatly and becomes negligible after three weeks at pH 1–2; at this acidity level cyanide is present mainly as HCN, which confirms our observations.

2. Water may also be excluded; in view of the standard redox potentials, a direct water/ferricyanide reaction should be excluded. Although a self-reduction process of Fe^{3+} has already been described in the literature (23):

$$[5] \quad Fe^{3+} + [Fe(CN)_6]^{3-} + 2H_2O \rightarrow Fe^{2+} + [Fe(CN)_5]^{3-} + NH_4^+ + CO_2$$

this reaction was not confirmed in our observations, since ammonium ion was not detected as a reaction product.

3. Traces of Cu^{2+} present as impurities could be responsible for the reduction of ferricyanide; in basic medium Cu^{2+} catalyzes the reduction of ferricyanide by cyanide (24). In the process, Cu^+ ions produced by reduction of Cu^{2+} by cyanide are oxidized again to Cu^{2+} by ferricyanide, which in turn is reduced to ferrocyanide; in this cyclic redox process, Cu^{2+} ions act simply as catalyst. However, the observed rate law (24) does

TABLE 8. Thermal and thermodynamic activation parameters of the decomposition reaction of ferricyanide

$[HClO_4]$ (M)	E_a (kJ mol^{-1})	$\Delta H_{\neq}$ (kJ mol^{-1})	$\Delta S_{\neq}$ (eu)
0.10	37.8 ± 3.7	37.3 ± 3.7	32.7 ± 11.6
4.00	29.8 ± 1.6	29.2 ± 1.6	10.0 ± 4.9
7.50	16.8 ± 2.0	16.3 ± 2.0	−27.5 ± 6.2
8.73	12.0 ± 0.3	11.4 ± 0.3	−38.9 ± 1.0
10.60	10.1 ± 0.6	9.5 ± 0.6	−42.9 ± 1.9

not agree with our results:

[6] $-d[Fey]/dt = k[Fey]^2[Cu]/[Feoy]$

where Fey stands for ferricyanide and Feoy for ferrocyanide; moreover, the initial addition of (2–4) × 10^{-5} M Cu^{2+} in the decomposition reaction of 10^{-4} M ferricyanide in 8.7 M $HClO_4$ did not affect the process, but the addition of 10^{-4} M Cu^{2+} into a 10^{-4} M ferricyanide solution in 1.0 M $HClO_4$ generated a yellow solid, cupric cyanide, which overlaps and obstructs the study. Thus this route appears to be unacceptable.

4. A fourth path may be considered, in which the aquo-cyanide complex of Fe^{3+}, generated during the course of the decomposition, undergoes reduction with HCN, generating the aquo-cyanide complex of Fe^{2+}; this, finally, looses the central atom Fe^{2+}, which undergoes a fast oxidation to Fe^{3+} by ferricyanide, forming ferrocyanide.

Reaction [7] takes place in basic medium (25)

[7] $2[Fe(CN)_5H_2O]^{2-} + CN^- + 2OH^- \rightarrow 2[Fe(CN)_5H_2O]^{3-} + CNO^- + H_2O$

but in acid medium this reaction is not possible, as happened in the reduction of ferricyanide by cyanide. In any event, in this type of reaction, the external addition of cyanide should accelerate the formation of an aquo-cyanide complex of Fe^{2+} and more ferricyanide would be consumed to oxidize it to Fe^{3+}; consequently, the rate of decomposition would increase, which is not in agreement with our observations. Thus, this path seems to be very improbable.

5. A last way lies in the possibility of causing the homolytic breakdown of HCN into H· and CN· radicals by the action of UV light. It is well known that hydrogen atoms reduce ferricyanide rapidly (26, 27); this route is not probable since the only light used in this investigation was selected at 416 nm, out of the UV region.

A more reasonable possibility would consist of both homolytic and heterolytic steps, where CN· and HCN· radicals and complex species of Fe^{2+} would be generated. Although this kind of rupture is unusual, a few references were found in the literature involving complexes of cobalt, chromium, and others (28–34); it was also found in the decomposition of hexacyanomanganate(III) and hexacyanomanganato(IV) ions in aqueous acid media (35, 36). However, the best proof was recently supplied (37): potassium ferricyanide is slowly reduced under dry air atmosphere, forming cyanogen and ferricyanide in small amounts, according to reactions [8]–[10]:

[8] $[Fe(CN)_6]^{3-} \rightarrow [Fe(CN)_5]^{3-} + CN\cdot$

[9] $CN\cdot + [Fe(CN)_6]^{3-} \rightarrow [Fe(CN)_5]^{3-} + C_2N_2$

[10] $2CN\cdot \rightarrow C_2N_2$

If water vapour is contained in the atmosphere, HCN and CNOH are produced according to

[11] $2CN\cdot + H_2O \rightarrow HCN + CNOH$

The predictions including homolytic and heterolytic steps are in agreement with our observations; thus, this route is suggested to explain the decomposition of ferricyanide.

Rhodes' test (38) for the detection of cyanogen was negative, which means that CN· and HCN· radicals disappear by the hydrolysis process. This hydrolysis may occur (22) either by reaction [12] or [13]:

[12] $(CN)_2 + 2OH^- \rightarrow CN^- + CNO^- + H_2O$

[13] $(CN)_2^- + xH_2O \rightarrow P + CN^-$

Reaction [12] may be discarded, since ammonium ion was not detected among the reaction products. On the other hand, the species P was identified containing C, N, O, and H, and underwent a further reaction, generating a polymeric material hardly recognizable. This matches our findings, since in very concentrated solutions of $K_3Fe(CN)_6$ the whole system forms a spongy dark blue polymer.

The following mechanism is proposed for the decomposition of ferricyanide in acid media:

[14] $[Fe(CN)_6]^{3-} + H_3O^+ \rightarrow [HFe(CN)_6]^{2-} + H_2O$

[15] $[HFe(CN)_6]^{2-} + H_3O^+ \rightarrow [H_2Fe(CN)_6]^- + H_2O$

[16] $[H_2Fe(CN)_6]^- + H_3O^+ \rightleftharpoons [H_3Fe(CN)_6] + H_2O$

[17] $[H_nFe(CN)_6]^{n-3} \xrightarrow[\text{slow}]{k_{het}(n)} [H_{n-1}Fe(CN)_5]^{n-3} + HCN$

[18] $[H_{n-1}Fe(CN)_5]^{n-3} + H_2O \xrightarrow[\text{fast}]{} [H_{n-1}Fe(CN)_5H_2O]^{n-3}$

[19] $[H_{n-1}Fe(CN)_5H_2O]^{n-3} + 5H_2O \xrightarrow[\text{fast}]{} [Fe(H_2O)_6]^{3+} + (n-1)HCN + (6-n)CN^-$

[20] $[H_nFe(CN)_6]^{n-3} \xrightarrow[\text{slow}]{k_{hom}(n)} [H_{n-1}Fe(CN)_5]^{n-4} + CN\cdot + H^+$

[21] (recombination and probable hydrolysis of CN·)

[22] $[H_{n-1}Fe(CN)_5]^{n-4} + H_2O \xrightarrow[\text{fast}]{} [H_{n-1}Fe(CN)_5H_2O]^{n-4}$

[23] $[H_{n-1}Fe(CN)_5H_2O]^{n-4} + 5H_2O \xrightarrow[\text{fast}]{} [Fe(H_2O)_6]^{2+} + (n-1)HCN + (6-n)CN^-$

[24] $[H_nFe(CN)_6]^{n-3} + [Fe(H_2O)_6]^{2+} \xrightarrow[\text{fast}]{} [H_nFe(CN)_6]^{n-4} + [Fe(H_2O)_6]^{3+}$

[25] $[H_nFe(CN)_6]^{n-4} + [Fe(H_2O)_6]^{3+} + K^+ \xrightarrow[\text{fast}]{} Fe^{III}K^+[Fe^{II}(CN)_6] + 6H_2O$

In steps [17] and [20] the linkage Fe^{3+}–CNH is considered to be weaker than Fe^{3+}–CN^-, so that the first of these is broken much more easily. Reactions [19] and [23] take place in several irreversible fast steps (39). Step [24] is fast and, in accordance with step [25], a Prussian Blue precipitate is formed at a given concentration. The rate-determining steps [17] and [20] are S_N1 dissociative processes, since the existence of six ligands around the central atom does not allow enough room for a seventh ligand. Dissociative processes are the most frequent in substitution reactions of octahedral complexes (40); moreover, the proton enables the cyanide ligand to be released (41).

Activation entropies decrease with increasing acidity, as

Can. J. Chem. Downloaded from www.nrcresearchpress.com by 91.144.44.67 on 09/07/12
For personal use only.

TABLE 9. Homolytic and heterolytic rate constants calculated

n	$[HClO_4]$ (M)	$k_{het}(n)(min^{-1})$	$k_{hom}(n)(min^{-1})$
0	0.1	0.00125	0.00031
1	4.0	0.00308	0.00077
2	7.0	0.00436	0.00109
3	11.5	0.09126	0.02281

observed in the decomposition of hexacyanomanganate(IV) (35), which was explained by considering an intramolecular hydrogen linkage in the activation step. From the above reaction mechanism, the following rate law is obtained:

$$[26] \quad -\frac{d[\text{hexacyanoferrate (III)}]_{total}}{dt} = \frac{d\sum_{n=0}^{3}[(H_nFe(CN)_6)^{n-3}]}{dt} = \sum_{n=0}^{3}[k_{het}(n) + k_{hom}(n)][(H_nFe(CN)_6)^{n-3}]$$

A quantitative analysis of the reaction products reveals that $k_{het} \sim 4k_{hom}$; if the acidity of the medium is selected so that only one species $[H_nFe(CN)_6]^{n-3}$ is predominant, it will be possible to determine the different k_{het} values. Table 9 collects the results obtained; k_{hom} and k_{het} increase similarly as n increases either from $n = 0$ to $n = 1$, or from $n = 1$ to $n = 2$. However, this is not the case when passing from $n = 2$ to $n = 3$. This surprising effect suggests a certain change in the reaction mechanism when $n = 3$. A possible reason, not yet sufficiently investigated, lies in the solvent effect on the rate-determining steps at acidity levels above 8 M, according to the observation that the use of ethanol–water mixtures accelerates the disappearance of the ferricyanide ions in 9 M $HClO_4$. This fact was explained by considering the oxidation of ethanol, since the oxidizing power of ferricyanide increases with increase in acidity; however, further investigation remains to be done.

Determination of the dissociation constants

The curves $A/[HClO_4]$ and $k_{obs}/[HClO_4]$ exhibited in Fig. 5 may be interpreted considering the [1]–[3] acid–base equilibria. In media containing a high concentration of mineral acid, the activity coefficients involved in the definition of pK cannot be calculated by means of the Debye–Hückel equation, so we need to resort to one of the general alternative methods; in this work the determination of pK was carried out by means of the Cox–Yates equation (42):

$$[27] \quad \log I - \log C_{H^+} = m^*X + pK$$

where X, the excess acidity function, which is the same for all the bases in a single system, is calculated by an iterative method based on the ionization of a large number of different bases; for aqueous perchloric acid, used in this investigation, the function X is determined by starting from the percentage of mineral acid (42). The ionization ratio I = [basic form]/[acid form], can be estimated by means of Gold–Hawes' equation (43):

$$[28] \quad I = (P_B - P)/(P - P_A)$$

where P, the property of the system, stands for the observed rate constant in the cases of equilibria [1] and [3], and for the absorbance at 416 nm in the case of equilibrium [2]; P_B is the property of the basic species and P_A that of the conjugate acid, each corresponding to the limits of acidity in which the equilibrium takes place; P is the property corresponding to intermediate acidities. The pK is obtained as the ordinate of the linear regression $(\log I - \log C_{H^+})/X$, while from the slope we obtain the parameter m^*, which is particular to each base and can be interpreted in terms of hydration.

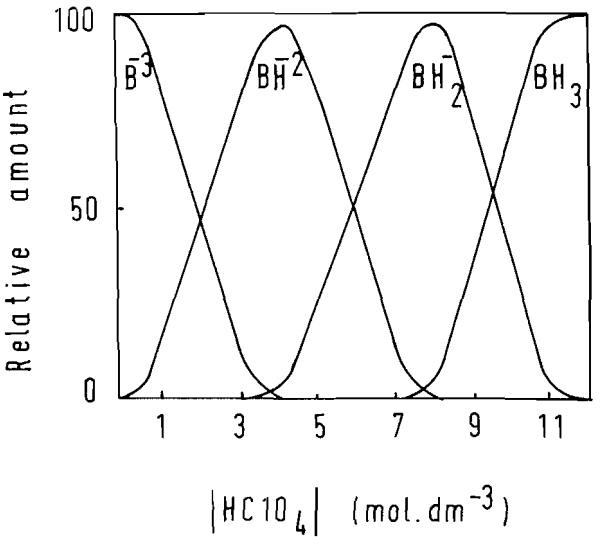

FIG. 6. Distribution of the various protonated forms of ferricyanide ions as a function of aqueous perchloric acid concentration.

In a previous paper (44), the separation method for overlapping equilibria was proposed and applied to investigate the successive protonations of the ferrocyanide ions (1). Although equilibria [1], [2], and [3] partially overlap, the procedure utilized in this work also includes measurements coming from the decomposition process, and avoids the need for using the separation method. Equilibrium [3] occurs in the range 0.1–4.0 M $HClO_4$ and the following values were obtained from the k_{obs} data: $pK_3 = -0.60 \pm 0.02$; $m_3^* = 1.01 \pm 0.04$; $r_{xy} = 0.9955$. Equilibrium [2] occurs in the range 3.5–8.5 M $HClO_4$, and the following values were obtained from the absorbance data: $pK_2 = -3.23 \pm 0.03$; $m_2^* = 0.99 \pm 0.01$; $r_{xy} = 0.9903$. Finally, equilibrium [1] occurs in the range 7.0–11.5 M $HClO_4$ and the following values were obtained from the k_{obs} data: $pK_1 = -6.25 \pm 0.10$; $m_1^* = 1.24 \pm 0.02$; $r_{xy} = 0.9983$. Figure 6 displays the distribution of the various protonated forms of ferricyanide ions as a function of aqueous perchloric acid concentration.

Conclusions

Due to the existence of two simultaneous processes, protonation and decomposition, the study of the acid–base protonation equilibria of the ferricyanide ions gives results more complicated than those of the ferrocyanide ions. Although the interpretation given in this paper is consistent with our own results, some additional experiments will complete a better knowledge of the acid–base behaviour of ferricyanide; thus, the influence of the solvent on the decomposition rate constant, using organic solvent – water mixtures, will provide useful information. On the other hand, the formal reduction potential of the ferricyanide/ferrocyanide pair was obtained at different acidity levels, being 0.410 V in pure water; 0.688 V in 1 M $HClO_4$; 0.798 V in 4 M $HClO_4$; 0.899 V in 7 M $HClO_4$; and 0.986 V in 10 M $HClO_4$. Thus, the oxidizing power of ferricyanide

Can. J. Chem. Downloaded from www.nrcresearchpress.com by 91.144.44.67 on 09/07/12
For personal use only.

Can. J. Chem. Downloaded from www.nrcresearchpress.com by 91.144.44.67 on 09/07/12
For personal use only.

increases with the acidity; this fact is important and should be taken into account, since certain organic solvents could be oxidized by ferricyanide in acid media. Finally, a deconvolution process by adaptation of characteristic vector analysis will be applied to the UV–VIS spectra of ferricyanide with the aim of separating them into independent bands and assigning the maxima wavelengths to the corresponding electronic transitions; the purpose is to evaluate the alterations in the spatial symmetry of ferricyanide as a consequence of the protonation reactions.

Experimental

Reactants

All reactants used were of analytical grade. When necessary, the ionic strength was controlled with sodium perchlorate in the kinetic experiments; in the spectrophotometric experiments, however, it was not necessary to control the ionic strength, since this factor is included in the excess acidity function method. All solutions were prepared with twice distilled and deionized water as solvent, over which nitrogen gas was made to flow before being used. In every case, the solutions used had been freshly prepared and kept out of the light. Values of C_{H^+} were calculated directly from molar concentrations of perchloric acid, since this species is fully ionized at least up to 60% w/w (42).

Equipment

The UV–VIS spectral curves were recorded with a Bodenseewerk Perkin Elmer 554 spectrophotometer with double beam, slit 1 nm, optic path 1 cm, and thermostatable cells; this permits multiple expansion in both absorbances and wavelengths and an accuracy of ± 0.001 in the absorbance readings. The reference cell contained the same solvent as the sample under measurement. The temperature of all solutions was kept constant with a P-Selecta thermostat. The kinetic experiments were followed with a Philips Pye Unicam 8600 spectrophotometer, furnished with a Pye Unicam cell temperature controller. The data processing was carried out with an Olivetti 240 computer.

General

In the decomposition of ferricyanide ions the reaction products were determined by analyzing solutions containing 0.05 g $K_3Fe(CN)_6$ in 20 mL of 1 M and 4 M $HClO_4$, respectively. After 48 h at 60°C a blue precipitate and a characteristic smell of HCN gas were observed.

1. This gas was bubbled with a nitrogen stream into a solution of $AgNO_3$ 10% w/w, acidified with HNO_3, and a white solid precipitated; this gas was also bubbled into a solution of NaOH containing Mohr salt, a few drops of $FeCl_3$, and, after 15 min, dilute H_2SO_4 for dissolving the ferrous and ferric hydroxides; a blue coloration and blue precipitate appeared. These facts indicate the formation of HCN.

2. Addition of ferricyanide to a sample of the liquid portion produced a red coloration, confirming the presence of ferric ions. This also confirms the absence of ferrous ions; otherwise, a blue coloration and blue precipitate would have appeared. On the other hand, addition of ferric ions generates a blue coloration, due to the presence of ferrocyanide; this evidence is also supported by the UV–VIS spectrum of a sample of the decomposition products in very dilute solutions of ferricyanide, where no precipitate was observed.

HCN undergoes a hydrolysis reaction when boiled, forming ammonium ions and formic acid. This reaction, however, was not confirmed, since a typical test for NH_4^+ led to negative results.

3. The blue precipitate, once recovered, isolated, and dried, gave an IR spectrum coincident with that of a sample of Prussian Blue obtained by mixing ferrocyanide and ferric ions, and also with that of a sample of Turnbull Blue obtained by mixing ferricyanide and ferrous ions; it is well known that both species are the same, ferric ferrocyanide, since ferricyanide oxidizes Fe^{2+} to Fe^{3+}, being itself reduced to ferrocyanide (45–48). There exist, in fact, two different types of Prussian Blue: (a) soluble Prussian Blue, $Fe^{III}M^+Fe^{II}(CN)_6$, which is formed when the alkaline ion M^+ is in excess, and (b) insoluble Prussian Blue, $Fe_4[Fe(CN)_6]_3$, when the alkaline and ferric ions are present in similar amounts (49, 50); the IR spectra of both species are identical.

During the process of decomposition, the concentration of K^+ ions is at any moment much higher than that of Fe^{3+} ions, which are released slowly, and the first of these becomes predominant; the Fe^{3+} ions released could, in the presence of ferricyanide, react to generate the red complex $FeFe(CN)_6$ (21, 51, 52); however, such coloration was not observed during the decomposition, and the UV–VIS spectrum of the reacting mixture showed no absorption above 500 nm, the spectral region of the red complex.

Several papers exist, reporting on the thermal decomposition of ferricyanide within the pH 0–14 region to generate $[Fe(CN)_5H_2O]^{2-}$ (17–19); the rate constant is 6×10^{-7} s^{-1} at 25°C and pH 4.6. The maximum band of this species is located at 565 nm (53); however, our reacting mixtures showed no noticeable absorption above 500 nm at any moment during the course of the decomposition.

The quantitative analysis of the reaction products in aqueous 1 M and 4 M $HClO_4$ was carried out by isolating the blue precipitate and collecting the HCN released over an NaOH solution, where the cyanide ions were titrated vs. $AgNO_3$, following the Liebig–Déniges' method (54). Independently of the acidity of the medium, the amount of HCN collected was about 75–80% of the total cyanide in the sample and the Prussian Blue collected was about 20–25% of the solid sample of $K_3Fe(CN)_6$ used. In media of 7 and 10 M $HClO_4$, $H_3Fe(CN)_6$ acid precipitates, this fact making advisable concentrations lower than 5×10^{-4} M; under these conditions, only small amounts of blue precipitate are collected, and the quantitative analysis of HCN is carried out as already described, the HCN being about 70–80% of the total cyanide in the sample. These results lead to the conclusion that about four fifths of the ferricyanide decomposes, producing HCN and ferric ions, and one fifth reduces, producing ferrocyanide.

Most chemicals contain traces of metal ions as impurities; the levels of Cu^{2+} detected by atomic absorption (324 nm) were 0.200 ppm in 0.303 M ferricyanide and 0.261 ppm in 0.267 M ferrocyanide. For this reason, the possibility of Cu^{2+} ions being responsible for the decomposition of ferricyanide was investigated.

Acknowledgements

This work was supported in part by Caja de Ahorros Municipal de Burgos.

1. P. L. Domingo, B. Garcia, and J. M. Leal. Can. J. Chem. **65**, 583 (1987).
2. J. Jordan and G. I. Ewing. Inorg. Chem. **1**, 587 (1962).
3. G. Charlot. Les réactions chimiques en solution. L'analyse qualitative minérale. Masson, Paris. 1969.
4. J. Brigando. Bull. Soc. Chim. Fr. 503 (1957).
5. A. K. Bhattacharjee and M. K. Mahanti. Indian J. Chem. **22B**, 74 (1983).
6. M. D. Lilani, G. K. Sharma, and R. Shanker. Indian J. Chem. **25A**, 370 (1986).
7. A. K. Bhattacharjee and M. K. Mahanti. Bull. Soc. Chim. Fr. 270 (1983).
8. A. K. Bhattacharjee and M. K. Mahanti. Korean Chem. Soc. **4**, 120 (1983).
9. A. K. Bhattacharjee and M. K. Mahanti. Int. J. Chem. Kinet. **14**, 113 (1982).
10. K. Sriraman, P. R. Nath, B. V. Sastry, and R. P. Rao. Z. Phys. Chem. Leipzig, **267**, 953 (1986).
11. A. K. Bhattacharjee and M. K. Mahanti. Gazz. Chim. Ital. **113**, 1 (1983).
12. G. Graver. Química Inorgánica preparativa. Reverté, Barcelona. 1958.
13. S. R. Cohen and R. A. Plane. J. Phys. Chem. **61**, 1096 (1957).
14. C. B. Monk. Ion association constants at zero ionic strength. *In* Chemical physics of ionic solutions. *Edited by* B. E. Conway and R. G. Barradas. John Wiley, New York. 1966.
15. W. A. Eaton, P. George, and G. I. H. Hanania. J. Phys. Chem. **71**, 2016 (1967).
16. R. J. Lemire and M. W. Lister. J. Solution Chem. **5**, 171 (1976).
17. A. G. McDiarmid and N. F. Hall. J. Am. Chem. Soc. **75**, 5203 (1953).

18. W. C. CROUSE, D. A. BENNETT, and D. W. MARGERUM. React. Kinet. Catal. Lett. **1**, 135 (1974).
19. J. DUPLESIS-LEGROS. C.R. Acad. Sci. Ser. C, **270**, 1768 (1970).
20. P. PASCAL. Nouveau traité de chimie minérale. Masson, Paris. 1959.
21. M. A. ALICH, D. T. HAWORTH, and M. F. JOHNSON. J. Inorg. Nucl. Chem. **29**, 1637 (1967).
22. A. W. ADAMSON. J. Phys. Chem. **56**, 858 (1952).
23. J. F. DE WET and R. ROLLE. Z. Anorg. Allgem. Chem. **336**, 96 (1965).
24. F. R. DUKE. Inorg. Nucl. Chem. Lett. **12**, 107 (1976).
25. A. ADAMSON, J. WELIER, and M. VOLPE. J. Am. Chem. Soc. **72**, 4030 (1950).
26. R. P. MITRA, D. V. S. JAIN, A. K. BANNERJEE, and K. V. RAGHAVACHARI. Nature, **200**, 163 (1963).
27. G. CZAPSKI, J. RABANI, and G. STEIN. Trans. Faraday Soc. **58**, 2160 (1962).
28. J. H. ESPENSON. Adv. Inorg. Bioinorg. Mech. **1**, 1 (1982).
29. A. R. SCHMIDT and T. W. SWADDLE. J. Chem. Soc. (A), 1927 (1970).
30. R. G. COOMBES and M. D. JOHNSON. J. Chem. Soc. (A), 177 (1966).
31. M. J. SISLEY, W. RINDERMANN, R. VAN ELDIK, and T. W. SWADDLE. J. Am. Chem. Soc. **106**, 7432 (1984).
32. R. VAN ELDIK. Inorg. Chem. **22**, 353 (1983).
33. W. E. JONES, L. R. CAREY, and T. W. SWADDLE. Can. J. Chem. **50**, 2739 (1972).
34. K. ISHIHARA and T. W. SWADDLE. Can. J. Chem. **64**, 2168 (1986).
35. G. LOPEZ-CUETO and C. UBIDE. Can. J. Chem. **64**, 2301 (1986).
36. G. LOPEZ-CUETO and G. DEL CAMPO. XX Reunion Bienal de Química. Castellón, Spain. 1984.
37. P. G. SIM and E. WHALLEY. J. Phys. Chem. **91**, 1877 (1987).
38. F. H. RHODES. Ind. Eng. Chem. **4**, 652 (1912).
39. G. EMSCHWILLER. C.R. Hebd. Seances Acad. Sci. **236**, 72 (1953).
40. F. BASOLO and R. JOHNSON. Química de los compuestos de coordinación. Reverté, Barcelona. 1967.
41. P. SOUCHAY and J. LEFEBVRE. Equilibres et réactivité des complexes en solution. Masson, Paris. 1969.
42. R. A. COX and K. YATES. J. Am. Chem. Soc. **100**, 3861 (1978).
43. V. GOLD and B. W. V. HAWES. J. Chem. Soc. 2102 (1951).
44. B. GARCIA, P. L. DOMINGO, and J. M. LEAL. Collect. Czech. Chem. Commun. **52**, 1087 (1987).
45. L. M. EPSTEIN. J. Chem. Phys. **36**, 2731 (1962).
46. J. F. DUNCAN and P. W. R. WIGLEY. J. Chem. Soc. 1120 (1963).
47. K. MAER, M. L. BEASLEY, R. L. COLLINGS, and W. O. MILLIGAN. J. Am. Chem. Soc. **90**, 3201 (1968).
48. A. ITO, M. SVENAGA, and K. ONO. J. Chem. Phys. **48**, 3597 (1968).
49. R. E. WILDE, S. N. GHOSH, and B. J. MARSHALL. Inorg. Chem. **9**, 2512 (1970).
50. J. F. KEGGIN and F. D. MILES. Nature, 577 (1936).
51. J. A. IBERS and N. DAVIDSON. J. Am. Chem. Soc. **73**, 476 (1951).
52. D. L. SINGLETON and J. H. SWINEHART. Inorg. Chem. **6**, 1536 (1967).
53. B. JASELSKIS. J. Am. Chem. Soc. **83**, 1082 (1981).
54. L. MEITES. Handbook of analytical chemistry. McGraw Hill, New York. 1963.

Can. J. Chem. Downloaded from www.nrcresearchpress.com by 91.144.44.67 on 09/07/12
For personal use only.

Thermodynamic behaviour of molten metal oxychlorides. 1. The $PbO–PbCl_2$ system

A. HACETOGLU[1] AND S. N. FLENGAS

Department of Metallurgy and Materials Science, University of Toronto, Toronto, Ont., Canada M5S 1A4

Received February 28, 1989[2]

A. HACETOGLU and S. N. FLENGAS. Can. J. Chem. **68**, 236 (1990).

Partial molar and integral molar properties of mixing for $PbO–PbCl_2$ melts have been investigated by using solid electrolyte galvanic cells of the type: Ni–NiO | $CaO–ZrO_2$ | $PbO–PbCl_2$ | Pb. Thermodynamic properties, such as activities and partial molar enthalpies of mixing, calculated from the measured cell potentials show pronounced negative deviations from ideality. To explain this behaviour and to predict the concentration dependence of the thermodynamic properties of these solutions, a theoretical model based on a number of possible reaction mechanisms has been developed. It is shown that in a non-ideal solution, the activity of any component A^+X^- is given as

$$a_{A_xB_y} = (N_{A^+}^x \cdot N_{B^-}^y)_{\text{equilibrium}}$$

where N_{A^+} and N_{B^-} are respectively the cation and anion fractions in a solution that has reached the ionic composition representing a specific reaction mechanism at equilibrium. From the activity data, the limiting experimental conditions for removing the oxygen impurity from $PbCl_2$ melts and for recovery of Pb and O_2 by fused salt electrolysis have been established.

Key words: oxychlorides, activities, solution properties, $PbO–PbCl_2$, EMF.

A. HACETOGLU et S. N. FLENGAS. Can. J. Chem. **68**, 236 (1990).

Utilisant des cellules galvaniques d'électrolytes solides du type : Ni–NiO | $CaO–ZrO_2$ | $PbO–PbCl_2$ | Pb, on a étudié les propriétés de mélanges molaires partiels et molaires intégrales de mélanges de $PbO–PbCl_2$ fondus. Les propriétés thermodynamiques, telles que les activités et les enthalpies molaires partielles qui ont été calculées à partir des potentiels mesurés, présentent des déviations négatives importantes par rapport à l'idéalité. Pour expliquer ce comportement et pour arriver à prédire la relation entre la concentration et les propriétés thermodynamiques de ces solutions, on a développé un modèle théorique qui est basé sur un certain nombre de mécanismes réactionnels possibles. On a démontré que dans une solution qui n'est pas idéale, l'activité de tout composant A^+X^- peut être représentée par l'équation suivante :

$$a_{A_xB_y} = (N_{A^+}^x \cdot N_{B^-}^y)_{\text{équilibre}}$$

dans laquelle N_{A^+} et N_{B^-} correspondent respectivement aux fractions cationiques et anioniques que l'on retrouve en solution lorsqu'on atteint la composition ionique représentant un mécanisme réactionnel spécifique à l'équilibre. À partir des données relatives à l'activité, on a déterminé les conditions expérimentales qui limitent l'enlèvement de l'oxygène présent sous forme d'impureté dans du $PbCl_2$ fondu ainsi que la récupération du Pb et du O_2 par électrolyse du sel fondu.

Mots clés : oxychlorures, activités, propriétés de solution, $PbO–PbCl_2$, FEM.

[Traduit par la revue]

Introduction

Molten solutions of $PbO–PbCl_2$ represent the only metal oxide – metal chloride system in which oxide solubility occurs over a wide concentration and temperature range at relatively low temperatures.

Recently the phase diagram of the system was revised by Renaud *et al.* (1) and significant differences from the earlier work by Ruer (2) and Varoni (3) were found. At a temperature of 973 K the range of liquid solutions extends from pure $PbCl_2$ to about 80 mol% PbO.

Activities of PbO in this system have been measured electrochemically by Sugawara *et al.* (4) at temperatures between 506 and 1063°C.

In the present investigation the reversible EMF of the cell,

$$(+)Pb_{(liq)}, PbO_x–PbCl_{2_{(1-x)}} \mid ZrO_2–CaO \mid NiO_s, Ni_s(-)$$

was measured for PbO compositions varying from pure PbO to 1 mol% PbO, and in the temperature range 723–1223 K. From the results, the thermodynamic properties of PbO and of $PbCl_2$ in the $PbO–PbCl_2$ melts have been calculated. In addition to its theoretical significance, the thermodynamic information has been used to predict the limiting equilibrium conditions for the chlorination of PbO at high temperatures, for the preparation of pure $PbCl_2$ through the electrochemical removal of an oxygen impurity, and for the recovery of metallic lead by fused salt electrolysis of the $PbO–PbCl_2$ solutions in the temperature range 773–873 K.

Experimental

The design of the cell for the EMF measurements is given in Fig. 1. The reference electrode consisted of a CaO stabilized zirconia tube containing 13 mol% CaO, closed at one end, having a total length of about 30 cm. To make this electrode, nickel wire 1 mm in diameter having a spiral end was inserted into the zirconia tube and was covered with 2–3 cm of a compacted mixture of Ni and predried NiO powders. The open end of this tube was closed with a glass bell cemented into place and the entire system could be evacuated and sealed under vacuum. During its operation the thermal decomposition of NiO at the temperature of the experiment established the oxygen gas pressure and the EMF measurements did not contain errors due to mixed potentials that are created by nonequilibrium oxygen pressure conditions (5).

The indicator electrode was molten lead in contact with the $PbO–PbCl_2$ melt contained in a zirconia crucible. Electrical contact to the lead was through iridium wire, about 1 mm in diameter and 10 cm long, connected to a platinum wire lead.

The entire electrode assembly, including the crucible with the salt mixture, was placed in a silica tube closed at one end. The top of this tube was covered with a nickel plate machined to contain entry ports for the various cell components, as shown in Fig. 1. A vacuum-tight seal was provided by De Khotinsky cement covering the entire surface of the top plate and all openings. To prevent the escape of the volatile $PbCl_2$ from the zirconia crucible containing the $PbO–PbCl_2$ melt, the

[1]Present address: Cyanamide of Canada, Niagara Falls, Ont., Canada.

[2]Revision received September 7, 1989.

Can. J. Chem. Downloaded from www.nrcresearchpress.com by 91.144.44.67 on 09/07/12
For personal use only.

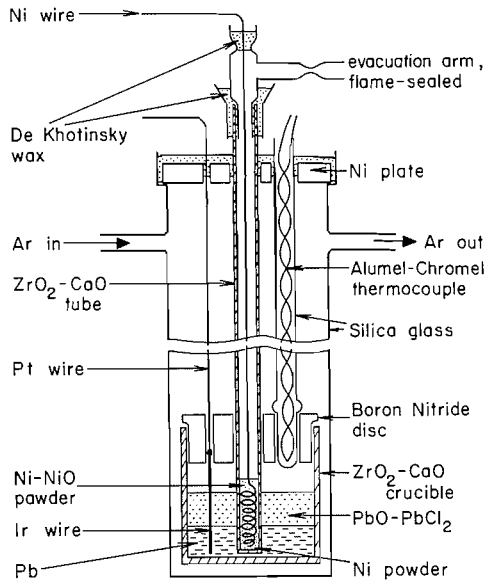

FIG. 1. Schematic drawing of the experimental EMF cell.

top of the crucible was also closed with a boron nitride lid machined to fit tightly. This lid had openings for the insertion of the reference electrode and the other cell components shown in Fig. 1. A further precaution against possible volatilization of $PbCl_2$ was provided by operating the indicator electrode compartment under a static blanket of purified argon. A gas valve, connected in parallel with the argon supply to the cell, maintained a slightly positive gas pressure while it prevented the flow of gas and created semistatic conditions.

Materials losses due to possible volatilization were determined by weighing the contents of the crucible before and after a run, during runs that duplicated the experimental conditions in terms of melt composition, temperature, and duration. No significant loss of materials was observed. For example, for a total melt weight of 50 g containing 70 mol% $PbCl_2$, at a temperature of 1023 K over a period of 10 h the weight loss was only 0.2 g. Accordingly, melt compositions did not have to be corrected for losses due to volatilization.

The PbO and $PbCl_2$ used for these experiments were anhydrous high purity reagents and argon was dehydrated and oxygen purified by using Ti pellets at 1273 K.

Potential measurements taken during a heating and cooling cycle at each composition were in agreement to within ±2 mV. Maximum duration of a run was about 10 h.

Results and data treatment

Reversible potentials were measured as a function of temperature and composition. The data have been treated by least squares to correspond to linear equations of the form:

$$[1] \qquad E\ (\text{in mV}) = A - BT$$

where A and B are constants for a given composition and T is given in degrees Kelvin. The constants, and the calculated standard and maximum deviations, are given in Table 1.

The activities of PbO were calculated from the Nernst equation given as

$$[2] \qquad E = (E^0_{NiO} - E^0_{PbO}) - RT/2F \ln a_{PbO}$$

where a_{PbO} is the activity of PbO calculated with respect to pure molten PbO as the standard state. R and F have the values of 8.3136 J mol^{-1} and 96 484 J $volt^{-1}$, respectively. E is given in volts and E^0_{NiO} and E^0_{PbO} are, respectively, the formation potentials of pure solid NiO and pure molten PbO at the same temperature as T. T is given in degrees Kelvin.

TABLE 1. EMF measurements representing the overall cell reaction $Ni_{(s)} + (PbO)_{\text{in } PbO\text{–}PbCl_2} = NiO_{(s)} + Pb_l$

		$E = A - BT$		
X_{PbO}	T Temp. range (K)	A (mV)	B	Standard deviation (mV)
0.01	778–914	−15.933	0.15322	±0.90
0.05	778–873	−39.228	0.05184	±1.16
0.1	762–874	−32.380	0.02944	±1.34
0.2	775–874	−14.103	0.00106	±0.92
0.3	474–926	19.579	0.01716	±2.08
0.4	781–935	29.452	0.000066	±0.30
0.5	921–1010	78.821	0.01374	±0.88
0.6	956–1062	117.207	0.02322	±0.51
0.7	967–1064	158.435	0.03938	±0.34
0.8	1016–1094	204.462	0.06705	±1.03
1.0	1160–1371	222.98	0.05052	±0.57

NOTE: Negative EMF values imply a reversal in the electrode reaction.

The formation potentials for pure solid NiO at various temperatures have been established in previous investigations (5–11). With regard to pure molten PbO, the standard Gibbs free energies reported by several investigators (12–14) and by Charette and Flengas (5) are in substantial agreement to within 2–4 mV. Accordingly, the standard formation potentials for NiO and for PbO used for the calculation of the activities from eq. [2] are those reported in our previous work (5). The latter were obtained by EMF measurements in closed cells similar to those used in the present investigation. The data for the standard potentials of NiO and PbO are given in Table 2.

The activities of PbO at the selected temperatures of 1023 and 1123 K are given in Table 3. The activities of $PbCl_2$, which are also included in Table 3, have been calculated using the well-known Gibbs–Duhem relationship (15).

The partial molar enthalpies of mixing for PbO, given in Table 3, have been calculated from the A constants that are presented in Table 1, using the readily derived expression:

$$[3] \qquad \overline{\Delta H}_{PbO} = 19.2968(A - 223.3)$$

These values are given in kJ mol^{-1}.

Activities of PbO in this system reported by Sugawara *et al.* (4) are in disagreement with the present results, particularly at high PbO contents. For solutions containing more than 80 mol% of PbO, the reported activities are greater than unity, which is thermodynamically impossible for the chosen reference states, which were the same as in the present calculations. For compositions lower than 30 mol% PbO, there is better agreement with the present results, although the temperature dependences of the EMFs differ.

Activity isotherms for the PbO and the $PbCl_2$ components are shown in Fig. 2. Activities calculated by Sugawara *et al.* (4) are also included for comparison.

Discussion

The pronounced negative deviations from ideality shown by the activity data in Table 3 and by the strongly exothermic partial molar heats of mixing for PbO are indicative of strong interactions between the solute ions in the PbO–$PbCl_2$ melts.

The result of such interactions could be the formation of complex oxychloride configurations of the general type $(Pb_pO_qCl_r)^{(2p-2q-2r)+}$ where p, q, and r are integers having

Can. J. Chem. Downloaded from www.nrcresearchpress.com by 91.144.44.67 on 09/07/12
For personal use only.

TABLE 2. Standard electrode potentials

Electrode	Temp. range (K)	Cell potential $E^0 = A^0 - B^0T$ A^0 (mV)	B^0	Standard deviation (mV)	Maximum deviation (mV)
$Ni_{(s)} + \frac{1}{2}O_{2(g,\ 1\ atm)} = NiO_{(s)}$ (5)	911–1376	1210.83	0.43993	±0.57	±1.0
$Pb_{(l)} + \frac{1}{2}O_{2(g,\ 1\ atm)} = PbO_{(l)}$ (5)	1160–1370	987.5	0.38941	±0.51	±0.8
$Pn_{(l)} + Cl_{2(g,\ 1\ atm)} = PbCl_{2(l)}$	773–1200	1742.5	0.602	—	—

TABLE 3. Isothermal activities as a function of melt composition

X_{PbO}	1023 K a_{PbO}	1023 K a_{PbCl_2}	1123 K a_{PbO}	1123 K a_{PbCl_2}	$\overline{\Delta H}_{PbO}$† (kJ mol^{-1})
0.1	0.005	0.890	0.008	0.899	−49.33
0.2	0.010	0.765	0.200	0.796	−45.81
0.3	0.022	0.620	0.035	0.660	−39.31
0.4	0.045	0.440	0.650	0.475	−37.40
0.50	0.085	0.240	0.115	0.300	−27.88
0.60	0.160	0.110	0.200	0.150	−20.47
0.7	0.280	0.035	0.325	0.060	−12.51
0.8	0.450	0.010	0.480	0.018	−3.63
0.9	—	—	(0.760)*	(0.001)*	

*Extrapolated.

†The uncertainty in the values of the partial molar heats of mixing is about ±4 kJ mol^{-1}.

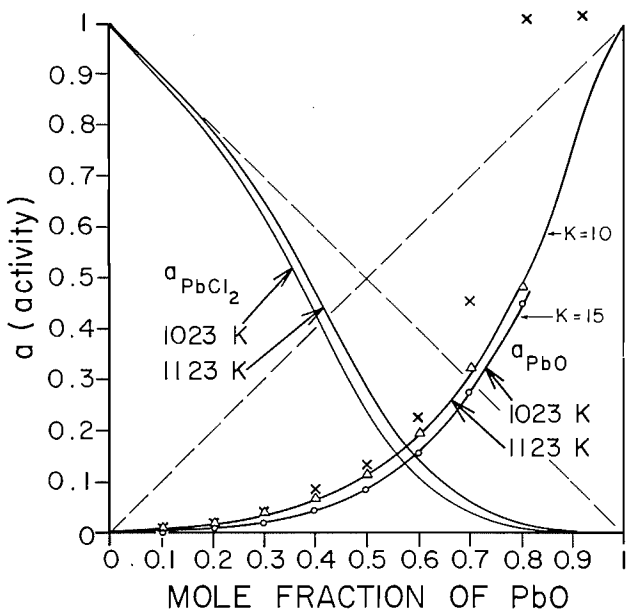

FIG. 2. Activity isotherms for PbO and $PbCl_2$ at 1023 K and 1123 K, respectively. Points (circles and triangles) are from experimental work. Solid lines are calculated from eqs. [10] and [11]. x's are experimental activity data for PbO reported by Sugawara *et al.* (4).

values greater than zero, as in the incongruently melting compounds $3PbCl_2.2PbO$, $PbCl_2.PbO$, $PbCl_2.2PbO$, and $PbCl_2.4PbO$, which have been identified as existing in a solid state within the phase diagram of the system (1–3).

Considering a solution that initially contains n_1 and n_2 moles of PbO and $PbCl_2$, respectively, it will be assumed that a complex forming reaction is taking place until equilibrium is reached.

If a is the fraction of the initial oxygen that has reacted and has been incorporated in the complex oxychloride, then the enthalpy change for the formation of the solution is given as

$$[4] \qquad \Delta H_m = n_1 a \Delta H_r^0$$

where ΔH_r^0 is the enthalpy change for the formation of one mole of oxychloride specie containing one gram-atom of oxygen, such as in a molten $(Pb_{p/q}\cdot O\cdot Cl_{r/q})^{(2p-2q-2r/q)+}$ type compound.

The "reaction" part of the enthalpy of mixing is considered to be a major contribution to the total energy released during mixing, and any other secondary interactions between the solute atoms in the reacted system will not be taken into account.

The total entropy of mixing is considered to consist of two major contributions: (*i*) the entropy for the formation of the amount of oxychloride complex present at equilibrium and (*ii*) the configurational contribution for the random mixing of the various specie i present at equilibrium.

The total entropy of mixing may be written as

$$[5] \qquad \Delta S_m = n_1 a \Delta S_r^0 - R\sum_i n_1 \ln N_i$$

where n_i and N_i are, respectively, the number of moles and the ionic fractions of species i present in the mixture at equilibrium.

Combination of eqs. [4] and [5] into the Gibbs–Helmholtz relationship yields the Gibbs free energy of mixing as

$$[6] \qquad \Delta G_m = n_1 a(\Delta H_r^0 - T\Delta S_r^0) + RT\sum_i n_i \ln N_i$$

where

$$[7] \qquad \Delta H_r^0 - T\Delta S_r^0 = -RT \ln K$$

K is the equilibrium constant for a given oxychloride formation reaction, which is dependent only on temperature.

The expression for the activities of PbO is obtained by partial differentiation of eq. [7] with respect to n_1 at constant n_2 and under the restriction that

$$[8] \qquad \sum_i N_i = 1, \qquad \text{at equilibrium,}$$

or

$$\sum_i \left| \frac{n_i}{N_i} \cdot \frac{dN_i}{dn_1} \right|_{n_2} = 0$$

The final equation takes the form:

$$[9] \qquad \ln a_{PbO} = \sum_i \left| \ln N_i \left(\frac{dn_i}{dn_1} \right)_{n_2} \right| - \left| n_i \left(\frac{da}{dn_1} \right)_{n_2} + a \right| \ln K$$

Can. J. Chem. Downloaded from www.nrcresearchpress.com by 91.144.44.67 on 09/07/12
For personal use only.

TABLE 4. Ionic composition of the PbO–$PbCl_2$ molten solutions representing the reaction $2Pb^{2+} + O^{2-} + 2Cl^- = Pb_2OCl^+ + Cl^-$

Unreacted melt			Melt composition when reaction has reached equilibrium	
Composition	No. of moles	Mole fractions	Mole numbers at equilibrium	Ion fractions
PbO	n_1	X_1	$n_{Pb^{2+}} = n_1 + n_2 - 2an_1$	$N_{Pb^{2+}} = \dfrac{1 - aX_1}{1 - 2aX_1}$
$PbCl_2$	n_2	X_2	$n_{Pb_2OCl^+} = an_1$	$N_{Pb_2OCl^-} = \dfrac{aX_1}{1 - aX_1}$
			$n_{O^{2-}} = n_1(1 - a)$	$N_{O^{2-}} = \dfrac{X_1(1 - a)}{1 + X_2 - 2aX_1}$
			$n_{Cl^-} = 2n_2 - an_1$	$N_{Cl^-} = \dfrac{2X_2 - aX_1}{1 + X_2 - 2aX_1}$

TABLE 5. Dependence of degree of reaction α on the equilibrium constant, K, at various compositions, for the reaction $Pb^{2+} + O^{2-} + Cl^- \rightarrow Pb_2OCl^+$

	α						
X_{PbO}	$K = 1$	$K = 10$	$K = 15$	$K = 100$	$K = 1000$	$K = 10\,000$	$K = \infty$
0.0	1	1	1	1	1	1	1
0.1	0.32183	0.81296	0.86579	0.97676	0.99762	0.99976	1
0.2	0.30941	0.78486	0.84143	0.97038	0.99691	0.99969	1
0.3	0.29576	0.74659	0.80520	0.95713	0.99525	0.99952	1
0.4	0.28035	0.69702	0.75367	0.92370	0.98886	0.99881	1
0.5	0.26216	0.63809	0.68849	0.84653	0.93307	0.96991	1
0.6	0.23926	0.57257	0.61545	0.74321	0.80369	0.82380	0.83333
0.7	0.20976	0.49620	0.53292	0.64094	0.69062	0.70674	0.71428
0.8	0.16765	0.37906	0.40544	0.47618	0.49709	0.49970	0.50000
0.9	0.09229	0.19302	0.20171	0.21883	0.22188	0.22219	0.22222
1.0	0	0	0	0	0	0	0

It is readily seen that the expression for the activity of PbO contains the equilibrium constant K as the only adjustable parameter.

The solution of eq. [9] is readily found by considering the mass balances representing various reaction mechanisms. Irrespective of the scheme chosen, the expression for the activity is always found to have the following form:

[10] $$a_{PbO} = (N_{Pb^{2+}} \cdot N_{O^{2-}})_{equilibrium}$$

In eq. [10], $N_{Pb^{2+}}$ and $N_{O^{2-}}$ are, respectively, the ionic fractions for Pb^{2+} and O^{2-} in a molten mixture of PbO and $PbCl_2$ that has reacted internally in accordance with a specific reaction mechanism and has reached a state of equilibrium.

From similar considerations it may be shown that the activity of $PbCl_2$ is given by the expression:

[11] $$a_{PbCl_2} = (N_{Pb^{2+}} \cdot N_{Cl^-}^2)_{equilibrium}$$

For the PbO–$PbCl_2$ solutions, several reaction mechanisms have been considered, such as the formation of the complex oxychlorides, Pb_2OCl^+, Pb_2O^{2+}, $PbCl_2O^{2-}$, as well as the compositions representing the various incongruently melting compounds mentioned earlier.

From all these possible schemes the experimental data appear to be best represented by the reaction:

[12] $$2Pb^{2+} + O^{2-} + Cl^- = Pb_2OCl^+$$

The mass balance representing eq. [12] is given in Table 4. The equilibrium constant is written as

[13] $$K = \frac{N_{Pb_2OCl^+}}{N_{Pb^{2+}}^2 \cdot N_{O^{2-}} \cdot N_{Cl^-}}$$

for which the expressions for the ionic fractions are given in Table 4.

Degrees of reaction α have been estimated for various selected K values from eq. [13], and are given in Table 5.

From the equilibrium ion fractions given in Table 4, the activities for PbO and $PbCl_2$ are readily calculated as

[14] $$a_{PbO} = \frac{1 - 2aX_1}{1 - aX_1} \cdot \frac{X_1(1 - a)}{1 + X_2 - 2aX_1}$$

and

[15] $$a_{PbCl_2} = \frac{1 - 2aX_1}{1 - aX_1} \cdot \left| \frac{2X_2 - aX_1}{1 + X_2 - 2aX_1} \right|^2$$

where X_1 and X_2 in these expressions are respectively the primary mole fractions of PbO and $PbCl_2$ in the "unreacted" mixture. Details for the mathematical treatment are given in Appendix A.

Can. J. Chem. Downloaded from www.nrcresearchpress.com by 91.144.44.67 on 09/07/12
For personal use only.

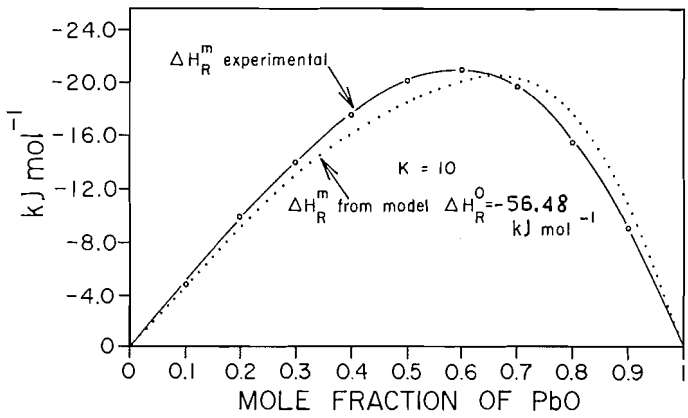

FIG. 3. Plot of the integral heat of mixing as a function of the PbO mole fraction in the PbO–$PbCl_2$ melts. Dotted line has been calculated from eq. [17] for $K = 10$.

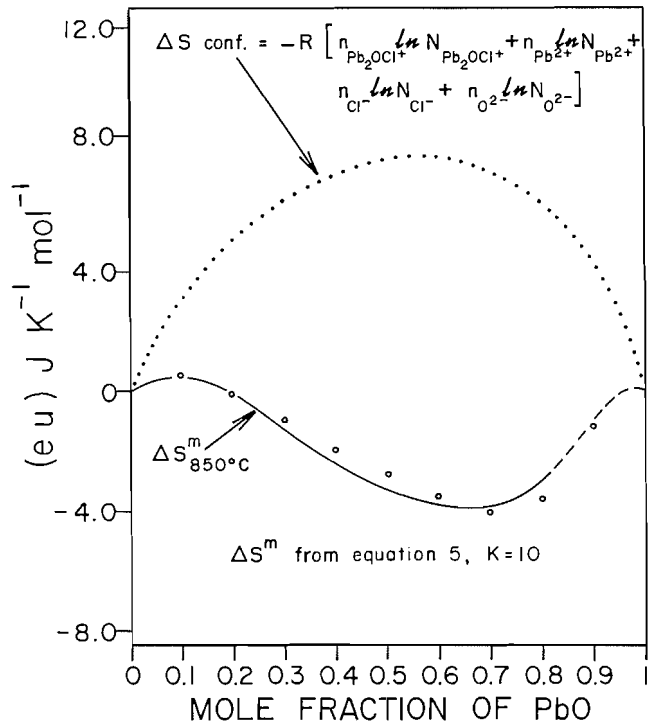

FIG. 4. Integral molar entropies of mixing plotted as a function of the PbO content in the PbO–$PbCl_2$ melts. Solid line represents the total entropy calculated from eq. [5] for $K = 10$. Points are from the experimental results. Dotted line represents the configurational component of the total entropy.

The activity isotherms shown in Fig. 2 were calculated from eqs. [14] and [15] (solid lines), while the points are experimental. The 1023 K isotherm was calculated from a values corresponding to $K = 15$. The isotherm at 1123 K was calculated from a values based on $K = 10$.

It should be noticed that at constant composition the activity of a_{PbO} increases as K decreases.

The integral enthalpy of mixing for the system was calculated from the expression:

$$[16] \quad \Delta H_m = X_1\overline{\Delta H}_{PbO} + X_2\overline{\Delta H}_{PbCl_2}$$

For the calculation, the partial molar enthalpies of mixing for $PbCl_2$ were obtained from the partial molar enthalpies of mixing of PbO using the Gibbs–Duhem relationship.

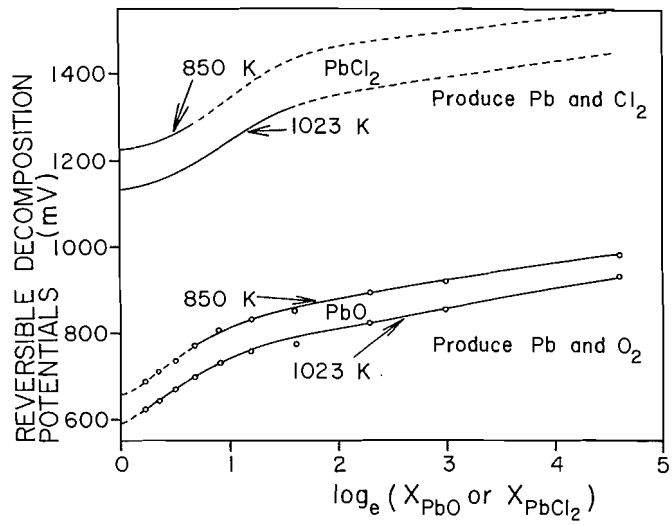

FIG. 5. Reversible decomposition potentials for PbO and $PbCl_2$ in the PbO–$PbCl_2$ melts at 850 K and 1023 K, respectively.

The results of these calculations are given in Fig. 3. On this graph the points are experimental, while the dotted line has been derived from eq. [4] written in the form:

$$[17] \quad \Delta H_m = aX_1\Delta H_r^0$$

which represents the enthalpy of mixing *per mole* of solution.

For the calculation, the degrees of reaction, based on reaction [12] for $K = 10$, have been used. The value for the ΔH_r^0 term, which must be common for all compositions, is -56.48 kJ mol^{-1}.

Entropies of mixing, calculated from the enthalpies of mixing and the corresponding Gibbs free energies, are plotted in Fig. 4 as a function of composition. Here the solid line represents the experimental values for the total integral entropy of mixing, while the points are calculated from eq. [5], as applied to reaction [12], for $K = 10$. For this calculation the a values that correspond to $K = 10$ and a common value of $\Delta S_r^0 = -32.34$ eu were found to satisfy the entire composition range. The dotted line in Fig. 4 represents only the configurational component of the total integral entropy of mixing.

Considering the uncertainty that is always present when calculating entropies, the agreement between the experimental and the theoretical entropies of mixing and, particularly, the correct prediction of their concentration dependence indicates the validity of the present thermodynamic model.

Electrolytic behaviour of the PbO–$PbCl_2$ melts

From eq. [2] and its equivalent for $PbCl_2$, it is possible to calculate the reversible potentials for the electrochemical separation of Pb and O_2, or of Pb and Cl_2, from a molten solution of PbO and $PbCl_2$.

For the reactions

$$[18] \quad Pb_{liq} + Cl_{2(g,\ 1\ atm)} = (PbCl_2)_{in\ solution}$$

and

$$[19] \quad Pb_{liq} + \tfrac{1}{2}O_{2(g,\ 1\ atm)} = (PbO)_{in\ solution}$$

the reversible electrode potentials at 850 and 1023 K, respectively, were calculated using the previously derived activity values and the standard potentials given in Table 2.

The results of these calculations are plotted in Fig. 5. Because of the wide potential separation, the electrolysis of the PbO–$PbCl_2$ is almost independent of melt composition and, consequently, lead chloride melts may be deoxygenated by pre-electrolysis.

Can. J. Chem. Downloaded from www.nrcresearchpress.com by 91.144.44.67 on 09/07/12
For personal use only.

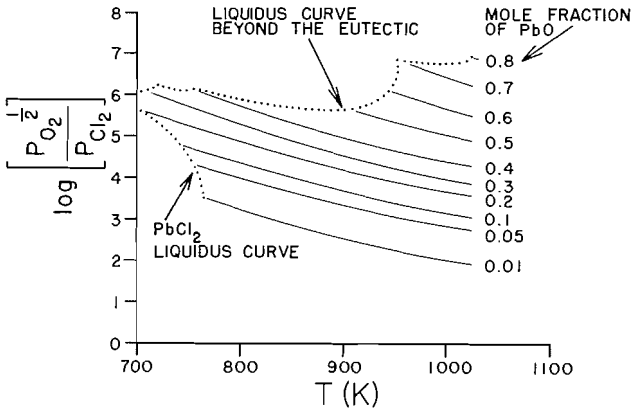

FIG. 6. Chlorination conditions for PbO in PbO–$PbCl_2$ molten solutions, at various temperatures and $P_{O_2}^{1/2}/P_{Cl_2}$ gas ratios.

Fused salt electrolysis of PbO dissolved in a $PbCl_2$ solvent is expected to produce lead and oxygen, respectively, as cathodic and anodic products.

Chlorination of PbO

The reaction of PbO in solution with gaseous chlorine at high temperatures may be written as

[20] $$(PbO) + Cl_{2(g)} \rightleftharpoons (PbCl_2) + \tfrac{1}{2}O_{2(g)}$$

where PbO and $PbCl_2$ are present as a molten solution.

Considering chlorination at constant temperature, in a closed system, equilibrium will be established between the molten solution and a gaseous mixture containing Cl_2 and O_2.

For reaction [20] the equilibrium constant is

[21] $$K = \frac{P_{O_2}^{1/2}}{P_{Cl_2}} \cdot \frac{a_{PbCl_2}}{a_{PbO}}$$

where K calculated from the standard potentials listed in Table 2 has the following values:

T (K)	K
725	3.5×10^{7}
850	5.3×10^{6}
960	5.9×10^{5}
1023	2.1×10^{5}

From the present results the activities of PbO and of $PbCl_2$ are readily calculated over the entire composition range at the same temperatures.

Accordingly, the equilibrium ratio P_{O_2}/P_{Cl_2} has been calculated from eq. [21] for various compositions and the results are given in Fig. 6, as an equilibrium predominant area type diagram in which the temperature–composition boundaries of the molten solutions correspond to those given in the phase diagram of the PbO–$PbCl_2$ system (1).

In any open system, the chlorination of PbO would require that the P_{O_2}/P_{Cl_2} ratios over the melts satisfy at all times the thermodynamic conditions given in Fig. 6. It is evident that chlorination of mixtures containing about 1 mol% at a low temperature of about 773 K is possible with a gaseous mixture containing chlorine at a partial pressure of only 10^{-4} atm (1 atm = 101.3 kPa).

Conclusions

The thermodynamic properties of the PbO–$PbCl_2$ molten solutions show pronounced negative deviations from ideality that are indicative of strong interactions between the ionic species in solution. To explain this behaviour and to predict the concentration dependence of the activities of PbO and of $PbCl_2$, of the enthalpies and of the entropies of mixing, a thermodynamic model based on the presence of strong complex oxychloride species has been developed. In this model the concentration dependence of the activities at each temperature requires the equilibrium constant K as the only adjustable parameter. The concentration dependence of the enthalpy of mixing is predicted from eq. [17] in which the only other adjustable parameter is the term ΔH_r^0, which, however, is constant over the entire composition range. The calculation of the entropies of mixing does not require any other adjustable parameters. K and ΔS_r^0 are related by eq. [7] and ΔS_r^0 cannot be adjusted independently.

It is shown that in non-ideal solutions the activity of any component A_xB_y is expressed by the simple relationship:

$$a_{A_xB_y} = (N_{A^{x+}}^{x} \cdot N_{B^{y-}}^{y})_{\text{equilibrium}}$$

In this expression $N_{A^{x+}}$ and $N_{B^{y-}}$ are the respective cation and anion fractions in a solution that has the ionic composition corresponding to a specific reaction mechanism *at equilibrium*.

Thus Temkin's rule (16) is of general validity for *ideal* and *non-ideal* solutions, providing that the correct reaction mechanism and dissociation schemes are formulated.

In this treatment non-ideality is attributed to changes in the composition of a solution as the result of complex forming reactions. The theory does not account for secondary interactions between the reaction products. Equilibrium ion fractions of the assumed ionic forms are used throughout, the basic assumption being that the reactivity of the simple ionic species like Pb^{2+}, O^{2-}, or Cl^- has been satisfied through the formation of the complex and that all other interactions are not too significant.

Under such circumstances, the equilibrium constant K is expected to be composition independent and to depend only on temperature over the composition range within which the above assumptions are valid.

Acknowledgements

The authors acknowledge the valuable contribution by Peter King to the initial part of this work. The financial assistance by the Natural Sciences and Engineering Research Council of Canada is also gratefully acknowledged.

1. M. RENAUD, E. POIDATZ, and F. E. CHAIX. Can. J. Chem. **48**, 2061 (1970).
2. R. RUER. Z. Anorg. Chem. **29**, 372 (1906).
3. A. VARONI. Atti Accad. Naz. Lincei, Classe Sci. Fis. Mat. Nat. Rend. **20**, 384 (1934).
4. H. SUGAWARA, K. NAGATA, and K. S. GOTO. Metall. Trans. B: **8B**, 511 (1977).
5. G. G. CHARETTE and S. N. FLENGAS. J. Electrochem. Soc. **115**, 796 (1968).
6. K. KIUKKOLA and C. WAGNER. J. Electrochem. Soc. **104**, 308 (1957); **104**, 379 (1957).
7. C. B. ALCOCK and T. N. BELFORD. Trans. Faraday Soc. **60**, 822 (1964).
8. J. F. ELLIOTT and M. GLEISER. Thermochemistry for steel making. Vol. 1. Addison–Wesley, 1960.
9. R. A. RAPP. Trans. Soc. Min. Eng. AIME, **227**, 371 (1965).
10. B. C. H. STEELE and C. B. ALCOCK. Trans. Soc. Min. Eng. AIME, **233**, 1359 (1965).
11. B. C. H. STEELE. *In* Electromotive force measurements in high temperature systems. *Edited by* C. B. Alcock. Elsevier, New York. 1968. pp. 3–27.

Can. J. Chem. Downloaded from www.nrcresearchpress.com by 91.144.44.67 on 09/07/12
For personal use only.

12. A. LEUNG and W. T. THOMPSON. Can. Metall. Q. **15**, 227 (1976).
13. M. IWASE, K. FUJIMURA, and T. MORI. Trans. Jpn. Inst. Met. **19**, 377 (1964).
14. Y. MATSUSHITA and K. GOTO. J. Fac. Eng. Univ. Tokyo Ser. B, **27**, 217 (1964).
15. D. R. GASKELL. Intro. Metall. Therm., 2nd ed. McGraw–Hill, New York. 1981. p. 327.
16. M. TEMKIN. J. Phys. Chem. USSR, **20**, 105 (1946).

Appendix A

Considering the reaction model

$$2Pb^{2+} + O^{2-} + Cl^- \rightleftharpoons Pb_2OCl^+$$

the activity of PbO is given by eq. [9], which may be written in an expanded form as

$$[A\text{-}1] \quad \ln a_{PbO} = -\left[x\left(\frac{\partial \alpha}{\partial n_1}\right)_{n_2} + \alpha \right] \ln K + \ln N_{Pb^{2+}}\left(\frac{\partial n_{Pb^{2+}}}{\partial n_1}\right) + \ln N_{Cl^-}\left(\frac{\partial n_{Cl^-}}{\partial n_1}\right)_{n_2} + \ln N_{O^{2-}}\left(\frac{\partial n_{O^{2-}}}{\partial n_1}\right)_{n_2} + \ln N_{Pb_2OCl^+}\left(\frac{\partial n_{Pb_2OCl^+}}{\partial n_1}\right)_{n_2}$$

where

$$[A\text{-}2] \quad K = \frac{N_{Pb_2OCl^+}}{N^2_{Pb^{2+}} \cdot N_{O^{2-}} \cdot N_{Cl^-}}$$

where the n's are mole numbers and α is the degree of reaction per mole of O^{2-}; n_1 and n_2 are, respectively, the moles of PbO and $PbCl_2$ initially present in the melt.

The expressions for the partial differentials given in eq. [A-1] are readily obtained as

$$[A\text{-}3] \quad \left(\frac{\partial n_{Pb^{2+}}}{\partial n_1}\right)_{n_2} = 1 - 2\alpha - 2n_1\left(\frac{\partial \alpha}{\partial n_1}\right)_{n_2}$$

$$[A\text{-}4] \quad \left(\frac{\partial n_{Cl^-}}{\partial n_1}\right)_{n_2} = -\alpha - n_1\left(\frac{\partial \alpha}{\partial n_1}\right)_{n_2}$$

$$[A\text{-}5] \quad \left(\frac{\partial n_{O^{2-}}}{\partial n_1}\right)_{n_2} = 1 - \alpha - n_1\left(\frac{\partial \alpha}{\partial x}\right)_{n_2}$$

and

$$[A\text{-}6] \quad \left(\frac{\partial n_{Pb_2OCl^+}}{\partial n_1}\right)_{n_2} = \alpha + n_1\left(\frac{\partial \alpha}{\partial n_1}\right)_{n_2}$$

Introduction of the expressions [A-2], [A-3], [A-4], [A-5], and [A-6] into expression [A-1] yields

$$a_{PbO} = (N_{Pb^{2+}} \cdot N_{O^{2-}})_{equilibrium}$$

It should be noted that an analytical expression for $\left(\frac{\partial \alpha}{\partial n_1}\right)_{n_2}$ may be obtained from the condition that, at constant temperature, $\left(\frac{\partial K}{\partial n_1}\right)_{n_2,T} = 0$.

All terms in eq. [A-1] that contain $\left(\frac{\partial \alpha}{\partial n_1}\right)_{n_2}$ cancel out.

Can. J. Chem. Downloaded from www.nrcresearchpress.com by 91.144.44.67 on 09/07/12
For personal use only.

Single-ion Setschenow coefficients for several hydrophobic non-electrolytes in aqueous electrolyte solutions

P. PEREZ-TEJEDA, A. MAESTRE,[1] AND P. DELGADO-COBOS
Departamento de Química Física, Universidad de Sevilla, Sevilla 41072, Spain
AND
J. BURGESS[1]
Department of Chemistry, University of Leicester, Leicester LE1 7RH, U.K.

Received July 1, 1988[2]

P. PEREZ-TEJEDA, A. MAESTRE, P. DELGADO-COBOS, and J. BURGESS. Can. J. Chem. **68**, 243 (1990).

Setschenow coefficients have been derived from solubility measurements on cyclohexane, benzene, naphthalene, 1-naphthol, 1,5-dihydroxynaphthalene, and anthracene in alkali halide, tetraalkylammonium bromide, and tetraphenylarsonium chloride aqueous solutions at 298.2 K. Single ion Setschenow coefficients have thence been obtained by an assumption involving extrapolation of the tetraalkylammonium bromide results to zero cation volume. Setschenow coefficients for the tetraalkylammonium cations correlate well with a hydrophobicity parameter based on their transfer chemical potentials from water into 1,2-dichloroethane.

Key words: solubilities, aqueous salt solutions, Setschenow coefficients.

P. PEREZ-TEJEDA, A. MAESTRE, P. DELGADO-COBOS et J. BURGESS. Can. J. Chem. **68**, 243 (1990).

On a évalué les coefficients de Setschenow, en se basant sur des mesures de solubilité du cyclohexane, de l'hexane, du benzène, du naphtalène, du 1-naphtol, du 1,5-dihydroxynaphtalène et de l'anthracène dans des solutions aqueuses d'halogénures alcalins, de bromure de tétraalkylammonium et de chlorure de tétraphénylarsonium effectuées à 298,2 K. On a ensuite déterminé les coefficients de Setschenow pour des ions uniques en utilisant une hypothèse impliquant une extrapolation, à un volume cationique de zéro, des résultats obtenus avec le bromure de tétraalkylammonium. Il existe une bonne corrélation entre les coefficients de Setschenow obtenus pour les cations tétraalkylammonium et un paramètre d'hydrophobicité basé sur les potentiels de transfert chimique de l'eau au 1,2-dichloroéthane.

Mots clés : solubilités, solutions aqueuses de sels, coefficients de Setschenow.

[Traduit par la revue]

Can. J. Chem. Downloaded from www.nrcresearchpress.com by 91.144.44.67 on 09/07/12
For personal use only.

Introduction

Salt effects on solubilities of non-electrolytes have been the focus of numerous studies for several decades. Several theories have been used to characterise the essential features of the salting phenomenon (1–3). The influence of a salt on the solubility of a non-electrolyte is usually characterised and quantified by the Setschenow coefficient, or salting constant, k_s. This is estimated by solubility, distribution, or vapour pressure experiments:

$$\log(S_0/S) = \log(D/D_0) = m_s k_s$$

Here m_s is the concentration of the dissolved electrolyte, S_0 and S are, respectively, the solubilities of the non-electrolyte in water and in the salt solution, or D_0 and D are the respective distribution ratios between water or salt solution and organic layer. On multiplication of k_s by $2.3RT$ one obtains the change in the standard Gibbs function or, in other words, the transfer chemical potential between water and salt solution. Setschenow coefficients are available for the effects of a number of electrolytes on solubilities of a range of non-electrolytes, but there have been relatively few attempts to determine single ion Setschenow coefficients. However, Fromon and Treiner have detailed two procedures for establishing single ion Setschenow coefficients from k_s values for electrolytes in their extensive study, by vapour pressure measurements, of solubilities of tetrahydrofuran in aqueous salt solutions (4).

In a previous paper (5) we reported Setschenow coefficients for naphthols, noting that k_s decreased with increasing hydrophilic character of the non-electrolyte for a given salt, and that the nature and location of substituents affected k_s in different ways. In the present paper we report extensions of this earlier investigation to the determination of k_s values for cyclohexane, benzene, naphthalene, 1-naphthol, 1,5-dihydroxynaphthalene, and anthracene in aqueous solutions of alkali halides, tetraalkylammonium bromides, and tetraphenylarsonium chloride. We derive Setschenow coefficients for each electrolyte, and discuss the division of these values into single ion components.

Experimental

Materials

1-Naphthol, naphthalene, and anthracene (Fluka puriss.) were used as received. 1,5-Dihydroxynaphthalene (Sigma) was purified by repeated recrystallisation from aqueous methanol. Cyclohexane was HPLC grade (Scharlau); benzene (Riedel De Haën, min. 99.9% GC) was kept over 4A molecular sieve.

Sodium chloride and sodium bromide (Merck p.a.) were dried at 150°C; Ph_4AsCl (Merck) was used as received. Me_4NBr, Et_4NBr, Pr_4NBr, and Bu_4NBr (Fluka) were purified by the method described by Conway *et al.* (6). All salts were kept in a vacuum desiccator prior to use.

Distribution measurements

Distribution ratios of a known amount of 1-naphthol (2.0×10^{-4} mol dm^{-3}) between water or salt solution and cyclohexane were determined after vigorous agitation of thermostatted small aliquots for 15 min. These were allowed to stand in the thermostat bath for a further 2 h before aliquots of the respective layers were taken and analysed spectrophotometrically (Perkin Elmer Lambda 5; $\varepsilon_{293.0} = 4.79 \times 10^3$ and $\varepsilon_{290.3} = 5.27 \times 10^3$ dm^3 mol^{-1} cm^{-1} for 1-naphthol in water and in cyclohexane respectively). These measurements were used to get preliminary estimates of k_s; the main series of experiments used solubility measurements (next paragraph) to obtain k_s values more directly.

[1]Authors to whom correspondence may be addressed.

[2]Revision received September 8, 1989.

TABLE 1. Setschenow coefficients, k_s (kg mol^{-1}) (molar scale)

Salt	Cyclohexane	Benzene	Naphthalene	Anthracene	1-Naphthol	1,5-Dihydroxynaphthalene
NaCl	0.171±0.009	0.186[a]	0.197±0.018	0.306±0.010	0.209±0.008	0.211±0.009
NaBr	0.163±0.010	0.150±0.010	0.144±0.018	0.303±0.015	0.180±0.010	0.155±0.016
Me_4NBr	0.018±0.002	−0.190[a]	−0.338±0.021	−0.673±0.080	−0.390±0.023	−0.498±0.049
Et_4NBr	−0.084±0.010	−0.300[a]	−0.836±0.066	−1.64±0.09	−1.18±0.03	−1.64±0.04
n-Pr_4NBr	−0.190±0.009	−0.480[a]	−1.25±0.08	−2.69±0.05	−1.88±0.18	—
n-Bu_4NBr	−0.293±0.024	−0.650[a]	−1.79±0.13	−3.70±0.34	−2.68±0.10	—
Ph_4AsCl	−5.48±0.26	−3.16±0.04	−5.77±0.41[b] −5.20±0.15[c]	—	−5.97±0.16	—

[a]Taken from ref. 11.
[b]Chromatographic method.
[c]Spectrophotometric method.

Solubility measurements

The solubilities of cyclohexane, benzene, naphthalene, 1-naphthol, 1,5-dihydroxynaphthalene, and anthracene in water and in salt solutions were determined in the following manner. An excess of the non-electrolyte was added to 40 cm^3 of water or salt solution in a Pyrex flask with a Teflon stopper, and allowed to equilibrate (at 298.2 K) for 30 min. The solutions were stirred at ca. 25 000 rpm for 8 min with a Virtis model 23 homogenizer. After equilibrium was reached, aliquots from these solutions were removed and the concentrations of the non-electrolytes were obtained by an appropriate technique.

Spectrophotometric measurement was used for naphthalene ($\varepsilon_{275} = 4.68 \times 10^3$) and for 1,5-dihydroxynaphthalene ($\varepsilon_{328.7} = 5.13 \times 10^3$) with all salts studied. The very low solubility of anthracene in water precluded the determination of an accurate extinction coefficient. To obtain k_s values for this non-electrolyte we plotted log(absorbance) vs. salt concentration and measured the slopes of these plots. This method was used for R_4NBr solutions (at $\lambda = 251.3$ nm). Solubilities of anthracene in water and in NaCl and NaBr solutions were obtained by fluorescence measurements (Perkin Elmer 650-40 spectrofluorimeter); the excitation and fluorescence wavelengths were chosen at 355 and 401 nm respectively. Aliquots were removed and diluted (50% by volume aqueous ethanol) prior to their quantification.

Chromatographic methods were used for determining solubilities of cyclohexane with all salts studied, of benzene in water and in Ph_4AsCl solution, and of naphthalene in water. A Hewlett-Packard model 5890 instrument equipped with a flame ionisation detector was used. A small amount of glass wool was introduced into the glass liner to trap the salts. A packed stainless steel column (2 m × 1/8 in.) filled with 10% FFAP/Chromosorb W-AW-DMCS (80/100 mesh) was used. Concentrations were determined by measuring areas under chromatographic peaks with a Hewlett–Packard 3390A integrating recorder, using the internal standard method.

Results and discussion

Solubilities of 6.63×10^{-4}, 2.28×10^{-2}, 2.64×10^{-4} (spectrophotometry) and 2.58×10^{-4} (chromatography), 9.39×10^{-3}, 1.46×10^{-3}, and 3.40×10^{-7} mol dm^{-3} were obtained for cyclohexane, benzene, naphthalene, 1-naphthol, 1,5-dihydroxynaphthalene, and anthracene respectively. These values agree within experimental uncertainty with those obtained by previous workers (7–10).

Values of k_s, for each salt on each non-electrolyte, on the molar scale, are given in Table 1. We have also included in this table data for benzene in NaCl and R_4NBr solutions (11). Uncertainties are given as $\pm t\sigma/\sqrt{N}$ (95% confidence limits). Our results are compatible with k_s values obtained by earlier workers for aromatic non-electrolytes in alkali and tetraalkylammonium halide solutions (1–5, 12). The data in this table provide a reasonably self-consistent assembly according to the "additivity rule", and it is thus not unreasonable to attempt to dissect the k_s values for the electrolytes into single ion values. Fromon and Treiner discussed two methods for such a dissection, and showed that in their system they gave very similar results. The first method involved the use of the ubiquitous TATB assumption (13), in this case simply that $k_s(Ph_4As^+) = k_s(BPh_4^-)$. The TATB assumption has been used in many aspects of electrochemistry and is favoured by many workers (14). Unfortunately we cannot use this assumption here, for several reasons. Most seriously, we are unable to obtain precise and reproducible values for k_s for solutions of non-electrolytes in $NaBPh_4$ solutions. This is mainly attributable to the low solubility of $NaBPh_4$ in water and the consequent short range of concentrations available for Setschenow plots. However, there are other problems with this salt, such as its small but significant solubility in several organic solvents, which precludes the use of distribution methods. The TATB assumption is also difficult to apply to anthracene, since both Ph_4As^+ and BPh_4^- cause quenching problems with the spectrofluorimetric determination of the anthracene, and to 1,5-dihydroxynaphthalene, where solubility measurements proved unsatisfactory in Ph_4AsCl (Table 1).

We therefore employed Fromon and Treiner's second method, based on extrapolation to zero molecular weight for results for Me_4N^+, Et_4N^+, Pr_4N^+, and Bu_4N^+ bromides (but not Ph_4As^+, see below). Plots of k_s for R_4NBr against the molecular weights of the cations (Fig. 1) when extrapolated to zero molecular weight give values of k_s (Br^-) for the respective non-electrolytes. Once these values have been established, they can be used with the whole salt values in Table 1 to obtain a complete set of single ion k_s values (Table 2). There is a general increase in magnitude of k_s with increasing size of the non-electrolyte, for the hydrocarbon solutes; the incorporation of a hydroxyl group also leads to a marked increase in k_s, both for cations and for anions. These qualitative trends are in accord with trends earlier observed in relation to k_s values for whole salts (12, 15). Table 2 also includes Fromon and Treiner's results for tetrahydrofuran (4), where k_s values are of a similar order of magnitude to those for cyclohexane for the halides. However, for cations, k_s values for tetrahydrofuran are smaller than those for all the compounds we have studied.

The salting-out effects of Cl^- and of Br^- may be considered in terms of the combined action of two factors (16). First, water molecules are usually more polarised by ionic fields than non-electrolyte molecules. Therefore water will be more attracted by these ions, resulting in an increase in the non-electrolyte activity coefficient (salting-out). This attraction follows the order of increasing ionic field, $Cl^- > Br^-$. Secondly, the overlap bet-

Can. J. Chem. Downloaded from www.nrcresearchpress.com by 91.144.44.67 on 09/07/12
For personal use only.

TABLE 2. Single-ion k_s values

Non-electrolyte	Cl^-	Br^-	Na^+	Me_4N^+	Et_4N^+	$n\text{-}Pr_4N^+$	$n\text{-}Bu_4N^+$	Ph_4As^+
Cyclohexane	0.163	0.155	0.008	−0.138	−0.239	−0.345	−0.448	−5.65
Benzene	0.066	0.035	0.120	−0.225	−0.335	−0.515	−0.685	−3.23
Naphthalene	0.364	0.292	−0.148	−0.630	−1.12	−1.54	−2.08	−6.13
1-Naphthol	0.632	0.603	−0.423	−0.993	−1.78	−2.48	−3.28	−6.55
Anthracene	0.685	0.682	−0.379	−1.35	−2.32	−3.37	−4.38	—
cf. THF[a]	0.164	0.091	0	−0.014	−0.091	−0.145	−0.204	−0.521

[a]Taken from ref. 4.

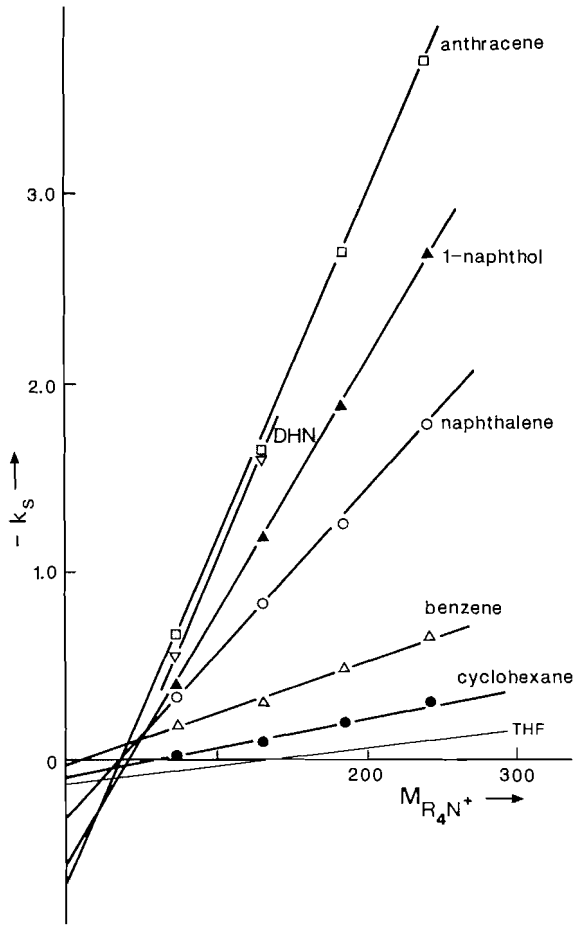

FIG. 1. Plots of Setschenow coefficients, k_s, against tetraalkylammonium molecular weight, $M_{R_4N^+}$ (R = Me, Et, *n*-Pr, *n*-Bu).

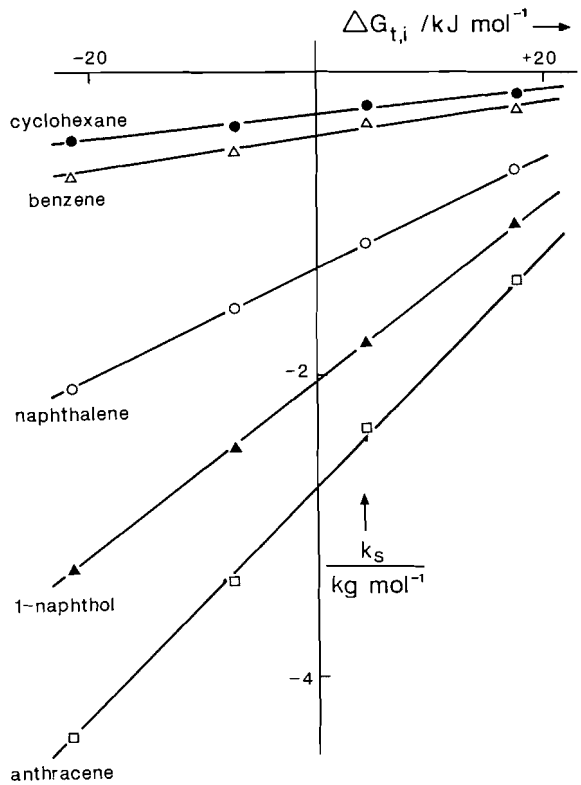

FIG. 2. Plots of single-ion Setschenow coefficients, k_S, against Gibbs free energies of transfer of R_4N^+ cations from water into 1,2-dichloroethane.

ween the cospheres around ions and non-electrolytes may produce a repulsive interaction, also resulting in salting-out (17, 18). However, these cosphere interactions are complicated, and it would be wise to wait until considerably more experimental data are available before attempting to produce a general rationalisation.

The decrease in single ion k_s values with increasing size of R_4N^+ ions is principally caused by the combined action of two factors, van der Waals dispersive forces and hydrophobic interactions. The former seems the more important, at least in the cases of cyclohexane and benzene. However, cyclohexane, being bigger and more hydrophobic than benzene, should show a stronger salting-in effect than benzene. A possible explanation for the observed (Table 2) salting-in difference between cyclohexane and benzene is that van der Waals interactions are higher in the case of benzene because of its aromatic character (19). In this connection we note that k_s for Ph_4As^+ in relation to cyclohexane is out of line with the overall pattern of values in Table 2. It is interesting to relate single ion k_s values for the R_4N^+ cations with other hydrophobicity parameters (20), such as their Gibbs free energies of transfer from water into an organic solvent such as 1,2-dichloroethane (21). Figure 2 indicates a linear correlation in this case; the hydrophobic nature of these R_4N^+ cations is manifested in a similar manner in these two parameters. The Ph_4As^+ cation cannot be included in these correlations; points for this cation lie a long way off the R_4N^+ correlation lines of Figs. 1 and 2. This is also true when Fromon and Treiner's data (4) for tetrahydrofuran are plotted in similar fashion. Again, a plot of k_s values for trisacetylacetonatocobalt(III) against partial molar volumes shows a marked discontinuity between the points for aliphatic R_4N^+ and aromatic Ph_4P^+ and BPh_4^- (22). Clearly, size is not the only factor for these large hydrophobic ions; various types of specific interactions must be invoked. In this context it is interesting to compare the k_s values of $Fe(CN)_2(bipy)_2$, $Fe(CN)_2(sbl)_2$, and $Fe(CN)_2(sb2)_2$ in 0.2 mol dm^{-3}

Can. J. Chem. Downloaded from www.nrcresearchpress.com by 91.144.44.67 on 09/07/12
For personal use only.

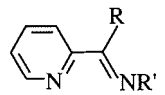

sb1 R = Me, R' = H
sb2 R = R' = Ph

Ph_4AsCl solution.[3] Salting-in is very much more marked for the complex containing the very hydrophobic Schiff base ligand (sb2) than for that containing 2,2′-bipyridyl, which in turn is salted-in slightly more efficiently than the smaller and less hydrophobic species $Fe(CN)_2(sbl)_2$; $k_s = 56$, 3.5, and 2.3 respectively. Ligand nature is very important here, as indeed was indicated in the earlier study of k_s values for compounds of this $Fe(CN)_2(LL)_2$ and related types (12). It seems likely that a wider range of non-electrolytes will need to be studied before it is possible to disentangle the various contributions to single-ion k_s coefficients. In particular, it will probably prove advantageous to expand the number and range of uncharged inorganic complexes, as well as of the organic solutes that have dominated this field for so long.

1. B. E. Conway and D. M. Novak. Symposium on Chemistry and Physics of Aqueous Gas Solutions. The Electrochemical Society. 1974. p. 115.
2. R. F. Cross and P. McTigue. J. Phys. Chem. **80**, 814 (1976).
3. C. V. Krishnan and H. L. Friedman. J. Solution Chem. **3**, 727 (1974).
4. M. Fromon and C. Treiner. J. Chem. Soc. Faraday Trans. 1, **75**, 1837 (1979).
5. M. Balon, A. Maestre, E. Muñoz de Miguel, and E. Soria del Hoyo. Can. J. Chem. **61**, 244 (1983).
6. B. E. Conway, R. E. Verral, and J. E. Desnoyers. Trans. Faraday Soc. **62**, 2738 (1966).
7. C. McAuliffe. J. Phys. Chem. **70**, 1267 (1966).
8. R. L. Bohon and W. F. Claussen. J. Am. Chem. Soc. **73**, 1571 (1951).
9. Ya. I. Korenman, E. I. Polumestroya, and E. M. Tishchenko. Russ. J. Phys. Chem. **54**, 1232 (1980).
10. R. S. Pearlman, S. H. Yalkowsky, and S. Banerjee. J. Phys. Chem. Ref. Data, **13**, 555 (1984).
11. J. E. Desnoyers, G. E. Pelletier, and C. Jolicoeur. Can. J. Chem. **43**, 3232 (1965).
12. M. J. Blandamer, J. Burgess, and J. C. McGowan. J. Chem. Soc. Dalton Trans. 616 (1980), and references therein.
13. G. Baugham, E. Grunwald, and G. Kohnstam. J. Am. Chem. Soc. **82**, 5801 (1960); E. M. Arnett and D. R. McKelvey. Rec. Chem. Progr. **26**, 185 (1965);Y. Marcus. Ion solvation. Wiley, New York. 1985.
14. Y. Marcus. J. Chem. Soc. Faraday Trans. 1, **83**, 2985 (1987).
15. F. A. Long and W. F. McDevit. Chem. Rev. **51**, 119 (1952).
16. B. E. Conway. Pure Appl. Chem. **57**, 263 (1980).
17. B. E. Conway. Ionic hydration in chemistry and biophysics. Elsevier, Amsterdam. 1981. Chap. 23.
18. J. E. Desnoyers, M. Arel, G. Perron, and C. Jolicoeur. J. Phys. Chem. **73**, 3346 (1969).
19. C. Tanford. The hydrophobic effect. 2nd ed. Wiley, New York. 1980.
20. G. Rose, A. R. Geselowitz, G. J. Lesser, R. H. Lee, and M. H. Zehfus. Science, **229**, 834 (1985).
21. J. Czapkiewicz and B. Czapkiewicz-Tutaj. J. Chem. Soc. Faraday Trans. 1, **76**, 1663 (1980).
22. E. Iwamoto, Y. Tanaka, H. Kimura, and Y. Yamamoto. J. Solution Chem. **9**, 841 (1980).

[3]J. Burgess. Unpublished observations.

Can. J. Chem. Downloaded from www.nrcresearchpress.com by 91.144.44.67 on 09/07/12
For personal use only.

Thermodynamic properties of the ternary Na–Cu–Te alloy by electromotive force measurements with an alumina solid electrolyte[1]

PETER J. TUMIDAJSKI[2] AND JOHN KUEHLER[3]

Argonne National Laboratory, Chemical Technology Division/Materials Science Program, 9700 South Cass Avenue, Argonne, IL 60439-4837, U.S.A.

Received July 13, 1989

PETER J. TUMIDAJSKI and JOHN KUEHLER. Can. J. Chem. **68**, 247 (1990).

Activity coefficients for sodium metal in the equimolar CuTe alloy were measured up to 54 at.% sodium at 913 K. The experimental technique consisted of an alloy concentration cell with a solid alumina electrolyte. The results indicated that the solutions were Henrian up to 1 at.% sodium. In addition, for dilute sodium concentrations, there is an exosolution effect. However, for the more concentrated solutions, there is some ionicity.

Key words: tellurides, thermodynamics, alkali metals.

PETER J. TUMIDAJSKI et JOHN KUEHLER. Can. J. Chem. **68**, 247 (1990).

Opérant à 913 K et jusqu'à 54 at.% de sodium, on a mesuré les coefficients d'activité du sodium moléculaire dans un alliage équimolaire de CuTe. La technique expérimentale implique une cellule à concentration d'alliage et un électrolyte d'alumine solide. Les résultats indiquent que les solutions obéissent à la loi de Henry jusqu'à 1 atome pourcent de sodium. De plus, pour des concentrations diluées de sodium, on observe un effet d'exosolution. Toutefois, pour les solutions plus concentrées, on observe un certain caractère ionique.

Mots clés : tellurures; thermodynamique; métaux alcalins.

[Traduit par la revue]

Introduction

Pure liquid tellurium occupies an unique position in the periodic table. Albeit commonly considered to be a metal, its electrical properties, like conductivity, cannot be adequately explained by the nearly free electron model for metals. Structurally, tellurium is different from other metals because it has mixed covalent and metallic bonding (1). A structure consisting of tellurium covalently bonded in a network of hexagonal rings or in chain-like assemblies has been proposed to account for many of the unusual properties (2).

The alloys of tellurium have recently attracted much attention because the tellurides exhibit metal-to-nonmetal transitions at specific compositions. A particularly interesting class of tellurium based alloys are the copper tellurides. The electronic properties of the liquid copper tellurides are unusual. The conductivities display a sharp minimum at the stoichiometric composition Cu_2Te_3 and a weak maximum near 15 at.% Cu. In fact, the conductivity of liquid Cu_xTe_{1-x} for alloys with $x < 0.2$ are greater than for pure liquid tellurium (3, 4). Warren, using an NMR technique (5), showed that charge transfer occurs between copper and tellurium, suggesting some ionicity for liquid copper tellurides. Enderby *et al.* (6–8) presented neutron scattering patterns for liquid copper tellurides. Subsequently, the results were interpreted (9, 10) as indicating the existence of Te^{2-} anions in a close packed assembly similar to the molten salt concept of a complex (11). However, there is direct copper-to-copper interaction, and, as a result of bond overlap, there is a significant effect on the bonding characteristics of copper tellurides. The thermodynamic measurements for copper tellurides (12–15) indicate that the chemical interactions are of a mixed metallic and covalent type in consonance with the NMR and neutron diffraction experiments.

The addition of alkali metal to bismuth tellurides has been found to dramatically influence the nature of chemical interactions (16). In this paper, we report on the thermodynamic behavior of sodium in equimolar copper tellurium alloy up to 54 at.% sodium at 913 K. The results provide further insight on how structure and the nature of interactions can be modified in chalcogenide alloys. To our knowledge, this is the first report on the thermodynamic behavior of sodium in copper tellurium alloys.

Experimental

The experimental apparatus and procedure has been described in previous publications (16, 17). The electromotive force cell was a simple alloy concentration cell described schematically as,

$$\underset{\text{(RE)}}{\text{Bi–Na}\|\beta\text{-}Al_2O_3\|}\underset{\text{(CE)}}{\text{Bi–Na}\|\beta\text{-}Al_2O_3\|}\underset{\text{(WE)}}{\text{(CuTe)–Na}}$$

The reference electrode (RE) contained 5 at.% alkali metal. Reference electrodes were calibrated against pure sodium metal using a similar concentration cell. All emfs are reported with pure liquid sodium metal as the reference. The composition of the working electrode (WE) was changed by coulometric titration. In this context, the counter electrode (CE) provided electrical contact, as well as a source or sink of alkali metal during coulometric titration.

Cells were loaded and operated under the protective atmosphere of a He glovebox. Approximately 1.8 g of CuTe were added to the cell in small pieces of vacuum-filtered copper and tellurium. Sodium was added to the WE by coulometric titration technique involving application of a potential across β-Al_2O_3 between the WE and CE. Overvoltages were always maintained to less than 250 mV. Sodium cations are transported through the β-Al_2O_3 solid electrolyte and are subsequently reduced to sodium metal at the WE. There is negligible electronic transport through the solid electrolyte and exactly one mole of the alkali metal will be transported for each Faraday of charge. The introduction of oxides and impurity ions into the WE is prevented, and compositional changes can be closely controlled.

[1]Work performed at Argonne National Laboratory and supported by the U.S. Department of Energy, Division of Materials Sciences, Office of Basic Energy Sciences, under Contract W-31-109-ENG-38. Accordingly, the U.S. Government retains a nonexclusive, royalty-free license to publish or reproduce the published form of this contribution, or allow others to do so, for U.S. Government purposes.

[2]Present address: Department of Materials Engineering, The University of Western Ontario, London, Ont., Canada N6A 5B9.

[3]Present address: Department of Physics and Astronomy, University of Oklahoma, Norman, OK 73019 U.S.A.

Printed in Canada / Imprimé au Canada

Can. J. Chem. Downloaded from www.nrcresearchpress.com by 91.144.44.67 on 09/07/12
For personal use only.

Can. J. Chem. Downloaded from www.nrcresearchpress.com by 91.144.44.67 on 09/07/12
For personal use only.

TABLE 1. Values of emf (with respect to pure Na) and activity coefficients for the Na–Cu–Te system

	X_{Na}	Emf (mV)	ln γ_{Na}
Expt. 1	0.02000	1696.8	−17.590
915.8 K	0.03021	1675.0	−17.726
	0.04035	1656.7	−17.783
	0.05026	1638.6	−17.774
	0.06019	1622.7	−17.752
	0.06998	1608.3	−17.720
	0.08135	1592.7	−17.673
	0.09003	1578.1	−17.589
	0.09999	1565.0	−17.528
	0.13133	1526.1	−17.309
	0.15080	1502.0	−17.141
	0.19092	1433.2	−16.505
	0.21145	1419.6	−16.435
	0.22031	1407.0	−16.316
	0.22569	1398.2	−16.230
	0.23581	1382.3	−16.071
	0.24999	1357.0	−15.809
	0.26000	1337.0	−15.595
	0.27034	1315.2	−15.358
	0.34999	1097.2	−12.854
	0.35999	1091.4	−12.808
	0.37114	1082.6	−12.728
	0.38499	1073.8	−12.652
	0.42008	1072.9	−12.728
	0.44008	1072.9	−12.774
	0.45007	1072.2	−12.789
	0.46003	1072.3	−12.811
	0.47995	1061.7	−12.719
	0.52003	593.4	−6.865
	0.53995	572.3	−6.636
Expt. 2	0.00500	1821.4	−17.868
912.4 K	0.00600	1807.5	−17.874
	0.00700	1795.6	−17.876
	0.00807	1785.2	−17.886
	0.01000	1769.0	−17.895
	0.02000	1720.3	−17.968
	0.03000	1686.3	−17.942
	0.04121	1657.9	−17.898
	0.04999	1639.0	−17.850
	0.06000	1622.0	−17.816
	0.06000	1621.8	−17.807
	0.07173	1592.5	−17.620
	0.08000	1580.0	−17.570
	0.08999	1566.0	−17.510
	0.10000	1552.4	−17.443
	0.11999	1526.7	−17.297
	0.14327	1502.3	−17.164
	0.14986	1494.2	−17.107
	0.18899	1454.3	−16.831
	0.20003	1429.3	−16.571
	0.21997	1401.8	−16.315
	0.24084	1370.4	−16.006
	0.24994	1356.1	−15.861
	0.25999	1338.8	−15.681
	0.28002	1297.0	−15.223
	0.30004	1258.4	−14.802
	0.32287	1093.9	−12.783
	0.33999	1088.7	−12.769
	0.36014	1083.2	−12.756
	0.38026	1071.1	−12.657
	0.40001	1068.7	−12.676
	0.41997	1067.3	−12.707
	0.43997	1066.7	−12.747
	0.46001	1066.1	−12.784
	0.48000	1065.8	−12.822
	0.48973	768.2	−9.057

TABLE 1 (*concluded*)

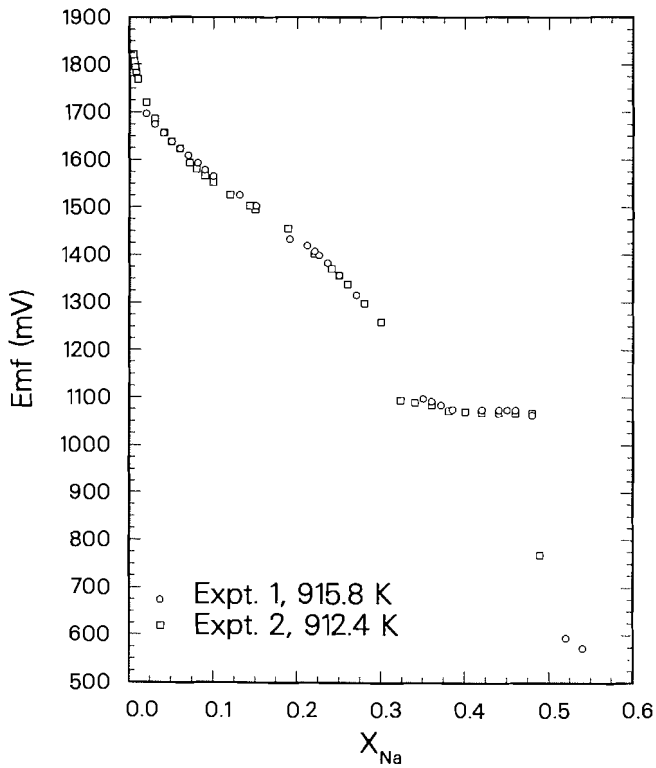

FIG. 1. Variation of cell voltage with composition for the Na–Cu–Te system.

Temperatures were measured with a calibrated (Pt–Pt 10 at.% Rh) thermocouple directly immersed into the CE.

Results and discussion

The cell reaction for the sodium metal concentration cell is,

[1] $Na_{(pure,\ l)} \rightleftarrows \underline{Na}$

where, the line beneath sodium denotes sodium in solution with an equimolar copper telluride. The corresponding Nernst expression is,

$$[2] \quad E = -\frac{RT}{F} \ln \gamma_{Na} - \frac{RT}{F} \ln X_{Na}$$

where F is the Faraday constant, R is the universal gas constant, T is the absolute temperature, and γ_{Na} and X_{Na} represent, respectively, the alkali metal activity coefficient and mole fraction. Figure 1 and Table 1 show the variation of cell voltage as a function of composition for both data sets. There are several interesting features in the Na–CuTe alloy system. There is a region ($0.3 < X_{Na} < 0.5$) where the cell voltage is almost

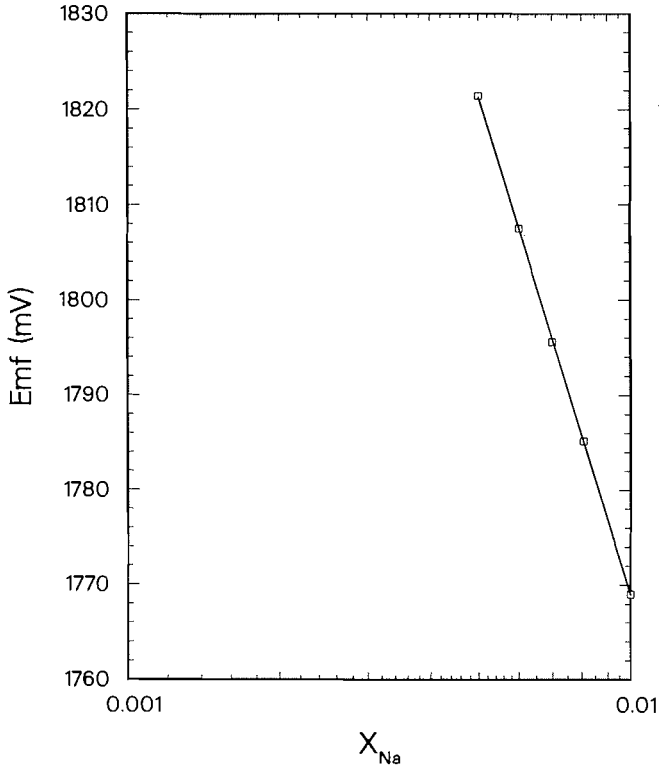

FIG. 2. Nernst plot for the Na–Cu–Te system at 912.4 K. The points represent experimental values; the line is the linear least squares line through the experimental data.

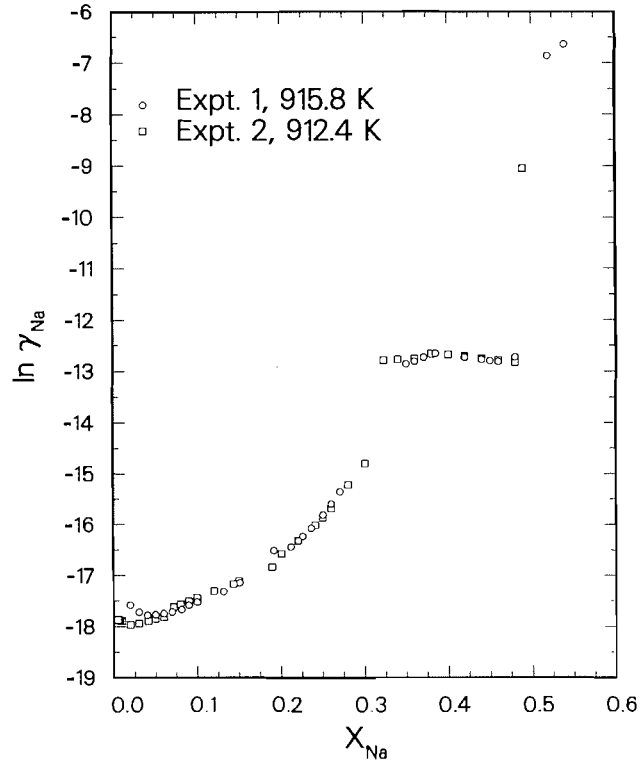

FIG. 3. Variation of ln γ_{Na} with X_{Na} in the Na–Cu–Te system.

composition independent. At $X_{Na} = 0.5$, the cell voltage changes very rapidly with composition, and it appears that for compositions greater than $X_{Na} = 0.5$, the cell voltage again tends to be a constant value. For compositions less than $X_{Na} = 0.30$, the cell voltage varies continuously with composition. The results will be discussed in detail later.

For dilute solutions, less than about $X_{Na} = 0.01$, Henry's law applies. In this case, eq. [2] simplifies to

$$[3] \quad E = E^0_{\underline{Na}} - \frac{RT}{F} \ln X_{Na}$$

where $E^0_{\underline{Na}}$ represents the limiting standard potential of sodium in the molten CuTe alloy. The limiting standard potential defines a hypothetical standard state where the mole fraction of sodium in the CuTe approaches unity, but the sodium metal behaves thermodynamically as if it were infinitely diluted. The Nernst plot at 912.4 K as expressed by eq. [3] is given in Fig. 2 where the emf is plotted against $\log_{10} X_{Na}$. It should be noted that the emf results were obtained for both directions of current in coulometric titration (i.e., $i > 0$, and $i < 0$). Least-squares fitting of the experimental data led to a value of 1.04 for the number of Faraday's transferred, compared to the expected result of one. The limiting standard potential at 912.4 K was calculated to be 1406 ± 2 mV. The corresponding value in the Na–Te binary alloy at 753 K was previously given as 1620 mV (18) and 1596 mV at 800 K (19). It is difficult to ascertain the influence on the sodium limiting standard potential when the solvent composition changes from pure tellurium to CuTe. Lack of data for the Na–Cu binary is compounded by the variances in temperatures in different investigations. However, the resistivity data (3, 4) show that the conductivity for the tellurium-rich side in liquid CuTe has a very weak dependence on composition. It appears that a similar situation exists for limiting standard potentials.

A thermodynamic property, related to limiting standard potential, is the limiting excess chemical potential defined by the expression,

$$[4] \quad \mu^E_0[\underline{Na}] = -FE^0_{\underline{Na}}$$

Accordingly, the value in the present Na–Cu–Te system is $-135.7\,\text{kJ mol}^{-1}$.

As can be seen from Fig. 2, Henrian behavior for sodium in liquid CuTe occurs below approximately $X_{Na} = 10^{-2}$. When the sodium metal content in the CuTe alloys increases, the deviations from Henry's law are significant. The activity coefficient, γ_{Na}, can be calculated at each alloy concentration from eq. [2] which is rearranged to

$$[5] \quad \ln \gamma_{Na} = \left(\frac{FE}{RT}\right) - \ln (X_{Na})$$

Figure 3 shows the isothermal compositional dependence of ln γ_{Na}. The Henrian activity coefficient has been calculated to be $\ln \gamma^h_{Na} = -17.8829$ at 912.4 K. There is a pronounced dip in the ln γ_{Na} values immediately following the Henrian regime. The Na–Te binary system exhibits the same trend (18). Furthermore, in agreement with the cell voltage values reported in Fig. 1, there is an almost negligible concentration dependence for ln γ_{Na} from $X_{Na} = 0.30$ to $X_{Na} = 0.50$, indicating a two-phase regime. It would appear that sodium complexes strongly with tellurium (18); at $X_{Na} = 0.30$, there is sufficient sodium to form sodium telluride. Any remaining sodium reacts less strongly with copper. As a result, the thermodynamic behavior of sodium is primarily determined by the value of sodium activity coefficient in the formed sodium telluride

Can. J. Chem. Downloaded from www.nrcresearchpress.com by 91.144.44.67 on 09/07/12
For personal use only.

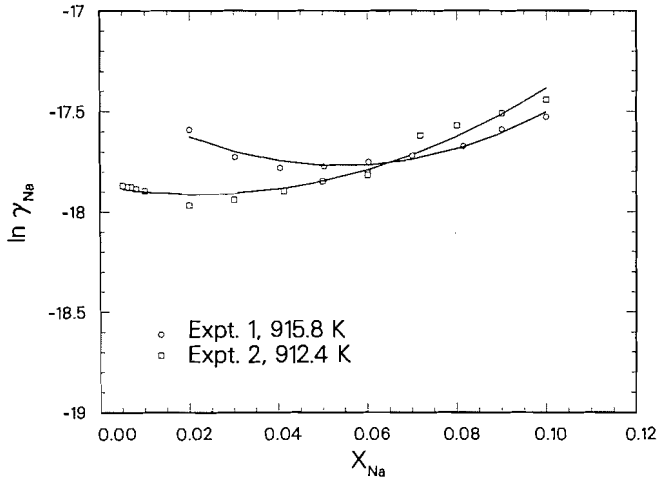

FIG. 4. Plot of ln γ_{Na} versus composition in the dilute solution range ($X_{Na} < 0.11$).

complex. At approximately $X_{Na} = 0.50$, there is a steep change in the sodium activity coefficient. At this composition, there is now sufficient sodium available, and a Na–Cu complex forms. Consequently, the activity coefficient of sodium is determined by its behavior in Na–Te and Na–Cu complexes.

According to the Kirkwood–Buff formalism (20), and subsequently reinterpreted by Saboungi and Corbin (21), the limiting slope, defined as,

$$[6] \quad \epsilon = \left(\frac{\partial \ln \gamma_{Na}}{\partial X_{Na}}\right)_{X_{Na}\to 0}$$

is related to the kind and degree of ordering within solutions. A positive value for ϵ is indicative of attraction between the sodium atoms and either copper or tellurium and a high probability of preferred coordination (i.e., complex formation) in the liquid state. A zero value for ϵ means that there is a random distribution for neighboring atoms. A negative ϵ value represents the situation where there are attractive forces between the sodium atoms, e.g., formation of Na_2 and repulsive forces between unlike atoms. Figure 4 is a plot of ln γ_{Na} versus composition in the dilute solution range ($X_{Na} < 0.11$). The experimental data points have been fitted to quadratic polynomial equations given as

$$[7] \quad \ln \gamma_{Na} = -17.402 - 13.662X_{Na} + 126.44X_{Na}^2$$

and

$$[8] \quad \ln \gamma_{Na} = -17.868 - 4.029X_{Na} + 88.517X_{Na}^2$$

for 915.8 K and 912.4 K, respectively. The limiting slopes, evaluated with eq. [6], are −13.662 and −4.029 for the 915.8 K and 912.4 K experiments, respectively. The values imply a segregation of sodium atoms in copper telluride. There is a demixing process very much like the onset of a miscibility gap, and the results would indicate pairing between sodium atoms occurs in dilute solutions. Consequently, for the dilute solutions, sodium in copper telluride is mainly covalently bonded. As the sodium content increases within the dilute solution range, the slopes of ln γ_{Na} versus composition become positive, suggesting that there is a development of a more ionic-like character.

Acknowledgment

The authors wish to thank Dr. M.-L. Saboungi for suggesting the topic and for many insightful discussions.

1. J. E. ENDERBY and M. GAY. J. Non-Cryst. Solids, **35**, 1269 (1980).
2. M. CUTLER. Phil. Mag. **24**, 381 (1971).
3. E. A. DANCY. Trans. Metall. Soc. AIME, **233**, 270 (1965).
4. J. OKADA, F. KAKINUMA, and S. OHNO. J. Phy. Soc. Jpn. **52**, 3526 (1983).
5. W. W. WARREN, JR. Proc. Int. Conf. Properties Liquid Metals, 2nd, Tokyo, 395 (1973).
6. J. E. ENDERBY and J. HAWKER. J. Non-Cryst. Solids **8**, 687 (1972).
7. I. HAWKER, R. A. HOWE, and J. E. ENDERBY. Proc. Liquid Metals Conf., Mexico, 1975. p. 85.
8. J. E. ENDERBY and M. GAY. J. Non-Cryst. Solids, **35**, 1296 (1980).
9. V. T. NGUYEN, M. GAY, J. E. ENDERBY, R. J. NEWPORT, and R. A. HOWE. J. Phys. C: Solid State Phys. **15**, 4627 (1982).
10. R. J. NEWPORT, R. A. HOWE, and J. E. ENDERBY. J. Phys. C: Solid State Phys. **15**, 4635 (1982).
11. S. N. FLENGAS and A. S. KUCHARSKI. Can. J. Chem. **49**, 3971 (1971).
12. B. PREDEL and J. PIEHL. Z. Metallkd. **66**, 33 (1975).
13. A. S. PASHINKIN, L. M. PAVLOVA, and R. A. AMIROV. Izv. Akad. Nauk SSSR Neorg. Mater. **21**, 2088 (1985).
14. J. TERPILOWSKI and B. FUGLEWICZ. Rocz. Chem. **48**, 1871 (1974).
15. R. BLACHNIK and B. GATHES. J. Chem. Therm. **15**, 401 (1983).
16. P. J. TUMIDAJSKI and M.-L. SABOUNGI. CALPHAD. To be published.
17. P. J. TUMIDAJSKI, A. PETRIC, T. TAKENAKA, M.-L. SABOUNGI, and A. D. PELTON. J. Phy. In press.
18. A. PETRIC, A. D. PELTON, and M.-L. SABOUNGI. Ber. Bunsenges. Phys. Chem. **93**, 18 (1989).
19. E. A. MAIOROVA and A. G. MORACHEVSKII. Elektrokhimiya, **11**, 821 (1975).
20. J. G. KIRKWOOD and F. P. BUFF. J. Chem. Phys. **19**, 774 (1951).
21. M.-L. SABOUNGI and T. P. CORBIN. J. Phys. F: Met. Phys. **14**, 13 (1984).

Can. J. Chem. Downloaded from www.nrcresearchpress.com by 91.144.44.67 on 09/07/12
For personal use only.

A study on excess functions and thermodynamic parameters of some bromoform-containing binary mixtures[1]

SHRIKANT S. JOSHI AND TEJRAJ M. AMINABHAVI[2]
Department of Chemistry, Karnatak University, Dharwad, India 580 003
AND
SHYAM S. SHUKLA
Department of Chemistry, Lamar University, Beaumont, P.O. Box 10022, Texas 77710, USA

Received May 8, 1989

SHRIKANT S. JOSHI, TEJRAJ M. AMINABHAVI, and SHYAM S. SHUKLA. Can. J. Chem. **68**, 251 (1990).

Densities and viscosities have been determined for six binary mixtures of bromoform, aniline, *n*-hexane, benzonitrile, butyronitrile, and benzylnitrile at different mole fractions and temperatures. The excess volumes V^E, apparent excess values of viscosity $\delta\eta$, excess Gibbs energy of activation of flow ΔG^{*E}, and partial molar volumes V_i, have been calculated from the experimental data. Furthermore, attempts were made to calculate theoretically the excess isobaric thermal expansion coefficient $\delta\alpha$, of the mixtures using the refractive index mixture rules. These results are in good agreement with the experimental data obtained from densities. Various excess functions and thermodynamic parameters have been used in the discussion of results to understand the nature and type of interactions in binary mixtures.

Key words: excess volume, refractive index mixture rules, interactions, bromoform, density, viscosity.

SHRIKANT S. JOSHI, TEJRAJ M. AMINABHAVI et SHYAM S. SHUKLA. Can. J. Chem. **68**, 251 (1990).

On a déterminé les densités et les viscosités de six mélanges binaires du bromoforme, de l'aniline, du *n*-hexane, du benzo-nitrile, du butyronitrile et du phénylacétonitrile, à diverses fractions molaires et à diverses températures. En se basant sur ces données expérimentales, on a calculé les volumes en excès, V^E, les valeurs des excès apparents de la viscosité, $\delta\eta$, l'énergie d'activation d'écoulement de Gibbs en excès, ΔG^{*E}, ainsi que les volumes molaires partiels, V_i. De plus, utilisant les règles de mélange des indices de réfraction, on a essayé de calculer d'une façon théorique le coefficient d'expansion thermique isobare, $\delta\alpha$, des mélanges. Ces résultats sont en bon accord avec les données expérimentales obtenues à l'aide des densités. On a utilisé diverses fonctions en excès et divers paramètres thermodynamiques pour discuter les résultats, dans le but de comprendre la nature et le type d'interactions présentes dans les mélanges binaires.

Mots clés : volume en excès, règles de mélange des indices de réfraction, interactions, bromoforme, densité, viscosite.
[Traduit par la revue]

Can. J. Chem. Downloaded from www.nrcresearchpress.com by 91.144.44.67 on 09/07/12
For personal use only.

Introduction

Solution properties of binary mixtures of bromoform with a number of organic solvents have been the subject of intensive research in view of their importance as media to study preferential adsorption of polymers in mixed solvents (1). Thermodynamic properties of a number of bromoform containing mixtures have been studied earlier in our laboratories (2–5). To the best of our knowledge, extensive thermodynamic data on mixtures of bromoform with aniline, benzonitrile, benzylnitrile, butyronitrile, and *n*-hexane have not been made. Such mixtures are of considerable interest from the viewpoint of the existence of intermolecular interactions between the mixing components.

In this paper, we report the density and viscosity data for five binary mixtures containing bromoform at different mole fractions and at 298.15, 303.15, 308.15, and 313.15 K. From the experimental results the excess volumes V^E, apparent excess values of the viscosity $\delta\eta$, excess Gibbs energy of activation of flow ΔG^{*E}, and partial molar volumes V_i, have been computed using the appropriate relations. From a temperature dependence of viscosity, enthalpy ΔH^{+} and entropy ΔS^{+}, of activation of flow have also been estimated using the theory of Eyring and co-workers (6). Furthermore, attempts have been made to compute the isobaric thermal expansion coefficient α_m, of the mixture using the available refractive index mixture rules. These data compare satisfactorily with the experimental data of α_m and are further used to predict the apparent excess values of the expansion coefficient $\delta\alpha$.

Experimental

Bromoform (Thomas Baker, Bombay) was obtained in its highest purity and was used as supplied. The remaining solvents were all purified by the standard procedures as described by Weissberger *et al.* (7). Density of pure liquids and their mixtures was determined by a pycnometer with an accuracy of ± 0.0001 g cm^{-3}. Viscosities were measured by using a Cannon–Fenske viscometer, size 100, and the accuracy was found to be ± 0.002 cP. Details of the procedures for these measurements have been given earlier (8). A thermostatically-controlled bath, constant to ± 0.02 K was used in all these measurements. The experimental densities and viscosities at 298.15, 303.15, 308.15, and 313.15 K have been measured for pure components and their mixtures over the entire range of mole fractions.[3] The observed data for pure liquids are in agreement with those available in the literature (7, 9).

Results

The values of V^E, $\delta\eta$, and ΔG^{*E} were calculated from the experimental data with the following equations (10).

$$[1] \quad V^E = V_m - \sum_{i=1}^{2} V_i x_i$$

[1]Based on the Ph.D. thesis of S.S.J. submitted to Karnatak University, Dharwad.

[2]Author to whom correspondences should be addressed.

[3]All numerical data may be purchased from the Depository of Unpublished Data, CISTI, National Research Council of Canada, Ottawa, Ont., Canada K1A 0S2.

TABLE 1. Computer evaluated parameters of eq. [7]

Function	Temperature (K)	A_0	A_1	A_2	A_3	σ
		(*i*) Bromoform (1) + aniline (2)				
V^E, cm^3 mol^{-1}	298.15	0.399	−0.127	0.176	0.485	0.006
	303.15	0.434	−0.129	−0.089	0.310	0.009
	308.15	0.434	−0.077	−0.053	0.061	0.006
	313.15	0.477	−0.066	−0.072	0.176	0.006
δη, cP	298.15	−0.347	−0.043	0.366	−0.827	0.004
	303.15	−0.168	−0.022	0.521	−0.649	0.009
	308.15	−0.060	−0.011	0.449	−0.495	0.006
	313.15	0.040	0.011	0.324	−0.487	0.008
ΔG^{*E}, J mol^{-1}	298.15	64.31	−17.14	113.4	−203.9	0.856
	303.15	66.92	−18.14	153.2	−186.6	1.968
	308.15	65.30	−14.79	140.0	−158.6	1.431
	313.15	75.20	−9.87	118.1	−170.7	2.187
V_1, cm^3 mol^{-1}	298.15	0.154	−0.284	0.037	−0.003	0.031
	303.15	0.214	−0.268	0.037	−0.045	0.021
	308.15	0.201	−0.256	0.034	−0.040	0.021
	313.15	0.231	−0.268	0.055	−0.056	0.014
V_2, cm^3 mol^{-1}	298.15	0.531	0.188	0.234	0.064	0.009
	303.15	0.396	0.022	0.115	0.050	0.006
	308.15	0.449	0.048	0.123	0.047	0.006
	313.15	0.451	0.005	0.063	0.030	0.003
		(*ii*) Bromoform (1) + *n*-hexane (2)				
V^E, cm^3 mol^{-1}	298.15	−1.818	0.472	0.994	−0.295	0.020
	303.15	−2.071	0.419	1.377	0.304	0.011
	308.15	−2.553	0.639	1.900	−0.142	0.039
	313.15	−2.771	0.871	2.051	−0.498	0.040
δη, cP	298.15	−1.585	0.581	−0.137	−0.020	0.004
	303.15	−1.470	0.531	−0.088	−0.078	0.004
	308.15	−1.396	0.515	−0.131	−0.057	0.002
	313.15	−1.243	0.458	−0.084	−0.093	0.004
ΔG^{*E}, J mol^{-1}	298.15	−187.5	−28.26	6.62	− 92.3	4.293
	303.15	−176.6	−32.43	21.88	− 98.1	3.604
	308.15	−166.7	−10.70	8.34	−117.8	2.715
	313.15	−155.9	4.47	12.67	−154.5	3.638
V_1, cm^3 mol^{-1}	298.15	−1.024	0.964	−0.216	0.350	0.074
	303.15	−1.227	1.037	−0.274	0.442	0.026
	308.15	−1.514	1.290	−0.275	0.554	0.078
	313.15	−1.644	1.454	−0.285	0.592	0.120
V_2, cm^3 mol^{-1}	298.15	−1.131	0.462	0.056	−0.106	0.016
	303.15	−1.079	0.778	0.388	−0.006	0.009
	308.15	−1.305	0.935	0.275	−0.120	0.023
	313.15	−1.395	0.955	0.147	−0.202	0.028
		(*iii*) Bromoform (1) + benzonitrile (2)				
V^E, cm^3/mol^{-1}	298.15	−0.211	0.31	0.12	−0.25	0.009
	303.15	−2.176	35.87	−17.45	−66.10	0.020
	308.15	−0.108	0.18	0.11	0.48	0.007
	313.15	−0.168	0.24	0.11	0.38	0.004
δη, cP	298.15	0.971	−0.713	−0.082	0.324	0.012
	303.15	0.814	−0.626	−0.116	0.331	0.019
	308.15	0.708	−0.580	−0.141	0.330	0.013
	313.15	0.582	−0.438	−0.024	0.102	0.011
ΔG^{*E}, J mol^{-1}	298.15	422.4	−159.0	−29.5	84.1	3.865
	303.15	384.5	−83.2	−163.5	−336.6	1.992
	308.15	377.7	−155.1	−65.2	110.4	4.755
	313.15	364.9	−121.6	−21.8	33.6	4.869
V_1, cm^3 mol^{-1}	298.15	−0.153	0.15	−0.018	0.053	0.017
	303.15	1.416	15.77	4.266	0.505	0.033
	308.15	−1.124	0.09	−0.109	0.020	0.020
	313.15	−0.158	0.14	−0.109	0.031	0.014

Can. J. Chem. Downloaded from www.nrcresearchpress.com by 91.144.44.67 on 09/07/12
For personal use only.

TABLE 1 (*concluded*)

Function	Temperature (K)	A_0	A_1	A_2	A_3	σ
V_2, cm^3 mol^{-1}	298.15	−0.009	0.05	0.07	−0.06	0.009
	303.15	−4.248	19.06	31.58	−12.57	0.017
	308.15	0.213	0.23	0.26	0.08	0.012
	313.15	0.169	0.21	0.22	0.06	0.009
		(*iv*) Bromoform (1) + benzylnitrile (2)				
V^E, cm^3 mol^{-1}	298.15	0.552	0.289	−0.089	−0.375	0.013
	303.15	0.523	0.234	0.010	−0.210	0.014
	308.15	0.625	0.326	−0.066	−0.359	0.008
	313.15	0.557	0.264	−0.152	−0.387	0.008
δη, cP	298.15	1.110	−0.089	−0.285	−0.376	0.005
	303.15	0.993	0.065	−0.448	−0.789	0.010
	308.15	0.823	0.044	−0.261	−0.732	0.009
	313.15	0.685	−0.075	−0.146	−0.294	0.008
ΔG^{*E}, J mol^{-1}	298.15	357.9	25.08	63.7	−120.3	1.396
	303.15	352.1	25.22	128.3	−264.5	3.194
	308.15	318.9	24.69	80.5	−266.0	3.006
	313.15	305.3	17.93	47.9	−123.6	3.270
V_1, cm^3 mol^{-1}	298.15	0.247	−0.185	0.088	−0.086	0.023
	303.15	0.209	−0.207	0.090	−0.060	0.010
	308.15	0.271	−0.212	0.096	−0.092	0.021
	313.15	0.262	−0.188	0.087	−0.094	0.024
V_2, cm^3 mol^{-1}	298.15	0.611	−0.078	−0.170	−0.076	0.015
	303.15	0.673	−0.037	−0.067	−0.050	0.009
	308.15	0.724	−0.055	−0.155	−0.074	0.015
	313.15	0.566	−0.115	−0.187	−0.075	0.015
		(*v*) Bromoform (1) + butyronitrile (2)				
V^E, cm^3 mol^{-1}	298.15	−1.134	−0.149	0.471	0.240	0.008
	303.15	−1.133	−0.070	0.450	0.479	0.006
	308.15	0.906	−1.363	−5.467	2.708	0.004
	313.15	−1.300	−0.160	0.426	0.580	0.003
δη, cP	298.15	0.016	−0.173	0.267	−0.020	0.005
	303.15	0.002	−0.169	0.246	−0.094	0.005
	308.15	−0.063	−0.216	0.139	0.195	0.003
	313.15	−0.062	−0.056	0.112	−0.032	0.008
ΔG^{*E}, J mol^{-1}	298.15	475.4	120.6	198.4	52.9	3.038
	303.15	466.4	104.2	173.7	17.2	2.843
	308.15	447.3	37.8	98.6	185.9	3.306
	313.15	431.9	152.1	136.5	14.8	5.079
V_1, cm^3 mol^{-1}	298.15	−0.578	0.483	−0.137	0.209	0.008
	303.15	−0.634	0.554	−0.191	0.219	0.034
	308.15	1.062	−0.262	−0.511	−0.626	0.036
	313.15	−0.677	0.571	−0.199	0.239	0.045
V_2, cm^3 mol^{-1}	298.15	0.966	0.235	0.164	0.024	0.008
	303.15	−0.748	0.335	0.278	0.059	0.018
	308.15	−1.679	−2.008	0.193	0.701	0.012
	313.15	−1.061	0.300	0.301	0.083	0.022

[2] $$\delta\eta = \eta_m - \sum_{i=1}^{2} \eta_i^0 x_i$$

[3] $$\Delta G^{*E} = RT[\ln \eta_m V_m - \sum_{i=1}^{2} (x_i \ln \eta_i^0 V_i^0)]$$

where x_i, V_i^0 and η_i^0 represent the mole fraction, molar volume, and viscosity of the ith pure component of the mixture; the subscript, m refers to the property of the mixture, and RT has the conventional meaning.

The molar volume V_m of the mixture was calculated from

[4] $$V_m = \sum_{i=1}^{2} x_i M_i / \rho_m$$

Where ρ_m is mixture density and M_i represent the molecular weight of component i in the mixture.

The partial molar volumes, V_1 and V_2, of components 1 and 2 were calculated from (11)

[5] $$V_1 = V_1^0 + V^E/x_1 + x_1x_2[\partial(V^E/x_1)/\partial x_1]$$

[6] $$V_2 = V_2^0 + V^E/x_2 + x_1x_2[\partial(V^E/x_2)/\partial x_2]$$

Can. J. Chem. Downloaded from www.nrcresearchpress.com by 91.144.44.67 on 09/07/12
For personal use only.

Can. J. Chem. Downloaded from www.nrcresearchpress.com by 91.144.44.67 on 09/07/12
For personal use only.

The various quantities $Y(V^E, \delta\eta, \Delta G^{*E}, V_1$, and $V_2)$ over the entire range of composition have been fitted to empirical equation (12):

$$[7] \quad Y = x_1x_2 \sum_{i=0}^{3} A_i(x_1 - x_2)^i$$

A nonlinear least-squares method (Marquardt algorithm) was used to estimate the coefficients, A_i. In each case, the optimum number of coefficients was ascertained from an examination of the variation of the standard error (σ) of the estimate with:

$$[8] \quad \sigma = [\Sigma(X^E_{obs} - X^E_{cal})^2/(n - P)]^{1/2}$$

where n is the total number of data points and P is the number of coefficients considered ($P = 4$ in the present calculation).

The last term of eqs. [5] and [6] was obtained by differentiating eq. [7] for V^E. Although this procedure is not adequate for small x_i, the results obtained can be considered valid since the contribution of the last term of eqs. [5] and [6] to the partial molar volume is less than 0.5% over the entire mole fraction scale. All these results are summarized in Table 1.

The isobaric thermal expansion coefficients, α_m of the mixture at a particular composition can be obtained either from the temperature variation of densities or by adding the contributions of the expansivities of each component in the mixture. Application of the latter method gives the relation for α_m of the mixture as:

$$[9] \quad \alpha_m = (1/\bar{V}_m)[\Sigma_i \frac{(M_ix_i)}{\bar{\rho}_i^0}\bar{\alpha}_i^0 + (\partial V^E/\partial T)_{P,x}]$$

where $\bar{V}_m$ is the average value of the molar volume of the mixture at each composition; $\bar{\rho}_i^0$ and $\bar{\alpha}_i^0$ are the average values of density and expansivity of pure components. Such average values are considered to be constant within the range of temperature used in this work. The values of $\bar{\alpha}_i^0$ were computed from the application of refractive index mixture rules (13, 14) using the known values of $(dn/dT)_i$ for ith liquid using the following relations:

For Gladstone–Dale (G–D) relation (15)

$$[10] \quad \bar{\alpha}_i^0(\text{G–D}) = -(1/n_i - 1)(dn/dT)_i$$

For Lorenz-Lorentz (L–L) relation (16)

$$[11] \quad \bar{\alpha}_i^0(\text{L–L}) = -[6n_i/(n_i^2 - 1)(n_i^2 + 2)](dn/dT)_i$$

For Eykman (Eyk) relation (17)

$$[12] \quad \bar{\alpha}_i^0(\text{Eyk}) = -[(n_i^2 + 0.8n_i + 1)/(n_i^2 - 1)(n_i + 0.4)](dn/dT)_i$$

For Oster (Ost) relation (18)

$$[13] \quad \bar{\alpha}_i^0(\text{Ost}) = -[2n_i(2n_i^4 + 1)/(n_i^2 - 1)(2n_i^4 + n_i^2)](dn/dT)_i$$

The values of $(dn/dT)_i$ for pure components needed in the above relations viz., eqs. [10]–[13], were either computed by extrapolation of the refractive index data over an interval of temperature or in some cases, these were directly obtained from the literature (9). On the other hand, experimentally, α_m can be obtained by using.

$$[14] \quad \alpha_m = -(\partial \ln \rho_m/\partial T)$$

The excess isobaric thermal expansion coefficient α^E of the mixture is a parameter which can be calculated from the following considerations:

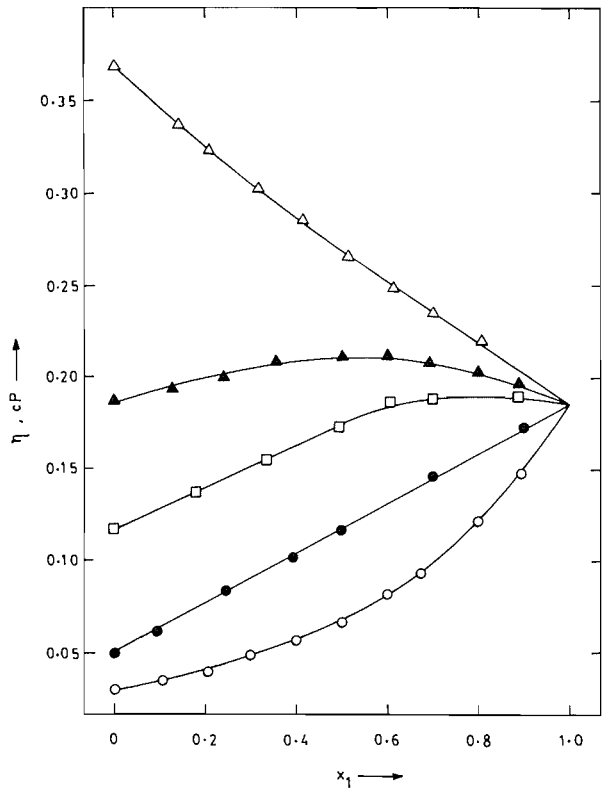

FIG. 1. Viscosity, η_m versus mole fraction, x_1 for binary mixtures at 298.15 K for mixtures of bromoform with (○) n-hexane; (△) aniline; (□) benzonitrile; (●) butyronitrile; (▲) benzylnitrile.

$$[15] \quad \alpha_m = \sum_{i=1}^{2} \bar{\alpha}_i^0 x_i + \Delta\alpha$$

As a first approximation, $\Delta\alpha$ may be described by means of a constant α^E according to:

$$[16] \quad \Delta\alpha = \alpha^E x_1x_2$$

Alternatively, α^E can be expressed more generally, as a function of x_1 and x_2 fitted to the experimental data by a polynomial. Thus,

$$[17] \quad \alpha_m = \sum_{i=1}^{2} \bar{\alpha}_i^0 x_i + x_1x_2 \sum_{i=1}^{3} A_i(x_1 - x_2)^i$$

Here, the values of $\bar{\alpha}_i^0$ have been calculated from the mixture rules. The fitted values of α^E are used to trace the plots of Figs. 7 and 8.

In view of the importance of enthalpy, $\Delta H^{\ddagger}$, and entropy, $\Delta S^{\ddagger}$, of activation of flow, we have calculated these quantities from the theory of Eyring *et al.* (6):

$$[18] \quad \eta_m = (N_Ah/V_m) \exp(\Delta H^{\ddagger}/RT - \Delta S^{\ddagger}/R)$$

Where N_A is Avogadro constant and h is Planck's constant. A plot of $\ln(\eta_mV_m/N_Ah)$ versus $1/T$ should be a straight line; the values of $\Delta H^{\ddagger}$ and $\Delta S^{\ddagger}$ were obtained from the slope and intercept, respectively.

To the best of our knowledge, there are no literature data on densities and viscosities of the studied mixtures with which the present results can be compared. Figures 1 and 2 show the dependence of viscosity and density of mixtures at 298.15 K.

However, the dependence of V^E, $\delta\eta$, and ΔG^{*E} on x_1 at

Can. J. Chem. Downloaded from www.nrcresearchpress.com by 91.144.44.67 on 09/07/12
For personal use only.

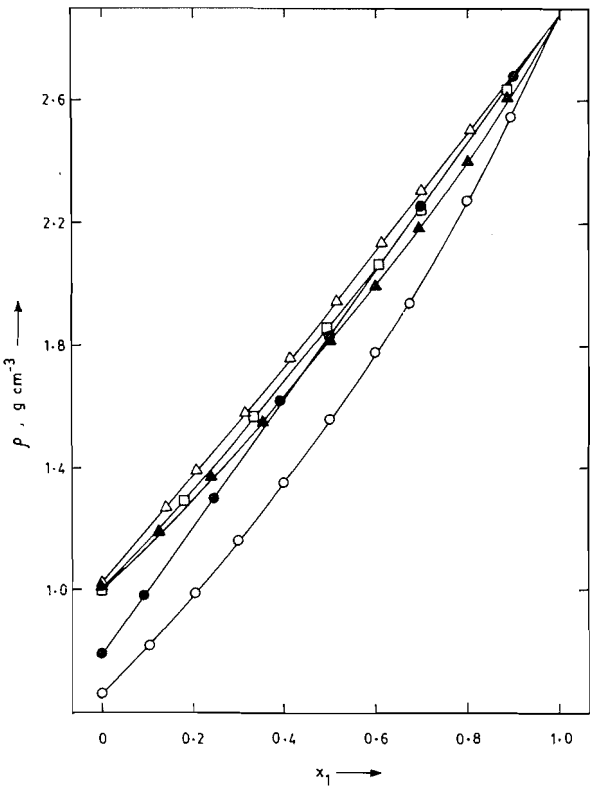

FIG. 2. Density, ρ_m versus mole fraction, x_1 at 298.15 K. All mixtures and symbols have the same meaning as in Fig. 1.

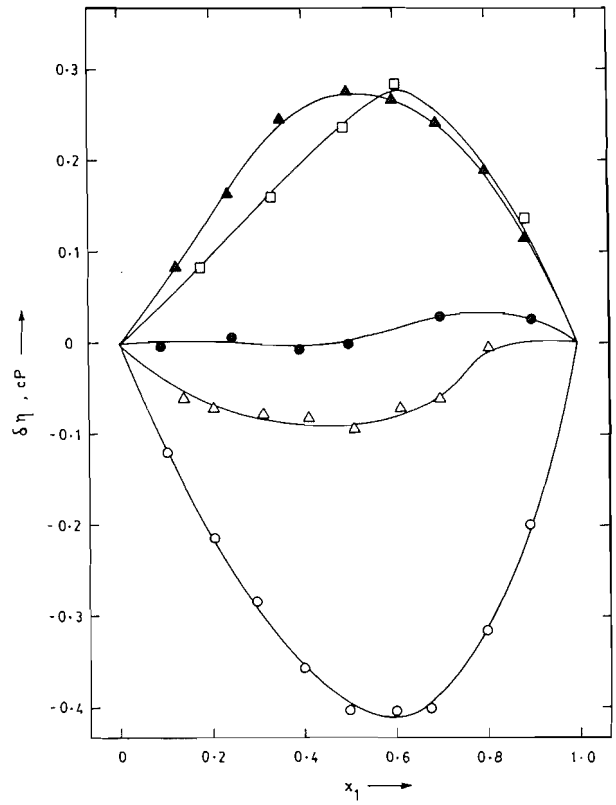

FIG. 4. Apparent excess values of viscosity, $\delta\eta$ versus mole fraction, x_1 at 298.15 K. All mixtures and symbols have the same meaning as in Fig. 1.

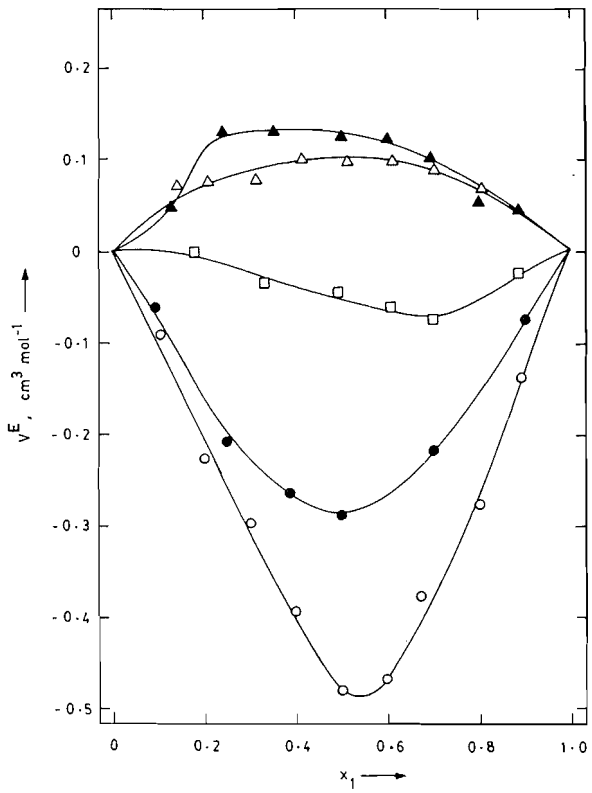

FIG. 3. Excess molar volume, V^E versus mole fraction, x_1 at 298.15 K. All mixtures and symbols have the same meaning as in Fig. 1.

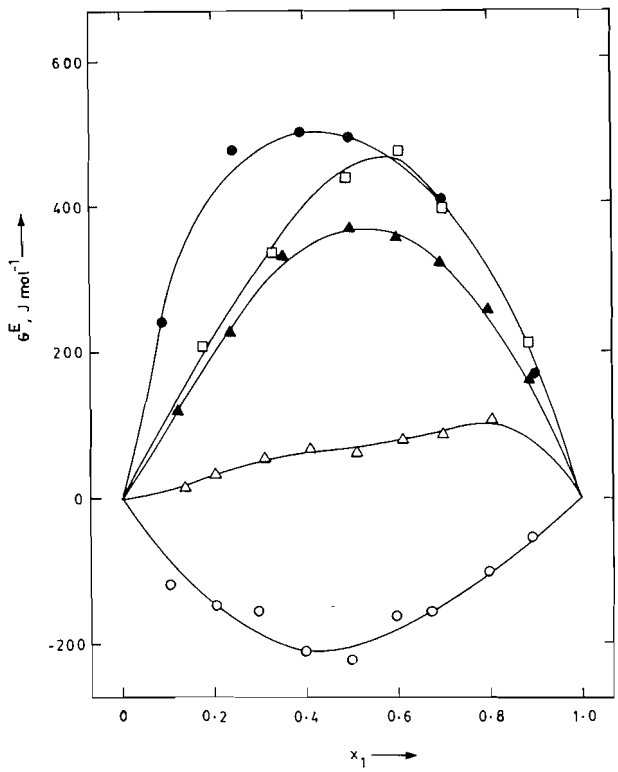

FIG. 5. Excess Gibb's energy of activation of flow, ΔG^{*E} versus mole fraction, x_1 at 298.15 K. All mixtures and symbols have the same meaning as in Fig. 1.

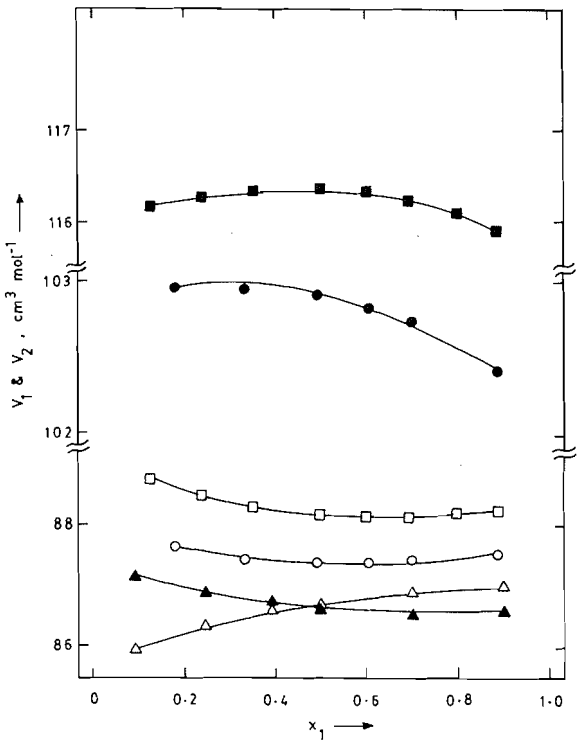

FIG. 6. Dependence of partial molar volumes, V_1 and V_2, on mole fraction, x_1 at 298.15 K for mixtures of bromoform with benzylnitrile (□) for V_1 and (■) for V_2; butyronitrile (△) for V_1 and (▲) for V_2; benzonitrile (○) for V_1 and (●) for V_2.

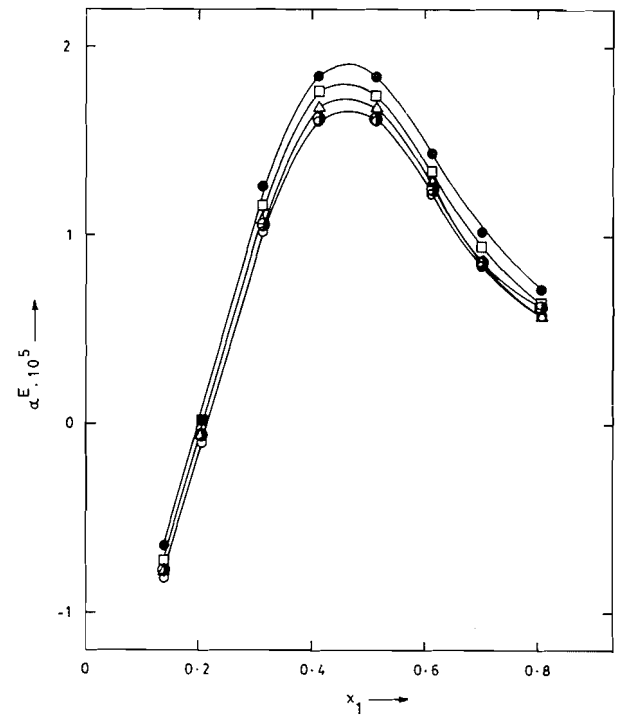

FIG. 7. Dependence of α^E on x_1 for bromoform + aniline mixture at 298.15 K. (○) Gladstone–Dale relation, (△) Lorenz–Lorentz relation, (□) Eykman relation, (◑) Oster relation, (●) density.

298.15 K for all the mixtures is shown in Figs. 3, 4, and 5. In Fig. 6, the dependence of V_1 and V_2 for a few typical mixtures is presented. The computed α^E values from the mixture rules, i.e., eqs. [10] to [13] and those of experimental α^E are presented in Figs. 7 and 8 for only a few typical mixtures.

Discussion

From a linear dependence of η_m on x_1, as shown in Fig. 1, it is found that the mixture, bromoform (1) + butyronitrile (2) exhibits an ideal behavior; this is due to their identical molar volumes (i.e., ~88 cm^3 mol^{-1} at 298.15 K). This is further confirmed by the linear variation of ρ_m with x_1 (Fig. 2). However, a large negative deviation as observed for bromoform (1) + *n*-hexane (2) in both viscosity and density profiles is attributed to their large differences in molar volumes (e.g., for bromoform, V_1^0 = 87.8 cm^3 mol^{-1}; for *n*-hexane V_2^0 = 131.2 cm^3 mol^{-1} at 298.15 K). Similarly, mixtures of bromoform with benzylnitrile and benzonitrile show significant deviations from linearity. On the other hand, for bromoform (1) + aniline (2), a slight deviation from linearity is prevalent for both ρ_m and η_m. This is because the molar volume of aniline (V_2^0 = 91.44 cm^3 mol^{-1} at 298.15 K) is somewhat close to that of bromoform. The same dependencies are observed at higher temperatures. However, to avoid overcrowding, these curves are not drawn.

Figure 3 shows the variation of excess molar volumes of the binaries at 298.15 K. For all mixtures, it is noticed that V^E tend to increase with an increase in temperature; this increase is somewhat insignificant for the chosen systems in the temperature interval of 298.15 to 313.15 K and thus, only the room temperature data are plotted. A close inspection of the V^E plots reveals positive V^E values for mixtures of bromoform with benzylnitrile and aniline; no sharp maxima are observed in both cases. The molecular interactions in these mixtures are thus characterized by dispersion type forces. Replacement of NH_2 group as in aniline by a more bulkier group like —CH_2CN as in benzylnitrile increases their steric repulsions with bromine atoms of bromoform. This would mean that benzylnitrile (due to its increased electron-donating capacity) will be attracted to the bromine atoms of bromoform leading to increased repulsion. Since V^E reflects the packing of the components of a binary mixture, it should be more positive for bulkier groups. This explains the observed higher V^E values of bromoform (1) + benzylnitrile (2) mixture as compared to bromoform (1) + aniline (2). Such observations can also be found in the literature (19).

A small but negative V^E as observed for bromoform (1) + benzonitrile (2) mixture may be due to the fact that benzonitrile (dipole moment, μ = 4.05 D at 303.15 K) is more polar than bromoform (μ = 0.99 D at 303.15 K). Thus, there is an induced dipole–dipole interaction leading to negative V^E (20). Similarly, mixtures of bromoform with *n*-hexane and butyronitrile suggest the existence of specific interactions as evidenced by large but negative values of V^E; sharp minima are observed around middle of the composition scale for both the mixtures. However, the highest negative V^E shown by bromoform (1) + *n*-hexane (2) mixture is attributed to a large difference in their molar volumes. In general, the trend in the variation V^E followed the sequence:

benzylnitrile > aniline > benzonitrile > butyronitrile > *n*-hexane

Figure 4 shows the dependence of $\delta\eta$ on x_1; mixtures of bromoform with aniline or with *n*-hexane exhibit negative $\delta\eta$. On the other hand, mixtures of bromoform with benzylnitrile or benzonitrile exhibit positive $\delta\eta$ with maxima or minima occurring around the middle of the composition scale. Surprisingly, the system bromoform (1) + butyronitrile (2) exhibits an entirely different behavior i.e., both positive and negative $\delta\eta$

Can. J. Chem. Downloaded from www.nrcresearchpress.com by 91.144.44.67 on 09/07/12
For personal use only.

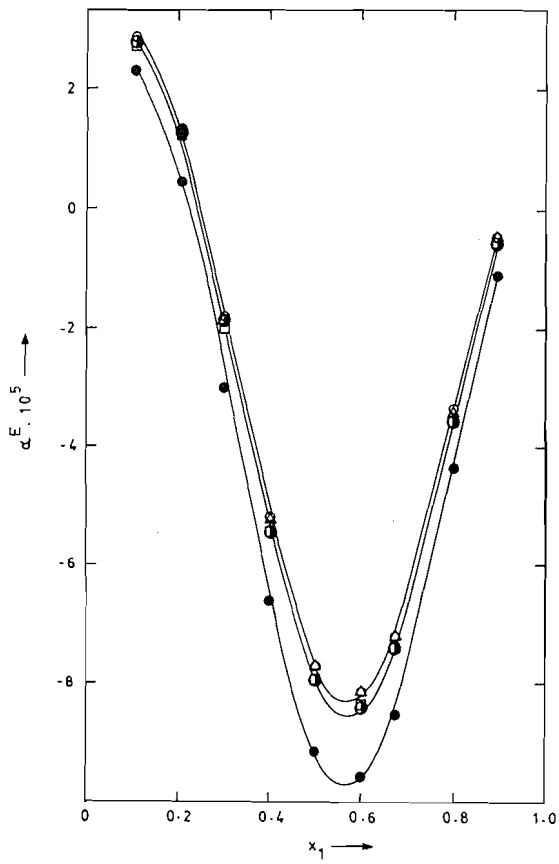

FIG. 8. Same as in Fig. 7 for bromoform + *n*-hexane mixture at 298.15 K. Symbols have the same meaning as in Fig. 7.

values are observed. Values of $\delta\eta$ increase with increase in temperature. This indicates that in these binary mixtures, the forces between pairs of unlike molecules are somewhat less than the forces between pairs of like molecules and that is why the mixture is less viscous (10).

Bromoform is less polar as compared to the three nitriles used here. Thus, in mixtures, it is expected that highly polar nitriles induce a dipole moment on somewhat less polar molecule like bromoform leading to the rupture of the molecular order as evidenced by the positive excess free energy of flow (Fig. 5). However, small but positive ΔG^{*E} for bromoform (1) + aniline (2) system is due to the less polar nature of the aniline ($\mu = 1.51$ and $\epsilon = 6.9$). The negative ΔG^{*E} for bromoform (1) + *n*-hexane (2) mixture indicates the absence of dipole–dipole type interactions because the dipole moment of *n*-hexane is smaller than bromoform. For all mixtures, except bromoform (1) + aniline (2), the ΔG^{*E} profiles are highly symmetric over the entire x_1 scale and the maxima or minima occurred for values of x_1 between 0.4 to 0.6.

The trend in the variation of $\delta\eta$ and that of ΔG^{*E}, vary respectively, in the following sequence: $\delta\eta$: benzylnitrile > benzonitrile > butyronitrile > aniline > *n*-hexane; ΔG^{*E}: butyronitrile > benzonitrile > benzylnitrile > aniline > *n*-hexane.

Thus, on the whole, it appears that there are strong specific interactions between bromoform and *n*-hexane in solution.

Figure 6 shows the variation of V_1 and V_2 with x_1 for some representative mixtures viz., nitriles with bromoform. It is seen that the convex shapes are observed for V_2 in case of mixtures of bromoform with benzonitrile and benzylnitrile whereas a reverse tendency is seen for the dependence of V_1. Similar observations are seen with other mixtures of bromoform except bromoform (1) + butyronitrile (2) wherein V_1 showed convex behavior and V_2 the concave shape.

Following the approach developed by Eyring and co-workers (6), the values of $\Delta H^{\neq}$ and $\Delta S^{\neq}$ are estimated for the mixtures considered here. It is found that in all cases, $\Delta S^{\neq}$ values are negative and small. Nitriles when mixed with bromoform produced almost identical $\Delta S^{\neq}$ values and vary generally in the range ~42 to 59 J mol^{-1} K^{-1}. However, no systematic variation of $\Delta S^{\neq}$ is seen with x_1 for many mixtures, except bromoform (1) + aniline (2), wherein $-\Delta S^{\neq}$ values increased systematically from ~27 to 52 J mol^{-1} K^{-1} with an increase in bromoform content of the mixture. In general, the negative $\Delta S^{\neq}$ values confirm the formation of activated weak molecular complexes leading to increased order as result of flow. For all the mixtures, the positive $\Delta H^{\neq}$ which range from ~5 to 2 kJ mol^{-1} K^{-1} suggest the endothermic nature of the mixing process.

The variation of α^E on x_1 for the system, bromoform (1) + aniline (2) at 298.15 K is shown in Fig. 7. It is found that Eykman relation agrees somewhat closer to the experimental α^E than the other mixture rules. Similar observations are also seen for the bromoform (1) + *n*-hexane (2) mixture (see Fig. 8) and other mixtures of bromoform with nitriles.

Acknowledgements

We thank the University Grants Commission, New Delhi, India, for major financial support (F.12-55/88-SR-III) and to the Robert A. Welch Foundation for partial support. We thank Dr. Keith Hansen, Chairman of Chemistry, and Dr. John Idoux, Dean, Lamar University, for their interest in this research.

1. T. M. AMINABHAVI. Ph.D. Dissertation, The University of Texas, Austin, USA. 1979.
2. T. M. AMINABHAVI, L. S. MANJESHWAR, and R. H. BALUNDGI. Indian J. Chem. **26A**, 641 (1987).
3. T. M. AMINABHAVI, L. S. MANJESHWAR, R. H. BALUNDGI, and M. V. MUDDAPUR. Indian J. Chem. **26A**, 106 (1987).
4. T. M. AMINABHAVI, L. S. MANJENHWAR, and R. H. BALUNDGI. J. Chem. Eng. Data, **32**, 50 (1987).
5. L. S. MANJESHWAR and T. M. AMINABHAVI. J. Chem. Eng. Data, **33**, 184 (1988).
6. S. GLASSTONE, K. J. LAIDLER, and H. EYRING. The theory of rate processes. McGraw Hill, New York. 1941.
7. A. WEISSBERGER, E. S. PROSKAUER, J. A. RIDDICK, and E. E. TOOPS. Organic solvents. Vol. VII. 2nd ed. Interscience, New York. 1955.
8. G. S. GOKAVI, J. R. RAJU, T. M. AMINABHAVI, R. H. BALUNDGI, and M. V. MUDDAPUR. J. Chem. Eng. Data, **31**, 15 (1986).
9. J. A. RIDDICK and W. B. BUNGER. Techniques of chemistry. Vol. II. Organic solvents. Wiley-Interscience, New York. 1970.
10. S. L. OSWAL. Can. J. Chem. **66**, 111 (1988).
11. J. R. GOATES, J. B. OTT, and J. F. MOELLMER. J. Chem. Thermodyn. **9**, 249 (1977).
12. O. REDLICH and A. T. KISTER. Ind. Eng. Chem. **40**, 345 (1948).
13. T. M. AMINABHAVI. J. Chem. Eng. Data, **29**, 54 (1984).
14. A. A. A. ABBEL-AZIM and P. MUNK. J. Phys. Chem. **91**, 3910 (1987).
15. J. H. GLADSTONE and T. P. DALE. Phil. Trans. **153**, 317 (1883).
16. J. R. PARTINGTON. An advanced treatise on physical chemistry. Vol. IV. Longmans, Green, London. 1953. p. 8.
17. J. F. EYKMAN. Recl. Trav Chim Pays-Bas. **14**, 185 (1895).
18. G. OSTER. Chem. Rev. **43**, 319 (1948).
19. M. G. PROLONGO, R. M. MASEGOSA, and I. HERNANDEZ-FUENTES. J. Phys. Chem. **88**, 2163 (1984).
20. L. S. MANJESHWAR. Ph.D. Thesis, Karnatak University, Dharwad, India. 1988.

Can. J. Chem. Downloaded from www.nrcresearchpress.com by 91.144.44.67 on 09/07/12
For personal use only.

Infrared and vibrational circular dichroism intensities of model systems CH_3OH, CH_3NH_2, NH_2NH_2, NH_2OH, and HOOH and the deuterated species, ND_2ND_2, DOOH, and DOOD: A theoretical study using the vibronic coupling formalism

ARVI RAUK,[1] REMO DUTLER, AND DANYA YANG
Department of Chemistry, University of Calgary, Calgary, Alta., Canada T2N 1N4

Received July 19, 1989

ARVI RAUK, REMO DUTLER, and DANYA YANG. Can. J. Chem. **68**, 258 (1990).

We have implemented at the *ab initio* level the vibronic coupling formalism for infrared and vibrational circular dichroism (VCD) intensities of Nafie and Freedman. We report here the results of a series of calculations on model systems. Hydrazine and hydrogen peroxide exist in chiral conformations. Although low barriers to racemization preclude the possibility of optical resolution of the parent compounds, the local *gauche* configuration at the heteroatom bond is preserved in substituted hydrazines and peroxides and these chiral fragments may contribute significantly to the vibrational chiroptical properties of the molecules in which they appear. The calculated VCD rotational strengths for the chiral *gauche* forms of both molecules suggest that the torsional mode is very intense in the VCD spectrum. In *gauche* hydrazine of P chirality, the in- and out-of-phase umbrella motions of the nitrogen atoms, $\nu 6$ and $\nu 12$, respectively, give rise to an intense CD couplet with negative rotational strength to the long wave length side. In hydrazine, all combinations of NH stretches are relatively weak in the IR but the highest frequency mode of b symmetry, $\nu 8$, has moderate positive strength. The in- and out-of-phase OOH bends of HOOH behave as a coupled oscillator system, exhibiting a strong bisignate CD pattern. The signals calculated for the OH stretches are not consistent with a coupled oscillator model. The nearly degenerate stretches result in a single band arising from the more intense negative rotational strength of the antisymmetric mode $\nu 5$, in HOOH of *P* chirality. An alternative model, based on induced charge flow along the chirally disposed skeleton (i.e., Nafie and Freedman's 3-bond electronic current model), explains the calculated sign of the antisymmetric mode, $\nu 5$. Significant changes in the VCD patterns due to deuterium substitution in both chiral molecules are discussed.

Key words: vibrational circular dichroism (VCD), *ab initio*, infrared intensities, molecular orbital, vibronic coupling theory, methanol, methanamine, hydrazine, hydroxylamine, hydrogen peroxide.

ARVI RAUK, REMO DUTLER et DANYA YANG. Can. J. Chem. **68**, 258 (1990).

On a implanté au niveau *ab initio* le formalisme de couplage vibronique développé par Nafie et Freedman pour les intensités infrarouges et du dichroïsme circulaire vibrationnel (DCV). On rapporte maintenant une série de calculs sur des systèmes modèles. L'hydrazine et le peroxyde d'hydrogène existent dans des conformations chirales. Même si les barrières à la racémisation sont tellement basses qu'il est impossible d'effectuer la résolution optique des composés parents, la configuration *gauche* locale de la liaison de l'hétéroatome est préservée dans des hydrazines et des peroxydes substitués et ces fragments chiraux peuvent contribuer d'une façon importante aux propriétés chiroptiques des molécules dans lesquelles ils apparaissent. Les forces rotationnelles calculées pour le DCV des formes *gauches* chirales de ces deux molécules suggèrent que le mode de torsion est très intense dans le spectre de DCV. Dans l'hydrazine *gauche* de chiralité *P*, les mouvements du parapluie des atomes d'azote qui sont ou qui ne sont pas en phase, respectivement $\nu 6$ et $\nu 12$, donnent lieu à un couplage de DC qui est intense et dont la force rotationnelle est négative jusqu'à la portion des grandes longueurs d'onde. Dans l'hydrazine, toutes les combinaisons des élongations NH sont relativement faibles dans l'IR; toutefois, le mode de symétrie b à la plus haute fréquence, $\nu 8$, possède une force positive d'intensité modérée. Les torsions dans le plan et hors du plan du OOH du HOOH se comportent comme un système oscillateur couplé présentant un DC fort à double signe. Les signaux calculés pour les élongations OH ne sont pas en accord avec un modèle d'oscillateur couplé. Dans le HOOH de chiralité *P*, les élongations pratiquement dégénérées sont le résultat d'une seule bande provenant de la force rotationnelle négative la plus intense du mode antisymétrique $\nu 5$. Un modèle alternatif, basé sur le flux de la charge induite le long du squelette disposée d'une façon chirale (soit le modèle actuel à trois liaisons électroniques de Nafie et Freedman), permet d'expliquer le signe calculé du mode antisymétrique, $\nu 5$. On discute des changements importants observés dans les DCV lorsqu'on introduit des atomes de deutérium dans ces deux molécules chirales.

Mots clés : dichroïsme circulaire vibrationnel (DCV), *ab initio*, intensités infrarouges, orbitales moléculaires, théorie du couplage vibronique, méthanol, méthanamine, hydrazine, hydroxylamine, peroxyde d'hydrogène.

[Traduit par la revue]

Introduction

Chiroptical measurements in the vibrational region of the electromagnetic spectrum promise to yield more structural information than other spectroscopic techniques but have suffered from the intractibility of the theory underlying the phenomenon and severe experimental difficulties. With the recent advent of Fourier transform methods (1) and other improvements in instrumentation, most of the vibrational region is amenable to measurements of both vibrational circular dichroism (VCD) and Raman optical activity (ROA), and numerous experimental results have emerged. Recent advances in the underlying theory (2–5) have kept pace with the advances in instrumentation. Semiempirical implementations of VCD theories have served to correlate some structural features and suggest new insights but have suffered from a general lack of predictability. Significant advances have had to await *ab initio* implementations. This was first accomplished by Stephens and co-workers (6) who reported the calculation of the CH and CD stretching IR and VCD intensities of *trans*-dideuteriocyclopropane and subsequently demonstrated encouraging agreement with experimentally measured values for *trans*-1,2-dideuteriocyclobutane and propylene oxide (7). Successive applications to a number of small model and real systems ensued (8).

[1]Author to whom correspondence should be addressed.

Can. J. Chem. Downloaded from www.nrcresearchpress.com by 91.144.44.67 on 09/07/12
For personal use only.

Can. J. Chem. Downloaded from www.nrcresearchpress.com by 91.144.44.67 on 09/07/12
For personal use only.

The vibronic coupling formalism for infrared (IR) and vibrational circular dichroism (VCD) intensities of Nafie and Freedman (4) has recently been implemented at the *ab initio* level (9) and the complete IR and VCD spectra of (*S*,*S*)-2,3-dideuterooxirane as well as the other deuterated isotopomers have appeared (10). This provides an alternative to the VCD formalism of Stephens (5). We report here the results of a series of calculations on model systems, methanol **1**, methanamine **2**, hydrazine **3**, hydroxylamine **4**, and hydrogen peroxide **5**. Some are intrinsically chiral, while others may be rendered so by virtue of isotopic substitution. All compounds contain polar bonds and are expected to exhibit strong IR and/or VCD activity. Hydrazine **3** and hydrogen peroxide **5** exist in chiral conformations. Low barriers to racemization preclude the possibility of optical resolution except in the solid state. However, the local *gauche* configuration at the heteroatom bond is preserved in substituted hydrazines and peroxides and these chiral units may contribute significantly to the vibrational chiroptical properties of the molecules in which they appear. We present here the results of an *ab initio* investigation using the vibronic coupling theory of Nafie and Freedman (4) of the IR intensities of **1**–**5**, as well as the VCD properties of the chiral systems, **3** and **5**, perdeuterio-**3** and -**5**, and monodeuterio-**5**.

Theory

The following is an abbreviated derivation of the vibronic theory of Nafie and Freedman (4). The dipole strength, $D_{g,e}$, and rotational strength, $R_{g,e}$, are given by:

$$[1] \qquad D_{g,e} = (\mu)_{g,e}(\mu)_{e,g} = (\langle\Phi_g|\mu_{el}|\Phi_e\rangle\langle\Phi_e|\mu_{el}|\Phi_g\rangle)$$

$$[2] \qquad R_{g,e} = (\mu)_{g,e}(m)_{e,g} = Im(\langle\Phi_g|\mu_{el}|\Phi_e\rangle\langle\Phi_e|\mu_{mag}|\Phi_g\rangle)$$

where Φ_g and Φ_e are the total molecular wavefunction of the ground state g and a vibrationally excited state e. The operators μ_{el} and μ_{mag}, the electric and magnetic dipole operators are given by:

$$[3] \qquad \mu_{el} = \mu^n_{el} + \mu^e_{el} = \Sigma_{n=1}^{n=n_{atoms}}\chi_n r_n + \Sigma_{i=1}^{i=n_{electrons}}\chi_i r_i$$

$$[4] \qquad \mu_{mag} = \mu^n_{mag} + \mu^e_{mag} = \Sigma_{n=1}^{n=n_{atoms}}\frac{\chi_n}{2m_n c}(r_n \times p_n) + \Sigma_{i=1}^{i=n_{electrons}}\frac{\chi_i}{2m_i c}(r_i \times p_i)$$

where μ^n_{el}, μ^e_{el}, μ^n_{mag}, and μ^e_{mag} denote the nuclear and electronic contributions of the electric and magnetic dipole transition moment operators, respectively. χ_k is the charge of particle k with mass m_k which is located at a point r_k relative to the origin of coordinates and moving with linear momentum p_k. The wavefunctions Φ_e and Φ_g may be represented as $\Phi_{0\nu'}$ and are expanded in terms of adiabatic Born–Oppenheimer functions $\{\Psi^a_e(r,Q)\phi_{e\nu}(Q)\}$:

$$[5] \qquad \Phi_{0\nu'} = \Psi^a_0\phi_{0\nu'} - \Sigma_{e\nu}\frac{\langle\Psi^a_e\phi_{e\nu}|T_N|\Psi^a_0\phi_{0\nu'}\rangle}{E_{e\nu} - E_{0\nu'}}\Psi^a_e\phi_{e\nu}$$

The variable ν' is either 0 or 1, denoting the vibrational ground or first excited state. The perturbation operator T_N is taken as that part of the nuclear kinetic energy operator which involves only first derivatives with respect to nuclear coordinates (normal modes) Q, acting separately on the electronic and nuclear parts of wavefunction, namely

$$[6] \qquad T_N = -\left(\frac{h}{2\pi}\right)^2\left(\frac{\partial}{\partial Q}\right)_{elec}\left(\frac{\partial}{\partial Q}\right)_{nuc}$$

The normal mode dependence of Ψ^a_0 is expressed as a Taylor expansion about the equilibrium geometry, keeping only the first order terms, and using the identity $1 = \Sigma_e|\Psi^a_e\rangle\langle\Psi^a_e|$,

$$[7] \qquad \Psi^a_0 = (\Psi^a_0)_0 + \left(\frac{\partial\Psi^a_0}{\partial Q}\right)_0 Q = (\Psi^a_0)_0 + \Sigma_e\langle\Psi^a_e\left|\frac{\partial}{\partial Q}\right|\Psi^a_0\rangle_0 Q\Psi^a_e$$

Use of eqs. [3]–[7], the approximation that the separation between vibrational levels of different electronic states is approximately equal to the difference between Born–Oppenheimer surfaces at the ground state equilibrium geometry, namely

$$[8] \qquad \frac{1}{E_{e\nu} - E_{01}} = \frac{1}{E^0_e - E^0_0}$$

and the expansion of the normal modes in terms of internal coordinates R_n,

$$[9] \qquad Q^j = \Sigma_{n=1}^{n_{atoms}} R_n s^j_n$$

allows one to obtain, after some algebra, expressions for the electric and magnetic dipole transition moments used in eqs. [1] and [2]. Specifically, for the jth normal mode, one obtains [4]

$$[10.1] \qquad \mu^{VC}_{(00,01)j} = \left(\frac{\hbar}{2\omega_j}\right)^{1/2}\left[\Sigma_{n=1}^{n_{atoms}}\chi_n s^j_n - 2\Sigma_{n=1}^{n_{atoms}}\Sigma_{i=1}^{n_{electrons}}\Sigma_{e=1}^{n_{ex}}\langle\Psi^a_0|r_i|\Psi^a_e\rangle\langle\Psi^a_e\left|\frac{\partial}{\partial R_n}\right|\Psi^a_0\rangle s^j_n\right]$$

$$[10.2] \qquad = \left(\frac{\hbar}{2\omega_j}\right)^{1/2}\left[\Sigma_{n=1}^{n_{atoms}}\chi_n s^j_n - 2\Sigma_{n=1}^{n_{atoms}}\Sigma_{i=1}^{n_{electrons}}\langle\Psi^a_0\left|r_i\frac{\partial}{\partial R_n}\right|\Psi^a_0\rangle s^j_n\right]$$

and

$$[11] \qquad m^{VC}_{(00,01)j} = \frac{1}{2c}\left(\frac{\hbar}{2\omega_j}\right)^{1/2}\left[i\Sigma_{n=1}^{n_{atoms}}\chi_n(R_n \times s^j_n) - 2\Sigma_{n=1}^{n_{atoms}}\Sigma_{i=1}^{n_{electrons}}\Sigma_{e=1}^{n_{ex}}\langle\Psi^a_0|r_i \times p_i|\Psi^a_e\rangle \times \langle\Psi^a_e\left|\frac{\partial}{\partial R_n}\right|\Psi^a_0\rangle s^j_n\frac{1}{E^0_e - E^0_0}\right]$$

The superscript VC denotes that these expressions describe a vibronic coupling mechanism for IR and VCD intensities. The subscript (00,01) signifies that the transition is between the $\nu = 0$ and $\nu = 1$ vibrational levels of the ground electronic state of the molecule. Electric dipole strengths derived from eq. [10] are formally equivalent to the Atomic Polar Tensor (APT) theory. Stephens circumvents the summation over excited states in eq. [11] by invoking the magnetic field dependence of the wavefunction, a procedure which requires solution of the perturbed Hartree–Fock equations in the presence of a magnetic field (5). In the present case, the sum over excited states which appears in eq. [10.2] and in the second term of eq. [11] is explicitly evaluated, in the first instance as a check for the "completeness" of the set of excited states (i.e. eqs. [10.1] and [10.2] should yield identical results), and in the second case out of necessity, since the presence of the energy dependence within the summation in eq. [11] precludes closure as is possible for eq. [10]. "Completeness" by the criterion that eqs. [10.1] and [10.2] give nearly identical results is only satisfied if the basis set is expanded by addition to it

of derivatives of the normal basis functions with respect to nuclear displacements (11).

Method

The geometries of **1**–**5** were determined by complete optimization at the restricted Hartree–Fock level of theory using the analytical procedures of the GAUSSIAN 82 system of programs (12) and the internal 6-31G** basis set (13). Normal coordinate analysis at the 6-31G** equilibrium geometry was carried out by analytical second differentiation of the Born–Oppenheimer RHF energy (14) using a basis set we designate as 6-31G~ (see below). Harmonic frequencies for isotopically substituted species, as well as IR and VCD (where appropriate) intensities were accomplished by the program system Freq85 (9), which implements the vibronic coupling theory of Nafie and Freedman (4) at the *ab initio* level. For improved agreement with experiment, frequencies were uniformly scaled by 0.9 (15). The intensity evaluations were accomplished using the 6-31G~ basis set, which is constructed by addition to the 6-31G basis set all non-redundant derivatives of the 6-31G basis functions with respect to nuclear displacements (11). Previous experience (9, 10) has shown that 6-31G~ geometries are very similar to 6-31G** geometries. Consequently, geometry optimization was not repeated with the 6-31G~ basis which is comparable in size to the larger standard 6-311G** basis set. The origin of coordinates in all intensity calculations was the molecular center of mass. Simulated IR and VCD spectra were obtained assuming a Lorentzian lineshape of half width 12 cm^{-1} and using uniformly scaled frequencies ($\times 0.9$).

Results and discussion

The RHF/6-31G** geometries are shown in Fig. 1. The structures of all systems agree reasonably well with corresponding experimental values (16, 17) and are virtually the same as the results of other *ab initio* calculations using large basis sets (18–20). At the present level of theory, bond angles generally agree to within 1.4° and bond lengths are underestimated by about 0.028 Å (18). Of the parent molecules, only hydrazine, **3**, and hydrogen peroxide, **5**, have chiral skeletons. The absolute configurations shown in Fig. 1 correspond to *P*, or right-handed, chirality. The other systems belong to molecular point group C_s. Simulated IR and VCD spectra of the parent systems are shown in Figs. 2, 4–6, and listed in Tables 1–5. The results are discussed separately below.

Methanol 1. The RHF/6-31G** geometry of **1** is shown in Fig. 1. The calculated geometry agrees well with experiment (C—O = 1.421 Å, O—H = 0.963 Å, ⟨C—H⟩ = 1.094 Å, C—O—H = 108.0° (16)) in all respects. The molecular point group is C_s. The C—H bond in the C—O—H plane is significantly shorter (1.082 Å) than the out-of-plane C—H bonds (1.088 Å). Raw and scaled harmonic frequencies and VC intensities calculated from the 6-31G~ force field are presented in Table 1. The simulated IR spectrum is shown in Fig. 2. The IR intensities agree quite well with qualitative experimental results (21) and the simulated spectrum resembles the experimental high pressure gas phase spectrum of Person (22) quite closely. The VC/6-31G~ results differ in some important respects from the CNDO/2 FORCE results of Kuczera (23) which are also given in Table 1. Specifically, with the present method, the intensities of the very strong band, $\nu 8$, and the very weak band, $\nu 5$, are qualitatively correct. Infrared intensities for **1** have been calculated by *ab initio* methods and using atomic polar tensors transferred from smaller molecules by Person (22). The main features of the experimental spectrum are very well reproduced in the simulated spectrum of Fig. 2.

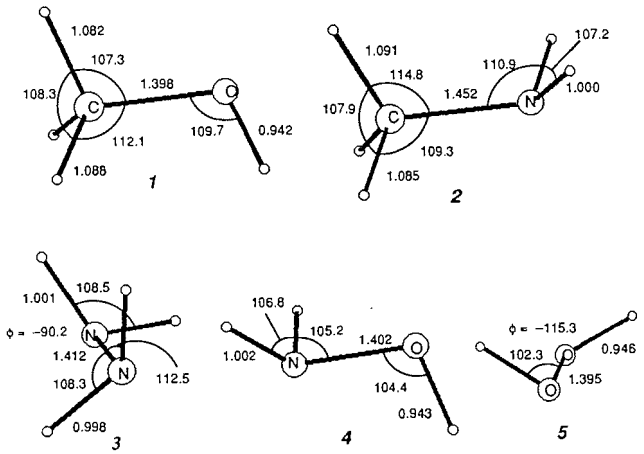

FIG. 1. The 6-31G** equilibrium structures (point groups) of methanol **1** (C_s), methanamine **2** (C_s), hydrazine **3** (C_2) hydroxylamine **4** (C_s), and hydrogen peroxide **5** (C_2). The absolute configurations of hydrazine and hydrogen peroxide shown have *P* chirality. Bond lengths are in Angstroms, bond and dihedral angles are in degrees.

Methanamine 2. The RHF/6-31G** geometry of **2** is shown in Fig. 1. The calculated geometry agrees well with experiment (C—N = 1.471 Å, N—H = 1.010 Å, ⟨C—H⟩ = 1.099 Å, C—N—H = 110.3° (16)) in all respects. The molecular point group is C_s. As in the case of **1**, the C—H bond opposite the lone pair is significantly longer (1.091 Å) than the other C—H bonds (1.085 Å). Raw and scaled harmonic frequencies calculated from the 6-31G~ force field are presented in Table 2. The simulated IR spectrum is shown in Fig. 2. The in- and out-of-phase N—H stretching modes, $\nu 1$ and $\nu 10$, at ~3400 cm^{-1} (scaled value) are very weak. The three methyl stretching distortions are separated by virtue of the interaction of one of the C—H bonds with the N non-bonded pair of electrons. The stretching mode at lowest frequency, $\nu 3$, formally the Me symmetric stretch, is more intense than the other two modes, and has a much larger component from the C—H bond which is *anti* to the N lone pair of electrons (Fig. 3*a*). The most intense band in the IR spectrum of **2** is calculated to arise from the pyramidal inversion motion at the nitrogen centre, $\nu 9$ (Fig. 3*b*), at 855 cm^{-1} (scaled). The torsion mode, $\nu 12$ (Fig. 3*c*), is relatively weak compared to the corresponding mode of **1**.

Hydrazine 3. The RHF/6-31G** geometry of **3** is shown in Fig. 1. The calculated geometry agrees well with experiment (N—N = 1.447 Å, ⟨N—H⟩ = 1.008 Å, N—N—H = 109.2°, H—N—H = 113.3°, ϕ = 88.9° (16)). The molecular point group is C_2. Raw and scaled harmonic frequencies calculated from the 6-31G~ force field are presented in Table 3. Hydrazine has been the subject of numerous IR and Raman investigations (24), as well as a thorough theoretical study by Morokuma and co-workers (25) who carried out a complete assignment of the vibrational spectrum based on *ab initio* force fields. The frequencies calculated using a CI–6-31G* force field and the association with observed bands shown in Table 3 are according to Morokuma and co-workers who revised a number of previous assignments (25). Our calculated frequencies (after uniform scaling) and our assignments agree entirely with theirs except in the NH stretching modes, $\nu 1$ and $\nu 8$, which we and they

Can. J. Chem. Downloaded from www.nrcresearchpress.com by 91.144.44.67 on 09/07/12
For personal use only.

TABLE 1. Frequencies and dipole strengths for methanol, CH_3OH, **1**

Normal mode			Frequency, cm^{-1}			Dipole strength, D[a]			
			Calc	Scal[e]	Exp[d]	Calc[b] ($esu^2\ cm^2$)[f]	Calc[b] (km/mol)	Calc[c] (km/mol)	(Exp)[d]
1	a″	ν12	367	330	272	1248.1	114.8	110.0	m
2	a′	ν8	1171	1054	1034	341.3	100.2	34.0	vs
3	a′	ν7	1192	1073	1077	95.5	28.5	13.0	w
4	a″	ν11	1287	1158	1157	8.7	2.8	14.0	
5	a′	ν6	1510	1359	1334	109.7	41.5	21.0	m
6	a′	ν5	1629	1466	1452	9.5	3.9	37.0	vw
7	a″	ν10	1645	1480	1466	8.3	3.4	0.0	w
8	a′	ν4	1656	1490	1473	13.1	5.4	2.0	w
9	a′	ν3	3138	2824	2847	71.5	56.2	42.0	m
10	a″	ν9	3183	2865	2962	85.9	68.5	72.0	m
11	a′	ν2	3253	2928	3006	44.4	36.2	51.0	m
12	a′	ν1	4112	3701	3667	45.8	47.2	27.0	m

[a]The dipole strength, D(km/mol), is derived from the calculated quantity, $D(esu^2\ cm^2 \times 10^{40})$ by $D(km/mol) = 0.0002507 \times D(esu^2\ cm^2 \times 10^{40}) \times \nu(cm^{-1})$ where ν is the calculated (unscaled) frequency.
[b]Present work, frequencies and intensities using 6-31G~ basis set at 6-31G** geometry.
[c]Reference 23.
[d]Reference 21.
[e]Calculated frequencies multiplied by 0.9 (ref. 15).
[f]$\times 10^{40}$.

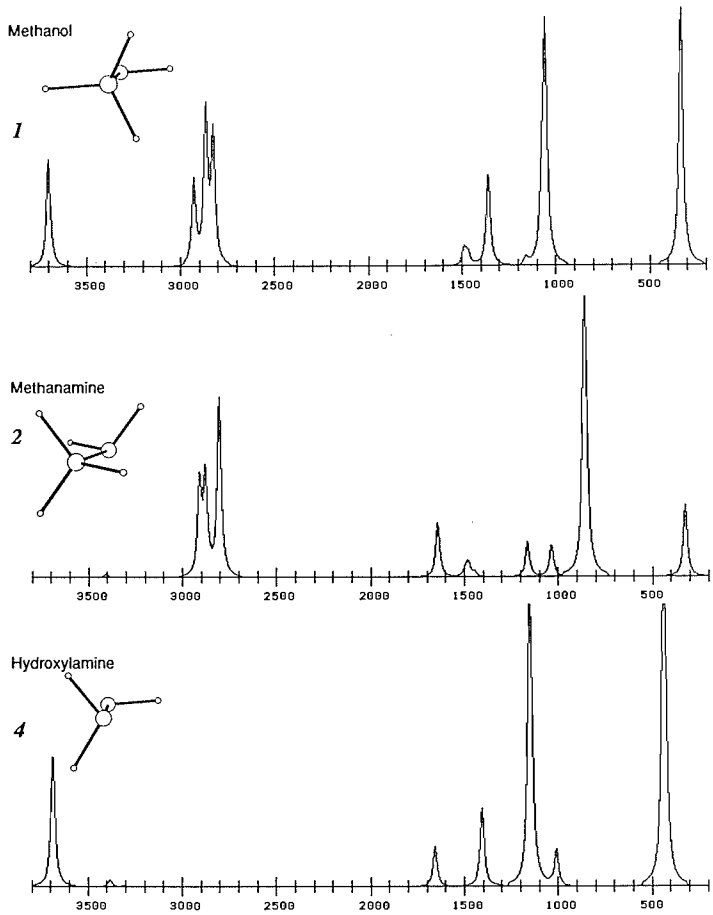

FIG. 2. Simulated IR spectra using uniformly scaled 6-31G~ frequencies. See text for a discussion.

calculate to be nearly degenerate and which are not resolved experimentally. Our IR and VCD intensities are tabulated in Table 3 and simulated spectra are displayed in Fig. 4. The most intense band in the IR spectrum, ν12 at 1001 cm^{-1} (scaled) corresponds to the out-of-phase umbrella motion of the two nitrogen atoms. The in-phase umbrella motion, ν6, at 873 cm^{-1} is also intense. These motions give rise to an intense conservative CD couplet in the VCD spectrum (Fig. 4*b*) of NH_2NH_2, as well as its tetradeuterio analogue, ND_2ND_2 (Fig. 4*a*). A symmetrical CD couplet is also predicted for the NH_2 rocking

Can. J. Chem. Downloaded from www.nrcresearchpress.com by 91.144.44.67 on 09/07/12
For personal use only.

TABLE 2. Frequencies and dipole strengths for methanamine, CH_3NH_2, **2**

Normal mode			Frequency, cm^{-1}			Dipole strength[a]		
			Calc	Scal[d]	Exp[c]	Calc[b] ($esu^2\ cm^2$)[e]	Calc[b] (km/mol)	(Exp)[c]
1	a″	ν15	359	323	264	350.7	31.6	s
2	a′	ν9	950	855	780	634.4	151.1	vs
3	a″	ν14	1066	959		0.0	0.0	vw
4	a′	ν8	1150	1035	1044	50.9	14.7	s
5	a′	ν7	1291	1162	1130	47.8	15.5	m
6	a″	ν13	1482	1334		0.1	0.0	vw
7	a′	ν6	1606	1445	1430	5.0	2.0	m
8	a′	ν5	1642	1478	1474	14.8	6.1	s
9	a″	ν12	1661	1495	1485	9.4	3.9	vw
10	a′	ν4	1825	1643	1623	52.6	24.1	s
11	a′	ν3	3114	2803	2820	100.7	78.6	vs
12	a′	ν2	3196	2876	2962	54.2	43.4	vs
13	a″	ν11	3231	2908	2985	50.0	40.5	s
14	a′	ν1	3708	3337	3360	0.3	0.3	w
15	a″	ν10	3785	3406	3424	1.9	1.8	s

[a]The dipole strength, D(km/mol), is derived from the calculated quantity, $D(esu^2\ cm^2 \times 10^{40})$ by $D(km/mol) = 0.0002507 \times D(esu^2\ cm^2 \times 10^{40}) \times \nu(cm^{-1})$ where ν is the calculated (unscaled) frequency.
[b]Present work, frequencies and intensities using 6-31G~ basis set at 6-31G** geometry.
[c]Reference 32.
[d]Calculated frequencies multiplied by 0.9 (ref. 15).
[e]$\times 10^{40}$.

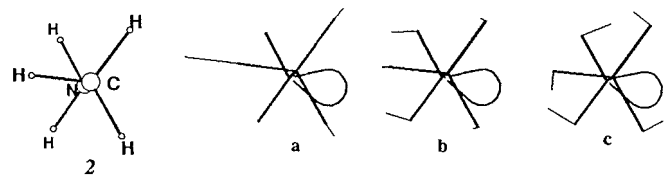

FIG. 3. Selected vibrational modes of methanamine: *a*, ν2 stretch of CH anti to N lone pair; *b*, ν9 pyramidal inversion at N; *c*, ν12 CN torsion.

modes, ν4 and ν11, near 1300 cm^{-1}. The effect of deuteration on IR and VCD spectra, besides the obvious frequency shift due to the increased mass, is to reduce the intensities of those modes where the motion of H/D dominates. Thus the VCD spectrum of ND_2ND_2 shown in Fig. 4 is only about one quarter as intense as the VCD spectrum of NH_2NH_2. The rocking modes of the ND_2 groups do not give rise to a CD couplet as was observed in the case of NH_2NH_2 since these modes are shifted closer to the N—N stretch, ν5, and the increased coupling of ν4 and ν5 redistributes their negative rotatory intensity to both sides of the positive CD band due to ν11. The VCD spectra of all of the deuterated isotopomers of **3** will be described in greater detail elsewhere (26).

Hydroxylamine ***4***. The RHF/6-31G** geometry of **4** is shown in Fig. 1. The calculated geometry agrees well with experiment (N—O = 1.453 Å, N—H = 1.016 Å, O—H = 0.962 Å, O—N—H = 103.2°, N—O—H = 101.4°, H—N—H = 107.1° (16)) except that the N—O bond length is shorter by 0.051 Å. The molecular point group is C_s. Raw and scaled harmonic frequencies calculated from the 6-31G~ force field are presented in Table 4 and the simulated IR spectrum is shown in Fig. 2. The strongest calculated absorption, ν9, corresponds to the torsional mode. This has been reported as *very weak* by Giguere and Liu (27). The second most intense absorption, ν5,

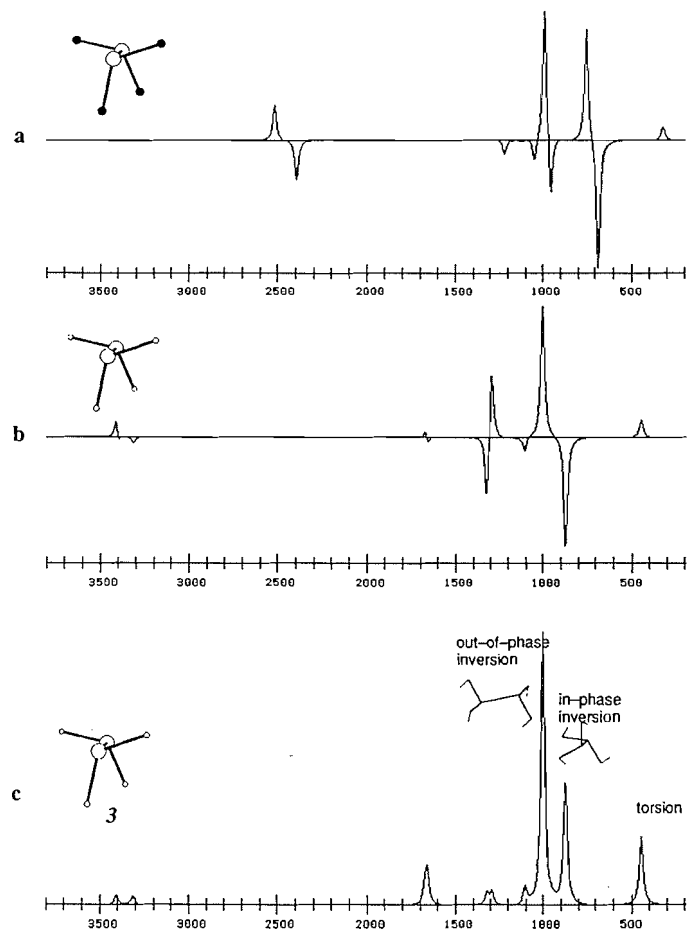

FIG. 4. Simulated IR and VCD spectra of hydrazine: *b*, *c* NH_2NH_2; *a*, ND_2ND_2. The spectrum *a* is magnified 4× relative to *b*.

Can. J. Chem. Downloaded from www.nrcresearchpress.com by 91.144.44.67 on 09/07/12
For personal use only.

TABLE 3. Frequencies, dipole strengths, and rotational strengths for hydrazine, NH_2NH_2, **3**

Normal mode			Frequency, cm^{-1}				Dipole strength[a]		Rotational strength ($esu^2\ cm^2$)[e]
			Calc[b]	Scal[c]	Exp[d]	Calc[d]	Calc[b] ($esu^2\ cm^2$)	Calc[b] (km/mol)	
1	*a*	ν7	498	448	377[f]	401	319.1	39.8	459.5
2	*a*	ν6	970	873	780[g]	898	301.9	73.4	−1495.8
3	*b*	ν12	1112	1001	937[i]	1045	562.1	156.7	1559.9
4	*a*	ν5	1226	1103	1098[g,h]	1167	30.4	9.3	−165.9
5	*b*	ν11	1437	1293	1283[j]	1320	22.1	8.0	685.8
6	*a*	ν4	1469	1322	1324[j]	1376	18.3	6.7	−627.0
7	*b*	ν10	1843	1659	1587[g,h]	1645	32.3	14.9	−68.4
8	*a*	ν3	1856	1670	1628[g,h]	1705	26.9	12.5	71.4
9	*b*	ν9	3682	3314	3297[k]	3287	4.9	4.5	−18.8
10	*a*	ν2	3691	3322		3300	0.4	0.4	−5.6
11	*a*	ν1	3781	3403		3413	1.7	1.6	−80.0
12	*b*	ν8	3788	3409	3390[k]	3402	4.5	4.3	111.2

[a]The dipole strength, D(km/mol), is derived from the calculated quantity, $D(esu^2\ cm^2 \times 10^{40})$ by D(km/mol) = $0.0002507 \times D(esu^2\ cm^2 \times 10^{40}) \times \nu(cm^{-1})$ where ν is the calculated (unscaled) frequency.
[b]Present work, frequencies and intensities using 6-31G~ basis set at 6-31G** geometry.
[c]Calculated frequencies multiplied by 0.9 (ref. 15).
[d]Ref. 25; calculated frequencies by CI–6-31G* force field.
[e]$\times 10^{45}$.
[f]Reference 24*e*.
[g]Reference 24*a*.
[h]Reference 24*c*.
[i]Reference 24*f*.
[j]Reference 24*d*.
[k]Reference 24*b*.

TABLE 4. Frequencies, and dipole strengths for hydroxylamine, NH_2OH, **4**

Normal mode			Frequency, cm^{-1}				Dipole strength[a]			
			Calc[b]	Calc[c]	Scal[e]	Exp[d]	Calc[b] ($esu^2\ cm^2$)[f]	Calc[b] (km/mol)	Calc[c] (km/mol)	(Exp)[d]
1	*a″*	ν9	482	434	434	430	1534.6	185.4	230.9	vw?
2	*a′*	ν6	1121	1122	1009	895	59.5	16.7	20.8	m
3	*a′*	ν5	1275	1276	1148	1120	479.2	153.2	164.4	vs
4	*a″*	ν8	1474	1482	1327	765	1.6	0.6	2.3	w
5	*a′*	ν4	1561	1556	1405	1357	88.8	34.8	30.0	s
6	*a′*	ν3	1841	1855	1657	1605	38.2	17.6	22.4	m
7	*a′*	ν2	3681	3718	3313	3297	0.6	0.6	5.2	m
8	*a″*	ν7	3760	3810	3384	3350	3.5	3.3	1.2	w
9	*a′*	ν1	4097	4204	3687	3656	57.3	58.9	70.1	s

[a]The dipole strength, D(km/mol), is derived from the calculated quantity, $D(esu^2\ cm^2 \times 10^{40})$ by D(km/mol) = $0.0002507 \times D(esu^2\ cm^2 \times 10^{40}) \times \nu(cm^{-1})$ where ν is the calculated (unscaled) frequency.
[b]Present work, frequencies and intensities using 6-31G~ basis set at 6-31G** geometry.
[c]6-31G** basis set, ref. 33.
[d]Reference 27.
[e]Our calculated frequencies multiplied by 0.9 (ref. 15).
[f]$\times 10^{40}$.

is calculated to be the out-of-phase combination of umbrella motion at N and the N—O—H bend, dominated by the former. The umbrella mode, ν5, of **4** is markedly shifted to higher frequency compared to ν9 of **2** or ν6 and ν12 of **3**, due to the repulsive 4-electron interaction between the non-bonding lone pair on N and the lower non-bonding electron pair on O. The NH_2 rocking mode, ν8, is extremely weak and is expected to occur near 1330 cm^{-1}. The N—O—H bend is the major component of the motion responsible for the band, ν4, at 1405 cm^{-1} (scaled), observed at 1357 cm^{-1} (27). The NH_2 scissor, ν3, occurs at 1657 cm^{-1} (scaled), 1605 cm^{-1} (observed (27)). The calculated position is very similar to the values obtained for the same mode in **2** (ν4, at 1643 cm^{-1}) and **3** (ν3, at 1670 cm^{-1}, and ν10, at 1659 cm^{-1}). As was the case for **2** and **3**, the NH stretches, ν2 and ν7, are calculated to be very weak.

Hydrogen peroxide **5**. The RHF/6-31G** geometry of **5** is shown in Fig. 1. The calculated geometry agrees reasonably well with experiment (O—O = 1.464 Å, O—H = 0.965 Å, O—O—H = 99.4°, ϕ = 121.6° (17)). Systematic deviations at the RHF level could be corrected by inclusion of electron

Can. J. Chem. Downloaded from www.nrcresearchpress.com by 91.144.44.67 on 09/07/12
For personal use only.

TABLE 5. Frequencies, dipole strengths, and rotational strengths for H_2O_2, **5**

Normal mode			Frequency, cm^{-1}			Dipole strength[a]				Rotational strength ($esu^2\ cm^2$)[f]
			Calc	Scal[d]	Exp[e]	Calc[b] ($esu^2\ cm^2$)	Calc[b] (km/mol)	Calc[c] (km/mol)	(Exp) (km/mol)	
1	$\nu 4$	*a*	426	383	317	1870.8	199.8	123.0		1904.6
2	$\nu 3$	*a*	1146	1031	864	2.8	0.8	0.1		−27.1
3	$\nu 6$	*b*	1504	1354	1266	301.3	133.6	101.0	84[g] 113[h]	202.6
4	$\nu 2$	*a*	1636	1472	1394	0.7	0.3	0.9		−127.7
5	$\nu 1$	*a*	4063	3657	3607	21.5	21.9	14.5		14.3
6	$\nu 5$	*b*	4064	3658	3608	93.2	94.9	46.2		−77.5

[a]The dipole strength, D(km/mol), is derived from the calculated quantity, $D(esu^2\ cm^2 \times 10^{40})$ by D(km/mol) = 0.0002507 × $D(esu^2\ cm^2 \times 10^{40}) \times \nu(cm^{-1})$ where ν is the calculated (unscaled) frequency.
[b]Present work, frequencies and intensities using 6-31G~ basis set at 6-31G** geometry.
[c]Reference 29.
[d]Calculated frequencies multiplied by 0.9, ref. 15.
[e]Reference 28.
[f]$\times 10^{45}$.
[g]Reference 34.
[h]Value quoted by ref. 27 as modified from ref. 35 by P. D. Maker.

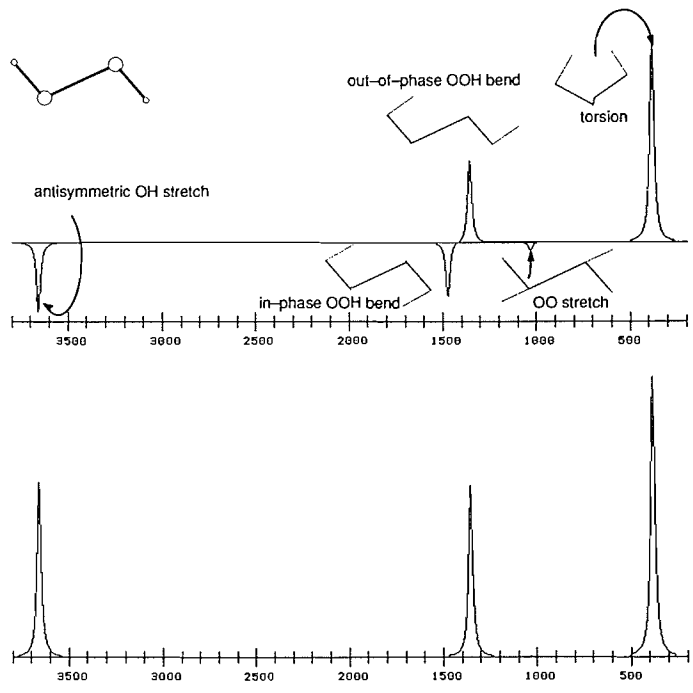

FIG. 5. Simulated IR and VCD spectra of hydrogen peroxide, **5**.

correlation in the calculations (18, 20) but this is beyond the scope of the present model studies. The molecular point group is C_2. Raw and scaled (by 0.9) harmonic frequencies calculated from the 6-31G~ force field are presented in Table 5 together with calculated IR and VCD intensities. It is noteworthy that even with the usual scaling factor, all of the calculated frequencies are higher than observed. Simulated IR and VCD spectra are shown in Fig. 5. Rogers and Hillman (29) have previously calculated absolute intensities for **5** by APT theory, using a combination of theoretical and empirical APTs for H_2O, CH_3OH, and HOCl. Their values, shown in Table 5, are in qualitative agreement with our 6-31G~ values. The most intense band in the IR is calculated to be the torsional mode, $\nu 4$. Its intensity may be exaggerated somewhat since the optimized torsional angle is too small by 6°.

The predicted VCD spectrum of *P*-H_2O_2 is shown in Fig. 5, and again in Fig. 6 for comparison to the predicted VCD spectra of the mono- and dideuterio isotopomers. The torsional mode, $\nu 4$, is calculated to give rise to the most intense VCD band (Fig. 4). The most striking feature of the VCD spectrum is the CD couplet between 1300 cm^{-1} and 1500 cm^{-1}. Polavarapu (30) has analysed the expected intensity distribution among symmetric and antisymmetric bending vibrational modes in A_2B_2 systems and has predicted that for H_2O_2 of *P* chirality, the higher frequency symmetric O—O—H bend, should be considerably weaker in the IR than the antisymmetric O—O—H bend, and have negative rotatory strength of about the same magnitude as the antisymmetric mode if the fixed-partial-charge (FPC) mechanism dominates. Our calculated VCD spectrum displays just these features, but with a two-fold asymmetry favouring the antisymmetric bending CD band, $\nu 6$. From Table 5, it is apparent that the symmetric and antisymmetric O—H stretching modes, $\nu 1$ and $\nu 5$, respectively, are not consistent with features expected from a simple coupled oscillator mechanism from which one would predict a negative rotatory strength for the symmetric O—H mode, $\nu 1$. The signs are reversed and there is a five-fold asymmetry favouring the antisymmetric band. The near degeneracy calculated and observed (28) of the frequencies of the two stretching modes has the effect of completely cancelling the weaker positive CD band. An explanation for the origin of the "anomalous" rotatory strength is offered in connection with the VCD spectrum of DOOH discussed below. Apparently, **5** does crystallize in a single enantiomeric form (31) so in principle the VCD spectrum can be measured.

The simulated VCD spectrum of dideuterio-**5** is shown in Fig. 5. The VCD intensities are greatly attenuated by deuterium substitution but the same features as were found in **5** are reproduced in the O—D stretching and torsional regions. The mid-IR region is predicted to be markedly different, however. The isotopic shift places the O—O—D bending frequencies into the vicinity of the O—O stretch and the strong mixture of the modes results in the disappearance of the CD couplet found for **5** itself.

The simulated VCD spectrum of DOOH is also shown in Fig. 5. In this system, the O—H and O—D stretches and

Can. J. Chem. Downloaded from www.nrcresearchpress.com by 91.144.44.67 on 09/07/12
For personal use only.

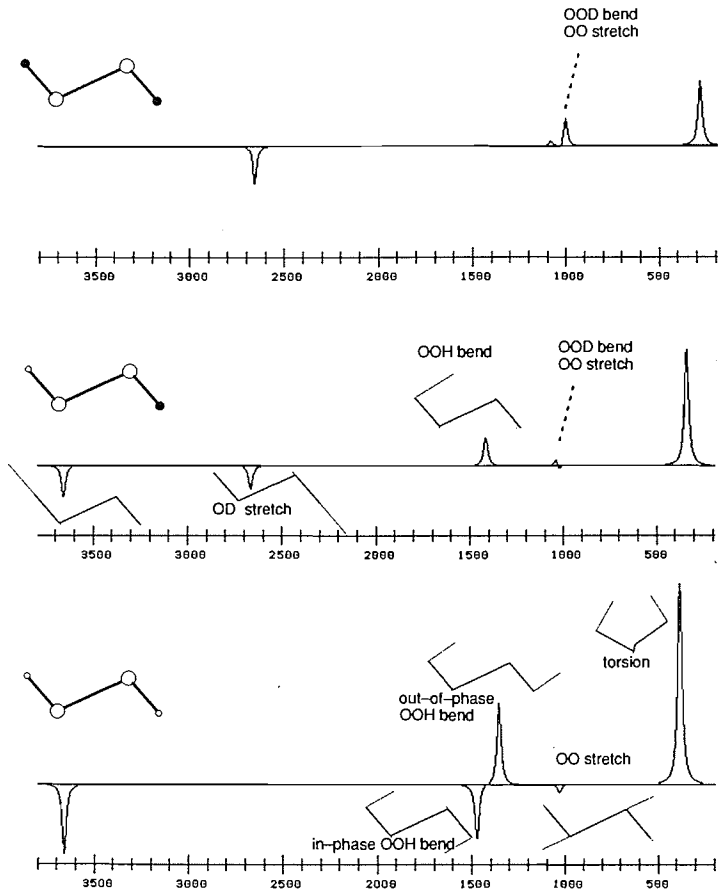

FIG. 6. Simulated VCD spectra of HOOH, HOOD, and DOOD, plotted on the same scale.

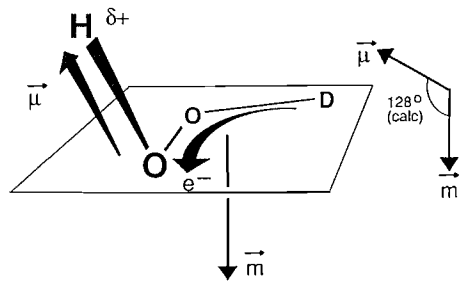

FIG. 7. Model for rotatory strength of O—H stretching vibration of HOOD of *P* chirality. Motion of the positive H away from the O—O—D group induces a flow of electrons toward it. The associated electric (μ) and magnetic (m) dipole transition moments are directed as shown. The calculated angle between the moments is −128°.

the O—O—H and O—O—D bends are well separated and essentially decoupled. Each of the isotopes, H or D, resides in a chiral environment of the same handedness. The O—O—H bend results in a positively signed band of similar intensity to the two stretches. The O—O—D bend and O—O stretch are almost degenerate and, as was the case for DOOD, the mixture of the two modes results in almost a complete cancellation of VCD intensity.

In DOOH, both stretching modes, O—H and O—D, yield a negative VCD signal, the origin of which may be explained by Nafie and Freedman's "3-bond electronic current model" (36) which is applied to DOOH in Fig. 7. The O—H bond is strongly polarized in the direction expected from electronegativity considerations. The bond dipole is positive and a stretch of the bond results in a positive change in the bond dipole (and the permanent molecular dipole moment) in the direction of the O—H(D) bond. The remainder of the molecule, the O—O—D(H) fragment, forms an arc along which negative charge is drawn toward the O—H(D) bond being stretched. The induced flow of charge around the arc is associated with an induced magnetic dipole moment perpendicular to the O—O—D(H) plane on the side opposite to the O—H(D) dipole. Thus the scalar product of the change in the electric dipole moment and the induced magnetic dipole moment is negative. The calculated angle between the electric and magnetic dipole transition moments is |128|°. In HOOH and DOOD where the stretching modes are coupled, the induced flow of charge along the bonds is cooperative in the case of the antisymmetric stretch, resulting in greater intensity for this mode.

Summary of VCD results

The calculated VCD rotational strengths for the *gauche* forms of *P* chirality shown in Fig. 1 for both chiral molecules, **3** and **4**, suggest that the torsional mode is very intense in the VCD spectrum. In hydrazine, the in- and out-of-phase umbrella motions of the nitrogen atoms, $\nu 6$ and $\nu 12$, respectively, give rise to an intense CD couplet with negative rotational strength to the long wave length side. The umbrella modes and the rocking modes of the NH_2 groups each form a coupled oscillator system which gives rise to very symmetrical CD couplets. This pattern is largely destroyed in ND_2ND_2 for the rocking modes because these are shifted into the region of, and mix with the NN stretch. In hydrazine, all combinations of NH stretches are relatively weak in the IR but the highest frequency mode of *b* symmetry, $\nu 8$, has moderate positive rotatory strength. The in- and

Can. J. Chem. Downloaded from www.nrcresearchpress.com by 91.144.44.67 on 09/07/12
For personal use only.

out-of-phase OH stretches of HOOH, $\nu 1$ and $\nu 5$, respectively, nominally also a coupled oscillator system, reveal a significant asymmetry and anomalous signs in the expected bisignate CD pattern. The higher frequency mode, $\nu 5$, has a negative rotational strength four times as intense as the lower frequency mode, $\nu 1$, and completely cancels it in the calculated VCD spectrum. The results of the calculations are explained in terms of a simple model (36) involving an induced flow of electrons around the O—O—H arc in the direction of the O—H bond being stretched.

Acknowledgments

The financial support of the Natural Sciences and Engineering Research Council of Canada is gratefully acknowledged. We also thank Supercomputer Services of the University of Calgary for a generous amount of time on the CDC Cyber 205.

1. (*a*) L. A. NAFIE and M. DIEM. Appl. Spectrosc. **33**, 130 (1979); (*b*) L. A. NAFIE and D. W. VIDRINE. *In* Fourier transform infrared spectroscopy. Vol. 3. *Edited by* J. R. Ferraro and L. J. Basile. Academic Press, New York. 1982. p. 38; (*c*) P. L. POLAVARAPU. Chem. Phys. Lett. **148**, 21 (1988).
2. (*a*) D. P. CRAIG and T. THIRUNAMACHANDRAN. Mol. Phys. **35**, 825 (1978); (*b*) D. P. CRAIG and T. THIRUNAMACHANDRAN. Can. J. Chem. **63**, 1773 (1985); (*c*) A. D. BUCKINGHAM, P. W. FOWLER, and P. A. GALWAS. Chem. Phys. **112**, 1 (1987).
3. L. A. NAFIE. J. Chem. Phys. **79**, 4960 (1983).
4. L. A. NAFIE and T. B. FREEDMAN. J. Chem. Phys. **78**, 7108 (1983).
5. P. J. STEPHENS. J. Phys. Chem. **89**, 748 (1985).
6. M. A. LOWE, G. A. SEGAL, and P. J. STEPHENS. J. Am. Chem. Soc. **108**, 248 (1986).
7. M. A. LOWE, P. J. STEPHENS, and G. A. SEGAL. Chem. Phys. Lett. **123**, 108 (1986).
8. (*a*) K. J. JALKANEN, P. J. STEPHENS, R. D. AMOS, and N. C. HANDY. J. Am. Chem. Soc. **109**, 7193 (1987); (*b*) K. J. JALKANEN, P. J. STEPHENS, R. D. AMOS, and N. C. HANDY. Chem. Phys. Lett. **142**, 153 (1987); (*c*) K. J. JALKANEN, P. J. STEPHENS, R. D. AMOS, and N. C. HANDY. J. Phys. Chem. **92**, 1781 (1988); (*d*) K. J. JALKANEN, P. J. STEPHENS, R. D. AMOS, and N. C. HANDY. J. Am. Chem. Soc. **110**, 2012 (1988); (*e*) R. W. KAWIECKI, F. DEVLIN, P. J. STEPHENS, R. D. AMOS, and N. C. HANDY. Chem. Phys. Lett. **145**, 411 (1988).
9. R. DUTLER. Ph.D. Dissertation. The University of Calgary, Calgary, Alta. 1988.
10. R. DUTLER and A. RAUK. J. Am. Chem. Soc. In press.
11. (*a*) A. J. SADLEJ. Chem. Phys. Lett. **47**, 50 (1977); (*b*) H. NAKATSUJI, K. KANDA, and T. YONEZAWA. Chem. Phys. Lett. **75**, 340 (1980).
12. (*a*) J. S. BINKLEY, M. J. FRISCH, D. J. DEFREES, K. RAGHAVACHARI, R. A. WHITESIDES, H. B. SCHLEGEL, E. M. FLUDER, and J. A. POPLE. Department of Chemistry, Carnegie-Mellon University, Pittsburgh, PA; (*b*) A. RAUK and R. DUTLER. J. Comput. Chem. **8**, 324 (1987).
13. (*a*) W. J. HEHRE, R. DITCHFIELD, and J. A. POPLE. J. Chem. Phys. **56**, 2257 (1972); (*b*) M. M. FRANCL, W. J. PIETRO, W. J. HEHRE, J. S. BINKLEY, M. S. GORDON, D. J. DEFREES, and J. A. POPLE. J. Chem. Phys. **77**, 3654 (1982).
14. P. PULAY. *In* Modern theoretical chemistry. Vol. 3. Methods of electronic structure theory. *Edited by* H. F. Schaefer III. Plenum, New York. 1977.
15. J. A. POPLE, H. B. SCHLEGEL, R. KRISHNAN, D. J. DEFREES, J. S. BINKLEY, M. J. FRISCH, R. A. WHITESIDE, R. F. HOUT, and W. J. HEHRE. Int. J. Quantum Chem. Symp. **15**, 269 (1981).
16. M. D. HARMONY, V. W. LAURIE, R. L. KUEZKOWSKI, R. H. SCHWENDEMAN, D. A. RAMSEY, F. L. LOVAS, W. J. LAFFERTY, and A. G. MAKI. J. Phys. Chem. Ref. Data, **8**, 619 (1979).
17. D. CREMER and D. CHRISTEN. J. Mol. Spectrosc. **74**, 480 (1979).
18. D. J. DEFREES, K. RAGHAVACHARI, H. B. SCHLEGEL, and J. A. POPLE. J. Am. Chem. Soc. **104**, 5576 (1982).
19. J. A. POPLE, K. RAGHAVACHARI, M. J. FRISCH, J. S. BINKLEY, and P. V. R. SCHLEYER. J. Am. Chem. Soc. **105**, 6389 (1983).
20. R. A. BLAIR and W. A. GODDARD III. J. Am. Chem. Soc. **104**, 2719 (1982).
21. A. SERRALLACH, R. MEYER, and Hs. H. GUNTHARD. J. Mol. Spectrosc. **52**, 94 (1974).
22. W. B. PERSON. Report 1982, N-82-25047; (CA 99:130590x).
23. K. KUCZERA. Acta Phys. Pol. A**70**, 797 (1986).
24. (*a*) P. A. GIGUERE and I. D. LIU. J. Chem. Phys. **20**, 136 (1952); (*b*) E. CATALANO, R. H. SANBORN, and J. W. FRAZER. J. Chem. Phys. **38**, 2265 (1963); (*c*) J. S. ZIOMEK and M. D. ZEIDLER. J. Mol. Spectrosc. **11**, 163 (1963); (*d*) J. DURIG, S. F. BASH, and E. E. MERCER. J. Chem. Phys. **44**, 4328 (1966); (*e*) A. YAMAGUCHI, I. ICHISHIMA, T. SHIMANOUCHI, and S. MIZUSHIMA. Spectrochim. Acta, **16**, 1471 (1960); (*f*) Y. HAMADA, A. Y. HIRAKAWA, K. TAMAGAKE, and M. TSUBOI. J. Mol. Spectrosc. **35**, 420 (1970).
25. N. TANAKA, Y. HAMADA, Y. SUGAWARA, M. TSUBOI, S. KATO, and K. MOROKUMA. J. Mol. Spectrosc. **99**, 245 (1983).
26. R. DUTLER, A. RAUK, and D. YANG. To be published.
27. P. A. GIGUERE and D. I. LIU. Can. J. Chem. **30**, 948 (1952).
28. P. A. GIGUERE and T. K. K. SRINIVASAN. J. Raman Spectrosc. **2**, 125 (1974).
29. J. D. ROGERS and J. J. HILLMAN. (*a*) J. Chem. Phys. **75**, 1085 (1981); (*b*) J. Chem. Phys. **76**, 4046 (1982).
30. P. L. POLAVARAPU. J. Chem. Phys. **87**, 4419 (1987).
31. R. SRINIVASAN. Curr. Sci. **39**, 130 (1970).
32. Y. HAMADA, N. TANAKA, Y. SUGAWARA, A. Y. HIRAKAWA, M. TSUBOI, S. KATO, and K. MOROKUMA. J. Mol. Spectrosc. **96**, 313 (1982).
33. G. A. YEO and T. A. FORD. J. Mol. Struct. **141**, 331 (1986).
34. F. P. J. VALERO, D. GOORVITCH, F. S. BONOMO, and R. W. BOESE. Appl. Opt. **20**, 4097 (1981).
35. H. NIKI, P. D. MAKER, C. M. SAVAGE, and L. P. BREITENBACH. Chem. Phys. Lett. **73**, 43 (1980).
36. L. A. NAFIE and T. B. FREEDMAN. J. Mol. Struct. In press.

Can. J. Chem. Downloaded from www.nrcresearchpress.com by 91.144.44.67 on 09/07/12
For personal use only.

The microwave and far-infrared spectra and the geometry of 8-oxabicyclo[3.2.1]octane

THOMAS EGGIMANN, TRACY L. SMITHSON, AND HAL WIESER
Department of Chemistry, University of Calgary, Calgary, Alta., Canada T2N 1N4

AND

PRIMOŽ LORENČAK, PAMELA BERGQUIST, HASSAN BADAWI, SCOTT P. SIBLEY, AND ROBERT L. KUCZKOWSKI
Department of Chemistry, University of Michigan, Ann Arbor, MI U.S.A. 48109-1055

Received May 29, 1989

THOMAS EGGIMANN, TRACY L. SMITHSON, HAL WIESER, PRIMOŽ LORENČAK, PAMELA BERGQUIST, HASSAN BADAWI, SCOTT P. SIBLEY, and ROBERT L. KUCZKOWSKI. Can. J. Chem. **68**, 267 (1990).

The structure of 8-oxabicyclo[3.2.1]octane was calculated by *ab initio* means at the STO-3G level, and the structural data used to assign the microwave spectrum of the title compound in the range of 26.5 to 40 GHz fitting 144 lines up to $J = 48$ by adjusting the rotational and three centrifugal distortion constants in the Watson *A* reduction. Structural parameters were deduced from the rotational constants by allowing all bond lengths and angles to vary in a least-squares manner. These parameters were in good agreement with those calculated at the STO-3G and 3-21G levels. Of many satellite lines observed, only the most intense could be utilized for locating the two lowest fundamental vibrations, estimated to occur at 190 and 240 cm^{-1}. The far-infrared spectrum is reported in the region of 80 to 300 cm^{-1}, exhibiting only one distinct sequence of Q branches at 264 cm^{-1}. On the basis of unscaled *ab initio* force fields at both levels of the theory the corresponding fundamentals are assigned, respectively, to a twisting (A'') and a bending (A') of the cycloheptane ring.

Key words: 8-oxabicyclo[3.2.1]octane, microwave and far-infrared spectra, *ab initio* STO-3G and 3-21G geometries.

THOMAS EGGIMANN, TRACY L. SMITHSON, HAL WIESER, PRIMOŽ LORENČAK, PAMELA BERGQUIST, HASSAN BADAWI, SCOTT P. SIBLEY et ROBERT L. KUCZKOWSKI. Can. J. Chem. **68**, 267 (1990).

Utilisant des méthodes *ab initio* au niveau STO-3G, on a calculé la structure du 8-oxabicyclo[3.2.1]octane et on a utilisé les données de structure ainsi obtenues pour attribuer 144 bandes, jusqu'à $J = 48$ dans la zone allant de 26,5 à 40 GHz, du spectre de micro-ondes du composé mentionné dans le titre en procédant à un ajustement de la constante de rotation et de trois constantes de centrifugation de la réduction A de Watson. On a pu déduire les paramètres de structure à partir des constantes de rotation et en permettant à toutes les longueurs de liaison et à tous les angles de varier selon le mode des moindres carrés. Ces paramètres sont en bon accord avec ceux calculés aux niveaux STO-3G et 3-21G. Parmi toutes les bandes satellites observées, seules les plus intenses ont pu être utilisées pour établir la location des deux vibrations fondamentales les plus basses qui se situeraient à 190 et 240 cm^{-1}. On a déterminé le spectre infrarouge lointain dans la région de 80 à 300 cm^{-1} et l'on n'a observé qu'une seule séquence de branches Q à 264 cm^{-1}. En se basant sur les champs de force *ab initio* des deux niveaux de la théorie, on a pu attribuer les bandes fondamentales correspondantes respectivement à une torsion (A'') et à une déformation (A') du noyau cycloheptane.

Mots clés : 8-oxabicyclo[3.2.1]octane, spectres de micro-ondes et infrarouge lointain, structures *ab initio* aux STO-3G et 3-21G.

[Traduit par la revue]

Introduction

Bicyclic compounds continue to be of considerable interest to mechanistic organic as well as to structural chemists probing, both experimentally and theoretically, the relationship between electronic structure and spectroscopic properties (1–5). As a continuation of related studies in our separate laboratories, we have investigated the microwave and far-infrared spectra of 8-oxabicyclo[3.2.1]octane, and compared the experimental geometry to that calculated by *ab initio* means at the STO-3G and 3-21G levels.

The analysis of the microwave spectrum was of interest especially for two reasons. First, the far-infrared spectra of several related bicyclo[3.2.1]octane molecules exhibit well resolved hot band sequences (6) normally characteristic of large amplitude anharmonic skeletal deformations which should lead to corresponding rotational lines in a number of excited vibrational states. Second, the interpretation of vibrational circular dichroism spectra of certain chiral analogs of the title compound, currently in progress, depends on a reliable force field best obtained by *ab initio* methods (7), for which in turn the geometry must be ascertained with commensurate accuracy. Only two experimental structures have been reported in the literature for related bicyclo[3.2.1]octane systems (8, 9) which could be compared with the *ab initio* geometries of the analog molecules of interest. As the experimental bond lengths contained in those reports differed widely from those we calculated by *ab initio* means, additional structural information from microwave spectra seemed appropriate.

Experimental and computational methods

Microwave spectra were obtained with a Hewlett-Packard 8460A spectrometer in the region 26.5 to 40 GHz. Frequency measurements were accurate to ±0.05 MHz. Radiofrequency–microwave double resonance (RFMWDR) spectra were obtained by replacing the Stark modulator with a tunable amplitude modulated radio frequency source covering 1–60 MHz at 50–5000 mW output.

The far-infrared spectrum was recorded with a Nicolet 8000 Fourier transform interferometer at 45 m path length in an optically matched long path cell, also manufactured by Nicolet (10). A globar was used as the light source in conjunction with a 3 μm Mylar beamsplitter and a liquid helium cooled bolometer, made by Infrared Laboratories, operating at 4.2 K and filtered to 400 cm^{-1}. With a resolution of 0.12 cm^{-1}, a moderate vapor pressure, and appropriate mirror velocity, 300 scans were deemed sufficient to give an adequate signal-to-noise ratio. Calibrated against standard water absorptions the reported peak positions are believed to be accurate to 0.03 cm^{-1}.

The Raman spectra including the polarization measurements were recorded with a Jarrell Ash model 25–100 double grating monochro-

Can. J. Chem. Downloaded from www.nrcresearchpress.com by 91.144.44.67 on 09/07/12
For personal use only.

TABLE 1. Selected structural parameters for 8-oxabicyclo[3.2.1]octane (in Å and degrees)

			Microwave[a]			
	Ab initio		Bond lengths fixed	Bond angles fixed	Bond lengths and angles varied	
Parameter	STO-3G	3-21G				cpoz[b]
C_1—C_2	1.554	1.531	1.543	1.523	1.527	1.528
C_2—C_3	1.547	1.545	1.539	1.544	1.543	1.540
C_1—O_8	1.442	1.452	1.432	1.437	1.438	1.414
C_1—C_7	1.557	1.548	1.543	1.549	1.547	—
C_6—C_7	1.552	1.561	1.548	1.537	1.541	—
C_1—H_9	1.093	1.078	1.093	1.103	1.093	1.091
C_2—H_{10}	1.088	1.084	1.087	1.115	1.109	1.089
C_2—H_{11}	1.088	1.085	1.088	1.091	1.091	1.093
C_3—H_{12}	1.088	1.084	1.088	1.087	1.103	1.090
C_3—H_{13}	1.087	1.084	1.087	1.051	1.060	1.097
C_6—H_{19}	1.086	1.081	1.085	1.022	1.031	—
C_6—H_{20}	1.086	1.081	1.085	1.133	1.116	—
$\angle C_1O_8C_5$	102.5	104.1	103.4	102.5	102.5	101.0
$\angle C_2C_3C_4$	111.1	110.7	111.1	111.1	111.1	110.3
$\angle C_1C_2C_3$	110.6	110.5	110.4	110.6	110.6	109.4
$\angle C_2C_1C_7$	112.6	112.4	112.1	112.5	112.5	—
$\angle C_1C_7C_6$	103.0	103.6	103.1	103.1	103.1	—
$\angle C_2C_1O_8$	109.0	107.7	109.1	109.0	109.0	110.4
$\angle O_8C_1C_7$	104.6	103.7	104.2	104.6	104.6	—
Ψ	39.9	42.5	40.7	39.5	39.7	40.8
Θ	113.6	113.0	114.2	113.4	113.5	113.6
Φ	134.5	135.1	134.4	134.8	134.7	136.7
Std. dev.[c]			0.247	0.058	0.057	—

[a]Structures by least squares fitting three moments of inertia and three principal axis conditions along with input predicate observables. Some of the latter were held fixed and others allowed to vary. See text.

[b]Cyclopentene ozonide (5).

[c]Rms standard deviation of the fit in amu Å^2.

Can. J. Chem. Downloaded from www.nrcresearchpress.com by 91.144.44.67 on 09/07/12
For personal use only.

mator using slit widths of 5 cm^{-1}. The incident beam was the 514.5 nm line of an argon ion laser (Coherent Radiation) with 300 mW power at the sample. The data were collected with a microcomputer interfaced to the instrument, allowing for co-adding of eight scans in the present case. Observed Raman lines were calibrated against liquid CCl_4. The solid sample was sealed into a capillary and melted in a special cell heated with a stream of hot air at 50°C.

8-Oxabicyclo[3.2.1]octane was prepared from cyclopentanone by a nine-step procedure involving in sequence, among other intermediates, 2-*N*-pyrrolidylbicyclo[3.2.1]octan-8-one, 5-cycloheptenol, and 8-oxabicyclo[3.2.1]octane-2-mercurial iodide. Details of this synthesis will be given elsewhere in due course (6). The final product was a waxy solid which was purified by sublimation at 85°C and atmospheric pressure to better than 99% as determined by analytical gc.

The GAUSSIAN 82 program package (11), running on a Cyber 205 supercomputer (12), was used for the computation with the STO-3G basis set. Due to computer disk limitations the later version, GAUSSIAN 86, as implemented on a Convex C120 was used for the calculations at the 3-21G level of theory. The equilibrium geometry of the molecule was evaluated by analytical gradient techniques based on *ab initio* Hartree–Fock molecular orbital calculations. No constraints were imposed in the calculations on the molecular structure other than C_s symmetry and starting the refinement process from a structure with the C_2—C_3—C_4 plane in the chair conformation. The optimization procedures in GAUSSIAN 82 and 86 in our experience are very reliable so that we can be certain that the rigid structure of this bicyclic molecule would not allow any minima other than the true one even with the low levels of theory. A second conceivable minimum could exist with the six-membered ring in the boat conformation. We have tested this hypothesis with 6,8-dioxabicyclo[3.2.1]octane obtaining an energy difference of about 1500 cm^{-1} between the two conformations, and no minima in-between (13). While we have not determined the magnitude of the barrier to inversion, it is reasonable to assume that it will be very much higher. Presumably the title compound will not be very different qualitatively. Vibrational frequencies were then obtained with unscaled harmonic force constants determined in the GAUSSIAN programs by analytical second differentiation of the energy at the stationary point.

Results and discussion

Microwave spectrum

Initially STO-3G *ab initio* structural parameters were used to predict a trial spectrum. The calculated geometry was later repeated at the 3-21G level. A selection of the most useful parameters is given in Table 1, while their complete listing is available as supplementary material (Table 1S).[1] Cartesian coordinates computed with the higher level of theory also have been deposited as supplementary material (Table 2S). The atom numbering used in these tables is explained in Fig. 1. Guided by the STO-3G predictions, five sets of doublets were observed between 36.7 and 39.0 GHz using RFMWDR techniques. One of these pairs, split by 102.5 MHz, was readily assigned to the μ_c K doublet 7(2,5) → 6(1,5) and 7(3,5) → 6(2,5), when pumped at this frequency. The remaining four doublets were split by 1.2 to 16.5 MHz. By trial and error the correct pair arising from the 7(1,6) → 6(0,6) and 7(2,6) → 6(1,6) transi-

[1]A complete set of data may be purchased from the Depository of Unpublished Data, CISTI, National Research Council of Canada, Ottawa, Ont., Canada K1A 0S2.

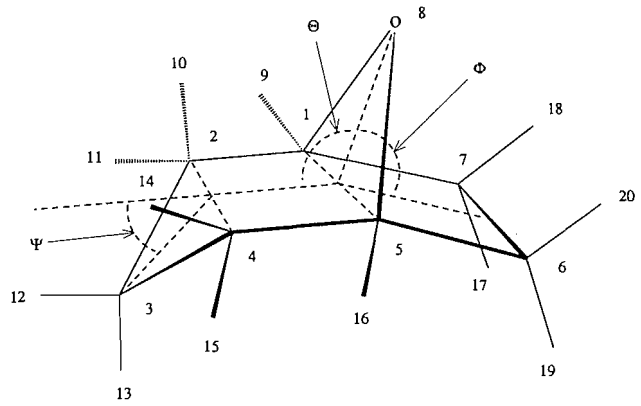

FIG. 1. Structure of 8-oxabicyclo[3.2.1]octane. Numbers correspond to atom numbering given in Table 1.

TABLE 2. Selected transitions of 8-oxabicyclo[3.2.1]octane

Transition	Frequency/MHz	$\Delta\nu^a$/MHz
5(5,0)–4(4,0)	28019.14	0.18
5(5,1)–4(4,1)	28037.74	0.01
5(4,1)–4(3,1)	26779.09	0.04
5(4,2)–4(3,2)	27059.57	−0.05
6(6,0)–5(5,0)	33742.99	−0.05
6(6,1)–5(5,1)	33748.13	−0.03
6(4,2)–5(3,2)	31302.08	0.01
6(4,3)–5(3,3)	31909.60	0.01
7(7,0)–6(6,0)	39461.70	0.09
7(7,1)–6(6,1)	39462.85	−0.13
7(6,1)–6(5,1)	38324.02	−0.03
7(6,2)–6(5,2)	38372.46	−0.04
26(25,2)–26(24,2)	26825.95	0.01
27(25,3)–27(24,3)	26707.57	−0.01
28(27,2)–28(26,2)	29035.06	−0.01
29(26,4)–29(25,4)	27682.43	0.00
30(28,3)–30(27,3)	30024.92	0.00
31(26,6)–31(25,6)	27372.10	−0.01
32(30,3)–32(29,3)	32235.91	0.02
33(31,3)–33(30,3)	33341.27	0.01
34(34,1)–34(33,1)	36867.20	0.01
34(33,2)–34(32,2)	35662.24	0.02
34(31,4)–34(30,4)	33218.20	0.01
34(30,5)–34(29,5)	31974.38	0.00
34(29,6)–34(28,6)	30711.76	0.01
37(30,8)–37(29,8)	31475.00	−0.01
38(31,8)–38(30,8)	32593.55	0.01
39(30,10)–39(29,10)	31054.14	0.01
40(30,11)–40(29,11)	30811.78	−0.01
41(30,12)–41(29,12)	30545.02	−0.02

[a] $\nu_{calc} - \nu_{obs}$.

tions was located. The identification of these four transitions led to the straightforward assignment of the crowded Stark modulated spectrum. Other prominent features in the Stark spectrum were strong Q branch μ_c transitions. A selection of transitions is given in Table 2, with the complete set of 144 assigned transitions available as supplementary material (Table 3S). The rotational and centrifugal distortion constants, listed in Table 3, were determined with the program ZFAP (14).

Second order Stark splittings were measured for several low J transitions. Since the spectrum was very crowded, resulting in interference with neighbouring lines, not all Stark shifts could be readily traced for different electric field settings. The fit of

TABLE 3. Rotational and centrifugal distortion constants[a] for 8-oxabicyclo[3.2.1]octane

	Value			
	Observed[b]		Calculated[c]	
Parameter	Ground state	First excited state[d]	STO-3G	3-21G
A/MHz	2858.186(1)	2860.926(3)	2831.67	2827.51
B/MHz	2458.657(1)	2482.415(2)	2437.72	2494.07
C/MHz	2041.973(3)	2038.142(14)	2012.48	2041.34
D_{JK}/Hz	246.4(8)	—		
D_K/Hz	−197.8(4)	—		
d_j/Hz	23.6(5)	—		
n^e	144	16		
$\Delta\nu^f$/kHz	36	20		
J_{max}^g	48	7		

[a] The constants from Watson's A reduction (19) were determined.
[b] The uncertainty in the last digits represents one standard deviation of the fit.
[c] Calculated with the coordinates from the theoretical calculations (see text).
[d] 190 ± 30 cm^{-1} from relative intensity measurements.
[e] Number of transitions.
[f] Standard deviation of the fit.
[g] The highest J of the measured transitions.

TABLE 4. Stark shifts[a] and dipole moment of 8-oxabicyclo-[3.2.1]octane

Transition	$\lvert M\rvert$	Observed	Calculated
6(4,2)–5(3,2)	1	0.432	0.458
7(4,3)–6(3,3)	1	0.717	0.714
7(4,3)–6(3,3)	2	3.075	3.073
7(5,2)–6(4,2)	1	0.375	0.389
7(5,2)–6(4,2)	2	2.025	2.019
$\mu_a = 0.382 \pm 0.002$ D			
$\mu_c = 1.557 \pm 0.004$ D			
$\mu_t = 1.603 \pm 0.013$ D			

[a] Units of $MHz/V^2\ cm^{-2} \times 10^6$.

the observed Stark shifts as a function of electric field to all three dipole moment components resulted in an imaginary μ_b consistent with the expected C_s symmetry. Holding $\mu_b = 0$ during the fitting process resulted in the dipole moment components given in Table 4.

The observed moments of inertia were used to test the structure determined from theoretical calculations. Lacking isotopically substituted data, 30 additional constraints involving structural parameters were employed during the fitting process with our modified version of Schwendeman's program STRFIT (15). In essence, this program will adjust those input structural assumptions which are allowed to vary, equivalent to a "predicate observables" or diagnostic least squares fitting procedure (16); see Appendix for a more detailed description of the fitting method and its reliability. Three fitting strategies were employed. If many bond distances were held fixed to the values from theoretical calculations (weight 20), the observed moments of inertia (weight 1) and assumed bond angles (weight 0.1) produced a reasonable fit (ΔI_{rms} = 0.247 amu Å^2, see Table 1) and bond angles close to those from theoretical calculations. When bond angles were held fixed and bond distances were allowed to vary, a nearly exact fit of the observed moments was obtained. However, this calculation produced

Can. J. Chem. Downloaded from www.nrcresearchpress.com by 91.144.44.67 on 09/07/12
For personal use only.

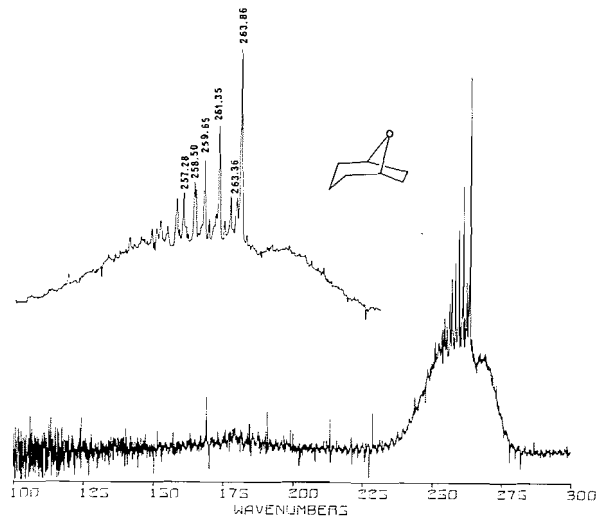

FIG. 2. Far-infrared spectrum of 8-oxabicyclo[3.2.1]octane, 0.12 cm^{-1} resolution, 3 μm Mylar beamsplitter, 300 scans, 45 m path length, and moderate vapour pressure.

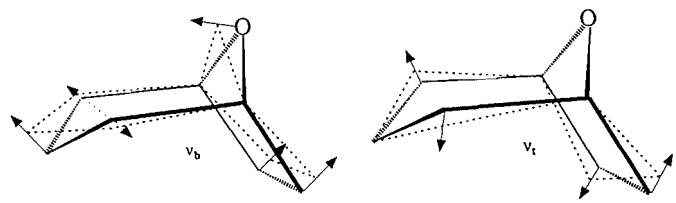

FIG. 3. Skeletal bending (ν_b) and twisting (ν_t) vibration of 8-oxabicyclo[3.2.1]octane.

some unreasonably short C—H distances (C_6—H_{19} = 1.022 Å) and poorly determined values for all dihedral angles involving hydrogen atoms. A similar fit to the observed moments was obtained when bond lengths and angles were allowed to vary. This fit gave reasonable values for most of the parameters. The structural parameters from all three calculations are given in Tables 1 and 1S.

It is interesting to note that the C_1—C_2 and C_2—C_3 bond distances from the last fit are 1.527 and 1.543 Å, respectively, compared to 1.528 and 1.540 Å in cyclopentene ozonide (5). Moreover, this fit predicts all *endo* C—H bond distances to be shorter than *exo* ones, similar to what has been observed for cyclobutene ozonide (16). The same order for the two C—C bonds is confirmed by the *ab initio* predictions using the 3-21G basis set, while STO-3G predicts the reverse order (Table 1). The corresponding bond lengths are 1.507 and 1.524 Å, respectively, for the 5,7-dimethyl-7-phenyl derivative of 6,8-dioxabicyclo[3.2.1]octane according to an X-ray study (9), while electron diffraction measurements for bicyclo[3.2.1]octane yielded 1.553 and 1.532 Å for C_1—C_2 and C_2—C_3, respectively (8), the order apparently agreeing with an MM2 geometry (18) which gave 1.540 and 1.537 Å, respectively.

Several low-lying vibrational states were observed in the microwave spectrum as weaker satellites to the ground state transitions. Sixteen low *J* transitions of the most intense satellite series were assigned (σ = 0.02 MHz). The rotational constants are reported in Table 3. Estimates of vibrational spacings were not as accurate as they could be in more ideal circumstances, since the spectrum for the low *J* lines was weak, crowded, and base line determinations were difficult. Nonetheless, relative intensities at room temperature of five of the most intense lines gave 190 ± 30 cm^{-1} as the lowest vibrational separation. The

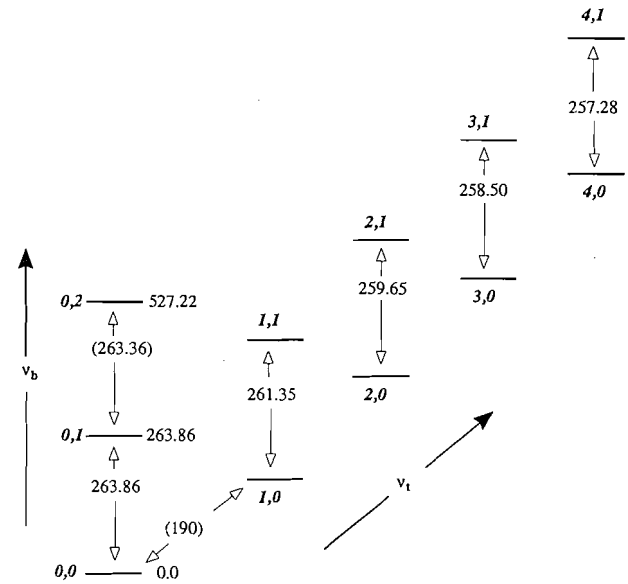

FIG. 4. Energy level diagram for skeletal bend and twist vibrations (ν_b and ν_t) of 8-oxabicyclo[3.2.1]octane. Energies in cm^{-1}.

next lowest state according to satellite intensities was estimated as 240 ± 40 cm^{-1} from the ground state.

Far-infrared spectrum

The far-infrared spectrum from 80 to 300 cm^{-1} is characterized by one series of pronounced Q bands starting at 263.86 cm^{-1} and extending to lower wavenumbers (Fig. 2). No other bands in this region are observed. The same fundamental is found in the Raman spectrum of the melted solid as a polarized line at 263 cm^{-1}, clearly corresponding to the 240 cm^{-1} absorption suggested by relative microwave intensities. *Ab initio* calculations of harmonic force constants at the STO-3G and 3-21G levels (unscaled) place this vibration at 270.7 and 287.5 cm^{-1}, respectively, and predict it to be an *A'* bending of the cyclopentane ring about the C—O—C bridge (Fig. 3) with its major contribution to the dipole moment change along the *C* rotational axis. The lowest transition, estimated near 190 cm^{-1} from microwave satellites, apparently has little intensity in the vapour phase infrared spectrum where it would have a *B* contour, but is seen in the Raman of the melted solid at 184 cm^{-1}. According to the *ab initio* predictions, it should occur at 191.2 and 183.0 cm^{-1} for the two levels of theory respectively, and arises from a twisting with *A"* symmetry of the cycloheptane ring (Fig. 3). The infrared intensities calculated with GAUSSIAN 86 from 3-21G atomic polar tensors are 94.8 × 10^3 and 10.0 × 10^3 cm/mol for the *A'* and *A"* modes, respectively, in qualitative agreement with the intensities observed in the vapour phase spectrum.

An assignment of the far-infrared sequence is suggested in Fig. 4. Only the most prominent members of the sequence can be assigned as bend (ν_b) transitions in consecutive excited states of the twist (ν_t). There are indications of additional sequences in this band (see Fig. 2), but their assignment is not corroborated by other information. The transitions are therefore not included in the energy level diagram. Additional series of microwave satellites which can be clearly seen but not assigned must originate from various other bend–twist excited states. Modeling of the potential energy surface to reproduce the far-infrared transitions would require at least these two coordinates. Of these, the ring bending mode may be thought of as leading to an inversion from the chair to the boat form of the six-membered

Can. J. Chem. Downloaded from www.nrcresearchpress.com by 91.144.44.67 on 09/07/12
For personal use only.

ring via a planar conformation of the C_1—C_2—C_3—C_4—C_5 skeletal fragment. Unfortunately, not enough of the transitions from either the far-infrared or microwave spectra are known to determine a best-fitting potential function and hence estimate the inversion barrier with an appropriate two-dimensional Hamiltonian.

Conclusions

As far as we are aware, this is the first documented evidence of vibrational anharmonicity in low energy skeletal deformations for a bicyclo-octane ring system. Evidence for this anharmonicity is observed in the rotational spectrum in the region of 26.5 to 40 GHz in terms of many satellite lines in vibrationally excited states, and in the vibrational spectrum in the region of 80 to 300 cm^{-1} in terms of a distinctive sequence of Q branches arising from the ring bending vibration (264 cm^{-1}) in excited states of a skeletal twist mode (190 cm^{-1}). The former in the extreme would lead to the inversion of the six-membered ring from the chair to the boat form. Assignment of the rotational lines in the vibrationally excited states is complicated by the inherent low intensities and by the density of the lines. The vibrational assignments are uniquely determined by an *ab initio* calculation of the force field using either the STO-3G or 3-21G levels of the theory.

The geometry deduced from the microwave rotational constants is reproduced well by the *ab initio* calculations with the two levels of theory differing only slightly in few respects. The ordering of the C—C bond lengths calculated with the 3-21G basis set is the same as that derived experimentally, with the exception of C_6—C_7 which 3-21G overestimates by 0.020 Å compared to the latter. The C_1—O_8 bond length and $\angle C_1O_8C_5$ bond angle are larger by 0.010 Å and 1.6°, respectively, for 3-21G than for STO-3G and the experimental values. Notwithstanding these minor differences, the agreement between the microwave and *ab initio* structures suggests that the latter constitute presently the best structural parameters available for the title molecule. With this assurance, it will be possible to approach the interpretation of the infrared absorption and VCD spectra with the commensurate confidence.

Acknowledgements

The microwave work was performed at the University of Michigan with the support of Grant CHE-8614340 from the National Science Foundation, Washington, D.C. We are grateful to Dr. Kurt W. Hillig II for assistance with the spectroscopic analysis.

The far-infrared spectroscopic work and the *ab initio* calculations were done at the University of Calgary supported by an Operating Grant from the Natural Sciences and Engineering Research Council of Canada. We gratefully acknowledge the substantial assistance from Drs. A. Rauk and R. Dutler with the calculations using the GAUSSIAN 82 and 86 systems of programs, and the Academic Computing Services and Supercomputer Committee of the University of Calgary for financially assisted access to the Convex C120 and the Cyber 205 supercomputer. We thank Mr. Ken Schmidt for the loan of a specially built variable temperature Raman cell, and Ms. Nan Ibrahim for preparing the compound under investigation.

1. P. Carrupt and P. Vogel. J. Mol. Struct. (Theochem.) **124**, 9 (1985).
2. C. R. Castro, R. Dutler, A. Rauk, and H. Wieser. J. Mol. Struct. (Theochem.) **152**, 241 (1987).
3. R. J. Abraham and J. Fisher. Magn. Res. Chem. **23**, 856 (1985).
4. Y. Senda, A. Ohno, J. Ishiyama, S. Imaizume, and S. Makiyama. Bull. Chem. Soc. Jpn. **60**, 613 (1987).
5. D. G. Borseth and R. L. Kuczkowski. J. Phys. Chem. **87**, 5381 (1983).
6. T. Eggimann, N. Ibrahim, T. L. Smithson, and H. Wieser. Unpublished results.
7. R. A. Shaw, N. Ibrahim, and H. Wieser. J. Phys. Chem. In press.
8. V. S. Mastryukov, E. L. Osina, L. V. Vilkov, and R. L. Hilderbrandt. J. Struct. Chem. **22**, 190 (1981).
9. B. P. Mundy, G. W. Dirks, R. D. Larson, and C. N. Caughlan. J. Org. Chem. **43**, 2347 (1978).
10. T. L. Smithson. Ph.D. Thesis, University of Calgary. 1982.
11. J. S. Binkley, M. J. Frisch, D. J. Defrees, K. Raghavachari, R. A. Whiteside, H. B. Schlegel, E. M. Fluder, and J. A. Pople. Department of Chemistry, Carnegie-Mellon University, Pittsburgh, PA. U.S.A.
12. A. Rauk and R. Dutler. J. Comp. Chem. **8**, 324 (1987).
13. T. Eggimann and H. Wieser. Unpublished results.
14. V. Typke. J. Mol. Spectrosc. **63**, 170 (1976).
15. R. H. Schwendeman. *In* Critical evaluation of chemical and structural information. *Edited by* D. R. Lide and M. A. Paul. National Academy of Sciences, Washington, D.C. 1974. pp. 94–115.
16. (*a*) L. S. Bartell, D. Romanesko, and T. C. Wong. *In* Molecular structure and diffraction methods. Spec. Per. Rep. Vol. 3. 1975. Chap. 4; (*b*) P. Nösberger, A. Bauder, and H. H. Günthard. Chem. Phys. **1**, 418 (1973); (*c*) J. J. Kierns and R. J. Curl, Jr. Chem. Phys. **48**, 3773 (1968).
17. D. B. Borseth, P. Lorenčak, H. M. Badawi, K. W. Hillig II, R. L. Kuczkowski, and G. D. Mendenhall. J. Mol. Struct. **190**, 125 (1988).
18. N. L. Allinger. J. Am. Chem. Soc. **99**, 8127 (1977).
19. J. K. G. Watson. *In* Vibrational spectra and structure, a series of advances. Vol. 6. *Edited by* J. R. Durig. Elsevier, New York. 1977. pp. 1–89.

Appendix

The determination of a unique set of structural parameters from the three rotational constants (observables) is, of course, impossible. The method of predicate observables provides the additional fitting equations necessary to determine a plausible structure consistent with the observables. The procedure distinguishes between real observables (moments of inertia) and predicate observables, i.e. structural parameters which are either held fixed to assumed values or permitted to vary from the assumption over a narrow but plausible range in order to arrive at ("determine") a structure which fits the rotational constants. The range of variance assigned to a predicate observable can be incorporated inversely as a weight assigned to the equation for that variable in the least squares fitting analysis, or the weight can be assigned ad hoc. An unlimited number of combinations of fixing some of the structural parameters and treating others as variables is feasible. The results in Table 1, column 4, were obtained by fixing all the bond lengths and allowing all the angles to vary, while in column 5 the angles were fixed and the bond lengths were varied. The results when all structural parameters were allowed to vary are in column 6. These procedures arrived at a generally sensible structure, consistent with the observables, but not necessarily the true structure. The structure is deemed sensible by comparison with other information such as the structure of cyclopentene ozonide (column 7) and the *ab initio* results (columns 2 and 3). The scatter in the distances and angles among the determinations in Table 1 (except for the CH distances) are a useful indicator of the range of structural parameters consistent with the observables, and of the uncertainty in the structure.

Can. J. Chem. Downloaded from www.nrcresearchpress.com by 91.144.44.67 on 09/07/12
For personal use only.

Structural studies of digitoxin and related cardenolides by two-dimensional NMR

TORBJÖRN DRAKENBERG
Department of Physical Chemistry 2, Lund Institute of Technology, Chemical Centre, 22100 Lund, Sweden
PETER BRODELIUS
Institute of Biotechnology, Swiss Federal Institute of Technology, Hönggerberg, CH-8093, Zürich, Switzerland
AND
DEANE D. MCINTYRE AND HANS J VOGEL[1]
Department of Biological Sciences, University of Calgary, Calgary, Alta., Canada T2N IN4

Received May 1, 1989

TORBJÖRN DRAKENBERG, PETER BRODELIUS, DEANE D. MCINTYRE, and HANS J. VOGEL. Can. J. Chem. **68**, 272 (1990).

The ^1H and ^{13}C NMR spectra of the cardenolides digitoxigenin, digoxigenin, digitoxin, and mono- and bis-digitoxigenin digitoxosides have been completely assigned by two-dimensional NMR spectroscopy. The techniques used include phase-sensitive COSY, multiple relay COSY, and carbon–proton correlation (HETCOR and HMQC) spectra. Various aspects of the solution conformation of the steroid moiety of digitoxin and digoxigenin could be determined from coupling constants and NOE difference experiments and they are indicative of an all-chair conformation. The carbohydrate rings in digitoxin and the mono- and bis-digitoxigenin digitoxosides are also in the chair conformation.

Key words: cardenolides, digitoxigenin, digitoxin, 2-dimensional NMR, conformational analysis.

TORBJÖRN DRAKENBERG, PETER BRODELIUS, DEANE D. MCINTYRE et HANS J. VOGEL. Can. J. Chem. **68**, 272 (1990).

Faisant appel à la RMN bidimensionnelle, on a pu attribuer l'ensemble des bandes des spectres RMN du ^1H et du ^{13}C des cardénolides digitoxigénine, digoxigénine, digitoxine et des digitoxosides des mono- et bis-digitoxigénines. Les techniques utilisées comprennent : COSY, COSY à relais multiples ainsi que les spectres (HETCOR et HMQC) de corrélation carbone–proton. En se basant sur les constantes de couplage et sur des expériences d'EON différentiel, on a pu déterminer divers aspects de la conformation en solution de la portion stéroïdale de la digitoxine et de la digoxigénine et ils suggèrent qu'il s'agit d'une conformation complètement chaise. Les cycles carbohydrates de la digitoxine et des digitoxosides des mono- et bis-digitoxigénines existent aussi dans la conformation chaise.

Mots clés : cardénolides, digitoxigénine, digitoxine, RMN bidimensionnelle, analyse conformationnelle.

[Traduit par la revue]

Introduction

The cardenolide digitoxin **4**, and related cardenolides such as digoxin, are steroidal compounds with a carbohydrate moiety in the 3β position that are isolated from the plant genus *Digitalis*. They have also been found in a number of unrelated species of plants (1). Cardenolides are of considerable importance in the treatment of heart disease (2) and have been used since ancient times as arrow poisons (3). Due to the toxicity of digitoxin and related cardenolides, considerable effort has been expended on the study of the biotransformation of these compounds by plant cell suspension cultures (4). Also, large numbers of plant species have been screened (5) in an attempt to separate the cardiotonic activity from the toxic side effects, but to date these have met with little success.

Nuclear magnetic resonance (NMR) spectroscopy has for the past quarter century been the method of choice in the elucidation of the chemical structure of new natural products of all types. However, for the cardenolides, as is the case with steroids generally, the complexity of the ^1H NMR spectrum has made a complete assignment of such spectra difficult due to excessive signal overlap in the 1.0–2.5 ppm chemical shift range (6). Carbon-13 NMR spectra of steroids generally do not suffer from this problem, because the signals are spread out over a much larger chemical shift range (7). However, the ^{13}C chemical shifts and couplings are somewhat less informative than the proton chemical shifts and the proton–proton coupling constants in studies leading to the determination of molecular conformations. As the latter determine the biological activity, it would be desirable to apply techniques by which the proton NMR spectra of steroids and other biomolecules can be analyzed. Once these have been assigned, the information about the solution conformation of the molecule can be obtained from qualitative internuclear distances and from dihedral angles between vicinal protons, which are determined from NOE data and proton–proton coupling constants respectively (6).

In this work we report two-dimensional NMR studies that have lead to the complete assignment of the proton NMR spectra of digitoxin **4**, its aglycon, digitoxigenin **1**, the related mono- and bis-digitoxigenin digitoxosides **2** and **3**, and the aglucon of diogoxin, digoxigenin **5**. These assignments have allowed us to determine various aspects of the conformation of digitoxin in solution. Attempts to correlate the biological activity with the conformation of the E ring relative to that of the D ring have been reported previously (8), as has a study of the binding of digitoxin to human serum albumin by NMR (9). Partial proton assignments of digitoxigenin and some related compounds have also recently been reported (10–12).

Experimental

NMR spectra were obtained on a Nicolet NT-360 WB (^1H, 360 MHz; ^{13}C, 90.4 MHz) or a Bruker AM-400 WB (^1H, 400.1 MHz; ^{13}C, 100.6 MHz) operating in the Fourier transform mode, at 25°C in $CDCl_3$ solutions using tetramethylsilane (TMS) as an internal reference for both nuclei. All compounds were commercially obtained: **1**, **4**, and **5** from the Sigma Chemical Company, St. Louis, MO, and **2**, and **3** from Carl Roth GmbH, Karlsruhe, FRG. Due to the limited solubility of **5** in chloroform, spectra of this compound were obtained in a 1:4 $(CD_3)_2SO/CDCl_3$ mixture. In the case of ^{13}C spectra, a relaxation delay of 2.0 s was used between the 70° pulses. The ^{13}C relaxation

[1]Author to whom correspondence may be addressed.

Can. J. Chem. Downloaded from www.nrcresearchpress.com by 91.144.44.67 on 09/07/12
For personal use only.

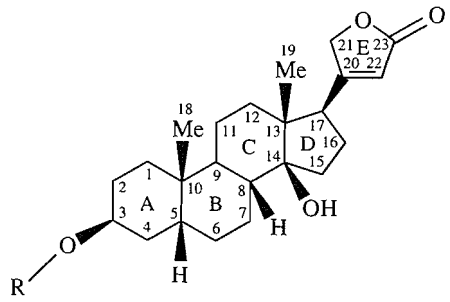

1, R = H

2, R =

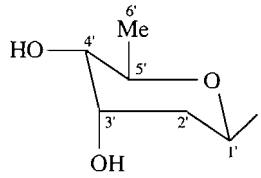

3, R =

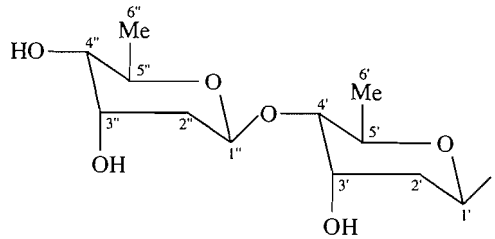

4, R =

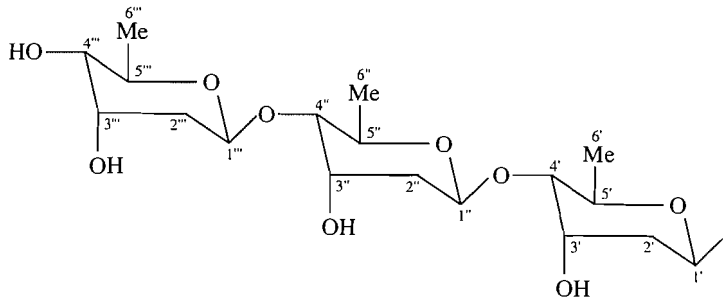

times were determined by the inversion–recovery method, using eight different delay times and delay list cycling, and were processed using standard Bruker software. A mixing time of 500 ms was used in the NOE difference experiments.

The two-dimensional COSY, relayed COSY, and HETCOR spectra were recorded using standard pulse sequences and Bruker Aspect 3000 software. The mixing time in all relayed COSY experiments was 60 ms. All two-dimensional spectra were weighted with a standard sine bell function and zero-filled along both axes prior to transformation. The phase-sensitive COSY spectrum was obtained using the Time-Proportional Phase Increment (TPPI) approach, with 1024 increments in $t1$, 16 scans each. The HMQC spectra were obtained in the phase-sensitive mode (TPPI), with a bilinear (BIRD) pulse (13). A delay of 0.4 s was inserted between the BIRD pulse and the first preparation pulse of the HMQC sequence. The number of increments in $t1$ was 128, and 128 scans (256 data points each) were collected per experiment. The resulting data were weighted with a sine bell squared function shifted $\pi/4$ radians in $t2$ (proton) and a Lorentz–Gauss function in $t1$ (carbon) and zero-filled twice in each dimension prior to transformation.

Results and discussion

Carbon-13 NMR

Our initial objective was to confirm whether we could reproduce the previously reported ^{13}C NMR spectral data (14–17) as these spectra would be an important tool in the assignment of the ^{1}H spectra via ^{13}C–^{1}H correlation experiments. The results (Table 1) for digitoxigenin **1**, digitoxin **4**, and digoxigenin **5** were in general in good agreement with those previously reported; small differences in chemical shift likely arise from the temperature dependence of the chemical shift. We also determined the ^{13}C spectra of the related mono- and di-glycosides **2** and **3** (see Table 1). In the case of digitoxin, an attached proton test (APT) (18) was performed to determine the number of protons attached to each carbon; these results were again in agreement with previously reported data. The ^{13}C relaxation

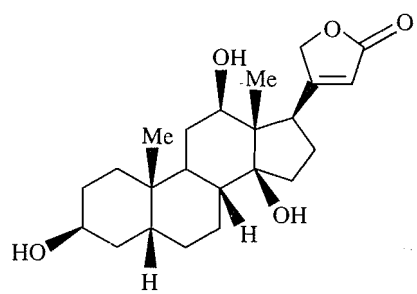

5

Can. J. Chem. Downloaded from www.nrcresearchpress.com by 91.144.44.67 on 09/07/12
For personal use only.

Can. J. Chem. Downloaded from www.nrcresearchpress.com by 91.144.44.67 on 09/07/12
For personal use only.

TABLE 1. Carbon-13 chemical shifts (ppm) for compounds **1–5**, and T_1 relaxation times (s) for **4**

	Chemical shifts (ppm)					
Carbon	**1**	**2**	**3**	**4**	**5**	**4** T_1(s)
1	29.65	29.90	29.84	29.84	29.78	0.33
2	27.93	26.67[a]	26.68[a]	26.68[a]	27.54	0.23
3	66.79	72.94	72.76	72.74	65.67	0.71
4	33.36	30.20	30.22	30.22	33.19	0.36
5	36.00[b]	36.30[b]	36.26[b]	36.25[b]	35.89	0.46
6	26.49	26.61[a]	26.57[a]	26.57[a]	26.54	0.27
7	21.19[c]	21.18[c]	21.18[c]	21.18[c]	21.54	0.29
8	41.84	41.84	41.88	41.89	40.86	0.57
9	35.52[b]	35.77[b]	35.78[b]	35.78[b]	32.06	0.73
10	35.41	35.19	35.18	35.18	35.09	2.4
11	21.37[c]	21.42[c]	21.42[c]	21.43[c]	29.64	0.42
12	40.06	40.08	40.10	40.11	73.65	0.32
13	49.62	49.60	49.61	49.60	55.93	3.1
14	85.54	85.48	85.61	85.63	85.08	9.6
15	33.16	33.12	33.20	33.20	32.78	0.24
16	26.91	26.93	26.92	26.92	27.19	0.38
17	50.95	50.95	50.97	50.97	45.50	0.68
18	15.79	15.78	15.79	15.79	9.25	0.91
19	23.72	23.63	23.62	23.61	23.68	1.04
20	174.49[d]	174.57[d]	174.55[d]	174.47[d]	176.07	[f]
21	73.44	73.48	73.45	73.43	74.09	0.47
22	117.63	117.62	117.62	117.64	119.70	0.70
23	174.42[d]	174.53[d]	174.48[d]	174.42	174.70	[f]
1′	—	95.40	95.38	95.38	—	0.45
1″	—	—	98.20	98.19[e]	—	0.67
1‴	—	—	—	98.25[e]	—	0.67
2′	—	38.29	37.88	37.85	—	0.33
2″	—	—	37.19	36.24	—	0.46
2‴	—	—	—	37.18	—	0.31
3′	—	68.17	66.49	66.38	—	0.39
3″	—	—	68.13	66.47	—	0.40
3‴	—	—	—	68.26	—	0.54
4′	—	72.71	82.67	82.20	—	0.54
4″	—	—	72.58	82.57	—	0.57
4‴	—	—	—	72.55	—	0.63
5′	—	69.22	68.06	68.10	—	[f]
5″	—	—	69.49	68.10	—	[f]
5‴	—	—	—	69.49	—	0.61
6′	—	18.14	18.19	18.19	—	[f]
6″	—	—	18.19	18.19	—	[f]
6‴	—	—	—	18.19	—	[f]

[a–e]Assignments within column may be interchanged.
[f]Could not be determined due to signal overlap.

times (T_1) were also determined for digitoxin, and are included in Table 1. They do not reveal large differences in mobility throughout the molecule.

*^{1}H NMR. Digitoxigenin **1**, **2**, and **3***

The proton NMR spectra of these compounds were assigned as described in detail for digitoxin **4** below. The assignments are given in Tables 2 and 3.

*^{1}H NMR. Digitoxin **4***

Due to the complexity of the ^{1}H NMR spectrum of digitoxin (Fig. 1) only the resonances downfield of 2.5 ppm, and the two methyl groups, are resolved from other signals, and can be readily assigned by inspection and comparison with model compounds. The methyl groups can be assigned as C-18 (0.87 ppm) and C-19 (0.92 ppm). The assignment of the downfield signals

TABLE 2. Chemical shifts (δ) and selected coupling constants (J) for the steroid protons of digitoxigenin **1**, digitoxin **4**, and digoxigenin **5**

Proton	Digitoxigenin (δ, ppm)	Digitoxin (δ, ppm)	Digitoxin (J, Hz)	Digoxgenin (δ, ppm)
1α	1.50	1.49		1.60
1β	1.50	1.48		1.43
2α	1.52	1.44	$J_{2\alpha,3}$ = 4 Hz	1.50
2β	1.57	1.57		1.50
3	4.12	4.02	$J_{3,4\beta}$ = 2 Hz	4.02
4α	1.34	1.45		1.32
4β	1.89	1.70		1.81
5	1.78	1.74		1.80
6α	1.87	1.87		1.84
6β	1.22	1.21		1.23
7α	1.25	1.26	$J_{7\alpha,7\beta}$ = 18 Hz	1.18
7β	1.68	1.66	$J_{8\beta,8}$ = 4 Hz	1.75
8	1.56	1.54	$J_{8,9}$ = 12 Hz	1.58
9	1.62	1.60	$J_{9,11\beta}$ = 4 Hz	1.61
11α	1.43	1.42		1.40
11β	1.38	1.38		1.23
12α	1.38	1.37	$J_{12\alpha,12\beta}$ = 18 Hz	3.31
12β	1.52	1.50		—
15α	2.12	2.12	$J_{15\alpha,15\beta}$ = 18 Hz	1.91
15β	1.70	1.70	$J_{15\beta,16\beta}$ = 10 Hz	1.52
16α	1.86	1.88	$J_{16\alpha,17}$ = 4 Hz	1.91
16β	2.15	2.16	$J_{16\beta,17}$ = 10 Hz	2.08
17	2.77	2.78	$J_{17,21}$ = 1 Hz	3.34
18	0.87	0.87		0.79
19	0.95	0.92		0.97
21	4.81, 4.98	4.82, 4.98	J = 9 Hz	4.82, 4.97
22	5.87	5.87	$J_{21,22}$ = 1 Hz	5.92

TABLE 3. Chemical shifts (δ, ppm) and coupling constants (Hz) for the carbohydrate protons of **2**, **3**, and **4**

	Chemical shifts (δ)			
Proton	**2**	**3**	**4**	Coupling constants (Hz)
1′	4.86	4.88	4.85	$J_{1',2\alpha'}$ = 2Hz, $J_{1',2\beta'}$ = 9 Hz
2α′	2.05	2.07	2.05	$J_{2\alpha',2\beta'}$ = 14 Hz, $J_{2\alpha',3'}$ = 4Hz
2β′	1.80	1.77	1.71	$J_{2\beta',3'}$ = 4 Hz
3′	4.13	4.26	4.24	$J3',4'$ = 4 Hz
3′-OH			3.04	
4′	3.35	3.25	3.24	$J_{4',5'}$ = 10 Hz
5′	3.70	3.79	3.78	$J_{5',6'}$ = 6 Hz
6′	1.25	1.30	1.28	
1″	—	4.93	4.88	$J_{1'',2\alpha''}$ = 2 Hz, $J_{1'',2\beta''}$ = 9 Hz
2α″	—	2.13	2.13	$J_{2\alpha'',2\beta''}$ = 14 Hz, $J_{2\alpha'',3''}$ = 4 Hz
2β″	—	1.77	1.71	$J_{2\beta'',3''}$ = 4 Hz
3″	—	4.14	4.25	$J_{3'',4''}$ = 4 Hz
3″-OH	—		2.98	
4″	—	3.32	3.21	$J_{4'',5''}$ = 10 Hz
5″	—	3.79	3.83	$J_{5'',6''}$ = 6 Hz
6″	—	1.23	1.22	
1‴	—	—	4.90	$J_{1''',2\alpha'''}$ = 2 Hz, $J_{1''',2\beta'''}$ = 9 Hz
2α‴	—	—	2.12	$J_{2\alpha''',2\beta'''}$ = 14 Hz, $J_{2\alpha''',3'''}$ = 4 Hz
2β‴	—	—	1.75	$J_{2\beta''',3'''}$ = 3 Hz
3‴	—	—	4.13	$J_{3''',4'''}$ = 4 Hz
3‴-OH	—	—	2.46	
4‴	—	—	3.30	$J_{4''',5'''}$ = 10 Hz
4‴-OH	—	—	2.20	
5‴	—	—	3.78	$J_{5''',6'''}$ = 6 Hz
6‴	—	—	1.22	

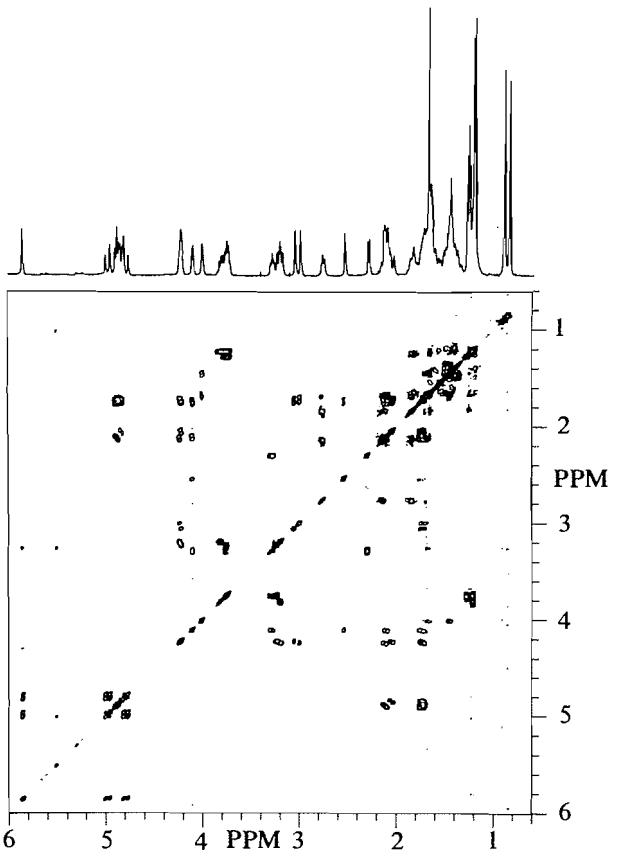

FIG. 1. One-dimensional and COSY proton NMR spectra of **4** in $CDCl_3$ solution at 25°C.

is as follows: H-22 (5.87 ppm), H-21 (4.82 and 4.98 ppm), H-3 (4.02 ppm), and H-17 (2.78 ppm). These assignments were confirmed by appropriate decoupling experiments. To assign, as far as possible, the signals in the 2.5–1.0 ppm region of the spectrum a proton 2-D correlation spectrum (COSY) (Fig. 1) was obtained. In this type of spectrum protons that are coupled to each other produce "cross peaks" at coordinates corresponding to the chemical shifts of the two protons involved. Starting from the previously assigned H-17 (2.78 ppm), we can assign resonances at 2.16 and 1.88 ppm as being due to protons 16β and 16α. As these signals also show correlation with signals at 2.12 and 1.70 ppm, the latter chemical shifts represent the 15α and 15β resonances. As axial protons usually absorb upfield of the equatorial proton attached to the same carbon atom, it is possible to assign the α and β protons of methylene groups by inspection of a molecular model of the compound (*vide infra*). These assignments were also confirmed by decoupling experiments.

With the assignment of the protons of the D and E rings complete, the next step was the considerably more difficult task of the assignment of the A, B, and C ring protons. These protons form one extended spin system, so in principle, once one is assigned (H-3 in this case), it should be possible to trace out the connectivity of the entire spin system by simple inspection of the COSY spectrum. In the case of steroids, however, this is not straightforward because of overlapping cross peaks and some cross peaks that may not be observed due to low intensity resulting from weak coupling. Starting from H-3 (4.02 ppm) in the magnitude mode COSY spectrum, signals at 1.70 and 1.57 ppm can be assigned to H-2 and (or) H-4 protons; however, due

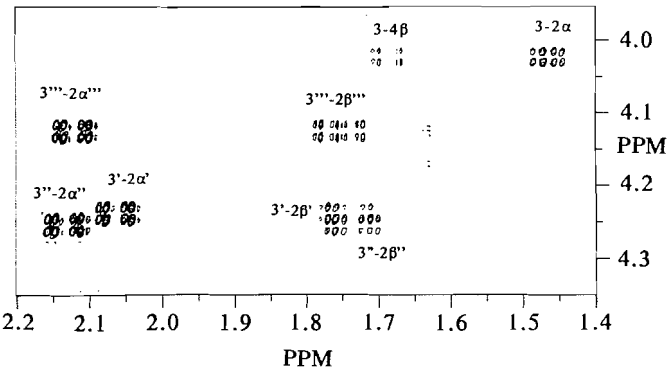

FIG. 2. Region of a phase-sensitive COSY spectrum of **4** in $CDCl_3$ at 25°C, illustrating the fine structure of selected crosspeaks, which were used to obtain the coupling constants.

to the complexity of the COSY spectrum, further assignments based solely on the magnitude mode COSY data would be doubtful. To resolve this difficulty, recourse was made to ^{13}C–^{1}H correlation (HETCOR) spectroscopy (19). In this type of spectrum, cross peaks are observed for each carbon at the coordinates of the ^{13}C chemical shift and the ^{1}H chemical shift of the attached proton(s); thus, quaternary carbons are not observed in this type of spectrum. Using the assignment of the ^{13}C spectrum reported by Habermehl *et al.* (17), and confirmed by us, as a starting point we can confirm that our previous proton assignments are correct. In addition, all remaining proton signals can be assigned, at least approximately (within 0.05 ppm), from the HETCOR spectrum. Once the approximate chemical shifts were known, careful inspection of the COSY and one-dimensional spectra, combined when necessary with decoupling experiments, gave reasonably accurate chemical shifts (within 0.02 ppm) for the remaining protons.

It was possible to obtain even more accurate chemical shifts, as well as coupling constants, from phase-sensitive COSY spectra (Fig. 2). This spectrum was recorded at fairly high resolution (ca. 1.0 Hz in the F-2 domain) so that the appropriate coupling constants necessary to define the conformation of the molecule could be obtained (*vide infra*). The chemical shifts and selected coupling constants are tabulated in Table 2. Due to the increased resolution, virtually the entire steroid could be assigned by inspection of the phase-sensitive COSY spectrum, independently of the more time-consuming HETCOR experiments.

The assignment of the carbohydrate portion of the spectrum of digitoxin from the phase-sensitive COSY (Fig. 2) was straightforward. Beginning with the anomeric protons, the connectivity for each digitoxose ring was readily traced out, including the -OH protons, which are in slow exchange in chloroform solution. The terminal ring was readily identified as such as it is the only one bearing an -OH at the 4 position. The ring bound to the steroid was identified on the basis of upfield chemical shifts for the 1′ and 2′α protons, and a downfield chemical shift for the methyl group, compared to the other two rings.

To further confirm the assignment of the carbohydrate resonances of digitoxin, a series of relayed coherence transfer (Relay) COSY spectra (20) were also obtained (Fig. 3). In these spectra, magnetization is transferred sequentially from proton to proton, thus giving rise to cross peaks between protons not directly coupled to each other. In all cases a total mixing time of 60 ms for each coherence transfer was employed for obtaining a relay, double-relay, and triple-relay COSY spectrum. This mixting time is optimal for the 8–10 Hz couplings that are observed

Can. J. Chem. Downloaded from www.nrcresearchpress.com by 91.144.44.67 on 09/07/12
For personal use only.

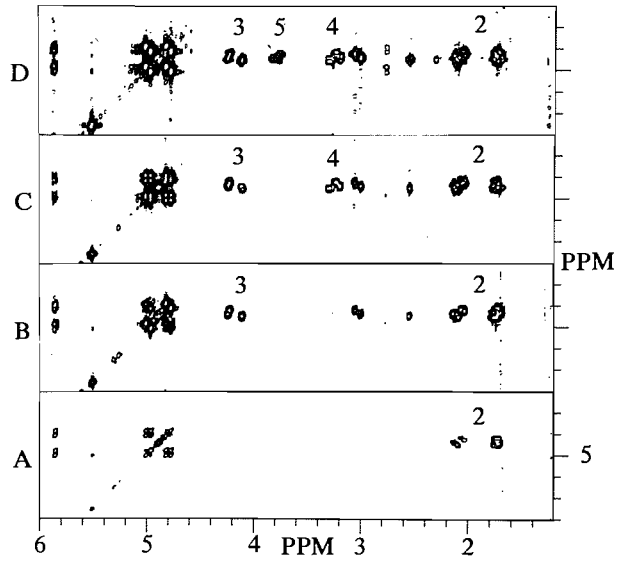

FIG. 3. Magnitude mode COSY and relay-COSY spectra of **4** in $CDCl_3$ solution at 25°C, showing the carbohydrate protons (a) COSY, (b) relay COSY, (c) double-relay COSY, (d) triple-relay COSY. New crosspeaks from the anomeric protons, which appear with each successive relay, are labeled. Note the overlap resulting from near chemical shift equivalence from corresponding protons in each of the three carbohydrate rings. Crosspeaks between 2.4 and 3.1 ppm arise from -OH protons.

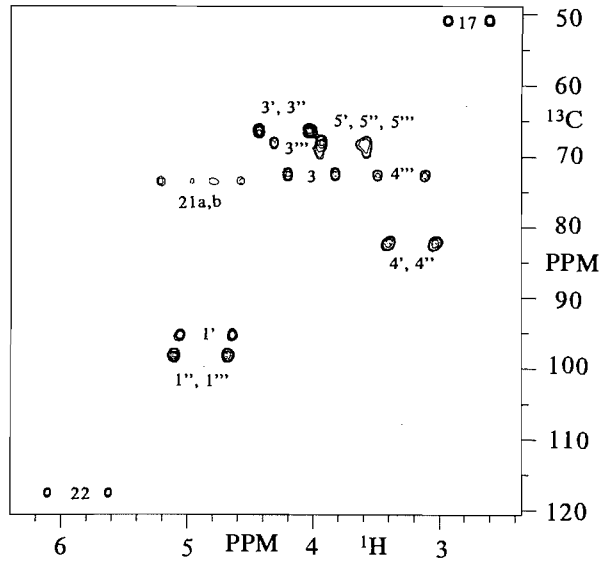

FIG. 4. Carbon-13–proton correlation (HMQC) spectrum of **4** in $CDCl_3$ solution at 25°C. Only the downfield region is shown. The spectrum was obtained without decoupling; thus all signals appear as doublets. The horizontal axis represents the proton chemical shifts; the vertical axis, the carbon chemical shifts.

between axial protons in carbohydrates. Despite the fact that H-3 is equatorial in the digitoxose ring system (and thus its coupling constant with the vicinal protons H-2 and H-4 is considerably less than 8 Hz), good multiple relayed COSY spectra were obtained. In the case of the triple-relay COSY spectrum, coherence transfer was observed between H-1 and H-5 for all three sugar rings. However, a quadruple-relay COSY spectrum did not show correlation between H-1 and H-6, probably due to loss of signal intensity through T_2 relaxation during the mixing periods and loss of magnetization resulting from multiple coherence transfer pathways (data not shown). These results demonstrate the utility of multiple relay COSY experiments for the assignment of carbohydrate spectra. Similar data can be obtained by using total correlation spectra such as HOHAHA (21) and TOCSY (22). Due to the diverse range of coupling constants between the steroid protons, the multiple relay COSY experiments were somewhat less useful in the assignment of the steroid protion of the spectra, although some assignments could be confirmed in this manner. In addition to the above, an HMQC (13) spectrum was obtained for digitoxin (Fig. 4). In principle, this proton-detected heteronuclear correlation experiment provides information that is similar to that obtained in the carbon-detected HETCOR experiment, but with much improved sensitivity. In this case, the spectrum was obtained without decoupling, and hence approximate coupling constants, useful in making assignments, can be obtained from the typical doublet appearance of the peaks. With digitoxin, considerble overlap was observed among some of the carbohydrate resonances.

As far as the complete assignment of the proton NMR spectrum of digitoxin is concerned, our results are in complete agreement with a previously reported partial assignment (23).

^1H and ^{13}C NMR. Digoxigenin 5

Digoxigenin **5**, the aglycon of digoxin, is 12β-OH-**1**. Using digitoxigenin as a model, the complete proton and carbon-13 assignments were obtained using HETCOR and COSY spectra. The results (Tables 1 and 2) indicate that substitution at the 12 position results in a large (0.56 ppm) downfield shift of H-17, and a large upfield shift of approximately 5 ppm for the C-17 (see also ref. 17). Steric compression (γ *gauche* effect) results in a large (approximately 6 ppm) upfield shift for C-18. Appreciable downfield shifts for both protons attached to C-15 were also observed.

Conformation

The X-ray structures of digitoxin and digitoxigenin have not been reported to our knowledge. However, the structure of two closely related compounds, 3-α digitoxigenin (24) (which differs from digitoxigenin only in the configuration at C-3) and dihydro digitoxigenin (25) (digitoxigenin with the C20—C22 double bond saturated), have been determined. In both compounds all the steroid six-membered rings adopt a chair conformation in the crystal lattice.

The coupling constant of 12 Hz measured between H-8 and H-9 indicated that they are *trans* to each other, as is common for a *trans*-ring junction. The $J_{9,11\beta}$ (4 Hz), $J_{7\beta,8}$ (4 Hz), and $J_{6\beta,7\beta}$ (8 Hz) couplings all support the view that the six-membered steroid rings B and C are in the chair conformation. By inspection of molecular models it is readily apparent that for reasons of steric hindrance, the A ring is most likely also in the chair conformation. This was confirmed by the use of NOE-difference experiments. Upon irradiation of the C-19 methyl protons at 0.87 ppm, an enhancement was observed in the intensity of the signals arising from the 1β and 6β protons; upon irradiation of the H-3 signal at 4.02 ppm, an enhancement was obtained for the 2α and 4α protons. These results confirm that the A ring indeed has a chair conformation. Unfortunately, due to excessive signal overlap, it was not possible to obtain accurate coupling constants for the A-ring protons from the phase-sensitive COSY spectrum. Thus it appears that the all-chair configuration of the steroid moiety found in the crystal lattice in this case is preserved in solution.

Can. J. Chem. Downloaded from www.nrcresearchpress.com by 91.144.44.67 on 09/07/12
For personal use only.

From the observed coupling constants (Table 2) for each digitoxose ring, the anomeric proton is *antiperiplanar* to one of the protons on C-2 and *gauche* to the other. All digitoxose H-3 protons are *gauche* to the vicinal protons 2α, 2β, and 4, and the latter proton is *antiperiplanar* to H-5 in all rings. Therefore, it can be concluded that the three digitoxose rings in digitoxin are all in the chair conformation, as are the digitoxose rings in the mono- and bis-digitoxigenin digitoxosides **2** and **3**. This is the same conformation as observed for free digitoxose (26).

Acknowledgements

This work was supported by the Swedish, Swiss, and Canadian national scientific research councils. The AM400 WB spectrometer was purchased with funds provided by the Alberta Heritage Foundation for Medical Research (AHFMR). H.J.V. is the recipient of a Scholarship from the AHFMR.

1. F. B. Salisburg and C. W. Ross. *In* Plant physiology. 3rd ed. Wadsworth, Belmont, CA. 1985.
2. W. H. Lewis and M. P. F. Elvin-Lewis. *In* Medical botany: plants affecting man's health. John Wiley and Sons, New York. 1977.
3. T. Robinson. *In* The organic constituents of higher plants. 4th ed. Cordus Press, North Amherst, MA. 1980.
4. A. W. Alfermann, H. M. Boy, P. C. Doller, W. Hagedorn, M. Heins, J. Wald, and E. Reinhard. *In* Plant tissue culture and its biotechnological application. *Edited by* W. Barz, E. Reinhard, and M. H. Zenk. Springer-Verlag, Berlin, Heidelberg, and New York. 1977. p. 125.
5. T. W. Guntert and H. H. A. Linde. Experientia, **33**, 697 (1977).
6. W. R. Croasmun and R. M. K. Carlson. *In* Two dimensional NMR spectroscopy: applications for chemists and biochemists. VCH, Weinheim, FRG. 1987. Chap. 7.
7. J. W. Blunt and J. B. Stothers. Org. Magn. Reson. **9**, 439 (1977).
8. R. Hintsche, R. Megges, D. Pfeiffer, H. J. Portius, W. Schoenfield, and K. R. H. Repke. Eur. J. Med. Chem.-Chim. Ther. **20**, 9 (1985).
9. T. J. Oida. Biochemistry (Tokyo), **100**, 99 (1986).
10. F. Tsutomu, K. Kiichiro, and M. Hirotani. Phytochemistry, **27**, 2129 (1988).
11. F. Tsutomu, K. Kiichiro, and M. Hirotani. Phytochemistry, **27**, 3475 (1988).
12. J. M. Beale, H. G. Floss, T. Lehmann, and M. Luckner. Phytochemistry, **27**, 3143 (1988).
13. A. Bax and S. Subramanian. J. Magn. Reson. **67**, 565 (1986).
14. K. Tori, H. Ishii, Z. W. Wolkowsky, C. Chachaty, M. Sangaé, F. Piriou, and G. Lukacs. Tetrahedron Lett. 1077 (1973).
15. H. T. A. Cheung, L. Brown, J. Boutagy, and R. Thomas. J. Chem. Soc. Perkin Trans 1, 1773 (1981).
16. L. Brown, H. T. Andrew, R. Thomas, T. R. Watson, and J. L. E. Nemorin. J. Chem. Soc. Perkin Trans. 1, 1779 (1981).
17. G. G. Habermehl, P. E. Mammann, and V. Wray. Magn. Reson. Chem. **23**, 951 (1985).
18. G. A. Morris and R. Freeman. J. Am. Chem. Soc. **101**, 760 (1979).
19. G. A. Morris and L. D. Hall. J. Am. Chem. Soc. **103**, 4703 (1981).
20. M. Ikura and K. Hikichi. Carbohydr. Res. **163**, 1 (1987).
21. D. G. Davis and A. Bax. J. Am. Chem. Soc. **107**, 2821 (1985).
22. L. Braunschweiler and R. R. Ernst. J. Magn. Reson. **53**, 521 (1983).
23. K. Wiesner, T. Y. R. Tsai, and H. Jin. Helv. Chim. Acta, **68**, 300 (1985).
24. A. Messerschmidt, E. Höhne, and R. Megges. Cryst. Struct. Commun. **10**, 149 (1981).
25. A. Messerschmidt, E. Höhne, and C. Lihdig. Cryst. Struct. Commun. **10**, 629 (1981).
26. B. Coxon. J. Carbohydr. Chem. **3**, 525 (1984).

Can. J. Chem. Downloaded from www.nrcresearchpress.com by 91.144.44.67 on 09/07/12
For personal use only.

The kinetics of formation of electron donor–acceptor complexes. A temperature-jump study

M. A. ZON, H. FERNANDEZ, L. SERENO, AND J. J. SILBER[1]

Departamento de Química y Física, Universidad Nacional de Río Cuarto, Estafeta No. 9, Río Cuarto, 5800, Córdoba, Argentina

Received June 12, 1989

M. A. ZON, H. FERNANDEZ, L. SERENO, and J. J. SILBER. Can. J. Chem. **68**, 278 (1990).

The kinetics of the Electron Donor–Acceptor (EDA) complex between *N,N,N′,N′*-tetramethyl-*p*-phenylenediamine and *m*-dinitrobenzene in acetonitrile has been studied by the temperature-jump technique. The magnitude of the rate constants of association and dissociation, although relatively large, is well below the diffusion control values. The calculated rates closely coincide with those obtained by chronoamperometry. An entropy control is suggested for this reaction. The results obtained in this work are useful to demonstrate that the concept about EDA complexes being formed by diffusion-controlled reactions should not be generalized.

Key words: electron donor–acceptor complexes, *m*-dinitrobenzene, *N,N,N′,N′*-tetramethyl-*p*-phenylenediamine, T-jump, kinetics.

M. A. ZON, H. FERNANDEZ, L. SERENO et J. J. SILBER. Can. J. Chem. **68**, 278 (1990).

Utilisant la technique des sauts de température, on a étudié la cinétique du complexe accepteur–donneur électronique (ADE) formé par la *N,N,N′,N′*-tetraméthyl-*p*-phénylènediamine et le *m*-dinitrobenzène dans l'acétonitrile. L'amplitude de la constante de vitesse, même si elle est relativement importante, est beaucoup plus faible que les valeurs attendues sur la base d'un contrôle par diffusion. Les vitesses calculées coïncident bien avec celles obtenues par chronoampérométrie. On suggère que cette réaction est contrôlée par l'entropie. Les résultats obtenus dans ce travail sont utiles pour démontrer que l'on ne devrait pas généraliser le concept selon lequel les complexes ADE se forment au cours de réactions contrôlées par la diffusion.

Mots clés: complexes accepteur–donneur électronique, *m*-dinitrobenzène, *N,N,N′,N′*-tétraméthyl-*p*-phénylènediamine, saut de température, cinétique.

[Traduit par la revue]

Introduction

Electron donor–acceptor (EDA) complexes play a considerable role in general chemistry reactivity as well as in biological and therapeutical reactions of living organisms (1, 2). Thus knowledge of the kinetic parameters of their formation becomes important for mechanistic studies.

It is generally considered that the forward and back reactions of the complex components are diffusion controlled (1, 3) or nearly so (4–6). However, actual measurements of these rates have been few. Moreover, several examples have been found in the literature (7–10) in which the rate constants are reported to be small enough to be measured by conventional techniques. Hence this matter appears to be somewhat controversial, particularly when considering that these kinetics seem to depend strongly on the donor and the acceptor structure and on the solvent medium (6, 11).

In a previous work we reported the application of an electrochemical technique, chronoamperometry, to measure the kinetic parameters of the EDA complex between *N,N,N′,N′*-tetramethyl-*p*-phenylenediamine (TMPD) and *m*-dinitrobenzene (MDB) in acetonitrile (ACN) (12). The magnitude of the rate constants obtained, although relatively large, is well below the diffusion control values. This was the first example of the use of chronoamperometry to evaluate kinetic parameters of EDA complexes and showed that this type of study could be very valuable provided that the lifetimes of complexation are within the time constant of the technique.

Nevertheless, our results were actually obtained in the detection limit of the chronoamperometry. Hence, considering that it is necessary to clarify some of the controversial ideas about the rates of EDA complexation, we decided to reinvestigate the system by a different technique. Thus in this work we report temperature-jump (T-jump) studies of the TMPD–MDB complex in ACN.

Results and discussion

The equilibrium that involves the formation of the complex studied can be represented by eq. [1]:

$$[1]\quad \mathrm{TMPD} + \mathrm{MDB} \underset{k_{-1}}{\overset{k_1}{\rightleftharpoons}} \mathrm{TMPD\text{–}MDB}$$

where TMPD–MDB represents the EDA complex and k_1 and k_{-1} are the association and dissociation rate constants, respectively. Previous studies of the thermodynamic parameters of this complex (13) demonstrated the formation of a 1:1 complex and the stability constant (K_s) was determined at different temperatures. The value of $\Delta H = -30$ kJ mol^{-1} obtained is acceptable for performing the kinetic analysis by T-jump experiments (14, 15). Thus solutions of the complex at varying concentrations of MDB and TMPD were subjected to temperature jumps and the ensuing relaxation effect was spectrophotometrically monitored.

One single relaxation time (τ) was observed, as expected, under all experimental conditions, Typical results of the semilog plots of the signal intensity (I_s) vs. time are shown in Fig. 1. As can be observed, good linear relationships are obtained. The relaxation time for this system is given by eq. [2]:

$$[2]\quad \tau^{-1} = k_1 ([\mathrm{TMPD}]_e + [\mathrm{MDB}]_e) + k_{-1}$$

where $[\mathrm{TMPD}]_e$ and $[\mathrm{MDB}]_e$ are the concentrations at the new equilibrium situation. Since the study was performed under pseudo first-order conditions, i.e., $[\mathrm{MDB}]_0 > [\mathrm{TMPD}]_0$, eq. [2] can be expressed as

$$[3]\quad \tau^{-1} = k_1 [\mathrm{MDB}]_0 + k_{-1}$$

where $[\mathrm{MDB}]_0$ is the initial concentration of the acceptor.

[1]Author to whom correspondence may be addressed.

Can. J. Chem. Downloaded from www.nrcresearchpress.com by 91.144.44.67 on 09/07/12
For personal use only.

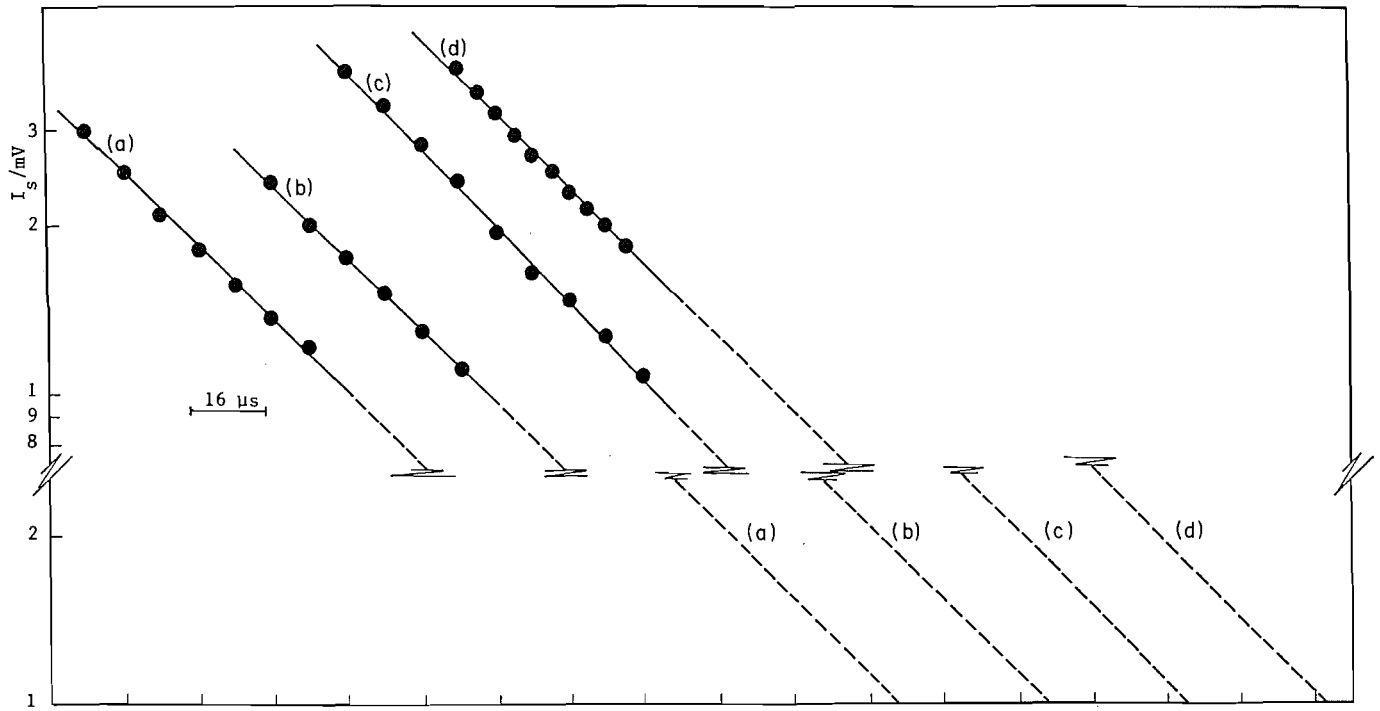

FIG. 1. Semilog plots of signal intensity (I_s) vs. time: (a)–(c) $[TMPD]_0 = 2.90 \times 10^{-3}$ M, $[MDB]_0 = 0.20$ M; (d) $[TMPD]_0 = 1.20 \times 10^{-3}$ M, $[MDB]_0 = 0.20$ M.

TABLE 1. Experimental relaxation times at different initial concentrations of MDB. $[TMPD]_0 = 2.90 \times 10^{-3}$ M; temperature = 20°C

$[MDB]_0$ (M)	$10^6 \tau$(s)					$10^{-3} \bar{\tau}^{-1a}$ (s^{-1})
0.10	52	50	53	51	50	19 ± 1
0.28	33	36	36	33	37	28 ± 2
0.40	31	29	31	26	32	34 ± 4
0.44	26	27	32	29	27	35 ± 4

[a] $\bar{\tau}$ is the average relaxation time. Errors are calculated from $e = (\sigma_{n-1}^2 + \varepsilon^2)^{1/2}$, where σ_{n-1} is the standard deviation and ε is the time scale precision.

Typical values of τ at different $[MDB]_0$ are gathered in Table 1. A plot of τ^{-1} vs. $[MDB]_0$ should be linear with slope k_1 and intercept k_{-1}. The ratio k_1/k_{-1} should agree with the values of K_s previously determined (13). Some of these plots, obtained at different temperatures, are shown in Fig. 2.

The values of the rate constants calculated through eq. [3] by a least-squares procedure are given in Table 2 along with the values previously obtained by an electrochemical technique (12). It should be pointed out that similar results are obtained if we use the previously measured values of K_s (13) in finding $k_1 = 1/(\tau\{[MDB]_0 + K_s^{-1}\})$ for each relaxation time.

As can be observed, the magnitudes of k_1 and k_{-1} for the complex, although relatively large, are well below the diffusion control values.

On the other hand, these values are in close agreement with those obtained by chronoamperometry. Moreover, the calculated K_s values agree with the ones previously calculated. Thus we believe that these are quite reliable results and give an indication that, at least for these complexes, the rates of formation (and dissociation) are relatively low compared with those expected for complexes of other nitro compounds with, for example, aliphatic amines (3, 4).

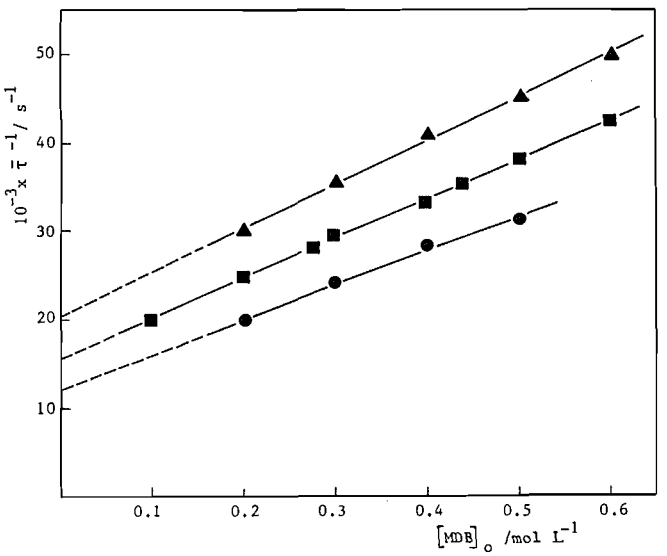

FIG. 2. $\bar{\tau}^{-1}$ as a function of $[MDB]_0$ and temperature: (●) 10°C; (■) 20°C; and (▲) 30°C.

Although the temperature range allowed by our experimental conditions is rather small for making precise calculations of the activation parameters, it is still possible to establish that they are in the order of the values obtained electrochemically (12). They have the characteristic of a low activation enthalpy, $\Delta H^{\neq}$, and of a large and highly negative value for the activation entropy, $\Delta S^{\neq}$, for the association process. This suggests that there is no activation-energy barrier but there is an entropy control for this reaction. An ubiquitous explanation for these results is not easy to ascertain. Either steric and (or) solvent reorganization effects may be adduced for such entropy control.

TMPD–MDB is a weak EDA complex, as inferred from the

Can. J. Chem. Downloaded from www.nrcresearchpress.com by 91.144.44.67 on 09/07/12
For personal use only.

TABLE 2. Values of rate constants and K_s obtained by T-jump at different temperatures. Uncertainties are standard deviations. The values obtained by chronoamperometry (12) are included for comparison

	Method					
	T-jump			Chronoamperometry		
T (°C)	$10^{-4}\ k_1$[a] ($M^{-1}\ s^{-1}$)	$10^{-4}\ k_{-1}$[b] (s^{-1})	K_s (M^{-1})	$10^{-4}\ k_1$ ($M^{-1}\ s^{-1}$)	$10^{-4}\ k_{-1}$ (s^{-1})	K_s (M^{-1})
0	—	—	—	3.18 ± 0.80	1.02 ± 0.25	3.1
10	3.8 ± 0.1	1.2 ± 0.1	3.1	3.16 ± 0.80	1.21 ± 0.30	2.6
20	4.6 ± 0.1	1.6 ± 0.1	2.9	3.12 ± 0.75	2.48 ± 0.62	1.2
30	4.9 ± 0.1	2.0 ± 0.1	2.4	—	—	—

[a]$\Delta H^{\ddagger} = 7 \pm 1$ kJ/mol and $\Delta S^{\ddagger} = -123 \pm 5$ J/K mol at 25°C.
[b]$\Delta H^{\ddagger} = 15 \pm 1$ kJ/mol and $\Delta S^{\ddagger} = -103 \pm 2$ J/K mol at 25°C.

hypsochromic shift of the λ_{max} of its charge transfer band and the decrease in the K_s value in polar solvents with respect to nonpolar ones (13, 16). Then, a small contribution of the dative (ionic) structure in the ground state of this complex is expected (17). In these cases is more probable that solvation is controlled by local polar centers on donor and acceptor than by the, usually small, ground state complex dipole. On these grounds solvent reorganization in the transition state should be more significant in the dissociation process.

On the other hand, although solvent reorganization around local dipoles generated by complex formation cannot be disregarded, a preferential orientation of the donor and the acceptor structures may be the dominant factor in the association process.

The need of preferred sites of approach of two moieties has been proposed (1) and is actually observed for several EDA complexes (18). Also, our previous studies of the complexes between dinitro and dicyanobenzenes with aliphatic amines show that preferred orientations determine the relative stabilities of the complexes (19).

For the TMPD–MDB complex, the steric and electronic effects exerted by the *N*-methyl groups of TMPD are assumed to be the cause of the entropy control in the complex formation. Such effects have also been adduced to explain the differences in the electronic interactions and thermodynamic stabilities observed by *N*-methyl substitutions in the EDA dimerizations of *p*-phenylenediamine cation radicals (20).

In summary, the kinetics of the TMPD–MDB complex in ACN, although fast, is not diffusion controlled, as proved by two completely different techniques. Thus we want to emphasize that no generalization can be made about the rates of EDA complexation.

Considering that EDA complexes are being proposed as the actual intermediates in the new mechanistic approach to several organic reactions believed to occur via electron transfer (21), the need for knowledge of the factors that influence their kinetic parameters becomes immediately apparent.

Experimental

ACN (Carlo Erba, R.P.) and $NaClO_4$ (Koch-Light A.R.) were purified as previously described (22). TMPD, obtained from its dihydrochloride (Fluka A.G.), and MDB (Carlo Erba R.P.) were purified as reported before (13).

The relaxation times were measured on a temperature-jump transient apparatus from Messanlagen Studiengesellschaft Gottingen, Germany. The solutions were subjected to temperature jumps of 4°C; the temperatures of the preequilibrated solutions were chosen to be 10, 20, and 30 ± 0.5°C respectively after the jump.

The concentration of MDB was varied in the range 0.1–0.6 M and that of TMPD from 1 to 3×10^{-3} M in ACN as solvent. The ionic strength was kept constant at 1 M by adding $NaClO_4$.

Relaxation curves were recorded at $\lambda = 480$ nm, which is the previously determined absorption maximum wavelength for the complex in this medium (13). The absorbance vs. time transients were stored in a Leader LBO-5825 digital storage oscilloscope and later recorded in a Houston 2000 *X–Y* instrument. The relaxation times were calculated as the average values from at least five relaxation curves, generated from the same solution, or often from separately prepared solutions, on different days. The estimated accuracy associated with each relaxation time was not greater than 10%.

Acknowledgements

This work was partially supported by grants from Consejo Nacional de Investigaciones Científicas y Técnicas (CONICET) and Consejo de Investigaciones Científicas y Tecnológicas de la Provincia de Córdoba (CONICOR), Argentina. The authors thank Drs. M. R. Feliz and A. L. Capparelli for their help in the T-jump measurements.

1. R. FOSTER. J. Phys. Chem. **84**, 2135 (1980), and references therein.
2. K. TAMARU. Catal. Rev. **4**, 161 (1970).
3. C. F. BERNASCONI. J. Am. Chem. Soc. **92**, 129 (1970).
4. J. E. ANDERSON and C. P. SMYTH. J. Am. Chem. Soc. **85**, 2904 (1963).
5. R. A. CRUMP and A. H. PRICE. Trans. Faraday Soc. **66**, 92 (1972).
6. E. F. CALDIN, J. E. CROOKS, D. O'DONNELL, D. SMITH, and S. TONER. J. Chem. Soc. Faraday Trans. 1, **68**, 849 (1972).
7. A. V. BRATCHIKOV and G. L. RYZHOVA. Russ. J. Phys. Chem. **48**, 480 (1974).
8. U. MURALIKRISHNA and M. KRISHNAMURTHY. Indian J. Chem. **22A**, 858 (1983).
9. U. MURALIKRISHNA, Y. V. S. K. SESHASAYI, and M. KRISHNAMURTHY. React. Kinet. Catal. Lett. **24**, 193 (1984).
10. M. A. SLIFKIN. Charge transfer interactions of biomolecules. Academic Press, New York. 1971. p. 46.
11. M. A. SLIFKIN, H. A. K. SAAID, and E. FERNANDEZ-DIAZ. Spectrochim. Acta, **42A**, 827 (1986).
12. M. A. ZON, H. FERNANDEZ, L. SERENO, and J. J. SILBER. Electrochim. Acta, **32**, 1733 (1987).
13. M. A. ZON, H. FERNANDEZ, L. SERENO, and J. J. SILBER. Electrochim. Acta, **32**, 71 (1987).

Can. J. Chem. Downloaded from www.nrcresearchpress.com by 91.144.44.67 on 09/07/12
For personal use only.

14. D. N. HAGUE. Fast reactions. Wiley Interscience, London, New York. 1971.
15. F. BERNASCONI. Relaxation kinetics. Academic Press, New York. 1976.
16. (*a*) R. FOSTER AND T. J. THOMPSON. Trans. Faraday Soc. **58**, 1747 (1962); (*b*) Trans. Faraday Soc. **59**, 2287 (1963).
17. K. M. DAVIS. *In* Molecular association. Vol. 1. *Edited by* R. Foster. Academic Press. New York. 1975, p. 151.
18. (*a*) R. FOSTER and C. A. FYFE. J. Chem. Soc. B, 926 (1966); (*b*) M. B. JURINSKI and P. A. D. DE MAINE. J. Am. Chem. Soc. **86**, 3217 (1964)
19. (*a*) J. O. SINGH, J. D. ANUNZIATA, and J. J. SILBER. Can. J. Chem. **63**, 905 (1985); (*b*) J. D. ANUNZIATA, N. S. GALAVERNA, J. O. SINGH, AND J. J. SILBER. Can. J. Chem. **64**, 1491 (1986).
20. (*a*) S. NAKAYAMA and K. SUSUKI. Bull. Chem. Soc. Jpn. **46**, 3694 (1973); (*b*) F. B. KAUFMAN. J. Am. Chem. Soc. **98**, 5339 (1976).
21. J. K. KOCHI. Angew. Chem. Int. Ed. Engl. **27**, 1227 (1988).
22. N. VETTORAZZI, J. J. SILBER, and L. SERENO. J. Electroanal. Chem. **125**, 459 (1981).

Can. J. Chem. Downloaded from www.nrcresearchpress.com by 91.144.44.67 on 09/07/12
For personal use only.

Hydroxylation of prostanoids by fungi. Synthesis of (−)-15-deoxy-19-(*R*)-hydroxy-PGE_1 and (−)-15-deoxy-18-(*S*)-hydroxy-PGE_1

HERBERT L. HOLLAND, FRANCES M. BROWN, P. CHINNA CHENCHAIAH, AND J. APPA RAO
Department of Chemistry, Brock University, St. Catharines, Ont., Canada L2S 3A1

Received August 21, 1989

HERBERT L. HOLLAND, FRANCES M. BROWN, P. CHINNA CHENCHAIAH, and J. APPA RAO. Can. J. Chem. **68**, 282 (1990).

A series of racemic substituted cyclopentanones, with alkyl groups corresponding to the upper prostanoid side chain and (or) the lower prostanoid side chain without the C-15 alcohol, has been synthesized. Using a steroid template for the prostanoid molecule as a basis for selection, fungi capable of hydroxylating steroids have been used to biotransform the prostanoid substrates. The predominant products were hydroxylated at the prostanoid C-18 and C-19 positions. The hydroxylations were enantioselective, with excesses in the range 10–60%, and in most cases the predominant configuration corresponded to that of the natural prostanoids. The stereochemistry of the C-19 hydroxyl group was found to be *R* by degradation of products to methyl 6-acetoxyheptanoate and comparison of that material with a resolved sample, obtained via crystallization of the brucine salt of ethyl 6-phthaloxyheptanoate. Hydroxylation at C-18 gave the *S* configuration of alcohol. Hydroxylation at prostanoid C-15 was observed, but in all cases this was accompanied by other reactions. Hydroxylation of *Rhizopus arrhizus* has been used in a preparation of (−)-15-deoxy-19-(*R*)-hydroxy-PGE_1 and (−)-15-deoxy-18-(*S*)-hydroxy-PGE_1.

Key words: biotransformation, hydroxylation, prostaglandins, prostanoids.

HERBERT L. HOLLAND, FRANCES M. BROWN, P. CHINNA CHENCHAIAH et J. APPA RAO. Can. J. Chem. **68**, 282 (1990).

On a synthétisé une série de cyclopentanones substituées racémiques portant des groupements alkyles correspondant à la chaîne latérale prostanoïde supérieure et (ou) à la chaîne latérale prostanoïde inférieure ne portant pas la fonction alcool en C-15. Utilisant comme base de sélection un gabarit stéroïdal pour représenter la molécule prostanoïde, on a fait appel à un champignon capable d'hydroxyler les stéroïdes pour effectuer la biotransformation des substrats prostanoïdes. Les produits principaux sont les prostanoïdes hydroxylés en positions C-18 et C-19. Les hydroxylations sont énantiosélectives, avec des excès de l'ordre de 10–60%, et, dans la plupart des cas, la configuration prédominante correspond à celle des prostanoïdes naturels. En se basant sur une dégradation des produits en 6-acétoxyheptanoate de méthyle et sur une comparaison de ce produit avec un échantillon résolu, obtenu par cristallisation du sel de brucine du 6-phtaloxyheptanoate d'éthyle, on a démontré que la stéréochimie du groupement hydroxyle en C-19 est *R*. L'hydroxylation en C-18 fournit un alcool de configuration *S*. On a observé une hydroxylation en C-15 du prostanoïde; toutefois, cette réaction est toujours accompagnée par d'autres réactions. On a fait appel à une hydroxylation par le *Rhizopus arrhizus* pour la préparation des (−)-15-désoxy-19-(*R*)-hydroxy-PGW_1 et (−)-15-désoxy-18-(*S*)-hydroxy-PGW_1.

Mots clés : biotransformation, hydroxylation, prostaglandins, prostanoïdes.

[Traduit par la revue]

Introduction

The prostaglandins constitute a small but extremely valuable group of human hormones. Prostaglandins of the PG_1 and PG_2 series (Fig. 1) have in common a *trans* relationship of substituents on a cyclopentane ring, and a C-15-(*S*) allylic alcohol. The necessity of achieving the correct absolute stereochemistry at both ring and chain substituents has resulted in many ingenious syntheses of prostaglandins (e.g., refs. 1 and 2), but final product costs are still high and, as a result, can limit the commercial development of prostanoids.

In view of the value of microbial, and particularly fungal, biotransformation as a means of introducing the hydroxyl group in a regio- and stereospecific manner into a wide range of organic molecules (3), especially steroids (4), we have undertaken a study of the fungal biotransformation of a series of simple racemic prostaglandin precursors and model compounds (**2**, **4**, **5**, **14**, **20**, and **29**). Although biotransformation of the natural prostanoids has been studied (5), and enzymic reactions such as ester hydrolysis (6), carbonyl/alcohol reduction/oxidation (7), and toluene dioxygenation (8) have been used to produce chiral prostaglandin synthons, the use of fungal biotransformation to enantioselectively hydroxylate simple racemic prostanoid precursors has not been reported by others.

The rationale behind our approach has been outlined elsewhere (9). The spatial and structural similarities between steroids and prostanoids of the PG_1 series outlined in Fig. 2 have been used to select fungi as candidates for testing for their ability

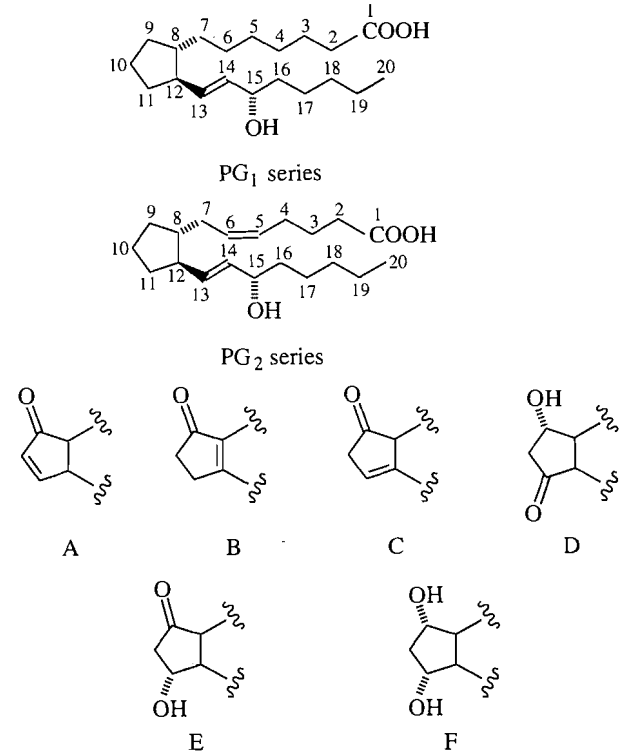

FIG. 1

Can. J. Chem. Downloaded from www.nrcresearchpress.com by 91.144.44.67 on 09/07/12
For personal use only.

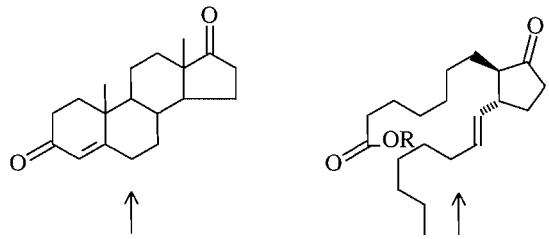

(a) (b)

FIG. 2 Structural similarities between steroids (a) and prostanoids (b).

to hydroxylate 15-deoxyprostanoids, based on the reported ability of such fungi to hydroxylate steroids at an analogous position.

It is remarkable that one of the commonest positions of hydroxylation of steroids by both fungal and mammalian enzymes, C-6β (10), corresponds to the C-15α hydroxyl of the natural prostaglandins using the relationship of Fig. 2. Fungi that are known to hydroxylate androstanes at C-6β, for example, might therefore be able to introduce a hydroxyl group at C-15α into a suitable prostanoid precursor. Furthermore, the correct prostanoid absolute stereochemistry of ring substituents, shown in Fig. 2(b), is a better fit into an enzyme active site designed for a steroid than the opposite stereochemistry would be, leading to the prediction that hydroxylation of racemic prostanoids carried out by a steroid hydroxylase should be enantioselective for the correct absolute stereochemistry of prostanoid product. The above relationships, and the fact that the solution conformation of natural prostaglandins is similar to that represented in Fig. 2(b) (11), were instrumental in the development of our approach to prostanoid hydroxylation.

The choice of hydroxylating fungi was also based on the relationship of Fig. 2. The steroid C-6β hydroxylating fungi *Rhizopus arrhizus* and *Rhizopus stolonifer* (10) were examined for hydroxylation at C-15 of the prostanoid precursors; *Aspergillus ochraceus* and *Curvularia lunata*, both hydroxylators of steroids at C-11 (12, 13) in addition to C-6, were selected for examination in the hope of also achieving hydroxylation at C-6 of the PG upper side chain (the site of oxygenation in prostacyclin); *Calonectria decora* was selected on the basis of its ability to hydroxylate a wide variety of steroidal substrates (12); and *Cunninghamella echinulata* var. *elegans* was examined because of its ability to perform allylic hydroxylation of 5(6)-unsaturated steroids (14).

Results

To avoid problems of solubility and pH maintenance, we opted to use substrates in their ester rather than acid forms, where appropriate. This is justified by the fact that PG esters are as efficient as the acids in many biological systems (15), and by the observation that rapid ester hydrolysis by the fungus would precede or accompany the hydroxylation reactions (16). To examine any stereoselection that might be attributable to esterase activity, we first examined the biotransformation of the model substrates **2** and **4**. The results of these and subsequent biotransformations are summarized in Table 1.

Both **2** and **4** were hydrolyzed by the fungi listed in Table 1 to give the acids **1** and **3**, respectively, re-isolated as the methyl esters following treatment with diazomethane. In all cases, low (5–10%) enantioselectivity was observed (based on optical rotation comparisons (17)), giving the 2-(*S*) enantiomer of **2** and the 2-(*R*) enantiomer of **4** (both configurations identical and opposite to that of the corresponding natural prostaglandin side chain). Such low stereoselection by esterases is unlikely to be a major factor in determining the stereoselectivity of any biotransformation process that may also involve hydroxylase enzymes.

Before proceeding with a study of the prostanoid substrates **20** and **29**, model substrates possessing only the lower prostanoid side chain, namely **5** and **14**, were examined. Hydroxylation

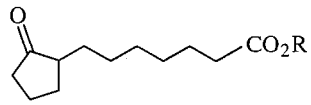

1: R = H
2: R = CH_3

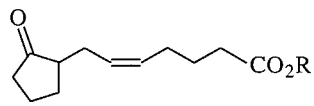

3: R = H
4: R = CH_3

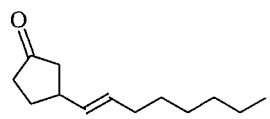

5

of racemic **5** by either *R. arrhizus* or *R. stolonifer* gave four products, **6**, **9**, **10**, and **11**, all of which carried a hydroxyl group at C-7′, corresponding to C-19 of the prostanoid skeleton. The structures of these products were determined by spectral analysis (see experimental section), with nmr data being particularly valuable. The position of the newly introduced hydroxyl group at C-7′ is apparent from the appearance of a doublet in the ^1H nmr attributable to the terminal methyl group, while the ^{13}C nmr data, presented in Table 2, confirm the proposed structures. Thus the presence of the C-7′ hydroxyl is reflected in the appearance of characteristic α, β, and γ shifts in the side chain, while the *cis* relative stereochemistry of ring substitution in product **9** is proposed on the basis of comparison of the chemical shifts of C-1 and C-3 with those of *cis* and *trans* substituted 3-alkyl cyclopentanols (18). The structure of **10** is based on analysis of its ^{13}C nmr spectrum (Table 2), the high field methylene signal at δ 21.7, assigned to C-5′ influenced by two upfield γ shifts due to the combined influence of the hydroxyl groups at C-3′ and C-7′, being particularly diagnostic.

The *trans* relative stereochemistry of the vicinal hydroxyl groups in product **11** is derived from ^{13}C nmr analysis. The absolute stereochemistry is tentatively assigned as 1(*S*),2(*S*) on the basis of comparison of the sign of rotation of **11** with those of similar cyclic *trans*-1,2-diols of known configuration (19, 20). The assignment of absolute stereochemistry at C-3 of the products **6**, **9**, and **10** was achieved by analysis of optical rotatory data. Thus a positive $n \rightarrow \pi^*$ Cotton effect in the cd spectrum of both **6** and its oxidation product **8** confirms the 3(*R*) absolute configuration for these two compounds (21), while the presence of a negative $n \rightarrow \pi^*$ Cotton effect in the spectrum of the diketone obtained by Jones' oxidation of **9** indicates that the latter compound has the (*S*) absolute stereochemistry at C-3 (21).

Can. J. Chem. Downloaded from www.nrcresearchpress.com by 91.144.44.67 on 09/07/12
For personal use only.

TABLE 1. Summary of biotransformations

Substrate	Fungus	Products (%)	ee (%)	Ring configuration
2	*R. arrhizus*	**2** (15)	5–10*	2*S*
	R. stolonifer	**2** (18)	5–10	2*S*
	C. lunata	**2** (7)	5–10	2*S*
	A. ochraceus	**2** (12)	5–10	2*S*
4	*R. arrhizus*	**4** (18)	5–10	2*R*
	R. stolonifer	**4** (20)	5–10	2*R*
	C. lunata	**4** (6)	5–10	2*R*
	A. ochraceus	**4** (5)	5–10	2*R*
5	*Rhizopus*	**6** (10)	20	3*R*
		9 (1)	20	3*S*
		10 (2)	27*	3*S*
		11 (14)	—	1*S*,2*S*
	C. lunata	Complex mixture		
	A. ochraceus	**6** (5)	—	—
		12 (5)	—	—
		plus other products		
	C. decora	**12** (9)	10	3*S*
	C. elegans	—	—	—
14	*Rhizopus*	**15** (18)	20	3*S*,4*R*
		17 (10)	Low	4*R*
		18 (20)	—	1*S*,3*S*,4*R*
	C. lunata	Complex mixture		
	A. ochraceus	**15** (5)	—	—
		19 (3)	—	—
	C. decora, *C. elegans*	**15**, **18**, plus other products		
20	*Rhizopus*	**21** (12)	26	2*R*,3*R*
		24 (10)	50	2*R*,3*R*
		26 + **27** (12)	—	—
		28 (4)	20*	2*R*,3*R*
	A. ochraceus	**21** + **24** (15)	—	—
	C. lunata	Complex mixture		
	C. decora	**21** (1.5)	14*	2*R*,3*R*
		24 (2)	22*	2*R*,3*R*
	C. elegans	**21** + **24** (10)	—	—
29	*Rhizopus*	**30** (12)	49*	2*R*,3*R*,4*R*
		32 (5)	60*	2*R*,3*R*,4*R*
		33 + **34** (2)	—	—

*Determined indirectly from rotation or cd values.

TABLE 2. ^{13}C nuclear magnetic resonance chemical shifts of mono-alkylated cyclopentanones

Carbon	Cyclopentanones												
	5	**6**	**8**	**9**	**10**	**11**†	**12**	**13**	**14**	**15**	**17**†	**18**	**19**
1	218.5	219.1	219.0	73.9	218.8	79.2*	219.0	219.0	215.4	215.0	209.1	78.5	207.8
2	44.8	45.0	44.9	43.0	44.7	39.7	45.0	44.9	43.2	43.3	41.6	41.0	134.1*
3	39.5	39.7	39.7	41.0	39.4	37.6	39.7	39.7	46.2	46.3	44.1	50.0	137.8
4	29.8*	30.0*	30.0	31.1	29.3	38.9	30.0	30.0	74.1	74.1	167.0	72.2	29.2
5	37.9	38.2	38.1	35.6	38.1	79.8*	38.2	38.2	48.1	48.3	132.4*	43.3	37.3
1′	131.9	132.3	132.5	134.8	133.1	134.8	132.4	133.0	133.4	133.0	133.3	131.8	132.2
2′	130.5	130.4	130.0	129.0	133.1	129.0	130.3	129.0	129.1	129.6	129.1	130.9	160.0
3′	32.3	32.4	32.2	32.4	72.5	32.3	32.5	31.9	32.6	32.4	32.4	32.4	70.0
4′	28.6*	29.4*	28.9	29.6	37.3	29.6	25.5	23.5	28.6	29.0	29.3	29.2	37.3
5′	29.2*	25.3	23.3	25.3	21.7	25.3	36.4	41.6	29.3	25.0	25.3	25.1	25.0
6′	31.5	39.2	43.5	39.3	39.0	39.3	73.2	210.0	31.7	39.0	39.2	39.0	31.0
7′	22.4	68.1	210.0	68.2	68.0	68.2	30.3	36.0	22.6	68.1	68.1	68.0	22.0
8′	13.8	23.6	29.7	23.5	23.6	23.5	9.9	7.9	14.1	23.6	23.6	23.5	14.0

*Chemical shifts in vertical columns marked with asterisks may be interchanged.
†Numbered here to conform with other entries in this table.

Can. J. Chem. Downloaded from www.nrcresearchpress.com by 91.144.44.67 on 09/07/12
For personal use only.

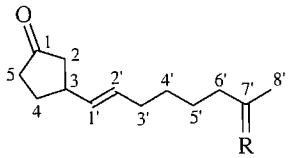

6: R = αH, βOH
7: R = αH, βOAc
8: R = O

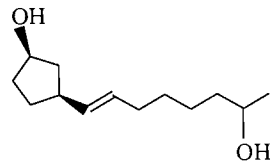

9

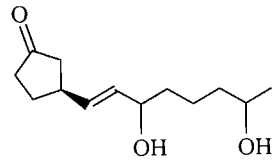

10

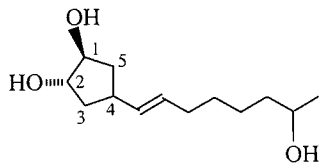

11

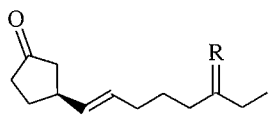

12: R = αH, βOH
13: R = O

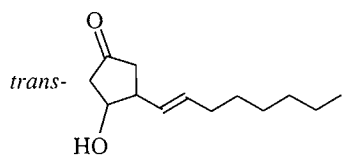

14

The enantiomeric excesses (ee) of compounds **6** and **9** at C-3 were determined following oxidation to the diketone **8**, and conversion of the latter to the bis(ketal) using 2(*R*),3(*R*)-butane-2,3-diol (22). The ^{13}C nmr spectrum of the bis(ketals) obtained from **6** and **9** showed pairs of signals attributable to the presence of diastereomeric components for C-2–C-5 and C-1′, and the enantiomeric excesses (shown in Table 1) were obtained directly from the signal intensities.

Product **10** is tentatively assigned the 3(*S*) configuration on the basis of a comparison of its optical rotation (−ve) with those of **6** (+ve) and the oxidation product of **9** (−ve), it having been shown that the configuration of substituent allylic hydroxyl groups on the alkyl chain of molecules such as **10** does not influence the overall sign of rotation of the molecule at longer wavelengths (7, 23, 24). The observation that the predominant configuration of **9** is different from that of **6**, from which it is presumably derived, is not exceptional: the enantiomeric excess of **6** is not high, and an enzyme converting **6** to **9** need not operate with the same enantioselectivity at C-3 as one that produces **6**, the enzymic functions of carbonyl reduction (by alcohol dehydrogenases) and hydroxylation (by mono-oxygenases) being unrelated.

The absolute stereochemistry of the newly introduced hydroxyl group at C-7′ in **6** has been determined to be (*R*) by conversion of **6** to the acetate **7** and oxidation of the latter to give, following methylation of the corresponding acid, (*R*)-(−)-methyl 6-acetoxyheptanoate (**39**). An authentic sample of this compound was prepared, as its (*S*)-(+) enantiomer, following resolution of ethyl 6-phthaloxyheptanoate (**37**) as the brucine salt. The (−) enantiomer of **39** is assigned the (*R*) absolute configuration by comparison with other methylcarbinol esters of different chain lengths but known configurations. In all cases, the (−) enantiomer has the (*R*) configuration at the carbinol centre (25). Within the experimental limits, the hydroxylation at C-7′ of **6** was found to be stereospecific. The absolute stereochemistry at other hydroxylation sites in this series of products has not been determined.

Of the other fungi used to biotransform **5**, *C. lunata* gave a complex mixture of products, while *C. elegans* gave no detectable products. *Aspergillus ochraceus* gave, in addition to other products, the 7′-alcohol **6** and a new product, **12**, identified as the 6′-alcohol on the basis of ^{13}C nmr (Table 2) and other spectral data (see Experimental). This latter product was also obtained as the sole metabolite of **6** by *C. decora*. In this case, the predominant absolute stereochemistry of **12** was identified as 3(*S*) by the observation of a negative $n \rightarrow \pi^*$ Cotton effect at 296 nm in the cd spectrum (21), and the enantiomeric excess determined following Jones' oxidation to the diketone **13** and conversion to the bis(ketal) with 2(*R*),3(*R*)-butane-2,3-diol as described above. The result is presented in Table 1.

The absolute configuration at the newly introduced C-6′ position of **12** was again determined by conversion to the acetate and oxidation to give, following diazomethane treatment of the resulting acid, (*S*)-(+)-methyl 5-acetoxyheptanoate (**40**). The absolute configuration of **40** is assigned by comparison of its sign of rotation with that of other ethylcarbinol esters with differing chain lengths: in all cases where the absolute configuration is known, the (*S*) enantiomer has a positive rotation (25).

The next model system to be studied was the PGE analogue **14**. The *Rhizopus* species again gave the same product profile: products **15**, **17**, and **18** all carried a newly introduced hydroxyl group at C-7′, and were identified largely by their ^{13}C nmr spectra (Table 2). It is probable that both **17** and **18** arise from **15**, by dehydration and reduction, respectively. The relative stereochemistry of ring substitution in **18** follows from ^{13}C nmr data. The *trans* relationship between the C-4 hydroxyl and C-3 alkyl groups is dictated by the substrate stereochemistry, while the *cis* relationship between the C-1 and C-3 substituents is determined by comparison of the ^{13}C nmr chemical shifts of C-1 and C-3 with those of equivalent carbons in *cis* and *trans*-1,3-alkyl cyclopentanols (18).

The ring absolute stereochemistry of **18** is tentatively assigned as 1(*S*),3(*S*),4(*R*) based on a comparison of its rotation (negative) with those of other alkyl substituted cyclic 1,3-diols of known configuration (26) and comparison with the absolute stereochemistry proposed for compound **9**. The absolute stereochemistry at C-3 and -4 of **15** is also based on

Can. J. Chem. Downloaded from www.nrcresearchpress.com by 91.144.44.67 on 09/07/12
For personal use only.

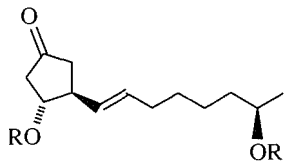

15: R = H
16: R = $COCH_3$

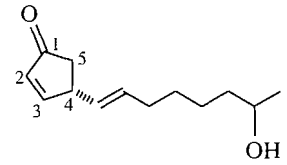

17

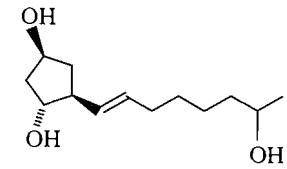

18

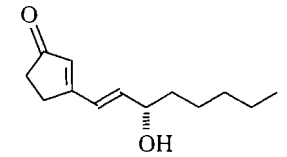

19

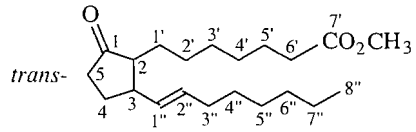

systematic numbering

20

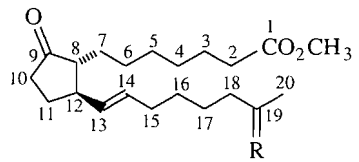

PG numbering

21: R = αH, βOH
22: R = αH, βOAc
23: R = O

optical data, the observation of a negative rotation confirming the predominant 3(*S*),4(*R*) configuration shown (21). In this case, the enantiomeric excess was determined to be 20% by chiral shift reagent analysis of the ^{1}H nmr spectrum of **15**. The absolute stereochemistry of **17** has not been determined, but the 4(*R*) configuration may be suggested by comparison of its sign of rotation with those of PGA compounds, which carry similar ring functionality (27).

The absolute stereochemistry of the C-7′ hydroxyl group in **15** was determined as outlined above for compound **6**, and was again found to be (*R*). Thus compounds **6** and **14** are both hydroxylated at the C-7′ position by *R. arrhizus* to give the 7′-(*R*) alcohol, although the enantioselectivity of conversion of the two substrates is different, presumably due to the presence of the C-4 alcohol functionality in **14**.

Products **15** and **18** were also obtained (along with other unidentified products) from *C. decora* and *C. elegans*. *Curvularia lunata* gave a complex product profile, but *A. ochraceus* gave only two products, **15** and **19**, the latter identified by its spectral data (see experimental section and Table 2). The appearance of a new signal at δ 4.15 in the ^{1}H nmr spectrum, assigned to an allylic hydrogen geminal to hydroxyl, the absence of the usual C-4 hydrogen signal, and ^{13}C nmr chemical shifts assigned to a conjugated cyclopentenone (see Table 2) suggested structure **19**. Dehydration of PGE structures such as **14** in aqueous medium at pH ≤4 or ≥8, giving rise to PGA and PGB systems (the latter via the PGC structure, see Fig. 1) is well documented (28), and *Aspergillus* growth medium is acidic, in this case pH 3.5. The absolute stereochemistry at C-3′ of **19** has not been determined, but (−)-alkenyl alkyl carbinols are known to have the (*S*) configuration at the carbinol carbon (25). The enantiomeric excess at C-3′ determined by chiral ^{1}H nmr shift reagent analysis was 35%.

As with the other substrates used in this study, the 11-deoxy-PGE analogue **20** gave the same product profile from both

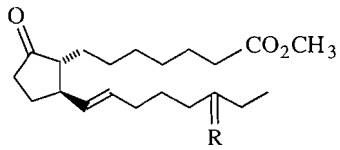

24: R = αH, βOH
25: R = O

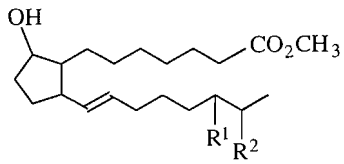

26: R^1 = H, R^2 = OH
27: R^1 = OH, R^2 = H

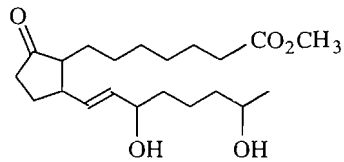

28

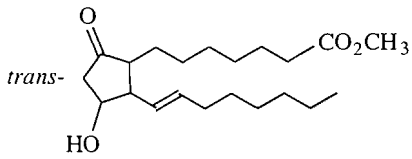

29

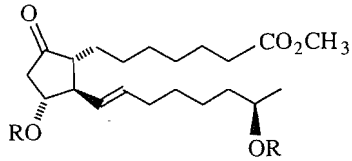

30: R = H
31: R = $COCH_3$

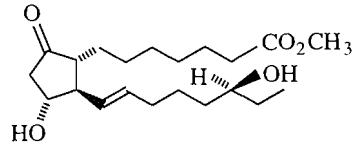

32

Can. J. Chem. Downloaded from www.nrcresearchpress.com by 91.144.44.67 on 09/07/12
For personal use only.

TABLE 3. ^{13}C nuclear magnetic resonance chemical shifts of dialkylated cyclopentanones

	Cyclopentanone							
Carbon†	**20**	**21**	**23**	**24**	**28**	**29**	**30**	**32**
1	174.3	173.8	174.0	173.7	175.5	174.1	174.2	174.0
2	34.1	34.1	34.1	32.8	33.2	33.8	33.8	34.0
3	24.9	24.9	23.1*	23.5	24.5	24.7	24.8	24.9
4	29.5	29.5	29.4	30.1	30.7	29.2	28.9	28.5
5	29.0	29.0	28.9	29.6	29.3	29.2	29.3	27.3
6	28.3	28.3*	28.2	29.3	28.4	27.5	27.7	27.8
7	26.7	26.7	26.4	26.3	24.4	26.5	26.6	26.5
8	54.8	53.6	53.6	54.4	52.9	54.4	54.4	54.2
9	220.0	219.1	219.4	219.0	218.9	215.4	215.1	215.0
10	37.7	37.4	37.5	37.4	36.8	46.0	46.1	48.0
11	27.7	28.1*	28.2	28.1	27.5	72.0	72.2	72.2
12	46.1	46.1	46.3	46.2	45.8	54.2	54.9	55.1
13	132.5	132.7	132.4	132.2	131.7	129.4	129.8	129.6
14	131.6	131.0	131.5	131.8	131.2	134.5	134.8	134.1
15	32.5	32.2	32.2	32.8	72.6	32.4	32.3	32.4
16	28.2	28.1	29.7	25.3	38.3	28.6	28.9	25.5
17	29.0	25.0	23.3*	36.3	22.7	28.9	25.0	36.4
18	31.7	39.1	43.6	72.9	36.8	31.5	38.7	73.0
19	22.7	67.0	210.0	30.1	67.6	22.4	68.0	30.2
20	14.1	23.5	29.9	9.8	24.2	13.9	23.6	9.8
Other	51.4	51.4	51.4	51.4	51.4	51.2	51.4	51.5

*Values in vertical columns so marked may be interchanged.
†PG numbering.

R. arrhizus and *R. stolonifer*. In addition to the C-6″ and C-7″ alcohols **21** and **24**, isolated and fully characterized by nmr and other spectral data (see experimental section and Table 3), and their corresponding reduction products, tentatively assigned structures **26** and **27** on the basis of ^{13}C nmr data, the dihydroxylated product **28** was obtained in low yield. The structure of **28** was deduced by comparison of its ^{13}C nmr spectral data (Table 3) with those of substrate **20** and product **10** (*vide supra* and Table 2).

The absolute configurations at C-2 and -3 of products **21** and **24** were determined by cd data. In both cases, the observation of a negative Cotton effect attributable to the $n \rightarrow \pi^*$ transitions at 296 and 297 nm for **21** and **24** respectively confirmed the 2(*R*),3(*R*) configuration shown (21). The enantiomeric excesses were determined as described above following oxidation to the ketones **23** and **25** and their conversion to the bis(ketals) with 2(*R*),3(*R*)-butane-2,3-diol. The ^{13}C nmr analysis of the ketals so obtained was used to determine the ee values given in Table 1. Product **28** was also assigned the 2(*R*),3(*R*) absolute configuration and an approximate ee of 20% based on the published negative rotation value of the corresponding C-7″-deoxy compound (7).

Products **21** and **24** were also obtained from incubation of **20** with *A. ochraceus*, *C. elegans*, and *C. decora*, but only characterized fully in the case of the latter fungus. The configuration and ee values listed in Table 1 were then derived from a comparison with the values determined for the corresponding products from *R. arrhizus*.

For both **21** and **24** derived from *R. arrhizus*, the configurations at the newly introduced carbinol centres were determined by acetylation, oxidation, and methylation as previously described to give the degradation products **39** and **40**, respectively. In both cases the results obtained were identical with those of earlier degradations, confirming that hydroxylation had occurred to give the C-7″(*R*) configuration in **21** and the C-6″(*S*) configuration in **24**.

The final compound used in this study was the PGE_1 precursor **29**. As a result of the experiments outlined above, which suggested that the *Rhizopus* species were the most efficient hydroxylating fungi of those studied for this series of compounds, biotransformation of **29** was limited to *R. arrhizus* and *R. stolonifer*. Two products were isolated and characterized as the C-19 alcohol **30** and the C-18 alcohol **32** (PG numbering). The structures followed from their ^{13}C nmr (Table 3) and other spectral data (see experimental section), the positions of hydroxylation being characterized by the shift parameters discussed above for products **6** and **12**. Unfortunately, no product of dihydroxylation at C-15 and C-18 or -19, corresponding to **28**, could be isolated, although ^{13}C nmr analysis of the minor products (see Experimental) indicated the possible presence of the reduction products **33** and **34**.

The absolute stereochemistry at C-2, -3, and -4 of **30** and **32** was determined, as before, by cd analysis (21), and the enantiomeric excesses were estimated by a comparison of the magnitudes of the $n \rightarrow \pi^*$ Cotton effects at 296 nm with that reported for natural PGE_1 (29): the C-15 allylic alcohol of the latter does not contribute appreciably to the $n \rightarrow \pi^*$ transition in the cd spectrum (23), and the effect of a hydroxyl group at C-18 or -19 unrelated to the carbonyl chromophore can be neglected. The configurations at the sites of hydroxylation were determined as before by conversion of the biotransformation products to the acetates, followed by oxidation and conversion of the resulting acids to the esters **39** (from **30**) and **40** (from **32**). As for previous hydroxylation products, the configurations were found to be 19(*R*) and 18(*S*) in **30** and **32**, respectively.

In view of the predominance of hydroxylation of the above substrates at the prostanoid C-18 and -19 positions, and the comparative rarity of hydroxylation at C-15, an attempt was made to suppress the former in favour of the latter by the use of the enzyme inhibitor 11-dodecynoic acid in the incubations of compound **5** with *R. arrhizus*. Such acetylenic fatty acids are known to be effective inhibitors of enzymes that hydroxylate at

Can. J. Chem. Downloaded from www.nrcresearchpress.com by 91.144.44.67 on 09/07/12
For personal use only.

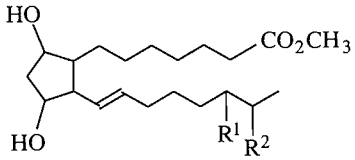

33: $R^1 = H, R^2 = OH$
34: $R^1 = OH, R^2 = H$

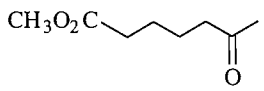

35

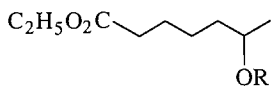

36: R = H

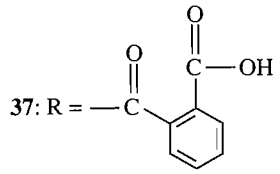

37: R =

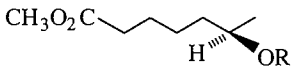

38: R = H
39: $R = COCH_3$

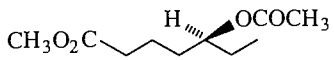

40

the terminal and penultimate positions of fatty acids and related compounds (30, 31), but in the present study no change in the product profile obtained from **5** and *R. arrhizus* was observed when the acetylenic fatty acid was added to the fungus prior to the addition of **5**.

In a series of experiments designed to suppress the activity of oxidoreductases (manifested by the frequent observation of carbonyl reduction accompanying hydroxylation) the solvent for the addition of **5** to *R. arrhizus* was changed from 95% ethanol to varying concentrations of DMF and DMSO. The absence of ethanol denies the fungus access to relatively large amounts of reducing equivalents, but neither these experiments, nor trials in which the substrate was added without any solvent, caused an appreciable change in the product profile.

Discussion

While no direct data on the nature of the enzymes responsible for the hydroxylation products obtained in this study exist, their identity may be speculatively assigned as fatty acid or steroid cytochrome P-450 dependent monooxygenases (12, 30, 32). Fatty acid hydroxylases typically produce terminal, penultimate, or peripenultimate alcohols (33–35), and are known to hydroxylate non-fatty acid substrates (35). On the other hand, a steroid C-6β hydroxylase operating as outlined in Fig. 3 could produce the major hydroxylation products discussed above, reaction from the "α" side giving the prostanoid C-19(*R*) or

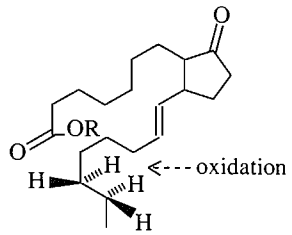

FIG. 3 Model for prostanoid C-18 or C-19 hydroxylation by a steroid hydroxylase.

C-18(*S*) alcohols. The steroid C-6β hydroxylase of *R. arrhizus* can hydroxylate from the α face in the absence of the steroid 3-keto-4-ene π system (10). This fact, together with the observation that highest yields of C-18 and -19 hydroxylated products were obtained from steroid C-6β hydroxylating fungi, the absence of terminal oxidation products, and the report that other natural products with long alkyl chains, e.g., cannabinoids, are also metabolized by steroid hydroxylating fungi to products with hydroxyl groups at the penultimate and peripenultimate (but not terminal) carbons of the alkyl chain (36), supports the model of Fig. 3.

Irrespective of the nature of the fungal hydroxylating enzymes, it is remarkable that their sites of attack, C-18 and -19, are identical with the sites of hydroxylation of natural prostaglandins by mammalian enzymes (37–43). Furthermore, the absolute stereochemistry at C-19 in the human metabolite 19-hydroxy-PGB_1 has been identified as (*R*) (44), identical to that observed in the present study. The 19-hydroxy-PG's, particularly in the PGE series (45), have greater physiological effects on smooth muscle than do the parent PG's (46), and are used in treatment of male infertility attributable to lack of seminal fluid PGE_1 metabolites (47).

In contrast to the 19-hydroxy-PGE's, whose formation and activities are understood, the 18-hydroxy-PGE's produced by mammalian PGE metabolism remain an enigma (43). They have no defined physiological role, and are of unknown configuration at C-18. In view of the correspondence of stereochemistries at C-19 between the mammalian metabolites and the products obtained in this study, it is tempting to speculate that the mammalian 18-hydroxy-PG's may have the 18(*S*) configuration.

The enantioselectivity observed in the fungal biotransformation of the PG precursors **20** and **29** was not high, but in view of the ease of their preparation, and the stereospecificity of their hydroxylation at C-18 or -19, fungal biotransformation must be considered a serious candidate for any synthetic route aimed at producing 18- or 19-hydroxy PG analogues.

Experimental

Apparatus, material, and methods

Melting points were determined on a Kofler heating stage and are uncorrected. Infrared spectra were recorded with an Analect 6260FX spectrometer. Proton nmr spectra were recorded at 200 MHz and carbon nmr spectra at 50.3 MHz (J MOD mode) with a Bruker AC200 spectrometer, using $CDCl_3$ as solvent and internal standard. Chiral shift reagent work used tris[3-(heptafluoropropylhydroxymethylene)-(+)-camphorato], europium(III) derivative in CCl_4 solution at relative concentrations of 0.1–0.3 M with respect to the compound under investigation. Mass spectra were obtained with an AEI MS30/Kratos DS55 system. Optical rotations were measured at 20°C in 95% ethanol solution using a Rudolph Autopol 3 polarimeter with a sample pathlength of 1 dm. The cd spectra were acquired by Dr. A. F. Drake

Can. J. Chem. Downloaded from www.nrcresearchpress.com by 91.144.44.67 on 09/07/12
For personal use only.

Can. J. Chem. Downloaded from www.nrcresearchpress.com by 91.144.44.67 on 09/07/12
For personal use only.

of the S.E.R.C. national CD service, Birkbeck College, University of London, U.K., or at the Department of Biochemistry, McMaster University, Hamilton, Ontario. The hplc analysis was performed on a Perkin–Elmer Series 3 chromatograph. Thin-layer chromatography was performed on Merck silica gel 60F-254, and flash column chromatography used silica gel (230–400 mesh, Merck 9385 or equivalent). Microanalysis was carried out by Guelph Analytical Laboratories.

Maintenance of microorganisms

Rhizopus arrhizus ATCC 11145 and *Rhizopus stolonifer* ATCC 6227b were maintained on malt agar slopes. *Aspergillus ochraceus* ATCC 18500 was maintained on Czapek's agar, *Curvularia lunata* ATCC 12017 on rabbit food agar, and *Calonectria decora* ATCC 14767 and *Cunninghamella echinulata* var. *elegans* ATCC 9245 on potato dextrose agar.

Synthesis of substrates

The following compounds were prepared by standard procedures and gave analytical and spectral data in agreement with those reported. The ^{13}C nmr data are reported in the tables. (±)-Methyl 2-oxocyclopentaneheptanoate (**2**) (48); (±)-methyl *Z*-7-(2′-oxocyclopentyl)-5-heptenoate (**4**) (48, 49); (±)-*trans*-2-(6′-carbomethoxyhexyl)-3-(*E*-1″-octenyl)-cyclopentanone ((±)-11,15-dideoxyprostaglandin E_1) (**20**) by diazomethane treatment of the acid (48); (±)-*trans,trans*-2-(6′-carbomethoxyhexyl)-3-(*E*-1″-octenyl)-4-hydroxycyclopentanone ((±)-15-deoxyprostaglandin E_1) (**29**) by diazomethane treatment of the acid (48).

*(±)-3-(*E*-1′-Octenyl)-cyclopentanone (**5**)*

A solution of *E*-1-iodo-1-octene (7) (6.69 g) in dry ether (100 mL) was cooled to −85°C and then treated with a solution of *tert*-butyllithium (30 mL, 1.9 M in pentane) over a period of 5 min. The resulting mixture was stirred at −78°C for 2 h, and then transferred under positive argon pressure into a flask containing a solution of copper(I) iodide (5.4 g) and tri-*n*-butyl phosphine (18.5 mL) in dry THF (360 mL) maintained at −78°C. The mixture was then stirred at −78°C for 15 min, and next treated over a period of 50 min with a cooled (−78°C) solution of 2-cyclopentenone (1.86 g) in dry THF (180 mL) under a positive pressure of argon. The reaction mixture was stirred at −78°C for a further period of 1 h, and then treated with aqueous ammonium chloride (270 mL) and the resulting mixture shaken vigorously for 10 min. The organic layer was then separated and the aqueous layer extracted with ether (3 × 150 mL). The combined organic material was dried and evaporated to yield a residue (16 g) that afforded a pure product **5** (2.5 g, oil) on chromatography (eluent hexane/ethyl acetate 7:1); ir ν_{max}: 1745 cm^{-1}; ^1H nmr included signals at δ 0.89 (3H, t, C-8′ CH_3) and 5.5 (2H, m, C-1′,2′ H's) ppm; ^{13}C nmr: see Table 2. *Anal.* calcd. for $C_{13}H_{22}O$: C 80.35, H 11.33%; found: C 80.14, H 11.45%.

*(±)-*trans*-3-(*E*-1′-Octenyl)-4-hydroxycyclopentanone (**14**)*

This was prepared by the route outlined below.

(±)-4-Hydroxy-2-cyclopentenone

This was most conveniently prepared by rearrangement of furfuryl alcohol (50). A solution of furfuryl alcohol (50 g) in 0.066 M phosphate buffer was adjusted to pH 4.1 by addition of phosphoric acid, and the mixture then maintained at reflux temperature under an atmosphere of argon for 15 h. The solution was then cooled and extracted twice with toluene (100 mL) and the aqueous layer then evaporated to dryness. The residue was then extracted with methylene chloride and the extract dried and evaporated to give an oil (22 g), which was purified by chromatography (eluent hexane/ethyl acetate 3:2) and afforded 18 g of (±)-4-hydroxy-2-cyclopentenone with spectral data identical to those reported (6).

(±)-4-Tetrahydropyranyloxy-2-cyclopentenone

This was prepared from the above alcohol (6 g) and dihydropyran (16 g) by the addition of concentrated HCl (3 drops); the mixture so produced was allowed to stand at room temperature for 3 h, and then worked up by the addition of ether and water to give the pyranyl ether in 95% yield. The ^1H nmr included signals at δ 1.5 (6H, m, tetrahydropyranyl hydrogens), 2.0–2.8 (2H, m, C-5 CH_2), 3.5–4.0 (2H, m, CH_2—O—), 4.8–5.0 (2H, m, C-4 H and O—CH—O), 6.1 (1H, d, C-2 H), and 7.5 (1H, m, C-3 H) ppm.

*(±)-*trans*-3-(*E*-1′-Octenyl)-4-hydroxycyclopentanone (**14**)*

This was prepared from the above THP ether (4.16 g) using the procedure outlined for the preparation of **5**. To the reaction product (2.9 g) was added a solution of acetic acid in water (65% vol/vol, 60 mL), and the cloudy suspension then made homogeneous by the addition of THF (6 mL). The resulting solution was stirred at 30°C for 12 h, and then neutralized (solid sodium bicarbonate) and extracted with ether. The extract was dried and evaporated to give an oil that, on chromatography (eluent hexane/ethyl acetate 1:1), afforded the title compound (1.9 g); ir ν_{max}: 1745, 3400 cm^{-1}; ^1H nmr included signals at δ 0.8 (3H, t, C-8′ CH_3), 4.1 (1H, dd, C-4 H), and 5.2–5.8 (2H, m, C-1′,2′ H's) ppm; ^{13}C nmr: see Table 2. *Anal.* calcd. for $C_{13}H_{22}O_2$: C 74.24, H 10.54%; found: C 74.02, H 10.28%.

Biotransformations

The results are summarized in Table 1. Incubations with the following fungi were performed as described, unless otherwise stated: *R. arrhizus* (51), *R. stolonifer* (51), *A. ochraceus* (52), *C. lunata* (13), *C. decora* (53), and *C. elegans* (54). Incubations were performed on a 1 g scale for a period of 3 days unless otherwise stated. Following the incubation period, the medium was extracted with dichloromethane (continuous extraction for 4 days). The extract was then dried and evaporated and, in the case of substrates **2**, **4**, **20**, and **29**, the residue treated with an excess of diazomethane in ether solution, and the resulting solution then evaporated. The final residue was subjected to chromatography to yield the products described below. Listed below under substrate headings and microorganism subheadings are conditions of incubation (if different from standard procedures); products; isolated yield (%); spectral and physical data. All products listed were homogeneous by chromatographic analysis (tlc, hplc), unless otherwise stated: no diastereomeric separations due to less than 100% ee of ring substituents were observed.

*(±)-Methyl 2-oxocyclopentaneheptanoate (**2**)*

Rhizopus arrhizus, R. stolonifer, Aspergillus ochraceus, Curvularia lunata

Methyl 2-oxocyclopentaneheptanoate; 10–20; identical with authentic material except $[\alpha]_D$ +6 to +10°.

*(±)-Methyl Z-7-(2′-oxocyclopentyl)-5-heptenoate (**4**)*

Rhizopus arrhizus, R. stolonifer, Aspergillus ochraceus, Curvularia lunata

Methyl *Z*-7-(2′-oxocyclopentyl)-5-heptenoate; 5–20; identical with authentic material except $[\alpha]_D$ +6 to +10°.

*(±)-3-(*E*-1′-Octenyl)-cyclopentanone (**5**)*

Rhizopus arrhizus, R. stolonifer

3-(*E*-1′-Octen-7′-olyl)-cyclopentanone (**6**); 10; ir ν_{max}: 1740, 3500 cm^{-1}; $[\alpha]_D$ +8.1° (*R. arrhizus*), +6.3° (*R. stolonifer*); ^{13}C nmr, see Table 2; ^1H nmr included signals at δ 1.17 (3H, d, C-8′ CH_3, collapsed to s on irradiation at δ 3.6–3.8 ppm), 3.6–3.8 (1H, m, C-7′ H), 5.3–5.7 (2H, m, C-1′,2′ H's) ppm; cd λ_{max}: 296 nm, Δε +0.028 (*R. arrhizus*); ms *m/e* (%): 192 ($M^+ - H_2O$, 3), 163 (7), 136 (60), 94 (68), 83 (85) relative to 80 (100). *cis*-3-(*E*-1′-Octen-7′-olyl)-cyclopentanol (**9**); 1; ir ν_{max}: 3345 cm^{-1}; $[\alpha]_D$ +7.0°; ^{13}C nmr, see Table 2; ^1H nmr included signals at δ 1.17 (3H, d, C-8′ CH_3), 3.5–3.9 (2H, m, C-1,7′ H's), 5.3–5.7 (2H, m, C-1′,2′ H's) ppm. Jones' oxidation of **9** (11 mg) gave 3-(7′-oxo-1′-octenyl)-cyclopentanone (**8**) (8 mg); ir ν_{max}: 1716, 1741 cm^{-1}; $[\alpha]_D$ −6.3°; ^{13}C nmr, see Table 2; ^1H nmr included signals at δ 2.15 (3H, s, C-8′ CH_3) and 5.5 (2H, br s, C-1′,2′ H's) ppm; ms *m/e* (%): 208 (20), 165 (5), 123 (50) relative to 95 (100). 3-(*E*-1′-Octen-3′,7′-diolyl)-cyclopentanone (**10**); 2; ir ν_{max}: 1738, 3400 cm^{-1}; $[\alpha]_D$ −8.3°; ^{13}C nmr, see Table 2; ^1H nmr included signals at δ 1.17 (3H, d, C-8′ CH_3), 3.0 (2H, br s, exchanges with D_2O, OH), 3.7–3.8 (1H, m, C-7′ H), 3.95 (1H, br s, C-3′ H), and 5.3–5.4 (2H, m, C-1′,-2′ H's) ppm; 4-(*E*-1′-Octen-7′-olyl)-

Can. J. Chem. Downloaded from www.nrcresearchpress.com by 91.144.44.67 on 09/07/12
For personal use only.

cyclopentane-*trans*-1,2-diol (**11**); 14; ir ν_{max}: 3460 cm^{-1}; $[\alpha]_D$ +24.0°; ^{13}C nmr, see Table 2; ^1H nmr included signals at δ 1.17 (3H, d, C-8′ CH_3), 3.3–3.9 (3H, m, C-1,-2,-7′ H's), 5.3–5.5 (2H, m, C-1′,-2′ H's) ppm.

Rhizopus arrhizus, R. stolonifer, *time and solvent studies*

Variation of the time of incubation of substrate with *R. arrhizus* and *R. stolonifer* using periods of 24, 36, 48, and 72 h produced only minor variations in yield of products. Change of the solvent for substrate addition from 95% ethanol to DMF or DMSO (0.020–1 mL per 75 mg of substrate), or the addition of substrate in the absence of a solvent, produced no change in the range of products produced.

Rhizopus arrhizus, *inhibitor studies*

11-Dodecynoic acid (31) (0.25 and 0.5 mg/mL in separate experiments) was added to the fungal culture following the normal growth period but prior to addition of substrate **5** at the normal concentration (6). Subsequent biotransformation of **5** proceeded to give the range of products described above.

Curvularia lunata

Incubation of **5** (1 g) with *C. lunata* gave an extract (0.8 g). Thin-layer chromatographic analysis indicated a complex, multicomponent mixture, which was not investigated further.

Aspergillus ochraceus

3-(*E*-1′-Octen-7′-olyl)-cyclopentanone (**6**); 5; spectral data as described above. 3-(*E*-1′-Octen-6′-olyl)-cyclopentanone (**12**); 5; ir ν_{max}: 1743, 3490 cm^{-1}; ^{13}C nmr, see Table 2; ^1H nmr included signals at δ 0.90 (3H, t, C-8′ CH_3), 4.02 (1H, m, C-7′ H), and 5.3–5.5 (2H, m, C-1′,-2′ H's) ppm. Additional, more polar, minor products were detected by tlc analysis, but not investigated further.

Calonectria decora

3-(*E*-1′-Octen-6′-olyl)-cyclopentanone (**12**); 9; spectral data as described above in addition to $[\alpha]_D$ +10.4°; cd λ_{max}: 296 nm, Δε −0.18; ms *m/e* (%): 193 (28), 192 (M − H_2O, 33), 177 (5), 163 (72), 136 (60) relative to 80 (100).

Cunninghamella elegans

Incubation of **5** (1 g) with *C. elegans* gave an extract (0.11 g) from the growth medium that, on analysis (tlc, nmr), was found to contain only endogenous fungal products. Extraction of the fungal biomass yielded the unchanged starting material.

*(±)-*trans*-3-(*E*-1′-Octenyl)-4-hydroxycyclopentanone (**14**)*

Rhizopus arrhizus, R. stolonifer

3-(*E*-1′-Octen-7′-olyl)-4-hydroxycyclopentanone (**15**); 18; ir ν_{max}: 1740, 3480 cm^{-1}; $[\alpha]_D$ −14.4°; ^{13}C nmr, see Table 2; ^1H nmr included signals at δ 1.15 (3H, d, C-8′ CH_3), 3.1 (2H, br s, exchanges with D_2O, OH), 3.6–3.8 (1H, m, C-7′ H), 4.0–4.2 (1H, d of t, C-4 H) and 5.2–5.6 (2H, m, C-1′,-2′ H's) ppm, chiral shift reagent analysis using the C-4 hydrogen signal indicated an ee of 20%; ms *m/e* (%): 208 (M − H_2O, 3), 189 (10), 181 (30) relative to 55 (100). 4-(*E*-1′-Octen-7′-olyl)-cyclopent-2-en-1-one (**17**); 10; ir ν_{max}: 1709 cm^{-1}; $[\alpha]_D$ −11.7°; ^{13}C nmr, see Table 2; ^1H nmr included signals at δ 1.17 (3H, s, C-8′ CH_3), 3.5–3.8 (1H, m, C-7′ H), 5.2–5.6 (2H, m, C-1′,-2′ H's), 6.20 (1H, d, C-5 H), and 7.57 (1H, d of d, C-4 H) ppm; ms *m/e* (%): 208 (3), 190 (4), 166 (3), 149 (6), 95 (90), 82 (40), 67 (55), relative to 55 (100). 3-(*E*-1′-Octen-7′-olyl)-cyclopentane-*trans*-1,4-diol (**18**); 20; ir ν_{max}: 3400 cm^{-1}; $[\alpha]_D$ −11.4°; ^{13}C nmr, see Table 2; ^1H nmr included signals at δ 1.15 (3H, d, C-8′ CH_3), 3.4–4.1 (3H, m, C-1,-4,-8′ H's), and 5.3–5.6 (2H, m, C-1′,-2′ H's) ppm.

Curvularia lunata

Incubation of **14** (0.95 g) with *C. lunata* gave an extract from the aqueous medium (0.45 g) that, upon tlc examination, was found to consist of multiple components, and was not examined further.

Aspergillus ochraceus

3-(*E*-1′-Octen-7′-olyl)-4-hydroxycyclopentanone (**15**); 5; spectral data identical with those listed above. 3-(*E*-1′-Octen-3′-olyl)-cyclopent-2-ene-1-one (**19**); 3; ir ν_{max}: 1710, 3450 cm^{-1}; $[\alpha]_D$ −2.7°; ^{13}C nmr, see Table 2; ^1H nmr included signals at δ 0.96 (3H, t, C-8′ CH_3), 4.15 (1H, m, C-3′ H), 5.80 (1H, d, C-2 H), 6.25 (1H, d, C-1′ H), and 7.75 (1H, d, C-2′ H) ppm, chiral shift reagent analysis indicated an ee at C-3′ of 35%; ms *m/e* (%): 208 (1), 190 (10), 166 (3) relative to 55 (100).

Calonectria decora, C. elegans

Incubation of **14** (1 g) with each of these fungi gave extracts from the aqueous media (0.35 and 0.65 g, respectively); tlc examination indicated the presence of **15** and **18** in both extracts, together with other unidentified products. These extracts were not examined further.

*(±)-*trans*-2-(6′-Carbomethoxyhexyl)-3-(*E*-1″-octenyl)-cyclopentanone (**20**)*

Rhizopus arrhizus, R. stolonifer

2-(6′-Carbomethoxyhexyl)-3-(*E*-1″-octen-7″-olyl)-cyclopentanone (**21**); 12; ir ν_{max}: 1738, 3450 cm^{-1}; $[\alpha]_D$ −4.7° (*R. arrhizus*), −6.0° (*R. stolonifer*); ^{13}C nmr, see Table 3; ^1H nmr included signals at δ 1.15 (3H, d, C-8″ CH_3), 3.6–3.8 (1H, m, C-7″ H), 3.63 (3H, s, OCH_3), and 5.25–5.7 (2H, m, C-1″,-2″ H's) ppm; cd λ_{max}: 296 nm, Δε −0.23 (*R. arrhizus*); ms *m/e* (%): 334 (M − H_2O, 2), 303 (3), 225 (2), 223 (2), 191 (3) relative to 55 (100). 2-(6′-Carbomethoxyhexyl)-3-(*E*-1″-octen-6″-olyl)-cyclopentanone (**24**); 10; ir ν_{max}: 1740, 3480 cm^{-1}; $[\alpha]_D$ −20.0 (*R. arrhizus*), −21.07 (*R. stolonifer*); ^{13}C nmr, see Table 3; ^1H nmr included signals at δ 0.90 (3H, t, C-8″ CH_3), 3.4–3.7 (1H, m, C-6″ H), 3.61 (3H, s, OCH_3), and 5.25–5.6 (2H, m, C-1″,-2″ H's) ppm; cd λ_{max}: 297 nm, Δε −0.52 (*R. arrhizus*); ms as reported above for compound **21**. 2-(6′-Carbomethoxyhexyl)-3-(*E*-1″-octen-3″,7″-diolyl)-cyclopentanone (**28**); 4; ir ν_{max}: 1735, 3450 cm^{-1}; $[\alpha]_D$ −8.5° (*R. arrhizus*), −6.8° (*R. stolonifer*); ^{13}C nmr, see Table 3; ^1H nmr included signals at δ 1.15 (3H, d, C-8″ CH_3), 3.6–4.0 (2H, m, C-3″,-7″ H's), 3.61 (3H, s, OCH_3), and 5.2–5.4 (2H, m, C-1″,-2″ H's) ppm. 2-(6′-Carbomethoxyhexyl)-3-(*E*-1″-octen-6″-olyl)-cyclopentanol (**27**) and 2-(6′-carbomethoxyhexyl)-3-(*E*-1″-octen-7″-olyl)-cyclopentanol (**26**), mixture, approximately 1:3; 12; ^{13}C nmr included peaks at δ 10.0 (C-8″ of **27**), 23.4 (C-8″ of **26**), 68.0 (C-7″ of **26**), 73.3 (C-6″ of **27**), 77.7 and 78.8 (C-1) ppm; ^1H nmr included signals at δ 0.90 (t, C-8″ CH_3 of **27**), 1.15 (d, C-8″ CH_3 of **26**) in the ratio 1:3, in addition to signals at 3.4–3.8 (m, -CHOH-), 3.58 (OCH_3), and 5.2–5.4 (olefinic H) ppm.

Aspergillus ochraceus, C. elegans

Incubation of **20** (1 g) with these fungi gave extracts (0.5 and 0.8 g, respectively). Initial chromatography to remove endogenous fungal products gave, in each case, oils that by tlc analysis appeared to consist of a mixture of **21** and **24** (15 and 10%, respectively). These mixtures were not separated further, but their identity was confirmed by ^{13}C and ^1H nmr analysis by comparison with the spectra of isolated materials (see above).

Curvularia lunata

Incubation of **20** (1 g) with *C. lunata* gave an extract (0.65 g) that was found by tlc analysis to consist of a complex mixture of components. This extract was not analysed further.

Calonectria decora

2-(6′-Carbomethoxyhexyl)-3-(*E*-1″-octen-7″-olyl)-cyclopentanone (**21**); 1.5; spectral data identical with those reported above except $[\alpha]_D$ −3.4°. 2-(6′-Carbomethoxyhexyl)-3-(*E*-1″-octen-6″-olyl)-cyclopentanone (**24**); 2; spectral data identical with those reported above except $[\alpha]_D$ −9.4°.

*(±)-*trans*-2-(6′-Carboxymethylhexyl)-3-(*E*-1″-octenyl)-4-hydroxycyclopentanone (**29**)*

Rhizopus arrhizus

2-(6′-Carboxymethylhexyl)-3-(*E*-1″-octen-7″-olyl)-4-hydroxycyclopentanone (15-deoxy-19-hydroxy-PGE_1, **30**); 12; ir ν_{max}: 1735, 1740, 3450 cm^{-1}; $[\alpha]_D$ −18°; ^{13}C nmr, see Table 3; ^1H nmr included signals at δ 1.15 (d, C-8″ CH_3), 3.60 (3H, s, OCH_3), 3.5–3.8 (1H, m, C-7″ H), 4.0 (1H, d of t, C-4 H), 5.3 and 5.6 (each 1H, m, C-1″ and -2″ H's) ppm; cd λ_{max}: 296, Δε −1.80; ms *m/e* (%): 332 (20, M − $2H_2O$), 301 (35), 300 (30) relative to 55 (100). 2-(6′-Carbomethoxyhexyl)-3-(*E*-1″-octen-6″-olyl)-4-hydroxycyclopentanone (15-deoxy-18-hydroxy-PGE_1, **32**); 5; $[\alpha]_D$ −25.4°; ^{13}C nmr, see Table 3, ^1H nmr included signals at δ 0.92 (3H, t, C-8″ CH_3), 3.55 (3H, s, OCH_3), 3.6–3.8 (1H, m, C-6″ H), 3.96 (1H, m, C-4 H), and 5.25–5.7 (2H, m, C-1″,-2″ H's) ppm; ms, see that reported for **30**, above. Other, more

Can. J. Chem. Downloaded from www.nrcresearchpress.com by 91.144.44.67 on 09/07/12
For personal use only.

polar products (total 2%), were obtained. The ^{13}C nmr spectra of the mixture contained, in addition to methylene and methine resonances, peaks at δ 10.0 and 23.6 (CH_3), and 68.1, 72.5, 78.6, and 79.0 (CHOH) ppm, but no ketone C=O, suggesting possible structures **33** and **34**, but these products were not investigated further.

Determination of enantiomeric excesses and absolute configuration

1. At ring carbons

The direct values reported in Table 1 were obtained by Jones' oxidation of the biotransformation products, followed by ^{13}C nmr analysis of the diastereomeric ketals obtained by reaction of the products of Jones' oxidation with 2*R*,3*R*-butane-2,3-diol.

*3-(*E*-1′-Octen-7′-olyl)-cyclopentanone (6) (from* R. arrhizus*).* The above alcohol (20 mg) was reacted with Jones' reagent in the usual way, and the reaction mixture worked up to give the corresponding ketone (**8**) (18 mg), spectral data identical with those reported above except $[\alpha]_D$ +6.0°, cd λ_{max}: 279 nm, Δε +0.022. The above dione (18 mg) was dissolved in dry benzene, and to this solution was added 2*R*,3*R*-butane-2,3-diol (30 mg) and *p*-toluene sulphonic acid (1 mg). The resulting mixture was refluxed for 7 h and then cooled, diluted with ether (50 mL), and washed with 10% sodium bicarbonate solution. The organic layer was then dried and evaporated, and the residue dissolved directly in $CDCl_3$ for nmr analysis; ^{13}C nmr: 16.6, 16.9, 17.0, 17.2 (ketal CH_3's), 23.5 (C-5′), 25.7 (C-8′), 29.8 (C-4′), 30.9 and 31.2 (ratio 40:60, C-4), 32.4 (C-3′), 37.8 and 38.1 (ratio 38:62, C-3), 40.4 (C-6′), 40.7 and 41.2 (ratio 41:59, C-5), 44.9 and 45.1 (ratio 35:65, C-2), 78.0, 78.3, 78.5, and 78.8 (ketal -O*C*H(CH_3)-), 109.3 (C-7′), 118.0 (C-1), 129.2 and 129.8 (ratio 60:40, C-1′), and 133.8 and 134.0 (ratio 58:42, C-2′) ppm, indicating an average diastereomeric ratio of 40:60, or an enantiomeric excess for **6** of 20%.

*3-(*E*-1′-Octen-7′-olyl)-cyclopentanol (9) (from* R. arrhizus*).* Jones' oxidation of **9** gave the dione **8**, $[\alpha]_D$ −6.0°, ketalization of which as described above gave a sample whose ^{13}C nmr spectrum was identical with that described above except for the peaks assigned to C-2, -3, -4, -5, -1′, and -2′. Analysis of the spectrum indicated an enantiomeric excess for **9** of 20%.

*3-(*E*-1′-Octen-6′-olyl)-cyclopentanone (12) (from* C. decora*).* Jones' oxidation of **12** (37 mg) gave the dione **13** (32 mg); $[\alpha]_D$ −6.0°; ^{13}C nmr, see Table 2; ^1H nmr included signals at δ 1.0 (3H, t, C-8′ CH_3), 2.38 (2H, q, C-7′ CH_2), and 5.3–5.6 (2H, m, C-1′,-2′ H's) ppm; cd λ_{max}: 295 nm, Δε −0.36, converted to the ketal with 2*R*,3*R*-butane-2,3-diol as described above; ^{13}C nmr, δ: 8.12 (C-8′), 16.6, 16.9, 17.0, and 17.2 (ketal CH_3's), 23.7 (C-4′), 29.7 (C-7′), 30.9 and 31.2 (ratio 53:47, C-4), 31.4 (C-3′), 32.7 (C-3′), 37.7 (C-5′), 38.1 and 37.7 (C-3, overlapping with C-5′), 40.7 and 41.3 (ratio 54:46, C-5), 44.9 and 45.1 (ratio 53:47, C-2), 78.3, 78.5, 78.6, and 78.7 (-*C*H(CH_3)O-), 111.2 (C-6′), 117.0 (C-1), 129.0 (C-2′), and 134.0 and 134.3 (ratio 54:46, C-1′) ppm, indicating an enantiomeric excess for **12** on ca. 10%.

*2-(6′-Carbomethoxyhexyl)-3-(*E*-1″-octen-7″-olyl)-cyclopentanone (21) (from* R. arrhizus*).* Oxidation of **21** (50 mg) with Jones' reagent gave the diketone **23** in quantitative yield; ^{13}C nmr, see Table 3; ^1H nmr included a signal at δ 2.0 (3H, s, C-8″ CH_3), 3.58 (3H, s, OCH_3), and 5.3–5.6 (2H, m, C-1″,-2″ H's) ppm, converted to the ketal with 2*R*,3*R*-butane-2,3-diol as described above; ^{13}C nmr included doubled signals at 46.1 and 46.3 (ratio 36:64, C-12), 49.9 and 50.1 (ratio 39:61, C-8), and 129.5 and 130.0 (ratio 65:35, C-1″) ppm, indicating an average ee for **21** of 26%.

*2-(6′-Carbomethoxyhexyl)-3-(*E*-1″-octen-6″-olyl)-cyclopentanone (24) (from* R. arrhizus*).* The diketone **25** obtained by Jones' oxidation of **24** was converted to the bis ketal as described above. The ^{13}C nmr included doubled signals at δ 46.9 and 47.2 (ratio 22:78, C-12), 51.0 and 51.2 (ratio 24:76), and 129.7 and 129.8 (ratio 72:28, C-1″) ppm, indicating an average ee for **24** of 50%.

2. At hydroxylation sites

(a) By chiral nmr shift reagent

This method as used on compounds **6** from *R. arrhizus* and *R. stolonifer*, **12** from *C. decora*, **21** from *R. arrhizus* and *R. stolonifer*, and **24** from *R. arrhizus* and *R. stolonifer*. No evidence for diastereomeric complex formation was observed at concentrations of shift reagent capable of moving the -CH(OH)- signal under observation to chemicals shift of δ 15–20 ppm. The same phenomenon was observed by monitoring the CH_3 signal of the methyl carbinols **6** and **21** (with decoupling irradiation of the -CH(OH)- resonance) over the range 3–7 ppm.

(b) By degradation

(i) Methyl carbinols 6, 15, 21, and 30 from R. arrhizus. These were converted to the corresponding acetates **7**, **16**, **22**, and **31**, and then to (−)-methyl 6-acetoxyheptanoate (**39**) by the procedure outlined below in the case of **21**. The alcohol **21** (47 mg) was dissolved in dry pyridine (1 mL), and treated with acetic anhydride (1 mL). The resulting solution was allowed to stand at room temperature overnight, and then worked up in the usual way to afford the acetate **22** (37 mg); ^{13}C nmr δ (PG numbering): 19.9 (C-20), 21.3 (acetate CH_3), 23.1 (C-17), 24.8 (C-3), 26.7 (C-7), 28.2 (2C, C-6,-11), 29.1 (C-5), 31.3 (C-4), 32.2 (C-15), 33.8 (C-2), 35.7 (C-18), 37.4 (C-10), 46.2 (C-12), 51.4 (OCH_3), 53.6 (C-8), 70.0 (C-19), 131.7, 132.4 (C-13,-14), 170.6 and 174.0 (ester C=O), and 219.0 (C-9) ppm; ^1H nmr included signals at δ 1.20 (3H, s, C-20 CH_3), 3.66 (3H, s, OCH_3), 4.8–5.1 (1H, m, C-19H), and 5.2–5.6 (2H, m, C-13,-14 H's) ppm. The above acetate was dissolved in acetone (20 mL), and to this solution was added solid potassium permanganate (0.8 g). The resulting mixture was stirred and heated under reflux for 18 h, then evaporated, and water (10 mL) was added to the residue. This mixture was treated with solid sodium bisulphite until the purple color was discharged, and then acidified (10% HCl) to give a clear solution, which was extracted with ether (3 × 10 mL). The combined extract was washed with water, and then extracted with saturated aqueous sodium bicarbonate (3 × 10 mL). The aqueous extract was washed with ether, then acidified (10% HCl), and extracted with ether (3 × 10 mL). The ethereal extract was then dried and evaporated to give a residue (22.9 mg), which was treated with excess ethereal diazomethane in the usual manner to give a further residue. This was chromatographed by elution with 5% ethyl acetate/hexane to afford (−)-methyl 6-acetoxyheptanoate (**39**) (9 mg), identical in spectral properties with an authentic sample of racemic material (see below) except $[\alpha]_D$ −8.1°. Samples of **39** obtained in an identical manner from **6**, **15**, and **30** had $[\alpha]_D$ −8.5, −8.0, and −8.8° respectively.

(ii) Ethyl carbinols 12 from C. decora *and 24 and 32 from* R. arrhizus. These were converted to the corresponding acetates as described above, and the latter then treated with potassium permanganate and the resulting acids esterified as also described above. Chromatography (elution with 5% ethyl acetate/hexane) gave *S*-(+)-methyl 5-acetoxyheptanoate (**40**); ^{13}C nmr δ: 9.3 (C-7), 20.8 (C-3), 21.3 (acetate CH_3), 26.1 (C-6), 32.4 (C-4), 33.1 (C-2), 51.4 (OCH_3), 76.4 (C-5), 170.6 and 173.4 (ester C=O) ppm; ^1H nmr, δ: 0.90 (3H, t, C-7 CH_3), 1.2–1.9 (6H, m, C-3,-4, and -6 CH_2's), 2.02 (3H, s, OAc), 2.30 (2H, t, C-2 H's), 3.68 (3H, s, CH_3-O), and 4.9–5.3 (1H, m, C-5 H) ppm. Samples of **40** obtained from **12**, **24**, and **32** had $[\alpha]_D$ +11.6, +13.8, and +12.3° respectively. Analysis by chiral nmr shift reagent failed to provide evidence for the existence of more than one enantiomer of **40**.

Resolution of ethyl 6-phthaloxyheptanoate and the preparation of (+)-methyl 6-acetoxyheptanoate

(±)-Ethyl 6-hydroxyheptanoate (36)

6-Oxoheptanoic acid (commercial sample) was converted to the methyl ester **35** by treatment with diazomethane in the usual manner. Sodium borohydride (0.5 g) was then dissolved in a solution **35** (5 g) in absolute ethanol (200 mL), and the resulting mixture allowed to stand at room temperature for 24 h and then poured onto water and extracted with ether. The extract was washed with 5% HCl and water, and then dried and evaporated to give **36** (4.8 g, oil); ^{13}C nmr, δ: 14.0 (ethyl CH_3), 23.3 (C-7), 24.7, 25.1 (C-3,-4), 34.1 (C-2), 38.7 (C-5), 60.0 (ethyl CH_2), 67.4 (C-6), and 173.6 (C-1) ppm; ^1H nmr, δ: 1.12 (3H, d, C-7 CH_3), 1.22 (3H, t, ethyl CH_3), 1.25–1.9 (6H, m, C-3,-4,-5 H's), 2.30 (2H, t, C-2 H's), 3.75 (1H, m, C-6 H), and 4.12 (2H, q, ethyl CH_2) ppm. Chiral nmr shift reagent analysis showed clear separation of the C-6 hydrogen signals of the diastereomeric complexes at chemical

Can. J. Chem. Downloaded from www.nrcresearchpress.com by 91.144.44.67 on 09/07/12
For personal use only.

shifts >13.0 ppm. *Anal.* calcd. for $C_9H_{18}O_3$: C 62.04, H 10.41%; found: C 61.95, H 10.50%.

(±)-Ethyl 6-phthaloxyheptanoate (37)

A solution of the alcohol **36** (5.22 g) and phthalic anhydride (4.44 g, freshly sublimed) in dry pyridine (40 mL) was allowed to stand at room temperature for 72 h, then poured onto 10% aqueous HCl and the mixture extracted with chloroform (3 × 200 mL). The chloroform solution was then washed (10% HCl), dried, and evaporated to give a residue that was dissolved in a mixture of ether and saturated aqueous sodium bicarbonate (200 mL of each). The ether layer was discarded, the aqueous layer washed further with ether (2 × 100 mL), and then acidified (10% HCl) and extracted with chloroform (3 × 100 mL). The final extract was dried and evaporated to give the half-ester **37** (7.5 g, oil); ^{13}C nmr, δ: 14.0 (ethyl CH_3), 19.4 (C-7), 24.6, 24.7 (C-3,-4), 34.0 (C-2), 35.2 (C-5), 60.3 (ethyl CH_2), 72.5 (C-6), 128.5, 129.4, 130.3, 130.5, 131.7, and 133.6 (aromatic C's), 167.6 (acid C=O), and 171.3 and 174.0 (ester C=O's) ppm; ^{1}H nmr, δ: 1.25 (3H, s, ethyl CH_3), 1.37 (3H, d, C-7 CH_3), 1.3–2.0 (6H, m, C-3,-4,-5 CH_2's), 2.35 (2H, t, C-2 H's), 4.10 (2H, q, ethyl CH_2), 5.0–5.3 (1H, m, C-6 H), and 7.4–7.9 (4H, aromatic H's) ppm. *Anal.* calcd. for $C_{17}H_{22}O_6$: C 63.34, H 6.88%; found: C 63.56, H 6.74%.

S-(+)-Ethyl 6-phthaloxyheptanoate

A mixture of the phthalate half-ester **37** (21 g), brucine dihydrate (30.42 g), and acetone (50 mL) was heated to boiling, and maintained under reflux conditions until a clear solution was obtained (ca. 10 min). The solution was then placed in a 4°C refrigerator for 48 h, and the resulting solid material (21 g) then collected by filtration. This was subsequently redissolved in acetone (50 mL) by heating, and the solution left undisturbed at 4°C for 24 h to produce 17.1 g of crystalline salt. Two further crystallizations from acetone (each 50 mL) resulted in 14.1 g of salt, mp 128–130°C, which was then shaken with a mixture of chloroform (100 mL) and 10% aqueous HCl (100 mL). The chloroform layer was removed and the aqueous layer extracted with further chloroform (3 × 100 mL); the combined organic extracts were dried and evaporated to yield *S*-(+)-**37** (4.9 g), with spectral data identical to those reported above except $[\alpha]_D$ +25.3°.

S-(+)-Methyl 6-hydroxyheptanoate (38)

Sodium borohydride (0.3 g) was added to a solution of the phthalate ester **37** (1 g) in absolute methanol (100 mL), and the resulting solution heated under reflux for 48 h. The solution was then evaporated, and the residue partitioned between 5% aqueous HCl and ether (50 mL of each). The ethereal layer was removed and the aqueous layer extracted further with ether (2 × 50 mL). The combined organic extract was then washed with saturated aqueous sodium bicarbonate, dried, and evaporated to give **38** (0.14 g, oil, ref. 55); $[\alpha]_D$ +21.9°; ^{13}C nmr, δ: 21.1 (ester CH_3), 23.2 (C-7), 24.7 and 25.0 (C-3,-4), 33.7 (C-2), 38.7 (C-5), 67.6 (C-6), and 173.0 (C-1) ppm; ^{1}H nmr, δ: 1.10 (3H, d, C-7 CH_3), 1.25–1.8 (6H, m, C-3,-4,-5 CH_2's), 2.27 (2H, t, C-2 H's), 3.4–3.8 (1H, m, C-6 H), and 3.60 (3H, s, OCH_3). Analysis by chiral nmr shift reagent showed no evidence for the existence of more than one enantiomer under conditions that shifted the C-6 hydrogen signal to 16.5 ppm. Conversion to the Mosher ester by reaction with 3,3,3-trifluoro-2-methoxy-2-phenylpropanoyl chloride and hplc analysis of the product were performed as described (56) and indicated an enantiomeric excess for **38** of ≥95%.

S-(+)-Methyl 6-acetoxyheptanoate

Treatment of the above alcohol with acetic anhydride in pyridine and work-up in the usual manner gave the acetate; $[\alpha]_{589}$ +8.5°, $[\alpha]_{546}$ +11.0°, $[\alpha]_{435}$ +18.7°, $[\alpha]_{405}$ +21.9° (*c* 0.31); ^{13}C nmr, δ: 19.7 (C-7), 24.6, 24.7 (C-3,-4), 33.8 (C-2), 35.4 (C-5), 51.4 (OCH_3), 70.5 (C-6), and 173.4 (C-1) ppm; ^{1}H nmr, δ: 1.20 (C-7 CH_3), 1.1–2.0 (6H, m, C-3,-4,-5 CH_2's), 2.32 (2H, t, C-2 H's), 3.65 (3H, s, OCH_3), and 4.8–5.6 (1H, m, C-6 H) ppm.

Acknowledgements

This work was funded through the Strategic Grants Programme of the Natural Sciences and Engineering Research Council of Canada. We are grateful to Mr. T. R. B. Jones for assistance with the acquisition of spectral data, and to Dr. A. F. Drake of Birkbeck College, University of London, U.K., and Dr. R. Epand, Department of Chemistry, McMaster University, Hamilton, Ontario, for their cooperation in the provision of cd spectral data.

1. R. F. Newton and S. M. Roberts. Tetrahedron, **36**, 2163 (1980).
2. R. Noyori and M. Suzuki. Angew. Chem. **23**, 847 (1984).
3. K. Kieslich (*Editor*). Biotechnology. Vol. 6a. Biotransformations. Verlag Chemie, Weinheim. 1984.
4. G. Nominé. Bull. Soc. Chim. Fr. II, 18 (1980).
5. A. Kergomard. *In* Biotechnology. Vol. 6a. Biotransformations. *Edited by* K. Kieslich, Verlag Chemie, Weinheim. 1984. p. 127.
6. T. Tanaka, S. Kurozumi, T. Toru, S. Miura, M. Kobayashi, and S. Ishimoto. Tetrahedron, **32**, 1713 (1976).
7. C. J. Sih, J. B. Heather, R. Sood, P. Price, G. Peruzzotti, L. F. H. Lee, and S. S. Lee. J. Am. Chem. Soc. **97**, 857 (1975).
8. T. Hudlicky, H. Luna, G. Barbieri, and L. D. Kwart. J. Am. Chem. Soc. **110**, 4735 (1988).
9. H. L. Holland, F. M. Brown, J. A. Rao, and P. C. Chenchaiah. Dev. Ind. Microbiol. **29**, 191 (1988).
10. H. L. Holland. Acc. Chem. Res. **17**, 398 (1984).
11. E. M. K. Loevey and N. H. Andersen. J. Am. Chem. Soc. **97**, 4148 (1975).
12. H. L. Holland. Chem. Soc. Rev. **11**, 371 (1982).
13. Y. Y. Lin, M. Shibahara, and L. L. Smith. J. Org. Chem. **34**, 3530 (1969).
14. T. A. Crabb, P. J. Dawson, and R. O. Williams. J. Chem. Soc. Perkin Trans. 1, 2535 (1980).
15. F. Suzuki, H. Hayashi, S. Ito, and O. Hayaishi. Biochim. Biophys. Acta, **917**, 224 (1987).
16. W. Marshek and M. Miyano. U.S. Pat. 3,878,046 (1975); Chem. Abstr. **83**, 76968 (1975).
17. J. J. Partridge, N. K. Chada, and M. R. Uskokovic. J. Am. Chem. Soc. **95**, 532 (1973).
18. (*a*) M. Cristl, H. J. Reich, and J. D. Roberts. J. Am. Chem. Soc. **93**, 3463 (1971); (*b*) E. Breitmaier and W. Voelter. Carbon-13 NMR Spectroscopy. VCH Publishers, Weinheim. 1987. p. 210.
19. Y. Yamamoto, M. Fushimi, J. Oda, and Y. Inouye. Agric. Biol. Chem. **39**, 2223 (1975).
20. A. C. Cope and A. S. Mehta. J. Am. Chem. Soc. **86**, 5626 (1964).
21. D. N. Kirk. Tetrahedron, **42**, 777 (1986).
22. H. Hiemstra and H. Wynberg. Tetrahedron Lett. 2183 (1977).
23. M. F. Ansell, M. P. L. Caton, A. F. Drake, and K. A. J. Stuttle. Tetrahedron Lett. **24**, 3017 (1983).
24. C. J. Sih, P. Price, R. Sood, R. G. Salomon, G. Peruzzotti, and M. Casey. J. Am. Chem. Soc. **94**, 3643 (1972).
25. P. Newman. Optical resolution procedures for chemical compounds. Vol. 3. Optical Resolution Information Centre, New York. 1984.
26. (*a*) J. Fried, M. M. Mehra, and Y. Y. Chan. J. Am. Chem. Soc. **96**, 6759 (1974); (*b*) E. J. Corey, K. C. Nicolaou, and M. Shibasaki. J. Chem. Soc. Chem. Commun. 658 (1975).
27. E. J. Corey and G. Moinet. J. Am. Chem. Soc. **95**, 6831 (1973).
28. J. S. Bindra. *In* The total synthesis of natural products. Vol. 4. *Edited by* J. W. ApSimon. Wiley, New York. 1981. pp. 356, 431.
29. O. Korver. Recl. Trav. Chim. Pays-Bas, **88**, 1070 (1969).
30. S. Shak, N. O. Reich, I. M. Goldstein, and P. R. Ortiz de Montellano. J. Biol. Chem. **260**, 13023 (1985).
31. P. R. Ortiz de Montellano and N. O. Reich. J. Biol. Chem. **259**, 4136 (1984).
32. A. S. Muerhoff, D. E. Williams, N. O. Reich, C. A. CaJacob, P. R. Ortiz de Montellano, and B. S. S. Masters. J. Biol. Chem. **264**, 749 (1989).
33. K. Wikvall. J. Biol. Chem. **259**, 3800 (1984).

34. L. O. NARHI and A. J. FULCO. J. Biol. Chem. **261**, 7160 (1986).
35. Y. MIURA, H. HISAKI, W. SIEMS, and S. ODA. Lipids, **22**, 987 (1987).
36. M. BINDER. Helv. Chim. Acta, **59**, 1674 (1976).
37. P. L. TAYLOR and R. W. KELLY. Nature, **250**, 666 (1974).
38. H. T. JONSSON, B. S. MIDDLEDITCH, and D. M. DESIDERIO. Science, **187**, 1093 (1975).
39. R. W. KELLY, P. L. TAYLOR, J. P. HEARN, R. V. SHORT, D. E. MARTIN, and J. H. MARSTON. Nature, **260**, 544 (1976).
40. K. P. VATSIS, A. D. THEOHARIDES, D. KUPFER, and M. J. COON. J. Biol. Chem. **257**, 11221 (1982).
41. K. A. HOLM, D. R. KOOP, M. J. COON, A. D. THEOHARIDES, and D. KUPFER. Arch. Biochem. Biophys. **243**, 135 (1985).
42. E. H. OLIW and Ö. JOHNSEN. Biochim. Biophys. Acta, **963**, 295 (1988).
43. E. H. OLIW. Prostaglandins, **35**, 523 (1988).
44. M. HAMBERG. Eur. J. Biochem. **6**, 147 (1968).
45. E. H. OLIW, A.-C. KINN, and U. KVIST. J. Biol. Chem. **263**, 7222 (1988).
46. C. H. SPILMAN, K. K. BERGSTROM, and A. D. FORBES. Prostaglandins, **13**, 795 (1977).
47. R. I. LEWY, T. K. BILLS, J. DALTON, J. B. SMITH, and M. J. SILVER. Prostaglandins Med. **2**, 367 (1979).
48. K. L. BERNADY, M. B. FLOYD, J. F. POLETTO, and M. J. WEISS. J. Org. Chem. **44**, 1438 (1979).
49. S. KUROZUMI and T. TORU. Synth. Commun. 427 (1977).
50. M. MINAI. Jap. Patent **55**, 138502 (1955); **57**, 62236 (1957).
51. H. L. HOLLAND and B. J. AURET. Can. J. Chem. **53**, 2041 (1975).
52. H. L. HOLLAND and B. J. AURET. Can. J. Chem. **53**, 845 (1976).
53. J. W. BLUNT, I. M. CLARK, J. M. EVANS, E. R. H. JONES, G. D. MEAKINS, and J. T. PINHEY. J. Chem. Soc. (C), 1136 (1971).
54. C. E. CERNIGLIA, J. C. MORGAN, and D. T. GIBSON. Biochem. J. **180**, 175 (1979).
55. S. ITO and M. MATSUMOTO. J. Org. Chem. **48**, 1133 (1983).
56. L. THIJS, P. P. WAANDERS, E. H. M. STOKKINGREEF, and B. ZWANENBURG. Recl. J. R. Neth. Chem. Soc. **105**, 332 (1986).

Can. J. Chem. Downloaded from www.nrcresearchpress.com by 91.144.44.67 on 09/07/12
For personal use only.

Thermodynamics of electrolyte solutions: activity coefficients of NaCl in the NaCl–$NiCl_2$–H_2O system at 25, 35, and 45°C

CH. VENKATESWARLU AND J. ANANTHASWAMY[1]

Department of Chemistry, Osmania University, Hyderabad – 500 007, India

Received June 9, 1989

CH. VENKATESWARLU and J. ANANTHASWAMY. Can. J. Chem. **68**, 294 (1990).

The activity coefficients of NaCl in the NaCl–$NiCl_2$–H_2O system were estimated at 25, 35, and 45°C and total ionic strengths of 0.5, 1.0, 2.0, and 3.0 *m* by an EMF method using a Na-ion selective electrode and a silver–silver chloride reference electrode. The Harned coefficients were calculated at all the temperatures studied. At 25°C the data were analysed using the Pitzer formalism. The osmotic coefficients and the excess free energies of mixing were also calculated at 25°C.

Key words: activity coefficients, sodium chloride, nickel chloride, Pitzer equations, thermodynamics.

CH. VENKATESWARLU et J. ANANTHASWAMY. Can. J. Chem. **68**, 294 (1990).

Opérant à des températures de 25, 35 et 45°C et à des forces ioniques totales de 0,5, 1,0, 2,0 et 3,0 *m* et faisant appel à une méthode de FEM utilisant une électrode sélective à l'ion Na et une électrode de référence d'argent/chlorure d'argent, on a évalué les coefficients d'activité du NaCl dans le système NaCl–$NiCl_2$–H_2O. On a calculé les coefficients de Harned à toutes les températures étudiées. À 25°C, on a analysé les données à l'aide d'un formalisme de Pitzer. On a aussi calculé les coefficients osmotiques et les énergies libres en excès, à 25°C.

Mots clés : coefficients d'activité, chlorure de sodium, chlorure de nickel, équations de Pitzer, thermodynamique.

[Traduit par la revue]

Can. J. Chem. Downloaded from www.nrcresearchpress.com by 91.144.44.67 on 09/07/12
For personal use only.

Introduction

Activity and osmotic coefficient data are essential for predicting the thermodynamic behaviour of mixed electrolyte solutions, and extensive data is available for mixtures of alkali and alkaline earth metal halides (1–5). However, very few studies have been reported on aqueous mixtures of alkali metal halides with transition metal halides. Recently, Rard (6) determined the osmotic and activity coefficients of pure aqueous $NiCl_2$ at 25°C using the isopiestic method. The heat capacities and volumes of aqueous nickel chloride were measured by Perron *et al.* (7). The osmotic coefficients of the NaCl–$NiCl_2$–H_2O system at 25°C were estimated by Filippov *et al.* using an isopiestic method (8). However, the activity coefficients of NaCl in aqueous mixtures of NaCl–$NiCl_2$ have not yet been estimated as a function of temperature. In continuation of our earlier studies (9) on ternary mixtures of the aqueous alkali metal halides with transition metal halides, we are now reporting the mean ion activity coefficients of NaCl in the system NaCl–$NiCl_2$–H_2O by an EMF method at 25, 35, and 45°C and total ionic strengths of 0.5, 1.0, 2.0, and 3.0 *m*.

Results and discussion

The experimental mean activity coefficients of NaCl in the NaCl–$NiCl_2$–H_2O system at all the ionic strengths ($I = m_{NaCl} + 3m_{NiCl_2}$) and at 25, 35, and 45°C are summarized in Table 1 at different values of y_B, where $y_B = 3m_{NiCl_2}/(m_{NaCl} + 3m_{NiCl_2})$. The $\log \gamma_\pm$ vs. y_B plots at 25°C are shown in Fig. 1.

The activity coefficient data at each ionic strength were fitted to the Harned equation (10)

$$[1] \quad \log \gamma_A = \log \gamma_A^0 - \alpha_{AB} y_B$$

where γ_A^0 is the activity coefficient of pure NaCl at the same ionic strength as the mixture. The Harned coefficient values, i.e., α_{AB}, along with the root-mean-square deviations (RMSD) are listed in Table 2.

At 25°C the activity coefficient data were also analysed using the Pitzer formalism (11–13). The values of the Pitzer coefficients for NaCl and $NiCl_2$ are given below.

$$\beta^0_{NaCl} = 0.07537;\ \beta^1_{NaCl} = 0.2770;\ C^\phi_{NaCl} = 0.001407$$

$$\beta^0_{NiCl_2} = 0.34991;\ \beta^1_{NiCl_2} = 1.5300;\ C^\phi_{NiCl_2} = -0.00471$$

The experimental activity coefficient data at 25°C were fitted to the Pitzer equations and the binary ($^s\theta_{NaNi}$) and ternary (ψ_{NaNiCl}) interaction coefficients were evaluated at each of the ionic strengths studied. These values are given in Table 3. Also, the common $^s\theta$, ψ values and corresponding RMSD values are listed in Table 3.

It may be possible to compare the ternary mixtures HCl–$CoCl_2$–H_2O with NaCl–$CoCl_2$–H_2O, and HCl–$NiCl_2$–H_2O with the present system. The binary interaction parameter of the second system (14), i.e., $^s\theta_{NaCo} = 0.0382$, is lower than that of the first system (14), i.e., $^s\theta_{HCo} = 0.0829$. A similar trend is exhibited by $^s\theta_{NaNi} = 0.06795$ obtained in the present work, as it is lower than the $^s\theta_{HNi} = 0.0895$ value (14). This may be due to the increase in ionic size as we go from H^+ to Na^+. The same decreasing trend is observed as well in the case of the ternary interaction parameters (ψ).

The common $^s\theta$ and ψ values ($^s\theta = 0.06795$; $\psi = -0.03026$) were used to calculate the osmotic coefficients of the mixture at various compositions using the Pitzer equations (15). Osmotic coefficients of the mixture at 25°C are listed in Table 4. These osmotic coefficients, up to $I = 3.0$, are in good agreement with the values reported by Filippov *et al.* (8), with an RMSD of 1.36×10^{-2}.

Then, the excess free energies of the mixture were calculated using the equation

$$\Delta_m G^E = -2.3026 y_A y_B RTI^2(\alpha_{AB} + \alpha_{BA})$$

where all the symbols have their usual significance (16). These excess free energies of mixing are listed in Table 5 at the ionic strengths studied.

Experimental

Analytical grade NaCl (GR:S Merck) and $NiCl_2$ (GR:S Merck) were used without further purification. All solutions were prepared by

[1]Author to whom correspondence may be addressed.

TABLE 1. Mean activity coefficients of NaCl in the NaCl–$NiCl_2$–H_2O system

I = 0.5		I = 1.0		I = 2.0		I = 3.0	
y_B	$-\log \gamma_\pm$	y_B	$-\log \gamma_\pm$	y_B	$-\log \gamma_\pm$	y_B	$-\log \gamma_\pm$
			T = 25°C				
0.0000	0.1667	0.0000	0.1823	0.0000	0.1749	0.0000	0.1466
0.0979	0.1659	0.1022	0.1808	0.1031	0.1733	0.0957	0.1467
0.1784	0.1653	0.1854	0.1799	0.1870	0.1721	0.1747	0.1470
0.2457	0.1649	0.2545	0.1792	0.2565	0.1712	0.2410	0.1471
0.3028	0.1646	0.3128	0.1787	0.3151	0.1705	0.2974	0.1472
0.3518	0.1643	0.3626	0.1783	0.3651	0.1699	0.3461	0.1474
0.3944	0.1641	0.4057	0.1779	0.4083	0.1695	0.3884	0.1476
0.4318	0.1639	0.4434	0.1777	0.4460	0.1691	0.4256	0.1478
0.4648	0.1637	0.4765	0.1775	0.4792	0.1688	0.4585	0.1479
0.4942	0.1636	0.5059	0.1773	0.5086	0.1686	0.4878	0.1481
0.4898	0.1636	0.4976	0.1774	0.4828	0.1688	0.4811	0.1480
0.5192	0.1635	0.5270	0.1772	0.5122	0.1685	0.5105	0.1482
0.5524	0.1634	0.5601	0.1771	0.5455	0.1683	0.5438	0.1484
0.5901	0.1633	0.5977	0.1770	0.5834	0.1680	0.5817	0.1486
0.6334	0.1631	0.6406	0.1768	0.6269	0.1677	0.6253	0.1488
0.6835	0.1630	0.6902	0.1767	0.6775	0.1674	0.6760	0.1492
0.7422	0.1629	0.7482	0.1767	0.7369	0.1671	0.7355	0.1496
0.8120	0.1628	0.8167	0.1767	0.8077	0.1668	0.8067	0.1501
0.8963	0.1627	0.8991	0.1768	0.8936	0.1666	0.8930	0.1508
			T = 35°C				
0.0000	0.1672	0.0000	0.1811	0.0000	0.1709	0.0000	0.1409
0.0914	0.1624	0.0916	0.1778	0.1251	0.1654	0.0941	0.1414
0.1675	0.1580	0.1678	0.1752	0.2223	0.1651	0.1721	0.1405
0.2319	0.1562	0.2322	0.1733	0.3001	0.1606	0.2377	0.1422
0.2870	0.1524	0.2873	0.1714	0.3638	0.1593	0.2936	0.1406
0.3347	0.1503	0.3351	0.1686	0.4168	0.1605	0.3419	0.1406
0.3765	0.1481	0.3768	0.1689	0.4617	0.1557	0.4211	0.1417
0.4133	0.1479	0.4464	0.1656	0.5002	0.1527	0.4540	0.1409
0.4460	0.1452	0.4756	0.1651	0.5335	0.1512	0.5096	0.1409
0.4752	0.1426	0.5020	0.1654	0.5884	0.1518	0.4645	0.1406
0.5016	0.1452	0.5126	0.1622	0.6317	0.1525	0.5534	0.1423
0.5283	0.1390	0.5419	0.1623	0.6668	0.1479	0.6343	0.1408
0.5575	0.1386	0.5748	0.1623	0.6958	0.1500	0.6844	0.1433
0.5901	0.1382	0.6120	0.1604	0.7201	0.1460	0.7430	0.1419
0.6268	0.1356	0.6543	0.1593	0.7409	0.1437	0.8126	0.1396
0.6684	0.1342	0.7029	0.1587	0.8000	0.1460	0.8966	0.1402
0.7159	0.1324	0.7593	0.1560	0.9000	0.1430	0.9455	0.1424
0.8344	0.1264	0.8256	0.1524				
0.9097	0.1235	0.9044	0.1511				
			T = 45°C				
0.0000	0.1686	0.0000	0.1816	0.0000	0.1699	0.0000	0.1389
0.0952	0.1674	0.0907	0.1783	0.0918	0.1676	0.1164	0.1432
0.1739	0.1656	0.1662	0.1752	0.1682	0.1662	0.2085	0.1360
0.2400	0.1637	0.2302	0.1725	0.2327	0.1644	0.2832	0.1404
0.2963	0.1642	0.2851	0.1700	0.2880	0.1632	0.3450	0.1396
0.3348	0.1625	0.3326	0.1682	0.3358	0.1620	0.3970	0.1412
0.3871	0.1618	0.3743	0.1672	0.3776	0.1604	0.4414	0.1447
0.4242	0.1616	0.4110	0.1653	0.4144	0.1600	0.4796	0.1418
0.4571	0.1612	0.4437	0.1633	0.4472	0.1576	0.5130	0.1404
0.4865	0.1612	0.4729	0.1634	0.4764	0.1592	0.5684	0.1411
0.5224	0.1595	0.4887	0.1615	0.4996	0.1568	0.6124	0.1455
0.5517	0.1590	0.5151	0.1596	0.5290	0.1566	0.6483	0.1449
0.6213	0.1592	0.5444	0.1591	0.5621	0.1572	0.6781	0.1467
0.6632	0.1584	0.5773	0.1578	0.5997	0.1539	0.7033	0.1426
0.7111	0.1578	0.6144	0.1565	0.6425	0.1552	0.7248	0.1480
0.8311	0.1552	0.6566	0.1544	0.6920	0.1534	0.8000	0.1465
		0.7050	0.1523	0.8180	0.1503	0.9000	0.1470
		0.7611	0.1504				
		0.8500	0.1470				
		0.9000	0.1450				

Can. J. Chem. Downloaded from www.nrcresearchpress.com by 91.144.44.67 on 09/07/12
For personal use only.

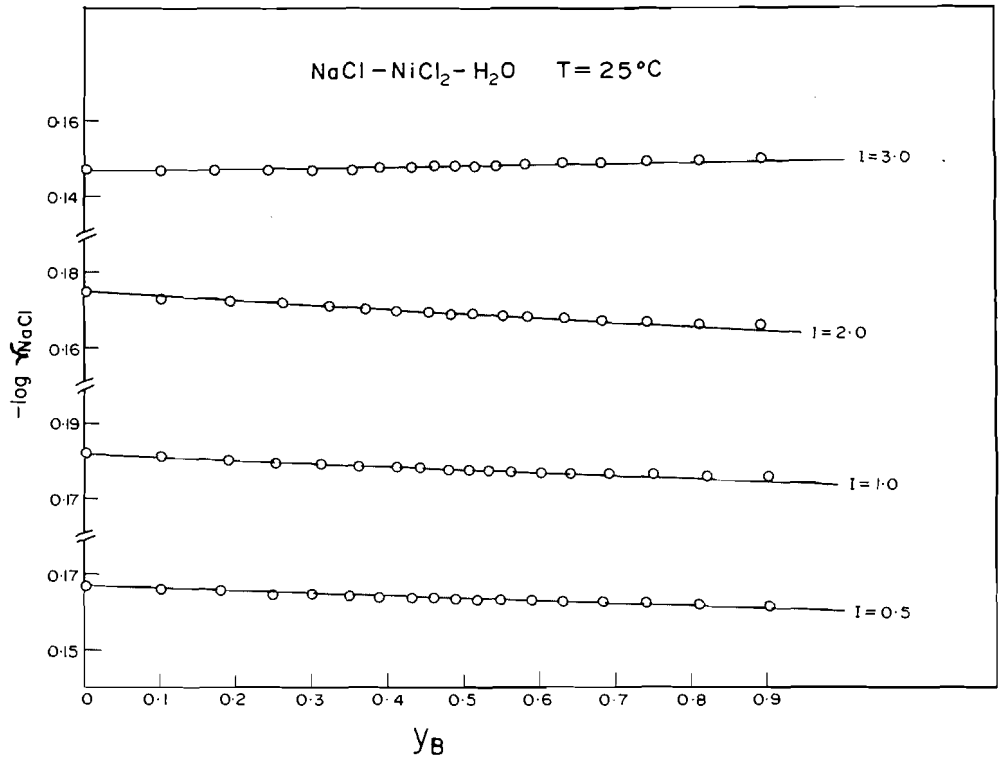

FIG. 1. Variation of $-\log \gamma_{NaCl}$ with y_B.

TABLE 2. Harned coefficients of NaCl in the $NaCl–NiCl_2–H_2O$ system

I	$\log \gamma_{NaCl}$	$\alpha_{AB} \times 10^2$	RMSD $\times 10^3$
		25°C	
0.5	−0.1667	−0.5872	0.4385
1.0	−0.1822	−0.9071	0.9268
2.0	−0.1749	−1.1879	0.7846
3.0	−0.1466	0.3361	0.4153
		35°C	
0.5	−0.1672	−4.950	1.063
1.0	−0.1811	−3.345	0.945
2.0	−0.1709	−3.265	1.731
3.0	−0.1409	0.066	0.9465
		45°C	
0.5	−0.1686	−1.679	0.8987
1.0	−0.1816	−4.070	0.4804
2.0	−0.1699	−2.431	0.7326
3.0	−0.1389	0.7982	2.267

TABLE 3. ${}^s\theta$ and ψ values obtained from the activity coefficient data of NaCl in the $NaCl–NiCl_2–H_2O$ system at 25°C

I	${}^s\theta_{NaNi}$	ψ_{NaNiCl}	RMSD $\times 10^5$	RMSD with common ${}^s\theta = 0.06795$, $\psi = -0.03026$
0.5	0.0640	0.0233	2.542	4.40×10^{-4}
1.0	0.0249	0.0545	2.727	8.60×10^{-4}
2.0	0.0344	0.0112	2.177	2.64×10^{-3}
3.0	0.0054	0.0015	2.803	3.08×10^{-3}

TABLE 4. Osmotic coefficients of the mixture $NaCl–NiCl_2–H_2O$ at 25°C

	Osmotic coefficient			
y_{NaCl}	$I = 0.5$	$I = 1.0$	$I = 2.0$	$I = 3.0$
0	0.8607	0.8907	0.9770	1.081
0.1	0.8732	0.9013	0.9805	1.074
0.2	0.8833	0.9095	0.9825	1.068
0.3	0.8915	0.9160	0.9837	1.062
0.4	0.8984	0.9212	0.9841	1.056
0.5	0.9041	0.9253	0.9842	1.052
0.6	0.9089	0.9286	0.9841	1.048
0.7	0.9130	0.9312	0.9839	1.046
0.8	0.9165	0.9333	0.9837	1.044
0.9	0.9194	0.9350	0.9837	1.044
1.0	0.9220	0.9363	0.9839	1.045

weight using double distilled conductance water. The NaCl and $NiCl_2$ solutions were standardized by volumetric titration against $AgNO_3$ using a potentiometer. All the stock solutions were prepared and standardized with utmost care to maintain an accuracy of five significant figures (±0.01%) in the molalities. Also, all titrations and dilutions were made using weight burettes.

The cell (17) consisted of a Na-ion selective electrode (Elico: India) of the glass membrane type and a silver – silver chloride electrode (18). These electrodes were immersed in a double walled glass vessel whose temperature was maintained constant by circulation of thermostated water. The temperature was maintained constant within ±0.01°C. The cell arrangement was

Na-ion selective electrode (glass membrane)	NaCl (m_A) + $NiCl_2$ (m_B)	Ag/AgCl electrode

Can. J. Chem. Downloaded from www.nrcresearchpress.com by 91.144.44.67 on 09/07/12
For personal use only.

TABLE 5. Excess free energies of mixing for the $NaCl–NiCl_2–H_2O$ system at 25°C

	$\Delta_m G^E$ (J kg^{-1} of water)			
y_{NaCl}	$I = 0.5$	$I = 1.0$	$I = 2.0$	$I = 3.0$
0.1	0.9327	11.07	82.96	146.1
0.2	1.658	19.68	147.5	259.7
0.3	2.176	25.83	193.6	340.9
0.4	2.487	29.52	221.2	389.6
0.5	2.591	30.75	230.5	405.8

The potentials were measured with a Keithly $5\frac{1}{2}$ digit electrometer/multimeter after processing the signals with a unit gain amplifier of input impedance $\simeq 10^{12}$ Ω. The accuracy of the EMF measurements was ±0.01 mV.

The EMF values of the Na-ion selective electrode vs. the Ag/AgCl electrode in $NaCl–NiCl_2$ mixtures are given by the relation

$$[2] \quad E = E_0 + k \log (a_{Na} a_{Cl} + K a_{Ni}^{1/2} a_{Cl})$$

where k is the Nernst slope and K is the selectivity coefficient of Na electrode for Ni^{2+} ions.

In pure NaCl solution, i.e., where $a_{Ni} = 0$,

$$[3] \quad E_{NaCl} = E_0 + k \log a_{Na} a_{Cl}$$

In pure $NiCl_2$ solutions, $a_{Na} = 0$ and, therefore,

$$[4] \quad E_{NiCl_2} = E_0 + k \log K a_{Ni}^{1/2} a_{Cl}$$

or

$$[5] \quad K^2 = (1/a_{NiCl_2}^3) \exp [4.606(E_{NiCl_2} - E_0)/k]$$

At each ionic strength in the first set, the EMFs of the aqueous NaCl solutions (E_{NaCl}) were measured and these EMFs were fitted to eq. [3] using the least-squares procedure to evaluate the E_0 and k values. The activity coefficients of pure NaCl are taken from NBS data (19). In the second set, the EMFs of the pure $NiCl_2$ solutions (E_{NiCl_2}) were measured and substituted in eq. [5] to estimate selectivity coefficient (K) values. The activity coefficients of pure $NiCl_2$ solution were taken from the work of Rard (6). These selectivity coefficient (K) values at all the ionic strengths studied were less than 1×10^{-4}. Therefore the second term within the parentheses on the right hand side of eq. [2] was neglected. The third set consisted of the EMF measurements ($E_{NaCl-NiCl_2}$) of the aqueous mixtures of NaCl and $NiCl_2$ solutions. Then, substituting these $E_{NaCl-NiCl_2}$ values in the following equations,

$$[6] \quad E_{NaCl-NiCl_2} = E_0 + k \log \{m_A (m_A + 2m_B) \gamma_\pm^2\}$$

or

$$[7] \quad \gamma_\pm^2 = (1/m_{Na} m_{Cl}) \exp \{2.303(E_{NaCl-NiCl_2} - E_0)/k\}$$

the activity coefficients of NaCl in aqueous $NaCl–NiCl_2$ mixtures were calculated. In eq. [6], the m_A and m_B represent the molalities of NaCl and $NiCl_2$ respectively in the mixture $NaCl–NiCl_2–H_2O$. Further experimental details were given earlier (17).

Acknowledgements

The authors wish to thank Prof. T. Navaneeth Rao, Vice-Chancellor, Osmania University, Hyderabad, and Prof. B. Subrahmanyam, Head, Department of Chemistry, for constant encouragement and many helpful discussions. Ch.V. is grateful to C.S.I.R. for the award of a Science Research Fellowship.

1. R. D. LANIER. J. Phys. Chem. **69**, 3992 (1965).
2. P. G. CHRISTENSON. J. Chem. Eng. Data, **18**, 286 (1973).
3. D. R. JR. WHITE, R. A. ROBINSON, and R. G. BATES. J. Solution Chem. **9**, 457 (1980).
4. K. H. KHOO. J. Chem. Soc. Faraday Trans. 1, **82**, 1 (1986).
5. J. ANANTHASWAMY and G. ATKINSON. J. Chem. Eng. Data, **30**, 120 (1985).
6. J. A. RARD. J. Chem. Eng. Data, **32**, 334 (1987).
7. G. PERRON, A. ROUX, and J. E. DESNOYERS. Can. J. Chem. **59**, 3049 (1981).
8. V. K. FILIPPOV, N. A. CHARYKOV, and YU. A. FEDOROV. Russ. J. Inorg. Chem. **31**, 1071 (1986).
9. CH. VENKATESWARLU and J. ANANTHASWAMY. Indian J. Chem. **27A**, 768 (1988).
10. H. S. HARNED and B. B. OWEN. The physical chemistry of electrolyte solutions. 3rd ed. Reinhold, New York. 1958. Chap. 14.
11. K. S. PITZER. J. Phys. Chem. **77**, 268 (1973).
12. K. S. PITZER and J. J. KIM. J. Am. Chem. Soc. **96**, 5701 (1974).
13. J. ANANTHASWAMY and G. ATKINSON. J. Chem. Eng. Data, **29**, 81 (1984).
14. H. T. KIM and W. J. FREDERICK. J. Chem. Eng. Data, **33**, 278 (1988).
15. K. S. PITZER. J. Solution Chem. **4**, 249 (1975).
16. A. MUKHERJEE and M. SENGUPTA. Electrochim. Acta, **26**, 1569 (1981).
17. J. ANANTHASWAMY and G. ATKINSON. J. Solution Chem. **11**, 509 (1982).
18. D. J. IVES and G. J. JANZ. Reference electrodes. Academic Press, New York. 1961. Chap. 4.
19. W. J. HAMER and YUNG CHI WU. J. Phys. Chem. Ref. Data, **1**, 1047 (1972).

Can. J. Chem. Downloaded from www.nrcresearchpress.com by 91.144.44.67 on 09/07/12
For personal use only.

Structure of 2-methoxy-3,5-dinitropyridine

G. PUNTE[1] AND B. E. RIVERO[2]

Depto. de Física, Facultad de Ciencias Exactas, UNLP, C.C.67, (1990) La Plata, Argentina

AND

S. CERDEIRA AND N. S. NUDELMAN[1]

Depto. de Química Orgánica Facultad de Ciencias Exactas y Naturales, UBA, Pabellón II, Ciudad Universitaria, (1428) Buenos Aires, Argentina

Received March 22, 1989

G. PUNTE, B. E. RIVERO, S. CERDEIRA, and N. S. NUDELMAN. Can. J. Chem. **68**, 298 (1990).

2-Methoxy-3,5-dinitropyridine, $C_6N_3O_5H_5$, crystallizes in the monoclinic system, space group $P2_1/n$, with cell parameters a = 7.496(5), b = 18.38(1), c = 6.068(2) Å, β = 77.18(4)°, V = 815(1) Å^3, and four molecules per unit cell. Its structure was solved by direct methods and refined by least-squares procedures to a final R = 4.99%, R_w = 5.42%, for 753 observed independent reflections. The molecule is not planar, a rotation of the methoxy and 3-nitro groups out of the pyridine ring (7° and 16°, respectively) is observed. The methoxy group is located *syn* to the ring nitrogen atom to avoid repulsion with the 3-NO_2 group and adopts a geometry different from the mean reported in the literature for methoxyaromatic groups. Geometrical parameters suggested by Domenicano and Murray-Rust and Norrestam and Schepper are used to analyze substituent effects on the pyridine shape and the possible causes of non-additivity of substituent effects are discussed. The relation of molecular conformation with reactivity of the title compound with amines is examined.

Key words: methoxy pyridine, substituted nitropyridines, crystal structure.

G. PUNTE, B. E. RIVERO, S. CERDEIRA et N. S. NUDELMAN. Can. J. Chem. **68**, 298 (1990).

Les cristaux de la 2-méthoxy-3,5-dinitropyridine, $C_6N_3O_5H_5$, sont monocliniques et ils appartiennent au groupe d'espace $P2_1/n$, avec a = 7,496(5), b = 18,38(1) et c = 6,068(2) Å, β = 77,18(4)°, V = 815(1) Å^8 et Z = 4. On a résolu la structure par des méthodes directes et on l'a affinée par la méthode des moindres carrés jusqu'à une valeur finale de R = 0,0499 et R_w = 0,0542 pour 753 réflexions observées d'une façon indépendante. La molécule n'est pas plane; on a observé que les groupements méthoxy et 3-nitro sont déplacés hors du plan du noyau pyridine par 7 et 16° respectivement. Afin d'eviter une répulsion de la part du groupement 3-nitro, le groupement méthoxy est *syn* par rapport à l'atome d'azote du cycle et sa géométrie est différente de celle généralement rapportée dans la littérature pour les groupements méthoxyaromatiques. On a utilisé les paramètres géométriques suggérés par Domenicano et Murray-Rust et par Norrestam et Schepper pour analyser l'effet des substituants sur la forme de la pyridine et on discute des causes qui pourraient expliquer la non-additivité des effets de substituant. On a aussi examiné la relation entre la conformation moleculaire et la réactivité des amines avec le composé mentionné dans le titre.

Mots clés : méthoxypyridine, nitropyridine, conformation moleculaire.

[Traduit par la revue]

Introduction

Several X-ray single crystal (1, 2–5), quantum-chemical (1, 6, 7), kinetic (7), and spectroscopic (8–10) studies have been performed on methoxyaromatic compounds to establish the relationship between either reactivity or pharmacological activity and the orientation of methoxy group with respect to the aromatic ring in solid state, gas phase, and solution. Some of these studies (1, 4, 5, 10) have shown that *ortho* disubstitution has a strong effect on methoxy orientation.

In fact, in methoxyphenyl systems with no *ortho* substitution, the favoured conformation for the methoxy group is coplanar with the ring (1, 6, 11) and *ortho* monosubstituted anisoles (1, 5) and veratroles (4) in solid state present the methoxy group only slightly twisted out of the benzene ring; by contrary, in 2,6-disubstituted anisoles the methoxy group tends to be almost perpendicular to the aromatic ring (4, 5, 7, 10). Nuclear magnetic resonance studies of 2,6-disubstituted methoxybenzenes (8) have indicated that for these compounds in solution, the perpendicular conformation tends to be preferred. X-ray single crystal study of 2,6-dinitroanisol (5) has shown, as expected, that the influence of two nitro groups adjacent to the methoxy group forces it out of the benzene ring. Contrary to anisoles, structural studies on methoxypyridines are scarce. Therefore we report here an X-ray single crystal examination of 2-methoxy-3,5-dinitropyridine to add to the understanding of the effect of di-*ortho* substitution on methoxyaromatic geometry in the pyridine series.

Experimental

The title compound was synethesized from 2-chloro-3,5-dinitropyridine by treatment with 0.39 *M* sodium methoxide in anhydrous methanol. After 2 h refluxing, the solvent was distilled at reduced pressure, the orange residue was treated with a small amount of distilled water, and white crystals appeared. They were crystallized from anhydrous methanol until constant mp 89–91°, Talik and Plazck reported mp 88–89° (12). The product was recrystallized by slow evaporation from methanol. It must be mentioned that it was rather difficult to get crystals of acceptable quality for intensity collection. Preliminary photographic studies using CuK_α radiation showed the crystals presented either short order arrangements or thermal disorder since intensities decayed quite quickly with increased θ. Besides, the crystals proved to react with several types of adhesives, the reaction being apparently enhanced by X-ray exposure. Therefore, after several tries a needle-shaped crystal of approximate dimensions 0.15 × 0.20 × 0.5 mm, fixed with water soluble plastic glue, was used for data collection. The measurements were done at T = 296 K in an automatic four-circle Huber diffractometer with graphite-monochromated MoK_α radiation (λ = 0.71073 Å), $\mu(MoK_\alpha)$ = 1.38 cm^{-1}. Calculated density D_X = 1.622 g cm^{-3}. Lattice parameters were obtained from the setting angles of twenty reflections in the range $10° < 2\theta < 28°$. Systematic absences, $h0l$, $h + l$ odd and $0k0$, k odd, indicated the space group $P2_1/n$, unique axis b.

[1]Member of Carrera del Investigador Científico, CONICET, Argentina.

[2]Member of Carrera del Investigador Científico, CICPBA, Argentina.

Can. J. Chem. Downloaded from www.nrcresearchpress.com by 91.144.44.67 on 09/07/12
For personal use only.

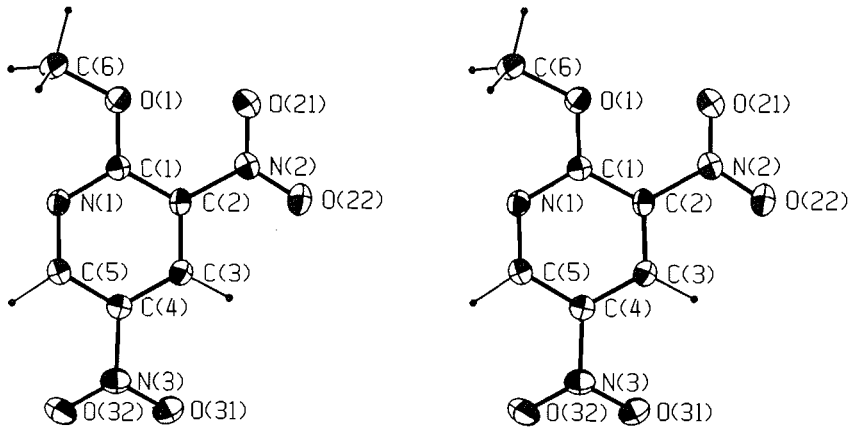

FIG. 1. Stereoscopic ORTEP drawing of the molecule, thermal ellipsoids 20%, showing non-hydrogen atoms labelling.

TABLE 1. Fractional positional parameters and equivalent isotropic thermal parameters (Å^2), esd's in parentheses

Atom	x/a	y/b	z/c	B_{eq}*
N(1)	0.1000(4)	0.0738(2)	0.7814(6)	4.8
N(2)	0.3571(5)	0.2349(2)	0.4989(8)	5.6
N(3)	0.4472(6)	0.0835(2)	1.1248(7)	5.8
O(1)	0.0492(4)	0.1449(1)	0.4927(5)	5.5
O(21)	0.2992(5)	0.2399(2)	0.3276(7)	7.7
O(22)	0.4599(6)	0.2783(2)	0.5516(7)	9.4
O(31)	0.5844(5)	0.1187(2)	1.1302(7)	8.4
O(32)	0.3925(4)	0.0340(2)	1.2562(6)	7.2
C(1)	0.1469(5)	0.1298(2)	0.6414(8)	4.3
C(2)	0.2997(5)	0.1736(2)	0.6524(7)	4.4
C(3)	0.3986(5)	0.1603(2)	0.8117(7)	4.6
C(4)	0.3453(5)	0.1023(2)	0.9551(7)	4.5
C(5)	0.1976(5)	0.0600(2)	0.9335(8)	4.8
C(6)	−0.1184(5)	0.1047(3)	0.5030(9)	6.2

*Defined according to Hamilton (16).

X-ray data were collected in the ω step scan mode, with scan width 1°, min–max scan speed 0.77–4.62° min^{-1}, to $2\theta_{max} = 50°$, index range: h −8, 8; k 0, 21; l 0,7. Three standard reflections (111, $\bar{2}82$, $27\bar{2}$) measured each 90 min showed only random intensity variations, max: 4%. Lorentz and polarization corrections were applied. Isotropic secondary extinction correction of the form $F' = F(1 - CF^2 \sin\theta)$ was applied on F_c, refined C value: 8.5×10^{-3}. No absorption correction was done. $F(000)$ value: 408. Of the 1952 measured intensities (1431 unique, $R_{int} = 0.034$) 753 were considered observed using the criterion: $I > 2\sigma(I)$, where $\sigma(I)$ is the standard deviation based on counting statistics.

The structure was solved using direct methods, Multan-80 (13). From the partial model obtained all non-hydrogen atoms were located and refined from alternated difference Fourier syntheses and isotropic least-squares refinement cycles. After refinement by full-matrix least-squares, based on F's and employing anisotropic thermal parameters, the hydrogens were stereochemically positioned (with C—H = 1.08 Å, ideal tetrahedral H—C—C and H—C—H angles for Me group and ideal trigonal H—C—C and H—C—H for CH groups) and refined, isotropically, with their positions riding on the bonded atoms; an overall temperature factor for hydrogens of the methoxy group was refined.

The final refinement, with 131 parameters, converged to $R = 0.0499$, $R_w = 0.0542$, weighting scheme: $w = 1/[\sigma^2(F_0) + 0.00035F_0^2]$, maximum shift/esd = 2×10^{-3}. Minimum and maximum values of the residual electron density were −0.23 and 0.19 e Å^{-3}, respectively. Scattering factors for H and scattering factors and anomalous dispersion corrections for O, C, and N were taken from SHELX76 (14). Calculations were carried out on a MicroVAXII system using the programs MULTAN80 (13), SHELX76 (14), and ORTEP (15).

Fractional atomic parameters with equivalent isotropic thermal parameters for the non-hydrogen atoms are given in Table 1.[3] The numbering scheme is shown in a stereoscopic view of the molecule, Fig. 1. Table 2 shows intramolecular bond lengths and angles.

Discussion

As can be observed from Fig. 1 the main feature of the molecular conformation is the location of the OMe group *syn* to the ring nitrogen, N(1), to avoid repulsion with the 3-nitro group. A methoxy group in a position *anti* to the 2-nitro group has been reported for 2,4-dinitroanisole from X-ray single crystal data (5). ^{1}H and ^{13}C nmr spectra of the title compound in $CDCl_3$ solution (9) suggest that the methoxy group may adopt the same conformation in solution. Nuclear magnetic resonance spectra of 2-methoxy-3-nitropyridine in solution would also indicate the same conformation (9, 10).

The pyridine ring is planar within 3σ[3] and the sum of the internal angles is 720°. The methoxy–oxygen and the nitrogens N(2) and N(3) from the 3-nitro and 5-nitro groups are bent out of the mean ring plane ($\Delta = -0.045(3)$, 0.025(4), and 0.018(4) Å, respectively).

The dihedral angles of the methoxy and nitro groups with the aromatic ring were determined from their least-squares planes.[3] The 5-nitro group makes a small angle with the ring, 3.9°, whereas the methoxy and 3-nitro groups are twisted out of the mean ring plane making angles of 7.4 and 15.6°, respectively.

The effect of the different substituents on the pyridine system can be analyzed from the comparison of the geometry adopted by the ring in the title compound (**I**) with that observed in pyridine from microwave spectroscopy (**II***a*) (17) and from single crystal X-ray study (**II***b*) (18) and with single-crystal X-ray data reported by Destro, Pilati, and Simonetta (19) for 3,5-dinitropyridine (**III**), see Table 3.

It is well known that substitution causes redistribution of the electrons of aromatic rings and thus affects both intramolecular angles and bonds. A systematic study of the effects of different substituents on the benzene ring have been performed by Domenicano and Murray-Rust (DMR) (20) and by Norrestand and Schepper (NS) (21). These last authors have studied heterocyc-

[3]List of structure factors, H-atoms parameters, anisotropic thermal parameters, and best least-squares planes may be purchased from the Depository of Unpublished Data, CISTI, National Research Council of Canada, Ottawa, Ont., Canada. K1A 0S2.

Can. J. Chem. Downloaded from www.nrcresearchpress.com by 91.144.44.67 on 09/07/12
For personal use only.

Can. J. Chem. Downloaded from www.nrcresearchpress.com by 91.144.44.67 on 09/07/12
For personal use only.

TABLE 2. Bond distances (Å) and angles (deg) within the molecule, esd's in parentheses

Bond	Distance (Å)
N(1)—C(1)	1.331(6)
N(1)—C(5)	1.323(5)
N(2)—O(21)	1.216(6)
N(2)—O(22)	1.201(6)
N(2)—C(2)	1.464(6)
N(3)—O(31)	1.222(6)
N(3)—O(32)	1.219(5)
N(3)—C(4)	1.453(6)
O(1)—C(1)	1.312(5)
O(1)—C(6)	1.447(5)
C(1)—C(2)	1.414(5)
C(2)—C(3)	1.364(6)
C(3)—C(4)	1.378(6)
C(4)—C(5)	1.383(5)

Bonds	Angle (deg)
C(1)—N(1)—C(5)	119.0(4)
O(21)—N(2)—O(22)	123.3(4)
O(21)—N(2)—C(2)	119.5(4)
O(22)—N(2)—C(2)	117.2(4)
O(31)—N(3)—O(32)	122.7(4)
O(31)—N(3)—C(4)	118.1(4)
O(32)—N(3)—C(4)	119.2(4)
C(1)—O(1)—C(6)	118.3(3)
N(1)—C(1)—O(1)	119.6(4)
N(1)—C(1)—C(2)	120.8(4)
O(1)—C(1)—C(2)	119.6(4)
N(2)—C(2)—C(1)	122.3(4)
N(2)—C(2)—C(3)	117.3(4)
C(1)—C(2)—C(3)	120.3(4)
C(2)—C(3)—C(4)	117.3(4)
N(3)—C(4)—C(3)	120.5(4)
N(3)—C(4)—C(5)	119.4(4)
C(3)—C(4)—C(5)	120.1(4)
N(1)—C(5)—C(4)	122.5(4)

lic six-member rings as well. Therefore we have used the angular parameters of NS for the hetero N and NO_2 groups and those proposed by DMR for OMe in order to examine the data presented in Table 3. The predicted values are shown in Table 4.

The additivity of the substituent effects on valence angles in the ring was studied analyzing $\Sigma|\theta_c - \theta_o|_i$ for the three compounds. In the cases of compounds **II***a*, **II***b*, and **III** the value of the summations (1.59, 1.07, and 1.69°, respectively) indicate that additivity is held within experimental errors. Inclusion of the OMe substituent, however, seems to modify the ring geometry in a way that it is not accounted for by the predictions of the NS and DMR models. In fact, both models predict stronger angular deformations than the actually observed ones. The methoxy geometry found in **I** is different from the mean one reported by various authors based on surveys of methoxyaromatic groups (1, 11). Besides, conflicting interactions between the methoxy and 3-nitro groups are observed. Therefore, it can be assumed that the OMe parameters proposed by DMS may be unsuitable for describing the OMe group effect on ring geometry in the title compound. This would explain the observed non additivity of the effects of the substituents ($\Sigma|\theta_c - \theta_o|_i = 7.1°$).

The examination of the methoxy geometry in the title compound shows that the C(1)—O(1) distance, 1.312(5) Å, is

TABLE 3. Geometries adopted by pyridine ring. in **I**, **II**, and **III**, bond angles in deg, bond lengths in Å, and esd's in parentheses

	Angle (deg)			
Bonds	**I***	**II***a*†	**II***b*‡	**III**§
C(5)—N(1)—C(1)	119.0(4)	116.83	116.6(2)	117.4(2)
N(1)—C(1)—C(2)	120.8(4)	123.88	123.8(5)	122.2(2)
C(1)—C(2)—C(3)	120.3(4)	118.53	118.6(1)	121.4(2)
C(2)—C(3)—C(4)	117.3(4)	118.33	118.8(2)	115.8(2)
C(3)—C(4)—C(5)	120.1(5)	118.53	118.5(2)	121.2(2)
C(4)—C(5)—N(1)	122.5(4)	123.88	123.5(2)	122.2(2)
	Length (Å)			
Bond	**I***	**II***a*†	**II***b*‡	**III**§
N(1)—C(1)	1.331(6)	1.3402	1.337(1)	1.327(4)
C(1)—C(2)	1.414(5)	1.3944	1.382(2)	1.373(4)
C(2)—C(3)	1.364(6)	1.3945	1.376(7)	1.361(3)
C(3)—C(4)	1.378(6)	1.3945	1.379(3)	1.370(3)
C(4)—C(5)	1.383(5)	1.3944	1.379(7)	1.374(4)
C(5)—N(1)	1.323(5)	1.3402	1.334(3)	1.330(3)

*This work.
†Pyridine. Microwave data (17).
‡Pyridine. X-ray single crystal data. Mean value from the four crystallographically inequivalent molecules (18).
§3,5-Dinitropyridine. X-ray single crystal data (19).

TABLE 4. Predicted bond angles (deg) from NS model (21), angle parameters for OMe group taken from DMR (20)

	Angle (deg)		
Bonds	**I***	**II**†	**III**‡
C(5)—N(1)—C(1)	116.6(2)	117.2(1)	117.2(1)
N(1)—C(1)—C(2)	122.6(5)	123.5(1)	122.4(3)
C(1)—C(2)—C(3)	120.9(3)	118.5(1)	121.4(2)
C(2)—C(3)—C(4)	116.2(4)	118.8(1)	115.1(3)
C(3)—C(4)—C(5)	120.3(4)	118.5(1)	121.4(2)
C(4)—C(5)—N(1)	123.5(5)	123.5(1)	122.4(3)

*2-Methoxy-3,5-dinitropyridine.
†Pyridine.
‡3,5-Dinitropyridine.

shorter than the mean, 1.37(2) Å (1), that the N(1)—C(1)—O(1) angle, 119.6(4)°, is smaller than the mean, 124(1)° (1), and that the C(2)—C(1)—O(1) angle, 119.6(4)°, is larger than the mean, 115(1)° (1). The shortening of the C(1)—O(1) bond suggests a certain degree of double bond and a strong resonance with the 5-nitro group. This assumption is reinforced by the fact that the dihedral angle between the 5-nitro group and the aromatic ring is smaller than the angle between the 3-nitro group and the aromatic ring as has been described above.

On the other hand, the C(1)—C(2) bond length, 1.414(5) Å, is larger than the mean value for the other four C—C bonds: 1.38(1) Å. Besides, an increase in the exocyclic N(2)—C(2)—C(1) bond angle, 122.3(4)° and a corresponding shrinking of the N(2)—C(2)—C(3) angle, 117.3(4)°, from their expected sp^2 value are observed. These deviations from ideal aromatic ring geometry clearly tend to relieve steric compression.

In spite of these ring deformations and the rotation of 3-nitro group out of the pyridine ring a rather short intramolecular distance involving O(1) and O(21) atoms (d = 2.594(4) Å) is

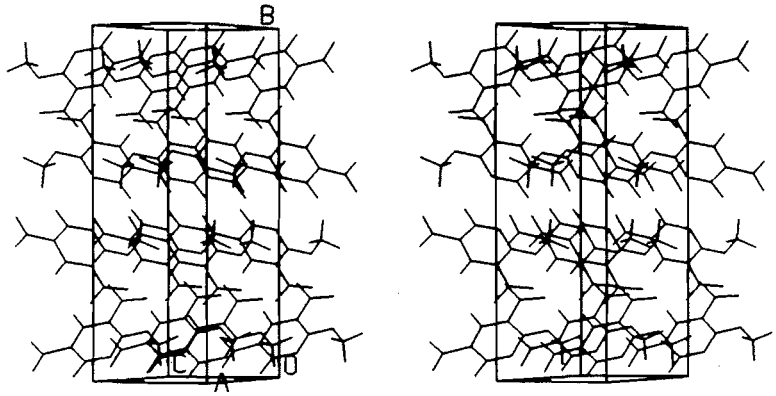

FIG. 2. Stereoscopic view of the molecular packing.

TABLE 5. Angles (deg) between least-squares planes of aromatic ring and OMe and *o*-nitro groups. O(OMe)-O(*o*-nitro) distance, *d* (Å), esd's in parentheses

	o-nitro	OMe	*d*
I	7	16	2.594(45)
V (molecule A)*	32	13	2.637(6)
V (molecule B)	24, −20	5	2.546(9), 2.705(8)
VI (molecule A)†	14	79	2.585(6)
VI (molecule B)	14	72	2.671(5)
VII‡	41	7	2.70(1)
VII§	32	89	2.74(3)

*2,4-Dinitroanisole (5), molecule B present its *o*-nitro group disordered.
†2,6-Dinitroanisole (5).
‡α-Chloro-α-chlorosulfenyl-4-nitro-2,5-dimethoxyphenylacetyl chloride (22).
§Methoxy 2,4,6-trinitrophenetole (23).

observed. We have retrieved data from some mono- and di-nitro *ortho* substituted methoxyaromatic compounds and we have found that though the orientation of methoxy and *o*-nitro groups are quite different in **I**, in 2,4-dinitroanisole (**V**) (5), in 2,6-dinitroanisole (**VI**) (5), in α-chloro-α-chlorosulfenyl-4-nitro-2,5-dimethoxyphenylacetyl chloride (**VII**) (22) and in methoxy-2,4,6-trinitrophenetole (**VIII**) (23), short distances, less than the sum of oxygen van der Waals radii, 1.4 Å (24), between the O of the OMe group and at least one oxygen of the *o*-nitro group are observed, see Table 5.

The manifest interaction between the 2-OMe and the 3-nitro groups mentioned above could be the reason of the observed enhanced reactivity of the 2-methoxy-3-nitropyridine with amines when compared with the 2-methoxy-5-nitropyridine (25) in spite of the greater steric hindrance. In fact, when forming the zwitterionic intermediate the sp^3 configuration that C(1) holds relieves strain in the 3-nitro substituted compound.

A stereoscopic view of crystal packing is shown in Fig. 2. Assuming as van der Waals radii for carbon, nitrogen, oxygen, hydrogen, and methyl group the values 1.6, 1.5, 1.4, 1.2, and 2.0 Å, respectively, according to Pauling (24), only N(1)...H(5) [x, y, 2 − z] and O(31)...H(61) [1 + x, y, 1 + z] distances (2.625(5) and 2.561(7) Å, respectively) would indicate some intermolecular interactions. Packing forces involving O(31) might cause the deviations of N(3) from mean aromatic ring plane in spite of the conjugation effects mentioned above.

Acknowledgments

S.C. is a grateful recipient of a fellowship from the Argentine Research Council (CONICET). The authors thank CONICET and CICPBA for financial support.

1. C. M. ANDERSON III, P. A. KOLLMAN, L. N. DOMELMSMOTH, and K. N. HOUK. J. Am. Chem. Soc. **101**, 2344 (1979) and references therein.
2. C. H. FAERMAN, H. NEGRI, G. PUNTE, A. A. VITALE, and N. S. NUDELMAN. Can. J. Chem. **61**, 2001 (1983).
3. S. C. NYBURG, C. H. FAERMAN, G. PUNTE, B. E. RIVERO, A. A. VITALE, and N. S. NUDELMAN. Can. J. Chem. **63**, 3374 (1985).
4. K. RISSANSEN, J. VALKONEN, and J. KNUNTINEN. Acta Crystallogr. C**43**, 1966 (1987).
5. S. C. NYBURG, C. H. FAERMAN, L. PRASAD, D. R. PALEROS, and N. S. NUDELMAN. Acta Crystallogr. C**43**, 686 (1987).
6. H. KONSCHIN. J. Mol. Struct. **105**, 213 (1983).
7. N. S. NUDELMAN and D. R. PALLEROS. J. Chem. Soc. Perkins Trans. II, 805 (1985).
8. J. N. NUNTIEN and I. O. O. KORHONEN. Org. Magn. Reson. **21**, 38 (1983).
9. N. S. NUDELMAN and S. B. CERDEIRA. Magn. Res. Chem. **24**, 507 (1986).
10. W. J. P. BLONSKI, F. E. HUNSKA, and T. A. WILDMAN. Org. Magn. Reson. **22**, 505 (1984).
11. S. C. NYBURG and C. H. FAERMAN. J. Mol. Struct. **140**, 347 (1986).
12. Z. TALIK and E. PLAZCK. Bull. Acad. Pol. Ser. Sci. Chim. **8**, 219 (1960).
13. P. MAIN, S. J. FISKE, S. E. HULL, L. LESSINGER, G. GERMAIN, and M. M. WOOLFSON. MULTAN80. A system of computer programs for automatic solution of crystal structures from X-ray diffraction data. Univs. of York, England and Louvain-la-Nouve, Belgium. 1980.
14. G. M. SHELDRICK. SHELX76. Program for crystal structure determination, Univ. of Cambridge, England. 1976.
15. C. K. JOHNSON. ORTEP. Report ORNL-3794. Oak Ridge National Laboratory, TN. 1965.
16. W. C. HAMILTON. Acta Crystallogr. **12**, 609 (1959).
17. B. BAK, L. HANSEN-NYGAARD, and J. RASTRRUP-ANDERSEN. J. Mol. Struct. **140**, 347 (1958).
18. D. MOOTZ and H. G. WUSSOW. J. Chem. Phys. **75**, 1517 (1981).
19. R. DESTRO, T. PILATI, and M. SIMONETTA. Acta Crystallogr. B**30**, 2071 (1974).
20. A. DOMENICANO and P. MURRAY-RUST. Tetrahedron Lett. **24**, 2283 (1979).
21. R. NORRESTAM and L. SCHEPPER. Acta Chem. Scand. A**35**, 91 (1981).
22. M. S. SIMON, J. B. ROGERS, W. SAENGER, and J. ZANOS GOUGOUTAS. J. Am. Chem. Soc. **89**, 5838 (1967).
23. C. M. GRAMACCIOLI, R. DESTRO, and M. SIMONETTA. Acta Crystallogr. B**24**, 129 (1968).
24. L. PAULING. The nature of the chemical bond 3rd. ed. Cornell Univ. Press, Ithaca. 1960.
25. S. CERDEIRA. Diss. Abstr. (UBA), 1 (1986).

Can. J. Chem. Downloaded from www.nrcresearchpress.com by 91.144.44.67 on 09/07/12
For personal use only.

Inert films on electrodes. Electrochemical properties of carbon fibre electrodes modified by α- and β-naphthol electropolymerization

PANTELIS KARABINAS

Laboratory of Physical Chemistry, Aristotelian University of Thessaloniki, 540 06, Thessaloniki, Greece

Received July 13, 1989

PANTELIS KARABINAS. Can. J. Chem. **68**, 302 (1990).

Modification of carbon fibre electrodes has been achieved by electropolymerization of α- and β-naphthols. The formation of the film was followed spectrophotometrically by probing the decrease of the concentration of the corresponding monomer in dilute solutions. The electrochemical behaviour of several depolarizers on the modified electrodes showed that the charge transfer takes place at the electrode–film interface. The film structure can be satisfactorily described by the "pin-hole" model.

Key words: carbon fibres, inert film, electromodification, α-naphthol, β-naphthol.

PANTELIS KARABINAS. Can. J. Chem. **68**, 302 (1990).

On a modifié des électrodes en fibre de charbon en effectuant une électropolymérisation des α- et β-naphthols. On a suivi la formation du film par spectrophotométrie en déterminant l'abaissement de la concentration du monomère correspondant dans des solutions diluées. Le comportement électrochimique de plusieurs dépolarisants sur les électrodes modifiées montre que le transfert de charge se produit à l'interface film-électrode. On peut décrire la structure du film d'une façon satisfaisante à l'aide du modèle du «trou d'aiguille».

Mots clés : fibres de carbon, film inert, électromodification, α-naphthol, β-naphthol.

[Traduit par la revue]

Can. J. Chem. Downloaded from www.nrcresearchpress.com by 91.144.44.67 on 09/07/12
For personal use only.

Introduction

There is much current interest focused on the electrochemical applications of modified electrodes especially in electrocatalysis or passivation of electrodes to corrosion. Films formed by polmerization of radicals obtained during the oxidation of phenol or naphthol derivatives show catalytic or inhibitory behaviour depending on the presence or absence of active redox groups. Moreover, carbon fibres (c.f.) have nowadays been used successfully in numerous fields of technology, mostly as reinforced composites. The permeability and the roughness of a film on c.f. are the major factors that define the quality of the modified fibres as matrix for the attachment of epoxy resins.

Dubois *et al.* proposed the protective coating of metallic surfaces with a polyphenylene oxide film obtained by the electrooxidation of disubstituted phenols from concentrated alkaline aqueous-methanolic solutions (1). The polymerization mechanism suggested the propagation of the film by head-to-tail coupling of the phenate radicals. In recent studies 5-hydroxy-1,4-naphthoquinone and its derivatives have been found to follow the same electropolymerization mechanism on carbon, Pt, and Au electrodes (2–4). The film obtained showed catalytic effect on oxygen reduction due to the presence of the redox quinone group.

Furthermore, the electrosorption of nitro- and nitroso- derivatives of α- and β-naphthol has been studied lately (5, 6). It was found that the irreversible oxidation of the —OH group of 2-nitroso-1-naphthol results in the formation of a film, while in the case of reversible oxidation of 1-nitroso-2-naphthol no modification is observed.

The stability of the polymeric film depends on the substituent, pH and solvent composition. Thus, the polynaphthoquinone film is not stable in alkaline solutions and films bearing nitro- or nitroso- groups are stable only up to the reduction potential of the corresponding groups.

In all of the above cases the surface coverage exceeds a monolayer. Submonolayer coverage has been found for the electrosorption of β-naphthol, performed at a negative potential range where no oxidation of the —OH group occurs. In this case the adsorption increases at less negative potentials and follows the Langmuir adsorption isotherm (7).

Recently, Zinger *et al.* (8) suggested the electropolymerization of hydroxyalkyl-methacrylates and aniline for the improvement of the interlaminar shears strength of the c.f.

In the present paper the electrooxidation and electropolymerization of α- and β-naphthol is studied, since phenol — the parent compound of the monocyclic series — follows mainly dimerization reactions during its electrooxidation (9, 10). Our objective is to verify the electrochemical formation, the stability and the properties of films which have no functional groups attached to highly oriented c.f. electrodes. The amount of naphthol electrosorbed was calculated from its bulk concentration decrease. The permeability of the film in relation to the film thickness is investigated on the basis of the electrochemical behaviour of several reactants with various molecular sizes. The structure of the film is interpreted according to the existing theories.

Experimental

The PAN-based carbon fibres (Celion GY-70) used in this study were product of Celanese Corporation U.S.A.

The fibres were pretreated with ethanol or acetone in a Soxhlet-type apparatus for 2 h, washed with water, and vacuum dried to remove the adhesive resins which were deposited during the production process.

Absorbance values of the electrosorption experiments were measured with a PMQ-3 Zeiss spectrophotometer at 292 nm and 224 nm for α- and β-naphthol, respectively.

Micrographs were taken in the Physics Department using the JEOL-CX electron microscope in the SEM mode.

Cyclic voltammetric measurements were carried out using a conventional set up consisting of a voltage scan generator Wenking VSG 72 (G. Bank), a standard potentiostat Wenking ST 72 (G. Bank) and an X-Y recorder Servogor 733 B.B.C. (Goertz).

Current densities are expressed per mg fibres. All potential values are referred to the aqueous calomel electrode (SCE). A Pt sheet was used as counter electrode. Both the counter and the reference electrodes were separated from the working electrode compartment by glassy diaphragms.

α- and β-Naphthols puriss. p.a. (Fluka) were used after recrystal-

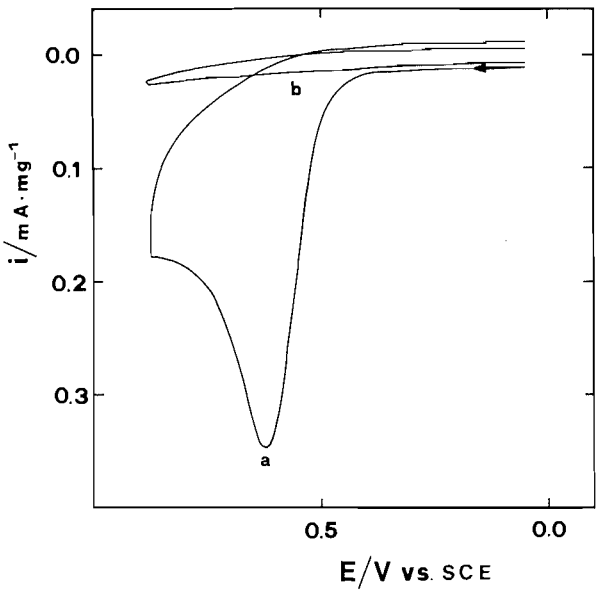

FIG. 1. Cyclic voltammogram of β-naphthol (C = 1 mM, pH = 4) on (a) bare electrode and (b) modified electrode with 1.7 × 10^{-8} mole cm^{-2} (u = 100 mV s^{-1}).

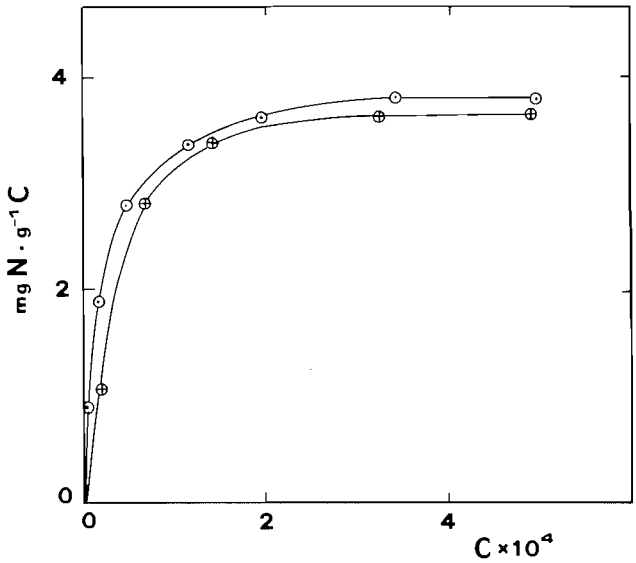

FIG. 2. Concentration dependence of the electrosorbed quantity of (α-) ○ and (β-) ⊕ naphthol (pH = 4).

lization from 80% ethanol. The study was carried out at 25 ± 0.1°C in aqueous 5% methanolic Britton–Robinson buffered solutions (pH = 1–12) prepared with triply distilled water.

Results and discussion

The electrosorption experiments were carried out on large bundles of highly oriented carbon fibres and the applied electrosorption potential covered a wide range of positive values. The concentration decrease, after the adsorption equilibrium, was followed spectrophotometrically. The largest amount of naphthol electrosorbed was observed at the potential where the oxidation of the naphthol at the corresponding pH takes place.

Figure 1 curve a represents the cyclic voltammogram of β-naphthol on carbon fibre electrodes at pH = 4. The i_p value varies linearly with the square root of the potential scan rate, as is expected for diffusion-controlled processes. The E_p is shifted 0.059 V per pH unit towards more negative values up to pH = 9 i.e. for pH < pK (p$K_{\beta\text{-N}}$ = 9.57). This behaviour suggests that a one-electron oxidation takes place, resulting in the formation of the naphthoxy radical. α-Naphthol exhibits exactly the same electrochemical behaviour.

The naphthoxy radical formed on the electrode surface undergoes further reactions, depending on the naphthol concentration. At high concentrations the polymerization through head-to-tail coupling is the predominant process (1–4), while at lower concentrations tail-to-tail dimerization (9, 10) as well as addition of water molecule (10, 11) can also take place.

Controlled potential electrolysis at 180–200 mV more positive than the E_p of the wave of Fig. 1 and simultaneous determination of the bulk concentration decrease showed that the amount of naphthol electropolymerized levels off to a limiting value with increasing electrolysis time. Each limiting value, which is attained at greater electrolysis time as the concentration of naphthol in the solution is decreased, suggests termination of the polymerization. These limiting values, expressed in mg naphthol per g of c.f., obtained from various naphthol concentrations (5×10^{-4}–10^{-6} M) reach a maximum as in Fig. 2. It may also be concluded from Fig. 2 that the

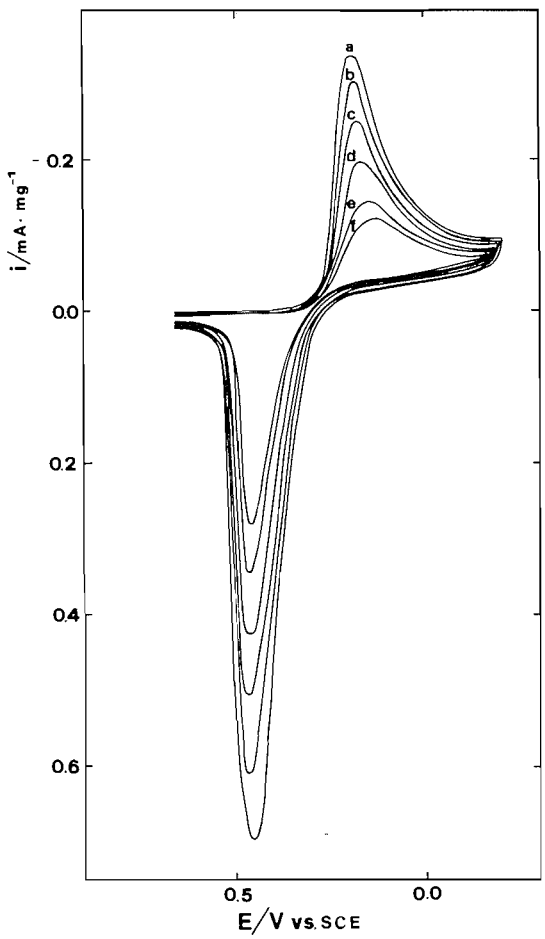

FIG. 3. Cyclic voltammogram of $AgNO_3$ (u = 100 mV s^{-1}, C = 1 mM, pH = 4) on electrodes modified with β-naphthol charged from the following concentrations: (a) without naphthol, (b) 10^{-5} M, (c) 5×10^{-5} M, (d) 10^{-4} M, (e) 2×10^{-4} M, and (f) 5×10^{-4} M.

Can. J. Chem. Downloaded from www.nrcresearchpress.com by 91.144.44.67 on 09/07/12
For personal use only.

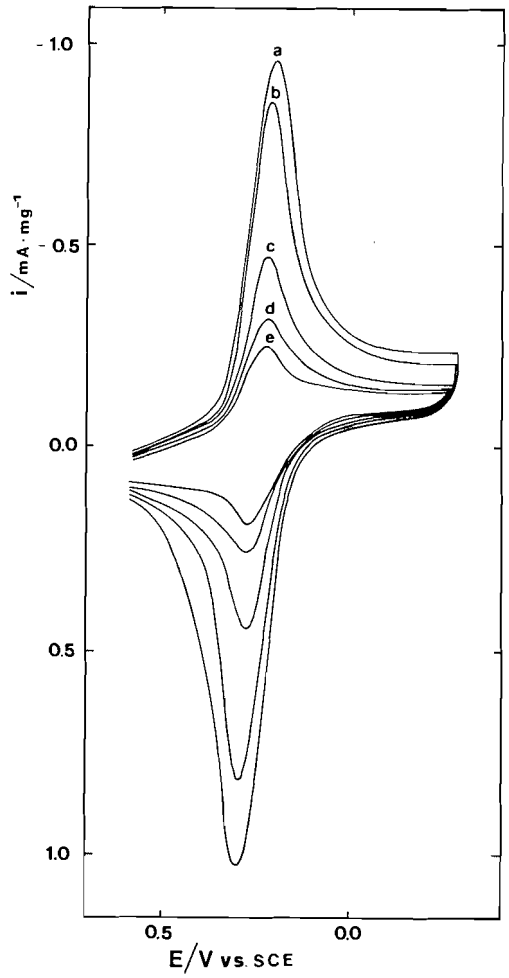

FIG. 4. Cyclic voltammogram of $K_4Fe(CN)_6$ (u = 100 mV s^{-1}, C = 2 mM, pH = 4) on electrodes modified with β-naphthol charged from the following concentrations: (*a*) bare electrode, (*b*) 5×10^{-6} M, (*c*) 2×10^{-5} M, (*d*) 5×10^{-4} M, (*e*) 10^{-4} M.

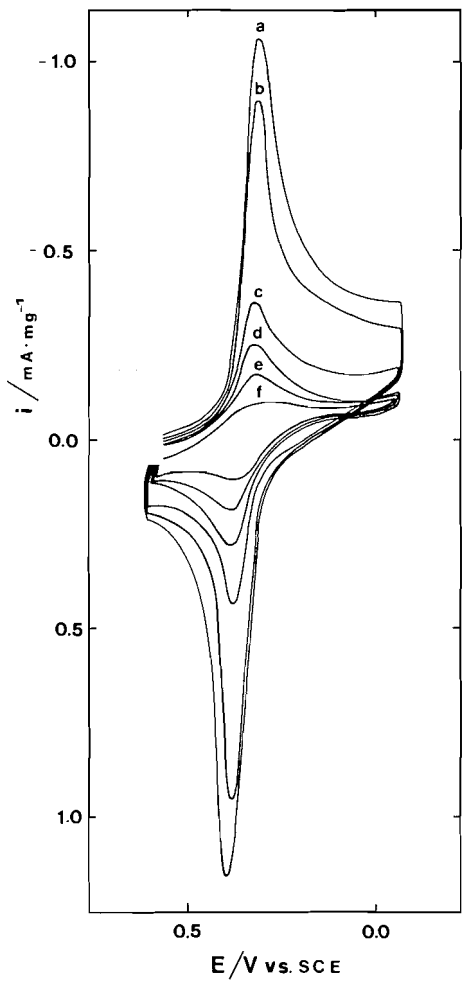

FIG. 5. Cyclic voltammogram of *p*-benzoquinone (u = 100 mV s^{-1}, C = 1 mM, pH = 4) on electrodes modified with β-naphthol charged from the following concentrations: (*a*) bare electrode, (*b*) 10^{-6} M, (*c*) 5×10^{-5} M, (*d*) 10^{-4} M, (*e*) 2×10^{-4} M, and (*f*) 5×10^{-4} M.

maximum amount of naphthol electropolymerized is achieved for concentrations greater than 3×10^{-4} M. This behaviour suggests that the film formed from relatively low concentrations can not exceed a critical thickness.

Projected molecular areas for both naphthols of 6.6×10^{-15} cm^2 and 2.6×10^{-15} cm^2 in the planar and perpendicular orientations (12, 13) yield values for surface coverage of 70 and 25 equivalent monolayers, respectively. These values were obtained taking into account that 1 mg of carbon fibres correspond to 1.5 cm^2 of effective area (14).

On an electrode bearing the limiting amount of the film the oxidation of naphthol itself is totally hindered, as curve *b* in Fig. 1 shows.

The film remains strongly attached to the carbon fibre over a wide potential range of about 2.5 V and is removed only after prolonged remaining at potentials where extreme hydrogen evolution occurs. After the film detachment the oxidation and electrosorption of naphthol can be carried out again on the regenerated fibre. The film is very stable in aqueous solutions (pH = 1–12) and in benzene. However, it is removed after remaining for 24 h in 1 M NaOH solution and by immersion of the fibre in ethanol, acetone, and acetonitrile.

Cyclic voltammetry has been employed to verify the film structure. It was found that at the whole potential range where

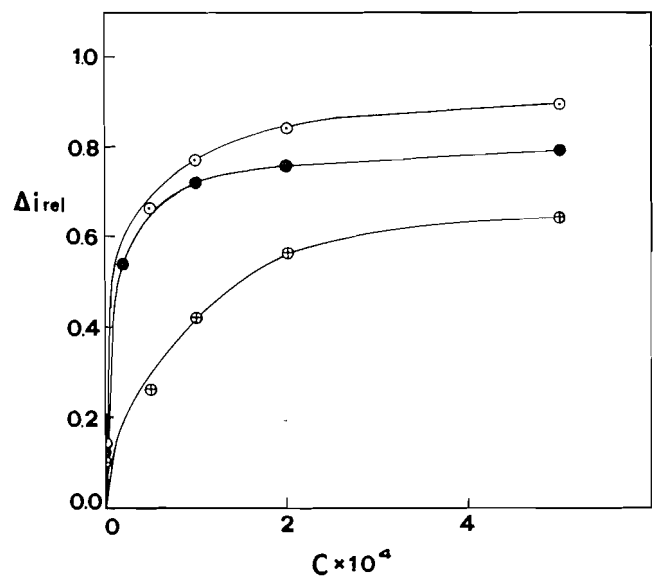

FIG. 6. Dependence of Δi_{Prel} for ○ $AgNO_3$, ● $K_4Fe(CN)_6$, and ⊕ *p*-Benzoquinone on the bulk equilibrium concentration of β-naphthol employed for modification.

Can. J. Chem. Downloaded from www.nrcresearchpress.com by 91.144.44.67 on 09/07/12
For personal use only.

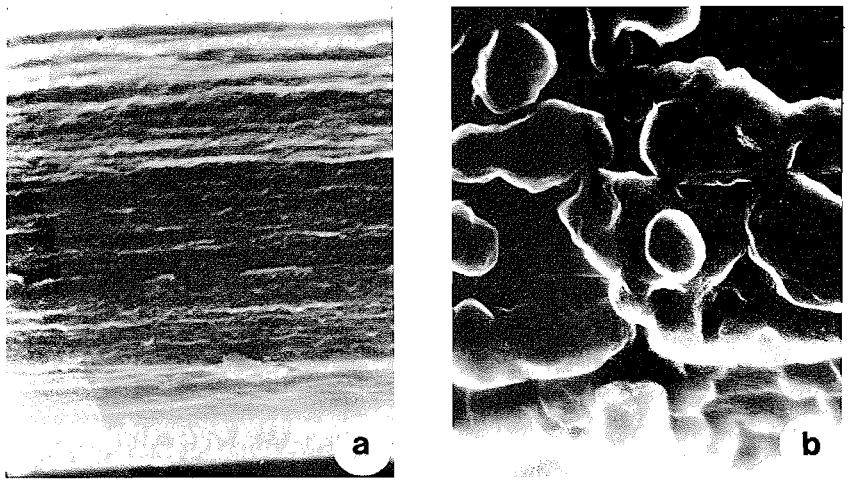

FIG. 7. Scanning electron micrograph of (*a*) bare carbon fibre (×30 000) and (*b*) partially modified fibre with β-naphthol (×40 000).

the film exists, several electrochemical reactions are considerably hindered, with the magnitude of inhibition depending on the extent of modification.

Figures 3, 4, and 5 show the gradual i_p decrease with increasing film thickness for three different depolarizers Ag^+, $Fe(CN)_6^{4-}$, and benzoquinone. It can be seen that in all cases the redox potential remains constant and the shape of the wave is the same, independent of the film thickness. On the other hand, on electrodes with the same modification a different inhibition is observed depending on the molecular size of the reactant. Thus, for an electrode coated with 1.7×10^{-8} mole β-naphthol cm^{-2} the Ag^+ reduction is almost 65% inhibited, whereas the Fe^{2+}/Fe^{3+} and quinone/hydroquinone reactions are inhibited about 80% and 90%, respectively.

The plot of $(\Delta i)_{rel} = i_p - i_m/i_p$, where i_p and i_m represent the peak current on pristine and modified fibres respectively, vs. the concentration of β-naphthol employed for modification, results in the curves presented in Fig. 6. It is observed that, for low β-naphthol concentrations, the limiting value of $(\Delta i)_{rel}$ is different for each depolarizer depending on its diffusion through the film.

Three possibilities can be considered for the reduction of the above depolarizers: (*a*) electron exchange taking place at the film–solution interface considering electron propagation through the film (15–18), (*b*) diffusion of the species through pores or channels (pin-hole model) (19–21) or through the film itself (membrane model) (22) with electron exchange at the electrode–film interface (23), and (*c*) diffusion of the species and propagation of the electrons with electron exchange in the film (24, 25). It must be noted that the film under consideration is inactive due to the absence of functional groups.

If the reduction of the depolarizer occurred at the film–solution interface (case *a*), the electrons had to diffuse through the film and the electrochemical reaction should occur at a potential different than that for a bare electrode (17). It follows that the magnitude of inhibition should be the same for each depolarizer depending only on the film thickness.

If electron propagation and species diffusion simultaneously occurred in the film (case *c*) a shift of the redox potential and a change of the shape of the wave should be observed. These effects should be more pronounced as the film thickness is increased (16, 24).

In case *b*, where the species is diffused through the film, the redox potential remains unaffected by the extent of modification

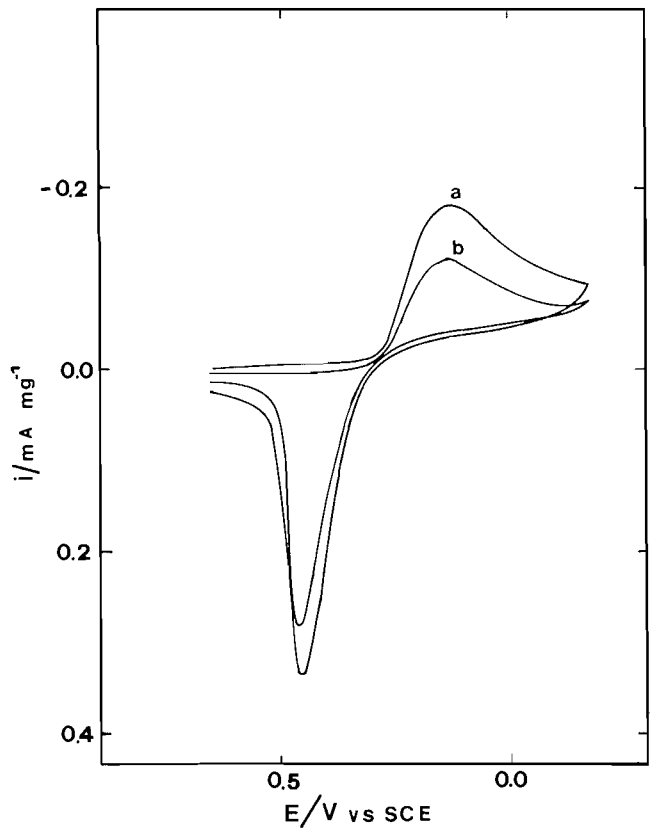

FIG. 8. Cyclic voltammogram of $AgNO_3$ (u = 100 mV s^{-1}, C = 1 mM, pH = 4) on modified electrodes (15 min electrolysis in a 1 mM β-naphthol solution at 0.75 V for different supporting electrolyte concentrations (*a*) CH_3COOH 1.6 M, CH_3COONa 0.4 M, and (*b*) CH_3COOH 0.16 M, CH_3COONa 0.04 M.

and the process is kinetically controlled by the diffusion of the species through the film (case "S" in the Andrieux and Savéant notation) (16).

As it has already been pointed out, in the case of films derived from naphthol electropolymerization, the redox potential of the depolarizers remains unaffected by the film thickness and is the same as that on a bare electrode. This indicates that the charge transfer takes place at the electrode–film interface and the height of the wave reflects merely the magnitude of the species

Can. J. Chem. Downloaded from www.nrcresearchpress.com by 91.144.44.67 on 09/07/12
For personal use only.

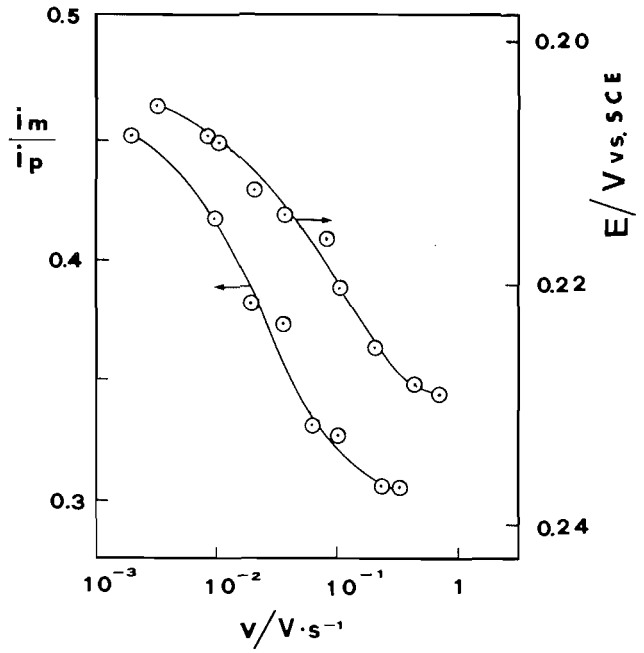

FIG. 9. Variation of the ratio i_m/i_p and of E_{pa} vs. u for $K_4Fe(CN)_6$ electrooxidation on a modified electrode bearing 1.5×10^{-8} mole β-naphthol cm^{-2}.

penetration through the film. Thus, it may be considered that on a modified electrode there are still active regions on the surface which are exposed to the solution.

The film formation may be described as an island growth of inactive regions on the electrode, so that the surface becomes inhomogeneous and the active species from the solution penetrates the film only through pores or channels. As the film thickness increases the size of the holes and the distribution of active sites decrease significantly and a smaller wave is observed. This also explains why for the same film thickness the inhibition is proportional to the molecular size of the corresponding reactant and even though the surface coverage exceeds several monolayers the electrochemical reaction is still observed. The structure suggested is very similar to that presented in the scanning electron micrographs of Fig. 7. Figure 7*a* shows a top view of pristine c.f. and Fig. 7*b* shows an image of the polymer particles deposited on the electrode where pores are clearly observed. The deposit appears distally brightened due to its insulating properties.

Further evidence is provided by the effect of the concentration of the supporting electrolyte on the film compactness. At high concentrations the film is swelled with solvent and electrolyte ions. This results in an increase of holes and/or channels in the film and consequently the peak current of the depolarizer is increased (Fig. 8).

In Fig. 9 the variation of the ratio i_m/i_p vs. u for the ferrocyanide on an electrode modified with 1.5×10^{-8} mole β-naphthol/cm^2 is given. This variation is rather in agreement with the theory predicted by Gueshi *et al.* (21) and further supports that the film structure fits the pin-hole model.

When the modification is performed from a concentrated solution of naphthol (10^{-2} *M* in 10% MeOH) the film becomes compact, the naphthol molecule is unable to reach the electrode surface and termination of the electropolymerization occurs. In this case channels and/or pores are blocked and the film exhibits properties of an impermeable inert insulator. These properties are different from those predicted by the membrane model since in the latter the current is governed by the extraction and diffusion coefficients of the species in the two phases (26).

1. F. BRUNO, M. C. PHAM, and J. E. DUBOIS. Electrochim. Acta, **22**, 451 (1977).
2. M. C. PHAM, A. HACHEMI, and J. E. DUBOIS. J. Electroanal. Chem. **161**, 199 (1984).
3. M. C. PHAM, A. HACHEMI, and M. DELAMAR. J. Electroanal. Chem. **184**, 197 (1985).
4. M. C. PHAM and J. E. DUBOIS. J. Electroanal. Chem. **199**, 153 (1986).
5. E. THEODORIDOU, P. KARABINAS, and D. JANNAKOUDAKIS. Z. Naturforsch. **37***b*, 112 (1982).
6. S. ANTONIADOU, A. D. JANNAKOUDAKIS, P. KARABINAS, and E. THEODORIDOU. J. Electroanal. Chem. **207**, 203 (1986).
7. R. S. EISING and R. C. ALKIRE. J. Electrochem. Soc. **130**, 85 (1983).
8. B. ZINGER, S. SHKOLNIK, and H. HÖCKER. Polymer, **30**, 628 (1989).
9. W. A. WATERS. J. Chem. Soc. (B), 2026 (1971).
10. F. P. BUB, K. WISSER, W. J. LORENZ, and W. HEIMANN. Ber. Bunsenges. Phys. Chem. **77**, 823 (1973).
11. L. FIESER and M. A. PETERS. J. Am. Chem. Soc. **53**, 793 (1931).
12. R. S. EISING and R. C. ALKIRE. J. Electroanal. Chem. **112**, 327 (1980).
13. L. BLOMGREN, J. O'M. BOCKRIS, and C. JESCH. J. Phys. Chem. **65**, 2000 (1961).
14. A. D. JANNAKOUDAKIS and E. THEODORIDOU. Z. Phys. Chem. N.F. **136**, 225 (1983).
15. C. P. ANDRIEUX and J. M. SAVÉANT. J. Electroanal. Chem. **111**, 377 (1980).
16. C. P. ANDRIEUX and J. M. SAVÉANT. J. Electroanal. Chem. **142**, 1 (1982).
17. E. LAVIRON. J. Electroanal. Chem. **131**, 61 (1982); **112**, 1 (1980).
18. E. LAVIRON, L. ROULLIER, and C. DEGRAND. J. Electroanal. Chem. **112**, 11 (1980).
19. A. MERZ and A. J. BARD. J. Am. Chem. Soc. **100**, 3222 (1978).
20. T. GUESHI, K. TOKUDA, and H. MATSUDA. J. Electroanal. Chem. **89**, 247 (1978).
21. T. GUESHI, K. TOKUDA, and H. MATSUDA. J. Electroanal. Chem. **101**, 29 (1979).
22. P. J. PEERCE and A. J. BARD. J. Electroanal. Chem. **112**, 97 (1980).
23. M. DELAMAR, M. C. PHAM, P. C. LACAZE, and J. E. DUBOIS. J. Electroanal. Chem. **108**, 1 (1980).
24. C. P. ANDRIEUX, J. M. DUMAS-BUCHAT, and J. M. SAVÉANT. J. Electroanal. Chem. **114**, 159 (1980); **131**, 1 (1982).
25. K. N. KUO and R. N. MURRAY. J. Electroanal. Chem. **131**, 37 (1982).
26. K. H. MANCY, D. A. OKUN, and C. N. REILLEY. J. Electroanal. Chem. **4**, 65 (1962).

Can. J. Chem. Downloaded from www.nrcresearchpress.com by 91.144.44.67 on 09/07/12
For personal use only.

Étude cinétique de la N-chloration de l'acide cyanurique en phase aqueuse

DENISE MATTE,[1] BERNARD SOLASTIOUK, ANDRÉ MERLIN ET XAVIER DEGLISE[2]
Université de Nancy I, Laboratoire de photochimie appliquée (Unité associée n° 238 du Centre national de la recherche scientifique), Boite postale 239, 54506 Vandœuvre-les-Nancy CEDEX, France

Reçu le 10 février 1988

DENISE MATTE, BERNARD SOLASTIOUK, ANDRÉ MERLIN et XAVIER DEGLISE. Can. J. Chem. **68**, 307 (1990).

Nous présentons une étude des mécanismes et déterminons les constantes de vitesse des N-chlorations d'acide cyanurique en milieu aqueux basique. Les énergies d'activation des processus mis en cause ont été déterminées. Ces cinétiques rapides ont été étudiées sur spectrophotomètre à écoulement bloqué. Dans le domaine de pH étudié nos résultats expérimentaux sont en accord avec un modèle cinétique comprenant la contribution de deux couples de processus indiscernables.

$$H_3Cy + ClO^- \xrightarrow{k_2} \text{produits}$$

ou

$$H_2Cy^- + ClOH \xrightarrow{k_3} \text{produits}$$

et

$$H_2Cy^- + ClO^- \xrightarrow{k_4} \text{produits}$$

ou

$$HCy^{2-} + ClOH \xrightarrow{k_5} \text{produits}$$

Les valeurs limites des constantes de vitesse dans le cas où, pour chaque couple, un seul des processus participe à la cinétique de chloration sont les suivantes :

$$k_2 = (5{,}4 \times 10^{11}) \exp(-35500/RT)\ M^{-1}\ s^{-1}$$

$$k_3 = (2{,}0 \times 10^{11}) \exp(-36700/RT)\ M^{-1}\ s^{-1}$$

$$k_4 = (1{,}4 \times 10^{13}) \exp(-55200/RT)\ M^{-1}\ s^{-1}$$

$$k_5 = 2{,}2 \times 10^7\ M^{-1}\ s^{-1} \text{ (à 298 K)}$$

À partir de ces valeurs, nous avons pu calculer les constantes de vitesse d'hydrolyse des dérivés monochlorés de l'acide cyanurique.

Mots clés : cinétique, N-chloration, 1,3,5-triazine 2,4,6-trione, phase aqueuse, spectrophotométrie à écoulement bloqué.

DENISE MATTE, BERNARD SOLASTIOUK, ANDRÉ MERLIN, and XAVIER DEGLISE. Can. J. Chem. **68**, 307 (1990).

A complete kinetic study of the N-chlorination, in basic aqueous medium, of cyanuric acid by the stopflow spectrophotometric method is presented. Our experimental results can be interpreted by two pairs of kinetically indistinguishable mechanisms.

$$H_3Cy + ClO^- \xrightarrow{k_2} \text{products}$$

or

$$H_2Cy^- + ClOH \xrightarrow{k_3} \text{products}$$

and

$$H_2Cy^- + ClO^- \xrightarrow{k_4} \text{products}$$

or

$$HCy^{2-} + ClOH \xrightarrow{k_5} \text{products}$$

The rate constants and their corresponding activation energies were determined in the limiting case where one of the elementary steps in each pair is involved alone in the kinetics of reaction.

$$k_2 = (5.4 \times 10^{11}) \exp(-35500/RT)\ M^{-1}\ s^{-1}$$

$$k_3 = (2.0 \times 10^{11}) \exp(-36700/RT)\ M^{-1}\ s^{-1}$$

$$k_4 = (1.4 \times 10^{13}) \exp(-55200/RT)\ M^{-1}\ s^{-1}$$

$$k_5 = 2.2 \times 10^7\ M^{-1}\ s^{-1} \text{ (at 298 K)}$$

The rate constants for hydrolysis of the monochlorinated cyanuric acid derivatives were derived from our experimental values.

Key words: kinetics, N-chlorination, 1,3,5-triazine-2,4,6-trione, aqueous medium, stopped flow.

---

1. Adresse actuelle : Département de génie chimique, Université Laval, Québec (Québec), Canada G1K 7P4.
2. Auteur à qui adresser toute correspondance.

Printed in Canada / Imprimé au Canada

Can. J. Chem. Downloaded from www.nrcresearchpress.com by 91.144.44.67 on 09/07/12
For personal use only.

Can. J. Chem. Downloaded from www.nrcresearchpress.com by 91.144.44.67 on 09/07/12
For personal use only.

Introduction

Les dérivés N-chlorés de la triazine-1,3,5 trione-2,4,6 ou acide cyanurique (H_3Cy) sont des sources sèches de chlore couramment utilisées dans les détergents et les eaux de piscines.

Mises en solution, ces molécules constituent un réservoir de chlore actif pouvant être libéré par leurs hydrolyses successives :

$$Cl_{(3-x)}CyH_x + H_2O \rightleftarrows HOCl + Cl_{(2-x)}CyH_{(x+1)}$$

où x est compris entre 0 et 2.

Suivant les conditions de pH, la concentration en ions chlorures et le rapport [chlore]/[Cy] et compte tenu des propriétés acido-basiques de ces dérivés, on peut recenser en solution dix composés comprenant un noyau cyanurique en présence de différentes espèces du chlore libre (Cl_2, ClOH, ClO^-).

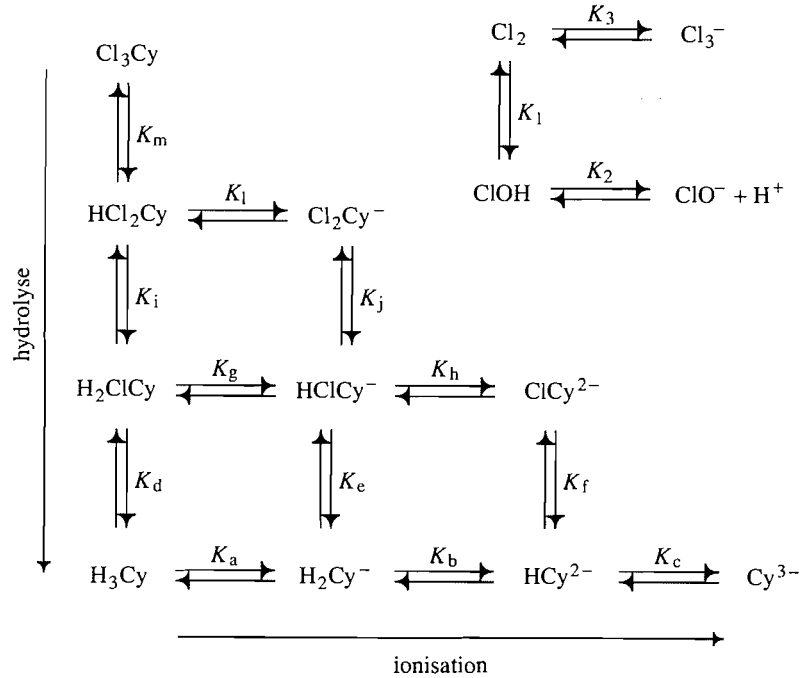

Les constantes d'équilibre entre ces composés ont été déterminées par O'Brien *et al.* (1, 2). À partir de ces valeurs, nous avons mis au point un mode de calcul appliqué à la micro-informatique permettant de déterminer la composition complète de ce système dans des conditions variées (3).

Ce calcul permet de vérifier qu'en milieu basique, le système précédent se simplifie notablement, en particulier un excès d'acide cyanurique permet de ne tenir compte que de la réaction de première chloration de celui-ci :

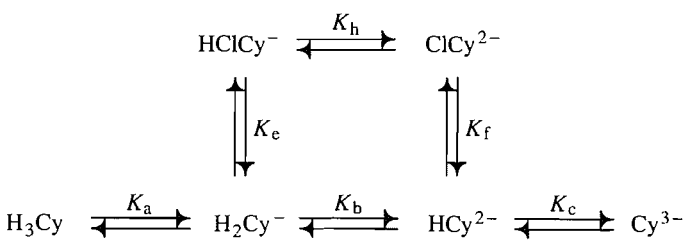

Pour le chlore libre, dans ces mêmes conditions, on ne tient compte que de l'équilibre entre l'acide hypochloreux et les ions hypochlorites :

$$ClOH \xrightleftharpoons{K_2} ClO^- + H^+$$

À ces pH, la composition de ce milieu ne dépend donc pas des ions chlorures en dehors d'un effet de force ionique.

Il n'existait pas de données cinétiques ou mécanistiques sur ces réactions rapides et équilibrées. Nous nous sommes donc intéressés à l'étude cinétique de la première chloration de l'acide cyanurique en milieu basique.

Techniques expérimentales (réf. 4)

Nous avons suivi la chloration de l'acide cyanurique par des solutions diluées d'ions hypochlorites. Le maximum d'absorption de ClO^- se situant à 290 nm et les dérivés monochlorés de H_3Cy absorbant à des longueurs d'onde plus faibles, nous avons pu, par *spectrophotométrie à écoulement bloqué*, déterminer les paramètres cinétique de cette réaction en observant la disparition de ClO^- à cette longueur d'onde.

En opérant en large excès d'acide cyanurique par rapport au chlore, nous avons pu mesurer une constante de vitesse expérimentale du pseudo-premier ordre (k_{obs}), pente de la droite $\ln(A - A_\infty)$ en fonction du temps (A est la densité optique de la solution à un instant donné). Dans ces conditions, le chlore est totalement consommé et la réaction s'arrête à la formation du composé monochloré.

Résultats expérimentaux

Nous avons tout d'abord vérifié que les résultats obtenus dans les conditions précédemment décrites étaient parfaitement représentés par le modèle d'une cinétique du pseudo-premier ordre. La relation liant $\ln(A - A_\infty)$ avec le temps étant linéaire, la réaction est du premier ordre par rapport à la concentration en chlore total $[Cl]_t$. La vitesse globale de réaction s'exprime donc, en présence d'un excès d'acide cyanurique ($[Cy]_t \gg [Cl]_t$), par :

$$[1] \quad v = -\frac{d[Cl]_t}{dt} = k_{obs}[Cl]_t$$

À pH constant, nous avons observé que k_{obs} est proportionnelle à la concentration totale d'acide cyanurique (fig. 1).

La réaction est donc globalement du second ordre et d'ordre

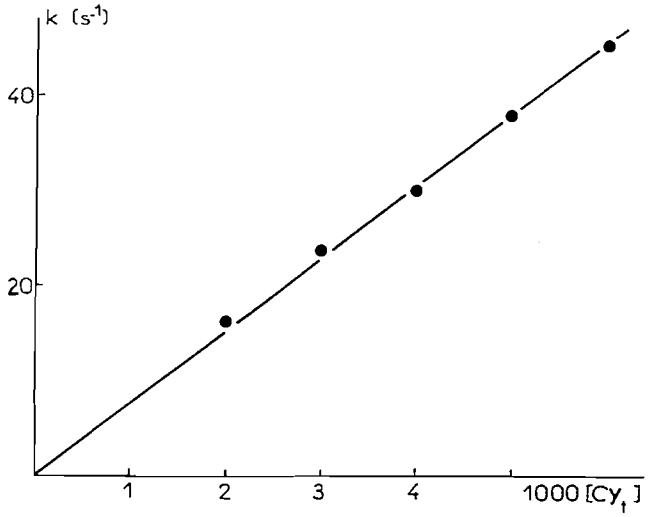

FIG. 1. Influence de la concentration en acide cyanurique : T = 298 K; pH = 8,60; $Cl_t = 3{,}5 \times 10^{-4}$ M pour $[Cy_t] < 4 \times 10^{-3}$ M; $Cl_t = 7{,}0 \times 10^{-4}$ M pour $[Cy_t] \geq 4 \times 10^{-3}$ M. k pente de la droite $\ln(A - A_\infty)$ en fonction du temps.

1 par rapport à chacun des deux réactifs

[2] $\quad v = k_{exp}[Cy]_t[Cl]_t$

où k_{exp} la constante de vitesse globale du second ordre s'exprime simplement pour nos conditions expérimentales à partir de [1] et [2] :

[3] $\quad k_{exp} = \dfrac{k_{obs}}{[Cy]_t}$

Les variations de k_{exp} en fonction du pH à 25°C sont représentées sur la figure 2.

Nous avons aussi suivi l'influence de la température sur ce paramètre à différents pH (fig. 3). Les relations exprimant $\ln(k_{exp})$ en fonction de la température pour les pH étudiés sont regroupées dans le tableau 1.

Interprétation

L'acide cyanurique est un triacide faible que l'on peut trouver en solution sous les quatre formes H_3Cy, H_2Cy^-, HCy^{2-} et Cy^{3-} en équilibre dans des proportions qui dépendent du pH (fig. 4). Corrélativement la concentration totale en acide cyanurique sera la somme des concentrations de ces espèces :

[4] $\quad [Cy]_t = [H_3Cy] + [H_2Cy^-] + [HCy^{2-}] + [Cy^{3-}]$

Compte tenu du domaine de pH des solutions utilisées (pH > 8) et de la vitesse de la réaction qui exclut qu'une espèce trop minoritaire intervienne dans le mécanisme, nous considérons le chlore libre sous forme d'acide hypochloreux ou d'ions hypochlorites qui sont les espèces majoritaires de ce milieu (fig. 5) :

[5] $\quad [Cl]_t = [ClOH] + [ClO^-]$

Les concentrations de ces différentes espèces peuvent être exprimées en fonction des constantes d'équilibre K_2, K_a, K_b et K_c, de leurs coefficients d'activité (γ_i), du pH et de $[Cy]_t$ et $[Cl]_t$. Le détail de ce calcul qui conduit aux expressions [6]–[9] est présenté en annexe.

[6] $\quad [H_3Cy] = \dfrac{1}{\mathscr{A}}[Cy]_t$

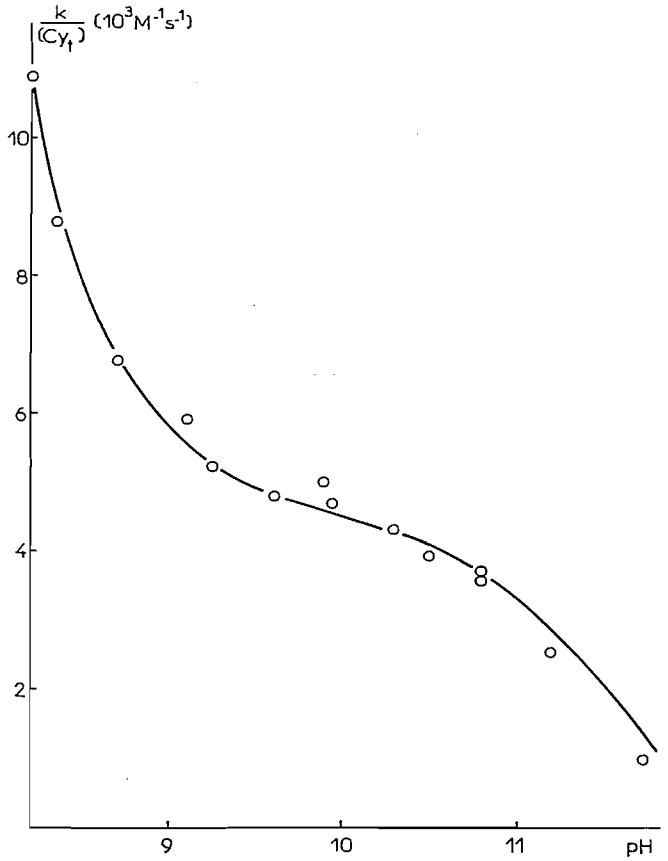

FIG. 2. Constante de vitesse expérimentale de chloration de l'acide cyanurique en fonction du pH; T = 298 K; $[Cy_t] = 5 \times 10^{-3}$ M; $[Cl_t] = 7 \times 10^{-4}$ M.

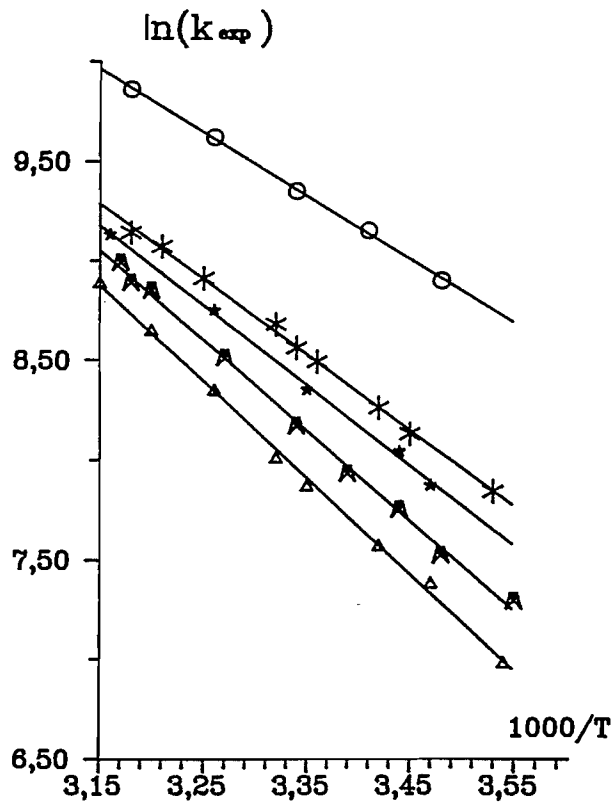

FIG. 3. Énergies d'activation globales à différents pH. ○ : pH = 8,15; ✳ : pH = 9,30; * : pH = 10,05; A : pH = 10,80; Δ : pH = 11,15.

Can. J. Chem. Downloaded from www.nrcresearchpress.com by 91.144.44.67 on 09/07/12
For personal use only.

Can. J. Chem. Downloaded from www.nrcresearchpress.com by 91.144.44.67 on 09/07/12
For personal use only.

TABLEAU 1. Énergies d'activation globales de la chloration de l'acide cyanurique à différents pH

pH	$\ln(k_{exp}/M^{-1}s^{-1})$	Énergie d'activation globale (kJ mol^{-1})
8,15	$-(3190/T) + 20,0$	26,5
9,30	$-(3800/T) + 21,3$	31,6
10,05	$-(4070/T) + 22,0$	33,8
10,80	$-(4540/T) + 23,4$	37,7
11,15	$-(4850/T) + 24,2$	40,3

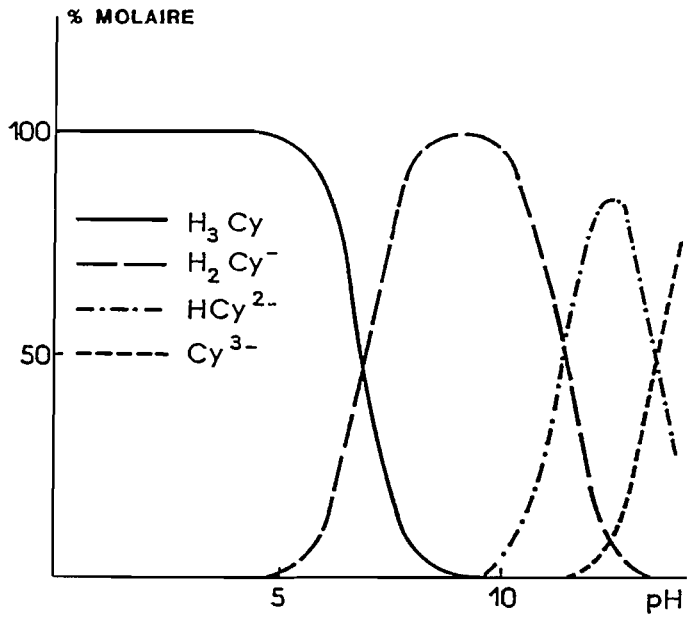

FIG. 4. Fractions molaires de chaque espèce dans une solution aqueuse d'acide cyanurique en fonction du pH (courbes calculées).

$$[7]\quad [H_2Cy^-] = \frac{K_a\gamma_{H_3Cy}}{\mathcal{A}(H^+)\gamma_{H_2Cy^-}}[Cy]_t$$

$$[8]\quad [HCy^{2-}] = \frac{K_aK_b\gamma_{H_3Cy}}{\mathcal{A}(H^+)^2\gamma_{HCy^{2-}}}[Cy]_t$$

$$[9]\quad [Cy^{3-}] = \frac{K_aK_bK_c\gamma_{H_3Cy}}{\mathcal{A}(H^+)^3\gamma_{Cy^{3-}}}[Cy]_t$$

Pour le chlore en posant : $d = K_a\gamma_{ClOH} + (H^+)\gamma_{ClO^-}$

$$[10]\quad [ClOH] = \frac{(H^+)\gamma_{ClO^-}}{d}[Cl]_t$$

et

$$[11]\quad [ClO^-] = \frac{K_a\gamma_{ClOH}}{d}[Cl]_t$$

Les équilibres de protonation et d'ionisation caractérisés par les constantes K_2, K_a, K_b et K_c sont rapides devant la cinétique de chloration et les relations [4]–[11] restent vérifiées au cours de la réaction.

Compte tenu de la mise en évidence expérimentale d'un ordre un par rapport à chacun des réactifs, nous pouvons envisager huit processus différents susceptibles de limiter la vitesse globale de réaction :

$P_1 : H_3Cy + ClOH \longrightarrow$ produits
$P_2 : H_3Cy + ClO^- \longrightarrow$ produits
$P_3 : H_2Cy^- + ClOH \longrightarrow$ produits
$P_4 : H_2Cy^- + ClO^- \longrightarrow$ produits
$P_5 : HCy^{2-} + ClOH \longrightarrow$ produits
$P_6 : HCy^{2-} + ClO^- \longrightarrow$ produits
$P_7 : Cy^{3-} + ClOH \longrightarrow$ produits
$P_8 : Cy^{3-} + ClO^- \longrightarrow$ produits

Le comportement de la constante de vitesse expérimentale en fonction du pH (fig. 2) semblant indiquer la participation de plusieurs processus à la cinétique globale de la réaction, nous envisagerons tout d'abord une participation ($v_{(P_i)}$) de chacun des processus P_1–P_8.

$$v = \frac{d[CyCl]_t}{dt} = v_{(P_1)} + v_{(P_2)} + v_{(P_3)} + v_{(P_4)} + v_{(P_5)} + v_{(P_6)} + v_{(P_7)} + v_{(P_8)}$$

Pour un processus bimoléculaire en solution réelle ($A + B \leftrightarrows C^{\neq} \rightarrow$) où $C^{\neq}$ est le complexe activé du processus :

$$[12]\quad v_{(P_1)} = k_1^0\frac{\gamma_A\gamma_B}{\gamma_{C^{\neq}}}[A][B]$$

d'où :

$$v = k_1^0\frac{\gamma_{H_3Cy}\gamma_{ClOH}}{\gamma_{Cl^{\neq}}}[H_3Cy][ClOH] + k_2^0\frac{\gamma_{H_3Cy}\gamma_{ClO^-}}{\gamma_{C2^{\neq}}}[H_3Cy][ClO^-] + \ldots$$

À partir des relations [6]–[11] donnant les concentrations des différentes espèces et en posant

$$X = \frac{\gamma_{H_3Cy}\gamma_{ClOH}\gamma_{ClO^-}}{\mathcal{A}d}$$

nous obtenons l'expression de la vitesse globale de réaction en fonction de $[Cy]_t$ et $[Cl]_t$:

$$v = \left[\frac{k_1^0}{\gamma_1^{\neq}}(H^+) + \left(\frac{k_2^0}{\gamma_2^{\neq}}K_2 + \frac{k_3^0}{\gamma_3^{\neq}}K_a\right) + \left(\frac{k_4^0}{\gamma_4^{\neq}}K_2K_a + \frac{k_5^0}{\gamma_5^{\neq}}K_aK_b\right)\frac{1}{(H^+)} + \left(\frac{k_6^0}{\gamma_6^{\neq}}K_2K_aK_b + \frac{k_7^0}{\gamma_7^{\neq}}K_aK_bK_c\right)\frac{1}{(H^+)^2} + \frac{k_8^0}{\gamma_8^{\neq}}K_2K_aK_bK_c\frac{1}{(H^+)^3}\right]X[Cy]_t[Cl]_t$$

Cette expression permet de regrouper les processus en fonction de la dépendance de leur contribution vis à vis de l'activité du proton hydraté : P_1; (P_2, P_3); (P_4, P_5); (P_6, P_7) et P_8.

Pour chacun des couples, (P_2, P_3), (P_4, P_5) et (P_6, P_7), nous pouvons vérifier que les deux complexes activés à l'intérieur de chaque couple ont même charge et même composition. Ainsi leurs coefficients d'activité peuvent être considérés comme égaux ou en tout cas comme variant de façon identique avec la force ionique du milieu. Comme le pH influe de la même manière sur leurs contributions à la vitesse globale de réaction, les pro-

Can. J. Chem. Downloaded from www.nrcresearchpress.com by 91.144.44.67 on 09/07/12
For personal use only.

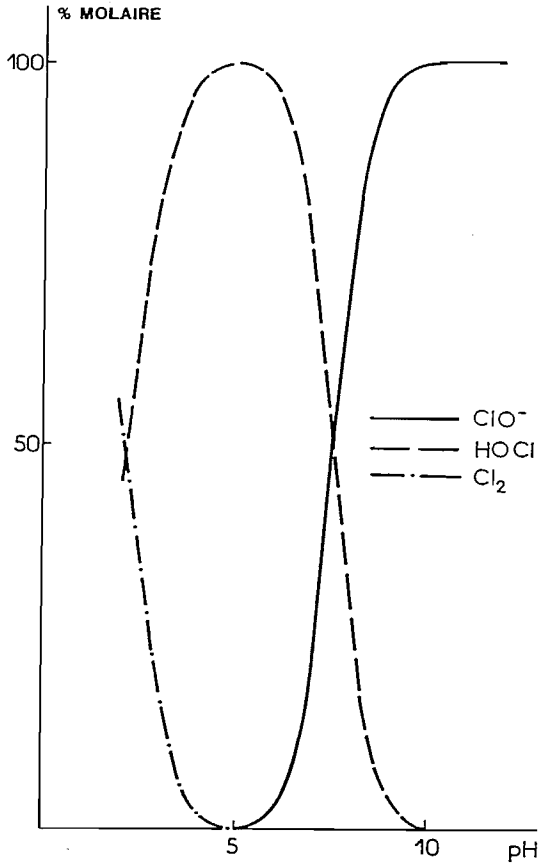

FIG. 5. Fractions molaires de chaque espèce du chlore en solution aqueuse en fonction du pH (courbes calculées).

cessus sont indiscernables à l'intérieur de chaque couple et notre étude se ramène à cinq cas : P_1; P_2 ou P_3; P_4 ou P_5; P_6 ou P_7 et P_8.

Nous avons déjà observé et décrit ce phénomène d'indiscernabilité de processus pour la N-chloration d'amines secondaires (4, 8).

En notant F les facteurs caractérisant ces contributions (les facteurs F ne dépendent pas du pH et restent constants à force ionique constante) nous obtenons :

$$v = \left(F_1(H^+) + F_{2\text{-}3} + \frac{F_{4\text{-}5}}{(H^+)} + \frac{F_{6\text{-}7}}{(H^+)^2} + \frac{F_8}{(H^+)^3}\right) X[Cy]_t[Cl]_t$$

et en identifiant à la relation [2] une expression théorique de la constante de vitesse expérimentale :

$$k_{exp} = \left(F_1(H^+) + F_{2\text{-}3} + \frac{F_{4\text{-}5}}{(H^+)} + \frac{F_{6\text{-}7}}{(H^+)^2} + \frac{F_8}{(H^+)^3}\right) X$$

Soit Y, obtenu à partir de nos points expérimentaux et des valeurs de X calculées pour les conditions correspondantes, défini par :

$$Y = \frac{k_{exp}}{X} = \left(F_1(H^+) + F_{2\text{-}3} + \frac{F_{4\text{-}5}}{(H^+)} + \frac{F_{6\text{-}7}}{(H^+)^2} + \frac{F_8}{(H^+)^3}\right)$$

En portant $\log_{10}(Y)$ en fonction du pH (fig. 6), nous pouvons déterminer les facteurs qui influencent la cinétique de réaction.

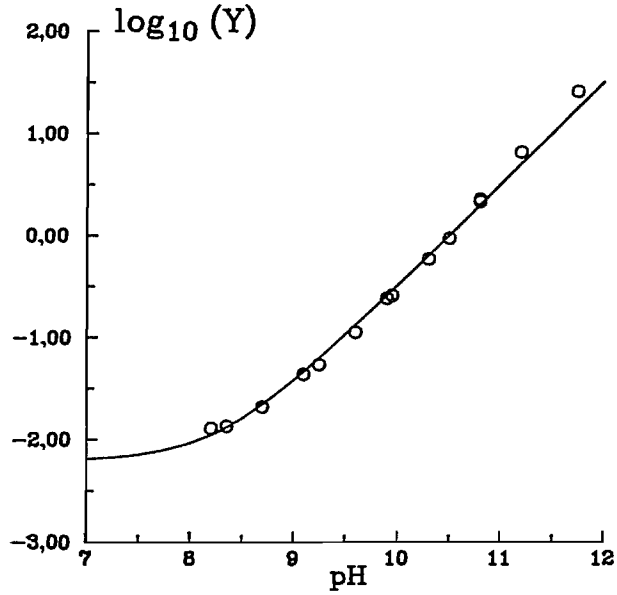

FIG. 6. $\text{Log}_{10}(Y)$ en fonction du pH

$$Y = k_{exp}\frac{\mathcal{A}d}{\gamma_{H_3Cy}\gamma_{ClOH}\gamma_{ClO^-}}$$

À pH > 10, les points obtenus sont portés par une droite de pente 1, ce qui indique une participation exclusive dans ce domaine des processus 4 ou 5. Pour des pH plus faibles, l'amortissement de la courbe indique que la participation des processus 2 ou 3 est prépondérante (pH < 8,5). Il apparaît donc que, dans le domaine de pH étudié, les résultats expérimentaux sont correctement décrits en considérant une expression de la forme :

$$[13]\quad Y = k_{exp}\frac{\mathcal{A}d}{\gamma_{H_3Cy}\gamma_{ClOH}\gamma_{ClO^-}} = \left(F_{2\text{-}3} + \frac{F_{4\text{-}5}}{(H^+)}\right)$$

Une optimisation permet de trouver les valeurs de ces paramètres à 298 K :

$$F_{2\text{-}3} = \frac{k_2^0}{\gamma_2^{\neq}}K_2 + \frac{k_3^0}{\gamma_3^{\neq}}K_a = 11{,}5 \times 10^{-3}\,s^{-1}$$

$$F_{4\text{-}5} = \frac{k_4^0}{\gamma_4^{\neq}}K_2K_a + \frac{k_5^0}{\gamma_5^{\neq}}K_aK_b = 2{,}35 \times 10^{-11}\,M\,s^{-1}$$

Dans le cas limite où l'un des processus de chaque couple devient prépondérant, nous pouvons calculer la valeur théorique maximale des constantes de vitesse à 25°C :

si $\frac{k_2^0}{\gamma_2^{\neq}}K_2 \gg \frac{k_3^0}{\gamma_3^{\neq}}K_a$ $\quad k_2^0 = 3{,}25 \times 10^5\,M^{-1}\,s^{-1}$

si $\frac{k_2^0}{\gamma_2^{\neq}}K_2 \ll \frac{k_3^0}{\gamma_3^{\neq}}K_a$ $\quad k_3^0 = 7{,}27 \times 10^4\,M^{-1}\,s^{-1}$

si $\frac{k_4^0}{\gamma_4^{\neq}}K_2K_a \gg \frac{k_5^0}{\gamma_5^{\neq}}K_aK_b$ $\quad k_4^0 = 2{,}92 \times 10^3\,M^{-1}\,s^{-1}$

si $\frac{k_4^0}{\gamma_4^{\neq}}K_2K_a \ll \frac{k_5^0}{\gamma_5^{\neq}}K_aK_b$ $\quad k_5^0 = 2{,}16 \times 10^7\,M^{-1}\,s^{-1}$

La détermination des constantes de vitesse expérimentales obtenues pour une série de pH constants à des températures variant de 10 à 45°C (tableau 1) a permis l'étude de l'influence de ce facteur sur les paramètres $F_{2\text{-}3}$ et $F_{4\text{-}5}$. Le calcul des

Can. J. Chem. Downloaded from www.nrcresearchpress.com by 91.144.44.67 on 09/07/12
For personal use only.

TABLEAU 2. Les valeurs de $F_{2\text{-}3}$ et $F_{4\text{-}5}$ sont obtenues par optimisation à partir des expressions du tableau 1 et de la relation [13]. Pour chaque température, une valeur de ces paramètres correspond à deux valeurs limites de la constante de vitesse selon le processus envisagé. Pour calculer les coefficients d'activité des espèces chargées nous utilisons la loi limite de Debye et Hückel en tenant compte de l'effet de la force ionique et de la température.

Temperature (°C)	$F_{2\text{-}3}$ (s^{-1})	$F_{4\text{-}5}$ ($M^{-1}s^{-1}$)	k_2^0 ($M^{-1}s^{-1}$)	k_3^0 ($M^{-1}s^{-1}$)	k_4^0 ($M^{-1}s^{-1}$)	k_5^0 ($M^{-1}s^{-1}$)
10	$3{,}4\times10^{-3}$	$5{,}1\times10^{-12}$	$1{,}3\times10^{5}$	$3{,}0\times10^{4}$	$1{,}2\times10^{3}$	$2{,}4\times10^{7}$
15	$5{,}3\times10^{-3}$	$9{,}2\times10^{-12}$	$1{,}9\times10^{5}$	$4{,}0\times10^{4}$	$1{,}6\times10^{3}$	$2{,}2\times10^{7}$
20	$8{,}0\times10^{-3}$	$1{,}6\times10^{-11}$	$2{,}5\times10^{5}$	$5{,}3\times10^{4}$	$2{,}1\times10^{3}$	$2{,}2\times10^{7}$
25	$1{,}2\times10^{-2}$	$2{,}8\times10^{-11}$	$3{,}2\times10^{5}$	$7{,}3\times10^{4}$	$2{,}9\times10^{3}$	$2{,}2\times10^{7}$
30	$1{,}6\times10^{-2}$	$4{,}7\times10^{-11}$	$3{,}9\times10^{5}$	$8{,}5\times10^{4}$	$4{,}2\times10^{3}$	$2{,}1\times10^{7}$
35	$2{,}2\times10^{-2}$	$7{,}9\times10^{-11}$	$5{,}0\times10^{5}$	$1{,}1\times10^{5}$	$6{,}2\times10^{3}$	$2{,}2\times10^{7}$
40	$2{,}7\times10^{-2}$	$1{,}4\times10^{-10}$	$6{,}0\times10^{5}$	$1{,}4\times10^{5}$	$9{,}7\times10^{3}$	$2{,}5\times10^{7}$
45	$3{,}4\times10^{-2}$	$2{,}4\times10^{-10}$	$7{,}0\times10^{5}$	$1{,}7\times10^{5}$	$16{,}2\times10^{3}$	$3{,}0\times10^{7}$

TABLEAU 3. Constantes de vitesse, énergies d'activation, $\Delta H^{\neq}$ et $\Delta S^{\neq}$ des processus de chloration de l'acide cyanurique

Processus	$k^0_{(298)}$ ($M^{-1}s^{-1}$)	E_a (kJ mol^{-1})	$\Delta H^{\neq}$ (kJ mol^{-1})	$\Delta S^{\neq}$ (J K^{-1} mol^{-1})
$P_2: H_3Cy + ClOH \rightarrow$	$3{,}25\times10^{5}$	35,2	33,0	−12
$P_3: H_2Cy^- + ClOH \rightarrow$	$7{,}27\times10^{4}$	36,7	34,3	−10
$P_4: H_2Cy^- + ClO^- \rightarrow$	$2{,}92\times10^{3}$	55,2	52,7	15
$P_5: HCy^{2-} + ClOH \rightarrow$	$2{,}16\times10^{7}$	—	—	—

coefficients $\mathcal{A}$ et d dans cette gamme de températures a été fait en utilisant pour expression des constantes d'ionisation les relations :

$$pK_2 = (3000/T) - 10{,}0686 + 0{,}0253T \text{ (réf. 5)}$$

$$pK_a = 31{,}08 - 0{,}154T + (2{,}441\times10^{-4})T^2 \text{ (réf. 6)}$$

$$pK_b = 35{,}86 - 0{,}1215T + (1{,}39\times10^{-4})T^2 \text{ (réf. 6)}$$

$$pK_c = pK_{c(298)}(298/T) \text{ (réf. 6)}$$

Les valeurs des constantes de vitesse déduites de ce calcul sont reportées dans le tableau 2.

Pour les processus P_2, P_3 et P_4 le logarithme des constantes de vitesse versus $1/T$ est porté par des droites dont les pentes donnent les énergies d'activation des processus.

$$\ln(\dot{k}_2) = -\frac{4272}{T} + 27 \qquad E_2^{\neq} = 35{,}5\text{ kJ/mol}$$

$$\ln(\dot{k}_3) = -\frac{4419}{T} + 26 \qquad E_3^{\neq} = 36{,}7\text{ kJ/mol}$$

$$\ln(\dot{k}_4) = -\frac{6640}{T} + 30{,}3 \qquad E_4^{\neq} = 55{,}2\text{ kJ/mol}$$

$\dot{k}_5$ apparait constant avec la température dans la limite des erreurs expérimentales.

Le tableau 3 résume les résultats obtenus : constantes de vitesse des processus à 298 K, énergies d'activation des différents processus ($d\ln k/dT = E^{\neq}/RT^2$) et valeurs $\Delta H^{\neq}$ et $\Delta S^{\neq}$ calculées en identifiant les expressions tirées de l'expérience aux valeurs de la dérivée de la constante de vitesse exprimée par la relation $k = (k_bT/h)K^{\neq}$.

Calcul des constantes de vitesse d'hydrolyse

Nos résultats nous permettent à partir des valeurs des constantes d'équilibre ($pK_d = 4{,}07$, $pK_e = 5{,}62$, $pK_f = 6{,}90$ (1, 2)) de calculer les constantes de vitesse d'hydrolyse des différentes formes de dérivés monochlorés de l'acide cyanurique :

$$H_2CyCl + HO^- \underset{k_2}{\overset{k_{-2}}{\rightleftharpoons}} ClO^- + H_3Cy$$

$$\left(K_{II} = \frac{k_{-2}}{k_2} = K_d\frac{K_2}{K_w}\right)$$

$$HCyCl^- + H_2O \underset{k_3}{\overset{k_{-3}}{\rightleftharpoons}} ClOH + H_2Cy^-$$

$$\left(K_e = \frac{k_{-3}}{k_3}\right)$$

$$HCyCl^- + HO^- \underset{k_4}{\overset{k_{-4}}{\rightleftharpoons}} ClO^- + H_2Cy^-$$

$$\left(K_{II} = \frac{k_{-4}}{k_4} = K_e\frac{K_2}{K_w}\right)$$

$$CyCl^{2-} + H_2O \underset{k_5}{\overset{k_{-5}}{\rightleftharpoons}} ClOH + HCy^{2-}$$

$$\left(K_f = \frac{k_{-5}}{k_5}\right)$$

où K_w est la constante de dissociation de l'eau, et K_2 la constante d'ionisation de ClOH. Nous obtenons à 25°C les valeurs suivantes :

$$k_{-2} = 8\times10^{7}\,M^{-1}\,s^{-1}$$

$$k_{-3} = 0{,}17\,s^{-1}$$

$$k_{-4} = 2\times10^{4}\,M^{-1}\,s^{-1}$$

$$k_{-5} = 2{,}72\,s^{-1}$$

Conclusions

Les résultats obtenus pour la première chloration de l'acide cyanurique peuvent être comparés aux valeurs correspondantes des amines aliphatiques. Nous avons aussi étudié précédemment (8) la N-chloration de la diéthylamine :

$$Et_2NCl + H_2O \underset{k_{ClOH}}{\overset{k_h}{\rightleftharpoons}} Et_2NH + ClOH$$

$$\left(K = \frac{k_h}{k_{ClOH}} = 5{,}89 \times 10^{-16}\,M \text{ (réf. 7)}\right)$$

et $k_{ClOH} = 5{,}3 \times 10^7\,M^{-1}\,s^{-1}$ à 25°C (8).

Ce qui correspond à une constante d'hydrolyse $k_h = 4{,}3 \times 10^{-8}\,s^{-1}$, soit un temps de demi réaction de 4500 h.

Comparativement les temps de demi-réaction des hydrolyses des chlorocyanuriques n'excédent pas quelques secondes.

Du point de vue cinétique et thermodynamique, le chlore fixé par un noyau cyanurique apparaît beaucoup plus labile qu'un chlore lié à une amine.

Sachant de plus que dans l'utilisation habituelle de ces produits, en présence d'un excès d'acide cyanurique (25–60 ppm d'acide cyanurique pour 1 ppm de chlore dans une eau de piscine), la majeure partie du chlore est sous forme d'acide monochlorocyanurique et est ainsi protégée de la photolyse due au rayonnement solaire (3). Nos résultats confirment que dérivés chlorocyanuriques sont une excellente source de chlore *actif* pour la désinfection et *stabilisé* vis à vis des pertes par photolyse.

Remerciements

Les auteurs remercient la société ORKEM et le C.N.R.S. pour l'aide apportée à l'un d'entre eux (D.M.) dans la réalisation de ce travail.

1. J. E. O'Brien. Thèse, Harvard University, Cambridge, MA. 1972.
2. J. E. O'Brien, J. C. Morris et J. N. Butler. Chem. Water Supply Treat. Distrib. Symp. 1973. *Editeur* : Alan J. Rubin. Ann Arbor Sci., Ann Arbor, MI. 1974. pp. 333–358.
3. B. Solastiouk et X. Deglise. Can. J. Chem. **66**, 2188 (1988).
4. D. Matte. Thèse, Université de Nancy I, Nancy. 1986.
5. J. Carrel Morris. J. Phys. Chem. **70**, 3798 (1966).
6. B. Solastiouk. Thèse de l'Institut National Polytechnique de Lorraine, Nancy. 1989.
7. R. A. Robinson et R. H. Stokes. Electrolyte solutions. 2è ed. Butterworth, London. 1970.
8. D. Matte, B. Solastiouk, A. Merlin et X. Deglise. Can. J. Chem. **67**, 786 (1989).

Annexe

Les expressions des concentrations des différentes espèces plus ou moins ionisées de l'acide cyanurique sont établies d'une part à partir du bilan en acide cyanurique total :

$$[Cy]_t = [H_3Cy] + [H_2Cy^-] + [HCy^{2-}] + [Cy^{3-}]$$

et d'autre part à partir des trois lois d'action de masse correspondant aux équilibres acido-basiques :

$$K_a = \frac{[H_2Cy^-](H^+)}{[H_3Cy]}\,\frac{\gamma_{H_2Cy^-}}{\gamma_{H_3Cy}}$$

$$K_b = \frac{[HCy^{2-}](H^+)}{[H_2Cy^-]}\,\frac{\gamma_{HCy^{2-}}}{\gamma_{H_2Cy^-}}$$

$$K_c = \frac{[Cy^{3-}](H^+)}{[HCy^{2-}]}\,\frac{\gamma_{Cy^{3-}}}{\gamma_{HCy^{2-}}}$$

Par substitutions successives dans ces relations d'équilibre, nous obtenons l'expression des concentrations des espèces ionisées en fonction de celle de H_3Cy.

$$[H_2Cy^-] = [H_3Cy]\,\frac{K_a\gamma_{H_3Cy}}{(H^+)\gamma_{H_2Cy^-}}$$

$$[HCy^{2-}] = [H_2Cy^-]\,\frac{K_b\gamma_{H_2Cy^-}}{(H^+)\gamma_{HCy^{2-}}} = [H_3Cy]\,\frac{K_aK_b\gamma_{H_3Cy}}{(H^+)^2\gamma_{HCy^{2-}}}$$

$$[Cy^{3-}] = [HCy^{2-}]\,\frac{K_c\gamma_{HCy^{2-}}}{(H^+)\gamma_{Cy^{3-}}} = [H_3Cy]\,\frac{K_aK_bK_c\gamma_{H_3Cy}}{(H^+)^3\gamma_{Cy^{3-}}}$$

D'où la relation liant $[Cy]_t$ à $[H_3Cy]$:

$$[Cy]_t = [H_3Cy]\left(1 + \frac{K_a\gamma_{H_3Cy}}{(H^+)\gamma_{H_2Cy^-}} + \frac{K_aK_b\gamma_{H_3Cy}}{(H^+)^2\gamma_{HCy^{2-}}} + \frac{K_aK_bK_c\gamma_{H_3Cy}}{(H^+)^3\gamma_{Cy^{3-}}}\right)$$

En posant

$$\mathcal{A} = 1 + \frac{K_a\gamma_{H_3Cy}}{(H^+)\gamma_{H_2Cy^-}} + \frac{K_aK_b\gamma_{H_3Cy}}{(H^+)^2\gamma_{HCy^{2-}}} + \frac{K_aK_bK_c\gamma_{H_3Cy}}{(H^+)^3\gamma_{Cy^{3-}}}$$

nous retrouvons la relation [6] : $[H_3Cy] = [Cy]_t/\mathcal{A}$, puis par déductions successives les relations [7]–[9] du texte.

Can. J. Chem. Downloaded from www.nrcresearchpress.com by 91.144.44.67 on 09/07/12
For personal use only.

Enantioselectivity of carbonic anhydrase catalyzed hydrolysis of mandelic methyl esters

ROBERT CHÊNEVERT[1] AND MARTIN LÉTOURNEAU

Département de chimie, Faculté des sciences et de génie, Université Laval, Québec (Québec), Canada G1K 7P4

Received March 20, 1989

ROBERT CHÊNEVERT and MARTIN LÉTOURNEAU. Can. J. Chem. **68**, 314 (1990).

We report the first enantioselective hydrolysis of esters catalyzed by carbonic anhydrase. We found that mandelic methyl esters are good substrates for carbonic anhydrase. The *R* enantiomers are better substrates and enantiomeric excess values are moderate (40–51%).

Key words: carbonic anhydrase, mandelic esters, enantioselectivity, hydrolysis.

ROBERT CHÊNEVERT et MARTIN LÉTOURNEAU. Can. J. Chem. **68**, 314 (1990).

Nous avons découvert que les esters mandéliques sont des substrats de l'anhydrase carbonique. L'enzyme est stéréosélectif pour les énantiomères *R* et les valeurs de l'excès énantiomère sont modérées (40–51%). Il s'agit de la première étude sur l'énantiosélectivité de l'anhydrase carbonique.

Mots clés : anhydrase carbonique, esters mandeliques, énantiosélectivité, hydrolyse.

Can. J. Chem. Downloaded from www.nrcresearchpress.com by 91.144.44.67 on 09/07/12
For personal use only.

Carbonic anhydrase (EC 4.2.1.1) is a zinc-containing metalloenzyme. The sole natural function of this ubiquitous enzyme is to catalyze the reversible hydration of carbon dioxide (eq. [1])

[1] $CO_2 + H_2O \rightleftharpoons HCO_3^- + H^+$

(1–3). In addition to its known physiological role, carbonic anhydrase catalyses in vitro the reversible hydration of carbonyl compounds (4, 5) and the hydrolysis of some esters (5–12), among other reactions (12–16). The unnatural substrates used in the previous studies were achiral and as far as we know the enantioselectivity of carbonic anhydrase has never been investigated. We report here the first enantioselective hydrolysis of esters catalyzed by bovine carbonic anhydrase (BCA). We found that mandelic methyl esters are good substrates for BCA and offer a good opportunity to investigate the enantioselectivity of this enzyme.

The racemic ester substrates **1**–**7** were prepared by esterification of the commercially available corresponding acids with methanol in the presence of 2,2-dimethoxypropane and *p*-toluenesulfonic acid. Preparative-scale enzyme catalyzed hydrolyses were performed on 2 mmol of the substrates with 40 mg of BCA in a phosphate buffer at pH 7.5. The reaction was indicated by the decrease of pH, which was maintained at its initial value by the addition of a dilute NaOH solution. The reactions were monitored from the consumption of the base and terminated when 50% of the substrate was hydrolyzed. The unreacted esters were recovered from the reaction mixtures by extraction with diethyl ether at the initial pH. The product acids that are present in the aqueous phase as sodium salts were extracted with ether after acidification to pH 2.0.

The results are summarized in eq. [2] and Table 1. Recovery yields ranged from 70 to 91%. Optical purities and absolute configurations were determined by comparison with the optical rotations reported in the literature (17–22). Optical purities (enantiomeric excess values) were further confirmed by ^{1}H nmr analysis using tris[3-(heptafluoropropylhydroxymethylene)-*d*-camphorato]ytterbium as a chiral shift reagent (23). Samples of the acids were converted to their methyl esters by the method mentioned above before nmr analysis. Substituted mandelic methyl esters **2**–**6** are hydrolyzed more rapidly than the parent compound **1**. In every case, the absolute configuration of the preferentially hydrolyzed enantiomer is *R*, and ee values cover a range from 37 to 55%. The enantioselectivity of the enzyme is slightly better than indicated by the ee value. In control experiments, we found that esters **1**–**7** are slowly hydrolyzed in the buffer at pH 7.5 in the absence of the enzyme (5–10% of the esters was hydrolyzed in 24 h). Enzymatic hydrolyses at pH 7.0 did not give a better enantioselectivity and the reaction times were 2.5 times longer.

Since the values of enantiomeric excess increase with the extent of conversion (24), it is possible to improve the optical purity of the unreacted ester by extending reaction times, but at the expense of decreased yield. For example, BCA-catalyzed hydrolysis of methyl *p*-chloromandelate **3** gave a 55% ee value at 50% conversion and a 73% ee value at 60% conversion. Acids can be prepared with higher values of ee by carrying hydrolysis to low conversions. Methyl phenyllactate **7**, which is a homolog of the mandelic esters, is also a good substrate, but the enantioselectivity of its hydrolysis drops significantly

[2] 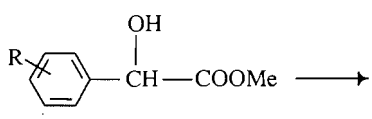

RS

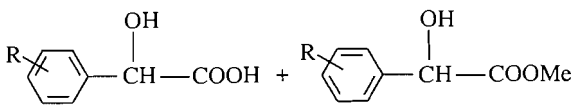

R *S*

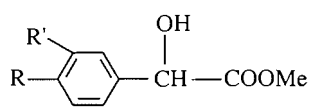

1 R = H R' = H
2 R = F R' = H
3 R = Cl R' = H
4 R = Br R' = H
5 R = OMe R' = H
6 R = H R' = OMe

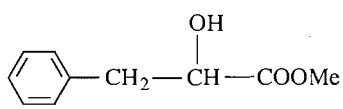

7

[1]Author to whom correspondence may be addressed.

TABLE 1. BCA-catalyzed hydrolysis of esters **1–7**

Substrate	Time (h)	Recovered ester[a] Yield (%)	ee (%)[b]	Absolute configuration	Acid product[a] Yield (%)	ee (%)[b]	Absolute configuration
1	16	74	51	*S*	76	40	*R*
2	4	91	42	*S*	70	48	*R*
3	3	78	55	*S*	78	51	*R*
4	4	89	37	*S*	81	40	*R*
5	6.7	76	38	*S*	72	40	*R*
6	4	91	41	*S*	72	42	*R*
7	4.5	81	15	*S*	76	13	*R*

[a]Average values of three runs.
[b]Determined by ^{1}H nmr (200 MHz) using the chiral shift reagent Yb(hfc)$_3$; the accuracy of this method is ±3%.

(13–15%). Other related compounds such as methyl lactate **8**, tropic acid methyl ester **9**, and methyl 2-phenoxypropionate **10** are not substrates for BCA. Finally, to check that the enzymatic activity was not caused by the presence of hydrolases as impurities, the hydrolyses were repeated and found strongly inhibited in the presence of acetazolamide. It is well documented that acetazolamide is a strong inhibitor of carbonic anhydrase activity with respect to both hydration and hydrolysis (1, 3, 6).

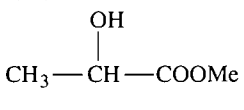

8

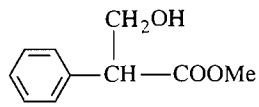

9

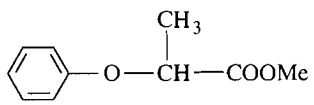

10

BCA is a stable enzyme commercially available in a pure lyophilized form. The substrate specificity and the enantioselectivity of BCA is not yet well known but this enzyme could be useful as a catalyst in organic syntheses. A search of highly enantioselective hydrolyses is in progress.

Experimental

Carbonic anhydrase (from bovine erythrocytes, dialyzed and lyophilized, 2500 W-A units/mg) was purchased from Sigma. Methyl mandelate **1**, substituted mandelic acid, and phenyllactic acid were obtained from Aldrich or from Lancaster Synthesis. NMR studies were performed on a Varian XL-200 spectrometer on $CDCl_3$ solutions with TMS as internal standard. Samples for ee measurements were prepared by dissolving 30 mg of the ester in 1 mL of dry $CDCl_3$, to which solid Yb(hfc)$_3$ (150 mg) was then added incrementally. The ester methyl ($COOCH_3$) was shifted downfield and the enantiomeric shift difference was in the range 11–18 Hz. Optical rotations were measured with a Jasco DIP-360 digital polarimeter. Mass spectra were recorded on a Hewlett–Packard 5992 spectrometer.

Esterification of mandelic acids, general procedure

The acid (0.125 mol), 2,2-dimethoxypropane (0.185 mol), and a catalytic amount of *p*-toluenesulfonic acid (15 mg) were dissolved in dry methanol (0.185 mol). The solution was stirred magnetically overnight at 55°C under a dry atmosphere. Acetone and methanol were evaporated and the crude ester was dissolved in dichloromethane (250 mL). The organic phase was washed successively with 5% $NaHCO_3$ (50 mL) and saturated brine (50 mL). Dichloromethane was dried over magnesium sulfate and evaporated. The crude ester was purified by recrystallization or distillation.

*Methyl (±)-*p*-fluoromandelate* **2**

Crystallization from light petroleum ether, mp 44–45°C (lit. (25) mp 45°C); yield 62%; ir (KBr) ν_{max}: 3475, 2950, 1735, 1603, 1508, 1220, 1080, 835, 815 cm^{-1}; ^{1}H nmr δ: 3.49 (1H, d, J = 5.5 Hz), 3.78 (3H, s), 5.16 (1H, d, J = 5.5 Hz), 7.05 (2H, m), 7.39 (2H, m); ^{13}C nmr δ: 52.99, 72.14, 115.15, 115.58, 128.13, 128.30, 133.94, 160.09, 173.70; ms *m/e* (rel. intensity): 184 (20%), 125 (100%), 95 (20%).

*Methyl (±)-*p*-chloromandelate* **3**

Crystallization from light petroleum ether, mp 51–54°C (lit. (25) mp 55°C); yield 68%; ir (KBr) ν_{max}: 3360, 2960, 1740, 1598, 1490, 1215, 1180, 1090, 825, 770 cm^{-1}; ^{1}H nmr δ: 3.52 (1H, d, J = 5.1 Hz), 3.76 (3H, s), 5.16 (1H, d, J = 5.1 Hz), 7.35 (5H, m); ^{13}C nmr δ: 53.06, 72.13, 127.79, 128.57, 134.15, 136.52, 173.46; ms *m/e* (rel. intensity): 202 (2.9%), 200 (9%), 143 (13%), 141 (42%).

*Methyl (±)-*p*-bromomandelate* **4**

Crystallization from light petroleum ether, mp 58–60°C (lit. (25) mp 58°C); yield 67%; ir (KBr) ν_{max}: 3460, 2955, 1740, 1590, 1488, 1210, 1185, 1080, 1015, 820, 770 cm^{-1}; ^{1}H nmr δ: 3.63 (1H, s), 3.75 (3H, s), 5.13 (1H, s), 7.30 (2H, d, J = 8.4 Hz), 7.49 (2H, d, J = 8.4 Hz); ^{13}C nmr δ: 53.17, 72.22, 122.38, 128.13, 131.57, 137.05, 173.43; ms *m/e* (rel. intensity): 246 (14%), 244 (13%), 187 (80%), 185 (100%), 157 (35%), 155 (12%).

*Methyl (±)-*p*-methoxymandelate* **5**

Crystallization from light petroleum ether/ether, mp 30–33°C (lit. (25) mp 32°C); yield 63%; ir (KBr) ν_{max}: 3460, 2995, 2950, 2830, 1735, 1610, 1585, 1510, 1455, 1440, 1245, 1175, 1075, 1030, 830, 795 cm^{-1}; ^{1}H nmr δ: 3.41 (1H, d, J = 5.5 Hz), 3.75 (3H, s), 3.80 (3H, s), 5.13 (1H, d, J = 5.5 Hz), 6.89 (2H, d, J = 8.8 Hz), 7.33 (2H, d, J = 8.8 Hz); ^{13}C nmr δ: 52.75, 55.15, 72.40, 113.84, 127.72, 130.33, 159.47, 173.99; ms *m/e* (rel. intensity): 196 (16%), 137 (100%).

*Methyl (±)-*m*-methoxymandelate* **6**

Crystallization from light petroleum ether/ether, mp 34–35°C (lit. (25) mp 35°C); yield 64%; ir (KBr) ν_{max}: 3450, 2990, 2950, 2830, 1735, 1600, 1585, 1490, 1435, 1250, 1150, 1065, 1040, 780 cm^{-1}; ^{1}H nmr δ: 3.49 (1H, d, J = 5.0 Hz), 3.76 (3H, s), 3.81 (3H, s), 5.15 (1H, d, J = 5.0 Hz), 6.87 (1H, m), 7.00 (2H, m), 7.28 (1H, m); ^{13}C nmr δ: 52.86, 55.14, 72.73, 111.83, 113.94, 118.75, 129.42, 139.57, 159.53, 173.68; ms *m/e* (rel. intensity): 196 (33%), 137 (100%).

Methyl (±)-phenyllactate **7**

Distillation, bp 125°C/7.5 Torr (1 Torr = 133.3 Pa) (lit. (20) bp 86°C (0.3 Torr)); yield 71%; ir (film) ν_{max}: 3480, 3080, 3060, 3020, 2950, 1738, 1600, 1592, 1452, 1435, 1215, 1092, 740 cm^{-1};

Can. J. Chem. Downloaded from www.nrcresearchpress.com by 91.144.44.67 on 09/07/12
For personal use only.

^{1}H nmr δ: 2.80 (1H, d, J = 6.2 Hz), 2.98 (1H, dd, J_{AB} = 13.9 Hz, J_{AX} = 6.6 Hz), 3.13 (1H, dd, J_{AB} = 13.9 Hz, J_{BX} = 4.4 Hz), 3.76 (3H, s), 4.45 (1H, dd, J_{AX} = 6.6 Hz, J_{BX} = 4.4 Hz), 7.26 (5H, m); ^{13}C nmr δ: 40.46, 52.30, 71.20, 126.66, 128.21, 129.26, 136.17, 174.30; ms *m/e* (rel. intensity): 180 (5%), 121 (11%), 92 (21%), 91 (100%).

BCA-catalyzed hydrolyses of esters 1–7, general procedure

The ester (2 mmol) was suspended in a buffered aqueous solution (50 mL, phosphate pH 7.5) at room temperature (25°C). The enzyme (40 mg, 100 000 units) was added and the pH was maintained at its initial value by addition of 0.1 M aqueous NaOH from a burette. The reaction was stopped at the 50%-of-hydrolysis point. The mixture was first extracted at initial pH with ether (3 × 50 mL) to remove the unchanged ester. The aqueous mixture was then acidified to pH 2.0 with 2 M hydrochloric acid and was again extracted with ether (3 × 50 mL) to remove the product acid. The ether extracts were dried on magnesium sulfate and evaporated. The physical and spectral properties of the recovered esters were identical with those reported above, and properties of the acid products were identical with those of commercially available samples, except for the magnitudes of their rotations. The $[\alpha]_D^{25}$ values observed for recovered esters and acid products were as follows.

Substrate **1**: recovered ester, [α] +89.2° (*c* 2.6, $CHCl_3$); commercially available sample, [α] 174.2° (*c* 2.5, $CHCl_3$). Acid, [α] −61.1° (*c* 2.1, acetone); commercially available sample, [α] −154.3° (*c* 2.1, acetone).

Substrate **2**: recovered ester, [α] +47.5° (*c* 2.6, acetone); lit. (18): [α] +113.8° (*c* 1, acetone). Acid, [α] −67.4° (*c* 2.6, acetone); lit. (17) [α] −140° (*c* 1, acetone).

Substrate **3**: recovered ester, [α] +54.3° (*c* 1.4, acetone); lit. (18) [α] +99.6° (*c* 0.9, acetone). Acid, [α] −69.4° (*c* 2.1, acetone); lit. (17) [α] −136° (*c* 0.7, acetone).

Substrate **4**: recovered ester, [α] +32.9° (*c* 2.1, acetone); lit. (18) [α] +88.2° (*c* 1, acetone). Acid, [α] −46.5° (*c* 2.3, acetone); lit. (17) [α] −115° (*c* 0.6, acetone).

Substrate **5**: recovered ester, [α] +69.8° (*c* 2.3, ethanol); lit. not available. Acid, [α] −57.0° (*c* 0.4, water), lit. (19) [α] −141° (*c* 0.3, water).

Substrate **6**: recovered ester, [α] +44.5° (*c* 2.2, ethanol); lit. not available. Acid, [α] −48.8° (*c* 2.6, ethanol); lit. (19) [α] −117° (*c* 0.3, ethanol).

Substrate **7**: recovered ester, [α] −1.9° (*c* 2.5, benzene); lit. (20) [α] −12.6° (*c* 2.4, benzene). Acid, [α] +3.5° (*c* 2.0, acetone); commercially available sample, [α] +27.7° (*c* 2, acetone).

Acknowledgments

We acknowledge the financial support of this work by the Natural Sciences and Engineering Research Council of Canada and the Ministère de l'éducation du Québec.

1. D. N. Silverman and S. Lindskog. Acc. Chem. Res. **21**, 30 (1988).
2. Y. Pocker and N. Janjie. J. Am. Chem. Soc. **111**, 731 (1989).
3. S. Lindskog. *In* Zinc enzymes. *Edited by* T. G. Spiro. Wiley, New York. 1983. p. 77.
4. Y. Pocker and J. E. Meany. Biochemistry, **4**, 2535 (1965).
5. Y. Pocker, J. E. Meany, and R. C. Jones. J. Am. Chem. Soc. **104**, 4885 (1982).
6. Y. Pocker, J. E. Meany, B. C. Davis, J. Arrigoni, and J. E. Stein. J. Am. Chem. Soc. **100**, 2883 (1978).
7. Y. Pocker and N. Watamori. Biochemistry, **12**, 2475 (1973).
8. J. M. Gulian, D. Faure, J. Buc, and M. Charrel. Biochimie, **60**, 473 (1978).
9. J. A. Verpoorte, S. Mehta, and J. T. Edsall. J. Biol. Chem. **242**, 4221 (1967).
10. Y. Pocker and M. W. Beug. Biochemistry, **11**, 698 (1972).
11. Y. Pocker and T. L. Deits. J. Am. Chem. Soc. **104**, 2424 (1982).
12. Y. Pocker and S. Sarkanen. Biochemistry, **17**, 1110 (1978).
13. P. Henkart, G. Guidotti, and J. T. Edsall. J. Biol. Chem. **243**, 2447 (1968).
14. P. C. Harrington and R. G. Wilkins. J. Chem. Soc. Chem. Commun. 638 (1977).
15. Y. Pocker and L. J. Guilbert. Biochemistry, **11**, 180 (1972).
16. G. Sanyal, J. L. Ferrero, and T. M. Maren. Biochim. Biophys. Acta, **744**, 171 (1983).
17. A. Collet and J. Jacques. Bull. Soc. Chim. Fr. 3330 (1973).
18. A. Schoofs, R. Weidmann, A. Collet, and A. Horeau. Bull. Soc. Chim. Fr. 2031 (1976).
19. J. R. E. Hoover, G. L. Dunn, D. R. Jakas, L. L. Lam, J. J. Taggart, J. R. Guarini, and L. Philipps. J. Med. Chem. **17**, 34 (1974).
20. S. G. Cohen, B. Torem, V. Vaidya, and A. Ehret. J. Biol. Chem. **251**, 4722 (1976).
21. S. A. Macdonald, C. G. Willson, M. Chorev, F. S. Vernacchia, and M. Goodman. J. Med. Chem. **23**, 413 (1980).
22. M. S. Silver and S. L. T. James. J. Biol. Chem. **255**, 555 (1980).
23. R. R. Fraser. *In* Asymmetric synthesis. Vol. 1. *Edited by* J. D. Morrison. Academic Press, New York. 1983. p. 173.
24. C. S. Chen, Y. Fujimoto, G. Girdaukas, and C. J. Sih. J. Am. Chem. Soc. **104**, 7294 (1982).
25. O. Korver. Tetrahedron, **26**, 5507 (1970).

Can. J. Chem. Downloaded from www.nrcresearchpress.com by 91.144.44.67 on 09/07/12
For personal use only.

The synthesis of protected 5-azido-5-deoxy-D-gluconononitriles as precursors of glycosidase inhibitors

P. BIRD, D. H. DOLPHIN, AND S. G. WITHERS[1]

Department of Chemistry, University of British Columbia, Vancouver, B.C., Canada V6T 1Y6

Received May 30, 1989

P. BIRD, D. H. DOLPHIN, and S. G. WITHERS. Can. J. Chem. **68**, 317 (1990).

The successful syntheses of 5-azido-2,3,4,6-tetra-*O*-benzyl-5-deoxy-D-gluconononitrile and 2,3,4,6-tetra-*O*-benzyl-5-deoxy-5-trifluoroacetamido-D-gluconononitrile starting from D-glucose are described. Unsuccessful attempts were made to convert these two compounds into a protected 5-amino-5-deoxy-D-gluconononitrile and to subsequently cyclize them to an amidine analogue of glucose as a possible glycosidase inhibitor.

Key words: synthesis, amino-sugars, glycosidase inhibitors.

P. BIRD, D. H. DOLPHIN et S. G. WITHERS. Can. J. Chem. **68**, 317 (1990).

On décrit des synthèses réalisables des 5-azido-2,3,4,6-tétra-*O*-benzyl-5-désoxy- et 2,3,4,6-tétra-*O*-benzyl-5-désoxy-5-trifluoroacétamido-D-gluconononitriles à partir du D-glucose. On a essayé sans succès de transformer ces deux composés en un 5-amino-5-désoxy-D-gluconononitrile et éventuellement de les cycliser en une amidine analogue du glucose qui aurait pu être évaluée comme inhibiteur de la glycosidase.

Mots clés : synthèse, amino-sucres, inhibiteurs de la glycosidase.

[Traduit par la revue]

Can. J. Chem. Downloaded from www.nrcresearchpress.com by 91.144.44.67 on 09/07/12
For personal use only.

Introduction

Considerable effort has been expended in recent years in the design and synthesis of glycosidase inhibitors. These synthetic endeavours have been motivated by the discovery of a number of naturally occurring glycosidase inhibitors such as nojirimycin (1) and acarbose (2) and by their possible use in the treatment of diabetes and obesity (3, 4). These inhibitors are often nitrogen-containing analogues of glucose and glucooligosaccharides and their effectiveness as glycosidase inhibitors can be understood in terms of the generally accepted mechanism (5) of such enzymes where protonation of the glycosidic oxygen and departure of the protonated aglycone generate a glycosyl enzyme intermediate via an oxocarbonium ion transition state stabilized by interaction with an enzyme carboxylate group. Hydrolysis of this intermediate completes the reaction. Tight binding of aminoglycoside inhibitors presumably results from protonation of the nitrogen atom, generating an ammonium/carboxylate ion pair in the active site. In addition, a number of these inhibitors contain a partially planar ring, which may mimic the conformation of the transition state in the enzymic reaction. Glycosylamines, containing an exocyclic nitrogen atom at the anomeric centre, have also been shown (6) to be good inhibitors of a number of glycosidases. This suggested that a compound that combined the endo- and exo-cyclic nitrogen atoms in an unsaturated ring system might be an excellent glycosidase inhibitor. An example of such a compound is **1**, the amidine analogue of glucose.

A retrosynthetic analysis (7) gives two reasonable routes. The one that we attempted involves intramolecular attack of an amine on a nitrile (8), itself synthesized using an appropriately protected precursor such as an azido nitrile or an amino nitrile. An alternative route (not followed) could start with a protected 5-amino-5-deoxy-D-gluconolactam (9, 10), which could be converted to the desired amidine by first converting it to an *N*-alkylimino ester (11) or imidate (12), and then reacting this with an amine.

This paper describes the synthesis of the intermediates necessary for the first route, namely the azido nitrile and the amido nitrile. It also describes attempts at selective reductions of the azide moiety to give the desired amino nitrile.

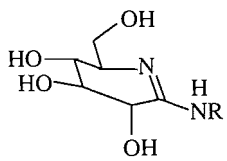

1

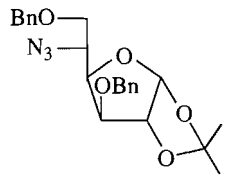

2

Results and discussion

Several slightly different routes to the desired protected 5-azido-5-deoxy-D-gluconononitrile were followed, all of which originated from the same starting material, the azido acetonide derivative (**2**). This was prepared from glucose according to literature procedures (13–15).

The first route attempted involved the formation of an oxime derivative at C-1, which could then be converted to the desired azido nitrile by an elimination reaction. Thus, the acetonide **2** was hydrolysed using aqueous trifluoroacetic acid to yield the hemiacetal **3**, which, on treatment with hydroxylamine (16), gave a mixture of the *E*- and *Z*-oximes **7**. Since these oximes could not be separated readily, the mixture was subjected to acetylation under basic conditions (17), effecting the facile elimination of the *Z*-oxime to give the desired nitrile (**8**) as the major product. The *E*-oxime, however, was inert to elimination and was isolated as the acetoxime **9**. Since the next step was to be the selective reduction of the azide to an amine, to which the acetate protecting groups would migrate, it was necessary to change protecting groups. Numerous attempts (e.g., 10% H_2SO_4/EtOH (18), KCN/MeOH (19)) were made to remove the acetates under neutral to acid conditions to avoid cyanohydrin decomposition, but none were successful. The direct dehydration of the unprotected oximes **7** was also attempted under a variety of conditions, but without success: e.g., treatment with selenium dioxide (20) regenerated the hemiacetal **3** while copper(II) acetate (21) gave degradation products.

Although ultimately unsuccessful, this approach demonstrated that a protected azido nitrile could be formed using this chemistry, so further attempts were made in which the desired

[1]Author to whom correspondence may be addressed.

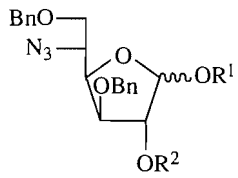

	R^1	R^2
3	H	H
4	Me	H
5	Me	Bn
6	H	Bn

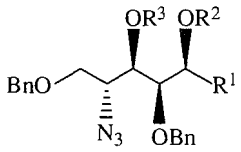

	R^1	R^2	R^3
7	C=NOH	H	H
8	CN	Ac	Ac
9	C=NOAc	Ac	Ac
10	C=NOH	Bn	H
11	CN	Bn	H
12	C=NOMe	H	H
13	C=NOMe	Bn	Bn

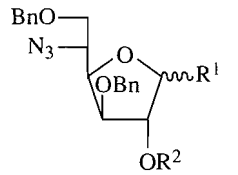

	R^1	R^2
14	β-SEt	H
15	α-SEt	H
16	α/β-SEt	Bn

hydroxyl protecting groups were inserted prior to nitrile formation. Selective protection of the C-2 hydroxyl was achieved by conversion of the hemiacetal **3** to the methyl furanosides **4**, then benzylation of the free C-2 hydroxyl using sodium hydride and benzyl bromide to give the tribenzyl ether **5**. Hydrolysis of the acetal (trifluoroacetic acid/water) yielded the hemiacetal **6**, which was converted into the oximes (**10**) by treatment with hydroxylamine. Unfortunately, it proved impossible to convert this oxime to the nitrile either by the previous protocol, or by using more reactive reagents such as trifluoroacetic anhydride (22), 2,4,6-trichloro-*s*-triazine (23), or carbonyldiimidazole (24), all of which gave complex mixtures. Presumably the bulky benzyl group at C-2 hinders the elimination process, rendering the less reactive reagents inactive. Failure of the more reactive reagents (which led to decomposition) was probably a result of reaction at, and elimination of, the C-4 hydroxyl or intramolecular attack of the free C-4 hydroxyl on the C-1 nitrile or the activated oxime (16).

Protection of the C-4 hydroxyl would alleviate these problems, making the use of the more vigorous dehydrating agents more feasible. The hemiacetal **3** was therefore reacted with methoxylamine hydrochloride yielding the methoximes **12** in which both the C-2 and the C-4 hydroxyls are exposed. Benzylation of **12** yielded the tetrabenzyl ether **13**, which we planned to either convert directly to the desired nitrile by elimination of methanol from the methoxime, or at least to convert it back to the aldehyde whence the nitrile could be formed. However, hydrolysis of **13** under acidic conditions (25) led to extensive decomposition, while attempted exchange with semicarbazide hydrochloride (26) failed completely. Direct formation of the nitrile from **13** by treatment with base (27) under a variety of conditions also failed, since either no reaction occurred, or there was extensive decomposition.

Failure of this approach necessitated a new strategy wherein the aldehyde is protected temporarily as the dithioacetal while the free hydroxyl groups are benzylated, the aldehyde then being regenerated and converted back into the nitrile. Treatment of the hemiacetal **3** with ethanethiol in concentrated hydrochloric acid (28) resulted in formation of the β-thiofuranoside **14** as the major product, with the α-thiofuranoside **15** and the desired dithioacetal **17** being produced as minor components. Considerable effort was expended in an attempt to produce a dithioacetal as the major product. This included changes (29) in temperature, reaction time, acid catalysts (e.g., zinc chloride, *p*-toluenesulfonic acid, boron trifluoride etherate), solvents, and thiol reagents (1,2-ethanedithiol, 1,3-propanedithiol), but all failed to significantly improve the yield of dithioacetal. Resubjecting the isolated major product (**14**) to the reaction conditions resulted in a slow conversion to **15** and **17** along with decomposition products. Since these could not be separated easily by column chromatography, the crude mixture was benzylated directly to give the benzyl ethers **16** and **18**, which were readily separable by chromatography. Hydrolysis of the dithioacetal **18** was accomplished in good yield using mercury(II) chloride (30), and the resulting aldehyde was converted directly to the oximes (**20**) by treatment with hydroxylamine. Reaction of these oximes with methanesulfonyl chloride in pyridine yielded the desired azido nitrile **21**.

While this route was ultimately successful, the yield of the dithioacetal was poor. An alternative approach was therefore explored, involving reduction of the aldehyde group in **3**, selective protection of the primary hydroxyl thus generated, and benzylation of the free hydroxyls at C-2 and C-4. Subsequent selective removal of the C-1 protecting group and oxidation should yield the desired aldehyde **19**. Therefore, hemiacetal **3** was reduced with sodium borohydride (31) to furnish the triol **22**, which was selectively protected at C-1 by treatment with pivaloyl chloride (32), giving the pivaloate ester **23** in good yield. Benzylation of the free hydroxyl groups yielded the tribenzyl ether **24**, which was then treated with sodium methoxide in methanol to remove the pivaloate ester at C-1 and expose the primary alcohol (**25**). Oxidation of this primary alcohol with pyridinium chlorochromate (33) proceeded reasonably smoothly to give the aldehyde **19**. This latter route proved to be the more efficient in terms of both yield and time.

The next step in the synthesis required the selective reduction of the azide in the presence of the nitrile to yield an amino nitrile, the required precursor to the amidine. Reductions were attempted under a number of conditions, as follows. No reaction whatsoever was observed with tin(II) chloride (34), or upon transfer hydrogenation with ammonium formate over palladium (35). Both hydrogen sulfide (36) and sodium ethoxide reacted preferentially with the nitrile moiety. Complex reaction mixtures were obtained with 1,3-propanedithiol (37), triphenylphosphine (38), and upon transfer hydrogenation with cyclohexene over palladium (39). Treatment with more vigorous

Can. J. Chem. Downloaded from www.nrcresearchpress.com by 91.144.44.67 on 09/07/12
For personal use only.

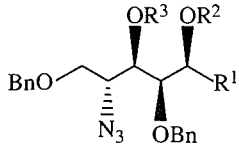

	R^1	R^2	R^3
17	$CH(SEt)_2$	H	H
18	$CH(SEt)_2$	Bn	Bn
19	CHO	Bn	Bn
20	C=NOH	Bn	Bn
21	CN	Bn	Bn
22	CH_2OH	H	H
23	CH_2OPiv	H	H
24	CH_2OPiv	Bn	Bn
25	CH_2OH	Bn	Bn

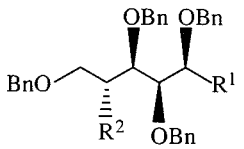

	R^1	R^2
26	CH_2OH	NH_2
27	CH_2OH	$NHCOCF_3$
28	CHO	$NHCOCF_3$
29	C=NOH	$NHCOCF_3$
30	CN	$NHCOCF_3$

reducing reagents such as lithium aluminum hydride (40) or sodium borohydride (41) resulted in the reduction of both the azide and the nitrile moieties.

Since selective reduction had proved more difficult than anticipated, an alternative route involving reduction of the azide and acylation of the resultant amine prior to formation of the nitrile was attempted. Treatment of the azido pivaloate **24** with lithium aluminum hydride resulted in the reduction of the azide and removal of the pivaloate ester, yielding the amino alcohol **26** in one step. Selective protection of the amine by reaction with trifluoroacetic anhydride, then with methanol, yielded the desired trifluoroacetamide **27** with a free primary alcohol. This was oxidized using pyridium chlorochromate to yield the protected aldehyde **28**, which was directly converted to the mixture of oximes (**29**) by treatment with hydroxylamine. Dehydration of the oximes was again achieved using methanesulfonyl chloride in pyridine, producing the desired trifluoroacetamido nitrile **30**.

Attempted removal of the trifluoroacetamide protecting group was unsuccessful. Treatment of **30** with potassium carbonate in aqueous methanol (42) or with sodium borohydride in boiling ethanol (43) yielded a mixture of at least four products, while no reaction was observed on treatment with triethylamine.

These attempts were therefore unsuccessful in generating the desired amino nitrile for cyclization to the amidine. However, they did generate viable routes to the precursor azido nitrile and amido nitrile, compounds that may have other applications in amino sugar chemistry.

Experimental

Thin-layer chromatography (tlc) was performed on Merck silica gel $60F_{254}$ aluminum backed plates. Chromatograms were visualized by charring with 10% sulphuric acid in methanol. Flash chromatography was carried out on Merck silica gel (230–400 mesh). The ^1H nmr spectra were recorded either on a Bruker WH-400 spectrometer, a Varian 300 MHz spectrometer, or a modified Bruker/Nicolet 270 MHz spectrometer, using $CDCl_3$ solutions and tetramethylsilane as an internal standard, unless otherwise stated. Chemical shifts are expressed as d and coupling constants (J) are given in hertz (s = singlet, d = doublet, t = triplet, m = multiplet).

2,4-Di-O-acetyl-5-azido-3,6-di-O-benzyl-5-deoxy-D-gluconononitrile (8)

The acetonide (15) **2** (1 g, 2.35 mmol) was suspended in trifluoroacetic acid (12 mL)/water (8 mL) and stirred for 3.5 h. Water (10 mL) was added, the mixture concentrated by evaporation, and the residue further dried by dissolving in toluene (25 mL), then concentrating by evaporation of solvent, three times over. The dark syrup obtained slowly solidified on standing at 4°C, and was usually used directly in subsequent reactions. Chromatography on silica gel (1:1 ethyl acetate–hexane) gave a light yellow syrup of 5-azido-3,6-di-*O*-benzyl-5-deoxy-α/β-D-glucofuranose **3**, which solidified (723 mg, 80%); $[\alpha]_D$ −2.9° (*c* 0.018, $CHCl_3$); ν_{max}(KBr): 3412 cm^{-1} (OH), 2100 cm^{-1} (N_3); ^1H nmr (300 MHz, $CDCl_3/D_2O$) δ: 7.44–7.24 (m, 10 H, C_6H_5), 5.47 (d, $J_{1,2}$ 3.7 Hz, H-1β), 5.09 (s, H-1α), 4.70–4.54 (m, $C_6H_5CH_2$), 4.24 (s, H-2α), 4.18 (dd, $J_{1,2}$ 3.7 Hz, H-2β), 4.15, 4.04–3.85, 3.75–3.62 (m, 5H, H-3,4,5,6,6′).

The hemiacetal **3** (904 mg, 2.35 mmol) in dry pyridine (20 mL) containing hydroxylamine hydrochloride (350 mg, 5.0 mmol) was kept at room temperature for 24 h. The solvent was evaporated and the residue concentrated from toluene (20 mL) three times over, dissolved in $CHCl_3$ (100 mL), washed with $NaHCO_3$ (40 mL), saturated brine (40 mL), and dried (Na_2SO_4). The syrup was chromatographed on silica (1:1 ethyl acetate – hexane) to give a mixture of *E*- and *Z*-5-azido-3,6-di-*O*-benzyl-5-deoxy-D-glucose oxime **7** (800 mg, 85%); $[\alpha]_D$ −7.7° (*c* 0.008, $CHCl_3$); ν_{max}(KBr): 3400 cm^{-1} (OH), 2100 cm^{-1} (N_3); ^1H nmr (270 MHz, $CDCl_3/D_2O$) δ: 7.52–7.14 (m, 10 H, C_6H_5), 7.49 (d, $J_{1,2}$ 5 Hz, H-1 *E* isomer), 6.90 (d, $J_{1,2}$ 7 Hz, H-1 *Z* isomer), 4.79–4.42 (m, 4H, $C_6H_5CH_2$), 3.98 (dd, 1H, H-2), 3.91–3.80 (m, 2H, H-3,4), 3.75–3.61 (m, 2H, H-5,6), 3.54 (m, 1H, H-6′).

To the oximes **7** (110 mg, 0.275 mmol) in dry pyridine (5 mL) was added acetic anhydride (1 mL) and triethylamine (1 mL). After standing at room temperature for 1 h, the solution was heated at 30°C for 20 h, then cooled and stirred with aqueous sodium bicarbonate (16 mL) for 2 h. The solution was extracted with $CHCl_3$ (40 mL), washed with $NaHCO_3$ (20 mL) and water (20 mL), and dried (Na_2SO_4). Evaporation of the solvent left a thick syrup, which was chromatographed on silica (1:3 ethyl acetate – hexane). The early fractions contained (*E*)-2,4-di-*O*-acetyl-5-azido-3,6-di-*O*-benzyl-5-deoxy-D-glucose acetoxime **9** (20 mg, 14%) as a colourless syrup; $[\alpha]_D$ +4.4° (*c* 0.001, $CHCl_3$); ν_{max}(KBr): 2100 cm^{-1} (N_3), 1760 cm^{-1} (OAc); ^1H nmr (300 MHz, $CDCl_3$) δ: 7.58–7.14 (m, 11H, C_6H_5, H-1 *E* isomer, H-1 *Z* isomer), 6.35 (br s, 3H, NOAc), 5.34 (br s, 1H, H-2), 4.79 (m, 1H, H-4), 4.70–4.53 (m, 4H, $C_6H_5CH_2$), 4.26 (m, 1H, H-3), 4.10–3.78 (m, 2H, H-5,6), 3.63 (m, 1H, H-6′), 2.15, 2.10–2.00 (2s + br s, OAc).

The later fractions contained the nitrile **8** (73 mg, 57%) as a colourless syrup; $[\alpha]_D$ +11.9° (*c* 0.0057, $CHCl_3$); ν_{max}(KBr): 2100 cm^{-1} (N_3), 1760 cm^{-1} (OAc); ^1H nmr (300 MHz, $CDCl_3$) δ: 7.44–7.35 (m, 10 H, C_6H_5), 5.48 (d, 1H, $J_{2,3}$ 6.5 Hz, H-2), 5.19 (dd, 1H, $J_{3,4}$ 2.0, $J_{4,5}$ 9.3 Hz, H-4), 4.78, 4.57 (2s, 4H, $C_6H_5CH_2$), 4.11 (dd, 1H, $J_{2,3}$ 6.5, $J_{3,4}$ 2.0 Hz, H-3), 3.96 (m, 1H, H-5), 3.66 (dd, 1H, $J_{5,6}$ 3.3, $J_{6,6'}$ 10.0 Hz, H-6), 3.60 (dd, 1H, $J_{5,6'}$ 7.3, $J_{6,6'}$ 10.0 Hz, H-6′), 2.15, 2.14 (2s, 6H, OAc); ^{13}C nmr (100.6 MHz, $CDCl_3$) δ: 169.7, 168.3 (CO), 137.3, 136.3 (Ar, C-1), 128.7, 128.6, 128.4, 128.3, 127.9, 127.8 (Ar), 114.8 (C≡N), 74.7, 74.6, 73.6, 69.6, 68.9 (*C*H, *C*-N_3), 59.7, 59.4 (CH_2), 20.7, 20.1 (*Me*).

(E,Z)-5-Azido-2,3,4,6-tetra-O-benzyl-5-deoxy-D-glucose methoxime (12)

The hemiacetal **3** (1.5 g, 3.89 mmol) in dry methanol (50 mL) containing Amberlite IR-120(H^+) resin (1.4 g) and 4 Å molecular sieves (1 g) was heated at reflux for 10 h. The cool solution was filtered, the solvent evaporated, and the resultant syrup dissolved in $CHCl_3$

Can. J. Chem. Downloaded from www.nrcresearchpress.com by 91.144.44.67 on 09/07/12
For personal use only.

Can. J. Chem. Downloaded from www.nrcresearchpress.com by 91.144.44.67 on 09/07/12
For personal use only.

(100 mL), washed with $NaHCO_3$ (40 mL), then with brine (40 mL), and dried (Na_2SO_4). Evaporation gave a syrup, which was chromatographed on silica (1:2 ethyl acetate – hexane) to give the product as an anomeric mixture (1.19 g, 77%).

The early fractions contained the β-anomer: $[\alpha]_D$ +10.2° (*c* 0.01, $CHCl_3$); ^1H nmr (300 MHz, $CDCl_3$) δ: 7.49–7.10 (m, 10 H, C_6H_5), 5.02 (d, 1H, $J_{1,2}$ 4.4 Hz, H-1), 4.74–4.58 (m, 4H, $C_6H_5CH_2$), 4.23 (ddd, 1H, $J_{1,2}$ 4.4, $J_{2,3}$ 0.4, $J_{2,OH}$ 3.1 Hz, H-2), 4.11 (dd, 1H, $J_{3,4}$ 4.3, $J_{4,5}$ 9.2 Hz, H-4), 3.97 (m, 2H, H-3,5), 3.87 (dd, 1H, $J_{5,6}$ 2.5, $J_{6,6'}$ 10 Hz, H-6), 3.64 (dd, 1H, $J_{5,6'}$ 7.4, $J_{6,6'}$ 10 Hz, H-6'), 3.46 (s, 3H, OMe), 2.84 (d, 1H, $J_{OH,2}$ 3.1 Hz, OH).

The later fractions contained the α-anomer: $[\alpha]_D$ −13.8° (*c* 0.023, $CHCl_3$); ^1H nmr (300 MHz, $CDCl_3$) δ: 7.48–7.21 (m, 10 H, C_6H_5), 4.77 (s, 1H, H-1), 4.70–4.61 (m, 4H, $C_6H_5CH_2$), 4.20 (s, 1H, H-2), 4.17 (dd, 1H, $J_{3,4}$ 5.1, $J_{4,5}$ 9.7 Hz, H-4), 4.03 (m, 1H, H-5), 3.91 (m, 2H, H-3,6), 3.67 (dd, 1H, $J_{5,6'}$ 7.2, $J_{6,6'}$ 10.1 Hz, H-6'), 3.33 (s, 3H, OMe), 1.8 (br s, 1H, OH).

The alcohol **4** (1.19 g, 2.98 mmol) in dry DMF (20 mL) was stirred at 0°C under an argon atmosphere, sodium hydride (115 mg, 4.79 mmol) was rapidly added, and the mixture stirred for 1 h. Benzyl bromide (0.4 mL, 3.34 mmol) was added and the mixture slowly warmed to room temperature. After 4 h, dry methanol (4 mL) was added dropwise and stirred for 1 h. The solution was concentrated, the residue partitioned between chloroform (100 mL) and aqueous sodium bicarbonate (50 mL), and the organic phase washed with saturated brine (50 mL), dried (Na_2SO_4), and the solvent evaporated. Chromatography on silica (1:6 ethyl acetate – hexane) gave the methyl 5-azido-2,3,6-tri-*O*-benzyl-5-deoxy-α/β-D-glucofuranosides **5** as a colourless syrup (1.23 g, 84%); $[\alpha]_D$ +40.0° (*c* 0.006, $CHCl_3$); ν_{max}(KBr): 2100 cm^{-1} (N_3); ^1H nmr (300 MHz, CCl_3) δ: 7.38–7.25 (m, 15H, C_6H_5), 4.88 (s, H-1α), 4.87 (d, $J_{1,2}$ 4 Hz, H-1β), 4.67–4.52 (m, 6H, $C_6H_5CH_2$), 4.20–3.83 (m, 5H, H-2,3,4,5,6), 3.70–3.59 (m, 1H, H-6'), 3.38, 3.34 (2s, OMe).

The methyl glycosides **5** (1.13 g, 2.31 mmol) in trifluoroacetic acid (14 mL)/water (6 mL) were stirred for 6 h at room temperature. The solution was diluted with water (15 mL) and the solvent evaporated to give a dark residue, which was dried by evaporation from toluene (3 × 20 mL). The thick syrup was dissolved in chloroform (60 mL), washed with $NaHCO_3$ (100 mL), saturated brine (40 mL), dried (Na_2SO_4), concentrated, and chromatographed on silica (1:4 ethyl acetate – hexane) to give 5-azido-2,3,6-tri-*O*-benzyl-5-deoxy-α/β-D-glucofuranose **6** as a light yellow syrup (910 mg, 83%); $[\alpha]_D$ −3.8° (*c* 0.015, $CHCl_3$); ν_{max}(KBr): 3400 cm^{-1} (OH), 2100 cm^{-1} (N_3); ^1H nmr (270 MHz, $CDCl_3$) δ: 7.56–7.13 (m, 15H, C_6H_5), 5.45 (dd, $J_{1,2}$ 4, $J_{1,OH}$ 11 Hz, H-1β), 5.21 (d, $J_{1,OH}$ 12 Hz, H-1α), 4.70–4.41 (m, 6H, $PhCH_2$), 4.11–3.79 (m, 5H, H-2,3,4,5,6), 3.71–3.58 (m, 2H, H-6', OH), 3.37 (d, 1H, $J_{1,OH}$ 12 Hz, OH).

Hemiacetal **6** (461 mg, 0.97 mmol) was treated in the same manner as for the preparation of compound **7**. Chromatography on silica (1:2 ethyl acetate – hexane) gave (*E*,*Z*)-5-azido-2,3,6-tri-*O*-benzyl-5-deoxy-D-glucose oxime **10** as a colourless syrup (394 mg, 83%); $[\alpha]_D$ −31.2° (*c* 0.008, $CHCl_3$); ν_{max}(KBr): 3400 cm^{-1} (OH, NOH), 2100 cm^{-1} (N_3); ^1H nmr data (300 MHz, $CDCl_3/D_2O$) δ: 7.49–7.14 (m, C_6H_5, H-1 *Z* isomer), 6.89 (d, H-1 *E* isomer), 4.95–4.18 (m, 7H, $C_6H_5CH_2$, H-2), 4.01–3.80 (m, 2H, H-3,4), 3.73–3.43 (m, 3H, H-5,6,6').

To hemiacetal **3** (164 mg, 0.42 mmol) in dry pyridine (6 mL) was added methoxylamine hydrochloride (100 mg, 1.19 mmol). After 22 h at room temperature the solution was concentrated, the residue dissolved in $CHCl_3$ (50 mL), washed with $NaHCO_3$ (40 mL), brine (30 mL), dried (Na_2SO_4), and concentrated to a dark syrup. Chromatography on silica (1:2 ethyl acetate – hexane) gave (*E*,*Z*)-5-azido-3,6-di-*O*-benzyl-5-deoxy-D-glucose methoxime **12** as a colourless syrup (163 mg, 93%); $[\alpha]_D$ +18° (*c* −0.006, $CHCl_3$); ^1H nmr (300 MHz, $CDCl_3/D_2O$) δ: 7.49 (dd, H-1 *Z* isomer), 7.51–7.40 (m, 10 H, C_6H_5), 6.88 (dd, H-1 *E* isomer), 4.91, 4.82–4.48 (m, 7H, H-2,3,4; $C_6H_5CH_2$), 3.98–3.51 (m, 3H, H-5,6,6'), 3.89 (s, OMe, *Z* isomer), 3.85 (s, OMe, *E* isomer).

Diol **12** (120 mg, 0.289 mmol) was benzylated using the same procedure as for compound **5**. Chromatography on silica (1:8 ethyl acetate – hexane) gave the product (*E*,*Z*)-5-azido-2,3,4,6-tetra-*O*-benzyl-5-deoxy-D-glucose methoxime **13** as a light yellow syrup (132 mg, 77%); $[\alpha]_D$ +5.0° (*c* 0.01, $CHCl_3$); ν_{max}(KBr): 2100 cm^{-1} (N_3), 1640 cm^{-1} (C=N); ^1H nmr (270 MHz, $CDCl_3$) δ: 7.69–7.07 (m, C_6H_5, H-1 *Z* isomer), 6.88 (d, H-1 *E* isomer), 4.79–4.40 (m, 9H, $C_6H_5CH_2$, H-2), 4.35–4.28 (m, 2H, H-3,4), 3.88–3.47 (m, 3H, H-5,6,6'), 3.85 (s, 3H, OMe). Exact mass calcd. for $C_{35}H_{38}N_4O_5$: 594.2842; found: 594.2849.

*5-Azido-2,3,4,6-tetra-*O*-benzyl-5-deoxy-D-glucononitrile (**21**)*

Hemiacetal **3** (1 g, 2.59 mmol) in ethanethiol (20 mL) was cooled to 0°C, concentrated hydrochloric acid (1 mL) was added, and the mixture stirred at 0°C for 4 h. The mixture was poured into aqueous sodium bicarbonate (100 mL) and the solution extracted with $CHCl_3$ (50 mL). The organic phase was washed with $NaHCO_3$ (40 mL), water (40 mL), dried (Na_2SO_4), the solvent evaporated, and the dark syrup chromatographed on silica (2:7 ethyl acetate – hexane) to give a colourless syrup (948 mg) containing ethyl 5-azido-3,6-di-*O*-benzyl-5-deoxy-1-thio-β-D-glucofuranoside (**14**), the -α-D-anomer (**15**), and 5-azido-3,6-di-*O*-benzyl-5-deoxy-D-glucose diethyldithioacetal (**17**).

Early fractions were enriched with the β-anomer (**14**): ^1H nmr (400 MHz, $CDCl_3$) δ: 7.41–7.26 (m, 10 H, C_6H_5), 5.39 (d, 1H, $J_{1,2}$ 4 Hz, H-1), 4.65, 4.58 (2s, 4H, $C_6H_5CH_2$), 4.28 (ddd, 1H, $J_{1,2}$ 4, $J_{2,3}$ 1, $J_{2,OH}$ 5 Hz, H-2), 4.15–3.96 (m, 3H, H-3,4,5), 3.89 (dd, 1H, $J_{5,6}$ 2.5, $J_{6,6'}$ 10 Hz, H-6), 3.63 (dd, 1H, $J_{5,6}$ 7.5, $J_{6,6'}$ 10 Hz, H-6'), 2.64 (q, 2H, *J* 7 Hz, SCH_2), 2.43 (d, 1H, $J_{2,OH}$ 5 Hz, OH), 1.28 (t, 3H, *J* 7 Hz, SCH_2CH_3).

The middle fractions were enriched with **17**: ^1H nmr (270 MHz, $CDCl_3$) δ: 7.39–7.27 (m, 10 H, C_6H_5), 4.91–4.77 (m, 2H, $C_6H_5CH_2$), 4.58 (s, 2H, $C_6H_5CH_2$), 4.22 (dd, 1H, H-2), 4.14–3.70 (m, 5H, H-1,3,4,5,6), 3.59 (m, 1H, H-6'), 3.25, 3.14 (2 br s, 2H, OH), 2.65 (q, 4H, *J* 8 Hz, SCH_2), 1.26 (t, 6H, *J* 8 Hz, SCH_2CH_3).

A mixture of **14**, **15**, and **17** (410 mg) was benzylated in the same manner as for compound **5**. Chromatography on silica (1:12 ethyl acetate – hexane) gave 5-azido-2,3,4,6-tetra-*O*-benzyl-5-deoxy-D-glucose diethyldithioacetal **18** (135 mg) as a colourless syrup; $[\alpha]_D$ −6.8° (*c* 0.003, $CHCl_3$); ν_{max}(KBr): 2100 cm^{-1} (N_3); ^1H nmr (300 MHz, $CDCl_3$) δ: 7.40–7.14 (m, 20 H, C_6H_5), 4.88–4.50 (m, 8H, $C_6H_5CH_2$), 4.13 (dd, 1H, $J_{2,3}$ 6.7, $J_{3,4}$ 4.3 Hz, H-3), 4.01 (dd, 1H, $J_{2,3}$ 6.7, $J_{1,2}$ 3.8 Hz, H-2), 3.92–3.83 (m, 3H, H-1,4,5), 3.72 (m, 2H, H-6,6'), 2.70, 2.54 (2 dq, 4H, SCH_2), 1.22, 1.16 (2t, 6H, SCH_2CH_3). The later fractions contained ethyl-5-azido-2,3,6-tri-*O*-benzyl-5-deoxy-1-thio-α/β-D-glucofuranose **16** as a colourless syrup (360 mg); $[\alpha]_D$ −10.3 (*c* 0.0015, $CHCl_3$); ν_{max}(KBr): 2100 cm^{-1} (N_3); ^1H nmr (300 MHz, $CDCl_3$) δ: 7.47–7.23 (m, 15H, C_6H_5), 5.48 (d, $J_{1,2}$ 4.5 Hz, H-1β), 5.06 (d, $J_{1,2}$ 2.3 Hz, H-1α), 4.64–4.42 (m, 6H, $C_6H_5CH_2$), 4.15–3.85 (m, 5H, H-2,3,4,5,6), 3.63 (m, 1H, H-6'), 2.66, 2.63 (2q, *J* 7.4 Hz, SCH_2), 1.28, 1.26 (2t, *J* 7.4 Hz, SCH_2CH_3).

To the dithioacetal **18** (127 mg, 0.189 mmol) in acetonitrile (6 mL)/water (1 mL) was added calcium carbonate (111 mg, 1.11 mmol) and mercury(II) chloride (260 mg, 0.957 mmol). After stirring at room temperature for 4 h, the solids were removed by filtration through a Celite plug and washed with $CHCl_3$ (2 × 50 mL). The combined filtrate was washed with sodium iodide (1 mol dm^{-3}, 2 × 30 mL), dried (Na_2SO_3), and concentrated to a colourless syrup of 5-azido-2,3,4,6-tetra-*O*-benzyl-5-deoxy-D-glucose **19** (95 mg, 89%), which was used immediately in subsequent reactions.

Crude aldehyde **19** (106 mg, 0.189 mmol) was reacted with hydroxylamine hydrochloride in the same manner as for the preparation of compound **7**. Chromatography on silica (1:4 ethyl acetate – hexane) gave (*E*,*Z*)-5-azido-2,3,4,6-tetra-*O*-benzyl-5-deoxy-D-glucose oxime **20** as a colourless syrup (74 mg, 68%); $[\alpha]_D$ +17.5° (*c* 0.0033, $CHCl_3$); ν_{max}(KBr): 3390 cm^{-1} (NOH), 2100 cm^{-1} (N_3); ^1H nmr data (270 MHz, $CDCl_3$) δ: 7.57–7.10 (m, C_6H_5, H-1 *Z* isomer), 6.95 (d, H-1 *E* isomer), 4.77–4.33 (m, 9H, $C_6H_5CH_2$, H-2), 4.27 (dd, 1H, $J_{2,3}$ 6, $J_{3,4}$ 7.7 Hz, H-3), 3.94–3.48 (m, 4H, H-4,5,6,6').

The oximes **20** (123 mg, 0.212 mmol) in dry pyridine (2.5 mL) were

Can. J. Chem. Downloaded from www.nrcresearchpress.com by 91.144.44.67 on 09/07/12
For personal use only.

cooled to 0°C under an argon atmosphere, methanesulphonyl chloride (0.1 mL, 1.29 mmol) was added dropwise, and the solution kept on ice for 0.25 h, then at room temperature for 1 h. Saturated $NaHCO_3$ (3 mL) was added dropwise and, after concentration, the residue was partitioned between $CHCl_3$ (50 mL) and $NaHCO_3$ (40 mL). The aqueous phase was extracted with $CHCl_3$ (2 × 20 mL), and the combined organic phase washed with water (20 mL), dried, and evaporated. Chromatography on silica (1:5 ethyl acetate – hexane) gave 5-azido-2,3,4,6-tetra-*O*-benzyl-5-deoxy-D-glucononitrile **21** as a colourless syrup (112 mg, 94%); $[\alpha]_D$ +37.0° (*c* 0.004, $CHCl_3$); ν_{max}(KBr): 2100 cm^{-1} (N_3, C≡N); ^1H nmr (300 MHz, $CDCl_3$) δ: 7.40–7.18 (m, 20 H, C_6H_5), 4.89–4.47 (m, 8H, $C_6H_5CH_2$), 4.34 (d, 1H, $J_{2,3}$ 6.8 Hz, H-2), 3.94 (m, 2H, H-4,5), 3.81 (dd, 1H, $J_{2,3}$ 6.8, $J_{3,4}$ 2 Hz, H-3), 3.74–3.63 (m, 2H, H-6,6′); ^{13}C nmr (75 MHz, $CDCl_3$) δ: 137.37, 137.24, 137.09, 135.29 (4s, Ar), 128.71–127.76 (14s, Ar), 116.63 (1s, C≡N), 78.07, 76.99, 68.52, 60.49 (4s, C-2,3,4,5), 75.29, 74.98, 73.32, 72.81, 68.90 (5s, C-6, $PhCH_2O$). Exact mass calcd. for $C_{34}H_{34}N_4O_4$: 562.2580; found: 562.2579.

*2,3,4,6-Tetra-*O*-benzyl-5-deoxy-5-trifluoroacetamido-D-glucitol (27)*

To hemiacetal **3** (1.75 g, 4.55 mmol) in absolute ethanol (50 mL) was added sodium borohydride (166 mg, 4.36 mmol) and water (4 mL) and the solution heated at reflux for 3 h. The cooled solution was acidified with glacial acetic acid and concentrated. The residue was partitioned between dilute HCl (50 mL) and $CHCl_3$ (50 mL), the aqueous phase extracted with $CHCl_3$ (2 × 25 mL), then the combined organic phase was washed with $NaHCO_3$ (50 mL) and dried (Na_2SO_4). Evaporation of solvent gave a dark syrup, which was chromatographed on silica (1:1 ethyl acetate – hexane) to give 5-azido-3,6-di-*O*-benzyl-5-deoxy-D-glucitol **22** as a thick colorless syrup (1.25 g, 71%); $[\alpha]_D$ −53.3° (*c* 0.0075, $CHCl_3$); ν_{max}(KBr): 3420 cm^{-1} (OH), 2100 cm^{-1} (N_3); ^1H nmr data (270 MHz, $CDCl_3/D_2O$) δ: 7.56–7.22 (m, 10 H, C_6H_5), 4.69–4.58 (m, 4H, $C_6H_5CH_2$), 3.94–3.50 (m, 8H, H-1,1′,2,3,4,5,6,6′).

The triol **22** was acetylated (Ac_2O, pyridine, room temp.) to give 1,2,4-tri-*O*-acetyl-5-azido-3,6-di-*O*-benzyl-5-deoxy-D-glucitol; $[\alpha]_D$ 7.4° (*c* 0.004, $CHCl_3$); ν_{max}(KBr): 2100 cm^{-1} (N_3), 1750 cm^{-1} (OAc); ^1H nmr (300 MHz, $CDCl_3$) δ: 7.39–7.20 (m, 10 H, C_6H_5), 5.26 (m, 1H, $J_{1,2}$ 2.8 Hz, H-2), 5.08 (dd, 1H, $J_{3,4}$ 2.8, $J_{4,5}$ 8.3 Hz, H-4), 4.72 (m, 2H, $C_6H_5CH_2$), 4.53 (d, 2H, *J* 5.2 Hz, $C_6H_5CH_2$), 4.40 (dd, 1H, $J_{1,1'}$ 12.3, $J_{1,2}$ 2.8 Hz, H-1), 4.02 (m, 2H, H-1′,3), 3.87 (m, 1H, H-5), 3.61 (dd, 1H, $J_{5,6}$ 3.7, $J_{6,6'}$ 10 Hz, H-6), 3.54 (dd, 1H, $J_{5,6'}$ 7.1, $J_{6,6'}$ 10 Hz, H-6′), 2.04, 1.99, 1.96 (3s, 9 H, OAc).

The triol **22** (1.12 g, 2.89 mmol) in dry pyridine (20 mL) was cooled to −40°C under an argon atmosphere. Pivaloyl chloride (0.356 mL, 2.89 mmol) was added dropwise and the solution kept at −40°C for 1 h, then slowly warmed to room temperature over 1.5 h. Methanol (0.1 mL) was added, solvent evaporated, and the residue was then dissolved in $CHCl_3$ (100 mL), washed with $NaHCO_3$ (40 mL), brine (40 mL), dried (Na_2SO_4), and concentrated. The crude syrup of 5-azido-3,6-di-*O*-benzyl-5-deoxy-1-*O*-pivaloyl-D-glucitol **23** (1.36 g, 100%) was further dried by concentration from toluene (3 × 15 mL) and used directly in the formation of compound **24**; $[\alpha]_D$ −38.2° (*c* 0.008, $CHCl_3$); ν_{max}(KBr): 3460 cm^{-1} (OH), 2100 cm^{-1} (N_3), 1730 cm^{-1} (CO).

Diol **23** (1.35 g, 2.86 mmol) was benzylated using the same procedure as for compound **5**. Chromatography on silica (1:6 ethyl acetate – hexane) gave a colourless syrup of 5-azido-2,3,4,6-tetra-*O*-benzyl-5-deoxy-1-*O*-pivaloyl-D-glucitol **24** (1.69 g, 90%); $[\alpha]_D$ +0.4° (*c* 0.0176, $CHCl_3$); ν_{max}(KBr): 2100 cm^{-1} (N_3), 1735 cm^{-1} (CO); ^1H nmr (270 MHz, $CDCl_3$) δ: 7.36–7.14 (m, 20 H, C_6H_5), 4.76–4.41 (m, 8H, $C_6H_5CH_2$), 4.36–4.17 (2dd, 2H, $J_{1,1'}$ 12 Hz, H-1,1′), 3.83–3.63 (m, 6H, H-2,3,4,5,6,6′), 1.20 (s, 9H, Me_3C).

A solution of sodium (50 mg, 2.17 mmol) dissolved in dry methanol (3 mL) was rapidly added to compound **24** (310 mg, 0.47 mmol) in dry methanol (10 mL). After heating at 45°C for 4 days, the cooled solution was neutralized with glacial acetic acid, concentrated, dissolved in $CHCl_3$ (50 mL), washed with $NaHCO_3$ (30 mL) and brine (20 mL), dried (Na_2SO_4), and the solvent evaporated. Chromatography on silica (1:3 ethyl acetate – hexane) gave recovered **24** (75 mg) and the syrupy product, 5-azido-2,3,4,6-tetra-*O*-benzyl-5-deoxy-D-glucitol **25** (170 mg, 63%); $[\alpha]_D$ −2.7° (*c* 0.002, $CHCl_3$); ν_{max}(KBr): 3460 cm^{-1} (OH), 2100 cm^{-1} (N_3); ^1H nmr (270 MHz, $CDCl_3$) δ: 7.56–7.10 (m, 20 H, C_6H_5), 4.81–4.31 (m, 8H, $C_6H_5CH_2$), 3.91 (m, 2H, H-2,4), 3.85 (m, 1H, H-3), 3.77, 3.73 (2 br s, 2H, H-1,1′), 3.55 (dd and m, 2H, $J_{5,6}$ 5, $J_{6,6'}$ 9.5 Hz, H-5,6), 3.41 (dd, 1H, $J_{5,6'}$ 7, $J_{6,6'}$ 9.5 Hz, H-6′).

The alcohol **25** (43 mg, 0.075 mmol) in dry dichloromethane (2 mL) was stirred at room temperature, pyridinium chlorochromate (36 mg, 0.167 mmol) was added, and stirring was continued for 3 h. The mixture was diluted with 1:4 ethyl acetate – hexane (10 mL) and applied to a short silica column. Elution with 1:4 ethyl acetate – hexane gave 5-azido-2,3,4,6-tetra-*O*-benzyl-5-deoxy-D-glucose **19** (30 mg, 71%), which was used immediately in subsequent reactions: ν_{max}(KBr): 2100 cm^{-1} (N_3), 1685 cm^{-1} (CHO).

To the azido ester **24** (86 mg, 0.132 mmol) in dry oxolane (10 mL) was added lithium aluminium hydride (15 mg, 0.39 mmol) and the mixture stirred at room temperature for 1.5 h. Sodium sulphate decahydrate (50 mg) was added; the solids were removed by filtration and then washed with $CHCl_3$ (4 × 10 mL). The combined filtrates were concentrated and the syrup dissolved in dry acetonitrile (6 mL). After cooling to 0°C, trifluoroacetic anhydride (0.1 mL, 0.70 mmol) was added dropwise, and the solution kept on ice for 5 min, then at room temperature for 5 min. The solvent was evaporated and the syrup dissolved in $CHCl_3$ (20 mL), washed with $NaHCO_3$ (20 mL), saturated brine (10 mL), dried (Na_2SO_4), and concentrated to a syrup of the bistrifluoroacetyl derivative; ν_{max}(KBr): 3390 cm^{-1} (NH), 1790 cm^{-1} ($OCOCF_3$), 1730 cm^{-1} ($NCOCF_3$). This syrup was dissolved in dry methanol (10 mL) and heated at 45°C for 8 h. Evaporation of solvent gave a crude syrup, which was chromatographed on silica (1:3 ethyl acetate – hexane) to give 2,3,4,6-tetra-*O*-benzyl-5-deoxy-5-trifluoroacetamido-D-glucitol **27** as a colourless syrup (49 mg, 58%); $[\alpha]_D$ +2.8° (*c* 0.0083, $CHCl_3$); ν_{max}(KBr): 2390 cm^{-1} (OH), 1730 cm^{-1} (CO); ^1H nmr (270 MHz, $CDCl_3$) δ: 7.54–7.17 (m, 20 H, C_6H_5), 4.72–4.34 (m, 8H, $C_6H_5CH_2$), 4.60 (m, 1H, H-5), 3.93 (m, 2H, H-3,4), 3.85 (m, 1H, H-2), 3.76 (dd, 1H, $J_{1,1'}$ 12, $J_{1,2}$ 3.5 Hz, H-1), 3.55 (2dd, 2H, $J_{1,1'}$ 12, $J_{1,2}$ 4 Hz, H-1′, $J_{5,6}$ 5, $J_{6,6'}$ 9.5 Hz, H-6), 3.42 (dd, 1H, $J_{5,6'}$ 6.5, $J_{6,6'}$ 9.5 Hz, H-6′). Exact mass calcd. for $C_{36}H_{38}NF_3O_6$: 637.2651; found: 637.2627.

*2,3,4,6-Tetra-*O*-benzyl-5-deoxy-5-trifluoroacetamido-D-glucononitrile (30)*

Alcohol **27** (42 mg, 0.065 mmol) was oxidized in the same manner as for the preparation of aldehyde **19**. The crude reaction mixture was filtered through a short silica column, eluting with 1:3 ethyl acetate – hexane to give 2,3,4,6-tetra-*O*-benzyl-5-deoxy-5-trifluoroacetamido-D-glucose **28** as a colourless syrup (31 mg, 76%), which was immediately used in subsequent transformations; ν_{max}(KBr): 1730 cm^{-1} ($NHCOCF_3$), 1690 cm^{-1} (CHO); ^1H nmr (270 MHz, $CDCl_3$) δ: 9.67 (s, 1H, CHO), 7.62–7.07 (m, 20 H, C_6H_5), 4.88–4.09 (m, 9H, H-5, $C_6H_5CH_2$), 4.09, 3.96 (2dd, 2H, *J* 2.5, *J* 5.5 Hz, H-3,4), 3.99 (d, 1H, $J_{2,3}$ 5.5 Hz, H-2), 3.54 (dd, 1H, $J_{5,6}$ 4.5, $J_{6,6'}$ 9.5 Hz, H-6), 3.33 (dd, 1H, $J_{5,6'}$ 7, $J_{6,6'}$ 9.5 Hz, H-6′).

The aldehyde **28** (41 mg, 0.065 mmol) was treated in the same manner as for the preparation of compound **3**. Chromatography on silica (1:3 ethyl acetate – hexane) gave (*E*,*Z*)-2,3,4,6-tetra-*O*-benzyl-5-deoxy-5-trifluoroacetamido-D-glucose oxime **29** as a colourless syrup (30 mg, 71%); $[\alpha]_D$ +10.0° (*c* 0.01, $CHCl_3$); ν_{max}(KBr): 3390 cm^{-1} (NOH), 1728 cm^{-1} (CO); ^1H nmr (270 MHz, $CDCl_3$) δ: 7.60–7.12 (m, 21H, C_6H_5, H-1 *E* isomer, H-1 *Z* isomer), 4.80–4.24 (m, 9H, $C_6H_5CH_2$, H-2), 4.57 (m, 1H, H-5), 3.99–3.89 (m, 2H, H-3,4), 3.52 (dd, 1H, $J_{5,6}$ 4.5, $J_{6,6'}$ 9.5 Hz, H-6), 3.30 (dd, 1H, $J_{5,6'}$ 7.5, $J_{6,6'}$ 9.5 Hz, H-6). Exact mass calcd. for $C_{36}H_{37}N_2F_3O_6$: 650.2604; found: 650.2604.

The oximes **29** (42 mg, 0.064 mmol) were treated in the same manner as for the preparation of compound **21**. Chromatography on silica (1:3 ethyl acetate – hexane) gave 2,3,4,6-tetra-*O*-benzyl-5-deoxy-5-trifluoroacetamido-D-glucononitrile **30** as a colourless syrup

(31 mg, 76%); $[\alpha]_D$ +23° (*c* 0.025, $CHCl_3$); ν_{max}(KBr): 3390 cm^{-1} (NH), 2100 cm^{-1} (CN), 1729 cm^{-1} (NHCO); ^1H nmr (270 MHz, $CDCl_3$) δ: 7.50–7.06 (m, 20 H, C_6H_5), 4.89–4.24 (m, 8H, $C_6H_5CH_2$), 4.67 (m, 1H, H-5), 4.57 (d, 1H, $J_{2,3}$ 7 Hz, H-2), 4.11 (dd, 1H, $J_{3,4}$ 3, $J_{4,5}$ 5 Hz, H-4), 4.05 (dd, 1H, $J_{2,3}$ 7, $J_{3,4}$ 3 Hz, H-3), 3.53 (dd, 1H, $J_{5,6}$ 5.5, $J_{6,6'}$ 9.5 Hz, H-6), 3.34 (dd, 1H, $J_{5,6'}$ 8, $J_{6,6'}$ 9.5 Hz, H-6′). Exact mass calcd. for $C_{36}H_{35}N_2F_3O_5$: 632.2478; found: 632.2488.

Acknowledgements

We thank the Natural Sciences and Engineering Research Council of Canada for financial support.

1. S. Inouye, T. Tsurnoka, and T. Niida. J. Antibiot. **19**, 288 (1966).
2. D. D. Schmidt, W. Frommer, B. Junge, L. Muller, W. Wingender, E. Truscheit, and D. Schafer. Naturwissenschaften, **64**, 535 (1977).
3. W. Puls, E. Keupe, H. P. Krause, L. Muller, D. D. Schmidt, C. Thomas, and E. Truscheit. Front. Horm. Res. **7**, 235 (1980).
4. K. Schoffling, I. Hillebrand, and P. Berchtold. Front. Horm. Res. **7**, 248 (1980).
5. M. L. Sinnott. *In* The chemistry of enzyme action. *Edited by* M. I. Page. Elsevier, New York. 1984. pp. 389–431.
6. P. Lalegerie, G. Legler, and J. M. Yon. Biochimie, **64**, 977 (1982).
7. J.-A. Gautier, M. Miocque, and C. C. Farnoux. *In* The chemistry of amidines and imidates. *Edited by* S. Patai. John Wiley and Sons, New York. 1975. Chap. 7. pp. 283–348.
8. R. Kwok and P. Pranc. J. Org. Chem. **32**, 738 (1967).
9. S. Hanessian. J. Org. Chem. **34**, 675 (1969).
10. S. Inouye, T. Tsuruoka, T. Ito, and T. Niida. Tetrahedron, **23**, 2125 (1968).
11. L. Weintraub, S. R. Oles, and N. Kalish. J. Org. Chem. **33**, 1679 (1968).
12. S. R. Sandler and W. Karo. Organic functional group preparations. Academic Press, New York. 1972. pp. 217–222.
13. R. L. Whistler and W. C. Lake. Methods Carbohydr. Chem. **6**, 286 (1972).
14. R. L. Whistler and R. E. Gramera. J. Org. Chem. **29**, 2609 (1964).
15. H. Saeki and E. Ohki. Chem. Pharm. Bull. **16**, 2477 (1968).
16. J. G. Buchanan, K. A. Maclean, R. H. Wightman, and H. Paulsen. J. Chem. Soc. Perkin Trans. 1, 1463 (1985).
17. V. Deulofeu. Adv. Carbohydr. Chem. **4**, 119 (1949).
18. G. Zemplen. Ber. Dtsch. Chem. Ges. **60**, 171 (1927).
19. J. Herzig, A. Nudelman, H. E. Gottlieb, and B. Fischer. J. Org. Chem. **51**, 727 (1986).
20. G. Sosnovsky and J. A. Krogh. Synthesis, 703 (1978).
21. O. Attanasi, P. Palma, and F. Serra-Zanetti. Synthesis, 741 (1983).
22. A. Cavrotti, F. Campagna, and R. Ballini. Synthesis, 56 (1979).
23. J. K. Chakrabarti and T. M. Hotten. J. Chem. Soc. Chem. Commun. 1226 (1972).
24. H. G. Foley and D. R. Dalton. J. Chem. Soc. Chem. Commun. 628 (1973).
25. M. Heller, F. J. McEvoy, and S. Bernstein. J. Org. Chem. **28**, 1523 (1963).
26. J. H. Fried and A. N. Nutile. J. Org. Chem. **27**, 914 (1962).
27. J. March. Advanced organic chemistry. 3rd ed. John Wiley and Sons, New York. 1985. p. 931.
28. M. L. Wolfrom and K. Anno. J. Am. Chem. Soc. **74**, 6150 (1952).
29. D. Askin, C. Angst, and S. Danishefsky. J. Org. Chem. **52**, 622 (1987).
30. E. J. Corey and B. W. Erickson. J. Org. Chem. **36**, 2553 (1971).
31. M. L. Wolfrom and H. B. Wood. J. Am. Chem. Soc. **73**, 2933 (1951).
32. M. J. Robins, S. D. Hawrelak, T. Kanai, J.-M. Siefert, and R. Mengel. J. Org. Chem. **44**, 1317 (1979).
33. E. J. Corey and J. W. Suggs. Tetrahedron Lett. 2647 (1975).
34. S. N. Maiti, M. P. Singh, and R. G. Micetich. Tetrahedron Lett. **27**, 1423 (1986).
35. T. Gartiser, C. Selre, and J.-J. Delpuech. Tetrahedron Lett. **24**, 1609 (1983).
36. T. W. Doyle. Can. J. Chem. **55**, 2714 (1977).
37. H. Bayley, D. N. Standring, and J. R. Knowles. Tetrahedron Lett. **39**, 3633 (1978).
38. M. Vaultier, N. Knouzi, and R. Carrié. Tetrahedron Lett. **24**, 763 (1983).
39. G. Brieger and T. J. Nestrick. Chem. Rev. **74**, 567 (1974).
40. J. H. Boyer and F. C. Canter. Chem. Rev. **54**, 1 (1954).
41. J. H. Boyer and S. E. Ellzey. J. Org. Chem. **23**, 127 (1958).
42. H. Newman. J. Org. Chem. **30**, 1287 (1965).
43. F. Weygand and E. Frauendorfer. Chem. Ber. **103**, 2437 (1970).

Can. J. Chem. Downloaded from www.nrcresearchpress.com by 91.144.44.67 on 09/07/12
For personal use only.

Structure of an acidic polysaccharide elaborated by *Bacillus polymyxa*-1231-ATCC 842

SALAH M. ABDEL-KADER,[1] MOHAMADY A. ISSA, AND MOHAMED A. EL-SHAFEI
Agricultural Chemistry Department, Faculty of Agriculture, EL-Minia University, EL-Minia, Egypt

Received August 12, 1989

SALAH M. ABDEL-KADER, MOHAMADY A. ISSA, and MOHAMED A. EL-SHAFEI. Can. J. Chem. **68**, 323 (1990).

An extracellular acidic polysaccharide, elaborated by *Bacillus polymyxa*, was composed of D-glucose, D-mannose, D-galactose, and D-glucuronic acid (approximate molar ratio of 4:3:1:1). Methylation and fragmentation analysis by partial acid hydrolysis indicated that the polysaccharide had a complicated, highly branched structure, consisting mainly of β(1 → 3) and (1 → 4) D-glycosidic linkages. The backbone chain containing D-glucose, D-mannose, and D-glucuronic acid residues is attached at the C-4, C-3, and C-4 positions, respectively, one out of every three glucose residues being substituted at the C-2 position to form two kinds of branches at the C-2 and C-4 positions, with side chains of single or a few carbohydrate units that are terminated by D-glucose and (or) D-mannose residues.

Key words: acidic polysaccharide, *Bacillus polymyxa*.

SALAH M. ABDEL-KADER, MOHAMADY A. ISSA et MOHAMED A. EL-SHAFEI. Can. J. Chem. **68**, 323 (1990).

Un polysaccharide acide extra-cellulaire obtenu à partir du *Bacillus polymyxa* est composé de D-glucose, de D-mannose, de D-galactose et d'acide D-glucuronique (rapport molaire approximatif de 4 : 3 : 1 : 1). Une analyse de la méthylation et de la fragmentation effectuée en faisant appel à une hydrolyse acide partielle indique que la structure du polysaccharide comporte de nombreuses ramifications complexes formées principalement de liaisons D-glycosidiques β(1 → 3) et (1 → 4). Le squelette de la chaine contient des résidus de D-glucose, de D-mannose et d'acide D-glucuronique qui sont attachés respectivement aux positions C-4, C-3 et C-4; un résidu glucose sur trois est substitué en position C-2 et il en résulte deux sortes de ramifications, en positions C-2 et C-4, comportant des chaines latérales avec une ou quelques unités de carbohydrates qui se terminent par des résidus de D-glucose et (ou) de D-mannose.

Mots clés : polysaccharide acide, *Bacillus polymyxa*.

[Traduit par la revue]

Can. J. Chem. Downloaded from www.nrcresearchpress.com by 91.144.44.67 on 09/07/12
For personal use only.

Introduction

Some microorganisms belonging to *Bacillus* species have been known to produce extracellular polysaccharides, such as cellulose (1), dextran (2), levan (3), and an acidic polysaccharide (4). A previous study (5) showed that an extracellular acidic polysaccharide produced by a newly isolated microorganism, designated *Bacillus polymyxa*, reduced the cholesterol levels in serum and liver of hypercholesterolemic rats (6). Recently, some plant polysaccharides, such as pectin, guar gum, and sodium alginate have attracted attention for their hypocholesterolemic effects on experimental rats. In the course of study, it has been found that some strains of *Bacillus* sp. were capable of producing new types of acidic heteropolysaccharides composed of D-glucose, D-mannose, D-galactose, D-glucuronic acid, and D-mannuronic acid in a complicated highly branched structure, consisting mainly of (1 → 3) and (1 → 4) D-glycosidic linkages.

This work was conducted to study the possible structural features of the acidic polysaccharide produced by *Bacillus polymyxa*, as revealed by methylation and also fragmentation analysis as a result of partial acid hydrolysis.

Materials and methods

General methods

The procedure of concentration by evaporation was carried out under reduced pressure at 35–40°C. Paper chromatography was carried out on Whatman No. 1 filter paper by the descending technique with the following systems (v/v): (a) 1-butanol – acetic acid – water (4:1:5); (b) ethyl acetate – acetic acid – water (7:1:1); (c) ethyl acetate – acetic acid – formic acid – water (18:3:1:4); and (d) benzene–ethanol–water (190:50:5), for methylated sugars, which were detected on the chromatogram by spraying with alkaline silver nitrate (7) and *p*-anisidine hydrochloride reagent (8).

Gas–liquid chromatography (glc) was performed with a Shimadzu model GC-GAM gas chromatography apparatus fitted with a flame ionization detector, with a glass column (0.4 × 200 cm) packed with 5% OV-101, at 180°C. Analysis was done at 175°C at a nitrogen flow rate of 15 mL/min. Polysaccharides (2–5 mg) were hydrolyzed in sealed tubes with 1 M sulfuric acid for 8 h using a boiling water bath. Total carbohydrate was determined by the phenol – sulfuric acid method (9). Colorimetric determination of uronic acid was done by the carbazole method (10).

Production and purification of polysaccharide

Bacillus polymyxa was grown in a medium (7 L, pH 6.8) by the method of Holding and Collee (11) for 5 days at 28°C in a 10-L jar fermenter with vigorous aeration. The culture broth (500 mL) was diluted with 0.01 M sodium hydroxide (500 mL), sterilized for 5 min at 75°C, clarified by filtration, deionized with Amberlite IR-120, and then lyophilized to give a crude polysaccharide (10–13 g).

For purification of the polysaccharide, the crude polysaccharide (10 g) was dissolved in 0.03 M sodium sulfate (1000 mL), and selectively precipitated by gradual addition of cetylpyridinium chloride (CPC, 12 g) until no more precipitate was formed. The precipitated CPC complex was collected by centrifugation, washed several times with ethanol, and dissolved in 10% sodium chloride (500 mL). The solution was filtered, dialyzed, and concentrated to 300 mL (Fraction A). The purified polysaccharide precipitated upon the addition of ethanol (900 mL) was redissolved in warm water and precipitated again with ethanol, yielding a white powder (6.5 g) of an acidic polysaccharide.

The supernatant solution of the precipitate was dialyzed, concentrated (Fraction B), and then poured into ethanol, yielding a neutral polysaccharide (2.1 g), which was kept for further study.

Fehling's solution (50 mL) was added to fraction A (200 mL) and the mixture was allowed to stand for 7 days. The resulting copper complex (2.6 g) was separated by centrifugation, washed several times with alcohol, and dried in a desiccator. *Anal.* calcd. for $[C_{1.6}H_{2.4}O_{1.4}-0.1Cu(NH_3)_2]n$: Cu 11.94%; found : Cu 14.08%.

The polysaccharide was recovered from the copper complex by treatment with 1 M hydrochloric acid (50 mL) with stirring and pouring into ethanol (150 mL). The white precipitate was filtered off, washed successively with ethanol and ether, then dried under reduced pressure; $[\alpha]_D$ +78° (*c*, 0.1% in H_2O).

[1]Author to whom correspondence may be addressed.

Can. J. Chem. Downloaded from www.nrcresearchpress.com by 91.144.44.67 on 09/07/12
For personal use only.

Identification of sugar components

The polysaccharide (300 mg) was hydrolyzed with 1 M sulfuric acid (15 mL) for 8 h in a boiling water bath. After neutralization with $BaCO_3$, filtration, deionization on Rexyn-101(H^+) resin, and concentration, the mixture of acidic and neutral sugars was fractionated on a column of IR-48 resin. The column was eluted, first with 250 mL of water to remove the neutral sugars, followed by gradient elution with ethanolic ammonia (100 mL) to obtain the uronic acids.

(a) Neutral sugars (9)

The column eluates were concentrated, and on examination on paper chromatograms they were found to contain three components. These gave the same colour reactions, moved to the same extent, and were indistinguishable from authentic samples of D-galactose (R_f 0.11), D-glucose (R_f 0.13), and D-mannose (R_f 0.15) respectively (solvent a). The ratio of sugars was determined after eluting the corresponding zones from the paper chromatogram, with solvent a, by the phenol – sulfuric acid method.

(b) Uronic acid fraction (10)

This was indistinguishable from an authentic sample of D-glucuronic acid (R_f 0.07). The proportion of glucuronic acid was estimated after eluting the corresponding zone, by colorimetric determination with carbazole reagent (uronic acid 12.77%).

Methylation analysis of polysaccharide

The polysaccharide (500 mg) was methylated by the method of Hakomori (12) with methylsulfinyl carbanion and methyl iodide. The reaction mixture was dialyzed exhaustively against water and evaporated to dryness. Successive methylation processes were required until complete methylation was achieved, as judged from the ir spectrum (elimination of free hydroxyl groups). *Anal.* calcd. for 93.4% methylation, $[C_{3.2}H_{3.77}O_{1.3}–(OCH_3)_{1.43}]n$: OMe 41.37%; found: OMe 41.54%.

Methylated polysaccharide (300 mg) was hydrolyzed with 90% formic acid (2 mL) for 16 h at 100°C, followed by heating with 2 M trifluoroacetic acid (1 mL) for 5 h. Acids were removed by evaporation, and the product was examined by paper chromatography using solvent d, and found to contain at least nine components with R_f values of 0.016, 0.12, 0.23, 0.45, 0.59, 0.69, 0.71, 0.84, and 0.88. The methylated sugars in the hydrolyzate were converted into their corresponding alditol acetates by the usual manner (13) and then analyzed by glc.

The glucuronic acid was confirmed by reduction of polysaccharide, using the method of Taylor and Conrad (14).

An aqueous solution of the native polysaccharide (50 mg in 100 mL of water) was adjusted to pH 4.7 with 0.1 M hydrochloric acid, followed by the addition of 1-ethyl-3-(3-dimethylaminopropyl) carbodiimide (500 mg), and the stirred reaction mixture was maintained at pH 4.7 for 3 h by the addition of 0.02 M hydrochloric acid. After addition of sodium borohydride (500 mg) and one drop of *n*-octanol, the mixture was kept overnight with stirring, dialyzed exhaustively, deionized with Amberlite IR-120(H^+ form), and evaporated to dryness. The methylation of reduced polysaccharide was carried out by the method of Hakomori (12).

The partially methylated sugars in the hydrolyzate were converted into the corresponding alditol acetates as described previously (13) and then analyzed by glc.

Partial acid hydrolysis of polysaccharide

The polysaccharide (3.5 g) was heated with 0.5 M trifluoroacetic acid (300 mL) for 3 h at 100°C. After evaporation of the acid, the hydrolyzate was dissolved in water (100 mL), ethanol (300 mL) was added to the solution, and the resultant precipitate was collected by centrifugation to give a degraded polysaccharide. The supernatant was evaporated to a small volume, passed through a column of Dowex-1 × 4) resin (5 × 20 cm, formate form), and washed with water to give a mixture of neutral oligosaccharides (1500 mL). Acidic oligosaccharides absorbed on the column were eluted with 1 M formic acid (1000 mL).

The neutral oligosaccharides were fractionated by a column (2 × 30 cm) of activated charcoal. After washing the column with water, the oligosaccharides were eluted stepwise with 4%, 7%, 12%, and 25% aqueous ethanol, and finally with warm 50% ethanol. Each fraction was evaporated to dryness and further purified by preparative paper chromatography using Whatman No. 1 filter paper (solvents a and c).

Structural analysis of oligosaccharides

The neutral oligosaccharides (1.5–3 mg each) were hydrolyzed with 2 M TFA for 6 h at 100°C. After the acid was evaporated, monosaccharides in the hydrolyzate were examined by paper chromatography. Methylation of the oligosaccharides was done by the method of Hakomori (12) as described previously. After evaporating the methyl iodide, the methylated oligosaccharide was extracted with chloroform and purified on a Sephadex LH-20 column (1 × 20 cm) by elution with chloroform to give the purified methylated product. The methylated oligosaccharide was hydrolyzed successively with 90% formic acid and 2 M TFA as described previously, and then analyzed by glc after converting into its alditol acetate.

Each of the acidic oligosaccharides (2–4 mg) was methylated in the same manner. It was dissolved in diethyl ether and treated with diazomethane. The resulting methyl esters of the uronic acid residues were reduced with lithium aluminium hydride (10 mg) in diethyl ether by heating with refluxing for 4 h, after which water was added dropwise to decompose the excess reagent. After filtration, the residue was washed repeatedly with acetone and dried *in vacuo*. The methylated carboxyl-reduced oligosaccharide was remethylated by the method of Hakomori (12), hydrolyzed, and then analyzed by glc as described previously.

Periodate oxidation and Smith degradation

The polysaccharide (150 mg) was oxidized with 0.3 M sodium metaperiodate (225 mL) at room temperature in the dark (15). Aliquots (5 mL) were removed after 18 h and the consumption of periodate and production of formic acid were determined (16, 17). The results, based on 163.75 g of polysaccharide in the glucose–mannose–galactose – glucuronic acid (ratios of 2.7:2.3:0.4:0.8), were as follows: periodate consumed, 0.78 mole; formic acid produced, 0.26 mole.

After complete oxidation (5 days), the oxidation was stopped by the addition of ethylene glycol and the solution dialyzed. The polyaldehyde was reduced with excess of $NaBH_4$ at room temperature overnight. The reaction was terminated by addition of ice-cold 4 N acetic acid and the solution was again dialyzed and lyophilized (120 mg polysaccharide-polyalcohol). A portion of the resulting polysaccharide-polyalcohol was hydrolyzed with 1 M sulfuric acid for 6 h at 100°C. The hydrolyzate was neutralized ($BaCO_3$), centrifuged, concentrated to a syrup, examined by paper chromatography using solvent a, and finally analyzed by glc after conversion into the corresponding alditol acetate.

The remainder of the polysaccharide-polyalcohol (90 mg) (18) was hydrolyzed with 0.05 M sulfuric acid for 18 h at 40°C. The mild hydrolysis product (oligosaccharide components) was isolated by paper chromatography (solvent a), and its structure was examined by methylation analysis as described previously.

Results and discussion

When *Bacillus polymyxa* was grown for 5 days at 28°C in a medium containing 2% sucrose, appropriate amounts of nitrogen compounds, and inorganic nutrients, the culture medium became viscous due to the production of an extracellular polysaccharide. The procedure for fractionation is shown in Scheme 1. The crude polysaccharide was extracted successively with 0.01 M sodium hydroxide at 75°C for 5 min. The crude polysaccharide dissolved in sodium sulfate was further fractionated by treatment with CPC, to give an acidic polysaccharide (Fraction A) and a neutral polysaccharide (Fraction B; for further study).

The acidic polysaccharide was purified by repeated fractional precipitations with ethanol, and then via its copper complex. In addition, the polysaccharide contained one kind of aldouronic acid, as shown by paper chromatography.

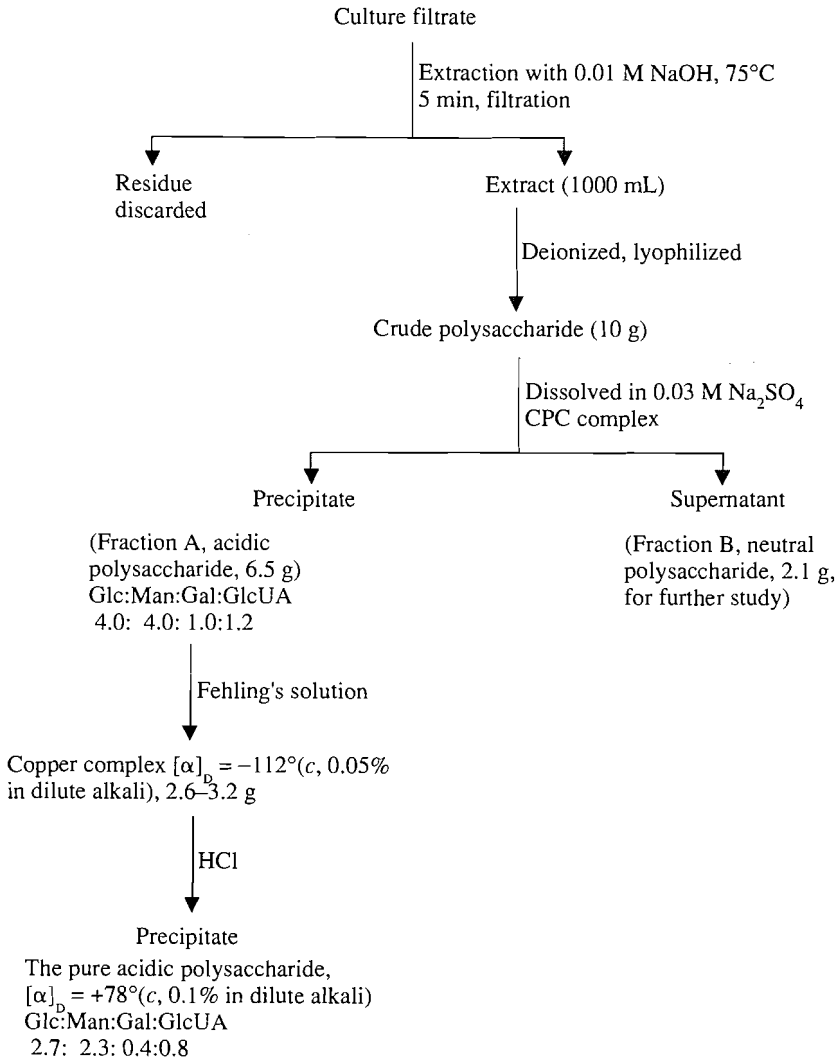

SCHEME 1. Fractionation of polysaacharide from *Bacillus Polymyxa*.

In another experiment, the polysaccharide was treated with carbodiimide and sodium borohydride by the method of Taylor and Conrad (14), and the resulting carboxyl-reduced polysaccharide was hydrolyzed with acid and quantitatively analyzed by paper chromatography (9) as described previously. The comparison of sugar compositions of the native and carboxyl-reduced polysaccharides indicated that the original polysaccharide was composed of D-glucose, D-mannose, D-galactose, and D-glucuronic acid (Glc UA) in a molar ratio of 2.7:2.3:0.4:0.8.

This polysaccharide is unique, containing a small but significant amount of D-glucuronic acid, which usually occurs in plant gum polysaccharides such as arabic gum and khaya gums (19) but is rare in microbial polysaccharides, such as Pneumococci (for a survey up to about 1959, see ref. 20).

Methylation study

To obtain information on the mode of glycosidic linkages of these sugar residues, the native and carboxyl-reduced polysaccharides were methylated by the method of Hakomori (12). The polysaccharides exhibited considerable resistance towards complete methylation and successive methylation processes were required to yield methylated products containing 0.934 OCH_3 and 0.971 OCH_3 per hydroxyl group in the native and carboxyl-reduced polysaccharides respectively (as judged from the ir spectrum, by the absence of the OH band at 3400–3600 cm^{-1}). The comparison of methylated sugars of the native and carboxyl-reduced polysaccharides was made by glc after hydrolysis with acid and conversion into the corresponding alditol acetates.

As shown in Table 1, D-glucose, D-mannose, and D-glucuronic acid residues in the inner chains of the polysaccharide are linked mainly with (1 → 3) and (1 → 4) D-glycosidic linkages, as indicated by the presence of 2,4,6-tri-*O*-methyl-D-mannose and 2,3,6-tri-*O*-methyl-D-glucose and -D-galactose. The identification of 2,3,4,6-tetra-*O*-methyl derivatives of D-mannose and D-glucose indicates that the polysaccharide has a highly branched structure and the side chains are terminated with D-mannose and also with D-glucose residues. In addition, the presence of 3,6-di-*O*-methyl-D-glucose suggests that some of the (1 → 4)-linked D-glucose residues might form branch points.

As regards the glycosidic linkages of D-glucuronic acid residues, the methylated carboxyl-reduced polysaccharide, but *not* the native polysaccharide, gave, on acid hydrolysis, 2,6-di-*O*-methyl-D-glucose, indicating that D-glucuronic acid residues are located in the main chain at the branch point by double substitutions at the O-3 and O-4 atoms.

However, in view of the failure to detect any tetra-*O*-methyl-

Can. J. Chem. Downloaded from www.nrcresearchpress.com by 91.144.44.67 on 09/07/12
For personal use only.

TABLE 1. Molar ratio of methylated sugar fragments from hydrolyzates of methylated native and carboxyl-reduced polysaccharide

O-Methylated sugar (alditol acetate)	Mode of linkage	Retention time*	Molar ratio	
			Native	Carboxyl reduced
2,3,4,6-Tetra-*O*-methyl-D-glucose	Glc(1→	1.0	0.14	0.12
2,3,6-Tri-*O*-methyl-D-glucose	→4)Glc(1→	2.19	0.21	0.18
2,6-Di-*O*-methyl-D-glucose	→3,4)Glc(1→	3.0	—	0.14
3,6-Di-*O*-methyl-D-glucose	→2,4)Glc(1→	3.65	0.12	0.11
3-Mono-*O*-methyl-D-glucose	→2,4,6)Glc(1→	7.50	Trace	Trace
2,3,4,6-Tetra-*O*-methyl-D-mannose	Man(1→	0.98	0.13	0.11
2,4,6-Tri-*O*-methyl-D-mannose	→3)Man(1→	2.09	0.30	0.26
2,3,6-Tri-*O*-methyl-D-galactose	→4)Gal(1→	1.51	0.07	0.07

*Retention time of alditol acetate relative to 1,5-di-*O*-acetyl-2,3,4,6-tetra-*O*-methyl-D-glucitol.

TABLE 2. Hydrolysis products of methylated neutral oligosaccharides isolated from partial hydrolyzate of the polysaccharide

Oligosaccharide	Yield* (mg)	R_{Glc}†	*O*-Methyl sugar	Molar ratio
(**1**) Disaccharide $[\alpha]_D^T$ +25.6°	7.2	0.69	2,3,4,6-Tetra-*O*-methyl-D-mannose	1.0
			2,4,6-Tri-*O*-methyl-D-mannose	1.2
(**2**) Disaccharide $[\alpha]_D^T$ +35°	9.3	0.61	2,3,4,6-Tetra-*O*-methyl-D-glucose	1.2
			2,3,6-Tri-*O*-methyl-D-glucose	1.0
(**3**) Trisaccharide $[\alpha]_D^T$ +23°	12	0.33	2,3,4,6-Tetra-*O*-methyl-D-mannose	1.2
			2,4,6-Tri-*O*-methyl-D-mannose	1.1
			2,3,6-Tri-*O*-methyl-D-glucose	0.9
(**4**) Tetrasaccharide $[\alpha]_D^T$ +10°	5	0.21	2,3,4,6-Tetra-*O*-methyl-D-mannose	1.1
			2,4,6-Tri-*O*-methyl-D-mannose	1.0
			2,3,4,6-Tetra-*O*-methyl-D-glucose	0.9
			2,6-Di-*O*-methyl-D-glucose	0.71

*The polysaccharide (3.5 g) was partially hydrolyzed with 0.5 M TFA for 3 h at 100°C.
†R_{Glc}: paper-chromatographic mobility relative to that of D-glucose (solvent a).

D-galactose in the hydrolyzate of the methylated product of the native and carboxyl-reduced polysaccharides, it has been suggested that the reason for the presence of most of the tri-*O*-methyl-D-galactose may be complete methylation of the polysaccharide, and demethylation during hydrolysis. Another reason could be the presence of a "start point" for establishing a repeating unit. The isolation of mono-*O*-methyl-D-glucose as a trace quantity of D-glucose derivative is suggestive of branching at positions 2 and (or) 6 of the glucose units. Nevertheless, the presence of mono-*O*-methyl-D-glucose may be due to incomplete methylation or to demethylation. Other authors (21, 22) have reported similar observations.

Fragmentation of polysaccharide by partial acid hydrolysis

To investigate the sequential arrangement of the sugar residues, the polysaccharide was subjected to partial acid hydrolysis. After the acid was distilled off, the high molecular weight fraction (degraded polysaccharide) was separated by precipitation with ethanol (3 volumes). The oligosaccharides in the supernatant solution were fractionated by a column of Dowex-1 × 4) and charcoal, and were respectively isolated by preparative paper chromatography. These procedures afforded four kinds of neutral oligosaccharides (**1**–**4**) and an acidic oligosaccharide (**5**). They were characterized mainly by methylation analysis.

As shown in Table 2, the two neutral disaccharides were characterized as 3-*O*-D-mannopyranosyl-D-mannose (**1**) and 4-*O*-D-glucopyranosyl-D-glucose (**2**).

Oligosaccharide **2** gave 2,3,4,6-tetra-*O*- and 2,3,6-tri-*O*-methyl-D-glucose in a molar ratio 1.0:1.2 on methylation followed by acid hydrolysis (1 M H_2SO_4 for 6 h). This oligosaccharide had $[\alpha]_D^T$ +35°, while the authentic cellobiose had $[\alpha]_D^T$ +34.6° (*c*, 0.1% in water); as well, it has the same R_f as an authentic sample (R_f 0.35, solvent a).

The trisaccharide (**3**) was shown to contain one nonreducing terminal D-mannose residue and the substituted D-mannose residue at the O-3 position. Since its specific rotation, $[\alpha]_D^T$ +23°, was lower than that of the disaccharide (**1**), both terminal D-mannose residues must have the β-configuration. In addition, the tetrasaccharide (**4**) was shown to contain two nonreducing termini of D-glucose and D-mannose residues, and the double substituted D-glucose residue at the O-2 and O-4 positions, as revealed by methylation analysis (Table 2). Since its specific rotation, $[\alpha]_D^T$ +10°, was lower than that of the trisaccharide (**3**), both terminal D-glucose and D-mannose residues must have the β-configuration. On consideration of the structure of the related di- and trisaccharides (**1**, **2** and **3**), the tetrasaccharide is tentatively characterized as shown in **4**.

The acidic oligosaccharide fraction was a mixture of three major components, as detected by paper chromatography with solvent c. Their mobilities on a paper chromatogram were R_{GlcA}

Can. J. Chem. Downloaded from www.nrcresearchpress.com by 91.144.44.67 on 09/07/12
For personal use only.

β-D-Manp(1→3)-D-Manp (**1**)

β-D-Glcp(1→4)-D-Glcp (**2**)

β-D-Manp(1→3)-β-D-Manp(1→4)-DGlcp (**3**)

β-D-Manp(1→3)-β-D-Manp(1→4)-D-Glcp (**4**)
2
↑
β-D-Glcp

β-D-Glcp(1→4)-α-D-GlpAp(1→3)-D-Manp (**5**)

β-D-Glcp(1→3)-α-D-GlcAp(1→2)-erythritol (**6**)

α-D-GlcAp(1→3)-β-D-Manp(1→3)-β-D-Manp(1→4)-α-D-GlcAp(1→2)-erythritol (**7**)

FIG. 1. Structural formulas of oligosaccharides.

0.31, 0.35, and 0.43 respectively. Among them, oligosaccharide **5** (R_{GlcA} 0.31 and $[\alpha]_D^T$ +46), adsorbed on a Dowex-1 × 4 (formate form) column and eluted with 1 N formic acid, was purified by paper chromatography. The acidic oligosaccharide **5** was methylated, carboxyl-reduced, and hydrolyzed, and 2,3,4,6 tetra-*O* and 2,3-di-*O*-methyl-D-glucose and 2,4,6-tri-*O*-methyl-D-mannose (ratio 1:1:1.1) were identified, while the corresponding carboxyl-reduced oligosaccharide gave, on remethylation and acid hydrolysis, 2,3,4,6-tetra-*O*- and 2,3,6-tri-*O*-methyl-D-glucose and 2,4,6-tri-*O*-methyl-D-mannose in a ratio 1:1.05:1. From these results, the acidic oligosacharide **5** was characterized as 4-*O*-β- D-glucopyranosyl-3*O*-α-D-glucopyranosyl uronic acid-D-mannose. The highly positive $[\alpha]_D^T$ values (+78° and +16.8° respectively) for the unmethylated and methylated polysaccharides, and the presence of an absorption band at 890 cm^{-1} in the infrared spectrum, are characteristic of β-configuration (23).

The sequential arrangements of the sugar residues in the (galacto-glucurono-manno-glucan) polysaccharide were also examined by Smith degradation. On complete Smith degradation it gave D-glucose, D-mannose, and D-glucuronic acid in addition to erythritol and glycerol, as shown in Table 3.

Smith degradation and methylation products of the original polysaccharide together may indicate that D-glucose, D-mannose, and D-glucuronic acid should have arisen from a branching unit, and joined to other units at (1 → 2)-linked D-glucose, and (1 → 3)-linked D-mannose and D-glucuronic acid residues. Comparison of the molar ratio of D-glucose and D-mannose to D-glucuronic acid in the hydrolyzate of the complete Smith degradation product and in the original polysaccharide (0.65: 1.13: 0.79 and 2.7:2.3:0.80 respectively) may indicate that all glucuronic acid units are resistant to oxidation by periodate.

The glycerol and erythritol should have arisen from the nonreducing terminal sugar units; in addition the polysaccharide contains (1 → 4)- and (1 → 2)-linked D-glucose, and (1 → 3)-linked D-mannose residues.

Furthermore, comparison of the unit ratio of mannose and glucose to glucuronic acid in the hydrolyzate of the periodate-oxidized polysaccharide with branching units in the original polysaccharide (0.8:1.4:1.0 and 1.0:2.0:1.0 respectively) may indicate that some mannose and glucose units were lost (20%) during overoxidation.

TABLE 3. Complete Smith degradation products from the native polysaccharide

Degradation product	Molar ratio
D-Mannose	1.13
D-Glucose	0.65
D-Glucuronic acid	0.79
Erythritol	1.48
Glycerol	1.56

The polysaccharide-polyalcohol derived from the native polysaccharide was hydrolyzed under mild conditions with 0.05 M sulfuric acid for 18 h at 40°C. After neutralization with $BaCO_3$ as described previously, the high molecular weight fraction was separated by precipitation with ethanol (3 volumes). The water soluble fraction gave, on the paper chromatogram with solvent a, at least one spot, having R_{GlcA} 0.97.

On acid hydrolysis, it yielded D-glucose, D-glucuronic acid, and erythritol (ratio 1.0:1.1:0.9). By methylation and then acid hydrolysis, it gave 2,3,4,6-tetra-*O*-methyl-D-glucose and 2,4-di-*O*-methyl-D-glucose. Therefore, this oligosaccharide should have the structure shown as **6**. On consideration of the results of methylation analysis of the polysaccharide and the structures of oligosaccharides **4**, **6** might have arisen from the following sequence of sugar residue in the side chain of the polysaccharide.

The water-insoluble fraction comprised mainly D-mannose, D-glucuronic acid, and erythritol (ratio 2:1:1). This fraction might be a mixture of oligosaccharides or a degraded polysaccharide containing D-glucuronic acid and D-mannose; this oligo-

Can. J. Chem. Downloaded from www.nrcresearchpress.com by 91.144.44.67 on 09/07/12
For personal use only.

β-D-Manp(1→3)-β-D-Manp(1→4)-β-D-Glcp(1→3)-D-GlcAp(1→
2
↑
1
β-D-Glcp

saccharide should have the structure shown as **7**. However, the details of the structure have not been studied. Since the D-glucuronic acid residues must be located in the main chain to form branch points, a part of the sequential arrangement of sugar residues in the backbone chain may be elucidated as follows:

→3)-β-D-Manp(1→4)-D-Glcp(1→
3
↑
1
→3)-β-D-Manp(1→4)-D-Glcp

The aforementioned results indicate that the polysaccharide has a complicated branched structure, where major portions of both D-glucose and D-mannose residues are linked by β(1 → 4) and β(1 → 3) bonds, respectively. The minor portions of D-glucuronic acid residues are joined by α-D linkages with both D-glucose and D-mannose residues. The minor portions of D-glucuronic acid are located in the main chain by α(1 → 3) and (1 → 4) linkages with both D-mannose and D-glucose residues. There are two kinds of side chains, one consisting of β(1 → 3)-linked D-glucose and glucuronic acid residues and the other consisting of the β-D-glycopyranosyl-(1 → 2)-D-glucose unit, attached at the C-3 positions of the D-glucuronic acid residues. However, similarly, a small proportion of D-glucose residues must be located in the side chain to form branch points.

On reacting the polysaccharide with Fehling's solution, a copper complex that contained one-third atomic equivalent of copper per mole of sugar unit was formed. Comparison of the specific rotation of the galacto-glucurono-manno-glucan in dilute alkali (+78°) with that in cuprammonium (−112°), showed that a levorotatory complex was formed in cuprammonium. This has been shown (24) to occur in reactions involving the 2- and 3-hydroxyl groups in both D-glucopyranoside and -galactopyranoside as well as the 2- and 3- or the 3- and 4-OH groups of D-mannopyranoside. Such shifts in the case of starch and glycogen, where reaction involves all the sugar units, are from +375° to −715° and from +366° to −597°, respectively (24).

In the acidic polysaccharide of *Bacillus polymyxa*, the copper complex isolated involves only 36.25% of the sugar units and the levorotatory shift is about one third (36.25%) of the starch or glycogen.

Acknowledgments

The authors wish to express their thanks to Dr. Safwat, M.S.A. and Dr. EL-dahtory, Th., Microbiology Department, EL-Minia University, for their help, particularly in providing the purified culture of *Bacillus polymyxa*.

1. S. HESTRIN, M. ASCHNER, and J. MAGER. Nature (London), **159**, 64 (1947).
2. M. S. LOITSYANSKAYA and TR. PETERGOF. Leningr. Gos. Univ. Ser. Biol. **19**, 20 (1965).
3. E. J. HEHRE and D. M. HAMILTON. J. Biol. Chem. **192**, 161 (1951).
4. J. R. CALVIN, L. CHÉNÉ, L. C. SOWDEN, and M. TAKAI. Can. J. Biochem. **55**, 1057 (1977).
5. A. MISAKI, M. KAKUTA, and H. OKAMATSU. Abstracts of Papers. 37th Annual Meeting of the Japanese Society of Nutrition and Food Science. Osaka, May, 1983. p. 35.
6. H. FUKUI, M. TANAKA, and A. MISAKI. Agric. Biol. Chem. **49**, 2343 (1985).
7. E. W. TREVELYAN, D. P. PROCTER, and J. S. HARRISON. Nature, **166**, 444 (1950).
8. R. C. BEAN and G. G. PORTWE. Anal. Chem. **31**, 1929 (1959).
9. M. DUBOIS, K. A. GILLES, J. R. HAMILTON, P. A. REBERS, and F. SMITH. Anal. Chem. **28**, 350 (1956).
10. Z. DISCH. J. Biol. Chem. **196**, 189 (1947).
11. J. A. HOLDING and G. J. COLLEE. Methods in microbiology. 6A. *Edited by* J. R. Norris and D. W. Ribbons. Academic Press, London. 1971. pp. 1–32.
12. S. HAKOMORI. J. Biochem. **55**, 205 (1964).
13. E. A. DAVIDSON. Carbohydrate chemistry. R. Holt and Winston, New York. 1967. Chap. 5. pp. 108–112.
14. R. L. TAYLOR and H. E. CONRAD. Biochemistry, **11**, 1383 (1972).
15. H. C. SRIVASTAVA and G. A. ADAMS. Can. J. Chem. **40**, 1415 (1962).
16. G. NEUMULLER and E. VASSEUR. Ark. Kemi, **5**, 235 (1953).
17. T. G. HALSALL, E. L. HIRST, and J. K. N. JONES. J. Chem. Soc. 1427 (1947).
18. G. F. O'DEA and R. A. GIBBONS. Biochem. J. **55**, 580 (1953).
19. G. O. ASPINALL and J. M. MCNAB. J. Chem. Soc. 845 (1969).
20. M. STACEY and S. A. BARKER. Polysaccharides of microorganisms. Oxford University Press, Oxford. 1960.
21. G. O. ASPINALL, E. L. HIRST, and R. S. MOHAMED. J. Chem. Soc. 1734 (1954).
22. C. P. J. GLAUDEMANS and T. E. TIMELL. J. Am. Chem. Soc. **80**, 1209 (1958).
23. I. R. SIDDIQUI and P. J. WOOD. Carbohydr. Res., **53**, 85 (1977).
24. R. E. REEVES. Adv. Carbohydr. Chem. **6**, 108 (1951).

Can. J. Chem. Downloaded from www.nrcresearchpress.com by 91.144.44.67 on 09/07/12
For personal use only.

Structural characterization of the capsular polysaccharide and *O*-chain of the lipopolysaccharide of *Actinobacillus pleuropneumoniae* serotype 8 (strain 405)[1]

ELEONORA ALTMAN, JEAN-ROBERT BRISSON, AND MALCOLM B. PERRY[2]
Division of Biological Sciences, National Research Council of Canada, Ottawa, Ont., Canada K1A 0R6

Received August 22, 1989

ELEONORA ALTMAN, JEAN-ROBERT BRISSON, and MALCOLM B. PERRY. Can. J. Chem. **68**, 329 (1990).

The capsular polysaccharide of *Actinobacillus pleuropneumoniae* serotype 8 (strain 405) was found to be a teichoic acid type polysaccharide composed of 2-acetamido-2-deoxy-D-galactose (two parts), glycerol (one part), and phosphate (one part). From hydrolysis, dephosphorylation, methylation, and ^{1}H and ^{13}C nuclear magnetic resonance studies, the polysaccharide was found to be a high molecular weight linear polymer having the structure:

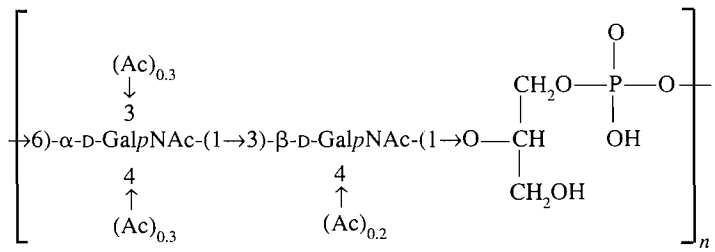

The lipopolysaccharide *O*-antigen of *A. pleuropneumoniae* serotype 8 was shown to be a high molecular weight unbranched linear polymer of a repeating pentasaccharide unit having the structure identical to that produced by *A. pleuropneumoniae* serotype 3, as follows:

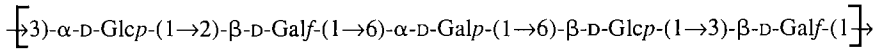

Key words: *Actinobacillus pleuropneumoniae* polysaccharide, lipopolysaccharide, NMR.

ELEONORA ALTMAN, JEAN-ROBERT BRISSON et MALCOLM B. PERRY. Can. J. Chem. **68**, 329 (1990).

On a trouvé que la polysaccharide capsulaire de l'*Actinobacillus pleuropneumoniae* du sérotype 8 (souche 405) est un polysaccharide du type de l'acide teichoïque qui est composé de 2-acétamido-2-désoxy-D-galactose (deux parties), de glycérol (une partie) et de phosphate (une partie). En se basant sur des études d'hydrolyse, de déphosphorylation, de méthylation et de résonance magnétique nucléaire du ^{1}H et du ^{13}C, on a trouvé que le polysaccharide est une polymère de poids moléculaire élevé de structure :

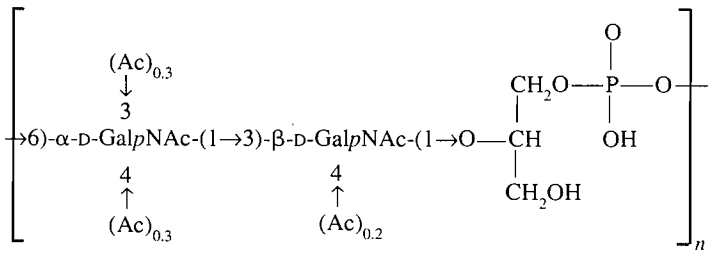

On a montré que le liposaccharide du *O*-antigène du *A. pleuropneumoniae* du sérotype 8 est un polymère linéaire sans ramification de poids moléculaire élevé contenant une unité pentasaccharide qui se répète, qui possède une structure identique à celle produite par l'*A. pleuropneumoniae* du sérotype 3 et qui correspond à la suivante :

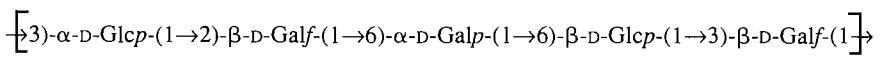

Mots clés : polysaccharide de l'*Actinobacillus pleuropneumoniae*, lipopolysaccharide, RMN.

[Traduit par la revue]

Introduction

Actinobacillus pleuropneumoniae (APP) infections cause severe respiratory disease in pigs. The organism is encapsulated and 12 serotypes based on the structurally distinct polysaccharide capsular antigens (CPS) have been identified (1–4). In addition, similar to other Gram-negative bacterial pathogens, *A. pleuropneumoniae* have cell wall lipopolysaccharides (LPS) that play a significant role in the interaction between the bacteria and the host, on the serological identification of the organisms, and in the pathogenesis of disease.

Because the immunobiological properties of the LPS and CPS are only explainable at a molecular level in terms of their three-dimensional structures, a complete analysis of these major antigens produced by 12 known serotypes of *A. pleuropneumoniae* has been undertaken. This paper reports the structural analysis of the CPS and *O*-polysaccharide component of the LPS produced by *A. pleuropneumoniae* serotype 8 (strain 405).

[1]NRCC Publication No. 30980.
[2]Author to whom correspondence may be addressed.

Can. J. Chem. Downloaded from www.nrcresearchpress.com by 91.144.44.67 on 09/07/12
For personal use only.

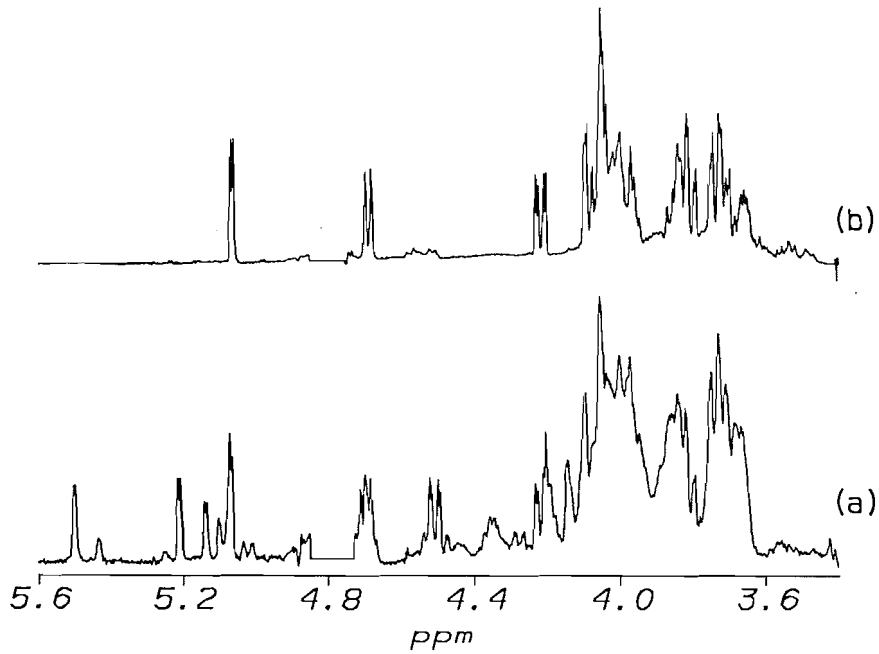

FIG. 1. The ^{1}H nmr spectra (24°C, 500 MHz) of the capsular polysaccharide of *A. pleuropneumoniae* serotype 8. (a) Native polysaccharide, (b) *O*-deacetylated polysaccharide.

Experimental

Production of the capsular polysaccharide and of the O*-polysaccharide*

Actinobacillus pleuropneumoniae serotype 8 (strain 405) cells were grown in Difco brain heart infusion (BHI) (37 g/L) supplemented with β-NAD (Sigma) (50 μg/L) and D-glucose (1% final concentration) (yield ~ 3 g wet weight/L).

The LPS was isolated from the aqueous phase of the phenol extract by ultracentrifugation. A solution of LPS (0.2 g) in aqueous 2% acetic acid (100 mL) was kept at 100°C for 2 h, the precipitated liquid A was removed by low speed centrifugation, and the *O*-polysaccharide was recovered by Sephadex G-50 filtration as previously described (5).

The CPS was isolated from the above ultracentrifugate via its insoluble cetyltrimethylammonium complex as previously described (6) and it was obtained pure by Sephadex G-50 gel filtration followed by ion-exchange chromatography on a DEAE–Sephacel column, from which it was eluted as a single peak with approximately 0.13 M NaCl (6).

Analytical methods

Quantitative methods for glycose analysis and glc and glc–ms methods used were the same as previously described (6).

Samples (0.5 mg) of oligo- and polysaccharides were hydrolyzed with 2 M hydrochloric acid (1 mL) or with 1 M sulfuric acid for 17 h at 100°C. Glycoses were determined by glc of their alditol acetate derivatives (7) using *myo*-inositol as an internal standard. The configuration of glycoses was established by capillary glc of their acetylated (−)-2-butyl glycosides (8). Lipids were identified by glc–ms of their methyl esters as previously described (6). Gel filtration was performed on columns of Sephadex G-50 (2 × 100 cm) or Bio-Gel P-2 (1.6 × 100 cm) (200–400 mesh) (Bio-Rad Labs). SDS-PAGE and methylation analyses were made under previously reported conditions (6).

Polysaccharide dephosphorylation with aqueous hydrofluoric acid

Polysaccharide (16.1 mg) was dissolved in cold 40% hydrofluoric acid (1 mL) and kept at 4°C for 24 h. The solution was concentrated to dryness in high vacuum over NaOH and the residue was neutralized with 5% ammonium hydroxide and lyophilized. The products were fractionated by gel filtration on the Bio-Gel P-2 column.

Nuclear magnetic resonance

Decoupled ^{13}C nmr 125-MHz spectra were recorded at 27°C for a 25-kHz spectral width, using a $\pi/2$ pulse and a 32K data set with a Bruker AM-500 spectrometer. DEPT experiments (9) were performed for a 12.5-kHz spectral width using a $3\pi/2$ pulse to distinguish between CH and CH_2 resonances. The delay between pulses $(2J)^{-1}$ was set at 3.4 ms. Chemical shifts were expressed relative to internal acetone (1%, 31.07 ppm). Proton spectra at 500 MHz were recorded at 24°C and 34°C using a spectral width of 2.5 kHz, a $\pi/2$ pulse, and a 16K data set for digital resolution of 0.3 Hz/point. Chemical shifts were expressed relative to internal acetone (0.1%, 2.225 ppm). Coupling constants are reported in hertz.

Proton homonuclear-correlated 2D-nmr experiments, phase-sensitive COSY (10, 11) and relay COSY (12), were performed at 24°C, using the standard software provided by Bruker (DISNMR), and all experiments were done in the magnitude mode. The heteronuclear ^{13}C–^{1}H shift correlated spectrum (13, 14) was recorded at 24°C on a polysaccharide sample of 40 mg/mL in a 5-mm tube with proton decoupling in the F_1 domain.

Results and discussion

Actinobacillus pleuropneumoniae serotype 8 CPS was obtained via its precipitated cetyltrimethylammonium salt complex from the 1% saline washings of the aqueous phase crude LPS isolated by the phenol extraction procedure (yield: 10 mg of purified CPS/100 g cells (wet weight)). The crude CPS was applied to the Sephadex G-50 gel filtration column from which it eluted as a single peak (K_{av} 0.03), indicating that it had a high molecular weight, and was homogeneous across the collected fractions with respect to neutral glycose, aminodeoxyglucose, and phosphate. Pure CPS was obtained by ion-exchange chromatography using a DEAE–Sephacel column from which it was eluted by approximately 0.13 M sodium chloride. It was readily soluble in water and had $[\alpha]_D$ +52° (*c* 0.8, water) (Anal. found C 38.31, H 5.30, N 5.00, ash 5.7%). Analysis of component sugars by glc of their derived alditol acetates showed that the CPS

Can. J. Chem. Downloaded from www.nrcresearchpress.com by 91.144.44.67 on 09/07/12
For personal use only.

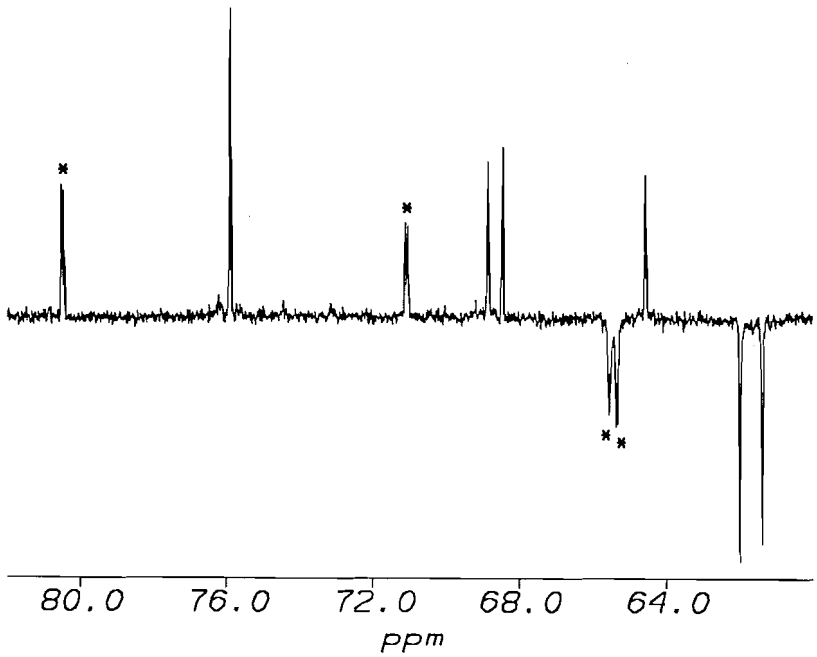

FIG. 2. Partial ^{13}C DEPT spectrum of the *O*-deacetylated capsular polysaccharide from *A. pleuropneumoniae* serotype 8, recorded at 27°C. Carbon–phosphorus couplings are marked with asterisks.

was composed of 2-amino-2-deoxy-D-galactose and glycerol (2.0:0.4). The D configuration of 2-amino-2-deoxygalactose was established by glc of its acetylated (−)-2-butyl glycosides by comparison with authentic reference derivatives according to the method of Leontein *et al.* (8).

The ^1H nmr spectrum of the native CPS (Fig. 1a) (24°C, 500 MHz) exhibited multiple signal patterns of differing intensities due to partial *O*-acetylation. This was further substantiated by analysis of the ^{13}C nmr spectrum of the native CPS (27°C, 125 MHz), which displayed signals for three *O*-acetyl groups at δ 20.86, 20.98, 21.16, 172.62, 173.82, and 174.18 ppm. The ^{13}C nmr spectrum of the native CPS was less complex and showed the presence of two anomeric carbons of equal intensity at δ 94.33 and 102.25 ppm, indicating that two sugar residues were involved in the repeating unit of the CPS.

The *O*-deacetylation of the native CPS significantly simplified its ^1H nmr spectrum (24°C, 500 MHz), which now showed two signals in the anomeric region at δ 5.07 (d, 1H, $J_{1,2}$ 4.0 Hz) and 4.69 (d, 1H, $J_{1,2}$ 8.5 Hz) ppm, and two signals at 2.04 (s, 3H) and 2.08 (s, 3H) ppm corresponding to the CH_3 of the *N*-acetyl group, confirming that both sugar residues were aminodeoxyglycoses (Fig. 1b). The ^{13}C nmr spectrum (27°C, 125 MHz) of the *O*-deacetylated CPS contained 18 carbon signals, indicating that in addition to two 2-acetamido-2-deoxy-D-galactopyranose residues, a three-carbon fragment was also present. The presence of four phosphorus coupled carbons (Fig. 2) suggested that the CPS was of a teichoic acid type involving glycerophosphate linkages.

An attempted dephosphorylation of the CPS with 48% hydrofluoric acid (4°C, 48 h) resulted in cleavage of the glycerol moiety, yielding, almost exclusively, a reducing disaccharide. The unusual lability of the *O*-glycosidic bond between the 2-acetamido-2-deoxy-β-D-glucopyranosyl or galactopyranosyl residue and an acyclic polyol was reported earlier (15). Dephosphorylation of the CPS was achieved using 40% hydrofluoric acid (4°C, 24 h), followed by purification of the

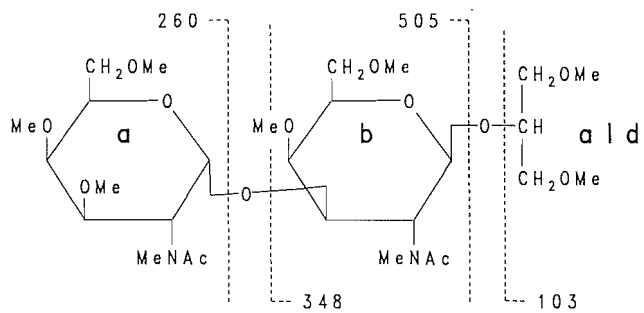

FIG. 3. The glc–ms of methylated oligosaccharide obtained during dephosphorylation of the capsular polysaccharide from *A. pleuropneumoniae* serotype 8 with some primary fragments.

resulting product by Bio-Gel P-2 gel filtration, which yielded a non-reducing disaccharide glycoside (K_{av} 0.40, 1.8 mg) that had $[\alpha]_D$ +38.7° (*c* 0.16, water) and afforded 2-acetamido-deoxy-D-galactose and glycerol on hydrolysis (2.0:0.4). Partial ^1H nmr (27°C, 500 MHz) showed signals at δ 5.07 (d, 1H, $J_{1,2}$ 3.8 Hz), 4.66 (d, 1H, $J_{1,2}$ 8.5 Hz), 2.06 (s, 3H, $NHCOCH_3$), and 2.04 (s, 3H, $NHCOCH_3$) ppm. Partial ^{13}C nmr (27°C, 125 MHz) showed signals at δ 175.41 ($NHCOCH_3$), 101.79 (anomeric C), 94.24 (anomeric C), 22.96 ($NHCOCH_3$), and 22.74 ($NHCOCH_3$) ppm.

Consistent with the nmr and compositional data, glc–ms of the permethylated oligosaccharide (16) (Fig. 3) confirmed presence of two 2-acetamido-2-deoxyhexosyl residues and a glycerol moiety: a base peak at *m/z* 260 (aA_1), peaks at *m/z* 228 (aA_2), 505 (abA_1); those of the glycerol moiety were *m/z* 103 (ald A_1), 163 (bald J_1), and 348 (bald). Hydrolysis of the permethylated oligosaccharide yielded products that after reduction ($NaBD_4$) and acetylation on glc analysis (program B) were identified as 1,5-di-*O*-acetyl-2-deoxy-2-(*N*-methylacetamido)-3,4,6-tri-*O*-methyl-D-galactitol-1-*d*, and 1,3,5-tri-*O*-acetyl-2-deoxy-2-(*N*-methylacetamido)-4,6-di-*O*-methyl-D-galactitol-

Can. J. Chem. Downloaded from www.nrcresearchpress.com by 91.144.44.67 on 09/07/12
For personal use only.

TABLE 1. ^{1}H chemical shifts[a] for the *O*-deacetylated capsular polysaccharide of *Actinobacillus pleuropneumoniae* serotype 8

Proton	Unit **a** →6)-α-D-Gal*p*NAc-(1→	Unit **b** →3)-β-D-Gal*p*NAc-(1→	Unit **c** →2)-Gly-(1→
H-1	5.07 (4.0)	4.69 (8.5)	3.98
H-1′	—	—	4.08
H-2	4.20	4.06	4.00
H-3	3.81	3.83	3.73
H-3′	—	—	3.85
H-4	4.05	4.06	
H-5	3.95	3.63	
H-6	3.98	3.75	
H-6′	4.07	3.67	

[a]In ppm measured at 24°C in D_2O with internal reference (2.225 ppm).
[b]$J_{1,2}$ in hertz.

TABLE 2. ^{13}C chemical shifts[a] for the *O*-deacetylated capsular polysaccharide of *Actinobacillus pleuropneumoniae* serotype 8

Carbon atom	Unit **a** →6)-α-D-Gal*p*NAc-(1→	Unit **b** →3)-β-D-Gal*p*NAc-(1→	Unit **c** →2)-Gly-(1→
C-1	94.34	102.26	65.29[c] (3.7)[d]
C-2	50.19	51.78	80.47 (8.2)[b]
C-3	68.44	75.89	61.97
C-4	68.84	64.57	
C-5	71.05 (9.3)[b]	75.89	
C-6	65.52[c] (3.6)[d]	61.37	

[a]In ppm measured at 24°C with 1% internal acetone (31.07 ppm).
[b]$^3J_{^{31}P,^{13}C}$ in Hz.
[c]Assignments may be reversed.
[d]$^2J_{^{31}P,^{13}C}$ in Hz.

1-*d* (1.0:0.3). Consideration of the composition, glc–ms data, and nmr evidence allows an oligosaccharide to be identified as D-Gal*p*NAc-(1→3)-D-Gal*p*NAc-(1→2)-glycerol. The anomeric configurations of the component monosaccharides were confirmed by 2D-nmr studies.

The position of the monophosphate diester linkage was established by 2D-nmr studies of the *O*-deacetylated CPS. A complete assignment of the proton resonances in the ^{1}H nmr spectrum was made from phase-sensitive COSY (10, 11) and relay COSY (12) experiments, and, following convention, the anomeric signals were labelled **a**–**c** in order of their decreasing chemical shifts. Most of the proton resonances could be assigned through their cross-peaks (Table 1). The assignments of the proton resonances corresponding to the hydroxymethyl groups were confirmed by correlation with the corresponding ^{13}C resonances via a ^{13}C–^{1}H shift correlated experiment (13, 14), which also enabled a complete assignment of the resonances in the ^{13}C nmr spectrum of polymer (Table 2) to be made. Based on the polymer composition, proton chemical shift data, and $J_{1,2}$ values (4.0 Hz), unit **a** was assigned to the 2-acetamido-2-deoxy-α-D-galactopyranosyl residue and **b** to the 2-acetamido-2-deoxy-β-D-galactopyranosyl residue ($J_{1,2}$ 8.5 Hz). The ^{13}C–^{31}P couplings for C-6**a** ($^2J_{^{31}P,^{13}C}$ 3.6 Hz) and C-1**c** ($^2J_{^{31}P,^{13}C}$ 3.7 Hz) and the large three-bond coupling for C-5**a** (9.3 Hz) and C-2**c** (8.2 Hz) located the monophosphate diester group at the *O*-6 position of the 2-acetamido-2-deoxy-α-D-galactopyranosyl residue and at *O*-1 of the glycerol moiety. The above evidence leads to the conclusion that the *O*-deacetylated CPS of *A. pleuropneumoniae* serotype 8 is a linear polymer having the structure

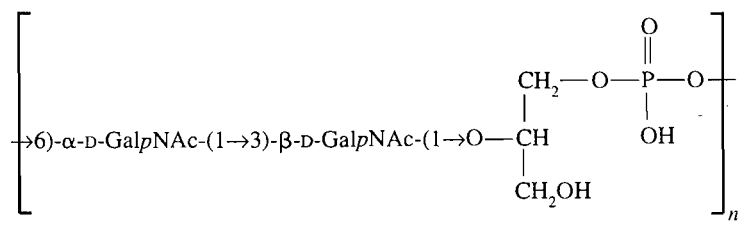

The *O*-acetyl substitution pattern of the native CPS, derived by comparison of its ^{13}C nmr and ^{13}C DEPT experimental spectral data with those of the *O*-deacetylated material, specified that both sugar residues were partially *O*-acetylated. The substitution pattern of residue **a** was complex since it carried two *O*-acetyl groups on the positions *O*-3 and *O*-4 (~30%, based on the ^{13}C nmr resonance intensities). The C-4**a** resonance exhibited a downfield shift of 2.35 ppm and the C-5**a** resonance

Can. J. Chem. Downloaded from www.nrcresearchpress.com by 91.144.44.67 on 09/07/12
For personal use only.

was upfield shifted by 1.97 ppm. The C-3**a** resonance experienced a downfield shift of 1.35 ppm, which reflected a cumulative effect of a positive increment due to the *O*-acetylation of C-3**a** and negative increment due to the presence of an *O*-acetyl group on the adjacent carbon (C-4**a**). Similarly, C-2**a** exhibited an upfield shift of 2.13 ppm due to the *O*-acetylation of the adjacent C-3**a** carbon. The *O*-acetylation pattern of the residue **b** was less obvious. Partial *O*-acetylation of the C-4**b** (~20%, based on the carbon-13 resonance intensities) was derived from its downfield shift by 2.45 ppm together with the upfield shift of the C-5**b** (4.19 ppm). The carbon resonance corresponding to the expected upfield shift of C-3**b** could not be located, although the cumulative effect of several *O*-acetyl groups could be difficult to predict (17).

In conclusion, the primary structure of the native capsular polysaccharide of *Actinobacillus pleuropneumoniae* serotype 8 (strain 405) was established as

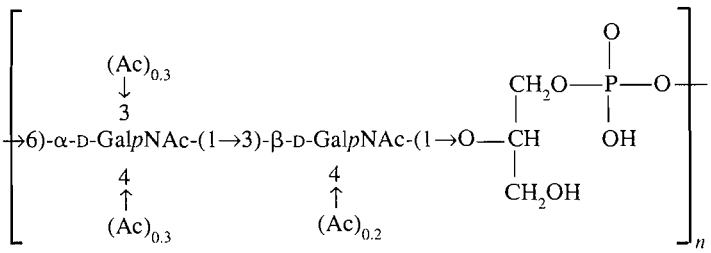

Structural studies were also made on the *O*-chain liberated by mild acid hydrolysis of the aqueous phase LPS, which was extracted by the lysozyme phenol–water method from saline-washed cells of *A. pleuropneumoniae* serotype 8. The purified *O*-chain had $[\alpha]_D$ +3° (*c* 1.2, water) (Anal. found: C 37.64, H 5.56, N 0.08, ash 0%). On the basis of glc of the derived alditol acetates and the acetylated derivatives of their (−)-2-butyl glycosides, the *O*-polysaccharide was found to be composed of D-glucose and D-galactose in the molar ratio ~ 2:3. The results of methylation studies and the analysis of ^1H and ^{13}C nmr spectra of the *O*-chain showed it to be identical with the *O*-chain of the *A. pleuropneumoniae* serotype 3 (ATCC 33590) (6) previously determined to have the structure:

→[3)-α-D-Glc*p*-(1→2)-β-D-Gal*f*-(1→6)-α-D-Gal*p*-(1→6)-β-D-Glc*p*-(1→3)-β-D-Gal*f*-(1→]

Serological cross-reactions between *A. pleuropneumoniae* serotypes 3, 6, and 8 have been reported (18). Our structural studies show that the apparent serotype cross-reactions could be due to the common epitopic features shared by the *O*-polysaccharide chains of these serotypes (6, 19). The study of the cross-reactions at the ultrastructural level using immunostabilization technique (20) also suggested that the observed cross-reactivity may be due to the somatic antigens. Only the capsules of serotypes 6 and 8 were completely cross-immunostabilized by the corresponding heterologous antisera when examined by transmission electron microscopy (20). The results of the present study show that although the CPS of serotypes 6 (21) and 8 have similar structural features, which probably contribute to the observed cross-reactivity, they are sufficiently distinct to allow the production of serotype specific antisera.

Acknowledgements

We thank Mr. F. P. Cooper for the glc–ms analyses and Mr. D. W. Griffith for the large-scale production of cells.

1. A. Gunnarsson, E. L. Biberstein, and B. Hurrell. Am. J. Vet. Res. **38**, 1111 (1977).
2. S. Rosendal and D. A. Boyd. J. Clin. Microbiol. **16**, 840 (1982).
3. R. Nielsen and P. J. O'Connor. Acta Vet. Scand. **25**, 96 (1984).
4. R. Nielsen. Acta Vet. Scand. **27**, 453 (1987).
5. E. Altman, J.-R. Brisson, and M. B. Perry. Carbohydr. Res. **179**, 245 (1988).
6. E. Altman, J.-R. Brisson, and M. B. Perry. Biochem. Cell Biol. **64**, 707 (1986).
7. S. W. Gunner, J. K. N. Jones, and M. B. Perry. Can. J. Chem. **39**, 1892 (1961).
8. K. Leontein, B. Lindberg, and J. Lönngren. Carbohydr. Res. **62**, 359 (1978).
9. D. M. Doddrell, D. T. Pegg, and M. R. Bendall. J. Magn. Reson. **48**, 323 (1982).
10. D. Marion and K. Wüthrich. Biochem. Biophys. Res. Commun. **113**, 967 (1983).
11. G. Bodenhausen, H. Kogler, and R. R. Ernst. J. Magn. Reson. **58**, 370 (1984).
12. A. Bax and G. Drobny. J. Magn. Reson. **61**, 306 (1985).
13. A. Bax. J. Magn. Reson. **53**, 517 (1983).
14. A. Bax and G. A. Morris. J. Magn. Reson. **42**, 501 (1981).
15. H. J. Jennings and C. Lugowski. Can. J. Chem. **58**, 2610 (1980).
16. N. K. Kochetkov and O. S. Chizhov. Adv. Carbohydr. Chem. **21**, 39 (1966).
17. K. Bock and C. Pedersen. Adv. Carbohydr. Chem. Biochem. **41**, 27 (1983).
18. K. R. Mittal, R. Higgins, and S. Larivière. J. Clin. Microbiol. **26**, 985 (1988).
19. E. Altman, J.-R. Brisson, and M. B. Perry. Can. J. Chem. **67**, 703 (1989).
20. M. Jacques, B. Foiry, R. Higgins, and K. R. Mittal. J. Bacteriol. **170**, 3314 (1988).
21. E. Altman, J.-R. Brisson, and M. B. Perry. Carbohydr. Res. **183**, 321 (1988).

Can. J. Chem. Downloaded from www.nrcresearchpress.com by 91.144.44.67 on 09/07/12
For personal use only.

On the unusual hydrolysis reaction of 8-acetamido-2,4,4,8-tetramethyl-3-azanium-bicyclo[3.3.1]non-2-ene perchlorate

J. A. CARAM[1]

Instituto de Investigaciones Físicoquímicas Teóricas y Aplicadas, C.C. 16, Suc. 4, 1900 La Plata, Argentina

B. E. RIVERO[2] AND O. E. PIRO[3]

Laboratorio de Cristalografía, Departamento de Física, Universidad Nacional de La Plata, 47 y 115, 1900 La Plata, Argentina

E. G. GROS[3]

Departamento de Química Orgánica, Facultad de Ciencias Exactas y Naturales, Universidad de Buenos Aires, Pabellón II, Ciudad Universitaria, 1428 Buenos Aires, Argentina

AND

C. M. MARSCHOFF[2,4]

Departamento de Ingeniería Química, Facultad de Ingeniería, Universidad de Buenos Aires, Pabellón de Industrias, Ciudad Universitaria, 1428 Buenos Aires, Argentina

Received July 11, 1988[5]

J. A. CARAM, B. E. RIVERO, O. E. PIRO, E. G. GROS, and C. M. MARSCHOFF. Can. J. Chem. **68**, 334 (1990).

The recently synthesized iminium salt 8-acetamido-2,4,4,8-tetramethyl-3-azanium-bicyclo[3.3.1]non-2-ene perchlorate (ATABNEP) shows unusual reluctance to undergo hydrolysis. It was established that ATABNEP is not attacked by water in acid or neutral media but readily reacts in alkaline solutions yielding the corresponding imine by direct abstraction of the iminium proton. The imine crystallizes as a monohydrate. Crystals belong to the monoclinic space group $P2_1$ with a = 6.915(2) Å, b = 8.459(4) Å, c = 13.287(6) Å, β = 92.53(3)°. Crystal structure of this compound was determined by X-ray diffraction using direct methods and refined to an R factor of 5.6%. As expected, the organic molecule structure is practically the same as that of ATABNEP. The imine molecules are arranged in sheets parallel to the *ab* plane linked, within a sheet, through a net of hydrogen bonds via the water protons and the hydrogen atom of the acetamido group.

Key words: iminium salt, hydrolysis, X-ray diffraction, molecular structure.

J. A. CARAM, B. E. RIVERO, O. E. PIRO, E. G. GROS et C. M. MARSCHOFF. Can. J. Chem. **68**, 334 (1990).

Le perchlorate de 8-acétamido-2,4,4,8-tetramethyl-3-azanium-bicyclo[3.3.1]non-2-ène (ATABNEP) présente une remarquable résistance à s'hydrolyser. On a établi que l'ATABNEP ne réagit pas dans les milieux acides ou neutres, mais réagit par abstraction du proton du groupe iminium en solution alcaline, en donnant l'imine correspondante. Ce produit crystallise comme un monohydrat. La structure crystalline de ce composé a été étudié par diffraction des rayons X. Il appartient au groupe spatial monoclinique $P2_1$ avec a = 6,915(2) Å, b = 8,459(4) Å, c = 13,287(6) Å, β = 92,53(3)°. La structure a été déterminée par méthodes directes et affinée jusqu'à une valeur du facteur d'accord R de 5,6%. Comme attendu, la structure du produit d'hydrolyse est pratiquement la même que celle du sel d'origine. Les molécules d'imine sont arrangées en couches parallèles au plan *ab*, liées par des ponts hydrogène faisant intervenir les protons de la molécule d'eau et l'hydrogène du groupe acétamide.

Mots clés : sel iminium, hydrolyse, diffraction des rayons X, structure moléculaire.

Introduction

Iminium salts have received increasing attention during the last 15 years because of the important role they play in many reactions that occur both in the laboratory and in nature (1–3). However, potential applications of these compounds have been limited because, as is well known (4), the iminium group is quite sensitive to hydrolysis, yielding a secondary ammonium salt and a carbonyl compound. This reaction is quite fast and therefore iminium salts cannot be stored under ambient conditions.

We recently reported the synthesis of a new iminium salt, namely, 8-acetamido-2,4,4,8-tetramethyl-3-azanium-bicyclo-[3.3.1]non-2-ene perchlorate (ATABNEP) (5), which shows an unusual stability when exposed to the laboratory atmosphere. Moreover, the solid salt not only showed no changes after several days of being exposed to air but was also recrystallized from neutral aqueous solutions.

Because of this behaviour, ATABNEP is thus the first iminium compound, to our knowledge, that might be considered for practical uses and, in fact, it has been proposed that the dielectric properties of this and related compounds should be studied (6). It was, therefore, considered of interest to have a better understanding of the hydrolysis behaviour of this salt, particularly with regard to its pH dependence.

Experimental

In a first series of experiments, some crystals of ATABNEP were dissolved in 10% H_2SO_4 and refluxed for 1 h. Surprisingly enough, the organic salt was quantitatively recovered when the experiment was over. In another group of experiments ATABNEP was first dissolved in 10% H_2SO_4 and then 20% NaOH was added dropwise: when pH values higher than 7 were reached, a colourless precipitate was obtained. Following these preliminary observations, this product was synthesized under controlled conditions and its molecular formula was solved by means of the usual analytical techniques. X-ray diffraction analysis was employed in solving the crystal structure of the new compound.

Thus (1*S*,5*R*,8*R*) 8-acetamido-2,4,4,8-tetramethyl-3-aza-bicyclo-[3.3.1]non-2-ene perchlorate, obtained as described elsewhere (5) (0.722 g), was dissolved in 10% H_2SO_4 (20 mL) and 20% NaOH was

[1]Student fellow of the Consejo Nacional de Investigaciones Científicas y Técnicas (CONICET).

[2]Member of the Carrera del Investigador Científico of the Comisión de Investigaciones Científicas de la Provincia de Buenos Aires.

[3]Member of the Carrera del Investigador Científico of CONICET.

[4]Author to whom correspondence may be addressed.

[5]Revision received October 19, 1989.

Can. J. Chem. Downloaded from www.nrcresearchpress.com by 91.144.44.67 on 09/07/12
For personal use only.

Can. J. Chem. Downloaded from www.nrcresearchpress.com by 91.144.44.67 on 09/07/12
For personal use only.

added dropwise until complete precipitation of a white product. The precipitate (0.378 g) was recrystallized from hexane.

Melting points are uncorrected. The IR spectrum was registered in KBr pellets using a Beckman IR-33 spectrophotometer. FT-NMR spectra (^{1}H and ^{13}C) were recorded at 100 MHz and 25.2 MHz with a Varian XL-100-15 spectrometer. Mass spectra were obtained at 70 eV (direct inlet) with a Varian-Mat CH7-A spectrometer interfaced to a Varian-Mat Data System 166 computer. X-ray data were obtained with a Huber four-circle diffractometer used with graphite monochromated MoKα radiation (λ = 0.7093 Å).

Results and discussion

The compound obtained had mp 155–156°C, $[\alpha]_D^{20}$ −144.1° (*c* 1.3, chloroform), and spectral data were as follows. IR: 3330 (OH), 3050 (NH), 1670 (C=N), 1650, 1560 (—N—C=O), 1300 (C—CO—NH···OH$_2$); ^{1}H NMR ($CDCl_3$–TMS), δ: 1.16 (3H, s, Me-4), 1.28 (3H, s, Me-4), 1.47 (3H, s, Me-8), 1.50–1.80 (8H, m, CH_2CH), 2.00 (3H, s, Me-C=O), 2.10 (3H, s, Me-C=N); ^{13}C NMR ($CDCl_3$–TMS), δ: 23.8 (*Me*-CO), 23.9 (Me-4), 24.3 (Me-4), 26.0 (C-6), 27.0 (Me-8), 29.3 (*Me*-C=N), 31.4 (C-7), 32.6 (C-9), 33.7 (C-5), 40.2 (C-1), 55.4 (C-4), 57.5 (C-8), 166.4 (C=N), 169.6 (C=O); MS (*m/z*, %): 236 (M^+, 37), 221 (*M* − 15, 12), 177 (*M* − 59, 35), 162 (177 − 15, 26), 150 (177 − 27, 29), 136 (177 − 41, 38), 122 ($C_8H_{12}N$, 82), 43 (C_2H_5N, 56), 42 (C_2H_4N, 100).

According to these results the solid was identified as a previously unreported imine, namely, 8-acetamido-2,4,4,8-tetramethyl-3-aza-bicyclo[3.3.1]non-2-ene (ATABNE), and the molecular formula $C_{14}H_{24}N_2O.H_2O$ and structure **2** were proposed in view of the following considerations.

The mass spectrum is almost identical to that of ATABNEP (5) and this strongly suggests that the structure of the new compound, after losing a fragment of 18 amu, is the same as that of compound **1** after losing the $HClO_4$ molecule. This conclusion is supported by the resonances at δ 1.16, 1.28, and 1.47 in the ^{1}H NMR spectrum, which indicate that the bicyclic structure of the original cation is maintained. The IR band at 1670 cm^{-1} points to the existence of an imine group, without signals of olefinic protons in the ^{1}H NMR spectrum, confirmed by the resonance at 166.4 ppm in the ^{13}C NMR spectrum. On the other hand, the IR band at 3330 cm^{-1} suggests the existence of O—H bonds, while those at 3050, 1650, and 1560 cm^{-1} correspond to the acetamide group and the one at 1300 cm^{-1} might be ascribed to the existence of a hydrogen bond with the amidic nitrogen, which approaches then the behaviour of a secondary amide.

Elemental analysis carried out on the crystals obtained agrees with this proposal as shown by the resulting data, which are given as follows. *Anal.* calcd. for $C_{14}H_{24}N_2O.H_2O$: C 66.10, H 10.30, N 11.01; found: C 66.07, H 10.34, N 10.91.

Structure **2**, as a monohydrate, was confirmed by X-ray diffraction analysis performed under the following conditions. A complete data set was obtained from a prismatic crystal of approximate dimensions 0.3 × 0.2 × 0.4 mm. The unit cell dimensions and orientation matrix for data collection were produced from 16 centred reflections by least-squares refinement. The reflections in the $\pm h$, $+k$, $-l$ reciprocal space quadrant having θ in the range 0–25° were measured by the ω-scan technique, working in the constant precision mode. Intensities of two standard reflections, which were monitored every 180 min, were essentially constant within 1% throughout the experiment.

The crystal structure was established from 935 independent reflections such that $I > 2\sigma(I)$. $\sigma(I)$ are based on counting statistics. Data were corrected for Lorentz, polarization, and extinction effects but not for absorption. The structure was solved employing direct methods to locate a fragment of the molecule. The remaining non-hydrogen atoms were positioned by isotropic least-squares refinement and difference Fourier syntheses. The two hydrogen atoms of the water molecule and some of the hydrogen atoms in the organic molecule were located in a difference Fourier synthesis phased on the positions of the non-hydrogen atoms. The remaining hydrogen atoms were located on stereochemical grounds. All hydrogen atoms were refined riding on the bonding atoms, with the following B_{iso} values (in Å^2): 6.2 (8) (CH and NH), 6.6 (9) (CH_2), 9.9 (7) (CH_3), and 6.2 (1) (H_2O). The quantity minimized was $M = \Sigma w[|F_o| - |F_c|]^2$ with $w = 0.85[\sigma^2(F_o) - 0.0028(F_o)^2]^{-1}$. The number of independent reflections per parameter was 4.8 and the final difference Fourier synthesis is essentially flat (maximum and minimum peaks were 0.24 and −0.28 e/Å^3, respectively). Final agreement factors were R = 5.6% and R_w = 6.1%.[6] The atomic dispersion scattering factors of Cromer and Waber (10) and the anomalous dispersion coefficients of Cromer and Ibers (11) were employed in the calculations. Most of these calculations were performed on a PDP 11/34 computer with the SHELX program (12). The projection was drawn with the program ORTEP (13).

Crystal data are as follows:

$C_{14}H_{24}N_2O.H_2O$ FW = 254.4

Monoclinic, space group $P2_1$, a = 6.915(2) Å, b = 8.459(4) Å, c = 13.287(6) Å, β = 92.53(3)°, V = 776.4(8) Å^3, z = 2, ρ_c = 1.088 g cm^{-3}, ρ_m = 1.05(1) g cm^{-3}, μ(MoKα) = 0.41 mm^{-1}, and F(000) = 280 electrons. Final positional parameters and equivalent isotropic temperature factors computed following Hamilton (7) are given in Table 1 for all non-hydrogen atoms. Bond lengths and bond and torsional angles for these atoms are listed in Table 2 and interatomic distances and angles involving the hydrogen bonds are shown in Table 3. In Fig. 1, a schematic

TABLE 1. Fractional positional parameters and equivalent isotropic thermal parameters for ATABNE

Atom	*X/a*	*Y/b*	*Z/c*	B_{eq} (Å^2)
C(1)	0.9451(9)	0.0486(7)	0.7447(0)	3.8
C(2)	1.0052(9)	0.2226(8)	0.7296(7)	4.1
N(3)	1.0039(8)	0.3246(6)	0.7986(7)	4.2
C(4)	0.9576(11)	0.2895(8)	0.9036(7)	4.4
C(5)	0.8825(11)	0.1151(9)	0.9243(8)	4.8
C(6)	0.6681(10)	0.0772(8)	0.9070(8)	4.7
C(7)	0.6039(10)	0.1031(9)	0.7996(8)	4.3
C(8)	0.7211(8)	0.0176(7)	0.7227(8)	3.8
C(9)	0.9919(10)	0.0079(9)	0.8551(7)	4.5
C(10)	1.0836(12)	0.2688(9)	0.6276(8)	5.7
C(11)	0.8080(13)	0.4071(10)	0.9384(8)	6.4
C(12)	1.1467(12)	0.3220(10)	0.9618(8)	6.0
C(13)	0.6681(12)	0.0697(9)	0.6166(8)	4.9
N(14)	0.6940(7)	−0.1561(6)	0.7290(7)	4.2
C(15)	0.5222(10)	−0.2385(9)	0.7171(9)	5.0
C(16)	0.5333(11)	−0.4164(8)	0.7137(10)	6.7
O(17)	0.3664(7)	−0.1758(6)	0.7029(8)	6.7
O(18)	0.0222(7)	−0.3451(6)	0.7347(9)	7.7

[6]Structure factor tables, anisotropic thermal parameters, and H-atom coordinates may be purchased from the Depository of Unpublished Data, CISTI, National Research Council of Canada, Ottawa, Ont., Canada K1A 0S2.

TABLE 2. Bond distances (Å) and bond and torsional angles (deg) in ATABNE

(a) Bond distances

Bond	Distance	Bond	Distance
C(1)—C(2)	1.525(9)	C(5)—C(6)	1.582(10)
C(1)—C(8)	1.587(8)	C(5)—C(9)	1.593(12)
C(1)—C(9)	1.544(9)	C(6)—C(7)	1.513(15)
C(2)—N(3)	1.259(11)	C(7)—C(8)	1.508(12)
C(2)—C(10)	1.506(13)	C(8)—C(13)	1.527(14)
N(3)—C(4)	1.460(12)	C(8)—N(14)	1.475(7)
C(4)—C(5)	1.566(10)	N(14)—C(15)	1.361(9)
C(4)—C(11)	1.534(12)	C(15)—C(16)	1.511(10)
C(4)—C(12)	1.535(12)	C(15)—O(17)	1.235(9)

(b) Bond angles

Bond	Angle	Bond	Angle
C(2)—C(1)—C(8)	111.0(5)	C(6)—C(5)—C(9)	107.0(7)
C(2)—C(1)—C(9)	106.8(5)	C(5)—C(6)—C(7)	113.6(7)
C(8)—C(1)—C(9)	110.6(5)	C(6)—C(7)—C(8)	113.8(7)
C(1)—C(2)—N(3)	123.8(7)	C(1)—C(8)—C(7)	109.7(6)
C(1)—C(2)—C(10)	116.7(6)	C(1)—C(8)—C(13)	111.6(6)
N(3)—C(2)—C(10)	119.4(7)	C(1)—C(8)—N(14)	113.1(7)
C(2)—N(3)—C(4)	124.4(6)	C(7)—C(8)—C(13)	110.3(6)
N(3)—C(4)—C(5)	114.9(7)	C(7)—C(8)—N(14)	113.1(7)
N(3)—C(4)—C(11)	107.8(6)	C(13)—C(8)—N(14)	108.6(7)
N(3)—C(4)—C(12)	105.3(6)	C(1)—C(9)—C(5)	109.0(6)
C(5)—C(4)—C(11)	110.7(7)	C(8)—N(14)—C(15)	125.0(6)
C(5)—C(4)—C(12)	108.9(7)	N(14)—C(15)—C(16)	115.6(6)
C(11)—C(4)—C(12)	109.0(7)	N(14)—C(15)—O(17)	123.8(7)
C(4)—C(5)—C(6)	116.8(7)	C(16)—C(15)—O(17)	120.5(7)
C(4)—C(5)—C(9)	107.6(7)		

(c) Torsional angles

Atoms	Angle
C(9)—C(1)—C(8)—C(7)	52.9(7)
C(9)—C(1)—C(8)—N(14)	−68.1(8)
C(9)—C(1)—C(8)—C(13)	175.3(6)
C(2)—C(1)—C(8)—C(7)	−65.5(7)
C(2)—C(1)—C(8)—N(14)	173.6(6)
C(2)—C(1)—C(8)—C(13)	57.0(7)
C(8)—C(1)—C(9)—C(5)	−62.0(7)
C(2)—C(1)—C(9)—C(5)	58.8(7)
C(8)—C(1)—C(2)—N(3)	90.9(8)
C(8)—C(1)—C(2)—C(10)	−93.8(7)
C(9)—C(1)—C(2)—N(3)	−29.7(8)
C(9)—C(1)—C(2)—C(10)	145.6(6)
C(1)—C(8)—C(7)—C(6)	−48.1(8)
N(14)—C(8)—C(7)—C(6)	66.9(8)
C(13)—C(8)—C(7)—C(6)	−171.4(6)
C(1)—C(8)—N(14)—C(15)	178.7(9)
C(7)—C(8)—N(14)—C(15)	60.1(10)
C(13)—C(8)—N(14)—C(15)	−62.6(12)
C(8)—C(7)—C(6)—C(5)	53.7(8)
C(7)—C(6)—C(5)—C(9)	−59.6(8)
C(7)—C(6)—C(5)—C(4)	61.0(10)
C(6)—C(5)—C(9)—C(1)	63.5(8)
C(4)—C(5)—C(9)—C(1)	−62.8(8)
C(6)—C(5)—C(4)—N(3)	−83.9(10)
C(6)—C(5)—C(4)—C(11)	38.5(12)
C(6)—C(5)—C(4)—C(12)	158.3(8)
C(9)—C(5)—C(4)—N(3)	36.3(9)
C(9)—C(5)—C(4)—C(11)	158.7(7)

Can. J. Chem. Downloaded from www.nrcresearchpress.com by 91.144.44.67 on 09/07/12
For personal use only.

TABLE 2 (*concluded*)

Atoms	Angle
C(9)—C(5)—C(4)—C(12)	−81.5(9)
C(5)—C(4)—N(3)—C(2)	−7.1(10)
C(11)—C(4)—N(3)—C(2)	−131.0(7)
C(12)—C(4)—N(3)—C(2)	112.7(8)
C(4)—N(3)—C(2)—C(1)	4.1(10)
C(4)—N(3)—C(2)—C(10)	−171.1(7)
C(8)—N(14)—C(15)—O(17)	−2.6(18)
C(8)—N(14)—C(15)—C(16)	172.8(10)

TABLE 3. Hydrogen bond distances (Å) and angles (deg) for $C_{14}H_{24}N_2O.H_2O$. Donor and acceptor atoms are indicated by D and A, respectively

D	H	A	D—H	D····A	H····A	D—H···A
O(18)—H(181)···N(3)^{i}			0.98	2.918(8)	1.94	173
O(18)—H(182)···O(17)			1.04	2.756(7)	1.71	179
N(14)—H(141)···O(18)^{ii}			1.08	2.756(7)	1.85	149

Symmetry code: (*i*) $x-1, y-1, z$; (*ii*) $x+1, y, z$

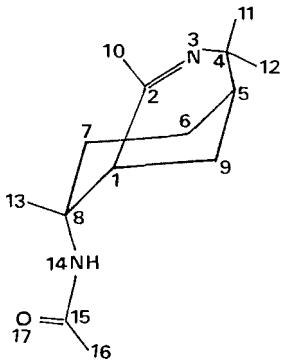

FIG. 1. Schematic drawing of the ATABNE molecule with heavy atoms numbering.

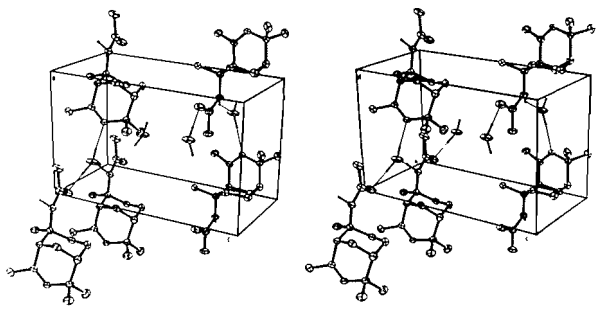

FIG. 2. Stereoscopic view of the structure and crystal packing of ATABNE.

drawing of the molecule with the numbering of the heavy atoms is given, while in Fig. 2 a stereoscopic view showing the structure and crystal packing of the new imine, including H-bonding atoms, is displayed.

The six-carbon ring of the imine has a well-defined chair configuration with a mean C—C distance of 1.53(3) Å and a mean C—C—C angle of 111(3)°. The other ring, which contains the imine group, has five of its atoms, i.e., C(1), C(2), N(3), C(4), and C(5), as well as the substituting carbon C(10) almost in the same plane (within 0.06 Å). As expected, these structural data are in very close agreement with those obtained for the organic cation in the unhydrolyzed salt (9). Crystal analysis also shows that the imine molecules are arranged in sheets parallel to the *ab* plane, with molecules linked to each other within the sheet through a network of hydrogen bonds involving the water protons and the hydrogen in the acetamido group (see Fig. 2 and Table 3). Neighbouring sheets are held together by van der Waals interaction.

Regarding the mechanism through which compound **2** is formed, it must be recalled that the electronic structure of the iminium group is best described by admitting contributions from two resonance forms, which correspond, respectively, to a pure iminium cation and a carbonium ion (8):

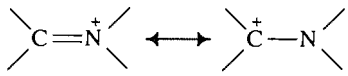

Thus, formation of the imine could proceed via direct abstraction of the iminium proton or, alternatively, by addition of an OH group on the carbon, followed by the loss of a water molecule. The much larger contribution of the iminium form in ATABNEP (9) suggests that the first path should be preferred. This conclusion is confirmed by theoretical calculations,[7] which indicate that the activation energy for OH addition is much larger than that for H abstraction. Consequently, Scheme 1 is proposed as a description for the reaction mechanism.

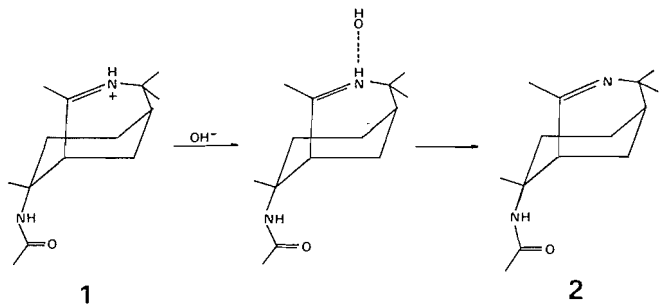

SCHEME 1

[7]H. O. Villar and E. A. Castro. To be published.

Can. J. Chem. Downloaded from www.nrcresearchpress.com by 91.144.44.67 on 09/07/12
For personal use only.

The present study shows that ATABNEP is unusually stable when compared to other iminium compounds, a fact that must be related to the bicyclic nature of the organic cation, which leads to low contribution of the carbonium ion resonance form (9). This, in turn, suggests that related iminium salts, obtained from the same monoterpenes but employing different nitriles, should also be stable to hydrolysis and, thus, able to be stored and handled without special care. This conclusion has been experimentally confirmed in several cases, as will be reported in future papers.

Acknowledgments

We are indebted to UMYMFOR for the spectra and elemental analysis and to the Organization of the American States and the Comisión de Investigaciones de la Provincia de Buenos Aires for partial financial support.

1. H. BÖHME and H. G. VIEHE (*Editors*). Iminium salts in organic chemistry. Part 1. John Wiley & Sons, New York. 1976.
2. H. BÖHME and H. G. VIEHE (*Editors*). Iminium salts in organic chemistry. Part 2. John Wiley & Sons, New York. 1979.
3. P. S. MARIANO. Tetrahedron, **39**, 3845 (1983).
4. H. BÖHME and N. HAABE. *In* Iminium salts in organic chemistry. Part 1. *Edited by* H. Böhme and H. G. Viehe. John Wiley & Sons, New York. 1976. p. 156.
5. J. A. CARAM, M. E. MARTINS, C. M. MARSCHOFF, L. F. R. CAFFERATA, and E. G. GROS. Z. Naturforsch. B: Anorg. Chem. Org. Chem. **39B**, 972 (1984).
6. J. A. CARAM, E. G. GROS, and C. M. MARSCHOFF. XVII Argentine Congress on Chemistry, Bahía Blanca, Argentina. 1985.
7. W. C. HAMILTON. Acta Crystallogr. **12**, 609 (1959).
8. P. A. KOLLMAN. *In* Iminium salts in organic chemistry. Part 1. *Edited by* H. Böhme and H. G. Viehe. John Wiley & Sons, New York. 1976. p. 4.
9. H. R. VITURRO, B. E. RIVERO, O. E. PIRO, J. A. CARAM, M. E. MARTINS, and C. M. MARSCHOFF. Can. J. Chem. **65**, 2000 (1987).
10. D. T. CROMER and J. T. WABER. *In* International tables for X-ray crystallography. Vol. IV. Kynoch Press, Birmingham. 1974. pp. 71–98.
11. D. T. CROMER and J. A. IBERS. *In* International tables for X-ray crystallography. Vol. IV. Kynoch Press, Birmingham. 1974. p. 149.
12. G. M. SHELDRICK. SHELX. A program for crystal structure determination. Univ. of Cambridge, England. 1976.
13. C. K. JOHNSON. ORTEP, Report ORNL-3794. Oak Ridge National Laboratory, Oak Ridge, TN. U.S.A. 1965.

Can. J. Chem. Downloaded from www.nrcresearchpress.com by 91.144.44.67 on 09/07/12
For personal use only.

Computations and measurements of the structures and conformations of 2- and 3-fluorobenzaldehyde in the gas and in solution

TED SCHAEFER AND CRAIG S. TAKEUCHI
Department of Chemistry, University of Manitoba, Winnipeg, Man., Canada R3T 2N2

Received September 7, 1989

TED SCHAEFER and CRAIG S. TAKEUCHI. Can. J. Chem. **68**, 339 (1990).

Precise ^1H and ^{19}F nuclear magnetic resonance chemical shifts and spin–spin coupling constants are reported for 4 mol% solutions of 2-fluorobenzaldehyde (2FB) and 3-fluorobenzaldehyde (3FB) in $CS_2/C_6D_{12}/TMS/C_6F_6$ and acetone-d_6/TMS/C_6F_6 solvent mixtures at 300 K. A small amount of the *O-cis* conformer of 2FB is present even in the nonpolar solvent mixture, corresponding to a free energy difference of 7.6(3) kJ/mol between the planar *O-cis* and *O-trans* conformers. In the polar solvent, this number decreases to 4.5(2) kJ/mol. The *O-cis* and *O-trans* conformers of 3FB have very similar abundances in the two solvent mixtures, the former being favored by a free energy difference of 0.38(4) kJ/mol in the nonpolar medium and, unexpectedly, considering its highly polar nature, by only 0.27(4) kJ/mol in the polar environment. STO-3G MO computations, with geometry optimization, of the internal rotational potentials of 2FB and 3FB confirm the planarity of the *O-cis* conformer of 2FB, that is, that the planar form is more stable than a somewhat twisted conformer. 6-31G MO calculations for the four planar conformers yield structures of potential use in the fitting of rotational spectra in the vapor. Extrapolation of the ^1H nmr data for 2FB implies a free energy difference of 11.5 ± 0.6 kJ/mol at 300 K in the vapour favoring the *O-trans* form, midway between the two theoretical estimates. The present experiments and computations are compared with the latest rotational, vibrational, and electronic spectra and with other assessments of the relative conformer stabilities in the vapor and in solution.

Key words: NMR for 2- and 3-fluorobenzaldehyde; conformations in solution and vapor, for 2- and 3-fluorobenzaldehyde; MO calculations, 2- and 3-fluorobenzaldehyde.

TED SCHAEFER et CRAIG S. TAKEUCHI. Can. J. Chem. **68**, 339 (1990).

Opérant à 300 K, dans des mélanges de solvant $CS_2/C_6D_{12}/TMS/C_6F_6$ et acétone-d_6/TMS/C_6F_6, on a déterminé d'une façon précise les déplacements chimiques et les constantes de couplage spin–spin observées des spectres de résonance magnétique nucléaire du ^1H et du ^{19}F de solutions à 4 mol% de 2-fluorobenzaldéhyde (2FB) et de 3-fluorobenzaldéhyde (3FB). Même dans le mélange de solvants non-polaires, on peut observer la présence de faibles quantités du conformère *O-cis* du produit 2FB; on peut donc établir que la différence d'énergie entre les conformères *O-cis* et *O-trans* est de 7,6(3) kJ/mol. Dans le solvant polaire, cette valeur diminue à 4,5(2) kJ/mol. Les abondances relatives des conformères *O-cis* et *O-trans* du produit 3FB sont assez constantes dans les deux mélanges de solvants; le premier est favorisé par une différence d'énergie libre de 0,38(4) kJ/mol dans le milieu non-polaire et par seulement 0,27(4) kJ/mol dans le milieu polaire ce qui est très surprenant compte tenu de la nature très polaire de ce mélange de solvants. Des calculs d'OM STO-3G, avec optimisation de la géométrie, ont été effectués sur les potentiels à la barrière de rotation interne des composés 2FB et 3FB; les résultats de ces calculs confirment le fait que le conformère *O-cis* du produit 2FB est plan, c'est à dire que la forme plane est plus stable qu'un conformère légèrement déformé. Des calculs d'OM au niveau 6-31G effectués sur les quatre conformères plans fournissent des structures de potentiel qui ont été utilisées pour ajuster le spectre de rotation en phase vapeur. Une extrapolation des données de la rmn du ^1H pour le composé 2FB implique que, à 300 K, en phase gazeuse la différence d'énergie libre favorise la forme *O-trans* par 11,5 ± 0,6 kJ/mol, valeur à mi-chemin entre les deux évaluations théoriques. On compare les expériences et les calculs réalisés ici avec les derniers spectres de rotation, de vibration et électroniques disponibles ainsi qu'avec d'autres évaluations des stabilités relatives des conformères tant en phase vapeur qu'un solution.

Mots clés : RMN de 2- et 3-fluorobenzaldehyde; conformations, en solution et en phase vapeur, de 2- et 3-fluorobenzaldéhyde; calculs d'OM sur 2- et 3-fluorobenzaldéhyde.

[Traduit par la revue]

Introduction

The conformational behaviour of 2-fluoro- and 3-fluorobenzaldehyde is again a topic of discussion (1) in connection with the microwave spectra of these compounds in the gas phase. Only the spectrum of the *O-trans* conformer is detected (1) for 2-fluorobenzaldehyde (2FB). From relative intensity measurements of certain rotational transitions in the spectrum of 3-fluorobenzaldehyde (3FB), the free energy difference between the conformers is assessed at 1.25 ± 0.84 kJ/mol at 260 K, the *O-cis* form being present in greater abundance (1). The microwave spectra also establish the planarity of the three detected conformers (1). These conclusions follow a long history of disagreement about the conformational equilibria of these compounds.[1]

[1]In the following discussion, only the latest reference to a given technique is cited; the disagreements have been repeatedly rehearsed and can be found in the present citations.

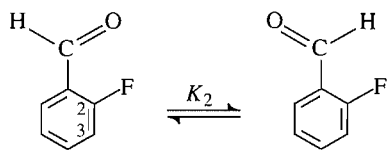

The latest (2) of numerous dipole moment measurements are interpreted to mean that, in CCl_4 at 298 K, 3FB exists as a roughly equimolar mixture of the two conformers, the *O-cis* form being present to the extent of 53 ± 5%. The *O-trans* conformer of 2FB is considered to be strongly and probably exclusively favoured (2).

Perhaps the most marked disagreements about conformational stabilities of 2FB and 3FB arose from vibrational spectra. The most recent data (3) for the liquids and for solutions imply the existence of both conformers for each of 2FB and 3FB, but afford no evidence concerning their relative proportions.

In acetone-d_6 solutions at 303 K containing 30 mol% of the

Can. J. Chem. Downloaded from www.nrcresearchpress.com by 91.144.44.67 on 09/07/12
For personal use only.

TABLE 1. The ^{1}H nmr and ^{19}F nmr spectral data for 2-fluorobenzaldehyde and 3-fluorobenzaldehyde at 300 K

Parameter	Compound			
	2FB(CS_2)[a]	2FB(acetone)[b]	3FB(CS_2)[a]	3FB(acetone)[b]
ν(CHO)	3084.387(1)[c]	3101.312(0)	2976.177(1)[d]	3019.310(1)
ν_2	11195.234(1)[d]	11624.356(0)[d]	2235.248(1)	2292.475(1)
ν_3	2128.056(1)	2198.112(0)	14548.555(1)[d]	14417.336(1)[d]
ν_4	2261.646(1)	2325.958(0)	2171.259(1)	2245.897(1)
ν_5	2162.600(1)	2217.376(0)	2240.805(1)	2302.890(1)
ν_6	2289.307(1)	2361.382(0)	2278.199(1)	2341.111(1)
$^3J_{23}$	10.278(1)[e,f]	10.855(1)[f]	8.445(1)[f]	8.851(1)[f]
$^3J_{34}$	8.377(1)	8.413(1)	8.127(1)[f]	8.708(1)[f]
$^3J_{45}$	7.334(1)	7.380(1)	8.230(1)	8.291(1)
$^3J_{56}$	7.762(1)	7.746(1)	7.568(1)	7.600(1)
$^4J_{24}$	5.332(1)[f]	5.406(1)[f]	2.686(1)	2.729(1)
$^4J_{26}$	6.993(1)[f]	7.116(1)[f]	1.429(1)	1.420(1)
$^4J_{35}$	1.028(1)	1.008(1)	5.209(1)[f]	5.377(1)[f]
$^4J_{46}$	1.886(1)	1.880(1)	1.042(1)	1.015(1)
$^5J_{25}$	−0.226(1)[f]	−0.167(1)[f]	0.423(1)	0.429(1)
$^5J_{36}$	0.390(1)	0.395(1)	0.138(1)[f]	0.237(1)[f]
^4J(2, CHO)	−0.216(1)	−0.411(1)	−0.001(1)	−0.058(1)
^4J(6, CHO)	−0.144(1)	−0.166(1)	−0.137(1)	−0.133(1)
^5J(3, CHO)	0.039(1)	0.117(1)	1.889(1)	1.866(1)
^5J(5, CHO)	0.830(1)	0.733(1)	0.398(1)	0.407(1)
^6J(4, CHO)	−0.001(1)	−0.001(1)	0.045(1)	0.050(1)
Calcd. transitions	192	192	205	192
Assigned transitions	192	190	180	191
Peaks observed	167	157	182	176
Largest difference	0.014	0.014	0.015	0.019
RMS deviation	0.004	0.002	0.004	0.005

[a]4.0 mol% in CS_2, containing also 10 mol% of C_6D_{12}, 0.5 mol% of TMS, and 0.25 mol% of C_6F_6.
[b]4.0 mol% in acetone-d_6, containing also 0.5 mol% of TMS and 0.25 mol% of C_6F_6.
[c]The ^{1}H nmr chemical shifts are in Hz at 300.135$_2$ MHz to high frequency of internal TMS.
[d]The ^{19}F nmr chemical shifts are in Hz at 282.363 MHz to high frequency of internal C_6F_6.
[e]Numbers in parentheses are the standard deviations in the last significant figure.
[f]The solvent dependence of $^nJ(^1H, ^{19}F)$ in aromatic systems is documented (28).

benzaldehyde derivatives, stereospecific long-range spin–spin coupling constants (4) yield an 86% abundance of the *O-trans* form of 2FB, that is, K_2 above is 6.1; K_3 is found as unity for 3FB (4). However, at 123 K, the ^{13}C nmr spectra of 0.5 M solutions of 2FB and 3FB in a mixture of CCl_2F_2 and $CHCl_2F$ provide no evidence for the *O-cis* conformer of 2FB. The fraction of the *O-trans* form of 3FB is 0.26 (K_3 = 0.35), the interconversion of the two conformers being slow on the nmr chemical shift time scale at 123 K (5).

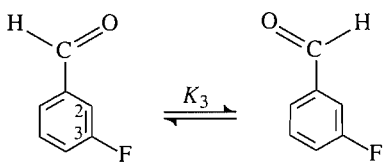

The emissive and absorptive $n\pi^*$ electronic spectra of 2FB and 3FB in the vapour phase (5), studied as to their vibrational fine structure, are analyzed to mean that the *O-trans* conformer is dominant for both compounds in the ground electronic state. A disagreement with the microwave spectrum of 3FB is apparent.

The most recent semiempirical and, apparently, geometry unoptimized STO-6G computations for 3FB predict (7) equal energies for the two planar conformers. The STO-6G calculations have the *O-cis* conformer of 2FB as 5.1 kJ/mol more stable than the *O-trans* (7), whereas the INDO method has the latter as more stable by 3.9 kJ/mol (4).

Three comments are appropriate. First, the four conformers in question have significantly different dipole moments so that perturbations of the conformational equilibria by the solvent are probable; these are likely to be most easily probed by the highly precise nmr measurements possible with modern instruments. Second, *ab initio* molecular orbital calculations with a minimal basis set (8) happen to be reliable for the internal motion in benzaldehyde and may well be useful for the prediction of the relative energies of the planar conformers of 2FB and 3FB *if* geometry optimization is included. Third, the microwave spectra have been fit to assumed structures (1); here 6-31G computations may well provide a fairly reliable basis for the refinement of such structures (9).

Accordingly, this paper reports precise ^{1}H nmr and ^{19}F nmr spectral parameters for dilute solutions of 2FB and 3FB in the nonpolar solvent mixture, CS_2/C_6D_{12}, and in the polar solvent, acetone-d_6. In addition, geometry optimized STO-3G and 6-31G MO structures and energies are given for the two compounds. Comparisons with solution and gas phase data are thereby facilitated.

Experimental

Dilute solutions (see Table 1) of 2FB and 3FB (Aldrich) in CS_2/C_6D_{12}/TMS/C_6F_6 and acetone-d_6/TMS/C_6F_6 solvent mixtures were filtered into 5 mm o.d. nmr sample tubes. The solutions were then degassed by numerous freeze–pump–thaw cycles and the sample tubes were sealed under vacuum. The ^{1}H nmr and ^{19}F nmr spectra were

Can. J. Chem. Downloaded from www.nrcresearchpress.com by 91.144.44.67 on 09/07/12
For personal use only.

Can. J. Chem. Downloaded from www.nrcresearchpress.com by 91.144.44.67 on 09/07/12
For personal use only.

acquired on a Bruker AM300 spectrometer, in a manner previously described (10), at a probe temperature of 300 K.

STO-3G (11) and 6-31G MO (12) computations employed the program Gaussian 86 (13) on an Amdahl 5870 system. The geometry optimization procedures allowed all bond angles and lengths to vary, with the constraint, however, that the nuclei of the benzene moiety remain in a plane. The STO-3G energies were computed in steps of 15°, between 0° and 180°, in the angle of the rotation about the exocyclic C_{sp^2}—C_{sp^2} bond. The minimal basis set happens to reproduce the internal barrier to rotation in benzaldehyde much more reliably than do the split-valence bases, even those with polarization functions (8). The 6-31G computations were done for the planar conformers only.

Results and discussion

The nmr spectra were analyzed with the program Numarit (4). The ensuing chemical shifts and spin–spin coupling constants appear in Table 1. The signs of the coupling constants are known from the earlier experiments (4) at lower magnetic field intensities. Figure 1 demonstrates the resolution obtainable in the spectra.

The conformational equilibria in solution

(i) 2-Fluorobenzaldehyde

The crucial coupling constant is ^5J(H, CHO) over five bonds and involving the aldehydic and ring protons. A recent analysis of the ^{1}H nmr spectra of benzaldehyde in the same solvent mixtures (apart from a tiny amount of C_6F_6) as in Table 1 gave ^5J(H, CHO) as 0.431(2) and 0.430(1) Hz in CS_2/C_6D_{12} and acetone-d_6, respectively (15). The methyl group-replacement procedure (16) showed (15) that ^5J(H, CHO) is a pure σ electron coupling (for these essentially planar benzaldehyde derivatives) and hence ^5J(H-5, CHO) is expected to vanish in the *O-cis* forms above, as it does in 2-hydroxybenzaldehyde (17) and, from recent unpublished work in this laboratory, in 3-fluoro-2-hydroxybenzaldehyde. In each of the latter two compounds, the strong intramolecular hydrogen bond ensures the exclusive existence at 300 K of the conformation analogous to *O-cis* above. In benzaldehyde, therefore, it is safe to write ^5J(H, CHO) as 0.861(5) Hz for an all-*trans* arrangement of the intervening bonds, applicable to either solvent.

For 2FB in CS_2/C_6D_{12}, the sum of the two ^5J(H, CHO) values is 0.869(2) Hz. The salient fact is the finite value of ^5J(H-3, CHO); at 0.039(1) Hz it demonstrates the presence of a small proportion of the *O-cis* form. If ^5J(H, CHO) for this form is taken as 0.869(2) Hz, then 4.5% of the 2FB molecules exists as the *O-cis* conformer, corresponding to a K_2 of 21.3(1.3) at 300 K and a free energy difference of 7.6(2) kJ/mol between the *O-cis* and *O-trans* forms. This conclusion assumes that the fluorine substituent does not perturb the extrema in ^5J(H, CHO). As pointed out above, all available evidence indicates the absence of ^5J(H, CHO) in the non-zigzag bond arrangement for planar conformers. However, suppose that the fluorine substituent, appended to the coupling pathway for ^5J(H-3, CHO) in 2FB, increases the extremum in ^5J(H-3, CHO) to 0.877 Hz, leaving the extremum in ^5J(H-5, CHO) unchanged from its value in benzaldehyde. Then the fractional population of the *O-trans* conformer becomes 0.830(1)/0.861(5) = 0.964(7) and that of the *O-cis* conformer is 0.039(1)/0.877 = 0.044(1), compatible within experimental error. It appears that a free energy difference of 7.6 ± 0.3 kJ/mol will encompass uncertainties in the extrema of ^5J(H, CHO).

In acetone-d_6 solution, the sum of the ^5J(H, CHO) numbers is 0.850(2) Hz, 0.01 Hz smaller than for benzaldehyde. Furthermore, ^5J(H-3, CHO) has increased to 0.117(1) Hz, indicating a significant enhancement of the population of the *O-cis* conformer. Qualitatively, it is expected that the more polar *O-cis* form, whose dipole moment is estimated from group moments as 4.35 D (2), as compared to the estimate of 3.15 D for the *O-trans* form, will be stabilized by the polar acetone-d_6 (18); a reaction field model in first order (18), treating the medium as a dielectric continuum, implies that the *O-cis* conformer is stabilized by 2.7 kJ/mol when 2FB transferred from CS_2 to acetone-d_6. The ^5J(H, CHO) values are in rough agreement with this implication, to be seen as follows.

If the extrema in ^5J(H, CHO) are both 0.850(2) Hz, the sum of the two values in acetone-d_6 solution, then the fractional population of the *O-trans* conformer is 0.733(1)/0.850(2) or 0.862(4) and that of the *O-cis* conformer is 0.117(1)/8.50(2) or 0.138(2). Hence, at 300 K, the free energy difference is 4.6 kJ/mol. However, if the extremum in ^5J(H-5, CHO) is unchanged from its value in benzaldehyde, then the population of the *O-trans* form becomes 0.733(1)/0.861(5) or 0.851(5) and hence that of the *O-cis* form is 0.149(5). This result entails a value of 0.785 Hz for ^5J(H-3, CHO) in the *O-cis* conformer, just the opposite trend assumed above for the CS_2 solution. The free energy difference is now 4.3 kJ/mol. Suppose the extremum in ^5J(H-3, CHO) is 0.877 Hz. Then the population of the *O-cis* conformer becomes 0.133 and implies a value of 0.846 Hz for the extremum in ^5J(H-5, CHO). The free energy difference is now 4.7 kJ/mol. It seems that a free energy difference of 4.5 ± 0.2 kJ/mol is a reliable value. The stabilization by 3.1 ± 0.5 kJ/mol of the *O-cis* conformer in the polar solvent, *relative* to the nonpolar solvent, agrees reasonably well with the reaction field model in first order (dipole terms only). This result may well be coincidental because quadrupolar terms (18) in the reaction field model are not small. However, as demonstrated in calculations for 2-pyridine aldehyde (19), uncertainties in the dipole moments of the individual conformers and in the origin for the estimation of quadrupole moments, themselves calculated from dipole vector components, not to speak of other corrections (18), introduce errors as large as 2.5 kJ/mol into the

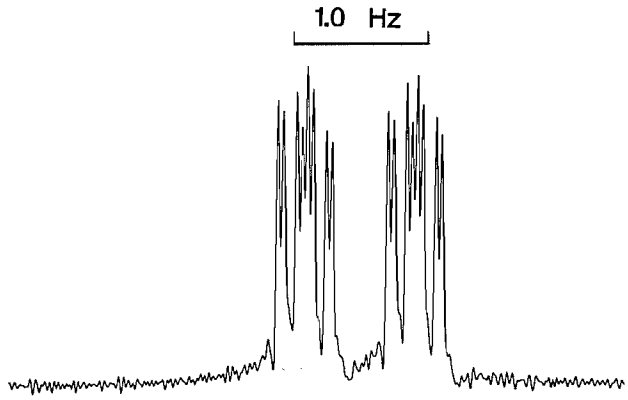

FIG. 1. The aldehyde proton magnetic resonance spectrum, at 300.135 MHz and 300 K, is shown for a 4.0 mol% solution of 2-fluorobenzaldehyde in a $CS_2/C_6D_{12}/TMS/C_6F_6$ solvent mixture. The 16 peaks arise from spin–spin coupling to H-3, H-5, H-6, and F-2 (see Table 1 for the magnitudes of the coupling constants). The small splitting of 0.039(1) Hz, as given by the spectral analysis, arises from an interaction over five bonds with H-3. This splitting is also cleanly resolved in the ^{1}H nmr spectrum of the latter, which is relatively isolated from the spectra of the other ring protons (Table 1) and does not display artifacts near the base line due to bad field shimming; such artifacts are evident in the figure above.

Can. J. Chem. Downloaded from www.nrcresearchpress.com by 91.144.44.67 on 09/07/12
For personal use only.

computed differences in the solvation energies for the two solvents. Hence the calculations were not pursued further. It may be noted that the dipolar and the quadrupolar interactions both act to increase the stability of the *O-cis* form of 2FB in polar solvents so that, qualitatively, the model agrees with the present experimental data.

The dielectric constant of the $CF_2Cl_2/CHFCl_2$ mixture at 123 K will lie between that of the CS_2 and acetone-d_2 solutions. Therefore an energy difference of, say, 5 kJ/mol between the conformers in the former mixture corresponds to a population of less than 1% for the *O-cis* form at 123 K. Its absence (5) in the ^{13}C nmr spectrum is therefore anticipated.

The discussion in this section has been somewhat elaborate; it is meant to illustrate the reliability of precise ^5J(H-5, CHO) numbers in applications to conformational analysis.

3-Fluorobenzaldehyde

In 3FB the substituent is further removed from the coupling pathway for ^5J(H, CHO) and should therefore minimally perturb its extreme value. In CS_2 solution, ^5J(H-5, CHO) is 0.398(1) Hz (Table 1). If ^5J(H-5, CHO) is 0.851(5) Hz for the *O-trans* conformer, as in benzaldehyde, then its population is 0.462(4) and K_3 is 0.859(14). The free energy difference at 300 K follows as 0.38(4) kJ/mol, the *O-cis* conformer being favoured. For the acetone-d_6 solution, this difference becomes 0.27(4) kJ/mol.

(iii) Comparison with other conformational data

In CCl_4 solution the population of the *O-trans* conformer of 3FB was determined as 0.47(5) from dipole moment measurements (2). The intensities of the rotational transitions in the gas phase gave the free energy difference as 1.25 ± 0.84 kJ/mol at 260 K (1). Within experimental error this number agrees with that for the CS_2 solution at 300 K. One might have expected that the *O-cis* conformer, with an estimated (2) dipole moment of 3.47 D, would be less stable in the gas phase than the *O-trans* form, with an approximate dipole moment of 1.73 D; the arrangement of the bond dipoles in the former should lead to an electrostatic repulsion. Worse, the polar acetone-d_6 solution causes an insignificant change in the conformer distribution. In the reaction field model, the quadrupolar now opposes the dipolar term and acts to stabilize the *O-trans* form (19). It seems rather unlikely that the two terms cancel to the same extent in the two solvents. Within experimental error, the microwave, dipole moment, and coupling constant data imply a state-independent conformational equilibrium for 3FB. The striking exception to this implication is the ^{13}C nmr result at 123 K (5). The population of the *O-trans* conformer, being 0.26, has the free energy difference between the conformers as 2.6 kJ/mol, *O-cis* favored.

An attempt at the resolution of the disparate results for 3FB goes as follows. If all these data are treated on an equal footing it follows that the enthalpy of the *O-trans* form of 3FB is 4.10 ± 0.52 kJ/mol larger than that of the *O-cis* form and, furthermore, that its entropy is 11.8 ± 2.2 J deg^{-1} mol^{-1} larger. This result is unlikely (see the molecular orbital calculations below and, for example, the various contributions to the entropy of benzaldehyde at 298.15 K (20)). One possibility is that, for the 0.5 M solution of 3FB in $CF_2Cl_2/CHFCl_2$ at 123 K, the much more polar *O-cis* conformer undergoes a significant degree of self-association, hence its *apparent* lower enthalpy and entropy in the egalitarian approach above. Another possibility is that the more polar *O-cis* form is more stabilized by specific dipole–dipole interactions with solvent molecules than is the *O-trans* form (18), also compatible with the *apparent* lower entropy of the former. It is also noted that on solidification (in a mull) no significant change occurs in the vibrational spectrum of 3FB, implying no change in the conformational equilibrium found in the liquid (3). A third possibility concerns the well-known π complexes formed between benzene and the polar C—H bond in chloroform molecules. It is therefore conceivable that, at 123 K, the $CHFCl_2$ molecules in the solvent mixture preferentially interact with the π electron cloud of the *O-cis* conformer of 3FB, thereby increasing its population.

TABLE 2. STO-3G MO energies for various conformations of 2-fluoro- and 3-fluorobenzaldehyde

θ/degrees[a]	2FB	3FB	θ/degrees	2FB	3FB
0	0.000[b,c]	0.000[b,c]	105	18.386	21.697
15	1.203	1.483	120	13.907	17.408
30	4.614	5.616	135	7.858	11.537
45	9.618	11.477	150	1.881	5.692
60	14.935	17.464	165	−2.441	1.551
75	18.892	21.814	180	−3.999	0.019
90	20.185	23.332			

[a]θ = 0° corresponds to the *O-cis* conformer for both compounds.
[b]Relative energies in kJ/mol, the *O-cis* conformer having a total energy of −436.578 586 au for 2FB and −436.580 023 au for 3FB.
[c]The relative energies are fit by Fourier series, as given by eqs. [1] and [2] of the text.

As to 2FB, the ^5J(H-5, CHO) data leave no doubt of the existence of the *O-cis* conformer in both polar and nonpolar solutions at 300 K, as do the vibrational spectra of the liquid (3). The dipole moment in CCl_4 (2) at 298 K is compatible with the result for the CS_2 solution in the present work. In the vapor phase the fraction of the *O-cis* conformer at 260 K, judging by ^5J(H, CHO) in the CS_2 solution, will be less than 4% and perhaps not detectable by microwave spectroscopy (1). This matter is further discussed below.

Molecular orbital calculations

(i) STO-3G MO internal barriers

Table 2 presents the energies of 2FB and 3FB as a function of the internal angle of rotation about the exocyclic C_{sp^2}—C_{sp^2} bond. According to this minimal basis, the planar conformers do indeed represent minima in the internal potential, even for the *O-cis* conformer of 2FB, calculated as 4.00 kJ/mol higher in energy than the *O-trans* form. The two planar conformers of 3FB are computed to be essentially isoenergic.

The energies in Table 2 can be fit to composite sinusoidal potentials, as in eq. [1] for 2FB and in eq. [2] for 3FB.

$$[1]\quad V/\text{kJ mol}^{-1} = -3.28\sin^2(\theta/2) + 22.23\sin^2\theta - 0.67\sin^2(3\theta/2) - 0.36\sin^2 2\theta - 0.06\sin^2 3\theta$$

$$[2]\quad V/\text{kJ mol}^{-1} = 0.02\sin^2(\theta/2) + 23.38\sin^2\theta + 0.03\sin^2(3\theta/2) - 0.17\sin^2 2\theta - 0.08\sin^2 3\theta$$

In these equations, θ is zero for the *O-cis* conformer and the standard error in the fit is 0.04 kJ/mol in each term of eq. [1] and 0.03 kJ/mol in each term of eq. [2]. These numbers may be compared with the STO-3G computations for benzaldehyde (8), which yield the twofold term, in $\sin^2\theta$, as 24.28(3) kJ/mol and the fourfold term, in $\sin^2 2\theta$, as −0.30(3) kJ/mol. According to Table 2, the internal barriers in 2FB and 3FB are both somewhat lower than in benzaldehyde (8). The computed decrease of 1.0 kJ/mol for 3FB roughly agrees with some free energies of

TABLE 3. Fractional populations of the *O-cis* conformers of 2-fluorobenzaldehyde and 3-fluorobenzaldehyde as obtained by various methods

Population			
2FB	3FB	Method	State
~0	0.64(9)	Rotational spectrum (1)	Vapor, 260 K
~0	0.53(5)	Dipole moment (2)	CCl_4, 298
0.045(5)	0.538(4)	^1H nmr, ^5J(H, CHO)	CS_2/C_6D_{12}, 300 K
0.140(7)	0.527(4)	^1H nmr, ^5J(H, CHO)	Acetone-d_6, 300 K
~0	0.74	^{13}C nmr (5)	$CF_2Cl_2/CHFCl_2$, 123 K
Present[a]	Present[a]	Vibrational spectra (3)	Liquid, solution
0.17[b]	0.50[b]	STO-3G MO	Free molecule
0	0.49[b]	6-31G MO	Free molecule

[a]Not informative about the actual population.

[b]On the assumption that differences in zero point energies and corrections for enthalpies at finite temperatures are negligible. See ref. 29, for example, for indications of how such corrections could be made, given enough information. In our opinion, these corrections would not alter the populations by more than about 5%.

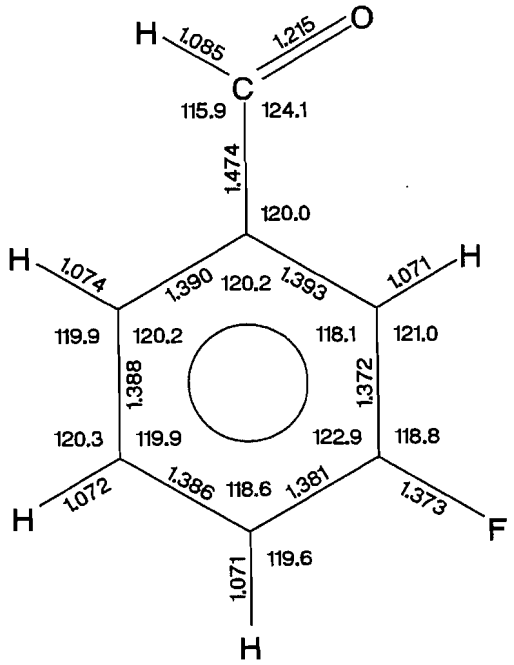

FIG. 2. The 6-31G MO geometry of the *O-cis* conformer of 3-fluorobenzaldehyde is shown. Its total energy is computed as −442.120 139 au. The geometry within the aldehyde group is not very different from that computed for benzaldehyde (8). The geometry of the *O-trans* conformer, not shown, is very similar to that of the *O-cis* form, apart from the orientation of the CHO group.

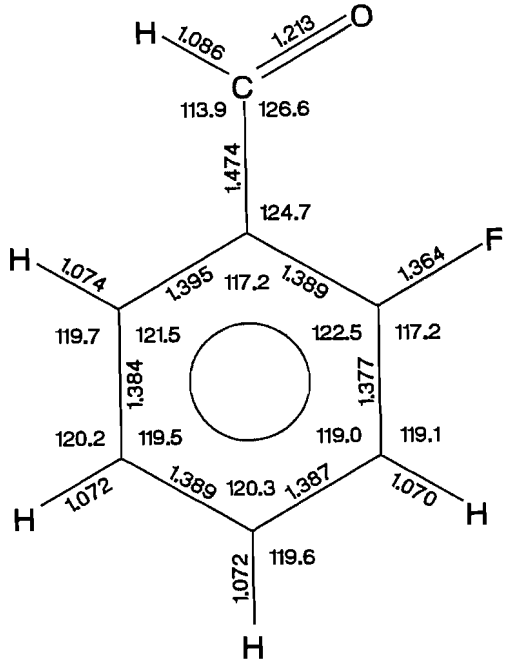

FIG. 3. The 6-31G structure of the *O-cis* conformer of 2-fluorobenzaldehyde displays a geometry in the vicinity of the aldehyde group indicative of strong repulsion between the C=O and C—F bonds, as expected. Its total energy, at −442.112 822 au, is 20.22 kJ/mol higher than that calculated for the *O-trans* conformer.

activation measured in solution (5, 21). No experimental value for the internal barrier is known for 2FB.

(ii) STO-3G and 6-31G MO energies of the planar conformers and extrapolation from solution

The STO-3G energy difference between the two conformers of 2FB, at 4.0 kJ/mol, is too small to explain the apparent absence of the *O-cis* conformer in the vapor phase. The 6-31G MO energies have the *O-trans* conformer of 2FB as 20.2 kJ/mol more stable than the *O-cis*. A simple extrapolation of a plot of the log of the equilibrium constants in the CS_2 and acetone-d_6 solutions versus $(\varepsilon - 1)/(2\varepsilon + 1)$, where ε is the dielectric constant, implies a K_2 of 100 at 300 K in the vapor phase, that is, for $\varepsilon = 1$. The reaction field model actually yields free energy differences (22, 23), so that this estimate is reasonable in principle. Allowance for uncertainties in the dielectric constants of the dilute solutions in Table 1, and for small correction terms to the dielectric function used above (examine in detail eq. 13.18 in ref. 18 and the many examples), suggests that K_2 in the vapor is 100 ± 20. Hence the free energy difference at 300 K in the vapor for 2FB is 11.5 ± 0.6 kJ/mol, *O-trans* more stable. If the entropy difference between the conformers is small, then K_2 is 200 ± 50 at 260 K, accounting for the absence of the microwave spectrum of the *O-cis* conformer at this temperature. The experimental estimate above lies midway between the two theoretical energy differences.

The essentially equal stabilities of the two planar forms of 3FB at the STO-3G level of MO theory, while the 6-31G basis

Can. J. Chem. Downloaded from www.nrcresearchpress.com by 91.144.44.67 on 09/07/12
For personal use only.

TABLE 4. Computed and estimated dipole moments[a] of the planar conformers of 2-fluoro- and 3-fluorobenzaldehyde

	2-FB			3-FB		
Method	*O-cis*	*O-trans*		*O-cis*	*O-trans*	
STO-3G MO	2.78	1.98	(2.02)[e]	2.25	0.97	(1.78)[f]
6-31G MO	5.94	4.12	(4.22)[e]	4.74	1.79	(3.68)[f]
INDO MO[b]	4.32	2.95	(0.03)[e]	3.47	1.13	(2.66)[f]
Estimated[c]	4.35	3.15		3.47	1.74	
Experiment[d]	3.12			2.80		

[a]In debyes.
[b]Reference 4.
[c]Vector addition of group moments (2).
[d]In CCl_4 solution at 298 K (2)
[e]Predicted on the basis of an *O-cis* population of 4.5% (Table 3).
[f]Predicted on the basis of an *O-cis* population of 53.8% (Table 3).

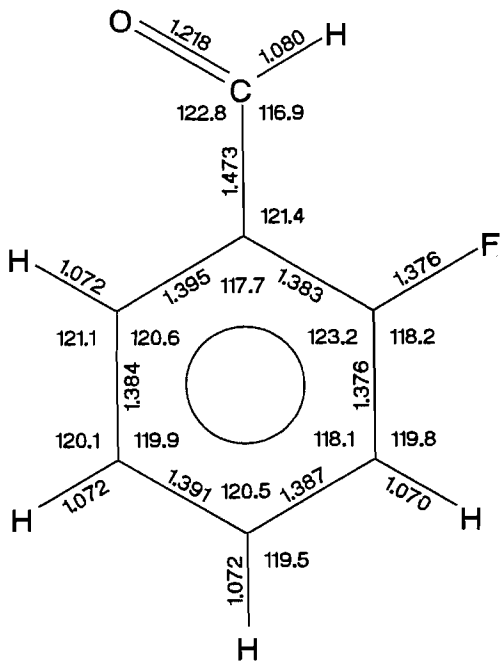

FIG. 4. The 6-31G structure of the *O-trans* conformer of 2-fluorobenzaldehyde is the one relevant to spectroscopic studies in the vapor phase, it probably being about 11.5 kJ/mol more stable than the *O-cis* form (see text).

implies the *O-trans* form as more stable by 0.12 kJ/mol, are not congruent with the microwave data (Table 3) unless the latter assumed somewhat incorrect dipole moment components. The $n\pi^*$ electronic spectra (6), in contrast to the microwave spectra, imply a greater abundance of the *O-trans* form (temperature not given). The coupling constants in Table 1 indicate very nearly equal populations of the two conformers in the CS_2 and acetone-d_6 environments (Table 3) and therefore that the conformer ratio will be the same in the vapor. This result is compatible with the theoretical stabilities.

(iii) The 6-31G MO geometries

These are given in Figs. 2–4 and should be useful to molecular spectroscopists, if it is remembered that the C—F bond length is computed as too long by about 0.02 A (24) with the 6-31G basis. The bond angles in the ring are probably reliable (8, 24–27).

(iv) Dipole moments

Table 4 collects some theoretical dipole moments for the planar conformers of 2FB and 3FB and also gives those estimated from group moments. To assess the reliability of these numbers, it will be assumed that the populations of the *O-cis* and *O-trans* conformers in CCl_4 solution are the same as those in the CS_2 solutions (Table 3). This assumption is probably correct to within one or two percent. Immediately clear is the underestimate of the dipole moments by the STO-3G and a corresponding overestimate by the 6-31G basis. As it turns out, the mean of the dipole moments of a conformer given by the two basis sets is very nearly correct. Thus, the dipole moment for 2FB in CCl_4 solution is then predicted as 3.12 D, as measured, while that for 3FB is predicted as 2.61 D, the measured value being 2.80 D. The moments obtained from INDO MO calculations (4) yield predicted dipole moments in solution that are rather close to experiment.

Discussions (30, 31) about the relative merits of the various basis sets for the computation of charge distributions in aromatic systems are available. Of course, the computed dipole moments depend on the way in which the overlap populations are divided among the atomic sites; the standard Mulliken procedure is used here.

Acknowledgments

We thank the Natural Sciences and Engineering Research Council of Canada for financial assistance and the referees for helpful criticism.

1. J. L. ALONSO and R. M. VILLAMAÑÁN. J. Chem. Soc. Faraday Trans. 2, **85**, 137 (1989).
2. E. A. W. BRUCE, G. L. D. RITCHIE, and A. J. WILLIAMS. Aust. J. Chem. **27**, 1809 (1974).
3. J. H. S. GREEN and D. J. HARRISON. Spectrochim. Acta, Part A, **32**, 1265 (1976).
4. R. WASYLISHEN and T. SCHAEFER. Can. J. Chem. **49**, 3216 (1971).
5. T. DRAKENBERG, R. JOST, and J. M. SOMMER. J. Chem. Soc. Perkin Trans. 2, 1682 (1975).
6. M. K. HAQUE and S. N. THAKUR. Chem. Phys. Lett. **66**, 561 (1979).
7. A. LAKSHMI, S. WALKER, B. J. MCCLELLAND, and J. H. CALDERWOOD. J. Mol. Struct. **95**, 249 (1982).
8. G. H. PENNER, P. GEORGE, and C. W. BOCK. J. Mol. Struct. (Theochem), **152**, 201 (1987).

Can. J. Chem. Downloaded from www.nrcresearchpress.com by 91.144.44.67 on 09/07/12
For personal use only.

9. C. W. BOCK, A. DOMINICANO, P. GEORGE, I. HARGITTAI, G. PORTALONE, and G. SCHULTZ. J. Phys. Chem. **91**, 6120 (1987), and references therein.
10. T. SCHAEFER, J. PEELING, and R. SEBASTIAN. Can. J. Chem. **63**, 3219 (1985).
11. W. J. HEHRE, R. DITCHFIELD, R. F. STEWART, and J. A. POPLE. J. Chem. Phys. **52**, 2769 (1970).
12. W. H. HEHRE, R. DITCHFIELD, and J. A. POPLE. J. Chem. Phys. **56**, 2257 (1972).
13. M. J. FRISCH, J. S. BINKLEY, H. B. SCHLEGEL, K. RAGHAVACHARI, C. F. MELIUS, R. L. MARTIN, J. J. P. STEWARD, F. W. BOBROWICZ, C. F. ROHLFING, L. R. KHAN, D. J. DEFREES, R. SEEGER, R. A. WHITESIDE, D. J. FOX, E. M. FLUDER, and J. A. POPLE. Carnegie–Mellon Quantum Publishing Unit, Pittsburgh, PA. 1984.
14. J. S. MARTIN, A. R. QUIRT, and K. E. WORVILL. The NMR program library. Daresbury Laboratory, Daresbury, U.K.
15. T. SCHAEFER AND C. S. TAKEUCHI. Can. J. Chem. **67**, 827 (1989).
16. R. A. HOFFMAN. Mol. Phys. **1**, 325 (1958).
17. T. SCHAEFER, R. SEBASTIAN, R. LAATIKAINEN, and S. R. SALMAN. Can. J. Chem. **62**, 326 (1984).
18. R. J. ABRAHAM and E. BRETSCHNEIDER. *In* Internal rotation in molecules. *Edited by* W. J. Orville-Thomas. J. Wiley and Sons, New York. 1974. Chap. 13.
19. W. DANCHURA, T. SCHAEFER, J. B. ROWBOTHAM, and D. J. WOOD. Can. J. Chem. **52**, 3986 (1974).
20. D. AMBROSE, J. E. CONNETT, J. H. S. GREEN, J. L. HALES, A. J. HEAD, and J. F. MARTIN. J. Chem. Thermodyn. **7**, 1143 (1975).
21. T. DRAKENBERG, R. JOST, and J. M. SOMMER. J. CHEM. SOC. CHEM. COMMUN. 1011 (1974).
22. J. J. MOURA RAMOS, L. DUMONT, M. L. STIEN, and J. REISSE. J. Am. Chem. Soc. **102**, 4150 (1980).
23. A. Y. MEYER. J. Mol. Struct. **195**, 147 (1989).
24. O. L. STIEFVATER. Z. Naturforsch. A: Phys. Phys. Chem. Kosmophys. **43A**, 155 (1988).
25. J. E. BOGGS, F. PANG, and P. PULAY. J. Comput. Chem. **3**, 344 (1982).
26. G. PORTALONE, G. SCHULTZ, A. DOMENICANO, and I. HARGITTAI. J. Mol. Struct. **118**, 53 (1984).
27. C. W. BOCK, M. TRACHTMAN, and P. GEORGE. J. Mol. Struct. **122**, 155 (1985); J. Comput. Chem. **6**, 592 (1985).
28. H. M. HUTTON, B. RICHARDSON, and T. SCHAEFER. Can. J. Chem. **45**, 1795 (1967).
29. K. B. WIBERG and M. A. MURCKO. J. Am. Chem. Soc. **110**, 8029 (1988).
30. S. MARRIOTT, T. SILVESTRO, R. D. TOPSOM, and C. W. BOCK. J. Mol. Struct. (Theochem), **151**, 15 (1987).
31. S. MARRIOTT, A. SILVESTRO, and R. D. TOPSOM. J. Chem. Soc. Perkin Trans. 2, 457 (1988).

Can. J. Chem. Downloaded from www.nrcresearchpress.com by 91.144.44.67 on 09/07/12
For personal use only.

Synthesis and characterization of a new crystalline tin(IV) arsenophosphate ion exchanger

K. V. SURENDRA NATH AND S. N. TANDON[1]

Department of Chemistry, University of Roorkee, Roorkee-247 667, India

Received May 6, 1989

K. V. SURENDRA NATH and S. N. TANDON. Can. J. Chem. **68**, 346 (1990).

A new crystalline layered inorganic ion exchanger tin(IV) arsenophosphate with the formula $Sn(HAsO_4)(HPO_4).H_2O$ has been prepared by refluxing the amorphous precursor. This exchanger has been characterized by X-ray powder pattern, chemical analysis, IR spectra, and thermal dehydration. Its ion exchange behaviour towards sodium ions is reported. The exchanger has an exchange capacity of 5.36 mequiv./g for Na^+. The performance of tin(IV) arsenophosphate is compared with crystalline tin(IV) phosphate and arsenate.

Key words: cation exchanger, crystalline tin(IV) arsenophosphate, ion exchange, thermal behaviour, X-ray studies.

K. V. SURENDRA NATH et S. N. TANDON. Can. J. Chem. **68**, 346 (1990).

En portant au reflux son précurseur amorphe, on a préparé un nouvel arsénophosphate d'étain(IV) cristallin qui peut agir comme échangeur d'ions inorganique et dont la formule est $Sn(HAsO_4)(HPO_4).H_2O$. On a caractérisé cet échangeur par le patron de diffraction des rayons-X par sa poudre, par une analyse chimique, par son spectre infrarouge et par une déshydratation thermique. On a déterminé son comportement comme échangeur d'ions et il possède une capacité d'échange de 5,36 méquiv./g de Na^+. On a comparé la performance de l'arsénophosphate d'étain(IV) à celles des phosphate et arsénate d'étain(IV).

Mots clés : échangeur de cations, arsénophosphate d'étain(IV) cristallin, échange d'ions, comportement thermique, études par rayons-X.

[Traduit par la revue]

Introduction

Over the years efforts have been directed towards synthesizing crystalline inorganic ion exchangers of the type $M(IV)(HXO_4)_2.H_2O$ (M = tetravalent metal and X = P, As), primarily for a better understanding of their ion exchange reactions (1, 2). These materials also have great potential for use as membranes for proton conduction, as superion conductors and as catalysts (1, 3). Crystalline materials are preferred over amorphous exchangers because of their high ion exchange capacity and resistance towards hydrolysis.

Every layered material is expected to have its own characteristic behaviour towards diffusion of the counter ions and thermal properties. However, among several known insoluble acid salts of tetravalent metals, α-layered zirconium phosphate (α-ZrP) and its other salt forms have received the maximum attention. In this series of compounds two new mixed layered materials, namely, zirconium–titanium phosphate (4, 5) and zirconium arsenophosphate (6) have been synthesized and studied for their ion exchange properties. These mixed salts are reported to be isomorphous with the parent single salts, nevertheless, they do show some variations in ion exchange and thermal properties. α-Zirconium arsenophosphate is obtained in almost complete miscible phases though it contains two anions of different sizes.

Ion exchange studies on α-tin(IV) phosphate (α-SnP) and α-tin(IV) arsenate (α-SnAs) (7) reveal that they behave more or less in a similar fashion but in some respects differently from α-ZrP and other similar compounds. Thus, it is of sufficient interest to synthesize crystalline tin(IV) arsenophosphate to determine how the presence of two anions of different dimensions affects the crystalline structure, vis-a-vis the ion exchange and thermal properties of the material. Crystalline tin(IV) arsenophosphate has been synthesized and the reproducibility and chemical stability of the exchanger checked. Its ion exchange behaviour towards sodium ions is reported together with phase changes which occur at different degrees of exchange and temperatures. The results thus obtained have been compared with those of α-SnP and α-SnAs.

[1]To whom correspondence should be addressed.

Experimental

Chemicals

All the chemicals used were analytical grade.

Preparation of the exchangers

(i) Tin(IV) hydrogen arsenate hydrogen phosphate

A 250 mL of 0.30 *M* $SnCl_4$ solution was added under stirring at room temperature to a 250 mL solution containing 15 mL of 14.5 *M* H_3PO_4 and 34.5 g of As_2O_5. A white gel was immediately formed. To it 250 mL of 15.5 *M* HNO_3 were added and the slurry was refluxed for 100 h. The solid thus obtained was filtered off, washed with distilled water till pH 4.5, and dried over $CaCl_2$ under vacuum to constant weight.

(ii) Tin(IV) hydrogen arsenate and tin(IV) hydrogen phosphate

These were prepared as described (6) by refluxing the slurries obtained by taking As/Sn = 2 and P/Sn = 30 molar ratios in over all 4 *M* HNO_3 for 100 h.

Analytical procedures

The composition of the tin(IV) arsenophosphate (SnAsP) samples was determined as follows: About 300 mg of the exchanger was boiled in 25 mL of 1.0 *M* NaOH; 10 mL of concentrated HCl was added to ensure complete solubility. This solution was then diluted to 100 mL with distilled water. Sn, As, and P contents were determined using Inductively Coupled Plasma-Atomic Emission Spectrometer (ICP-AES) Model LABTAM (Australia).

Na^+ ions and the As and P released to the external solutions during titration of the samples were also estimated by ICP-AES.

The solids (at various degrees of exchange) obtained from the titration were washed and conditioned over $CaCl_2$ under vacuum. X-Ray powder diffraction patterns were taken on a Phillips PW 1130 diffractometer using nickel-filtered Cu-Kα radiation. Thermogravimetric (TG) and differential thermal analysis (DTA) measurements were carried out on a Stanton Redcroft STA 780 at a heating rate of 10°C min^{-1}. Infrared spectra were taken on KBr pellets on a Beckmann IR-20 spectrophotometer.

Can. J. Chem. Downloaded from www.nrcresearchpress.com by 91.144.44.67 on 09/07/12
For personal use only.

TABLE 1. X-Ray powder diffraction patterns of different forms of crystalline tin(IV) arsenophosphate

$Sn(HAsO_4)(HPO_4).4H_2O$[a]		$Sn(HAsO_4)(HPO_4)$[b]		Layered $SnAsPO_7$[c]		Cubic $SnAsPO_4$[d]		$SnNa_2(HAsO_4)(PO_4).4H_2O$[a]	
d/Å	*I*/%	*d*/Å	*I*/%	*d*/Å	*I*/%	*d*/Å	*I*/%	*d*/Å	*I*/%
7.97	75	7.76	93	7.50	100	6.81	26	10.17	100
4.31	33	4.31	54	4.31	48	4.87	21	4.31	47
3.51	100	3.51	100	4.02	15	4.19	100	3.77	31
3.20	6	2.70	11	3.65	52	3.74	45	3.56	38
2.67	17	2.67	10	2.54	82	3.40	38	3.47	27
2.53	46	2.52	72	2.17	22	2.93	40	3.08	18
2.46	17	2.43	18			2.70	13	2.75	40
2.41	12	2.18	5			2.61	36	2.64	40
						2.50	60	2.54	40
						2.38	23	2.48	27
						2.34	11		
						2.32	11		
						2.28	13		
						2.20	13		

[a]Dried over $CaCl_2$.
[b]Heated at 300°C.
[c]Heated at 500°C.
[d]Heated at 800°C.

Ion exchange capacity

The ion exchange capacity was determined by the batch method. Several samples of exchanger (~0.5 g) in H^+ form were equilibrated with 100 mL of 0.10 *M* (NaCl + NaOH) solutions in various mixing ratios. The titrant was added in small increments to minimize hydrolysis. The solutions were shaken intermittently for 5 days at room temperature. The solutions were centrifuged and the supernatant liquid was analysed for alkali metal, arsenate, and phosphate contents; its pH was also measured.

Results and discussion

The composition of samples of three representative preparations shows reproducible results. The mean weight percentages of Sn, As, P, and H_2O in the samples dried at 50 ± 1°C for 24 h are 31.58, 20.13, 8.32, and 10.0 with standard deviation 0.18, 0.19, 0.61, and 0.33, respectively as against theoretical values 31.86, 20.11, 8.31, and 9.66 calculated for the formula $Sn(HAsO_4)(HPO_4).H_2O$.

The X-ray powder diffraction pattern for the H^+ form of the sample shown in the Fig. 2(*a*) (corresponding *d* values are listed in Table 1) shows a great similarity with those of α-$Sn(HPO_4).H_2O$ and α-$Sn(HAsO_4).H_2O$. The first *d* value at 7.97 Å is assumed as the distance between two adjacent planes of tin atoms (d_{002}).

Infrared spectra

The IR spectra for SnAsP samples show five characteristic absorption bands corresponding to interstitial water and hydroxyl groups (3700–2600 cm^{-1}), interstitial water (1800–1500 cm^{-1}), phosphate groups (1300–1000 cm^{-1}), arsenate groups (1000–750 cm^{-1}), and Sn—O bond (650–300 cm^{-1}).

Ion exchange behaviour of crystalline $Sn(HAsO_4)(HPO_4).H_2O$ towards sodium ions

The sodium uptake curve (Fig. 1) gives an ion exchange capacity of 4.49 mequiv./g at pH 7.3. Since 0.87 mmol of arsenate and phosphate are released at this pH to the external solution, the total ion exchange capacity of the sample can be taken as 5.36 mequiv./g. This value is in good agreement with the theoretical exchange capacity (5.37 mequiv./g) calculated by considering two exchangeable hydrogens per formula weight of $Sn(HAsO_4)(HPO_4).H_2O$. The observed exchange capacity for SnAsP falls in between α-SnP (6.08 mequiv./g) and α-SnAs (4.8 mequiv./g). The sodium exchange takes place appreciably in the pH range 5–6 and at pH 7 and beyond severe hydrolysis of the product takes place with consequent loss of Na^+ to the

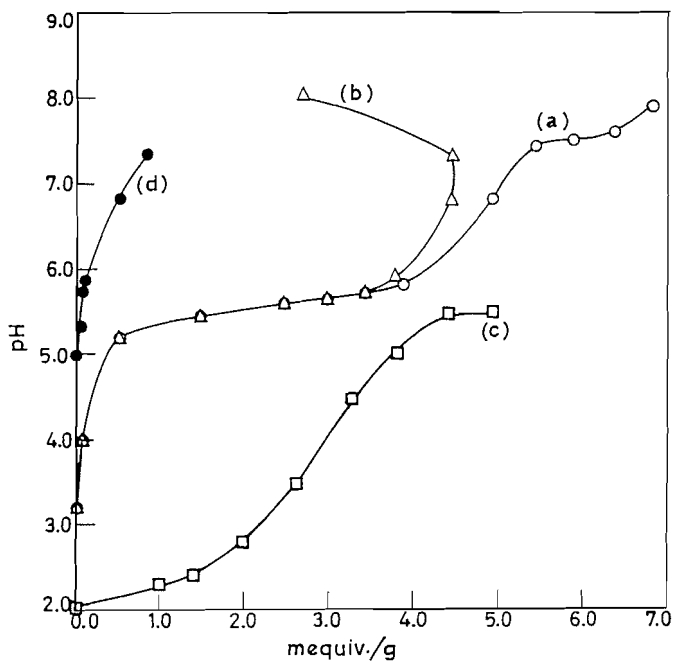

FIG. 1. Titration-uptake curves for $Sn(HAsO_4)(HPO_4).H_2O$. (*a*) Forward titration: titrant 0.1 *M* NaCl + 0.1 *M* NaOH; (*b*) Na^+ ion uptake; (*c*) reverse titration: titrant 0.1 *M* NaCl + 0.1 *M* HCl; and (*d*) mmol/g of arsenate and phosphate released to solution.

Can. J. Chem. Downloaded from www.nrcresearchpress.com by 91.144.44.67 on 09/07/12
For personal use only.

Can. J. Chem. Downloaded from www.nrcresearchpress.com by 91.144.44.67 on 09/07/12
For personal use only.

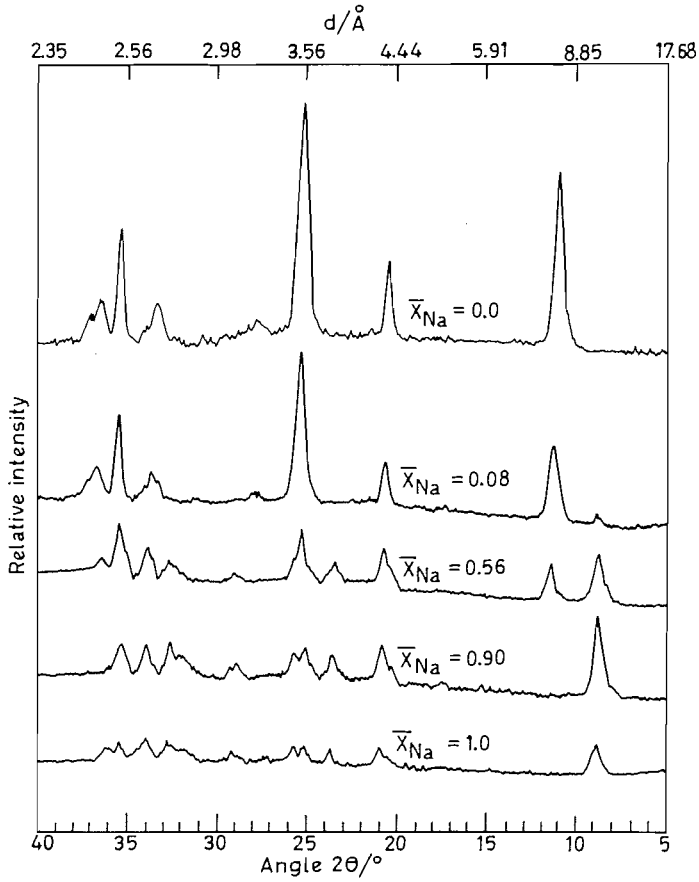

FIG. 2. X-Ray powder patterns of samples at different Na^+ loadings, expressed in molar fraction of sodium content in the solid ($\bar{X}_{Na}$).

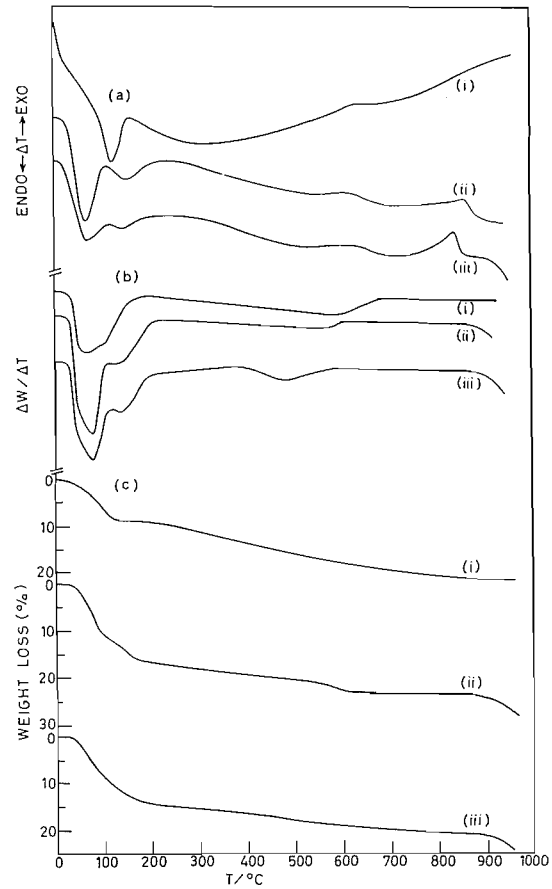

FIG. 3. (*a*) DTA, (*b*) DTG, and (*c*) TG curves of (*i*) $SnH_2(PO_4)_2.4H_2O$, (*ii*) $SnH_2(AsO_4)(PO_4).4H_2O$, and (*iii*) $SnH_2(AsO_4)_2.4H_2O$.

solution (Fig. 1(*b*)). The initial rise of pH from 3.2 to 5.0 in the titration curve signifies that the Na^+ is going into solid solution up to about 0.5 mequiv./g. X-Ray diffraction patterns of the sample at various degrees of Na^+ uptake shown in Fig. 2 are in good agreement with the shape of the titration curve. Beyond 0.5 mequiv./g of Na^+ uptake a second phase with an interlayer distance of 10.17 Å starts appearing and coexists with the first phase at 7.97 Å along the plateau of the titration curve. At the end of $Na^+ \rightarrow H^+$ process the first phase completely vanishes and only the second phase remains unchanged. This process of change from hydrogen to disodium form in one stage is also apparent from the single plateau obtained in the sodium exchange titration curve. A similar behaviour of one-stage transformation is observed in the case of α-SnP and α-SnAs (7). In contrast, α-ZrP and like compounds exhibit two plateaus, indicating the formation of mono- and disodium phases. The exchange of hydrogen ions in these materials in two stages is not due to the presence of protons at two different acidic sites but attributed to the two-phase changes involved in $Na^+ \rightarrow H^+$ process (8). All the hydrogen ions present in the SnP, SnAsP, and SnAs are supposed to be available for exchange to take place in a single step. The sodium exchange titration curve exhibits a shorter plateau and wider slope. It is known that the lower the degree of crystallinity of the material, the shorter is the plateau and therefore, the wider is the step involving the solid solution formation (slope) (9). The broadness of the peaks obtained in the X-ray patterns (Fig. 2(*a*)) is due to a lower degree of crystallinity in the sample. The fully exchanged sodium phase used for the back titration has more or less the same Sn:As:P ratio as the sample in H^+ form and the reverse titration of this material shows a marked hysteresis (Fig. 1(*c*)). The replacement of Na^+ ions by protons occurs at a lower pH than that required for forward reaction and yields a highly hydrated phase.

Thermal behaviour

The TG, DTG, and DTA curves of the samples in H^+ form and fully exchanged sodium forms are shown in Figs. 3 and 4, respectively. The samples dried over $CaCl_2$ show a total weight loss of about 20–22% up to 600°C. The weight loss at 35–200°C is ascribed to the loss of water of crystallization (~4 mol), and the loss at 350–600°C to condensation of phosphate and arsenate groups (~1 mol of H_2O). The DTG curve reveals that the dehydration of water of crystallization occurs in two stages and the corresponding two endothermic peaks in DTA curves are obtained in the range 35–100°C and 100–200°C. The third endothermic peak in DTA and weight loss in DTG curves corresponds to the condensation of arsenate and phosphate groups and the process takes place in the range 350–600°C. The analogous processes for SnP and SnAs occur in the ranges 350–650°C and 375–570°C, respectively. However, for these compounds the dehydration steps in TG curves are not distinct as the weight loss is continuous throughout the range up to 600°C. Constantino and Gasperoni (7) observed analogous behaviour on α-SnP and α-SnAs and demonstrated that the condensation of phosphate and arsenate groups begins before the water of crystallization is completely lost. Nevertheless, the

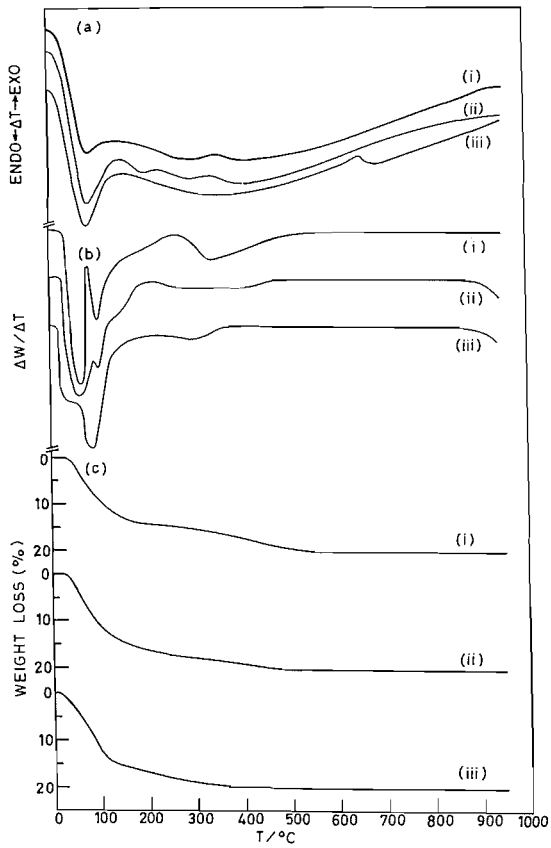

FIG. 4. (*a*) DTA, (*b*) DTG, and (*c*) TG curves of (*i*) $SnNa_2(PO_4)_2.4H_2O$, (*ii*) $SnNa_2(AsO_4)(PO_4).4H_2O$, and (*iii*) $SnNa_2(AsO_4)_2.4H_2O$.

samples heated up to 300°C still maintained the same layered structure in X-ray diffraction (Table 1(*b*)) indicating that the water held up to 300°C in the exchanger can be assumed only to be the constitution water. After the condensation process a layered tin pyroarsenophosphate is formed; above 800°C, this transforms into a cubic pyrocompound (Table 1, columns 3 and 4). The exothermic peak around 800°C in DTA curves (Figs. 3 and 4) signifies the phase transformation of the layered pyro-compounds to cubic pyro-compounds. The weight loss after 900°C in SnAsP and SnAs samples is related to the loss of arsenic pentoxide.

In the dehydration process of the sodium exchanged materials water molecules are lost at lower temperatures than the exchangers in H^+ form. The decrease in the temperatures of dehydration process can be attributed to the weaker bonds of water and to some degradation in the crystallinity of the fully exchanged sodium forms (Fig. 2(*e*)). The interlayer spacings in the samples vary with the degree of water of crystallization. The sample with 4 mol of water of crystallization has larger interlayer spacing (7.97 Å) than the dehydrated product (7.76 Å) (Table 1, columns 1, 2).

Although the structure of the new mixed compound is not known precisely, its X-ray powder diffraction pattern shows a great similarity to those of α-SnP and α-SnAs. From its chemical analysis, ion exchange, and thermal behaviour, this material can be classified as an α-type layered structure.

The investigations indicate that it is possible to prepare a tin(IV) based mixed ion exchanger with a single crystalline phase containing phosphate and arsenate anions in 1:1 ratio. The material, $Sn(HAsO_4)(HPO_4).H_2O$, shows a wide miscibility and is isostructural with α-$Sn(HPO_4).H_2O$ and α-$Sn(HAsO_4).H_2O$. It possesses an interlayer spacing of 7.97 Å intermediate between the parent single acid salts.

Acknowledgement

Financial assistance of U.G.C. (India) to K. V. S. Nath is gratefully acknowledged.

1. A. CLEARFIELD. Inorganic ion-exchange materials. CRC Press, Boca Raton, FL. 1982. Chap. 1.
2. A. CLEARFIELD, G. H. NANCOLLAS, and R. H. BLESSING. New inorganic ion exchangers, ion exchange and solvent extraction. *Edited by* J. A. Marinsky and Y. Marcus. Marcel Dekker, New York. 1973. Chap. 1.
3. A. LA GINESTRA, P. PATRONO, M. L. BERARDELLI, P. GALLI, C. FERRAGINA, and M. A. MASSUCCI. J. Catal. **103**, 346 (1987).
4. A. CLEARFIELD and T. N. FRIANEZA. J. Inorg. Nucl. Chem. **40**, 1925 (1978).
5. Y. YAZAWA, T. EGUCHI, K. TAKAGUCHI, and I. TOMITA. Bull. Chem. Soc. Jpn. **52**(10), 2923 (1979).
6. L. BERARDELLI, P. GALLI, A. LA GINESTRA, M. A. MASSUCCI, and K. G. VARSHNEY. J. Chem. Soc. Dalton Trans. 1737 (1985).
7. U. COSTANTINO and A. GASPERONI. J. Chromatogr. **51**, 289 (1970).
8. A. CLEARFIELD, W. L. DUAX, A. S. MEDINA, G. D. SMITH, and J. R. THOMAS. J. Phys. Chem. **73**, 3424 (1969).
9. G. ALBERTI, U. COSTANTINO, S. ALLULLI, M. A. MASSUCCI, and M. PELLICCIONI. J. Inorg. Nucl. Chem. **35**, 1347 (1973).

Can. J. Chem. Downloaded from www.nrcresearchpress.com by 91.144.44.67 on 09/07/12
For personal use only.

1,3,5-Trimethylbenzene(mesitylene) adducts with selected tin(II) compounds: the syntheses of $Sn(SO_3F)_2 \cdot C_9H_{12}$ and $Sn(SbF_6)_2 \cdot 2C_9H_{12}$

D. Y. Gin, M. S. R. Cader, J. R. Sams, and F. Aubke[1]

Department of Chemistry, The University of British Columbia, Vancouver, B.C., Canada V6T 1Y6

Received August 1, 1989

D. Y. Gin, M. S. R. Cader, J. R. Sams, and F. Aubke. Can. J. Chem. **68**, 350 (1990).

Addition of 1,3,5-trimethylbenzene (mesitylene or mes) to the tin(II) salts, $Sn(SO_3F)_2$ and $Sn(SbF_6)_2$, results in the formation of adducts of the composition $Sn(SO_3F)_2 \cdot$mes and $Sn(SbF_6)_2 \cdot 2$mes in very high yield. The adducts are characterized by chemical analysis and infrared spectra. The adduct formation is followed by ^{119}Sn Mössbauer spectroscopy. It appears that only tin(II) compounds with large, weakly nucleophilic anions are capable of forming mesitylene adducts, while $SnCl_2$, SnF_2, and stannocene do not give any indication of adduct formation under similar conditions.

Key words: tin(II)–mesitylene complexes, synthesis, vibrational study, ^{119}Mössbauer spectra.

D. Y. Gin, M. S. R. Cader, J. R. Sams et F. Aubke. Can. J. Chem. **68**, 350 (1990).

L'addition de 1,3,5-triméthylbenzène (mésitylène ou mes) aux sels d'étain(II), $Sn(SO_3F)_2$ et $Sn(SbF_6)_2$, fournit des adduits de composition $Sn(SO_3F)_2 \cdot$mes et $Sn(SbF_6)_2 \cdot 2$mes, avec des rendements très élevés. On a caractérisé les adduits par des analyses chimiques et par leurs spectres infrarouges. On a suivi la formation des adduits à l'aide de la spectroscopie Mössbauer du ^{119}Sn. Il semble que seuls les composés de l'étain(II) portant des anions faiblement nucléophiles et volumineux peuvent former des adduits avec le mésitylène; dans des conditions semblables, il ne semble pas y avoir de formation d'adduits avec le $SnCl_2$, le SnF_2 et le stannocène.

Mots clés : complexes de l'étain(II)–mésitylène, synthèse, spectres de vibration, spectres Mössbauer du ^{119}Sn.

[Traduit par la revue]

Can. J. Chem. Downloaded from www.nrcresearchpress.com by 91.144.44.67 on 09/07/12
For personal use only.

Introduction

Arene π-complexes, where low valent post-transition metal centers act as acceptors, and benzene or various alkyl benzenes, function as π-donors, form a small but interesting group of weakly bound complexes. Structural and bonding aspects of these compounds have become more widely known through the work of Amma and co-workers (1), and Schmidbaur (2). A review on the more general topic of π-complexes of main group elements has also appeared recently (3).

Within this group of π-complexes, interest has focussed mainly on arene complexes with univalent metal centers such as Ag(I), Cu(I), Hg(I), Ga(I), In(I), and Tl(I) and comparatively little is known about similar compounds with the group 14 centers such as Sn(II) (4–7) and Pb(II) (1, 8). There are commonly two reasons given for the paucity of arene π-complexes in group 14. As exemplified by the structural chemistry of divalent tin (9), the $5s^2$ pair is stereochemically far more active than in compounds of isoelectronic In(I), with the Sn(II) derivatives apparently less inclined to form π-complexes with arenes (2). In addition, lattice energies for Sn(II) and Pb(II) -salts tend to be considerably higher than those of Ga(I), In(I), or Tl(I) salts. The non-polar, π-donating arenes are normally incapable of breaking up such lattices effectively. To reduce the lattice energy and to facilitate complex formation, salts with large, univalent anions are chosen and the vast majority of arene π-complexes reported so far feature tetrahalometallate(III) anions of the type MX_4^- with M = B, Al, Ga, In, or Tl, and X = Cl or Br (1–8) as counter anions, however, weakly basic anions like $OTeF_5^-$ appear to be suitable as well (10).

The tin(II)–π-arene complexes reported so far are limited largely to mono-arene complexes with either Sn^{2+} (4) or the chloride-bridged moieties $(Sn_2Cl_2)^{2+}$ (5) or $(Sn_4Cl_4)^{4+}$ (7) as acceptors, but very recently a bis(arene) complex has been reported: $[(\eta^6\text{-}C_6H_6)_2SnCl(AlCl_4)]_2$ (6). Benzene functions primarily as donor, bonded to tin in the η^6-mode, and $AlCl_4^-$ is the counter anion, with Cl atoms bridging to tin. Frequently, however, arenes are also present in the lattice, without being coordinated to tin (4, 6, 7). Detailed crystal structures are reported for all compounds (4–7) and have been used in the development of bonding concepts based on MO theory (1, 4, 5).

We have been interested in the chemistry of tin for some time now, with two specific related objectives: (*a*) the use of ^{119}Sn Mössbauer spectroscopy as a structural tool and (*b*) stemming from our interest in superacids, the stabilisation of "bare", non- or very weakly coordinated cations like Sn^{2+} (11) or R_2Sn^{2+} (12). Two recent objects of our investigation (13), tin(II) bis(fluorosulfate), $Sn(SO_3F)_2$, and tin(II) bis(hexafluoroantimonate), $Sn(SbF_6)_2$, both originally reported by Gillespie and co-workers (14), seemed to us to be potentially capable to function as acceptors in arene π-complexes. Both give rise to broad line ^{119}Sn Mössbauer spectra with large positive isomer shifts relative to SnO_2, and, in case of $Sn(SO_3F)_2$, a small quadrupole splitting (11, 14) suggesting non-directional, nearly spherical distribution of the $5s^2$ electron pair. The anions, SO_3F^- and SbF_6^-, function frequently as weakly coordinated, tridentate ligands towards divalent metal ions giving rise to layer structures, based on the $CdCl_2$-prototype. This structural type is commonly found for most sulfonates of divalent metals, and the reported structure of $Ca(SO_3CH_3)_2$ (15) provides an example. The recently reported structure of $Ag(SbF_6)_2$ (16) may serve as an example for the layer structure formed by $M(SbF_6)_2$. Both SO_3F^- and SbF_6^- are very weakly basic, and covalent contributions to the lattice energies of their tin(II) salts should be small. Alternatively, both anions may stabilize arene complexes of tin with the help of oxygen or fluorine bridges. As donor, 1,3,5-trimethylbenzene (mesitylene) is chosen, because it is expected and found (2) to be a better donor than benzene. ^{119}Sn Mössbauer spectroscopy is found to be a useful tool during this investigation. Its application to the study of tin(II) compounds has recently been reviewed (17).

[1]Author to whom correspondence should be addressed.

Can. J. Chem. Downloaded from www.nrcresearchpress.com by 91.144.44.67 on 09/07/12
For personal use only.

Experimental

(a) Chemicals

1,3,5-Trimethylbenzene (mesitylene) obtained from Aldrich was dried over CaH_2 and distilled *in vacuo* before use. Fluorosulfuric acid technical grade was obtained from Orange County Chemicals and doubly distilled at atmospheric pressure as described previously (18). Antimony(V) fluoride (Ozark Mahoning-Pennwalt) was purified by repeated distillation, first at atmospheric pressure in a stream of dry N_2 and subsequently *in vacuo*. $Sn(SO_3F)_2$ was obtained from $SnCl_2$ (B.D.H.) and HSO_3F as described (19), and $Sn(SbF_6)_2$ resulted from the solvolysis of $Sn(SO_3F)_2$ in an excess of SbF_5 as reported recently (13). Stannocene, $(\eta^5\text{-}C_5H_5)_2Sn$, was synthesized from $SnCl_2$ and NaC_5H_5 (Aldrich). The crude product was purified by sublimation and the purity checked by microanalysis. SnF_2 and $SnCl_2$ were obtained from Matheson Coleman & Bell in 98 and 98.5% purity, respectively.

(b) Instrumentation

Infrared spectra were obtained on either a Perkin-Elmer 1710 FT-IR spectrometer or a Perkin Elmer 598 spectrometer. Samples were contained as thin, solid films between AgBr plates. For the recording of Raman spectra a Spex Ramalog 5 instrument equipped with an Ar^+ Laser was available. Ultraviolet–visible spectra of Nujol mulls were obtained on a Hewlett Packard 8452-A diode array spectrophotometer with the mull contained in an air-tight cell fitted with quartz windows. ^1H nmr spectra were recorded on a Varian XL-300 spectrometer.

Mössbauer spectra were collected on a constant acceleration spectrometer, using $Ba^{119}SnO_3$ as the γ-ray source. Data counts were acquired on a Tracer-Northern multichannel analyzer linked to the mainframe computer via an IBM-PC. The relative velocity scale was calibrated with an iron foil absorber and a ^{57}Co source.

Standard vacuum line techniques were used for the transport of volatile materials. Filtration apparatus, similar in design to equipment described by Shriver (20), was used for product isolation.

All moisture-sensitive solids were handled in a Vacuum Atmospheres Corp. "Dri-Lab" Model No. He-493, filled with purified dry nitrogen and equipped with a Dri-Train circulating unit. The reactions were performed in Pyrex reaction vessels of about 50-mL capacity made from round bottom flasks fitted with Kontes Teflon stem valves and equipped with Teflon-coated spin bars. The reactions were monitored by weight. Chemical analysis was carried out by the Analytische Laboratorien, Gummersbach, West Germany, and by Mr. P. Borda of this Department.

(c) Synthetic reactions

(i) Synthesis of $Sn(SO_3F)_2 \cdot 1,3,5\text{-}(CH_3)_3C_6H_3$

To a one-part reactor a sample of $Sn(SO_3F)_2$ (1.06 g, 3.35 mmol) was added and after evacuation of the reactor, dry mesitylene (ca. 7 mL, ~50 mmol) was transferred into the reaction vessel via a distillation bridge. The white suspension was stirred *in vacuo* at room temperature for 3 days. Excess mesitylene was removed *in vacuo* at −20 to −15°C (ice/NaCl bath) over a period of 3 days yielding 1.39 g of a white powder, of the composition $Sn(SO_3F)_2 \cdot$mes with a decomposition point of 97.2–98°C.

Anal. calcd. for $C_9H_{12}F_2O_6S_2Sn$: C 24.74, H 2.77, F 8.70, S 14.67, Sn 27.16; found: C 25.77, H 2.87, F 8.53, S 14.84, and Sn 27.10.

An alternate preparation with mesitylene removed *in vacuo* at −5°C gave the following analysis:

Anal. Calcd: C 24.74, H 2.77, S 14.67; found: C 24.97, H 2.80, S 14.55.

Infrared bands and estimated intensities: (cm^{-1}) 2910w,b, 2860vw, 1760vw, 1604m, 1575w,sh, 1446w, 1337w, 1191vs, 1127w,sh, 1054vs, 888s, 786w, 667w, 589ms, 544m, 507vw, and 405m.

(ii) Synthesis of $Sn(SbF_6)_2 \cdot 2[1,3,5\text{-}(CH_3)_3C_6H_3]$

To the bottom portion of a two-part reactor, freshly prepared $Sn(SbF_6)_2$ (3.11 g, 5.27 mmol) was added. The flask was then fitted to the bottom end of the filtration apparatus. On the top end of the filtration apparatus a second 100-mL flask was fitted and the entire apparatus was then evacuated. Through a Teflon valve in the bottom chamber of the apparatus mesitylene (15 mL, 108 mmol) was transferred via a distillation bridge. Upon exposure to the mesitylene vapor, the white powder immediately turned yellow and then during the filtration, pale, off-white. When the mesitylene distillation was complete, the suspension was stirred *in vacuo* for 1.5 h. The apparatus was inverted, and the mixture filtered. The filtrate flask was cooled to −10°C (salt/ice bath) and the mixture was left to filter for 17 h. When gravity filtration was complete, the filtrate chamber of the apparatus was evacuated to dry the solid further. The apparatus was refilled with dry nitrogen, and the filtrate chamber was evacuated again. This drying procedure was repeated three more times, giving a pale, off-white solid (4.18 g, or 5.04 mmol, 95.5% yield) and yellow–green filtrate, which was discarded. The product was transferred to a two-part reactor and was further dried *in vacuo* for 24 h at room temperature. No further weight change was observed. The solid decomposed between 69.5 and 71.5°C to a greenish yellow liquid.

Anal. calcd. for $C_{18}H_{24}F_{12}Sb_2Sn$: C 26.03, H 2.91, F 27.45, Sb 29.32, Sn 14.29; found: C 26.87, H 3.00, F 27.31, Sb 29.05, Sn 14.20; total 100.43.

Infrared bands and estimated intensities (cm^{-1}): 2920mw, 2860w, 1601m, 1580m, 469w, 1384m, 1168vw, 1080vw, 1040vw, 1007w, 960vw,b, 860w, 687s, 671vs, 635s,sh, 580m,b, 544m, 512w, 440w, and 395w.

Results and discussion

(a) Synthesis

The previously reported synthesis of Sn(II) containing benzene π-complexes (4–7) involves either the reaction of $SnCl_2$ and $AlCl_3$ at different mole ratios and temperatures (4, 5), or of molten $Sn(AlCl_4)_2$ (6, 7) with the arene to give either Sn^{2+}, $(Sn_2Cl_2)^{2+}$, or $(Sn_4Cl_4)^{4+}$ containing complexes as white colorless crystals. Crystals suitable for single crystal X-ray diffraction studies are obtained (4–7) in all instances. The course of the reaction appears to be influenced in part by the mole ratios of the reactants used and in part by the reaction temperature. The different products, with Sn^{2+} or $(Sn_nCl_n)^{n+}$, $n = 2$ or 4, are not totally surprising since in the binary system $SnCl_2$–$AlCl_3$, phase studies (9) have revealed the existence of two distinct phases: $SnCl_2 \cdot AlCl_3$ and $SnCl_2 \cdot 2AlCl_3$. It appears that the same two phases crystallise now in the form of π-arene complexes with $AlCl_4^-$ as coordinated counter ion and in several instances with lattice arene present (4, 6, 7).

The synthetic reactions reported here differ in a number of ways. Binary rather than tertiary reaction mixtures are used, the reaction temperature is room temperature and the tin(II) substrates are synthesized and characterized prior to their reaction with mesitylene.

Addition of mesitylene occurs smoothly according to:

$$[1]\quad Sn(SO_3F)_2 + \text{mes} \xrightarrow[\text{mesitylene}]{25^\circ C} Sn(SO_3F)_2 \cdot \text{mes}$$

or

$$[2]\quad Sn(SbF_6)_2 + 2\ \text{mes} \xrightarrow[\text{mesitylene}]{25^\circ C} Sn(SbF_6)_2 \cdot 2\ \text{mes}$$

mes = mesitylene or 1,3,5-trimethylbenzene, and the two complexes are formed in nearly quantitative yield. Solid material remains present throughout the reaction and in case of $Sn(SO_3F)_2$ as acceptor, there is no visible sign of a reaction, except for an increase in the bulk of the solid residue. Complete removal of excess mesitylene *in vacuo* is difficult to judge and the conditions quoted in the Experimental section are arrived at by trial and error. It does appear that samples submitted

Can. J. Chem. Downloaded from www.nrcresearchpress.com by 91.144.44.67 on 09/07/12
For personal use only.

for microanalysis (C, H, and S contents) immediately after isolation had small amounts of residual mesitylene trapped while samples sent to Germany for further analysis (S, Sn, Sb, and F contents) seemed to have lost the excess reactant.

The reaction of mesitylene with $Sn(SbF_6)_2$ differs even further. A 2:1 complex forms and a color change to bright yellow is noted as soon as the tin salt is exposed to mesitylene vapor. However, the color of the solid quickly fades during product isolation and an off-white solid is obtained in very high yield together with a yellow–green filtrate. The origin of the initially observed color is unclear. A uv–visible spectrum taken as Nujol mull on a solid sample at this stage shows an intense uv-absorption at ~240 nm tailing off in the visible region with weak shoulders 486, 580, and 656 nm, respectively. Observations made during product isolation suggest that the intense color is due to a by-product, which is very soluble in excess mesitylene. A complex formed by mesitylene and small, residual amounts of SbF_5 becomes a distinct possibility and addition of mesitylene to pure SbF_5 results in an intensely colored dark brown solid, which is not investigated further. There is little doubt that the final product like other arene complexes of group 13 and 14 metals (1–8) is white.

The use of gravity filtration as a means of product isolation is important in case of the $Sn(SbF_6)_2 \cdot 2mes$ synthesis. Attempts to isolate this compound by slow, careful removal of excess mesitylene *in vacuo* or in a stream of dry N_2 at room temperature and at −5°C result in partial decomposition and materials that analyse as $Sn(SbF_6)_2 \cdot 1.5mes$. In addition the product has a slight yellow tint.

The thermal stability of both mesitylene complexes described here is limited. $Sn(SO_3F)_2 \cdot mes$ melts with decomposition at 97–98°C while $Sn(SbF_6)_2 \cdot 2mes$ has a decomposition range of 69.5–71.5°C, where a greenish yellow liquid forms.

Attempts to extend the mesitylene addition reaction to three other tin(II) compounds are unsuccessful. Both $SnCl_2$ and SnF_2 are recovered unchanged. Both salts have Sn^{2+} in distorted octahedral environments (7) and the structures of $SnCl_2$ (21) and orthorhombic SnF_2 (14, 22), one of the two polymorphic forms, may be regarded as layer structures. It must be concluded that the lattice energies of both compounds are too high and adduct formation does not occur.

Stannocene, $(\eta^5\text{-}C_5H_5)_2Sn$, has a molecular structure with a tilted arrangement of the C_5H_5-rings (23) and presumably a stereochemically active electron pair. Its ^{119}Sn Mössbauer spectrum shows a detectable quadrupole splitting of 0.86 mm s^{-1} (24). It dissolves well in mesitylene, but stannocene is again recovered unchanged after removal of the arene *in vacuo*. The ^1H nmr spectrum of stannocene in mesitylene is studied down to −40°C, but only rather subtle changes are noted. The principle resonance due to stannocene (25) shifts from 5.96 ppm in $CDCl_3$ to 5.91 ppm relative to TMS in the presence of mesitylene while $J(^1H\text{–}^{119/117}Sn)$ changes from 15.76 to 15.16 Hz. Beginning at −20°C and more pronounced at −40°C, a second, smaller, and rather broad resonance at 5.88 ppm emerges with a similar separation of the satellite peaks. Mesitylene resonances appear virtually in the same positions as in pure mesitylene as single lines at 2.28 (CH_3) and 6.78 (C—H) ppm and do not shift with decreasing temperature. While there may be a weak interaction between stannocene and mesitylene at reduced temperature, all attempts to isolate a reaction product by low temperature filtration have failed.

Hence it appears that tin(II) is sufficiently acidic only when bulky and very weakly nucleophilic anions like $AlCl_4^-$, SO_3F^-, and SbF_6^- are present, and when lattice energies are reduced in the resulting layer structures. From a correlation of ^{119}Sn Mössbauer data of dimethyltin(IV) salts (12) it appears that SbF_6^- is the weaker nucleophile of the two fluoroanions, and formation of a 2:1 complex with mesitylene is not unexpected, while $Sn(SO_3F)_2$ forms a 1:1 complex only. Complex formation by addition of mesitylene to a solid tin(II) salt as described here does not allow the formation of single crystals suitable for structural studies. Hence evidence for the presence of π-arene complexes has to come from ^{119}Sn Mössbauer and vibrational spectra. They will be discussed subsequently.

(b) ^{119}Sn Mössbauer spectra

Isomer shifts, relative to SnO_2 for tin(II) compounds, fall within the range of ~2.1 mm s^{-1}, viewed as the borderline between Sn(II) and Sn(IV), and calculated values of about 5.1–7.7 mm s^{-1} for a "bare" Sn^{2+} with a spherically distributed $5s^2$ electron pair (9, 26). Experimental values have not reached the ionic limit. The highest values reported so far are 4.69 mm s^{-1} for the tin(II) moiety in $Sn(II)[Sn(IV)(SO_3CF_3)_6]$ (27) and 4.66 mm s^{-1} for $Sn(SbF_6)_2 \cdot 2AsF_3$ (28) where an X-ray diffraction study reveals a distorted nine-coordinated environment for Sn^{2+}.

In these close approaches to a Sn^{2+} ion no quadrupole splitting is observed (27, 28), however, with decreasing isomer shift first line broadening, already evident for $Sn(SbF_6)_2$, is noted and eventually small but well resolved quadrupole splittings are found (29). Hence ^{119}Sn Mössbauer spectroscopy provides two criteria for the ionic character of Sn(II) compounds: the isomer shift which should be high, close to, or in excess of 4.69 mm s^{-1} relative to SnO_2 and the quadrupole splitting which should be zero.

Some ^{119}Sn Mössbauer data for Sn(II) compounds of interest in this study are listed in Table 1. Of the five tin(II) compounds studied here $Sn(SO_3F)_2$ (4.18 mm s^{-1}) and $Sn(SbF_6)_2$ (4.44 mm s^{-1}) have the highest isomer shifts of those listed and only the former has a small, resolvable quadrupole splitting. Not unexpectedly the more acidic $Sn(SbF_6)_2$ is the better acceptor, seemingly capable of coordinating two mesitylene donors, while $Sn(SO_3F)_2$ forms a 1:1 complex only.

Upon arene uptake the isomer shift is reduced, for $Sn(SO_3F)_2$ by 0.17 mm s^{-1} and for $Sn(SbF_6)_2$ by 0.40 mm s^{-1}. This reduction suggests that mesitylene is interacting with Sn(II) and, judging by the magnitude of the shift, that in case of $Sn(SbF_6)_2 \cdot 2mes$ both mesitylene molecules are probably coordinated to tin. A similar isomer shift of 3.93 mm s^{-1} is reported for $(\pi\text{-}C_6H_6)Sn(AlCl_4)_2 \cdot C_6H_6$ (4*c*) but no Mössbauer data appear to have been reported for the two $SnCl_2$–$AlCl_3$ phases (9), to allow an estimate of the decrease on arene addition. The reduction in isomer shift upon binding to mesitylene is accompanied by an increase in quadrupole splitting to 1.04 mm s^{-1} for $Sn(SO_3F)_2 \cdot mes$ while in case of $Sn(SbF_6)_2 \cdot 2mes$ a slightly asymmetrical doublet results (see Fig. 1) and a ΔE_Q value of 1.13 mm s^{-1} is obtained. These findings are consistent with trends in δ and ΔE_Q summarized above. The occurrence of quadrupole splitting suggests increasing asymmetry in the coordination environment of tin(II) when coordination to only oxygen or fluorine changes to include coordination to the arene as well. For both mesitylene adducts the ^{119}Sn Mössbauer parameters obtained remain well within the range reported for typical tin(II) compounds (17). The addition of mesitylene to Sn^{2+}, as suggested by the ^{119}Sn Mössbauer data, is expected to cause a change in the manner in which the anions coordinate

TABLE 1. ^{119}Sn Mössbauer parameter of relevant tin(II) compounds at 80 K[a]

Compound	Isomer shift δ (mm s^{-1}) rel to SnO_2[a]	Quadrupole splitting ΔE_Q (mm s^{-1})[a]	Reference
SnF_2 (orthorhombic)	3.30	2.15	[b]
SnF_2 (monoclinic)	3.49	1.61	[b]
$(\eta^5\text{-}C_5H_5)_2Sn$	3.74	0.86	[c]
$(\pi\text{-}C_6H_6)Sn(AlCl_4)_2\cdot C_6H_6$	3.93	0	[d]
$SnCl_2$	4.08	0.66	[e]
$Sn(SO_3F)_2$	4.18	0.68	[b]
$Sn(SO_3F)_2\cdot$mes	4.01	1.04	[f]
$Sn(SbF_6)_2$	4.44	0	[b]
$Sn(SbF_6)_2\cdot$2mes	4.04	1.13	[f]

[a]Accuracy limits for δ and ΔE_Q are ± 0.03 mm s^{-1}.
[b]Reference 14.
[c]Reference 24*a*.
[d]Reference 4*c*.
[e]Reference 26*a*.
[f]Present study.

to tin. This change in anion denticity is probed by infrared spectroscopy and discussed in the subsequent section.

(c) Infrared spectra

Attempts to obtain Raman spectra of both mesitylene adducts are unsuccessful and quick darkening of areas exposed to laser light indicates thermal degradation is occurring even at very low laser power. Hence evidence rests on infrared spectra obtained on solid films between silver halide windows.

Both infrared and Raman spectra for $Sn(SO_3F)_2$ (14, 19) and $Sn(SbF_6)_2$ (14) have been reported previously, and for tridentate SbF_6-groups present in $M(SbF_6)_2$ compounds a useful vibrational assignment has been presented (13, 30). To account for the observed spectral complexity in the SbF-stretching region, a subdivision into metal coordinated, through fluorine bridges Sb—F^b, and non-coordinated or terminal Sb—F^t stretches is suggested with the former usually between 550 and 650 cm^{-1} and the latter above 650 cm^{-1} (30). Vibrational bands reported for $Sn(SbF_6)_2$ (14) allow such a division as well, even though a distorted environment around tin introduces additional complexity. Assignments for $Sn(SO_3F)_2$ have suggested the presence of ionic SO_3F^- with the symmetry of the anion reduced from C_{3v} for the free ion to C_s due to coordination to tin (14, 19), but there are still unresolved problems, best reflected in the occurrence of two equally intense bands at ~770 and 830 cm^{-1} possibly due to $\nu SF(A_1)$ and a splitting found for $\delta SO_3(A_1)$. It seems more appropriate to us to view the spectrum as being due to two non-equivalent SO_3F groups with approximately C_{3v} symmetry with some band overlap in the area of deformation modes. This implies either ionic groups or more likely O-tridentate groups.

Addition of mesitylene to both Sn(II) compounds has two general effects: (*a*) the infrared spectrum is dominated in both instances by bands due to the SO_3F and SbF_6 groups, respectively, with all mesitylene bands of very low intensity, and (*b*) the vibrational spectra of the anions appear to change, and at least the SbF_6 bands reflect a change in anion coordination. Low intensity of vibrational bands due to organic groups is commonly found for organotin(IV) salts (31), and this feature appears to extend to the mesitylene adducts of tin(II) salts as well.

The observed infrared frequencies for the two mesitylene adducts are listed in the Experimental section together with

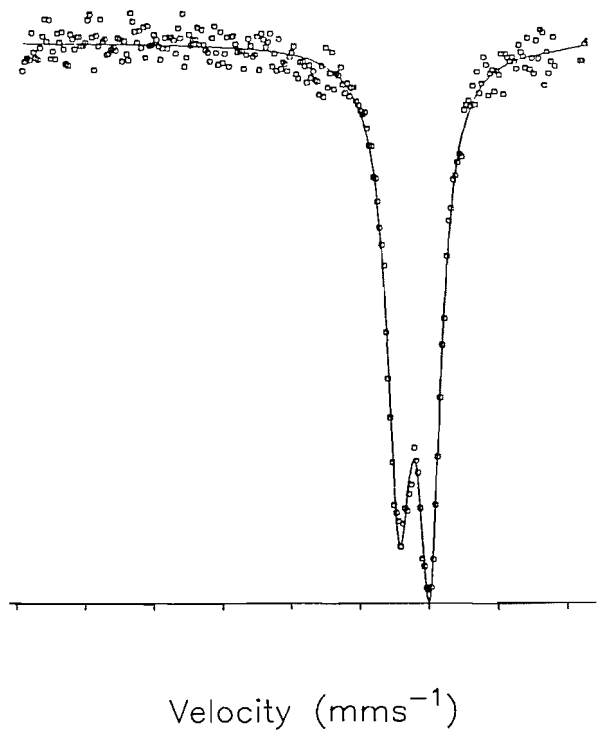

FIG. 1. ^{119}Sn Mössbauer spectrum of $Sn(SbF_6)_2\cdot 2$ mes at 77 K.

estimated relative intensities. The discussion in this section will center around two aspects, (*i*) the mesitylene bands in neat mesitylene and in the complexes, and (*ii*) the "anion" bands before and after mesitylene addition to $Sn(SO_3F)_2$ and $Sn(SbF_6)_2$, respectively. Vibrational bands attributed to mesitylene are listed in Table 2 for both adducts and compared to bands observed for liquid mesitylene. The listing of bands for the adducts is incomplete because of the very low intensity mentioned above which causes medium and weak bands to be unobservable and in case of $Sn(SO_3F)_2\cdot$mes partial overlap of mesitylene bands with more intense anion bands, in particular in the region of 800–1300 cm^{-1}.

In regions where no anion bands are expected, small band shifts are observed, mostly to lower frequencies. The aromatic C=C stretch at 1608 cm^{-1} in free mesitylene is a good

Can. J. Chem. Downloaded from www.nrcresearchpress.com by 91.144.44.67 on 09/07/12
For personal use only.

Can. J. Chem. Downloaded from www.nrcresearchpress.com by 91.144.44.67 on 09/07/12
For personal use only.

TABLE 2. Infrared bands of liquid mesitylene and bands attributed to mesitylene in the adducts $Sn(SO_3F)_2 \cdot mes$ and $Sn(SbF_6)_2 \cdot 2mes$[a]

Mesitylene (cm^{-1})	$Sn(SO_3F)_2 \cdot mes$ (cm^{-1})	$Sn(SbF_6)_2 \cdot 2mes$ (cm^{-1})
3018s		
2921vs	2910w,b	2920mw
2860s	2860vw	2860vw
2730m		
1760m–w	1760vw	
1715m–w		
1608vs	1604m, 1575w,sh	1601m, 1580m
1512w		
1473s	1446w	1469w
1442m,sh		
1375m–s		1384m
1170vw		1168vw
1037s		1080vw, 1040vw, 1007w
932vw		960vw,b
882vw		860w
835vs	786w	
687vs	667w	687ms
561w,b		544m
515w	507vw	512w
443m		440w
421m		
411m		395w

[a]s = strong, m = medium, w = weak, v = very, sh = shoulder, b = broad.

example. This peak is shifted to 1604 and 1601 cm^{-1} for $Sn(SO_3F)_2 \cdot mes$ and $Sn(SbF_6)_2 \cdot 2mes$, respectively. The lower frequency indicates a very slight withdrawal of π electron density of the aromatic ring towards tin.

Interestingly, some bands assigned to bonded mesitylene appear to be split compared with those of free mesitylene. This is noticeable in the 1570–1610 cm^{-1} region of both spectra, and especially in the 1000–1200 cm^{-1} region for $Sn(SbF_6)_2 \cdot 2mes$. The splitting can be attributed to a reduction in symmetry of the bonded mesitylene, and/or the presence of two non-equivalent mesitylenes in particular in $Sn(SO_3F)_2 \cdot mes$, but some solid state splitting is possible as well.

All features affecting bands due to mesitylene are subtle, and the observed features are in general consistent with a very weak interaction between the arene and the two Sn(II) salts.

The infrared bands attributed to the anion are summarized in Table 3 and are compared to the reported values for the parent compounds $Sn(SO_3F)_2$ (14, 19) and $Sn(SbF_6)_2$ (14). For $Sn(SO_3F)_2 \cdot mes$ the ir spectrum is dominated by an intense broad band centered at 1054 cm^{-1} and two bands at 1191 and 1127 cm^{-1}. These are assigned collectively as SO_3 stretching modes, probably masking some of the less intense motions of the mesitylene component in the adduct.

The most noticeable change appears to have occurred in the S—F stretching region. The two intense bands at 772 cm^{-1} and 833 cm^{-1} in $Sn(SO_3F)_2$ (Table 3) are now replaced by a single strong band at 888 cm^{-1}, with a weak band at 786 cm^{-1} (possibly due to mesitylene).

From this overall band distribution and the increased wavenumber of the νS—F band, it appears that a change in denticity of the anion has taken place during mesitylene adduct formation. The findings are consistent with a bidentate, possibly bridging configuration tentatively formulated as $[(\eta^6\text{-mes})Sn(SO_3F)_2]_n$ rather than an ionic (perturbed) or tridentate grouping (32).

Compared to the rather complicated pattern observed for $Sn(SbF_6)_2$ in the region of 520–750 cm^{-1} (Table 3), the band pattern displayed by the anion in the adduct $Sn(SbF_6)_2 \cdot 2mes$ is very simple: a very strong band at 671 cm^{-1}, a sharp, medium band at 635 cm^{-1}, and a weak band at 580 cm^{-1} are found. For

TABLE 3. Infrared frequencies for $Sn(SO_3F)_2$ and $Sn(SbF_6)_2$ and bands attributed to the anions in the mesitylene adducts $Sn(SO_3F)_2 \cdot mes$ and $Sn(SbF_6)_2 \cdot 2mes$[d]

Infrared frequency			Infrared			
			$Sn(SbF_6)_2$[b]		$Sn(SbF_6)_2 \cdot 2mes$	
$Sn(SO_3F)_2$[a] (cm^{-1})	$Sn(SO_3F)_2 \cdot mes$ (cm^{-1})	Approximate band description for C_{3v}	Frequency (cm^{-1})	Assignment[c]	Frequency (cm^{-1})	Assignment
1290s,sh	1137w	νSO_3 (E)	741m,sh			
1240vs	1191vs		713s	Sb—F[t]	671vs	νSbF_6
1180s,sh	1127w,sh		676ms	in- and out-	635s,sh	as. (E_{1u})
			650s	of-phase		
1062s	1054vs	νSO_3 (A_1)	629s	Sb—F[b]		
			~613sh	in- and out-		
833s	888s	νSF (A_1)	~575sh	of-phase	580m,b	νSbF_6 (E_{2g})
606m		δSO_3 (E)	477w	SbF_6^-		
592m	589ms		313sh	deformations		
			292m			
573s	544m	δSO_3 (A_1)	271m			
554s						
403m	405m	δSO_3F (E)				
395sh						

[a]Reference 19.
[b]Reference 14.
[c]See refs. 13 and 30 for details.
[d]s = strong, m = medium, w = weak, v = very, sh = shoulder, b = broad, as = asymmetric, t = terminal, b = bridging.

a free SbF_6^- anion, a peak at ~660 cm^{-1} is attributed to the asymmetric stretch with Raman-active bands observed at ~660 again and at 575 cm^{-1}. The pattern observed for $Sn(SbF_6)_2 \cdot 2mes$ suggests the presence of a weakly coordinated SbF_6^- anion. Peak splitting in the SbF_6^- stretching region produces bands at 671 and 635 cm^{-1}, with the loss of a symmetry center allowing detection of a Raman-active fundamental at 580 cm^{-1} (33).

It appears then that addition of mesitylene has a different effect on the anion bands in $Sn(SO_3F)_2 \cdot mes$ and $Sn(SbF_6)_2 \cdot 2mes$, respectively. In the former adduct the SO_3F group appears to be still coordinated to tin, but more likely in a bidentate, possibly bridging manner. In $Sn(SbF_6)_2 \cdot 2mes$ only weak coordination of the SbF_6 group is evident and any departure from an ionic SbF_6^- with O_h symmetry is rather slight. It is unfortunate that, particularly for this compound, support from Raman spectroscopy is lacking.

The findings for $Sn(SbF_6)_2 \cdot 2mes$ are consistent with the view that both mesitylene groups are coordinated to tin, which in turn is supported also by the ^{119}Sn Mössbauer spectra.

Conclusions

Direct addition of an arene, in this case mesitylene, to suitable Sn(II) salts like $Sn(SO_3F)_2$ and $Sn(SbF_6)_2$ at room temperature, and product isolation well below room temperature, allow the high yield synthesis of very weakly bound mesitylene complexes. However, only microcrystalline materials result which precludes structural studies by single crystal X-ray diffraction. Alternatively, ^{119}Sn Mössbauer spectroscopy allows not only product characterisation, but also, using the isomer shift and the absence of quadrupole splitting as criteria, the identification of other suitable substrates for complex formation.

Acknowledgements

Financial support by the Natural Sciences and Engineering Research Council of Canada is gratefully acknowledged. Professor Dr. H. Willner is thanked for helpful discussions.

1. A. G. GASH, P. F. RODSILER, and E. L. AMMA. Inorg. Chem. **13**, 2429 (1974).
2. H. SCHMIDBAUR. Angew. Chem. Int. Ed. (Engl.) **24**, 893 (1985).
3. P. JUTZI. Adv. Organomet. Chem. **26**, 217 (1986).
4. (*a*) TH. AUEL and E. L. AMMA. J. Am. Chem. Soc. **90**, 5941 (1968); (*b*) H. LÜTH and E. L. AMMA. J. Am. Chem. Soc. **91**, 7515 (1969); (*c*) P. F. RODSILER, TH. AUEL, and E. L. AMMA. J. Am. Chem. Soc. **97**, 7405 (1975).
5. (*a*) M. S. WEININGER, P. F. RODSILER, A. G. GASH, and E. L. AMMA. J. Am. Chem. Soc. **94**, 2135 (1972); (*b*) M. S. WEININGER, P. F. RODSILER, and E. L. AMMA. Inorg. Chem. **18**, 751 (1979).
6. H. SCHMIDBAUR, T. PROBST, B. HUBER, O. STEIGELMANN, and G. MÜLLER. Organomet. **8**, 1567 (1989).
7. H. SCHMIDBAUR, T. PROBST, B. HUBER, G. MÜLLER, and C. KRÜGER. J. Organomet. Chem. **365**, 53 (1989).
8. TH. AUEL and E. L. AMMA. J. Am. Chem. Soc. **90**, 5941 (1968).
9. J. D. DONALDSON. Prog. Inorg. Chem. **8**, 287 (1967) and references therein.
10. S. H. STRAUSS, M. D. NOIROT, and O. P. ANDERSON. Inorg. Chem. **25**, 3851 (1986).
11. S. P. MALLELA, S. T. TOMIC, K. LEE, J. R. SAMS, and F. AUBKE. Inorg. Chem. **25**, 2939 (1986).
12. S. P. MALLELA, S. YAP, J. R. SAMS, and F. AUBKE. Inorg. Chem. **25**, 4327 (1986).
13. M. S. R. CADER and F. AUBKE. Can. J. Chem. In press.
14. T. BIRCHALL, P. A. W. DEAN, and R. J. GILLESPIE. J. Chem. Soc. A, 1777 (1971).
15. F. CHARBONIER, R. FAURE, and H. LOISELEUR. Acta Crystallogr. B 33, 1478 (1977).
16. D. GANTAR, I. LEBAN, B. FRLEC, and J. H. HOLLOWAY. J. Chem. Soc. Dalton Trans. 2379 (1987).
17. R. V. PARISH. *In* Mössbauer spectroscopy applied to inorganic chemistry. Vol. I. *Edited by* G. J. Long. Plenum Press, New York. 1984. p. 527 ff.
18. J. BARR, R. J. GILLESPIE, and R. C. THOMPSON. Inorg. Chem. **3**, 1149 (1964).
19. C. S. ALLEYNE, K. O'SULLIVAN MAILER, and R. C. THOMPSON. Can. J. Chem. **52**, 336 (1974).
20. D. F. SHRIVER. The manipulation of air-sensitive compounds. McGraw-Hill, New York. 1969.
21. R. E. RUNDLE and D. H. OLSON. Inorg. Chem. **3**, 596 (1964).
22. J. D. DONALDSON, R. OTENG, and B. J. SENIOR. Chem. Commun. 618 (1965).
23. A. ALMENNINGEN, A. HAALAND, and T. MOTZFELD. J. Organomet. Chem. **7**, 97 (1967).
24. (*a*) P. G. HARRISON and J. J. ZUCKERMAN. J. Am. Chem. Soc. **92**, 2577 (1970); (*b*) T. S. DORY and J. J. ZUCKERMAN. J. Organomet. Chem. **264**, 295 (1984).
25. L. D. DAVE, D. F. EVANS, and G. WILKINSON. J. Chem. Soc. 3684 (1959).
26. (*a*) P. A. FLINN, G. K. SCHENOY, and F. E. WAGNER (*Editors*). Mössbauer isomer shifts. North-Holland Publishing, Amsterdam. 1978. p. 593 ff; (*b*) J. D. DONALDSON and B. J. SENIOR. J. Chem. Soc. A, 1821 (1967).
27. R. J. BATCHELOR, J. N. R. RUDDICK, J. R. SAMS, and F. AUBKE. Inorg. Chem. **16**, 1414 (1977).
28. A. J. EDWARDS and K. I. KHALLOW. J. Chem. Soc. Chem. Commun. 50 (1984).
29. (*a*) J. G. STEVENS and V. E. STEVENS. *In* Mössbauer effect data index. Plenum Press, New York. 1958; (*b*) J. J. ZUCKERMAN. *In* Chemical Mössbauer spectroscopy. *Edited by* R. H. Herber. Plenum Press, New York. 1984.
30. K. O. CHRISTE, W. W. WILSON, R. BOUGON, and P. CHARPIN. J. Fluor. Chem. **20**, 385 (1982).
31. P. A. YEATS, J. R. SAMS, and F. AUBKE. Inorg. Chem. **11**, 2634 (1972).
32. W. W. WILSON and F. AUBKE. Inorg. Chem. **13**, 326 (1974).
33. A. M. QURESHI, A. H. HARDIN, and F. AUBKE. Can. J. Chem. **49**, 816 (1971).

Can. J. Chem. Downloaded from www.nrcresearchpress.com by 91.144.44.67 on 09/07/12
For personal use only.

Poly(vinyl acetate) as a template for polymerization of methacrylic acid

NEETA TEWARI AND A. K. SRIVASTAVA[1]
Department of Chemistry, H.B. Technological Institute, Kanpur 208002, India
Received June 5, 1989

NEETA TEWARI and A. K. SRIVASTAVA. Can. J. Chem. **68**, 356 (1990).

The template polymerization (TP) of methacrylic acid (MAA) using polyvinyl acetate (PVAc) of $\bar{M}_v$ 66 400 at 60°C for 120 minutes in dimethyl formamide (DMF) has been studied dilatometrically to study the effect of template, and of the monomer and initiator (α-α′ azobisisobutyronitrile) concentrations upon the kinetics. Viscometric measurements showed that complexation between PVAc and PMAA was maximum when the template/polymer ratio was 1:1, and the time required for complete complexation was 7 minutes. The overall energy of activation was the same, i.e., 115 kJ/mol, in the presence and absence of template. The overall system follows mechanism II.

Key words: template polymerization, polyvinyl acetate, methacrylic acid, α,α′-azobisisobutyronitrile, relative rate of polymerization.

NEETA TEWARI et A. K. SRIVASTAVA. Can. J. Chem. **68**, 356 (1990).

Dans le but d'évaluer l'effet du gabarit, des concentrations du monomère et de l'initiateur (α,α′-azobisisobutyronitrile) sur la cinétique de la réaction, faisant appel à la dilatométrie et opérant à 60°C, dans le diméthylformamide (DMF), on a étudié pendant 120 minutes la polymérisation sur gabarit (TP) de l'acide méthacrylique (AMA) sur de l'acétate de polyvinyle (AcPV). Des mesures de viscosité ont montré que la complexation entre l'AcPV et l'APMA est maximale lorsque le rapport de gabarit/polymère est égal à 1 : 1 et que le temps requis pour la complexation totale n'est que de 7 minutes. La valeur globale de l'énergie d'activation est la même, soit 115 kJ/mol, que le gabarit soit présent ou non. Le système global suit le mécanisme II.

Mots clés : gabarit de polymérisation, acétate de polyvinyle, acide méthacrylique, α,α′-azabisisobutyronitrile, vitesse relative de polymérisation.
[Traduit par la revue]

Introduction

A search of the literature reveals that template polymerization (TP) of MAA using isotactic poly(methyl methacrylate) (1), poly(*N*-vinyl pyrrolidone) (2), poly(ethylene oxide) (3), poly(4-vinyl pyridine) (4), poly(2-vinyl pyridine) (5), poly(1-lysine) (6), ionene (7), and polyethylene glycol (8) as templates has been extensively reported. However, data regarding applications of PVAc as template for polymerization of vinyl monomers is still scarce. In this paper we report the first results of the TP of MAA in the presence of PVAc templates, obtained using a dilatometric technique, at 60°C.

Experimental

Reagent grade vinyl acetate (Loba), methacrylic acid (Ranbaxy), and solvents were distilled under reduced pressure before use. α-α′ Azobisisobutyronitrile (AIBN) (Loba) was recrystallized twice before use. PVAc was prepared by polymerizing [VAc] = 5.4 M in inert solvent benzene under nitrogen in a three-necked flask at 60°C using [AIBN] = 0.01 M. The polymerized content was precipitated in *n*-hexane and dried. It was purified by reprecipitation from its acetone solution into *n*-hexane and finally dried. The viscosity-average molecular weights ($\bar{M}_v$) of PVAc were calculated by means of the relationship (9) $[\eta] = 22 \times 10^{-5} \bar{M}_v^{0.65}$ (dL/g), the intrinsic viscosity being determined viscometrically in benzene at 30°C.

Kinetic measurements

Rates of polymerization were measured isothermally at 60°C by employing a modified dilatometric apparatus for 120 min under an inert atmosphere of N_2. Dilatometric measurements were carried out by injecting the reaction mixture of PVAc and MAA and AIBN in DMF into the dilatometer and noting the progress of the reaction, monitored as volume contraction (meniscus movement in cm per unit volume per unit time), with the help of a cathetometer. The polymerized content was precipitated in diethyl ether and dried to a constant weight. The weight of the daughter polymer was obtained by subtracting the weight of template from that of precipitated polymers. The template and daughter polymers were separated by refluxing the polymers with water; percentage separation was about 30%. The rate of polymerization (R_p) was calculated from the slope of conversion–time plots (Fig. 3). The $\bar{M}_v$ of the daughter polymers were calculated by means of the relationship (10) $[\eta] = 24.2 \times 10^{-4} \bar{M}_v^{0.51}$, the intrinsic viscosity (in dL/g) being determined viscometrically in methanol at 26°C. An Ubbelhode type viscometer was used.

[1]Author to whom correspondence may be addressed.

Results and discussion

Viscometric measurements

To investigate complexation between PVAc and PMAA, the polymers were dissolved separately in DMF and mixed just before the measurements. The total polymer concentration was 0.1 g dL^{-1}. The change in reduced viscosity, $\eta_{red}(= \eta_{sp}/c)$, of the mixture of PVAc and PMAA in DMF as a function of composition is shown in Fig. 1. The minimum in both the cases lies at a percentage by weight of PVAc corresponding to a 1:1 base molar ratio. Complexation was very fast, as illustrated in Fig. 2. The rapid drop of η_{red} within less than 7 min down to a level that remained constant for 2 h signifies that complexation was virtually completed within 7 min. Early reports regarding complex formation in template polymerization (11–13) also show that the time required for complete complex formation is generally 10–20 min.

Effect of template concentration

The influence of [template](PVAc) upon the polymerization of MAA was investigated by comparing the initial rate of polymerization in the absence and presence of various concentrations of PVAc from 9.07×10^{-2} to 90.75×10^{-2} base M. The results are compiled in Table 1 and shown in Fig. 4.

The influence of the template is expressed as a relative rate of polymerization, V_R, defined as

$$V_R = \frac{\text{rate of a TP system}}{\text{rate of the blank system}}$$

It is clear from Table 1 that the rate of polymerization is enhanced in the presence of the template due to the growing contribution of template propagation. A study of Fig. 4 further reveals a sudden rise in R_p between [T] 63.52×10^{-2} and 72.60

Can. J. Chem. Downloaded from www.nrcresearchpress.com by 91.144.44.67 on 09/07/12
For personal use only.

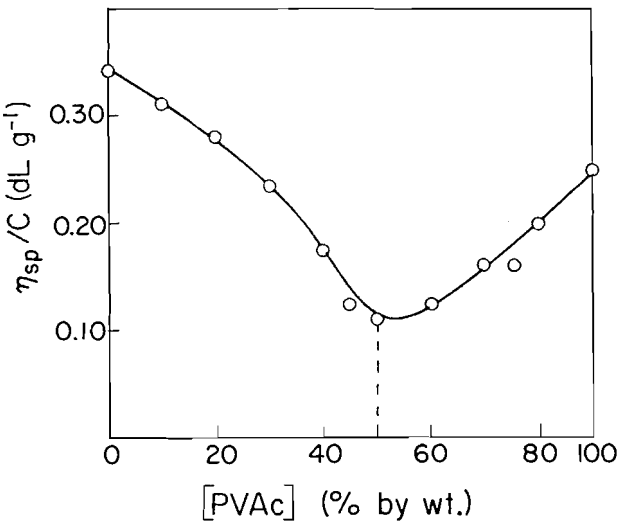

FIG. 1. Reduced viscosity (η_{sp}/c) as a function of weight percentage of PVAc for PVAc/PMAA mixtures in DMF, with PVAc ($\bar{M}_v$ = 66 400) and PMAA ($\bar{M}_v$ = 20 600). The temperature used was 60°C and the total polymer concentration 0.1 g dL^{-1}.

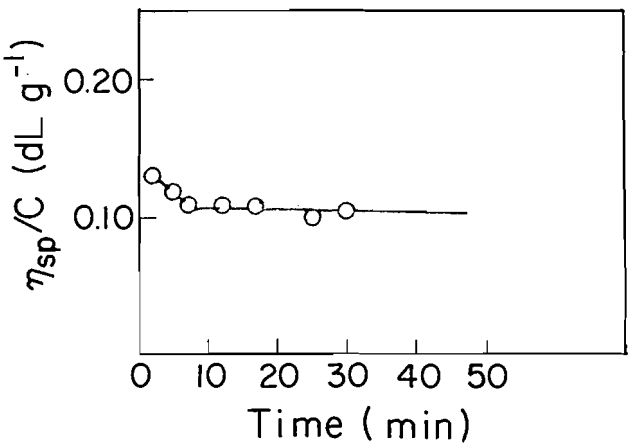

FIG. 2. Reduced viscosity, η_{sp}/c versus time t as a function of molar mass of PMAA for PVAc/PMAA mixtures (1:1 base mole ratio) in DMF, with PVAc ($\bar{M}_v$ = 66 400). The temperature used was 60°C and the total polymer concentration 0.1 g dL^{-1}.

$\times 10^{-2}$ base M. It may be caused by jumping of propagating chain radicals from one template coil to another as has already been reported by Gons *et al.* (14) for other template systems. The increase stops only at a stage when the whole reaction volume is homogeneously occupied by template coils, i.e., at [T] = 72.60 $\times 10^{-2}$ base M. Above this value only template propagation takes place, hence the rate remains constant. The course of the relative rate of polymerization as a function of template concentration at constant [MAA] (Fig. 4) gave insight into the mechanism of the present system, which follows mechanism II (15) and is characterized by a constant maximum value of V_R above the critical concentration of beginning coil overlap, whereby every growing chain can find a template with which to complex.

The enhancement of V_R is a result of the decrease of termination rate due to strongly hindered segmental mobility of polymer radical chains adsorbed on the template. The rate of complexation of polymer radicals is assumed to be first order in both free radical and template concentration. The diffusion of the chain towards the template limits the buildup of template-

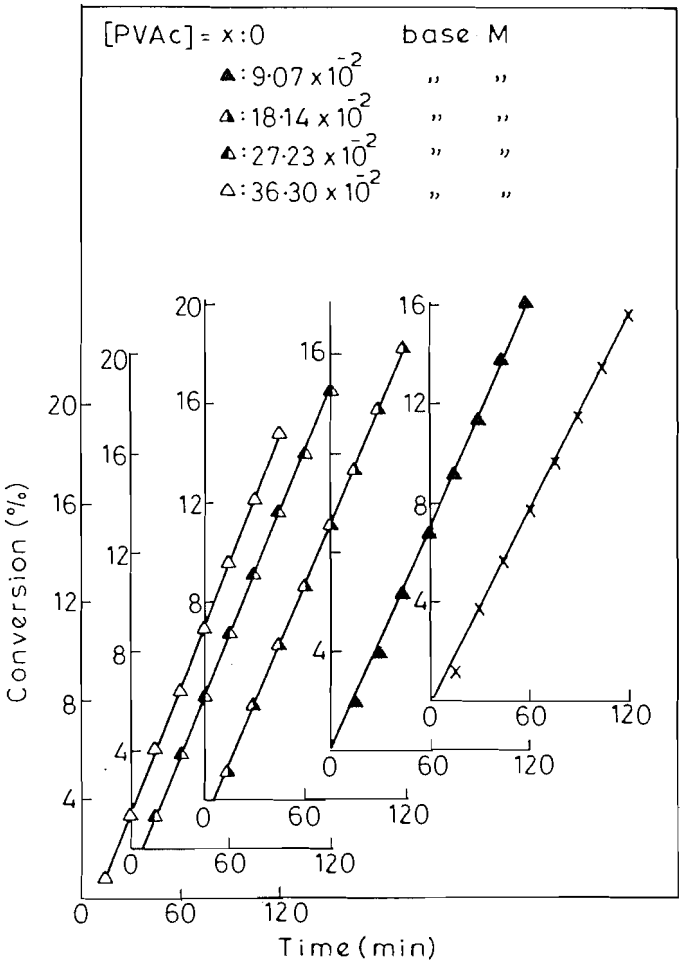

FIG. 3. Time-conversion plots showing effect of [PVAc] for MAA polymerization initiated by AIBN in the presence of template (PVAc) at 60°C in DMF using 23.82 $\times 10^{-3}$ mol L^{-1} of [AIBN] and 0.78 mol L^{-1} of [MAA].

associated radicals. To be certain that the influence is due to the polymeric character of the template, the rate was also determined in the presence of a low molecular weight analogue of PVAc, i.e., ethyl acetate, which had no effect on R_p. The viscosity average molecular weight $\bar{M}_v$ of the daughter polymers increases as the concentration of template increases. Table 2 shows the effect of $\bar{M}_v$ of the templates on V_R and $\bar{M}_v$ of the daughter polymers. As expected for the template effect, the V_R increases as the $\bar{M}_v$ of template increases.

Effect of monomer concentration

The influence of monomer concentration on the template polymerization rate was investigated by varying the concentration of MAA from 0.39 to 1.18 mol L^{-1} at fixed [template] = 72.60 $\times 10^{-2}$ base M and [AIBN] = 23.82 $\times 10^{-3}$ mol L^{-1}. The results are summarized in Table 3 and Fig. 5. V_R is a direct function of [MAA]. From Fig. 5 it is clear that there is no preferential adsorption of monomer on the template site, since in that case the shape of the curve would have been concave. It has already been reported in the literature (16) that if there is preferential adsorption of monomer by template sites (mechanism I), then a plot between [monomer] and V_R must show a concave curve due to lowering of monomer concentration in the bulk solution, thereby decreasing the blank rate as well as the template "pick-up" propagation rate. Thus oligomers created

Can. J. Chem. Downloaded from www.nrcresearchpress.com by 91.144.44.67 on 09/07/12
For personal use only.

Can. J. Chem. Downloaded from www.nrcresearchpress.com by 91.144.44.67 on 09/07/12
For personal use only.

TABLE 1. Effect of [PVAc] template on radical polymerization of methacrylic acid in DMF at 60°C

[PVAc] × 10^2 (base M)	Conversion in %	$R_p \times 10^6$ (mol L^{-1} s^{-1})	V_R	$\bar{M}_v$ (daughter polymer)
0	15.56	23.15	1	20 600
9.07	18.38	24.69	1.07	22 900
18.14	18.45	25.92	1.12	25 400
27.23	18.61	27.78	1.20	27 750
36.30	18.77	29.17	1.26	35 972
45.37	18.85	30.55	1.32	40 250
54.45	19.16	31.00	1.34	46 920
63.52	19.39	32.33	1.40	55 780
68.40	19.45	37.04	1.60	—
72.60	22.83	46.30	2.00	66 360
81.61	21.74	45.84	1.98	—
86.21	20.33	45.75	1.98	66 358
90.75	19.86	45.60	1.97	66 356

*[MAA] = 0.78 mol L^{-1}; [AIBN] = 23.82 × 10^{-3} mol L^{-1}; PVAc ($\bar{M}_v$ = 66 400); time = 120 min.

TABLE 2. Effect of polyvinyl acetate of different molecular weights on radical polymerization of methacrylic acid in DMF at 60°C

PVAc (template)	(PVAc) $\bar{M}_v$	Conversion in %	$R_p \times 10^6$ (mol L^{-1} s^{-1})	V_R	$\bar{M}_v$ (daughter polymer)
PVAc-1	66 400	22.83	46.30	2	66 360
PVAc-2	55 830	21.70	45.72	1.97	48 000
PVAc-3	47 000	19.46	43.98	1.90	45 400
PVAc-4	40 580	18.85	30.50	1.32	35 520
PVAc-5	35 600	18.78	29.19	1.27	32 800

*[MAA] = 0.78 mol L^{-1}; [AIBN] = 23.82 × 10^{-3} mol L^{-1}; [PVAc] = 72.60 × 10^{-2} base M.

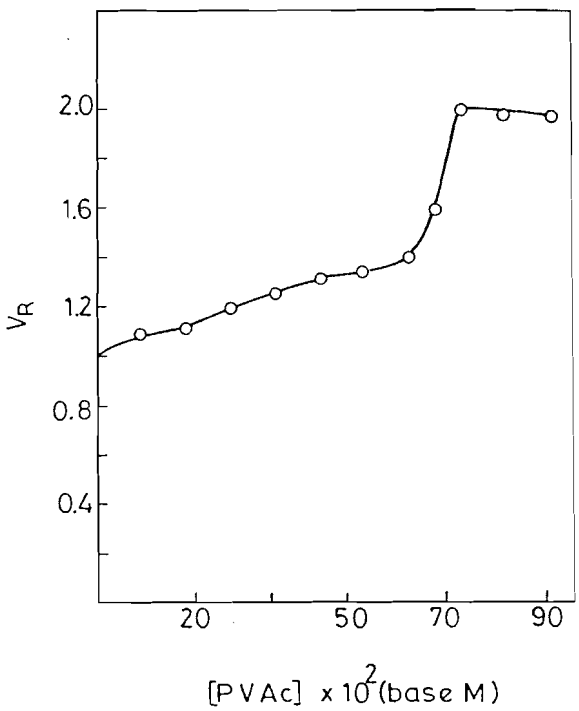

FIG. 4. Relative polymerization rate, V_R, vs. [PVAc] template concentration for MAA polymerization in DMF at 60°C. Blank polymerization rate: 23.15 × 10^{-6} mol L^{-1} s^{-1}; [MAA] = 0.78 mol L^{-1}; [AIBN] = 23.82 × 10^{-3} mol L^{-1}.

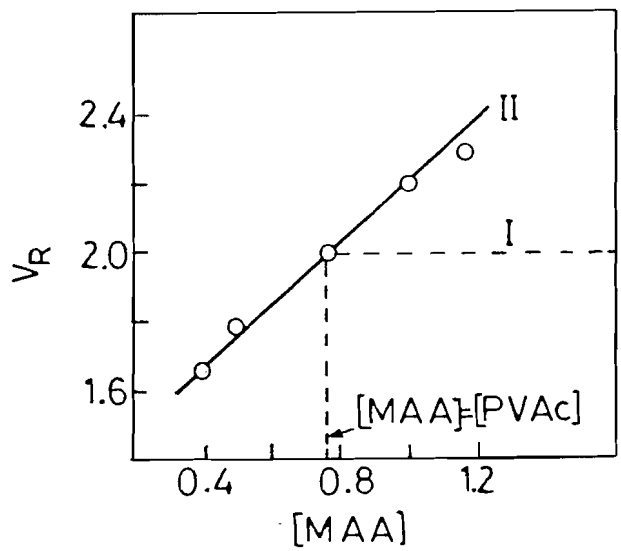

FIG. 5. Relative polymerization rate, V_R, vs. [MAA] for MAA polymerization in DMF at 60°C, at constant template concentration [PVAc] = 72.60 × 10^{-2} base M.

during polymerization get complexed with the template, and propagation proceeds. This also supports that the present system follows mechanism II.

Effect of temperature

The overall energy of activation was the same in the presence

TABLE 3. Effect of [MAA] on its radical polymerization along polyvinyl acetate template in DMF at 60°C

[MAA] (mol L^{-1})	Conversion in (%)		$R_p \times 10^6$(mol L^{-1} s^{-1})		
	Blank	With template	Blank	With template	V_R
0.39	10.17	12.20	11.75	19.50	1.66
0.50	11.88	18.00	14.79	26.30	1.78
0.78	15.56	22.83	23.15	46.30	2.00
1.00	25.45	30.62	29.51	64.56	2.19
1.18	27.00	35.58	34.67	79.43	2.29

*[PVAc] = 72.60 × 10^{-2} base M; [AIBN] = 23.82 × 10^{-3} mol L^{-1}; time = 120 min.

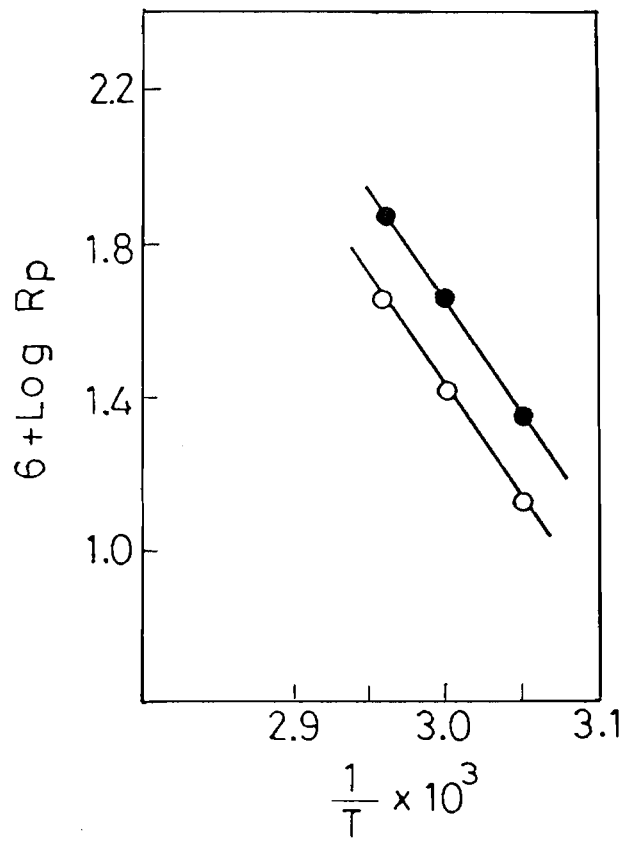

FIG. 6. Arrhenius plot for the polymerization of MMA initiated by AIBN in the absence (○) and presence (●) of PVAc (template) in DMF using 23.82 × 10^{-3} mol L^{-1} of [AIBN], 0.78 mol L^{-1} of [MAA], and 72.60 × 10^{-2} base M [PVAc].

and in the absence of PVAc, i.e., 115 kJ/mol, as shown by the Arrhenius plot in Fig. 6.

Conclusion

The present system proceeds through mechanism II.

Acknowledgements

The authors thank Prof. A. K. Vasishtha, Director, and Prof. R. S. Tewari, Head, Chemistry Department, H.B. Technological Institute, Kanpur, for encouragement. Financial assistance by the Department of Science and Technology, New Delhi, for support of the project entitled "Studies on Template Polymerization," and DST no. SP/S1/G08/85 are gratefully acknowledged.

1. J. G. H. M. LOHMEYER, Y. Y. TAN, and G. CHALLA. J. Macromol. Sci. Chem. **A14**, 945 (1980).
2. N. SHAVIT and J. COHEN. *In* Polymerization of organized systems. *Edited by* H. G. Elias, Gordon and Breach, London. 1977. p. 213.
3. Y. OSADA, A. D. ANTIPINA, I. M. PAPISOV, V. A. KABANOV, and V. A. KARGIN. Dokl. Akad. Nauk SSSR, **191**, 339 (1970); I. M. PAPISOV, V. A. KABANOV, Y. OSADA, M. LESKARNO-BRITO, J. RICHMOND, and A. N. GVOZDETSKII. Vysokmol. Soedin, Ser. A, **14**, 2402 (1972).
4. K. FUJIMORI. Makromol. Chem. **180**, 1743 (1979).
5. J. SMID, Y. Y. TAN, and G. CHALLA. Eur. Polym. J. **19**, 853 (1983).
6. O. A. ALEKSINA, I. M. PAPISOV, K. I. BOLYACHEVSKAYA, and A. B. ZEZIN. Vysokomol. Soedin, Ser. A, **15**, 1463 (1973).
7. E. TSUCHIDA and Y. OSADA. J. Polym. Sci. Polym. Chem. Ed. **13**, 551 (1975).
8. J. MATUSZEWSKA-CZERWIK and S. POLOWINSKI. Eur. Polym. J. **24**, 791 (1988).
9. J. BRANDRUP and E. H. IMMERGENT. Polymer handbook. 2nd ed. A Wiley–Interscience Publication, John Wiley and Sons, New York. 1975. IV-15.
10. N. M. WIEDERKORN and A. R. BROWN. J. Polym. Sci. **81**, 651 (1957).
11. J. SMID, Y. Y. TAN, and G. CHALLA. Polym. Commun. **27**, 148 (1986).
12. J. MATUSZEWSKI-CZERWIK and S. POLOWINSKI. Polym. Bull. **19**, 149 (1988).
13. I. ILLIOPOULOS and R. AUDEBERT. Eur. Polym. J. **24**, 2 (1988).
14. J. GONS, L. J. P. STRAATMANN, and G. CHALLA. J. Polym. Sci. Polym. Chem. Ed. **16**, 427 (1978).
15. G. CHALLA and Y. Y. TAN. Pure Appl. Chem. **53**, 627 (1981).
16. J. SMID, Y. Y. TAN, and G. CHALLA. Eur. Polym. J. **20**, 1099 (1984).

Can. J. Chem. Downloaded from www.nrcresearchpress.com by 91.144.44.67 on 09/07/12
For personal use only.

Microwave acid dissolution of soil samples for elemental analysis

BYRON KRATOCHVIL[1] AND SIPHO MAMBA[2]
Department of Chemistry, University of Alberta, Edmonton, Alta., Canada T6G 2G2

Received June 9, 1989

BYRON KRATOCHVIL and SIPHO MAMBA. Can. J. Chem. **68**, 360 (1990).

Closed vessel microwave acid dissolution is compared with conventional open vessel methods for the determination of trace zinc and copper in a series of soil samples collected from sugarcane fields in Swaziland. Analytical measurements by flame atomic absorption spectroscopy show that all the zinc and copper in the samples is released within 7 min in a commercial microwave oven at 400 W. Up to seven 500-mg portions can be handled at a time. Attention must be paid to the amount of organic matter present in a soil so that excess pressure build up does not occur during dissolution.

Key words: microwave dissolution, soil analysis, trace metal determination, atomic absorption spectroscopy.

BYRON KRATOCHVIL et SIPHO MAMBA. Can. J. Chem. **68**, 360 (1990).

Pour la détermination de traces de zinc et de cuivre dans une série d'échantillons de sols provenant de champs de canne à sucre du Swaziland, on a comparé la méthode conventionnelle utilisant des contenants ouverts avec celle inpliquant une dissolution acide effectuée dans des contenants fermés et faisant appel à des micro-ondes. Des mesures analytiques faisant appel à la spectroscopie d'absorption atomique à flamme démontrent que tout le zinc ainsi que tout la cuivre des échantillons est dissous en moins de 7 min lorsqu'on utilise un four à micro-onde commercial de 400 W. On peut traiter jusqu'à sept échantillons de 500 mg à la fois. On doit s'assurer que la quantité de substances organique présente dans les sols ne créera pas un excés de pression au cours de la dissolution.

Mots clés : dissolution à l'aide de microondes; analyse des sols, détermination de traces de métaux, spectroscopie d'absorption atomique.

[Traduit par la revue]

Can. J. Chem. Downloaded from www.nrcresearchpress.com by 91.144.44.67 on 09/07/12
For personal use only.

Introduction

In trace element analysis of soil by flame atomic absorption spectroscopy (FAAS), sample dissolution is often the most time-consuming step. While HNO_3 alone may be sufficient to liberate metals which are bound to organic matrices, Jackson and Newman (1) warn against its use for metals in inorganic material. Unless HF and hot, concentrated $HClO_4$ are used, metals contained in crystal lattices of unweathered primary minerals resist conventional open vessel digestions (2, 3). The best alternative, dissolution using $HClO_4$, requires careful supervision and special fume hoods equipped with wash-down facilities. The introduction of microwave ovens for analytical sample dissolution (4) has allowed many of the problems associated with conventional methods to be overcome (5–9). Several types of closed vessels for microwave digestions have been used. These provide the elevated pressures and temperatures necessary for rapid decomposition of samples. In this work, the completely closed type (CCT) vessels described by Berman and co-workers (10) were used for the treatment of a weathered tropical soil prior to analysis for zinc and copper. These vessels of Teflon PFA are suitable for samples containing small quantities of organic matter.

Experimental section

Apparatus

The microwave oven was a 700 W Sears Kenmore (Model 87751) operating at a frequency of 24.5 MHz. It has a timing cycle ranging from 1 s to 100 min in 1 s increments and a heating cycle based on power settings ranging from 0% (0 W) to 100% (700 W) in 1% increments. Up to eight 60-mL digestion vessels were handled at a time. These screw-cap, wide-mouth vessels were made of Teflon PFA with a fully fluorinated alkoxy-side chain (Savillex Corp. Minnetonka, MN, USA). A microwave-transparent rotating platform (Litton Corp.) was used to avoid hot spots due to inhomogeneities in microwave energy inside the cavity.

Atomic absorption measurements were performed on a microprocessor-controlled atomic absorption spectrophotometer with deuterium background correction (SpectrAA-10, Varian Techtron). Acetylene (flow rate of 1.5 L/min) was used as fuel and air (12 L/min) as oxidant. The 324.8 and 213.9 nm lines for Cu and Zn respectively were used.

Reagents and samples

All blanks and standard solutions were prepared using distilled demineralized water. All volumetric ware was soaked in 3:1 v/v H_2O/HNO_3 (analytical reagent, BDH Chemicals) before use. 70% $HClO_4$ (analytical reagent, Mallinckrodt Chemical Works), 49% HF (reagent grade, Fisher), and 65% HNO_3 (Seastar Chemicals, Sidney, BC, Canada, produced by double sub-boiling distillation in quartz) were used for all ashing procedures. Solutions were stored prior to measurement in 60-mL polyethylene bottles (Nalgene).

The soil samples were collected in a systematic grid pattern from a sugarcane field of the Royal Swaziland Sugar Corporation (Field 201, Simunye Plantation, Kingdom of Swaziland). The 500-mg increments were dried and sterilized by heating for a week at 110°C, then transferred to polyethylene bottles for shipment to Canada. The dry samples were gound in a motorized mortar and pestle to allow 95% passage through a 150-mesh seive. Canadian (CCRMP) certified reference soil standards SO-2, SO-3, and SO-4 were used to evaluate the validity of the procedures.

Analytical procedures

Open vessel dissolution of soil using HNO_3, HF, and $HClO_4$

To a finely divided 500-mg test portion of soil in a Teflon digestion vessel were added 6 mL HNO_3, 3 mL HF, and 2 mL $HClO_4$. The vessel was tightly capped and placed in a boiling water bath for 2.5 h. After cooling the contents were transferred to a Teflon beaker and fumed to near dryness at 200°C inside a stainless steel perchloric acid fume hood. (CAUTION: Use only a system specifically designed for $HClO_4$ fumes.) The resulting residue was dissolved in 2 mL HNO_3 and 2 mL $HClO_4$ and fumed again to near dryness. The colorless residue was re-dissolved in 2 mL HNO_3 to give a clear solution which was diluted to

[1]To whom all correspondence should be addressed.

[2]Present address: Department of Chemistry, University of Swaziland, PB Kwaluseni Campus, Swaziland.

TABLE 1. Zinc and copper concentrations in soil samples digested with $HClO_4$, by open vessel control method*

Sample†	Zinc, μg/g	Copper, μg/g
201-01 (3)	103 ± 3	137 ± 2
201-11 (3)	104 ± 2	130 ± 2
201-22 (4)	101 ± 1	125 ± 1
201-24 (4)	92 ± 1	129 ± 1
201-32 (4)	98 ± 4	146 ± 2
SO-4 (1)	95 ± 2‡	22 ± 2
Certified value for SO-4	94 ± 2	22 ± 1

*Uncertainties are given as one standard deviation.
†Values in parentheses represent number of replicate samples analyzed.
‡Uncertainty is that of the standard additions plot intercept.

100 mL. A blank, prepared by running the acid mixtures without the sample through all the procedures, was included with each set of samples run.

Closed vessel microwave acid digestion using HNO_3 and HF

A maximum of 500 mg of soil was weighed into Savillex Teflon vessels. To each vessel was added 4 mL HNO_3 and 7 mL HF and the lids tightened with a plastic wrench. Eight vessels, including one blank, were positioned in a ring in a 4-L polyethylene container with a tight fitting lid to contain fumes from possible leakage. This container was then placed in the microwave oven. A beaker containing 400 mL of water was also placed in the oven and the power and time settings adjusted. (CAUTION: Excessive gas generation within closed container may cause vessel rupture and explosion. The use of vessels with safety rupture disks, which have recently become commercially available, is strongly recommended.)

After digestion and cooling, the contents of each vessel were transferred to 100-mL polyethylene volumetric flasks and diluted to volume with deionized water.

Standard additions and AAS measurements

For each sample, four 20-mL aliquots of solution were pipetted into four 50-mL polyethylene volumetric flasks. A Socorex micropipet was used to transfer 5 to 75 μL volumes of 1000 ppm Zn^{2+} and Cu^{2+} stock solutions into the flasks. Standard additions plots, together with calculated values for the concentration axis intercepts using linear regression, were obtained from an on-line Epson (Spectrum LX-80) printer.

Results and discussion

Validity of conventional open vessel technique

Several 500-mg portions from selected samples of Swaziland soil were digested with $HClO_4$ and analyzed by standard additions. Reference soil sample SO-4 was included to evaluate the accuracy of the dissolution scheme. The results obtained are presented in Table 1.

All samples were completely dissolved after 10–12 h. The SO-4 results are in good agreement with certified values at the 95% confidence level. This method is therefore reliable, and can be used as a control method for testing the accuracy of the microwave procedure.

Microwave acid dissolution vs. control method

A preliminary study using HNO_3 and HF digestion gave the results presented in Table 2. The scheme used in this initial study involved an initial 15-min exposure to microwave energy at 15% power, followed by cooling and venting of the Teflon vessels. The venting step was necessary to release pressure build up by acid fumes and gaseous oxidation products. After retightening, the vessels were heated for a further 60 min at 30% microwave power.

TABLE 2. Comparison of Zn and Cu results obtained by control method to those by microwave method for 2 selected soil samples*

	Sample 201-32		Sample 201-24	
Method	Zn, μg/g	Cu, μg/g	Zn, μg/g	Cu, μg/g
Microwave†	95 ± 4	144 ± 3	90 ± 2	128 ± 3
Control‡	98 ± 4	146 ± 2	92 ± 1	129 ± 1

*Uncertainties given as one standard deviation.
†Number of replicates = 5 for 201-32 and 2 for 201-24.
‡Number of replicates = 4.

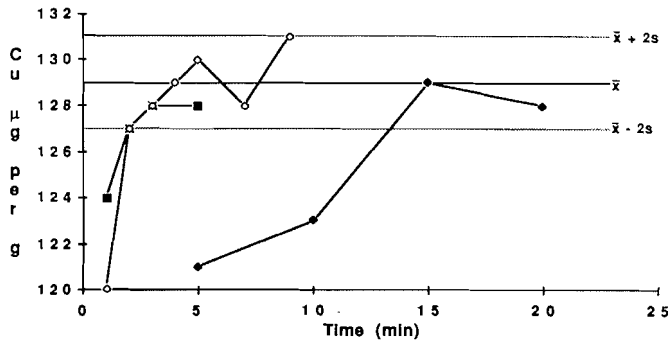

FIG. 1. Copper results vs. time for microwave digestion of sample 201-24 at 35 (◆), 50 (◇), and 100% (■) power. Dotted lines are 95% confidence limits for average obtained by control method.

The data in Table 2 show that results obtained by both methods fall within one standard deviation of each other. The microwave scheme is therefore as efficient as the control method at extracting Zn and Cu from the soil matrix. The effect of longer dissolution times is shown in Table 3. The reported times do not include an initial 15% power–15 min venting stage. For these runs, venting was necessary every 30 min during the first 2 h of digestion and every 60 min thereafter. The results indicate that no advantage is gained by using digestion periods longer than 1 h at 30% microwave power; in fact, time constraints and deterioration of the digestion vessels mitigate against extended times. Even with pressure release each 30 min, pressure build up during the digestion caused the vessels to bulge permanently around the seals. Some residue remained even after 6 h digestion; the extraction of Zn and Cu was complete, however.

Effect of microwave power

Higher power settings were investigated with the aim of finding optimum conditions for complete extraction of Zn and Cu from the soil matrix in the shortest possible time and with minimum pressure build up. Plots of the results obtained for Cu and Zn analyses at power settings of 35% (300 W), 50% (400 W), and 100% (700 W) are shown in Figs. 1 and 2. In both figures the solid horizontal line represents mean estimates obtained by the control method and microwave digestions of test portions, while the broken lines are the 95% confidence limits based on the standard deviation estimates. The plots show a decrease in the time required to achieve complete extraction of Zn and Cu as microwave power increases. At the same time, however, risks of sample loss, container deformation and explosion increase. Full power (700 W) is not recommended for sample digestions by this method. On the basis of convenience, safety, and fast dissolution, 50% power (400 W) was found to be a satisfactory compromise. Even though complete recovery

Can. J. Chem. Downloaded from www.nrcresearchpress.com by 91.144.44.67 on 09/07/12
For personal use only.

TABLE 3. Effect of time on microwave closed vessel digestion of soil samples*

	Sample 201-32		Sample 201-24		
Time (h)	Zn, μg/g	Cu, μg/g	Zn, μg/g	Cu, μg/g	% Dissolution
1	93	143	90 ± 2	128 ± 3	95
2	95	142	89 ± 1	127 ± 1	94
3	98	143	91 ± 3	127 ± 0	95
4	95	142			92
6	84†	143			90
Control method	98 ± 4	146 ± 2	92 ± 1		

*Sample 201-32 results are based on one test portion at each time period; sample 201-24 results are based on two test portions.

†Error likely due to local heterogeneity since the Cu result on the same portion falls within acceptable limits.

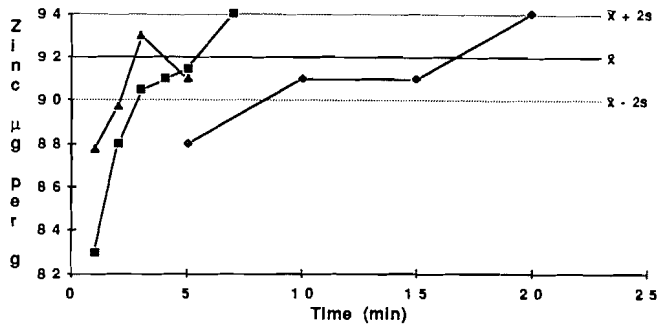

FIG. 2. Zinc results vs. time for microwave digestion of sample 201-24 at 35 (◆), 50 (■), and 100% (▲) power. Dotted lines are 95% confidence limits for average obtained by control method.

TABLE 4. Comparison of control dissolution method and microwave closed vessel acid digestion at 50% power for 7 min for the determination of zinc and copper in soils.*

	Zinc (ppm)		Copper (ppm)	
Sample†	Control method	Microwave digestion	Control method	Microwave digestion
201-32	98 ± 3 (4)	95 ± 2 (2)	146 ± 2	144 ± 1
201-22	101 ± 1 (4)	100 ± 1 (2)	125 ± 1	125 ± 1
201-24	92 ± 1 (4)	94 (1)	128 ± 2	128
201-11	104 ± 2 (3)	101 ± 1 (2)	129 ± 1	124 ± 1
201-14	90 (1)	88 ± 2 (2)	117	118 ± 2
201-06	103 (1)	97 ± 1 (2)	118	119 ± 1
201-06	103 (1)	96 ± 1 (2)	137	135 ± 2
201-17	84 (1)	83 (1)	119	119
201-48	103 (1)	97 (1)	149	150
SO-2[1]	—	125 (1)	—	9
SO-3[2]	—	51 (1)	—	19
SO-4[3]	95	95 (1)	25	24

*Numbers in parentheses are number of test portions analyzed.

†Certified values: [1]Zn = 124 ± 5, Cu = 7 ± 1; [2]Zn = 52 ± 3, Cu = 17 ± 1; [3]Zn = 94 ± 3, Cu = 22 ± 1.

of Zn and Cu is observed after 4 to 5 min digestion at a 50% power setting, 7 min was chosen for subsequent sample preparation to provide a safety margin.

Reliability of microwave acid dissolution

Standard reference materials SO-2, SO-3, SO-4, and several randomly selected samples from the field were analyzed using the HF-HNO_3 scheme at 400 W for 7 min. In Table 4, the results are compared with those obtained by total dissolution with $HClO_4$, and also with certified values. There is no significant difference between the means obtained by the two methods for Zn and Cu, and the results by microwave dissolution are in good agreement with certified values for the standard reference soils.

Conclusions

The microwave acid dissolution procedure described gives the same results as conventional total dissolution, but is faster and has less likelihood of contamination than open vessel methods which employ HF, HNO_3, and $HClO_4$. However, since 100% dissolution of test portions may not be achieved by this method, tests should be performed to ensure that the insoluble residue does not contain significant quantities of the element(s) being investigated. Other soil types besides the ones investigated in this study may require different dissolution conditions, and hence the optimum conditions described here should be used only as a guide. Pressure build up inside the digestion vessels may cause leakage of contents and possibly explosions if the samples being digested contain large quantities of organic matter. Therefore caution and close supervision are recommended for all digestions under closed conditions. After this work was completed commercial vessels provided with rupture disks became available. Use of such vessels is highly recommended.

Acknowledgments

Financial support from the Natural Sciences and Engineering Research Council of Canada, the University of Alberta, and the Canadian International Development Agency are gratefully acknowledged.

1. K. JACKSON and P. NEWMAN. Analyst (London), **108**, 261 (1983).
2. M. BERROW and M. STEIN. Analyst (London), **108**, 277 (1983).
3. J. CANSUL, T. FRIES, and P. LAMONTHE. Anal. Chem. **58**, 1881 (1986).
4. A. ABU-SARMA, S. KOIRTYOHANN, and J. MORRIS. Anal. Chem. **47**, 1475 (1975).
5. R. NARDKARNI. Anal. Chim. Acta, **135**, 363 (1982).
6. L. JASSIE and H. KINGSTON. Anal. Chem. **58**, 2534 (1986).
7. P. ANDERSON, P. AYSOLA, and C. LANGFORD. Anal. Chem. **59**, 1582 (1987).
8. J. BOZIC, B. COUSINS, W. FLORA, and F. SMITH. Anal. Chim. Acta, **177**, 243 (1985).
9. J. M. LABRECQUE. *In* Introduction to microwave sample preparation. *Edited by* H. M. Kingston and L. B. Jassie. American Chemical Society. Washington, D.C. 1988. Chap. 10.
10. S. BERMAN, S. NAKASHIMA, R. STURGEON, and S. WILLIE. Analyst (London), **113**, 159 (1988).

Can. J. Chem. Downloaded from www.nrcresearchpress.com by 91.144.44.67 on 09/07/12
For personal use only.

Excess volumes, isentropic compressibilities, and viscosities of binary mixtures containing cyclohexene

P. RAJA SEKAR, R. VENKATESWARLU, AND KALLURU S. REDDY
Department of Chemistry, Sri Venkateswara University, Tirupati 517 502, India

Received July 13, 1989

P. RAJA SEKAR, R. VENKATESWARLU, and KALLURU S. REDDY. Can. J. Chem. **68**, 363 (1990).

Excess volumes, excess isentropic compressibilities, and excess viscosities have been reported for the binary liquid mixtures of cyclohexene with *n*-hexane, cyclohexane, benzene, trichloromethane, tetrachloromethane, and 1,4-dioxane at 303.15 K. V^E results are negative for mixtures of cyclohexene with *n*-hexane and tetrachloromethane and are positive for the remaining systems. k_S^E values are negative for mixtures of cyclohexene with *n*-hexane and positive for all other systems. The data of $\Delta \ln \eta$ are positive for cyclohexene with cyclohexane and tetrachloromethane, and negative for the remaining systems. Prigogine–Patterson–Flory equation of state theory has been applied to predict excess volumes and excess enthalpies, and the viscosity relations proposed by Bloomfield are used to calculate free energy and free volume contributions to excess viscosity.

Key words: excess volumes, excess isentropic compressibilities, excess viscosities.

P. RAJA SEKAR, R. VENKATESWARLU et KALLURU S. REDDY. Can. J. Chem. **68**, 363 (1990).

Opérant à 303,15 K, on a mesuré les volumes en excès, les compressibilités isentropiques en excès et les viscosités en excès de mélanges liquides binaires de cyclohexène avec le *n*-hexane, le cyclohexane, le benzène, le trichlorométhane, le tétrachlorométhane et le 1,4-dioxane. Les valeurs de V^E sont négatives pour les mélanges de cyclohexène avec le *n*-hexane et le tétrachlorométhane alors qu'elles sont positives avec les autres systèmes. Les valeurs de k_S^E sont négatives pour les mélanges de cyclohexène avec le *n*-hexane et elles sont positives pour tous les autres systèmes. Les données de $\Delta \ln \eta$ sont positives pour le cyclohexène avec le cyclohexane et avec le tétrachlorométhane et elles sont négatives pour tous les autres systèmes. On a utilisé l'équation de Prigogine–Patterson–Flory relative à la théorie de l'état pour prédire les volumes et les enthalpies en excès alors qu'on a utilisé les relations de viscosité proposées par Bloomfield pour calculer les contributions d'énergie libre et de volume libre à la viscosité en excès.

Mots clés : les volumes en excès, les compressibilités isentropique en excès, les viscosités en excès.

[Traduit par la revue]

Introduction

As a part of our study on thermodynamic and physical properties of liquid mixtures, here we report excess volumes, excess isentropic compressibilities, and excess viscosities for mixtures containing an unsaturated hydrocarbon. The properties have been measured at 303.15 K for the following binary mixtures: cyclohexene with *n*-hexane, cyclohexane, benzene, trichloromethane, tetrachloromethane, and 1,4-dioxane. These systems have been selected with a view to study the nature of interaction of π electrons of cyclohexene in different mixtures in which the second components vary systematically from nonpolar to polar. Excess enthalpies for these systems have been reported in the literature (1–5) but there is no such measurements on the properties selected here except excess volumes for some systems at 298.15 K (6).

The experimental excess volumes are analysed in light of the Prigogine–Patterson–Flory theory (7–10). The various contributions to excess volume are evaluated and the importance of cohesive energy factor in the prediction of excess volumes is discussed. The viscosity relation proposed by Bloomfield and Dewan (11, 12) is also used to calculate the free volume and the free energy contributions to excess viscosity.

Experimental

Analar samples of benzene (SD's), tetrachloromethane (SD's), *n*-hexane (SD's), cyclohexane (BDH), and 1,4-dioxane (BDH) were purified by the methods described earlier (13–15). Trichloromethane was dried over calcium chloride for 2 days and fractionally distilled. Cyclohexene was purified by refluxing over sodium for 7 h and fractionally distilled. The purity of the samples was ascertained by comparing boiling points and densities with the literature data (16, 17) and are shown in Table 1.

Excess volumes were measured using batch dilatometer technique described earlier (18) and were accurate to ± 0.003 cm^3 mol^{-1}.[1] Densities were calculated from excess volumes using the relation

$$[1] \qquad \rho = \frac{x_1 M_1 + x_2 M_2}{x_1 V_1 + x_2 V_2 + V^E}$$

for mixtures, and with the aid of a bicapillary pycnometer for pure components. Densities of mixtures and of pure components were accurate to $\pm 5 \times 10^{-5}$ g cm^{-3}.

Isentropic compressibilities were calculated using the relation

$$[2] \qquad k_S = 1/u^2\rho$$

The sound velocities, u, were measured with an accuracy of $\pm 0.1\%$ using an ultrasonic interferometer at a fixed frequency of 1 MHz. Viscosities were measured using an Ostwald viscometer and the values were accurate to $\pm 0.5\%$.

[1]Nomenclature used in this article is as follows: C_P, molar heat capacity at constant pressure; ΔG^R, residual free energy; H^E, excess enthalpy; ΔH^M, enthalpy of mixing; k_S, isentropic compressibility; k_T, isothermal compressibility; P_i^*, characteristic pressure of component $i = \alpha T \tilde{v}^2 k_T^{-1}$; ΔS^R, residual entropy; $\tilde{T}_i$, reduced temperature of component $i = (\tilde{v}_i^{1/3} - 1)\tilde{v}_i^{-4/3}$; T_i^*, characteristic temperature of component $i = T\tilde{T}_i^{-1}$; U_i^*, characteristic energy of component $i = P_i V_i^*$; V_i, molar volume of component i; V_i^*, characteristic volume of component $i = V_i \tilde{v}_i^{-1}$; $\tilde{v}_i$, reduced volume of component

$$i = \left[\frac{(3 + 4\alpha_i T)}{3(1 - \alpha_i T)}\right]^3$$

V^E, excess volume; x_i, mole fraction of component i; X_{12}, Flory interaction parameter; α, thermal expansion coefficient; η, viscosity; ϕ_i, segment fraction of component $i = x_i V_i^* / \Sigma x_i V_i^*$; ψ_i, energy fraction of component $i = x_i U_i^* / \Sigma x_i U_i^*$; θ_2, surface fraction of component $2 = x_2 V_2^{*2/3} / (x_1 V_1^{*2/3} + x_2 V_2^{*2/3})$; σ, standard deviation.

Printed in Canada / Imprimé au Canada

Can. J. Chem. Downloaded from www.nrcresearchpress.com by 91.144.44.67 on 09/07/12
For personal use only.

TABLE 1. Boiling points and densities at 303.15 K for pure compounds

Compound	Density (g cm^{-3})		Boiling point (K)	
	Present work	Refs. 10, 11	Present work	Ref. 10
Cyclohexene	0.80172	0.8017	356.65	356.13
n-Hexane	0.65110	0.65055	341.35	341.89
Cyclohexane	0.77013	0.76928	353.25	353.88
Benzene	0.86856	0.86850	352.85	353.25
Trichloromethane	1.47090	1.47060	349.45	349.90
Tetrachloromethane	1.57480	1.57480	334.45	334.30
1,4-Dioxane	1.02056	1.02230	373.65	374.47

Theory

Excess volumes were predicted using the following relation (7) developed on the basis of Van der Waals model used by Flory (19, 20) for the dependence of energy on volume.

$$[3]\quad \frac{V^E}{x_1V_1^* + x_2V_2^*} = \tilde{T}\frac{\partial\tilde{\nu}}{\partial\tilde{T}}\psi_1\theta_2X_{12}/P_1^* + (\tilde{\nu}_1 - \tilde{\nu}_2)(\psi_1 - \phi_1) - \frac{1}{2}\left[\frac{\tilde{\nu}_1 - \tilde{\nu}_2}{\partial\tilde{\nu}/\partial\tilde{T}}\right]^2\frac{\partial\tilde{\nu}}{\partial\tilde{T}^2}\left\{\psi_1\psi_2 + (\psi_1 - \phi_1)^2\right\}$$

where $\tilde{\nu} = \phi_1\tilde{V}_1 + \phi_2\tilde{V}_2$ and $\tilde{T}$ corresponds to $\tilde{\nu}$. The first term in the equation is represented as $V^E(X_{12})$ which is the excess volume contribution arising from interactional, steric hindrance, and disorder effects. The second term represents $V^E(P^*)$, it is the excess volume contribution due to cohesive energy difference between unlike components. The third term, V^E(f.v.) depends on the difference between free volumes of unlike components.

An appropriate form of the Prigogine–Patterson–Flory theory has been used to evaluate the interactional and free volume (f.v.) contributions of excess enthalpy. The free volume contribution is defined as

TABLE 2. Mole fraction of cyclohexene x_1 and excess volumes V^E at 303.15 K*

x_1	V^E (cm^3 mol^{-1})	ΔV^E (cm^3 mol^{-1})	x_1	V^E (cm^3 mol^{-1})	ΔV^E (cm^3 mol^{-1})
		Cyclohexene + *n*-hexane			
0.1718	−0.040	−0.000	0.5946	−0.070	−0.001
0.2792	−0.054	−0.001	0.6859	−0.062	−0.002
0.3914	−0.064	0.001	0.8067	−0.046	0.004
0.5249	−0.074	−0.005	0.9032	−0.031	−0.001
		Cyclohexene + cyclohexane			
0.1133	0.021	0.000	0.4866	0.060	0.002
0.2435	0.038	−0.003	0.5820	0.055	−0.001
0.3293	0.052	0.002	0.7181	0.042	−0.004
0.3919	0.057	0.002	0.8663	0.026	0.001
		Cyclohexene + benzene			
0.1198	0.060	0.002	0.4904	0.122	0.001
0.2756	0.100	−0.008	0.6697	0.115	0.004
0.3442	0.115	−0.001	0.7561	0.010	−0.008
0.4509	0.130	0.009	0.8665	0.070	0.002
		Cyclohexene + trichloromethane			
0.1005	0.012	0.000	0.4917	0.034	−0.001
0.2478	0.026	0.000	0.6290	0.031	−0.001
0.3282	0.031	−0.001	0.7454	0.023	−0.002
0.4351	0.039	0.004	0.8452	0.017	0.001
		Cyclohexene + tetrachloromethane			
0.1014	−0.032	−0.001	0.5562	−0.081	−0.002
0.2018	−0.051	0.002	0.6526	−0.074	0.002
0.3213	−0.067	0.002	0.7514	−0.063	0.003
0.4018	−0.076	−0.001	0.9049	−0.035	−0.001
0.5046	−0.082	−0.003			
		Cyclohexene + 1,4-dioxane			
0.1067	0.174	−0.005	0.5637	0.394	−0.011
0.2617	0.363	0.006	0.6603	0.332	−0.001
0.3551	0.424	0.010	0.7706	0.243	−0.001
0.4267	0.438	0.007	0.8678	0.146	0.006
0.4787	0.424	−0.005			

*$\Delta V^E = V^E$(exp) − V^E(eq. [15]).

Can. J. Chem. Downloaded from www.nrcresearchpress.com by 91.144.44.67 on 09/07/12
For personal use only.

TABLE 3. Mole fraction of cyclohexene x_1, density ρ, sound velocity u, isentropic compressibility k_S, viscosity η, excess isentropic compressibility k_S^E, and excess viscosity Δ ln η at 303.15 K

x_1	ρ (g cm^{-3})	u (ms^{-1})	k_S (TPa^{-1})	η (cP)	k_S^E (TPa^{-1})	Δ ln η
			Cyclohexene + *n*-hexane			
0.0000	0.65110	1055	1380	0.320	—	—
0.1718	0.67215	1081	1273	0.348	−29	−0.020
0.2792	0.68615	1104	1196	0.365	−47	−0.032
0.3914	0.70154	1126	1124	0.387	−58	−0.037
0.5249	0.72100	1150	1049	0.418	−61	−0.038
0.5946	0.73164	1162	1012	0.438	−57	−0.034
0.6859	0.74165	1178	972	0.464	−44	−0.028
0.8067	0.76645	1200	906	0.503	−28	−0.017
0.9032	0.78364	1226	849	0.536	−15	−0.010
1.0000	0.80172	1253	795	0.573	—	—
			Cyclohexene + cyclohexane			
0.0000	0.77013	1233	854	0.799	—	—
0.1133	0.77336	1232	852	0.772	3	0.005
0.2435	0.77718	1234	845	0.745	4	0.011
0.3293	0.77977	1239	835	0.725	5	0.014
0.3919	0.78161	1237	836	0.720	6	0.015
0.4866	0.78455	1242	826	0.684	5	0.015
0.5820	0.78760	1242	823	0.678	5	0.014
0.7181	0.79208	1245	815	0.654	3	0.010
0.8663	0.79712	1247	807	0.620	2	0.005
1.0000	0.80172	1253	795	0.573	—	—
			Cyclohexene + benzene			
0.0000	0.86856	1282	701	0.574	—	—
0.1198	0.85892	1274	717	0.570	4	−0.005
0.2756	0.84742	1263	740	0.568	11	−0.010
0.3442	0.84250	1261	747	0.569	12	−0.011
0.4509	0.83510	1256	759	0.566	13	−0.013
0.4904	0.83248	1256	762	0.566	12	−0.013
0.6697	0.82095	1254	775	0.568	9	−0.010
0.7561	0.81573	1254	780	0.568	6	−0.009
0.8665	0.80912	1254	786	0.571	3	−0.004
1.0000	0.80172	1253	795	0.573	—	—
			Cyclohexene + tetrachloromethane			
0.0000	1.57480	907	772	0.906	—	—
0.1014	1.49346	920	791	0.875	17	0.011
0.2018	1.41347	938	804	0.839	27	0.016
0.3213	1.31916	962	819	0.800	40	0.023
0.4018	1.25619	918	827	0.775	46	0.027
0.5046	1.17641	1009	835	0.740	52	0.029
0.5562	1.13662	1026	836	0.722	51	0.027
0.6526	1.06274	1063	833	0.688	46	0.024
0.7514	0.98769	1107	826	0.653	37	0.018
0.9049	0.87239	1190	810	0.603	18	0.008
1.0000	0.80172	1253	795	0.573	—	—
			Cyclohexene + trichloromethane			
0.0000	1.47090	967	727	0.635	—	—
0.1005	1.38797	989	737	0.620	2	−0.013
0.2478	1.27393	1022	752	0.604	5	−0.025
0.3282	1.21517	1041	759	0.595	6	−0.031
0.4351	1.14055	1069	767	0.585	7	−0.037
0.4917	1.10255	1086	769	0.581	6	−0.038
0.6290	1.01445	1126	778	0.575	5	−0.034
0.7454	0.94398	1163	783	0.573	4	−0.027
0.8452	0.88634	1196	789	0.571	3	−0.020
1.0000	0.80172	1253	795	0.573	—	—

TABLE 3 (*concluded*)

x_1	ρ (g cm^{-3})	u (ms^{-1})	k_S (TPa^{-1})	η (cP)	k_S^E (TPa^{-1})	Δ ln η
			Cyclohexene + 1,4-dioxane			
0.0000	1.02056	1323	560	1.023	—	—
0.1067	0.99149	1304	593	0.932	4	−0.032
0.2617	0.95184	1283	638	0.833	9	−0.054
0.3551	0.92953	1274	663	0.789	10	−0.056
0.4267	0.91358	1268	681	0.754	12	−0.057
0.4787	0.90242	1265	693	0.734	11	−0.053
0.5637	0.88458	1260	712	0.702	10	−0.050
0.6603	0.86508	1255	734	0.668	8	−0.042
0.7706	0.84353	1254	754	0.634	6	−0.032
0.8678	0.82662	1253	771	0.606	3	−0.020
1.0000	0.80172	1253	795	0.573	—	—

[4] $$H^E(\text{f.v.})/(x_1U_1^* + x_2U_2^*) = \tilde{C}_P(\tilde{T}_U)[\psi_1\tilde{T}_1 + \psi_2\tilde{T}_2 - \tilde{T}_U]$$

where $\tilde{T}_U$ is the average reduced temperature for the solution appropriate to the energy $\tilde{U}$ and is given by

[5] $$\tilde{U}(\tilde{T}_U) = \psi_1\tilde{U}(\tilde{T}_1) + \psi_2\tilde{U}(\tilde{T}_2)$$

Applying the Van der Waals model used by Flory, $\tilde{T}_U$ is obtained with the relation

[6] $$\tilde{T}_U = \tilde{V}_U^{-1}(1 - V_U^{-1/3})$$

where $\tilde{V}_U^{-1} = (\psi_1/\tilde{V}_1 + \psi_2/\tilde{V}_2)$ and $\tilde{C}_P(\tilde{T}_U)$ in eq. [4] is defined as $(\frac{4}{3}\tilde{V}_U^{-1/3} - 1)^{-1}$.

The interactional contribution to H^E is defined in terms of the Flory parameter X_{12} which also includes the contributions due to disorder and steric hindrance effects. The X_{12} parameter was correlated using the following relation

[7] $$\frac{H^E(\text{exp}) - H^E(\text{f.v.})}{x_1U_1^* + x_2U_2^*} = \frac{X_{12}}{P_1}\psi_1\theta_2 f(\tilde{V}_U)$$

where $f(\tilde{V}_U)$ is defined by $(4\tilde{V}_U - 3\tilde{V}_U^{4/3})^{-1}$.

The theory is applied to predict excess volumes for all the mixtures at equimolar composition using eq. [3]. The interaction parameter X_{12} required in this equation is obtained from experimental excess enthalpies (1–5). Similarly, H^E values were predicted using eqs. [4] and [7] with X_{12} values taken from experimental excess volumes.

According to Bloomfield and Dewan (11), theoretical excess viscosity is represented as

[8] $$\ln\eta - (x_1\ln\eta_1 + x_2\ln\eta_2) = -\frac{\Delta G^R}{RT} + \left[\frac{1}{\tilde{\nu} - 1} - \frac{x_1}{\tilde{\nu}_1 - 1} - \frac{x_2}{\tilde{\nu}_2 - 1}\right]$$

[9] $$\Delta\ln\eta_{\text{the}} = \ln\eta_G + \ln\eta_v$$

where $\ln\eta_G$ and $\ln\eta_v$ are the viscosity contributions to theoretical excess viscosity according to absolute rate and free volume theories, respectively. Equation [9] can be written as

[10] $$\Delta\ln\eta_{\text{the}} = \ln\eta_H + \ln\eta_S + \ln\eta_v$$

where

Can. J. Chem. Downloaded from www.nrcresearchpress.com by 91.144.44.67 on 09/07/12
For personal use only.

Can. J. Chem. Downloaded from www.nrcresearchpress.com by 91.144.44.67 on 09/07/12
For personal use only.

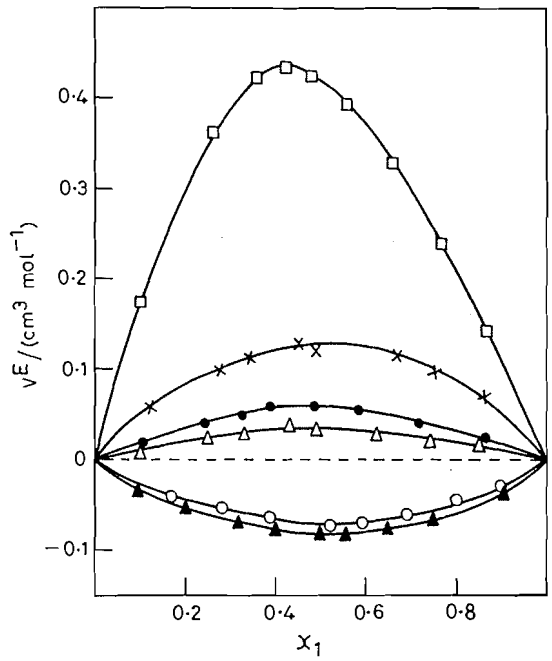

FIG. 1. Excess volumes versus mole fraction of cyclohexene for the systems cyclohexene + *n*-hexane (○), + cyclohexane (●), + benzene (×), + trichloromethane (△), + tetrachloromethane (▲) and + 1,4-dioxane (□) at 303.15 K.

$$\ln \eta_H = -\frac{H^E}{RT},$$

$$\ln \eta_S = \frac{\Delta S^R}{R}$$

and

$$\ln \eta_V = \frac{1}{\tilde{v} - 1} - \frac{x_1}{\tilde{v}_1 - 1} - \frac{x_2}{\tilde{v}_2 - 1}$$

The enthalpy contributions, $\ln \eta_H$, to theoretical excess viscosity are calculated from the experimental excess enthalpies (1–5). The residual entropy of mixing, ΔS^R, required in the calculation of entropy contribution to theoretical excess viscosity, is obtained from the Flory (18) equation,

[11] $$\Delta S^R = -3\left[\frac{x_1 P_1^* V_1^*}{T_1^*} \ln \frac{\tilde{v}_1^{1/3} - 1}{\tilde{v}^{1/3} - 1} + \frac{x_2 P_2^* V_2^*}{T_2^*} \ln \frac{\tilde{v}_2^{1/3} - 1}{\tilde{v}^{1/3} - 1}\right]$$

Reduced volumes for the mixture and for the pure components are calculated with experimental densities using the equations

[12] $$\tilde{v} = \frac{V}{(x_1 V_1^* + x_2 V_2^*)}, \quad \tilde{v}_i = \frac{V_i}{V_i^*} \qquad (i = 1, 2)$$

The parameters of the pure components used in the above equations have the same significance as described by Flory (18, 19) and are defined in the list of symbols (see footnote 1).

Results and discussion

Excess volumes are given in Table 2. Excess isentropic compressibilities are calculated using the relation

[13] $$k_S^E = k_{S,\text{mix}} - (\phi_1 k_{S_1} + \phi_2 k_{S_2})$$

where ϕ_1 and ϕ_2 are volume fractions. Excess isentropic

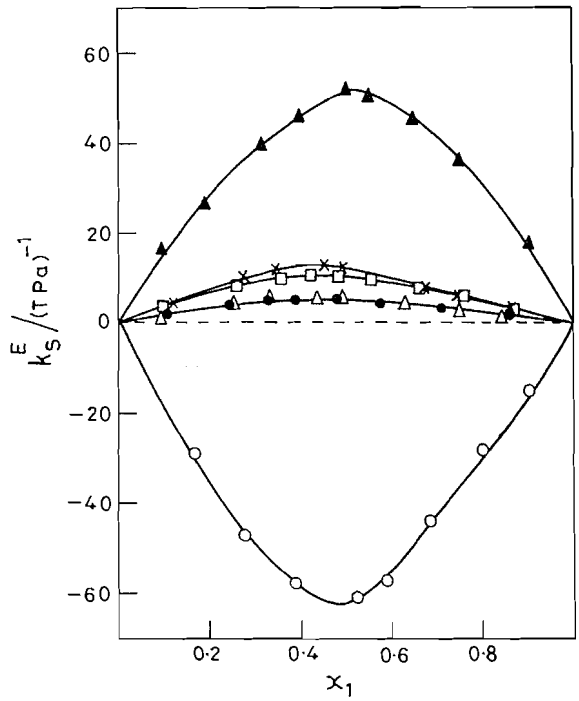

FIG. 2. Excess isentropic compressibilities versus mole fraction of cyclohexene for the systems cyclohexene + *n*-hexane (○), + cyclohexane (●), + benzene (×), + trichloromethane (△), + tetrachloromethane (▲), and + 1,4-dioxane (□) at 303.15 K.

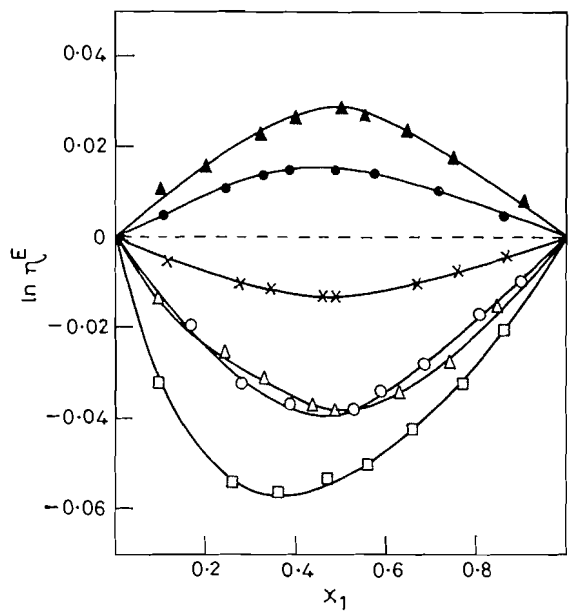

FIG. 3. Excess viscosities versus mole fraction of cyclohexene for the systems cyclohexene + *n*-hexane (○), + cyclohexane (●), + benzene (×), + trichloromethane (△), + tetrachloromethane (▲), and + 1,4-dioxane (□) at 303.15 K.

compressibilities, densities, and sound velocities are given in Table 3. Excess viscosities are calculated using the relation

[14] $$\Delta \ln \eta = \ln \eta_{\text{mix}} - (x_1 \ln \eta_1 + x_2 \ln \eta_2)$$

and are included in Table 3. Excess properties as a function of mole fraction are shown in Figs. 1 to 3 and are also fitted into an empirical equation

[15] $$x^E = x_1(1 - x_1)[a_1 + a_2(1 - 2x_1) + a_3(1 - 2x_1)^2]$$

The parameters a_1, a_2, and a_3 are calculated by the method of

TABLE 4. Least square parameters and standard deviation $\sigma(x^E)$

Property	a_1	a_2	a_3	$\sigma(x^E)$
Cyclohexene + *n*-hexane				
V^E (cm^3 mol^{-1})	−0.2769	−0.0319	−0.0559	0.003
k_S^E (TPa^{-1})	−241.33	19.09	99.61	1.6
$\Delta \ln \eta$	−0.1484	0.0165	0.0491	0.002
Cyclohexene + cyclohexane				
V^E (cm^3 mol^{-1})	0.2317	0.0026	−0.0360	0.003
k_S^E (TPa^{-1})	20.25	−7.67	4.34	0.3
$\Delta \ln \eta$	0.0609	−0.0084	−0.0258	0.001
Cyclohexene + benzene				
V^E (cm^3 mol^{-1})	0.4849	−0.0223	0.2225	0.006
k_S^E (TPa^{-1})	49.31	−12.46	−25.99	0.7
$\Delta \ln \eta$	−0.0491	0.0144	−0.0025	0.001
Cyclohexene + trichloromethane				
V^E (cm^3 mol^{-1})	0.1417	−0.0107	−0.0251	0.002
k_S^E (TPa^{-1})	24.48	−4.88	−3.21	0.5
$\Delta \ln \eta$	−0.1458	−0.0063	0.0011	0.001
Cyclohexene + tetrachloromethane				
V^E (cm^3 mol^{-1})	−0.3147	−0.0325	−0.0885	0.002
k_S^E (TPa^{-1})	197.53	19.04	−6.78	1.9
$\Delta \ln \eta$	0.1067	−0.0340	0.0025	0.005
Cyclohexene + 1,4-dioxane				
V^E (cm^3 mol^{-1})	1.7039	−0.4440	−0.2877	0.009
k_S^E (TPa^{-1})	42.89	−11.06	−13.09	0.4
$\Delta \ln \eta$	−0.2129	0.1014	−0.0698	0.001

least squares and are given in Table 4 along with the standard deviation $\sigma(x^E)$. x^E represents V^E, k_S^E, and $\Delta \ln \eta$.

The values of the parameters of pure components required in the prediction of V^E, H^E, and $\Delta \ln \eta$ are given in Table 5. The values of the interaction parameter X_{12} and various contributions to excess volume are included in Table 6 along with the experimental V^E for equimolar mixtures. The comparison of theoretical and experimental excess enthalpies at $x_1 = 0.5$ are shown in Table 7, along with the interaction parameter X_{12}. Excess viscosity results for all the mixtures at $x_1 = 0.5$ are compared in Table 8.

Excess volumes are negative for the systems cyclohexene with *n*-hexane and tetrachloromethane and positive for the remaining systems over the entire range of mole fraction. k_S^E values are negative for mixtures containing *n*-hexane and positive in all other systems. $\Delta \ln \eta$ are positive for the systems cyclohexene with cyclohexane and tetrachloromethane and negative in the remaining systems. The results show no simple pattern and cannot be interpreted only in terms of π–π, π–H, and π–n interactions.

The results presented in Table 6 reveal that the experimental and theoretical excess volumes at $x_1 = 0.5$ agree in sign in all the systems except in the mixtures containing tetrachloromethane. Quantitative agreements is also satisfactory in the systems of cyclohexene with cyclohexane and 1,4-dioxane. In the system, cyclohexene + *n*-hexane, the interactional contribution to excess volumes is positive but it is dominated by the negative contributions due to $V^E(P^*)$ and V^E(f.v.). This suggests that the contributions to V^E(calc) due to packing effects are dominant over the interactional contributions. Further, the large negative $V^E(P^*)$ indicate that *n*-hexane with low P^* (less cohesive) contracts more in the solutions and hence

TABLE 5. Parameters of the pure compounds at 303.15 K

Compound	$\alpha \times 10^3$ [a] / K^{-1}	k_T [b] / (TPa)$^{-1}$	$\tilde{v}$	V^* / cm^3 mol^{-1}	P^* / J cm^{-3}	$\tilde{T}$
Cyclohexene	1.191	1076.5	1.2894	79.466	557.6	0.06300
n-Hexane	1.404	1780.9	1.3292	99.574	422.2	0.06808
Cyclohexane	1.230	1169.1	1.2969	84.263	536.4	0.06401
Benzene	1.248	1010.5	1.3004	69.162	633.1	0.06447
Trichloromethane	1.263	1058.1	1.3032	62.277	614.5	0.06483
Tetrachloromethane	1.241	1114.9	1.2990	75.193	569.4	0.06428
1,4-Dioxane	1.104	768.8	1.2723	67.855	704.7	0.06063

[a] Values were calculated from measured density using the relation $\alpha_1 = (\rho_1 - \rho_2)/\rho_2(T_2 - T_1)$.
[b] k_T values were obtained from measured density and sound velocity with the equation $k_T = k_s + \alpha^2 TV/Cp$, heat capacities at 303.15 K were evaluated from extrapolation of literature values (16, 17, 21).

TABLE 6. Calculated and experimental excess volumes of equimolar mixtures at 303.15 K

Cyclohexene +	X_{12} [a] / J cm^{-3}	$V^E(x_{12})$ / cm^3 mol^{-1}	$V^E(P^*)$ / cm^3 mol^{-1}	V^E(f.v.) / cm^3 mol^{-1}	V^E(calc) / cm^3 mol^{-1}	V^E(exp) / cm^3 mol^{-1}
n-Hexane	7.67	0.173	−0.247	−0.098	−0.172	−0.074(−0.105)[b]
Cyclohexane	4.18	0.082	−0.006	−0.0001	0.076	0.060(0.094)[b]
Benzene	15.96	0.239	0.026	−0.002	0.263	0.122(0.248)[b]
Trichloromethane	−5.23	−0.077	0.023	−0.004	−0.058	0.034
Tetrachloromethane	−2.08	−0.034	0.004	−0.004	−0.034	−0.082
1,4-Dioxane	45.78	0.619	−0.077	−0.002	0.540	0.424

[a] Calculated with excess enthalpies using eq. [3].
[b] The values given in parentheses are excess volumes at 298.15 K for equimolar mixtures (6).

Can. J. Chem. Downloaded from www.nrcresearchpress.com by 91.144.44.67 on 09/07/12
For personal use only.

TABLE 7. Calculated and experimental excess enthalpies of equimolar mixtures at 303.15 K

Cyclohexene +	X_{12}[a] / J cm^{-3}	$H^E(X_{12})$ / J mol^{-1}	H^E(f.v.) / J mol^{-1}	H^E(calc) / J mol^{-1}	H^E(exp)[b] / J mol^{-1}
n-Hexane	−12.13	−275.5	−9.2	−284.7	165.0
Cyclohexane	3.57	76.5	0.1	76.6	90.2
Benzene	6.47	129.5	0.2	129.7	320.0
Trichloromethane	1.44	28.1	−2.2	25.9	−105.0
Tetrachloromethane	−5.21	−107.6	−0.2	−107.8	−231.0
1,4-Dioxane	38.70	766.0	−5.3	760.7	901.0

[a]Calculated with experimental excess volumes using eq. [7].
[b]H^E values are at 298.15 K, taken from the literature (1–5).

TABLE 8. Entropy ln η_S, enthalpy ln η_H, free volume ln η_v, and free energy ln η_G contributions to viscosity. Theoretical Δ ln η_{the} and experimental Δ ln η_{exp} excess viscosities, and reduced volume $\tilde{v}$, for equimolar mixtures at 303.15 K

Cyclohexene +	$\tilde{v}$	ln η_S	ln η_H	ln η_G	ln η_v	Δ ln η_{the}	Δ ln η_{exp}
n-Hexane	1.3107	0.018	−0.065	−0.047	−0.028	−0.075	−0.038
Cyclohexane	1.2940	0.009	−0.036	−0.027	−0.010	−0.037	0.015
Benzene	1.2961	0.013	−0.127	−0.114	−0.015	−0.129	−0.013
Trichloromethane	1.2960	0.002	0.042	0.044	0.002	0.046	−0.038
Tetrachloromethane	1.2930	0.012	0.092	0.104	0.013	0.117	0.029
1,4-Dioxane	1.2873	0.074	−0.357	−0.283	−0.083	−0.366	−0.052

molecules have more compact arrangement. In all other systems $V^E(P^*)$ contributions are small so that the sign and magnitude of V^E(calc) depend mainly on interactional contributions. The results in Table 7 reveal that the theoretical and experimental excess enthalpies are in semiquantitative agreement in cyclohexene with cyclohexane and 1,4-dioxane, and in sign agreement in the systems cyclohexene with benzene and tetrachloromethane. However, the H^E results are not even in qualitative agreement in the other two systems.

The data presented in Table 8 indicate that the free volume contribution to excess viscosity are nearer to the experimental excess viscosity in all the systems than the free energy contribution to excess viscosity or theoretical excess viscosity. Even here ln η_v and ln η_{exp} are not in sign agreement for the systems cyclohexene with cyclohexane and tetrachloromethane; however, in other systems the results are semiquantitative.

Acknowledgement

The authors are grateful to University Grants Commission, New Delhi, for financial support.

1. W. WOYCICKI. J. Chem. Thermodyn. **11**, 727 (1979).
2. W. WOYCICKI. J. Chem. Thermodyn. **12**, 165 (1980).
3. W. WOYCICKI. J. Chem. Thermodyn. **12**, 761 (1980).
4. J. P. E. GROLIER, A. INGLESE, and E. WILHELM. J. Chem. Eng. Data, **27**, 333 (1982).
5. K. GUENZEL and H. J. BITTRICH. Z. Phys. Chem. **258**, 1073 (1977).
6. T. M. LETCHER. J. Chem. Thermodyn. **7**, 205 (1975).
7. D. PATTERSON and G. DELMAS. Discuss. Faraday Soc. **49**, 98 (1970).
8. D. PATTERSON and HUUTRAVAN. J. Solution Chem. **11**, 793 (1982).
9. M. COSTAS and D. PATTERSON. J. Solution Chem. **11**, 807 (1982).
10. B. RIEDL and G. DELMAS. Can. J. Chem. **61**, 1876 (1983).
11. V. A. BLOOMFIELD and R. K. DEWAN. J. Phys. Chem. **75**, 3113 (1971).
12. T. JAYALAKSHMI and K. S. REDDY. Can. J. Chem. **63**, 2824 (1985).
13. K. P. RAO and K. S. REDDY. Can. J. Chem. Eng. **66**, 474 (1988).
14. K. S. REDDY and P. R. NAIDU. Indian J. Chem. **19A**, 942 (1980).
15. K. S. REDDY and D. V. S. JAIN. Thermochim. Acta, **107**, 383 (1986).
16. J. A. RIDDICK and W. B. BUNGER. Organic solvents. Vol. II, 3rd. ed. Weisberger, Interscience Publishers, New York. 1970.
17. J. TIMMERMANS. Physico-chemical constants of pure organic compounds. Elsevier Publishing Co., Amsterdam. 1950.
18. K. S. REDDY and P. R. NAIDU. Can. J. Chem. **55**, 76 (1977).
19. P. J. FLORY. J. Am. Chem. Soc. **87**, 1833 (1965).
20. A. ABE and P. J. FLORY. J. Am. Chem. Soc. **87**, 1838 (1965).
21. J. P. E. GROLIER, A. INGLESE, and E. WILHELM. J. Chem. Thermodyn. **16**, 67 (1984).

Can. J. Chem. Downloaded from www.nrcresearchpress.com by 91.144.44.67 on 09/07/12
For personal use only.

Andre G. Michel, Chakib Ameziane-Hassani, Gaston Boulay et Gilles Lajoie. Étude structurale de la liaison thioamide : Synthèse et conformation de dérivés de la thioalanine et de la thioglycine. Can. J. Chem. **67**, 1312 (1989).

Page 1316. La structure **1** devrait lire :

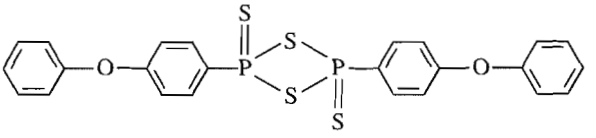

Can. J. Chem. Downloaded from www.nrcresearchpress.com by 91.144.44.67 on 09/07/12
For personal use only.

Sesquiterpene alkaloids from *Tripterygium wilfordii* (Hook): a nuclear magnetic resonance study of 1-desacetylwilfordine, 1-desacetylwilfortrine, and 2-debenzoyl-2-nicotinoylwilforine

LI YA AND GEORGE M. STRUNZ[1]
Forestry Canada — Maritimes Region, P.O. Box 4000, Fredericton, N.B., Canada E3B 5P7
AND
LARRY A. CALHOUN
Department of Chemistry, University of New Brunswick, Fredericton, N.B., Canada E3B 6E2

Received August 29, 1989

LI YA, GEORGE M. STRUNZ, and LARRY A. CALHOUN. Can. J. Chem. **68**, 371 (1990).

1-Desacetylwilfordine, **8**, 1-desacetylwilfortrine, **9**, and 2-debenzoyl-2-nicotinoylwilforine, **10**, have been isolated from root extracts of the Chinese medicinal and insecticidal plant *Tripterygium wilfordii*. Analysis of the ^1H and ^{13}C NMR spectra of **8** and **10**, with the aid of COSY, HCCOSY, and COLOC experiments, has allowed unambiguous chemical shift assignments of all protons and carbons of these alkaloids.

Key words: alkaloids, sesquiterpene, Celastraceae, *Tripterygium*, NMR.

LI YA, GEORGE M. STRUNZ et LARRY A. CALHOUN. Can. J. Chem. **68**, 371 (1990).

On a isolé le wilfordine-désacétyl-1, **8**, le wilfortrine-désacétyl-1, **9**, et le wilforine-débenzoyl-2-nicotinoyl-2, **10**, des extraits de racines de la plante médicinale et insecticide chinoise, *Tripterygium wilfordii*. L'analyse des spectres RMN du ^1H et ^{13}C, des composés **8** et **10**, à l'aide des expériences COSY, HCCOSY et COLOC a permis d'attribuer de façon définitive tous les déplacements de tous les protons et de tous les atomes de carbone de ces alcaloïdes.

Mots clés : alcaloïdes, sesquiterpène, Celastraceae, *Tripterygium*, RMN.

Introduction

The presence of alkaloids in plants of the Celastraceae family has been recognized for more than 50 years (1). It was not, however, until 1970 that the first complete structures were announced for members of this large group of sesquiterpene alkaloids (2). The Thunder God Vine, *Tripterygium wilfordii* Hook, belonging to the Celastraceae family, is widely distributed in southern China and has been utilized in traditional Chinese medicine for treatment of cancer, rheumatism, and lupus (3). The insecticidal properties of *T. wilfordii* are also noteworthy, and this species, as well as *T. forrestii*, were commonly used as contact insecticides in rural China (1). A number of alkaloids, including wilfordine, wilforine, wilforzine, wilforgine, and wilfortrine, were isolated from *T. wilfordii* by Beroza (refs. cited in ref. 1). The structure of wilfordine, **1**, $C_{43}H_{49}NO_{19}$, was elucidated by Yamada *et al.* (4), and structures of wilforine, **2**, and wilfortrine, **3**, postulated by Smith (1) on the basis of Beroza's earlier research (refs. cited in ref. 1), were established by Wu *et al.* (5, 6).

In recent studies, a group at the Shanghai Institute of Materia Medica, including one of us (Li Ya), has reisolated these alkaloids from *T. wilfordii*, and proved the structure of wilforgine, **4**, postulated earlier by Smith (1), and that of wilforzine, **5** (7). An alkaloid, designated wilformine, was found (7) to be identical with euonine, **6**, previously isolated from *Euonymus sieboldiana* (8). The Shanghai researchers have, in addition, established the structure of the new alkaloid wilforidine, **7** (9).

In this communication, we report the isolation and structure determination of three additional related alkaloids from *T. wilfordii*. The chemical shifts of *all* protons and carbons in the NMR spectra of two of these alkaloids are unambiguously assigned.

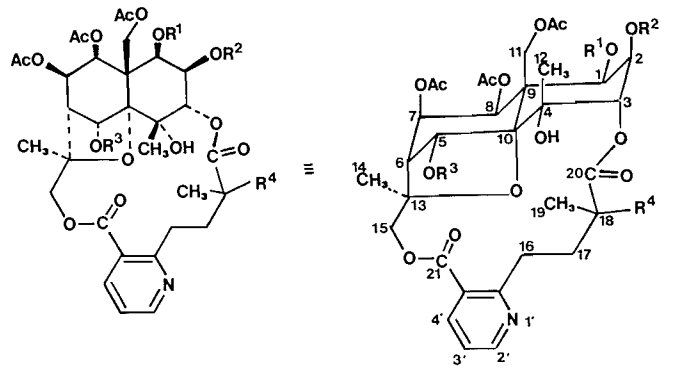

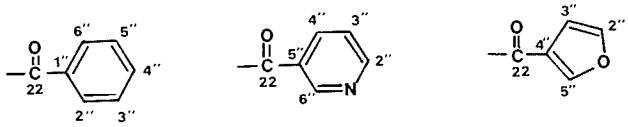

Wilfordine (**1**) R^1 = Ac, R^2 = benzoyl, R^3 = Ac, R^4 = OH
Wilforine (**2**) R^1 = Ac, R^2 = benzoyl, R^3 = Ac, R^4 = H
Wilfortrine (**3**) R^1 = Ac, R^2 = 3-furanoyl, R^3 = Ac, R^4 = OH
Wilforgine (**4**) R^1 = Ac, R^2 = 3-furanoyl, R^3 = Ac, R^4 = H
Wilforzine (**5**) R^1 = Ac, R^2 = benzoyl, R^3 = H, R^4 = H
Wilformine = Euonine (**6**) R^1 = Ac, R^2 = Ac, R^3 = Ac, R^4 = H
Wilforidine (**7**) R^1 = Ac, R^2 = H, R^3 = Ac, R^4 = OH
1-Desacetylwilfordine (**8**) R^1 = H, R^2 = benzoyl, R^3 = Ac, R^4 = OH
1-Desacetylwilfortrine (**9**) R^1 = H, R^2 = 3-furanoyl, R^3 = Ac, R^4 = OH
2-Debenzoyl-2-nicotinoylwilforine (**10**) R^1 = Ac, R^2 = nicotinoyl, R^3 = Ac, R^4 = H

[1]Author to whom correspondence may be addressed.

Can. J. Chem. Downloaded from www.nrcresearchpress.com by 91.144.44.67 on 09/07/12
For personal use only.

TABLE 1. ^{1}H NMR spectral data

Proton	Alkaloid 1	8	9	10
1	5.75 (d, 3.2)	4.59 (overlapping H-11)	4.54 (dd, 7.6, 3.7)	5.76 (d, 3.5)
2	5.47 ("t", 3.0)	5.36 ("t", 3.1)	5.24 (dd, 3.7, 2.8)	Envelope 5.40–5.58
3	~5.09 (d, 2.9)	5.14 (d, 2.9)	5.08 (d, 2.7)	5.08 (d, ~2.8) (overlapping OH)
5	6.86 (s)	6.52 (s)	6.66 (s)	6.96 (s)
6	2.40 (d, 3.8)	2.44 (d, 3.5)	2.41 (d, 3.6)	2.37 (3.6)
7	~5.54 (overlapping H-11)	5.57–5.62 (overlapping H-8 and H-11)	5.53–5.63 (overlapping H-8 and H-11)	Envelope 5.40–5.58
8	5.40 (d, 5.7)	5.57–5.62 (overlapping H-7 and H-11)	5.53–5.63 (overlapping H-7 and H-11)	Envelope 5.40–5.58
11	4.41, 5.57 (ABq, 13.0)	4.60, 5.59 (ABq, 12.2)	4.47, 5.52 (ABq, 13.1)	4.37, Envelope 5.40–5.58, ABq (13.2)
12	1.73 (s)	1.69 (s)	1.44 (s), 1.61 (s) or 1.67 (s)	1.65 (s) or 1.69 (s)
14	1.65 (s)	1.68 (s)	1.44 (s), 1.61 (s) or 1.67 (s)	1.65 (s) or 1.69 (s)
15	3.76, 5.83 (ABq, 12.1)	3.75, 5.77 (ABq, 12.0)	3.71, 5.81 (ABq, 12.0)	3.78, 5.79 (ABq, 11.8)
16	2.89 (m), 4.08 (m)	~2.9 (m), ~4.0 (m)	~2.86 (m), ~4.0 (m)	~2.94 (m), ~4.0 (m)
17	~2.25 (m), 2.50 (m)	~2.25 (m), ~2.50 (m)	~2.25 (m), ~2.50 (m)	~1.8 (m), ~2.4 (m)
19	1.51 (s)	1.46 (s)	1.44 (s), 1.61 (s) or 1.67 (s)	1.24 (d, 6.0)
2′	8.70 (dd, 4.8, 1.7)	8.70 (dd, 4.7, 1.7)	8.70 (dd, 4.8, 1.8)	8.77 (dd, 4.7, 1.7)
3′	7.22 (dd, 7.9, 4.9)	7.22 (dd, 7.8, 4.9)	7.21 (dd, 7.9, 4.8)	7.29 (dd, 7.9, 4.7)
4′	8.14 (dd, 7.9, 1.7)	8.13 (dd, 7.9, 1.8)	8.12 (dd, 7.9, 1.8)	8.36 (overlapping H-4″)
2″	8.08 (d, 8.0)	8.03 (d, 7.6)	7.50 ("t", 1.7)	8.85 ("d", 2.6)
3″	7.52 ("t", 7.3)	7.50 ("t", 7.6)	6.79 ("t", ~1.3)	7.48 (dd, 7.7, 5.0)
4″	7.64 ("t", 7.3)	7.64 ("t", 7.4)	—	8.36 (overlapping H-4′)
5″	7.52 ("t", 7.3)	7.50 ("t", 7.6)	8.20 ("t", ~1.2)	—
6″	8.08 (d, 8.0)	8.03 (d, 7.6)	—	9.31 (br s)
1-OAc	1.88 (s)	—	—	1.86 (s)
5-OAc	2.21 (s)	2.22 (s)	1.97 (s), 2.16 (s)	2.24 (s)
7-OAc	2.11 (s)	1.94 (s)		2.18 (s)
8-OAc	1.95 (s)	2.20 (s)	2.19 (s), 2.21 (s)	2.19 (s)
11-OAc	2.20 (s)	1.97 (s)		1.96 (s)1

Chromatography of the crude crystalline alkaloid mixture obtained from extracts of *T. wilfordii* afforded the previously reported alkaloids followed, in later fractions, by additional compounds, three of which could readily be separated by preparative thin-layer chromatography on silica gel. On the basis of its mass spectrum (*m/z* 841; $C_{41}H_{47}NO_{18}$), it was surmised that the most mobile of these (solvent system ethyl acetate – chloroform, 4:1) was a desacetylwilfordine. The relationship with wilfordine was confirmed when acetylation of the new compound yielded the parent alkaloid.

The proton NMR data and chemical shift assignments for wilfordine (cf. ref. 6, 9) and desacetylwilfordine are listed in Table 1. The assignments are based on ^{1}H–^{1}H shift correlation (COSY) experiments (10). The placement of the distinguishing unacetylated hydroxyl group of desacetylwilfordine at C-1, as in **8**, follows, *inter alia*, from the 1.16-ppm upfield shift of H-1 relative to its position in wilfordine.

The carbon-13 NMR data and chemical shift assignments are listed in Table 2. As expected, the carbon-13 spectra of wilfordine, **1**, and 1-desacetylwilfordine, **8**, are very similar; however, carbons 2 and 11 of wilfordine are significantly shielded in comparison with those of 1-desacetylwilfordine, whereas carbon 1 does not display the anticipated 2-ppm shift associated with acetylation (11). These observations suggest that a conformational change may occur in the B ring of wilfordine upon deacetylation at position 1, resulting in a partial release of steric compression.

The assignments of the hydrogen-bearing carbons were established by ^{1}H–^{13}C shift correlation (HCCOSY) experiments (12). Quaternary carbons were assigned by the COLOC (13) experiment, which allows proton–carbon correlations over two and three bonds. Thus the placement of the benzoate group at C-2 was confirmed by the detection of chemical shift correlations between the protons at δ_H 5.36 (H-2) and δ_H 8.03 (H-2″, H-6″) ppm and the carbonyl (C-22) at δ_C 165.88 ppm. The resonance at δ_C 172.19 ppm could be assigned to C-20 by a correlation to δ_H 5.14 ppm (H-3). This, in turn, allowed the assignment of δ_H 1.46 ppm to the 19-methyl group by an observed correlation to C-20. The positions and assignments of the acetate groups were also discernible by an analysis of the COLOC experiment. For example, the methyl carbon at δ_C 20.95 ppm was correlated with the methyl protons at δ_H 1.97 ppm by the HCCOSY experiment. The COLOC *F*1 trace at δ_C 169.47 ppm showed correlations with δ_H 1.97, 4.60 (H-11a), and 5.59 (H-11b) ppm, placing this acetate group at the C-11 position. Similarly, the other acetate groups could be assigned to positions C-5, C-7, and C-8, confirming the placement of the distinguishing hydroxyl group at C-1.

Thus, an analysis of the proton, carbon-13, COSY, HCCOSY, and COLOC spectra of wilfordine and 1-

Can. J. Chem. Downloaded from www.nrcresearchpress.com by 91.144.44.67 on 09/07/12
For personal use only.

TABLE 2. Carbon-13 NMR multiplicities and assignments[a]

Carbon	Alkaloid 1	8	9	10
1	73.20 (d)	72.94 (d)	72.65 (d)	73.34 (d)
2	69.25 (d)	73.50 (d)	72.65 (d)	70.69 (d)
3	76.86 (d)	76.49 (d)	76.46 (d)	75.76 (d)
4	69.78 (s)	69.72 (s)	69.65 (s)	69.71 (s)
5	73.60 (d)	73.76 (d)	73.67 (d)	73.57 (d)
6	51.04 (d)	50.79 (d)	50.88 (d)	51.15 (d)
7	68.93 (d)	69.40 (d)	69.25 (d)	68.89 (d)
8	70.78 (d)	72.38 (d)	71.98 (d)	70.32 (d)
9	51.89 (s)	51.35 (s)	51.66 (s)	52.06 (s)
10	94.01 (s)	93.64 (s)	93.77 (s)	93.79 (s)
11	60.57 (t)	62.63 (t)	61.88 (t)	60.30 (t)
12	22.98 (q)	23.61 (q)	23.19 (q)	23.03 (q)
13	84.77 (s)	84.79 (s)	84.68 (s)	84.53 (s)
14	17.88 (q)	17.90 (q)	17.91 (q)	18.02 (q)
15	69.78 (t)	69.72 (t)	69.71 (t)	70.58 (t)
16	31.42 (t)	31.07 (t)	31.11 (t)	32.62 (t)[b]
17	38.40 (t)	38.18 (t)	38.15 (t)	33.31 (t)
18	77.67 (s)	77.40 (s)	77.49 (s)	38.31 (d)
19	28.03 (q)	28.52 (q)	28.56 (q)	18.90 (q)
20	172.48 (s)	172.19 (s)	172.10 (s)	174.95 (s)
21	167.99 (s)	169.74 (s)	169.77 (s)	166.30 (s)
22	164.91 (s)	165.88 (s)	161.99 (s)	163.72 (s)
2′	152.23 (d)	152.03 (d)	152.21 (d)	152.23 (d)[b]
3′	120.58 (d)	120.71 (d)	120.60 (d)	121.64 (d)
4′	137.82 (d)	138.05 (d)	137.81 (d)	139.81 (d)[b]
5′	125.48 (s)	125.57 (s)	125.48 (s)	124.77 (s)
6′	164.77 (s)	164.22 (s)	164.44 (s)	163.90 (s)
1″	128.66 (s)	128.66 (s)	—	—
2″	129.85 (d)	129.76 (d)	144.41 (d)	151.03 (d)
3″	128.79 (d)	128.84 (d)	109.53 (d)	124.89 (d)
4″	133.86 (d)	133.99 (d)	118.22 (s)	137.46 (d)
5″	128.79 (d)	128.84 (d)	148.76 (d)	123.71 (s)
6″	129.85 (d)	129.76 (d)	—	154.03 (d)
1-Ac	20.50 (q), 169.84 (s)	—	—	20.50 (q), 169.85 (s)
5-Ac	21.57 (q), 169.83 (s)	20.95 (q), 169.78 (s)	21.11 (q), 170.02 (s)	21.60 (q), 169.31 (s)
7-Ac	20.99 (q), 170.13 (s)	20.66 (q),[c] 169.66 (s)[d]	20.70 (q), 169.86 (s)	21.03 (q), 170.10 (s)
8-Ac	20.45 (q), 168.97 (s)	21.54 (q),[c] 170.13 (s)[d]	21.53 (q), 170.11 (s)	20.50 (q), 169.02 (s)
11-Ac	20.99 (q), 170.06 (s)	20.95 (q), 169.47 (s)	20.99 (q), 168.02 (s)	21.14 (q), 170.39 (s)

[a]Multiplicities were determined by DEPT (14) experiments.
[b]Broadened lines.
[c,d]May be interchanged due to the proton chemical shift degeneracy of H-7 and H-8 (δ_H 5.60 ppm).

desacetylwilfordine resulted in a complete, unambiguous chemical shift assignment of all protons and carbons of these alkaloids, as well as providing confirmation of their structures.

The FAB mass spectrum of the second new alkaloid (m/z 832, $C_{39}H_{45}NO_{19}/H$; 95, C_5H_3O) was indicative of a desacetylwilfortrine, and the relationship between the new alkaloid and its known acetylated relative (6, 15) was confirmed by an acetylation experiment. Proton NMR data and chemical shift assignments for desacetylwilfortrine, based on comparison with the previously reported spectrum of wilfortrine (15) and confirmed by COSY experiments, are compiled in Table 1. Carbon-13 data are in Table 2.

The salient feature of the ^1H spectrum of desacetylwilfortrine is the 1.16-ppm upfield shift of the H-1 signal relative to its position in the spectrum of wilfortrine. Thus the unacetylated hydroxyl group is again at C-1, establishing the new compound as 1-desacetylwilfortrine, **9**.

The mass spectrum of the least mobile of the new alkaloids (m/z 868, $C_{42}H_{48}N_2O_{18}$) suggested that it might be 2-debenzoyl-2-nicotinoyl wilforine, **10**,[2] and this hypothesis was confirmed by ^1H and ^{13}C NMR analysis (cf. Tables 1 and 2). Proton NMR assignments were established by a COSY (10) experiment, while the carbon assignments were made by comparison with those of wilfordine. With the obvious exception of the nicotinoyl moiety, carbons 17, 18, and 19 of the macrocyclic ring, and the site of attachment at C-3, the NMR data for compound **10** are in excellent agreement with those of wilfordine. The analysis of the carbon-13 spectrum of **10** was complicated initially by the "fluctional" behavior of the macrocyclic ring in this molecule, which resulted in broadened lines for carbons 16, 2′, and 4′. Re-recording of the spectrum at temperatures of 35 and 40°C resulted in a progressive sharpening

[2]While this manuscript was in preparation, a paper came to our attention reporting the isolation of compound **10**, designated wilfornine, from *T. wilfordii* (16).

Can. J. Chem. Downloaded from www.nrcresearchpress.com by 91.144.44.67 on 09/07/12
For personal use only.

of these lines as the fast exchange limit was reached. The fluctionable behavior was not observed in wilfordine, 1-desacetylwilfordine, and 1-desacetylwilfortrine. Whereas this may reflect conformational changes that are too rapid to be observed on the NMR time scale, a more likely explanation may be that in **1**, **8**, and **9**, where R^4 = OH, hydrogen bonding involving this C-18 hydroxyl group locks the macrocyclic ring into a more rigid conformation.

Experimental

Melting points were determined on a hot-stage apparatus and are uncorrected. Infrared spectra were recorded on a Philips Pye Unicam PU9516 infrared spectrophotometer. FAB mass spectra were provided by Dr. A. Hogg, University of Alberta. Accurate mass measurements were made on a Kratos MS-50 instrument. All NMR spectra were recorded in $CDCl_3$ on a Varian XL-200 spectrometer operating at frequencies of 200.068 MHz for ^1H and 50.308 MHz for ^{13}C. Tetramethylsilane was used as an internal standard. The COSY and HCCOSY spectra were obtained using standard Varian software. COLOC spectra were recorded twice for compounds **1** and **8**, with constant evolution time period, T_1, values of 60 and 100 ms. The refocussing delay time, $\Delta 2$, was 30 ms. For each spectrum, 256 transients were recorded for each of 128 t_1 increments with a recycle delay time of 1 s/transient for a total experiment time of 14 h. The digital resolution was 0.06 and 0.09 ppm in F_1 and F_2, respectively.

Isolation of alkaloids

Air-dried roots of *T. wilfordii* were milled to a coarse powder. Powdered root material (5 kg) was moistened with 10% NH_4OH solution and then extracted with refluxing ether. The mixture, when cold, was filtered at the pump, and the residue was reextracted with ether four times. The combined extracts were reduced to a small volume *in vacuo*, and then washed four times with equal volumes of 2.5% HCl solution. The aqueous phase was adjusted to pH 9 by addition of concentrated NH_4OH solution, and the resulting precipitate was collected by filtration at the pump. The yield of crude amorphous alkaloidal material thus obtained was 13.0 g (0.26%). The white powdery alkaloid mixture was dissolved in hot methanol and the resulting solution, on standing for several days at ambient temperature, deposited crystals (10% of crude mixture).

The crystalline alkaloid mixture was chromatographed on a column of silica gel (100–120 mesh), using chloroform–acetone (4:1) as eluent.

Fractions displaying similar mobilities on TLC were pooled, and four groups of compounds were thus separated. Fractions 1–3, rechromatographed on a column of silica gel H (30–40 μm) under a pressure of 1.5 kg cm^{-2} with EtOAc–$CHCl_3$ (4:1) as eluent, afforded wilformine[3] (7). The second group, fractions 4–6, chromatographed on silica gel H (or G) (10–40 μm) under 1.5 kg cm^{-2} pressure with cyclohexane–acetone (3:2) as eluting solvent, yielded wilforine (5) and wilforgine (7). Rechromatography of the third group in the same manner produced wilforzine (7), wilfordine (4), and wilfortrine (6). The fourth group, fractions 28–29, was subjected to flash chromatography using EtOAc–$CHCl_3$ (3:2) as eluent, and yielded wilforidine[3] (9), plus a mixture of three new alkaloids, which were separated by preparative thin-layer chromatogrphy.

1-Desacetylwilfordine, obtained in a yield of 185 mg, melted at 182–184°C; IR ($CHCl_3$): *inter alia*, 3680, 3550, 3480, 3040, 3000, 2960, 1750, 1730, 1600, 1590, and 1570 cm^{-1}; ^1H and ^{13}C NMR, see text; mass spectrum (FAB, Cleland matrix): *inter alia*, *m/z* 842 $(MH)^+$, $(C_{41}H_{47}NO_{18}/H)^+$; 105 $(C_7H_5O)^+$, $(PhCO)^+$.

[3]All of the known alkaloids were identified by comparison of their physical and spectroscopic characteristics with those of authentic material, or with literature data.

1-Desacetylwilfortrine, obtained in a yield of 44 mg, melted at 179–182°C; IR ($CHCl_3$): *inter alia*, 3690, 3550, 3480, 3040, 2960, 1745, 1735 (sh), 1602, and 1572 cm^{-1}; ^1H and ^{13}C NMR, see text; mass spectrum (FAB, Cleland matrix): *inter alia*, *m/z* 832 (MH^+), $(C_{39}H_{45}NO_{19}/H^+)$; 95 $(C_5H_3O)^+$, $(Furan\text{-}3\text{-}CO)^+$.

2-Debenzoyl-2-nicotinoylwilforine, obtained in a yield of 20 mg, melted at 177–178°C; IR ($CHCl_3$): *inter alia*, 3680, 3530, 3450, 3040, 2980, 2960, 2880, 1745, 1735 (sh), 1590, and 1570 cm^{-1}; ^1H and ^{13}C NMR, see text; mass spectrum, (FAB, Cleland matrix): *inter alia*, 869 $(MH)^+$, $(C_{42}H_{48}N_2O_{18}/H)^+$;106 $(C_6H_4NO)^+$, $(Pyr\text{-}3\text{-}CO)^+$. Exact mass calcd. for $C_{42}H_{48}N_2O_{18}$: 868.2888; found: 868.2871.

Conversion of 1-desacetylwilfordine to wilfordine

A solution of 1-desacetylwilfordine (34 mg) in pyridine (1.5 mL) and acetic anhydride (0.15 mL) was stirred under anhydrous conditions at ambient temperature for 7 h. Additional acetic anhydride (1.5 mL) was then added and the mixture was set aside with stirring for a further 16 h. Work-up, followed by chromatography of the crude product on preparative layer silica gel plates with cyclohexane–acetone (3:2) as eluting solvent, afforded amorphous wilfordine (33 mg, 92%), Crystallization from methanol gave crystals, mp 174–177°C, identical in all respects with an authentic specimen of wilfordine. No depression of the melting point was observed on admixture with authentic wilfordine.

Conversion of 1-desacetylwilfortrine to wilfortrine

A solution of 1-desacetylwilfortrine (28 mg) in pyridine (1.5 mL) and acetic anhydride (0.5 mL) was stirred under anhydrous conditions at ambient temperature for 16 h.

Work-up and preparative layer chromatography on silica gel plates with EtOAc–$CHCl_3$ (4:1) as eluent afforded 25 mg (85%) of a product, mp 233–235°C, identical with an authentic specimen of wilfortrine. No depression of melting point was observed on admixture with authentic wilfortrine.

1. R. M. Smith. The alkaloids. Vol. 16. Academic Press, New York 1977.
2. S. M. Kupchan, R. M. Smith, and R. F. Bryan. J. Am. Chem. Soc. **92**, 6667 (1970).
3. J. Li. Yaoxue Tongbao, **20**, 101 (1985).
4. (a) Y. Shizuri, K. Yamada, and Y. Hirata. Tetrahedron Lett. 741 (1973); (b) K. Yamada, Y. Shizuri, and Y. Hirata. Tetrahedron, **34**, 1915 (1978).
5. D.-G. Wu, L. Liu, and K.-C. Chen. Acta Bot. Yunnanica, **3**, 471 (1981).
6. D.-G. Wu. Acta Bot. Yunnanica, **8**, 343 (1986).
7. Z.-S. He, Y. Li, S.-D. Fang, and S.-H. Hong. Acta Chim. Sin. **45**, 510 (1987).
8. K. Sugiura, K. Yamada, and Y. Hirata. Tetrahedron Lett. 113 (1973).
9. Z.-S. He, S.-H. Hong, Y. Li, H. Sha, and X.-G. Yu. Acta Chim. Sin. **43**, 593 (1985).
10. A. Bax, R. Freeman, and G. Morris. J. Magn. Reson. **42**, 164 (1981).
11. F. W. Wehrli and T. Nishida. Fortschr. Chem. Org. Naturst. **36**, 1 (1979).
12. A. Bax and G.A. Morris. J. Magn. Reson. **42**, 501 (1981).
13. H. Kessler, C. Griesinger, J. Zarbock, and H. R. Loosi. J. Magn. Reson. **57**, 331 (1984).
14. D. M. Doddrell, D. T. Pegg, and M.R. Bendell. J. Magn. Reson. **48**, 323 (1982).
15. Z.-S. He, Y. Li, S.-D. Fang, and S.-H. Hong. Acta Chim. Sin. **47**, 178 (1989).
16. F. Deng, J. Cao, Z. Xia, S. Lin, and Z. Wang. Zhiwu Xuebao, **29**, 523 (1987); Chem. Abstr. **108**, 87738S (1988).

Can. J. Chem. Downloaded from www.nrcresearchpress.com by 91.144.44.67 on 09/07/12
For personal use only.

Flash photolysis production of the tetrahedral intermediate of the methanolysis of methyl benzoate. Direct measurement of the rate of breakdown of the conjugate base form

ROBERT A. MCCLELLAND,[1] V. M. KANAGASABAPATHY, AND STEEN STEENKEN
Department of Chemistry, University of Toronto, Toronto, Ont., Canada M5S 1A1
and
Max-Plank-Institut für Strahlenchemie, D-4330 Mulheim–Ruhr, West Germany

Received May 30, 1989

Can. J. Chem. Downloaded from www.nrcresearchpress.com by 91.144.44.67 on 09/07/12
For personal use only.

ROBERT A. MCCLELLAND, V. M. KANAGASABAPATHY, and STEEN STEENKEN. Can. J. Chem. **68**, 375 (1990).

Laser flash photolysis in aqueous basic solutions of the ortho acid derivatives 1-(phenyldimethoxymethyl)benzimidazole **2** and 4-bromo-1-(phenyldimethoxymethyl)imidazole **3** results in production of the phenyldimethoxymethyl cation, which has λ_{max} at 260 nm. The cation decays in reactions with water ($k = 9.9 \times 10^4\ s^{-1}$) and hydroxide ion ($2.5 \times 10^8\ M^{-1}\ s^{-1}$) to finally yield methyl benzoate, whose formation was monitored at 234 nm. In solutions with pH 10–12, rate constants measured at this wavelength are the same as those obtained at 260 nm, but with pH >13 and pH <9, rate constants at 234 nm are smaller. With pH 9–10 and pH 12–13, single exponential kinetics are not observed at 234 nm. This behavior is interpreted in terms of a scheme where at each pH there are two consecutive first-order reactions, cation → phenyldimethoxyhydroxymethane (**5**) → ester, and the pH dependencies of the rate constants are such that they cross twice over the pH range of this study. The intermediate **5** is the tetrahedral intermediate formed in the methanolysis of methyl benzoate, and the 234-nm buildup at pH >13 and pH <9 directly measures its breakdown. At pH >13 the rate constant is independent of pH with $k = 9 \times 10^6\ s^{-1}$. This represents the rapid expulsion of methoxide from the conjugate base of **5**. At pH <9 the rate constants are proportional to hydroxide ion concentration, with $k_{OH^-} = 7.5 \times 10^9\ M^{-1}\ s^{-1}$. In these solutions the neutral intermediate predominates and the dependence on [OH^-] of its rate of conversion to ester is interpreted in terms of breakdown of the anion and protonation of this species by water occurring at comparable rates. Thus, k_{OH^-} represents a situation where there is partial rate-limiting deprotonation of the neutral intermediate by hydroxide. The intermediate of this study bears a close resemblance to the tetrahedral intermediate of the hydrolysis of methyl benzoate. The observation that the anionic forms of such intermediates undergo breakdown at rates similar to those associated with the establishment of proton transfer equilibrium explains why the ester undergoes carbonyl oxygen exchange in base at a rate slower than hydrolysis.

Key words: tetrahedral intermediate, flash photolysis, ester hydrolysis.

ROBERT A. MCCLELLAND, V. M. KANAGASABAPATHY et STEEN STEENKEN. Can. J. Chem. **68**, 375 (1990).

La photolyse éclair au laser de solutions basiques aqueuses de dérivés d'ortho acides (1-(phényldiméthoxyméthyl)-benzimidazole **2** et 4-bromo-1-(phényldiméthoxyméthyl)imidazole **3**), conduit à la formation du cation phényldiméthoxy-méthyle qui présente un λ_{max} à 260 nm. Le cation se décompose par réaction avec l'eau ($k = 9{,}9 \times 10^4\ s^{-1}$) et l'ion hydroxyde ($2{,}5 \times 10^8\ M^{-1}\ s^{-1}$) pour donner finalement du benzoate de méthyle dont on détermine la formation en suivant la progression de la bande à 234 nm. Dans des solutions dont le pH varie de 10 à 12, les constantes de vitesse telles que mesurées à cette longueur d'onde sont identiques à celles que l'on obtient à 260 nm; toutefois, à des pH >13 ou <9, les constantes de vitesse évaluées à 234 nm sont plus faibles. À 234 nm et à des pH de 9 à 10 ou de 12 à 13, on n'observe pas de cinétiques exponentielles uniques. On interprète ce comportement en fonction d'un schéma selon lequel il existe, pour chaque pH, deux réactions consécutives du premier ordre : cation → phényldiméthoxyhydroxyméthane (**5**) → ester, et les variations des constantes de vitesse en fonction du pH sont telles qu'elles se coupent deux fois sur la plage de pH examinée au cours de cette étude. Le composé **5** correspond à l'intermédiaire tétraédrique qui se forme lors de la méthanolyse du benzoate de méthyle et l'accumulation observée à 234 nm, pour des pH >13 ou <9, mesure directement sa décomposition. À un pH >13, la constante de vitesse est indépendante du pH et $k = 9 \times 10^6\ s^{-1}$. Cette valeur représente une expulsion rapide du méthylate à partir de la base conjuguée du composé **5**. À des pH <9, les constantes de vitesse sont proportionnelles à la concentration en ion hydroxyde et $k_{OH^-} = 7{,}5 \times 10^9\ M^{-1}\ s^{-1}$. Dans ces solutions, l'intermédiaire neutre prédomine et on interprète la relation qui existe entre la concentration en ions OH^- et sa vitesse de conversion en ester en fonction de deux réactions compétitives, soit une décomposition de l'anion et une protonation de cette espèce par l'eau, qui se produiraient à des vitesses comparables. Ainsi, le k_{OH^-} représenterait une situation dans laquelle il existerait une déprotonation partielle de l'intermédiaire neutre par l'ion hydroxyde qui limiterait la vitesse de la réaction. L'intermédiaire observé au cours de cette étude ressemblerait beaucoup à l'intermédiaire tétraédrique impliqué au cours de l'hydrolyse de benzoate de méthyle. L'observation que les formes anioniques de tels intermédiaires subissent des décompositions à des vitesses semblables à celles associées avec l'établissement d'un équilibre de transfert protonique explique pourquoi, en milieu basique, l'ester subit un échange de l'oxygène du carbonyle à une vitesse inférieure à celle de l'hydrolyse.

Mots clés : intermédiaires tétraédriques, photolyse éclair, hydrolyse des esters.

[Traduit par la revue]

Hemiorthoesters **1** are the tetrahedral intermediates of ester interchange reactions (R′ = alkyl), and obviously bear a close relationship to tetrahedral intermediates of ester hydrolysis (R′ = H).

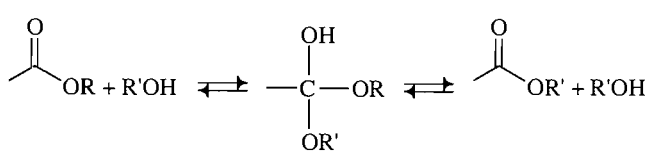

1

[1]Author to whom correspondence may be addressed.

Can. J. Chem. Downloaded from www.nrcresearchpress.com by 91.144.44.67 on 09/07/12
For personal use only.

The same intermediates **1** are also encountered in the three-stage hydrolysis of ortho esters and appropriate derivatives, arising from the hydration of an initially formed dialkoxycarbocation.

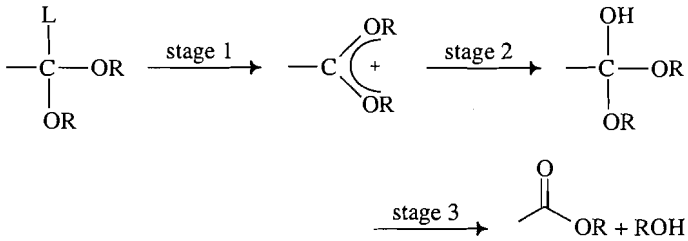

These latter systems have the interesting feature that with some derivatives, under some conditions, stage 3 has been found to be the slowest step in the overall reaction (1–3). When this occurs, the hemiorthoester **1** actually accumulates and can be observed, and rate constants for its breakdown to the final products can then be directly measured. Such kinetic information is normally unobtainable from an investigation of the appropriate ester interchange reaction, where only immeasurably small stationary state concentrations of the tetrahedral intermediate are formed.

For **1** to accumulate it is necessary that both stage 1 and stage 2 in the reaction sequence be faster than stage 3. Stage 2, the hydration of the dialkoxycarbocation, is normally fast (4–6). There is, however, an efficient base catalysis of stage 3, while stage 1 usually occurs only with acid catalysis. The consequence is that, regardless of the relative rates of stage 1 and stage 3 in acidic solutions, stage 1 is invariably the slowest step in neutral and basic solutions and, in such solutions, kinetic information for the hemiorthoester decomposition can no longer be obtained.

One way of overcoming the problem of the slow first stage would be to have this reaction occur photochemically, thus providing a rapid entry into stages 2 and 3, whose kinetic behavior could then be monitored using the technique of laser flash photolysis. We have recently described experiments involving short-lived carbenium ions being generated by photoheterolysis and photoprotonation (7–10), and dialkoxycarbocations being generated by radical cation fragmentation (6). With the latter system we recognized that the immediate product of the reaction of the cation with water was a hemiorthoester, and wondered whether it might be possible to find conditions to study its decomposition. In this paper we report such an investigation, from the photolysis of the ortho ester derivatives **2** and **3**. These compounds undergo a photoheterolysis, generating as an observable intermediate the phenyldimethoxymethyl cation **4**. Hydration of this produces the hemiorthoester **5**,

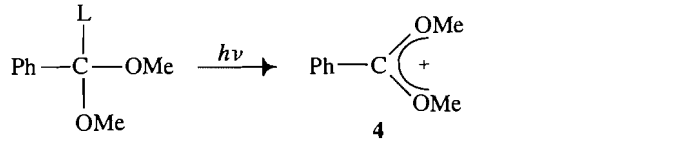

4

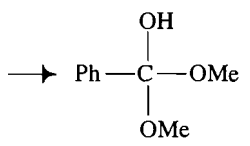

5

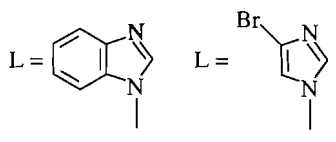

2 3

whose decomposition can be followed even under strongly basic conditions where it exists in its conjugate base anionic form.

Experimental

Substrates

The ortho ester derivatives **2** and **3** were prepared by the reaction of a two- to threefold excess of trimethyl orthobenzoate with benzimidazole and 4(5)-bromoimidazole. The mixture was stirred at 120°C for 6 h, with the methanol that was released in the reaction being allowed to distil off. After cooling to 40–50°C the mixture was evacuated to 0.1 Torr (1 Torr = 133.3 Pa) to remove excess trimethyl orthobenzoate. Compound **2** was purified by column chromatography on neutral alumina, eluting progressively with diethyl ether in hexanes; **2** had mp 90–92°C; ^{1}H NMR ($CDCl_3$) δ: 3.25 (s, 6H), 7.1–7.8 (m, 9H), 8.55 (s, 1H); mass spectrum, *m/e*: 268 (M^+, 2%), 237 ($M^+ - OCH_3$, 5%), 151 ($PhC(OCH_3)_2^+$, 100%), 105 ($PhCO^+$, 23%). Anal. calcd. for $C_{16}H_{16}N_2O_2$: C 71.62, H 6.01; found: C 72.03, H 6.16. Compound **3** was purified by column chromatography on alumina, eluting progressively with ethyl acetate in hexanes; **3** had mp 81–83°C; ^{1}H NMR ($CDCl_3$) δ: 3.19 (s, 6H), 6.87 (d, J = 1.3 Hz, 1H), 7.35–7.5 (m, 5H), 7.72 (d, J = 1.3 Hz, 1H); ^{13}C NMR δ: 49.2, 106.3, 115.6, 116.3, 126.4, 128.6, 129.7, 135.5, 137.5; mass spectrum, *m/e*: 265/267 ($M^+ - OCH_3$, 1.4%), 151 ($PhC(OCH_3)_2^+$, 100%), 136 ($PhCOOMe^+$, 12.5%), 105 ($PhCO^+$, 34%). Anal. calcd. for $C_{12}H_{13}BrN_2O_2$: C 48.50, H 4.41, N 9.43; found: C 48.65, H 4.47, N 9.43. The reaction conditions and spectral and analytical data are consistent with the structure **3** as written above or with the isomer with the bromine attached to the 5-position in the imidazole ring. The two possibilities cannot be distinguished with the data available; we favor the 4-bromo isomer on steric grounds.

Flash photolysis experiments

Aqueous solutions were prepared with water from a Millipore-Q system, with the pH adjusted by the addition of sodium hydroxide (pH >9.5) or 1 mM borate buffer (pH <9.5). Stock solutions with concentration ~ 1 M of the substrates in acetonitrile were prepared. The appropriate volume to give a final concentration of 0.1 mM substrate was added to the aqueous solution shortly before irradiation and the pH recorded. Photolyses were carried out with ~20 ns pulses of 248 nm light (KrF) from a Lambda Physik EMG 103 MSC excimer laser. Descriptions of the detection and analyzing systems have been given elsewhere (7).

Results

Figure 1 shows absorption spectra recorded in 0.001 M NaOH after laser photolysis of the substrate **3**. Immediately after the flash there appeared two bands, one centered at 300 nm and a second at 260 nm. Although these decayed at approximately the same rate in the solution employed in generating Fig. 1, they must be due to different transient species, since the decay at 300 nm was markedly accelerated by oxygen while there was no effect at 260 nm. We have not identified the 300 nm transient, since this is not the one of interest, and its decay did not interfere with our desired kinetic studies. The quenching by oxygen implies that it is a radical, or possibly a triplet. One possibility is that it is a radical derived from homolysis of the carbon–bromine bond. A piece of evidence that is at least consistent with this explanation is that this transient was not observed with the benzimidazole derivative **2**, where there is no bromine.

The 260 nm transient, on the other hand, can be identified as the phenyldimethoxymethyl cation **4**. An authentic spectrum of this ion obtained by the addition of trimethyl orthobenzoate to concentrated sulfuric acid is shown in Fig. 2. In this solution **4** is formed from the ortho ester and is stable to further reaction (4, 11); it can be unambiguously identified by ^{1}H and ^{13}C NMR spectroscopy (4, 12). Decay of the transient cation followed good exponential kinetics, with the rate constant unchanged in

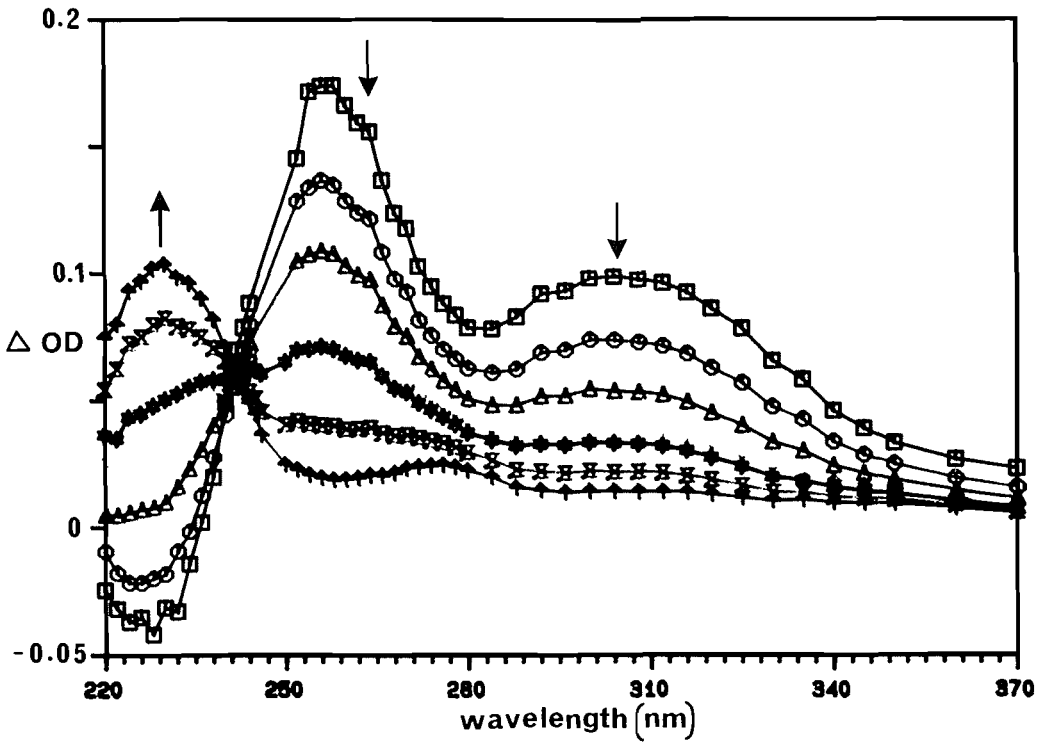

FIG. 1. Transient absorption spectra following 248-nm excitation of the bromoimidazole amide acetal **3** in argon-saturated 0.002 M sodium hydroxide. Spectra were recorded in the windows 200–300 ns, 1.2–1.6 μs, 2.4–2.8 μs, 5.6–6.0 μs, 9.6–10 μs, and 36–40 μs after the flash. The arrows indicate the direction of the change in optical density with time.

Can. J. Chem. Downloaded from www.nrcresearchpress.com by 91.144.44.67 on 09/07/12
For personal use only.

oxygen-saturated solutions, but dependent on the concentration of hydroxide ion.

Also apparent from Fig. 1 is that immediately after the laser pulse there was a negative signal in the region around 230 nm, arising from bleaching of the precursor that absorbs in this region. However, as the cation decayed, an absorbance built in, and after disappearance of the cation there was a net positive signal. This absorbance was permanent and can be assigned to methyl benzoate, the final product of the reaction of the cation. For comparison, the spectrum of this ester in water is shown in Fig. 2. The ester also has absorbance at ~280 nm and this could also be seen at long times in the photolysis experiments. One further comment about Fig. 1 is that in this particular solution the exponential increase at 230 nm had the same rate constant as that for the decrease at 260 nm, and there was a good isosbestic point at 242 nm. As will be discussed, such behavior was not always observed.

An identical pattern, a transient at 260 nm whose decay was matched by an increase in absorbance at 230 nm, was also observed with **2**. This precursor obviously must give the same cation as **3**, and the kinetic behavior with the two compounds was identical. As noted above, the benzimidazole derivative gave none of the second transient at longer wavelength. However, for the purpose of the detailed kinetic studies described below, **3** was preferred since it was more soluble in 100% aqueous solution. It should also be noted that there was ground state hydrolysis with both compounds. As discussed previously in kinetic studies of the hydrolysis of imidazole amide acetals of this type (13, 14), this occurs by reversible protonation of the imidazole or benzimidazole ring, and at high pH (> ~7) the rate constant is proportional to H^+ concentration. The consequence of this hydrolysis is that flash photolysis experiments could only be carried out at high pH where the substrates were reasonably stable, the limits being pH >9 with **2** and pH >7.5 with **3**.

Our other method for generating dialkoxycarbocations involved C—C fragmentation of photochemically generated radical cations (6). The cation **4** has been studied by this method, using the acetal precursor shown below, and decay rate constants agree well with those obtained from the two heterocyclic precursors.

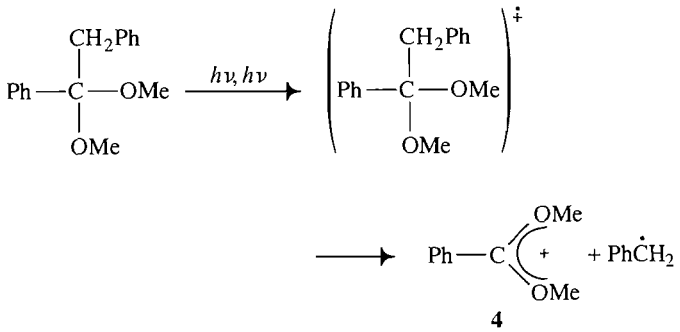

4

The mechanism for the formation of **4** from the heterocyclic systems appears to involve a straightforward photoheterolysis (15, 16). This means that the final products are methyl benzoate (and methanol) and the N-1 unsubstituted heterocycle. This point was established for the benzimidazole derivative **2** by photolysis at 254 nm in a Rayonet reactor in a solution in 0.001 M sodium hydroxide. After photolysis appeared complete, as judged by the observation of no further change in the UV spectrum of the solution, the pH was adjusted to 7, and the solution was extracted with methylene chloride. After separation and removal of the organic solvent, a 200 MHz ^{1}H NMR spectrum was recorded, showing only the signals of methyl benzoate and benzimidazole.

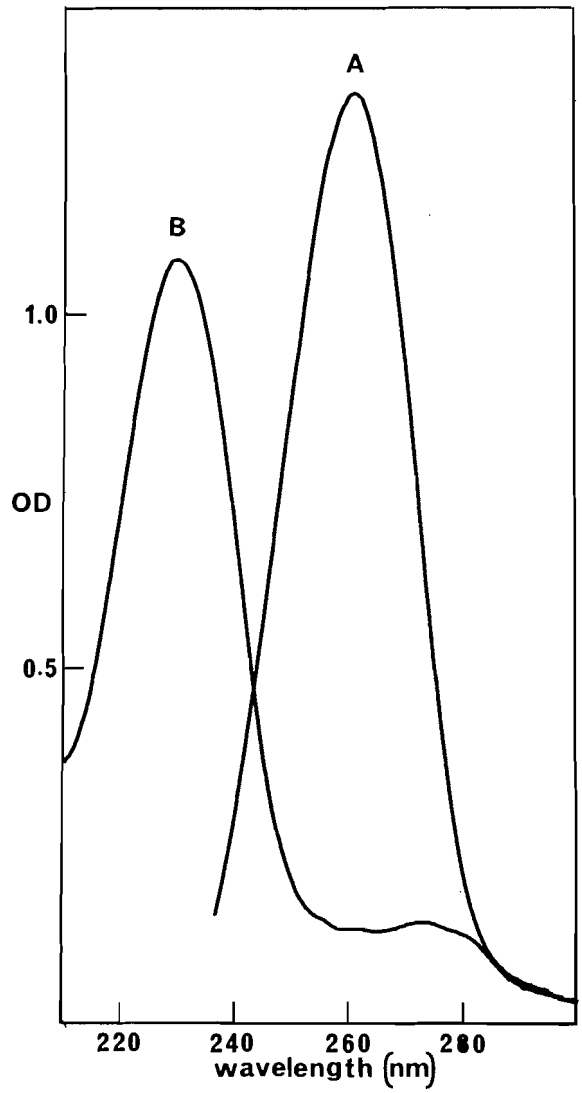

FIG. 2. Absorption spectra of 0.1 mM solutions of (A) trimethyl orthobenzoate (phenyldimethoxymethyl cation **4**) in 96% H_2SO_4 and (B) methyl benzoate in water.

A flash photolysis experiment with time-resolved AC conductivity detection corroborates the mechanistic conclusion. In this experiment **2** was photolyzed in 0.0001 M aqueous sodium hydroxide. A rapid conductivity increase, occurring within the resolution of the conductance method, was observed, followed by a slower exponential decrease to the original conductivity level, the latter occurring with the same rate constant as measured at 260 nm in this solution using optical detection. The initial increase represents the formation of the two ions, with the benzimidazole anion (pK_a of benzimidazole is ~12 (17)) then being rapidly protonated by water to give hydroxide. Reaction of the cation then consumes the hydroxide and the conductivity returns to its original level.

A mechanism that is not excluded by either the product or conductivity results involves nitrogen protonation in the excited state, followed by C—N bond breaking to give the cation and the neutral heterocycle. There is substantial evidence that heterocyclic compounds in the singlet excited state are considerably more basic than in their ground state (18).

Figure 3 summarizes rate constants, obtained mainly with **3**, measured following the decay in absorbance at 260 nm, and the increase at 234 nm. At the higher wavelength, good exponential kinetics were seen in all solutions, with the rate constants independent of pH below pH 10, and increasing at higher pH until at pH >13 the decay was complete within the laser flash and could not be observed. In these very basic solutions, however, the increase at 234 nm was still seen. (This rules out the possibility that the photoheterolysis does not occur at high pH as an explanation for the failure to observe the 260 nm decay.) The 234 nm increase at high pH was very rapid, with rate constants, within experimental error, constant. On decreasing pH the 234 nm traces went through a region centered around pH 12.5 where good exponential behavior was not observed. This was followed by an extended region (pH 10–12) where reasonable exponential behavior was again seen, with rate constants within experimental error identical to those measured at 260 nm. A second non-exponential region, this time centered around pH 9.5, then followed. Finally at low pH (<8.8) good exponential behavior was again observed, with the rate constants measured at 234 nm smaller than those measured at 260 nm. Representative kinetic traces are shown in Fig. 4.

Discussion

Kinetic analysis

The kinetic behavior can be described by a system where at each pH there are two consecutive first-order reactions, with the neutral and conjugate base forms of the hemiorthoester as intermediate species.

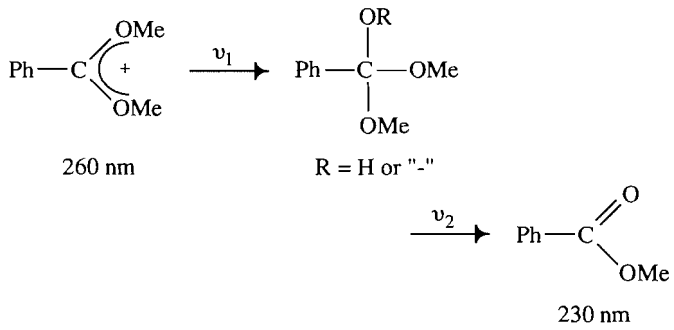

The equations relating concentration and time for this general kinetic system are well established (19). Under all conditions the disappearance of the starting material is expected to follow exponential kinetics, as is observed here at 260 nm, with a first-order rate constant equal to the rate constant of the first step. With this system this is the parameter υ_1 of the above equation. This constant does vary with pH since both solvent and hydroxide ion can act as nucleophiles. Rate constants for these two reactions are $9.9 \times 10^4\ s^{-1}$ and $2.5 \times 10^8\ M^{-1}\ s^{-1}$ respectively. (The water rate constant was calculated as the average value of the observed rate constants in solutions with pH <9.5. The hydroxide ion rate constant was obtained from linear regression of k_{obs} versus $[OH^-]$ in solutions with pH <12.3. The k_{obs} values for cation decay in solutions with higher pH show small negative deviations from this line, but this can be ascribed to an ionic strength effect.)

The equation for the appearance of product is more complex, taking the form of a double exponential (19). Single exponential behavior is, however, found when there are significant differences in the magnitudes of υ_1 and υ_2, in which case product forms in a first-order fashion with a rate constant equal to that of the slower process. Using idealized concentration–time data calculated with the appropriate equation (19), we found that a factor of 5 difference in υ_1 and υ_2 was sufficient to produce a

Can. J. Chem. Downloaded from www.nrcresearchpress.com by 91.144.44.67 on 09/07/12
For personal use only.

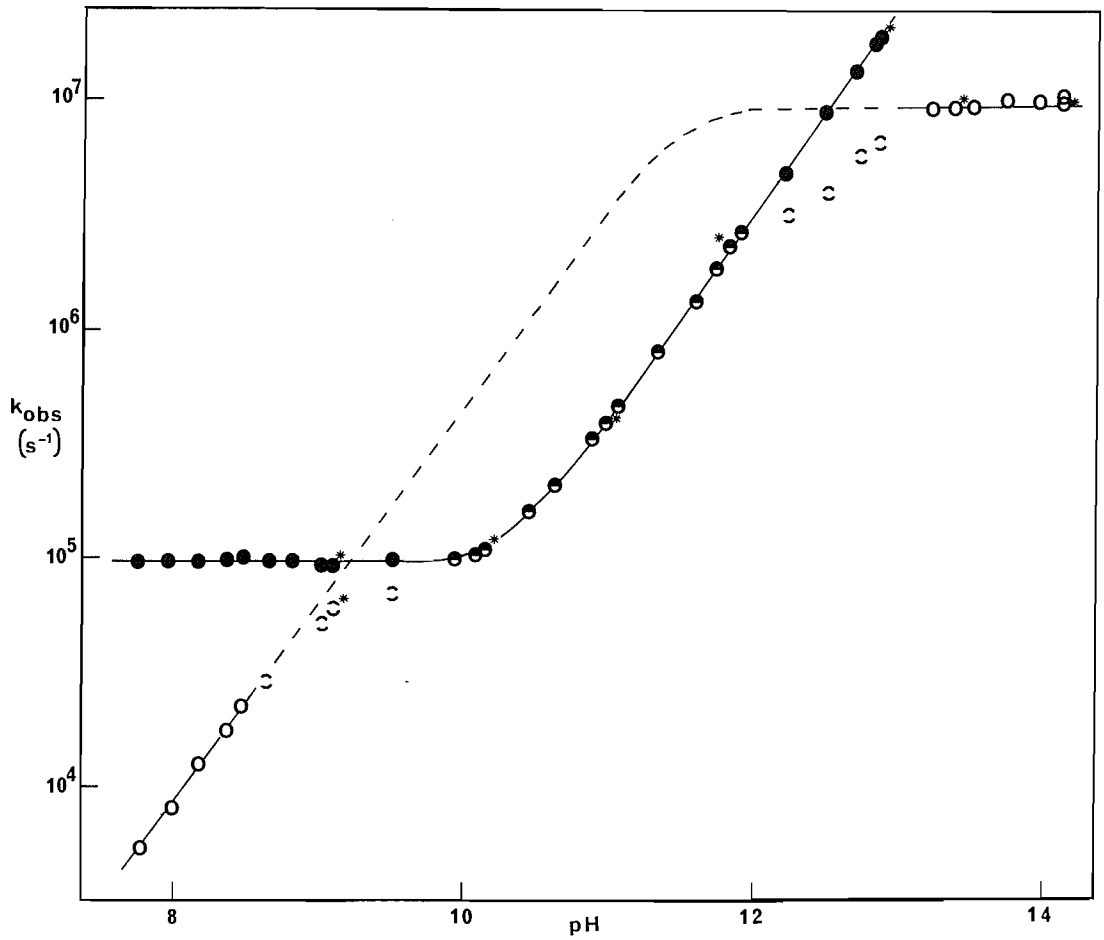

FIG. 3. First-order rate constants measured at 260 nm and 234 nm following laser photolysis of the bromoimidazole amide acetal **3**. Explanation of symbols: (●) monitoring exponential decay at 260 nm; (◓) monitoring exponential decay at 260 nm and exponential rise at 234 nm. In these solutions rate constants measured at 234 nm are within 5% of rate constants measured at 260 nm. (○) monitoring exponential rise at 234 nm. In these solutions reasonable exponential behavior is observed at this wavelength, but the rate constants are smaller than those measured at 260 nm. (◌) monitoring the rise at 234 nm, but poor adherence to single exponential behavior (see Fig. 4). Rate constant given in figure as (◌) was obtained from single exponential fit to data. Points indicated with an asterisk were obtained with the benzimidazole amide acetal **2**. The curve through the 260-nm points represented by both the symbols (●) and (◓) has the formula $(9.9 \times 10^4) + (2.5 \times 10^8)[OH^-]$. The curve through the 234-nm points represented by the symbol (○) has the formula $(9.0 \times 10^6)[OH^-]/(1.2 \times 10^{-3} + [OH^-])$.

reasonable fit to a single exponential, with the first-order rate constant within 10% of the smaller of υ_1 and υ_2.

Thus when $\upsilon_1 < \upsilon_2$, the situation which exists here between pH 10 and 12, rate constants measured for product appearance are υ_1, the same number as are obtained following reactant disappearance. In these solutions the hemiorthoester is reacting faster than it is formed, and it does not accumulate, at least to any significant extent. When $\upsilon_1 > \upsilon_2$, however, product appearance and reactant disappearance are uncoupled, the intermediate must accumulate during the reaction, and the rate constant measured following product appearance is υ_2. The indicator of such behavior is that the ester forms more slowly than the cation disappears. This is obviously then the situation at both very high pH and at neutral pH. As shown by the curves drawn in Fig. 3, the pH dependencies of υ_1 and υ_2 are such that the two cross twice in the region pH 7 – pH 14. In the crossover regions, where the two constants are similar in magnitude, single exponential behavior in product appearance is not observed, as is demonstrated in Fig. 4D. In such solutions the rate constants measured by forcing a single exponential on the data have no significance, being smaller than both υ_1 and υ_2. In principle, the absorbance–time data in the crossover regions could have been fit using multiple regression analysis to the double exponential expression. In practice we found that this procedure was not very satisfactory, the values of the two constants not agreeing particularly well with those estimated by extrapolation from the regions where single exponential kinetics were observed. The problem of a multiparameter fit to a curve where there is a single monotonic change has been noted in a review of computer methods of kinetic analysis (20). It can also be noted that the intermediate is not observed, since it is not expected to have a significant absorbance above 220 nm. For example trimethyl orthobenzoate, an appropriate model, has only a weak absorbance with λ_{max} ~260 nm and extinction coefficient ~400. The cation and ester have extinction coefficients on the order of 10^4, and their spectral changes therefore dominate.

Hemiorthoester breakdown

The two regions with the condition $\upsilon_1 > \upsilon_2$ provide a direct measure of the rate of decay of the hemiorthoester to product. These show different types of behavior: at pH >13, the reaction being independent of pH, with a rate constant of 9×10^6 s^{-1}; and at pH <9, the reaction being first order in hydroxide

Can. J. Chem. Downloaded from www.nrcresearchpress.com by 91.144.44.67 on 09/07/12
For personal use only.

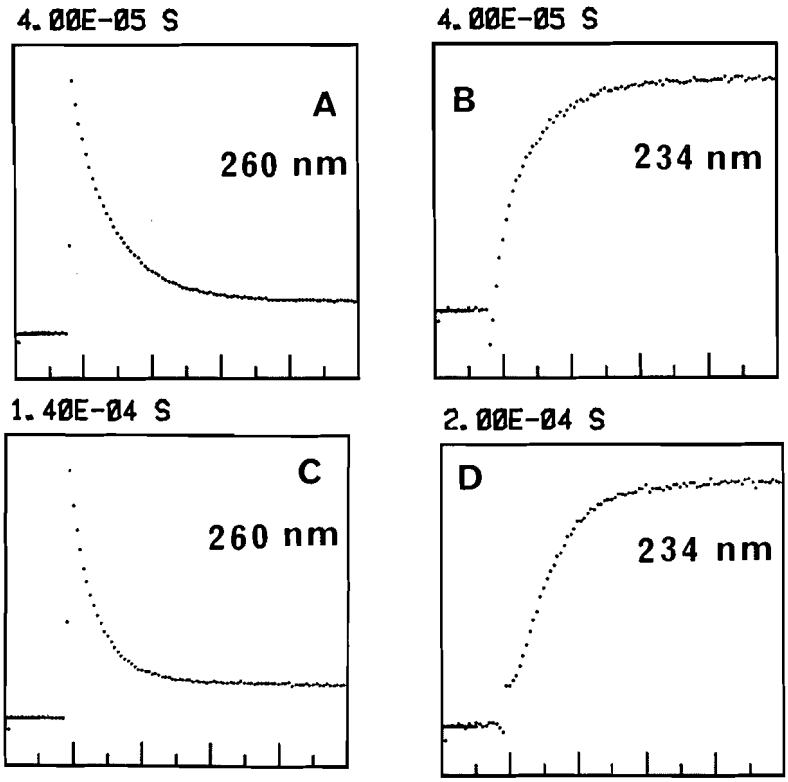

FIG. 4. Changes in optical density with time at 260 nm (A, C) and 234 nm (B, D) following 248-nm photolysis of **3** in aqueous solutions with pH = 10.7 (A, B) and 9.1 ((C, D). Traces A and B are exponential, with rate constants $2.09 \times 10^5\ s^{-1}$ and $2.15 \times 10^5\ s^{-1}$ respectively. Trace C is also exponential with a rate constant of $9.6 \times 10^4\ s^{-1}$. Trace D cannot be fit with a single exponential. The number indicated at the top of each trace is the time for the full range.

ion concentration, rate = k_{OH^-}[hemiorthoester][OH^-], with a second-order rate constant k_{OH^-} of $7.5 \times 10^9\ M^{-1}\ s^{-1}$.

The mechanism normally accepted for the hydroxide ion mediated decomposition of hemiorthoesters involves deprotonation to its conjugate base, followed by expulsion of alkoxide (1–3).

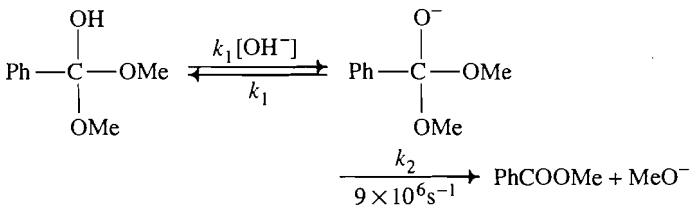

The pH independent reaction that is observed at high pH must therefore represent a situation where the anion predominates in the initial equilibrium reaction, and what is being measured is the breakdown of this species. With the high concentrations of hydroxide ion that are present in these solutions, it is not unreasonable that an initially formed neutral hemiorthoester will deprotonate very rapidly (see later). Hydroxide ion addition to the cation to form this neutral adduct is also rapid, as seen in the failure to observe the cation when [OH^-] > 0.1 M. What is present therefore after the 20-ns laser pulse is the anionic hemiorthoester, and what is observed kinetically is the breakdown of this species by expulsion of methoxide ion. Thus the pH-independent rate constant observed at high pH is equal to k_2 of the above reaction.

The interpretation normally made of the OH^--dependent reaction at lower pH is that the neutral hemiorthoester predominates in the deprotonation equilibrium, and there is rate-limiting breakdown of the anionic species present in small quantities in the equilibrium. According to such a mechanism, the observed k_{OH^-} is equal to k_2K_a/K_w, where K_a is the acidity constant for the neutral intermediate and K_w is the autoprotolysis constant of water. Unlike the situation in most investigations, k_2 is known from the high pH data, so that with this interpretation the acidity constant can actually be calculated, as 11.08 (as the pK_a value).

This number for the acidity constant of a tetrahedral intermediate is reasonable. For example, Guthrie and Cullimore (21), using a linear free energy equation originally suggested by Hine and Koser (22) based upon data for carbonyl hydrates, have estimated the pK_a of $PhC(OH)_2OMe$ to be 11.01. For $PhC(OMe)_2OH$ itself, an alternative relationship of Fox and Jencks (23), with a simple alcohol as a starting point, provides a pK_a value of 10.90. Moreover there is a measured value of 10.4 for the more stable derivative 2-hydroxy-2-(4-nitrophenyl)-4,4,5,5-tetramethyl-1,3-dioxolane (24).

However, a closer examination reveals that the assumption of a rapid equilibrium of the neutral and ionic forms of the hemiorthoester cannot be correct. This equilibrium at basic pH will have deprotonation with hydroxide ion, while the microscopic reverse protonation will occur with solvent water molecules as the acid. The equation relating the acidity constant to the individual rate constants is therefore $K_a = k_1K_w/k_{-1}$. With p$K_a \sim 11$, the deprotonation with hydroxide ion is the reaction in the thermodynamically favored direction, and k_1 must be of the order of $10^{10}\ M^{-1}\ s^{-1}$, and $k_{-1} \sim 10^7\ s^{-1}$. This, however, means that k_2 and k_{-1} are of the same order of magnitude, and the condition is not obeyed that is required for a

Can. J. Chem. Downloaded from www.nrcresearchpress.com by 91.144.44.67 on 09/07/12
For personal use only.

TABLE 1. Values of constants for the equilibrium of the hemiorthoester $PhC(OMe)_2OH$ with its conjugate base, which satisfy the experimental parameters k_2 (at high pH) = 6×10^9 s^{-1} and $k_{OH} = 7.5 \times 10^9$ M^{-1} s^{-1} and the assumption of a stationary state in the hemiorthoester anion at low pH

pK_a	k_1, M^{-1} s^{-1}	k_{-1}, s^{-1}
10.20	8.6×10^9	1.4×10^6
10.40	9.5×10^9	2.4×10^6
10.60	1.1×10^{10}	4.5×10^6
10.80	1.6×10^{10}	1.0×10^7
10.90	2.2×10^{10}	1.8×10^7
11.00	4.5×10^{10}	4.5×10^7
11.05	1.2×10^{11}	1.3×10^8
11.07	3.4×10^{11}	4.2×10^8
11.08	-4×10^{12}	

rapid pre-equilibrium, namely that k_2 be significantly smaller than k_{-1}. A further indication of the inconsistency of the pre-equilibrium assumption is that the observed k_{OH^-} is of the same order of magnitude as the value expected for k_1, the rate constant for deprotonation with hydroxide ion.

In consequence, this system at lower pH must be treated by making a stationary state assumption in the hemiorthoester anion, leading to the equation

$$\text{Rate} = \left(\frac{k_1 k_2}{k_{-1} + k_2}\right)[\text{hemiorthoester}][OH^-]$$

where the experimentally observed k_{OH^-}, 7.5×10^9, is given by the term in parentheses. Although the individual k_1, k_{-1}, and K_a values cannot be obtained, only one of these is independent, since k_2 is known from the high pH data. Possible combinations of these three constants that satisfy the experimental parameters are given in Table 1. It can be noted that there is an upper limit on pK_a of 11.07 which satisfies the data; higher values require negative values for k_1 and k_{-1}. A pK_a value of 10.5–11.0 seems to most reasonably fit the data, and at the same time to satisfy the previous estimates and determinations of the acidity of tetrahedral intermediates. Eigen lists a rate constant of 1.4×10^{10} M^{-1} s^{-1} for the reaction of hydroxide ion with phenol (25), an OH acid whose acidity is not dissimilar to the one of this study. Such a value for k_1 requires a pK_a value of 10.75.

Despite the uncertainty in the magnitudes of these constants, it can be concluded that decomposition of the hemiorthoester anion competes with protonation by water, and, starting from neutral hemiorthoester, deprotonation by hydroxide ion is partially rate limiting in the breakdown to products. Such a conclusion has been reached previously with other tetrahedral adducts (14, 26–28), based upon examinations of the effects of catalyzing buffers, or observations of k_{OH^-} values approaching 10^{10} M^{-1} s^{-1}. The novel feature of this study is the direct determination of the rate constant for the breakdown of the anion, with this demonstration that this process is very fast.

Comparison with hydrolysis of methyl benzoate

The hemiorthoester of this study bears a close resemblance to the tetrahedral intermediate formed in the hydrolysis of methyl benzoate. The mechanistic tool introduced by Bender to identify the intermediacy of tetrahedral adducts in the hydrolysis of acyl derivatives involved the demonstration of carbonyl oxygen exchange in unreacted starting material isolated after partial hydrolysis (29, 30). Alkyl benzoates do undergo such exchange, during both their acid and base hydrolysis (29, 31, 32). However, a careful reexamination of the latter has shown that hydrolysis dominates, the k_{hyd}/k_{ex} ratio for methyl benzoate in 100% water being 28, with the ratio increasing as dioxane is added (32). As seen in the mechanism,

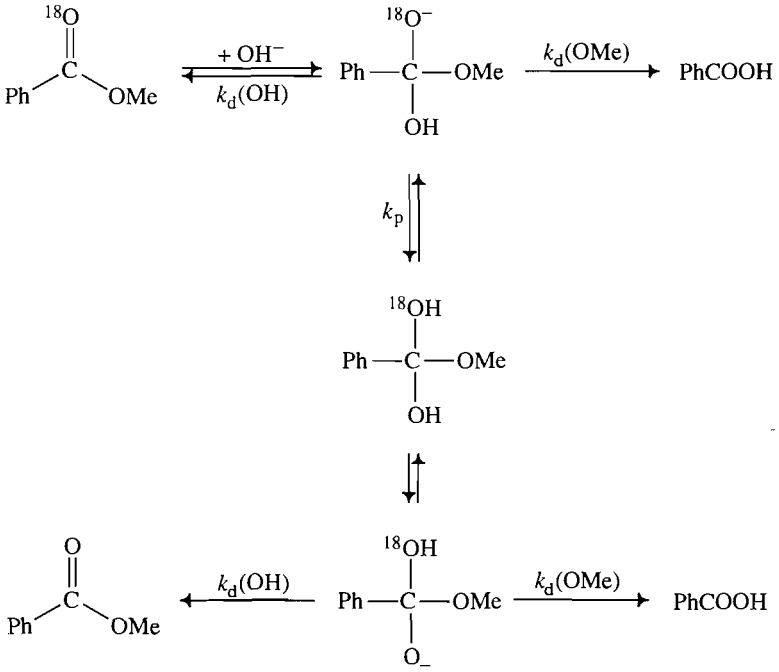

Can. J. Chem. Downloaded from www.nrcresearchpress.com by 91.144.44.67 on 09/07/12
For personal use only.

there are two explanations for the high ratio, either that methoxide is a better leaving group than hydroxide, so that the intermediate prefers to go on to products, or that the intermediate is sufficiently short lived that the protonic equilibrium required for exchange does not occur. The importance of these two factors is seen in the equation

$$\frac{k_{hyd}}{k_{ex}} = \left(\frac{k_d(OMe)}{k_d(OH)}\right)\left(\frac{k_d(OH) + k_d(OMe) + 2k_p}{k_p}\right)$$

derived from a stationary state treatment in the intermediates with neglect of $^{18}O/^{16}O$ isotope effects. The first term in parentheses represents the competition between hydroxide and methoxide leaving groups, and the second term reflects the competition between breakdown and protonation. If $k_p > (k_d(OMe) + k_d(OH))$, the intermediates are at equilibrium, and the hydrolysis–exchange ratio is determined solely by the partitioning factor, $k_{hyd}/k_{ex} = 2k_d(OMe)/k_d(OH)$, with the factor of 2 appearing since, half the time, return to ester results in the same carbonyl oxygen as was there initially. If, however, protonation is not fast compared to breakdown, k_{hyd}/k_{ex} is larger than the partitioning ratio. The intermediate can return to starting ester, but the ^{18}O exchange does not reflect this, since proton transfer is necessary to expel the original carbonyl oxygen. The results of this study clearly suggest that this latter situation is likely to hold. Unfortunately it is not possible to put exact numbers on the various rate constants, since the tetrahedral intermediates are not exactly the same. Our results suggest that protonation by water and breakdown occur at comparable rates, and if this were to be true for the ester intermediate, the effect would be to increase k_{hyd}/k_{ex}, but not by a large factor. We conclude therefore that the failure to achieve proton transfer equilibrium does contribute to the large k_{hyd}/k_{ex}, but the effect is probably not sufficient to account for the entire ratio; therefore $k_d(OMe)$ must be larger than $k_d(OH)$. (A reviewer has suggested that this may occur since the expulsion of the methoxide group can be assisted by simultaneous protonation by the intramolecular OH group (perhaps through a chain of solvent molecules), while no such assistance is available for the OH group when it departs.)

Acknowledgment

Acknowledgment is made to the donors of the Petroleum Research Fund, administered by the ACS, for support of this research.

1. B. Capon, A. K. Ghosh, and D. M. A. Grieve. Acc. Chem. Res. **14**, 306 (1981).
2. R. A. McClelland and L. J. Santry. Acc. Chem. Res. **16**, 306 (1983).
3. B. Capon, M. I. Dosunmu, and M. N. Matos Sanchez. Adv. Phys. Org. Chem. **21**, 37 (1985).
4. R. A. McClelland and M. Ahmad. J. Am. Chem. Soc. **100**, 7031 (1978).
5. R. A. McClelland and S. Steenken. J. Am. Chem. Soc. **110**, 5860 (1988).
6. S. Steenken and R. A. McClelland. J. Am. Chem. Soc. **111**, 4967 (1989).
7. R. A. McClelland, N. Banait, and S. Steenken. J. Am. Chem. Soc. **108**, 7023 (1986).
8. R. A. McClelland, V. M. Kanagasabapathy, and S. Steenken. J. Am. Chem. Soc. **110**, 6913 (1988).
9. R. A. McClelland, N. Banait, and S. Steenken. J. Am. Chem. Soc. **111**, 2929 (1989).
10. R. A. McClelland, V. M. Kanagasabapathy, N. Banait, and S. Steenken. J. Am. Chem. Soc. **111**, 3966 (1989).
11. B. G. Ramsey and R. W. Taft. J. Am. Chem. Soc. **88**, 3058 (1966).
12. H. Perst. Oxonium ions in organic chemistry. Verlag Chemie/Academic, Weinheim. 1971.
13. R. S. Brown and J. G. Ulan. J. Am. Chem. Soc. **105**, 2382 (1983).
14. R. A. McClelland. J. Am. Chem. Soc. **106**, 7579 (1984).
15. S. J. Cristol and T. H. Bindel. *In* Organic photochemistry. Vol. 6. *Edited by* A. Padwa. Marcel Dekker, New York. 1983. pp. 327–415.
16. P. J. Kropp. Acc. Chem. Res. **17**, 131 (1984).
17. D. D. Perrin. Dissociation constants of organic bases in aqueous solution. Butterworths, London. 1965. p. 262.
18. E. Nachliel, Z. Ophir, and M. Gutman. J. Am. Chem. Soc. **109**, 1342 (1987).
19. E. Rosenbaum. Physical chemistry. Meredith Corporation, New York. 1970. pp. 406–408.
20. K. B. Wiberg. *In* Investigation of rates and mechanisms of reactions. 3rd ed. *Edited by* E. S. Lewis. Wiley–Interscience, New York. 1974. pp. 741–766.
21. J. P. Guthrie and P. A. Cullimore. Can. J. Chem. **58**, 1281 (1980).
22. J. Hine and G. F. Koser. J. Org. Chem. **36**, 1348 (1971).
23. J. P. Fox and W. P. Jencks. J. Am. Chem. Soc. **96**, 1436 (1974).
24. R. A. McClelland, N. E. Seaman, and D. Cramm. J. Am. Chem. Soc. **106**, 4511 (1984).
25. M. Eigen. Angew. Chem. Int. Ed. Engl. **3**, 1 (1964).
26. T. Okuyama and T. Fueno. J. Am. Chem. Soc. **107**, 4224 (1985).
27. R. A. McClelland, D. B. Devine, and P. Sorensen. J. Am. Chem. Soc. **107**, 5459 (1985).
28. P. E. Sorensen, K. J. Pedersen, P. R. Pedersen, V. M. Kanagasabapathy, and R. A. McClelland. J. Am. Chem. Soc. **110**, 5118 (1988).
29. M. L. Bender. J. Am. Chem. Soc. **73**, 1626 (1951).
30. D. Samuel and B. L. Silver. Adv. Phys. Org. Chem. **3**, 123 (1965).
31. M. L. Bender, R. D. Ginger, and J. P. Unik. J. Am. Chem. Soc. **80**, 1044 (1958).
32. S. A. Shain and J. F. Kirsch. J. Am. Chem. Soc. **90**, 5848 (1968).

Can. J. Chem. Downloaded from www.nrcresearchpress.com by 91.144.44.67 on 09/07/12
For personal use only.

Bacteriorhodopsin analogue from anthryl chromophores

ANIL K. SINGH[1] AND MITA ROY

Department of Chemistry, Indian Institute of Technology, Powai, Bombay 400 076, India

Received May 18, 1989

ANIL K. SINGH and MITA ROY. Can. J. Chem. **68**, 383 (1990).

Preparation and properties of the bacteriorhodopsin (bR) analogue having the 3,7-dimethyl-9-(9-anthryl)-2*E*,4*E*,6*E*,8*E*-nonatetraenal (**12**) chromophore is described. Synthesis of the chromophore has been achieved by successive introduction of C_5 units to 9-anthraldehyde (**3**) via the Horner reaction. The all-*trans* chromophore has been characterized by its ultraviolet–visible and ^1H nuclear magnetic resonance spectra. Incubation of **12** with bacterioopsin suspension (prepared by photobleaching of bR isolated from *Halobacterium halobium*) at ambient temperature in the dark gave the new bR analogue **15**, which showed an absorption band at 545 nm, and an opsin shift of 5575 cm^{-1}. The new pigment is stable to hydroxyl amine in the dark. It showed light–dark adaptation with the light-adapted form absorbing at a slightly red-shifted value of 550 nm. All-*trans*-retinal did not replace the anthryl chromophore in competitive bindings. Photolysis of the bR analogue **15**, followed by difference spectrophotometric analysis, indicated formation of a photoproduct with an absorption band near 400 nm. The results are discussed in terms of the stereoelectronic requirements of the bR reaction centre.

Key words: bacteriorhodopsin (bR), retinal analogue, reconstitution, opsin shift (OS), external point charge model (EPC).

ANIL K. SINGH et MITA ROY. Can. J. Chem. **68**, 383 (1990).

On décrit la préparation et les propriétés d'un analogue de la bactériorhodopsine (bR) possédant le chromophore 3,7-diméthyl-9-(9-anthryl)-2*E*,4*E*,6*E*,8*E*-nonatétraènal (**12**). On a réalisé la synthèse du chromophore en faisant appel à la réaction de Horner pour introduire des unités successives en C_5 sur le 9-anthraldéhyde (**3**). On a établi le caractère complètement *trans* du chromophore à l'aide de données d'UV–VIS et de RMN du ^{13}C. L'incubation, à la température ambiante et en l'absence de lumière, du composé **12** avec une suspension de bactérioopsine (préparée par photoblanchiment d'une bR isolée à partir de *Halobacterium halobium*) fournit le nouvel analogue **15** de la bR qui présente une bande d'absorption à 545 nm et un déplacement opsine de 5575 cm^{-1}. Le nouveau pigment ne réagit pas avec l'hydroxylamine, en l'absence de lumière. Il présente une adaptation de la lumière à la noirceur; la forme adaptée à la lumière absorbe à une valeur de 550 nm, qui est légèrement déplacée vers le rouge. Le rétinal complètement *trans* ne remplace pas le chromophore anthryle dans les sites où ils sont en compétition. La photolyse de la bR analogue **15**, suivie par une analyse spectrophotométrique différentielle, indique qu'il y a formation d'un photo-produit possédant une bande d'absorption près de 400 nm. On discute des résultats en fonction des facteurs stéréoélectroniques inhérents au centre réactionnel de la bR.

Mots clés : bactériorhodopsine (bR), analogue rétinal, reconstitution, déplacement opsine, modèle de point-charge externe.

[Traduit par la revue]

Introduction

Bacteriorhodopsin (bR), the sole protein component of the purple membrane (pm) of *Halobacterium halobium* (1, 2), is produced by the bacterial cell in response to oxygen starvation. The protein displays some characteristic features in terms of its colour and physiological functions. These aspects of bR have been the subject of intense investigations in recent years. The primary and secondary structures of bR are known (3, 4). The three-dimensional structure of bR has been elucidated to a resolution of 7–14 Å (5). The chromophore of bR is a retinal molecule attached to the ε-amino group of lysine-216 (4) of the apoprotein, bacterioopsin (bOP), via a protonated Schiff base (PSB) (6) linkage (Fig. 1). There are two forms of bR, the light-adapted bR (bR^{LA}, λ_{max} 570 nm) and the dark-adapted bR (bR^{DA}, λ_{max} 560 nm), the chromophores of which are respectively all-*trans*-retinal and a 1:1 mixture of all-*trans*- and 13-*cis*-retinal. Absorption of photons by bR leads to a photochemical cycle (7), which begins with the photochemical all-*trans* to 13-*cis* isomerization of the retinyl prosthetic group in the pigment. The pigment then decays through the K_{610} and L_{550} intermediates, and the Schiff base nitrogen deprotonates, producing the blue-shifted M_{412} species. The photocycle of bR drives the extrusion of protons from the cell to generate a proton gradient, which is then utilized by the Halobacteria to fuel active transport and ATP synthesis.

Specific active-site interactions (8, 9) between chromophore and apoprotein are believed to be responsible for the characteristic features of bR. An approach to the study of the nature of chromophore–apoprotein interactions has been to strip the natural pigment of its chromophore and then to incubate the apoprotein with suitably tailored retinal analogue to generate bioorganic models of bR (8). Such studies have greatly enhanced our understanding of the absorption behaviour of rhodopsins. However, several aspects of the structure, and mechanism of function, of bR are not yet fully understood.

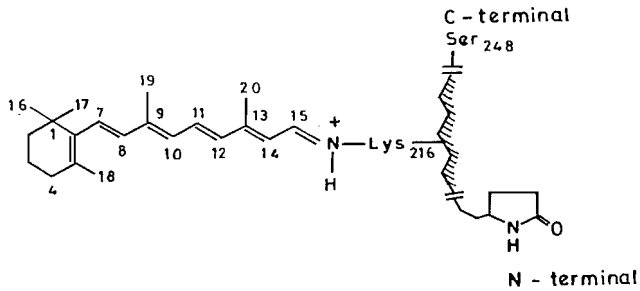

FIG. 1. All-*trans* retinal bound to bR apoprotein via a protonated Schiff base linkage.

The chromophore of bR has three distinct regions, the ring, the side chain, and the Schiff base region. To investigate the nature of the binding site in these regions, a bR analogue with a chromophore having modifications in a particular region can be prepared. The stereoelectronic properties of the ring binding site can thus be studied if bR analogues can be prepared from chromophores that have been suitably modified in the ring portion of the natural chromophore. In our earlier work (10) it

[1]Author to whom correspondence may be addressed.

Can. J. Chem. Downloaded from www.nrcresearchpress.com by 91.144.44.67 on 09/07/12
For personal use only.

Can. J. Chem. Downloaded from www.nrcresearchpress.com by 91.144.44.67 on 09/07/12
For personal use only.

was observed that the iodophenyl retinal analogue binds rapidly to bOP and shows a dramatically altered opsin shift (OS). An anthryl dienal chromophore (**6**) was also found to bind bOP readily, and showed an OS unexpected for a bR analogue having a chromophore with only two double bonds in its side chain. The results were explained in terms of the External Point Charge (EPC) model (8, 9) wherein opsin-bound charges are evoked to electrostatically interact with the chromophore's excited state positive charge near the β-ionyl ring. Thus, EPC attributes the OS to an interaction through space with a negative charge introduced by the protein, in addition to the Schiff base counterion. In bR (OS, 4870 cm^{-1}), it has been suggested that the negative charge is located in the vicinity of the β-ionyl moiety.

The present communication deals with the preparation and properties of the bR analogue from the anthryl chromophore (**12**) in which all four double bonds of the side chain are present, as in the natural chromophore, but the trimethyl cyclohexenyl ring has been replaced by an anthryl moiety.

Experimental

C_5-Phosphonate, methyl-4-(diethyl phosphono)-3-methyl-2-butenoate, was synthesized by following the procedures indicated in standard text (11). AR grade organic solvents were from Spectrochem, Bombay, and were purified before use. Other chemicals were either from Aldrich (USA) or Sigma (USA), and were used as received. Activated manganese dioxide (MnO_2) was prepared by following the published procedure (12). Sodium hydride (NaH) was used as a 50% oil dispersion, which was washed with two portions of anhydrous petroleum ether (40–60°C) prior to use. Horner reactions were carried out under an inert atmosphere of dry nitrogen gas, with anhydrous conditions. All the operations pertaining to retinal and related light-sensitive compounds were performed in a dark room having a dim red light. Column chromatography was done by using 100–200 mesh silica gel (SISCO Laboratories, Bombay). Flash column chromatography was performed on 230–400 mesh silica gel (Merck) according to the reported procedure (13).

Ultraviolet–visible spectra were recorded either on Beckman DU 6 or on Shimadzu UV 260 spectrophotometers. The ir spectra were recorded with a Perkin Elmer 681 IR spectrophotometer. Proton nmr spectra were taken either on Bruker 80 and 500 MHz or on Varian 100 MHz nmr spectrometers. Mass spectra were measured on a Shimadzu QP 1000 mass spectrometer. High pressure liquid chromatographic (hplc) analyses were carried out on a Beckman 110 A instrument using a Microporacil (10 μm, 4.5 × 250 mm, Si-60) column, and spectrophotometric detection. Ultracentrifugations were done on a Beckman L-8-55 M ultracentrifuge. Sonications were performed on a Branson B-12 sonifier. pH measurements were made on a Radiometer PHM-84 pH meter with GK 2401C electrodes.

Isolation of bR, from the cells of *Halobacterium halobium* grown under low oxygen tension and illumination conditions, was done according to the reported procedure (14). The apoprotein was prepared by photobleaching of bR in the presence of hydroxylamine at 4°C.

*9-Anthraldehyde (**3**)*

Anthracene (8.9 g, 0.05 mol), *N*,*N*-dimethyl formamide (DMF, 3.5 mL), phosphorous oxychloride (8.75 mL), and *ortho*-dichlorobenzene (20 mL) were placed in a round-bottomed flask fitted with a reflux condenser and mechanical stirrer. The mixture was heated at 90–95°C for 40 min with simultaneous stirring. Anthracene dissolved during this period to give a deep red solution. The reaction mixture was further refluxed for 3 h and then allowed to cool. The cold mixture was poured into an aqueous solution of sodium acetate (140 g/250 mL), and kept in a refrigerator overnight. Solid material deposited in the flask was recovered by filtration. The crude solid was further purified by column chromatography (5% ethyl acetate in petroleum ether, 40–60°C). Recrystallization of the column-purified material from glacial acetic acid, and further washing of the crystalline material with methanol, gave yellow needle-shaped crystals of 9-anthraldehyde; 6 g, 50%; mp 101–102°C; ir (KBr), ν: 2860, 1670, 1555, 1448, 900, 872, 851 cm^{-1}; uv (MeOH), λ_{max}, nm (ε): 390 (5748), 261 (68 210); ^1H nmr ($CDCl_3$, 100 MHz) δ: 7.60 (4H, m), 8.10 (2H, m), 8.80 (1H, s), 9.10 (2H, m), 11.70 (1H, s); ms, EI (*m*/*e*, % rel. int.): 206 (M^+, 86), 177 (M^+ − CHO, 100); hplc (5% ethyl acetate in hexane, 1.5 mL/min, 360 nm) R_t, 4.6 min.

Methyl 3-methyl-5-(9-anthryl)-2 E,*4* E*-pentadienoate (**4**)*

A solution of C_5-phosphonate (2.33 g, 8.9 mmol) in dry tetrahydrofuran (THF, 10 mL) was added dropwise to a suspension of NaH (0.43 g, 17.8 mmol) in 15 mL dry THF maintained at 0°C. The mixture was stirred (Teflon) for 1 h under N_2. The colour of the mixture turned gradually from colourless to pale yellow and then to dark yellow. A solution of 9-anthraldehyde (**3**, 1.83 g, 8.9 mmol) in 10 mL THF was added dropwise to the yellow reaction mixture at 0°C. The reaction mixture was further stirred for 1 h. The reaction was quenched with brine at 0°C, and the contents taken up in ether. The ethereal layer was separated, washed with brine, and dried over anhydrous sodium sulphate. Removal of ether under diminished pressure on a Rota-vapour gave a solid, which was purified by column chromatography (5% ethyl acetate in petroleum ether, 40°C–60°C). Crystallization of the column-purified material from a mixture of petroleum ether and ethyl acetate (5:1) yielded yellow crystals of ester **4**; 1.10 g, 50%; mp 90–92°C; ir (KBr), ν: 1721, 1170 (ester), 1621, 1525, 1451, 851 (aromatic) cm^{-1}; uv (MeOH), λ_{max}, nm (ε): 387 (18 287), 254 (216 286); ^1H nmr ($CDCl_3$, 80 MHz) δ: 2.76 (3H, s, 3-CH_3), 3.70 (3H, s, -$COOCH_3$), 6.04 (1H, s, H-2), 6.78 (1H, d, J = 16 Hz, H-4), 7.52 (4H, m, arom.), 7.94 (1H, d, J = 16 Hz, H-5), 8.20 (4H, m, arom.), 8.56 (1H, s, 10-H, arom.); ms, EI (*m*/*e*, % rel. int.): 302 (M^+, 71), 256 (100); hplc (5% ethyl acetate in petroleum ether, 1.5 mL/min) R_t, 4.2 min.

3-Methyl 5-(9-anthryl)-2 E,*4* E*-pentadienal (**6**)*

An ethereal solution (15 mL) of pentadiene ester **4** (1 g, 3 mmol) was added dropwise to a suspension of lithium aluminum hydride (LAH) (0.22 g, 5.7 mmol) in 20 mL dry ether. The mixture was stirred (Teflon) for 1 h at −10°C. Reaction was quenched by dropwise addition of water at the same temperature. Ether was added to the reaction mixture, and the aqueous layer was separated. The ethereal layer was washed with brine, and dried over anhydrous sodium sulphate. Ether was then removed under reduced pressure. The resultant alcohol, 3-methyl 5-(9-anthryl)-2*E*,4*E*-pentadien-1-ol (**5**) was stirred with MnO_2 (2.03 g, 24 mmol) in 20 mL THF under N_2 at ambient temperature for 2.5 h. The dark brown mixture was filtered through a G-3 filter. THF was then removed by careful distillation on a Rota-vapour under reduced pressure. The resultant aldehyde **6** was purified by flash column chromatography (7% ethyl acetate in petroleum ether, 40°C–60°C). Further purification of the compound by crystallization from a mixture of ethyl acetate/petroleum ether (1:5) yielded dark-yellow-coloured crystals of **6**; 0.30 g, 40%; mp 70–72°C; ir (KBr) ν: 2860, 1668 (aldehyde), 1625, 1515, 1440, 850 (aromatic) cm^{-1}; uv (MeOH), λ_{max}, nm (ε): 387 (11 252), 252.6 (205 286); ^1H nmr ($CDCl_3$, 80 MHz) δ: 2.68 (3H, s, 3-CH_3), 6.18 (1H, d, J = 11.8 Hz, H-2), 6.80 (1H, d, J = 16.5 Hz, H-4), 7.35 (1H, d, J = 16.5 Hz, H-5), 7.53 (4H, m, arom.), 8.23 (4H, m, arom.), 8.44 (1H, s, 10-H, arom.), 10.32 (1H, d, J = 11.8 Hz, H-1); ms, EI, (*m*/*e*, % rel. int.): 272 (M^+, 84.7), 257 ($M^+ - CH_3$, 77), 243 (M^+ − CHO, 50.5), 228 ($M^+ - C_2H_4O$, 100); hplc (5% ethyl acetate in petroleum ether 40°C–60°C, 1.5 mL/min) R_t, 4.4 min.

Methyl 3,7-dimethyl-9-(9-anthryl)-2 E,*4* E,*6* E,*8* E*-nonatetraenoate (**10**)*

A solution of C_5-phosphonate (0.562 g, 2.23 mmol) in 10 mL dry THF was added to a suspension of NaH (0.107 g, 4.46 mmol) in 20 mL dry THF. The mixture was stirred (Teflon) at 0°C in the dark under N_2 for 1 h. A solution of compound **6** (0.5 g, 1.84 mmol) in 15 mL dry THF was syringed in slowly over a period of 30 min while stirring was continued. After complete addition of the aldehyde, the reaction

Can. J. Chem. Downloaded from www.nrcresearchpress.com by 91.144.44.67 on 09/07/12
For personal use only.

mixture was further stirred at 0°C for 1 h, and then allowed to warm up to ambient temperature over a period of 3 h. At the end of the 3 h period, the reaction mixture was again brought to the low temperature (−10°C), and worked up by addition of brine and ether. The ethereal layer was washed throughly with brine and water, and further dried over anhydrous sodium sulphate in the dark. Removal of ether gave a viscous material, which was subjected to multiple flash column chromatography (7% ethyl acetate in petroleum ether, 40°C–60°C). Repetitive flash column separations gave ester **10** (0.029 g) as a yellowish gummy material; ir (KBr) ν: 1721, 1170 (ester), 1621, 1525, 1451, 851 (aromatic) cm^{-1}; ^1H nmr ($CDCl_3$, 500 MHz) δ: 2.19 (3H, s, 3-CH_3), 2.30 (3H, s, 7-CH_3), 3.75 (3H, s, -OCH_3), 5.80 (1H, s, H-2), 5.82 (1H, d, J = 15 Hz, H-4), 6.29 (1H, d, J = 11 Hz, H-6), 6.74 (1H, d, J = 16 Hz, H-8), 6.79 (1H, d, J = 16 Hz, H-9), 7.10 (1H, dd, J = 11 Hz, 15 Hz, H-5), 7.14–8.42 (9H, m, arom.); ms, EI, (m/e, % rel. int.): 367 (M^+, 67); hplc (7% ethyl acetate in petroleum ether, 40°C–60°C, 1.5 mL/min) R_t, 4.3 min.

*3,7-Dimethyl-9-(9-anthryl)-2*E*,4*E*,6*E*,8*E*-nonatetraenal (12)*

An ethereal solution (15 mL) of nonatetraenoate **10** (0.22 g, 0.76 mmol) was added to a suspension of LAH (0.057 g, 1.5 mmol) in 10 mL dry ether at −10°C. The reaction mixture was stirred (Teflon) at that temperature in the dark for 30 min. Reaction was terminated by careful addition of about 2 mL of brine to the reaction mixture maintained at −10°C. Ether was added, and the aqueous layer was removed. The ethereal layer was washed with brine and water, and dried over anhydrous sodium sulphate. About two thirds of the ether was removed from the yellow solution on a Rota-vapour under reduced pressure, and the remaining ether was evaporated by gentle N_2 jet. The dark yellowish viscous alcohol **11** obtained was immediately treated with a 20 mL THF suspension of MnO_2 (0.61 g, 6.75 mmol) in the dark under N_2. After 3 h of stirring (Teflon) at ambient temperature, the mixture was filtered through a G-3 filter, and finally through a Celite column (2 cm, in a 5-mm pipette). Most of the THF was removed on a Rota-vapour, and the residue was subjected to flash column chromatography (5% ethyl acetate in petroleum ether, 40°C–60°C), when an orange viscous material (0.1 g) was recovered from the effluent. High pressure liquid chromatographic analysis (7% ethyl acetate in petroleum ether, 40°C–60°C, 1.5 mL/min) showed it to contain approximately 60% of the desired aldehyde **12**; ir (KBr), ν: 2770, 1668 (CHO), 1621, 1528, 1451, 851 (aromatic) cm^{-1}; uv (MeOH), λ_{max}: 410 nm; ^1H nmr ($CDCl_3$, 500 MHz) δ: 2.34 (3H, s, 3-CH_3), 2.37 (3H, s, 7-CH_3), 6.00 (1H, d, J = 8.00 Hz, H-2), 6.35 (1H, d, J = 11 Hz, H-6), 6.43 (1H, d, J = 15.20 Hz, H-4), 6.75 (1H, d, J = 16.30 Hz, H-9), 6.76 (1H, d, J = 16.30 Hz, H-8), 7.26 (1H, d, J = 15.20 and 11.00 Hz, H-5), 7.40–8.42 (9H, m, arom.), 10.13 (1H, d, J = 8.00 Hz, H-1); hplc, R_t, 4.5 min.

Protonated Schiff bases (PSB, 8 and 14)

The PSBs were prepared by addition of dry, freshly distilled *n*-butyl amine to methanolic solutions of the respective aldehydes. The reaction was carried out over 4 Å molecular sieves at 0°C under N_2 in the dark. After 12 h, the methanol and excess *n*-butyl amine were removed under vacuum, and the semisolid residue was redissolved in anhydrous methanol. Protonation of the Schiff bases thus prepared was accomplished by addition of methanol saturated with dry hydrogen chloride gas. Protonation of the Schiff bases was indicated by a red shift in their absorption spectra.

The bR analogue (15)

An ethanolic solution of anthryl retinal analogue **12** was incubated with freshly prepared bOP at ambient temperature in the dark over a period of 24 h. The final ethanol concentration was ≤1% v/v. The growth of the pigment was followed by periodic recording of the absorption spectrum of the mixture. A new peak at 545 nm appeared as a result of binding of anthryl analogue **12** with bOP. The competitive displacement experiments were done by adding an aliquot of ethanolic solution of all-*trans*-retinal to the synthetic pigment. The synthetic pigment was purified by washing of excess chromophore by ultracentrifugation (*n*-hexane, 50 000 g, 10 min).

Preparation of light- and dark-adapted pigments

The dark-adapted bR analogue (bR^{DA}_{545}-**15**) suspensions were irradiated with a 500 W tungsten lamp at a distance of 5 cm using 1% $CuSO_4$–H_2O solution as filter at 4°C. The sample was continuously stirred with a small Teflon bar. The photolysed sample showed an absorption band at 550 nm corresponding to the light-adapted form of **15** (bR^{LA}_{550}-**15**). Incubation of bR^{LA}-**15** in the dark over a period of 24 h regenerated bR^{DA}-**15**.

Photolysis of bR analogue 15 at low temperature

bR-Analogue **15** was suspended in a solution containing 3 mL of 25% NaCl and 75% glycerol. The pH of the sample was adjusted to 9.0 by adding 0.5 M NaOH solution. The sample was cooled to 0°C, and light adapted as described in the previous section. The light-adapted sample was further cooled to −60°C, and irradiation was continued. The difference uv–vis spectrum was obtained by recording the absorption spectra of photostationary and initial-stage samples. A new species with absorption near 400 nm was detected from the difference spectrum. A control experiment was performed by observing changes in the cooled non-irradiated sample.

Results and discussion

Synthesis of retinal analogue 12

The procedure adapted for the synthesis of analogue **12** is outlined in Scheme 1. 9-Anthraldehyde (**3**) was prepared (15) by formylation of anthracene in 50% yield. The adduct **2**, formed as a dark red liquid, was hydrolysed with aqueous sodium acetate solution, and the mixture was allowed to stand overnight at 4°C. This resulted in the solidification of aldehyde **3** as a yellow solid. *ortho*-Dichlorobenzene did not hinder solidification; rather, it helped in partially purifying the desired compound by dissolution of the products in the last step. Thus the purity of the aldehyde was improved by allowing it to solidify in the presence of dichlorobenzene, such that it retained the unreacted anthracene. Long needle-shaped crystals of **3** gave satisfactory physicochemical analysis.

The desired C_5-phosphonate was synthesized starting from 3,3-dimethyl acrylic acid (11). Esterification of the acid involved the usual preparation of its acyl chloride followed by its *in situ* reaction with dry methanol. Allylic bromination of the acrylate with *N*-bromosuccinimide in carbon tetrachloride under reflux conditions, followed by fractional distillation of the reaction residue, afforded the extremely lachrymatic bromoester, methyl 4-bromo-3-methyl-2-butenoate. Reaction of the bromoester with triethyl phosphite at 180°C for 1 h gave the desired phosphonate, which was isolated from the reaction mixture by fractional distillation. The ^1H nmr analysis of the phosphonate showed it to be a 2:3 mixture of 2-*cis*- and 2-*trans* butenoate. The identity of the isomers was established by the appearance of two singlets, in the nmr spectrum, at δ 2.30 and 2.05, corresponding to 3-CH_3 protons of 2-*cis* and 2-*trans* isomers, respectively. The allylic methylene protons at C-4 adjacent to the phosphonate group appeared at δ 3.25 and δ 2.90 for the two isomers. All other intermediate compounds also showed satisfactory data conforming to their structure.

Condensation of 9-anthraldehyde (**3**) with C_5-phosphonate in the presence of NaH gave the diene ester **4**. It could be purified by flash column chromatography, and gave the expected physicochemical analyses. It showed an intense, sharp uv band at 254 nm due to ^1B transition, and weak but structured bands centered at 387 nm due to transversely polarized ^1L_a transitions. The ir spectrum of **4** exhibited an intense band at 1721 cm^{-1} featuring an ester carbonyl. Mass spectroscopic analysis of **4** revealed the molecular ion peak at m/e 302, and the base peak at m/e 256 corresponding to $M^+ - C_2H_6O$. Another prominent

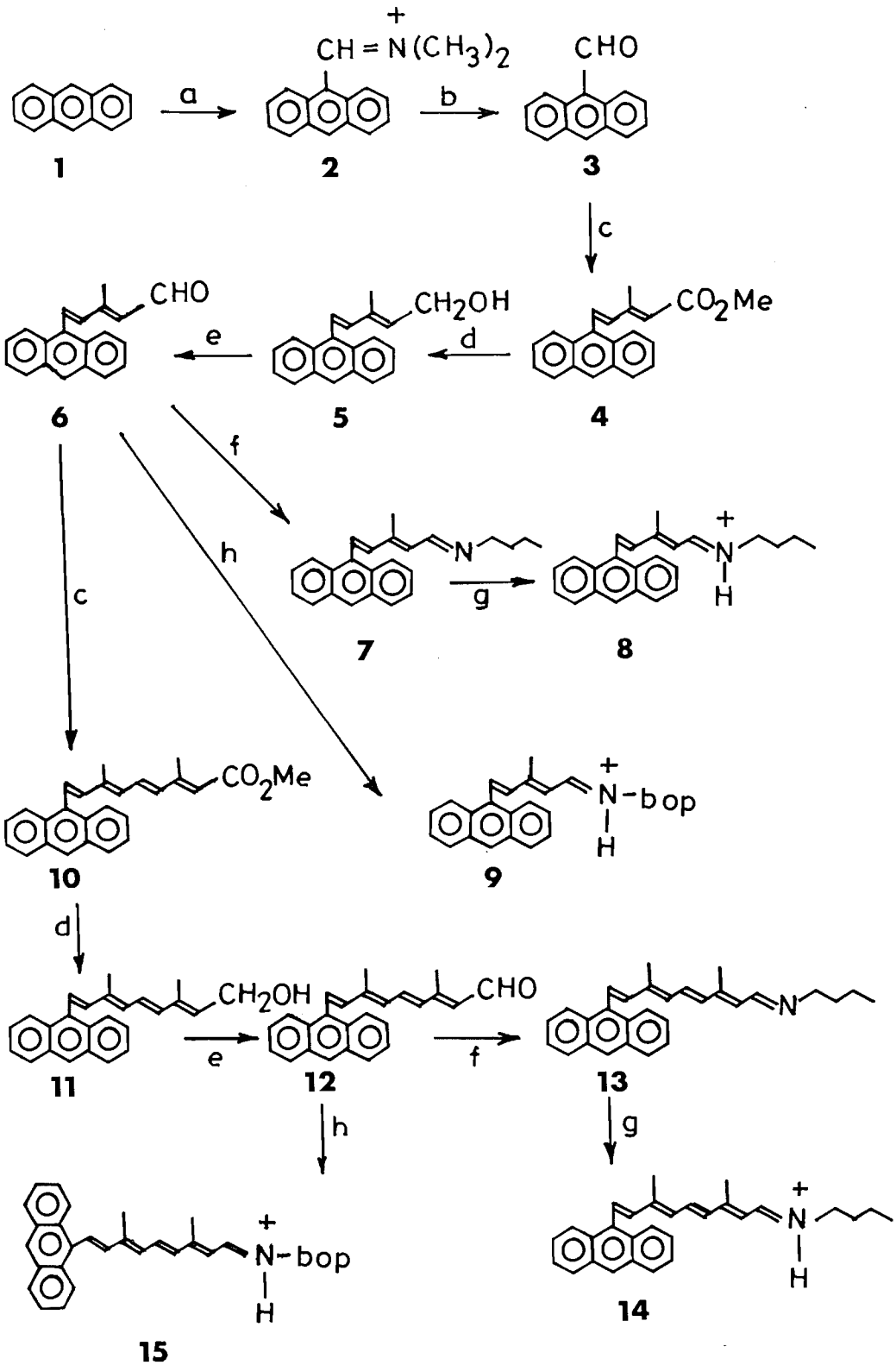

SCHEME 1. (a) DMF–$POCl_3$, *o*-dichlorobenzene; (b) NaOAc; (c) $(EtO)_2POCH_2.(CH_3)CH{=}CH.COOMe$, THF, NaH; (d) $LiAlH_4$–Et_2O; (e) MnO_2–THF; (f) *n*-butyl amine, MeOH; (g) MeOH–HCl, dry; (h) bOP, HEPES, dark.

mass peak was observed at *m/e* 271 due to the $M^+ - OMe$ fragment. The proton nmr spectrum of **4** showed the expected singlets at δ 3.70 (-COOMe), δ 2.76 (-3-CH_3), and δ 6.04 (H-2). The coupling constant of 16 Hz between protons at C-4 and C-5 was indicative of a *trans* configuration between the C_4—C_5 double bond. The anthryl ring showed three signals. The two multiplets at δ 7.52 and 8.20 corresponded to four protons each. The C-10 proton of the anthryl ring was observed as a singlet at δ 8.56.

Reduction of the ester function in **4** by LAH required low temperature and early termination of the reaction. Reactions at ambient temperature resulted in the formation of several side

Can. J. Chem. Downloaded from www.nrcresearchpress.com by 91.144.44.67 on 09/07/12
For personal use only.

TABLE 1. Ultraviolet–visible absorption data for anthryl chromophores in methanol

Compound	λ_{max}, nm (ε)
1	380 (9000), 254 (180 000)
6	387 (11 252), 254 (205 285)
7	386, 254
8*	454, 254
12	410 (24 794), 261 (80 561)
13	393, 260
14*	418, 261

*Chloride salts.

products that did not analyse for the desired dienol group. Prolonged reaction even at low temperatures gave similar undesired results. The alcohol **5** obtained from the careful reduction of **4** was oxidised by MnO_2 to aldehyde **6**. Dienal **6** was purified by a combination of flash column chromatography and crystallization. Both the reduction of ester **4** and oxidation of the resulting alcohol proceeded with no detectable stereochemical change as evidenced by homogeneous hplc patterns and by spectral analyses. The ir spectrum of **6** showed characteristic bands for an aldehyde group at 1668 and 2860 cm^{-1}. Significant features in the ^1H nmr spectrum of **6** were the appearance of a doublet at δ 6.18 with a coupling constant of 11.80 Hz for the C-2 proton (which was a singlet at 6.04 in the ester **4**) that arose due to coupling of the adjacent proton at C-1. As expected, the configuration at the C_4—C_5 double bond was *trans*, with a coupling constant of 16 Hz between protons at C-5 and C-4. Mass spectrometric analysis showed a fragmentation pattern characteristic of a dienal.

Further elongation of the chain of **6** was done by adding one more C_5 unit to it. The resulting ester **10** could be purified by flash column chromatography. While its intense ir band at 1721 cm^{-1} was very characteristic of an ester carbonyl group, the 500 MHz ^1H nmr spectrum provided confirmation of its configurational structure. The tetraenyl chain showed the expected signals for its *trans*-coupled protons. LAH reduction of **10**, followed by MnO_2 oxidation of the resulting alcohol **11**, gave tetraenal **12**, which could be satisfactorily characterized by its uv–vis and ^1H nmr analyses. As expected, the tetraenyl compound was obtained as a mixture of several configurational isomers. The all-*trans* analogue showed characteristic nmr signals for olefinic and aldehydic protons. The aldehyde proton for the all-*trans* compound resonated at δ 10.13 as a doublet with a coupling constant of 8 Hz. The corresponding H-2 proton is seen at δ 6.00, also as a doublet with a *J* value of 8.00 Hz. The *trans* coupling between the H-4 and H-5 protons and *s-trans* coupling between H-5 and H-6 were observed to be 15.2 and 11.0 Hz, respectively. Compound **12** showed the characteristic aldehyde peak at 1668 cm^{-1}. Expected uv–vis absorption bands at 410 and 261 nm due to ^1L_a and ^1B transitions, respectively, confirmed the conjugated nature of the elongated side chain. The absorption properties of the anthryl chromophores are discussed in the following section.

Ultraviolet–visible absorption properties of anthryl chromophores

The uv–vis absorption data for the anthryl compounds are given in Table 1. The spectrum of parent anthracene, a *cata*-condensed nucleus, shows an intense peak at 254 nm (ε, 180 000) due to ^1B transitions. The other major band in the spectrum of anthracene is due to ^1L_a transitions, and consists of a series of five vibrational sub-bands, the longest of which occurs at about 380 nm with ε of 9000. Introduction of an olefinic chain at C-9 in anthracene did not result in any major change in the shape of the spectrum. With the introduction of a chain at the C-9 position, an increase in the resonance stabilization of the vertically polarized excited states could be anticipated and the absorption band associated with this transition (^1L_a) should be shifted to longer wavelength. However, only a small shift of 7 nm was observed. The failure to observe a significant red shift may be due to less resonance coupling between the chain and the nucleus. This could be a result of increased size of the substituent, and accordingly enhanced potentialities for steric interference with resonance. As the steric strain in aldehyde **6** gets relieved due to twisting of the essentially single bond between the anthracene ring and the diene chain, departure from coplanarity is experienced, and thus the absence of a significant red shift in the absorption spectrum of **6**. On further extension of the chain, as in compound **12**, a bathochromic shift of the ^1L_a band to 410 nm was observed, probably due to an increased conjugation in the chain.

The Schiff base (SB) of aldehyde **6** and *n*-butyl amine in MeOH showed a ^1L_a band only at 386 nm. On the other hand, the SB of aldehyde **12** and *n*-butyl amine showed a 17-nm blue-shifted absorption band as compared to the parent aldehyde. On protonation, however, a red shift of 68 nm for the transversely polarized band was observed for the protonated Schiff base (PSB) **8** of dienal **6**. However, the PSB **14** of tetraenal **12** showed a red shift of only 25 nm for the transversely polarized band. The additional resonance energy acquired by the conjugation with the powerful chromophore ($=\overset{+}{N}HR$) acts to rotate the substituent in the PSB of dienal **6** into the plane of the anthracene ring, and thus accounts for the marked bathochromic shift. In the PSB of tetraenal, however, the resonance effect acting to bring the chain to coplanarity is opposed by the steric overlap of the methyl group with the hydrogens in the anthryl ring.

The bR analogue

Synthesis of the new pigment is carried out by combining a concentrated ethanolic solution of the retinal analogue with freshly bleached protein. Apoprotein, when incubated with retinal analogue **12**, resulted in the formation of a new bR analogue, which showed an absorption band at 545 nm in its dark-adapted form. Most of the binding occurred in the first 30 min of the incubation (Fig. 2). Further characterization of the pigment was done by determining the opsin shift (OS) value.

OS is expressed by the λ_{max} of PSB in cm^{-1} minus the λ_{max} of the pigment in cm^{-1} (8). The PSB is usually prepared by reacting the retinal or its analogues with *n*-butyl amine, followed by its production with HCl. The bR regenerated from all-*trans* retinal shows an OS of 4870 cm^{-1}. Following a similar procedure, the OS of bR analogue **15** has been determined to be 5575 cm^{-1}. The bR analogue prepared from dienal **6** exhibited an OS of 3911 cm^{-1} (Table 2). It is interesting to note that bR analogues can be prepared by a chromophore having only two double bonds in the side chain. The bR active site is thus found to be quite flexible and nonspecific, at least in the ring binding site. The bR analogue prepared from 11,12-dihydro retinal, essentially a dienal, has no measurable OS in the uv–vis region (8). The 9,10-dihydro retinal, a trienal, has an OS of only 300 cm^{-1} (8). In view of these results, the OS shown by anthryl dienal-based bR is quite interesting. The anthryl analogue may be considered as having some of the required double bonds in the anthryl ring. This imparts a more planar conformation to the

Can. J. Chem. Downloaded from www.nrcresearchpress.com by 91.144.44.67 on 09/07/12
For personal use only.

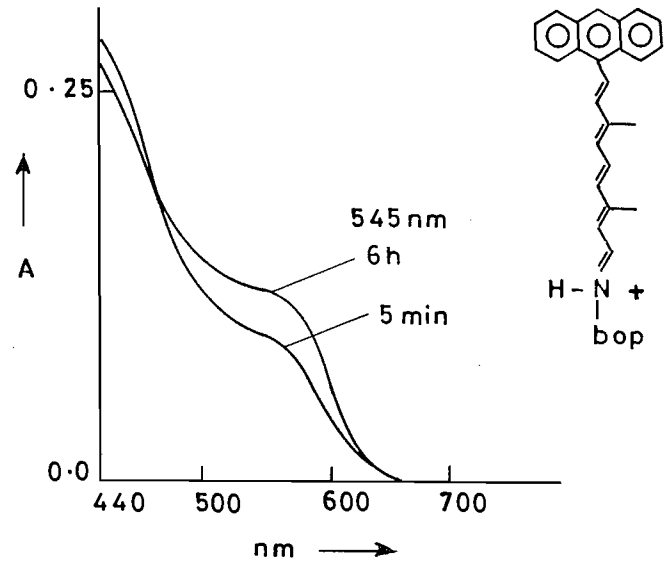

FIG. 2. Formation of bR analogue **15** from anthryl retinal analogue **12**.

TABLE 2. Opsin shifts (cm^{-1}) for bR analogues

Compound	λ_{max}, nm			Opsin shift
	CHO	PSB	bR	
Anthryl pentadienyl retinal analogue	387	454	550	3911*
Anthryl tetraenyl retinal analogue	410	418	545	5575
Retinal	380	440	560	4870

*Reference 10.

chromophore. Besides, as has been observed, the protonated anthryl dienyl chromophore shows more of planar characteristics. In addition, the dienyl chromophore may be undergoing interactions with opsin-bound charges present in the vicinity of the flattened anthryl moiety at the active site. The anthryl ring could be disposed in the region of the active site, which is occupied by C-8 to C-10 of the natural chromophore, retinal. According to the EPC model, electronic and steric perturbations at the active site are expected to strongly influence the absorption spectra of the protein. The PSB of dienal **6** and tetraenal **12** showed absorption bands at 454 and 418 nm respectively. However, when these aldehydes were attached to lysine-216 of the protein in the form of a protonated Schiff base, they exhibited absorption bands at 550 (10) and 545 nm respectively. The longer chromophore **12** shows absorption that is now only 5 nm blue-shifted as compared to the shorter chromophore. The source of the 96-nm shift in dienyl anthryl-based bR (as compared to the absorption of *n*-butyl amine PSB of dienal) and the 127-nm shift in tetraenal anthryl-based bR (as compared to the absorption of *n*-butyl amine PSB of tetraenal) has to be partly due to additional interactions between the anthryl chromophore and opsin-bound charges. In this context, it is important to note the recent suggestion (16) that the bR active site has opsin-bound charges in the form of ion pairs. A comparison of the absorption data of native bR and the bR analogues prepared from anthryl retinal analogues **6** and **12** indicates that there is less conjugation in the polyene chain and

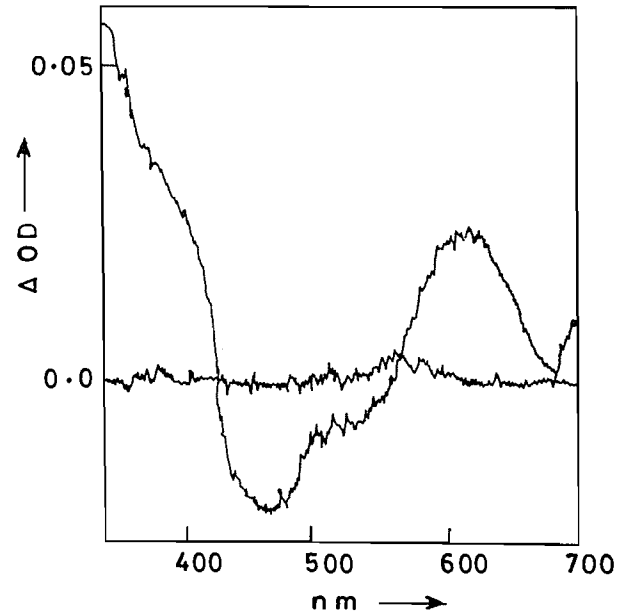

FIG. 3. Difference uv–vis absorption spectrum of the photolysed bR analogue **15** at −60°C.

the anthryl ring in the case of the chromophore in bR analogue **15**. Similar observations were made in the absorption behaviour of chromophore **14** in solution. However, decreased interactions between the twisted chromophore and the now more distant opsin-bound charges can also be partly responsible for such behaviour of the chromophore in the protein.

It has been found that the ring binding site readily accepts acyclic polyenes (17). The ring binding site appears to be quite unrestrictive, as large groups such as aromatic derivatives and 4-substituted analogues (18) can be easily accommodated by bR. Bioorganic models of bR from retinal analogues with a locked 6-*s*-*trans* conformation (9), the phenyl (10, 19) and naphthyl (18, 20, 21) compounds, have suggested a view of the binding site in which the bR protein appears to bind the chromophore in its planar conformation.

Stability of the bR analogue

Stability of the pigment can be inferred from competitive binding with all-*trans* retinal, and with the behaviour of the bR analogue towards hydroxylamine. It was found that addition of all-*trans* retinal did not displace the anthryl chromophore, as the appearance of the bR band at 560 nm was not more than 5%. Similarly, addition of hydroxylamine to bR analogue and incubation in the dark did not significantly alter the 545 nm absorption of the pigment. However, it was found that the bR analogue with the anthryl tetraenyl chromophore was relatively more stable (>24 h) than the bR analogue with anthryl dienal chromophore (~8 h). It can thus be inferred that a complete longitudinal fitting of the chromophore at the active site is necessary for the stability of bR. This also suggests that the longitudinal chain binding site is more important than the ring binding site.

The anthryl bR analogue **15** also showed expected light and dark adaptation. Thus, on illumination, dark-adapted **15** showed a red-shifted absorption band at 550 nm.

The M intermediate generation

During the photocycle of bR a blue-shifted M intermediate with absorption band at 412 nm is formed. Concomitantly a

Can. J. Chem. Downloaded from www.nrcresearchpress.com by 91.144.44.67 on 09/07/12
For personal use only.

proton is released in the medium. This proton is later taken up in the photocycle with the decay of the M intermediate. To see whether such an intermediate is generated for the anthryl bR analogue, photolysis of analogue **15** was carried out at low temperature. For measuring the absorption spectra of the blue-shifted intermediate a temperature of −60°C, high salt concentration, and a pH of 9.0 was maintained. Difference uv–vis analysis (Fig. 3) of the photomixture showed the appearance of a band near 400 nm, which could be due to the unprotonated Schiff base chromophore of the M anthryl bR formed during the photolysis of bR-**15**. Thus it is apparent that the presence of the trimethyl cyclohexenyl moiety may not be essential for bR to undergo the photocycle.

Conclusions

Thus, synthetic retinal analogue **12** binds to bacterioopsin to give a new bR analogue. It is found that the ring binding site is unrestrictive and nonspecific. The binding site of bR prefers to bind the chromophore in a planar conformation. The longitudinal chain binding site appears to play a more important role than the ring binding site. Both resonance and steric compatibility of the chromophore seem to play important roles in the regulation of the absorption behaviour of bR. The presence of the trimethyl cyclohexenyl ring does not seem to have much effect on the functional properties of the protein. However, a proper fit of the chromophore at the active site seems to be important for both the structural and functional features of bR.

Acknowledgements

Financial assistance from the Department of Science and Technology, Government of India, is gratefully acknowledged. Our thanks are due to the Tata Institute of Fundamental Research, Bombay, for providing the 500 MHz nmr facility. We are also grateful to the project advisory committee of the DST for useful suggestions.

1. D. Oesterhelt and W. Stoeckenius. Nature (London) New Biol. **233**, 149 (1971).
2. (*a*) W. Stoeckenius, R. Lozier, and R. A. Bogomolni. Biochim. Biophys. Acta, **505**, 215 (1978); (*b*) W. Stoeckenius and R. A. Bogomolni. Ann. Rev. Biochem. **52**, 587 (1982); (*c*) P. Lester. Biomembranes. Part I. Visual pigments and purple membranes. Methods in enzymology. 2nd ed. Academic Press, New York. 1982; (*d*) J. B. C. Findlay and D. J. C. Pappin. Biochem. J. **238**, 625 (1986); (*e*) C. Sandorfy and D. Vocelle. Can. J. Chem. **64**, 2251 (1986).
3. Y. A. Ovchinnikov, N. G. Abdulaev, M. Y. Feigina, A. V. Kiselev, and N. A. Lobanov. FEBS Lett. **100**, 219 (1979).
4. H. G. Khorana, G. E. Gerber, W. C. Herlihi, C. P. Gray, R. J. Anderegg, K. Nihei, and K. Bieman. Proc. Natl. Acad. Sci. U.S.A. **76**, 5046 (1979).
5. (*a*) R. Henderson and P. N. T. Unwin. Nature (London), **257**, 28 (1975); (*b*) D. Leifer and R. Henderson. J. Mol. Biol. **163**, 451 (1983).
6. (*a*) K. Rothschild and H. Marrero. Proc. Natl. Acad. Sci. U.S.A. **79**, 4045 (1982); (*b*) K. Bagley, G. Dollinger, L. Eisenstein, A. K. Singh, and L. Zimanyi. Proc. Natl. Acad. Sci. U.S.A. **79**, 4972 (1982).
7. D. Oesterhelt and W. Stoeckenius. Proc. Natl. Acad. Sci. U.S.A. **70**, 2853 (1973).
8. (*a*) K. Nakanishi, V. Balog-Nair, M. Arnaboldi, K. Tsujimoto, and B. Honig. J. Am. Chem. Soc. **102**, 7945 (1980); (*b*) F. Derguini, D. Dunn, L. Eisenstein, K. Nakanishi, K. Odashima, V. J. Rao, L. Shastry, and J. Termini. Pure Appl. Chem. **58**, 719 (1986).
9. R. van-der Stein, P. L. Bieshevel, R. A. Mathies, and J. Lugtenburg. J. Am. Chem. Soc. **108**, 6410 (1986).
10. A. K. Singh, M. Roy, S. M. Sonar, and M. M. Kapil. J. Biosci. **13**, 55 (1988).
11. H. Mayer and O. Isler. *In* Carotenoids. *Edited by* O. Isler. Birkhauser, Basel. 1971. p. 325.
12. A. J. Fatiadi. Synthesis, 65 (1976).
13. W. C. Still, M. Kahn, and H. Mitra. J. Org. Chem. **43**, 2923 (1978).
14. D. Oesterhelt and W. Stoeckenius. Methods Enzymol. **31**, 667 (1974).
15. E. Compaigne and W. L. Archer. J. Am. Chem. Soc. **95**, 989 (1953).
16. (*a*) J. L. Spudich, D. A. McCain, K. Nakanishi, M. Okabe, N. Shimuzu, H. Rodman, B. Honig, and R. A. Bogomolni. Biophys. J. **49**, 479 (1986); (*b*) J. Lugtenburg, M. Mauradin-Szweykowska, G. S. Harbinson, S. O. Smith, C. Heeremans, J. A. Pardoen, J. Herzfeld, R. G. Griffin, and R. A. Mathies. J. Am. Chem. Soc. **108**, 3104 (1986).
17. (*a*) J. Zingoni, Y. S. Or, and R. K. Crouch. Biochemistry, **25**, 2022 (1986); (*b*) R. K. Crouch, Y. S. Or, and S. Ghent. J. Am. Chem. Soc. **106**, 8325 (1984); (*c*) V. Rao, J. Zingoni, R. K. Crouch, M. Denny, and R. S. H. Liu. Photochem. Photobiol. **41**, 171 (1985).
18. (*a*) R. K. Crouch, R. Scott, S. Ghent, R. Govindji, C.-H. Chang, and T. Ebrey. Photochem. Photobiol. **43**, 297 (1986); (*b*) U. Sonnewald, S. Seltzer, A. E. Robinson, and L. Packer. Photochem. Photobiol. **41**, 303 (1985); (*c*) M. Sheves, T. Bassov, N. Friedman, M. Ottolenghi, R. Feinmann-Weinburg, V. Rosenbach, and B. Ebrenbeng. J. Am. Chem. Soc. **106**, 2435 (1984).
19. H. Bayley, R. Radhakrishnan, K. S. Huang, and H. G. Khurana. J. Biol. Chem. **256**, 3797 (1981).
20. M. Akhtar, L. Jallo, and A. H. Johnson. J. Chem. Soc. Chem. Commun. 44 (1982).
21. T. Iwasa, M. Tako, M. V. K. Tsujimoto, and F. Tokunaga. Biochemistry, **23**, 838 (1984).

Can. J. Chem. Downloaded from www.nrcresearchpress.com by 91.144.44.67 on 09/07/12
For personal use only.

The effects of metal salts on the photosensitized (electron transfer) carbon–carbon bond cleavage of the 2,2-diphenylethyl ether system[1]

LAURIE J. LAMONT AND DONALD R. ARNOLD[2]
Department of Chemistry, Dalhousie University, Halifax, N.S., Canada B3H 4J3

Received September 11, 1989

LAURIE J. LAMONT and DONALD R. ARNOLD. Can. J. Chem. **68**, 390 (1990).

Irradiation of an acetonitrile solution of *para*-dicyanobenzene (**1**), 3,3-diphenyltetrahydrofuran (**2**), and magnesium perchlorate leads to the formation of 4,4-diphenyl-1,3-dioxane (**7**). Similarly, irradiation of an acetonitrile solution of **1**, methyl 2,2-diphenylcyclopentyl ether (**5**), and magnesium perchlorate leads to the formation of 6,6-diphenyl-2-methoxytetrahydropyran (**8**). The mechanism proposed for these reactions involves formation of the radical cations $\mathbf{2}^{+\cdot}$ and $\mathbf{5}^{+\cdot}$ with the first excited singlet state of **1** acting as the photosensitizer (electron transfer). The radical cations $\mathbf{2}^{+\cdot}$ and $\mathbf{5}^{+\cdot}$ then cleave to give 1,5 radical cations. Reaction of the cationic site with water, followed by futher oxidation of the radical site by the perchlorate anion, gives the diphenylalkyl carbocation that can cyclize via a six-membered intermediate to the observed products **7** and **8**. While the addition of other perchlorate salts (lithium and tetra-*n*-butylammonium) also lead to the formation of **7** and **8**, lithium trifluoroacetate is ineffective. The proposal that water is involved as the nucleophile is supported by incorporation of ^{17}O in the products **7** and **8** when ^{17}O-enriched water was added to the reaction mixture.

Key words: photosensitization, electron transfer, radical cations, bond cleavage, 2,2-diphenylethyl ether.

LAURIE J. LAMONT et DONALD R. ARNOLD. Can. J. Chem. **68**, 390 (1990).

L'irradiation d'une solution d'acétonitrile contenant du *para*-dicyanobenzène (**1**), du 3,3-diphényltétrahydrofurane (**2**) et du perchlorate de magnésium conduit à la formation de 4,4-diphényl-1,3-dioxane (**7**). De la même manière, l'irradiation d'une solution d'acétonitrile contenant du produit (**1**), du 1-méthoxy-2,2-diphénylcylopentane (**5**) et du perchlorate de magnésium conduit à la formation du 6,6-diphényl-2-méthoxytétrahydropyrane (**8**). Le mécanisme proposé pour ces réactions implique la formation des cations radicaux $\mathbf{2}^{+\cdot}$ et $\mathbf{5}^{+\cdot}$ par le biais de réactions au cours desquelles le premier état singulet excité du composé **1** agit comme photosensibilisateur (transfert d'électron). Les cations radicaux $\mathbf{2}^{+\cdot}$ et $\mathbf{5}^{+\cdot}$ se clivent alors pour donner les cations radicaux 1,5. La réaction du site cationique avec de l'eau, suivie par une oxydation additionnelle du site radicalaire par l'anion perchlorate, fournit le carbocation diphénylalkyle qui peut se cycliser par le biais d'un intermédiaire à six chaînons pour fournir les produits observés **7** et **8**. Alors que l'addition d'autres perchlorates (lithium et tétra-*n*-butylammonium) conduit aussi à la formation des produits **7** et **8**, le trifluoroacétate de lithium est inefficace. La proposition selon laquelle l'eau est impliquée comme nucléophile est corroborée par l'incorporation de ^{17}O dans les produits **7** et **8** lorsqu'on additionne de l'eau enrichie en ^{17}O au mélange réactionnel.

Mots clés: photosensibilisation, transfert d'électron, cations radicaux, clivage de liaison, 2,2-diphényléthyl éther.
[Traduit par la revue]

Can. J. Chem. Downloaded from www.nrcresearchpress.com by 91.144.44.67 on 09/07/12
For personal use only.

Introduction

The photosensitized (electron transfer) carbon–carbon bond cleavage of 2,2-diphenylethyl ethers is a well-known reaction (1,3). For example, irradiation of an acetonitrile–methanol (3:1) solution of *para*-dicyanobenzene (**1**) (an electron-accepting photosensitizer) and 3,3-diphenyltetrahydrofuran (**2**) results in the formation of methyl 3,3-diphenylpropyl formaldehyde acetal (**3**) (60% yield after 20% conversion) (reaction 1) (1*b*). The mechanism for this reaction (Scheme 1) involves carbon–carbon bond cleavage of the radical cation of **2** to give an intermediate 1,5 radical cation. The cationic site is trapped by nucleophilic solvent (methanol), the radical site is reduced to the carbanion by electron transfer from the radical anion of the photosensitizer ($\mathbf{1}^{-\cdot}$), and the carbanion is protonated to give the observed product. When the solvent is acetonitrile–water (3:1), 3,3-diphenylpropanol (**4**) is formed (1*b*). This product results from an analogous reaction, trapping of the carbocation with water, followed by hydrolysis of the initially formed hemiacetal. When this irradiation is carried out in the absence of a nucleophile, no reaction occurs.

Reaction 1

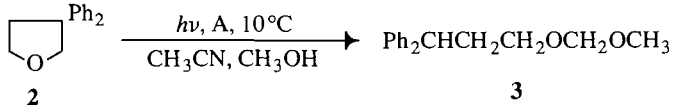

2 **3**

A = 1,4-Dicyanobenzene (**1**)

Similar irradiation of an acetonitrile–methanol (3:1) solution of *para*-dicyanobenzene (**1**) and methyl 2,2-diphenylcyclopentyl ether (**5**) also results in carbon–carbon bond cleavage to yield 5,5-diphenylpentanal dimethyl acetal (**5**) (reaction 2) (1*b*). Again, when the irradiation is carried out in the absence of added nucleophile, no reaction takes place.

Metal salts are known to have a profound effect on photoinduced electron transfer reactions (4). However, the mode of action of the salt has not always been firmly established. It has been suggested that separation of the initially formed radical ion pair ($A^{-\cdot}$ ... $D^{+\cdot}$), to the solvent dissociated radical ions ($A^{-\cdot}$) and ($D^{+\cdot}$) may be facilitated by the addition of salts serving as alternative counterions. Metal salts, particularly magnesium perchlorate, are also known to enhance the lifetime of the radical ion pair, by slowing down the back electron transfer from the sensitizer radical anion to the donor radical cation, presumably through stabilizing ionic interactions of the cation with the radical anion.

One of the main objectives of this work was to determine the effect of added metal salts on the photosensitized (electron transfer) reactions involving the radical cations of 3,3-diphenyltetrahydrofuran (**2**), and methyl 2,2-diphenylcyclopentyl ether

[1]This is part 25 of the series Radical Ions in Photochemistry. Preceding publications in these series are refs 1. and 2.

[2]Author to whom correspondence may be addressed.

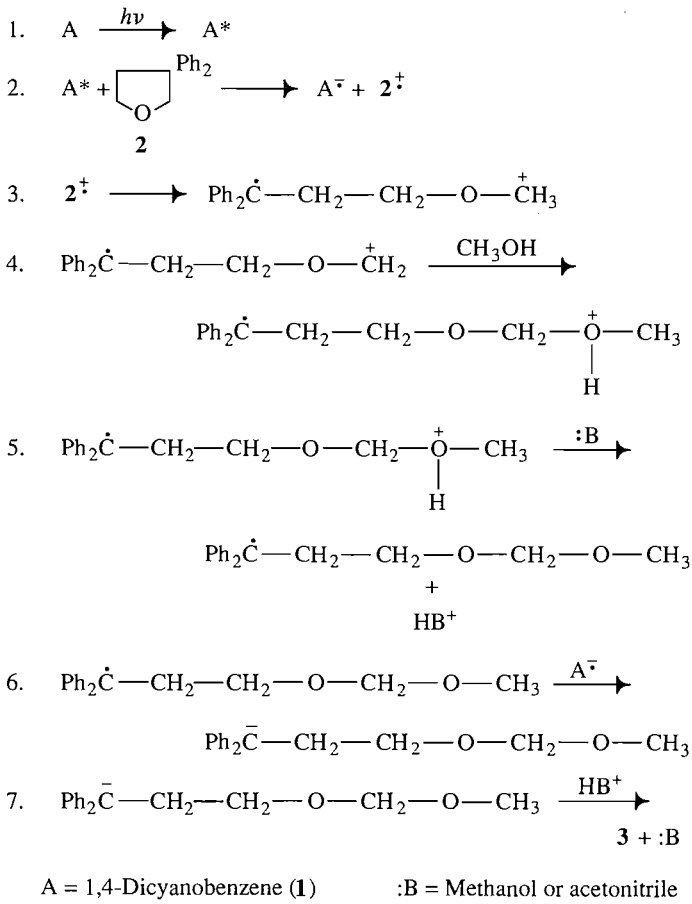

A = 1,4-Dicyanobenzene (**1**) :B = Methanol or acetonitrile

SCHEME 1

(**5**). Our initial thought was that an increase in the lifetime of the 1,5 radical cation might lead to intramolecular cyclization into the terminal phenyl ring, providing a new synthesis of seven-membered ring compounds. There are several examples of this cyclization involving 1,4 radical cations, but this reaction has yet to be observed with 1,5 radical cations (5).

Reaction 2

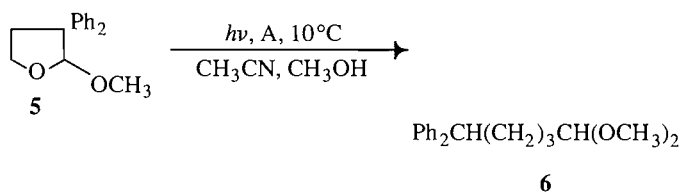

A = 1,4-Dicyanobenzene (**1**)

Results

The irradiation procedure was similar to that used for reactions 1 and 2 except that the solvent was pure acetonitrile, dried in the usual way, and the salt (0.3 M) was added. Progress of the reaction was followed by capillary column gas chromatography using a mass selective detector (gc/ms).

The irradiation of an acetonitrile solution of *para*-dicyanobenzene (**1**) (0.02 M), 3,3-diphenyltetrahydrofuran (**2**) (0.02 M), and magnesium perchlorate (0.3 M) leads to the formation of 4,4-diphenyl-1,3-dioxane (**7**) (45% yield at 86% conversion). A trace of 3,3-diphenylpropanol (**4**) was also detected (gc/ms) (reaction 3). When water (1 M) was added to the solution, the two products **7** and **4** were formed in almost equal amounts, and when the water concentration was increased further (4 M), **4** was the only product. The structural assignment of **7** was based on spectral (^{1}H and ^{13}C nmr, and mass spectra) evidence, in comparison with reported data (6).

Reaction 3 was repeated after having added an equivalent (0.02 M) of water isotopically labelled with ^{17}O (16% enriched). Mass spectral analysis of the isolated product **7** established the fact that ^{17}O (ca. 10%) had been incorporated at the 3-position.

Other perchlorate salts, lithium and tetra-*n*-butyl ammonium, had a similar effect on the photosensitized (electron transfer) reaction of **2**. The major products were **7** and **4** in both reactions. A metal salt with a different anion, lithium trifluoroacetate, was also tried and no **7** was detected after the usual irradiation period.

Reaction 3

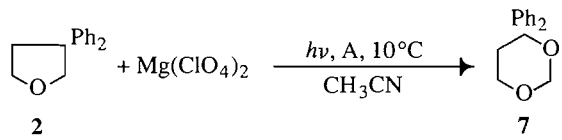

A = 1,4-Dicyanobenzene (**1**)

The irradiation of an acetonitrile solution of **1**, methyl 2,2-diphenylcyclopentyl ether (**5**), and magnesium perchlorate led to formation of 6,6-diphenyl-2-methoxytetrahydropyran (**8**) in 30% yield (reaction 4). The structure of **8**, a new compound, was established by spectral and elemental analyses. The proton at the 2-position appears in the ^{1}H nmr spectrum as a doublet of doublets at 4.44 ppm with coupling constants of 2.17 and 9.69 Hz. This is indicative of a proton shifted downfield by two adjacent oxygen atoms and in the axial position, coupled by an axial–equatorial and an axial–axial proton interaction. From

Reaction 4

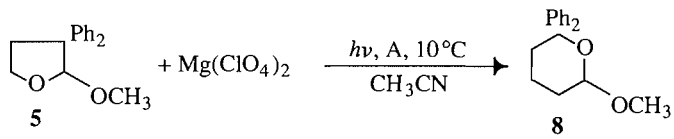

A = 1,4-Dicyanobenzene (**1**)

this we infer that the favoured conformation of this compound places the methoxy group in the equatorial position. This conformation minimizes the repulsive 1,3-diaxial interaction at the expense of the stabilizing anti-periplanar interaction of the polar carbon–oxygen bond of the methoxy group with a nonbonding pair of electrons on the oxygen of the tetrahydropyran ring—the anomeric effect (7).

This irradiation was also carried out in the acetonitrile–water-^{17}O (0.02 M) solution. Mass spectral analysis of the product **8** indicated that ^{17}O (ca. 10%) was incorporated at the 1-position.

In marked contrast to these results observed with the cyclic systems **2** and **5**, the irradiation of the acyclic analogue, methyl 2,2-diphenylethyl ether, under conditions identical to those used for reactions 3 and 4 gave a complex mixture with diphenylmethane as the major product; benzhydrol and methyl diphenylmethyl formaldehyde acetal were only minor products.

Discussion

The mechanism summarized in Scheme 1 is adequate to describe the formation of **3** and **4** from **2** (reaction 1) and **6** from **5** (reaction 2) (1*b*). The additional aspects of the mechanism, required to account for the formation of **7** and **8** (reactions 3 and

Can. J. Chem. Downloaded from www.nrcresearchpress.com by 91.144.44.67 on 09/07/12
For personal use only.

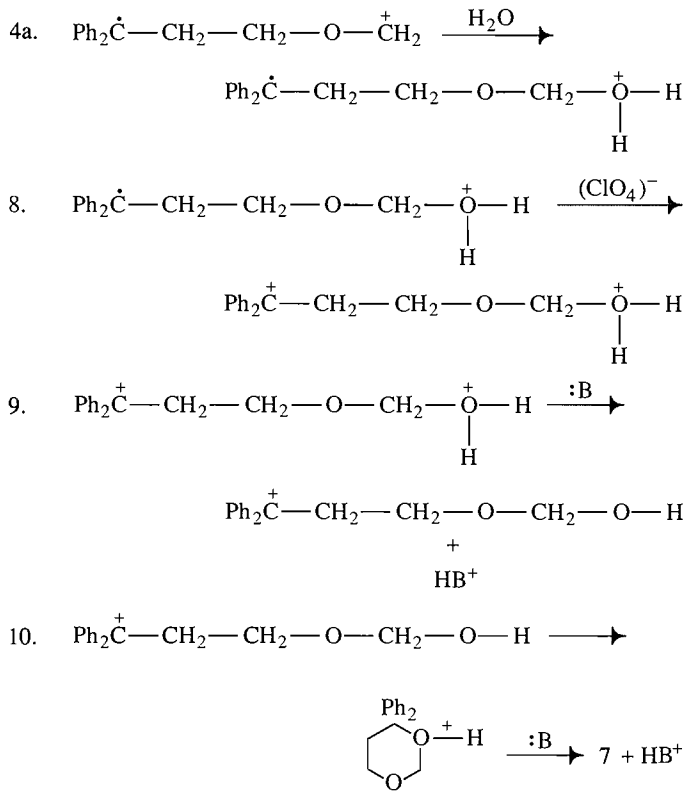

SCHEME 2

4), are outlined in Scheme 2. The initial steps, up to the formation of the 1,5 radical cation, are essentially the same with or without added salts.

Step 4a represents the nucleophilic attack on the cationic site of the 1,5 radical cation by adventitious water. The perchlorate salts that were added to the reaction mixture are hydrated. The procedure used to dry, store, and transfer the acetonitrile may also be inadequate to prevent the introduction of the small amount of water sufficient to trap the carbocation. The involvement of water is indicated by the isotopic oxygen incorporation when an equivalent amount of ^{17}O-enriched water was added to the reaction mixture. An alternative possibility, incorporation of oxygen from the perchlorate anion, seems unlikely; the perchlorate anion is a poor nucleophile.

The key step in the proposed mechanism for formation of **7** and **8** is the further one-electron oxidation of the radical to generate the diphenylalkyl cation (step 8). The most likely oxidant in the reaction mixture is the perchlorate anion, which is known to be a powerful oxidant in acidic media. The acidity of the reaction mixture is difficult to estimate; however, reaction of the cationic site of the 1,5 radical cation with water leads to the distonic 1,6 radical cation that is protonated on the oxygen. The lifetime of this intermediate may be long enough to influence the oxidation potential of the perchlorate anion. The diphenylalkyl radical has a relatively low oxidation potential (ca. 0.23 V) (8). The proximity of the acidic proton in the distonic 1,6 radical cation may account for the fact that these cyclic systems undergo this reaction much more efficiently than the acyclic analogue.

The final step, cyclization of the carbocation to the oxygen through a six-membered cyclic intermediate, is a favourable process (step 10). Cleavage of the acyclic analogue leads rapidly to solvent-separated species and reencounter is less likely.

These reactions are unusual. The photosensitized (electron transfer) process generally involves only a single electron. Products resulting from the transfer of two electrons in the same direction are rarely observed (9). This reaction will add a useful extension to the synthetic utility of the photoinduced electron transfer process. We continue to search for conditions that will favour cyclization of a 1,5 radical cation.

Experimental

General information

The mass spectral analyses were performed on a VG Analytical Instruments double focusing mass spectrometer (reverse geometry), model ZAB-E (ion source: electron impact; accelerating voltage: 8000 V; instrument resolution: 1000; high mass: 300; and low mass: 100). The ^1H nmr spectra were recorded on a Nicolet Magnetics Corp. narrow bore 360 MHz spectrometer and are reported in parts per million downfield from TMS. The ^{13}C nmr spectra were recorded on the Nicolet spectrometer operating at 90 MHz. Infrared spectra were recorded on an air-purged Perkin Elmer 180 grating spectrometer and are reported in wave numbers. The gc/ms analyses were done on an Hewlett Packard 5890A GC/5970 mass selective detector interfaced with an H. P. 9816 microcomputer. The column was 25 m × 0.2 mm, 5% phenyl methyl silicone on fused silica with a film thickness of 0.25 μm. Combustion analysis was performed by Canadian Microanalytical Services Ltd., Vancouver, B.C. Acetonitrile (Fisher ACS grade) was distilled successively from sodium hydride and phosphorus pentoxide, and was then passed through a column of basic alumina, refluxed over calcium hydride for 24 h (under a nitrogen atmosphere), and fractionally distilled. The preparation of **2** and **5** and the conditions for the irradiation have been described (1).

Irradiations

Irradiation of 3,3-diphenyltetrahydrofuran (2)

A solution of 3,3-diphenyltetrahydrofuran (**2**) (168 mg, 7.49×10^{-4} mol), *para*-dicyanobenzene (**1**) (84 mg, 6.5×10^{-4} mol), and magnesium perchlorate (1.272 g) in 30 mL acetonitrile was irradiated at 10°C for 50 h. Flash column chromatography using 90% methylene chloride and 10% hexanes was employed to separate the product, 4,4-diphenyl-1,3-dioxane (**7**), from the starting material **2** and the photosensitizer **1**. At 86% conversion, the acetal **7** was obtained in 45% yield; ^1H nmr (360 MZ) in $CDCl_3$: 7.22–7.39(m, 10H), 4.94(s, 2H), 3.96(t, 2H, J = 5.4 Hz), 2.52(t, 2H, J = 5.4 Hz) (in agreement with the reported spectrum (6)); ^{13}C nmr (90 Mz) in $CDCl_3$: 144.6, 132.3, 128.4, 127.8, 127.0, 126.2, 89.3, 79.4, 63.9, 35.5. Trace amounts of 3,3-diphenylpropanol (**4**) and benzonitrile were detected (gc/ms) and were identified by comparison (mass spectra and retention times) with authentic samples.

Incorporation of ^{17}O in the reaction product 7

Conditions similar to those described above were used except one mole equivalent of water-^{17}O (16% enriched) was added to the reaction mixture. The product, **7**, was isolated as described above and mass spectral analyses were done using the ZAB-E mass spectrometer. The ^{17}O-enriched product showed an increase in the $M+1$ peak relative to the molecular ion peak of 8.2 ± 0.6% relative to the unenriched product, **7**. An increase in the mass peak (m/z) 211 relative to 210, corresponding to a loss of formaldehyde, of 9.6 ± 2.1% was observed relative to the unenriched product **7**. The mass peak 183 relative to 182 (loss of C_3H_6O) showed an increase of 11.5 ± 3.2% relative to the unenriched product **7**.

Irradiation of methyl 2,2-diphenylcyclopentyl ether (5)

A solution of methyl 2,2-diphenylcyclopentyl ether (**5**) (502 mg, 1.99×10^{-3} mol), *para*-dicyanobenzene (**1**) (255 mg, 1.99×10^{-3} mol), and magnesium perchlorate (1.34 g) in 30 mL acetonitrile was irradiated at 10°C for 24 h. Gradient medium pressure liquid chromatography (mplc) using methylene chloride and hexanes as eluent separated the product, 2,2-diphenyl-6-methoxytetrahydropyran (**8**), from the photosensitizer **1**. Trace amounts of benzonitrile were detected by

Can. J. Chem. Downloaded from www.nrcresearchpress.com by 91.144.44.67 on 09/07/12
For personal use only.

gc/ms. The acetal (**8**) was recrystallized from ethanol–water to yield colourless needles (mp 74–76°C) in 30% yield; ir (PE 180) neat: 3090(m), 3065(m), 3025(m), 2990(m), 2955(s), 2845(m), 1595(m), 1495(s), 1460(s), 1445(s), 1395(s), 1355(s), 755(s), 695(s); ^{1}H nmr (360 MHz) in $CDCl_3$: 7.49–7.09(m, 10H), 4.44 (dd, 1H, J = 2.17 Hz, 9.69 Hz), 3.57 (s, 3H), 2.67–2.62 (m, 1H) 1.87–1.74 (m, 5H); ^{13}C nmr (90 MHz) in $CDCl_3$: 148.6 (t, J = 7.4 Hz),143.0 (dt, J = 6.9 Hz, 13.2 Hz), 128.6 (dd, J = 7.6 Hz, 160.2 Hz), 127.9 (dd, J = 7.7 Hz, 159.7 Hz), 127.1 (dt, J = 7.1 Hz, 157.7 Hz), 126.9 (dt, J = 7.6 Hz, 160 5 Hz), 126.3 (dt, J = 7.5 Hz, 160.3 Hz), 124.8 (dt, J = 6.8 Hz, 159.3 Hz), 98.7 (dm, J = 154.0 Hz), 80.7 (s), 55.8 (dq, J = 4.3 Hz, 142.2 Hz), 34.4 (mt, J = 5.6 Hz, 110 Hz, 129.5 Hz), 30.9(mt, J = 3.5 Hz, 7.1 Hz, 128.8 Hz), 19.8 (mt, J = 128.1 Hz); ms: 268, 252, 236, 208, 203, 180, 165, 152, 128, 115, 105, 91, 77. Anal. calcd. for $C_{18}H_{20}O_2$: C 80.56, H 7.51; found: C 80.62, H 7.69.

Incorporation of ^{17}O in the reaction product 8

Irradiation of similar mixtures of **1**, **5**, and $Mg(ClO_4)_2$ in acetonitrile containing one mole equivalent of water-^{17}O (16% enrichment) led to the incorporation of ^{17}O in the product **8**, which was isolated by the procedure described above. Mass spectral analyses were carried out using the ZAB-E mass spectrometer on the product, and the ratio of relevant peaks was compared with the ratio observed from the unenriched product. The molecular ion was not normally observed in this case. The relative abundance of the peak (m/z) 237 to 236 (loss of methanol) showed an increase of 2.3 ± 5.1% relative to the unenriched **8**. Mass peaks 209/208 (loss of C_3H_8O) showed an increase of 9.1 ± 0.3% and the mass peaks of 181/180 showed an increase of 5.0 ± 0.3% relative to the unenriched product **8**.

Acknowledgments

Acknowledgment is made to the Natural Sciences and Engineering Research Council of Canada for support of this work. We thank Dr. D. L. Hooper and the Atlantic Regional Magnetic Resonance Centre at Dalhousie University for the 360 MHz nmr spectra and for help in the preparation of the manuscript. We also thank Dr. R. K. Boyd and Mr. D. J. Embree at the Atlantic Regional Laboratories of the National Research Council of Canada for the mass spectra run on the ZAB-E spectrometer.

1. (*a*) D. R. Arnold and L. J. Lamont, Can. J. Chem. **67**, 2119 (1989); (*b*) D. R. Arnold, B. J. Fahie, L. J. Lamont, J. Wierzchowski, and K. M. Young. Can. J. Chem. **65**, 2734 (1987).
2. (*a*) R. Popielarz and D. R. Arnold, J. Am. Chem. Soc. In press; (*b*) X. Du and D. R. Arnold. J. Am. Chem. Soc. **111**, 7666 (1989).
3. D. R. Arnold and A. J. Maroulis. J. Am. Chem. Soc. **98**, 5931 (1976).
4. (*a*) C. Pac, T. Ohtsuki, T. Fukunaga, S. Yanagida, and H. Sakurai. Chem. Lett. 1855 (1985); (*b*) T. Gotoh, M. Kato, M. Yamamoto, and Y. Nishijima. J. Chem. Soc. Chem. Commun. 90 (1981); (*c*) K. Mizuno, N. Ichinose, and Y. Otsuji. Chem. Lett. 455 (1985); (*d*) B. E. Goodson and G. B. Schuster. J. Am. Chem. Soc. **106**, 7254 (1984); (*e*) D. R. Arnold and M. S. Snow. Can. J. Chem. **66**, 3012 (1988); (*f*) F. O. Lewis and J. R. Petisce. Tetrahedron, **42**, 6207 (1986).
5. (*a*) R. A. Neunteufel and D. R. Arnold. J. Am. Chem. Soc. **95**, 4080 (1973); (*b*) D. R. Arnold, R. M. Borg, and A. Albini. J. Chem. Soc. Chem. Commun. 138 (1981); (*c*) A. J. Maroulis and D. R. Arnold. J. Chem. Soc. Chem. Commun. 351 (1979); (*d*) S. L. Mattes and S. Farid. J. Am. Chem. Soc. **105**, 1386 (1983); (*e*) T. Asanuma, T. Gotoh, A. Tsuchida, M. Yamamoto, and Y. Nishijima. J. Chem. Soc. Chem. Commun. 485 (1977); (*f*) K. Yamaguchi, S.-C. Oh, and Y. Shirota. Chem. Lett. 1445 (1986).
6. R. Todesco, D. Van Bockstaele, J. Gelan, H. Martens, J. Put, and F. C. DeSchryver. J. Org. Chem. **48**, 4963 (1983).
7. (*a*) P. Deslongchamps. Stereoelectronic effects in organic chemistry. Pergamon Press, Toronto. 1983. Chap. 2; (*b*) H. Booth, T. B. Grindley, and K. A. Khedhair. J. Chem. Soc. Chem. Commun. 1047 (1982).
8. D. D. M. Wayner, D. J. McPhee, and D. Griller. J. Am. Chem. Soc. **110**, 132 (1988).
9. K. Mizuno, J. Ogawa, H. Kagano, and Y. Otsuji. Chem. Lett. 437 (1981).

Can. J. Chem. Downloaded from www.nrcresearchpress.com by 91.144.44.67 on 09/07/12
For personal use only.

Abietinarins A and B, cytotoxic metabolites of the marine hydroid *Abietinaria* sp.[1]

CHARLES PATHIRANA AND RAYMOND J. ANDERSEN[2]
Departments of Chemistry and Oceanography, University of British Columbia, Vancouver, B.C., Canada V6T 1W5
AND
JEFFREY L. C. WRIGHT
National Research Council of Canada, Atlantic Research Laboratory, Halifax, N.S., Canada B3H 3Z1

Received September 20, 1989

CHARLES PATHIRANA, RAYMOND J. ANDERSEN, and JEFFREY L. C. WRIGHT. Can. J. Chem. **68**, 394 (1990).

Abietinarins A (**1**) and B (**2**), two new 1-[4*H*]-anthracenone derivatives, have been isolated from the Northeastern Pacific marine hydroid *Abietinaria* sp. The proposed structures for abietinarins A (**1**) and B (**2**) are based on spectroscopic analysis. Abieitinarin A (**1**) exhibited significant cytotoxicity in an in vitro L1210 bioassay.

Key words: cytotoxic, hydroid, abietinarins, metabolites, marine.

CHARLES PATHIRANA, RAYMOND J. ANDERSEN et JEFFREY L. C. WRIGHT. Can. J. Chem. **68**, 394 (1990).

À partir de l'*Abietinaria* sp., un hydroïde marin du nord-ouest du Pacifique, on a isolé deux nouveaux dérivés 1-[4*H*]-anthracénones, les abiétinarines, A (**1**) et B (**2**). Les structures proposées pour les abiétinarines A (**1**) et B (**2**) son basées sur des analyses spectroscopiques. L'abiétinarine A (**1**) présente une cytotoxicité importante dans des bioessais in vitro avec le L1210.

Mots clés : cytotoxique, hydroïde, abiétinarines, métabolites, marin.

[Traduit par la revue]

Can. J. Chem. Downloaded from www.nrcresearchpress.com by 91.144.44.67 on 09/07/12
For personal use only.

The smallest common members of the invertebrate phylum Cnidaria are the marine hydroids (class Hydrozoa). Very little is known about the taxonomy and natural history of most hydroids and there is a corresponding lack of knowledge about hydroid secondary metabolism. The handful of hydroids examined to date have yielded a variety of polyhydroxylated steroids (1), a series of halogenated monoterpenoids (2), a family of brominated β-carbolines (3), a group of polyketide derived aromatic antibiotics (4), and a cytotoxic diphenyl-*p*-menthane derivative (5). A broad screening program carried out by the Atlantic Research Laboratory of the National Research Council of Canada, designed to discover bioactive metabolites in marine invertebrates collected from Canadian coastal waters, uncovered weak antiviral activity and host-cell cytotoxicity in extracts of the hydroid *Abietinaria* sp. Bioassay-guided fractionation of the *Abietinaria* sp. extracts led to the isolation of two new cytotoxic metabolites, abietinarins A (**1**) and B (**2**), whose structures we now wish to report.

Samples of *Abietinaria* sp. were collected by hand using SCUBA off the southern coast of Vancouver Island, B.C. Freshly collected hydroid specimens were immediately frozen and stored below −5°C until needed. Thawed samples of *Abietinaria* sp. (1 kg dry wt.) were extracted whole with methanol at room temperature for 24 h prior to the removal of the solids by vacuum filtration. Concentration of the methanol filtrate *in vacuo* gave an aqueous suspension that was exhaustively extracted with dichloromethane. Fractionation of the dichloromethane soluble material by Sephadex LH 20 chromatography (MeOH) gave a crude mixture of the abietinarins. Further separation of this crude mixture by silica gel high performance liquid chromatography (CH_3CN/CH_2Cl_2 3:97) gave pure samples of abietinarins A (**1**) (4 mg) and B (**2**) (2.5 mg).

Abietinarin A (**1**), obtained as a yellow solid, gave a parent ion in the electron impact high resolution mass spectrum (EIHRMS) at *m/z* 314.1520 Da appropriate for a molecular formula of $C_{19}H_{22}O_4$ (ΔM +0.2 mmu). Prominent peaks at *m/z* 296.1405 ($C_{19}H_{20}O_3$; ΔM −0.7 mmu) and *m/z* 281.1170 ($C_{18}H_{17}O_3$; ΔM −0.7 mmu) Da in the mass spectrum of **1** were assigned to ($M^+ - H_2O$) and ($M^+ - H_2O - CH_3$) fragment ions, respectively. The limited amount of abietinarin A available prevented us from obtaining a satisfactory ^{13}C NMR spectrum. Fortunately, however, the information obtained from a series of ^1H NMR experiments, when combined with the IR and mass spectral data, proved sufficient to define the structure of abietinarin A (**1**).

The observation of a series of scalar and dipolar $^1H/^1H$ couplings identified the naphthalenic fragment "**i**" in abietinarin A. Double resonance experiments showed that a pair of aromatic proton resonances at δ 6.84 (H7) and 6.99 (H5) were *meta* coupled (J = 2.5 Hz). The upfield resonance (δ 6.84; H7) was also scalar coupled to an aromatic methyl resonance that appeared at δ 2.86 (Me14), indicating that the methyl group was *ortho* to the aromatic proton. Irradiation of this aromatic methyl resonance induced a nOe in the upfield aromatic resonance (δ 6.84: H7) in agreement with this assignment. Irradiation of the downfield aromatic resonance (δ 6.99: H5) induced nOe's in a deshielded methyl resonance (δ 3.89: OMe), assigned to an aromatic methyl ether, as well as in a third aromatic proton resonance at δ 7.06 (H10). The lack of scalar coupling between this latter aromatic resonance and the two other aromatic resonances indicated that the methyl ether had to occupy the position between the *meta* coupled protons, and that the third aromatic proton (δ 7.06: H10) had to be on an adjacent ring as shown in "**i**". A nOe observed between the aromatic methyl resonance at δ 2.86 (Me14) and a highly deshielded resonance at δ (15.45 (OH9), assigned to a chelated phenolic proton, revealed the spatial proximity of the methyl and phenolic functionalities as shown.

The remaining fragment of abietinarin A had to account for an elemental composition of $C_7H_{12}O_2$ and two sites of unsaturation. An intense band at 1619 cm^{-1} in the IR spectrum of **1** was assigned to a carbonyl stretching vibration. The frequency of the band was nearly identical to that observed for the C1 ketone functionality (1620 cm^{-1}) in the previously reported metabolite

[1]NRCC No. 30853.
[2]Author to whom correspondence may be addressed.

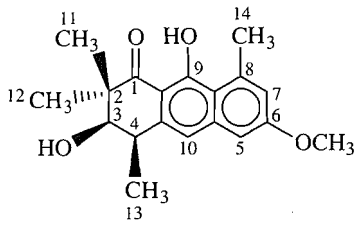

1

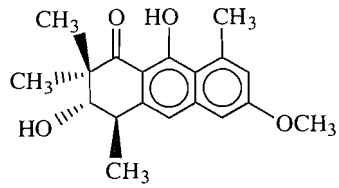

2

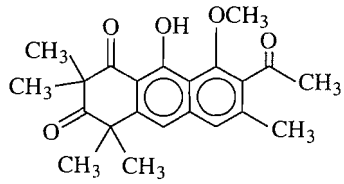

3

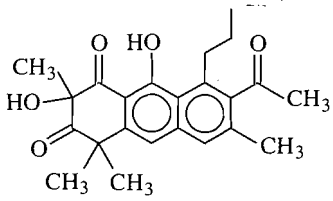

4

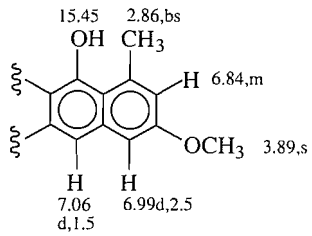

"i"

garveatin C (**3**) (4*a*). This similarity in carbonyl stretching frequencies suggested that there was a ketone functionality (C1) attached *ortho* to the phenolic hydroxyl in fragment "**i**" of abietinarin A. The downfield shift of the phenolic OH resonance (δ 15.45: OH9) was consistent with intramolecular hydrogen bonding between the phenol and C1 ketone, as expected in this arrangement of functional groups. Double resonance experiments identified a seven spin system in the ^{1}H NMR spectrum of abietinarin A that consisted of a methine resonance at δ 3.70 (H3), coupled to an exchangeable resonance at δ 2.99 (OH3) and to another methine resonance at δ 3.37 (H4), which was in turn coupled to a methyl resonance at δ 1.48 (Me13) and to the previously assigned aromatic resonance at δ 7.06 (H10) (Table 1). The scalar coupling between the methine resonance at δ 3.37 (H4) and the aromatic resonance at δ 7.06 (H10) was assigned to allylic coupling, which required that a methine carbon (C4), bearing a methyl group (Me13) and another methine carbon (C3), be attached *ortho* to H10 on fragment "**i**". The most deshielded resonance in this spin system (δ 3.70: H3) was assigned to a carbinol methine residue on the basis of its chemical shift and its observed scalar coupling to an exchangeable resonance at δ 2.99, assigned to an alcohol proton. The remaining carbon and hydrogen atoms (C_3H_6) in abietinarin A could be accounted for by a pair of geminal methyls (δ 1.24, s, Me12: 1.32, s, Me11) and an attached quaternary carbon. Linking the quaternary carbon to the C1 ketone and the C3 methine carbons created a six-membered ring, which accounted for the final site of unsaturation in abietinarin A (**1**).

The relative stereochemistry of the hydroxyl and methyl groups at C3 and C4 in abietinarin A (**1**) was assigned as *cis* on the basis of the 2.5 Hz vicinal coupling observed between H3 and H4. In either possible half-chair conformation of the aliphatic ring, the H3 and H4 protons have pseudoequatorial/pseudoaxial relationships with each other resulting in a dihedral angle of approximately 60°, which is consistent with the small vicinal H3/H4 coupling constant. Irradiation of the Me12 resonance at δ 1.24 induced nOe's in H3 (δ 3.70) and H4 (δ 3.37) in agreement with the assigned stereochemistry. The nOe results also indicated that the preferred conformation of the aliphatic ring has the C3 hydroxyl in a pseudoaxial orientation and the C4 methyl in a pseudoequatorial orientation.

TABLE 1. ^{1}H NMR data for abietinarins A (**1**) and B (**2**). Recorded in CD_3CN at 400 MHz. Chemical shifts are in ppm from internal TMS

Proton	Abietienarin A (**1**)	Abietinarin B (**2**)
H3	3.70, dd, J = 2.5, 5.2 Hz	3.48, d, J = 11 Hz
H4	3.37, ddq, J = 1.5, 2.5, 7 Hz	2.93, ddq, J = 1.5, 11, 7 Hz
H5	6.99, d, J = 2.5 Hz	7.01, d, J = 2.5 Hz
H7	6.84, m	6.82, m
H10	7.06, d, J = 1.5 Hz	7.19, d, J = 1.5 Hz
OH3	2.99, d, J = 5.5 Hz	—
OH9	15.45, s	15.53, s
Me11	1.32, s	1.14, s
Me12	1.24, s	1.14, s
Me13	1.48, d, J = 7 Hz	1.52, d, J = 7 Hz
Me14	2.86, bs	2.86, bs
OMe	3.89, s	3.88, s

Abietinarin B (**2**), isolated as a pale yellow oil, gave a parent ion in the EILRMS at m/z 314 Da, suggesting that it had the same molecular formula as abietinarin A (**1**). The ^{1}H NMR (Table 1) and IR spectra of abietinarin B (**2**) closely resembled the corresponding spectra of abietinarin A (**1**), revealing that the two metabolites were very similar in structure. In particular, the aromatic resonances were virtually identical in the ^{1}H NMR spectra of both metabolites, indicating that they contained identical naphthalenic fragments "**i**". A series of upfield resonances in the ^{1}H NMR spectrum of abietinarin B (**2**) could be assigned to the *gem*-dimethyl (**2**: δ 1.14, s, 6H: Me11 and

Can. J. Chem. Downloaded from www.nrcresearchpress.com by 91.144.44.67 on 09/07/12
For personal use only.

Me12), carbinol methine (**2**: δ 3.48, d, J = 11 Hz: H3) benzylic methine (**2**: δ 2.93, br dq, J = 11, 7 Hz: H4) and secondary methyl (**2**: δ 1.52, d, J = 7 Hz: Me13) functionalities found in the aliphatic ring of abietinarin A (**1**). The coupling constant observed between H3 and H4 in abietinarin B (**2**) (J = 11 Hz) implied that both of these protons occupied pseudoaxial orientations and, therefore, that the C3 hydroxyl and Me13 were *trans* to each other. Double resonance and nOe experiments confirmed the proposed connectivities in abietinarin B (**2**) just as they had in abietinarin A (**1**). Hence, abietinarin B (**2**) is simply a diastereomer of abietinarin A (**1**), having the opposite configuration at either C3 or C4.

Abietinarins A (**1**) and B (**2**) are closely related to the garveatins (e.g., garveatin C (**3**)) and the garvins (e.g., 2-hydroxygarvin A (**4**)) previously isolated from the Northeastern Pacific hydroid *Garveia annulata* (4*b*). *Abietinaria* sp. thus becomes the second hydroid known to elaborate 1-[4*H*]-anthracenone-based polyketide-derived metabolites. Abietinarin A (**1**) exhibited significant cytotoxicity in an in vitro L1210 bioassay (ED_{50} <10 μg/mL).[3] The small amount of abietinarin B (**2**) available prevented us from testing its cytotoxicity.

Experimental

Abietinarins A(**1**) and B(**2**) were extracted and purified as described in the text.

[3]Carried out by Dr. T. Allen, Department of Pharmacology, University of Alberta, Edmonton.

Abietinarin A(1): pale yellow amorphous solid; IR (film): 3384, 1619, 1606, 1462, 1389, 1309, 1256, and 1201 cm^{-1}; ^1H NMR, see Table 1, ^{13}C NMR (CD_3CN, 75 MHz: only intense aliphatic resonances were observed) δ: 17.3, 22.5, 25.3, 34.8, 56.2, 81.5; LRMS m/z: M^+ 314 (base peak), 296, 281, 253; CIMS (CH_4) m/z: MH^+ 315, 314; EIHRMS m/z: M^+ 314.1520 ($C_{19}H_{22}O_4$; ΔM +0.2 mmu).

Abietinarin B(2): pale yellow amorphous solid; IR (film): 3380, 1619 cm^{-1}; ^1H NMR, see Table 1; EILRMS m/z: M^+ 314 (base peak), 296, 281, 253.

Acknowledgements

This work was funded by a DSS contract (no. 31028-7-8442) and the National Cancer Institute of Canada.

1. (*a*) A. Aiello, E. Fattorusso, and S. Magno. J. Nat'l Prod. **50**, 191 (1987); (*b*) E. Fattorusso, V. Lanzotti, S. Magno, and E. Novellino. J. Org. Chem. **50**, 2868 ((1985); (*c*) G. Cimono, S. De Rosa, S. De Stephano, and G. Sodano. Tetrahedron Lett. **21**, 3303 (1980).
2. L. De Napoli, E. Fattorusso, S. Magno, and L. Mayol. Biochem. Syst. Ecol. **12**, 321 (1984).
3. A. Aiello, E. Fattorusso, S. Magno, and L. Mayol. Tetrahedron, **43**, 5929 (1987).
4. (*a*) E. Fahy, R. J. Andersen, C. F. Xu, and J. Clardy. J. Org. Chem. **51**, 5145 (1986); (*b*) E. Fahy and R. J. Andersen. Can. J. Chem. **65**, 376 (1987); (*c*) E. Fahy, R. J. Andersen, G. D. Van Duyne, and J. Clardy. J. Org. Chem. **51**, 57 (1986).
5. C. Pathirana, R. J. Andersen, and J. C. L. Wright. Tetrahedron Lett. **30**, 1487 (1989).

Can. J. Chem. Downloaded from www.nrcresearchpress.com by 91.144.44.67 on 09/07/12
For personal use only.

The chlorination of isobutyrophenone: determination of its pK_a value and of the course of the reaction

J. PETER GUTHRIE[1] AND JOHN COSSAR
Department of Chemistry, University of Western Ontario, London, Ont., Canada N6A 5B7

Received July 4 1989

J. PETER GUTHRIE and JOHN COSSAR. Can. J. Chem. **68**, 397 (1990).

Chlorination of isobutyrophenone in alkaline aqueous solution leads to formation of α-hydroxyisobutyrophenone as the first detectable intermediate; a slow subsequent oxidation gives benzoate. From the rates of the initial chlorinations we have been able to determine the pK_a value for the ketone as 18.18 ± 0.50. α-Chloroisobutyrophenone undergoes surprisingly rapid alkaline hydrolysis, $k_{OH} = 71.9 \pm 1.5\ M^{-1}\ s^{-1}$.

Key words: isobutyrophenone, chlorination, enolization, pK_a, hydrolysis.

J. PETER GUTHRIE et JOHN COSSAR. Can. J. Chem. **68**, 397 (1990).

La chloration de l'isobutyrophénone, réalisée en solution alcaline, conduit à la formation de l'α-hydroxyisobutyrophénone comme premier intermédiaire détectable; une oxydation ultérieure lente conduit au benzoate. Sur la base des vitesses initiales de chloration, on a déterminé que la valeur du pK_a pour la cétone est égale à 18,18 ± 0,50. La vitesse d'hydrolyse alcaline de l'α-chloroisobutyrophénone est étonnamment rapide, $k_{OH} = 71{,}9 \pm 1{,}5\ M^{-1}\ s^{-1}$.

Mots clés : isobutyrophénone, chloration, énolisation, pK_a, hydrolyse.

[Traduit par la revue]

Can. J. Chem. Downloaded from www.nrcresearchpress.com by 91.144.44.67 on 09/07/12
For personal use only.

Introduction

We have developed a method for determining pK_a values of simple ketones by analysis of the kinetics of chlorination in alkaline solution (1, 2). This method has been applied to a series of ring substituted acetophenones (3). We now wish to report its application to isobutyrophenone. Isobutyrophenone would have been expected to undergo ready monochlorination to produce α-hydroxyisobutyrophenone. We found that in fact α-hydroxyisobutyrophenone is the only detectable intermediate, and that this undergoes further reaction with hypochlorite to give benzoate.

Results

Biphasic kinetics were observed, with an initial rapid reaction followed by a tenfold slower reaction. The overall kinetics of chlorination of isobutyrophenone could be followed by UV, and showed two well-separated phases. A product isolation experiment after the first reaction had run to completion (about 14 half-lives for the first reaction and one for the second) showed 43% α-hydroxyisobutyrophenone and 57% benzoic acid, with no other detectable components. In the initial kinematics experiments the progress of reaction was followed at 292 nm, λ_{max} for OCl^-. At this wavelength there is an initial rapid decrease in absorbance followed by a larger, slower decrease. Interpretation of the absorbance change was simpler when reaction was followed at 230 nm, where the extinction coefficient of OCl^- is small. At 230 nm there was an initial decrease in absorbance followed by a slower increase. In both cases the integrated rate law was of the form:

$$[1]\quad \text{Absorbance} = a_1 + a_2 \exp(-a_3 t) + a_4 \exp(-a_5 t)$$

For a reaction of the type:[2]

$$\text{iBP} \xrightarrow{k_1} \text{HBP} \xrightarrow{k_2} \text{BA}$$

where k_1 and k_2 are pseudo-first-order rate constants including $[OCl^-]$, which is effectively constant within an experiment, we find that:

$$[\text{iBP}] = [\text{iBP}]_0 \exp(-k_1 t)$$

$$[\text{HBP}] = [\text{iBP}]_0\{k_1/(k_2 - k_1)\} \times \{\exp(-k_1 t) - \exp(-k_2 t)\}$$

$$[OCl^-] = [OCl^-]_0 - n[\text{iBP}]_0 + [\text{iBP}]_0(1 + k_2 n/(k_2 - k_1)) \exp(-k_1 t) + [\text{iBP}]_0 n k_1/(k_2 - k_1) \exp(-k_2 t)$$

$$[\text{BA}] = [\text{iBP}]_0\{1 + 1/(k_1 - k_2)\} \times \{k_2 \exp(-k_1 t) - k_1 \exp(-k_2 t)\}$$

$$[2]\quad \text{Absorbance}/l = \epsilon_{\text{iBP}}[\text{iBP}] + \epsilon_{\text{HBP}}[\text{HBP}] + \epsilon_{OCl}[OCl^-] + \epsilon_{\text{BA}}[\text{BA}]$$

$$= \epsilon_{OCl}\{[OCl]_0 - n[\text{iBP}]_0\} + \epsilon_{\text{BA}}[\text{iBP}]_0 + \exp(-k_1 t)\{\epsilon_{\text{iBP}}[\text{iBP}]_0 + \epsilon_{\text{HBP}} k_1[\text{iBP}]_0/(k_2 - k_1) + \epsilon_{OCl}[\text{iBP}]_0(1 + nk_2/(k_2 - k_1)) + \epsilon_{\text{BA}} k_2/(k_1 - k_2)\} + \exp(-k_2 t)\{-[\text{iBP}]_0 k_1/(k_2 - k_1)\}\{\epsilon_{\text{HBP}} + n\epsilon_{OCl} - \epsilon_{\text{BA}}\}$$

$$n = (a_1/(l\epsilon_{OCl}) - [OCl^-]_0)/[\text{iBP}]_0$$

where n = the number of moles of hypochlorite consumed per mole of isobutyrophenone in the complete reaction; we assume that the first phase consumes one mole of hypochlorite per mole of ketone. The validity of this assumption is shown by the good agreement of observed and calculated values of a_2: see below.

For kinetics followed at 230 nm the expression for absorbance is simplified by setting ϵ_{OCl} to zero; for kinetics followed at 292 nm the expression is simplified by setting ϵ_{BA} to zero.

For experiments at 292 nm, n can be calculated for the runs

[1]Author to whom correspondence may be addressed.

[2]Abbreviations used: iBP, isobutyrophenone; HBP, α-hydroxyisobutyrophenone; BA, benzoic acid.

Can. J. Chem. Downloaded from www.nrcresearchpress.com by 91.144.44.67 on 09/07/12
For personal use only.

where both exponential terms were evaluated. The values so obtained are found in Table 1. These values require that more than one mole of hypochlorite be consumed as a result of the second phase of reaction. Upon reflection it is clear that in addition to the cleavage of α-hydroxyisobutyrophenone, which is expected to consume one mole of hypochlorite, there should also be a rapid consumption of the acetone produced as a by-product with a stoichiometry of 2 moles of hypochlorite per acetone at a high $[OCl^-]/[OH^-]$ ratio, and 3 moles of hypochlorite at a low $[OCl^-]/[OH^-]$ ratio (2). This expectation is approximately fulfilled, although some runs showed higher than expected stoichiometries. It is possible to calculate values of the parameters a_2 and a_4 from n, the rate constants, and the extinction coefficients. When this is done the values obtained are in reasonable agreement with the observed values. The average ratios of calculated to observed parameters were a_2, 0.96 ± 0.17; a_4, 1.03 ± 0.06. One reason for imperfect agreement is that the very slow second phase was not followed as long as would be desirable, and often to only one or two half-lives, so that the least-squares parameters are uncertain, and subject to correlation. For runs in part (a) of Table 1, the initial excess of OCl^- is often too small to preserve good pseudo-first-order conditions throughout the second phase, although it is always large enough for the first phase to be pseudo first order. That this was the case became clear only as the stoichiometry was determined. In consequence, the rate constants determined in these experiments are bound to be less accurate. For runs in part (b) of Table 1, the excess of OCl^- is larger and these problems do not arise. There is no obvious trend when data from both sets are compared in plots, so we have used all of the data in the least-squares analysis presented below.

For reactions followed at 230 nm, the interpretation of a_1, a_2, and a_4 is simpler:

$$a_1/l[\text{iBP}]_0 = \epsilon_{BA}$$

$$a_2/l[\text{iBP}]_0 = \epsilon_{iBP} + \epsilon_{HBP}k_1/(k_2 - k_1)$$

$$a_4/l[\text{iBP}]_0 = -k_1/(k_2 - k_1)\{\epsilon_{HBP} - \epsilon_{BA}\}$$

The calculated values are in reasonable accord with the parameters from least-squares fitting. The average ratios of calculated to observed values were a_1, 0.98 ± 0.07; a_2, 1.16 ± 0.04; a_4, 1.19 ± 0.04.

We prepared α-chloroisobutyrophenone and measured its rate of hydrolysis to confirm that this was rapid relative to its formation by chlorination of isobutyrophenone. We also prepared α-hydroxyisobutyrophenone and showed that its rate of reaction with hypochlorite matched the second phase of reaction of isobutyrophenone.

For low concentrations of hydroxide it was necessary to use quite low concentrations of hypochlorite to make chlorination the rate determining step for the initial phase of the reaction; this made both phases slow, and the second phase very slow indeed. Kinetics under conditions where chlorination was clearly rate limiting were needed to determine the pK_a of isobutyrophenone; these kinetics were not possible by the UV method because the low concentrations of hypochlorite involved (with hypochlorite in excess) led to very small absorbance changes. By HPLC we could follow either the disappearance of isobutyrophenone (with OCl^- in excess) or the appearance of α-hydroxyisobutyrophenone (with ketone in excess). In the latter situation, $d[\text{HBP}]/dt = k_{obs}[\text{iBP}][OCl^-]$ and, since [iBP] is essentially fixed, pseudo-first-order conditions prevail. For isobutyrophenone there can be no question but that the stoichiometry number is 1 for the initial reaction. In general one must remember that the observed rate includes the stoichiometry number, for ketine in excess conditions, but not for hypochlorite in excess conditions (1). All of these rate constants are found in Table 1.

For substituted acetophenones we have found that the first chlorination step was rate determining under the usual conditions for chlorination kinetics (3), and the observed rates followed the rate law given in eq. [3]:

$$[3] \quad \begin{aligned} v &= k_{obs}[\text{Ketone}] \\ k_{obs} &= \{k_{II}^0 + k_{II}^-[OH^-]\}[OCl^-] \end{aligned}$$

If the same rate law applied for isobutyrophenone, then in terms of Scheme 1,

$$k_{II}^0 = k_{12}k_{23}^0K_w/k_{21}K_a^{HOCl}, \quad \text{and} \quad k_{II}^- = k_{12}k_{23}^-/k_{21}.$$

For the initial phase of the kinetics, where the rate of chlorination of isobutyrophenone is being followed, it was found that the pseudo-first-order rate constants for a set of experiments at fixed hydroxide concentration were not linearly dependent upon hypochlorite concentration, but showed a tendency to level off at high $[OCl^-]$. Thus, for isobutyrophenone enolate, halogenation and reprotonation are competitive. For this situation we may derive the expression for the rate law given in eq. [4]:

$$[4] \quad k_{obs} = \frac{k_{12}(k_{23}^0K_w/K_a^{HOCl} + k_{23}^-[OH^-])[OCl^-]}{k_{21} + (k_{23}^0K_w/K_a^{HOCl} + k_{23}^0[OH^-])[OCl^-]}$$

This may be transformed into a form convenient for fitting to the data, shown in eq. [5]:

$$[5] \quad k_{obs} = (a_1 + a_2[OH^-])/(1/[OCl^-] + a_1/a_3[OH^-] + a_2/a_3)$$

where $a_1 = k_{II}^0$, $a_2 = k_{II}^-$, and $a_3 = k_{12}$. The data from Table 1 were fitted to eq. [5]. Figure 1 shows the dependence of the corresponding second-order rate constants upon the concentrations of hydroxide and hypochlorite. For the determination of the pK_a it was more satisfactory to use the directly measured second-order rate constants at low $[OCl^-]$ for low $[OH^-]$ and extrapolated values at high $[OH^-]$ to give a fit to eq. [3]; the extrapolation was carried out by fitting data at constant $[OH^-]$ to eq. [6], and calculating the apparent second-order rate con-

$$[6] \quad k_{obs} = b_1/(1 + b_2/[OCl^-])$$

stant from the parameters so obtained. Simple algebra shows that b_1/b_2 from eq. [6] is equal to $a_1 + a_2[OH^-]$ from eq. [5]. Within the uncertainties of the parameters, as calculated by the least-squares procedure, the same parameter values were obtained in fitting to eq. [3] with or without the extrapolated values, but the uncertainties were smaller if the extrapolated values were included. This treatment of the data is shown in Fig. 2 and Table 2.

Table 3 contains the rate constants for the hydrolysis of α-chloroisobutyrophenone. The rate of this reaction is first order in hydroxide ion, with a second-order rate constant of 71.9 ± 1.5. In the same table are rate constants for the further reaction of α-hydroxyisobutyrophenone with alkaline hypochlorite. This reaction occurs at the same rate as the second phase of the overall reaction of isobutyrophenone. The rate law for this reaction has two terms, one zero order in $[OH^-]$ and one first order in $[OH^-]$; both are first order in $[OCl^-]$. This is equivalent to

TABLE 1. Kinetics of chlorination of isobutyrophenone[a]

(a) Reactions followed at 292 nm

$[OH^-]$ (M)	$[OCl^-]$ (10^4 M)	[Ketone] (10^4 M)	a_1	a_2	a_3 (10^4 s^{-1})	a_4	a_5 (10^4 s^{-1})	l	n
0.975	23.2	2.33	0.486	0.096	11.64(0.070)	0.413	0.144(0.00046)	1	4.0
0.99	18.6	0.91	0.496	0.036	10.75(0.73)	0.191	0.112(0.0033)	1	5.0
0.987	10.50	0.859	0.744	0.069	6.96(0.069)			1	
0.420	16.2	1.26	0.624	0.101	3.511(0.042)	0.606	0.0713(0.0044)	2	5.8
0.426	33.2	1.08	0.940	0.042	5.844(0.123)	0.268	0.144(0.0073)	1	5.6
0.424	11.4	0.859	0.797	0.0726	2.827(0.067)			1	
0.198	20.2	1.80	0.487	0.059	2.42(0.055)	0.309	0.099(0.0012)	1	3.5
0.199	31.0	2.16	0.732	0.057	3.17(0.051)	0.467	0.126(0.00076)	1	4.7
0.184	33.4	2.49	0.715	0.0807	2.884(0.038)	0.564	0.119(0.0015)	1	5.3
0.190	16.1	1.26	0.714	0.0942	1.819(0.018)	0.512	0.0659(0.0009)	2	4.7
0.193	7.23	0.559	0.841	0.128	0.945(0.011)	0.510	0.0443(0.0012)	5	4.4
0.195	3.51	0.275	0.777	0.149	0.456(0.003)	0.511	0.0272(0.0003)	10	4.7
0.0985	7.71	0.559	0.877	0.0849	0.841(0.018)	0.608	0.0435(0.0011)	5	4.9
0.0236	1.83	19.5	1.321	0.0749	1.02(0.010)				
					0.0957(0.0093)[b]				

(b) Reactions followed at 230 nm[c]

$[OH^-]$ (M)	$[OCl^-]$ (10^4 M)	[Ketone] (10^4 M)	a_1	a_2	a_3 (10^4 s^{-1})	a_4	a_5 (10^4 s^{-1})
0.943	84.0	1.47	1.229	0.213	20.07(0.08)	−0.478	0.612(0.0013)
0.451	81.0	1.47	1.157	0.226	8.36(0.03)	−0.475	0.497(0.0010)
0.977	111.	1.58	1.199	0.225	23.70(0.09)	−0.497	0.727(0.0013)
0.977	90.6	1.58	1.161	0.214	20.20(0.09)	−0.483	0.633(0.0012)
0.977	62.7	1.55	1.226	0.208	17.30(0.07)	−0.472	0.422(0.0010)
0.490	113.	1.58	1.130	0.229	10.77(0.07)	−0.508	0.636(0.0018)
0.489	85.4	1.58	1.371	0.235	9.58(0.06)	−0.527	0.493(0.0015)
0.488	63.7	1.58	1.089	0.214	8.92(0.07)	−0.472	0.357(0.0014)

(c) Reactions followed by HPLC[d]

$[OH^-]$ (M)	$[OCl^-]$ (10^4 M)	[Ketone] (10^4 M)	a_1	a_2	a_3 (10^4 s^{-1})
0.987	10.50	0.859	0.003	7.609	7.12(0.61)
0.424	11.40	0.859	0.002	1.828	3.21(0.097)
0.425	93.7	1.450	0.003	3.183	9.054(0.28)
0.425	1000.	17.60	0.0004	1.078	13.20(0.21)
0.196	51.5	3.91	0.011	1.571	3.69(0.15)
0.0485	8.28	0.56	−0.009	1.194	0.535(0.027)
0.023	2.95	0.288	0.002	0.881	0.389(0.033)
0.023	3.25	0.288	−0.003	9.666	0.250(0.015)
0.023	3.39	0.281	−0.010	1.141	0.259(0.0061)
0.023	0.59	19.5	0.911	−0.915	1.078(0.022)
					0.0326(0.00067)[b]
0.057	1.13	18.9	2.087	−2.104	1.439(0.038)
					0.0860(0.0023)[b]
0.107	1.34	17.8	2.503	−2.516	2.066(0.153)
					0.156(0.012)[b]
0.193	1.21	16.1	1.991	−2.014	2.649(0.086)
					0.199(0.0065)[b]

[a]In aqueous solution at 25°C, ionic strength 1.0 (KCl). Followed by absorbance measurements at 292 or 230 nm unless otherwise stated. Absorbance–time data were fitted to $y = a_1 + a_2 \exp(-a_3 t) + a_4 \exp(-a_5 t)$. l is the path length for the cell used. n is the stoichiometry, calculated from eq. [2].

[b]k_{II}[OCl], calculated from k_ψ[OCl]/[ketone], for comparison with kinetics carried out with hypochlorite in excess.

[c]All reactions carried out in 1-cm cells.

[d]HPLC data were fitted to $y = a_1 + a_2 \exp(-a_3 t)$.

Can. J. Chem. Downloaded from www.nrcresearchpress.com by 91.144.44.67 on 09/07/12
For personal use only.

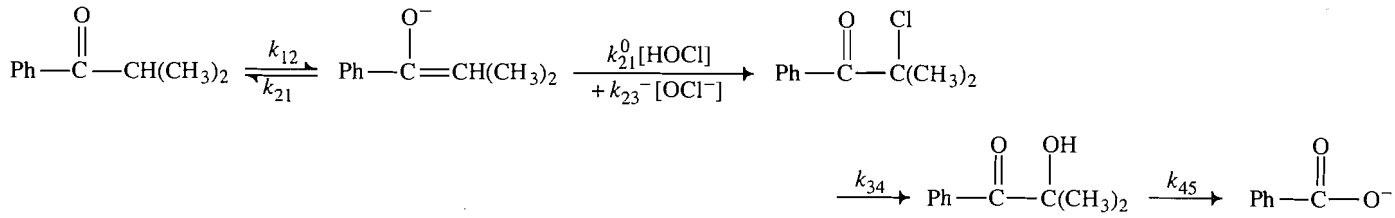

SCHEME 1

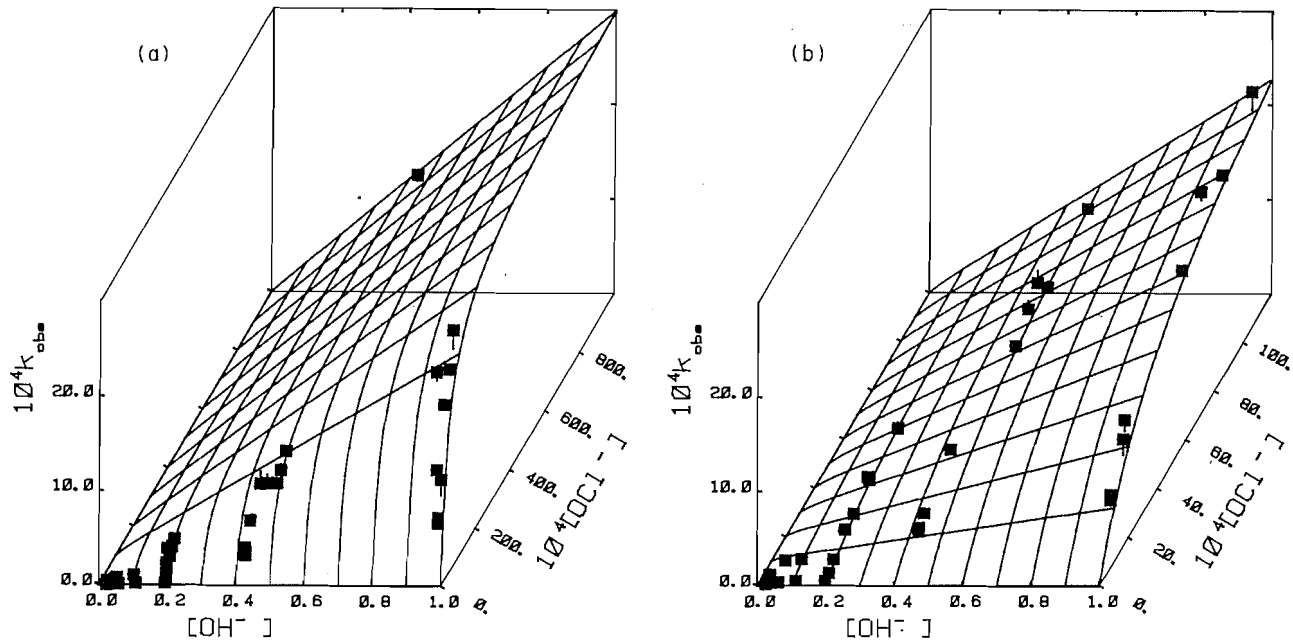

FIG. 1. Chlorination of isobutyrophenone, initial phase; k_{obs} as a function of $[OCl^-]$ and $[OH^-]$. The surface is calculated using parameters determined by least-squares fitting. (a) All data included. (b) Only data for $[OCl^-] \leq 0.012$ M included.

TABLE 2. Least-squares parameters and derived pK_a values for isobutyrophenone[a]

(a) Results of least-squares fitting of kinetics of chlorination

Reaction	Equation	a_1	a_2	a_3
Isobutyrophenone,				
first phase	[5]	0.0458(0.0085)	0.651(0.084)	0.00312(0.00028)
first phase[b]	[3]	0.0363(0.0008)	0.695(0.013)	
first phase[c]	[3]	0.0356(0.0009)	0.709(0.0172)	
second phase	[3]	0.00421(0.0008)	0.00284(0.0013)	

(b) pK_a values derived from kinetics

Compound	k_{II}^0	k_{II}^-	pK_a	$\log k_2^-$
PhCOiPr	0.0363±0.0008	0.695±0.013	18.18±0.50	4.02±0.50

[a]All in aqueous solution at 25°C.
[b]Data at all $[OH^-]$, including values extrapolated to low $[OCl^-]$.
[c]Data at low $[OH^-]$ and low $[OCl^-]$ only.

eq. [3]. All of the data for this reaction, both from experiments starting with isobutyrophenone and from experiments starting with α-hydroxyisobutyrophenone, were fitted by least squares to eq. [3]. Figure 3 illustrates these concentration dependences. A plausible pair of transition state structures corresponding to the compositions indicated by the kinetics is shown in Scheme 2.

Discussion

For isobutyrophenone the absorbance–time curves could only be described by using two exponential terms. This contrasts with the behavior seen for acetone or acetophenone where the first chlorination step is clearly rate limiting under similar conditions. This complexity arises because of slower reaction of

Can. J. Chem. Downloaded from www.nrcresearchpress.com by 91.144.44.67 on 09/07/12
For personal use only.

TABLE 3. Kinetics of further reactions of α-chloro and α-hydroxy-isobutyrophenones[a]

(a) Hydrolysis of α-chloroisobutyrophenone[b]

[Ketone] (10^4 M)	pH	[OH^-] (10^4 M)	a_1	a_2	a_3 (10^3 s^{-1})	k_{II} (M^{-1} s^{-1})
3.24	10.00	1.00	2.839	−0.45	7.224(0.40)	72.2
1.56	10.06	1.15	1.440	−0.221	8.364(0.21)	72.9
1.56	10.30	2.00	1.406	−0.195	14.45(0.43)	72.4
1.56	10.70	5.01	1.364	−0.207	35.82(2.06)	71.5
1.56	9.12	0.132	1.420	−0.245	0.911(0.020)	69.1
					ave.	71.9(1.5)

(b) Reaction of α-hydroxyisobutyrophenone with hypochlorite[c]

[Ketone] (10^4 M)	[OCl^-] (10^4 M)	[OH^-] (M)	a_1	a_2	a_3 (10^4 s^{-1})
1.26	17.8	0.983	0.929	−0.312	0.162(0.0019)[d]
1.74	118.	0.986	1.334	−0.501	0.857(0.0011)
1.74	61.1	0.492	1.163	−0.497	0.379(0.0010)

[a]All in aqueous solution at 25°C. Data are fitted by least squares to: absorbance = $a_1 + a_2 \exp(-a_3 t) + a_4 t$. $k_{II} = a_3/[OH^-]$.
[b]Reactions carried out in 1-cm cells, and followed at 248 nm.
[c]Reactions carried out in 10-cm cells unless otherwise noted, and followed at 230 nm.
[d]Reaction carried out in a 2-cm cell.

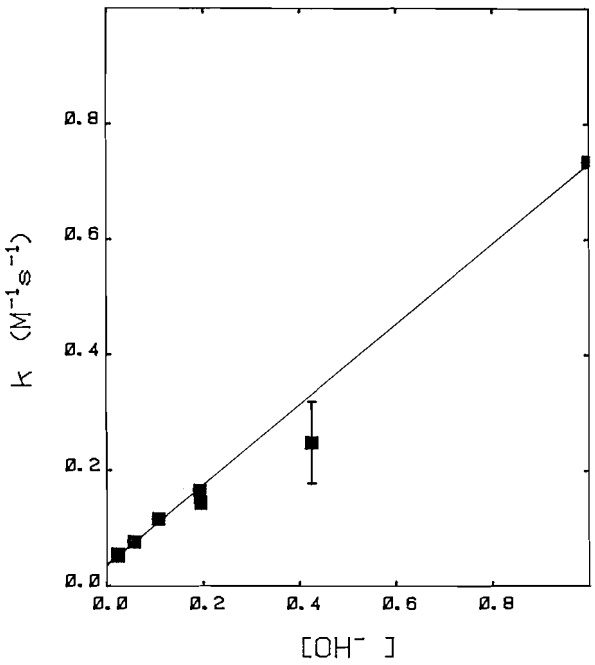

FIG. 2. Chlorination of isobutyrophenone: k_2 at low concentrations of [OCl^-] as a function of [OH^-]. The line is calculated using parameters determined by least-squares fitting. All data used, including extrapolated values from experiments at high [OH^-].

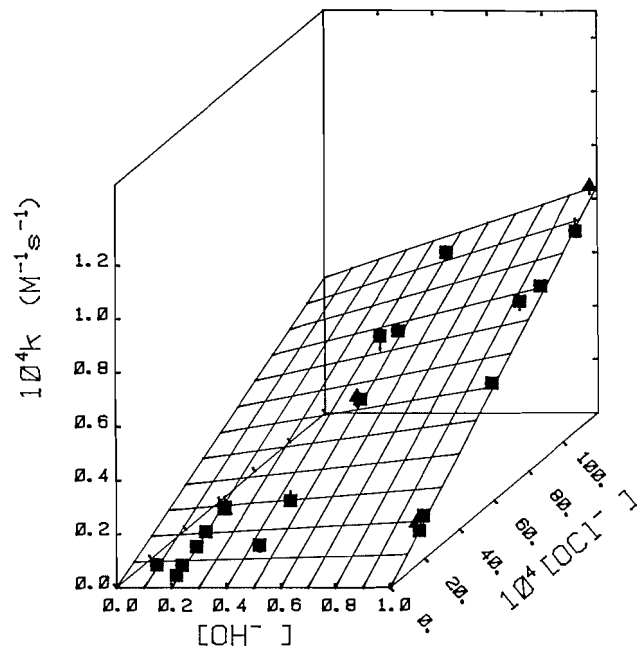

FIG. 3. Chlorination of isobutyrophenone, second phase; k_{obs} for a function of [OH^-] and [OCl^-]. The surface is calculated using parameters determined by least-squares fitting to eq. [5].

the hydroxyketones formed by hydrolysis of the monochlorinated starting material. It is perhaps surprising that the subsequent oxidative cleavage is as fast as it is, and also that the hydrolysis of the chloroketone is so rapid.

α-Hydroxyisobutyrophenone accumulated as the only detectable intermediate in the reaction. The initial reaction is expected to be chlorination to give α-chloroisobutyrophenone; we have shown that hydroxide-catalyzed hydrolysis of this chloroketone is rapid. The hydrolysis of α-chloroisobutyrophenone is remarkably fast, with a rate constant of 71.9 M^{-1} s^{-1}, compared to 1.19 M^{-1} s^{-1} for monochloroacetone (2).

This hydrolysis would be expected to be slow by the classical S_N2 mechanism, because it takes place at a tertiary center (4). It would also be expected to be slow by the classical S_N1 solvolysis mechanism because reaction occurs next to a carbonyl group. Although S_N1 reactions at tertiary centers next to a carbonyl are known, they occur at rates similar to the analogous secondary centers with the acyl function replaced by hydrogen

Can. J. Chem. Downloaded from www.nrcresearchpress.com by 91.144.44.67 on 09/07/12
For personal use only.

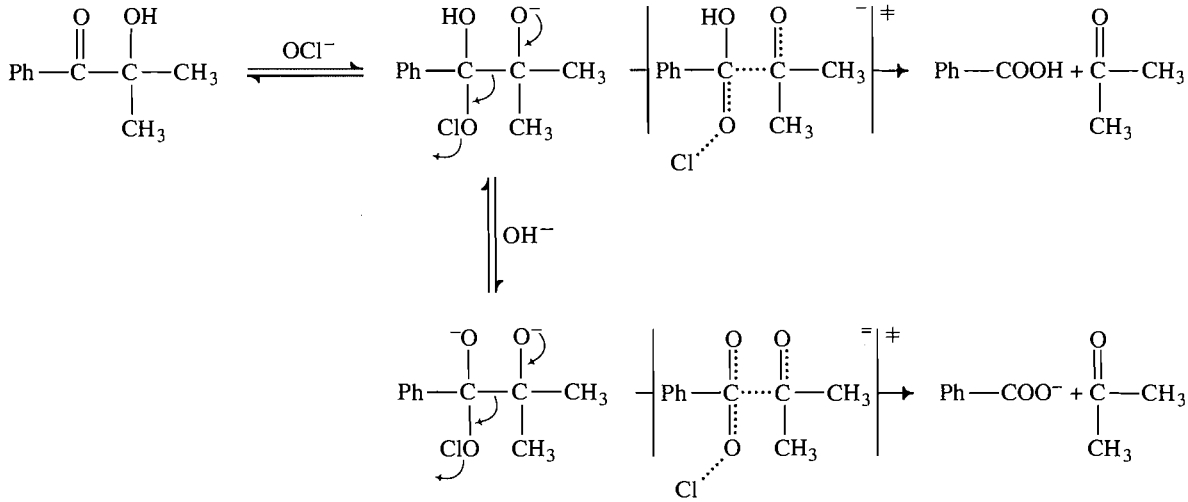

SCHEME 2

(5). In any case the reaction rate is first order in hydroxide so that it cannot be solvolysis. A plausible mechanism is addition of hydroxide, followed by intramolecular substitution.

This oxidation of α-hydroxyisobutyrophenone is unexpected and somewhat puzzling. When it first became clear that there was a second oxidation occurring, we wondered if the first step might be an alkaline ketol rearrangement to 3-hydroxy-3-phenyl-2-butanone, which could then undergo halogenation and haloform cleavage to atrolactic acid, or more likely (by analogy with acetophenone) halogenation, hydrolysis, and rearrangement to 2,3-dihydroxy-3-phenylbutanoic acid; or by addition of hypochlorite to the carbonyl, followed by fragmentation to give acetone and benzoic acid; or by hypochlorite ester formation, followed by hydroxide addition to the carbonyl and fragmentation to acetone and benzoic acid. When HPLC analysis, monitoring the absorptions due to aromatic compounds, was used to follow the course of the chlorination of isobutyrophenone, the only species observed were the starting material, the hydroxyketone, and benzoic acid. The rate of benzoic acid formation is first order in hypochlorite and approximately zero order in hydroxide (there is a term first order in hydroxide and first order in hypochlorite but this is less important); thus the rate determining step cannot be a hydroxide-catalyzed rearrangement, and since neither 3-hydroxy-3-phenyl-2-butanone (the product of an alkaline ketol rearrangement) nor atrolactic acid (derived from 3-hydroxy-3-phenyl-2-butanone by a standard haloform reaction) were observed to accumulate, rearrangement cannot be a pre-equilibrium step followed by rate determining cleavage by hypochlorite. Thus regardless of whether atrolactic acid or 2,3-dihydroxy-3-phenylbutanoic acid is stable to the reaction conditions, we can state that an alkaline ketol rearrangement is not part of the mechanism. We can rule out these paths on the basis of the observed product as well, because any plausible route to benzoate would have to pass through acetophenone as an intermediate, and acetophenone would give extensive formation of mandelate under at least some of the experimental conditions used (3). The remaining ambiguity is whether addition of hypochlorite to the carbonyl or esterification at the α-hydroxyl initiates the cleavage reaction. Esterification seems inherently unlikely in alkaline solution; although *tert*-butyl hypochlorite is synthesized in alkaline solution (6), the equilibrium is doubtless displaced towards the ester by phase separation. *tert*-Butyl hypobromite is prepared from *tert*-butyl alcohol and hypobromous acid and is destroyed by carbonate (7). The most probable mechanism appears to be addition of hypochlorite to the carbonyl to give an anionic adduct, which then undergoes fragmentation. An analogous mechanism has been proposed for the oxidative cleavage of α-ketols by alkaline hydrogen peroxide (8).

For the reasons outlined above, we suggest that the reactions occurring are as shown in Scheme 2.

The rate of enolization of isobutyrophenone which we determined was $0.0031\ M^{-1}\ s^{-1}$ at 1.0 M ionic strength, which is in satisfactory agreement with a direct measurement by Kresge and co-workers, $0.00243\ M^{-1}\ s^{-1}$ at 0.1 M ionic strength (9). The pK_a value which we found, 18.18, is very similar to the more precise value determined by Kresge, 18.26 (9). Thus our method has again been shown to lead to valid pK_a results, with relatively simple kinetics measurements.

The very old-fashioned reaction of ketones with chlorine in alkaline solution has abundant surprises still to be found. The hydrolysis of α-chloroketones is well known to be fast, but that the process can be faster for a tertiary than for a primary center seems startling. The cleavage of an α-hydroxyketone by hypochlorite is a reminder of how powerful the thermodynamic driving force for chlorine oxidations really is.

Experimental

Materials

Sodium hydroxide and potassium chloride were reagent grade, used without further purification. Sodium hypochlorite solutions were prepared by bubbling chlorine into aqueous sodium hydroxide; the hypochlorite concentration of the resulting solution was determined either by the absorbance at 292 nm or by titration (2). The sodium hydroxide concentration of kinetics solutions was determined by titration (2).

Isobutyrophenone, Aldrich "97%", was purified by distillation, bp 117–118°C (25 Torr; 1 Torr = 133.3 Pa). UV spectrum in water: $\lambda_{max} = 245.5$, $\epsilon_{max} = 12\,000$; $\epsilon_{292} = 760$.

α-Chloroisobutyrophenone

Isobutyrophenone, 3.00 g (20.2 mmol) in ether, 50 mL, containing aqueous HCl, 1 mL, was treated with excess chlorine gas for 2 h with cooling in an ice bath and then 2 h at room temperature. The ether solution was washed once with conc. aq. Na_2SO_4 and once with conc. aq. $NaHCO_3$, dried (Na_2SO_4), and evaporated. The residue was purified by Kugelrohr distillation (70–75°C, 0.5 Torr) to give 3.49 g of

Can. J. Chem. Downloaded from www.nrcresearchpress.com by 91.144.44.67 on 09/07/12
For personal use only.

viscous liquid. ^{1}H NMR analysis showed it to be ca. 90% product and 10% starting material. A pure sample was obtained by column chromatography on silica gel, eluting with 1:1 $CHCl_3$:CCl_4. UV: λ_{max} 252, ϵ_{max} 7700 in H_2O; λ_{max} 247.5, ϵ_{max} 8100 in 0.1 M aq. NaOH. ^{1}H NMR ($CDCl_3$) δ: 1.92, (s, 6H), C*H*$_3$-C, 7.5, 8.2, (m, total of 5H), aromatic C-*H*. Literature (10) bp 69–70°C, 0.4 Torr; (11) bp 119–120°C, 18 Torr; ^{1}H NMR (CCl_4) δ: 1.80 (6H, s), 7.7 (5H, m).

α-Hydroxyisobutyrophenone

α-Chloroisobutyrophenone, 413 mg (2.26 mmol) was stirred for 3 days at room temperature in 0.1 M aq. $NaHCO_3$, 300 mL. The pH of the solution was ca. 8.6; solution of the starting material was complete after 12 h. Extraction with ether, 3 × 150 mL, drying of the extracts (Na_2SO_4), and evaporation gave 366 mg of viscous liquid; 98%. UV: λ_{max} 247.5, ϵ_{max} 9600 in H_2O; λ_{max} 247.5, ϵ_{max} 9600 in 0.1 M aq. NaOH; λ_{max} 244.5, ϵ_{max} 11700, log ϵ_{max} 4.07 in 95% ethanol; lit. (12) λ_{max} 245, log ϵ_{max} 4.05 in 90% ethanol. ^{1}H NMR ($CDCl_3$) δ: 1.60, (s, 6H), C*H*$_3$-C, 7.7 and 8.0 (m, total of 5H), aromatic C-*H*. Literature (8) ^{1}H NMR (CCl_4) δ: 1.52 (6H, s), 7.2–7.5 and 7.8–8.0 (total of 5H, m).

Methods

TLC was carried out using Analtech 250 μm silica gel GF plates or Macherey–Nagel, Polygram SIL G/UV precoated plastic sheets (0.25 mm). Column chromatography was carried out using Terochem silica gel, no. 1918.

HPLC analyses were carried out using C18 reverse phase columns (Waters Radial Pak), with mixtures of aqueous buffers and methanol as eluting solvent, and UV detection.

Least-squares calculations were carried out using FORTRAN programs written for the purpose; non-linear least squares and the Marquardt algorithm (13) were used for other than straight line correlations.

Kinetics procedures

All reactions were studied in aqueous solution at 25°C and ionic strength 1.0 M (KCl) using apparatus and procedures previously described (2). Reactions were initiated by injecting (Hamilton syringe) a known amount of a stock solution of the ketone into thermally equilibrated hydroxide/hypochlorite solution in a quartz UV cell.

Hydrolysis of chloroisobutyrophenone

A stock solution was prepared in 80% methanol:20% water. Freshly prepared hydroxide solutions, ionic strength 1 M with KCl, were titrated immediately before use and immediately after the runs, with 0.05 M HCl standardized against tris base. Kinetics were initiated by injecting a suitable amount of stock solution of chloroketone into hydroxide solution previously thermostatted in 5 or 10 cm quartz cells, and were followed by monitoring absorbance at 247 nm, the λ_{max} of the product. pH values were taken at the end of the reaction and had changed by no more than 0.01 pH unit.

Chlorination of isobutyrophenone and hydroxyisobutyrophenone

Reactions monitored by UV absorbance were carried out as described above. Reactions monitored by HPLC were carried out in a thermostatted flask and samples were taken and injected at suitable intervals using an autosampler. In some cases 1.0-mL samples were taken manually and quenched ($NaHSO_3$ and H_3PO_4) for later analysis. The peaks for HPP and HPA were assigned by comparison with those for authentic samples prepared as described above.

Product studies

Isobutyrophenone (0.00107 M), NaOH (0.1 M), KCl (0.9 M), and NaOCl (0.003 M), in a volume of 1 L, were allowed to stand for 20 h, which is 17 half-lives for the initial reaction based on the starting concentration of hypochlorite, and about one half-life for the second reaction. Extraction with ether, 3 × 200 mL, drying of the extracts (Na_2SO_4), and evaporation gave 112 mg, shown by ^{1}H NMR analysis to be 70% α-hyroxyisobutyrophenone and 30% benzoic acid. Only two UV positive spots were detected by TLC analysis. No isobutyrophenone was detectable. Treatment of the aqueous reaction solution with 0.5 g $NaHSO_3$ and acidification with HCl, followed by extraction with ether, 3 × 200 mL, drying of the extracts, and evaporation gave 39 mg, shown by NMR and TLC analysis to be benzoic acid. The mass balance was 99.9%.

Acknowledgments

We thank the Natural Sciences and Engineering Research Council of Canada for financial support of this work. We thank Professor A. J. Kresge for communicating results to us prior to publication.

1. J. P. GUTHRIE, J. COSSAR, and A. KLYM. J. Am. Chem. Soc. **106**, 1351 (1984).
2. J. P. GUTHRIE and J. COSSAR. Can. J. Chem. **64**, 1250 (1986).
3. J. P. GUTHRIE, J. COSSAR, and A. KLYM. Can. J. Chem. **65**, 2154 (1987).
4. A. STREITWIESER, JR. Solvolytic displacement reactions. McGraw–Hill, New York. 1962. p. 16.
5. X. CREARY. J. Am. Chem. Soc. **106**, 5568 (1984).
6. H. M. TEETER and E. W. BELL. Org. Synth. Coll. Vol. **4**, 125 (1963).
7. L. F. FIESER and M. FIESER. Reagents for organic synthesis. Wiley, New York. 1967. p. 90.
8. Y. OGATA, Y. SAWAKI, and M. SHIROYAMA. J. Org. Chem. **42**, 4061 (1977).
9. P. PRUSZYNSKI, Y. CHIANG, A. J. KRESGE, N. P. SCHEPP, and P. A. WALSH. J. Phys. Chem. **90**, 3760 (1986).
10. J. S. PIZEY and K. SYMEONIDES. Phosphorus Sulfur, **1**, 41 (1976).
11. H. RIVIERE. Bull. Soc. Chim. Fr. 1389 (1962).
12. Organic electronic spectral data. Vol. IX. p. 196.
13. P. R. BEVINGTON. Data reduction and error analysis for the physical sciences. McGraw–Hill, New York. 1969.

Can. J. Chem. Downloaded from www.nrcresearchpress.com by 91.144.44.67 on 09/07/12
For personal use only.

Synthesis and transannular Diels–Alder reaction of a 13-membered macrocyclic triene having a tetrasubstituted enol ether as dienophile

GERVAIS BÉRUBÉ[1] AND PIERRE DESLONGCHAMPS

Laboratoire de synthèse organique, Départment de chimie, Faculté des sciences, Université de Sherbrooke, Sherbrooke (Québec), Canada J1K 2R1

Received July 17, 1989

GERVAIS BÉRUBÉ and PIERRE DESLONGCHAMPS. Can. J. Chem. **68**, 404 (1990).

The syntheses of the acyclic triene *trans–trans–cis* **27** and *trans–trans–trans* **31** are described. Macrocyclization and concomitant transannular Diels–Alder reaction were performed with the chloride derivative obtained from the *trans–trans–cis* triene alcohol **27** yielding a mixture of the tricyclic compounds *trans–syn–trans* **33** and *cis–syn–cis* **34**. On the other hand, macrocyclization of the chloride derived from *trans–trans–trans* triene **31** was not successful.

Key words: transannular process, Diels–Alder reaction, macrocyclic triene, macrocyclization, tricyclic compounds, organic synthesis.

GERVAIS BÉRUBÉ et PIERRE DESLONGCHAMPS. Can. J. Chem. **68**, 404 (1990).

La synthèse des triènes acycliques *trans–trans–cis* **27** et *trans–trans–trans* **31** est décrite. Une réaction de macrocyclisation suivie d'une réaction de Diels–Alder transannulaire a été observée en partant du dérivé chlorure du triène *trans–trans–cis* alcool **27** donnant un mélange des composés tricycliques *trans–syn–trans* **33** et *cis–syn–cis* **34**. Par contre, la macrocyclisation du dérivé chlorure du triène *trans–trans–trans* alcool **31** n'a pas été réussie.

Mots clés : procédés transannulaires, réaction Diels–Alder, triènes macrocycliques, macrocyclisation, composés tricycliques, synthèse organique.

Can. J. Chem. Downloaded from www.nrcresearchpress.com by 91.144.44.67 on 09/07/12
For personal use only.

The synthesis of polycyclic natural products like steriods and terpenes is a well-documented subject (1). These compounds can be obtained via numerous methods such as aldol condensation (2), biomimetic cyclization of polyenes (3), or by intramolecular Diels–Alder reaction (4*a–c* (reviews), 4*d–h* (specific examples)). We (5) and others (6) have recently been investigating a new strategy for the construction of such polycyclic compounds, which makes use of the transannular Diels–Alder process on a macrocyclic triene, i.e., **1** → **2** (Scheme 1).

To demonstrate the feasibility of this new strategy, one[2] of the examples that we have examined is the reaction **3** → **4**, which should give rise to a tricyclic structure containing quaternary centers at positions 9 and 10 (steroid membering). This substitution pattern is found in nature in compounds such as germine (**5**) (Scheme 2), a steroid alkaloid of the Veratrum family (7), or batrachotoxin (**6**), one of the most poisonous compounds known (8). It can also be found in other compounds like rosenonolactone (**7**) (9) or forskolin (**8**) (10).

Synthesis of the acyclic triene precursors

The synthesis of the monosilylated derivative of *trans–trans*-hexa-2,4-diene-1,6-diol **14** (Scheme 3) was carried out starting from the *trans*-unsaturated aldehyde **10** (11). Emmons–Horner reaction of **10** with ethyl diisopropyl phosphonoacetate (12) gave the *trans–trans* diene ester **11**. The tetrahydropyranyl group in **11** was then replaced by a *tert*-butyl dimethyl silyl protecting group (PPTS, CF_3COOH, MeOH (13); *t*-Bu$(CH_3)_2SiCl$, imidazole, THF (14)) to produce the silylated diene ester **13** via intermediate formation of **12**. Reduction of **13** with diisobutyl aluminium hydride gave the required diene alcohol **14** which was then converted into the *trans–trans*-allylic chloride **15** (LiCl, CH_3SO_2Cl, *s*-collidine, DMF) (15), which is described in Scheme 4.

The dioxolane malonate **9** (Scheme 4) was prepared (16) from the Michael reaction of dimethyl malonate with methyl vinyl ketone followed by ketalization with ethylene glycol. Condensation of allylic chloride **15** with the sodium salt of dimethyl malonate **9** gave the corresponding diene **16** in 89% yield.

Decarbalkoxylation of **16** (17) gave the monoester **17**, which was reduced to the alcohol **18** with diisobutyl aluminium hydride and protected as the benzyl ether **19**. Acid hydrolysis of **19** with pyridinium *p*-toluenesulfonate (13) afforded the ketone alcohol **20**, which was reprotected as its silyl ether **21** (14). The Emmons–Horner reaction of the lithium salt of phosphonate **22** (18) with ketone **21** in toluene proceeded slowly (90–100 h) to give a mixture of α,β-unsaturated esters **23** (79%, *cis*:*trans* = 1:1 ratio) as shown by ^{1}H nmr. Reduction of **23** with diisobutyl aluminium hydride afforded a mixture of allylic alcohols, which were separated by chromatography, the *trans–trans–cis* alcohol **24** being less polar than the *trans–trans–trans* isomer **28**.

The *trans–trans–cis* triene acyclic precursor **27** was prepared from the *cis*-alcohol **24** in the following way: compound **24** was converted into the allylic chloride **25** (LiCl, CH_3SO_2Cl, *s*-collidine, DMF) (15), which was then treated with an excess of dimethyl sodium malonate to give the substituted malonate **26**. Cleavage of the silyl ether protecting group with fluoride ion (14) afforded the *trans–trans–cis* alcohol **27**. The *trans–trans–trans* triene acyclic precursor **31** was prepared from **28** using a similar procedure via the intermediate formation of **29** and **30**.

Macrocyclization and Diels–Alder reaction

The best results for macrocyclization and Diels–Alder reaction were obtained with the allylic chloride **32** (Scheme 5) derived from the *trans–trans–cis* triene alcohol **27** using a pseudo high-dilution technique. The crude allylic chloride **32** prepared (LiCl, CH_3SO_2Cl, *s*-collidine, DMF) (15) from alcohol **27** was dissolved in *N,N*-dimethylformamide (DMF) and added over a period of 22 h (syringe pump) directly into a suspension of sodium hydride in a mixture of tetrahydrofuran and DMF at 70°C. This produced compounds **33** and **34** along with a mixture of monodecarboxylated products **35** in a ratio of 13:6:3 and with an overall yield of 68%. These compounds were separated by chromatography and the structure of compound **33** was fully confirmed by X-ray crystallography (19). The general structure

[1]NSERCC (1980–1984) and FCAR (1981–1985) predoctoral fellowships. This work was abstracted from the Ph.D thesis of G. Bérubé.

[2]This work was reported in a preliminary form, see ref. 5*c*.

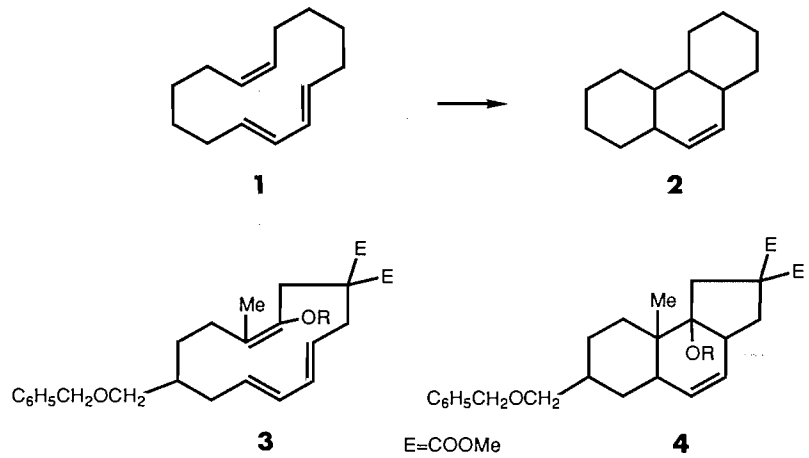

1 2 3 4

SCHEME 1

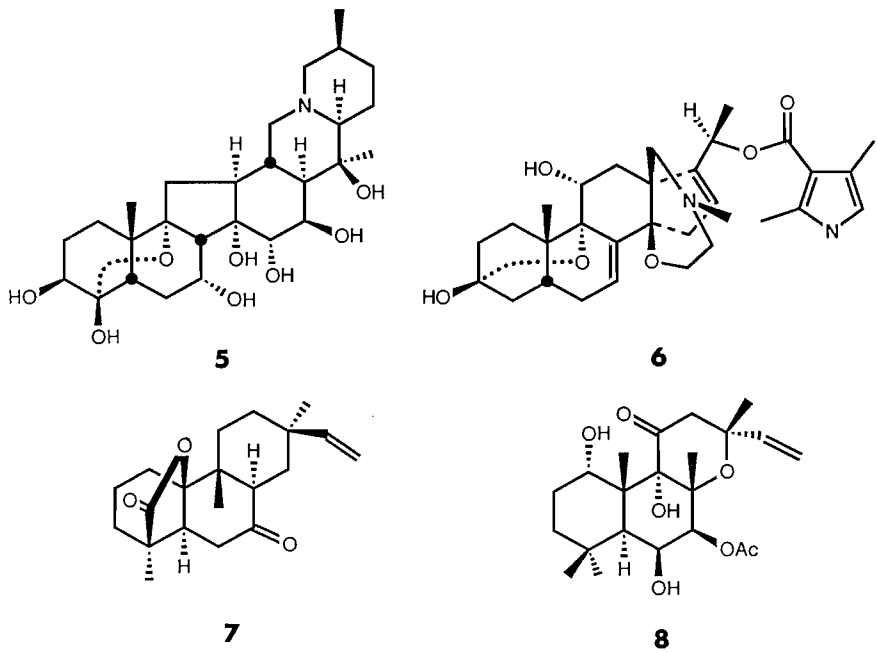

5 6 7 8

SCHEME 2

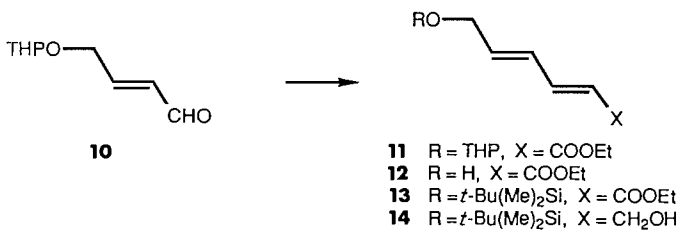

10

11 R = THP, X = COOEt
12 R = H, X = COOEt
13 R = *t*-Bu(Me)$_2$Si, X = COOEt
14 R = *t*-Bu(Me)$_2$Si, X = CH_2OH

SCHEME 3

of compounds **34** and **35** was established by their spectral data[3] relative to compound **33**.

The ^{1}H nmr spectrum of **33** shows the following characteristic signals: an angular methyl at 0.74 ppm (similar to an angular methyl at the ring junction of a *trans* decalin where the methyl is axial to both rings), and the methylene group of the methoxymethyl ether as an AB system (two doublets) at 4.53 ppm. The methylene protons are diastereotopic, have different chemical shifts, and appear as two doublets.

The ^{1}H nmr spectrum of **34** shows the following characteristics: an angular methyl at 1.05 ppm, and the methylene group of the methoxymethyl ether as a singlet at 4.67 ppm. The methylene protons are diastereotopic and should in principle appear as doublets; however, they have the same chemical shift. Being angular at a *cis* decalin ring junction, the angular methyl is shifted downfield at 1.05 ppm as it is normally observed. The relative stereochemistry of the *cis–syn–cis* tricycle **34** has not been rigorously established by X-ray crystallography since this compound is not crystalline, but its assignment is based on the preceding criteria and on the following analysis. Using molecular models, and assuming that the Diels–Alder reaction must take place via a boat-like transition state, it can be readily seen that the *trans–trans–cis* macrocyclic triene **36**, which must have been formed from **32**, can undergo two different transannular cycloadditions leading either to a *trans–syn–trans* (TSC) or a *cis–syn–cis* (CSC) tricycle with ring B in a boat form (cf. **33A** and **34A**), both of which have ring A in a chair

[3]The minor formation of monodecarboxylated products is presumably due to the presence of a small quantity of sodium hydroxide in the medium, which induced partial hydrolysis and decarboxylation.

Can. J. Chem. Downloaded from www.nrcresearchpress.com by 91.144.44.67 on 09/07/12
For personal use only.

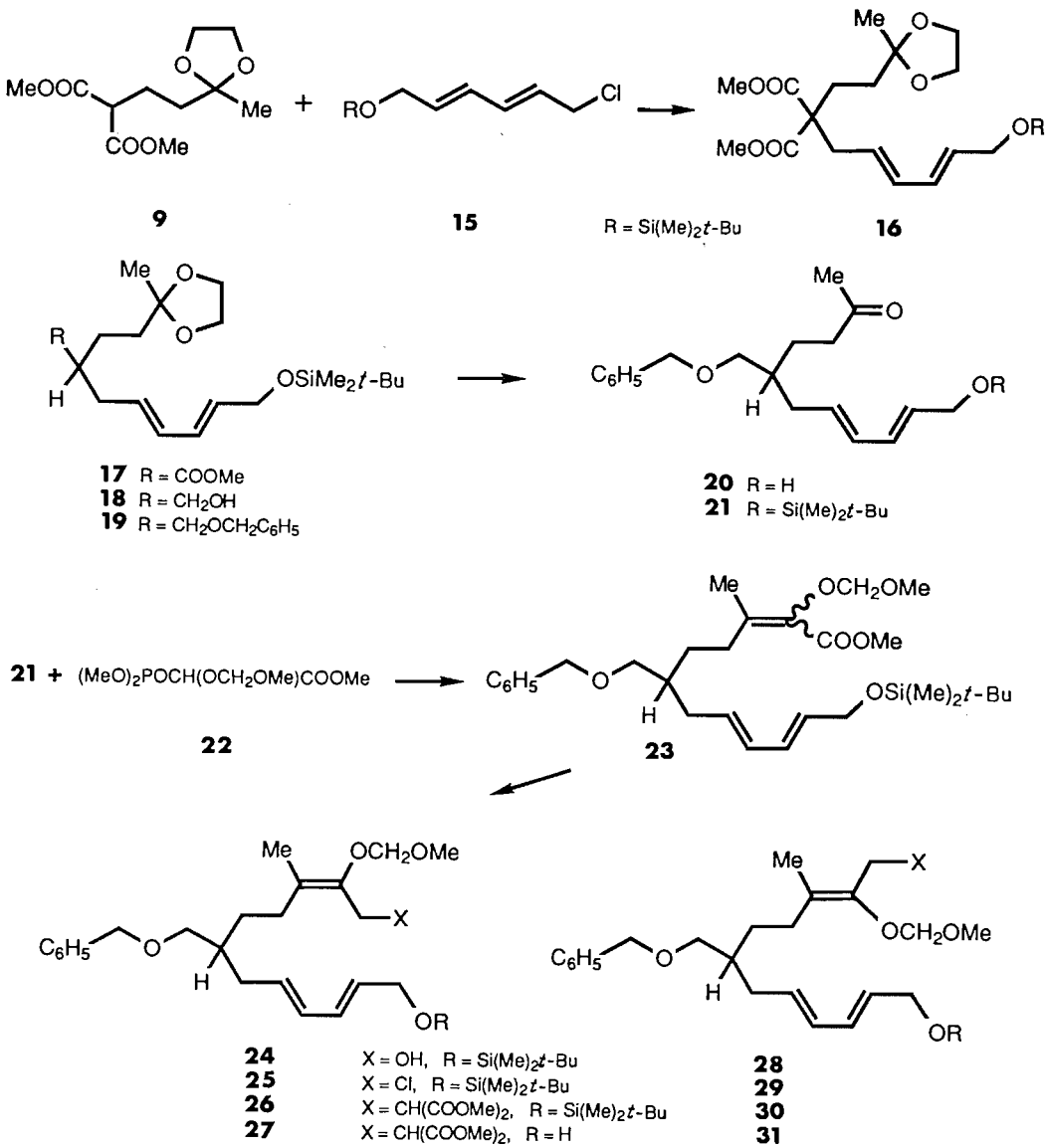

9 **15** **16**

17 R = COOMe
18 R = CH_2OH
19 R = $CH_2OCH_2C_6H_5$

20 R = H
21 R = $Si(Me)_2t$-Bu

22 **23**

24 **25** **26** **27** **28** **29** **30** **31**

SCHEME 4

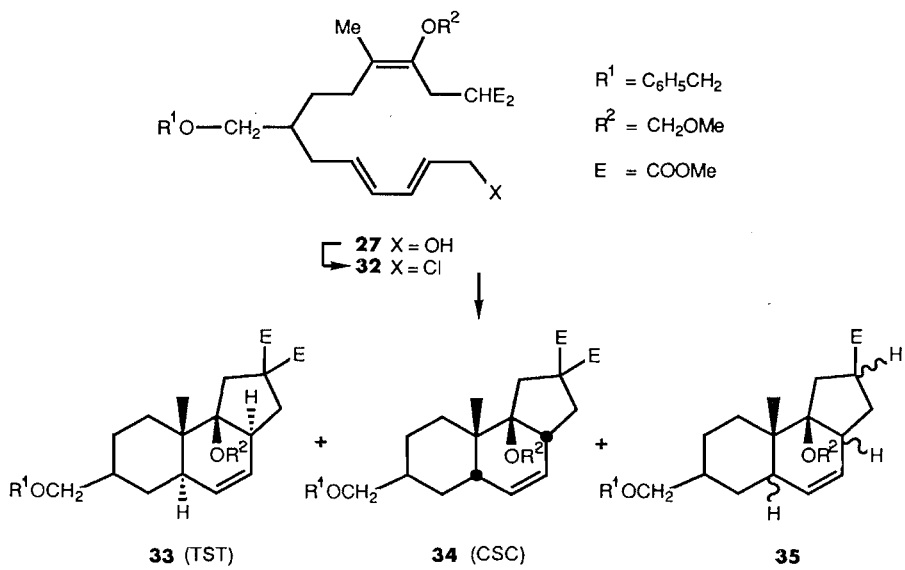

33 (TST) **34** (CSC) **35**

SCHEME 5

Can. J. Chem. Downloaded from www.nrcresearchpress.com by 91.144.44.67 on 09/07/12
For personal use only.

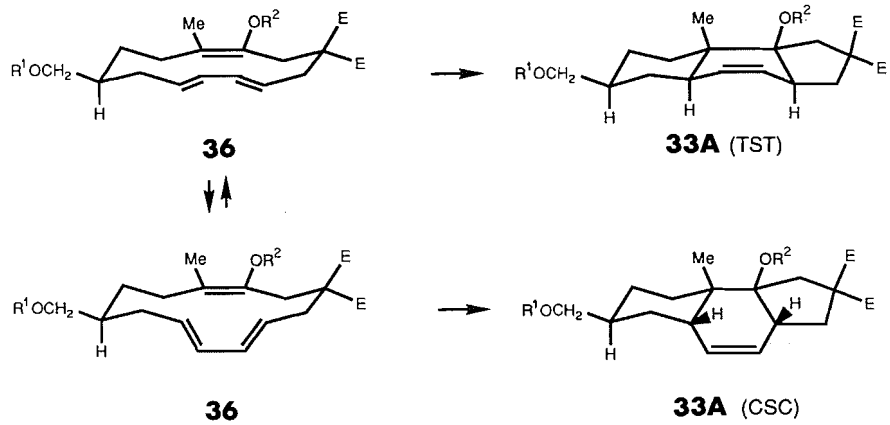

SCHEME 6

form with the benzyloxymethylene group in an equatorial position as shown in Scheme 6.[4]

To confirm that the above Diels–Alder reaction is the result of a transannular process, the mixture of α,β-unsaturated esters **23** dissolved in toluene was heated in a sealed tube at 210°C for 18 h. No Diels–Alder product was observed and starting material was recovered quantitatively. Since the isomeric compounds **23** have an activated dienophile (due to the conjugation with the ester function) and did not undergo an intramolecular Diels–Alder reaction at 210°C, this clearly confirms that transannular Diels–Alder can take place with much greater ease (70°C) and even with a poorly activated dienophile.

The *trans–trans–trans* acyclic precursor **31** was also converted into the corresponding allylic chloride and submitted to the above experimental conditions for macrocyclization. In this series, we failed to isolate any specific compounds having a macrocyclic or a tricyclic structure; rather we observed essentially complete decomposition of the starting material. This is likely due to the fact that the macrocyclization reaction must have failed. We have also observed in other series that the yield of macrocyclization of acyclic trienes having the *trans–trans–trans* geometry can indeed be low (5*e*).

In conclusion, we have shown in this work that the macrocyclization of an acyclic triene can yield a macrocycle that undergoes a very facile transannular Diels–Alder reaction by comparison with the simple intramolecular process. However, the success of the process depends on the ease of macrocyclization, which varies as a function of the geometry of the unsaturations (20). This work also shows that transannular Diels–Alder reaction on macrocycles is potentially a powerful strategy for the construction of polycyclic compounds (21). Further work in this direction is in progress.

Experimental

The ir spectra were taken on a Perkin–Elmer 681 spectrophotometer. Proton nmr spectra were recorded on a Bruker WP-80 or Bruker WM-250 instrument. The following abbreviations have been used: s, singlet; d, doublet; dd, doublet of doublets; dt, doublet of triplets; ddd, doublet of doublets of doublets; ddt, doublet of doublets of triplets; t, triplets; q, quartet; and m, multiplet. Chemical shifts are reported in δ values relative to tetramethylsilane or chloroform as internal standard. Carbon nuclear magnetic resonance spectra were recorded on a Bruker WP-80 or Bruker WM-250 instrument (chloroform as internal standard). Mass spectra were obtained on a Micromass ZAB-2F instrument. Melting points were determined on a Büchi M-50 or on a Reichert apparatus and are uncorrected.

Thin-layer chromatography was performed using silica gel 60 F-250. For flash chromatography, Merck Kieselgel 60 (230–400 mesh A.S.T.M.) was used. All solvents used in chromatography were distilled. Unless otherwise noted, starting materials and reactants were obtained commercially and were used as such or purified by standard means. All solvents and reactants purified and dried were stored under argon.

Anhydrous reactions were performed under an inert atmosphere of argon. Organic solutions were dried over magnesium sulfate, and were evaporated on a rotatory evaporator and under reduced pressure.

Dioxolane 9

Dimethyl malonate (18 mL, 20.8 g, 157 mmol) in dry benzene (200 mL) was stirred at room temperature with potassium carbonate (21.7 g, 151 mmol) and methyl vinyl ketone for 21 h. Water was added and the mixture was extracted with ether. The organic layer was dried, filtered, and the solvents evaporated. The crude product was then refluxed in benzene (250 mL, Dean–Stark) with ethylene glycol (9.6 mL, 10.68 g, 170 mmol) and *p*-toluenesulfonic acid (10 mg, 5.8×10^{-2} mmol) for 18 h. It was then washed with sodium bicarbonate solution (2×30 mL, 5% aqueous) and with distilled water (4×30 mL). The organic layer was dried, filtered, and the benzene evaporated. The residue was purified by flash chromatography (hexane:acetone, 4:1) to give the dioxolane **9** (26.3 g, 75% overall); ir ($CHCl_3$): 1740 (C=O), 1300–1120 (C—O), 1060 (C—O); nmr ($CDCl_3$) δ: 3.93 (4H, s, -OCH_2CH_2O-), 3.73 (6H, s, $2 \times$ -CO_2CH_3), 3.42 (1H, t, $J = 7.24$ Hz, -CH(CO_2CH_3)$_2$), 2.25–1.50 (4H, m, -CH_2CH_2-), 1.31 (3H, s, -CH_3); ms *m/e* (70 eV): 231 ($M^+ - CH_3$), 215 ($M^+ - OCH_3$). Exact mass calcd.: 231,0868 ($M^+ - CH_3$); found: 231,0868 ($M^+ - CH_3$).

trans-*Aldehyde 10*

A mixture of commercially available *cis*-2-butene-1,4-diol (22.04 g, 0.25 mol), 3,4-dihydro-2*H*-pyran (23.14 g, 0.27 mol), and *p*-toluenesulfonic acid (242 mg, 1.27 mmol) in dry ethyl acetate (500 mL) was stirred at 0°C for 40 min and at room temperature for 30 min. Then sodium bicarbonate (525 mg, 6.25 mmol) was added and the mixture was stirred for 30 min, filtered, and the solvent was evaporated. The crude oil was purified by flash chromatography. Elution with a mixture of ethyl acetate:hexane (15:85) gave the bis-tetrahydropyranyl derivative (9.55 g, 15%) and elution with a mixture of ethyl acetate:hexane (50:50) gave the mono-tetrahydropyranyl derivative (22.7 g, 53%).

Mono-derivative: ir ($CHCl_3$): 3620 (OH, free), 3650–3250 (OH, associated), 1025 (C—O); nmr ($CDCl_3$) δ: 6.20–5.50 (2H, m, -CH=CH-), 4.68 (1H, br s, -OCHO-), 4.60–3.30 (6H, m, -CH_2CH_2O-, $2 \times$ =CHCH_2O-), 2.18 (1H, br s, OH), 1.65 (6H, m, -$CH_2CH_2CH_2$O-).

Bis-derivative: ir ($CHCl_3$): 1025 (C—O); nmr ($CDCl_3$) δ: 5.75 (2H, t, $J = 4.0$ Hz, -CH=CH-), 4.63 (2H, br s, $2 \times$ -OCHO-), 4.55–3.20 (8H, m, $2 \times$ -CH_2CH_2O-, $2 \times$ =CHCH_2O-), 1.64 (12H, m, $2 \times$ -$CH_2CH_2CH_2CH_2$O-).

[4]With its *trans–syn–trans* geometry, ring B of compound **33** is locked in the boat conformation, and this is clearly revealed in the X-ray analysis (19).

Can. J. Chem. Downloaded from www.nrcresearchpress.com by 91.144.44.67 on 09/07/12
For personal use only.

Can. J. Chem. Downloaded from www.nrcresearchpress.com by 91.144.44.67 on 09/07/12
For personal use only.

A solution of the preceding alcohol (mono-tetrahydropyranyl derivative) (10 g, 58 mmol), sodium acetate (14.3 g, 174 mmol), crushed molecular sieves (3Å, 20 g), and pyridinium chlorochromate (PCC, 18.8 g, 87 mmol) in dry methylene chloride (250 mL) was stirred at 0°C for 30 min and at room temperature for 1 h. Then ether (250 mL) was added and the resulting mixture was filtered through Celite and sodium sulfate. The filtrate was then evaporated to give *trans*-aldehyde **10** (9.4 g, 95% crude), which was used without any purification; ir ($CHCl_3$): 2860 and 2740 (C—H, aldehyde), 1690 (C=O), 1645 (C=C), 1040 (C—O); nmr ($CDCl_3$) δ: 9.59 (1H, d, J = 7.6 Hz, -C*H*O-, 6.92 (1H, dt, J = 15.6 Hz, 3.6 Hz, -CH_2CH=), 6.36 (1H, ddt, J = 15.6 Hz, 7.4 Hz, 1.5 Hz, =C*H*CHO-), 4.69(1H, m, -OC*H*O-), 4.40 (2H, m, =CHCH_2O-), 4.15–3.15 (2H, m, -CH_2CH_2O-), 1.69 (6H, m, -$CH_2CH_2CH_2CH_2$O-).

Ester ***11***

To a stirred suspension of sodium hydride (2.6 g (60% in oil), 64.9 mmol) in anhydrous THF (100 mL) at 0°C was added via cannula a solution of ethyl diisopropylphosphonoacetate (17.8 g, 70 mmol) in anhydrous THF (50 mL). When gas evolution had ceased, the resulting solution was cooled to −50°C and a solution of *trans*-aldehyde **10** (9.2 g, 54 mmol) in anhydrous THF (50 mL) was added via cannula. The reaction was allowed to warm to 0°C and stirred for 2 h. After that period, ether (500 mL) and saturated ammonium chloride (100 mL) were added. The aqueous layer was separated and extracted with ether (3 × 50 mL). The combined organic layers were washed with brine (2 × 50 mL), dried, filtered, and evaporated. The residue was purified by flash chromatography (ethyl acetate:hexane, 1:9) to give the ester **11** (6.6 g, 50%); ir ($CHCl_3$): 1710 (C=O), 1650 and 1620 (C=C), 1140 and 1025 (C—O); nmr ($CDCl_3$) δ: 7.27 (1H, dd, J = 15.3 Hz, 11.0 Hz, -C*H*=CHCO_2Et), 6.40 (1H, ddt, J = 15.3 Hz, 11.0 Hz, 1.4 Hz, -CH_2CH=C*H*-), 6.17 (1H, dt, J = 15.3 Hz, 5.3 Hz, -CH_2CH=CH-), 5.86 (1H, d, J = 15.3 Hz, -CH=C*H*CO_2Et), 4.64 (1H, t, J = 3.3 Hz, -OC*H*O-), 4.34–4.08 (2 × 1H, ddd, J = 14.7 Hz, 5.3 Hz, 1.4 Hz, -CH_2OTHP), 4.21 (2H, q, J = 7.1 Hz, -CH_2CH_3), 3.84–3.50 (2 × 1H, m, -CH_2CH_2O-), 1.69 (6H, m, -$CH_2CH_2CH_2CH_2$O-), 1.28 (3H, t, J = 7.1 Hz, -CH_2CH_3); ms m/e (70 eV): 240 (M^+). Exact mass calcd.: 240.1362 (M^+); found: 240.1372 (M^+).

Hydroxy-ester ***12***

A solution of ester **11** (6.4 g, 26.6 mmol), pyridinium *p*-toluenesulfonate (PPTS, 670 mg, 2.6 mmol), and trifluoroacetic acid (TFA, one drop) in methanol (100 mL) was stirred at 50°C for 2.5 h. Then methanol was evaporated and the residue, dissolved in ether (10 mL), was filtered through silica. The filtrate was then evaporated to give hydroxy-ester **12** (4.1 g, 98% crude), which was used without any purification.

Silyl ether ***13***

To a solution of crude hydroxy-ester **12** (4.1 g, 26 mmol) in dry THF (300 mL) at 0°C was added *tert*-butyldimethysilyl chloride (7.9 g, 52 mmol) and imidazole (7.15 g, 105 mmol). The reaction mixture was allowed to warm to room temperature and stirred for 1 h. Ether (600 mL) was added and the organic phase was washed with distilled water (4 × 100 mL), dried, filtered, and evaporated to give silyl ether **13** (9.5 g crude, 130%), which was used without any purification.

Alcohol ***14***

Crude silyl ether **13** (9.5 g crude, theoretically 26 mmol), dissolved in dichloromethane (175 mL) at −78°C, was treated with a solution of diisobutylaluminium hydride (55 mL of 1 M solution in hexane, 55 mmol) and stirred for 45 min. Then the reaction mixture was quenched with saturated ammonium chloride (80 mL) and allowed to warm to room temperature. The viscous solution was filtered on a pad of Celite using ether as eluent. Solvents were evaporated and the residue was dissolved in ether (300 mL). The ethereal phase was washed with 5% aqueous sodium bicarbonate (3 × 50 mL) and with water (3 × 50 mL). The ethereal phase was dried, filtered, and evaporated to yield, after flash chromatography (hexane:acetone, 4:1), the alcohol **14** (5.8 g, 95% from ester **11**); ir ($CHCl_3$): 3620 (OH, free), 3660–3250 (OH, associated), 1665 and 1628 (C=C), 1255 (Si-CH_3), 1150–980 (C—O) and Si—O); nmr ($CDCl_3$) δ: 6.50–5.50 (4H, m, -C*H*=C*H*—C*H*=C*H*-), 4.19 (4H, m, -CH_2OH and -CH_2OSi$(CH_3)_2$C$(CH_3)_3$), 1.45 (1H, m, -CH_2O*H*), 0.92 (9H, s, -Si$(CH_3)_2$C$(CH_3)_3$), 0.08 (6H, s, -Si$(CH_3)_2$C$(CH_3)_3$).

Allylic chloride ***15***

To a solution of allyl alcohol **14** (987 mg, 4.33 mmol), *s*-collidine (640 μL, 586 mg, 4.83 mmol), and lithium chloride (224 mg, 5.28 mmol) in dry *N*,*N*-dimethylformamide (DMF, 10 mL), at 0°C, was added methanesulfonyl chloride (370 μL, 547 mg, 4.78 mmol). The reaction mixture was stirred at 0°C for 1 h and at room temperature for 1 h. Then the solution was poured in a funnel containing water and ice and extracted with a mixture of ether and hexane (1:4, 100 mL, 3 × 20 mL). The organic layers were combined and washed with water (3 × 20 mL), then dried, filtered, and the solvent evaporated. The crude product **15** (906 mg, 85%) was used without any purification since it decomposes on silica. Nevertheless the allylic chloride **15** can be stored in frozen benzene; ir ($CHCl_3$): 1660 and 1630 (C=C), 1255 (Si-CH_3), 1180–1050 (C—O and Si—O); nmr ($CDCl_3$) δ: 6.50–5.50 (4H, m, -C*H*=C*H*—C*H*=C*H*-), 4.18 (4H, two d, J = 5.5 Hz and 8.6 Hz, -CH_2-Cl and -CH_2O-), 0.92 and 0.08 (9H and 6H, two s, -Si$(CH_3)_2$C$(CH_3)_3$).

Diene ***16***

Sodium hydride (63.4 mg (60% in oil), 1.6 mmol) was added to a solution of dioxolane **9** (350 mg, 1.42 mmol) in a mixture of tetrahydrofuran (THF) and DMF (5:1, 8 mL) at 0°C. The reaction was allowed to warm to room temperature and stirred for 1 h. Then, at 0°C, a solution of crude allylic chloride **15** (395 mg, 1.6 mmol) in THF:DMF (5:1, 4 mL) was added. After addition, the mixture was stirred at room temperature for 12 h. The reaction mixture was then evaporated and the residue, dissolved in ether (50 mL), was washed with saturated ammonium chloride (40 mL). The aqueous layer was extracted with ether (3 × 10 mL). The combined organic layers were washed with brine (2 × 30 mL), dried, filtered, and evaporated. The crude oil was purified by flash chromatography (hexane:acetone, 4:1) to give the diene **16** (579 mg, 89%); ir ($CHCl_3$): 1730 (C=O), 1255 (Si-CH_3), 1055 (C—O); nmr ($CDCl_3$) δ: 6.16 (1H, ddt, J = 14.75 Hz, 10.0 Hz, 1.5 Hz, -C*H*=CHCH$_2$O-), 6.07 (1H, dd, J = 14.75 Hz, 10.0 Hz, -CH_2CH=C*H*-), 5.67 (1H, dt, J = 14.75 Hz, 5.0 Hz, -CH= C*H*CH_2O-), 5.47 (1H, dt, J = 14.75 Hz, 7.7 Hz, -CH_2CH=CH-), 4.19 (2H, d, J = 5.0 Hz, =CHCH_2O-), 3.92 (4H, m, -OCH_2CH_2O-), 3.71 (6H, s, 2 × -CO_2CH_3), 2.64 (2H, d, J = 7.7 Hz, -CH_2CH=CH-), 1.97 (2H, m, -CH_2CH_2C$(CO_2CH_3)_2$), 1.54 (2H, m, -CH_2CH_2C$(CO_2CH_3)_2$), 1.30 (3H, s, -CH_3), 0.90 and 0.06 (9H and 6H, two s, -Si$(CH_3)_2$C$(CH_3)_3$); ms m/e (70 eV): 456 (M^+), 441 (M^+-CH_3), 399 ($M^+-C(CH_3)_3$). Exact mass calcd.: 441.2308 (M^+-CH_3); found: 441.2296 (M^+-CH_3).

Ester ***17***

A solution containing diene **16** (5.05 g, 11 mmol), lithium chloride (1.03 g, 24.2 mmol), and water (250 μL, 250 mg, 13.8 mmol) in DMF (30 mL) was stirred at 165°C for 2.5 h. Then the solution was dried with magnesium sulfate and filtered on silica with ether as eluant. Evaporation of the solvent gave a crude oil, which was purified by flash chromatography (hexane:acetone, 85:15) to afford ester **17** (2.7 g, 61%); ir ($CHCl_3$): 1730 (C=O), 1255 (Si-CH_3), 1050 (C—O); nmr ($CDCl_3$ δ: 6.16 (1H, ddt, J = 14.5 Hz, 10.0 Hz, 1.5 Hz, -C*H*=CHCH$_2$O-), 6.05 (1H, dd, J = 14.5 Hz, 10.0 Hz, -CH_2CH=C*H*-), 5.66 (1H, dt, J = 14.5 Hz, 5.1 Hz, -CH=C*H*CH_2O-), 5.56 (1H, dt, J = 14.5 Hz, 7.3 Hz, -CH_2CH=CH-), 4.18 (2H, d, J = 5.1 Hz, =CHCH_2O-), 3.91 (4H, m, -OCH_2CH_2O-), 3.66 (3H, s, -CO_2CH_3), 2.50–2.20 (3H, m, -C*H*—CO_2CH_3 and -CH_2CH=CH-), 1.80–1.55 (4H, m, -CH_2CH_2CH—CO_2CH_3), 1.30 (3H, s, -CH_3), 0.90 and 0.06 (9H et 6H, two s, -Si$(CH_3)_2$C$(CH_3)_3$); ms m/e (70 eV): 398 (M^+), 383 (M^+-CH_3), 367 (M^+-OCH_3). Exact mass calcd.: 383.2253 (M^+-CH_3); found: 383.2251 (M^+-CH_3).

Alcohol ***18***

To a stirred solution of ester **17** (2.7 g, 6.78 mmol) in dichloromethane (100 mL), at −78°C, was added dropwise diisobutylaluminium hydride (DIBAH, 17 mL, 1.7 mmol, 1 M in hexane). The mixture was stirred for 30 min at −78°C after which it was quenched with aqueous

Can. J. Chem. Downloaded from www.nrcresearchpress.com by 91.144.44.67 on 09/07/12
For personal use only.

saturated NH_4Cl solution (60 mL), and allowed to warm to room temperature. The resulting slurry was filtered through Celite with ether as eluent. The filtrate was then evaporated and the residue, dissolved in ether (20 mL), was washed with 5% aqueous sodium bicarbonate (3 × 50 mL) and with water (3 × 50 mL). The ethereal phase was dried, filtered, and evaporated to yield, after flash chromatography (hexane:acetone, 4:1), the alcohol **18** (2.05 g, 82%); ir ($CHCl_3$): 3630 (OH, free), 3600–3350 (OH, associated), 1255 (Si-CH_3), 1050 (C—O); nmr ($CDCl_3$) δ: 6.20 (1H, ddt, J = 14.5 Hz, 10.0 Hz, 1.5 Hz, -C*H*=$CHCH_2O$-), 6.07 (1H, dd, J = 14.5 Hz, 10.0 Hz, -CH_2CH=C*H*-), 5.72–5.57 (2H, m, -C*H*=CH—CH=C*H*CH_2O-), 4.19 (2H, d, J = 5.1 Hz, =$CHCH_2O$-), 3.93 (4H, m, -OCH_2CH_2O-), 3.54 (2H, multiplet, -CH_2OH), 2.13 (2H, dd, J = 7.0 Hz, 6.8 Hz, -$CHCH_2CH$=), 1.77–1.35 (6H, m, -$CH_2CH_2CHCH_2OH$), 1.31 (3H, s, -CH_3), 0.91 and 0.06 (9H and 6H, two s, -$Si(CH_3)_2C(CH_3)_3$); ms m/e (70 eV): 371 (M^+-H), 355 (M^+-CH_3), 352 (M^+-H_2O). Exact mass calcd.: 355.2304 (M^+-CH_3); found: 355.2308 (M^+-CH_3).

Benzyl ether ***19***

To a stirred suspension of sodium hydride (378 mg (60% in oil), 9.45 mmol) in a mixture of THF:DMF (5:1, 30 mL), at 0°C, was added the alcohol **18** (2.23 g, 6 mmol) dissolved in the same solvent (18 mL). The reaction was allowed to warm to room temperature and was stirred for 1 h. Then freshly distilled benzyl bromide (860 μL, 1.24 g, 7.23 mmol) was added and the mixture stirred at room temperature for 17 h. The reaction mixture was quenched with aqueous saturated NH_4Cl solution (50 mL), and was extracted with ether:hexane (1:4, 200 mL). The aqueous phase was extracted again with the same solvent (2 × 50 mL). The combined organic layers were washed with brine (2 × 50 mL), dried, filtered, and evaporated. The residue was purified by flash chromatography (hexane:acetone,25:5) to give the benzyl ether **19** (2.53 g, 92%); ir ($CHCl_3$): 1255 (Si-CH_3), 1060 (C—O); nmr ($CDCl_3$ δ: 7.32 (5H, m, aromatic protons), 6.18 (1H, ddt, J = 15.0 Hz, 10.0 Hz, 1.5 Hz, -C*H*=$CHCH_2O$-), 6.03 (1H, dd, J = 15.0 Hz, 10.0 Hz, -CH_2CH=C*H*-), 5.70–5.53 (2H, m, -C*H*=CH—CH=C*H*CH_2O-), 4.48 (2H, s, -$CH_2\phi$), 4.20 (2H, dd, J = 5.1 Hz, 1.2 Hz, =$CHCH_2O$-), 3.91 (4H, m, -OCH_2CH_2O-), 3.33 (2H, d, J = 5.8 Hz, -$CHCH_2O$-), 2.16 (2H, m, -$CHCH_2CH$=), 1.80–1.35 (5H, m, -$CH_2CH_2CH_2CH_2O$-), 1.30 (3H, s, -CH_3), 0.91 and 0.07 (9H and 6H, two s, -$Si(CH_3)_3C(CH_3)_3$); ms m/e (70 eV): 460 (M^+), 445 (M^+-CH_3), 403 ($M^+-CH_3)_3$), Exact mass calcd.: 445.2773 (M^+-CH_3); found: 445.2773 (M^+-CH_3).

Ketol ***20***

A solution of benzyl ether **19** (1.8 g, 3.9 mmol) and pyridinium tosylate (28 mg, 0.39 mmol) in wet acetone (20 mL, 5% water) was stirred at 65°C for 5 h and then concentrated. The residue, dissolved in ether (200 mL), was washed with a solution of sodium bicarbonate (2 × 30 mL, 5% aqueous) and with brine (2 × 30 mL). The organic layer was dried and filtered, giving, after concentration, the crude ketol **20** (1.45 g), which was used without purification for the next step. An analytical sample was obtained by flash chromatography (hexane:acetone, 3:2); ir ($CHCl_3$): 3610 (OH, free), 3600–3300 (OH, associated), 1710 (C=O), 1080 (C—O); nmr ($CDCl_3$) δ: 7.32 (5H, m, aromatic protons), 6.21 (1H, ddt, J = 15.0 Hz, 10.0 Hz, 1.4 Hz, -C*H*=$CHCH_2OH$), 6.05 (1H, dd large, J = 15.0 Hz, 10.0 Hz, -CH_2CH=C*H*-), 5.73 (1H, dt, J = 15.0 Hz, 6.0 Hz, -CH=C*H*CH_2OH), 5.64 (1H, dt, J = 15.0 Hz, 7.4 Hz, -CH_2CH=CH-), 4.46 (2H, s, -$CH_2\phi$), 4.16 (2H, d, J = 6.0 Hz, =$CHCH_2OH$), 3.33 (2H, dd, J = 5.4 Hz, 1.6 Hz, -$CHCH_2O$-), 2.44 (2H, t apparent, J = 7.4 Hz, -$CHCH_2CH$=), 2.12 (2H, m, -$CH_2C(O)CH_3$), 2.10 (3H, s, -$C(O)CH_3$), 1.80–1.55 (4H, m, -$CHCH_2CH_2C(O)$-, -CH_2OH); ms m/e (CI, CH_4): 303 (M^++H), 285 (M^+-OH). Exact mass calcd.: 285.1855 (M^+-OH); found: 285.1858 (M^+-OH).

Silyl ether ***21***

To a solution of crude ketol **20** (1.45 g) in dry THF (30 mL) was added *tert*-butyldimethylsilyl chloride (1.3 g, 8.6 mmol) and imidazole (1.06 g, 15.6 mmol) at 0°C. The reaction mixture was allowed to warm to room temperature, stirred for 1 h, and then concentrated. The residue, dissolved in ether (200 mL), was washed with distilled water (4 × 40 mL), and the ethereal phase was dried, filtered, and evaporated to an oil. The residue was purified by flash chromatography (hexane:acetone, 9:1) to give silyl ether **21** (1.58 g, 97% yield from **19**); ir ($CHCl_3$): 1710 (C=O), 1255 (Si-CH_3), 1110 (C—O); nmr ($CDCl_3$) δ: 7.32 (5H, m, aromatic protons), 6.17 (1H, ddt, J = 15.0 Hz, 10.0 Hz, 1.4 Hz, -C*H*=$CHCH_2O$-), 6.04 (1H, dd, J = 15.0 Hz, 10.0 Hz, -CH_2CH=C*H*-), 5.65 (1H, dt, J = 15 Hz, 5.5 Hz, -CH=C*H*CH_2O-), 5.59 (1H, dt, J = 15.0 Hz, 7.4 Hz, -CH_2CH=CH-), 4.46 (2H, s, -$CH_2\phi$), 4.19 (2H, dd, J = 5.5 Hz, 1.3 Hz, =$CHCH_2O$-), 3.34 and 3.30 (2H, part AB of an ABX system, J_{AB} = 10.0 Hz, J_{AX} = 5.3 Hz, J_{BX} = 5.4 Hz, -$CHCH_2OBn$), 2.44 (2H, t apparent, J = 7.4 Hz, -$CHCH_2CH$=), 2.13 (2H, m, -$CH_2C(O)CH_3$), 2.10 (3H, s, -$C(O)CH_3$), 1.80–1.55 (3H, m, -$CHCH_2CH_2C(O)$-), 0.91 and 0.07 (9H and 6H, two s, -$Si(CH_3)_2C(CH_3)_3$); ms m/e (CI, CH_4): 417 (M^++H); 399 (M^+-OH); 359 ($M^+-C(CH_3)_3$). Exact mass calcd.: 417.2825 (M^++H); found 417.2819 (M^++H).

α,β-Unsaturated esters ***23***

To a stirred solution of phosphonate **22** (4.14 g, 17 mmol) in dry toluene (40 mL) was added *n*-butyllithium (7.34 mL of 2.2 M solution in hexane, 16 mmol) at 0°C. The reaction mixture was allowed to warm to room temperature and stirred for 15 min. The solution was then treated with ketone **21** (1.34 g, 3.23 mmol) dissolved in dry toluene (40 mL), and stirred at 0°C for 30 min and at room temperature for 90 h to 150 h, i.e., until the starting material has disappeared by thin-layer chromatography (toluene:acetone, 96:4). Then, distilled water (5 mL) was added and the toluene evaporated. The residue, dissolved in ether (300 mL), was washed with distilled water (4 × 50 mL). The ethereal layer was dried, filtered, and concentrated to an oil. The crude oil was purified by flash chromatography (toluene:acetone, 50:1) to give the esters **23** (1.37 g, 79%); ir ($CHCl_3$): 1715 (C=O), 1630 (C=C), 1255 (Si-CH_3), 1105 and 1060 (C—O); nmr ($CDCl_3$) δ: 733 (5H, m, aromatic protons), 6.26–5.97 (2H, m, -CH=C*H*—C*H*=$CHCH_2O$-), 5.72–5.54 (2H, m, -C*H*=CH—CH=C*H*CH_2O-), 4.79 and 4.76 (2H, two s, -OCH_2OCH_3), 4.19 and 4.48 (2H, two s, -$CH_2\phi$), 4.19 (2H, dd, J = 5.2 Hz, 1.2 Hz, =$CHCH_2O$-), 3.77 and 3.73 (3H, two s, -CO_2CH_3), 3.49 and 3.45 (3H, two s, -OCH_2OCH_3), 3.37 (2H, d, J = 5.7 Hz, -$CHCH_2OBn$), 2.51–2.12 (4H, m, -CH_2CH_2C= and -$CHCH_2CH$=), 2.00 and 1.87 (3H, two s, CH_3C=CCO_2CH_3), 1.72 (1H, m, -$CHCH_2CH_2C$=), 1.5 (2H, m, -$CHCH_2CH_2C$=), 0.91 and 0.07 (9H and 6H, two s, -$Si(CH_3)_2C(CH_3)_3$); ms m/e (CI, CH_4): 532 (M^+), 531 (M^+-H), 517 (M^+-CH_3). Exact mass calcd.: 517.2985 (M^+-CH_3); found: 517.2978 (M^+-CH_3).

Alcohols trans–trans–cis ***24*** *and* trans–trans–trans ***28***

The esters **23** (1.45 g, 2.7 mmol) dissolved in dichloromethane (50 mL) were treated, at −78°C, with a solution of diisobutylaluminium hydride (6.8 mL of 1 M solution in hexane, 6.8 mmol) and stirred for 15 min. Then the reaction mixture was quenched with Glauber's salt ($Na_2SO_4\cdot10H_2O$, 3.0 g) and was allowed to warm until the solution became cloudy. The mixture was dried with magnesium sulfate and was filtered on a pad of Celite using ether as eluent. The solvents were evaporated and the residue was purified by flash chromatography (hexane:acetone, 85:15) to give alcohols *trans–trans–cis* **24** (less polar) and *trans–trans–trans* **28** (more polar) (1.0 g, 73%, ≃1:1).

Alcohol trans–trans–cis ***24***: ir ($CHCl_3$): 3600 (OH, free), 3600–3320 (OH, associated), 1670 (C=C), 1255 (Si-CH_3), 1160–980 (C—O); nmr ($CDCl_3$) δ: 7.33 (5H, m, aromatic protons), 6.17 (1H, ddt, J = 14.8 Hz, 10.0 Hz, 1.5 Hz, -C*H*=$CHCH_2O$-), 6.03 (1H, dd, J = 14.8 Hz, 10.0 Hz, -CH_2CH=C*H*-), 5.64 (1H, dt, J = 14.8 Hz, 5.3 Hz, -CH=C*H*CH_2O-), 5.59 (1H, dt, J = 14.8 Hz, 8.1 Hz, -CH_2CH=CH-), 4.83 (2H, s, -OCH_2OCH_3), 4.48 (2H, -$CH_2\phi$), 4.19 (2H, d, J = 5.3 Hz, =$CHCH_2O$-), 4.10 (2H, d, J = 6.1 Hz, =CCH_2OH), 3.50 (3H, s, -OCH_2OCH_3), 3.35 (2H, d, J = 5.7 Hz, -$CHCH_2OBn$), 2.91 (1H, t, J = 6.1 Hz, =CCH_2OH), 2.28–2.00 (4H, m, -CH_2CH_2C= and -$CHCH_2CH$=), 1.70 (1H, m, -$CHCH_2CH_2C$=), 1.67 (3H, s, CH_3C=CCH_2OH), 1.43 (2H, m, -$CHCH_2CH_2C$=), 0.91 and 0.07 (9H and 6H, two s, -$Si(CH_3)_2C(CH_3)_3$); ms m/e (CI, CH_4): 487 (M^+-OH). Exact mass calcd.: 487.3244 (M^+-OH); found: 487.3244 (M^+-OH).

Alcohol trans–trans–trans ***28***: ir ($CHCl_3$): 3600 (OH, free), 3600–3320 (OH, associated), 1670 (C=C), 1255 (Si-CH_3), 1160–980 (C—O); nmr ($CDCl_3$) δ: 7.33 (5H, m, aromatic protons), 6.18 (1H, ddt, J = 15.0 Hz, 10.0 Hz, 1.5 Hz, -C*H*=CHCH$_2$O-), 6.04 (1H, dd, J = 15.0 Hz, 10.0 Hz, -CH$_2$CH=C*H*-), 5.65 (1H, dt, J = 15.0 Hz, 5.3 Hz, -CH=C*H*CH$_2$O-), 5.59 (1H, dt, J = 15.0 Hz, 7.8 Hz, -CH$_2$C*H*=CH-), 4.77 (2H, s, -OC*H*$_2$OCH$_3$), 4.48 (2H, s, -C*H*$_2$φ), 4.19 (2H, dd, J = 5.3 Hz, 1.3 Hz, =CHC*H*$_2$O-), 4.13 (2H, d, J = 5.7 Hz, =CC*H*$_2$OH), 3.47 (3H, s, -OCH$_2$OC*H*$_3$), 3.36 (2H, d, J = 5.7 Hz, -CHC*H*$_2$OBn), 2.96 (1H, t, J = 5.7 Hz, =CCH$_2$O*H*), 2.28–2.05 (4H, m, -CH$_2$C*H*$_2$C= and -CHC*H*$_2$CH=), 1.69 (1H, m, -C*H*CH$_2$-CH$_2$C=), 1.69 (3H, s, C*H*$_3$C=CH$_2$OH), 1.40 (2H, m, -CHC*H*$_2$-CH$_2$C=), 0.91 and 0.07 (9H and 6H, two s, -Si(C*H*$_3$)$_2$C(C*H*$_3$)$_3$); ms m/e (CI, CH_4): 487 (M^+−OH). Exact mass calcd.: 487.3244 (M^+−OH); found: 487,3244 (M^+−OH).

*Malonate **26***

*A. Allylic chloride **25***

To a solution of *trans–trans–cis* alcohol **24** (450 mg, 0.89 mmol), *s*-collidine (1.19 mL, 1.09 g, 9 mmol), and lithium chloride (380 mg, 8.9 mmol) in dry DMF (16 mL), at 0°C, was added methanesulfonyl chloride (350 μL, 518 mg, 4.5 mmol). The mixture was stirred at 0°C for 15 min and at room temperature for 1 h. Then the reaction mixture was poured over a solution of sodium bicarbonate (50 mL, 5% aqueous) and was extracted with ether (300 mL). The organic layer was washed with a saturated solution of copper nitrate (3 × 10 mL) and with water (4 × 50 mL). The ethereal phase was dried, filtered, and evaporated to an oil. The crude allylic chloride **25** was used without any purification since it decomposes on silica.

B. Alkylation

A suspension of sodium hydride (364 mg (60% in oil), 9.1 mmol) in a mixture of dry THF:DMF (2:1, 15 mL) cooled at 0°C was treated with dimethyl malonate (1.54 mL, 1.78 g, 13.4 mmol). Once hydrogen evolution ceased, the mixture was stirred 15 min to ensure reaction completion. Then, crude allylic chloride **25** dissolved in dry THF:DMF (2:1, 10 mL, 5 mL wash) was added via cannula. The reaction mixture was allowed to warm to room temperature and was stirred for 12 h. The solution was concentrated and ether (200 mL) was added. The ethereal phase was washed with water (5 × 40 mL), dried, filtered, and concentrated to an oil. The residue was purified by flash chromatography (hexane:acetone, 88:12) to give malonate **26** (426 mg, 77% (two steps)); ir ($CHCl_3$): 1750 and 1735 (C=O), 1680 (C=C), 1255 (Si-CH_3), 1170–980 (C—O); nmr ($CDCl_3$) δ: 7.33 (5H, m, aromatic protons), 6.17 (1H, ddt, J = 15.0 Hz, 10.0 Hz, 1.5 Hz, -C*H*=CHCH$_2$O-), 6.03 (1H, dd, J = 15.0 Hz, 10.0 Hz, -CH$_2$CH=C*H*-), 5.64 (1H, dt, J = 15.0 Hz, 5.3 Hz, -CH=C*H*CH$_2$O-), 5.60 (1H, dt, J = 15.0 Hz, 7.5 Hz, -CH$_2$C*H*=CH-), 4.74 (2H, s, -OC*H*$_2$OCH$_3$), 4.49 (2H, s, -C*H*$_2$φ), 4.19 (2H, dd, J = 5.3 Hz, 1.3 Hz, =CHC*H*$_2$O-), 3.71 and 3.70 (6H, two s, 2 × -CO$_2$C*H*$_3$), 3.70 (1H, t, J = 7.2 Hz, -C*H*(CO$_2$CH$_3$)$_2$), 3.46 (3H, s, -OCH$_2$OC*H*$_3$), 3.36 (2H, d, J = 5.7 Hz, -CHC*H*$_2$OBn), 2.84 (2H, d, J = 7.2 Hz, -C*H*$_2$CH(CO$_2$CH$_3$)$_2$), 2.17 (2H, m, -CH$_2$C*H*$_2$C=), 2.00 (2H, t apparent, J = 8.2 Hz, -CHC*H*$_2$CH=), 1.71 (1H, m, -C*H*CH$_2$CH$_2$C=), 1.64 (3H, s, C*H*$_3$C=CCH$_2$-), 1.38 (2H, m, -CHC*H*$_2$CH$_2$C=), 0.91 and 0.07 (9H and 6H, two s, -Si(C*H*$_3$)$_2$C-(C*H*$_3$)$_3$); ms m/e (70 eV): 816 (M^+), 603 (M^+−CH_3), 561 (M^+−C(CH$_3$)$_3$). Exact mass calcd.: 603.3353 (M^+−CH_3); found: 603.3353 (M^+−CH_3).

*Malonate **30***

*A. Allylic chloride **29***

The preparation of this allylic chloride was done as for allylic chloride **25** (*vide supra*) with the following quantities: *trans*-alcohol **28** (465 mg, 0.92 mmol), *s*-collidine (1.22 mL, 1.19 g, 9.2 mmol), lithium chloride (390 mg, 9.2 mmol), methanesulfonyl chloride (360 μL, 528 mg, 4.6 mmol), DMF (15 mL).

B. Alkylation

The alkylation of dimethylmalonate with crude allylic chloride **29** was done as for allylic chloride **25** (*vide supra*) with the following quantities: sodium hydride (369 mg (60% in oil), 9.2 mmol), dimethylmalonate (1.58 mL, 1.82 g, 13.8 mmol), THF:DMF (2:1, 15 mL), crude allylic chloride **29** in THF:DMF (2:1, 15 mL). This gave malonate **30** (503 mg, 88% (two steps)); ir ($CHCl_3$): 1750 and 1735 (C=O), 1680 (C=C), 1255 (Si-CH_3), 1170–980 (C—O); nmr ($CDCl_3$) δ: 7.32 (5H, m, aromatic protons), 6.25–5.96 (2H, m, -CH=C*H*—C*H*=CHCH$_2$O-), 5.70–5.53 (2H, m, -C*H*=CH—CH=C*H*CH$_2$O-), 4.71 (2H, s, -OC*H*$_2$OCH$_3$), 4.47 (2H, s, -C*H*$_2$φ), 4.19 (2H, dd, J = 5.3 Hz, 1.1 Hz, =CHC*H*$_2$φ), 3.71 and 3.70 (6H, two s, 2 × -CO$_2$C*H*$_3$), 3.69 (1H, t, J = 7.5 Hz, -C*H*(CO$_2$CH$_3$)$_2$), 3.42 (3H, s, -OCH$_2$OC*H*$_3$), 3.34 (2H, d, J = 5.7 Hz, -CHC*H*$_2$OBn), 2.84 (2H, d, J = 7.5 Hz, -C*H*$_2$CH(CO$_2$CH$_3$)$_2$), 2.17 (2H, m, -CH$_2$-CH$_2$C=), 2.08 (2H, t apparent, J = 8.1 Hz, -CHC*H*$_2$CH=), 1.66 (1H, m, -C*H*CH$_2$CH$_2$C=), 1.60 (3H, s, C*H*$_3$C=CCH$_2$-), 1.35 (2H, m, -CHC*H*$_2$CH$_2$C=), 0.91 and 0.07 (9H and 6H, two s, -Si(C*H*$_3$)$_2$C-(C*H*$_3$)$_3$); ms m/e (70 eV): 618 (M^+), 603 (M^+−CH_3), 561 (M^+−C(CH$_3$)$_3$). Exact mass calcd.: 603.3353 (M^+−CH_3); found: 603.3353 (M^+−CH_3).

trans–trans–cis *Triene alcohol **27***

To a solution of silyl ether **26** (426 mg, 0.68 mmol) in THF (15 mL), at 0°C, was added a solution of tetrabutylammonium fluoride (2.56 mL of a 1 M solution in THF, 2.56 mmol). The mixture was allowed to warm to room temperature and was stirred for 1 h. Then the solvent was evaporated and the residue dissolved in ether (100 mL). The ethereal phase was washed with water (5 × 25 mL), dried, filtered, and evaporated to an oil. The crude material was purified by flash chromatography (hexane:acetone, 3:2) to give the *trans–trans–cis* triene alcohol **27** (297 mg, 85% (65% overall, from alcohol **20**); ir ($CHCl_3$): 3610 (OH, free), 3620–3320 (OH, associated), 1750 and 1735 (C=O), 1680 (C=C), 1170–980 (C—O); nmr ($CDCl_3$) δ: 7.33 (5H, m, aromatic protons), 6.21 (1H, dd, J = 14.9 Hz, 10.0 Hz, -C*H*=CHCH$_2$OH), 6.07 (1H, dd, J = 14.9 Hz, 10.0 Hz, -CH$_2$CH=C*H*-), 5.73 (1H, dt, J = 14.9 Hz, 5.6 Hz, -CH=C*H*CH$_2$OH), 5.67 (1H, dt, J = 14.9 Hz, 7.4 Hz, -CH$_2$C*H*=CH-), 4.74 (2H, s, -OC*H*$_2$OCH$_3$), 4.49 (2H, s, -C*H*$_2$φ), 4.16 (2H, t apparent, J = 5.6 Hz, =CHC*H*$_2$OH), 3.71 and 3.70 (6H, two s, 2 × -CO$_2$C*H*$_3$), 3.70 (1H, t, J = 7.3 Hz, -C*H*(CO$_2$CH$_3$)$_2$), 3.46 (3H, s, -OCH$_2$OC*H*$_3$), 3.35 (2H, d, J = 5.8 Hz, -CHC*H*$_2$OBn), 2.82 (2H, d, J = 7.3 Hz, -C*H*$_2$CH(CO$_2$CH$_3$)$_2$), 2.19 (2H, m, -CH$_2$C*H*$_2$C=), 1.99 (2H, m, -CHC*H*$_2$CH=), 1.71 (1H, m, -C*H*CH$_2$CH$_2$C=), 1.64 (3H, s, C*H*$_3$C=CCH$_2$-), 1.53–1.22 (3H, m, -CHC*H*$_2$CH$_2$C= and -CH$_2$O*H*); ms m/e (70 eV): 487 (M^+−OH), 442 (M^+−CH_3OCH$_2$OH). Exact mass calcd.: 487.2696 (M^+−OH); found: 487.2696 (M^+−OH).

trans–trans–trans *Triene **31***

The cleavage of silyl ether **30** was done as for silyl ether **24** (*vide supra*) with the following quantities: silyl ether **30** (503 mg, 0.81 mmol), tetrabutylammonium fluoride (2.84 mL of a 1 M solution in THF, 2.84 mmol), THF (15 mL); this gave *trans–trans–trans* triene **31** (390 mg, 95%) (84% overall, from alcohol **28**); ir ($CHCl_3$): 3610 (OH, free), 3620–3320 (OH, associated), 1750 and 1735 (C=O), 1680 (C=C), 1170–980 (C—O); nmr ($CDCl_3$) δ: 7.32 (5H, m, aromatic protons), 6.21 (1H, dd, J = 14.9 Hz, 10.0 Hz, -C*H*=CHCH$_2$OH), 6.05 (1H, dd, J = 14.9 Hz, 10.0 Hz, -CH$_2$CH=C*H*-), 5.72 (1H, dt, J = 14.9 Hz, 5.8 Hz, -CH=C*H*CH$_2$OH), 5.61 (1H, dt, J = 14.9 Hz, 7.8 Hz, -CH$_2$C*H*=CH-), 4.71 (2H, s, -OC*H*$_2$OCH$_3$), 4.47 (2H, s, -C*H*$_2$φ), 4.16 (2H, t apparent, J = 5.8 Hz, =CHC*H*$_2$OH), 3.71 and 3.70 (6H, two s, 2 × -CO$_2$C*H*$_3$), 3.69 (1H, t, J = 7.6 Hz, -C*H*(CO$_2$CH$_3$)$_2$), 3.42 (3H, s, -OCH$_2$OC*H*$_3$), 3.35 (2H, d, J = 5.4 Hz, -CHC*H*$_2$OBn), 2.84 (2H, d, J = 7.6 Hz, -C*H*$_2$CH(CO$_2$CH$_3$)$_2$), 2.17 (2H, m, -CH$_2$C*H*$_2$C=), 2.09 (2H, t apparent, J = 7.8 Hz, -CHC*H*$_2$CH=), 1.66 (1H, m, -C*H*CH$_2$CH$_2$C=), 1.60 (3H, s, C*H*$_3$C=CCH$_2$-), 1.50–1.22 (3H, m, -CHC*H*$_2$CH$_2$C= and -CH$_2$O*H*); ms m/e (70 eV): 487 (M^+−OH), 442 (M^+−CH_3OCH$_2$OH). Exact mass calcd.: 487.2696 (M^+−OH); found: 487.2691 (M^+−OH).

Cyclization of trans–trans–cis *triene **27***

*A. Allylic chloride **32***

To a solution of *trans–trans–cis* triene alcohol **27** (100 mg, 0.2 mmol), *s*-collidine (270 μL, 247 mg, 2.0 mmol), and lithium chloride (90 mg, 2.1 mmol) in dry DMF (4 mL), at 0°C, was added

Can. J. Chem. Downloaded from www.nrcresearchpress.com by 91.144.44.67 on 09/07/12
For personal use only.

Can. J. Chem. Downloaded from www.nrcresearchpress.com by 91.144.44.67 on 09/07/12
For personal use only.

methanesulfonyl chloride (78 μL, 115 mg, 1.0 mmol). The mixture was stirred at 0°C for 15 min at room temperature for 1 h. Then the reaction mixture was poured over a solution of sodium bicarbonate (25 mL, 5% aqueous) and was extracted with ether (150 mL). The organic layer was washed with a saturated solution of copper nitrate (3 × 2 mL) and with water (4 × 25 mL). The ethereal phase was dried, filtered, and evaporated to an oil. The crude allylic chloride **32** was used without any purification since it decomposes on silica.

B. Alkylation

A suspension of sodium hydride (18 mg (60% in oil), 0.45 mmol) in a mixture of dry THF:DMF (1:1, 40 mL) was stirred at 70°C. The crude allylic chloride **32** dissolved in DMF (4 mL) was added, over 22 h (with a syringe pump), directly into the suspension of sodium hydride. Once the addition was complete, the mixture was stirred 1 h. The reaction mixture was concentrated under vacuum, then diluted with ether (200 mL). The organic phase was washed with a saturated solution of ammonium chloride (3 × 20 mL) and with water (5 × 25 mL), dried, filtered, and evaporated to an oil. The residue was purified by flash chromatography (hexane:acetone, 4:1) to give a mixture of Diels–Alder adducts (66 mg, 68%).

*Separation of Diels–Alder adducts **33, 34, 35***

The two main Diels–Alder adducts and the decarboxylated products were separated by flash chromatography. The mixtures of solvents used were acetone:hexane (1:4) and acetone:toluene (4:96) (**33:34:35** ≃ 13:6:3).

R_f of Diels–Alder adducts

Solvents	**33**	**34**	**35**
Acetone:hexane (1:4)	0.30	0.34	0.34 and 0.40
Acetone:toluene (4:96)	0.30	0.26	0.43

Compound **33**: ir ($CHCl_3$): 1730 (C=O), 1605 (C=C), 1170–1000 (C—O); nmr ($CDCl_3$) δ: 7.33 (5H, m, aromatic protons), 5.88 (1H, dt apparent, J = 8.3 Hz, 3.1 Hz, 7-H), 5.72 (1H, dt apparent, J = 8.3 Hz, 3.3 Hz, 6-H), 4.63 and 4.43 (2H, two d, parts A and B of an AB system, J_{AB} = 7.4 Hz, -OCH_2OCH_3), 4.51 (2H, s, -$CH_2\phi$), 3.74 and 3.70 (6H, two s, 2 × -CO_2CH_3), 3.34 (2H, d, J = 5.6 Hz, -$CHCH_2OBn$), 3.21 (3H, s, -OCH_2OCH_3), 2.78 (1H, dd, J = 13.3 Hz, 12.1 Hz, 13-H_β), 2.71 and 2.60 (2H, two d, parts A and B of an AB system, J_{AB} = 15.0 Hz, 11-H_2), 2.40 (1H, m, 8-H), 2.23 (1H, dd, J = 12.1 Hz, 6.4 Hz, 13-H_α), 1.85 (1H, m, 5-H), 1.80–1.35 (7H, m, -$CH_2CH_2CHCH_2$-), 0.74 (3H, s, -CH_3). ms m/e (70 eV): 486 (M^+), 471 (M^+-CH_3), 454 (M^+-CH_3OH), 424 ($M^+-CH_3OCH_2OH$). Exact mass calcd.: 486.2617; found: 486.2608.

Compound **34**: ir ($CHCl_3$): 1730 (C=O), 1130–1000 (C—O); nmr ($CDCl_3$) δ: 7.33 (5H, m, aromatic protons), 5.65 (1H, dt apparent, J = 10.1 Hz, 3.2 Hz, 7-H), 5.51 (1H, dt apparent, J = 10.1 Hz, 1.8 Hz, 6-H), 4.67 (2H, s, -OCH_2OCH_3), 4.49 (2H, s, -$CH_2\phi$), 3.76 and 3.71 (6H, two s, 2 × -CO_2CH_3), 3.29 (3H, s, -OCH_2OCH_3), 3.27 (2H, d, J = 6.2 Hz, -$CHCH_2OBn$), 3.01 (1H, m, 8-H), 2.86 and 2.58 (2H, two d, parts A and B of an AB system, J_{AB} = 16.5 Hz, 11-H_2), 2.53 (2H, m, 5-H and 13-H_β), 1.86 (1H, t apparent, J = 13.5 Hz, 13-H_α), 1.76–1.10 (7H, m, -$CH_2CH_2CHCH_2$-), 1.05 (3H, s, -CH_3); ms m/e (70 eV): 424 ($M^+-CH_3OCH_2OH$). Exact mass calcd.: 424.2250 ($M^+-CH_3OCH_2OH$); found: 424.2251 ($M^+-CH_3OCH_2OH$).

Compound **35**: ir ($CHCl_3$): 1730 (C=O), 1605 (C=C), 1170–1000 (C—O); nmr ($CDCl_3$) δ: mixture of isomers → decarboxylated tricyclic compounds; ms m/e (70 eV): 428 (M^+), 396 (M^+-CH_3OH), 366 ($M^+-CH_3OCH_2OH$). Exact mass calcd.: 366.2194 ($M^+-CH_3OCH_2$-OH); found: 366.2194 ($M^+-CH_3OCH_2OH$).

Following a similar experimental procedure *trans–trans– trans* triene alcohol **31** was converted into the corresponding allylic chloride and the macrocyclization was attempted as described above, but no specific products could be isolated from the resulting reaction mixture.

Acknowledgements

This research was supported by the Natural Sciences and Engineering Research Council of Canada (NSERCC) and by the "Ministère de l'Education (FCAR) du Québec".

1. (*a*) D. TAUB. *In* The total synthesis of natural products. Vol. 6. *Edited by* J. ApSimon. John Wiley and Sons, New York, NY. 1984. pp. 1–49; (*b*) K. NAKANISHI. *In* Natural products chemistry. Vol. 3. *Edited by* K. Nakanishi *et al.* Kodansha Ltd, Tokyo. 1983. Chap. 4; (*c*) *In* Natural products chemistry. Vol. 1. *Edited by* K. Nakanishi *et al.* Kodansha Ltd, Tokyo. 1974. pp. 421–545; (*d*) D. TAUB. *In* The total synthesis of natural products. Vol. 2. *Edited by* J. ApSimon. John Wiley and Sons, New York, NY. 1973. pp. 641–725.
2. (*a*) R. A. MITCHELI, Z. G. HAJOS, N. COHEN, D. R. PARRISH, L. A. PORTLAND, W. SCIAMANNA, M. A. SCOTT, and P. A. WHERLI. J. ORG. CHEM. **40**, 675 (1975); (*b*) Z. G. HAJOS and D. R. PARRISH. J. Org. Chem. **38**, 3244 (1973).
3. W. S. Johnson, B. E. McCarry, R. L. Harkezich, and S. G. BOOTS. J. Am. Chem. Soc. **102**, 352 (1980).
4. (*a*) T. KAMETANI and H. NEMOTO. Tetrahedron, **37**, 3 (1981); (*b*) W. OPPOLZER. Angew. Chem. Int. Ed. Engl. **16**, 10 (1977); (*c*) A. G. FALLIS. Can. J. Chem. **62**, 183 (1984), and references therein; (*d*) M. IHARA, I. SUDOW, and K. FUKUMOTO. J. Chem. Soc. Perkin Trans. 1, 117 (1986); (*e*) M. IHARA, I. SUDOW et K. FUKUMOTO. J. Org. Chem. **50**, 144 (1985); (*f*) M. E. JUNG and K. M. HALWEG. Tetrahedron Lett. 2121 (1984); (*g*) T. KAMETANI, K. SUZUKI, and H. NEMOTO. J. Org. Chem. **47**, 2331 (1982); (*h*) T. KAMETANI, H. MATSUMOTO, H. NEMOTO, and F. FUKUMOTO. J. Am. Chem. Soc. **100**, 6218 (1978).
5. (*a*) K. BAETTIG, C. DALLAIRE, R. PITTELOUD, and P. DESLONGCHAMPS. Tetrahedron Lett. **28**, 5249 (1987); (*b*) K. BAETTIG, A. MARINIER, R. PITTELOUD, and P. DESLONGCHAMPS. Tetrahedron Lett. **28**, 5253 (1987); (*c*) G. BÉRUBÉ and P. DESLONGCHAMPS. Tetrahedron Lett. **28**, 5255 (1987); (*d*) S. LAMOTHE, A. NDIBWAMI, and P. DESLONGCHAMPS. Tetrahedron Lett. **29**, 1639 (1988); (*e*) S. LAMOTHE, A. NDIBWAMI, and P. DESLONGCHAMPS. Tetrahedron Lett. **29**, 1641 (1988); (*f*) A. MARINIER and P. DESLONGCHAMPS. Tetrahedron Lett. **29**, 6215 (1988).
6. T. TAKAHASHI, K. SHIMIZU, T. DOI, and J. TSUJI. J. Am. Chem. Soc. **110**, 2674 (1988).
7. S. M. KUPCHAN and A. W. BY. *In* The alkaloids. Vol. X. *Edited by* R. H. F. Manske. 1968. Chap. 2. pp. 193–285.
8. T. TOKUYAMA, J. DALY, and B. WITKOP. J. Am. Chem. Soc. **91**, 3931 (1969).
9. A. J. BIRCH, R. W. RICHARDS, H. SMITH, A. HARRIS, and W. B. WHALLEY. Tetrahedron, **7**, 241 (1959).
10. S. V. BHAT, B. S. BAJWA, H. DORNAUER, N. J. DE SOUZA, and H.-W. FEHLHABER. Tetrahedron Lett. 1669 (1977).
11. E. J. COREY and J. W. SUGGS. Tetrahedron Lett. **31**, 2647 (1975).
12. H. NAGAOKA and Y. KISHI. Tetrahedron, **37**, 3873 (1981).
13. N. MIYASHITA, A. YOSHIKOSHI, and P. A. GRIECO. J. Org. Chem. **42**, 372 (1977).
14. E. J. COREY and A. VENKATESWARLU. J. Am. Chem. Soc. **94**, 6190 (1972).
15. E. W. COLLINGTON and A. I. MEYERS. J. Org. Chem. **36**, 3044 (1971).
16. B. M. TROST and W. C. VLADUCHICK. J. Org. Chem. **44**, 148 (1979).
17. A. P. KRAPCHO, J. F. WEIMASTER, J. M. ELRIDGE, E. C. E. JANHNGEN, JR., A. I. LOVEY, and W. P. STEPHENS. J. Org. Chem. **43**, 138 (1978).
18. E. NAKAMURA. Tetrahedron Lett. **22**, 663 (1981).
19. A. G. MICHEL, M. PROULX, and M. MICHEL-DEWEZ. Acta Crystallogr. Sect. C: Cryst, Struct. Commun. **C44**, 1646 (1988).
20. (*a*) P. DESLONGCHAMPS, S. LAMOTHE and H.-S. LIN. Can. J. Chem. **65**, 1298 (1987); (*b*) D. BRILLON and P. DESLONGCHAMPS. Can. J. Chem. **65**, 43 (1987); **65**, 56 (1987).
21. (*a*) P. DESLONGCHAMPS. Aldrichimica Acta, **17**, 59 (1984); (*b*) Bull. Soc. Chim. Fr. II, **9–10**, 349 (1984).

Alkylammonium lead halides. Part 2. $CH_3NH_3PbX_3$ (X = Cl, Br, I) perovskites: cuboctahedral halide cages with isotropic cation reorientation[1]

OSVALD KNOP, RODERICK E. WASYLISHEN, MARY ANNE WHITE, T. STANLEY CAMERON, AND MICHIEL J. M. VAN OORT

Department of Chemistry, Dalhousie University, Halifax, N.S., Canada B3H 4J3

Received April 27, 1989

OSVALD KNOP, RODERICK E. WASYLISHEN, MARY ANNE WHITE, T. STANLEY CAMERON, and MICHIEL J. M. VAN OORT. Can. J. Chem. **68**, 412 (1990).

Methylammonium lead(II) halides, $CH_3NH_3PbX_3$ (X = Cl, Br, I), have been investigated by single-crystal X-ray diffraction, ^2H and ^{14}N nmr, adiabatic calorimetry, and other methods. The chloride (CL) has transitions at 171.5 and 177.4 K, the bromide (BR) at 148.4, 154.2, and 235.1 K, and the iodide (IO) at 162.7 and 326.6 K. The respective entropies of transition (J K^{-1} mol^{-1}) are 11.0 and 5.1 for CL; 8.7, 3.4, and 5.3 for BR; and 16.1 and 1.9 for IO. The highest-temperature phase, phase *I*, of each halide is of the cubic (*Pm3m*) perovskite type. The cation in CL(*I*) and BR(*I*) could not be localized in the electron density maps; the thermal motion of the halogen atom is highly anisotropic. The ln $T_1(^2H)$ vs. T^{-1} plots (*N*-deuterated samples as well as $CD_3NH_3PbCl_3$) show significant departures from linearity: the temperature variation of $T_1(^2H)$ in BR(*II*) and IO(*II*) can be represented by functions of the type $\ln T_1(H) = k_0 - k_2T^{-2}$, which give adequate analytical representations of $T_1(^2H)$ and $T_1(^{14}N)$ in phase *I* as well. On cooling, BR(*II*) and IO(*II*) exhibit small quadrupole splittings QS(^2H), which can be represented to a high degree of correlation by $QS(^2H) = k(T_{tr} - T)^n$, i.e. they appear to exhibit critical behaviour with respect to *T*. The ^{14}N nmr results indicate that the C—N bond in phase *I* reorientates in an isotropic potential at a rate approaching that of the freely rotating methylammonium ion. Below phase *I* this motion takes place in an increasingly anisotropic potential in BR(*II*) and IO(*II*) and is essentially arrested in CL(*II*), BR(*III*), and IO(*III*). The temperature dependence of the activation energy E_a for the cation reorientation and other aspects of the non-Arrhenius behaviour are discussed, and the $CH_3NH_3PbX_3$ perovskites are compared with the corresponding $(CH_3NH_3)_2TeX_6$ halides, utilizing preliminary ^2H nmr results on $(CH_3ND_3)_2TeBr_6$. The electrical conductivity, between 0 and 95°C, of $CH_3NH_3PbI_3$ increases with temperature and exhibits no discontinuity at T_{tr} = 326.6 K; the activation energy for the conduction process is estimated as ~0.4 eV.

Key words: crystal structure, $MeNH_3PbCl_3$ and $MeNH_3PbBr_3$; heat capacity, $MeNH_3PbX_3$ (X = Cl, Br, I); methylammonium lead halides; solid-state NMR, ^2H and ^{14}N; spin-lattice relaxation, non-Arrhenius behaviour.

OSVALD KNOP, RODERICK E. WASYLISHEN, MARY ANNE WHITE, T. STANLEY CAMERON et MICHIEL J. M. VAN OORT. Can. J. Chem. **68**, 412 (1990).

On a étudié les halogénures de méthylammonium plomb(II), $CH_3NH_3PbX_3$ (X = Cl, Br ou I) par diffraction des rayons-X sur un monocristal, par rmn du ^2H et du ^{14}N, par calorimétrie adiabatique ainsi que par d'autres méthodes. Le chlorure (CL) a des transitions à 171,5 et 177,4 K, le bromure (BR) en présente à 148,4, 154,2 et 235,1 K alors que pour l'iodure (IO) elles se situent à 162,7 et 326,6 K. Les entropies respectives de ces transitions (J K^{-1} mol^{-1}) sont 11,0 et 5,1 pour le Cl, 8,7, 3,4 et 5,3 pour le Br et 16,1 et 1,9 pour le IO. Pour chacun des halogénures, la phase observée à la température la plus élevée, la phase *I*, est du type perovskite cubique (*Pm3m*). Les cations des formes CL(*I*) et BR(*I*) ne peuvent pas être localisés dans les sections de densités électroniques; le mouvement thermique de l'atome d'halogène est très anisotrope. Les courbes du ln $T_1(^2H)$ vs. T^{-1} (des échantillons *N*-deutérés ainsi que du $CD_3NH_3PbCl_3$) présentent des déviations importantes par rapport à la linéarité: pour les formes BR(*II*) et IO(*II*), la variation de $T_1(^2H)$ en fonction de la température peut être représentée par des fonctions du type ln $T_1(H) = k_0 - k_2T^{-2}$ qui fournissent aussi des représentations analytiques adéquates de $T_1(^2H)$ et $T_1(^{14}N)$ de la phase *I*. Lors de leur refroidissement, les formes BR(*II*) et IO(*II*) présentent de faibles couplages quadrupolaires, QS(^2H), qui peuvent être représentées avec un grand degré de corrélation par l'équation $QS(^2H) = k(T_{tr} - T)^n$, c'est-à-dire qu'elles semblent présenter un comportement critique par rapport à *T*. Les résultats de la rmn du ^{14}N indiquent que la liaison C—N de la phase *I* se réoriente dans un potentiel isotrope à une vitesse qui approche celle de l'ion méthylammonium qui tournerait librement. En dessous de la phase *I*, ce mouvement se produit dans un potentiel de plus en plus anisotrope pour les formes BR(*II*) et IO(*II*) et il est essentiellement arrêté pour les formes CL(*II*), BR(*III*) et IO(*III*). On discute de la relation qui existe entre la température et l'énergie d'activation E_a de la réorientation du cation ainsi que d'autres aspects du comportement qui ne se conforment pas à la loi d'Arrhénius; de plus, utilisant des données préliminaires de rmn du ^2H obtenues à l'aide du $(CH_3ND_3)_2TeBr_6$, on compare les perovskites $CH_3NH_3PbX_3$ avec les halogénures $(CH_3NH_3)_2TeX_6$ correspondants. Entre 0 et 95°C, la conductivité électrique du $CH_3NH_3PbI_3$ augmente avec une augmentation de la température sans présenter une discontinuité à la valeur de T_{tr} = 326,6 K; on évalue l'énergie d'activation du processus de conduction à environ 0,4 eV.

Mots clés : structure cristalline, $MeNH_3PbCl_3$ et $MeNH_3PbBr_3$; capacité thermique $MeNH_3PbX_3$ (X = Cl, Br, I); halogénures de methylammonium plomb; RMN de l'était solide, ^1H et ^{14}N; relaxation spin-réseau, comportement «non-Arrhenius».

[Traduit par la revue]

The cubic $CH_3NH_3PbX_3$ (X = Cl, Br, I) perovskites described by Weber (2) are compounds unusual in several respects. Their colour intensifies rapidly from the cream white chloride to the reddish-orange bromide and black iodide, pointing to a charge-transfer character of the Pb—X bonds and possibly to photoconduction (2). The $CH_3NH_3^+$ ion is nominally at the centre of a simple cubic cell (*Pm3m*, *Z* = 1, Pb in 1(*a*) − 000), i.e. at 1(*b*) − $\frac{111}{222}$ (site symmetry *m3m*) and inside a cuboctahedral cage formed by 12 nearest X neighbours at 3(*d*) − $\frac{1}{2}00$ etc. It is clear that if this is the crystallographically correct

[1]For Part 1, see ref. 1.

Can. J. Chem. Downloaded from www.nrcresearchpress.com by 91.144.44.67 on 09/07/12
For personal use only.

Can. J. Chem. Downloaded from www.nrcresearchpress.com by 91.144.44.67 on 09/07/12
For personal use only.

unit cell, then (*i*) the cation must be orientationally disordered in a manner consistent with the observed average symmetry;[2] (*ii*) the major component of the disorder would be expected to be dynamic; and (*iii*) reduction of the thermal motion of the cation on cooling is likely to result in the occurrence of transitions to phases of lower symmetry but closely related to the respective cubic phases. In this paper we report on our investigation of the validity of these expectations by single-crystal X-ray diffraction, solid-state ^2H and ^{14}N nmr, and adiabatic calorimetry, with minor assistance from other methods.[3]

The following abbreviations will be used: CL, $CH_3NH_3PbCl_3$; CLD, $CD_3NH_3PbCl_3$; BR, $CH_3NH_3PbBr_3$; IO, $CH_3NH_3PbI_3$.

Experimental

Preparation

BR and IO were prepared as described in ref. 2 (for IO cf. also ref. 1). They were authenticated by X-ray powder diffractometry and IO also by chemical analysis: a duplicate determination of Pb as $PbCrO_4$ gave 33.51 wt% Pb (theory, 33.42 wt%). The room-temperature lattice parameters of both (and of CL) agreed reasonably well with those of ref. 2. However, in the diffraction pattern of IO some of the lines corresponding to Weber's cubic IO (a = 6.27 Å) were split up or broadened, indicating that IO at room temperature is not strictly cubic.

CL was prepared by the method described in ref. 2 for BR, using CH_3NH_3Cl instead of CH_3NH_3Br, and also by direct conversion of solid $PbCl_2$ in an excess of hot concentrated aqueous solution of CH_3NH_3Cl. The method of ref. 2 modified for CL gave a pure product only when the molar CH_3NH_3/Pb ratio was at least 12. When a smaller excess was used, the product was pure white instead of cream-coloured as in the $PbCl_2$ method, but on standing it eventually discoloured. The powder diffraction pattern of the aged product contained a number of unidentified impurity lines, possibly of Pb(OH)Cl or a related compound.

Single crystals of CL and BR suitable for structure analysis were obtained by dissolving CL or BR in hot concentrated aqueous solution of the respective CH_3NH_3X halide and allowing the resulting solution to cool slowly. IO is the least soluble of the three halides and attempts to obtain in this way crystals of a size and quality suitable for single-crystal diffraction failed.

Partially *N*-deuterated samples of CL, BR, and IO required for the nmr studies were prepared using D-containing solutions. CLD was prepared by direct conversion of $PbCl_2$ using CD_3NH_3Cl.

X-ray diffraction

CAD-4 four-circle diffractometer; Mo $K\alpha_1$, λ = 0.70926 Å (graphite monochromator); T = ~18°C. Lorentz, polarization, and absorption corrections applied. Anisotropic temperature factor defined as $\exp[-2\pi^2(U_{11}h^2a^{*2} + U_{22}k^2b^{*2} + U_{33}l^2c^{*2} + 2U_{23}klb^*c^* + 2U_{13}hla^*c^* + 2U_{12}hka^*b^*)]$.

CH_6Cl_3NPb fw = 345.62

Cubic, *Pm3m* (no. 221) (systematic absences, none); a = 5.657(2) Å, V = 181.0(2) Å^3, Z = 1; θ-range, 2–40°, μ_{Mo} = 233 cm^{-1}, ρ_c = 3.171(4) g/cm^3, $F(000)$ = 152. Crystal, 0.22 × 0.32 × 0.38 mm^3. Reflections: total measured, 781; unique total, 150; unique used, 150 ($I > 2\sigma(I)$). R_{merg} = 11.5% before and 7.0% after absorption corrections.

CH_6Br_3NPb fw = 478.98

Cubic, *Pm3m* (no. 221) (systematic absences, none); a = 5.902(2) Å, V = 205.6(2) Å^3, Z = 1; θ-range, 2–40°, μ_{Mo} = 339 cm^{-1}, ρ_c = 3.818(7) g/cm^3, $F(000)$ = 206. Crystal, 0.22 × 0.26 × 0.26 mm^3. Reflections: total measured, 869; unique total, 166; unique used, 166 ($I > 2\sigma(I)$). Intensities collected twice, second collection used in refinement. R_{merg} = 12.2% before and 8.9% after absorption corrections.

Nmr measurements[4]

^2H spectra of all three compounds were obtained with partially *N*-deuterated material, $CH_3N(H, D)PbX_3$. The exact D content was not determined, nor was the effect of the deuteration on the transition temperatures. In addition, ^2H spectra were obtained with CLD. Samples (sealed in cylindrical thin-walled tubes of 0.9 cm o.d. and approximately 1 cm high) were placed in standard thin-walled 10 mm o.d. nmr tubes for all measurements.

Measurements were carried out at 8.48 T with a Nicolet 360NB spectrometer using a broad band (16–58 MHz) variable-temperature 10 mm probe supplied by Nicolet. The ^2H and ^{14}N frequencies were 55.427 and 26.083 MHz, respectively. Spin–lattice relaxation time experiments were performed using the inversion recovery pulse sequence, which employs compensating pulses (10); the ^2H and ^{14}N $\pi/2$ pulse widths were 30–40 and 45–60 μs, respectively. T_1 values were calculated from peak heights (obtained at ten or more delays) by a nonlinear, three-parameter least-squares fitting procedure available in the Nicolet software (11). As a check on possible frequency dependence $T_1(^2H)$ values in CL(I) and BR(I) at room temperature were also measured at 30.7 MHz on a Bruker MSL-200 spectrometer and found to be within experimental error (≤3%) of the corresponding values obtained at the higher frequency.

Calorimetry[4]

The heat capacities were measured in an adiabatic calorimeter from 30 to 345 K for CL, from 30 to 300 K for BR, and from 30 to 350 K for IO, using sample masses of 14.6883 g (CL), 12.8235 g (BR), and 17.9217 g (IO). The calorimeter was operated in the heat-pulse mode and gave direct values of $C_p = q/\Delta T$ from the measurement of the temperature increase ΔT for a measured heat pulse q; in most of the experiments it was used in the automated (12) mode. Temperatures were measured with a calibrated Pt resistance thermometer to an accuracy of 0.005 K. The accuracy of the overall determinations, as estimated from previous heat capacity measurements on NBS-49 benzoic acid (13), was ±1%.

Transition temperatures T_{tr} were defined by small ΔT measurements in the regions of the transitions. Transition enthalpies were measured by the long-heat method, and entropies of transition were evaluated as $\Delta T_{tr} = \int[C_p(\text{measured}) - C_p(\text{baseline})](dT/T)$ in the region of the transition (12). The results are summarized in Table 1.

Infrared spectra

In alkylammonium halides containing N—(H, D)···X bonds the spectral features of most interest are the NH and ND stretching absorptions, for their numbers and frequencies yield information concerning the type and strength of the hydrogen bonding. In this respect the spectra of partially *N*-deuterated $CH_3NH_3PbX_3$ samples were disappointing. The heavy continuous absorption in the 2000–4000 cm^{-1} region[5] increased from CL to IO and precluded the kind of examination of the individual ν(NH) and ν(ND) features that has proved so informative in other methylammonium (8, 14, 15) and especially ammonium (16) salts. Nevertheless, the spectra did permit qualitative estimates to

[2]In this respect the $CH_3NH_3PbX_3$ halides differ from $(CH_3NH_3)_2SnCl_6$ at room temperature, in which the cation is also surrounded by 12 Cl atoms (three at 3.46 Å and six at 3.59 Å from N) but *oriented*: the C—N bond coincides with a threefold rotation axis, consistent with the 3*m* site symmetry of the cation (3–8).

[3]Partial results of the nmr experiments were reported in a previous communication (9). The lattice parameters of the three halides and their variation with temperature will be reported and discussed in Part 3.

[4]The results of these measurements are in Tables A to E. Copies of this material can be purchased from the Depository of Unpublished Data, CISTI, National Research Council of Canada, Ottawa, Ont., Canada K1A 0S2.

[5]This absorption is largely due to the mismatch between the refractive indices of the mulling oil (Nujol, fluorolube) and the highly refracting sample powder.

TABLE 1. Calorimetric characteristics of the transitions in $CH_3NH_3PbX_3$ (ΔH_{tr} in J mol^{-1}, ΔS_{tr} in J K^{-1} mol^{-1})

Phase	T_{tr}, K	ΔH_{tr}	ΔS_{tr}	exp ($\Delta S_{tr}/R$)
		$CH_3NH_3PbCl_3$		
III				
II	171.49(2)	2140(20)	11.03(5)	3.77(2)
I	177.36(3)	902.5(9)	5.1(1)	1.85(3)
		$CH_3NH_3PbBr_3$		
IV				
III	148.35(5)	1293(10)	8.72(7)	2.85(3)
II	154.2(1)	519(12)	3.37(8)	1.50(2)
I	235.1(2)	951(7)	5.30(3)	1.89(1)
		$CH_3NH_3PbI_3$		
III				
II	162.68(3)	2577(17)	16.1(1)	6.93(9)
I	326.6(1)	506(5)	1.88(1)	1.25(1)

be made of the strength of the N—H···X bond, and the discontinuous changes with temperature which were observed in the profiles of certain absorption bands (not assigned in detail) in the 1300–1700 cm^{-1} region[6] for all three compounds testified to the existence of transitions. The temperatures of the latter were estimated as 175, 150, and 165 for CL, BR, and IO, respectively. The nature of these changes could not be ascertained from the ir evidence.

Electrical conductivity

To determine the conductivity of the black IO and its temperature variation the powder was pressed at ~7 kbar to wafers 5 × 25 mm^2 in area and about 1 mm thick. The wafers were visually of good quality but brittle, and the ease with which they fragmented on handling severely limited the scope of the experiment. A fragment approximately 4.7 × 17 × 1 mm^3 in size was fixed onto a sheet of mica with silicone grease and the mica sheet in turn was fixed onto a copper heater block. Copper wires 0.005″ diameter and 20 mm long were then attached to the sample at two silver-paint contacts 11 mm apart and connected to a Keithley 619 electrometer with 24 gauge copper leads. Temperature was measured with a chromel–alumel thermocouple with the measuring junction on the mica near the sample. The sample assembly was contained in a bell jar which was evacuted to ~10^{-5} Torr to prevent deterioration of the sample surface in the heating experiments. Without this precaution the surface was soon covered with a yellow coating (cf. ref. 1). Thermal history effects, possibly due to cracking, were seen in the absolute resistivity of the sample on thermal cycling.

Results

X-ray diffraction

The available X-ray evidence confirms *Pm*3*m* as the space group of CL(*I*) and BR(*I*). Since for $Z = 1$ this symmetry is incompatible with a unique orientation of the cation within the cuboctahedral X_{12} cage (see above), the cation must be disordered over at least six and at most 48 equivalent C—N orientations, not taking into account the H atoms. The effective contribution of the C and N atoms to the total diffracted intensity is thus very small relative to the contributions from Pb at (0, 0, 0) and X at (½, 0, 0) etc. Consistent with this expection, *F* maps phased[7] with Pb and X revealed no features that could be

[6]This region was relatively transparent from 10 to 300 K.

[7]With Pb and X placed as above, all the F_0 signs will be determined: in CL all will be positive and in BR the signs will be negative only when all three Br atoms contribute in antiphase to Pb.

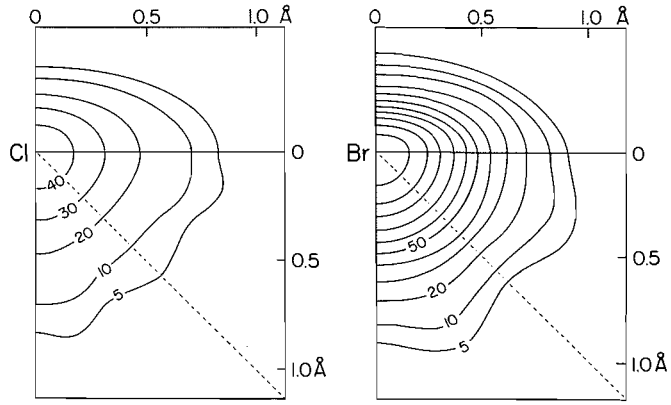

FIG. 1. Electron density (F_o) maps of $CH_3NH_3PbX_3$ (X = Cl, *left*; X = Br, *right*). Sections through X at (0, 0, ½), contours in e/Å^3, distances from X in axial directions in Å; a_1 direction down from X; a_2 direction horizontal to the right; a_3 axis up from X. Electron-density distribution in the Pb—X bond (*upper*, Pb at (0, 0, 1) up from X in the page) and perpendicular to the Pb—X bond (*lower*, Pb projecting onto X).

attributed with any confidence to the presence of the C and N atoms. The mean peak maxima (e/Å^3) in the *F* maps corresponded to Pb (906, 988) and X (44, 110) (first value CL, second value BR). In addition, small series-termination peaks associated with the Pb maxima were present, 21, 9, and 7 e/Å^3 in the CL map and 11–14 e/Å^3 in the BR map. Away from the Pb and X regions the maps were flat, with electron density values between 5 and −5 e/Å^3.

In these circumstances structure determinations were limited to refinements of the U_{iso}(Pb), U_{11}(X) (∥ to the Pb—X bond), and U_{33}(X) (⊥ to the Pb—X bond) parameters (Å^3). For CL this resulted in $R = 4.6\%$, $R_w = 3.6\%$, U_{iso}(Pb) = 0.0200(2), U_{11}(Cl) = 0.0212(19), U_{33}(Cl) = 0.1269(71), and U_{33}/U_{11} = 6.0(9). For BR, $R = 5.5\%$, $R_w = 4.6\%$, U_{iso}(Pb) = 0.0210(4), U_{11}(Br) = 0.0209(12), U_{33}(Br) = 0.1341(33), and U_{33}/U_{11} = 6.4(5). With the Pb atom so heavily dominating the scattering intensities, no attempt was made to determine whether the very large U_{ii}(X) anisotropy could be accounted for better on a model incorporating multiple positional disorder of the X atom, e.g. with X in 12(*h*) or 24(*l*) of *Pm*3*m*, although the flattening, along the broken lines in Fig. 1, of the electron density contours of X in planes perpendicular to the Pb—X bonds would suggest that such a disorder is a distinct possibility.

Existence of transitions

Discontinuous changes with temperature in the ^{2}H nmr spectra (see below) and in the ir spectra pointed to the existence of transitions in all three halides. The estimates of T_{tr} obtained from the nmr spectra (178(5) K for CL, 150(3) and 227(5) K for BR, and 168 and 321 K for IO) agreed quite well with those from the ir spectra (see Experimental). In particular, the existence of the transition above room temperature in IO confirmed the conclusion from X-ray powder diffraction that IO at room temperature is not cubic.

The transition temperatures were determined more accurately from heat capacity measurements (Figs. 2–4). These measurements revealed that the transition in CL and the lower transition in BR are in fact closely-spaced double transitions; the upper transitions in BR and IO are single (Table 1). All the transitions were reversible, highly reproducible, and independent of the thermal history of the sample. The number of phases that exist

Can. J. Chem. Downloaded from www.nrcresearchpress.com by 91.144.44.67 on 09/07/12
For personal use only.

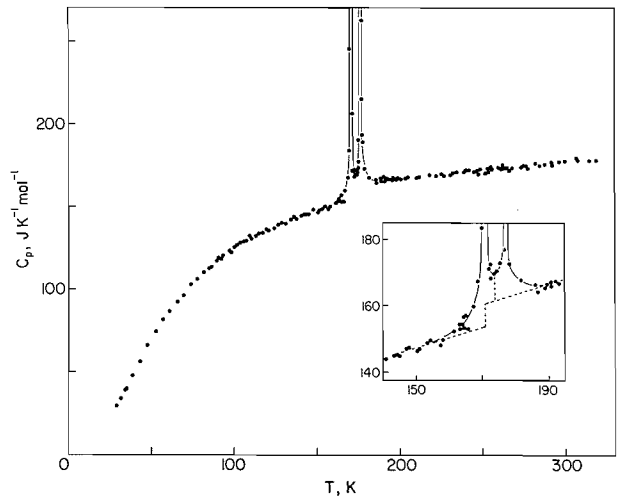

FIG. 2. Variation of C_p of $CH_3NH_3PbCl_3$ with temperature.

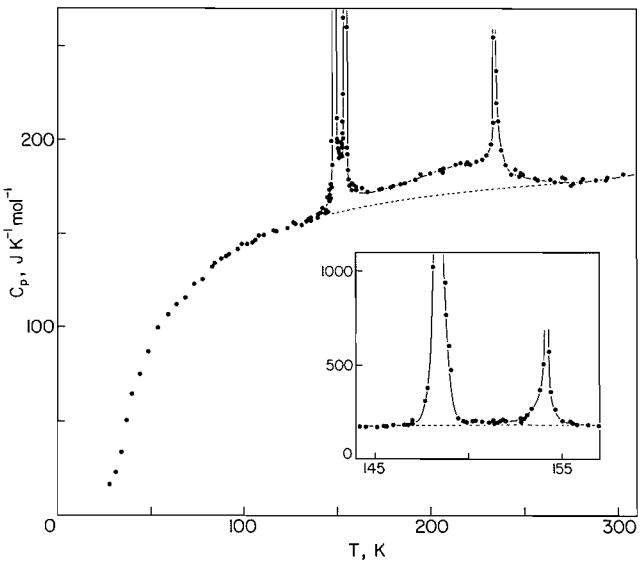

FIG. 3. Variation of C_p of $CH_3NH_3PbBr_3$ with temperature.

between 30 and 373 K is thus three for CL, four for BR, and three for IO. Phase *I* is cubic in all three compounds.

For brevity, the temperature of the upper ($I \leftrightarrow II$) transition will be referred to as $T_{tr,u}$ and that of the $II \leftrightarrow III$ transition as $T_{tr,l}$.

^2H nmr spectra

A single, sharp line was observed in the spectra of CL above 178(5) K, or BR above ~235 K, and of IO above ~318 K. On cooling below these temperatures the three compounds behaved differently. The single line in the CL spectrum split suddenly by ~40 kHz into a symmetric Pake doublet (17). A similar splitting was observed also in BR (~42 kHz) and IO (~39 kHz), but only on cooling below ~150 and ~165 K, respectively. In the intermediate range a small quadrupole splitting (QS) was seen in the spectra of BR and IO. This splitting, which developed with decreasing temperature but did not exceed 8 kHz, is described in detail below. These reproducible changes in the spectra were taken to be associated with transitions in the three solids and used to estimate T_{tr}.

The variation of the spin–lattice relaxation time $T_1(^2H)$ with T

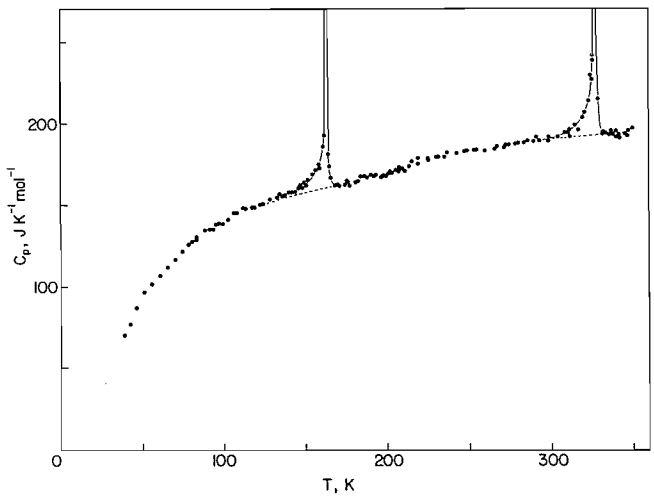

FIG. 4. Variation of C_p of $CH_3NH_3PbI_3$ with temperature.

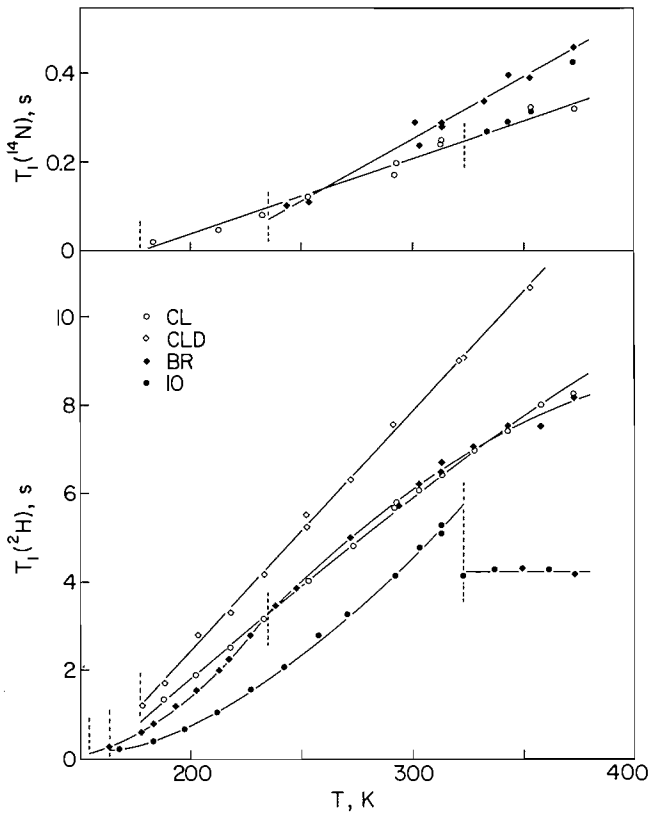

FIG. 5. Variation of $T_1(^2H)$ (*bottom*) and $T_1(^{14}N)$ (*top*) in $CH_3N(D, H)_3PbX_3$ with temperature. The transition temperatures of the undeuterated compounds are indicated by broken lines; $T_{tr,u}$(CLD) is taken to be the same as $T_{tr,u}$(CL).

in phase *I* could be represented by a straight line for CLD and by parabolas of only slight curvatures for CL and BR (Fig. 5). In contrast, the $T_1(^2H)$ variation with T in BR(*II*) and IO(*II*) was clearly nonlinear (parabolic fits gave $r^2 = 0.999$, $\sigma = 0.037$ s for BR(*II*) and $r^2 = 0.999$, $\sigma = 0.071$ s for IO(*II*)), and the $T_1(^2H)$ vs. T plot for IO(*I*) was different again in that its mean slope was zero.

The quasilinearity of the $T_1(^2H)$ vs. T plots implies nonlinearity of the corresponding Arrhenius plots ln $T_1(^2H)$ vs. T^{-1}. Indeed, the experimental points in the Arrhenius plots fall on

Can. J. Chem. Downloaded from www.nrcresearchpress.com by 91.144.44.67 on 09/07/12
For personal use only.

Can. J. Chem. Downloaded from www.nrcresearchpress.com by 91.144.44.67 on 09/07/12
For personal use only.

TABLE 2. Regressions of $\ln T_1$ on $k_0 - k_2T^{-2}$ (T_1 in s; cf. Fig. 6)*

Phase	n	k_0	k_2	r^2	σ
			^{2}H spectra		
CL(*I*)	14	2.749(7)	86922(445)	1.000	0.010
				0.993	0.051
CLD(*I*)	12	3.086(36)	90065(1940)	0.995	0.049
				0.982	0.098
BR(*I*)	11	2.709(27)	82635(2335)	0.993	0.025
				0.982	0.039
BR(*II*)	8	3.534(68)	128029(2516)	0.998	0.041
				0.992	0.076
IO(*II*)	11	2.941(18)	128489(880)	1.000	0.024
				0.994	0.085
			^{14}N spectra		
CL(*I*)	11	−0.132(47)	129906(2959)	0.996	0.063
				0.982	0.130
BR(*I*)	10	0.404(86)	161824(7666)	0.982	0.072
				0.977	0.084
IO(*I*)	4	0.975(315)	257497(38314)	0.958	0.051
				0.964	0.047

*Second-line entries under r^2 and σ: figures of merit for $\ln T_1 = k_0' - k_1'T^{-1}$ (Arrhenius) regressions. n, number of measurements.

upward convex curves in all five cases. Since at this stage it was considered futile to postulate a mechanism for the non-Arrhenius behaviour, we looked instead for an adequate empirical representation of the temperature variation of $T_1(^2H)$ that would be useful for manipulative purposes (smoothing) and retain the theoretical advantages offered by Arrhenius-type plots. After a number of trials it was found that *all* the $T_1(^2H),T$ pairs for CL(*I*), CLD(*I*), and BR(*I*) could be satisfactorily ($r^2 > 0.99$) fitted to quadratic polynomials $\ln T_1 = k_0 + k_1T^{-1} + k_2T^{-2}$, regression on cubic polynomials resulting in only marginal improvements. Further, it seemed reasonable to assume that as $T^{-1} \rightarrow 0$, the activation energy E_a for the reorientation of the D-containing groups in phase falls asymptotically to zero, i.e. $k_1 = -2k_2T^{-1}$ and $\ln T_1(^2H) = k_0 - k_2T^{-2}$. Refitting the data to this two-term quadratic gave r^2 and σ which differed only insignificantly from those obtained from the unconstrained quadratic regressions. This justified adoption of the two-term fits for phase *I*. In fact, the same applied to the data for IO(*II*), but for BR(*II*) the unconstrained quadratic regression gave $\sigma = 0.029$ compared to 0.041 for the two-term fit. Nevertheless, it was felt that it would be more consistent with the other sets of data to adopt the two-term fit for BR(*II*) also. Exponential and simple power regressions gave significantly poorer results for all the sets of Fig. 5. The coefficients and figures of merit of the expressions considered to be adequately faithful approximations to the (at present unknown) functional dependence of $\ln T_1$ on temperature are listed in Table 2. The rectified plots are shown in Fig. 6.

In contrast to the other four phases, in IO(*I*) the $T_1(^2H)$ values were considerably smaller than expected and practically independent of temperature (Fig. 5). This fall-off and the pseudo-constancy over the observation interval suggest intervention of an additional relaxation mechanism or, more likely, some modification of the cation reorientation mechanism operating in CL(*I*) and BR(*I*) (see below).

The small QS(^{2}H) in phase *II* increased gradually, on cooling, from zero at $T_{tr,u}$ to about 4 kHz at $T_{tr,1}$ in BR and about 7.5 kHz in IO. The temperature variation of this QS is suggestive of an

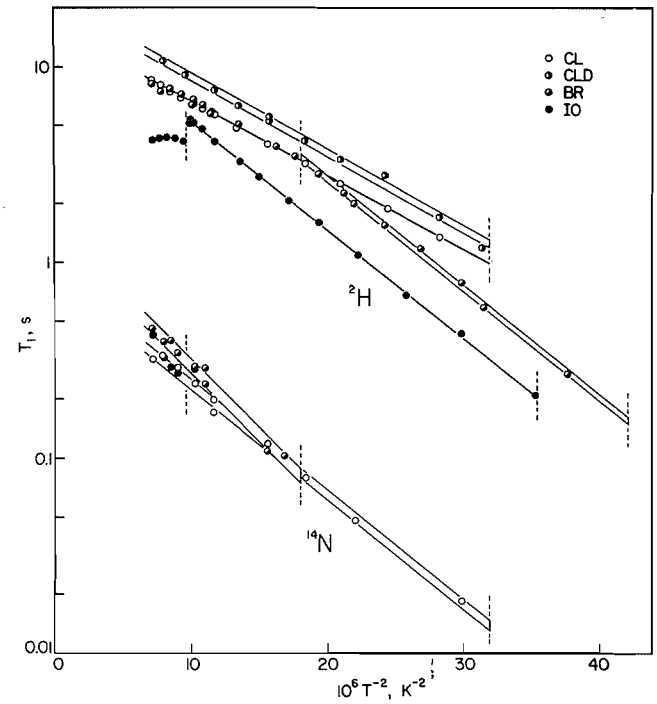

FIG. 6. Rectification of the data of Fig. 5

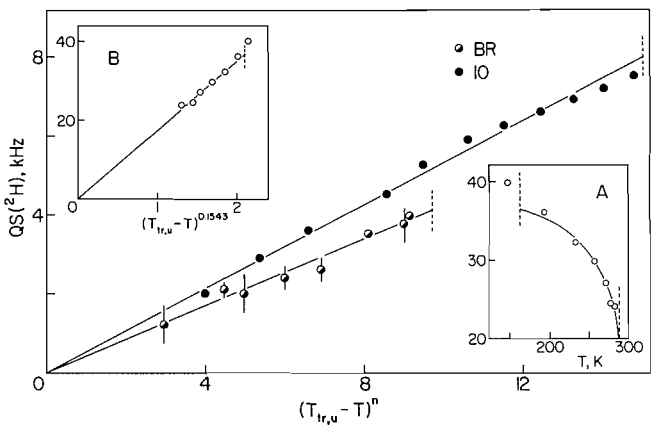

FIG. 7. Variation of the quadrople splitting QS(^{2}H) in BR(*II*) and IO(*II*) with $(T_{tr,u} - T)^n$ (see text). (*Inset A*) Variation of QS(^{2}H) in $(CH_3ND_3)_2TeBr_6$(*II*) with temperature. (*Inset B*) Variation of QS(^{2}H) in $(CH_3ND_3)_2TeBr_6$(*II*) with $(T_{tr,u} - T)^{0.1543}$ (rectification of plot *A*, see text). Transition temperatures of the undeuterated compounds are indicated by vertical broken lines.

ordering process, with QS(^{2}H) as an order parameter. Fitting the observed QS(^{2}H) to $k(T_{tr,u} - T)^n$ indeed resulted in a high degree of correlation (Fig. 7):[8]

BR: $k = 0.416$, $n = 0.517(36)$, $r^2 = 0.972$, $\sigma = 0.18$ kHz

IO: $k = 0.531$, $n = 0.532(11)$, $r^2 = 0.993$, $\sigma = 0.16$ kHz.

As noted above, on cooling through $T_{tr,1}$ the single line in the CL spectrum split suddenly to a symmetric doublet of ~40 kHz, and in the BR and IO spectra the splitting already present

[8]While these regressions are statistically highly significant, to demonstrate criticality with certainty requires having values of the order parameter as close to T_{tr} as possible. Unfortunately, extracting QS(^{2}H) from the close, poorly resolved doublets at sample temperatures closer to $T_{tr,u}$ than in Fig. 7 is so unreliable as to be of little value.

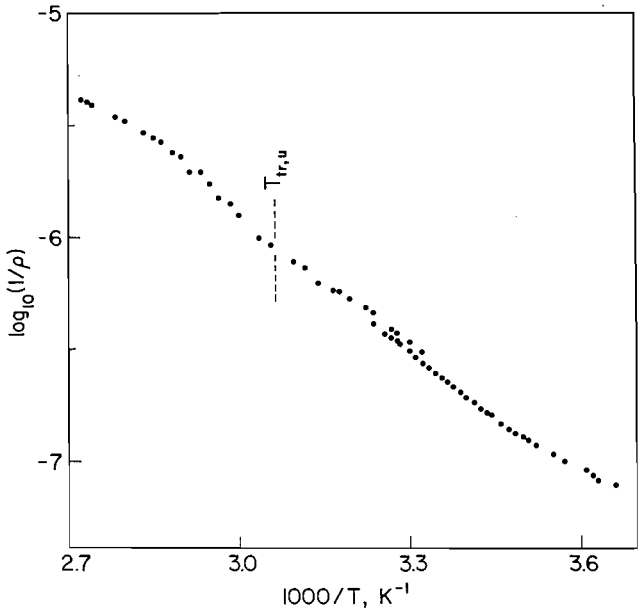

FIG. 8. Temperature dependence of the electrical resistivity ρ (Ω cm) of IO between 0 and 95°C (fourth cooling and fifth heating run, thermal hysteresis evident).

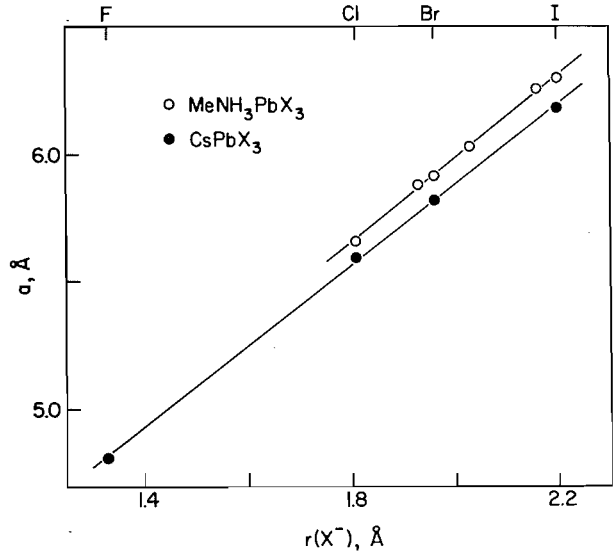

FIG. 9. Variation of the lattice parameter a of cubic $CH_3NH_3PbX_3$ and $CsPbX_3$ at room temperature with the ionic radius $r(X^-)$. $MeNH_3PbX_3$: single anion, this work; mixed anions, ref. 2. $CsPbX_3$: X = F, ref. 18; X = Cl, Br, I, ref. 19. Where a was measured above room temperature, the value has been adjusted by assuming a to change by 0.01%/K. For $MeNH_3PbI_3$ and $CsPbI_3$, where T_{tr} (cubic ↔ noncubic) > 293 K, $\bar{a} = (V/Z)^{1/3}$ is used in place of a.

suddenly increased to ~42 and ~39 kHz, respectively. These splittings remained practically constant on further cooling to 130 K, the lowest temperature attained in the present nmr measurements. The corresponding value for CLD was 37 kHz at 163 K.

^{14}N nmr spectra

These could only be obtained in phase *I*. The single-line signal disappeared at 173–183 K for CL, 233–238 K for BR, and 323–333 K for IO. The $\ln T_1(^{14}N)$ values showed a similar nonlinear variation with T^{-1} as the $\ln T_1(^2H)$ values and like the latter could be fitted, to a high degree of correlation, to $\ln T_1(^{14}N) = k_0 - k_2T^{-2}$ (Table 2, Fig. 6). Indeed, in this respect the same remarks apply to them as to $\ln T_1(^2H)$.

Electrical conductivity of IO

The resistivity of the pressed IO compact decreased on heating from ~1.3×10^7 Ω cm at 0°C to ~2.6×10^5 Ω cm at 94°C, i.e. 50-fold over the 100 K interval, and was unaffected by the presence or absence of daylight. The Arrhenius plot (Fig. 8) is essentially linear if the problems with the sample are taken into account. The activation energy for the conduction process obtained from the plot is 0.39 eV. There was no evidence of a discontinuity in the temperature variation of ρ at $T_{tr,u}$.

Discussion

In some respects the $CH_3NH_3PbX_3$ perovskites resemble the corresponding $CsPbX_3$ halides, while in others they differ considerably. In the following and in Part 3 we shall compare the two series wherever possible, in order to see to what extent the differences are due specifically to the composite nature of the $CH_3NH_3^+$ cation.

Volume properties

The room-temperature lattice parameter a of $CH_3NH_3PbX_3(I)$ varies linearly with the effective radius of X^- (Fig. 9). The straight line also accommodates Weber's (2) mixed cubic phases $CH_3NH_3Pb(Cl, Br)_3(I)$ and $CH_3NH_3Pb(Br, I)_3(I)$. This variation is similar to that observed for $CsPbX_3$. The regression lines for the two series are very nearly parallel, and that even when $CsPbF_3$ is included.

With the mean position of X taken as $3(d) - \frac{1}{2}00$ etc. of $Pm3m$, the Pb^{vi}—X distances in $CH_3NH_3PbX_3(I)$ are about 0.1 Å longer than those in the corresponding $CsPbX_3$, i.e. ~2.83 Å in CL, ~2.96 Å in BR, and ~3.15 Å in IO. This slight lengthening of the Pb—X bond over $CsPbX_3$ does not affect the character of the bond appreciably, judging by the similarity of colour: $CsPbCl_3$ is pale yellow (20) compared to the off-white CL, while the bromides are both orange and the iodides both black.

Electron-density distribution

The lack of cation features in the F maps of CL(I) and BR(I) confirms the indefiniteness of the cation position in the X_{12} cage, consistent with the expectation from the mismatch of the site symmetry at the centre of the cage and the symmetry of the cation.

The anisotropy of $U_{ii}(X)$ is commonly observed in cubic AMX_3 perovskites and their congeners (cf. ref. 21). It is associated with the volume of the X_{12} cage available to the cation (usually expressed in terms of the geometric tolerance factor $t = (r_A + r_X)/(r_M + r_X)\sqrt{2}$) and also with $T_{tr,u}$ (Fig. 27 of ref. 21). In the present case it is the magnitude of the $U_{ii}\perp/U_{ii}\parallel$ ratio which is noteworthy as well as the magnitude of the $U_{ii}\perp$ value itself. With $U_{ii}\perp = U_{33} \sim 0.13$ Å^2 significant interaction of the thermal motion of X with the cation motion is to be expected. Evidence of this is seen in the irregularity of the electron-density contours of X in planes containing X and perpendicular to the Pb—X bond (Fig. 1).

Transitions

The temperatures of the transition from the cubic phase I to phase II are related to the dimensions of the unit cell: $T_{tr,u}(K) = 1.202 \exp 0.891a$ ($r^2 = 0.994$, $\sigma = 7.5$ K). This relation, which can be interpreted in terms of the mean cation–anion distance $a\sqrt{3}/2$ or the X···X distance $a/\sqrt{2}$, does not appear to be accidental, for the $T_{tr,u}$ in the corresponding cubic $CsPbX_3$ (X =

Can. J. Chem. Downloaded from www.nrcresearchpress.com by 91.144.44.67 on 09/07/12
For personal use only.

Can. J. Chem. Downloaded from www.nrcresearchpress.com by 91.144.44.67 on 09/07/12
For personal use only.

Cl, Br, I) pervoskites (19, 20) can be represented similarly by $T_{tr,u} = 1.163 \exp 1.006a$ ($r^2 = 1.000$, $\sigma = 3$ K; the a value corrected to room temperature, cf. caption of Fig. 9).[9] The ratio $T_{tr,u}(CsPbX_3)/T_{tr,u}(CH_3NH_3PbX_3)$ for a given X is roughly 1.8. This parallel between the two series indicates that the nature of the cation (i.e. whether simple or composite, hydrogen-bonding or nonbonding) is at most a secondary factor responsible for the occurrence of the transition. The *cause* of the transition is to be sought in the lattice dynamics of the three-dimensional $[PbX_{6/2}]_\infty$ framework, although the *position* of the transition on the T scale is cation-sensitive and the effect on $T_{tr,u}$ of replacing a structureless cation with a composite one can be dramatic.[10]

Since a complete discussion of the dependence of $T_{tr,u}$ on the sizes and masses of the participating atoms would require detailed knowledge of the mechanism of the transition in each particular case — available only for a few compounds at present — empirical relationships like the above are not without value even though the reasons for their existence are not clear. Apart from the two Pb series the $T_{tr,u}$ of cubic $AMBr_3$ and AMI_3 are largely lacking, but for the few AMF_3, $AMCl_3$ pairs where both a and $T_{tr,u}$ are known the two regression parameters appear to be of the same order as for $CsPbX_3$ and $CH_3NH_3PbX_3$. In NH_4MF_3 (M = Mg, Mn, Co, Zn) the transition from the cubic $Pm3m$ phase on cooling involves a restriction on the reorientational freedom of the cation (22, 23) and the size of M would be expected to play a rôle, albeit a less direct one than the size of X. Indeed, $T_{tr,u}$ of NH_4MF_3 can be represented as $0.00057 \exp 2.983a$ ($r^2 = 0.952$, $\sigma = 7.7$ K ~ 10% of the $T_{tr,u}$ range).

Thermal properties

The shapes of the C_p peaks at ~175 K for CL and ~150 K for BR suggest that in each case both components of these double transitions are first-order. This is supported by the observation that the single crystal of BR used in the X-ray diffraction experiment shattered almost explosively on cooling through $T_{tr,1}$.

The $I \leftrightarrow II$ transition in BR is first-order with a long tail of pre-transition excess C_p. The evaluation of C_p(baseline) is necessarily somewhat uncertain and the overlap of the $II \leftrightarrow III$ transition peak with the excess C_p component is severe. Nevertheless, assuming that the C_p values between 80 and 130 K and between 270 and 303 do not contain significant excess contributions, the baseline between 80 and 303 K can be represented by a cubic polynomial ($f = 25$, $r^2 = 0.997$, $\sigma = 1.0$ J K^{-1} mol^{-1}). With this baseline approximation $\Delta C_p = C_p$(measured) − C_p(baseline) was estimated in the interval 200–235.2 K. Regressing ln ΔC_p on ln $[1 - (T/T_{tr})]$ ($r^2 = 0.95$, Fig. 10) gave 0.34(2) for the critical exponent. The excess C_p thus conforms to the same type of temperature dependence as QS(^{2}H) and represents another parameter of the ordering process in phase *II*. For IO this procedure for evaluating ΔC_p for the $I \leftrightarrow II$ transition is rendered uncertain owing to the difficulties in choosing a proper baseline (cf. Fig. 4). The pre-transition excess C_p associated with the $II \leftrightarrow III$ transition in IO does not appear to be proportional to a power of $T_{tr,1} - T$.

[9]Cubic $CsPbF_3$ is obtained by cooling the stoichiometric melt to room temperture (18). The existence of a phase transition at 615°C has been inferred from the shape of the liquidus line in the CsF–PbF_2 system, but no thermal effect was observed on cooling pure $CsPbF_3$ at normal cooling rates. Prolonged annealing of the cubic phase at 300°C produced a perovskite-like noncubic phase stable at room temperature.

[10]The effect of the cation on $T_{tr,u}$ in cubic AMX_3 alkali and ammonium perovskites and related halides is discussed in terms of the geometric tolerance factor t in ref. 21.

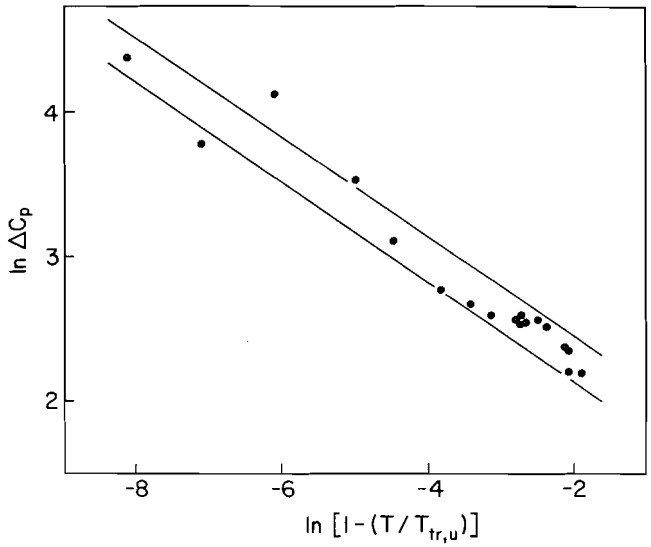

FIG. 10. Variation of ln ΔC_p of BR(*II*) with ln $[1 - (T/T_{tr,u})]$.

The total entropy of transition, $\Sigma\Delta S_{tr}$, increases only slightly from CL to IO: 16.1(2), 17.4(2), and 18.0(2) J K^{-1} mol^{-1}, pointing to similarity in the gross behaviour of the three systems, but the individual ΔS_{tr} sequences differ.

^{2}H nmr spectra

For a methylammonium ion with its C—N axis fixed in the structure the expected quadrupole splitting would be QS(^{2}H) = $\frac{3}{4}(e^2qQ/h) \sim 130$ kHz (24) if the ion does not undergo rotational reorientations about that axis (rigid-lattice spectrum), and QS(^{2}H) = $\frac{3}{8}(3\cos^2\beta - 1)(e^2qQ/h) \sim 43$ kHz (25) if such reorientations take place (C_3 jumps, β = CNH ~ 109.5°). An observed splitting smaller than the latter value would imply that the C—N axis is undergoing some motion. The single sharp line in the ^{2}H spectra of phase *I* of all three halides, the 40–42 kHz splitting below $T_{tr,u}$ in CL and at $T_{tr,1}$ in BR and IO, and the temperature dependent splitting of 0–8 kHz in BR(*II*) and IO(*II*) can then be interpreted as follows. In phase *I* the cation undergoes overall reorientations in an isotropic potential. In CL below $T_{tr,u}$ the C—N reorientation is suddenly frozen but the reorientation about the C—N axis persists. In BR and IO below $T_{tr,u}$, however, the C—N bond continues to reorientate. This motion is progressively slowed down on further cooling and, more importantly, takes place in an increasingly anisotropic potential until at $T_{tr,1}$ it suddenly stops.[11]

^{14}N nmr spectra

The absence of splitting on the single ^{14}N resonance line in phase *I* and the large values of $T_1(^{14}N)$ again indicate that the C—N bond in all three crystals undergoes very fast reorientations in an isotropic potential. Assuming $T_1^{-1} = \frac{3}{2}\pi^2\chi^2\tau_\perp$, χ = 1106.7(15) kHz (27), $\tau_\perp$ (s) = $5.512 \times 10^{-14} T_1^{-1}$, we have, at

[11]A very similar situation appears to exist in $CH_3NH_3SnBr_3$ (26): ^{81}Br nqr and ^{1}H nmr measurements indicate that the cubic ↔ noncubic transition occurs at ~232 K (235.1 K in BR) and another transition at ~180 K (154.2 K in BR). The second moment in the ^{1}H nmr spectrum was 0.5(1) G^2 in the cubic phase and 8.0(5) G^2 below 180 K, and in each phase was almost constant. However, in the intermediate phase it increased continuously with decreasing temperature from ~0.5 to ~8 G^2. The quadrupole splitting in the ^{119}Sn Mössbauer spectrum was ~0 at 293 K but 0.54(3) mm/s at 93 K, indicating a nonzero EFG at the Sn nucleus in the lowest phase. These observations are all consistent with the above interpretation for BR.

TABLE 3. Activation energies E_a(kJ/mol) = $0.01662k_2T^{-1} = CT^{-1}$ for the reorientation of ^2H and ^{14}N containing groupings*

Phase	C	E_a at $T_{tr,l}$	E_a at $T_{tr,u}$	E_a at 373 K	E_a at $T/T_{tr,u} = 1.14$
			^2H spectra		
CL(*I*)	1445(8)	—	8.15(5)	3.87(2)	7.12(4)
CLD(*I*)	1497(32)	—	8.46(18)	4.01(9)	7.38(16)
BR(*I*)	1373(39)	—	5.84(17)	3.68(10)	5.13(15)
BR(*II*)	2128(42)	13.80(27)	9.05(18)	—	—
IO(*II*)	2135(15)	13.13(9)	6.54(5)	—	—
			^{14}N spectra		
CL(*I*)	2159(49)		12.17(28)	5.79(13)	10.7(3)
BR(*I*)	2690(127)		11.44(54)	7.21(34)	10.0(5)
IO(*I*)	4280(637)		13.1(20)	11.5(17)	11.5(17)

*Since the T_{tr} of the partially *N*-deuterated samples are not known, the calorimetric T_{tr} of $CH_3NH_3PbX_3$ have been used instead. The isotopic effect on T_{tr} is probably quite small (cf. ref. 34).

the end of the observation intervals,

$T = 178$ K, $T_1 = 0.015(2)$ s, $\tau_\perp = 3.8(5)$ ps

$T = 373$ K, $T_1 = 0.34(5)$ s, $\tau_\perp = 0.16(3)$ ps

for CL and

$T = 235$ K, $T_1 = 0.080(14)$ s, $\tau_\perp = 0.67(12)$ ps

$T = 373$ K, $T_1 = 0.47(5)$ s, $\tau_\perp = 0.12(2)$ ps

for BR. For comparison, in $CH_3ND_3^+NO_3^-(I)$ at 355 K the corresponding T_1 and $\tau_\perp$ values are 0.0119 s and 4.7 ps, and in the melt at 393 K, 0.0168 s and 3.3 ps, respectively (28), i.e. reorientation rates about thirty times slower than in CL and BR. However, very fast overall cation reorientations comparable to those in $CH_3NH_3PbX_3(I)$ may be expected to occur in the cubic *anti*-fluorite quasi-perovskites $(CH_3NH_3)_2MX_6$ (29, 30); the two classes of compounds are compared below.

If the methylammonium ion is treated as a prolate spheroid (C—H = 1.08 Å, N—H = 1.02 Å, C—N = 1.48 Å, ∠HCN = ∠CNH = 109.5°), the correlation time $\tau_{\perp,free}$ for the inertial rotation of the free ion about an axis perpendicular to the C—N bond can be expressed (e.g. ref. 31)[12] as $\tau_{\perp,free} = (2I_\perp/3\pi k)^{\frac{1}{2}}T^{-\frac{1}{2}} = 2.34 \times 10^{-12}T^{-\frac{1}{2}}$ for $CH_3NH_3^+$ and $2.49 \times 10^{-12}T^{-\frac{1}{2}}$ for $CH_3ND_3^+$. From this, $\tau_{\perp,free} = 0.18$, 0.15, and 0.13 ps at $T = 178$, 235, and 373 K, respectively, for $CH_3NH_3^+$ and 0.19, 0.16, and 0.13 ps, respectively, for $CH_3ND_3^+$. These values indicate that the reorientations of the C—N axis in phase *I*, while not inertial, take place with a rapidity which at the upper limit of our experimental range approaches that calculated for the free ion.

The disappearance of the ^{14}N signal below $T_{tr,u}$ in all three halides is not inconsistent with the conclusion from the ^2H spectra. Any reduction in the isotropy of the potential in which the cation moves would introduce a quadrupole splitting which would be a fraction of the ~700 kHz value expected for a rigid-lattice spectrum (28). However, the QS(^{14}N) arising from even a modest reduction of the isotropy in phase *I* might still fall outside the available instrumental range, and this appears to be the case here.

[12]Calculations using the expression for $\tau_{inertial}$ of ref. 32 or other such expressions (cf. ref. 33) lead to very similar results.

Activation energy E_a *for rotational reorientation*

The inverse proportionality of E_a to T within the existence interval of a phase (Table 3) is a feature peculiar to the $CH_3NH_3PbX_3$ halides. Because of this temperature dependence E_a can be compared only when the structural situations are similar, i.e. at the same reduced temperatures $T/T_{tr,u}$ or $T/T_{tr,l}$ (Fig. 11).

At $T_{tr,u}$ the $E_a(^2H)$ values are about the same for CL(*I*) and CLD(*I*), while for BR(*I*) the $E_a(^2H)$ is only about 70% of that for CL(*I*). A similar reduction is observed between $E_a(^2H)$ of BR(*II*) and IO(*II*), while at $T_{tr,l}$ the two $E_a(^2H)$ values are very similar, E_a(BR, *II*)/E_a(IO, *II*) = 1.05(3). The reduction at $T_{tr,u}$ is to be expected, for the cuboctahedral Br_{12} cage is larger than the Cl_{12} and N—H···Br interactions are weaker than N—H···Cl interactions, thereby facilitating the reorientational process.

The $E_a(^2H)$ values for CL(*I*) are similar to those estimated from ^1H nmr studies of the trigonal $(CH_3NH_3)_2PtCl_6(I)$ (3, 4), 3.6(5) kJ/mol,[13] but much smaller than the corresponding values obtained for the NH_3 reorientation in the β and γ phases of CD_3NH_3Cl, 26.4 and 32.0 kJ/mol, respectively (35), pointing to stronger hydrogen bonding in methylammonium chloride (cf. ref. 15). The similarity of the $E_a(^2H)$ values in CL(*I*) and CLD(*I*) suggests that the CD_3 and ND_3 reorientations about the C—N bond are correlated, i.e. the activation energy for the rigid-body C_3 reorientation of the cation is significantly lower than that for internal rotation (cf. refs. 3 and 4 for a similar conclusion involving $(CH_3ND_3)_2PtCl_6(I)$ and $(CD_3NH_3)_2PtCl_6(I)$; also refs. 36 and 37).

The $E_a(II)/E_a(I)$ for ^2H at $T_{tr,u}$ is available only for BR, where it is 1.55(7), which corresponds to a difference of 3.2(3) kJ/mol. The reorientation of the cation is thus significantly more hindered in BR(*II*) even at temperatures ≤8 K of $T_{tr,u}$, i.e. within less than 10% of the existence range of BR(*II*).

At $T_{tr,u}$ (and at $T/T_{tr,u}$ up to 1.14) the activation energies $E_a(^{14}N)$ for C—N tumbling in phase *I* of all three halides are the same within the statistics (Fig. 11). This points to the mechanism of the C—N reorientation having essentially the same character in all three compounds.

[13]The C—N axis in these trigonal crystals coincides with the unique crystallographic C_3 axis (see below).

Can. J. Chem. Downloaded from www.nrcresearchpress.com by 91.144.44.67 on 09/07/12
For personal use only.

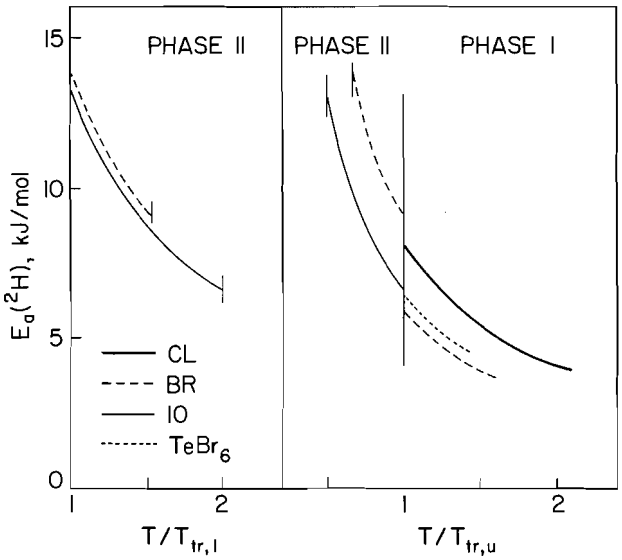

FIG. 11. Variation of the activation energy E_a for the reorientation of the ^2H and ^{14}N containing groupings of the methylammonium ion in CL, BR, IO, and the hexabromotellurate (smoothed data).

Relationship of the ^2H and ^{14}N nmr parameters in phase I

Using the analytical representations of Table 2 we obtain

$$[1]\quad T_1(^2H)/T_1(^{14}N) = A \exp C'T^{-2}$$

$$A = \exp [k_0(^2H) - k_0(^{14}N)],\ C' = -k_2(^2H) + k_2(^{14}N)$$

$$[2]\quad E_a(^{14}N)/E_a(^2H) = C(^{14}N)/C(^2H).$$

These expressions indicate that, to the extent to which the analytical representations are faithful, the reorientational behaviour of the ^2H and ^{14}N atoms as described by the spin–lattice relaxation time T_1 is mutually determined. In particular, the $E_a(^{14}N)/E_a(^2H)$ ratio for each crystal is constant over the experimental T interval: 1.49(4) for CL(*I*), 1.94(15) for BR(*I*).

The $T_1(^2H)/T_1(^{14}N)$ ratio in CL varies from 70(10) at $T_{tr,u}$ to 25(2) at 373 K; in BR, from 42(11) at $T_{tr,u}$ at 18(3) at 373 K. At $T_{tr,u}$(BR) the ratio is the same, within 1σ, for CL and BR. With increasing temperature a small difference appears to develop, but even at 373 K the two values are only $\sim 2\sigma$ from each other. In terms of $T/T_{tr,u}$, however, the $T_1(^2H)/T_1(^{14}N)$ vs. $T/T_{tr,u}$ curve for BR is only about 60% the height of the curve for CL.

The relaxation time $T_1(^2H)$(CL) increases, over the 177–373 K interval, from 0.98 to 8.37 s, i.e. about eightfold. In contrast, $T_1(^{14}N)$(CL) over the same interval increases from 0.015 to 0.34 s, i.e. about 23-fold. In attempting to rationalize this difference in the temperature dependence we recall that $T_1(^{14}N)$ and $T_1(^2H)$ probe different motions. The largest component of the ^{14}N EFG tensor lies along the C—N axis, hence $T_1(^{14}N)$ probes the reorientational motion of the C—N bond vector directly, and the $T_1(^{14}N)$ values are independent of reorientational motions of the ND_3 groups about the C—N axis. The largest component of the ^2H EFG tensor lies along the N—D axis; $T_1(^2H)$ thus probes the motion of the N—D bond vector, but here the $T_1(^2H)$ values will depend on the motions of the CD_3 and ND_3 groups about the C—N axis *as well as* on reorientations *of* the C—N axis.

Qualitatively, the greater temperature dependence of $T_1(^{14}N)$ relative to $T_1(^2H)$ indicates that at temperatures at which thermal activation of the C—N reorientation begins to become significant the reorientational motion of the N—D bond vector is already very rapid.

Similar conclusions apply to BR, for which $T_1(^2H)$ increases, from 235 to 373 K, by a factor of ~ 2.5 and $T_1(^{14}N)$ by a factor of ~ 6.

$T_1(^2H)$ anomaly in IO(I)

The $T_1(^2H)$ at $T > T_{tr,u}$ is lower than immediately below $T_{tr,u}$ and remains approximately constant over a 50 K interval, while simultaneously $T_1(^{14}N)$ increases with temperature at least as rapidly as in CL(*I*) and BR(*I*) (Figs. 5 and 6). This puzzling behaviour implies that the thermal activation energy for the ^2H reorientation above $T_{tr,u}$ is close to zero, while that for the C—N reorientation is comparable to those for CL(*I*) and BR(*I*) (Table 3). Since the main difference between IO(*I*) and the other two cubic halides is in the volume of the X_{12} cavity, we have the paradox that by making available to the cation a larger volume the reorientational motion of the *N*-hydrogens slows down.

The lowering of $T_1(^2H)$ is unlikely to be attributable to extraneous factors precisely because its onset coincides with $T_{tr,u}$. If it were due, for example, to the presence of a paramagnetic species, such species would have to be generated by the transition mechanism, a process difficult to envisage in the circumstances; the electrical conductivity of IO(*I*) varies smoothly through $T_{tr,u}$ (Fig. 8). Because the anomaly almost certainly involves the N—H···I bonding, we hope that we shall be able to elucidate its origin from a detailed comparison of $CD_3NH_3PbI_3$ and $CH_3ND_3PbI_3$ which is now being initiated.

Comparison with $(CH_3NH_3)_2MX_6$

Methylammonium hexahalometallates(IV) at room temperature are known to crystallize in one of the three structure types:[14] (*i*) *anti*-$CdCl_2$ (*anti*-*C*19, $R\bar{3}m$) (5, 39): X = Cl, M = Pd, Pt, Se, Sn, Pb; X = Br, M = Pd, Pt, Se, Sn; X = I, M = Pt; (*ii*) *anti*-CdI_2 (*anti*-*C*6, $P\bar{3}m1$) (40): X = Cl, M = Te; and (*iii*) *anti*-CaF_2 (*anti*-*C*1, $Fm3m$ or superstructure) (29): X = Br or I, M = Te. The C_{3v} cation site symmetry in the *anti*-$CdCl_2$ and *anti*-CdI_2 structures requires the C—N bond to be located in an oriented C_3 axis, hence 120° reorientations (CH_3 and NH_3 motions correlated or independent) about this fixed bond are naturally compatible with the respective space-group symmetries and indeed are observed in these phases (up to 400 K for X = Cl and M = Sn, Pt) (4, 29, 30).[15]

In contrast, in the *anti*-CaF_2 structure the crystallographic site symmetry of the cation in the $Fm3m$ cell is T_d and the cation is surrounded by four MX_6^{2-} anions with the M atoms at the alternate corners of cubes of $\frac{1}{2}a$ edge length. The 12 H atoms nearest to the cation form a cuboctahedron of T_d symmetry but with dimensions almost consistent with O_h symmetry. This situation thus resembles the cation coordination in $CH_3NH_3PbX_3$ but is more restrictive as regards reorientation: it is best understood by comparing $CH_3NH_3PbX_3$(*I*) and the *anti*-CaF_2 $(CH_3NH_3)_2TeX_6$ with the corresponding ammonium salts, NH_4MF_3 and $(NH_4)_2MX_6$, which are essentially isostructural with the respective $CH_3NH_3^+$ salts and have been extensively studied. From ir studies of the isotopically isolated NH_3D^+ ion (21, 41, 42) it is known that in the *anti*-CaF_2 $(NH_4)_2MX_6$ the N—H bonds avoid pointing at the corners of the

[14]The *C*19 structure type is topologically related to the *C*1 type, whereas the *C*6 type is not (38).

[15]The estimated $E_a(^1H)$ (kJ/mol) for the correlated C_3 rotations are 4.2(5) in the hexachlorostannate (4), 3.6(5) in the hexachloroplatinate (4), and 5–7 in the hexachlorotellurate (30); and for the uncorrelated rotations, 7.2(10) in the hexachlorostannate and 8.5(10) in the hexachloroplatinate (4).

Can. J. Chem. Downloaded from www.nrcresearchpress.com by 91.144.44.67 on 09/07/12
For personal use only.

Can. J. Chem. Downloaded from www.nrcresearchpress.com by 91.144.44.67 on 09/07/12
For personal use only.

$\frac{1}{2}a$ cube that are occupied by the M atoms. Instead, each points, along a C_3 diagonal, at an unoccupied corner to form a symmetrically trifurcated N—H···3X bond to X atoms belonging to different MX_6^{2-} ions each. In the *Pm3m* NH_4MF_3 perovskites, however, all eight corners of the cube are occupied by M atoms. The geometry of the $[MF_{6/2}]_\infty$ framework in these crystals being unfavourable to simultaneous formation of four equivalent, linear N—H···F bonds, the NH_4^+ ion strives to achieve such a bond *dynamically*, one at a time, by large-amplitude libration. Thus while the cation in both cases is inside an X_{12} cage of cubic symmetry, in $(NH_4)_2MX_6$ its *effective* symmetry coincides with the crystallographic site symmetry at the centre of the cage, whereas in NH_4MF_3 it is only D_{2d}. We may reasonably assume that in respect of hydrogen bonding $CH_3NH_3^+$ in these salts resembles the ammonium ion. This raises the question of how the structural difference between $CH_3NH_3PbX_3(I)$ and the *anti*-CaF_2 $(CH_3NH_3)_2TeX_6$ is reflected in the reorientational behaviour of the cation.

Cubic $(CH_3NH_3)_2TeBr_6$ is known (43) to undergo at $T_{tr,u}$ = 289 K a first-order transition to phase *II* (all Br atoms equivalent, cf. ref. 29) and another first-order transition, at $T_{tr,1}$ = 164 K, to phase *III*. Exploratory ^2H nmr measurements on the *N*-deuterated compound up to 413 K (M. Gruwel and R. E. Wasylishen, unpublished results) show that the variation of $T_1(^2H)$ with temperature in phase *I* can be represented as $\ln T_1 = 2.725(23) - 111210(2430)T^{-2}$ (T_1 in s, $f = 10$, $r^2 = 0.995$, $\sigma = 0.017 \sim 2.4\%$ of the $\ln T_1$ range), similar to CL(*I*), CLD(*I*), and BR(*I*).[16] Because of the relatively high $T_{tr,u}$ of this bromide the $T/T_{tr,u}$ at the end of the experimental temperature range was only 1.43, but within this range the E_a vs. $T/T_{tr,u}$ curve (Fig. 11) is seen to parallel the corresponding curve for BR(*I*); at $T_{tr,u}$, E_a = 6.40(14) kJ/mol, i.e. 0.56(22) kJ/mol higher than $E_a(T_{tr,u})$ of BR(*I*). This difference indicates that E_a is probably marginally higher in $(CH_3NH_3)_2TeBr_6(I)$, which would be consistent with the slightly smaller Br_{12} cage in this crystal (the difference in $\frac{1}{2}a$ at room temperature is 0.2 Å ~ 3.5%, cf. ref. 29), but it provides no information bearing on the above question.

The extent of dissimilarity in the reorientational behaviour of the two crystals can be assessed somewhat better in phase *II*. The QS(^2H) of the *N*-deuterated $(CH_3NH_3)_2TeBr_6$ at 283 K, the temperature closest to $T_{tr,u}$ = 289 K in the exploratory experiments, was 23.9(5) kHz. Further cooling increased QS(^2H) at a faster rate than in BR(*II*), or IO(*II*), the value at 193 K being 36.0(5) kHz (Fig. 7A). At 148 K in phase *III*, i.e. 16 K below $T_{tr,1}$, QS(^2H) was 39.9(5) kHz and thus indicative of a fixed C—N axis. From the currently available results it is not possible to determine the variation of QS(^2H) at temperatures closer to $T_{tr,u}$ than 6 K. Fitting the QS(^2H) (kHz) values to $k(T_{tr,u} - T)^n$ (Fig. 7B) gave k = 17.47, n = 0.1543, r^2 = 0.974, σ = 0.8 kHz, which would suggest that critical behaviour might be a possibility. This would not be inconsistent with the variation of C_p with T in phase *II* of this bromide (Figs. 2, 4, and 6 of ref. 43), although the steepness of the rise of QS(^2H) on cooling just below $T_{tr,u}$ and the coexistence of an unsplit single line of phase *I* with the sharp doublet with QS(^2H) ~ 24 kHz in the 283 K spectrum indicate that further work is required. However, regardless of whether the QS(^2H) develops from zero at $T_{tr,u}$ (as in BR(*II*) and IO(*II*)) and reflects a critical process, or jumps from zero directly to a substantial value on cooling through $T_{tr,u}$, the behaviour of the hexabromotellurate in this respect differs significantly from that of BR and IO. The combined observations imply that the structural change associated with the $I \rightarrow II$ transition results in an almost immmediate hindrance of the reorientation of the C—N bond, and that this hindrance is much stronger than in BR(*II*) at any reduced temperature. The C—N reorientation is completely arrested in phase *III*. This interpretation is consistent with the behaviour of the second moment in the ^1H nmr spectrum of the hexabromotellurate (29). Above $T_{tr,u}$ the moment was found to be small, 0.4(1) G^2 (0.5(1) G^2 for the iodo compound), but below $T_{tr,u}$ its temperature variation appeared to mimic that of the QS(^2H) (Fig. 7): only a few degrees below $T_{tr,u}$ its value was already ~3.5 G^2 and it continued to increase on further cooling to ~6 G^2 at $T_{tr,1}$.

Conclusions

The combined results of our X-ray diffraction, calorimetric, ^2H and ^{14}N nmr and other studies of the $CH_3NH_3PbX_3$ (X = Cl, Br, I) perovskites can be summarized as follows:

In addition to phase *I* (of *Pm3m* symmetry) which exists above the upper transition temperature $T_{tr,u}$, each of the three halides has low-temperature phases. The transition temperatures were determined and the transitions characterized by heat capacity measurements in the ~30 to ~350 K range (Table 1, Figs. 2–4). In phase *I* the cation is inside a cuboctahedral (O_h) cage formed by twelve X atoms undergoing strongly anisotropic thermal motions. X-ray diffraction (Fig. 1) has revealed that the cation is positionally highly disordered, and evidence from ^2H and ^{14}N nmr spectra shows that it reorientates in an isotropic potential at a rate which at 373 K approaches that expected for inertial rotation. In the chloride (CL), the tumbling of the C—N axis ceases on cooling through $T_{tr,u}$, whereas in the bromide (BR) and iodide (IO) it continues, at a decreasing rate and in an increasingly anisotropic potential, into phase *II* but ceases at the $II \rightarrow III$ transition. Reorientation *about* the C—N axis in all three halides persists down to the lower end of our nmr temperature range, ~150 K.

The spin–lattice relaxation time $T_1(^{14}N)$ probes directly the reorientational motion of the C—N axis, independently of the motions of the ND_3 or CD_3 groups about that axis. In contrast, $T_1(^2H)$ probes the motion of the N—D bond about *and with* the C—N axis. The temperature variation of $T_1(^2H)$ in CL(*I*), BR(*I*), BR(*II*), and IO(*II*), and that of $T_1(^{14}N)$ in CL(*I*), BR(*I*), and probably IO(*I*), display non-Arrhenius behaviour but can be represented analytically with good accuracy by expressions of the type $\ln T_1 = k_0 - k_2T^{-2}$ (Table 2, Fig. 6). The activation energies E_a for the reorientation of the H- and N-containing groups thus depend on temperature, $E_a = C/T$ (Table 3, Fig. 11). This implies that the reorientation is not a simple thermally activated process but is controlled by additional factors.[17] The similarity of $E_a(^2H)$ for *C*- and *N*-deuterated CL(*I*) suggests that the CH_3 and NH_3 reorientations about the C—N axis are correlated. The passage from BR(*I*) to BR(*II*) is accompanied by a significant increase in E_a, $E_a(II)/E_a(I) \sim 1.6$, which corresponds to a difference of ~3.2 kJ/mol. The temperature variation of the $T_1(^{14}N)/T_1(^2H)$ ratio in CL(*I*) and BR(*I*) indicates that at temperatures at which thermal activation of the C—N

[16]Regression of $\ln T_1$ on T^{-1} gave $r^2 = 0.989$, $\sigma = 0.026 \sim 3.6\%$ of the $\ln T_1$ range, with a temperature-independent E_a of 5.4(2) kJ/mol. However, the distribution of signs of the deviations from the regression line appeared to be biased. The transition temperatures of the *N*-deuterated hexabromotellurate were taken to be the same as those for the undeuterated compound.

[17]This matter will be dealt with more fully in Part 3, together with the results of our X-ray and neutron diffraction investigations.

reorientation begins to become significant the N—D reorientational motion is already very rapid. The $T_1(^2H)$ values in IO(*I*) show anomalous behaviour the reasons for which are not yet understood.

The quadrupole splitting QS(^{2}H) observed in the spectra of BR(*II*) and IO(*II*) develops from zero at $T_{tr,u}$ and increases with decreasing temperature to ~4 kHz at the $II \rightarrow III$ transition in BR and ~8 kHz in IO. Its variation with temperature can be represented by $QS(^2H) = k(T_{tr,u} - T)^n$: for BR, $n = 0.52(4)$, $r^2 = 0.972$, $\sigma = 0.18$ kHz; for IO, $n = 0.53(2)$, $r^2 = 0.993$, $\sigma = 0.16$ kHz. This is consistent with the temperature variation of the excess heat capacity in BR(*II*) (Fig. 10) and strongly suggests that QS(^{2}H) in BR(*II*) and IO(*II*) may be regarded as an order parameter of a critical ordering process.[17]

While N—H···X hydrogen bonding in phase *I*, as measured by the lowering of the ν(NH) frequency in the ir spectra, is weaker than in the simple CH_3NH_3X halides, it is stronger than in the previously (15) investigated trigonal $(CH_3NH_3)_2PtCl_6$: the estimated mean of the ν_s(NH) and ν_a(NH) frequencies in $CH_3NH_3PbCl_3$ falls about halfway between those in CH_3NH_3Cl and $(CH_3NH_3)_2PtCl_6$.

The present results for the $CH_3NH_3PbX_3$ perovskites are compared in some detail with the available corresponding results for the cubic $(CH_3NH_3)_2TeX_6$, both from the literature and from our preliminary investigation of $(CH_3NH_3)_2TeBr_6$.

Acknowledgments

We wish to thank Professor M. H. Jericho and Mr. A. M. Putnam for the electrical conductivity measurements; Dr. M. Falk for obtaining the ir spectra; and Dr. D. Adhikesavalu, Dr. A. Linden, Miss K. N. Robertson, Mr. M. L. H. Gruwel, and Mr. J. B. Macdonald for their contributions to particular aspects of this investigation. Research grants to the first four authors and a Graduate Scholarship to the fifth author from the Natural Sciences and Engineering Research Council of Canada are acknowledged.

1. B. R. Vincent, K. N. Robertson, T. S. Cameron, and O. Knop. Can. J. Chem. **65**, 1042 (1987).
2. D. Weber. Z. Naturforsch. **33b**, 1443 (1978).
3. Y. Kume, R. Ikeda, and D. Nakamura. J. Magn. Reson. **20**, 276 (1975).
4. R. Ikeda, Y. Kume, D. Nakamura, Y. Furukawa, and H. Kiriyama. J. Magn. Reson. **24**, 9 (1976).
5. Y. Furukawa, H. Kiriyama, and R. Ikeda. Bull. Chem. Soc. Jpn. **50**, 1927 (1977).
6. K. Kitahama, H. Kiriyama, and Y. Baba. Bull. Chem. Soc. Jpn. **52**, 324 (1979).
7. T. Matsuo, M. Ueda, and H. Suga. Chem. Phys. Lett. **82**, 577 (1981).
8. O. Knop, T. S. Cameron, M. A. James, and M. Falk. Can. J. Chem. **61**, 1620 (1983); (errata) **62**, 1227 (1984).
9. R. E. Wasylishen, O. Knop, and J. B. MacDonald. Solid State Commun. **56**, 581 (1985).
10. R. Freeman, S. P. Kempsell, and M. H. Levitt. J. Magn. Reson. **38**, 453 (1983).
11. G. C. Levy and I. R. Peat. J. Magn. Reson. **18**, 500 (1975).
12. M. J. M. Van Oort and M. A. White. J. Chem. Soc. Faraday 1, **81**, 3059 (1985).
13. M. A. White. Thermochim. Acta, **74**, 55 (1984).
14. I. A. Oxton and O. Knop. J. Mol. Struct. **37**, 59 (1977).
15. I. A. Oxton, O. Knop, and J. L. Duncan. J. Mol. Struct. **38**, 25 (1977).
16. O. Knop, I. A. Oxton, and M. Falk. Can. J. Chem. **57**, 404 (1979); (errata) **57**, 2003 (1979).
17. J. H. Davis. Biochim. Biophys. Acta, **737**, 117 (1983).
18. O. Schmitz-Dumont, G. Bergerhoff, and E. Hartert. Z. Anorg. Allg. Chem. **283**, 314 (1956).
19. C. K. Møller. Mat.-fys. Medd. Kgl. Danske Vid. Selsk. **32**, nos. 1 and 2 (1959).
20. C. K. Møller. Nature, **182**, 1436 (1958).
21. O. Knop, W. J. Westerhaus, M. Falk, and W. Massa. Can. J. Chem. **63**, 3328 (1985).
22. H. B. Brom and J. Bartolomé. Physica, **111B**, 183 (1981).
23. E. Palacios, J. Bartolomé, R. Navarro, J. García, D. González, and H. B. Brom. Ferroelectrics, **55**, 287 (1984).
24. M. J. Hunt and A. L. MacKay. J. Magn. Reson. **15**, 402 (1974).
25. N. Boden. Nmr studies of plastic crystals. *In* The plastically crystalline state. *Edited by* J. N. Sherwood. John Wiley and Sons, New York. 1979. p. 147.
26. K. Yamada, S. Nose, T. Umehara, T. Okuda, and S. Ichiba. Bull. Chem. Soc. Jpn. **61**, 4265 (1988).
27. P. Polatin, T. Barbara, and B. P. Dailey. J. Magn. Reson. **47**, 148 (1982).
28. R. E. Wasylishen. Can. J. Chem. **64**, 773 (1986).
29. Y. Kume, R. Ikeda, and D. Nakamura. J. Phys. Chem. **82**, 1926 (1978).
30. Y. Furukawa, H. Kiriyama, and R. Ikeda. Bull. Chem. Soc. Jpn. **54**, 103 (1981).
31. R. E. Wasylishen, B. Pettitt, and W. Danchura. Can. J. Chem. **55**, 3602 (1977).
32. W. A. Steele. J. Chem. Phys. **38**, 2404 (1963).
33. J. M. Lehn and J. P. Kintzinger. *In* Nitrogen nmr. *Edited by* M. Witanowski and G. A. Webb. Plenum Press, London and New York. 1973.
34. T. Matsuo, H.-K. Yan, and H. Suga. J. Phys. Chem. Solids, **49**, 85 (1988).
35. S. Albert and J. A. Ripmeester. J. Chem. Phys. **58**, 541 (1973).
36. C. J. Ludman, C. I. Ratcliffe, and T. C. Waddington. J. Chem. Soc. Faraday 2, **72**, 1759 (1976).
37. S. Forss, G. Bergström, and N. Meinander. *In* Raman spectroscopy, linear and nonlinear. *Edited by* J. Lascombe and P. V. Huong. J. Wiley and Sons, New York. 1982.
38. O. Knop. J. Solid State Chem. **45**, 223 (1982).
39. Y. Kume, R. Ikeda, and D. Nakamura. J. Magn. Reson. **33**, 331 (1979).
40. K. Kitahama and H. Kiriyama. Acta Crystallogr. A, **34**, S302 (1978).
41. O. Knop, I. A. Oxton, W. J. Westerhaus, and M. Falk. J. Chem. Soc. Faraday 2, **77**, 309 (1981).
42. O. Knop, I. A. Oxton, W. J. Westerhaus, and M. Falk. J. Chem. Soc. Faraday 2, **77**, 811 (1981).
43. N. Onoda, T. Matsuo, and H. Suga. J. Phys. Chem. solids, **47**, 211 (1986).

Can. J. Chem. Downloaded from www.nrcresearchpress.com by 91.144.44.67 on 09/07/12
For personal use only.

The direct electrochemical synthesis of d^{10} metal ion derivatives of some anionic bidentate oxygen donors

THEODORE A. ANNAN, CLOVIS PEPPE,[1] AND DENNIS G. TUCK[2]

Department of Chemistry and Biochemistry, University of Windsor, Windsor, Ont., Canada N9B 3P4

Received August 4, 1989

THEODORE A. ANNAN, CLOVIS PEPPE, and DENNIS G. TUCK. Can. J. Chem. **68**, 423 (1990).

The electrochemical oxidation of a sacrificial anode (M = Zn, Cd, Hg, In, Sn) in non-aqueous solutions of 3-hydroxyflavone, 1′-hydroxy-2′-acetonaphthone, or 2-ethoxyphenol (= HL) gives ZnL_2, CdL_2, HgL, InL_3, or SnL_2 (not all combinations). Adducts with 2,2′-bipyridine (bpy) or *N,N,N′,N′*-tetramethylethanediamine (tmen) have also been prepared in some cases. Certain zinc and cadmium compounds produce paramagnetic species on exposure to the atmosphere. The structure of $Zn(C_{15}H_9O_3)_2$tmen has been determined; the crystals are orthorhombic, space group *Pbcn*, cell dimensions a = 18.817(2) Å, b = 13.886(3) Å, c = 12.567(3) Å, Z = 4, R = 0.0758 for 773 unique observed reflections. The corresponding data for $Cd(C_{12}H_9O_2)_2$bpy are orthorhombic, space group *Pbca*, cell dimensions a = 20.338(4) Å, b = 30.473(5) Å, c = 9.316(2) Å, Z = 8, R = 0.0457 for 2623 unique observed reflections. Both molecules have MO_4N_2 kernels, but each shows significant differences in the two M—O bond lengths to the dioxo ligand, and there are concomitant effects in the C—O and C—C bond distances in the ligands.

Key words: electrochemical synthesis, d^{10} metal ions, X-ray crystallography, zinc complex, cadmium complex.

THEODORE A. ANNAN, CLOVIS PEPPE et DENNIS G. TUCK. Can. J. Chem. **68**, 423 (1990).

L'oxydation électrochimique d'une anode qui est sacrifiée (M = Zn, Cd, Hg, In et Sn) dans des solutions non-aqueuses de 3-hydroxyflavone, de l'hydroxy-2′-acétonaphtone ou de 2-éthoxyphénol (= HL) fournit les composés ZnL_2, CdL_2, HgL, InL_3 ou SnL_2 (pas nécessairement toutes les combinaisons). Dans quelques cas, on a aussi préparé les adduits avec la 2,2′-bipyridine (bpy) ou la *N,N,N′,N′*-tétraméthylèneéthanediamine (tmen). Lorsqu'on soumet un certain nombre de composés du zinc et du cadmium à l'atmosphère, on obtient des espèces paramagnétiques. On a déterminé la structure du produit $Zn(C_{15}H_9O_3)_2$tmen; les cristaux sont orthorhombiques, groupe d'espace *Pbcn*, avec a = 18,817(2), b = 13,886(3) et c = 12,567(3) Å, Z = 4 et R = 0,0758 pour 773 réflexions uniques qui ont été observées. Les données correspondantes pour le produit $Cd(C_{12}H_9O_2)_2$bpy sont cristaux orthorhombiques, groupe d'espace *Pbcn*, avec a = 20,338(4), b = 30,473(5) et c = 9,316(2) Å, Z = 8 et R = 0,0457 pour 2623 réflexions uniques qui ont été observées. Les deux molécules comportent un noyau de MO_4N_2; toutefois, chacune présente des différences importantes dans les deux longueurs des liaisons M—O conduisant au ligand dioxo et ces différences donnent lieu à des effets concomitants dans les longueurs des liaisons C—O et C—C de ces ligands.

Mots clés : synthèses électrochimiques, ions métalliques d^{10}, diffraction des rayons-X, complexe du zinc, complexe du cadmium.

[Traduit par la revue]

Introduction

The method of direct electrochemical synthesis developed in this laboratory consists in oxidizing a sacrificial metallic anode in a non-aqueous solution containing the appropriate ligand or ligand precursor to produce the appropriate metallic derivative, and a number of publications have established the wide applicability of this technique for the preparation of inorganic and organometallic derivatives of Main Group and transition metals. Recent studies have demonstrated the direct electrochemical synthesis of derivatives of many weak organic acids, including metal thiolates (1–4), metal acetylides (5), metal diethyldithiophosphates (6), metal dialkyldithiocarbamates (6), metal diphenylphosphides (7), and metal catecholates (8–10).

The present work was prompted by these last studies, which showed that under the conditions of the electrochemical experiment, the product tends to be in a low oxidation state, so that for example with catechol or other aromatic 1,2-diols, tin gave $Sn^{II}(O_2R)$ derivatives (9), and with indium, the products were the unusual $In^{I}[OR(OH)]$ derivatives (10). It therefore seemed appropriate to study compounds containing adjacent —OH and —OR groups, in the hope that these would also form chelate complexes of metals in unusual oxidation states. We have therefore investigated the electrochemical reactions of three weak organic acids, namely 3-hydroxyflavone ($C_{15}H_9O_3H$), 1′-hydroxy-2′-acetonaphthone ($C_{12}H_9O_2H$), and 2-ethoxyphenol ($C_8H_9O_2H$) with indium, tin, zinc, cadmium, and mercury.

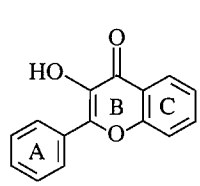

$C_{15}H_9O_3H$

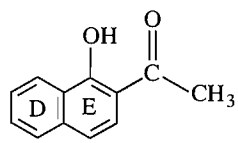

$C_{12}H_9O_2H$

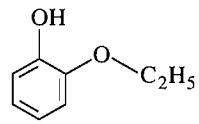

$C_8H_9O_2H$

The tin derivative was the hoped-for tin(II) species, but the final indium product proved to be the result of disproportionation. The zinc and cadmium derivatives show unusual redox properties. In the course of this work, we have also established the molecular structure of $Zn(C_{15}H_9O_3)_2$tmen and $Cd(C_{12}H_9O_2)_2$bpy, each of which shows a number of interesting features.

Experimental section

General

Metals, 3-hydroxyflavone, 2-ethoxyphenol, 1′-hydroxy-2′-aceto-

[1]Permanent address: Departamento de Quimica, Universidade Federal da Paraiba, Cidade Universitaria, Joao Pessoa-PB, Brazil 58000.

[2]To whom correspondence should be addressed.

Can. J. Chem. Downloaded from www.nrcresearchpress.com by 91.144.44.67 on 09/07/12
For personal use only.

Can. J. Chem. Downloaded from www.nrcresearchpress.com by 91.144.44.67 on 09/07/12
For personal use only.

TABLE 1. The electrochemical preparation of $M(C_{15}H_9O_3)_n$, $M(C_8H_9O_2)_n$, and $M(C_{12}H_9O_2)_n$ compounds and their bpy adducts

Compound	Initial ROH[a] (mg)	Initial bpy (mg)	Initial Current (mA)	Initial Voltage (V)	Time of electrol. (min)	Mass of metal dissolved (mg)	Mass of product (mg)	Yield (%)	E_F (mol F^{-1})
$Zn(C_{15}H_9O_3)_2$	419	—	30	32	100	63	380	73	0.52
$Zn(C_{15}H_9O_3)_2bpy$	509	333[d]	40	30	60	48	310	62	0.50
$Cd(C_{15}H_9O_3)_2$	510	—	20	27	120	81	360	71	0.48
$Cd(C_{15}H_9O_3)_2bpy$	502	329[d]	20	40	120	83	306	56	0.49
$Hg(C_{15}H_9O_3)$	488	—	12	40	120	[g]	204	[g]	[g]
$In(C_{15}H_9O_3)_3$	327	—	20	50	60	88	159	76	1.02
$Sn(C_{15}H_9O_3)_2$	391	—	30	40	60	71	171	48	0.53
$Zn(C_8H_9O_2)_2$	1000[b]	—	70	50	120	178	320	34	0.51
$Zn(C_8H_9O_2)_2bpy$	1030[c]	600[e]	38	20	120	[g]	550	[g]	[g]
$Cd(C_8H_9O_2)_2$	878[c]	—	32	28	80	91	290	92	0.51
$Sn(C_8H_9O_2)_2$	831[b]	—	50	38	100	195	230	36	0.53
$Zn(C_{12}H_9O_2)_2$	448[b]	—	20	24	140	54	250	70	0.47
$Zn(C_{12}H_9O_2)_2bpy$	470[b]	291[f]	30	25	100	70	347	55	0.57

[a]Dissolved in 40 mL CH_3CN + toluene (1:1, v/v), containing ca. 50 mg Et_4NClO_4.
[b]Solvent CH_3CN (40 mL).
[c]Solvent 40 mL CH_3CN + toluene (3:1, v/v).
[d]Mole ratio HL:bpy ≈ 1:1.
[e]Mole ratio HL:bpy ≈ 2:1.
[f]Mole ratio HL:bpy ≈ 1:1.
[g]Not recorded.

naphthone, 2,2′-bipyridine (bpy), and *N,N,N′,N′*-tetramethylethanediamine (tmen) were used as supplied (Aldrich). Tetraethylammonium perchlorate was prepared by mixing aqueous solutions of $NaClO_4$ and Et_4NBr; the product was recrystallized from hot aqueous ethanol (9:1, v:v). Solvent were dried and distilled before use, and stored over drying agents.

Metal analyses were by atomic absorption spectrophotometry, and microanalysis was performed by Guelph Chemical Laboratories. Infrared spectroscopy involved the use of samples as KBr discs with a Nicolet 5DX instrument. Nuclear magnetic resonance spectra were recorded on a Bruker AC 300 L spectrometer. Electron spin resonance spectra were measured with a Varian E12 instrument, using the calibration and solution handling techniques described elsewhere (11).

Electrochemical synthesis

The method of preparing these new compounds was essentially the same as those used in our previous papers (1–10). The solution phase was contained in a 100 mL round-bottomed flask with a Schlenk arm; a metal rod suspended through rubber septum formed the anode of the cell, and a platinum wire was the cathode. In the case of mercury, the element was contained in small cup into which a platinum wire was inserted. Details of solution composition are given in Table 1, and Table 2 gives the analytical results for each compound synthesized. The use of an atmosphere of dry nitrogen is critically important in the derivatives of 1′-hydroxy-2′-acetonaphthone, as is the use of freshly distilled oxygen-free solvents. These rigorous precautions are not necessary in the other systems studied, since the derivatives can be safely handled in air.

The isolation of the product varied according to the system in question. In only three did precipitation occur completely during the electrolysis; $Hg(C_{15}H_9O_3)$ and $Cd(C_8H_9O_2)_2$ were collected by filtration, washed with diethyl ether, and dried *in vacuo*, while $Zn(C_{12}H_9O_2)_2$ was collected, recrystallized from hot toluene, and dried. With Sn, Zn, and $Cd(C_{15}H_9O_3)_2$, $Zn(C_8H_9O_2)_2$ and $Zn(C_{12}H_9O_2)_2bpy$, precipitation did not begin until the electrolysis had proceeded for some time, but solid continued to form over a period of ca. 12 h after the end of the experiment. This material was collected, washed with diethyl ether, and dried. In the case of $Zn(C_{15}H_9O_3)_2bpy$, the clear solution obtained at the end of the electrolysis was evaporated to dryness, and the product washed successively with acetonitrile (to remove Et_4NClO_4), toluene, and diethyl ether, and dried. Similarly, for $Cd(C_{15}H_9O_3)_2bpy$ the clear solution obtained at the end of the electrolysis was reduced in volume by ca. 50%; addition of diethyl ether produced a solid which was collected and washed in the usual way. Finally, in the case of $In(C_{15}H_9O_3)_3$, the clear solution phase deposited finely divided indium as the electrolysis proceeded; at the end of the experiment, the filtrate from this reaction was cooled to 0°C, which caused the indium(III) species to precipitate. This material was collected, washed, and dried.

TABLE 2. Analytical results for metal–dioxo compounds

Compound	Colour	M% Found	M% Calcd.
$Zn(C_{15}H_9O_3)_2$	Yellow	12.7	12.1
$Zn(C_{15}H_9O_3)_2bpy$	Yellow	9.7	9.4
$Zn(C_{15}H_9O_3)_2tmen$	Yellow	10.0	10.0[a]
$Cd(C_{15}H_9O_3)_2$	Yellow	19.2	19.2
$Cd(C_{15}H_9O_3)_2bpy$	Yellow	15.1	15.1
$Cd(C_{15}H_9O_3)_2tmen$	Yellow	16.0	16.1[b]
$Hg(C_{15}H_9O_3)$	Yellow–green	47.0	45.8
$HgI(C_{15}H_9O_3).(1/2)C_7H_8$	Yellow	32.7	32.8[c]
$In(C_{15}H_9O_3)_3$	Yellow	13.9	13.9
$Sn(C_{15}H_9O_3)_2$	Yellow	20.0	20.0[d]
$Zn(C_8H_9O_2)_2$	White	19.2	19.2
$Zn(C_8H_9O_2)_2bpy$	White	13.6	13.2
$Cd(C_8H_9O_2)_2$	White	29.7	29.1
$Zn(C_{12}H_9O_2)_2$	Yellow[e]	14.9	15.0
$Zn(C_{12}H_9O_2)_2bpy$	Yellow[e]	11.2	11.0
$Cd(C_{12}H_9O_2)_2bpy$	Yellow[e]	17.0	17.6

[a]Found (calcd): C 65.1 (65.9), H 5.24 (5.22), N 4.44 (4.27).
[b]Found (calcd): C 61.2 (61.5), H 4.92 (4.87), N 4.70 (3.98).
[c]Found (calcd): C 36.0 (36.4), H 1.81 (2.14).
[d]Found (calcd): C 61.0 (60.8), H 3.33 (3.06).
[e]Compound becomes green in the presence of O_2.

TABLE 3. Summary of crystal data, intensity collection, and structural refinement

Parameter	Value	
	1	**2**
a (Å)	18.817(2)	20.338(4)
b (Å)	13.886(3)	30.473(5)
c (Å)	12.567(3)	9.316(2)
α (deg) = β = γ	90.0	90.0
V (Å^3)	3283.66(4)	5773.9(2)
Crystal system	orthorhombic	orthorhombic
Space group	Pbcn	Pbca
Molecular weight	656.02	638.97
Z	4	8
ρ_c (g cm^{-3})	1.33	1.47
ρ_0 (g cm^{-3})	1.33	1.49
Crystal dimensions (mm)	0.26 × 0.15 × 0.10	0.46 × 0.38 × 0.23
Absorption coefficient, μ (cm^{-1})	8.21	7.08
2θ angle (deg)	4–40	4–45
Background time/scan time	0.5	0.5
Total reflections measured	1546 ($+h$, $+k$, $+l$)	3798 ($+h$, $+k$, $+l$)
Unique data used ($I \geq 3\sigma(I)$)	773	2623
No. of parameters (NP)	104	200
$R = \Sigma\Delta/\Sigma\|F_o\|$	0.0758	0.0457
$R_w = [\Sigma w\Delta^2/\Sigma w\phi_0^2]^{1/2}$	0.0766	0.0483
Largest peak in final difference Fourier, e/Å^3	0.36	0.38
Largest shift/error value on final cycle	0.01	0.01

Crystallographic analysis

In both X-ray crystallographic studies, involving $Zn(C_{15}H_9O_2)_2$tmen (**1**) and $Cd(C_{12}H_9O_2)_2$bpy (**2**), the crystal was mounted along its longest dimension on a Syntex $P2_1$ automated diffractometer with Mo-Kα radiation (λ = 0.71069 Å) and a graphite monochromator. Data were collected (θ–2θ scan, width Kα_1 − 1° to Kα_2 + 1°, scan speeds 2.02–4.88° min^{-1}) at 21°C by the procedures described previously (12). The crystal of **1** was mounted on a glass fibre with epoxy resin adhesive, while **2** was sealed in a capillary tube, but the procedures were otherwise essentially the same in each case. The intensities of three check reflection were monitored at regular intervals, and no significant decay was observed during the time required for data collection. The cell parameters were measured, checked for dimensions and symmetry from axial photographs, and refined from data from 30 strong reflections in the range $15 < 2\theta < 25°$ reflections. Data used in the structure determinations were corrected for Lorentz and polarization effects, and analytically for absorption. Pertinent crystal and experimental data are given in Table 3. The densities were measured by the flotation method, using carbon tetrachloride – benzene mixtures.

The systematic absences for **1** ($0kl$ for $k = 2n$, $h0l$ for $l = 2n$, $hk0$ for $h + k = 2n$, $h00$ for $h = 2n$, $0k0$ for $k = 2n$, and $00l$ for $l = 2n$) identified the space group as *Pbcn*. For **2**, the space group *Pbca* was identified by the systematic absences $0kl$ for $k = 2n$, $h0l$ for $l = 2n$, $hk0$ for $h = 2n$, $h00$ for $h = 2n$, $0k0$ for $k = 2n$, and $00l$ for $l = 2n$. Direct methods and Fourier techniques were used to solve the structure in these centrosymmetric space groups, with refinement by full-matrix least-squares methods. In the final stages of the refinement of **1**, Zn, O, and N and the carbon atoms of the tmen ligand (C16—C18) were refined with anisotropic thermal parameters and the remaining carbon atoms isotropically; hydrogen atoms were fixed in idealized positions (r(C—H) = 0.95 Å), and assigned isotropic thermal parameters 10% higher than those of the bonding carbon atoms. Due to the small size of the crystal, and the consequent small unique data set used in the analysis, C10—C15 and C4—C9 were refined as rigid groups, using C—C bond lengths of 1.395 Å, and angles of 120°. Unit weights were used in the initial stages, while in the final cycles the weighting scheme used was of the form $W = \sigma^2(F) + 0.00001F^2$. The refinement, minimizing the function $\Sigma w(|F_o| - |F_c|)^2$, converged at R = 0.0758 and R_w = 0.0766; these values clearly reflect the restricted data set available.

For the final stages of the refinement of the structure of **2**, Cd, O, and N atoms were refined with anisotropic thermal parameters and the carbon atoms were treated isotropically. Hydrogen atoms were again fixed in idealized positions, and the weighting scheme was that used in the case of **1**. The refinement minimizing the function $\Sigma w(|F_o| - |F_c|)^2$ converged at R = 0.0457 and R_w = 0.0483.

The computer programs and the source of scattering factors were those used in earlier work (12). Fractional atomic coordinates are given in Tables 4 and 6, and bond lengths and angles in Tables 5 and 7. Tables of thermal parameters, hydrogen atom coordinates, and observed and calculated structure factor amplitudes, are available as supplementary data. The structures are shown in Figs. 1 and 2. The cell diagrams have been deposited.[3]

Results and discussion

Electrochemical

The electrochemical oxidation of the various metals investigated obviously provides a convenient route to the compounds listed in Table 2. As in the earlier systems studied in this laboratory, the products are obtained in a one-step high yield synthesis, and the method readily lends itself to working on a larger scale than that which we chose to use in the present studies. The electrochemical route is obviously simpler than that involving a sequence of reactions starting from metal salt + parent acid.

The stoichiometry of the electrochemical reactions is indicated by the electrochemical efficiency, defined as moles of

[3]A complete set of deposited material may be purchased from the Depository of Unpublished Data, CISTI, National Research Council of Canada, Ottawa, Ont., Canada K1A 0S2.

Can. J. Chem. Downloaded from www.nrcresearchpress.com by 91.144.44.67 on 09/07/12
For personal use only.

Can. J. Chem. Downloaded from www.nrcresearchpress.com by 91.144.44.67 on 09/07/12
For personal use only.

TABLE 4. Final fractional coordinates and isotropic thermal parameters[a] for non-hydrogen atoms for $Zn(C_{15}H_9O_3)_2tmen$, $C_{36}H_{34}N_2O_2Zn$, with standard deviations in parentheses

Atom	x	y	z	U_{eq} (Å × 10^3)
Zn	0.00000	0.18475(2)	0.25000	85.4(3)
O(1)	−0.0730(5)	0.2983(7)	0.3139(8)	56.6(7)
O(2)	0.0396(6)	0.2029(7)	0.3943(7)	58.4(7)
O(3)	0.0036(6)	0.3743(6)	0.6050(7)	46.3(7)
N(1)	0.0721(10)	0.0636(12)	0.2090(14)	74.1(13)
C(1)	−0.0504(9)	0.3230(12)	0.4048(13)	67.2(5)
C(2)	0.0105(9)	0.2728(11)	0.4512(12)	64.7(5)
C(3)	0.0353(8)	0.3038(11)	0.5459(12)	56.9(5)
C(4)	−0.0534(5)	0.4207(7)	0.5651(6)	51.5(5)
C(5)	−0.0827(5)	0.4011(7)	0.4654(6)	55.5(5)
C(6)	−0.1412(5)	0.4535(7)	0.4295(6)	60.5(5)
C(7)	−0.1704(5)	0.5256(7)	0.4933(6)	71.0(5)
C(8)	−0.1412(5)	0.5452(7)	0.5929(6)	85.7(6)
C(9)	−0.0827(5)	0.4011(7)	0.4654(6)	68.7(5)
C(10)	0.0991(5)	0.2669(7)	0.6006(8)	51.0(4)
C(11)	0.1097(5)	0.2867(7)	0.7083(8)	78.0(6)
C(12)	0.1743(5)	0.2633(7)	0.7564(8)	116.5(7)
C(13)	0.2281(5)	0.2201(7)	0.6969(8)	110.0(7)
C(14)	0.2175(5)	0.2004(7)	0.5893(8)	109.7(7)
C(15)	0.1529(5)	0.2238(7)	0.5411(8)	84.7(6)
C(16)	0.0986(12)	0.0702(14)	0.1009(16)	127.5(16)
C(17)	0.1333(12)	0.0611(15)	0.2800(16)	110.3(18)
C(18)	0.0270(18)	−0.0228(14)	0.2084(19)	169.2(27)

[a] $U_{eq} = \frac{1}{3}[\Sigma_i\Sigma_j U_{ij} a_i^* a_j^* \boldsymbol{a}_i \cdot \boldsymbol{a}_j]$; all carbon atoms other than C16–C18 were refined isotropically.

TABLE 5. Interatomic distances (Å) and angles (deg) for Zn-$(C_{15}H_9O_3)_2tmen$[a]

Bond	Distance	Bonds	Angle
Zn—O(1)	2.240(1)	O(1)—Zn—O(2)	79.3(4)
Zn—O(2)	1.980(1)	N(1)—Zn—O(1)	172.0(5)
Zn—N(1)	2.229(1)	N(1)—Zn—O(2)	94.2(5)
C(1)—O(1)	1.266(1)	C(1)—O(1)—Zn	107.6(9)
C(2)—O(2)	1.318(1)	C(2)—O(2)—Zn	115.7(9)
C(3)—O(3)	1.363(1)	C(4)—O(3)—C(3)	119.1(10)
C(4)—O(3)	1.351(1)	C(2)—C(1)—O(1)	120.0(10)
C(1)—C(2)	1.468(2)	C(5)—C(1)—O(1)	122.1(10)
C(1)—C(5)	1.455(2)	C(5)—C(1)—C(2)	117.9(10)
C(2)—C(3)	1.350(2)	C(1)—C(2)—O(2)	117.0(10)
C(3)—C(10)	1.474(2)	C(3)—C(2)—O(2)	125.0(10)
N(1)—C(16)	1.462(2)	C(3)—C(2)—C(1)	117.9(10)
N(1)—C(17)	1.450(2)	C(2)—C(3)—O(3)	124.3(10)
N(1)—C(18)	1.473(2)	C(10)—C(3)—O(3)	110.5(10)
C(18)—C(18)[b]	1.457(4)	C(10)—C(3)—C(2)	125.2(10)
		C(5)—C(4)—O(3)	123.6(5)
		C(4)—C(5)—C(1)	117.0(7)
		C(15)—C(10)—C(3)	119.4(6)
		C(16)—N(1)—Zn	111.1(10)
		C(17)—N(1)—Zn	111.4(10)
		C(18)—N(1)—Zn	104.9(10)
		C(18)—N(1)—C(16)	103.8(15)
		C(16)—N(1)—C(17)	107.6(17)
		C(18)—N(1)—C(17)	116.7(20)
		N(1)—Zn—N(1)[b]	82.0(10)

[a] Phenyl rings with carbon atom numberings of C(4) through C(9) and C(10) through C(15) were idealized to regular hexagons of side 1.395 Å and angles of 120 deg.

[b] A two-fold symmetry related atom within the molecule.

TABLE 6. Final fractional coordinates and isotropic thermal parameters[a] for non-hydrogen atoms for $Cd(C_{24}H_{18}O_4)bpy$, $C_{34}H_{26}N_2O_4Cd$, with standard deviations in parentheses

Atom	x	y	z	U_{eq} (Å × 10^3)
Cd	0.0749(1)	0.1402(1)	0.4677(2)	28.6(3)
O(1)	−0.0005(2)	0.1421(1)	0.6380(5)	30.8(2)
O(2)	0.1317(2)	0.1187(2)	0.6678(5)	41.6(3)
O(3)	0.1532(2)	0.1229(1)	0.3178(5)	35.9(3)
O(4)	0.0392(2)	0.0745(1)	0.3864(5)	39.8(3)
N(1)	0.0132(3)	0.1846(2)	0.3130(6)	30.8(3)
N(2)	0.1083(3)	0.2139(2)	0.4895(6)	30.9(4)
C(1)	−0.0069(3)	0.1195(2)	0.7536(7)	34.7(2)
C(2)	0.0445(3)	0.0969(2)	0.8247(7)	38.6(2)
C(3)	0.0288(3)	0.0720(2)	0.9509(7)	52.2(2)
C(4)	−0.0318(3)	0.0702(2)	1.0086(8)	55.7(2)
C(5)	−0.0849(3)	0.0932(2)	0.9428(7)	47.5(2)
C(6)	−0.0728(3)	0.1177(2)	0.8167(7)	38.5(2)
C(7)	−0.1246(3)	0.1413(2)	0.7523(8)	49.3(2)
C(8)	−0.1869(4)	0.1398(2)	0.8122(9)	62.6(2)
C(9)	−0.1991(4)	0.1154(3)	0.9341(8)	61.5(2)
C(10)	−0.1498(4)	0.0923(3)	0.9973(8)	58.7(2)
C(11)	0.1120(3)	0.0983(2)	0.7730(8)	47.8(2)
C(12)	0.1636(4)	0.0732(3)	0.8545(9)	73.3(2)
C(1A)	0.1723(3)	0.0856(2)	0.2711(7)	37.8(2)
C(2A)	0.1359(3)	0.0460(2)	0.2776(7)	40.1(2)
C(3A)	0.1659(3)	0.0063(2)	0.2220(8)	53.3(2)
C(4A)	0.2254(3)	0.0059(3)	0.1623(8)	58.5(2)
C(5A)	0.2640(3)	0.0447(2)	0.1498(7)	45.9(2)
C(6A)	0.2369(3)	0.0839(2)	0.2029(7)	38.5(2)
C(7A)	0.2725(3)	0.1226(2)	0.1856(7)	47.9(2)
C(8A)	0.3328(4)	0.1224(3)	0.1175(8)	58.8(2)
C(9A)	0.3605(4)	0.0829(3)	0.0722(8)	64.2(2)
C(10A)	0.3266(4)	0.0455(3)	0.0875(8)	61.0(2)
C(11A)	0.0695(3)	0.0436(2)	0.3310(7)	42.5(2)
C(12A)	0.0307(3)	0.0021(2)	0.3158(8)	54.2(2)
C(21)	0.0218(3)	0.2287(2)	0.3200(7)	45.6(2)
C(22)	−0.0172(4)	0.2561(3)	0.2357(8)	60.4(2)
C(23)	−0.0628(4)	0.2390(3)	0.1443(9)	69.4(2)
C(24)	−0.0697(4)	0.1950(3)	0.1353(9)	64.9(2)
C(25)	−0.0315(3)	0.1690(3)	0.2225(8)	56.9(2)
C(31)	0.0729(3)	0.2445(2)	0.4179(7)	45.6(2)
C(32)	0.0864(4)	0.2886(3)	0.4390(9)	68.9(2)
C(33)	0.1344(4)	0.3015(3)	0.5327(10)	84.4(3)
C(34)	0.1702(4)	0.2705(3)	0.6049(10)	79.4(3)
C(35)	0.1806(4)	0.2259(3)	0.5775(9)	66.3(2)

[a] $U_{eq} = \frac{1}{3}[\Sigma_i\Sigma_j U_{ij} a_i^* a_j^* \boldsymbol{a}_i \cdot \boldsymbol{a}_j]$; all carbon atoms were refined isotropically.

metal dissolved per Faraday of charge (E_F). The values in Table 1 show that for all R(OH) solutes with zinc, cadmium, and tin anodes, $E_F = 0.51 \pm 0.02$ mol F^{-1} which implies the reactions

Cathode

[1] $2R(OH) + 2e \rightarrow 2RO^- + H_2$

Anode

[2] $2RO^- + M \rightarrow M(OR)_2 + 2e$

corresponding to the formation of products with the metal in the +II state for these elements. For indium, $E_F = 1.02$ mol F^{-1}, implying the formation of an indium(I) species at the anode, but the subsequent disproportionation in solution is evidenced by the deposition of indium metal, and by the isolation of $In(C_{15}H_9O_3)_3$. For mercury and $C_{15}H_9O_2(OH)$, the product is formally a mercury(I) species, but we were not able to measure E_F with any degree of accuracy.

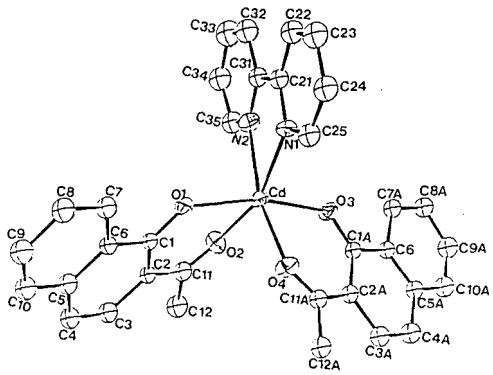

FIG. 1. The molecular structure of $Zn(C_{15}H_9O_3)_2$tmen (**1**); ORTEP diagram, with atoms drawn as 30% probability ellipsoids. The numbering system is shown; unlabelled and labelled atoms are related by a two-fold axis. Hydrogen atoms have been omitted for the sake of clarity.

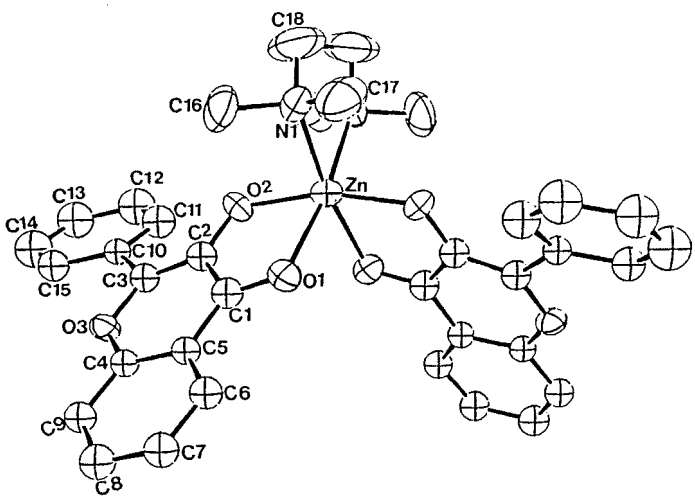

FIG. 2. The molecular structure of $Cd(C_{12}H_9O_2)_2$bpy (**2**); comments as in Fig. 1.

Preparative

(1) 3-Hydroxyflavone derivatives

Amongst the three organic compounds investigated, derivatives of 3-hydroxyflavone are the easiest to prepare. No deposition of metal on the electrode was detected during the electrolysis, except in the case of the indium compound (see below). All the compounds are air stable materials, and were obtained in high yields.

The compounds $M(C_{15}H_9O_3)_2$ (M = Zn, Cd) are the natural derivatives expected with the metal in its +II oxidation state. When the electrolysis was conducted in the presence of bpy, the 1:1 addition compounds $M(C_{15}H_9O_3)_2$bpy were obtained, and both $M(C_{15}H_9O_3)_2$ compounds reacted with tmen in acetonitrile or acetonitrile:toluene (1:1) to form the crystalline 1:1 addition compounds $M(C_{15}H_9O_3)_2$tmen in yields better than 80%. With tin and mercury, the products are those of the element in the low oxidation state, and in the case of tin, the stable $Sn(C_{15}H_9O_3)_2$ compound is isolated as a crystalline yellow solid. The electrochemical oxidation of mercury leads to the formation of the mercurous flavonate, in contrast to the behaviour of the other elements of the same group; $Hg(C_{15}H_9O_3)$ is readily oxidized to $HgI(C_{15}H_9O_3)$ by reaction with half an equivalent of I_2 in toluene.

[3] $2Hg(C_{15}H_9O_3) + I_2 \rightarrow 2HgI(C_{15}H_9O_3)$

supporting the assumption that the initial electrochemical reaction yields a mercury(I) derivative. The presence of toluene in the final product was demonstrated by the characteristic ν(C—H) infrared bands at 2839 + 2959 cm^{-1}.

The isolation of the indium(III) flavonate can be explained in terms of the initial formation of an indium(I) species electrochemically, followed by disproportionation according to the stoichiometry

[4] $3In(C_{15}H_9O_3) \rightarrow 2In + In(C_{15}H_9O_3)_3$

In keeping with this argument, during the initial stages of the electrolysis we observed the formation of a yellow solid, which quickly decomposes shortly after its formation with the deposition of metallic indium, which can be isolated in the quantity required by the stoichiometry of reaction [4].

(2) 2-Ethoxyphenol derivatives

During the electrochemical experiments with this compound, we observed considerable heating in the cell and a significant increase in the current flowing in the circuit, although this could be controlled by decreasing the applied voltage. A considerable deposition of metal on the cathode of the cell was also observed, especially in the preparation of $Cd(C_8H_9O_2)_2$. To overcome this difficulty, a small beaker (1 cm diameter, 1 cm height) was placed below the platinum cathode to collect the metal which is deposited during the electrolysis, and thereby avoid the contamination of the insoluble product which falls away from the area immediately below the electrode.

The results are similar to those for the flavonates discussed above. With zinc and cadmium, $M(C_8H_9O_2)_2$ and $Zn(C_8H_9O_2)_2$bpy are M^{II} complexes and call for no special comment. We were not able to achieve the electrochemical synthesis of $Cd(C_8H_9O_2)_2$bpy. In each of several attempts, large quantities of metallic cadmium deposited on the platinum cathode, and changing the solvent did not eliminate this deposition. It seems probable that the $Cd(C_8H_9O_2)_2$bpy compound formed electrochemically undergoes subsequent cathodic reduction to cadmium metal

[5] $Cd(C_8H_9O_2)_2bpy + 2e^- \rightarrow Cd + 2C_8H_9O_2^- + bpy$

It is also worth noting that this bipyridine adduct could not be prepared by a direct reaction between $Cd(C_8H_9O_2)_2$ and bpy in refluxing toluene, since the initial cadmium compound was recovered unchanged. This result suggests that the solid $Cd(C_8H_9O_2)_2$ has a homo-polymeric structure which is not easily broken down even by a strong bidentate donor.

Attempts to prepare indium ethoxyphenolato derivatives were unsuccessful; a considerable amount of metallic indium was deposited at the cathode, suggesting the *in situ* reduction of the indium compound formed electrochemically.

(3) 1′-Hydroxy-2′-acetonaphthone derivatives

The electrochemical reduction of 1′-hydroxy-2′-acetonaphthone, followed by the oxidation of anodic zinc, leads to $Zn(C_{12}H_9O_2)_2$, and to $Zn(C_{12}H_9O_2)_2$bpy when the bidentate ligand is present in the solution phase. The oxidation of cadmium produced a yellow compound, identified as $Cd(C_{12}H_9O_2)_2$. During the formation of this substance, the deposition of metallic cadmium at the cathode was observed, but the use of a small beaker under the electrode (see above) prevented any contamination of the final product. $Cd(C_{12}H_9O_2)_2$bpy was prepared from previously formed $Cd(C_{12}H_9O_2)_2$ by reaction with 2,2′-bipyridine in toluene; crystals suitable for X-ray diffraction were grown from this solution.

Can. J. Chem. Downloaded from www.nrcresearchpress.com by 91.144.44.67 on 09/07/12
For personal use only.

TABLE 7. Interatomic distances (Å) and angles (deg) for $Cd(C_{24}H_{18}O_4)bpy$

Bond	Distance	Bonds	Angle
Cd—O(1)	2.207(4)	O(1)—Cd—O(2)	76.8(2)
Cd—O(2)	2.289(5)	O(1)—Cd—O(3)	166.6(2)
Cd—O(3)	2.183(4)	O(1)—Cd—O(4)	93.2(2)
Cd—O(4)	2.260(4)	O(1)—Cd—N(1)	93.2(2)
Cd—N(1)	2.342(5)	O(1)—Cd—N(2)	96.5(2)
Cd—N(2)	2.355(5)	O(2)—Cd—O(3)	94.8(2)
O(1)—C(1)	1.284(7)	O(2)—Cd—O(4)	100.4(2)
O(3)—C(1A)	1.278(7)	O(2)—Cd—N(1)	159.6(2)
O(2)—C(11)	1.227(8)	O(2)—Cd—N(2)	93.3(2)
O(4)—C(11A)	1.237(7)	O(3)—Cd—O(4)	78.8(2)
C(1)—C(2)	1.417(8)	O(3)—Cd—N(1)	97.9(2)
C(1A)—C(2A)	1.417(8)	O(3)—Cd—N(2)	94.3(2)
C(1)—C(6)	1.466(8)	O(4)—Cd—N(1)	97.7(2)
C(1A)—C(6A)	1.459(8)	O(4)—Cd—N(2)	165.1(2)
C(2)—C(3)	1.435(9)	N(1)—Cd—N(2)	69.9(2)
C(2A)—C(3A)	1.450(9)	Cd—O(1)—C(1)	131.3(4)
C(2)—C(11)	1.457(9)	Cd—O(3)—C(1A)	130.9(3)
C(2A)—C(11A)	1.442(9)	Cd—O(2)—C(11)	129.1(4)
C(3)—C(4)	1.346(9)	Cd—O(4)—C(11A)	130.8(3)
C(3A)—C(4A)	1.331(9)	O(1)—C(1)—C(2)	125.3(5)
C(4)—C(5)	1.426(9)	O(3)—C(1A)—C(2A)	125.8(2)
C(4A)—C(5A)	1.425(9)	O(1)—C(1)—C(6)	116.7(5)
C(5)—C(6)	1.412(9)	O(3)—C(1A)—C(6A)	116.9(2)
C(5A)—C(6A)	1.406(8)	C(2)—C(1)—C(6)	118.0(5)
C(5)—C(10)	1.415(9)	C(2A)—C(1A)—C(6A)	117.3(6)
C(5A)—C(10A)	1.400(9)	C(1)—C(2)—C(3)	118.4(5)
C(6)—C(7)	1.409(9)	C(1A)—C(2A)—C(3A)	118.4(6)
C(6A)—C(7A)	1.393(9)	C(2)—C(3)—C(4)	123.5(6)
C(7)—C(8)	1.385(11)	C(2A)—C(3A)—C(4A)	122.6(7)
C(7A)—C(8A)	1.381(11)	C(3)—C(4)—C(5)	120.1(6)
C(8)—C(9)	1.382(12)	C(3A)—C(4A)—C(5A)	121.8(7)
C(8A)—C(9A)	1.394(12)	C(4)—C(5)—C(6)	119.1(6)
C(9)—C(10)	1.354(12)	C(4A)—C(5A)—C(6A)	117.5(6)
C(9A)—C(10A)	1.339(12)	C(5)—C(6)—C(1)	120.8(6)
C(11)—C(12)	1.501(11)	C(5A)—C(6A)—C(1A)	122.4(6)
C(11A)—C(12A)	1.498(9)	C(5)—C(6)—C(7)	119.6(6)
N(1)—C(21)	1.356(8)	C(5A)—C(6A)—C(7A)	118.3(6)
N(1)—C(25)	1.328(8)	C(6)—C(7)—C(8)	119.7(6)
N(2)—C(31)	1.355(9)	C(6A)—C(7A)—C(8A)	120.8(7)
N(2)—C(35)	1.313(9)	C(7)—C(8)—C(9)	120.7(8)
C(21)—C(22)	1.394(9)	C(7A)—C(8A)—C(9A)	120.0(7)
C(21)—C(31)	1.465(9)	C(8)—C(9)—C(10)	120.3(7)
C(31)—C(32)	1.383(12)	C(8A)—C(9A)—C(10A)	119.7(8)
C(22)—C(23)	1.361(12)	C(9)—C(10)—C(5)	121.5(7)
C(32)—C(33)	1.366(13)	C(9A)—C(10A)—C(5A)	121.8(7)
C(23)—C(24)	1.350(12)	C(10)—C(5)—C(6)	118.1(6)
C(33)—C(34)	1.370(14)	C(10A)—C(5A)—C(6A)	119.2(6)
C(24)—C(25)	1.373(12)	C(2)—C(11)—C(12)	118.4(6)
C(34)—C(35)	1.413(13)	C(2A)—C(11A)—C(12A)	120.3(6)
		Cd—N(1)—C(21)	118.2(4)
		Cd—N(2)—C(31)	117.5(4)
		Cd—N(2)—C(25)	123.4(4)
		Cd—N(2)—C(35)	122.0(5)
		C(21)—N(1)—C(25)	118.3(6)
		C(31)—N(2)—C(35)	120.3(6)
		N(1)—C(21)—C(22)	119.5(6)
		N(2)—C(31)—C(32)	119.5(7)
		N(1)—C(21)—C(31)	116.7(6)
		N(2)—C(31)—C(21)	117.2(6)
		C(22)—C(21)—C(31)	123.8(7)
		C(32)—C(31)—C(21)	123.3(7)
		C(21)—C(22)—C(23)	120.7(7)
		C(31)—C(32)—C(33)	120.8(8)
		C(22)—C(23)—C(24)	119.3(8)

Can. J. Chem. Downloaded from www.nrcresearchpress.com by 91.144.44.67 on 09/07/12
For personal use only.

TABLE 7 (*concluded*)

Bond	Distance	Bonds	Angle
		C(32)—C(33)—C(34)	119.6(9)
		C(23)—C(24)—C(25)	118.4(8)
		C(33)—C(34)—C(35)	117.4(9)
		C(24)—C(25)—N(1)	123.7(7)
		C(34)—C(35)—N(2)	122.3(8)
		C(24)—C(25)—N(1)	123.7(7)

Experiments using a tin anode lead to considerable deposition of metal at the cathode of the cell, and similarly with indium anodes. We observed deposition of indium metal in the cell. No compound of sensible formulation could be isolated in either case.

The structure of $Zn(C_{15}H_9O_3)_2tmen$ (1)

The molecular structure of this compound (Fig. 1) shows that it has the expected six-coordination at zinc, but an examination of the actual bond distances and angles (Table 6) reveals some interesting details. The most striking is the difference in the two Zn—O bond distances within the C_2O_2Zn ring of the flavonate ligand. The bond to O2, the phenolic oxygen of the parent compound (Zn—O2 = 1.980(1) Å), is significantly shorter than that to the ketonic oxygen (2.240(1) Å), and associated with this effect are different C—O bond distances (C2—O2 = 1.318(1) Å, C1—O1 = 1.266(1) Å), and a C—C bond (C1—C2 = 1.468(2) Å) which is longer than normal in conjugated systems. We return to the bond distances in the rings below. The Zn—O average bond length of 2.110 Å can be compared with values found in the determination of structures of similar molecules. In Zn_3(crotonate)$_6$(quinoline)$_2$ (13), both tetrahedral ZnO_3N and octahedral ZnO_6 kernels are found, with Zn_{tet}—O = 1.956 Å (av) over the range 1.938(2)–1.976(2) Å, and Zn_{oct}—O = 2.109 Å (av) over the range 2.038–2.177(2) Å. Very similar Zn_{tet}—O distances are reported for other related M_2Zn crotonate complexes. Similarly, in $Zn(C_7H_8O_5)(H_2O)_2$, the Zn—O bond distances to the oxygen atoms of the 4-oxoheptanedioato ligand are 2.179(2) and 2.213(3) Å (14), and in solvated Zn-propanedienate (15), the mean Zn—O distance in bonds involving the diketonate is 2.020(7) Å, so that the values reported in Table 6 agree well with the previous results. The Zn—N distance (2.229(1) Å) is similar to those reported for related species (e.g., refs. 13, 16). Equally, the N—Zn—N angle, and the C—C and C—N distances within the tmen ligand are reasonably close to those in other Main Group complexes (e.g., ref. 17).

The relevance of bond lengths within the ZnO_2C_2 ring to those in the C_5O ring (B) of the flavonate can now be addressed. We should first emphasise a point made in the Experimental section, that the small crystal size restricted the treatment of the experimental data. We found it necessary to fix the C—C bond lengths within rings A and C, so that the results in Table 6 are conditioned by this treatment. In a subsequent refinement in which this restriction was removed, the bond lengths and angles in ring B (and elsewhere) did not change significantly, but the ratio of data points to output results fell below an acceptable level. We believe that the values in Table 6 are sufficiently sound to support the conclusion that the Zn—O and C—O distances in the ZnO_2C_2 do indeed differ significantly. Equally, within ring B we identify two relatively long C—C bonds (C1—C2 = 1.468(2) and C1—C5 = 1.455(2) Å) and two shorter ones (C2—C3 = 1.350(2) and C4—C5 (constrained)). The C—O distances (av. 1.357(1) Å) are typical of those found in conjugated heterocyclic rings (18), and a particularly close analogy exists with the cadmium(II)-2,6-dimethyl-4*H*-pyran-4-one complex (19). The conclusion is that rings B and C involve not only the expected form **3** in which the positive charge is completely delocalized, but also a significant contribution from **4**

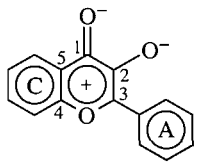

3

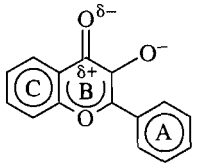

4

The effect of this charge distribution upon the chemistry of this and related molecules will be discussed elsewhere.

The structure of $Cd(C_{12}H_8O_2)_2bpy$ (2)

As in the case of the zinc compound just discussed, the structure of **2** (Fig. 2) is based on a six-coordinate cadmium atom with a CdO_4N_2 kernel. The Cd–bpy system is essentially identical to that in $Cd(S_2CSC_4H_9\text{-}n)_2bpy$ (20), and need not be discussed further.

The bond lengths in the CdO_2C_2 ring again establish the asymmetry of this system. The Cd—O bonds are 2.195(4) and 2.275(5) Å in length, and the relevant C—O bond distances are 1.281(7) and 1.232(8) Å. These and other averaged values are as shown

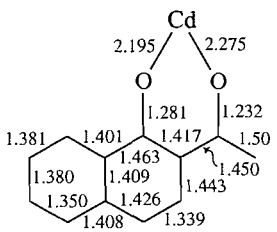

Ring D (see Fig. 2) shows insignificant deviations from the hexagonal symmetry of the aromatic C_6 ring, but in ring E there are two relatively long C—C bonds (C1—C6, av. 1.463(8) Å, and C2—C3, av. 1.443(9) Å), and one short bond (C3—C4, av. 1.339(9) Å). The interpretation of these results in terms of the contributing structures is that the delocalization which would give **6** is much less significant than one might have expected, and that **7** makes an important contribution to the overall structure and reactivity of this molecule.

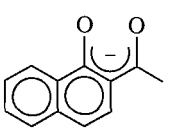

6

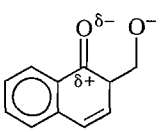

7

Can. J. Chem. Downloaded from www.nrcresearchpress.com by 91.144.44.67 on 09/07/12
For personal use only.

The average Cd—O bond distance of 2.235 Å (range 2.183(4)–2.289(5) Å) compares favourably with those in other six-coordinate cadmium species. The average value in $CdZn_2$-(crotonate)$_6$(quinoline)$_2$, which involves a CdO_6 kernel, is 2.266 Å (range 2.212(3)–2.314 Å) (13), and the bond to the neutral ligand in $Cd(NO_3)_2(C_7H_8O_2)_3$ ($C_7H_8O_2$ = 2,6-dimethyl-4*H*-pyran-4-one) is 2.283(4) Å (19). A range of 2.25–2.35 Å in CdO_6 species was suggested from an earlier review of the literature (21).

Although the effects are different from those identified in $Zn(C_{15}H_9O_3)_2$tmen, there are equally structural features in **2** which suggest interesting chemical properties. One of these is noted briefly below.

Spectroscopic information

The characterization of the products depended on elemental analysis and spectroscopic results. The most prominent feature in the ir spectra of these compounds, compared to the spectra of the parent compounds, is the absence of the O—H stretching absorption. In the derivatives of 3-hydroxyflavone and 1′-hydroxy-2′-acetonaphthone, we also observed a significant shift of the C=O stretching absorption to lower frequencies, from 1609 cm^{-1} to *ca.* 1550 cm^{-1} for 3-hydroxyflavone, and from 1625 cm^{-1} to *ca.* 1590 cm^{-1} for 1′-hydroxy-2′-acetonaphthone.

It was not possible to obtain the nmr spectrum of every compound prepared. The derivatives of 1′-hydroxy-2′-acetonaphthone form solutions which when in contact with air become paramagnetic, and the ethoxyphenolato complexes have poor solubility in most common organic solvents. The derivatives of 3-hydroxyflavone show in their ^1H nmr spectra (in d_6-DMSO) the characteristic absorptions of the ligands and the absence of the OH resonance found at 9.65 ppm in the parent compound. We have obtained ^{13}C nmr spectra for the bisflavonates of zinc and cadmium(II), and for the parent 3-hydroxyflavone, also in d_6-DMSO. The most important feature of these spectra is the downfield shift of the carbonyl resonances from 172.9 ppm in the parent compound to 178.0 (Cd derivative) and 178.2 ppm (Zn), which undoubtedly can be associated with the coordination of the oxygen to the metal centre as confirmed by the X-ray analysis.

The reaction of the Zn and Cd 1′-hydroxy-2′-acetonaphthone derivatives with air (*i.e.*, presumably O_2) to produce paramagnetic species has been briefly investigated by electron spin resonance (esr) spectroscopy. The spectrum of a sample of solid $Cd(C_{12}H_9O_2)$.bpy exposed to the air for ca. 10 min was a broad featureless singlet, very similar to that obtained when an alkaline solution of the parent $C_{12}H_9O(OH)$ was allowed to react with atmospheric oxygen. In contrast, the esr spectrum of a solution of $Cd(C_{12}H_9O_2)$.bpy after exposure to air has a number of sharp features. Further work on these systems is proceeding.

Acknowledgements

This work was supported by Operating Grants (to D.G.T.) from the Natural Sciences and Engineering Research Council of Canada. We thank Drs. Bruce R. McGarvey and Andrzej Ozarowski for their help with the esr spectroscopy. One of us (C.P.) thanks the Universidad da Paraiba for a leave of absence.

1. F. F. Said and D. G. Tuck. Inorg. Chim. Acta, **59**, 1 (1982).
2. J. L. Hencher, M. A. Khan, F. F. Said, R. Sieler, and D. G. Tuck. Inorg. Chem. **21**, 2787 (1982).
3. J. H. Green, R. Kumar, N. Seudeal, and D. G. Tuck. Inorg. Chem. **28**, 123 (1989).
4. C. Geloso, H. E. Mabrouk, and D. G. Tuck. J. Chem. Soc. Dalton Trans. 1759 (1989).
5. R. Kumar and D. G. Tuck. J. Organomet. Chem. **281**, C47 (1985).
6. C. Geloso, R. Kumar, J. R. Lopez-Grado, and D. G. Tuck. Can. J. Chem. **65**, 928 (1987).
7. T. A. Annan, R. Kumar, and D. G. Tuck. J. Chem. Soc. Chem. Commun. 446 (1988).
8. H. E. Mabrouk, D. G. Tuck, and M. A. Khan. Inorg. Chim. Acta, **129**, 75 (1987).
9. H. E. Mabrouk and D. G. Tuck. J. Chem. Soc. Dalton Trans. 2539 (1988).
10. H. E. Mabrouk and D. G. Tuck. Can. J. Chem. **67**, 746 (1989).
11. T. A. Annan, R. Chadha, B. R. McGarvey, A. Ozarowski, and D. G. Tuck. J. Chem. Soc. Dalton Trans. 439 (1989).
12. M. A. Khan, R. C. Steevensz, D. G. Tuck, J. G. Noltes, and P. W. R. Corfield. Inorg. Chem. **19**, 3409 (1980).
13. W. Clegg, W. R. Little, and B. P. Straughan. Inorg. Chem. **27**, 1916 (1988).
14. A. Karapides. Acta Crystallogr. C**39**, 1541 (1983).
15. X. Solans, M. Font-Altaba, J. L. Brianso, A. Llobet, F. Teixidor, and J. Casabo. Acta Crystallogr. C**39**, 1512 (1983).
16. T. Tatarowski, M. Kubiak, T. Glowiak, J. P. Morawiec, and H. Kozlowski. Inorg. Chim. Acta, **93**, L3 (1984).
17. M. A. Khan, C. Peppe, and D. G. Tuck. Organometallics, **5**, 525 (1986).
18. Interatomic distances, Special Publication No. 18, The Chemical Society, London. 1965. p. S21s.
19. A. Banerjee, C. J. Brown, P. C. Jain, and P. Gautman. Acta Crystallogr. C**40**, 1161 (1984).
20. S. J. Black, F. W. B. Einstein, P. C. Hayes, R. Kumar, and D. G. Tuck. Inorg. Chem. **25**, 4181 (1986).
21. D. G. Tuck. Rev. Inorg. Chem. **1**, 209 (1979).

Can. J. Chem. Downloaded from www.nrcresearchpress.com by 91.144.44.67 on 09/07/12
For personal use only.

Conductimetric titrations of symmetrical aliphatic dicarboxylic acids in solvents pyridine and pyridine–benzene mixtures

TURGUT GÜNDÜZ,[1] ESMA KILIÇ, MUSTAFA TASTEKIN, AND GÜLEREN OZKAN
Department of Chemistry, Faculty of Science, University of Ankara, Ankara, Turkey

Received July 18, 1989

TURGUT GÜNDÜZ, ESMA KILIÇ, MUSTAFA TASTEKIN, and GÜLEREN OZKAN. Can. J. Chem. **68**, 431 (1990).

Nine symmetrical aliphatic dicarboxylic acids, namely oxalic, malonic, succinic, glutaric, adipic, pimelic, suberic, azelaic, and sebacic acids, were titrated conductimetrically with tetrabutylammonium hydroxide in pyridine and pyridine–benzene mixtures ((2 + 1), (1 + 1), (1 + 2), (1 + 3), and (1 + 4)). Titration curves of the acids exhibited two distinct and stoichiometric end-points in media of dielectric constants 13.5, 10.0, 8.2, 6.3, 5.3, and 4.7, respectively. The closer investigations of the titration curves revealed that three factors mainly influence the shapes of the titration curves: dielectric constant of the medium, number of the methylene groups in the acid, and formation of hydrogen bonds between several species. As dielectric constant of the medium decreases, conductivity of the medium also decreases at any point in the titration curve. Increase in the number of methylene groups from one to five decreases conductivity of the medium linearly at the first end-points of the acids, from then the conductivity becomes practically constant in acids having five to eight methylene groups in pyridine and pyridine–benzene mixtures of 2 + 1 and 1 + 1 ratios.

Key words: conductimetric titration in pyridine, conductimetric titration in pyridine–benzene mixtures, symmetrical aliphatic dicarboxilic acids.

TURGUT GÜNDÜZ, ESMA KILIÇ, MUSTAFA TASTEKIN et GÜLEREN OZKAN. Can. J. Chem. **68**, 431 (1990).

Utilisant de l'hydroxyde de tétrabutylammonium, faisant appel à la conductimétrie et opérant dans la pyridine ainsi que dans des mélanges ((2 + 1), (1 + 1), (1 + 2), (1 + 3) et (1 + 4)) de pyridine–benzène, on a titre neuf acides dicarboxyliques aliphatiques symétriques, soit les acides oxalique, malonique, succinique, glutarique, adipique, pimélique, subérique, azélaïque et sébacique. Dans ces milieux dont les constantes diélectriques sont respectivement de 13,5, 10,0, 8,2, 6,3, 5,3 et 4,7, les courbes de titration des acides présentent chacune deux points distincts et stoechiométriques. Un examen plus approfondi des courbes de titration monter que trois facteurs principaux influencement la forme des courbes de titration, soit la constante diélectrique du milieu, le nombre de groupements méthylènes dans les molécules d'acides ainsi que la formation de liaisons hydrogènes entre diverses espèces. Une diminution de la constante diélectrique du milieu provoque une diminution de la conductivité du milieu à tous les points de la courbe de titration. Lorsque le nombre de groupements méthylène passe de un à cinq, on observe une diminution linéaire de la conductivité du milieu; pour les acides comportant de cinq à huit groupements méthylènes qui ont été examinés dans la pyridine ainsi que dans des mélanges 2 + 1 ainsi que 1 + 1 de pyridine–benzène, la conductivité devient toutefois pratiquement constante.

Mots clés : titrations conductimétriques dans la pyridine, titrations conductimétriques dans des mélanges pyridine–benzène, acides dicarboxyliques aliphatiques symétriques.

[Traduit par la revue]

Introduction

There are a number of publications on the titrations of dicarboxylic acids in nonaqueous media (1–9). However, with only one exception there is no systematic report on the titrations of these compounds in nonaqueous media; the exception being potentiometric titrations of the compounds in pyridine, 2-propanol, and their mixture with benzene (9). Here we report the results on conductimetric titrations of nine symmetrical aliphatic dicarboxylic acids: oxalic, malonic, succinic, glutaric, adipic, pimelic, suberic, azelaic, and sebacic. Solutions (0.001 M) of these compounds in solvent pyridine ($\epsilon = 13.6$) and in mixtures of pyridine and benzene ($\epsilon = 2.2$) ((2 + 1), (1 + 1), (1 + 2), (1 + 3), and (1 + 4)) were titrated conductimetrically with tetrabutylammonium hydroxide (0.036 M) dissolved in propan-2-ol. The conductimetric titration curves of the acids have exhibited two distinct end-points each corresponding to one carboxylic group in the medium of dielectric constants from 13.6 to 4.7. These are important observations in media of lower dielectric constants. Potentiometric (9) titrations did not yield the same information.

Experimental

Apparatus

An Orion Model 101 conductivity meter equipped with an Orion Cat No. 99.01.01 conductivity cell (cell constant of 1.04 cm^{-1}) was used. The conductimetric titrations were carried out in the same cell as in ref. 10.

Chemicals

Tetrabutylammonium hydroxide (TBAOH) was purchased from Merck AG as a 0.100 M solution in propan-2-ol-methanol and was diluted with pure, dry propan-2-ol to give an approximately 0.040 M solution. This solution was standardized against primary standard benzoic acid and its true concentration was found to be 0.036 M (mean value of five runs). The solution was kept in a dark-coloured ground glass stoppered flask in a refrigerator. Solutions prepared and kept under these conditions was found to be stable for at least six months.

Benzoic acid (sublimed) was purchased from Merck AG.

Pyridine and benzene were purchased from Merck AG and used after further purification (12).

Oxalic, malonic, and succinic acids were purchased from Merck AG (99% pure) and used as received.

Glutaric, pimelic, and suberic acids were purchased from Sigma and used as received. Adipic and azelaic acids were purchased from Fluka (purum, 99%) and used without further purification. Sebacic acid was purchased from Riedel de Haen (pure 99%) and used without further purification.

Results and discussion

The conductimetric titration curves of the nine symmetrical aliphatic dicarboxylic acids in solvent pyridine are shown in Fig. 1. The titration curves have been normalized (ordinate axis

[1]To whom correspondence to be addressed.

Can. J. Chem. Downloaded from www.nrcresearchpress.com by 91.144.44.67 on 09/07/12
For personal use only.

Can. J. Chem. Downloaded from www.nrcresearchpress.com by 91.144.44.67 on 09/07/12
For personal use only.

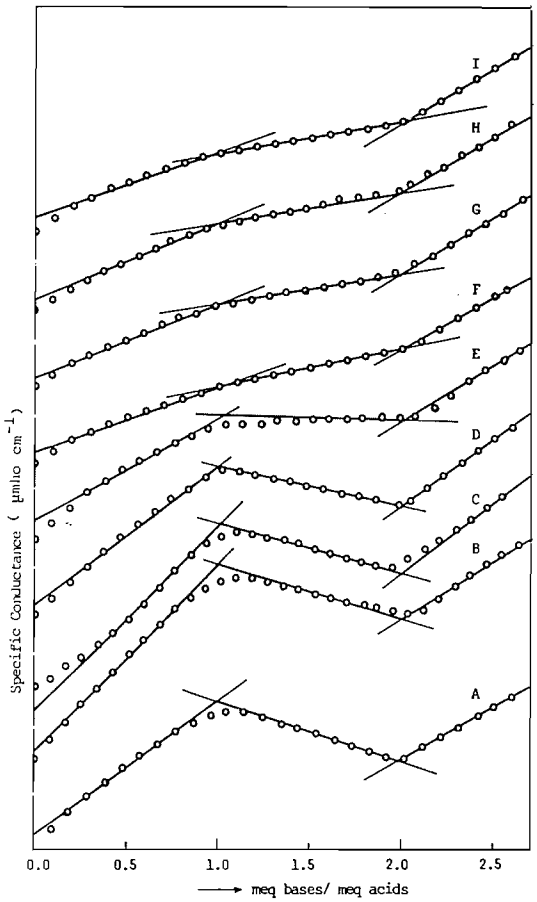

FIG. 1. Conductimetric titration of the solutions (0.001 M) of symmetrical aliphatic dicarboxylic acids with tetrabutylammonium hydroxide (0.036 M) in pyridine solvent at 25°C and under nitrogen atmosphere. Ordinate axis is not in scale. Curves are drawn for qualitative comparison only: (*A*) oxalic, (*B*) malonic, (*C*) succinic, (*D*) glutaric, (*E*) adipic, (*F*) pimelic, (*G*) suberic, (*H*) azelaic, (*I*) sebacic acids.

is not in scale). Titrations have been carried out under nitrogen at 25°C. As can be seen from the figure all acids show two stoichiometric and distinct end-points. This means that these compounds can be determined stepwise when they are dissolved in solvent pyridine in concentrations as low as 0.001 M.

Closer investigation of the titration curves revealed that several factors play important roles on the shape of the titration curves. These factors are (*i*) intra- and intermolecular hydrogen bonding, (*ii*) formation of ion-pairs, and (*iii*) number of methylene groups on the dicarboxylic acids. Only singly charged ions can be present in regions before the first end-point. Singly charged ions in nonaqueous aprotic solvents such as pyridine may form intra- (**I**) and intermolecular (**II**) hydrogen bonds as well as ion-pairs. Since titration curves up to first end-point show that the conductivity increases smoothly, there

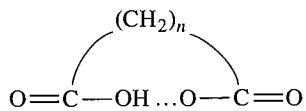

(**I**)

$$HOOC(CH_2)_nCOOH \cdots OOC(CH_2)_nCOOH$$

(**II**)

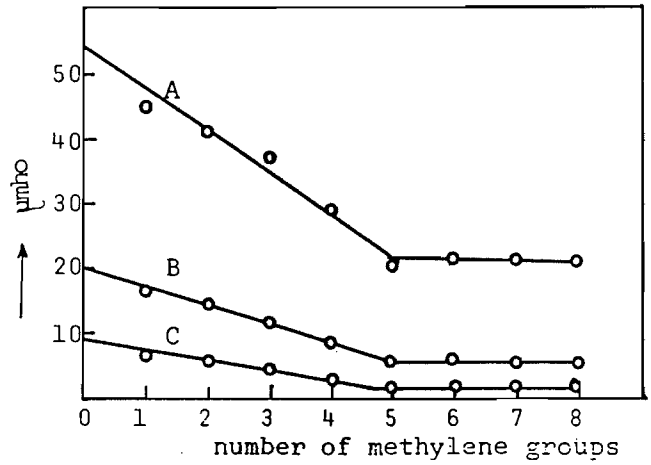

FIG. 2. The decrease in conductivities at the first end-points of symmetrical aliphatic dicarboxylic acids with increasing number of methylene group. (*A*) In pyridine solvent, (*B*) in 2 + 1 pyridine–benzene mixture, (*C*) in 1 + 1 pyridine–benzene mixture. Titrations were carried out under nitrogen at 25°C. Readings were taken in a standard solution of specific conductance (0.110 mol KCl per liter at 25°C) at 0.0129 mho cm^{-1}.

should be no intermolecular hydrogen bonds (**II**). Otherwise maxima at the half-neutralization points would appear before the first end-points (13–16).

Figure 1 further shows that the first end-points of acids having up to four methylene groups are very sharp; while those of acids having five to eight methylene groups are less sharp. A possible explanation is that for acids with up to four methylene groups, the mobility of the doubly charged ion is smaller than the mobility of the singly charged anion. Doubly charged anion can form two hydrogen bonds with propan-2-ol (propan-2-ol enters the media as the solvent of the titrant), $PrOH \cdots OOC(CH_2)_nCOO \cdots HOPr$, whereas the singly charged anion can form only one hydrogen bond, $PrOH \cdots OOC(CH_2)_nCOOH$. Since the former is bulkier than the latter, doubly charged entity is less mobile than the singly charged entity. Furthermore, doubly charged anions can form ion-pairs more readily than singly charged anions, as their electrical charge is higher. Anion of higher electrical charge attracts cations more readily to form ion-pairs. These factors are not as effective for dicarboxylic acids with five to eight methylene groups. However, the mobilities of doubly charged anions of these acids are very slightly more mobile than their singly charged anions. This can be explained by the increased number of methylene groups in these acids. As the number of methylene groups increases, the inductive effects between two carboxylic groups decreases. Consequently each carboxylic group of the dicarboxylic acid may react independently, as if they were monocarboxylic acids.

The second end-points of all acids are either sharp or very sharp. The slopes of the titration curves for the longer chainlength acids before the first end-point are practically identical, measuring 0.35, 0.38, 0.37, 0.37 for pimelic, suberic, azelaic, and sebacic acids respectively. This indicates that the inductive effects between the two carboxylic groups are negligible in acids having five or more methylene groups. After second end-points, the slopes of the titration curves are 0.57, 0.59, 0.58, and 0.58, respectively. Similar regularities are not observed for oxalic, malonic, succinic, glutaric, and adipic acids before the first end-point. However, past the second end-point the slopes of the titration curve of all acids are

Can. J. Chem. Downloaded from www.nrcresearchpress.com by 91.144.44.67 on 09/07/12
For personal use only.

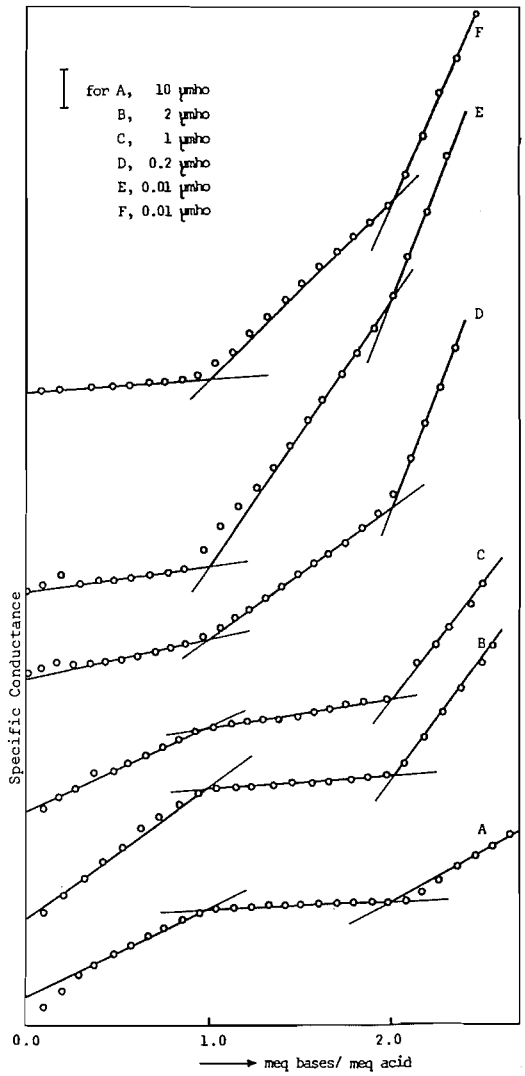

FIG. 3. The conductimetric titrations of adipic acid in pyridine (*A*) and pyridine–benzene mixtures of 2 + 1 (*B*) 1 + 1 (*C*) 1 + 2 (*D*) 1 + 3 (*E*), 1 + 4 (*F*). Dielectric constants of the media are 13.6, 10.0, 8.2, 6.3, 5.3, and 4.7 respectively. Titrations are carried out at 25°C under nitrogen.

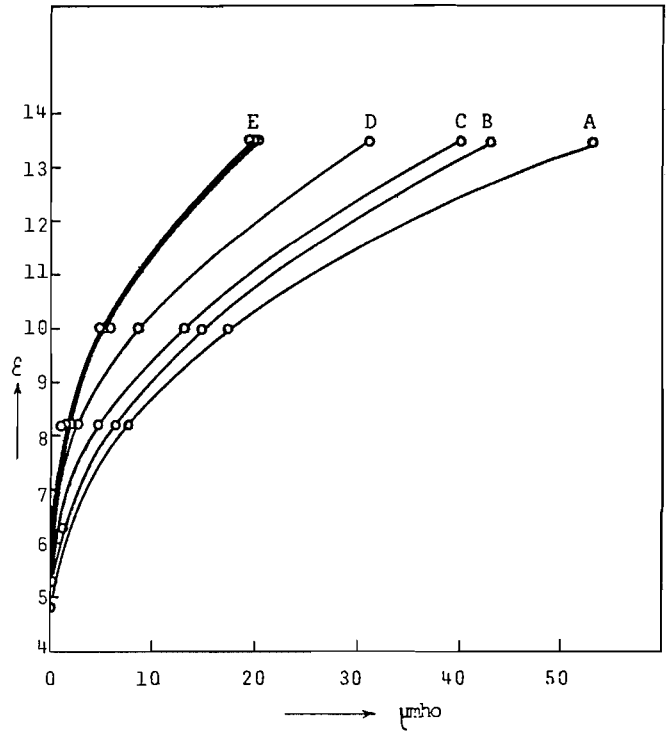

FIG. 4. Relationships between dielectric constants of solvents and conductivities of the solutions at first end-points (0.001 M) of (*A*) malonic, (*B*) succinic, (*C*) glutaric, (*D*) adipic, (*E*) pimelic, (*E*) suberic, (*E*) suberic, (*E*) azelaic, and (*E*) sebacic acids. Titrations were carried out in pyridine and pyridine–benzene mixtures of 2 + 1, 1 + 1, 1 + 2, 1 + 3, and 1 + 4 ratios at 25°C. Standard solution of tetrabutylammonium hydroxide (0.036 M) was used as titrant; titrations were carried out under nitrogen.

approximately the same. Here the composition of solutions are nearly the same; there are doubly charged anions of short or long chainlength irrespective of the presence of hydrogen bonding.

Except for oxalic acid the first end-point conductivities decrease monotonically with increasing number of methylene groups until the number of methylene group is five (pimelic acid) and then the conductivities become practically constant, Fig. 2*A*. This means that in pimelic, suberic, azelaic, and sebacic acids the carboxylic groups do not influence each other inductively; an observation in accordance with literature data (9, 11) obtained by potentiometric means.

Titrations of the acids in pyridine–benzene mixtures of ratios 2 + 1, 1 + 1, 1 + 2, 1 + 3, and 1 + 4 have also been carried out and two distinct, stoichiometric end-points for each acid have been obtained. Dielectric constants of these mixed solvents have been calculated by the equation (17)

$$\epsilon_{mixt} = x_1 \epsilon_1 + x_2 \epsilon_2$$

and found to be 10.0, 8.2, 6.3, 5.3, and 4.7, respectively. Titration curves for adipic acid in different media are given in Fig. 3. The curves are normalized to facilitate comparison. The figure clearly shows that carboxylic acids can be titrated in media of dielectric constants as low as 4.7 in mixed pyridine and benzene. In 2 + 1 and 1 + 1 pyridine–benzene mixtures, conductivities at first end-points decrease linearly with increasing number of methylene groups, up to five (pimelic acid) and then become a constant when for methylene number ranging from five to eight, Fig. 2*B* and *C*.

Another feature is the smooth relationship between the conductivities at first end-points and dielectric constants of the medium for each acid, Fig. 4. Figure 4 shows that the curves for pimelic, suberic, azelaic, and sebacic acids are nearly superimposed. The same relationship is observed between the first end-point conductivities of the acids and their number of methylene groups. This means that the methylene groups and dielectric constants both exert the same sort of effects on the symmetrical aliphatic dicarboxylic acids. The conductimetric titration curves of the dicarboxylic acids in solvent pyridine exhibit much more detailed and instructive curves than potentiometric titration curves. In the potentiometric titration of adipic acid, only one end-point corresponding to two equivalent protons is observed (9) in the same solvent. The higher homologues of adipic acid exhibit the same properties as adipic acid.

Conclusions

The following conclusions can be drawn from the conductimetric titration curves obtained for solution of nine symmetrical aliphatic dicarboxylic acids with tetrabutylammonium hy-

droxide in pyridine ($\epsilon = 13.6$) and pyridine–benzene mixtures, dielectric constant of benzene being 2.2

1. The titration curves obtained for the solutions of the symmetrical aliphatic dicarboxylic acids in pyridine and in pyridine–benzene mixtures show two distinct and stoichiometric end-points in media of dielectric constants between 13.6 and 4.7.

2. The conductivities at the first end-points of the symmetrical aliphatic dicarboxylic acids decrease almost linearly with increasing number of methylene group up to five and then becomes practically constant for pimelic, suberic, azelaic, and sebacic acids. A very similar trend is observed for media of decreasing dielectric constants. Pimelic, suberic, azelaic, and sebacic acids exhibit practically the same conductivity at the first end-points in the same media.

3. Doubly-charged anions of pimelic, suberic, azelaic, and sebacic acids are more mobile than their singly charged anions, because of decreasing inductive effects.

4. As for the shapes of the titration curves, hydrogen bonding between anions and propan-2-ol and the formation of ion-pairs play an important role.

5. The conductimetric titration curves of the dicarboxylic acids provide more details than their potentiometric titration curves. Thus in titrations conductimetric method should be preferred.

1. N. V. Meurs and E. A. M. F. Dahmen. Anal. Chim. Acta, **19**, 64 (1958); **21**, 443 (1959).
2. J. S. Fritz and L. W. Marple. Anal Chem. **34**, 921 (1962).
3. R. H. Cundiff and P. C. Markunas. Anal. Chem. **28**, 792 (1956).
4. E. S. Lane. Analyst, **80**, 675 (1955).
5. V. Z. Deal and G. E. A. Wild. Anal. Chem. **27**, 47 (1955).
6. I. M. Kolthoff and M. K. Chantooni. Jr. J. Am. Chem. Soc. **97**, 1376 (1975).
7. M. K. Chantooni Jr. and I. M. Kolthoff. J. Phys. Chem. **79**, 1176 (1975).
8. I. M. Kolthoff and M. K. Chantooni. Jr. Anal. Chem. **50**, 1440 (1978).
9. T. Gündüz, E. Kiliç, and G. Ozkan. Analyst, **113**, 1017 (1988).
10. T. Gündüz, N. Gündüz, E. Kiliç, F. Köseoglu, and S. G. Oztas. Analyst, **113**, 715 (1988).
11. T. Gündüz, E. Kiliç, O. Atakol, and A. Kenar. Analyst **112**, 1735 (1987).
12. D. D. Perrin, W. L. F. Amarego, and D. R. Perrin. Purifications of laboratory chemicals. Pergamon Press, London. 1966, pp. 79, 248.
13. M. M. Davis. Acid–base behavior in aprotic solvents. Natl. Bur. Stand. (US) Monogr., 105, Washington, D.C. 1968.
14. I. M. Kolthoff and M. K. Chantooni, Jr. J. Am Chem. Soc. **85**, 426 (1963); **85**, 2195 (1963).
15. I. M. Kolthoff. Anal. Chem. **46**, 1992 (1974).
16. F. J. R. Bryant and A. W. H. Wardrup. J. Chem. Soc. **169**, 895 (1957).
17. N. Van Meurs and E. A. M. F. Dahman. Anal. Chim. Acta **21**, 10, (1959).

Can. J. Chem. Downloaded from www.nrcresearchpress.com by 91.144.44.67 on 09/07/12
For personal use only.

Solubility of nonpolar gases in 2,6-dimethylcyclohexanone

MARIA ASUNCION GALLARDO, MARIA DEL CARMEN LOPEZ, JOSE SANTIAGO URIETA, AND CELSO GUTIERREZ LOSA
Química Física, Facultad de Ciencias, Universidad de Zaragoza, 50009-Zaragoza, Spain

Received April 19, 1989

MARIA ASUNCION GALLARDO, MARIA DEL CARMEN LOPEZ, JOSE SANTIAGO URIETA, and CELSO GUTIERREZ LOSA. Can. J. Chem. **68**, 435 (1990).

Solubility measurements of He, Ne, Ar, Kr, Xe, H_2, D_2, N_2, CH_4, C_2H_4, C_2H_6, CF_4, SF_6, and CO_2 in 2,6-dimethylcyclohexanone at temperatures 273.15 to 303.15 K and at a gas partial pressure of 101.33 kPa are reported. Standard changes in Gibbs energy, enthalpy, and entropy for the dissolution process at 298.15 K are also presented. Results for both solubility and thermodynamic functions are compared with those for cyclohexanone and 2-methylcyclohexanone. The scaled particle theory is used to obtain the effective Lennard–Jones (6,12) pair potential parameters for 2,6-dimethylcyclohexanone and, from these, the values it predicts for the solubility of the studied gases in the solvent are obtained.

Key words: gas solubility, Henry coefficient, 2,6-dimethylcyclohexanone, thermodynamic functions of solution, non-polar gases.

MARIA ASUNCION GALLARDO, MARIA DEL CARMEN LOPEZ, JOSE SANTIAGO URIETA et CELSO GUTIERREZ LOSA. Can. J. Chem. **68**, 435 (1990).

Opérant à des températures allant de 273,15 à 303,15 K et à une pression partielle de gaz de 101,33 kPa, on a mesuré les solubilités du He, du Ne, du Ar, du Kr, du Xe, du H_2, du D_2, du N_2, du CH_4, du C_2H_4, du C_2H_6, du CF_4, du SF_6 et du CO_2 dans la 2,6-diméthylcyclohexanone. On en a tiré les changements standard de l'énergie de Gibbs, de l'enthalpie et de l'entropie du processus de dissolution à 298,15 K. On a comparé les résultats obtenus tant pour les solubilités que pour les fonctions thermodynamiques avec celles rapportées antérieurement pour la cyclohexanone et la 2-méthylcyclohexanone. On a fait appel à la théorie de la particule scalaire pour déterminer les paramètres effectifs de Lennard–Jones (6,12) pour le potentiel de paire de la 2,6-diméthylcyclohexanone et, à partir de ceux-ci, les valeurs qu'elles permettent de prédire pour la solubilité des gaz étudiés dans ces solvants.

Mots clés : solubilité des gaz, coefficient de Henry, 2,6-diméthylcyclohexanone, fonctions thermodynamiques de solution, gaz non-polaires.

[Traduit par la revue]

Introduction

This paper is a continuation of our work on the solubility of non-polar gases (1–8) to study the influence exerted by the presence of different features in the solvent molecule. In this particular case we were interested in seeing how the solubility changes with the introduction of methyl groups as substituents in the solvent cyclohexanone. Previously, the solubility of fourteen non-polar gases in cyclohexanone and 2-methylcyclohexanone was measured and published in this journal (4, 7). Here we present the solubility of the same fourteen gases in 2,6-dimethylcyclohexanone. This solvent was chosen because it not only has one more methyl substituent but its relative position in the cycle is the same as that of the methyl group in 2-methylcyclohexanone. Therefore the molecule is "symmetrical" and both methyl groups are equivalent (the product used was a mixture of *cis–trans* stereoisomers). The values of the thermodynamic functions for the solution process are also reported and compared with those for the other cyclohexanones. Finally, using the scaled particle theory for solubility of gases (9, 10) the effective Lennard–Jones (6,12) pair potential parameters for the solvent will be calculated and our experimental results will be compared with the values predicted by that theory.

Experimental

In refs. 2, 11 details of the apparatus and the procedure have been given. The experimental technique is based on the determination of the volume of gas which dissolves in a known mass of solvent at a constant temperature and pressure. The total pressure is chosen to be such that the partial pressure of gas is about 101.33 kPa. The solute mole fraction in the liquid phase, x_2, was derived by assuming the gas phase to be ideal. The temperature of the air thermostatic bath holding the apparatus was controlled to within ±0.2 K. Temperature control in the solution vessel was to within ±0.05 K. Precision in the mole fraction x_2 is estimated to be ±0.7% with the exception of gases with low solubility (He and Ne) for which it is approximately ±2.0%. The non-ideality of the gas phase was not considered due to the lack of the necessary data to get the gas virial coefficients for the solvent and the mixture. However, empirical approaches (12, 13) were used to estimate the critical data for the solvent and the necessary parameters, and from these the mentioned virial coefficients in the case of the most soluble gases, to give an idea of the error introduced by considering ideal gas phase behaviour. In the least favourable instances, Xe, C_2H_4, C_2H_6, and SF_6, such estimations led to mole fractions about 1%, 1%, 1.5%, and 2.3%, respectively, higher than when ideality is assumed.

For CO_2 dry gas was used (the procedure was slightly different, see ref. 2) and the number of moles in the solution vessel at constant pressure and temperature was determined by taking into account the non-ideality of CO_2 by means of its second virial coefficient. The solute mole fraction in the liquid phase is obtained by subtracting the number of moles of CO_2 in the gas phase above the liquid from the number of moles of gas in the solution vessel. The volume of this gas phase is so small that any corrections to account for its non-ideality are certainly smaller than the experimental error.

All the gases were from Sociedad Española del Oxígeno, except Ne and CF_4, which were from Baker. Their mole-percentage purities were: He 99.995, Ne 99.9, Ar 99.9990, Kr 99.95, Xe 99.995, H_2 99.99, D_2 99.4, N_2 99.998, CH_4 99.95, C_2H_4 99.90, C_2H_6 99.0, CF_4 99, SF_6 99.5, and CO_2 99.998.

The solvent was 2,6-dimethylcyclohexanone (mixture of *cis–trans* stereoisomers) and was a Fluka product. Its purity was checked by GLC to be 98.2%. The main impurities were identified as cyclohexanone, 2-methylcyclohexanone, and some other methylated and dimethylated cyclohexanones, all of which are products that have similar gas solubilities to that of 2,6-dimethylcyclohexanone (4, 7). The refractive index was also measured (n_D(293.15 K) = 1.44686) but no literature values were found for it. The vapour pressures and the densities of 2,6-dimethylcyclohexanone were determined in the working temperature range and fitted by least squares to equations

Printed in Canada / Imprimé au Canada

Can. J. Chem. Downloaded from www.nrcresearchpress.com by 91.144.44.67 on 09/07/12
For personal use only.

TABLE 1. Experimental solubility of gases ($\times 2 \times 10^4$) in 2,6-dimethyl-cyclohexanone at 101.33 kPa partial pressure of gas between 273.15 and 303.15 K, values of the coefficients A_i in eq. [3] and standard deviations as defined by eq. [4]

	T (K)							
Gas	273.15	283.15	293.15	298.15	303.15	A_0	A_1	σ
He	0.834	0.951	1.069	1.148	1.213	5.6038	1035.39	0.0054
Ne	1.241	1.384	1.53	1.59	1.67	5.9916	819.81	0.0037
Ar	12.11	12.02	11.99	11.93	11.91	6.8807	−44.80	0.0013
Kr	43.0	39.8	37.1	36.1	35.0	7.5152	−563.46	0.0028
Xe	214	185	162	152	142	7.9498	−1121.25	0.0010
H_2	2.88	3.08	3.27	3.40	3.52	6.1745	540.70	0.0054
D_2	2.99	3.19	3.40	3.52	3.64	6.1170	546.91	0.0041
N_2	5.71	5.87	6.01	6.07	6.14	6.7455	197.14	0.0004
CH_4	29.6	28.0	26.7	26.1	25.6	7.2927	−401.28	0.0021
C_2H_4	220	186	159	148.4	137.3	8.5532	−1293.69	0.0027
C_2H_6	255	215	183	170	158	8.5100	−1322.04	0.0014
CF_4	7.50	7.47	7.44	7.44	7.43	7.2901	−25.74	0.0006
SF_6	44.0	39.8	36.4	35.0	33.8	8.1076	−731.60	0.0033
CO_2	267	218	181	168	154	9.1607	−1511.35	0.0053

[1] $\ln (p/\text{kPA}) = -3.87053 \times 10^3 (T/K)^{-1} + 12.861$

and

[2] $\rho/\text{g cm}^{-3} = -8.313 \times 10^{-4} (t/°\text{C}) + 0.9290$

respectively.

Results and discussion

Experimental equilibrium mole fraction of gas, x_2, in 2,6-dimethylcyclohexanone at temperatures between 273.15 and 303.15 K and at a gas partial pressure of 101.33 kPa are displayed in Table 1. These x_2 (101.33 kPa, T) data were fitted by a least-squares method to an equation of the form

[3] $-\ln x_2 = A_0 + A_1 \times T^{-1}$

Table 1 contains the coefficients A_i for the different gases. The standard deviation, σ, defined as

[4] $\sigma^2 = \Sigma [\ln x_{2,i} - (A_0 + A_1 \times T_i^{-1})]^2/(n-2)$

is also included in Table 1.

The standard changes in partial molar Gibbs energy, $\Delta G^0_{m,2}$, partial molar enthalpy, $\Delta H^0_{m,2}$, partial molar entropy, $\Delta S^0_{m,2}$, and Hildebrand entropy, ΔS_H, for the dissolution process were calculated using equations (14–16):

[5] $\Delta G^0_{m,2} = -RT \ln x_2(\text{sat})$

[6] $\Delta H^0_{m,2} = RT\left[\frac{\partial \ln x_2(\text{sat})}{\partial \ln T}\right]$

[7] $\Delta S^0_{m,2} = R\left[\frac{\partial \ln x_2(\text{sat})}{\partial \ln T} + \ln x_2\right]$

[8] $\Delta S_H = R\left[\frac{\partial \ln x_2(\text{sat})}{\partial \ln T}\right]_{\text{sat},P}$

where R is the gas constant, T is the absolute temperature, and x_2(sat) is the mole fraction of the gas in the liquid phase in equilibrium with the gas at a partial pressure of 101.33 kPa. In the derivations of eqs. [5]–[8] both ideal behaviour of the gas and validity of the laws for dilute solutions are assumed (14–16).

The values obtained for the thermodynamic functions of the solution of the studied gases in 2,6-dimethylcyclohexanone at 298.15 K are given in Table 2.

When comparing the solubility of the studied gases in 2,6-dimethylcyclohexanone, 2-methylcyclohexanone (7), and cyclohexanone (4), it is seen that the solubility of any of the studied gases is always higher in 2,6-dimethylcyclohexanone than in 2-methylcyclohexanone and higher in this solvent than in cyclohexanone in the temperature range studied (as an example, the solubility of He, Ar, Kr, and Xe in the three cycloketones as a function of $1/T$ is plotted in Fig. 1). The only exception is CO_2. For this gas the solubility in 2,6-dimethylcyclohexanone only becomes higher than in 2-methylcyclohexanone above a certain temperature in between 273.15 and 298.15 K.

Consequently with the solubility sequence, the more methyl groups the cyclohexanone has, the lower the partial molar Gibbs energy for the dissolution process becomes.

As far as the sequence of increasing solubility of gases in 2,6-dimethylcyclohexanone is concerned, it is found to be basically the same as for cyclohexanone and 2-methylcyclohexanone though there are some interchanges in the positions of some of the most soluble gases depending on the temperature, examples of which are SF_6 and Kr, Xe and C_2H_4, and C_2H_6 and CO_2.

Table 2 shows the variation of the standard partial molar enthalpy of solution, $\Delta H^0_{m,2}$, (this thermodynamic function is directly related via eq. [6] to the variation of solubility with temperature) with the solubility of gases. As in the case of other solvents (15), there is a tendency of the temperature coefficient of solubility to decrease with increasing solubility of the gas, e.g. the more soluble the gas, the smaller its standard partial molar enthalpy of solution. He, Ne, H_2, and D_2 show increasing solubilities with temperature and positive values for $\Delta H^0_{m,2}$, while the most soluble gases (Xe, C_2H_4, C_2H_6, and CO_2) have very negative values for $\Delta H^0_{m,2}$, and solubility decreases with temperature.

That the standard partial molar enthalpy $\Delta H^0_{m,2}$ decreases with the increase of solubility of gas holds for the three different solvents considered here (see Fig. 1). Moreover, according to

Can. J. Chem. Downloaded from www.nrcresearchpress.com by 91.144.44.67 on 09/07/12
For personal use only.

TABLE 2. Experimental and calculated (SPT) values for partial molar Gibbs energy, $\Delta G^0_{m,2}$, partial molar enthalpy, $\Delta H^0_{m,2}$, and partial molar entropy, $\Delta S^0_{m,2}$, and experimental partial molar Hildebrand entropy for the solution of gases in 2,6-dimethylcyclohexanone at 298.15 K and 101.33 kPa partial pressure of gas*

	$x_2 \times 10^4$		$\Delta G^0_{m,2}$ (kJ mol^{-1})		$\Delta H^0_{m,2}$ (kJ mol^{-1})			$\Delta S^0_{m,2}$ (kJ K^{-1} mol^{-1})			
						Calcd			Calcd		
Gas	Fitted	Calcd	Exp	Calcd	Exp	$l_1 = 1.48 \times 10^{-4}$	$l_1 = 0$	Exp	$l_1 = 1.48 \times 10^{-4}$	$l_1 = 0$	ΔS_H (kJ K^{-1} mol^{-1})
He	1.143	1.63	22.50	21.62	8.61	8.62	4.45	−0.047	−0.044	−0.058	0.029
Ne	1.60	4.84	21.67	18.92	6.82	6.25	1.68	−0.050	−0.043	−0.058	0.023
Ar	11.94	22.6	16.68	15.10	−0.37	3.85	−2.41	−0.057	−0.038	−0.059	−0.001
Kr	36.0	46.1	13.94	13.34	−4.68	2.77	−4.28	−0.062	−0.035	−0.059	−0.016
Xe	152	103	10.38	11.35	−9.32	1.62	−6.37	−0.066	−0.033	−0.060	−0.031
H_2	3.40	3.47	19.80	19.74	4.50	7.23	2.47	−0.051	−0.042	−0.058	0.015
D_2	3.52	3.72	19.71	19.57	4.55	7.06	2.29	−0.051	−0.042	−0.058	0.015
N_2	6.07	8.04	18.36	17.67	1.64	7.18	0.04	−0.056	−0.035	−0.059	0.005
CH_4	26.1	35.5	14.74	13.68	−3.34	3.50	−3.65	−0.061	−0.035	−0.059	−0.011
C_2H_4	147.9	121	10.45	10.93	−10.76	1.53	−6.84	−0.071	−0.032	−0.060	−0.036
C_2H_6	170	123	10.10	10.90	−10.99	2.48	−6.98	−0.071	−0.028	−0.060	−0.037
CF_4	7.44	7.70	17.86	17.77	−0.21	10.30	−0.21	−0.061	−0.025	−0.060	−0.001
SF_6	35.1	26.1	14.02	14.75	−6.08	10.55	−3.52	−0.067	−0.014	−0.061	−0.020
CO_2	167	64.4	10.14	12.51	−12.57	2.71	−5.21	−0.076	−0.033	−0.059	−0.042

*Theoretical values of $\Delta H^0_{m,2}$ and $\Delta S^0_{m,2}$ were calculated using both $l_1 = 1.48 \times 10^{-4}$ K^{-1} and $l_1 = 0$). Column 2 shows the fitted values of x_2 at 298.15 K from our experimental fitting coefficients in Table 1. Column 3 contains the values of x_2 at 298.15 K calculated via SPT

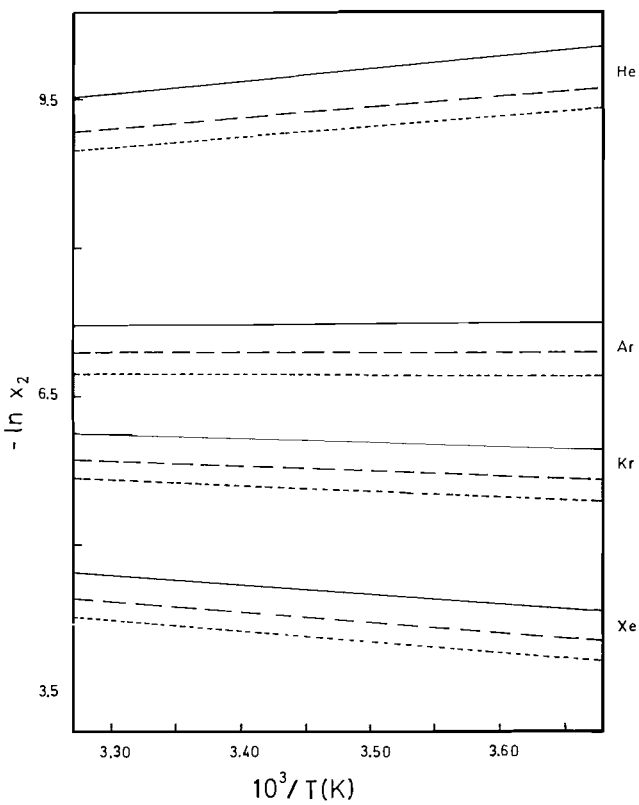

FIG. 1. The lines in the plot represent the fitting of experimental gas solubility data to eq. [3] for different solvents: — cyclohexanone (4), – – – 2-methyl-cyclohexanone (7), - - - 2,6-dimethylcyclohexanone.

the solubility sequence, for any given gas, $\Delta H^0_{m,2}$ at 298.15 K is always lower in 2,6-dimethylcyclohexanone than in 2-methylcyclohexanone and is lower in this solvent than in cyclohexanone; the only exception is CO_2.

The standard partial molar entropy $\Delta S^0_{m,2}$ for dissolution in 2,6-dimethylcyclohexanone of the gases studied follows the same pattern and has values similar to other organic solvents[1] but no tendencies are detected when comparing the values for a given gas in the three cyclohexanones (4, 7).

The scaled particle theory (SPT) allows an evaluation of effective Lennard–Jones pair potential parameters for the solvent from a knowledge of both gas solubility data and the corresponding parameters for gases (9, 10), and it has also been used to predict Henry coefficients of gases in different solvents (1–4, 6, 7, 9, 10, 17, 19, 20, and references therein) and the thermodynamic magnitudes associated with the solution process. The theory stipulates that dissolution takes place in two steps: (*a*) creation in the solvent of a cavity of the right size to accommodate the solute molecule, and (*b*) insertion of the solute molecule into the cavity, then the solute interacts with the solvent. The partial molar Gibbs energy for the cavity formation is calculated using the SPT expressions derived by Reiss *et al.* for hard spheres (10, 21). The calculation of the partial molar Gibbs energy coming from the interaction involves more approximations (10) and it is usually made on the basis of an effective Lennard–Jones (6,12) potential corrected with a term for dipole – induced dipole interactions. Objections can be made to the use of the induction contribution term obtained by this model, since pair additivity is assumed in deriving it. An option to avoid this would be the use of just a Lennard–Jones (6,12) pair potential, thus the effective parameters would include all the induction effects in them. In this work the Lennard–Jones pair potential parameters presented are those obtained when the first option is adopted to allow comparisons with other solvents, the parameters of which were obtained in the same way.

The properties of gases required for the calculations were

[1]See, for example, the review on thermodynamic functions for dissolution of gases in organic solvents by Wilhelm and Battino, ref. 14. Due to the hydrophobic effect for water the experimental values of $\Delta S^0_{m,2}$ are much more negative than for any other solvent (16–18).

Can. J. Chem. Downloaded from www.nrcresearchpress.com by 91.144.44.67 on 09/07/12
For personal use only.

TABLE 3. Effective Lennard–Jones (6,12) pair potential parameters for the solvents: effective hard sphere diameter at 298.15 K σ_1, and energy parameter ϵ_1/k

Compound	$\sigma_1 \times 10^{10}$ (m)	(ϵ_1/k) (K)
Cyclohexanone*	5.651	584
2-Methylcyclohexanone†	5.988	627
2,6-Dimethylcyclohexanone	6.292	665

*From ref. 3, 4.
†From ref. 7.

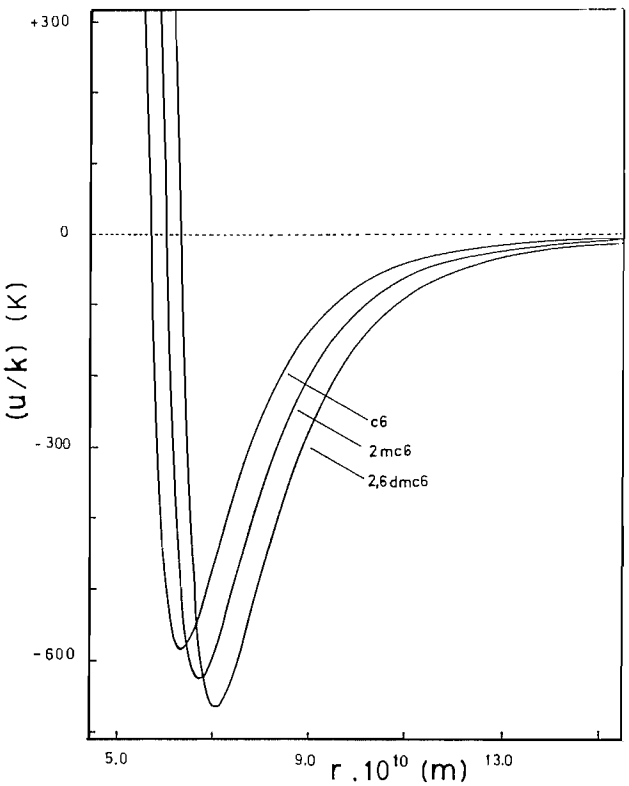

FIG. 2. Lennard–Jones (6,12) pair potential as a function of the interparticle distance for cyclohexanone (c6), 2-methylcyclohexanone (2mc6), and 2,6-dimethylcyclohexanone (2,6dmc6) with the parameters σ_1 and ϵ_1/k obtained from gas solubility data (refs. 4 and 7, and present work).

taken from the literature (22); the dipole moment of 2,6-dimethylcyclohexanone was estimated to be 3.13 D from dielectric permittivity measurements. The values found for the effective Lennard–Jones (6,12) pair potential parameters for 2,6-dimethylcyclohexanone are shown in Table 3. These values can be considered an average of the *cis* and *trans* stereoisomers since the product used in the experimental measurements was a mixture of the two. There is a clear increase in the distance parameter in the order cyclohexanone, 2-methylcyclohexanone, 2,6-dimethylcyclohexanone, as would be expected (given the increasing size of the molecule) since the distance parameter is, in a way, a measure of the diameter of the molecule.

The energy parameter also increases in the same sequence, meaning a deeper potential well as the cyclohexanone becomes more methylated. In Fig. 2, the Lennard–Jones (6,12) potential is represented for the three cyclohexanones using the parameters estimated from our gas solubility data.

The value obtained for the linear coefficient of the effective hard sphere diameter at 298.15 K of 2,6-dimethylcyclohexanone, $l_1 = (1/a_1)(\partial a_1/\partial T)_P$, was $l_1 = -1.58 \times 10^{-4}\ K^{-1}$ from the solubility data of rare gases at different temperatures (23), and $l_1 = -1.48 \times 10^{-4}\ K^{-1}$ from enthalpy solution data (24). The agreement between both methods is ordinary (4, 7, 24).

Once the parameters for the solvent were known, calculations were made to obtain the theoretical values of the thermodynamic functions in the solution process. The results obtained are shown in Table 2. The agreement between the calculated and experimental values for $\Delta G^0_{m,2}$ and x_2 follows the same pattern as for other solvents (1–4, 6, 7, 17, 20, 25) and can be considered satisfactory if one takes into account the simplifications in the theory. The same result as in literature is found for enthalpies and entropies of solution (4, 7, 24): the introduction of temperature dependence in the effective hard-sphere diameter of the solute ($l_1 \neq 0$) leads to $\Delta H^0_{m,2}$ and $\Delta S^0_{m,2}$ values that agree with the experimental values for gases closest to being hard-spheres (polarizability approaching zero): He and Ne. The use of $l_1 = 0$ leads to values for $\Delta H^0_{m,2}$ and $\Delta S^0_{m,2}$ more in agreement with the experimental ones for gases such as Ar, Kr, CH_4, or CF_4.

Acknowledgement

This project was financially supported by the Comisión Asesora de Investigación Científica y Técnica (Project number 1788/82), to which the authors are very grateful.

1. F. GIBANEL, J. S. URIETA, and C. GUTIERREZ LOSA. J. Chim. Phys. **78**, 171 (1981).
2. M. A. GALLARDO, J. S. URIETA, and C. GUTIERREZ LOSA. J. Chim. Phys. **80**, 621 (1983).
3. J. M. MELENDO, M. A. GALLARDO, J. S. URIETA, and C. GUTIERREZ LOSA. Acta Cient. Compostelana, **XXII**, 269 (1985).
4. M. A. GALLARDO, J. M. MELENDO, J. S. URIETA, and C. GUTIERREZ LOSA. Can. J. Chem. **65**, 2198 (1987).
5. M. C. LOPEZ, M. A. GALLARDO, J. S. URIETA, and C. GUTIERREZ LOSA. J. Chem. Eng. Data, **32**, 472 (1987).
6. F. GIBANEL, M. C. LOPEZ, M. A. GALLARDO, J. S. URIETA, and C. GUTIERREZ LOSA. Fluid Phase Equil. **42**, 261 (1988).
7. M. A. GALLARDO, M. C. LOPEZ, J. S. URIETA, and C. GUTIERREZ LOSA. Can. J. Chem. **67**, 809 (1989).
8. M. C. LOPEZ, M. A. GALLARDO, J. S. URIETA, and C. GUTIERREZ LOSA. J. Chem. Eng. Data, **34**, 198 (1989).
9. R. A. PIEROTTI. J. Phys. Chem. **69**, 281 (1965).
10. R. A. PIEROTTI. Chem. Rev. **76**, 717 (1976).
11. J. CARNICER, F. GIBANEL, J. S. URIETA, and C. GUTIERREZ LOSA. Rev. Acad. Cienc. (Zaragoza), **34**, 115 (1979).
12. R. C. REID, J. M. PRAUSNITZ, and B. E. POLING. The properties of gases and liquids. 4th ed. McGraw-Hill Book Company, New York, NY. 1987.
13. E. WILHELM. Pure Appl. Chem. **57**, 303 (1985).
14. E. WILHELM and R. BATTINO. Chem. Rev. **73**, 1 (1973).
15. H. L. CLEVER and R. BATTINO. *In* Weissberger: Techniques of chemistry. Vol. 8. Part 1. M. R. J. Dack, Wiley-Interscience, New York, NY. 1985.
16. E. WILHELM, R. BATTINO, and R. J. WILCOCK. Chem. Rev. **77**, 219 (1977).
17. T. R. RETTICH, Y. P. HANDA, R. BATTINO, and E. WILHELM. J. Phys. Chem. **85**, 3230 (1981).
18. R. CROVETTO, R. FERNANDEZ-PRINI, and M. L. JAPAS. J. Chem. Phys. **76**, 1077 (1982).

Can. J. Chem. Downloaded from www.nrcresearchpress.com by 91.144.44.67 on 09/07/12
For personal use only.

19. T. R. RETTICH, R. BATTINO, and E. WILHELM. J. Sol. Chem. **13**, 335 (1984).
20. T. TOMINAGA, R. BATTINO, H. K. GOROWARA, R. D. DIXON, and E. WILHELM. J. Chem. Eng. Data, **31**, 175 (1986).
21. H. REISS, H. L. FRISCH, and J. L. LEBOWITZ. J. Chem. Phys. **31**, 369 (1959).
22. E. WILHELM and R. BATTINO. J. Chem. Phys. **55**, 4012 (1971).
23. R. A. PIEROTTI. J. Phys. Chem. **71**, 2366 (1967).
24. B. A. COSGROVE and J. WALKLEY. Can. J. Chem. **60**, 1896 (1982).
25. J. E. BYRNE, R. BATTINO, and E. WILHELM. J. Chem. Thermodyn. **7**, 515 (1975).

Can. J. Chem. Downloaded from www.nrcresearchpress.com by 91.144.44.67 on 09/07/12
For personal use only.

Conformational analysis of [3.3.3](1,3,5)cyclophane systems[1]

TATSUYA MENO, KATSUYA SAKO, MASAHIKO SUENAGA, MIYUKI MOURI, TERUO SHINMYOZU,[2] AND TAKAHIKO INAZU[2]

Department of Chemistry, Faculty of Science, Kyushu University, Hakozaki 6-10-1, Higashi-ku, Fukuoka 812, Japan

AND

HIROYUKI TAKEMURA

Laboratory of Chemistry, College of General Education, Kyushu University, Ropponmatsu 4-2-1, Chuo-ku, Fukuoka 810, Japan

Received October 12, 1989

TATSUYA MENO, KATSUYA SAKO, MASAHIKO SUENAGA, MIYUKI MOURI, TERUO SHINMYOZU, TAKAHIKO INAZU, and HIROYUKI TAKEMURA. Can. J. Chem. **68**, 440 (1990).

2,2,11,11,20,20-Hexadeuterio[3.3.3](1,3,5)cyclophane **1**-d_6 and its precursor, [3.3.3](1,3,5)cyclophane-2,11,20-trione **2**, were synthesized and their conformational behavior was examined by a variable temperature ^{1}H NMR method; **1**-d_6 (ca. 1% CD_2Cl_2 solution) exists in a mixture of the conformer A (C_{3h}) and the conformer B (C_s) in a 27:73 ratio at −70°C with the energy barriers for the trimethylene bridge inversion processes (A ⇌ B, B ⇌ B) being 12.4 kcal/mol (T_c = −7°C, 270 MHz). Conformer B is more stable than A by 0.4 kcal/mol based on the populations of both conformers. In contrast to the conformational behavior of **1**, inversion of the tricarbon bridges of **2** is not frozen even at −90°C because of the increased flexibility of these tricarbon bridges.

Key words: conformational analysis, cyclophane, tri-*n*-butyltin deuteride.

TATSUYA MENO, KATSUYA SAKO, MASAHIKO SUENAGA, MIYUKI MOURI, TERUO SHINMYOZU, TAKAHIKO INAZU et HIROYUKI TAKEMURA. Can. J. Chem. **68**, 440 (1990).

On a synthétisé le 2,2,11,11,20,20-hexadeutéro[3.3.3](1,3,5)cyclophane (**1**-d_6) ainsi que son précurseur la [3.3.3](1,3,5)-cyclophane-2,11,20-trione (**2**) et on a examiné leur comportement conformationnel en faisant appel à une méthode de RMN VT ^{1}H; à −70°C, le **1**-d_6 en solution à environ 1% dans le CD_2Cl_2 existe sous la forme d'un mélange du conformère A (C_{3h}) et du conformère B (C_s) dans les proportions 27 : 73; les varrières d'énergie pour le processus d'inversion du pont triméthylène (A ⇌ B, B ⇌ B) sont de 12,4 kcal/mol (T_c = −7°C, 270 MHz). Sur la base des populations de chacun des conformères, on peut déduire que le conformère B est plus stable que le conformère A par environ 0,4 kcal/mol. Dû à une flexibilité accrue des ponts à trois atomes de carbones, le comportement conformationnel du composé **2** diffère de celui du composé **1**; à −90°C, l'inversion des ponts à trois carbones du composé **2** n'est pas figée.

Mots clés : analyse conformationnelle, cyclophane, deutérure tri-*n*-butyle d'étain.

[Traduit par la revue]

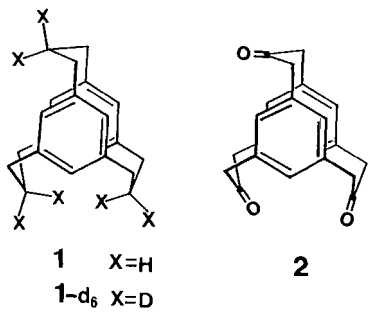

1 X=H
1-d_6 X=D

2

[3.3.3](1,3,5)Cyclophane **1**, one of the lowest homologs of the multibridged [3_n]cyclophanes, was first synthesized by Hübert in 1967 by internal cyclotrimerization of aromatic triyne on a Ziegler catalyst (1). Later, Misumi and co-workers reported an alternative three-step synthesis of **1** by sulfur elimination from 2,13,22-trithia[4.4.4](1,3,5)cyclophane in 8.6% overall yield (2). The stereochemical aspects of conformationally mobile multibridged [3_n]cyclophanes are of particular interest in connection with correlated trimethylene bridge inversion as exemplified by the inversion process of six trimethylene bridges (**3A** ⇌ **3B**) of our final target molecule, [3_6](1,2,3,4,5,6)cyclophane **3**. As a first step for the conformational study of multibridged [3_n]cyclophanes, we undertook the conformational analysis of [3_3](1,3,5)cyclophane systems, in which steric interactions among the trimethylene bridges would be a minimum in multibridged [3_n]cyclophanes.

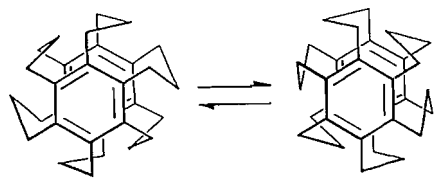

3A **3B**

FIG. 1. Correlated inversion process of the six trimethylene bridges in **3**.

So far, only one conformational study of an aza analog of **1**, *N*,*N*′,*N*″-tritosyl-2,11,20-triaza[3_3](1,3,5)cyclophane **4**, has been reported by Vögtle *et al.* (3); a single isomer was observed at low temperatures and the energy barrier for the trimethylene bridge inversion was estimated to be 12.6 kcal/mol. Crystal structures of 2,11,20-trithia[3_3]cyclophane **5** (4, 5) and trione **2**[3] show that they exist in the conformer with a C_s symmetry exclusively, although disorder of one of the sulfur bridges is observed in **5** (4). Reportedly the singlet of the benzylic protons of **5** remains unchanged as low as −110°C, suggesting a

[1]Conformational analysis of [3.3]cyclophanes, Part 3. For previous papers, see refs. 6*a* (Part 1) and 6*b* (Part 2).

[2]Authors to whom correspondence may be addressed.

[3]Y. Miyahara of our laboratory, unpublished results.

Printed in Canada / Imprimé au Canada

Can. J. Chem. Downloaded from www.nrcresearchpress.com by 91.144.44.67 on 09/07/12
For personal use only.

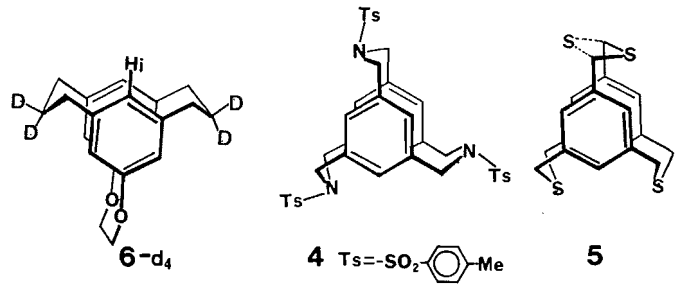

low energy barrier for the trimethylene bridge inversion (3*b*). Our work is the first complete conformational analysis of tribridged [3.3.3]cyclophane systems.

We report here the synthesis of 2,2,11,11,20,20-hexadeuterio[3_3](1,3,5)cyclophane **1**-d_6 and its precursor trione **2**, as well as their VT ^{1}H NMR study. This study certainly provides us with basic data for the understanding of the conformational behavior of more highly bridged [3_n]cyclophanes. In the preceding papers, we reported the conformational analyses of [3.3]*meta*- and *para*-cyclophanes (6*a*,*b*).

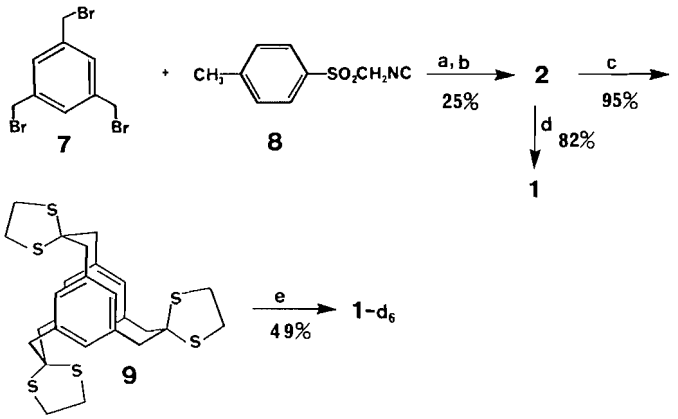

SCHEME 1. Synthetic route of **1**-d_6: (a) *n*-Bu_4NI, NaOH, CH_2Cl_2–H_2O; (b) conc. HCl; (c) $HSCH_2CH_2SH$, $BF_3 \cdot OEt_2$, AcOH; (d) 100% $NH_2NH_2 \cdot H_2O$, KOH, $HO(CH_2)_3OH$; (e) *n*-Bu_3SnD, AIBN, xylene.

The coupling reaction of *p*-tolylsulfonylmethyl isocyanide (TosMIC) **8** with 1,3,5-tris(bromomethyl)benzene **7**, followed by acid treatment, afforded the trione **2** in 25% yield. The Wolff–Kishner reduction of the carbonyl groups provided **1** in 82% yield (7*a*,*b*). Our method constitutes a simpler alternative method for the synthesis of **1**. The trione **2** was converted, by a conventional method in 95% yield, into thioacetal **9**, which was reduced with tri-*n*-butyltin deuteride in the presence of AIBN in refluxing xylene to afford **1**-d_6 in 49% yield (6, 8).

At 20°C, **1**-d_6 (270 MHz, ca. 1% solution in CD_2Cl_2) shows benzylic and aromatic protons at 2.71 (br s) and 6.51 (s) ppm, respectively. Both protons are strongly temperature dependent, as shown in Fig. 2. The aromatic signal broadens as the temperature is lowered. It becomes three broad peaks at −30°C, and finally it appears as three singlets at 6.36, 6.52, and 6.71 ppm with relative intensities being 1:2:1 at −70°C (Fig. 3).

Scheme 2 shows possible trimethylene bridge inversion processes for **1** (9). There are two discernible conformational isomers: the conformers A (C_{3h}) and B (C_s). Two types of isomerization processes are considered: isomerizations between two different conformers (A ⇌ B) and the same conformers (B ⇌ B). In principle, therefore, there should be two different free-energy barriers for the corresponding rate processes.

The aromatic proton signals are assigned as follows, based on the fact that inner aromatic protons (H_i) of 1,4-dioxa[4.3.3]-metacyclophane-d_4, **6**-d_4, experience a through-space deshielding, in the following order, from the bridge deuteriums of C-2 or C-11 constrained to proximity: boat–boat > chair–boat > chair–chair (6*a*). (Conformer A, H_a 6.52 ppm; B, H_c 6.36, $H_{a'}$ 6.52, and H_b 6.71 ppm.) Populations of the A and B isomers are estimated to be 27:73 on the basis of the integral of the aromatic signals: 6.36 (B, H_c) and 6.52 (A, H_a + B, $H_{a'}$) ppm.

As shown in Fig. 2, the benzylic signal broadens as the temperature is lowered. The broad signal begins to split into two broad peaks at −7°C, and finally it becomes four sets of an AB quartet. The four doublets due to the axial protons of a benzylic position appearing at a higher field at 2.43 (J = 13.7 Hz) ppm are overlapped with each other, whereas the equatorial

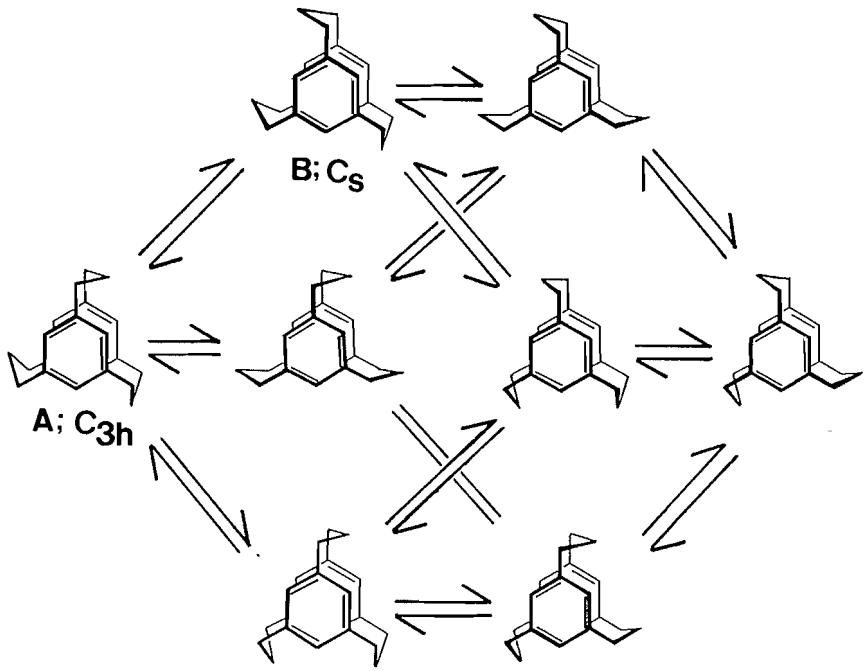

SCHEME 2. Possible trimethylene bridge inversion processes for **1**.

Can. J. Chem. Downloaded from www.nrcresearchpress.com by 91.144.44.67 on 09/07/12
For personal use only.

Can. J. Chem. Downloaded from www.nrcresearchpress.com by 91.144.44.67 on 09/07/12
For personal use only.

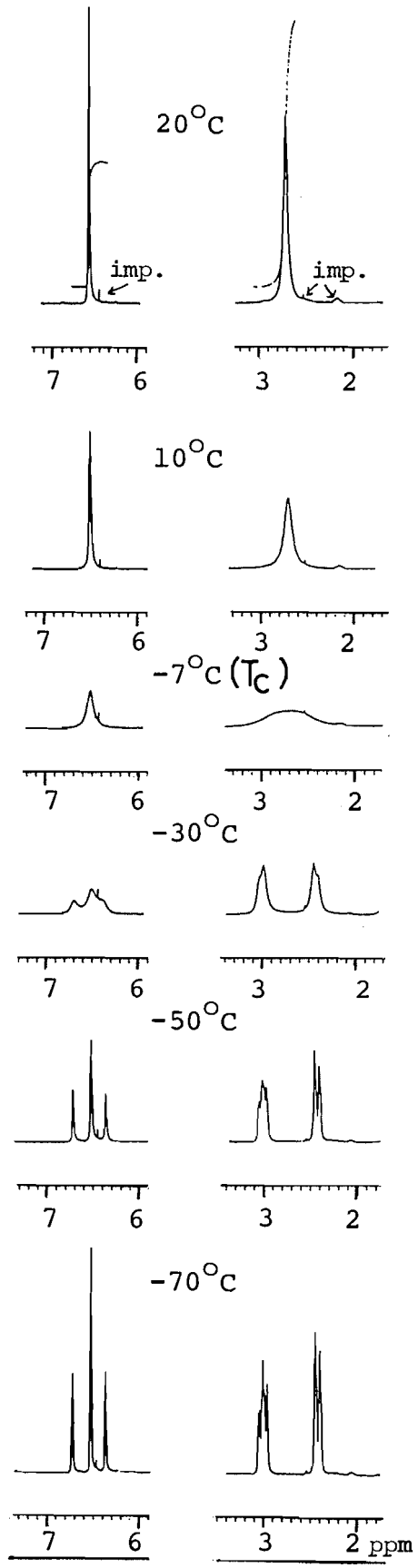

FIG. 2. The ^{1}H nmr spectra of **1** at various temperatures (270 MHz, CD_2Cl_2).

protons appear as four sets of a doublet. On the basis of the chemical shifts of the corresponding protons observed in **6**-d_4, the following assignments are made for the equatorial protons (Fig. 4): A, H_{eq} 2.99 (J = 13.7 Hz) ppm; B, H'''_{eq} 3.01 (J = 13.7 Hz), H'_{eq} 2.99 (J = 13.7 Hz), H''_{eq} 3.03 (J = 13.7 Hz) ppm.

The energy barriers for the trimethylene bridge inversion processes (A $\rightleftharpoons$ B, B $\rightleftharpoons$ B) are estimated to be ca. 12.4 kcal/mol due to the T_c = −7°C, chemical shift differences, and geminal coupling constants of the benzylic protons (10);[4] identical energy barriers are obtained for the two types of inversion processes. The value is comparable to those of **6**-d_4 (12.1–12.3 kcal/mol) (6*a*) and triaza analog **4** (12.6 kcal/mol) (3*a*) but is slightly higher than those of [3.3]*meta*- (11.6 (6*a*), 10–11 kcal/mol (11)) and *para*-cyclophane (12.0 (6*b*), 11.7 kcal/mol (12)). Populations of the isomers show that the B isomer is more stable than A by 0.4 kcal/mol. The structure of the preferred isomer B in solution is in agreement with those found in the crystalline state of the [3_3](1,3,5)cyclophane derivatives (ref. 4 and footnote 3). These results reveal that the trimethylene bridges in **1** do not undergo a correlated inversion process but move independently.

The trione **2** shows benzylic and aromatic protons at 3.76 and 6.85 ppm, respectively, as sharp singlets at room temperature (ca. 1% CD_2Cl_2 solution, 270 MHz). Both signals remain unchanged, except for slight broadening of the bands, even at −90°C, suggesting a much lower energy barrier for the tricarbon bridge inversion in **2** than in **1**. We qualitatively interpret this result as indicating that the torsional energy difference between the preferred conformer (**2e** for **2**, **1s** for **1**) and the transition conformer (**2s** for **2**, **1e** for **1**) is much less in **2** than in **1**. In the transition state four H/H eclipsed interactions in **1** (**1e**) whereas two CH_2/CO staggered interactions in **2** (**2s**) are regarded as significant for the major torsional energy, since the phenyl/benzyl eclipsed interactions of both conformers are estimated to be identical (Fig. 7). Therefore the energy barrier for the tricarbon bridge inversion is estimated to be much higher in **1** than in **2** according to the following data; the energy difference between eclipsed and staggered conformations of ethane is 3 kcal/mol, while that of acetaldehyde is only 1.1 kcal/mol (13).

On the other hand, the aromatic protons of the thioacetal **9** exhibit a very broad signal even at room temperature, as shown in Fig. 6, indicating an increased energy barrier for the bridge inversion due to the introduction of heavy 5-membered rings into the bridges.

A study on the correlated trimethylene bridge inversion of [3_3](1,2,3)cyclophane and the synthesis of the higher homologs is in progress.

Experimental

All melting points were uncorrected. Proton nuclear magnetic resonance (^{1}H nmr) spectra were recorded on either a Hitachi R-20B (60 MHz), a JEOL JNM-GSX 270 (270 MHz), or a JEOL JNM-GX 400 (400 MHz) spectrometer. Chemical shifts are reported as δ values (ppm) relative to internal Me_4Si. Mass spectra were obtained on a Hitachi RMU-6MG mass spectrometer at an ionization energy of 70 eV; m/z values reported include the parent ion peak. Infrared (ir) spectra were obtained on a JASCO IR-700 spectrophotometer as KBr disks. Elemental analyses were performed by the Service Centre of

[4] $\Delta G_c^{\ddagger}$ (kcal/mol) = $2.303 \times 1.987 T_c\ (10.319 - \log_{10} k_c + \log_{10} T_c)$ where $k_c = (\pi/\sqrt{2})[(\nu_A - \nu_B)^2 + 6J^2]^{1/2}$.

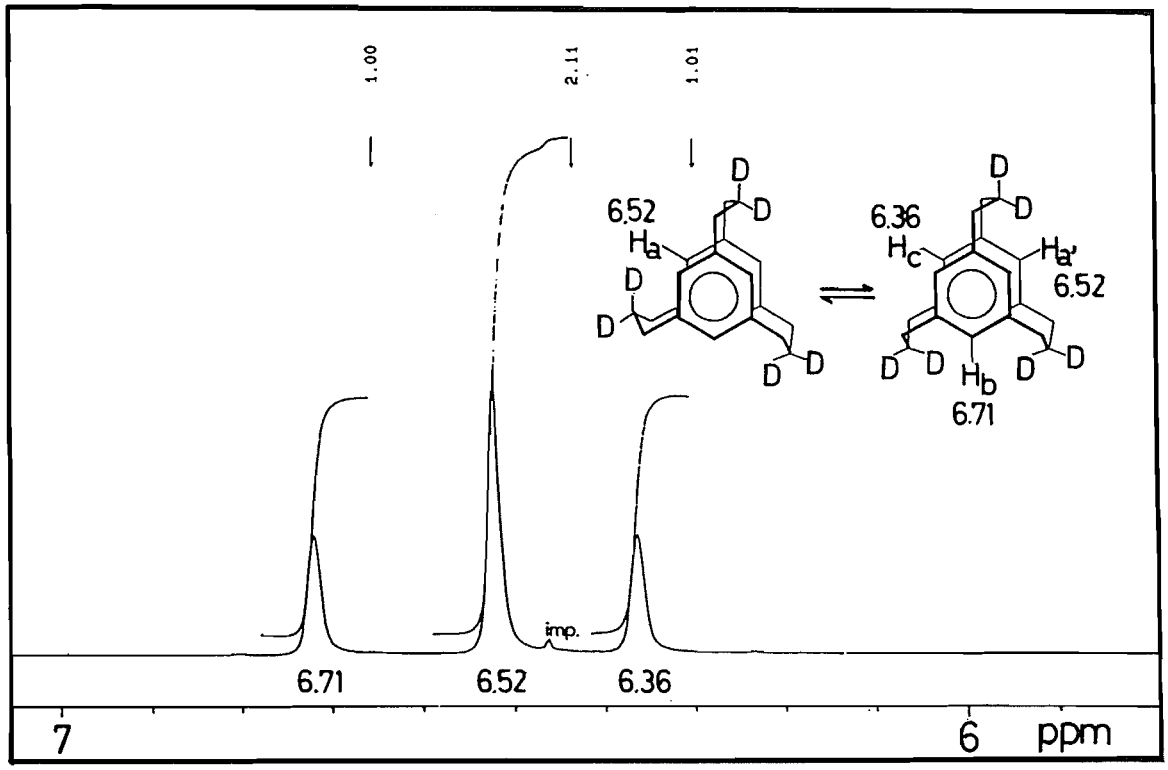

FIG. 3. Expanded ^{1}H nmr spectrum of the aromatic protons in **1** at −70°C (270 MHz, CD_2Cl_2).

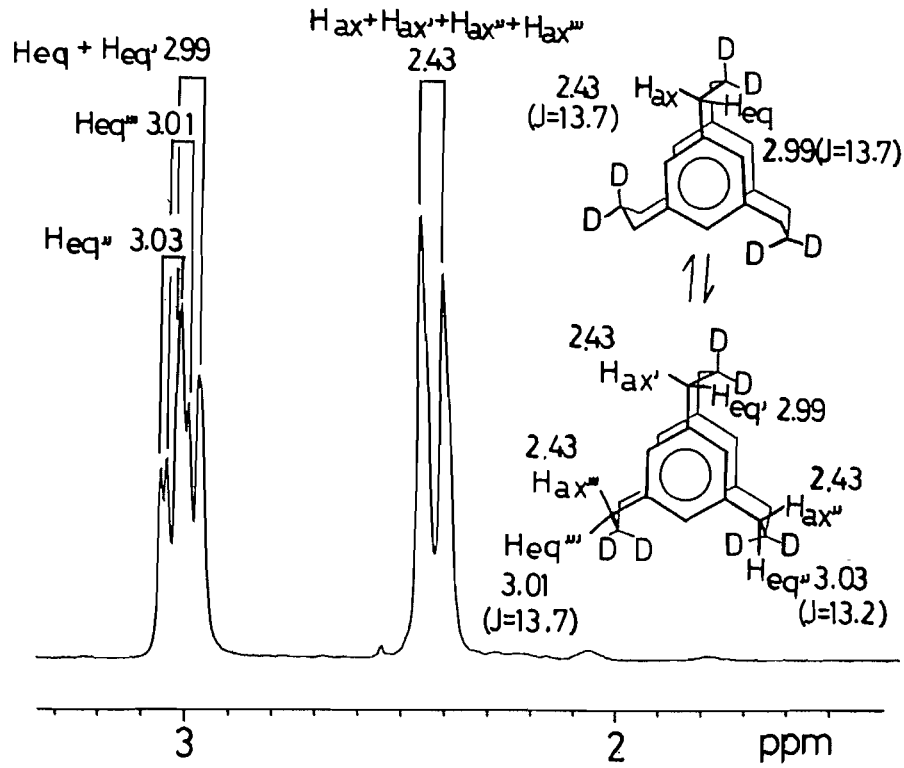

FIG. 4. Expanded ^{1}H nmr spectrum of the benzylic protons in **1** at −70°C (270 MHz, CD_2Cl_2).

Can. J. Chem. Downloaded from www.nrcresearchpress.com by 91.144.44.67 on 09/07/12
For personal use only.

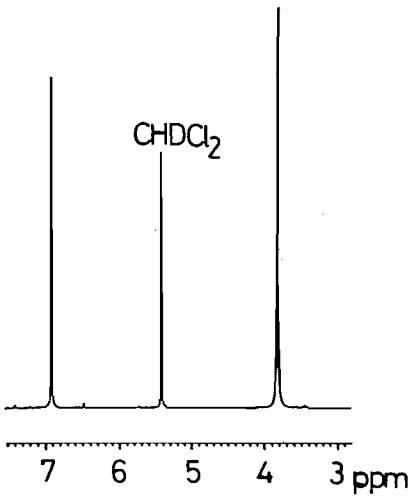

FIG. 5. the ^{1}H nmr spectrum of **2** at −90°C (270 MHz, CD_2Cl_2).

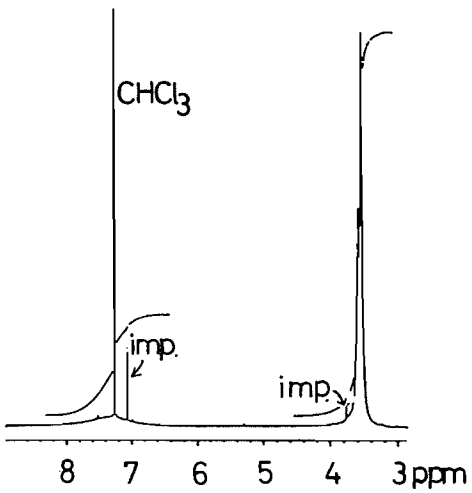

FIG. 6. the ^{1}H nmr spectrum of **3** at 20°C (400 MHz, $CDCl_3$).

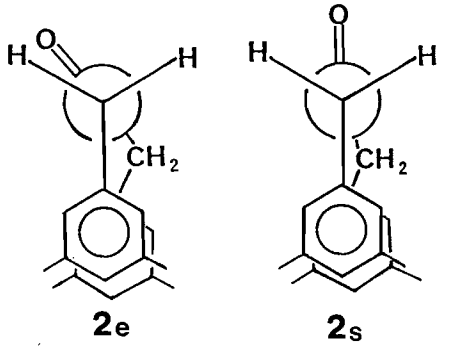

FIG. 7. Conformations of the tricarbon bridge in **2**: the most stable conformation (eclipsed) **2e** and the transition state (staggered) **2s**.

the Elementary Analysis of Organic Compounds affiliated with the Faculty of Science in Kyushu University.

Silica gel chromatography utilizes Daiso gel IR-60 and Merck silica gel 60 for column chromatography, Merck silica gel PF_{254} for preparative tlc, and Merck silica gel F_{254} (0.2 mm on aluminum) for analytical purposes.

1,3,5-Tris(bromomethyl)benzene **7** (*5a*) was prepared by the $LiAlH_4$ reduction of 1,3,5-tris(ethoxycarbonyl)benzene (quantitative), followed by bromination of the triol with PBr_3 in $CHCl_3$ (71%). *n*-Bu_3SnD was prepared by the $LiAlD_4$ reduction of *n*-Bu_3SnCl (14). Xylene was distilled from CaH_2. AIBN was recrystallized from MeOH.

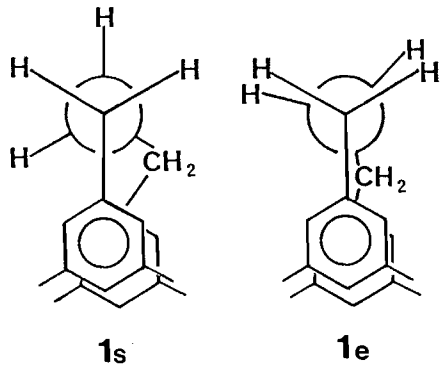

FIG. 8. Conformations of the trimethylene bridge in **1**: the most stable conformation (staggered) **1s** and the transition state (eclipsed) **1e**.

[3.3.3](1,3,5)Cyclophane-2,11,20-trione (2)

To a refluxing mixture of *n*-Bu_4NI (5 g), NaOH (70 g) dissolved in water (120 mL), and CH_2Cl_2 (1.5 L) was added dropwise a mixture of the bromide **7** (15.0 g, 42.0 mmol) and TosMIC **8** (12.3 g, 63.0 mmol) in CH_2Cl_2 (1.0 L) over a period of 8 h with vigorous stirring. After the addition, the mixture was stirred for an additional 2 h. After cooling, the mixture was washed with water (1.5 L × 4) and concentrated to a volume of ca. 600 mL. To the concentrate was added concentrated HCl (100 mL), and the mixture was stirred at room temperature for 2 h. The mixture was washed successively with water (200 mL × 3) and brine (200 mL), and concentrated to dryness to give brown semisolid material. Similar reactions were repeated three times on the same scale and the combined products were chromatographed on silica gel (250 g) with CH_2Cl_2. Concentration of the eluate afforded pale brown crystals, which were triturated with MeOH and collected by filtration to give **2** as colorless crystals (4.99 g, 25%). A sample was recrystallized from $MeOH/CH_2Cl_2$ (3:7) to provide colorless needles, mp 284.5°C; ir (KBr): 1698 (C=O) cm^{-1}; R_f (Si gel, CH_2Cl_2) 0.25; ms *m/z*: M^+ 318. Anal. calcd. for $C_{21}H_{18}O_3$: C 79.23, H 5.70; found: C 78.94, H 5.83.

2,2,11,11,20,20-Hexadeuterio[3.3.3](1,3,5)cyclophane (1-d_6)

A mixture of the trione **2** (970 mg, 3.05 mmol), 1,2-ethanedithiol (5.0 mL, 59.6 mmol), AcOH (50 mL), and $BF_3 \cdot Et_2O$ (0.3 mL, 2.38 mmol) was stirred at room temperature for a day. Then an additional amount of $BF_3 \cdot Et_2O$ (0.2 mL, 1.59 mmol) was added and the mixture was stirred for 3 h. The reaction was quenched by the addition of water (100 mL), and the mixture was extracted with $CHCl_3$ (300 mL × 1, 100 mL × 2). The combined organic portion was washed successively with saturated $NaHCO_3$ solution (200 mL) and water (400 mL × 4), dried over $MgSO_4$, and filtered. The filtrate was concentrated to dryness *in vacuo* and the resulting powder was collected by filtration, washed successively with MeOH and acetone, and recrystallized from xylene to give colorless crystals (1.58 g, 95%); mp 298.3–298.8°C; ^{1}H nmr (400 MHz, $CDCl_3$): 3.53 (s, 12H, —SCH_2CH_2S—), 3.58 (br s, 12H, benzylic H), 6.40–8.40 (br s, 6H, ArH); ms *m/z*: M^+ 546. Anal. calcd. for $C_{27}H_{30}S_6$: C 59.29, H 5.53; found: C 59.40, H 5.41.

A mixture of the thioacetal **9** (286 mg, 0.523 mmol), freshly prepared *n*-Bu_3SnD (3.0 mL, 11.2 mmol), AIBN (100 mg), and xylene (27 mL) was refluxed for a day with stirring under N_2. After cooling, the mixture was concentrated to a volume of ca. 10 mL and chromatographed on silica gel (50 g) with hexane. Concentration of the eluate gave **1**-d_6 as colorless crystals, which were further purified by preparative tlc (silica gel) with hexane (72 mg, 49%). A sample for microanalysis was sublimed (90°C, 1 Torr; 1 Torr = 133.3 Pa); mp 153–154.5°C; ir (KBr): 2182, 2142, 2098 (—CD_2—) cm^{-1}; R_f (Si gel, hexane) 0.28; ms *m/z*: M^+ 282. Anal. calcd. for $C_{21}H_{18}D_6$: C 89.30, H + 1/2D 8.56; found: C 89.31, H + 1/2D, 8.65.

Can. J. Chem. Downloaded from www.nrcresearchpress.com by 91.144.44.67 on 09/07/12
For personal use only.

[3.3.3](1,3,5)Cyclophane (1)

A stirred mixture of the trione **2** (318 mg, 1.0 mmol), 100% hydrazine hydrate (25 mL), KOH (5 g), and triethylene glycol (50 mL) was heated at 120°C for 2.5 h and then at 200°C for 2 h. After cooling, the mixture was poured into ice-water, acidified with diluted HCl, and extracted with CH_2Cl_2. The combined organic portion was washed successively with water, diluted $NaHCO_3$ solution, and brine, dried over $MgSO_4$, and filtered. Removal of the solvent afforded colorless crystals, which were passed through a silica gel column with CH_2Cl_2 to give **1** (226 mg, 82%) as colorless crystals; **1**: colorless plates from MeOH, mp 152.5–153.3°C (lit. (1) mp 140°C; lit. (2) mp 134–135.5°C); ^{1}H nmr ($CDCl_3$): 2.05–2.33 (m, 6H, —$CH_2CH_2CH_2$—), 2.75 (t, 12H, —$CH_2CH_2CH_2$—), 6.52 (s, 6H, ArH); ms *m/z*: M^+ 276. Anal. calcd. for $C_{21}H_{24}$: C 91.25, H 8.75; found: C 91.08, H 8.73.

1. A. J. HÜBERT. J. Chem. Soc. C, 6 (1967).
2. T. OTSUBO, M. KITASAWA, and S. MISUMI. Bull. Chem. Soc. Jpn. **52**, 1515 (1979).
3. (*a*) F. VÖGTLE and P. NEUMANN. J. Chem. Soc. Chem. Commun. 1464 (1970); (*b*) F. VÖGTLE and G. HOHNER. Top. Curr. Chem. **74**, 1 (1978).
4. A. W. HANSON and E. W. MACAULAY. Acta Crystallogr. Sect. B: Crystallogr. Cryst. Chem. **B28**, 1255 (1972).
5. (*a*) V. BOEKELHEIDE and R. A. HOLLINS. J. Am. Chem. Soc. **92**, 3512 (1970); (*b*) F. VÖGTLE. Liebigs Ann. Chem. **735**, 193 (1970).
6. (*a*) K. SAKO, T. HIRAKAWA, N. FUJIMOTO, T. SHINMYOZU, T. INAZU, and H. HORIMOTO. Tetrahedron Lett. **29**, 6275 (1988); (*b*) K. SAKO, T. MENO, H. TAKEMURA, T. SHINMYOZU, and T. INAZU. Chem. Ber. In press.
7. (*a*) K. KUROSAWA, M. SUENAGA, T. INAZU, and T. YOSHINO. Tetrahedron Lett. **23**, 5335 (1982); (*b*) T. SHINMYOZU, Y. HIRAI, and T. INAZU. J. Org. Chem. **51**, 1551 (1986).
8. C. G. GUTIERREZ, R. A. STRINGHAM, T. NITASAKA, and K. G. GLASSCOCK. J. Org. Chem. **45**, 3393 (1980).
9. J. C. COLL, D. R. CRIST, M. C. G. BARRIO, and N. J. LEONARD. J. Am. Chem. Soc. **94**, 7092 (1972).
10. R. J. KURLAND, M. B. RUBIN, and W. B. WISA. J. Chem. Phys. **40**, 2426 (1964); M. OKI, H. IWAMURA, and N. HAYAKAWA. Bull. Chem. Soc. Jpn. **37**, 1965 (1865).
11. M. F. SEMMELHACK, J. J. HARRISON, D. C. YOUNG, A. GUTIÉRREZ, S. RAFII, and J. CLARDY. J. Am. Chem. Soc. **107**, 7508 (1985).
12. (*a*) F. A. L. ANET and M. A. BROWN. J. Am. Chem. Soc. **91**, 2389 (1969); (*b*) R. BENN, N. E. BLANK, M. W. HAENEL, J. KLEIN, A. R. KORAY, K. WEIDENHAMMER, and M. L. ZIEGLER. Angew. Chem. Int. Ed. Engl. **19**, 44 (1980).
13. B. TESTA. *In* Principles of organic stereochemistry. *Edited by* P. G. Gassmann. Marcel Dekker, New York, Basel. 1979. pp. 82–147.
14. G. J. M. VAN DER KERK, J. G. NOLTES, and J. G. A. LUITJEN. J. Appl. Chem. **7**, 366 (1957); G. M. WHITESIDES and J. S. FILLIPPO, JR. J. Am. Chem. Soc. **92**, 6611 (1970).

Can. J. Chem. Downloaded from www.nrcresearchpress.com by 91.144.44.67 on 09/07/12
For personal use only.

Substituent effects in the bis(benzotriazolylmethylation) of aromatic amines

ALAN R. KATRITZKY,[1] STANISLAW RACHWAL, AND JING WU
Department of Chemistry, University of Florida, Gainesville, FL 32611, U.S.A.

Received April 17, 1989

ALAN R. KATRITZKY, STANISLAW RACHWAL, and JING WU. Can. J. Chem. **68**, 446 (1990).

1-(Hydroxymethyl)benzotriazole and aromatic amines react to give an equilibrium mixture of *N*-mono- and *N*,*N*-bis(benzotriazolylmethyl)arylamines. Electron-releasing substituents on the arylamine ring shift the equilibrium towards the *N*,*N*-bis(benzotriazolylmethylated) products, and removal of water formed in the reaction leads to these bis derivatives in quantitative yields. These products were isolated as mixtures of three isomers, the benzotriazolyl-1,1′, -1,2′, and -2,2′ derivatives; these mixtures were characterized by full assignment of their ^{13}C NMR spectra and by partial separation and enrichment. Electron-withdrawing substituents on the arylamine ring increase the isomer interconversion energy barriers and make *N*,*N*-bis(benzotriazolylmethyl)arylamines more resistant to hydrolysis. A strong influence of *ortho* alkyl groups on the stability and NMR spectral properties of *N*,*N*-bis(benzotriazolylmethyl)arylamines is interpreted on the basis of steric hindrance.

Key words: Mannich reaction, benzotriazole isomerization, substituent effects, anilines, bis(benzotriazolylmethyl)arylamines.

ALAN R. KATRITZKY, STANISLAW RACHWAL et JING WU. Can. J. Chem. **68**, 446 (1990).

Le 1-(hydroxyméthyl)benzotriazole et les amines aromatiques réagissent pour donner des mélanges à l'équilibre des *N*-mono- et *N*,*N*-bis(benzotriazolylméthyl)arylamines. La présence de substituants électrorépulsifs sur le noyau des amines aromatiques déplace l'équilibre vers les produits *N*,*N*-bis(benzotriazolylméthylés), et l'élimination de l'eau qui se forme au cours de cette réaction conduit à la formation de ces bis-dérivés avec un rendement quantitatif. On a isolé ces produits sous la forme de mélanges de trois isomères comprenant les dérivés benzotriazolyl-1,1′, -1,2′ et -2,2′; on a caractérisé ces mélanges en attribuant toutes les bandes des spectres RMN du ^{13}C ainsi que par des séparations et des enrichissements partiels. La présence de substituants électrodonneurs sur les amines aromatiques augmente l'énergie d'interconversion entre les isomères et rend les *N*,*N*-bis(benzotriazolylméthyl)arylamines plus résistantes à l'hydrolyse. Les groupements alkyles présents en *ortho* influencent fortement la stabilité et les propriétés spectrales des *N*,*N*-bis(benzotriazolylméthyl)arylamines; on interprète ces résultats en se basant sur des facteurs d'empêchement stérique.

Mots clés : réaction Mannich, isomérisation benzotriazole, effets de substituants, anilines, bis(benzotriazolylméthyl)arylamines.
[Traduit par la revue]

Can. J. Chem. Downloaded from www.nrcresearchpress.com by 91.144.44.67 on 09/07/12
For personal use only.

Introduction

Primary aromatic amines react rapidly with 1-(hydroxymethyl)benzotriazole in ethanolic solution (1) or in aqueous suspension (2) to give the corresponding mono-*N*-(benzotriazolylmethyl)arylamines regardless of the ratio of the reagents. The same result is obtained by mixing benzotriazole, formaldehyde, and arylamine (3); instead of formaldehyde, other alkyl- and aryl-aldehydes can be used (1, 2). All of these reactions proceed essentially quantitatively. In the case of primary aliphatic amines, the picture is more complex: *N*-mono(benzotriazolylmethyl)alkylamines, *N*,*N*-bis(benzotriazolylmethyl)alkylamines, and compounds of type $(BtCH_2NR)_2CH_2$ have all been isolated (4).[2]

Mannich reactions of arylamines with formaldehyde and N–H heterocyclic systems frequently lead to stable monoadducts with N—CH_2—N bonds. Several such reactions, e.g., with succinimides (5, 6) benzimidazoles (7–10), benzimidazolin-2-thiones (11–13), benzoxalin-2-ones (14), 4-oxothiazolidines (15, 16), 1,2,4-triazoline-3-thiones (17), 4-quinazolinones (18–20), 2-mercaptobenzothiazole (21), 5-chlorobenzotriazole (22), and 5-nitrobenzotriazole (23), have recently been reported, mainly due to pharmacological interest in the adducts. Under similar conditions, however, arylamines condense with two molar equivalents of 1-(hydroxymethyl)-3,5-dimethylpyrazole giving their *N*,*N*-bis(pyrazol-1-ylmethyl) derivatives (24, 25) with an N—CH_2—N(Ar)—CH_2—N group. At elevated temperatures, arylamines react with formaldehyde to give *N*,*N*′,*N*″-triphenylhexahydrotriazines (26).

[1]Author to whom correspondence may be addressed.
[2]A. R. Katritzky and B. Pilarski. Unpublished results.

Bis(benzotriazolylmethylation) of aromatic amines

The goal at the beginning of these investigations was the elucidation of a route to *N*,*N*-bis(benzotriazolylmethyl)arylamines, compounds that were expected to be convenient precursors for *N*,*N*-dialkylarylamines. We initially investigated 4-butylaniline and modified the reported procedure (1) for *N*-benzotriazolylmethylation of arylamines. Butyl substitution of the ring increased the solubility of the products and facilitated the investigations.

Monitoring an equimolar mixture of 1-hydroxymethylbenzotriazole (**1**) and *N*-(benzotriazol-1-ylmethyl)-4-butylaniline (**2***c*) by NMR revealed a fast reaction at 20°C. The strongest new peak in the spectrum at δ 6.25 (presumably from **5**) was observed after a few minutes; its intensity grew, while the methylene signals of **1** and **2** (both at δ 6.04–6.06) diminished in intensity. Thus, after 20, 60, 105 min, and 13 h, the intensity of the 6.25 peak was respectively 3, 7, 13, and 75% of that of the methylene signal of the starting reagent. Further reaction was slow, indicating an equilibrium between the products and the starting materials. Because other methylene singlets (of lower intensity) were also observed, more precise estimates of the ratio of the products to the starting materials were obtained using the butyl group signals (which did not change during the reaction) as a reference. The integral ratio of the signals at δ 6.05 to those of two butyl methylene groups at δ 1.20–1.60, representing percentage of the starting materials remaining in the mixture, was as follows: 98 (20 min), 89 (60 min), 82 (105 min), 55 (13 h), 46 (24 h), and 45% (4 days).

Mixtures of aromatic amines with 1-(hydroxymethyl)benzotriazole, monitored by the NMR technique, revealed the

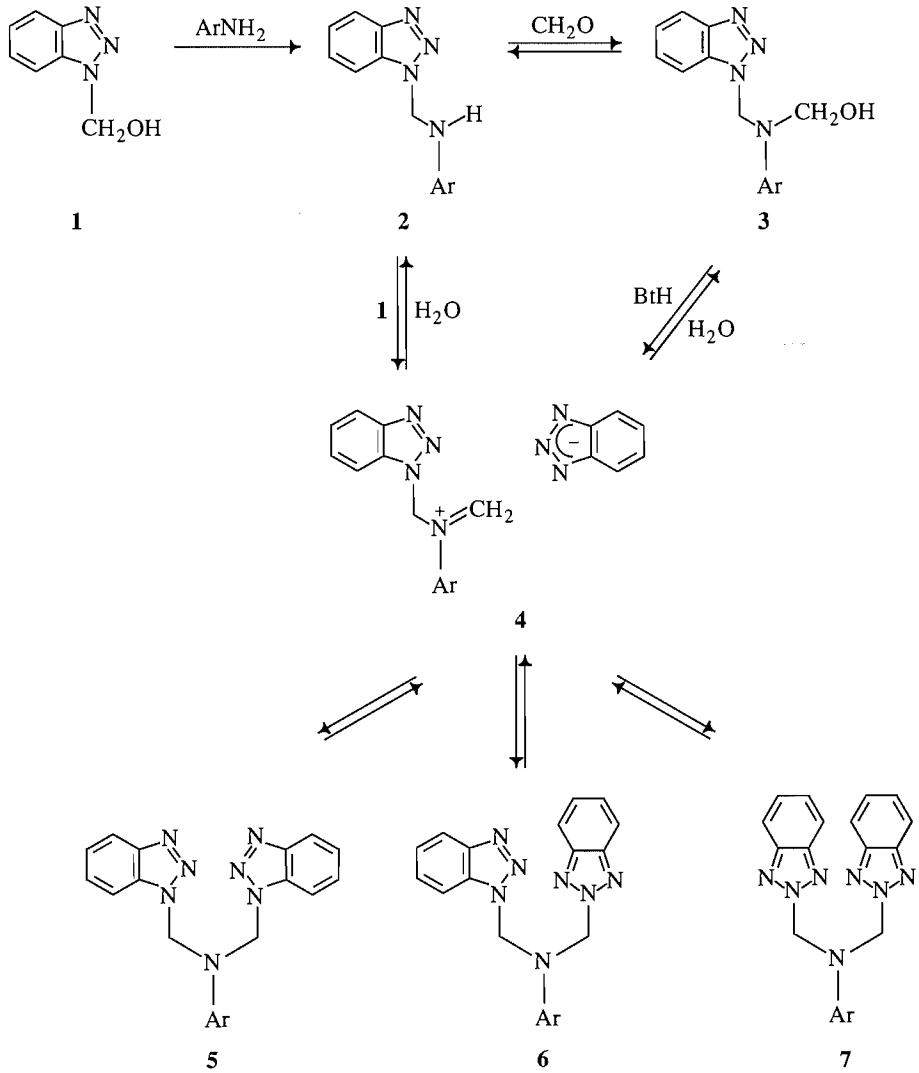

For the significance of *a–l* in the designation of Ar see Table 1

SCHEME 1

formation of compounds possessing isolated methylene groups. The strongest signal was usually recognized as that of the corresponding *N*-(benzotriazol-1-ylmethyl)arylamine **2**, by comparison of the spectrum of the reaction mixture with that of the authentic compound. Further signals at lower field, in order of decreasing intensity, were assigned to the three isomeric *N*,*N*-bisbenzotriazolylmethylated arylamines **5**, **6**, and **7**, respectively (Scheme 1). Other small methylene signals, of total intensity usually <5%, are attributed to unstable intermediates such as **3**. (Later in this paper, to avoid repetition, reference to **5** can mean a mixture of **5**, **6**, and **7**.)

For direct comparison of substituent effects, reaction mixtures of the same initial molar concentration were investigated at elevated temperatures to increase the rate of equilibration. Thus, a mixture of 1-(hydroxymethyl)benzotriazole (5 mmol) and aniline (2.5 mmol) in DMSO-d_6 (10 mmol) was kept at 100°C for 1 h. In addition to the 1-(hydroxymethyl)benzotriazole methylene singlet at δ 6.06, a doublet at δ 6.09 turning into a singlet upon addition of D_2O (methylene group of **2***a*), a singlet at δ 6.24 (**5***a*), a pair of equal singlets at δ 6.34 and 6.55 (**6***a*), and a small singlet at δ 6.58 (**7***a*) were assigned as indicated. Very small singlets were also observed at δ 6.25, 6.30, and 6.33 (possibly **3***a* and (or) similar structures). The molar ratios of the products at equilibrium for this, and for similar reaction mixtures, are given in Table 1.

As shown in Table 1, *para* electron-releasing substituents in the aniline ring favor formation of the *N*,*N*-bis(benzotriazolylmethylated) products (**5**, **6**, and **7**), whereas electron-withdrawing *para* or *meta* substituents shift the equilibrium towards *N*-mono(benzotriazolylmethylated) amines **2**. *ortho*-Alkyl anilines form an exception to this rule, as properties of the adducts cannot be directly correlated with the σ_o constants given in Table 1. Evidently, more complex parameters reflecting steric interactions (29, 30) should be used here. Thus, reaction of 1-(hydroxymethyl)benzotriazole with 2-methyl- or 2-ethylaniline leads to a product ratio similar to that obtained from 3-chloroaniline, because of steric hindrance. Whereas **2***i* and **2***j* are unstrained in the *anti* conformation, a second benzotriazolylmethyl substituent on the nitrogen atom (in **5***i* and **5***j*) causes steric repulsions with the *ortho* group in the planar conformation: hence **5***i* and **5***j* have higher energy and are less readily formed. Similar examples are commonplace, e.g.,

Can. J. Chem. Downloaded from www.nrcresearchpress.com by 91.144.44.67 on 09/07/12
For personal use only.

Can. J. Chem. Downloaded from www.nrcresearchpress.com by 91.144.44.67 on 09/07/12
For personal use only.

TABLE 1. Molar ratio between *N*-mono- (**2**) and *N,N*-bis(benzotriazolyl-methyl)arylamines (**5**, **6**, and **7**) in equilibrium mixtures formed from 1-(hydroxymethyl)benzotriazole and arylamines (2:1)[a]

No.	$ArNH_2$	Aniline[b] substituent[b] σ	Molar percentage of **2**	Molar percentage of **5** + **6** + **7**
a	$PhNH_2$	0.00	71	29
b	$4\text{-}MeC_6H_4NH_2$	−0.17	59	41
c	$4\text{-}BuC_6H_4NH_2$	−0.16	59	41
d	$4\text{-}MeOC_6H_4NH_2$	−0.27	58	42
e	$4\text{-}Me_2NC_6H_4NH_2$	−0.60	33	66
f	$4\text{-}ClC_6H_4NH_2$	0.23	84	16
g	$3\text{-}ClC_6H_4NH_2$	0.37	73	27
h	$3\text{-}NO_2C_6H_4NH_2$	0.71	86	14
i	$2\text{-}MeC_6H_4NH_2$	−0.12	72	28
j	$2\text{-}EtC_6H_4NH_2$	−0.17	73	27
k	$2,6\text{-}iPr_2C_6H_4NH_2$		20	80
l	$PhCH_2NH_2$		10	90

[a]For conditions see the experimental section.
[b]For σ_m and σ_p see ref. 27; σ_o are taken from ref. 28.

methylation of *p*-toluidine by a bulky methylating agent gave exclusively *N,N*-dimethyl-*p*-toluidine but, under the same conditions, *o*-toluidine formed only a mono-*N*-methylated derivative (31).

However, excessive steric hindrance can reverse the preference. In 2,6-diisopropylamine derivatives, even *N*-monosubstitution by the benzotriazolylmethyl group (**2***k*) causes rotation of the nitrogen-ring bond. The *N*-monosubstituted amine, having lost the conjugation of the lone pair with the ring, easily undergoes further benzotriazolylmethylation to give **5**–**7***k* (Fig. 1), just as occurs for aliphatic primary amines, e.g., benzylamine **2***l* (Table 1).

Under more stringent conditions (refluxing in toluene and trapping the water), aromatic amines react with 2 moles of **1** to form *N,N*-bis(benzotriazolylmethyl)arylamines in quantitative yields. Use of benzotriazole, an aromatic amine, and aqueous formaldehyde gives similar results. Alkylation of the amine nitrogen atom by **1**, leading in the first step to **2**, and then in a second step to **5** (or its isomer **6**), is a feasible reaction route. However, intermediate amine-formaldehyde adducts of type **3** are probably also involved, especially when the amine and benzotriazole react with aqueous formaldehyde. The *N,N*-bis(benzotriazolylmethyl)arylamines thus obtained were characterized by CHN analysis (Table 2).

The formation of **5** from **2** is reversible: decomposition of **5** to **1** and the mono-*N*-substituted aniline **2** was observed in moist DMSO solutions of **5** at elevated temperatures. 2-Ethylaniline derivative **5***j* could not be satisfactorily analyzed because of its rapid hydrolysis in air. However, in the crystalline state, adducts **5** are stable, and insensitive towards moist air, for months at room temperature.

Bis(benzotriazolylmethylation) fails for a few aromatic amines: 4-nitroaniline, and 2- and 4-aminopyridines, gave only the *N*-monosubstituted aromatic amines **2** under the standard conditions. Prolonged heating of *N*-(benzotriazolylmethyl)-4-nitroaniline with **1** at 150°C led only to benzotriazole as a product of decomposition of **1**. 4-Chloroaniline was easily bis(benzotriazolylmethylated), whereas 3-chloroaniline required an extended reaction time for bis(benzotriazolylmethylation) to be accomplished. Although 3-nitroaniline gave only its mono

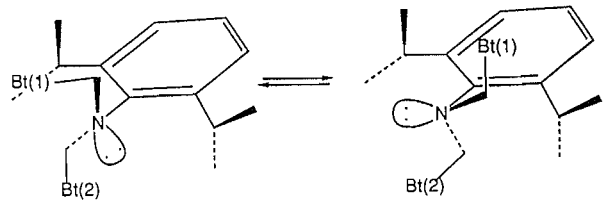

FIG. 1. Conformations of the molecules of **6***k*.

derivative **2***h* under standard reaction conditions, the *N,N*-bis isomer mixture (**5***h*, **6***h*, **7***h*) was formed upon prolonged reflux in toluene.

The behavior of the amine towards 1-(hydroxymethyl)benzotriazole (**1**) can be correlated with the amine basicity (32), cf. pK_a of 4-anisidine, 5.40; 4-toluidine, 5.15; aniline, 4.67; 4-chloroaniline, 4.05; 3-chloroaniline, 3.52; 3-nitroaniline, 2.52; and 4-nitroaniline, 1.13. The basicity of the amino groups in 2- and 4-aminopyridines cannot be measured directly, as the ring nitrogen atom is the more basic and undergoes preferential protonation (33); values estimated from the Hammett equation (34) are 2.3 for 2-amino- and 2.0 for 4-amino-pyridine. These examples suggest that amines with pK_a above 2.4 undergo *N,N*-bis(benzotriazolylmethylation) whereas less basic amines give only *N*-mono(benzotriazolylmethylated) derivatives **2** under the conditions applied.

Attempted use of aliphatic aldehydes other than formaldehyde to give *N,N*-bis(benzotriazolylalkylated) aromatic amines failed. Complex and undefined mixtures were always obtained (TLC, NMR), probably because of self-condensation, possibly catalyzed by benzotriazole and (or) amines. Heating benzotriazole with propionaldehyde in acetic acid formed 2,6-diethyl-4-(benzotriazol-1-yl)-5-methyl-1,3-dioxane (35). Attempted bis(benzotriazolylalkylation) of aliphatic amines was also previously reported to fail (1).[2]

Certain *o*-substituted anilines afford cyclic products: *o*-phenylenediamine with four molar equivalents of benzotriazole and excess of formaldehyde gave cycloadduct **8** instead of the expected tetra(benzotriazolylmethylated) derivative. Such tetraadducts resulted from Mannich reactions of *o*-phenylenediamine with pyrazoles (24). Similarly, bis(benzotriazolylmethylation) of 2-aminobenzyl alcohol gave adduct **9**.

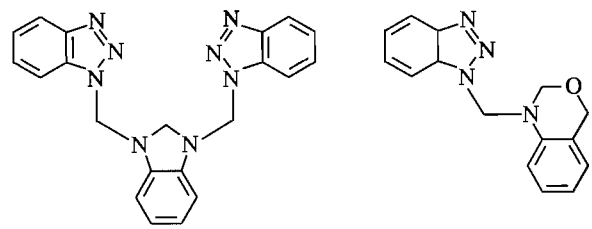

8 **9**

Structures **8** and **9**

Isomerization and stability of *N,N*-bis(benzotriazolylmethyl)anilines

The rapid equilibration of *N*-(1-benzotriazol-1-yl-alkyl)-amines with their benzotriazol-2-yl analogs in solution is well known (36, 37). As expected, we found that all three isomers **5**, **6**, and **7** are present in solutions of the newly synthesized *N,N*-bis(benzotriazolylmethyl)anilines. In the ^1H NMR spectra, the methylene groups of different isomers resonate as easily recognizable singlets at slightly different field; two singlets

TABLE 2. Analytical samples of mixtures of isomeric *N,N*-bis(benzotriazolylmethyl)arylamines **5**, **6**, and **7**

No.	Ar	Molecular formula	Recrystallization		Melting point (°C)	Yield[a] (%)	Analyses (%) Found (Calculated)		
			Solvent	Crystal form			C	H	N
a	Ph	$C_{20}H_{17}N_7$	Ether	Prisms	129	40	67.2 (67.6)	4.7 (4.8)	27.6 (27.6)
b	4-MeC_6H_4	$C_{21}H_{19}N_7$	Ether	Needles	139	25	67.9 (68.3)	5.1 (5.2)	26.5 (26.5)
c	4-BuC_6H_4	$C_{24}H_{25}N_7$		Oil	—	—	69.8 (70.0)	6.2 (6.1)	24.0 (23.8)
d	4-$MeOC_6H_4$	$C_{21}H_{19}N_7O$	THF	Prisms	120	55	65.7 (65.4)	5.0 (5.0)	25.7 (25.4)
e	4-$Me_2NC_6H_4$	$C_{22}H_{22}N_8$	THF	Needles	163	62	66.3 (66.3)	5.6 (5.6)	28.5 (28.1)
f	4-ClC_6H_4	$C_{20}H_{16}N_7Cl$	Dioxane	Polyhedrons	114	73	61.7 (61.6)	4.1 (4.1)	25.3 (25.2)
g	3-ClC_6H_4	$C_{20}H_{16}N_7Cl$	THF	Prisms	106	32	61.3 (61.6)	4.1 (4.1)	25.2 (25.2)
h	3-$O_2NC_6H_4$	$C_{20}H_{16}N_8O_2$	Methanol	Prisms	158	25	60.1 (60.0)	4.0 (4.0)	27.8 (28.0)
i	2-MeC_6H_4	$C_{21}H_{19}N_7$	Ether	Needles	115	58	68.5 (68.3)	5.2 (5.2)	26.4 (26.5)
j	2-EtC_6H_4	$C_{22}H_{21}N_7$		Oil	—	—	[b] (68.9)	[b] (5.5)	[b] (25.6)
k	2,6-$Me_2C_6H_3$	$C_{26}H_{29}N_7$	Ether	Prisms	168	68	70.9 (71.0)	6.7 (6.7)	22.3 (22.3)

[a]Yields calculated for the crystalline samples; oily mixtures of isomers **5**, **6**, and **7** were obtained in 100% yield.
[b]Rapid hydrolysis of the product in air made its CHN analysis impossible.

TABLE 3. Methylene proton resonances[a] and composition of the mixtures of *N,N*-bis(benzotriazolylmethyl)arylamine isomers **5**, **6**, and **7** formed initially and after recrystallization

No.	Ar	Chemical shifts				Composition (%) of crude mixtures			Composition (%) of anal. samples[b]		
		5	⟵ **6** ⟶		**7**	**5**	**6**	**7**	**5**	**6**	**7**
a	Ph	6.21	6.31	6.53	6.57	62	34	4	58	35	7
b	4-MeC_6H_4	6.23	6.33	6.56	6.60	58	40	2	94	6	0
c	4-BuC_6H_4	6.14	6.27	6.47	6.53	54	36	10	54	36	10
d	4-$MeOC_6H_4$	6.06	6.18	6.39	6.46	65	31	4	100	0	0
e	4-$Me_2NC_6H_4$	6.04	6.16	6.38	6.45	66	32	2	98	2	0
f	4-ClC_6H_4	6.14	6.22	6.40	6.47	43	45	12	50	40	10
g	3-ClC_6H_4	6.18	6.26	6.44	6.50	49	46	5	54	40	6
h	3-NO_2	6.36	6.40	6.55	6.60	52	46	2	75	32	3
i	2-MeC_6H_4	5.97	5.99	6.22	6.29	73	19	8	83	14	3
j	2-EtC_6H_4	6.00	6.01	6.14	6.31	67	22	11	[c]	[c]	[c]
k	2,6-$iPr_2C_6H_3$	6.13	6.16	6.27	6.28	69	28	3	68	29	3

[a]Deuteriochloroform solutions; chemical shifts, δ, are given in ppm from TMS.
[b]See Table 2.
[c]The product was not analyzed because of its instability in air.

of equal intensity are observed for isomers **6** due to the two different methylene groups present. The ratio of these methylene group integrals reflects the percentage of the isomers in the investigated sample. Data obtained from the ^1H NMR spectra of the crude products, isolated by simple evaporation of the solvent, are collected in Table 3. The *N,N*-bis(benzotriazol-1-yl) isomers **5** dominate strongly in the product mixtures deriving from anilines bearing electron-releasing groups. However, for the less basic anilines bearing electron-withdrawing groups, the dominance of **5** is less marked and, in some instances, isomers **6** can dominate (4-chloroaniline derivatives).

Surprisingly, in view of literature data (36), and of our previous experience (37, 38), the individual isomers of the *N,N*-bis(benzotriazolylmethyl)arylamines are relatively stable in solution, at room temperature. The crude oily or glassy mixtures of isomers **5**, **6**, and **7** could often be converted into crystalline materials by trituration at room temperature with ether; sometimes cooling to Dry Ice temperatures was required. Solutions of the crystalline samples so obtained, although

Can. J. Chem. Downloaded from www.nrcresearchpress.com by 91.144.44.67 on 09/07/12
For personal use only.

Can. J. Chem. Downloaded from www.nrcresearchpress.com by 91.144.44.67 on 09/07/12
For personal use only.

mixtures of the same isomers, were found to contain them in proportions different than those observed in the solutions of the crude amorphous materials. For example, a solution of the crude 4-toluidine derivative showed an isomer ratio 54:43:3, whereas a solution of the crystalline material showed 86:14:0, for isomers **5***b*, **6***b*, and **7***b* respectively. Recrystallization from THF gave a crystalline sample enriched in isomer **5***b*, which then showed in solution the ratio 94:6:0 (Table 3). Sometimes the pure isomers **5** could be obtained. Crystalline samples enriched in isomers **6** could then be isolated from the filtrates. These various crystalline samples of the *N*,*N*-bis(benzotriazolylmethyl)arylamines were characterized by C, H, N analysis and by melting points (Table 2).

Substituents on the aniline ring of the *N*,*N*-bis(benzotriazolylmethyl)anilines strongly influence the interconversion rates of the individual isomers. Thus, no isomerization was observed when solutions of the aniline (**5–7***a*) and 4-chloroaniline (**5–7***f*) derivatives in chloroform were stored at 25°C for several weeks, whereas fast equilibration (within hours) occurred in chloroform solutions of the 4-anisidine (**5–7***d*) and 4-dimethylaminoaniline (**5–7***e*) derivatives. The isomers in these last two series undergo relatively fast equilibration (days at 20°C) even in the solid state.

Isomerization of **5** to a benzotriazol-2-yl derivative **6** requires the benzotriazolyl N—CH_2 bond to undergo ionization giving the ion pair **4** (Scheme 1), and the ease or difficulty of this ionization determines the reaction barrier. Electron-withdrawing substituents on the aniline ring increase the barrier to isomerization by destabilizing cation **4**: hence the individual isomers are the most stable when derived from amines of low basicity.

The same ionization pattern as for **4** is required in the hydrolysis of *N*,*N*-bis(benzotriazolylmethyl)arylamines (**5–7**) to hydroxymethylbenzotriazole (**1**) and the *N*-mono(benzotriazolylmethyl)arylamines **2**. Indeed, a similar lowering of the hydrolysis rate by electron-withdrawing substituents on the arylamine ring is found. Thus, the *p*-anisidine derivative, **5***d*, undergoes fast hydrolysis in DMSO solution at room temperature, and the aniline derivative, **5***a*, is hydrolysed at 60°C over hours, whereas *N*,*N*-bis(benzotriazolylmethyl)-3-nitroaniline (**5***h*) is inert to hydrolysis even at 60°C. A similar substituent influence was reported previously for the hydrolysis of Mannich bases derived from arylamines and succinimide (6).

Hence the influence of substituents in the aniline ring is diametrically different on (i) the equilibria between the mono- (**2**) and bis-(benzotriazolylmethylated) (**5–7**) arylamines and (ii) the reaction barriers between these products. Electron-releasing substituents on the aniline ring make the amine more basic, and favor formation of the bis(benzotriazolylmethylated) products under the equilibrium conditions, but also cause these products to be less stable (reactive) when the conditions are changed.

Proton and carbon NMR spectra of *N*,*N*-bis(benzotriazolylmethyl)arylamine isomers. Structural considerations

The *N*,*N*-bis(benzotriazolylmethyl)arylamines (isomers **5–7**) show characteristic N—CH_2—N methylene group resonances in their ^{1}H NMR spectra (Table 3). A downfield shift of a methylene group attached to a benzotriazolyl N(2) atom, of about 0.2 ppm in comparison with the isomer with the group at N(1), is a well-established characteristic for the benzotriazolyl series. Thus 1-ethylbenzotriazole (39) exhibits its methylene quartet at δ 4.67 and 2-ethylbenzotriazole (39) at δ 4.82. This behavior is caused by a stronger diamagnetic anisotropy of the 2-benzotriazolyl system. This diamagnetic influence of the 2-benzotriazolyl moiety acts over a long range, causing significant shifts even of the signals of quite distant groups. In isomers **6**, not only is the resonance of the methylene group adjacent to the 2-benzotriazolyl moiety shifted in comparison with isomers **5**, but also that of the 1-benzotriazolylmethyl group is moved downfield by about 0.1 ppm.

Full analysis of the ^{1}H NMR spectra was possible for the *N*,*N*-bis(benzotriazol-1-ylmethyl)arylamines **5**, the major components of the isomer product mixtures (Table 4). Small differences in chemical shifts of the methylene groups of **5** given in Tables 3 and 4 may result from different isomer concentrations in the product samples used. Spectra of the isomerically purest **5** were used for the assignments of Table 4, whereas other isomers of *N*,*N*-bis(benzotriazolylmethyl)arylamines present in the crude product mixtures (Table 3) could have some influence on the chemical shifts of **5**.

The benzotriazolyl H(4) signals are easily distinguished in medium resolution spectra near δ 8.00 ppm, as a doublet with $J_{4,5}$ (average value 8.2 Hz) the same as in 1-methylbenzotriazole (40). The benzotriazolyl H(5)–H(7) form a 6H multiplet regardless of substituent on the arylamine ring.

The two benzotriazol-1-ylmethyl substituents on the arylamine nitrogen atom strongly influence the arylamine ring proton signals. Significant downfield shifts of the *ortho* and *para* proton resonances (Table 7) reflect the electron-withdrawing effect of the benzotriazol-1-ylmethyl moieties, rather than the diamagnetic anisotropy of the benzotriazole system, as they depend strongly on the arylamine ring substituent. The opposite shift of the 6-position proton signals in the two *ortho*-substituted products, **5***i* and **5***j*, compared to all other compounds **5**, is explained by the different geometry caused by steric hindrance.

Although, in the ^{13}C NMR, the 1-benzotriazolylmethylene carbons of isomer **6** resonate at almost the same field as the analogous methylene carbons of isomer **5**, the carbon NMR spectra could nevertheless be fully analyzed even for unseparated isomer mixtures of **5**, **6**, and **7**. (In the proton spectra, overlapping aromatic signals precluded analysis.)

^{13}C NMR spectra of the isolated bis(1,1′-benzotriazolyl) derivatives from aniline (**5***a*), *p*-toluidine (**5***b*), *p*-anisidine (**5***d*), and *p*-*N*,*N*-dimethylaniline (**5***e*), identified the six resonances of the 1-benzotriazolyl moiety. These chemical shifts are close to the values reported for 1-methylbenzotriazole (14), allowing the assignment to the individual 1-benzotriazole carbons (Table 5).

Because of low solubility in chloroform, spectra of the 3-nitroaniline derivatives, **5***h* and **6***h*, were taken in DMSO-d_6. The influence of the nitro group allowed full assignments of the ^{13}C NMR resonances for isomer **6***h*. The strong signals at δ 118.0 and 126.6, and a weak signal at 143.7 in the spectra of **6***h*, by comparison with 2-methylbenzotriazole (41) (117.5, 125.9, and 144.3), were assigned to the carbon pairs C-4,7, C-5,6, and C-3a,7a, respectively. Solvent and the *N*-substituent thus have little influence on the 2-benzotriazolyl carbon shifts. This assumption for the 1-benzotriazolyl system allowed assignment, by comparison with 1-methylbenzotriazole (41), of six of the resonances of **6***h* (Table 6). The remaining six resonances, at δ 110.7, 115.0, 121.1, 130.2, 146.0, and 148.6, were assigned (42) to the 3-nitroaniline ring carbons 2, 4, 6, 5, 1, and 3, respectively.

Comparison of the spectra of adducts **5** and **6** (usually as mixtures of both) with those of the starting arylamines allowed complete assignment of the benzotriazolyl and amine ring

TABLE 4. ^{1}H NMR spectra[a] of *N,N*-bis(benzotriazol-1-ylmethyl)arylamines **5**

No.	N—CH_2—N (s, 4H)	Benzotriazole moiety 4 (d, 2H)	Benzotriazole moiety 5,6,7 (m, 6H)	Ar *ortho*	Ar *meta*	Ar *para*	Substituents
a	6.19	8.01 (8.2)	7.38	7.16 (d, 8.3, 2H)	7.25 (dd, 6.6 and 8.4, 2H)	7.01 (t, 6.6, 1H)	—
b	6.16	8.05 (8.1)	7.38	7.02 (d, 8.7, 2H)	7.08 (d, 8.7, 2H)	—	2.28 (s, 3H)
c	6.14	8.06 (8.1)	7.34	7.04 (d, 8.5, 2H)	7.07 (d, 8.5, 2H)	—	0.91 (t, 7.5, 3H) 1.31 (m, 2H) 1.52 (m, 2H) 2.52 (q, 7.6, 2H)
d	6.09	8.00 (8.3)	7.34	6.95 (d, 9.0, 2H)	6.73 (d, 9.0, 2H)	—	3.68 (s, 3H)
e	6.00	7.98 (7.9)	7.31	6.83 (d, 8.9, 2H)	6.50 (d, 8.9, 2H)	—	2.78 (s, 6H)
f	6.19	8.05 (8.3)	7.41	7.15 (d, 8.0, 2H)	7.23 (d, 8.0, 2H)	—	—
g	6.18	8.01 (8.4)	7.38	6.98 (d, 7.9, 1H) 7.25 (t, 2.1, 1H)	7.18 (t, 8.2, 1H)	7.10 (d, 8.2, 1H)	—
h[b]	6.78	7.99 (d, 8.3, 2H) 7.90 (d, 8.4, 2H) 7.52 (t, 8.4, 2H) 7.38 (t, 8.2, 2H)		8.28 (t, 2.4, 1H) 7.79 (d, 7.7, 1H)	7.46 (t, 8.2, 1H)	7.68 (d, 8.1, 1H)	—
i	5.98	8.04 (8.1)	7.35	6.53 (d, 7.9, 1H)	7.19 (m, 2H)	6.91 (t, 7.3, 1H)	2.11 (s, 3H)
j	5.99	8.02 (8.3)	7.34	6.49 (d, 8.0, 1H)	7.15 (m, 2H)	6.86 (t, 7.8, 1H)	0.99 (t, 7.6, 3H) 2.46 (q, 7.6, 2H)
k	6.13	8.07 (8.5)	7.34	—	7.01 (d, 7.6, 2H)	7.25 (t, 7.6, 1H)	0.70 (d, 6.8, 12H) 2.34 (heptet, 6.8, 2H)

[a]Deuteriochloroform solutions, chemical shifts, δ, are given in ppm from TMS signal, coupling constants *J* (in parentheses) are given in Hz; only the largest coupling constants of the individual signals were considered.
[b]Spectrum taken in DMSO-d_6.

TABLE 5. ^{13}C NMR spectra[a] of *N,N*-bis(benzotriazol-1-yl-methyl)arylamines **5**

No.	CH_2	Benzotriazole moiety C(4)	C(5)	C(6)	C(7)	C(7a)	C(3a)	Ar *ipso*	Ar *ortho*	Ar *meta*	Ar *para*	Substituents
5*a*	63.5	119.9	124.8	127.9	109.6	132.8	146.0	145.6	120.1	129.9	123.7	—
5*b*	63.9	120.0	124.1	127.8	109.8	132.8	146.0	143.1	120.0	130.3	133.6	20.6
5*c*	63.9	119.8	124.2	127.7	109.9	132.8	145.9	143.3	120.4	129.7	138.7	13.9, 22.1, 33.5, 34.7
5*d*	64.5	119.6	123.9	127.5	109.7	132.7	145.8	138.7	123.7	114.7	156.7	55.2
5*e*	64.9	119.3	123.8	127.3	109.9	132.7	145.6	134.8	123.9	113.1	148.0	40.3
5*f*	63.4	129.9	124.3	128.0	109.5	132.6	145.9	144.4	120.6	129.7	128.7	—
5*g*	63.1	120.0	124.5	128.2	109.5	132.6	145.8	146.7	116.9 119.1	130.8 135.6	123.4	—
5*h*[b]	63.2	119.3	124.0	127.6	110.5	132.5	145.3	145.6	115.3 122.0	130.1 148.7	119.4	—
5*i*	64.3	119.8	124.1	127.7	109.6	133.1	145.9	144.0	126.2 134.9	127.2 131.6	127.0	17.7
5*j*	64.9	119.7	124.2	127.7	109.7	133.1	145.7	143.3	126.4 141.0	127.3 129.6	126.9	14.5, 22.8
5*k*	65.8	119.7	123.9	127.6	109.1	132.9	145.7	139.6	147.2	124.6	128.3	24.1, 28.0

[a]Deuteriochloroform solutions; chemical shifts, δ, are given in ppm from the TMS signal.
[b]A solution in DMSO-d_6.

carbon resonances. Peak intensities helped in these assignments. Thus, for the symmetrical molecules of **5**, resonances of the benzotriazole carbons carrying protons and those of *ortho* or *meta* amino ring carbons gave peaks of similar intensity. Derivatives of *ortho*- or *meta*-monosubstituted amines gave arylamine ring signals of intensity half those of the benzotriazolyl C(4)–C(7) carbons. Similar reasoning was applied for isomers **6**. In the mixtures, the exact ratio of **5**:**6** was known from the proton NMR.

As seen in Table 7, in the *N,N*-bis-benzotriazol-1-ylmethyl isomers **5**, the amine *ortho* and *para* carbon resonances are shifted 4–8 and 5–9 ppm downfield, respectively, whereas the *meta* peaks were shifted less than 1 ppm, all compared to the parent arylamines. Dependence of these shifts on other *para* or *meta* substituents in the arylamine ring indicates nonadditive substituent effects on the carbon-13 NMR spectra (42, 43). The benzotriazol-2-ylmethyl substituent possesses an opposite, although smaller, effect as the observed shifts of the *ortho* and

Can. J. Chem. Downloaded from www.nrcresearchpress.com by 91.144.44.67 on 09/07/12
For personal use only.

TABLE 6. ^{13}C NMR spectra[a] of *N*-(benzotriazol-1-ylmethyl)-*N*-(benzotriazol-2-ylmethyl)arylamines **6**

No.	$CH_2Bt(1)$	$CH_2Bt(2)$	Bt(1)	Bt(2)	Arylamine ring				Substituents
					ipso	*ortho*	*meta*	*para*	
6*a*	63.8	70.4	109.6, 120.1, 124.2, 128.0, 132.9, 146.0	118.3, 126.8, and 144.4	145.5	116.4	129.6	122.0	—
6*b*	64.2	70.8	109.8, 120.0, 124.1, 127.9, 132.9, 146.0	118.3, 126.7, and 144.4	143.2	117.0	130.1	131.7	20.4
6*c*	64.1	70.7	109.8, 120.0, 124.0, 127.9, 132.9, 146.0	118.3, 126.7, and 144.4	143.5	116.9	129.5	136.7	13.9, 22.2, 33.5, 34.6
6*d*	64.8	71.7	109.8, 119.9, 124.1, 127.8, 132.9, 146.0	118.3, 126.7, and 144.4	139.2	120.5	114.7	155.6	55.5
6*e*	65.0	71.8	109.9, 119.5, 123.7, 127.3, 132.6, 145.7	118.0, 126.3, and 144.1	135.6	121.0	113.4	147.1	40.5
6*f*	63.5	70.3	109.5, 120.0, 124.3, 128.1, 132.9, 145.9	117.8, 127.0, and 143.9	144.3	118.3	129.4	127.1	—
6*g*	63.3	70.0	109.5, 120.1, 124.5, 128.2, 133.0, 145.9	118.3, 127.0, and 144.5	146.9	114.4 116.6	130.6 135.3	122.0	—
6*h*[b]	63.1	70.3	109.5, 119.2, 124.0, 127.5, 132.6, 145.2	118.0, 126.6, and 143.7	146.0	110.7 121.1	148.6 130.2	115.0	—
6*i*	65.7	72.3	111.3, 119.3, 122.9, 127.6, 133.1, 146.0	118.4, 126.7, and 144.3	143.7	126.5 135.3	127.5 131.5	126.9	17.5
6*j*	66.1	73.0	110.3, 119.5, 124.1, 127.5, 133.0, 145.9	118.3, 126.7, and 144.4	141.4	126.7 141.4	127.4 129.4	126.8	13.2, 23.8
6*k*	66.0	74.1	109.1, 119.6, 123.8, 127.5, 132.9, 145.7	118.1, 126.5, and 144.4	139.6	147.4	124.5	128.2	23.6, 24.5, and 27.9

[a]Deuteriochloroform solutions; the chemical shifts are given in ppm from TMS signal.
[b]The spectra taken in DMSO-d_6.

TABLE 7. Shifts of proton (**5**) and carbon (**5** and **6**) arylamine ring resonances in relation to free amines

No.	Aniline substituents	Proton NMR[a]			Carbon-13 NMR[b]				Ref.[c]
		ortho	*meta*	*para*	*ipso*	*ortho*	*meta*	*para*	
a	H	0.54	0.13	0.27	−2.9 (−3.0)	5.8 (2.1)	0.9 (0.6)	7.4 (5.7)	46
b	4-Me	0.44	0.13	—	−2.8 (−2.7)	5.6 (2.6)	1.0 (0.8)	5.9 (3.7)	46
c	4-Bu	0.47	0.13	—	−0.7 (−0.5)	5.2 (1.7)	0.6 (0.4)	5.8 (3.8)	[d]
d	4-MeO	0.33	0.02	—	−3.6 (−3.1)	8.4 (5.2)	0.0 (0.0)	5.7 (4.6)	46
e	4-Me_2N	0.16	−0.11	—	−3.2 (−2.4)	7.4 (4.5)	−2.5 (−2.2)	3.3 (2.4)	[d]
f	4-Cl	0.59	0.02	—	−0.8 (−0.9)	4.3 (2.0)	0.7 (0.4)	5.9 (4.3)	47
g	3-Cl	0.50	0.16	0.41	−1.2 (−1.0)	3.6, 4.3 (1.1, 1.8)	0.5, 1.0 (0.3, 0.5)	5.3 (3.9)	47
h[e]	3-NO_2	0.81 0.80	0.25	0.29	−3.3 (−2.9)	7.6, 1.9 (3.0, 1.0)	0.9, 0.1 (1.0, 0.0)	8.8 (4.4)	[d]
i	2-Me	−0.10	0.17 0.18	0.22	−2.4 (−2.7)	11.8, 13.5 (12.1, 13.9)	0.5, 1.4 (0.8, 1.3)	10.2 (10.1)	46
j	2-Et	−0.15	0.10 0.10	0.22	−2.9 (−1.0)	11.3, 13.4 (11.0, 13.0)	0.7, 1.1 (0.6, 1.3)	8.2 (8.3)	47
k	2,6-iPr_2	—	−0.10	0.47	−0.7 (−0.7)	15.0 (15.2)	2.0 (1.9)	9.8 (9.7)	47

[a]Data from Table 4 were compared with the spectra of arylamines taken for their $CDCl_3$ solution (0.5 M).
[b]Data for isomer **6** are given in parentheses.
[c]Literature data on ^{13}C NMR of N-unsubstituted arylamines taken for comparison.
[d]^{13}C NMR spectra of the reference amines were taken in this laboratory.
[e]Spectrum in DMSO-d_6.

Can. J. Chem. Downloaded from www.nrcresearchpress.com by 91.144.44.67 on 09/07/12
For personal use only.

Can. J. Chem. Downloaded from www.nrcresearchpress.com by 91.144.44.67 on 09/07/12
For personal use only.

para carbon resonances of **6** were only 2–5 and 3–6 ppm, respectively. The *ipso* carbons were usually shifted about 1–3 ppm downfield, in relation to the starting amines, in both **5** and **6**. For comparison, substitution of the aniline amino protons by two methyl groups shifts the *ipso*, *ortho*, *meta*, and *para* carbon-13 NMR signals (44) 4.3, −2.0, 0.1, and −1.5 ppm, respectively. Therefore the benzotriazol-1-ylmethyl substituent is electron withdrawing, whereas the benzotriazol-2-ylmethyl group demonstrates weak electron-releasing ability. Benzotriazol-2-yl as a substituent on the benzene ring was reported (45) to possess a strong electron-withdrawing influence (σ_p = 0.5).

Much stronger shifts of the *ortho* and *para* carbon signals in the spectra of the mono- and di-*ortho*-substituted products, **5***i–k* and **6***i–k*, result from steric hindrance at the amino group, which causes distortion of the $(BtCH_2)_2N$ group around the N—C(aryl) bond to such degree that overlapping of the nitrogen electron pair with the aryl π orbital is at least significantly decreased (Fig. 1). Similarly, the *ortho* and *para* carbon resonances of *N*,*N*-2,6-tetramethylaniline (48) are shifted downfield by 14.2 and 7.3 ppm, respectively, in comparison with 2,6-dimethylaniline. The isopropyl groups of **6***j* show as two methyl doublets in the ^{1}H NMR (δ 0.69 and 0.77, J = 6.8 Hz) and as two peaks in the ^{13}C NMR spectra (δ 23.6 and 24.5), which lends strong support to the structure proposed (Fig. 1).

Experimental

Melting points were determined with a hot-stage microscope and are uncorrected. The ^{1}H and ^{13}C NMR spectra were recorded on a Varian VXR-300 instrument in $CDCl_3$ solution (except when stated otherwise) with $(CH_3)_4Si$ as internal standard. Dry ether or THF means the solvent refluxed with sodium–benzophenone and distilled prior to use. 1-(Hydroxymethyl)benzotriazole was prepared according to the literature method (49). Benzotriazole and all amines used were commercial specimens.

Preparation of N-*(benzotriazol-1-ylmethyl)-4-butylaniline (2*c*)*

To a stirred solution of benzotriazole (7.36 g, 60 mmol) and 4-butylaniline (8.96 g, 60 mmol) in water (60 mL) and ethanol (20 mL) was added 37% formaldehyde (4.50 mL, 60 mmol). A white precipitate started to form immediately. The mixture was stirred at 25°C for 2 h and then stored at 5°C overnight. The precipitate was filtered off, washed with aqueous ethanol (1:1, 20 mL) followed by ethanol (10 mL), and dried in air at room temperature to give pure **2***c* (15.89 g, 94%) as white needles, mp 136°C; ^{1}H NMR (DMSO-d_6) δ: 0.86 (t, J = 7.3 Hz, 3H), 1.27 (hextet, J = 7.5 Hz, 2H), 1.46 (quintet, J = 8.1 Hz, 2H), 2.41 (t, J = 7.3 Hz, 2H), 6.05 (d, J = 8.0 Hz, 2H), 6.40 (t, J = 8.0 Hz, 1H, NH), 6.79 (d, J = 8.6 Hz, 2H), 6.92 (d, J = 8.4 Hz, 2H), 7.31 (t, J = 6.9 Hz, 1H), 7.41 (t, J = 6.9 Hz, 1H), 7.88 (d, J = 8.3 Hz, 1H), 7.95 (d, J = 8.4 Hz, 1H); ^{13}C NMR (DMSO-d_6) δ: 13.9, 22.1, 33.7, 34.5, 58.2, 110.4, 113.2, 119.3, 124.0, 127.4, 129.0, 132.4, 132.9, 143.2, 146.0. Anal. calcd. for $C_{17}H_{20}N_4$: C 72.83, H 7.19, N 19.98; found: C 72.68, H 7.22, N 20.15.

Other N-*(benzotriazol-1-ylmethyl)anilines 2 prepared according to the procedure given for 4-butylaniline*

N-(Benzotriazol-1-ylmethyl)aniline (**2***a*) was obtained in 82% yield as white needles, mp 139°C (lit. (4) mp 138–139°C); ^{1}H NMR (DMSO-d_6) δ: 6.07 (d, J = 7.1 Hz, 2H), 6.61 (t, J = 7.3 Hz, 1H), 6.85 (d, J = 7.7 Hz, 2H), 7.09 (m, 3H), 7.31 (t, J = 8.2 Hz, 1H), 7.45 (dd, J = 7.3 and 8.3 Hz, 1H), 7.94 (d, J = 8.3 Hz, 1H), 8.01 (d, J = 8.3 Hz, 1H); ^{13}C NMR (DMSO-d_6) δ: 57.2, 110.9, 112.8, 117.9, 119.0, 123.7, 126.9, 128.9, 132.2, 145.5, 145.7.

N-*(Benzotriazol-1-ylmethyl)*-p-*anisidine (2*d*)* was obtained in 87% yield as colorless needles, mp 140°C; ^{1}H NMR (DMSO-d_6) δ: 3.59 (s, 3H), 6.12 (d, J = 7.5 Hz, 2H), 6.73 (d, J = 9.0 Hz, 2H), 6.80 (d, J = 9.0 Hz, 2H), 7.00 (t, J = 7.5 Hz, 1H, NH), 7.38 (t, J = 8.0 Hz, 1H), 7.54 (t, J = 8.0 Hz, 1H), 8.03 (d, J = 8.3 Hz, 1H), 8.09 (d, J = 8.2 Hz, 1H); ^{13}C NMR (DMSO-d_6) δ: 55.4, 58.5, 110.8, 114.3, 114.6, 119.2, 123.8, 127.0, 132.3, 139.3, 145.9 and 152.5. Anal. calcd. for $C_{14}H_{14}N_4O$: C 66.13, H 5.55, N 22.03; found: C 66.11, H 5.54, N 22.18.

N-*(1-Benzotriazol-1-ylmethyl)-3-chloroaniline (2*g*)* was obtained in 92% yield as colorless prisms, mp 176°C; ^{1}H NMR (DMSO-d_6) δ: 6.09 (d, J = 7.1 Hz, 2H, CH_2), 6.60 (d, J = 7.9 Hz, 1H), 6.78 (d, J = 7.9 Hz, 1H), 6.89 (s, 1H), 7.04 (t, J = 8.0 Hz, 1H), 7.35 (dd, J = 8.4 and 7.3 Hz, 1H), 7.50 (m, 2H), 7.97 (d, J = 8.4 Hz, 1H), 8.02 (d, J = 8.4 Hz, 1H); ^{13}C NMR (DMSO-d_6) δ: 56.6 (CH_2), 110.9, 111.3, 112.4, 117.4, 119.1, 123.8, 127.1, 130.2, 132.1, 134.0, 145.6, and 147.2. Anal. calcd. for $C_{13}H_{10}ClN_4$: C 60.59, H 3.91, N 21.74; found: C 60.98, H 4.23, N 21.64.

N-*(Benzotriazol-1-ylmethyl)-2-methylaniline (2*i*)* was obtained in 93% yield as colorless prisms, mp 146°C; ^{1}H NMR (DMSO-d_6) δ: 2.16 (s, 3H), 6.14 (d, J = 6.8 Hz, 2H), 6.8 (m, 2H), 6.94 (m, 3H), 7.32 (t, J = 8.2 Hz, 1H), 7.45 (dd, J = 8.3 and 7.0 Hz, 1H), 7.95 (d, 8.4 Hz, 1H), 8.05 (d, 8.4 Hz, 1H); ^{13}C NMR (DMSO-d_6) δ: 17.7, 57.4, 110.2, 111.2, 117.7, 119.0, 122.2, 123.7, 126.6, 126.9, 130.1, 132.2, 143.4, 145.6. Anal. calcd. for $C_{14}H_{14}N_4$: C 70.57, H 5.92, N 23.51; found: C 70.19, H 5.85, N 23.57.

N-*(Benzotriazol-1-ylmethyl)-2-ethylaniline (2*j*)* was obtained in 92% yield as colorless needles, mp 110°C; ^{1}H NMR δ: 1.14 (t, J = 7.5 Hz, 3H), 2.50 (q, J = 7.5 Hz, 2H), 5.36 (t, J = 7.0 Hz, 1H), 6.12 (d, J = 7.0 Hz, 2H), 6.70 (m, 1H), 7.01 (m, 3H), 7.28 (t, J = 8.3 Hz, 1H), 7.37 (t, J = 8.0 Hz, 1H), 7.71 (d, J = 8.2 Hz, 1H), 7.98 (d, J = 8.0 Hz, 1H); ^{13}C NMR δ: 13.1 (Et), 23.7 (Et), 58.1 (N—CH_2—N), 109.9, 111.5, 119.4, 119.4, 119.6, 123.9, 126.9, 127.3, 128.3, 128.6, 132.4, 142.2, 146.1. Anal. calcd. for $C_{15}H_{16}N_4$: C 71.40, H 6.39, N 22.21; found: C 71.81, H 6.34, N 22.23.

Reaction of N-*(benzotriazol-1-ylmethyl)-4-butylaniline (2*c*) with 1-(hydroxymethyl)benzotriazole at 22°C*

A mixture of 1-(hydroxymethyl)benzotriazole (0.75 g, 5 mmol) and **2***c* (1.40 g, 5 mmol) was dissolved in DMSO-d_6/$CDCl_3$ (3 + 3 mL). A sample of such solution (0.2 mL) diluted with deuteriochloroform (0.4 mL) was transferred into an NMR tube and the reaction monitored by ^{1}H NMR. The sample was stored at 22°C in intervals between the NMR measurements. With time, the intensity of the methylene signals of the starting materials (both at δ ca. 6.05) decreased, whereas new signals at a lower field (the major one at δ 6.25) appeared and grew in intensity. Integrals representing the percentage of the starting materials in the reaction mixture as a function of time are given in the discussion part of the paper.

Investigation of the reaction equilibria between 1-(hydroxymethyl)-benzotriazole and arylamines in DMSO

A solution of arylamine (2.5 mmol), 1-(hydroxymethyl)benzotriazole (0.75 g, 5 mmol), and DMSO-d_6 (0.71 mL, 10 mmol) was heated at 100°C under argon for 1 h. A sample of the solution obtained (0.1 mL) was diluted with deuteriochloroform (0.5 mL) and the NMR spectrum was taken with precise integrals to get the molar ratio between the compounds in the mixture. In general, the NMR region that usually focused most attention was that at δ 6.00–6.60, where resonances of the methylene groups of the products and starting materials were observed. Very often, analysis of other signals in the spectra (aryl protons, substituents on the amine ring) gave help and further support in the estimation of percentage of the starting materials and products present in the reaction mixtures. In some instances, integrals of the carbon resonances in the ^{13}C NMR spectra of the mixtures were used for the same purpose. The data obtained are collected in Table 1.

Reaction of N-*(benzotriazol-1-ylmethyl)-4-butylaniline (2*c*) with 1-(hydroxymethyl)benzotriazole (1) in refluxing toluene*

A solution of **1** (1.49 g, 10 mmol) and **2***c* (2.80 g, 10 mmol) in

toluene (30 mL) was heated at reflux for 3 h under a Dean–Stark water trap. The solvent was evaporated at 90°C (rotary vacuum evaporator) to give analytically pure *N*,*N*-bis(benzotriazolylmethyl)-4-butylaniline in 100% yield as a viscous oil (Table 2).

N,N-*Bis(benzotriazolylmethylation) of aromatic amines with benzotriazole and aqueous formaldehyde. General procedure*

A mixture of benzotriazole (11.91 g, 100 mmol), an aromatic amine (50 mmol), 37% formaldehyde (11.2 mL, 150 mmol), and toluene (50 mL) was stirred at 60°C for 1 h and then refluxed with a Dean–Stark trap for 3 h. Water (about 11 mL) separated in the trap. The solvent was evaporated under reduced pressure and the residue was heated in vacuum at 90°C for 2 h (by means of a rotary vacuum evaporator) to remove traces of toluene. The viscous oil obtained usually became glassy after cooling to room temperature. The glass could be reversibly liquefied by heating to 100–120°C. In many instances, the glassy product was turned into a crystalline material upon trituration with dry ether. Isomer mixtures **5**, **6**, **7***a–g* and *k* (Tables 2 and 3) were obtained by this procedure.

N,N-*Bis(benzotriazolylmethylation) of 3-nitroaniline*

A mixture of benzotriazole (23.82 g, 200 mmol), 3-nitroaniline (13.81 g, 100 mmol), 37% formaldehyde (17.98 mL, 240 mmol), and toluene (200 mL) was stirred and heated to reflux under a Dean–Stark trap for 2 weeks. The precipitate obtained was filtered off from the hot mixture, washed with ether, and dried in a vacuum oven to give analytically pure *N*-(benzotriazol-1-ylmethyl)-3-nitroaniline **2***h* (5.02g, 19%) as yellow needles, mp 209°C; ^{1}H NMR (DMSO-d_6) δ: 6.19 (d, J = 7.1 Hz, 2H, CH_2), 7.25 (ddd, J = 8.2, 2.1, and 1.1 Hz, 1H, aniline-H(6)), 7.32 (t, J = 7.8 Hz, 1H, aniline-H(5)), 7.37 (td, J = 8.2 and 1.0 Hz, 1H, Bt-H(5)), 7.44 (ddd, J = 7.8, 2.2, and 1.2 Hz, 1H, aniline-H(4)), 7.53 (td, J = 8.1 and 1.0 Hz, 1H, Bt-H(6)), 7.72 (t, J = 2.1 Hz, 1H, aniline-H(2)), 7.88 (t, J = 7.1 Hz, 1H, N-H), 7.98 (dt, J = 8.4 and 0.9 Hz, 1H, Bt-H(7)), 8.03 (dt, J = 8.4 Hz and 0.9 Hz, 1H, Bt-H(4)); ^{13}C NMR (DMSO-d_6) δ: 56.1 (CH_2), aniline: 106.6, 112.0, 118.9, 121.9, 146.8 and 148.5, Bt: 110.6, 118.8, 123.7, 127.0, 131.9 and 145.4 ppm. Anal. calcd. for $C_{13}H_{11}N_5O_2$: C 58.0, H 4.1, N 26.0; found: C 58.3, H 4.1, N 26.4%.

The filtrate was kept at room temperature for 1 h. The precipitate was filtered off, washed with ether, and dried in a vacuum oven (50°C, 30 Torr; 1 Torr = 133.3 Pa) to give an analytically pure mixture of the isomers containing 75% of *N*,*N*-bis(benzotriazol-1-yl-methyl)-3-nitroaniline **5***h* (14.25 g, 36%).

The filtrate obtained from the above sample was stored in a freezer for 3 days. The precipitate obtained was filtered off, washed with ether, and dried in a vacuum oven to give an analytically pure sample of the isomers containing 80% of *N*-(benzotriazol-2-ylmethyl)-*N*-(benzotriazol-1-ylmethyl)-3-nitroaniline **6***h* (7.81 g, 20%).

N,N-*Bis(benzotriazolylmethylation) of 2-methylaniline*

A stirred mixture of benzotriazole (2.38 g, 20 mmol), *o*-toluidine (1.07 mL, 10 mmol), 37% formaldehyde (4.0 mL, 53 mmol), and cyclohexane (30 mL) was heated at reflux under a Dean–Stark water trap for 4 h. The solvent was evaporated (rotary vacuum evaporator) and the residual oil was triturated under argon with dry ether (20 mL). The crystalline material obtained was filtered off and dried in a vacuum oven to give an analytically pure mixture of isomeric *N*,*N*-bis(benzotriazolylmethyl)-2-methylanilines **5–7***i* (1.17 g, 31%) (Table 2).

N,N-*Bis(benzotriazolylmethylation) of 2-ethylaniline*

A solution of *N*-(benzotriazol-1-ylmethyl)-2-ethylaniline (1.26 g, 5 mmol) and 1-(hydroxymethyl)benzotriazole (0.74 g, 5 mmol) in toluene (20 mL) was heated at reflux under a Dean–Stark trap for 2 h. The solvent was evaporated by heating the solution at 90°C under pressure of 35 Torr. According to ^{1}H NMR, the product obtained was a mixture of *N*,*N*-bis(benzotriazolylmethyl)-2-ethylaniline, *N*-(benzotriazol-1-ylmethyl)-2-ethylaniline, and benzotriazole in a molar ratio of 1:1:1.

A solution of *N*-(benzotriazol-1-ylmethyl)-2-ethylaniline (2.52 g, 10 mmol) and 1-(hydroxymethyl)benzotriazole (1.49 g, 10 mmol) in chloroform (100 mL) was refluxed for 8 h in a Soxhlet apparatus filled with anhydrous magnesium sulfate (6.00 g, 50 mmol) to trap the water formed. The solvent was evaporated to give analytically pure *N*,*N*-bis(benzotriazolylmethyl)-2-ethylaniline, as a mixture of its three isomers (Table 3).

Condensation of benzotriazole with formaldehyde and o-phenylenediamine. Preparation of 1,3-bis(benzotriazol-1-yl-methyl)-2,3-dihydrobenzimidazole (8)

To a stirred solution of *o*-phenylenediamine (5.41 g, 50 mmol) and benzotriazole (11.19 g, 100 mmol) in toluene (50 mL) was added a 37% solution of formaldehyde (14.98 mL, 200 mmol) and the mixture obtained stirred at 60°C for 1 h followed by reflux under a Dean–Stark trap for 16 h. The solvent was evaporated (vacuum rotary evaporator) to give an oil, which turned into a glassy material upon cooling to room temperature. The crude product was dissolved in boiling ethanol–dioxane (200 + 200 mL) and the solution was stored at −5°C for 24 h to give **8** (4.26 g, 22%) as colorless prisms, mp 178–179°C; ^{1}H NMR δ: 4.94 (s, 2H), 5.87 (s, 4H), 6.82 (m, 4H), 7.34 (m, 2H), 7.42 (m, 4H), 8.01 (d, J = 8.2 Hz, 2H); ^{13}C NMR δ: 58.9, 71.4, 106.8, 108.9, 118.9, 118.8, 119.7, 123.3, 127.0, 131.8, 137.9, 145.0. Anal. calcd. for $C_{21}H_{18}N_8$: C 65.95, H 4.74, N 29.30; found: C 65.76, H 4.73, N 29.08.

*Condensation of benzotriazole with formaldehyde and 2-aminobenzyl alcohol: formation of 1-(benzotriazol-1-ylmethyl)-1,4-dihydro-2*H*-3,1-benzoxazine (9)*

A mixture of 2-aminobenzyl alcohol (4.92 g, 40 mmol), benzotriazole (4.48 g, 40 mmol), 37% formaldehyde (7.49 mL, 100 mmol), and toluene (40 mL) was stirred at 60°C for 1 h followed by reflux under a Dean–Stark trap for 2 h. The solvent was evaporated under reduced pressure (rotary vacuum evaporator) and the residue was dried at 90°C under vacuum (50 Torr) for 30 min.

The crude product was obtained as a very sticky oil (10.99 g), and crystallized from ethanol to give pure **9** (7.20 g, 67%), colorless prisms, mp 122°C; ^{1}H NMR δ: 4.68 (s, 2H, $ArCH_2O$), 4.87 (s, 2H, NCH_2O), 6.09 (s, 2H, NCH_2N), 6.89 (d, J = 7.8 Hz, 1H, Ar), 6.98 (m, 1H, Ar), 7.26 (m, 2H, Ar), 7.34 (m, 3H, Bt), 8.04 (d, J = 7.7 Hz, 1H, Bt) ppm; ^{13}C NMR δ: 66.0 (CH_2), 67.2 (CH_2), 79.9 (CH_2), Bt: 109.9, 120.0, 123.9, 127.5, 132.6, and 146.2, Ar: 118.6, 122.2, 125.3, 127.7, and 141.7 ppm. Anal. calcd. for $C_{15}H_{14}N_4O$: C 67.65, H 5.30, N 21.04; found: C 67.57, H 5.26, N 21.16.

Hydrolysis of N,N-*bis(benzotriazolylmethyl)arylamines by deuterium oxide*

To a solution of an *N*,*N*-bis(benzotriazolylmethyl)arylamine (0.05 mmol) in DMSO-d_6 (0.5 mL) was added deuterium oxide (0.09 mL, 5 mmol) and the solution kept at elevated temperature for the period of time specified below. NMR spectra (^{1}H and ^{13}C) taken for the solution allowed estimation of the percentage of *N*,*N*-bis(benzotriazolylmethyl)arylamine (isomers **5**, **6**, and **7**) as well as those of the hydrolysis products (O or N deuterated) analogues of **1** and **2**) in the reaction mixture. The results obtained are as follows:

4*d* (Ar = 4-$MeOC_6H_4$):	complete hydrolysis at 20°C within 2 h
5*b* (Ar = 4-MeC_6H_4):	no reaction at 20°C after 24 h, 32% (15 min) and 88% (60 min) of hydrolysis at 60°C
5*a* (Ar = Ph):	8.5% (1 h) and 37% (12 h) of hydrolysis at 60°C
5*f* (Ar = 4-ClC_6H_4):	46% (4 h) and 76% (12 h) of hydrolysis at 60°C
5*h* (Ar = 3-$NO_2C_6H_4$)	no evidence of hydrolysis after 24 h at 60°C

1. (*a*) R. S. VARMA. Indian J. Chem. Sect. B: **14B**, 718 (1976); (*b*) A. R. KATRITZKY, S. RACHWAL, and B. RACHWAL. J. Chem. Soc. Perkin Trans. 1, 799 (1987).
2. A. R. KATRITZKY and B. PILARSKI. Org. Prep. Proced. Int. In press.

Can. J. Chem. Downloaded from www.nrcresearchpress.com by 91.144.44.67 on 09/07/12
For personal use only.

3. J. J. LICARI, L. W. HARTZEL, G. DOUGHERTY, and F. R. BENSON. J. Am. Chem. Soc. **77**, 5386 (1955).
4. A. R. KATRITZKY, B. PILARSKI, and L. UROGDI. J. Chem. Soc. Perkin Trans. 1. In press.
5. G. CHEN and W. ZHONG. Gaodeng Xuexiao Huaxue Xuebao, **2**, 450 (1981); Chem. Abstr. **96**, 217672n (1982).
6. H. BUNDGAARD and M. JOHANSEN. Int. J. Pharm. **8**, 183 (1981).
7. S. BAHADUR, A. K. GOEL, and R. S. VARMA. J. Indian Chem. Soc. **53**, 1163 (1976).
8. M. GORCZYCA, B. LUCKA-SOBSTEL, A. ZEJC, I. ZGORNIAK-NOWOSIELSKA, M. MARCISZEWSKA, and A. GATKIEWITZ. Acta Pharm. Jugosl. **28**, 143 (1978).
9. X. XU and G. CHEN. Hauxue Xuebao, **40**, 362 (1982).
10. V. B. KUMAR, B. A. RAO, and M. V. REDDY. Indian J. Chem. Sect. B, **24B**, 889 (1985).
11. R. S. VARMA and D. CHATTERJEE. J. Indian Chem. Soc. **60**, 1077 (1983).
12. R. S. VARMA, V. A. SINGH, H. N. VERMA, and M. M. A. A. KHAN. J. Indian Chem. Soc. **62**, 475 (1985).
13. R. S. VARMA and V. A. SINGH. J. Chem. Soc. Pak. **6**, 133 (1984).
14. R. S. VARMA and A. KAPOOR. Curr. Sci. **46**, 779 (1977); Chem. Abstr. **88**, 62321f (1978).
15. R. R. MOHAN, R. AGARWAL, and V. S. MISRA. Indian Drugs, **21**, 90 (1983).
16. S. YU. SOLOVEVA, S. M. RAMSH, and A. I. GINAK. Khim. Geterotsikl. Soedin. 1204 (1983).
17. G. MAZZONE, F. BONINA, and G. BLANDINO. Farmaco, Ed. Sci. **36**, 1004 (1981); Chem. Abstr. **96**, 122698 (1982).
18. R. S. VARMA, S. BAHADUR, and A. K. AGNIHOTRI. J. Chem. Eng. Data, **26**, 103 (1981).
19. R. S. VARMA. Curr. Sci. **47**, 416 (1978).
20. R. S. VARMA and A. K. AGNIHOTRI. J. Indian Chem. Soc. **56**, 162 (1979).
21. E. HOLBOVA, V. SUTORIS, and G. BLOCKINGER. Chem. Zvesti, **30**, 195 (1976).
22. L. C. LEE, K. C. LIU, and T. T. HSIE. T'ai-wan Yao Hsueh Tsa Chih, **30**, 63 (1978).
23. K. C. LIU, H. H. CHEN, C. H. HONG, and K. N. LEUNG. T'ai-wan Yao Hsueh Tsa Chih, **34**, 108 (1982).
24. W. L. DRIESSEN. Recl. Trav. Chim. Pays-Bas, **101**, 441 (1982).
25. H. L. BLONK, W. L. DRIESSEN, and J. REEDIJK. J. Chem. Soc. Dalton Trans. 1699 (1985).
26. E. VERTESI, B. NAGY, Z. NAGY, A. VASS, L. KULCSAR, J. BESAN, and V. MIHALYFI. Hung. Pat. 34, 103 (1985); Chem. Abstr. **104**, 129929e (1986).
27. H. H. JAFFE. Chem. Rev. **53**, 191 (1953).
28. R. E. HESS. J. Org. Chem. **36**, 2201 (1971).
29. M. CHARTON. J. Am. Chem. Soc. **91**, 6649 (1969).
30. M. CHARTON. J. Org. Chem. **36**, 882 (1971).
31. G. P. BOLDRINI, M. PANUNZIO, and A. UMANIRONCHI. Synthesis, 733 (1974).
32. J. M. VANDENBELT, C. HENRICH, and S. G. VANDENBERG. Anal. Chem. **25**, 726 (1954).
33. J. ELGUERO, C. MARZIN, A. R. KATRITZKY, and P. LINDA. The tautomerism of heterocycles. Academic Press, New York. 1976. p. 154.
34. R. STEWART and M. G. HARRIS. J. Org. Chem. **43**, 3123 (1978).
35. A. R. KATRITZKY, S. RACHWAL, and B. RACHWAL. J. Chem. Soc. Perkin Trans. 1, 791 (1987).
36. I. R. L. SMITH and J. S. SADD. J. Chem. Soc. Perkin Trans. 1, 1181 (1975).
37. A. R. KATRITZKY, K. YANNAKOPOULOU, W. KUZMIERKIEWICZ, J. M. AURRECOECHEA, G. J. PALENIK, A. E. KOZIOL, and M. SZCZESNIAK. J. Chem. Soc. Perkin Trans. 1, 2673 (1987).
38. A. R. KATRITZKY and K. YANNAKOPOULOU. Heterocycles, **28**, 1121 (1989).
39. P. J. ABBOTT, R. M. ACHESON, M. W. FOXTON, N. R. RAULINS, and G. E. ROBINSON. J. Chem. Soc. Perkin Trans. 1, 2182 (1972).
40. M. H. PALMER, R. H. FINDLAY, S. M. F. KENNEDY, and P. S. MCINTYRE. J. Chem. Soc. Perkin Trans. 2, 1695 (1975).
41. J. ELGUERO, R. M. CLARAMUNT, R. GARCERAN, S. JULIA, L. AVILA, and J. M. DEL MAZO. Magn. Reson. Chem. **25**, 260 (1987).
42. J. BROMILOW, R. T. C. BROWNLEE, D. J. CRAIK, and M. SADEK. Magn. Reson. Chem. **24**, 862 (1986).
43. J. BROMILOW, R. T. C. BROWNLEE, D. J. CRAIK, M. SADEK, and R. W. TAFT. J. Org. Chem. **45**, 2429 (1980).
44. D. E. EWING. Org. Magn. Reson. **12**, 499 (1979).
45. I. CEPCIANSKY and J. MAJER. Collect. Czech. Chem. Commun. **34**, 72 (1969).
46. A. T. BALABAN, A. DINCULESCU, J. ELGUERO, and R. FAURE. Magn. Reson. Chem. **23**, 553 (1985).
47. Sadtler Standard Carbon-13 NMR Spectra Catalog. 1976; (*a*) 200C; (*b*) 190C; (*c*) 230C; (*d*) 3017C.
48. P. C. LAUTERBUR. J. Chem. Phys. **38**, 1415 (1963).
49. J. H. BURCKHALTER, V. C. STEPHENS, and L. A. R. HALL. J. Am. Chem. Soc. **74**, 3868 (1952).

Can. J. Chem. Downloaded from www.nrcresearchpress.com by 91.144.44.67 on 09/07/12
For personal use only.

A versatile method for the *N,N*-dialkylation of aromatic amines via Grignard reactions on *N,N*-bis(benzotriazolylmethyl)arylamines

ALAN R. KATRITZKY,[1] STANISLAW RACHWAL, AND JING WU
Department of Chemistry, University of Florida, Gainesville, FL 32611, U.S.A.

Received April 17, 1989

ALAN R. KATRITZKY, STANISLAW RACHWAL, and JING WU. Can. J. Chem. **68**, 456 (1990).

Grignard reactions of *N,N*-bis(benzotriazolylmethyl)arylamines afford the corresponding *N,N*-dialkylarylamines in high yields. Electron-releasing substituents on the aryl ring facilitate the reaction. Arylamines are *N,N*-dialkylated with two different alkyl groups by a stepwise procedure: *N*-benzotriazolylmethylation of an amine followed by a Grignard reaction to introduce the first alkyl group, and repetition of the same procedure to introduce the second alkyl group. Grignard reagents derived from 1,4-dihalobutane, upon reaction with *N,N*-bis(benzotriazolylmethyl)arylamines, give the corresponding *N*-aryl-hexahydroazepines together with acyclic products.

Key words: azepine, tertiary arylamines.

ALAN R. KATRITZKY, STANISLAW RACHWAL et JING WU. Can. J. Chem. **68**, 456 (1990).

Les *N,N*-bis(benzotriazolylméthyl)arylamines soumises à des réactions de Grignard fournissent les *N,N*-dialkylarylamines correspondantes avec des rendements élevés. La présence de substituants électrodonneurs sur les noyaux aryles facilite la réaction. Pour arriver à la *N,N*-dialkylation des arylamines par deux groupements alkyles différents, on procède par étapes : la benzotriazolylméthylation de l'amine suivie par une réaction de Grignard permet d'introduire le premier groupement alkyle et la répétition de la même séquence d'introduire le second groupement. Les réactifs de Grignard obtenus à partir de 1,4-dihalobutane réagissent avec les *N,N*-bis(benzotriazolylméthyl)arylamines pour conduire aux *N*-aryl-hexahydroazépines correspondantes aux côtés de produits acycliques.

Mots clés : azépine, arylamines tertiaires.

[Traduit par la revue]

Introduction

Arylamines condense with 1-(hydroxymethyl)benzotriazole under mild conditions to give the corresponding *N*-(benzotriazolylmethyl)arylamines in high yields (1). Treatment of these adducts with Grignard reagents leads to substitution of the benzotriazolyl moiety by an alkyl or aryl group, and this is in many cases the preferred method for the *N*-monoalkylation of arylamines (2). Under similar conditions, alkylamines, hydroxylamines, and hydrazines give their *N,N*-bis(benzotriazolylmethylated) derivatives, which upon treatment with Grignard reagents are transformed into the corresponding *N,N*-dialkylated alkylamines (3), hydroxylamines (3), and hydrazines (4).

Tertiary dialkylarylamines are products of interest in many areas of applied chemistry. Several reports have appeared recently on their preparation: (i) by nucleophilic substitution of aromatic halides with dialkylamines (5) or (dialkylamino)-tributyltin (6); (ii) by dealkylation of quaternary ammonium salts (7), (iii) by dialkylation of arylamines with alcohols (8–13) or ethers (14, 15), (iv) by reductive dialkylation of arylamines with aldehydes on a Pd/C catalyst (16), and (v) by reductive transformation of nitroarenes into dialkylaminoarenes using aldehydes and carbon monoxide (17) or aldehydes and hydrogen in the presence of a noble metal catalyst (18).

All these methods, however, suffer limitations, especially when complex alkyl groups have to be introduced. 4-Chloronitrobenzene reacted with dibutylamine to give *N,N*-dibutyl-4-nitroaniline in only 15% yield and not at all with diisopropylamine (5). Dealkylations of quaternary ammonium salts are limited to *N*-methyl and *N*-ethyl substituents (7). Aniline dialkylation in the presence of a ruthenium catalyst was successful with *n*-alkyl alcohols, but failed for secondary alcohols (8). Reductive dialkylation of nitrobenzene with isobutyraldehyde and carbon monoxide gave only 10% of *N,N*-diisobutylaniline (17). Nitrobenzene with butyraldehyde, hydrogen, and a platinum catalyst gives *N,N*-dibutylaniline, but isobutyraldehyde forms only the *N*-monoalkylated product (18).

Our recently disclosed method for the *N,N*-bis(benzotriazolylmethylation) or arylamines (19) prompted us to subject these adducts to Grignard reagents. We now report that this provides a superior method for the *N,N*-dialkylation of aromatic amines.

Results and discussion

Preparation of symmetrical N,N-*dialkylarylamines (**7**, $R^1 = R^2$)*

Similarly to *N*-mono(benzotriazolylmethylated) arylamines (2), *N,N*-bis(benzotriazolylmethyl)arylamines **1** are easily reduced by sodium borohydride and react readily with Grignard reagents to produce *N,N*-dimethyl- or *N,N*-dialkyl-arylamines **7**, respectively (Scheme 1). The alkyl groups in the product contain an extra methylene as compared to the Grignard reagent and this method is therefore especially valuable when effective alkylating agents for direct alkylation of the amine are not easily available (e.g., neopentyl), or for alkylating agents that easily undergo elimination in basic solution. Thus, we now report the synthesis of *N,N*-di(β-phenethyl)anilines, a previously unknown class. Again, 3-butenyl bromide, although less susceptible to elimination than phenethyl bromide, gave only 37% of *N,N*-bis(3-butenyl)aniline (**7***h*) in the direct dialkylation of aniline (20). Under our conditions, product **7***h* was obtained quantitatively, and analytically pure, from the reaction of *N,N*-bis(benzotriazolylmethyl)aniline with allylmagnesium bromide.

N,N-Dialkylarylamines prepared by this new method can be generally obtained in good yields (Table 1). The products were fully characterized by their ^{1}H and ^{13}C NMR spectra (Tables 2, 3). The method and the results obtained are comparable to those reported previously for the reaction of *N,N*-bis(phenylthiomethyl)aniline with Grignard reagents (21), but with the great advantages of the easier preparation of starting *N,N*-bis(benzo-

[1]Author to whom correspondence may be addressed.

Can. J. Chem. Downloaded from www.nrcresearchpress.com by 91.144.44.67 on 09/07/12
For personal use only.

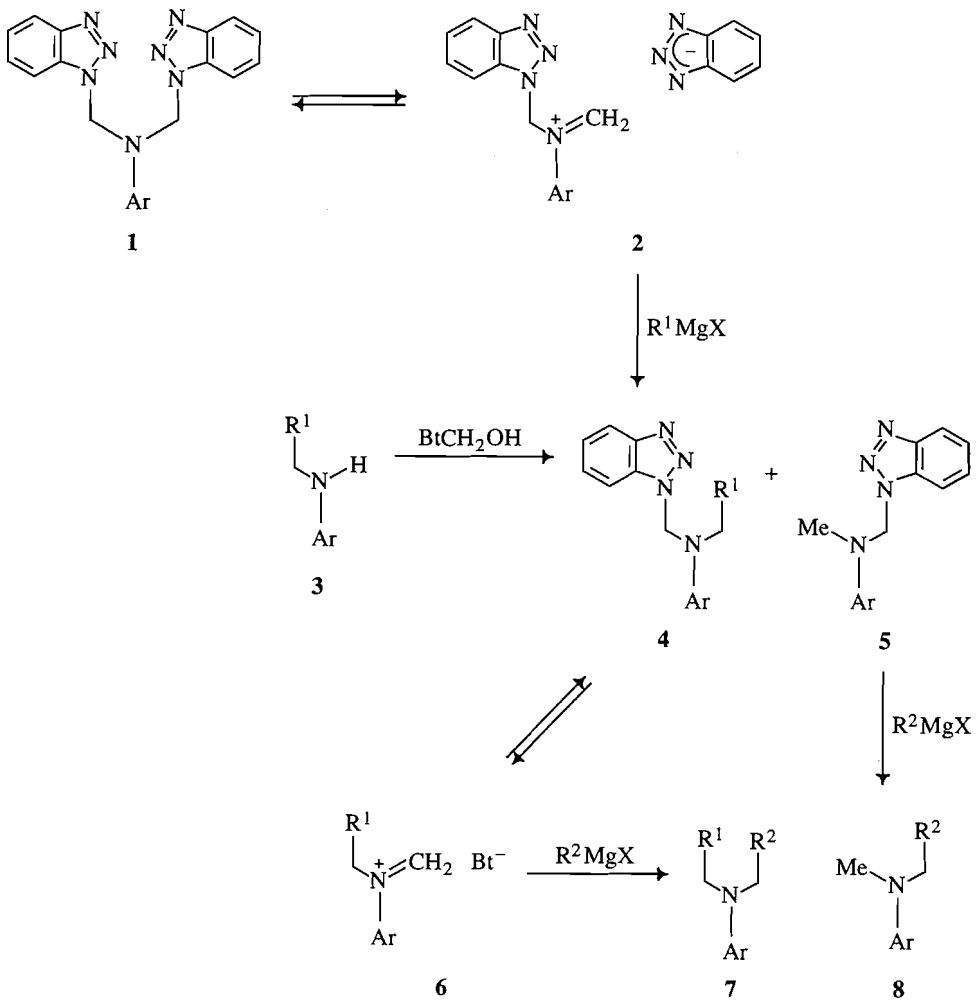

SCHEME 1

Can. J. Chem. Downloaded from www.nrcresearchpress.com by 91.144.44.67 on 09/07/12
For personal use only.

triazolylmethyl)anilines in comparison with their phenylthiomethyl analogs, and of the avoidance of harmful and unpleasant thio reagents, intermediates, and side products.

The only limitations of our new method, Tables 1, 3, are the following:

(a) The alkyl groups of the prepared *N*,*N*-dialkylarylamines are all linked to the nitrogen by a methylene group. No secondary or tertiary alkyl groups can be introduced.

(b) Protection is required for arylamines bearing substituents sensitive towards Grignard reagents.

(c) The crude amines **7** obtained are sometimes contaminated by *N*-alkyl-*N*-methylamines **8**, especially when secondary alkyl Grignard reagents (22, 23) are used.

Several recent reports on the successful use of 1,4-bis(halomagnesio)butane in organic synthesis, e.g., preparation of 1-(*o*-aminophenyl)cycloalkanols (26), oximes of 3-(hydroxycyclopentyl)-2-alkanones (27), 1-*tert*-butylcyclopentanol (28), spirolactones derived from pyridine and pyrazine 2,3-dicarboxylic acids (29), and 1-(3-hydroxypropyl)cyclopentanols (30, 31), prompted us to try 1,4-bis(halomagnesio)butane reagents in reactions with *N*,*N*-bis(benzotriazolylmethyl)arylamines **1**. Direct application of reaction conditions similar to those used previously in the reactions of **1** with ordinary Grignard reagents gave complex mixtures. Vacuum fractional distillation and (or) column chromatography gave the expected hexahydroazepines (32, 33) **9** together with acyclic products **10–12**. In the successful reactions of 1,4-di(bromomagnesio)butane, intramolecular coordination of the magnesium atom in the active intermediate by an oxygen atom seems to be required for high yields of the cyclic products. This could not happen in our case, leading to low yields of **9**.

We believe that molecules of the intermediate *N*-(benzotriazol-1-ylmethyl)-*N*-(4-halomagnesiobutyl)aniline, because of weak magnesium coordination at the reaction center, were attacked further by Grignard reagent giving *N*,*N*-dialkylated products **11** and **12** (and more complex molecules), as the main reaction course. The intermediate is also reduced by a second molecule of the Grignard reagent giving the *N*-methyl derivative **10**.

Substituent influences

We failed to get two different groups in the final product **7** by stepwise Grignard reaction of **1** via **4**. Thus, *N*,*N*-bis(benzotriazolylmethyl)-4-anisidine, when reacted with 1 molar equivalent of isopropylmagnesium bromide, gave exclusively *N*,*N*-diisobutyl-4-anisidine together with the unchanged starting material **1**. None of intermediate **4** was detected, indicating that the cation **6** forms from the molecule of **4** much more easily than **2** from **1** (destabilizing effect of the electron-withdrawing benzotriazolyl group), causing the reaction **4** → **7** to be much faster than the reaction **1** → **4** (Scheme 1). This illustrates the decisive influence of substituents on the stability of the ion pair intermediate **2**.

For a direct comparison of the reactivity towards Grignard

TABLE 1. Characterization of obtained amines **7**

No.	Ar	R^1	R^2	Molecular formula	Grignard reagent[a]	Yield (%)	Picrates: Melting point (°C)	Picrates: Found (Calcd.) (%) C	H	N
a	Ph	*i*-Pr	*i*-Pr	$C_{14}H_{23}N$	*i*-PrMgBr	87[b]	138	55.4 (55.3)	6.0 (6.0)	13.0 (12.9)
b	4-MeC_6H_4	$PhCH_2$	$PhCH_2$	$C_{23}H_{25}N$	$PhCH_2MgCl$	85	116	63.6 (64.0)	5.1 (5.2)	10.3 (10.3)
c	4-BuC_6H_4	$PhCH_2$	$PhCH_2$	$C_{26}H_{31}N$	$PhCH_2MgCl$	76	104	65.4 (65.5)	5.8 (5.8)	9.8 (9.6)
d	4-$MeOC_6H_4$	*i*-Pr	*i*-Pr	$C_{15}H_{25}NO$	*i*-PrMgBr	68	102	53.9 (54.3)	6.0 (6.1)	12.0 (12.1)
e	3-ClC_6H_4	$PhCH_2$	$PhCH_2$	$C_{22}H_{22}ClN$	$PhCH_2MgCl$	56	118	59.8 (59.5)	4.5 (4.5)	9.8 (9.9)
f	4-ClC_6H_4	*i*-Pr	*i*-Pr	$C_{14}H_{22}ClN$	*i*-PrMgBr	39	*f*	*f*	*f*	*f*
g	Ph	Cyclohexyl	Cyclohexyl	$C_{20}H_{31}N$	$C_6H_{11}MgBr$	33	86[g]	84.3[g] (84.2)	11.1[g] (11.0)	4.8[g] (4.9)
h	Ph	$CH_2CH{=}CH_2$	$CH_2CH{=}CH_2$	$C_{14}H_{19}N$	$CH_2{=}CHCH_2MgBr$	99[c]	93	55.5 (55.8)	5.2 (5.2)	13.0 (13.0)
i	2-EtC_6H_4	H	H	$C_{10}H_{15}N$	$NaBH_4$	77[d]	135	50.8 (50.8)	4.8 (4.8)	14.8 (14.8)
j	4-Pyridyl	$PhCH_2$	$PhCH_2$	$C_{21}H_{22}N_2$	$PhCH_2MgCl$	21[e]	162	61.3 (61.0)	4.7 (4.7)	13.2 (13.2)
k	Ph	H	$PhCH_2$	$C_{15}H_{17}N$	$PhCH_2MgCl$	99	114	57.2 (57.3)	4.5 (4.6)	12.7 (12.7)
l	Ph	Me	$PhCH_2$	$C_{16}H_{19}N$	$PhCH_2MgCl$	87	122	57.8 (58.2)	4.8 (4.9)	12.3 (12.3)
m	Ph	Pr	$PhCH_2$	$C_{18}H_{23}N$	$PhCH_2MgCl$	38[e]	oil[g]	85.3[g] (85.3)	9.2[g] (9.2)	5.5[g] (5.5)

[a]Instead of a Grignard reagent, sodium borohydride was used in the case of **7***i*.
[b]Reported (24) yield 86%.
[c]Reported (20) yield 37%.
[d]Reported (25) yield 8%.
[e]Total yield from the two-step synthesis starting from the appropriate arylamine.
[f]Problems with preparation of the picrate; the compound was characterized by HR MS; accurate mass calcd. for $C_{14}H_{22}NCl$: 239.1440; found: 233.1417.
[g]Data for the free amine, not its picrate.

reagents of *N*,*N*-bis(benzotriazolylmethyl)anilines **1** bearing different substituents on the aniline ring, a mixture of one mole each of *N*,*N*-bis(benzotriazolylmethylated) 4-anisidine and 4-chloroaniline was reacted with two molar equivalents of isopropylmagnesium bromide. The derivative of 4-anisidine proved to be much more reactive than that of 4-chloroaniline as, after work-up of the reaction, *N*,*N*-diisopropyl-4-anisidine was found by the NMR technique to be present to the extent of 28 mol% compared to only 8 mol% of *N*,*N*-diisobutyl-4-chloroaniline in a mixture with unreacted starting materials. This phenomenon can be explained in terms of the relative reactivity of cation **2**: the chlorine substituent on the aryl group ($\sigma = 0.23$, ref. 34) effectively destabilizes cation **2**, whereas the methoxy group ($\sigma = -0.27$, ref. 34) has just the opposite effect.

Asymmetrically N,N-*dialkylated arylamines. Stepwise procedure*

Although the above experiment excluded the possibility of the preparation of *N*,*N*-dialkylated arylamines with two different alkyl groups by stepwise Grignard reactions on **1**, such dialkylation of arylamines succeeds well on applying a stepwise procedure. Mono-benzotriazolylmethylation of an arylamine and subsequent Grignard reaction to **3** were described in our previous papers (1–2). Further benzotriazolylmethylation of secondary alkylarylamine to **4** followed by its Grignard reaction to **7** is now demonstrated to be a good route to *N*,*N*-dialkylarylamines having two different alkyl groups (**7***k*–**7***m*).

Additionally, such a stepwise route also allows for dialkylation of the electron-poor amines, which do not form adducts **1**. Thus, 4-aminopyridine was transformed into 4-(benzotriazolylmethyl)aminopyridine, then by reaction with benzylmagnesium chloride to 4-phenethylaminopyridine **3***j*, which by repeated benzotriazolylmethylation followed by a second Grignard reaction gave the final product 4-(*N*,*N*-diphenethylamino)pyridine (**7***j*) in the overall total yield of 21% (four steps).

A unique phenomenon was observed in this case, which is responsible for the corresponding low yield of **7***j*. Thus, reaction of 4-(benzotriazolylmethyl)aminopyridine with benzylmagnesium chloride afforded, apart from the expected 4-phenethylaminopyridine (70%), another product, 4-(2-methylbenzylamino)pyridine (17%). Although the fact that benzyl Grignard reagents can also undergo reactions with electrophiles as their mesomeric forms, with the negative charge localized on the *ortho* carbon, is well known (35, 36), such a reaction course was never observed in any of our other cases where benzyl Grignard reagent was used. The reason seems to be the difference in a steric hindrance of cation **2** and an analogous cation derived from a mono(benzotriazolylmethylated) aniline. A nucleophilic attack of the benzyl anion by its more sheltered

Can. J. Chem. Downloaded from www.nrcresearchpress.com by 91.144.44.67 on 09/07/12
For personal use only.

TABLE 2. Proton NMR spectra[a] of obtained amines **7**

No.	Ar[b] *ortho*	Ar[b] *meta*	Ar[b] *para*	Ar[b] Subst.	CH_2R^1	CH_2R^2	R^1, R^2
a	6.64d (8.3, 2H)	7.18t (8.4, 2H)	6.61t (7.3, 1H)	—	3.13d (7.3)	3.13d (7.3)	0.89d (6.8, 12H) 2.08heptet (6.8, 2H)
b	6.71d (8.3, 2H)	7.08d (8.3, 2H)	—	2.27s (3H)	3.42t (8.1)	3.42t (8.1)	2.78t (7.7, 4H), 7.16m (6H) 7.26m (4H)
c	6.72d (8.8, 2H)	7.10d (8.8, 2H)	—	2.54t[c] (7.8, 2H)	3.45t (7.6)	3.45t (7.6)	2.81t (7.8, 4H) 7.19m (6H), 7.28m (4H)
d	6.64d (9.1, 2H)	6.80d (9.1, 2H)	—	3.74s (3H)	3.02d (7.1)	3.02d (7.1)	0.88d (6.6, 12H) 1.98m (2H)
e	6.61d (7.8, 1H) 6.70t (2.0, 1H)	7.21t (7.7, 1H)	6.66d (7.8, 1H)	—	3.41t (7.9)	3.41t (7.9)	2.78t (8.0, 4H) 7.14t (8.0, 2H) 7.16d (7.0, 4H) 7.29t (7.7, 4H)
f	6.54d (9.0, 2H)	7.10d (9.0, 2H)	—	—	3.10d (7.3)	3.10d (7.3)	0.87d (6.7, 12H) 2.03m (2H)
g	6.61d (8.1, 2H)	7.19t (7.3, 2H)	6.65t (7.5, 1H)	—	3.14d (6.6)	3.14d (6.6)	0.91m (4H), 1.16m (6H) 1.69m (12H)
h	6.67d (8.1, 2H)	7.22m (2H)	6.65t (7.6, 1H)	—	3.36t (7.8)	3.36t (7.8)	2.34q (7.2, 4H) 5.08m (4H), 5.83m (2H)
i	7.07d (9, 1H)	7.20d (7.5, 1H) 7.16t (9, 1H)	7.01t (9, 1H)	1.25t (7.5, 3H) 2.73q (7.4, 2H)	2.67s	2.67s	—
j	6.52d (6.2, 2H)	8.24 (6.2, 2H)	—	—	3.41t (8.0)	3.41t (8.0)	2.78t (7.9, 4H), 7.13d (7.1, 4H) 7.23m (2H), 7.28t (7.8, 4H)
k	6.67–6.76m	7.16–7.32m	6.67–6.76m	—	3.55t (7.6)	2.87s	R^2: 2.84t (7.5, 2H) 7.16–7.32m (5H)
l	6.72d (8.1, 2H)	7.15–7.33m	6.67t (7.2, 1H)	—	3.49t (7.8)	3.30q (7.1)	R^1: 1.11t (7.1, 3H) R^2: 2.86t (7.8, 2H) 7.15–7.33m (5H)
m	6.66–6.73m	7.17–7.33m	6.66–6.73m	—	3.50t (7.6)	3.21t (7.5)	R^1: 0.92t (7.3, 3H) 1.32sextet (7.9, 2H) R^2: 1.53quintet (8.1, 2H) 2.85t (8.1, 2H) 7.17–7.33m (5H)

[a]Chemical shifts, δ, in ppm from TMS signal, coupling constants (in parentheses) in Hz.
[b]Only the highest coupling constants are considered.
[c]Other signals: 0.94t (7.3, 3H), 1.37hextet (7.5, 2H), and 1.58m (2H).

ortho carbon atom can be effective only when there is enough space around the electrophile.

In general, however, a 2-phenylethyl group (or two such groups) can be efficiently introduced on the arylamine nitrogen atom by a reaction of the benzotriazolylmethylated intermediate with a benzyl Grignard reagent, giving a 2-phenylethylamino function. This application of our method is of special interest, as 2-phenylethylamine and its derivatives are important for their biological activity and wide natural occurrence (37–45).

Experimental

Melting points were determined on a Thomas–Hoover capillary melting point apparatus and were not corrected. NMR spectra (^1H and ^{13}C) were taken on a Varian VXR-300 instrument in $CDCl_3$ solvent with tetramethylsilane as the internal standard for ^1H and ^{13}C. Low and high resolution mass spectra were determined at 70 eV with an A.E.I. MS-30 mass spectrometer operating with a Kratos DS-55 data system. Elemental analyses were performed in house under the supervision of Mr. M. Courtney. Ether and THF for the Grignard reaction were dried by reflux under argon with sodium/benzophenone and distilled immediately prior to use. Silica gel used for column chromatography was 230–400 mesh.

Reaction of N,N-*bis(benzotriazolylmethyl)aniline with isopropylmagnesium bromide. Preparation of* N,N-*diisobutylaniline (7a)*

To a solution of isopropylmagnesium bromide prepared from isopropyl bromide (2.92 g, 120 mL) and magnesium turnings (2.92 g, 120 mmol) in ether (40 mL) was added a suspension of *N,N*-bis(benzotriazolylmethyl)aniline (10.00 g, 28 mmol) in ether–toluene (20 + 10 mL). The mixture obtained was stirred under argon for 16 h and then poured into ice water (400 g), neutralized with acetic acid, and the organic layer separated. The water phase was washed twice with ether (2 × 100 mL). The combined organic phase was washed with water (100 mL), followed by 10% sodium hydroxide (100 mL) and again by water (100 mL). The solution was dried over anhydrous potassium carbonate and the solvent was evaporated by means of a rotary vacuum evaporator to give crude *N,N*-bis(2-methylpropyl)aniline (**7***a*) as an oily substance of purity about 80% (according to NMR, from the ratio of integrals of **7***a* protons, calculated on the basis of the resonance at δ 3.13, to the sum of the integrals observed in the spectrum) (6.24 g, 87%). The product was characterized in Tables 1–3. Similar processes were used for the preparation of amines **7***b*–**7***e*.

Preparation of the picrate of N,N-*bis(2-methylpropyl)aniline (7a)*

A mixture of crude *N,N*-bis(2-methylpropyl)aniline (5.0 g, 19.5 mmol) and 65% picric acid (8.81 g, 25 mmol) was heated under

Can. J. Chem. Downloaded from www.nrcresearchpress.com by 91.144.44.67 on 09/07/12
For personal use only.

TABLE 3. Carbon-13 NMR spectra[a] of obtained amines **7**

No.	Ar					$CH_2(1)$, $CH_2(2)$	R^1, R^2
	ipso	*ortho*	*meta*	*para*	Subst.		
a	148.2	112.4	129.0	115.0	—	60.4	20.4, 26.3
b	145.2	112.3	130.0	125.2	20.2	53.4	33.6, 126.1, 128.5, 128.7, 139.8
c	145.4	112.0	129.3	130.4	34.5[b]	53.4	33.7, 126.1, 128.5, 128.7, 139.8
d	143.5	114.6[c]	114.8[c]	150.9	55.8	61.3	20.5, 26.4
e	148.8	110.3	130.7	116.1	—	53.5	33.8, 126.7, 128.9, 129.1, 139.6
		112.1	135.7				
f	146.8	113.5	128.7	119.8	—	60.4	20.3, 26.2
g	148.2	112.0	129.0	114.6	—	59.2	35.8, 31.3, 26.6, 26.0
h	147.6	111.9	129.3	115.6	—	50.6	31.7, 116.4, 135.8
i	152.4	119.1	126.3	123.3	14.8	45.1	—
		138.7	128.9		23.4		
j	151.9	106.5	150.0	—	—	52.2	33.1, 126.5, 128.6, 128.7, 138.7
k	148.8	112.1	129.2	116.1	—	38.4	—
						54.7	32.9, 126.1, 128.5, 128.8, 139.8
l	147.5	111.8	129.3	115.6	—	45.0	12.3
						52.3	33.8, 126.1, 128.4, 128.7, 139.7
m	147.7	111.7	129.3	115.5	—	50.9	14.0, 20.3, 29.5
						52.9	33.5, 126.1, 128.5, 128.7, 139.7

[a]Chemical shifts, δ, in ppm from TMS signal.
[b]Additional signals of the butyl group are at δ 14.0, 22.4, 34.0.
[c]Tentative assignments.

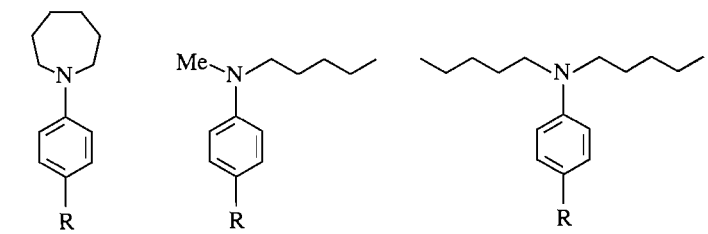

9 **10** **11**

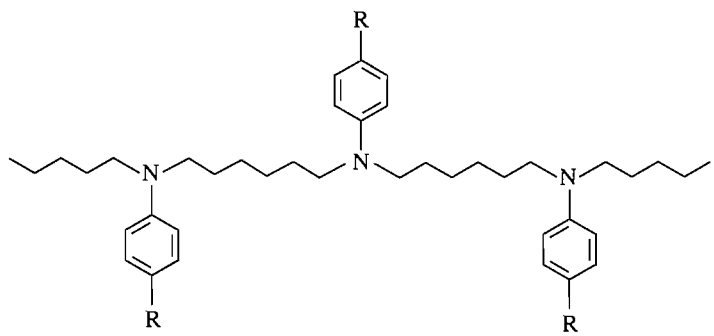

12

a R = H
b R = Me

vacuum to evaporate the water. The semisolid material obtained was stirred with methanol (15 mL) at −5°C for 5 h. The precipitate obtained was filtered off, washed with cold (−5°C) methanol (10 mL), and recrystallized from absolute ethanol (5 mL) to give an analytically pure sample of the picrate of **7***a* (2.20 g, 26%).

The picrates of **7***b*–**7***e* were obtained from the analytical samples purified by column chromatography (silica gel; toluene/hexane, 1:1).

*Preparation of 4-chloro-*N,N*-diisobutylaniline (7*f*)*

37% Aqueous formaldehyde (22.8 mL, 0.3 mol) was added to a solution of benzotriazole (23.83 g, 200 mmol) and *p*-chloroaniline (12.76 g, 100 mmol) in toluene (150 mL) heated to 60°C. Much heat was evolved and the solution started to boil. After stirring for 1 h, the content was refluxed under a Dean–Stark water trap for 3 h and allowed to cool to room temperature. To this solution was added isopropylmagnesium bromide prepared from isopropyl bromide (36.90 g, 300 mmol) and magnesium turnings (9.72 g, 400 mmol) in ether (150 mL). Much solid precipitated and the solution began to boil. The mixture was stirred and heated at reflux under argon for 2 h and then poured into ice water (200 g). The mixture obtained was neutralized with acetic acid and extracted twice with ether (2 × 200 mL). The ethereal solution was washed with water (2 × 400 mL), 10% sodium

Can. J. Chem. Downloaded from www.nrcresearchpress.com by 91.144.44.67 on 09/07/12
For personal use only.

Can. J. Chem. Downloaded from www.nrcresearchpress.com by 91.144.44.67 on 09/07/12
For personal use only.

hydroxide (2 × 200 mL), and again with water (2 × 400 mL), and dried over sodium carbonate monohydrate (50 g) for 3 h. The solvent was removed (rotary vacuum evaporator) to give crude **7***f* (20.35 g) as a reddish-brown viscous liquid.

According to its ^{1}H and ^{13}C NMR spectra, the crude product consisted of 4-chloro-*N*,*N*-diisobutylaniline (**7***f*) (40%, characteristic doublet of the methylene group at δ 3.10), starting 4-chloro-*N*,*N*-bis(benzotriazol-1-ylmethyl)aniline (**1***f*) (30%, methylene singlet at δ 6.18), 4-chloro-*N*-isobutylaniline (**3***f*) (19%, CH_2 doublet at δ 2.88), and 4-chloro-*N*-isobutyl-*N*-methylaniline (**5***f*) (10%, CH_2 doublet at δ 3.15 and CH_3 singlet at δ 2.90).

An analytical sample of 4-chloro-*N*,*N*-diisobutylaniline (**7***f*) (0.06 g) was prepared from the crude mixture by column chromatography (30 g of silica gel and a 1:1 hexane/benzene as the eluent).

Preparation of N,N-*bis(cyclohexylmethyl)aniline (7g)*

To a stirred solution of *N*,*N*-bis(benzotriazol-1-ylmethyl)aniline (**1***a*) (7.15 g, 20 mmol) in dry THF (20 mL) was added dropwise a Grignard reagent prepared by a reaction of cyclohexyl chloride (7.11 mL, 60 mmol) with magnesium turnings (1.94 g, 5 mmol) in ether (40 mL). The mixture obtained was stirred under argon for 50 h, and then poured into a 20% solution of ammonium chloride (100 mL). The resulting mixture was shaken with toluene (100 mL) and the toluene extract was washed with water (100 mL) followed by 10% sodium hydroxide (100 mL), again with water, and finally dried over anhydrous sodium carbonate. Evaporation of the solvent under reduced pressure afforded a crude product (9.66 g) consisting, according to its NMR spectra, of *N*,*N*-bis(cyclohexylmethyl)aniline (**7***g*) and *N*-(cyclohexylmethyl)-*N*-methylaniline (**8***g*) in a molar ratio of 3:1. Column chromatography (80 g, of silica gel; 2:1 hexane/benzene) of a crude sample (1.47 g) afforded pure **7***g* (0.38 g). The second fraction gave **8***g* (0.04 g); ^{1}H NMR δ: 0.86–1.02 (m, 2H), 1.12–1.30 (m, 3H), 1.62–1.81 (m, 6H), 2.94 (s, 3H), 3.11 (d, J = 6.7 Hz, 2H), 6.62–6.73 (m, 3H), 7.18–7.28 (m, 2H); ^{13}C NMR δ: 26.0, 26.6, 31.1, 36.9, 39.6, 59.7, 111.6, 115.4, 129.0, 149.5. Exact mass calcd. for $C_{14}H_{21}N$: 203.1674; found: 203.1674.

Preparation of N,N-*bis(1-buten-4-yl)aniline (7h)*

N,*N*-Bis(benzotriazol-1-ylmethyl)aniline (**1***a*) (10.66 g, 30 mL) dissolved in dry THF (250 mL) was added to a solution of the Grignard reagent prepared from allyl bromide (17.31 mL, 200 mmol) and magnesium turnings (6.05 g, 250 mmol) in dry ether (120 mL). The mixture was stirred and heated at reflux under argon for 50 h. The ether slowly evaporated and, after 24 h of heating, the temperature of the reaction mixture reached 60°C and then continued to grow slowly to finally reach 72°C. The reaction mixture was poured onto crushed ice (200 g) and toluene (100 mL) was added, followed by sodium bicarbonate (16.8 g, 200 mmol). The mixture obtained was stirred at 20°C for 12 h. The precipitate was filtered off and washed with ethanol (50 mL), followed by ethyl acetate (2 × 100 mL). The filtrate and the washings were collected and the organic phase was separated. The aqueous phase was washed additionally with ethyl acetate (100 mL) and the solution obtained, in ethyl acetate, was added to the main organic fractions. The toluene/ethyl acetate solution of the product mixture was then washed with 10% sodium hydroxide (200 mL), followed by water (200 mL), and dried over anhydrous potassium carbonate. The solvent was evaporated (rotary vacuum evaporator) to give almost analytically pure **7***h* (6.01 g) as a yellowish oil. The compound was characterized as its picrate (Table 1).

Sodium borohydride reduction of N,N-*bis(benzotriazol-1-ylmethyl)-2-ethylaniline. Preparation of* N,N-*dimethyl-2-ethylaniline (7i)*

A mixture of 2-ethylaniline (6.06 g, 50 mmol), benzotriazole (11.91 g, 100 mmol), 37% aqueous formaldehyde (9.12 mL, 120 mmol), and toluene (100 mL) was stirred for 2 h at 20°C and then stirred and heated under reflux for 3 h with a Dean–Stark water trap. The solvent was removed to give a clear orange oil (19.44 g). A solution of this oil (19.28 g) and sodium borohydride (1.77 g, 46.8 mmol) in 1,4-dioxane (50 mL) was heated under reflux for 4.5 h. The reaction mixture was diluted with ether (200 mL) and washed with 5% sodium hydroxide (100 mL). The organic layer was separated, washed with water (2 × 100 mL), and dried over anhydrous sodium carbonate (10 g). The solvent was evaporated to give crude **7***i* (6.16 g) as an orange liquid. The compound was characterized as its picrate (Table 1).

Preparation of 4-(phenethylamino)pyridine (3, R^1 = $PhCH_2$, Ar = 4-pyridyl) and 4-(2-methylbenzylamino)pyridine (3, R^1 = o-$CH_3C_6H_4$, Ar = 4-pyridyl)

A mixture of 4-aminopyridine (9.41 g, 100 mmol), benzotriazole (11.91 g, 100 mmol), and 37% formaldehyde (8.24 mL, 110 mmol) in toluene (100 mL) was stirred at 60°C for 1 h, followed by reflux under a Dean–Stark trap for 3 h. To the obtained suspension of 4-(benzotriazol-1-ylmethylamino)pyridine in toluene was added a solution of benzylmagnesium chloride obtained from magnesium turnings (8.50 g, 350 mmol) and benzyl chloride (34.5 mL, 300 mmol) in ether (100 mL). Evolution of heat was observed and the mixture started to boil. The mixture was stirred at reflux for 16 h and then poured into ice water (500 mL) and ammonium chloride (100 g). Acetic acid was added dropwise to the mixture until the precipitate of magnesium hydroxide dissolved. The organic layer was separated and the water phase was washed twice with ether (2 × 100 mL). The combined organic solutions were washed with water (100 mL), 10% sodium hydroxide (100 mL), and finally with water (100 mL). The solution was dried over anhydrous sodium carbonate (5 g) and the solvent was evaporated under reduced pressure. The oil obtained was dissolved in ether–hexane (50 + 50 mL) and stored at 0°C for 3 days. The deposited prisms were filtered off, washed with ether, and dried in a vacuum oven to give analytically pure 4-(2-methylbenzylamino)pyridine (3.37 g, 17%), mp 118°C; ^{1}H NMR δ: 2.35 (s, 3H), 4.30 (d, J = 5.1 Hz, 2H), 4.46 (bt, 1H), 6.46 (d, J = 6.5 Hz, 2H), 7.22 (m, 4H), 8.19 (d, J = 6.4 Hz, 2H); ^{13}C NMR δ: 18.9, 45.1, 107.6, 126.3, 127.9, 128.1, 130.6, 135.5, 136.2, 150.1, and 153.3. Anal. calcd. for $C_{13}H_{14}N_2$: C 78.75, H 7.12, N 14.13; found: C 78.50, H 7.07, N 14.09.

The filtrate and the washings were combined and stored in a freezer for 2 weeks. The crystals obtained were filtered off, washed with hexane, and dried in a vacuum desiccator at 20°C to give 4-(phenethylamino)pyridine (13.88 g, 70%), of purity about 90%; ^{1}H NMR δ: 2.91 (t, J = 7.0 Hz, 2H), 3.43 (dt, J = 6.0 and 7.0 Hz, 2H), 4.38 (bt, 1H), 6.42 (d, J = 6.4 Hz, 2H), 7.25 (m, 5H), and 8.15 (d, J = 6.4 Hz, 2H); ^{13}C NMR δ: 35.1, 43.7, 107.6, 126.7, 128.7 (4 C, *ortho* and *meta*), 138.5, 149.8, 153.2.

4-(Phenethylamino)pyridine picrate recrystallized from ethanol as orange prisms, mp 136°C. Anal. calcd. for $C_{19}H_{17}N_5O_7$: C 53.40, H 4.01, N 16.39; found: C 53.00, H 3.93, N 16.21.

Preparation of N,N-*diphenethyl-4-pyridinamine (7j)*

4-(Phenethylamino)pyridine (9.33 g, 47 mmol), benzotriazole (5.96 g, 50 mmol), and 37% formaldehyde (5.00 mL, 67 mmol) in toluene (200 mL) were stirred and heated at reflux under a Dean–Stark water trap for 18 h. Excess formaldehyde and part of the toluene were distilled off to concentrate the solution to 100 mL. To the solution was added a Grignard reagent prepared from benzyl chloride (34.5 mL, 300 mmol) and magnesium turnings (8.5 g, 350 mmol) in dry ether (80 mL). The mixture obtained was stirred at reflux (about 65°C) for 16 h and poured into ice water (500 g). Chloroform (300 mL) and sodium carbonate monohydrate (50 g) were added and the whole was stirred at 20°C for 1 h. The solution was filtered and the precipitate was washed thoroughly with chloroform (2 × 50 mL). The filtrate and the washings were washed with 10% sodium hydroxide (100 mL) and dried over anhydrous potassium carbonate. Evaporation of the solvent afforded crude *N*,*N*-diphenethyl-4-pyridineamine (21.47 g) as a brownish oil. A sample of the crude product (2.25 g) was subjected to column chromatography (silica gel, methylene chloride) to give biphenyl (0.43 g) as the first fraction. The second fraction gave *N*,*N*-diphenethyl-4-pyridinamine (**7***j*) as a colorless oil (0.49 g) (total yield 4.68 g, 33%). Amine **7***j* is characterized in Tables 1–3. The third fraction afforded the recovered starting *N*-phenethyl-4-pyridinamine (0.21 g, 22%).

Preparation of N-*methyl*-N-*phenethylaniline (7k)*

A mixture of *N*-methylaniline (10.72 g, 100 mmol), benzotriazole (11.91 g, 100 mmol), aqueous formaldehyde (37%, 9.12 mL,

Can. J. Chem. Downloaded from www.nrcresearchpress.com by 91.144.44.67 on 09/07/12
For personal use only.

120 mmol), and toluene (100 mL) was stirred for 2 h and then heated under reflux for 3 h with a Dean–Stark water trap. The solvent was removed (rotary vacuum evaporator) to give a mixture (23.86 g) of *N*-(benzotriazol-1-ylmethyl)-*N*-methylaniline and *N*-(benzotriazol-2-ylmethyl)-*N*-methylaniline (84% and 16%, respectively, according to the NMR spectra). To a solution of benzylmagnesium chloride prepared from benzyl chloride (2.30 mL, 20 mmol) and magnesium turnings (1.23 g, 30 mmol) in ether (30 mL) was added a solution of the isomeric mixture of *N*-methyl-*N*-(benzotriazolylmethyl)anilines (2.38 g, 10 mmol) in THF (20 mL) at a rate to keep a gentle reflux. After stirring at room temperature for 24 h, the reaction mixture was poured into 10% ammonium chloride (100 mL) and extracted with toluene (100 mL, 2 × 50 mL). The combined organic solutions were washed with water (50 mL), 10% sodium hydroxide (50 mL), and again with water (2 × 50 mL), and dried over anhydrous sodium carbonate (10 g). Evaporation of the solvent gave *N*-methyl-*N*-phenethylaniline (**7***k*) as a yellow liquid. The compound was characterized as the picrate (Table 1).

Preparation of N-*butyl*-N-*phenethylaniline (7*m*)*

To a stirred solution of benzotriazole (37.65 g, 316 mmol) and aniline (29.58 g, 316 mmol) in 95% ethanol (200 mL) was added butyraldehyde (27.61 g, 379 mmol). Precipitation of a white solid occurred. The mixture was stirred at 20°C for 3 h. The precipitate formed was filtered off, washed with 1:1 ether/hexane (3 × 20 mL), and dried in a vacuum desiccator to give *N*-(1-benzotriazolylbutyl)aniline (37.66 g). To a stirred warm solution of this compound (35.00 g) in dry THF (150 mL) was added sodium borohydride (2.49 g, 65.7 mmol). The mixture was heated under reflux for 27 h. The semi-clear solution obtained was washed with 10% NaOH (100 mL) and diluted with THF (100 mL). The organic substances were extracted into chloroform (2 × 100 mL), and dried over anhydrous sodium carbonate followed by molecular sieves (3 Å). Removal of the solvent afforded *N*-butylaniline (21.80 g) as a clear yellow liquid. The ^{1}H NMR spectrum of the product was in accordance with the reported data (46).

The *N*-butylaniline obtained was *N*-(benzotriazolylmethylated) and then the adduct obtained was subjected to a Grignard reaction with benzylmagnesium chloride, applying procedures similar to those given above for preparation of **7***k*, to give *N*-butyl-*N*-phenethylaniline (**7***m*) (Table 1).

Reaction of N,N-*bis(benzotriazol-1-ylmethyl)aniline with less than an equimolar amount of isopropylmagnesium bromide*

To a stirred solution of *N,N*-bis(benzotriazol-1-ylmethyl)aniline (10.66 g, 30 mmol) in dry ether (40 mL) was added a solution of the Grignard reagent prepared from 2-bromopropane (3.75 mL, 40 mmol) and magnesium turnings (1.21 g, 50 mmol) in ether (20 mL). The mixture was stirred at 25°C for 40 h, poured into ice water (100 mL), neutralized with acetic acid, and extracted with methylene chloride (2 × 100 mL). The solution was washed with water (100 mL) followed by 10% sodium carbonate and dried over anhydrous potassium carbonate. Evaporation of the solvent gave a mixture consisting of the starting material (63% mol; a characteristic methylene singlet in the ^{1}H NMR spectrum at δ 6.22) and *N,N*-diisobutylaniline (37% mol; a characteristic methylene doublet at δ 3.15). Neither the mixed (half-reacted) product, *N*-(benzotriazol-1-ylmethyl)-*N*-isobutylaniline, nor its hydrolysis product, *N*-isobutylaniline, was detected in the reaction mixture.

Reaction of a mixture of N,N-*bis(benzotriazolylmethyl)*-p-*anisidine and* N,N-*bis(benzotriazolylmethyl)-4-chloroaniline with isopropylmagnesium bromide*

To a stirred suspension of *N,N*-bis(benzotriazolylmethyl)-*p*-anisidine (1.02 g, 2.6 mmol) and *N,N*-bis(benzotriazolylmethyl)-4-chloroaniline (1.15 g, 2.9 mmol) in dry ether (40 mL) was added an ethereal solution of isopropylmagnesium bromide (4.16 mL, 5.0 mmol). Concentration of the Grignard reagent was estimated on the basis of the volume of propane evolved after treatment of a sample of the Grignard solution with water. The reaction mixture was stirred at 25°C for 20 h. The mixture was then poured into ice water and extracted with chloroform (2 × 50 mL). The chloroform solution was washed with water and dried over anhydrous magnesium sulfate. Evaporation of the solvent afforded a semisolid material (1.20 g), which according to ^{1}H NMR consisted of *N,N*-bis(benzotriazol-1-ylmethyl)-4-chloroaniline and its Bt,Bt-1,2 isomer (total 49 mol%; the characteristic methylene singlets at δ 6.20, 6.29, and 6.48; Bt,Bt-1,1 and -1,2 isomers, respectively), *N,N*-bis(benzotriazol-1-ylmethyl)-*p*-anisidine (15 mol%; the characteristic methylene singlet at δ 6.09), *N,N*-diisobutyl-4-chloroaniline (8 mol%; characteristic methylene doublet at δ 3.11), and *N,N*-diisobutyl-*p*-anisidine (28 mol%; characteristic doublet at δ 3.02).

Reaction of N,N-*bis(benzotriazolylmethyl)aniline with 1,4-di(bromomagnesio)butane*

A mixture of aniline (9.31 g), benzotriazole (23.83 g), and toluene (150 mL) heated to about 60°C turned into a clear solution. After 1 h, 37% aqueous formaldehyde was added and the stirring at 60°C was continued for an additional hour, followed by reflux under a Dean–Stark water trap for 2 h. To this solution was added the Grignard reagent prepared from 1,4-dibromobutane (43.19 g, 200 mmol) and magnesium turnings (12.15 g, 500 mmol) in dry ether (150 mL). Evolution of heat and formation of precipitate was observed. The mixture obtained was refluxed for 3.5 h under argon. The reaction mixture was poured into ice water (500 mL), neutralized with acetic acid, and extracted with ether (2 × 250 mL). The ethereal solution was washed with water (500 mL) followed by 10% sodium hydroxide (300 mL) and water (500 mL), and dried over anhydrous magnesium sulfate (40 g). Evaporation of the solvent (rotary vacuum evaporator) afforded a dark oil (10.50 g), which was partially separated by distillation. A fraction of yellow liquid (0.68 g, bp 68–75°C/0.03 Torr; 1 Torr = 133.3 Pa) was subjected to column chromatography (90 g silica gel, 2:1 hexane/benzene) to give pure *1-phenylhexahydroazepine* **9***a* (0.02 g) as a yellow liquid; ^{1}H NMR δ: 1.51–1.59 (m, 4H), 1.74–1.83 (m, 4H), 3.45 (t, *J* = 5.9 Hz, 4H), 6.62 (t, *J* = 9 Hz, 1H), 6.69 (d, *J* = 7.9 Hz, 2H); ^{13}C NMR δ: 27.1, 27.8, 49.0, 111.1, 115.1, 129.2, 148.9. Exact mass calcd. for $C_{12}H_{17}N$: 175.1361; found: 175.1354. The second fraction gave pure N-*methyl*-N-*pentylaniline (26)* **10***a* (0.02 g) as a colorless liquid; ^{1}H NMR δ: 0.90 (t, *J* = 6.8 Hz, 3H), 1.25–1.41 (m, 4H), 1.57 (quintet, *J* = 7.3 Hz, 2H), 2.92 (s, 3H), 3.29 (t, *J* = 7.4 Hz, 2H), 6.63–6.75 (m, 3H), 7.19–7.28 (m, 2H); ^{13}C NMR δ: 14.1, 22.6, 26.3, 29.4, 38.2, 52.8, 112.0, 115.7, 129.1, 149.4. Exact mass calcd. for $C_{12}H_{19}N$: 177.1518; found: 177.1522. The third fraction gave pure N-*pentylaniline (47)* (0.03 g) as a colorless liquid; ^{1}H NMR δ: 0.92 (t, *J* = 6.9 Hz, 3H), 1.32–1.41 (m, 4H), 1.61 (quintet, *J* = 2.6 Hz, 1H), 3.09 (t, *J* = 7.1 Hz, 2H), 3.58 (br, 1H), 6.59 (d, *J* = 7.6 Hz, 2H), 6.68 (t, *J* = 7.3 Hz, 1H), 7.17 (t, *J* = 7.4 Hz, 2H); ^{13}C NMR δ: 14.0, 22.5, 29.2, 29.3, 43.9, 112.6, 117.0, 129.2, 148.5. Exact mass calcd. for $C_{11}H_{17}N$: 163.1361; found: 163.1347.

Reaction of N,N-*bis(benzotriazol-1-ylmethyl)-4-toluidine with 1,4-di(iodomagnesio)butane*

A mixture of *p*-toluidine (1.07 g, 10 mmol), 37% aqueous formaldehyde (2.3 mL, 30 mmol), benzotriazole (2.38 g, 10 mmol), and toluene (50 mL) was stirred at 60°C for 1 h, followed by reflux under a Dean–Stark water trap for 11 h. The obtained solution of *N,N*-bis(benzotriazolylmethyl)-4-toluidine was added dropwise to a solution of the Grignard reagent obtained from 1,4-diiodobutane (6.20 g, 20 mmol) and magnesium turnings (1.22 g, 50 mmol) in ether (140 mL). The mixture obtained was refluxed under argon for 21 h, then poured into ice water (100 mL), and neutralized with acetic acid. The organic layer was separated, washed with water (100 mL) followed by 10% NaOH (2 × 100 mL), and dried over anhydrous sodium carbonate (25 g) for 10 h. After the solvent was removed, a yellow liquid (2.72 g) was obtained.

A sample of the reaction mixture (1.79 g) was separated by column chromatography (80 g silica gel, 1:1 hexane/benzene) to give as the first fraction N,N-*diamyl-4-toluidine* **11** (0.13 g); ^{1}H NMR δ: 0.88 (t, *J* = 6.5 Hz, 6H), 1.20–1.35 (m, 8H), 1.5–1.6 (m, 4H), 2.23 (s, 3H), 3.21 (t, *J* = 7.1 Hz, 4H), 6.56 (d, *J* = 8.5 Hz, 2H), 7.00

(d, J = 8.3 Hz, 2H). ^{13}C NMR δ: 14.1, 20.1, 22.7, 29.4, 31.9, 51.3, 112.1, 124.3, 129.7, 146.2. Exact mass calcd. for $C_{17}H_{29}N$: 247.2300; found: 297.2293. The second fraction gave *1-(p-methylphenyl)hexahydroazepine* **9***b* (0.11 g); ^{1}H NMR δ: 1.50–1.60 (m, 4H), 1.72–1.82 (m, 4H), 2.23 (s, 3H), 3.41 (t, J = 5.9 Hz, 4H), 6.60 (d, J = 8.6 Hz, 2H), 7.00 (d, J = 8.7 Hz, 2H); ^{13}C NMR δ: 20.2, 27.2, 27.8, 49.2, 111.2, 124.0, 129.8, 146.8. Exact mass calcd. for $C_{13}H_{19}N$: 189.1518; found: 189.1514. The third fraction gave *N-amyl-N-methyl-p-toluidine* **10***b* (0.01 g); ^{1}H NMR δ: 0.90 (t, J = 6.9 Hz, 3H), 1.24–1.40 (m, 4H), 1.50–1.65 (m, 2H), 2.23 (s, 3H), 2.88 (s, 3H), 3.17–3.29 (m, 2H), 6.54–6.66 (m, 2H), 6.99–7.07 (m, 2H); ^{13}C NMR δ: 14.1, 20.2, 22.6, 26.2, 29.7, 38.4, 53.1, 112.6, 125.1, 129.6, 147.5. Exact mass calcd. for $C_{13}H_{21}N$: 191.1674; found: 191.1668. The fourth fraction gave a mixture of oligomers (0.04 g) in which **12***b* dominated; ^{1}H NMR δ: 0.85–0.93 (m, 6H), 1.23–1.36 (m, 16H), 1.46–1.60 (m, 12H), 2.23 (s, 9H), 3.14–3.25 (m, 12H), 6.55–6.64 (dd, 6H), 7.00 (d, J = 8.6 Hz, 6H).

1. A. R. KATRITZKY, S. RACHWAL, and B. RACHWAL. J. Chem. Soc. Perkin Trans. 1, 799 (1987).
2. A. R. KATRITZKY, S. RACHWAL, and B. RACHWAL. J. Chem. Soc. Perkin Trans. 1, 805 (1987).
3. A. R. KATRITZKY, K. YANNAKOPOULOU, P. LUE, D. RASALA, and L. UROGDI. J. Chem. Soc. Perkin Trans. 1. 225 (1989).
4. A. R. KATRITZKY and M. S. C. RAO. J. Chem. Soc. Perkin Trans. 1. In press.
5. T. IBATA, Y. ISOGAMI, and J. TOYODA. Chem. Lett. 1187 (1987).
6. M. KOSUGI, M. KAMEYAMA, H. SANO, and T. MIGITA. Nippon Kagaku Kaishi, 547 (1985); Chem. Abstr. **104**, 129990t (1986).
7. G. R. NEWKOME, V. K. MAJESTIC, and J. D. SAUER. Org. Prep. Proced. Int. **12**, 345 (1980).
8. Y. WATANABE, Y. TSUJI, and Y. OHSUGI. Tetrahedron Lett. **22**, 2667 (1981).
9. V. PESCARU. Rom. Pat. 65,766 (1978); Chem. Abstr. **92**, 110644v (1980).
10. W. SCHULTE-HUERMANN and H. P. HEMMERICH. Ger. Pat. 2,918,023 (1980); Chem. Abstr. **99**, 156513w (1981).
11. N. VERVUTA, C. PREDOIU, I. KESERU, I. PUIAN, I. VASILESCU, A. MARIAN, and N. BALCACEAN. Rom. Pat. 89,025 (1986); Chem. Abstr. **107**, 9314r (1987).
12. K. TAKAHATA, T. MURASHIGE, and S. HIROKANE. Jpn. Pat. 61,238,768 (1986); Chem. Abstr. **106**, 138074r (1987).
13. H. KASHIWAGI and S. ENOMOTO. Nippon Kagaku Kaishi, 279 (1980). Chem. Abstr. **93**, 25372f (1980).
14. D. C. HARGIS. Eur. Pat. 240,631 (1987); Chem. Abstr. **108**, 188882q (1988).
15. D. C. HARGIS. U.S. Pat. 4,721,810 (1988); Chem. Abstr. **108**, 186309j (1988).
16. T. PAPENFUHS and W. KUEHN. Ger. Pat. 3,528,262 (1987); Chem. Abstr. **106**, 156042h (1987).
17. Y. WATANABE, N. SUZUKI, Y. TSUJI, S. C. SHIM, and T. MITSUDO. Bull. Chem. Soc. Jpn. **55**, 1116 (1982).
18. M. V. KLYUEV and M. L. KHIDEKEL. J. Org. Chem. USSR (Engl. Transl.), **17**, 2316 (1981).
19. A. R. KATRITZKY, S. RACHWAL, and JING WU. Can. J. Chem. **68**, 446 (1990).
20. C. L. MCCORMICK and G. B. BUTLER. J. Org. Chem. **41**, 2803 (1976).
21. I. E. POLLAK and G. F. GRILLOT. J. Org. Chem. **32**, 2892 (1967).
22. J. MILLER, G. GREGORIOU, and H. S. MOSHER. J. Am. Chem. Soc. **83**, 3966 (1961).
23. F. C. WHITMORE and R. S. GEORGE. J. Am. Chem. Soc. **64**, 1239 (1942).
24. P. CAUBERE and N. DEROZIER. Bull. Soc. Chim. Fr. 1737 (1969).
25. J. WROBEL and A. M. KONOWAL. Rocz. Chem. **39**, 1437 (1965).
26. P. CANONNE, R. BOULANGER, and B. CHANTEGREL. Tetrahedron, **43**, 663 (1987).
27. P. CANONNE, D. THIBEAULT, and G. FYTAS. Tetrahedron, **42**, 4203 (1986).
28. A. FADEL and J. SALAUN. Tetrahedron, **41**, 1267 (1985).
29. P. CANONNE and M. BELLEY. Can. J. Chem. **65**, 1885 (1987).
30. P. CANNONE, G. B. FOSCOLOS, and D. BELANGER. J. Org. Chem. **45**, 1828 (1980).
31. N. E. SCHORE and M. J. KNUDSEN. J. Org. Chem. **52**, 569 (1987).
32. D. BARBRY and B. HASIAK. Synth. Commun. **12**, 733 (1982).
33. R. E. WALKUP and S. SEARLES. Tetrahedron, **41**, 101 (1985).
34. H. H. JAFFE. Chem. Rev. **53**, 191 (1953).
35. R. A. BENKESER and W. DETALVO. J. Am. Chem. Soc. **89**, 2141 (1967).
36. S. SIEGEL, M. W. BOYER, and R. R. JAY. J. Am. Chem. Soc. **73**, 3237 (1951).
37. K. BAILEY and D. LEGAULT. Org. Magn. Reson. **21**, 391 (1983).
38. K. W. BENTLEY. Alkaloids (London), **12**, 94 (1982).
39. K. W. BENTLEY. Nat. Prod. Rep. **3**, 153 (1986).
40. B. G. BAKER, R. T. COUTTS, and T. S. RAO. Br. J. Pharmacol. **92**, 243 (1987).
41. M. A. J. S. VAN BOEKEL and A. P. ARENTSEN-STASSE. J. Chromatogr. **389**, 267 (1987).
42. R. BRETTLE, N. A. HILTON, and S. SHIBIB. J. Chem. Res. Synop. 379 (1984).
43. L. G. BEREGI and P. HUGON. Biochem. Pharmacol. Obes. 203 (1983).
44. M. E. WOLF and A. D. MOSNAIM. Gen. Pharmacol. **14**, 385 (1983).
45. G. B. BAKER, J. T. F. WONG, R. T. COUTTS, and F. M. PASUTTO. J. Chromatogr. **392**, 317 (1987).
46. L. H. P. MEIJER, J. C. G. VAN NIEL, and U. K. PANDIT. Tetrahedron, **40**, 5185 (1984).
47. L. E. OVERMAN and R. M. BURK. Tetrahedron Lett. **25**, 1635 (1984).

Can. J. Chem. Downloaded from www.nrcresearchpress.com by 91.144.44.67 on 09/07/12
For personal use only.

Bromation régiosélective en série aromatique. II. Approche théorique du mécanisme de la substitution électrophile par l'ion tribromure Br_3^-

JACQUES BERTHELOT,[1] CATHERINE GUETTE, PAUL-LOUIS DESBÈNE ET JEAN-JACQUES BASSELIER
Laboratoire de chimie organique structurale, Unité associé n° 455, Université Pierre et Marie Curie, Batiment F, 4 Place Jussieu, 75252 Paris CEDEX 05, France

ET

PATRICK CHAQUIN ET DANIEL MASURE
Laboratoire de chimie organique théorique, Unité associé n° 506, Université Pierre et Marie Curie, Batiment F, 4 Place Jussieu, 75252 Paris CEDEX 05, France

Reçu le 16 février 1989[2]

JACQUES BERTHELOT, CATHERINE GUETTE, PAUL-LOUIS DESBÈNE, JEAN-JACQUES BASSELIER, PATRICK CHAQUIN et DANIEL MASURE. Can. J. Chem. **68**, 464 (1990).

Une étude théorique (SCF PS-HONDO + CI) de la stabilité de l'anion tribromure Br_3^- a été réalisée. À partir de considérations orbitalaires qualitatives et de calculs MNDO, nous proposons une première approche du mécanisme de substitution électrophile par Br_3^-. Il implique une attaque axiale de l'ion linéaire Br_3^-, dont les sites les plus électrophiles sont les atomes de brome terminaux, bien qu'ils portent une charge négative. Ce modèle suggère des arguments rendant compte de la sélectivité en position *para* observée expérimentalement. Des calculs effectués sur une série de systèmes MBr_3 mettent en évidence l'importance de la nature du contre-ion pour la vitesse et la sélectivité de la réaction.

Mots clés : bromation, tribromure, mécanisme, parabromophénol.

JACQUES BERTHELOT, CATHERINE GUETTE, PAUL-LOUIS DESBÈNE, JEAN-JACQUES BASSELIER, PATRICK CHAQUIN, and DANIEL MASURE. Can. J. Chem. **68**, 464 (1990).

A theoretical study (SCF PS-HONDO + CI) of the stability of the tribromide anion Br_3^- has been carried out. On the basis of qualitative MO arguments and MNDO calculations, we propose a first approach to the mechanism of electrophilic aromatic substitution by Br_3^-. It involves an axial attack of linear Br_3^-, the most electrophilic sites of which are terminal bromine atoms, although they bear a negative charge. This model suggests some arguments to explain the *para* versus *ortho* selectivity experimentally observed. Calculations performed on a series of MBr_3 systems emphasize the importance of the countercation for the rate of the reaction as well as for its selectivity.

Key words : bromination, tribromide, mechanism, parabromophenol.

Introduction

Dans un précédent mémoire (1), nous avons montré tout l'intérêt d'utiliser le tribromure de tétrabutylammonium ($TBABr_3$) comme agent très sélectif de bromation en *para* de composés aromatiques activés. Cette réaction s'effectue dans des conditions douces avec d'excellents rendements et inhibition totale des polybromations quand le solvant employé, dont le rôle est essentiel, ne présente aucun caractère acide ou basique. La plupart des auteurs (2) supposaient une dissociation préalable de l'ion Br_3^- avec formation de dibrome selon :

$$Br_3^- \rightleftharpoons Br_2 + Br^-$$

le dibrome libéré étant alors l'agent réel de la bromation. Dans les solvants protiques ou basiques, ou si le milieu réactionnel est acidifié, l'équilibre est fortement déplacé vers la formation du dibrome (1) qui est alors responsable de la bromation. Par contre, dans les solvants sans caractère acido-basique, tels que le chloroforme, l'acétonitrile ou le tétrachlorure de carbone, les mesures de la constante de dissociation de l'anion Br_3^- ont montré que cet ion est très peu dissocié. En outre, il a été prouvé (3) que si le pouvoir électrophile du dibrome est plus élevé que celui de Br_3^-, ce dernier permet des bromations plus sélectives. En nous basant sur cette importante sélectivité de l'attaque électrophile, quand $TBABr_3$ est employé, nous pensons que l'ion tribromure est bien l'agent bromant.

En utilisant le tribromure de pyridinium, Sharma *et al.* (4) ont postulé que Br_3^- et Br_2 réagissaient tous les deux en concurrence sur un même composé phénolique et se fixaient sur des pôles différents : Br_3^- bromerait en *para*, tandis que Br_2 le ferait en *ortho*. L'explication, considérant principalement la taille des entités réactives et l'encombrement respectif des positions *ortho* et *para*, ne nous semble pas entièrement satisfaisante en l'absence de données sur la géométrie d'approche des réactifs.

Nous pensons que des calculs de répartition de charges et la théorie des orbitales moléculaires peuvent permettre une approche plus satisfaisante du mécanisme de la réaction de bromation des composés aromatiques par l'ion tribromure.

Avant d'aborder cette étude, il est nécessaire de préciser la nature du réactif, Br_3^-, et de rappeler certains résultats déjà établis.

La structure et les propriétés physico-chimiques des polyhalogénures d'ammonium ont déjà fait l'objet de nombreuses études. Il s'agit de composés ioniques (5) formés d'un cation R_4N^+ et d'un anion trihalogénure X_3^-. Certains tribromures ont déjà été étudiés par diffraction X (6*a*–*c*) et par spectroscopie de résonance nucléaire quadrupolaire (6*d*, 7). Ces examens ont confirmé que ces composés sont ioniques, que le groupe Br_3^- est linéaire, et que ses liaisons sont plus longues (2,78 Å) que dans la molécule Br_2 (2,28 Å), mais la distribution de la densité électronique dans ces anions n'est pas encore bien précisée. De plus, dans les études cristallographiques, les valeurs trouvées pour l'ion Br_3^- associé au cation R_4N^+ à l'état solide, pourraient ne pas refléter exactement celles de l'ion libre Br_3^- en solution. Ces résultats ont d'ailleurs été l'objet d'avis divergents (8). Il nous semble normal d'avoir affaire à des anions Br_3^- plus ou moins symétriques selon leur degré d'association

1. Auteur à qui adresser toute correspondance.
2. Révision reçue le 26 octobre 1989.

Can. J. Chem. Downloaded from www.nrcresearchpress.com by 91.144.44.67 on 09/07/12
For personal use only.

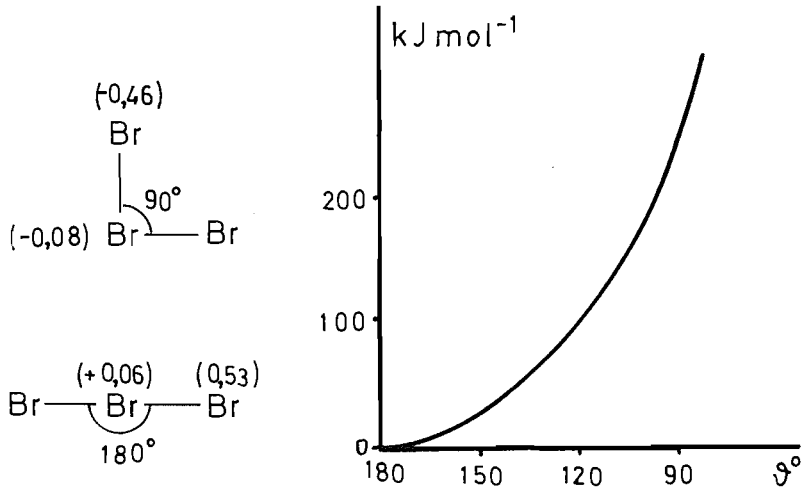

FIG. 1. Variation de l'énergie SCF de Br_3^- en fonction de l'angle Br—Br—Br, pour des longueurs de liaison de 2,67 Å. Les charges nettes (SCF) sont indiquées entre parenthèses.

avec le cation correspondant. En outre, il existe différentes formes cristallines qui possèdent une structure symétrique ou non symétrique, avec une certaine possibilité d'ambiguïté pour les deux symétries.

En ce qui nous concerne, nous avons déjà mis en évidence la stabilité de $TBABr_3$, supérieure à celle des tribromures de pyridinium et de triméthylphénylammonium, en phase gazeuse, dans un spectromètre de masse. Nous avons identifié la présence de l'ion Br_3^- (9). Dans les conditions de l'ionisation chimique par des ions négatifs, $TBABr_3$ présente un plasma d'anions Br_3^- majoritaires qui se sont révélés être d'excellents agents bromants, d'une façon sélective, de phénols et d'amines aromatiques (10). Cette analogie des résultats en phase gazeuse et condensée permet de minimiser le rôle du solvant, dans le cas où il assure la stabilité de Br_3^-, et justifie une première approche théorique du mécanisme de cette réaction.

Résultats

1. Description de l'ion Br_3^- (méthode PS-HONDO)

(a) Choix de la méthode de calcul

L'obtention de données quantitatives avec une marge d'erreur acceptable pour des espèces telles que l'anion Br_3^-, se heurte à deux difficultés :

Le nombre des électrons présents dans le système rend difficile l'utilisation d'une méthode du type *ab initio* auto-cohérente (SCF) classique. Aussi avons-nous choisi une méthode dans laquelle seuls les électrons de la couche externe sont traités *ab initio*, les électrons internes étant remplacés par un potentiel (11). C'est la méthode des pseudo-potentiels PS-HONDO 1 (12).

Une autre difficulté provient de la présence d'espèces chargées négativement qui impliquent la présence d'orbitales diffuses occupées. Nous avons donc enrichi la base interne du programme HONDO d'un ensemble d'orbitales *s*, *p*, *d*, soit finalement 11 Gaussiennes contractées en deux orbitales *s*, deux orbitales *p*, et une orbitale *d*. L'étape SCF a été suivie d'une interaction de configuration (IC) suivant la méthode des perturbations de Möller–Plesset (13) que a été réalisée à l'aide du programme CIPSI (14).

(b) Résultats

Les résultats sont présentés dans le tableau 1 : les longueurs de liaison ont été optimisées au niveau SCF pour Br_2, et Br_3^- avec une géométrie linéaire, qui est la plus stable, comme le montre la figure 1. La distance internucléaire d'équilibre calculée pour Br_2 est de 2,33 Å contre une valeur expérimentale de 2,28 Å (14).

Les caractéristiques géométriques sont en accord avec les données cristallographiques (6). Il est important de noter que les

TABLEAU 1. Energie de référence des systèmes

	Longueur de la liaison Br—Br (Å)	Energie (ua) SCF	Energie (ua) SCF + IC
Br^-		−13,09958	−13,18905
Br—Br	2,33	−26,04177	−26,21403
$(Br—Br—Br)^-$	2,67	−39,17532	−39,43703

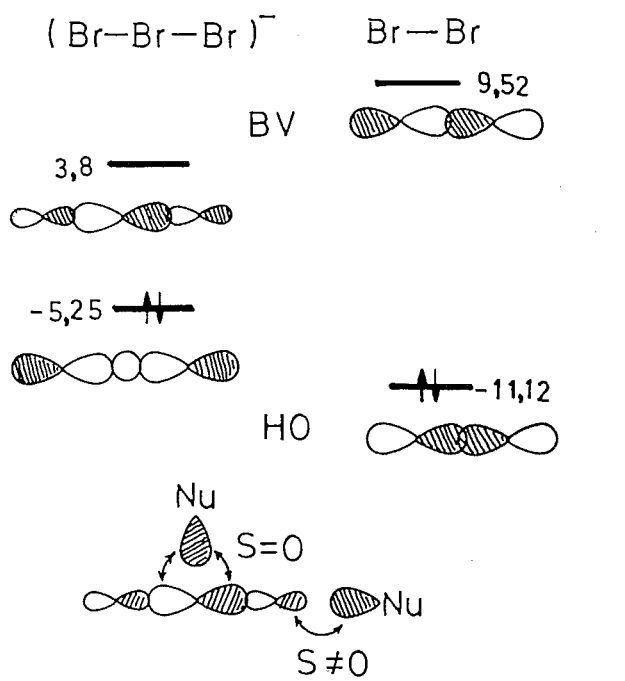

FIG. 2. Orbitales frontalières de Br_3^- et Br_2 (PS-HONDO, énergies en eV) et géométrie d'approche d'un nucléophile Nu (symbolisé par une orbitale *p*).

Can. J. Chem. Downloaded from www.nrcresearchpress.com by 91.144.44.67 on 09/07/12
For personal use only.

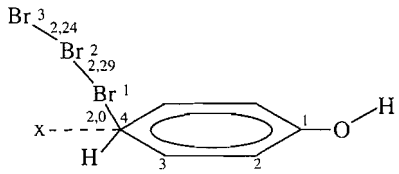

Br(1)—C(4)—x = 63°
H—C(4)—x = 34°
C(4)—Br(1)—Br(2) = 154°
Br(1)—Br(2)—Br(3) = 172°

1

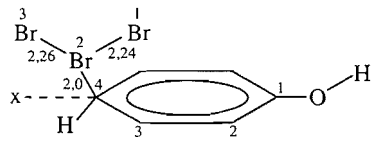

Br(2)—C(4)—x = 77°
H—C(4)—x = 39°
C(4)—Br(2)—Br(1) = 103°
Br(1)—Br(2)—Br(3) = 156°

2

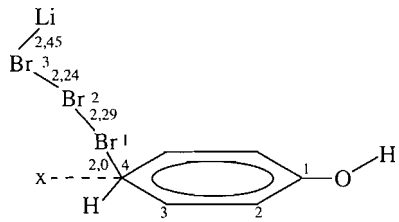

Br(1)—C(4)—x = 69°
H—C(4)—x = 38°
C(4)—Br(1)—Br(2) = 176°
Br(1)—Br(2)—Br(3) = 179°
Br(2)—Br(3)—Li = 74°

3

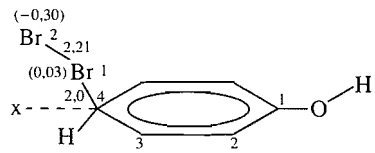

H—C(4)—x = 30°
Br(1)—C(4)—x = 109°
C(4)—Br(1)—Br(2) = 111°

4

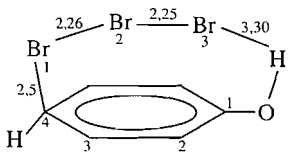

C(1)—C(4)—Br(1) = 103°
C(4)—Br(1)—Br(2) = 100°
Br(3)—H—O = 144°

E = 76,7 kJ mol^{-1}

5

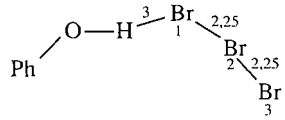

Br(1)—H—O = 173°
Br(2)—Br(1)—H = 105°

6

FIG. 3. Approches modèles de la position *para* du phénol. Les valeurs des paramètres optimisés correspondent à une distance C—Br de 2 Å. Les autres paramètres ont été maintenus constants avec les valeurs suivantes : C—C = 1,43 Å, C—O = 1,36 Å, O—H = 0,96 Å, C—H = 1,08 Å, C—O—H = 110°.

sommets 1 et 3 portent une charge (charge atomique nette résultant du calcul SCF) légèrement supérieure à un demi-électron et que, corrélativement, le brome central est très légèrement positif. Si la molécule se plie, on prévoit une diminution des charges négatives aux extrémités de la molécule : à la limite, pour un angle de 60°, on aurait une symétrie d'ordre 3 et chaque brome porterait 1/3 de charge électronique négative. Neanmoins cet effet est peu marqué au voisinage de 180°, puisque jusqu'à 90° la répartition des charges n'est pas profondément perturbée. L'énergie de stabilisation calculée de Br_3^- par rapport à (Br_2 + Br^-) est de 89 kJ mol^{-1}.

(c) Aspect orbitalaire de la réactivité de Br_3^- ; comparaison avec Br_2

On sait que les interactions acido-basiques peuvent être classées en deux catégories : les interactions « dures », de type électrostatique, et les interactions « molles » de type orbitalaire.

La charge positive de l'atome central (+0,06) est trop faible pour que ce site présente un caractère électrophile dur notable.

Si on examine maintenant les orbitales frontalières de Br_3^- (figure 2), on constate que la plus basse orbitale vacante (BV) est antisymètrique : elle ne peut donc présenter de recouvrement important avec un nucléophile, symbolisé par une orbitale atomique (OA) *p*, que le long de l'axe moléculaire. L'éventualité d'une intervention de la seconde OM vacante doit être écartée, compte tenu de son niveau d'énergie trop élevé. Ainsi, Br_3^- présente deux sites acides mous en 1 et 3. Comparée à celle de Br_2 (voir figure 2), l'orbitale BV de Br_3^- est sensiblement plus basse en énergie. Or Br_2 est considéré comme un acide mou dans les réactions envisagées, et de ce point de vue, Br_3^- se présenterait donc comme un acide plus mou que Br_2.

L'examen des orbitales moléculaires conduit donc à un résultat apparemment paradoxal : Br_3^- ne manifeste des propriétés électrophiles qu'au niveau des atomes terminaux qui sont chargés négativement.

II. Étude de la réactivité de l'ion Br_3^- sur le phénol (méthode MNDO)

Afin d'étayer les conclusions suggérées par l'examen des OM de l'ion tribromure et d'interpréter les principaux résultats

Can. J. Chem. Downloaded from www.nrcresearchpress.com by 91.144.44.67 on 09/07/12
For personal use only.

Can. J. Chem. Downloaded from www.nrcresearchpress.com by 91.144.44.67 on 09/07/12
For personal use only.

expérimentaux, un certain nombre de calculs modèles ont été effectués.

En raison de la taille du système étudié, la méthode semi-empirique MNDO dans sa version 4.00 (16) a été choisie. Nous avons utilisé les paramètres atomiques publiés par les auteurs suivants : Dewar et Thiel (17) pour C, H, N, O; Dewar et Healy (18) pour Br; Thiel (19) pour Li. Il ne faut pas attendre d'une telle technique une bonne précision sur l'énergie absolue, en l'absence, notamment, de fonctions diffuses et de corrélation électronique : c'est pourquoi nous avons évité d'argumenter à partir de données thermodynamiques que nous n'avons signalées qu'exceptionnellement et à titre purement indicatif. A fortiori, nous n'avons pas tenté de déterminer la structure et l'énergie des états de transition. Ceci, outre les causes d'erreur précédentes, eût nécessité l'optimisation complète des nombreux paramètres géométriques; d'autre part, certaines étapes de la réaction impliquent des séparations de paires d'ions dont l'énergie, en l'absence de solvant, serait très largement surévaluée. Tout cela rendrait très aléatoire la validité des résultats.

Nous pensons, en revanche, que les variations d'énergie pour diverses configurations relatives des réactifs sont un guide semi-quantitatif utile pour l'élucidation de ce mécanisme.

(a) Réactivité comparée des pôles 1 et 2 de l'ion tribromure et géométrie optimale d'approche des réactifs

Nous avons effectué une simulation du début de la coordonnée réactionnelle correspondant à l'approche en *para* du phénol des pôles 1 et 2 de Br_3^-, respectivement. Pour cela, nous avons fait varier la distance C(4)—Br(1) ou C(4)—Br(2) de 2,5 à 2,0 Å, en optimisant les paramètres géométriques des atomes les plus directement impliqués (figure 3, structures **1** et **2**). À titre indicatif, la distance C(4)—Br a été trouvée égale à 1,91 Å dans le «complexe σ» $(Br\phi OH)^+$. On constate (figure 4) que l'approche du pôle 1 de Br_3^- est beaucoup plus aisée que celle du pôle 2; le gain d'énergie atteint plus de 80 kJ mol^{-1} à 2 Å. De plus, Br_3^- adopte une géométrie grossièrement perpendiculaire au plan du cycle ce qui assure un bon recouvrement de sa BV avec la HO du phénol, en éloignant autant que possible de ce dernier les atomes Br(2) et Br(3), ce qui minimise les répulsions entre orbitales occupées des deux entités. Ainsi se trouve confirmée l'hypothèse selon laquelle ce sont les atomes terminaux du tribromure qui, bien que chargés négativement, présentent un caractère électrophile. La conséquence immédiate est que l'on peut attendre de cet ion une réactivité sensiblement plus faible que celle du dibrome. L'approche de Br_2, réalisée dans les mêmes conditions, le montre clairement (figure 4).

Une troisième géométrie d'approche est envisageable, qui pourrait justifier la sélectivité en *para* par l'intervention d'une liaison hydrogène Br—H—O, selon le mécanisme de la figure 5. Nous avons donc calculé l'énergie du système **5** (figure 3), dans lequel la distance C(4)—Br(1) (2,5 Å) et la distance H—Br(3) (3,0 Å, valeur justifiée plus loin) ont été maintenues constantes, alors que les distances Br—Br et tous les angles et dièdres de la chaîne C(4)—Br(1)—Br(2)—Br(3)—H ont été optimisés. L'énergie de ce système se situe à 76,7 kJ mol^{-1} au dessus de celle des réactifs à distance infinie, soit 23,6 kJ mol^{-1} au dessus de la géométrie d'approche la plus favorable **1**, pour une même distance C(4)—Br de 2,5 Å. Ce mécanisme apparait donc comme improbable.

La géométrie optimale du complexe phénol–tribromure est plane (structure **6** de la figure 3), avec une distance H—Br de 3 Å. La liaison hydrogène apporte dans cette structure une stabilisation calculée de 16,7 kJ mol^{-1}. Cette valeur est très insuffisante pour compenser la perte de coplanéité du groupement phénol (6,27 kJ mol^{-1}, calcul MNDO), la répulsion entre les systèmes du phénol et de l'ion tribromure, et la diminution du recouvrement entre la BV du tribromure et la HO du phénol imposés par la structure **5**.

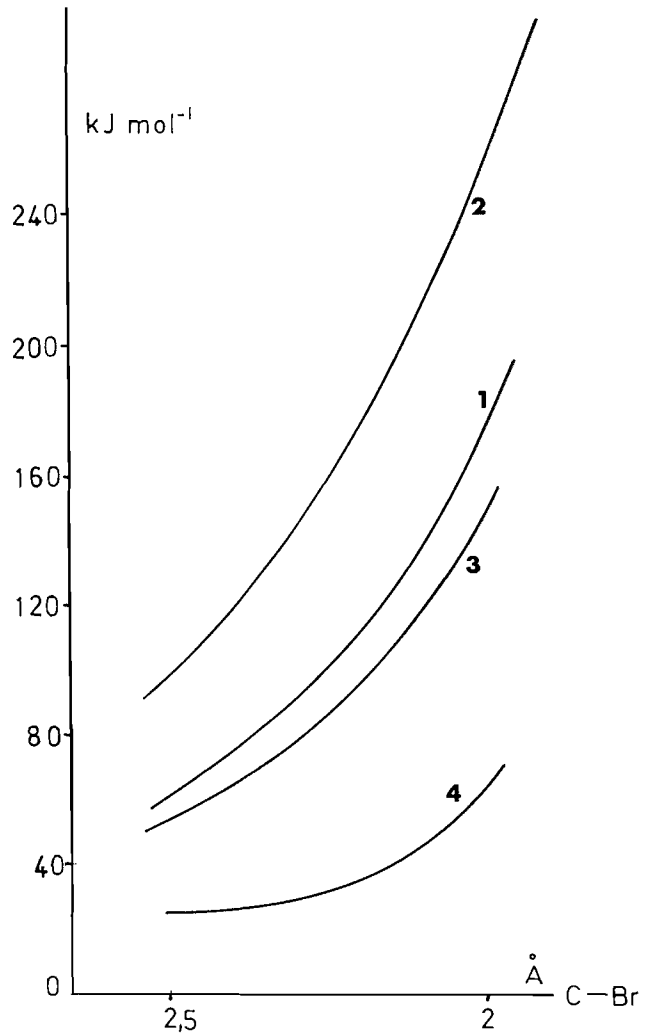

FIG. 4. Variation de l'énergie MNDO des structures 1–4 (figure 3) en fonction de la distance C—Br. L'origine des énergies correspond aux deux réactifs à distance infinie.

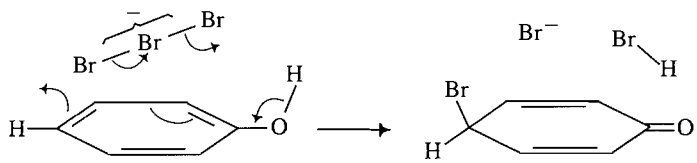

FIG. 5. Mécanisme concerté faisant intervenir une liaison hydrogène.

(b) Rôle du contre-ion ou de molécules polaires

La figure 6 rassemble les résultats des calculs MNDO de Br_3^- et de systèmes MBr_3 où M = H^+, Li^+, H_2O, NH_4^+, et $(CH_3)_4N^+$. L'effet de ces ions ou entités polaires est d'affaiblir la liaison Br(2)—Br(3) qui s'allonge de 2,25 Å (valeur optimisée pour Br_3^-) à 2,47 Å quand M = H^+. De façon concomitante, la liaison Br(1)—Br(2) se raccourcit jusqu'à 2,18 Å, tendant vers 2,17 Å (valeur optimisée pour Br_2). Il faut noter que, selon ce calcul, Br_3H ne se dissocie pas spontanément en HBr + Br_2; cette réaction ne demande cependant qu'une faible énergie (19,6 kJ mol^{-1}). (Expérimentalement, on

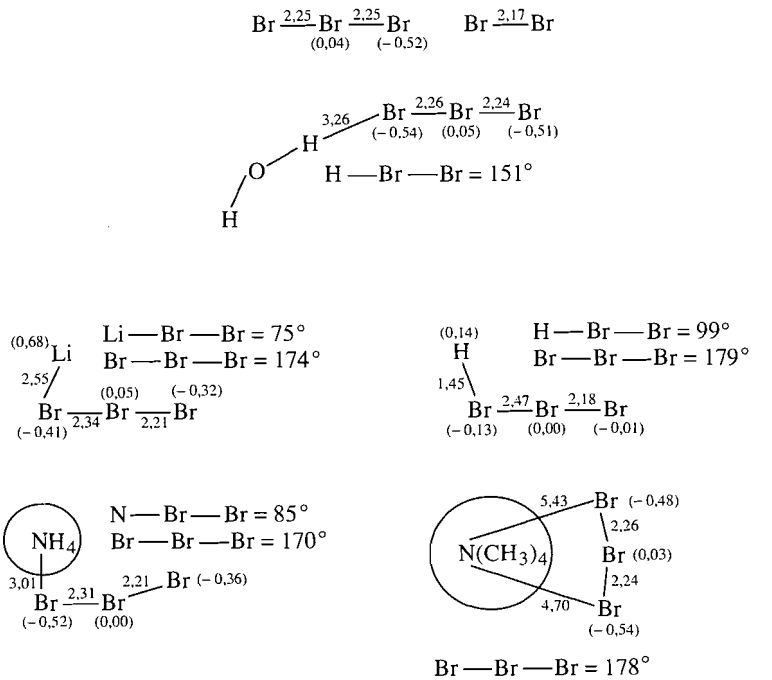

FIG. 6. Structures optimisées (MNDO) de systèmes du type MBr_3. Les charges atomiques nettes résultant du calcul SCF-MNDO sont indiquées entre parenthèses.

observe une libération de Br_2 par Br_3^- en solution acide.) À l'inverse, un gros cation, comme le tétraméthylammonium, ne perturbe que faiblement l'entité Br_3^- et s'associe de façon pratiquement symétrique avec les deux bromes terminaux.

Afin de déterminer le rôle du contre-ion dans la réactivité de Br_3^-, nous avons analysé le système $LiBr_3$ + ϕOH dans l'approche optimale (structure **3** de la figure 3 et de la figure 4). Le cation lithium (17) a été choisi en raison de son pouvoir polarisant élevé, afin d'exalter les différences éventuelles avec Br_3^- seul, modèle de MBr_3 où M serait le cas limite du très gros cation (situé à l'infini).

Nous constatons que l'approche est plus facile que dans le cas de Br_3^- seul : ceci était prévisible si on remarque (figure 6) que la présence de Li^+ diminue la charge négative de Br(1). Ensuite, la structure **3** (figure 3) montre que la liaison Br(2)—Br(3) s'allonge sensiblement, avec 2,45 Å contre 2,34 Å dans $LiBr_3$. La rupture de cette liaison ne demande plus qu'une énergie très faible (7,5 kJ mol^{-1}). En revanche, la structure **1** (figure 3) présente une distance Br(2)—Br(3) de 2,24 Å pratiquement inchangée par rapport à Br_3^-. Au contraire, c'est la liaison Br(1)—Br(2) qui tend, dans ce dernier cas, à s'affaiblir.

Ainsi, si on assimile la coordonnée réactionnelle à la distance C(4)—Br(1), il ressort que le système contenant un petit cation tend à se comporter, dès le début de la réaction, comme Br_2 + ϕOH.

À l'inverse, les systèmes à gros cations ne tendent pas à la formation de Br_2. Dans ce cas, le départ de $Br(3)^-$, d'une part est donc plus tardif, et d'autre part entraîne une inversion de polarisation spectaculaire du groupement Br(1)—Br(2) (cf. structure **4**, figure 3), de sorte que le départ des ions $Br(3)^-$ et $Br(2)^-$ est probablement quasi-synchrone. On peut raisonnablement supposer que, bien que le complexe σ $(Br\phi OH)^+$ soit commun aux bromations par Br_2 et par Br_3^-, dans le cas de Br_3^- isolé ou avec un contre-ion peu polarisant, l'étape cruciale est la rupture de Br(2)—Br(3); en revanche, lors de la bromation par Br_2 ou par Br_3^- en présence d'un cation fortement polarisant, cette étape serait la rupture de Br(1)—Br(2). Bien entendu,

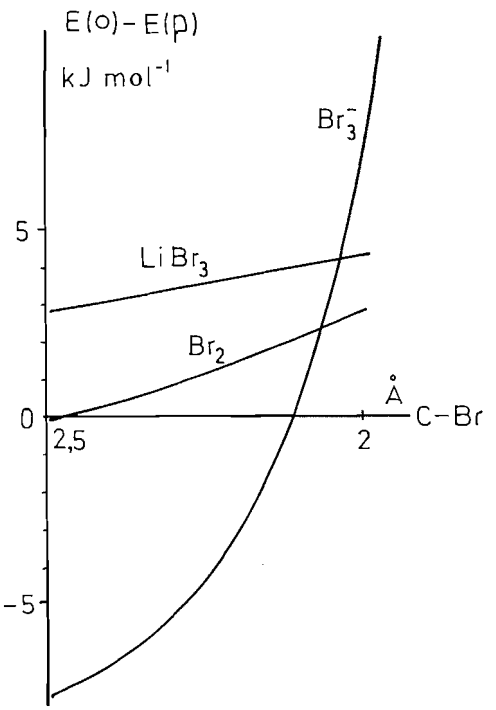

FIG. 7. Différence d'énergie calculée (MNDO) entre les approches optimales des pôle *ortho* et *para* de Br_3^-, Br_3Li et Br_2, en fonction de la distance C—Br.

avec des cations intermédiaires, un spectre d'états de transition compris entre ces deux cas limites peut être attendu.

Ainsi, plus le pouvoir polarisant du cation augmente, plus la réaction ressemblera à celle du dibrome lui-même, avec pour conséquences principales la perte de sélectivité et l'augmentation de la vitesse.

(c) Sélectivité ortho/para

L'étude théorique de ce point est beaucoup plus délicate : il

Can. J. Chem. Downloaded from www.nrcresearchpress.com by 91.144.44.67 on 09/07/12
For personal use only.

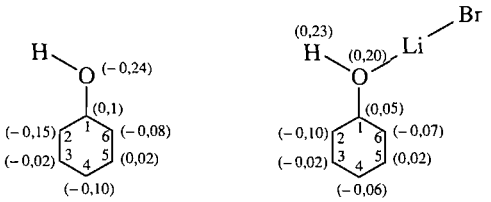

FIG. 8. Charges nettes calculées (MNDO) pour la molécule de phénol et l'agrégat phénol + LiBr.

suffit en effet de moins de 10 kJ mol^{-1} de différence d'énergie d'activation entre deux réactions concurrents pour assurer une très large sélectivité.

Les calculs MNDO montrent, à une distance C(4)—Br(1) de 2,0 Å, que l'approche de Br_3^- est plus facile en position *para* qu'en position *ortho*, la différence étant de 6,9 kJ mol^{-1}. Ce résultat est conforme aux données expérimentales et d'un ordre de grandeur satisfaisant, alors que l'état de transition n'est pas encore atteint. Néanmoins, il doit être considéré avec prudence, compte tenu du fait que tous les paramètres n'ont pas été optimisés. Plus que les valeurs absolues de l'énergie, nous considérons que le gradient énergétique en début de réaction est un élément de discussion utile. Nous avons donc porté, figure 7, la différence d'énergie entre les approches en *ortho* et *para* des trois entités Br_3^-, $LiBr_3$ et Br_2, pour une distance C—Br(3) variant de 2,5 à 2,0 Å. Les paramètres optimisés sont ceux présentés sur la structure **1** (figure 3), pour l'approche *para*, et les paramètres correspondants, pour l'approche *ortho*. Nous avons cependent, en outre, optimisé l'angle dièdre C(2)—C(1)—O—H pour permettre une éventuelle stabilisation électrostatique entre Br(1) et l'atome d'hydrogène de la fonction phénol, lors de l'approche en *ortho*.

Deux remarques peuvent être faites.

(i) La géométrie optimale de l'approche qui fait intervenir le brome terminal et une conformation de Br_3^- quasi perpendiculaire au plan du cycle amène à considérer comme secondaire le rôle des effets stériques lorsqu'un petit contre-ion est utilisé. En effet, dans ce cas, il se forme une liaison localisée avec un seul des atomes de brome terminaux, laissant l'autre disponible (cf. figure 7). En revanche, un gros cation comme $(CH_3)_4N^+$ s'associe presque symétriquement avec les deux bromes terminaux, augmentant l'encombrement stérique, et favorisant ainsi la substitution en *para*.

(ii) Si on considère (figure 7) la différence d'énergie des approches *para* et *ortho* de Br_3^- en fonction de la distance C—Br, on constate qu'il semble exister une corrélation entre la sélectivité et la charge du brome terminal. Le gradient des courbes obtenues croît en effet de Br_2 à $LiBr_3$ et à Br_3^-, ce qui montre que les interactions électrostatiques jouent également un rôle dans la sélectivité. L'examen des charges nettes calculées du phénol (MNDO, figure 8) montre une situation complexe. Le pôle le moins chargé est le carbone 6 *ortho*. En fait, pour Br_3^- isolé, C(2) est préféré à C(6) par suite de la possibilité d'une interaction stabilisante avec l'hydrogène phénolique. Celui-ci tend en effet à sortir du plan du cycle pour se rapprocher de Br(1). C'est d'ailleurs ce qui explique qu'au début de l'approche, vers 2,5 Å (figure 7), le pôle 2 est favorisé par rapport au pôle *para* lui-même, cette préférence disparaissant si on bloque l'hydrogène phénolique en position *anti* par rapport à C(2). Quand la distance C—Br atteint environ 2 Å, le pôle *ortho* se trouve défavorisé par les interactions du brome terminal avec C(2) et l'oxygène fortement négatif.

Ces deux points sont en accord avec les résultats expérimentaux obtenus par l'action de $TBABr_3$ en présence de LiBr, en milieu biphasique : la sélectivité au profit du pôle *para* diminue (*para* : *ortho* = 78 : 22). Le cation lithium peut avoir trois effets allant dans ce sens. Par association avec Br_3^-, il diminue la charge du brome terminal et le dégage de la proximité du gros cation TBA^+; par association avec le phénol selon $(\phi\text{-OHLi})^+$ Br^-, il diminue les charges négatives sur l'ensemble de la molécule de phénol (figure 8), en particulier en position 2 et sur l'atome d'oxygène.

Conclusion

La structure orbitalaire de l'anion tribromure montre que les pôles terminaux, quoique chargés négativement, sont les plus électrophiles. Cette considération qualitative est corroborée par les calculs modèles (MNDO) des systèmes correspondant aux deux approches des pôles 1 et 2 du tribromure de la position *para* du phénol. Cette situation paradoxale explique en premier lieu la lenteur de la bromation du phénol par les tribromures, comparée à la bromation par le dibrome. La nature du contre-ion apparaît comme très importante du point de vue de la vitesse et de la sélectivité. Un cation fortement polarisant diminue la charge négative du pôle électrophile et favorise une scission précoce de Br_3^- en Br^- et Br_2, la réaction se rapprochant alors de celle du dibrome lui-même. Inversement, un cation volumineux, peu polarisant, diminue la vitesse de réaction, retarde la libération du premier ion Br^-, et favorise la sélectivité en *para* en exaltant les interactions électrostatiques.

La géométrie préférentielle d'attaque de Br_3^-, pratiquement perpendiculaire au plan du phénol, semble minimiser l'importance de facteurs stériques, qui demeurent ainsi comparables à ceux du dibrome. Ces facteurs peuvent cependant être indirectement invoqués en présence d'un gros cation qui encombre simultanément les deux pôles électrophiles de l'ion tribromure, ce qui favorise aussi la bromation en position *para*.

Remerciements

Nous remercions le Pr. W. Thiel (Bergische Universität Gesamthochschule, Wuppertal) pour nous avoir communiqué, avant publication, les paramètres du lithium.

1. J. BERTHELOT, C. GUETTE, P. L. DESBENE, P. CHAQUIN, J. J. BASSELIER et D. MASURE. Can. J. Chem. **67**, 2061 (1989).
2. W. J. WILSON et E. G. SOPER. J. Chem. Soc. 3376; (1949); L. ALTSCHULER et E. BERLINER. J. Am. Chem. Soc. **88**, 5837 (1966).
3. J. J. AARON et J. E. DUBOIS. Bull. Soc. Chim. Fr. 604 (1971).
4. S. SHARMA, J. RAJARAM et J. C. KURIACOSE. Indian J. Chem. **15B**, 274 (1977).
5. T. H. READE. J. Chem. Soc. 148 (1924).
6. (*a*) R. C. L. MOONEY. Z. Kristallogr. **100**, 519 (1939); (*b*) O. ANDRESEN et C. RONNING. Acta Chem. Scand. **16**, 1882 (1962); (*c*) G. L. BRENEMAN et R. D. WILLETT. Acta Crystallogr. **B25**, 1073, (1969); (*d*) W. BABES, D. J. STUFKENS et H. GERDING. J. Mol. Struct. **20**, 343 (1974).
7. G. A. BOWMAKER, P. D. BOYD et R. J. SORRENSON. J. Chem. Soc. Faraday Trans 2, **80**, 1125 (1984).
8. J. ESTIENNE. Acta Crystallogr. **C42**, 1614 (1986).
9. C. LANGE, C. GUETTE, J. BERTHELOT et J. J. BASSELIER. Org. Mass Spectrm. **22**, 123 (1987).
10. J. BERTHELOT, C. GUETTE et C. LANGE. Org. Mass Spectrom. **23**, 54 (1988).
11. J. C. BARTHELAT et P. DURAND. Gazz. Chim. Ital. **108**, 225 (1978).
12. Version modifiée du programme HONDO (Programme QCPE n° 338).

Can. J. Chem. Downloaded from www.nrcresearchpress.com by 91.144.44.67 on 09/07/12
For personal use only.

13. C. MÖLLER et M. S. PLESSET. Phys. Rev. **46**, 618 (1934).
14. B. HURON, J. P. MALRIEU et P. RANCUREL. J. Chem. Phys. **58**, 5745 (1973); J. P. MALRIEU. Theor. Chim. Acta, **62**, 163 (1982); S. EVANGELISTI, J. P. DAUDEY et J. P. MALRIEU. J. Chem. Phys. **75**, 91 (1983).
15. C. HERZBERG. Molecular spectra and molecular structure. I. Spectra of diatomic molecules. D. Van Nostrand Company, New York, 1966.
16. F. J. SEILER. Res. Lab., U.S. Air Force Academy, Colorado Springs, CO. 80840.
17. M. J. S. DEWAR et W. THIEL. J. Am. Chem. Soc. **99**, 4899 (1977).
18. M. J. S. DEWAR et J. HEALY. J. Comput. Chem. **4**, 542 (1983).
19. W. THIEL. Quantum Chemistry Program Exchange, Indiana University, Bloomington, IN. 1982. Program no. 438.

Can. J. Chem. Downloaded from www.nrcresearchpress.com by 91.144.44.67 on 09/07/12
For personal use only.

Redistribution reactions of alkoxy- and siloxysilanes, catalyzed by dimethyltitanocene

SHIXUAN XIN, CLARE AITKEN, JOHN F. HARROD, AND YING MU
Department of Chemistry, McGill University, Montreal, P.Q., Canada H3A 2K6

AND

E. SAMUEL
Laboratoire de Chimie Organométallique de l'ENSCP (U.A. 403, CNRS), 11 rue P. et M. Curie, 75005 Paris, France

Received May 15, 1989

SHIXUAN XIN, CLARE AITKEN, JOHN F. HARROD, YING MU, and E. SAMUEL. Can. J. Chem. **68**, 471 (1990).

Dimethyltitanocene is an excellent catalyst for the redistribution of alkoxy- and siloxyhydrosilanes. The redistribution reactions of triethoxysilane, diethoxymethylsilane, 1,3,5,7-tetramethylcyclotetrasiloxane, pentamethyldisiloxane, and H—$(SiMe_2O)_n$—$SiMe_2H$ (n = 1 to 3) are described. The mechanism of these reactions is discussed in terms of TiH mediated displacements. The possibility of both Ti(III) and Ti(IV) mediated displacements are considered and a mechanism involving the former, which fits all of the experimental data, is proposed.

Key words: siloxanes, alkoxysilanes, redistribution, catalysis, dimethyltitanocene.

SHIXUAN XIN, CLARE AITKEN, JOHN F. HARROD, YING MU et E. SAMUEL. Can. J. Chem. **68**, 471 (1990).

Le diméthyltitanocène est un excellent catalyseur pour la redistribution des alcoxy- et siloxyhydrosilanes. On décrit les réactions de redistribution du triéthoxysilane, du diéthoxyméthylsilane, du 1,3,5,7-tétraméthylcyclotétrasiloxane, du pentaméthyldisiloxane et des H—$(SiMe_2O)_n$—$SiMe_2H$ (n = 1 à 3). On discute du mécanisme de ces réactions en fonction de déplacements effectués sous l'influence du TiH. On a considéré la possibilité que les déplacements s'effectuent sous l'influence du Ti(III) ainsi que du Ti(IV) et on propose une mécanisme impliquant le premier qui permet d'expliquer l'ensemble des données expérimentales.

Mots clés : siloxanes, alcoxysiloxanes, redistribution, catalyse, diméthyltitanocène.

[Traduit par la revue]

Introduction

We have recently described the use of dimethyltitanocene, **1**, as a catalyst for the oligomerization of organosilanes (1). In the course of a wider study of the reactions of silicon hydrides with group 4 metallocenes and their derivatives, we have now found that **1** is also a very effective catalyst for the redistribution of alkoxy- and siloxysilanes. The catalysis of siloxane redistribution by platinum group metal complexes has been previously studied in detail by Curtis *et al.* (2).

In this paper we describe the reactions of a number of alkoxy and siloxysilanes with **1** and show how these reactions may be exploited for the synthesis of polysiloxanes.

Results

Reactions of alkoxysilanes with dimethyltitanocene

Commercial trimethoxysilane is usually deliberately contaminated with small amounts of chlorosilanes to inhibit the slow but dangerous disproportionation to methylsilicate and silane. These contaminants are difficult to remove and impaired our attempts to identify the products resulting from reaction of **1** with trimethoxysilane. We therefore attempted to use **1** to scavenge the active chlorine from a sample of trimethoxysilane. As long as the amount of **1** was less than sufficient to remove all active chlorine the strategy worked and it was rapidly converted to insoluble dichlorotitanocene (identified by comparison of its IR spectrum with that of an authentic sample). If the amount of **1** exceeded the amount necessary to remove all of the active chlorine, reduction of the excess **1** to the previously reported blue–black titanocene(III) complexes occurred (1, 3). These reduced titanocene species proved to be a potent catalyst for the disproportionation reaction and the trimethoxysilane was rapidly and completely converted to methylsilicate and silane.

Reaction of diethoxymethylsilane with a catalytic amount of **1** led to the rapid conversion of the reactant to triethoxymethylsilane and methylsilane, according to reaction [1]. When the

[1] $3\,(EtO)_2MeSiH \longrightarrow MeSiH_3 + 2\,(EtO)_3MeSi$

Cp_2TiMe_2 reaction was carried out on a synthetic scale with a 1:2 ratio of **1** to diethoxymethylsilane, dark blue needles of what appeared to be a pure compound crystallized out from the reacting solution. The crystals were slightly soluble in toluene-d_8 and the dark blue solution gave an ^{1}H-NMR spectrum corresponding to a mixture of the *cis*- and *trans*-isomers of the dimer **2**. The assignment was made by comparison of the spectrum with that of a sample of **2**, made by reaction of methylsilane with **1**, and by comparison with the spectrum of the previously characterized phenylsilyl analogue (1).

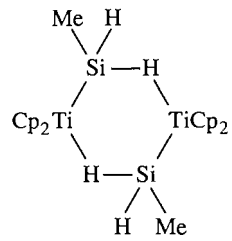

2

The ^{1}H-NMR resonances were assigned as follows: *cis*-isomer: Cp, 4.69 and 4.58; Si—H (terminal), 4.91 (q), $J_{H—H}$ = 3.65 Hz; CH_3, 0.88 (d); Si—H (bridge), −10.11 (broad s); *trans*-isomer: Cp, 4.68 and 4.61; Si—H (terminal), 5.00, $J_{H—H}$ = 3.65 Hz; CH_3, 0.855 (d); Si—H (bridge), −10.11 (broad s). The spectral parameters for the Si—H (terminal) and CH_3 resonances are cited for the spectrum observed while decoupling at −10.11 ppm. Without this decoupling the resonances are poorly resolved multiplets. The Si—H (bridge) resonances of the two isomers are not resolved at 200 MHz even with the methyl resonance decoupled. By integration of the Cp resonances, the *cis*/*trans* isomer ratio is ca. 1.2.

An X-ray crystallographic study of the dark blue needles

Can. J. Chem. Downloaded from www.nrcresearchpress.com by 91.144.44.67 on 09/07/12
For personal use only.

gave the same crystal parameters and diffraction pattern as a sample of bis[bis(cyclopentadienyl)-μ-ethoxytitanium(III)].[1] The latter compound, which is dark green in the pure state, is virtually insoluble in toluene. It may be reasonably concluded that the crystalline product of the reaction of **1** with diethoxymethylsilane is a mixture of titanocene(III) ethoxide with **2**, and that **2** is selectively extracted from the mixture by trituration with toluene. The presence of **2** is also evident from the NMR spectrum of the mother liquor from which the crystalline product precipitates.

Reaction of 1,3,5,7-tetramethylcyclotetrasiloxane (D_4') with ***1***

A reaction of **1** with a several molar excess of D_4' in hydrocarbon solvent resulted in the rapid transformation of the orange **1** into dark blue reduced titanium species and subsequently to the formation of dark blue needles. Attempts to separate the crystals revealed that they were coated with a gelatinous material which rendered their purification impossible.

The origin of the gelatinous material became obvious when a reaction of pure D_4' was carried out in the presence of a catalytic amount of **1**. In this case, the change in color from yellow to blue was again observed, together with the evolution of a steady stream of gas bubbles. The evolved gas was collected and shown by IR spectroscopy to be mainly methylsilane. After some time, the reaction mixture became an immobile gel and after about 24 h a rigid, blue colored glass was obtained.

Examination of the reaction mixture by NMR in the period prior to gelation revealed the presence of methylsilane in solution and also the presence of **2**. These observations lead to the conclusion that the catalytic reaction being observed is that shown in reaction [2]:

$$[2] \quad 3\text{—}(MeHSiO)_4\text{—} \xrightarrow{Cp_2TiMe_2} 8\text{—}(MeSiO_{3/2})\text{—} + 4\,MeSiH_3$$

The catalytic disproportionation of 1,1,3,3-tetramethyldisiloxane (E′E′) and some related compounds[2]

Reaction of pure E′E′ with a catalytic amount of **1** leads to the usual color change from yellow to blue and a vigorous evolution of gas. The gas was shown to be dimethylsilane by IR spectroscopy. The composition of the liquid phase was monitored by GC and the disappearance of E′E′ was initially accompanied by a very rapid production of E′DE′ and E′D_2E′. The cyclics D_n were produced much more slowly and in smaller amounts. The profile of such a reaction is shown in Fig. 1. After several hours the viscosity of the reaction mixture had increased considerably. Removal of volatile material at this point by pumping under high vacuum left a rigid, rubbery, but still soluble residue, corresponding to about a 70% yield based on E′E′. By GPC, this polymer was shown to have a polystyrene-equivalent number average molecular weight of ca. 9500 Dalton, with a polydispersity of 1.6. The ^{1}H- and ^{29}Si-NMR and the IR spectra of this material were indistinguishable from those of an authentic sample of linear poly(dimethylsiloxane). The volatile fraction consisted of a mixture of lower molecular weight ring and chain siloxanes whose mole fraction decreased

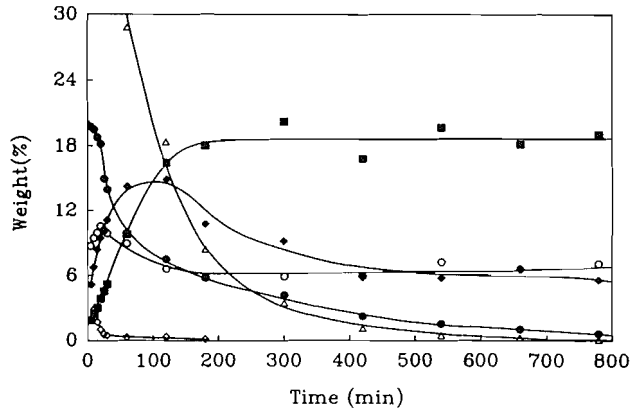

FIG. 1. Reaction profile for the catalytic redistribution of E′E′. [Cp_2TiMe_2] = 0.05 *M* in neat [E′E′] at 20°C. ◇, E′E′; △, E′DE′; ●, E′D_2E′; ◆, D_3; ■, D_4; ○, D_5.

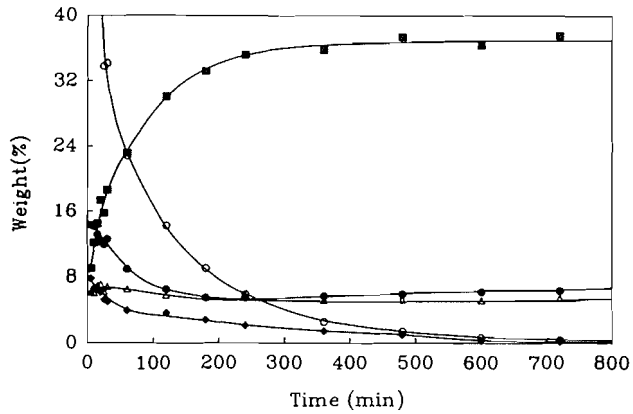

FIG. 2. Reaction profile for the catalytic redistribution of E′DE′. [Cp_2TiMe_2] = 0.056 *M* in neat [E′DE′] at 20°C. ○, E′DE′; ◆, E′D_2E′; △, D_3; ■, D_4; ●, D_5.

rapidly with increasing molecular weight and became vanishingly small above Si_{10}.

The redistribution of E′DE′ was also studied and a typical profile of reaction products is shown in Fig. 2. The rate of reaction of E′DE′ is between one and two orders of magnitude slower than that of E′E′. The most striking difference in the initial product composition is the enhancement in production of D_4 and D_5 and the diminution of the amount of E′D_2E′ in the E′DE′ reaction compared to the E′E′ reaction. This suggests a greater propensity for direct formation of small cyclics, relative to linear products, in the E′DE′ reaction. The trend appears to continue throughout the reaction, but it is likely that depolymerization equilibria contribute to the small cyclics at later stages in the reaction.

This interpretation is supported by the results of a run in which the initial reactant consisted of an equimolar mixture of E′E′ and E′DE′, shown in Fig. 3. In this reaction, the E′E′ had almost completely reacted by the time of the first measurement. At this point the amount of E′DE′ was slightly greater than the initial amount, but much less than would be expected if the conversion of E′E′ to E′DE′ was proceeding at the same rate as in the reaction shown in Fig. 1. The amounts of small cyclics are more like those in Fig. 2 than in Fig. 1 and both D_3 and D_5 pass through a minimum, reinforcing the hypothesis that the small cyclics are produced by depolymerization in the later stages of the reaction.

The influence of ligand chain length on intramolecular ring

[1]The crystal parameters for this compound are as follows: tetragonal, *P*-4*n*2, a = 8.238(1) Å, c = 15.717(2) Å, V = 1066.7 Å^3.

[2]We adopt the same abbreviations for methylsiloxanes as used by Curtis and Epstein (2). In this formalism the following labels are used: $Me_3SiO_{1/2}$ (E), $Me_2HSiO_{2/2}$ (E′) (E′), $Me_2SiO_{2/2}$ (D), $MeHSiO_{2/2}$ (D′).

Can. J. Chem. Downloaded from www.nrcresearchpress.com by 91.144.44.67 on 09/07/12
For personal use only.

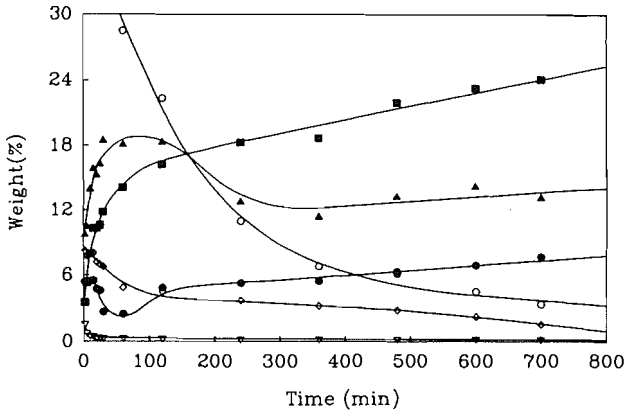

FIG. 3. Reaction profile for the catalytic redistribution of an equimolar mixture of E′E′ and E′DE′. [Cp_2TiMe_2] = 0.05 *M*; [E′E′] = 1.0 *M* in benzene at 20°C. ▽, E′E′; ○, E′DE′; ◇, E′D_2E′; ▲, D_3; ■, D_4; ●, D_5.

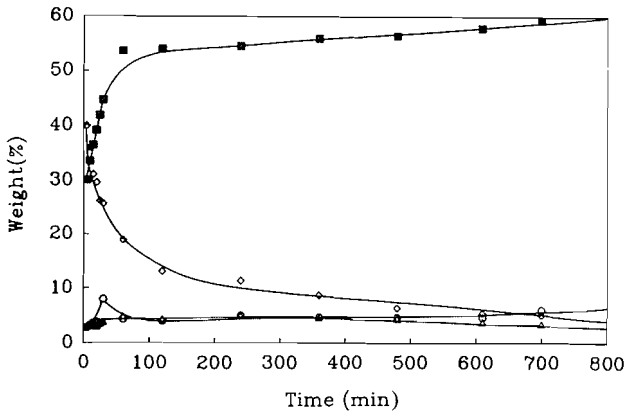

FIG. 4. Catalytic cyclization of E′D_2E′. [Cp_2TiMe_2] = 0.05 *M*; [E′D_2E′] = 1.0 *M*. In benzene at 20°C. ◇, E′D_2E′; ■, D_3; ○, D_4; △, D_6.

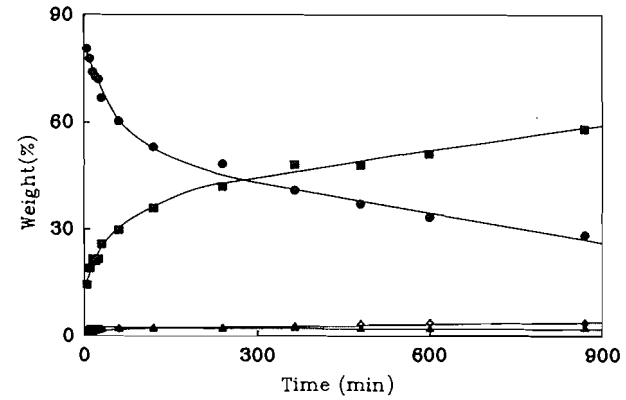

FIG. 5. Reaction profile for the reaction of EE′. [Cp_2TiMe_2] = 0.05 *M*; [EE′] = 2 *M* in benzene at 20°C. ●, EE′; ■, EDE; △, EE; ◇, ED_2E.

closure is dramatically illustrated by the results of a reaction of E′D_2E′, shown in Fig. 4. In this case, the reactant is converted almost exclusively into D_3 in the early stages of the reaction. There are, however, small amounts of D_4 and D_6 and a trace of D_5 produced.

The reaction of EE′ leads almost exclusively to the formation of Me_2SiH_2 and EDE, with only trace amounts of heavier products. A profile for this reaction is shown in Fig. 5.

It was of interest to establish whether or not ring-opening polymerization of small cyclics could be a source of the high molecular weight product. To this end a reaction of D_3 with a catalyst generated by reaction of dimethyltitanocene with E′E′ was followed. The reaction was very slow compared to the reactions of the Si—H containing reactants and even after 50 h almost all of the reacted D_3 could be accounted for by the small cyclic products D_4, D_5, and D_6. It may therefore be concluded that ring-opening polymerization plays no significant part in the redistribution reactions.

Discussion

The catalytic redistribution of siloxanes under the influence of noble metal complexes, such as Vaska's and Wilkinson's complexes, has been studied very thoroughly by Curtis and his collaborators (2). It is essential therefore that the results obtained in the present study be compared to those reported by Curtis. The titanocene catalysts described herein are considerably more reactive than the noble metal complexes and they give larger amounts of small ring products. Nevertheless the gross features of the reactions are sufficiently similar to presume that there may be mechanistic similarities between the two types of system.

The entry of the dimethyltitanocene into the catalytic cycle to give an initial complex analogous to that proposed by Curtis *et al.* could occur by the reactions shown in [3]–[5].

[3] $Cp_2TiMe_2 + HMe_2SiOSiMe_2H \longrightarrow Cp_2TiMe(SiMe_2OSiMe_2H) + CH_4$

[4] $Cp_2TiMe(SiMe_2OSiMe_2H) \longrightarrow Cp_2Ti + Me_3SiOSiMe_2H$

[5] $Cp_2Ti + HMe_2SiOSiMe_2H \longrightarrow Cp_2Ti(H)SiMe_2OSiMe_2H$

3

This proposition is supported by the detection of both methane and EE′ in the initial reaction products.

Although the intermediate **3** could in principle lose H_2 to give a four-membered metallocycle, **4**, again analogous to that

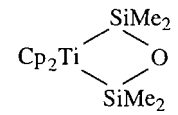

4

proposed by Curtis *et al.*, we have not been able to devise a plausible mechanism involving such an intermediate, which at the same time would be expected to give the experimentally observed extremely high conversion rate of E′E′ to E′DE′. Furthermore, it is impossible to accommodate an additional hydride ligand in the coordination sphere of **4** without exceeding the normal oxidation limit of Ti. Such an additional hydride ligand is an explicit requirement of the Curtis mechanism, as proposed for Ir (Rh).

Rather than conversion of **4** to the next Curtis-type intermediate, **5**, it is simpler to assume a direct rearrangement of **3** through hydride (TiH) displacement of the $OSiMe_2H$. An even

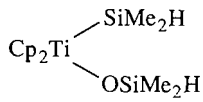

5

Can. J. Chem. Downloaded from www.nrcresearchpress.com by 91.144.44.67 on 09/07/12
For personal use only.

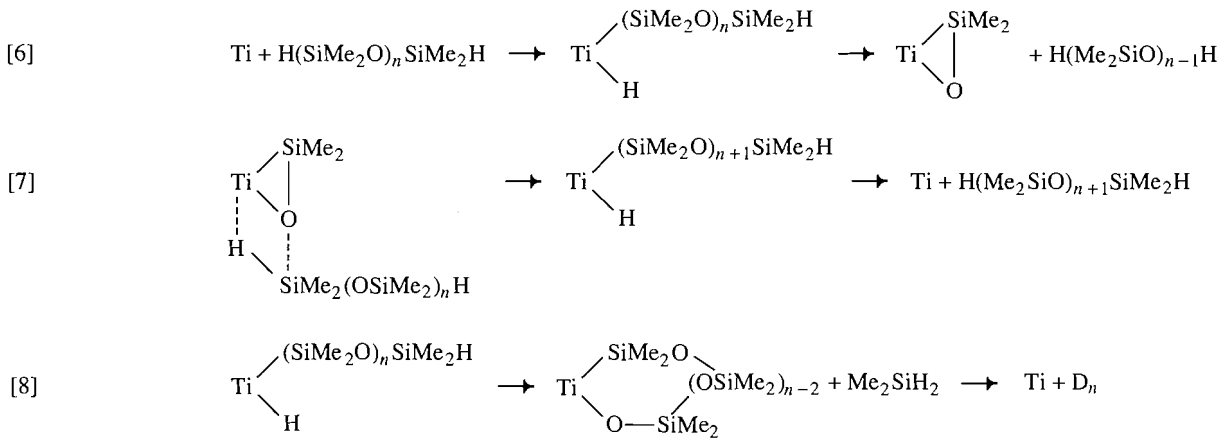

SCHEME 1. Mechanism involving σ-bond metathesis at Ti(IV).

more direct route to **5** would be via the oxidative addition of E′E′ to Cp_2Ti by cleavage of the Si—O linkage. To be favored, such an oxidative addition would require that the sum of the bond energies for the new Ti—Si and Ti—O bonds, plus the positive $T\Delta S$ for the associative process, exceed the energy of the sacrificed Si—O bond. Given the general oxophilicity of Ti(IV) and the fact that titanium is observed in the present study to acquire alkoxy and siloxy groups from silicon, this seems a reasonable assumption. For much the same reasons as adduced by Curtis, it is difficult to avoid the involvement of a silanone intermediate if one is restricted to a mechanism involving monomeric Ti(IV). Such a silanone may be generated either directly from **3**, by hydride (TiH) displacement of Me_2SiH_2, or by elimination of Me_2SiH_2 from **5**. A simple mechanism which fits most of the experimental observations is illustrated in the following scheme (Cp ligands omitted for clarity). See Scheme 1.[3]

Reaction [7] accounts for the linear chain propagation. Reaction [8] accounts for the formation of ring compounds. The highly selective conversion of E′D_2E′ to D_3 strongly supports this type of mechanism. The intermediate metallocycle is expected to be most stable for small values of n. The high yield of D_4 from the reaction of E′DE′ suggests the intermediacy of a metallocycle with $n = 4$ (reaction [8]). This metallocycle would most likely arise from the sequence of steps:

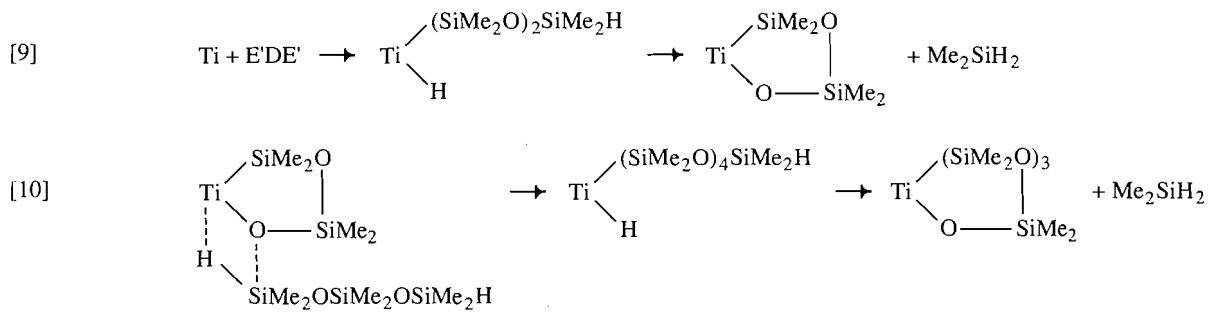

It is interesting to compare the evolution of the reactions shown in Figs. 1 and 2 in view of the fact that there is about the same amount of E′DE′ after 5 min of reaction of E′E′ as there is after 10 min reaction of E′DE′, yet the amounts of other species present and subsequently appearing in the mixture are rather different. The results show that the simultaneous presence of both E′E′ and E′DE′ promotes the formation of larger amounts of E′D_2E′ than are produced when E′E′ is absent. This is fully in line with the above mechanism, since E′D_2E′ is the product of reaction of E′DE′ with the dimethylsilanone complex. Since the latter is only generated directly from E′E′, absence of the E′E′ would suppress formation of E′D_2E′. The formation of rings is also suppressed by the presence of the highly reactive E′E′ since the rate of the ring-opening reactions, e.g. [7] and [10], when the attacking reagent is E′E′ is apparently faster than the putative ring-forming reductive elimination reactions [8].

The rate of reaction [8] will decrease rapidly with increasing siloxane chain length and eventually analogous intermolecular reactions will compete. The extension of longer polymer chains is therefore most likely to occur by attack of the terminal Si—H of a longer chain species with a small ring metallocycle, at least until the reaction is very well advanced.

A mechanism based on Ti(IV) intermediates presents a number of serious problems, not least of which is our failure to observe any Ti(IV) species during either catalytic or stoichiometric reactions. The absence of NMR observable species strongly suggests that most, if not all of the titanium is in the Ti(III) state. In the case of the alkoxysilane redistribution reactions, most of the titanium is demonstrably present as Ti(III).

A fatal objection to the mechanism shown in reactions [6] to

[3]The suggestion that σ-bond metathesis is important in the catalytic reactions of group 14 hydrides with group 4 metallocenes is due to T. D. Tilley, personal communication. The σ-bond metathesis mechanism has been proposed to explain a number of early transition metal and lanthanide reactions (4).

Can. J. Chem. Downloaded from www.nrcresearchpress.com by 91.144.44.67 on 09/07/12
For personal use only.

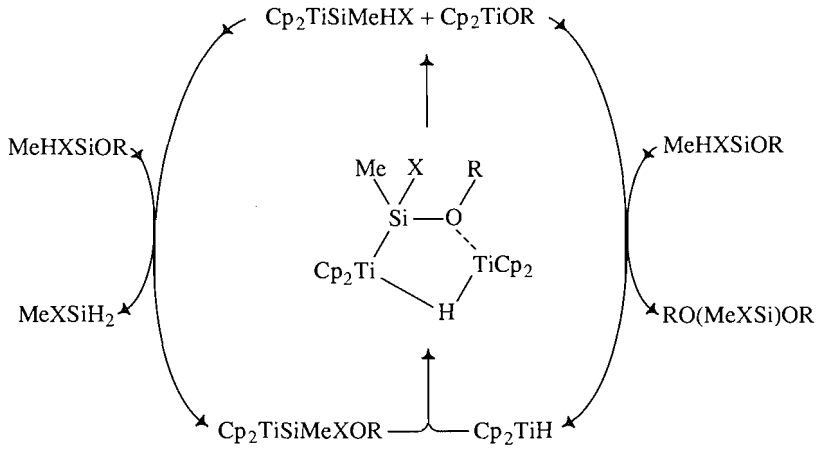

SCHEME 2. Mechanism involving bimetallic Ti(III) intermediates.

[10] is its inability to account for the products of the EE′ reaction. The steps shown in [6] would lead to the formation of Me_3SiH and EDE′ as initial products, whereas the observed products are Me_2SiH_2 and EDE. It is worth noting that Curtis *et al.* obtained ED′E as the principal product from this reaction catalyzed by Vaska's complex (2). They attributed the formation of the D′ units to metal-catalyzed Me_3SiO/Me exchange, a process notably absent in the titanocene-catalyzed reaction.

A final difficulty with the Ti(IV)-based σ-bond metathesis mechanism is that we have been unable to accommodate the results of alkoxysilane redistribution reactions in such a scheme. In Scheme 2, which invokes the intermediacy of bimetallic Ti(III) intermediates, we illustrate a mechanism which seems to satisfy all of the experimental observations. In this scheme, when R = Et and X = OEt, we have the diethoxymethylsilane case. When X = Me and R = $SiMe_2H$ we have the tetramethyldisiloxane case and when X and R are both part of a D_4' ring system we have the D_4' polymerization case (in this case the TiOR and TiSiMeHX remain joined together throughout the cycle). The products of the EE′ reaction find a natural explanation in this scheme as does the failure to detect Ti(IV) species in the system.

The formation of cyclics in the E′E′ redistribution reaction would require an intramolecular metathesis of the Ti—O bond by the terminal Si—H group of the R ligand rather than intermolecular attack in the right hand loop of Scheme 2. All of the arguments applied above to the pattern of cyclics formation in the σ-bond metathesis mechanism apply equally to the mechanism of Scheme 2.

We are continuing attempts to isolate titanium-containing intermediates from the E′E′ redistribution reaction to obtain more substantive evidence in favor of this or some related type of mechanism.

Experimental

All solvents were dried and degassed by standard techniques prior to use. Dimethyltitanocene was synthesized by a literature procedure (5). The following compounds were obtained from Petrarch Systems Inc.: E′E′, E′E, E′DE′, E′D_2E′, E′D_3E′, D_4, D_4', D_5, $(MeO)_3SiH$, and $Me(EtO)_2SiH$. The E′E′ was further purified by distillation prior to use, the other siloxanes were used as received.

Gas chromatography

Analyses of the products of the E′E′ redistribution reactions were carried out on a Shimadzu GC-8A chromatograph equipped with a H_2 flame detector and a DB-5 30 m capillary column. Stationary phase: 95% dimethyl-, 5% diphenylpolysiloxane. Inlet port temperature 300°C. Column temperature 100–300°, programmed at 8°C per min. Carrier gas flow rate 0.5 mL min^{-1}. Calibration was carried out with the commercial siloxane compounds listed above. Products heavier than pentasiloxanes were identified by GC-MS.

Products of the methyldiethoxysilane–dimethyltitanocene reaction

(i) Catalytic reaction

A sample of diethoxymethylsilane (10 g, 75 mmol) was placed in a reactor which had previously been purged with argon and charged with dimethyltitanocene (100 mg). The reactor was warmed to 50°C and the evolved gas was collected in a liquid nitrogen cooled receiver. After 30 min the reaction was stopped and the condensate was distilled twice by allowing the receiver to warm slowly to −10°C and collecting the product in a new receiver at liquid nitrogen temperature. The resulting distillate (1.00 g; 22 mmol; 87%) had NMR and IR spectra indistinguishable from an authentic sample of $MeSiH_3$.

The undistilled residue was then distilled at ambient pressure to remove catalyst residues. The product (bp = 123–125°C/15 mm Hg; 8.50 g; 48 mmol; 96%) was shown by comparison with an authentic sample to be triethoxymethylsilane. The yields are based on reactant, assuming reaction [1].

(ii) Stoichiometric reaction

A sample of dimethyltitanocene (50 mg) was dissolved in previously degassed toluene (5 mL) in a Schlenk tube and methyldiethoxysilane (0.1 mL) was added. After about 5 min gas evolution was observed and the solution rapidly turned from orange to dark blue. The reaction mixture was left undisturbed for 12 h and then the supernatant liquid was decanted to leave a residue of well formed blue–black crystals. The product was partially dissolved in toluene-d_8 (0.5 mL), filtered, and its ^{1}H-NMR spectrum was measured. The spectrum was identical to that of a sample of **2** prepared *in situ* by bubbling methylsilane through a solution of dimethyltitanocene (10 mg) in toluene-d_8 (1 mL).

Redistribution reactions

In a typical redistribution reaction, a sample of dimethyltitanocene (50 mg) was placed in a 20 mL capacity Schlenk tube, equipped with a rubber septum and a magnetic stirrer. After the reactor was purged with argon, previously degassed reactant (5 mL) was injected and the catalyst was rapidly dissolved. Within a few minutes the catalyst color changed from yellow to dark blue, or (in the case of tetramethyldisiloxane) olive green. The color change was accompanied by gas evolution and the gas was periodically sampled by syringe and analysed by GC and IR spectroscopy. The presence of CH_4, SiH_4 (the $(MeO)_3SiH$ reaction), $MeSiH_3$ (D_4' and $(EtO)_2MeSiH$ reactions), and Me_2SiH_2 (E′E′ and E′DE′ reactions) in the gaseous products was established by comparison of IR spectra and GC retention times with authentic samples.

In the case of tetramethyldisiloxane redistribution, the liquid fraction of the reaction mixture was also periodically sampled and analysed by GC. The products up to Si_5 were identified by calibration with authentic standards. Products of higher mass were identified by GC/MS.

Can. J. Chem. Downloaded from www.nrcresearchpress.com by 91.144.44.67 on 09/07/12
For personal use only.

Acknowledgements

Financial support from the Natural Sciences and Engineering Research Council of Canada and the Fonds FCAR de Québec are gratefully acknowledged. This work was also partially supported under U.S. Office of Naval Research Grant No. NOO14-K-O305. One of us (S.X.) thanks the government of the Peoples Republic of China for support as a Visiting Scholar. We thank J. Hénique for technical assistance.

1. C. AITKEN, J. F. HARROD, and E. SAMUEL. J. Am. Chem. Soc. **108**, 4059 (1986); J. F. HARROD. Am. Chem. Soc. Symp. Ser. No. 360, Am. Chem. Soc. Washington DC. 1988. pp. 89–99.
2. M. D. CURTIS and P. S. EPSTEIN. Adv. Organomet. Chem. **19**, 213 (1981) and references therein.
3. E. SAMUEL and J. F. HARROD. J. Am. Chem. Soc. **106**, 1859 (1984).
4. M. E. THOMPSON, S. M. BAXTER, A. R. BULLS, B. BURGER, M. C. NOLAN, B. D. SANTARSIERO, W. P. SCHAEFER, J. BERCAW. J. Am. Chem. Soc. **109**, 203 (1987).
5. K. CLAUS and K. BESTIAN. Justus Liebig's Ann. Chem. **654**, 8 (1962).

Can. J. Chem. Downloaded from www.nrcresearchpress.com by 91.144.44.67 on 09/07/12
For personal use only.

Fluorination of sulfur-containing amino acids: Reaction of xenon difluoride with cysteine derivatives

XIAOLING HUANG,[1] BARRY J. BLACKBURN,[2] STEVE C. F. AU-YEUNG, AND ALEXANDER F. JANZEN
Department of Chemistry, University of Manitoba, Winnipeg, Man., Canada R3T 2N2

Received May 26, 1989

XIAOLING HUANG, BARRY J. BLACKBURN, STEVE C. F. AU-YEUNG, and ALEXANDER F. JANZEN. Can. J. Chem. **68**, 477 (1990).

The reaction of XeF_2 with cysteine derivatives $RSCH_2CH(NHR)COOR$, i.e., *S*-benzyl-*N*-trifluoroacetyl-L-cysteine methyl ester, *S*-benzyl-*N*-carbobenzoxy-L-cysteine *p*-nitrophenyl ester, and *S*-methyl-*N*-trifluoroacetyl-L-cysteine methyl ester is described. The fluorinated products $PhCHFSCH_2CH(NHR)COOR$, $PhCH_2SCHFCH(NHR)COOR$, and $FCH_2SCH_2CH(NHR)COOR$ were identified by ^1H and ^{19}F nuclear magnetic resonance spectroscopy. $PhCH_2SCHFCH(NHR)COOR$ loses HF within 24 hours to give *Z*- and *E*-$PhCH_2SCH{=}C(NHR)COOR$. If the reaction with XeF_2 is carried out in the presence of moisture the sulfoxide $RS(O)CH_2CH(NHR)COOR$ and sulfone $RSO_2CH_2CH(NHR)COOR$ are produced.

Key words: fluorination, XeF_2, amino acids, cysteine.

XIAOLING HUANG, BARRY J. BLACKBURN, STEVE C. F. AU-YEUNG et ALEXANDER F. JANZEN. Can. J. Chem. **68**, 477 (1990).

On décrit la réaction du XeF_2 avec des dérivés de la cystéine, $RSCH_2CH(NHR)COOR$, comme l'ester méthylique de la *S*-benzyl-*N*-trifluoroacétyl-L-cystéine, l'ester *p*-nitrophénylique de la *S*-benzyl-*N*-carbobenzoxy-L-cystéine et l'ester méthylique de *S*-méthyl-*N*-trifluoroacétyl-L-cystéine. Utilisant la résonance magnétique nucléaire du ^1H et du ^{19}F, on a identifié les produits fluorés $PhCHFSCH_2CH(NHR)COOR$, $PhCH_2SCHFCH(NHR)COOR$ et $FCH_2SCH_2CH(NHR)COOR$. Le composé $PhCH_2SCHFCH(NHR)COOR$ perd du HF en moins de 24 heures pour donner les *Z*- et *E*-$PhCH_2SCH{=}C(NHR)COOR$. Si l'on effectue la réaction avec le XeF_2, en présence d'humidité, il se forme du sulfoxyde $RS(O)CH_2CH(NHR)COOR$ et de la sulfone $RSO_2CH_2CH(NHR)COOR$.

Mots clés : fluoration, XeF_2, acides aminés, cystéine.

[Traduit par la revue]

Can. J. Chem. Downloaded from www.nrcresearchpress.com by 91.144.44.67 on 09/07/12
For personal use only.

Results and discussion

The reaction of XeF_2 with organosulfides (1–5) has been applied previously to biotin (6), methionine, and methionylglycine derivatives (7), and as a continuation of our work on sulfur-containing amino acids we have carried out reactions with several cysteine derivatives **1–3**.

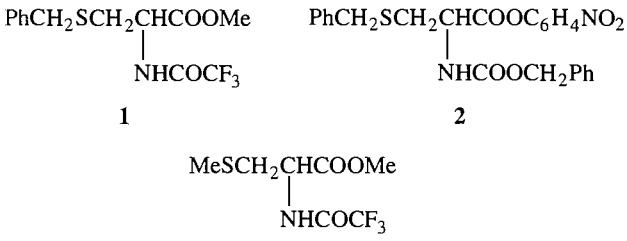

1

2

3

Reaction of **1** with XeF_2 was carried out at 0–5°C in acetonitrile solution over a period of 1 h. Monofluorination of both $-CH_2-$ groups in **1** occurred to give products **4** and **5** in approximately a 1:1 ratio in a combined yield of 70–80%. Products **4** and **5** were identified by ^1H and ^{19}F nmr spectroscopy (Table 1) and the nmr data are in agreement with earlier assignments of fluoromethionine (7) and fluoroalkylsulfides (2–5). Both **4** and **5** contain two chiral centers and the presence of diastereomers (A and B) is confirmed by ^1H and ^{19}F nmr (Table 1). The vicinal couplings $^3J(HH)$ and $^3J(HF)$, which reflect the rotamer populations, and the ^1H and ^{19}F nmr chemical shifts differ significantly for the diastereomers of **4** and **8**, but for **5**, where the chiral centers are separated by three bonds, only the ^{19}F nmr chemical shifts differ significantly.

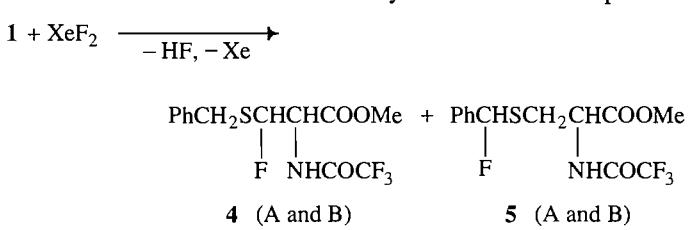

4 (A and B) **5** (A and B)

Products **4** and **5** were not separated and purified because of moderately rapid decomposition, complete within 24 h at 20°C. Decomposition could not be prevented by lowering the temperature to 0°C or by removing HF from the reaction mixture under reduced pressure or by bubbling a stream of nitrogen through the reaction mixture, or by chemical treatment with NaF, $NaHCO_3$, Et_3N, or $(Me_3Si)_2NH$ (8), all of which failed to stop decomposition of **4** and **5**.

Decomposition of **4** gave mainly alkenes *E*-**6** and *Z*-**6**, which are stable indefinitely and were separated by tlc and characterized by elemental analysis, mass spectrometry, and ^1H and ^{19}F nmr. The chemical shifts of the olefinic hydrogens of *Z*-**6** (8.47 ppm) and *E*-**6** (7.64 ppm) differ significantly and the higher field resonance may tentatively be assigned to the *E* isomer (9).

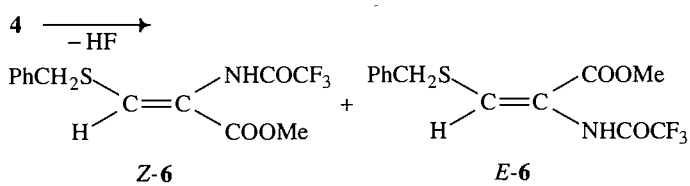

Z-**6** *E*-**6**

Product **5**, which contains a fluorobenzyl substituent, gave more complex decomposition products, including [MeOC(O)-

[1]Department of Chemistry, Wuhan University, Wuhan, China.
[2]Department of Chemistry, University of Winnipeg, Winnipeg, Man., R3B 2E9.

TABLE 1. The ^1H and ^{19}F nmr data for some cysteine derivatives in CD_3CN[a]

Compound	Chemical shift (ppm)		Coupling constant (Hz)		
	δH(CHF)	δF(CHF)	^2J(HF)	^3J(HH)	^3J(HF)
4 $PhCH_2SCHFCH(NHCOCF_3)COOMe$					
Isomer A	6.13	−157.7	53.6	3.5	12.0
Isomer B	5.95	−160.3	53.3	4.9	24.4
5 $PhCHFSCH_2CH(NHCOCF_3)COOMe$					
Isomer A	6.81	−144.6	55.2		
Isomer B	6.81	−147.2	55.2		
7 $PhCH_2SCHFCH(NHCOOCH_2Ph)COOC_6H_4NO_2$					
Isomer A	6.26	−158.4	54.5	3.4	11.3
Isomer B	6.09	−160.6	54.1	5.0	24.1
10 $FCH_2SCH_2CH(NHCOCF_3)COOMe$	5.57	−180.6	52.8		

[a]Chemical shifts were measured relative to internal CHD_2CN (1.93 ppm) and C_6F_6 (−162.9 ppm) and converted to the TMS and $CFCl_3$ scales. CF_3 groups in **4**, **5**, and **10** are found in the range −74.5 to −75.2 ppm.

$CH(NHCOCF_3)CH_2S-]_2$, $PhCH_2SSCH(NHCOCF_3)COOMe$, $PhCH_2SSCH_2Ph$, and PhC(O)H.

Fluorination of **2** proceeded in the same manner as **1**, except that product **8** appeared to decompose even faster than **5** and therefore reliable nmr spectra of **8** could not be obtained.

$$\mathbf{2} + XeF_2 \xrightarrow[-HF,\,-Xe]{} PhCH_2SCH(F)CH(NHCOOCH_2Ph)COOC_6H_4NO_2 + PhCH(F)SCH_2CH(NHCOOCH_2Ph)COOC_6H_4NO_2$$

7 (A and B) **8**

However, **7** was stable enough for ^1H and ^{19}F nmr identification and both diastereomers (A and B) were detected by nmr (Table 1). HF elimination within 24 h converted **7** to alkene *E*-**9** and the latter was identified by mass spectrometry and ^1H nmr.

$$\mathbf{7} \xrightarrow[-HF]{} PhCH_2SCH{=}C(COOC_6H_4NO_2)NHCOOCH_2Ph$$

E-**9**

Loss of the nitrophenyl protecting group during the reaction with XeF_2 and during subsequent work-up made **2** a more difficult compound to study than **1**.

The reaction of **3** with XeF_2 was briefly studied and the product **10** was identified by ^1H and ^{19}F nmr (Table 1). This reaction confirms the result obtained with methionine and methionylglycine (7), namely, that fluorination with XeF_2 occurs preferentially at a primary rather than a secondary hydrogen.

$$\mathbf{3} + XeF_2 \xrightarrow[-HF,\,-Xe]{} CH_2SCH(F)CH_2CHCOOMe\ (NHCOCF_3)$$

10

The postulated intermediate in the α-fluorination of organosulfides is a sulfur(IV) difluoride R_2SF_2 (2–5). Since it is known that R_2SF_2 undergoes rapid hydrolysis, e.g., Ph_2SF_2 to Ph_2SO (3, 4) or Me_2SF_2 to Me_2SO (5), a test for intermediate **11** was carried out by reacting **1** with XeF_2 at 0–5°C, followed by immediate addition of water. The sulfoxide **12** was indeed formed, as expected if **11** is an intermediate in the fluorination reaction. On occasion, this reaction also produced the sulfone $PhCH_2SO_2CH_2CH(NHCOCF_3)COOMe$ **13**, and sulfones have

$$\mathbf{1} + XeF_2 \xrightarrow[-Xe]{} [PhCH_2SCH(F)CH_2CHCOOMe\ (F)\ (NHCOCF_3)]$$

11

$$\xrightarrow[-2HF]{H_2O} PhCH_2S(=O)CH_2CHCOOMe\ (NHCOCF_3)$$

12

been identified previously in related reactions of XeF_2 (3). In a similar reaction of **3** with XeF_2 in the presence of small amounts of water, the sulfoxide $MeS(O)CH_2CH(NHCOCF_3)COOMe$ **14** was formed.

Experimental

The ^1H and ^{19}F nmr spectra were recorded on a Bruker WH90 spectrometer at 90 and 84.66 MHz, respectively. The reaction progress, involving disappearance of XeF_2 and appearance of fluorinated products and HF (as well as BF_4^- from reaction with glass nmr tubes), was routinely monitored by ^{19}F nmr. Mass spectra were obtained on a Finnigan 1015 quadrupole instrument at 70 eV and samples were introduced on the solids probe. Elemental analyses were performed by Galbraith Laboratories, Knoxville, Tenn.

The tlc separations were carried out on silica gel plates using a petroleum ether:benzene:chloroform:methanol = 2:1:0.8:0.05 mixture.

The following compounds were commercial samples: XeF_2 (PCR/SCM), *S*-benzyl-*N*-carbobenzoxy-L-cysteine *p*-nitrophenyl ester **2** (Sigma), *S*-benzyl-L-cysteine (Aldrich), and *S*-methyl-L-cysteine (Aldrich).

S-Benzyl-*N*-trifluoroacetyl-L-cysteine was prepared from *S*-benzyl-L-cysteine by the method of Weygand and Geiger (10). Esterification was carried out by dissolving *S*-benzyl-*N*-trifluoroacetyl-L-cysteine (0.53 g, 1.7 mmol) in 1,2-dichloroethane (3 mL), adding p-$MeC_6H_4SO_3H \cdot H_2O$ (30 mg) in anhydrous methanol (0.9 mL), and heating the mixture for 7 h. The solvent was pumped off, methanol added twice, and the mixture pumped off to dryness. The residue was washed with cold and warm (40°C) water, dried in air, and purified by two sublimations at 100–104°C/0.5 Torr (1 Torr = 133.3 Pa) to give *S*-benzyl-*N*-trifluoroacetyl-L-cysteine methyl ester **1** (477 mg, 85%, mp 64°C, lit. (11) mp 62–64°C), identified by ^1H and ^{19}F nmr and

Can. J. Chem. Downloaded from www.nrcresearchpress.com by 91.144.44.67 on 09/07/12
For personal use only.

Can. J. Chem. Downloaded from www.nrcresearchpress.com by 91.144.44.67 on 09/07/12
For personal use only.

ms m/z: 321 (M^+). *S*-Methyl-L-cysteine (1 g) was esterified (12) with 15 mL of 2 M methanolic HCl for 2 h at 60°C and, after removal of excess methanol, treated with trifluoroacetic anhydride in CH_2Cl_2 at 0–25°C for 30 min followed by removal of volatile material to give *S*-methyl-*N*-trifluoroacetyl-L-cysteine methyl ester **3**, identified by nmr and ms m/z: 245 (M^+).

Reaction of XeF_2 with S-*benzyl*-N-*trifluoroacetyl*-L-*cysteine methyl ester* ***1***

In a typical reaction, XeF_2 (34.5 mg, 0.20 mmol) was weighed into a PTFE bottle which was then cooled to 5–10°C and CD_3CN (0.2 mL) added. Cysteine **1** (60 mg, 0.18 mmol) in CD_3CN (0.7 mL) was added with stirring within 5 min. The reaction mixture was stirred for 50 min and the solution allowed to reach room temperature. During this time, the solution turned slightly yellow. The mixture was transferred into an nmr tube and the fluorocysteine products **4** and **5** were identified at this stage by ^1H and ^{19}F nmr (Table 1).

After standing for 24 h at 25 or 0°C, the ^{19}F nmr signals of **4** and **5** disappeared and the HF peak appeared. The solution now contained *Z*-**6** and *E*-**6**, as described below.

(Z)- and (E)-Methyl N-*trifluoroacetyl*-3-*benzylthio*-2-*amino*-2-*propenoate* ***6***

Typically, the reaction of **1** with XeF_2 was carried out as described above, and the mixture allowed to stand for 24 h or longer. HF was then pumped off and the mixture separated by tlc. The major components were *E*-**6** and *Z*-**6** in about a 3:1 ratio. Anal. calcd. for $C_{13}H_{12}F_3NO_3S$: C 48.91, H 3.79, N 4.38; found: C 49.4, H 3.9, N 4.2. *E*-**6**, ^1H nmr ($CDCl_3$) δ: 3.80 (CH_3), 4.10 (CH_2), 7.35 (Ph), 7.56b (NH), 7.64 (CH); ^{19}F nmr ($CDCl_3$) δ: −76.36 (CF_3). *Z*-**6**, ^1H nmr ($CDCl_3$) δ: 3.90 (CH_3), 4.00 (CH_2), 7.35 (Ph), 8.3 (b, NH), 8.47 (CH); ^{19}F nmr ($CDCl_3$) δ: −77.05 (CF_3). Mass spectrum m/z: 319 (M^+).

To simplify the preparation of *Z*-**6** and *E*-**6**, the reaction of XeF_2 with **1** was carried out for 30 min (as described above), after which dry nitrogen gas was bubbled through the reaction mixture for 15 min (to remove HF) and the products *Z*-**6** and *E*-**6** separated by tlc.

A small amount of solid was separated by tlc and tentatively identified as the cystine derivative $[MeOC(O)CH(NHCOCF_3)CH_2S\text{-}]_2$ on the basis of nmr and ms m/z: 460 (M^+), 401 ($M^+ - CO_2Me$).

S-*Benzyl*-N-*trifluoroacetyl*-L-*cysteine sulfoxide methyl ester* ***12*** *and sulfone* ***13***

XeF_2 (44 mg, 0.26 mmol) was dissolved in CH_3CN (0.6 mL) in a PTFE bottle that had been set on a cold plate at 5–10°C. A solution of **1** (75 mg, 0.23 mmol) in CH_3CN was added with stirring within 5 min. The reaction solution was stirred for 30 min at 5–10°C and then 1 mL cold water was added. The solution was neutralized with a clear solution of $Ca(OH)_2$ until pH 8. The solution was extracted twice with CH_2Cl_2. The combined extracts were dried with 4A molecular sieve and the solvent removed under vacuum. Recrystallization of the solid residue from 1:1 benzene:petroleum ether gave sulfoxide **12** (9 mg, 12%), identified by nmr and ms m/z: 337 (M^+). Anal. calcd. for $C_{13}H_{14}F_3NO_4S$: C 46.29, H 4.18, N 4.15; found: C 46.3, H 4.4, N 4.6.

In some reactions, separation of the above mixture by tlc gave an additional minor component tentatively identified as sulfone **13** ms m/z: 353 (M^+). Anal. calcd. for $C_{13}H_{14}F_3NO_5S$: C 44.19, H 3.99, N 3.96; found: C 45.7, H 4.1, N 4.0.

Reaction of XeF_2 with S-*benzyl*-N-*carbobenzoxy*-L-*cysteine* p-*nitrophenyl ester* ***2***

Reactions of XeF_2 with **2** were typically carried out as described above for **1**, but the loss of the nitrophenyl protecting group during reaction with XeF_2 and during subsequent work-up made **2** a more difficult compound to study than **1**. Product **7** (diastereomers A and B) was identified by nmr (Table 1). On standing, an olefinic ^1H peak appears at 7.71 ppm assigned to *E*-**9**, ms m/z: 464 (M^+).

The ms and ^1H nmr of additional products that were separated by tlc suggested the presence of $PhCH_2SSCH_2Ph$ m/z 246 (M^+), $PhCH_2SSSCH_2Ph$ m/z 278 (M^+), and benzaldehyde.

Reaction of XeF_2 with S-*methyl*-N-*trifluoroacetyl*-L-*cysteine methyl ester* ***3***

The reaction was carried out as described above for **1** and **2** and the product $FCH_2SCH_2CH(NHCOCF_3)COOMe$ **10** was identified by ^1H and ^{19}F nmr (Table 1) and ms m/z: 263 (M^+), but purification was not successful. Various reaction mixtures also showed the presence of (*E*)- and (*Z*)-$MeSCH{=}C(NHCOCF_3)COOMe$ with olefinic ^1H nmr peaks at 7.66 and 8.33 ppm, respectively, and ms m/z: 243 (M^+), 196 ($M^+ - CH_2S$). Additional ms peaks at m/z 261 and 277 are assigned to $CH_3S(O)CH_2CH(NHCOCF_3)COOMe$ **14** and $CH_3SO_2CH_2CH(NHCOCF_3)COOMe$ **15**. The yield of sulfoxide **14** could be increased by carrying out the reaction of XeF_2 and **3** in the presence of small amounts of water. Evidently, the reaction with XeF_2 did not stop at the monofluorination stage and the reaction was not pursued further.

Acknowledgement

The financial assistance of the Natural Sciences and Engineering Research Council of Canada is gratefully acknowledged.

1. J. A. GIBSON, R. K. MARAT, and A. F. JANZEN. Can. J. Chem. **53**, 3044 (1975).
2. M. ZUPAN. J. Fluorine Chem. **8**, 305 (1976); R. MINKWITZ and A. WERNER. J. Fluorine Chem. **39**, 141 (1988); T. B. PATRICK and S. NADJI. J. Fluorine Chem. **39**, 415 (1988).
3. M. ZUPAN and B. ZAJC. J. Chem. Soc. Perkin Trans. 1, 965 (1978).
4. R. K. MARAT and A. F. JANZEN. Can. J. Chem. **55**, 3031 (1977).
5. A. M. FORSTER and A. J. DOWNS. J. Chem. Soc. Dalton Trans. 2827 (1984).
6. A. F. JANZEN and X. HUANG. 7th Winter Fluorine Conference, Orlando, Florida. Feb. 3–8, 1985.
7. A. F. JANZEN, P. M. C. WANG, and A. E. LEMIRE. J. Fluorine Chem. **22**, 557 (1982).
8. A. F. JANZEN, J. A. GIBSON, and D. G. IBBOTT. Inorg. Chem. **11**, 2853 (1972).
9. R. M. SILVERSTEIN, G. C. BASSLER, and T. C. MORRILL. Spectrometric identification of organic compounds. 3rd ed. John Wiley and Sons, New York. 1974. p. 223.
10. F. WEYGAND and R. GEIGER. Chem. Ber. **89**, 647 (1956).
11. F. WEYGAND, A. PROX, E. C. JORGENSEN, R. AXEN, and P. KIRCHNER. Z. Naturforsch. **18B**, 93 (1963).
12. R. H. WHITE and F. B. RUDOLPH. Biochem. Biophys. Acta, **542**, 340 (1978).

Dielectric polarization and molecular interaction. Part III. Styrene, benzene, and ethyl vinyl ether – acrylonitrile – cyclohexane systems

GAMAL R. SAAD, MAGDI M. NAOUM, AND HANNA A. RIZK[1]
Department of Chemistry, Faculty of Science, University of Cairo, Cairo, Egypt

Received April 21, 1989

GAMAL R. SAAD, MAGDI M. NAOUM, and HANNA K. RIZK. 1990. Can. J. Chem. **68**, 480 (1990).

The apparent molecular polarization at infinite dilution of acrylonitrile in constant-ratio mixtures of styrene, benzene, and ethyl vinyl ether in cyclohexane leads to the inference of the equilibrium constants of the association process between the acid and the base, and the dipole moments of the complexes formed. The results are mainly consistent with the concept of dipole–dipole interaction.

Key words: dielectric polarization, molecular interaction, styrene, acrylonitrile, cyclohexane.

GAMAL R. SAAD, MAGDI M. NAOUM et HANNA K. RIZK. Can. J. Chem. **68**, 480 (1990).

La polarisation moléculaire apparente à dilution infinie de l'acrylontrile dans des mélanges à rapport constant de tyrène, de benzène et d'éthoxybutène dans le cyclohexane permet d'évaluer les constantes d'équilibre du processus d'association entre l'acide et la base ainsi que les moments dipolaires des complexes qui se forment. Les résultats sont généralement en accord avec le concept d'une interaction dipole.

Mots clés: polarisation diélectrique, interactions moléculaires, styrène, acrylonbitrile, cyclohexane.

[Traduit par la revue]

Can. J. Chem. Downloaded from www.nrcresearchpress.com by 91.144.44.67 on 09/07/12
For personal use only.

In Part I (1) and Part II (2) of this series the systems used for molecular interaction investigation using dielectric polarization measurements (3) were those in which hydrogen bonding (4, 5) was dominant in complex formation, the acids being ketoanilides and diketones, and the base triethylamine. This work extends the investigation to three bases, namely, styrene, **2**, benzene, **3**, and ethyl vinyl ether, **4**, using the same acid acrylonitrile, **1**, and the inert, non-polar solvent cyclohexane, so that other types of interacions (6, 7) leading to association complexes could be studied.

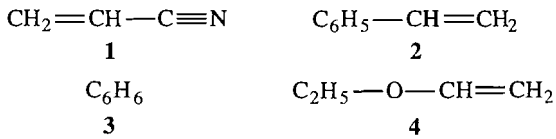

1 **2** **3** **4**

Experimental

Acrylonitrile (B.D.H.), styrene (Merck), benzene (Analar), ethyl vinyl ether (Merck), and cyclohexane (PROLABO, France) were purified according to recommended procedures (8). The purity of these compounds was checked by comparing their physical constants with those in literature (8).

Preparation of solutions, and measurements at 30°C of dielectric constant, ϵ, density, d, refractive index for the sodium-D line, n_D, were carried out as described before (1, 9).

Results

To calculate the equilibrium constant, K, of the association process, and the dipole moment, μ_{AB}, of the complex, the following original equation of Few and Smith (3) was applied:

$$[1] \quad \frac{\Delta P}{P^*_A - P_A} = 1 + \frac{M_B}{KW_B d}$$

Here P^*_A = molecular polarization at infinite dilution of the acid, A, in a constant-ratio mixture of the active polar base, B, and the inert, non-polar solvent, cyclohexane, S; P_A = molecular polarization at infinite dilution of the acid, A, in the inert solvent cyclohexane, S; ΔP = increase in molecular polarization at infinite dilution associated with the formation of 1 mol of the association complex, AB, i.e., equals $P_{AB} - P_A - P_B$; W_B = weight fraction of the base, B, in a given solvent mixture, BS, which, at the same time, was considered to be approximately equal to that of th base in very dilute solutions of the acid in the same solvent mixture; M_B = molecular weight of the base, B; d = density of the solvent mixture, BS, which was also taken to be approximately equal to the density of very dilute solutions of the acid in the same solvent mixture, and K = equilibrium constant of the association process A + B = AB, where the active masses were expressed in terms of their concentrations in mol per cm^3.

However, it was found that in the two systems styrene–acrylonitrile–cyclohexane and ethyl vinyl ether – acrylonitrile – cyclohexane, the values of the molecular polarization, P^*_A, at infinite dilution of acrylonitrile in the various constant-ratio solvent mixtures were sufficiently close to one another, and to the value of its molecular polarization, P_A, at infinite dilution in the inert solvent cyclohexane. The fact that this behaviour was not observed in the system benzene–acrylonitrile–cyclohexane, for which the dielectric constant of the base benzene (2.272) differs only slightly from that of the inert solvent cyclohexane (2.007), whereas it appeared in the former two systems, for which the dielectric constants of the bases styrene and ethyl vinyl ether (2.46 and 4.06, respectively) differ markedly from that of cyclohexane, might lead one to suggest that it is due to solvent effect. An approximate correction for this effect has thus been made only for these two systems. That is, the molecular polarizations of acrylonitrile at various concentrations in a constant-ratio mixture of the base, B, in the inert solvent, S, were graphically interpolated at a dielectric constant value equal to that of cyclohexane. The polarization so obtained for acrylonitrile was denoted as P^*_A(corr.); this term was substituted for P^*_A in eq. [1] when the base was either styrene or ethyl vinyl ether.

A summary of the results is given in Tables 1–3 for styrene, benzene, and ethyl vinyl ether – acrylonitrile – cyclohexane systems, respectively.[2]

[1]To whom correspondence should be addressed.

[2]A complete set of Tables 4 to 12 may be purchased from the Depository of Unpublished Data, CISTI, National Research Council of Canada, Ottawa, Ont., Canada K1A 0S2.

TABLE 1. Polarization data of acrylonitrile (A) in styrene (B) – cyclohexane (S) mixtures

% Styrene (= w_B)	d_{BS} (g/cm^3)	$P^*_{A(corr.)}$ (cm^3)	R^*_A (cm^3)	$1/(P^*_A - P_A)$ (corr.)	$1/w_B d_{BS}$	μ_2 (D)
0.000	0.7698	236.0	16.68	—	—	3.28
2.047	0.7718	244.5	16.66	0.1177	63.30	3.34
3.206	0.7729	248.8	16.65	0.0782	40.36	3.37
6.242	0.7759	258.9	16.61	0.0437	20.15	3.44
8.308	0.7777	263.5	16.34	0.0364	15.48	3.48
9.348	0.7787	265.4	16.40	0.0341	13.74	3.49

$M_B/K\Delta P$ (slope)	$1/\Delta P$ (intercept)	ΔP (cm^3)	K (cm^3/mol)	P_{AB} (cm^3)	R_{AB} (cm^3)	μ_{AB} (D)
1.70×10^{-3}	9.83×10^{-3}	101.7	606.6	372.2	54.4	3.98

TABLE 2. Polarization data of acrylonitrile (A) in benzene (B) – cyclohexane (S) mixtures

% Benzene (= w_B)	d_{BS} (g/cm^3)	P^*_A (cm^3)	R^*_A (cm^3)	$1/(P^*_A - P_A)$	$1/w_B d_{BS}$	μ_2 (D)
0.000	0.7698	236.0	—	—	—	3.28
5.056	0.7731	251.2	16.43	0.0657	25.58	3.29
8.037	0.7748	256.3	16.23	0.0493	16.06	3.43
10.498	0.7764	264.0	16.67	0.0357	12.27	3.48
14.840	0.7792	267.8	15.99	0.0315	8.65	3.51
17.656	0.7809	272.6	15.88	0.0274	7.25	3.52

$M_B/K\Delta P$ (slope)	$1/\Delta P$ (intercept)	ΔP (cm^3)	K (cm^3/mol)	P_{AB} (cm^3)	R_{AB} (cm^3)	μ_{AB} (D)
2.1×10^{-3}	1.24×10^{-2}	80.7	457.5	342.1	42.8	3.83

TABLE 3. Polarization data of acrylonitrile (A) in ethyl vinyl ether (B) – cyclohexane mixtures

% Ether (= w_B)	d_{BS} (g/cm^3)	$P^*_{A(corr.)}$ (cm^3)	R^*_A (cm^3)	$1/(P^*_A - P_A)$ (corr.)	$1/w_B d_{BS}$	μ_2 (D)
0.000	0.7698	236.0	16.68	—	—	3.28
3.686	0.7684	240.6	18.03	0.2174	35.31	3.34
6.053	0.7675	242.4	18.02	0.1563	21.53	3.37
10.258	0.7659	247.3	17.93	0.0888	12.73	3.44
13.410	0.7647	251.0	17.99	0.0666	9.75	3.48
15.933	0.7637	253.0	17.97	0.0556	8.22	3.49

$M_B/K\Delta P$ (slope)	$1/\Delta P$ (intercept)	ΔP (cm^3)	K (cm^3/mol)	P_{AB} (cm^3)	R_{AB} (cm^3)	μ_{AB} (D)
5.9×10^{-3}	1.52×10^{-2}	66.0	185.1	354.7	40.3	3.93

Discussion

Tables 1–3 show that the apparent solution moment, μ_2, of acrylonitrile in the various constant-ratio solvent mixtures for each system increases with increasing concentration of the base, signifying an increase in complex formaion. This suggests an estimate can be made of the fraction of acrylonitrile introduced in the constant-ratio mixture of the base in cyclohexane, which is complexed with the base at infinite dilution. For this purpose, the following equation also suggested by Few and Smith (3) has been used, except that P^*_A(corr.) was substituted for P^*_A when the base is either styrene or ethyl vinyl ether.

[2] $P^*_A - P_A = \Delta P(\Delta W_A/W_A)$

The values of this fraction expressed as $\Delta W_A/W_A$ are listed in Table 13. Here W_A is the weight fraction of acrylonitrile in a constant-ratio mixture of the base and cyclohexane, and ΔW_A the amount of A which passes into the form of the complex AB. It is obvious from Table 13 that an increase in the proportion of

Can. J. Chem. Downloaded from www.nrcresearchpress.com by 91.144.44.67 on 09/07/12
For personal use only.

TABLE 13. Fractions of acrylonitrile introduced in different solvent mixtures (BS) which pass into the form of complex at infinite dilution

Styrene		Benzene		Ethyl vinyl ether	
% Base	$\left(\frac{\Delta w_A}{w_A}\right)$	% Base	$\left(\frac{\Delta w_A}{w_A}\right)$	% Base	$\left(\frac{\Delta w_A}{w_A}\right)$
2.047	0.084	5.056	0.189	3.686	0.070
3.206	0.126	8.037	0.252	6.053	0.097
6.242	0.225	10.498	0.347	10.258	0.171
8.308	0.270	14.840	0.394	13.410	0.228
9.348	0.289	17.656	0.453	15.933	0.272

the base in the solvent mixture favours complex formation, as is to be expected. Moreover, for a given solvent mixture, the tendency toward complex formation with acrylonitrile is highest for styrene, **2**, and least with ethyl vinyl ether, **4**. This is consistent with the fact that the equilibrium constant, K, of the association complex, as determined in the present work, decreases in the sequence

$$2 > 3 > 4$$

To account for these results, it may first be assumed that acrylonitrile interacts with styrene in cyclohexane by means of local dipole – induced dipole force. That is, the electron-deficient sites of local dipoles in any of these two types of molecules are approached by the electron-rich centers in the molecule of the other type. Thus, while the methylene hydrogen atoms of acrylonitrile are approached by the styrene phenyl groups, those of styrene itself are directed toward the electron-rich centers at the nitrogen atom of acrylonitrile. At the same time, it might be expected that the stereospecific approach of the styrene molecule with its phenyl groups directed toward the methylene group of acrylonitrile is favoured, because of the location of the latter group with respect to the negative end of the molecular dipole moment. The assumption that the interaction between acrylonitrile and styrene is mainly governed by long-range forces might be extended to the case of benzene as a base. That is, the benzene molecules solvate the electron-deficient sites in acrylonitrile. This means again that the benzene rings are mainly directed toward the methylene hydrogen atoms of acrylonitrile, whereby interactions occur between these hydrogens as positive sites of local dipoles, and the π-electron cloud of benzene.

It is thus evident from above that whilst the orientations of styrene molecules with references to an acrylonitrile molecule are determined by dipole – induced dipole interactions at the negative end of the dipole moment of acrylontrile, and also by local dipole – induced dipole interactions at the positive end of this moment, the orientations of benzene molecules with respect to an acrylonitrile molecule are only determined by local dipole – induced dipole interactions. Accordingly, the observed greater equilibrium constant of the association process between acrylonitrile and styrene than that between acrylonitrile and benzene in cyclohexane could be ascribed to the stronger dipole – induced dipole forces in the former case.

Furthermore, the assumption of local dipole – induced dipole interaction may also be extended to the ethyl vinyl ether molecule as a base. Here, the ethoxy and methylene groups would be, respectively, directed toward the methylene and cyano groups of the acrylonitrile molecule. However, owing to the non-planarity of the ether molecule in contrast to the styrene and benzene molecules, the association complexes formed would not involve parallel alignment of molecules, so that the equilibrium constant of these complexes would be lower than that of complexes involving either styrene or benzene molecules, as is observed.

Finally, it may be added that although the orientations of the base molecules with reference to the acrylonitrile molecule in cyclohexane seem to be dominated by dipole–dipole forces, other forces are also quite possible.

1. M. M. NAOUM, G. R. SAAD, M. M. ABDEL MOTELEB, H. G. SHINOUDA, and H. A. RIZK. Can. J. Chem. **65**, 2760 (1987).
2. G. R. SAAD, M. M. NAOUM, and H. A. RIZK. Can. J. Chem. **67**, 284 (1989).
3. A. V. FEW and J. W. SMITH. J. Chem. Soc. 2781 (1949).
4. A. S. N. MURTY and C. N. R. RAO. J. Mol. Struct. **6**, 253 (1970).
5. P. SHUSTER. Intern. J. Quantum Chem. **3**, 851 (1969).
6. R. S. MÜLLIKEN. J. Am. Chem. Soc. **74**, 811 (1952).
7. H. A. BENESI and J. H. HILDBRAND. J. Am. Chem. Soc. **70**, 3978 (1948).
8. A. WEISSBERGER and E. PROSKAUER. Organic solvents, physical constants, and methods of purification. The Clarendon Press, Oxford. 1935.
9. A. R. TOURKY, H. A. RIZK, and Y. M. GIRGIS. J. Phys. Chem. **64**, 565 (1960).

Can. J. Chem. Downloaded from www.nrcresearchpress.com by 91.144.44.67 on 09/07/12
For personal use only.

The simultaneous influence of organic solvent and salt on the iodide-peroxodisulphate reaction

MANUEL BALÓN AND CARMEN CARMONA[1]

Departamento de Química Física, Facultad de Farmacia, Universidad de Sevilla, 41012 Sevilla, Spain

Received August 14, 1989

MANUEL BALÓN and CARMEN CARMONA. Can. J. Chem. **68**, 483 (1990).

To study the additivity of medium effects, the rates of reaction between peroxodisulphate and iodide ions have been measured in several salt – water – organic solvent mixtures. The results are consistent with Symons's hypothesis of the influence of salts and organic solvents on the equilibrium between bound water, free OH, and lone pair groups.

Key words: medium effects, kinetics, iodide, peroxodisulphate.

MANUEL BALÓN et CARMEN CARMONA. Can. J. Chem. **68**, 483 (1990).

Dans le but de vérifier l'hypothèse d'une additivité dans effets de solvants, on a mesuré les vitesses de réaction des ions peroxodisulfate et iodure, dans plusieurs mélanges de sel – eau – solvants organiques. Les résultats sont en accord avec l'hypothèse de Symon sur l'influence des sels et des solvants organiques sur l'équilibre entre l'eau et les groupements OH libres et les paires d'électrons libres.

Mots clés : effets de solvants, cinétique, iodure, peroxodisulfate.

[Traduit par la revue]

Can. J. Chem. Downloaded from www.nrcresearchpress.com by 91.144.44.67 on 09/07/12
For personal use only.

Introduction

The influence of the medium on peroxodisulphate–iodide reaction has been reported previously (1–8). The effects of different added salts on this reaction were shown to be very specific and dependent upon the nature and concentration of the cations (5). Although this fact has sometimes been explained on the basis of ion pair formation, it is, in general, difficult to accurately interpret the data for this reaction in terms of ionic association. Some recent studies support the above statement. However, in spite of the importance of ion pair formation in media of low dielectric constant, this assumption can not explain the experimental results (7).

On the other hand, the kinetic salt effects (5) and the reactivity in water – organic solvent mixtures (8) has been successfully explained by modification on the water structure because of the presence of salt and organic solvent, respectively. Solvent mixtures with positive excess Gibbs free energy of mixing and structure-making salts diminish or just slightly increase the rate constant (2, 8), while evident rate constant increases are observed for structure-breaking salts and solvent mixtures with negative Gibbs free energy of mixing (5, 8). However, the simultaneous influence of both factors, i.e., organic solvent and salt, has never been studied. Thus in the present work, we have followed the reactivity in water–organic solvent–salt mixtures to analyze the additivity of medium effects. Mixtures of organic solvent and salt belonging to the two different groups mentioned above have been selected (9, 10).

Experimental

All reagents were of AnalaR grade and were used without further purification. Kinetic runs were carried out as described in literature (7). The concentrations of reactants were $|KI| = 0.25\ mol\ dm^{-3}$ and $|K_2S_2O_8| = 2 \times 10^{-4}\ mol\ dm^{-3}$. The solutions also contained $K_2(H_2edta)$ (edta = ethylendiaminetetraacetate) to prevent catalysis by some metal ions that could be present as impurities ($|K_2(H_2edta)| = 5 \times 10^{-4}\ mol\ dm^{-3}$). The organic solvents and compounds used were *tert*-butyl alcohol (TBA), acetonitrile (acn), dimethysulfoxide (dmso), *N*,*N*′-dimethylformamide (dmf), and sucrose. The water–organic compound mixtures were prepared by weight and the dielectric constant data are taken from the literature (11, 14). In each case the organic solvent was found to be inert in relation to the reactants and products. The salts were LiCl, KCl, KF, KBr, Me_4NBr, and Et_4NBr. In every case, the salt concentrations were 0.025, 0.050, 0.075, and $0.100\ mol\ dm^{-3}$.

Rate constants in duplicate or triplicate runs were reproducible to within better than 2%.

Results and discussion

The rate constants in the water – organic compound – salt mixtures are recorded in Table 1 and those in water – dmso and water – dmf in Table 2. As can be seen, the general pattern of the rate constants for all systems is remarkably similar. Thus, inorganic salts behave as sucrose, i.e., they produce an increase in rate constant, while TBA, acn, and tetralkylammonium salts decrease the rate constant. However, before trying any explanation on the experimental results, the following fact should be realized. On interpreting the medium effect on reaction rates between ions of the same charge sign, one point should be taken into account (15, 16). The addition of salts increases the ionic strength and thereby increases the rate constant. This effect could mask the real behavior of the system and lead to mistaken interpretation of experimental results. Thus, to make clear the existence of specific effects on this reaction, it is of interest to examine the results by applying a standard allowance for the long-range Debye–Hückel interactions and to obtain a corrected rate constant $k^{0\prime}$, defined by the following equation

$$[1] \quad \log k^{0\prime} = \log k - 2AZ_AZ_B\frac{\sqrt{I}}{1+\sqrt{I}}$$

where $A = 1.814 \times 10^6/(DT)^{3/2}$, D is the macroscopic dielectric constant, Z_A and Z_B the charges of the reactants, and the other symbols have their usual meaning.

The values of the corrected rate constants $k^{0\prime}$ and the slopes, m, of some representative plots (not shown) of $k^{0\prime}$ against salt concentration are recorded in Table 2. As can be seen in this table, a rather different pattern is now observed. While tetralkylammonium salts produce a decrease in rate constant on increasing salt concentration, the effect of LiCl is just the

[1]Author to whom correspondence may be addressed.

TABLE 1. Observed rate constants ($k \times 10^3/\text{min}^{-1}$ at 298 K) in several water – organic compound – salt mixtures

Cosolvent wt%	Salt concentration (M)	$k \times 10^3$/min when salt =					
		LiCl	KCl	KF	KBr	Me_4NBr	Et_4NBr
			Water–sucrose				
0	0	112.23					
	0.025	116.50	120.40	119.18	119.60	110.53	104.00
	0.050	—	128.09	124.69	127.16	108.07	98.00
	0.075	122.22	132.71	130.16	132.58	105.92	90.98
	0.100	125.58	139.98	135.86	139.73	104.74	87.23
18.62	0	137.88					
	0.025	132.94	147.74	145.63	146.47	121.52	119.49
	0.050	134.28	156.38	152.19	156.69	120.34	111.71
	0.075	135.14	164.75	155.66	163.71	116.47	104.03
	0.100	137.20	173.43	165.86	171.44	115.60	98.06
32.74	0	159.02					
	0.025	159.38	168.13	167.66	168.78	158.48	123.90
	0.050	163.87	177.33	178.83	178.82	154.55	117.71
	0.075	165.71	187.22	187.02	186.52	144.74	112.60
	0.100	167.66	198.44	196.77	198.64	142.66	105.99
			Water – t-butyl alcohol				
5	0	96.17					
	0.025	98.49	103.56	101.82	104.85	94.07	100.24
	0.050	100.69	110.49	108.24	112.40	91.41	95.51
	0.075	100.93	117.27	114.05	119.54	88.82	86.86
	0.100	102.28	122.72	119.43	128.04	86.89	83.36
14.6	0	78.77					
	0.025	75.41	86.37	83.06	84.06	75.55	74.38
	0.050	76.70	93.04	89.40	89.96	71.31	69.73
	0.075	77.36	99.90	94.31	97.50	68.36	64.42
	0.100	—	106.30	98.89	101.95	66.80	58.88
27.0	0	78.93					
	0.025	76.28	86.60	83.50	85.30	72.80	73.65
	0.050	76.90	93.16	92.75	91.73	69.46	65.86
	0.075	78.38	102.23	97.71	97.74	64.64	58.74
	0.100	—	108.30	103.74	106.73	61.71	55.60
			Water–acetonitrile				
20.2	0.025		28.09		28.09		18.30
	0.050		30.33		30.33		17.27
	0.075		31.92		31.92		16.39
	0.100		33.32		33.32		15.70
41.1	0.025	13.27	13.96		14.76	12.67	12.02
	0.050	13.46	15.17		15.51	11.26	11.54
	0.075	13.66	16.20		16.07	10.98	10.74
	0.100	13.64	17.37		—	10.31	10.24

opposite of that observed before and the other inorganic salts do not seem to bring about any important change in the rate constant. Moreover, the increase in rate constant due to the increase of sucrose concentration is lost and the $k^{0\prime}$ values in sucrose–water mixtures are only slightly higher than those in pure water.

Thus, substances which diminished the rate constant still maintain the same effect (TBA, acn, or tetralkylammonium salts), but those which increased k (except $k^{0\prime}$ for LiCl) have no effect or just a minor positive effect on $k^{0\prime}$. Therefore, the significant rate increase of k with increasing inorganic salt concentration was apparently due to an ionic strength effect. This effect was strong enough to overcompensate the real behaviour of LiCl which is similar, although less pronounced (16), to that observed for Me_4NBr and Et_4NBr.

As can be seen in Table 2, the effect of salts has near zero or negative influence on the rate constant in sucrose–water mixtures independent of the sucrose concentration. However, in TBA and acn–water mixtures the negative effect decreases with

Can. J. Chem. Downloaded from www.nrcresearchpress.com by 91.144.44.67 on 09/07/12
For personal use only.

TABLE 2. Corrected rate constants ($k^{0\prime} \times 10^4/\text{min}^{-1}$) in several water – organic compound – salt mixtures

Cosolvent wt%	Salt concentrations (M)	$k^{0\prime} \times 10^4$/min when salt =					
		LiCl	KCl	KF	KBr	Me_4NBr	Et_4NBr
				Water–TBA			
5	0	175.4					
	0.025	170.4	179.1	176.1	181.4	162.7	173.4
	0.050	165.6	181.7	178.0	184.8	150.3	157.1
	0.075	158.5	184.2	179.1	187.7	139.5	136.4
	0.100	153.4	184.0	179.1	192.0	130.3	127.0
		$m=-0.023$ ±0.004				$m=-0.043$ ±0.006	$m=-0.070$ ±0.01
14.6	0	104.8					
	0.025	94.07	107.7	103.6	104.9	94.24	92.78
	0.050	90.11	109.3	105.0	105.7	83.78	81.93
	0.075	86.00	111.1	104.8	108.4	76.00	71.62
	0.100	—	112.1	104.3	107.5	70.43	62.08
						$m=-0.032$ ±0.01	$m=-0.041$ ±0.003
27	0	56.30					
	0.025	50.05	56.82	54.79	55.97	47.77	48.33
	0.050	46.55	56.39	56.15	55.53	42.05	39.87
	0.075	44.18	57.62	55.07	55.09	36.43	33.11
	0.100	—	56.97	54.57	56.14	32.18	29.25
						$m=-0.021$ ±0.003	$m=-0.026$ ±0.029
				Water–sucrose			
0	0	237.2					
	0.025	234.2	242.5	240.0	240.8	222.6	209.4
	0.050	—	245.8	239.2	244.0	207.4	188.0
	0.075	225.0	244.3	239.6	244.0	195.0	167.5
	0.100	221.8	247.2	239.9	246.8	185.0	154.1
						$m=-0.050$ ±0.01	$m=-0.070$ ±0.02
18.62	0	251.5					
	0.025	230.5	256.2	252.5	254.0	210.7	207.2
	0.050	221.3	257.7	250.8	258.3	198.3	184.1
	0.075	212.7	259.3	245.0	257.7	183.3	163.7
	0.100	206.2	260.7	249.3	257.7	173.8	147.4
		$m=-0.033$ ±0.006				$m=-0.050$ ±0.009	$m=-0.08$ ±0.01
				Water–acn			
32.7	0	251.5					
	0.025	237.4	250.4	249.7	251.4	236.0	184.5
	0.050	230.9	250.0	252.0	252.0	217.8	165.9
	0.075	222.0	250.8	250.5	249.9	193.9	150.8
	0.100	214.0	253.3	251.2	253.6	182.1	135.3
		$m=-0.032$ ±0.004				$m=-0.070$ ±0.02	$m=-0.065$ ±0.007
10.8 (D=74)	0	65.3					
20.23	0.025		41.83		40.30		27.26
	0.050		42.74		40.21		24.34
	0.075		42.76		39.25		21.96
	0.100		42.53		42.25		20.04
							$m=-0.010$ ±0.002

Can. J. Chem. Downloaded from www.nrcresearchpress.com by 91.144.44.67 on 09/07/12
For personal use only.

TABLE 2. (*Concluded*)

Cosolvent wt%	Salt concentrations (M)	$k^{0\prime} \times 10^4$/min when salt = LiCl	KCl	KF	KBr	Me_4NBr	Et_4NBr
41.12	0.025	12.07	12.70		11.53		10.94
	0.050	11.40	12.85		9.54		9.77
	0.075	10.88	12.90		8.74		8.55
	0.100	10.21	12.99		7.71		7.66
							$m = -0.004$ ± 0.0006
			Water–dmso				
56.32 (D=74)	0.000	1.95					
			Water–dmf				
20.6 (D=74)	0.000	25.7					

TABLE 3. Observed and corrected rate constant for the iodide–peroxodisulphate reaction in Et_4NClO_4 and NaCl solutions

Et_4NClO_4 concentration	$k^a(M^{-1}\,s^{-1}) \times 10^3$	$k^{0\prime b}(M^{-1}\,s^{-1}) \times 10^4$	NaCl concentration	$k^c(M^{-1}\,s^{-1}) \times 10^3$	$k^{0\prime b}(M^{-1}\,s^{-1}) \times 10^4$
0.01	1.389	4.77	0	1.26	9.71
0.02	1.442	4.69	0.02	1.77	9.35
0.05	1.635	4.61	0.04	2.12	9.17
0.10	1.523	3.57	0.10	2.84	8.54
		$m = -0.001$ ± 0.0009			

[a]Taken from ref. 2.
[b]Corrected using eq. [1].
[c]Taken from ref. 27.

increasing organic solvent content. In fact, the differences observed between Me_4NBr and Et_4NBr at low mole fraction TBA are mitigated at high alcohol proportions. Although no clear conclusions can be drawn from the sucrose – water – salts mixtures, owing to the small influence on reactivity of sucrose concentration, it can be said that in TBA–water–LiCl or tetralkylammonium salts these is a cancellation of added cosolvent and salt effects. The existence of such cancellation could be due to the dominance of hydration effects on reactivity patterns)17).

Therefore, the interpretation of experimental results has to be based on the different interactions between organic solvents and salts with water. Although there are several ways of interpretation that such interaction leads to a classification of salts and cosolvents into different groups (18–23), the present results are better explained using Symons's theory (24) on the influence of salts and organic solvents on the equilibrium between bound water and $(OH)_{free}$ or $(LP)_{free}$ groups. Assuming that a fundamental step in the reaction studied must be an electron transfer from the iodide to the peroxodisulphate ion (1) and that this transfer will be favoured through solvation from $(OH)_{free}$ groups of water, the reactivity pattern could be explained. The substances that diminish $(OH)_{free}$ concentration should produce a decrease in rate constant and those that increase $(OH)_{free}$ concentration an increase in rate constant. According to Symons (24), alcohol and bases cause a loss of $(OH)_{free}$ groups and hence a decrease in rate constant. Tetralkylammonium salts can also induce a great decrease in $(OH)_{free}$ concentration, an effect so pronounced that their influence on rate constant is not compensated by the ionic strength effect. This gives rise to an overall decrease in rate constant even after the ionic strength correction. As would be expected (24), the alkali halide salts induce minor changes in $k_{0\prime}$, the differences between KCland LiCl or NaCl (see Tables 2 and 3) probably being due to the slight differences in solvation of the respective cations. These changes in solvation could also explain the smaller influence of the weakly solvated ClO_4^-anion (24) (see Table 3) (Et_4NCLO_4) as compared with the Br^- anion (Et_4NBr).

Since sucrose is a weak polybasic acid (25) for which two dissociation constants have been determined, it can be suggested that sucrose interacts with water to cause a slight increase of $(OH)_{free}$ groups and hence a small increase in rate constant. In this sense, it can be said that the spectroscopic changes induced by addition of sucrose to water are, in general, small and similar to those produced by potassium nitrate (26).

Finally, if the decrease of the OH groups concentration gives rise to a decrease in the reactivity, solvents such as dmso or dmf should also decrease the rate constant. As can be seen in Table 2, the observed order is

$$k^{0\prime}_{H_2O} > k^{0\prime}_{acn} > k^{0\prime}_{dmf} > k^{0\prime}_{dmso}$$

which qualitatively agrees with the effective base-strength of the cosolvents in water (24).

Can. J. Chem. Downloaded from www.nrcresearchpress.com by 91.144.44.67 on 09/07/12
For personal use only.

1. A. INDELLI and E. S. AMIS. J. Am. Chem. Soc. **82**, 332 (1960).
2. A. INDELLI, F. SECCO, and M. L. FERNANDEZ CASTAÑON. Ann. Chim. **56**, 207 (1966).
3. M. C. CARMONA GUZMAN, P. PEREZ TEJEDA, F. SANCHEZ BURGOS, and J. HIDALGO. React. Kinet. Catal. Lett. **27**(2), 329 (1985).
4. J. BURGESS. J. Chem. Soc. a, 2531 (1970).
5. F. SÁNCHEZ, F. DE PABLOS, E. DOBARGANES, and J. RODRIGUEZ. An. Quim. **80**, 683 (1984).
6. A. INDELLI and J. E. PRUE. J. Chem. Soc. 107 (1959).
7. C. CARMONA, J. RODRIGUEZ, F. SÁNCHEZ, and J. HIDALGO. J. Chem. Soc. Dalton Trans. 31 (1985).
8. C. CARMONA, F. SÁNCHEZ, and J. RODRIGUEZ. J. Chem. Soc. Faraday Trans. 1, **80**, 3429 (1984).
9. F. FRANKS. *In* Water: a comprehensive treatise. Vol. 1. *Edited by* F. Franks. Plenum Press, New York.
10. J. B. TAYLOR and J. S. ROWLINSON. Trans. Faraday Soc. **51**, 1183 (1955).
11. C. G. MALMBERG and A. A. MARYOTT. J. Res. Natl. Bur. Stand. Sect. A, **45**, 229 (1950).
12. G. AKERLOF. J. Am. Chem. Soc. **54**, 4125 (1932).
13. G. J. JANZ and R. P. T. TOMKINS. Nonaqueous electrolytes Handbook. Vol 1. Academic Press. 1972.
14. C. G. MALMBERG and A. A. MARYOTT. J. Res. Natl. Bur. Stand. **45**, 4 (1950).
15. A. MERETOJA. Ann. Acad. Sci. Fennic. Chem. **24**, 5 (1947).
16. A. D. PETHYBRIDGE and J. E. PRUE. Prog. Inorg. Chem. **17**, 327 (1972).
17. N. F. ASHFORD, M. J. BLANDAMER, J. BURGESS, D. LAYCOCK, M. WATERS, P. WELLINGS, and R. WOODHEAD. J. Chem. Soc. Dalton Trans. 869 (1979).
18. J. JUILLARD. J. Chem. Soc. Faraday Trans. 1, **78**, 43 (1982).
19. J. JUILLARD. J. Chem. Soc. Faraday Trans. 1, **78**, 37, (1982).
20. Y. MARCUS. *In* Ion solvation. John Wiley and Sons Ltd. 1985.
21. S. TANIEWSKA-OSINSKA, L. BARTEL, H. PIEKARSKI, A. PIEKARSKA, and J. WOZNICKA. Acta Univ. Lodz. 3 (1985).
22. M. R. J. DACK. Aust. J. Chem. **29**, 779 (1976).
23. D. W. JAMES and R. L. FROST. J. Phys. Chem. **78**, 1754 (1974).
24. M. C. R. SYMONS. J. Chem. Res. (s), 140 (1978); M. C. R. SYMONS. Acc. Chem. Res. **14**, 179 (1981); Y. Y. LIM, A. SMITH, and M. C. R. SYMONS. J. Chem. Soc. Faraday, 1, **72**, 2876 (1976); S. E. JACKSON, E. A. SMITH, and M. C. R. SYMONS. Faraday Discuss. Chem. Soc. **64**, 173 (1977).
25. A. T. ALLEN, R. M. WOOD, and M. P. MCDONALD. Sugar Technol. Rev. **2**, 165 (1974).
26. D. W. JAMES and R. L. FROST. J. Phys. Chem. **78**, 17 (1974), **78**, 1754 (1974).
27. A. INDELLI and J. E. PRUE. Atti Accad. Sci. Ferrara, **35**, 1(1957).

Can. J. Chem. Downloaded from www.nrcresearchpress.com by 91.144.44.67 on 09/07/12
For personal use only.

Phenylfluorophosphoranes: axial–equatorial fluorine exchange in $RC_6H_4PF_3H$ and intermolecular exchange in the $PhPF_2(H)OMe$–MeOH–base system

LEONARD J. KRUCZYNSKI, ALBERTA E. LEMIRE,[1] KIRK MARAT, AND ALEXANDER F. JANZEN
Department of Chemistry, University of Manitoba, Winnipeg, Man., Canada R3T 2N2

Received June 14, 1989

LEONARD J. KRUCZYNSKI, ALBERTA E. LEMIRE, KIRK MARAT, and ALEXANDER F. JANZEN. Can. J. Chem. **68**, 488 (1990).

Activation parameters for axial–equatorial fluorine exchange in arylfluorophosphoranes $RC_6H_4PF_3H$, where R = *o*-CF_3, *m*-CF_3, *p*-CF_3, *m*-CH_3, were studied by the dynamic nmr technique: $\Delta G^{\ddagger}_{298}$ varied between 53 and 56 kJ mol^{-1}.

The synthesis of difluoromethoxyphenylphosphorane, $PhPF_2(H)OMe$, from $PhPF_2$ and MeOH is catalyzed by small amounts of Et_3N, pyridine, $PhPF_3H$, or HF. Rapid intermolecular ligand exchange occurs in $PhPF_2(H)OMe$ after addition of methanol and a base such as triethylamine or pyridine. Under these conditions, exchange of fluorine, hydrogen, and methoxy ligands occurs, as shown by ^1H, ^{19}F, and ^{31}P nmr. From a line shape analysis of the $^{31}P\{^1H\}$ nmr spectrum, the rate of P—F cleavage was found to be first order (1.17 ± 0.2) in Et_3N concentration, with $\Delta G^{\ddagger}_{298}$ = 50 kJ mol^{-1} and $\Delta S^{\ddagger}$ = −67 J mol^{-1} deg^{-1}.

An equilibrium constant of 1.8 at 25°C was found for the reaction of $PhPF_2(H)OMe$ with $PhPF_2$.

Key words: axial–equatorial fluorine exchange in $RC_6H_4PF_3H$ intermolecular exchange in the $PhPF_2(H)OMe$–MeOH–base system; ^{31}P and ^{19}F nmr study of ligand exchange in phosphoranes.

LEONARD J. KRUCZYNSKI, ALBERTA E. LEMIRE, KIRK MARAT et ALEXANDER F. JANZEN. Can. J. Chem. **68**, 488 (1990).

Faisant appel à la technique de la rmn dynamique, on a déterminé les paramètres d'activation de l'échange axial–équatorial du fluor dans des arylfluorophosphanes, $RC_6H_4PF_3H$, dans lesquels R = *o*-CF_3, *m*-CF_3, *p*-CF_3 et *m*-CH_3; la valeur du $\Delta G^{\ddagger}_{298}$ varie de 53 à 56 kJ mol^{-1}.

La synthèse des difluorométhoxyphénylphosphoranes, $PhPF_2(H)OMe$, à partir du $PhPF_2$ et du MeOH est catalysée par de faibles quantités de Et_3N, de pyridine, de $PhPF_3H$ ou de HF. L'addition de méthanol et d'une base, comme la triéthylamine ou la pyridine, provoque un échange intermoléculaire rapide de ligands dans le $PhPF_2(H)OMe$. Dans ces conditions, on a pu montrer par rmn du ^1H, du ^{19}F et du ^{31}P qu'il se produit un échange des ligands fluor, hydrogène et méthoxy. En se basant sur une analyse de la forme des bandes du spectre rmn du $^{31}P\{^1H\}$, on a trouvé que la vitesse de clivage de la liaison P—F est du premier ordre (1,17 ± 0,2) en Et_3N alors que le $\Delta G^{\ddagger}_{298}$ = 50 kJ mol^{-1} et le $\Delta S^{\ddagger}$ = −67 J mol^{-1} deg^{-1}.

Par la réaction du $PhPF_2(H)OMe$ avec le $PhPF_2$, à 25°C, on a trouvé que la constante d'équilibre est égale à 1,8.

Mots clés : échange axial–équatorial du fluor dans des $RC_6H_4PF_3H$ échange intermoléculaire dans le système $PhPF_2(H)OMe$–MeOH–base; étude en rmn du ^{31}P et du ^{19}F de l'échange de ligands dans les phosphoranes.

[Traduit par la revue]

Stereoselective bond-cleavage is difficult to observe in five- and six-coordinate compounds if accompanied by axial–equatorial scrambling of ligands, as illustrated by the $PhPF_3H$–$PhPF_4H^-$ or $PhPF_4$–$PhPF_5^-$ systems (1, 2), although the introduction of three phenyl substituents can avert this problem, as demonstrated by the Ph_3TeF_3–$Ph_3TeF_2^+$ or Ph_3TeF_2Cl–Ph_3TeFCl^+ systems (3). In this paper we describe another, albeit unsuccessful, attempt at slowing down axial–equatorial ligand exchange, namely, by the introduction of trifluoromethyl or methyl substituents into the phenyl ring of $PhPF_3H$. The role of catalysts in phosphorane synthesis, as well as intermolecular ligand exchange in phosphoranes, was studied in the $PhPF_2(H)OMe$–MeOH–base system and the results compared to a previous study of intra- and intermolecular ligand exchange in the $PhPF_3H$–$PhPF_4H^-$ system (1).

Axial–equatorial exchange in phosphoranes $RC_6H_4PF_3H$

The phosphoranes $RC_6H_4PF_3H$ were prepared by the addition of HF to the corresponding aryldifluorophosphines (4)

[1] $RC_6H_4PF_2 + HF \longrightarrow RC_6H_4P(F^a)(H)(F^e)(F^a)$

R = *o*-CF_3, *m*-CF_3, *o*-CF_3, *m*-CH_3

and the compounds identified by ^{31}P nmr (Table 1), as well as ^{19}F and ^1H nmr. During some preparations, impurities $RC_6H_4P(O)F_2$ and $RC_6H_4P(O)FH$ were observed and their ^{31}P nmr data are also recorded in Table 1, but these impurities do not interfere with the axial–equatorial exchange process.

Addition of small amounts of Et_3N to $RC_6H_4PF_3H$ leads to the formation of $RC_6H_4PF_2$ and the onset of intermolecular fluorine exchange, and reactions [2] and [3] are consistent with the behavior reported for $PhPF_3H$ (1).

[2] $2RC_6H_4PF_3H + Et_3N \rightarrow RC_6H_4PF_2 + Et_3NH^+\ RC_6H_4PF_4H^-$

[3] $RC_6H_4PF_3H + RC_6H_4PF_4H^- \rightleftharpoons RC_6H_4PF_3H\text{-}F\text{-}PF_3HC_6H_4R^-$

In the absence of a base, axial–equatorial fluorine exchange in $RC_6H_4PF_3H$ may be studied by comparing the variable-temperature $^{31}P\{^1H\}$ nmr spectra with line shapes calculated by the method described previously for $PhPF_3H$ (1). A least-squares analysis of the data gave the activation parameters for axial–equatorial exchange listed in Table 2, with $\Delta G^{\ddagger}_{298}$ values in the range 52.9 to 56.0 kJ mol^{-1}, which may be compared to 55.6 kJ mol^{-1} for $PhPF_3H$ (1). These results show that trifluoromethyl or methyl substituents have only a slight effect on the activation barriers, and our attempt to slow down axial–equatorial scrambling in five-coordinate species by this approach was not successful, therefore $RC_6H_4PF_3H$ is not a suitable "rigid" probe of site-specific bond cleavage at ambient temperature.

Intermolecular exchange in the $PhPF_2(H)OMe$–MeOH–base system

The synthesis of $PhPF_2(H)OMe$ was found to be catalyzed

[1] Present address: Whiteshell Nuclear Research Establishment, Pinawa, Man., Canada R0E 1L0.

Can. J. Chem. Downloaded from www.nrcresearchpress.com by 91.144.44.67 on 09/07/12
For personal use only.

TABLE 1. ^{31}P nmr data of some phosphorus compounds in 2:1 toluene–C_6D_6 at 303 K*

	$RC_6H_4PF_2{}^aF^eH$ (250 K)†			$RC_6H_4P(O)F_2$		$RC_6H_4P(O)FH$		$RC_6H_4PF_2$	
R	δP	$^1J(PF^a)$	$^1J(PF^e)$	δP	$^1J(PF)$	δP	$^1J(PF)$	δP	$^1J(PF)$
o-CF_3	−23	973	838	+6	1107	+25	1025	+195	1198
m-CF_3	−34	973	839	+8	1104	+29	1018	+201	1176
p-CF_3	−33	974	840	+8	1106	+29	1010	+202	1177
m-CH_3	−32	969	830	+11	1102	+33	1011	+208	1162

*Coupling constants are reported in Hz and chemical shifts in ppm relative to $CFCl_3$ and 85% H_3PO_4.
†a = axial, e = equatorial.

TABLE 2. Activation parameters for axial–equatorial fluorine exchange in some phosphoranes in 2:1 toluene–C_6D_6*

Compound	$\Delta G^{\ddagger}_{298}$ (kJ mol^{-1})	$\Delta H^{\ddagger}$ (kJ mol^{-1})	$\Delta S^{\ddagger}$ (J K^{-1} mol^{-1})
$C_6H_5PF_3H$†	55.6±2.1	52.7±1.7	−8.8±5.4
o-$CF_3C_6H_4PF_3H$	52.9±0.4	47.9±1.9	−16.9±7.2
m-$CF_3C_6H_4PF_3H$	53.6±0.4	45.0±1.8	−28.5±6.6
p-$CF_3C_6H_4PF_3H$	53.7±0.3	44.6±0.7	−30.5±2.6
m-$CH_3C_6H_4PF_3H$	56.0±0.4	44.1±1.2	−39.9±4.2

*Temperature range for $^{31}P\{^1H\}$ nmr study: 250–300 K.
†Reference 1.

by the addition of small amounts of Et_3N, pyridine, $PhPF_3H$, or HF.

[4] $PhPF_2 + MeOH \xrightarrow[PhPF_3H \text{ or } HF]{Et_3N,\ pyr}$ 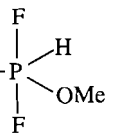

Without an added catalyst, the formation of $PhPF_2(H)OMe$ at 27°C from $PhPF_2$ (0.65 *M*) and MeOH (0.65 *M*) is complete within about 1 h, as seen in Fig. 1, with a half-life of formation of 28 min, but addition of Et_3N (3.6×10^{-3} *M*) or $PhPF_3H$ (6.8×10^{-2} *M*) reduces the half-life to 6.6 and 2.5 min, respectively. The reaction of HF with $PhPF_2$ is rapid and occurs on mixing in an nmr tube while MeOH (1.2 *M*) reacts more rapidly with $PhPF_3H$ (1.2 *M*) than with $PhPF_2$, the reaction being complete within 2 min. Catalysis by HF and $PhPF_3H$ can thus be accounted

[5] $PhPF_2 + HF \rightarrow PhPF_3H$

[6] $PhPF_3H + MeOH \rightarrow PhPF_2(H)OMe + HF$

for by the more rapid reactions [5] and [6] as compared to the uncatalyzed formation of $PhPF_2(H)OMe$. Pyridine also catalyzes reaction [4] and the synthesis of $PhPF_2(H)OMe$ with 1% added pyridine was complete within 5 min at −10°C, but the mechanism of pyridine or Et_3N catalysis remains unclear.

$PhPF_2(H)OMe$ is chemically stable below 10°C and undergoes no intermolecular ligand exchange in solvents such as C_6H_6, CH_2Cl_2, or CH_3CN, but above 10°C decomposition slowly sets in after about 5 h. A sample of $PhPF_2(H)OMe$ plus 10% MeOH, without solvent or base, shows no exchange below 2°C, however, with excess MeOH there is rapid exchange above 2°C but the equilibrium remains essentially towards the $PhPF_2(H)OMe$ side.

The $PhPF_2(H)OMe$–MeOH–base system (5) is of some interest because hydrogen, fluorine, and methoxy exchange can be observed by ^1H, ^{19}F, and ^{31}P nmr. A typical sample made

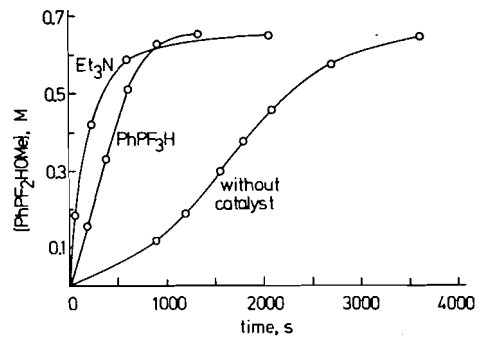

FIG. 1. Formation of $PhPF_2(H)OMe$ from $PhPF_2$ (0.65 *M*) and MeOH (0.65 *M*) without catalysts and with catalysts Et_3N (3.6×10^{-3} *M*) and $PhPF_3H$ (6.8×10^{-2} *M*) at 300 K in C_6H_6 solution.

up from $PhPF_2(H)OMe$ (1 *M*), MeOH (1 *M*), and Et_3N (0.09 *M*) contains $PhPF_2(H)OMe$ (80%), PhPFOMe (1%), and $PhP(OMe)_2$ (7%) at equilibrium, plus some PhP(O)(H)OMe and PhP(O)F(OMe). Kinetic information may be obtained by studying the line broadening of nmr peaks due to $PhPF_2(H)OMe$ in $PhPF_2(H)OMe$–MeOH–base samples and comparing experimental and calculated nmr spectra.

The rate of P—F cleavage in a $PhPF_2(H)OMe$–MeOH–Et_3N sample was studied by $^{31}P\{^1H\}$ nmr and from the variable-temperature spectrum it was found that $E_a = 33$ kJ mol^{-1} and $\Delta S^{\ddagger} = -67$ J mol^{-1} deg^{-1} (Fig. 2). By varying the Et_3N concentration, it was found that the exchange process is first order (1.17 ± 0.2) in Et_3N concentration. Variable-temperature ^{19}F nmr spectra of a $PhPF_2(H)OMe$ (0.67 *M*) – MeOH (0.30 *M*) – pyridine (0.04 *M*) sample in C_6D_6 over the temperature range −49 to 8°C, gave $E_a = 39$ kJ mol^{-1}. By keeping the concentration of $PhPF_2(H)OMe$ (1 *M*) and Et_3N (0.14 *M*) constant, but varying that of MeOH (1.47 to 3.94 *M*), it was possible to show by $^{31}P\{^1H\}$ nmr that the rate of P—F bond cleavage is independent of MeOH concentration. These results suggest a

Can. J. Chem. Downloaded from www.nrcresearchpress.com by 91.144.44.67 on 09/07/12
For personal use only.

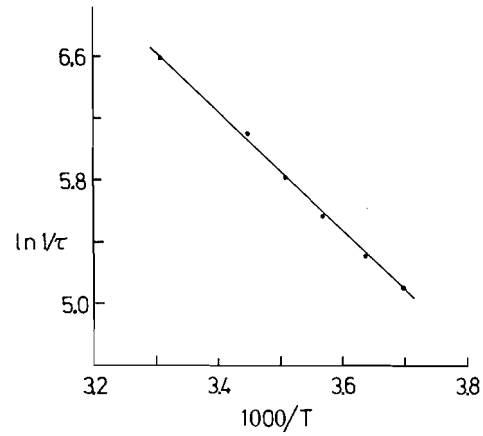

FIG. 2. Plot of ln $1/\tau$ vs. $1/T$ for $PhPF_2(H)OMe$–MeOH–base system. $^{31}P\{^1H\}$ nmr sample contained $PHPF_2(H)OMe$ (1 *M*), MeOH (1 *M*), and Et_3N (0.14 *M*) in CD_2Cl_2 (2 mL).

mechanism very similar to that proposed for base-initiated P—F bond cleavage in the $PhPF_3H$–$PhPF_4H^-$ system (1), namely, the slow production of PhPFOMe and anion $PhPF_3(H)OMe^-$, reaction [7], followed by rapid fluorine exchange between five- and six-coordinate phosphorus species, reaction [8]. Since the nmr spectral lines of PhPFOMe show no line broadening

[7] $2PhPF_2(H)OMe + base \rightarrow PhPF(OMe) + baseH^+\ PhPF_3(H)OMe^-$

[8] $PhPF_2(H)OMe + PhPF_3(H)OMe^- \rightleftharpoons PhPF_2(H)OMe—F—PhPF_2(H)OMe^-$

throughout the exchange process, a simple base-promoted loss of HF (to give PhPFOMe) from $PhPF_2(H)OMe$ is ruled out as a mechanism of rapid exchange in the $PhPF_2(H)OMe$–MeOH–base system.

The appearance of PhPFOMe and $PhP(OMe)_2$ indicates that P—OMe and P—H bond cleavage also occurs in $PhPF_2(H)OMe$–MeOH–base samples. That bond cleavage is rapid and reversible was demonstrated by ^1H and ^{19}F nmr. For example, the methoxy signal in $PhPF_2(H)OMe$ at 16°C changes from a doublet $^3J(HP) = 14.8$ Hz of triplets $^4J(HF) = 1.1$ Hz to a single peak, averaged with the MeOH peak, in a $PhPF_2(H)OMe$–MeOH–base sample, but at −42°C exchange is stopped and separate methoxy peaks are observed for $PhPF_2(H)OMe$ and MeOH.

In an attempt to gain information about the relative rates of P—F versus P—OMe and P—H bond cleavage, variable-temperature ^{19}F nmr spectra of $PhPF_2(H)OMe$–MeOH–pyridine samples were recorded from −49 to 10°C and compared with calculated spectra based on different exchange mechanisms (Fig. 3). Unfortunately, the fast exchange limit, where clear differences are predicted by the calculated line shapes, required temperatures well above 10°C, but these led to decomposition of the $PhPF_2(H)OMe$–MeOH–base samples. Therefore, the mechanism of P—OMe and P—H bond cleavage remains unclear. The fact that the rate of P—F cleavage is independent of MeOH concentration (*vide supra*), plus the demonstration that P—F cleavage in the $PhPF_3H$–$PhPF_4H^-$ system (1) is not accompanied by P—H bond cleavage leads us to assume that cleavage of P—F bonds occurs more rapidly than P—OMe or P—H bonds in the $PhPF_2(H)OMe$–MeOH–base system.

$PhPF_2(H)OMe$ may be converted to $PhP(OMe)_2$ by adding a base and an excess of MeOH, reaction [9]. Thus a sample containing $PhPF_2(H)OMe$ (1 *M*), MeOH (2.5 *M*), and Et_3N (0.7 *M*) at 37°C gave $PhP(OMe)_2$ in 90% yield. On the other hand, adding $PhPF_2$ to $PhPF_2(H)OMe$, reaction [10],

[9] $PhPF_2(H)OMe + MeOH + Et_3N \rightarrow PhP(OMe)_2 + Et_3N\cdot(HF)_n$

[10] $PhPF_2(H)OMe + PhPF_2 \rightleftharpoons PhPFOMe + PhPF_3H$

or mixing $PhPF_2$ and MeOH in a 2:1 ratio, results in the formation of PhPFOMe (5). Since $PhPF_2(H)OMe$ can be prepared *in situ* from $PhPF_2$ and MeOH, therefore, controlling the amounts of $PhPF_2$, MeOH, and base leads to convenient synthesis of either PhPFOMe or $PhP(OMe)_2$.

Equilibrium [10] involves fluorine exchange which is very slow on the nmr time scale and all species gave well-resolved

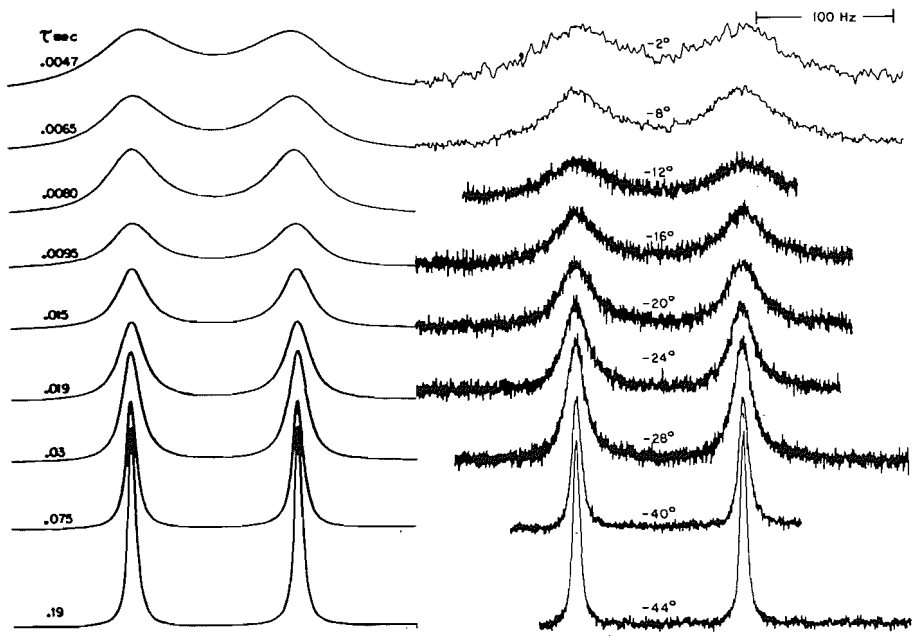

FIG. 3. Typical temperature-dependent experimental (right) and calculated (left) ^{19}F nmr spectra of $PhPF_2(H)OMe$–MeOH–base system. Sample contained $PhPF_2(H)OMe$ (0.67 *M*), MeOH (0.29 *M*), and pyridine (0.04 *M*) in C_6D_6 (2 mL) (F—P coupling omitted).

Can. J. Chem. Downloaded from www.nrcresearchpress.com by 91.144.44.67 on 09/07/12
For personal use only.

nmr signals, hence from ^{19}F and ^{1}H nmr peak integrations an equilibrium constant of 1.8 at 25°C was calculated.

Experimental

The nmr spectra were recorded on a Bruker WH90 spectrometer at 90(^{1}H), 84.66(^{19}F) and 36.44(^{31}P) MHz. Line-shapes were calculated using a modified version of the program EXCHSYS (6), as described for the $PhPF_3H$–$PhPF_4H^-$ system (1), and temperatures were calibrated by the method of Van Geet (7).

o-, *m*-, and *p*-Bromobenzotrifluoride were obtained from Aldrich Chemical Co. and $PhPF_2(H)OMe$ (5) and *o*-$CF_3C_6H_4PF_2$ (8) were prepared as described previously. $(Et_2N)_2PCl$ was made in 61% yield from PCl_3 (28 g, 0.20 mol) and Et_2NH (58 g, 0.79 mol) in petroleum ether (275 mL) at −78 to 25°C, according to the method of Burg and Slota (9). $PhP(OMe)_2$ was made from $PhPCl_2$, HOMe, and pyridine in petroleum ether (10); it was also prepared in 90% yield from $PhPF_2(H)OMe$ (2 mmol), MeOH (5 mmol), and Et_3N (1.4 mmol) at 37°C in an nmr tube. HF solutions were prepared by condensing 1–2 g of anhydrous HF into 10 mL acetonitrile. The following compounds were identified by their nmr spectra: $PhPF_2$ (11), $PhP(O)F_2$ (12), PhPF(OMe) (5), $PhP(OMe)_2$ (12), PhP(O)H(OMe) (12), PhP(O)F(OMe) (11), and $PhPF_3H$ (1, 13).

m-*$CF_3C_6H_4PCl_2$*

m-$CF_3C_6H_4Br$ (25 g, 0.11 mol) in ether (25 mL) was added to Mg turnings (2.8 g) in ether (5 mL) and the reaction initiated with an iodine crystal and periodically cooled to 0°C to slow down the rate of reaction. After the addition was complete, the mixture was stirred for 1 h and then $(Et_2N)_2PCl$ (23 g, 0.11 mmol) added dropwise with stirring at 0°C. After standing at 25°C for 12 h, the mixture was cooled to −78°C and gaseous HCl bubbled in. The ether layer was decanted off and the precipitate washed twice with 30 mL of ether. Extracts were combined and more HCl bubbled in. The ether layer was again decanted off and evaporated on rotary evaporator to give *m*-$CF_3C_6H_4PCl_2$ (14) (15 g, 72% yield).

A similar procedure was used for *o*-, *p*-$CF_3C_6H_4PCl_2$ and *m*-$CH_3C_6H_4PCl_2$.

m-*$CF_3C_6H_4PF_2$*

NaF (14 g, 0.33 mol) was dried under vacuum with a flame for 15 min and added to dry sulfolane (25 mL). *m*-$CF_3C_6H_4PCl_2$ (15 g, 61 mmol) in sulfolane (10 mL) was added and the reaction mixture heated at 120–140°C for 4 h under N_2 atmosphere. After a further 12 h at 25°C, ^{31}P nmr confirmed the presence of *m*-$CF_3C_6H_4PF_2$ and some *m*-$CF_3C_6H_4P(O)F_2$, but no unreacted *m*-$CF_3C_6H_4PCl_2$. Distillation under vacuum gave *m*-$CF_3C_6H_4PF_2$ (5 g, 30%) and some *m*-$CF_3C_6H_4P(O)F_2$.

A similar procedure was used for *o*-, *p*-$CF_3C_6H_4PF_2$ and *m*-$CH_3C_6H_4PF_2$.

m-*$CF_3C_6H_4PF_3H$*

HF (1.2 equiv.) in acetonitrile was added to *m*-$CF_3C_6H_4PF_2$ (2.6 g, 12 mmol), prepared as described above. Excess HF and acetonitrile was removed under vacuum and distillation under reduced pressure gave a central fraction containing *m*-$CF_3C_6H_4PF_3H$ and some *m*-$CF_3C_6H_4P(O)F_2$. Since the latter oxide did not interfere with the axial–equatorial exchange process, this fraction was used for the nmr study. A typical nmr sample contained *m*-$CF_3C_6H_4PF_3H$ (2.1 mmol) in 2 mL of 2:1 v/v toluene–C_6D_6.

A similar procedure was used for *o*-, *p*-$CF_3C_6H_4PF_3H$ and *m*-$CH_3C_6H_4PF_3H$.

Samples of $RC_6H_4PF_3H$ and $RC_6H_4PF_2$ were stored in sealed tubes in a freezer until required for nmr studies.

Acknowledgement

Financial support from the Natural Sciences and Engineering Research Council of Canada is gratefully acknowledged.

1. R. K. Marat and A. F. Janzen. Inorg. Chem. **19**, 798 (1980).
2. C. Wang and A. F. Janzen. Can. J. Chem. **62**, 1563 (1984).
3. A. S. Secco, K. Alam, B. J. Blackburn, and A. F. Janzen. Inorg. Chem. **25**, 2125 (1986); A. F. Janzen, K. Alam, M. Jang, B. J. Blackburn, and A. S. Secco. Can. J. Chem. **66**, 1308 (1988); A. F. Janzen and M. Jang. Can. J. Chem. **67**, 71 (1989).
4. G. I. Drozd, S. Z. Ivin, V. V. Sheluchenko, B. I. Tetel'baum, and A. D. Varshavskii. Zh. Obshch. Khim. **38**, 567 (1968); Chem. Abstr. **69**, 43972k (1968).
5. A. F. Janzen and L. J. Kruczynski. Can. J. Chem. **57**, 1903 (1979).
6. J. K. Krieger. Ph.D. Thesis. Massachusetts Institute of Technology, Cambridge, MA. 1971.
7. A. L. Van Geet. Anal. Chem. **42**, 679 (1970).
8. T. Schaefer, K. Marat, A. Lemire, and A. F. Janzen. Org. Magn. Res. **18**, 90 (1982).
9. A. B. Burg and P. J. Slota. J. Am. Chem. Soc. **80**, 1107 (1958).
10. A. E. Arbuzov and A. I. Razumov. Izv. Akad. Nauk SSSR. 854 (1952); Chem. Abstr. **47**, 9903c (1953).
11. R. Schmutzler. Chem. Ber. **98**, 552 (1965).
12. G. Mavel. Ann. Rep. NMR Spect. **5B**, 1 (1973).
13. E. L. Muetterties, W. Mahler, K. J. Packer, and R. Schmutzler. Inorg. Chem. **3**, 1298 (1964).
14. T. Weil, B. Prijs, and H. Erlenmeyer. Helv. Chim. Acta, **35**, 1412 (1952).

Can. J. Chem. Downloaded from www.nrcresearchpress.com by 91.144.44.67 on 09/07/12
For personal use only.

Pentacarbonylmanganese enolate and dienolate complexes. Preparative and mechanistic considerations

ANDREW P. MASTERS AND TED S. SORENSEN
The Department of Chemistry, University of Calgary, Calgary, Alta., Canada T2N 1N4

Received June 5, 1989

ANDREW P. MASTERS and TED S. SORENSEN. Can. J. Chem. **68**, 492 (1990).

Reactions of pentacarbonyl manganate anion with 4-halocrotonate esters or 2-halocarboxylate esters result in a complex set of inorganic and organic products, usually including the expected dienolate (or enolate) complexes. The reaction variables include the counterion, solvent, and halo group. The mechanism of the reaction has been investigated by conducting a thorough characterization of the reaction products under various conditions and also by carrying out model reactions. One can rationalize most of the non-organometallic products using either a radical or carbanion mechanism, but the latter seems to fit the available data better. Experimental procedures for optimizing the yield of the organometallic dienolate or enolate complexes have been worked out.

Key words: pentacarbonyl manganate, metalate nucleophilicity, enolate complex, nucleophilic substitution, ^{55}Mn NMR spectroscopy.

ANDREW P. MASTERS et TED S. SORENSEN. Can. J. Chem. **68**, 492 (1990).

Les réactions de l'anion pentacarbonyl manganate avec les esters 4-halocrotonates ou 2-halocarboxylates conduisent à la formation d'un ensemble de complexes de produits organiques et inorganiques qui contiennent généralement les complexes diénolates (ou énolates) attendus. Les facteurs qui influencent la réaction comprennent le contre-ion, le solvant et la nature de l'halogène. Dans le but de déterminer le mécanisme de la réaction, on a procédé à un examen minutieux des produits obtenus au cours de réactions réalisées sous diverses conditions et on a réalisé diverses réactions modèles. On peut rationaliser la formation de la plupart des produits qui ne sont pas des organométalliques par des mécanismes soit radicalaires ou carbanioniques; toutefois, ces derniers semblent mieux accommoder les données disponibles. On a déterminé les conditions expérimentales appropriées pour obtenir les meilleurs rendements possibles de complexes diénolates ou énolates.

Mots clés : pentacarbonyl manganate, nucléophilicité métallate, complexe énolate, substitution nucléophile, spectroscopie RMN du ^{55}Mn.

[Traduit par la revue]

Can. J. Chem. Downloaded from www.nrcresearchpress.com by 91.144.44.67 on 09/07/12
For personal use only.

The metal-centered anion $Mn(CO)_5^-$ has been extensively used to prepare $R\text{-}Mn(CO)_5$ type compounds (R = alkyl, perfluoroalkyl, etc.). However, there are numerous instances where eq. [1] fails, where the yields are inexplicably poor, or

[1] $M^+Mn(CO)_5^- + RX \rightarrow RMn(CO)_5 + X^- + M^+$

where other products such as $Mn_2(CO)_{10}$ are formed. In fact the present study evolved when we had difficulties in applying eq. [1] to the synthesis of a simple ester dienolate complex (R = dienolate).

For a background to transition-metal enolate complexes, the recent papers of Heathcock and co-workers (1) provide an extensive bibliography. Dienolate complexes of transition metals have even more potential bonding modes, including the straightforward η^1-, η^3-, or η^5-complexes **1**, **2**, or **3**. The initial intent of our work was to study the synthetic utility of the η^3-complex, with the expectation that the geometry in these could be controlled via the η^5-complex, as indicated below:

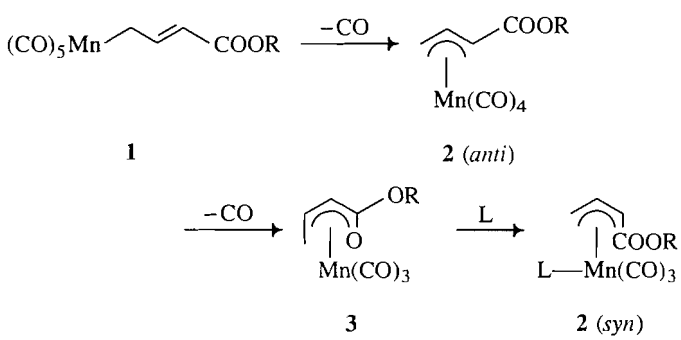

1 **2** (*anti*)

3 **2** (*syn*)

However, the most common and practicable route to the η^3-complexes of $Mn(CO)_4$ involves the initial preparation of the η^1-complex.

Mechanistically, the eq. [1] reaction has been shown to occur with at least some inversion of configuration in the case of 2-bromopropionate (2), and other metallate anions have shown similar S_N2 (or S_N2-like) reactivity. There is, however, some literature discussion at present concerning the role of single electron transfer (S.E.T.) in nucleophilic substitution reactions. The radical chain ($S_{RN}1$) mechanism can be tested for in well-defined ways, but substitutions where the overall process is envisioned as two closely timed events (S.E.T. followed by leaving group loss and geminate recombination) can be virtually indistinguishable from S_N2 mechanisms (the recent papers of Bordwell and Wilson (3) provide an extensive bibliography of work in this area).

The overall aims of this study were (1) to carry out a reasonably complete analysis of all of the products and by-products of eq. [1], where R = ester enolate or dienolate. This includes varying a number of experimental parameters to optimize the yields of the desired products. (2) In conjunction with (1), to formulate mechanisms to account for all of the products and by-products observed. This study also involves carrying out extra experiments designed simply to answer certain mechanistic questions.

Results and discussion

The reaction between $Mn(CO)_5^-$ and commercially available ethyl 4-bromocrotonate **4** seemed a likely method for preparing the parent η^1-dienolate ester complex **5** (eq. [2]). For example,

allyl chloride gives the corresponding η^1-adduct in good yield (4).

[2] $Mn(CO)_5^- + Br\text{-}CH_2$ (H, H, COOEt) → $(CO)_5Mn\text{-}CH_2$ (H, H, COOEt) + Br^-

4 5

$Mn(CO)_5Br$ $OC\text{—}Mn\text{—}Mn\text{—}CO$ (CO, CO, CO, CO, CO, CO, CO, CO)

6 7

However, initial attempts at this reaction gave $Mn_2(CO)_{10}$ as the main isolable manganese product (column chromatography). At this point it was assumed that $Mn_2(CO)_{10}$ was a decomposition product of a labile η^1-adduct **5**. Because of such potential work-up problems, we moved to an *in situ* examination of reaction mixtures using ^{55}Mn NMR spectroscopy and IR spectroscopy. This allows one to rapidly examine the manganese products formed and to therefore rapidly monitor the effect of various experimental variables connected with the eq. [2] reaction.

^{55}Mn NMR spectroscopy shows broad but separate resonances for a number of different manganese carbonyl environments. The most extensive study in this area is by Calderazzo *et al.* (5), showing chemical shifts varying over nearly 3000 ppm. Line widths vary from a few Hz (MnO_4^-) to many kHz. The manganese compounds of relevance in this work are listed in Tables 1 and 2, together with our measured chemical shifts and $W_{1/2}$ values. A few other compounds that were available to us are also included in these tables. These agree reasonably well with the older data (5) in those cases where we have repeated some of the measurements. The use of ^{55}Mn NMR as an analytical tool is hampered because very broad lines are difficult to observe on a high resolution spectrometer. However, we have invariably backed up the ^{55}Mn assignments using IR spectroscopy, even though this may not be explicitly discussed in the text.

A tetrahydrofuran (THF) solution of $Na^+Mn(CO)_5^-$ at 25°C shows a single ^{55}Mn peak at −2675 ppm, $W_{1/2}$ ca. 7000 Hz (the anion). Rapid mixing with ethyl 4-bromocrotonate results in the immediate formation of a precipitate of sodium bromide, and the ^{55}Mn NMR spectrum (Fig. 1) showed the loss of the −2675 peak and the formation of three new resonances at −1156, −1929, and −2281 ppm, corresponding to $Mn(CO)_5Br$ **6**, the η^1-complex **5** (subsequently verified), and $Mn_2(CO)_{10}$ **7**, respectively. The relative yields by integration (using a variable correction factor, as discussed in the Experimental) gave 25% **6**, 34% **5**, and 42% **7**. The products of this reaction could be separated by flash chromatography, confirming the NMR identifications. The η^1-complex **5** was isolated as a pale yellow air-sensitive oil in ca. 20% yield and was fully characterized.

Using the above analytical procedures, most of the eq. [1] experimental conditions were then varied. This included changing

TABLE 1. ^{55}Mn NMR chemical shift data for inorganic manganese carbonyls in THF

	Shift[a]	$W_{1/2}$ (Hz)
$(CO)_5MnCl$	−985	450
$(CO)_5MnBr$	−1156	790
$(CO)_5MnI$	−1450	1156
$(CO)_4MnBr_2^-$	−618	3800
$(CO)_4MnI_2^-$	−1011	4810
$(CO)_5MnH$	−2500	4105
$PPN^+[Mn(CO)_5^-]$	−2690	6500
$Li^+[Mn(CO)_5^-]$	−2694	6500
$Na^+[Mn(CO)_5^-]$	−2675	7100
$K^+[Mn(CO)_5^-]$	−2666	6800
$Mn_2(CO)_{10}$	−2281(−2325)[b]	74(83)[b]

[a]In ppm with respect to $KMnO_4$ in D_2O, ±4 ppm.
[b]Literature value (5).

the solvent, the counterion, the halogen leaving group, and the relative stoichiometry of $Mn(CO)_5^-$ and halo ester. These results are summarized in Table 3 and there are several obvious conclusions:

1. The chloride leaving group gives the best yield of **5**.
2. The lithium counterion (which had been used in the initial work) is particularly bad. The Na^+, K^+, and PPN^+ (bistriphenylphosphineiminium) counterions give quite similar results, although PPN^+ is best.
3. The use of a cation complexing crown ether is useful, as is the addition of 5% dimethylformamide or 4% HMPA. There has been much related work in this area (6).
4. It is not very convenient to vary the solvent in the case of the Li^+, Na^+, or $K^+Mn(CO)_5^-$ salts, since these are usually prepared *in situ* in THF. However, the PPN^+ salt is soluble in a variety of solvents. Comparing THF and $CHCl_3$ (Table 3), there is very significantly less η^1-adduct **5** and much more $Mn_2(CO)_{10}$ in the latter case.

Overall, the best results are obtained using $PPN^+Mn(CO)_5^-$ together with the chloride leaving group and THF solvent, giving a near quantitative yield of the η^1-complex. Obviously, in this case, one uses a 1:1 stoichiometric ratio of both reactants. However, in those reactions where one obtains significant amounts of $Mn(CO)_5Br$ and $Mn_2(CO)_{10}$, it is not clear that a 1:1 stoichiometry is the best choice. We therefore conducted a study where the reactant stoichiometry was varied, and this is summarized in Table 4. As expected, the chloride leaving group results are not much affected, but for the bromide there are substantial changes in products, particularly in the amount of $Mn(CO)_5Br$ being formed. The results shown in Tables 3 and 4 also indicate a clearcut difference between bromo and chloro esters, since the latter *never* give any $Mn(CO)_5Cl$ product.

The purely organic products

From flash chromatography of a crude reaction mixture involving a significant yield of $Mn(CO)_5Br$ (see Table 3), a diethyl ether eluant was found to yield a colorless oil containing the purely organic compounds. This material was a complex mixture but could be separated by preparative GLC into the individual components, identified by MS and NMR spectroscopy as compounds **8**, **9**, **10**, and **11**. Diesters **8** and **9** are known (7) and the reported ^1H NMR spectra agree with those found here. Compound **11** was isolated as a single geometric isomer (assigned *trans*), but consisted of a mixture of two

Can. J. Chem. Downloaded from www.nrcresearchpress.com by 91.144.44.67 on 09/07/12
For personal use only.

TABLE 2. ^{55}Mn NMR chemical shift data for various alkyl, allyl, and cyclopentadienyl manganese carbonyl complexes

	Shift[a]	$W_{1/2}$ (Hz)	Solvent
$(CO)_5MnCH_3$	$(-2265)^b$	$(3040)^b$	THF
$(CO)_5MnCH_2CH'=CH_2$	−2065	2010	THF
$(CO)_5MnCH_2CH'=CHC_6H_5$	−2043	3050	THF
$(CO)_5MnCH_2CH'=CHCOOEt$	−1949	3400	THF
$(CO)_5MnCH_2CH'=CHCOOC_6H_5$	−1929	3800	THF
$(CO)_5MnCH_2CH'=CHCOMe$	−1939	3000	THF
$(CO)_5MnCH_2COOC_2H_5$	−1929	2250	THF
$(CO)_5MnCH_2COOC_2H_5$	−1921	2900	$CHCl_3$[c]
$(CO)_5MnCHCH_3COOC_2H_5$	−1900	2010	THF
$(CO)_5MnCHCH_3COOC_2H_5$	−1891	2600	$CHCl_3$[c]
η^3-$(CO)_4Mn(CH_2CHCH_2)$	−2275	1600	THF
η^3-$(CO)_4Mn(CH_2CHCHCOOC_2H_5)$	−1981	3000	THF
η^3-$(CO)_4Mn(CH_2CHCHCOOC_6H_5)$	−1941	3100	THF
$(CO)_3MnCp$	−2195	9200	THF
$(CO)_3MnCpMe$	−2188	10560	THF

[a]In ppm with respect to $KMnO_4$ in D_2O, ±4 ppm.
[b]Corrected literature value (5).
[c]Solution also contained PPN^+Cl^-.

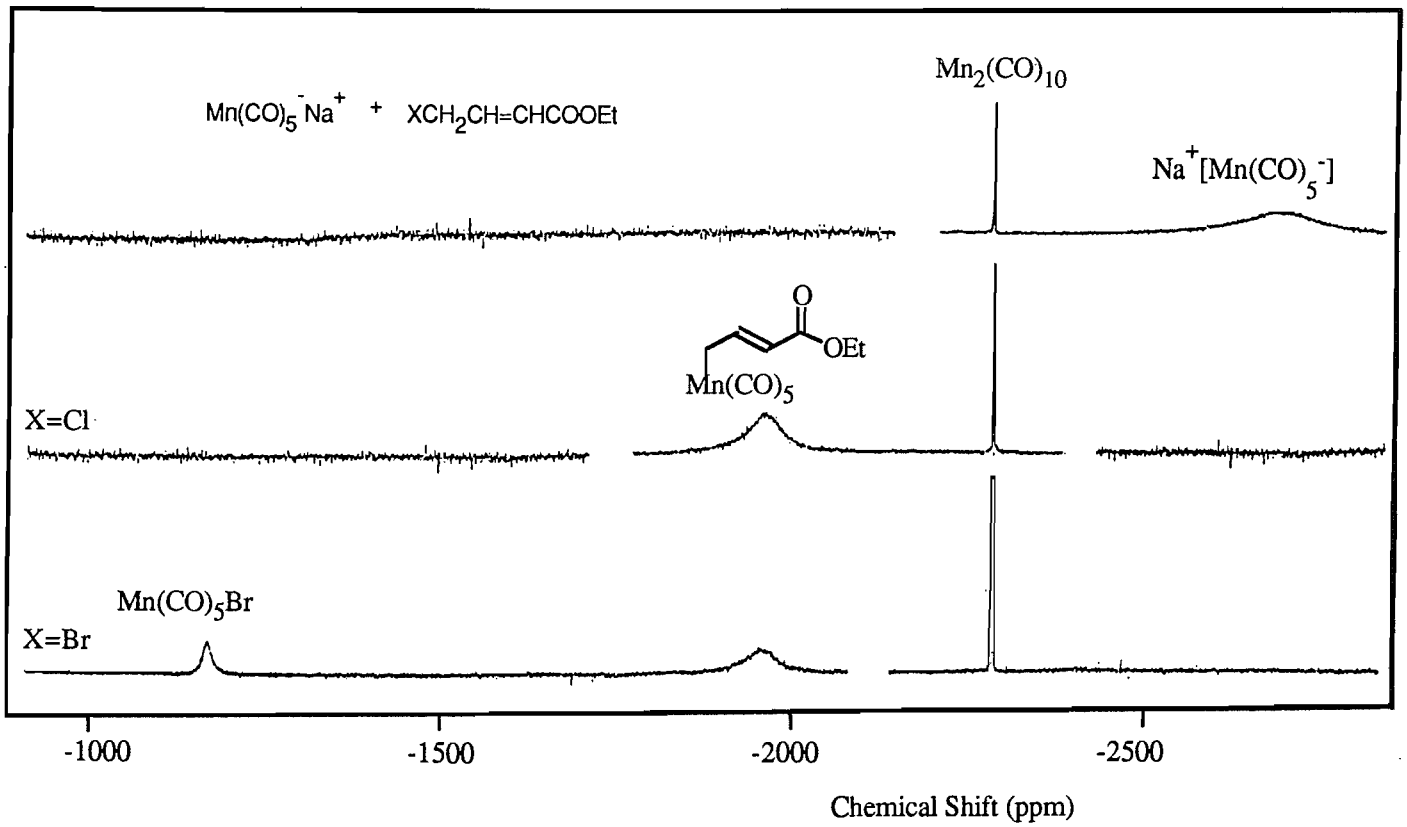

FIG. 1. *In situ* ^{55}Mn NMR spectra for the reaction of $Mn(CO)_5^-$ with ethyl-4-halocrotonate (THF, 25°C).

diastereomers, only partly resolved by GLC. Nevertheless, by careful fraction cutting, enough pure material could be obtained for an ^{1}H NMR spectrum of the pure diastereomers, although we were not able to make a definitive assignment from this.

The reaction of $Mn(CO)_5^-$ with 2-halocarboxylate esters

Given the variable product distributions found for the 4-halocrotonate esters, it was decided to conduct a study of the reactions of simple 2-halocarboxylate esters. This involved the organic compounds $R^1R^2XCCOOEt$, where X was Cl, Br, and I, and R^1 and R^2 were H,H; H,CH_3; and CH_3,CH_3. There are two previous reports dealing with the title reactions, a communication in which 2-bromopropionate was used (2) and a later study using methyl 2-chloroacetate (8).

In our study, the $Mn(CO)_5^-$ was used as the sodium salt in THF, or as the PPN^+ salt in THF or chloroform. The reactions were carried out by rapid mixing of one equivalent of $Mn(CO)_5^-$ with one equivalent of the 2-haloester (unless otherwise

Can. J. Chem. Downloaded from www.nrcresearchpress.com by 91.144.44.67 on 09/07/12
For personal use only.

Can. J. Chem. Downloaded from www.nrcresearchpress.com by 91.144.44.67 on 09/07/12
For personal use only.

TABLE 3. Products for the reaction of manganese pentacarbonyl anion with ethyl 4-halocrotonate determined by ^{55}Mn NMR (% manganese compound)

$M^+[Mn(CO)_5^-] + XCH_2CH{=}CHCOOEt$

Solvent, tetrahydrofuran; 25°C; concentration, 0.12 M

M^+	X	$XMn(CO)_5$	$RMn(CO)_5$	$Mn_2(CO)_{10}$
K	Cl	0	85	15
K	Br	27	42	31
Na	Cl	0	88	12
Na	Br	25	34	42
Na/18c6[a]	Br	*	(86)	(14)
Li	Cl	0	67	33
Li	Br	*	0	56[b]
PPN	Cl	0	98	2
PPN	Br	21	78	1
PPN[c]	Br	24	53	24

[a]One equivalent of the crown ether 18-crown-6 added to the anion solution. Addition of 5% dimethylformamide or hexamethylphosphoramide had the same effect.
[b]Determined by isolation.
[c]In $CDCl_3$.
*Signal corresponding to $Mn(CO)_4Br_2^-$ was observed but not quantified.

TABLE 4. Variation of manganese products[a] with stoichiometry for the reaction of $Mn(CO)_5^-$ with 4-halocrotonate

Solvent, tetrahydrofuran; 25°C; concentration, 0.12 M

Ratio = $Na^+[Mn(CO)_5^-]$:$XCH_2CH{=}CHCOOEt$

Ratio	X	$XMn(CO)_5$	$RMn(CO)_5$	$Mn_2(CO)_{10}$
1:1	Cl	0	85	15
1:2	Cl	0	88	13
1:0.5	Br	0	21	79
1:1	Br	25	34	42
1:2	Br	51	35	14

[a]Determined by ^{55}Mn NMR.

specified) at room temperature. The yields of the various manganese species were determined by ^{55}Mn NMR spectroscopy, IR spectrometry, or by actual isolation. *In situ* proton NMR spectroscopy was used as well in some instances.

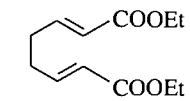

8 (14%)

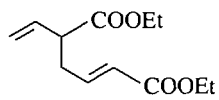

9 (21%)

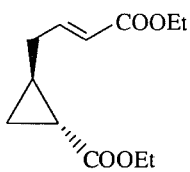

10 (21%)

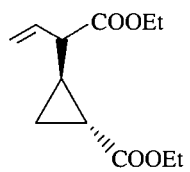

11 (43%)

Using the sodium salt in THF, the results of this reaction are given in Table 5. The general trends in the primary system parallel those found for crotonates, i.e., high yields of the η^1-adduct with Cl, poor yields with Br, together with considerable $Mn(CO)_5Br$ and $Mn_2(CO)_{10}$. The primary iodo compound gave no η^1-adduct, a result also verified for a 1:2 or a 1:0.5

TABLE 5. Manganese products[a] for the reaction of $Na^+Mn(CO)_5^-$ with 2-halocarboxylate esters

$M^+[Mn(CO)_5^-] + X\text{-}CR^1R^2COOEt$

$M^+ = Na^+$; solvent, tetrahydrofuran; 25°C

R^1	R^2	X	$XMn(CO)_5$	$RMn(CO)_5$	$Mn_2(CO)_{10}$
H	H	Cl	0	94	6
H	H	Br	39	39	22
H	H	I	74	0	26
H	CH_3	Cl	No reaction[b]		
H	CH_3	Br	6	63	31
H	CH_3	I	33	35	32
CH_3	CH_3	Cl	No reaction		
CH_3	CH_3	Br	0	0	100
CH_3	CH_3	I	40	0	60

[a]Determined by ^{55}Mn NMR.
[b]Some alkyl product was observed after prolonged reaction times.

TABLE 6. Manganese products[a] for the reaction of $PPN^+Mn(CO)_5^-$ with 2-halocarboxylate esters in tetrahydrofuran

$M^+[Mn(CO)_5^-] + X\text{-}CR^1R^2COOEt$

$M^+ = PPN^+$; solvent, tetrahydrofuran; 25°C

R^1	R^2	X	$XMn(CO)_5$	$RMn(CO)_5$	$Mn_2(CO)_{10}$
H	H	Cl	0	99	1
H	H	Br	0	100	0
H	H	I	15	85	0
H	CH_3	Cl	No reaction[c]		
H	CH_3	Br	24[b]	76	0
H	CH_3	I	32[b]	68	0
CH_3	CH_3	Cl	No reaction		
CH_3	CH_3	Br	100[d]	0	0
CH_3	CH_3	I	100[d]	0	0

[a]Determined by ^{55}Mn NMR spectroscopy.
[b]Signal rapidly disappeared due to the conversion to $Mn(CO)_4X_2^-PPN^+$.
[c]Some alkyl product was observed after prolonged reaction times.
[d]The only signals observed for these reactions corresponded to $[Mn(CO)_4X_2]^-PPN^+$ and unreacted $Mn(CO)_5^-$. The extra X^- must come from the "organic reactions".

stoichiometric ratio of $Mn(CO)_5^-$ to iodoacetate. In the first case, the $Mn(CO)_5I$:$Mn_2(CO)_{10}$ product ratio was 86:14, while in the latter, the figures were 0:100. The tertiary system was unreactive when X was Cl, gave only $Mn_2(CO)_{10}$ for X = Br, and a mixture of $Mn(CO)_5I$ and $Mn_2(CO)_{10}$ for X = I. For the secondary system with X = Cl, only a very slow reaction occurred to give a trace of η^1-adduct after several days but with X = Br or I, all three products were formed (η^1-adduct, $Mn(CO)_5X$, and $Mn_2(CO)_{10}$).

The reaction of the nine halo esters with the PPN^+ salt in THF gave the results shown in Table 6. A noteworthy observation is the virtual absence of $Mn_2(CO)_{10}$ in any of these reactions, a result which was also seen in the crotonate system using the same salt and solvent. Yields of the η^1-adduct are excellent for either primary chloride or bromide, and even the secondary systems give reasonable yields. In those cases where there is some initial $Mn(CO)_5Br$ or $Mn(CO)_5I$ formed, one sees a rapid subsequent reaction with the also present Br^- or I^- (from the displacement reaction) giving $Mn(CO)_4Br_2^-$ or $Mn(CO)_4I_2^-$ salts, which are both polar and nonvolatile (9). A simple flash chromatography gave good isolated yields of pure primary and secondary η^1-enolates, which were fully characterized (see Experimental).

Can. J. Chem. Downloaded from www.nrcresearchpress.com by 91.144.44.67 on 09/07/12
For personal use only.

TABLE 7. Manganese products[a] for the reaction of $PPN^+Mn(CO)_5^-$ with 2-halocarboxylate esters in $CDCl_3$

$M^+[Mn(CO)_5^-] + X\text{-}CR^1R^2COOEt$

$M^+ = PPN^+$; solvent, deuterochloroform; 25°C

R^1	R^2	X	$XMn(CO)_5$	$RMn(CO)_5$	$Mn_2(CO)_{10}$
H	H	Cl	0	99	1
H	H	Br	14	75	11
H	H	I	17	67	16
H	CH_3	Cl	No reaction[b]		
H	CH_3	Br	4	39	57
H	CH_3	I	20	56	24
CH_3	CH_3	Cl	No reaction		
CH_3	CH_3	Br	5	0	95
CH_3	CH_3	I	77	0	23

[a]Determined by ^{55}Mn NMR.
[b]Some alkyl product was observed after prolonged reaction times.

TABLE 8. Variation of manganese products[a] with stoichiometry for the reaction of $PPN^+Mn(CO)_5^-$ with 2-halocarboxylate esters in $CDCl_3$

Ratio = $Mn(CO)_5^-$:X-CR^1R^2COOEt

Ratio	R^1	R^2	X	$XMn(CO)_5$	$RMn(CO)_5$	$Mn_2(CO)_{10}$
11:0.5	H	CH_3	Br	0	40	60
1:1	H	CH_3	Br	4	39	57
1:2	H	CH_3	Br	4	50	45
1:4	H	CH_3	Br	5	54	41
1:1	H	CH_3	I	20	56	24
1:2	H	CH_3	I	18	66	16
1:1	CH_3	CH_3	Br	7	0	93
1:2	CH_3	CH_3	Br	10	0	90
1:1	CH_3	CH_3	I	77	0	23
1:2	CH_3	CH_3	I	88	0	7

[a]Determined by ^{55}Mn NMR.

Using the PPN^+ salt in $CHCl_3$ (Table 7) gave markedly different results from the THF solvent, in that $Mn_2(CO)_{10}$ was again a major product. This solvent, as $CDCl_3$, was useful, however, for *in situ* ^1H NMR studies. This same counterion–solvent system was also used to vary the stoichiometry of the reactants (Table 8).

The purely organic products

This section refers to the characterization of the purely organic products derived from reactions where $Mn(CO)_5X$ (or $Mn_2(CO)_{10}$) is the manganese species formed. The products observed are actually very dependent on the solvent system (THF vs. $CDCl_3$) and both series will be discussed.

Because the primary system gives relatively large amounts of substitution in most cases, the secondary and tertiary halo esters are the most convenient for this study. Using the PPN^+ salt in $CDCl_3$, the deuterochloroform appears to serve as an efficient "trapping agent". *In situ* ^1H NMR spectroscopic examination of the secondary system reaction products in $CDCl_3$ (Br or I) shows a mixture of ethyl 2-deuteropropionate and the η^1-adduct. For the tertiary esters, the bromo system gives ethyl 2-deutero-2-methylpropionate (54%) and unreacted starting material, whereas the iodo system gives 74% of the deutero ester. Although the primary system was dominated by the η^1-adduct, it was possible to also observe the characteristic ^1H triplet for CDH_2COOEt, in addition to some starting material. These ^1H assignments were further verified by preparative GLC isolation

TABLE 9. Organic products[a] for the reaction of $PPN^+Mn(CO)_5^-$ with 2-halocarboxylate esters in $CDCl_3$

$M^+[Mn(CO)_5^-] + X\text{-}CR^1R^2COOEt$

$M^+ = PPN^+$; solvent, deuterochloroform; 25°C

R^1	R^2	X	XCR^1R^2COOEt	DCR^1R^2COOEt	$RMn(CO)_5$
H	H	Cl	11	0	89
H	H	Br	10	19	71
H	H	I	0	25	75
H	CH_3	Cl	100	0	0
H	CH_3	Br	49	19	32
H	CH_3	I	20	16	64
CH_3	CH_3	Cl	100	0	0
CH_3	CH_3	Br	46	54	0
CH_3	CH_3	I	26	74	0

[a]Determined by ^1H NMR, ±3%.
[b]By GC/MS it is possible to detect some unidentified chlorine containing compounds, presumably resulting from CCl_3^- decomposition.

of the deutero esters in the secondary and tertiary cases, followed by both MS and a further ^1H NMR spectrum, this time of the pure compound. In the primary case, the deutero ethyl acetate and solvent were codistilled from the manganese compounds, and a ^1H NMR spectrum of the pure ester obtained. All of this data is summarized in Table 9.

Using the PPN^+ salt in THF gives a very different set of organic products, apparently because THF does not "trap" the reactive organic intermediate formed. In the tertiary bromo case, where no η^1-adduct was present, approximately 80% of the theoretical organic molecular weight was distillable from the crude reaction mixture. GLC analysis (including preparative GLC where needed) indicated the following compounds and abundances:

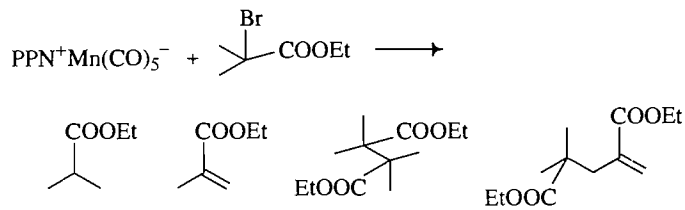

12 (35%) **13** (6%) **14** (36%) **15** (3%)

Using the sodium salt in THF, very similar results were obtained, except that 25% of starting material was present in addition to **12**–**15** (36%, 16%, 14%, 1%, respectively).

With the primary and secondary systems, some thermally labile η^1-adduct was always present and the distillation procedure was difficult to implement. However, we believe that products related to **12**–**15** are also formed here.

Possible mechanisms for the $Mn(CO)_5^-$ reactions

Initially, it was believed that the 4-bromocrotonate **4** results could be explained on the basis of a "single" primary mechanism, starting with electron transfer (mechanism 1). The various products formed would then represent a case of later competitive cage vs. non-cage reactions. However, this mechanism does not account very well for some aspects of the $Mn_2(CO)_{10}$ formation, nor are the purely organic products entirely consistent with a radical mechanism, at least in the case of the $CDCl_3$ solvent (see later). We therefore considered a second mechanism (Mechanism 2) in which somewhat different competing reactions are postulated. Although Mechanism 2 is shown with an initial S.E.T. step (1′) and a geminate recombination (3′), these

Can. J. Chem. Downloaded from www.nrcresearchpress.com by 91.144.44.67 on 09/07/12
For personal use only.

two steps could be replaced by a single and separate S_N2 displacement (shown as 3a'). The competition is between steps 2' and 3' (or 2' and 3a'). Other key differences in Mechanisms 1 and 2 involve how $Mn_2(CO)_{10}$ is formed, and the mechanism by which the organic dimers are produced.

The formation of transition metal carbonyl bromides from anions is obviously a halogen–metal exchange (H.M.E.) reaction but this terminology does not imply any particular mechanism and, as shown in Mechanisms 1 and 2, several possible routes seem reasonable in our particular case, providing yet another differentiation between these two overall schemes.

Mechanism 1

(1) $Mn(CO)_5^- + Br\text{-}CH_2\text{-}CH{=}CHCOOEt \xrightarrow{S.E.T.} Mn(CO)_5^{\bullet} + [Br\text{-}CH_2\text{-}CH{=}CH\text{-}COOEt]^{\bullet -}$

(2) $Mn(CO)_5^{\bullet} + [Br\text{-}CH_2\text{-}CH{=}CHCOOEt]^{\bullet -} \xrightarrow{cage} Mn(CO)_5^{\bullet} + Br^- + \dot{C}H_2\text{-}CH{=}CHCOOEt$

(3) Geminate recombination $\xrightarrow{cage} Mn(CO)_5\text{-}CH_2\text{-}CH{=}CHCOOEt + Br^-$ **5**

(4) $Mn(CO)_5^{\bullet} + BrCH_2CH{=}CHCOOEt \xrightarrow{non\text{-}cage} Mn(CO)_5Br + \dot{C}H_2\text{-}CH{=}CHCOOEt$

(5) $2\,Mn(CO)_5^{\bullet} \xrightarrow{non\text{-}cage} Mn_2(CO)_{10}$

(6) $2\,\dot{C}H_2\text{-}CH{=}CH\text{-}COOEt \xrightarrow{non\text{-}cage}$ dimers

Mechanism 2

(1') $Mn(CO)_5^- + Br\text{-}CH_2\text{-}CH{=}CHCOOEt \xrightarrow{S.E.T.} Mn(CO)_5^{\bullet} + [Br\text{-}CH_2\text{-}CH{=}CH\text{-}COOEt]^{\bullet -}$

(2') $Mn(CO)_5^{\bullet} + [Br\text{-}CH_2\text{-}CH{=}CHCOOEt]^{\bullet -} \xrightarrow{cage} Mn(CO)_5Br + \bar{C}H_2\text{-}CH{=}CH\text{-}COOEt$

(3) $Mn(CO)_5^{\bullet}\,[Br\text{-}CH_2\text{-}CH{=}CH\text{-}COOEt]^{\bullet -} \xrightarrow[recombination]{geminate} Mn(CO)_5\text{-}CH_2CH{=}CH\text{-}COOEt + Br^-$ **5**

or

(3a') $Mn(CO)_5^- + Br\text{-}CH_2\text{-}CH{=}CH\text{-}COOEt \xrightarrow[S_N2\ reaction]{after\ Br^-\ loss}$ **5**

(4) $Mn(CO)_5^- + Mn(CO)_5Br \longrightarrow Mn(CO)_{10} + Br^-$

(5) $\bar{C}H_2CH{=}CH\text{-}COOEt + Br\text{-}CH_2\text{-}CH{=}CH\text{-}COOEt \xrightarrow[S.E.T.\ "mechanism"]{probable}$ dimers + Br^-

In attempting to distinguish between Mechanisms 1 and 2, we should make it clear that we are not primarily concerned with the mechanism of the "S_N2" substitution reaction, i.e., whether S.E.T. is, or is not, involved. Studies of $(CH_3)_3Sn^-$ nucleophilic reactions (10) and Bordwell's recent studies (3) illustrate the complexities involved in such a case. Our major concern is to understand how the other "aberrant" reactions are occurring, i.e., the formation of $Mn(CO)_5X$, $Mn_2(CO)_{10}$, organic dimers, etc., since the curtailment of these reactions would obviously result in better yields of the desired product.

Reactions designed to differentiate between Mechanisms 1 and 2

The nature of the organic dimerization reactions

Experiments designed to probe the nature of the reactive organic intermediates have been performed in both the crotonate and simple carboxylate series. In the former, we have attempted to separately generate both the radical and the carbanion of debrominated **4**, and to observe what dimeric products are formed.

$Mn_2(CO)_{10} \xrightarrow{h\nu} 2\,Mn(CO)_5^{\bullet}$

$Mn(CO)_5^{\bullet} + \mathbf{4} \longrightarrow Mn(CO)_5Br + \dot{C}H_2CH{=}CH\text{-}COOEt$

$2\,\dot{C}H_2\text{-}CH{=}CH\text{-}COOEt \longrightarrow$ **8** and **9**

The photolysis of $Mn_2(CO)_{10}$ is known (11) to give $Mn(CO)_5^{\bullet}$ radicals, which in turn have been shown to abstract halide from organohalides (11). Using this procedure on 4-bromocrotonate **4**, followed by work-up of the reaction and analysis by GLC, shows only two dimeric products, the previously observed diesters **8** and **9** in a ratio of ca. 36:64. These two esters are easily rationalized as direct coupling products of the corresponding radical. Since four dimers are observed in the $Mn(CO)_5^-$ reaction, of which **8** and **9** are in the minority, one could conclude that a radical intermediate was not involved here. However, attempts using the corresponding carbanion were also ambiguous. The carbanion could not be prepared in pure THF and a THF–HMPA mixture had to be used. Reaction of the carbanion with the bromocrotonate gave only one major product, the dimer **16**, a reaction previously reported (12).

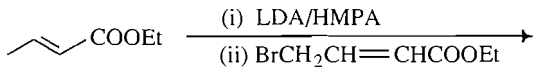

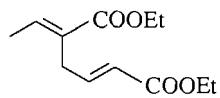

16

This dimer may in fact arise from a base-catalyzed rearrangement of **9**. In any case, neither of these reactions resembles the product mixture found for the $Mn(CO)_5^-$ reaction. In both cases the cyclopropyl products are not formed. The most probable mechanism for forming cyclopropyl products involves a Michael addition of the dienolate (or radical) to the bromocrotonate, followed by displacement of Br^- or $Br^{\bullet}$. The actual conditions in the $Mn(CO)_5^-$ reaction more closely resemble those of the photolysis experiment, so the lack of cyclopropyl products **10** and **11** in this case is probably more noteworthy than in the model carbanion case. In the latter we are not only using a different solvent mixture but the relative concentrations of carbanion and bromoester are probably very different, i.e., we are adding the completely formed dienolate to an equimolar amount of bromocrotonate in the model reaction. Overall, however, these two model experiments are disappointingly ambiguous.

Experiments were also carried out with the simple halocarboxylate esters. We particularly wanted to see if radical

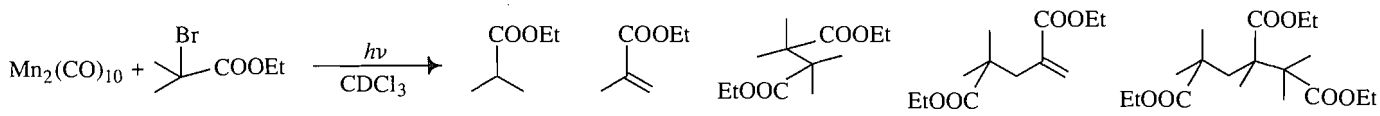

12 (13%) **13** (5%) **14** (36%) **15** (4%) **17** (9%)

intermediates were "quenched" by $CDCl_3$. Photolysis experiments were therefore carried out on the primary, secondary, and tertiary bromocarboxylate esters, together with $Mn_2(CO)_{10}$, in $CDCl_3$ at ca. 25°C. The tertiary system was also photolyzed for comparison in THF solvent.

In the primary case, the main products were ca. 50% diethyl succinate and 11% ethyl acetate. No detectable (less than 3% of the total) $CH_2DCOOEt$ was observed in the latter compound. In the secondary case, the products were 47% diethyl 2,3-dimethylsuccinate (1:1 *meso-d,l*) and 21% ethyl propionate, in addition to 27% recovered starting material. In the tertiary case, diethyl 2,2,3,3-tetramethylsuccinate **14** was the major product (36%), together with 13% ethyl 2-methylpropionate **12**, 5% ethyl methacrylate **13**, 4% dimer **15**, and 9% of the trimeric structure **17**. A similar pattern of products was found for the THF solvent system. These products are in good agreement with those previously reported for radical reactions of $(CH_3)_2\dot{C}$-COOEt (13), where the radical is produced by a completely different process.

There is obviously a striking difference in $CDCl_3$ solvent between the behavior of the photolysis-generated organic intermediate (expected to be a radical) and the intermediate produced in the $Mn(CO)_5^-$ reactions. In the latter case, the $CDCl_3$ efficiently trapped the intermediate and no dimeric products were formed. In the photolysis experiments, some hydrogen atom abstraction appears to be occurring, since debrominated esters are found, but this abstraction is occurring from the starting material or products thereof, and to the apparent exclusion of the much more abundant $CDCl_3$ solvent. In agreement, no trace of hexachloroethane was detected by GLC in any of the systems studied. No attempt was made to generate the simple enolates in $CHCl_3$, but the base abstraction of the chloroform proton is a well-known reaction. Attempts to trap a dichlorocarbene–cyclohexane adduct were unsuccessful, but it is quite possible that CCl_3^- would be relatively stable in nonpolar solvents (i.e., loss of Cl^- requires solvation).

Tentative conclusions on radical vs. enolate intermediates

Even though the deuterium abstraction reactions favor an enolate mechanism, most of the products formed in the $Mn(CO)_5^-$/THF reaction (tertiary bromide) are identical to those seen in the corresponding photolysis reaction. However, the tetramethyl succinate **14** has previously been prepared from the enolate and bromide (14) or via radical coupling (12), and one can explain the formation of dehalogenated ester **12** and methacrylate **13** by invoking either a radical or enolate mechanism. However, diester **15** (3% yield) formation seems unlikely via an enolate mechanism, but the Michael addition of the radical to **13**, followed by disproportion (e.g., with the simple radical), would yield **15**, and indeed this ester is also a product of the photolysis reaction (in fact to a much larger extent). The formation of the trimeric ester **17** is exclusive to the photolysis reaction and corresponds to the coupling of the simple radical with the Michael addition radical discussed above. Overall, the available evidence is somewhat contradictory, but the balance of evidence favors a carbanion (enolate) model (Mechanism 2) for the majority of the reaction products.

The $Mn_2(CO)_{10}$ forming reactions

There are several observations from Tables 3–8 that relate directly to the question of how $Mn_2(CO)_{10}$ is formed. We have also carried out additional control experiments.

From studies where the $Mn(CO)_5^-$:RX stoichiometry was varied, e.g., Table 4 (X = Br), one notes that a 2:1 excess of $Mn(CO)_5^-$ gave no $Mn(CO)_5Br$ and 79% $Mn_2(CO)_{10}$, whereas a reverse 1:2 molar ratio gave 51% $Mn(CO)_5Br$ and only 14% $Mn_2(CO)_{10}$. This suggests that under the reaction conditions (THF, Na^+ salt, 25°C) $Mn(CO)_5^-$ reacts with RBr in a competitive manner (as outlined in Mechanism 2) to produce both $RMn(CO)_5$ and $Mn(CO)_5Br$. However, the latter is also reactive with $Mn(CO)_5^-$ to give $Mn_2(CO)_{10}$ and this third competing reaction builds up as one forms more of the $Mn(CO)_5Br$. Where there is enough $Mn(CO)_5^-$, this latter reaction then goes to completion, but in the normal course, one is depleted in $Mn(CO)_5^-$ before all of the $Mn(CO)_5Br$ is consumed.

The other observation is that $Mn_2(CO)_{10}$ formation is strongly solvent and counterion dependent. Using the PPN^+ $Mn(CO)_5^-$ salt in THF produces essentially no $Mn_2(CO)_{10}$, whereas the Na^+ salt produces large amounts. As well, the PPN^+ salt in $CDCl_3$ (Table 7) also produces large amounts of $Mn_2(CO)_{10}$ in some cases.

To verify that these conclusions were sound, we have separately studied the reaction of $Mn(CO)_5^-$ and $Mn(CO)_5X$ (X = Br or I) in both chloroform and THF solvents. Both the PPN^+ and Na^+ salts of $Mn(CO)_5^-$ were used.

When $Na^+Mn(CO)_5^-$ was reacted with $Mn(CO)_5Br$ in THF, a rapid reaction took place and ^{55}Mn NMR and IR spectroscopies confirmed the essentially quantitative formation of $Mn_2(CO)_{10}$. The PPN^+ salt also reacted rapidly with both $Mn(CO)_5Br$ and $Mn(CO)_5I$ in $CDCl_3$, *but in THF the reaction required about 4 h*. In addition, the reaction was accompanied by CO evolution and the major stoichiometry appeared to be

$$Mn(CO)_5^- + 2Mn(CO)_5Br \rightarrow Mn_2(CO)_{10} + Mn(CO)_4Br_2^- + 2CO$$

A competitive experiment was also carried out involving the PPN^+ salt in $CDCl_3$ and a mixture of both $Mn(CO)_5Br$ and $Mn(CO)_5I$. The latter reacted about 10% faster.

The reaction of $NaMn(CO)_5$ with $Mn(CO)_5I$ in THF has been studied by Wilkinson, Hursthouse, and co-workers (15*a*). They used a 2:1 ratio of the compounds and reported the formation of the trimeric anion $Mn_3(CO)_{14}^-$ in 31% yield after an extended reaction time. These results are not inconsistent with those reported here if one assumes that the reaction proceeds:

$$Mn(CO)_5^- + Mn(CO)_5I \rightarrow Mn_2(CO)_{10} + I^- \rightarrow Mn_2(CO)_9I^- + CO \xrightarrow{Mn(CO)_5^-} Mn_3(CO)_{14}^- + I^-$$

i.e., that an "excess" of $Mn(CO)_5^-$ is required in this case. The mixed $MnRe(CO)_{10}$ and ligand-substituted derivatives of $Mn_2(CO)_{10}$ have also been prepared by similar reactions to those we reported here (15*b*).

Clearly, the solvent–counterion effects in these model reactions resemble those encountered in the main reactions and

Can. J. Chem. Downloaded from www.nrcresearchpress.com by 91.144.44.67 on 09/07/12
For personal use only.

Can. J. Chem. Downloaded from www.nrcresearchpress.com by 91.144.44.67 on 09/07/12
For personal use only.

it seems to us that most of the $Mn_2(CO)_{10}$ must be formed from a reaction of $Mn(CO)_5^-$ and $Mn(CO)_5X$, i.e., as outlined in Mechanism 2, rather than by the radical coupling mechanism shown in Mechanism 1. Therefore, both the $Mn_2(CO)_{10}$ and the organic products formed seem better accommodated by Mechanism 2. If we assume Mechanism 2 for the moment, there are a few other comments which are relevant with regard to the results presented in the various tables.

1. The formation of $Mn(CO)_5Br$ seems to be slower than that of $Mn(CO)_5I$. Since both react at a similar rate with $Mn(CO)_5^-$, one gets more $Mn_2(CO)_{10}$ in the bromo cases (the $Mn(CO)_5^-$ is present for a longer time) (see Tables 5 and 7).

2. With the 1:1 RX:$Mn(CO)_5^-$ stoichiometry, one conversely gets more recovered starting material in the bromide case (Table 9) compared to iodide ($Mn(CO)_5^-$ is lost in forming $Mn_2(CO)_{10}$).

Overall conclusions for preparing $Mn(CO)_5$-enolates or -dienolates

1. In RX + $Mn(CO)_5^-$ reactions, the X = Cl leaving group is preferred if it is reactive enough. If not, X = Br is better than X = I.

2. If the bromide is used, one may have to carefully adjust the stoichiometry of the starting materials to maximize the yield of $RMn(CO)_5$.

3. The PPN^+ salt in THF solvent is particularly favorable for cases where bromides or iodides are used. Lithium salts are particularly unfavorable and may give no $RMn(CO)_5$ product.

Concluding discussion

Preliminary experiments were also carried out between $Mn(CO)_5^-$ and several allylic bromides. Although allyl bromide and other primary bromides worked quite well, secondary allylic bromides usually gave extensive coupling of the organic product. These results mirror the 2-halocarboxylate and 4-halocrotonate results to some extent and indicate the rather fine dividing line between the substitution and H.M.E. reactions.

Experimental

All procedures involving organometallic species were performed under an atmosphere of argon or nitrogen. A combination of syringe, transfer needle, and Schlenk techniques were used.

Infrared analysis was performed using a Perkin–Elmer 467 or a Nicolet 5DX FT instrument. Mass spectrometric analyses were obtained on a Kratos MS80, and ^1H, ^{55}Mn, and ^{13}C NMR spectra on a Varian XL-200. The ^{55}Mn NMR chemical shifts are reported with respect to potassium permanganate in D_2O, and were calculated using the signal for dimanganese decacarbonyl as a secondary reference. For very broad signals in a conventional high-resolution spectrometer one loses signal intensity in the FID during the pulse time itself and in the subsequent dead time before the receiver is turned on. This signal loss was not a major problem in our work but we have attempted to correct for these intensity errors. Integration of signals was performed using manually set parameters and the values thus obtained were then adjusted using calibration parameters determined for mixtures of organometallic species of known concentration, i.e., very similar to a GC calibration. Gas chromatographic (GC) analyses were carried out using a Hewlett–Packard 5890.

THF was distilled from benzophenone ketyl under nitrogen and deuterated solvents were dried over molecular sieve dust prior to use. The majority of compounds were available from commercial sources and were used without further purification, except ethyl 4-bromo-2-butenoate, which was obtained as technical grade (Aldrich) and distilled prior to use (spinning band). Ethyl 2-iodoethanoate, ethyl 2-iodopropanoate, and ethyl 2-iodo-2-methylpropanoate were prepared by treating the corresponding bromo-ester with sodium iodide in acetone. Ethyl 2-chloropropanoate and ethyl 4-chloro-2-butenoate were obtained from the corresponding bromides using lithium chloride in dimethylformamide. The anions $PPN^+[Mn(CO)_5^-]$ (16), $Li^+[Mn(CO)_5^-]$ (16, 17), $Na^+[Mn(CO)_5^-]$ (18), and $K^+[Mn(CO)_5^-]$ (19) were prepared according to literature procedures from $Mn_2(CO)_{10}$ (Strem Chemicals).

In situ *reactions of $M^+[Mn(CO)_5^-]$ with halo-esters*

Solutions of the anions (0.128 molar) were filtered, and transferred to a nitrogen-purged graduate cylinder fitted with a rubber septum; known volumes (ca. 2 mL) of the solution were transferred by syringe into a 10 mm NMR tube containing a known amount of halo-ester, and shaken. Where the reaction was carried out in the presence of 18-crown-6 (Aldrich), this was added to the anion solution prior to mixing.

The reaction of $Na^+[Mn(CO)_5^-]$ with ethyl 4-bromocrotonate ***4***

In a 10-mL round-bottom flask fitted with a rubber septum, 4 mL of $Na^+[Mn(CO)_5^-]$ solution (prepared from 0.96 g of $Mn_2(CO)_{10}$ (0.245 mmol) in 4 mL of THF) was added with stirring to 0.96 g (0.50 mmol) of ethyl 4-bromocrotonate in 2 mL of THF. The reaction mixture was then stirred for 30 min after which the solvent was removed at reduced pressure and the residue then extracted with 2 × 5 mL of pentane. The extracts were combined and the solvent evaporated. The residue was applied to a 1 × 15 cm flash chromatography column of silica gel and eluted with methylene chloride. After initial bands of $Mn_2(CO)_{10}$, followed by $Mn(CO)_5Br$ and a small quantity (0.001 g) of the η^3-complex **2** (R = Et), the η^1-complex **5** eluted as a broad pale-yellow band (0.0492 g). The infrared and ^1H NMR of the last fraction indicated that the sample was pure (33% yield). Further elution of the column with diethyl ether yielded 0.0135 g of a colourless liquid, the GC of which (3% OV17, 2 mm × 2 m glass column) indicated the presence of four organic products. Samples of these were isolated by GC (3% OV17, 4 mm × 2 m glass column) and identified as follows:

Ethyl trans*-2-(2-carbethoxycyclopropyl)-3-butenoate* ***11*** (43% of total "organic" product)

Diastereomer A: ^1H NMR ($CDCl_3$): 1.22 (t, J = 7.1 Hz, 3H), 1.24 (t, J = 7.0 Hz, 3H), 2.58 ("t", J = 8 Hz, 1H), 4.13 (q, J = 7.0 Hz, 2H), 4.18 (q, J = 7.0 Hz, 2H), 5.1 and 5.2 (d × 2, J = 16.4 and 11.2 Hz, 2H), 5.85 (m, 1H), 0.82 (m, 1H), 1.62 (m, 1H), 1.75 (m, 1H). One proton is hidden by the methyl peaks.

Diastereomer B: The *trans* stereochemistry in this compound was inferred from the coupling constants, which in turn were arrived at by extensive decoupling experiments and computer simulations. The following numbering system is arbitrarily used here:

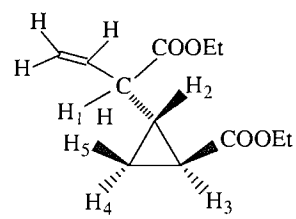

Chemical shifts	Coupling constants (Hz)
1. 2.54	J_{12} = 8
2. 1.79	J_{23} = 4
3. 1.48	J_{24} = 8
4. 1.2–1.3 (peak is obscured)	J_{25} = 6
5. 0.92	J_{34} = 4
	J_{35} = 8
	J_{45} = −4

$COOEt(CH_3)$	1.24, t, J = 7
	1.26, t, J = 7
(CH_2)	4.16, q, J = 7
	4.19, q, J = 7
Vinyl	5.17, d, J = 16.8
	5.19, d, J = 10.0
	5.88, m

Can. J. Chem. Downloaded from www.nrcresearchpress.com by 91.144.44.67 on 09/07/12
For personal use only.

The coupling between H_2 and H_3 is 8 Hz, which is in the range expected for a *trans* orientation of protons on a cyclopropane ring (20).

Ethyl E-*5-carbethoxy-2,6-heptadienoate* **9** (21%): ^{1}H NMR ($CDCl_3$): 1.24 (t, J = 7.3 Hz, 3H), 1.26 (t, J = 7.2, 3H), 2.34–2.8 (m, 2H), 3.17 (dt, J = 8.1 and 6.2 Hz, 1H), 4.18 (q, J = 7.2 Hz, 2H), 4.2 (q, J = 7.1 Hz, 2H), 5.21 (m, 2H), 5.72–5.96 (m, 2H), 6.88 (dt, J = 10 and 15 Hz, 1H); GC–MS (*m/e*, % base peak): 226 (3, M^+), 181 (55), 180 (68), 153 (81), 152 (78), 134 (66), 125 (69), 113 (70), 108 (35), 107 (88), 106 (73), 97 (67), 85 (97), 81 (92), 80 (79), 79 (100), 78 (76), 77 (77), 69 (35), 68 (82), 67 (79), 57 (64), 55 (61), 54 (47), 53 (67), 43 (49), 41 (78). See ref. 7.

Ethyl E-*4-(2'-carbethoxycyclopropyl)-2-butenoate* **10** (21%): ^{1}H NMR ($CDCl_3$): 1.25 (t, J = 6.9 Hz, 3H), 1.28 (t, J = 7.1 Hz, 3H), 2.2 (m, 2H), 4.14 (q, J = 7.0 Hz, 2H), 4.21 (q, J = 7.0 Hz, 2H), 5.85 (d, J = 15.6 Hz, 1H), 6.94 (dt, J = 6.4 and 15.6 Hz, 1H), 0.70–0.95 (m, 2H), 1.45 (m, ca. 1H); GC–MS (*m/e*, % base peak): 226 (1, M^+), 181 (80), 153 (45), 152 (80), 135 (29), 134 (73), 125 (37), 123 (28), 107 (79), 106 (63), 98 (66), 97 (80), 85 (55), 81 (100), 80 (47), 79 (92), 78 (79), 77 (48), 68 (65), 67 (46), 66 (27), 57 (30), 55 (90), 54 (38), 53 (65), 43 (30), 41 (50).

Ethyl E,E-*2,6-octadien-1,8-dioate* **8** (14%): ^{1}H NMR ($CDCl_3$): 1.28 (t, J = 7.1 Hz, 6H), 2.37 ("d", J = 6.8 Hz, 4H), 4.17 (q, J = 7.2 Hz, 4H), 5.85 (d, J = 15.5 Hz, 2H), 6.96 (dt, J = 6.7 and 15.7 Hz, 2H); GC–MS (*m/e*, % base peak): 226 (1, M^+), 181 (87), 153 (56), 152 (94), 135 (30), 134 (28), 125 (42), 114 (25), 113 (25), 111 (38), 107 (80), 106 (30), 97 (28), 86 (44), 85 (100), 76 (77), 75 (30), 74 (92), 73 (54), 72 (35), 69 (25), 68 (95), 67 (48), 57 (77), 55 (68), 53 (40), 43 (28), 41 (55). See ref. 7.

η^1-4-Oxo-4-ethoxy-2-butenyl manganese pentacarbonyl **5**: Infrared (methylene chloride, cm^{-1}): 2110 (w), 2018 (m), 2005 (s), 1690 (w), 1610 (w); ^{1}H NMR ($CDCl_3$): 1.27 (t, J = 7.1 Hz, 3H), 1.88 (d, J = 9.6 Hz, 2H), 4.17 (q, J = 7.0 Hz, 2H), 5.65 (d, J = 15.1 Hz, 1H), 7.45 (dt, 1H); $\{^1H\}^{13}$C NMR ($CDCl_3$): 8.1 (CH_2), 14.4 (CH_3), 59.7 (CH_2), 111.5 (CH), 158.5 (CH); MS (*m/e*, % base peak): 224 (5), 196 (30), 168 (80), 124 (45), 100 (95), 68 (80), 55 (100). Anal. calcd. for $C_{11}H_9MnO_7$: C 42.88, H 2.94%; found: C 39.78, H 3.25%. The elemental analysis for this compound could not be improved, even by repeated purification.

The reaction of ethyl 2-bromo-2-methylpropanoate with $PPN^+[Mn(CO)_5^-]$ in THF

In a 10-mm NMR tube 0.11 g, (0.15 mmol) of $PPN^+[Mn(CO)_5^-]$ was added to 0.05 g (0.26 mmol) of ethyl 2-bromo-2-methylpropanoate in 3 mL of THF, and the mixture shaken. The solution was then allowed to stand for 5 h. GC analysis of the crude reaction mixture indicated that **12**, **13**, **14**, and **15** were formed in the reaction. These volatile components were obtained by distillation (trap to trap, ca. 0.1 Torr; 1 Torr = 133.3 Pa) from the reaction mixture. The first three were easily identified by comparison to the known compounds (retention time, MS fragmentation, and ^{1}H NMR). Compound **15** was isolated by preparative GC and identified on the basis of the MS and the reported (13) ^{1}H NMR spectrum. The residue from this distillation was dissolved in 4 mL of THF, filtered, and pentane slowly added to the filtrate. Oily material formed, which was separated by decantation and washed with pentane. This oil solidified to a resinous material (0.04 g) that could not be crystallized. The infrared spectrum of this oil contained bands (in THF) at 2081 (w), 2007 (s), 1973 (s), 1925 (s), and 1907 (sh), which probably correspond to $PPN^+[Mn(CO)_4Br_2^-]$.

Ethyl 2-methylpropanoate **12**: GC–MS (*m/e*, % base peak): 116 (50), 89 (51), 88 (55), 73 (55), 71 (70), 43 (100).

Ethyl 2-methyl-2-propenoate **13**: GC–MS (*m/e*, % base peak): 114 (52), 99 (55), 86 (68), 70 (60), 69 (100), 41 (90).

Diethyl 2,2,3,3-tetramethylsuccinate **14**: ^{1}H NMR ($CDCl_3$): 1.23 (s, 12H), 1.26 (t, J = 7.1 Hz, 6H), 4.10 (q, J = 7.1 Hz, 4H); GC–MS (*m/e*, % base peak): 185 (50), 157 (51), 116 (97), 88 (90), 87 (100), 84 (55), 83 (90), 70 (50), 69 (85), 59 (77), 57 (45), 55 (60), 43 (90), 42 (47), 41 (95).

Diethyl 2,2-dimethyl-4-methylenepenta-1,5-dioate **15** (13): ^{1}H NMR ($CDCl_3$): 1.18 (s, 6H), 1.264 and 1.31 (t × 2, J = 7.1, 7.1 Hz, 6H), 2.64 (s, 2H), 4.11 (q, J = 7.1 Hz, 2H), 4.2 (q, J = 7.1, 2H), 5.53 ("s", 1H), 6.22 (d, J = 1.6 Hz, 1H); GC–MS (*m/e*, % base peak): 228 (4), 155 (59), 154 (50), 127 (25), 109 (87), 81 (100), 68 (30), 67 (32), 59 (37), 43 (45), 41 (94).

Photolysis of dimanganese decacarbonyl with halo-esters

The photolyses were carried out, using a G.E. 250-W sun lamp, in Pyrex tubes fitted with septa placed in a water cooled jacket.

Ethyl 4-bromo-2-butenoate

Dimanganese decacarbonyl (0.2 g, 0.51 mmol) and ethyl 4-bromo-2-butenoate (0.2 g, 1.04 mmol) in 8 mL of THF were irradiated for 4.5 h. The infrared spectrum of the crude reaction mixture indicated that some $Mn(CO)_5Br$ and $Mn_2(CO)_8Br_2$ were formed, in addition to a considerable amount of an insoluble white solid. After removing the THF solvent, the residue was extracted with 3 × 20 mL of pentane, and the extracts combined, filtered, and evaporated to give 0.08 g of a yellow oil from which flash chromatography (silica/methylene chloride) yielded 0.07 g colourless oil. The GC (10-m methyl silicone column) and ^{1}H NMR spectrum of this fraction indicated that it contained ethyl 5-carboethoxy-2,6-heptadienoate **9** (64%) and ethyl 2,6-octadien-1,8-dioate **8** (36%).

Ethyl 2-bromoethanoate

Dimanganese decacarbonyl (0.10 g, 0.26 mmol), and ethyl 2-bromoethanoate (0.081 g, 0.49 mmol) in 3 mL of deuterochloroform were irradiated for 3 h. The colourless solution was filtered to remove the white powder that formed. A singlet in the ^{1}H NMR spectrum of the filtered solution at 2.63 ppm was assigned to diethyl succinate (50% yield) and this was confirmed by GC analysis (3% OV1, 2 mm × 2 m glass column) and comparison with authentic material. Unreacted ethyl 2-bromoethanoate was also present (29%). One resonance in the ^{1}H NMR spectrum (singlet, 3.28 ppm, 8% of the total integration as CH_2 protons) remained unidentified.

The reaction of $Mn(CO)_5^-$ with $Mn(CO)_5Br$

(i) $Na[Mn(CO)_5]$ and $Mn(CO)_5Br$ in THF solvent

A THF solution of $Na[Mn(CO)_5]$ (0.128 M) was prepared from $Mn_2(CO)_{10}$, as previously referred to, and this was added rapidly to an equimolar amount of $Mn(CO)_5Br$. Clean conversion of the $Mn(CO)_5Br$ to $Mn_2(CO)_{10}$ was observed by ^{55}Mn NMR and IR spectroscopy within 10 min. The solution was filtered, evaporated, and the residue applied to a 1 cm × 15 cm flash chromatography column (silica gel, methylene chloride). The first yellow band yielded $Mn_2(CO)_{10}$ in 84% yield.

(ii) $PPN[Mn(CO)_5]$ and $Mn(CO)_5Br$ in chloroform

The salt $PPN[Mn(CO)_5]$, 0.1476 g (0.202 mmol), was dissolved in 2.0 mL of $CHCl_3$ and added to solid $Mn(CO)_5Br$, 0.0535 g (0.195 mmol), and the mixture shaken. The reaction was complete within a few minutes and IR and ^{55}Mn NMR spectroscopy showed that $Mn_2(CO)_{10}$ was the major product formed.

(iii) $PPN[Mn(CO)_5]$ and $Mn(CO)_5Br$ in THF

This reaction was performed as in (ii) but in this case there was no observable reaction after 10 min (IR spectroscopy). However, after ca. 4 h, the IR and ^{55}Mn NMR spectra indicated the presence of both $[Mn(CO)_4Br_2^-]PPN^+$ and $Mn_2(CO)_{10}$.

(iv) $PPN[Mn(CO)_5]$ and $Mn(CO)_5Br$–$Mn(CO)_5I$ in chloroform

This reaction was performed as in (ii) using approximately equimolar ratios of the three compounds. ^{55}Mn NMR spectroscopy of the residual $Mn(CO)_5Br$ and $Mn(CO)_5I$ was used for the analytical determination (see previous section on ^{55}Mn peak integration methods).

Ethyl 2-bromopropanoate

This photolysis was carried out in the same way as that described above for ethyl 2-bromoethanoate using 0.1 g (0.26 mmol) of dimanganese decacarbonyl and 0.09 g (0.50 mmol) of ethyl 2-bromopropanoate.

The ^{1}H NMR spectrum of the crude reaction mixture contained resonances that were assigned to 1:1 *meso-d,l* diethyl 2,3-dimethylsuccinate (47%), unreacted ethyl 2-bromopropanoate (21%), and ethyl propanoate (21%). The assignments were confirmed by comparison with authentic materials (GC and ^{1}H NMR analysis).

Ethyl 2-bromo-2-methylpropanoate

Dimanganese decacarbonyl and 0.05 g (0.13 mmol) of ethyl

2-bromo-2-methylpropanoate in 3 mL of freshly distilled THF (or $CDCl_3$) were irradiated for 30 min. The solvent was then removed under reduced pressure and the oily residue extracted with hexane, filtered, and evaporated. GC analysis indicated that the extract contained six components, of which starting material (8%), ethyl 2-methylpropanoate **12** (17%), ethyl 2-methyl-2-propenoate **13** (12%), diethyl 2,2,3,3-tetramethyl succinate **14** (45%), and diethyl 2,2-dimethyl-4-methylenepenta-1,5-dioate **15** (5%) were readily identified by GC–MS (see section where these same products were produced from $Mn(CO)_5^-$ reaction). The remaining component was isolated by preparative GC and shown to be diethyl 3-carbethoxy-2,2,3,5,5-pentamethylhexa-1,6-dioate **17** (13%), by comparison of the ^1H NMR spectrum to that previously reported (13).

Acknowledgements

We thank the Natural Sciences and Engineering Research Council of Canada for generous support.

1. E. R. Burkhardt, J. J. Doney, R. G. Bergman, and C. H. Heathcock. J. Am. Chem. Soc. **109**, 2022 (1987).
2. R. W. Johnson and R. G. Pearson. Chem. Commun. 986 (1970).
3. F. G. Bordwell and C. A. Wilson. J. Am. Chem. Soc. **109**, 5470 (1987).
4. W. R. McClellan, H. H. Hoehn, H. N. Cripps, E. L. Muetterties, and B. W. Howk. J. Am. Chem. Soc. **83**, 1601 (1961).
5. F. Calderazzo, E. A. C. Lucken, and D. F. Williams. J. Chem. Soc. (A), 154 (1967).
6. M. Y. Darensbourg. Prog. Inorg. Chem. **33**, 221 (1985).
7. Y. Ito, T. Konoike, T. Harada, and T. Saegusa. J. Am. Chem. Soc. **99**, 1487 (1977).
8. J. Engelbrecht, T. Greiser, and E. Weiss. J. Organomet. Chem. **204**, 79 (1981).
9. M. F. Farona and L. M. Frazee. J. Inorg. Nucl. Chem. **29**, 1814 (1967).
10. (*a*) M. S. Alnajjar and H. G. Kuivila. J. Am. Chem. Soc. **107**, 416 (1985); (*b*) E. C. Ashby, W.-Y. Su, and T. N. Pham. Organometallics, **4**, 1493 (1985).
11. G. L. Geoffrey and M. S. Wrighton. Organometallic photochemistry. Academic Press, New York. 1972. p. 89.
12. P. Prempree, S. Radviroongit, and Y. Thebtaramonth. J. Org. Chem. **48**, 3553 (1983).
13. S. Bizilj, D. P. Kelly, A. K. Serelis, D. H. Solomon, and K. E. White. Aust. J. Chem. **38**, 1657 (1985).
14. N. Petragnani and M. Yonashiro. Synthesis, 710 (1980).
15. (*a*) R. Poli, G. Wilkinson, M. Motevalli, and M. B. Hursthouse. J. Chem. Soc. Dalton Trans. 931 (1985); (*b*) D. L. Morse and M. S. Wrighton. J. Organomet. Chem. **125**, 71 (1977).
16. (*a*) D. N. Duffy and B. K. Nicholson. J. Organomet. Chem. **164**, 227 (1979); (*b*) J. A. Gladysz, G. M. Williams, W. Tam, D. L. Johnson, D. W. Parkes, and J. C. Selover. Inorg. Chem. **18**, 553 (1979).
17. T. L. Brown and C. D. Pribalen. J. Organomet. Chem. **71**, 415 (1974).
18. W. Hieber and G. Wagner. Z. Naturforsch. **13B**, 339 (1959).
19. J. E. Ellis and E. A. Flour. J. Organomet. Chem. **99**, 263 (1975).
20. K. B. Wiberg, D. E. Barth, and P. H. Schertler. J. Org. Chem. **38**, 378 (1973).

Can. J. Chem. Downloaded from www.nrcresearchpress.com by 91.144.44.67 on 09/07/12
For personal use only.

The preparation and reactions of ω-bromoacylmanganese pentacarbonyls

ANDREW P. MASTERS AND TED S. SORENSEN
The Department of Chemistry, University of Calgary, Calgary, Alta., Canada T2N 1N4

Received July 10, 1989

ANDREW P. MASTERS and TED S. SORENSEN. Can. J. Chem. **68**, 502 (1990).

The reaction of ω-bromoacyl chlorides Br—CH_2—$(CH_2)_n$—COCl and $Mn(CO)_5^-$ is reported. In the case of $n = 0$, one obtains ketene, $Mn(CO)_5Br$, and chloride ion. In contrast, the corresponding chloro compound gives the known chloroacyl manganese complex. With $n = 1$, 2, or 3, one can isolate the corresponding ω-bromoacylmanganese complexes. On mild heating, the $n = 1$ complex produces only ethylene and $Mn(CO)_5Br$. The $n = 2$ and 3 complexes are also relatively labile on heating in THF solution and produce the 1-alkene as the major organic product. In chloroform solution, the corresponding ω-bromoalkyl complex is produced initially on heating, but further heating again produces mainly the 1-alkene. However, the $n = 2$ complex also produces appreciable amounts of cyclopropane.

Key words: bromoacylmanganese pentacarbonyl, pentacarbonyl manganate, ethylene, cyclopropane.

ANDREW P. MASTERS et TED S. SORENSEN. Can. J. Chem. **68**, 502 (1990).

On a étudié les réactions des chlorures de ω-bromoacyles (Br—CH_2—$(CH_2)_n$—COCl) avec le $Mn(CO)_5^-$. Dans le cas où $n = 0$, on obtient du cétène, du $Mn(CO)_5Br$ et de l'ion chlorure. Par opposition, le composé chloré correspondant fournit le complexe chloroacyl manganèse connu. Lorsque $n = 1$, 2 ou 3, on peut isoler les complexes ω-bromoacylmanganèse correspondants. Lorsqu'on le chauffe légèrement, le complexe dans lequel $n = 1$ ne conduit qu'à d'éthylène et de $Mn(CO)_5Br$. Les complexes dans lesquels $n = 2$ ou 3 sont aussi relativement labiles; lorsqu'on les soumet à un chauffage, en solution dans le THF, le produit organique majeur est le 1-alcène. En solution dans le chloroforme, il y a formation des complexes ω-bromoalkyles correspondants; mais, si l'on continue le chauffage, il y a principalement formation du 1-alcène. Toutefois, le complexe dans lequel $n = 2$ conduit à la formation d'une quantité appréciable de cyclopropane.

Mots clés: bromoacylmanganèse pentacarbonyl, pentacarbonyl manganate, éthylène, cyclopropane.

[Traduit par la revue]

Can. J. Chem. Downloaded from www.nrcresearchpress.com by 91.144.44.67 on 09/07/12
For personal use only.

Acylmanganese pentacarbonyls **1** are a very well-known class of organometallic compounds (1). The readily lose carbon monoxide to form the alkyl complex **2** and the mechanism of this reversible reaction has been elegantly determined by labelling studies (2) and supported by later theoretical calculations (3).

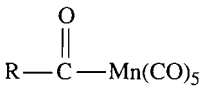

1

2

A great many derivatives of **1** are known, but there has been no systematic study of cases where R = —$(CH_2)_n$—CH_2Br, **3**, although most of the corresponding chloro compounds have been prepared. The fact that the first member of this series ($n = 0$) reacted in a totally different way compared to the chloro analog makes the extension to the bromo analogs non-trivial. Our interest was mainly in the fate of the organic part of these complexes when they were subjected to thermolysis, i.e., unsaturated ($16e^-$) organometallics often add oxidatively to a C—Br bond. It was planned to study acyl system **3** where n was varied from 0 to 3. The usual route for preparing such complexes is to react the corresponding acyl halide with $Mn(CO)_5^-$ salts.

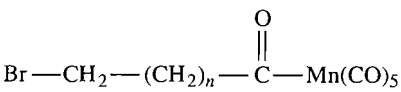

3

Results

2-Bromoacetyl chloride (or bromide) **4** reacts with sodium pentacarbonylmanganate to give a near quantitative yield of ketene, $Mn(CO)_5Br$, and sodium chloride (bromide).

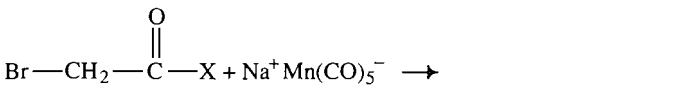

4 X = Cl or Br

This reaction is in fact a very general ketene synthesis, which has been described in other publications (4). The reaction of $Mn(CO)_5^-$ with acyl chlorides to give acylmanganese organometallics is normally a rapid reaction and it is surprising in this case to find this process completely superseded by the ketene-forming reaction. One might postulate that the acyl manganese complex corresponding to **3** ($n = 0$) is initially formed and that this then rapidly eliminates $Mn(CO)_5Br$, but the evidence is against this (4). The 2-chloroacyl manganese compound **5** can in fact be prepared in the normal way, as previously reported (5), and repeated in this study. This compound on heating gives the alkyl species **6** together with other unidentified material.

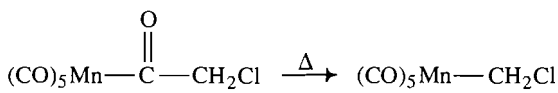

5 **6**

This experience with **5** suggests that **3** ($n = 0$) might be a reasonably stable species, once formed, but we have not explored possible alternative approaches to this synthesis.

3-Bromopropanoyl chloride **7** reacts with $Mn(CO)_5^-$ to give the crystalline acyl complex **3** ($n = 1$). The complex was characterized by ^1H and ^{55}Mn NMR spectroscopy, and by IR spectroscopy. When **3** ($n = 1$) was heated above the melting point, gas evolution occurred at ca. 62°C and the color changed from

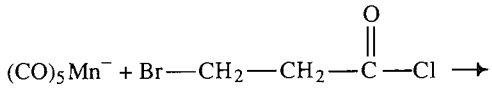

7

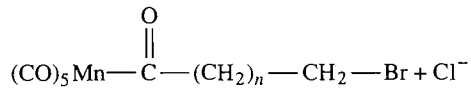

3 ($n = 1$)

pale yellow to orange. The formation of the orange $Mn(CO)_5Br$ was confirmed by TLC separation and comparison of the IR spectrum to that of the authentic compound. Heating a solution of **3** ($n = 1$) in deuterochloroform at 75°C for 4 h (sealed NMR tube) produced only one ^1H NMR product peak, at 5.38 ppm, assigned to ethylene and confirmed along with carbon monoxide by gas chromatography. The only manganese-containing species was $Mn(CO)_5Br$. In tetrahydrofuran solution (THF), the reaction of **3** ($n = 1$) was more rapid ($t_{1/2}$ ca. 10 min at 60°C) but the products produced were the same. All of these results are consistent with the following reaction stoichiometry.

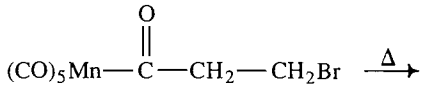

$$Mn(CO)_5Br + CH_2{=}CH_2 + CO$$

The preparation of 4-bromobutanoylmanganese pentacarbonyl **3** ($n = 2$) proceeded as for the $n = 1$ case, but the compound was relatively air and (or) moisture sensitive. The major products from the air interaction were $Mn(CO)_5Br$ and δ-butyrolactone **8**. Heating **3** ($n = 2$) above the melting point led to gas evolution and the formation of an orange residue. Flash chromatography led to an 81% recovered yield of $Mn(CO)_5Br$ and 4% of a second orange solid. This product had ν_{CO} peaks at 2097(m), 2027(sh), 2013(s), and 1967(s) and ^1H NMR peaks at δ 2.09 (t, t), 2H; 4.18 (t, $J = 7.9$ Hz), 2H; and 5.21 (t, $J = 9.0$ Hz), 2H. These results are consistent with the carbene complex **9**, in that the spectral data are very similar to the previously reported (6) iodo complex of **9**. Complex **9** was also produced in very low yields by heating a THF solution of **3** ($n = 2$) and lithium bromide or by irradiating **3** ($n = 2$) in deuterochloroform with a sun lamp.

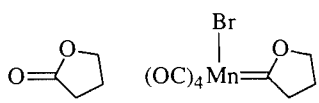

8 9

$$(OC)_5Mn{-}CH_2{-}CH_2{-}CH_2{-}Br$$

10

Heating a chloroform-*d* solution of **3** ($n = 2$) at 75°C for 3 h in a sealed NMR tube cleanly produced the corresponding alkyl complex **10**, showing a characteristic ^1H NMR spectrum (particularly the high field peak at 0.90 ppm for CH_2 bound to manganese). On standing overnight at room temperature, partial conversion back to the acyl complex was seen. If the solution is heated to 125°C for 1 h, considerable decomposition occurs and the manganese shows up as an insoluble brown powder of unknown composition. The ^1H NMR spectrum showed a singlet at 0.24 ppm, assigned to cyclopropane (12%), and peaks attributable to propene (38%). Both of these identifications were confirmed by gas chromatography. When **3** ($n = 2$) was heated in THF-d_8 solution at 60°C for 2 h, no intermediate alkyl complex **10** was seen. The major organic product was propene, with a trace (<1%) of cyclopropane. The manganese was mainly in the form of $Mn(CO)_5Br$, as judged by IR spectroscopy.

The formation of 5-bromopentanoylmanganese pentacarbonyl **3** ($n = 3$) proceeded in good yield and this solid was characterized in a similar way to the lower members. Heating the solid above the melting point at 70°C gave a fairly clean conversion to $Mn(CO)_5Br$. Heating a deuterochloroform solution at 70°C for 3.5 h gave the haloalkyl complex **11**, characterized as for

$$(CO)_5Mn{-}CH_2{-}CH_2{-}CH_2{-}CH_2Br$$

11

10 by the distinctive ^1H NMR spectrum. As with **10**, complex **11** was partly converted back to the acyl complex on cooling overnight. Heating the solution at 120°C for 1 h gave 85% 1-butene and an unidentified manganese-containing product (insoluble brown powder). Heating **3** ($n = 3$) in THF-d_8 at 60°C for 4 h gave directly 90% 1-butene, and $Mn(CO)_5Br$ was the major manganese-containing product. No alkyl complex **11** was observed nor was any cyclobutane observed.

Discussion

The n = *1 case*

Under all three reaction conditions (melt, chloroform, or THF solvent) ethylene is readily produced and we believe that a fragmentation process is the most likely here. One possibility is the direct fragmentation of **3** ($n = 1$), eq. [1], but no sign of $Mn(CO)_6^+$ (7) was observed in the *in situ* ^{55}Mn spectrum when this reaction was monitored by NMR spectroscopy. A more likely reaction is the initial loss of CO, and then fragmentation, eq. [2], perhaps even involving a cyclic transition state. The fragmentation of an alkyl complex intermediate is a third alternative (eq. [3]).

[1] 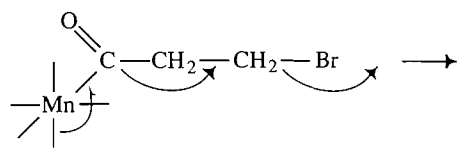

$$H_3C{=}CH_2 + [Mn(CO)_6^+\ Br^-]$$

[2] 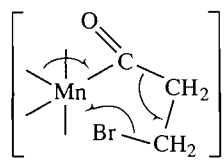 $CH_2{=}CH_2 + Mn(CO)_5Br$

[3] 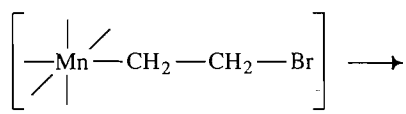

$$CH_2{=}CH_2 + Mn(CO)_5Br$$

Although a cationic ethylene complex, $Mn(CO)_5(\eta^2\text{-}C_2H_4)BF_4$, is known (8), there is no evidence for a similar complex (bromide anion) in our case.

The n = *2 case*

The formation of δ-butyrolactone **8** on air/water exposure of

Can. J. Chem. Downloaded from www.nrcresearchpress.com by 91.144.44.67 on 09/07/12
For personal use only.

3 (n = 2) is consistent with the formation of the cationic carbene intermediate **12** (eq. [4]). When **12** loses CO, one obtains the relatively air-stable neutral complex **9**.

Stone and co-workers (6) have previously prepared the chloro analog of **3** (n = 2) and also the chloroalkyl analog of **10**. Although their chloroacyl compound is unreactive, the monophosphine analog reacts with silver tetrafluoroborate to give a cationic carbene complex that is an isolatable monophosphine-substituted derivative of **12**.

In our case, it is not really clear why one sees no evidence for **12** in the absence of air. It is possible that one has an equilibrium of **3** (n = 2) and **12** which is favorable to the former, but that by removing **12** by oxidation one can eventually produce large amounts of butyrolactone and $Mn(CO)_5Br$. In fact, the abnormal O_2 sensitivity of **3** (n = 2) can be nicely accounted for with this assumption.

[4] 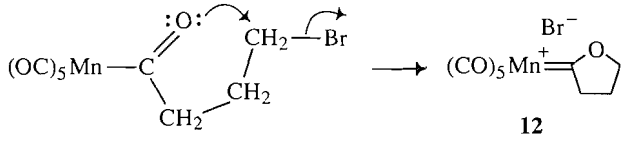

12

$\xrightarrow{O_2/H_2O}$ $Mn(CO)_5Br$ + **8**

However, the major reaction occurring in solution in the absence of oxygen is not likely to involve **12**. The formation of the alkyl complex **10** in chloroform solution and the fact that **10** is not seen in THF solution implies that a stabilizing THF coordination of unsaturated intermediates is involved at some point in the reaction mechanism. One route for such stabilization could involve $16e^-$ intermediates such as **13**, **14**, **15**, or **16**. In eq. [5], we show a plausible route to the organic products involving a metallocycle intermediate **14**, although other mechanisms are certainly not ruled out. The route shown as eq. [5] has much analogy in platinum metallocycle chemistry, where metallocycles are well characterized and details of the thermolysis reactions have been investigated (9).

The fact that the chloroform solution reactions require a much higher temperature than those in THF, and the fact that considerable cyclopropane is formed in the former case, can be accounted for by the eq. [5] mechanism, i.e., **13** and **14** can be stabilized by weak THF coordination. Also, since the propene-forming route might involve further intermediates **15** and **16**, there is probably more chance for the direct reductive elimination of cyclopropane from **14** (or an $18e^-$ equivalent), compared to THF solution. The formation of an insoluble manganese "powder" in chloroform solution is also consistent with the presence of very reactive unsaturated manganese species, whereas in THF such species "hold together" long enough for $Mn(CO)_5Br$ to be the eventual manganese product.

The postulate of a metallocycle intermediate, while reasonable, is certainly not a requirement since the cyclopropane could be formed by a concerted 1,3-elimination much like that shown in eq. [1] or eq. [2].

The n = *3 case*

The formation of 1-butene here parallels the observations made for the n = 2 situation (propene). The 1-butene can be explained using the eq. [5] mechanism but the evidence for a metallocyclic intermediate would have been stronger if some cyclobutane had been observed.

Other possible routes to 1-butene (or propene) could involve β-hydride abstraction (10) in the alkyl complexes to give $Mn(CO)_5H$ ($Mn(CO)_4H$) and alkenyl bromide, followed by re-

[5] 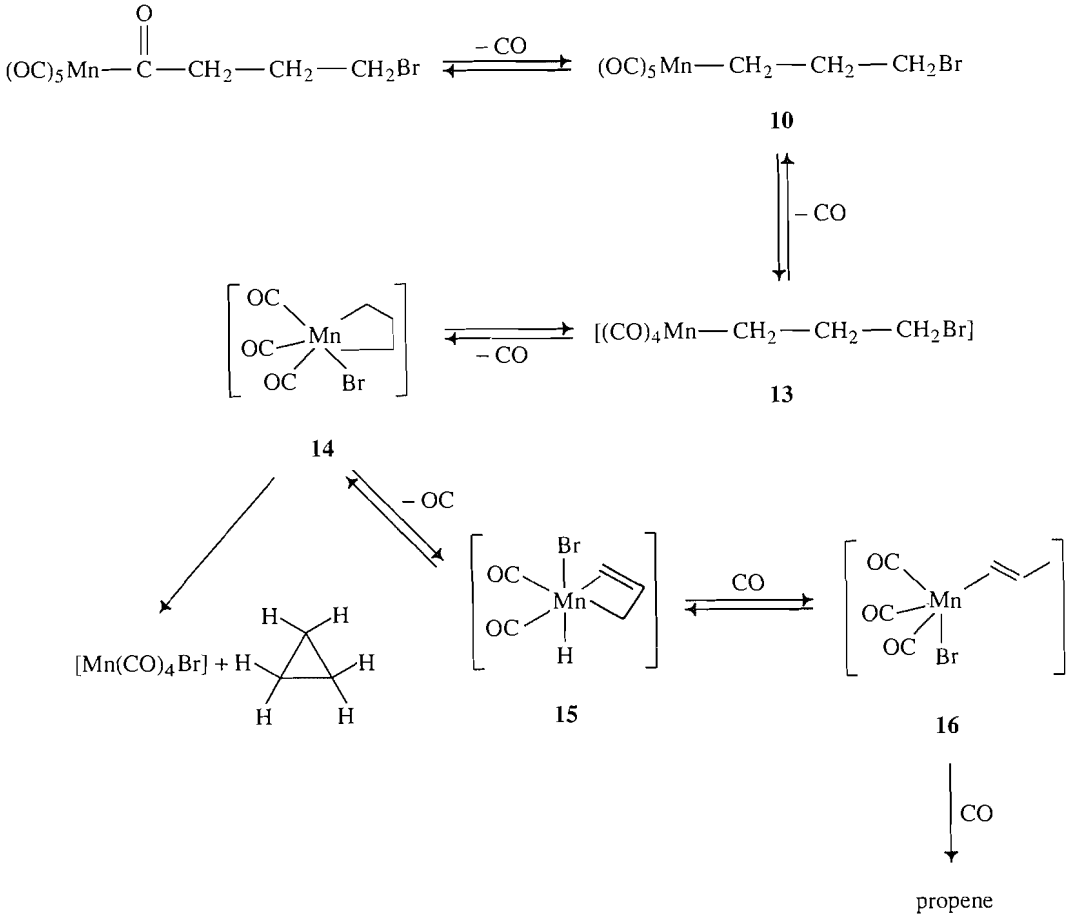

Can. J. Chem. Downloaded from www.nrcresearchpress.com by 91.144.44.67 on 09/07/12
For personal use only.

duction of the latter by the $Mn(CO)_4H$ ($Mn(CO)_5H$). However, in chloroform solution $Mn(CO)_5H$ might have also reduced the solvent (11), which was not observed. Furthermore, no evidence for $Mn(CO)_5H$ was seen in *in situ* ^{55}Mn NMR studies.

Another possibility might involve reversible rearrangement of **10** or **11** to the bromoalkylmanganese complex **17** (10), followed by the same fragmentation process described for the $n = 1$ case.

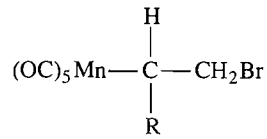

17 R = Me or Et

Conclusion

A ω-bromoacylmanganese pentacarbonyl complex **3** ($n = 0$) is not formed from $Mn(CO)_5^-$ and the bromoacyl halide. One can, however, form the 3-bromopropionyl complex **3** ($n = 1$). This complex is readily fragmented to ethylene in a relatively low temperature process involving the loss of both the bromine atom and the carbonyl group. ω-Bromoacylmanganese pentacarbonyl complexes **3** with $n = 2$ or 3 show no tendency to reductively eliminate a cycloalkanone (even though one sees decarbonylation on heating, the a priori possibility of this reaction was not ruled out in a sealed tube experiment). The $n = 2$ case produces some cyclopropane, perhaps from a metallocycle intermediate. However, the major thermolysis product in both cases is the 1-alkene.

Experimental

All procedures involving the preparation and reactions of $Mn(CO)_5^-$ were performed under an atmosphere of argon or nitrogen (purified by passing the gases through columns of silica gel and molecular sieves). A combination of syringe, transfer needle, and Schlenk techniques was used (12). The acyl complexes are much more air stable and were handled without using dry box or vacuum line techniques, although some non-rigorous inert gas protection was used as a precaution, particularly with **3** ($n = 2$). Infrared analysis was performed using a Perkin–Elmer 467 or a Nicolet 5DX FT instrument, using 0.1-mm liquid cells. NMR spectroscopy was performed on a Varian XL-200 instrument. For ^{55}Mn NMR (49.33 MHz), chemical shifts are reported with respect to potassium permanganate in D_2O. However, this reference is well outside the window (50 kHz) for the ^{55}Mn signal in the acyl complexes, and the "sharp" signal for a very small amount of $Mn_2(CO)_{10}$ was used as a secondary reference. The high receptivity of ^{55}Mn allows one to use ca. 0.1 M solutions of the acyl complexes. The ^{55}Mn chemical shift tabulations of Calderazzo *et al.* (13) were used as a guide in setting up the spectrometer offsets. Gas analysis was performed on a Carle gas chromatograph designed for gas sampling. All melting points are uncorrected. Flash chromatography was performed according to literature procedures (14) using 0.040–0.063 mm silica gel (E. Merck 9385) and methylene chloride (distilled from P_2O_5) as eluant (unless otherwise noted). THF was distilled from benzophenone ketyl under nitrogen or argon. $CDCl_3$ was dried over molecular sieve 3A powder (3–5 μM) prior to use.

The ω-bromoacyl chlorides were either commercially available or were prepared from the commercially available acid using thionyl chloride.

3-Bromopropanoylmanganese pentacarbonyl **3** (n = *1*)

Dimanganese decacarbonyl (0.20 g, 0.51 mmol) was reduced with 1% sodium amalgam in 10 mL THF. The solution was transferred by syringe to 0.18 g 3-bromopropanoyl chloride (1.05 mmol) in 2 mL THF and stirred for 30 minutes at room temperature, by which time a white precipitate had formed in the yellow solution. The solvent was then removed at reduced pressure and the oily residue extracted with two 10-mL aliquots of hexane, filtered, and the volume of the combined extracts reduced to ca. 10 mL. The product crystallized upon cooling to 0°C and after filtering and washing with cold hexane yielded 0.19 g white needles (57% yield), mp 57.5°C; Infrared (hexane, cm^{-1}): 2117(m), 2055(m), 2016(s), 1648(m); ^1H NMR ($CDCl_3$): 3.45 (m, $-CH_2CH_2-$) ppm; $\{^1H\}^{13}C$ NMR ($CDCl_3$): 25.8 ($-CH_2CO$), 67.5 ($-CH_2Br$), and 144 (CO) ppm; ^{55}Mn NMR (THF): −1830 ppm, $W_{1/2} = 6100$ Hz. Anal. calcd. for $C_8H_4BrMnO_6$: C 29.03, H 1.22%; found: C 27.58, H 1.41%.

4-Bromobutanoylmanganese pentacarbonyl **3** (n = *2*)

This complex was prepared in a similar way to 3-bromopropanoylmanganese pentacarbonyl. Thin-layer chromatography indicated that the yellow solid isolated was contaminated with manganese pentacarbonyl bromide. Flash chromatography (methylene chloride/silica) of the crude material, followed by recrystallization from hexane, gave pale yellow needles in 19% isolated yield, mp 55°C. The crude yield of product was considerably higher but purification of the somewhat fragile and atmosphere-sensitive product resulted in some loss of material. Infrared (methylene chloride, cm^{-1}): 2117(m), 2052(m), 2013(s), 1638(m); ^1H NMR ($CDCl_3$): 2.01 (dt, 2H), 3.12 (t, J = 6.7 Hz, 2H), 3.39 (t, J = 6.3 Hz, 2H); ^{55}Mn NMR (THF): −1874 ppm, $W_{1/2} = 7250$ Hz. Anal. calcd. for $C_9H_6BrMnO_6$: C 31.33, H 1.75%; found: C 31.45, H 1.81%.

5-Bromopentanoylmanganese pentacarbonyl **3** (n = *3*)

The procedure followed for the preparation of this compound was the same as that described for 3-bromopropanoylmanganese pentacarbonyl. White needles were isolated in 71% yield, mp 52.5°C; Infrared (hexane, cm^{-1}): 2115(m), 2052(m), 2009(s), 1659(m); ^1H NMR ($CDCl_3$): 1.5–1.9 (m, 4H), 2.96 (t, J = 6.7 Hz, 2H), 3.35 (t, J = 6.6 Hz, 2H); $\{^1H\}^{13}C$ NMR ($CDCl_3$): 23.2 ($-CH_2CO$), 31.9 ($-CH_2-$), 33.2 ($-CH_2-$), 65.9 ($-CH_2Br$), 143.9 (CO); ^{55}Mn NMR (THF): −1880 ppm, $W_{1/2} = 7300$ Hz. Anal. calcd. for $C_{10}H_8BrMnO_6$: C 33.45, H 2.25%; found: C 32.47, H 2.29%.

The thermal decomposition of 3-bromopropanoylmanganese pentacarbonyl **3** (n = *1*)

In 5-mm NMR tubes, 20 mg (0.06 mmol) 3-bromopropanoylmanganese pentacarbonyl **3** ($n = 1$) was dissolved in 0.5 mL deuterochloroform or 0.5 mL THF-d_8. The solutions were degassed by several freeze–thaw cycles and sealed under vacuum (0.1 Torr; 1 Torr = 133.2 Pa) and then placed in an oil bath at 75°C. The decomposition was followed by ^1H NMR (200 MHz), the tubes being inverted and centrifuged prior to running the spectrum. The only peak observed was a signal at δ 5.38 ppm (ethylene). When the decomposition was complete, the samples were opened while connected to a manifold, and the released gases analysed by GC.

The thermal decomposition of 4-bromobutanoylmanganese pentacarbonyl **3** (n = *2*)

This was carried out in a similar fashion to the experiment described for **3** ($n = 1$) using 5.0 mg (0.015 mmol) of acyl compound. In $CDCl_3$ after heating for 3 h at 75°C, the ^1H NMR spectrum showed only the alkyl complex **10**, δ 0.90, t (J = 8.0 Hz), 2H ($Mn-CH_2-$); 2.16, dt, 2H; 3.34, t (J = 7.5 Hz), 2H ($-CH_2Br$). Continued heating for 1 h at 125°C led to considerable decomposition, but ^1H peaks at 0.24 ppm (cyclopropane) and 1.72, d (J = 6.2 Hz), 3H; 4.95, d (J = 12) 1H; 5.05, d (J = 19) 1H; and 5.88, m, 1H (propene) accounted for 12 and 38% of the total proton integration. The reaction was cleaner in THF-d_8, giving propene and only a trace of cyclopropane.

The thermal decomposition of 5-bromobutanoylmanganese pentacarbonyl **3** (n = *3*)

This was carried out in a similar fashion to the experiment for **3** ($n = 1$), using 25 mg (0.070 mmol) of acyl compound. After heating for 3 h at 75°C in $CDCl_3$, ^1H NMR peaks were observed at δ: 0.97, t (J = 7.5), 2H ($Mn-CH_2$); 1.90 (m), 4H; 3.43, t (J = 6.5), 2H ($-CH_2Br$). On heating the solution to 120°C for 1 h, a reasonably clean (85%) spectrum of 1-butene was observed (also confirmed by GC gas analysis). An even cleaner spectrum of 1-butene was observed in THF-d_8 after heating the acyl complex for 4 h at 60°C.

Can. J. Chem. Downloaded from www.nrcresearchpress.com by 91.144.44.67 on 09/07/12
For personal use only.

2-Chloroacetylmanganese pentacarbonyl ***5***

This was prepared by a literature procedure (5) and purified by flash chromatography and recrystallization from hexane, mp 35°C; Infrared ($CDCl_3$): 2123(w), 2054(m), 2024(s), 1658(w); reported in heptane (5): 2117, 2055, 2014, 2007, 1654; ^1H NMR ($CDCl_3$) δ: 4.35(s); reported (5) 4.37.

The thermal decomposition of ***5***

In a 5-mm NMR tube, 10 mg of **5** was dissolved in 0.5 mL of $CDCl_3$ and the tube was sealed. After heating for 5 min at 70°C, about half of **5** had been converted to the alkyl complex **6** (^1H NMR, δ: 3.60, s; reported (15) 3.52. After heating for 30 min, little of **5** remained. However, new resonances at 3.0, 2.2, and 1.85 ppm had appeared in addition to the peak for **6** at 3.60 ppm.

Bromo carbene complex ***9***

This complex was formed in only very small yields, the 4% from heating the pure liquid acyl complex at 70°C being the highest. The complex **9** was isolated as an orange solid by flash chromatography of the melt material. The infrared and ^1H NMR data are reported in the Results section. The data reported for the corresponding iodo complex are quite similar (7), but the data for a dimeric carbene complex origi-
are quite similar (7), but the data for a dimeric carbene complex (16) are considerably different. The small quantities involved here did not allow for a confirmatory elemental analysis.

Acknowledgements

We thank the Natural Sciences and Engineering Research Council of Canada for generous financial support.

1. P. M. Tretichel. *In* Comprehensive organometallic chemistry. Vol. 4. *Edited by* G. Wilkinson, F. G. A. Stone, and E. W. Abel. Pergamon, New York. 1980.
2. A. Wojcicki. Adv. Organomet. Chem. **11**, 87 (1973).
3. T. Ziegler, L. Verlius, and V. Tschinke. J. Am. Chem. Soc. **108**, 612 (1986).
4. (*a*) A. P. Masters, T. S. Sorensen, and T. Ziegler. J. Org. Chem. **51**, 3558 (1986); (*b*) A. P. Masters, T. S. Sorensen, and P. M. Tran. Can. J. Chem. **65**, 1409 (1987); (*c*) A. P. Masters, T. S. Sorensen, and T. Ziegler. Organometallics, **8**, 1088 (1989).
5. (*a*) M. Dilgassa and M. D. Curtis. J. Organomet. Chem. **172**, 177 (1979); (*b*) F. Calderazzo, K. Noack, and U. Schaerer. J. Organomet. Chem. **6**, 265 (1966).
6. C. H. Game, M. Green, J. R. Moss, and F. G. A. Stone. J. Chem. Soc. Dalton Trans. 351 (1974).
7. D. Rehder, H. C. Bechthold, A. Kececi, H. Schmidt, and M. Siewing. Z. Naturforsch. B: Anorg. Chem. Org. Chem. **37B**, 631 (1982).
8. M. L. H. Green, A. G. Massey, J. T. Moelwyn-Hughes, and P. L. I. Nagy. J. Organomet. Chem. **8**, 511 (1967).
9. (*a*) J. Y. McDermott, J. F. White, and G. M. Whitesides. J. Am. Chem. Soc. **98**, 6521 (1976); (*b*) T. H. Johnson and S. Cheng. J. Am. Chem. Soc. **101**, 5277 (1979).
10. (*a*) C. P. Casey, C. R. Cyr, and J. A. Grant. Inorg. Chem. **13**, 910 (1974); (*b*) C. P. Casey, W. R. Brunsvold, and J. Koch. Inorg. Chem. **15**, 1991 (1976).
11. B. L. Booth and R. N. Haszeltine. J. Chem. Soc. (A), 157 (1966).
12. D. F. Shriver. The manipulation of air sensitive compounds. McGraw–Hill, New York. 1969.
13. F. Calderazzo, E. A. C. Lucken, and D. F. Williams. J. Chem. Soc. (A), 154 (1967).
14. K. A. M. Kremer and P. Helquist. Organometallics, **3**, 1743 (1984).
15. C. Botha, J. R. Moss, and S. Pelling. J. Organometal. Chem. **220**, C21 (1981).
16. R. B. King. J. Am. Chem. Soc. **85**, 1922 (1963); C. P. Casey and R. L. Anderson. J. Am. Chem. Soc. **93**, 3554 (1971).

Can. J. Chem. Downloaded from www.nrcresearchpress.com by 91.144.44.67 on 09/07/12
For personal use only.

2,2′-Bipyridyl adducts of tungsten oxide fluorides: preparation and characterization of WOF_4.bipy and WO_2F_2.bipy; crystal structure of WO_2F_2.bipy

LUCILE ARNAUDET, ROLAND BOUGON,[1] BUU BAN, PIERRETTE CHARPIN, JACQUES ISABEY, MONIQUE LANCE, MARTINE NIERLICH, AND JULIEN VIGNER

Département des Lasers et de la Physico-Chimie, Service de Chimie Moléculaire, Unité de Recherches Associée n° 331 – Centre National de la Recherche Scientifique, Commissariat à l'Energie Atomique Centre d'Etudes Nucléaires de Saclay, 91191 Gif sur Yvette Cédex, France

Received July 26, 1989

LUCILE ARNAUDET, ROLAND BOUGON, BUU BAN, PIERRETTE CHARPIN, JACQUES ISABEY, MONIQUE LANCE, MARTINE NIERLICH, and JULIEN VIGNER. Can. J. Chem. **68**, 507 (1990).

WOF_4.bipy was prepared from the reaction of WOF_4 with 2,2′-bipyridyl (bipy) in the melt or in solution in CH_2Cl_2 or CH_3CN.

The adduct, which is not moisture-sensitive at room temperature, was characterized by elemental analysis, X-ray powder data, and vibrational spectroscopy. WOF_4.bipy is almost insoluble in the usual organic solvents, and the species which were observed in CH_2Cl_2 or CH_3CN by ^1H NMR and Raman spectroscopy resulted from the dismutation of WOF_4.bipy into WO_2F_2.bipy and WF_6.bipy.

This transformation in solution was revealed by the slow growing of crystals identified as WO_2F_2.bipy and by the ^1H NMR spectrum which displayed lines assigned to the independently synthesized and characterized species WF_6.bipy. Unlike the WOF_4 adduct, the tungstyl adduct is moisture-sensitive, its crystal structure showed that the tungsten atom is surrounded by a very distorted octahedron of ligands with each nitrogen of the bipy ligand *trans* to one oxygen atom and the two fluorine atoms *trans* to each other. The space group, unit cell parameters, and R factor for $C_{10}H_8F_2N_2O_2W$ are as follows: monoclinic, $P2_{1/n}$ (No. 14) (alternate setting of the standard space group $P2_{1/c}$), $a = 8.637(1)$ Å, $b = 13.823(2)$ Å, $c = 9.526(2)$ Å, $\beta = 109.98(2)°$, $V = 1068.8(6)$ Å^3, $Z = 4$, and $R = 0.044$ for 806 ($I > 3\sigma(I)$) of 1471 total reflections and 94 parameters.

Key words: 2,2′-bipyridyl adducts, tungsten oxide tetrafluoride, tungsten dioxide difluoride.

LUCILE ARNAUDET, ROLAND BOUGON, BUU BAN, PIERRETTE CHARPIN, JACQUES ISABEY, MONIQUE LANCE, MARTINE NIERLICH et JULIEN VIGNER. Can. J. Chem. **68**, 507 (1990).

WOF_4.bipy a été préparé par réaction de WOF_4 avec le 2,2′-bipyridyl (bipy) à l'état fondu ou en solution dans CH_2Cl_2 ou CH_3CN.

L'adduit, qui n'est pas sensible à l'humidité à la température ambiante, a été caractérisé par analyse élémentaire, le diagramme de diffraction X de poudre et la spectroscopie vibrationnelle. WOF_4.bipy est presque insoluble dans les solvants organiques courants, et les espèces observées dans CH_2Cl_2 ou CH_3CN par RMN ^1H et spectroscopie Raman proviennent d'une dismutation de WOF_4.bipy en WO_2F_2.bipy et WF_6.bipy.

Cette transformation en solution est révélée par la croissance lente de cristaux identifiés comme étant WO_2F_2.bipy et par le spectre RMN ^1H qui indique la présence de raies attribuables à l'espèce WF_6.bipy synthétisée et caractérisée par ailleurs. Contrairement à l'adduit du WOF_4, le dérivé du tungstyle est sensible à l'humidité atmosphérique, la détermination de sa structure par diffraction des rayons X a montré que le tungstène s'y trouve entouré d'un octaèdre très déformé de ligands, chaque atome d'azote du ligand bipy est en position *trans* d'un atome d'oxygène, et les deux atomes de fluor sont en position *trans* l'un par rapport à l'autre. Le groupe d'espace, les paramètres de la maille élémentaire et le facteur R sont comme suit : $C_{10}H_8F_2N_2O_2W$, monoclinique, $P2_{1/n}$ (N° 14) (variante d'orientation du groupe d'espace standard $P2_{1/c}$), $a = 8{,}637(1)$ Å, $b = 13{,}823(2)$ Å, $c = 9{,}526(2)$ Å, $\beta = 109{,}98(2)°$, $V = 1068{,}8(6)$ Å^3, $Z = 4$, et $R = 0{,}044$ pour 806 ($I > 3\sigma(I)$) reflections sur un total de 1471 et 94 paramètres.

Mots clés : adduits du 2,2′-bipyridyl, oxytétrafluorure de tungstène, dioxydifluorure de tungstène.

Introduction

The ability of tungsten oxide tetrafluoride to form adducts with a nitrogen-base such as pyridine (py) has been recently (1) demonstrated. The stability of the adducts was found to be dependent on the coordination number of the tungsten atom. For instance, the adduct WOF_4.2py with a seven-fold coordination of the tungsten atom was found to decompose easily into the WOF_4.py adduct for which the coordination number of the tungsten atom is six. The effect of the coordination number and of the nature of the nitrogen-base on the stability and reactivity of the tungsten oxide tetrafluoride adducts has been further investigated using the bidentate molecular ligand 2,2′-bipyridyl (bipy).

Experimental

Apparatus

Volatile fluorides were manipulated in an all-metal vacuum line equipped with Teflon or metal valves. Other volatile materials were purified and transferred in a glass vacuum line designed to handle highly moisture-sensitive materials. Solid products were handled in glove boxes flushed with dry nitrogen. Infrared spectra were recorded in the range 4000–200 cm^{-1} on a Perkin-Elmer Model 283 spectrophotometer. Spectra of solids were obtained by using small crystals pressed between AgCl windows in an Econo press (Barnes Engineering Co), or ground and pressed in KBr pellets.

Raman spectra of the solutions contained in 5 mm o.d. NMR tubes, or of powders in 0.5 mm o.d. glass capillaries were recorded on a Coderg Model T 800 spectrophotometer using the 514.5 nm exciting line of an Ar ion Spectra Physics laser filtered with a Coderg premonochromator. Below 2000 cm^{-1}, the frequency accuracy was estimated to be approximately ±3 cm^{-1} for the infrared spectra, and ±1 cm^{-1} for the Raman spectra; above 2000 cm^{-1}, the accuracy was estimated to be twice these values. The ^{19}F and the ^1H NMR spectra of the solutions in standard tubes were obtained on a Varian NV 14 spectrometer and a Bruker WP spectrometer operating at 56.4 and 60 MHz, respectively. Samples were referenced externally with respect to $Si(CH_3)_4$ (^1H) and $CFCl_3$ (^{19}F). A positive chemical shift

[1]Author to whom correspondence may be addressed.

Printed in Canada / Imprimé au Canada

Can. J. Chem. Downloaded from www.nrcresearchpress.com by 91.144.44.67 on 09/07/12
For personal use only.

Can. J. Chem. Downloaded from www.nrcresearchpress.com by 91.144.44.67 on 09/07/12
For personal use only.

denotes a resonance occurring at high frequency of the reference compound. The chemical shift accuracy was estimated to be approximately ±0.05 ppm.

X-ray diffraction

X-ray powder diffraction patterns of the samples sealed in 0.3 mm o.d. glass capillaries were obtained by using a Phillips camera (diameter 11.46 cm) using Ni-filtered CuKα radiation. Crystals suitable for structural determination were selected in the dry box under a microscope and sealed inside 0.3 mm o.d. glass capillaries to protect them from the atmosphere. X-ray diffraction was carried out using an Enraf-Nonius CAD4 automated diffractometer. Cell dimensions were obtained by a least-squares refinement of the setting angles of 25 reflections with θ between 8 and 12°. Intensities were corrected for Lorentz polarization and absorption by using successively the empirical methods based on ψ-scans of top reflections (0.963 to 1) and DIFABS (2) (0.777 to 1.311). The structure was solved by the heavy-atom method and refined by full-matrix least squares (F) with W, F, and O atoms refined anisotropically. H atoms were included in the refinement at calculated positions: they were not refined but constrained to ride on their C atoms. All calculations were performed on a Micro VAX II computer with the Enraf-Nonius structure determination package (3). Analytical scattering factors for neutral atoms (4) were corrected for both $\Delta f'$ and $\Delta f''$ components of anomalous dispersion. Other experimental details appear with the crystal data in Table 3 and in the supplementary material.[2]

Materials

Tungsten oxide tetrafluoride was obtained by the literature (5) procedure and purified by sublimation *in vacuo* at ca. 50°C. Tungsten hexafluoride used for this preparation was obtained from Comurhex. 2,2′-Bipyridyl from Aldrich-Chemie was sublimed under vacuum at ca. 50°C; methylene chloride (Prolabo) was dried over Na–Pb alloy under reflux. Acetonitrile (Prolabo) was dried over P_2O_5 followed by treatment and storage on 5A molecular sieves. To avoid consumption of material, acetonitrile-d_3 was only treated with, and stored on, 5A molecular sieves. Microanalyses were carried out by Analytische Laboratorien, Elbach, West Germany.

Preparation of WOF_4.bipy and formation of WO_2F_2.bipy

To obtain single crystals for X-ray structure determination, several preparative methods were used. In a typical preparation, 0.1902 g (0.689 mmol) of WOF_4 in 10 cm^3 of dichloromethane was poured under vacuum onto a solution of 0.2152 g (1.378 mmol) of 2,2′-bipyridyl in 10 cm^3 of dichloromethane. The white crystalline powder that instantly precipitated was filtered off and washed under vacuum with dichloromethane to remove the excess of 2,2′-bipyridyl. The powder was finally pumped to dryness at room temperature. Other preparations were achieved using either 2,2′-bipyridyl in the melt, or in a solution in acetonitrile. For the latter either an excess of 2,2′-bipyridyl or the stoichiometric amount was used. All the solid products so prepared were found to have the same X-ray powder pattern. *Anal.* calcd. for $WOF_4.C_{10}H_8N_2$: W 42.55, F 17.59, C 27.80, H 1.87, N 6.48; found: W 42.30, F 17.47, C 27.63, H 1.83, N 6.40.

The attempts that were made to grow single crystals of WOF_4.bipy by very slow evaporation of the solvent from saturated solutions or drop to drop mixing of the reagents were not successful as far as the initial purpose was concerned. The few small colorless crystals which grew in CH_2Cl_2 or CH_3CN on standing over WOF_4.bipy for several days were identified as WO_2F_2.bipy from the X-ray single crystal study.

Results and discussion

Tungsten oxide tetrafluoride reacts with 2,2′-bipyridyl either in the melt or in solvents such as CH_3CN or CH_2Cl_2 to yield the adduct WOF_4.bipy. This adduct was found to be stable in the open air, and its X-ray powder pattern (Table 1) did not show signs of alteration after exposure of the solid to the atmospheric moisture for several days. When heated under vacuum in a sealed tube, WOF_4.bipy was found to decompose at 180°C and crystals of 2,2′-bipyridine sublimed onto the cold part of the tube.

TABLE 1. X-ray powder data for WOF_4.bipy[a]

d, Å	Intensity	*d*, Å	Intensity
6.80	m	2.882	w
6.28	m	2.748	vw
5.90	s	2.646	w,br
5.82	s	2.600	vvw
5.52	s	2.544	mw
4.40	m	2.526	mw
4.25	mw	2.434	w
4.13	m	2.415	w
3.90	vw	2.225	m
3.69	m,br	2.149	vw
3.411	m	2.102	vw
3.258	ms	2.070	mw
3.092	w		
3.025	w		

[a]s = strong, m = medium, w = weak, v = very, br = broad.

The adduct WO_2F_2.bipy has been reported (6) as being obtained from the reaction of $WOF_2(OC_2H_5)_2$, 2,2′-bipyridyl, and HF in ethanol solution. Some properties including some of the vibrational data and an X-ray diffraction pattern were also given (6) but no structural determination was presented. This tungstyl adduct was obtained from dismutation of WOF_4.bipy during the work reported here and its crystal structure was determined. The circumstances of its formation are discussed in the last part of this section.

Vibrational spectra

The frequencies observed for the infrared and Raman spectra of the solid adducts WOF_4.bipy and WO_2F_2.bipy and for free bipy are summarized in Table 2. These data show that the formation of the adducts leads to a significant change from the spectra of the free ligand. Comparable changes, observed in the infrared absorption spectra of adducts having 2,2′-bipyridyl as ligand, have already been described and discussed. Due to the abundant literature regarding the complexes of bipy, only illustrative references are quoted here (7–30). The interpretation of the spectra given by the authors was based on those published for bipy and other heteroaromatic compounds (7, 28–30). The bands in the range 3150–3050 cm^{-1} have been assigned to the C—H stretches, in the range 1650–1300 cm^{-1} to C—C and C—N stretches of the ring and the deformations of the C—C—H angles, in the range 1250–1000 cm^{-1} to the in-plane deformations of the C—H bonds, in the range 1030–990 cm^{-1} to the breathing vibrations of the ring, in the range 980–700 cm^{-1} to the out-of-plane deformations of the C—H bonds, in the range 650–600 cm^{-1} to the in-plane ring bending, and in the range 750–400 cm^{-1} to the out-of-plane deformations of the ring.

A striking feature brought about by the donor–acceptor interaction is the shift of the breathing vibration (11) of the ring, observed at 995 cm^{-1} in the Raman spectrum of the free ligand versus 1027 and 1028 cm^{-1} for WOF_4.bipy and WO_2F_2.bipy, respectively. Also characteristic of the coordination of the

[2]A complete set of material may be purchased from the Depository of Unpublished Data, CISTI, National Research Council of Canada, Ottawa, Ont., Canada K1A 0S2.

Can. J. Chem. Downloaded from www.nrcresearchpress.com by 91.144.44.67 on 09/07/12
For personal use only.

TABLE 2. Vibrational data[a] for WOF_4.bipy and WO_2F_2.bipy; comparison with those of 2,2′-bipyridyl (bipy)

Infrared			Raman[b]			Infrared			Raman[b]		
bipy	WOF_4.bipy	WO_2F_2.bipy	bipy	WOF_4.bipy	WO_2F_2.bipy[c]	bipy	WOF_4.bipy	WO_2F_2.bipy	bipy	WOF_4.bipy	WO_2F_2.bipy[c]
	3150mw		3140(1)				1122mw				1120(5)
	3115m	3110m	3116(1)				1106mw	1100sh	1091(3)		
3090mw		3090m	3082(3)	3088(2)		1090ms	1082m	1080s			
			3073(7)			1065m					1061(3)
3060mw		3060m	3064(11)			1043ms	1046w	1045vw	1043(15)		
			3045(6)				1033m	1032ms		1027(35)	1028(100)
		3020mw	3028(2)				1016m	1017w			
3010w			3006(3)			996m	987mw		995(97)		
	2930w					975sh	968ms	960s		965(11)	958(50)
2295w							923ms	915s			918(10)
1990w		2010w				895m	900mw	905sh			
1965mw							795w	795sh	813(15)	795(2)	
1895mw						755vs	775s	767s	763(5)	775(2)	769(20)
1870mw		1875w				740m	735w	740vw			
1803mw							725ms	733ms		725(2)	
1715mw						652ms	657mw	650ms		657(4)	660(5)
1695mw							645vw				
1665mw			1673(2)				633s	635mw			
					1640(2)	616ms			612(25)	622(8)	
			1628(2)		1630(2)		580s	575s			
	1610ms	1610sh	1612(3)		1615sh		527s				
		1600s	1587(100)	1605(100)	1597(100)			508mw			
1580s	1573ms	1570m	1572(80)				494ms	495vw			
1557ms				1566(29)	1562(39)	462w					
1529vw		1530w					453m	450ms			
						422w	422s		437(3)		
	1510mw			1507(33)				410mw			
1503w	1500	1495m		1497(7)	1493(68)	396s		390mw			
	1480ms	1473ms	1480(41)				365s	363ms			368(10)
1453s	1462w						350w	350sh			342(3)
	1440s	1445s	1440(72)	1440(2)			330w				330(2)
1417s		1420sh		1427(4)	1426(5)		307mw			310(2)	300(5)
1397sh							285mw	290ms			
					1380(3)					265(2)	
				1332(70)							254(26)
	1323s	1320ms		1317(7)	1318(63)					240(2)	
		1313			1312(63)				222(25)		220(3)
1306w	1300w		1300(43)							205(6)	
1270w			1290sh	1275(4)	1265(3)					190(3)	180(2)
1253ms	1243s	1245ms									165(2)
	1230s	1220w	1235(48)							133(17)	140(2)
1215mw	1205w		1216(12)								
1170w	1173mw	1173sh									
1142m	1153m	1155m	1145(2)		1148(5)						

[a]Frequencies in cm^{-1}. Abbreviations used: sh, shoulder; br, broad; v, very; s, strong; m, medium; w, weak.
[b]Uncorrected Raman intensities based on relative peak heights are given in parentheses.
[c]Due to the high noise level of this spectrum, the lines expected around 3090 cm^{-1} could not be observed, and the relative intensities of the weak lines are only approximate.

Can. J. Chem. Downloaded from www.nrcresearchpress.com by 91.144.44.67 on 09/07/12
For personal use only.

TABLE 3. Crystallographic data for $WO_2F_2.bipy$

Parameter	Value	Parameter	Value
Formula	$WO_2F_2.C_{10}H_8N_2$	Formula weight	410.03
a, Å	8.637(1)	Space group $P2_1/n$	(No. 14)
b, Å	13.823(2)	T_K	295
c, Å	9.526(2)	λ, Å	0.71073
β, deg	109.98(2)	ρ_{calcd}, g cm^{-3}	2.548(2)
V, Å^3	1068.8(6)	μ, cm^{-1}	110.59
Z	4	Absorption correction	
		min–max	0.777–1.311
		R(F)	0.044
		R_w(F)	0.055

TABLE 4. Positional parameters and their estimated standard deviations for $WO_2F_2.bipy$

Atom	x	y	z	B, Å^2
W	0.2778(1)	0.3632(1)	0.2897(1)	3.51(2)*
F(1)	0.2016(14)	0.2385(10)	0.2851(14)	3.3(3)*
F(2)	0.2736(15)	0.4958(9)	0.3173(11)	3.5(3)*
O(1)	0.4734(16)	0.3418(15)	0.3954(16)	4.0(4)*
O(2)	0.2683(17)	0.3652(14)	0.1124(14)	3.6(3)*
N(1)	0.2056(16)	0.3662(13)	0.4979(14)	1.4(3)
N(2)	−0.0025(18)	0.3887(12)	0.2223(17)	1.8(3)
C(1)	0.0489(20)	0.3714(16)	0.4853(18)	1.5(3)
C(2)	−0.0002(24)	0.3609(20)	0.6062(21)	2.8(4)
C(3)	0.1211(30)	0.3466(21)	0.7437(29)	4.5(6)
C(4)	0.2773(29)	0.3411(17)	0.7572(25)	3.6(5)
C(5)	0.3191(25)	0.3510(18)	0.6344(22)	2.8(4)
C(6)	−0.0666(21)	0.3889(13)	0.3297(20)	1.4(4)
C(7)	−0.2339(24)	0.4016(14)	0.3001(21)	2.1(4)
C(8)	−0.3328(29)	0.4154(19)	0.1520(25)	3.6(5)
C(9)	−0.2613(26)	0.4133(18)	0.0420(25)	3.2(5)
C(10)	−0.0951(27)	0.4045(18)	0.0828(25)	3.3(5)

[a] Values with asterisks denote anisotropically refined atoms for which $B_{equiv} = (4/3)\Sigma_{ij}\beta_{ij}\boldsymbol{a}_i\boldsymbol{a}_j$.

TABLE 5. Selected bond lengths (Å) and angles (deg) for $WO_2F_2.bipy$

Bond	Length	Bond	Length
W—F(1)	1.840(6)	N(1)—C(1)	1.32(1)
W—F(2)	1.854(6)	N(1)—C(5)	1.35(1)
W—O(1)	1.671(7)	N(2)—C(6)	1.32(1)
W—O(2)	1.663(6)	N(2)—C(10)	1.31(1)
W—N(1)	2.274(6)	C(1)—C(6)	1.50(1)
W—N(2)	2.310(7)		
		C—C(cycle)	1.37(2)

Bonds	Angle	Bonds	Angle
F(1)—W—F(2)	154.8(3)	O(1)—W—O(2)	107.7(3)
F(1)—W—O(1)	97.3(3)	O(1)—W—N(1)	90.0(3)
F(1)—W—O(2)	95.7(4)	O(2)—W—N(2)	91.9(3)
F(1)—W—N(1)	80.5(3)	N(1)—W—N(2)	70.5(2)
F(1)—W—N(2)	78.7(3)		
F(2)—W—O(1)	98.9(4)	C(1)—N(1)—C(5)	118.8(7)
F(2)—W—O(2)	97.5(4)	C(6)—N(2)—C(10)	120.9(8)
F(2)—W—N(1)	80.4(3)		
F(2)—W—N(2)	79.6(2)	C—C—C(cycle)	119.8(1)
		N(1)—C(1)—C(6)	114.5(7)
		N(2)—C(6)—C(1)	117.0(7)

ligand is the appearance (7, 11, 22) in the infrared spectrum of molecular adducts of bipy of a strong band in the range 1310–1319 cm^{-1}. This band was reported to be missing in the infrared spectrum of free bipy. In line with these observations, the present study showed that strong new infrared bands appeared at 1323 cm^{-1} and 1313–1320 cm^{-1} for $WOF_4.bipy$ and $WO_2F_2.bipy$, respectively, and that these bands corresponded to the strong Raman bands found at 1300 cm^{-1} for free bipy, at 1332 cm^{-1} for $WOF_4.bipy$, and at 1312–1318 cm^{-1} for $WO_2F_2.bipy$. The very weak infrared band found at 1306 cm^{-1} for free bipy probably corresponds to the same vibration. As a whole, the bands due to the ring stretches and the deformations of the C—C—H angles as well as those of the C—H stretches are shifted to higher frequencies in the spectra of the adducts. Judged from the massif of infrared bands in the range 3150–3050 cm^{-1}, the positive shift of the C—H stretching frequencies was found to be more pronounced for $WOF_4.bipy$ than for $WO_2F_2.bipy$. The transfer of electronic density from the nitrogen lone-pair to the tungsten atom may account for the positive shifts of the frequencies of the ligand bipy.

Due to the numerous bands of bipy, the vibrations associated with the W, F, or O atoms are somewhat difficult to assign. However, a comparison with the infrared spectra of similar adducts of bipy (6, 19, 20, 21, 23, 25) made it possible to propose the following assignments for $WOF_4.bipy$: W—F

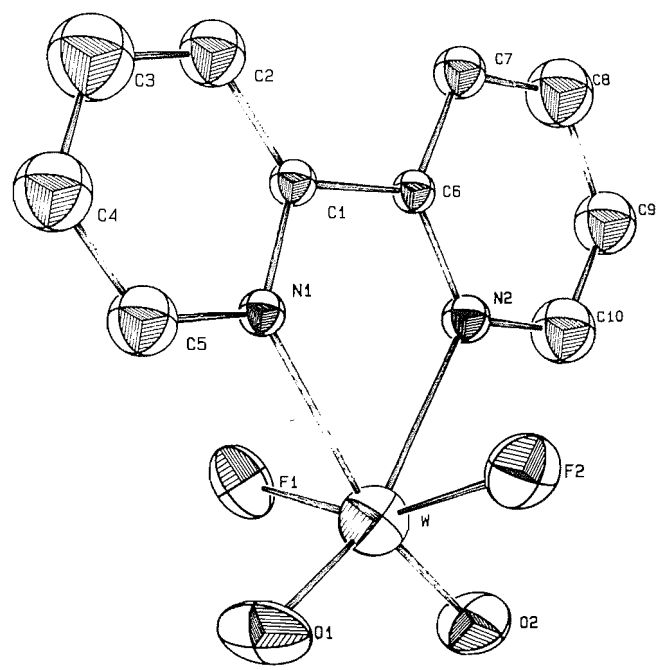

FIG. 1. ORTEP drawing of the molecular unit $WO_2F_2.bipy$ with the hydrogen atoms omitted.

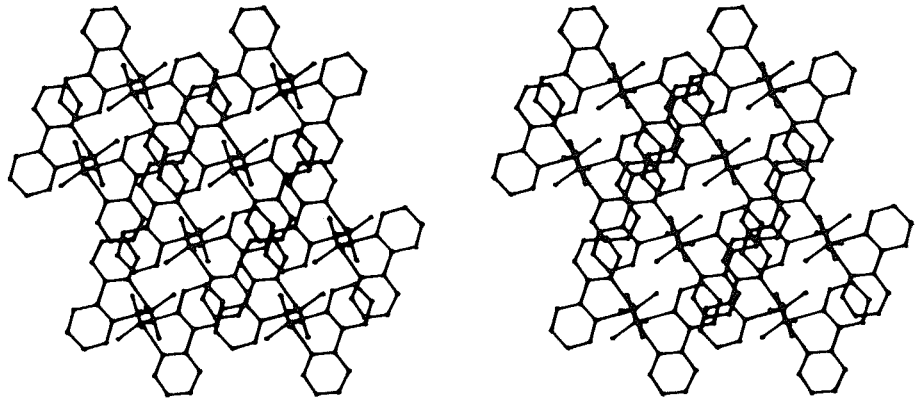

FIG. 2. Stereoscopic view of the molecular packing of WO_2F_2.bipy.

TABLE 6. ^1H NMR data[a] for a solution obtained by saturation[b] of acetonitrile with WOF_4.bipy; comparison with those for bipy or WF_6.bipy in acetonitrile

	Chemical shifts[c]				Coupling constants[c]					
	δ_3	δ_4	δ_5	δ_6	J_{34}	J_{35}	J_{36}	J_{45}	J_{46}	J_{56}
bipy	8.48	7.94	7.42	8.71	7.81	1.23	0.98	7.53	1.79	4.87
WF_6.bipy[d]	8.5	8.4	7.9	8.85	8	5.3	1.2	3.4	1.2	5.3
WO_2F_2.bipy[e]	8.88	8.5	8	9.41	5.2	1.3	1.3	3.7	1.5	5.1

[a]Chemical shifts δ in ppm from TMS, and coupling constant J in Hz at 303 K obtained from a first-order approximation analysis (33) of the spectra.

[b]Saturation obtained by stirring WOF_4.bipy with CH_3CN at room temperature and filtration of the excess of solid.

[c]Subscripts 3, 4, 5, 6 refer to hydrogen atom positions with 6, 5, 4 indicating ortho, meta, and para position to the nitrogen atom respectively.

[d]Data obtained for a solution of WF_6.bipy synthesized (34) by reaction of WF_6 with bipy in acetonitrile (ABXY-type spectrum).

[e]Data (ABXY-type spectrum) for the solution of WOF_4.bipy in acetonitrile after removal of the lines assigned to WF_6.bipy (see text).

vibrations at 494 cm^{-1}, 527 cm^{-1}, 580 cm^{-1}, and 638 cm^{-1} (IR); W—O vibration at 968 cm^{-1} (IR) (965 cm^{-1} (R)), and for WO_2F_2.bipy: W—F vibration at 495 cm^{-1}, 508 cm^{-1}, 575 cm^{-1}, and 635 cm^{-1}; tungsten–oxygen vibrations at 918 cm^{-1}, 958 cm^{-1} (R), (915 cm^{-1}, 960 cm^{-1} (IR)). The infrared bands previously reported by Buslaev *et al.* (6) for WO_2F_2.bipy were at 925 cm^{-1} and 976 cm^{-1} for the W—O vibrations and at 596 cm^{-1} for the strongest W—F vibration.

Crystal structure of WO_2F_2.bipy

The molecular stereochemistry of the adduct WO_2F_2.bipy was established by a single-crystal study. Crystal data are given in Table 3. Final positional and thermal parameters with their estimated standard deviations are given in Table 4. The relevant distances and angles are given in Table 5. Figure 1 shows the molecular unit and atomic labeling scheme, and Fig. 2 gives a stereoscopic view of the molecular packing.

The coordination polyhedron of the tungsten atom is a very distorted octahedron with each nitrogen of the bipy ligand *trans* to one oxygen atom. The F(1)—W—F(2) axis is strongly bent (154.8°) due to the steric effect of the tungsten oxygen double bond, while the angle O(1)—W—O(2) in the equatorial plane is very much larger (107.7°) than the angle N(1)—W—N(2) (70.5°). Because of the significant difference in the two sets of bond lengths and based on the usual (1, 31) relative lengths of the bonds W—O(terminal) and W—F(terminal), the sets with mean bond distances of 1.667 Å and 1.847 Å are unambiguously attributed to the W—O and W—F bonds, respectively.

Solution studies

From the ^1H and ^{19}F NMR signal intensities, it would appear that the solubility of the adduct WOF_4.bipy in the usual organic solvents is very low. In fact, no ^{19}F NMR signals could be observed with the CW type instrument which was used. However, use of an FT instrument allowed ^1H NMR spectra to be observed for proton signals of saturated solutions of WOF_4.bipy in CH_3CN or CH_2Cl_2. The signals of the bipyridyl ligand were found to be shifted downfield from those of the free ligand in the same solvent by an average of 0.55 ppm, and to be temperature independent in the range 303–243 K. The peaks observed for a solution in CH_3CN are listed in Table 6. The Raman spectra of these solutions also displayed lines shifted from those of the free ligand. One of them, observed at 1315 cm^{-1}, was more in correspondence with that observed at 1312–1318 cm^{-1} for WO_2F_2.bipy in the solid than that of WOF_4.bipy observed at 1332 cm^{-1} in the solid. Since the lines of the free ligand were found to be not significantly shifted from the solid to the solutions, it is inferred that the ^1H NMR and Raman signals observed for the solutions are those of the ligand bound to WO_2F_2 rather than to WOF_4. The growing of crystals of WO_2F_2.bipy from these solutions gives further support to this conclusion. The assumption by which a slow hydrolysis of WOF_4.bipy is taking place would be an obvious explanation for the formation of the WO_2F_2 adduct. However, as mentioned above, WOF_4.bipy is not moisture-sensitive in the solid, and according to the study performed by Il'in *et al.* (32), the hydrolysis of WOF_4 in acetonitrile requires more than traces of

Can. J. Chem. Downloaded from www.nrcresearchpress.com by 91.144.44.67 on 09/07/12
For personal use only.

water to yield species containing the tungstyl group. The use of dry materials as well as sealed tubes does not favor the assumption of an accidental hydrolysis. As an alternate mechanism, a solvent-assisted dismutation of WOF_4.bipy yielding WO_2F_2.bipy and WF_6.bipy was considered. The direct synthesis (34) of WF_6.bipy which was achieved gave support to this assumption as the lines of this species were found together with those of WO_2F_2.bipy in the ^1H NMR spectrum of the solution of WOF_4.bipy.

Conclusion

Tungsten oxide tetrafluoride forms a one-to-one molecular adduct with the bidentate ligand 2,2′-bipyridyl. Owing to the negligible solubility of this adduct in the usual organic solvents, and to its low vapor pressure below its decomposition temperature, the crystal structure of WOF_4.bipy could not be obtained. However, the structure of the corresponding tungstyl adduct which was formed from slow solvent assisted dismutation of the WOF_4 adduct was determined. One driving force for this dismutation to occur might be the lowering in the coordination number of the tungsten atom from seven in WOF_4.bipy to six in WO_2F_2.bipy. Such a stabilization through reduction of the coordination number has already been observed (1) for the adduct of WOF_4 with the monodentate ligand pyridine. However, this effect is probably limited to the oxide fluoride derivatives since the coordination number of the tungsten atom in WF_6.bipy must be at least eight. The absence of short ligand–tungsten bonds probably accounts for the higher coordination number in this adduct.

1. L. Arnaudet, R. Bougon, Buu Ban, P. Charpin, J. Isabey, M. Lance, M. Nierlich, and J. Vigner. Inorg. Chem. **28**, 257 (1989).
2. N. Walker and D. Stuart. Acta Crystallogr. A**39**, 158 (1983).
3. B. A. Frenz. SDP users guide (Version of Jan. 6, 1983). Enraf-Nonius: Delft, The Netherlands. 1983.
4. International tables for X-ray crystallography. Vol. IV. Kynoch, Birmingham, England. 1974.
5. W. W. Wilson and K. O. Christe. Inorg. Synth. **24**, 37 (1986).
6. Yu. A. Buslaev, Yu. V. Kokunov, and V. A. Bochkareva. Russ. J. Inorg. Chem. (*Engl. Transl.*) **20**, 495 (1975).
7. A. A. Shilt and R. C. Taylor. J. Inorg. Nucl. Chem. **9**, 211 (1959).
8. B. Martin, W. R. McWhinnie, and G. M. Waind. J. Inorg. Nucl. Chem. **23**, 207 (1961).
9. R. G. Inskeep. J. Inorg. Nucl. Chem. **24**, 763 (1962).
10. M. Allbutt, K. Feenan, and G. W. A. Fowles. J. Less-Common Metals, **6**, 299 (1964).
11. S. P. Shinha. Spectrochim. Acta, **20**, 879 (1964).
12. A. D. Adley, P. H. Bird, A. R. Fraser, and M. Onyszchuk. Inorg. Chem. **11**, 1402 (1972).
13. W. R. McWhinnie. J. Inorg. Nucl. Chem. **26**, 15 (1964).
14. R. J. H. Clark and C. S. Williams. Spectrochim. Acta, **21**, 1861 (1965).
15. J. R. Ferraro, L. J. Basile, and D. L. Kovacic. Inorg. Chem. **5**, 391 (1966).
16. G. C. Kulasingam, W. R. McWhinnie, and R. R. Thomas. Spectrochim. Acta, **22**, 1365 (1966).
17. J. R. Ferraro and W. R. Walker. Inorg. Chem. **4**, 1382 (1965).
18. G. W. A. Fowles, D. J. Tidmarsh, and R. A. Walton. J. Chem. Soc. A, 1546 (1969).
19. R. Kergoat and J. E. Guerchais. Bull. Soc. Chim. Fr. **8/9**, 2932 (1970).
20. C. Djordjevic and V. Katovic. J. Chem. Soc. A, 3382 (1970).
21. R. Kergoat and J. E. Guerchais. Bull. Soc. Chim. Fr. **2**, 494 (1973).
22. L. M. Mikheeva, A. I. Grigor'ev, and A. I. Tarasova. Russ. J. Inorg. Chem. (*Engl. Transl.*), **19**, 1277 (1974).
23. J. Y. Calves, J. Sala-Pala, J. E. Guerchais, A. J. Edwards, and D. R. Slim. Bull. Soc. Chim. Fr. **3/4**, 517 (1975).
24. Yu. A. Buslaev, Yu. V. Kokunov, and V. A. Bochkareva. Russ. J. Inorg. Chem. (*Engl. Transl.*), **20**, 495 (1975).
25. M. E. Ignatov, D. B. Grebeshkov, and E. G. Il'in. Russ. J. Inorg. Chem. (*Engl. Transl.*), **28**, 345 (1983).
26. L. V. Ostapchuk, L. A. Gavrilova, V. O. Gel'mbol'dt, and A. A. Ennan. Russ. J. Inorg. Chem. (*Engl. Transl.*), **33**, 813 (1988).
27. J. S. Strukl and J. L. Walter. Spectrochim. Acta, **27A**, 223 (1971).
28. A. R. Katritzky. Q. Rev. Chem. Soc. **13**, 353 (1959).
29. J. S. Strukl and J. L. Walter. Spectrochim. Acta, **27A**, 209 (1971).
30. A. I. Popov, J. C. Marshall, F. B. Stute, and W. B. Person. J. Am. Chem. Soc. **83**, 3586 (1961).
31. P. A. Tucker, P. A. Taylor, J. H. Holloway, and D. R. Russell. Acta Crystallogr. Sect. B, **31**, 906 (1975).
32. E. G. Il'in, B. V. Golovanov, M. E. Ignatov, V. D. Butskii, and Yu. Buslaev. Dokl. Akad. Nauk SSSR, **289**, 624 (1986).
33. F. A. Jr. Kramer and R. West. J. Phys. Chem. **69**, 673 (1965).
34. L. Arnaudet, R. Bougon, Buu Ban, J. Isabey, M. Lance, and M. Nierlich. Unpublished results.

Can. J. Chem. Downloaded from www.nrcresearchpress.com by 91.144.44.67 on 09/07/12
For personal use only.

Repulsive *gauche* conformational effect. Analysis of seven-membered rings containing *endo* and *exo* sulfur atoms

P. DIONNE AND M. ST-JACQUES[1]

Département de chimie, Université de Montréal, C.P. 6128, Succ. A, Montréal (Québec), Canada H3C 3J7

Received September 21, 1989

P. DIONNE and M. ST-JACQUES. Can. J. Chem. **68**, 513 (1990).

The so-called repulsive *gauche* conformational effect associated with sulfur is investigated through a study of 3-methylthio-1,5-benzodioxepin (**1**) and 3-methylthio-1-benzoxepin (**2**), together with 3-fluoro- and 3-chloro-1,5-benzodithiepins (**3** and **4**), by ^{13}C and ^{1}H dynamic nuclear magnetic resonance methods. The results show that, while compounds **2**, **3**, and **4** exhibit a large amount of the C_e conformation, the *TB* form predominates for compound **1**. Intramolecular stereoelectronic $\sigma-\sigma^*$ orbital interactions are analyzed, together with several other factors (steric, electrostatic, and solvation), to explain the observed conformational behaviour.

Key words: *gauche* effect, seven-membered rings, 1,5-benzodithiepins, variable temperature NMR, orbital interactions.

P. DIONNE et M. ST-JACQUES. Can. J. Chem. **68**, 513 (1990).

On a étudié l'effet conformationnel *gauche* répulsif associé à l'atome de soufre en examinant la 3-méthylthio-1,5-benzodioxépine (**1**), la 3-méthylthio-1-benzoxépine (**2**) ainsi que les 3-fluoro- et 3-chloro-1,5-benzodithiépines (**3** et **4**), par des méthodes de résonance magnétique nucléaire dynamique du ^{13}C et du ^{1}H. Les résultats démontrent que, alors que l'on détecte la présence de quantités importantes de la conformation C_e dans les composés **2**, **3** et **4**, la forme *TB* prédomine pour le composé **1**. On a analysé les interactions stéréoélectroniques intramoléculaires des orbitales $\sigma-\sigma^*$ ainsi que plusieurs autres facteurs (stérique, électrostatique et de solvatation) afin de pouvoir expliquer le comportement conformationnel observé.

Mots clés : effet *gauche*, cycles à sept chaînons, 1,5-benzodithiépines, RMN à température variable, interactions orbitales.

[Traduit par la revue]

Introduction

Over the last few years, we have been interested in the mechanism of the *gauche* effect (1) and the underlying molecular interactions as revealed by the conformational analysis of some 3-substituted 1,5-benzodioxepins (2, 3) and 1-benzoxepins (4, 5). These results have shown that the seven-membered heterocycles can provide information complementary to analogous six-membered molecules because of the greater ring flexibility, giving rise to the twist boat (*TB*) form in addition to the axial chair (C_a) and the equatorial chair (C_e) conformations. Such studies unravelled the nature of the molecular orbital interaction involved. According to the rationalizations formulated earlier by Zefirov *et al.* (6) from studies of six-membered ring molecules, the conformational feature of the oxygen-containing seven-membered rings studied (2–5) was characteristic of attractive or negligible *gauche* effects. Our present aim is to analyze the repulsive *gauche* effect (6, 7) through the conformational study of seven-membered rings containing *endo* and *exo* sulfur atoms interacting with other heteroatoms such as in the series **1**–**6**.

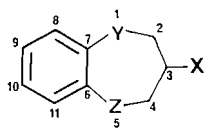

1 Y = Z = O ; X = SCH_3

2 Y = O ; Z = CH_2 ; X = SCH_3

3 Y = Z = S ; X = F

4 Y = Z = S ; X = Cl

5 Y = Z = S ; X = OCH_3

6 Y = O ; Z = CH_2 ; X = OCH_3

[1]Author to whom correspondence may be addressed.

We therefore report the high-field variable temperature ^{13}C nmr spectral analyses of 3-methylthio-1,5-benzodioxepin (**1**), 3-methylthio-1-benzoxepin (**2**), 3-fluoro-1,5-benzodithiepin (**3**), and 3-chloro-1,5-benzodithiepin (**4**). The data are completed with 3-methoxy-1,5-benzodithiepin (**5**), reported earlier by Ménard and St-Jacques (8), 3-methoxy-1-benzoxepin (**6**) from the work of Lachapelle and St-Jacques (4), and the trends observed are discussed in the framework of a theoretical model for the *gauche* effect (9, 10).

Results and spectral analyses

The high-field ^{13}C nmr spectra of compounds **1**–**4** were obtained at temperatures varying between 0 and −135°C. The solvents used were CHF_2Cl (more polar solvent) and CH_3OCH_3 (less polar solvent), both containing some CD_2Cl_2 for nmr locking purposes.

Figure 1 shows the 100.62 MHz ^{13}C spectral modifications observed in CHF_2Cl at low temperature for compound **1**. Each carbon signal has been assigned using as reference published chemical shifts obtained for the 1,5-benzodioxepin family (3). The aromatic C-6,7 carbons, being quite remote from the site of substitution, give signals characteristic of the nature of the ring conformation (*C* or *TB*) adopted. Thus, the most deshielded C-6,7 signal corresponds to the *C* form while the upfield signal is characteristic of the *TB* form (3). In contrast, the C-3 carbon provides information on the axial–equatorial nature of the *C* forms (C_a or C_e). For example, it is found that the C-3 signal of the C_a form is more deshielded than that of the *TB* and C_e forms, while the signal of the C_e form is the most shielded of the three conformations (3). The above information, and the unequal intensity of the signals corresponding to each of the three forms at −135°C, allows complete assignment of the other chemical shifts as given in Table 1.

In the less polar CH_3OCH_3 solvent, the ^{13}C nmr spectrum of compound **1** at −135°C shows only two lines, indicating a

Can. J. Chem. Downloaded from www.nrcresearchpress.com by 91.144.44.67 on 09/07/12
For personal use only.

Can. J. Chem. Downloaded from www.nrcresearchpress.com by 91.144.44.67 on 09/07/12
For personal use only.

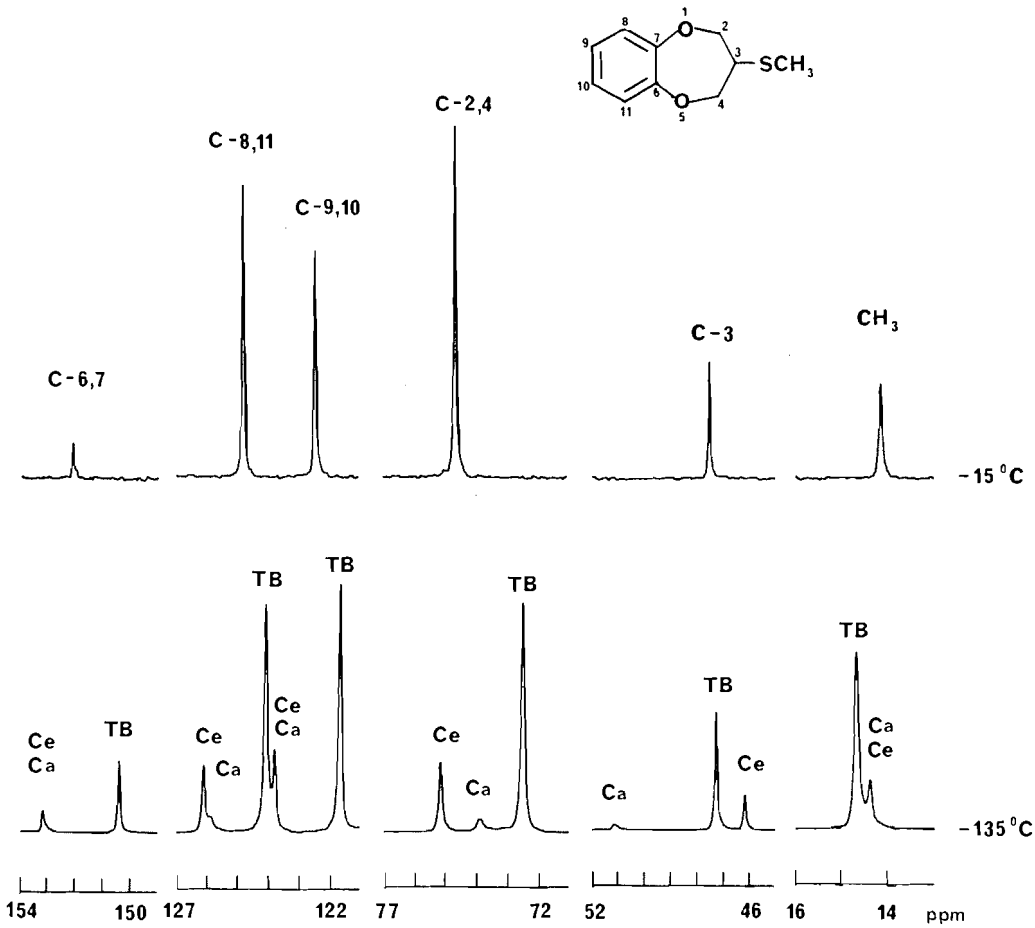

FIG. 1. 100.62 MHz ^{13}C spectra of **1** in CHF_2Cl at −15°C and −135°C (C_e = equatorial chair, C_a = axial chair, and *TB* = twist boat).

C_e:*TB* population ratio of 36:64. Indeed, in the C-3 region, the signal corresponding to the chair form at 46.17 ppm identifies the C_e conformation (46.14 ppm in CHF_2Cl). However, the signal of the *TB* form located at 47.22 ppm in CHF_2Cl has shifted to 45.44 ppm in CH_3OCH_3, corresponding to a shielding of 1.78 ppm. The solvent change also affects the chemical shifts of the CH_3 signals for the two forms, C_e (shielding of 1.15 ppm) and *TB* (shielding of 1.65 ppm) as shown in Table 1.

Figure 2 illustrates the 100.62 MHz ^{13}C nmr spectral modifications observed at low temperature for compound **2** in CHF_2Cl. At −20°C, all signals have been assigned, using the results from the $^1H/^{13}C$ Heteronuclear shift Correlation experiment (HC COSY) (11), carried out at room temperature in $CDCl_3$, in order to distinguish between the C-4 and C-5 carbons whose signals are too close to be assigned with confidence by the above method. All pertinent data are reported in Table 1.

At −120°C, several carbon signals have split into two lines of intensity ratio 9:91. Based on earlier results for the 1-benzoxepin family (4, 5), the two close signals, found in the C-6 region at 137.33 and 136.88 ppm, indicate the presence of two chair forms. Indeed, the nmr spectrum of 3-methoxy-1-benzoxepin (**6**) (4) at −125°C revealed that the C-6 signal of the *TB* form is found at 130.54 ppm while the C_e and C_a forms are located at 137.04 and 137.95 ppm respectively. Thus, a difference of more than 6 ppm exists between the *C* and the *TB* signals.

The association of each family of signals is best carried out using the C-4 and C-5 signals as probe because previous results showed that the C_a signal is the more shielded (5). Therefore, the signals in the C-4 and C-5 region of **2** are assigned as follows: in the C-4 region, the intense signal (91%) at 33.56 ppm represents the C_e form while the upfield signal (30.44 ppm) integrating for 9% corresponds to the C_a form, and similarly for the C-5 signals. The chemical shifts for the complete analysis are summarized in Table 1.

In the less polar solvent, CH_3OCH_3, the C_a:C_e population ratio of **2** at −120°C is 4:96. All pertinent data are reported in Table 1.

As for the published 1,5-benzodioxepin (3) and 1-benzoxepin families (4, 5), the aromatic C-8,11 and C-9,10 signals of the 1,5-benzodithiepin derivatives (**3**–**5**) can also provide information on the seven-membered ring conformation, whereby the *TB* signal is always found upfield from that of the *C* form (8). Finally, the C-3 signals reveal the nature of the three forms C_a, C_e, or *TB*, whereby the C_a signal is the most shielded, the C_e signal is the most deshielded, and the *TB* signal is found in between.

Figure 3 shows the 100.62 MHz ^{13}C nmr spectral changes observed for compound **3** in CH_3OCH_3. Firstly, it is important to note that this compound contains C–F coupling constants $^1J_{C-F} \approx 170$–180 Hz (12) and $^2J_{C-F} \approx 20$–25 Hz (13). At 0°C, the signals are broadened due to the slowing down of the conformational interconversion process. Lowering the temperature to −120°C yields a well-resolved spectrum in which the various carbons show signals with two or three peaks in a ratio of 7:90:3. Using the C-8,11 signals as conformational probe, the following analysis can be carried out: the downfield signals

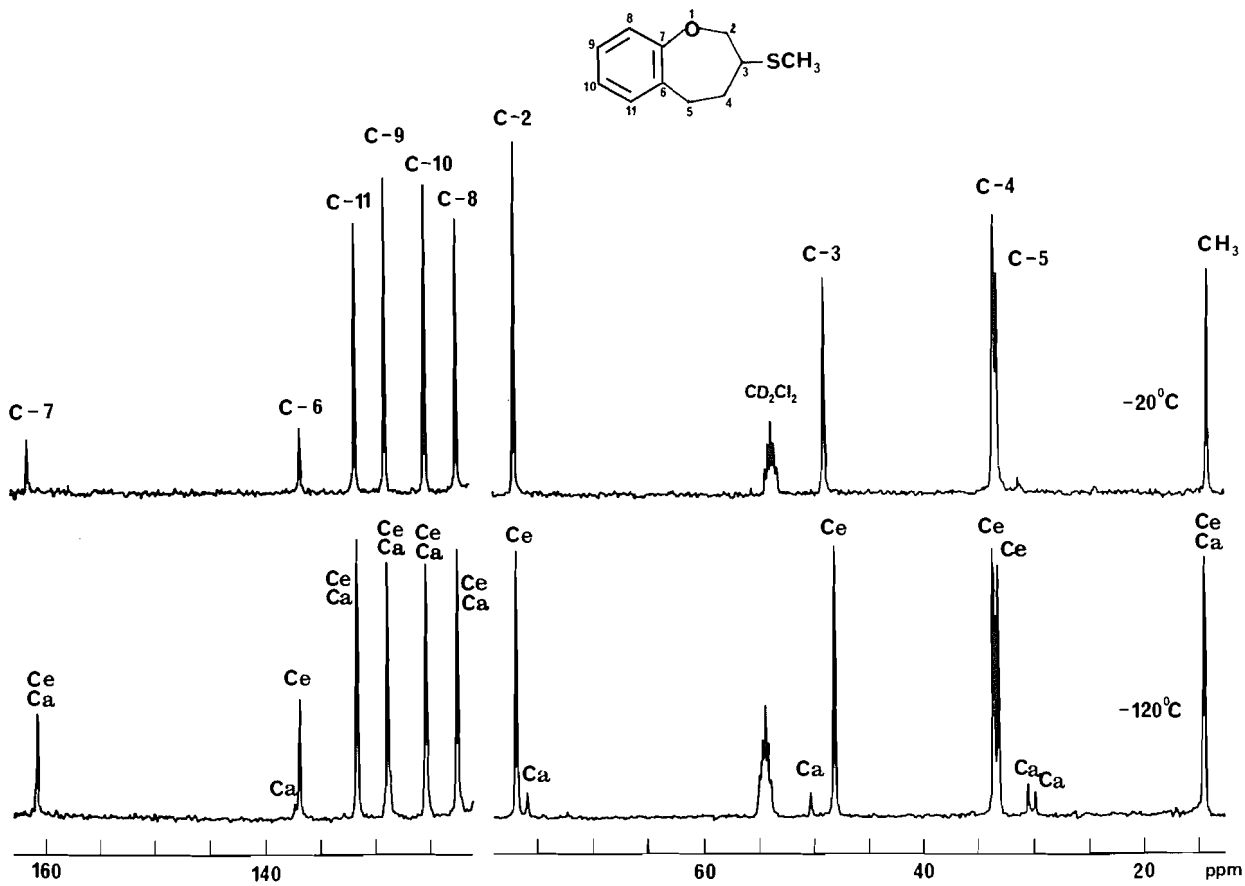

FIG. 2. 100.62 MHz ^{13}C spectra of **2** in CHF_2Cl at −20°C and −120°C.

at 135.23 and 135.54 ppm are deemed characteristic (8) of the *C* forms while the signal at 131.70 ppm corresponds to the *TB* form. Furthermore, the C-3 carbon signals identify each form. The most intense signal (90%) at 95.72 ppm is characteristic of the C_e form while the upfield signal at 86.13 ppm corresponds to the C_a form (7%). Between the C_a and the C_e forms appears the *TB* signal at 90.62 ppm. The chemical shifts of all other carbons have been assigned by integration and the results are reported in Table 1.

In the more polar CHF_2Cl solvent at −120°C, compound **3** reveals a C_a:C_e:*TB* population ratio of 20:79:1, as indicated in Table 1.

Spectral modifications have also been observed for compound **4** and the assignment of all signals has been made using the same procedure as described for compound **3**. Three conformations have been found in the polar CHF_2Cl solvent in a ratio of 6:92:2 for the C_a:C_e:*TB* forms, while in the less polar CH_3OCH_3 solvent, only the C_e form is detected. The results are also summarized in Table 1.

Discussion

The SCH_3 substituent is well known to exhibit an important steric effect (14). For example, the data in Table 2 (6, 14–16) show that the equatorial preference of cyclohexylmethyl sulfide is higher than that of the heavy halogen and methoxy substituents. But when the SCH_3 substituent interacts with a vicinal polar OCH_3 substituent, as in *trans*-1-methylthio-2-methoxycyclohexane, a conformational population change occurs that is larger than predicted on steric grounds (32% of axial conformation in CCl_4, $-\Delta G^\circ = 0.4$ kcal/mol) (6). It was suggested by Zefirov *et al.* (6) that this additional perturbation originates from an O/S repulsive *gauche* effect.

In comparison, Eliel and Juaristi (17) have studied this same interaction in 5-methylthio-1,3-dioxane and 5-methoxy-1,3-dithiane. Their results suggested that the O/S interaction is attractive for the 5-methylthio-1,3-dioxane while the S/O interaction is repulsive for 5-methoxy-1,3-dithiane (the following convention is used in the present paper: O/S indicates that the oxygen atom is located inside the ring and the sulfur atom is outside the ring and conversely for S/O). The repulsive S/O interaction was explained in terms of a probable repulsive overlap of the filled $3p$ orbital on sulfur with the $2sp^3$ filled orbital on oxygen. However the apparently conflicting results between the S/O and O/S interactions have left the issue unresolved.

Earlier works (3, 5) aimed at characterizing the O/O *gauche* effect in the seven-membered rings have shown that σ–σ^* orbital interactions play a significant role and it appears important to assess the O/S and S/O *gauche* interaction in light of this underlying framework.

It is therefore advantageous to divide the analysis of our results in two parts. The first part will consider compounds **1** and **2** for which the sulfur atom is located outside the ring, in the SCH_3 substituent (models for the O/S interaction), while the second part focuses on derivatives from the 1,5-benzodithiepin family (**3**, **4**, and **5**), containing *endo* sulfur atoms (model for the S/O interaction).

The O/S interaction

Unlike the analogous six-membered compounds, the particu-

Can. J. Chem. Downloaded from www.nrcresearchpress.com by 91.144.44.67 on 09/07/12
For personal use only.

Can. J. Chem. Downloaded from www.nrcresearchpress.com by 91.144.44.67 on 09/07/12
For personal use only.

TABLE 1. Carbon-13 chemical shifts of

Compound	Solvent	Temperature (°C)	Conformations	%	C-2	C-3
1	CHF_2Cl	−15			74.64	47.50
(X = SCH_3)		−135	C_a	7	73.90	51.17
			C_e	22	75.76	46.14
			TB	71	72.49	47.22
	CH_3OCH_3	−20			74.45	46.59
		−135	C_e	36	74.51	46.17
			TB	64	73.01	45.44
2	CHF_2Cl	−20			76.78	49.02
(X = SCH_3)		−120	C_a	9	75.88	50.30
			C_e	91	76.84	48.11
	CH_3OCH_3	−20			76.71	48.76
		−120	C_a	4	76.33	50.59
			C_e	96	76.33	48.01
3	CHF_2Cl	−20			37.50(^2J = 16.98)	[a]
(X = F)		−120	C_a	20	37.37(^2J = 20.97)	86.86(^1J = 173.52)
			C_e	79	36.73(^2J = 24.38)	96.04(^1J = 176.55)
			TB	1	34.20(^2J = 22.98)	[b]
	CH_3OCH_3	0			37.04(^2J = 24.63)	[a]
		−120	C_a	7	36.80(^2J = 20.73)	86.13(^1J = 174.56)
			C_e	90	36.08(^2J = 24.51)	95.72(^1J = 176.98)
			TB	3	33.92(^2J = 22.35)	90.62(^1J = 180.66)
4	CHF_2Cl	−20			41.52	63.00
(X = Cl)		−120	C_a	6	41.24	59.33
			C_e	92	40.50	62.92
			TB	2	[b]	59.84
	CH_3OCH_3	0			40.97	[a]
		−120	C_e	<98	39.67	63.50
5	CHF_2Cl	0			37.31	84.51
(X = OCH_3)		−120	C_a	33	36.77	74.82
			C_e	61	36.77	84.77
			TB	6	33.47	79.23

[a]These signals were not observed because of coalescence.
[b]These signals were not observed, either because of peak overlapping or too small signal-to-noise ratio.
[c]Compound **5** exists as a mixture of three conformations C_e, C_a, and *TB* in ratio 88:8:4 respectively, in the CH_3OCH_3 solvent (8).

lar seven-membered system represented by compounds **1** and **2** is characterized by the presence of the *TB* conformation, in addition to the C_a and C_e forms.

For compound **1**, three conformations (C_a:C_e:*TB* = 7:22:71) are observed in CHF_2Cl but only two forms, *TB* and C_e (64:36), have been detected in the less polar CH_3OCH_3 solvent. Because increasing solvent polarity should attenuate the repulsive electrostatic interactions (18), the more polar C_a form is observed (MMX calculations (19) reveal that dipole moments are C_a, μ = 3.34D; C_e, μ = 1.09D; and *TB*, μ = 1.77D). Furthermore, in each of the two solvents, compound **1** exists predominantly in the *TB* form, as also found for the analogous methoxy derivative (2). But the presence of the C_e form for compound **1** contrasts with the methoxy derivative for which the C_e form is never observed.

Recent studies of 1-benzoxepin derivatives (4, 5) have shown that the *TB* form is not stabilized relative to the chair form in this family. Our results for compound **2** reveal that it exists predominantly in the C_e form while the *TB* form is not detected. By comparison, the relative populations of the conformers for the analogous methoxy derivative are C_a:C_e:*TB* = 70:20:10 in CHF_2Cl (4). Is this greater C_e preference shown by **2** indicative of some change in the underlying orbital interactions (9) as the OCH_3 substituent is replaced by SCH_3?

Before assessing the bond–antibond molecular orbital interactions present in the conformations of **1** and **2**, it is useful to review briefly the theory of the σ–σ^* interactions (9, 20, 21).

The stabilization energy resulting from an interaction between a doubly occupied bonding molecular orbital (σ) and an empty antibonding orbital (σ^*) is proportional to $S^2/\Delta E$, where S is the overlap integral and ΔE is the energy difference between the σ and σ^* orbitals. These two terms can either decrease or increase the stabilization energy as follows:

(a) First, for a series of compounds, the ΔE term increases stabilization as the energy level of the bonding orbital σ increases and (or) the energy level of the antibonding orbital σ^* decreases (22).

(b) Second, the effect of the overlap S term is best illustrated using a polar C—X bond. The electronic density in the molecular orbital σ_{C-X} is concentrated on the most electronegative atom X whereas, in the σ^*_{C-X} orbital, the electronic density is concentrated on the less electronegative atom C and it increases with increasing electronegativity of X (9, 22). Thus, overlap is increasingly effective with increasing electronegativity of X for interactions of the type σ–σ^*_{C-X}.

The overlap contribution is therefore predicted to be more stabilizing for the σ_{C-H}–σ^*_{C-X} interaction and less stabilizing for σ_{C-X}–σ^*_{C-H} relative to the σ_{C-H}–σ^*_{C-H} interaction (9).

compounds **1–5** at high and low temperatures

C-4	C-5	C-6	C-7	C-8	C-9	C-10	C-11	CH_3
74.64		152.12	152.12	124.76	122.42	122.42	124.76	14.16
73.90		153.15	153.15	125.96	123.77	123.77	125.96	[b]
75.16		153.15	153.15	126.09	123.77	123.77	126.09	14.39
72.49		150.39	150.39	124.05	121.63	124.05	124.05	14.68
74.45		151.88	151.88	124.08	122.00	122.00	124.08	13.47
74.51		153.33	153.33	125.29	123.40	123.40	125.29	13.44
73.01		150.45	150.45	123.40	121.19	121.19	123.40	13.03
33.42	33.14	136.55	161.35	122.24	128.77	125.09	131.53	14.15
30.45	29.82	137.33	160.85	122.44	128.60	125.31	131.64	14.38
33.56	33.13	136.88	160.85	122.44	128.84	125.31	131.64	14.38
33.51	33.14	135.99	161.39	121.93	128.40	124.55	131.06	13.74
29.72	29.43	136.11	161.01	121.99	128.18	124.73	131.06	13.65
33.39	33.26	136.11	161.01	121.99	128.48	124.73	131.06	13.65
37.50(^2J = 16.98)		[a]	[a]	135.76	130.25	130.25	135.76	
37.37(^2J = 20.97)		142.61	142.61	135.74	130.26	130.26	135.74	
36.73(^2J = 24.38)		141.54	141.54	136.02	130.59	130.59	136.02	
34.20(^2J = 22.09)		[b]	[b]	132.03	127.41	127.41	132.03	
37.04(^2J = 24.63)		[a]	[a]	135.05	129.47	129.47	135.05	
36.80(^2J = 20.73)		143.28	143.28	135.23	129.65	129.65	135.23	
36.08 (^2J = 24.51		142.05	142.05	135.54	130.05	130.05	135.54	
33.92(^2J = 22.35)		[b]	[b]	131.70	126.93	126.93	131.70	
41.52		[a]	[a]	135.75	130.35	130.35	135.75	
41.24		142.70	142.70	[b]	[b]	[b]	[b]	
40.50		141.77	141.77	135.83	130.54	130.54	135.83	
[b]		[b]	[b]	132.07	127.56	127.56	132.07	
40.97		[a]	[a]	135.34	129.78	129.78	135.34	
39.67		142.39	142.39	135.31	129.74	129.74	135.31	
37.31		141.94	141.94	135.02	129.39	129.39	135.02	57.14
36.77		143.10	143.10	135.60	129.88	129.88	135.60	56.63
36.77		142.23	142.23	135.78	130.22	130.22	135.78	57.45
33.47		[b]	[b]	131.90	127.15	127.15	131.90	60.82

For a given compound existing in several different conformations, the dominant orbital interaction for each conformer can be determined as follows:

1. All orbital interactions about the C(α)—C(β) bond are listed for each conformation (the α carbon is the site of substitution).

2. The σ–σ* interactions having a weak overlap are neglected and the other σ–σ* interactions are considered potentially more stabilizing. For each of the remaining interactions, the σ orbital is associated with the C—Y bond having the least electronegative Y atom, while the σ* orbital originates from the C—X bond having the most electronegative X atom (i.e., σ_{C-Y}–σ^*_{C-X}, where X is more electronegative than Y).

3. When more than one interaction remains for a given conformation: (a) If the S term is similar for these interactions, then the ΔE parameter determines which is the dominant interaction. (b) On the other hand, if the differences in the ΔE values are comparable, then the S term is determinant. (c) Finally, if both terms, ΔE and S, are significantly different, then the situation becomes complex when the effects of ΔE and S oppose each other.

Figure 4 shows the relative order of the energy levels of the σ_{C-X} and σ^*_{C-X} orbitals for the bonds involved in the analysis of compounds **1–6**. These data were derived from the results of CNDO/2 and *ab initio* calculations (10), from the analysis of ionization potentials of CH_3X molecules (23, 24), and from photoelectron spectra (25). Together, they allow qualitative predictions regarding the importance of the various σ–σ* orbital interactions potentially significant in each of the observed conformations.

The σ–σ* interactions involving at least one polar bond for conformations C_e and C_a are listed under structures **7** and **8**. Because of poor overlap, the σ_{C-O}–σ^*_{C-S} interaction in **7** and the σ_{C-O}–σ^*_{C-H}, σ_{C-H}–σ^*_{C-S}, and σ_{C-S}–σ^*_{C-H} interactions in **8** are neglected (for each structure, the interactions in parentheses are excluded because of poor overlap). Then the most stabilizing (or dominant) interactions are σ_{C-S}–σ^*_{C-O} for the C_e form (**7**) and σ_{C-H}–σ^*_{C-O} for the C_a form (**8**). Now, the difference between these two interactions is located in the σ orbital (σ_{C-H} and σ_{C-S}). Theoretical studies (9) indicate that the relative strength of the overlap contribution in σ–σ* interactions depends most sensitively on the nature of the antibonding rather than the bonding orbital. Furthermore, the small differences between the electronegativity of the hydrogen and sulfur atoms (2.1 and 2.5 respectively (26)) suggest that the overlap contribution is similar for both interactions. Since the ΔE term is smaller for the σ_{C-S}–σ^*_{C-O} interaction, the greater strength of the σ_{C-S}–σ^*_{C-O} interaction should favor the C_e

Can. J. Chem. Downloaded from www.nrcresearchpress.com by 91.144.44.67 on 09/07/12
For personal use only.

Can. J. Chem. Downloaded from www.nrcresearchpress.com by 91.144.44.67 on 09/07/12
For personal use only.

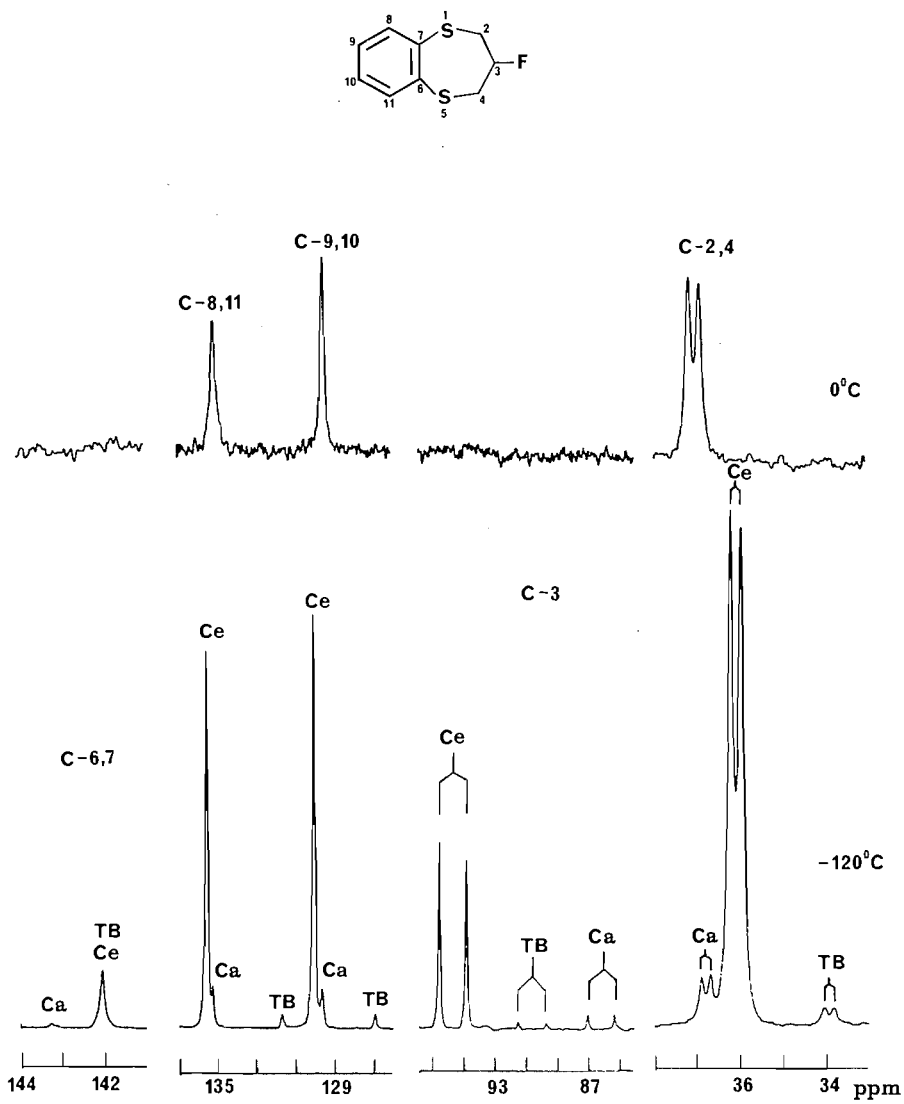

FIG. 3. 100.62 MHz ^{13}C spectra of **3** in CH_3OCH_3 at 0°C and −120°C.

form over the C_a form. In contrast, the *TB* conformation (**9**) involves all the stabilizing σ–σ* interactions found in both the C_a and C_e forms. The fact that *TB* is the major form observed is in agreement with orbital interactions being operative. In addition, the *TB* form avoids any steric interactions present in the C_a form.

Similarly, compound **2** possesses the same σ–σ* orbital interactions as compound **1** for which the σ_{C-S}–σ^*_{C-O} interaction in C_e is strongest. Because the *TB* ring conformation is not accessible to compound **2**, the C_e form should then be more stabilized than C_a by this interaction, as observed. However, this feature for **2** is different from that of the analogous methoxy derivative **6** for which the C_a form is favored (4). Indeed, the data in Table 2 suggest that the SCH_3

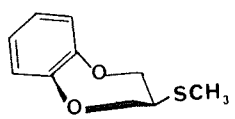

7

$\sigma_{C-S} - \sigma^*_{C-O}$

$(\sigma_{C-O} - \sigma^*_{C-S})$

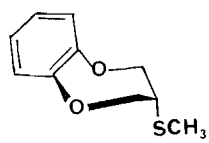

8

$\sigma_{C-H} - \sigma^*_{C-O}$

$(\sigma_{C-O} - \sigma^*_{C-H})$

$(\sigma_{C-H} - \sigma^*_{C-S})$

$(\sigma_{C-S} - \sigma^*_{C-H})$

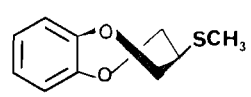

9

$\sigma_{C-H} - \sigma^*_{C-O}$

$(\sigma_{C-O} - \sigma^*_{C-H})$

$(\sigma_{C-H} - \sigma^*_{C-S})$

$(\sigma_{C-S} - \sigma^*_{C-H})$

$\sigma_{C-S} - \sigma^*_{C-O}$

$(\sigma_{C-O} - \sigma^*_{C-S})$

Can. J. Chem. Downloaded from www.nrcresearchpress.com by 91.144.44.67 on 09/07/12
For personal use only.

TABLE 2. $-\Delta G°$ values of some 1-substituted cyclohexanes and 5-substituted benzocycloheptenes

Compound	$-\Delta G°$ (kcal/mol)	Ref.
Cyclohexylmethyl sulfide	1.07	14
Cyclohexylmethyl ether	0.60	15
Cyclohexyl chloride	0.50	6
Cyclohexyl fluoride	0.25	6
5-Methoxybenzocycloheptene	−0.13	16
5-Chlorobenzocycloheptene	0.03	16

substituent in compound **2** should prefer the C_e position on steric grounds. But the similarity of the C_a:C_e ratio for **2** and cyclohexylmethyl sulfide, in view of steric interaction with one electron lone pair in **2**, suggests that a contribution of the σ_{C-S}–σ^*_{C-O} interaction is present but not overly dominant.

The S/O, S/F, and S/Cl interactions

Recent studies of 1,5-benzodithiepin derivatives (8) have shown that the *TB* form is not stabilized specifically in this system and the parent compound exists exclusively in the chair conformation. For compounds **3**, **4**, and **5**, Table 1 reveals a large amount of the C_e form and small quantities of the *TB* form together with an intermediate quantity of the C_a form.

The experimental conformational data describing the axial–equatorial equilibrium in cyclohexane derivatives, summarized in Table 2, suggest that the amount of the C_e form should be similar for compounds **4** (X = Cl) and **5** (X = OCH_3) and less abundant for **3** (X = F). In contrast, dipolar interactions should contribute to invert this order for F and Cl in the seven-membered heterocycles. Indeed, because the C—F bond is more polar than the C—Cl bond, there exists a greater dipole–dipole destabilization of the C_a form, which leads to an increase in the amount of the C_e form. Furthermore, the orientation of the dipole moment of the halogen substituents is different from that of the methoxy group (the dipole moment of the halogen is located along the C—X bond, while that of the methoxy group bisects the C—O—C angle of the most stable rotamer). For these reasons it is more useful, in the absence of precise geometrical information, to compare the conformational behavior of compounds **3**, **4**, and **5** in the more polar solvent, assuming that under these conditions dipolar interactions are sufficiently attenuated to be of minimal importance (18).

Based on steric interactions alone, the relative populations of the C_e form should follow the order $OCH_3 \approx Cl > F$, which contrasts with the experimental populations as shown in Table 1. The fact that the C_e form is found to be predominant for these three compounds (in the two solvents used), as well as published considerations (6, 8), suggests that part of the stabilization of the C_e form should arise from a repulsive *gauche* effect. Accordingly, the bond–antibond orbital interactions will be examined to identify the origin of the repulsive feature.

Structures **10** and **11** show the σ–σ^* orbital interactions present in the C_a and C_e forms for compounds **3–5**. For the C_a form (**10**), the σ_{C-H}–σ^*_{C-X} interaction is dominant and is a function of each X substituent. On the other hand, the dominant interaction in the C_e form (**11**) is σ_{C-S}–σ^*_{C-X}. Then, this interaction stabilizing the C_e form (**11**) should be stronger and should contribute to the trend observed for compounds **3–5**.

Taking into account the nature of X in compounds **3–5**, the specific dominant interaction for each C_e form is σ_{C-S}–σ^*_{C-F}, σ_{C-S}–σ^*_{C-Cl}, and σ_{C-S}–σ^*_{C-O} respectively. Variations in overlap (*S* term) caused by changes in the σ^*_{C-X} orbitals

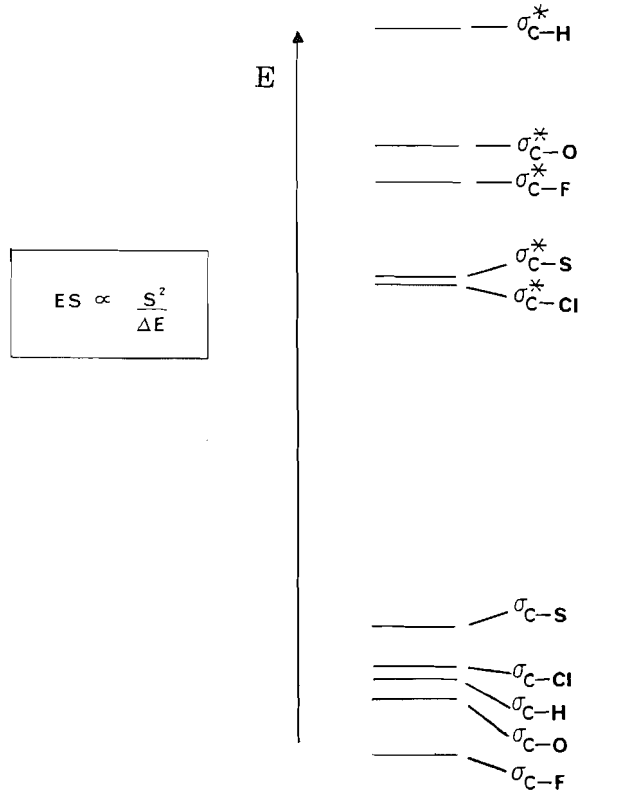

FIG. 4. Relative order of the bonding and antibonding orbital energies of the C—X bonds in various X-CH_2CH_2-Y and CH_3X molecules.

10

$\sigma_{C-H} - \sigma^*_{C-X}$

$(\sigma_{C-X} - \sigma^*_{C-H})$

$(\sigma_{C-H} - \sigma^*_{C-S})$

$(\sigma_{C-S} - \sigma^*_{C-H})$

11

$\sigma_{C-S} - \sigma^*_{C-X}$

$(\sigma_{C-X} - \sigma^*_{C-S})$

suggest that the stabilizing order should be Cl < O < F, whereas the ΔE term predicts a different one: O < F < Cl. Then, both the *S* and the ΔE terms indicate that the σ_{C-S}–σ^*_{C-F} interaction should be more stabilizing than the σ_{C-S}–σ^*_{C-O} interaction, as supported by the experimental results showing that the C_e populations for compounds **3** (X = F) and **5** (X = OCH_3) are 79% and 61% respectively in CHF_2Cl.

In contrast, the magnitude of the σ_{C-S}–σ^*_{C-Cl} interaction is determined by a competition between opposing ΔE and *S* terms. Accurate evaluation of each term is not possible for these compounds, but a comparison of the C_e populations for Cl, F, and OCH_3 (92%, 79%, and 61% respectively) suggests that the ΔE term, favoring the C_e form, is more important and is responsible in a large part for the trend observed.

Comparison of the S/O and O/S interactions

The molecular orbital σ_{C-S}–σ^*_{C-O} interaction is found to be common to compounds **1** and **2** (O/S interaction) as well as to

Can. J. Chem. Downloaded from www.nrcresearchpress.com by 91.144.44.67 on 09/07/12
For personal use only.

5 (S/O interaction) and it stabilizes the C_e form for all three molecules. The strength of this interaction can also usefully be pointed out using the six-membered compounds **12** and **13** as described below.

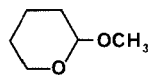

12

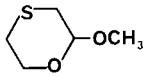

13

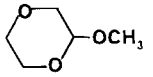

14

While the axial preference (80% in MeCN) for the 2-methoxytetrahydropyran (**12**) (27) is due to the anomeric effect (28), it is observed that introducing a sulfur atom at position 4 of the ring, as in **13**, stabilizes the C_e form and reduces the axial population to 56% in MeCN (29). This observation cannot be explained by dipole–dipole repulsion between the substituent and the sulfur atom because when the sulfur atom is replaced by an oxygen atom, as in **14**, the C_a form (73% in MeCN) is favored (29, 30). The results of the present work on σ–σ^* molecular orbital interactions suggests that the significant σ_{C-S}–σ^*_{C-O} interaction present in the C_e form (**13**), which opposes the η_O–σ^*_{C-O} interaction, is largely responsible for its behavior.

We can now address the question of whether the σ_{C-S}–σ^*_{C-O} interaction is of different intensity when the sulfur atom changes from an *endo* to an *exo*cyclic position (S/O or O/S) because of different angle constraints?

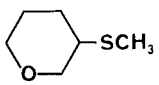

15

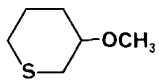

16

Firstly, the σ_{C-S}–σ^*_{C-O} interaction is involved in both six-membered cyclic compounds **15** and **16**. In a polar solvent (acetone), the $-\Delta G°$ values of **15** and **16** are 1.30 ± 0.19 and 1.19 ± 0.03 kcal/mol at 183 K and 178 K respectively (31, 32). Several contributing factors are involved in these compounds. For example, in a polar solvent the dipole–dipole interactions are attenuated, favoring the C_a form, and the steric interactions are generally stronger for the SCH_3 substituent than for OCH_3. The recently published method (33) of estimating the strength of the *gauche* interactions in 3-aminothiacyclohexane provides a useful framework for the analysis of **15** and **16**. It was suggested that the *gauche* interaction between a substituent X and the heterocyclic atom Y can be estimated from the following equation: $(X/Y) = -\Delta G° - (X/CH_2)_{gauche}$ where the $(X/CH_2)_{gauche}$ interaction is considered empirically as half of the *A* value of the X group. Applying this method to compounds **15** and **16**, the following values are obtained: (S/O) = 0.77 kcal/mol and (O/S) = 0.89 kcal/mol.

Furthermore, for each $(X/Y)_{gauche}$ interaction, the contributions from steric interactions are estimated as follows (33). For compound **15**, the $(O/CH_2)_{gauche}$ interaction (0.30 kcal/mol) is 0.34 times the $(Me/CH_2)_{gauche}$ interaction and the term $\Delta = (X/Y) - [(X/CH_2) \times (Y/CH_2)/(Me/CH_2)]$ then corresponds to the difference between the (X/Y) interaction and the value from an "exclusively steric" point of view. The Δ terms obtained for compound **15** and **16** are 0.59 and 0.70 kcal/mol respectively and correspond to the (S/O) and (O/S) interactions other than steric. Furthermore, the positive sign of Δ indicates that these interactions are repulsive.

Considering the approximate nature of this method, it appears that the calculated (S/O) and (O/S) *gauche* interactions are similar for compounds **15** and **16**. Even though this method is limited quantitatively, it provides a useful reference point and offers an indication as to the presence of interactions other than steric ones.

In the light of the above analysis, the σ_{C-S}–σ^*_{C-O} interaction should in principle be independent of the location of the S atom in compounds **1** and **5**, assuming that the angles between the two interacting orbitals are similar in the C_e form of both compounds. Indeed, MMX calculations (19) reveal that the dihedral angles between the C—O and C—S bonds in the C_e form are 172° and 166° for compounds **1** and **5** respectively. But the presence of the *TB* form for compound **1** prevents a definitive conclusion from being reached. Indeed, the stabilization of this form is most likely due to the fact that its flexibility allows the interacting σ orbitals to adopt a near-perfect antiperiplanar arrangement.

Conclusion

In studies of the *gauche* effect, repulsive or attractive interactions have been invoked to explain specific conformational preferences. Results presented herein indicate that the origin of this effect involves molecular orbital interactions associated with at least one polar bond. In addition to the steric and electrostatic interactions, it appears that the underlying σ–σ^* interactions are important in conformational analysis and, together with the anomeric effect (n–σ^*), constitute important features of the general theory of stereoelectronic molecular orbital interactions.

Experimental

Routine ^1H nmr spectra were recorded on a Bruker WH-90 spectrometer as solutions in $CDCl_3$ (10% w/v) containing Me_4Si as reference.

The 2D proton–carbon heteronuclear chemical shift correlation (HC COSY) spectrum was obtained using the standard pulse sequence (9). The experiment was performed on a Varian VXR-300 spectrometer operating at 75.431 MHz for ^{13}C with F_2 = 299.949 MHz in the second dimension. The spectrum was acquired with 256 × 1K data points.

The low temperature ^1H nmr spectra at 400.13 MHz and ^{13}C nmr spectra at 100.62 MHz were obtained using a Bruker WH-400 spectrometer equipped with a B-VT-1000 variable temperature unit. Calibration using a thermocouple inside a solvent-containing nmr tube indicates that the low temperatures reported are accurate within ±3°C.

Proton samples in standard 5-mm tubes (degassed and sealed) were recorded as solutions in CHF_2Cl and CF_2Cl_2 (10–20 mg in 0.55 mL of solution) containing Me_4Si and about 15–20% of CD_2Cl_2 or CD_3COCD_3 for field locking purposes. For proton spectra, the typical instrumental parameters used are as follows: flip angle = 10°–70°; scan width (SW) = 5000 Hz; data size = 8 and 16K; aquisition time (AQ) = 0.8–1.0 s; relaxation delay (RD) = 0.01 s.

For all ^{13}C nmr spectra, the following parameters are typical: flip angle = 20°–60°; SW = 20 000 Hz; data size = 8–16K; AQ = 0.43 s; RD = 0.6 s. The ^{13}C samples were studied at low temperature, as solutions in CHF_2Cl or CH_3OCH_3 (100–150 mg in 2.2 mL of solution) containing Me_4Si and about 15–20% of CD_2Cl_2 as locking agent, in standard 10-mm tubes that had been degassed and sealed. Integrations were carried out by using Bruker software and are precise within ±2% (34).

The high resolution mass spectra were taken using a modified MS-9 spectrometer at 70 eV.

The dipole moments and dihedral angles were obtained by MMX molecular mechanics calculations on an IBM/AT computer, using the PCMODEL program (19) purchased from Serena Software, Box 3076, Bloomington, IN 47402-3076.

2H-2,3-Dihydro-3-methylthio-1,5-benzodioxepin (**1**)

A round-bottomed flask containing 10 mL of dry ether, fitted with a magnetic stirrer, rubber septum, and maintained under argon was

Can. J. Chem. Downloaded from www.nrcresearchpress.com by 91.144.44.67 on 09/07/12
For personal use only.

cooled to 0°C in an ice bath. Afterwards, 4.8 mL (0.082 mol) of methanethiol was added. Commercial methyllithium (1.4 M) (Aldrich) (60 mL, 0.082 mol) was introduced via syringe at a rate such that gas (CH_4) evolution did not become excessively violent. During the course of the addition of CH_3Li, a white solid separated. When the addition of CH_3Li was completed, the ether and unreacted CH_3SH were removed by an argon current at room temperature.

Afterwards, a solution of 50 mL of dry THF and 2.0 g (0.016 mol) of 2*H*-2,3-dihydro-3-mesyl-1,5-benzodioxepin (3) was added and the mixture was heated at ~50°C for 2 days. The solution was cooled to room temperature, filtered, and the solvent was evaporated. The product was purified by flash chromatography on silica gel by using 25% dichloromethane and 75% hexane as eluent, giving 2.8 g (88%) of a colorless liquid; ^{1}H nmr δ($CDCl_3$): 6.98 (4H, s, Ar), 4.56 (2H, dd, CH_2), 4.07 (2H, dd, CH_2), 3.3 (1H, m, CH), 2,2 (3H, s, CH_3). Exact mass calculated for $C_{10}H_{12}O_2S$: 196.0558; found (70 eV): 196.0557.

2,3,4,5-Tetrahydro-3-methylthio-1-benzoxepin (**2**)

This product was prepared by a method similar to that for compound **1** from 1.04 g (0.0043 mol) of 2,3,4,5-tetrahydro-3-mesyl-1-benzoxepin (4). Purification by flash chromatography on silica gel using a 15:85 mixture of dichloromethane and hexane gave 375 mg (45%) of a colorless liquid; ^{1}H nmr δ($CDCl_3$): 7.0–7.2 (4H, m, Ar), 4.3–4.5 (1H, m, H-2), 3.60 (1H, dd, H-2) 2.7–3.0 (4H, m, H-4, H-5, H-3), 2.15 (3H, s, CH_3), 1.5–1.6 (1H, m, H-4). Exact mass calculated for $C_{11}H_{14}OS$: 194.0765; found (70 eV): 194.0764.

1,3-Dibromo-2-fluoropropane (ref. 35)

This product was made using the method described in ref. 36.

3-Fluoro-1,5-benzodithiepin (**3**)

A mixture of 4.03 g of K_2CO_3 and 10 mL of pentanol was brought to reflux. Afterwards, 0.912 g (0.007 mol) of 1,3-dibromo-2-fluoropropane was added. The reflux was maintained for 10 h. The mixture was cooled to room temperature, filtered, and extracted with ether and brine. The organic layer was dried with $MgSO_4$, filtered, and the solvent was evaporated. The yellow oil was purified by flash chromatography with 10:90 dichloromethane:hexane as eluent to give 0.381 g (26%) of a colorless liquid; ^{1}H nmr δ($CDCl_3$): 7.72–7.17 (4H, m, Ar), 5.03 (1H, m, CH), 3.23–2.75 (4H, m, CH_2). Exact mass calculated for $C_9H_9S_2F$: 200,0130; found (70 eV): 200.0101.

2-Chloro-1,3-propanediol

This product was made and characterized using the method described in ref. 37.

2-Chloro-1,3-ditosylate propane

This compound was synthesized by a standard method (38), using the 2-chloro-1,3-propanediol as starting product.

3-Chloro-1,5-benzodithiepin (**4**)

At 0°C, to 0.50 g (0.004 mol) of benzenedithiol was added 1.4 M commercial methyllithium (5.4 mL, 0.008 mol) via syringe at a rate such that gas (CH_4) evolution did not become excessively violent. A white solid was formed. Afterwards, a solution of 1.4 g (0.004 mol) of 2-chloro-1,3-ditosylate propane in 10 mL of THF was added. The mixture was stirred for 4 h, filtered, and the solvent was evaporated. The product was purified by flash chromatography on silica gel by using 95:5 hexane:dichloromethane as eluent. A colorless liquid was obtained, 0.12 g (14%); ^{1}H nmr δ($CDCl_3$): 7.74–7.20 (4H, m, Ar), 4.50 (1H, m, CH), 3.36 (2H, dd, CH_2). Exact mass calculated for $C_9H_9S_2Cl$: 215.9834; found (70 eV): 215.9841.

Acknowledgments

We acknowledge the assistance of Dr. Phan Viet Minh Tan, manager of the Laboratoire Régional de RMN à Haut Champ in Montréal. We thank the Natural Sciences and Engineering Research Council of Canada for financial assistance.

1. S. Wolfe. Acc. Chem. Res. **5**, 102 (1972).
2. D. Ménard and M. St-Jacques. J. Am. Chem. Soc. **106**, 2055 (1984).
3. P. Dionne and M. St-Jacques. J. Am. Chem. Soc. **109**, 2616 (1987).
4. A. Lachapelle and M. St-Jacques. Can. J. Chem. **65**, 2575 (1987).
5. P. Dionne and M. St-Jacques. Can. J. Chem. **67**, 11 (1989).
6. N. S. Zefirov, L. G. Gurvich, A. S. Shashkov, M. Z. Krimer, and E. A. Vorob'eva. Tetrahedron, **32**, 1211 (1976).
7. E. Juaristi. J. Chem. Educ. **56**, 438 (1979).
8. D. Ménard and M. St-Jacques. Can. J. Chem. **64**, 2142 (1986).
9. T. K. Brunk and F. Weinhold. J. Am. Chem. Soc. **101**, 1700 (1979).
10. N. D. Epiotis, W. R. Cherry, S. Shaik, R. Yates and F. Bernardi. Top. Curr. Chem. **70** (1977).
11. (*a*) G. Bodenhausen and R. Freeman. J. Magn. Reson. **28**, 471 (1977); (*b*) A. Bax and G. A. Morris. J. Magn. Reson. **42**, 501 (1981).
12. (*a*) G. P. Van Der Kelen and Z. Eeckhaut. J. Mol. Spectrosc. **10**, 141 (1963); (*b*) A. C. Blizzard and D. P. Santry. J. Chem. Phys. **55**, 950 (1971).
13. J. W. Emsley, L. Phillips, and L. Wray. Prog. Nucl. Magn. Reson. Spectrosc. **10**, 83 (1975); (*b*) F. J. Weigert and J. D. Roberts. J. Am. Chem. Soc. **93**, 2361 (1971).
14. F. R. Jensen, C. H. Bushweller, and B. H. Beck. J. Am. Chem. Soc. **91**, 344 (1969).
15. D. Hofner, S. A. Lesko, and G. Binsh. Org. Magn. Reson. **11**, 179 (1978).
16. D. Ménard and M. St-Jacques. Tetrahedron, **39**, 1041 (1983).
17. E. L. Eliel and E. Juaristi. J. Am. Chem. Soc. **100**, 6114 (1978).
18. M. K. Kaloustian. J. Chem. Educ. **51**, 777 (1974).
19. N. L. Allinger. Adv. Phys. Org. Chem. **13**, 1 (1976).
20. T. A. Albright, J. K. Burdett, and M. H. Whangbo. Orbital interactions in chemistry. John Wiley & Sons, New York. 1985.
21. N. D. Epiotis, R. L. Yates, J. R. Larson, C. R. Kirmaier, and F. Bernardi. J. Am. Chem. Soc. **99**, 8379 (1977).
22. V. Minkin, B. Simkine, and R. Mihiaev. Théorie de la structure moléculaire (couches électroniques). French translation. Mir, Moscow. 1982.
23. K. Kimura, S. Ktsumata, Y. Achiba, T. Y. Amazaki, and S. Iwaka. Handbook of HeI photoelectron spectra of fundamental molecules. Japan Scientific Soceieties Press, Tokyo; Halsted Press, New York. 1981.
24. R. C. Bingham. J. Am. Chem. Soc. **97**, 6743 (1975).
25. Y. Uehara, N. Saito, and T. Yonezawa. Chem. Lett. 495 (1973).
26. L. Pauling. *In* The chemical bond. Cornell University Press, Ithaca, N.Y. 1967.
27. N. S. Zefirov, V. S. Blagoveschensky, I. V. Kazimirchik, and N. S. Surova. Tetrahedron, **27**, 3111 (1971).
28. (*a*) A. J. Kirby. *In* The anomeric effect and related stereoelectronic effect at oxygen. Springer-Verlag, Berlin; Heidelberg; New York. 1983; (*b*) P. Deslongchamps. *In* Stereoelectronic effects in organic chemistry. Vol. 1. Pergamon Press, Oxford. 1983.
29. N. S. Zefirov, M. A. Fedorovskaya, V. S. Blagovshenskii, and I. V. Kazimirchik. Zh. Org. Khim. **4**, 1498 (1968).
30. N. S. Zefirov and M. A. Fedorovskaya. Zh. Org. Khim. **5**, 158 (1969).
31. J. L. G. Ruano, J. Rodriguez, F. Alcudia, J. M. Liera, E. M. Olefirowicz, and E. L. Eliel. J. Org. Chem. **52**, 4099 (1987).
32. E. Brunet and E. L. Eliel. J. Org. Chem. **51**, 677 (1986).
33. E. Brunet and P. Azpetia. Tetrahedron, **44**, 1751 (1988).
34. G. D. Christian. Analytical chemistry. 3rd ed. John Wiley & Sons, New York. 1980.
35. F. L. M. Pattison, D. A. V. Peters, and F. H. Dean. Can. J. Chem. **43**, 1689 (1965).
36. P. J. Card and G. S. Reddy. J. Org. Chem. **48**, 4734 (1983).
37. P. Maroni, L. Cazaux, G. Chassaing, I. Prejzner, and T. Le Trang. Bull. Soc. Chim. 1258 (1975).
38. J. J. Baldwin, A. W. Raab, K. Mensler, B. H. Arison, and D. E. McClure. J. Org. Chem. **43**, 4876 (1978).

The substrate- and stereoselectivity of microbial reductions of 1,4-dithiaspiro[4.5]decanones and 1,5-dithiaspiro[5.5]undecanones

TETSUO TAKEMURA,[1] YOSHIKO HOSOYA, AND NOBUO MORI

Department of Chemistry, Science University of Tokyo, Kagurazaka, Shinjuku-ku, Tokyo 162, Japan

Received August 8, 1989

TETSUO TAKEMURA, YOSHIKO HOSOYA, and NOBUO MORI. Can. J. Chem. **68**, 523 (1990).

The title spirocyclic ketones, possessing possible substitution patterns 1,4-dithiaspiro[4.5]decan-6-one (**1***a*), -7-one (**3***a*), and -8-one (**5***a*), and 1,5-dithiaspiro[5.5]undecan-7-one (**2***a*), -8-one (**4***a*), and -9-one (**6***a*), have been reduced with new strains of yeast (*Saccharomyces cerevisiae*, JCM 1819 and JCM 2214). Reductions of the prochiral ketones **1***a*–**4***a* occur with high enantiofacial selectivity on the preparative scale (up to 99% ee). The product alcohols (1,4-dithiaspiro[4.5]decan-6-ol (**1***b*) and -7-ol (**3***b*) and 1,5-dithiaspiro[5.5]undecan-7-ol (**2***b*) and -8-ol (**4***b*)) have the *S* configuration, as confirmed by 2D COSY experiments of the (*S*)-MTPA esters of **1***b*–**4***b* using the configuration correlation model of Mosher.

Key words: microbial reduction, *Saccharomyces cerevisiae*, dithiaspiro ketones, substrate- and stereoselectivity, H,H-COSY spectra.

TETSUO TAKEMURA, YOSHIKO HOSOYA et NOBUO MORI. Can. J. Chem. **68**, 523 (1990).

Utilisant de nouvelles variétés de levures (*Saccharomyces cerevisiae*, JCM 1819 et JCM 2214), on a réduit les cétones spirocycliques mentionnées dans le titre et possédant divers types de substituants (les 1,4-dithiaspiro[4.5]décan-6-one (**1***a*), -7-one (**3***a*) et -8-one (**5***a*) ainsi que les 1,5-dithiaspiro[5.5]undécan-7-one (**2***a*), -8-one (**4***a*) et -9-one (**6***a*)). À l'échelle préparative, les réductions des cétones prochirales **1***a*–**4***a* se produisent avec une haute énantiosélectivité. Les alcools obtenus (les 1,4-dithiaspiro[4.5]décan-6-ol (**1***b*) et -7-ol (**3***b*) ainsi que les 1,5-dithiaspiro[5.5]undécan-7-ol (**2***b*) et -8-ol (**4***b*)) possèdent la configuration *S*; cette conclusion découle d'expériences COSY en 2D effectuées sur les esters (*S*)-MTPA des composés **1***b*–**4***b* en utilisant le modèle de configuration de Mosher.

Mots clés : réduction microbiologique, *Saccharomyces cerevisiae*, dithiaspiro cétones, substrats et stéréosélectivité, spectres COSY du H,H.

[Traduit par la revue]

Biocatalysts have already demonstrated high utility and potential in certain areas of current importance in preparative organic chemistry (1). The asymmetric microbial reduction of the carbonyl group is one of the viable biological methods because of the broad substrate specificity involving dehydrogenase (or reductase) enzymes available in microorganisms. The most promising and popular microorganism for this purpose is *Saccharomyces cerevisiae* (e.g., common bakers' yeast) (1, 2). Bakers' yeast mediated reductions of acyclic ketones for the preparation of chiral building blocks have been extensively documented (2). Cyclic ketones as substrates of biocatalysts are also important for their stereochemical aspects (1, 3). Although several microbial reductions of cyclic ketones have recently been reported (4), no systematic study on spiro cyclic ketones has so far been undertaken (3*b*, 3*d*, 4*e*). There is a current interest in defining rules for the structural limits of acceptability of nonconventional substrates by synthetically useful biocatalysts.

In this paper we report on the structural- and stereospecificity of microbial reductions, by two new strains of *Saccharomyces cerevisiae*, of 1,4-dithiaspiro[4.5]decanones (**1***a*, **3***a*, and **5***a*) and 1,5-dithiaspiro[5.5]undecanones (**2***a*, **4***a*, and **6***a*), which include all possible patterns of these spiroketone skeletons. In addition, the present approach provides the features of the biocatalytic reductions of cyclic ketones possessing synthetically important protective groups, i.e., five- and six-membered thioketals.

Results

The substrate ketones **1***a*–**6***a* were obtained in 20–67% yields from 1,2-, 1,3-, and 1,4-cyclohexanediones (**7**, **8**, and **9** respectively) and 1,2-ethane- and 1,3-propanedithiols (**10** and **11** respectively) by the usual acetalization procedure (5). The racemic alcohols (±)-**1***b*–**4***b* and achiral alcohols **5***b* and **6***b* required for reference purposes were prepared by reduction of **1***a*–**6***a* with lithium aluminum hydride.

Screening various strains of *Saccharomyces cerevisiae* proved that type cultures JCM 1819 and JCM 2214 (microorganisms A and B respectively) were sufficiently active toward spiroketones **1***a*–**6***a*.[2] In each case, the sole product of the microbial reduction was the corresponding alcohol as shown in Scheme 1. The substrate specificities of the microbial reductions of ketones **1***a*–**6***a* (reaction time vs. % conversion) are summarized in Table 1.

The prochiral spiroketones **1***a*–**4***a* were each subjected to preparative scale (151–642 mg) microbial reduction under the usual aerobic conditions (substrate concentration, 30 mg/100 mL). Ketones **5***a* and **6***a* were omitted because both the substrates and products are achiral. Each reaction was terminated when GLC analysis[3] showed it to be an appropriate conversion level (82–100%). The product alcohols and, in some cases, unchanged ketones were easily purified by PTLC. Optically active **1***b*–**4***b* are unknown substances. Their structures were confirmed by comparisons with the racemic compounds characterized earlier. The results obtained are also summarized in Scheme 1 and Table 1.

The ee's of the optically active alcohols were determined by chiral HPLC analysis of their 3,5-dinitrophenyl urethanes (6) and (or) by preparing their MTPA esters (7*a*) and monitoring the 400 MHz ^{1}H NMR absorptions of the externally diastereo-

[1]Author to whom correspondence may be addressed.

[2]Bakers' yeast (purchased from Oriental Yeast Co. Ltd., Japan) showed much less reactivity toward these ketones under the same reaction conditions.

[3]The total loss of material for the GLC analysis was less than 1% in each preparative run.

Printed in Canada / Imprimé au Canada

Can. J. Chem. Downloaded from www.nrcresearchpress.com by 91.144.44.67 on 09/07/12
For personal use only.

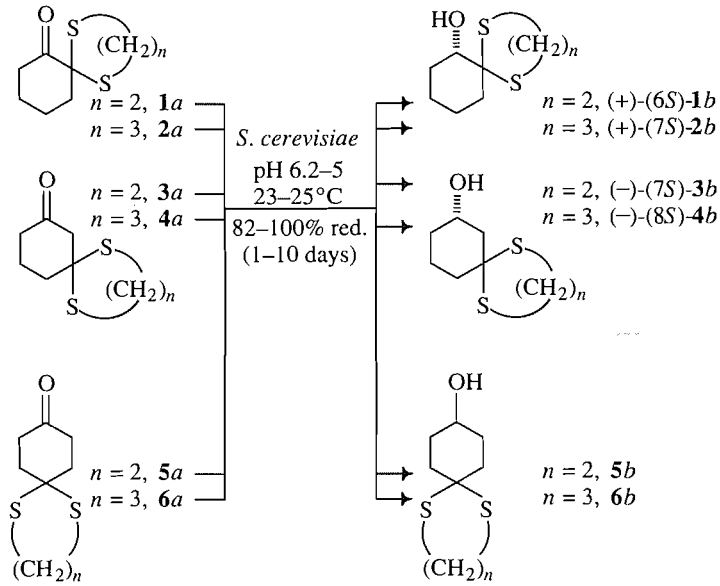

SCHEME 1

TABLE 1. Results of the microbial reduction of spirocyclic ketones **1***a*–**6***a*

Run	Substrate	Strain[a]	Reaction time (days)	% conversion[b]	$[\alpha]_D$[c]	% ee HPLC	% ee NMR
1[e]	**1***a*	A	3.6	95 (93)	+6.4	87	—
2[e]		B	3.5	82 (77)	+7.0	86	87
3	**2***a*	A	1.7	100 (91)	+38.3	99	>97
4		B	1.1	99 (98)	+35.5	96	—
5[e]	**3***a*	A	1.0	100 (92)	−2.9	97	93
6		B	3.8	97 (83)	−3.5	96	91
7[e]	**4***a*	A	6.9	95 (81)	−8.3	92	90
8[e]		B	10.0	93 (75)	−5.7	83	86
9	**5***a*	A	3.9	100 [d]			
10		B	4.7	100 [d]			
11	**6***a*	A	6.9	92 [d]			
12		B	1.9	100 [d]			

[a]Strains of *Saccharomyces cerevisiae*, A:JCM 1819, B:JCM 2214.
[b]Parentheses denote isolated yields.
[c]All specific rotations were measured in $CHCl_3$.
[d]The preparative experiment was not carried out.
[e]Repeated experiments under similar conditions (at least once) gave similar results; e.g., 93% conv./10.0 days – 65% conv./3.0 days, 83–93% ee for run 7.

meric protons specified in the experimental section. The ee values determined by these procedures are also given in Table 1.

The absolute configurations of the product alcohols depicted in Scheme 1 were deduced from the Mosher rule (7*b*) analyses of their MTPA esters (**1***c*–**4***c*) obtained by treatment of the corresponding optically active and racemic alcohols with freshly prepared (*S*)-α-methoxy-α-trifluoromethylphenylacetyl chloride (7). The ^1H NMR chemical shifts of the esters were assigned on the basis of two-dimensional (2D) homonuclear proton correlation spectroscopy (COSY) experiments. The partial 2D ^1H COSY contour plots (400 MHz; $CDCl_3$) for the (*S*)-MTPA esters of (−)- and (±)-**4***b* are shown (aromatic proton resonances omitted) in Fig. 1 as examples of the model for (*S*)-MTPA esters of (*S*)- and (*R*)-**4***b* as an example of the analysis. The ^1H NMR chemical shift differences (Δδ values) for the diastereomeric MTPA esters (**1***c*–**4***c*) used for the configuration determinations are summarized in Table 2.

Discussion

A standard procedure as given in the experimental section was used for the incubation of the spirocyclic ketones **1***a*–**6***a* in growing cultures of *S. cerevisiae* to compare differences in enzymatic reduction resulting from the structural variations of the substrates. It is very important that although the reaction rate varied, the spiroketones examined were all good substrates, irrespective of the ring members of thioketal moieties, the position of the carbonyl group, and the microorganisms used. The substrate specificity of the enzyme systems is fairly broad.

Can. J. Chem. Downloaded from www.nrcresearchpress.com by 91.144.44.67 on 09/07/12
For personal use only.

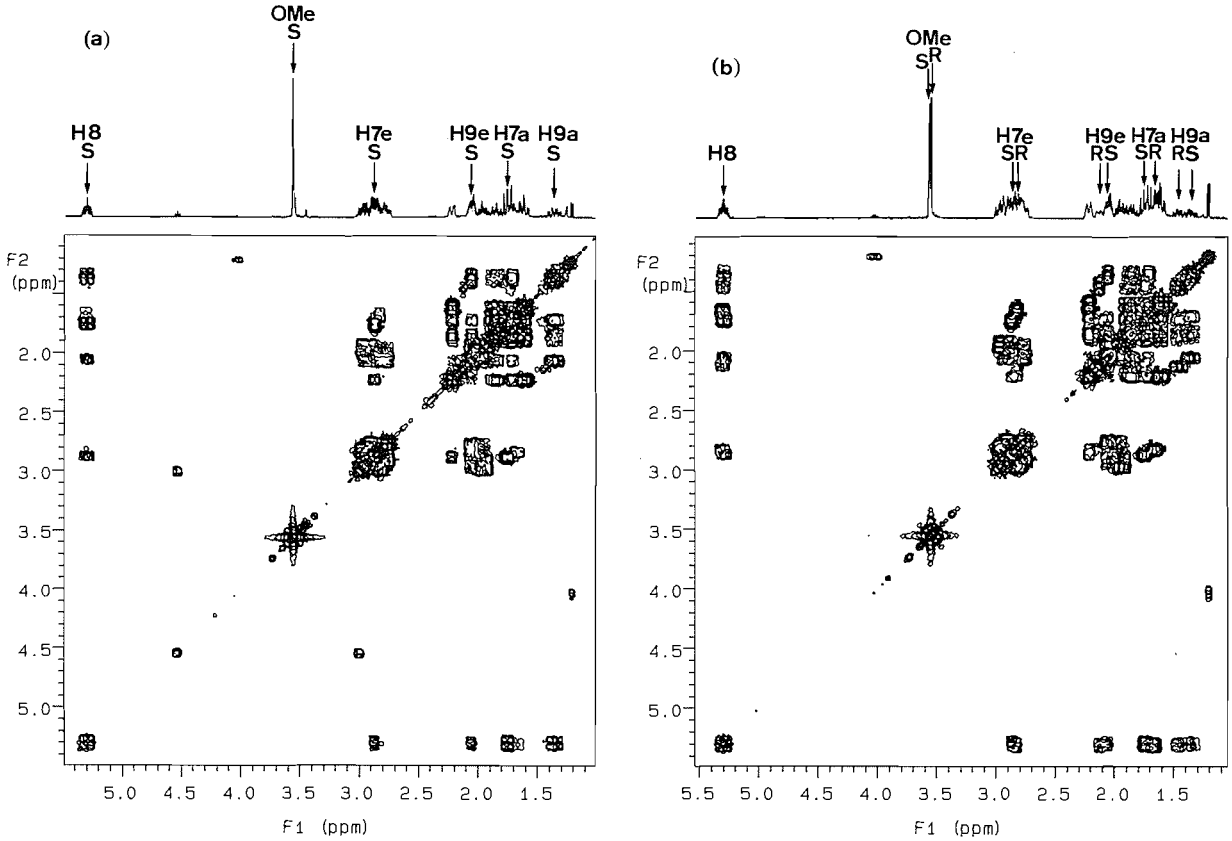

FIG. 1. Partial 2D ^{1}H COSY contour plots for the (*S*)-MTPA esters of (a) (−)- and (b) (±)-**4***b* (400 MHz; $CDCl_3$).

TABLE 2. ^{1}H NMR chemical shift differences for the diastereomeric MTPA esters[a]

Compound	Proton[b] chemical shift difference, Δδ (I − II) in ppm		
	R_L moiety	R_S moiety	Methoxyl
1*c*	2,3 (+0.16)	7a (−0.043), 7e (−0.035)	(+0.029)
2*c*	2a (+0.354), 2e (+0.234)	8a (−0.056), 8e (−0.08)	(+0.010)
	4a (−0.08),[c] 4e (+0.068)		
3*c*	2,3 (+0.009)	8a (−0.115), 8e (−0.09)	(+0.006)
	6a (+0.089), 6e (+0.061)	9a (−0.036), 9e (−0.038)	
4*c*	7a (+0.088), 7e (+0.063)	9a (−0.090), 9e (−0.07)	(+0.015)

[a]Values in parentheses are differences in δ(Δδ), ppm, obtained by subtracting the chemical shift of the indicated protons of diastereomer II from that of the corresponding protons in I.
[b]The symbols "a" and "e" are used to denote axial and equatorial protons respectively.
[c]An exceptional upfield shift of R_L moiety.

While **4***a* against strain B (93% conv./10 days) was the poorest substrate of all substrate–microorganism combinations, its rate of reduction was still fast enough to permit a preparative scale reaction. No substantial amounts of by-products were detected by TLC and GLC in the reaction mixture, indicating that the reaction is chemoselective. Hence the recovery of material was virtually quantitative by this method, with the total yields of isolated, purified products being 75–98%.

As observed in entries 1–8, both strains A and B showed the same tendency to give the optically active alcohol products of high optical purities (83–99% ee). The ketone **2***a* (99–100% conv./1.1–1.7 days, 96–99% ee) possessing a flexible 6-membered ring gave better results compared to **1***a* (82–95% conv./3.5–3.6 days, 86–87% ee) possessing a less flexible (i.e., a smaller change in shape would be expected) 5-membered ring (8). The opposite is true where the prochiral center is further separated from the spiro-carbon atom (i.e., **3***a* (97–100% conv./1.0–3.8 days, 96–97% ee) vs. **4***a* (93–95% conv./6.9–10 days, 83–92% ee)). In this case, the higher %ee was obtained for **3***a* with the less flexible 5-membered ketal moiety β to the carbonyl. This substrate dependence on both rate and enantioselectivity (i.e., **2***a* > **1***a* and **3***a* > **4***a*) of the reaction are probably due to the preferable binding modes[4] (3*a*) of

[4]The fact that bakers' yeast mediated reduction of flexible open chain analogs of **2***a* (2*l*) and **4***a* (2*f*) constantly gave excellent %ee's (>96% ee and >99% ee respectively) may support the contribution of better fitting of substrates at the active sites of enzyme systems.

Can. J. Chem. Downloaded from www.nrcresearchpress.com by 91.144.44.67 on 09/07/12
For personal use only.

Can. J. Chem. Downloaded from www.nrcresearchpress.com by 91.144.44.67 on 09/07/12
For personal use only.

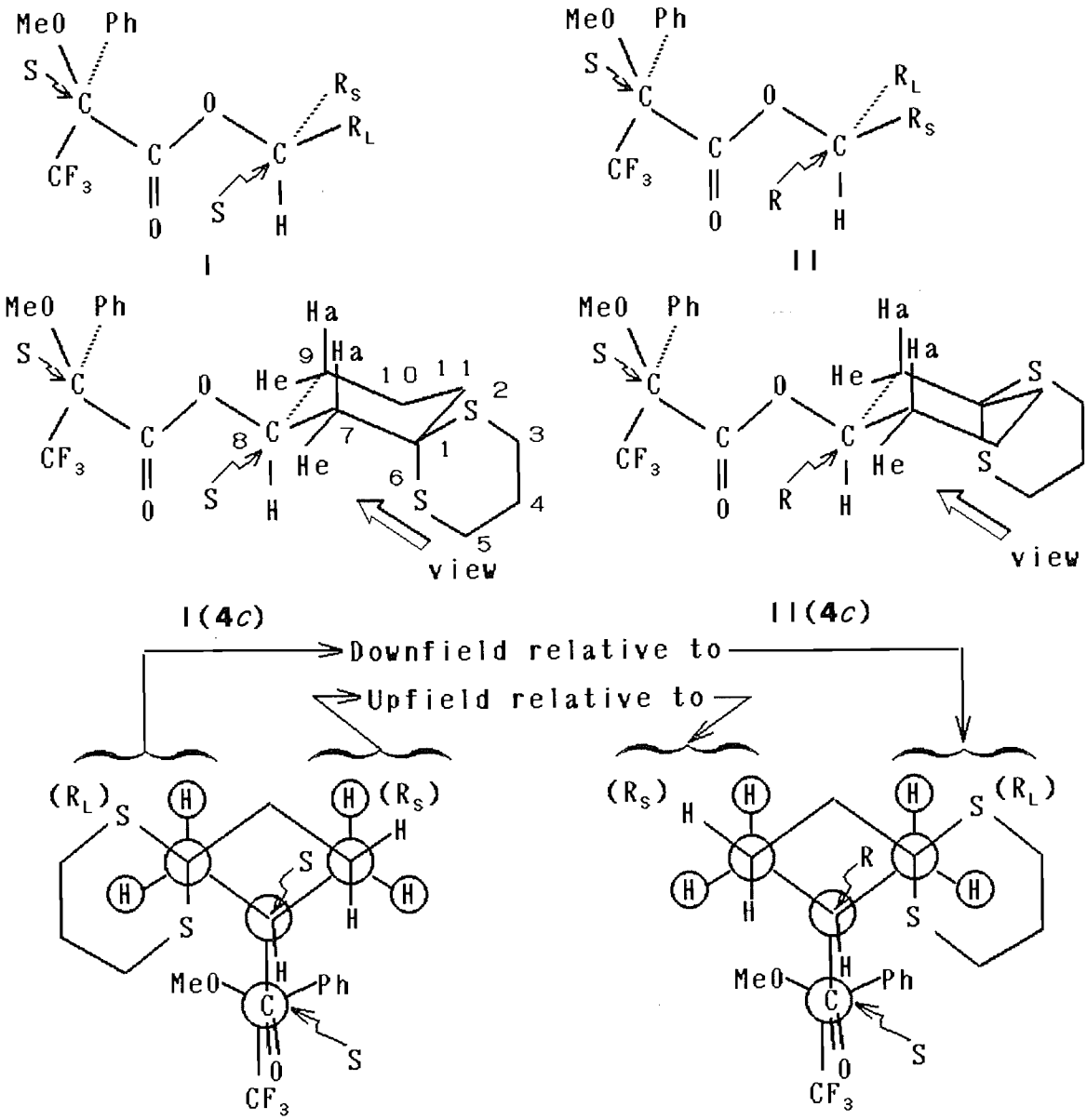

FIG. 2. Configurational correlation model for (*S*)-MTPA esters of (*S*)- and (*R*)-**4***b*.

the substrates **2***a* and **3***a* to the enzyme systems of the microorganisms.

2D COSY analysis was employed as a reliable technique for the assignment of otherwise difficult NMR absorptions of the MTPA esters **1***c*–**4***c*. ^{1}H 2D COSY spectra clearly depicted the H6—H7 correlation of **1***c* and the H7—H8 correlation of **2***c*. Similarly, the 2D technique was also found effective in the assignment of the H6—H7—H8 and H7—H8—H9 networks of **3***c* and **4***c* (see Fig. 1) respectively. The H2—H3 (**1***c* and **3***c*) or H2—H3—H4 (**2***c* and **4***c*) networks on thioketal rings have been successfully assigned, since these networks are independent of other proton networks in the ^{1}H COSY spectra. The absolute configurations of product alcohols **1***b*–**4***b* were then deduced based on the ^{1}H NMR chemical shift differences for the diastereomeric MTPA esters (Table 2). According to Dale and Mosher (7*b*), the most populated conformation, the *S,S* diastereomer I, would have the R_S moiety eclipsed with the phenyl group and the R_L moiety (thioketal side) with the methoxyl group as shown in Fig. 2 (7*b*). Owing to shielding effects of the phenyl group, the $R_S(R_L)$ moiety of I should appear upfield (downfield)[5] in the ^{1}H NMR spectrum relative to that of the *S,R* diastereomer II, as was observed for each of the MTPA esters **1***c*–**4***c* derived from the present microbial reductions. The observed downfield shifts of the methoxyl protons of *S,S* diastereomer I compared to those of II in all cases examined ($\Delta\delta$ +0.006 to +0.029 ppm as shown in Table 2) would be attributable to the deshielding effect of the thioketal rings due to the anisotropy of the carbon–sulfur bonds in the rings (9).[6] Accordingly, the absolute configurations of all

[5]Although an exceptional upfield shift (−0.08 ppm) was observed for H4a of the R_L moiety in **2***c*, the downfield shift of this moiety as a whole is still apparent from the summation (+0.576 ppm) of all chemical shift differences of the moiety in **2***c*.

[6]Since the anisotropy of the carbon–sulfur single bond is opposite in sense to that of the carbon–carbon single bond, the axial hydrogens of thioketal rings in **2***c* and **4***c* also resonate at lower field than the equatorial hydrogens of the same rings (see experimental section for the assignments based on their coupling constants) as suggested for α-trithioacetaldehyde (9).

Can. J. Chem. Downloaded from www.nrcresearchpress.com by 91.144.44.67 on 09/07/12
For personal use only.

microbial products **1***b*–**4***b* can be determined to be *S*. Thus, the present reductions of prochiral ketones **1***a*–**4***a* occur with predictable stereochemistry, i.e., hydride delivery to the Re face of the carbonyl group, in accord with Prelog's rule (10). The same configuration was also reported for (+)-(1*S*)-1-spiro[4.4]nonanol prepared by microbial reductions of the corresponding carbocyclic spiroketones with *Curvularia lunata* and *Rhodotorula rubra* (3*d*). Since the stereochemical course of reduction is dependent on the relative steric bulk of the substituents attached to the carbonyl group, it is reasonable to extend Prelog's rule to the prediction of the stereochemical outcome for the microbial reductions toward spirocyclic compounds.

Experimental

Melting points were determined on a Yamato Scientific apparatus and are uncorrected. IR and MS spectra were recorded on Hitachi 215 and Hitachi M-80 (70 eV) instruments, respectively. NMR spectra were obtained on the following instruments using $(CH_3)_4Si$ as internal standard: ^1H (100 MHz) and ^{13}C (25 MHz) spectra, JEOL JNM-FX100; ^1H (400 MHz) spectra, Varian XL-400; ^1H (400 MHz) 2D correlation spectra, Varian UNITY-400. Optical rotations were measured on a Jasco DIP-181 digital polarimeter. HPLC was carried out on Shimadzu LC-3A liquid chromatograph equipped with Shimadzu SPD-6A UV spectrophotometric detector. GLC analyses were performed on Shimadzu GC-4CM or GC-14A instruments using Chemipack A, 3% Silicone OV-17 on Chromosorb W AW DMCS, or 10% Silicone GE SE-30 on Celite 545 columns, and TLC analyses with Merck silica gel 60 F_{254}. The optical densities (OD, with 1-cm pathlength glass cuvette at λ = 660 nm) of the culture mediums were monitored using a Shimadzu UV-250 spectrophotometer. Preparative TLC was carried out with silica gel 60 PF_{254} (Merck Art 7747 or 7749). 1,2-Cyclohexanedione (**7**) and 1,2-ethanedithiol (**10**) were purchased from Tokyokasei Kogyo, and 1,3- and 1,4-cyclohexanedione (**8** and **9** respectively) and 1,3-propanedithiol (**11**) from Aldrich. All substrates used were GLC-pure. Unless otherwise indicated, IR spectra were determined on KBr pellets and ^1H and ^{13}C NMR spectra and optical rotations in C^2HCl_3 and $CHCl_3$ solutions, respectively.

*Preparations of dithiaspiro ketones (**1**a–**6**a)*

*1,4-Dithiaspiro[4.5]decan-7-one (**3**a)*

A mixture of 27.9 g (0.25 mol) of dione **8**, 12.5 g (0.132 mol) of dithiol **10**, and 12.1 g (0.064 mol) of *p*-toluenesulfonic acid monohydrate (*p*-TsOH·H_2O) in 600 mL of benzene was heated under reflux in a Dean–Stark apparatus for 3.5 h, water (ca. 2 mL) formed during the reaction being continuously removed. The reaction mixture was then washed with two 400-mL portions of 5% aqueous Na_2CO_3. The aqueous layer was extracted with two 400-mL portions of benzene. All the benzene solutions were combined, washed twice with 1000 mL of water, dried ($MgSO_4$), and then evaporated. The oily residue was chromatographed on silica gel with benzene elution to give **3***a* as a crystalline solid (9.25 g, 37.2% yield). Kugelrohr distillation of the solid afforded pure **3***a*: 7.25 g (29.2% yield); bp 160°C/0.6 Torr (1 Torr = 133.3 Pa); mp 40–41°C; IR: 1715 cm^{-1}; ^1H NMR δ: 1.80–2.16 (2H, m), 2.16–2.44 (4H, m), 2.90 (2H, br s), and 3.34 (4H, s) ppm; ^{13}C NMR δ: 24.92 (C-9), 39.37 (C-2,3), 39.96 (C-10), 40.66 (C-8), 57.63 (C-6), 68.16 (C-5), and 206.63 (C-7) ppm; MS *m/e* (rel. int.): 188 (100), 160 (27), 145 (42), 131 (99), and 118 (34). Anal. calcd. for $C_8H_{12}OS_2$: C 51.03, H 6.42, S 34.05; found: C 51.05, H 6.43, S 33.67.

The remaining substrates were prepared by the same basic procedure.

*1,4-Dithiaspiro[4.5]decan-6-one (**1**a)* (lit. (11)) (from dione **7** and dithiol **10**): 66.7% yield; bp 125°C/0.8 Torr (lit. (11*b*) bp 94°C/0.2 Torr); mp 57.2–57.8°C (lit. (11*b*) mp 57.5°C); IR: 1695 cm^{-1}; ^1H NMR δ: 1.45–2.05 (4H, m), 2.38 (2H, m, $W_{1/2}$ = 11 Hz), 2.70 (2H, m, $W_{1/2}$ = 10 Hz), and 3.29 (4H, s) ppm.

*1,5-Dithiaspiro[5.5]undecan-7-one (**2**a)* (lit. (12)) (from dione **7** and dithiol **11**): 37.8% yield; bp 130–145°C/0.24 Torr (lit. (12*b*) bp 140°C/0.001 Torr); mp 53.2–53.6°C (lit. (12*b*) mp 53–54°C); IR: 1700 cm^{-1}; ^1H NMR δ: 1.55–3.50 (m) ppm.

*1,5-Dithiaspiro[5.5]undecan-8-one (**4**a)* (from dione **8** and dithiol **11**): 25.6% yield; bp 150°C/0.3 Torr; mp 73.0°C; IR: 1720 cm^{-1}; ^1H NMR δ: 1.68–2.46 (8H, m) and 2.60–3.0 (6H, m) ppm; ^{13}C NMR δ: 21.30 (C-10), 25.10 (C-3), 26.09 (C-2,4), 36.56 (C-11), 40.31 (C-9), 50.78 (C-6), 52.71 (C-7), and 206.63 (C-8) ppm; MS *m/e* (rel. int.): 202 (100), 159 (15), 145 (33), and 128 (44). Anal. calcd. for $C_9H_{14}OS_2$: C 53.43, H 6.98, S 31.69; found: C 53.43, H 6.99, S 31.38.

*1,4-Dithiaspiro[4.5]decan-8-one (**5**a)* (lit. (13)) (from dione **9** and dithiol **10**): 25.5% yield; bp 118°C/1.2 Torr (lit. (13*a*) 100–102°C/0.1 Torr); IR (CCl_4): 1714 cm^{-1}; ^1H NMR δ: 2.15–2.68 (8H, m) and 3.40 (4H, m) ppm; ^{13}C NMR δ: 38.9 (C-2,3), 40.8 (C-7,9), 42.1 (C-6,10), 66.3 (C-5), and 209.3 (C-8) ppm.

*1,5-Dithiaspiro[5.5]undecan-9-one (**6**a)* (from dione **9** and dithiol **11**): 19.5% yield; bp 146–160°C/0.77 Torr; mp 102.7–103.2°C; IR: 1712 cm^{-1}; ^1H NMR δ: 1.80–2.19 (2H, m), 2.19–2.65 (8H, m), and 2.65–2.96 (4H, m) ppm; ^{13}C NMR δ: 25.8 (C-3), 26.4 (C-2,4), 37.4 (C-7,11), 37.6 (C-8,10), 48.3 (C-6), and 209.5 (C-9) ppm; MS *m/e* (rel. int.): 202 (98), 145 (96), 127 (62), 99 (21), and 74 (100). Anal. calcd. for $C_9H_{14}OS_2$: C 53.43, H 6.98, S 31.69; found: C 53.22, H 6.90, S 31.54.

*Preparation of alcohols **1**b–**6**b*

The same procedure was used for each. The appropriate dithiaspiro ketone (**1***a*–**6***a*, 0.005 mol) in dry ether (20 mL) was added dropwise with stirring to a cooled (0°C) suspension of lithium aluminum hydride (0.005 mol) in dry ether (5 mL). The resulting mixture was stirred for 1 h and water (0.2 mL) was then added carefully, followed by 10% aqueous sodium hydroxide (0.32 mL) and further water (0.4 mL). The mixture was filtered and the filtrate dried ($MgSO_4$), evaporated, and Kugelrohr distilled. The products obtained were as follows.

*1,4-Dithiaspiro[4.5]decan-6-ol ((±)-**1**b)* (lit. (14)): 95.5% yield; bp 90°C/0.8 Torr; IR (CCl_4): 3445 cm^{-1}; ^1H NMR δ: 1.00–2.66 (9H, m), 3.27 (4H, s), and 3.48–3.46 (1H, m) ppm; ^{13}C NMR δ: 25.7 (C-9), 32.6 (C-8), 39.0 (C-2,3), 39.1 (C-7), 40.3 (C-10), 75.3 (C-5), and 75.8 (C-6) ppm; MS *m/e* (rel. int.): 190 (88.6), 131 (100), and 105 (50.0).

*1,5-Dithiaspiro[5.5]undecan-7-ol ((±)-**2**b)* (lit. (15)): 96.4% yield; bp 102°C/0.8 Torr; IR (CCl_4): 3450 cm^{-1}; ^1H NMR δ: 1.00–2.28 (10H, m), 2.28–3.20 (5H, m), and 4.03 (1H, m, $W_{1/2}$ = 10.5 Hz) ppm; ^{13}C NMR δ: 20.3 (C-10), 21.2 (C-9), 25.2 (C-2,4), 26.0 (C-3), 27.6 (C-11), 34.5 (C-8), 55.8 (C-6), and 69.4 (C-7) ppm; MS *m/e* (rel. int.): 204 (100), 145 (76.0), 119 (36.9), and 106 (34.7).

*1,4-Dithiaspiro[4.5]decan-7-ol ((±)-**3**b)*: 97.5% yield; bp 151°C/3.8 Torr; mp 82–84°C; IR: 3245 cm^{-1}; ^1H NMR δ: 1.00–2.52 (9H, m), 3.29 (4H, s), and 3.54–3.96 (1H, m) ppm; ^{13}C NMR δ: 23.2 (C-9), 33.9 (C-10), 38.0 (C-2), 39.0 (C-3), 41.8 (C-8), 50.5 (C-6), 66.9 (C-5), and 69.5 (C-7) ppm; MS *m/e* (rel. int.): 190 (93), 147 (100), 105 (39), and 97 (52). Anal. calcd. for $C_8H_{14}OS_2$: C 50.49, H 7.41, S 33.69; found: C 50.39, H 7.39, S 33.64.

*1,5-Dithiaspiro[5.5]undecan-8-ol ((±)-**4**b)* (lit. (16)): 98.3% yield; bp 135°C/1.0 Torr; mp 64–66°C (lit. (16) mp 67.0–68.6°C; IR: 3270 cm^{-1}; ^1H NMR δ: 1.0–2.24 (9H, m), 2.32–3.14 (6H, m), and 3.96 (1H, m, $W_{1/2}$ = 16 Hz) ppm; ^{13}C NMR δ: 19.5 (C-10), 25.8 (C-3), 26.3 (C-2,4), 34.8 (C-9), 37.4 (C-11), 45.0 (C-7), 49.4 (C-6), and 66.7 (C-8) ppm; MS *m/e* (rel. int.): 204 (100), 130 (23), 129 (24), 112 (30), 97 (51), and 74 (50).

*1,4-Dithiaspiro[4.5]decan-8-ol (**5**b)* (lit. (12*b*, 13*c*)): 91.9% yield; bp 98°C/0.75 Torr; mp 84.2–84.5°C (lit. (13*c*) mp 83–85°C); IR: 3260 cm^{-1}; ^1H NMR δ: 1.20–2.40 (9H, m), 3.38 (4H, m), and 3.56–3.88 (1H, m) ppm; ^{13}C NMR δ: 34.4 (C-7,9), 38.3 (C-2), 38.7 (C-3), 39.5 (C-6,10), 67.6 (C-5), and 68.0 (C-8) ppm.

*1,5-Dithiaspiro[5.5]undecan-9-ol (**6**b)*: 97.0% yield; bp 140°C/0.7 Torr; mp 79.8–80.5°C; IR: 3370 cm^{-1}; ^1H NMR δ: 1.73–2.07 (9H, m), 2.07–2.24 (2H, m), 2.32–2.47 (4H, m), and 3.75 (1H, m, $W_{1/2}$ = 15.2 Hz) ppm; ^{13}C NMR δ: 25.9 (C-3), 26.0 (C-2), 26.4 (C-4), 30.3 (C-7,11), 34.7 (C-8,10), 49.3 (C-6), and 68.7 (C-9) ppm; MS *m/e* (rel. int.): 204 (100), 145 (62), 112 (72), 79 (62), and 41 (74). Anal. calcd. for $C_9H_{16}OS_2$: C 52.90, H 7.89, S 31.38; found: C 52.92, H 7.86, S 31.17.

Can. J. Chem. Downloaded from www.nrcresearchpress.com by 91.144.44.67 on 09/07/12
For personal use only.

General incubation procedure for microbial reductions

The cultures of *Saccharomyces cerevisiae* (JCM 1819 and JCM 2214) were obtained from the Japan Collection of Microorganisms, JCM, Wako, Saitama, Japan. The culture medium (pH 6.2) for these microorganisms was prepared by dissolving 42 g of Difco dehydrated YM broth in 2 L of distilled water and was sterilized at 120°C for 20 min before incubation. The yeast was precultivated in a Sakaguchi flask containing 100 mL of the above medium at 24–25°C with shaking. This culture (OD = 1.2–2.8) was transferred into a 10-L jar fermenter containing 1.9 L of the same medium for preparative runs, and incubation was maintained for another 3–5 h at 24°C. Then the substrate ketone (151–642 mg) in EtOH (10–40 mL) was added to the culture (OD = 0.2–1.2, logarithmic phase) and the incubation was continued for a suitable period (0.8–10 days) at 23–25°C with good agitation and aeration. A part of the incubation mixture (3 mL) was pipetted out and extracted with ether at a regular time interval. Each ether extract was subjected to GLC. The products were identified by comparison with authentic samples. Yields of the products were determined on the basis of the peak areas on GLC and are expressed as the relative percent for the total amount of a whole reaction product extracted. Small scale reactions (substrate: EtOH: medium = 30 mg: 2 mL: 100 mL) in Sakaguchi flasks were performed with basically the same procedure.

Isolation of metabolites in preparative scale reactions

The following general procedure was employed. When sufficient (82–100%) reduction had occurred, the mixture was brought to pH 7 with 10% aqueous NaOH (pH usually moved downward to show ca. 5 at harvest), then filtered through Celite, saturated with NaCl, and extracted with dichloromethane (2–3 L). The dried ($MgSO_4$) dichloromethane extract was evaporated and the residual oil (ca. quantitative recovery) was separated into its components by PTLC on silica gel with hexane/ethyl acetate (2:1–3:1) development followed by Kugelrohr distillation. The overall data are summarized in Table 2. The individual reactions gave the following results; IR and NMR spectra for each product were identical with those detailed above.

Reduction of 1,4-dithiaspiro[4.5]decan-6-one

Run 1: The spiroketone (**1***a*, 597 mg, 3.17 mmol) with JCM 1819 for 3.6 days (95% conversion) gave spiroalcohol (+)-(6*S*)-**1***b* (561.6 mg, 93.1% yield, 86.6% ee), bp 110°C/0.8 Torr; $[\alpha]_D^{23}$ +6.37° (*c* 1.020, *l* = 0.1).

Run 2: The ketone (**1***a*, 600.8 mg, 3.19 mmol) with JCM 2214 for 3.5 days (82% conversion) gave unchanged **1***a* (61.7 mg, 10.3% yield) and alcohol (+)-(6*S*)-**1***b* (466.9 mg, 76.9% yield, 85.8% ee), bp 160°C/2.1 Torr; $[\alpha]_D^{23}$ +6.96° (*c* 1.150, *l* = 0.1).

Reduction of 1,5-dithiaspiro[5.5]undecan-7-one

Run 3: The ketone (**2***a*, 597.4 mg, 2.95 mmol) with JCM 1819 for 1.7 days (100% conversion) gave alcohol (+)-(7*S*)-**2***b* (546 mg, 90.5% yield, 99.4% ee), bp 119°C/0.8 Torr; $[\alpha]_D^{22.5}$ +38.3° (*c* 1.175, *l* = 0.1).

Run 4: The ketone (**2***a*, 642.1 mg, 3.17 mmol) with JCM 2214 for 1.1 days (99% conversion) gave alcohol (+)-(7*S*)-**2***b* (637.5 mg, 98.4% yield, 96.4% ee), bp 130–139°C/0.24 Torr; $[\alpha]_D^{24.2}$ +35.5° (*c* 2.36, *l* = 1.0).

Reduction of 1,4-dithiaspiro[4.5]decan-7-one

Run 5: The ketone (**3***a*, 602.1 mg, 3.20 mmol) with JCM 1819 for 1.0 days (100% conversion) gave alcohol (−)-(7*S*)-**3***b* (559.4 mg, 91.9% yield, 97.2% ee), bp 150°C/0.6 Torr; mp 56–58°C; $[\alpha]_D^{27}$ −2.94° (*c* 1.020, *l* = 0.1).

Run 6: The ketone (**3***a*, 601.1 mg, 3.19 mmol) with JCM 2214 for 3.8 days (97% conversion) gave unchanged **3***a* (13.5 mg, 2.25% yield) and alcohol (−)-(7*S*)-**3***b* (503.5 mg, 82.9% yield, 95.6% ee), bp 150°C/0.6 Torr; mp 59°C; $[\alpha]_D^{27}$ −3.48° (*c* 1.005, *l* = 0.1).

Reduction of 1,5-dithiaspiro[5.5]undecan-8-one

Run 7: The ketone (**4***a*, 150.6 mg, 0.744 mmol) with JCM 1819 for 6.9 days (95% conversion) gave alcohol (−)-(8*S*)-**4***b* (122.8 mg, 80.7% yield, 92.4% ee), bp 100°C/0.7 Torr; $[\alpha]_D^{25}$ −8.3° (*c* 5.540, *l* = 0.1).

Run 8: The ketone (**4***a*, 150.6 mg, 0.744 mmol) with JCM 2214 for 10.3 days (93% conversion) gave alcohol (+)-(8*S*)-**4***b* (113.7 mg, 74.8% yield, 83.1% ee), bp 100°C/0.7 Torr; $[\alpha]_D^{25}$ −5.65° (*c* 4.690, *l* = 0.1).

Enantiomeric excess determinations of microbial products **1**b–**4**b

The optical purities of alcohols **1***b*–**4***b* were determined by the HPLC analyses of the corresponding 3,5-dinitrophenylurethane (DNPU) derivatives, employing a chiral stationary phase. A Sumipax OA 1000 5-μm 4 mm × 50 cm column (Sumitomo Chemical Co., Ltd., Osaka) was used with hexane-1,2-dichloroethane-ethanol (100:20:5 for **1***b*–**3***b* derivatives or 100:20:1 for **4***b* derivatives) as solvent; flow rate 1.0 mL/min (60–80 kg/cm^2).

Absolute configuration determinations of microbial products **1**b–**4**b

The optically active and racemic alcohols **1***b*–**4***b* were converted to their MTPA esters **1***c*–**4***c* in quantitative yields by the standard literature procedure (7) using freshly prepared (−)-(2*S*)-α-methoxy-α-trifluoromethylphenyl acetyl chloride: $[\alpha]_D^{22.2}$ −130.9° (*c* 1.725, *l* = 1.0, CCl_4) (lit. (7) $[\alpha]_D$ 129.0 ± 0.2° (*c* 5.17, CCl_4)). The absolute configurations of the alcohols **1***b*–**4***b* derived from the microbial reductions were then determined by 1D and 2D ^{1}H NMR (400 MHz) examination of the signals from the specified protons of the MTPA esters (see Fig. 1 and Table 1). The esters of the racemic alcohols were used to provide the necessary reference peaks (i.e., *S*,*R*-diastereomers) for determining the Δδ values including shift direction for each pair of diastereotopic protons (7*b*). The chemical shifts of reference peaks are shown in brackets, if assignable, after each chemical shift of the following MTPA esters (i.e., *S*,*S*-diastereomers) of the microbial products. The peaks used also in ee determination are marked with a dagger.

*MTPA ester of 1,4-dithiaspiro[4.5]decan-6-ol (**1**c)*: IR (CCl_4): 1741 cm^{-1}; ^{1}H NMR (400 MHz) δ: 1.358 [1.358] (1H, m, H-8a), 1.57 (1H, m, H-9a), 2 (1H, m, H-9e), 1.817 [1.860] (1H, ddt, *J*(7a,7e) = 14.2, *J*(6,7a) = 6.3, *J*(7a,8e) = 5.2, H-7a), 1.98 [1.98] (1H, m, H-9a), 2.005 [2.04] (1H, m, H-7e), 2.185 [2.185] (2H, ddd, *J*(10a,10e) = 14.3, *J*(9a,10a) = 9.0, *J*(9e,10a) = 4.6, H-10a; dt, *J*(10a,10e) = 14.3, *J*(9e,10e) = *J*(9a,10e) = 4.6, H-10e), 3.220 [3.060]† (4H, m, H-2,3), 3.622 [3.593]† (3H, m, -OMe), and 5.178 [5.190] (1H, dd, *J*(6,7a) = 6.3, *J*(6,7e) = 3.0, H-6) ppm.

*MTPA ester of 1,5-dithiaspiro[5.5]undecan-7-ol (**2**c)*: IR (CCl_4): 1745 cm^{-1}; ^{1}H NMR (400 MHz) δ: 1.39 [1.4] (1H, m, H-9a), 1.41 [1.4] (1H, m, H-9e), 1.506 [1.5] (1H, m, H-10a), 1.7 [1.78] (1H, m, H-8e), 1.73 [1.7] (1H, m, H-10e), 1.85 [1.85] (1H, m, H-11a), ca. 1.87 [ca. 1.87] (1H, m, H-3e), 1.9 [1.9] (1H, m, H-11e), 2.045 [2.04] (1H, m, H-3a), 2.267 [2.323] (1H, ddq, *J*(8a,8e) = 14.8, *J*(7a,8a) = 10.4, *J*(8a,9a) = 5.2, *J*(8a,9e) = 2.4, H-8a), 2.558 [2.49] (1H, ddt, *J*(4a,4e) = 14.4, *J*(3a,4e) = 3.2, *J*(3e,4e) = 1.6, H-4e), 2.686 [2.452] (1H, ddt, *J*(2a,2e) = 14.4, *J*(2e,3a) = 3.2, *J*(2e,3e) = 1.6, H-2e), 2.964 [2.61] (1H, ddd, *J*(2a,2e) = 14.4, *J*(2a,3a) = 10.8, *J*(2a,3e) = 3.2, H-2a), 3.056 [3.136] (1H, ddd, *J*(4a,4e) = 14.4, *J*(3a,4a) = 10.8, *J*(3e,4a) = 3.2, H-4a), 3.634 [3.624] (3H, m, -OMe), and 5.62 [5.57]† (1H, m, H-7) ppm.

*MTPA ester of 1,4-dithiaspiro[4.5]decan-7-ol (**3**c)*: IR (CCl_4): 1749 cm^{-1}; ^{1}H NMR (400 MHz) δ: 1.295 [1.41] (1H, ddt, *J*(8a,8e) = 12.8, *J*(7,8a) = *J*(8a,9a) = 10.8, *J*(8a,9e) = 4.2, H-8a), 1.634 [1.67] (1H, m, H-9a), 1.83 [1.83] (1H, m, H-10a), 1.832 [1.87] (1H, m, H-9e), 2.005 [2.005] (1H, m, H-10e), 2.01 [2.1] (1H, m, H-8e), 2.064 [1.975] (1H, dd, *J*(6a,6e) = 12.8, *J*(6a,7) = 11.0, H-6a), 2.523 [2.462]† (1H, ddt, *J*(6a,6e) = 12.8, *J*(6e,7) = 4.2, *J*(6e,8e) = *J*(6e,10e) = 2.0, H-6e), 3.325 [3.316] (4H, m, H-2,3), 3.554 [3.548] (3H, m, -OMe), and 5.139 [5.134] (1H, tt, *J*(6a,7) = *J*(7,8a) = 10.8, *J*(6e,7) = *J*(7,8e) = 4.2, H-7) ppm.

*MTPA ester of 1,5-dithiaspiro[5.5]undecan-8-ol (**4**c)*: IR (CCl_4): 1745 cm^{-1}; ^{1}H NMR (400 MHz) δ: 1.356 [1.45] (1H, ddt, *J*(9a,9e) = 12.8, *J*(8a,9a) = *J*(9a,10a) = 10.8, *J*(9a,10e) = 4.4, H-9a), 1.613 [1.61] (1H, m, H-11a), 1.706 (1H, m, H-10a), 1.750 [1.662] (1H, dd, *J*(7a,7e) = 12.8, *J*(7a,8) = 10.8, H-7a), 1.84 (1H, m, H-10e), 1.966 (1H, m, H-3e), 2.05 [2.12] (1H, dq, *J*(9a,9e) = 12.8, *J*(8,9) = *J*(9,10) = 4.4, H-9e), 2.05 (1H, m, H-3a), 2.220 [2.23] (1H, m, H-11e), 2.764 (1H, ddd, *J*(2a,2e) = 14.4, *J*(2,3) = 7.4 and 3.4,

H-2e), 2.804 (1H, ddd, J(4a,4e) = 14.4, J(3,4) = 7.4 and 3.4, H-4e), 2.86 [2.80] (1H, dd, J(7a,7e) = 12.8, J(7e,8) = 4.4, H-7e), 2.903 (1H, ddd, J(4a,4e) = 14.4, J(3a,4a) = 9.5, J(3e,4a) = 3.4, H-4a), 2.975 (1H, ddd, J(2a,2e) = 14.4, J(2a,3a) = 9.5, J(2a,3e) = 3.4, H-2a), 3.560 [3.545]† (3H, m, -OMe), and 5.296 [5.305] (1H, tt, J(7a,8) = J(8,9a) = 10.8, J(7e,8) = J(8,9e) = 4.4, H-8) ppm.

Acknowledgments

We are grateful to Drs. Kazuo Komagata and Takashi Nakase, JCM, for the slants of type cultures as well as to Mr. Katsuhiko Kushida, Magnetics Application Manager, Varian Instruments Ltd., Shinjuku-ku, Tokyo, for the 2D COSY experiments. We are also indebted to Mr. Yoshinori Yamanaka for his assistance in checking the runs 2, 5, and 7 of microbial reductions.

1. (*a*) J. B. Jones. Tetrahedron, **42**, 3351 (1986); (*b*) R. Porter and S. Clark (*Editors*). Enzymes in organic synthesis. Ciba Foundation symposium 111. Pitman, London. 1985; (*c*) R. Bowen and S. Pugh. Chem. Ind. 323 (1985); (*d*) J. Tramper, H. C. van der Plas, and P. Linko (*Editors*). Studies in organic chemistry: Biocatalysts in organic syntheses. Elsevier, Amsterdam. 1985; (*e*) H. Simon, J. Bader, H. Gunther, S. Neumann, and J. Thanos. Angew. Chem. Int. Ed. Engl. **24**, 539 (1985); (*f*) G. M. Whitesides and C.-H. Wong. Angew. Chem. Int. Ed. Engl. **24**, 617 (1985); (*g*) C. J. Sih and C.-S. Chen. Angew. Chem. Int. Engl. **23**, 570 (1984); (*h*) C. J. Suckling (*Editor*). Enzyme chemistry, impact and applications. Chapman and Hall, London. 1984; (*i*) A. Kergomard. *In* Biotechnology. Vol. 6a; Biotransformations. *Edited by* H.-J. Rehm and G. Reed. Verlag Chemie, Weinheim, Basel. 1984. pp. 128–205; (*j*) J. A. Lepoivre. Janssen Chim. Acta, **2**, 20 (1984).
2. (*a*) K. Nakamura, T. Miyai, A. Nagar, S. Oka, and A. Ohno. Bull. Chem. Soc. Jpn. **62**, 1179 (1989); (*b*) M. Christen and D. H. G. Crout. J. Chem. Soc. Chem. Commun. 264 (1988); (*c*) C. Fuganti, P. Grasselli, and S. Servi. J. Chem. Soc. Perkin Trans. 1, 3061 (1988); (*d*) A. Manzocchi, A. Fiecchi, and E. Santaniello. J. Org. Chem. **53**, 4405 (1988); (*e*) A. Fauve and H. Veschambre. J. Org. Chem. **53**, 5215 (1988); (*f*) M. Utaka, E. Nishiyama, H. Furutani, and A. Takeda. J. Org. Chem. **52**, 1359 (1987); (*g*) R. Bernardi, R. Cardillo, D. Ghiringhelli, and O. V. de Pava. J. Chem. Soc. Perkin Trans. 1, 1067 (1987); (*h*) H. Ohta, K. Ozaki, and G. Tsuchihashi. Chem. Lett. 2225 (1987); (*i*) C.-Q. Han, D. DiTullio, Y.-F. Wang, and C. J. Sih. J. Org. Chem. **51**, 1253 (1986); (*j*) H. Akita, H. Matsukura, and T. Oishi. Tetrahedron Lett. 5397 (1986); (*k*) G. Guanti, L. Banfi, A. Guaragna, and E. Narisano. J. Chem. Soc. Chem. Commun. 138 (1986); (*l*) D. Seebach and M. Eberle. Synthesis, 37 (1986); (*m*) T. Fujisawa, E. Kojima, T. Itoh, and T. Sato. Chem. Lett. 1751 (1985); (*n*) B. Wipf, E. Kupfer, R. Bertazzi, and H. G. W. Leuenberger. Helv. Chim. Acta, **66**, 485 (1983).
3. (*a*) A. R. Krawczyk and J. B. Jones. J. Org. Chem. **54**, 1795 (1989); (*b*) T. Kitahara and K. Mori. Tetrahedron Lett. 451 (1985); (*c*) M. Kasai and H. Ziffer. J. Org. Chem. **48**, 712 (1983); (*d*) M. Nakazaki, H. Chikamatsu, and M. Asao. J. Org. Chem. **46**, 1147 (1981).
4. (*a*) A. P. Kozikowski and B. B. Mugrage. J. Org. Chem. **54**, 2275 (1989); (*b*) K. Mori and M. Fujiwhara. Tetrahedron, **44**, 343 (1988); (*c*) D. J. Kertesz and A. F. Kluge. J. Org. Chem. **53**, 4962 (1988); (*d*) T. Sato, H. Maeno, T. Noro, and T. Fujisawa. Chem. Lett. 1739 (1988); (*e*) D. W. Brooks, M. Wilson, and M. Webb. J. Org. Chem. **52**, 2244 (1987); (*f*) S. Butt, H. G. Davies, M. J. Dawson, G. C. Lawrence, J. Leaver, S. M. Roberts, M. K. Turner, B. J. Wakefield, W. F. Wall, and J. A. Winders. J. Chem. Soc. Perkin Trans. 1, 903 (1987).
5. K. Sakane, Y. Otsuji, and E. Imoto. Bull. Chem. Soc. Jpn. **47**, 2410 (1974).
6. N. Ōi and H. Kitahara. J. Chromatogr. **265**, 117 (1983).
7. (*a*) J. A. Dale, D. L. Dull, and H. S. Mosher. J. Org. Chem. **34**, 2543 (1969); (*b*) J. A. Dale and H. S. Mosher. J. Am. Chem. Soc. **95**, 512 (1973).
8. M. T. Barros, C. F. G. C. Geraldes, C. D. Maycock, and M. I. Silva. Tetrahedron, **44**, 2283 (1988).
9. E. Campaigne, N. F. Chamberlain, and B. E. Edwards. J. Org. Chem. **27**, 135 (1962).
10. V. Prelog. Pure Appl. Chem. **9**, 119 (1964).
11. (*a*) R. B. Woodward, I. J. Pachter, and M. L. Scheinbaum. Org. Synth. **54**, 37 (1974); (*b*) R. H. Jaeger and H. Smith. J. Chem. Soc. 160 (1955).
12. (*a*) B. M. Trost, K. Hiroi, and L. N. Jungheim. J. Org. Chem. **45**, 1839 (1980); (*b*) R. B. Woodward, I. J. Pachter, and M. L. Scheinbaum. Org. Synth. **54**, 39 (1974); (*c*) M. E. Kuehne. J. Org. Chem. **28**, 2124 (1963).
13. (*a*) V. L. Bell, A. B. Holmes, S.-Y. Hsu, G. A. Mock, and R. A. Raphael. J. Chem. Soc. Perkin Trans. 1, 1507 (1986); (*b*) V. L. Bell and A. B. Holmes. Synth. Commun. **12**, 323 (1982); (*c*) R. A. Moss and C. B. Mallon. J. Org. Chem. **40**, 1368 (1975).
14. S. Takano, S. Yamada, K. Tanigawa, S. Hatakeyama, and K. Ogasawara. Heterocycles, **4**, 953 (1976).
15. (*a*) N. H. Andersen, D. A. McCrae, D. B. Grotjahan, S. Y. Gabhe, L. J. Theodore, R. M. Ippolito, and T. K. Sarkar. Tetrahedron, **37**, 4069 (1981); (*b*) D. B. Grotjahn and N. H. Andersen. J. Chem. Soc. Chem. Commun. 306 (1981); (*c*) W. Lottenbach and W. Graf. Helv. Chim. Acta, **61**, 3087 (1978).
16. D. Seebach, I. Willert, A. K. Beck, and B.-T. Grobel. Helv. Chim. Acta, **61**, 2510 (1978).

Can. J. Chem. Downloaded from www.nrcresearchpress.com by 91.144.44.67 on 09/07/12
For personal use only.

Conformational isomerism in squaraines: saturation transfer NMR studies on hydroxy squaraines

PETER M. KAZMAIER, GORDON K. HAMER, AND RICHARD A. BURT
Xerox Research Centre of Canada, 2660 Speakman Drive, Mississauga, Ont., Canada L5K 2L1

Received July 31, 1989

This paper is dedicated to the memory of Professor Don Tavares

PETER M. KAZMAIER, GORDON K. HAMER, and RICHARD A. BURT. Can. J. Chem. **68**, 530 (1990).

The proton and ^{13}C NMR of azulene and dialkylaminohydroxyphenyl squaraines have been investigated. The four-membered ring carbon resonances occur in the 180–190 ppm range and are attributed to the cyclobutenediylium character of this structure. Some charge delocalization from the central ring to the pendent aromatic substituents was also observed, indicative of a substituent effect of the squaraine moiety on aminoaromatic systems equivalent to that of a formyl or acetyl group. Hydroxy squaraines **10** and **11** show the presence of two isomeric squaraine species in the proton NMR in deuterochloroform. Saturation transfer experiments confirm that these species are readily interconverted, and *cis/trans* isomerism (**9***a* ⇆ **9***b*) is consistent with these observations. The free energy difference between the two isomers at 318 K is calculated to be 3.0 and 3.2 kJ/mol for hydroxysquaraines **10** and **11** respectively.

Key words: squaraines, saturation transfer, NMR.

PETER M. KAZMAIER, GORDON K. HAMER et RICHARD A. BURT. Can. J. Chem. **68**, 530 (1990).

On a examiné les spectres RMN du proton et du ^{13}C de l'azulène et des dialkylaminohydroxyphényl squaraïnes. Les résonances des carbones du cycle à quatre chaînons sont observées dans la plage allant de 180 à 190 ppm et elles sont attribuées au caractère cyclobutènediylium de cette structure. On a aussi observé une certaine délocalisation de la charge du noyau central vers les substituants attachés au noyau aromatique; ces observations suggèrent qu'il existe un effet de substituant de la portion squaraïne sur les systèmes aminoaromatiques équivalent à celui d'un groupement formyle ou acyle. Dans les spectres RMN du proton des hydroxy squaraïnes **10** et **11** en solution dans le deutérochloroforme, on observe la présence de deux espèces isomères. Des expériences de transfert de saturation confirment que ces espèces se transforment facilement l'une dans l'autre; une isomérie *cis/trans* (**9***a* ⇆ **9***b*) est en accord avec ces observations. On a calculé que, à 318 K, les différences d'énergie libre entre les deux isomères sont de 3,0 et de 3,2 kJ/mol respectivement pour les hydroxysquaraïnes **10** et **11**.

Mots clés : squaraïnes, transfert de saturation, RMN.

[Traduit par la revue]

Introduction

Squaraines are 1,3-derivatives of squaric acid **1** in which the substituents are amines or highly electron-donating aromatic or heterocyclic groups (1). Since the discovery of these compounds by Treibs and Jacob in 1965 (2), their electronic structure has been the subject of considerable discussion. Treibs and Jacob depicted the structure of bis-2-pyrrylsquaraines by **2** because the properties of **2** were similar to the properties of the trimethine cyanine dyes (3) (for example compare the structures of **3** and **4**). At a later time Sprenger and Ziegenbein (4) described the electronic structures as either **5** or a hybrid of **5** and **6**. Canonical form **5** is particularly attractive because it corresponds to a Hückel aromatic system ($N = 0$).

More recently the consensus has shifted back to the original Treibs and Jacob proposal (5, 6), i.e., that a dipolar cyanine structure (e.g., **3**) and not a cyclobutenediylium structure best represents the electronic configuration of these compounds. The evidence for this conclusion rests on several observations.

1. The visible spectra of squaraines show close similarity to cyanine dyes (7).
2. The solubility of squaraines, like cyanines, is very low in most organic solvents consistent with a dipolar structure.
3. Squaraines, like cyanines, readily undergo addition with nucleophilic reagents.[1]
4. More recently, semiempirical molecular orbital (MNDO) studies (7) on **3** have shown a distinct polyene character to the squaraine chromophore. This quinoid character is enhanced when explicit solute/solvent interactions are taken into account.

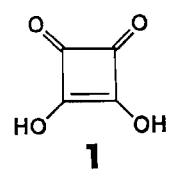

1

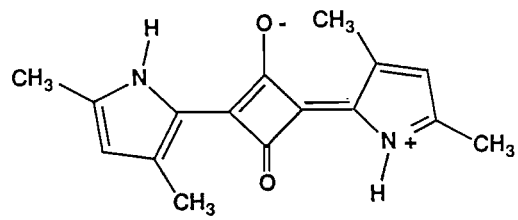

2

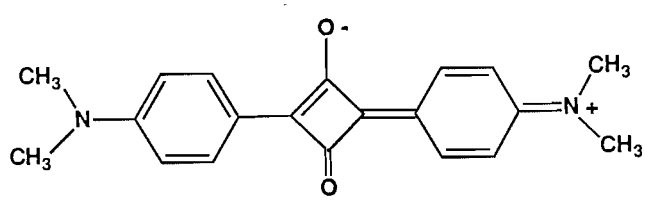

3

[1]P. M. Kazmaier and G. K. Hamer. Unpublished results.

Can. J. Chem. Downloaded from www.nrcresearchpress.com by 91.144.44.67 on 09/07/12
For personal use only.

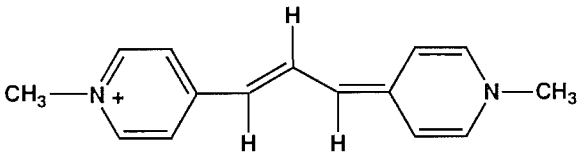

4

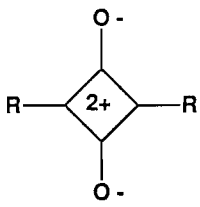

5

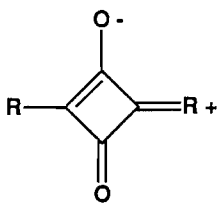

6

Support for this description can also be gleaned from work on amino squaraines. Both experimental and theoretical studies (9, 10) on a related series of aminosquaraine compounds (**7** and **8**) indicated that these compounds experience considerable C—N π-bonding between the central four-membered ring and the amino substituents, supporting the MNDO evidence presented for aryl squaraines.

The conclusion that canonical form **6** best approximates the electronic structure of squaraines leads to a number of implications for the NMR of these compounds. If the central ring has the charge distribution of **6** rather than **5**, then one would expect this ring to behave more like an α,β-unsaturated ketone than an aromatic system.

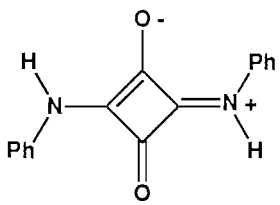

7

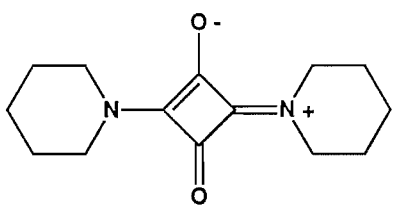

8

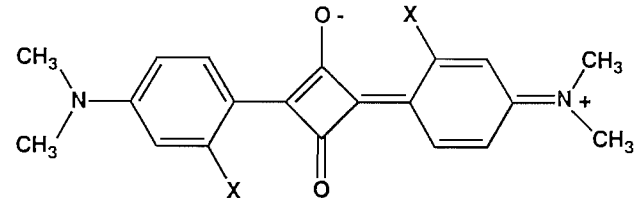

9a

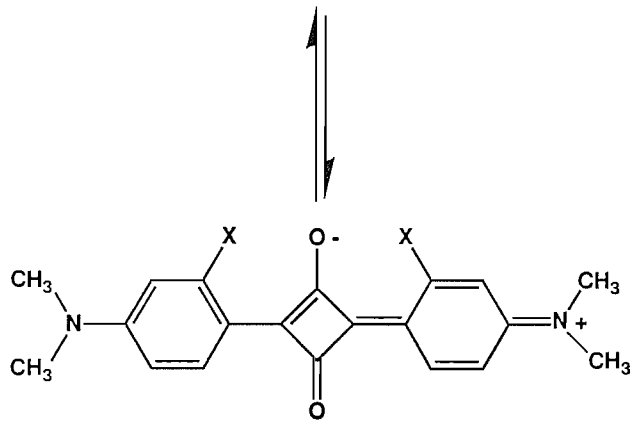

9b

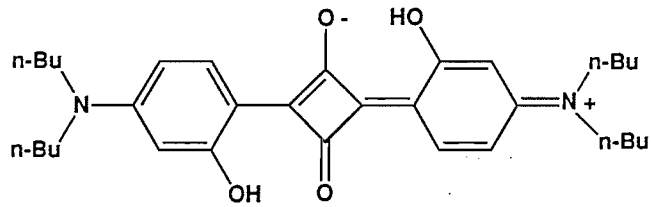

10

Secondly, canonical representation **6** indicates that the positive charge is delocalized to the pendent aromatic groups and that these groups would have a pseudo-quinoid structure.

Thirdly, if one considers squaraines such as **9**, then the dipolar canonical structure **6** predicts that the partial double bond character in the bond connecting the 4-membered ring to the 6-membered ring would make this rotational barrier high and, if the thermodynamics permit it, both isomers should be observable by NMR. Although many of these predictions are amenable to validation by ^{1}H or ^{13}C NMR, no ^{13}C NMR study of these materials has been reported. In this paper we report our findings on the ^{1}H and ^{13}C NMR of squaraines and report the observation of squaraine rotational isomers for the first time.

Experimental

Compounds were prepared by methods described in the literature (1, 4, 12, and 13) or as described below. Carbon NMR spectra were run on dilute (saturated) solutions (10^{-1} to 10^{-3} M) in $CDCl_3$ on a Bruker WM-250 spectrometer operating at 62.9 MHz. No attempt was made to standardize the concentrations since the solubilities of the squaraines varied widely. Proton spectra were also recorded in $CDCl_3$ solution on the same spectrometer at 250.13 MHz. Tetramethylsilane (TMS) was used as an internal chemical shift reference for both ^{1}H and ^{13}C spectra. Infrared spectra were recorded on a Beckman IR-4250. Combustion analyses were performed by Galbraith Laboratories, Knoxville, Tennessee.

Can. J. Chem. Downloaded from www.nrcresearchpress.com by 91.144.44.67 on 09/07/12
For personal use only.

Can. J. Chem. Downloaded from www.nrcresearchpress.com by 91.144.44.67 on 09/07/12
For personal use only.

Preparation of 3-(dibutylamino)phenol

A single-neck 250-mL round-bottomed flask with an air condenser, water condenser, nitrogen inlet, and magnetic stirbar was charged with 3-aminophenol (21.8 g, 0.2 mol) and tributyl phosphate (53.2 g, 0.2 mol). While stirring, the reaction mixture was heated to 120°C and then cautiously to 210°C to avoid an excessive exotherm. After heating at 210°C for 2.5 h, the reaction mixture was cooled. When the increase in viscosity made stirring difficult, aqueous sodium hydroxide (200 mL of 3.6 M solution) was added quickly and the mixture heated (80°C) until homogeneous, and then stirring was continued overnight. The mixture was transferred to a 1-L separatory funnel, extracted with ether (3 × 500 mL), and then the ether solution was dried over sodium sulfate. The product was isolated by rotary evaporation (35.2 g, 80%). Since this amino phenol oxidizes readily, it was passed through a column of silica gel just prior to use in the squaraine formation reaction. IR (CCl_4): 3410 br, 2980, 2960, 2900, 1633, 1592, 1517, 1380, 1206 cm^{-1}. ^1H NMR ($CDCl_3$, TMS) δ: 0.94 (t, 6H, CH_3), 1.3 (m, 4H, CH_2), 3.2 (m, 4H, NCH_2), 5.6 (br s, 1H, OH), 6.2 (m, 3H, Bz), 7.02 (t, 1H, BzH5, J_{12} = 8.09).

*Preparation of bis(4-dibutylamino-2-hydroxyphenyl)squaraine (**10**)*

A 3-necked 500-mL round-bottomed flask equipped with a thermometer, magnetic stirbar, and a 10-mL Dean–Stark trap topped with a condenser and nitrogen inlet was charged with squaric acid (4.38 g, 36.0 mmol), toluene (60 mL), and 1-butanol (150 mL). The mixture was stirred rapidly and heated to 100°C over 15 min at which time the squaric acid started to dissolve. When solution was complete, the 3-dibutylaminophenol (17 g, 76.9 mmol) was added dropwise in toluene (80 mL) over 20 min. A color change to red, then black, indicated that squaraine formation was underway. The reaction mixture was heated rapidly to reflux (internal temperature 105°C) and reflux was maintained for 2 h. Upon cooling to room temperature, the crystals were isolated by filtration and were thoroughly washed with ethyl acetate before drying under vacuum to constant weight (7.4 g, 40%); mp 196–197°C. UV–visible ($CHCl_3$, λ_{max} (log ε)): 668 (5.45). IR (KBr): 1610 cm^{-1} (squaraine carbonyl). Anal. calcd. for $C_{32}H_{44}N_2O_4$: C 73.81, H 8.52, N 5.38; found: C 73.88, H 8.30, N 5.30.

*Preparation of bis(8-hydroxy-9-julolidinyl)squaraine (**11**)*

A 3-necked 300-mL round-bottomed flask equipped with a thermometer, magnetic stirbar, and a 10-mL Dean–Stark trap topped with a condenser and nitrogen inlet was charged with squaric acid (1.72 g, 15.1 mmol), toluene (75 mL), and 1-butanol (75 mL). The mixture was stirred rapidly and heated to 100°C over 15 min at which time the squaric acid started to dissolve. When solution was complete, the amine (5.72 g, 30.2 mmol) was added in one portion. A color change to blue-green indicated that squaraine formation was underway. The reaction mixture was heated rapidly to reflux (internal temperature 105°C) and refluxed for 2 h. Upon cooling to room temperature, the crystals were isolated by filtration and thoroughly washed with ethyl acetate before drying under vacuum to constant weight (95%); mp 255°C (dec.). UV–visible (CH_3CN, λ_{max} (log ε)): 645 (5.51). IR (KBr): 1625 cm^{-1} (squaraine carbonyl). Anal. calcd. for $C_{28}H_{28}N_2O_4$: C 73.66, H 6.18, N 6.14; found: C 73.02, H 6.34, N 6.02.

Preparation of bis(9-julolidinyl)squaraine

Bis(9-julolidinyl)squaraine was prepared by a procedure identical to that described for **11**. The isolated yield was 49%; mp 226°C (dec.). UV–visible ($CHCl_3$, λ_{max} (log ε)): 660 (5.45). IR (KBr): 1603 cm^{-1} (squaraine carbonyl). Anal. calcd. for $C_{28}H_{28}N_2O_2$: C 79.22, H 6.65, N 6.60; found: C 79.32, H 6.71, N 6.62.

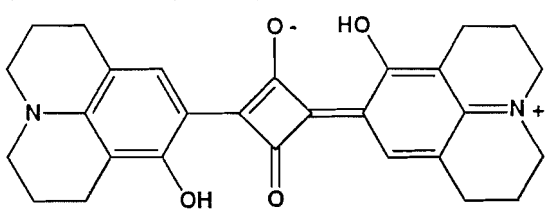

11

TABLE 1. A comparison of the carbon chemical shifts of bisguaiazulenylsquaraine and guaiazulene

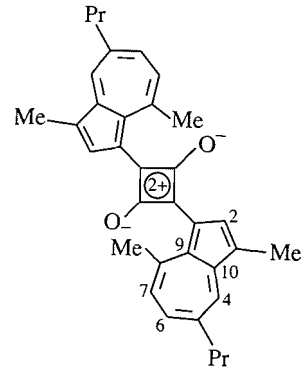

Carbon	Chemical shifts (ppm) GSq	G	Δ[a]
1	121.97	112.82	9.15
2	139.26	136.15	3.11
3	130.49	125.26	5.23
4	133.94	133.24	0.70
5	149.90	139.91	9.99
6	137.67	134.80	2.87
7	135.48	125.05	10.43
8	152.66	144.24	8.42
3-CH_3	12.90	12.83	0.07
8-CH_3	28.15	24.00	4.15
5-*C*H—$(CH_3)_2$	38.37	38.31	0.06
5-CH—$(CH_3)_2$	24.26	24.78	−0.52
9	142.50	137.44	5.06
10	147.15	136.39	10.76
Sq *C*	183.09		
Sq *C*—O	183.43		

[a]Δ = GSq − G.

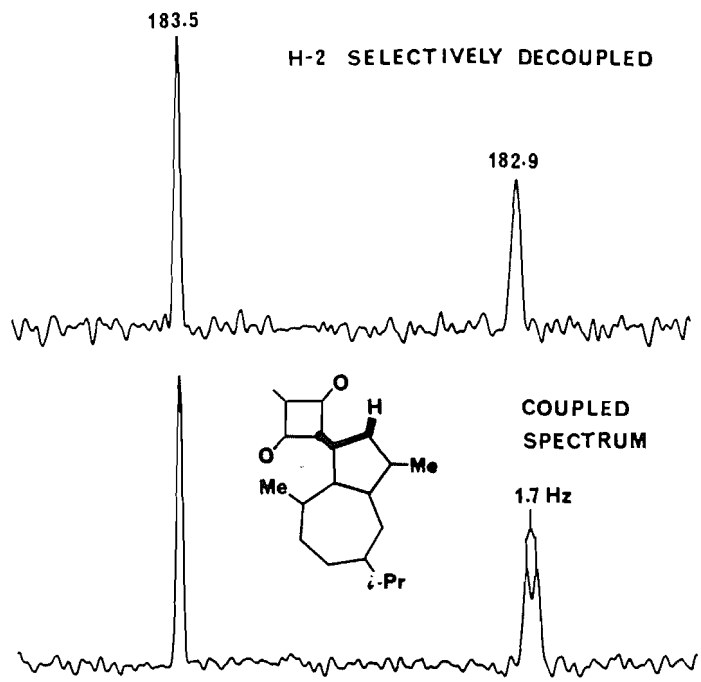

FIG. 1. Selective decoupling experiments for the assignment of the chemical shifts of squaraine carbons C2 and C4.

Can. J. Chem. Downloaded from www.nrcresearchpress.com by 91.144.44.67 on 09/07/12
For personal use only.

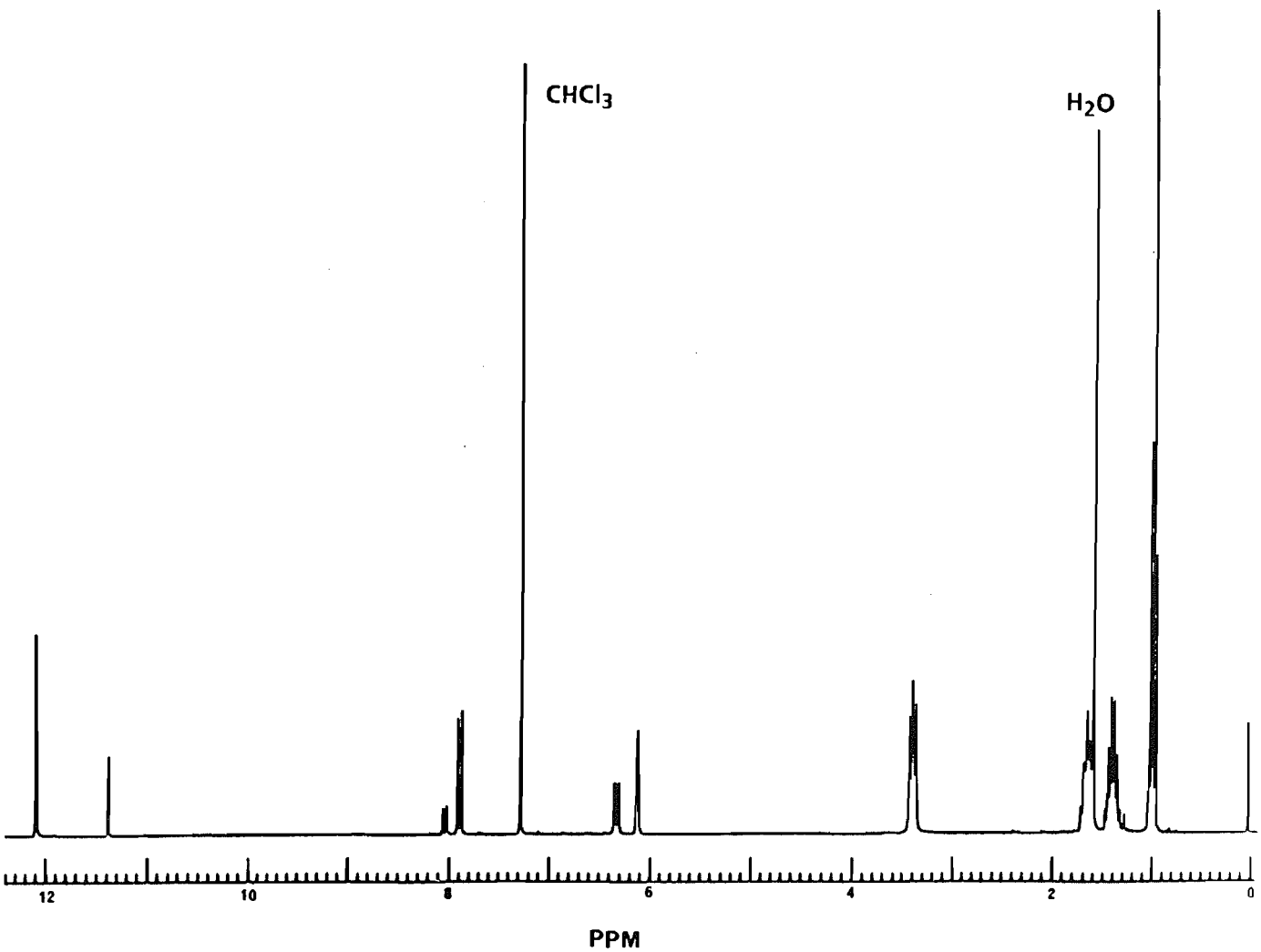

FIG. 2. The 250 MHz ^{1}H NMR spectrum of bis(4-dibutylamino-2-hydroxyphenyl)squaraine.

Results and discussion

Although many squaraines have been prepared (11–13) in our laboratory, most of these compounds are too insoluble to permit the accumulation of solution ^{13}C NMR spectra. Some compounds initially appear soluble enough but crystallize out of solution after several hours before spectrum accumulation is complete. For these reasons fewer ^{13}C NMR spectra are available than proton spectra.

Table 1 compares the ^{13}C chemical shifts of bisguaiazulenylsquaraine to the parent guaiazulene. Since the complete proton spectrum can be assigned for this molecule, it was straightforward to assign the carbon resonances by a series of selective heteronuclear low-power decoupling experiments. The quaternary carbons 9 and 10 were assigned by long-range coupling to the guaiazulene ring protons. The squaraine carbons appear at 183.09 ppm and 184.43 ppm in this compound. The two signals can be assigned by long-range coupling as shown in Fig. 1. The oxygen-bearing carbons are not coupled to any protons in the guaiazulene groups while the other 4-membered ring carbon is coupled to proton H2 ($^3J_{CH}$ = 1.7 Hz).

The strong deshielding observed for these carbons is not only restricted to bisguaiazulenylsquaraine. Table 2 summarizes the chemical shifts of the 4-membered ring resonances for three other compounds. In all cases the chemical shifts for these resonances fall in the range 180–190 ppm. This strong deshield-

TABLE 2. C-13 chemical shifts of the 4-membered ring carbons

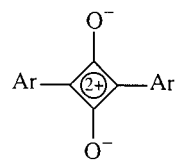

Aryl group	δ, 4-membered ring carbons
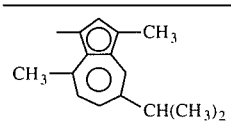	183.5 (C—O), 182.9
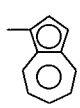	183.5, 183.5
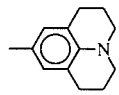	184.7, 184.2
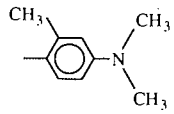	190.3, 182.5

Can. J. Chem. Downloaded from www.nrcresearchpress.com by 91.144.44.67 on 09/07/12
For personal use only.

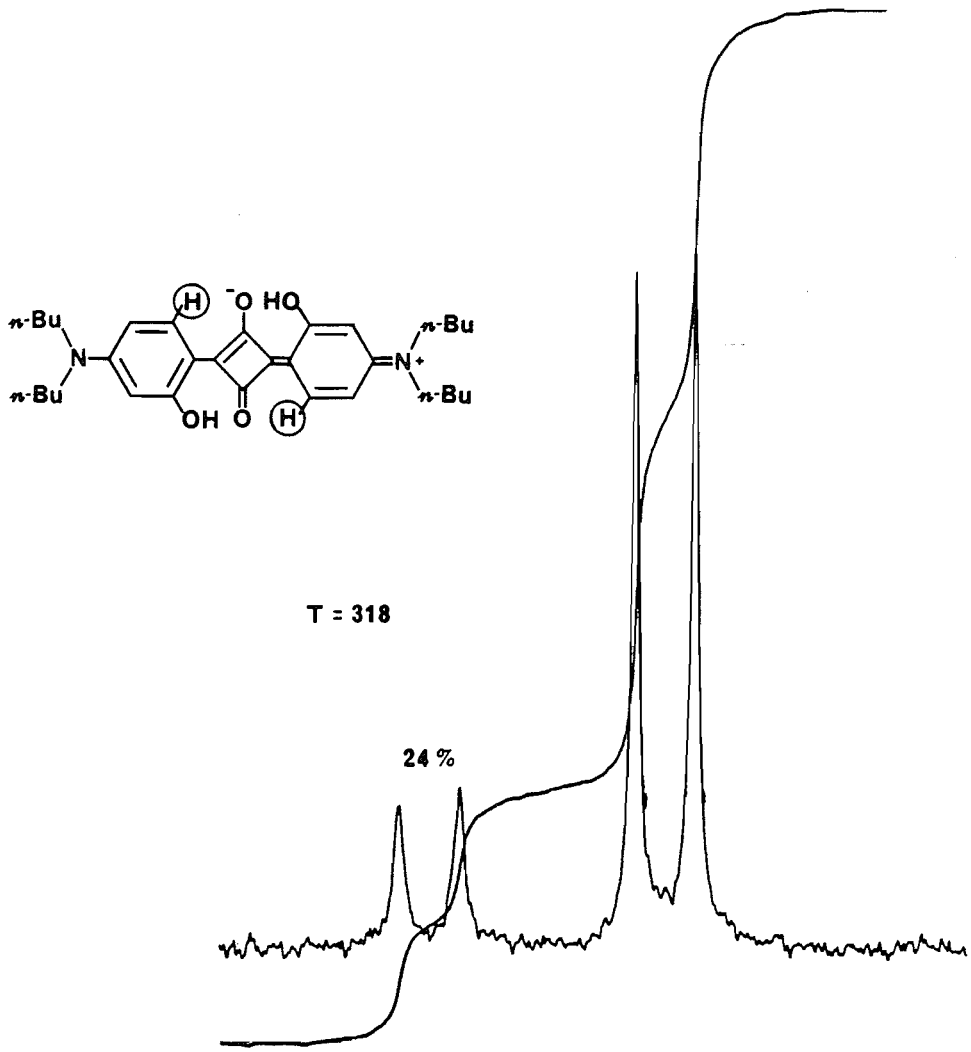

FIG. 3. The relative intensities of the *ortho* hydrogen resonances in bis(4-dibutylamino-2-hydroxyphenyl)squaraine.

TABLE 3. A comparison of the carbon chemical shifts for bisjulolidinylsquaraine to julolidine

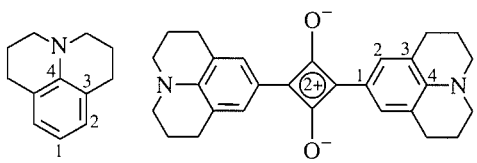

Carbon	Julolidine	Squaraine	Δδ
C-1	115.8	119.5	3.7
C-2	126.9	130.0	3.1
C-3	121.6	121.8	0.2
C-4	143.0	149.2	6.2

ing for the ring is consistent with substantial cyclobutendiylium character for this moiety (14–17).

If one turns one's attention to the pendent guaiazulene groups in bisguaiazulenylsquaraine (Table 1), then several carbons show sizeable downfield (10 ppm) shifts from the parent guaiazulene. If one compares these shifts observed for bisguaiazulenylsquaraine to the shifts reported for 1-substituted azulene (18–20), then 10-ppm substituent shifts in the 7-membered ring are only observed on mono nitration. These results suggest that some positive charge is delocalized into the 7-membered ring. The methyl group on C-8 is strongly deshielded (4.15 ppm) because of the strong steric interaction between this methyl group and the squaraine oxygen.

Table 3 summarizes the chemical shifts for the julolidine group in bis-9-julolidinylsquaraine. In this compound the chemical shifts of the julolidine group in the squaraine are similar to the parent julolidine. The shift differences are approximately what one would expect if a carbonyl substituent were placed on julolidine (e.g., formyl or acetyl) *para* to the nitrogen.

In conclusion then, the ^{13}C NMR of squaraines investigated suggests that the squaraine ring system has substantial cyclobutendiylium character. Chemical shift changes in the pendent aromatic substituents are consistent with some electron density donation to the squaraine moiety. The magnitude of the electron density donation is approximately that experienced by aromatic aminoaldehydes.

A study of Dreiding and CPK models of the compounds described in Table 2 suggests that, whereas the azulene and julolidine squaraines are planar, the guaiazulene and bis(4-dimethylamino-2-methylphenyl)squaraines are decidedly nonplanar. The relative insensitivity of the squaraine carbon

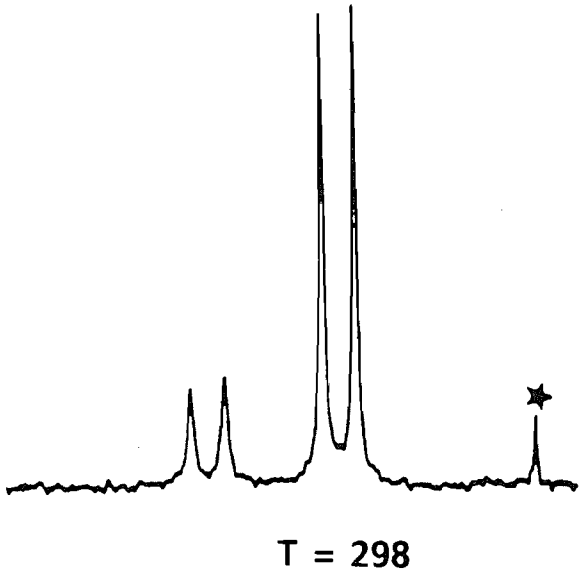

FIG. 4. The unperturbed *ortho* hydrogen resonances before irradiation at 298 K.

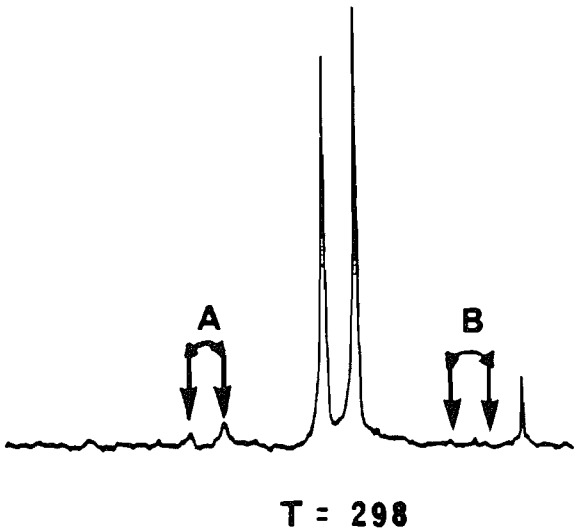

FIG. 5. The effect of decoupling at frequency A at 298 K.

resonances to chromophore planarity and the small squaraine-induced shifts in the julolidine (Table 3) and guaiazulene squaraines (Table 1) suggests that π-donation is relatively unimportant as a means of stabilization.

In the introduction it was pointed out that for squaraines such as **10**, a dipolar canonical structure such as **6** would predict that two isomers (*cis* and *trans*) would be observable if thermodynamics were to permit it. The 250-MHz ^{1}H NMR spectrum of bis(4-dibutylamino-2-hydroxyphenyl)-squaraine **10** is shown in Fig. 2. For both the OH (δ = 12.09, 11.38) and *ortho* protons (δ = 8.02, 7.87) two resonances are observed. Figure 3 shows the *ortho* protons clearly as two doublets ($^1J_{HH}$ = 9.2 Hz). The minor isomer makes up 24% of the total; a similar result is obtained from integration of the OH resonances.

To establish that the major and minor components do, in fact, arise from equilibrating conformational isomers, a series of ^{1}H saturation transfer experiments were carried out. The results are shown in Figs. 4–7 for the *ortho* proton doublets. Figure 4 shows the unperturbed spectrum; the starred peak is a ^{13}C

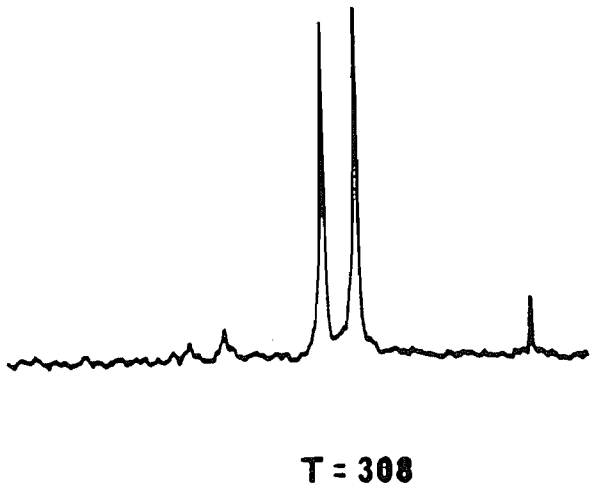

FIG. 6. The effect of decoupling at frequency A at 308 K.

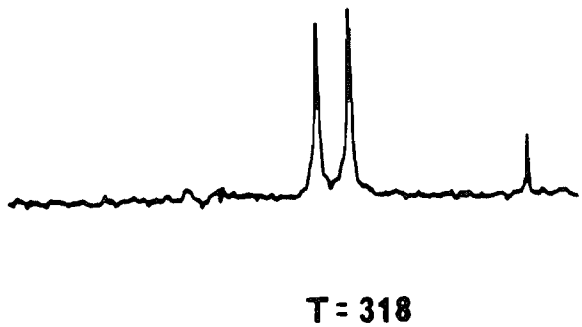

FIG. 7. The effect of decoupling at frequency A at 318 K.

satellite of the residual $CHCl_3$ of the $CDCl_3$ solvent and serves as a convenient internal intensity standard. In the saturation transfer experiment the minor isomer resonance (Fig. 5, A) was saturated by rapidly shifting the frequency of the low power decoupler between the two peaks of the doublet (21). After ca. 100 frequency-shift cycles the decoupler was gated off and the spectrum acquired in the normal way. As shown in Fig. 5, the minor resonance is almost completely suppressed by this technique and the intensity of major doublet is decreased. To confirm that this effect is the result of saturation transfer and not "spill-over" from the decoupler, the decoupler frequency was shifted an equal distance to the low frequency side of the major doublet (B) and the experiment repeated; the result was identical to the control spectrum, Fig. 4. Further evidence of conformational isomerism is provided by Figs. 6 and 7. As one expects, at higher temperatures the rate of interconversion is increased and consequently saturation transfer becomes more efficient.

Molecular models suggest that *cis,trans* isomerism is not an unreasonable explanation for this phenomenon. This compound is not unique in demonstrating this kind of isomerism. Compound **11** shows a similar behaviour. The magnitude of the rotational barrier could not be determined because of the low solubility of these compounds at low temperatures. However, the success of the saturation transfer, and the observation that addition of a hydrogen-bonding solvent such as CD_3OD to a $CDCl_3$ solution of **10** collapses the pair of doublets to a single doublet, suggests that the barrier is smaller than the 49–74 kJ/mol barrier normally associated with cyanines (8, 22).

Can. J. Chem. Downloaded from www.nrcresearchpress.com by 91.144.44.67 on 09/07/12
For personal use only.

The free energy difference between the two isomers at 318 K is calculated to be 3.0 and 3.2 kJ/mol for hydroxysquaraines **10** and **11** respectively.

Acknowledgements

We thank Anne Dewar for typing the manuscript.

1. A. H. SCHMIDT. Synthesis, 961 (1980).
2. A. TREIBS and K. JACOB. Angew. Chem. **77**, 680 (1965).
3. E. J. VAN LARE. *In* Kirk–Othmer Encyclopedia of Chemical Technology. Vol. 6. *Edited by* A. Standen. John Wiley and Sons, New York. 1965. pp. 605–624.
4. H. E. SPRENGER and W. ZIEGENBEIN. Angew. Chem. Int. Ed. Engl. **7**, 530 (1968).
5. A. H. SCHMIDT. *In* Oxocarbons. *Edited by* R. West. Academic Press, New York. 1980. pp. 185–231.
6. H. FALK, O. HOFER, and A. LEODOLTER. Monatsh. Chem. **106**, 983 (1975).
7. R. W. BIGELOW and H. J. FREUND. Chem. Phys. **107**, 159 (1986).
8. S. SAEBOE and J. ALMLOEF. Acta Chem. Scand. **A34**, 651 (1980).
9. E. W. NEUSE and B. R. GREEN. J. Am. Chem. Soc. **97**, 3987 (1975).
10. P. H. M. BUDSELAAR, H. DIETRICH, J. MACHELEID, R. WEISS, and P. VON R. SCHLEYER. Chem. Ber. **118**, 2118 (1985).
11. R. O. LOUTFY, C. K. HSIAO, and P. KAZMAIER. Photogr. Sci. Eng. **27**, 5 (1983).
12. P. M. KAZMAIER, R. BURT, G. DIPAOLA-BARANYI, C. K. HSIAO, T. BLUHM, G. K. HAMER, M. TAYLOR, R. O. LOUTFY, and T. I. MARTIN. J. Imaging Sci. **32**, 1 (1988).
13. G. DIPAOLA-BARANYI, C. K. HSIAO, P. M. KAZMAIER, R. BURT, R. O. LOUTFY, and T. I. MARTIN. J. Imaging Sci. **32**, 60 (1988).
14. T. CHIANG, R. C. KERBER, S. D. KIMBALL, and J. W. LAUHER. Inorg. Chem. **18**, 1687 (1979).
15. E. V. DEHMLOW. Tetrahedron Lett. 203 (1975).
16. G. A. OLAH and J. S. STARAL. J. Am. Chem. Soc. **98**, 6290 (1976).
17. G. A. OLAH, J. M. BOLLINGER, and A. M. WHITE. J. Am. Chem. Soc. **91**, 3667 (1969).
18. P. R. WELLS, K. G. PENMAN, and I. D. RAE. Aust. J. Chem. **33**, 2221 (1980).
19. T. A. HOLAK, S. SADIGH-ESFANDIARY, F. R. CARTER, and D. J. SARDELLA. J. Org. Chem. **45**, 2400 (1980).
20. J. R. LLINAS, D. ROARD, M. DERBESY, and E. J. VINCENT. Can. J. Chem. **53**, 2911 (1975).
21. S. FORSEN and R. A. HOFFMAN. J. Chem. Phys. **39**, 2892 (1963).
22. J. DALE, R. G. LICHTENHALER, and G. TEIEN. Acta Chem. Scand. **B33**, 141 (1979).

Can. J. Chem. Downloaded from www.nrcresearchpress.com by 91.144.44.67 on 09/07/12
For personal use only.

Kinetics of the reduction of the tropylium and xanthylium cations by 1,4-dihydropyridine derivatives

JOHN W. BUNTING AND M. MORGAN CONN
Department of Chemistry, University of Toronto, Toronto, Ont., Canada M5S 1A1

Received June 14, 1989

JOHN W. BUNTING and M. MORGAN CONN. Can. J. Chem. **68**, 537 (1990).

The pH-dependences of the apparent second-order rate constants (k_2^{app}) for the reduction of 2,4,6-cycloheptatrien-1-ol and 9-xanthydrol by each of 1-benzyl-1,4-dihydronicotinamide (BNH) and 10-methyl-9,10-dihydroacridine (MAH) have been measured in 20% acetonitrile – 80% water, at 25°C and ionic strength 1.0. For each of these reactions, the pH-dependence of k_2^{app} is only consistent with reduction occurring via the aromatic cation (either tropylium or xanthylium) that is present in equilibrium with these alcoholic species. The relative second-order rate constants (k_2^{BNH}/k_2^{MAH}) for reductions by these two reducing agents (1700 for tropylium and 770 for xanthylium) are similar for these two cations. These ratios are also similar to those observed for a variety of nitrogen heteroaromatic hydride acceptors, even though the absolute magnitudes of these rate constants vary by 10^{10}-fold. The second-order rate constants for the reductions of the tropylium and xanthylium cations are predicted reasonably well by their pK_{R^+} values, with the latter cation being (7×10^5)-fold more reactive than its π-isoelectronic *N*-methyl acridinium cation. The xanthylium cation has the greatest k_2^{BNH}/k_{OH} ratio yet observed for any heteroaromatic cation, and this value further extends the known range of this ratio as a function of reactivity.

Key words: hydride transfer, kinetics of reduction, 1,4-dihydropyridine derivatives, tropylium cation, xanthylium cation.

JOHN W. BUNTING et M. MORGAN CONN. Can. J. Chem. **68**, 537 (1990).

Opérant à 25°C et à une force ionique de 1,0, dans des solutions contenant 20% d'acétonitrile et 80% d'eau, on a mesuré la relation qui existe entre le pH et les constantes apparentes de vitesse du deuxième ordre (k_2^{app}) pour la réduction du cyclohepta-2,4,6-trièn-1-ol et du xanthydr-9-ol soit par le 1-benzyl-1,4-dihydronicotinamide (BNH) ou par la 10-méthyl-9,10-dihydroacridine (MAH). Pour chacune de ces réactions, la relation entre le pH et le k_2^{app} ne correspond qu'à celle attendue pour une réduction se produisant par le biais d'un cation aromatique (soit tropylium ou xanthylium) qui est présent à l'équilibre dans ces espèces alcooliques. Les constantes relatives des vitesses de réaction du second ordre (k_2^{BNH}/k_2^{MAH}) pour les réductions par ces deux agents réducteurs (1700 pour le tropylium et 770 pour le xanthylium) sont semblables pour ces deux cations. Même si les valeurs absolues de ces constantes de vitesse varient par des facteurs allant jusqu'à 10^{10}, ces rapports sont aussi similaires à ceux observés pour un grand nombre de dérivés hétéroaromatiques azotés accepteurs d'hydrure. Utilisant les valeurs des pK_{R^+} des cations, on peut aussi prédire assez correctement les constantes de vitesse du deuxième ordre pour les réductions des cations tropylium et xanthylium; ce dernier cation est environ 7×10^5 fois plus réactif que le cation *N*-méthyl acridinium qui lui est π-isoélectronique. La valeur du rapport k_2^{BNH}/k_{OH} du cation xanthylium est la plus élevée à avoir été observée jusqu'à maintenant et cette valeur élargit la plage connue de ce rapport en fonction de la réactivité.

Mots clés : transfert d'hydrure, cinétique de la réduction, dérivés 1,4-dihydropyridines, cation tropylium, cation xanthylium.

[Traduit par la revue]

Can. J. Chem. Downloaded from www.nrcresearchpress.com by 91.144.44.67 on 09/07/12
For personal use only.

Kinetic studies of the hydride transfer reaction described by eq. [1] are currently under active investigation in many laboratories (1–10). This reaction formally involves hydride transfer from a donor (DH) to an acceptor (A^+), and can be considered a hydride transfer between two heteroaromatic cations, when a dihydropyridine derivative (DH) is used to reduce a nitrogen heteroaromatic cation (A^+).

[1] $A^+ + DH \rightarrow AH + D^+$

Reactions of this type originally attracted interest as mechanistic probes of the chemistry of enzymic reactions employing the nicotinamide coenzyme redox couple (NAD(P)H–NAD(P)$^+$) (11, 12). More recently, rate–equilibrium correlations of such reactions have been vigorously explored in connection with the application of Marcus theory to the hydride transfer process (1, 13–15). There is now a significant body of literature relating to the reduction of a variety of pyridinium, quinolinium, isoquinolinium, acridinium, and phenanthridinium cations (2). Various 1,2- and 1,4-dihydropyridine derivatives have been used as the hydride donor species, with 1,4-dihydronicotinamides and 9,10-dihydroacridines being the most commonly investigated hydride donors. We felt that a significant addition to this area would be provided by a quantitative investigation of the rates of reduction of a wider variety of cationic acceptor species (A^+) than has been the case up until now. As an initial effort towards such an extension, we have chosen to measure the rates of reduction of the tropylium (**1**) and xanthylium (**2**) cations by both 1-benzyl-1,4-dihydronicotinamide (**3** = BNH) and 10-methyl-9,10-dihydroacridine (**4** = MAH).

1

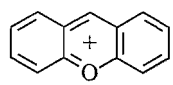

2

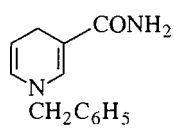

3

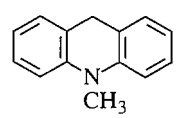

4

Several considerations were involved in the choice of these two cations. Firstly, we wished to include aromatic cations other than the nitrogen heteroaromatic species that have been predominantly investigated to date. Secondly, we required cations for which the second-order rate constants for hydroxide ion attack were available (16, 17), since we wished to continue our comparisons (18) of the rates of reduction with the rates of reaction with hydroxide ion as a standard nucleophile. Thirdly, we wished to choose cations that might be expected to be more reactive than the cations investigated to date. Because the tropylium (16) and xanthylium (19) cations have pK_{R^+} values

Can. J. Chem. Downloaded from www.nrcresearchpress.com by 91.144.44.67 on 09/07/12
For personal use only.

considerably lower than any of the nitrogen heterocyclic cations previously studied, they should fulfill this third criterion since linear free energy relationships between the second-order rate constant for reduction and pK_{R^+} have been established for other series of cations (18, 20, 21). Fourthly, the xanthylium cation is an attractive acceptor, since it is π-isoelectronic with the acridinium cations that have been the subjects of numerous investigations in this area.

The choice of 1-benzyl-1,4-dihydronicotinamide and 10-methyl-9,10-dihydroacridine as hydride donors was based upon our earlier observations (2) of an approximately constant relative reactivity for these two donors towards several acceptor cations. We wished to explore whether this relative reactivity would also be applicable to two quite different cationic acceptors chosen according to the criteria indicated above.

Experimental

Materials

Tropylium tetrafluoroborate and 9-hydroxyxanthene (9-xanthydrol) were both obtained from Aldrich Chemical Co. They were recrystallized from ethanol and aqueous ethanol, respectively, and characterized by ^{1}H NMR spectroscopy. The tropylium salt displayed a clean singlet δ 9.34 (in CF_3CO_2H relative to $(CH_3)_4Si$), and 9-hydroxyxanthene showed δ 2.25 (br s, OH), 5.68 (s, 1H), 6.90–7.60 (m, 8H) (in $CDCl_3$). 1-Benzyl-1,4-dihydronicotinamide and 10-methyl-9,10-dihydroacridine were synthesized as previously reported (2, 22). All compounds were stored in dark bottles in a vacuum desiccator over Drierite. Potassium chloride, potassium hydroxide, and all buffer species (CH_2ClCO_2H/KOH (pH = 2.5–3.7), CH_3CO_2H/KOH (pH = 4.0–5.5), NaH_2PO_4/Na_2HPO_4 (pH = 6.2–7.2), and $(HOCH_2)_3CNH_2$/HCl (pH = 7.7–8.7)) were the best commercially available grades. Acetonitrile was spectroscopic grade.

Kinetic studies

All rate data were obtained in buffered aqueous solutions containing 20% or 30% acetonitrile (v/v) (see below), at 25°C and ionic strength 1.0 (KCl). Stock solutions of reagents for kinetic studies were kept in the dark when not in use and discarded after a maximum of 48 h. Care was taken to ensure that complete solubility of the reactants and products was maintained before and during all kinetic runs. Solubility limitations were the major consideration in defining the highest accessible concentration of the excess component in each reaction system. The reaction between **2** and **3** proved to be incompatible with 20% acetonitrile containing phosphate buffer, although solubility was maintained under these conditions in 30% acetonitrile. The choice of specific experimental conditions was sometimes influenced by the occurrence of slow reactions of one or more of the individual components. In all cases, conditions were chosen so that such background reactions occurred at less than 1% of the rate of the reduction under investigation.

All reactions were followed spectrophotometrically under pseudo-first-order conditions with 17- to 200-fold excesses of the acceptor species over the hydride donors ([BNH] = 0.04 mM and [MAH] = 0.02 mM). Most reactions were followed on a Varian Cary 210 spectrophotometer, with digitized absorbance data being recorded on a Commodore 4048 computer. Occasional runs were also followed on a Unicam SP-1800 spectrophotometer equipped with a Unicam AR-25 linear recorder. Data were collected for at least 95% of each reaction, with the exception of some very slow reactions between **2** and **3** in which data were only obtained over the first 75% of the reaction. The pH was measured at the end of each kinetic run on a Radiometer PHM82 pH meter equipped with a GK2401B combination electrode.

Pseudo-first-order rate constants were calculated by fitting the absorbance (A) at time (t) to the relationship:

$$A = A_f + (A_i - A_f)\exp(-k_{obs}t)$$

via the Marquardt algorithm, treating the initial absorbance (A_i), the final absorbance (A_f), and the pseudo-first-order rate constant as parameters to be evaluated.

Results

In aqueous solutions, the tropylium ($pK_{R^+} = 4.76$ (16)) and xanthylium ($pK_{R^+} = -0.83$ (19)) cations exist in equilibrium with their hydroxide adducts (**5** and **6**, respectively). The alcohols **5** and **6** are the predominant species present in most of the reactions in the current study, although the tropylium cation is the major species in the most acidic solutions investigated for the reaction with MAH. The predominance of these alcoholic species in these reactions had both advantages and disadvantages. The advantage lay in the fact that what proved to be very fast reactions of these cationic acceptors could be studied under routine pseudo-first-order conditions in which only low equilibrium concentrations of the acceptor species were present. The disadvantage lay in the limited solubilities of **5** and **6** in the predominantly aqueous media in use. Clean kinetic data were only obtainable below 3.5 mM for **5** and below 2.2 mM for **6**.

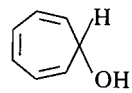

5

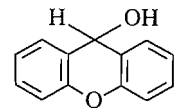

6

1-Benzyl-1,4-dihydronicotinamide (**3**, λ_{max} = 357 nm) and the 10-methylacridinium cation (the oxidation product from **4**) are the only species with significant absorbances above 300 nm in the current studies. Reactions of BNH were followed by the disappearance of the absorbance due to this species at 357 nm. Reactions of MAH produced the very characteristic absorption spectrum (23) of the 10-methylacridinium cation over the range 330–450 nm. Kinetic data were obtained by following the increase in absorbance at the intense maximum at 356 nm.

Pseudo-first-order rate constants (k_{obs}) were evaluated at six acceptor concentrations at each pH. In all cases k_{obs} was found to be cleanly proportional to the total concentration ($[A^+] + [AOH]$) of the acceptor species in solution (e.g., Figs. 1 and 2). Apparent second-order rate constants (k_2^{app}) were evaluated from the slopes of plots of k_{obs} vs. ($[A^+] + [AOH]$) at each pH. Standard errors in each k_2^{app} were in the range ±2%–±6%. The pH dependences of k_2^{app} are displayed in Figs. 3 and 4.

The pH-dependent pseudo-second-order rate constants are defined by:

$$-\frac{d[DH]}{dt} = k_2^{app}([A^+] + [AOH])[DH]$$

$$= k_2^{app}(1 + K_{R^+}/[H^+])[A^+][DH]$$

$$= k_2[A^+][DH]$$

$$[2] \qquad k_2^{app} = k_2/(1 + K_{R^+}/[H^+])$$

The pH-dependence shown in Fig. 3 for the reaction of **1** with **4** was fitted to eq. [2], with $k_2 = 15.1(\pm 0.6)\ M^{-1}\ s^{-1}$ and $pK_{R^+} = 4.82(\pm 0.05)$. For the other three reactions, log k_2^{app} appears to be linear in pH with negative unit slope. These latter three reactions were investigated over pH ranges for which $K_{R^+} \gg [H^+]$, and under this condition eq. [2] simplifies to $k_2^{app} = k_2[H^+]/K_{R^+}$; i.e.,

$$\log k_2^{app} = \log k_2 + pK_{R^+} - pH$$

Thus for each of these reactions, k_2 may be readily evaluated from the experimental data in Figs. 3 and 4.

The second-order rate constants (k_2) for each of these four reactions are summarized in Table 1. Data for the reaction of **2** with **3** in 30% acetonitrile have been corrected to 20%

Can. J. Chem. Downloaded from www.nrcresearchpress.com by 91.144.44.67 on 09/07/12
For personal use only.

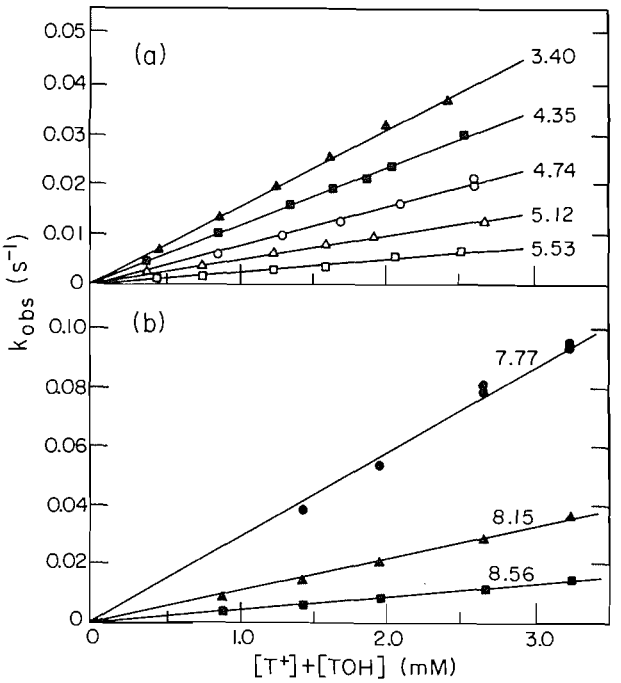

FIG. 1. Concentration dependence of the pseudo-first-order rate constants for reduction of the tropylium cation (T^+) in equilibrium with its hydroxide adduct (TOH): (a) by 10-methyl-9,10-dihydroacridine (0.02 mM); (b) by 1-benzyl-1,4-dihydronicotinamide (0.04 mM) in solutions with pH as indicated. All data are in 20% acetonitrile – water.

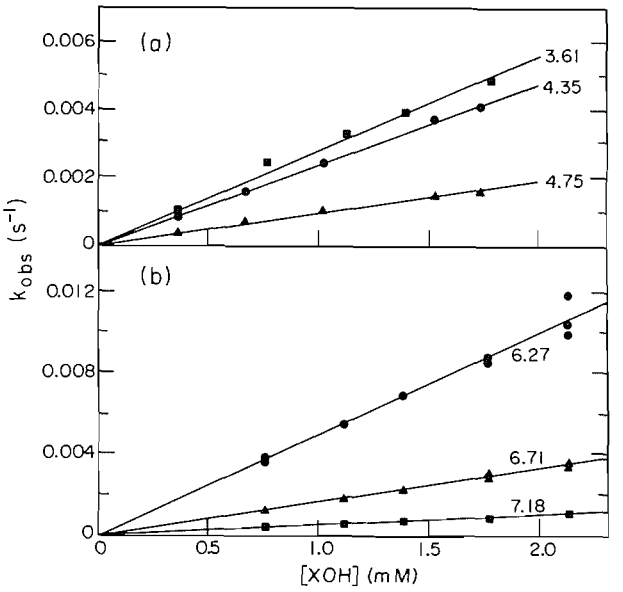

FIG. 2. Concentration dependence of the pseudo-first-order rate constants for the reduction of 9-xanthydrol (XOH): (a) by 10-methyl-9,10-dihydroacridine (0.02 mM); (b) by 1-benzyl-1,4-dihydronicotinamide (0.04 mM) in solutions with pH as indicated. Data for pH 3.61 in (a) and all data in (b) are in 30% acetonitrile – water; other data are in 20% acetonitrile – water.

acetonitrile using a factor of 4.6. This factor was obtained from the observation that k_2^{app} for the reaction of **2** with **4** is 4.6-fold smaller in 30% acetonitrile than in 20% acetonitrile at pH 3.6. We have assumed that the solvent effects on the reduction of the xanthylium cation will be similar for the two different reductants.

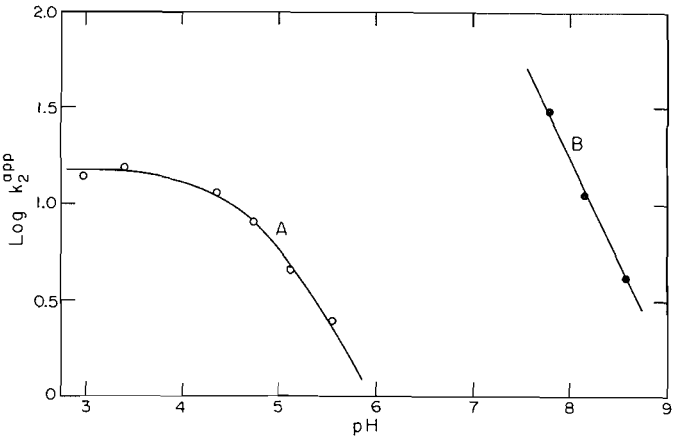

FIG. 3. The pH-dependence of k_2^{app} for the reduction of the tropylium cation: (A) by 10-methyl-9,10-dihydroacridine (the curve is eq. [2] with k_2 = 15.1 and pK_{R^+} = 4.82); (B) by 1-benzyl-1,4-dihydronicotinamide (the line has slope −1). All data in 20% acetonitrile – water.

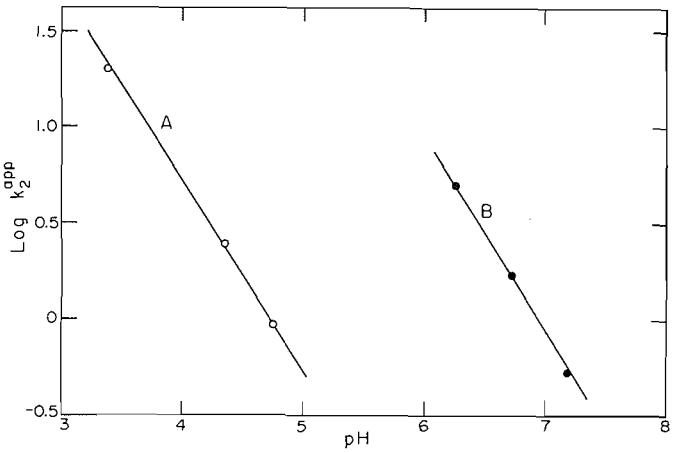

FIG. 4. The pH-dependence of k_2^{app} for the reduction of 9-xanthydrol: (A) by 10-methyl-9,10-dihydroacridine (20% acetonitrile – water); (B) by 1-benzyl-1,4-dihydronicotinamide (30% acetonitrile – water). Both lines have slope −1.

TABLE 1. Second-order rate constants for reduction of tropylium and xanthylium cations[a]

Oxidant	Reductant	$k_2(M^{-1}\ s^{-1})$
Tropylium cation	MAH	15.1(±0.6)
	BNH	$2.5(\pm0.3)\times10^4$
Xanthylium cation	MAH	$3.5(\pm0.3)\times10^5$
	BNH	$2.7(\pm0.2)\times10^8$
	BNH	$5.9(\pm0.5)\times10^7$ [b]

[a]At 25°C, in 20% CH_3CN – 80% H_2O, ionic strength 1.0 (unless stated otherwise).
[b]At 25°C, in 30% CH_3CN – 70% H_2O, ionic strength 1.0.

Discussion

The pH–rate profiles shown in Figs. 3 and 4 are consistent with a reaction that occurs as outlined in Scheme 1. This scheme generates the rate constant relationship given in eq. [2].

Of the four reactions included in the current study, only one reaction appears to have been investigated previously. Grishin and Yasnikov (24) reported a kinetic investigation of the

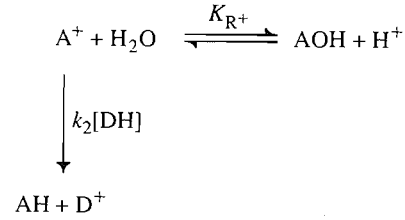

SCHEME 1

reaction of the tropylium cation with three N-substituted 1,4-dihydronicotinamides in 50% ethanol – water at 25°C. For the *N*-benzyl derivative (**3**), they reported a third-order rate constant, $k_3 = 5.4 \times 10^8\ M^{-2}\ min^{-1}$, which was defined in a way that is equivalent to eq. [3] at neutral pH. This equation is equivalent to eq. [4], and so a second-order rate constant $k_2 = k_3K_{R^+}$ can be evaluated provided that pK_{R^+} for the tropylium cation can be evaluated in 50% ethanol – water. If one uses $pK_{R^+} = 3.1$ for this cation in this solvent (25), then $k_2 = 7000\ M^{-1}\ s^{-1}$, which is only 28% of the value obtained for this same reaction in 20% acetonitrile – water in the current study. In this light, the 4.6-fold decrease in rate reported above, for the reaction of the xanthylium cation with MAH upon going from 20% to 30% acetonitrile, is not unreasonable. Other dramatic rate changes with small changes in solvent polarity have also been reported in related reductions (26, 27), although, in general, solvent effects seem to be quite variable for this type of reaction (5, 28).

$$[3]\quad \text{Rate} = k_3[DH][AOH][H^+]$$

$$[4]\quad = k_3K_{R^+}[DH][A^+]$$

As anticipated above, the tropylium and xanthylium cations proved to be much more reactive than any of the nitrogen heteroaromatic cations that have previously been examined with these two reductants. For instance, the 10-methylacridinium cation reacts with 1-benzyl-1,4-dihydronicotinamide with $k_2 = 400\ M^{-1}\ s^{-1}$ under the current experimental conditions (29). Thus, the xanthylium cation reacts with this reductant (7×10^5)-fold faster than does the π-isoelectronic acridinium cation. Interestingly, $\Delta(\log k_2)/\Delta pK_{R^+} = -0.54$ when one compares these two cations reacting with this reductant. This value is similar to the slopes of the relationships in eqs. [5] and [6], respectively, for the reduction of quinolinium (21) and isoquinolinium (20) cations by BNH.

$$[5]\quad \log k_2 = -0.56\ pK_{R^+} + 7.3$$

$$[6]\quad \log k_2 = -0.50\ pK_{R^+} + 4.9$$

The reactivity of the tropylium cation with BNH is predicted reasonably well by the linear free energy relationship for C-4 reduction of quinolinium cations. Thus extrapolation of eq. [5] to $pK_{R^+} = 4.82$ gives $k_2 = 4.0 \times 10^4\ M^{-1}\ s^{-1}$ compared with the value of $2.5 \times 10^4\ M^{-1}\ s^{-1}$ that is experimentally observed. The tropylium cation is much more reactive than predicted by eq. [6] for isoquinolinium cations ($k_2 = 310\ M^{-1}\ s^{-1}$ for $pK_{R^+} = 4.82$). The 10-methylacridinium cation and the xanthylium cation are both somewhat more reactive (8-fold and 5-fold, respectively) than predicted by eq. [5] for quinolinium cations.

The k_2^{rel} values for the reduction of the tropylium (1700) and xanthylium cations (770) by BNH and MAH are given in Table 2. This table also includes all literature data that we have been able to locate for the reduction of a common oxidant by these two reductants. With two exceptions, the k_2^{rel} values in this table lie within the range 770–1700. One of these exceptions (the 2-methyl-5-nitroisoquinolinium cation with $k_2^{rel} = 120$) is not unexpected since the reduction of this cation by BNH is known to be complicated by the presence of nonproductive complexation between these two reactants (2, 22). The other exception involves the 10-methylacridinium cation for which k_2^{rel} appears to be "normal" in acetonitrile solution (4) but is reported to be threefold larger in 80% 2-propanol – 20% water (13). Thus, aside from these two exceptions, k_2^{rel} varies by only twofold despite the fact that the individual reactivities of these oxidants vary by 10^{10}-fold with either of these reducing agents individually. Note that the neutral oxidant, **7**, shows the same k_2^{rel} as the cationic oxidants in Table 2. There is almost constant selectivity towards these two reducing agents over a 10^{10}-fold change in reactivity. This phenomenon represents a further expression of a Ritchie N^+ correlation (31) for organic cation reactivity.

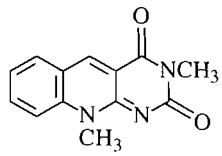

7

Although these organic cations show essentially constant selectivity towards two reducing agents, such a constant selectivity is not observed if one compares the relative reactivities of these same cations towards one of these reducing agents and nucleophilic attack by hydroxide ion. Such a comparison is presented in Table 3 for reduction by 1-benzyl-1,4-dihydronicotinamide. This table includes data for the xanthylium and tropylium cations, and also data for several nitrogen heteroaromatic cations for which both k_{OH} and k_2 (for reduction by BNH in 20% acetonitrile – 80% water) are available. The k_2/k_{OH} ratios vary (9×10^6)-fold. Enhanced k_2/k_{OH} reactivities have previously been demonstrated (18) for cations that give 1,4-dihydropyridine reduction products when compared with the *N*-methyl isoquinolinium cation, which gives a 1,2-dihydropyridine. In that work it was also noted that the k_2/k_{OH} ratio shows a significant increase with increasing reactivity (k_2). Consistent with this conclusion, we now find that the xanthylium cation, which is the most reactive cation in reductions by BNH, also displays by far the largest k_2/k_{OH} ratio (= 7.7). The tropylium cation has k_2/k_{OH} smaller than might have been expected in terms of this reactivity–selectivity relationship. Nevertheless, this cation does display k_2 consistent with its pK_{R^+}, and k_2/k_{OH} is greater for this cation than for any *N*-heteroaromatic cation other than the *N*-methyl acridinium ion.

We have recently suggested (32) that the order of k_2/k_{OH} ratios that is observed for cations generating 1,4-dihydropyridine reduction products can be traced to the importance of charge-transfer interactions between the cation and reductant. Other workers have also concluded that such charge-transfer species may lie on the reaction coordinate for these formal hydride transfer processes (3, 30). It should be noted that it has been established (32–34) that the order of charge-transfer absorption maxima (λ_{max}) with a common donor species follows the order: xanthylium > tropylium > 10-methylacridinium > 1-methylquinolinium > 1-methylpyridinium. Fur-

Can. J. Chem. Downloaded from www.nrcresearchpress.com by 91.144.44.67 on 09/07/12
For personal use only.

TABLE 2. Relative reactivities of 1-benzyl-1,4-dihydronicotinamide (BNH) and 10-methyl-9,10-dihydroacridine (MAH) in hydride transfer reactions

Cationic oxidant	$k_2^{BNH}(M^{-1}\,s^{-1})$	$k_2^{MAH}(M^{-1}\,s^{-1})$	k_2^{rel} $(= k_2^{BNH}/k_2^{MAH})$	Conditions	Ref.
Xanthylium	2.7×10^{8}	3.5×10^{5}	770	20% CH_3CN/80% H_2O 25°C, I = 1.0	[a]
Tropylium	2.5×10^{4}	15.1	1700	20% CH_3CN/80% H_2O 25°C, I = 1.0	[a]
10-Methylacridinium	210	0.043	4900	80% Me_2CHOH/20% H_2O 25°C	13
	79.9	0.051	1600	CH_3CN, 30°C	4
3-Cyano-1-methylquinolinium	121	0.103	1200	20% CH_3CN/80% H_2O 25°C, I = 1.0	2
4-Cyano-2-methylisoquinolinium	29	0.033	880	20% CH_3CN/80% H_2O 25°C, I = 1.0	2
2-Methyl-5-nitroisoquinolinium	0.12	0.001	120	20% CH_3CN/80% H_2O 25°C, I = 1.0	2
Compound **7**[b]	0.032	1.9×10^{-5}	1700	80% Me_2CHOH/20% H_2O 25°C	30

[a]Current work.
[b]1,5-Dihydro-3,10-dimethyl-5-deazaisoalloxazine.

TABLE 3. Relative reactivities of aromatic cations towards reduction by 1-benzyl-1,4-dihydronicotinamide and attack by hydroxide ion

Cation	pK_{R^+}	$k_{OH}(M^{-1}\,s^{-1})$	$k_2^{BNH}(M^{-1}\,s^{-1})$[a]	k_2^{BNH}/k_{OH}	Rel. k_2^{BNH}/k_{OH}
N-Me pyridinium(C-4)[b]	20.5	0.011	4.2×10^{-7}	3.8×10^{-5}	45
N-Me quinolinium(C-4)[c]	17.4	2	5.0×10^{-3}	2.5×10^{-3}	2900
N-Me isoquinolinium[d]	16.3	940	8×10^{-4}	8.5×10^{-7}	(1)
N-Me acridinium[e]	10.0	550	400	0.73	8.6×10^{5}
Tropylium[f]	4.76	3.1×10^{5}	2.5×10^{4}	0.081	9.5×10^{4}
Xanthylium[g]	−0.83	3.5×10^{7}	2.7×10^{8}	7.7	9.1×10^{6}

[a]At 25°C, in 20% CH_3CN – 80% H_2O, ionic strength 1.0.
[b]Data from refs. 18, 35.
[c]Data from refs. 21, 36.
[d]Data from refs. 20, 37.
[e]Data from refs. 29, 38.
[f]Data from ref. 16 and current work; k_{OH} at 23°C.
[g]Data from refs. 17, 19 and current work; k_{OH} at 20°C.

thermore, this order also reflects the order of stabilities of charge-transfer complexes between these cations and a common donor species (32). It therefore transpires that the choice of the xanthylium and tropylium cations for the current study has provided a valuable extension of the general structure–reactivity relationships that are emerging with respect to hydride transfer reactions of the type described by eq. [1].

Acknowledgements

We appreciate the continued support of this work by the Natural Sciences and Engineering Research Council of Canada.

1. M. M. KREEVOY, D. OSTOVIC, I. H. LEE, D. A. BINDER, and G. W. KING. J. Am. Chem. Soc. **110**, 524 (1988).
2. J. W. BUNTING and M. L. LUSCHER. Can. J. Chem. **66**, 2524 (1988).
3. T. T. ROMOFF, N. S. SAMPSON, and P. VAN EIKEREN. J. Org. Chem. **52**, 4454 (1987).
4. M. F. POWELL and T. C. BRUICE. J. Am. Chem. Soc. **105**, 7139 (1983).
5. A. VAN LAAR, H. J. VAN RAMESDONK, and J. W. VERHOEVEN. Recl. Trav. Chim. Pays-Bas, **102**, 157 (1983).
6. A. OHNO, T. SHIO, H. YAMAMOTO, and S. OKA. J. Am. Chem. Soc. **103**, 2045 (1981).
7. R. SRINIVASAN, R. T. MEDARY, H. F. FISHER, D. J. NORRIS, and R. STEWART. J. Am. Chem. Soc. **104**, 807 (1982).
8. C. I. F. WATT. Adv. Phys. Org. Chem. **24**, 57 (1988).
9. S. YASUI and A. OHNO. Bioorg. Chem. **14**, 70 (1986).
10. S. ZEHANI and G. GELBARD. Nouv. J. Chim. **10**, 511 (1986).
11. R. J. KILL and D. A. WIDOWSON. *In* Bioorganic chemistry. Vol. IV. *Edited by* E. van Tamalen. Academic Press, New York. 1978. Chap. 8.
12. D. J. SIGMAN, J. HAJDU, and D. J. CREIGHTON. *In* Bioorganic chemistry. Vol. IV. *Edited by* E. van Tamalen. Academic Press, New York. 1978. Chap. 14.
13. R. M. G. ROBERTS, D. OSTOVIC, and M. M. KREEVOY. Faraday Discuss. Chem. Soc. **74**, 257 (1982).

Can. J. Chem. Downloaded from www.nrcresearchpress.com by 91.144.44.67 on 09/07/12
For personal use only.

14. M. M. KREEVOY and I. H. LEE. J. Am. Chem. Soc. **106**, 2550 (1984).
15. M. M. KREEVOY, D. OSTOVIC, D. G. TRUHLAR, and B. C. GARRETT. J. Phys. Chem. **90**, 3766 (1986).
16. C. D. RITCHIE and H. FLEISCHHAUER. J. Am. Chem. Soc. **94**, 3481 (1972).
17. R. A. MCCLELLAND, N. BANAIT, and S. STEENKEN. J. Am. Chem. Soc. **111**, 2929 (1989).
18. J. W. BUNTING and J. L. BOLTON. Tetrahedron, **42**, 1007 (1986).
19. J. C. MARTIN and R. G. SMITH. J. Am. Chem. Soc. **86**, 2252 (1964).
20. J. W. BUNTING, V. S. F. CHEW, and G. CHU. J. Org. Chem. **47**, 2303 (1982).
21. J. W. BUNTING and N. P. FITZGERALD. Can. J. Chem. **63**, 655 (1985).
22. J. W. BUNTING and S. SINDHUATMADJA. J. Org. Chem. **46**, 4211 (1981).
23. J. W. BUNTING and W. G. MEATHREL. Can. J. Chem. **52**, 981 (1974).
24. O. M. GRISHIN and A. A. YASNIKOV. Ukr. Khim. Zh. **34**, 70 (1968); Soviet Prog. Chem. (Engl. Transl.), **34**, 62 (1968).
25. K. OKAMOTO, K. TAKEUCHI, K. KOMATSU, Y. KUBOTA, R. OHARA, M. ARIMA, K. TAKAHASHI, Y. WAKI, and S. SHIRAI. Tetrahedron, **39**, 4011 (1983).
26. R. H. ABELES, R. F. HUTTON, and F. H. WESTHEIMER. J. Am. Chem. Soc. **79**, 712 (1957).
27. P. VAN EIKEREN and D. L. GRIER. J. Am. Chem. Soc. **98**, 4655 (1976).
28. J. HAJDU and D. S. SIGMAN. Biochemistry, **16**, 2841 (1977).
29. J. W. BUNTING, V. S. F. CHEW, G. CHU, N. P. FITZGERALD, A. GUNASEKARA, and H. T. P. OH. Bioorg. Chem. **12**, 141 (1984).
30. I. H. LEE, D. OSTOVIC, and M. M. KREEVOY. J. Am. Chem. Soc. **110**, 3989 (1988).
31. C. D. RITCHIE. Pure Appl. Chem. **50**, 1281 (1978); Can. J. Chem. **64**, 2239 (1986).
32. J. W. BUNTING and M. L. LUSCHER. Can. J. Chem. **66**, 2532 (1988).
33. H. J. DAUBEN, JR. and J. D. WILSON. Chem. Commun. 1629 (1968).
34. M. FELDMAN and S. WINSTEIN. Theor. Chim. Acta, **10**, 86 (1968).
35. J. W. BUNTING. Tetrahedron, **43**, 4277 (1987).
36. J. W. BUNTING and N. P. FITZGERALD. Can. J. Chem. **62**, 1301 (1984).
37. J. W. BUNTING, V. S. F. CHEW, and S. SINDHUATMADJA. Can. J. Chem. **59**, 3195 (1981).
38. J. W. BUNTING and W. G. MEATHREL. Can. J. Chem. **51**, 1965 (1973).

Can. J. Chem. Downloaded from www.nrcresearchpress.com by 91.144.44.67 on 09/07/12
For personal use only.

NMR study of π–σ* stereoelectronic interactions in 3-substituted benzocycloheptene derivatives

Y. AUBIN AND M. ST-JACQUES[1]

Département de chimie, Université de Montréal, C.P. 6128, Succ. A, Montréal (Québec), Canada H3C 3J7

Received July 4, 1989

Y. AUBIN and M. ST-JACQUES. Can. J. Chem. **68**, 543 (1990).

Dynamic NMR methods are used to study 3-substituted benzocycloheptene derivatives, useful models for investigating the conformational effect of the stereoelectronic π–σ* orbital interaction. The 11 compounds studied are divided in two subgroups, the first one containing mainly halogenated derivatives (F, Cl, Br, and OCH_3) and the second consisting of oxy derivatives (OCH_3, OCH_2CH_3, $OCH{=}CH_2$, OAc, *p*-OPh-R, where R = H, OCH_3, and NO_2). The results for the first series show the presence of two chair conformations (C_a and C_e) characterized by a decreasing C_a population with increasing electronegativity of the substituent. This trend suggests the presence of a dominant π–σ* interaction for Cl and Br stabilizing the C_a form. The larger C_e population observed for F suggests that a strong attractive interaction with the aromatic *peri* hydrogen is present in this compound. Finally, in the oxy-substituent series, the populations trend does not correspond to that predicted from the π–σ* orbital interaction, but the individual population perturbations appear to be caused primarily by electrostatic interactions involving the nonsymmetrical polar substituents.

Key words: low temperature NMR, conformational analysis, seven-membered rings, orbital interactions, benzocycloheptene derivatives.

Y. AUBIN et M. ST-JACQUES. Can. J. Chem. **68**, 543 (1990).

On a utilisé des méthodes de RMN dynamique pour étudier des benzocycloheptènes substitués en position 3 qui sont de bons modèles pour évaluer l'effet conformationnel de l'interaction stéréoélectronique de l'orbitale π–σ*. Les 11 composés étudiés ont été divisés en deux sous-groupes : le premier comprend principalement des dérivés halogénés (F, Cl, Br et OCH_3) alors que le second est formé de dérivés oxygénés (OCH_3, OCH_2CH_3, $OCH{=}CH_2$, OAc et *p*-OPh-R dans lequel R = H, OCH_3 et NO_2). Les résultats obtenus avec la première série de composés démontrent que deux conformations chaises (C_a et C_e) sont présentes et que la population de la conformation C_a diminue avec une augmentation de l'électronégativité du substituant. Cette tendance suggère que, pour les substituants Cl et Br, il existe une interaction π–σ* dominante qui stabilise la forme C_a. La présence d'une population plus élevée de C_e avec le F suggère que, dans ce composé, l'hydrogène aromatique en *péri* exerce une forte interaction attractive. Enfin, dans les composés oxygénés, les variations des populations ne correspondent pas à celles que l'on pourrait prévoir en se basant sur l'interaction de l'orbitale π–σ*; toutefois, les perturbations dans les populations individuelles semblent refléter principalement des interactions électrostatiques impliquant les substituants polaires qui ne sont pas symétriques.

Mots clés : RMN à basse température, analyse conformationnelle, cycles à sept chaînons, interactions orbitales, dérivés de benzocycloheptène.

[Traduit par la revue]

Introduction

Earlier results on derivatives of methylenecyclohexane (1) predict, for α-halogens (**1**), an increase in the population of the axial chair conformation (C_a) with the size of the halogen substituent. This prediction was based on the contribution from two interactions: the first one (allylic strain or $A^{(1,3)}$ strain) destabilizes the C_e conformer while the second stabilizes the C_a form through a π–σ* orbital interaction as proposed by Lessard and co-workers (2).

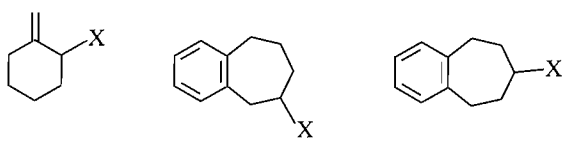

1 **2** **3**

Results for analogous oxy derivatives of methylenecyclohexane show that substituents containing an unsaturated moiety show greater preference for the C_e form than predicted by the π–σ* interaction (2). This apparent deviation was rationalized in terms of an unsaturation effect (2).

Our aim was to investigate the conformational consequence of the π–σ* interaction and the unsaturation effect through a study of 3-substituted derivatives of benzocycloheptene. This system, having a chair geometry, is complementary to methylenecyclohexane and can more easily be studied by low temperature NMR techniques such as were used to characterize the conformational properties of 4- and 5-substituted derivatives (3) represented by structures **2** and **3**. Two groups of substituents were selected: the first comprises mainly the halogen substituents (compounds **5**–**8**) whereas the second contains saturated and unsaturated 3-oxy derivatives (**8**–**14**). It was believed that the first group should reveal the effect of electronegativity on the π–σ* interaction while the second might shed some light on the unsaturation effect and, if confirmed, permit its characterization.

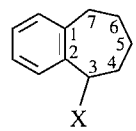

4 X = CH_3
5 X F
6 X = Cl
7 X = Br
8 X = OCH_3
9 X = OCH_2CH_3
10 X = $OCH{=}CH_2$
11 X = OAc
12 X = OPh
13 X = *p*-$OPhOCH_3$
14 X = *p*-$OPhNO_2$

Results

*Spectral analysis and stable conformations of compounds **4**–**14***

The carbon-13 NMR spectra of compounds **4**–**14** (except for compound **7** (X = Br)) show spectral changes at low temperature. Only the aliphatic regions have been analyzed

[1]Author to whom correspondence may be addressed.

Can. J. Chem. Downloaded from www.nrcresearchpress.com by 91.144.44.67 on 09/07/12
For personal use only.

TABLE 1. Carbon-13 chemical shifts[a] and populations of several 3-substituted benzocycloheptene derivatives at high and low temperatures[b]

Compound	Solvent	Temp. (°C)	Conf./Pop. (%)		C-3	C-4	C-5	C-6	C-7
4 (X = CH_3)	CHF_2Cl	0			39.60	37.76	31.52	29.46	37.61
		−120	C_e	90	37.37	37.37	32.74	28.43	36.67
			C_a	10	42.87	34.37	26.28	29.60	36.60
	CH_3OCH_3	0			38.25	37.34	32.02	29.09	37.31
		−120	C_e	90	37.15	37.49	32.86	28.57	36.48
			C_a	10	48.80	34.49	26.44	29.67	37.29
5 (X = F)	CHF_2Cl	0			96.23	35.90	28.39	28.75	36.90
					J = 172.0[c]	J = 22.0	J = 9.3		
		−120	C_e	90	95.43	36.02	28.74	27.71	36.30
					J = 171.4	J = 21.0	J = 14.0		
			C_a	10	98.89	33.05	26.04	29.02	36.69
					J = 166.3	J = 23.3	J = 4.4		
	CH_3OCH_3	0			95.15	35.85	28.31	28.74	36.56
					J = 174.2	J = 22.0	J = 11.0		
		−120	C_e	85	94.02	36.04	28.62	27.81	35.77
					J = 173.1	J = 21.6	J = 13.7		
			C_a	15	97.16	32.99	26.05	29.09	36.27
					J = 168.9	J = 23.6	J = 4.3		
6 (X = Cl)	CHF_2Cl	−20			68.32	37.07	27.33	29.31	36.88
		−120	C_a	>99	69.02	36.54	26.75	28.90	36.02
	CH_3OCH_3	−20			67.51	36.51	27.54	29.25	36.52
		−120	C_e	>1	[d]	40.89[e]	31.30	27.30	36.70[e]
			C_a	<99	67.91	36.09	26.75	28.93	35.90
7 (X = Br)	CHF_2Cl	−20			61.70	37.60	28.42	29.27	37.02
		−120	C_a	100	62.47	36.88	28.17	28.96	36.67
	CH_3OCH_3	−20			61.65	36.80	28.24	28.84	36.22
		−120	C_a	100	60.84	37.31	28.22	29.10	36.54
8 (X = OCH_3)	$CHFCl_2$	25			84.55	34.31	27.62	28.66	36.00
		−103	C_e	60	82.51	35.73	29.65	27.62	35.73
			C_a	40	85.31	32.54	25.59	28.78	32.54
	CH_3OCH_3	0			84.69	34.69	27.84	29.30	36.23
		−120	C_e	44	85.15	33.39	26.05	29.37	35.82
			C_a	56	82.37	36.15	28.29	30.10	35.61
9 (X = OEt)	CHF_2Cl	0			83.27	35.66	28.72	29.36	36.72
		−120	C_e	80	84.24	36.05	30.20	28.26	37.06
			C_a	20	81.50	32.97	26.09	29.41	36.22
	CH_3OCH_3	0			83.06	35.25	28.08	29.47	36.39
		−120	C_e	50	80.06	35.64	30.21	28.44	36.78
			C_a	50	83.73	33.52	26.07	29.51	35.87
10 (X = $OCHCH_2$)	CHF_2Cl	0			82.84	35.34	29.03	29.03	36.75
		−120	C_e	83	80.95	35.97	29.89	28.03	36.18
			C_a	17	84.88	32.63	26.04	29.21	[d]
	CH_3OCH_3	0			82.02	35.14	28.68	28.99	36.39
		−120	C_e	82	79.53	35.67	29.66	28.19	35.88
			C_a	18	83.44	32.60	26.01	29.28	[d]
11 (X = OAc)	$CHFCl_2$	25			76.77	34.13	27.88	28.35	36.29
		−103	C_e	65	75.13	35.03	29.21	27.36	35.95
			C_a	35	78.58	31.46	25.85	28.57	[d]
	CH_3OCH_3	0			76.44	34.71	28.92	28.47	26.59
		−120	C_e	71	74.66	35.61	29.66	28.00	35.87
			C_a	29	78.17	31.86	26.30	29.17	36.21
12 (X = OPh)	THF-d_8	−15			80.37	35.10	28.52	28.52	35.90
		−120	C_e	89	79.15	35.30	29.43	28.16	35.92
			C_a	11	80.92	32.06	[d]	[d]	[d]

Can. J. Chem. Downloaded from www.nrcresearchpress.com by 91.144.44.67 on 09/07/12
For personal use only.

TABLE 1 (*concluded*)

Compound	Solvent	Temp. (°C)	Conf./Pop. (%)		C-3	C-4	C-5	C-6	C-7
13 (X = OPhOMe)	CHF_2Cl	−15			81.28	35.87	29.26	28.97	36.77
		−120	C_e	89	79.19	36.15	30.04	28.14	36.38
			C_a	11	81.63	32.27	25.90	29.38	[d]
	CH_3OCH_3	−15			80.63	35.67	28.90	28.90	36.34
		−120	C_e	88	78.02	35.58	29.82	28.28	36.32
			C_a	12	80.06	32.51	25.94	29.42	35.94
	THF-d_8	−20			79.67	35.48	28.70	28.70	36.07
		−120	C_e	86	77.88	35.68	29.75	28.36	36.15
			C_a	14	80.53	32.52	[d]	[d]	[d]
14 (X = $OPhNO_2$)	THF-d_8	−15			79.04	35.51	28.86	28.61	36.02
		−90	C_e	88	77.78	35.65	29.69	28.30	36.19
			C_a	12	79.62	32.42	[d]	29.48	36.00

[a]Chemical shifts relative to TMS.
[b]Spectrum recorded in solutions containing CD_2Cl_2 and CHF_2Cl or CH_3OCH_3 (20:80) and TMS.
[c]Coupling constants calculated in Hz.
[d]Overlapping of two signals.
[e]The assignment of this signal is uncertain.

and the spectral parameters are listed in Table 1. Because carbon–fluorine couplings in the spectrum of compound **5** facilitate the assignation of its ^{13}C NMR spectrum at high and low temperatures, it is considered first.

Figure 1 illustrates the proton-decoupled 100.62 MHz carbon-13 NMR spectrum of **5** in CH_3OCH_3 at 0 and −120°C. At low temperature each signal has separated into two components of unequal intensity (15:85) indicative of two conformers. The signal identification at 0°C is done directly, using the carbon–fluorine coupling constants. The largest C—F coupling is observed for the C3 carbon at 95.15 ppm ($^1J_{C3-F}$ = 174.2 Hz). The C4 signal (35.85 ppm) can be distinguished from that of C7 (36.15 ppm) by a splitting arising from the coupling constant $^2J_{C4-F}$ = 22.0 Hz. Similarly the C5 signal is assigned to the doublet at 28.31 ppm ($^3J_{C5-F}$ = 9.3 Hz) and the C6 carbon to the singlet at 28.74 ppm.

The known stereodependence (4) of $^3J_{CF}$ can be used to determine the nature of the conformers of **5** in addition to assigning the signals of the ^{13}C NMR spectrum at −120°C. The magnitude of this coupling constant depends on the dihedral angle F—C3—C4—C5, and for this purpose angles were calculated, using the Still–Steliou MODEL 2.93 program to model the geometry of the C_e and C_a conformers: the values obtained are 158° and 45° respectively. According to ref. 4, the large coupling constant $^3J_{C5e-F}$ = 13.7 Hz observed for the doublet at 28.62 ppm is indicative of an angle near 160–180° and therefore identifies C5 of the C_e form (represented by C5e) while the C5a carbon is found at 26.05 ppm (doublet with $^3J_{C5a-F}$ = 4.3 Hz).

The carbon-13 chemical shift substituent effects[2] were calculated and listed in Table 2; these parameters are useful in assigning the signals of each of the two conformers for some of the other compounds. Thus, for **5** (X = F), the γ-*gauche* effect involving C5 is −6.97 ppm and γ-*anti* is −4.40 ppm.

Another way to characterize the conformers is provided by the magnitude of the proton–proton coupling constant $^3J_{H3-H4}$ measured from the ^1H NMR spectra at low temperature. In a previous ^1H NMR study of benzocycloheptene, St-Jacques and Vaziri (6) measured proton coupling constants from partially deuterated derivatives of benzocycloheptene, and the two coupling constants of interest are $^3J_{3e-4e}$ = 6.6 Hz and $^3J_{3a-4a}$ = 12.6 Hz. The corresponding coupling constants determined for compound **5** (X = F) from the ^1H NMR spectrum in CHF_2Cl at −120°C are $^3J_{3e-4e}$ = 5.0 Hz for the minor form (C_a) and $^3J_{3a-4a}$ = 11.5 Hz for the major conformer (C_e). Integration revealed an intensity ratio of 15:85 for C_a:C_e.

Knowing the nature of the major and minor conformers, the other signals of the ^{13}C NMR spectrum of **5** (X = F) at −120°C can now be assigned. The C3 signals are readily located at 94.02 ppm (C_e) and 97.16 ppm (C_a), whereas C4e is observed at 36.04 ppm ($^2J_{C4e-F}$ = 21.6 Hz) and C4a at 32.99 ppm

TABLE 2. Carbon-13 chemical shift substituent effects of some 3-substituted benzocycloheptene derivatives calculated from the ^{13}C NMR spectra recorded at −120°C in CH_3OCH_3 and relative to the chemical shifts of benzocycloheptene

X	Conf.	α	β	γ_{C5}	δ	γ_{C7}
CH_3	C_e	0.56	9.22	−0.16	0.30	−0.11
	C_a	12.21	6.22	−6.58	1.40	0.70
F	C_e	57.61	7.77	−4.40	−0.46	−0.82
	C_a	60.57	4.72	−6.97	0.82	−0.32
Cl	C_e	[a]	[a]	[a]	[a]	[a]
	C_a	31.32	7.82	−6.27	0.66	−0.69
Br	C_a	24.25	9.04	−4.80	0.83	−0.05
OCH_3	C_e	45.78	7.87	−4.73	1.83	−0.98
	C_a	48.56	5.12	−6.97	1.10	−0.77
OAc	C_e	38.66	7.34	−3.36	−0.27	−0.72
	C_a	41.58	3.59	−6.72	0.90	−0.38
OPh	C_e	42.56	7.03	−3.59	−0.11	−0.67
	C_a	44.33	3.79	[a]	[a]	[a]
$OPhOCH_3$	C_e	41.43	7.31	−3.20	0.01	−0.27
	C_a	43.47	4.24	−7.08	1.15	−0.65
$OPhNO_2$	C_e	41.19	7.38	−3.33	0.03	−0.40
	C_a	43.62	4.15	[a]	1.21	−0.59

[a]This signal was not detected, and the substituent effect was not calculated.

[2]Calculated using the chemical shifts of benzocycloheptene as reference, see ref. 3.

Can. J. Chem. Downloaded from www.nrcresearchpress.com by 91.144.44.67 on 09/07/12
For personal use only.

Can. J. Chem. Downloaded from www.nrcresearchpress.com by 91.144.44.67 on 09/07/12
For personal use only.

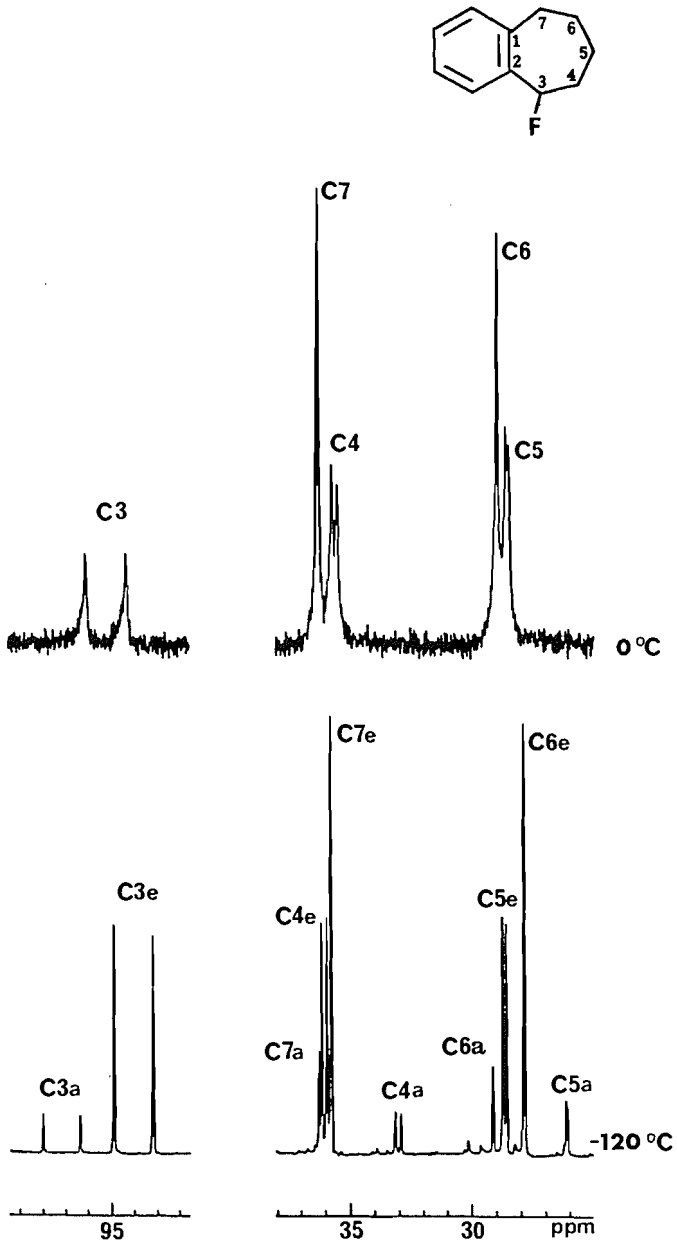

FIG. 1. The 100.62 MHz ^{13}C spectra of **5** at 0°C and −120°C (e = equatorial chair and a = axial chair).

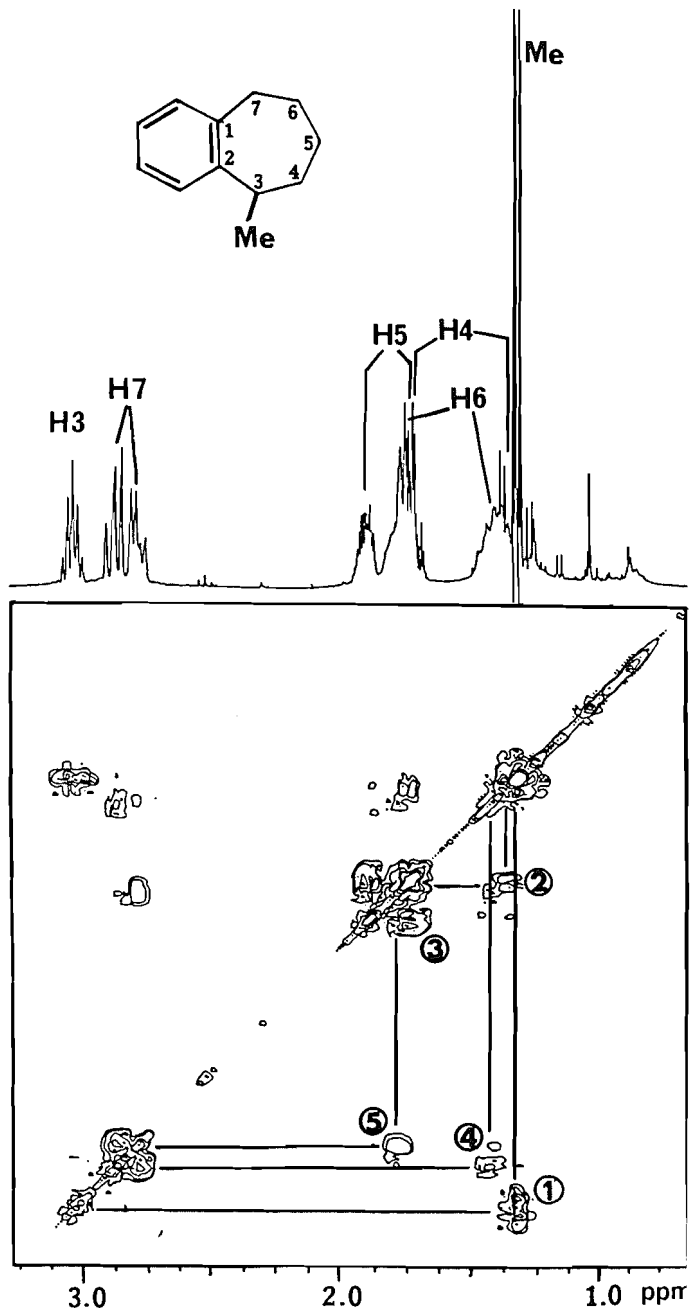

FIG. 2. The 400 MHz two-dimensional ^1H NMR (COSY) spectrum of **4** in $CDCl_3$ at room temperature.

($^2J_{C4a-F}$ = 23.6 Hz). These two last signals show a separation of 3 ppm, arising from differences in β effects. This parameter was used to identify the conformers of other compounds. Finally, the C6 signals are found at 29.09 ppm (C_a) and 27.81 (C_e) while the C7 carbons are at 36.27 ppm (C_a) and 35.77 ppm (C_e).

The spectral analysis of **4**, **6**, **12**, **13**, and **14** required two-dimensional NMR techniques such as a COSY-45 experiment (7) and a heteronuclear correlation (HETCOR) (8, 9) experiment performed at 25°C in $CDCl_3$. The experimental details of these experiments are described in the experimental section. The results, used to assign the signals of the carbon-13 NMR spectra at high temperature, are exemplified by the spectral analysis of derivative **4** (X = CH_3).

Figure 2 shows both 2D-NMR plots as recorded for **4** (X = CH_3) on a WH-400 (COSY-45) and a VXR-300 (HETCOR) spectrometer. In the 2D COSY contour spectrum, the off-diagonal signals represent correlations between coupled protons whose chemical shifts are obtained from peaks along the diagonal line. The H3 proton, being a benzylic methyne, is the most downfield aliphatic proton (3.00 ppm) and the H7 protons are easily assigned at 2.84 ppm (H7) and 2.74 ppm (H7′) because they are deshielded by the aromatic ring. These three proton signals serve as reference for the analysis. The correlation peak 1 arises from coupling between H3 with H4 at 1.36 ppm and the methyl group at 1.29 ppm. Correlation 2 arises from coupling between H4 with H4′ and H5 at 1.68 ppm, while the coupling of H5 with H5′ (1.87 ppm) gives rise to a part of the correlation peak 3. While H7 and H7′ are readily assigned, the correlation peaks 4 and 5 arise from the coupling

Can. J. Chem. Downloaded from www.nrcresearchpress.com by 91.144.44.67 on 09/07/12
For personal use only.

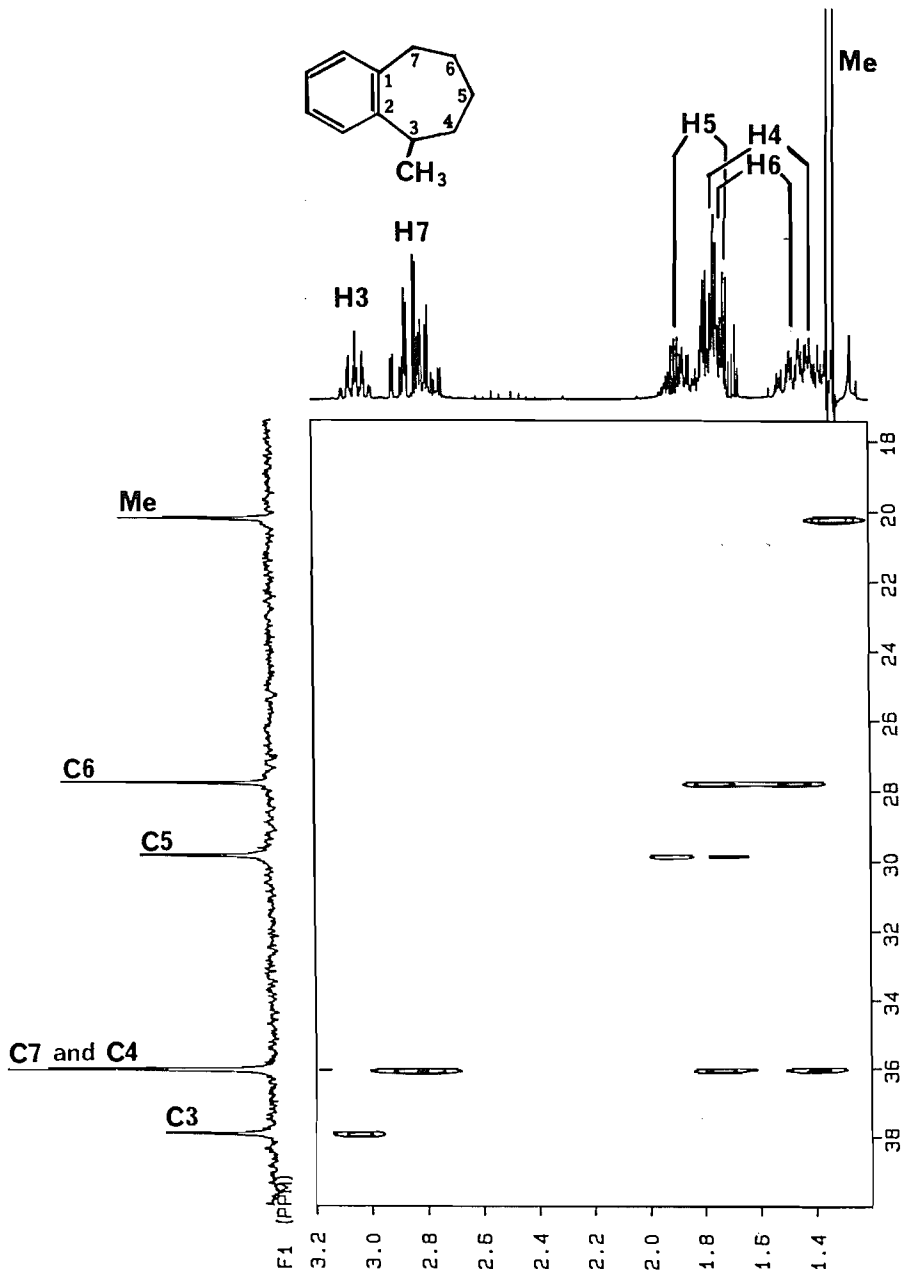

FIG. 3. 2D proton–carbon heteronuclear chemical shift correlation (HETCOR) of **4** in $CDCl_3$ at room temperature at 75.431 MHz for ^{13}C with F_2 = 299.949 MHz in the second dimension.

of H7 with H6 (1.43 ppm) and H7′ with H6′ (1.76 ppm) respectively. The correlation peak 3 also indicates the coupling between H5 and H6′.

Using the known proton chemical shifts, the ^{13}C NMR signals can then be identified by the HETCOR experiment at 25°C. The experiment performed in $CDCl_3$ cannot differentiate between C4 and C7 because the signals overlap. However, the ^{13}C NMR spectrum at 0°C in the CH_3OCH_3 (Fig. 3) reveals two distinct signals, a sharp one (37.31 ppm) and a broadened signal slightly upfield (37.34 ppm), representing C7 and C4 respectively. The signals of the ^{13}C spectra at low temperature were identified using substituent effects. The γ and δ substituent effects derived from the C5 and C6 signals provide useful information on the major conformer, in this case C_e. All substituents studied produce similar γ and δ effects on the chemical shifts of the carbons on the benzocycloheptene ring listed in Table 2. Integration of the spectra in CHF_2Cl and CH_3OCH_3 at −120°C gave 10% of the C_a form of **4** in each solvent.

The very small intensity of the ^{13}C lines of the minor form in the NMR spectrum of derivative **6** (X = Cl) at −120°C required an analysis using substituent effects to assign its lines. The nature of the major form (C_a) is confirmed by the proton–proton coupling constant $^3J_{H3-H4}$ of 5.2 Hz measured in the ^1H NMR spectrum at −120°C in CH_3OCH_3. Integration revealed ≈99% of the C_a form and 1% of C_e form for which several signals are identified. Changing the solvent to CHF_2Cl causes the minor signals of **6** to disappear. Similarly, in both solvents the spectra of compound **7** (X = Br) show signals of the C_a conformer only.

The analysis of the ^{13}C spectra of compounds **8**–**14** at high

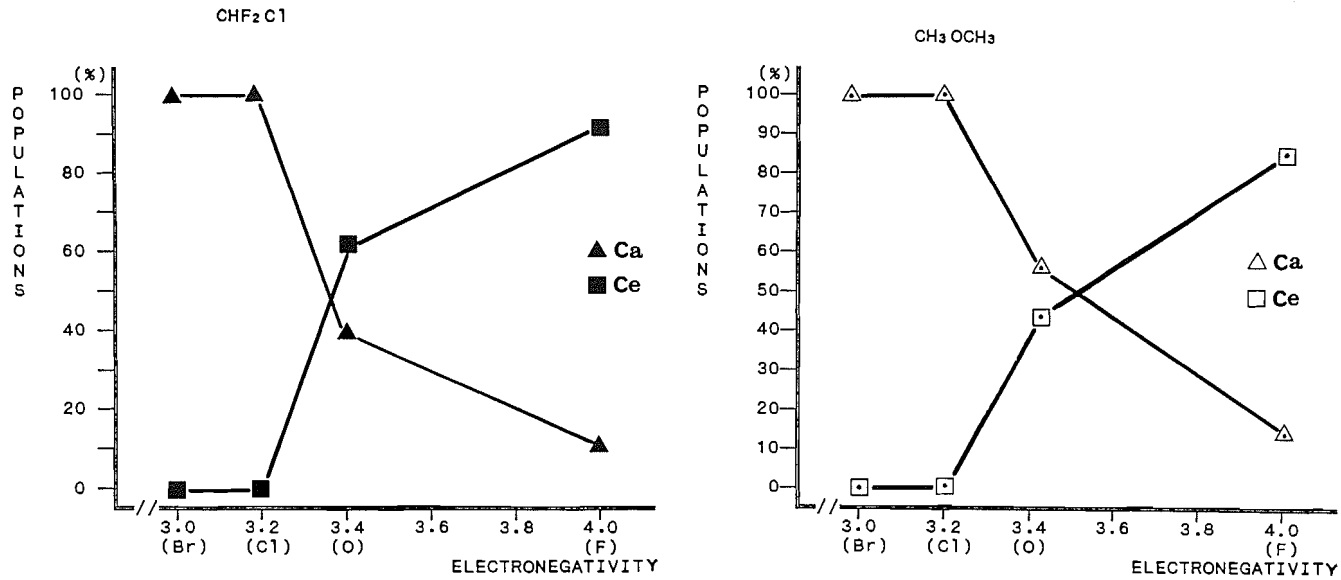

FIG. 4. Plots of the population of the C_e and C_a forms versus the electronegativity of Br, Cl, and F in CH_3OCH_3 and CHF_2Cl solutions. Data for OCH_3 are included as references for oxygen.

and low temperatures is based on chemical shift substituent effects and a close resemblance of all the spectral behavior observed for the derivatives studied. Their chemical shifts and populations are summarized in Table 1.

Discussion

The ^{13}C NMR spectra of derivatives **4–14** (except **7**) revealed the presence of two conformations (C_a and C_e) whose relative populations, given in Table 1, are quite different from those of the families of benzocycloheptene (3) represented by compounds **2** and **3**. The ratio of the two forms should be influenced by electrostatic interactions, steric interactions, solvation effects, and stereoelectronic $\pi-\sigma^*$ orbital interactions. Such orbital interactions were not possible for families **2** and **3**.

Information on steric repulsion is provided by the data obtained for **4** (X = CH_3). The two steric interactions found in the methylenecyclohexane system, allylic strain ($A^{(1,3)}$) and *syn*-diaxial repulsion, are also found in the 3-substituted benzocycloheptene derivatives, as illustrated by structures **15** and **16**, in which allylic strain becomes benzylic strain.

C_e C_a

15 **16**

The presence (3) of 10% of the C_a form for **4** suggests that the benzylic strain of the methyl group in **15** is less destabilizing for the C_e form than the *syn*-diaxial interactions (1,3 and 1,4, as illustrated in **16**) are destabilizing for the C_a form.

To explain the results obtained for the polar substituted derivatives (**5–14**), it is useful to divide them into two subgroups: the first one includes mainly the halogen compounds (**5–8**) while the second contains the oxy derivatives (**8–14**). The OCH_3 substituent (**8**) is included in both subgroups for reference purposes, as will be explained below.

The first subgroup: compounds 5–8

Figure 4 illustrates the population change of the C_a and C_e forms with substituent electronegativity in two solvents, the more polar CHF_2Cl and the less polar CH_3OCH_3. It is seen that in each solvent the population of the C_a form decreases as the substituent electronegativity increases. The large C_a populations for the Cl and Br derivatives cannot be explained by steric arguments. The ΔG^0 values given by Jensen and Bushweller (10) for the substituents of the first group in cyclohexane (0.5 kcal/mol for Br and Cl, 0.3 kcal/mol for F, and 0.6 kcal/mol for OCH_3) cannot account for the observed trend for these four substituents because the predicted C_a populations, based solely on steric arguments, should be F > Cl $\approx$ Br > OCH_3. Furthermore, the $A^{(1,3)}$ effect, also of steric origin, should counterbalance this trend, producing a levelling effect. It therefore appears clear that these effects are not dominant.

In addition, electrostatic effects would be determined by the orientations of two dipole moments (3, 11) present in these benzocycloheptene derivatives, as illustrated by structures **17** and **18**. The C_e form (with parallel dipoles) is expected to be

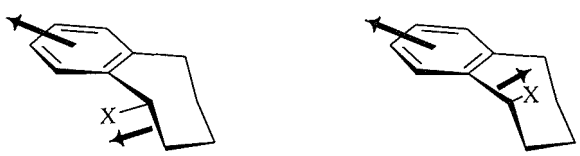

C_e C_a

17 **18**

more polar than the C_a form with oppositely oriented dipoles, and the latter should be favored in a nonpolar solvent (3, 11). Calculations using the Still–Steliou MODEL 2.93 program have confirmed that the C_e form is the more polar one. Thus, as substituent electronegativity increases, the C_a form should also increase, contrary to observations for the first subgroup. Furthermore, a change of solvent from CH_3OCH_3 to CHF_2Cl should stabilize C_e more than C_a and shift the equilibrium toward C_e (4). This solvent effect is indeed observed for **5**

Can. J. Chem. Downloaded from www.nrcresearchpress.com by 91.144.44.67 on 09/07/12
For personal use only.

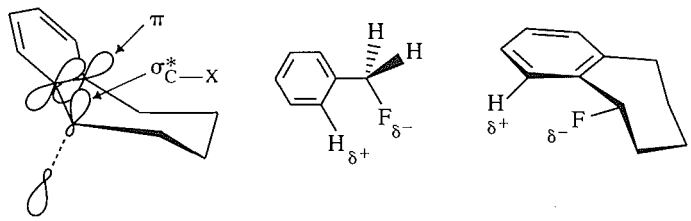

19 20 21

(X = F) and **8** (X = OCH_3) but not for **6** (X = Cl) and **7** (X = Br). Therefore the high proportion of the C_a form for **6** and **7** does not appear to be determined by dominant electrostatic interactions, although these no doubt contribute.

In light of the preceding arguments, the π–σ* stereoelectronic effect is required to explain the conformational behavior of the Cl and Br substituents. The relevance of this interaction was suggested from studies of oxy derivatives of methylenecyclohexane by Lessard and co-workers (2).

Generally, an occupied molecular orbital near an unoccupied molecular orbital can lead, under proper conditions, to a stabilizing interaction between them (12, 13). For the π–σ* interaction in the benzocycloheptene derivatives considered in this work, the orbitals involved are the π orbital of the benzo ring (at the C2 position) and the σ* anti-bonding orbital of the carbon-substituent bond at C3, as illustrated by structure **19**. For maximum interaction, two conditions are needed: (1) the π and σ* orbitals must be parallel for effective overlap to occur and (2) the energy difference (or energy gap) between the π and σ* orbitals should be as small as possible. These conditions are represented by the following expression:

$$E \propto -S^2/|e_1^0 - e_2^0|$$

where E is the stabilization energy, S is the overlap integral, and e_i^0 is the energy of orbital i.

According to the requirement for effective overlap, the geometry of the C_a form is better than that of C_e. For derivatives **5**–**7** (X = F, Cl, and Br), the calculated (using the Still–Steliou MODEL 2.93 program) π—C2—C3—σ* dihedral angles of the C_a form vary from 23° to 17° as we pass from F to Br. Moreover, the S term is influenced by the substituent electronegativity whereby increasing substituent electronegativity produces greater electronic density localized at the carbon atom of σ*, and thus stabilization will be greater (13).

The fact that the C_a population decreases with increasing substituent electronegativity (Fig. 4) suggests that the energy gap ($e_1^0 - e_2^0$) might be more important than the S term in the π–σ* interaction.

The relevant energy orbitals, determined by *ab initio* and CNDO/2 calculations (14) and supported by ionization potentials of molecules of type CH_3X (15, 16), are schematically represented in Fig. 5. The relative order of the $\sigma^*_{C—X}$ orbital energies suggests (assuming the $|e_1^0 - e_2^0|$ term is predominant) that the population of the C_a form should decrease with an energy gap increase. Thus, the relative order of the C_a populations should be Br > Cl > F > OCH_3, instead of the relative order observed: Br ≥ Cl ≫ OCH_3 > F. This inversion of F and OCH_3 suggests the existence of either a particular stabilizing effect in the C_e form of the F derivative (**5**) or the presence of a destabilizing effect in the C_e form of the OCH_3 derivative (**8**). In fact, it was shown previously (in the analysis of CH_3 derivative **4**) that the benzylic strain $A^{(1,3)}$ is destabilizing for the C_e form.

Penner *et al.* (17) have published results on the benzylic

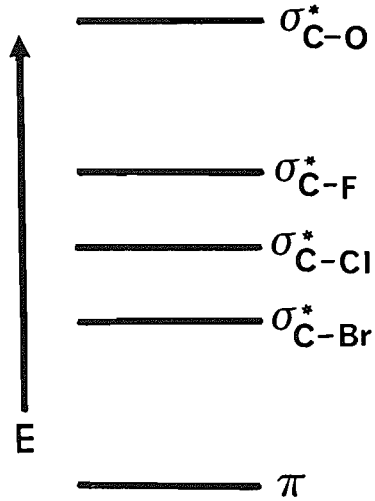

FIG. 5. Relative order of antibond orbital energies of C—X bond in various X—CH_2—CH_2—Y and CH_3—X molecules.

"anomeric" effect in benzyl fluoride and benzyl chloride. Their calculations show a significant stabilization of the expected unfavored planar geometry **20**, resulting from a coulombic attraction between the fluorine atom and the *ortho* hydrogen on the aromatic ring. The fluorine atom bears a negative charge of −0.401 electron while the hydrogen has a positive charge of +0.227 electron, which results in a stabilization of 62.9 kJ mol^{-1} for the planar conformation. The C_e form of **5** (X = F) has a geometry (**21**) quite similar to that found stabilizing for benzyl fluoride, and thus it is possible that the OCH_3–F inversion, noted in Fig. 4, is due to an interaction of this type.

Penner *et al.* (17) also reported an attractive coulombic interaction for the benzyl chloride, but less stabilizing than for benzyl fluoride. For the halogen derivatives (**6**, X = Cl, and **7**, X = Br), this effect should stabilize the C_e form. Thus the large C_a population found for both derivatives is compatible with a strong π–σ* interaction that overrides any attractive coulombic interaction.

In conclusion, the data obtained for the first subgroup show evidence for the π–σ* interaction as the major stabilizing factor for the C_a form of **6** and **7** (X = Cl and Br). The analysis of **5** (X = F) points out an attractive coulombic interaction, which is strongly stabilizing for the C_e form. The data suggest that **8** (X = OCH_3) is borderline and its $C_a \rightleftharpoons C_e$ equilibrium is determined by the balance of several interactions.

The second subgroup: compounds 8–14

First of all, the analysis of the oxy derivatives, within the framework of the π–σ* interaction, should be based on the effective electronic density at the oxygen atom of each substituent, that is to say, on the electron-withdrawing ability of the R part of the -OR substituents. Thus the electronic density should be greater on the oxygen atom if R is a methyl group and, as a consequence, the energy of the anti-bonding orbital $\sigma^*_{C—OCH_3}$ should be higher. Because of electron delocalization in the acetyl group, the electronic density on oxygen should be lower and, equally so, the energy of the $\sigma^*_{C—OAc}$ orbital. Thus, the energy of the $\sigma^*_{C—OR}$ orbitals should increase in the following order: $\sigma^*_{C—OAc} < \sigma^*_{C—OPh} < \sigma^*_{C—OCH_3}$. Therefore, the populations of the C_a form, if determined by the π–σ* interaction, should be in the increasing order OCH_3 < OPh < OAc, because the smaller the energy gap between the π

Can. J. Chem. Downloaded from www.nrcresearchpress.com by 91.144.44.67 on 09/07/12
For personal use only.

Can. J. Chem. Downloaded from www.nrcresearchpress.com by 91.144.44.67 on 09/07/12
For personal use only.

and the $\sigma^*_{C—OR}$ orbitals, the stronger is the stability obtained from the π–σ^* interaction.

The oxy derivatives of methylenecyclohexane (2) show a C_a trend (OAc < OPh < OCH_3) that is opposite to that predicted from the π–σ^* interaction. The inversion of OCH_3 and OAc could not be explained by the authors, who have proposed an unsaturation effect as a specific interaction characterizing an oxy derivative with a substituent containing an unsaturated moiety. However, no details of its mechanism of action were proposed.

Our system shows a specific trend for the five oxy derivatives studied (OCH_3 **8**, OCH_2CH_3 **9**, $OCH{=}CH_2$ **10**, OAc **11**, and OPh **12**) and, for the three substituents mentioned above, the increasing order of axial populations is OPh < OAc < OCH_3. This trend is different from both that observed in the methylenecyclohexane family and that predicted from the effective electronegativity of the oxygen atom in the π–σ^* framework.

Comparison of OCH_3 and OCH_2CH_3 (8 and 9)

Now let us analyze the conformational trends of the OCH_3 (**8**) and the OCH_2CH_3 (**9**) derivatives. The C_e population of the OCH_2CH_3 derivative changes from 50% in CH_3OCH_3 to 80% in $CHFCl_2$ whereas for the OCH_3 substituent the trend is similar, but the total conformational change is reduced to 16%, that is, from 44% (CH_3OCH_3) to 60% (CHF_2Cl). The two derivatives differ only by a -CH_2- unit, which should not induce electronic perturbation on the oxygen atom. These substituents should also have a similar steric effect, but it is observed that the C_a population for OCH_2CH_3 is less than that for OCH_3 in the two solvents: 56% for OCH_3 and 50% for OCH_2CH_3 in the CH_3OCH_3 compared to 40% for OCH_3 and only 20% for OCH_2CH_3 in CHF_2Cl. The population difference is most probably due to electrostatic interactions associated with the characteristic rotamer difference between the two groups, which could affect the overall dipole moment.

Comparison of OCH_2CH_3 and $OCH{=}CH_2$ (9 and 10)

In the polar solvent (CHF_2Cl), the OCH_2CH_3 (**9**) and the $OCH{=}CH_2$ (**10**) derivatives show, respectively, 80% and 83% of the C_e form. Stabilization is therefore similar for these two derivatives and thus no unsaturation effect appears to be manifest. On the other hand, in the less polar solvent (CH_3OCH_3), the populations of the C_e form become 50% (OCH_2CH_3) and 82% ($OCH{=}CH_2$). Thus for the OCH_2CH_3 derivative an increase of the solvent polarity induces a great change in the C_e population: from 50% to 80%, but for the $OCH{=}CH_2$ substituent the solvent polarity increase has essentially no effect on the C_e amount. In the latter case, the observed behavior is similar to that noted for the *p*-$OPhOCH_3$ (**13**) derivative, as will be discussed further.

The phenoxy derivatives 12–14

The *para* hydrogen on the phenoxy ring (OPh) was replaced by an electron-withdrawing group (NO_2) and an electron-donating group (OCH_3). The results in THF-d_8 (Table 1) show 86% of the C_e form for the *p*-$OPhOCH_3$ derivative, 89% for OPh, and 88% for *p*-$OPhNO_2$. The constancy of these values suggests that delocalization involving the unsaturated part of the substituents is not a significant factor.

Behavior of the OAc derivative (11)

The observed C_e populations for OAc (**11**) and OCH_3 (**8**) are respectively 71% and 44% in the less polar solvent (CH_3OCH_3), while in the more polar solvent (CHF_2Cl) they become 65% (OAc) and 60% (OCH_3). These data show a small increase in the C_a population of OAc with an increase in the solvent polarity, but an increase in the C_e population of OCH_3. Therefore the more polar solvent stabilizes the C_a form for the OAc derivative and stabilizes the C_e form for OCH_3. Moreover, when the polarity of the solvent is increased, the C_a population of OAc (35% in CHF_2Cl) tends toward the C_a population of OCH_3 (40% in CHF_2Cl). These observations suggest, firstly, that the C_a form of OAc is more polar than the C_e form (as was confirmed by calculations using the Still–Steliou MODEL 2.93 program), contrary to what is calculated for compounds of the first subgroup, and, secondly, that the C_a form is destabilized by electrostatic interactions (11), which are responsible for the equatorial tendency of this substituent. It would therefore appear that in a polar solvent the electrostatic interactions are attenuated and only the intrinsic interactions of the molecule are operating, that is to say, the steric and orbital interactions. Therefore the particular behavior of the OAc derivative appears not to be due to an unsaturation effect but is caused by specific electrostatic interactions. Moreover, OAc is a complex group, and a change of 6% is too small to be used as evidence for a special effect.

Conclusion

The results obtained for both classes of substituents show a strong π–σ^* interaction for Cl and Br substituents but do not provide evidence for a novel effect arising from unsaturation in the oxygenated substituents of the 3-substituted benzocycloheptene family. The conformational behavior of the oxy derivatives can be rationalized from contributions of steric and electrostatic origin whereas the F substituent shows a strong attractive coulombic interaction.

Experimental

Melting points are uncorrected and were determined with a Thomas–Hoover (Uni-melt) melting point apparatus. High resolution MS spectra at 70 eV were recorded by using a Kratos MS-50 spectrometer.

Routine ^1H NMR spectra were taken on a Bruker WH-90 or a Varian VXR-300 spectrometer: solutions were typically 10% in $CDCl_3$ containing TMS as reference.

The variable temperature ^1H NMR spectra at 400.13 MHz and ^{13}C NMR spectra at 100.62 MHz were obtained by using a Bruker WH-400 spectrometer equipped with a variable temperature B-VT-1000 unit. Calibration, using a thermocouple inside a solvent-containing NMR tube, indicates that the low temperatures reported are exact within 3°C.

All ^{13}C NMR spectra were recorded with broadband proton decoupling, and the following instrumental parameters are typical: flip angle, 79°; SW = 20 000 Hz, data size = 16 K, AQ = 0.41 s. The spectra were recorded as solutions in CHF_2Cl, CH_3OCH_3, or THF-d_8 (100–150 mg in 2.2 mL of solution) containing TMS and about 15–20% of CD_2Cl_2 as locking agent, in standard 10-mm tubes that have been degassed and sealed.

^1H NMR spectra were recorded as solutions in CHF_2Cl, CF_2Cl_2, or THF-d_8 (5–10 mg in 0.55 mL of solution) containing TMS and about 15–20% of CD_2Cl_2 or CD_3COCD_3 (for locking purposes), in standard 5-mm tubes, which were degassed and sealed. The typical instrumental parameters used are as follows: flip angle = 30–87°; SW = 5000 Hz; data size = 8 and 16 K; AQ = 0.90–1.82 s.

Integrations were carried out by using Bruker software. The uncertainty is estimated as ±2% from standard deviation (18).

For the 2D COSY experiment, the following pulse sequence (7) was used: RD–90°–t_1–45°–acq. A spectral width of 2100 Hz was used with quadrature detection to collect a 256 × 1K data matrix. The

Can. J. Chem. Downloaded from www.nrcresearchpress.com by 91.144.44.67 on 09/07/12
For personal use only.

matrix was zero-filled in the t_1 dimension and transformed in the magnitude mode by using the sine-bell square function.

The heteronuclear correlations were performed by using the HETCOR sequence (8, 9). Spectral widths of 300 Hz in the proton dimension and 1680 Hz in the carbon dimension were used to collect 128 FID in quadrature detection. The matrix was zero-filled in the t_1 dimension and transformed in the magnitude mode by using a Gaussian function to obtain a pseudo-echo shape of the peak.

*3-Methylbenzocycloheptene (**4**)*

This compound was prepared by catalytic hydrogenation of 3-methylenebenzocycloheptene (obtained by Wittig reaction (19) on benzosuberone) over palladium–charcoal (10%) at 35 psi (1 psi = 6.9 kPa) in AcOEt. The product obtained was identical to that described in ref. 20.

3-Hydroxybenzocycloheptene

Benzosuberone was reduced by $LiAlH_4$ in Et_2O using the standard procedure (21). ^1H NMR, δ($CDCl_3$): 1.80 (7H), 2.80 (2H), 4.25 (1H), 7.26 (4H).

*3-Fluorobenzocycloheptene (**5**)*

To a solution of 3-hydroxybenzocycloheptene (2 g, 12.3 mmol) in 100 mL of anhydrous CH_2Cl_2 at −25°C, 2.6 mL (36.9 mmol) of DAST ($(C_2H_5)_2NSF_3$) was added. The mixture was stirred overnight at room temperature, was afterwards cooled at −25°C, and 80 mL of methanol was added; the resulting solution was poured onto 800 mL of saturated aqueous $NaHCO_3$. This aqueous mixture was extracted with CH_2Cl_2 and the organic layer was washed with 5% HCl and brine. The organic layer was dried over $MgSO_4$ and the solvent was evaporated. The residue was distilled with a Kugelrohr distillation apparatus at 78°C/1 Torr (1 Torr = 133.3 Pa), and 1.2 g (63%) of a colorless liquid was obtained. ^1H NMR, δ($CDCl_3$): 1.70 (6H), 2.61 (2H), 5.60 (1H), 7.30 (4H); mass spectrum, calcd. for $C_{11}H_{13}F$, *M*: 164.1001; found (70 eV): 164.1002 (M^+), 144 ($M - HF)^+$.

*3-Chlorobenzocycloheptene (**6**)*

This compound was prepared as described by Huigsen *et al.* (21) from 3-hydroxybenzocycloheptene.

*3-Bromobenzocycloheptene (**7**)*

At 0°C, 1.33 mL (14.2 mmol) of PBr_3 was added to 2 g (12.3 mmol) of neat 3-hydroxybenzocycloheptene. After 2 h of stirring, 100 mL of hexane was added and the resulting organic layer was washed with the same amount of water. The organic layer was dried over $MgSO_4$ and the solvent was evaporated to give 2.5 g (89%) of yellow liquid. ^1H NMR, δ($CDCl_3$): 2.06 (7H), 3.30 (1H), 5.47 (1H), 7.14 (4H); mass spectrum, calcd. for $C_{11}H_{13}Br$, *M*: 224.0200; found (70 eV): 224.0220 (M^+), 144 ($M - HBr)^+$.

*3-Methoxybenzocycloheptene (**8**)*

This compound was prepared by alkylation of the alkoxide ion of 3-hydroxybenzocycloheptene with methyl iodide to obtain the product described in ref. 22.

*3-Ethoxybenzocycloheptene (**9**)*

This compound was prepared by the procedure for **8**. ^1H NMR, δ($CDCl_3$): 1.24 (3H, t), 1.70 (5H), 2.04 (1H), 2.67 (1H), 2.98 (1H), 3.44 (2H, q), 4.41 (1H), 7.15 (4H); mass spectrum, calcd. for $C_{13}H_{18}O$, *M*: 190.1358; found (70 eV): 190.1336 (M^+).

*3-Vinyloxybenzocycloheptene (**10**)*

This compound was prepared using the method described by Kodama *et al.* (5). ^1H NMR, δ($CDCl_3$): 1.85 (5H), 2.79 (1H), 2.89 (1H), 4.48 (1H), ABX: 4.38 (1H, A, dd), 4.11 (1H, B, dd), 6.45 (1H, X, dd), 7.20 (4H); mass spectrum, calcd. for $C_{13}H_{16}O$, *M*: 188.1201; found (70 eV): 188.1199 (M^+).

*3-Acetoxybenzocycloheptene (**11**)*

Esterification of 3-hydroxybenzocycloheptene by acetic anhydride in pyridine give the desired compound, described in ref. 5.

*3-Phenoxy, 3-paramethoxy, and 3-paranitrobenzocycloheptene (**12**, **13**, and **14**)*

These three compounds were prepared by the same method as next described for **12**. To a suspension of 0.53 g (22 mmol) of NaH in 25 mL of THF, a solution of 2.1 g (21 mmol) of phenol in 25 mL of THF was added dropwise. After the addition, a solution of 4 g (22 mmol) of 3-chlorobenzocycloheptene (**6**) and 0.6 g (3 mmol) of 18-crown-6 ether in 250 mL of anhydrous DMSO was added dropwise. The reaction mixture was heated at 70°C overnight, after which the solution was cooled to room temperature and 250 mL of water was added. The resulting solution was extracted with Et_2O. The organic layers were dried over $MgSO_4$ and the solvent was evaporated. The residue was chromatographed on silica gel with hexane/AcOEt to give 560 mg (11%) of a white solid, mp 83–84°C, which is the compound **12**. ^1H NMR, δ($CDCl_3$): 1.93 (6H), 2.90 (2H), 5.35 (1H), 7.10 (9H); mass spectrum, calcd. for $C_{17}H_{18}O$, *M*: 238.1358; found (70 eV): 238.1369 (M^+), 145 ($M - OPh)^+$.

Characteristics of compound **13**: white solid, mp 48.5–49.5°C; ^1H NMR, δ($CDCl_3$): 1.63 (6H), 2.85 (2H), 3.70 (3H, s), 5.22 (1H), 7.13 (4H, s), 7.20 (4H); mass spectrum, calcd. for $C_{18}H_{20}O_2$, *M*: 268.1463; found (70 eV): 268.1470 (M^+), 145 ($M - OPhOCH_3)^+$.

Characteristics of compound **14**: pale yellow solid, mp 117°C; ^1H NMR, δ($CDCl_3$): 1.70 (6H), 2.91 (2H), 5.45 (1H), 7.17 (4H), AB: 7.54 (4H); mass spectrum, calcd. for $C_{17}H_{17}NO_3$, *M*: 283.1208; found (70 eV): 283.1194 (M^+), 145 ($M - OPhNO_2)^+$.

Acknowledgments

We thank Professor K. Steliou from our department for a copy of the MODEL program and useful discussions. We acknowledge the assistance of Dr. Phan Viet Minh Tan, manager of the "Laboratoire régional de RMN à haut champ" at the Université de Montréal. We acknowledge helpful discussions with Professor Lessard, Université de Sherbrooke. We thank the Natural Sciences and Engineering Research Council of Canada for financial support.

1. N. S. Zefirov and I. V. Baraneskov. Tetrahedron, **39**, 1769 (1983).
2. (*a*) J. Lessard, M. T. Phan Viet, R. Martino, and J. K. Saunders. Can. J. Chem. **55**, 1014 (1977); (*b*) M. T. Phan Viet, J. Lessard, and J. K. Saunders. Tetrahedron Lett. 317 (1979); (*c*) J. Lessard, J. K. Saunders, and M. T. Phan Viet. Tetrahedron Lett. **23**, 2059 (1982); (*d*) A. Ouedraogo, M. T. Phan Viet, J. K. Saunders, and J. Lessard. Can. J. Chem. **65**, 1761 (1987).
3. D. Ménard and M. St-Jacques. Tetrahedron, **39**, 1041 (1983).
4. H.-J. Schneider, W. Gschwendtner, D. Heiske, V. Hoppen, and F. Thomas. Tetrahedron, **33**, 1769 (1977).
5. M. Kodama, Y. Shiobara, H. Sumitomo, K. Furuzumi, H. Minami, and Y. Miyamoto. J. Org. Chem. **53**, 1437 (1988).
6. M. St-Jacques and C. Vaziri. Org. Magn. Reson. **4**, 77 (1972).
7. A. Bax, R. Freeman, and G. A. Morris. J. Magn. Reson. **42**, 169 (1981).
8. A. Bax and G. A. Morris. J. Magn. Reson. **42**, 501 (1981).
9. A. Bax. J. Magn. Reson. **52**, 512 (1983).
10. F. K. Jensen and C. H. Bushweller. Adv. Alicylic. Chem. **3**, 139 (1970).
11. M. K. Kaloustian. J. Chem. Educ. **51**, 777 (1974).
12. N. D. Epiotis, L. R. Yates, J. R. Larson, C. R. Kirmaier, and F. Bernardi. J. Am. Chem. Soc. **99**, 8379 (1977).
13. T. A. Albright, J. K. Burdett, and M. Whangho. Orbital interactions in chemistry. John Wiley & Sons, New York. 1985.
14. N. D. Epiotis, W. R. Cherry, S. Shaik, R. L. Yates, and F. Bernardi. Top. Curr. Chem. 70 (1977).
15. R. C. Bingham. J. Am. Chem. Soc. **97**, 6473 (1975).
16. K. Kimura, S. Ktsumata, Y. Achiba, T. Y. Amazaki, and S. Iwaka. Handbook of HeI photoelectron spectra of fundamental

organic molecules. Japan Scientific Societies Press, Tokyo; Halsted Press, New York. 1981.
17. G. H. PENNER, T. SCHAEFER, R. SEBASTIAN, and S. WOLFE. Can. J. Chem. **65**, 1845 (1987).
18. G. D. CHRISTIAN. Analytical chemistry. 3rd ed. John Wiley & Sons, New York. 1980.
19. WITTIG and SCHOLLKOPF. Chem. Ber. **87**, 1318 (1954).
20. N. A. NELSON, J. H. FASSNACHT, and J. U. PIPER. J. Am. Chem. Soc. **83**, 206 (1961).
21. R. HUIGSEN, W. RAPP, I. UGI, H. WALZ, and MERGENTHALER. Ann. **586**, 1 (1954).
22. S. FUJITA, T. NOMI, and H. NOZAKI. Tetrahedron Lett. **40**, 3557 (1969).

Can. J. Chem. Downloaded from www.nrcresearchpress.com by 91.144.44.67 on 09/07/12
For personal use only.

Solvatation des électrons en excès dans les solvants polaires : corrélation entre les valeurs de ϵ_{max}, $W_{1/2}$ et E_{Amax}

J.-P. JAY-GERIN

Groupe du Conseil de recherches médicales du Canada en sciences des radiations et Département de médecine nucléaire et de radiobiologie, Faculté de médecine, Université de Sherbrooke, Sherbrooke (Québec), Canada J1H 5N4

ET

C. FERRADINI

Laboratoire de chimie-physique, Université René Descartes, 45, Rue des Saints-Pères, 75270 Paris CEDEX 06, France

Reçu le 1[cr] août 1989

J.-P. JAY-GERIN et C. FERRADINI. Can. J. Chem. **68**, 553 (1990).

D'après les données de la littérature, nous montrons qu'une corrélation peut être établie entre le coefficient d'extinction molaire au maximum du spectre d'absorption optique de l'électron solvaté (ϵ_{max}), la largeur de celui-ci à mi-hauteur ($W_{1/2}$) et l'énergie correspondant à ce même maximum (E_{Amax}).

Mots clés : électrons solvatés, solvants polaires, spectres d'absorption optique.

J.-P. JAY-GERIN and C. FERRADINI. Can. J. Chem. **68**, 553 (1990).

On the basis of data found in the literature, it is shown that a correlation exists between the molar extinction coefficient at the maximum optical absorption of the solvated electron (ϵ_{max}), its width at half height ($W_{1/2}$), and the energy corresponding to that maximum (E_{Amax}).

Key words: solvated electrons, polar solvants, optical absorption spectra.

[Journal translation]

Les spectres d'absorption optique correspondant à des électrons en excès complètement relaxés dans un liquide polaire ont été déterminés expérimentalement pour un grand nombre de solvants, ainsi que nous l'avons déjà souligné (1). Il nous est donc apparu possible, sur la base des données disponibles actuellement, de tenter d'élargir la systématique concernant ces spectres, par exemple en essayant d'établir une corrélation entre le coefficient d'extinction molaire au maximum du spectre (ϵ_{max}), la largeur à mi-hauteur de celui-ci ($W_{1/2}$) et l'énergie (E_{Amax}) correspondant à ce même maximum. Sur le plan pratique, il serait intéressant, tout particulièrement, de pouvoir exprimer ϵ_{max} et $W_{1/2}$ en fonction de E_{Amax}. En effet, cela permettrait d'obtenir une caractérisation a priori de la forme du spectre d'électrons solvatés dans n'importe quel solvant polaire à partir de la seule détermination expérimentale de la longueur d'onde correspondant au maximum d'absorption.

Dans le tableau 1, nous avons rassemblé les données expérimentales trouvées dans la littérature pour 43 solvants de polarités diverses à la température ambiante (2–54). Les solvants sont classés par ordre des valeurs croissantes de ϵ_{max}. On peut remarquer que les valeurs de ϵ_{max} et de $W_{1/2}$ varient respectivement entre 0,6 et $5 \times 10^4\ M^{-1}\ cm^{-1}$ et entre 1,63 et 0,41 eV, alors que celles de E_{Amax} sont comprises entre 2,33 et 0,5 eV.

Nous avons tracé dans un diagramme semi-logarithmique (figure 1) la variation de ϵ_{max} en fonction de E_{Amax}. Une corrélation linéaire décrit de façon satisfaisante les données expérimentales. La relation entre ces deux paramètres peut donc s'écrire sous la forme

$$[1] \quad \epsilon_{max} = \epsilon^0_{max} \exp(-\alpha E_{Amax})$$

Un ajustement utilisant la méthode des moindres carrés conduit à $\epsilon^0_{max} = 5{,}48 \times 10^4\ M^{-1}\ cm^{-1}$ et pour la valeur de la pente de la droite à $\alpha = 0{,}81\ eV^{-1}$ avec un coefficient de corrélation égal à 0,914. Afin de mieux visualiser la relation ainsi établie, nous avons reporté sur la figure 2 quelques spectres typiques

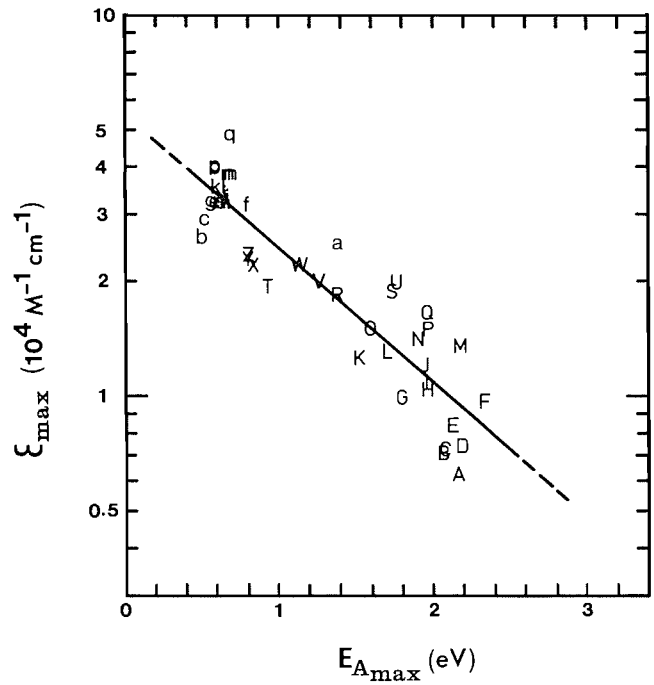

FIG. 1. Diagramme semilogarithmique montrant la variation de ϵ_{max} en fonction de E_{Amax}. La droite en trait plein a été obtenue à l'aide d'un ajustement par la méthode des moindres carrés de l'équation [1] aux données expérimentales trouvées dans la littérature pour 43 solvants de polarités diverses à la température ambiante (voir tableau 1).

d'électrons solvatés, ainsi que la courbe exponentielle représentant la relation [1].

Il est intéressant de souligner ici que l'existence d'une telle corrélation entre ϵ_{max} et E_{Amax} implique une importante conséquence. En effet, si nous appelons dN_{max} la variation de la concentration en électrons solvatés susceptibles d'absorber un

Printed in Canada / Imprimé au Canada

Can. J. Chem. Downloaded from www.nrcresearchpress.com by 91.144.44.67 on 09/07/12
For personal use only.

TABLEAU 1. Valeurs, pour des solvants de polarités diverses, du coefficient d'extinction molaire au maximum du spectre d'absorption optique de l'électron solvaté (ϵ_{max}), de la largeur de celui-ci à mi-hauteur ($W_{1/2}$) et de l'énergie correspondant à ce même maximum (E_{Amax})[a]

Solvant	ϵ_{max} ($10^4\ M^{-1}\ cm^{-1}$)	$W_{1/2}$ (eV)	E_{Amax} (eV)	Symbole[b]	Références
Propanediol-1,3	0,62[c]	1,46	2,16	A	2, 3
Butanediol-1,4	0,71[c]	1,54	2,06	B	2, 3
Butanediol-1,3	0,73[c]	1,46	2,08	C	2, 3
Propanediol-1,2	0,74[c]	1,52	2,18	D	2–4
Butanediol-2,3	0,84[c]	1,60	2,12	E	2, 3
Glycérol	0,97	1,41	2,33	F	4–6
Éthanol	0,99	1,59	1,80	G	7–10
Méthanol	1,04	1,43	1,96	H	7–12
Propanol-1	1,09	1,63	1,95	I	9, 10
Butanol-1	1,21	1,57	1,95	J	3, 4, 8–10
Propanol-2	1,25	1,45	1,51	K	3, 4, 7–9, 11, 13
Méthoxy-2 éthanol	1,3	1,63	1,70	L	11, 14
Éthylène glycol	1,35	1,43	2,17	M	2, 4, 7, 11, 15
Décanol-1	1,4	1,5	1,90	N	8, 11
Butanol-2	1,5[c]	1,57	1,59	O	3, 9, 16
Octanol-1	1,5	1,55	1,96	P	8, 9, 17
Méthyl-2 propanol-1	1,65[c]	1,61	1,97	Q	3, 9, 15, 16
Amino-2 éthanol	1,84	1,16	1,38	R	3, 4, 18, 19
H_2O	1,88	0,85	1,73	S	9, 10, 19–23
Diamino-1,2 éthane	1,95	0,88	0,93	T	24–28
D_2O	1,99	0,80	1,76	U	22, 29–31
Hydrazine	2,0	0,76	1,26	V	32–34
Méthyl-2 propanol-2	2,2	0,95	1,14	W	3, 4, 35, 36
Diamino-1,3 propane	2,2	0,73[c]	0,83	X	14, 37
Diméthyl-1,3 imidazolidinone-2	2,3[c]	—	0,80	Y	3, 38
Diméthyl-1,3 oxohexahydropyrimidine-2	2,35[c]	—	0,80	Z	3, 38
Butanone-2[d]	2,5	0,5	1,38	a	18, 39
Éther *n*-butylique	2,6	0,55[c]	0,50	b	40, 41
Éther *n*-propylique	2,9	0,5[c]	0,52[c]	c	40, 41
Diéthylamine	3,2	0,52[c]	0,63	d	26, 37, 42
Isopropylamine	3,2	0,56	0,58	e	43
N-Méthyl-pyrrolidinone	3,2	0,5[c]	0,80	f	38
Hexaméthylphosphoramide	3,2	0,45	0,56	g	44, 45
n-Propylamine	3,2	0,74	0,65	h	34, 46
Méthylamine	3,3	0,6	0,66	i	43, 47
Diglyme	3,4	0,58	0,65	j	37, 48
Éther éthylique	3,5	0,5	0,58	k	26, 37, 41, 42, 49
Diméthoxy-1,2 éthane	3,6	0,50	0,65	l	26, 37, 42, 48–50
Éthylamine	3,8	0,63	0,67	m	14, 26, 27, 43, 47
Triglyme	3,8	0,63	0,67	n	48, 49
Méthyl-2 tétrahydrofuranne	3,95	0,45	0,58	o	37, 49, 50
Tétrahydrofuranne	4,0	0,43	0,59	p	26, 28, 37, 41, 47, 50, 51
Ammoniac	4,8	0,41	0,68	q	43, 46, 52–54

[a]Valeurs sélectionnées à la température ambiante.
[b]Utilisé dans les figures 1, 3 et 4.
[c]Valeur estimée.
[d]Les cétones captent les électrons. Il est possible que le spectre obtenu dans le butanone-2 (point a) corresponde à celui d'un radical anion (G. R. Freeman, communication personnelle).

photon dont l'énergie est comprise entre E_{Amax} et $E_{Amax} + dE_{Amax}$ lorsqu'on passe d'un solvant au suivant,

[2] $$d\epsilon_{max} = \beta\, dN_{max} = \gamma \epsilon_{max}\, dE_{Amax}$$

le nombre d'électrons étant proportionnel à l'élément de surface sous la courbe $\epsilon_{max}(E_{Amax})$. Dans le cas général, on s'attendrait à ce que β et γ soient fonctions de la nature du solvant et donc de E_{Amax}. Il n'en est cependant rien puisque la relation [2] est identique à la relation expérimentale [1] avec $\gamma = -\alpha$. Par conséquent, la variation de ϵ_{max} avec E_{Amax} provient essentiellement de la modification concomitante de la forme des spectres, chaque électron solvaté contribuant de la même manière à la valeur de ϵ_{max} quelle que soit la nature du solvant. Ceci n'est valable que dans la mesure évidemment où la relation [1] est vérifiée. La dispersion des points expérimentaux de la figure 1 pourrait traduire la part due à l'influence de la nature du solvant.

À notre connaissance, aucun modèle théorique n'a prédit jusqu'ici une variation exponentielle de ϵ_{max} avec E_{Amax}. Il faut dire à ce sujet que la nature des transitions optiques responsables du spectre d'absorption de l'électron solvaté reste encore à ce jour relativement mal comprise. On sait en effet qu'un

Can. J. Chem. Downloaded from www.nrcresearchpress.com by 91.144.44.67 on 09/07/12
For personal use only.

Can. J. Chem. Downloaded from www.nrcresearchpress.com by 91.144.44.67 on 09/07/12
For personal use only.

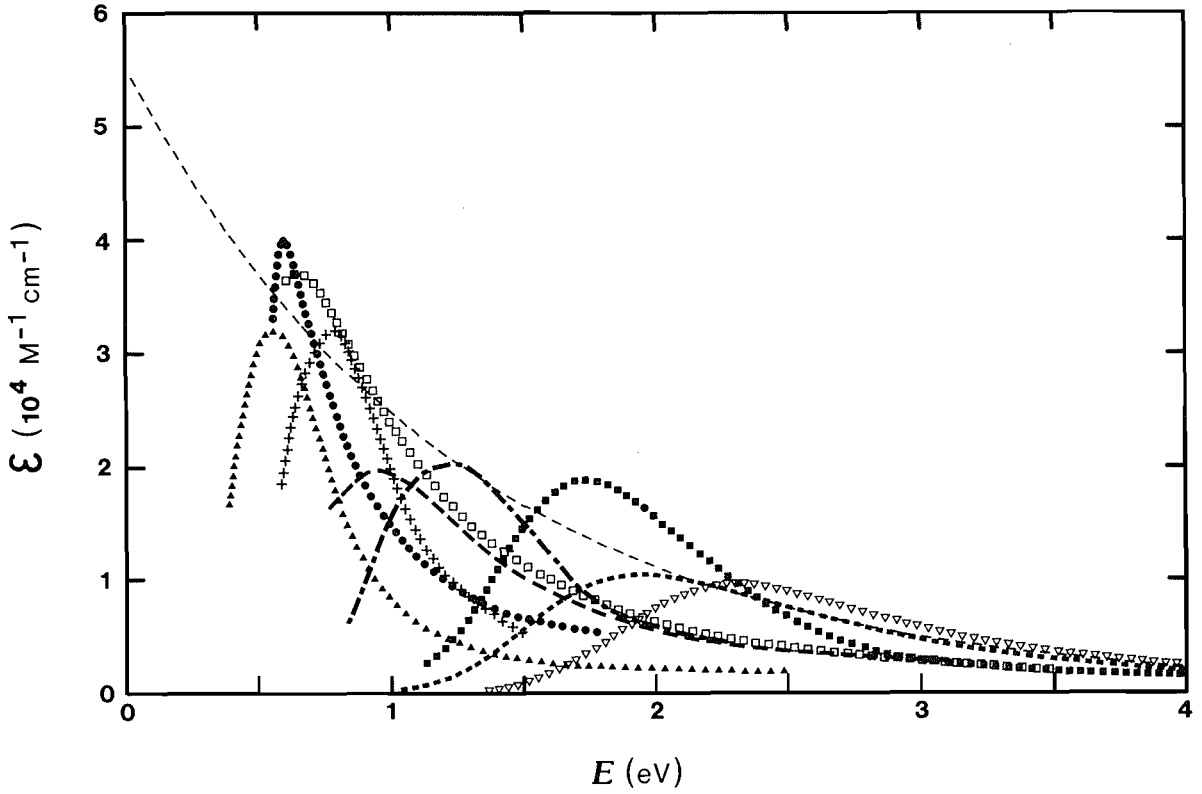

FIG. 2. Spectres typiques d'absorption d'électrons solvatés $\epsilon(E)$, à la température ambiante, dans divers solvants : ▲▲▲, hexaméthylphosphoramide; ●●●, tétrahydrofuranne; □□□, *n*-propylamine; + + +, *N*-méthylpyrrolidinone; ––, diamino-1,2 éthane; - - -, hydrazine; ■■■, H_2O; ---, méthanol; ▽▽▽, glycérol. La courbe exponentielle en tirets représente le lieu géométrique des maxima ϵ_{max} des différents spectres tel que donné par la relation [1].

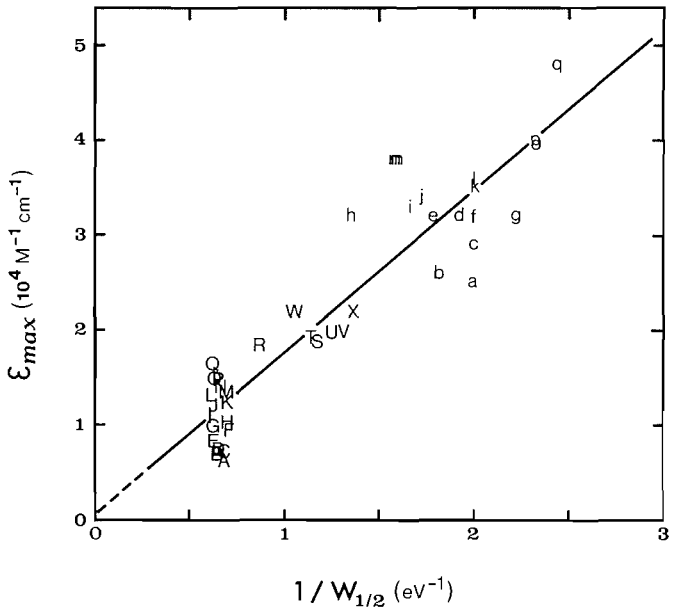

FIG. 3. Variation de ϵ_{max} en fonction de $1/W_{1/2}$. La droite en trait plein a été obtenue à l'aide d'un ajustement par la méthode des moindres carrés de l'équation [3] aux données expérimentales trouvées dans la littérature pour 41 solvants de polarités diverses à la température ambiante (voir tableau 1).

désaccord persiste entre les auteurs en ce qui concerne la nature physique des états électroniques finals, la question posée restant de savoir si les transitions mises en jeu se font vers des états liés, ou bien vers un continuum d'états délocalisés (55). Puisque ϵ_{max} reflète une mesure de la section efficace d'interaction entre un électron solvaté et un photon d'énergie E_{Amax}, la relation [1] obtenue dans ce travail, bien qu'approximative, pourrait apporter un indice utile à notre quête d'une meilleure compréhension de la nature du spectre d'absorption de l'électron solvaté.

Dans la figure 3 nous avons tracé la variation de ϵ_{max} en fonction de $1/W_{1/2}$. Une corrélation linéaire est observée, dont l'extrapolation aux faibles valeurs de $1/W_{1/2}$ passe pratiquement par l'origine. Une telle relation peut donc s'écrire sous la forme

$$[3] \quad \epsilon_{max} = \eta\left(\frac{1}{W_{1/2}}\right) + \mu$$

Un ajustement par la méthode des moindres carrés conduit à $\eta = 1{,}71 \times 10^4\ M^{-1}\ cm^{-1}\ eV$ et $\mu = 0{,}054 \times 10^4\ M^{-1}\ cm^{-1}$ avec un coefficient de corrélation égal à 0,921.

Cette corrélation linéaire entre ϵ_{max} et $1/W_{1/2}$ pouvait être attendue. En effet, de nombreux auteurs, et en particulier Freeman et coll. (4, 10, 41, 56), ont signalé que la valeur de la force d'oscillateur (f) correspondant au spectre d'absorption de l'électron solvaté varie peu lorsqu'on passe d'un solvant à l'autre. f est défini par (57)

$$[4] \quad f = 3{,}49 \times 10^{-5} \int_0^\infty \epsilon(E)\, dE$$

où $\epsilon(E)$ est le coefficient d'extinction molaire à l'énergie E (eV). L'intégrale de la relation [4], qui représente l'aire totale sous la courbe $\epsilon(E)$, peut être calculée avec une bonne approximation par l'équation

$$[5] \quad \int_0^\infty \epsilon(E)\, dE \simeq \epsilon_{max} W_{1/2}$$

Can. J. Chem. Downloaded from www.nrcresearchpress.com by 91.144.44.67 on 09/07/12
For personal use only.

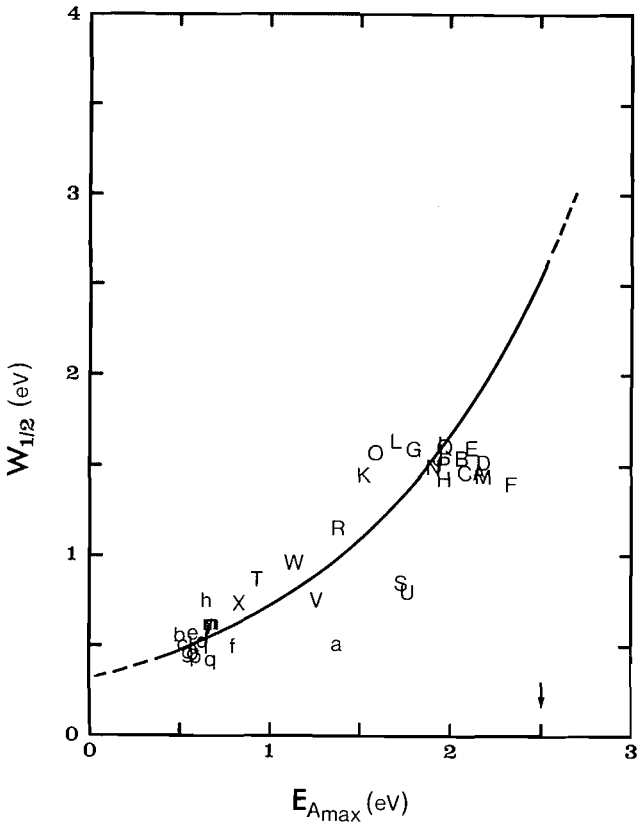

FIG. 4. Variation de $W_{1/2}$ en fonction de E_{Amax}. La courbe en trait plein illustre la relation [6]. Les données expérimentales du tableau 1 sont également représentées afin de vérifier la validité de la loi $W_{1/2}(E_{Amax})$ trouvée. La flèche indique la limite supérieure pour E_{Amax} (~2,5 eV), telle que suggérée par Freeman (58).

D'après les relations [4] et [5], on s'attend donc bien à ce que le produit $\epsilon_{max} W_{1/2}$ soit peu modifié d'un solvant à l'autre, et par conséquent à ce que ϵ_{max} varie de façon sensiblement inversement proportionnelle avec $W_{1/2}$.

On peut calculer, en utilisant les relations [3]–[5] et en prenant en compte l'ensemble des solvants considérés dans cette étude, une valeur moyenne de f. Si l'on s'en tient à la détermination précédente de η et μ, on obtient $f \simeq 0{,}62$. Une telle valeur s'accorde bien avec les données de la littérature concernant les différents solvants.

L'existence d'une corrélation, d'une part entre ϵ_{max} et E_{Amax}, et d'autre part entre ϵ_{max} et $W_{1/2}$, implique comme conséquence une corrélation entre $W_{1/2}$ et E_{Amax}. Les relations [1] et [3] donnent en effet immédiatement

$$[6] \quad W_{1/2} = \frac{1}{a \exp(-\alpha E_{Amax}) - b}$$

avec $a = \epsilon^0_{max}/\eta = 3{,}20\ \text{eV}^{-1}$ et $b = \mu/\eta = 0{,}032\ \text{eV}^{-1}$, et où $W_{1/2}$ et E_{Amax} sont exprimés en eV. La relation [6] est représentée figure 4. Afin de vérifier la validité de la loi $W_{1/2}(E_{Amax})$ ainsi trouvée, nous avons également porté sur cette même figure les données expérimentales (voir tableau 1). Comme on peut le voir, l'accord obtenu est satisfaisant.

En conclusion, nous avons montré, sur la base des données de la littérature, qu'il est possible d'établir une corrélation entre le coefficient d'extinction molaire au maximum du spectre d'absorption optique de l'électron solvaté, la largeur à mi-hauteur de celui-ci et l'énergie correspondant à ce même maximum. Cette corrélation est intéressante sur un plan pratique, car elle permet une estimation a priori de la forme du spectre d'électrons solvatés dans un solvant polaire donné. Sur un plan plus fondamental, elle pourrait apporter un élément utile à la compréhension de la nature du spectre de l'électron solvaté.

Remerciements

Les auteurs tiennent à exprimer leurs remerciements au Conseil de recherches médicales du Canada et au Programme de coopération franco-québécoise en recherche médicale pour l'aide financière qu'ils leur ont apportée.

1. J.-P. JAY-GERIN and C. FERRADINI. J. Chem. Phys. **91**, 3275 (1989).
2. K. OKAZAKI, K. M. IDRISS-ALI et G. R. FREEMAN. Can. J. Chem. **62**, 2223 (1984).
3. J.-P. JAY-GERIN et C. FERRADINI. Radiat. Phys. Chem. **33**, 251 (1989).
4. F.-Y. JOU et G. R. FREEMAN. Can. J. Chem. **57**, 591 (1979).
5. S. ARAI et M. C. SAUER, JR. J. Chem. Phys. **44**, 2297 (1966).
6. T. KAJIWARA et J. K. THOMAS. J. Phys. Chem. **76**, 1700 (1972).
7. M. C. SAUER, JR., S. ARAI et L. M. DORFMAN. J. Chem. Phys. **42**, 708 (1965).
8. G. E. HALL et G. A. KENNEY-WALLACE. Chem. Phys. **32**, 313 (1978).
9. A.-D. LEU, K. N. JHA et G. R. FREEMAN. Can. J. Chem. **61**, 1115 (1983).
10. F.-Y. JOU et G. R. FREEMAN. J. Phys. Chem. **81**, 909 (1977).
11. R. R. HENTZ et G. A. KENNEY-WALLACE. J. Phys. Chem. **78**, 514 (1974).
12. T. A. CHUBAKOVA et N. A. BAKH. Khim. Vys. Energ. **12**, 373 (1978). (Traduction anglaise: High Energy Chem. **12**, 315 (1979)).
13. R. S. DIXON et V. J. LOPATA. Radiat. Phys. Chem. **19**, 495 (1982).
14. J. F. GAVLAS, F. Y. JOU et L. M. DORFMAN. J. Phys. Chem. **78**, 2631 (1974).
15. A. V. RUDNEV, A. V. VANNIKOV et N. A. BAKH. Khim. Vys. Energ. **6**, 473 (1972) (Traduction anglaise : High Energy Chem. **6**, 416 (1973)).
16. K. OKAZAKI et G. R. FREEMAN. Can. J. Chem. **56**, 2305 (1978).
17. F.-Y. JOU et G. R. FREEMAN. J. Phys. Chem. **83**, 261 (1979); **88**, 3900 (1984).
18. A. V. VANNIKOV. Usp. Khim. **44**, 1931 (1975) (Traduction anglaise: Russ. Chem. Rev. **44**, 906 (1975)).
19. A. M. BRODSKY et A. V. TSAREVSKY. Int. J. Radiat. Phys. Chem. **8**, 455 (1976).
20. J. P. KEENE. Radiat. Res. **22**, 1 (1964).
21. E. J. HART et M. ANBAR. The hydrated electron. Wiley, New York, NY. 1970. p. 39.
22. A. SINGH, W. J. CHASE et J. W. HUNT. Faraday Discuss. Chem. Soc. **63**, 28 (1978).
23. G. V. BUXTON, C. L. GREENSTOCK, W. P. HELMAN et A. B. ROSS. J. Phys. Chem. Ref. Data, **17**, 513 (1988).
24. J. L. DYE, M. G. DEBACKER et L. M. DORFMAN. J. Chem. Phys. **52**, 6251 (1970).
25. J. L. DYE, M. G. DEBACKER, J. A. EYRE et L. M. DORFMAN. J. Phys. Chem. **76**, 839 (1972).
26. M. T. LOK, F. J. TEHAN et J. L. DYE. J. Phys. Chem. **76**, 2975 (1972).
27. J. A. DELAIRE et J. R. BAZOUIN. Can. J. Chem. **57**, 2013 (1979).
28. T. H. TRAN-THI, A. M. KOULKÈS-PUJO, J. SUTTON et O. ANITOFF. Radiat. Phys. Chem. **23**, 77 (1984).
29. E. M. FIELDEN et E. J. HART. Radiat. Res. **33**, 426 (1968).
30. R. S. DIXON et V. J. LOPATA. Radiat. Phys. Chem. **11**, 135 (1978).
31. F.-Y. JOU et G. R. FREEMAN. J. Phys. Chem. **83**, 2383 (1979).

32. J. DELAIRE, P. CORDIER, J. BELLONI, F. BILLIAU et M. O. DELCOURT. J. Phys. Chem. **80**, 1687 (1976).
33. W. A. SEDDON, J. W. FLETCHER et F. C. SOPCHYSHYN. Can. J. Chem. **54**, 2807 (1976).
34. J. DELAIRE. Doctorat ès-sciences physiques (Chimie), Université de Paris-Sud, Orsay, France. 1980.
35. G. G. TEATHER et N. V. KLASSEN. Int. J. Radiat. Phys. Chem. **7**, 475 (1975).
36. A.-D. LEU, K. N. JHA et G. R. FREEMAN. Can. J. Chem. **60**, 2342 (1982).
37. L. M. DORFMAN et F. Y. JOU. *Dans* Electrons in fluids. The nature of metal–ammonia solutions. *Éditeurs* : J. Jortner et N. R. Kestner. Springer, Berlin, Allemagne de l'Ouest. 1973. p. 447.
38. J. R. LANGAN, K. J. LIU, G. A. SALMON, P. P. EDWARDS, A. ELLABOUDY et D. M. HOLTON. Proc. R. Soc. London, A : **421**, 169 (1989).
39. A. V. VANNIKOV, E. I. MAL'TSEV, V. I. ZOLOTAREVSKY et A. V. RUDNEV. Int. J. Radiat. Phys. Chem. **4**, 135 (1972).
40. J.-P. DODELET et G. R. FREEMAN. Can. J. Chem. **53**, 1263 (1975).
41. F.-Y. JOU et G. R. FREEMAN. Can. J. Chem. **54**, 3693 (1976).
42. L. M. DORFMAN, F. Y. JOU et R. WAGEMAN. Ber. Bunsen-Ges. Phys. Chem. **75**, 681 (1971).
43. W. A. SEDDON, J. W. FLETCHER et F. C. SOPCHYSHYN. Can. J. Chem. **56**, 839 (1978).
44. J. M. BROOKS et R. R. DEWALD. J. Phys. Chem. **72**, 2655 (1968).
45. E. A. SHAEDE, L. M. DORFMAN, G. J. FLYNN et D. C. WALKER. Can. J. Chem. **51**, 3905 (1973).
46. F.-Y. JOU et G. R. FREEMAN. Can. J. Chem. **60**, 1809 (1982).
47. W. A. SEDDON, J. W. FLETCHER et R. CATTERALL. Can. J. Chem. **55**, 2017 (1977).
48. W. A. SEDDON, J. W. FLETCHER, F. C. SOPCHYSHYN et R. CATTERALL. Can. J. Chem. **55**, 3356 (1977).
49. F. Y. JOU et L. M. DORFMAN. J. Chem. Phys. **58**, 4715 (1973).
50. M. F. FOX et E. HAYON. Chem. Phys. Lett. **25**, 511 (1974).
51. G. A. SALMON, W. A. SEDDON et J. W. FLETCHER. Can. J. Chem. **52**, 3259 (1974).
52. J. BELLONI et J. FRADIN DE LA RENAUDIÈRE. Nature, **232**, 173 (1971).
53. FARHATAZIZ, L. M. PERKEY et R. R. HENTZ. J. Chem. Phys. **60**, 4383 (1974).
54. J. BELLONI et J. L. MARIGNIER. Radiat. Phys. Chem. **34**, 157 (1989).
55. T. R. TUTTLE, JR., S. GOLDEN et G. ROSENFELD. Radiat. Phys. Chem. **32**, 525 (1988).
56. K. N. JHA, G. L. BOLTON et G. R. FREEMAN. J. Phys. Chem. **76**, 3876 (1972).
57. N. J. TURRO. Modern molecular photochemistry. Benjamin/Cummings, Menlo Park, CA. 1978. Chap. 5. p. 76.
58. G. R. FREEMAN. J. Phys. Chem. **77**, 7 (1973).

Can. J. Chem. Downloaded from www.nrcresearchpress.com by 91.144.44.67 on 09/07/12
For personal use only.

Synthesis and substitution chemistry of some bis(dithiolate) complexes of molybdenum, $Mo(S_2C_6H_3R)_2(PMePh_2)_2$, R = H, Me

NATALIE J. LAZAROWYCH AND ROBERT H. MORRIS

Department of Chemistry and the Scarborough Campus, University of Toronto, Toronto, Ont., Canada M5S 1A1

Received September 5, 1989

NATALIE J. LAZAROWYCH and ROBERT H. MORRIS. Can. J. Chem. **68**, 558 (1990).

The new bis(dithiolate) complexes $Mo(1,2\text{-}S_2\text{-}4\text{-}R\text{-}C_6H_3)_2(PMePh_2)_2$, R = H, Me, are readily synthesized from three different types of starting materials: *trans*-$Mo(N_2)_2(PMePh_2)_4$, $MoCl_4(PMePh_2)_2$, and $MoOCl_2(PMePh_2)_3$. The ^{31}P NMR spectra of the dithiolate complexes at low temperature are consistent with a *cis* stereochemistry of the $PMePh_2$ ligands and isomerism with respect to inversion at sulfur and relative positioning of the methyl groups on the chelating $1,2\text{-}S_2\text{-}4\text{-}Me\text{-}C_6H_3$ ligands. The singlet in the ^{31}P NMR spectrum at room temperature arises from rapid interconversion of these isomers. Substitution of one or two of the $PMePh_2$ ligands in the dithiolate complexes proceeds under mild conditions to give the complexes $Mo(S_2C_6H_4)_2(CO)(PMePh_2)$, $Mo(S_2C_6H_4)_2(CN\text{-}t\text{-}Bu)(PMePh_2)$, $Mo(S_2C_6H_3Me)_2(dppe)$, $Mo(S_2C_6H_4)_2(depe)$, $Mo(S_2C_6H_4)_2(PMePh_2)(PMe_3)$, $Mo(S_2C_6H_4)_2(PMePh_2)(P(OMe)_3)$, and $Mo(S_2C_6H_4)_2(P(OMe)_3)_2$. The ^{31}P and ^{13}C NMR spectroscopy of these bis(dithiolate) complexes suggest that they have monodentate ligands *cis* disposed.

A reversible equilibrium exists between $Mo(S_2C_6H_4)_2(PMePh_2)_2$ and $Mo(S_2C_6H_4)_2(CO)(PMePh_2)$ in the presence of carbon monoxide in solution. Isolation of $Mo(S_2C_6H_4)_2(CO)(PMePh_2)$ is facilitated by use of CH_3I as a "phosphine sponge" reagent. If the sulfur ligands are viewed as dianions, then this is the first thermally stable carbonyl complex of molybdenum(IV).

Keywords: molybdenum, dithiolate, diphenylmethylphosphine, carbonyl, NMR.

NATALIE J. LAZAROWYCH et ROBERT H. MORRIS. Can. J. Chem. **68**, 558 (1990).

De nouveau complexes bis(dithiolate), $Mo(1,2\text{-}S_2\text{-}4\text{-}R\text{-}C_6H_3)_2(PMePh_2)_2$ dans lesquels R = H ou Me, peuvent facilement être synthétisés à partir des composés suivants : *trans*-$Mo(N_2)_2(PMePh_2)_4$, $MoCl_4(PMePh_2)_2$, et $MoOCl_2(PMePh_2)_3$. Les spectres RMN du ^{31}P des complexes dithiolates, réalisés à basse température, correspondent à une stéréochimie *cis* des ligands $PMePh_2$ et à une isomérie par rapport à l'inversion au niveau du soufre et aux positions relatives des groupements méthyles sur les ligands chélatants $1,2\text{-}S_2\text{-}4\text{-}Me\text{-}C_6H_3$. Le singulet observé dans le spectre RMN du ^{31}P enregistré à la température ambiante provient d'une interconversion rapide de ces isomères. La substitution de l'un ou des deux ligands $PMePh_2$ des complexes dithiolates peut se faire dans des conditions douces pour conduire aux complexes $Mo(S_2C_6H_4)_2(CO)(PMePh_2)$, $Mo(S_2C_6H_4)_2(CN\text{-}t\text{-}Bu)(PMePh_2)$, $Mo(S_2C_6H_3Me)_2(dppe)$, $Mo(S_2C_6H_4)_2(depe)$, $Mo(S_2C_6H_4)_2(PMePh_2)(PMe_3)$, $Mo(S_2C_6H_4)_2(PMePh_2)(P(OMe)_3)$ et $Mo(S_2C_6H_4)_2(P(OMe)_3)_2$. Les spectres RMN du ^{31}P et du ^{13}C de ces complexes bis(dithiolates) suggèrent que les ligands monodentates sont disposés d'une façon *cis*.

En solution, en présence de monoxyde de carbone, il existe un équilibre réversible entre le $Mo(S_2C_6H_4)_2(PMePh_2)_2$ et le $Mo(S_2C_6H_4)_2(CO)(PMePh_2)$. Pour isoler le $Mo(S_2C_6H_4)_2(CO)(PMePh_2)$ plus facilement, on peut utiliser du CH_3I comme « éponge de phosphine ». Si l'on considère les ligands sulfurés comme des dianions, on peut alors considére ces complexes comme les premiers complexes du molybdène(IV)-carbonyle qui soient thermiquement stables.

Mots clés : molybdène, dithiolate, diphénylméthylphosphine, carbonyle, RMN.

[Traduit par la revue]

Introduction

Some important industrial chemical processes like hydrodesulfurization and biological processes like nitrogen fixation involve complexes where molybdenum is ligated primarily by sulfur donors. In the course of our studies of the properties of such complexes that also contain hydride ligands (1, 2), we identified the complexes $Mo(S_2C_6H_3R)_2(PMePh_2)_2$, R = H (**1***a* with the benzene-1,2-dithiolato ligand) and R = Me (**1***b* with the toluene-3,4-dithiolato ligand) as the products of the reaction of the hydride complexes $Mo(H)_2(S_2C_6H_3R)(PMePh_2)_3$ with excess dithiol ligand (reaction [1]).

[1] $Mo(H)_2(S_2C_6H_3R)(PMePh_2)_3 + (HS)_2C_6H_3R \rightarrow Mo(S_2C_6H_3R)_2(PMePh_2)_2 + 2\ H_2 + PMePh_2$

This is a report on the spectroscopy and chemistry of complexes **1** that have not been previously investigated.

The only directly related work is by Sellmann and Reisser (3). The complex $Mo(S_2C_6H_4)_2(PMe_3)_2$ was prepared via the dealkylation of $NaSC_6H_4S(CH_2)_2SC_6H_4SNa$ (Na_2dttd) upon reaction of this potentially tetradentate ligand with $MoCl_2(PMe_3)_4$ (reaction [2]).

[2] $MoCl_2(PMe_3)_4 + NaSC_6H_4S(CH_2)_2SC_6H_4SNa \rightarrow Mo(S_2C_6H_4)_2(PMe_3)_2 + 2\ NaCl + 2\ PMe_3 + C_2H_4$

The stereochemistry of $Mo(S_2C_6H_4)_2(PMe_3)_2$ was not elucidated. Other formally Mo(IV) complexes with four nonbridging thiolate ligands include $Mo(S\text{-}t\text{-}Bu)_4$ (4), $Mo(TIPT)_4$ (5), $Mo(TIPT)_4(RC{\equiv}CR)$ (TIPT = S-2,4,6-$C_6H_2(CHMe_2)_3$) (6), and $Mo(S_2C_6H_4)_3^{2-}$ (7). There is a wealth of chemistry associated with complexes of Mo(II) coordinated by four sulfur atoms and, usually, three other ligands like $Mo(dttd)(CO)_2(PMe_3)$ (8), $Mo(S_2PPh_2)_2(CO)_2(PPh_3)$ (9), and $Mo(S_2CNR_2)_2(CO)(PMe_3)_2$ (10).

Experimental

General

All manipulations were performed using Schlenk flasks or a glove-box filled with pure nitrogen. Literature procedures that were used to make *trans*-$Mo(N_2)_2(PMePh_2)_4$ (11–13), $Mo(H)_4(PMePh_2)_4$ (14), $MoOCl_2(PMePh_2)_3$ (15), $MoOCl_2(PEtPh_2)_3$ (15), and $1,2\text{-}(SH)_2\text{-}C_6H_4$ (16) have been described. $MoCl_5$ (resublimed) was purchased from Alfa Chemicals (Danvers) and used as such. Other ligands were purchased from Aldrich Chemical Company (Milwaukee, WI), or from Strem Chemicals (Newbury Port, MA).

Solvents other than alcohols were dried over and distilled from sodium benzophenone ketyl and were degassed before use. Alcohols were distilled from their magnesium alkoxides. Tetrahydrofuran (THF) was further dried over and vacuum distilled from $LiAlH_4$.

The infrared spectra were obtained by use of a Nicolet 5DX FTIR

Can. J. Chem. Downloaded from www.nrcresearchpress.com by 91.144.44.67 on 09/07/12
For personal use only.

Can. J. Chem. Downloaded from www.nrcresearchpress.com by 91.144.44.67 on 09/07/12
For personal use only.

spectrometer (±2 cm^{-1}) as mineral oil mulls on NaCl plates or as solutions in 0.1 mm KBr cells.

The NMR spectra were recorded by use of a Varian XL200 spectrometer operating at 80.98 MHz for ^{31}P, 200 MHz for ^{1}H, or a Varian XL400 operating at 161.98 MHz for ^{31}P and 400 MHz for ^{1}H. ^{31}P chemical shifts were recorded relative to 1% $P(OMe)_3$ in C_6D_6 in a coaxial capillary. ^{1}H chemical shifts were measured relative to residual non-deuterated solvent peaks or silicone grease (0.297 ppm in C_6D_6), and then reported relative to TMS. All resonances are singlets unless otherwise stated. All spectra were obtained at 22°C unless otherwise indicated.

Microanalyses were performed by Canadian Microanalytical Services, Vancouver, B.C.

Visible absorption spectra were recorded using a Perkin Elmer Lambda 3B UV/visible spectrophotometer and a Perkin Elmer R100 recorder.

Mass spectra were obtained using a VG 70-250S instrument. Xe atom flux was used along with nitrophenyl octyl ether (NPOE) or nitrobenzyl alcohol (NBA) as the matrices (17). The matrices were degassed before use. The compounds were stored in vials with septa under nitrogen or argon and usually added as solids to the matrix that had been applied to the target, these applications being performed as quickly as possible in air.

Preparation of cis-$Mo(S_2C_6H_3Me)_2(PMePh_2)_2$ *from* $MoOCl_2(PMePh_2)$

$MoOCl_2(PMePh_2)_3$ (0.510 g, 0.651 mmol) was suspended in benzene (20 mL) and frozen 1,2-$(SH)_2$-4-CH_3-C_6H_3 (0.203 g, 1.30 mmol) was added. The green suspension was stirred to yield a red slurry-solution within 2 min. The mixture then became a red solution as it stirred for 2.7 h. The solvent was reduced in volume, using vacuum, to 2 mL and the resulting red solid was separated by filtration (0.41 g, 0.50 mmol, 77% yield) and recrystallized from benzene/pentanes. The sample was contaminated with silicone stopcock grease. Anal. calcd. for $MoS_4P_2C_{40}H_{38}\cdot 0.2SiO(CH_3)_2$: C 59.20, H 4.82; found: C 59.09, H 4.88. FAB^+ MS (toluene/NPOE matrix): 806.2 maximum corresponding to $^{98}Mo(S_2C_6H_3Me)_2(PMePh_2)_2$ isotopomer. Superior signal-to-noise ratio spectra were obtained when a toluene slurry was dabbed onto the target, which was coated with NPOE, as opposed to using a solution of the compound in toluene/NPOE. $^{31}P\{^{1}H\}$ NMR (red-orange C_6H_6 solution) δ: −102.7. $^{31}P\{^{1}H\}$ NMR (90% toluene/10% C_6D_6, 161.98 MHz, −70°C): three sets of complex multiplets (each of approximately equal integration) having maxima at δ −98.42 (A), −98.38 (B), −101.23 (C) ppm, the most discernable peaks occurring at −98.0, −98.42, −98.60; −99.18, −99.38, −99.5, −99.71; −100.93, −101.24, −101.46; see discussion section for structures of A, B, and C.

Preparation of cis-$Mo(S_2C_6H_4)_2(PMePh_2)_2$

Method A

$MoOCl_2(PMePh_2)_3$ (0.51 g, 0.65 mmol) and 1,2-$(SH)_2$-C_6H_4 (0.20 g, 1.41 mmol) were reacted in a similar fashion to the 1,2,-S_2-4-$CH_3C_6H_3$ derivative (see above). The mixture appeared as a red slurry-solution, then a homogeneous red solution, and then a red solution with red and black precipitate. Dinitrogen purge reduced the solvent volume to 10 mL. The red solid was separated from the red liquid using filtration (0.38 g, 0.49 mmol, 75% yield). The red solid was recrystallized from benzene/pentanes. Anal. calcd. for $MoS_4P_2C_{38}H_{34}\cdot C_6H_6$: C 61.82, H 4.72; found: C 61.78, H 4.79. ^{1}H NMR (C_6D_6, 200 MHz) δ: 2.01 (br, 6H, PMe); 6.73(br), 7.081, 7.089, 7.096, 7.104, 8.347(br) (32 H (expect 28), aromatic protons of thiol and phosphine ligands). $^{31}P\{^{1}H\}$ NMR (orange-red C_6H_6 solution) δ: −102.6 ppm. $^{31}P\{^{1}H\}$ NMR (toluene, −75.5°C, lock methanol-d_4 in insert, ref. external $P(OMe)_3$ in acetone-d_6, approximate integrations in parentheses) δ: −97.98 (1), A; −98.94(1), B; −100.65(0.5), C; −100.76(0.5), C. See discussion for structures of conformers A, B, and C. λ_{max} (pale orange benzene solution, quartz cells): 421 nm, 360 nm (less intense maximum).

Method B

An orange solution of $Mo(N_2)_2(PMePh_2)_4$ (3.2 g, 3.4 mmol) in benzene (100 mL) was degassed with hydrogen (three cycles of evacuation and backfill with gas) and then left to stir under hydrogen for 45 min at 75°C. The solvent was removed from the resultant yellow solution using vacuum, leaving $MoH_4(PMePh_2)_4$ as a dirty yellow solid. Benzene (70 mL) and 1,2-$(SH)_2$-C_6H_4 (1.0 g, 7.0 mmol) were added and the yellow solution was stirred for 40 min, during which time it became a very dark red colour. The solvent was concentrated to 5 mL, using vacuum, to give a red precipitate. Recrystallization of this material from benzene/hexanes afforded a red solid (70% yield). $^{31}P\{^{1}H\}$ NMR δ: −102.82.

Crude molecular weight determination of cis-$Mo(S_2C_6H_4)_2(PMePh_2)_2$

The Signer method for molecular weight determination was employed (18, 19). The sample solution of $Mo(S_2C_6H_4)_2(PMePh_2)_2$ (0.020 g, 0.0257 mmol) in THF (2.503 g), and the reference solution of benzophenone (0.054 g, 0.296 mmol) in THF (3.007 g) were prepared. An equal volume (1.00 mL) of each of the sample and reference solutions was transferred into the appropriate compartment of the Signer apparatus. The solutions were freeze–thaw degassed three times. The initial volumes of each solution were marked on the arms of the apparatus using a fine felt-tipped glass marker. The solutions were drained from the arms into the round-bottom compartments of the apparatus and the vapours were allowed to equilibrate between compartments. After 5, 12, 13, 27, and 50 days of equilibration the solutions were drained into the arms of the apparatus, the volume marked, and the solution returned into the round-bottom compartment. The volume did not change between 27 and 50 days. On the 50th day the solutions were removed and the volume markings calibrated using microlitre syringes and dichloromethane. The approximate molecular weight, as determined by partial vapour pressure equilibration of the two solutions, is 970 ± 200 (calcd. 804).

Preparation of cis-$Mo(S_2C_6H_4)_2(CO)(PMePh_2)$

$Mo(1,2\text{-}S_2\text{-}C_6H_4)_2(PMePh_2)_2$ (1.58 g, 2.043 mmol) was partially dissolved in benzene (200 mL). The flask was evacuated and filled with carbon monoxide (1 atm (101.3 kPa)) three times. Iodomethane (320 μL, 0.73 g, 5.14 mmol) was then added to the orange-red mixture. After stirring for 10 min, the reaction solution turned deep pink. The solution was stirred under carbon monoxide for 3 days and then stored at −20°C for 3 days. The solvent was then reduced to 150 mL by N_2 purge at 20°C. Diethyl ether (200 mL) was added. The white precipitate ($[PMe_2Ph_2]I$, see below) that formed was filtered off along with a small amount of starting complex. All except a small amount of the solvent was removed from the pink filtrate using a carbon monoxide purge. The deep pink solid was then filtered off and washed with ether (0.71 g, 1.17 mmol, 57% yield). Anal. calcd. for $MoS_4POC_{26}H_{21}$: C 51.65, H 3.50; found: C 51.32, H 3.58. $^{31}P\{^{1}H\}$ NMR (benzene) δ: −95.51 ppm. ^{13}C NMR ($CDCl_3$, all resonances not assigned arise from carbons on the aromatic dithiolate ligand, or carbons of the phenyl groups on the phosphine ligand) δ: 230.3 (doublet, J_{PC} = 11.9 Hz, MoCO); 184.3 (weak); 156.0; 135.0; 134.1; 132.9 (doublet, J = 9.5 Hz); 130.4 (doublet, J = 2.2 Hz); 129.3; 128.4 (doublet, J = 10.0 Hz); 124.1; 18.3 (doublet, J_{PC} = 33.4 Hz, PCH_3). FAB^+ MS (NBA or NPOE matrix): 578 largest peak due to $^{98}Mo(S_2C_6H_4)_2(PMePh_2)$ (i.e., $M^+ - CO$). The ion current for the 578 peak (and hence the observed intensity) was much greater when NBA was used as the matrix. IR(mineral oil mull), ν_{CO}: 1977 cm^{-1}. Characterization of $[PMe_2Ph_2]I$, the white solid recovered (0.4 g, 1.2 mmol, 60% yield), was as follows. $^{31}P\{^{1}H\}$ NMR (colourless acetone/acetone-d_6 solution) δ: −114.3. ^{1}H NMR (C_6D_6) δ: 2.76 (doublet, J_{PH} = 13.9 Hz, 6H, PMe_2); 7.83–7.49 (multiplet, 10H, PPh_2).

Preparation of cis-$Mo(S_2C_6H_4)_2(CN\text{-}t\text{-}Bu)(PMePh_2)$

$Mo(S_2C_6H_4)_2(PMePh_2)_2$ (0.2 g, 0.26 mmol) and *tert*-butyl isonitrile (0.021 g, 0.25 mmol) were stirred together in 20 mL benzene for 1.5 h. The tomato-juice-red coloured slurry-solution of $Mo(S_2C_6H_4)_2(PMePh_2)_2$ became a clear dark cranberry-red coloured solution almost

Can. J. Chem. Downloaded from www.nrcresearchpress.com by 91.144.44.67 on 09/07/12
For personal use only.

immediately upon addition of the isonitrile. Vacuum was used to reduce the solvent volume to 2 mL and then pentanes were added to cause precipitation of a red solid. The solid, collected by filtration, was recrystallized using benzene and pentanes at room temperature. The resultant solid was dried *in vacuo* (0.04 g, 24%). Anal. calcd. for $MoS_4PNC_{30}H_{30}$: C 54.62, H 4.58, N 2.12; found: C 54.72, H 4.63, N 2.13. $^{31}P\{^1H\}$ NMR (benzene) δ: −94.0. ^1H NMR (C_6D_6, 200 MHz) δ: 0.83 (9H, *t*-Bu); 2.39 (d, J_{PH} = 7.6 Hz, 3H, PMe); 6.7–7.3 (multiplet, 10H); 7.04, 7.06, 7.07, 7.09, 8.36, 8.38, 8.39, 8.41 (8H, part of AA′XX′ pattern due to similar environments of thiol ligands). IR(mineral oil mull), ν_{CN}: 2138 cm^{-1}.

Generation of $Mo(S_2C_6H_3Me)_2(dppe)$ from $MoCl_4(dppe)$

$MoCl_4(dppe)$, dppe = $PPh_2CH_2CH_2PPh_2$, was prepared by slight modification of the method of Butcher and Chatt (15). $MoCl_4(THF)_2$ (20) was used in the preparation instead of $MoCl_4(EtCN)_2$. To a tawny-orange solution-slurry of $MoCl_4(dppe)$ (0.057 g, 0.090 mmol) in 20 mL benzene was added 1,2-$(SH)_2$-4-CH_3-C_6H_3 (0.028 g, 0.179 mmol). The reaction was allowed to sir overnight under a dynamic N_2 atmosphere during which time the solvent evaporated. The following morning a green oily solid, which was relatively insoluble, remained in the flask. $^{31}P\{^1H\}$ NMR (green C_6H_6 solution) δ: −75.6 (weak). FAB^+ MS (slurry in NPOE matrix), calcd. mass of isotopomer, relative amount: 798, 40; 799, 20; 800, 40; 801, 60; 802, 80; 803, 70; 804, 100; 805, 48; 806, 52; 807, 20; 808, 10; found: 798, 40; 799, 30; 800, 50; 801, 70; 802, 81; 803, 70; 804, 100; 805, 58; 806, 56; 807, 20; 808, 10; the maximum at 804 corresponds to $^{98}Mo(S_2C_6H_3Me)_2(dppe)$.

Generation of $Mo(S_2C_6H_3Me)_2(dppe)$ from $Mo(S_2C_6H_3Me)_2(PMePh_2)_2$

$Mo(S_2C_6H_3Me)_2(PMePh_2)_2$ (0.33 g, 0.41 mmol) was dissolved in benzene (5 mL). 1,2-Bis(diphenylphosphino)ethane (dppe, 0.18 g, 0.45 mmol) was added to this red solution and the solution turned green over 3 days. $^{31}P\{^1H\}$ NMR (benzene) δ: −76.0 ($Mo(S_2C_6H_3Me)_2$-(dppe); −168 (free $PMePh_2$).

Observation of $Mo(S_2C_6H_4)_2(depe)$ by ^{31}P NMR

$Mo(S_2C_6H_4)_2(PMePh_2)_2$ (0.20 g, 0.26 mmol) and depe, Et_2PCH_2-CH_2PEt_2 (0.053 g, 0.26 mmol), were stirred together in 20 mL benzene. The reaction mixture rapidly changed from tomato juice colour to a clear red solution within seconds. After 0.5 h of reaction time the solution turned red-brown. After 1.75 h all solvent was removed in vacuum to yield a red oily solid. $^{31}P\{^1H\}$ NMR (benzene) δ: −79.7 ($Mo(depe)(S_2C_6H_4)_2$); −168 (free $PMePh_2$).

Observation of $Mo(S_2C_6H_4)_2(PMePh_2)(PMe_3)$ by NMR

$Mo(1,2\text{-}S_2\text{-}C_6H_4)_2(PMePh_2)_2$ (0.20 g, 0.26 mmol) and PMe_3 (0.026 mL, 0.020 g, 0.26 mmol) were stirred together in 30 mL benzene. The orange-red slurry changed to a clear red solution within minutes. The reaction was stirred for 1 day and then the $^{31}P\{^1H\}$ NMR spectrum was recorded. $^{31}P\{^1H\}$ NMR (C_6H_6/C_6D_6) δ: −99.0 (br weak, Mo-$PMePh_2$); −126.1 (br weak, Mo-PMe_3); −168 (free $PMePh_2$). ^1H NMR (C_6D_6, 200 MHz) δ: 0.99 (d, J_{PH} = 9 Hz, 8H, PMe_3); 1.25 (d, J_{PH} = 9 Hz, 3H, $PMePh_2$); 3.34 (br, 2H); 6.57–7.24 (multiplet, 10H, P-Ph); 7.10, 7.11, 7.13, 7.15, 8.38, 8.39, 8.41, 8.42 (8H, part of AA′XX′ pattern of thiol ligands).

Preparation of $Mo(S_2C_6H_4)_2(PMePh_2)(P(OMe)_3)$

$Mo(S_2C_6H_4)_2(PMePh_2)_2$ (0.20 g, 0.26 mmol) and $P(OMe)_3$ (0.033 g, 0.27 mmol) were reacted as for the PMe_3 derivative. The orange-red slurry changed to a clear, deeper red solution within 40 min. The ^{31}P NMR spectrum was recorded after 1 day. The solvent was removed using vacuum to leave a red oily solid. $^{31}P\{^1H\}$ NMR (C_6H_6 solution, 80.98 MHz) δ: 23.76 (d, J_{PP} = 33 Hz, Mo-$P(OMe)_3$), −99.24 (d, J_{PP} = 33 Hz, Mo-$PMePh_2$). ^1H NMR (C_6D_6, 200 MHz) δ: 1.24 (3H, P**Me**Ph_2); 2.86 (d, J_{PH} = 15 Hz, 7H, P(O**Me**)$_3$); 6.64–7.32 (multiplet, 11 H, PMe**Ph$_2$**); 7.08, 7.10, 7.11, 7.12, 8.40, 8.42, 8.43, 8.45 (9H, part of AA′XX′ pattern of thiol ligands). FAB^+ MS (NPOE matrix): 702, M^+ for $^{98}Mo(S_2C_6H_4)_2(PMePh_2)(P(OMe)_3)$.

Observation of $Mo(S_2C_6H_4)_2P(OMe)_3)_2$ by ^{31}P NMR

$Mo(S_2C_6H_4)_2(PMePh_2)_2$ (0.200 g, 0.257 mmol) and $P(OMe)_3$ (0.12 g, 0.97 mmol) were reacted as for the PMe_3 derivative. The red solution was reduced in volume and the resultant red solid filtered off and washed with pentanes. $^{31}P\{^1H\}$ NMR (C_6H_6) δ: 30.3.

Reaction of $Mo(S_2C_6H_3Me)_2(PMePh_2)_2$ with $LiAlH_4$

$LiAlH_4$ (0.023 g, 0.605 mmol) was slowly added to the orange-red solution of $Mo(S_2C_6H_3Me)_2(PMePh_2)_2$ (0.497 g, 0.617 mmol) in 50 mL THF. After 15 min the solution had turned amber. After stirring for 21 h the solution was dark brown. The solvent was removed using vacuum, and then trituration with hexanes resulted in a clear yellow solution and a green-brown precipitate. The yellow solution was removed using a pipette and discarded, and the green-brown residue was dried *in vacuo*. ^1H NMR (amber C_6D_6 solution) δ: −2.33 ppm (quartet, J_{PH} = 55.5 Hz, Mo-H). $^{31}P\{^1H\}$ NMR (benzene, 80.98 MHz) δ: −87.93, −88.93 ppm.

Reaction of $Mo(S_2C_6H_3CH_3)_2(PMePh_2)_2$ with $LiAlH_4$ and methyldiphenylphosphine

$Mo(S_2C_6H_3Me)_2(PMePh_2)_2$ (0.84 g, 1.0 mmol) was dissolved in THF (20 mL) to give a red solution. To this solution was added $PMePh_2$ (0.21 g, 1.0 mmol) and $LiAlH_4$ (0.039 g, 1.0 mmol). The addition of $LiAlH_4$ was accompanied by gas evolution. When the gas evolution ceased the solution looked amber. The solution was stirred for 14.5 h and then the solvent was removed using vacuum. The yellow-brown residue was scraped out of the flask and into a frit using hexanes and pentanes washings. ^1H NMR (C_6D_6) δ: −0.24; −0.64; −2.29 (quartet, J_{PH} = 55.15 Hz, Mo-H of $Mo(H)_2(S_2C_6H_3Me)(PMePh_2)_3$); −2.04 (quintet, J_{PH} = 32.4 Hz, Mo-H of $Mo(H)_4(PMePh_2)_4$); −7.7 (br).

Results

Reaction of $MoOCl_2(PMePh_2)_3$ with 1,2-$(SH)_2$-4-CH_3-C_6H_3 is the preferred method of preparation of pure $Mo(S_2C_6H_3Me)_2$-$(PMePh_2)_2$ (reaction [3], R = Me; see also Scheme 1).

[3] $MoOCl_2(PMePh_2)_3$ + 2 1,2-$(SH)_2$-4-R-C_6H_3 → $Mo(S_2C_6H_3R)_2(PMePh_2)_2$ + 2 HCl + H_2O + $PMePh_2$

$Mo(S_2C_6H_3Me)_2(PMePh_2)_2$ can also be prepared from $Mo(N_2)_2(PMePh_2)_4$ (reaction [4]):

[4] $Mo(N_2)_2(PMePh_2)_4$ + 2 1,2-$(SH)_2$-4-CH_3-C_6H_3 → $Mo(S_2C_6H_3Me)_2(PMePh_2)_2$ + 2 $PMePh_2$ + 2 N_2 + 2 H_2

In fact, a mixture of $Mo(S_2C_6H_3Me)_2(PMePh_2)_2$ and $Mo(H)_2$-$(S_2C_6H_3Me)(PMePh_2)_3$ (1) was obtained as the initial crude product, but recrystallization and purification afforded only $Mo(S_2C_6H_3Me)_2(PMePh_2)_2$.

Room temperature and elevated temperature ^1H NMR spectra of $Mo(S_2C_6H_3Me)_2(PMePh_2)_2$ are consistent with the formula as proposed. However, a somewhat unusual feature, observable in the ^1H NMR spectrum of the bis(dithiolate) derivatives, is the broadness and low field position of the PCH_3 methyl resonance (*vide infra*). The ^1H NMR resonances were not useful in assigning stereochemistry. The room temperature ^{31}P NMR spectra is a simple singlet for $Mo(S_2C_6H_3Me)_2(PMePh_2)_2$, the signal occurring in the same chemical shift range as all other bis(dithiolate) complexes prepared herein (Table 1). Low temperature ^{31}P NMR spectra of this complex were much more complicated than the room temperature spectra, displaying three sets of complex multiplets due to conformers with different dithiolate ring orientations (see Discussion). This supports a *cis* stereochemistry for the complex.

Reaction [3], R = H, gave the best yield of $Mo(S_2C_6H_4)_2$-$(PMePh_2)_2$. $Mo(S_2C_6H_4)_2(PMePh_2)_2$ can also be produced by reaction of $MoH_4(PMePh_2)_4$ with 2 equivalents of 1,2-$(SH)_2$-C_6H_4 (reaction [5]):

[5] $Mo(H)_4(PMePh_2)_4$ + 2 1,2-$(SH)_2$-C_6H_4 → $Mo(S_2C_6H_4)_2(PMePh_2)_2$ + 2 $PMePh_2$ + 4 H_2

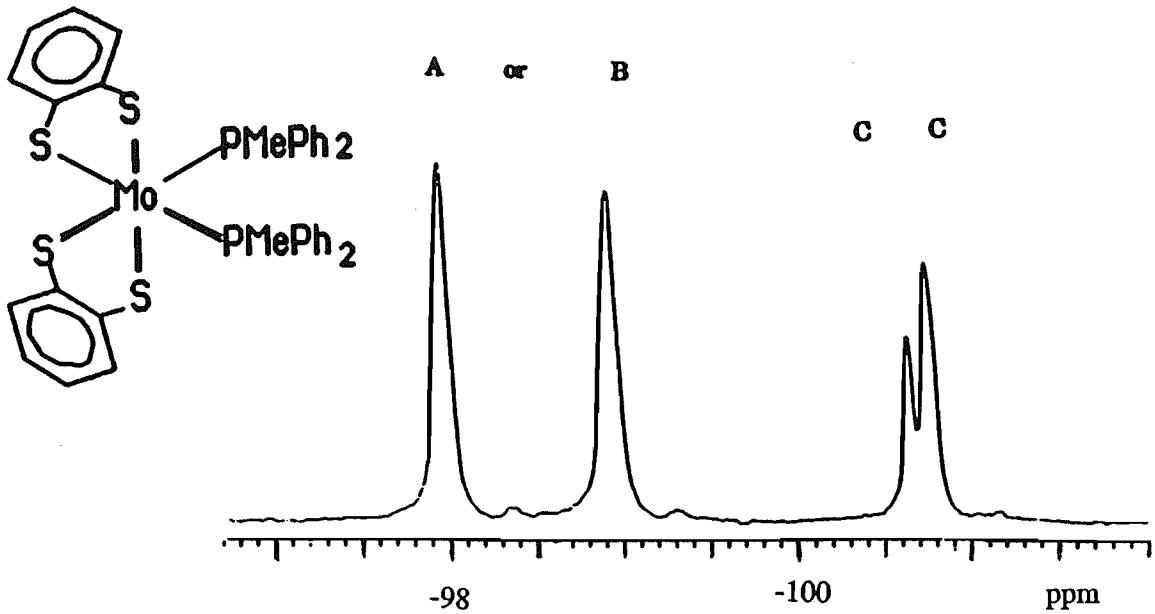

FIG. 1. $^{31}P\{^1H\}$ NMR spectrum (162 MHz) of $Mo(S_2C_6H_4)_2(PMePh_2)_2$ in toluene at −75.5°C. See Discussion for assignments of conformers A, B, and C.

TABLE 1. ^{31}P NMR resonances of bis(dithiolate) complexes

Complex	δ (ppm, vs. $P(OMe)_3$)
$Mo(S_2C_6H_4)_2(PMePh_2)_2$	−102.56
$Mo(S_2C_6H_3Me)_2(PMePh_2)_2$	−102.30
$Mo(S_2C_6H_4)_2(CO)(PMePh_2)$	−95.51
$Mo(S_2C_6H_4)_2(CN\text{-}t\text{-}Bu)(PMePh_2)$	−93.96
$Mo(S_2C_6H_4)_2(depe)$	−79.70
$Mo(S_2C_6H_3Me)_2(dppe)$	−75.23
$Mo(S_2C_6H_3Me)_2(PMePh_2)(PMe_3)$	−98.99[a]
	−126.08[b]
$Mo(S_2C_6H_3Me)_2(PMePh_2)(P(OMe)_3)$	−99.24[c]
	+23.76[d]
$Mo(S_2C_6H_3Me)_2(P(OMe)_3)_2$	+30.33

[a]br, weak, $PMePh_2$.
[b]br, weak, PMe_3.
[c]d, $PMePh_2$, $^2J_{PP}$ = 32 Hz.
[d]d, $P(OMe)_3$, $^2J_{PP}$ = 32 Hz.

The low temperature ^{31}P NMR of $Mo(S_2C_6H_4)_2(PMePh_2)_2$ displayed four signals (Fig. 1), again due to different conformers, which suggest a *cis* stereochemistry for the complex. The Signer method of molecular weight determination established that the compound is monomeric. This evidence indicates that the complicated low temperature spectra do not arise from some type of monomer–dimer equilibrium.

The reaction of $Mo(S_2C_6H_4)_2(PMePh_2)_2$ in benzene with CO is reversible, the CO being extremely labile in the product complex (reaction [6]).

[6] $Mo(S_2C_6H_4)_2(PMePh_2)_2 + CO \rightleftarrows Mo(S_2C_6H_4)_2(CO)(PMePh_2) + PMePh_2$

Reaction [6] proceeds to the right in 10 min, with the colour of the solution changing from orange-red to a burgundy pink. On application of vacuum to effect solvent reduction and product isolation, the colour becomes progressively more orange-red. The complex $Mo(S_2C_6H_4)_2(CO)(PMePh_2)$ was obtained (as a red solid) contaminated by $Mo(S_2C_6H_4)_2(PMePh_2)_2$ by this procedure. Repeated equilibration under a carbon monoxide atmosphere, and discarding the filtrate (without application of vacuum), resulted in incremental percentage enrichment of the product mixture along with considerable loss of product. The preparation of pure $Mo(S_2C_6H_4)_2(CO)(PMePh_2)$ in good yield may be achieved by adding iodomethane to the reaction mixture (eq. [7]):

[7] $Mo(S_2C_6H_4)_2(PMePh_2)_2 + CO + MeI \rightarrow Mo(S_2C_6H_4)_2(CO)(PMePh_2) + [PMe_2Ph_2]I$

The MeI reagent acts as a "phosphine sponge" (21) by selectively precipitating the dissociating $PMePh_2$ as its phosphonium salt. The work-up of the monocarbonyl complex must be carried out under a CO atmosphere.

The carbonyl ligand dissociates from $Mo(S_2C_6H_4)_2(CO)(PMePh_2)$ in the mass spectrometer, even with "soft" FAB ionization. Regardless of the matrix used, the highest mass peak observed does not correspond to the parent ion, but instead to $Mo(S_2C_6H_4)_2(PMePh_2)^+$. The infrared spectrum of pure $Mo(CO)(S_2C_6H_4)_2(PMePh_2)$ shows a strong, sharp absorption due to ν(CO) at 1977 cm^{-1}. No reaction was observed when H_2 instead of CO was used in eq. [7].

Preparation of high purity $Mo(S_2C_6H_4)_2(CN\text{-}t\text{-}Bu)(PMePh_2)$ may be achieved by the simple reaction of equimolar amounts of $Mo(S_2C_6H_4)_2(PMePh_2)_2$ and CN-*t*-Bu (Scheme 2). A phosphine sponge is not required to drive the reaction to the right. The formation of an isonitrile adduct is confirmed by the ν(CN) stretch at 2138 cm^{-1} of the ir spectrum and a strong singlet due to the *tert*-butyl group in the ^1H NMR spectrum.

$Mo(S_2C_6H_3Me)_2(dppe)$ may be prepared from $MoCl_4(dppe)$, reaction [8], or by substitution of the two monodentate ligands in $Mo(S_2C_6H_3Me)_2(PMePh_2)_2$ by dppe (Scheme 2).

[8] $MoCl_4(dppe) + 2\ 1,2\text{-}(SH)_2\text{-}4\text{-}CH_3\text{-}C_6H_3 \rightarrow Mo(S_2C_6H_3Me)_2(dppe) + 4\ HCl$

The FAB MS spectrum was extremely useful in the identification of this insoluble complex. The isotopomer distribution is correct with the 804 peak, due to the species with ^{98}Mo, being most intense. $Mo(S_2C_6H_4)_2(depe)$ may similarly be generated

Can. J. Chem. Downloaded from www.nrcresearchpress.com by 91.144.44.67 on 09/07/12
For personal use only.

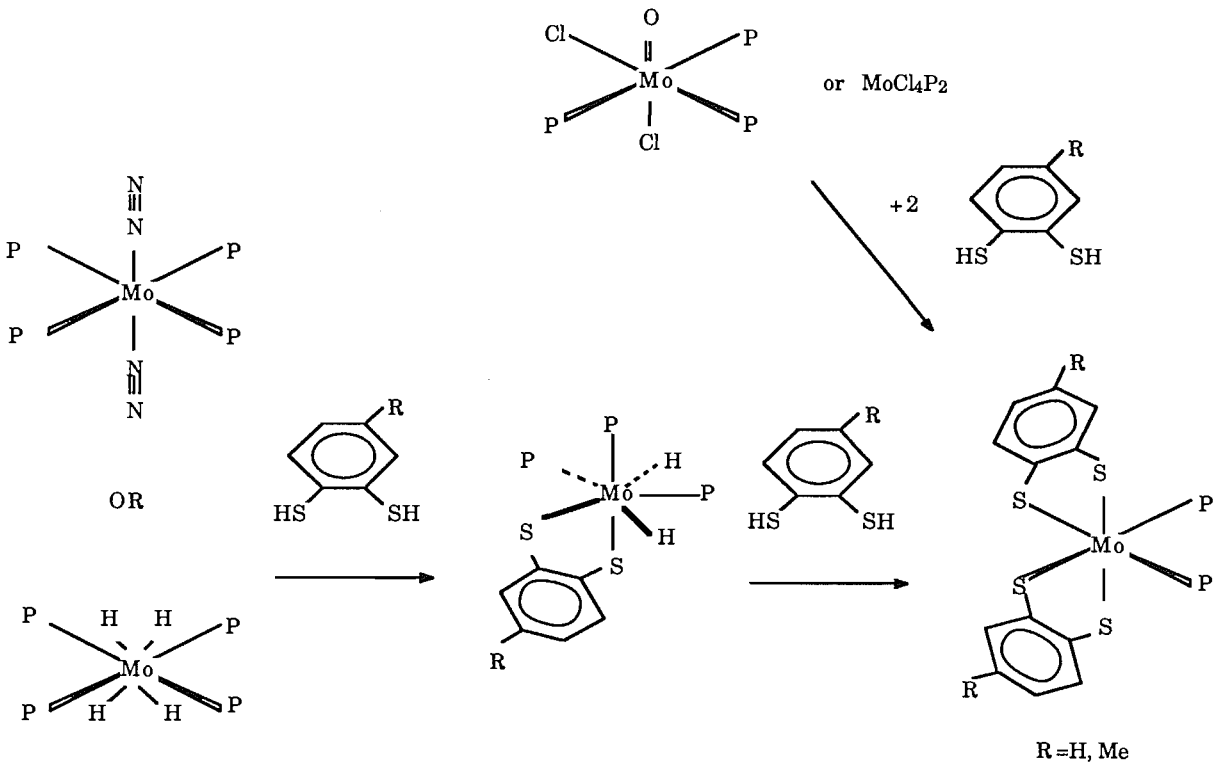

SCHEME 1. Preparation of bis(dithiolate)bis(phosphine) complexes of molybdenum.

from $Mo(S_2C_6H_4)_2(PMePh_2)_2$ and depe; depe = 1,2-bis(diethylphosphino)ethane.

When $Mo(S_2C_6H_4)_2(PMePh_2)_2$ is reacted with 1 equivalent of PR_3, R = Me, OMe, the monosubstitution product $Mo(S_2C_6H_4)_2(PR_3)(PMePh_2)$ is obtained (Scheme 2). The ^{31}P NMR spectrum of $Mo(S_2C_6H_4)_2(P(OMe)_3)(PMePh_2)$ displays two doublets with $^2J_{PP}$ = 32 Hz, while that of $Mo(S_2C_6H_4)_2(PMe_3)(PMePh_2)$ gives two broad signals (see Table 1). If 2 equivalents of $P(OMe)_3$ are reacted with $Mo(S_2C_6H_4)_2(PMePh_2)_2$ the disubstituted product, $Mo(S_2C_6H_4)_2(P(OMe)_3)_2$, is formed (Scheme 2).

The reactions of complexes $Mo(S_2C_6H_3R)_2(PMePh_2)_2$ with $LiAlH_4$ generate a mixture of hydride species, one of which is identified by ^1H and ^{31}P NMR as $Mo(H)_2(S_2C_6H_3R)(PMePh_2)_3$ (1). The ^1H and ^{31}P chemical shifts were slightly different from those of pure samples of $Mo(H)_2(S_2C_6H_3R)(PMePh_2)_3$, possibly because of interactions with unidentified aluminium-containing species. The reaction of $Mo(S_2C_6H_3Me)_2(PMePh_2)_2$ with equimolar amounts of $LiAlH_4$ and methyldiphenylphosphine yields not only $Mo(H)_2(S_2C_6H_3Me)(PMePh_2)_3$ but also $Mo(H)_4(PMePh_2)_4$ and other unidentified species.

A few other reactions were attempted. $Mo(S_2C_6H_4)_2(PMePh_2)_2$ does not react with H_2O at 22°C but does react with acetylene to give a plethora of products. It does not react with equimolar amounts of 1,2-dichloroethane or 1,3-dibromopropane, unlike the complex $[Mo(CO)_3(SC_2H_4SC_2H_4S)]^{2-}$ (22).

Discussion

Bis(phosphine)bis(dithiolate) complexes of molybdenum were initially obtained in poor yield from decomposition of the novel dihydrides, $Mo(H)_2(S_2C_6H_3R)(phosphine)_3$ with R = Me, or H (1). Once it was established that the decomposition products were not oxo-species, such as $Mo(O)(SR)_4$ (23), but instead unknown bis(dithiolate) species, high yielding routes to these complexes were sought so that their chemical properties could be investigated.

Bis(dithiolate) complexes of molybdenum were prepared using four different starting materials: bis(dinitrogen), tetrahydrido, bis(phosphine)tetrachloro, and oxo-dichloro-tris(phosphine) complexes of molybdenum (Scheme 1).

Routes involving $MoOCl_2(phosphine)_3$ and $MoCl_4(phosphine)_2$ species are superior (in terms of both yield and simplicity) for generation of bis(dithiolate)bis(phosphine) species. Routes involving dinitrogen or tetrahydride starting materials result in less tractable product mixtures since the excess phosphine that is generated impairs product crystallization and isolation. Addition of a base such as triethylamine to deprotonate and activate the thiol was not necessary.

The substitution reactions of these complexes with mono- or bidentate phosphorus donor ligands or *tert*-butyl isonitrile give either the mono- or disubstituted complexes depending on how many equivalents of donor were added (Scheme 2).

The room temperature ^{31}P NMR spectrum (Table 1) of the monosubsituted $P(OMe)_3$ derivative is most informative as to the stereochemistry of the complexes. The magnitude of the coupling constant $^2J_{PP}$ (32 Hz) observed in the ^{31}P NMR spectra of $Mo(S_2C_6H_4)_2(PMePh_2)(P(OMe)_3$ and the magnitude of $^2J_{P-CO}$ (11.8 Hz) observed in the ^{13}C NMR of $Mo(S_2C_6H_4)_2(CO)(PMePh_2)$ suggest that the complexes have *cis* monodentate ligands (24). For comparison with the above values, the complex $Mo(CO)_4(dppe)$ has a *cis* $^2J_{PC}$ coupling of 8.4 Hz and a *trans* $^2J_{PC}$ coupling of 24 Hz; the complex $Mo(N_2)_2(PMePh_2)_3(P(OMe)_3)$ has a *cis* $^2J_{PP}$ coupling of 30 Hz and a *trans* $^2J_{PP}$ coupling of 173 Hz (12). At ambient temperature, a $^2J_{PP}$ value cannot be clearly observed in the ^{31}P NMR of $Mo(S_2C_6H_4)_2(PMePh_2)(PMe_3)$.

The low temperature ^{31}P NMR spectra of the Mo(dithiolate)$_2$(PMePh$_2$)$_2$ complexes are consistent with phosphine

Can. J. Chem. Downloaded from www.nrcresearchpress.com by 91.144.44.67 on 09/07/12
For personal use only.

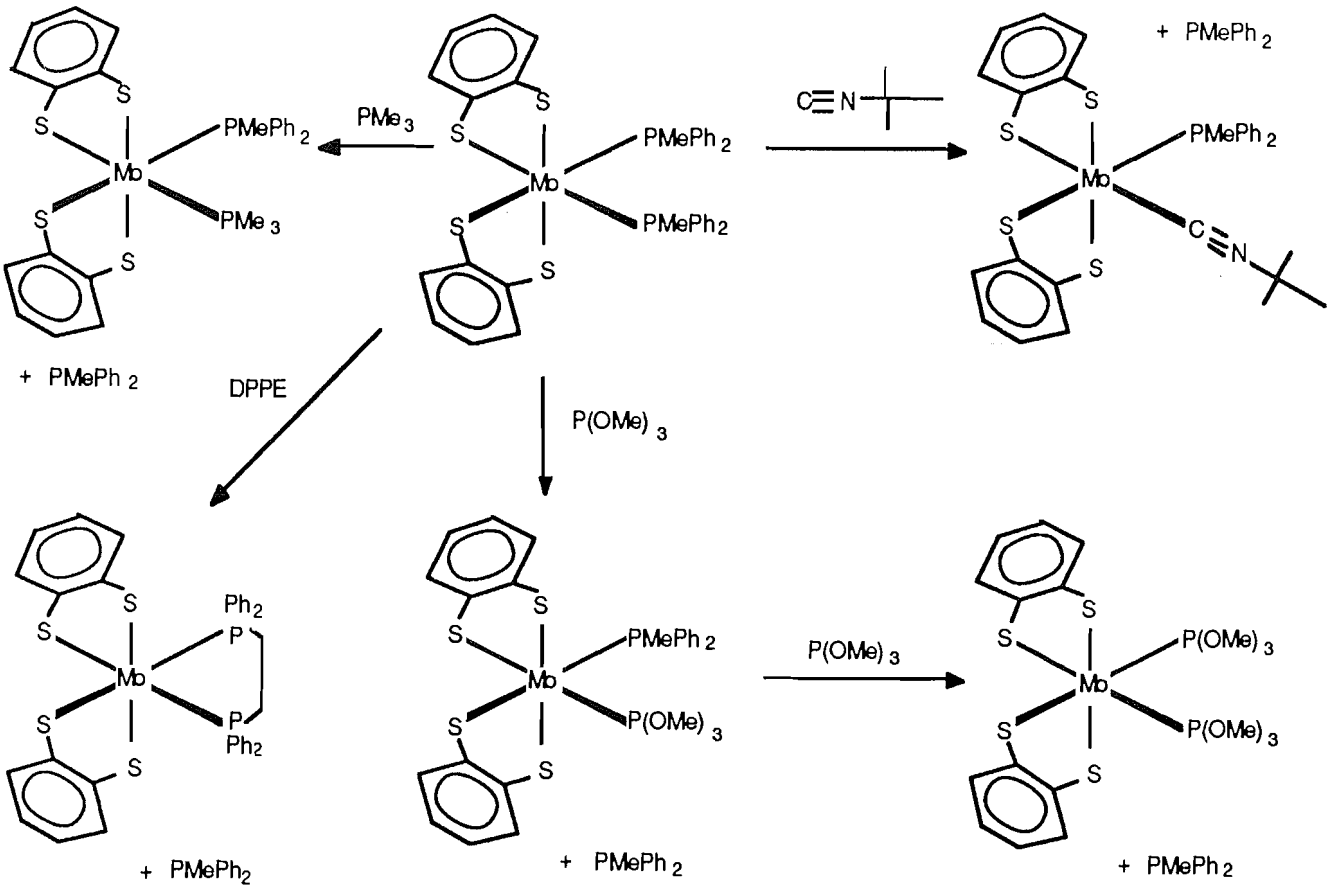

SCHEME 2. The substitution reactions of $Mo(S_2C_6H_4)_2(PMePh_2)_2$.

ligands *cis* disposed in isomers arising due to various conformations of the dithiolate ligands, as depicted in Fig. 2. Consider the low temperature ^{31}P NMR spectrum of $Mo(S_2C_6H_4)_2(PMePh_2)_2$ (Fig. 1), which consists of four signals. One phosphorus resonance arises from the isomer where both aromatic rings are flipped in towards the phosphines (and both phosphines are equivalent) (isomer A); another resonance arises from the isomer with both aromatic rings flipped away from the phosphines (and both phosphines are again equivalent; isomer B); the last two resonances arises from the other possible isomer where one ring is flipped towards the phosphorus ligands, and one away (in which the two phosphines are inequivalent; isomer C). The assignments of resonances arising from isomers A and B are tentative and may be reversed. Introduction of one methyl group in $Mo(PMePh_2)_2(S_2C_6H_3Me)(S_2C_6H_4)$ or two methyl groups in $Mo(PMePh_2)_2(S_2C_6H_3Me)_2$ gives the opportunity for geometric isomers regarding the position(s) of the methyl group(s) (almost *trans* to a phosphorus donor, or almost *trans* to a sulfur donor, and also their position relative to the other methyl group). Hence, more complicated low temperature ^{31}P spectra are obtained when the aromatic ring is substituted.

The simple one-resonance ^{31}P NMR spectra observed at room temperature for the $Mo(S_2C_6H_3R)_2(PMePh_2)_2$ complexes are the averaged signals arising from rapid interconversion of isomers by ring-flipping as the sulfur configurations invert. It is assumed that the small differences in chemical shift due to differences in position of methyl substitution are not resolved at room temperature. Otherwise a second mechanism of isomer interconversion, a Bailar twist, has to be invoked to explain the equivalence of ^{31}P resonances of isomers that differ in position of methyl substitution. Kopf and Klapotke (25) have described this type of ring-flip isomerism, which results in nonequivalence of the Cp rings at low temperatures, in the complexes $M(Cp)_2(Se_2C_6H_4)$ (where M = Ti, Zr, Hf, Mo, W). The barrier to interconversion between the isomers of $Mo(S_2C_6H_3Me)_2(PMePh_2)_2$ is expected to be much lower than $MoCp_2(Se_2C_6H_4)$, which has a barrier slightly greater than 80 kJ/mol.

The complex $Mo(S_2C_6H_4)_2(CO)(PMePh_2)$ is intriguing in that the CO can be readily removed under vacuum when $PMePh_2$ is present (cf. reaction [6]). It is not surprising that the parent ion cannot be seen in the FAB^+ mass spectrum where the sample is under vacuum; the highest mass peak corresponds to $[M - CO]^+$. Although the oxidation state of this monocarbonyl complex is ambiguous because of π delocalization in the dithiolene ligands (26, 27), an oxidation state closer to Mo(IV) than to Mo(II) is consistent with the physical properties of the complex. Thus the stretching frequency ν(CO) of 1977 cm^{-1} is higher than for comparable Mo(II) complexes such as $Mo(S_2CNC_4H_4)_2(CO)_2$ with ν(CO) = 1956, 1879 cm^{-1} (28), $Mo(S_2CNC_6H_4)_2(CO)_2(PPh_3)$ (1947, 1878 cm^{-1} (28)), and $Mo(S_2CNMe_2)_2(CO)(PMe_3)_2$ (1760 cm^{-1} (10)). The ease of displacement of CO from $Mo(CO)(PMePh_2)(S_2C_6H_4)_2$ also suggests that it can be considered as a carbonyl of Mo(IV), the first thermally stable example of its type. The other known Mo(IV) carbonyl complex, *trans*-$Mo(O)_2(CO)_4$, which was generated at 10 K, might be stable above 20 K; it has an e_u carbonyl stretching mode at 2110 cm^{-1} (29). Iodomethane can be used in reaction [7] as a phosphine sponge because the Mo(IV) complexes involved are not readily oxidized and the coordinated sulfurs are not very nucleophilic. In cases where the

Can. J. Chem. Downloaded from www.nrcresearchpress.com by 91.144.44.67 on 09/07/12
For personal use only.

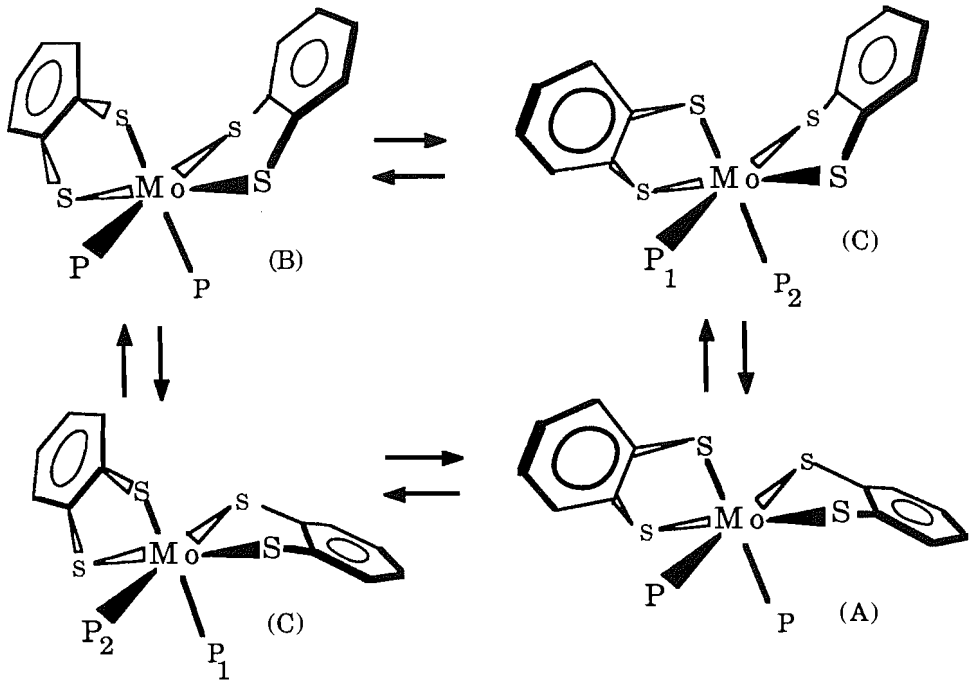

FIG. 2. Three conformations of the bis(dithiolate) complexes.

complexes are likely to be oxidized, the phosphine sponge reagent 9-BBN has been recommended (21).

The binding site of $Mo(S_2C_6H_4)_2(PMePh_2)$ has poor back-bonding capability as judged by the high ν(CO) of the monocarbonyl adduct. This explains why we were not able to isolate a dihydrogen adduct of the type $Mo(S_2C_6H_4)_2(H_2)(PMePh_2)$. Dihydrogen complexes of d^6 octahedral metals are expected to be stable when the range of ν(CO) for the corresponding carbonyl complex falls in the range 1860–1960 cm^{-1} (30). Similarly, a complex like $Mo(S_2C_6H_4)_2(N_2)(PMePh_2)$ is not expected to be stable.

Conclusions

The spectroscopic properties of the oxygen sensitive complexes $Mo(S_2C_6H_3R)_2(PMePh_2)_2$ are most consistent with an octahedral, *cis* stereochemistry. These complexes can exist as conformational isomers with respect to the MoS_2(arene) "hinges". These isomers readily interconvert at room temperature but can be observed at low temperature by ^{31}P NMR. Geometric isomerism with respect to the placement of the methyl groups on the dithiolate ligands in the complex $Mo(S_2C_6H_3Me)_2(PMePh_2)_2$ can also be detected by ^{31}P NMR at low temperature. The $PMePh_2$ ligands are labile in these complexes and are readily substituted, even by weakly coordinating carbon monoxide (in the case of Mo(IV) to give a range of products, again with *cis* stereochemistry. If the dithiolates are viewed as dianions, then $Mo(S_2C_6H_4)_2(CO)(PMePh_2)$ is the first thermally stable carbonyl complex of Mo(IV).

Acknowledgements

This research was supported by grants from NSERC Canada and Imperial Oil Ltd.

1. N. J. LAZAROWYCH and R. H. MORRIS. J. Chem. Soc. Chem. Commun. 1865 (1987).
2. N. J. LAZAROWYCH. Ph.D. Thesis, University of Toronto, 1989.
3. D. SELLMANN and W. REISSER. J. Organomet. Chem. **294**, 333 (1985).
4. S. OTSUKA, M. KAMATA, K. HIROTSU, and T. HIGUCHI. J. Am. Chem. Soc. **103**, 3011 (1981).
5. E. ROLAND, E. C. WALBORSKY, J. C. DEWAN, and R. R. SCHROCK. J. Am. Chem. Soc. **107**, 5797 (1985).
6. E. E. WALBORSKY, D. E. WIGLEY, E. ROLAND, J. C. DEWAN, and R. R. SCHROCK. Inorg. Chem. **26**, 1615 (1988).
7. D. SELLMANN and L. ZAPF. Z. Naturforsch. B: Anorg. Chem. Org. Chem. **40B**, 380 (1985).
8. D. SELLMANN and J. SCHWARZ. J. Organomet. Chem. **214**, 343 (1983).
9. C. Y. CHOU and E. A. MAATTA. Inorg. Chem. **23**, 2912 (1984).
10. E. CARMONA, K. DOPPERT, J. M. MARIN, M. L. POVEDA, L. SANCHEZ, and R. SANCHEZ-DELGADO. Inorg. Chem. **23**, 530 (1984).
11. T. A. GEORGE and C. D. SEIBOLD. Inorg. Chem. **12**, 2548 (1973).
12. N. J. LAZAROWYCH, R. H. MORRIS, and J. M. RESSNER. Inorg. Chem. **25**, 3926 (1985).
13. N. J. LAZAROWYCH. M.Sc. Thesis, University of Toronto, 1985.
14. L. J. ARCHER and T. A. GEORGE. Inorg. Chem. **18**, 2079 (1979).
15. A. V. BUTCHER and J. CHATT. J. Chem. Soc. (A), 2652 (1970).
16. L. DEGANI and R. FOCHI. Synthesis, 471 (1976).
17. R. L. COCHRAN. Appl. Spectrosc. Rev. **22**, 137 (1986).
18. R. SIGNER. Justus Liebigs Ann. Chem. **478**, 246 (1930).
19. E. P. CLARK. Ind. Eng. Chem., Anal. Ed. **13**, 820 (1941).
20. J. R. DILWORTH and R. L. RICHARDS. Inorg. Synth. **20**, 121 (1980).
21. R. L. LUCK and R. H. MORRIS. Inorg. Chem. **23**, 1489 (1984).
22. D. SELLMANN and L. ZAPF. Angew. Chem. Int. Ed. Engl. **23**, 807 (1984).
23. S-L. SOONG, V. CHEBOLU, S. A. KOCH. T. O'SULLIVAN, and M. MILLAR. Inorg. Chem. **25**, 4068 (1986), and references therein.
24. P. S. BRATERMAN, D. W. MILNE, E. W. RANDALL, and E. ROSENBERG. J. Chem. Soc. Dalton Trans. 1027 (1973).
25. H. KOPF and T. KLAPOTKE. J. Organomet. Chem. **310**, 303 (1986).
26. D. SELLMANN, G. BINKER, and F. KNOCH. Z. Naturforsch. B: Anorg. Chem. Org. Chem. **42B**, 1298 (1987).
27. F. A COTTON and G. WILKINSON. Advanced inorganic chemistry. 4th ed. John Wiley and Sons, Toronto. 1980. pp. 187, 180, 346.
28. R. S. HERRICK and J. L. TEMPLETON. Inorg. Chem. **25**, 1270 (1986).
29. J. A. CRAYSTON, M. J. ALMOND, A. J. DOWNS, M. POLIAKOFF, and J. J. TURNER. Inorg. Chem. **23**, 3051 (1984).
30. R. H. MORRIS, K. A. EARL, R. L. LUCK, N. J. LAZAROWYCH, and A. SELLA. Inorg. Chem. **28**, 2672 (1987).

Can. J. Chem. Downloaded from www.nrcresearchpress.com by 91.144.44.67 on 09/07/12
For personal use only.

Rhodium induced titanium–sulfur bond cleavage: crystal and molecular structure of $((COD)Rh(\mu\text{-}SMe))_2$

TERESA A. WARK[1] AND DOUGLAS W. STEPHAN[2]

Department of Chemistry and Biochemistry, University of Windsor, Windsor, Ont., Canada N9B 3P4

Received September 25, 1989

TERESA A. WARK and DOUGLAS W. STEPHAN. Can. J. Chem. **68**, 565 (1990).

Reactions of Ti(III) and Ti(IV) thiolates with Rh complexes have been investigated. In the reaction of $Cp_2Ti(SMe)_2$ and $[(COD)_2Rh]BF_4$ or $[(COD)Rh(sol)_2]PF_6$, thiolate abstraction yields $((COD)Rh(\mu\text{-}SMe))_2$, **1**. Reaction of $(Cp_2Ti(\mu\text{-}SMe))_2$ with $((COD)Rh(\mu\text{-}Cl))_2$ results in ligand exchange affording $(Cp_2Ti(\mu\text{-}Cl))_2$ and **1**. The complex **1** crystallizes in the monoclinic space group $P2_1/n$, with $a = 8.551(2)$ Å, $b = 10.058(3)$ Å, $c = 22.187(4)$ Å, $\beta = 92.54(1)°$, $Z = 4$, and $V = 1906(1)$ Å^3. The structural data show a relatively short approach between the Rh centres (2.948 Å) and between the bridging sulfur atoms (2.888 Å). The implications of these structural features in terms of metal–metal and sulfur–sulfur bonding are discussed. In addition, the implications of these results with respect to the formation of thiolato-bridged, early–late heterobimetallics is considered.

Key words: thiolate abstraction, rhodium thiolate bridged dimer.

TERESA A. WARK et DOUGLAS W. STEPHAN. Can. J. Chem. **68**, 565 (1990).

On a étudié les réactions des thiolates du Ti(III) et du Ti(IV) avec des complexes du Rh. Lors de la réaction du $Cp_2Ti(SMe)_2$ avec le $[(COD)_2Rh]BF_4$ ou le $[(COD)Rh(sol)_2]PF_6$, la réaction d'abstraction du thiolate fournit du $((COD)Rh(\mu\text{-}SMe))_2$, **1**. La réaction du $((Cp_2)Ti(\mu\text{-}SMe))_2$ avec le $((COD)Ti(\mu\text{-}Cl))_2$ conduit à un échange de ligands et à la formation de $((Cp_2)Ti(\mu\text{-}Cl))_2$ et du composé **1**. Le complexe **1** cristallise dans le groupe d'espace monoclinique $P2_1/n$, avec $a = 8{,}551(2)$, $b = 10{,}058(3)$ et $c = 22{,}187(4)$ Å, $\beta = 92{,}54(1)°$, $Z = 4$ et $V = 1906(1)$ Å^3. Les données structurales montrent que les centres Rh (2,948 Å) et les atomes de soufre agissant comme ponts (2,888 Å) sont relativement rapprochés. On discute des implications de ces caractéristiques structurales en fonction des liaisons métal–métal et soufre–soufre. De plus, on considère les implications de ces résultats par rapport à la formation de pont thiolato dans les hétérobimétalliques du début et de la fin.

Mots clés : enlèvement de thiolates, dimère ponté du thiolate de rhodium.

[Traduit par la revue]

Introduction

Our interest in early–late heterobimetallics (1–14) has included an extensive investigation of synthetic routes to thiolato-bridged mixed metal species (2–7). We have recently described the utilization of titanocene dithiolates as metalloligands for Cu(I) (5) and Ni(0) (6). Analogous chemistry yielding thiolato-bridged V(IV)–Cu(I) species has been described (7); however, reaction of vanadocene dithiolates with Ni(0) species led to redox chemistry, ligand exchange, and the isolation of Ni(II) thiolate hexamers (6). In related studies, we have described the synthesis of the complex $[Cp_2Ti(\mu\text{-}SCH_2CH_2CH_2PPh_2)_2Rh]^+$ and its redox partner $[Cp_2Ti(\mu\text{-}SCH_2CH_2CH_2PPh_2)_2Rh]^0$ (3). Preliminary studies of related phosphido-bridged systems show that the Ti(III)/Rh(I) species $Cp_2Ti(\mu\text{-}PR_2)_2Rh(COD)$ form readily.[3] We have also previously shown that related bridged Zr/Rh complexes are active catalysts for hydroformylation (10). In attempting to extend the chemistry of such heterobimetallic systems towards further applications in catalysis, it seemed that an interesting system would be one in which simple thiolate bridges link Ti and Rh. In this paper, we describe our initial investigations of the reaction of $Cp_2Ti(SMe)_2$ with $[(COD)_2Rh]BF_4$ and the reaction of $((COD)Rh(\mu\text{-}Cl))_2$ with $(Cp_2Ti(\mu\text{-}SMe))_2$. Ti—S bond cleavage was evident in both cases, yielding the species $((COD)Rh(\mu\text{-}SMe))_2$, **1**. This product is also readily prepared directly from the reaction of $((COD)Rh(\mu\text{-}Cl))_2$ and NaSMe. The complex **1** was structurally characterized by X-ray crystallography. The results confirm the dimeric nature of the Rh species in which the thiolates bridge the two Rh centres. The small steric demands of the thiolate substituents apparently allow for a relatively close approach of the metal centres. The implications of these structural features in terms of metal–metal and sulfur–sulfur bonding are discussed. In addition, the implications of the results of this initial study with respect to the formation of thiolato-bridged, early–late heterobimetallics are considered.

Experimental

All preparations were done under an atmosphere of dry, O_2-free N_2. Solvents were reagent grade, distilled from the appropriate drying agents under N_2 and degassed by the freeze–thaw method at least three times prior to use. $^{31}P\{^1H\}$ NMR experiments were performed using a Bruker AC 200-MHz spectrometer employing external 85% H_3PO_4 as the reference. EPR experiments were performed with a Varian E-12 spectrometer using DPPH as the reference. PCy_3 was purchased from the Strem Chemical Co. NaSMe (6), $(Cp_2Ti(\mu\text{-}Cl))_2$ (16), $((COD)Rh(\mu\text{-}Cl))_2$ (17), and $[(COD)_2Rh]BF_4$ (18) were prepared by the literature methods.

Reaction of $Cp_2Ti(SMe)_2$ and $[(COD)_2Rh]BF_4$

To a 30 mL THF suspension of $[(COD)_2Rh]BF_4$ (149 mg, 0.37 mmol) was added PCy_3 (208 mg, 0.74 mmol) and the mixture stirred for 30 min. A 10 mL THF solution of $Cp_2Ti(SMe)_2$ (100 mg, 0.37 mmol) was added to the reaction mixture, resulting in a colour change from purple to orange over 1 h of stirring. $^{31}P\{^1H\}$ NMR (THF), δ: 10.82 (s). The solvent was removed *in vacuo* and the orange residue washed with 2 × 10 mL pentane, leaving an orange solid and an orange pentane solution.

Generation of $[(COD)Rh(sol)_2]PF_6$

To a 20 mL THF solution of $((COD)Rh(\mu\text{-}Cl))_2$ (100 mg, 0.20 mmol) was added $AgPF_6$ (103 mg, 0.40 mmol) and the solution stirred for 10 min. The silver chloride was filtered off, leaving a clear, yellow solution of the solvated rhodium cation.

[1]Present address: Department of Chemistry, University of New Mexico, Albuquerque, New Mexico.

[2]Author to whom correspondence may be addressed.

[3]D. G. Dick and D. W. Stephan. Unpublished results.

Can. J. Chem. Downloaded from www.nrcresearchpress.com by 91.144.44.67 on 09/07/12
For personal use only.

Can. J. Chem. Downloaded from www.nrcresearchpress.com by 91.144.44.67 on 09/07/12
For personal use only.

Reaction of $Cp_2Ti(SMe)_2$ and $[(COD)Rh(sol)_2]PF_6$

To a 20 mL THF solution of $[(COD)Rh(sol)_2]PF_6$ (0.40 mmol) was added $Cp_2Ti(SMe)_2$ (109 mg, 0.40 mmol) and the solution immediately changed from purple to orange-red. The mixture was stirred for 1 h and then stripped to dryness. The resulting oil was washed with pentane, giving an orange solution and an oil. The pentane solution was stripped to dryness. ^1H NMR (acetone-d_6), δ: 4.04 (br s, 4H), 2.28 (br m, 8H), 1.51 (s, 3H).

Preparation of $(Cp_2Ti(\mu\text{-}SMe))_2$

To a THF solution of $(Cp_2Ti(\mu\text{-}Cl))_2$ (100 mg, 0.24 mmol) was added NaSMe (33 mg, 0.48 mmol) and the mixture stirred overnight. The reaction mixture was filtered, the solvent removed *in vacuo*, and the residue washed with 2 × 10 mL pentane. The mixture was filtered and the purple, microcrystalline solid dried under vacuum. Yield: 74 mg, 80%; EPR (THF): $g = 1.979$, $a\langle^{47}Ti/^{49}Ti\rangle = 12.5$ G.

Reaction of $(Cp_2Ti(\mu\text{-}SMe))_2$ and $((COD)Rh(\mu\text{-}Cl))_2$

To a 30 mL THF solution of $((COD)Rh(\mu\text{-}Cl))_2$ (100 mg, 0.20 mmol) was added $(Cp_2Ti(\mu\text{-}SMe))_2$ (92 mg, 0.20 mmol) and the mixture stirred for 1 h during which time the colour changed from purple to yellow-green. EPR (THF): $g = 1.979$, $a\langle^{47}Ti/^{49}Ti\rangle = 10.0$ G.

Preparation of $((COD)Rh(\mu\text{-}SMe))_2$

To a 20 mL THF solution of $(COD)Rh(\mu\text{-}Cl))_2$ (30 mg, 0.061 mmol) was added NaSMe (8.5 mg, 0.12 mmol) and the mixture was stirred for 1 h. The reaction mixture was filtered and then the yellow-orange solution stripped to dryness, yielding **1**, 35%. X-ray quality crystals were obtained by diffusion of hexane into a THF solution of **1**. ^{1}NMR (benzene-d_6), δ: 4.04 (br s, 4H), 2.29 (m, 8H), 1.52 (s, 3H). Anal. calcd.: C 41.87, H 5.86; found: C 41.50, H 5.80.

X-ray data collection and reduction

Diffraction experiments were performed on a four-circle Syntex $P2_1$ diffractometer with graphite-monochromatized Mo Kα radiation (λ = 0.71069 Å). The initial orientation matrix was obtained from 15 machine-centred reflections selected from a rotation photograph. These data were used to determine the crystal system. Partial rotation photographs around each axis were consistent with a monoclinic crystal system for **1**. The final lattice parameters and the orientation matrix were determined from 24 high-angle data measurements ($20° < 2\theta < 25°$). The observed extinctions were consistent with the space group $P2_1/n$. $\pm h, +k, +l$ data were collected ($4.5° < 2\theta < 45.0°$), with three standard reflections recorded every 197 reflections. Their intensities showed no statistically significant change over the duration of the data collection. The data were processed using the SHELX-76 program package.

Structure solution and refinement

Non-hydrogen atomic scattering factors were taken from the literature tabulations (19–21). The heavy atom positions were determined using direct methods. The remaining non-hydrogen atoms were located from successive difference Fourier map calculations. The refinement was carried out by using full-matrix least-squares techniques on F, minimizing the function $w(|F_o| - |F_c|)^2$ where the weight, w, is defined as $4F_o^2/2\sigma(F_o^2)$ and F_o and F_c are the observed and calculated structure factor amplitudes. In the final cycles of refinement, the rhodium, sulfur, and methyl carbons were assigned anisotropic temperature factors. The methyl hydrogen atom positions were calculated and allowed to ride on the carbon to which they are bonded assuming a C—H bond length of 0.95 Å; however, the cyclooctadiene hydrogens were located from a difference map. Hydrogen atom temperature factors were fixed at 1.10 times the isotropic temperature factor of the carbon atom to which they are bonded. The hydrogen atom contributions were calculated, but not refined. The residual electron densities were of no chemical significance. Crystal data and data collection parameters are summarized in Table 1. Tables of positional parameters (Table 2) and selected bond distances and angles (Table 3) are reported. Thermal parameters (Table 1A), hydrogen atom parameters (Table A2), and calculated and observed structure factors (Table A3) have been deposited.[4]

TABLE 1. Crystallographic parameters

Formula	$C_{18}H_{30}Rh_2S_2$
Crystal color, form	Orange blocks
Crystal system	Monoclinic
a (Å)	8.551(2)
b (Å)	10.058(3)
c (Å)	22.187(4)
β (deg)	92.54(1)
Space group	$P2_1/n$
Volume (Å^3)	1906(1)
Density (g cm^{-3}) calcd.	1.80
Z	4
Crystal dimensions (mm)	0.12 × 0.19 × 0.23
Absorption coefficient, μ (cm^{-1})	17.72
Radiation, λ (Å)	Mo Kα (0.71069)
Temperature (°C)	24
Scan speed (deg/min)	2.0–5.0(θ/2θ scan)
Scan range (deg)	1.0 below Kα1 1.0 above Kα2
Background scan time ratio	0.5
Data collected	2762
No. of unique data $F_o^2 > 3\sigma(F_o^2)$	1666
No. of variables	199
R (%)	3.82
Rw (%)	4.14
Largest Δ/σ in the final least-squares cycle	0.002
Maximum residual electron density (e/Å^3)	0.59
Atom associated	Rh1, Rh2

Results and discussion

Reaction of the rhodium solvated species $[(COD)Rh(sol)_2]PF_6$ with $Cp_2Ti(SMe)_2$ was the initial attempt to prepare the desired Ti/Rh heterobimetallic species. A similar route was used previously by Green and co-workers to prepare mixed metal species, $[(C_5H_4CH_2CH_2S\text{-}n\text{Pr})_2Mo(\mu\text{-}S\text{-}n\text{Pr})_2Rh(COD)]^+$ (22). Addition of $Cp_2Ti(SMe)_2$ to the yellow THF solution containing the rhodium cation caused an immediate colour change from yellow to orange. The pentane soluble species exhibited a ^{1}H NMR spectrum consistent with that of the rhodium thiolato species with the empirical formula (COD)Rh(μ-SMe). The degree of aggregation was confirmed as the dimer $((COD)Rh(\mu\text{-}SMe))_2$, **1**, by X-ray crystallography (*vide infra*).

Similarly, reactions of $[(COD)_2Rh]BF_4$ with $Cp_2Ti(SMe)_2$, in the presence of phosphine, yielded complex **1**. Despite the fact that ^{31}P NMR spectra of mixtures of $[(COD)_2Rh]BF_4$ and PPh_3 indicate the expected initial coordination of phosphine to Rh, the ^{31}P NMR spectrum of the orange reaction mixture, following addition of the $Cp_2Ti(SMe)_2$, showed only a single resonance corresponding to free phosphine. This result suggests that the phosphine is displaced by the thiolate of the metalloligand and then the thiolate is abstracted by the rhodium centre.

[4]Tables of thermal and hyrogen atom parameters and values of 10 F_o and 10 F_c have been deposited. These tables may be purchased from the Depository of Unpublished Data, CISTI, National Research Council of Canada, Ottawa, Ont., Canada K1A 0S2.

TABLE 2. Positional parameters[a]

Atom	x	y	z	Atom	x	y	z
Rh1	687(1)	2678(1)	6889(1)	Rh2	2692(1)	2480(1)	5846(1)
S1	2545(3)	1059(2)	6676(1)	S2	2945(3)	3910(2)	6689(1)
C1	1839(13)	−625(9)	6554(5)	C2	2633(11)	5667(9)	6540(4)
C11	−1005(10)	4231(8)	6763(4)	C12	−544(10)	4175(8)	7368(4)
C13	−1380(13)	3547(10)	7867(5)	C14	−1827(13)	2152(10)	7777(5)
C15	−964(11)	1424(9)	7315(5)	C16	−1331(11)	1471(9)	6716(4)
C17	−2622(15)	2277(11)	6411(6)	C18	−2576(12)	3725(10)	6523(5)
C21	2467(11)	3984(9)	5159(4)	C22	3977(12)	3513(9)	5207(5)
C23	4686(16)	2535(11)	4759(6)	C24	3656(13)	1368(11)	4617(5)
C25	2683(12)	989(10)	5163(5)	C26	1207(11)	1435(9)	5235(4)
C27	288(13)	2439(9)	4845(5)	C28	1233(12)	3600(10)	4672(5)

[a]Positions multiplied by 10^4.

TABLE 3. Selected bond distances and angles

Bond	Distance (Å)	Bond	Distance (Å)	Bond	Distance (Å)
Rh1..Rh2	2.948(1)	Rh1—S1	2.338(2)	Rh1—S2	2.353(2)
Rh2—S1	2.340(2)	Rh2—S2	2.363(2)	S1—C1	1.815(10)
S2—C2	1.815(9)	Rh1—C11	2.138(8)	Rh1—C12	2.145(9)
Rh1—C15	2.144(10)	Rh1—C16	2.131(9)	Rh2—C21	2.149(9)
Rh2—C22	2.104(10)	Rh2—C25	2.132(10)	Rh2—C26	2.098(10)
C11—C12	1.381(12)	C12—C13	1.486(13)	C13—C14	1.466(13)
C14—C15	1.483(13)	C15—C16	1.353(12)	C16—C17	1.506(14)
C17—C18	1.478(13)	C11—C18	1.512(12)	C21—C22	1.375(12)
C22—C23	1.542(14)	C23—C24	1.493(14)	C24—C25	1.548(13)
C25—C26	1.356(12)	C26—C27	1.525(13)	C27—C28	1.480(13)
C21—C28	1.526(13)				

Bonds	Angle (deg)	Bonds	Angle (deg)	Bonds	Angle (deg)
S1—Rh1—S2	76.0(1)	S1—Rh2—S2	75.8(1)	Rh1—S1—Rh2	78.1(1)
Rh1—S2—Rh2	77.4(1)	C1—S1—Rh1	117.1(4)	C1—S1—Rh2	118.8(3)
C2—S2—Rh1	115.6(3)	C2—S2—Rh2	116.1(3)		

Dimerization yields **1**. This hypothesis is supported by the ability of allylic aryl sulfides to displace triphenylphosphine from $RhH(PPh_3)_4$ to give rhodium thiolate dimers and olefins (23). Abstraction of thiolate from Ti is expected to give a cationic Ti intermediate of the form $[Cp_2Ti(THF)SMe]^+$.

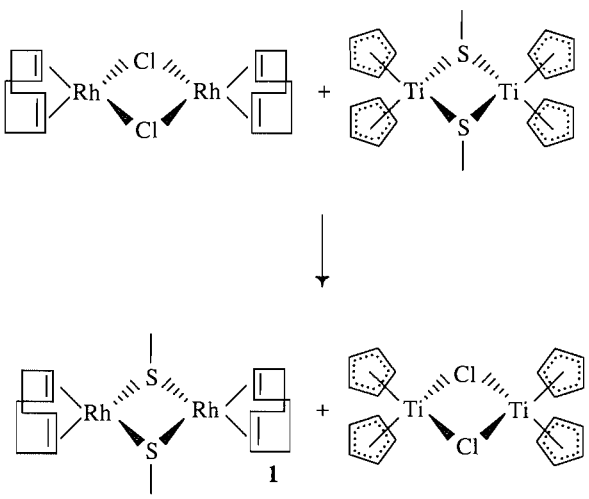

SCHEME 1

Jordan *et al.* have established that such Ti cations react rapidly with BF_4^- or PF_6^- to give a Ti–F species (24). Although this speculation appears consistent with known chemistry, the precise nature of the Ti containing products was not confirmed in the present reactions.

Attempts to incorporate Ti(III) and Rh(I) in a heterobimetallic complex involved the reaction of $(Cp_2Ti(\mu\text{-}SMe))_2$ with $((COD)Rh(\mu\text{-}Cl))_2$. The EPR spectrum of the reaction mixture showed a singlet with a g value of 1.980, indicative of the presence of the species $(Cp_2Ti(\mu\text{-}Cl))_2$ (25). This result implies that complete bridging ligand exchange between the titanium and rhodium dimers has occurred, affording the rhodium containing product, **1** (Scheme 1).

The compound **1** was previously prepared by heating together $((CO)_2Rh(\mu\text{-}SMe))_2$ and cyclooctadiene (26). However, a more direct route to **1** involves the reaction of $((COD)Rh(\mu\text{-}Cl))_2$ with NaSMe. Yields of **1** via this route appear quantitative by NMR.

X-ray quality crystals of $((COD)Rh(\mu\text{-}SMe))_2$ were obtained by cooling a pentane solution of **1** to −10°C. The crystallographic study showed that the crystal is made up of monoclinic unit cells containing four formula units per cell. The closest approach between any of these molecules is 2.252 Å (H1B—H27B). ORTEP drawings of the dimer appear in Fig. 1. Each

Can. J. Chem. Downloaded from www.nrcresearchpress.com by 91.144.44.67 on 09/07/12
For personal use only.

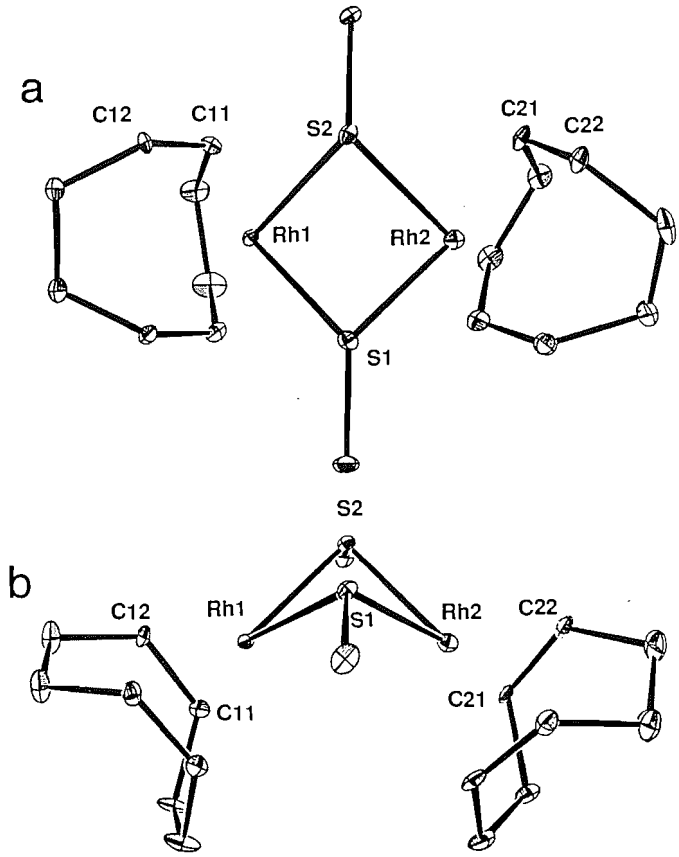

FIG. 1. (a) ORTEP drawing of molecule **1**, 20% thermal ellipsoids are shown. Hydrogen atoms are omitted for clarity; (b) ORTEP drawing of **1**; this view is rotated 90° about the Rh–Rh vector relative to the view in (a).

rhodium is π-bonded to the double bonds of a cyclooctadiene molecule and to two bridging methanethiolates in a pseudo-square-planar geometry. Each of the cyclooctadiene rings has a boat configuration, with a mean carbon–carbon double bond length of 1.366 Å, which is less than that of 1.425 Å found for $((COD)Rh(\mu\text{-}Cl))_2$ (27). In the crystal structure of the latter, the authors reported that the double and single bonds of the olefin could not be distinguished. In **1**, there is a significant difference between the single and double bond lengths, as expected. The average Rh—S distance of 2.349 Å is smaller than that found for $(Rh(SPh)(CO)(PMe_3))_2$ (2.388 Å) (28), but larger than 2.306 Å found in $(CpRh(\mu\text{-}SPh))_2$ (29). The methyl groups on the sulfurs adopt an *exo* arrangement with respect to the RhS_2Rh core. The Rh—Rh separation of 2.948 Å found in **1** is considerably shorter than the Rh—Rh distance of 3.498 Å found in $((COD)Rh(\mu\text{-}Cl))_2$ (27). It is also smaller than the Rh—Rh separation observed in $(Rh(\mu\text{-}SPh)(CO)(PMe_3))_2$ (3.061 Å) (28) or $(CO)_2Rh(\mu\text{-}SPh)_2Rh(COT)$ (3.12 Å) (26). In the related complex $(Rh(\mu\text{-}SPh)(CO)(PMe_3))_2$, a metal–metal interaction has been proposed to account for the relatively close approach of the Rh centres (28).

The S—Rh—S angles found in **1** (76.0(1)° and 75.8(1)°) are smaller than those found for $(Rh(SPh)(CO)(PMe_3))_2$ (81.0(1)° and 80.9(1)°), as are the Rh1—S—Rh2 angles of 78.1(1)° and 77.4(1)° compared to 80.2(1)° and 79.2(1)° (28). The small angle at the rhodium centres and the relatively short S—S separation of 2.888 Å in **1** suggest some degree of sulfur–sulfur interaction. Disulfide bonding character has been suggested in other metal systems where coordination of *cis* thiolato groups is present. For example, in $Cp_2Nb(SPh)_2$, the S—S distance of 3.08 Å was described as an indication of interaction between the sulfur centres (15). The existence of some degree of disulfide bonding character in **1** further suggests some degree of metal–metal interaction, thus accounting for the relatively short Rh—Rh distance. Such Rh–Rh interactions may be inhibited by the steric demands of the bridging thiophenolate groups in $(Rh(\mu\text{-}SPh)(CO)(PMe_3))_2$ (28) or $(CO)_2Rh(\mu\text{-}SPh)_2Rh(COT)$ (26).

In summary, we have described several reactions between titanium thiolate species and Rh complexes. Thiolate abstraction and ligand exchange reactions have been observed. In the present cases, the net effect has been the cleavage of Ti—S bonds and the formation of the rhodium thiolate species **1**. The inability to isolate stable Ti/Rh species is somewhat surprising in view of the numerous heterobimetallic complexes in which simple thiolates bridge divergent transition metals (1, 5, 6, 15). Apparently, the thermodynamic stability of the $Rh(\mu\text{-}SMe)_2Rh$ core is a driving force in the reactions described herein. Present research is aimed at the development of synthetic routes to stable thiolato-bridged Ti/Rh complexes.

Acknowledgements

Financial support from NSERC of Canada is gratefully acknowledged.

1. D. W. STEPHAN. Coord. Chem. Rev. **95**, 41 (1989).
2. G. S. WHITE and D. W. STEPHAN. Inorg. Chem. **24**, 1499 (1985).
3. G. S. WHITE and D. W. STEPHAN. Organometallics, **6**, 2169 (1987).
4. G. S. WHITE and D. W. STEPHAN. Organometallics, **7**, 903 (1988).
5. T. A. WARK and D. W. STEPHAN. Inorg. Chem. **26**, 363 (1987).
6. T. A. WARK and D. W. STEPHAN. Organometallics, **8**, 2836 (1989).
7. T. A. WARK and D. W. STEPHAN. Inorg. Chem. In press.
8. L. GELMINI and D. W. STEPHAN. Inorg. Chim. Acta, **111**, L17 (1986).
9. L. GELMINI and D. W. STEPHAN. Inorg. Chem. **25**, 1222 (1986).
10. L. GELMINI and D. W. STEPHAN. Organometallics, **7**, 849 (1988).
11. L. GELMINI, L. C. MATASSA, and D. W. STEPHAN. Inorg. Chem. **24**, 2585 (1985).
12. L. GELMINI and D. W. STEPHAN. Organometallics, **7**, 1515 (1988).
13. P. Y. ZHENG, T. T. NADASDI, and D. W. STEPHAN. Organometallics, **8**, 1393 (1989).
14. P. Y. ZHENG and D. W. STEPHAN. Can. J. Chem. **67**, 1584 (1989).
15. M. Y. DARENSBOURG, R. SILVA, J. REIBENSPIES, and C. K. PROUT. Organometallics, **8**, 1315 (1989).
16. L. MANZER. Organomet. Chem. **110**, 291 (1976).
17. G. GIORDANA and R. H. CRABTREE. Inorg. Synth. **9**, 218 (1979).
18. R. R. SCHROCK and J. A. OSBORN. J. Am. Chem. Soc. **93**, 3089 (1971).
19. D. T. CROMER and J. B. MANN. Acta Crystallogr. Sect. A: Cryst. Phys. Diffr. Theor. Gen. Crystallogr. **A24**, 324 (1968).
20. D. T. CROMER and J. B. MANN. Acta Crystallogr. Sect. A: Cryst. Phys. Diffr. Theor. Gen. Crystallogr. **A24**, 390 (1968).
21. D. T. CROMER and J. T. WABER. International tables for X-ray crystallography. Kynoch Press, Birmingham, England. 1974.
22. D. O'HARE, M. L. H. GREEN, and F. G. N. CLOKE. J. Organomet. Chem. **282**, 225 (1985).

Can. J. Chem. Downloaded from www.nrcresearchpress.com by 91.144.44.67 on 09/07/12
For personal use only.

23. K. OSAKADA, K. MATSUMOTO, T. YAMAMOTO, and A. YAMAMOTO. Organometallics, **4**, 857 (1985).
24. (*a*) R. F. JORDAN, W. E. DASHER, and S. F. ECHOLS. J. Am. Chem. Soc. **108**, 1718 (1986); (*b*) R. F. JORDAN, C. S. BAJGUR, R. WILLETT, and B. SCOTT. J. Am. Chem. Soc. **108**, 7410 (1986); (*c*) R. F. JORDAN, R. E. LAPOINTE, C. S. BAJGUR, S. F. ECHOLS, and R. WILLETT. J. Am. Chem. Soc. **109**, 4111 (1987).
25. R. S. P. COUTTS and P. C. WAILES. Aust. J. Chem. **26**, 2101 (1973).
26. R. HILL, B. A. KELLY, F. G. KENNEDY, S. A. R. KNOX, and P. WOODWARD. J. Chem. Soc. Chem. Commun. 434 (1977).
27. J. A. IBERS and R. G. SYNDER. Acta Crystallogr. **15**, 923 (1962).
28. J. J. BONNET, P. KALCK, and R. POILBLANC. Inorg. Chem. **16**, 1514 (1977).
29. N. G. CONNELLY, G. A. JOHNSON, B. A. KELLY, and P. WOODWARD. J. Chem. Soc. Chem. Commun. 436 (1977).

Can. J. Chem. Downloaded from www.nrcresearchpress.com by 91.144.44.67 on 09/07/12
For personal use only.

An ICR mass spectrometry study of ion/molecule reactions in mixtures of methylamine with ethylamine, propylamine, or butylamine

GUOYING XU, JAN A. HERMAN, AND LESZEK WÓJCIK[1]

C. R. A. M. et le département de chimie, Université Laval, Québec (Qué.), Canada G1K 7P4

Received August 7, 1989

GUOYING XU, JAN A. HERMAN, and LESZEK WÓJCIK. Can. J. Chem. **68**, 570 (1990).

Ion/molecule reactions of protonated alkylamine ion species, RNH_3^+, were studied in mixtures of methylamine with ethylamine, propylamine, or butylamine by ICR mass spectrometry at 10^{-5} Torr. The occurrence of methyl group transfer from methylamine to higher protonated alkylamine ion species was observed. The rate constants of some bimolecular reactions occurring in these systems were estimated by numerical simulation.

Key words: ion/molecule reactions, methylamine, ethylamine, propylamine, butylamine, ICR mass spectrometry.

GUOYING XU, JAN A. HERMAN et LESZEK WÓJCIK. Can. J. Chem. **68**, 570 (1990).

Faisant appel à la spectrométrie de masse ICR et opérant dans des mélanges de méthylamine contenant de l'éthylamine, de la propylamine ou de la butylamine, à une pression totale de 10^{-5} Torr, on a étudié les réactions ion/molécule des espèces ioniques, alkylamines protonées, RNH_3^+. On a observé un transfert du groupement méthyle de la méthylamine vers les espèces ioniques des homologues supérieurs des alkylamines protonées. On a évalué les constantes de vitesse de quelques réactions bimoléculaires se produisant dans ces systèmes.

Mots clés : réactions ion/molécule, méthylamine, éthylamine, propylamine, butylamine, spectrométrie de masse ICR.

[Traduit par la revue]

Can. J. Chem. Downloaded from www.nrcresearchpress.com by 91.144.44.67 on 09/07/12
For personal use only.

Introduction

The gas-phase ion chemistry of methylamine and some higher alkylamines has been studied extensively in high-pressure or ICR mass spectrometers in the pressure range 10^{-5} to 2 Torr (1–7). In this pressure range the main reaction is protonation of the molecular ion, followed only at higher gas densities by condensation processes:

[1] $RNH_2^+ + RNH_2 \rightarrow RNH_3^+ + RNH$

[2] $RNH_3^+ + RNH_2 \xrightarrow{M} (RNH_2)_2H^+ + NH_3$

Depending on the nature of the alkylamine, reaction [1] is exothermic by 20 to 50 kJ/mol in terms of the available ground state energetics (8). Condensation reaction [2] is a termolecular process. In the case of methylamine its kinetics was thoroughly analysed by Meot-Ner and Field (9), Brauman and co-workers (10), Bowers and co-workers (11), and Chang and Golden (12). For higher alkylamines the experiments were mainly focussed on the mechanism of reaction [1] (13–18). No studies on further solvation reactions of RNH_3^+ with its neutral RNH_2 (R = C_2H_5, C_3H_7, C_4H_9) were reported.

Experimental evidence suggests that ion/molecule reactions in amines proceed through an activated intermediate also called a collision or reaction complex (19). In the case of methylamine the decomposition of the chemically activated intermediate cannot proceed through a four-centered front site displacement mechanism, because the single lone electron pair of nitrogen is involved in a strong hydrogen bond. Therefore, a back attack in a nucleophilic displacement reaction is expected, but such a process should be characterized by a low rate constant

[3] $CH_3NH_3^+ + CH_2NH_2 \rightarrow [(CH_3NH_2)_2H]^{*+} \rightarrow (CH_3)_2NH_2^+ + NH_3$

If process [3] in methylamine is slow, it may be obscured by the fast proton transfer reactions from $CH_3NH_3^+$ to dimethyl- and trimethylamines, which are usually present as impurities (a few tenths of a percent) but are difficult to remove. Therefore, process [3] cannot be unambiguously studied in methylamine.

In the case of mixtures of methylamine with higher alkylamines the decomposition of the collision complexes may form product ions with alkyl groups other than the methyl group. These product ions may be distinguishable by their mass from protonated dimethyl- or trimethylamine ion species or other impurities. It is the purpose of this work to explore the processes occurred between methylamine and higher alkylamines ($C_2H_5NH_2$, $C_3H_7NH_2$, and $C_4H_9NH_2$) leading to formation of ions having the general formula $(R_xR_yNH_{3-x-y})^+$.

Experimental

The pulsed ICR mass spectrometer used in this work has been described (20). The usual pulse sequence started with a 2 ms ionizing pulse of 70 eV electrons followed by a variable delay (5–500 ms) during which ion/molecule processes take place. Then a 1.5 ms resonant RF frequency excitation pulse of 0.5 V, followed immediately by a 4 ms detection pulse, terminate the measured events. The pulse sequence ended with a quenching pulse, which swept out all remaining ions in the cell. The magnetic field was set up at 0.8 Tesla allowing ions in mass range 26 to 150 amu to be scanned within a frequency range of 80 to 450 kHz. Due to the proximity of one of the trapping plates to the emission filament the temperature of the cell cannot be uniform. We estimate the average cell temperature to be around 50°C.

The pressure at which all experiments were performed was $(1.0 \pm 0.1) \times 10^{-5}$ Torr (1.33×10^{-5} mbar). At that pressure ions can be kept in the reaction cell for about 2 s, but practical measurements of the ion intensities were limited to 0.5 s.

Methyl- and ethylamines from Matheson were of the best available purity (~99%). A gas-chromatographic analysis of methylamine showed impurities amounting to less than 1%. The propyl-, isopropyl-, and butylamines from Aldrich were better than 99% pure and were used as such.

The mixtures of alkylamines were prepared in a known ratio in a separate high vacuum manifold, which was baked each time between preparation of gaseous samples.

Results and discussion

In mixtures of methylamine with ethylamine, propylamine, or butylamines, the proton affinity of methylamine is the smallest (21). Furthermore, if the fast proton transfer processes

[1]Visiting scientists 1986–1987. Permanent address: Institute of Physics, Maria Curie Skłodowska University, Lublin, Poland.

TABLE 1. Rate constants for the formation of some protonated amine ions

Reaction	Rate constants (10^{10} cm^3 molecule^{-1} s^{-1})					
	This work	Ref. 1	Ref. 3	Ref. 6	Ref. 7	Ref. 2
$CH_3NH_2^+ + MeNH_2 \rightarrow CH_3NH_3^+ + MeNH$	9.0	9.0	14		16.4	19
$CH_2NH_2^+ + MeNH_2 \rightarrow CH_3NH_3^+ + CH_2NH$	5.0	7.0	4.0			12
$CH_2N^+ + MeNH_2 \rightarrow CH_3NH_3^+ + CHN$	7.0	9.0	5.0			16
$C_2H_5NH_2^+ + EtNH_2 \rightarrow C_2H_5NH_3^+ + EtNH$	15.0			18.3		
$C_2H_4NH_2^+ + EtNH_2 \rightarrow C_2H_5NH_3^+ + C_2H_4NH$	9.0					
$CH_3NH_2^+ + EtNH_2 \rightarrow C_2H_5NH_3^+ + MeNH$	7.8					
$CH_2NH_2^+ + EtNH_2 \rightarrow C_2H_5NH_3^+ + CH_2NH$	10.0			19.7		
$CH_3NH_3^+ + EtNH_2 \rightarrow C_2H_5NH_3^+ + MeNH_2$	3.6					
$C_3H_7NH_2^+ + ProNH_2 \rightarrow C_3H_7NH_3^+ + ProNH$	15.6			15.6		
$CH_3NH_2^+ + ProNH_2 \rightarrow C_3H_7NH_3^+ + MeNH$	8.3					
$CH_2NH_2^+ + ProNH_2 \rightarrow C_3H_7NH_3^+ + CH_2NH$	16.7			22.4		
$CH_3NH_3^+ + ProNH_2 \rightarrow C_3H_7NH_3^+ + MeNH_2$	4.2					
$C_4H_9NH_2^+ + BuNH_2 \rightarrow C_4H_9NH_3^+ + BuNH$	11.0					
$CH_3NH_2^+ + BuNH_2 \rightarrow C_4H_9NH_3^+ + MeNH$	9.0					
$CH_3NH_3^+ + BuNH_2 \rightarrow C_4H_9NH_3^+ + MeNH_2$	5.0					

in amines are taken into account, it can be expected that in a very short time the only ion species left will be the protonated alkylamine ion, RNH_3^+, where R is a C_2H_5, C_3H_7, or C_4H_9 group. Therefore, these mixtures can be used to study the reactions of protonated alkylamine ions RNH_3^+ with methylamine neutral molecules.

If the rate of formation of RNH_3^+ by charge- and proton-transfer processes in these mixtures can be measured from the rate of disappearance of primary ion species, then the subsequent slow reactions of RNH_3^+ with neutral molecules might be estimated by straightforward kinetic modeling. To that end we have used the numerical simulation written by Robichaud (22) to find solutions for a system of first, second, and/or third order kinetic differential equations. To run this program the initial concentrations (at $t = 0$) have to be known and the reaction mechanisms and rate constants have to be assumed. The initial concentrations of neutral reactants are known from the total pressure and mixture ratios. The relative initial concentrations of primary ions were obtained by extrapolating their fractional intensities to zero time. Since the total absolute initial concentration of primary ion species is not known, it was arbitrarily chosen to be 1% of the neutral concentration, which is small enough to maintain the concentration of neutral reactants constant during the experimental reaction time. If more realistic values of 0.1% or 0.01% for the initial concentration of primary ion species were used, the calculation time increases correspondingly without improving the results.

If the simulation results were reasonably close to experiment then the proposed mechanism and assumed rate constants were considered to be acceptable. An additional test for the assumed rate constants was the requirement that the experimental data agreed with calculated results at different mixture ratios. In general they agreed to within a factor of 2 for most of the product ion species, except for the less abundant ones (<6%). However, the fractional intensities of these latter ion species are also subject to more significant errors of measurement.

The rate constants of formation of protonated alkylamines from the literature and those measured in our experiments and used in the numerical simulation are reported in Table 1. It can be seen that these values often differ by nearly one order of magnitude depending on the method used for their measurements.

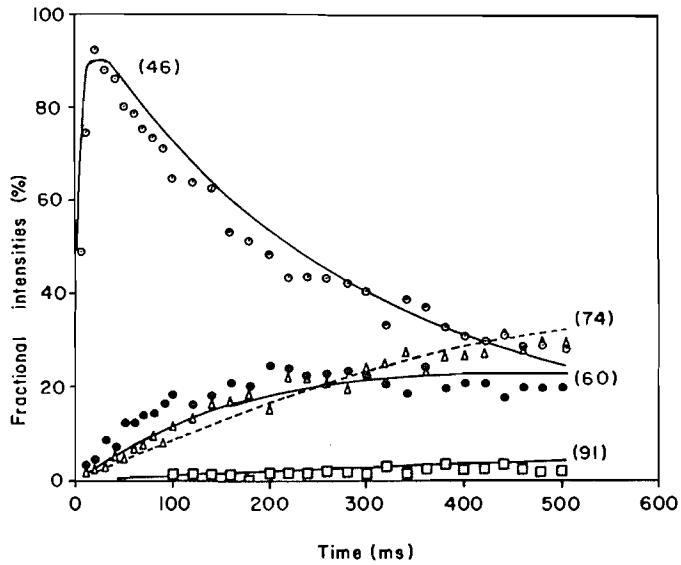

FIG. 1. Fractional intensities of ion species formed in a 8:1 mixture of $C_2H_5NH_2/CH_3NH_2$ as a function of time: (46) $C_2H_6NH_3^+$, (60) $[C_2H_5NH_2CH_3]^+$, (74) $[(C_2H_5)_2NH_2]^+$ and $[C_2H_5NH(CH_3)_2]^+$, (91) $(C_2H_5NH_2)_2H^+$. Solid lines represent simulation results.

Mixtures of ethylamine ($EtNH_2$) with methylamine ($MeNH_2$)

Mixtures of $EtNH_2$:$MeNH_2$ = 1:1, 2:1, 4:1 and 8:1, respectively, were investigated for their ion/molecule reactions occurring after ionization by 70 eV electrons.

In Fig. 1 is shown the time evolution of fractional intensities of ion species formed in ion/molecule reactions in $EtNH_2$:$MeNH_2$ = 8:1 mixture. We did not draw the disappearance of primary ions or other fragments as function of time, because all these species vanish very quickly in proton transfer processes to form the protonated ethylamine ion, $(C_2H_5NH_3)^+$, which at 30 ms is practically the sole species left in the mass spectrum.

We assume that the observed ions at longer time (>30 ms) are $[C_2H_5NH_2CH_3]^+$ at m/z = 60, $[C_4H_{10}N]^+$ at m/z = 72, $[C_2H_5NH(CH_3)_2]^+$ or $[(C_2H_5)_2NH_2]^+$ at m/z = 74, $[C_2H_5N(CH_3)_3]^+$ at m/z = 88, and $(C_2H_5NH_2)_2H^+$ at m/z = 91, respectively. The fractional intensities of ions at m/z = 72 and 88 are small and are not shown in Fig. 1. The fractional intensities of the m/z = 60 and 74 ion species are higher in

Can. J. Chem. Downloaded from www.nrcresearchpress.com by 91.144.44.67 on 09/07/12
For personal use only.

mixtures with larger methylamine content. Even in the mixture $EtNH_2$:$MeNH_2$ = 8:1 the maximum fractional intensity of m/z = 60 ion species is larger than that in pure ethylamine.

The methyl group transfer processes may explain the formation of higher mass species:

[4] $C_2H_5NH_3^+ + CH_3NH_2 \rightarrow [CH_3NH_2..C_2H_5NH_3]^{*+} \rightarrow [C_2H_5NH_2CH_3]^+ + NH_3$

$C_2H_5NH_3^+ + C_2H_5NH_2 \rightarrow [C_2H_5NH_2...H^+...NH_2C_2H_5]^* \rightarrow$

[5] $\rightarrow [C_2H_5NH_2CH_3]^+ + CH_3NH_2$

[6] $\rightarrow [(C_2H_5)_2NH^+NH_2]^+ + NH_3$

[7] $\rightarrow C_4H_{10}N^+ + NH_3 + H_2$

[8] $\xrightarrow{M} (C_2H_5NH_2)_2H^+$

In addition the following sequence of methyl group transfers from methylamine could also contribute to the formation of m/z = 74 and 88 ion species:

[9] $[C_2H_6NH_2CH_3]^+ \xrightarrow{MeNH_2} [C_2H_5NH(CH_3)_2]^+ + NH_3$

$\xrightarrow{MeNH_2} [C_2H_5N(CH_3)_3]^+ + NH_3$

The results from these experiments allow the approximate calculation of the contribution of processes [4], [6], and [9] to the formation of the $C_4H_{12}N^+$ (m/z = 74) species.

The calculated rate constants for some of these reactions occurring in $EtNH_2$:$MeNH_2$ = 8:1 mixture are shown in Table 2.

Mixtures of propylamine ($PrNH_2$) with methylamine ($MeNH_2$)

The experimental data for all four mixture ratios of $PrNH_2$ with $MeNH_2$, 1:1, 2:1, 4:1, and 8:1, were more scattered than for the corresponding *n*-butyl- or ethylamine systems. We have no explanation for such behaviour.

The experimental results for the $PrNH_2$:$MeNH_2$ = 8:1 mixture are shown in Fig. 2. In this figure the fate of primary and their fragment ion species are not shown, because they all react very efficiently in proton transfer processes with neutral propylamine (PA = 912 kJ/mol) (20*b*), leaving in the mass spectrum at less than 50 ms only the protonated propylamine species (m/z = 60). The observed product ions are $C_4H_{12}N^+$ (m/z = 74), $C_5H_{14}N^+$ (m/z = 88), and $C_6H_{16}N^+$ (m/z = 102). We assume that the corresponding structures are $(C_3H_7NH_2CH_3)^+$ for m/z = 74, $[C_3H_7NH(CH_3)_2]^+$ or $[C_3H_7NH_2C_2H_5]^+$ for m/z = 88, and $[(C_3H_7)_2NH_2]^+$ for m/z = 102, respectively. The formation of 5 or 6 carbon cyclic structures should also be considered, the enthalpy of formation of such ions being usually lower than the corresponding acyclic species (8). Therefore, only the sequence of reactions between $C_3H_7NH_3^+$ and methyl- and propylamines have to be considered:

[10] $C_3H_7NH_3^+ + CH_3NH_2 \rightarrow [CH_3NH_2..C_3H_7NH_3]^{*+} \rightarrow [C_3H_7NH_2CH_3]^+ + NH_3$

$C_3H_7NH_3^+ + C_3H_7NH_2 \rightarrow [C_3H_7NH_2...H^+...NH_2C_3H_7]^* \rightarrow$

[11] $\rightarrow [C_3H_7NH_3CH_3]^+ + C_2H_5NH_2$

[12] $\rightarrow [C_3H_7NH_2C_2H_5]^+ + CH_3NH_2$

[13] $\rightarrow [(C_3H_7)_2NH_2]^+ + NH_3$

[14] $\xrightarrow{M} (C_3H_7NH_2)_2H^+$

[15] $(C_3H_7NH_2CH_3)^+ + CH_3NH_2 \rightarrow [C_3H_7NH(CH_3)_2]^+ + NH_3$

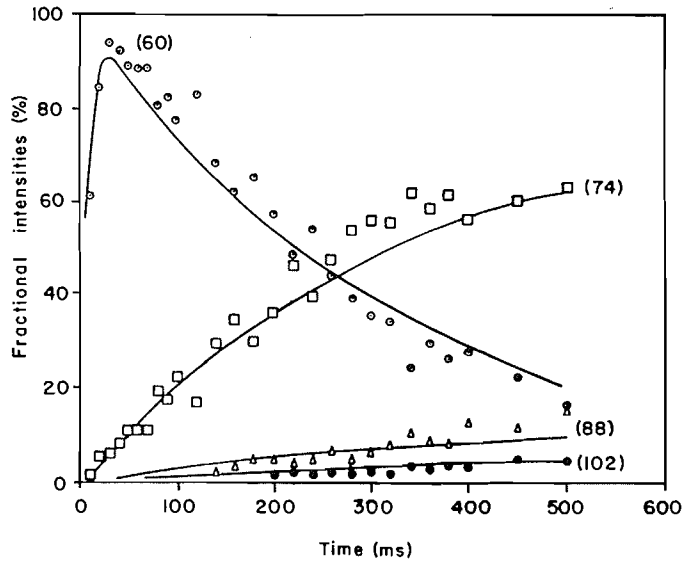

FIG. 2. Fractional intensities of ion species formed in a 8:1 mixture of $C_3H_7NH_2/CH_3NH_2$ as a function of time: (60) $C_3H_7NH_3^+$, (74) $[C_3H_7NH_2CH_3]^+$, (88) $[C_3H_7NH_2C_2H_5]^+$ and $[C_3H_7NH(CH_3)_2]^+$, (102) $[(C_3H_7)_2NH_2]^+$. Solid lines represent simulation results.

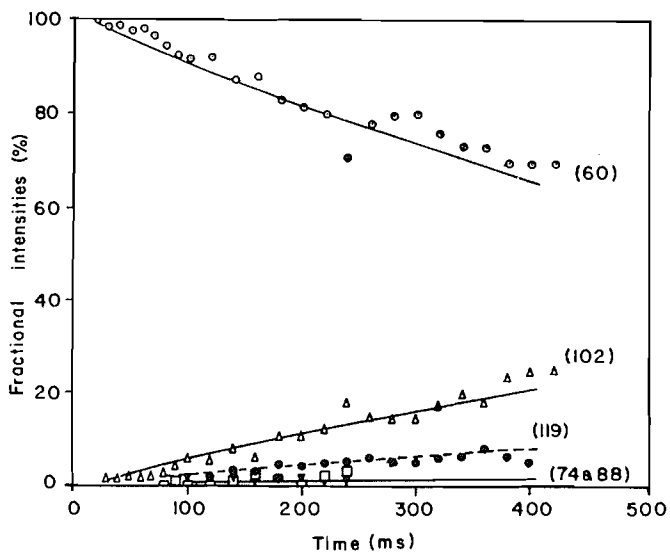

FIG. 3. Fractional intensities of ion species formed in pure propylamine as a function of time: (60) $C_3H_7NH_3^+$, (74) $[C_3H_7NH_2CH_3]^+$, (88) $[C_3H_7NH_2C_2H_5]^+$, (102) $[(C_3H_7)_2NH_2]^+$, (119) $(C_3H_7NH_2)_2H^+$. Solid lines represent simulation results.

If one compares these results with those in pure propylamine (Fig. 3), one can see that although ions with m/z = 74 and 88 are the major products in the 8:1 mixture (the same is true for 1:1, 2:1, and 4:1 mixtures), these ions occur only in small amounts in pure propylamine. The main product ions in pure propylamine are species with m/z = 102 and 119, which are assumed to be $[(C_3H_7)_2NH_2]^+$ and $(C_3H_7NH_2)_2H^+$, respectively. In contrast, at longer times, these ions account for less than 5% of the mass spectrum of the $PrNH_2$:$MeNH_2$ = 8:1 mixture and much less in methylamine-richer mixtures. These results imply that the dominant ion/molecule processes are methyl group transfer from methylamine to the protonated propylamine ion species (reactions [10] and [15]).

The calculated rate constants of some reactions for the mixture $PrNH_2$:$MeNH_2$ = 8:1 are shown in Table 2.

Can. J. Chem. Downloaded from www.nrcresearchpress.com by 91.144.44.67 on 09/07/12
For personal use only.

TABLE 2. List of rate constants

Reaction	Rate constant[a] (10^{10} cm^3 molecule^{-1} s^{-1})
$C_2H_5NH_3^+ + MeNH_2 \rightarrow [C_2H_5NH_2CH_3]^+ + NH_3$	0.28
$C_2H_5NH_3^+ + EtNH_2 \rightarrow [C_2H_5NH_2CH_3]^+ + MeNH_2$	0.03
$\rightarrow [(C_2H_5)_2NH_2]^+ + NH_3$	0.04
$\rightarrow [C_4H_{10}N]^+ + NH_3 + H_2$	0.02
$[C_2H_5NH_2CH_3]^+ + MeNH_2 \rightarrow [C_2H_5NH(CH_3)_2]^+ + NH_3$	0.31
$C_3H_7NH_3^+ + MeNH_2 \rightarrow [C_3H_7NH_2CH_3]^+ + NH_3$	0.34
$C_3H_7NH_3^+ + PrNH_2 \rightarrow [C_3H_7NHCH_3]^+ + EtNH_2$	0.05
$\rightarrow [C_3H_7NH_2C_2H_5]^+ + MeNH_2$	0.01
$\rightarrow [(C_3H_7)_2NH_2]^+ + NH_3$	0.03
$[C_3H_7NH_2CH_3]^+ + MeNH_2 \rightarrow [C_3H_7NH(CH_3)_2]^+ + NH_3$	0.06
$C_4H_9NH_3^+ + MeNH_2 \rightarrow [C_4H_9NH_2CH_3]^+ + NH_3$	0.08
$C_4H_9NH_3^+ + BuNH_2 \rightarrow [C_4H_9NH_2CH_3]^+ + PrNH_2$	0.01
$\rightarrow [C_4H_9NH_2C_2H_5]^+ + EtNH_2$	0.01
$\rightarrow [(C_4H_9)_2NH_2]^+ + NH_3$	0.007
$[C_4H_9NH_2CH_3]^+ + MeNH_2 \rightarrow [C_4H_9NH(CH_3)_2]^+ + NH_3$	0.09

[a]These rate constants are within a factor of 2.

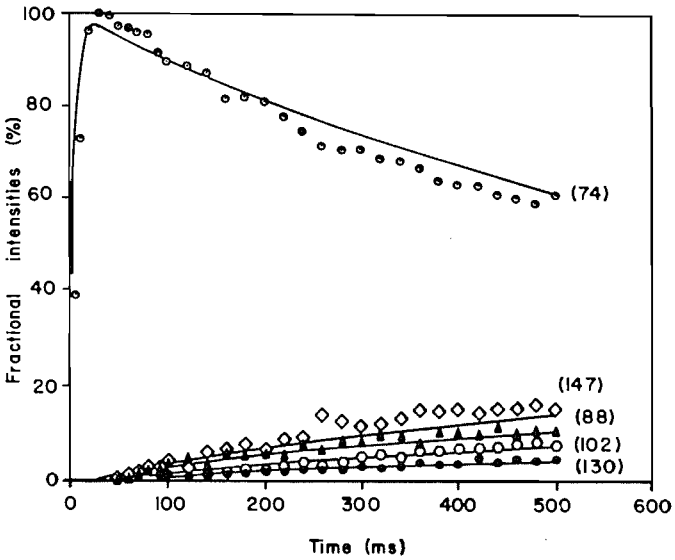

FIG. 4. Fractional intensities of ion species formed in a 8:1 mixture of n-$C_4H_9NH_2/CH_3NH_2$ as a function of time: (74) $C_4H_9NH_3^+$, (88) $[C_4H_9NH_2CH_3]^+$, (102) $[C_4H_9NH_2C_2H_5]^+$ and $[C_4H_9NH(CH_3)_2]^+$, (130) $[(C_4H_9)_2NH_2]^+$, (147) $(C_4H_9NH_2)_2H^+$. Solid lines represent simulation results.

Mixtures of butylamine ($BuNH_2$) with methylamine ($MeNH_2$)

The mixtures of $BuNH_2$:$MeNH_2$ = 1:1, 2:1, 4:1, and 8:1 respectively were investigated for their reactions occurring after ionization by 70 eV electrons.

Figure 4 shows the fractional intensities of some ion species formed in an 8:1 mixture as a function of time. The proton affinity of n-butylamine (PA = 914 kJ/mol) is larger than that of methylamine (PA = 896 kJ/mol) (21*b*) and because the proton transfer in amines is very fast (at almost collision rate) the primary ions: $CH_3NH_2^+$, CH_3NH^+, $C_4H_9NH_2^+$ ... etc., formed by electron impact quickly are transformed to protonated butylamine ions. One can see, indeed, that after 50 ms the only species practically present in the system is $(C_4H_9NH_3)^+$, and the resulting sequence of ion/molecule reactions are processes between this ion and neutral component molecules of the mixture (Fig. 4).

The observed ion products are assumed to be $(C_4H_9NH_2CH_3)^+$ at m/z = 88, $(C_4H_9NH_2C_2H_5)^+$ or $[C_4H_9NH(CH_3)_2]^+$ at m/z = 102, $[(C_4H_9)_2NH_2]^+$ at m/z = 130, and $(C_4H_9NH_2)_2H^+$ at m/z = 147. The fractional intensities of ions of m/z = 88 and m/z = 147 depends on the mixture ratio. The former dominates when the mixture ratio is $BuNH_2$:$MeNH_2$ = 1:1, whereas the latter ion dominates for a mixture ratio of 8:1 respectively. These results imply that $(C_4H_9NH_2CH_3)^+$ species are mainly formed in reaction [16]. On the other hand, the $(C_4H_9NH_2)_2H^+$ ions are apparently formed mainly in reaction [20], if we assume that the dibutylamine impurity is only in trace amounts.

The suggested mechanism is shown below:

[16] $C_4H_9NH_3^+ + CH_3NH_2 \rightarrow [CH_3NH_2..C_4H_9NH_3]^{*+} \rightarrow [C_4H_9NH_2CH_3]^+ + NH_3$

$C_4H_9NH_3^+ + C_4H_9NH_2 \rightarrow [C_4H_9NH_2...H^+...NH_2C_4H_9]^* \rightarrow$

[17] $\rightarrow [(C_4H_9)_2NH_2]^+ + NH_3$

[18] $\rightarrow [C_4H_9NH_2C_2H_5]^+ + C_2H_5NH_2$

[19] $\rightarrow [C_4H_9NH_2CH_3]^+ + C_2H_5NH_2$

[20] $\xrightarrow{M} (C_4H_9NH_2)_2H^+$

In addition the following reaction may contribute to the formation of the $C_6H_{16}N^+$ (m/z = 102) species:

[21] $(C_4H_9NH_2CH_3)^+ + CH_3NH_2 \rightarrow [C_4H_9NH(CH_3)_2]^+ + NH_3$

The apparent rate constants for these reactions are summarized in Table 2.

The comparison of rate constants for methyl group transfer reactions [4], [10], and [16] involving the three alkylamines (Table 2) indicates that butylamine is the least reactive and that ethylamine and propylamine have similar reactivities. In the case of methyl group transfer to $CH_3NH_3^+$ ion species its rate constant is estimated to be $(0.2 \pm 0.1) \times 10^{-10}$ cm^3 molecule^{-1} s^{-1}, which is close enough to the rate constants of reactions [4] and [10], indicating that these processes proceed through a similar mechanism involving the C—N bond cleavage. The lower rate constant for methyl group transfer to protonated butylamine (reaction [16]) may reflect steric effects. On the other hand, reactions [5] to [7], [11] to [13], [17] to [19] involving a C—C bond rupture to release neutral alkylamine have rate constants one order of magnitude smaller (Table 2).

The lowest rate constants in Table 2 have to be taken

Can. J. Chem. Downloaded from www.nrcresearchpress.com by 91.144.44.67 on 09/07/12
For personal use only.

cautiously. If one assumes reasonable rate constants for proton transfer reactions, it requires appropriate impurities at the level of about 0.1% to account for the products in reactions [5], [7], [11], [12], [18], and [19]. However, we were unable to identify and to measure at this level the impurities contained in the available amines.

Conclusion

The present results indicate that with increasing methylamine concentration in mixtures the fractional intensities of product ions of general formula $(RNH_2CH_3)^+$ is notably increased. Therefore, it appears that methyl group transfer reactions occur from methylamine to higher protonated alkylamine ions. The calculated rate constant for these methyl group transfer processes are between 50 and 100 times smaller than the rate constants for proton transfer reactions. Therefore, the eventual presence of small amounts of dimethyl- or trimethylamines impurities can hinder very efficiently the methyl group transfer processes from methylamine. This is the reason why these processes were not observed unambiguously in the mass spectrum of methylamine.

Acknowledgements

The authors are grateful to the National Sciences and Engineering Research Council of Canada and to the Fonds FCAR for financial support.

1. M. S. B. Munson. J. Phys. Chem. **70**, 2034 (1966).
2. E. G. Jones and A. G. Harrison. Can. J. Chem. **45**, 3119 (1967).
3. T. J. Zielinska and H. Wincel. Nukleonika, **15**, 343 (1970).
4. T. Su and M. T. Bowers. J. Am. Chem. Soc. **95**, 7611 (1973).
5. L. Hellner and L. W. Sieck. Int. J. Chem. Kinet. **5**, 177 (1973).
6. J. M. Bupbacher, C. J. Eagle, and E. Tschuikow-Roux. J. Phys. Chem. **79**, 671 (1975).
7. T. B. McMahon and J. L. Beauchamp. J. Phys. Chem. **81**, 593 (1977).
8. S. G. Lias, J. E. Bartmess, J. F. Liebman, J. L. Holmes, R. D. Levin, and W. G. Mallard. J. Phys. Chem. Ref. Data, **17**, Suppl. 1 (1988).
9. M. Meot-Ner and F. H. Field. J. Am. Chem. Soc. **97**, 5339 (1975).
10. W. N. Olmstead, M. Lev-On, D. M. Golden, and J. I. Brauman. J. Am. Chem. Soc. **99**, 992 (1977).
11. P. V. Nielsen, M. T. Bowers, M. Chan, W. R. Davidson, and D. H. Aue. J. Am. Chem. Soc. **100**, 3649 (1978).
12. J. S. Chang and D. M. Golden. J. Am. Chem. Soc. **103**, 496 (1981).
13. T. J. Zielinska and H. Wincel. Chem. Phys. Lett. **25**, 354 (1974).
14. M. S. B. Munson. J. Am. Chem. Soc. **87**, 2332 (1965).
15. J. I. Brauman and L. K. Blair. J. Am. Chem. Soc. **93**, 3911 (1971).
16. J. I. Brauman, J. M. Riveros, and L. K. Blair. J. Am. Chem. Soc. **93**, 3914 (1971).
17. E. M. Arnett, F. M. Jones III, M. Taagepera, W. G. Henderson, J. L. Beauchamp, D. Holts, and R. W. Taft. J. Am. Chem. Soc. **94**, 4724 (1972).
18. J. P. Briggs, R. Yamdagni, and P. Kebarle. J. Am. Chem. Soc. **94**, 5130 (1972).
19. J. L. Beauchamp. *In* Interactions between ions and molecules. *Edited by* P. Ausloos. Plenum Press, New York, NY. 1975. pp. 413–444 and references therein.
20. J. A. Herman, R. Neagu-Plesu, and L. Wojcik. Can. J. Chem. **67**, 97 (1989).
21. (*a*) R. Walder and J. L. Franklin. Int. J. Mass Spectrom. Ion Phys. **36**, 85 (1980); (*b*) S. G. Lias, J. F. Liebman, and R. D. Levin. J. Phys. Chem. Ref. Data, **13**, 695 (1984).
22. J. P. L. Robichaud. Research rapport, DIUL-RR, Université Laval. To be published.

Can. J. Chem. Downloaded from www.nrcresearchpress.com by 91.144.44.67 on 09/07/12
For personal use only.

Facile 5-*endo* ring closures to the azo group. A free radical synthesis of indazoles

CHERYL P. A. KUNKA AND JOHN WARKENTIN[1]
Department of Chemistry, McMaster University, Hamilton, Ont., Canada L8S 4M1

Received August 25, 1989

CHERYL P. A. KUNKA and JOHN WARKENTIN. Can. J. Chem. **68**, 575 (1990).

Five 1-alkyl-3-methylindazoles were prepared by treatment of 1-(2-bromophenyl)-1-methoxy-1-(2-alkylazo)ethanes with tri-*n*-butyl stannane and AIBN at 80°C in benzene. Yields in the radical cyclization step ranged from 39 to 92%. 1-Phenyl-3-methylindazole was prepared by an analogous route but in very poor yield (<5%). Rate constants for the 5-*endo* radical closures ($k_{5\text{-}en}^{80°C}$), estimated by the radical clock method, were $5.2 \times 10^9\ s^{-1}$ and $9.2 \times 10^8\ s^{-1}$ for two of the alkyl systems. Rate constants for analogous 5-*endo* cyclizations of aryl radicals onto C—C double bonds are much smaller than those for cyclizations to the azo functional group.

Key words: cyclization, radical; azo group, radical closure to; indazoles, radical synthesis of.

CHERYL P. A. KUNKA et JOHN WARKENTIN. Can. J. Chem. **68**, 575 (1990).

On a préparé cinq 1-alkyl-3-méthylindazoles en faisant réagir des 1-(2-bromophényl)-1-méthoxy-1-(2-alkylazo)éthanes avec du tri-*n*-butyl stannane et du AIBN, à 80°C, dans le benzène. Les rendements obtenus au cours de la cyclisation radicalaire varient de 39 à 92%. Utilisant une voie analogue, on a aussi préparé le 1-phényl-3-méthylindazole avec un très mauvais rendement (<5%). Pour deux des systèmes alkylés, les constantes de vitesse des cyclisations radicalaires 5-*endo* ($k_{5\text{-}en}^{80°C}$), telles qu'évaluées par la méthode de l'horloge radicalaire, sont égales à $5{,}2 \times 10^9\ s^{-1}$ et $9{,}2 \times 10^8\ s^{-1}$. Les constantes de vitesse des cyclisations 5-*endo* analogues des radicaux aryles sur les doubles liaisons C—C sont beaucoup plus faibles que celles des cyclisations sur le groupement fonctionnel azo.

Mots clés : cyclisation radicalaire; cyclisation radicalaire sur un groupement azo; synthèse radicalaire d'indazoles.

[Traduit par la revue]

Can. J. Chem. Downloaded from www.nrcresearchpress.com by 91.144.44.67 on 09/07/12
For personal use only.

Introduction

Intramolecular reaction of a free radical with a suitably placed site of unsaturation leads to the formation of a cyclic isomer of the initial radical. Such radical cyclizations now occupy a prominent place among methods for the construction of five- and six-membered rings. In the most common applications the site of unsaturation is a carbon–carbon multiple bond[2] but examples of closures to the carbonyl (8–10) and cyano groups (8, 11) as well as to imino (12) and azo (13, 14) functionality have been reported. Recently it was found (14) that cyclizations of aryl radicals onto the azo functional group are faster than corresponding alkene cyclizations and do not show the high selectivity for formation of a five-membered ring, rather than a six-membered ring, that is fairly characteristic of the latter. Very little else is known about radical cyclizations to the azo group and there are no examples of 5-*endo* closures. Therefore we decided to explore the utility of that reaction for the construction of the indazole ring system. We now report that some 5-*endo* cyclizations to azo nitrogen are facile and useful.

Methods, results, and discussion

An attractive system for studying 5-*endo* ring closures to azo nitrogen is the family of substrates **3**. They are readily available from hydrazones **2** by oxidation with lead tetraacetate (LTA) in methanol, Scheme 1. Moreover, the anticipated products (**6**) of cyclization were expected to lose methanol spontaneously to afford indazoles (**7**), (Scheme 1). Finally, authentic samples of the expected by-products (**8**) can by synthesized readily in two steps from acetophenone.

The yields of 12 hydrazones of 2-bromoacetophenone (**2**) or of acetophenone (**9**), together with their ^{1}H NMR spectra are listed in Tables 1 and 2. An interesting feature of the compounds **2** is that two isomers were observed in each case by ^{1}H NMR spectroscopy, whereas the acetophenone hydrazones (**9**) did not show isomerism. Several explanations of those phenomena are possible and discussion of them is deferred until after additional experiments are completed.

Oxidation of **2** with lead tetraacetate in methanolic solution (Scheme 1) afforded azoethers (**3**, Table 3), which were purified without difficulty by chromatography, to remove the azoacetate by-product. Reference compounds **8** (Scheme 1) were similarly prepared from the appropriate acetophenone hydrazones. Yields and spectral data of azoethers **3** and **8** are in Table 3.

Solutions of **3**, with benzene containing AIBN and excess $HSnBu_3$ in sealed tubes, were heated at 80°C to afford indazoles **7**, azoethers **8**, methanol, and products derived from **8**, including the appropriate hydrazone of acetophenone and, in some cases, acetophenone. The presumed precursors (**6**) of the indazoles could not be detected and are assumed to be short-lived under the conditions of their formation. Spectra of the indazoles **7** are in Table 4.

Control experiments, in which indazole **7** was subjected to the radical cyclization conditions, indicated that the indazole products are not affected by the other species present. Analogous experiments with **8**, however, revealed that they are not inert to the reaction conditions, but are partially converted to a mixture of products, including the parent hydrazone and acetophenone. A mechanism that could account, in part, for the disappearance of **8** is given in Scheme 2. Tributylstannyl radicals can presumably add to the azo group to form radical **10**. The latter would then afford **11** and **12** in sequence and **12** could lead to **9** during work-up. There is precedent for protiodestannylation of a vinyltin compound (16) during chromatography on silica with dichloromethane.

The initial addition of $Bu_3Sn\cdot$ (Scheme 2) could also occur with the alternative regiochemistry, leading to a regioisomer of **11** that could also afford **9** during the work-up. Acetophenone could arise during the work-up from hydrolysis of **9**, although alternative pathways, including decomposition of an azohydro-

[1]Author to whom correspondence may be addressed.

[2]The literature on this subject has been reviewed many times. Only some of the more recent reviews are cited here (1–7).

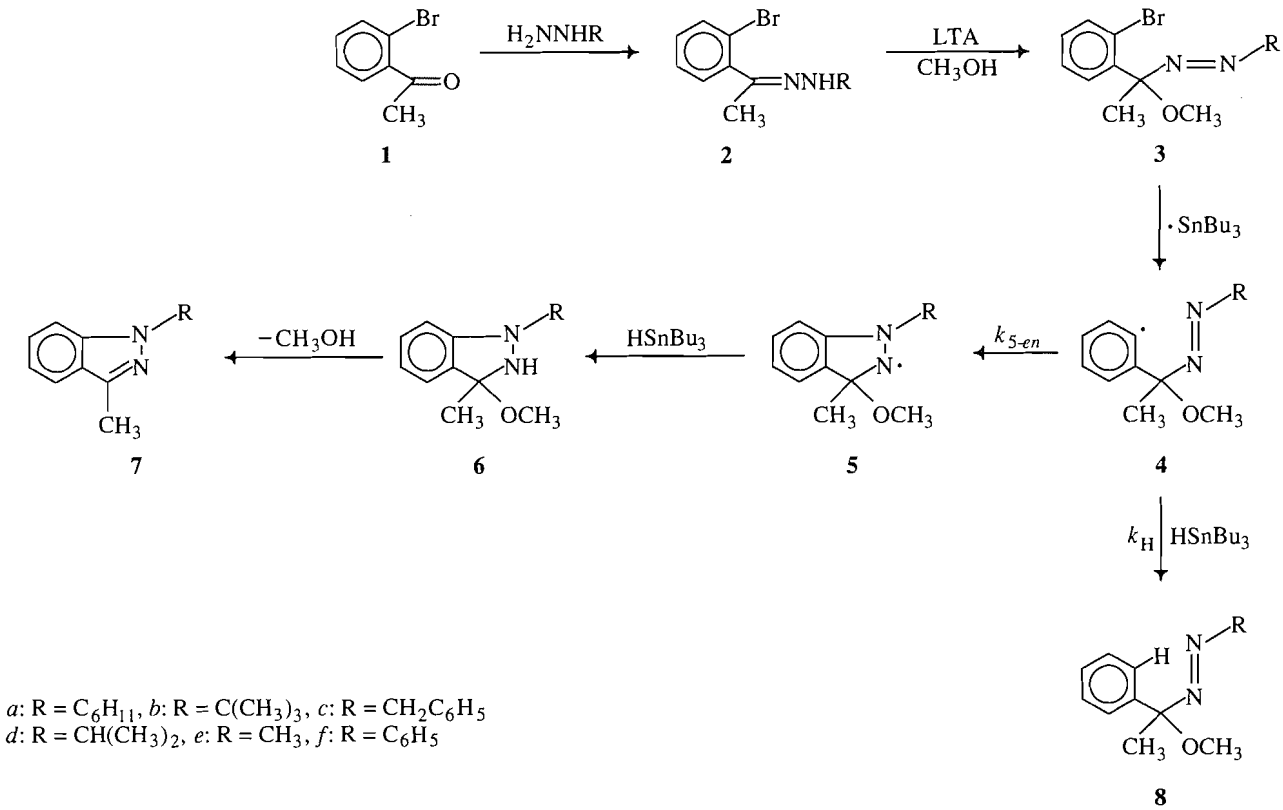

a: R = C_6H_{11}, *b*: R = $C(CH_3)_3$, *c*: R = $CH_2C_6H_5$
d: R = $CH(CH_3)_2$, *e*: R = CH_3, *f*: R = C_6H_5

SCHEME 1

TABLE 1. Hydrazones of 2-bromoacetophenone

Compound	Yield (%)[a]	Isomer ratio (a/b)	^{1}H NMR (δ)[b] Isomer (a)[c]	Isomer (b)[c]
2*a*, R = *c*—C_6H_{11}	82	1.5	0.64–2.35 (m, 13H)[d] 3.24 (m, 1H) 7.02–7.78 (m, 4H)	
2*b*, R = $C(CH_3)_3$	92	1.4	1.12 (s, 9H)[e] 2.09 (s, 3H) 7.02–7.82 (m)	1.25 (s, 9H)[e] 2.18 (s, 3H)
2*c*, R = $CH_2C_6H_5$	85	1.6	2.10 (s, 3H) 4.32 (s, 2H) 6.88–7.82 (m)	2.18 (s, 3H) 4.50 (s, 2H)
2*d*, R = $CH(CH_3)_2$	82	1.4	1.08 (d, 6H) 2.18 (s, 3H) 3.50 (sept)[f] 7.00–7.77 (m)	1.25 (d, 6H) 2.12 (s, 3H)
2*e*, r = CH_3	90	1.4	2.08 (s, 3H) 2.88 (s, 3H) 7.00–7.80 (m)	2.18 (s, 3H) 3.06 (s, 3H)
2*f*, R = C_6H_5	[g]	[g]	2.18 (s, 3H) 6.80–8.00 (m)	2.25 (s, 3H)

[a]Yields of isolated material.
[b]Solvent $CDCl_3$, TMS ref. Coupling to H of NH was not visible.
[c]See text concerning the isomerism. Separate signals are listed in the isomer columns. Composite signals are listed between those columns.
[d]Two singlets at δ 2.10 and 2.17, totalling 3H, are included with ten cyclohexyl protons.
[e]Integrations of resolved signals are relative for each isomer and do not reflect the isomer ratio. Integrals of composite signals were satisfactory.
[f]Although seven quite sharp lines are visible, the intensity ratio is not that of a true septet but rather closer to the expected intensity ratio of two superimposed septets, one displaced from the other by twice the coupling constant.
[g]Not determined.

Can. J. Chem. Downloaded from www.nrcresearchpress.com by 91.144.44.67 on 09/07/12
For personal use only.

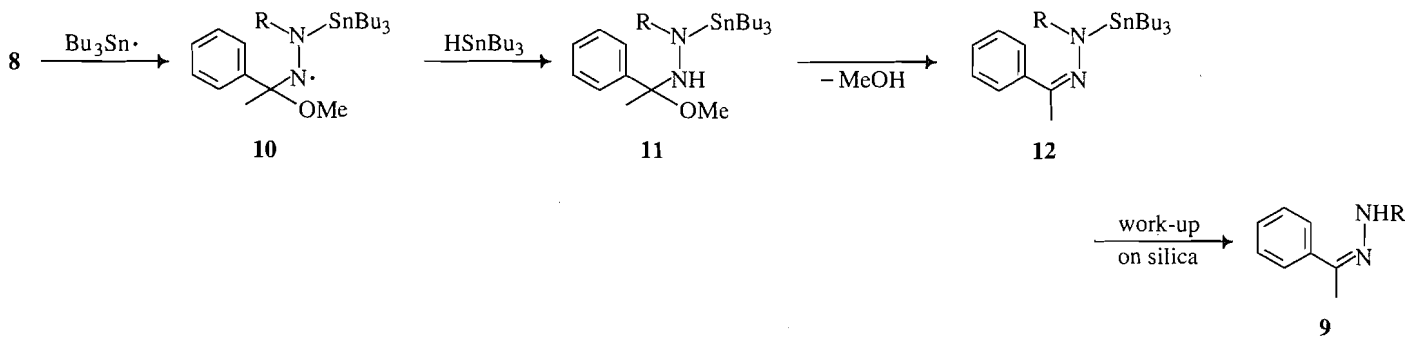

SCHEME 2

TABLE 2. Hydrazones of acetophenone

Compound	Yield (%)[a]	^{1}H NMR (δ)[b]
8*a*, R = *c*—C_6H_{11}	81	0.72–2.40 (m, 13H)[c]; 3.24 (m, 1H); 7.18–8.10 (m, 5H)
8*b*, R = $C(CH_3)_3$	75	1.28 (s, 9H); 2.08 (s, 3H); 7.12–7.92 (m, 5H)
8*c*, R = $CH_2C_6H_5$	84	2.08 (s, 3H); 4.54 (s, 2H); 7.06–8.08 (m, 5H)
8*d*, R = $CH(CH_3)_2$	86	1.24 (d, 6H); 2.10 (s, 3H); 3.61 (sept, 1H); 7.25–7.63 (m, 5H)
8*e*, R = CH_3	57	2.05 (s, 4H); 3.08 (s, 3H); 7.12–7.82 (m, 5H)
8*f*, R = C_6H_5	55	2.20 (s, 3H); 6.72–8.04 (m, 10H)

[a]Isolated.
[b]Solvent $CDCl_3$, TMS ref. Coupling to H of NH was not visible.
[c]A methyl group singlet at δ ≃ 2.06 is superimposed on the multiplet corresponding to ten cyclohexyl protons.

peroxide formed from **12** by reaction with oxygen, cannot be excluded.

Analogous addition of $Bu_3Sn\cdot$ to **3** does not compete effectively with debromination, in general, as indicated by the yields of indazoles that can be obtained. However, the very poor yield of indazole from **3***f* suggests that either addition to the phenylazo functional group, to form the phenyl-conjugated hydrazyl radical, or methoxyl abstraction, is faster than abstraction of Br from **3***f*. The competition with halogen abstraction is serious, for use of the 2-iodo analogue of **3***f* did not raise the yield of indazole **7***f* significantly.

The instability of **8** under the reaction conditions made it difficult to estimate cyclization rate constants, $k_{5\text{-}en}$ (Scheme 1). Those are normally obtained from product analysis and a knowledge of the magnitude of k_H. In this case, quantitative analysis for **8**, and for numerous products derived from it, was not possible and it was necessary to resort to the assumption that all of the non-indazole material should be counted as **8**. In other words, the yield of **8** was estimated by difference, as 100 minus the yield of **7**, eq. [1]. The assumption should lead to minimum values of $k_{5\text{-}en}$, because the denominator in eq. [1] will presumably be equal to, or larger than, the percentage of **4** that went to **8**. A second problem has to do with the actual value of k_H. Although k_H for the phenyl radical has been measured directly (17), the published value ($k_H^{80°C} = 8.9 \times 10^8\ M^{-1}\ s^{-1}$) is now known to be in error and it was necessary to use a value ($k_H^{80°C} = 3.5 \times 10^8\ M^{-1}\ s^{-1}$) from a secondary source (18).

$$[1] \quad k_{5\text{-}en} = k_H \frac{[HSnBu_3]\ (\text{yield of } \mathbf{7})}{(100 - (\text{yield of } \mathbf{7}))}$$

Values of $k_{5\text{-}en}$ for the two cases that gave the best yields, and for which eq. [1] is most likely to be a good approximation, are in Table 5. In view of the way in which those values had to be obtained, the uncertainty in them is quite large, possibly as much as a factor of five. Nevertheless, there is a strong indication that cyclization of the alkylazo aryl radicals (**4***a*–**4***e*) is fast, with $k_{5\text{-}en} \geq 10^9\ s^{-1}$ at 80°C. The phenylazo-substituted aryl radical, **4***f*, either cyclizes more slowly, resulting in the very poor yield of **7***f* (Table 4), or else **4***f* is not formed efficiently, as was discussed above.

[2] 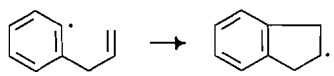

13

Fast 5-*endo* cyclization of radicals **4***a*–**4***e* is a striking result. Analogous cyclization of *ortho* alkenylaryl radicals (**13**, eq. [2]) is very much slower,[3] with $k_{5\text{-}en}^{80°C} \simeq 1.0 \times 10^3\ s^{-1}$. In fact, the 5-*endo* cyclizations reported here are at least as fast as 5-*exo*

[3] 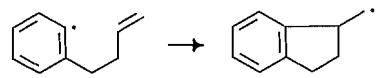

14

cyclizations of **14** (eq. [3]) for which $k^{80°C} = 3.7 \times 10^8\ s^{-1}$ (18), and are comparable to the rates of 5-*exo* and 6-*endo* cyclizations of radical **15**, eq. [4].

[4] 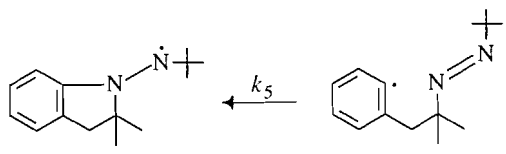

15

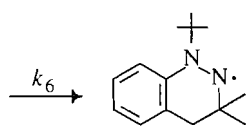

[3]The rate constant is an estimate based on the fact that ring closures of aryl radicals are some two to three orders of magnitude faster than those of alkyl radicals (19). The rate constant for 5-*endo* cyclization of 4-pentenyl at 60°C is believed to be no larger than $1.0\ s^{-1}$ (20).

Can. J. Chem. Downloaded from www.nrcresearchpress.com by 91.144.44.67 on 09/07/12
For personal use only.

TABLE 3. Azoethers **3** and **8**

Compound	Yield (%)[a]	^{1}H NMR (δ)[b]	UV (λ_{max}, log ε)
3*a* (R = C_6H_{11})	73	1.06–2.19 (m, 13H)[c] 3.24 (s, 3H), 3.68 (m, 1H) 7.05–7.84 (m, 4H)	220 (3.61) 259 (2.67)
3*b* (R = $C(CH_3)_3$	43	1.29 (s, 9H), 1.74 (s, 3H) 3.24 (s, 3H), 7.06–7.84 (m, 4H)	202 (2.82) 218 (3.69)
3*c* (R = $CH_2C_6H_5$)	45	1.69 (s, 3H), 3.24 (s, 3H) 5.12 (s, 2H), 7.02–7.75 (m, 9H)	222 (3.91) 258 (3.08)
3*d* (R = $CH(CH_3)_2$)	70	1.32 (d, 6H), 1.67 (s, 3H) 3.25 (s, 3H), 3.92 (sept, 1H) 7.02–7.80 (m, 4H)	218 (2.88) 256 (2.05) 262 (2.03) 360 (1.69)
3*e* (R = CH_3)	64	1.69 (s, 3H), 3.25 (s, 3H) 3.94 (s, 3H), 7.00–7.82 (m, 4H)	216 (3.83) 258 (3.17) 358 (2.88)
3*f* (R = C_6H_5)	d	1.86 (s, 3H), 3.38 (s, 3H) 7.08–8.04 (m, 9H)	216 (4.21) 264 (4.13)
8*a* (R = C_6H_{11})	59	0.76–2.08 (m, 13H)[e] 3.30 (s, 3H), 3.60 (m, 1H) 7.10–7.70 (m, 5H)	220 (3.30) 250 (2.37)
8*b* (R = $C(CH_3)_3$)	56	1.28 (s, 9H), 1.66 (s, 3H) 3.30 (s, 3H), 7.20–7.74 (m, 5H)	216 (4.06)
8*c* (R = $CH_2C_6H_5$)	36	1.60 (s, 3H), 3.30 (s, 3H) 5.05 (s, 2H), 6.91–8.15 (m, 10H)	212 (3.83) 216 (3.85)
8*d* (R = $CH(CH_3)_2$)	54	1.24 (d, 3H), 1.32 (d, 3H) 1.59 (s, 3H), 3.30 (s, 3H 3.85 (sept, 1H), 7.10–7.64 (m, 5H)	216 (3.76) 260 (3.05)
8*e* (R = CH_3)	58	1.65 (s, 3H), 3.36 (s, 3H) 3.94 (s, 3H), 7.21–7.78 (m, 5H)	216 (3.61) 255 (2.92)
8*f* (R = C_6H_5)	52	1.68 (s, 3H), 3.34 (s, 3H) 7.02–7.90 (m, 10H)	216 (3.87) 262 (3.89)

[a]Yields of chromatographically purified product.
[b]$CDCl_3$, TMS ref.
[c]The C-CH_3 singlet, included in this multiplet, is at δ 1.68.
[d]Not determined.
[e]The C-CH_3 singlet, included in this multiplet, is at δ 1.57.

For **15**, $k_5 = 1.5 \times 10^9\ s^{-1}$ and $k_6 = 2.3 \times 10^9\ s^{-1}$ at 82°C (14).

Although 5-membered rings result from radicals **4**, there are actually two ways in which **4** can rearrange to **5** (Scheme 1). Besides direct 5-*endo* closure there could be 4-*exo* cyclization followed by neophyl rearrangement, Scheme 3. Although neophyl rearrangement of hydrazyls was reported recently (21), we consider the mechanism of Scheme 3 to be unlikely. First, 4-*exo* closure of radicals **4** is unlikely to have a rate constant as large as $10^8\ s^{-1}$ at 80°C, given that cyclizations to form cyclobutylcarbinyl radicals are virtually unknown (20). Moreover, even if such a large rate constant were accepted, it is unlikely that the neophyl rearrangement could be fast enough to prevent **16** from abstracting from $HSnBu_3$ during their lifetimes. The rate constant for rearrangement of the neophyl (2-methyl-2-phenylpropyl) radical is about $1.6 \times 10^4\ s^{-1}$ at 80°C (22). Therefore, if more than 50% of **16** were to advance to **17** at $[HSnBu_3] = 3.49\ M$ (neat $HSnBu_3$), k_H for the step **16** → **18** would have to be less than $4.6 \times 10^3\ M^{-1}\ s^{-1}$ at 80°C.

We were unable to detect intermediates, such as **18**, by ^{1}H NMR spectroscopy of partially converted samples of **3**, and we are led to conclude that **18** are either not involved in the overall process or else that they are short-lived and rearrange to **7** by a mechanism such as that involving ylide **19**. In short, the probability that the rate constants in Table 5 are really those for 4-*exo* cyclization is small. That mechanism is not ruled out, however, because the properties of **16** and **18** are unknown.

Indazoles can be prepared readily by non-radical methods (23). The fact that the four indazoles **7***a*–**7***d* were unknown when this work was begun suggests that the approach based on

Can. J. Chem. Downloaded from www.nrcresearchpress.com by 91.144.44.67 on 09/07/12
For personal use only.

TABLE 4. Indazoles, 7[a, b]

Compound	Yield (%)[c]	^{1}H NMR (δ)[d]	^{13}C NMR (δ)[e]	MS[f]
7a	92	1.05–2.24 (m, 10H) 2.56 (s, 3H), 4.32 (m, 1H), 6.94–7.78 (m, 4H)	140.6, 123.3, 120.4 119.4, 125.7, 108.9 139.6, 11.9, 57.8 32.7, 25.8, 25.9	214.1470 214.1463
7b	80	1.75 (s, 9H), 2.58 (s, 3H), 6.95–7.84 (m, 4H)	139.5, 125.2, 120.4 119.0, 124.8, 112.0 139.0, 13.5, 59.0 11.8	188.1313 188.1321
7c	70	2.60 (s, 3H), 5.54 (s, 2H), 6.95–7.84 (m, 9H)	141.7, 123.7, 119.7 120.3, 126.2, 109.1 140.4, 11.9, 52.5 137.2, 127.5, 128.6 127.0	222.1157 222.1166
7d[g]	49	1.56 (d, 6H), 2.58 (s, 3H), 4.76 (sept, 1H), 7.00–7.97 (m, 4H)	140.9, 123.4, 120.4 119.4, 125.7, 108.9 139.4, 13.5, 49.9 22.1	174.1157 174.1160
7e	39	2.56 (s, 3H), 3.98 (s, 3H) 6.98–7.82 (m, 4H)	[h]	[i]
7f	<5[k]	2.66 (s, 3H), 7.05–8.94 (m, 9H)	[h]	[j]

[a]New compounds, *7a–7d*.

[b]The ultraviolet spectra of *7a–7e* in hexane have two bands, $\lambda_{max} \simeq 220$ nm, log ε = 3.4–4.0; 296 nm, log ε = 3.8–4.4. For *7b*, *7d*, and *7e*, a shoulder, at 308 nm, on the long wavelength band was visible. The ultraviolet spectrum of *7f* consisted of three bands: 214 (3.90), 250 (4.15), and 306 (3.74)..

[c]Isolated, except as noted. These yields are for preparative runs, with $HSnBu_3$ in 1.1 to 1.3-fold excess; initial $[HSnBu_3] = 0.1–0.2$ M.

[d]$CDCl_3$, TMS.

[e]In order of increasing number according to the numbering system shown for *7a*. Assigned by means of spin sort and analogy (15) and subject to possible reversal for atoms with very similar shifts. Referenced to $CHCl_3$ at δ 77.0 relative to TMS.

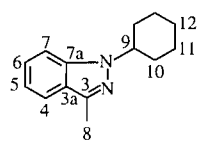

7a

[f]High resolution. The numbers are in the order calculated/found.

[g]Melting point 56–57°C.

[h]Not determined.

[i]Low resolution ms: $m/z = 146$.

[j]Low resolution ms: $m/z = 208$.

[k]Yield estimated by ^{1}H nmr spectroscopy, relative to methyl acetate added to the chromatographic fraction containing the heterocycle.

TABLE 5. Rate constants for cyclization of radicals **4**

Indazole	Yield (%)[a]	k_{5-en}/k_H (M)[b]	$k_{5-en}^{80°C}$ (s^{-1})[c]
7a (R = C_6H_{11})	81	14.9	5.2×10^9
7b (R = $C(CH_3)_3$)	43	2.6	9.2×10^8

[a]From reactions run in neat $HSnBu_3$ (ca. 3.49 M) with $HSnBu_3$ in more than tenfold excess.

[b]Obtained from eq. [1] by using the initial value of $[HSnBu_3]$..

[c]From eq. [1] with $k_H = 3.5 \times 10^8$ M^{-1} s^{-1} at 80°C (17).

radical cyclization holds promise as an alternative synthetic route. However, much more important is the general promise for the construction of heterocyclic rings that is suggested by the high reactivity of the azo group in 5-*endo* as well as in 5-*exo* and 6-*endo* cyclizations (14).

Experimental

Ultraviolet spectra (hexane) were obtained with a Hewlett Packard model 8451A diode array spectrophotometer. Proton magnetic resonance spectra were recorded with a Varian EM-390 spectrometer. Deuterochloroform was the solvent and TMS was the internal reference. Carbon-13 NMR spectra were obtained with a Bruker AM-500 instrument operating at 125.76 MHz and were calibrated against the ^{13}C signal of the $CDCl_3$ solvent at 77.20 ppm. Mass spectra were obtained with a VG 70-70F, double focusing, or a VG ZAB-E, triple focusing, mass spectrometer. Samples were introduced by means of a direct insertion probe and the energy of the ionizing electrons was 70 eV.

Separations were generally carried out by means of centrifugal chromatography, with a Chromatotron (model 7924T) device fitted with a silica coated (Merck, Kieselgel 60 PF_{254}, 2 mm thickness) glass plate. The eluting solvent was ethyl acetate (2%) in low boiling petroleum ether, both distilled before use.

Can. J. Chem. Downloaded from www.nrcresearchpress.com by 91.144.44.67 on 09/07/12
For personal use only.

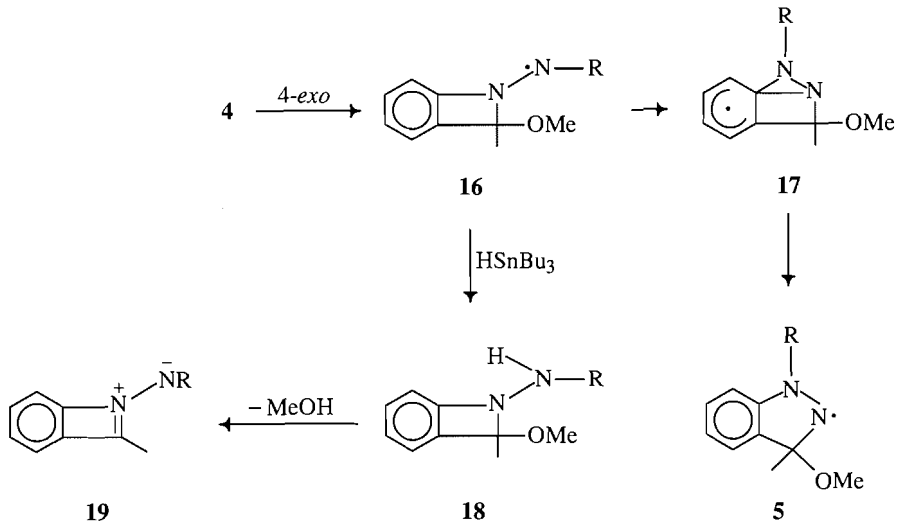

SCHEME 3

Syntheses

The straightforward syntheses of azoethers **3** are illustrated with a detailed procedure for **3***a*.

Cyclohexylhydrazine was prepared by the dropwise addition of cyclohexyl bromide (25.08 g, 0.15 mol) in 25 mL of ethanol to hydrazine hydrate (50 g, 1.0 mol) in 50 mL of ethanol. The resulting solution was heated to 74°C for 27.5 h before the ethanol was removed and the residue was extracted with ether (300 mL) for 2 days in a continuous extractor. The ether layer was dried over magnesium sulfate and the ether was evaporated to leave cyclohexylhydrazine (3.12 g, 18%), satisfactory for the next step; ^{1}H NMR (90 MHz, $CDCl_3$) δ:0.48–2.80 (m, 10H), 3.14–4.18 (m, 4H).

o-Bromoacetophenone cyclohexylhydrazone (**2***a*) was prepared by refluxing a solution of *o*-bromoacetophenone (2.13 g, 0.011 mol) and cyclohexylhydrazine (1.45 g, 0.013 mol) in 25 mL of ether, with stirring, under nitrogen for 41 h. Drying over $MgSO_4$ and evaporation of the ether yielded **2***a* (3.16 g, 82%) as a 60:40 mixture of isomers.

1-(*o*-Bromopheny)-1-cyclohexylazo-1-methoxyethane (**3***a*) was prepared by addition of a solution of **2***a* (3.16 g, 0.011 mol) in 25 mL of methanol through a dropping funnel to an ice-cold solution of lead tetraacetate (5.83 g, 0.013 mol) in 30 mL of methanol. Stirring and cooling were continued for 8 h. Most of the solvent was removed with a rotary evaporator, ice water (50 mL) and dichloromethane were added, and both phases were filtered through a bed of Celite. The organic layer was separated and the aqueous phase was extracted twice more with dichloromethane. The combined organic extract was washed sequentially with ice water, with dilute, cold bicarbonate solution, with ice water, and with cold brine before it was dried over magnesium sulfate. Evaporation of the solvent left crude **3***a*, which was purified in lots of ca. 200 mg by centrifugal chromatography. Spectral data for **3***a*, as well as for analogs prepared by similar methods, are in Tables 1–3.

Cyclizations to indazoles

The procedure described below for the case of **7***a* is representative.

A solution of **3***a* (512 mg, 1.66 mmol), tri-*n*-butyltin hydride (576 mg, 1.98 mmol), and azobisisobutyronitrile (13.5 mg, 0.08 mmol) in benzene (10 mL) was sealed into a glass tube after three cycles of freeze–pump–thaw degassing. The tube was immersed in an oil bath controlled at 80°C. After 30 h the tube was cooled and opened, and most of the benzene was distilled from the reaction products. Centrifugal chromatography of the residue afforded **7***a* (327 mg, 92%). Yields, and spectral data for all of the indazoles, are in Table 4.

1. A. L. J. BECKWITH, C. J. EASTON, and A. K. SERALIS. J. Chem. Soc. Chem. Commun. 482 (1980).
2. F. MINISCI and A. CITTERIO. Advances in free radical chemistry. Vol. 6. *Edited by* G. H. Williams. Heyden, London. 1980. p. 65.
3. J. M. SURZUR. *In* Reactive intermediates. Vol. 2. *Edited by* R. A. Abramovitch. Plenum Press, New York. 1982. pp. 121–295.
4. D. J. HART. Science, **223**, 883 (1984).
5. B. GIESE. Angew. Chem. Int. Ed. Engl. **24**, 553 (1985).
6. B. GIESE. Radicals in organic synthesis: Formation of carbon–carbon bonds. Permagon Press, New York. 1986.
7. M. RAMAIAH. Tetrahedron, **43**, 3541 (1987).
8. S. W. WESTWOOD. J. Am. Chem. Soc. **110**, 2565 (1988).
9. A. L. J. BECKWITH and B. P. HAY. J. Am. Chem. Soc. **111**, 2674 (1989).
10. A. R. FORRESTER, J. SKILLING, and R. H. THOMPSON. J. Chem. Soc. Perkin Trans. 1, 2161 (1974).
11. D. GRILLER, P. SCHMID, and K. U. INGOLD. Can. J. Chem. **57**, 831 (1979).
12. D. D. TANNER and P. M. RAHIMI. J. Org. Chem. **44**, 1674 (1979).
13. (*a*) L. BENATI, G. PLACUCCI, P. SPAGNOLO, A. TUNDO, and G. ZANARDI. J. Chem. Soc. Perkin Trans. 1, 1684 (1977); (*b*) L. BENATI and P. C. MONTEVICHI. J. Org. Chem. **46**, 4570 (1981).
14. A. L. J. BECKWITH, S. F. WANG, and J. WARKENTIN. J. Am. Chem. Soc. **109**, 5289 (1987).
15. J. ELGUERO, R. M. CLARAMUNT, R. GARCERÁN, S. JULIÀ, L. AVILA, and J. M. DEL MAZO. Magn. Reson. Chem. **25**, 260 (1987).
16. G. STORK and R. MOOK, JR. J. Am. Chem. Soc. **109**, 2829 (1987).
17. L. J. JOHNSTON, J. LUSZTYK, D. D. M. WAYNER, A. N. ABEYWICKREMA, A. L. J. BECKWITH, J. C. SCAIANO, and K. U. INGOLD. J. Am. Chem. Soc. **107**, 4594 (1985).
18. A. N. ABEYWICKREMA, A. L. J. BECKWITH, and S. GERBA. J. Org. Chem. **52**, 4072 (1987).
19. A. N. ABEYWICKREMA and A. L. J. BECKWITH. J. Chem. Soc. Chem. Commun. 464 (1986).
20. A. L. J. BECKWITH and K. U. INGOLD. *In* Rearrangements in ground and excited states. *Edited by* P. de Mayo. Academic Press, New York. 1980. p. 200.
21. S. F. WANG, L. MATHEW, and J. WARKENTIN. J. Am. Chem. Soc. **110**, 7235 (1988).
22. J. A. FRANZ, R. D. BARROWS, and D. M. CAMAIONI. J. Am. Chem. Soc. **106**, 3964 (1984).
23. J. ELGUERO. *In* Comprehensive heterocyclic chemistry. Vol. 5. *Edited by* K. T. Potts. Permagon Press, Oxford. 1984. p. 273.

Can. J. Chem. Downloaded from www.nrcresearchpress.com by 91.144.44.67 on 09/07/12
For personal use only.

Experimental and theoretical estimates of the internal rotational barrier of benzyl fluoride in the vapor phase

TED SCHAEFER, CHRISTIAN BEAULIEU, RUDY SEBASTIAN, AND GLENN H. PENNER[1]
Department of Chemistry, University of Manitoba, Winnipeg, Man., Canada R3T 2N2

Received November 14, 1989

TED SCHAEFER, CHRISTIAN BEAULIEU, RUDY SEBASTIAN, and GLENN H. PENNER. Can. J. Chem. **68**, 581 (1990).

The twofold barrier to rotation about the C_{sp^2}—C_{sp^3} bond in benzyl fluoride is deduced from the long-range $^1H,^1H$; $^1H,^{19}F$; and $^{13}C,^{19}F$ nuclear spin–spin coupling constants in solution. The barrier changes from 3.2(2) kJ/mol in the polar solvent, acetonitrile-d_3, to 0.7(2) kJ/mol in the nonpolar environment provided by cyclohexane-d_{12}. In all solutions the conformer of greatest stability has the C—F bond in a plane perpendicular to that of the phenyl group. Extrapolation of the barrier to the vapor phase, using a simple reaction field model, indicates that the most stable conformer for the free (unclustered) molecule is now that with the C—F bond in the phenyl plane and that the barrier to internal rotation is 1.1(7) kJ/mol. Molecular orbital calculations with the basis sets STO-3G, 4-21G, 4-31G, 6-31G, and 6-31G* all predict the latter conformer as that of lowest energy. However, they disagree significantly among themselves as to the height of the internal barrier. The complete geometries are given for both conformers, as computed with the 6-31G basis, and the side-chain geometries are tabulated for the planar and perpendicular conformers, as given by all the bases.

Key words: benzyl fluoride, internal rotational potential; $^{13}C,^{19}F$ spin–spin coupling constants in benzyl fluoride; benzyl fluoride, molecular orbital computations.

TED SCHAEFER, CHRISTIAN BEAULIEU, RUDY SEBASTIAN et GLENN H. PENNER. Can. J. Chem. **68**, 581 (1990).

En se basant sur les constantes de couplage nucléaire spin–spin à longue distance entre ^1H et ^1H, entre ^1H et ^{19}F et entre ^{13}C et ^{19}F mesurées en solution, on a déterminé la valeur de la barrière binaire à la rotation autour de la liaison C_{sp^2}—C_{sp^3} dans le fluorure de benzyle. Cette barrière varie de 3,2(2) kJ/mol dans le solvant polaire, l'acétonitrile-d_3, à 0,7(2) kJ/mol dans l'environnement non-polaire fournit par le cyclohexane-d_{12}. Dans toutes les solutions, le conformère le plus stable est celui dans lequel la liaison C—F se trouve dans un plan perpendiculaire à celui du groupement phényle. L'extrapolation de la barrière à la phase vapeur, utilisant un modèle simple de champ de réaction, indique que le conformère le plus stable de la molécule libre (non encombrée) est celui dans lequel la liaison C—F se trouve dans le plan du groupement phényle et que la barrière à la rotation interne est de 1,1(7) kJ/mol. Des calculs d'orbitales moléculaires effectués à l'aide des bases STO-3G, 4-21G, 4-31G, 6-31G et 6-31G* prédisent tous que ce dernier possède l'énergie la plus faible. Toutefois, ces calculs diffèrent beaucoup entre eux concernant la valeur absolue de la barrière interne. On rapporte les géométries complètes des deux conformères telles que calculées avec la base 6-31G et l'on fournit des tables rapportant les géométries des chaînes latérales des conformères plans et perpendiculaires telles qu'elles ont été évaluées par chacun des ensembles.

Mots clés : fluorure de benzyle, potentiel de la rotation interne; constantes de couplage nucléaire spin–spin entre ^{13}C et ^{19}F en fluorure de benzyle; calculs d'orbitales moléculaires pour le fluorure de benzyle.

[Traduit par la revue]

Introduction

The barrier to rotation about the C_{sp^2}—C_{sp^3} bond in benzyl fluoride has been assessed theoretically and experimentally, with diverse results. Geometry-optimized STO-3G MO computations (1) indicate that the barrier is 1.4 kJ/mol in magnitude and twofold in nature, **1** being the conformation of lowest energy. Electron diffraction patterns of the vapor, together with molecular mechanics calculations (2), imply a minimum in the internal rotation potential near a ψ of 60° and a barrier height of 1.7 kJ/mol. The geminal proton coupling constant, ^2J(H,H), for a $CDCl_3$ solution suggests a conformation intermediate between **1** and **2**, with a small barrier (2), while ^5J(C,F) indicates essentially free internal rotation (3). Nuclear spin-lattice relaxation times in solution are consistent with rather different internal barriers, perhaps as large as 11 kJ/mol (4, 5). ^{19}F nuclear magnetic resonance chemical shifts, as a function of temperature in acetone solution (6), can be interpreted to mean that **2** is 1.7 kJ/mol more stable than **1**.

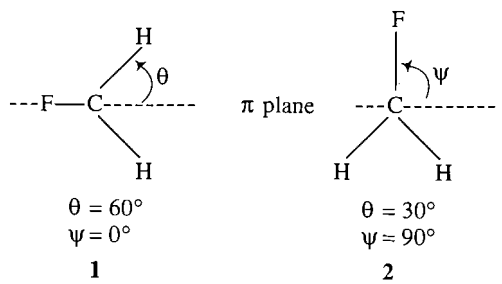

1 **2**

More recently (1), ^5J(C,F), ^6J(H,H), and ^6J(H,F) in benzyl fluoride, in a number of solvents, suggest strongly that, if the barrier is twofold, then **2** is stabilized by about 2 kJ/mol in passing from CS_2 to acetone-d_6 solution; in CS_2 solution the internal potential is rather flat and may be completely so at 300 K. The latest investigation, for solutions in liquid crystalline solvents (7), finds a twofold barrier of 0.3 ± 0.02 kJ/mol in one such solvent and a barrier of 1.5 ± 0.08 kJ/mol in another, more polar, liquid crystal environment. In both instances, at 300 K the stable conformer is **2** (7).

The latter work has encouraged us to reexamine our data for ^6J(H,H) and ^6J(H,F), to remeasure ^nJ(C,F) in a number of solvents, and to attempt an extrapolation of these data to the vapor phase. The results are reported below. It appears that **1** is the most stable conformer for the free molecule, and this conclusion is in agreement with a series of molecular orbital calculations, also reported below.

Experimental

Benzyl fluoride was prepared as dilute solutions in the solvents given in Table 2. The solutions were transferred to 5 mm od nmr sample

[1]Present address: Department of Chemistry and Biochemistry, University of Guelph, Guelph, Ontario.

Can. J. Chem. Downloaded from www.nrcresearchpress.com by 91.144.44.67 on 09/07/12
For personal use only.

Can. J. Chem. Downloaded from www.nrcresearchpress.com by 91.144.44.67 on 09/07/12
For personal use only.

TABLE 1. ^{13}C nuclear magnetic resonance parameters for benzyl fluoride at 300 K

Parameter	C_6D_{12}[a]	CS_2[b]	CCl_4[c]	CD_2Cl_2[a]	$(CD_3)_2C{=}O$[d]	CD_3CN[a]
$\delta_{(CH_2)}$[e]	84.10	83.61	83.47	85.04	85.11	85.57
δ_1	137.50	136.40	136.34	136.74	137.53	137.48
δ_2	127.36	126.90	126.88	127.94	128.48	128.76
δ_3	128.75	128.36	128.18	128.92	129.34	129.75
δ_4	128.69	128.30	128.17	129.09	129.46	129.57
$-^1J$(C,F)[g]	170.38	170.39	169.41	164.97	163.62	162.33
^2J[f]	17.64	17.46	17.68	16.94	16.91	16.65
^3J[f]	5.98	5.93	5.98	5.78	5.74	5.70
$(-)^4J$[f]	0.85	0.92	0.94	1.41	1.41	1.57
^5J[f]	2.70	2.76	2.77	3.14	3.11	3.27

[a]4.0 mol% containing also 0.5 mol% TMS.
[b]2.3 mol%, containing also 10 mol% of C_6D_{12}, 0.5 mol% TMS, and a tiny amount of C_6F_6.
[c]4 mol%, containing also 10 mol% of C_6D_{12} and 0.5 mol% TMS.
[d]2.8 mol%, 0.5 mol% TMS, and a tiny amount of C_6F_6.
[e]In ppm relative to internal TMS, measured at 75.486 MHz.
[f]With a digital resolution of 0.003–0.005 Hz/point.
[g]With a digital resolution of 0.006–0.008 Hz/point.

TABLE 2. Internal barriers in benzyl fluoride in various solutions

Solvent	$\langle\sin^2\psi\rangle$[a]	V_2(kJ/mol)[b]	ϵ[c]	$(\epsilon-1)/(2\epsilon+1)$
C_6D_{12}	0.536(10)	0.7(2)	2.11	0.21_3
CS_2/C_6D_{12}	0.548(10)	0.9(2)	2.62	0.26_0
CCl_4/C_6D_{12}	0.550(10)	1.1(2)	2.31	0.23_3
CD_2Cl_2	0.624(12)	2.8(2)	8.76	0.41_9
Acetone-d_6	0.618(12)	2.6(2)	20.3	0.46_4
CD_3CN	0.649(12)	3.2(2)	37.4	0.48_0

[a]At 300 K, based on ^5J(C,F) in Table 1 and a $^5J_{90}$ of 5.03(13) Hz (see text). **2** is the stable form if $\langle\sin^2\psi\rangle > 0.5$.
[b]From tables of $\langle\sin^2\psi\rangle$ as a function of V_2, computed from a hindered rotor model, although a classical average yields the same results for such barriers at 300 K. The error of 0.2 kJ/mol is given as twice that implied by the error in $\langle\sin^2\psi\rangle$.
[c]The static dielectric constant, or permittivity, estimated for the solution by assuming molar additivity of the constituents, including benzyl fluoride (see text).

tubes. The latter were degassed by the freeze–pump–thaw procedure, employing at least four cycles, and were then flame-sealed. The ^{13}C nmr spectra were obtained on an AM300 spectrometer at a probe temperature of 300 K in a manner described previously (1). The digital resolution was 0.004–0.005 Hz/point.

Molecular orbital computations with partial geometry optimization (see Table 3) were performed on benzyl fluoride as a function of the angle of rotation about the C_{sp^2}—C_{sp^3} bond. The basis sets included the STO-3G, 4-21G, 4-31G, 6-31G, and 6-31G* (5*d* orbitals on each heavy atom), as described (8). The GAUSSIAN 82 computer algorithms (9) were employed on an Amdahl 5870 system. Some STO-3G MO calculations were also done for some derivatives of benzyl fluoride (Table 3).

Results and discussion

The ^{13}C nmr chemical shifts of benzyl fluoride for six solvents are presented in Table 1, as are the values of ^nJ(C,F) for n = 1–5. The signs of all but ^4J(C,F) are known (1). That of ^4J(C,F) is almost certainly negative (1), as expected on the basis of spin correlation (10, 11).

The internal barrier in CS_2/C_6D_{12} and acetone-d_6 solutions

The following argument depends on the $\sigma-\pi$ nature of ^6J(H,H) and ^6J(H,F). This matter has been discussed in detail (1) for benzyl fluoride and it is concluded that ^6J(H,H) and ^6J(H,F) are proportional to $\sin^2\theta$ and $\sin^2\psi$, respectively. To a very good approximation, therefore, one may write that $\langle\sin^2\theta\rangle = 0.75 - 0.5\langle\sin^2\psi\rangle$, angular brackets indicating expectation values. These expectation values can be had from the measured values of ^6J if ^6J is known at its extremum, that is, when θ and ψ are 90°. In the present instance, recognizing that the polar and nonpolar solutions cause different values for the two expectation values, one has two equations in two unknowns, the extrema in ^6J(H,H) and ^6J(H,F). The former is −0.452(2) and −0.409(2) Hz in CS_2/C_6D_{12} and acetone solutions, respectively (1), whereas the latter is −1.539(2) and −1.800(2) Hz in the two solutions at 300 K. Thus, for the CS_2/C_6D_{12} solution, $\langle\sin^2\theta\rangle = -0.452(2)/^6J_{90}$(H,H) and $\langle\sin^2\psi\rangle = -1.539(2)/^6J_{90}$(H,F). The ensuing relationships yield $^6J_{90}$(H,H) as −0.941(4) Hz and $^6J_{90}$(H,F) as −2.856(4) Hz. The former number is very close to the −0.95 Hz estimated by other methods and in other connections.[2] The values of $\langle\sin^2\theta\rangle$ follow as 0.480(4) and 0.435(4) in the polar and nonpolar media, respectively, whereas those of $\langle\sin^2\psi\rangle$ are 0.538(2) and 0.630(2).

Tables of expectation values as a function of the twofold barrier, derived from a hindered rotor model (15), then yield the barrier as 0.8(2) kJ/mol in the CS_2/C_6D_{12} and as 2.7(2) kJ/mol in the acetone-d_6 solution. The $\langle\sin^2\psi\rangle$ values, of course, must yield the same estimates; formally, the error estimates, at 0.1 kJ/mol, are somewhat lower than given.

Note that the minimum in the sinusoidal potential well occurs at ψ = 90°, that is, conformer **2** is the most stable in both solutions; in the liquid crystalline solvents, **2** is also most stable (7). For a vanishing barrier the expectation values are 0.5, so that **2** immediately follows as the stable conformer from the fact that $\langle\sin^2\psi\rangle$ is larger than 0.5; for a rigid conformer, **2**, $\langle\sin^2\psi\rangle$ would be unity, of course.

The analysis of the ^1H nmr and ^{19}F nmr spectra at 300 and 282 MHz, respectively, is not an easy matter (1); for example, in CS_2 solution the internal chemical shift between the *ortho* and

[2]Thus, $^6J_{90}$ depends on the electronegativity, E_X, of the substituent, X, on the methyl group and is −1.02 Hz for X = OCH_3 (12, 13) and −1.20 Hz for X = H (14). If E_H, E_O, and E_F are 2.1, 3.5, and 4.0, respectively, then a linear dependence of $^6J_{90}$ on E_X implies $^6J_{90}$ as −0.95 Hz in benzyl fluoride.

TABLE 3. Theoretical components of the internal rotational potential (in kJ/mol) for benzyl fluoride

Basis	V_2	V_4	V_6	$-E$(minimum)/au	$\langle\sin^2\psi\rangle^c$
STO-3G[a]	1.637(3)	0.074(3)	−0.068(3)	363.921 977	0.419
STO-3G[b]	1.477(4)	0.063(4)	−0.063(4)	363.922 039	0.426
4-21G[b]	15.92(3)	−0.03(3)	−0.79(3)	367.795 330	0.097
4-31G[b]	4.62(1)	−0.51(1)	−0.22(1)	368.085 500	0.300
6-31G[b]	3.22(1)	−0.56(1)	−0.21(1)	368.467 610	0.354
6-31G*[a,d]	3.16(7)	−0.87(7)	—	368.586 292	0.343
4-CH_3[a,f]	1.220(1)	0.075(1)	−0.070(1)	402.506 014	0.439
4-NH_2[a,e]	0.71	—	—	418.242 898	—
4-NO_2[a,e]	3.05	—	—	564.630 562	—
3,5-diCl[a]	2.41(2)	0.13(2)	—	1271.926 487	0.381

[a]Nuclei in the phenyl group held coplanar and the ring as a hexagon, conformer **1** (text) being stable (F in plane).
[b]Hexagonal constraint is relaxed, otherwise as in footnote *a*.
[c]At 300 K.
[d]At only 0°, 30°, 60°, and 90° for ψ, unlike the 15° intervals in ψ for the other bases; ψ is zero when the C—F bond lies in plane.
[e]At ψ = 0° and 90°, only, therefore not a true V_2.
[f]For benzyl fluoride derivatives the STO-3G basis set was used.

para protons is 0.26 Hz. However, ^5J(C,F), for example, is relatively easily measured and, as a σ−π coupling constant (1), can also be used to find V_2.

^{5}J(C,F) and the solvent dependence of V_2

In Table 1, ^5J(C,F) is tabulated for solvents of varying polarity. In the CS_2 and acetone-d_6 solvent mixtures, those for which ^6J(H,H) and ^6J(H,F) were extracted from the ^{1}H nmr and ^{19}F nmr spectra (same sample tubes), ^5J(C,F) is 2.76(1) and 3.11(1) Hz, respectively. The values of $\langle\sin^2\psi\rangle$ obtained from ^6J(H,F) above then yield $^5J_{90}$(C,F) as 5.13(3) and 4.94(3) Hz for the two solutions. The mean, 5.03 ± 0.13 Hz, is in reasonable agreement with that of 5.2 ± 0.3 Hz, deducible from a rigid model compound, 1-fluorindan (3). The error in $^5J_{90}$, at less than 3%, assumes that ^5J(C,F) is a pure σ−π parameter, that is, that it is proportional to $\sin^2\psi$.

The values of $\langle\sin^2\psi\rangle$ then follow for the solutions in Table 1 and are given in Table 2, which also reports the twofold barriers. In all solutions, including that with the least polar C_6D_{12} as solvent, the most stable conformer is **2**. The internal barrier drops from 3.2(2) kJ/mol in the polar CD_3CN environment to 0.7(2) kJ/mol in C_6D_{12}.

The barrier of 0.3 ± 0.02 kJ/mol found in the liquid crystal solvent, 1-(3-fluoro-4′-ethylbiphenyl)-2-(4-*n*-pentylphenyl) ethane (7), is perhaps in reasonable congruence with that of 0.7(2) kJ/mol in C_6D_{12}, derived from ^5J(C,F).

Extrapolation to the vapor phase

The size of V_2 (Table 2) appears to be determined predominantly by the dielectric constant or polarity of the solvent, probably modified by some specific molecular interactions. Qualitatively, because the dipole moment of conformer **2** is most likely larger than that of **1** (1), the higher stability of **2** in the more polar solvents is expected on the basis of a dielectric continuum model based on the reaction field (16). The most straightforward application of that model to the present data (see eq. 13.18 and the discussion on p. 562 of ref. 16) assumes a linear dependence of V_2 on $(\epsilon - 1)/(2\epsilon + 1) \equiv x$, where ϵ is the dielectric constant of the medium. Allowing for the error of 0.2 kJ/mol in the V_2 values, the result is that V_2(kJ/mol) = $-1.14(36) + 8.77(99)x$, with a correlation coefficient of 0.976. The quantity, x, in Table 2 is estimated on the assumption of molar additivity of the dielectric constants of the solution components, including benzyl fluoride. The effective dielectric constant of the latter appears to be similar to that of chloroform, judging by the value (1) of ^5J(C,F). Actually, if the dielectric constant of the solution is taken as that of the major constituent, a very similar value, −0.97(34) kJ/mol, is obtained for V_2 in the vapor phase, that is, when $x = 0$.

For the free molecule (unclustered) one has the result that **1** is now the most stable conformer (negative sign in the linear relationship) and that the twofold barrier is 1.1(7) kJ/mol, where the doubling of the standard error is meant to allow for uncertainties in x and other small corrections (16) to the model. This result should be of interest to microwave, infrared, and other spectroscopists. It may be noted that in 3-fluoropropene the most stable conformer in the vapor phase also has the C—F bond lying *cis* to the double bond and in the plane of the molecule (17, 18) and that in the liquid the stability of this conformer decreases relative to other conformers.

^{4}J(C,F) as a check on V_2

A previous discussion (1) of ^4J(C,F) asserts that ^4J(C,F) = $^4J^\pi\langle\sin^2\psi\rangle + {}^4J^\sigma\langle\sin^2(\psi/2)\rangle$; the σ−π component, $^4J^\pi$, is negative while the σ electron component is positive. For a barrier consisting of evenfold components, the multiplier of $^4J^\sigma$ is 0.5. If the values of ^4J(C,F) for the C_6D_{12} and CD_3CN solutions are used in this equation, then $^4J^\pi$ follows as −6.37 Hz and $^4J^\sigma$ as 5.13 Hz.[3] This parametrization reproduces ^4J(C,F) for the other solutions (using again the $\langle\sin^2\psi\rangle$ values in Table 2) to within a mean deviation of 0.01 Hz. Furthermore, for 3,5-dichlorobenzyl fluoride, the ^5J(C,F) of 2.0 Hz in CS_2 solution (1) entails a ^4J(C,F) of 0.0 Hz and, indeed, this coupling constant appears to vanish (1). Hence the ^4J(C,F) numbers are consistent with the conformational conclusions based on ^6J(H,H), ^6J(H,F), and ^5J(C,F).

^{1}J(C,F), ^{2}J(C,F), and ^{3}J(C,F)

^1J(C,F) varies considerably (Table 1) and correlates reasonably well (r = 0.967) with the dielectric function, x. For unit dielectric constant, ^1J(C,F) extrapolates as −176.9(9) Hz, much different from its value of −162.3 Hz in acetonitrile

[3]It follows that ^4J(C,F) will become positive if **1** is sufficiently stable, that is, if $\langle\sin^2\psi\rangle < 0.4$, corresponding to a barrier of 2.0 kJ/mol or more.

Can. J. Chem. Downloaded from www.nrcresearchpress.com by 91.144.44.67 on 09/07/12
For personal use only.

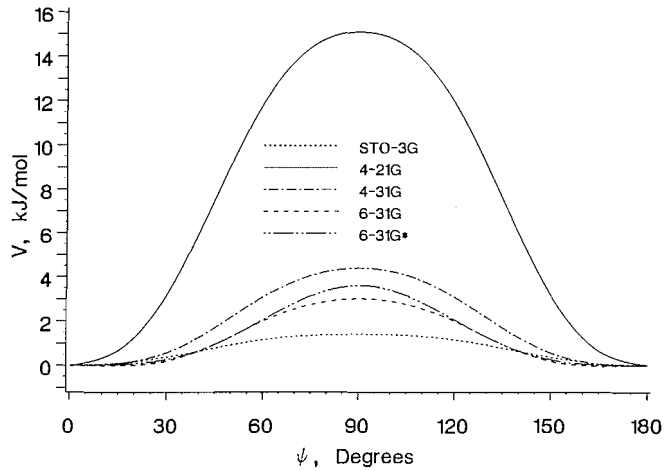

FIG. 1. The internal rotational potentials, obtained from the various basis sets (Table 3), are plotted against the angle, ψ, by which the C—F bond of benzyl fluoride twists out of the plane of the phenyl group. The minimal basis set agrees best with the experimental estimates described in the text.

solution. A possible experiment could involve the preparation of benzyl fluoride-α-^{13}C and the measurement of ^1J(C,F) in the vapor phase via ^{19}F nmr. If the vapor were dense, it would be necessary to know its dielectric constant.

^2J(C,F) correlates at least as well with x as does ^1J(C,F) and is predicted to be 18.4(1) Hz in a medium of unit dielectric constant. ^3J ($r = 0.992$) extrapolates to 6.21(2) Hz at $x = 0$ and, as a Karplus-like coupling constant, is expected to be largest in a planar conformation (1); hence its larger value in the gas phase.

Molecular orbital computations

Table 3 presents the n-fold components of the theoretical potential, V/kJ mol^{-1} = $\Sigma_n V_n \sin^2 n(\psi/2)$, where ψ is the angle by which the C—F bond twists out of the phenyl plane. The quoted errors are the standard deviations in the fits to seven computed energies, at intervals of 15° in ψ. Conformer **1**, with the C—F bond in the phenyl plane, is computed as most stable with all five basis sets. The computed relative stability of **1**, however, varies considerably from basis to basis, the minimal basis set corresponding to the lowest, essentially twofold, barrier at 1.4 kJ/mol; this value is closest to the experimental estimate above. A similar situation holds for the computations of the internal rotational potential for benzaldehyde, for which the minimal basis set agrees best with experiment (19), while the split-valence bases, including the one with polarization functions, 6-31G*, imply much too large a magnitude for the barrier; furthermore, the larger split-valence bases approach most closely the value predicted with the minimal basis. As can be seen in Table 3, relaxation of the hexagonal constraint does not drastically alter the computed potential for the STO-3G basis. The cpu time for the calculations on benzyl fluoride was over 215 h, so that the hexagonal constraint was retained for the 6-31G* optimizations.

The minimal basis set suggests a predominantly twofold barrier, equal in magnitude, within experimental error, to that obtained above by extrapolation from the solution state. The smallest barrier, obtained from the most complete geometry optimization with this basis, is 1.41 kJ/mol (V_4 does not contribute to the height of barrier whereas V_6 contributes negatively). Omission of the small fourfold and sixfold components in Table 3 alters the value of $\langle \sin^2 \psi \rangle$ at 300 K by only as much as 0.004, except for the 6-31G* results where the larger V_4 component increases it by 0.01.

The large barrier of over 15 kJ/mol at the 4-21G level of theory is rejected on the basis of the experimental results. A significant negative fourfold component, amounting to as much as 20% of the twofold in magnitude, is predicted with

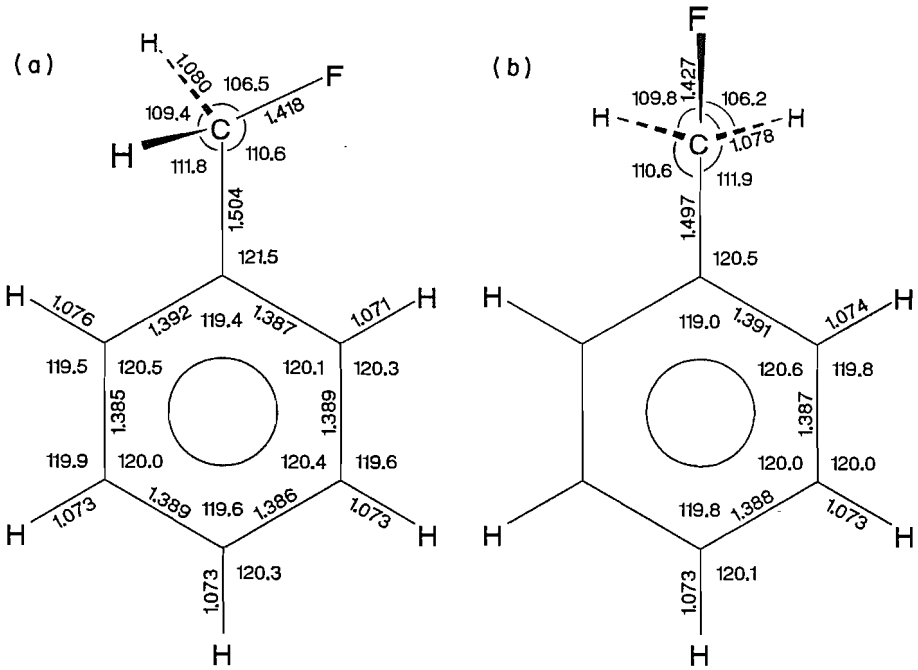

FIG. 2. The geometries of the (a) planar and (b) perpendicular conformers of benzyl fluoride are shown and were obtained with the 6-31G basis set, the largest for which the carbon atoms of the phenyl group were not constrained to a regular hexagon. The geometry of the side chain is somewhat different when computed with the 6-31G* basis, particularly the C—F bond length; see Table 4. During the geometry optimization procedures, the exocyclic C—C bond was constrained to lie in the phenyl plane.

Can. J. Chem. Downloaded from www.nrcresearchpress.com by 91.144.44.67 on 09/07/12
For personal use only.

TABLE 4. The computed side-chain geometry and the dipole moment of benzyl fluoride in the planar and perpendicular conformations as given by various basis sets

	STO-3G[b,c]		4-21G		4-31G		6-31G		6-31G*	
Parameter[a]	0°	90°	0°	90°	0°	90°	0°	90°	0°	90°
r(C—F)	1.384	1.389	1.409	1.413	1.415	1.424	1.418	1.427	1.368	1.374
r(C—H)	1.100	1.099	1.081	1.079	1.077	1.077	1.080	1.078	1.083	1.082
r(C—C)	1.541	1.538	1.509	1.507	1.502	1.495	1.504	1.497	1.510	1.506
$\angle C_2C_1C_\alpha$[d]	120.7	120.5	119.9	120.5	121.3	120.5	121.5	120.5	121.1	120.0
∠CCF	111.9	111.3	109.8	111.4	110.6	110.6	110.6	110.6	111.2	110.7
∠CCH	109.7	109.7	110.9	110.5	111.7	111.8	111.8	111.9	110.9	111.1
∠HCH	107.0	107.8	109.1	108.8	109.5	109.8	109.4	109.8	108.9	108.9
∠HCF	109.4	109.2	108.1	107.8	106.6	106.3	106.5	106.2	107.6	107.4
μ	1.063	1.197	2.003	2.405	2.334	2.776	2.349	2.780	1.737	2.102

[a]Bond lengths in angstroms, bond angles in degrees, and dipole moments in debyes.
[b]The planar conformation with the C—F bond in the phenyl plane is defined by 0°.
[c]For all but the 6-31G* basis, all bond angles and lengths are optimized. For the polarized basis, the carbon atoms of the phenyl group are constrained to a regular hexagon.
[d]As in Fig. 1.

the larger basis sets. Because $(2V_2 + 8V_4) > 0$, there is no computed barrier to planarity, that is, conformer **1** represents the minimum in the internal potential. The height of the barrier is 3.0 and 3.6 kJ/mol, respectively, according to the 6-31G and 6-31G* bases. In our opinion these magnitudes are too large and, furthermore, at present no experimental evidence exists for sizeable, higher than twofold, components of the barrier. Figure 1 displays the computed internal potential curves for the various basis sets.

It does not follow, of course, that the large basis sets do not yield reasonably reliable equilibrium geometries for the conformers of benzyl fluoride. Figure 2 displays the geometries of conformers **1** and **2**, as computed with the 6-31G basis. Table 4 displays the side-chain geometries of the planar and perpendicular conformers as obtained from the various basis sets. Judging from a recent comparison (21) of geometries from various basis sets, the geometry of the side chain in benzyl fluoride should be further refined at the MP2 level of corrections for electron correlation. Some comparisons with experimental data go as follows. It is deduced (22) from microwave data that the C—F bond length in ethyl fluoride is 1.383(7) Å, while the HCF angle is 107.3(4)°; the latter value is close to that found with the 6-31G* basis. Again, the HCH angle is 108.8°, as deduced from the nmr studies in nematic solutions (7), very close to the 6-31G* results. However, the former have the CCF angle as 105.3° (7), the latter giving 110.7°. It may be that this angle would increase from 105.3° were the C—C_α bond taken as rather shorter than the 1.54 Å assumed in the experimental work.

Of all the computed dipole moments in Table 4, those obtained from the polarized basis with the usual Mulliken procedure best fit the experimental value of 1.77(5) D; the latter refers to a benzene solution at 298 K (23).

The perturbation of the internal rotational potential by ring substituents was simulated by a limited set of computations, also presented in Table 3, employing the STO-3G basis. Substantial perturbations are predicted, the π electron donor, the amino group at the *para* position, causing a reduction in V_2 whereas the 4-nitro, electron-accepting substituent, increases V_2. The *meta* chlorine substituents also enhance V_2. The most simple rationalization is that the electrostatic stabilization of the planar conformer, **1**, by attraction of the C^+—F^- to the *ortho* C^-—H^+ bond (20), is enhanced by the electronegative chlorine and nitro substituents but reduced by the amino and methyl groups; the latter may well reduce the polarity of the C—H bond. That **1** is indeed stabilized in 3,5-dichlorobenzyl fluoride has been demonstrated for a CS_2 solution (1).

The computations imply that each benzyl fluoride derivative will have its own, significantly distinct, internal rotational potential. The experimental results for benzyl fluoride imply a medium effect on each rotational potential. Hence such compounds present a challenge to the various spectroscopies in the vapor and liquid states.

1. T. SCHAEFER, J. PEELING, and R. SEBASTIAN. Can. J. Chem. **63**, 3219 (1985).
2. R. J. ABRAHAM, R. A. HEARMON, M. TRAETTEBERG, and P. BAKKEN. J. Mol. Struct. **57**, 149 (1979).
3. W. ADCOCK and A. N. ABEYWICKREMA. Aust. J. Chem. **33**, 181 (1980).
4. C. BÉGUIN and R. DUPEYRE. J. Magn. Reson. **44**, 294 (1981).
5. R. DUPEYRE and C. BÉGUIN. J. Chim. Phys. **78**, 363 (1981).
6. R. T. C. BROWNLEE and D. J. CRAIK. Tetrahedron Lett. **21**, 1681 (1980).
7. G. CELEBRE, G. DELUCA, M. LONGERI, and J. W. EMSLEY. Mol. Phys. **67**, 239 (1989).
8. W. J. HEHRE, L. RADOM, P. V. R. SCHLEYER, and J. A. POPLE. *Ab initio* molecular orbital theory. Wiley and Sons, New York. 1986.
9. J. S. BINKLEY, M. J. FRISCH, D. J. DEFREES, K. RAGHAVACHARI, R. A. WHITESIDE, H. B. SCHLEGEL, E. M. FLUDER, and J. A. POPLE. GAUSSIAN 82. Department of Chemistry, Carnegie–Mellon University, Pittsburgh, PA.
10. H. M. MCCONNELL. J. Chem. Phys. **30**, 126 (1959).
11. T. SCHAEFER, K. MARAT, J. PEELING, and R. P. VEREGIN. Can. J. Chem. **61**, 2779 (1983).
12. R. LAATIKAINEN. Magn. Reson. Chem. **24**, 588 (1986).
13. R. LAATIKAINEN and K. TUPPURAINEN. J. Chem. Soc. Perkin Trans. **2**, 121 (1987).
14. T. SCHAEFER, R. SEBASTIAN, and G. H. PENNER. Can. J. Chem. **63**, 2597 (1985).
15. W. J. E. PARR and T. SCHAEFER. Acc. Chem. Res. **13**, 400 (1980).
16. R. J. ABRAHAM and E. BRETSCHNEIDER. *In* Internal rotation in

Can. J. Chem. Downloaded from www.nrcresearchpress.com by 91.144.44.67 on 09/07/12
For personal use only.

molecules. *Edited by* N. J. Orville-Thomas. Wiley and Sons, New York. 1974. Chap. 13.
17. J. R. DURIG, M. ZHEN, and T. S. LITTLE. J. Chem. Phys. **81**, 4259 (1984).
18. J. R. DURIG, M. ZHEN, H. L. HEUSEL, P. J. JOSEPH, P. GRONER, and T. S. LITTLE. J. Phys. Chem. **89**, 2877 (1985).
19. G. H. PENNER, P. GEORGE, and C. W. BOCK. J. Mol. Struct. (Theochem), **152**, 201 (1987).
20. G. H. PENNER, T. SCHAEFER, R. SEBASTIAN, and S. WOLFE. Can. J. Chem. **65**, 1845 (1987).
21. H. GUO and M. KARPLUS. J. Chem. Phys. **91**, 1719 (1989).
22. P. NOSBERGER, A. BAUDER, and Hs. H. GÜNTHARD. Chem. Phys. **1**, 418 (1973).
23. M. T. ROGERS. J. Am. Chem. Soc. **69**, 457 (1947).

Can. J. Chem. Downloaded from www.nrcresearchpress.com by 91.144.44.67 on 09/07/12
For personal use only.

Oxidation products of 5-ethenyl-4-methyl-3-pyridinecarbonitrile and 2- and 4-methylpyridines

JAHANGIR, JIAN WANG, RICHARD W. SMITH, AND DAVID B. MACLEAN[1]
Department of Chemistry, McMaster University, Hamilton, Ont., Canada L8S 4M1
AND
HERBERT L. HOLLAND
Department of Chemistry, Brock University, St. Catharines, Ont., Canada L2S 3A1

Received August 24, 1989

JAHANGIR, JIAN WANG, RICHARD W. SMITH, DAVID B. MACLEAN, and HERBERT L. HOLLAND. Can. J. Chem. **68**, 587 (1990).

The anion of 5-ethenyl-4-methyl-3-pyridinecarbonitrile **1** undergoes oxidative coupling on treatment with dibenzoyl peroxide affording 1,2-bis-(5′-ethenyl-3′-cyano-4′-pyridyl)-ethane, **2**. It is also shown that the anions of 2- and 4-methylpyridine undergo oxidative coupling. In the latter case, however, the coupling reaction is accompanied by addition to the carbonyl group of dibenzoyl peroxide. The addition products have been identified as phenacyl pyridines and dipicolyl phenyl carbinols. The ethenyl side chain of **1** has been hydrated by way of the oxymercuration–reduction process and the secondary alcohol oxidized to a ketone. Both the alcohol and ketone in protected form are potentially useful intermediates in alkaloid synthesis.

Key words: oxidative coupling, 2- and 4-methylpyridines, dibenzoyl peroxide, oxymercuration–reduction.

JAHANGIR, JIAN WANG, RICHARD W. SMITH, DAVID B. MACLEAN et HERBERT L. HOLLAND. Can. J. Chem. **68**, 587 (1990).

Sous l'action du peroxyde de dibenzoyle, l'anion du 5-éthènyl-4-méthyl-3-pyridinecarbonitrile (**1**) subit un couplage oxydant conduisant au 1,2-bis-(5′-éthènyl-3′-cyano-4′-pyridyl)-éthane (**2**). On a aussi démontré que les anions des 2- et 4-méthylpyridines subissent des couplages oxydants. Dans ces derniers cas, la réaction de couplage est accompagnée d'une addition sur le groupement carbonyle du peroxyde de dibenzoyle. On a identifié les phénacylpyridines et les dipicolylphénylcarbinols comme produits d'addition. La chaîne latérale de produit **1** a été hydratée par le biais d'une réaction d'oxymercuration suivie d'une réduction et l'alcool secondaire ainsi obtenu a été oxydé en cétone. Les formes protégées de l'alcool ainsi que la cétone sont des intermédiaires qui peuvent s'avérer utiles dans des synthèses d'alcaloïdes.

Mots clés : couplage oxydant, 2- et 4-méthylpyridines, peroxyde de dibenzoyle, oxymercuration–réduction

[Traduit par la revue]

Can. J. Chem. Downloaded from www.nrcresearchpress.com by 91.144.44.67 on 09/07/12
For personal use only.

The synthesis of 5-ethenyl-4-methyl-3-pyridinecarbonitrile **1** was reported by Govindachari *et al.* (1) in 1957 and was used by them in the synthesis of gentianine. Some years later Kametani *et al.* (2) prepared **1** using a slightly different procedure, and converted it to gentianine and to 5-ethenyl-1-oxo-1*H*-pyrano[3,4-*c*]pyridine-3-carboxylic acid ethyl ester. The latter compound was used in the synthesis of the indole alkaloid, angustine. We have found that **1**, as its anion, is an effective intermediate for the synthesis of several benzopyridoquinolizines (3) and indolopyridoquinolizines (3*a*, 4), including a number of alkaloids of each ring system as illustrated in Scheme 1 for the former group of compounds. We describe here other transformations of **1**, namely, the oxidative coupling of its anion upon treatment with dibenzoyl peroxide to give 1,2-bis(3′-cyano-5′-ethenyl-4′-pyridyl)-ethane **2**, and the conversion of **1** to 5-(1′-hydroxyethyl)-4-methyl-3-pyridine carbonitrile **3** and to 5-acetyl-4-methyl-3-pyridinecarbonitrile **4**. We show also that the anions of 2- and 4-methylpyridine undergo oxidative coupling upon treatment with dibenzoyl peroxide and that the coupling reaction is accompanied by formation of phenacyl pyridines and dipicolyl phenyl carbinols.

Results and discussion

Oxidative coupling

The oxidative coupling of the lithium salt of **1** to give 1,2-bis-(3′-cyano-5′-ethenyl-4′-pyridyl)-ethane **2** upon treatment with dibenzoyl peroxide was discovered in the course of experiments directed toward the synthesis of **5**. We had investigated a variety of methods for converting the methyl group of **1** to CH_2OH in order to prepare **5**. Azaphthalides of this type were used previously to prepare the benzopyridoquinolizine ring system (5). Initially an attempt was made to prepare the alcohol by way of a halide. However, the introduction of a halogen using *N*-bromosuccinimide under a variety of reaction conditions was unsuccessful. Similarly, attempts to halogenate the lithium salt of **1** with chlorine or bromine failed. In an attempt to introduce a benzoate group we treated the lithium salt of **1** with dibenzoyl peroxide but only traces of benzoate ester were formed. Instead, the major product was the coupled product **2** formed in an overall yield of 77% based on **1**. The structure of **2** is based upon its spectroscopic properties. The mass spectrum has a molecular ion at m/z 286 at twice the mass of the starting anion. The ^{1}H nmr spectrum of **2** shows the same number of signals as the starting material **1** reflecting the symmetrical character of the product. The C-methyl signal present in the spectrum of **1** is absent in the "dimer", **2**. However, a new signal is present at δ 3.22, which is ascribed to the newly formed methylenes joining the two pyridine rings.

Under the same reaction conditions as those used to prepare **2** we have shown that the lithium salts of 2-methylpyridine and 4-methylpyridine also form dimeric products. The properties of the products of these reactions, namely, 1,2-bis-(2′-pyridyl)-ethane **6** (6) and 1,2-bis-(4′-pyridyl)-ethane **7** (7), agree with those described in the literature. The mechanism of the coupling reaction has not been studied but it is likely that it proceeds by a free radical mechanism.

The initial experiments were conducted using equimolar amounts of dibenzoyl peroxide and lithium salt. However, the

[1]Author to whom correspondence may be addressed.

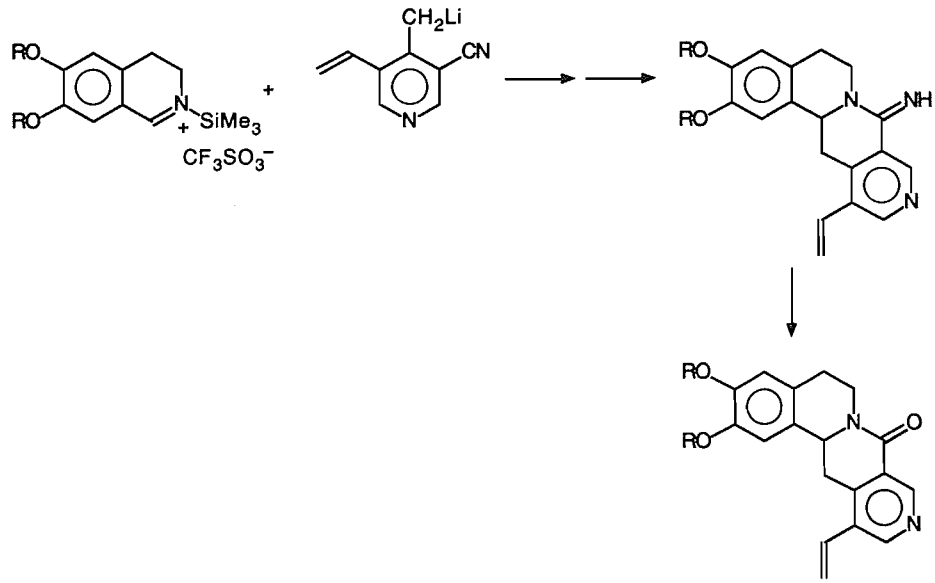

SCHEME I

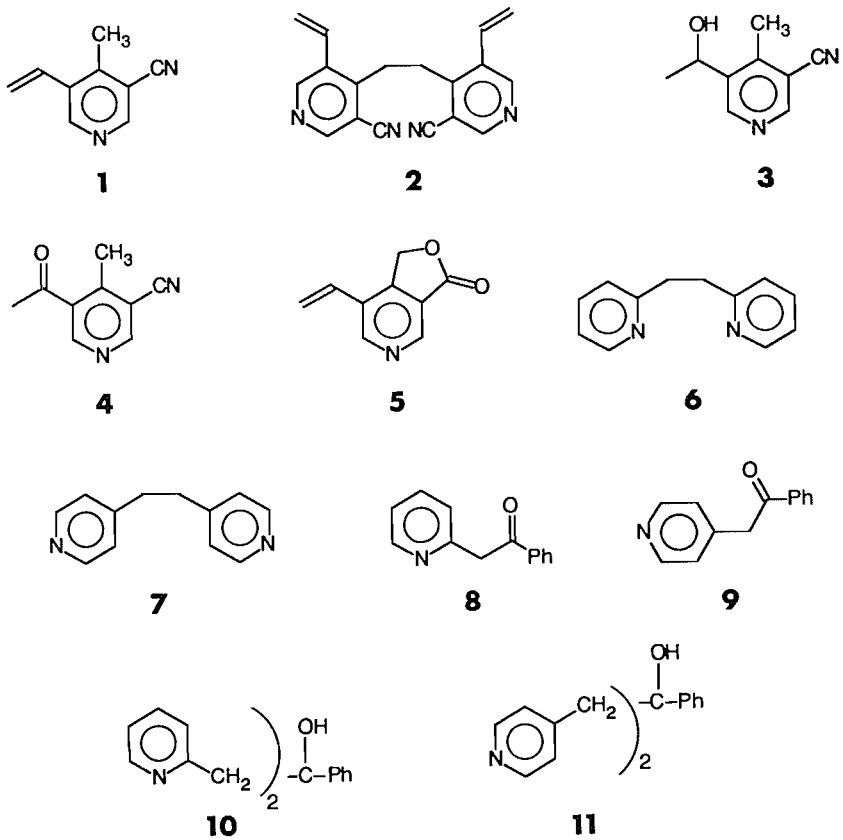

coupling reaction proceeds equally well with a molar ratio of lithium salt to dibenzoyl peroxide equal to 2:1 as shown in eq. [1]. Benzoic acid was recovered from the reaction mixtures in a yield roughly equivalent to that of the coupled products when the molar ratio of starting materials was 2:1.

[1] $2\ ArCH_2Li + C_6H_5CO_2O_2CC_6H_5 \rightarrow ArCH_2CH_2Ar + 2\ C_6H_5CO_2Li$

Ar = 2-pyridyl, 4-pyridyl, or 3-cyano-5-ethenyl-4-pyridyl

Additional products isolated from the reactions of the lithium salts of 2-methylpyridine and 4-methylpyridine with dibenzoyl peroxide were identified as the respective phenacylpyridines, **8** and **9**, and the bis-1,3-dipyridyl-2-phenyl-2-propanols, **10** and **11**. The spectroscopic properties of the compounds isolated in these reactions were identical with those of reference samples prepared here (see experimental section for details). The ketones may arise from the reaction of the lithium salts of the picolines with the lithium salts of benzoic acid (see eq. [1]) as illustrated in eq. [2].

However, the alcohols are unlikely to be derived from ketones **8** and **9**. It has been stated that intermediates of type (a) are stable and are converted to ketones only on hydrolysis (8).

Can. J. Chem. Downloaded from www.nrcresearchpress.com by 91.144.44.67 on 09/07/12
For personal use only.

Can. J. Chem. Downloaded from www.nrcresearchpress.com by 91.144.44.67 on 09/07/12
For personal use only.

[2] $C_6H_5CO_2Li + ArCH_2Li \rightarrow$ 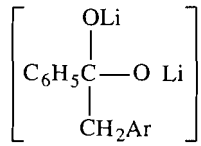

(a)

$\xrightarrow{H_2O}$ $C_6H_5COCH_2Ar + 2LiOH$

8, Ar = 2-pyridyl
9, Ar = 4-pyridyl

Moreover, if the ketones were to form in the reaction mixture it is known that they form enols with lithio reagents in preference to undergoing addition to the carbonyl group (9).

It is possible therefore that the alcohols form as a result of addition of the lithium reagent to the carbonyl group of dibenzoyl peroxide, followed by a substitution reaction as shown in eq. [3]. Such a mechanism has been proposed for the synthesis of alcohols from acid chlorides (10).

Ketones **8** and **9** might also be derived from hydrolysis of intermediate (b) of eq. [3].

[3] $ArCH_2Li + C_6H_5CO_2O_2CC_6H_5 \rightarrow$

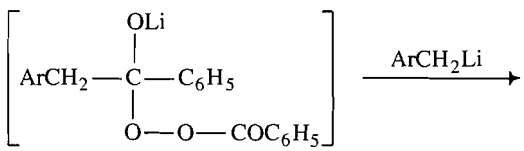

$\xrightarrow{ArCH_2Li}$

(b)

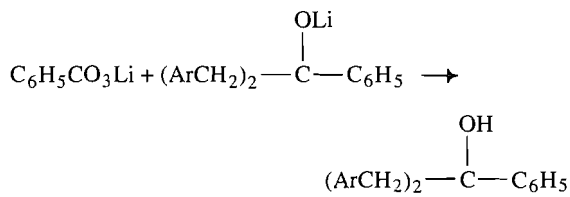

10, Ar = 2-pyridyl
11, Ar = 4-pyridyl

The coupling of lithium salts of methyl pyridines has been previously effected with a variety of reagents. For example, coupling has been reported by treatment of solutions of lithio 2-methylpyridine with air (11), oxygen (6), bromine (12), and CuCl or $CuBr_2$ (13). Recently, it has been shown that lithio 2,6-di-*tert*-butyl-4-methylpyridine undergoes coupling upon treatment with iodine (14). The last two procedures provide coupled products in yields comparable to those obtained with dibenzoyl peroxide.

*Oxymercuration–reduction of the vinyl side chain: preparation of alcohol **3** and ketone **4***

The preparation of benzopyridoquinolizine alkaloids bearing a vinyl side chain on the pyridine ring is illustrated in Scheme 1. Alkaloids are known in which the vinyl side chain has been replaced by a CH_3CHOH- or a CH_3CO- side chain. The latter alkaloids have not been prepared by the route outlined in Scheme 1, although syntheses by other approaches have been reported (15). We have been able to effect the hydration of the vinyl group of **1** to CH_3CHOH- using the oxymercuration–reduction method developed by Brown and Geoghegan (16) and to oxidize the latter compound to the methyl ketone. In the course of this work we found that variable and often poor yields of the desired alcohol were obtained when the reduction step was carried out in a flask open to the atmosphere. Besides the desired secondary alcohol, small amounts of glycol were obtained. The replacement of the HgX group by an OH group, required for glycol formation, was reported previously and is attributed to the formation of peroxy compounds in the hydride reduction step (17, 18). The oxymercuration step is considered to proceed by an ionic mechanism but the reduction step by a radical mechanism. The carbon radicals formed in the reduction of the carbon–mercury bond will react with oxygen in the medium to generate peroxides, which are reduced to alcohols. Other more complex products were apparently formed from the radical intermediate but were not identified. Much better results were obtained by us when the reduction reaction was conducted in an argon atmosphere. Under these conditions reproducible yields of 50% of **3** were obtained and very little glycol was formed.

The ketone **4** was derived from alcohol **3** by Jones' oxidation in a yield of 77%. Therefore the way is now open to the synthesis of benzopyridoquinolizine and indolopyridoquinolizine alkaloids containing an oxygenated side chain using these two starting materials in suitably protected form. Furthermore, the opportunity now exists to prepare enantiomerically pure alcohol **3** from ketone **4**. This may open the was to enantioselective synthesis of alkaloids by the route of Scheme 1.

Experimental

Apparatus, materials, and methods

The ^1H nmr spectra were recorded on a Varian EM 390 spectrometer. Unless otherwise specified, the samples were dissolved in chloroform-*d* using tetramethylsilane (TMS) as internal standard. Chemical shifts, quoted as δ values, were measured in relation to TMS. The symbols s, singlet, d, doublet, t, triplet, q, quartet, br, broad, and m, multiplet are used in reporting spectra. The ^{13}C nmr spectra were recorded at 125.76 MHz on a Bruker WM 500 FT spectrometer at ambient temperature.

EI mass spectra were recorded at 70 eV with a source temperature of ca. 200°C on a VG Analytical ZAB-E mass spectrometer equipped with a VG 11-250J data system. High resolution mass spectra (hrms) were recorded on the same instrument. Samples were introduced with a direct insertion probe. Infrared spectra were run on a Perkin–Elmer 283 spectrometer. Melting points were determined using a Gallenkamp apparatus and are uncorrected. Thin-layer chromatography (tlc) was performed using Polygram Sil G/UV_{254} or Polygram Alox N/UV_{254} plates. For flash column chromatography Kieselgel 60 (230–400 mesh) was used.

Compound **1** was prepared using the literature procedure (1). Reference samples of **9** and **11** were prepared by a modification of the procedure of Fryer *et al.* (10) in which *n*-BuLi was used instead of phenyl lithium to generate the picolyl lithium. Compounds **8** and **10** were prepared from 2-methylpyridine in a similar manner.

*1,2-Bis(3'-cyano-5'-vinyl-4'-pyridyl)-ethane **2***

To a stirred solution of diisopropylamine (0.31 mL, 2.2 mmol) in dry THF (2 mL) at −20°C was added a solution of *n*-BuLi (1.37 mL, 1.6 M in hexane, 2.2 mmol) under an argon atmosphere; the resulting LDA solution was stirred at this temperature for a further 10 min. The LDA solution was cooled to −78°C (Dry Ice – acetone bath) and treated dropwise with a solution of compound **1** (288 mg, 2 mmol) in dry THF (3 mL), producing a red solution. The mixture was stirred at −78°C for 20 min, and then treated dropwise with a solution of dibenzoyl peroxide (484 mg, 2 mmol) in dry THF (3 mL). The red colour of the solution was completely discharged at the end of the addition, and stirring of the mixture was continued at −78°C for a further 2 h; it was then allowed to warm to room temperature and stirred overnight. The reaction mixture was then treated with 10% aqueous sodium sulphite solution (1 mL)

Can. J. Chem. Downloaded from www.nrcresearchpress.com by 91.144.44.67 on 09/07/12
For personal use only.

and concentrated to a thick paste under vacuum. The residue was basified with saturated Na_2CO_3 solution (aqueous) and thoroughly extracted with chloroform. The combined chloroform extract was washed with saturated sodium chloride, dried over anhydrous Na_2SO_4, and evaporated to dryness. The crude product was purified by column chromatography on silica gel using hexane–CH_2Cl_2 (1:1) as eluant to give the dimeric compound **2** (220 mg, 77%), which was crystallized from acetone; mp 189–191°C; R_f 0.33 (alumina, $CHCl_3$); ^{1}H nmr (90 MHz), δ: 3.22 (4H, s, -CH_2CH_2-), 5.60 (1H, d, J = 11.5 Hz, -CH=CH_2), 5.80 (1H, d, J = 18.0 Hz, -CH=CH_2), 7.05 (1H, dd, J = 18.0 and 11.5 Hz, -CH=CH_2), 8.80 (1H, s, C-6′, or C-2′ H), and 8.90 (1H, s, C-2′ or C-6′ H); ms (EI), m/z (rel.int., %): 286 (81), 285 (76), 272 (22), 271 (100), 258 (14), 253 (13), 149 (16), 143 (46), 142 (38), and 116 (18). Anal. calcd. for $C_{18}H_{14}N_4$: C 75.52, H 4.90, N 19.58%; found: C 75.10, H 5.24, N 19.63%.

Treatment of 2-picolyl lithium with dibenzoyl peroxide

A solution of diisopropylamine (0.68 mL, 4.8 mmol) in THF (4.0 mL) was treated dropwise with stirring with *n*-BuLi (3.0 mL, 1.6 M in hexane, 4.8 mmol) at −20°C, and kept at this temperature for 10 min. The solution was then cooled to −78°C, 2-picoline (372 mg, 4 mmol) in THF (5 mL) was added dropwise, and the mixture stirred for 20 min at −78°C. A solution of dibenzoyl peroxide (484 mg, 2 mmol) in THF (5 mL) was added dropwise, the mixture was stirred at −78°C for 2 h, allowed to warm to room temperature, and stirred overnight before work-up. The reaction mixture was treated with a 10% aqueous solution of concentrated sodium sulphite, then with aqueous sodium carbonate, and extracted with dichloromethane. The extract was washed with saturated sodium chloride solution, dried over anhydrous sodium sulphate, and evaporated to give a residue, which was chromatographed on alumina (16 g). Elution with methylene chloride – cyclohexane (1:1) gave, in order of elution: compound **8**[2] (0.084 g, 11%), mp 52–54°C (lit. (9) mp 52–54°C; lit. (10) mp 59–60°C); ir (ν_{max}, $CDCl_3$): 1600, 1625, 1680 cm^{-1}; ^{1}H nmr (90 MHz) included signals at δ: 4.50 (s, CH_2), 6.06 (s, enolic -CH=), and 6.8–8.6 (m, aromatic hydrogens); ms (EI), m/z (rel.int., %): 197 (15), 196 (20), 169 (30), 168 (36), 120 (8), 105 (100), 92 (13), and 77 (68); compound **10** (0.058 g, 7%), mp 79–80°C (hexane) (lit. (19) mp 59°C); ir (ν_{max}, Nujol): 1590, 3300 cm^{-1}; ^{1}H nmr (90 MHz), δ: 3.2 and 3.4 (4H, overlapping ABq, J = 15 Hz, α-CH_2), 6.9–7.6 (11H, m, aromatic hydrogens), and 8.4 (2H, overlapping d, pyridyl α-H's); ms (NH_3CI), m/z (rel.int., %): 291 (33), 198 (100); compound **6** (0.143 g, 39%), mp 44–46°C (ethyl acetate – hexane) (lit. (6) mp 48–49°C); ^{1}H nmr (90 MHz), δ: 3.25 (4H, s, -CH_2-), 7.00–7.65 (6H, m, aromatic H's), and 8.53 (2H, d, pyridyl α-H's); ms (EI), m/z (rel.int., %): 184 (48), 183 (30), 169 (6), 106 (100), 92 (16), 91 (6), 78 (15).

Treatment of 4-picolyl lithium with dibenzoyl peroxide

The procedure described above for 2-picoline was followed and gave the following, in order of elution: compound **9** (0.026 g, 3%), mp 110–112°C (lit. (10) mp 113–115°C), ir (ν_{max}, Nujol): 1685 cm^{-1}; ^{1}H nmr (90 MHz), δ: 4.28 (2H, s, CH_2), 7.1–8.1 (7H, m, aromatic hydrogens), and 8.52 (2H, m, pyridyl α-H's); ms (EI), m/z (rel.int., %): 197 (8), 105 (100), 77 (42); compound **7** (0.15 g, 41%), mp 104–106°C (lit. (7*a*) mp 106–109°C; (7*b*) mp 110–111°C; (7*c*) mp 114.5–116°C); ^{1}H nmr (90 MHz), δ: 2.95 (4H, s, -CH_2's). 7.03–7.20 (4H, m, C-3′ H's), and 8.50–8.64 (4H, m, C-2′ H's); ms (EI), m/z (rel.int., %): 184 (100), 92 (64), 65 (33); compound **11** (0.075 g, 13%), mp 118–120°C (lit. (10) quotes various samples as melting from 92–99°C to 166–168°C, including one sample with mp 117–118°C ir (ν_{max}, Nujol): 1620, 3200 cm^{-1}; ^{1}H nmr (90 MHz), δ: 3.06, 3.28 (4H, ABq, -CH_2's), 6.86 (4H, d, pyridyl β-H's), 7.25 (5H, s, phenyl H's), and 8.28 (4H, d, pyridyl α-H's); ms (EI), m/z (rel.int., %): 290 (4), 289 (7), 198 (32), 105 (100), 92 (17), 77 (78), 65 (18).

Preparation of 5-(1′-hydroxyethyl)-4-methyl-3-pyridinecarbonitrile **3** *and 5-(1′,2′-dihydroxyethyl)-4-methyl-3-pyridinecarbonitrile*

Mercuric acetate (2.39 g, 7.5 mmol) was dissolved in water (7.5 mL) and THF (17.5 mL) was added to this solution. A solution of vinyl compound **1** (0.72 g, 5 mmol) in THF (5 mL) was added dropwise to the mercuric acetate solution over a period of 5 min and this was followed by the addition of 0.22 mL (2.5 mmol) of 70% $HClO_4$. The reaction mixture was stirred at room temperature under argon for 24 h and then cooled in an ice bath. An aqueous solution of 3 M sodium hydroxide (15 mL) was added slowly via syringe while maintaining the temperature at 0-5°C, after which the cooled solution was treated dropwise, also via a syringe, with 7.5 mL of a 0.5 M solution of sodium borohydride prepared in 3 M sodium hodroxide. The mercury formed in the reaction was separated from the supernatant solution by decantation. The solution was saturated with sodium chloride and the organic (THF) layer was separated. The remaining aqueous layer was then extracted several times with ether and the ether extract combined with the THF extract. The combined extracts were dried over Na_2SO_4 (anhydrous), filtered, and evaporated to dryness. The residual oil was chromatographed on silica (30 g) using ethyl acetate – hexane (4:6) as eluant. Starting material (0.064 g, 9%) and the alcohol **3** (0.414 g, 51%) were eluted under these conditions. An analytical sample was prepared by recrystallization from ether, mp 103–104°C; ir (ν_{max}, Nujol): 3210 (OH), 2220 (CN) cm^{-1}; ^{1}H nmr (90 MHz), δ: 1.52 (3H, d, J = 7.5 Hz, CH_3CH), 2.55 (3H, s, ArCH_3), 3.44 (1H, br s, OH), 5.15 (1H, m, CHOH), 8.66 (1H, s, H-2 or H-6), 8.89 (1H, s, H-2 or H-6); ^{13}C nmr (125.8 MHz, $CDCl_3$), δ: 16.7, 23.9, 65.1, 111.1 116.0, 140.0, 147.3, 150.0, 151.1; ms (EI), m/z, (rel.int., %): 162 (14), 147 (100), 145 (5), 144 (5), 143 (6), 119 (24), 92 (7). Exact mass (hrms). calcd. for $C_9H_{10}N_2O$: 162.0793; found: 162.0799.

Further elution of the column with ethyl acetate gave a brown oil from which the diol was obtained in low yield by crystallization from acetone, mp 140°C; ir (ν_{max}, Nujol): 3425, 3350 (sh), and 3160 (OH), 2212 (CN) cm^{-1}; ^{1}H nmr (90 MHz, DMSO-d_6 + D_2O), δ: 2.50 (3H, s, CH_3), 3.57 (2H, d, $J \approx$ 6 Hz, CH_2OH), 4.92 (1H, t, $J \approx$ 6 Hz, CHOH), 8.77 (2H, overlapping s's, H-2 and H-6); ^{13}C nmr (125.8 MHz, acetone-d_6), δ: 17.1, 67.1, 70.6, 111.5, 117.0, 138.0, 148.6, 152.1, 152.4; ms (EI) m/z (rel.int., %); 178 (4), 148 (42), 147 (100), 133 (5), 132 (4), 119 (23), 103 (4), 92 (10). Exact mass (hrms) calcd. for $C_9H_{10}N_2O_2$: 178.0742; found: 178.0746.

Preparation of 5-acetyl-4-methyl-3-pyridinecarbonitrile **4**

A solution of the alcohol **3** (0.324 g, 2 mmol) in acetone (8 mL) was treated rapidly with stirring with Jones' reagent (1.8 mL). The mixture was stirred an additional 24 h. The excess reagent was destroyed by the addition of methanol and the solution neutralized with aqueous ammonia. A precipitate of chromium compounds was removed by filtration and the filtrate heated to remove acetone. The residual solution was extracted with methylene chloride, the extract dried over Na_2SO_4 (anhydrous), the solution filtered, and the filtrate taken to dryness. The pale yellow solid residue was purified by chromatography on a silica column (10 g) using ethyl acetate – hexane (1.5:8.5) as eluant. Yield, 0.238 g, 74%; mp 64–65°C after recrystallization from hexane; ir (ν_{max}, Nujol): 2200 (CN), 1690 (C=O) cm^{-1}; ^{1}H nmr (90 MHz), δ: 2.67 (3H, s, CH_3CO), 2.76 (3H, s, Ar-CH_3), 8.90 (1H, s, H-2 or H-6), 9.05 (1H, s, H-2 or H-6); ^{13}C nmr (125.8 MHz, $CDCl_3$), δ: 19.1, 29.8, 113.2, 115.4, 133.6, 151.3, 152.3, 154.6, 198.1; ms (EI), m/z (rel.int., %): 160 (35), 145 (100), 117 (96), 90 (24), 63 (23). Exact mass (hrms) calcd. for $C_9H_8N_2O$: 160.0637; found: 160.0642.

[2]In solution in chloroform compound **8**, 2-phenacylpyridine, exists as a mixture of keto and enol forms (19). In the solid state, however, based upon ir evidence, only the enol form is present (20). We have confirmed this result using solid state ^{13}C nmr. In the solid state ^{13}C nmr spectrum of **8**, signals that might be attributed to a carbonyl carbon and a methylene carbon are absent. These signals were present in the solution spectrum at δ 196.7 and 48.2, respectively. A signal in the solid state and in solution appearing at δ 94.1 has been assigned to the enolic carbon bearing the hydrogen atom.

Acknowledgements

We thank the Natural Sciences and Engineering Research Council of Canada for financial support for this research.

1. T. R. GOVINDACHARI, K. NAGARAJAN, and S. RAJAPPA. J. Chem. Soc. 2725 (1957).
2. T. KAMETANI, M. TAKESHITA, M. IHARA, and K. FUKUMOTO. J. Org. Chem. **41**, 2542 (1976).
3. (*a*) JAHANGIR, D. B. MACLEAN, M. A. BROOK, and H. L. HOLLAND. J. Chem. Soc. Chem. Commun. 1608 (1986); (*b*) JAHANGIR, D. B. MACLEAN, M. A. BROOK, and H. L. HOLLAND. Can. J. Chem. **65**, 2362 (1987).
4. (*a*) JAHANGIR, M. A. BROOK, D. B. MACLEAN, and H. L. HOLLAND. Tetrahedron, **43**, 5761 (1987); (*b*) D. B. REPKE, JAHANGIR, R. D. CLARK, and D. B. MACLEAN. J. Chem. Soc. Chem. Commun. 439 (1988); (*c*) D. B. REPKE, JAHANGIR, R. D. CLARK, J. T. NELSON, and D. B. MACLEAN. Tetrahedron, **45**, 2541 (1989).
5. JAHANGIR, D. B. MACLEAN, and H. L. HOLLAND. Can. J. Chem. **64**, 1031 (1986).
6. A. M. JONES and C. A. RUSSEL. J. Chem. Soc. (C), 2246 (1969).
7. (*a*) R. G. COOMBES, M. D. JOHNSON, and N. WINTERTON. J. Chem. Soc. 7029 (1965); (*b*) H. I. THAYER and B. B. CORSON. J. Am. Chem. Soc. **70**, 2330 (1948; (*c*) E. D. BERGMANN, F. E. CRANE, and R. M. FUOSS. J. Am. Chem. **74**, 5979 (1952).
8. M. J. JORGENSON. Organic reactions. Vol. XVIII. John Wiley and Sons, New York. 1970. p. 1.
9. N. N. GOLDBERG, L. B. BARKLEY, and R. LEVINE. J. Am. Chem. Soc. **73**, 4301 (1951).
10. R. I. FRYER, B. BRUST, J. V. EARLEY, and L. H. STERNBACH. J. Org. Chem. **31**, 2415 1966.
11. W. M. EDWARDS and P. L. TEAGUE. J. Am. Chem. Soc. **71**, 3548 (1949).
12. P. G. CAMPBELL and P. C. TEAGUE. J. Am. Chem. Soc. **76**, 1371 (1954).
13. T. KAUFFMANN, G. BEISSNER, E. KÖPPELMANN, D. KUHLMANN, A. SCHOTT, and H. SCHRECKEN. Angew. Chem. Int. Ed. Engl. **7**, 131, (1968).
14. M. E. WRIGHT and L. Y. YAMADA. Synth. Commun. **18**, 1449 (1988).
15. (*a*) T. NAITO, O. MIYATA, I. NINOMIYA, and S. C. PAKRASHI. Heterocycles, **16**, 725 (1981); (*b*) I. NINOMIYA, T. NAITO, and H. TAKASUGI. J. Chem. Soc. Perkin Trans. **1**, 1865 (1976); (*c*) I. NINOMIYA and T. NAITO. Heterocycles, **2**, 607 (1974).
16. H. C. BROWN and P. J. GEOGHEGAN, JR. J. Org. Chem. **35**, 1844 (1970).
17. C. L. HILL and G. M. WHITESIDES. J. Am. Chem. Soc. **96**, 870 (1974).
18. R. P. QUIRK and R. E. LEA. J. Am. Chem. Soc. **98**, 5973 (1976).
19. E. PROFFT and F. SCHNEIDER. J. Prakt. Chem. **2**, 316 (1955).
20. R. F. BRANCH, A. H. BECKETT, and D. B. COWELL. Tetrahedron, **19**, 401 (1963).

Can. J. Chem. Downloaded from www.nrcresearchpress.com by 91.144.44.67 on 09/07/12
For personal use only.

Intercalation of basic molecules into niobyl-vanadyl phosphate

L. García-Ponce, L. Moreno-Real, and A. Jiménez-López[1]

Departamento de Química Inorgánica, Facultad de Ciencias, Universidad de Málaga, Apartado 59, 29071 Málaga, Spain

Received September 5, 1989

L. García-Ponce, L. Moreno-Real, and A. Jiménez-López. Can. J. Chem. **68**, 592 (1990).

Mixed niobyl-vanadyl phosphate $(V_{0.14}Nb_{0.86})OPO_4 \cdot 2.7H_2O$, VNbP, is a moderately acid solid that intercalates strong basic molecules such as branched alkylamines, allylamine, cyclohexylamine, piperidine, and diethylamine, giving rise to bilayers of inclined molecules. In the case of molecules of medium basicity, such as pyridine, the intercalated amounts are small at room temperature and they present a planar orientation. A special behaviour was found with ethylenediamine and butylenediamine, strong basic diamines, which also present a planar disposition in the interlayer space.

Key words: mixed niobyl-vanadyl phosphate, layered compounds, phosphates, intercalation, pyridine.

L. García-Ponce, L. Moreno-Real et A. Jiménez-López. Can. J. Chem. **68**, 592 (1990).

Le phosphate mixte de niobyle et de vanadyle $(V_{0,14}N_{0,86})OPO_4 \cdot 2,7H_2O$, VNbP, est un solide modérément acide qui intercale des molécules fortement basiques comme des alkylamines ramifiées, de l'allylamine, de la cyclohexylamine, de la pipéridine et de diéthylamine pour donner des bicouches de molécules inclinées. Dans le cas de molécules de basicité moyenne, comme la pyridine, les quantités intercalées à la température de la pièce sont faibles et elles se présentent dans une orientation planaire. On a observé un comportement spécial avec l'éthylènediamine et la butylènediamine, des diamines fortement basiques, qui présentent aussi une disposition planaire dans l'espace entre les couches.

Mots clés : phosphate mixte de niobyle et de vanadyle, composés en couches, phosphates, intercalation, pyridine.

[Traduit par la revue]

Introduction

The phosphates of the family $MO(AO_4) \cdot nH_2O$ (M = V, Nb; A = As, P) are layered, isostructural compounds. In their tetragonal forms, the layers consist of octahedrally coordinated metal atoms, four of the coordination positions being occupied by PO_4^{3-} groups and the other two by an oxygen atom bonded to the metal via a double bond and by a water molecule. The resulting layers interact through hydrogen bonds established by the water molecules that occupy the interlayer space.

The isostructural nature of niobyl and vanadyl phosphates and the similarity between the sizes of both elements facilitate the synthesis of mixed phosphates, which are in fact solid solutions of vanadyl phosphate in its niobyl counterpart. The maximum tolerated degree of replacement of niobyl by vanadyl ion in the phosphate of the latter is 21% (1).

These mixed phosphates can undergo redox reactions similar to those of their precursors (2, 3), as well as intercalate neutral molecules of basic nature (4, 5). Thus the mixed phosphate with 14% vanadium undergoes the intercalation of *n*-alkylamines, which form a molecular bilayer at an angle of 58° with respect to the layers (6). The mechanism of this intercalation process was established to be a proton-transfer reaction between the water molecules, both coordinated to the metal and of zeolitic type, and those of the amine.

The aim of this work has been to contribute new data on the interaction of basic molecules with the aforesaid mixed phosphate in general, and to determine the influence of branched chains and the basic strength of the amines on the orientation and extent of intercalation in particular.

Experimental

The synthesis and characterization of the VNbP (14% V) used has been described elsewhere (1). All bases used were of reagent quality, without further purification. The bases to intercalate into VNbP were as follows: (a) branched amines of the same main chain length, such as *sec*-butylamine (*sec*-BA), *iso*-butylamine (*iso*-BA), neopentylamine (*neo*-PtA), and allylamine (AA); (b) a secondary amine, such as diethylamine (DEA); (c) three cyclic bases, cyclohexylamine (CHA), piperidine (Pi), and pyridine (Py); (d) two diamines with basic groups of different strength, ethylenediamine (EDA) and butylenediamine (BDA); and (e) a very weakly basic substance, dimethyl sulphoxide (DMSO).

The liquid bases were in contact with the VNbP (0.25–0.4 g in 5–10 mL of pure base) at 25°C for 24–72 h. Then the suspensions were filtered and the solids were washed with ether until the excess amine was removed. The products were vacuum dried.

Pyridine and DMSO were sorbed from the vapour phase at 25 and 60°C, respectively. Another pyridine intercalate was obtained by placing the base in contact with VNbP for 3 weeks under reflux.

Amounts of the intercalated substances were determined by CHN analysis and (or) Kjeldahl microanalysis; the water contents were calculated from TG–DTA curves. The TG–DTA analyses were carried out in air on a Rigaku Thermoflex instrument using calcined alumina as internal reference and heating from room temperature to 1273 K at a rate of 3 or 10 K/min. Platinum crucibles and Pt/Pt–Rh thermocouples were used.

Powder X-ray diffraction patterns were obtained with an automated Siemens diffractometer using graphite monochromated CuK_α radiation. IR spectra were recorded by a Perkin–Elmer 883 double beam spectrophotometer using KBr pellets containing 2% of the products. The diffuse reflectance (UV–VIS) spectra were obtained on a Kontron Uvikon 810 instrument; the UV–VIS–nIR spectra were recorded on a Shimadzu UV 3100 double beam spectrophotometer, always using barium sulphate as reference.

Results and discussion

Table 1 lists the compositions of the different intercalates prepared, their basal spacings, and the pK_a of each intercalated base. As can be seen, the amine contents of the intercalates with branched amines of the same main chain length, namely *sec*-BA, *iso*-BA, and *neo*-PtA, are lower than those found for the *n*-alkylamine of the same chain length (1.5 mol *n*-propylamine per mol of phosphate) (6), as one would expect from the more extensive "coverage" by such molecules. Nevertheless, among the three branched amines, *sec*-BA is intercalated to a lesser extent than *iso*-BA as it has a methyl group in the α position that covers a larger surface than its β counterpart. An increase in the molecular volume (*neo*-PtA) results in a

[1]Author to whom correspondence may be addressed.

Printed in Canada / Imprimé au Canada

Can. J. Chem. Downloaded from www.nrcresearchpress.com by 91.144.44.67 on 09/07/12
For personal use only.

TABLE 1. Composition, basal spacing of intercalation compounds $(V_{0.14}Nb_{0.86})OPO_4 \cdot x$ (base)$\cdot y$ H_2O, and pK_a of intercalated bases

Intercalate	Symbol	x	y	d_1 (Å)	pK_a
iso-Butylamine	*iso*-BA	1.4	2.1	15.19	10.72
sec-Butylamine	*sec*-BA	1.2	1.7	15.37	—
Neopentylamine	*neo*-PtA	1.1	2.1	16.44	—
Diethylamine	DEA	0.7	1.8	13.17	11.04
Allylamine	AA	1.3	1.8	15.35	—
Cyclohexylamine	CHA	1.2	1.8	16.86	10.68
Piperidine	Pi	1.1	2.3	14.40	11.12
Ethylenediamine	EDA	0.4	1.8	7.04	9.92/6.84
Butylenediamine	BDA	0.3	1.8	7.08	10.80/9.35
Pyridine (vapour)	Py	0.5	1.1	8.70	5.25
Pyridine (reflux)	Py	0.8	2.4	9.90	5.25
Dimethylsulphoxide (vapour)	DMSO	0.1	1.6	6.80	0.40
$(V_{0.14}Nb_{0.86})OPO_4$(r.t.)	VNbP	—	2.7	7.9	
$(V_{0.14}Nb_{0.86})OPO_4$(100–140°C)	VNbP	—	1.0	6.2	
$(V_{0.14}Nb_{0.86})OPO_4$($t > 240$°C)	VNbP	—	0	4.1	

concomitant decrease in the intercalation content. On the other hand, the basal spacing for these four amines is close to that of *n*-propylamine (15.1 Å) (6). In fact, as can be seen in Table 1, the basal spacings are all of the same order, which allows one to assume that these molecules arrange themselves in an interlaminar bilayer with their main axis forming a 58° angle with respect to the layers. However, the greater steric hindrance posed by the three methyl groups of *neo*-PtA seems to result in slightly more staggered molecules and hence in a slightly wider spacing (16.4 Å).

The influence of steric hindrance is even more marked in the case of DEA, whose large extent of coverage results in a lower content compared with those of the other amines. The basal spacing of its corresponding intercalate is also indicative of the formation of a molecular bilayer in the interlayer space. Of the three cyclic bases, viz., CHA, piperidine, and pyridine, the last, on account of its special behaviour, will be discussed later. The composition of the intercalates of the other two is consistent with their similar steric hindrances: their basal spacings also suggest the formation of a bilayer, with a larger spacing for the exocyclic amine, as one would expect.

The amine content in all of the intercalates discussed above depends on the extent of coverage of the molecules, though not on their base strength as they are all strong bases. On the other hand, the X-ray diffractograms of the intercalates show a single swelling phase with various orders (001) and a clear (200) reflection, which is indicative of a preserved crystal structure.

The amine contents for the intercalates of the diamines (EDA and BDA) are clearly lower than those found for the above-mentioned amines: 0.4 and 0.3 mol per mole of phosphate, respectively. Bearing in mind that they are diamines, one should expect the formation of a monolayer of staggered molecules as a result of the simultaneous interaction of their two amine groups with the two neighbouring layers (7). On the other hand, the basal spacings found (7.0 and 7.1 Å, respectively) indicate that the molecules are oriented with the plane containing the carbon chain lying parallel to the layers and the molecules themselves occupying the structural vacancies. In addition, the amine content of these two intercalates depends on their size; thus, the ratio between the chain lengths of EDA and BDA (6.76 Å/9.28 Å) is consistent with the reciprocal of the ratio between their contents in the intercalates (0.75). The fact that these compounds form no perpendicular monolayer might be related to their base strength; their lower pK_{a2} could only allow a single protonation of the amines, so that the interaction with the upper layer would be rather weak, the energy released would be insufficient to induce the swelling, and the molecules would arrange themselves parallel to the layers. This point will be confirmed later in discussing IR and nIR spectra.

The water content of all the intercalates obtained was close to 2 mol per mol of phosphate and similar to those values found for *n*-alkylamines [6]. These water molecules play a major role in the intercalation process.

The intercalation of a weaker base, pyridine (pK_a 5.25), was effected by two methods, which resulted in two different intercalates, namely, in the vapour phase (4 months) and under reflux (3 weeks), yielding intercalates containing 0.5 mol pyridine and 1 mol water, and 0.78 mol pyridine and 2.4 mol water per mol of phosphate, respectively. Their basal spacings (8.7 and 9.9 Å, respectively) are consistent with these compositions and are larger than those obtained by other authors for the precursor phosphates (5, 8). On the other hand, the intercalate obtained under reflux, unlike that prepared by Johnson under other conditions, has a high water content, although both have similar basal spacings (8).

Taking into account that the van der Waals thickness of a pyridine ring is 3.7 Å and that the spacing of the intercalate synthesized in the vapour phase was 8.7 Å, we may assume that pyridine lies horizontally in the interlayer space. The composition is consistent with the molecular coverage (43 $Å^2$) and the area of the cell unit, $Z = 2$ (41.6 $Å^2$), so that the theoretical composition would be 0.48 mol per mol of phosphate (i.e., very close to the experimental value).

When pyridine was intercalated under more drastic conditions (e.g., under reflux), the base content was higher and the basal spacing increased up to 9.9 Å, which seems to indicate that the pyridine molecules lean slightly to accommodate themselves in the interlayer.

The DTA curves (Fig. 1) show the different thermal behaviour of these two pyridine intercalates. Thus, that obtained by the vapour reaction shows three steps in the TG curve corresponding to two endothermic effects and one exothermic effect. The first endothermic effect, between 80 and 100°C, corresponds to the partial removal of pyridine, which is weakly

Can. J. Chem. Downloaded from www.nrcresearchpress.com by 91.144.44.67 on 09/07/12
For personal use only.

TABLE 2. Selected vibration bands of the IR spectra of intercalates

Intercalate	ν(OH)	$\nu(NH^+)$	δ(OH) and (or) $\delta_a(NH_3^+)$	$\delta(NH^+)$	$\delta_s(NH_3^+)$
iso-BA	3425	3020	1616–1630		1518, sh1530
sec-BA	3408	3020	1602–1620		1500, sh1530
neo-PtA	3412	3020	1601–1618		1500, sh1530
AA	3418	3030	1617–sh1650		1517, sh1550
DEA	3430	3020	1630	sh1560–1500	
CHA	3409	3007	1600–1633		1520–1540
Pi	3427	2953	1628	1584	
EDA	3400	3176 3020	1615		1507, sh1540
BDA	3410	3220 3090 3020	1628		1495, 1505, sh1540

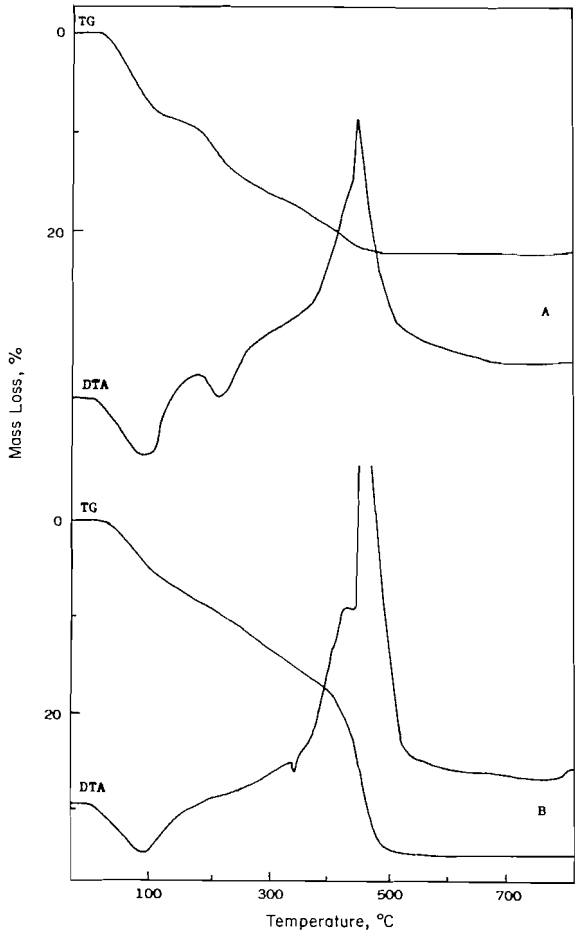

FIG. 1. DTA–TG curves for pyridine intercalates: (A) vapour phase; (B) reflux.

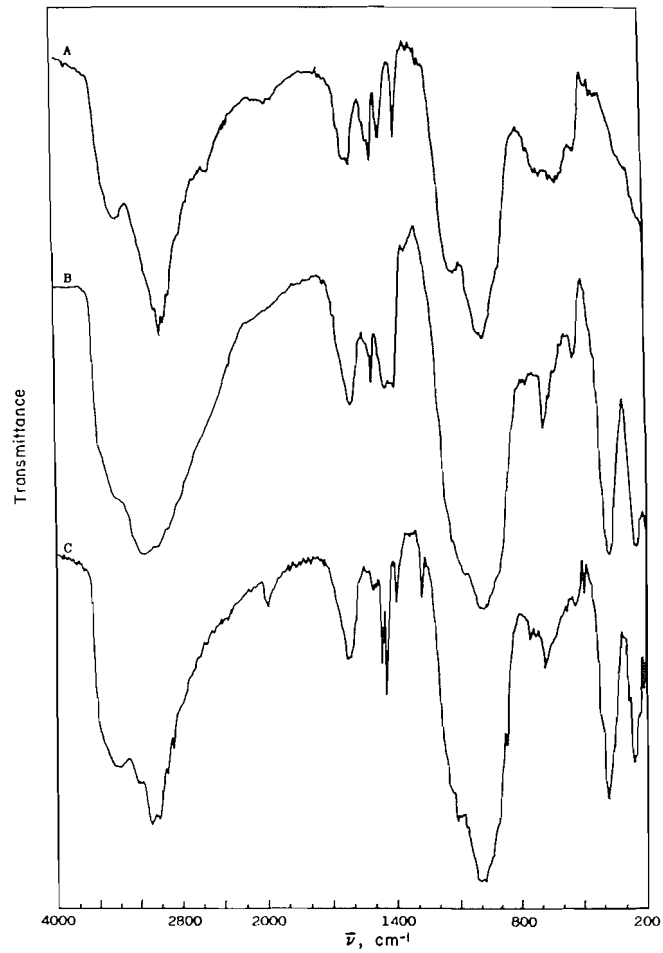

FIG. 2. Infrared spectra of intercalates of (A) *sec*-butylamine; (B) ethylenediamine; (C) butylenediamine.

retained; this is followed by the endothermic removal of coordinated water at 220°C and, finally, by a strong exothermic effect at 430°C corresponding to the combustion of the base. These results are consistent with those of the elemental CHN analysis. The steps of the intercalate obtained under reflux are not so well defined. The first, up to 170°C, corresponds to the loss of zeolitic water (1.4 mol per mol of phosphate); this stage is overlapped with the following, which corresponds to the loss of coordinated water and part of the strongly retained pyridine, which undergoes combustion at 460°C.

Finally, DMSO, very weakly basic (pK_a 0.4), is sorbed to a very small extent (0.1 mol per mol of phosphate). The composition and basal spacing of its intercalate seem to indicate that it is only retained superficially.

Infrared and nIR spectroscopy are the most useful techniques for establishing the intercalation mechanism of basic species. Table 2 gathers the most salient absorptions of the different intercalates obtained. The intercalates of all the monoamines (Fig. 2) show a typical band of symmetric deformation of the

Can. J. Chem. Downloaded from www.nrcresearchpress.com by 91.144.44.67 on 09/07/12
For personal use only.

Can. J. Chem. Downloaded from www.nrcresearchpress.com by 91.144.44.67 on 09/07/12
For personal use only.

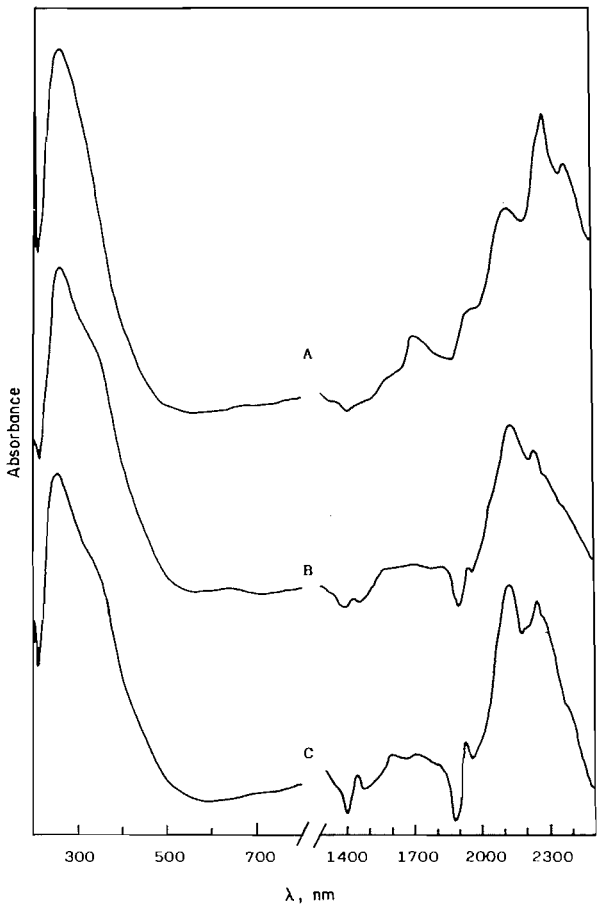

FIG. 3. Diffuse reflectance spectra in the 200–2500 nm region of intercalates of (A) *sec*-butylamine; (B) ethylenediamine; (C) butylenediamine.

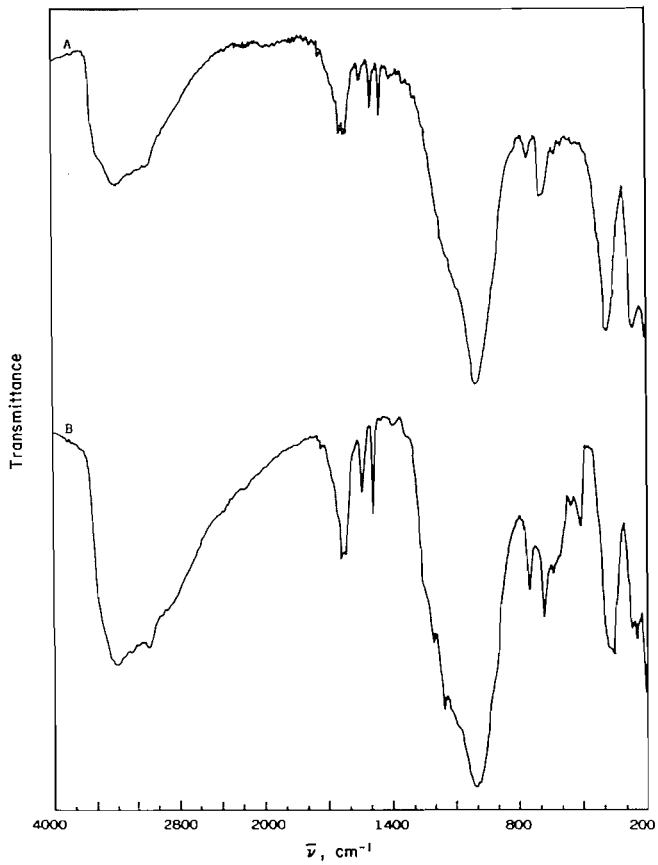

FIG. 4. Infrared spectra of pyridine intercalates: (A) vapour phase; (B) reflux.

$-NH_3^+$ group in the region 1500–1520 cm^{-1} (9), which indicates that the molecules lying in the interlayer space are protonated by the water molecules according to eq. [1]

[1] $H_2O + R\text{-}NH_2 \rightarrow R\text{-}NH_3^+ + OH^-$

The resulting *n*-alkylammonia ions interact via hydrogen bonds with the hydroxyl ions and the remaining water molecules; hence the appearance of a shoulder at 1530–1560 cm^{-1} in all cases. This protonation is also consistent with the fact that the NH stretching vibration appears at lower frequencies (3020 cm^{-1}) than that of a nonprotonated amine. The spectra of DEA and piperidine intercalates show a NH_2^+ deformation band at 1500 and 1584 cm^{-1}, respectively, which indicates that both amines are also protonated.

As far as the diamines are concerned, the IR spectrum of the BDA intercalate (Fig. 2), in addition to the above-mentioned bands at 1520–1560 cm^{-1} of the monoamines, shows other bands at 3220, 3090, and 3020 cm^{-1}, but not that at 3330 cm^{-1} corresponding to the ν(NH) of the pure amine, which seems to indicate that the BDA molecules in the interlayer space are fully protonated. This situation would make the diamine equivalent to two molecules of ethylamine, so it should arrange itself in a monolayer staggered with respect to the layers. The parallel orientation of this molecule in the interlayer space may arise from the fact that both of the amino groups may interact with polar groups of the same layer, which is the energetically most favourable arrangement. This is in contrast to the arrangement of monoamines, which are fixed to the layer by the basic group, while the hydrophobic group is directed to the center of the interlayer space. As this group cannot interact with the upper layer, the compound takes in another amine molecule, which interacts with the second water molecule, giving rise to a molecular bilayer intercalate.

The IR spectrum of the EDA intercalate, on the other hand, shows a single band in the region 3400–3200 cm^{-1}, which does not allow the bands corresponding to the ν(NH) of the nonprotonated amino groups to be clearly observed. However, the UV–VIS–nIR spectrum (Fig. 3) confirms the full protonation of EDA as it shows a combination band ($\nu(NH^+)$ + $\delta(NH_3^+)$) at 2164 nm (10). This spectrum is very similar to that of the BDA intercalate, so that this molecule also arranges itself in parallel with the layer.

Figure 3 also shows a single band at 245–255 nm for the monoamines, but not those at 335 and the shoulder at 400 nm; these two are responsible for the yellow colour of the original matrix, so the intercalates are white (1). The spectra of the intercalates with lower content of guest molecules (EDA, BDA, and DEA) exhibit a shoulder at 335 nm because of some vanadium-coordinated water molecules that do not interact with amines.

Figure 4 shows the IR spectra of the two pyridine intercalates. The spectrum obtained in the vapour phase shows a band at 1538 cm^{-1} indicative of the occurrence of protonated pyridine, and another at 1445 cm^{-1} corresponding to nonprotonated pyridine (11). The presence of these two types of pyridine molecules in the interlayer is consistent with the thermal behaviour of the intercalate, from which nonprotonated pyri-

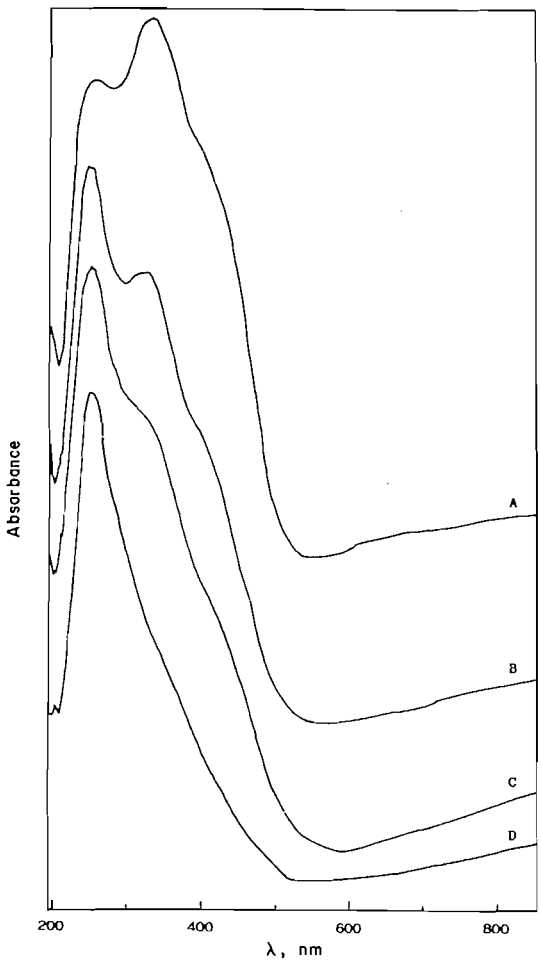

FIG. 5. Diffuse reflectance spectra in the 200–800 nm region of pyridine intercalates: (A) NbVP; (B) vapour phase (3 months); (C) vapour phase (4 months); (D) reflux.

dine was removed at a low temperature while protonated pyridine was lost at higher temperatures. The spectrum of the intercalate obtained under reflux, however, shows only the band at 1538 cm^{-1}, which indicates that all the pyridine molecules are protonated; this is also consistent with the thermal behaviour of this intercalate.

The diffuse reflectance spectra of these two intercalates between 200 and 800 nm are indicative of the same situation (Fig. 5). Thus, the spectrum of the pyridine intercalate obtained in the vapour phase shows a maximum at 330 nm that decreases until the intercalation process is completed, and is preserved as a shoulder in the 8.6 Å intercalate. However, such a shoulder completely disappears in the spectrum of the intercalate obtained under reflux, which indicates that the water molecules coordinated in the vanadium interact with pyridine, either through protonation or through hydrogen bonds.

We may conclude that the mixed VNbP is a solid of medium acidity liable to react to a great extent with monoamines, yielding molecular bilayers. The extent of intercalation of the diamines EDA and BDA is only partial and the molecules arrange themselves with their chains horizontal and parallel to the layers. Pyridine (pK_a 5.25) in the vapour phase intercalates in a ratio of 0.5 mol per mol of phosphate and its molecules lie parallel to the layers. Although the extent of intercalation under reflux is somewhat greater, the complete intercalation and a vertical arrangement of the molecules with respect to the layer (i.e., as with highly acidic solids such as uranyl hydrogen phosphate (12) or solids with a high surface charge density such as vermiculite (13)) is never reached. Finally, very weakly basic molecules (e.g., DMSO) are not intercalated at all.

Acknowledgment

We thank CICYT (Spain), Project PB 86-0244, for financial support.

1. A. L. García-Ponce, L. Moreno-Real, and A. Jiménez-López. Inorg. Chem. **27**, 3372 (1988).
2. M. Martínez-Lara, A. Jiménez-López, L. Moreno-Real, S. Bruque, B. Casal-Piga, and E. Ruiz-Hitzky. Mater. Res. Bull. **20**, 549 (1985).
3. A. J. Jacobson, J. W. Johnson, J. F. Brody, J. C. Scanlon, and J. T. Lewandowski. Inorg. Chem. **24**, 1782 (1985).
4. M. Martínez-Lara, L. Moreno-Real, A. Jiménez-López, S. Bruque, and A. Rodríguez García. Mater. Res. Bull. **21**, 13 (1986).
5. K. Beneke and G. Lagaly. Inorg. Chem. **22**, 1503 (1983).
6. A. L. García-Ponce, L. Moreno-Real, and A. J. Jiménez-López. Solid State Chem. In press.
7. E. Rodriguez-Castellón, P. Olivera-Pastor, A. Jiménez-López, P. Maireles-Torres, M. J. Hudson, and P. Sylvester. Can. J. Chem. **67**, 2095 (1989).
8. J. W. Johnson, A. J. Jacobson, J. F. Brody, and S. M. Rich. Inorg. Chem. **21**, 3820 (1982).
9. J. J. Fripiat, A. Servais, and A. Leonard. Bull. Soc. Chim. Fr. 635 (1962).
10. R. F. Goddu and D. A. Delker. Anal. Chem. **32**, 140 (1960).
11. V. C. Farmer and M. M. Mortland. J. Chem. Soc. (A), 344 (1966).
12. L. Moreno-Real, R. Pozas-Tormo, M. Martínez-Lara, and S. Bruque. Mater. Res. Bull. **22**, 19 (1987).
13. J. M. Serratosa. Clays Clay Miner. **14**, 145 (1966).

Can. J. Chem. Downloaded from www.nrcresearchpress.com by 91.144.44.67 on 09/07/12
For personal use only.

Conformational analysis of 1-oxaspiro[5.5]undecanes. A powerful probe for the *endo* and the *exo* anomeric effects in acetals

PIERRE DESLONGCHAMPS[1] AND NORMAND POTHIER

Laboratoire de synthèse organique, Département de chimie, Faculté des sciences, Université de Sherbrooke, Sherbrooke (Québec), Canada J1K 2R1

Received August 1, 1989

PIERRE DESLONGCHAMPS and NORMAND POTHIER. Can. J. Chem. **68**, 597 (1990).

A ^{13}C nuclear magnetic resonance spectroscopy study of 1-oxaspiro[5.5]undecanes **1**, **4**, and **5** as a function of temperature is reported. Compound **1** exists as a rapidly equilibrating mixture of a major and a minor conformer (**1***a* and **1***b*) at room temperature that can be observed at low temperature. By comparison, 1,7-dioxaspiro[5.5]undecane **2** is conformationally rigid in a single conformation (**2***a*) at room temperature. This completely different behavior demonstrates the importance of the *endo* and the *exo* anomeric effects in the acetal function.

Key words: spiro ethers, conformational analysis, ^{13}C NMR.

PIERRE DESLONGCHAMPS et NORMAND POTHIER. Can. J. Chem. **68**, 597 (1990).

Une étude par spectroscopie de résonance magnétique nucléaire du ^{13}C en fonction de la température des 1-oxaspiro[5.5]undécanes **1**, **4** et **5** est rapportée. Le composé **1** est un mélange de deux conformères, l'un majoritaire (**1***a*) et l'autre minoritaire (**1***b*) à la température ambiante que l'on peut observer à basse température. Par comparaison, le 1,7-dioxaspiro[5.5]undécane **2** est complètement rigide existant dans une seule conformation (**2***a*) à la température ambiante. Ce comportement différent démontre clairement l'importance des effets *endo* et *exo* anomères de la fonction acétale.

Mots clés : spiroéthers, analyse conformationnelle, RMN ^{13}C.

Introduction

Although α- and β-glycosides can theoretically exist as three different rotamers each, they are known to exist in the crystalline state (1) as rotamers A_1 and E_1 respectively as illustrated in Scheme 1. This conformational preference, as well as the greater stability of α- over β-glycosides, is currently explained by a combination of steric and stereoelectronic effects (2) known as the *endo* and the *exo* anomeric effects (3).

The conformation of glycosides in solution (4, 5) is similar to that found in the crystalline state. It is, however, difficult experimentally to rigorously establish the relative population of the rotamers of glycosides in solution because the energy barrier between the various rotamers is too weak. The precise evaluation of the *endo* and the *exo* anomeric effects with these compounds is thus difficult. On the other hand, Kishi and co-workers (6) have recently demonstrated that the side chain in *C*-glycosides[2] exists predominantly in solution in a conformation similar to that observed in normal *O*-glycosides. In *C*-glycosides, the preference is of course due to steric effects only, and this raised the question (6) of what is the real importance of the *exo* anomeric effect in the control of population of rotamers in normal *O*-glycosides.

We have previously reported a study on 1,7-dioxaspiro-[5.5]undecane and various substituted derivatives (7). These compounds were found suitable for the estimation of the *endo* and the *exo* anomeric effects because the energy barrier associated with the conformational equilibrium is sufficiently high between each conformer that their detection and relative abundance could be determined with precision at low temperature by ^{13}C nmr spectroscopy. For instance the unsubstituted 1,7-dioxaspiro[5.5]undecane can theoretically adopt the three conformations illustrated in Scheme 2, but it was shown to exist solely in conformation **2***a* *even at room temperature*. This result was explained by the fact that conformation **2***a* is sterically and stereoelectronically more stable than conformations **2***b* and **2***c*. This study allowed us to conclude that the minimum value for the *endo* and (or) *exo* anomeric effect must be close to 1.4 kcal/mol.[3]

It appeared to us that it would be interesting to compare the conformational behavior of 1,7-dioxaspiro[5.5]undecane with spiro compounds having only one oxygen atom next to the quaternary center. This comparison should be useful to probe the importance of stereoelectronic effects because steric effects can be readily evaluated with six-membered compounds. Also, these spiro ethers can be considered good models for *C*-glycosides just as the spiro ketals are excellent models for the normal *O*-glycosides. We have therefore synthesized the 1-oxaspiro[5.5]undecanes **1** (8), **4**, and **5** (Schemes 3) (8) and have carried out their conformational analysis at room and low temperatures using ^{13}C nmr spectroscopy as the analytical technique. We wish to report this study and to compare these results with those already reported for 1,7-dioxaspiro-[5.5]undecane **2** (7) and spiro[5.5]undecane **3** (9).

Synthesis

Spiro ethers **1**, **4**, and **5** were prepared as follows (Scheme 3). The lithium acetylide derivative of acetylenic tosylate **6** was reacted with cyclohexanone to give the adduct **7**, which was hydrogenated catalytically (H_2/PtO_2) to give hydroxy-tosylate **8**. This compound was then cyclized (*n*-Buli, THF) to give spiro ether **1** (8). Using the same procedure with 4-*tert*-butylcyclohexanone as starting ketone provided a 1:9 mixture of spiro ethers **4** and **5**, which were separated by chromatography.

[1]Author to whom correspondence may be addressed.

[2]In *C*-glycosides, the oxygen atom of the OR group at C_1 is replaced by a CH_2 group.

[3]**2***a* is energetically favored over **2***b* and **2***c* for steric and stereoelectronic reasons. *Steric*: **2***a* has two oxygens axially oriented (4 × 0.4 = 1.6 kcal/mol), while **2***b* has one oxygen and one methylene axially oriented ((2 × 0.4) + (2 × 0.9) = 2.6 kcal/mol) whereas **2***c* has two methylene groups axially oriented (4 × 0.9 = 3.6 kcal/mol). *Stereoelectronic*: **2***a* has two anomeric effects (2 × (−1.4) = −2.8 kcal/mol), **2***b* has one anomeric effect (−1.4 kcal/mol), and **2***c* has no anomeric effect (0 kcal/mol). The relative stability is therefore **2***a* = 0, **2***b* = 2.4, and **2***c* = 4.8 kcal/mol.

Can. J. Chem. Downloaded from www.nrcresearchpress.com by 91.144.44.67 on 09/07/12
For personal use only.

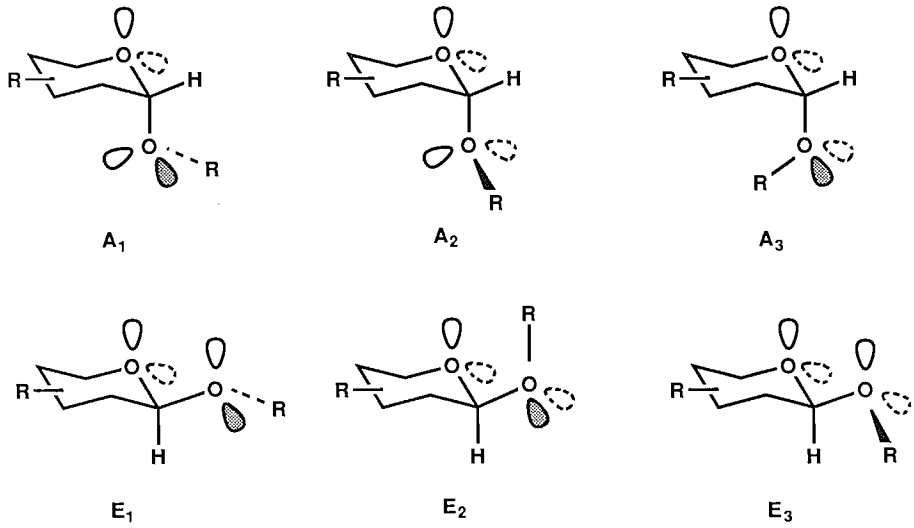

SCHEME 1

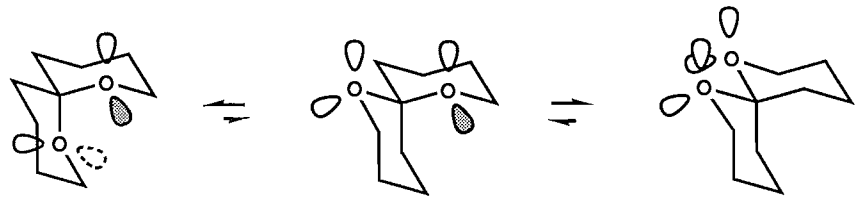

SCHEME 2

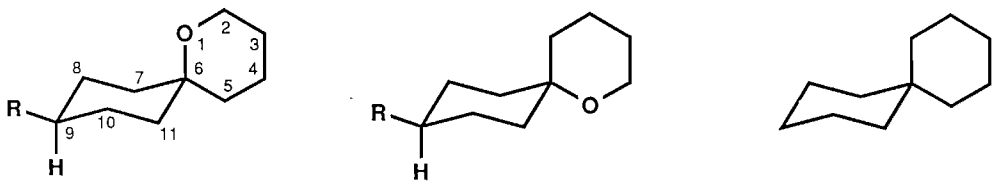

SCHEME 3

Can. J. Chem. Downloaded from www.nrcresearchpress.com by 91.144.44.67 on 09/07/12
For personal use only.

TABLE 1. ^{13}C chemical shift data for compounds **1**–**5** in ppm from TMS

Compound	C-1	C-2	C-3	C-4	C-5	C-6	C-7	C-8	C-9	C-10	C-11	C-12	CH_3
1[a]		60.8	26.8	19.4	36.2	71.8	35.2	22.1	26.8	22.1	35.2		
1[b]		60.7	26.8	19.4	36.5	71.7	35.2	21.9	26.8	21.9	35.2		
1*a*[c]		60.7	26.8	19.4	37.8	71.7	28.7	21.2	26.7	21.8	40.4		
1*b*[c]		61.0	26.8	19.6	30.4	73.5	30.9	23.3	26.7	23.8	41.4		
2[d]		60.3	25.4	18.6	35.8	94.9							
3[e]	37.6	22.0	27.5	22.0	37.6	32.7							
3[f]	32.2	22.0	27.6	22.0	43.0	32.7							
4[g]		61.0	26.7	19.5	37.6	71.2	35.2	22.2	48.8	22.2	35.2	32.8	28.0
4[b]		60.5	26.8	19.4	37.5	71.6	35.2	22.0	49.0	22.0	35.2	32.4	27.2
4[h]		60.8	26.8	19.4	37.4	71.4	29.0	21.8	48.7	22.5	40.7	33.0	27.2
5[g]		61.6	26.8	19.5	31.1	73.2	36.2	24.1	48.5	24.1	36.2	32.6	28.0
5[b]		61.0	26.8	19.4	31.1	72.7	36.2	24.0	48.7	24.0	36.2	32.2	27.2
5[h]		61.4	26.8	19.4	30.4	73.6	30.8	23.7	48.4	24.3	41.5	32.7	27.2

[a]In CD_2Cl_2 at 298 K.
[b]In 10% V/V CD_2Cl_2:CF_2Br_2 at 298 K.
[c]In 10% V/V CD_2Cl_2:CF_2Br_2 at 148 K.
[d]In 10% V/V CD_2Cl_2:$CHFCl_2$ at 310 K and 160 K at 100 Mz (see ref. 7).
[e]Room temperature (see ref. 9).
[f]Low temperature (see ref. 9).
[g]In $CDCl_3$ at 298 K.
[h]In 10% V/V CD_2Cl_2:CF_2Br_2 at 163 K.

Formation of the major isomer **5** results from the preferential axial addition of acetylide **6** on 4-*tert*-butylcyclohexanone (10).

Results and discussion

The ^{13}C nmr spectrum of 1-oxaspiro[5.5]undecane **1** was obtained at room temperature (298 K). The known chemical shifts of 1,7-dioxaspiro[5.5]undecane **2** (7) and spiro[5.5]undecane **3** (Scheme 4) (9) were used as references (Table 1) for the assignment of the carbon chemical shifts of compound **1** at ring A and ring B respectively.

The correlation for the chemical shifts for C_2, C_4, C_5, C_8, C_9, and C_{10} is very good, the observed difference being <1 ppm (cf. Scheme 4 for numbering). There are larger differences for C_3, C_6, C_7, and C_{11} but those are expected since the structures of compounds **1**, **2**, and **3** are basically different, having respectively one, two, and zero oxygen atoms.

For compound **1**, the chemical shifts for C_2 and C_6 are easily assigned since both have an oxygen atom. The single frequency off-resonance decoupling spectrum (SFORD) shows a triplet (CH_2, C_2-O) at 60.7 ppm and a singlet (C quaternary, C_6-O) at 71.7 ppm. For model compounds **2** and **3**, C_6 is observed at 94.9 and 32.7 ppm respectively, in agreement with the fact that the former has two oxygen atoms while the latter has none. The chemical shifts for C_2 in **1** and **2** are essentially identical. In the spectrum of **1**, the intensity of the signals observed at 21.9 and 35.2 ppm is indicative that each corresponds to two carbon atoms. The first signal must correspond to C_8 and C_{10} while the second one corresponds to C_7 and C_{11}. At room temperature, these carbons must be equivalent since compound **1** is conformationally mobile. Indeed, rapid inversion of ring A (tetrahydropyran ring) renders ring B (cyclohexane ring) symmetrical to it. As a result, the chemical shifts for C_7 and C_{11} as well as those of C_8 and C_{10} are respectively averaged. Also, by comparison with compound **3**, where C_1 = C_5 = C_7 = C_{11} = 37.0 ppm and C_2 = C_4 = C_8 = C_{10} = 22.0 ppm because of the symmetry imposed by its conformational mobility (9), it becomes obvious that C_7 and C_{11} on one hand and C_8 and C_{10} on the other must absorb at 35.2 and 21.9 ppm respectively in compound **1**.

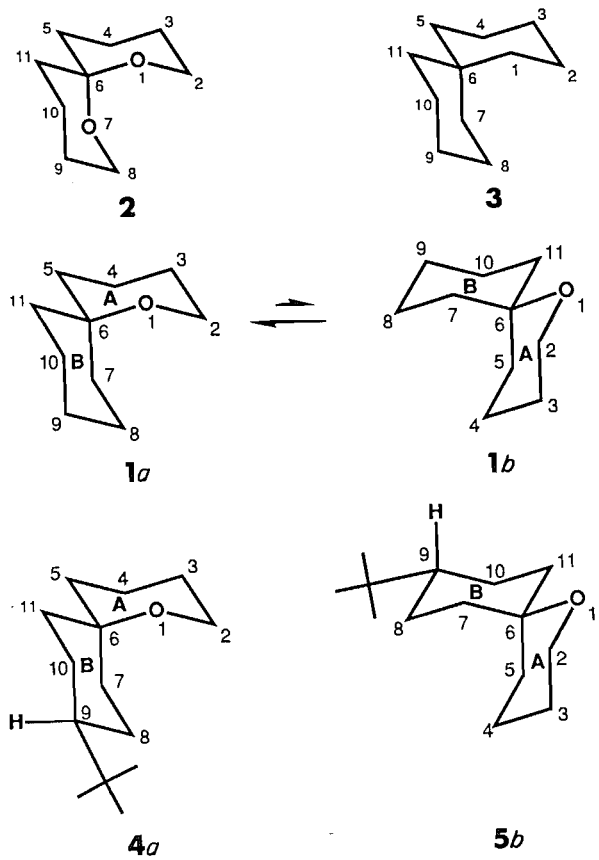

SCHEME 4

The two very close peaks at 26.8 ppm of **1** are assigned to C_3 and C_9 in agreement with the absorption of C_3 and C_9 in compounds **2** and **3**. For compounds **2** and **3**, C_3 and C_9 are identical by symmetry, and are observed at 25.4 and 27.5 ppm

Can. J. Chem. Downloaded from www.nrcresearchpress.com by 91.144.44.67 on 09/07/12
For personal use only.

respectively. The chemical shifts for C_3 and C_9 can also be compared with other compounds: for example, cyclohexane at 27.7 ppm (11), C_3 of tetrahydropyran at 26.8 ppm (11), and C_5 of 2-methyltetrahydropyran at 26.8 ppm (7).

The signal at 19.4 ppm for compound **1** is assigned to C_4 and is also in good agreement with C_4 of compound **2**, which is observed at 18.6 ppm. Finally, the chemical shifts for C_5 in compounds **1** and **2** are quite similar (35.8 and 36.5 ppm). This, a priori, is surprising since compound **2** is conformationally rigid and compound **1** is not (*vide infra*). However, it will be shown that the most stable conformer of **1** has essentially a conformation (**1***a*) identical to that observed for compound **2**, so the close chemical shift at C_5 for **1** and **2** is thus readily understood.

The ^{13}C nmr spectrum of compound **1** was obtained at low temperature (148 K). Figures 1 and 2 illustrate the 15–45 ppm region of the room and low temperature spectra. This result clearly demonstrates that compound **1** must exist as a mixture of two rapidly equilibrating conformers at room temperature, which can be observed at low temperature. Relative line intensities further indicate that one of the conformers must be predominant. Examination of molecular models suggests that these two conformers must correspond to conformers **1***a* and **1***b* (Scheme 4), which are interconvertible by inversion of ring B. Inversion of ring A is also possible and must also take place at room temperature, but that leads to the mirror image conformers of **1***a* and **1***b* and is not important for our analysis. This interconversion of course can be detected by ^{13}C nmr at low temperature (see C-7, C-8, C-10, and C-11 for **1***a*, **1***b*, **4**, and **5** in Table 1).

Using straightforward steric arguments, it can be further predicted that conformer **1***a*, which has the oxygen atom axially oriented towards ring B, must be more stable than conformer **1***b* in which the heteroatom has been replaced by the sterically more demanding C_5 methylene group in that same axial position. Thus, **1***a* and **1***b* must correspond to the major and the minor conformers. Furthermore, it is possible to assign a chemical shift for each carbon of both conformers and show that they fit with the major and minor absorptions observed in the low temperature ^{13}C nmr spectra of compound **1**. The carbon chemical shift assignments for **1***a* and **1***b* are described in Table 1.

Considering the semiempirical methods for the determination of chemical shift in ^{13}C nmr (7, 12) and the analysis of the steric effects observed in each conformer, we can predict that major differences will be observed, in terms of chemical shifts for C_5, C_7, and C_{11}. Effectively, at room temperature, C_7 and C_{11} are averaged at 35.2 as well as C_8 and C_{10} at 21.9 ppm. At low temperature, C_7 and C_{11} in **1***a* appear at 28.7 and 40.4 ppm respectively while C_7 and C_{11} in **1***b* appear at 30.9 and 41.4 ppm respectively. Similarly, C_8 and C_{10} appear at 21.2 and 21.8 pm in **1***a*, and at 23.3 and 23.8 ppm in **1***b* respectively. This indicates clearly that ring A is rigid in **1***a* and **1***b* at low temperature. The fact that C_5, which is averaged at 36.5 ppm at room temperature and shows two absorptions at 37.8 and 30.4 ppm at low temperature (assigned for C_5 in **1***a* and **1***b* respectively), indicates that ring B is also rigid at low temperature.

The chemical shift assignment for conformers **1***a* and **1***b* was rigorously confirmed by comparison with the ^{13}C nmr spectra of the *tert*-butyl spiro ethers **4** and **5**. Indeed, these two isomers are excellent rigid models for conformers **1***a* and **1***b*. Their low and room temperature ^{13}C nmr spectra are reported in Table 1.

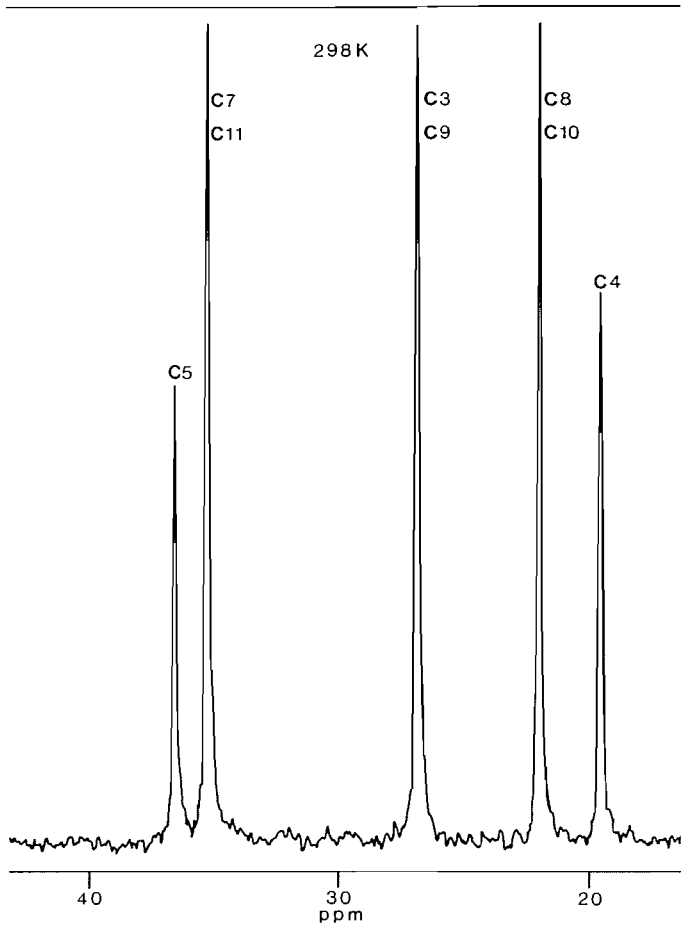

FIG. 1. The 15–45 ppm region of the ^{13}C nmr spectrum of 1-oxaspiro[5.5]undecane and chemical shift assignments in 10% CD_2Cl_2: CF_2Br_2 at 298K.

The presence of the *tert*-butyl group at C_9 renders ring B of **4** and **5** conformationally rigid at room temperature and these isomers must exist in conformations **4***a* and **5***b* respectively. However, ring A of isomers **4***a* and **5***b* must undergo rapid inversion at that temperature, which leads to the formation of the mirror image conformations of **4***a* and **5***b* respectively. The consequence of this rapid inversion is that the chemical shift at C_7 and C_{11}, on one hand, and at C_8 and C_{10} on the other, must be averaged in two single absorptions in isomer **4** as well as in isomer **5**. Of course, the chemical shift values of these carbons should differ in isomers **4** and **5**. The chemical shift assignments for C_7 and C_{11}, as described in Table 1 for the room temperature spectra of **4** and **5**, are in agreement with this discussion.

At low temperature, the rapid chair–chair interconversion of ring A in **4***a* and **5***b* is expected to slow down considerably, at least on the nmr scale. On that basis, different chemical shifts should now appear for C_7, C_8, C_{10}, and C_{11} in both isomers. Again, the exact values for these chemical shifts must be different in **4** and **5**. Furthermore, the four different signals for isomers **4** and **5** must now be very similar to those of conformers **1***a* and **1***b* respectively because **4** has a conformation (**4***a*) identical to **1***a* and the same is true for **5** (i.e., **5***b*) versus **1***b*. The spectral data described in Table 1 clearly show that with the expected exception of C_9 and the *tert*-butyl group, the low temperature spectra of **4** and **5** are indeed essentially superimposable with those of **1***a* and **1***b* respectively.

At 148 K, we have the spectra of conformers **1***a* and **1***b* as

Can. J. Chem. Downloaded from www.nrcresearchpress.com by 91.144.44.67 on 09/07/12
For personal use only.

Can. J. Chem. Downloaded from www.nrcresearchpress.com by 91.144.44.67 on 09/07/12
For personal use only.

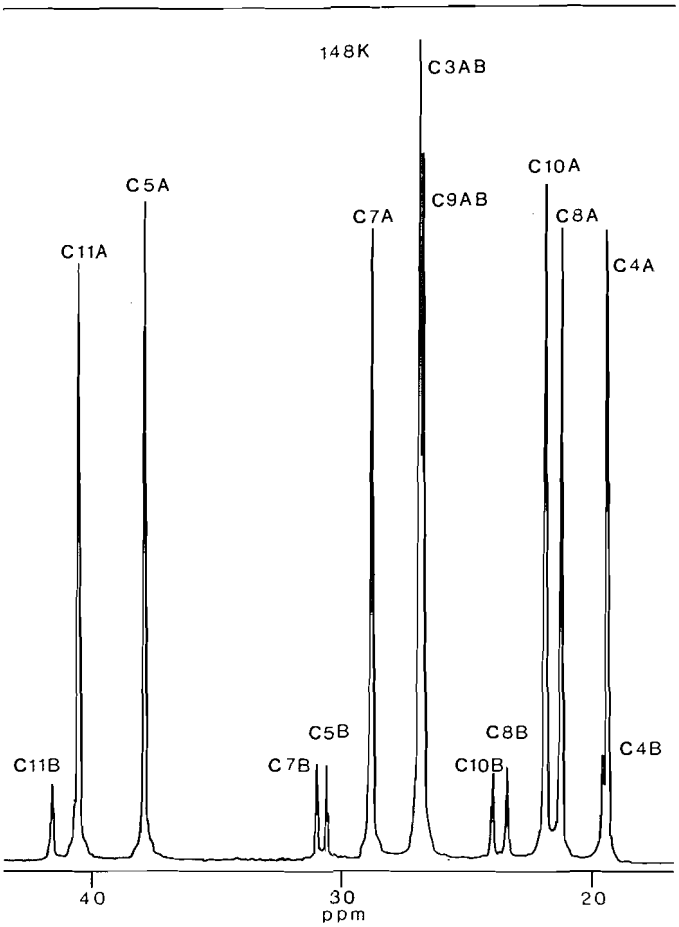

FIG. 2. The 15–45 ppm region of the ^{13}C nmr spectrum of 1-oxaspiro[5.5]undecane and chemical shift assignments in 10% CD_2Cl_2: CF_2Br_2 at 148 K.

well as the chemical shift of each carbon atom for each conformer. At 298 K, we have the average chemical shifts for the corresponding carbon atoms of the two conformers at equilibrium. The averaged chemical shifts at equilibrium depend on the chemical shifts for each carbon atom of each conformer at 148 K, and their relative population at 298 K. The relative population is related to the free energy difference, ΔG^0, between the two conformers and this can be calculated from the observed chemical shifts at 298 and 148 K using the following equation (13) where K_{298} is the population ratio of conformers **1***a* and **1***b* at 298 K.

$$K_{298} = \frac{P_{1a}^{298}}{P_{1b}^{298}} = \frac{\delta_{obs}^{298} - \delta_{1b}^{148}}{\delta_{1a}^{148} - \delta_{obs}^{298}}$$

Using the C_5 chemical shift values ($\delta_{obs}^{298} = 36.5$, $\delta_{1a}^{148} = 37.8$, and $\delta_{1b}^{148} = 30.4$ ppm), the calculated value for K_{298} is equal to 4.7. This value shows that the relative percentage of the two conformers at 298 K is 82% of **1***a* and 18% of **1***b*. ΔG_{298}^0 can be calculated from the usual equation, $\Delta G_{298}^0 = -RT \ln K_{298}$, and this gives a value of $\Delta G_{298}^0 = -0.9$ kcal/mol.

Using molecular models, we can now estimate the steric effects occurring in **1***a* and **1***b* utilizing steric parameters identical to those previously used in our analysis of the 1,7-dioxaspiro[5.5]undecane **2**. In conformer **1***b* these are two methylene groups (C_5 and C_7) oriented axially, and in conformer **1***a* there is one oxygen and one methylene group (C_7) axially oriented. When a methylene group is axially oriented, it corresponds to two *gauche* forms of butane evaluated at 0.9 kcal/mol each (14). When an oxygen is axially oriented, it corresponds to two *gauche* forms of *n*-propyl ether (O-CH_2-CH_2-CH_2) evaluated at 0.4 kcal/mol each (15). Using these values, the steric effects for conformers **1***a* and **1***b* are estimated to be 2.6 and 3.6 kcal/mol. The calculated difference in free energy, ΔG^0, between conformers **1***a* and **1***b* is thus 1.0 kcal/mol in favor of conformer **1***a*. This value is essentially identical to the experimental value of 0.9 kcal/mol. This analysis thus indicates that the values chosen for the steric effects are essentially correct. As one would expect, this also confirms that there is no need to consider parameters other than the steric one to understand the conformational behavior of compounds like spiro ethers **1**, **4**, and **5**.

The importance of the above work in relation to the *endo* and the *exo* anomeric effects stems from the completely different conformational behavior of spiro ether **1**, compared with that of spiro ketal **2**. The first compound is conformationally mobile at room temperature whereas spiro ketal **2** is not. Furthermore, spiro ether **1** exists as a mixture of a major and a minor conformer whereas spiro ketal **2** exists solely in a single rigid conformation.

First, the results obtained with **1** confirm that the steric parameters previously used for the analysis of spiro ketal **2** must be essentially correct.[4] On that basis, as discussed previously (7) (cf. footnote 3), the relative stabilities of conformers **2***a*, **2***b*, and **2***c* would be 0, 1, and 2 kcal/mol respectively, indicating that this compound could not exist in a single rigid conformation. However, if stereoelectronic effects are taken into consideration, and a value of 1.4 kcal/mol is chosen for each anomeric effect (i.e., two in **2***a*, one in **2***b*, and zero in **2***c*), the relative stabilities of conformers **2***a*, **2***b*, and **2***c* become 0, 2.4, and 4.8 kcal/mol, values that indicate that compound **2** must exist essentially in one single conformation, both at room as well as at low temperature, in accord with the experimental results.

Finally, in concluding, it is important to point out that although steric effects alone are sufficient to favor almost exclusively rotamers A_1 and E_1 in some α- and β-*C*-glycosides (6), the preferred occurrence of these rotamers in normal α- and β-*O*-glycosides *must be a result of a combination of steric and stereoelectronic effects as previously concluded.*

Experimental

All the reactions, with the exception of hydrogenation, were executed under an atmosphere of argon and were monitored by thin-layer chromatography (tlc). The intermediates were purified by flash chromatography (17) (silica gel; AcOEt in hexanes) and the final spiro ethers **1**, **4**, and **5** were purified by preparative vapor-phase chromatography (vpc). Spiro ethers **1** and **5** were obtained pure and spiro ether **4** in a mixture along with spiro ether **5**.

Vapor-phase chromatographic analysis and separations were carried out on a Varian Aerograph 920 chromatograph equipped with a thermal conductivity detector and using a 10% SE-30 on Chromosorb W column (6 ft × 3/8 in.). The infrared (ir) spectra were recorded neat or in chloroform on a Perkin–Elmer 681 spectrophotometer. Mass spectra (ms) were obtained on Micromass ZAB-1F spectrometer. Proton and carbon-13 nuclear magnetic resonance (^1H and ^{13}C nmr) spectra were recorded on a Brüker WM-250 spectrometer equipped with an Aspect 2000 computer and operating at 250 MHz for proton and 63 MHz for carbon-13. The free induction decays (FIDs) were sampled over 3000 Hz for proton and 10 000 Hz for carbon-13 using 16 384 data points. For ^1H nmr, the samples were run in deuterochloroform using the signal from residual chloroform (7.26 ppm) as an internal standard.

[4]It was suggested recently that such values might be incorrect (16).

Can. J. Chem. Downloaded from www.nrcresearchpress.com by 91.144.44.67 on 09/07/12
For personal use only.

For ^{13}C nmr, spiro ether **1** was run in CD_2Cl_2 at 298 K, and the signal observed at 26.8 ppm from TMS, corresponding to the absorption for C_3, has been used as an internal standard for all the other experiments executed at room temperature or at low temperature with spiro ethers **1**, **4**, and **5** (see Table 1). Spiro ethers **4** and **5** have also been run in deuterochloroform at 293 K with the signal from solvent at 77.0 ppm being used as an internal standard. For all experiments executed in dibromodifluoromethane (CBr_2F_2) the samples were prepared as follows. Spiro ethers **1**, **4**, and (or) **5** (~125 mg) were dissolved in bidistilled CBr_2F_2 containing 10% V/V CD_2Cl_2 for locking purposes. The spectra of spiro ether **1** were recorded at 298 and 148 K, whereas those of spiro ethers **4** and (or) **5** were recorded at 298 and 163 K, the desired temperature being maintained with a precision of ±1 K. Below 160 K, spiro ethers **4** and **5** were slightly insoluble in the mixture of solvents used.

The following abbreviations are used: RT (room temperature); s (singlet); d (doublet); t (triplet); q (quartet); m (multiplet); rf (rate of flow); δ (ppm from TMS).

Acetylenic tosylate 6

To a stirred solution of *p*-toluenesulfonyl chloride (22 mmol, 4.2 g) in CH_2Cl_2 (45 mL) at RT, is added triethylamine (29 mmol, 4 mL). After 5 min stirring, commercially available 3-butyn-1-ol (20 mmol, 1.5 mL) is added dropwise and the resulting mixture is stirred overnight. After that period, the reactional mixture is diluted to 100 mL with CH_2Cl_2 and the organic phase is washed with aqueous 1 N HCl (2 × 25 mL), saturated $NaHCO_3$ (2 × 25 mL), and saturated NaCl (1 × 25 mL). The organic phase is then dried ($MgSO_4$), filtered, and the solvent is evaporated under reduced pressure. Acetylenic tosylate **6** (4.3 g, 95% yield) is obtained pure and used without further purification; ^1H nmr δ: 1.98 (1H, t, J = 2.5 Hz, H-C≡C), 2.45 (3H, s, CH_3), 2.56 (2H, t of d, J = 7.0 Hz, 2.5 Hz, $CH_2C{\equiv}C$), 4.10 (2H, t, J = 7.0 Hz, CH_2O), 7.35 (2H, d, J = 7.2 Hz, aromatic), 7.80 (2H, d, J = 7.2 Hz, aromatic); ms m/e: 224 (M^+).

Hydroxy-tosylate 8

The acetylenic tosylate **6** (20 mmol, 4.48 g) is dissolved in anhydrous THF (50 mL) and that solution is stirred during 30 min at −78°C (Dry Ice: acetone). Then *n*-butyllithium (20 mmol, 12.5 mL, solution 1.6 M in hexane) is added dropwise and, after addition, the purple solution is stirred at −78°C for a further 30 min. A solution of cyclohexanone (20 mmol, 2.07 mL) in anhydrous THF (25 mL) is then added dropwise, slowly, and after addition the reactional mixture is stirred at −78°C during 2 h. After that period, the reaction is quenched with water (1 mL) and the resulting mixture is allowed to warm to RT. The mixture is diluted with Et_2O (100 mL) and the organic phase is dried ($MgSO_4$), filtered, and the solvent is evaporated under reduced pressure. Flash chromatography (AcOEt/hexane:silica gel) of the crude oil (6.3 g) gives pure acetylenic hydroxy-tosylate **7** (5.0 g, 78% yield); ^1H nmr δ: 1.3–2.0 (11H, m, cyclohexanol ring), 2.48 (3H, s, CH_3), 2.60 (2H, t, J = 7.0 Hz, $CH_2C{\equiv}C$), 4.10 (2H, t, J = 7.0 Hz, CH_2O), 7.35 (2H, d, J = 7.2 Hz, aromatic), 7.80 (2H, d, J = 7.2 Hz, aromatic). The triple bond of the acetylenic hydroxy-tosylate **7** (15.5 mmol, 5.0 g) is then completely hydrogenated by reaction with H_2 over PtO_2 catalyst at 40 psi (1 psi = 6.9 kPa) during 4 h in dry MeOH. After hydrogenation the reactional mixture is filtered, MeOH is evaporated under reduced pressure, and flash chromatography (AcOEt/hexane:silica gel) of the resulting crude oil gives pure hydroxy-tosylate **8** (2.53 g, 50% yield); ^1H nmr δ: 1.1–1.8 (17H, m, cyclohexanol ring, 3 chain CH_2), 2.46 (3H, s, CH_3), 4.05 (2H, t, J = 6.8 Hz, CH_2O), 7.35 (2H, d, J = 8.0 Hz, aromatic), 7.80 (2H, d, J = 8.0 Hz, aromatic).

1-Oxaspiro[5.5]undecane 1

The hydroxy-tosylate **8** (3.5 mmol, 1.14 g) is dissolved in anhydrous THF (20 mL) and that solution is stirred 30 min at −78°C. Then *n*-butyllithium (3.5 mmol, 2.2 mL, solution 1.6 M in hexane) is added slowly and, after addition, the reactional mixture is allowed to warm to RT and stirred for a further 2 h. Anhydrous $NaHCO_3$ (500 mg) is then added, the mixture is filtered, and the solvent evaporated under reduced pressure. The volatile spiro ether **1** (300 mg, 55% yield) is then obtained from the residual oil and purified by preparative vpc. The purification is realized using a 10% SE-30 on Chromosorb W column (6 ft × 3/8 in.); rf: 4.5 min at 160°C; ir: 2990, 2930, 2860, 1490, 1210, and 1075 cm^{-1}; ^1H nmr δ: 1.1–1.8 (16H, m, 8 CH_2), 3.56 (2H, t, J = 8.0 Hz, CH_2O); ^{13}C nmr (in CD_2Cl_2 at 298 K) δ: 71.8 (s), 60.8 (t), 36.2 (t), 35.2 (t), 26.8 (t, two very close peaks), 22.1 (t), 19.4 (t); ms m/e: 154 (M^+).

Hydroxy-tosylates 10

The hydroxy-tosylates **10** were obtained from 4-*tert*-butylcyclohexanone and the acetylenic tosylate **6**, following exactly the same experimental procedure as the one used to obtain hydroxy-tosylate **8**, with a 33% overall yield.

Intermediate acetylenic hydroxy-tosylates **9**; ^1H nmr δ: 0.85 (9H, s, *tert*-butyl), 0.9–2.0 (10 H, m, cyclohexanol ring), 2.45 (3H, s, CH_3), 2.60 (2H, t, J = 7.0 Hz, $CH_2C{\equiv}C$), 4.10 (2H, t, J = 7.0 Hz, CH_2O), 7.35 (2H, d, J = 7.2 Hz, aromatic), 7.80 (2H, d, J = 7.2 Hz, aromatic); the ^1H nmr spectrum does not show the presence of the two possible isomers.

Hydroxy-tosylates **10**: ^1H nmr δ: 0.85 (9H, s, *tert*-butyl), 0.9–2.0 (16H, m, cyclohexanol ring, 3 chain CH_2), 2.45 (3H, s, CH_3), 4.03 (2H, t, J = 6.8 Hz, CH_2O), 7.35 (2H, d, J = 7.0 Hz, aromatic), 7.80 (2H, d, J = 7.0 Hz, aromatic); once again there is no evidence for the presence of both hydroxy-tosylates **10**.

9-tert-Butyl-1-oxaspiro[5.5]undecanes 4 and 5

The spiro ethers **4** and **5** were obtained from the hydroxy-tosylates **10**, following exactly the same experimental procedure as the one used to obtain spiro ether **1**, with a 65% overall yield, total for both isomers, with a 9:1 ratio in favor of isomer **5**.

Spiro ethers **4** and **5**, mixture ~1:1; rf: 5.1 min (**4**) and 5.8 min (**5**) at 185°C; ir: 2935, 2780, 1450, 1165, and 1090 cm^{-1}; ^1H nmr δ: 0.85 (18H, s, *tert*-butyl (**4** and **5**), 0.9–2.0 (30 h, m, 2 CH, 14 CH_2 (**4** and **5**)), 3.60 (2H, t, J = 8.0 Hz, CH_2O (**4**)), 3.70 (2H, t, J = 8.0 Hz, CH_2O (**5**)); ms m/e: 210 (M^+).

Spiro ether **4**; ^{13}C nmr (in $CDCl_3$ at 298 K), δ: 71.2 (s), 61.0 (t), 48.8 (d), 37.6 (t), 35.2 (t), 32.8 (s), 28.0 (q), 26.7 (t), 22.2 (t), 19.5 (t).

Spiro ether **5**; ^{13}C nmr (in $CDCl_3$ at 298 K), δ: 73.2 (s), 61.6 (t), 48.5 (d), 36.2 (t), 32.6 (s), 31.1 (t), 28.0 (q), 26.8 (t), 24.1 (t), 19.5 (t).

Spiro ether **5**, pure; rf: 5.8 min at 185°C; ir: 2940, 2860, 1450, 1365, and 1090 cm^{-1}; ^1H nmr δ: 0.85 (9H, s, *tert*-butyl), 0.9–2.0 (15H, m, CH, 7 CH_2), 3.70 (2H, t, J = 8.0 Hz, CH_2O); ^{13}C nmr (in $CDCl_3$ at 298 K) δ: 73.2 (s), 61.6 (t), 48.5 (d), 36.2 (t), 32.6 (s), 31.1 (t), 28.0 (q), 26.8 (t), 24.1 (t), 19.5 (t); ms m/e: 210 (M^+).

Acknowledgements

This research was supported by the Natural Sciences and Engineering Research Council of Canada (NSERCC, Ottawa) and by the "Ministère de l'Éducation" (FCAR, Québec).

1. B. Fuchs, L. Schleifer, and E. Tartakovsky. Nouv. J. Chim. **5**, 275 (1984); H. M. Berman, S. S. Chu, and G. A. Jeffrey. Science, **157**, 1576 (1967).
2. P. Deslongchamps. Stereoelectronic effects in organic chemistry. Organic chemistry series. Vol. 1. *Edited by* J. E. Baldwin. Pergamon Press, Oxford, England. 1983; A. J. Kirby. The anomeric effect and related stereoelectronic effects at oxygen. Springer Verlag, Berlin. 1983.
3. R. U. Lemieux, S. Koto, and D. Voisin. The *exo* anomeric effect. *In* Anomeric effect, origin and consequences. *Edited by* W. A. Szarek and D. Horton. ACS Symposium Series 87. Washington, DC. 1979. p. 17; R. U. Lemieux and S. Koto. Tetrahedron, **30**, 1933 (1974).
4. R. U. Lemieux. Ann. N.Y. Acad. Sci. **222**, 915 (1973).
5. A. J. de Hoog, H. R. Buys, C. Altona, and E. Havinga. Tetrahedron, **25**, 3365 (1969); A. J. de Hoog and H. R. Buys. Tetrahedron Lett. 4175 (1969); M. Gelin, Y. Bahurel, and G. Descotes. Bull. Soc. Chim. Fr. 3723 (1970).

6. T. C. WU, P. G. GOEKJIAN, and Y. KISHI. J. Org. Chem. **52**, 4819 (1987); P. G. GOEKJIAN, T. C. WU, H. Y. KANG, and Y. KISHI. J. Org. Chem. **52**, 4823 (1987); S. A. BABIRAD, Y. WANG, P. G. GOEKJIAN, and Y. KISHI. J. Org. Chem. **52**, 4825 (1987); Y. WANG, P. G. GOEKJIAN, D. M. RYCKMAN, and Y. KISHI. J. Org. Chem. **53**, 4151 (1988).
7. P. DESLONGCHAMPS, D. D. ROWAN, N. POTHIER, G. SAUVE, and J. K. SAUNDERS. Can. J. Chem. **59**, 1105 (1981); P. DESLONGCHAMPS, D. D. ROWAN, N. POTHIER, and J. K. SAUNDERS. Can. J. Chem. **59**, 1122 (1981); N. POTHIER, D. D. ROWAN, P. DESLONGCHAMPS, and J. K. SAUNDERS. Can. J. Chem. **59**, 1132 (1981).
8. P. CANONNE, G. B. FOSCOLOS, and D. BÉLANGER. J. Org. Chem. **45**, 1828 (1980); J. C. COMBRET, M. LARCHEVEQUE, and Y. LEROUX. Bull. Soc. Chim. Fr. **10**, 3501 (1971).
9. D. K. DALLING, D. M. GRANT, and E. G. PAUL. J. Am. Chem. Soc. **95**, 3718 (1973).
10. G. STORK and J. M. STRYKER. Tetrahedron Lett. **24**, 4887 (1983); J. C. RICHER. J. Org. Chem. **30**, 324 (1965).
11. J. B. STOTHERS. Carbon 13 NMR spectroscopy. Academic Press, New York, NY. 1972.
12. H. BEIERBECK, J. K. SAUNDERS, and J. W. APSIMON. Can. J. Chem. **55**, 2813 (1977).
13. E. L. ELIEL. Chem. Ind. 568 (1959); E. L. ELIEL and R. J. L. MARTIN. J. Am. Chem. Soc. **90**, 682 (1968); **90**, 689 (1968).
14. H. BOOTH and J. R. EVERETT. J. Chem. Soc. Chem. Commun. 278 (1976); F. A. L. ANET, C. H. BRADLEY, and G. W. BUCHANAN. J. Am. Chem. Soc. **93**, 258 (1971).
15. H. J. SCHNEIDER and V. HOPPEN. Tetrahedron Lett. 579 (1974).
16. K. B. WIBERG and M. A. MURCKO. J. Am. Chem. Soc. **111**, 4821 (1989).
17. W. C. STILL, M. KAHN, and A. MITRA. J. Org. Chem. **43**, 2923 (1978).

Can. J. Chem. Downloaded from www.nrcresearchpress.com by 91.144.44.67 on 09/07/12
For personal use only.

Phase transitions in solid cycloheptene

JULIAN HAINES AND D. F. R. GILSON[1]

Department of Chemistry, McGill University, 801 Sherbrooke St. W., Montreal, Que., Canada H3A 2K6

Received October 16, 1989

JULIAN HAINES and D. F. R. GILSON. Can. J. Chem. **68**, 604 (1990).

The phase transition behaviour of cycloheptene has been investigated by differential scanning calorimetry, proton spin-lattice relaxation, and vibrational spectroscopy (infrared and Raman). Two solid–solid phase transitions were observed, at 154 and 210 K, with transition enthalpies and entropies of 5.28 and 0.71 kJ mol^{-1} and 34.3 and 3.4 J K^{-1}, respectively. Cycloheptene melted at 217 K with an entropy of melting of 4.5 J K^{-1} mol^{-1}. The bands in the vibrational spectra of the two high temperature phases were broad and featureless, characteristic of highly disordered phases. The presence of other conformers, in addition to the chair form, was indicated from bands in the spectra. The ring inversion mode was highly phase dependent and exhibited soft mode type behaviour prior to the transition from the low temperature phase. The low frequency Raman spectra (external modes) of these phases indicated that the molecules are undergoing isotropic reorientation. In the low temperature phase, the vibrational bands were narrow; the splitting of the fundamentals into two components and the presence of nine external modes are consistent with unit cell symmetry of either C_2 or C_s with two molecules per primitive unit cell. A glassy state can be produced from the intermediate phase and the vibrational spectra were very similar to those of the high temperature phases, indicating that static disorder was present. The barriers to reorientation, as obtained from proton spin-lattice relaxation measurements, are 9.0 kJ mol^{-1} in both the high temperature phases, and 15.4 kJ mol^{-1} in the low temperature, ordered phase.

Key words: cycloheptene, phase transition, differential scanning calorimetry, NMR, vibrational spectroscopy.

JULIAN HAINES et D. F. R. GILSON. Can. J. Chem. **68**, 604 (1990).

Utilisant la calorimétrie à balayage différentiel, la relaxation protonique spin-réseau et la spectroscopie de vibration (infrarouge et Raman), on a étudié le comportement du cycloheptène à ses transitions de phase. On a observé deux transitions de phase solide–solide, l'une à 154 K et l'autre à 210 K; les enthalpies et les entropies de transition sont respectivement de 5,28 et 0,71 kJ mol^{-1} et de 34,3 et 3,4 J K^{-1} mol^{-1}. Le cycloheptène fond à 217 K avec une entropie de fusion de 4,5 J K^{-1} mol^{-1}. Les bandes observées dans les spectres de vibration des deux phases de température élevée sont larges et sans traits marquants, caractéristiques de phases hautement désordonnées. La présence d'autres conformères, en plus de la forme chaise, peut être déduite de la présence d'autres bandes dans les spectres. Le mode d'inversion de cycle dépend fortement de la phase et, avant la transition de la phase de basse température, il présente une comportement typique d'un mode souple. Les spectres Raman de basse fréquence (modes externes) de ces phases indiquent que des molécules subissent une réorientation isotrope. Dans la phase de basse température, les bandes de vibration sont étroites; on observe un couplage des bandes fondamentales en deux composantes ainsi que neuf modes externes qui sont en accord avec symétrie C_2 ou C_s d'une maille qui comporterait deux molécules par maille primitive. On peut produire un état vitreux à partir de l'état intermédiaire et ses spectres de vibration sont semblables à ceux observés avec les phases de température plus élevée; ces résultats indiquent qu'un désordre statique est présent. Pour chacune des deux phases de température élevée, les barrières à la réorientation, telles qu'obtenues par des mesures de relaxation protonique spin-réseau, sont égales à 9,0 kJ mol^{-1} alors que cette barrière est de 15,4 kJ mol^{-1} pour la phase ordonnée de basse température.

Mots clés : cycloheptène, transition de phase, calorimétrie à balayage différentiel, RMN, spectroscopie de vibration.

[Traduit par la revue]

Introduction

Order–disorder transitions, known to occur in saturated cyclic hydrocarbons, also occur in some of their unsaturated analogues (1, 2). A differential thermal analysis (DTA) investigation of cycloheptene (3) indicated that a phase transition occurs at 153 K, well below the melting point of 217 K. The same study also showed that cycloheptene could form a glassy crystal, which exhibits a glass transition temperature of 100 K. This behaviour is similar to that of many other cyclic hydrocarbons with ring puckering vibrations, for which glassy crystals are readily formed. These include cyclohexene, cycloheptane, and 1,3,5-cycloheptatriene (3, 4).

The infrared and Raman spectra of gaseous, liquid, and solid cycloheptene have been investigated previously, and have indicated that, in the liquid at room temperature, an equilibrium exists between the chair and boat conformations, with the chair being favoured (5). The same study also indicated that, in the low temperature solid, cycloheptene exists in the chair form. The emphasis of this investigation was to perform a normal coordinate analysis and vibrational assignment, and hence no mention was made of the solid–solid phase transitions. The solid state spectrum was obtained from samples quenched at liquid nitrogen temperature and subsequently annealed. Force field calculations (6) have indicated that the chair conformation is more stable than the boat by 3.37 kJ mol^{-1}. A recent electron diffraction study confirmed that the chair form is the favoured conformation (7).

Previous work on order–disorder transitions in solids (8–10) has demonstrated the effectiveness of various combinations of calorimetric, variable-temperature vibrational spectroscopy, and proton spin-lattice relaxation time measurements, in investigating the phase transition behaviour of a given compound. In the case of cycloheptene, very little information is available on the solid phases, and the present investigation provides a better understanding of the phase transition behaviour of this compound.

Experimental

Cycloheptene (Wiley Organics, purity 99%) was repeatedly distilled under vacuum prior to use. Cycloheptene (Aldrich Chemical Co., purity 97%), distilled under vacuum was used in some of the Raman experiments.

[1]Author to whom correspondence may be addressed.

Can. J. Chem. Downloaded from www.nrcresearchpress.com by 91.144.44.67 on 09/07/12
For personal use only.

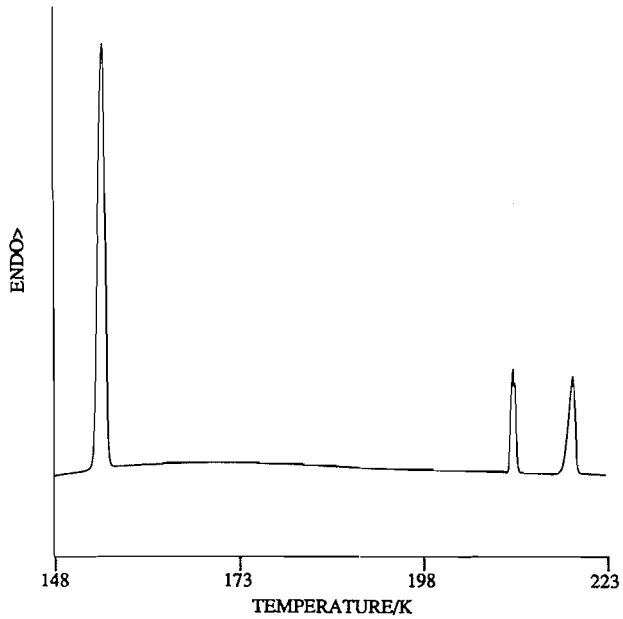

FIG. 1. DSC scan of annealed cycloheptene upon heating.

Differential scanning calorimetric (DSC) measurements down to 123 K were performed on a Perkin–Elmer DSC 7 calorimeter, which was calibrated on the solid–solid phase transition of cyclohexane (Aldrich Chemical Co. "Gold Label"). The calibration was found not to depend on the scan rate used (2.5 and 5 K min^{-1}). Samples, typically between 5 and 10 mg, were weighed on a Cahn microbalance and sealed in aluminum DSC pans. Spin-lattice relaxation times were measured by the inversion–recovery sequence using a Spin-lock CPS-2 spectrometer operating at 33 MHz. Sample temperature was varied by a stream of cold nitrogen gas.

Raman spectra were recorded on an Instruments S.A. spectrometer with a Jobin–Yvon Ramanor U-1000 1.0 m double monochromator, using a Spectra Physics model 164 argon-ion laser for excitation. The resolution was typically 1 or 2 cm^{-1}. Infrared spectra (1 cm^{-1} resolution) were acquired on a Nicolet 6199 FT-IR spectrometer. The sample temperature was controlled for both FT-IR and Raman experiments, with a Cryodyne Cryocooler model 21 cryostat (Cryogenics Technology Inc.), and measured using a silicon-diode temperature sensor attached to a Cryophysics model 4025 controller. The Raman spectra were obtained by cooling liquid samples in sealed glass capillary tubes, which were mounted onto the cold finger of the cryostat using indium foil as a conducting junction. The infrared spectra were measured on thin films sprayed on a potassium bromide window.

Results and discussion

DSC results, Fig. 1, indicate the presence of two solid–solid phase transitions in cycloheptene. Transition temperatures, enthalpies, and entropies are listed in Table 1. The phases are numbered in sequence from high to low temperature. The entropy of melting of 4.5 J K^{-1} mol^{-1} is very low, indicating that phase I is highly disordered, and the sum of the entropies of melting and the II → I transition is, in fact, very close to the values reported for the entropy of melting of cyclohexane (11) and of cycloheptane (12). Upon cooling, cycloheptene was found to supercool from the liquid down, through the melting point, to between 201 and 203 K with the I → II transition occurring 2–6 K below this temperature. The ΔS values for the freezing and I → II transitions were found to be −3.4 and −4.7 J K^{-1} mol^{-1}, respectively, the reverse of those obtained on heating. Phase II was also found to supercool well below the II → III transition temperature, and to transform irreversibly to phase III at 129 K upon heating. This supercooling and subsequent irreversible transition to phase III are consistent with previous DTA results (3). The II → I transition was found to occur reversibly with no significant thermal hysteresis.

TABLE 1. DSC results for cycloheptene

Transition	T_{onset} (K)	ΔH (kJ mol^{-1})	ΔS (J K^{-1} mol^{-1})
III → II	154	5.28	34.3
II → I	210	0.71	3.4
I → liquid	217	0.97	4.5

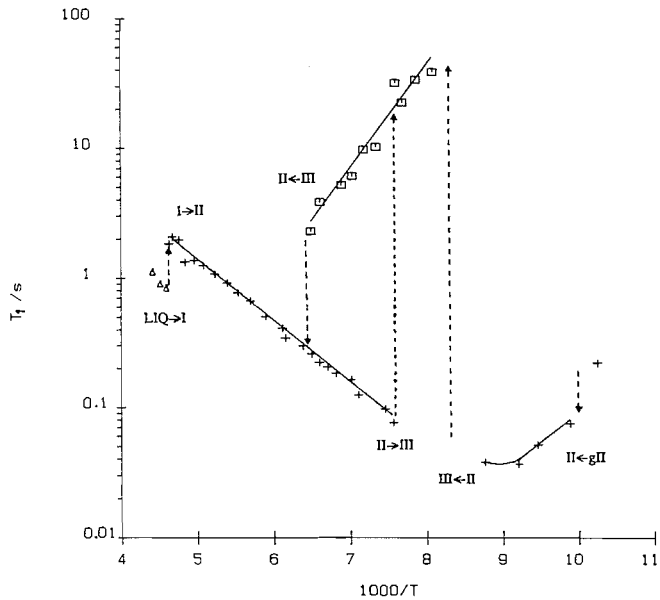

FIG. 2. Proton spin-lattice relaxation times in cycloheptene.

Transition entropies can be related to the disordering occurring at a phase transition by using the Guthrie–McCullough expression (13), $\Delta S = R \ln (N_1/N_2)$, where R is the gas constant and N_1 and N_2 are the number of distinguishable orientations in the high and low temperature phases, respectively. Applying this expression to the III → II and II → I transitions, entropy changes equivalent to $R \ln 62$ and $R \ln 1.5$ were obtained, respectively. While a 62-fold disordering process is unrealistic, the 1.5-fold or 6/4-fold disordering at the II → I transition could be due to a transition from a lattice of cubic to one of hexagonal symmetry. An alternative interpretation of the III → II transition can be made if the approach of Clarke *et al.* (14, 15) is taken, in which a contribution of approximately 10.3 J K^{-1} mol^{-1} is subtracted from the entropy of transition to account for the slackening of the lattice. This approach would produce a value of $R \ln 18$ for the configurational entropy, and hence an 18-fold disordering at the transition. This disordering contains both orientational and conformational contributions. The chair, boat, and twist-chair conformations of cycloheptene as well as the corresponding inverted structures are all of similar energy (6), and therefore interconversion between them could contribute to the total disorder.

Proton spin-lattice relaxation times, Fig. 2, were measured from just above the melting point down to 98 K, the temperature limit of the instrument. An increase in T_1 was observed at the freezing point, followed by continuous decrease in T_1 down to

Can. J. Chem. Downloaded from www.nrcresearchpress.com by 91.144.44.67 on 09/07/12
For personal use only.

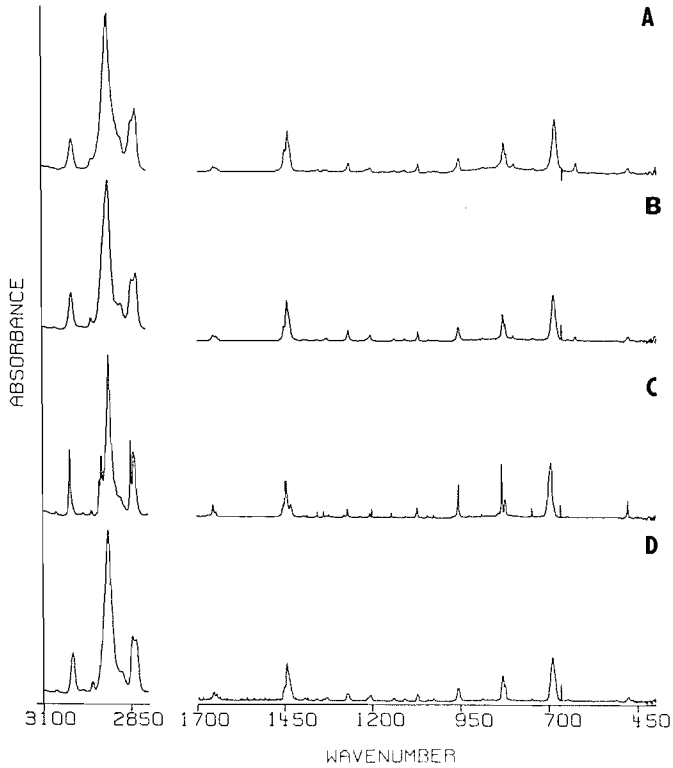

FIG. 3. Comparison of the infrared spectrum of cycloheptene: (A) phase I at 210 K; (B) phase II at 165 K; (C) phase III at 60 K; and (D) phase gII at 86 K (not to scale).

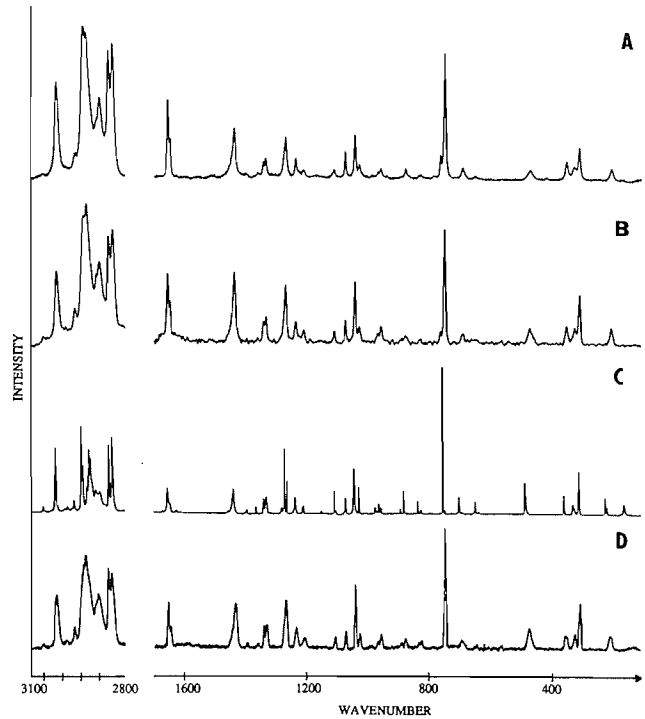

FIG. 4. Comparison of the Raman spectrum of cycloheptene: (A) phase I at 215 K; (B) phase II at 165 K; (C) phase III at 47 K; and (D) phase gII at 54 K (not to scale).

131 K. At this temperature, a sharp increase in T_1 was observed as supercooled phase II transformed to phase III. Phase III exhibited a decrease in T_1 with increasing temperature. Upon rapidly cooling phase II down to 98 K, the glassy crystal, phase gII, was formed. This phase reverted to phase II above the glass transition at 100 K, at which point the value of T_1 decreased abruptly. The supercooled phase II formed in this manner showed a decrease in T_1 with increasing temperature until the irreversible transition to phase III was observed.

Barriers to reorientation were calculated from the linear portions of the plots of ln T_1 versus reciprocal temperature. The results obtained are 15.4 kJ mol^{-1} for phase III and 9.0 kJ mol^{-1} for both phases I and II. A value of 8.7 kJ mol^{-1} was obtained for phase II below 120 K. The barrier in phase III is lower than the barrier for ring inversion of 20.9 kJ mol^{-1}, obtained in solution (16). However, ring inversion or a related motion, possibly involving interconversion between different conformers, is the most likely candidate for the motion occurring in this phase. The transition to phase II occurred before a T_1 minimum was reached, but phase II, on the other hand, appeared to reach a T_1 minimum upon heating from the glassy crystal. The value obtained, 0.035 s, corresponds to a C value, the constant from the BPP equation, of 6.3×10^9 rad^2 s^{-2}. This would be equivalent to a decrease in second moment of the resonance line of 8.8 G^2 at the III $\rightarrow$ II transition. A change of this magnitude could be the result of a transition in overall motion from ring inversion, or a related process that was not as yet fully developed, to isotropic rotation and lattice diffusion, although no definite conclusion can be made to this effect.

The vibrational spectra of phases I and II contained broad featureless bands and were characteristic of disordered solids, Figs. 3–5. Many bands were observed that were not present or were extremely weak in the low temperature phase III. These include the bands at 803 and 629 cm^{-1} in the infrared spectrum and those at 762 and 420 cm^{-1} in the Raman spectrum of phase II, Table 2. The band at 629 cm^{-1} has previously been assigned to a vibration of the boat conformation (5). The band at 327 cm^{-1} was also assigned to a vibration of the boat conformation, but no decrease in intensity was observed in the Raman spectrum upon passing to phase III. Conversely, the weak band at 420 cm^{-1}, which was not present in the Raman spectrum of phase III, was assigned as a fundamental vibration of the chair form. The present results would favor the band at 420 cm^{-1} being due to a conformation other than the chair and that at 327 cm^{-1} being due to the most stable conformation, presumably the chair form. The presence of additional bands in the spectra of these two upper phases indicated that a mixture of conformers in equilibrium with one another was present.

The spectra of the glassy crystal, phase gII, were very similar to those of phase II, with the main differences being that some of the bands had shoulders and were shifted slightly in frequency, and that there was a broad band in the low frequency Raman spectrum. In addition, the bands due to conformations other than the chair form were less intense than in phase II. This indicates that, as the temperature decreases, the equilibrium shifts in favor of the chair form. The ease with which cycloheptene supercools and forms this glassy crystal is related to the large degree of conformational disorder present in phase II.

The transformation of phase gII to phase III after passing through its glass transition can be seen from the changes in infrared linewidth of ν_{18} and ν_{45}, Fig. 6. These vibrations are both mixtures of a C—C stretch and various CH_2 vibrations. A marked decrease in the linewidth of both bands upon transition to phase III was observed, followed by an increase at the III $\rightarrow$ II transition temperature.

Can. J. Chem. Downloaded from www.nrcresearchpress.com by 91.144.44.67 on 09/07/12
For personal use only.

Can. J. Chem. Downloaded from www.nrcresearchpress.com by 91.144.44.67 on 09/07/12
For personal use only.

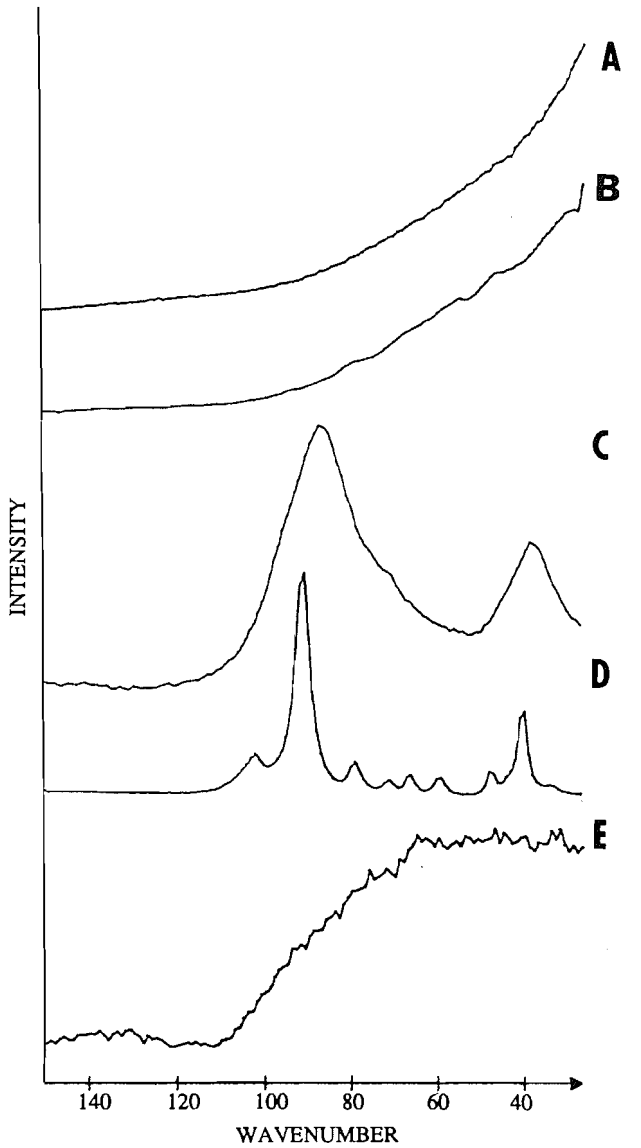

FIG. 5. Comparison of the low frequency Raman spectrum of cycloheptene: (A) phase I at 215 K; (B) phase II at 165 K; (C) phase III at 140 and (D) at 47 K; and (E) phase gII at 54 K (not to scale).

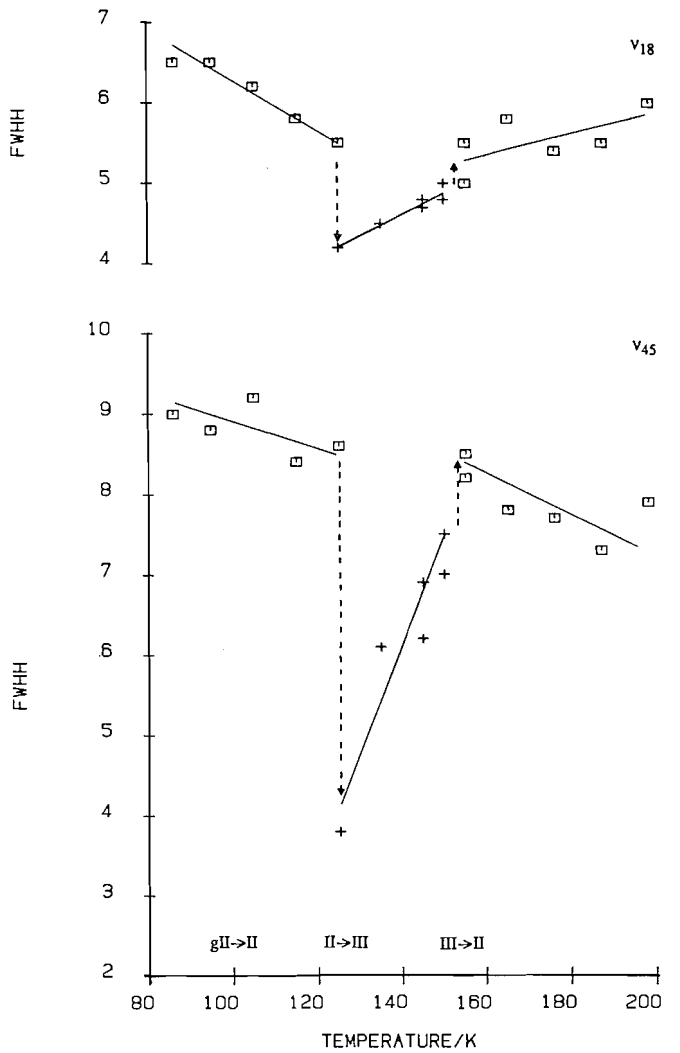

FIG. 6. Temperature dependence of the infrared linewidth (FWHH) in cm^{-1} of ν_{18} and ν_{45}.

The spectra of phase III were markedly different from those of the other phases. The bands were sharp, and the majority were split into at least two components. In particular, ν_{36} and ν_{42}, both a mixture of a CH_2 wag and a C—C stretch, split into two components in the IR and the Raman spectrum. In addition, many bands exhibited shifts in frequency, especially the out-of-plane vibrations. The lowest frequency out-of-plane vibration, ν_{28}, the ring inversion, was observed at 163 cm^{-1} in phase III, at 114 cm^{-1} in phase II, and at 132 cm^{-1} in phase gII. Such large shifts in the frequencies of the out-of-plane vibrations result from the closer packing the molecules experience in the high density, ordered phase III, which increases the barrier to the motion. In phase III, this band shifted by 8 cm^{-1} between 47 and 150 K and broadened significantly, Figs. 7 and 8; it then exhibited a decrease in frequency of more than 40 cm^{-1} at the phase transition. This behaviour is similar to that observed for the ring inversion modes in cyclohexene (9) and pentamethylene sulfide (10), except in this case the magnitude of the frequency shift is much greater. The frequency shift and broadening observed prior to the phase transition are indicative of the role played by the ring inversion vibration in the phase transition process. The linear relationship between the square of the frequency of ν_{28} and temperature, Fig. 9, is typical of soft mode type behaviour, indicating that this vibration is involved in driving the phase transition.

The infrared and Raman bands in phase III are coincident within experimental error, indicating that mutual exclusion does not apply and therefore the crystal belongs to a non-centrosymmetric space group. The point group of cycloheptene, C_s, restricts the possible site groups to C_1 and C_s. This, the observed splitting of the internal modes, and the presence of nine distinct external modes restrict the crystal to non-centrosymmetric monoclinic and orthorhombic space groups with at least two molecules per primitive unit cell. The most probable candidates are the monoclinic space groups with C_2 and C_s symmetry and two molecules located on the general positions. This presence of the molecules on the general positions prevents any further limitation of the choice of possible space groups.

The absence of external modes in the low frequency Raman spectra of phases I and II is consistent with the presence of isotropic molecular reorientation (17–19), as was proposed on the basis of the NMR results. Further evidence in support of this

TABLE 2. Vibrational data (cm^{-1}) for cycloheptene

Raman				Infrared				
Phase III (47 K)	Phase II (165 K)	Phase I (215 K)	Phase gII (54 K)	Phase III (60 K)	Phase II (165 K)	Phase I (210 K)	Phase gII (86 K)	Assignment[a]
3064w	3065vw	3065w	3065w	3064w	3065w		3064w	ν_{29}
3024vs	3019s	3020s	3018s	3025s	3019s	3019s	3018s	ν_1
2994w	2992w	2992w	2996w	2994w	2992w		2989w	
2986w			2988w	2986w			2986w	
2964w	2962w	2961w	2963w	2964w	2962m	2962m	2962m	ν_2
2939vs				2941m				
2935s	2930vs	2930vs	2928sh	2935m				ν_3
2921m	2920vs	2920vs	2920vs	2919vvs	2919vvs	2917vvs	2919vvs	
2914vs	2915sh		2912sh	2915vvs				ν_{31}
2910s								
2906sh	2907sh	2906sh						
2893m	2889m	2887m	2889sh					
2880m	2880m	2879m	2881s	2887sh	2880m	2880m	2880m	
2873sh	2873sh							ν_4
2864sh								
2850vs	2849s	2849s	2847vs					ν_5
				2852s	2849s	2848s	2848s	ν_{32}
				2844s				
				2841s	2837s	2837s	2838s	ν_{33}
2839vs	2835s	2835s	2836vs					
2830sh								ν_7
1654m	1656s	1655s	1655s	1654m	1656m	1654m	1653m	ν_8
1647mw	1647s	1647s	1646s	1646w	1684m	1647m	1646m	
1624mw				1626mw				
1456w	1451sh	1452sh		1457sh	1453m	1453m	1452sh	
				1454m				ν_9
1446m	1445sh	1445sh	1446sh	1447s	1445s	1445s	1445s	ν_{34}
1441w								ν_{10}
1438m	1437s	1437s	1435s	1439m	1439sh	1439sh	1437sh	ν_{35}
1433sh	1427sh			1433m				ν_{11}
1397w	1397vw	1397vw	1396vw	1396w	1395w		1394w	
1394w				1392vw				ν_{36}
				1386w	1385vw		1386w	
1362w	1359w	1359w	1360vw	1361w	1359w	1359w	1361vw	
				1357w				ν_{37}
1340sh	1340m	1340m	1340m	1339w	1340w		1340w	
1338m								ν_{12}
1331m	1332m	1331m	1331m	1333vw	1332w	1332w	1330w	ν_{13}
1329m				1327w				
1325m				1324w				ν_{38}
1279w				1281w				
1273sh								
1269vs	1268s	1269s	1269s	1272w	1271m	1271m	1272m	ν_{14}
1260m				1262vw		1260m		ν_{15}
1238w								

Can. J. Chem. Downloaded from www.nrcresearchpress.com by 91.144.44.67 on 09/07/12
For personal use only.

TABLE 2 (*continued*)

Raman				Infrared				
Phase III (47 K)	Phase II (165 K)	Phase I (215 K)	Phase gII (54 K)	Phase III (60 K)	Phase II (165 K)	Phase I (210 K)	Phase gII (86 K)	Assignment[a]
1234m	1234m	1234m	1235m	1235w	1237vw 1219w	1237vw 1219w	1236vw 1214sh	ν_{16}
1209w 1206w	1209w	1209w	1207m	1208w	1208w	1209w	1207w	ν_{40}
				1202w				ν_{17}
1185vw	1188vw	1188w	1185vw	1185vw		1182vw		
1148vw				1145w	1139w	1143w	1141w	ν_{41}
1106 1102w	1109w	1109w	1108m	1106w 1104sh	1109w	1111w	1108w	ν_{42}
1072sh 1069m	1073m	1073m	1073m	1073m	1072m	1073m	1073w	ν_{18}
1041s	1041s	1042m	1042vs	1042w	1041w	1042w	1042w	ν_{19}
1025m	1027m	1027m	1027m	1025w	1026w	1027w	1026w	ν_{43}
972w 970sh	968w	967w	969w	968vvw			968sh	$2\nu_{25}$
964sh 960w	957m	957m	957m	960sh 956m	958m	958m	957m	ν_{45}
953w 951sh								
	920w		922w	924vw				
889w	888vw		889w	889w	889w	889w	888w	ν_{46}
878m 876sh	876w	876w	876w	879w	874w	873w		ν_{21}
			845w	843sh	846w			$\nu_{28} + \nu_{24}$
833m	829w	829w	832w	833s	833m	833m	832s	ν_{47}
824w 823w			825w	825m 823m	826w	826m	825m	ν_{22}
					803w	804w		
762vvw	762w	762w	761vvw	762vvw				[b]
751vvs	749vvs	749vvs	750vvs	748s	748w	749w	748w	ν_{23}
741w				745w				
	717w	717w						
699m 689vw	691m	691m	695m	699sh 696s	690s	690s	692s	ν_{24}
653w 647m	647vw	649vw	647w	652w 647w	648vw	649vw	652w 649vw	$\nu_{28} + \nu_{49}$
635vw			632vw	627vvw	629w	630w		[b]
	565vw	566vw						
484m 482m				484sh 479m	480m	481w	477w	ν_{25}
474w	473m	473m	475m					ν_{49}
	420w	419w	420vw	418vw	418vw			[b]
361sh 359m	355m	356m	359m 354m					ν_{26}

Can. J. Chem. Downloaded from www.nrcresearchpress.com by 91.144.44.67 on 09/07/12
For personal use only.

TABLE 2 (*concluded*)

Raman				Infrared				
Phase III (47 K)	Phase II (165 K)	Phase I (215 K)	Phase gII (54 K)	Phase III (60 K)	Phase II (165 K)	Phase I (210 K)	Phase gII (86 K)	Assignment[a]
329m 326m	327m	327m	327m					ν_{27}
308m 298s	312m	311w	310s					ν_{50}
224m 219w	209m	209m	212m					ν_{51}
163m	114sh	110sh	132w,br					ν_{28}
102m 91vs 80m 72w 68w 59w 48m 40s 31w			46s,br					Intermolecular vibrations

[a]Following ref. 5.
[b]Bands corresponding to conformations other than the chair form.

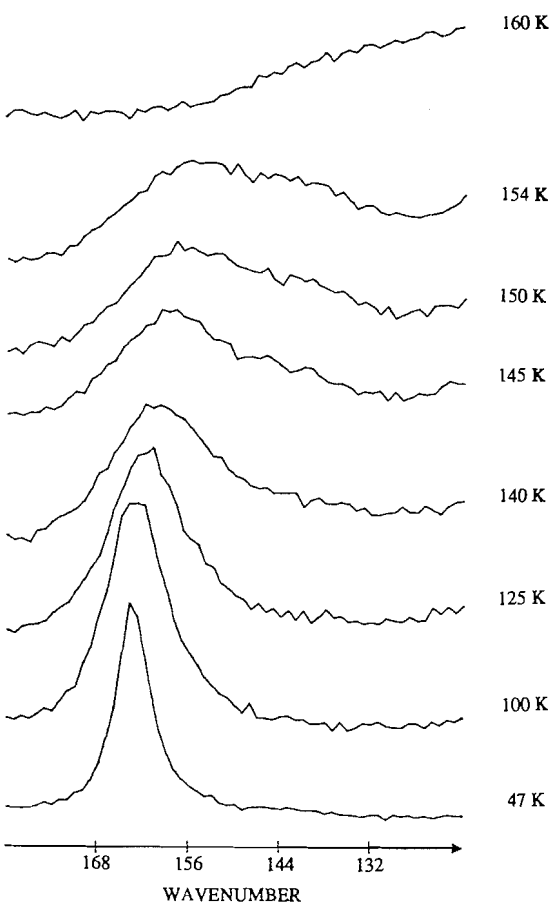

FIG. 7. Temperature dependence of the ring inversion mode of cycloheptene.

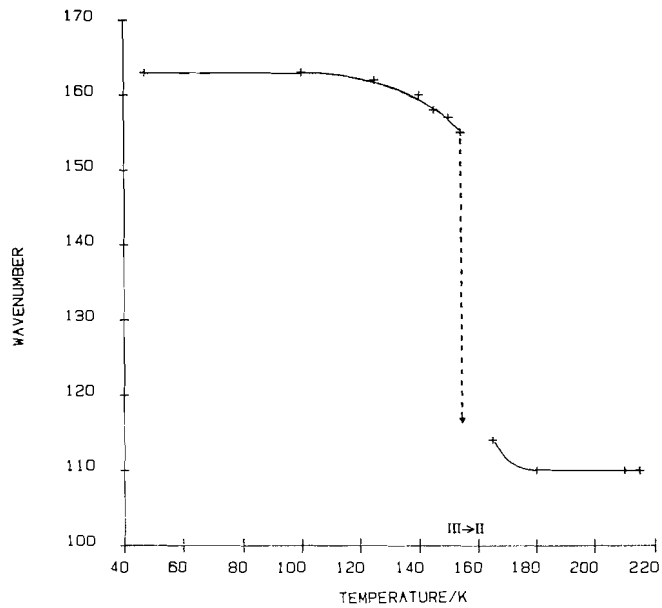

FIG. 8. Temperature dependence of the ring inversion mode frequency in cm^{-1} of cycloheptene.

conclusion is that τ, the correlation time for this motion as calculated from the proton T_1 measurements, was found to vary from 1.8×10^{-10} s at 154 K to 2.4×10^{-11} s at the melting point.

That discrete external modes were observed for phase III is indicative of an ordered crystal. These bands shifted slightly with temperature, Fig. 10, and broadened considerably. The broad band in the low frequency spectrum of phase gII indicated that static disorder was present, corresponding to a freezing-in

Can. J. Chem. Downloaded from www.nrcresearchpress.com by 91.144.44.67 on 09/07/12
For personal use only.

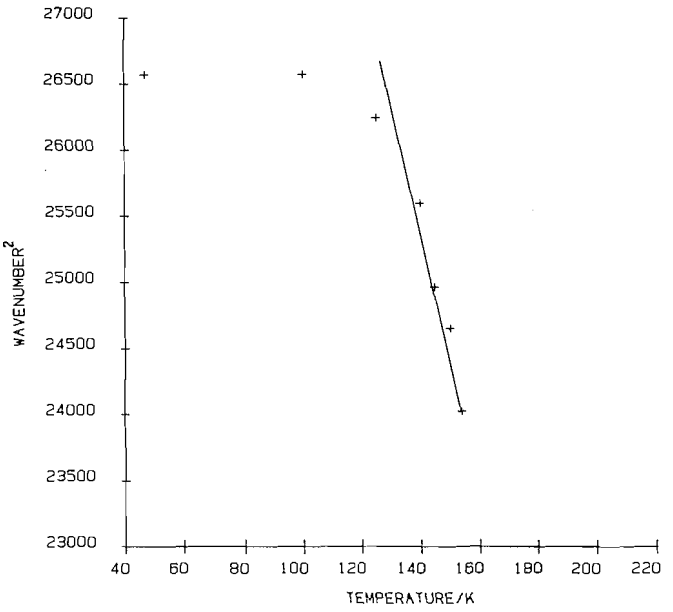

FIG. 9. Temperature dependence of the square of the ring inversion mode frequency in cm^{-2} of cycloheptene.

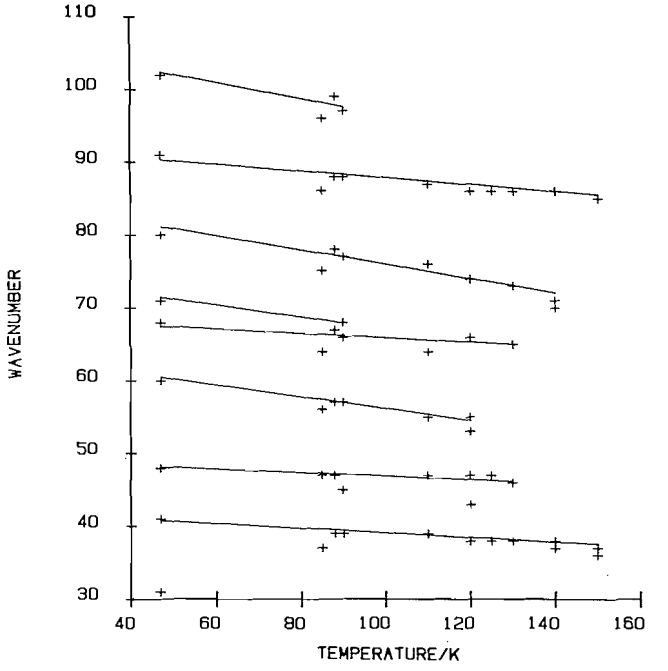

FIG. 10. Temperature dependence of the low frequency Raman spectrum of cycloheptene.

of the disorder in phase II. This spectrum was similar to that of glassy crystalline cyclohexanol (20), which has a disordered structure of cubic symmetry. In contrast, the low frequency Raman spectra of the glassy crystalline phases of cyclohexene were found to contain many overlapping bands, indicating that these phases are of lower symmetry (9). These phases arise from the cooling of the metastable phase III and the high temperature phase I, both of which are characterized by anisotropic disorder.

Acknowledgements

This research was supported by grants from the Natural Sciences and Engineering Research Council of Canada. J.H. acknowledges the award of a scholarship from NSERC.

1. N. G. PARSONAGE and L. A. K. STAVELEY. Disorder in crystals. Clarendon, Oxford. 1978.
2. H. M. HUFFMAN, M. EATON, and G. D. OLIVER. J. Am. Chem. Soc. **70**, 2911 (1948).
3. K. ADACHI, H. SUGA, and S. SEKI. Bull. Chem. Soc. Jpn. **43**, 1916 (1970).
4. H. SUGA and S. SEKI. J. Non-Cryst. Solids, **16**, 195 (1974).
5. N. NETO, C. DI LAURO, and S. CALIFANO. Spectrochim. Acta, **26A**, 1489 (1970).
6. N. L. ALLINGER and J. T. SPRAGUE. J. Am. Chem. Soc. **94**, 5734 (1972).
7. L. I. ERMOLAEVA, V. S. MASTRYUKOV, N. L. ALLINGER, and A. ALMENNINGEN. J. Mol. Struct. **196**, 151 (1989).
8. J. HAINES and D. F. R. GILSON. J. Phys. Chem. **93**, 20 (1989).
9. J. HAINES and D. F. R. GILSON. Can. J. Chem. **67**, 941 (1989).
10. J. HAINES and D. F. R. GILSON. J. Phys. Chem. **93**, 6237 (1989).
11. J. G. ASTON, G. J. SZASZ, and H. L. FINKE. J. Am. Chem. Soc. **65**, 1135 (1943).
12. H. L. FINKE, D. W. SCOTT, M. E. GROSS, J. F. MESSERLEY, and G. WADDINGTON. J. Am. Chem. Soc. **78**, 5469 (1956).
13. J. B. GUTHRIE and J. P. MCCULLOUGH. J. Phys. Chem. Solids, **18**, 28 (1961).
14. T. CLARK, H. MACKLE, M. A. MCKERVEY, and J. J. ROONEY. J. Chem. Soc. Faraday Trans. 1, **70**, 1279 (1974).
15. T. CLARK, T. MCO. KNOX, H. MACKLE, and M. A. MCKERVEY. J. Chem. Soc. Faraday Trans. 1, **73**, 1224 (1977).
16. M. ST-JACQUES and C. VAZIRI. Can. J. Chem. **49**, 1256 (1971).
17. S. S. BUKALOV and L. A. LEITES. Proc. Int. Conf. Raman Spectrosc. **8**, 611 (1982).
18. J. L. SAUVAJOL. J. Chim. Phys. **82**, 219 (1985).
19. G. N. ZHIZHIN, YU. N. KRASJUKOV, E. I. MUKHTAROV, V. N. ROGOVOI, and N. V. SIDEROV. Croat. Chem. Acta, **61**, 685 (1988).
20. D. W. JAMES, H. F. SHURVELL, and R. M. PARRY. J. Raman Spectrosc. **5**, 201 (1976).

Can. J. Chem. Downloaded from www.nrcresearchpress.com by 91.144.44.67 on 09/07/12
For personal use only.

Photooxidation of 9,10-diethoxyanthracene: mechanistic dichotomies between homogeneous solution and reverse micelle photoprocesses

R. J. DeVoe,[1] M. R. V. Sahyun,[1] and E. Schmidt[2]
3M Science Research Laboratory, St. Paul, MN 55144, U.S.A.

and

D. K. Sharma
Canadian Centre for Picosecond Laser Flash Spectroscopy, Concordia University, Montréal, Qué., Canada H3G 1M8

Received June 21, 1989

R. J. DeVoe, M. R. V. Sahyun, E. Schmidt, and D. K. Sharma. Can. J. Chem. **68**, 612 (1990).

We have compared the photooxidation of the title compound, DEA, by diphenyliodonium salts in homogeneous acetonitrile (AN) and in heptane/AOT/water reverse micelle solutions. The reaction is efficient, which we attribute to rapid (ca. 10 ps) deethylation of the DEA radical cation, initially formed by photoinduced electron transfer. In AN, the electron transfer occurs from singlet excited DEA, but in reverse micelles it is gated by intersystem crossing to triplet DEA. Under these conditions, DEA fluorescence quenching by the iodonium cation may still be observed; we infer operation of the external heavy atom effect as the primary mechanism.

Key words: anthracene, electron transfer, reverse micelle, photochemistry, picosecond.

R. J. DeVoe, M. R. V. Sahyun, E. Schmidt et D. K. Sharma. Can. J. Chem. **68**, 612 (1990).

On a comparé la photo-oxydation du composé mentionné dans le titre, le DEA, par des sels de diphényliodonium en solution homogène dans l'acétonitrile (AN) et dans des solutions micellaires inversées d'heptane/AOT/eau. La réaction est efficace et on attribue cette caractéristique à une dééthylation rapide (environ 10 ps) du cation radiocalaire DEA qui se forme originalement par un transfert d'électron photoinduit. Dans l'AN, le transfert d'électron se produit à partir d'un singulet excité du DEA; toutefois, dans les micelles inversées, cette réaction se produit par le biais d'un échange intersystème vers l'état triplet du DEA. Dans ces conditions, on peut encore observer le piégeage de la fluorescence du DEA par le cation iodonium. On en conclut que l'effet d'un atome lourd extérieur agit comme mécanisme primaire.

Mots clés : anthracène, transfert d'électron, micelle inversée, photochimie, picoseconde.

[Traduit par la revue]

Introduction

We previously (1) studied the anthracene sensitized photolyses of both diphenyliodonium and triphenylsulphonium salts in solution using both steady-state and laser flash photolysis techniques. Photoproducts, namely phenylated anthracenes along with iodobenzene or diphenylsulphide, respectively, were obtained from both salts with quantum efficiencies of ca. 0.1 at 375 nm. Accordingly we inferred the intermediacy of diphenyliodo and triphenylsulphur radicals formed by single electron transfer from the singlet excited anthracene (1), and we developed a comprehensive model of this chemistry. The overall reaction scheme is shown in Fig. 1, and the estimated rate constants for each significant step are listed in Table 1.

In the present work, we extend our observations to 9,10-diethoxyanthracene, DEA (2), as electron-transfer sensitizer for the diphenyliodonium cation. This system is not only of theoretical interest, but of technological importance as well (3). Our starting point was to make use of the reaction scheme of Fig. 1, with the goal of evaluating the corresponding rate constants when DEA substituted for anthracene. We recognized that blocking the 9- and 10-positions on the anthracene nucleus should inhibit the radical-wasting recombination pathway, which leads with anthracene, itself, principally to coupling at the 9-position (1). As will be seen, the major difference between anthracene and DEA sensitization involves active participation of the latter in the chemistry immediately consequent to the primary electron-transfer process.

The resulting highly efficient destruction of the anthracene nucleus provides a convenient monitor for electron-transfer events, which proved convenient for the study of interfacial electron transfer in a reverse micellar system. This phenomenon is of considerable current interest (4–9), particularly with respect to possibilities of enhanced efficiency of electron transfer at phase boundaries (5, 9) and the rectifying behaviour of an interface between media of differing polarity (6). In particular, we chose to make a comparative study of the photooxidation of DEA by diphenyliodonium cation in acetonitrile solution and in the heptane/Aerosol-OT/water reverse micellar system, which is well characterized (7–10).

Experimental

Diphenyliodonium hexafluorophosphate (11), mp 136°C, was purified by recrystallization from isopropanol. The DEA, mp 136–149°C, was prepared (2) by D. E. Vogel, Graphic Research Laboratory, 3M. Spectral quality, glass-distilled acetonitrile, AN (EM OmniSolv®), and glass-distilled heptane were used for solution preparation.

Reverse micelles were made using ion-exchanged, glass-distilled water and recrystallized sodium *bis*-(2-ethylhexyl)sulphosuccinate (Aldrich Aerosol-OT, AOT), which had been taken up in heptane, dried over activated molecular sieves, and recovered by removal of solvent on a rotary evaporator. The residue was dried in a vacuum oven and stored in a vacuum desiccator. No luminescent impurities were detected in either the solvents or the surfactant. The procedures for making the reverse micellar solutions were as previously described (10); DEA was incorporated 1×10^{-4} M in the heptane.

Fluorescence intensities were recorded on a Perkin Elmer MPF-44B

[1]Authors to whom correspondence may be addressed at 3M Center, 201-3N-05, St. Paul, MN 55144, U.S.A. This is contribution no. 1705 from the 3M Corporate Research Laboratories.

[2]Undergraduate research participant, University of Wisconsin, River Falls, WI; present address, Department of Chemistry, Michigan State University, E. Lansing, MI 48824, U.S.A.

Printed in Canada / Imprimé au Canada

Can. J. Chem. Downloaded from www.nrcresearchpress.com by 91.144.44.67 on 09/07/12
For personal use only.

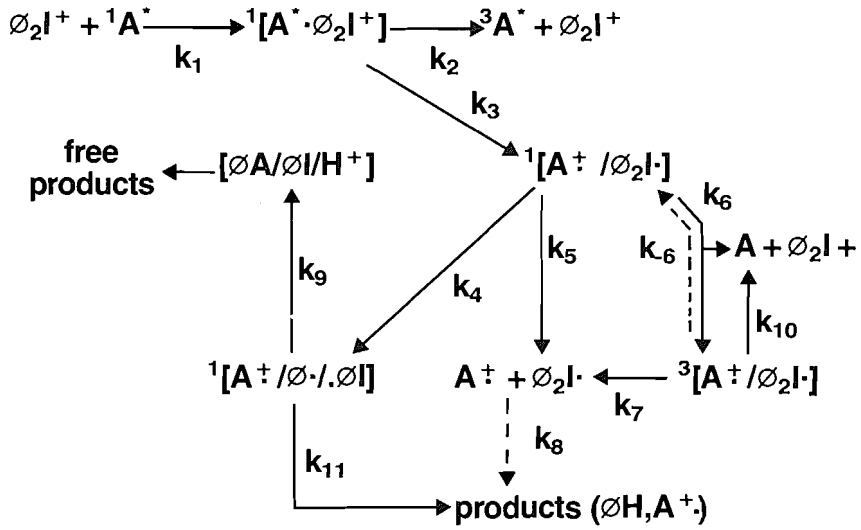

FIG. 1. Mechanistic scheme for anthracene sensitized photolysis of diphenyliodonium cation (from ref. 1); rate constants refer to Table 1.

TABLE 1. Parameters of the mechanistic schemes of Figs. 1 and 9

Variable	Anthracene[a]	DEA
Parameters:		
$k_1 = k_d[Ph_2I^+]$	$2 \times 10^{10}[Ph_2I^+]\ s^{-1}$	
k_2	1×10^8	ca. 0
k_3[b]	1×10^9	1×10^9
k_c	—	ca. 10^{11}
k_4	5×10^9	5×10^9
$k_5 = k_x$	5×10^8	5×10^8
k_6	5×10^{10}	$\leq 3 \times 10^{10}$
k_9	1×10^9	ca. 2×10^9
k_{11}	5×10^8	—

[a]From ref. 1.
[b]Assumed to be the same for both anthracene and DEA.

fluorescence spectrophotometer. The data for the Stern–Volmer plots, Figs. 3 and 4, are based on emission intensities at 450 nm of 0.3 mM anthracene solutions, excited by 370 nm radiation.

The photo-CIDNP spectra were obtained using the proton probe on a Varian XL-100 magnetic resonance spectrometer, with the probe modified to allow direct irradiation of the sample at the receiver coil. Typical sample composition was 0.0055 M 'onium salt and 0.0026 M DEA in acetonitrile-d_3. The light source was a 300-W Xe arc operating at full power, focused on the receiver coil using quartz optics on an optical rail. Heating of the sample was a problem, as infrared filtration decreased the light intensity too much to observe CIDNP. Consequently, photo-CIDNP spectra were recorded in the Fourier transform mode of the XL-100, collecting two transients over ca. 5 s exposure time, during which heating was minimal. Samples (2 mL volume) were deoxygenated by nitrogen purge, and dark spectra were taken before and after irradiation.

Quantum yields were measured with no more than 20% conversion of DEA on solutions 3×10^{-4} M in DEA and 0.005–0.10 M in the 'onium salt. The solutions were deoxygenated by dry argon purge, as required. Aliquots (3 mL) in a 1-cm quartz spectrophotometer cell were required at 366 ± 10 nm on an optical bench with light from the Xe arc lamp, passed through a monochromator with the slits adjusted to allow a 20-nm bandpass. The output of the source was calibrated by means of potassium ferrioxalate actinometry (12) and continuously monitored with a radiometer. Typical fluxes of 5×10^{-8} einstein min^{-1} resulted in ca. 20% conversion after 5 min irradiation. Ultraviolet absorption spectra were recorded on the samples in the reaction vessel before and after irradiation. For gas chromatographic analyses, the photolysis mixtures obtained after up to 10% conversion were diluted with 5 mL of 1 M aqueous sodium chloride and extracted with 1 mL cyclohexane containing 1×10^{-4} M dodecane as internal standard.

The instrumentation available at the Canadian Centre for Picosecond Laser Flash Spectroscopy has already been described in detail (13). The double-beam, mode-locked Nd-YAG laser system employed a silicon intensified target Vidicon detector. Light pulses at 355 nm were obtained by frequency-tripling; typical irradiances were ca. 2 mJ per pulse focused to a 2 mm diameter spot on the face of a 2-mm quartz sample cuvette. The pulse width was 30 ps (FWHM). Individual experiments utilized 0.6-mL aliquots of solutions 4×10^{-4} M in DEA and 0.10 M in the 'onium salt; the solutions were deoxygenated by dry argon purge prior to irradiation.

Results

Fluorescence quenching. AN solution

Like anthracene, DEA is highly fluorescent. Its absorption and fluorescence spectra are shown in Fig. 2. In carefully deoxygenated AN (but not hydrocarbon solvents), a room temperature phosphorescence spectrum may also be observed (Fig. 2). The fluorescence lifetime of DEA, determined in AN by time-correlated single photon counting, is 12.4 ns, about threefold longer than for anthracene itself. Accordingly, its fluorescence quantum yield is considerably higher, 0.68, by measurement in comparison with anthracene itself as 0.27 (14).

The quenching of DEA fluorescence, followed as the first-order fluorescence decay lifetime as a function of iodonium cation concentration in AN, is shown in Fig. 3. Quenching obeyed the Stern–Volmer relationship, with a slope of 201 ± 5 M^{-1}, close to the value expected for diffusion control.

Fluorescence quenching. Reverse micelles

The quenching of DEA fluorescence by (water-soluble) diphenyliodonium chloride in the reverse micelle system was next investigated. The water/AOT molar ratio, w, was taken as a variable in this study, and iodonium salt concentration was adjusted so that P, the average number of iodonium cations per water pool, remained within a reasonable range:

[1] $P = (nw[Ph_2I^+]/55)$

Can. J. Chem. Downloaded from www.nrcresearchpress.com by 91.144.44.67 on 09/07/12
For personal use only.

Can. J. Chem. Downloaded from www.nrcresearchpress.com by 91.144.44.67 on 09/07/12
For personal use only.

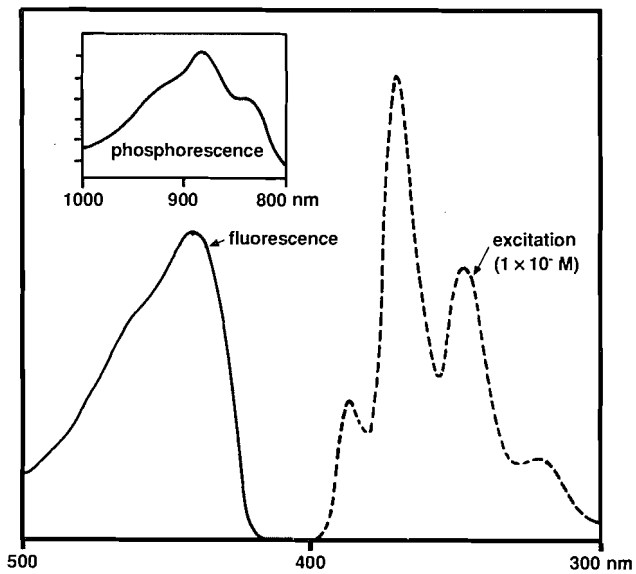

FIG. 2. Absorption and emission spectra of DEA in argon-purged AN.

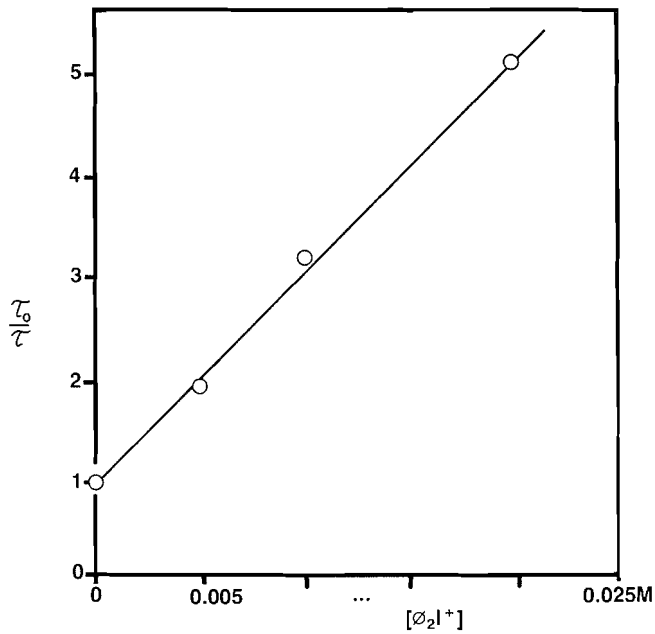

FIG. 3. Stern–Volmer plot for quenching of DEA fluorescence by diphenyliodonium hexafluorophosphate in AN.

The degree of aggregation of the AOT, n, i.e., the average number of AOT molecules associated with a typical micelle, had previously (10) been determined in luminescence probe experiments.

Under these conditions we expect that DEA would be entirely within the organic phase, while diphenyliodonium cation would be localized in the water droplets. The extent of fluorescence quenching at a given AOT concentration is accordingly

$$[2] \quad (I_0/I - 1) = k_d\Phi_q p\tau[\mathrm{AOT}]/n$$

so that the slope of the Stern–Volmer plots is given by

$$[3] \quad \mathrm{d}(I_0/I)/\mathrm{d}[\mathrm{AOT}] = k_d\Phi_q p\tau/n$$

where k_d is the rate constant for diffusional encounter of an

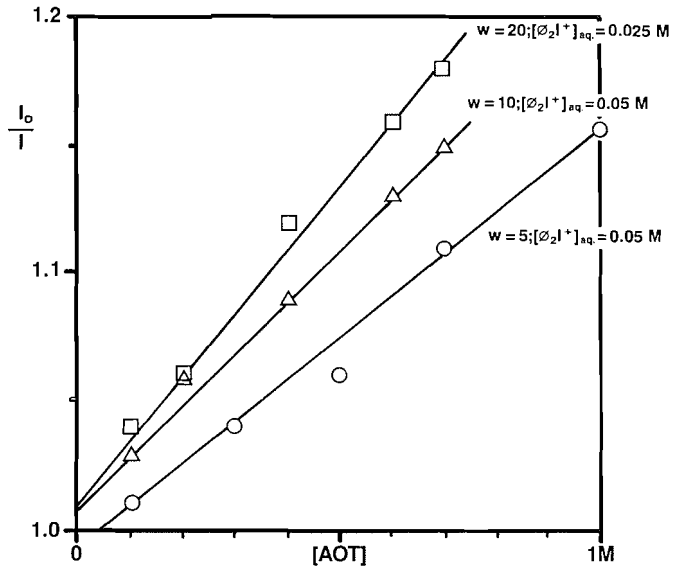

FIG. 4. Stern–Volmer plots for quenching of DEA fluorescence in heptane/AOT/water reverse micelle system; conditions of w = 5, 10, and 20 (see Table 2).

TABLE 2. DEA Fluorescence quenching by iodonium cation in reverse micelles

Parameter	$w = 5$	$w = 10$	$w = 20$
$[Ph_2I^+]$	0.050 M	0.050 M	0.025 M
n^a	33	48	80
p	0.14	0.35	0.52
$\mathrm{d}(I_0/I)/\mathrm{d}[\mathrm{AOT}]$	0.16 M^{-1}	0.20 M^{-1}	0.25 M^{-1}
Φ_q	0.31	0.22	0.31
r^b	0.989	0.994	0.995

[a] From ref. 10.
[b] Correlation coefficient for the Stern–Volmer analysis, Fig. 4.

excited DEA molecule with a water pool, numerically taken as $1 \times 10^{10}\,M^{-1}\,s^{-1}$, one half the usual bimolecular diffusion encounter rate constant in heptane, i.e., we assume diffusion of the micelle to be negligible in comparison with the diffusion of the DEA molecule; τ is the radiative lifetime of DEA in the absence of quencher, 12.4 ns; and p is the probability that any individual micelle contains one or more iodonium cation. From the Poisson distribution

$$[4] \quad p = 1 - \exp(-P)$$

so that Φ_q, the quenching probability, can be estimated directly from experimental data.

Typical Stern–Volmer plots are shown in Fig. 4 and the appropriate experimental parameters, along with the estimates of Φ_q from eq. [3], are listed in Table 2. The overall fluorescence intensity for DEA in heptane was essentially the same as in AN; the fluorescence was not quenched by AOT alone or by AOT/water micelles in the absence of added iodonium cation. The average value of Φ_q from Table 1, 0.27 ± 0.05, indicates that electron transfer quenching is substantially *less* efficient in the biphasic system than in homogeneous solution, in contradiction to our expectations from previously published studies (7).

Quantum yields. Homogeneous solution

Quantum yield determinations on the DEA sensitized (3 ×

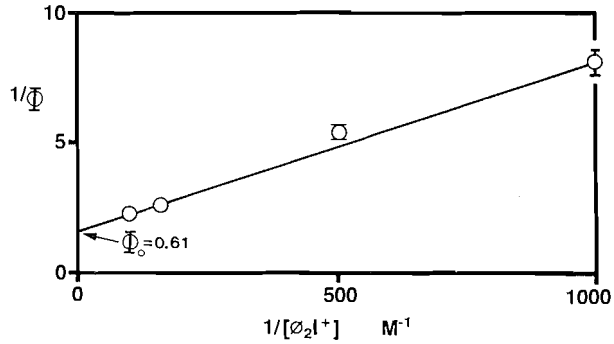

FIG. 5. Double reciprocal plot, $1/\Phi$ versus $1/[Ph_2I^+]$, for photooxidation of DEA by diphenyliodonium hexafluorophosphate in AN.

10^{-4} M in DEA) photolyses of diphenyliodonium hexafluorophosphate at 366 nm in AN were complicated by the complex mixture of reaction products detected by gas chromatographic analysis, none of which appeared to be formed stoichiometrically with iodonium salt or DEA disappearance. Iodobenzene, the principal product from diphenyliodonium cation decomposition under anthracene sensitization, did not appear in the product mixture in significant proportion, except on exhaustive photolysis.

A quantum yield for DEA photooxidation could be inferred from its spectrophotometric disappearance, e.g., at 366 nm, the irradiation wavelength. These data are shown in the form of a "double reciprocal plot" in Fig. 5. From the reciprocal of the intercept, the limiting quantum yield, Φ_0, of 0.60 is estimated. The ratio of the intercept to the slope of the plot is 240 M^{-1}, in reasonable agreement with the slope of the Stern–Volmer plot, Fig. 3, indicating mechanistic commonality of the quenching and bleaching phenomena in homogeneous solution. Determination of DEA disappearance by gas chromatographic analysis was less precise (±20%), but indicated in general that the spectrophotometric measure underestimated the extent of reaction by ca. 25%, i.e., the actual Φ_0 for the electron-transfer sensitized photolysis of the iodonium cation is better estimated as 0.75. Comparing the efficiency of fluorescence quenching, above, we conclude that essentially every quenching event leads to photochemistry in homogeneous solution.

Photo-CIDNP studies

Photochemically induced dynamic nuclear polarization (photo-CIDNP) spectra obtained with both anthracene and DEA (Fig. 6) sensitization of diphenyliodonium hexafluorophosphate photolysis in AN reveal emissions corresponding to both benzene and iodonium cation. Following the interpretation of the results with anthracene (1) in accord with Kaptein's Rules (15), we infer that benzene is a cage-escape product from a singlet radical pair while we assign the iodonium salt polarization to back electron transfer involving magnetic field induced T_-–S_0 mixing in a triplet radical pair. (There is no evidence that this occurs in the absence of the applied magnetic field, or even that triplet radical pairs form under normal circumstances.) Insofar as it competes with observable photochemistry, we expect back electron transfer entirely within the singlet manifold to be transparent to the CIDNP probe. We attribute the absence of photo-CIDNP signals corresponding to DEA and DEA-derived products to exchange broadening by interaction of the arene radical cations with the neutral hydrocarbons (16).

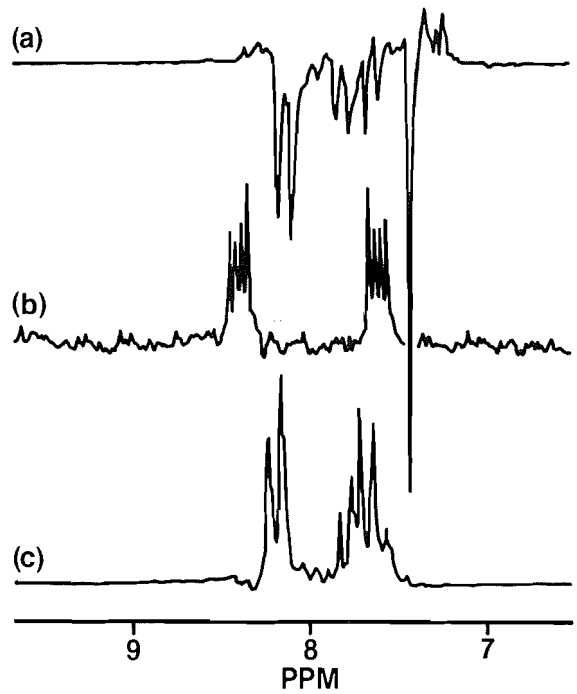

FIG. 6. (a) Photo-CIDNP spectrum for DEA, 2.6×10^{-3} M, sensitized photolysis of diphenyliodonium hexafluorophosphate, 5.5×10^{-3} M in AN-d_3; (b) reference proton nmr spectrum of DEA, 0.010 M in AN-d_3; (c) reference spectrum of diphenyliodonium cation, 0.15 M in AN-d_3.

Product identification

The mixture of products from the AN photolysis was further probed by high resolution gas chromatography in tandem with mass spectrometry. On a mixture corresponding to ca. 20% conversion, based on DEA, in addition to the remaining DEA and iodobenzene, in low yield, significant products exhibiting *m/e* ratios of 314, 342, and 374 were observed. (Other peaks corresponding to fragmentation products of DEA were also observed.) The first of these, which can be observed by gas chromatography from the start of the photoreaction, corresponds to $C_{22}H_{18}O_2$, and may be represented as either the anthrone, EAO, or an anthrol:

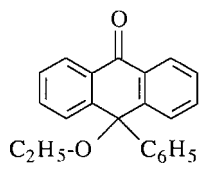

EAO

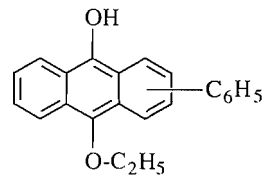

Anthrol

We prefer the former assignment, as it readily accounts for the disappearance of the DEA chromophore, almost quantitatively, at ca. 10% conversion. Its formation represents formal loss of an ethyl group from DEA, presumably in the radical cation state, and addition of a phenyl radical, presumably from the iodonium salt.

We accordingly synthesized an authentic sample of EAO according to the procedure of Awad, Fateen, and Zayed (17); the melting point of our product agreed with that reported by these authors and its identity was confirmed by proton nmr. This material was inseparable from the 314 molecular weight photoproduct by high resolution, capillary column, gas chromatography.

The second product corresponds to 1- or 2-phenyl-DEA.

Can. J. Chem. Downloaded from www.nrcresearchpress.com by 91.144.44.67 on 09/07/12
For personal use only.

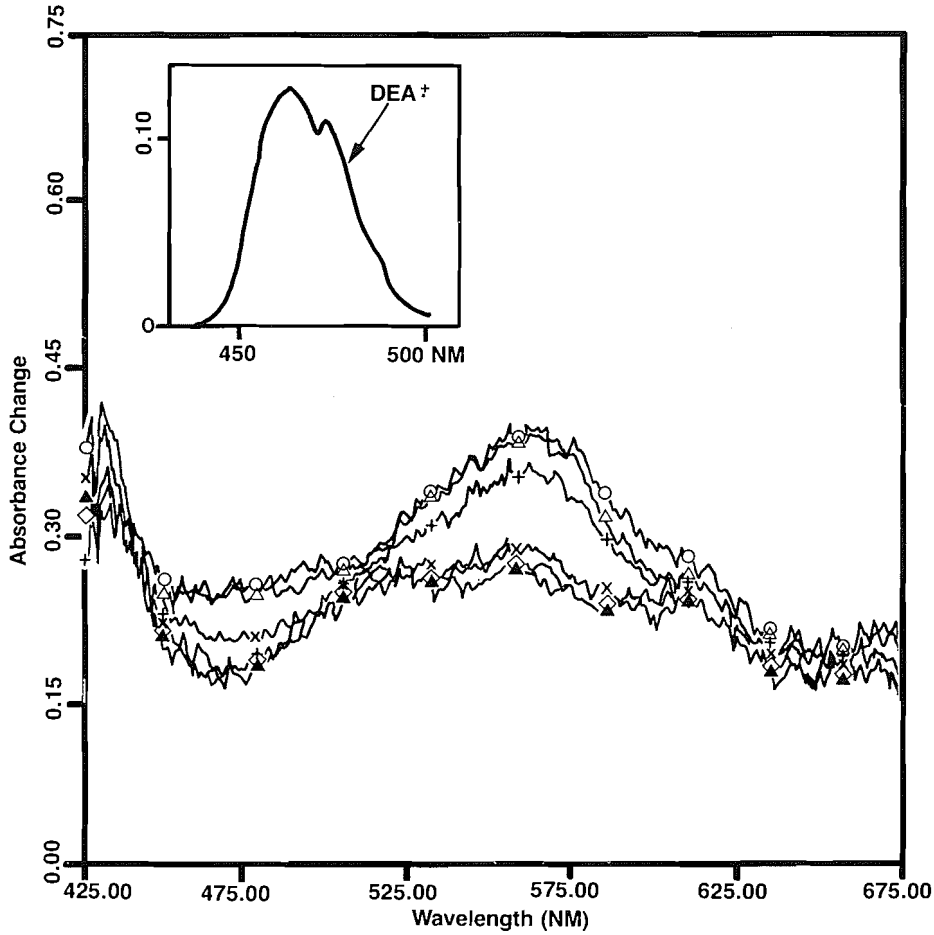

FIG. 7. Transient absorption spectra observed 50 ps (○), 200 ps (△), 500 ps (+), 2 ns (×), 5 ns (◇), and 10 ns (▲) after 355 nm laser flash photolysis of DEA in the presence of diphenyliodonium hexafluorophosphate in AN. Inset shows difference spectrum revealing weak absorption assigned to $DEA^{+\cdot}$.

The phenyl-DEA disappears on exhaustive photolysis, indicating that it also functions as a sacrificial sensitizer, undergoing similar chemistry to DEA. The third product observed in the gc/ms analysis corresponds to $C_{28}H_{22}O$, i.e., an ethoxydiphenylanthracene, most likely a secondary product, derived from phenyl-DEA. We did not attempt to identify products from the reverse micelle system.

Transient absorption spectroscopy

Absorption spectra of some of the transient intermediates observed on the 50 ps – 10 ns time scale in the DEA sensitized photolysis of the diphenyliodonium salt in AN were recorded under conditions of 355 nm laser flash photolysis. Transients observed on photolysis of a solution 3×10^{-4} M DEA and 0.1 M diphenyliodonium hexafluorophosphate in AN are shown in Fig. 7. The initially observed absorptions at 430 and 570 nm were also seen on flash illumination of DEA in the absence of the iodonium salt. In that case, the shorter wavelength absorption persisted over the lifetime of the experiment, while the longer wavelength transient decayed with a time constant comparable to the observed fluorescence lifetime for DEA (above). By analogy to similar peaks in transient absorption spectra of photoexcited anthracene, we assign them to the DEA triplet (18) and singlet (19) excited states, respectively.

We observe in Fig. 7 that the ^{1}DEA absorption decays faster than the measured radiative rate, with a time constant, in fact, of the same order of magnitude as that expected for diffusion controlled quenching by 0.1 M iodonium (2×10^9 s^{-1}). Unlike the case of anthracene, itself, the triplet absorption also decays comparably, indicating that both singlet and triplet excited states of DEA are able to enter into the electron-transfer sensitization process. This implies that the lowest triplet state of DEA is significantly more reducing than that of anthracene.

At the same time, a new absorption band emerges with an apparent maximum at ca. 475 nm. (A calculated differential absorption spectrum is shown as an inset in Fig. 7.) By analogy to anthracene and dimethoxyanthracene (20), we assign this band to $DEA^{+\cdot}$; its absorption is two- to threefold less intense than that of the anthracene radical cation observed under the same conditions (1), and the absorption maximum is, somewhat surprisingly, blue shifted relative to that for the dimethoxyanthracene radical cation (20).

Quantum yields. Reverse micelles

The lability of the DEA radical cation provides a convenient means for detecting one-electron oxidation of photoexcited DEA taking place at the water–heptane interface. When nitrogen-purged, reverse micellar solutions of similar preparation and composition to those used in the fluorescence quenching study were irradiated at 366 nm and monitored spectrophotometrically, we saw that DEA did indeed disappear. Double reciprocal plots of the quantum yields for DEA disappearance versus AOT concentration are shown in Fig. 8. Parameters for the Stern–Volmer kinetic analysis are given in Table 3. The prin-

Can. J. Chem. Downloaded from www.nrcresearchpress.com by 91.144.44.67 on 09/07/12
For personal use only.

TABLE 3. Parameters for photodisappearance of DEA in reverse micelles

Parameter	$w = 5$	$w = 10$	$w = 20$
$[Ph_2I^+]$	0.050 M	0.050 M	0.025 M
Φ_0	0.42	0.14	0.081
$d(1/\Phi)/d\{1/[AOT]\}$	0.097 M	0.78 M	1.26 M
r^a	0.995	0.983	0.984
$p\Phi_q k_d \tau/n$	0.91 M^{-1}	1.14 M^{-1}	1.36 M^{-1}
k_d	535 M^{-1}	580 M^{-1}	748 M^{-1}
k_s ($\times 10^7$)	20 ± 8 $cm^2 s^{-1}$	4 ± 1 $cm^2 s^{-1}$	5 ± 1 $cm^2 s^{-1}$

[a]Correlation coefficient for the double reciprocal plot, Fig. 8.

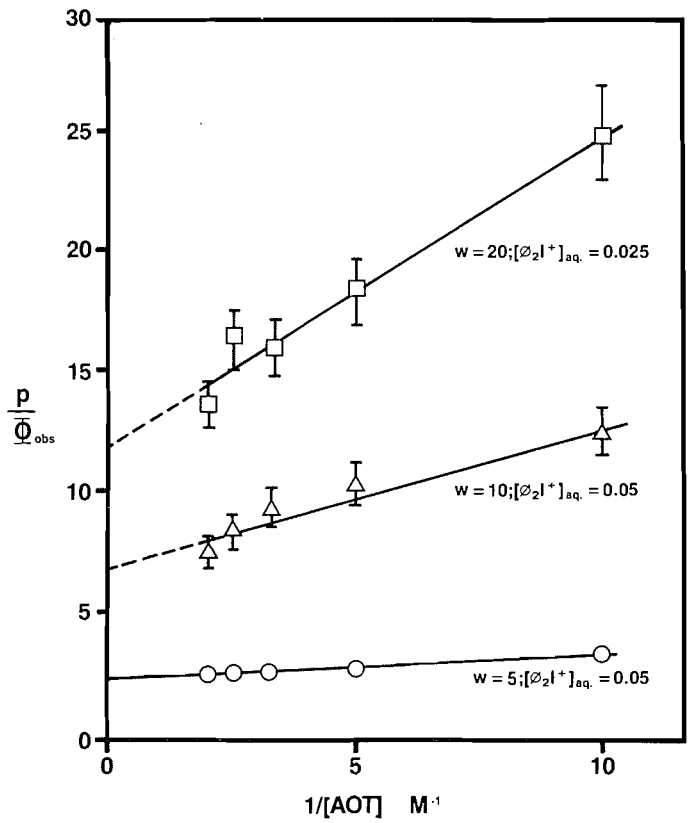

FIG. 8. Double reciprocal plots, $1/\Phi$ versus $1/[AOT]$, for photooxidation of DEA by diphenyliodonium chloride in the heptane/AOT/water reverse micelle system (see Table 3).

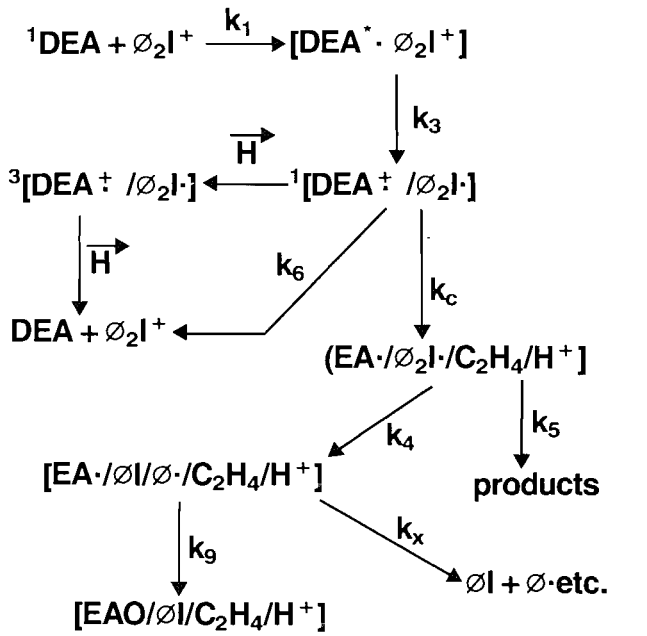

FIG. 9. Mechanistic scheme for photooxidation of DEA with diphenyliodonium cation in homogeneous solution; rate constants refer to Table 1. EA· designates the 9-ethoxy-10-anthroxyl radical.

cipal observation is that the limiting quantum yield, Φ_0, is inversely related to the average water pool size, wn; similar behaviour was *not* observed for the fluorescence quenching. A qualitatively similar inverse relationship between water pool size and efficiency of photooxidation of Mg porphyrin in a reverse micellar environment was observed by Pileni and coworkers (9).

$$[5] \quad (1/\Phi_0)\, d\{1/[AOT]\}/d(1/\Phi) = k_d\tau/n$$

When the intercept-to-slope ratios of the plots of Fig. 8 are multiplied by $p\Phi_q$, from Table 2, the products should be equal to the Stern–Volmer slopes for fluorescence quenching given in the same table, *if* the photochemistry arises from the emissive state of the DEA. Comparison of Tables 3 and 2 indicates that clearly this is not the case. The average Stern–Volmer slope for DEA bleaching (Table 3), $k_d\tau = 620 \pm 90\ M^{-1}$, requires an excited state of ca. 60 ns lifetime.

Discussion

Homogeneous solution photochemistry

A comprehensive mechanistic scheme for the photochemistry occurring in homogenous AN solution is shown in Fig. 9. Steps corresponding to those occurring in Fig. 1 are similarly numbered. Estimates of rate constants for the various steps are listed in Table 1.

The relatively weak absorption of $DEA^{\ddagger}$ in Fig. 7 (in comparison to that observed for the anthracene radical cation under similar conditions (1)) is of significance; we infer that a correspondingly reduced concentration of $DEA^{\ddagger}$ obtains at steady state. Kinetic analysis of the formation and destruction of $DEA^{\ddagger}$ then requires that the principal pathway for decomposition of $DEA^{\ddagger}$ occurs two- to threefold faster than for the anthracene radical cation. This latter species is destroyed primarily by back electron transfer from the diphenyliodo radical, with a pseudo first-order rate constant of ca. $5 \times 10^{10}\ s^{-1}$ (see Table 1); $DEA^{\ddagger}$ thus appears to have a lifetime under our conditions of the order of only 10 ps. This estimate is also consistent with the initial cleanliness of the reaction, i.e., absence of cage-escape products, which, in turn, requires that decomposition of $DEA^{\ddagger}$

Can. J. Chem. Downloaded from www.nrcresearchpress.com by 91.144.44.67 on 09/07/12
For personal use only.

occurs quickly in comparison to that of the diphenyliodo radical, which requires ca. 250 ps (1).

Decomposition of $DEA^{\ddagger}$ to yield EAO involves formal loss of an ethyl cation and addition of a phenyl radical, derived from the diphenyliodo radical. We hypothesize that the process occurring on the 10 ps time scale involves cleavage of a carbon–oxygen single bond in $DEA^{\ddagger}$ to yield the 9-ethoxy-10-anthroxyl radical ($EA^{\bullet}$). A similar deethylation of $DEA^{\ddagger}$ has been observed by Farid *et al.* (21) consequent to photolysis of DEA in the presence of electron-accepting aromatic hydrocarbons, e.g., 1,4-dicyanonaphthalene. This reaction may occur either by an S_E1 pathway, involving deprotonation of the ethyl group and elimination of ethylene (22), or by S_N2 reaction of an adventitious nucleophile, possibly water, at the methylene carbon. In support of operation of the S_E1 mechanism, rapid deprotonation tends to be a general fate of substituted aryl radical cations in polar media; as the rate constant for deprotonation of the toluene radical cation in water is of the order of $10^7\ s^{-1}$ (23*a*), it is doubtful that deprotonation of $DEA^{\ddagger}$ occurs with a rate of the order of $10^{11}\ s^{-1}$ (k_c). Alternatively, an 8-membered cyclic transition state, analogous to the 7-membered cyclic transition state proposed by Tolbert and Khanna (23*b*) for deethylation of the 9-ethyl-10-methylanthracene radical cation, may be involved.

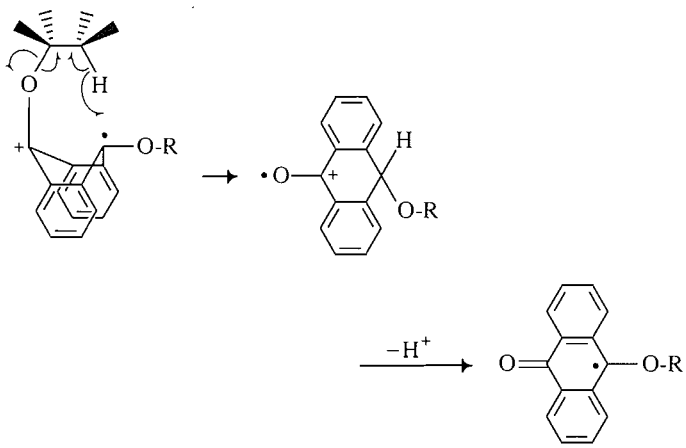

As the rate of quenching approaches the diffusion controlled limit,

[6] $\Phi_0 = k_c/(k_c + k_6)$

Given that the limiting quantum yield for DEA disappearance is $\Phi_0 = 0.75$, we estimate k_6, the rate constant for back electron transfer in the encounter complex, to be no larger than $3 \times 10^{10}\ s^{-1}$, comparable to the value previously (1) estimated for the anthracene radical cation – diphenyliodo radical pair.

The cage-escape processes, k_5 and k_x, can be described by the usual value for AN cage relaxation (24); since cage escape competes with k_9 for the radical coupling process, we assign it a comparable value, although the high initial yield of EAO (above) indicates that k_9 must be somewhat greater than k_x.

Reverse micelle photochemistry

The decomposition of DEA, initiated, presumably, by one-electron oxidation, proceeds out of an excited state of at least 60 ns lifetime in the reverse micelle system. Insofar as the fluorescence lifetime of DEA is unaltered in this medium from its value in homogeneous solution, we assign this longer lived excited state as triplet DEA; this assignment is independent of, but consistent with, the observation of DEA phosphorescence (Fig. 2), and the observed quenching of DEA triplet by diphenyliodonium cation in homogeneous solution.

This assignment implies that the principal pathway for quenching of DEA fluorescence in the reverse micelle system does not involve electron transfer — otherwise it would lead to photochemistry. We propose that the fluorescence quenching observed in the reverse micelles involves the external heavy atom effect (25) and results in DEA intersystem crossing, thus providing an additional reservoir of ^{3}DEA, which can undergo interfacial oxidation. Recent results on the mechanism and distance dependence of the external heavy atom effect (26) suggest that it can operate over distances of at least 6 Å. It is thus not unreasonable to expect an enhanced rate of intersystem crossing in photoexcited DEA in contact with a water pool of up to 10 Å radius ($w = 20$) containing one diphenyliodonium cation.

This interpretation is also consistent with the quantum yields of Table 3; at least at $w = 5$, the limiting quantum yield exceeds the yield of ^{3}DEA formed by the normal intersystem crossing pathway, ≤ 0.32, based on the measured fluorescence quantum yield. Accordingly we estimate the overall limiting triplet yield where fluorescence quenching occurs by external heavy atom mediated intersystem crossing as 0.50 ± 0.04, sufficient to account for the observed values of Φ_0.

[7] $\Phi_3 = \Phi_q + (1 - \Phi_q)(1 - \Phi_f)$

We may furthermore speculate as to the basis for the apparent lack of significant electron-transfer photochemistry for singlet excited DEA in the reverse micelle environment, as it proceeds with high efficiency in homogeneous solution. This result is the opposite of our expectation from proposals for enhanced efficiency of electron transfer at interfaces (7). Pileni and co-workers (9) have also observed that photooxidation of (organic soluble) Mg porphyrin occurs efficiently in a similar reverse micellar system when the oxidant is an alkylviologen, which they expect to be part of the interfacial layer, but not with viologen sulfonate, which is freely soluble in the water pool.

A simple model is embodied in eq. [8]:

[8] $\Phi_0 = \Phi_3 k_s\tau(4\pi R^2)^{-1}/[k_s\tau(4\pi R^2)^{-1} + 1]$

so that

[8*a*] $k_s = \Phi_0 4\pi R^2/[\tau(\Phi_3 - \Phi_0)]$

We assume that diphenyliodonium cation is electrostatically bound to the anionic micellar interface but freely diffuse on this surface; ^{3}DEA is, on the other hand, immobilized in the surfactant phase, but its rate of desorption is slow compared to its lifetime; k_s is then the rate constant for diffusion of the iodonium cation on the micellar interface. We estimate the water pool radius, R, from the volume, wn, and the molecular volume of water, $3.0 \times 10^{-24}\ cm^3$, to evaluate k_s. Values of k_s, included in Table 3, are of the order of $10^{-6}\ cm^2\ s^{-1}$, a reasonable value. According to this picture, the singlet DEA is relatively unreactive at the interface owing to its shorter lifetime: for $\tau = 10$ ns and $w = 5$, eq. [8] with $k_s = 1 \times 10^{-6}\ cm^2\ s^{-1}$ predicts a contribution to Φ_0 or Φ_q of ca. 0.1. This contribution may account for the anomalously high estimate of k_s in the case of $w = 5$.

Conclusions

We have compared the mechanistic features of the photooxidation of DEA by diphenyliodonium cation in homogeneous AN solution and a heptane/AOT/water reverse micelle system. Electron-transfer photochemistry in AN proceeds out of the singlet manifold of DEA. The photoreaction differs from

Can. J. Chem. Downloaded from www.nrcresearchpress.com by 91.144.44.67 on 09/07/12
For personal use only.

that of anthracene itself owing to the lability of the DEA radical cation, for which we estimate a lifetime under our conditions of the order of 10 ps; its principal decomposition pathway appears to involve deethylation.

In the reverse micelles, DEA fluorescence quenching does not appear to proceed primarily by electron transfer; we infer operation of the external heavy atom effect. Efficiency of this process does not depend on water pool size. Photooxidation of DEA under these conditions, on the other hand, involves a longer lived excited state, which we assign as the triplet. Efficiency of electron transfer depends inversely on water pool size. We have accommodated the experimental results with a model that assumes that diffusional encounter of electrostatically bound Ph_2I^+ with relatively immobile ^{3}DEA on the micelle interface is rate limiting.

Acknowledgments

We thank Profs. N. Serpone, Concordia University, Montréal, Laren M. Tolbert, Georgia Institute of Technology, D. G. Whitten, Center for Photoinduced Electron Transfer, University of Rochester, and Drs. B. B. Wright and M. Z. Ali of 3M Graphic Research Laboratories, St. Paul, for helpful discussion. Dr. J. Schroepfer and Mr. J. R. Hill, 3M Analytical and Properties Research Laboratory, assisted with the gas chromatography – mass spectrometric analyses and the photo-CIDNP experiments, respectively. We appreciate the expert technical assistance of Mr. Reza Danesh at Concordia University and of Ms Gwen Crooks in St. Paul. The work in Montréal was supported in part by the Natural Sciences and Engineering Research Council of Canada and in part by 3M Canada, Ltd.

1. R. J. DeVoe, M. R. V. Sahyun, E. Schmidt, N. Serpone, and D. K. Sharma. Can. J. Chem. **66**, 319 (1988); R. J. DeVoe, M. R. V. Sahyun, and E. Schmidt. *In* Photochemistry for imaging. *Edited by* A. J. Herbert. SPSE, Springfield, VA. 1988. p. 21ff.
2. J. S. Meek, P. A. Monroe, and C. J. Bouboulis. J. Org. Chem. **28**, 2576 (1963).
3. S. P. Pappas. J. Imaging Technol. **11**, 146 (1985); S. P. Pappas, B. C. Pappas, L. R. Gatechair, and W. Schnabel. J. Polym. Sci. Polym. Chem. Ed. **22**, 69 (1984); S. P. Pappas, L. R. Gatechair and J. Jilek. J. Polym. Sci. Polym. Chem. Ed. **22**, 77 (1984).
4. C. A. Backer and D. G. Whitten. J. Phys. Chem. **91**, 865 (1987).
5. J. M. Furois, P. Brochette, and M.-P. Pileni. J. Colloid Interface Sci. **31**, 423 (1980).
6. M. Calvin. Acc. Chem. Res. **11**, 369 (1978).
7. M. A. Rodgers and P. C. Lee. J. Phys. Chem. **88**, 3938 (1984).
8. M. Kotlarchyk, J. S. Huang, and S.-H. Chen. J. Phys. Chem. **89**, 4382 (1985).
9. J. M. Furois, P. Brochette, and M.-P. Pileni. J. Colloid Interface Sci. **97**, 552 (1984); P. Brochette, T. Zemb, P. Mathis, and M.-P. Pileni. J. Phys. Chem. **91**, 1444 (1987).
10. M. R. V. Sahyun. J. Phys. Chem. **92**, 6028 (1988).
11. J. V. Crivello and J. H. W. Lam. Macromolecules, **10**, 1307 (1977).
12. J. G. Calvert and J. N. Pitts, Jr. Photochemistry. John Wiley, New York. 1966.
13. G. Ponterini, N. Serpone, M. A. Bergkamp, and T. L. Netzel. J. Am. Chem. Soc. **105**, 4639 (1983); N. Serpone, T. L. Netzel, and M. Gouterman. J. Am. Chem. Soc. **104**, 246 (1982); T. L. Netzel, M. A. Bergkamp, and C.-K. Chang. J. Am. Chem. Soc. **104**, 1952 (1982); N. Serpone and M. Z. Hoffman. J. Phys. Chem. **91**, 1737 (1987).
14. I. B. Berlman. Handbook of fluorescence spectra of organic molecules. Academic Press, New York. 1965. p. 123.
15. R. Kaptein. (*a*) Adv. Free Radical Chem. **5**, 381 (1975); (*b*) *In* Chemically induced magnetic polarization. *Edited by* L. T. Muus, P. W. Atkins, K. A. McLauchlan, and J. B. Peterson. Riedel, Boston, MA. 1977. pp. 13–14.
16. H. D. Roth and A. A. Lamola. J. Am. Chem. Soc. **96**, 6270 (1974).
17. W. I. Awad, A. K. Fateen, and M. A. Zayed. J. Org. Chem. **25**, 358 (1960).
18. D. S. Kliger and A. C. Albrecht. J. Chem. Phys. **53**, 4059 (1970).
19. D. Bebelaar. Chem. Phys. **3**, 205 (1974).
20. Z. H. Zaidi and B. N. Khanna. J. Chem. Phys. **53**, 4059 (1970); J. M. Masnovi, J. K. Kochi, E. F. Hilinski, and P. M. Rentzepis. J. Am. Chem. Soc. **108**, 1126 (1986).
21. S. Farid, D. P. Specht, N. F. Haley, and R. E. Moody. Paper presented at SPSE's 41st Annual Conference, Arlington, VA, May 1988; see Advance printing of paper summaries. SPSE, Springfield, VA. 1988. p. 77.
22. R. C. Lum and J. J. Grabowski. J. Am. Chem. Soc. **110**, 8568 (1988).
23. (*a*) K. Sehested, J. Holcman, and E. J. Hart. J. Phys. Chem. **81**, 1363 (1977); K. Sehested and J. Holcman. J. Phys. Chem. **82**, 651 (1978); (*b*) L. M. Tolbert and R. K. Khanna. J. Am. Chem. Soc. **109**, 3477 (1987).
24. K. Schulten, H. Staerk, A. Weller, H.-J. Werner, and B. Nickel. Z. Phys. Chem. NF**101**, 371 (1976).
25. S. P. McGlynn, T. Azumi, and M. Kinoshita. Molecular spectroscopy of the triplet state. Prentice–Hall, Englewood Cliffs, NJ. 1969.
26. E. Haselbach, D. Pilloud, and P. Suppan. Abstracts of the XII IUPAC Symposium on Photochemistry. Institute FRAE–CNR, Bologna, Italy. 1988. Paper PK28.

Can. J. Chem. Downloaded from www.nrcresearchpress.com by 91.144.44.67 on 09/07/12
For personal use only.

Synthèse stéréosélective de (±) boschnialactone, (±) 7-épiteucriumlactone et (±) 7-épiisoiridomyrmécine. Étude de la stéréochimie par spectroscopie de résonance magnétique nucléaire

B. HANQUET, B. TABYAOUI, J.-C. CAILLE, M. FARNIER ET R. GUILARD[1]

Laboratoire de synthèse et d'électrosynthèse organométallique, associé au Centre national de la recherche scientifique (Unité associé n° 33), Faculté des sciences «Gabriel», 6, Bd. Gabriel, 21100 Dijon, France

Reçu le 21 décembre 1988[2]

B. HANQUET, B. TABYAOUI, J.-C. CAILLE, M. FARNIER et R. GUILARD. Can. J. Chem. **68**, 620 (1990).

Les synthèses stéréosélectives de la (±) boschnialactone **1**, la (±) 7-épiteucriumlactone **2** et la (±) 7-épiisoiridomyrmécine **3** sont décrites. Les préparations font appel à la réaction de Stetter suivie de l'addition nucléophile d'énolates de lithium d'esters convenables. L'étape de lactonisation utilise des réactifs silylés et les rendements obtenus sont compris entre 63 et 78%. L'analyse structurale proposée est en désaccord avec les résultats antérieurs. Les paramètres de résonance magnétique nucléaire sont précisés en utilisant les techniques de RMN ^1H et ^{13}C à une et deux dimensions.

Mots clés : synthèse stéréosélective, boschnialactone, 7-épiteucriumlactone, 7-épiisoiridomyrmécine, RMN ^1H et ^{13}C.

B. HANQUET, B. TABYAOUI, J.-C. CAILLE, M. FARNIER, and R. GUILARD. Can. J. Chem. **68**, 620 (1990).

The stereoselective syntheses of (±) boschnialactone **1**, (±) 7-epiteucriumlactone **2**, and (±) 7-epiisoiridomyrmecine **3** are described. Their preparation involved Stetter's reaction followed by nucleophilic addition of lithium enolates of suitable esters. Silylated reagents are used in the lactonisation step and the observed yields are between 63 and 78%. The proposed structural analysis is not in accord with the results of a previous study. The nuclear magnetic resonance data are determined using 1D and 2D proton and carbon NMR experiments.

Key words: stereoselective synthesis, boschnialactone, 7-epiteucriumlactone, 7-epiisoiridomyrmecine, ^1H and ^{13}C NMR.

Introduction

Au cours des 20 dernières années, la chimie des iridoïdes a connu un essor remarquable et a suscité un nombre considérable de travaux. De nombreux iridoïdes sont des constituants des plantes (1, 2) mais leur présence a également été mise en évidence dans les secrétions de certaines fourmis du genre iridomyrmex (3). Ainsi cette classe de composés est impliquée dans diverses fonctions biologiques et joue un rôle fondamental lors de la biosynthèse d'alcaloïdes indoliques (4).

Dans ce travail, nous avons limité notre objectif à la synthèse de trois composés d'arrangement structural proche du squelette fondamental des iridoïdes : la (±) boschnialactone **1**, la (±) 7-épiteucriumlactone **2** et la (±) 7-épiisoiridomyrmécine **3**.

Si la boschnialactone **1**, ou noriridomyrmécine, et la teucriumlactone **4** n'ont suscité qu'un nombre restreint de travaux, l'iridomyrmécine **5** et l'isoiridomyrmécine **6** ont fait l'objet de nombreuses études.

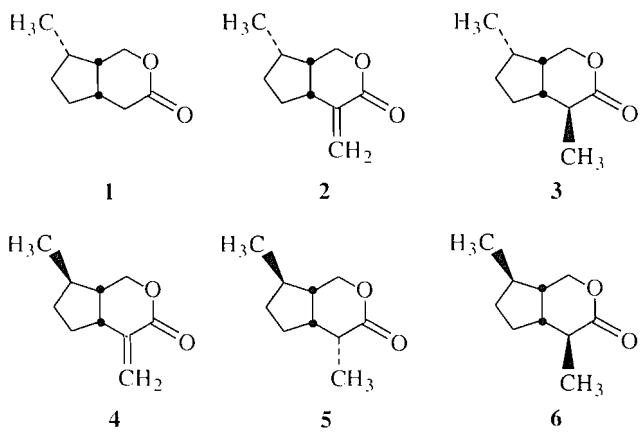

1 **2** **3**

4 **5** **6**

Comme préparations originales nous pouvons citer pour l'isoiridomyrmécine **6** celle réalisée au départ du L-citronellal selon une séquence «biomimétique» (5) ou la méthode de Wender et Dreyer (6) qui opère au départ d'une cétone tricyclique. Une voie d'accès très aisée à l'iridomyrmécine **5** procède via une réaction d'hétéro Diels–Alder au départ du méthyl-5 cyclopentène-1 carboxaldéhyde (7). Le même dérivé **5** peut également être synthétisé en mettant en œuvre le diméthyl-1,5 cyclooctadiène-1,5 qui résulte de l'isomérisation de l'isoprène (8).

Sakan *et al.* (1) ont décrit une méthode de synthèse spécifique de la boschnialactone sous forme d'un mélange d'épimères mais Callant *et al.* (9) en mettant à profit la géométrie convexe de norbornanones substituées ont proposé une synthèse stéréospécifique de la boschnialactone et de la teucriumlactone.

Résultats

Dans une publication préliminaire (10), nous avons décrit une synthèse rapide et stéréosélective de la (±) boschnialactone **1** en mettant en œuvre la méthoxyméthyl-2 méthyl-3 cyclopentène-2 one-1 **7**. Ce dérivé, aisément accessible par aldocrotonisation de la méthoxy-7 heptanedione-2,5 préparée selon la méthode de Stetter (11), constitue un remarquable synthon de départ pour élaborer une méthode générale de synthèse de composés comportant le squelette octahydrocyclopenta(*c*)pyrannique. Cette méthode nous permet ainsi de proposer une préparation aisée des trois molécules cibles **1**, **2** et **3**.

L'addition nucléophile (voir schéma 1) de l'énolate de lithium de l'acétate de tertiobutyle ou de l'acétate d'éthyle sur la cétone **7** dans le tétrahydrofuranne anhydre à −78°C suivie d'une hydrolyse acide conduit respectivement et régiospécifiquement aux diènes **8***a* et **8***b* avec des rendements de 76 et 80%. Par action de l'énolate de lithium du propanoate d'éthyle sur la cétone **7**, on accède au diène **10** avec un rendement de 54%.

Le rendement relativement faible observé dans le cas du

1. Auteur à qui adresser toute correspondance.
2. Révision reçue le 28 septembre 1989.

Printed in Canada / Imprimé au Canada

Can. J. Chem. Downloaded from www.nrcresearchpress.com by 91.144.44.67 on 09/07/12
For personal use only.

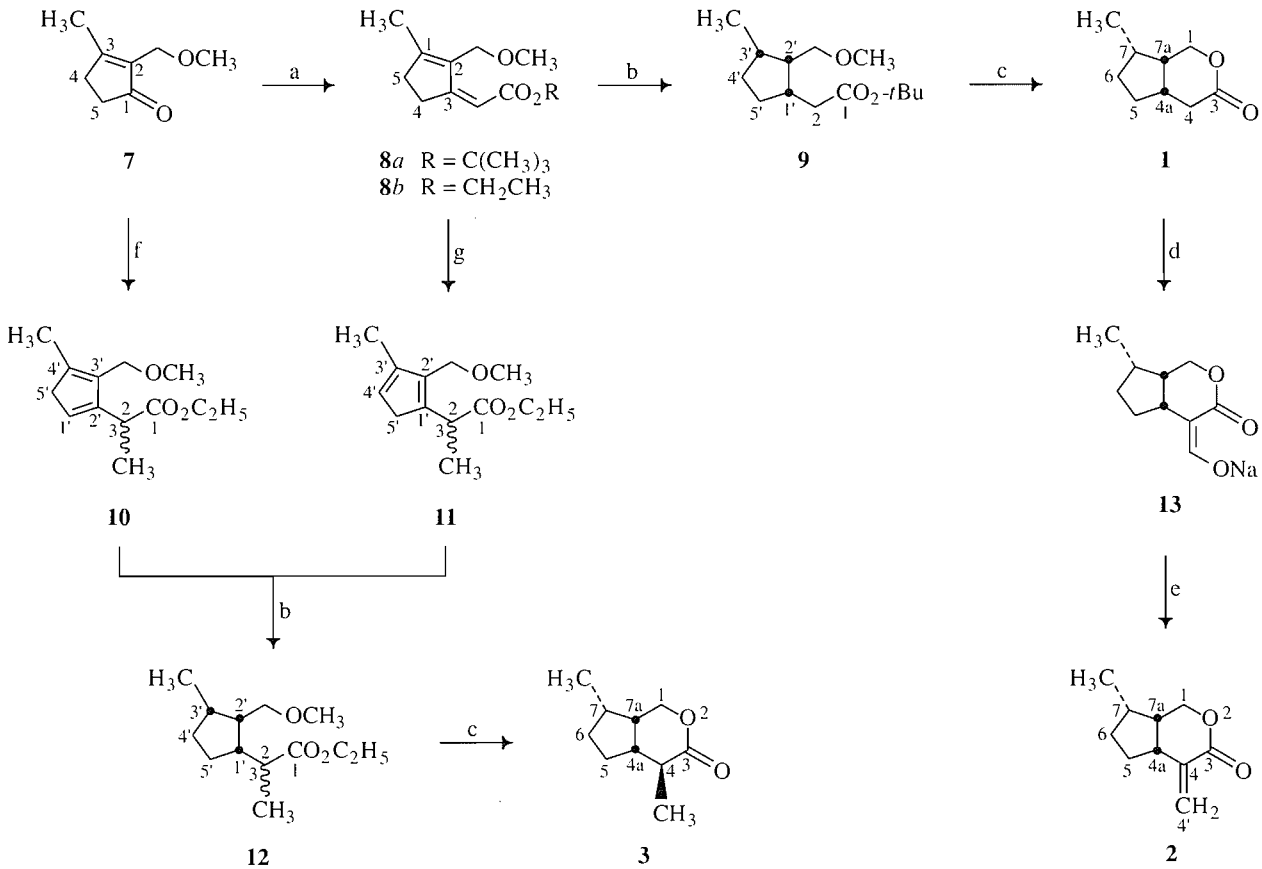

Reactifs : (a) LDA, THF, −78 °C, H_3CCO_2R; (b) H_2, PtO_2, AcOEt;
(c) $ClSiMe_3$, NaI, H_3CCN,Δ ; (d) NaH, HCO_2Et;
(e) HCHO 30%, THF; (f) LDA, THF, −78 °C, $H_3CCH_2CO_2Et$;
(g) LDA; THF : HMPT (80:20), −78 °C, ICH_3, −20 °C.

SCHÉMA 1

propanoate nous a incité à modifier cette stratégie de synthèse pour préparer le dérivé portant un groupe méthyle en position α du reste ester. La substitution nucléophile du sel de lithium de l'ester **8***b* par l'iodure de méthyle (12) dans le tétrahydrofuranne à −20°C conduit au mélange des deux diènes **10** et **11** en proportions égales avec un rendement de 66%. En opérant dans le mélange hexaméthylphosphorotriamide–tétrahydrofuranne à 20% et dans les mêmes conditions de température, on isole spécifiquement le diène **11** avec un rendement de 76%.

L'hydrogénation des diènes **8***a*, **10** et **11**, réalisée en présence d'oxyde de platine, conduit aux cyclopentanes trisubstitués **9** et **12** sous forme de mélange de deux diastéréoisomères. La stéréosélectivité de la réaction d'hydrogénation a pu être évaluée grâce aux rapports des intégrations des signaux de résonance attribués aux protons du groupe méthyle lié au noyau cyclopentanique. Dans le cas du composé **9** le diastéréoisomère présentant la configuration souhaitée est le composé majoritaire (80%). Pour le composé **12** l'existence d'un centre chiral porteur d'un groupe méthyle (C_2) induit une plus grande stéréospécificité de la réaction d'hydrogénation et seule la formation de deux diastéréoisomères est observée. Le composé majoritaire (80%) conduit à la lactone **3** attendue.

Cette étape de lactonisation implique l'utilisation des réactifs silylés préconisés par Olah *et al.* (13) pour régénérer les fonctions acide et alcool à partir d'ester ou d'éther. L'iodure de triméthylsilyle qui représente «l'entité réactive» est généré *in situ* au départ du chlorure correspondant. La réaction de lactonisation est ainsi réalisée en une seule étape avec un rendement voisin de 63% pour **1** ou **3** en opérant au reflux de l'acétonitrile en présence d'iodure de triméthylsilyle et au départ des cyclopentanes trisubstitués **9** ou **12**. La 7-épiteucriumlactone **2** a été isolée avec un rendement de 78% par α-méthylénation de la boschnialactone selon la méthode décrite par Murray et Reid (14).

Étude structurale

À l'exception des trois lactones objet du présent article, les caractéristiques RMN des composés synthétisés sont regroupées dans la partie expérimentale.

En ce qui concerne les trois lactones synthétisées, l'étude RMN a pour but de déterminer les paramètres de glissement chimique et de couplage pour préciser la conformation privilégiée qu'adoptent ces trois molécules. Un travail déjà ancien (15) a utilisé la RMN protonique (60 MHz) et la spectroscopie infrarouge pour l'analyse conformationnelle de molécules voisines. Se basant sur les données infrarouge, les auteurs proposent une structure flexible qu'ils rattachent à deux types possibles de conformation bateau pour le cycle lactonique. Le choix de la conformation préférentielle est effectué en considérant les constantes de couplage entre le méthylène lactonique et un des protons lié à un atome de carbone commun aux deux cycles. Notre propre étude est en désaccord avec les conclusions de ces auteurs.

Nous avons procédé à une analyse très détaillée du spectre

Can. J. Chem. Downloaded from www.nrcresearchpress.com by 91.144.44.67 on 09/07/12
For personal use only.

Can. J. Chem. Downloaded from www.nrcresearchpress.com by 91.144.44.67 on 09/07/12
For personal use only.

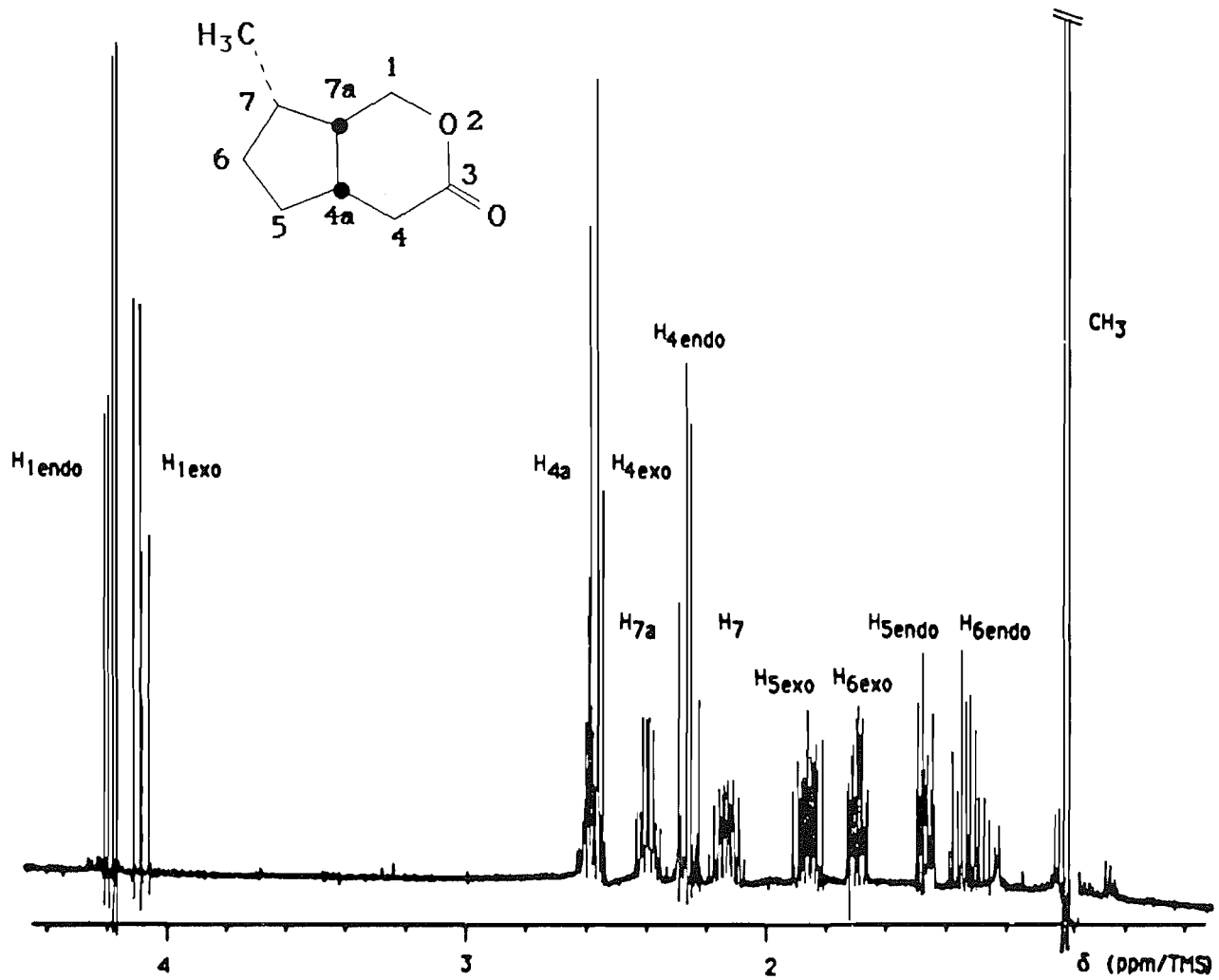

FIG. 1. Spectre de RMN ^1H (400 MHz, $CDCl_3$) de la (±) boschnialactone **1**.

de la boschnialactone et les résultats de cette étude ont servi de base à l'analyse des données concernant la 7-épiteucriumlactone et à l'analyse plus délicate de la 7-épiisoiridomyrmécine.

1. Boschnialactone

(a) Spectres à une dimension (1D)

Le spectre protonique de la boschnialactone enregistré à 400 MHz (voir figure 1) présente 14 protons répartis en 11 massifs distincts. L'examen direct du spectre ne permet d'attribuer aisément que cinq protons. Deux protons déblindés à 4,09 et 4,19 ppm correspondent au groupement méthylène $(CH_2)_1$ et les trois protons du reste méthyle apparaissent à 1,00 ppm.

Le spectre de RMN ^{13}C INEPT (16) indique la présence de neuf atomes de carbone non-équivalents. Un groupement carbonyle à 174,4 ppm, le méthylène lactonique $(CH_2)_1$ à 68,2 ppm et le reste méthyle à 15,4 ppm sont attribués sans ambiguïté. Le spectre révèle également l'existence de trois groupes méthylène voisins et de trois restes méthine entre 33,5 et 40,0 ppm. Il est à noter qu'un des restes méthine présente une constante de couplage très élevée (179 Hz) traduisant une contrainte de cycle importante (17).

Les informations fournies par les spectres à une dimension ne permettent cependant pas d'effectuer une attribution de tous les signaux en raison des forts couplages entre les protons des deux cycles. Seule l'analyse des spectres à deux dimensions conduit à une attribution certaine des différents signaux de résonance.

(b) Spectres à deux dimensions (2D)

Le spectre COSY (18) de la boschnialactone est reproduit sur la figure 2. Il montre que chacun des deux protons du groupe méthylène $(CH_2)_1$ donne une tache de connexion avec un unique proton H_{7a}. Le proton H_7 présente un couplage important avec le reste méthyle et est ainsi aisément attribué. Il reste à préciser les positions des protons géminés en 4, 5 et 6. Les protons du reste méthylène en 4 sont déblindés par suite de la proximité du groupement carbonyle et résonnent à 2,26 et 2,57 ppm. Les quatre protons portés par les atomes de carbone 5 et 6 sont tous couplés entre eux. La présence de deux taches de connexion entre deux de ces protons et H_7 permet d'attribuer ceux-ci au méthylène en 6. En revanche, les protons géminés en 5 sont seulement couplés avec H_{4a} précédemment identifié.

L'analyse complète du spectre COSY permet donc une attribution non ambigüe de l'ensemble des protons de la boschnialactone. Cette analyse va être mise à profit pour proposer une affectation des résonances carbone-13 non attribuées. Le spectre corrélé proton–carbone (19) permet de lever ces incertitudes et d'assigner les signaux de résonance aux différents atomes de carbone (voir figure 3).

Can. J. Chem. Downloaded from www.nrcresearchpress.com by 91.144.44.67 on 09/07/12
For personal use only.

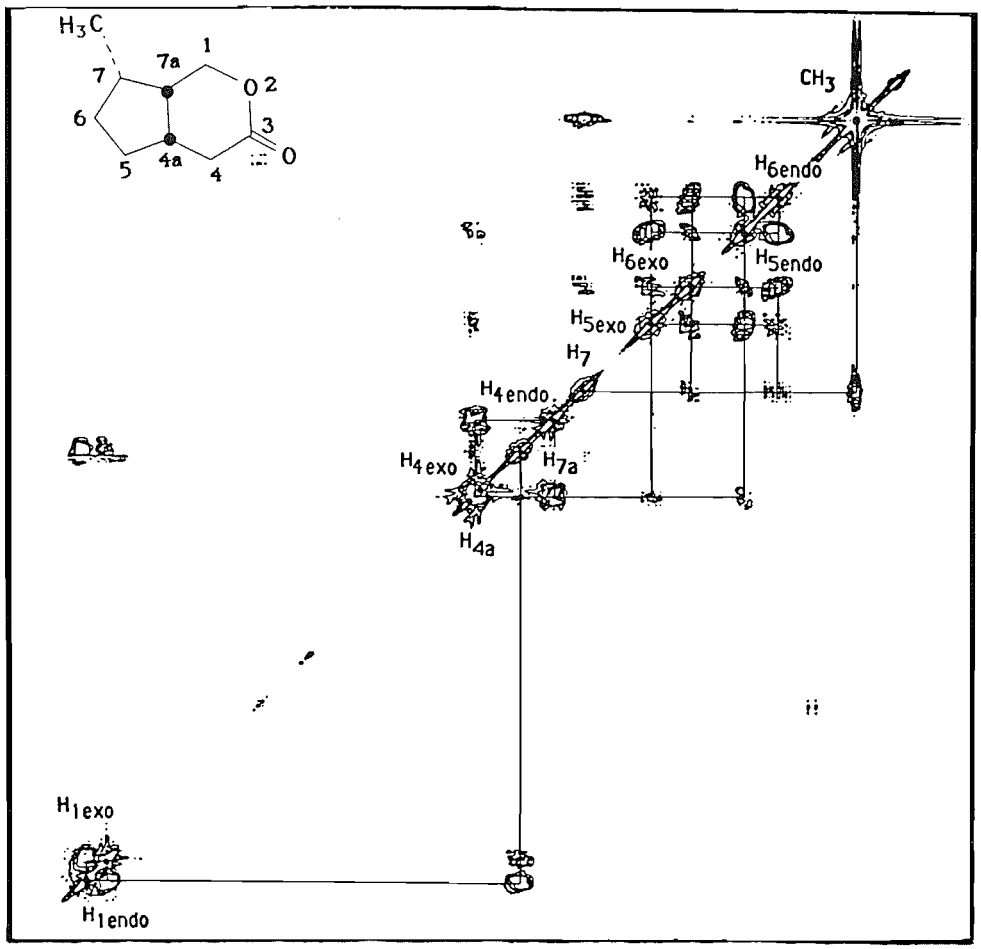

FIG. 2. Spectre de COSY (400 MHz, $CDCl_3$) de la (±) boschnialactone **1**.

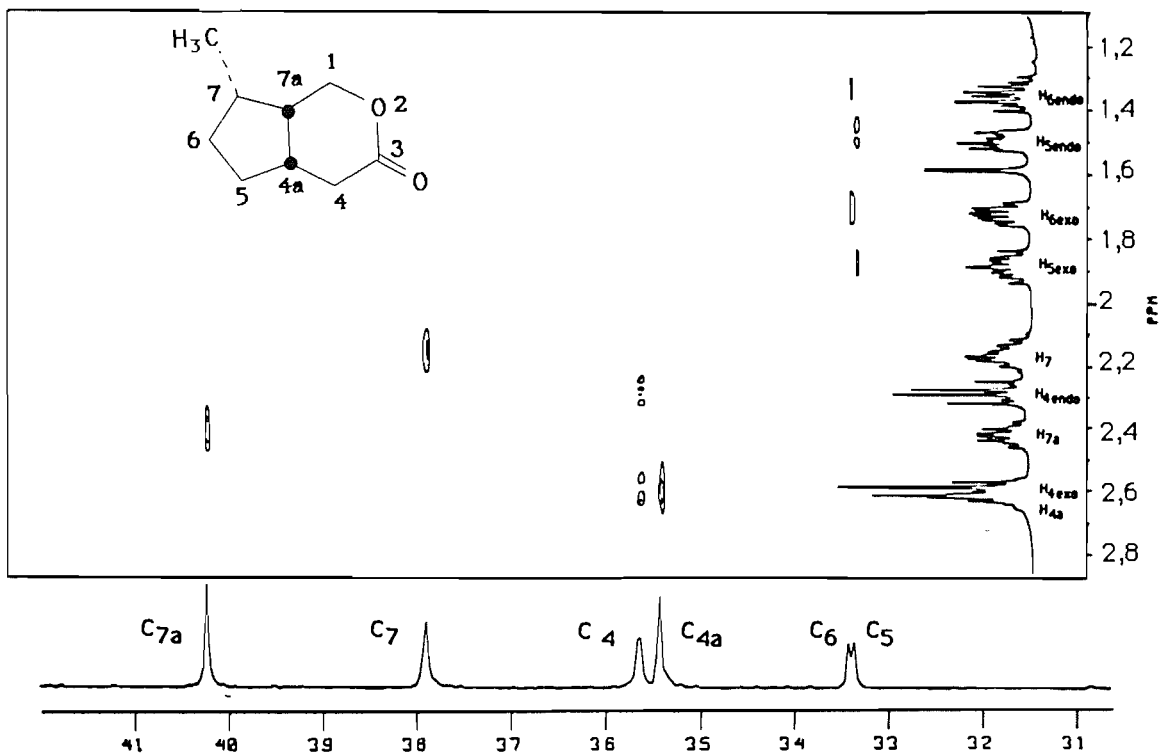

FIG. 3. Spectre corrélé $^1H-^{13}C$ de la (±) boschnialactone **1**.

TABLEAU 1. Caractéristiques RMN ^1H (400 MHz, $CDCl_3$) des lactones **1**, **2** et **3**

Composé	Déplacements chimiques (ppm)										
	H_{1exo}	H_{1endo}	**1** : H_{4exo} **2** : $H_{1'a}$ **3** : H_4	**1** : H_{4endo} **2** : $H_{1'b}$	H_{4a}	H_{5exo}	H_{5endo}	H_{6exo}	H_{6endo}	H_7	H_{7a}	$(CH_3)_7$	$(CH_3)_4$
(±) Boschnialactone, **1**	4,19 dd/1H	4,09 dd/1H	2,57 m/1H	2,26 m/1H	2,58 m/1H	1,86 m/1H	1,47 m/1H	1,70 m/1H	1,33 m/1H	2,13 m/1H	2,40 qd/1H	1,00 d/3H	
(±) 7-Épiisoiridomymécine, **3**	4,40 d/1H	4,22 dd/1H	2,75 m/1H		2,66 m/1H	1,74 m/1H	1,61 m/1H	1,68 m/1H	1,49 m/1H	2,16 m/1H	2,40 m/1H	1,06 d/3H	1,19 d/3H
(±) 7-Épiteucriumlactone, **2**	4,19 dd/1H	4,10 dd/1H	6,20 t/1H	5,53 t/1H	3,13 m/1H	2,10 m/1H	1,74 m/1H	1,83 m/1H	1,34 m/1H	2,24 m/1H	2,43 m/1H	1,03 d/3H	

TABLEAU 2. Valeurs des constantes de couplage (en Hz) de la (±) boschnialactone, **1**

$J_{H_{1endo}-H_{1exo}} = \|11,6\|$	$J_{H_{1endo}-H_{7a}} = 8,8$	$J_{H_{1exo}-H_{7a}} = 5,4$
$J_{H_{4endo}-H_{4exo}} = \|14,9\|$	$J_{H_{4endo}-H_{4a}} = 8,7$	$J_{H_{4exo}-H_{4a}} = 6,6$
$J_{H_{4a}-H_{7a}} = 9,3$	$J_{H_{4a}-H_{5exo}} = 9,0$	$J_{H_{4a}-H_{5endo}} = 2,4$
$J_{H_{5endo}-H_{5exo}} = \|13,3\|$	$J_{H_{5exo}-H_{6exo}} = 6,7$	$J_{H_{5exo}-H_{6endo}} = 11,3$
$J_{H_{5endo}-H_{6exo}} = 2,6$	$J_{H_{5endo}-H_{6endo}} = 6,8$	$J_{H_{6endo}-H_{6exo}} = \|12,5\|$
$J_{H_{6exo}-H_7} = 6,2$	$J_{H_{6endo}-H_7} = 11,4$	$J_{H_7-H_{7a}} = 8,6$
$J_{H_7-(CH_3)_7} = 7,1$		

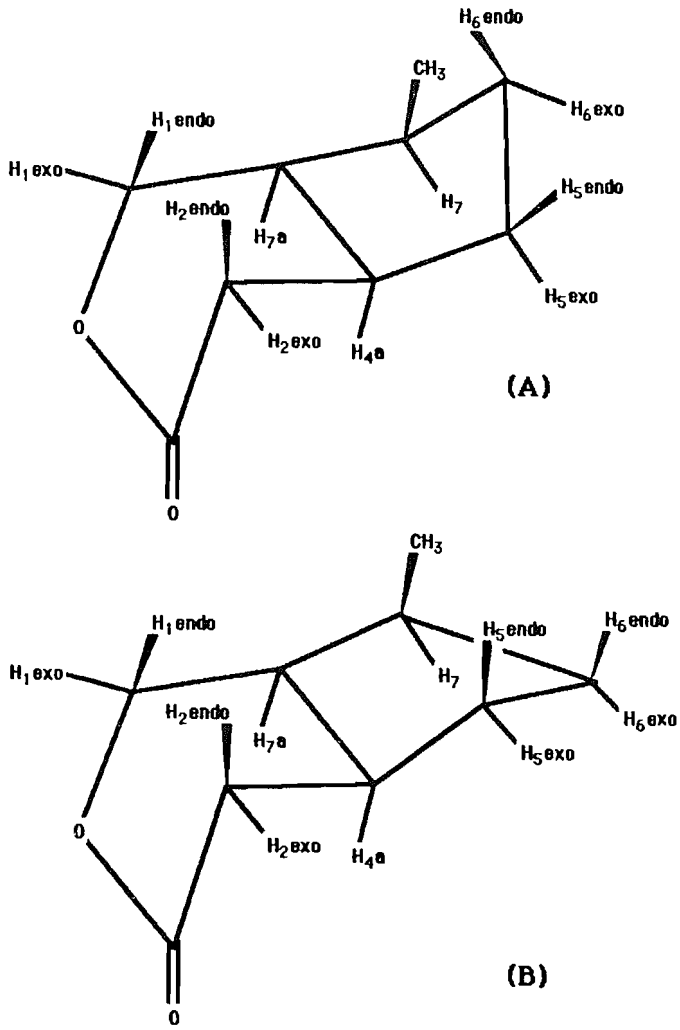

FIG. 4. Conformations enveloppe (A) ou (B) de la (±) boschnialactone **1**.

(c) Détermination de la stéréochimie de la boschnialactone

L'ensemble des paramètres RMN de la boschnialactone apparaît dans les tableaux 1 et 2. L'examen de la valeur des constantes de couplage ^3J permet, à l'aide de l'équation de Karplus (20), de déterminer la valeur de l'angle dièdre H—C—C—H et par suite de préciser la stéréochimie des différents protons.[3]

3. Sur la base de structures optimisées par des calculs théoriques, pour lesquels nous sommes redevables à Monsieur le Professeur L. D. Colebrook de l'Université Concordia, Montréal, Québec, Canada, il apparaît que la conformation (A) présente une plus grande stabilité que la conformation (B) (resp. 21,67 et 20,82 kcal/mol). La corrélation des constantes de couplage expérimentales et calculées la plus satisfaisante est donc obtenue pour la conformation (A).

Can. J. Chem. Downloaded from www.nrcresearchpress.com by 91.144.44.67 on 09/07/12
For personal use only.

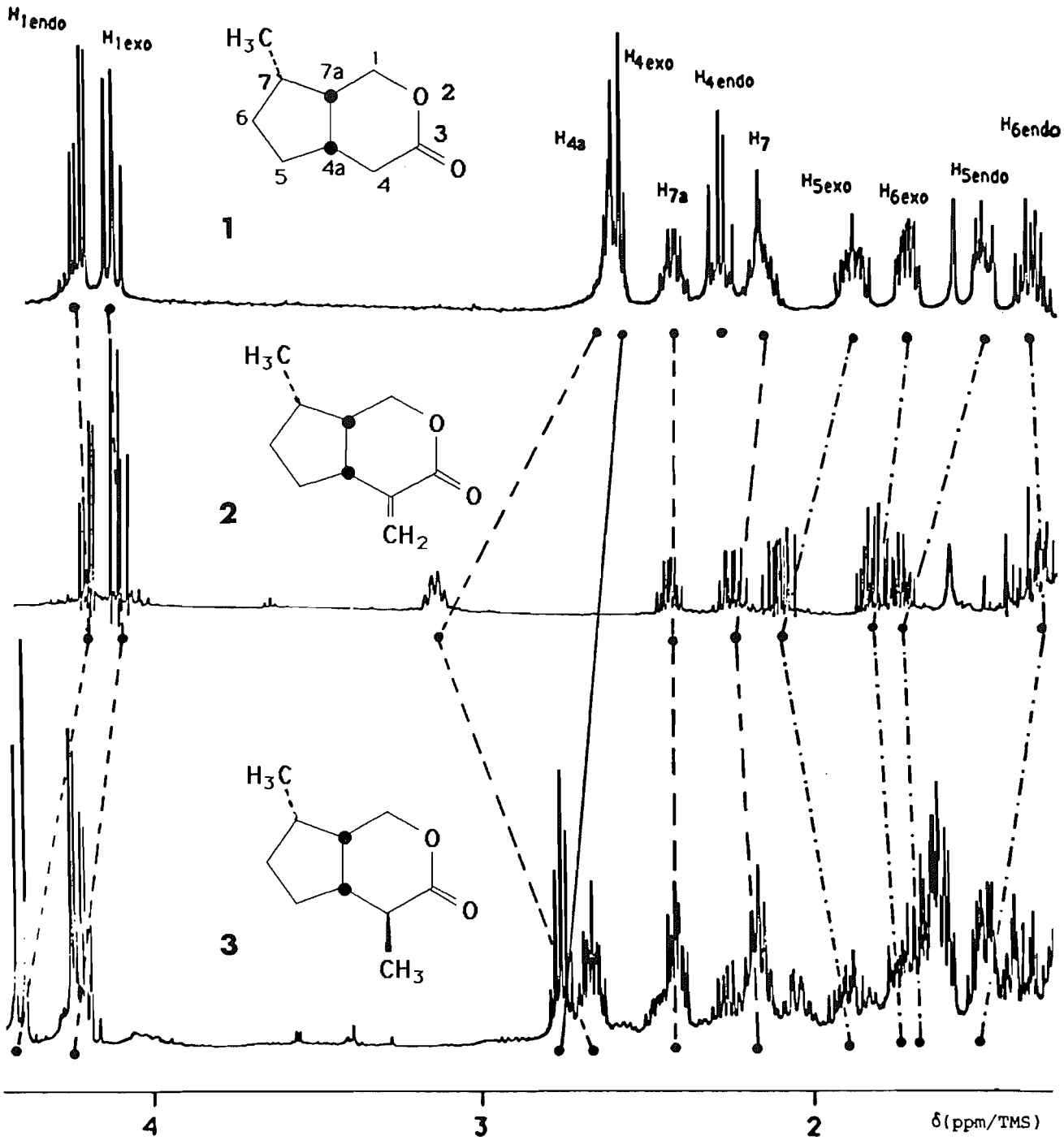

FIG. 5. Partie haut champ des spectres de RMN ^1H (400 MHz, $CDCl_3$) de la (±) boschnialactone **1**, de la (±) 7-épiteucriumlactone **2** et de la (±) 7-épiisoiridomyrmécine **3**.

La voie de synthèse de la boschnialactone fait appel à une préparation utilisant une hydrogénation catalytique et conduit ainsi à un produit de stéréochimie non ambigüe quant à la jonction des deux cycles de nature *cis* et quant à la configuration du reste méthyle en *trans* par rapport aux protons communs aux deux cycles.

L'examen des constantes de couplage ($^3J_{H_{7a}-H_{4a}}$ = 9,3 Hz et $^3J_{H_7-H_{7a}}$ = 8,6 Hz) confirme la position relative *cis*-diaxiale des protons H_{4a}–H_{7a}, H_7 et H_{7a}. La conformation de chacun des deux cycles peut également être précisée. Le carbocycle à cinq chaînons peut adopter deux conformations enveloppe (A) ou (B) (voir figure 4). Cependant l'existence d'un reste méthyle fait que l'une d'elles est privilégiée : il s'agit de celle correspondant au substituant en position équatoriale. Dans la conformation (A) seul l'un des protons en 6 présente deux fortes interactions *trans*-diaxales avec ses voisins, entraînant par là-même l'existence de deux couplages importants : $^3J_{H_{5exo}-H_{6endo}}$ = 11,3 Hz et $^3J_{H_{6endo}-H_7}$ = 11,4 Hz. Dans l'autre conformation enveloppe (B), aucun des protons en 6 ne présenterait de tels couplages. Par conséquent, H_{5exo} et H_{4a} présentent un couplage *cis*-diaxial (9 Hz). De plus, H_{5endo} et H_{4a} d'une part et H_{6exo} et H_{5endo} d'autre part ne sont que faiblement couplés (respectivement 2,4 et 2,6 Hz).

L'ensemble de ces résultats milite en faveur de l'enveloppe

Can. J. Chem. Downloaded from www.nrcresearchpress.com by 91.144.44.67 on 09/07/12
For personal use only.

TABLEAU 3. Valeurs des constantes de couplage (en Hz) de la (±) 7-épiteucriumlactone, **2**

$J_{H_{1endo}-H_{1exo}} = \|11,4\|$	$J_{H_{1endo}-H_{7a}} = 8,9$	$J_{H_{1exo}-H_{7a}} = 4,6$
$J_{H_{1'a}-H_{1'b}} = 1,5$	$J_{H_{1'a}-H_{4a}} = 1,4$	$J_{H_{1'b}-H_{4a}} = 1,5$
$J_{H_{4a}-H_{7a}} = 7,7$	$J_{H_{4a}-H_{5endo}} = 8,4$	$J_{H_{4a}-H_{5exo}} = 8,7$
$J_{H_{5endo}-H_{5exo}} = \|13,3\|$	$J_{H_{5endo}-H_{6endo}} = 7,1$	$J_{H_{5endo}-H_{6exo}} = 4,8$
$J_{H_{5exo}-H_{6endo}} = 9,8$	$J_{H_{5exo}-H_{6exo}} = 8,1$	$J_{H_{6endo}-H_{6exo}} = \|11,6\|$
$J_{H_{6exo}-H_7} = 7,6$	$J_{H_{6endo}-H_7} = 10,1$	$J_{H_7-H_{7a}} = 8,8$
$J_{H_7-(CH_3)_7} = 7,1$		

TABLEAU 4. Valeurs des constantes de couplage (en Hz) de la (±) 7-épiisoiridomyrmécine, **3**

$J_{H_{1endo}-H_{1exo}} = \|12,3\|$	$J_{H_{1exo}-H_{7a}} \simeq 0$	$J_{H_{1endo}-H_{7a}} = 4,8$
$J_{H_4-(CH_3)_4} = 7,0$	$J_{H_4-H_{4a}} = 5,9$	$J_{H_{4a}-H_{5exo}} = 7,9$
$J_{H_{4a}-H_{5endo}} = 6,5$	$J_{H_{5endo}-H_{5exo}} = *$	$J_{H_{5endo}-H_{6exo}} = 6,9$
$J_{H_{5endo}-H_{6endo}} = *$	$J_{H_{5exo}-H_{6exo}} = 2,7$	$J_{H_{5exo}-H_{6endo}} = 8,3$
$J_{H_{6endo}-H_{6exo}} = *$	$J_{H_{6exo}-H_7} = 5,6$	$J_{H_{6endo}-H_7} = 3,6$
$J_{H_{4a}-H_{7a}} = 9,8$	$J_{H_7-H_{7a}} = 8,8$	$J_{H_7-(CH_3)_7} = 7,1$

*Ces constantes de couplage n'ont pu être déterminées avec certitude en raison des difficultés d'attribution des signaux des protons du chaînon $(CH_2)_5$–$(CH_2)_6$.

(A) en contradiction avec l'interprétation proposé par Sisido (15).

2. Analyse comparative des paramètres RMN des trois lactones

À partir des données de RMN de la boschnialactone, il est possible d'analyser les spectres des deux molécules voisines que sont la 7-épiteucriumlactone et la 7-épiisoiridomyrmécine. La figure 5 reproduit la partie haut champ des spectres de RMN de ces trois composés et l'ensemble des paramètres RMN des lactones **2** et **3** est rassemblé dans les tableaux 1, 3 et 4. Certains motifs sont peu sensibles à la substitution : c'est le cas des protons H_7 et H_{7a}. Le proton H_{4a} est également peu modifié par la présence du groupe $(CH_3)_4$ de la 7-épiisoiridomyrmécine mais il est beaucoup plus affecté par le groupe $=CH_2$ de la 7-épiteucriumlactone. De plus pour la 7-épiisoiridomyrmécine, les signaux des protons H_{1exo}, H_{1endo}, H_{4exo} et H_{6endo} subissent un déblindage comparable, probablement dû à la présence du reste $(CH_3)_4$. En ce qui concerne le chaînon $(CH_2)_5$–$(CH_2)_6$, l'attribution des quatre protons H_{5endo}, H_{5exo}, H_{6endo} et H_{6exo} de la 7-épiisoiridomyrmécine reste incertaine. Nous proposons une attribution de ces signaux par analogie avec le spectre de RMN protonique de la boschnialactone.

Partie expérimentale

Les analyses centésimales ont été effectuées par le Service central d'analyse du C.N.R.S. Les mesures de R_f ont été réalisées après élution sur des plaques de gel de silice Merck 60 F_{254}.

Les spectres infra-rouge ont été relevés sur un appareil Perkin–Elmer 580B à partir de films d'échantillons (lames de NaCl).

Les spectres de masse ont été obtenus par bombardement électronique sur un appareil Finnigan 3300, tension d'accélération 70 eV, courant d'ionisation 0,4 mA, température de source 25–150°C.

Les spectres de RMN ^1H ont été relevés à 100 MHz (Jeol FX-100) et à 400 MHz (Bruker WM400) sur des solutions de 4–10 mg de composé dissous dans 0,4 cm^3. Les spectres ^{13}C ont été enregistrés à 100 MHz (Bruker WM400) sur des solutions de 20–30 mg de produit dans 2,5 cm^3 de solvant deutérié. Les déplacements chimiques sont donnés en partie par million (ppm) par rapport à $SiMe_4$ et les constantes de couplage en Hz. Les multiplicités sont indiquées comme suit : s (singulet), d (doublet), t (triplet), q (quadruplet), m (multiplet). Les séquences multi-impulsionnelles citées sont celles données en standard dans la bibliothèque des logiciels Bruker.

La synthèse de la méthoxyméthyl-2 méthyl-3 cyclopentène-2-one-1, **7**, a été effectuée selon la méthode citée en référence 10.

*Méthode générale de synthèse des diènes esters **8** et **10***

À une solution de diisopropylamidure de lithium (2 mmol) dans le tétrahydrofuranne anhydre (10 cm^3), on ajoute goutte à goutte à −78°C l'ester (1,5 mmol) dans 1 cm^3 de tétrahydrofuranne anhydre. On maintient le milieu réactionnel à −78°C pendant 15 min, puis on ajoute lentement la cyclopentènone **7** (1 mmol) en solution dans le tétrahydrofuranne anhydre (2 cm^3). Après addition, le milieu réactionnel est agité 1 h à −78°C puis hydrolysé par une solution d'acide chlorhydrique 1 M de façon à obtenir un pH de 1. Après retour à température ambiante puis agitation durant 15 min, le mélange est extrait par l'éther éthylique (3 × 20 cm^3) et la phase organique lavée et évaporée. Le résidu est chromatographié sur colonne de gel de silice par le mélange éther éthylique – hexane (1 : 1).

*Méthoxyméthyl-2 méthyl-1 [*tert*-butyloxycarbonylméthylène]-3 cyclopentène-1, **8**a*

On condense 0,52 g (4,5 mmol) d'acétate de tertiobutyle avec 0,42 g (3 mmol) de la cyclopentènone **7** selon le mode opératoire décrit ci-dessus. On isole après purification 0,54 g (Rdt 76%) du diène ***8a*** sous forme d'huile incolore; Eb_3 = 140°C; R_f = 0,67 (éther éthylique – hexane, 1 : 1); IR ν_{max} (film) cm^{-1} : 1698 (C=O), 1615 (C=C), 1145 (OtBu); RMN ($CDCl_3$, 100 MHz) δ : 5,74 (m, 1H, C=*CH*); 4,08 (s, 2H, CH_2—OCH_3); 3,34 (s, 3H, O—CH_3); 3,00 et 2,56 (2m, 4H, méthylènes cyclopenténiques); 1,99 (s, 3H, C—CH_3); 1,48 (s, 9H, *t*-Bu); SM *m/z* (%) : 238 (14,9), 182 (40,5), 165 (38,0), 150 (100,0), 149 (97,5). Anal. calc. pour $C_{14}H_{22}O_3$: C 70,56, H 9,30, O 20,14; tr. : C 70,34, H 9,10, O 20,24.

*Méthoxyméthyl-2 méthyl-1 [éthyloxycarbonylméthylène]-3 cyclopentène-1, **8**b*

Par condensation de 0,53 g (6 mmol) d'acétate d'éthyle sur 0,56 g (4 mmol) de cyclopentènone **7** selon le mode opératoire cité précédemment, on isole 0,76 g (Rdt 81%) du diène ***8b***, sous forme d'huile incolore; Eb_3 = 110°C; R_f = 0,53 (éther éthylique – hexane, 1 : 1); IR ν_{max} (film) cm^{-1} : 1698 (C=O), 1645 (C=C), 1151 (OEt); RMN ($CDCl_3$, 100 MHz) δ : 5,76 (m, 1H, C=*CH*); 4,16 (q, 2H, CH_2—CH_3); 4,09 (s, 2H, CH_2—OCH_3); 3,34 (s, 3H, O—CH_3); 3,00 et 2,56 (2m, 4H, méthylènes cyclopenténiques); 1,99 (s, 3H, C—CH_3); 1,28 (t, 3H, O—CH_2—CH_3); SM *m/z* (%) : 210 (15,0), 195 (29,2), 165 (40,4), 91 (100,0). Anal. calc. pour $C_{24}H_{18}O_3$: C 68,54, H 6,63, O 22,83; tr. : C 68,39, H 6,72, O 22,80.

*[(Méthoxyméthyl-3' méthyl-4') cyclopentadiène-1', 3' yl-2']-2 propanoate d'éthyle, **10***

Par condensation de 1,53 g (15 mmol) de propanoate d'éthyle sur 1,4 g (10 mmol) de cyclopentènone **7**, selon le même mode opératoire, on isole après purification 1,21 g (54%) du diène **10**, sous forme d'une huile incolore; Eb_3 = 66°C; R_f = 0,61 (éther éthylique – hexane, 1 : 1). IR ν_{max} (film) cm^{-1} : 1738 (C=O), 1638 (C=C); RMN ($CDCl_3$, 100 MHz) δ : 5,94 (s élargi, 1H, $H_{1'}$); 4,16 (s, 2H, CH_2—OCH_3); 4,13 (m, 2H, CO_2—CH_2CH_3); 3,61 (m, 1H, H_2); 3,31 (s, 3H, OCH_3); 2,91 (s élargi, 2H, $(CH_2)_{5'}$); 2,01 (s, 3H, $C_{4'}$—CH_3); 1,39 (d, 3H, C_2—CH_3); 1,21 (t, 3H, CO_2—CH_2CH_3); SM *m/z* (%) : 224 (25,3), 192 (40,4), 119 (100,0), 91 (29,2). Anal. calc. pour $C_{13}H_{20}O_3$: C 69,61, H 8,99, O 21,40; tr. : C 69,15, H 9,02, O 21,32.

*[Méthoxyméthyl-2' méthyl-3' cyclopentadiène-1', 3' yl-1']-2 propanoate d'éthyle, **11***

À une solution de diisopropylamidure de lithium (3,6 mmol) dans le mélange hexaméthylphosphorotriamide tétrahydrofuranne (20 : 80), on ajoute à −78°C et très lentement le diène ***8b*** (0,63 g, 3 mmol) dans 3 cm^3 de tétrahydrofuranne. Après agitation à −78°C pendant 30 min, on ajoute goutte à goutte 0,64 g (4,5 mmol) d'iodométhane fraîchement distillé dans 2 cm^3 de tétrahydrofuranne. À la fin de l'ajout on laisse la température s'élever jusqu'à −20°C puis on maintient le milieu réactionnel 1 h à cette même température. Après hydrolyse par une solution saturée de chlorure d'ammonium et extraction par l'éther

Can. J. Chem. Downloaded from www.nrcresearchpress.com by 91.144.44.67 on 09/07/12
For personal use only.

Can. J. Chem. Downloaded from www.nrcresearchpress.com by 91.144.44.67 on 09/07/12
For personal use only.

éthylique, la phase organique est lavée puis séchée. Le solvant est évaporé et le résidu élué sur colonne de gel de silice par le mélange éther éthylique – hexane (1 : 6). On isole 2,52 g (Rdt 76%) du cyclopentadiène **11** sous forme d'une huile incolore; Eb_3 = 68°C, R_f = 0,73 (éther éthylique – hexane, 1 : 1); IR ν_{max} (film) cm^{-1}: 1732 (C=O), 1631 (C=C); RMN ($CDCl_3$, 100 MHz) δ : 6,05 (s élargi, 1H, $H_{4'}$); 4,16 (s, 2H, CH_2—OCH_3); 4,13 (m, 2H, CO_2—CH_2CH_3); 3,61 (m, 1H, H_2); 3,31 (s, 3H, O—CH_3); 2,90 (s élargi, 2H, $(CH_2)_{5'}$); 2,02 (s, 3H, $C_{3'}$—CH_3); 1,41 (d, 3H, C_2—CH_3); 1,25 (t, 3H, CO_2—CH_2CH_3); SM *m/z* (%) : 224 (25,3), 192 (40,4), 119 (100,0), 91 (29,2). Anal. calc. pour $C_{13}H_{20}O_3$: C 69,61, H 8,99, O 21,40; tr. : C 69,96, H 9,03, O 21,18.

Méthode générale d'hydrogénation

Une solution du diène (2 mmol) dans 2 cm^3 d'acétate d'éthyle est hydrogénée à température ambiante sous pression d'hydrogène de 1 atmosphère (101,3 kPa) en présence de 0,05 g d'oxyde de platine pendant 24 h. La solution est filtrée sur Célite 545 puis évaporée et l'huile résiduelle chromatographiée sur colonne de gel de silice en utilisant l'éluant éther éthylique – hexane (1 : 1). Le produit hydrogéné est isolé avec un rendement de 98%.

[Méthoxyméthyl-2' méthyl-3' cyclopentyl-1']-2 propanoate d'éthyle, ***12***

L'hydrogénation des diènes **10** ou **11** (0,456 g, 2 mmol) est effectuée conformément à la méthode citée ci-dessus. On isole après purification 0,46 g d'une huile incolore; Eb_3 = 100°C; R_f = 0,78 (éther éthylique – hexane, 1 : 1); IR ν_{max} (film) cm^{-1}: 1735 (C=O), 1151 (OEt); RMN ($CDCl_3$, 100 MHz) δ : 4,33 (q, 2H, CH_2—CH_3); 3,33 (m, 2H, CH_2—OCH_3); 3,27 (s, 3H, O—CH_3); 2,49 (m, 1H, H_2); 2,28 (m, 1H); 2,14 et 1,80 (2m, 4H, méthylènes cyclopentaniques); 1,36 (m, 1H); 1,27 (m, 1H); 1,21 (t, 3H, O—CH_2CH_3); 1,18 et 1,12 (2d, 3H, J = 6,8 Hz et J = 7,1 Hz, CH_3—C—CO_2Et); 1,04 et 1,00 (2d, 3H, J = 6,8 Hz et J = 7,1 Hz, C—CH_3); SM *m/z* (%) : 228 (1,07), 199 (62,4), 94 (100,0). Anal. calc. pour $C_{13}H_{24}O_3$: C 68,42, H 10,52, O 21,05; tr. : C 68,40, H 10,28, O 21,36.

[Méthoxyméthyl-2' méthyl-3' cyclopentyl-1']-2 éthanoate de tert*-butyle,* ***9***

Ce composé est préparé selon le méthode citée en référence 10.

Méthode générale de lactonisation

À une suspension d'iodure de sodium (0,33 g, 2,2 mmol) dans l'acétonitrile (20 cm^3) sont ajoutés, sous courant d'azote, 0,24 g (2,2 mmol) de chlorotriméthylsilane et 1 mmol des esters **9** ou **12**. Le mélange est porté au reflux de l'acétonitrile pendant 16 h puis hydrolysé par 20 cm^3 d'eau. Après extraction par l'éther éthylique, la phase organique est lavée à l'eau puis par une solution saturée de thiosulfate de sodium. Après évaporation du solvant, le résidu est élué sur colonne de gel de silice par le mélange éther éthylique – hexane (1 : 1).

(±) Boschnialactone, ***1***

L'ester **9** (0,5 g, 2,05 mmol) est traité selon la méthode décrite ci-dessus. On récupère après purification 0,203 g (Rdt 63%) de la (±) boschnialactone; Eb_3 = 130°C; R_f = 0,36 (éther éthylique – hexane, 1 : 1); IR ν_{max} (film) cm^{-1}: 2935, 1745, 1460, 1245, 1055; SM *m/z* (%) : 154 (100,0), 136 (12,9), 124 (15,3), 111 (13,3), 108 (13,7), 95 (60,8), 81 (64,7). Anal. calc. pour $C_9H_{14}O_2$: C 70,13, H 9,09, O 20,78; tr. : C 69,98, H 9,04, O 20,70.

(±) 7-Épiisoiridomyrmécine, ***3***

L'ester **12** (0,5 g, 2,2 mmol) est traité comme décrit plus haut. On obtient après purification 0,5 g (Rdt 64%) de la lactone **3**; Eb_3 = 170°C; R_f = 0,54 (éther éthylique – hexane, 1 : 1); IR ν_{max} (film) cm^{-1}: 2930, 1745, 1458, 1147, 1117; SM *m/z* (%) : 168 (49,3), 150 (11,5), 109 (77,2), 95 (100,0), 81 (66,8). Anal. calc. pour $C_{10}H_{16}O_2$: C 71,43, H 9,52, O 19,05; tr. : C 71,23, H 9,38, O 19,01.

(±) 7-Épiteucriumlactone, ***2***

À 0,3 g d'hydrure de sodium mis en suspension dans 20 cm^3 d'éther anhydre, on ajoute goutte à goutte mais rapidement le mélange de boschnialactone (0,2 g, 1,29 mmol) et 10 cm^3 de méthanoate d'éthyle. À la fin de l'addition on ajoute 5 cm^3 d'éthanol absolu. Le mélange réactionnel est ensuite agité à température ambiante durant 1 nuit. On isole après filtration 0,26 g (Rdt 100%) du sel sodique **13** sous forme d'une poudre blanche utilisée sans aucune autre purification pour la suite de la synthèse.

À une solution du sel **13** (0,26 g, 1,29 mmol) dans 20 cm^3 de tétrahydrofuranne anhydre, sont ajoutés 10 cm^3 de formaldéhyde en solution à 30% dans l'eau. Le mélange réactionnel est porté au reflux du tétrahydrofuranne pendant 18 h. Après hydrolyse avec une solution d'acide chlorhydrique 4 M et extraction par l'éther éthylique, la phase organique est lavée à l'eau puis séchée et le solvant évaporé. Le résidu obtenu est chromatographié sur colonne de gel de silice par le mélange éther éthylique – hexane (1 : 1) pour donner 0,17 g (Rdt 78%) de la lactone **2** sous forme d'une huile; R_f = 0,78 (éther éthylique – hexane, 1 : 1); IR ν_{max} (film) cm^{-1} : 2930, 1732, 1625, 1458, 1147, 1117; SM *m/z* (%) : 166 (24,5), 167 (13,7), 150 (100,0), 138 (13,7), 109 (34,5), 95 (57,1), 81 (48,2). Anal. calc. pour $C_{10}H_{14}O_2$: C 72,29, H 8,43, O 19,28; tr. : C 72,20, H 8,23, O 19,26.

Remerciements

Les auteurs remercient très sincèrement Monsieur le Professeur L. D. Colebrook de l'Université Concordia, Montréal, pour ses suggestions et les calculs de mécanique moléculaire.

1. T. Sakan, F. Murai, Y. Hayashi, Y. Honda, T. Shono, M. Nakajima et M. Kato. Tetrahedron, **23**, 4635 (1967).
2. U. M. Pagnoni, A. Pinetti, R. Trave et L. Garanti. Aust. J. Chem. **29**, 1375 (1976).
3. (*a*) M. Pavan. Ric. Sci. **19**, 1011 (1949); Chem. Abstr. **45**, 5869g (1951); (*b*) R. Fusco, R. Trave et A. Vercellone. Chim. Ind. Milan, **37**, 958 (1955); Chem. Abstr. **50**, 6737b (1956).
4. (*a*) J. D. Philipson et M. H. Zenk (*Éditeurs*). Indole and biogenetically related alkaloids 3. Academic Press, London. 1980; (*b*) L. F. Tietze. Angew. Chem. Int. Ed. Engl. **22**, 828 (1983).
5. K. J. Clark, G. I. Fray, R. H. Jaeger et R. Robinson. Tetrahedron, **6**, 217 (1959).
6. P. A. Wender et G. B. Dreyer. Tetrahedron Lett. **24**, 4543 (1983).
7. F. Korte, J. Falbe et A. Zschocke. Tetrahedron, **6**, 201 (1959).
8. R. S. Matthews et J. K. Whitesell. J. Org. Chem. **40**, 3312 (1975).
9. P. Callant, P. Storme, E. van der Eycken et M. Vandewalle. Tetrahedron Lett. **24**, 5797 (1983).
10. J.-C. Caille, B. Tabyaoui, R. Guilard et F. D. Bellamy. Synth. Commun. **15**, 669 (1985).
11. H. Stetter. Angew. Chem. Int. Ed. Engl. **15**, 639 (1976).
12. M. W. Rathke et D. Sullivan. Tetrahedron Lett. **41**, 4249 (1972).
13. (*a*) G. A. Olah, S. C. Narang, B. G. Balaram Gupta et R. Malhotra. J. Org. Chem. **44**, 1247 (1979); (*b*) G. A. Olah, H. Husain, B. G. Balaram Gupta et S. C. Narang. Angew. Chem. Int. Ed. Engl. **20**, 690 (1981); (*c*) G. A. Olah, A. Husain, B. P. Singh et A. K. Mehrotra. J. Org. Chem. **48**, 3667 (1983).
14. A. W. Murray et R. G. Reid. J. Chem. Soc. Chem. Commun. 132 (1984).
15. K. Sisido, K. Inomata, T. Kageyema et K. Utimoto. J. Org. Chem. **33**, 3149 (1968).
16. O. W. Sorensen et R. R. Ernst. J. Magn. Reson. **51**, 477 (1983).
17. K. B. Wilberg, G. M. Lampman, R. P. Ciula, D. S. Connor, P. Schertler et J. Lavanish. Tetrahedron, **21**, 2749 (1965).
18. W. P. Aue, I. Bartholdi et R. R. Ernst. J. Chem. Phys. **64**, 2229 (1978).
19. R. Freeman et G. A. Morris. J. Chem. Soc. Chem. Commun. 684 (1978).
20. M. Karplus. J. Chem. Phys. **30**, 11 (1959).

The crystal and molecular structure of the coordinatively unsaturated Ni(0) species $Ni(PPh_3)_3$

DAVID G. DICK AND DOUGLAS W. STEPHAN[1]

Department of Chemistry and Biochemistry, University of Windsor, Windsor, Ont., Canada N9B 3P4

AND

CHARLES F. CAMPANA

Siemens Analytical X-ray Instruments, Inc., 6300 Enterprise Lane, Madison, WI 53719-1173, U.S.A.

Received October 10, 1989

DAVID G. DICK, DOUGLAS W. STEPHAN, and CHARLES F. CAMPANA. Can. J. Chem. **68**, 628 (1990).

The disproportionation of the complex $(Et_2N)_3Ti(\mu\text{-}PCy_2)Ni(PPh_3)$ affords the coordinatively unsaturated species $Ni(PPh_3)_3$, **1**. This compound crystallizes in the triclinic space group $P\bar{1}$, with $a = 18.483(4)$ Å, $b = 16.203(3)$ Å, $c = 17.783(4)$ Å, $\alpha = 105.85(2)°$, $\beta = 117.33(3)°$, $\gamma = 92.33(3)°$, $Z = 4$, and $V = 4464(2)$ Å^3. Full-matrix least-squares refinement of 1042 variables using 6484 data ($F_o^2 > 3\sigma F_o^2$) gave $R = 0.0441$ and $R_w = 0.0438$. The two crystallographically independent molecules are essentially identical, each exhibiting a trigonal planar coordination sphere at Ni. The most interesting feature of the structure is the close approach (2.744–3.094 Å) of three *ortho* hydrogens of the PPh_3 groups to the Ni centres. The implications of the structural data regarding *ortho* metallation and the known instability of **1** are discussed.

Key words: coordinatively unsaturated, nickel phosphine complex.

DAVID G. DICK, DOUGLAS W. STEPHAN et CHARLES F. CAMPANA. Can. J. Chem. **68**, 628 (1990).

La disproportionation du complex $(Et_2N)_3Ti(\mu\text{-}PCy_2)Ni(PPh_3)$ fournit le $Ni(PPh_3)_3$, **1**, une espèce non-saturée du point de vue de la coordination. Ce composé cristallise dans le groupe d'espace triclinique $P\bar{1}$, avec $a = 18{,}483(4)$, $b = 16{,}203(3)$ et $c = 17{,}783(4)$ Å, $\alpha = 105{,}85(02)$, $\beta = 117{,}33(3)$ et $\gamma = 92{,}33(3)°$, $Z = 4$ et $V = 464(2)$ Å^3. Un affinement de 1042 variables effectué sur 6484 données ($F_o^2 > 3\sigma F_o^2$) par la méthode des moindres carrés sur la matrice entière conduit à des valeurs de $R = 0{,}0441$ et $R_w = 0{,}0438$. Les deux molécules, qui sont indépendantes d'un point de vue cristallographique, sont essentiellement identiques et chacune présente une sphère de coordination trigonale plane au niveau du Ni. La caractéristique la plus intéressante de cette structure est la close proximité (2,744–3,094 Å) des trois hydrogènes *ortho* des groupement PPh_3 attachés aux centre Ni. On discute des implications des données de la structure sur la métallation en *ortho* et sur l'instabilité bien connue du composé.

Mots clés : non-saturé d'un point de vue de la coordination, complexe du nickel avec des phosphines.

[Traduit par la revue]

Introduction

Zerovalent metals of the Ni triad readily form coordinatively unsaturated complexes with sterically demanding phosphine ligands (1–14). Structural studies have confirmed coordination numbers of two and three for several complexes of Pt and Pd including $Pt(PPh(t\text{-}Bu)_2)_2$ (1), $Pd(PPh(t\text{-}Bu)_2)_2$ (1, 2), $Pd(PCy_3)_2$ (2), $Pt(PCy_3)_2$ (3), and $Pt(PPh_3)_3$ (4). The related compound $(Cy_3P)_2Ni(\mu\text{-}N_2)Ni(PCy_3)_2$ (5) is the only example of a coordinatively unsaturated Ni(0) species where the formulation has been confirmed by crystallography. The stability of this complex was attributed to the cage of cyclohexyl rings that surrounds the bridging nitrogen molecule. Other coordinatively unsaturated Ni-phosphine complexes have been known and studied spectroscopically for years (15); however, there have been no reports of structural studies of complexes of the form $Ni(PR_3)_3$ or $Ni(PR_3)_2$. During the course of our investigation of the chemistry of heterobimetallic complexes (16–20), we isolated the complex $Ni(PPh_3)_3$, **1**. This red-brown complex was previously prepared by Tolman *et al.* (15) via the Zn reduction of $NiCl_2$ in the presence of PPh_3; however, it was reportedly extremely unstable and proved to be most difficult to characterize. In this paper, we describe the serendipitous isolation and subsequent crystallographic study of $Ni(PPh_3)_3$, **1**. This report represents the first structural study of a coordinatively unsaturated Ni-perphosphine complex. The structural data presented herein are consistent with the interactions of the Ni centre with *ortho* phenyl protons of PPh_3. Such interactions may account for the difficulty of preparation of **1** and its observed instability.

Experimental

Isolation of crystals of 1

To a solution of $Ni(COD)_2$ (0.005 g, 0.018 mmol) was added $(Et_2N)_3Ti(PCy_2)$[2] (0.018 g, 0.039 mmol) and PPh_3 (0.010 g, 0.038 mmol). The intermediate product was formulated as $(Et_2N)_3Ti(\mu\text{-}PCy_2)Ni(PPh_3)$ on the basis of $^{31}P\{^1H\}$ NMR spectroscopy. This product was extracted into pentane. On standing at 20°C over 4 days, disproportionation led to the crystallization of $Ni(PPh_3)_3$, **1**. The crystals were isolated by decantation of the solvent. The crystals were handled in an inert atmosphere glove box in an atmosphere of O_2-free N_2. The crystals were immediately mounted and sealed in 0.5-mm capillaries.

X-ray data collection and reduction

Diffraction experiments were performed on a four-circle Syntex $P2_1$ diffractometer with graphite-monochromatized Mo Kα radiation ($\lambda = 0.71069$ Å). The initial orientation matrix was obtained from 15 machine-centred reflections selected from a rotation photograph. These data were used to determine the crystal system. Partial rotation photographs around each axis were consistent with a triclinic crystal system for **1**. The final lattice parameters and the orientation matrix were determined from 58 high-angle data ($20° < 2\theta < 25°$). The diffraction data were consistent with the space group $P\bar{1}$. $\pm h, \pm k, +l$ data were collected ($4.5° < 2\theta < 45.0°$), with three standard reflections recorded every 197 reflections. Their intensities showed no statistically significant change over the duration of the data collection. The data were processed, and the solution obtained was refined using the SHELX-86 program on a Micro VAX II computer in the Siemens Analytical X-ray Laboratories in Madison, WI.

Structure solution and refinement

Non-hydrogen atomic scattering factors were taken from the literature tabulations (21–23). The heavy atom positions were deter-

[1]Author to whom correspondence may be addressed.

[2]D. G. Dick and D. W. Stephan, unpublished results.

Printed in Canada / Imprimé au Canada

Can. J. Chem. Downloaded from www.nrcresearchpress.com by 91.144.44.67 on 09/07/12
For personal use only.

Can. J. Chem. Downloaded from www.nrcresearchpress.com by 91.144.44.67 on 09/07/12
For personal use only.

TABLE 1. Crystallographic parameters

Formula	$C_{18}H_{45}NiP_3$
Crystal color, form	Brown blocks
Crystal system	Triclinic
a(Å)	18.483(4)
b(Å)	16.203(3)
c(Å)	17.783(4)
α(deg)	105.85(2)
β(deg)	117.33(3)
γ(deg)	92.33(3)
Space group	$P\bar{1}$
Volume (Å^3)	4464(2)
Density (g cm^{-3}) calcd.	1.258
Z	4
Crystal dimensions (mm)	0.35 × 0.40 × 0.45
Absorption coefficient, μ (cm^{-1})	5.75
Radiation, λ (Å)	Mo Kα (0.71069)
Temperature (°C)	24
Scan speed (deg/min)	2.0–5.0(θ/2θ scan)
Scan range (deg)	1.0 below Kα1 1.0 above Kα2
Background/scan time ratio	0.5
Data collected	8738
No. of unique data $F_o^2 > 3\sigma(F_o^2)$	6484
No. of variables	1042
R (%)	4.41
R_w (%)	4.38
Largest Δ/σ in the final least-squares cycle	0.002
Maximum residual electron density (e/Å^3)	0.41
Atom associated	Ni(1)

mined using direct methods. The remaining non-hydrogen atoms were located from successive difference Fourier map calculations. Following the refinement of the structure in which all non-hydrogen atoms were included with isotropic thermal parameters, an empirical absorption correction was applied to the data, employing the program XABS. The final cycles of refinement were carried out by using full-matrix least-squares techniques on F, minimizing the function $w(|F_o| - |F_c|)^2$ where the weight, w, is defined as $4F_o^2/2\sigma(F_o^2)$ and F_o and F_c are the observed and calculated structure factor amplitudes. In the final cycles of refinement, all non-hydrogen atoms were assigned anisotropic temperature factors. The hydrogen atom positions were calculated and allowed to ride on the carbon to which they are bonded assuming a C—H bond length of 0.95 Å. Hydrogen atom temperature factors were fixed at 1.10 times the isotropic temperature factor of the carbon atom to which they are bonded. The hydrogen atom contributions were calculated, but not refined. Due to the large number of variables, it was necessary to employ an modified version of SHELXTL to complete the final cycles of full-matrix refinement. The residual electron densities were of no chemical significance. Crystal data and data collection parameters are summarized in Table 1. Tables of positional parameters (Table 2) and selected bond distances and angles (Table 3) are reported. Thermal parametes (Table S1), hydrogen atom parameters (Table S2), a complete listing of the bond distances and angles (Table S3), and calculated and observed structure factors (Table S4) have been deposited.[3]

[3]Tables of thermal and hydrogen atom parameters, complete listings of the bond distances and angles, and values of 10 F_o and 10 F_c may be purchased from the Depository of Unpublished Data, CISTI, National Research Council of Canada, Ottawa, Ont., Canada K1A 0S2.

The tables of hydrogen atom parameters and of bond distances and angles have also been deposited with the Cambridge Crystallographic Data Centre. They can be obtained on request from the Director, Cambridge Crystallographic Data Centre, Univerity Chemical Laboratory, Lensfield Road, Cambridge CB2 1EW, UK.

Results and discussion

Conventional synthetic routes to **1** have been previously described by other authors (13, 15). Tolman *et al.* (15), in their solution study of Ni(0) bis- and trisphosphine complexes, indicated that such species were "most difficult to characterize". Furthermore they stated that as a result of their "extreme sensitivity to O_2" these complexes decomposed over several hours, even under rigorously O_2-free conditions. In the present report, crystals of **1** are formed from a solution of the species $(Et_2N)_3Ti(\mu\text{-}PCy_2)Ni(PPh_3)$[1] in pentane. $^{31}P\{^1H\}$ NMR spectra showed no evidence of free PPh_3 in the solution immediately after extraction, rather only the Ti-Ni species formulated above. This suggests that the formation of **1** occurs via disproportionation; however, the nature of the Ti containing product(s) is not known. In hindsight, it seems that the use of the ligand $(Et_2N)_3Ti(PCy_2)$ may solubilize the resulting Ni complex in pentane, permitting the ligand dissociation reaction that yields **1**. Crystallization as a result of the low solubility of **1** in pentane precludes degradation processes that could occur in solution. X-ray quality crystals of **1** were obtained on standing of the solution under strictly anaerobic conditions.

The crystallographic study showed that the crystals of **1** are made up of triclinic unit cells each containing four discrete molecules. The cell volume and centre of symmetry required by the space group $P\bar{1}$ are consistent with the presence of two independent molecules in the asymmetric unit. ORTEP drawings of the two independent molecules are shown in Fig. 1. In each molecule the pseudotrigonal coordination sphere of Ni is composed of three phosphorus atoms of the triphenylphosphine groups. The angles about the Ni centres, that is, the P—Ni—P angles, sum to 360.0 and average 120(1)° for both of the independent molecules of the asymmetric unit, consistent with a trigonal planar geometry. The Ni—P bond distances were found to range from 2.139(1) to 2.156(1) Å. This range of values presumably reflects the steric interactions between the phenyl rings on adjacent phosphine groups and the effectiveness with which the interleaving of these substituents reduces such contacts. The average Ni—P value of 2.147(6) Å is shorter than 2.17(1) Å found for $(Cy_3P)_2Ni(\mu\text{-}N_2)Ni(PCy_3)_2$ (5), 2.19(2) Å for $(Ph_3P)_2Ni(C_2H_4)$ (24, 25), 2.26(1) Å for $(Ph_3P)_3Ni(SO_2)$ (26), and the 2.222(3) Å for $(Ph_3P)_2Ni(N(SiMe_3)_2)$ (27). The shorter average Ni—P distance is consistent with the lesser steric demands of Ph_3P versus Cy_3P as well as the coordinative unsaturation of the Ni centre. The P—C and C—C bond lengths as well as the angles about the triphenylphosphine groups were typical of those found in other structural studies of compounds containing the triphenylphosphine ligand.

The disposition of the phenyl rings in each triphenylphosphine moiety appears to be guided by the approximately parallel alignment of pairs of phenyl rings on adjacent phosphine ligands. This arrangement of aromatic rings was also observed for a single pair of rings in $Pt(PPh_3)_3$ (4). The shorter metal–phosphorus distances in **1** apparently demand more effective interleaving of the phosphine substituents, thus encouraging pseudo-stacking of the phenyl rings. Comparison of the two molecules of the asymmetric unit indicates some variability in the specific orientation of the corresponding phenyl rings. This suggests that while ring stacking may be comparable in magnitude to crystal packing forces, it seems that any stabilization energy that arises from ring stacking is relatively low.

The most interesting feature of the present stuctural study is the observation of the relatively close approach of *ortho* phenyl

TABLE 2. Positional parameters ($\times 10^4$)

Atom	x	y	z	Atom	x	y	z
Ni(1)	1294(1)	3752(1)	2541(1)	Ni(2)	3966(1)	1339(1)	7603(1)
P(1)	1935(1)	4636(1)	2233(1)	P(4)	4923(1)	1748(1)	7344(1)
C(1)	1931(3)	5809(3)	2598(3)	C(55)	4455(3)	2072(3)	6340(3)
C(2)	1223(3)	6056(3)	2589(3)	C(56)	3654(3)	1639(3)	5675(3)
C(3)	1173(4)	6925(4)	2842(4)	C(57)	3260(3)	1870(4)	4913(4)
C(4)	1824(4)	7565(4)	3129(4)	C(58)	3652(5)	2530(5)	4815(5)
C(5)	2520(4)	7336(4)	3143(4)	C(59)	4422(5)	2950(4)	5462(5)
C(6)	2575(3)	6475(3)	2867(4)	C(60)	4831(3)	2729(3)	6217(4)
C(8)	3415(3)	4388(3)	3485(3)	C(61)	5744(3)	2708(3)	8170(3)
C(7)	3050(3)	4624(3)	2731(3)	C(62)	5523(3)	3489(3)	8423(3)
C(9)	4250(4)	4354(3)	3884(4)	C(63)	6102(3)	4220(3)	9084(3)
C(10)	4726(3)	4558(3)	3537(4)	C(64)	6916(4)	4184(4)	9490(4)
C(11)	4380(3)	4807(3)	2795(4)	C(65)	7154(3)	3421(4)	9249(4)
C(12)	3547(3)	4836(3)	2391(3)	C(66)	6574(3)	2685(3)	8590(4)
C(13)	1636(3)	4470(3)	1061(3)	C(67)	5544(3)	974(3)	7103(3)
C(14)	1173(3)	4976(3)	589(4)	C(68)	5682(3)	819(3)	6391(4)
C(15)	899(3)	4779(4)	−318(4)	C(69)	6165(4)	231(4)	6260(5)
C(16)	1089(3)	4063(4)	−764(3)	C(70)	6518(3)	−205(4)	6850(6)
C(17)	1547(3)	3547(3)	−311(4)	C(71)	6388(3)	−70(4)	7567(5)
C(18)	1816(3)	3736(3)	589(3)	C(72)	5890(3)	510(3)	7681(3)
P(2)	995(1)	4215(1)	3597(1)	P(5)	3499(1)	2332(1)	8230(1)
C(19)	765(3)	3465(3)	4104(3)	C(73)	2425(3)	2120(3)	8022(3)
C(20)	1369(3)	3025(3)	4513(3)	C(74)	2183(3)	1445(3)	8254(3)
C(21)	1252(4)	2480(3)	4938(3)	C(75)	1372(3)	1237(3)	8067(4)
C(22)	514(4)	2345(3)	4935(4)	C(76)	793(3)	1680(4)	7638(3)
C(23)	−103(3)	2760(3)	4511(4)	C(77)	1007(3)	2336(3)	7387(3)
C(24)	16(3)	3319(3)	4100(3)	C(78)	1828(3)	2554(3)	7590(3)
C(25)	12(3)	4583(3)	3115(3)	C(79)	3539(3)	3401(3)	8074(3)
C(26)	−599(3)	4072(3)	2263(4)	C(80)	3853(3)	4193(3)	8756(3)
C(27)	−1373(3)	4285(4)	1863(4)	C(81)	3910(3)	4963(3)	8581(4)
C(28)	−1545(4)	5020(5)	2312(5)	C(82)	3628(3)	4958(4)	7723(5)
C(29)	−949(4)	5531(4)	3143(4)	C(83)	3300(3)	4181(4)	7033(4)
C(30)	−180(3)	5320(3)	3545(3)	C(84)	3264(3)	3406(3)	7202(3)
C(31)	1655(3)	5133(3)	4637(3)	C(85)	4108(3)	2586(3)	9438(3)
C(32)	1569(3)	5300(3)	5398(4)	C(86)	3821(3)	2916(3)	10036(4)
C(33)	2053(3)	6005(4)	6151(3)	C(87)	4333(5)	3066(4)	10942(4)
C(34)	2649(3)	6557(3)	6169(4)	C(88)	5124(5)	2896(4)	11243(5)
C(35)	2749(3)	6399(4)	5429(4)	C(89)	5402(4)	2582(4)	10664(5)
C(36)	2254(3)	5692(3)	4679(3)	C(90)	4901(3)	2431(3)	9775(4)
P(3)	889(1)	2396(1)	1711(1)	P(6)	3439(1)	−12(1)	7193(1)
C(37)	1597(3)	1937(3)	1324(4)	C(91)	3962(3)	−849(3)	6836(3)
C(38)	2431(4)	2245(3)	1888(4)	C(92)	4027(3)	−895(3)	6083(3)
C(39)	2995(5)	1959(5)	1627(7)	C(93)	4428(3)	−1487(3)	5785(4)
C(40)	2744(7)	1370(6)	818(8)	C(94)	4789(3)	−2036(3)	6251(4)
C(41)	1926(6)	1050(5)	256(6)	C(95)	4741(3)	−2002(3)	6990(4)
C(42)	1353(4)	1336(4)	507(4)	C(96)	4334(3)	−1413(3)	7293(3)
C(43)	−81(3)	2123(3)	651(3)	C(97)	3278(3)	−381(3)	8001(4)
C(44)	−222(3)	2701(3)	180(4)	C(98)	2624(3)	−1005(4)	7783(4)
C(45)	−908(4)	2507(4)	−661(5)	C(99)	2537(5)	−1222(5)	8440(6)
C(46)	−1462(4)	1745(5)	−1024(5)	C(100)	3109(6)	−829(6)	9314(6)
C(47)	−1343(4)	1178(4)	−571(5)	C(101)	3757(4)	−216(5)	9543(4)
C(48)	−653(4)	1357(4)	262(4)	C(102)	3840(3)	10(3)	8891(4)
C(49)	705(3)	1568(3)	2157(3)	C(103)	2412(3)	−341(3)	6207(3)
C(50)	1197(4)	965(4)	2351(4)	C(104)	2066(3)	−1184(3)	5616(4)
C(51)	1082(5)	393(5)	2751(5)	C(105)	1279(4)	−1386(4)	4887(4)
C(52)	465(6)	433(5)	2970(5)	C(106)	831(3)	−749(5)	4735(4)
C(53)	−50(5)	1005(5)	2767(5)	C(107)	1165(3)	93(4)	5310(4)
C(54)	82(4)	1583(3)	2389(4)	C(108)	1945(3)	293(3)	6032(3)

Can. J. Chem. Downloaded from www.nrcresearchpress.com by 91.144.44.67 on 09/07/12
For personal use only.

TABLE 3. Selected bond distances and angles

Bond	Distance (Å)	Bond	Distance (Å)	Bond	Distance (Å)
Ni(1)—P(1)	2.154(2)	Ni(1)—P(2)	2.148(2)	Ni(1)—P(3)	2.156(1)
P(1)—C(1)	1.835(5)	P(1)—C(7)	1.836(5)	P(1)—C(13)	1.830(5)
P(2)—C(19)	1.838(6)	P(2)—C(25)	1.826(5)	P(2)—C(31)	1.843(4)
P(3)—C(37)	1.835(7)	P(3)—C(43)	1.826(7)	P(3)—C(49)	1.828(4)
Ni(2)—P(4)	2.143(2)	Ni(2)—P(5)	2.144(2)	Ni(2)—P(6)	2.139(1)
P(4)—C(55)	1.827(5)	P(4)—C(61)	1.842(4)	P(4)—C(67)	1.831(5)
P(5)—C(73)	1.843(5)	P(5)—C(79)	1.830(5)	P(5)—C(85)	1.819(5)
P(6)—C(91)	1.836(5)	P(6)—C(97)	1.835(7)	P(6)—C(103)	1.820(4)

Bonds	Angle (deg)	Bonds	Angle (deg)
P(1)—Ni(1)—P(2)	121.2(1)	P(1)—Ni(1)—P(3)	118.5(1)
P(2)—Ni(1)—P(3)	120.2(1)	P(4)—Ni(2)—P(5)	118.0(1)
P(4)—Ni(2)—P(6)	121.7(1)	P(5)—Ni(2)—P(6)	120.3(1)

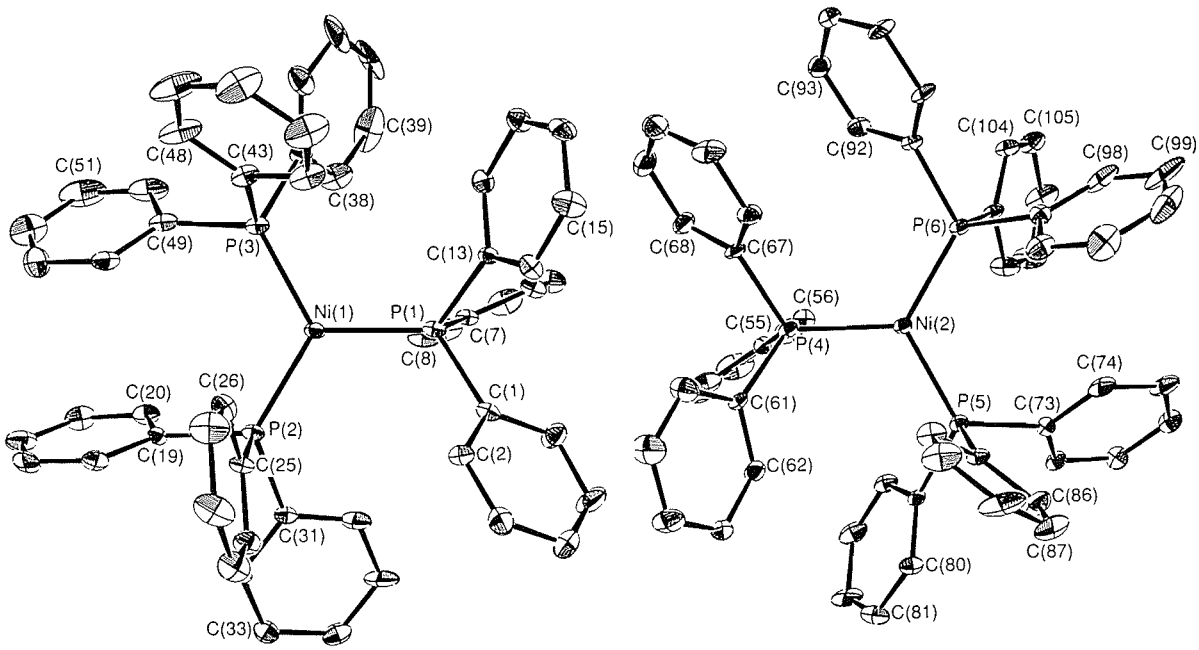

FIG. 1. ORTEP drawings of the two molecules of the asymmetric unit, showing the numbering scheme. 20% thermal elipsoids are shown and hydrogens are omitted for clarity.

ring protons to the Ni atom in each of the two independent molecules. In the case of Ni(1) and H(8), H(26), and H(38), the Ni—H distances are found to be 2.93, 2.91, and 3.09 Å, respectively, while for Ni(2) and H(56), H(90), and H(108) the analogous distances are found to be 2.87, 2.74, and 2.91 Å (Fig. 2). These Ni—H distances are much longer than those attributed to "agostic" interactions (1.9–2.3 Å) (28), suggesting that the approaches observed in the present case arise from ligand–ligand repulsions and not from Ni—(CH) bonding. These close approaches of the *ortho* protons to Ni are comparable to the *ortho*-hydrogen to Pd distances of 2.73 Å seen in $Pd(PPh(t\text{-}Bu)_2)_2$ (2). In that case, the authors noted that the substituent orientation that brings about this contact is sterically favoured, although a bonding interaction between the hydrogen and the metal was also suggested. Such interactions may precede the process of *ortho* metallation, the initial step suggested in the degradation of **1** to the species $(Ph_3P)Ni(\mu\text{-}PPh_2)Ni(PPh_3)$ (15). Interestingly, such *ortho*-hydrogen – metal interactions are not seen in the more stable $Pt(PPh_3)_3$ (4). The relatively close approach of three *ortho* hydrogens to the Ni in **1** may imply that *ortho* metallation is indeed facile. These observations may account for the previously reported instability of the compound and the difficulties in preparation and characterization of the coordinatively unsaturated Ni complex **1** (15).

The present study is the first in which the structure of a coordinatively unsaturated Ni(0)-perphosphine complex has been reported. Furthermore, structural studies of three-coordinate Ni complexes are not common in general. With the exception of the several Ni-olefin complexes (27), the species $(Cy_3P)_2Ni(\mu\text{-}N_2)Ni(PCy_3)_2$ (5) and $(Ph_3P)_2Ni(N(SiMe_3)_2)$ (27) are the only truly three-coordinate Ni species that have been structurally characterized prior to this report.

Can. J. Chem. Downloaded from www.nrcresearchpress.com by 91.144.44.67 on 09/07/12
For personal use only.

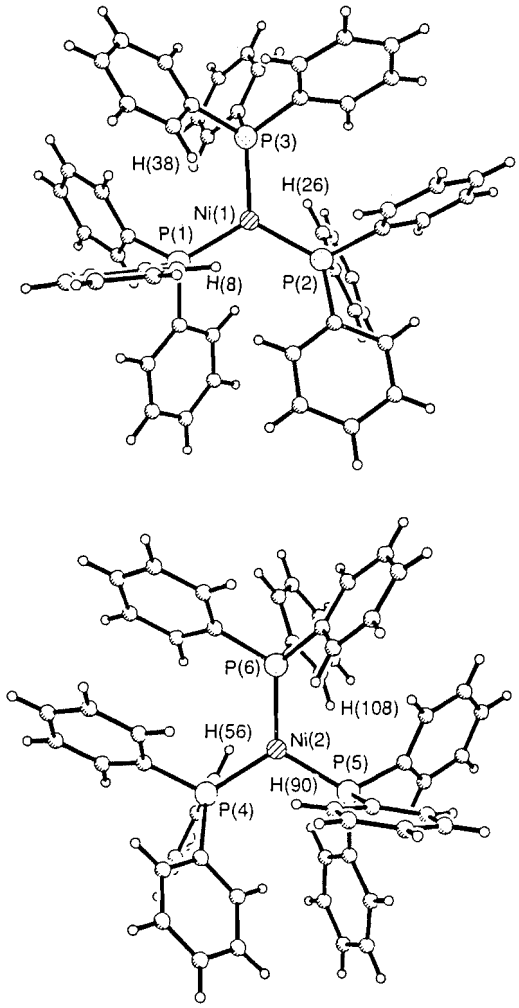

FIG. 2. PLUTO drawings of the two molecules of the asymmetric unit. Hydrogen atoms that are closest to the Ni centres are labelled (see discussion).

Acknowledgements

Financial support from NSERC of Canada is gratefully acknowledged. D.G.D. is grateful for the award of an NSERC of Canada Postgraduate scholarship.

1. S. OTSUKA, T. YOSHIDA, M. MATSUMOTO, and K. NAKATSU. J. Am. Chem. Soc. **98**, 5850 (1976).
2. A. IMMIRZI and A. MUSCO. J. Chem. Soc. Chem. Commun. 400 (1974).
3. A. IMMIRZI, A. MUSCO, P. ZAMBELLI, and G. CARTURAN. Inorg. Chim. Acta, **13**, L13 (1975).
4. V. ALBANO, P. L. BELLON, and V. SCATTURIN. J. Chem. Soc. Chem. Commun. 507 (1966).
5. P. W. JOLLY, K. JONAS, C. KRUGER, and Y. H. TSAY. J. Organomet. Chem. **33**, 109 (1971).
6. R. UGO, F. CARIATI, and G. LAMONICA. Inorg. Synth. **11**, 105 (1968).
7. A. SEN and J. HALPERN. Inorg. Chem. **19**, 1073 (1980).
8. R. UGO. Coord. Chem. Rev. **3**, 319 (1968).
9. L. MALATESTA and M. ANGOLETTA. J. Chem. Soc. 1186 (1957).
10. L. MALATESTA and M. ANGOLETTA. J. Chem. Soc. 2323 (1958).
11. R. VAN DER LINDE and R. O. DEJONGH. J. Chem. Soc. 563 (1971).
12. R. UGO and G. LAMONICA. J. Chem. Soc. 868 (1966).
13. P. HEIMBACH. Angew. Chem. Int. Ed. Engl. **3**, 648 (1964).
14. P. GIANNOCCARO, G. A. SACCO, and G. VASAPOLLO. Inorg. Chim. Acta, **37**, L455 (1979).
15. C. A. TOLMAN, W. C. SEIDEL, and D. H. GERLACH. J. Am. Chem. Soc. **94**, 2669 (1972), and references therein.
16. D. W. STEPHAN. Coord. Chem. Rev. **95**, 41 (1989), and references therein.
17. T. A. WARK and D. W. STEPHAN. Organometallics, **8**, 2836 (1989).
18. T. A. WARK and D. W. STEPHAN. Inorg. Chem. In press.
19. P. Y. ZHENG, T. T. NADASDI, and D. W. STEPHAN. Organometallics, **8**, 1393 (1989).
20. P. Y. ZHENG and D. W. STEPHAN. Can. J. Chem. **67**, 1584 (1989).
21. D. T. CROMER and J. B. MANN. Acta Crystallogr. Sect. A: Cryst. Phys. Diffr. Theor. Gen. Crystallogr. **A24**, 324 (1968).
22. D. T. CROMER and J. B. MANN. Acta Crystallogr. Sect. A: Cryst. Phys. Diffr. Theor. Gen. Crystallogr. **A24**, 390 (1968).
23. D. T. CROMER and J. T. WABER. International tables for X-ray crystallography. Kynoch Press, Birmingham, England. 1974.
24. P. T. CHENG, C. D. COOK, S. C. NYBURG, and K. Y. WAN. Inorg. Chem. **10**, 2210 (1971).
25. C. D. COOK, C. H. KOO, S. C. NYBURG, and M. T. SHIOMI. J. Chem. Soc. Chem. Commun. 426 (1967).
26. D. C. MOODY and R. R. RYAN. Inorg. Chem. **18**, 223 (1979).
27. P. G. ELLER, D. C. BRADLEY, M. B. HURSTHOUSE, and D. W. MEEK. Coord. Chem. Rev. **24**, 1 (1977), and references therein.
28. F. A. COTTON and R. L. LUCK. Inorg. Chem. **28**, 3210 (1989), and references therein.

Can. J. Chem. Downloaded from www.nrcresearchpress.com by 91.144.44.67 on 09/07/12
For personal use only.

The reaction of aluminum atoms with methane

HENGTAI YU[1] AND JOHN D. GODDARD[2]
Department of Chemistry and Biochemistry, University of Guelph, Guelph, Ont., Canada N1G 2W1

Received July 24, 1989

HENGTAI YU and JOHN D. GODDARD. Can. J. Chem. **68**, 633 (1990).

Ab initio SCF and CISD calculations with split valence and larger basis sets have been carried out for several possible reactions of ground state (^2P) aluminum atoms with methane. In particular, the barriers to insertion of Al into a CH bond to give a CH_3AlH intermediate and the abstraction of a hydrogen by Al to give AlH and CH_3 have been studied. At the SCF level, transition state structures have been located and verified by vibrational analyses. In addition, intrinsic reaction coordinates (IRC) have been followed from the transition state geometries down to reactants and to products. Calculated vibrational frequencies and lowest excitation energy for the CH_3AlH intermediate are in good agreement with matrix isolation experimental results. As anticipated on the basis of MO natural correlation symmetry arguments, the energy barrier to the insertion reaction is high (~50 kcal mol^{-1} at the CI level). The energy requirement for the abstraction reaction is similar.

$Al + CH_4 \rightarrow HAlCH_3$ Insertion
$Al + CH_4 \rightarrow HAl + CH_3$ Abstraction

Key words: Al, CH_4, $HAlCH_3$, insertion and abstraction reactions.

HENGTAI YU et JOHN D. GODDARD. Can. J. Chem. **68**, 633 (1990).

Utilisant des ensembles avec de larges bases, on a effectué des calculs *ab initio* SCF et CISD de plusieurs réactions possibles entre des atomes d'aluminium dans l'état fondamental (^2P) et du méthane. On a étudié particulièrement les barrières à l'insertion du Al dans une liaison CH pour donner un intermédiaire CH_3AlH et à l'enlévement d'un hydrogène par un Al pour donner du AlH et du CH_3. Au niveau SCF, on a localisé les structures des états de transition et on les a vérifiées par des analyses vibrationnelles. De plus, on a suivi les coordonnées intrinsèques de la réaction (CIR) des géometries de l'état de transition jusqu'aux réactifs et aux produits. Les fréquences vibrationnelles calculées ainsi que l'énergie d'excitation la plus basse pour l'intermédiaire CH_3AlH sont en bon accord avec les résultats expérimentaux obtenus avec des matrices isolées. Tel qu'on pouvait le prévoir sur la base d'arguments de symétrie des corrélations naturelles des OM, la barrière d'énergie à la réaction d'insertion est élevée (~50 kcal mol^{-1}, au niveau de IC). Les énergies requises pour les réactions d'enlévement sont semblables.

$Al + CH_4 \rightarrow HAlCH_3$ Insertion
$Al + CH_4 \rightarrow HAl + CH_3$ Abstraction

Mots clés : Al, CH_4, $HAlCH_3$, réactions d'insertion et d'abstraction.

[Traduit par la revue]

Introduction

The photochemically initiated reactions of matrix isolated aluminum atoms with methane have been the subject of a recent extensive study by Parnis and Ozin (1–4). The formation of methylaluminum hydride, CH_3AlH, from photoexcited aluminum atoms reacting with methane was conclusively demonstrated and the intermediate well characterized spectroscopically (1, 2). *Ab initio* SCF calculations on the geometry of the CH_3AlH species were reported (2) and orbital and state symmetry based discussions of possible reaction mechanisms were presented (4). A computational SCF study of the CH_3AlH molecule and of other possible reaction products, AlH and $AlCH_3$, has appeared (5). The general area of metal atom – small molecule chemistry has seen considerable activity by quantum chemists and a few references are given in ref. 6. A pioneering study of organoaluminum species is especially noteworthy (7). Interest in metal atom chemistry has been motivated both by the intrinsically fascinating problem of understanding the fine details of a chemical reaction and the view that understanding such prototypes may aid in unravelling important catalytic processes.

The present research focuses on establishing to semiquantitative accuracy the ground state potential energy surface for Al + CH_4 including transition state structures for various insertion or abstraction reactions. The features of this surface may be illustrated by the following scheme:

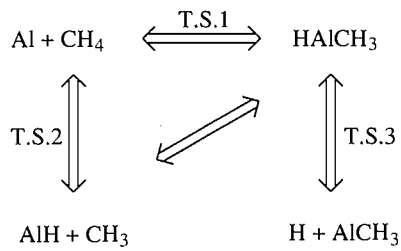

SCHEME 1

Such knowledge of the ground state surface is a necessary prerequisite to the study of the direct excited state chemistry of $Al^*(^2S) + CH_4$.

All geometries were optimized with modest but generally fairly reliable split valence basis sets, 3-21G* and 6-31G + d(Al). Restricted open shell SCF methods were used to eliminate any spin contamination difficulties that might be encountered with UHF. CISD calculations with ~10 000 configurations in C_1 symmetry were carried out to give preliminary indications of the effects of electron correlations on relative energies. The excited states of the Al atom and of the CH_3AlH were examined with comparable SCF + CI computations. The energies of these excited states relative to the various barrier heights on the ground state surface are crucial to the possibility of hot ground state chemistry following possible internal

[1]Permanent address: Institute of Theoretical Chemistry, Jilin University, Changchun, People's Republic of China.

[2]Author to whom correspondence may be addressed.

Can. J. Chem. Downloaded from www.nrcresearchpress.com by 91.144.44.67 on 09/07/12
For personal use only.

Can. J. Chem. Downloaded from www.nrcresearchpress.com by 91.144.44.67 on 09/07/12
For personal use only.

conversion of initially excited species to the ground state surface.

Computational methods

Calculations were performed with the GAMESS codes (8, 9). The Celerity UNIX version was modified slightly and run on the SUN3/280 workstations of the Guelph–Waterloo Chemistry and Physics computing facility. The standard 3-21G* set and a 6-31G + *d* on Al basis (exponent = 0.325) were employed in the SCF calculations (10, 11). Restricted open shell Hartree–Fock calculations were used to describe open shell species. To examine the possibility that a diffuse basis function might be required for an adequate description of the excited states,[3] an *s*-type function of exponent 0.014 (13) was added to the 3-21G* basis to give a set denoted 3-21G* + 4*s*. Geometries were optimized at the SCF level using the methods of Schlegel or Baker (14) as implemented in GAMESS. Starting from two of the transition state structures, intrinsic reaction coordinates, IRC, were followed to reactants and products (15). Configuration interaction calculations, CISD, employed the unitary group CI codes (16) included in GAMESS. Five doubly and one singly occupied orbitals were excited from, and 11 virtuals were kept active to yield, 9972 singly and doubly excited configurations in C_1 symmetry. Dissociation limits such as Al + CH_4 or $AlCH_3$ + H were treated as super molecules in the CISD with the fragments separated by ~7 Å. Such an approach will reduce size consistency errors in comparing the CH_3AlH species to its fragments.

Results and discussion

Qualitative considerations

Parnis and Ozin (4) have presented the argument that the reaction of a ground state aluminum atom with methane is forbidden on the basis of a state symmetry correlation diagram. Figure 1 presents both a MO natural correlation diagram (17) and the more conventional MO correlation (18) for the Al + $CH_4 \rightarrow HAlCH_3$ reaction. Either approach to the symmetry character of this reaction agrees with earlier work (4) in predicting that the ground state process is forbidden. Focusing on the MO natural correlation diagram (17) in Fig. 1, the reaction is an Al atom insertion into a CH bond in methane. As the reaction proceeds, the CH bond is stretched and the σCH bonding orbital ($2a''$) increases in energy in an attempt to correlate with the σCH* antibonding orbital ($4a''$) of the CH_3AlH product. Simultaneously, the σCH* orbital decreases in energy and attempts to correlate with the $2a''$ orbital. Thus an avoided crossing point is reached since both the σCH and σCH* orbitals have the same a'' symmetry. Another avoided crossing occurs involving the $8a'$ and $9a'$ orbitals of the CH_3AlH product and the $9a'$ and $11a'$ orbitals of the Al + CH_4 reactants. Thus, orbital correlations suggest a high energy barrier to the ground state reaction.

Energies

The total SCF energies from 3-21G*, 3-21G* + 4*s*, and 6-31G + *d*(Al) calculations are given in Table 1. The energies in kcal mol^{-1} relative to the ground state of the CH_3AlH intermediate are also presented. Table 2 contains the 3-21G* + 4*s* CISD and CISD + Davidson's correlation energies along with the coefficient of the SCF reference function in the CI expansion. Figure 2 illustrates the relative energies in kcal mol^{-1} of all species examined in this study.

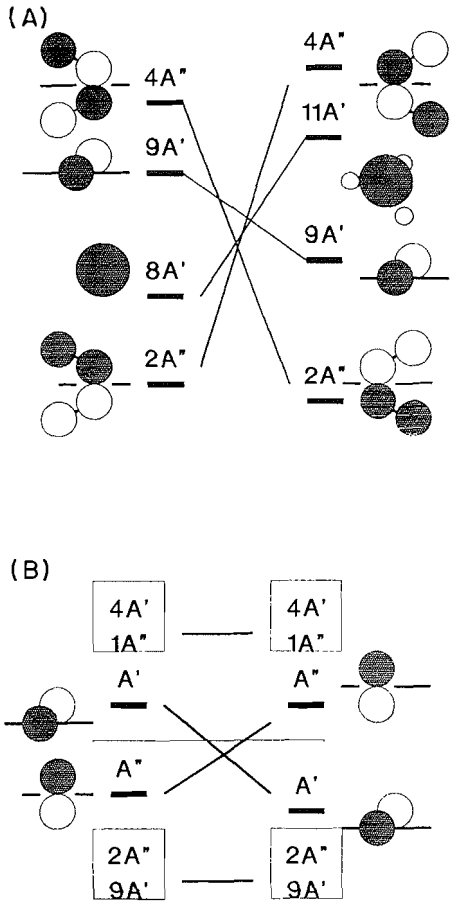

FIG. 1. The symmetry forbidden Al + CH_4 ground state reaction. A. MO natural correlation. B. Hoffmann MO correlation.

Parnis and Ozin have used the results of previous calculations (e.g., ref. 7) to suggest that the dissociation energies of both the CH_3Al—H and H_3C—AlH bonds are likely to be about 45 kcal mol^{-1}. The 3-21G* + 4*s* CISD + Davidson's correction values in Table 2 are 36.0 kcal mol^{-1} for the Al—H bond dissociation energy and 39.2 kcal mol^{-1} for the Al—C energy in methylaluminum hydride. The calculated values are 6–9 kcal mol^{-1} less than the earlier estimates (4). Certainly, the underestimation of a dissociation energy by the modest basis set and configuration interaction calculations is to be expected. Nonetheless the agreement is reasonable. It has been indicated (4) that the reaction of Al ground state (^2P) atoms with methane is 10–11 kcal mol^{-1} exothermic. The calculated exothermicity in this work is 5.4 kcal mol^{-1} or ~5 kcal mol^{-1} less. Thus, the relative energies of various minima on the potential energy surface agree within 5–10 kcal mol^{-1} with previous suggestions. (These energy quantities do *not* include corrections for zero point vibrational energy changes.)

Two energetic quantities of importance in comparison with the experimental results (1–4) are the $^2S \leftarrow {}^2P$ excitation energy of the Al atom and the excited state energy of the CH_3AlH intermediate. The experimental value for the Al $^2S \leftarrow {}^2P$ excitation energy is 72.5 kcal mol^{-1} in the gas phase. The 3-21G* + 4*s* CISD value was determined as the second root of a CI matrix built from ground state orbitals and was 82.3 kcal mol^{-1}. Thus, the calculated value is almost 10 kcal mol^{-1} too

[3]The $^2S \leftarrow {}^2P$ excitation of Al involves a transition to an *s* orbital of higher principal quantum number $3s^23p^1 \rightarrow 3s^24s^1$.

TABLE 1. Total and relative SCF energies with the 3-21G*, 3-21G* + 4s, and 6-31G + d(Al) basis sets. Calculations are at 3-21G* or 6-31G + d(Al) SCF optimized geometries. Relative energies are in kcal mol^{-1} with respect to the ground state of the CH_3AlH intermediate

	3-21G*		3-21G* + 4s		6-31G + d(Al)	
	$E(-280.)$	ΔE	$E(-280.)$	ΔE	$E(-281.)$	ΔE
CH_3AlH	0.57517	0.0	0.57597	0.0	1.04350	0.0
CH_3AlH excited state	0.52353	32.4	0.52415	32.5	0.99186	32.4
Al + CH_4	0.56382	7.1	0.56186	8.9	1.03753	3.7
AlH + CH_3	0.50601	43.4	0.50628	43.7	0.98148	38.9
$AlCH_3$ + H	0.50413	44.6	0.50538	44.3	0.97362	43.9
T.S. 1	0.47949	60.0	0.48017	60.1	0.94853	59.6
T.S. 2	0.47747	61.3	0.47817	61.4	0.94743	60.3
T.S. 3	0.50206	45.9	0.49451	51.1	0.96582	48.7

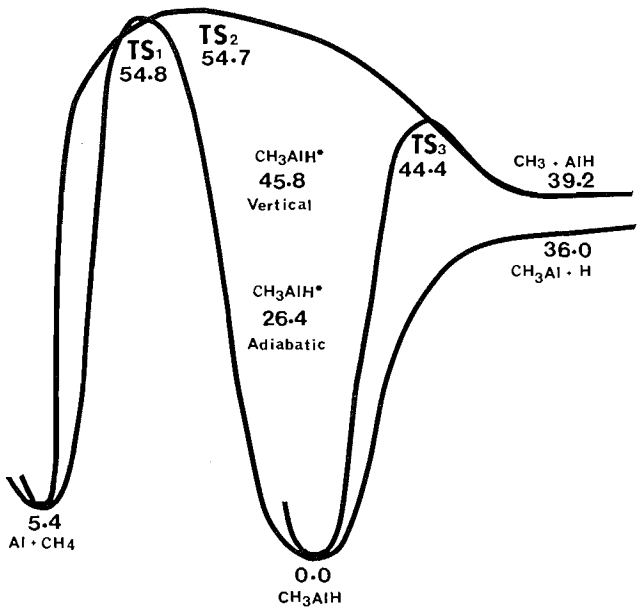

FIG. 2. A schematic illustration of the ground state potential energy surface for Al + CH_4. Energy differences shown are in kcal mol^{-1} relative to the ground state of the CH_3AlH intermediate and are from the 3-21G* + 4s CISD + Davidson's correction calculations.

large but still modestly accurate. The CISD + Davidson's correction vertical excitation energy of CH_3AlH, corresponding to $3a'' \leftarrow 10a'$, is calculated to be 45.8 kcal mol^{-1} after a separate excited state SCF before the CI. Previous computations yielded a value of 44–49 kcal mol^{-1} for this excitation energy (5). In a methane matrix, Parnis and Ozin assign an absorption at 525 nm or 54.5 kcal mol^{-1} to the $^2A'' \leftarrow {}^2A'$ energy difference in CH_3AlH. The geometry of the $^2A''$ excited state of CH_3AlH has been optimized and thus an adiabatic CI excitation energy of 26 kcal mol^{-1} can be predicted. In fact, as this excited state has the CAlH atoms essentially linear, it is degenerate (one component of an ^2E state) with the ground state at the linear structure.

The energies of the transition states at the 3-21G* + 4s CISD with Davidson's correction level will be noted here but discussed further under Reactivity. Transition state 3 (T.S. 3) represents a small barrier of ~5 kcal mol^{-1} to the reaction of H with $AlCH_3$ to form ground state methylaluminum hydride. A

TABLE 2. Total and relative energies at the CISD and CISD+ Davidson's correction levels with the 3-21G* + 4s basis set. The coefficient, c_0, of the SCF reference configuration in the CI expansion is also given

	CISD		CISD + Davidson correction		
	$E(-280.)$	ΔE	$E(-280.)$	ΔE	$\lvert c_0 \rvert$
CH_3AlH	0.62342	0.0	0.62685	0.0	0.970
CH_3AlH excited state	0.58158	26.3	0.58481	26.4	0.972
Al + CH_4	0.61516	5.2	0.61832	5.4	0.970
AlH + CH_3	0.56067	39.4	0.56433	39.2	0.965
$AlCH_3$ + H	0.56539	36.4	0.56953	36.0	0.965
T.S. 1	0.53526	55.3	0.53956	54.8	0.960
T.S. 2	0.53558	55.1	0.53963	54.7	0.964
T.S. 3	0.55268	44.4	0.55829	43.0	0.951

similar barrier was sought for CH_3 + AlH but could not be located. The barrier to Al insertion into CH_4 to yield CH_3AlH (T.S. 1) is ~49.4 kcal mol^{-1}, which is (a) lower by 23–33 kcal mol^{-1} than Al*(^2S) + CH_4 depending on whether the experimental or calculated atomic excitation energy is used, and (b) essentially equal to the vertical excitation energy of CH_3AlH. The barrier for Al abstracting hydrogen from CH_4 to give methyl radical and aluminum hydride is ~50 kcal mol^{-1}. The reverse reaction, i.e., CH_3 abstracting H from AlH, faces a barrier of ~11 kcal mol^{-1}.

Although the energy barriers to the Al atom insertion abstraction reaction are high, the energy requirements are less than or approximately equal to the energy available upon excitation to the lowest excited state of Al or of CH_3AlH.

Structures

The geometries of the aluminum containing molecules, namely AlH, $AlCH_3$, and CH_3AlH (ground and excited state) at the 3-21G* and 6-31G + d(Al) SCF levels are shown in Fig. 3. As expected, the 3-21G* and 6-31G + d(Al) SCF geometries are quite similar. This fact promoted the use of only the 3-21G* basis in locating the transition state structures presented in Fig. 4.

The calculated AlH bond lengths of 1.649 Å (3-21G*) and 1.652 Å (6-31G + d(Al)) are within 0.006 Å of the experimental (19) r_e value of 1.6459 Å. The 3-21G* and 6-31G + d(Al) SCF predictions of the AlC bond length in $AlCH_3$ are 2.004 and

Can. J. Chem. Downloaded from www.nrcresearchpress.com by 91.144.44.67 on 09/07/12
For personal use only.

Can. J. Chem. Downloaded from www.nrcresearchpress.com by 91.144.44.67 on 09/07/12
For personal use only.

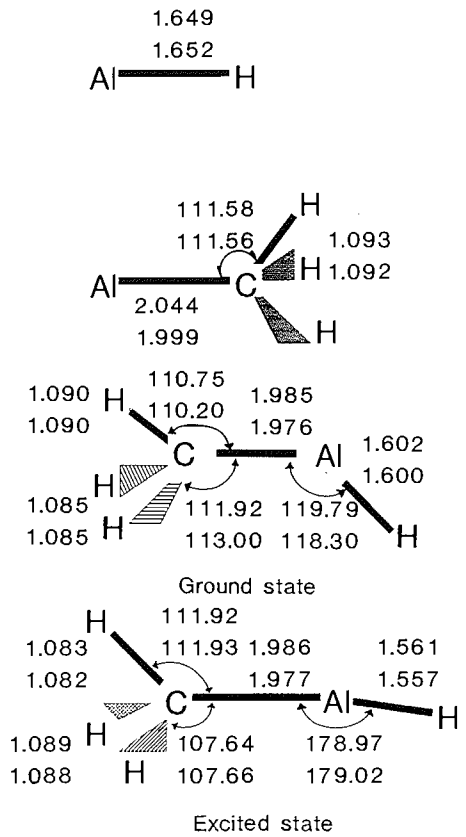

FIG. 3. Calculated geometries for AlH, $AlCH_3$, and the ground and lowest excited states of CH_3AlH at the 3-21G* and 6-31G + d(Al) SCF levels.

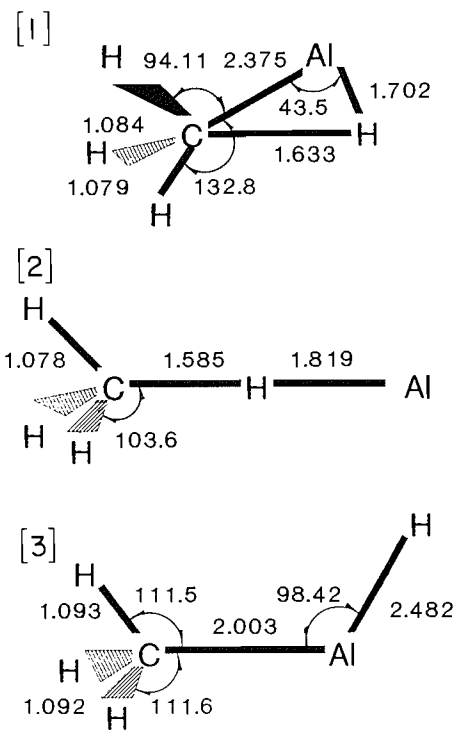

FIG. 4. Calculated transition state structures at the 3-21G* SCF level for the reactions:

[1] $Al + CH_4 \rightarrow CH_3AlH$
[2] $Al + CH_4 \rightarrow AlH + CH_3$
[3] $CH_3AlH \rightarrow CH_3Al + H$

1.999 Å, in good agreement with the previously calculated value 2.013 Å (7). In the ground electronic state of CH_3AlH both the AlC and AlH bonds are shorter than in monovalent aluminum species, $AlCH_3$ and AlH. Such a shortening of these bonds in a divalent aluminum compound may be rationalized by a "hybridization" argument (20). In AlH or $AlCh_3$ the Al uses a $3p$ orbital in bonding while in CH_3AlH sp^2 hybrids are a more appropriate qualitative description of the interactions. The 3-21G* and 6-31G + d(Al) SCF distances for the C—Al bond are 1.985 and 1.976 Å, which are close to the 6-31G** result of 1.981 Å in ref. 2 or 1.980 Å in ref. 5. The AlH distances of 1.602 Å (3-21G*) or 1.600 Å (6-31G + d(Al)) are also in excellent agreement with the previously calculated values of 1.598 or 1.600 Å (2, 5) for methylaluminum hydride. The predicted C—Al—H angles of 119.70° or 118.30° are both close to the 120° expected for sp^2 hybridization and in agreement with previous, calculated results (2, 5).

The lowest excited electronic state of CH_3AlH involves excitation from an in-plane sp^2 hybrid orbital $10a'$ to a $p\pi$ orbital $3a''$. The C—Al—H angle increases dramatically from ~120° to essentially 180° with this orbital change. The AlH distance shortens from 1.600 Å (6-31G + d(Al)) in the ground state or 1.557 Å in this excited state, while the AlC distance remains essentially unchanged. The change to a linear geometry with excitation from an a' to an a'' orbital is consistent with the Walsh diagram type arguments for a 5-valence electron AH_2-like system (21).

The 3-21G* ROHF transition state structures will be discussed briefly here, then examined further when reactivity is considered. Figure 4 illustrates T.S. 1 for the insertion of Al into a CH bond, T.S. 2 for the abstraction of a H from CH_4, and T.S. 3 for CH_3AlH fragmenting to CH_3Al and H. In the insertion transition state the Al interacts more strongly with the H at a distance of 1.702 Å as compared to the Al to C length of 2.375 Å. The CH bond into which the Al is inserting is stretched to 1.633 Å. In fact, at the transition state the reactive hydrogen is approximately equidistant from C and Al. The abstraction reaction T.S. 2 involves a head-on approach of Al to the CH bond (CHAl angle of 180°). At the transition state the CH has lengthened to 1.585 Å, which is ~45% greater than its equilibrium value. The Al to H distance of 1.819 Å is ~0.17 Å or ca. 10% greater than the equilibrium bond length in the diatomic AlH. Thus, the reaction is late in the AlH coordinate as would be expected on Hammond postulate grounds for a strongly endoergic (+33.8 kcal mol^{-1}) one.

T.S. 3 for the dissociation of CH_3AlH to CH_3Al and H has a CH_3Al moiety nearly at its equilibrium geometry with the exception of a C–Al distance slightly longer by ~0.04 Å. The hydrogen atom that is formed is ~2.5 Å removed from the Al.

Vibrational frequencies

The 3-21G* SCF level vibrational frequencies for AlH, $AlCH_3$, and CH_3AlH are collected in Table 3. Both the calculated harmonic frequencies and these values scaled by 0.9 to approximately correct both for anharmonicity and for the SCF method (22) are given. For AlH, the scaled frequency of 1621 cm^{-1} is 50 cm^{-1} lower than the experimental value (19). Previous calculated (and unscaled) frequencies for $AlCH_3$ (5) may be compared with the harmonic computed values in this study. The largest discrepancy is less than 40 cm^{-1} and the average absolute difference between the two sets of frequencies is 23 cm^{-1}.

Seven of the 12 vibrational frequencies of CH_3AlH have been

TABLE 3. Calculated vibrational frequencies for AlH, $AlCH_3$, and ground state CH_3AlH at the 3-21G* SCF level

	ν		Harmonic calculated	0.9* Calcd. scaled	Previous calculation[b] experiment;[a] computed/scaled
AlH	1	σ	1805	1625	1683; 1676
$AlCH_3$	1	e	3155	2840	— ; 3146
	2	a_1	3091	2782	— ; 3075
	3	e	1615	1453	— ; 1576
	4	a_1	1404	1264	— ; 1374
	5	a_1	617	555	— ; 602
	6	e	574	517	— ; 598
CH_3AlH	1	a'	3253	2928	2938; 3205/2980
	2	a''	3182	2864	2886; 3164/2940
	3	a'	3132	2819	— ; 3105/2910
	4	a'	1964	1768	1764, 1746; 1904/1785
	5	a''	1632	1469	— ; 1595/1472
	6	a'	1626	1463	— ; 1584/1462
	7	a'	1414	1272	1162; 1392/1178
	8	a'	847	762	730; 855/716
	9	a''	658	592	610; 673/620
	10	a'	648	583	— ; 647/540
	11	a'	515	463	— ; 518/455
	12	a''	116	104	— ; 86/86

[a] CH_3AlH (2); AlH (19).
[b] Reference 5.

TABLE 4. Calculated vibrational frequencies for the transition state structure at the 3-21G* SCF level

	T.S. 1		T.S. 2		T.S. 3	
	Harmonic	0.9* calcd.	Harmonic	0.9* calcd.	Harmonic	0.9* calcd.
1	3332	2999	3371	3034	3189	2870
2	3286	2957	3351	3016	3171	2854
3	3182	2865	3223	2901	3112	2801
4	1726	1553	1600	1440	1617	1455
5	1622	1460	1599	1439	1616	1454
6	1564	1408	1159	1043	1403	1263
7	1253	1128	832	749	619	557
8	796	716	832	749	597	537
9	612	551	365	329	580	522
10	278	250	288	259	183	165
11	241	217	288	259	107	96
ν*12	1306i	1175i	2317i	2085i	541i	487i

assigned on the basis of the matrix isolation experiments (2). The scaled 3-21G* values of this work differ by an average absolute value of 29 cm^{-1} from experiment. Only ν7, a CH_3 deformation, which is calculated to occur at 1272 cm^{-1} but is observed at 1162 cm^{-1}, is significantly in error. Presumably more flexibility in the C and H basis sets could resolve this difference (12). Previous calculated vibrational frequencies (5) showed the same overall good agreement with experiment.

The single imaginary frequencies for the stationary points in Table 4 verify that these are transition states. The imaginary frequency also provides information on the reaction coordinate at the transition structure. For the insertion reaction, T.S. 1, ν* is 1175i cm^{-1} and is a mode involving considerable bending of the CAlH angle. The reaction coordinate for abstraction is strongly dominated by motion of the H (CH stretching and AlH compression) and has a larger ν* of 2085i cm^{-1}. The T.S. 3 ν* of 487i cm^{-1} is consistent with the small barrier of ~5 kcal mol^{-1} relative to CH_3 + AlH.

Reactivity

Qualitative aspects of the reactions along with mention of the energies, structures, and imaginary vibrational frequencies of the transition states have already been presented. In this section, these results will be expanded upon with reference to the experiments (1–4), and the intrinsic reaction coordinates, Figs. 5 and 6, will be discussed.

The intrinsic reaction coordinates (e.g., ref. 15) shown in Figs. 5 and 6 verify that T.S. 1 connects Al + CH_4 to CH_3AlH and T.S. 2 links Al + CH_4 with CH_3 + AlH. The energy differences summarising the energetics are from the CI calculations at the 3-21G* + 4*s* CISD level although the actual points computed on the IRC were from 3-21G* SCF computations.

Can. J. Chem. Downloaded from www.nrcresearchpress.com by 91.144.44.67 on 09/07/12
For personal use only.

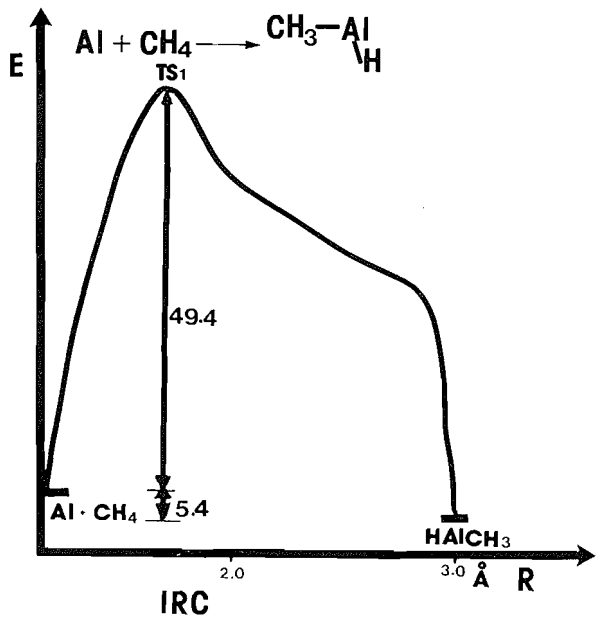

FIG. 5. The 3-21G* SCF intrinsic reaction coordinate connecting Al + CH_4 to AlH + CH_3.

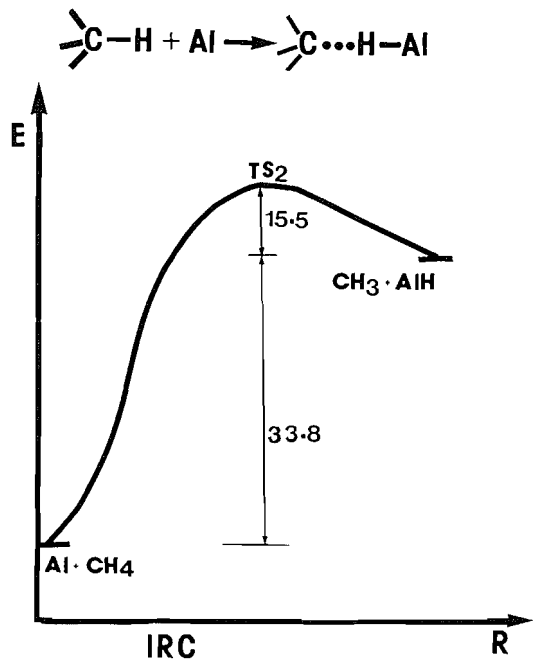

FIG. 6. The 3-21G* SCF intrinsic reaction coordinate connecting Al + CH_4 to CH_3AlH.

The high barrier of ~50 kcal mol^{-1} for the insertion provides computational confirmation of the orbital and state symmetry arguments for a forbidden ground state reaction of Al with CH_4. The abstraction reaction also faces a barrier of comparable height. These barriers are both less than the energy available once the Al is photoexcited (72.5 kcal mol^{-1} experiment or ~82 kcal mol^{-1} calculated). Thus, the possibility of hot ground state chemistry following a nonradiative relaxation from ^2S to ^2P by Al is open. Note that this "thermalization" mechanism is *not* favoured by Parnis and Ozin (4).

The prediction that the hydrogen abstraction barrier is equal to that of the insertion barrier is puzzling. Parnis and Ozin (4) presented the negative result that no evidence for formation of CH_3 was found on the Al/CH_4 system despite the high sensitivity of ESR to the detection of methyl radicals. The calculations indicate a small barrier to CH_3 and AlH recombining to yield CH_3AlH, which should inhibit the reaction and allow CH_3 to be trapped.

The regeneration of Al atoms following absorption at >450 nm by the CH_3AlH could be explained. The vertical excitation energy of the intermediate was calculated to be ~46 kcal mol^{-1} or less than 5 kcal mol^{-1} below the barriers to insertion or abstraction. Some quantum mechanical tunnelling of H may assist in the formation of Al + CH_4. Experimental evidence (4) that is at least suggestive of a role for tunnelling is the much lower yield of Al atoms in the $CD_3AlD \rightarrow Al + CD_4$ reaction.

Conclusions

The results of this study on the ground state reaction of Al atoms with CH_4 are consistent with earlier computations (1, 5) and with many of the experimental results. In particular, the high reaction barriers of ~50 kcal mol^{-1} to insertion or abstraction in the ground state verify the forbidden nature of these reactions. The possibility of hot ground state reactions following photoexcitation of Al cannot be excluded on energetic grounds. The suggestion by Parnis and Ozin (4) of a more direct excited state reaction involving a Rydberg state like Al with CH_4 will require further MCSCF or CI calculations. Such a study is planned.

Acknowledgements

Prof. G. A. Ozin kindly provided preprints of refs. 2–4. Financial support of this research by the Natural Sciences and Engineering Research Council of Canada through an operating grant to J.D.G. is acknowledged.

1. J. M. PARNIS and G. A. OZIN. J. Am. Chem. Soc. **108**, 1699 (1986).
2. J. M. PARNIS and G. A. OZIN. J. Phys. Chem. **93**, 1204 (1989).
3. J. M. PARNIS and G. A. OZIN. J. Phys. Chem. **93**, 1215 (1989).
4. J.M. PARNIS and G. A. OZIN. J. Phys. Chem. **93**, 1220 (1989).
5. G. E. QUELCH and I. H. HILLIER. J. Chem. Soc. Faraday Trans. 2, **83**, 2227 (1987).
6. P. CHAQUIN, A. SEVIN, and H. YU. J. Phys. Chem. **89**, 2813 (1985); R. A. POIRIER, M. R. PETERSON, and M. MENZINGER. J. Chem. Phys. **78**, 4592 (1983); N. ADAMS, W. H. BRECKENRIDGE, and J. SIMONS. Chem. Phys. **56**, 327 (1981).
7. D. J. FOX, D. RAY, P. C. RUBESIN, and H. F. SCHAEFER III. J. Chem. Phys. **73**, 3246 (1980).
8. M. DUPUIS, D. SPANGLER, and J. J. WENDOLOSKI. NRCC Software Catalog, 1. 1980. Program QG01.
9. M. W. SCHMIDT, J. A. BOATZ, K. K. BALDRIDGE, S. KOSEKI, M. S. GORDON, S. T. ELBERT, and B. LAM. Quantum Chemistry Program Exchange Bulletin, **7**, 115 (1987).
10. J. S. BINKLEY, J. A. POPLE, and W. J. HEHRE. J. Am. Chem. Soc. **102**, 939 (1980); M. S. GORDON, J. S. BINKLEY, J. A. POPLE, W. J. PIETRO, and W. J. HEHRE. J. Am. Chem. Soc. **104**, 2797 (1982); W. J. PIERTRO, M. M. FRANCL, W. J. HEHRE, D. J. DEFREES, J. A. POPLE, and J. S. BINKLEY. J. Am. Chem. Soc. **104**, 5039 (1982).
11. W. J. HEHRE, R. DITCHFIELD, and J. A. POPLE. J. Chem. Phys. **56**, 2257 (1972); M. M. FRANCL, W. J. PIETRO, W. J. HEHRE, J. S. BINKLEY, M. S. GORDON, D. J. DEFREES, and J. A. POPLE. J. Chem. Phys. **77**, 3654 (1982); P. C. HARIHARAN and J. A. POPLE. Theor. Chim. Acta, **28**, 213 (1973).
12. J. N. MURRELL and K. J. LAIDLER. Trans. Faraday Soc. **64**, 371 (1968).

Can. J. Chem. Downloaded from www.nrcresearchpress.com by 91.144.44.67 on 09/07/12
For personal use only.

13. T. H. DUNNING, JR. and P. J. HAY. *In* Methods of electronic structure theory. *Edited by* H. F. Schaefer III. Plenum, New York. 1977. Chap. 1. p. 1.
14. H. B. SCHLEGEL. J. Comput. Chem. **3**, 214 (1982); J. BAKER. J. Comput. Chem. **7**, 385 (1986).
15. M. W. SCHMIDT, M. S. GORDON, and M. DUPUIS. J. Am. Chem. Soc. **107**, 2585 (1985).
16. B. BROOKS and H. F. SCHAEFER III. J. Chem. Phys. **70**, 5092 (1979); B. BROOKS, W. LAIDLIG, P. SAXE, N. HANDY, and H. F. SCHAEFER III. Phys. Scr. **21**, 312 (1980).
17. A. DEVAQUET, A. SEVIN, and B. BIGOT. J. Am. Chem. Soc. **100**, 2009 (1978).
18. R. B. WOODWARD and R. HOFFMANN. The conservation of orbital symmetry. Academic Press, New York. 1969.
19. G. HERZBERG. Spectra of diatomic molecules. Van Nostrand Reinhold, New York. 1950.
20. M. L. MCKEE and W. N. LIPSCOMB. J. Am. Chem. Soc. **103**, 4673 (1981); R. H. NOBES, W. J. BOUMA, and L. RADOM. Chem. Phys. Lett. **89**, 497 (1982); J. S. YADAV and J. D. GODDARD. Int. J. Quantum Chem. **29**, 519 (1986).
21. T. A. ALBRIGHT, J. K. BURDETT, and H.-H. WHANGBO. Orbital interactions in chemistry. Wiley, New York. 1985. pp. 93–95.
22. J. A. POPLE, H. B. SCHLEGEL, R. KRISHNAN, D. J. DEFREES, J. S. BINKLEY, M. J. FRISCH, R. A. WHITESIDE, R. F. HOUT, and W. J. HEHRE. Int. J. Quantum Chem. Quantum. Chem. Symp. **15**, 269 (1981).

Can. J. Chem. Downloaded from www.nrcresearchpress.com by 91.144.44.67 on 09/07/12
For personal use only.

Electron spin resonance detection of heterogeneous reactions of Pigment Red 122

MARY JANE WALZAK[1] AND JOHN R. HARBOUR
Xerox Research Centre of Canada, 2660 Speakman Dr., Mississauga, Ont., Canada L5K 2L1

Received April 3, 1989[2]

MARY JANE WALZAK and JOHN R. HARBOUR. Can. J. Chem. **68**, 640 (1990).

Electron spin resonance spectroscopy (ESR) has been used to investigate the electrochemical and photolytic behaviour of particulate C.I. Pigment Red 122. Heterogeneous electrochemical reduction and oxidation of the pigment resulted in different reversible ESR signals with the radical cation giving a signal of ΔH_{pp} = 2.3 G and *g*-factor of 2.0033 and the radical anion giving ΔH_{pp} = 3.2 G and *g*-factor 2.0039. On exposure to light the inherent ESR signal, which was determined to be a two-component signal, increased in intensity by a factor of 2.4 but did not change in linewidth or *g*-factor. This light-induced signal was reversible and decayed to initial levels in the dark. The mechanism of these reactions is discussed.

Key words: ESR, pigment, electrochemistry, photo effects.

MARY JANE WALZAK et JOHN R. HARBOUR. Can. J. Chem. **68**, 640 (1990).

On a utilisé spectroscopie de résonance paramagnétique électronique (RPE) pour étudier les comportements électrochimique et photolytique du pigment rouge 122 à l'état de particule. La réduction électrochimique hétérogène et l'oxydation du pigment ont conduit à des signaux réversibles différents de RPE; le cation radical donne lieu à un signal comportant un ΔH_{pp} = 2,3 G et un facteur-*g* de 2,0033 alors que l'anion radical donne lieu à un signal comportant un ΔH_{pp} = 3,2 G et un facteur-*g* de 2,0039. Lorsqu'on le soumet à la lumière, on a observé que l'intensité du signal RPE inhérent — qui est formé par la superposition de deux signaux — est augmentée par un facteur de 2,4; toutefois, la largeur de la bande ou le facteur-*g* ne changent pas. Ce signal induit par la lumière est réversible et il retourne aux niveaux initiaux lorsqu'on le place à la noirceur. On discute du mécanisme de ces réactions.

Mots clés : RPE, pigment, éléctrochimie, effets photo.

[Traduit par la revue]

Can. J. Chem. Downloaded from www.nrcresearchpress.com by 91.144.44.67 on 09/07/12
For personal use only.

Introduction

For several years we have been studying the electron transfer to and from small particles. Our goal was to demonstrate charge exchange and to gain insight into the way in which particles accept or donate electrons. We used electron spin resonance spectroscopy (ESR) to monitor electron transfer with particles as they were electrochemically reduced and oxidized. Electron spin resonance has proven to be a viable technique for detecting changes in the number of spins with these systems. These changes are of the same order of magnitude as the number of charges exchanged during triboelectrification in the xerographic development process.

Initial efforts were focussed on carbon black particles (1–4) and demonstrated that carbon blacks in dispersion can accept electrons and that these electrons are observable by ESR. From this study it was demonstrated that chemical oxidation of the carbon black creates surface sites which accept electrons on electroreduction.

ZnO particles were also found to manifest an ESR signal, due to trapped electrons, on electroreduction (5). In addition to the ESR signal there was a dielectric loss increase on electroreduction leading to a decrease in the Q of the ESR cavity. Both observations were reversible.

The redox reactions of metal-free phthalocyanine (*x*-H_2Pc) have also been investigated (6). The results show that these pigment particles can also accept and donate electrons and that they manifest different ESR signals upon electroreduction and oxidation.

We have now extended this work by studying the redox behaviour of a quinacridone pigment, C.I. Pigment Red 122 (Structure **1**; quino[2,3-*b*]acridine-7,14-dione-5,12-dihydro-2,9-dimethyl). Colour Index Pigment Red 122 is bright bluish-red in colour and is used in plastics as a colourant, in organic solar cell applications (7), as a photoconductive pigment (8), and as a pigment in coloured toners (9, 10).

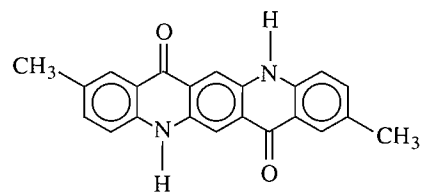

1, C.I. Pigment Red 122

Experimental

The sample of Pigment Red 122 was a commercial sample obtained from Hoechst. This sample had a surface area of 71.4 m^2/g (N_2 B.E.T.) and a stated particle size of 0.2 μm. A Bruker ESP300 EPR spectrometer was used to obtain the data. DPPH was used as the standard for the determination of the number of spins. The internal standard used was the Mn^{2+} impurity in strontium oxide powder in a sealed capillary tube. This provided a reference for both *g*-factor calculations and any changes in cavity Q. The electrochemical cell employed in this work has been described previously (1) and was used with minor modifications. The cell is composed of a capillary with a glass wool plug at the bottom. Pigment Red 122 was placed on top of this plug and a thick platinum wire inserted from the top into the pigment layer. The entire electrode was inserted into an ESR tube containing the electrolyte solution (0.05 *M* tetrabutylammonium perchlorate in methylene chloride) and a thin platinum counter electrode in a separate capillary tube. Since the pigment is insoluble in methylene chloride the redox reactions are heterogeneous rather than homogeneous. The dispersion was purged of oxygen by bubbling thoroughly with nitrogen gas. There was no mechanical stirring in the system. The two electrode system was run with an applied voltage of −6 V for the electroreduction and +6 V for the electrooxidation. This system contains no reference electrode; therefore, the real potential is unknown. The reduction and oxidation were run for 2.5 to 3 h with no

[1]To whom correspondence should be addressed. Present address: Surface Science Western, Natural Sciences Centre, Suite 6, University of Western Ontario, London, Ont., Canada N6A 5B7.

[2]Revision received December 4, 1989.

plateau or saturation of the signal. The temperature dependence of the ESR spectrum was obtained in the frozen state to minimize the possibility of signal decay when the applied potential was removed. Spectra for the electrochemically generated signals were asymmetric and so a lineshape was difficult to assign. However, the signal from the oxidation was very close to Gaussian in shape. The photolytic experiments were carried out in situ by irradiating a flat cell containing a suspension of Pigment Red 122 in Isopar G, using light from a 150 W Xe lamp filtered through a Corning 3-75 filter. This filter cuts off >99.5% of the light with wavelengths shorter than 365 nm and transmits >40% of the light of wavelength longer than 405 nm.

Results and discussion

Inherent signal

Pigment Red 122 in its solid powdered form exhibits an asymmetric ESR signal of ΔH_{pp} of 8.6 ± 0.2 G at an apparent g-factor of 2.0037 ± 0.0002 measured at the crossover point. The intensity, as compared to a DPPH standard, represents a spin concentration of approximately 7.8×10^{16} spins/g or 1 spin per 20 000 molecules. This inherent signal appears to be a mixture of two components, one of narrower linewidth and lower g-factor superimposed on one of broader linewidth and higher g-factor. The g-factors are typical of an interaction of the unpaired electron with heteroatoms oxygen and nitrogen. Because of the mixed nature of the signal a power saturation study was performed. The lineshape, g-factor, and linewidth of the signal at powers from 50 μW to 200 mW were determined. The signal shape changed significantly between these two powers as did the apparent g-factor (Fig. 1). At 50 μW the signal has a g-factor of 2.0037 and a linewidth of 10.3 G, while at 200 mW the signal has a g-factor of 2.0034 and a linewidth of 4.4 G. The results show that the broader signal saturates at lower powers than the narrower signal. This is consistent with the inherent ESR signal in the Pigment Red 122 having at least two components. The ESR response is temperature dependent. At lower temperature the combined signal intensity increases and the spectrum becomes broader (approximately 13 G) and more symmetrical.

Electroreduction

Pigment Red 122 was reduced at an applied potential of −6 V; this reaction produced a slightly asymmetrical ESR signal of linewidth 3.2 G at a g-factor of 2.0039 ± 0.0002 (Fig. 2*a*). The lineshape is very nearly Lorentzian despite the slight asymmetry. The signal intensity was 21 times larger than the inherent signal, representing a spin concentration of approximately 1.6×10^{18} spins/g (Table 1) or 1 spin per 950 molecules. This increase, although significant, is well below the value of 1 spin per 4 molecules previously observed in metal-free phthalocyanine (6). The temperature dependence of the signal, which follows the Curie law (Fig. 3), suggests that it arises from localized states. An alternative explanation (as pointed out by a referee) is that the experiments were performed at temperatures above the degeneracy temperature of the semiconductor and therefore give a Curie law behaviour. Further experiments at lower temperatures would be required to differentiate between the two possibilities. The signal is unstable when the applied voltage is removed, decaying within 1 min. The observed g-factor is typical of molecules containing oxygen and nitrogen.

Electrooxidation

Electrochemical oxidation of Pigment Red 122 at +6 V applied potential resulted in a slightly asymmetrical ESR signal of nearly Gaussian lineshape (Fig. 2*b*). The signal had a linewidth of 2.3 G and a g-factor of 2.0033 ± 0.0001. The increase in signal intensity was approximately 23 times that of the inherent signal corresponding to a spin concentration of approximately 1.8×10^{18} spins/g (Table 1) or 1 spin per 870 molecules. This increase in spin concentration is similar to that observed on reduction. Since the particles are small (0.2 μm) and have a surface area of 71 m^2/g it is possible that the electrochemically generated spins can be accommodated by surface states. The nearly Gaussian lineshape is contrary to our previous experience with pigment materials where the signals due to both reduced and oxidized species were Lorentzian in shape, a result of homogeneous broadening. Furthermore, the plot of inverse intensity versus temperature has a non-zero intercept (Fig. 3). Such a non-zero intercept can be accounted for by an exchange interaction. It is therefore difficult to understand the nature of the spins giving rise to this signal. The

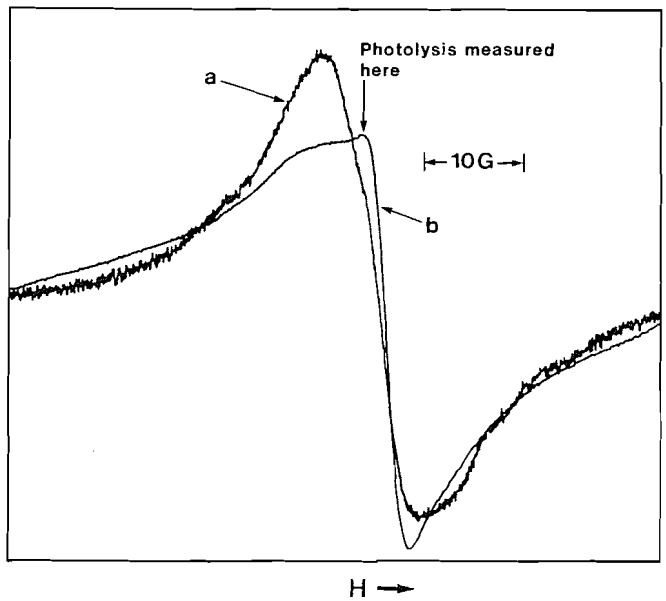

FIG. 1. Inherent ESR signal of Pigment Red 122: (*a*) gain = 1×10^6, modulation amplitude 1.6 G, power 49 μW, (*b*) gain = 1.6×10^5, modulation amplitude 1.0 G, power 200 mW.

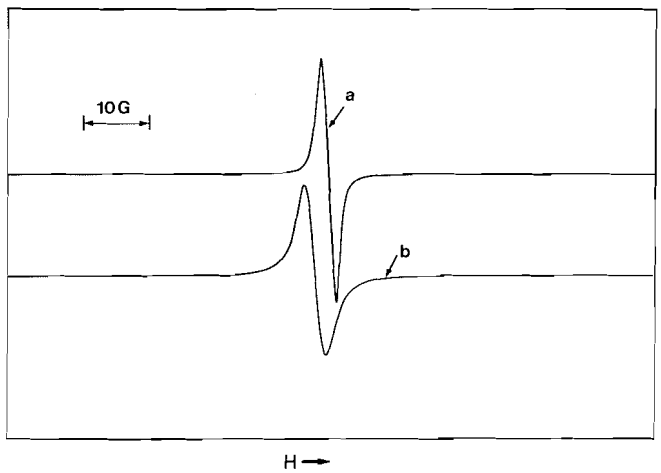

FIG. 2. Resultant ESR signals from reduction and oxidation of Pigment Red 122: (*a*) after 150 min of reduction, gain = 8×10^3, modulation amplitude = 2.8 G, power = 10 mW, (*b*) after 175 min of oxidation, gain = 5×10^3, modulation amplitude = 1.0 G, power = 10 mW.

Can. J. Chem. Downloaded from www.nrcresearchpress.com by 91.144.44.67 on 09/07/12
For personal use only.

TABLE 1. Comparison of the inherent, reduced, and oxidized signals

Signal type	Spins/g	g-factor	ΔH_{pp} (G)
Inherent	7.8×10^{16}	2.0037	8.6
Reduction	1.6×10^{18}	2.0039	3.2
Oxidation	1.8×10^{18}	2.0033	2.3

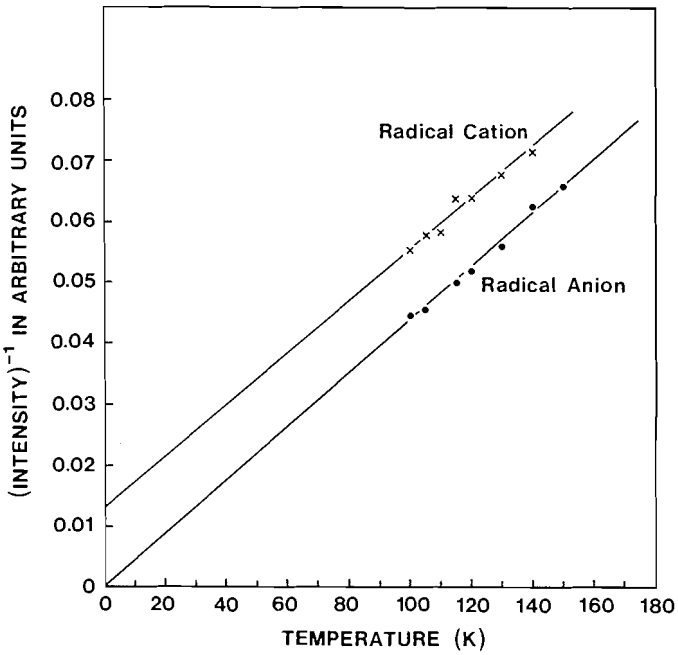

FIG. 3. Graph of inverse intensity (in arbitrary units) versus absolute temperature for the Pigment Red 122 radical anion and cation.

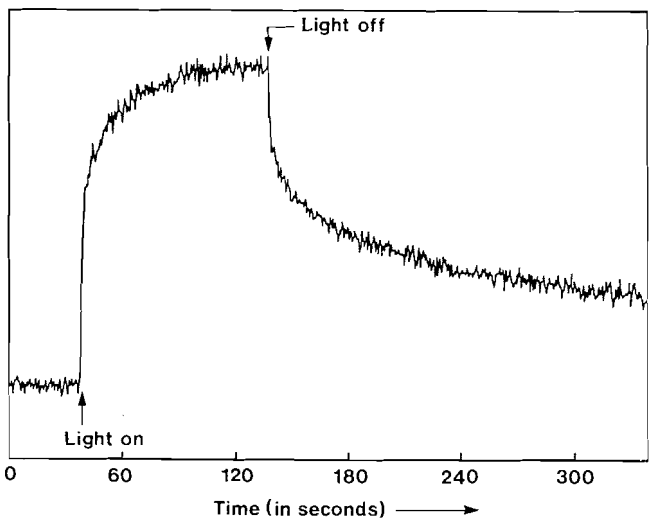

FIG. 4. Effects of irradiation on the intensity of the inherent ESR signal of Pigment Red 122 at 25°C with respect to time in seconds. Refer to Fig. 1 for the field position at which the spectrum was measured.

g-factor of the oxidized species is significantly lower than that of the reduced species. This result is consistent with the g-factors for radical ions generated from chlorophyll (2.0025 radical cation (11), 2.0028 radical anion (12)) and from soluble phthalocyanine (2.0020 radical cation (13), 2.0031 radical anion (14)). In contrast to the electroreduction signal, the electrooxidation signal is stable even 3 h after the applied voltage has been removed.

Photolysis

Pigment Red 122 has been used in a number of photolytic applications including that of a photoconductive pigment on composite electrophotographic plates (8) and as a photoactive pigment in organic solar cells (7). Consequently, the effect of light on the inherent ESR signal was investigated.

On illumination of the pigment sample ($\lambda > 365$ nm), the ESR signal increased by approximately 2.4 times with an initial sharp increase followed by a slower increase to a plateau (Fig. 4). The lineshape, apparent g-factor and linewidth obtained under illumination were identical to the values observed for the inherent signal. When the light was turned off the ESR signal initially decreased rapidly, then more slowly to the original dark level (Fig. 4). Furthermore, both the narrow and broad components of the signal grew and decayed equally in response to light.

Conclusions

C.I. Pigment Red 122 can undergo reversible electrochemical oxidation and reduction to give markedly different ESR signals. The radical anion has an ESR signal which is unstable when the voltage is removed and which follows the Curie law, indicating that it arises from localized states. Alternatively, it is possible that the experiments were performed above the degeneracy temperature of the semiconducting pigment and as a consequence the signal could arise from conduction electrons. The ESR signal from the radical cation is stable for several hours. The nature of the cation radical is difficult to determine from the present data. The non-zero intercept of the inverse temperature dependence of the signal intensity and the nearly Gaussian signal lineshape differ from our previous experiments on pigment materials. The number of spins generated in the reduction and oxidation are consistent with a surface phenomenon but a bulk effect can not be ruled out on the basis of the present evidence alone.

The inherent signal appears to be a composite of two ESR signals with g-factors similar to those of the anion and cation radicals. Photolysis of the pigment increases the composite signal intensity by a factor of 2.4. Since photoexcitation of this pigment results in charge separation, the origin of this signal is consistent with a superposition of radical cation and anion signals. However, the linewidths and temperature dependence of the inherent signal are not consistent with the linewidths and temperature dependences of the electrochemically generated anion and cation radicals. One possibility is a limited number of defect sites at which charge separation occurs. A distribution of recombination rates then accounts for the observed decay of the signal. The environment of such sites would have to be different from the sites that either donate or accept electrons electrochemically to account for the observed differences.

The significant difference in the ESR signals between the cation and anion radicals is important in our ongoing study of triboelectrifiction. These differences allow us to readily differentiate a pigment particle which has accepted an electron from a particle which has donated an electron. This will be particularly useful for experiments designed to monitor charge exchange between dry powders which have been subjected to mixing.

1. J. R. HARBOUR and M. J. WALZAK. Carbon, **22**, 191 (1984).
2. J. R. HARBOUR, M. J. WALZAK, and P. JULIEN. Carbon, **23**, 185 (1985).

Can. J. Chem. Downloaded from www.nrcresearchpress.com by 91.144.44.67 on 09/07/12
For personal use only.

3. J. R. HARBOUR and M. J. WALZAK. Carbon, **23**, 687 (1985).
4. J. R. HARBOUR and M. J. WALZAK. Carbon, **24**, 743 (1986).
5. J. R. HARBOUR and M. J. WALZAK. Photogr. Sci. Eng. **28**, 224 (1984).
6. J. R. HARBOUR and M. J. WALZAK. Langmuir, **2**, 788 (1986).
7. M. TOMIDA and S. KUSABAYASHI. Chem. Lett. 1305 (1984).
8. Mita Industrial Co. Ltd., Jpn. Kokai Tokkyo Koho, JP 57,179,853 [82,179,853], 05 Nov. 1982.
9. K. K. CANON and JPH. KOKAI TOKKYO KOHO. JP 58,189,652 [83,189,652], 05 Nov., 1983.
10. Konishiroku Photo Industry Col, Ltd., Jpn, Kokai Tokkyo Koho, JP8175,660, 22 June, 1981.
11. D. BORG, J. FAJER, R. H. FELTON, and D. DOLPHIN. Proc. Natl. Acad. Sci. U.S.A. **67**, 813 (1970).
12. J. FAJER, A. FORMAN, M. S. DAVIS, L. D. SPAULDING, B. C. BRUNE, and R. H. FELTON. J. Am. Chem. Soc. **99**, 4134 (1977).
13. J. B. RAYNOR, M. ROBSON, and A. S. M. TORRENS-BURTON. J. Chem. Soc. Dalton Trans. 2360 (1977).
14. C. M. GUZY, J. B. RAYNOR, L. P. STODULSKI, and M. C. R. SYMONS. J. Chem. Soc. A, 997 (1969).

Can. J. Chem. Downloaded from www.nrcresearchpress.com by 91.144.44.67 on 09/07/12
For personal use only.

Thiophenophane metal complexes. III. Preparation, X-ray structure, and properties of 2,5,7,10-tetrathia[12] (2, 5) thiophenophane, L, and $[Ag_2L_2]^{2+}$, its dinuclear silver complex cation[1]

C. Robert Lucas,[2] Shuang Liu, and Michael J. Newlands
Department of Chemistry, Memorial University of Newfoundland, St. John's, Nfld., Canada A1B 3X7

and

Jean-Pierre Charland and Eric J. Gabe
Division of Chemistry, National Research Council of Canada, Ottawa, Ont., Canada K1A 0R9

Received October 2, 1989

C. Robert Lucas, Shuang Liu, Michael J. Newlands, Jean-Pierre Charland, and Eric J. Gabe. Can. J. Chem. **68**, 644 (1990).

Preparations of the thiophenophane $C_{12}H_{18}S_5$ (L3), and its binuclear silver(I) complex cation $[Ag_2(L3)_2]^{2+}$ are described. The ^{13}C and ^1H nmr spectra of L3 and the ir and fast atom bombardment mass spectra of the complex are reported. X-ray structures of L3 and $[Ag_2(L3)_2](ClO_4)_2$ have been determined. For L3: space group $P2_1/n$, a = 10.8866(2), b = 9.4419(4), c = 14.9608(2) Å, β = 97.132(1)°, Z = 4, R_f = 0.057, R_w = 0.045. For $[Ag_2(L3)_2][ClO_4]_2$: space group $P2_1/n$, a = 9.2717(3), b = 19.8697(2), c = 10.2654(4) Å, β = 100.592(2)°, Z = 2, R_f = 0.036, R_w = 0.030. The effect of structure on the ligand's ability to form complexes is discussed. The centrosymmetric dinuclear cation has slightly distorted trigonal bipyramidal coordination geometry about each silver. The silver atoms are linked by one bridging thioether sulfur from each ligand. The remaining three sites on each silver are occupied by two terminal thioether sulfurs from one ligand molecule and one from the other ligand molecule. The complex is remarkably stable photochemically and chemically but under certain specific conditions reacts with loss of ligand. This stability is discussed with respect to structure.

Key words: binuclear silver(I) thiophenophane complex.

C. Robert Lucas, Shuang Liu, Michael J. Newlands, Jean-Pierre Charland et Eric J. Gabe. Can. J. Chem. **68**, 644 (1990).

On décrit des préparations du thiophénophane, $C_{12}H_{18}S_5$ (L3), et de son complexe cationique binucléaire de l'argent(I), $[Ag_2(L3)_2]^{3+}$. On a déterminé les spectres rmn du ^{13}C et du ^1H du composé L3 ainsi que les spectres ir et de masse par bombardement avec des atomes rapides du complexe. On a déterminé les structures des composés L3 et $[Ag_2(L3)_2](ClO_4)_2$ par diffraction des rayons-X. Pour L3 : groupe d'espace $P2_1/n$, a = 10,8866(2), b = 9,4419(4) et c = 14,9608(2) Å, β = 97,132(1)°, Z = 4, R_f = 0,057, R_w = 0,045. Pour $[Ag_2(L3)_2](ClO_4)_2$: groupe d'espace $P2_1/n$, a = 9,2717(3), b = 19,8697(2) et c = 10,2654(4) Å, β = 100,592(2)°, Z = 2, R_f = 0,036, R_w = 0,030. On discute de l'effet de la structure sur la facilité qu'a le ligand à former des complexes. Le cation binucléaire centrosymétrique possède une géométrie de coordination trigonale bipyramidale déformée autour de chacun des atomes d'argent. Les atomes d'argent sont liés par un pont formé d'un soufre du thioéther de chacun des ligands. Les trois autres sites de chacun des atomes d'argent sont occupés par deux soufres de thioéthers terminaux provenant d'une molécule de ligand et d'un autre provenant de l'autre molécule de ligand. Le complexe est remarquablement stable d'un point de vue photochimique et chimique; toutefois, dans certaines conditions spécifiques, il peut réagir en perdant un ligand. On discute de cette stabilité en fonction de la structure.

Mots clés : complexe thiophénophane binucléaire de l'argent(I).

[Traduit par la revue]

Introduction

We have recently described preparations and studies of the ligands and complexes $[Cu(L1)_2]^+$, $[CuCl_2L1]_2$, and $[CuCl_2L2]_2$ (1–3).

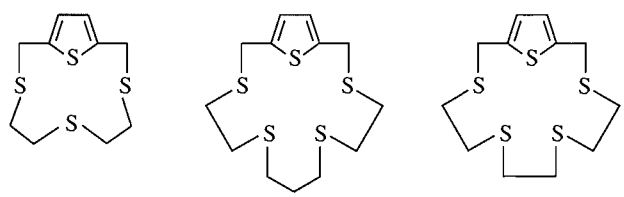

L1 L2 L3

As a continuation of that study we now report the synthesis of thiophenophane, L3, which has a different cavity and different flexibility than L1 or L2 and of its silver(I) complex ion $[Ag_2(L3)_2]^{2+}$. This dinuclear ion contains silver(I) with a trigonal bipyramidal coordination sphere that is only slightly distorted. Until recently, examples of silver(I) with coordination numbers greater than two were relatively rare (4) and often (5–8) exhibited moderate or even severe distortions from idealized coordination geometries, in contrast to $[Ag_2(L3)_2]^{2+}$ which is only slightly distorted from trigonal bipyramidal geometry. Use of macrocyclic thioethers as ligands by several researchers has, however, led to recent preparation of new examples of silver(I) complexes with higher than usual coordination numbers. For example, Wieghardt has reported a complex salt consisting of cations $[AgL_2]^+$ and $[Ag_3L_3]^{3+}$ (L = 1,4,7-trithiacyclononane) in which the silver ions are coordinated by thioether sulfurs in distorted octahedral and tetrahedral arrays, respectively (9). In the latter, a rare example of a bridging crown thioether sulfur, like that in our $[Ag_2(L3)_2]^{2+}$, is found. Likewise, Schröder has described a distorted six coordinate complex $[AgL']^+$ (L' = 1,4,7,10,13,16-hexathiacyclooctadecane) and has studied its electrochemical and chemical oxidation to a Ag(II) species (10). In contrast, our

[1]NRCC No. 31164.

[2]To whom all correspondence should be addressed.

Can. J. Chem. Downloaded from www.nrcresearchpress.com by 91.144.44.67 on 09/07/12
For personal use only.

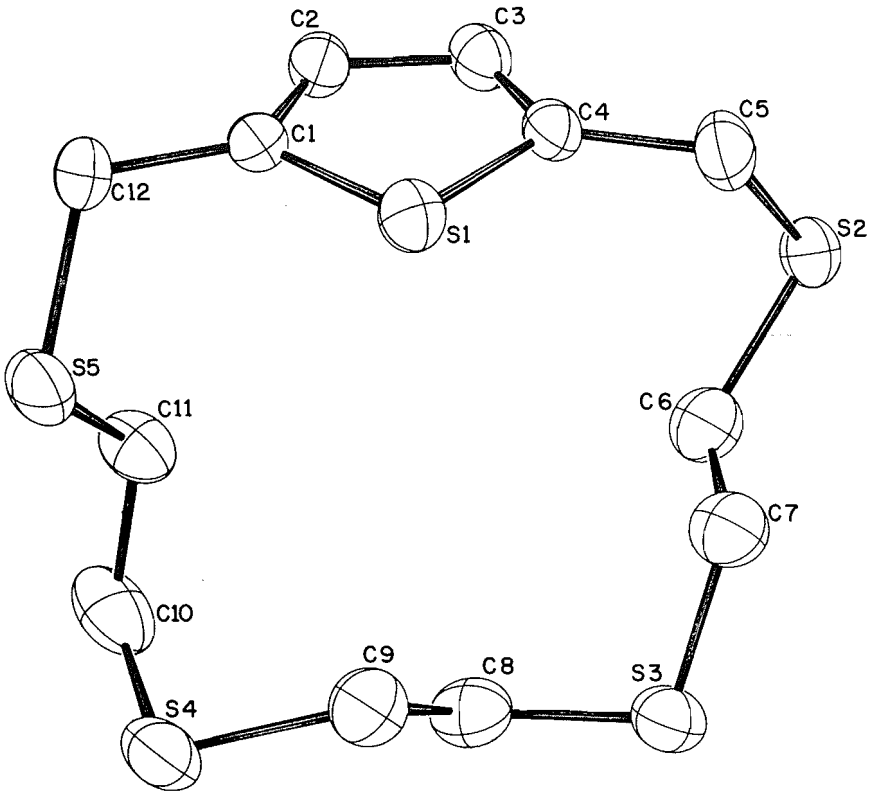

FIG. 1. ORTEP drawing of L3.

$[Ag_2(L3)_2]^{2+}$ is either unreactive or is completely decomposed under similar conditions.

Experimental

Commercially available reagents were obtained from the Aldrich Chemical Co. Inc. or from Morton Thiokol, Alfa Products Inc., and were used without further purification. Spectroscopic data were obtained using the following instruments: ir, Perkin Elmer Model 283; nmr, General Electric 300-NB; mass spectra, VG micromass 7070HS. FAB spectra were obtained using a saddle-field FAB gun on the VG 7070HS mass spectrometer equipped with a VG2035 data system. The standard VG argon atom source was operated at 8 keV and the silver salt was introduced as a mull in glycerol/*para*-toluensulfonic acid (approximately 3:1). X-ray diffraction data were collected using an Enraf-Nonius CAD-4 (L3) or a Picker ($[Ag_2(L3)_2][ClO_4]_2$), diffractometer. Analyses were performed by Canadian Microanalytical Service Ltd.

Preparative

(a) $C_{12}H_{18}S_5$ (ligand L3)

The 2,5-bis(chloromethyl)thiophene (11) used in this preparation must be purified or the overall yield of L3 will be low. Purification can be achieved by washing the crude brown liquid with saturated sodium carbonate solution and then water until the washings are neutral, drying over anhydrous $MgSO_4$, and recrystallizing from petroleum ether or by distilling under reduced pressure. Sodium (1.15 g, 50.0 mmol) was dissolved in commercial absolute ethanol (500 mL) under an atmosphere of dry nitrogen and 1,4,7,10-tetrathiadecane (12) (5.38 g, 25.0 mmol) was added slowly. The mixture was refluxed for an additional 10 min and then to the refluxing mixture a solution of purified 2,5-bis(chloromethyl)thiophene (4.53 g, 25.0 mmol) in commercial absolute ethanol (200 mL) was added dropwise over 8 h with stirring. When the addition was complete, refluxing and stirring were continued for a further 4 h. Volatiles were removed on a rotary evaporator and the residue was taken up in CH_2Cl_2, washed with water several times, dried over anhydrous $CaCl_2$, filtered, and taken to dryness. Recrystallization from benzene and then $CHCl_3$ gave white crystals. Melting point 90–91°C. Yield 4.4 g (56%). Mass spectrum: parent ion = 322 $[C_{12}H_{18}S_5]^+$. Nuclear magnetic resonance ($CDCl_3$, ppm from TMS internal standard, assignments from $^{13}C-^1H$ heteronuclear correlation and attached proton test, position identification from Fig. 1), ^{13}C: 141.9 C1—C4, 126.2 C2—C3, 32.5 C8—C9, 31.8 C7—C10, 31.0 C5—C12, 30.9 C6—C11; ^1H: 6.85 (s, 2H) C2—C3, 3.93 (s, 4H) C5—C12, 2.66 (m, 4H) C6—C11, 2.58 (m, 4H) C7—C10, 2.53 (s, 4H) C8—C9.

(b) $[Ag_2(L3)_2][ClO_4]_2$

NOTE: *Perchlorate salts are often treacherously explosive (13) and although we have been unable to cause this compound to detonate from shock or heat we recommend suitable precautions be taken whenever perchlorates are handled.*

To a solution of $AgClO_4$ (0.052 g, 0.25 mmol) in acetonitrile (10 mL) was added a solution of L3 (0.080 g, 0.25 mmol) in dichloromethane (5 mL). The resulting solution was filtered immediately and the filtrate was left in a beaker to evaporate slowly, giving eventually white crystals that were collected by filtration, washed with acetonitrile, and dichloromethane and dried in air. Yield 1.0 g (80%), mp 175–178°C (dec). Infrared: (Nujol mull) 1413 (s), 1403 (s), 1370 (s), 1302 (w), 1252 (s), 1187 (sh), 1180 (w), 1150 (w), 1080 (vs), 1028 (s), 1000 (sh), 922 (sh), 906 (w), 898 (w), 880 (w), 862 (vw), 852 (w), 838 (m), 810 (s), 743 (sh), 720 (sh), 704 (s), 685 (w), 658 (vw), 642 (m), 619 (vs), 600 (w), 580 (w), 570 (w), 480 (w), 395 (vw), 350 (vw), 275 (w), 245 (s), 225 (s) cm^{-1}. *Anal.* calcd. for $C_{24}H_{36}Ag_2Cl_2O_8S_{10}$: C 27.18, H 3.42, Ag 20.36; found: C 27.22, H 3.41, Ag 19.16.

(c) $[Ag_2(L3)_2][X]_2$ ($X = BF_4$, CF_3SO_3)

A procedure similar to that above was followed giving yields of 72% (BF_4), mp 142–145°C (dec); 89% (CF_3SO_3), mp 177–180°C (dec). *Anal.* calcd. for $C_{24}H_{36}Ag_2B_2F_8S_{10}$: C 27.85, H 3.51, Ag 20.86; found: C 27.88, H 3.50, Ag 21.29; calcd. for $C_{26}H_{36}Ag_2F_6O_6S_{12}$: C 26.94, H 3.13, Ag 18.61; found: C 27.34, H 3.21, Ag 19.50.

Infrared spectra (Nujol mulls) are similar to that of the perchlorate

Can. J. Chem. Downloaded from www.nrcresearchpress.com by 91.144.44.67 on 09/07/12
For personal use only.

Can. J. Chem. Downloaded from www.nrcresearchpress.com by 91.144.44.67 on 09/07/12
For personal use only.

TABLE 1. Crystal data for L3 and $[Ag_2(L3)_2][ClO_4]_2$

Parameter	Value	
	L3	$[Ag_2(L3)_2][ClO_4]_2$
Empirical formula	$C_{12}H_{18}S_5$	$C_{24}H_{36}Ag_2Cl_2O_8S_{10}$
Formula weight	322.40	1059.42
Crystal dimensions, mm	0.12 × 0.17 × 0.31	0.20 × 0.40 × 0.40
Space group	Monoclinic, $P2_1/n$	Monoclinic, $P2_1/n$
a, Å	10.8866(2)[a]	9.2717(3)[a]
b, Å	9.4419(4)	19.8697(2)
c, Å	14.9608(2)	10.2654(4)
β, deg	97.132(1)	100.592(2)
Z (molecules/cell)	4	2
F (0,0,0) electrons	680.27	1063.94
V, Å^3	1525.71	1858.93
d_{calc}, g/cm^3	1.404	1.893
Linear absorption coefficient (μ)mm^{-1}	6.73	1.77
Radiation, Å	λ = 1.54056 (CuKα$_1$)	λ = 0.70930 (MoKα$_1$)
2θ(max), deg	139	45.0
No. reflections measured	2950	2570
No. unique reflections	2871	2433
No. unique refl. $I_{net} > n\sigma I_{net}$	2278 (n = 3.0)	1940 (n = 2.5)
Last least sq. cycle calcd. with	35 atoms 227 parameters 2278 reflections	41 atoms 281 parameters 1940 reflections
R_f (sig. refl.)	0.057[b]	0.036[b]
R_w (sig. refl.)	0.045[c]	0.030[c]
Goodness of fit (last cycle)	4.349[d]	3.657[d]
R_f (all refl.)	0.069[b]	0.050[b]
R_w (all refl.)	0.046[c]	0.030[c]
Max. shift/σ	0.063	0.110
Last D-map		
deepest hole, e/Å^3	−0.470	−0.580
highest peak, e/Å^3	0.560	0.540
Sec. ext. coeff.	7.21	0.44(3)

[a]Throughout this work esd's are in parentheses and refer to the last digit printed.
[b]$R_f = \Sigma||F_o| - |F_c||/\Sigma|F_o|$.
[c]$R_w = [\Sigma w(|F_o| - |F_c|)^2/\Sigma(w|F_o|)^2]^{1/2}$ where $w = 1/\sigma^2 I$.
[d]Goodness of fit = $[\Sigma w(|F_o| - |F_c|)^2/(\text{No. of reflections} - \text{No. of parameters})]^{1/2}$.

salt except that bands at 1080 (vs) and 619 (vs) cm^{-1} have been replaced by bands at 1040 (s) and 521 (w) cm^{-1} (X = BF_4) or 1250 (s, br), 1140 (s), 1036 (sh), 1025 (m), 830 (m), 750 (m), 720 (m), 635 (s), 570 (m), and 515 (m) cm^{-1} (X = CF_3SO_3).

X-ray studies

A summary of crystal data for L3 and $[Ag_2(L3)_2][ClO_4]_2$ is given in Table 1. The diffraction intensities were collected at 295 K using the θ/2θ scan technique with profile analysis (14) at a scan speed of 4°/min. Three standards were measured after every 100 reflections and no significant crystal decay was detected. Space groups were determined by systematic absences. Unit cell parameters in Table 1 were obtained by a least-squares refinement of the setting angles for 25 reflections (91° ≤ 2θ ≤ 96°) for L3 and 25 reflections (90° ≤ 2θ ≥ 96°) for $[Ag_2(L3)_2][ClO_4]_2$. Lorentz and polarization factors were applied. Corrections were made for absorption in L3 but not in $[Ag_2(L3)_2][ClO_4]_2$.

The structures were solved with MULTAN (15) plus a difference Fourier map and refined by full-matrix least squares with counting statistics weights. H-atom positions were calculated but their parameters were not refined. All heavier atoms were refined anisotropically. All calculations were performed with the NRC VAX Crystal Structure programs (16). Scattering factors were taken from the usual source (17). The final atomic positional parameters, the equivalent isotropic temperature factors and important bond lengths and angles are listed in Tables 2–6. Anisotropic thermal parameters, a full listing of bond lengths and bond angles and final structure factors are available as supplementary data.[3] Figures 1 and 2 show views of the structures and their atomic numbering schemes.

Results and discussion

Synthesis of L3 was achieved in 56% yield by a high dilution S_N2 cyclization. Figure 1 suggests an open cavity in the macrocycle's center and the S—S distances of 5–7 Å across the cavity (Table 3) seem to confirm that suggestion making the cavity apparently suitable to accept one or more metal atoms. The solid state conformation, however, involves an exocyclic arrangement of the thioether sulfur lone pairs as is frequently found for simple thiocrown ligands (18). The exocyclic arrangement of lone pairs in thiocrowns is presumed to be due to a preference for *anti* arrangement of S—C—C—S systems as a result of steric and electronic effects (18). In L3, only 2/3 of the S—C—C—S systems have *anti* configurations but the ring still has exocyclic thioether lone pairs. In itself, this need not

[3]A complete set of data may be purchased from the Depository of Unpublished Data, CISTI, National Research Council of Canada, Ottawa, Ont., Canada K1A 0S2.

Can. J. Chem. Downloaded from www.nrcresearchpress.com by 91.144.44.67 on 09/07/12
For personal use only.

TABLE 2. Positional and thermal parameters and equivalent isotropic temperature factors for L3, ($C_{12}H_{18}S_5$)

Atom	x	y	z	B_{iso}[a]
S1	0.01106(11)	0.21463(14)	0.21386(7)	3.98(5)
S2	0.22355(11)	0.32829(15)	0.01704(8)	4.66(6)
S3	−0.12439(12)	0.15873(15)	−0.12700(8)	4.80(6)
S4	−0.43278(12)	0.20268(19)	0.03922(8)	5.72(8)
S5	−0.29062(10)	0.27837(15)	0.24476(8)	4.49(6)
C1	−0.0433 (4)	0.3570 (5)	0.26905(24)	3.29(21)
C2	0.0289 (4)	0.4709 (6)	0.2614 (3)	3.58(21)
C3	0.1298 (4)	0.4441 (6)	0.2132 (3)	3.55(21)
C4	0.1335 (4)	0.3127 (5)	0.1821 (3)	3.13(19)
C5	0.2228 (5)	0.2454 (6)	0.1268 (3)	4.3 (3)
C6	0.0614 (5)	0.3174 (7)	−0.0329 (3)	5.0 (3)
C7	0.0204 (5)	0.1728 (7)	−0.0504 (4)	4.9 (3)
C8	−0.2438 (6)	0.2362 (7)	−0.0715 (4)	5.0 (3)
C9	−0.2825 (6)	0.1468 (7)	0.0034 (4)	5.5 (3)
C10	−0.4071 (5)	0.3757 (8)	0.0815 (5)	6.0 (3)
C11	−0.2944 (5)	0.4018 (6)	0.1515 (4)	4.6 (3)
C12	−0.1565 (5)	0.3501 (7)	0.3152 (3)	4.5 (3)

[a] B_{iso} is the mean of the principal axes of the thermal ellipsoid.

TABLE 3. Selected bond lengths and angles in L3 ($C_{12}H_{18}S_5$)

Bond	Distance (Å)	Bonds	Angle (deg)
S(1)—C(1)	1.720(5)	C(1)—S(1)—C(4)	92.03(22)
S(1)—C(4)	1.737(4)	C(5)—S(2)—C(6)	103.4(3)
S(2)—C(5)	1.820(5)	C(7)—S(3)—C(8)	107.4(3)
S(2)—C(6)	1.833(6)	C(9)—S(4)—C(10)	105.1(3)
S(3)—C(7)	1.836(5)	C(11)—S(5)—C(12)	98.4(3)
S(3)—C(8)	1.783(6)	S(1)—C(1)—C(2)	110.2(3)
S(4)—C(9)	1.859(6)	S(1)—C(1)—C(12)	122.9(4)
S(4)—C(10)	1.762(8)	C(2)—C(1)—C(12)	126.9(5)
S(5)—C(11)	1.815(5)	C(1)—C(2)—C(3)	113.6(5)
S(5)—C(12)	1.822(5)	C(2)—C(3)—C(4)	114.0(5)
C(1)—C(2)	1.345(7)	S(1)—C(4)—C(3)	110.2(3)
C(1)—C(12)	1.487(6)	S(1)—C(4)—C(5)	119.9(4)
C(2)—C(3)	1.409(6)	C(3)—C(4)—C(5)	129.9(4)
C(3)—C(4)	1.327(7)	S(2)—C(5)—C(4)	113.1(3)
C(4)—C(5)	1.495(6)	S(2)—C(6)—C(7)	112.7(4)
C(6)—C(7)	1.450(9)	S(3)—C(7)—C(6)	113.7(4)
		S(3)—C(8)—C(9)	113.9(4)
		S(4)—C(9)—C(8)	113.2(4)
		S(4)—C(10)—C(11)	118.2(5)
		S(5)—C(11)—C(10)	111.2(4)
		S(5)—C(12)—C(1)	113.5(3)

necessarily preclude complex formation since orientation of the lone pairs with respect to each other is such that a metal atom could perch above the cavity by bonding to only some of the sulfur atoms. Approach to L3's cavity in its solid state conformation is, however, largely blocked by H atoms of the methylene groups. In addition to these conformational consequences, the rigidity of the thiophene subunit and its two attached methylenes keeps S2 and S5 (Fig. 1) well separated (6.92 Å) and projecting away from the plane of the thiophene ring. These two sulfurs are thus placed appropriately to coordinate to two different metal atoms except that their lone pairs are directed towards opposite sides of the macrocycle in the solid state conformation. Clearly, this molecule has considerable latent potential as a ligand but will only form complexes in which it is binucleating, or polydentate if

TABLE 4. Torsion angles in L3 ($C_{12}H_{18}S_5$)

Bonds	Angle (deg)
C(1)—S(1)—C(4)—C(3)	0.25(3)
C(4)—S(1)—C(1)—C(12)	179.03(2)
C(5)—S(2)—C(6)—C(7)	65.83(3)
C(7)—S(3)—C(8)—C(9)	73.58(3)
C(10)—S(4)—C(9)—C(8)	63.07(4)
C(11)—S(5)—C(12)—C(1)	56.42(3)
S(5)—C(12)—C(1)—S(1)	50.85(5)
S(1)—C(4)—C(3)—C(2)	1.11(7)
S(1)—C(4)—C(5)—S(2)	117.63(6)
C(4)—C(3)—C(2)—C(1)	1.70(6)
C(12)—C(1)—C(2)—C(3)	179.69(6)
S(3)—C(7)—C(6)—S(2)	164.23(7)
C(1)—S(1)—C(4)—C(5)	179.28(6)
C(4)—S(1)—C(1)—C(2)	0.69(5)
C(6)—S(2)—C(5)—C(4)	55.92(6)
C(8)—S(3)—C(7)—C(6)	65.36(5)
C(9)—S(4)—C(10)—C(11)	50.62(4)
C(12)—S(5)—C(11)—C(10)	175.56(5)
S(5)—C(12)—C(1)—C(2)	127.20(4)
C(5)—C(4)—C(3)—C(2)	178.36(4)
C(3)—C(4)—C(5)—S(2)	61.80(3)
S(1)—C(1)—C(2)—C(3)	1.44(2)
S(3)—C(8)—C(9)—S(4)	164.20(3)
S(5)—C(11)—C(10)—S(4)	52.20(3)

TABLE 5. Positional parameters[a] and equivalent isotropic temperature factors for $[Ag_2(L3)_2][ClO_4]_2$

Atom	x	y	z	B_{iso}[b]
Ag	1.01780(7)	0.00548(3)	−0.19497(5)	5.08(3)
Cl	0.3847(2)	0.1767(1)	0.3432(2)	4.21(9)
O(1)	0.3583(7)	0.1108(2)	0.2974(5)	9.4(4)
O(2)	0.3746(7)	0.2213(2)	0.2362(5)	9.0(4)
O(3)	0.5297(7)	0.1814(3)	0.4122(6)	9.5(4)
O(4)	0.2926(7)	0.1965(3)	0.4253(7)	11.1(5)
S(1)	0.6583(2)	0.0384(1)	−0.0982(2)	4.06(8)
S(2)	0.8281(2)	0.0371(1)	−0.4009(2)	4.06(9)
S(3)	1.1867(2)	0.0924(1)	−0.3117(2)	4.62(10)
S(4)	1.0877(2)	0.0878(1)	0.0034(2)	3.45(8)
S(5)	0.8468(2)	0.1049(1)	0.2209(2)	4.25(9)
C(1)	0.6292(7)	0.0820(3)	−0.2471(6)	3.5(3)
C(2)	0.5961(8)	0.1473(4)	−0.2242(8)	4.1(4)
C(3)	0.5966(8)	0.1624(4)	−0.0910(8)	4.5(4)
C(4)	0.6303(7)	0.1090(3)	−0.0091(7)	3.9(4)
C(5)	0.6443(10)	0.0492(4)	−0.3740(8)	4.7(5)
C(6)	0.8895(9)	0.1236(3)	−0.4114(7)	3.8(4)
C(7)	1.0412(9)	0.1272(4)	−0.4378(7)	4.7(4)
C(8)	1.2087(10)	0.1578(4)	−0.1873(8)	4.4(4)
C(9)	1.2390(9)	0.1289(4)	−0.0487(8)	4.1(4)
C(10)	0.9653(9)	0.1581(4)	0.0081(8)	4.2(4)
C(11)	0.9316(10)	0.1717(4)	0.1428(8)	4.6(4)
C(12)	0.6550(9)	0.1081(5)	0.1375(8)	5.2(5)

[a] The x, y, z parameters of the atoms of the symmetry related half of the molecule are $2 - x$, $2 - y$, $-z$.

[b] B_{iso} is the mean of the principal axes of the thermal ellipsoids.

conformational change first occurs in its flexible thioether chain. In this respect L3 is similar to L1 and L2 (2).

Inspection of the structure of $[Ag_2(L3)_2]^{2+}$ (Fig. 2) reveals that the dinucleating capability of the ligand has been utilized with S2 and S5 of the ligand coordinating in the equatorial positions of two separate silver atoms. Pairs of thioether sulfurs

TABLE 6. Selected bond lengths and angles in $[Ag_2(L3)_2]^{2+}$

Bond	Distance (Å)	Bonds	Angle (deg)
Ag—S(2)	2.567(2)	S(2)—Ag—S(3)	81.15(5)
Ag—S(3)	2.750(3)	S(2)—Ag—S(4)	121.69(5)
Ag—S(4)	2.600(2)	S(2)—Ag—S(4)′	115.79(6)
Ag—S(4)′	2.995(2)	S(2)—Ag—S(5)′	113.47(6)
Ag—S(5)′	2.564(2)	S(3)—Ag—S(4)	82.31(6)
Cl—O(1)	1.396(5)	S(3)—Ag—S(4)′	162.94(5)
Cl—O(2)	1.401(5)	S(3)—Ag—S(5)′	99.37(5)
Cl—O(3)	1.402(6)	S(4)—Ag—S(4)′	86.55(5)
Cl—O(4)	1.364(6)	S(4)—Ag—S(5)′	124.27(6)
S(1)—C(1)	1.735(6)	S(4)′—Ag—S(5)′	76.35(5)
S(1)—C(4)	1.720(7)	Ag—S(4)′—Ag′	93.45(5)
S(2)—C(5)	1.792(10)	C(1)—S(1)—C(4)	92.6(3)
S(2)—C(6)	1.820(7)	Ag—S(2)—C(5)	115.7(3)
S(3)—C(7)	1.825(7)	Ag—S(2)—C(6)	92.1(2)
S(3)—C(8)	1.807(8)	C(5)—S(2)—C(6)	101.5(4)
S(4)—C(9)	1.787(8)	C(7)—S(3)—C(8)	101.7(4)
S(4)—C(10)	1.805(7)	Ag—S(4)—C(9)	98.6(3)
S(5)—C(11)	1.804(8)	Ag—S(4)—C(10)	116.1(3)
S(5)—C(12)	1.828(8)	C(9)—S(4)—C(10)	100.8(4)
C(1)—C(2)	1.364(10)	Ag—S(5)—C(11)	108.8(3)
C(1)—C(5)	1.486(11)	Ag—S(5)—C(12)	115.8(3)
C(2)—C(3)	1.400(12)	C(11)—S(5)—C(12)	103.4(4)
C(3)—C(4)	1.355(10)	S(1)—C(4)—C(3)	110.5(5)
C(4)—C(12)	1.481(11)	S(1)—C(4)—C(12)	121.4(6)
C(6)—C(7)	1.483(12)	S(1)—C(1)—C(2)	109.1(5)
C(8)—C(9)	1.512(11)	S(1)—C(1)—C(5)	121.9(5)
C(10)—C(11)	1.497(12)	S(2)—C(5)—C(1)	116.0(5)
		S(2)—C(6)—C(7)	119.9(5)
		S(3)—C(8)—C(9)	111.7(6)
		S(3)—C(7)—C(6)	117.0(5)
		S(4)—C(9)—C(8)	115.8(6)
		S(4)—C(10)—C(11)	113.8(6)
		S(5)—C(11)—C(10)	117.3(6)
		S(5)—C(12)—C(4)	115.6(5)
		C(1)—C(2)—C(3)	114.3(7)
		C(2)—C(3)—C(4)	113.4(6)
		C(2)—C(1)—C(5)	128.9(6)
		C(3)—C(4)—C(12)	127.9(7)

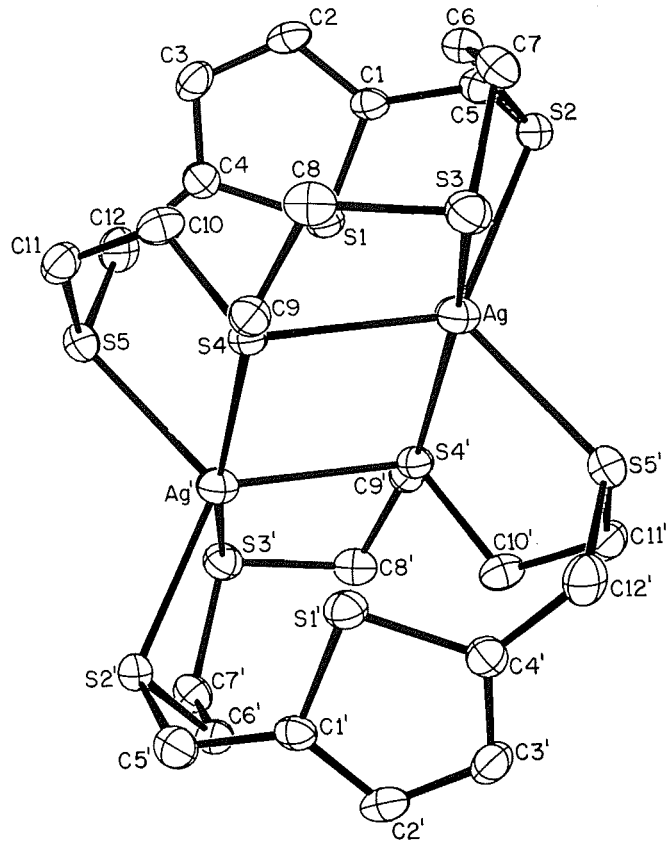

FIG. 2. ORTEP drawing of $[Ag_2(L3)_2]^{2+}$.

separated by two methylene groups are known (19) to have a tendency to form five-membered chelate rings with S—M—S bond angles close to 90°. Therefore, bearing in mind the total number of donors available the remainder of the available sulfur sites are poised for formation of trigonal–bipyramidal coordination about each silver atom. Conformational rearrangement in the thioether chain has occurred from C5 to C9 inclusive so that the lone pairs on the thioether sulfurs are oriented into the cavity towards the silver atoms. The dipositive complex cation (Fig. 2), which is centrosymmetric, consists of two silver atoms 4.082(3) Å apart (compared to 2.88 Å in metallic silver) and each is surrounded by a slightly distorted trigonal bipyramidal array of thioether sulfurs from two molecules of ligand. Neither ligand's thiophene sulfur is bonded to silver. The Ag—S (thiophene) distances are 3.7069(8) Å to the nearer thiophene and 3.9384(7) Å to the more distant one. The latter may be compared to 3.50 Å which is the sum of the van der Waals' radii (20). Sufurs S2 and S5 which hang below their thiophene's plane, bond to equatorial sites of separate silver atoms and one sulfur in each ligand (S4) bridges the two metals assuming an axial position with respect to one and an equatorial with respect to the other. The remaining two sites of a particular silver (an axial and an equatorial) are filled by adjacent sulfurs (S2 and S3) of one ligand so that a five-membered chelate ring with an S—Ag—S angle of 81.15(6)° is formed. The coordination sphere of each silver is distorted somewhat from idealized trigonal bipyramidal geometry. This is revealed most obviously by the S3—Ag—S4′ angle between axial positions which is 162.94(5)° instead of 180°. As a result, one equatorial-to-axial angle (S2—Ag—S4′) is also larger (115.79(6)°) than expected (90°). Each silver lies 0.62 Å out of the plane defined by the three equatorial S-donors and is part of three five-membered chelate rings with angles at Ag of 81.15(6), 82.31(5), and 76.35(5)°. These represent half the axial-to-equatorial angles about each silver. The other half involves a further three inter-ligand S—Ag—S angles, one of which (S4—Ag—S4′ = 86.55(5)°) is part of the Ag_2S_2 bridging system and two of which (S5′—Ag—S3 = 99.37(6); S2—Ag—S4′ = 115.79(6)°) are not part of a ring and so are relatively free to open as required to relieve any stereochemical strain.

The Ag—S lengths with an average of 2.695 Å and a range of 2.564–2.995 Å are comparable to those in other Ag(I) thioether complexes (7, 8). They show the usual slight (~11%) lengthening of average axial over average equatorial distances but the axial Ag—S4′ length is significantly longer (0.245 Å) than the other axial bond length (Ag—S3), presumably because S4′ is bridging whereas S3 is terminal and also because it reduces interaction of a hydrogen on C9 with S1′ of the other ligand.

Characterizing the cation by methods other than X-ray diffraction is difficult since most conventional spectroscopic techniques give no indication of its dinuclear nature. Fast atom bombardment mass spectroscopy has been applied to non-volatile thermally fragile organometallics (21) and we had hoped to apply it successfully to detect $[Ag_2(L3)_2]^{2+}$. The

Can. J. Chem. Downloaded from www.nrcresearchpress.com by 91.144.44.67 on 09/07/12
For personal use only.

Can. J. Chem. Downloaded from www.nrcresearchpress.com by 91.144.44.67 on 09/07/12
For personal use only.

spectrum finally obtained, however, consisted of two peaks of equal intensity with m/e = 429 and 431 corresponding to ions containing ^{107}Ag (51.8% relative abundance) and ^{109}Ag (48.2% relative abundance), respectively. These values of m/e and the relative peak intensities are consistent with $[Ag(L3)]^+$ from cleavage of the dinuclear cation into two monomer fragments. It is of interest to note that no spectrum was obtained when the matrix was glycerol and only when *p*-toluenesulfonic acid was added to the matrix was a spectrum of the complex silver cation detected. It seems reasonable to speculate, therefore, that the role of the acid is to add a proton to the anion of the silver salt, thereby freeing the complex cation so that it may be accelerated from the source into the mass-analyzing sections of the spectrometer.

Although the dimer cleaves in the mass spectrometer it is surprisingly robust under normal chemical conditions. For example, unlike macrocyclic polynitrogen ligand complexes and many other Ag(I) salts, crystalline samples or solutions in benzonitrile of the perchlorate salt can be subjected to uv radiation from a 100 W Hanovia lamp for 24 h with no sign of darkening. Stirred aqueous suspensions of the perchlorate salt containing sodium thiosulfate, ammonia or hydrochloric acid show no reaction after several hours and even a heated solution in benzonitrile of the perchlorate salt and *p*-thiocresol shows only limited reaction after 24 h. In contrast, solutions of the ion seem highly reactive in the presence of a base such as pyridine. For example, when pyridine is added to the unreactive solutions of *p*-thiocresol and $[Ag_2(L3)_2][ClO_4]_2$, a yellow precipitate of $(AgSC_6H_4CH_3)_n$ is formed rapidly in 93% yield. This insoluble mercaptide was identified by elemental analysis, and by its ir spectrum which is devoid of any bands attributable to L3 but contains bands typical of *p*-thiocresol.

It has been observed that coordinated thioethers generally stabilize low oxidation states (22). Exceptions (8) have been attributed to special geometric considerations or in complexes having large coordination numbers to high electron density on silver which should make oxidation relatively easy. Following this reasoning, we attempted unsuccessfully to oxidize the perchlorate salt by both chemical and electrochemical means. Use of ceric ammonium nitrate in methanol caused precipitation of a solid which appears to be the less soluble nitrate salt of $[Ag_2(L3)_2]^{2+}$ while electrochemical oxidation of an acetonitrile solution using a saturated calomel reference electrode gave a precipitate of silver chloride. This result stands in contrast to the inertness to chloride mentioned previously and may be a consequence of the special geometric requirements of the ligand. For example silver(II) is usually found in square or distorted octahedral environments as expected for a d^9 system. Either of these geometries would be difficult to attain from the distorted trigonal bipyramidal structure of $[Ag_2(L3)_2]^{2+}$ due to the rigidity of the thiophenophane. Thus, attempted oxidation could lead to destruction of the dinuclear complex and release of one or more silver(I) ions that would precipitate as AgCl. It would appear therefore that the special geometric requirements of L3 stabilize Ag(I). Thus, unlike cyclam which promotes disproportionation to Ag(0) and Ag(II) (23, 24) or 1,4,7-trithiacyclononane (8) which provides a coordination sphere compatible with both Ag(I) and Ag(II), leading to reversible oxidation of low electrochemical potential for its Ag(I) complex. The ligand L3 provides a coordination geometry particularly favourable to Ag(I) thereby stabilizing that oxidation state.

Acknowledgments

Assistance by Dr. B. Gregory and Miss M. Baggs with the FAB/MS is gratefully acknowledged as is that of K. Grebneff and H. Bassler with aspects of the reactivity studies. Financial support was provided by Memorial University in the form of a Hatcher Scholarship (S.L.) and an operating grant (C.R.L.). Funding was also provided by NSERC and the Canadian government's Challenge '89 summer student program (H.B.).

1. C. R. Lucas, S. Liu, M. J. Newlands, J. P. Charland, and E. J. Gabe. Can. J. Chem. **66**, 1506 (1988).
2. C. R. Lucas, S. Liu, M. J. Newlands, J. P. Charland, and E. J. Gabe. Can. J. Chem. **67**, 639 (1989).
3. C. R. Lucas, S. Liu, and L. K. Thompson. Inorg. Chem. **29**, 85 (1990).
4. F. A. Cotton and G. Wilkinson. Advanced inorganic chemistry. 5th ed. Wiley, Toronto. 1988. p. 941.
5. S. M. Nelson, S. G. McFall, M. G. B. Drew, and A. H. B. Othman. J. Chem. Soc. Chem. Commun. 370 (1977).
6. S. M. Nelson, S. G. McFall, M. G. B. Drew, A. H. B. Othman, and N. B. Mason. J. Chem. Soc. Chem. Commun. 167 (1977).
7. H. W. Roesky, H. Hofmann, P. G. Jones, W. Pinkert, and G. M. Sheldrick. J. Chem. Soc. Dalton Trans. 1215 (1983).
8. J. Clarkson, R. Yagbasan, P. J. Blower, S. G. Rawle, and S. R. Cooper. J. Chem. Soc. Chem. Commun. 950 (1987).
9. H. J. Küppers, K. Wieghardt, Y. T. Tsay, C. Krüger, B. Nuber, and J. Weiss. Angew. Chem. Int. Ed. **26**, 575 (1987).
10. A. J. Blake, R. O. Gould, A. J. Holder, T. I. Hyde, and M. Schröder. Polyhedron, **8**, 513 (1989).
11. J. M. Griffing. J. Am. Chem. Soc. **70**, 3416 (1948).
12. W. Rosen and D. H. Bush. J. Am. Chem. Soc. **91**, 4694 (1969).
13. H. J. Küppers, K. Wieghardt, B. Nuber, J. Weiss, E. Bill, and A. X. Trautwein. Inorg. Chem. **26**, 3762 (1987).
14. D. F. Grant and E. J. Gabe. J. Appl. Crystallogr. **11**, 114 (1978).
15. G. Germain, P. Main, and M. M. Woolfson. Acta Crystallogr. **A27**, 368 (1971).
16. E. J. Gabe, F. L. Lee, and Y. LePage. *In* Crystallographic computing 3. *Edited by* G. Sheldrick, C. Kruger, and R. Goddard. Clarendon Press, Oxford. 1985. p. 167.
17. International tables for X-ray crystallography. Vol. IV. Kynoch Press, Birmingham, England. 1974. p. 99. Table 2.2B.
18. R. E. Wolf, J. R. Hartman, J. M. E. Storey, B. M. Foxman, and S. R. Cooper. J. Am. Chem. Soc. **109**, 4328 (1987).
19. P. W. R. Corfield, C. Ceccarelli, M. D. Glick, I. Wei-Yu Moy, L. A. Ochrymowycz, and D. B. Rorabacher. J. Am. Chem. Soc. **107**, 2399 (1985).
20. A. Bondi. J. Phys. Chem. **68**, 441 (1964).
21. B. Gregory, C. R. Jablonski, and Y. P. Wang. J. Organomet. Chem. **269**, 75 (1984).
22. S. G. Murray and F. R. Hartley. Chem. Rev. **81**, 365 (1981).
23. T. Ito, H. Ito, and K. Toriumi. Chem. Lett. 1101 (1981).
24. K. B. Mertes. Inorg. Chem. **17**, 49 (1978).

Synthetic applications and spectroscopic investigations of the $(NSCl)_3$–SO_2Cl_2 system

ALLEN APBLETT and TRISTRAM CHIVERS[1]
Department of Chemistry, The University of Calgary, Calgary, Alta., Canada T2N 1N4

Received June 22, 1989

ALLEN APBLETT and TRISTRAM CHIVERS. Can. J. Chem. **68**, 650 (1990).

Solutions of $(NSCl)_3$ in the presence of excess SO_2Cl_2 behave as a source of the synthetic equivalent "$NSCl_3$" in reactions with methacrylonitrile or thioacetamide to give 4-cyanoisothiazole (78%) or 5-methyl-1,3,2,4-dithiadiazolium chloride (63%), respectively. In the reaction of this reagent with thiobenzamide both 5-phenyl-1,3,2,4-dithiadiazolium chloride (42%) and 3,5-diphenyl-1,2,4-thiadiazole (51%) are produced. The treatment of the $(NSCl)_3$–SO_2Cl_2 system with 2-aminobenzenethiol yields 2,4-$C_6H_3Cl_2NSCl_2$, which is converted to 2,4-$(C_6H_3Cl_2N)_2S$ upon heating at 80°C in toluene or by reduction with Ph_3Sb or mercury. The reaction of 2-aminobenzenethiol with excess SO_2Cl_2, in the absence of $(NSCl)_3$, produces 2,4,6-$C_6H_2Cl_3NSCl_2$. Attempts to characterize the active species in the $(NSCl)_3$–SO_2Cl_2 system by ^{14}N and ^{33}S nmr, Raman and infrared spectroscopy are also described.

Key words: cyclotrithiazyl chloride, isothiazole, dithiadiazolium, arylimidosulfurous dichloride, ^{14}N nmr.

ALLEN APBLETT et TRISTRAM CHIVERS. Can. J. Chem. **68**, 650 (1990).

En présence d'un excès de SO_2Cl_2, les solutions de $(NSCl)_3$ se comportent comme une source de "$NSCl_3$" et elles réagissent avec le méthacrylonitrile ou le thioacétamide pour donner respectivement le 4-cyanoisothiazole (78%) et le chlorure de 5-méthyl-1,3,2,4-dithiadiazolium (63%). Lors de la réaction de ce réactif avec le thiobenzamide, il se forme du chlorure de 5-phényl-1,3,2,4-dithiadaizolium (42%) ainsi que du 3,5-diphényl-1,2,4-thiadiazole (51%). Lorsqu'on soumet le 2-aminobenzénethiol au système $(NSCl)_3$–SO_2Cl_2, on obtient du 2,4-$C_6H_3Cl_2NSCl_2$ qui se transforme en 2,4-$(C_6H_3Cl_2N)_2S$ lorsqu'on le chauffe à 80°C dans le toluène ou qu'on le réduit par le Ph_3Sb ou le mercure. La réaction du 2-aminobenzènethiol avec un excès de SO_2Cl_2, en l'absence de $(NSCl)_3$, il se forme du 2,4,6-$C_6H_2Cl_3NSCl_2$. On décrit aussi les essais qui ont été effectués pour caractériser, à l'aide de la rmn du ^{14}N et du ^{33}S ainsi que par les spectroscopies infrarouge et Raman, les espèces actives du système $(NSCl)_3$–SO_2Cl_2.

Mots clés : chlorure de cyclotrithiazyle; isothiazole; dithiazolium; dichlorure d'arylimidosulfureux; rmn du ^{14}N.

[Traduit par la revue]

Introduction

Compounds of the type NSX_3 (X = halogen) are potentially useful reagents for the synthesis of carbon–nitrogen–sulfur heterocycles in cyclocondensation reactions with appropriate organic substrates. Reactions of this type have not been reported, however, for the kinetically and thermodynamically stable molecule NSF_3 (1). We have observed that solutions of $(NSCl)_3$ in the presence of excess SO_2Cl_2 behave as the reagent "$NSCl_3$" in reactions with methacrylonitrile or thioacetamide to give 4-cyanoisothiazole, **2** (R = CN), and 5-methyl-1,3,2,4-dithiazolium chloride, **3***a*, respectively, in good yields (2).[2] This direct synthesis of **2** (R = CN) is a marked improvement over the usual four-step synthesis from the parent ring system (3). Consequently we have investigated the generality of this route to **2**. The preparation of **3***a* from "$NSCl_3$" provides an alternative to the cycloaddition of $NS_2^+AsF_6^-$ to organic nitriles (4) for the synthesis of the 1,3,2,4-dithiazolium ring and produces soluble products. We have now extended this approach to the synthesis of **3***b* from thiobenzamide and "$NSCl_3$". The reaction of 2-aminobenzenethiol with "$NSCl_3$" has also been examined as a possible route to benzo-1,3-dithia-2,4-diazine, **4**, (5). Mechanisms are proposed to rationalize the formation of **2** and **3** in cyclocondensation reactions of methacrylonitrile or thioamides, respectively, with "$NSCl_3$". Attempts to characterize the active species in "$NSCl_3$" solutions by infrared, Raman, and ^{14}N, ^{17}O, and ^{33}S nmr spectroscopies are also described.

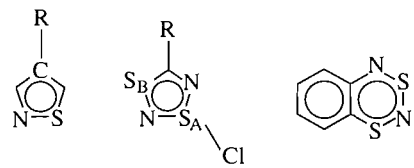

2 **3***a* (R = Me) **4**
3*b* (R = Ph)

Experimental

Reagents and general procedures

All experimental procedures were performed under an atmosphere of dry nitrogen. Solvents were dried by heating at reflux with the appropriate drying agent and then distilled before use.

The following reagents were commercial products used as received: methacrylonitrile, methacrolein, methyl methacrylate, 2-chloropropene, thioacetamide, thiobenzamide, 2-aminobenzenethiol, and triphenylantimony (all from Aldrich) and mercury (Fisher). SO_2Cl_2 (Aldrich) was distilled before use. $(NSCl)_3$ was prepared from $S_3N_2Cl_2$ by a modification of the literature procedure (6). After the second chlorination of $S_3N_2Cl_2$, the crude $(NSCl)_3$ was ground to a powder and a third chlorination with Cl_2 was followed by the addition of sufficient SO_2Cl_2 to cover the solid product. This mixture was stirred for 12 h and then volatile products were removed *in vacuo* to give pure $(NSCl)_3$ mp 91°C (cf. lit. (7) mp 92°C).

Instrumentation

Infrared spectra (4000–400 cm^{-1}) were recorded as Nujol or Fluorolube mulls (CsI windows) on a Nicolet 5DX FT-IR spectrophotometer. Ultraviolet–visible spectra were obtained by using a Cary 219 spectrophotometer and cuvettes which were sealed with rubber septa. Mass spectra were measured on a Kratos MS80RFA instrument (EI/70 eV).

[1]To whom correspondence should be addressed.

[2]The designation "$NSCl_3$" will be used to represent the reagent formed when an excess of SO_2Cl_2 is added to solutions of $(NSCl)_3$. This designation is not intended to imply a preference for structure **1***a* rather than **1***b* (X = Y = Z = Cl).

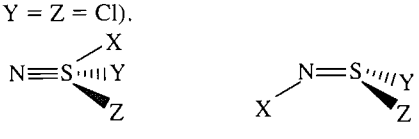

1*a* **1***b*

Can. J. Chem. Downloaded from www.nrcresearchpress.com by 91.144.44.67 on 09/07/12
For personal use only.

Can. J. Chem. Downloaded from www.nrcresearchpress.com by 91.144.44.67 on 09/07/12
For personal use only.

Experimental details for the measurement of Raman spectra have been described (8). In this work the spectra were obtained at *ca.* 25°C by using exciting radiation at 514.5 nm and a laser power of 300 mW.

^1H and ^{13}C nmr spectra were obtained on a Bruker ACE 200 spectrometer and chemical shifts are reported relative to Me_4Si in $CDCl_3$. All other nmr spectra were obtained on a Bruker AM-400 narrow bore nmr spectrometer operating in the FT mode at a frequency of 28.915 MHz for ^{14}N, 54.244 MHz for ^{17}O, and 30.690 MHz for ^{33}S, using a 10 mm broad-band probe. Conditions for acquisition of ^{14}N nmr spectra were a 90° pulse, a sweep width of 30 000 Hz, 4K data points and a recycle time of 0.07 s. Those for ^{17}O nmr spectra were a 90° pulse, a sweep width of 84 000 Hz, 4K data points and a recycle time of 0.025 s, while a 90° pulse, a sweep width of 50 000 Hz, 2K data points, and a recycle time of 0.02 s were utilized for ^{33}S nmr spectra. A dead time of 100 μS was used in all cases in order to negate the effects of probe ringing and all FIDs were zero filled to 16K prior to transformation. Sufficient scans were collected in order to obtain a signal-to-noise ratio of at least 100 to one. Samples were sealed under a dry nitrogen atmosphere in 10 mm Pyrex tubes equipped with Teflon-lined screw-caps. ^{14}N, ^{17}O, and ^{33}S nmr chemical shifts are reported relative to $MeNO_2$(l), H2O(l), and SO_4^{2-}(aq.), respectively.

Chemical analyses were performed by the Analytical Services Division, Department of Chemistry, The University of Calgary, and by Canadian Microanalytical Service, New Westminster, B.C.

Generation of "$NSCl_3$"

The reagent "$NSCl_3$" was generated for synthetic applications by the addition of at least a ten-fold excess of SO_2Cl_2 to a solution of $(NSCl)_3$ in CH_2Cl_2 or $CHCl_3$. This solution was stirred for at least 1 h prior to the addition of the other reactant.

Preparation of 4-cyanoisothiazole

Methacrylonitrile (0.67 g, 10 mmol) was added via syringe to a solution of $(NSCl)_3$ (0.81 g, 3.33 mmol) in chloroform (25 mL) and SO_2Cl_2 (10 mL). The reaction mixture was heated at reflux for 16 h. Volatile materials were removed under vacuum to give an orange–red residue from which colorless crystals of 4-cyanoisothiazole (0.86 g, 7.8 mmol) mp 95°C were obtained by sublimation at 50°C/0.1 Torr. *Anal.* calcd. for $C_4H_2N_2S$: C 43.62, H 1.83, N 25.44; found: C 43.74, H 1.85, N 25.51. *Mol. wt.* calcd. for $C_4H_2N_2S$: 109.9939; found (ms): 109.9930. Mass spectroscopy: *m/e* (relative intensity > 20%): 110(M^+,100), 83(M^+ − HCN,80), 45(30), 38(20), 32(25). ^1H nmr ($CDCl_3$)δ: 9.22(s,1H), 8.70(s,1H). ^{13}C nmr ($CDCl_3$)δ: 157.7, 156.0, 112.4 and 109.3. ^{14}N nmr (CH_2Cl_2) δ: −80 ppm, $\nu_{1/2}$ 505 Hz (*SN*), −117 ppm, $\nu_{1/2}$ 645 Hz (*CN*). Ultraviolet (MeCN, 25°C) λ_{max} (log ε): 264(3.97). Infrared (Nujol) ν_{max}: 2234(s,C≡N) cm^{-1}.

Preparation of 5-methyl-1,3,2,4-dithiadiazolium chloride

Thioacetamide (2.66 g, 35.4 mmol) was added rapidly to a solution of $(NSCl)_3$ (2.86 g, 11.8 mmol) in $CHCl_3$ (25 mL) and SO_2Cl_2 (10 mL). An immediate reaction occurred with the slow evolution of HCl and SO_2 and the solution became orange. The reaction mixture was heated at 60°C for 16 h and then volatile materials were removed under vacuum to give an orange–red oil. The addition of acetonitrile (15 mL) produced 5-methyl-1,3,2,4-dithiadiazolium chloride (2.85 g, 18.6 mmol) as an orange solid mp 210°C (dec.). A second crop (0.58 g, 3.8 mmol) was obtained by the addition of diethyl ether (50 mL) to the filtrate. *Anal.* calcd. for $C_2H_3ClN_2S_2$: C 15.53, H 1.96, N 18.12, found: C 15.44, H 2.14; N 18.28. ^1H nmr ($CDCl_3$) δ: 1.22. ^{14}N nmr (acetone): −271, −286 ppm. Mass spectroscopy: *m/e* (relative intensity > 20%): 119(M^+ − Cl,20), 78(NS_2^+,50), 73(MeCNS$^+$,25), 46(NS^+,25). Infrared (Nujol) ν_{max}: 1407 s, 1373 m, 1350 m, 1091 s, 1032 s, 1019 s, 860 vs, 848 vs, 794 s, 677 m, 597 m, 591 m, 535 s, 516 m, 389 m cm^{-1}.

Preparation of 5-phenyl-1,3,2,4-dithiadiazolium chloride

Thiobenzamide (1.37 g, 10 mmol) was added to a stirred solution of $(NSCl)_3$ (0.81 g, 3.33 mmol) in CH_2Cl_2 (30 mL) and SO_2Cl_2 (10 mL). The solution immediately became orange and there was a slow evolution of gas. The reaction was stirred for 36 h at 23°C and then volatile materials were removed under vacuum to give a yellow–orange solid from which 3,5-diphenyl-1,2,4-thiadiazole (0.61 g, 2.55 mmol) mp 88°C (lit. (9) 90°C) was obtained by sublimation at 70°C/10^{-1} Torr. *Anal.* calcd. for $C_{14}H_{10}N_2S$: C 70.56, H 4.23, N 11.76; found: C 70.59, H 4.32, N 11.80. ^{14}N nmr (CH_2Cl_2) δ: −86, −124 ppm. Mass spectroscopy: *m/e* (%), 238(20) ($C_6H_5)_2C_2N_2S^+$, 135(100) $C_6H_5CNS^+$, 103(30) $C_6H_5CN^+$, 77(25) $C_6H_5^+$. Infrared (Nujol): 1442 m, 1416 s, 1329 s, 1275 m, 1241 m, 1118 s, 1096 m, 1070 s, 1026 s, 988 s, 898 s, 832 m, 782 m, 761 vs, 681 vs, 637 s, 615 m, 479 m cm^{-1}.

The residue after sublimation was recrystallized from acetonitrile (20 mL) to give 5-phenyl-1,3,2,4-dithiadiazolium chloride (0.91 g, 4.2 mmol) mp 169°C. *Anal.* calcd. for $C_7H_5ClN_2S_2$: C 38.79; H 2.32; N 12.92; S 29.59; found: C 39.26; H 2.30, N 12.79, S 29.60. ^{14}N nmr (acetone) −277 ppm. Mass spectroscopy: *m/e* (relative intensity > 20%): 181 (M^+ − Cl,80), 135 ($C_6H_5CNS^+$,50), 103 ($C_6H_5CN^+$,50), 78 (NS_2^+,95), 46 (NS^+,55). Infrared (Nujol): 1599 m, 1397 s, 1151 s, 1031 m, 923 s, 889 s, 844 s, 783 s, 698 vs, 547 s cm^{-1}.

Reaction of 2-aminobenzenethiol with "$NSCl_3$"

A solution of 2-aminobenzenethiol (2.50 g, 20 mmol) in CH_2Cl_2 (10 mL) was added rapidly by syringe to a solution of $(NSCl)_3$ (1.63 g, 6.66 mmol) in CH_2Cl_2:SO_2Cl_2 (1:1, 60 mL) at −78°C. A strongly exothermic reaction occurred to give a dark red–black solution with the evolution of HCl. The reaction mixture was stirred and allowed to reach 20°C slowly (16 h). Volatile materials were removed under vacuum to give a reddish black oil, which was extracted with *n*-hexane (100 mL). The hexane solution was cooled to −30°C for 72 h to give yellow–orange needles of 2,4-dichlorophenylimidosulfurous dichloride (1.49 g, 5.6 mmol) mp 81°C (lit. (10) mp 78–80°C). A second crop (0.92 g, 2.4 mmol) was obtained by reducing the volume of the filtrate to *ca.* 25 mL and cooling this solution to −30°C. *Anal.* calcd. for $C_6H_3Cl_4NS$: C 27.40, H 1.15, N 5.53, S 12.19, Cl 53.93; found: C 27.58, H 1.20, N 5.38, S 11.85, Cl 53.51. ^{14}N nmr (CH_2Cl_2): −160 ppm, $\nu_{1/2}$ 605 Hz. Mass spectroscopy: *m/e* (relative intensity > 20%): 226(M^+ −Cl,50), 191(M^+ − 2Cl,100), 156(M^+ − 3Cl,80), 145($C_2H_3Cl_2^+$,40), 124($C_6H_3ClN^+$,95), 109($C_6H_2Cl^+$,75), 46(NS^+,60), 36(HCl^+,60). Infrared (Nujol): 1569 m, 1555 m, 1387 m, 1359 s, 1119 vs, 1102 s, 1047 m, 1018 m, 871 vs, 827 s, 813 vs, 701 m, 684 s, 634 s, 549 m, 425 vs, 400 vs cm^{-1}.

Reaction of 2-aminobenzenethiol with SO_2Cl_2

The procedure and observations were as described above for the reaction with "$NSCl_3$" except that no $(NSCl)_3$ was present and 2.00 g (16.0 mmol) of 2-aminobenzenethiol was used. The extraction of the crude product with *n*-hexane (150 mL) followed by cooling of this solution to −30°C produced yellow needles of 2,4,6-trichlorophenylimidosulfurous dichloride (1.70 g, 5.7 mmol) mp 56°C (lit. (10) mp 58°C) ^{14}N nmr (CH_2Cl_2): −167 ppm, $\nu_{1/2}$ 745 Hz. *Anal.* calcd. for $C_6H_2Cl_5NS$: C 24.23, H 0.68, N 4.71; found: C 24.30, H 0.74, N 4.77.

Preparation of bis(2,4-dichlorophenyl)sulfur diimide

(a) By reaction of 2,4-dichlorophenylimidosulfurous dichloride with mercury

Aliquots of mercury (0.25 g, 1.25 mmol) were added to a solution of 2,4-$Cl_2C_6H_3NSCl_2$ (0.66 g, 2.5 mmol) in CH_2Cl_2 (3 mL) in a 10 mm nmr tube. After each addition the tube was shaken vigorously and an ^{14}N nmr spectrum was recorded. The resonance at −160 ppm for 2,4-$Cl_2C_6H_3NSCl_2$ was gradually replaced by a new resonance at −89 ppm, $\nu_{1/2}$ 1300 Hz. The reaction was complete after the addition of four aliquots mercury (1.00 g, 5.0 mmol). The red solution was then filtered to remove Hg_2Cl_2 (1.12 g, 2.4 mmol) and the solvent was removed under vacuum to give a red solid, which was recrystallized from acetonitrile (5 mL) to give red filamentous crystals of bis(2,4-dichlorophenyl)sulfur diimide (0.40 g, 1.1 mmol) mp 133°C. *Anal.* calcd. for $C_{12}H_6Cl_4N_2S$: C 40.94, H 1.72, N 7.96, S 9.10, Cl 40.28; found: 40.42, H 1.56, N 7.92, S 9.27, Cl 41.05. Mass spectroscopy: *m/e* (relative intensity > 20%) 350(M^+,10), 315(M^+ − Cl,40), 191($C_6H_3Cl_2NS^+$,80), 159($C_6H_3Cl_2N^+$,100), 124($C_6H_3ClN^+$,35). Infrared (Nujol): 1599 m, 1300 s (ν_{as} NSN), 1150 m, 1102 vs (ν_s NSN), 1089 s, 818 vs, 722 s cm^{-1}.

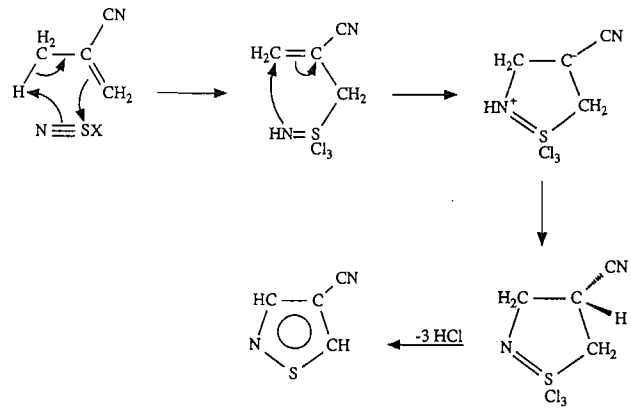

FIG. 1. Proposed mechanism for the reaction of methacrylonitrile with "$NSCl_3$".

(b) By thermolysis of 2,4-dichlorophenylimidosulfurous dichloride

A solution of 2,4-$Cl_2C_6H_3NSCl_2$ (0.50 g, 1.9 mmol) in toluene (3 mL) in a 10 mm nmr tube sealed with a Teflon-lined screwcap was heated at 80°C for 12h. The ^{14}N nmr spectrum indicated complete conversion to (2,4-$Cl_2C_6H_3$)NSN($C_6H_3Cl_2$-2,4) ($\delta(^{14}N)$ −92 ppm), which was obtained as an orange–red solid (0.32 g, 0.91 mmol) upon removal of solvent and volatile products (SCl_2 and Cl_2) under vacuum. The ir spectrum of this product was identical to that of an authentic sample prepared by procedure (*a*).

Results and discussion

Preparation of 4-cyanoisothiazole by the reaction of "$NSCl_3$" with methacrylonitrile[2]

Methacrylonitrile reacts with "$NSCl_3$" in chloroform to give 4-cyanoisothiazole, **2** (R = CN), in 78% yield. The reaction formally involves a triple cyclocondensation with the loss of three moles of HCl. The proposed mechanism in shown in Fig. 1. The first step is an ene reaction, which involves abstraction of an allylic proton with concurrent nucleophilic attack of the >C=C< bond on the sulfur atom of "$NSCl_3$"). An ene reaction has previously been postulated to explain the formation of an isothiazole from cholesteryl acetate and $(NSCl)_3$ in the presence of pyridine (11). In the present case the involvement of "$NSCl_3$" (i.e. X = Cl_3 in Fig. 1) rather than NSCl in the ene reaction is proposed because the reaction of methacrylonitrile with NSCl *in the absence of a chlorinating agent* produces mainly $[S_4N_3]Cl$. The second step is an intramolecular Michael addition to give a five-membered ring. The subsequent loss of three moles of HCl yields 4-cyanoisothiazole.

Attempts to extend this method to the synthesis of other 4-substituted isothiazoles bearing electronegative substituents were unsuccessful. The reaction of 2-chloropropene with "$NSCl_3$" gave a complex mixture of products which exhibited ^{14}N nmr resonances in the region −320 to −360 ppm indicative of amines (12). By contrast the reaction of methacrylonitrile with "$NSCl_3$" produced only a small amount of amine. The addition of methacrolein or methyl methacrylate to "$NSCl_3$" produced an exothermic reaction, but ^{14}N nmr spectroscopy indicated very little consumption of the sulfur–nitrogen reagent. Thus these alkenes appear to react preferentially with SO_2Cl_2.

Reactions of "$NSCl_3$" with thioamides

The cyclocondensation of "$NSCl_3$" with thioacetamide or thiobenzamide yields 5-methyl- or 5-phenyl-1,3,2,4-dithiadiazolium chloride, **3***a* or **3***b*, in 68% and 42% yields, respectively. The yield of **3***b* is lower due to a competing reaction between thiobenzamide and SO_2Cl_2 to give 3,5-diphenyl-1,2,4-thiadiazole, which can also be prepared by treatment of thiobenzamide with iodine (9). The cyclocondensation reaction of thioamides with "$NSCl_3$" formally involves the evolution of 2 mol of HCl and a possible reaction scheme is given in Fig. 2.

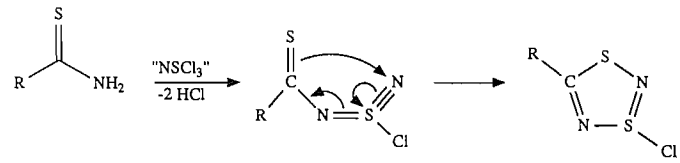

FIG. 2. Proposed mechanism for the reaction of thioamides with "$NSCl_3$".

The compounds **3***a* and **3***b* exhibit characteristic mass spectra in which the $\overline{RCNSNS}^+$ cation undergoes two major fragmentation pathways involving either the loss of NS^+ (and RCNS) or NS_2^+ (and RCN). The reverse of the second process, i.e. cycloaddition of NS_2^+ with organic nitriles, has been used for the preparation of cations of the type $\overline{RCNSNS}^+$ (4). The ir and ^{14}N nmr spectra of **3***a* and **3***b* are sufficiently different from those of the corresponding AsF_6^- salts (4) to propose a covalent structure for **3***a* and **3***b*. This contention is supported by the solubility of **3***a* and **3***b* in non-polar organic solvents and the observation of strong bands at 535 and 547 cm^{-1} in the ir spectra of **3***a* and **3***b*, respectively, attributable to ν(S—Cl). In a covalent structure the chlorine atom in **3** can be attached to either S_A or S_B. Since the sulfur atom between the two nitrogens should bear the higher positive charge in the cation, the chlorine atom is probably attached to S_A in **3***a* and **3***b*. By contrast, 4-phenyl-1,2,3,5-dithiadiazolium chloride, a structural isomer of **3***b*, is insoluble in non-polar solvents and is assumed to have an ionic structure (13). Attempts to obtain crystals of **3***a* or **3***b* suitable for an X-ray structural determination have been unsuccessful.

Reaction of 2-aminobenzenethiol with "$NSCl_3$"

Benzo-1,3-dithia-2,4-diazine, **4**, has been obtained as deep blue crystals in low yield by the reaction of $PhNSNSiMe_3$ with SCl_2 in a 1:1 molar ratio (5). We have investigated the reaction of 2-aminobenzenethiol with the trifunctional reagent "$NSCl_3$" as an alternative route to **4**. However, this approach produces an orange solid with the empirical formula $C_6H_3NSCl_4$ on the basis of C, H, N, S, and Cl analyses. ^{13}C and ^{13}C DEPT nmr spectroscopy established that the aromatic ring consists of three quaternary (δ 137.3, 134.6, and 131.0 ppm) and three tertiary carbon atoms (δ 130.0, 128.0 and 121.7 ppm). Thus the substitution of one of the hydrogen atoms on the original C_6H_4 ring has occurred. A similar electrophilic aromatic substitution takes place at the position *para* to the amino group in the reaction of aniline with S_2Cl_2 (14). Since the reduction of the orange solid with Ph_3Sb or Hg shows that only two of the chlorine atoms are labile (*vide infra*), this product is identified as 2,4-dichlorophenylimidosulfurous dichloride, **5**. This compound was previously prepared by the reaction of 2,4-$C_6H_3Cl_2NSO$ with PCl_5 (10), but the only characterization reported was the mp.

Compound **5** exhibits a single line at −160 ppm in the ^{14}N nmr spectrum (lit. (16) $\delta(^{14}N)$ $C_6F_5NSCl_2$, −112 ppm). A band at 1110 cm^{-1} in the ir spectrum of $ClSO_2NSCl_2$ has been assigned to the S=N stretching frequency and the asymmetric and symmetric SCl_2 stretching vibrations occur at 548 and 440 cm^{-1}, respectively (15). The corresponding ir absorptions for **6**

Can. J. Chem. Downloaded from www.nrcresearchpress.com by 91.144.44.67 on 09/07/12
For personal use only.

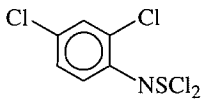

5

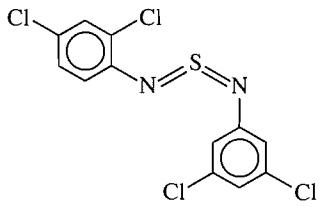

6

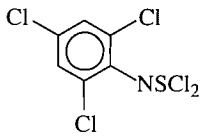

7

are observed at 1119, 549, and 426 cm^{-1}. The latter two bands disappear upon reduction of **5** with Ph_3Sb or mercury to give bis(2,4-dichlorophenyl)sulfur diimide, **6**, which exhibits a singlet in the ^{14}N nmr spectrum at −89 ppm (lit. (12) $\delta(^{14}N)$ ArNSNAr, −83 to −120 ppm). It is likely that the reduction of **5** occurs via a thionitrosoarene (eq. [1]), which dimerizes with loss of sulfur in the absence of a trapping agent (16). The observed thermolysis of **5** at 80±C in toluene to give **6** is in contrast to the previously reported thermal decomposition of $RCONSCl_2$ to yield acyl chlorides and NSCl (17).

$$[1]\quad 2ArNSCl_2 \xrightarrow[-2HgCl_2]{2Hg} 2[ArNS] \xrightarrow{-S} ArNSNAr$$

The production of **5** from 2-aminobenzenethiol does not involve the incorporation of additional sulfur or nitrogen. This suggests that **5** is formed by the reaction of 2-aminobenzenethiol with SO_2Cl_2. In fact, we found that this reaction produces the known compound 2,4,6-$C_6H_2Cl_3NSCl_2$, **7**, (10) in 36% yield. The C_2 symmetry of this product is demonstrated by ^{13}C and ^{13}C DEPT nmr spectroscopy, which reveals a single resonance for the two tertiary carbon atoms at 128.7 ppm and three signals for quaternary carbons at 130.2(2C), 133.6(1C) and 135.1(1C). The ^{14}N nmr spectrum exhibits a single resonance at −167 ppm.

A possible sequence for the formation $ArNSCl_2$ from 2-aminobenzenethiol and SO_2Cl_2 is shown in Fig. 3. The initial steps involve the well known oxidation of an aromatic thiol to an arylsulfur trichloride in the presence of excess chlorinating agent (18) followed by an intramolecular cyclocondensation reaction.[3] It is not known at which point the chlorination of the aromatic ring occurs or how the presence of NSCl limits the extent of chlorination.

Spectroscopic characterization of "$NSCl_3$"

Two isomers, **1***a* and **1***b*, are possible for molecules involving a sulfur–nitrogen multiple bond and three substituents. The isomer $FNSF_2$ (**1***b*, X = Y = Z = F) has been identified (19), but it is thermodynamically less stable than NSF_3 (**1***a*, X = Y = Z = F) by *ca.* 64 kJ mol^{-1} according to *ab initio* SCF calculations (20). Surprisingly, NSF_2Cl (**1***a*, X = Cl; Y = Z = F) is unknown, but the isomer $ClNSF_2$ (**2**, X = Cl; Y = Z = F) is obtained either by the reaction of $Hg(NSF_2)_2$ with Cl_2 (21) or by the treatment of NSF with chlorine monofluoride in the gas phase (22). By contrast, the addition of ClF to NSCl gas produces NSF, presumably by elimination of Cl_2, rather than **1***a* or **1***b* (X = Y = Cl; Z = F) (22). The molecule $NSCl_3$ has not been

[3]Alternatively, the cyclocondensation could occur via an intermolecular process.

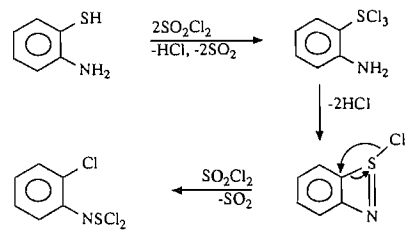

FIG. 3. The formation of an arylimidosulfurous dichloride from 2-aminobenzenethiol and SO_2Cl_2.

characterized in either of the isomeric forms, **1***a* or **1***b* (X = Y = Z = Cl), and *ab initio* SCF calculations indicate that the former isomer is thermodynamically unstable with respect to NSCl + Cl_2, but kinetically stable at low temperatures (20).

Passmore and Schriver have established by ^{14}N nmr spectroscopy that NSCl monomer is formed via dissociation of $(NSCl)_3$ in solution and that the extent of this dissociation depends on the temperature, the nature of the solvent, and the purity of $(NSCl)_3$ (7).

$$[2]\quad (NSCl)_3 \rightleftharpoons 3NSCl$$

We have used ^{14}N nmr and ir spectroscopy in an attempt to detect the formation of **1***a* or **1***b* in solutions of $(NSCl)_3$ in the presence of an excess of a chlorinating agent, e.g. SO_2Cl_2, $PhICl_2$, or Cl_2. The ^{14}N nmr spectrum of a pale green solution of $(NSCl)_3$ in $CDCl_3$ (*ca.* 0.1 *M*) at 25°C shows a dominant resonance at −261 ppm, $\nu_{1/2}$ 380 Hz (lit. (23) $\delta(^{15}N)$ $(NSCl)_3$ in $CHCl_3$, −261.5 ppm) and a very weak resonance (<5%) at 339 ppm attributed to NSCl (lit. (7) $\delta(^{14}N)$ NSCl (in CCl_4) 348–352 ppm, $\nu_{1/2}$ 70–80 Hz; $\delta(^{14}N)$ NSCl (in SO_2) 323 ppm, $\nu_{1/2}$ 60 Hz).[4] The addition of an excess of SO_2Cl_2 to this solution causes the growth of the resonance of *ca.* 339 ppm ($\nu_{1/2}$ 100 Hz) and a concomitant decrease in the intensity of the resonance due to $(NSCl)_3$. Similar behaviour was observed when $PhICl_2$ was used as the chlorinating agent. No other resonances are apparent in the ^{14}N nmr spectra except that of dissolved N_2 at −71 ppm (24). When "$NSCl_3$" solutions (*ca.* 0.005 *M* $(NSCl)_3$ in pure SO_2Cl_2 or a 50:50 mixture of SO_2Cl_2 and $CDCl_3$ or CH_2Cl_2) are cooled to −50°C the narrow resonance at 339 ppm is replaced by broader resonances at −148 and −261 ppm ($(NSCl)_3$). The former is well outside the range of chemical shifts (135–350 ppm) observed for triply bonded sulfur–nitrogen species (7, 8) but much closer to that of $ClNSF_2$, **1***b* (X = Cl; Y = Z = F) (lit. (25) $\delta(^{14}N)$ −232). Thus the −148 ppm resonance may be due to $ClNSCl_2$, **1***b* (X = Y = Z = Cl).[5] A saturated solution of $(NSCl)_3$ in liquid chlorine exhibits ^{14}N nmr spectra similar to those observed for SO_2Cl_2 solutions except for the appearance at 25°C of a weak resonance at −176 ppm in addition to the resonance for NSCl at 337 ppm. At −50°C the latter resonance disappears, while that at −176 ppm is much stronger. This resonance may be due to $ClNSCl_2$ shifted as a result of solvent effects (cf. NSCl (7)).

The ir spectrum of a solution of $(NSCl)_3$ in SO_2Cl_2 at 23°C exhibits bands at 1338 and 1331 cm^{-1}. The molecules SO_2 (ν_3 of SO_2 in H_2O occurs at 1332 cm^{-1} (27)) and NSCl (ν(SN) in CS_2 occurs at 1322 cm^{-1} (28)) are possible sources of these vibra-

[4]Although it is common practice to quote $\nu_{1/2}$ values for ^{14}N nmr signals, it should be noted that these values are dependent on factors such as temperature and solvent viscosity.

[5]A change of 135 ppm in the ^{14}N nmr chemical shift is observed in going from $C_6F_5NSF_2$ to $C_6F_5NSCl_2$ (26).

Can. J. Chem. Downloaded from www.nrcresearchpress.com by 91.144.44.67 on 09/07/12
For personal use only.

tions, but definite assignments cannot be made. The Raman spectra of solutions $(NSCl)_3$ in SO_2Cl_2 or liquid Cl_2 did not reveal the presence of S—N species other than NSCl or $(NSCl)_3$.

Both ^{33}S and ^{17}O nmr spectroscopy provide evidence for the formation of SO_2 in solutions of $(NSCl)_3$ in the presence of an excess of SO_2Cl_2. In the ^{33}S nmr spectrum a solution of $(NSCl)_3$ in CH_2Cl_2 exhibits a signal at 252 ppm ($\nu_{1/2}$ 950 Hz) for NSCl, but the resonance for $(NSCl)_3$ is too broad to be observed. The addition of SO_2Cl_2 to this solution causes a shift of the NSCl signal to 258 ppm and the appearance of resonances of −44 ($\nu_{1/2}$ 665 Hz) and 369 ppm attributed to SO_2Cl_2 (lit. (39) −45 ppm) and SO_2 (lit. (39) 375 ppm), respectively. The latter signal is not observed in the ^{33}S nmr spectrum of liquid SO_2Cl_2. The formation of SO_2 in these solutions is confirmed by the observation of a signal at 514 ppm (lit. (30) 513 ppm) in the ^{17}O nmr spectrum in addition to the resonance at 296 ppm (lit. (30) 304 ppm) for SO_2Cl_2.

In summary, the detection of SO_2 by ^{17}O and ^{33}S nmr spectroscopy indicates that SO_2Cl_2 behaves as a chlorinating agent upon addition to $(NSCl)_3$, but convincing spectroscopic evidence for the formation of $ClNSCl_2$ or $NSCl_3$ has not been obtained.

Conclusions

Solutions of $(NSCl)_3$ in the presence of an excess of SO_2Cl_2 behave as though they contain the synthetic equivalent "$NSCl_3$" upon treatment with methyacrylonitrile or thioamides and these reactions provide useful syntheses of 4-cyanoisothiazole or 5-methyl(or phenyl)-1,3,2,4-dithiadiazolium chloride, respectively. With other substrates, however, the reaction with excess SO_2Cl_2 predominates and this is likely to be a limiting factor in the application of the "$NSCl_3$" reagent to the synthesis of S—N heterocycles. Matrix isolation experiments will be necessary to characterize the active species in "$NSCl_3$" solutions.

Acknowledgements

We thank Dr. T. G. Back for helpful discussions. Financial support from NSERC (Canada) and postgraduate awards to A. A. from NSERC, the Alberta Heritage Scholarship Fund, and the Killam Foundation (The University of Calgary) are gratefully acknowledged.

1. O. Glemser and R. Mews. Angew. Chem. Int. Ed. Engl. **19**, 883 (1980).
2. A. Apblett and T. Chivers. J. Chem. Soc. Chem. Commun. 1889 (1987); 508 (1988).
3. K. R. H. Woolridge. Adv. Heterocycl. Chem. **14**, 1 (1972) and references therein.
4. (*a*) G. K. Maclean, J. Passmore, M. N. S. Rao, M. J. Schriver, and P. S. White. J. Chem. Soc. Dalton Trans. 1405 (1985); (*b*) N. Burford, J. P. Johnson, J. Passmore, M. J. Schriver, and P. S. White. J. Chem. Soc. Chem. Commun. 966 (1986).
5. (*a*) H. Koenig and R. T. Oakley. J. Chem. Soc. Chem. Commun. 73 (1983); (*b*) A. W. Cordes, M. Hojo, H. Koenig, M. C. Noble, R. T. Oakley, and W. T. Pennington. Inorg. Chem. **25**, 1137 (1986).
6. A. Apblett and T. Chivers. Inorg. Chem. **28**, 4544 (1989).
7. J. Passmore and M. Schriver. Inorg. Chem. **27**, 2751 (1988).
8. T. Chivers, D. D. McIntyre, K. J. Schmidt, and H. J. Vogel. Can. J. Chem. **67**, 1788 (1989).
9. A. W. Hofmann and H. Gabriel. Ber. **25**, 1578 (1892).
10. E. S. Levchenko and I. E. Sheinkman. J. Gen. Chem. USSR, **36**, 446 (1965).
11. D. H. R. Barton and W. A. Bubb. J. Chem. Soc. Perkin I. 916 (1977).
12. W. Witanowski, L. Stefaniak, and G. A. Webb. Annual reports on NMR spectroscopy. Vol. 18. Nitrogen NMR spectroscopy. London, Academic Press. 1986.
13. (*a*) G. G. Alange, A. J. Banister, B. Bell, and P. W. Millen. Inorg. Nucl. Chem. Lett. **13**, 143 (1977); (*b*) G. G. Alange, A. J. Banister, B. Bell, and P. W. Millen. J. Chem. Soc. Perkin I, 1192 (1979).
14. L. D. Huestis, M. I. Walsh, and N. Hahn. J. Org. Chem. **30**, 2763 (1965).
15. H. W. Roesky. Angew. Chem. Int. Ed. Engl. **80**, 43 (1968).
16. M. R. Bryce and P. C. Taylor. J. Chem. Soc. Chem. Commun. 950 (1988).
17. L. M. Markovskii, G. S. Fedyuk, E. S. Levchenko, and A. W. Kirsanov. J. Org. Chem. Russ. **9**, 2522 (1973).
18. W. R. Hardstaff and R. F. Langler. *In* Sulfur in organic and inorganic chemistry. Vol. 4. *Edited by* A. Senning. Marcel Dekker, Inc., New York, NY, U.S.A. 1982.
19. O. Glemser and R. Mews. Adv. Inorg. Chem. Radiochem. **14**, 333 (1972).
20. C. Ehrhardt and R. Ahlrichs. Chem. Phys. **108**, 429 (1986).
21. O. Glemser, R. Mews, and H. W. Roesky. Chem. Ber. **102**, 1523 (1969).
22. A. J. Banister, R. G. Hey, J. Passmore, and M. N. S. Rao. J. Fluorine Chem. **21**, 429 (1982).
23. T. Chivers, R. T. Oakley, O. J. Scherer, and G. Wolmershäuser. Inorg. Chem. **20**, 914 (1981).
24. D. D. McIntyre, A. W. Apblett, P. Lundberg, K. J. Schmidt, and H. J. Vogel. J. Magn. Res. **83**, 377 (1989), and references therein.
25. J. Mason, W. van Bronswijk, and O. Glemser. J. Phys. Chem. **82**, 463 (1978).
26. G. G. Furin, A. I. Rezvukhin, M. A. Fedotov, and G. G. Yacobson. J. Fluorine Chem. **22**, 231 (1983).
27. L. H. Jones and E. McLaren. J. Chem. Phys. **28**, 995 (1958).
28. J. Nelson and H. G. Heal. Inorg. Nucl. Chem. Lett. **6**, 429 (1970).
29. R. E. Wasylishen, C. Connor, and J. O. Friedrich. Can. J. Chem. **62**, 981 (1984).
30. B. N. Figgis, R. S. Kidd, and R. S. Nyholm. Proc. R. Soc., London, A. **269**, 469 (1962).

Can. J. Chem. Downloaded from www.nrcresearchpress.com by 91.144.44.67 on 09/07/12
For personal use only.

Thermodynamique de la solvatation d'acides protoniques et des bases conjuguées en milieux hydroorganiques riches en eau à 25°C

HENRI GILLET

Laboratoire de chimie physique des solutions, Université Blaise Pascal (Clermont-Ferrand II), Ensemble Universitaire des Cézeaux, 63177 Aubière CEDEX, France

Reçu le 9 août 1989

HENRI GILLET. Can. J. Chem. **68**, 655 (1990).

Nous avons mesuré à 25°C les enthalpies de dissolution des acides acétique, benzoïque et valérianique et de leurs sels de potassium dans les mélanges eau – alcool *tert*-butylique contenant jusqu'a 40% en masse de cosolvant organique. Nous avons aussi déterminé ces grandeurs pour le phénol, l'aniline et la pyridine dans les mêmes mélanges et pour l'acide acétique, l'aniline et la pyridine dans les mélanges eau–DMSO, eau–acétone, et eau–urée pour les mêmes teneurs en cosolvant. Nous avons, à partir de ces données, calculé les enthalpies standard de dissolution, les grandeurs de transfert correspondantes et les enthalpies de solvatation. Quand les enthalpies de dissolution sont difficiles ou impossibles à mesurer nous avons montré que les enthalpies de transfert pouvaient être calculées à partir de grandeurs de transfert judicieusement choisies obtenues à partir de mesures expérimentales, De cette manière nous avons déterminé les enthalpies de transfert du phénate de potassium et des chlorures et bromures d'anilinium et de pyridinium dans les divers mélanges. Les enthalpies de solvatation ont été séparées en enthalpies de formation d'une cavité dans le solvant et en enthalpies d'interaction. Ces dernières grandeurs ont fait l'objet d'un essai d'interprétation en rapport avec les structures des solutés et la nature des mélanges hydroorganiques.

Mots clés : enthalpies, dissolution, solvatation, acides–bases, solvants hydroorganiques.

HENRI GILLET. Can. J. Chem. **68**, 655 (1990).

We have measured at 25°C the enthalpies of solution of acetic, benzoic, and valeric acids and of their potassium salts in water – *tert*-butyl alcohol mixtures containing up to 40% by weight of organic cosolvent. We have also determined these quantities for phenol, aniline, and pyridine in the same mixtures and for acetic acid, aniline, and pyridine in water–DMSO, water–acetone, and water–urea in the zone rich in water. Using these data we have calculated the standard enthalpies of solution, the corresponding transfer quantities, and the enthalpies of solvation. When the enthalpies of solution are difficult or impossible to measure we have shown that the enthalpies of transfer can be calculated from judiciously selected transfer quantities obtained from experimental measurements. In this way we have worked out the enthalpies of transfer of potassium phenolate and of anilinium and pyridinium chlorides and bromides in the various mixtures. The enthalpies of solvation have been separated into enthalpies of formation of a cavity in the solvent and enthalpies of interaction. From these last quantities an attempt at interpretation in terms of solute and aqueous-organic media structures was made.

Key words: enthalpies, solution, solvation, acids–bases, aqueous-organic media.

Can. J. Chem. Downloaded from www.nrcresearchpress.com by 91.144.44.67 on 09/07/12
For personal use only.

I. Introduction

Dans un précédent mémoire (1) nous avons donné les valeurs des constantes de dissociation acide et des enthalpies de neutralisation des acides acétique, benzoïque et valérianique, du phénol et des ions anilinium et pyridinium dans les mélanges eau – alcool *tert*-butylique, eau–DMSO, eau–acétone et eau–urée contenant jusqu'à 40% en masse de cosolvant organique. Nous avons fait l'analyse de l'évolution des grandeurs thermodynamiques standard ΔG_d^θ, ΔH_d^θ et ΔS_d^θ relatives à la dissociation, et des grandeurs de transfert correspondantes, avec la teneur en cosolvant.

Pour accéder à l'enthalpie molaire standard de solvatation d'une molécule dans un milieu solvant déterminé il faut connaître son enthalpie molaire standard de dissolution dans ce solvant et son enthalpie de vaporisation. Les enthalpies de dissolution peuvent être obtenues par mesure calorimétrique directe pour certaines espèces ou par un processus plus complexe pour d'autres. Les enthalpies de vaporisation sont données par la littérature. La valeur de l'enthalpie de solvatation rend compte de la variation de l'énergie interne des molécules et des énergies d'interaction avec le solvant lors de la mise en solution. Les enthalpies de solvatation des ions peuvent être déduites de celles des molécules en utilisant les valeurs des enthalpies de dissociation en phase gazeuse et en solution des acides protoniques correspondants. Si l'enthalpie de solvatation du proton est connue dans le mélange considéré, on peut accéder à celle des autres ions; dans le cas contraire nous n'obtiendrons cette grandeur que pour un couple d'ions. L'enthalpie de solvatation peut être séparée en enthalpie de formation d'une cavité dans le solvant, convenable pour accueillir le soluté, et en enthalpie d'interaction. La théorie des particules calibrées (S.P.T.) nous permet d'estimer « l'enthalpie de cavité ».

Si l'on veut mettre en évidence l'influence de la nature du cosolvant organique et de la teneur du mélange sur la solvatation, il faut calculer les grandeurs de transfert pour les enthalpies d'interaction. Ces grandeurs rendent compte des variations de l'énergie interne des espèces en solution et des énergies d'interaction lors du passage de l'eau pure à un mélange hydroorganique.

En considérant à la fois la structure du soluté et la composition du solvant il est possible de faire un essai d'interprétation des enthalpies d'intéraction et des grandeurs de transfert correspondantes en essayant de déterminer les interactions existantes quand le solvant est l'eau et de voir comment se comportent ces interactions lorsqu'on ajoute un cosolvant organique.

Les chimistes organiciens sont très intéressés par l'influence du milieu solvant sur le déroulement des réactions. Dans les mélanges hydroorganiques de nombreux paramètres ont été proposés pour rendre compte de cette influence : la constante de réaction de Hammett (2), le paramètre Y du « postulat de Grunwald–Winstein » (3), le paramètre de solubilité de Hildebrand (4), le paramètre de Kosower (5), etc. Les enthalpies d'interaction peuvent aussi apporter des renseignements dans ce domaine en rendant compte de l'influence de la composition du mélange solvant et de la nature du cosolvant. On peut calculer l'enthalpie d'une réaction dans un mélange hydroorga-

Printed in Canada / Imprimé au Canada

nique si l'on connait l'enthalpie de cette réaction dans l'eau et les enthalpies de transfert des réactifs et des produits de l'eau au mélange utilisé.

II. Partie théorique

1. Enthalpie de dissolution et enthalpie de transfert des espèces

Toutes les variations d'enthalpie sont des grandeurs molaires.

L'enthalpie standard de dissolution ΔH_s^θ est la variation d'enthalpie mise en jeu lors du passage d'une molécule de soluté de l'état liquide ou solide à l'état de solution infiniment diluée dans le solvant s.

Dans le cas d'un acide non chargé, il faut tenir compte de sa dissociation en solution. Si ΔH_s est la variation d'enthalpie mesurée, nous avons

$$[1] \quad \Delta H_s^\theta(\mathrm{AH}) = \Delta H_s - \alpha \Delta H_d^\theta(\mathrm{AH})$$

α est le degré de dissociation de l'acide et $\Delta H_d^\theta(\mathrm{AH})$ son enthalpie standard de dissociation.

Dans le cas d'une base, il faut tenir compte de la dissociation de l'acide cationique conjugué ce qui donne, en négligeant la dissociation propre de l'eau :

$$[2] \quad \Delta H_s^\theta(\mathrm{B}) = \Delta H_s - \alpha[\Delta H_d^\theta(\mathrm{H_2O}) - \Delta H_d^\theta(\mathrm{BH^+})]$$

Dans le cas d'un sel AM on le suppose entièrement dissocié en solution et on peut accéder à la valeur standard :

$$[3] \quad \Delta H_s^\theta(\mathrm{AM}) = \Delta H_s - \Phi_L$$

Φ_L étant calculé par la relation donnée par Juillard et Morel (6).

Les enthalpies standard de dissolution dans les différents solvants permettent de calculer les enthalpies standard de transfert des espèces dissoutes i de l'eau (w) à ce solvant (s). En effet :

$$[4] \quad \Delta^s H_s^\theta(i) = {}^s\bar{H}^\theta(i) - H^0(i)$$

H^0 étant l'enthalpie molaire du soluté pur et $\bar{H}^\theta$ l'enthalpie molaire partielle du soluté en solution infiniment diluée. Donc :

$$[5] \quad {}^s\delta\bar{H}^\theta(i) = {}^s\delta\Delta H_s^\theta(i)$$

l'opérateur ${}^s\delta$ symbolisant le transfert.

Pour certains composés peu solubles ou difficiles à obtenir purs et anhydres, il est impossible de mesurer expérimentalement les enthalpies de dissolution, mais il est possible de calculer ces grandeurs.

Considérons deux acides A_1H et A_2H et leurs sels de potassium A_1K et A_2K. Nous pouvons facilement obtenir la relation :

$$[6] \quad {}^s\delta\bar{H}^\theta(\mathrm{A_2H}) = {}^s\delta\Delta H_d^\theta(\mathrm{A_1H}) - {}^s\delta\Delta H_d^\theta(\mathrm{A_2H}) + {}^s\delta\Delta H_s^\theta(\mathrm{A_2K}) - {}^s\delta\Delta H_s^\theta(\mathrm{A_1K}) + {}^s\delta\Delta H_s^\theta(\mathrm{A_1H})$$

Nous voyons que si nous choisissons un couple tel que toutes les grandeurs du membre de droite soient mesurables, il est possible d'accéder à ${}^s\delta\bar{H}^\theta(\mathrm{A_2H})$.

Au lieu de choisir un couple de deux acides, nous pouvons écrire :

$$[7] \quad {}^s\delta\bar{H}^\theta(\mathrm{AH}) = {}^s\delta\Delta H_s^\theta(\mathrm{A^-, K^+}) - {}^s\delta\Delta H_d^\theta(\mathrm{AH}) - {}^s\delta\Delta H_s^\theta(\mathrm{Cl^-, K^+}) + {}^s\delta\Delta H_s^\theta(\mathrm{Cl^-, H^+})$$

Si nous connaissons l'enthalpie de transfert de la réaction de dissociation de l'acide et les enthalpies de transfert de l'acide chlorhydrique, du chlorure de potassium et du sel AK, nous pouvons calculer ${}^s\delta\bar{H}^\theta(\mathrm{AH})$.

Dans le cas d'un acide cationique, nous pouvons écrire :

$$[8] \quad {}^s\delta\Delta H_d^\theta(\mathrm{BH^+}) = {}^s\delta\Delta H_s^\theta(\mathrm{B}) + {}^s\delta\Delta H_s^\theta(\mathrm{H^+, Cl^-}) - {}^s\delta\Delta H^\theta(\mathrm{BH^+, Cl^-})$$

Si nous connaissons l'enthalpie de transfert de la réaction de dissociation de l'acide, l'enthalpie de transfert de l'acide chlorhydrique et l'enthalpie de transfert de la molécule de base, nous pouvons calculer l'enthalpie de transfert du couple (BH^+, Cl^-).

2. Enthalpie de solvatation

L'enthalpie molaire standard de solvatation ΔH_{solv}^θ est l'enthalpie mise en jeu lors du passage d'une mole de soluté de l'état gazeux à l'état de solution infiniment diluée. On a la relation :

$$[9] \quad \Delta H_{solv}^\theta = \Delta H_s^\theta - \Delta H_{vap}^0$$

où ΔH_s^θ est l'enthalpie molaire standard de dissolution et ΔH_{vap}^0 l'enthalpie molaire standard de vaporisation du soluté correspondant au passage d'une mole de l'état liquide ou solide à l'état idéal gazeux monomère. Dans le cas d'un acide AH on peut écrire :

$$\Delta H_{d,g}^0(\mathrm{AH}) + \Delta H_{solv}^\theta(\mathrm{A^-, H^+}) = \Delta H_{solv}^\theta(\mathrm{AH}) + \Delta H_{d,sol}^\theta(\mathrm{AH})$$

$(\Delta H_{d,g}^0)$ est l'enthalpie molaire standard de dissociation en phase gazeuse, ΔH_{solv}^θ l'enthalpie molaire standard de solvatation et $\Delta H_{d,sol}^\theta$ l'enthalpie molaire standard de dissociation en solution. D'où la relation :

$$[10] \quad \Delta H_{solv}^\theta(\mathrm{A^-}) = \Delta H_{solv}^\theta(\mathrm{AH}) - \Delta H_{solv}^\theta(\mathrm{H^+}) + \Delta H_{d,sol}^\theta(\mathrm{AH}) - \Delta H_{d,g}^0(\mathrm{AH})$$

Si l'on connaît $\Delta H_{d,g}^0(\mathrm{AH})$ on peut accéder à $\Delta H_{solv}^\theta(\mathrm{A^-})$ dans l'eau et les mélanges où l'on connaît $\Delta H_{solv}^\theta(\mathrm{H^+})$. Dans les mélanges où cette dernière grandeur n'est pas connue, on peut seulement accéder à $\Delta H_{solv}^\theta(\mathrm{A^-, H^+})$.

Dans le cas d'un acide du type BH^+ nous pouvons écrire :

$$[11] \quad \Delta H_{d,g}^0(\mathrm{BH^+}) + \Delta H_{solv}^\theta(\mathrm{BH^+}) = \Delta H_{solv}^\theta(\mathrm{BH^+}) + \Delta H_{d,sol}^\theta(\mathrm{BH^+})$$

et

$$\Delta H_{solv}^\theta(\mathrm{BH^+}) = \Delta H_{d,g}^0(\mathrm{BH^+}) + \Delta H_{solv}^\theta(\mathrm{B}) + \Delta H^\theta{}_{solv}(\mathrm{H^+}) - \Delta H_{d,sol}^\theta(\mathrm{BH^+})$$

Là aussi, si l'on connaît $\Delta H_{d,g}^0(\mathrm{BH^+})$ on peut obtenir $\Delta H_{solv}^\theta(\mathrm{BH^+})$ dans l'eau et les mélanges où l'on connait $\Delta H_{solv}^\theta(\mathrm{H^+})$. Dans les autres mélanges on peut seulement accéder à $\Delta H_{solv}^\theta(\mathrm{BH^+}) - \Delta H_{solv}^\theta(\mathrm{H^+})$.

Pour la dissociation d'un acide AH en phase gazeuse nous avons

$$[12] \quad \mathrm{PA(A^-)} = \mathrm{D(AH)} - \mathrm{EA(A^\cdot)} + \mathrm{IP(H^\cdot)}$$

où EA(X) est l'affinité électronique de X (énergie négative), PA(X) est l'affinité pour le proton de X (énergie négative), IP(X) est le potentiel d'ionisation de X (positif) et D(AH) est l'énergie de coupure homolytique de la liaison A—H. McMahon et Kebarle (49) ont étudié par spectrophotométrie de masse des réactions d'échange du proton du type

$$\mathrm{A_1H + A_2^- = A_1^- + A_2H} \quad (1)$$

$$\mathrm{B_1H^+ + B_2 = B_1 + B_2H^+} \quad (2)$$

Can. J. Chem. Downloaded from www.nrcresearchpress.com by 91.144.44.67 on 09/07/12
For personal use only.

À 600 K ils obtiennent $\delta_R\Delta G^0_{d,g}$; ils font l'hypothèse $\Delta S^0_{d,g} \simeq 0$ donc :

$$\delta_R\Delta G^0_{d,g}(600\,K) \simeq \delta_R\Delta G^0_{d,g}(298\,K) \simeq \delta_R\Delta H^0_{d,g}$$

Comme nous avons

[13] $\Delta G^0_{d,g} = \Delta H^0_{d,g} = PA(A^-) = D(AH) - EA(A^\bullet) + IP(H^\bullet)$

nous pouvons écrire pour une réaction d'échange du proton du type (1) :

[14] $\delta_R\Delta H^0_{d,g} = D(A_2H) - EA(A_2^\bullet) - D(A_1H) + EA(A_1^\bullet)$

Connaissant D(AH) et EA(A•) pour HCl et H_2S, Kebarle a évalué D(AH) − EA(A•) pour d'autres acides.

Pour la dissociation d'un acide BH^+ en phase gazeuse nous avons

[15] $PA(B) = HA(B^{\bullet+}) - IP(B) + IP(H^\bullet)$

et

[16] $PA(B) = D(BH^+) - EA(B^{\bullet+}) + IP(H^\bullet) = \Delta H^0_{d,g}(BH^+)$

HA(X) est l'affinité pour l'hydrogène de X (énergie négative).

Pour une réaction d'échange du type (2) nous pouvons écrire

[17] $\delta_R\Delta H^0_{d,g} = D(B_2H^+) - EA(B_2^{\bullet+}) - D(B_1H^+) + EA(B_1^{\bullet+})$

3. Enthalpie de cavité et d'interaction

Pour une espèce en solution, on peut écrire :

[18] $\Delta H^\theta_{solv} = \Delta H_c + \Delta H^\theta_i$

ΔH_c est l'enthalpie de formation d'une cavité dans le solvant de dimension convenable pour accueillir le soluté.

Cette grandeur peut être évaluée à l'aide de la théorie des particules calibrées (scaled-particle theory) (7, 8) :

[19] $$\Delta H_c = \frac{\alpha RT^2}{(1-\xi_3)}\left\{\xi_3 + \frac{3\xi_2}{(1-\xi_3)}\,b + \frac{3\xi_1}{(1-\xi_3)}\,b^2 + \frac{9\xi_2^2}{(1-\xi_3)^2}\,b^2\right\}$$

avec

$$\xi_k = \frac{N}{6}\,\Pi \sum_{i=1}^{m} \rho_i a_i^k$$

m est le nombre d'espèces dans le mélange solvant, ρ_i est le nombre de particules i de diamètre a_i dans l'unité de volume, b le diamètre du soluté, k prend les valeurs 1, 2 ou 3, N est le nombre d'Avogadro, R la constante des gaz parfaits, α le coefficient de dilatation isobare du mélange solvant et T la température absolue. Le terme faisant intervenir la pression est négligé.

ΔH^θ_i rend compte des interactions soluté–solvant lorsque la cavité créée est occupée par le soluté.

III. Techniques expérimentales

1. Produits utilisés

Les solvants et les solutés ont été purifiés comme nous l'avons indiqué dans des publications précédentes (1, 9, 10).

2. Mesure de l'enthalpie de dissolution des acides, des bases et des sels

Nous avons utilisé un calorimètre LKB type 8700 à dissolution. La cellule contient 100 cm^3 de solvant. L'ampoule contient le soluté en quantité telle que la concentration finale soit $0{,}02 < m < 0{,}03$.

Plusieurs cas se sont présentés :

(a) La dissolution est rapide (durée <5 min). La courbe est exploitée par la méthode de Dickinson (11). C'est la majorité des cas.

(b) La dissolution est lente (durée >5 min). La courbe est exploitée par la méthode de Regnault–Pfaundler (12). Un exemple est la dissolution de l'aniline dans l'eau ou dans les mélanges très riches en eau.

(c) Dissolution avec existence temporaire de deux phases aqueuses. Un exemple est la dissolution de l'acide *n*-valérianique dans l'eau ou dans les mélanges très riches en eau : on obtient d'abord une élévation de température et ensuite une diminution; la température finale est inférieure à la température initiale.

(d) Substance peu soluble et à dissolution très lente, l'enthalpie de dissolution ne peut pas être mesurée avec le matériel dont nous disposons. La valeur pourra être obtenue par le calcul. C'est le cas de l'acide benzoïque dans les mélanges dont la teneur en alcool *tert*-butylique est inférieure à 25%.

(e) Cas d'une substance soluble mais hygroscopique. $^s\delta\Delta H_s$ est obtenu par dilution d'une solution concentrée de cette substance. Nous avons utilisé cette méthode pour l'acétate de potassium. La cellule contenait 100 cm^3 de mélange et l'ampoule une quantité de solution du sel, de molalité $m = 4{,}579\ mol\,kg^{-1}$, telle que la molalité de la solution finale soit de l'ordre de $2 \times 10^{-2}\ mol\,kg^{-1}$. La méthode ne permet que d'atteindre directement la valeur de transfert $^s\delta\Delta H^\theta_s(AK)$ que l'on peut calculer (13) par la formule :

[20] $$^s\delta\Delta H^\theta_s(AK) = \Delta^s H - \Delta^w H - \frac{n_w}{n_i}\,\bar{L}(H_2O) + {}^w\Phi_L - {}^s\Phi_L$$

$\Delta^s H$ et $\Delta^w H$ sont les effets thermiques obtenus expérimentalement dans le mélange et dans l'eau. $\bar{L}(H_2O)$ est l'enthalpie molaire partielle relative de l'eau dans le mélange (9). n_w/n_i rapport du nombre de mole d'eau au nombre de mole d'acétate dans la solution concentrée contenue dans l'ampoule.

La connaissance de la valeur de $\Delta^w H^\theta_s(AK)$ nous permet de calculer $\Delta^s H^\theta_s(AK)$ dans les mélanges.

IV. Résultats

1. Enthalpies de dissolution des acides, des amines et des sels

Les valeurs des enthalpies molaires standard de dissolution sont données dans les tableaux 1 et 2, elles ont été déterminées à environ 200 $J\,mol^{-1}$ près.

Les molalités finales sont comprises entre 0,02 et 0,03; nous avons assimilé les enthalpies déterminées à ces concentrations aux enthalpies standard de dissolution ΔH^θ_s. Nichols et Wadsö (22) montrent que pour la dissolution dans l'eau du phénol, du *p*-crésol, de l'alcool benzylique, de l'aniline et de la benzylamine, l'enthalpie de dissolution mesurée dans le domaine $0{,}01 < m < 0{,}06$ ne dépend pas de la concentration. Avedikian *et al.* (18) ont fait la même approximation pour la dissolution d'acides carboxyliques. Les valeurs obtenues dans l'eau ont été confrontées aux valeurs de la littérature pour les acides acétique (14–18), valérianique (16), benzoïque (19), le phénol (20–22, 26), l'aniline (22–24) et la pyridine (25). Nos mesures sont en bon accord avec ces valeurs.

Dans les mélanges solvants étudiés peu de valeurs de ΔH^θ_s relatives aux solutés utilisés dans cette étude ont été publiées. Les seules valeurs à notre disposition sont celles données par Avedikian *et al.* (18) pour l'acide acétique dans les mélanges eau – alcool *tert*-butylique. Nous avons eu seulement à faire des mesures pour 35 et 40% de cosolvant. Rochester et Sclosa (27) ont publié des valeurs d'enthalpie standard de dissolution du phénol dans ces mêmes mélanges; ces valeurs sont en bon accord avec les nôtres. Rodante *et al.* (28) ont fait des mesures d'enthalpie de dissolution de l'acide benzoïque dans les mélanges eau–DMSO mais ils ne donnent qu'une seule valeur dans la zone riche en eau que nous étudions.

Pour l'acétate de potassium dans les mélanges eau – alcool *tert*-butylique nous avons utilisé la méthode exposée en III.2(e) qui nous a permis d'accéder à l'enthalpie de transfert du sel.

Can. J. Chem. Downloaded from www.nrcresearchpress.com by 91.144.44.67 on 09/07/12
For personal use only.

TABLEAU 1. Enthalpies standard de dissolution (en kJ mol^{-1}) des acides, des sels de potassium et des amines dans les mélanges eau–alcool *tert*-butylique à 25°C

X (%)	MeCOOH	MeCOOK	BuCOOH	BuCOOK	ϕCOOH	ϕCOOK[d]	ϕOH	ϕNH$_2$	Π
0	−1,2	−15,3[b]	−0,4	−8,6	22,5[c]	7,0	12,7	1,9	−9,6
5	0,7[a]	−13,7	3,2	−5,5	26,6[c]	10,2	15,6	4,2	−6,8
10	3,0[a]	−11,1	8,7	−0,6	33,0[c]	14,9	19,8	8,1	−2,9
15	5,3[a]	−7,9	17,2	6,9	41,8[c]	21,1	25,4	13,3	1,7
17,5	6,1[a]	−5,7	20,6	11,4	44,1[c]	24,0	27,7	15,6	3,2
20	6,4[a]	−3,8	21,3	14,4	41,4[c]	25,7	27,1	16,3	3,5
25	5,8[a]	−2,1	16,7	16,5	33,3	25,7	22,6	14,4	2,1
30	5,1[a]	−1,6	12,3	16,2	27,6	23,9	18,4	11,9	0,7
35	4,4	−1,5	9,1	15,5	23,6	22,4	15,6	9,9	−0,5
40	3,7	−1,8	7,3	14,3	21,8	20,9	13,5	8,7	−1,5

[a]Référence 18.
[b]Référence 29.
[c]Valeurs calculées.
[d]Référence 30.
MeCOOH: acide acétique; BuCOOH: acide valérianique; ϕCOOH: acide benzoïque; ϕOH: phénol; ϕNH$_2$: aniline; Π: pyridine.

TABLEAU 2. Enthalpies standard de dissolution (en kJ mol^{-1}) de l'acide acétique, de l'aniline et de la pyridine dans les mélanges eau–DMSO, eau–acétone et eau–urée à 25°C

	Acide acétique			Aniline			Pyridine		
X(%)	Eau–DMSO	Eau–acétone	Eau–urée	Eau–DMSO	Eau–acétone	Eau–urée	Eau–DMSO	Eau–acétone	Eau–urée
0	−1,2	−1,2	−1,2	1,9	1,9	1,9	−9,6	−9,6	−9,6
5	−0,6	−0,1*	−1,6*	2,3*	3,3*	1,9*	−8,7*	−8,0*	−9,5*
10	0,1*	0,9	−1,9	2,8	4,7	1,8	−7,8	−6,3	−9,5
15	0,7	1,7	−2,3*	3,4*	6,0*	1,9*	−6,9*	−4.9*	−9,5*
20	1,3	2,3	−2,5	4,0	7,1	1,9	−6,0	−3,8	−9,5
25	1,8*	2,6	−2,8*	4,5*	7,6*	1,9*	−5,1*	−3,1*	−9,5*
30	2,3	2,6	−3,1	5,0	7,6	1,8*	−4,3	−2,7	−9,5
35	2,7*	2,4	−3,3*	5,4*	7,2*	1,8*	−3,4*	−2,5*	−9,5*
40	3,0	2,0	−3,5	5,7	6,5	1,8	−2,6	−2,5	−9,4

*Valeurs interpolées.

Pour avoir les valeurs des enthalpies de dissolution du sel dans les mélanges, nous avons utilisé la valeur de l'enthalpie de dissolution de l'acétate de potassium dans l'eau donné par Parker (29).

Pour le benzoate de potassium dans les mêmes mélanges, nous avons utilisé les valeurs données par Dollet et Juillard (30).

2. Calcul des grandeurs non mesurables

Nous avons déjà vu que certaines grandeurs thermodynamiques ne pouvaient être déterminées expérimentalement mais qu'il était possible de les calculer à partir de grandeurs mesurées.

Nous avons essayé un tel calcul sur le couple acide acétique, acide valérianique en milieu eau – alcool *tert*-butylique. Si A_2H représente l'acide valérianique, nous pouvons calculer ${}^{s}\delta\bar{H}^{\theta}(A_2H)$ par la relation [6] puisque tous les termes de droite peuvent être obtenus par l'expérience. Nous pouvons aussi calculer l'enthalpie de transfert de A_2H par la relation [7] en utilisant les enthalpies de transfert de HCl et de KCl données par Pointud *et al.* (13, 31). Les valeurs obtenues par ces deux voies sont comparées entre elles et aux valeurs expérimentales sur la figure 1. Nous voyons sur cette figure que ce sont les valeurs obtenues par la relation [7] qui concordent en général le mieux avec les valeurs expérimentales.

C'est donc cette relation que nous avons utilisée pour calculer les enthalpies de transfert de l'acide benzoïque de l'eau aux mélanges eau – alcool *tert*-butylique consignées dans le tableau 1. Nous avons d'autre part mesuré ses enthalpies de dissolution pour $X \geqq 25\%$ et avons déduit de ces résultats l'enthalpie de dissolution de l'acide benzoïque dans l'eau; la valeur trouvée, 22,5 kJ mol^{-1}, est assez différente de celle égale à 26,8 kJ mol^{-1} proposée par Fernandez et Hepler (19) et généralement utilisée. Nous avons ensuite calculé les enthalpies de dissolution pour $X < 25\%$ (tableau 1).

Pour le phénate de potassium, les difficultés rencontrées pour avoir le produit pur et en raison de son hygroscopicité nous ont fait préférer le calcul par la formule [7]. Ce calcul nous permet seulement d'obtenir l'enthalpie de transfert. Il n'existe pas à notre connaissance de valeur de l'enthalpie de dissolution dans l'eau.

De même pour les chlorures et les bromures d'anilinium et de pyridinium, nous avons calculé les enthalpies de transfert par la relation [8] en utilisant les enthalpies de transfert de HCl et de HBr données par la littérature (9, 13, 32–37). Pour pouvoir calculer les enthalpies de dissolution dans les mélanges, il faut connaître l'enthalpie de dissolution dans l'eau. Pour le chlorure d'anilinium il n'existe, à notre connaissance, que la valeur déterminée par Berthelot (38), $\Delta^{w}H_s = 11{,}43$ kJ mol^{-1}. Pour le chlorure de pyridinium nous ne connaissons aucune valeur.

Can. J. Chem. Downloaded from www.nrcresearchpress.com by 91.144.44.67 on 09/07/12
For personal use only.

TABLEAU 3. Enthalpies standard de transfert calculées du phénate de potassium, des chlorures et bromures d'anilinium et de pyridinium dans les mélanges eau – alcool *tert*-butylique et eau–acétone à 25°C (en kJ mol^{-1})

	Eau – alcool *tert*-butylique					Eau–acétone	
X (%)	ϕOK	ϕNH_3^+, Cl^-	ϕNH_3^+, Br^-	ΠH^+, Cl^-	ΠH^+, Br^-	ϕNH_3^+, Br^-	ΠH^+, Br^-
0	0	0	0	0	0	0	0
5	3,2	2,5	2,7	1,7	1,9	0,2	−0,5
10	7,9	5,9	6,0	3,9	4,0	0,4	−0,6
15	13,7	9,2	9,1	6,0	5,9	0,2	−0,9
17,5	16,3	10,7	—	6,9	—	—	—
20	19,1	11,2	10,3	7,2	6,3	0	−1,0
25	21,0	10,6	9,3	7,5	6,2	−0,7	−1,3
30	19,8	9,5	7,6	7,4	5,5	−1,3	−1,5
35	18,8	8,4	6,3	7,1	5,0	−3,5	−1,8
40	18,1	7,4	5,2	6,8	4,6	−7,7	−3,6

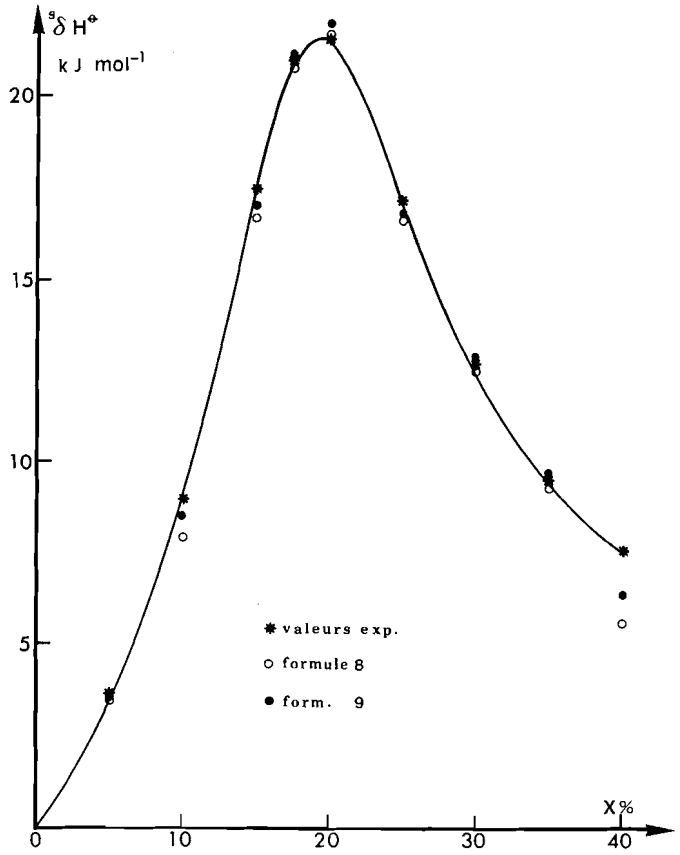

FIG. 1. Enthalpies de transfert de BuCOOH dans les mélanges eau – alcool *tert*-butylique à 25°C.

Les valeurs de transfert calculées des différentes espèces sont données dans les tableaux 3 et 4.

3. Enthalpie de solvatation, « enthalpie de cavité » et enthalpie d'interaction

Nous avons vu que la relation [9] permet de calculer l'enthalpie de solvatation si l'on connaît les enthalpies de dissolution et de vaporisation d'une espèce. L'enthalpie de solvatation peut être décomposée (voir relation [18]) en un terme ΔH_c, qui est l'enthalpie de formation d'une cavité dans le solvant, et un terme ΔH_i qui rend compte des interactions soluté–solvant.

Dans l'eau nous obtenons les résultats indiqués dans le tableau 5. Les enthalpies standard de vaporisation sont tirées de la littérature. Le terme ΔH_c a été calculé par la relation [19] sauf pour l'acide valérianique dont la structure en chaîne rend difficile le calcul de b. Pour l'eau nous avons pris $a = 2{,}73$ Å (39).

L'enthalpie de solvatation des anions est donnée par la relation [10], celle des ions BH^+ par la relation [11].

Pour les acides AH, McMahon et Kebarle (49) donnent les valeurs de D(AH) − EA(A$^\cdot$). Pour l'acide valérianique, ce terme est évalué par extrapolation à partir des valeurs données pour les acides acétique, propionique et butyrique (54, 55). On obtient PA(A^-) en ajoutant à ces valeurs IP(H$^\cdot$) comme le montre la relation [12]. La littérature donne IP(H$^\cdot$) = 1312,1 kJ mol^{-1} (49).

Pour les acides cationiques différents auteurs donnent directement la valeur de PA(B) pour NH_4^+ (50–52). Kebarle et coll. (53) donnent les valeurs de $\delta_R \Delta G^0_{d,g}$ pour les relations d'échange.

$$NH_4^+ + B = NH_3 + BH^+$$

On peut calculer $\Delta H^0_{d,g}(BH^+)$ par les relations [16] et [17] et ΔH_c pour les ions par la S.P.T. en prenant le diamètre de l'ion égal à celui de la molécule et obtenir ainsi le terme ΔH_i^θ.

Pour ce dernier calcul nous avons pris comme diamètre du cosolvant les valeurs suivantes : 5,07 Å pour l'alcool *tert*-butylique (56), 4,91 Å pour le DMSO (48), 4,76 Å pour l'acétone (48) et 4,41 Å pour l'urée (57).

Dans les solvants hydroorganiques nous pouvons calculer de la même façon les enthalpies de solvatation des molécules, les enthalpies de formation des cavités dans le solvant et les enthalpies d'interaction ΔH_i^θ.

Si l'on connaît l'enthalpie de solvatation de l'ion H^+ dans un solvant donné, on peut calculer l'enthalpie de solvatation des anions A^- par la relation [10] et celle des cations BH^+ par la relation [11]. L'enthalpie standard de solvatation du proton obtenue à l'aide de diverses hypothèses extrathermodynamiques n'est connue que dans l'eau (40, 59), dans les mélanges eau – alcool *tert*-butylique (58) et eau–DMSO (9, 33). Dans les autres mélanges nous pouvons seulement accéder aux enthalpies d'interaction $\Delta H_i^\theta(A^-, H^+)$ des couples (A^-, H^+) et aux différences $\Delta H_i^\theta(BH^+) - \Delta H_i^\theta(H^+)$.

V. Discussion

Les enthalpies standard d'interaction sont des grandeurs qui rendent compte principalement des énergies d'interaction soluté–solvant en tenant compte des modifications éventuelles de la nature des liaisons dans la molécule ou l'ion en solution. Elles

Can. J. Chem. Downloaded from www.nrcresearchpress.com by 91.144.44.67 on 09/07/12
For personal use only.

TABLEAU 4. Enthalpies standard de transfert calculées des chlorures et bromures d'anilinium et de pyridinium dans les mélanges eau–DMSO et eau–urée à 25°C (en kJ mol^{-1})

	Eau–DMSO				Eau–urée			
X (%)	ϕNH_3^+, Cl^-	ΦNH_3^+, Br^-	ΠH^+, Cl^-	ΠH^+, Br^-	ϕNH_3^+, Cl^-	ΦNH_3^+, Br^-	ΠH^+, Cl^-	ΠH^+, Br^-
0	0	0	0	0	0	0	0	0
5	0,8	0,4	0,7	0,3	−0,6	−0,9	−1,9	−2,2
10	1,5	0,7	1,1	0,3	−1,4	−1,7	−3,6	−3,9
15	2,0	1,1	1,4	0,5	−2,3	−2,3	−5,3	−5,3
20	2,9	1,8	2,0	0,9	−2,6	−2,9	−6,1	−6,4
25	3,8	2,2	2,9	1,3	−2,5	−3,4	−6,5	−7,4
30	4,6	2,6	3,7	1,7	−2,7	−3,9	−7,2	−8,4
35	5,6	3,2	4,8	2,4	−3,5	−4,2	−8,8	−9,5
40	5,5	2,7	5,3	2,5	−4,5	−4,4	−10,6	−10,5

TABLEAU 5. Enthalpies standard d'hydratation et d'interaction des acides protoniques et des bases conjugées dans l'eau à 25°C (en kJ mol^{-1}). $\Delta H^{\theta}_{hydr}(H^+) = -1104$ kJ mol^{-1} (40)

	ΔH^0_{vap}	$\Delta H^0_{d,g}$ (AH) ou (BH^+)	ΔH^{θ}_{hydr}	b (Å)	ΔH_c	ΔH^{θ}_i
MeCOOH	51,6[a]	1453,5[g]	−52,8	4,4[i]	4,2	−57,0
BuCOOH	62,4[b]	1443,0[g]	−62,8			
ϕCOOH	91,4[c]	1419,6[g]	−68,9	5,9[j]	7,2	−76,1
ϕOH	68,7[d]	1459,8[g]	−56,0	5,4[j]	6,1	−62,1
ϕNH_2	55,8[e]	911,7[h]	−53,9	5,6[i]	6,5	−60,4
Π	40,2[f]	952,3[h]	−49,8	5,3[j]	5,9	−55,7
$MeCOO^-$			−402,4	4,4	4,2	−406,6
$BuCOO^-$			−404,0			
ϕCOO^-			−384,1	5,9	7,2	−391,3
ϕO^-			−388,8	5,4	6,1	−394,9
ϕNH_3^+			−276,5	5,6	6,5	−283,0
ΠH^+			−221,7	5,3	5,9	−227,6

[a]Référence 41.
[b]Référence 42.
[c]Référence 43.
[d]Référence 44.
[e]Référence 45.
[f]Référence 46.
[g]Référence 49.
[h]D'après les références 50–53.
[i]Référence 47.
[j]Valeurs évaluées d'après celles données pour le benzène, le nitrobenzène, le toluène (48) et l'acétophénone (47).

sont donc des grandeurs de choix pour l'étude de la contribution énergétique au phénomène de solvatation et la valeur de transfert correspondante nous renseigne sur les variations de ces interactions lors du passage de l'eau à un solvant mixte.

Les résultats présentés ici nous montrent que les enthalpies de solvatation sont négatives pour les molécules et les ions et que les valeurs absolues de ces enthalpies sont beaucoup plus grandes pour les ions que pour les molécules et plus grandes pour les anions que pour les cations du type BH^+.

Nous avons vu que ΔH^{θ}_{solv} peut être considéré comme la somme des deux termes ΔH_c et ΔH^{θ}_i (relation [18]). La S.P.T. donne des valeurs de ΔH_c satisfaisantes quand les solutés sont des sphères rigides qui ne donnent pas d'interactions spécifiques avec le solvant. Treiner (60) et Morel-Desrosiers (61) ont montré que ce calcul donne de bons résultats avec des solutés de taille importante tels que l'ion tétrabutylammonium (b = 7,74 Å) et l'adamantane (b = 6,36 Å). Les espèces que nous étudions ont des diamètres de l'ordre de 5–6 Å, leur taille ne semble donc pas être un obstacle à une application correcte de la théorie. Elles sont toutes peu déformables, mais n'ont pas une configuration sphérique et peuvent donner, comme nous le verrons par la suite, des interactions spécifiques du type liaison hydrogène avec les molécules du solvant. Ces deux derniers points nous permettent de penser que les valeurs de ΔH_c obtenues ne sont qu'approximatives mais donnent quand même un ordre de grandeur correct de l'enthalpie de formation de la cavité. Si l'on considère les valeurs de ces enthalpies pour les différents solutés dans les divers solvants on se rend compte que l'enthalpie de formation de la cavité a une valeur relativement faible, surtout dans le cas des ions, devant celle de l'enthalpie d'interaction, tout du moins dans l'eau et les mélanges très riches en eau. Quand la teneur en cosolvant organique augmente cette disparité diminue mais l'enthalpie d'interaction reste la grandeur prépondérante. Ceci veut dire que les interactions solutés–solvants apportent la contribution énergétique principale au phénomène de solvatation. Si maintenant nous

Can. J. Chem. Downloaded from www.nrcresearchpress.com by 91.144.44.67 on 09/07/12
For personal use only.

TABLEAU 6. Répartition électronique dans les molécules et enthalpie d'interaction

	N ou C_0[a]	C1	C2[b] ou C6[b]	C3[b] ou C5[b]	C4[b]	H(OH)[c]	H(NH)[c]	O(C=O)[a]	O(OH)[a]	Réf.	Types liaisons hydrogène possibles	ΔH_i^θ (kJ mol^{-1})
MeCOOH	0,714	−0,517[a]				0,438		−0,579	−0,682	62	I–III	−57,0
ΦCOOH	0,389	−0,040[b]	0,031	−0,006	0,024	0,261		−0,351	−0,263	63–67 70	I–III V–VI	−76,1
ΦOH		0,049[b]	−0,059	0,023	−0,039	0,236			−0,422	64	I–III V–VI	−62,1
ΦNH_2	−0,268	0,057[b]	−0,066	0,026	−0,045		0,105			64	II–IV V–VI	−60,4
Π	−0,130		0,030	−0,020	0,040					65	IV–V VI	−55,7
$MeCOO^-$	0,686	−0,508[a]						−0,779	−0,785	62	III	−406,6
ΦCOO^-	0,355	0,068[b]	0,005	−0,023	−0,037			−0,557	−0,556	70	III–V VI	−391,3
ΦO^-		0,087[b]	−0,082	−0,009	−0,074				−0,698	66	III–V VI	−394,9
ΦNH_3^+	−0,422	−0,164[b]	0,013	0,031	0,074		0,330			68, 69	II–IV V–VI	−283,0
ΠH^+	0,040		0,100	0	0,180		0,200			65	II–IV V–VI	−227,6

[a]Charges $\pi + \sigma$.
[b]Charges π.
[c]Charges σ; Charges en électrons (charges nettes).

Numérotation des carbones : 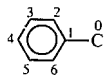

examinons les enthalpies de transfert relatives à la solvatation nous voyons que le terme $^s\delta\Delta H_c$ prend une importance beaucoup plus grande par rapport au terme $^s\delta\Delta H_i^\theta$, il devient du même ordre de grandeur, et, comme il est positif, l'energie nécessaire à la formation de la cavité est en partie compensée pour celle qui résulte de la modification des interactions solutés–solvants (fig. 2). Dans certains cas, cette compensation est totale, c'est le cas de l'aniline et de la pyridine dans les mélanges eau–urée; l'enthalpie de solvatation reste constante quand la teneur en cosolvant croît.

Il nous a paru intéressant d'étudier le rapport existant entre la répartition électronique dans les molécules et les ions et l'enthalpie standard d'interaction ΔH_i^θ des espèces en solution. Nous avons trouvé dans la littérature de nombreuses études théoriques donnant la répartition des charges sur les différents atomes; ces données sont consignées sur le tableau 6. Les valeurs de ces charges sont difficilement comparables entre elles quand elles ne viennent pas des mêmes auteurs parce que les méthodes de calcul sont en général différentes. Par contre les rapports de ces charges peuvent être comparés d'un auteur à l'autre. Les espèces étudiées sont des solutés mixtes, c'est à dire qui possèdent des groupements polaires (hydrophiles) et non polaires (hydrophobes). L'enthalpie d'interaction d'une molécule peut être considérée comme étant la somme de trois termes (71): l'enthalpie ΔH_{VDW} due aux interactions de van der Waals entre le soluté et le solvant, le terme ΔH_{LH} qui est l'enthalpie de formation de liaisons hydrogène entre ces deux entités et enfin le terme ΔH_{MS} dû à la modification de la structure du solvant par le soluté en excluant la formation de la cavité. Ce dernier terme est presque uniquement associé aux effets des groupes non polaires du soluté sur la structure du solvant; si ce dernier est l'eau ce sont des interactions hydrophobes. Nous avons donc :

$$\Delta H_i = \Delta H_{VDW} + \Delta H_{LH} + \Delta H_{MS}$$

Les types de liaison hydrogène qui peuvent se former entre l'eau et les molécules étudiées ici (72, 73) sont consignées ainsi que les enthalpies correspondantes dans le tableau 7. Dans les mélanges hydroorganiques il y a aussi possibilité de formation de liaisons hydrogène avec les molécules de cosolvant. Les enthalpies des liaisons hydrogènes sont faibles par rapport aux liaisons covalentes normales. Par exemple pour la liaison O...HOH l'enthalpie est environ 20 fois inférieure à celle de la liaison covalente O—H. Nous pouvons ajouter que plus l'electronégativité d'un atome est élevée plus son aptitude à former des liaisons hydrogène est grande. L'oxygène dont l'électronégativité est 3,5 dans l'échelle de Pauling donne des liaisons hydrogènes plus fortes que l'azote dont l'électronégativité est 3. Les enthalpies des différentes liaisons hydrogène rencontrées dans cette étude sont données dans le tableau 7.

Les deux atomes d'oxygène de l'acide acétique portent de fortes charges négatives et l'atome d'hydrogène du groupement OH une forte charge positive. Scheraga et coll. (62) ont montré que l'acide acétique forme en solution aqueuse des liaisons hydrogène avec deux molécules d'eau; ils ont écarté la structure cyclique avec une seule molécule de solvant. Ces liaisons s'établissent entre l'oxygène du carbonyle et un hydrogène de l'eau et entre l'hydrogène du groupement OH de l'acide et l'oxygène d'une molécule d'eau. Ces auteurs signalent aussi l'existence d'une liaison hydrogène relativement faible entre l'oxygène du groupement hydroxyle et une molécule d'eau. Dans l'eau, le terme ΔH_{MS}, dû aux interactions hydrophobes du groupement CH_3, peut être évalué à $-6\,kJ\,mol^{-1}$ ce qui est l'écart entre l'enthalpie d'hydratation de l'acide acétique et

Can. J. Chem. Downloaded from www.nrcresearchpress.com by 91.144.44.67 on 09/07/12
For personal use only.

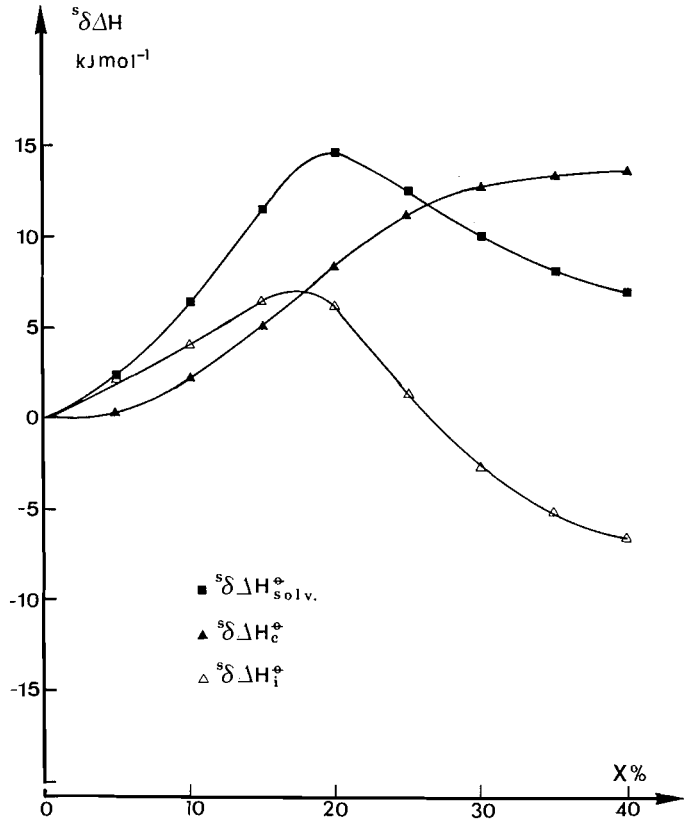

FIG. 2. Enthalpies de transfert pour la solvatation de l'aniline dans les mélanges eau – alcool *tert*-butylique à 25°C.

TABLEAU 7. Enthalpies standard des diverses liaisons hydrogènes

Type de liaison	$-\Delta H^0$ (kJ mol^{-1})
O—H...OH_2 type I ou O...HOH type III	21–29[a]
N—H...OH_2 type II	8–13[a]
N...HOH type IV	18–29[a]
ϕ...HOH type V ϕ...OH_2 type VI	$\cong 5$[b]

[a]Référence 74.
[b]Référence 75.

celle de l'acide formique (76). La somme des enthalpies de formation des trois liaisons hydrogènes et du terme ΔH_{VDW} est donc $\Delta H = -51$ kJ mol^{-1}.

En solution aqueuse la molécule d'acide benzoïque exerce un effet hydrophobe sur les molécules d'eau. Le groupement hydrophile COOH forme des liaisons hydrogène directes avec les molécules de solvant. Peut être existe-t-il aussi des liaisons de types V et VI. À l'inverse de ce qui se produit pour l'acide acétique la charge négative sur l'oxygène du carbonyle est plus importante que sur l'oxygène du groupement OH; ceci est dû à la présence du cycle, il y a «pompage» des électrons du cycle par l'oxygène du carbonyle. Le pouvoir accepteur de proton de cet oxygène est donc augmenté. Tout ceci se traduit par une enthalpie d'interaction relativement forte $\Delta H_i^{\theta} = -76{,}1$ kJ mol^{-1}, l'acide benzoïque est la molécule la plus «hydratée» de celles étudiées ici.

Le phénol par son groupement hydroxyle est à la fois donneur et accepteur de proton, il a donc la possibilité de se lier à deux molécules d'eau par liaison hydrogène. Le noyau exerce un effet hydrophobe et l'on peut envisager un processus de solvatation analogue à celui de l'acide benzoïque.

L'aniline possède une charge négative relativement forte sur l'azote et des hydrogènes chargés positivement. On peut donc envisager pour son «hydratation» une liaison du type N...HOH, deux liaisons du type NH...OH_2 et des liaisons des types V et VI. La présence du noyau provoque aussi des interactions hydrophobes. Toutes ces liaisons correspondent bien à un ΔH_i^{θ} d'environ -60 kJ mol^{-1}.

Del Bene (cité par la réf. 77) a évalué l'enthalpie ΔH_{LH} de liaison de la pyridine avec l'eau à $-19{,}7$ kJ mol^{-1} ce qui correspond à une liaison N...HOH faible. Il y a possibilité de formation de liaisons de type V et VI (-10 kJ mol^{-1}). La valeur de ΔH_i^{θ} étant de $-55{,}7$ kJ mol^{-1}, il reste -26 kJ mol^{-1} pour les interactions hydrophobes et les interactions de van der Waals.

Lors du transfert des molécules de l'eau aux solvants hydro-organiques nous constatons qu'elles ont un comportement différent suivant le cosolvant utilisé. Dans les mélanges eau – alcool *tert*-butylique (fig. 3) elles ont le comportement déjà décrit par de nombreux auteurs (1, 9, 13, 18, 30, 32, 58). Nous constatons que $^{s}\delta\Delta H_i^{\theta}$ est positif pour $0 < X < 25\%$ et passe par un maximum pour $X = 15\%$, ce qui veut dire que les solutés ont plus de difficultés à former des liaisons hydrogène avec l'eau que dans l'eau pure à cause d'une plus grande structuration du solvant. Pour $X > 25\%$ $^{s}\delta\Delta H_i^{\theta}$ est négatif, la structure du solvant est désorganisée et les solutés ont beaucoup plus de facilité pour former des liaisons hydrogène avec l'eau et l'alcool *tert*-butylique. Pour les mélanges eau–DMSO nous avons $^{s}\delta\Delta H_i^{\theta}$ négatif et croissant en valeur absolue ce qui veut dire que la formation de liaisons hydrogène est plus facile que dans l'eau. Ceci peut être interprété par le fait que le DMSO détruit les liaisons hydrogène existant entre les molécules d'eau pour participer à la structure du solvant et empêche les solutés hydrophobes de promouvoir des liaisons hydrogène entre les molécules d'eau dans leur voisinage (78). Il y a donc plus de molécules d'eau disponibles pour former des liaisons hydrogène avec le soluté et le DMSO peut donner lui aussi de telles liaisons par son oxygène. Dans les mélanges eau–acétone on constate aussi la croissance de l'enthalpie d'interaction avec la teneur en cosolvant mais la variation est moins rapide dans le domaine où X est inférieur à 20%. Nous proposons la même explication que pour les mélanges eau–DMSO (78). Dans les mélanges eau–urée l'enthalpie d'interaction croît aussi avec la teneur en cosolvant ce qui est normal puisque l'urée détruit la structure de l'eau et empêche la solvatation hydrophobe. Les molécules d'eau sont donc disponibles pour former des liaisons hydrogène avec les solutés. L'urée peut elle même donner de telles liaisons par ses groupements NH_2 et sa fonction carbonyle.

Les enthalpies de solvatation des ions organiques en solution aqueuse sont difficiles à interpréter. Chaque ion a une structure et une répartition des charges qui lui est propre et sa structure est en général complexe. Comme nous l'avons vu pour les molécules, l'enthalpie d'interaction est la somme de plusieurs termes. Pour les ions il faut ajouter aux trois termes déjà cités un quatrième ΔH_{ES} dû à la solvatation électrostatique et dans lequel est incluse l'électrostriction du solvant c'est à dire la diminution de son volume sous l'influence du champ électrique créé par la charge de l'ion.

Les cations se comportent comme des accepteurs d'électrons

Can. J. Chem. Downloaded from www.nrcresearchpress.com by 91.144.44.67 on 09/07/12
For personal use only.

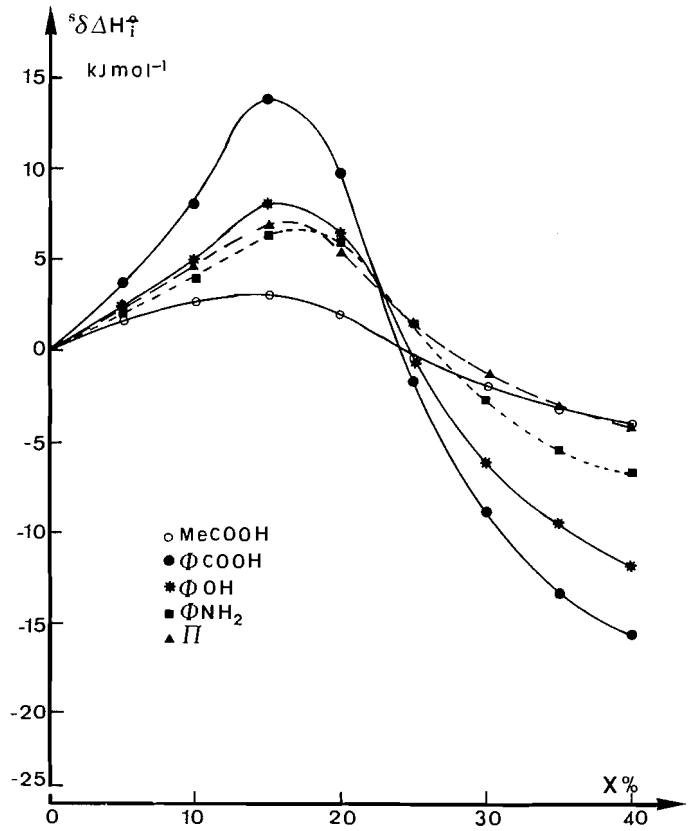

FIG. 3. Valeurs de transfert pour l'enthalpie d'interaction des acides et des amines dans les mélanges eau – alcool *tert*-butylique à 25°C.

vis à vis des atomes donneurs du solvant. Autour d'un cation BH^+ en solution aqueuse la configuration d'énergie minimum est celle dans laquelle les deux doublets électroniques libres de l'atome d'oxygène de l'eau sont orientés vers l'ion et forment une liaison «hydrogène ionique» (79) qui est plus une coordinence qu'une véritable liaison hydrogène (80). Les sphères de coordination des cations organiques sont en général mal définies. Les cations qui ont une grande variété de tailles ont des configurations qui s'adaptent elles-mêmes à la structure de l'eau environnante.

Les ions anilinium et pyridinium portent des charges positives sur les hydrogènes liés à l'azote. Ces hydrogènes peuvent donner des liaisons hydrogène ioniques avec les molécules d'eau. Dans ce cas le terme ΔH_{ES} est partagé entre l'enthalpie de formation de telles liaisons ΔH_{LHI} et l'électrostriction du solvant qui peut entrer dans le terme ΔH_{MS}. Jorgensen et Gao (81) ont évalué par la méthode de Monte Carlo l'importance des liaisons hydrogène ioniques dans l'hydratation des ions ammonium et méthylammonium. Leur étude montre que chaque hydrogène porté par l'azote est lié à 1,2 molécules d'eau et que chaque liaison hydrogène met en jeu une énergie de $-54{,}4$ kJ. Si nous faisons l'hypothèse qu'il en est de même pour les ions anilinium et pyridinium nous avons $\Delta H_{LHI} = -195{,}8$ kJ mol^{-1} pour le premier et $-65{,}3$ kJ mol^{-1} pour le second. Il reste donc pour les autres termes $\Delta H_{VDW} + \Delta H_{LH} + \Delta H_{MS}$, $-87{,}2$ kJ mol^{-1} pour l'ion anilinium et $-162{,}3$ kJ mol^{-1} pour l'ion pyridinium. Le terme ΔH_{LH} correspond ici a des liaisons entre le noyau aromatique et l'eau et peut-être aussi à des liaisons N...HOH si elles sont possibles.

Les anions ont des doublets électroniques à donner, ils sont solvatés par les solvants qui sont accepteurs de doublets. Ils forment aussi des liaisons hydrogène avec les solvants protiques. Autour des anions les hydrogènes des molécules d'eau qui portent des charges positives s'orientent vers l'ion. Dans cette situation les positions possibles des molécules d'eau les plus proches apparaissent plus étroitement dépendantes de la taille de l'ion qu'elles le sont pour les cations.

Les molécules d'eau tendent à orienter une de leur liaison O—H vers la charge négative de l'ion pour former une coordinence, elles ont ainsi la possibilité de former des liaisons hydrogène avec trois autres molécules d'eau (82). L'enthalpie d'hydratation des anions est toujours plus grande que celle des cations de même taille et de même charge. Verwey (83) explique cette différence par le fait que le centre de la charge positive du dipôle formé par la molécule d'eau est plus près de la surface que le centre de la charge négative et que l'interaction d'un ion négatif est donc plus forte que celle d'un ion positif.

L'anion acétate est un ion structuré, anisotrope, possédant deux sites négatifs équivalents, une polarisabilité et une électronégativité élevées. La structure bidentate n'existant pas en solution (81, 84) aqueuse, l'hydratation de cet ion peut être envisagée de la façon suivante (81) : liaison de molécules d'eau par coordinence sur chaque atome d'oxygène et fixation d'autres molécules d'eau par liaison hydrogène sur les précédentes. Jorgensen et Gao (81) évaluent à 3,3 le nombre de molécules d'eau liées à chacun des deux oxygènes de l'ion et l'énergie d'une liaison hydrogène ionique entre un oxygène et l'eau à $-57{,}0$ kJ. Donc pour l'ion acétate $\Delta H_{LHI} = -376{,}2$ kJ mol^{-1} et il reste $-29{,}7$ kJ mol^{-1} pour la somme des autres termes ΔH_{LH}, ΔH_{VDW} et ΔH_{MS}. Ces auteurs évaluent les interactions hydrophobes à environ -7 kJ mol^{-1}.

L'ion benzoate a aussi des charges négatives importantes équivalentes sur les oxygènes mais il est beaucoup plus gros que l'ion acétate ce qui peut géner l'approche des charges négatives par les molécules d'eau. La présence du cycle peut permettre la formation de liaisons hydrogène spécifiques et aussi provoquer un effet hydrophobe sur les molécules de solvant. L'ion benzoate est un peu moins bien «hydraté» que l'ion acétate.

L'ion phénate a une charge négative importante sur l'oxygène mais aussi une délocalisation de cette charge sur le cycle. L'enthalpie d'interaction de cet ion étant à peu près égale à celle de l'ion benzoate, nous pouvons donc penser que la diminution d'enthalpie correspondant à l'absence d'un deuxième oxygène est compensée par une plus grande importance de l'effet du cycle sur l'hydratation.

Nous voyons sur la figure 4 comment se comportent les divers ions faisant l'objet de cette étude lorsqu'on ajoute de l'alcool *tert*-butylique à l'eau. Nous pouvons séparer ce graphe en trois zones. Dans la première ($X < 12{,}5\%$) l'addition d'alcool ne produit aucun changement important dans les interactions entre l'eau et les ions. Dans la seconde ($12{,}5 < X < 30\%$) nous rencontrons les maximums (cations) et les minimums (anions) de $^s\delta\Delta H_i^\theta$ déjà rencontrés pour des systèmes chimiques voisins par de nombreux auteurs et expliqués par une structure particulière du solvant. Dans la troisième zone ($X > 30\%$) quand la teneur en alcool croît l'enthalpie d'interaction devient de plus en plus négative pour les cations et de moins en moins négative et même positive pour les anions. Le lecteur se reportera à la publication de Juillard (58) pour avoir une analyse plus complète de la solvatation dans les mélanges eau – alcool *tert*-butylique riches en eau.

Les mélanges eau–DMSO se comportent jusqu'à $X = 35\%$ comme des mélanges fortement structurés et au delà comme le

Can. J. Chem. Downloaded from www.nrcresearchpress.com by 91.144.44.67 on 09/07/12
For personal use only.

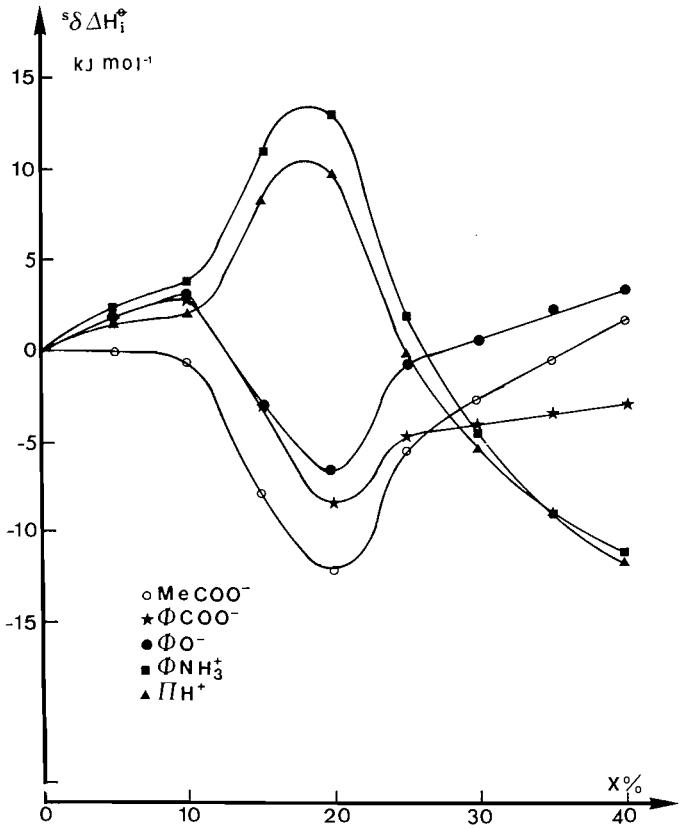

FIG. 4. Valeurs de transfert pour l'enthalpie d'interaction des anions et des cations dans les mélanges eau – alcool *tert*-butylique à 25°C.

DMSO pur, solvatant plus fortement les cations que les anions et davantage les petits cations que les gros.

Dans les mélanges eau–acétone et eau–urée nous ne pouvons étudier la solvatation que de couples d'ions. Les interactions y sont plus fortes que dans l'eau et leur force croît avec X. L'étude des couples $MeCOO^-,H^+$ et BH^+,H^+ nous montre que c'est dans les mélanges eau–urée que la force des interactions augmente le plus vite avec la teneur en cosolvant.

VI. Conclusions

Les valeurs des enthalpies d'interaction pour les molécules, les ions et les couples d'ions en solution aqueuse dépendent à la fois de la structure des espèces en solution et de la nature du solvant.

Dans le cas des molécules les interactions soluté–solvant avec un solvant protique sont en majorité des liaisons hydrogène mais il peut exister aussi des interactions hydrophobes. Les enthalpies d'interaction sont relativement faibles (−56 à −76 kJ mol^{-1}).

Pour les ions la solvatation est assurée essentiellement par des «liaisons hydrogène ioniques» qui sont des coordinences. Il peut exister aussi des liaisons hydrogène et des interactions hydrophobes. Les enthalpies d'interaction sont grandes, leurs valeurs sont situées entre −395 et −407 kJ mol^{-1} pour les anions et entre −228 et −283 kJ mol^{-1} pour les cations.

En ce qui concerne l'influence des solvants sur la solvatation, nos observations sont bien en accord avec ce que nous connaissons déjà sur eux. L'alcool *tert*-butylique organise fortement la structure de l'eau pour les teneurs comprises entre 12,5 et 25%. Le DMSO et l'acétone en participant à la structuration du solvant et en empêchant la solvatation hydrophobe permettent une solvatation plus importante des molécules par liaison hydrogène. On obtient le même résultat avec l'urée qui détruit la structure de l'eau et empêche donc aussi la solvatation hydrophobe.

Remerciements

Nous remercions Monsieur le Professeur Jean-Pierre Morel pour les conseils qu'il nous a donné pour la rédaction de ce mémoire.

1. H. GILLET. J. Chim. Phys. **84**, 475 (1987).
2. L. P. HAMMETT. Physical organic chemistry. 2^e ed. McGraw–Hill, New York. 1970.
3. E. GRUNWALD et S. WINSTEIN. J. Am. Chem. Soc. **70**, 846 (1948).
4. J. H. HILDEBRAND, J. M. PRAUSNITZ et R. L. SCOTT. Regular and related solutions. Van Nostrand Reinhold, New York. 1970.
5. M. E. KOSOWER. An introduction to physical organic chemistry. Wiley, New York. 1968.
6. J. JUILLARD et J. P. MOREL. C. Rend. Acad. Sci. Paris, C, **277**, 825 (1973).
7. M. LUCAS et A. FEILLOLAY. Bull. Soc. Chim. Fr. **4**, 1267 (1970).
8. M. LUCAS et A. FEILLOLAY. J. Phys. Chem. **75**, 2330 (1971).
9. H. GILLET, L. AVEDIKIAN et J. P. MOREL. Can. J. Chem. **53**, 455 (1975).
10. J. JUILLARD, J. P. MOREL et L. AVEDIKIAN. J. Chim. Phys. **69**, 787 (1972).
11. H. C. DICKINSON. Natl. Bur. Standards (U.S.) Bull. **11**, 189 (1915).
12. J. M. STURTEVANT. *Dans* Physical methods of organic chemistry. Vol. 1. 3^e ed. *Éditeur*: A. Weissberger, Interscience Publishers, New York, London. 1959. Part 1.
13. Y. POINTUD, J. P. MOREL et J. JUILLARD. J. Phys. Chem. **80**, 2381 (1976).
14. J. KONICEK et I. WADSÖ. Acta Chem. Scand. **25**, 1541 (1971).
15. I. WADSÖ. Acta Chem. Scand. **16**, 479 (1962).
16. E. M. ARNETT et J. V. CARTER. Cités dans la référence 14.
17. R. AVEYARD et R. W. MITCHELL. Trans. Faraday Soc. **64**, 1757 (1968).
18. L. AVEDIKIAN, J. JUILLARD, J. P. MOREL et M. DUCROS. Thermochim. Acta, **6**, 283 (1973).
19. L. P. FERNANDEZ et L. G. HEPLER. J. Phys. Chem. **63**, 110 (1959).
20. L. P. FERNANDEZ et L. G. HEPLER. J. Am. Chem. Soc. **81**, 1783 (1959).
21. J. H. PARSONS, C. H. ROCHESTER et C. E. C. WOOD. J. Chem. Soc. (B), 533 (1971).
22. N. NICHOLS et I. WADSÖ. J. Chem. Thermodyn. **7**, 329 (1975).
23. E. M. ARNETT, J. J. BURKE, J. V. CARTER et C. F. DOUTY. J. Am. Chem. Soc. **94**, 7 (1972).
24. W. J. O'HARA, H. C. KO, M. N. ACKERMAN et L. G. HEPLER. J. Phys. Chem. **71**, 3107 (1967).
25. L. SACCONI, P. PAOLETTI et M. CIAMPOLINI. J. Am. Chem. Soc. **82**, 3828 (1960).
26. G. H. PARSONS et C. H. ROCHESTER. J. Chem. Soc. Faraday Trans. 1, **71**, 1069 (1975).
27. C. H. ROCHESTER et S. A. SCLOSA. J. Chem. Soc. Faraday Trans. 1, **77**, 575 (1981).
28. F. RODANTE, F. RALLO et P. FIORDIPONTI. Thermochim. Acta, **9**, 269 (1974).
29. V. B. PARKER. Thermal properties of aqueous univalent electrolytes. NSRDS, NBS 2, Washington, DC. 1965.
30. N. DOLLET et J. JUILLARD. J. Solution Chem. **5**, 77 (1976).
31. Y. POINTUD, J. JUILLARD, J. P. MOREL et M. DUCROS. Thermochim. Acta, **8**, 423 (1974).
32. Y. POINTUD et J. JUILLARD. J. Chem. Soc. Faraday Trans. 1, **73**, 1907 (1977).
33. R. FUCHS et C. P. HAGAN. J. Phys. Chem. **77**, 1797 (1973).

Can. J. Chem. Downloaded from www.nrcresearchpress.com by 91.144.44.67 on 09/07/12
For personal use only.

34. B. G. Cox, R. Natarajan et W. E. Waghorne. J. Chem. Soc. Faraday Trans. 1, **75**, 1780 (1979).
35. I. Mekjavic' et I. Tominic'. Electrochem. Acta, **22**, 99 (1977).
36. K. K. Kundu et K. Mazumdar. J. Chem. Soc. Faraday Trans. 1, **69**, 806 (1973).
37. K. K. Kundu et K. Mazumdar. J. Chem. Soc. Faraday Trans. 1, **71**, 1422 (1975).
38. M. Berthelot. Ann. Chim. Phys. **21**, 355 (1890).
39. J. S. Rowlinson. Trans. Faraday Soc. **47**, 120 (1951).
40. B. E. Conway. J. Solution Chem. **7**, 721 (1978).
41. J. Konicek et I. Wadsö. Acta Chem. Scand. **24**, 2612 (1970).
42. C. G. De Kruif et H. A. J. Oonk. J. Chem. Thermodyn. **11**, 287 (1979).
43. M. Davies et J. I. Jones. Trans. Faraday Soc. **50**, 1042 (1954).
44. R. J. L. Andon, D. P. Biddiscombe, J. D. Cox, R. Handley, D. Harrop, E. F. G. Herington et J. F. Martin. J. Chem. Soc. 5246 (1960).
45. W. E. Hatton, D. L. Hildebrand, G. C. Sinke et D. R. Stull. J. Chem. Eng. Data, **7**, 229 (1962).
46. J. P. McCullough, D. R. Douslin, J. F. Messerly, J. A. Hossenlopp, T. C. Kincheloe et G. Waddington. J. Am. Chem. Soc. **79**, 4289 (1957).
47. H. Reiss. Adv. Chem. Phys. **9**, 1 (1964).
48. E. Wilhelm et R. Battino. J. Chem. Phys. **55**, 4012 (1971).
49. T. B. McMahon et P. Kebarle. J. Am. Chem. Soc. **99**, 2222 (1977).
50. E. M. Arnett, F. M. Jones III, M. Taagepera, W. G. Henderson, J. L. Beauchamp, D. Holtz et R. W. Taft. J. Am. Chem. Soc. **94**, 4724 (1972).
51. D. H. Aue, H. M. Webb et M. T. Bowers. J. Am. Chem. Soc. **94**, 4726 (1972).
52. W. G. Henderson, M. Taagepera, D. Holtz, R. T. McIver, Jr., J. L. Beauchamp et R. W. Taft. J. Am. Chem. Soc. **94**, 4728 (1972).
53. J. P. Briggs, R. Yamdagni et P. Kebarle. J. Am. Chem. Soc. **94**, 5128 (1972).
54. R. Yamdagni et P. Kebarle. J. Am. Chem. Soc. **95**, 4050 (1973).
55. R. Yamdagni et P. Kebarle. Can. J. Chem. **52**, 861 (1974).
56. W. A. Adams et K. J. Laidler. Can. J. Chem. **45**, 123 (1967).
57. N. Desrosiers et J. E. Desnoyers. Can. J. Chem. **54**, 3800 (1976).
58. J. Juillard. J. Chem. Soc. Faraday Trans. 1, **78**, 43 (1982).
59. Y. Marcus. J. Chem. Soc. Faraday Trans. 1, **83**, 339 (1987).
60. C. Treiner. Can. J. Chem. **55**, 682 (1977).
61. N. Morel-Desrosiers et J. P. Morel. J. Solution Chem. **8**, 579 (1979).
62. S. Kim, M. S. Jhon et H. A. Scheraga. J. Phys. Chem. **92**, 7216 (1988).
63. J. C. Baum et D. S. McClure. J. Am. Chem. Soc. **101**, 2340 (1979).
64. G. R. Howe. J. Chem. Soc. (B), 984 (1971).
65. M. L. Bailey et J. P. Bailey. Theor. Chim. Acta, **16**, 303 (1970).
66. K. Nishimoto et L. S. Forster. J. Phys. Chem. **72**, 914 (1968).
67. W. J. Hehre, L. Radom et J. A. Pople.J. Am. Chem. Soc. **94**, 1496 (1972).
68. W. F. Reynolds, T. A. Modro et P. G. Mezey. J. Chem. Soc. Perkin Trans. 2, 1066 (1977).
69. K. D. Summerhays, S. K. Pollack, R. W. Taft et W. J. Hehre. J. Am. Chem. Soc. **99**, 4585 (1977).
70. C. Nagata, T. Hasegawa et S. Tanaka. J. Chem. Soc. Jpn. 1087 (1977).
71. C. V. Krishnan et H. L. Friedman. J. Phys. Chem. **73**, 1572 (1969).
72. P. L. Huyskens et J. J. Tack. J. Phys. Chem. **79**, 1654 (1975).
73. A. Gomez, J. Mullens et P. Huyskens. J. Phys. Chem. **76**, 4011 (1972).
74. A. Julg. Chimie théorique. Dunod, Paris. 1964.
75. D. Joesten. J. Chem. Educ. **59**, 362 (1982).
76. F. Franks et D. S. Reid. *Dans* Water, a comprehensive treatise. Vol. 2. *Éditeur* : F. Franks. Plenum Press, New York, London. 1973. Chap. 5.
77. E. M. Arnett, B. Chawla, L. Bell, M. Taagepera, W. J. Hehre et R. W. Taft. J. Am. Chem. Soc. **99**, 5729 (1977).
78. M. J. Mastroianni, M. J. Pikal et S. Lindenbaum. J. Phys. Chem. **76**, 3050 (1972).
79. M. Meot-Ner (Mautner). J. Am. Chem. Soc. **106**, 1257 (1984).
80. Y. Marcus. Ion solvation. John Wiley, New York. 1985.
81. W. L. Jorgensen et J. Gao. J. Phys. Chem. **90**, 2174 (1986).
82. J. L. Kavanau. Water and solute–water interactions. Holden-Day, San Francisco, London. 1964.
83. E. J. W. Verwey. Recl. Trav. Chim. Pays-Bas, **61**, 127 (1942).
84. J. Gao, D. S. Garner et W. L. Jorgensen. J. Am. Chem. Soc. **108**, 4784 (1986).

Can. J. Chem. Downloaded from www.nrcresearchpress.com by 91.144.44.67 on 09/07/12
For personal use only.

Reaction mechanism of 1,2-hydrogen migration of hydrogen peroxide

ENRIC BOSCH, JOSÉ M. LLUCH,[1] AND JUAN BERTRÁN
Departament de Química, Universitat Autònoma de Barcelona, 08193 Bellaterra (Barcelona), Spain

Received July 1, 1989

ENRIC BOSCH, JOSÉ M. LLUCH, and JUAN BERTRÁN. Can. J. Chem. **68**, 666 (1990).

The 1,2-hydrogen migration of hydrogen peroxide has been investigated by *ab initio* methods and the Intrinsic Reaction Coordinate (IRC) has been constructed. An analysis of the evolution of the electron distribution along the reaction path has shown that the shifting hydrogen behaves as a proton. This transferring proton polarizes the O—O bond of the hydrogen peroxide that becomes broken at the transition state. If a water molecule is allowed to participate in the reaction, the energy barrier is noticeably lowered, this water molecule acting as a bifunctional catalyst.

Key words: 1,2-hydrogen migration, hydrogen peroxide, proton transfer, bifunctional catalyst, Intrinsic Reaction Coordinate.

ENRIC BOSCH, JOSÉ M. LLUCH et JUAN BERTRÁN. Can. J. Chem. **68**, 666 (1990).

Faisant appel à des méthodes *ab initio*, on a étudié la migration-1,2 d'hydrogène dans le peroxyde d'hydrogène et on a construit la Coordonnée Réactionnelle Intrinsèque (CRI). Une analyse de l'évolution de la distribution électronique en fonction de l'évolution de la réaction a permis de démontrer que l'hydrogène qui se déplace se comporte comme un proton. Le proton qui migre polarise la liaison O—O du peroxyde d'hydrogène et elle se brise dans l'état de transition. Si une molécule d'eau peut participer à la réaction, la barrière d'énergie est considérablement abaissée; cette molécule d'eau agit comme un catalyseur bifonctionnel.

Mots clés : migration-1,2 d'hydrogène, peroxyde d'hydrogène, transfert de proton, catalyseur bifonctionnel, Coordonnée Réactionnelle Intrinsèque.

[Traduit par la revue]

I. Introduction

Hydrogen-transfer reactions are a crucial step in many fundamental chemical and biochemical processes (1, 2). The elucidation of the actual nature of the transferring hydrogen is essential for understanding the mechanism of these reactions. As the reaction proceeds, very different electron rearrangement patterns take place depending on whether a hydride, an atomic hydrogen radical, or a proton is transferred.

Recently the 1,2-hydrogen migration of acetylene to form vinylidene has been studied theoretically (3) by an *ab initio* method and localized molecular orbital analysis. It was found that the shifting hydrogen behaves as a hydride. An interesting question is whether the nature of the migrating hydrogen depends on the identity of the hydrogen-donor and hydrogen-acceptor atoms or not. For this reason we deal in this paper with the 1,2-hydrogen migration between oxygen atoms, which are more electronegative than the carbon atoms. To this purpose we have chosen the simplest process of this type as a model: the intramolecular hydrogen transfer in hydrogen peroxide, which is in this respect an analogous system to acetylene, but involving oxygen atoms. In addition we have also investigated whether one water molecule can intervene in this process, in this way modifying the gas phase reaction mechanism. It is worthy of note that several hydrogen transfer reactions in which water molecules noticeably alter the molecular mechanism have been previously described (4–13).

From the analysis of the results obtained in this work we expect to understand how the electron reorganization takes place as the 1,2-hydrogen shift progresses. Furthermore, it is well known that H_2O_2 decomposes into water and molecular oxygen in the presence of an adequate homogeneous or heterogeneous catalyst. However, in the absence of catalyst hydrogen peroxide is stable indefinitely at room temperature (14). One can observe that the reaction proposed in this work could constitute one of the possible routes of decomposition into water and atomic oxygen, which could recombine later to form molecular oxygen. The results obtained will enable us to assess the feasibility of that process.

The organization of this paper is as follows. In the next section the theoretical method is described. The 1,2-hydrogen migration of hydrogen peroxide in the gas phase is studied in Sect. III. The effect of adding one water molecule is examined in Sect. IV. Finally, our principal conclusions are summarized in Sect. V.

II. Theoretical method

Ab initio self-consistent field (SCF) calculations have been carried out with the GAUSSIAN 86 series of programs (15), using the triply split valence basis set 3-21+G (16, 17), which contains a diffuse *sp* shell on atoms other than hydrogen.

All the geometrical parameters have been completely optimized at each stage of the hydrogen transfers. Geometry optimization and direct location of stationary points have been done with the Schlegel gradient optimization algorithm (18). Analytical second derivatives of the energy with respect to the Cartesian coordinates (19) were computed to test the nature of each stationary point: no negative eigenvalue for an equilibrium structure and one negative eigenvalue for a transition state.

Thermodynamic magnitudes were also computed by using the partition functions as provided by the statistical thermodynamic formulas within the ideal gas, rigid rotor, and harmonic oscillator models (20) as implemented in the GAUSSIAN 86 package. A pressure of 1 atm (101.3 kPa) and a temperature of 298.15 K were assumed in the calculations. The second derivatives of the energy were used for the determination of vibrational frequencies. For transition states the imaginary frequency is neglected in the thermodynamic evaluation.

To test the effect of expanding the basis sets, the energies of the stationary points were recalculated using 6-31+G and 6-31+G (D,P) basis sets, the 3-21+G geometries being kept unchanged. Moreover the influence of correlation energy was determined by using the Møller–Plesset perturbation theory to second (MP2) and third orders (MP3) (21).

Very useful information about the reaction mechanism can

[1]Author to whom correspondence may be addressed.

Printed in Canada / Imprimé au Canada

Can. J. Chem. Downloaded from www.nrcresearchpress.com by 88.85.125.76 on 09/07/12
For personal use only.

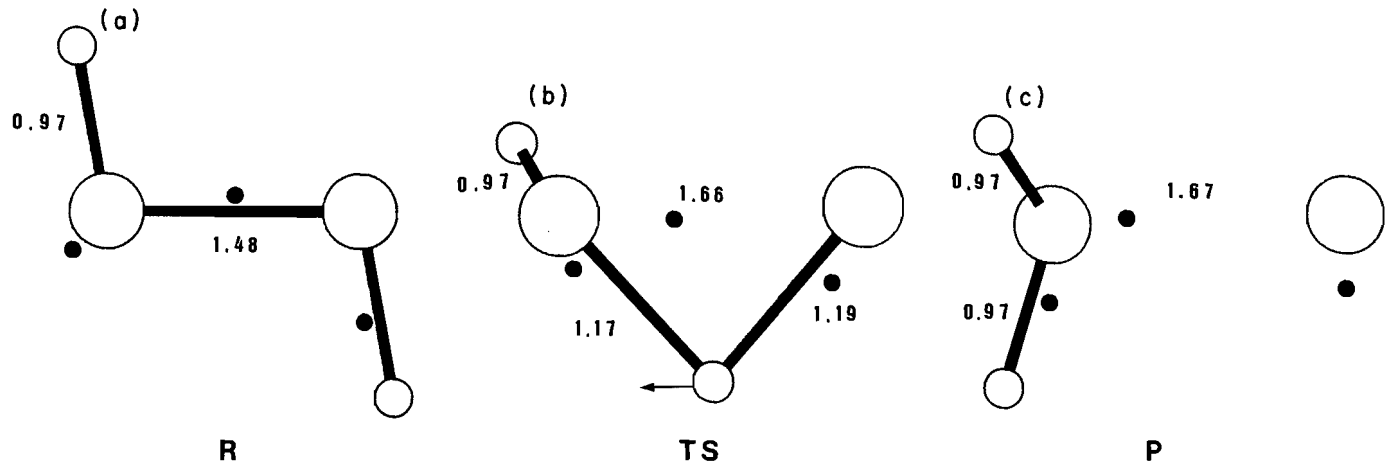

FIG. 1. Geometries of the reactant (R), transition state (TS), and product (P) for the 1,2-hydrogen migration of hydrogen peroxide in the gas phase. The arrow in the transition state structure indicates the transition vector. The positions of the three centroids of charge involved directly in the changing bonds have been marked by means of dots.

be obtained by following the evolution of the geometrical and electronic parameters of the system along the reaction path. To do this we have constructed the Intrinsic Reaction Coordinate (IRC) (22–24). The IRC has been computed with the GAMESS program (25), going downhill from the transition state in mass-weighted Cartesian coordinates (26, 27). The unique mode with imaginary frequency determines the starting direction away from the transition state. Assuming the harmonic approximation, we choose the initial step size Δs that produces the appropriate energy lowering $k(\Delta s)^2/2$, where k is the negative force constant associated with the imaginary frequency. Then the IRC is followed, taking successive very small steps in the direction of the negative gradient, which is equivalent to the Euler method. An initial energy lowering of 0.0005 hartrees and then successive steps of $\Delta s = 0.05$ amu$^{1/2}$ bohr have been used for both hydrogen transfer reactions.

III. 1,2-Hydrogen migration of hydrogen peroxide in gas phase

The geometries of the hydrogen peroxide, transition state, and product localized on the 3-21+G potential energy hypersurface are depicted in Fig. 1. The bond distances of the hydrogen peroxide agree well with the experimental values (28, 29) (1.475 and 0.95 Å for O—O and O—H bonds respectively). However, a dihedral angle of 180° corresponding to the *trans* conformation is obtained here, while it is known that in the gas phase the H_2O_2 adopts a skew configuration with a dihedral equilibration angle of 111.5° (infrared). This dihedral angle is particularly sensitive to the surroundings as values spanning the complete range from 90° to 180° have been found for various solid phases containing molecular H_2O_2 (28). Since the experimental (28, 30) *trans* barrier height is only 1.1 kcal/mol, we think that this discrepancy will not affect significantly the main results of the present work.

The transition state is nonplanar, both bond distances from the transferring hydrogen to the oxygen donor and the oxygen acceptor atoms being very similar. For this structure we have also represented the eigenvector associated with the imaginary frequency (1991i cm^{-1}), which indicates the direction of the reaction coordinate at this point. One can see that it corresponds completely to the hydrogen transfer, the rest of the atoms remaining fixed. Finally, the product is also nonplanar, both hydrogen atoms being bonded to the same oxygen atom. As will be mentioned later, the electronic distribution in this product suggests that it can dissociate to a singlet oxygen atom and a water molecule. It should be noted here that a multireference wave function would be needed to describe a free singlet oxygen atom. However, since the product of the hydrogen migration is only a precursor of a singlet oxygen atom, the RHF + MPn level of calculation is expected to be suitable to characterize the essential features of the hydrogen shift in the hydrogen peroxide.

TABLE 1. Classical potential energy,[a] enthalpy,[a] entropy,[b] and free-enthalpy[a] barriers for the forward and backward 1,2-hydrogen migration of hydrogen peroxide in the gas phase

	Forward	Backward
$\Delta E^{\ddagger}$ (3-21+G//3-21+G)	52.1	28.8
$\Delta E^{\ddagger}$ (6-31+G//3-21+G)	55.4	34.1
$\Delta E^{\ddagger}$ (6-31+G (D,P)//3-21+G)	58.2	21.9
$\Delta E^{\ddagger}$ (MP2/6-31+G//3-21+G)	49.0	7.9
$\Delta E^{\ddagger}$ (MP2/6-31+G (D,P)//3-21+G)	51.3	−4.8
$\Delta E^{\ddagger}$ (MP3/6-31+G//3-21+G)	53.5	16.7
$\Delta E^{\ddagger}$ (MP3/6-31+G (D,P)//3-21+G)	55.2	3.8
$\Delta H^{\ddagger}$ (3-21+G)	48.3	25.3
$\Delta S^{\ddagger}$ (3-21+G)	−0.9	−0.8
$\Delta G^{\ddagger}$ (3-21+G)	48.6	25.6

[a]In kcal/mol.
[b]In cal/(mol K).

Table 1 presents the classical potential energy, enthalpy, entropy, and free-enthalpy barriers for the forward and backward reactions obtained at different levels of calculation. The first row shows the classical potential energy barrier obtained at the 3-21+G level, the stationary points having been localized on the 3-21+G potential energy hypersurface. The values of the classical potential energy barriers recalculated using larger basis sets and then including electron correlation, the 3-21+G geometries being kept unchanged, are exhibited in the second to the seventh rows. It should be remembered that the classical potential energy barrier does not contain the zero-point vibrational energy (ZPE). Finally, the last three rows reflect the enthalpy, entropy, and free-enthalpy barriers computed at the 3-21+G level.

The first thing one can observe in Table 1 is that the energy barrier for the forward reaction is very high at all levels of

Can. J. Chem. Downloaded from www.nrcresearchpress.com by 88.85.125.76 on 09/07/12
For personal use only.

Can. J. Chem. Downloaded from www.nrcresearchpress.com by 88.85.125.76 on 09/07/12
For personal use only.

TABLE 2. 3-21+G IRC for the 1,2-hydrogen migration of hydrogen peroxide in the gas phase. O and O′ stand for the hydrogen-donor and hydrogen-acceptor oxygen atoms respectively. H denotes the transferring hydrogen

Point	s^a	Energy^b	R(O—O′)^c	R(O—H)^c	R(O′—H)^c
R		0.0	1.48	0.97	1.91
50	−2.5	0.2	1.48	0.97	1.92
32	−1.6	5.0	1.56	0.97	1.84
25	−1.3	12.6	1.60	0.98	1.72
17	−0.9	25.8	1.63	0.99	1.55
10	−0.5	39.8	1.64	1.04	1.39
TS	0.0	52.1	1.66	1.19	1.17
6	0.3	48.1	1.67	1.33	1.06
15	0.8	38.4	1.69	1.55	0.99
19	1.0	34.4	1.69	1.65	0.98
27	1.4	28.2	1.69	1.85	0.97
37	1.9	24.1	1.68	2.07	0.97
P		23.4	1.67	2.18	0.97

[a]In amu$^{1/2}$ bohr.
[b]Relative energy with respect to reactant in kcal/mol.
[c]In Angstroms.

calculation, as is also the case for the 1,2-hydrogen migration of acetylene (3). Expansion of the basis set and the introduction of electron correlation, respectively, slightly increases and decreases the barrier height. The effect of electron correlation is especially important for the backward reaction, the energy barrier being very small at the highest level of calculation. As expected, for all cases the MP2 level tends to overdo the electron correlation effect. Furthermore, it is noted that the reaction going from the hydrogen peroxide to the product is clearly endothermic. As a consequence of the trends of the energy barriers described above, the positive value of the energy reaction becomes very high at the MP3/6-31+G (D,P)//3-21+G level. Finally, regarding the thermodynamic properties, the 3-21+G enthalpy and free-enthalpy barriers for both the direct and the reverse reactions at 298.15 K are somewhat lower than the classical 3-21+G potential energy barriers at 0 K, mainly due to the fact that the ZPE at the transition state is smaller than that corresponding to both minima.

We have built up the 3-21+G IRC starting from the transition state (TS) and going to both the hydrogen peroxide (R) and the product (P) in order to follow the evolution of the reaction along the reaction path. The distance measured along the IRC is denoted by s, whose units are amu$^{1/2}$ bohr. The transition state is located at $s = 0$, and negative or positive values of s indicate the reactant or product region of the reaction respectively. The relative energies with respect to the reactant and the most relevant bond distances at selected points along the IRC are given in Table 2. The points have been numbered in both directions starting from the transition state, which is considered as point 0. Hydrogen-donor and hydrogen-acceptor oxygen atoms are respectively denoted by O and O′. Hereafter in this section H denotes the transferring hydrogen.

On the basis of the evolution of the geometrical parameters along the IRC one can say that the reaction takes place in three phases. Firstly, the O—O′ bond distance is lengthened while the O—H bond distance remains nearly fixed. The accompanying decrease in the O′—H bond distance arises from the diminution of the HOO′ angle. This phase finishes approximately at $s = -0.9$, requiring about 26 kcal/mol, one half of the energy barrier. In a second phase both oxygen atoms separate only a little more, while the O—H and O′—H bond distances are respectively lengthened and shortened in such a way that both become very similar at the transition state. One can consider that this second phase concludes at $s = 0.8$, when the new O′—H bond is almost completely formed. Finally, the third phase consists essentially in the variation of the OO′H angle so that the transferred hydrogen can attain its final position at the product. Notice that a slight OO′ bond contraction occurs in this period.

To analyze the electron-density rearrangement that takes place along the reaction path, a study of the topology of the total electronic charge density $\rho(\boldsymbol{r})$, according to Bader's methodology (31), has been performed. Figure 2 presents the isodensity contour plots of $\rho(\boldsymbol{r})$ in the plane defined by the transferring hydrogen and the oxygen atoms at selected points along the IRC. The positions of the bond critical points have been marked by means of dots. A bond critical point is a minimum along a single pair of gradient paths, which originated at the critical point and end one at each of the nuclei of the neighboring atoms, but is a maximum with respect to any orthogonal displacement. The existence of such a point indicates that the neighboring atoms are bonded to one another.

It can be seen in Fig. 2 that on going from the hydrogen peroxide to the transition state the O—O′ bond is weakened and becomes broken at the transition state, where the H atom is bonded to both oxygen atoms. Then when the H atom has been already transferred, the O—O′ bond is recovered. The product could be envisaged as an electrophilic singlet oxygen atom O nucleophilically solvated by a water molecule, the charge transfer being of 0.24 au towards the singlet O.

At this point the actual nature of the transferring hydrogen should be clarified. The net charge arising from a Mulliken population analysis on the migrating hydrogen changes from +0.47 (hydrogen peroxide) through +0.55 (transition state) to +0.52 (product). Note that the net charge peaks at the transition state. These values suggest that the moving hydrogen behaves as a proton. A localized molecular orbital analysis based on the localization method of Foster–Boys (32) confirms this idea. The localized molecular orbitals have been obtained and the positions of the centroids of negative charge associated with them have been determined. Given that the hydrogen peroxide is a closed-shell molecule containing 18 electrons, 9 centroids are found. The positions of the most relevant centroids have been marked by a dot in Fig. 1. For the sake of simplicity we have shown only the three centroids involved directly in the changing bonds. The main feature is that no centroid exists near the moving hydrogen at the transition state. In particular, one can see that the centroid related to the initial O—H bond does not follow the hydrogen atom as the reaction proceeds. Therefore one can state that, in effect, a 1,2-proton transfer takes place. This conclusion is consistent with the evolution of the $\rho(\boldsymbol{r})$ observed in Fig. 2. When the proton moves, an important polarization of the bonds that lie in the proximity of the proton trajectory occurs. As a consequence, the O—O′ bond is broken at the transition state, the electron density shifting towards the proton. Afterwards, when the proton is away from the O—O′ bond region, this bond is somewhat restored. The appearance of intense electron density redistributions accompanying a proton transfer has been already described in other works (33–36).

IV. 1,2-Hydrogen migration in the water – hydrogen peroxide complex

In the presence of a water molecule the 1,2-hydrogen migration takes place through a double proton exchange. The

Can. J. Chem. Downloaded from www.nrcresearchpress.com by 88.85.125.76 on 09/07/12
For personal use only.

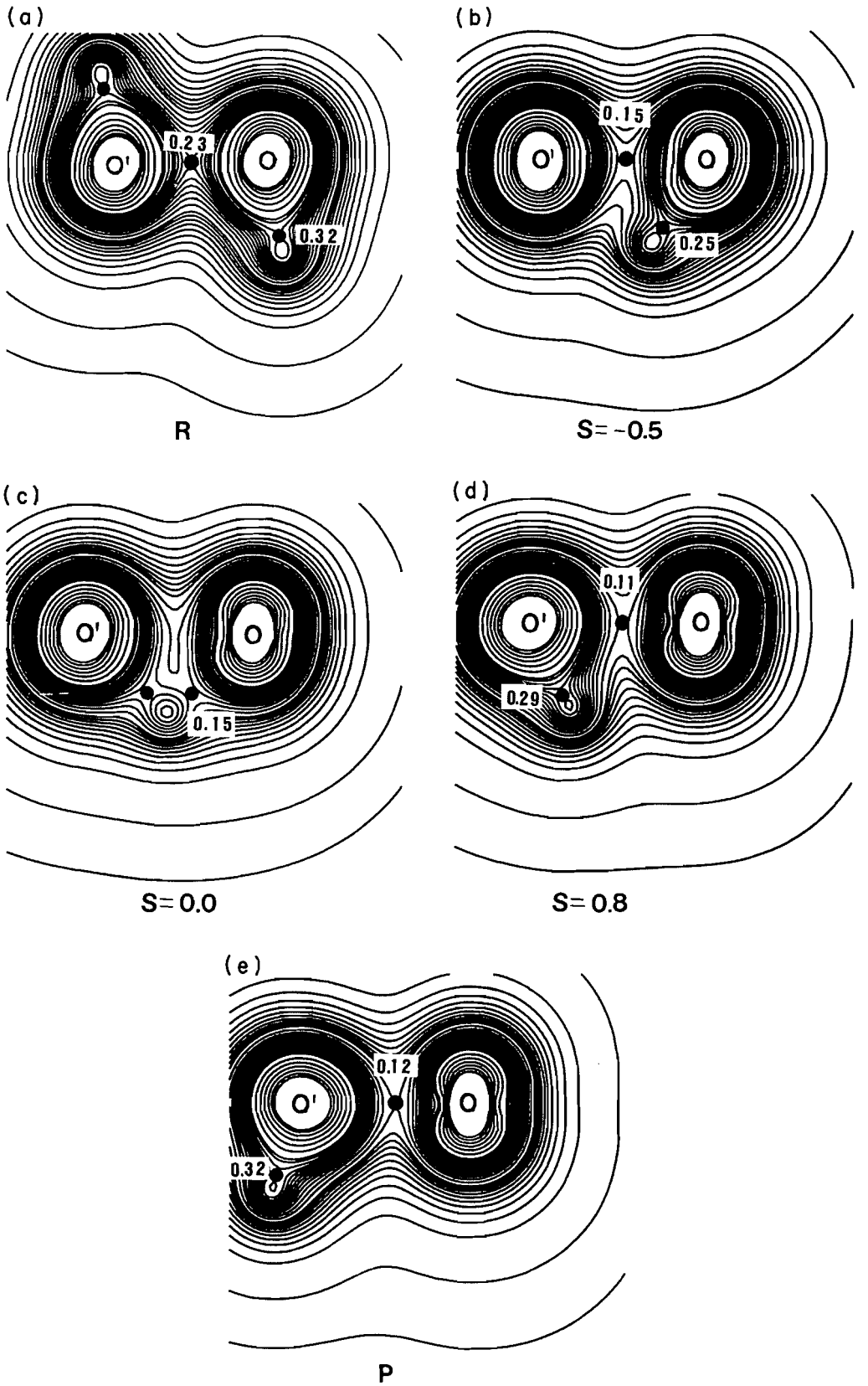

FIG. 2. Isodensity contour plots of $\rho(r)$ in the plane defined by the transferring hydrogen and the oxygen atoms at selected points along the IRC. O and O′ stand for the proton-donor and proton-acceptor oxygen atoms respectively.

reaction can be represented in Scheme 1, where we have introduced the numbering that will be used in this section. The structures of the reactant, transition state, and product localized on the 3-21+G potential energy hypersurface are shown in Fig. 3. The reactant corresponds to a hydrogen peroxide solvated by a water molecule. Only a transition state has been found, indicating that the reaction proceeds in just one step. At this transition state both hydrogen atoms 4 and 5 are being

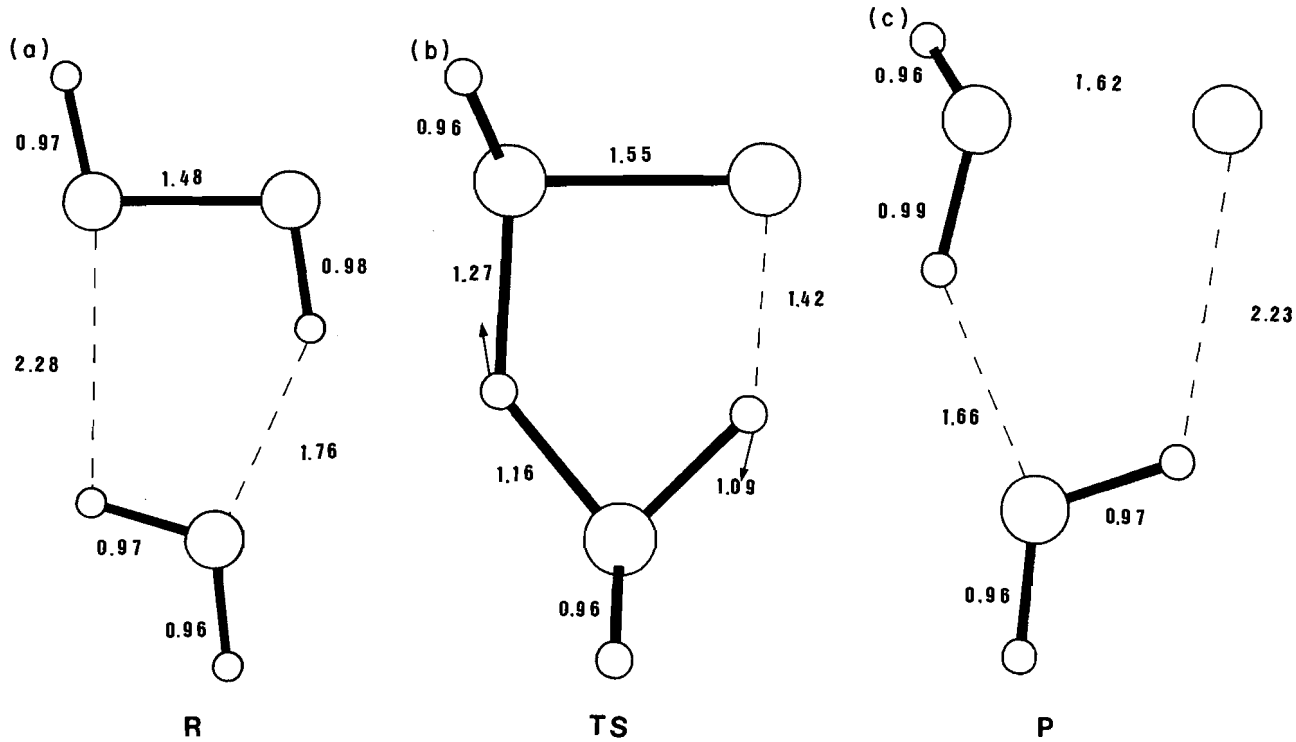

FIG. 3. Geometries of the reactant (R), transition state (TS), and product (P) for the water – hydrogen peroxide complex. The arrows in the transition state structure indicate the main components of the transition vector.

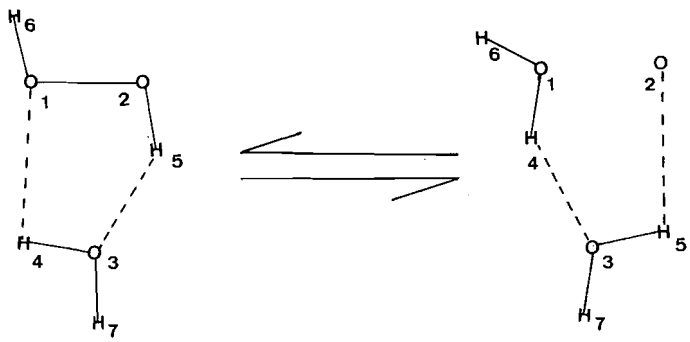

SCHEME 1

transferred, as is indicated by the eigenvector associated with the imaginary frequency (1517i cm^{-1}). The product consists of a singlet oxygen atom solvated by a chain of two water molecules.

From the energetic point of view, Table 3 displays the classical potential energy, enthalpy, entropy, and free-enthalpy values for the forward and backward processes, obtained at different levels of calculation. The most relevant point is that the intervention of a water molecule noticeably decreases the energy barriers for the forward reaction. However, these barriers remain very large, mainly due to the fact that the direct reaction is highly endothermic. On the other hand, the backward reaction occurs through a very small barrier. Finally, it can be noted that, in general, the same trends described in the gas phase, for the energy barriers when the basis set is expanded or the electron correlation is introduced and for the thermodynamic properties, are found here too.

To gain some insight into the mechanism of the double exchange, the 3-21+G IRC has been set up. The relative energies with respect to the reactant and the main bond distances

TABLE 3. Classical potential energy,[a] enthalpy,[a] entropy,[b] and free-enthalpy[a] barriers for the forward and backward 1,2-hydrogen migration in the water – hydrogen peroxide complex

	Forward	Backward
$\Delta E^{\ddagger}$ (3-21+G//3-21+G)	32.2	13.2
$\Delta E^{\ddagger}$ (6-31+G//3-21+G)	39.0	21.3
$\Delta E^{\ddagger}$ (6-31+G (D,P)//3-21+G)	49.1	18.0
$\Delta E^{\ddagger}$ (MP2/6-31+G//3-21+G)	35.8	4.1
$\Delta E^{\ddagger}$ (MP2/6-31+G (D,P)//3-21+G)	41.1	−3.4
$\Delta E^{\ddagger}$ (MP3/6-31+G//3-21+G)	40.4	9.7
$\Delta E^{\ddagger}$ (MP3/6-31+G (D,P)//3-21+G)	44.2	2.8
$\Delta H^{\ddagger}$ (3-21+G)	28.2	9.5
$\Delta S^{\ddagger}$ (3-21+G)	−7.7	−6.8
$\Delta G^{\ddagger}$ (3-21+G)	30.4	11.5

[a]In kcal/mol.
[b]In cal/(mol K).

at selected points along the IRC are presented in Table 4. As mentioned above, the points have been numbered in both directions starting from the transition state, which is considered as point 0.

From the values in Table 4 several consecutive phases can be distinguished in the reaction. Firstly, a motion of the water molecule occurs in such a way that H5 and H4 approach O3 and O1 respectively, the O2H5 and O3H4 bond distances remaining almost unchanged. Then the H5 transfer from O2 to O3 begins. At the transition state both H5 and H4 are moving. Lastly, when the double exchange has nearly been completed, the water molecule corresponding to O3 goes to its final position at the product. During the process the O1O2 bond distance corresponding to hydrogen peroxide is progressively lengthened.

Let us turn our attention to the electronic aspects of the

Can. J. Chem. Downloaded from www.nrcresearchpress.com by 88.85.125.76 on 09/07/12
For personal use only.

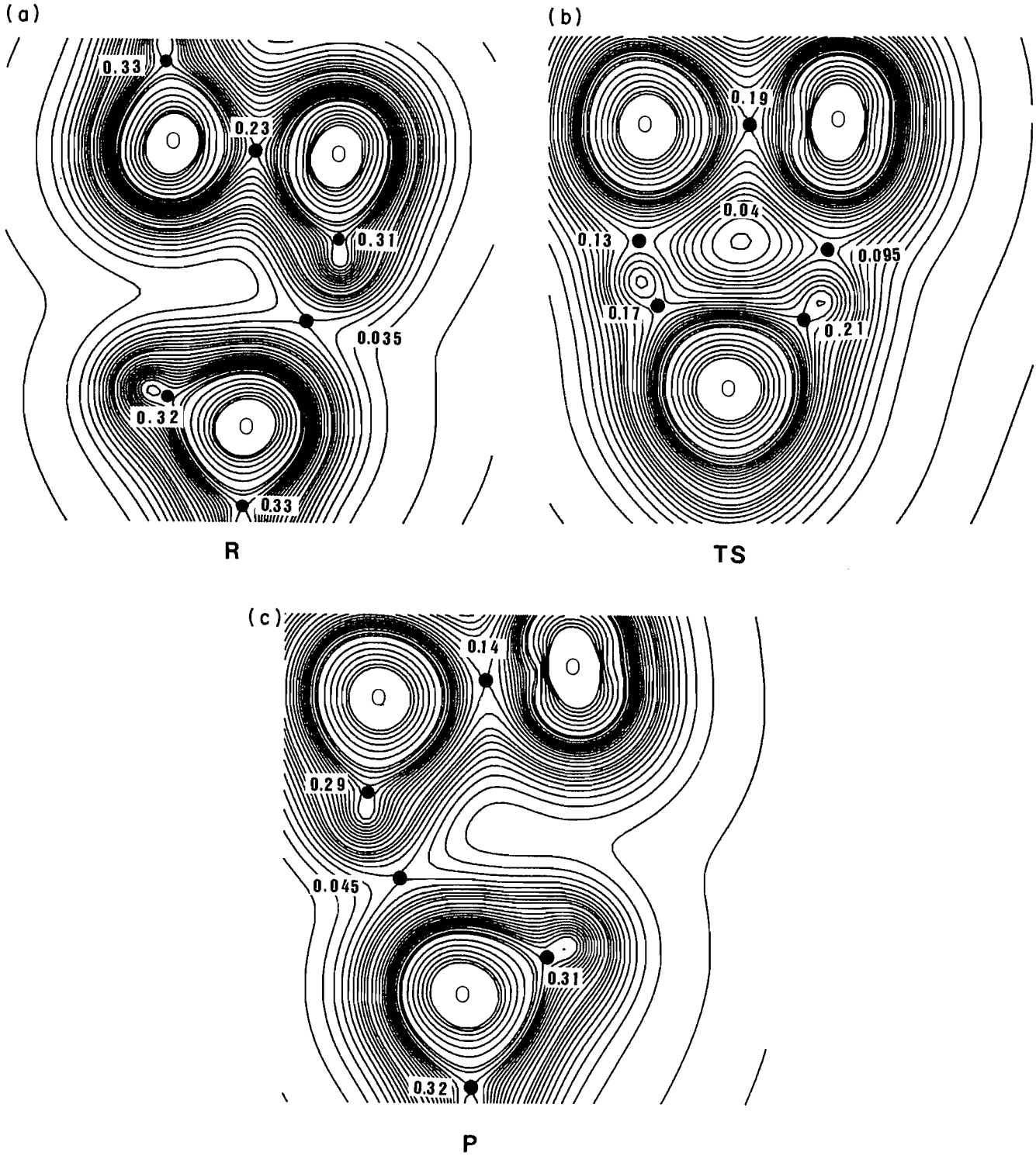

FIG. 4. Isodensity contour plots of $\rho(r)$ in the plane defined by the oxygen atoms at the reactant (R), transition state (TS), and product (P) for the water – hydrogen peroxide complex.

reaction. First of all, it should be noted that both transferring hydrogen atoms possess a net charge over +0.56 au at the transition state, which confirms their proton-like behaviour. Moreover, Fig. 4 displays the isodensity contour plots of $\rho(r)$ in the plane defined by the oxygen atoms at the reactant, transition state, and product. Two well-defined units corresponding to hydrogen peroxide and water exist at the reactant. Between them two hydrogen bonds are formed, but only the O3—H5 bond has a very weak covalent contribution. At the transition state one can see that H5 has already been transferred while H4 still "belongs" to O3. Thus, again, two structural entities can be distinguished, corresponding now to a hydronium cation and a hydroperoxide anion, with overall net charges of +0.66 and −0.66 au, respectively. A pair of covalent hydrogen bonds appears between them. H7 and H6 do not lie on the plane being considered and are not shown in the drawing. It should be emphasized that the intervention of the water molecule prevents the breaking of the O1—O2 bond of hydrogen peroxide at the

Can. J. Chem. Downloaded from www.nrcresearchpress.com by 88.85.125.76 on 09/07/12
For personal use only.

TABLE 4. 3-21+G IRC for the 1,2-hydrogen migration in the water – hydrogen peroxide complex

Point	s^a	Energy^b	R(O1—O2)^c	R(O1—H4)^c	R(O2—H5)^c	R(O3—H4)^c	R(O3—H5)^c
R		0.0	1.48	2.28	0.98	0.97	1.76
53	−2.6	3.4	1.48	1.84	0.99	0.97	1.66
33	−1.6	6.9	1.49	1.71	0.99	0.97	1.58
19	−0.9	13.8	1.52	1.54	1.03	0.98	1.45
13	−0.6	21.2	1.53	1.47	1.16	1.01	1.32
7	−0.3	28.8	1.54	1.39	1.29	1.06	1.20
TS	0.0	32.2	1.55	1.27	1.42	1.16	1.09
6	0.3	29.5	1.55	1.14	1.51	1.28	1.04
13	0.6	26.1	1.56	1.03	1.60	1.42	1.00
19	0.9	24.1	1.58	1.01	1.67	1.49	0.98
43	2.1	21.4	1.60	1.00	1.78	1.57	0.98
59	2.9	20.7	1.60	1.00	1.83	1.60	0.98
P		19.0	1.62	0.99	2.23	1.66	0.97

[a]In amu$^{1/2}$ bohr.
[b]Relative energy with respect to reactant in kcal/mol.
[c]In Angstroms.

transition state. As a consequence, a ring point appears in the middle of the system. This ring point is a minimum of $\rho(\boldsymbol{r})$ on the plane considered, but a maximum in the orthogonal direction, and indicates the existence of a closed chain of bond paths linking the five nuclei around it. Finally, at the product the O2 atom is nucleophilically solvated by a water molecule and linked to the other by a hydrogen bond.

From the results presented in this section we can conclude that the water molecule intervenes very actively in the 1,2-hydrogen migration, modifying the gas phase reaction mechanism. The water molecule acts as a bifunctional catalyst, first accepting and then transferring a proton, the energy barrier being noticeably lowered. Similar behaviour has also been found for the intramolecular proton transfer in the water – hydroperoxide anion complex. In that case (36), the water molecule first gives and then takes a proton, in such a way that a hydroxide anion rather than a hydronium cation is formed.

V. Conclusions

In this paper the 1,2-hydrogen migration of hydrogen peroxide has been studied. It has been shown that the transferring hydrogen behaves as a proton. This result contrasts with the case of the 1,2-hydrogen transfer of acetylene, recently investigated by Sakai and Morokuma (3), wherein a hydride moves. The difference perhaps can be attributed to the fact that a carbon atom is a much weaker proton-donating center than the more electronegative oxygen atom.

The 1,2-hydrogen migration of hydrogen peroxide proceeds through a very high energy barrier mainly due to two factors: the reaction is clearly endothermic and the moving proton polarizes the O—O bond that becomes broken at the transition state.

If a water molecule is allowed to intervene in the reaction, the energy barrier is noticeably lowered, but it still remains high. The water molecule acts as a bifunctional catalyst, first accepting and then transferring a proton.

Finally, it should be remarked that the high values of the energy barriers obtained in this work justify why the 1,2-hydrogen migration is not a reliable route for decomposition of hydrogen peroxide into water and atomic oxygen.

1. E. F. CALDIN and V. GOLD (*Editors*). Proton-transfer reactions. Chapman and Hall, London. 1975.
2. M. T. PAGE. The chemistry of enzyme action. Elsevier, Amsterdam. 1974.
3. S. SAKAI and K. MOROKUMA. J. Phys. Chem. **91**, 3661 (1987).
4. A. LLEDÓS and J. BERTRÁN. Tetrahedron Lett. **22**, 775 (1981).
5. A. LLEDÓS and J. BERTRÁN. J. Mol. Struct. Theochem. **120**, 73 (1985).
6. T. YAMABE, K. YAMASHITA, M. KAMINOYAMA, M. KOIZUMI, A. TACHIBANA, and K. FUKUI. J. Phys. Chem. **88**, 1459 (1984).
7. O. N. VENTURA, A. LLEDÓS, R. BONACCORSI, J. BERTRÁN, and J. TOMASI. Theor. Chim. Acta, **72**, 175 (1987).
8. P. RUELLE, V. W. KESSELRING, and H. NAM-TRAN. J. Am. Chem. Soc. **108**, 371 (1986).
9. P. RUELLE. J. Comput. Chem. **8**, 158 (1987).
10. P. RUELLE. J. Am. Chem. Soc. **109**, 1722 (1987).
11. I. H. WILLIAMS, D. SPANGLER, D. A. FEMEC, G. M. MAGGIORA, and R. L. SCHOWEN. J. Am. Chem. Soc. **105**, 31 (1983).
12. I. H. WILLIAMS. J. Am. Chem. Soc. **109**, 6299 (1987).
13. J. L. ANDRÉS, M. DURÁN, A. LLEDÓS, and J. BERTRÁN. Chem. Phys. Lett. **124**, 177 (1986).
14. E. A. V. EBSWORTH, J. A. CONNOR, and J. J. TURNER. *In* Comprehensive inorganic chemistry. Vol. 2. *Edited by* J. C. Bailar, H. J. Emeléus, R. Nyholm, and A. F. Trotman-Dickenson. Pergamon Press, Oxford. 1973. p. 685.
15. M. J. FRISCH, J. S. BINKLEY, H. B. SCHLEGEL, K. RAGHAVACHARI, C. F. MELIUS, R. L. MARTIN, J. J. P. STEWART, F. W. BOBROWICZ, C. M. ROHLFING, L. R. KAHN, D. J. DEFREES, R. SEEGER, R. A. WHITESIDE, D. J. FOX, E. M. FLEUDER, and J. A. POPLE. Gaussian 86. Carnegie–Mellon Quantum Chemistry Publishing Unit, Pittsburgh, PA. 1984.
16. G. W. SPITZNAGEL, T. CLARK, J. CHANDRASEKHAR, and P. VON R. SCHLEYER. J. Comput. Chem. **3**, 363 (1982).
17. T. CLARK, J. CHANDRASEKHAR, G. W. SPITZNAGEL, and P. VON R. SCHLEYER. Comput. Chem. **4**, 294 (1983).
18. H. B. SCHLEGEL. J. Comput. Chem. **3**, 214 (1982).
19. J. A. POPLE, R. A. KRISHNAN, H. B. SCHLEGEL, and J. S. BINKLEY. Int. J. Quantum Chem. Quantum Chem. Symp. **13**, 225 (1979).
20. D. A. MCQUARRIE. Statistical mechanics. Harper and Row, New York. 1976.
21. J. A. POPLE, J. S. BINKLEY, and R. SEEGER. Int. J. Quantum Chem. Quantum Chem. Symp. **10**, 1 (1976).
22. D. G. TRUHLAR and A. KUPPERMAN. J. Am. Chem. Soc. **93**, 1840 (1971).
23. K. FUKUI. J. Phys. Chem. **74**, 4161 (1970).
24. K. FUKUI. Pure Appl. Chem. **54**, 1825 (1982).
25. M. DUPUIS, D. SPANGLER, and J. J. WENDOLOSKI. National Resource for Computations in Chemistry Software Catalogue Program QG01. Lawrence Berkeley Laboratory, University of California, Berkeley, CA. 1980.

Can. J. Chem. Downloaded from www.nrcresearchpress.com by 88.85.125.76 on 09/07/12
For personal use only.

26. M. W. SCHMIDT, M. S. GORDON, and M. DUPUIS. J. Am. Chem. Soc. **107**, 2585 (1985).
27. B. C. GARRETT, M. J. REDMON, R. STECKLER, D. G. TRUHLAR, K. K. BALDRIDGE, D. BARTAL, M. W. SCHMIDT, and M. S. GORDON. J. Phys. Chem. **92**, 1476 (1988).
28. N. N. GREENWOOD and A. EARNSHAW. Chemistry of the elements. Pergamon Press, Oxford. 1986. p. 742.
29. R. L. REDINGTON, W. B. OLSON, and P. C. CROSS. J. Chem. Phys. **36**, 1311 (1962).
30. R. H. HUNT, R. A. LEACOCK, C. W. PETERS, and K. T. HECHT. J. Chem. Phys. **42**, 1931 (1965).
31. R. F. W. BADER, Y. TAL, S. G. ANDERSON, and T. T. NGUYEN-DANG. Isr. J. Chem. **19**, 8 (1980).
32. J. M. FOSTER and S. F. BOYS. Rev. Mod. Phys. **32**, 296 (1960); **32**, 300 (1960).
33. S. SCHEINER. J. Chem. Phys. **77**, 4039 (1982).
34. S. SCHEINER. J. Phys. Chem. **86**, 376 (1982).
35. E. A. HILLENBRAND and S. SCHEINER. J. Am. Chem. Soc. **106**, 6266 (1984).
36. E. BOSCH, J. M. LLUCH, and J. BERTRÁN. J. Am. Chem. Soc. In press.

Can. J. Chem. Downloaded from www.nrcresearchpress.com by 88.85.125.76 on 09/07/12
For personal use only.

Conductimetric and potentiometric investigation of effect of acidity on formation of homoconjugates in acetonitrile solvent

TURGUT GÜNDÜZ,[1] ESMA KILIÇ, GÜLEREN ÖZKAN, MUHAMMED F. AWAAD, AND MUSTAFA TASTEKIN
Department of Chemistry, Faculty of Science, University of Ankara, Ankara, Turkey

Received June 22, 1989

TURGUT GÜNDÜZ, ESMA KILIÇ, GÜLEREN ÖZKAN, MUHAMMED F. AWAAD, and MUSTAFA TASTEKIN. Can. J. Chem. **68**, 674 (1990).

In the present work, 11 aromatic and nine aliphatic carboxylic acids, namely benzoic, 2-nitrobenzoic, 3-nitrobenzoic, 4-nitrobenzoic, 2,4-dinitrobenzoic, 3,5-dinitrobenzoic, 2-aminobenzoic, 3-aminobenzoic, 4-aminobenzoic, *o*-phthalic, salicylic, formic, acetic, monochloroacetic, dichloroacetic, trichloroacetic, propionic, *n*-butyric, caprylic, and myristic acids, were titrated conductimetrically and potentiometrically with triethylamine in acetonitrile solvent, under a nitrogen atmosphere, at 25°C. Closer investigation of the conductimetric titration curves of these acids showed that the acidity of an acid, rather than the basicity of its conjugate base, plays a major part in the formation of homoconjugate ions, at least in acetonitrile solvent. If the acid is strong enough, there is a maximum before the experimental end point at about the half-neutralization point. To determine the minimum strength for an acid to show this maximum before the end point, all acids were also titrated potentiometrically. It was found that those acids which have half-neutralization potentials over −85 mV give a strong homoconjugation reaction and show a maximum before the experimental end point. Moreover, the acids that show maxima before the experimental end point in the conductimetric titration also show rather well-shaped potentiometric titration curves.

Key words: nonaqueous media, conductimetric titrations, potentiometric titrations, titration in acetonitrile, acidity and homoconjugation.

TURGUT GÜNDÜZ, ESMA KILIÇ, GÜLEREN ÖZKAN, MUHAMMED F. AWAAD et MUSTAFA TASTEKIN. Can. J. Chem. **68**, 674 (1990).

Opérant à 25°C et sous un atmosphère d'azote, utilisant de la triéthylamine dans de l'acétonitrile comme solvant et faisant appel à la conductimétrie et à la potentiométrie, on a titré 11 acides carboxyliques aromatiques et neuf acides aliphatiques, soit les acides benzoïque, 2-nitrobenzoïque, 3-nitrobenzoïque, 4-nitrobenzoïque, 2,4-dinitrobenzoïque, 3,5-dinitrobenzoïque, 2-aminobenzoïque, 3-aminobenzoïque, 4-aminobenzoïque, *o*-phtalique, salicylique, formique, acétique, monochloroacétique, dichloroacétique, trichloroacétique, propanoïque, butyrique, caprylique et myristique. Un examen plus approfondi des courbes de titrations conductimétriques a permis de démontrer que, dans l'acétonitrile, c'est l'acidité de l'acide plutôt que la basicité de son base conjugué qui est principalement responsable de la formation des ions homoconjugués. Si l'acide est suffisamment fort, il présente un maximum avant le point de virage expérimental, aux alentours du point de demi-neutralisation. Afin de déterminer quelle est la force minimale d'un acide qui donnera lieu à un maximum avant le point de virage, on a aussi titré tous les acides d'une façon potentiométrique et on a trouvé que les acides dont les potentiels de demi-neutralisation dépassent −85 mV donnent lieu à une forte réaction d'homoconjugaison et qu'ils présentent un maximum avant le point de virage expérimental. On a aussi observé que les acides qui présentent des maxima avant le point de virage expérimental dans les titrations potentiométriques présentent aussi des courbes de titrations potentiométriques qui sont plutôt bien définies.

Mots clés : milieux non-aqueux, titrations conductimétriques, titrations potentiométriques, titrations dans l'acétonitrile, acidité, homoconjugaison.

[Traduit par la revue]

Introduction

When an acid of intermediate strength is titrated conductimetrically with a base of intermediate strength, in a solvent of low or relatively low dielectric constant that is a non-hydrogen bond donor, a homoconjugation reaction takes place and homoconjugates are formed.

$$A^- + HA \rightarrow AH...A^-$$

At present it is a generally accepted fact that, in the formation of these homoconjugates, the basicity of the base rather than the acidity of the acid plays a major part (1–12). We have carried out the present work to verify this fact and to investigate it further. We selected 11 aromatic and nine aliphatic carboxylic acids, namely, benzoic, 2-nitrobenzoic, 3-nitrobenzoic, 4-nitrobenzoic, 2,4-dinitrobenzoic, 3,5-dinitrobenzoic, 2-aminobenzoic, 3-aminobenzoic, 4-aminobenzoic, *o*-phthalic, salicylic, formic, acetic, monochloroacetic, dichloroacetic, trichloroacetic, propionic, *n*-butyric, caprylic, and myristic acids, and titrated their 0.003 M solutions with a 0.100 M solution of triethylamine (an intermediate base) in acetonitrile solvent, which has a dielectric constant of 36 and is a non-hydrogen bond donor. All titrations were carried out under a nitrogen atmosphere, at 25°C.

[1]Author to whom correspondence may be addressed.

Experimental

Apparatus

The apparatus used in this work has been described in ref. 13.

Chemicals

Triethylamine was purchased from Fluka AG in 98% purity.

Acetonitrile was purchased from Merck AG (Reinst) and purified further as follows: Anhydrous phosphorus pentoxide (5 g) was added to 1 L of solvent in a stoppered flask and, after shaking the flask for 15 min, the solvent was filtered and distilled in a tall fractionating column at atmospheric pressure. The middle distillate was collected and stored in a dark-coloured flask.

Propan-2-ol: the pure Merck product was used after distillation over CaO.

Benzoic acid was purchased from Merck AG, and was used after being sublimed.

2-Nitrobenzoic acid was prepared from 2-nitrotoluene by the method given in ref. 14.

3-Nitrobenzoic acid was prepared from 3-nitrobenzaldehyde (BDH, in 99% purity) by the method given in ref. 15.

Can. J. Chem. Downloaded from www.nrcresearchpress.com by 91.144.44.67 on 09/07/12
For personal use only.

TABLE 1. Half-neutralization potentials (hnp) of 0.003 M solutions of some aromatic and aliphatic carboxylic acids titrated with a 0.100 M solution of triethylamine in acetonitrile solvent, under a nitrogen atmosphere, at 25°C

Aromatic acids	hnp/mV	Shape	Aliphatic acids	hnp/mV	Shape
Benzoic	−180	None*	Formic	−315	None*
2-Nitrobenzoic	−30	S	Acetic	−220	None*
3-Nitrobenzoic	−85	S	Monochloroacetic	−75	S
4-Nitrobenzoic	−78	S	Dichloroacetic	80	S
2,4-Dinitrobenzoic	75	S	Propionic	−225	None*
3,5-Dinitrobenzoic	10	S	*n*-Butyric	−245	None*
2-Aminobenzoic	−190	None*	Caprylic	−235	None*
3-Aminobenzoic	−195	None*	Myristic	−255	None*
4-Aminobenzoic	−213	None*	Trichloroacetic	—	—
o-Phthalic	125	S			
Salicylic	12	S			

*Half-neutralization potentials have been found from the calculated stoichiometry.

4-Nitrobenzoic acid was purchased from Merck AG in 99% purity and was used without further purification.

2,4-Dinitrobenzoic acid was purchased from Schering Kahlbaum (pure) and was used without further purification.

3,5-Dinitrobenzoic acid was purchased from Merck AG in 99% purity and was used without further purification.

2-Aminobenzoic acid was purchased from Riedel–de Häen in 99.5% purity and was used without further purification.

3-Aminobenzoic acid was purchased from Fluka AG in 99% purity and was used without further purification.

4-Aminobenzoic acid was purchased from Riedel–de Häen in 99% purity and was used without further purification.

o-Phthalic acid was purchased from Hyden Chemical Corporation (pure).

Salicylic acid was purchased from Merck AG in 99.5% purity.

Formic acid was purchased from Merck AG in 98–100% purity and was used without further purification.

Acetic acid was purchased from Merck AG (Zur Analyse) in 99–100% purity and was used without further purification.

Monochloroacetic acid was purchased from Riedel–de Häen (pure Cryst).

Dichloroacetic acid was purchased from Schering–Kahlbaum AG.

Trichloroacetic acid was purchased from Fluka AG in 98% purity and was used without further purification.

Propionic acid was purchased from Riedel–de Häen AG and was used without further purification.

n-Butyric acid was purchased from Dr. Praenkel and Dr. Landau (Normel Gereinigt) and was used without further purification.

Caprylic acid was purchased from Schering–Kahlbaum AG (pure) and was used without further purification.

Myristic acid was purchased from BDH in 99% purity and was used without further purification.

Results and discussion

The acids titrated conductimetrically and potentiometrically with triethylamine in acetonitrile solvent are given in Table 1. One of the acids titrated in this work is benzoic acid. The initial specific conductivity of its 0.003 M solution is extremely low (1 μmho), but increases rather sharply upon addition of a 0.100 M solution of titrant, Fig. 1A.

As can be seen from the titration curve, benzoic acid shows neither a maximum at about the half-neutralization point, nor a linear increase, until the experimental end point. This clearly indicates that benzoic acid has little tendency to form homoconjugate ions with its conjugate base (benzoate ions). So its simple salt and conjugate salt remain as ion-pairs or ion-aggregates in the medium. This can be formulated as follows.

$$HA + B \rightarrow BH^+A^- \rightarrow BH^+ + A^-$$

$$BH^+A^- + HA \rightarrow BH^+HA_2^- \rightarrow BH^+ + HA_2^-$$

On the other hand, the initial specific conductivity of the 0.003 M solution of 4-nitrobenzoic acid, which is a stronger acid than benzoic acid, is also very low, but it increases more sharply than the specific conductivity of benzoic acid on addition of triethylamine (titrant). In addition, in contrast to the titration curve of benzoic acid, the titration curve of 4-nitrobenzoic acid shows a maximum at about the half-neutralization-point, Fig. 1B. The maximum is approximately symmetrical on both sides of the half-neutralization point and the end point is rather well shaped. This clearly indicates that 4-nitrobenzoic acid has a rather strong tendency to form homoconjugate ions with its conjugate base. In addition, the specific conductivity of 4-nitrobenzoic acid at any neutralization point on the titration curve is greater than the specific conductivity of the benzoic acid at the corresponding neutralization point. Possibly this is due to the higher dissociation of its homoconjugate salt ($BH^+HA_2^-$) than that of its simple salt (BH^+A^-). As is known, homoconjugate salts generally dissociate more readily than their unhomoconjugated or simple salts because the negative charge on such species is effectively dissipated over the entire larger ions, the coulombic attraction forces are reduced, and, consequently, the dissociation is increased. The titration curves of the 2-nitrobenzoic and 3-nitrobenzoic acids are very similar to the titration curve of 4-nitrobenzoic acid.

2,4-Dinitrobenzoic acid shows a very similar titration curve to the titration curve of 4-nitrobenzoic acid. But the specific conductivity of the former at any neutralization point in the titration curve is greater than the specific conductivity of the latter at the corresponding neutralization point, Fig. 1C. Moreover, 3,5-dinitrobenzoic acid gives a very similar titration curve to that of 2,4-dinitrobenzoic acid. Despite the fact that the benzoate ion is a stronger base than the mono- and dinitrobenzoate ions, it has a lesser tendency to form homoconjugate ions than the mono- and dinitrobenzoate ions, at least in acetonitrile solvent. This observation cannot be explained with the generally accepted fact that the anion of an acid plays a major part in the formation of homoconjugates. Otherwise, on the titration curve of benzoic acid a higher and sharper maximum would be observed than the maxima observed on the titration curves of mono- and dinitrobenzoic acids. In addition,

Can. J. Chem. Downloaded from www.nrcresearchpress.com by 91.144.44.67 on 09/07/12
For personal use only.

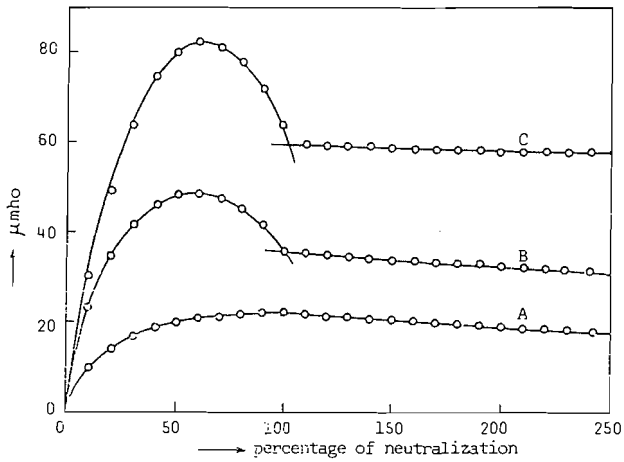

FIG. 1. Conductimetric titration curves of 0.003 M solutions of benzoic acid (A), 4-nitrobenzoic acid (B), and 2,4-dinitrobenzoic acid (C) with a 0.100 M solution of triethylamine in acetonitrile solvent. Titrations were carried out under a nitrogen atmosphere at 25°C. The specific conductivity of a 0.1000 ± 0.0005 M solution of KCl was taken as standard.

the specific conductivity of the salt of benzoic acid would be greater than the specific conductivity of the mono- and dinitrobenzoic acid salts at any point on the titration curves. As is well known, a dinitrobenzoic acid is a stronger acid than a mononitrobenzoic acid; in turn, a mononitrobenzoic acid is a stronger acid than benzoic acid. Thus anions of the nitrobenzoic acids should be weaker bases than the anion of benzoic acid. All these observations indicate that in homoconjugation reactions the acidity of an acid rather than the basicity of its conjugate base plays a major part, at least in acetonitrile solvent.

To support this observation, we also titrated aminobenzoic acids, namely, 2-amino-, 3-amino-, and 4-aminobenzoic acids. The titration curves of these acids showed a very similar pattern to that of the benzoic acid, except that their specific conductivities are relatively lower than the specific conductivity of the benzoic acid at any point in their titration curves. The anions of these are even stronger bases than the anion of benzoic acid, yet they do not undergo a homoconjugation reaction to an appreciable extent and as a result they do not show maxima before the end point owing to the weaknesses of their acids.

To further support the importance of acidity over basicity in the formation of homoconjugates, we also titrated *o*-phthalic acid and salicylic acid under the same conditions. The initial conductivity of *o*-phthalic acid solution was also low, but it increased linearly up to the end point upon addition of the titrant and then decreased very slowly, Fig. 2A. That is, it did not show a maximum at about the half-neutralization point. However, this acid is expected to show a maximum before the experimental end point because of its strong acidic character, Table 1. Such a maximum was not observed, owing to its molecular structure. Because of its special structure, *o*-biphthalate ion is very prone to give an intramolecular, rather than an intermolecular, hydrogen bond. So, up to the end point only BH^+ and intramolecular hydrogen-bonded *o*-phthalate ion are present in the medium. In addition, the experimental end point is exactly identical to the calculated or theoretical end point. The initial conductivity of the solution of salicylic acid is low; however, it increases rather sharply, but not linearly, as is the case with *o*-phthalic acid, upon addition of titrant, and gives a maximum

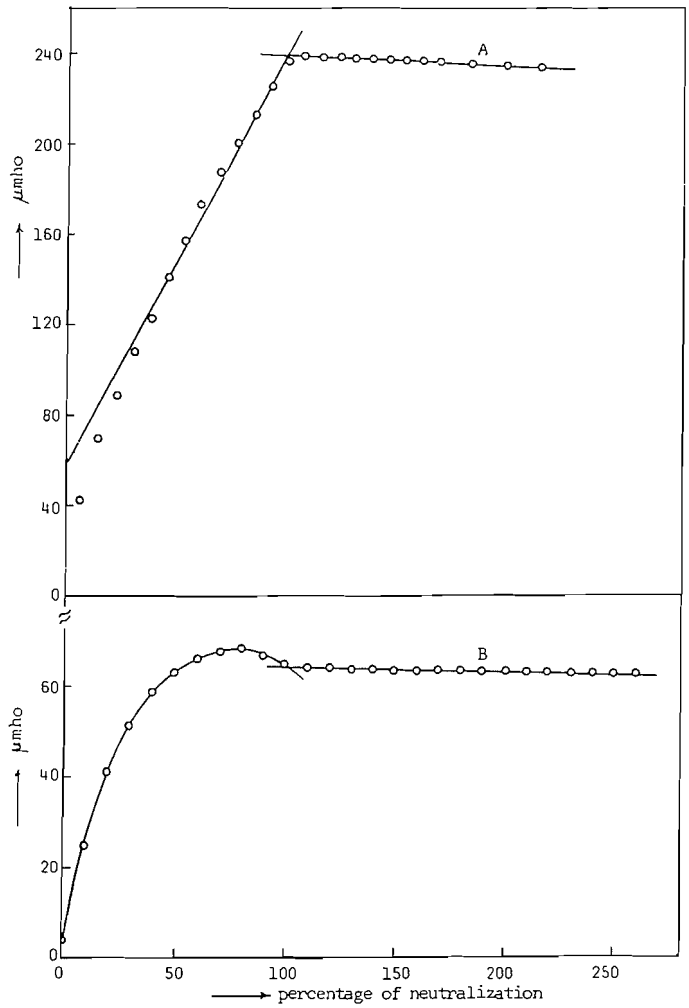

FIG. 2. Conductimetric titration of 0.003 M solutions of *o*-phthalic acid (A) and salicylic acid (B) with a 0.100 M solution of triethylamine in acetonitrile solvent. In the titrations the specific conductivity of a 0.1000 ± 0.0005 M solution of KCl was accepted as standard.

before the experimental end point, Fig. 2B. The reason that the salicylic acid shows a maximum before the end point is the weakness of the acidity of its phenolic hydroxy group. Thus, due to the weaker acidity of the hydroxy group than that of the carboxy group, salicylate ion does not give, or gives at best to a small extent, an intramolecular H-bond; instead it gives an intermolecular H-bond and consequently shows a maximum at about the half-neutralization point. The results obtained for *o*-phthalic acid and salicylic acid also supported strongly the observation given above.

To support this observation further, we also titrated some stronger and weaker aliphatic carboxylic acids, Table 1. Under the same conditions, the titration curve of acetic acid showed neither a maximum nor a conspicuous end point, Fig. 3A. On the other hand, monochloroacetic acid, a slightly stronger acid than acetic acid, showed a rather strong maximum before the end point, at about the half-neutralization point. Dichloroacetic acid behaved exactly as did monochloroacetic acid, but its specific conductivity at any point on the titration curve is greater than the corresponding specific conductivity of monochloroacetic acid, Figs. 3B and 3C. Despite the fact that the acetate ion possesses the strongest basicity among the anions of these

Can. J. Chem. Downloaded from www.nrcresearchpress.com by 91.144.44.67 on 09/07/12
For personal use only.

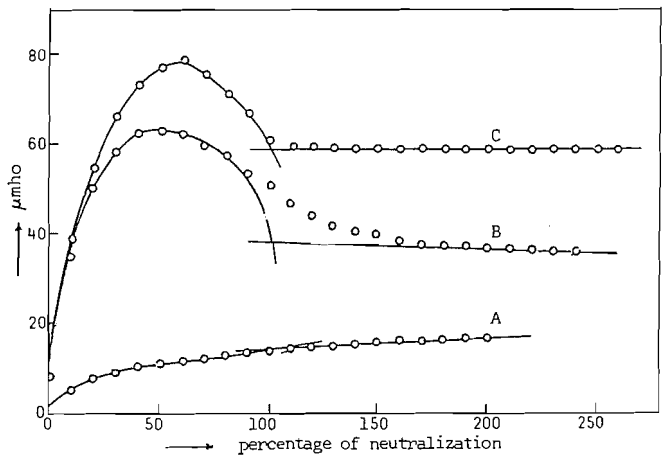

FIG. 3. Conductimetric titration curves of the solutions (0.003 M) of acetic (A), monochloroacetic (B), and dichloroacetic acids (C) with a solution (0.100 M) of triethylamine in acetonitrile solvent at 25°C. The conductivity of a 0.1000 ± 0.0005 M KCl solution was taken as standard.

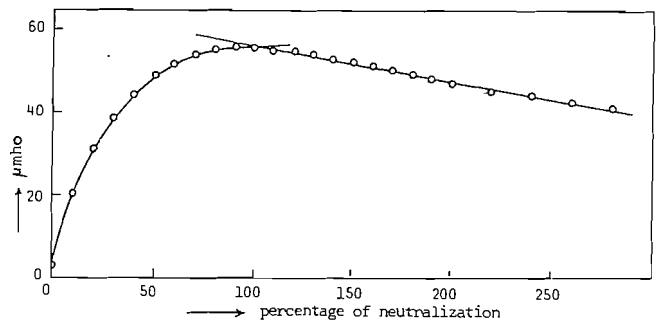

FIG. 4. Conductimetric titration curve of a 0.003 M solution of formic acid with a 0.100 M solution of triethylamine in acetonitrile solvent, under a nitrogen atmosphere at 25°C. In the titrations the specific conductivity of 0.1000 ± 0.0005 M KCl was taken as standard.

three acids, acetate ions do not form homoconjugate ions, at least to an appreciable extent, due to the weaker acidity of acetic acid than the mono- and dichloroacetic acids. This observation also strongly indicates that acidity rather than basicity of the species plays an important part in the formation of homoconjugates in acetonitrile solvent. Under the same conditions, trichloroacetic acid decomposes at the earlier stage of the titration. We also titrated formic acid, which is stronger than acetic and weaker than monochloroacetic acid, and obtained no well-defined maximum, but a rather well-defined end point, Fig. 4. The result indicates that even formic acid, though stronger than acetic acid, is not strong enough to give homoconjugate ions to an appreciable extent. Lastly, we titrated propionic, *n*-butyric, caprylic, and myristic acids, but none showed a maximum before the stoichiometric end point. These data also supported our view.

To determine the minimum acidity level for the formation of homoconjugates at appreciable concentration to give a maximum before the end point, we titrated potentiometrically all the acids given in Table 1, under the same experimental conditions, and obtained some interesting results. The acids that showed well-shaped or rather well-shaped maxima upon conductimetric

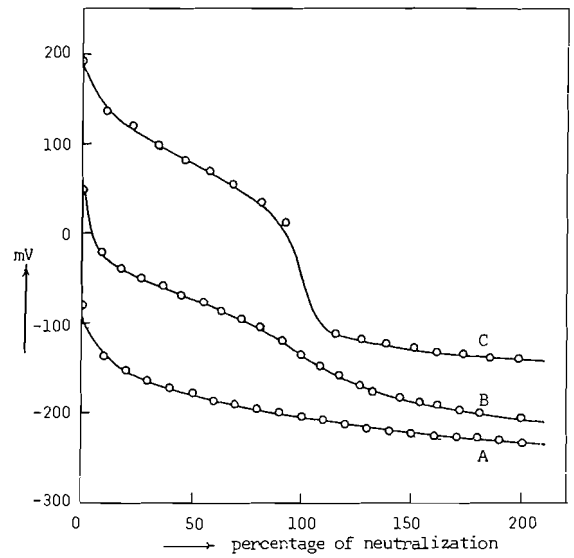

FIG. 5. Potentiometric titration curves of 0.003 M solutions of benzoic (A), 4-nitrobenzoic (B), and 2,4-dinitrobenzoic acids (C) with triethylamine in acetonitrile solvent, under a nitrogen atmosphere at 25°C.

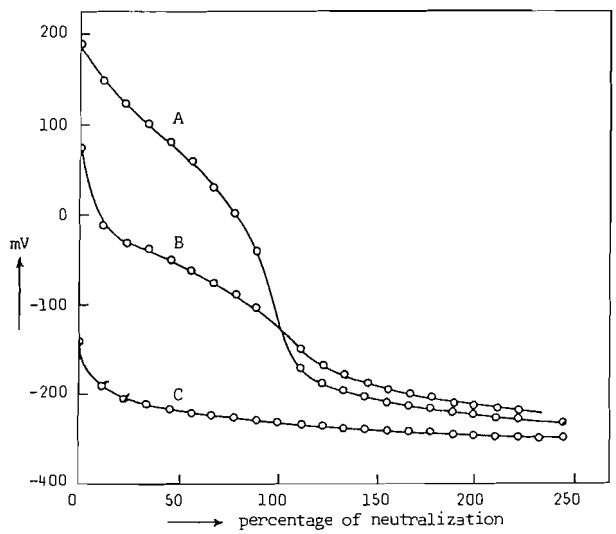

FIG. 6. Potentiometric titration curves of 0.003 M solutions of dichloroacetic (A), monochloroacetic (B), and acetic acids (C), under a nitrogen atmosphere at 25°C.

titration also gave rather well-shaped potentiometric titration curves. The rest did not even show characteristic titration curves. The half-neutralization potentials (hnp) of the acids obtained in this work have also been collected in Table 1. The acids that showed a half-neutralization potential over −85 mV gave well-shaped or rather well-shaped potentiometric titration curves, and also gave well-shaped or rather well-shaped maxima at about the half-neutralization points. To illustrate the potentiometric results, the titration curves of the benzoic, 4-nitrobenzoic, and 2,4-dinitrobenzoic acids and those of acetic, monochloroacetic, and dichloroacetic acids are given in Figs. 5 and 6.

The potentiometric titration curves of *o*-phthalic and salicylic acids are given in Fig. 7. As is easily seen from the shape of the titration curves, *o*-phthalic acid is a much stronger acid than

Can. J. Chem. Downloaded from www.nrcresearchpress.com by 91.144.44.67 on 09/07/12
For personal use only.

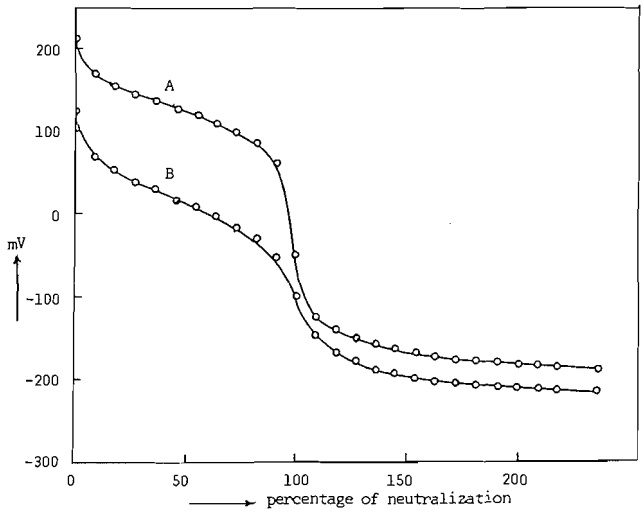

FIG. 7. Potentiometric titration of 0.003 M solutions of *o*-phthalic acid (A) and salicylic acid (B) in acetonitrile solvent, under a nitrogen atmosphere at 25°C.

salicylic acid. The half-neutralization potentials are given in Table 1. Closer examination of this table shows that the order of the acidity of certain acids, in contrast to the order of acidity in water, is as follows:

o-phthalic acid > acetic acid > formic acid

Conclusions

In the present work, we have tried to show that the acidity of an acid rather than the basicity of its conjugate base plays a major part in the formation of homoconjugates, in contrast to what has generally been believed, at least in acetonitrile solvent. The stronger the acid, the greater the concentration of homoconjugates with respect to its simple anion, at least in acetonitrile solvent, which has a relatively low dielectric constant ($\varepsilon = 36$) and is a non-hydrogen bond donor solvent.

The acids that show maxima in their conductimetric titration curves also show well-shaped or rather well-shaped potentiometric titration curves, due to their sufficiently strong acidity. For an acid to show a maximum, which is a great help in accurately determining the end point, it should have a minimum half-neutralization potential of −85 mV, under our experimental conditions.

1. P. J. BRYANT and A. W. H. WARDROP. J. Chem. Soc. 895 (1957).
2. D. B. BRUSS and G. A. HARLOW. Anal. Chem. **30**, 1836 (1958).
3. I. M. KOLTHOFF and M. K. CHANTOONI, JR. J. Am. Chem. Soc. **87**, 1004 (1965).
4. J. F. GOETZEE, G. PADMANABHAN, and G. CUMINGHAM. Talanta, **11**, 93 (1964).
5. I. M. KOLTHOFF and M. K. CHANTOONI, JR. J. Am. Chem. Soc. **85**, 426 (1963).
6. L. W. MARPLE and G. J. SCHEPPERS. Anal. Chem. **38**, 553 (1966).
7. I. M. KOLTHOFF and S. BRUCKENSTEIN. J. Am. Chem. Soc. **78**, 1 (1956).
8. G. A. HARLOW. Anal. Chem. **34**, 1482 (1962).
9. K. IZUTSU, I. M. KOLTHOFF, T. FUJINAGA, M. HATTORI, and M. K. CHANTOONI, JR. Anal. Chem. **49**, 503 (1977).
10. I. M. KOLTHOFF. Anal. Chem. **46**, 1992 (1974).
11. T. GÜNDÜZ, E. KILIÇ, F. KÖSEOĞLU, and S. G. ÖZTAS. Analyst, **113**, 1313 (1988).
12. N. GÜNDÜZ, T. GÜNDÜZ, E. KILIÇ, M. TÜZÜN, L. S. SHAW, and R. A. SHAW. J. Chem. Soc. Dalton Trans. 925 (1987).
13. T. GÜNDÜZ, N. GÜNDÜZ, E. KILIÇ, F. KÖSEOĞLU, and S. G. ÖZTAS. Analyst, **113**, 715 (1988).
14. M. REIMER and E. S. GATEWOOD. J. Am. Chem. Soc. **42**, 1475 (1920).
15. A. I. VOGEL. Vogel's textbook of practical organic chemistry. 4th ed. Longman, London. 1981.

Can. J. Chem. Downloaded from www.nrcresearchpress.com by 91.144.44.67 on 09/07/12
For personal use only.

The application of trifluoroacetic anhydride – sodium iodide (TFAA-I) system for quantitative determination of nitrones

WITOLD CIESIELSKI, ZBIGNIEW H. KUDZIN,[1] AND MACIEJ TASZ
Institute of Chemistry, University of Łódź, Łódź 80-136, Narutowicza 68, Poland

JÓZEF DRABOWICZ
Center of Molecular and Macromolecular Studies, Polish Academy of Sciences, Łódź 80-363, Sienkiewicza 112, Poland

Received July 17, 1989[2]

WITOLD CIESIELSKI, ZBIGNIEW H. KUDZIN, MACIEJ TASZ, and JÓZEF DRABOWICZ. Can. J. Chem. **68**, 679 (1990).

Trifluoroacetic anhydride – sodium iodide mixture (TFAA-I) reacts with nitrones with the release of iodine. Since stoichiometrical amounts of iodine are formed with respect to starting nitrones, TFAA-I reagent can be used for analytical determination of nitrones. Two procedures for the determination of nitrones (on μmole and on nmole scale) have been described.

Key words: nitrones determination, TFAA-I reagent.

WITOLD CIESIELSKI, ZBIGNIEW H. KUDZIN, MACIEJ TASZ et JÓZEF DRABOWICZ. Can. J. Chem. **68**, 679 (1990).

Les nitrones réagissent avec un mélange d'anhydride trifluoroacétique et d'iodure de sodium pour dégager de l'iode. La quantité d'iode dégagée par rapport aux nitrones de départ étant stoechiométriques, on peut donc utiliser le réactif ATFA-I pour déterminer les nitrones d'une façon analytique. On décrit deux méthodes permettant de déterminer la présence de nitrones aux niveaux de la μmole et de la nmole.

Mots clés : détermination des nitrones; réactif ATFA-I.

[Traduit par la revue]

Can. J. Chem. Downloaded from www.nrcresearchpress.com by 91.144.44.67 on 09/07/12
For personal use only.

Introduction

Nitrones are useful reagents in organic synthesis (for a review of nitrone chemistry, see ref. 1) and are often used as spin trap reagents in EPR work (2). However, quantitative determination of these compounds is considered part of nitrogen analytical chemistry (3).

Recently we have published on the application of trifluoroacetic anhydride – sodium iodide (TFAA-I) system for microdetermination of sulphoxides (4) and for qualitative detection of sulphoxides and sulphimides by TLC chromatography (5). TFAA-I has also been used in the deoxygenation of quinoxalines 1,4-dioxides (6), its reactivity has been examined in reactions with other *N*-oxy compounds, including nitrones (7). Recently (8), we have established that aldonitrones react rapidly with TFAA-I, even under "analytical conditions" (0 to 20°C, approximately 5-fold excess of TFAA) forming compounds **4** and iodine according to eq. [1]:[3]

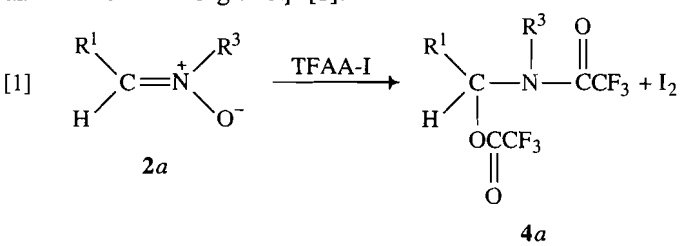

2*a* **4***a*

Reaction [1] proceeds with quantitative formation of iodine in very broad range of nitrones concentrations (10^{-1} to 10^{-6} M). Thus it can be used for quantitative determination of nitrones. The sensitivity of this procedure seems to be limited only by the method of iodine determination. Here we would like to present our approach for aldonitrones determination in which the use of TFAA-I reagent is combined with (*a*) the thiosulphate titration of released iodine with starch as an indicator and visual detection of the end point (μmole level of nitrones), and (*b*) the spectrophotometric determination of released iodine (nmole level of nitrones).

Experimental

Materials

Amine oxides — trimethylamine-*N*-oxide dihydrate, pyridine-*N*-oxide, 2-picoline-*N*-oxide, 3-picoline-*N*-oxide, and quinoline-*N*-oxide hydrate were purchased from Aldrich (Milwaukee, WI, USA). Trimethylamine-*N*-oxide, pyridine-*N*-oxide, picolines-*N*-oxide, and quinoline-*N*-oxide were dehydrated by double vacuum distillation. Quinoxaline-*N*-oxide was prepared according to ref. 6 and was of the same purity as previously reported.

Nitrones **2** were prepapred according to ref. 9 (**2***a* (9*a*), **2***b*, **2***c* (9*b*), **2***d* (9*c*), **2***e* (9*d*), **2***f* (9*e*), and **2***g* (9*f*). Nitrones **2***a–d* were purified by recrystallization to constant melting points: **2***a*: mp 85–86°C (84–86°C) (9*a*), **2***b*: mp 113–114°C (114°C) (9*b*), **2***c*: mp 115–117°C (116°C) (9*b*); **2***d*: mp 104–106°C (105°C) (9*c*). Nitrones **2***e–g* were purified by vacuum double distillation: **2***e*; bp 70–71°C/0.9 Tr, mp 29°C (66°C/0.6 Tr) (9*d*), **2***f*; bp 57–58.5°C/0.15 Tr, mp approx. 20°C, n_D^{20} = 1.4893 (9*e*), **2***g*; n_D^{22} = 1.4945 (9*f*).

Trifluoroacetic anhydride (TFAA) was purchased from Aldrich. Acetone was distilled over phosphorus pentoxide, redistilled over anhydrous potassium carbonate, and stored over molecular sieves, type 3A. Sodium iodide (Aldrich) was predried in a vacuum desiccator over phosphorus pentaoxide before use.

Solutions

NaI: 0.5 M solution of sodium iodide in anhydrous acetone.

TFAA: 0.5 M solution of trifluoroacetic anhydride in anhydrous acetone (the solution was prepared immediately before use).

Nitrones: 0.1 M solutions of nitrones **2***a–g* in anhydrous acetone. Working solutions of nitrones for spectrophotometric determinations were 5×10^{-4} *M* and were prepared immediately before use by dilution of 0.1 M solutions with anhydrous acetone.

Instruments

The absorption spectra were scanned on an instrument Specord UV-VIS, the absorbances were measured on a spectrophotometer VSU-2P (both Zeiss, Jena).

[1]To whom correspondence should be addressed.

[2]Revision received December 7, 1989.

[3]The structures of **3***a* and **4***a* were confirmed by GLC-MS measurements of corresponding reaction (TFAA-I and nitrone **2***a*) mixtures. Compounds **3***a* was also isolated from reaction mixture and compared with authentic imide **3***a*, synthesized independently. The results of mechanistic investigative reaction of TFAA-I and nitrones will be published in a separate paper.

TABLE 1. Comparison of the reaction course of TFAA–I with amine *N*-oxides **1** and nitrones **2**

Compound	Structure	Taken (μmoles)	Iodine determined (μmoles) 1 min	20 min	30 min	90 min	Solvent
1*a*	$Me_3\overset{+}{N}—O^-$ $(2H_2O)$	50	—	—	—	—	Acetone or AcOH–Ac_2O (90:10)
1*b*	$n\text{-}Pr_3\overset{+}{N}—O^-$	50	—	—	—	—	Acetone
1*c*	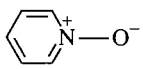	50	24	49.5	49.6		Acetone or AcOH–Ac_2O
1*d*	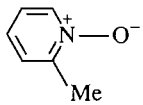	50	25	45	45		Acetone
1*e*	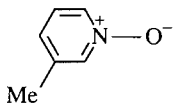	50	24	45	45		Acetone
1*f*	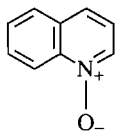	50	40	40	40		Acetone
1*g*	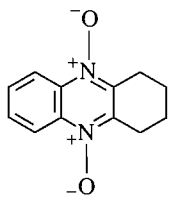	50	50	80	91	91	Acetone
2*a*	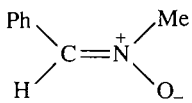	50	49.8	49.8			Acetone
2*e*	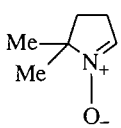	50	46 (47.8 $^{2\ min}$)	48	48	48	Acetone
2*f*	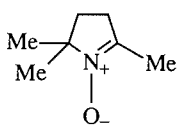	50	20	28.5	30	33	Acetone
2*g*	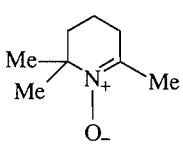	50	16	26	29		Acetone

Can. J. Chem. Downloaded from www.nrcresearchpress.com by 91.144.44.67 on 09/07/12
For personal use only.

Can. J. Chem. Downloaded from www.nrcresearchpress.com by 91.144.44.67 on 09/07/12
For personal use only.

TABLE 2. Comparison of the reaction course (μmoles of released iodine as a function of time) of various acylating agent – sodinm iodide systems with amine *N*-oxides **1** and nitrones **2**

Compound	Structure	Amount (μmoles)	Ac_2O–NaI			AcCl–NaI			PhC(O)Cl–NaI			TFAA–I		
			1 min	10 min	30 min	1 min	10 min	30 min	1 min	10 min	30 min	1 min	10 min	30 min
1*c*	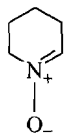	50	—	—	—	2.5	6.0	18.0	—	—	—	12	37.5	47
1*e*	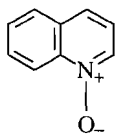	50	—	—	—	1.0	5.0	15.0	—	—	—	40	40	40
2*a*	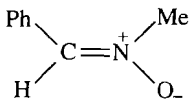	50	—	—	—	6.5	17.0	23.0	10.0	15.0	22.5	49.8	49.7	49.8
2*f*	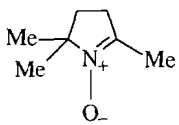	50	—	—	—	0.9	1.1	1.7	—	—	0.5	20	24	26.5

TABLE 3. The results of iodometric determination of nitrones using TFAA-I reagent

Compound	Structure	R^1	R^2	R^3	Taken (μmol)	Found (μmol)	Error (%)	R.S.D. ($n = 6$)
					20.0	19.9	−0.5	0.0066
2*a*		Ph	H	Me	50.0	49.7	−0.6	0.0050
					100.0	99.6	−0.4	0.0027
					20.0	19.9	−0.5	0.0076
2*b*	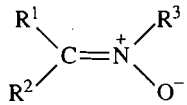	Ph	H	Ph	50.0	49.8	−0.4	0.0044
					100.0	100.2	+0.2	0.0032
					20.0	19.8	−1.0	0.0072
2*c*		*m*Cl—C_6H_4—	H	Ph	50.0	49.0	−2.0	0.0040
					100.0	98.8	−1.2	0.0026
					20.0	19.9	−0.5	0.0064
2*d*		*p*MeO—C_6H_4—	H	Ph	50.0	49.5	−1.0	0.0048
					100.0	99.4	−0.6	0.0030

Procedure

Iodometric titration

A known amount of nitrone (20–100 μmol contained in 200–100 μL 0.1 M solutions) is put into a 100 mL Erlenmayer flask and 1 mL of 0.5 M solution of NaI in acetone, followed by 0.8 mL of 0.5 M solution of TFAA in acetone are added. Iodine is immediately formed. After gentle mixing for 0.5 min the contents are diluted with 20 mL of 0.1 M solution of KI and titrated at once with sodium thiosulphate. At the end of titration, starch (0.5% aq. solution) is added.

Spectrophotometric determination

A known amount of nitrone (10 to 500 nmol) contained in 20 to 1000 μL of working solution is taken into a 10 mL volumetric flask and 1 mL of 0.5 M solution of NaI in acetone, followed by 100 μL of 0.5 M solution of TFAA in acetone are added. The reaction mixture is well mixed and diluted with acetone to 10 mL. Part of this solution is taken to a quartz type cuvette (for amounts of nitrone 10 to 50 nmol cuvettes with 50 mm light path and for 50 to 500 nmol cuvettes with 10 mm light path were used) and the reaction mixture absorbance (A) was measured after 2 min (since TFAA had been added), against acetone as a reference ($\lambda = 362$ nm, $t = 20$°C). The blank correction measurement (A_0) was performed also after 2 min for the reaction mixture of 1 mL of 0.5 M solution of NaI and 100 μL of 0.5 *M* solution of TFAA, diluted to 10 mL with anhydrous acetone, against acetone as a reference. The relation $A' = A - A_0$ as a function of nitrone quantity constituted the calibration line which was established on the base of nitrone **2***a* determinations (in the range of 10 to 500 nmol **2***a* — linear course) and was used in determinations of other nitrones.

Results and discussion

Apparent analytical feature of the reaction of nitrones with TFAA-I (Table 1) led to some additional investigations on the factors influencing the reaction course. One of the factors examined was the influence of the activity of acylation agents related to TFAA. Our results, summarized in Table 2, clearly reveal the change in reactivity in the following order: TFAA > AcCl > PhC(O)Cl > Ac_2O, which is in agreement with their relative acylation power. The results in Tables 1 and 2 also show that nitrones react faster than amines *N*-oxides and the reactivities of both nitrones and amines *N*-oxides are strongly dependent on the nature of the substituents. Thus, trialkylamine *N*-oxide treated with TFAA-I does not release iodine at all, whereas heterocyclic amines *N*-oxides react with nearly stoichiometric formation of iodine, showing the following reaction rate – structure dependence: quinoline *N*-oxide > quinoxaline *N*-oxide > pyridine *N*-oxide ~ picolines *N*-oxides. Similar differences are observed in reactions ot TFAA-I with nitrones: cyclic nitrones seem to be less reactive than acyclic, especially when bearing aryl substituents (Tables 1 and 2). It should be noted that the order of reagent addition strongly influences the reaction course, and consequently iodine formation. Thus, if the nitrone solution is first treated with TFAA and sodium iodide is added to this mixture later, only a small amount (approximately 10% of theoretical) of iodine is formed. This suggests that in the absence of iodide, acylated nitrone intermediate **2***A* rearranges to imide **3**, which is totally unreactive in further iodide oxidation (9) (eq. [2]).

[2] 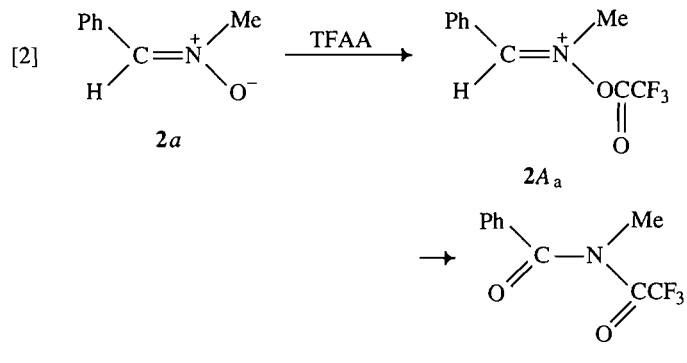

2*a* **2***A*$_a$ **3***a*

The results of nitrones determination by iodometric titration and spectrophotometric determination are summarized in Tables 3 and 4, respectively.

The iodometric titration of the iodine released permits one to determine nitrones at the 20 to 100 μmol level with an average deviation up to ±1% (R.S.D. 0.0027 to 0.0076). Because of the relatively high molecular absorbance of triiodide, formed *in situ* from released iodine and dissolved sodium iodide (Fig. 1) ($\epsilon = 2.5 \times 10^4$ mol L^{-1} cm^{-1} at 362 nm in acetone) this system also allows spectrophotometric determination of nitrones (equivalent to released iodine) at the 500 to 50 nmol level in standard ($l = 1$ cm) and at the 50 to 10 nmol level using cuvette with path light $l = 5$ cm. The average deviation of these determinations is ±2.8% and R.S.D. ($n = 6$) 0.022 to 0.066.

In principle, eq. [1] shows the reaction of TFAA-I with nitrones should be completed when exactly 1 mol trifluoroacetic anhydride (TFAA) and 2 mol sodium iodide are consumed.[4]

[4]In the case of ketonitrones (**2***f*, **2***g*), stoichiometry and the rate of reaction with TFAA-I are different (see Tables 1, 2).

Can. J. Chem. Downloaded from www.nrcresearchpress.com by 91.144.44.67 on 09/07/12
For personal use only.

TABLE 4. The results of spectrophotometric determination of nitrones using TFAA-I reagent ($\lambda(I_2)$ = 362 nm, l = 1 cm, n = 6)

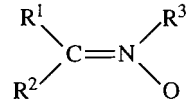

Compound	R^1	R^2	R^3	Taken (nmol)	Found (nmol)	Error (%)	R.S.D. × 10^{-3}
				50.0	51.0	+2.0	46
2*a*	Ph	H	Me	200.0	199.0	−0.5	36
				500.0	490.0	−2.0	24
				50.0	51.0	+2.0	46
2*b*	Ph	H	Ph	200.0	198.0	−1.0	30
				500.0	486.0	−2.8	22
				50.0	49.0	2.0	44
2*c*	*m*Cl—C_6H_4—	H	Ph	200.0	205.0	2.5	32
				500.0	492.0	1.6	26
				50.0	48.0	4.0	56
2*d*	*p*MeO—C_6H_4—	H	Ph	200.0	196.0	2.0	37
				500.0	510.0	2.0	30
2*a*	(l = 5 cm)			10.0	10.4	+4.0	84
				20.0	19.2	−4.0	66
				30.0	30.6	+2.0	34
				40.0	39.0	−2.5	27
				50.0	50.8	+1.6	20

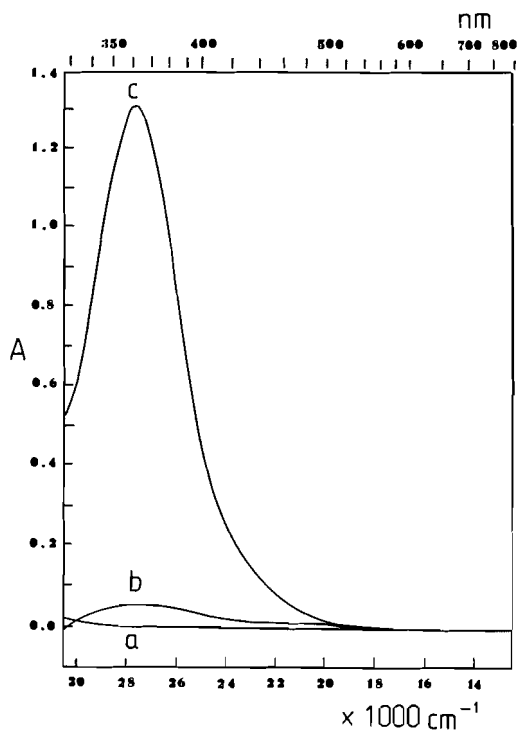

FIG. 1. Ultraviolet absorbance curves: (*a*) nitrones, (*b*) TFAA-I reagent, and (*c*) mixture of TFAA-I and nitrone. These curves were taken at standard conditions (2 min, 20°C, light path l = 1 cm) for solutions (*a*) 5 × 10^{-3} M of nitrone **2***a* or **2***b* (500 nmol nitrone in 10 mL acetone; (*b*) standard solution of TFAA-I in acetone (without nitrone); (*c*) standard reaction mixture containing 500 nmol of nitrone **2***a* (in 10 mL of acetonic solution).

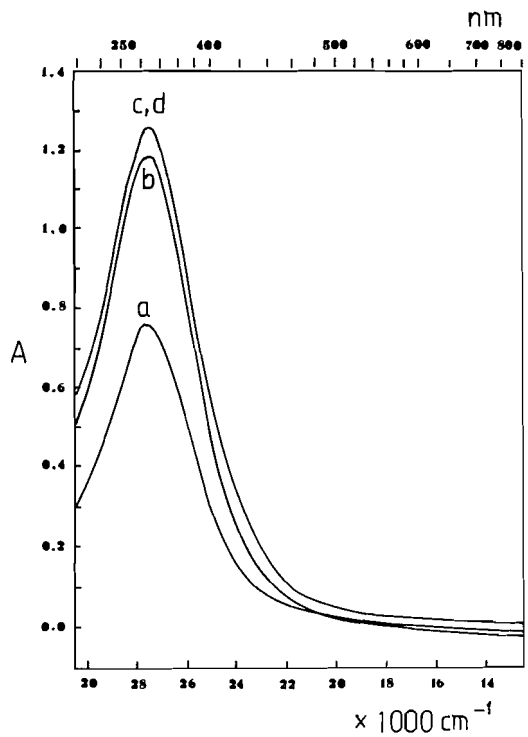

FIG. 2. The influence of sodium iodide on the uv absorbance of elemental iodine: (*a*) solution of iodine (500 nmol) in acetone (10 mL) (prepared by dilution of 50 μL of 0.01 M solution of iodine in acetone to 10 mL); (*b–d*) solutions of iodine (500 nmol) in 0.01 M (*b*), 0.05 M (*c*), and 0.1 M (*d*) acetone solutions of sodium iodide (10 mL).

However, TFAA is very easily hydrolyzed and to ensure that the reaction is completed in "analytical time" we have used at least four molar excess of TFAA and 2.5 molar excess of sodium iodide for determination on the μmole scale (with iodometric titration), and 100-fold excess of TFAA and 1000-fold excess of sodium iodide for spectrophotometric determination on nanomole level (Fig. 2). The low acidity of the reaction mixture (0.04 mmol TFAA) involves only marginal side-reaction of aerial oxidation of iodide, thus practically eliminates the

Can. J. Chem. Downloaded from www.nrcresearchpress.com by 91.144.44.67 on 09/07/12
For personal use only.

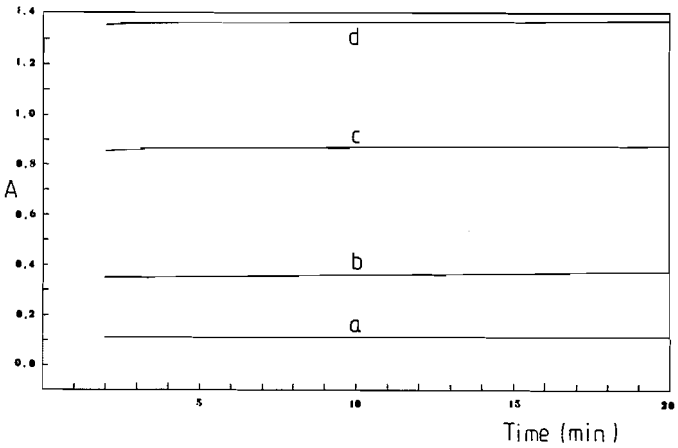

FIG. 3. The dependence of released iodine quantity as a function of the exposed time. The reaction mixture contains (*a*) standard solution of TFAA-I (without nitrone). The standard reaction mixture contains (*b*) 100 nmol, (*c*) 300 nmol, (*d*) 500 nmol nitrone **2***a*.

requirement of blank titration in titrimetric determinations of nitrones. However, in the spectrophotometric method, blank correction is needed since the iodine from aerial iodide oxidation constitutes a perceptible part of the total released iodine. Thus an examination of the course of iodine release as a function of time (Fig. 3) reveals that the reaction is completed in a few seconds after mixing the solutions, with slow gradual increase in iodine level caused by further air oxidation (A = 0.02 to A = 0.03 in 20 min). For this reason, blank correction was determined from the separate measurement of TFAA-I absorbance (standard condition: 2 min exposure, with acetone as reference) and this value was subtracted from measurements of nitrone determinations. The very low molecular absorbance of nitrones in the analytical wavelength region (Fig. 1) practically eliminates the requirement of additional correction of absorbance measurements.

Acknowledgements

This project was financially supported by the Polish Academy of Sciences under project CPBP 01.13. We are grateful to Dr. R. Nazarski of University of Łódź, Institute of Chemistry, for nitrones **2***e* and **2***f*. The authors also thank Professor M. Mikołajczyk for his interest in this work and his helpful discussion.

1. (*a*) E. BREUER. The chemistry of amino, nitroso and nitro compounds and their derivatives. *Edited by* S. Patai. John Wiley, New York. 1982. p. 458; (*b*) G. TENNANT. Comprehensive organic chemistry. *Edited by* D. H. Barton and W. D. Ollis. Vol. 2. Pergamon Press, New York. 1979. p. 500; (*c*) S. R. SANDLER and W. KARO. Organic functional group preparations. Vol. 2. Academic Press, New York. 1972. p. 301; (*d*) J. J. TUFARIELLO. 1,3-Dipolar cycloaddition chemistry. Vol. 2. *Edited by* A. Padwa. Wiley-Interscience, New York. 1984. Chap. 9.
2. (*a*) Special collection of papers on spin trapping chemistry. Can. J. Chem. **60**, 1379–1636 (1982); (*b*) C. A. EVAN. Aldrichim. Acta, **12**, 23 (1979).
3. (*a*) C. A. STREULI and P. R. AVERELL. The analytical chemistry of nitrogen and its compounds. Vol. 28. Wiley-Interscience, New York. 1970. p. 316; (*b*) E. HOFT and H. SCHULTZE. J. Prakt. Chem. **4**, 17 (1962).
4. W. CIESIELSKI, J. DRABOWICZ, W. JĘDRZEJEWSKI, Z. H. KUDZIN, and R. SKOWROŃSKI. Talanta, **35**, 969 (1988).
5. J. DRABOWICZ, A. KOTYŃSKI, and Z. H. KUDZIN. J. Chromatogr. **447**, 225 (1988).
6. F. R. HOMAIDAN, C. H. ISSIDORIDES. Heterocycles, **16**, 411 (1981).
7. W. CIESIELSKI, J. DRABOWICZ, W. JĘDRZEJEWSKI, Z. H. KUDZIN, and R. SKOWROŃSKI. Paper presented at the 31st International Congress of IUPAC. Sophia. 1987.
8. W. CIESIELSKI, J. DRABOWICZ, W. JĘDRZEJEWSKI, Z. H. KUDZIN, and R. SKOWROŃSKI. Paper presented on The Polish Chemical Society Congress, Łódź, Poland. 1988.
9. (*a*) P. DE SHONG and C. M. DICKEN. J. Org. Chem. **47**, 2047 (1982); (*b*) O. H. WHEELER and P. H. GORE. J. Am. Chem. Soc. **78**, 3363 (1956); (*c*) E. A. MEDIANCEVA, J. M. ANDRIJEVA, and W. L. MINKIN. Zh. Org. Khim. **8**, 146 (1972); (*d*) D. L. HAIRE, G. W. HILBORN, and E. G. JANZEN. J. Org. Chem. **51**, 4298 (1986); (*e*) R. B. NAZARSKI and R. SKOWROŃSKI. J. Chem. Soc. Perkin Trans. **1**, 1603 (1989); (*f*) M. R. TASZ, F. PLENAT, H. J. CRISTAU, and R. SKOWROŃSKI. Phosphorus Sulfur. To be published.

Can. J. Chem. Downloaded from www.nrcresearchpress.com by 91.144.44.67 on 09/07/12
For personal use only.

Reactions of confacial bioctahedral ditungsten(III) species: Product distribution in reactions of the μ-hydrido-(bis-μ-dimethylsulfide)bis(trichlorotungstate(III)) ion, and trichlorotungsten(III)(μ-hydrido)bis(μ-dimethylsulfide)(dimethylsulfide)-dichlorotungsten(III) with benzyl bromide and bromide ion[1]

JOANNE M. BALL, P. MICHAEL BOORMAN,[2] AND KELLY J. MOYNIHAN
Department of Chemistry, University of Calgary, Calgary, Alta., Canada T2N 1N4

Received September 13, 1989

JOANNE M. BALL, P. MICHAEL BOORMAN, and KELLY J. MOYNIHAN 1990. Can. J. Chem. **68**, 685 (1990).

Reactions of compound $Cl_3W(\mu\text{-}H)(\mu\text{-}Me_2S)_2WCl_2(Me_2S)$, **1**, and salts of derived chloro anion $[Cl_3W(\mu\text{-}H)(\mu\text{-}Me_2S)_2WCl_3]^-$, **2**, with bromide ion and with benzyl bromide are described. **1** was previously shown (1) to exist as a mixture of *meso* (C_{2v}) and DL-pair (C_1) of isomers, with the C_{2v} isomer being the more stable. Displacement of the terminal dimethyl sulfide ligand of **1** by bromide ion results in the formation of the analogous isomers of ion $[Cl_3W(\mu\text{-}H)(\mu\text{-}Me_2S)_2WCl_2Br]^-$, with retention of stereochemistry. The ^1H NMR spectra of compounds in this series are uniquely informative as to the isomers present since the two environments of the methyl groups in the bridging dimethyl sulfide ligands (axial and equatorial) provide a probe for the ion stereochemistry. This is used to show that in reactions of **2** with benzyl bromide, after replacement of μ-H by Br, Br exchanges with terminal chlorides to give a mixture of isomers. Reactions of **1** with benzyl bromide are further complicated by the fact that both terminal dimethyl sulfide and μ-H are replaced by bromides which then redistribute over all possible terminal sites.

Key words: hydride, confacial bioctahedral complexes, tungsten, bromocarbons.

JOANNE M. BALL, P. MICHAEL BOORMAN, et KELLY J. MOYNIHAN 1990. Can. J. Chem. **68**, 685 (1990).

On décrit les réactions du produit $Cl_3W(\mu\text{-}H)(\mu\text{-}Me_2S)_2WCl_2(Me_2S)$, **1**, et des sels du chloro anion $[Cl_3W(\mu\text{-}H)(\mu\text{-}Me_2S)_2WCl_3]^-$, **2**, avec l'ion bromure et avec le bromure de benzyle. Il a été démontré antérieurement (1) que le produit **1** existe sous la forme d'un mélange d'un isomère *méso* (C_{2v}) et d'une paire d'isomères-DL (C_1) et que l'isomère C_{2v} est le plus stable. Le déplacement du ligand sulfure de diméthyle terminal du produit **1** par l'ion bromure conduit à la formation des isomères analogues de l'ion $[Cl_3W(\mu\text{-}H)(\mu\text{-}Me_2S)_2WCl_2Br]^-$, avec rétention de la stéréochimie. Les spectres RMN du ^1H des composés de cette série fournissent des informations uniques sur la nature des isomères présents puisque les deux environnements des groupements méthyles des ligands sulfures de diméthyle agissant comme ponts (axial et équatorial) fournissent une sonde pour la stéréochimie de l'ion. On a utilisé ces sondes pour démontrer que, lors des réactions du composé **2** avec le bromure de benzyle suivie d'un remplacement du μ-H par un Br, le Br s'échange avec les chlorures terminaux pour donner un mélange d'isomères. Les réactions du composé **1** avec le bromure de benzyle sont encore plus compliquées par le fait que les deux sulfures de diméthyle terminaux ainsi que le μ-H sont remplacés par de ions bromures et qu'ils se redistribuent alors sur tous les sites possibles.

Mots clés : hydrure; complexes bioctaédriques confaciaux; tungtène; bromures de carbone.

[Traduit par la revue]

Introduction

The reactivity of confacial bioctahedral transition metal complexes has recently attracted considerable attention. Interconversion between edge-sharing and face-sharing bioctahedra in the presence of excess ligands is one method by which stereochemical rearrangements can take place (1). A second mechanism was recently demonstrated by Cotton and Luck (2), who showed that the interconversion between *syn* and *gauche* forms of the $[(PMe_3)Cl_2Mo(\mu\text{-}Cl)_3MoCl_2(Me_3P)]^-$ ion occurs through phosphine dissociation.

Cases involving an intramolecular exchange process between bridging and terminal ligands are less well documented; hence the observation of an example of this phenomenon in our laboratories (3) stimulated our interest in examining the factors which contribute to this kind of fluxionality. Processes of this type could be relevant to the potential catalytic properties of binuclear complexes possessing confacial bioctahedral structures, since coordinative unsaturation of one of the metal atoms can be achieved by bridge opening. The inclusion of hydride ligands in the coordination sphere of these M_2L_9 complexes would also be expected to enhance their potential reactivity. In an earlier publication (3) we reported the synthesis and characterization of the ditungsten(III) complex $Cl_3W(\mu\text{-}H)(\mu\text{-}Me_2S)_2WCl_2(Me_2S)$, **1** which, on the basis of a ^1H NMR study, was shown to exist as a mixture of two stereoisomers. As can be seen in Fig. 1, the C_{2v} isomer (*meso*) possesses just two pairs of environments (axial and equatorial) for the CH_3 groups of the two $\mu\text{-}Me_2S$ ligands whereas in the DL-pair of isomers (C_1 symmetry), the pairs of axial and equatorial CH_3 groups become inequivalent and as a result, four separate methyl resonances should be observed. However, we found that the DL-pair of enantiomers interconverted at room temperature in halocarbon solvents, via a fluxional process involving exchange of the terminal Me_2S ligand with the $\mu\text{-}Me_2S$ ligand *trans* to it. Through a different, and as yet undetermined route, the *meso* isomer was slowly produced from the C_1 isomers after extended periods in solution, and thus appears to be thermodynamically more stable. We then conducted a study of the reactivity of this compound with a variety of ligands and reagents and showed that the terminal Me_2S was readily displaced by Cl^- to yield anion $[Cl_3W(\mu\text{-}H)(\mu\text{-}Me_2S)_2WCl_3]^-$, **2** whose structure was determined crystallographically as the tetraphenylphosphonium salt (3). Subsequently, we reported (4) on the reactivity of **1** and **2** with chlorocarbons and several neutral ligands such as pyridine and MeCN, which resulted in a number of new W(III) binuclear complexes. In this paper we describe the reactivity of

[1]Taken in part from the Ph.D Theses of K. J. Moynihan, University of Calgary, 1983, and J. M. Ball, University of Calgary, 1988.

[2]Author to whom correspondence should be addressed.

Can. J. Chem. Downloaded from www.nrcresearchpress.com by 91.144.44.67 on 09/07/12
For personal use only.

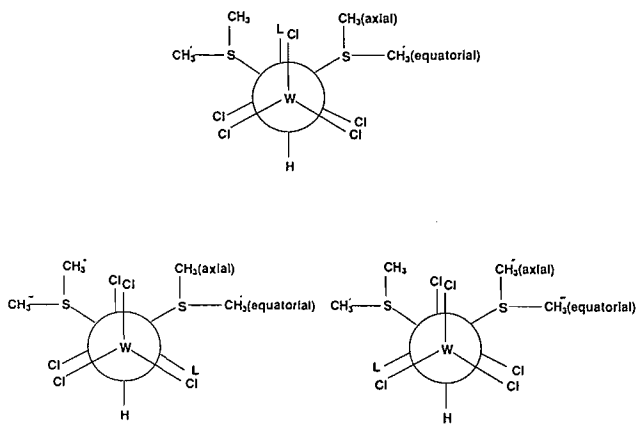

FIG. 1. Newman-type projection (along the W—W bond) of (*top*) the *meso* (C_{2v}) isomer of the confacial bioctahedral complex, $Cl_3W(\mu\text{-}H)(\mu\text{-}Me_2S)_2WCl_2L$, showing the two types of environment for the methyl groups of the bridging dimethyl sulfides; (*bottom*) the DL (C_1) pair of isomers, showing the four methyl environments.

TABLE 1. ^1H NMR spectral data (−70°C) for the two isomers of the anion $[Cl_3W(\mu\text{-}Cl)(\mu\text{-}Me_2S)_2WCl_2Br]^-$ in CD_2Cl_2. Ratio of C_s:C_1 is ~2:1.

Chemical shift (ppm)	Integration	Assignment
3.66	3	C_1 Me
3.56	12	C_s Me (axial)
3.51	3	C_1 Me
3.31	1	C_1 μ-H
3.18	12	C_s Me (equatorial)
3.10	3	C_1 Me
3.05	3	C_1 Me
2.77	2	C_s μ-H

1 and **2** with bromide ion and with benzyl bromide. It was anticipated that the reactivity pattern would be similar to that observed with Cl^- and with benzyl chloride (4). The latter compound reacts with the neutral complex **1** to yield the salt $[PhCH_2SMe_2][Cl_3W(\mu\text{-}Cl)(\mu\text{-}Me_2S)_2WCl_3]$, along with toluene. However, a more detailed understanding of the stereochemistry of these reactions would result from the distinction between the incoming bromide and the existing chloride ligands in the molecule.

Results

Reactions of neutral compound **1** can be divided into two types; namely, those involving displacement of the terminal dimethyl sulfide ligand and those which also involve the bridging hydride.

Initially we examined the reaction of **1** with tetraphenylphosphonium bromide in chlorocarbon solvents at ambient temperatures. It was anticipated that by analogy with the reaction of **1** with chloride ion under the same conditions the product would be the tetraphenylphosphonium salt of anion $[Cl_3W(\mu\text{-}H)(\mu\text{-}Me_2S)_2WCl_2Br]^-$. However, the stereochemistry would be distinguishable in this case since replacement of the terminal Me_2S from the C_s isomer would yield a product with C_s symmetry, whereas the C_1 isomeric pair would yield a pair of enantiomeric product ions with the same C_1 symmetry. The ^1H NMR spectra of the C_s isomer would consist of two methyl resonances of equal intensity stemming from the axial and equatorial Me groups of the $\mu\text{-}Me_2S$ groups, whereas the C_1 isomeric pair would be expected to produce four different methyl resonances (Fig. 1). The spectral data for the recrystallised product obtained from the reaction of **1** with PPh_4Br are given in Table 1. Resonances due to the phosphonium cation are not included, but the total integrations were consistent with the assignments given here. These assignments, for μ-H and axial/equatorial methyl groups of the bridging methyl sulfide ligands, are based on those reported earlier (3). As shown in Fig. 2 the spectrum is temperature dependent, and is best resolved at −70°C. Hence this is the spectrum reported in Table 1. The assignments for this bromo anion are based on those given earlier for the analogous chloro anion of **1** (3). The spectrum shows that both the more symmetric C_s isomer and the C_1 pair are produced, in approximately the same 2:1 ratio as in the starting material **1**. Thus the displacement of the terminal dimethyl sulfide ligand (confirmed by the presence of a signal due to the free ligand) occurs without significant change of configuration of the tungsten. Even in the presence of an excess of bromide there is no evidence that displacement of the terminal chloride ligands of **1** to give anions of the general formula $[W_2(\mu\text{-}H)(\mu\text{-}Me_2S)_2Cl_{6-n}Br_n]^-$ occurs. This is in contrast to the reactions of anion **2** with arylthiolate anions which rapidly displace chloride (5). In the spectral assignments given in Fig. 2 it is noteable that resonances due to μ-H ligands of the stereoisomers of bromo anion occur in the same general region of the spectrum as methyl resonances, rather than upfield of TMS. This phenomenon has been observed for other μ-hydrido complexes of tungsten (3, 6). By comparison with the ^1H NMR behavior of **1** and **2**, these hydride resonances were expected to display a temperature dependence. As shown in Fig. 2, at −70°C the C_s isomer displays a sharp hydride resonance at δ 2.77, while the C_1 pair has a hydride resonance at δ 3.31 ppm. With increasing temperature, these resonances broaden and move to lower field. This phenomenon appears to be common to all the complexes we have studied which contain the $W(\mu\text{-}H)(\mu\text{-}Me_2S)_2W$ entity. In previous work (3), we showed that $^{183}W—^1H$ coupling constants remained constant at ca. 105 Hz over the accessible temperature range, suggesting that the temperature dependence of δ was not caused by any process involving W—H bond cleavage. Chemical shifts of methyl sulfide resonances are independent of temperature, and are not involved in any exchange processes with the terminal ligand, in contrast to the behavior of C_1 isomers of precursor molecule **1** (3).

The thermodynamic stability of M—Cl bonds is, in general, greater than that of equivalent M—Br bonds. Consequently the reaction of solutions of mixed isomers of the $[BrCl_2W(\mu\text{-}H)(\mu\text{-}Me_2S)_2WCl_3]^-$ ion with tetraphenylphosphonium chloride in CD_2Cl_2 solution gave rise to a quantitative conversion to the perchloro anion, $[Cl_3W(\mu\text{-}H)(\mu\text{-}Me_2S)_2WCl_3]^-$. The characteristic ^1H NMR resonances of this anion (two singlets of equal intensity at δ 3.10 and 3.56 ppm), completely replace the group of six resonances in this region due to the two isomers of the bromoanion precursor. This helped to verify the identity of the bromo anion, but the availability of good quality crystals of tetraphenylphosphonium salt of this species prompted us to attempt to carry out an X-ray crystallographic investigation. Identity of bromo anion **3** was confirmed,[3] but the structure determination was complicated by the weighted disorder of the bromine atom among the six possible terminal ligand positions.

[3]Crystal data: formula: $[PPh_4][Cl_3W(\mu\text{-}H)(\mu\text{-}Me_2S)_2WCl_2Br]$; space group orthorhombic, $P2_1nb$; a = 12.041(3), b = 13.221(2), c = 22.782(3) Å

Can. J. Chem. Downloaded from www.nrcresearchpress.com by 91.144.44.67 on 09/07/12
For personal use only.

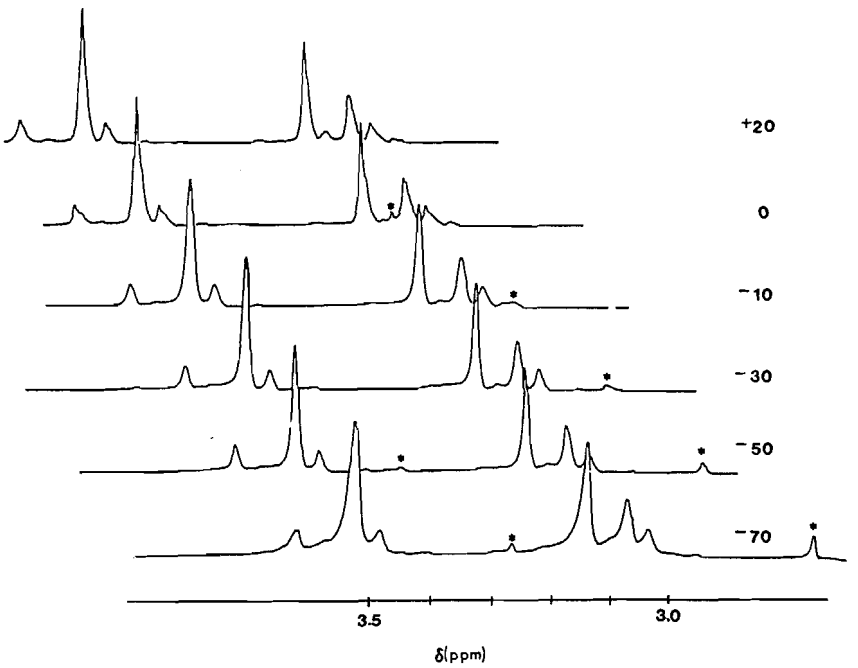

FIG. 2. Variable temperature (°C) 200 MHz ^{1}H NMR spectrum of $[Ph_4P][Cl_3W(\mu\text{-}H)(\mu\text{-}Me_2S)_2WCl_2Br]$ in CD_2Cl_2 solution. The asterisk denote the resonances assigned to the μ-H species for the two isomers; see assignments in Table 1.

Can. J. Chem. Downloaded from www.nrcresearchpress.com by 91.144.44.67 on 09/07/12
For personal use only.

Since the ^{1}H NMR spectrum of the solution had indicated that the compound is a mixture of two isomers, this form of disorder in the crystal structure might have been anticipated. Because the crystal contains a mixture of two stereoisomers, bond length and bond angle data will all be averages, and therefore would provide no definitive structural comparisons with the analogous chloro anion, **2**. This structure will be reported separately (7), since its refinement is of greater crystallographic than chemical interest.

Reactions of 1 and 2 with benzyl bromide

It was shown previously that the bridging hydride in **1** and **2** was capable of reducing various chlorocarbons at elevated temperatures (i.e. ca. 80°C) to yield an alkane and the anion $[Cl_3W(\mu\text{-}Cl)(\mu\text{-}Me_2S)_2WCl_3]^-$ (4). The replacement of μ-H by μ-Cl enabled us to make direct structural comparisons between these two binuclear anions, thus affording an opportunity to examine the effect of this type of ligand substitution on the W—W bond length. It was therefore anticipated that other halide ions might be introduced into the bridging position of the binuclear framework by suitable selection of reactive halocarbon. In addition, reactions of this type would provide information on the possible exchange between bridging and terminal sites during the reaction. The simplest of these reactions is that between RX and anion **2**, which can be represented (in the absence of halide scrambling) as:

$$[1]\quad [Cl_3W(\mu\text{-}H)(\mu\text{-}Me_2S)_2WCl_3]^- + RX \xrightarrow{\Delta} [Cl_3W(\mu\text{-}X)(\mu\text{-}Me_2S)_2WCl_3]^- + RH$$

The neutral compound **1** is subject to replacement of terminal dimethyl sulfide as well as replacement of hydride. Alkylation of terminal dimethyl sulfide yields sulfonium cation:

$$[2]\quad Cl_3W(\mu\text{-}H)(\mu\text{-}Me_2S)_2WCl_2(Me_2S) + 2RX \xrightarrow{\Delta} [RMe_2S]^+[Cl_3W(\mu\text{-}X)(\mu\text{-}Me_2S)_2WCl_2X]^- + RH$$

We carried out both types of reactions for RX = benzyl bromide. First, the compound $\{[Ph_4P][Cl_3W(\mu\text{-}H)(\mu\text{-}Me_2S)_2WCl_3]\}\cdot 2CH_2Cl_2$ was dissolved in $C_2H_4Cl_2$ with an excess of benzyl bromide and refluxed for ca. 2 h (see Experimental). Toluene was identified in the reaction volatiles as expected. After removal of the solvent and recrystallization of the reaction product from dichloromethane, the ^{1}H NMR spectrum of the resulting orange–brown crystals was obtained in CD_2Cl_2. This is shown in Fig. 3(*a*). Instead of the simple pattern expected for axial and equatorial methyl group protons in $[Cl_3W(\mu\text{-}Br)(\mu\text{-}Me_2S)_2WCl_3]^-$, (i.e. two singlets of equal intensity corresponding to the two equivalent pairs of environments), a complex multiplet is observed for each site, with the pattern being identical in both multiplets. This clearly indicated that bromine scrambling in the ditungsten(III) species had occurred. The three possible isomeric forms for the ion $[W_2Cl_6Br(Me_2S)_2]^-$ are shown in Fig. 4. It is clear that these three forms are inadequate to account for the spectrum observed, and that in all probability small amounts of dibromo- and possibly more highly substituted analogs, along with perchloro anion, were formed. It would therefore appear that redistribution of the bromide among the possible sites has occurred, and that there is some further substitution of chloride by bromide. There is, however, no indication that substitution reactions displace the μ-Me_2S ligands.

A plausible mechanism for this reaction is given in Scheme 1. In view of the elevated temperature required for any of the halocarbons to react with μ-hydride, the likely first step is the cleavage of a W—H bond, thereby generating the more reactive terminal hydride ligand. In the presence of benzyl bromide, in dichloroethane solvent, this hydride will have two possible C—X bonds to react with, but that with the more labile C—Br bond will be preferred. The coordinatively unsaturated intermediate so produced could then return to a confacial bioctahedral structure by either of two the pathways shown in Scheme 1. This could occur before the hydride reacts, as depicted in the

Can. J. Chem. Downloaded from www.nrcresearchpress.com by 91.144.44.67 on 09/07/12
For personal use only.

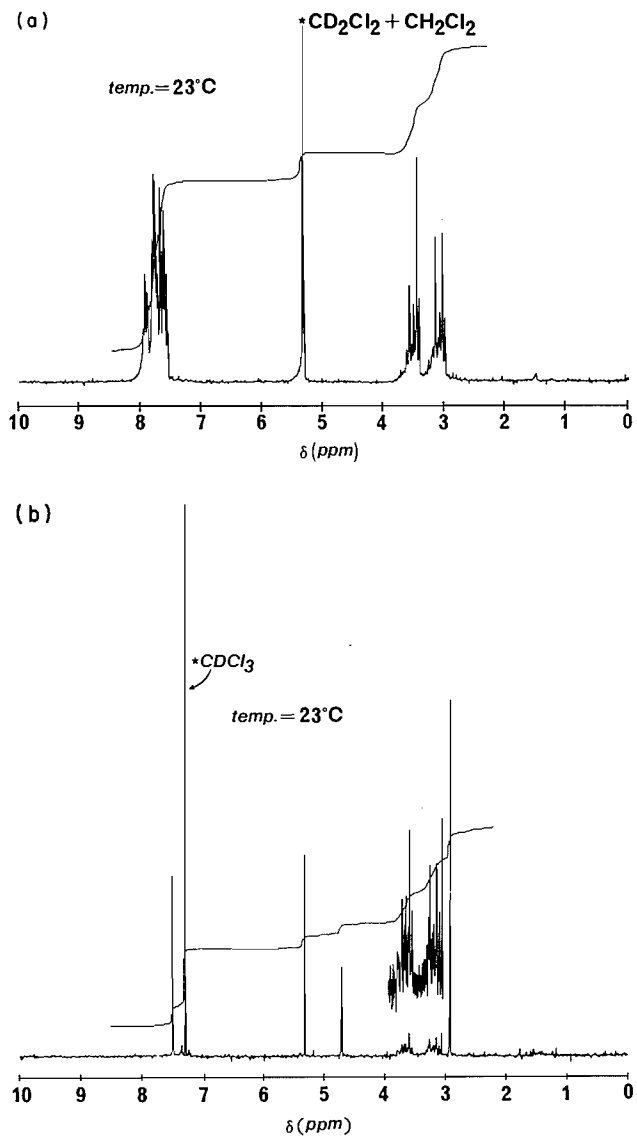

FIG. 3. (*a*) 200 MHz ^{1}H NMR spectrum (in CD_2Cl_2) of the product of reaction of **2** with benzyl bromide, $[Ph_4P][W_2Cl_{7-n}Br_n(Me_2S)_2]\cdot CH_2Cl_2$, ($n \sim 1$); (*b*) 200 MHz ^{1}H NMR spectrum (in CD_2Cl_2) of the product of reaction of **1** with benzyl bromide, $[PhCH_2SMe_2][W_2Cl_{7-n}Br_n(Me_2S)_2]\cdot CH_2Cl_2$, ($n \sim 2$). Resonances due to the axial and equatorial methyl groups of the μ-Me_2S groups have been expanded for clarity. Other signals are due to the sulfonium cation and CH_2Cl_2 of solvation.

central portion of the scheme. A similar mechanism was proposed by us earlier to account for the exchange between terminal and bridging Me_2S in **1**.[3] The interconversion between isomer **A**, **B**, and **C** could be explained on the same basis.

By analogy with this system, the spectrum of the product from the elevated temperature reaction between benzyl bromide and neutral compound 1 (as in [2] above) would be expected to possess an even more complex pattern in the methyl resonance region of the ^{1}H NMR spectrum, since a minimum of two bromines will be present in ditungsten(III) anion. A species with formula $[W_2Cl_5Br_2(\mu\text{-}Me_2S)_2]^-$ can be shown to exist as eight geometric isomers, three of which are enantiomeric. As shown in Fig. 3(*b*) the two multiplets in the μ-Me_2S region are indeed more complex, but to account for this spectrum, possible isomers of the dibromo anion alone are inadequate. Small amounts of more highly substituted isomers must also be present, along with monobromo and perchloro anions. These findings are of interest from two points of view. Firstly the binuclear anion retains its basic structural pattern even though there is a substantial change in the ligand set. This has been observed previously in confacial bioctahedral ditungsten(III) complexes by Hawkins and Garner, who studied chloride exchange in the $W_2Cl_9^{3-}$ anion and concluded that all sites were equivalent (8). More recently, it has been shown that halide ions can be replaced by chalcogenide ions in the basic octahedral cluster unit of $M_6X_8^{4+}$ (9). The second aspect worthy of comment is that, by implication, binuclear clusters might be capable of catalyzing the exchange of halide groups between benzyl molecules. This would logically ensue from the following implied reaction.

$$\text{W-Cl} + \text{Bz-Br} \leftrightharpoons \text{W-Br} + \text{Bz-Cl}$$

Small amounts of perchloro anion may be generated, a result of halide-generated exchange process in the chlorocarbon solvent.

Experimental

Starting materials **1** and **2** were prepared as described in ref. 3; a freshly prepared sample of **1** was used in each reaction, since it loses its terminal dimethyl sulfide over extended periods of time. All reactions and handling procedures were carried out in an atmosphere of pure dry nitrogen, by using standard Schlenk tube and glovebox techniques. Reagents, sources and drying procedures/agents were as follows: benzyl bromide (B.D.H.), dried over $MgSO_4$; tetraphenylphosphonium bromide (Aldrich), dried at 100°C *in vacuo*; acetonitrile (Fisher), dried over P_2O_5, then CaH_2; all other solvents and reagents were dried and degassed before use, as previously described (3, 4). Mass spectra were obtained using a Varian MAT CH-5 spectrometer, and ^{1}H NMR spectra were obtained using a Varian XL-200 or a Bruker ACE-200 MHz spectrometer.

Preparation of $[Ph_4P][BrCl_2W(\mu\text{-}H)(\mu\text{-}Me_2S)_2WCl_3]$

$Cl_3W(\mu\text{-}H)(\mu\text{-}Me_2S)_2WCl_2(Me_2S)$ (0.544 g, 0.74 mmol) and Ph_4PBr (0.31 g, 0.74 mmol) were placed in a Schlenk tube with dichloromethane (30 mL) and stirred for 30 min. A darkening in color of the reaction mixture indicated that the desired displacement of dimethyl sulfide by bromide ion had occurred, consistent with the results of an NMR study of this reaction. The solution was filtered after 12 h, and the resulting purple filtrate was reduced in volume to 15 mL. Hexane (15 mL) was slowly added to this solution. Cooling the solution to 10°C yielded a purple microcrystalline material, which after recrystallization from dichloromethane/hexane yielded crystals of X-ray quality. Yield: 0.75 g, 94% based on W. *Anal.* calcd for $W_2Cl_5BrPS_2C_{28}H_{32}$: C 30.80, H 3.05, S 5.88; found (M.H.W. Labs.): C 30.86, H 3.05, S 5.91.

Preparation of $[Ph_4P][W_2Cl_{7-n}Br_n(Me_2S)_2] \sim 1.5\ CH_2Cl_2$ (n ~ 1)

Reaction of neat benzyl bromide (ca. 1mL) with $[Ph_4P][Cl_3W(\mu\text{-}H)(\mu\text{-}Me_2S)_2WCl_3]\cdot 2CH_2Cl_2$ (0.27 g, 0.22 mmol) in $C_2H_4Cl_2$ (30 mL) at reflux temperature (~80°C) for a period of 2 h yielded an orange–red solid solution which was evaporated to dryness under vacuum. The solid product was recrystallized from a dichloromethane–hexane mixture to give the crystalline product. Yield: 0.19 g. The compound was characterized by its ^{1}H NMR spectrum as described above, but the labile nature of the CH_2Cl_2 of solvation precluded good elemental analysis. Toluene (GC analysis of the reaction volatiles) was found to be produced in the reaction, as expected.

Preparation of $[Me_2SCH_2Ph][W_2Cl_{7-n}Br_n(Me_2S)_2]\cdot CH_2Cl_2$ (n ~ 2)

1 (0.15 g, 0.20 mmol) was dissolved in $C_2H_4Cl_2$ (30 mL) and reacted with benzyl bromide (0.6 mL) at reflux temperature (~80°C) for 2 h. The orange–red solution was filtered, and the solvent removed under vacuum. The product was redissolved in CH_2Cl_2 (15 mL)

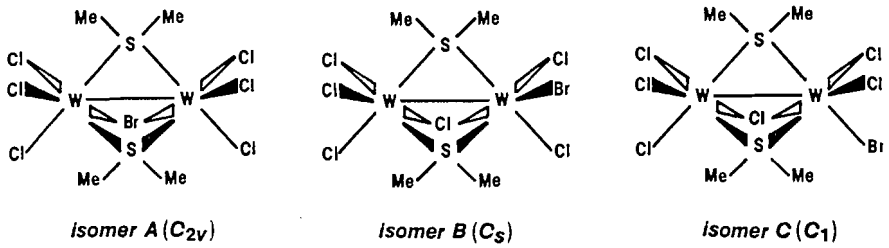

FIG. 4. Possible isomeric forms of the ion $[W_2Cl_6Br(\mu\text{-}Me_2S)_2]^-$.

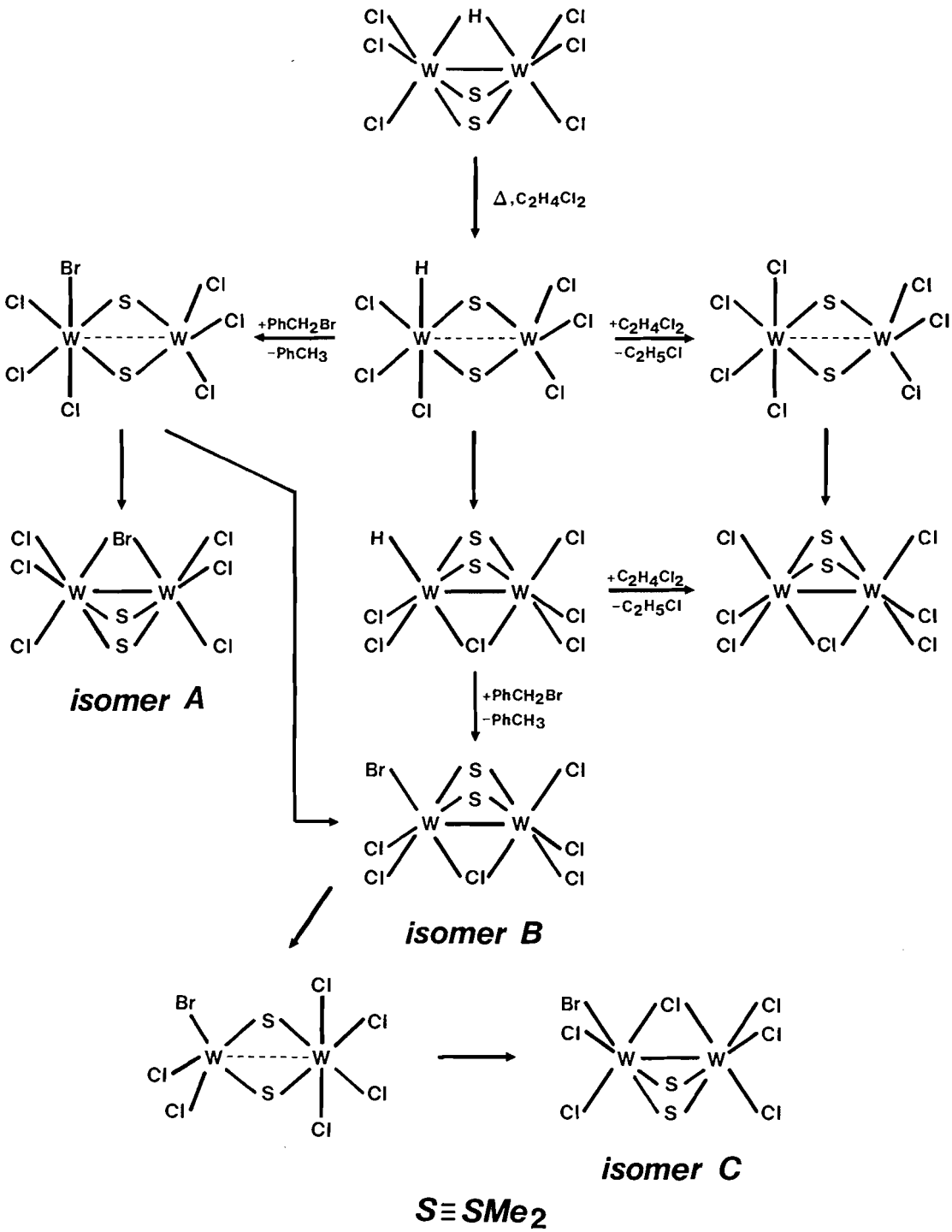

SCHEME 1. Postulated mechanism for the formation of halogenated products from anion **2**.

Can. J. Chem. Downloaded from www.nrcresearchpress.com by 91.144.44.67 on 09/07/12
For personal use only.

and hexane added (ca. 3 mL). After cooling to −20°C the solution deposited orange–red crystals which proved to be the above compound. Yield: 0.13 g. Reproducible analytical data were precluded by the labile nature of the solvent of crystallization. ^{1}H NMR data for this complex were discussed in the text.

Acknowledgements

The authors thank the Natural Sciences and Engineering Research Council of Canada for financial support (to P. M. B., J. M. B., and K. J. M.) and Dr R. Yamdagni for assistance in obtaining variable temperature N.M.R. data. Dr J. F. Fait's co-operation in providing information on the disordered crystal structure of the bromo anion is also gratefully acknowledged.

1. S. T. Chacon, M. H. Chisholm, W. E. Streib, and W. Van der Sluys. Inorg. Chem. **28**, 6 (1989).
2. F. A. Cotton and R. L. Luck. Inorg. Chem. **28**, 182 (1989).
3. P. M. Boorman, K. J. Moynihan, V. D. Patel, and J. F. Richardson. Inorg. Chem. **24**, 2989 (1985).
4. P. M. Boorman, K. J. Moynihan, and J. F. Richardson. Inorg. Chem. **27**, 3207 (1988).
5. J. M. Ball. Ph.D. Thesis, Univ. of Calgary, Calgary, Alta. 1988.
6. M. Akiyama, M. H. Chisholm, F. A. Cotton, M. W. Extine, D. A. Haitko, J. Leonelli, and D. Little. J. Am. Chem. Soc. **103**, 779 (1981).
7. J. F. Fait. Acta Crystallogr. To be submitted.
8. G. L. Hawkins and C. S. Garner. J. Am. Chem. Soc. **80**, 2946 (1958).
9. J. B. Michel and R. E. McCarley. Inorg. Chem. **21**, 1862 (1982).

Can. J. Chem. Downloaded from www.nrcresearchpress.com by 91.144.44.67 on 09/07/12
For personal use only.

Effect of substituents on the solvatochromism of stilbazolium merocyanines

MALGORZATA NIEDBALSKA[1] AND ILONA GRUDA[2]

Département de chimie–biologie, Université du Québec à Trois-Rivières, Trois-Rivières (Québec), Canada G9A 5H7

Received April 10, 1989[3]

MALGORZATA NIEDBALSKA and ILONA GRUDA. Can. J. Chem. **68**, 691 (1990).

The visible spectra of a series of merocyanines, derivatives of 4-[(4-oxocyclohexa-2,5-dienylidene)ethylidene]-1,4-dihydropyridine, have been investigated in a number of solvents and solvent mixtures. The effect of substituents on the solvatochromic behaviour of these compounds is described. All investigated merocyanines exhibited a strong negative solvatochromism. Inverse solvatochromism was observed in solvents of very low polarity for polar dyes, and in polar solvents for dyes containing hydrophobic substituents. This inversion of the solvatochromic behaviour is attributed to aggregation phenomena.

Key words: merocyanines, solvatochromism, betaine, aggregation.

MALGORZATA NIEDBALSKA et ILONA GRUDA. Can. J. Chem. **68**, 691 (1990).

Opérant dans un certain nombre de solvants et de mélanges de solvants, on a déterminé les spectres visibles d'une série de mérocyanines dérivées de la 4-[(4-oxocyclohexa-2,5-dièny1dène)éthylidène]-1,4-dihydropyridine. On décrit l'effet solvatochromique de ces composés. Toutes les mérocyanines étudiées présentent un solvatochromisme fortement négatif. On a observé un solvatochromisme inverse avec des solvants de très basse polarité mis en présence de colorants polaires et avec des solvants polaires mis en présence de colorants contenant des substituants hydrophobes. On attribue cette inversion dans le comportement solvatochromique à un phénomène d'agrégation.

Mots clés : mérocyanines, solvatochromisme, bétaïne, agrégation.

[Traduit par la revue]

Can. J. Chem. Downloaded from www.nrcresearchpress.com by 91.144.44.67 on 09/07/12
For personal use only.

Introduction

Merocyanine dyes of the stilbazolium betaine type (Table 1) have attracted much attention because of the extreme sensitivity of their electronic spectra to the medium (1–3). These spectra are strongly dependent on pH and polarity of their microenvironment and also on the external electric field (4, 5). The model compound, **1***a*, exhibits a very strong negative solvatochromism. This behaviour indicates that the ground state of the dye (much more polar than its excited state) acquires extra stabilization with increased polarity of the solvent. It has been reported recently that in solvents of very low polarity (E_T < 34.6) **1***a* undergoes an inverted solvatochromism, which implies a significant structural change of **1***a* in this kind of solvent (6).

We have shown previously (7) that the introduction of alkyl substituents into the quinonoid ring of stilbazolium betaines strongly influences the solvatochromic behaviour of these compounds. However, no systematic study has been done on the effect of substituents on the spectral properties of stilbazolium betaines. In this article we report the results obtained for several stilbazolium merocyanines substituted by electron-withdrawing or electron-donating groups. To cover a large scale of polarities, we used two solvent mixtures: pyridine–water and pyridine–cyclohexane.

Experimental

Melting points were taken on a Fisher–Johns melting point apparatus and are uncorrected. All merocyanines were synthesized according to the procedure described earlier (7). Compounds **1***b*, **1***c*, **1***d*, **1***g*, and **1***h* were described previously, as shown in Table 1. IR spectra were taken on a Perkin–Elmer model 597 spectrometer. Elemental analyses were performed by Guelph Chemical Lab. Ltd., Guelph, Ontario.

*1-(6-Hydroxyhexyl)-4-[(3-nitro-4-oxocyclohexa-2,5-dienylidene)ethylidene]-1,4-dihydropyridine (***1**e**)* was synthesized from the corresponding pyridinium salt (8) and 3-nitro-4-hydroxybenzaldehyde. The solid was twice recrystallized from ethanol – aqueous ammonia, treated with 10% NaOH, and washed several times with concentrated ammonium hydroxide; 84% yield, dark red solid with metallic luster, mp 218–220°C; IR (KBr): 3400, 1640, 1590, 1520, 1460, 1420, 1330, 1260, 1230, 1160, 1060, 1040, 960 cm^{-1}; ^1H NMR (Me_2SO-d_6) δ: 1.30 (m, 8), 3.30 (t, 2), 4.35 (t, 2), 6.33 (d, 1), 6.70 (d, 1), 7.50 (d, 1), 7.80 (m, 5), 8.60 (d, 1). Anal. calcd. for $C_{19}H_{22}N_2O_4$: C 66.67, H 6.43, N 8.19; found: C 67.05, H 6.82, N 8.26.

TABLE 1. Structure of merocyanines

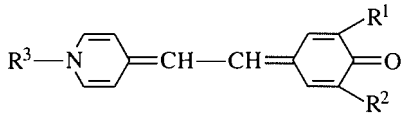

1

Compound	R^1	R^2	R^3	Ref.
1*a*	H	H	CH_3	1
1*b*	H	H	$(CH_2)_6OH$	7
1*c*	*t*-Bu	*t*-Bu	$(CH_2)_6OH$	7
1*d*	OCH_3	OCH_3	$(CH_2)_6OH$	9
1*e*	H	NO_2	$(CH_2)_6OH$	*
1*f*	NO_2	NO_2	$(CH_2)_6OH$	*
1*g*	CH_3	CH_3	$(CH_2)_6OH$	7
1*h*	*t*-Bu	*t*-Bu	$(CH_2)_{11}OH$	10
1*i*	*t*-Bu	*t*-Bu	$(CH_2)_{15}CH_3$	*

*Synthesized in this work. See experimental section.

*1-(6-Hydroxyhexyl)-4-[(3,5-dinitro-4-oxocyclohexa-2,5-dienylidene)ethylidene]-1,4-dihydropyridine (***1**f**)* was synthesized similarly from 3,5-dinitro-4-hydroxybenzaldehyde. The product was twice recrystallized from pyridine–ethanol; 60% yield, red solid, mp 252–255°C; IR (KBr): 3400, 1640, 1590, 1540, 1500, 1460, 1420, 1340, 1320, 1260, 1230, 1200, 1160, 1100, 1040, 960 cm^{-1}; ^1H NMR (Me_2SO-d_6) δ: 1.30 (m, 8), 4.32 (t, 2), 7.10 (d, 1), 7.90 (d, 1), 8.00 (m, 4), 8.75 (d, 2). Anal. calcd. for $C_{19}H_{21}N_3O_6$: C 58.90, H 5.42, N 10.85; found: C 59.60, H 5.51, N 10.93.

*1-Hexadecyl-4-[(3,5-di-*tert*-butyl-4-oxocyclohexa-2,5-dienylidene)ethylidene]-1,4-dihydropyridine (***1**i**)* was synthesized similarly from the corresponding pyridinium salt (3) and 3,5-di-*tert*-butyl-4-

[1]On study leave. Permanent address: Institut of Physics, Poznan Technical University, Poznan, Poland.

[2]Author to whom correspondence may be addressed.

[3]Revision received January 2, 1990.

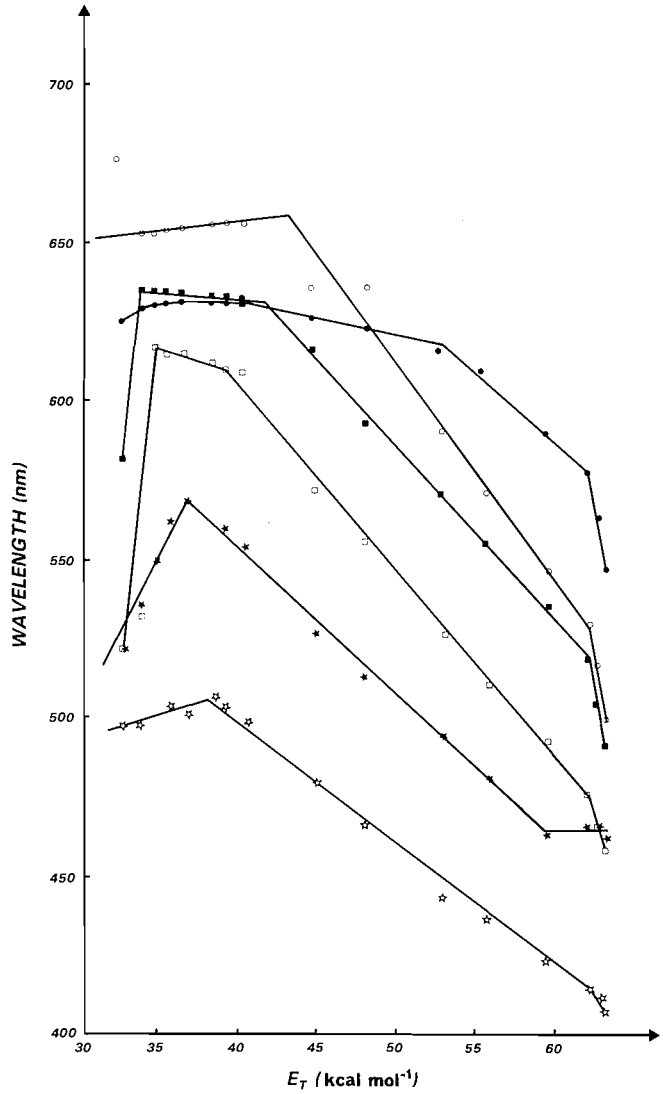

FIG. 1. Effect of the solvent polarity on the long wavelength absorption band of merocyanines: **1***b*, □; **1***c*, ●; **1***d*, ○; **1***e*, *; **1***f*, ☆; **1***g*, ■.

hydroxybenzaldehyde. The product was recrystallized twice from pyridine – aqueous ammonia; 67% yield, dark brown solid with metallic luster, mp 87–90°C; IR (KBr): 2900, 2850, 1640, 1600, 1560, 1500, 1460, 1420, 1320, 1250, 1150, 1010, 950 cm^{-1}; ^{1}H NMR (Me_2SO-d_6) δ: 0.95 (t, 3), 1.33 (s, 18), 1.40 (m, 28), 3.70 (t, 2), 6.10 (d, 1), 6.70 (d, 1), 7.20 (m, 6). Anal. calcd. for $C_{37}H_{59}NO$: C 83.30, H 11.07, N 2.63; found: C 82.75, H 10.73, N 2.80.

Spectra

Absorption spectra were recorded on a Perkin–Elmer Lambda 4B spectrophotometer. Cyclohexane (Fisher) and pyridine (Aldrich) were spectrophotometric grade and were used without further purification. Solutions (10^{-5} M) of merocyanines **1***b*–**1***i* were prepared in the following solvents and solvent mixtures: cyclohexane–pyridine, v/v (90, 80, 70, 60, 50, 30, and 20%), pyridine, 0.5% aq. NaOH – pyridine, v/v (5, 10, 20, 30, 50, 80, 90, 95%). We used 0.5% NaOH in order to avoid the protonation of merocyanines that occurs in pure water (7).

Results

Table 1 shows the compounds studied in this work. Compounds **1***b*–**1***g* were dissolved in anhydrous pyridine and solutions of various polarities were prepared by adding appropriate amounts of pyridine and 0.5% NaOH or cyclohexane. Figure 1 shows the changes in λ_{max} of the long wavelength absorption band as a function of the E_T parameter, which is considered to be an appropriate measure of solvent polarity for spectral studies (11). We calculated the E_T for the mixtures of solvents assuming molar additivity of this parameter. A similar pattern of curves was obtained when dielectric constants were used as a measure of polarity.

TABLE 2. Spectral properties of merocyanines

Compound	λ_{max} I	λ_{max} II	$\Delta\lambda_{max}$
1*b*	617.5	458.7	158.8
1*c*	631.9	547.1	84.8
1*d*	655.9	506.3	149.6
1*e*	567.6	463	104.6
1*f*	508.1	408.2	99.9
1*g*	633.9	491.9	142.0

Table 2 gives the two extreme values of λ_{max} (λ_{max} I in the least polar solvent and λ_{max} II in the most polar solvent), and $\Delta\lambda_{max}$, which was considered in this work as a measure of solvatochromism. It may be seen from Table 2 and Fig. 1 that strongly electron-withdrawing substituents like NO_2 (**1***e*, **1***f*) exert two effects: (1) a hypsochromic shift of the whole spectrum and (2) a decrease in the extent of solvatochromism, as measured by $\Delta\lambda_{max}$. Electron-donating groups such as CH_3 (**1***g*) and OCH_3 (**1***d*) cause a bathochromic shift of the spectrum and affect only slightly the extent of solvatochromism. In this aspect the compound with two *t*-Bu substituents (**1***c*) is an exception, with a much lower $\Delta\lambda_{max}$.

Inverted solvatochromism was apparently observed in media of very low polarity for all compounds in Fig. 1. However, this effect must be attributed to an aggregation phenomenon rather than to a change in the structure of merocyanines. Figure 2 shows the spectra of **1***f* in mixtures of 20, 30, and 50% cyclohexane in pyridine. It is seen that the hypsochromic shift in 50% cyclohexane is related to emergence of a new absorption band, which has to be attributed to an aggregated species. **1***f* is a very polar compound; therefore, in solvents of low polarity it forms aggregated species. Dilution experiments give additional data showing that these spectral changes are related to the formation of aggregated species (Fig. 3).

We then examined the spectra of a strongly lipophilic dye, **1***h*, in very polar media. Figure 4 shows the spectra of **1***h* recorded in mixtures of 80, 90, and 95% of 0.5% NaOH in pyridine. A phenomenon similar to that in Fig. 2 was observed, i.e., emergence of a new absorption band for the aggregated species, which, in this case, is red-shifted with respect to the monomeric dye. For a still more lipophilic compound (**1***i*) we observed (Fig. 5) similar behaviour beginning in a less polar solvent (70% NaOH in pyridine).

Discussion

The extreme solvatochromism of stilbazolium merocyanines, together with electrochromism (5) and the nonlinearity of their optical properties (4, 12), makes this class of compounds very promising with respect to technical applications.

Here we show that appropriate design of molecular structure allows construction of compounds that absorb in a very broad region of the visible spectra. Additional shifts may be obtained by inducing molecular aggregation. Strongly electron-with-

Can. J. Chem. Downloaded from www.nrcresearchpress.com by 91.144.44.67 on 09/07/12
For personal use only.

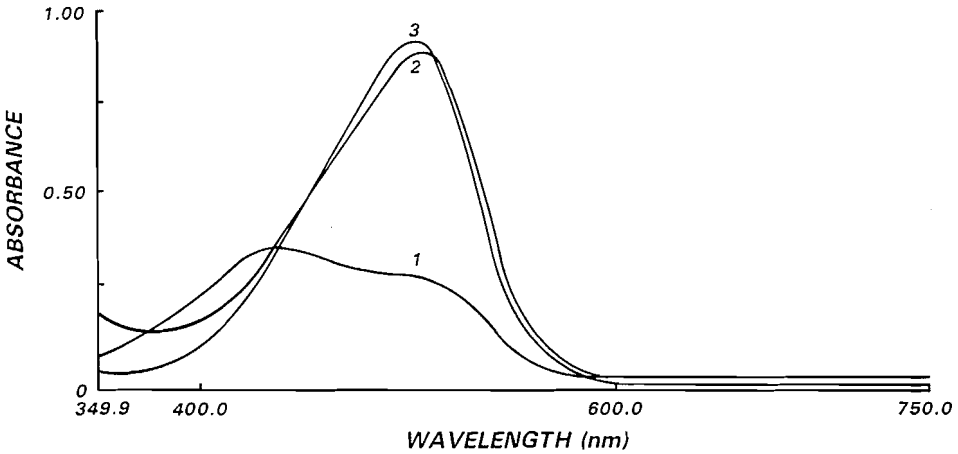

FIG. 2. Absorption spectra of merocyanine **1***f* in 50% cyclohexane–pyridine (1); 30% cyclohexane–pyridine (2); and 20% cyclohexane–pyridine (3).

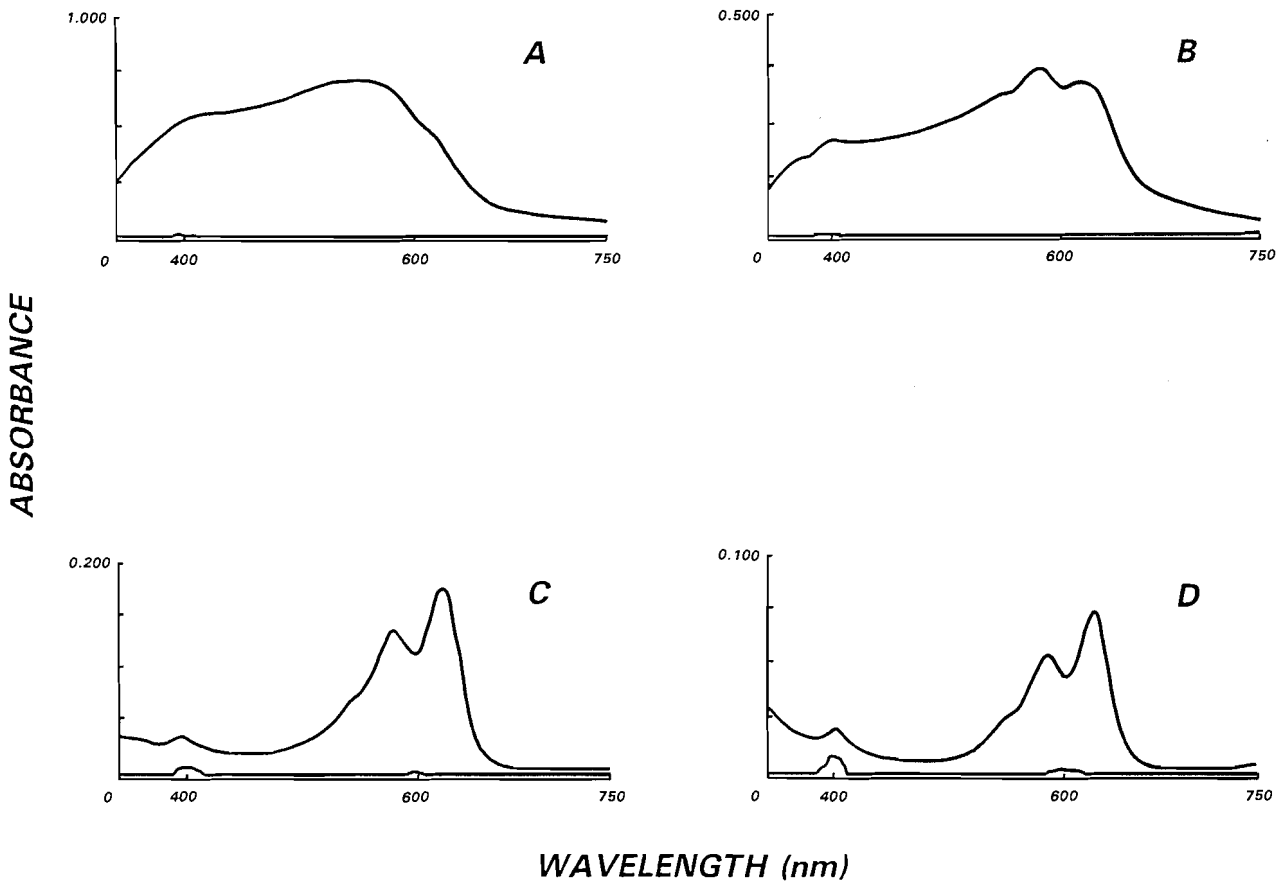

FIG. 3. Absorption spectra of merocyanine **1***b* in 70% cyclohexane–pyridine at dye concentrations of 5×10^{-5} M (A); 10^{-5} M (B); 5×10^{-6} M (C); and 10^{-6} M (D).

drawing substituents shift the absorption to shorter wavelengths, and electron-donating substituents to longer wavelengths, which is the normal contribution of substituents in conjugated systems. The extent of solvatochromy is reduced by NO_2 groups. This effect can be attributed to partial dispersion of the negative charge located on the carbonyl oxygen to the nitro groups as shown in Scheme 1.

This makes the solvation of the betaine structure B by polar solvents less efficient. Therefore the relative stability of ground and excited states is less affected by the increase in polarity of the medium.

One would expect an opposite effect, i.e., an increase of solvatochromy, by electron-donating groups, which should increase the negative charge on oxygen. It may be thought that this effect exists, but is reduced by a steric hindrance to solvation that, very important in the case of *t*-Bu substituents, is also present in the case of CH_3 and OCH_3 substituted derivatives. Therefore, for merocyanines substituted by electron-

Can. J. Chem. Downloaded from www.nrcresearchpress.com by 91.144.44.67 on 09/07/12
For personal use only.

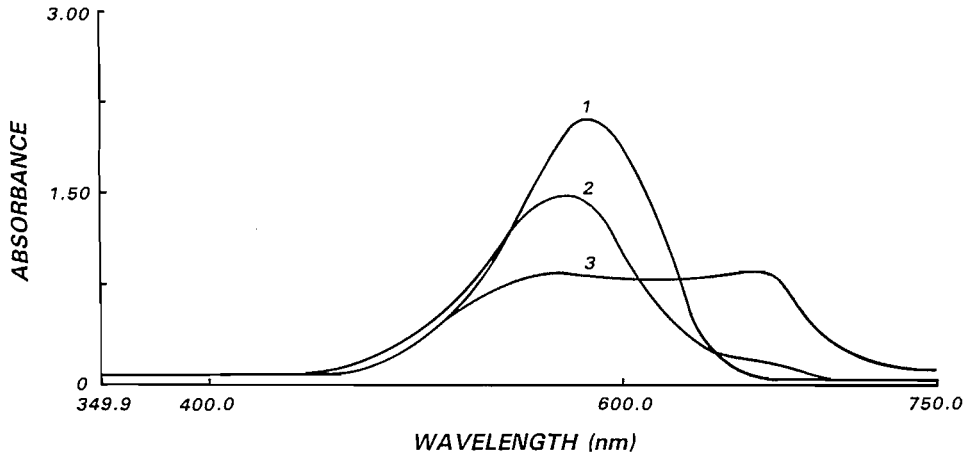

FIG. 4. Absorption spectra of merocyanine **1***h* in 80% aqueous NaOH (0.5%) – pyridine (1); 90% aqueous NaOH (0.5%) – pyridine (2); and 95% aqueous NaOH (0.5%) – pyridine (3).

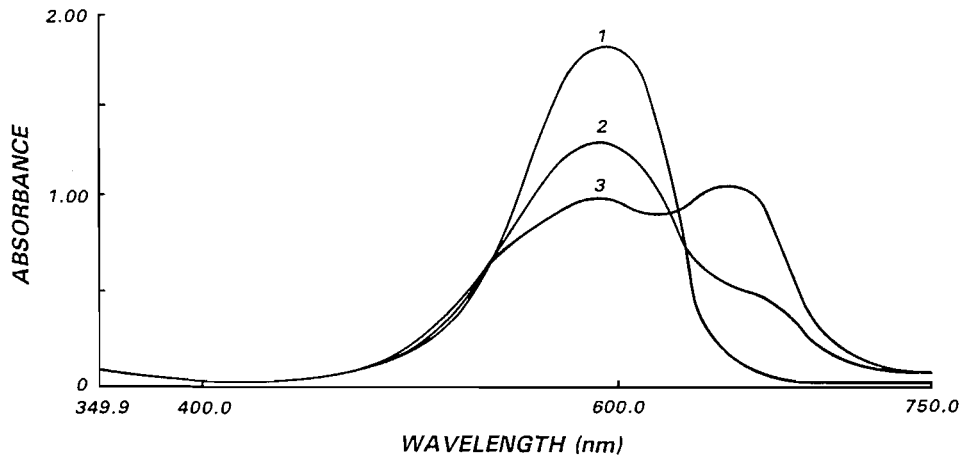

FIG. 5. Absorption spectra of merocyanine **1***i* in 60% aqueous NaOH (0.5%) – pyridine (1); 70% aqueous NaOH (0.5%) – pyridine (2); and 80% aqueous NaOH (0.5%) – pyridine (3).

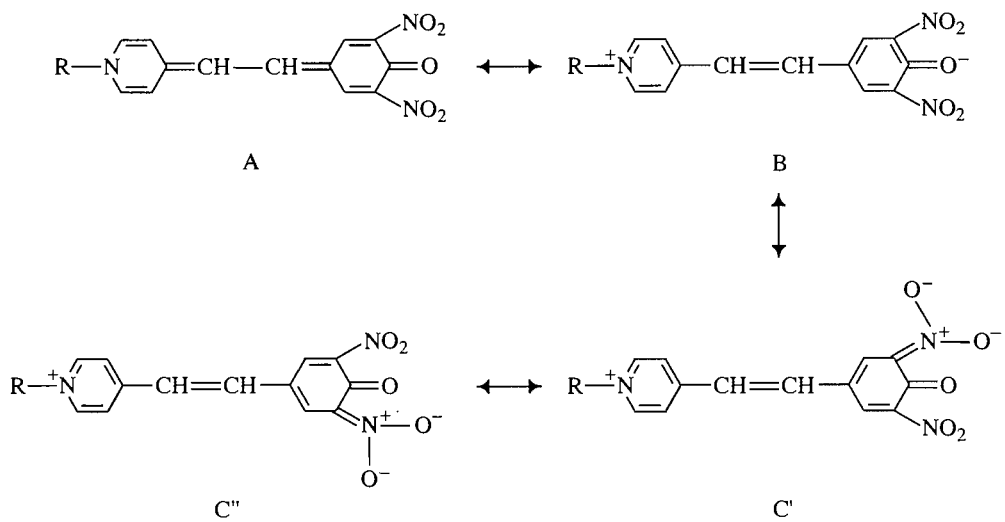

SCHEME 1

Can. J. Chem. Downloaded from www.nrcresearchpress.com by 91.144.44.67 on 09/07/12
For personal use only.

donating groups, we can observe a shift to longer wavelengths but no increase in the $\Delta\lambda_{max}$.

Two types of aggregates were observed in this study. Aggregation of polar merocyanines in solvents of very low polarity gave rise to an absorption band hypsochromic to the monomer band. Therefore we have to envisage here a card-packing head-to-tail arrangement of monomeric units. The main attraction force between monomers in this species should be the dipole–dipole interaction, which will preferentially stabilize the ground state molecules, and hence shift λ_{max} to lower wavelengths.

Aggregation of dyes containing many hydrophobic substituents in highly aqueous solvents resulted in a bathochromic shift of the spectrum, which may be attributed to a micelle-type association of monomers. The dipolar merocyanine portions of these molecules would be held on the micellar surface in a roughly head-to-head and tail-to-tail orientation so that the ground state is destabilized. This would account for the bathochromic shift on association (13, 14).

Acknowledgments

The authors express their gratitude to the Cancer Research Society Inc. for financial support.

1. L. G. S. Brooker, G. H. Keyes, and D. W. Heseltine. J. Am. Chem. Soc. **73**, 5350 (1951).
2. S. Hünig and O. Rosental. Liebigs Ann. Chem. **592**, 161 (1955).
3. K. F. Donchi, G. P. Rober, B. Ternai, and P. J. Derrick. Aust. J. Chem. **33**, 2199 (1980).
4. I. Gruda, S. Hotchandani, and D. Frackowiak. Photobiochem. Photobiophys. **12**, 267 (1986).
5. D. Franckowiak, M. Niedbalska, M. Romanowski, and I. Gruda. Stud. Biophys. **123**, 135 (1988).
6. P. Jacques. J. Phys. Chem. **90**, 5535 (1986).
7. I. Gruda and F. Bolduc. J. Org. Chem. **49**, 3300 (1984).
8. I. Gruda, M. Pagé, F. Bolduc, S. Laliberté, and C. Noël. Anticancer Res. **7**, 1125 (1987).
9. M. Pagé, I. Gruda, S. Laliberté, A. Pépin, C. Noël, and F. Grenier. 2nd Int. Conference of Anticancer Research, October 11–15, 1988. Saronis, Greece.
10. F. Dion, F. Bolduc, and I. Gruda. J. Colloid Interface Sci. **106**, 466 (1985).
11. C. Reichardt. Solvent effects in organic chemistry. Verlag Chemie, Weinheim, FRG. 1979.
12. I. Gruda, S. Laliberté, M. Niedbalska, and D. Frackowiak. J. Lumin. **39**, 1 (1987).
13. E. G. McRae and M. Kasha. *In* Physical processes in radiation biology. *Edited by* L. G. Augenstein, R. Masson, and B. Rosenberg. Academic Press, New York. 1964.
14. K. Fukuda and H. Nakahara. J. Colloid Interface Sci. **98**, 555 (1984).

Can. J. Chem. Downloaded from www.nrcresearchpress.com by 91.144.44.67 on 09/07/12
For personal use only.

Enzymic hydroxylation and sulfoxidation of cyclopropyl compounds by fungal biotransformation

HERBERT L. HOLLAND, MICHAEL J. CHERNISHENKO, MORGAN CONN, ANTHONY MUNOZ, T. SAMUEL MANOHARAN, AND MICHAEL A. ZAWADSKI

Department of Chemistry, Brock University, St. Catharines, Ont., Canada L2S 3A1

Received October 6, 1989

HERBERT L. HOLLAND, MICHAEL J. CHERNISHENKO, MORGAN CONN, ANTHONY MUNOZ, T. SAMUEL MANOHARAN, and MICHAEL A. ZAWADSKI. Can. J. Chem. **68**, 696 (1990).

A series of compounds containing a cyclopropyl ring adjacent to the position of oxidation during fungal biotransformation has been prepared and subjected to enzymic oxidation using *Mortierella isabellina* or *Rhizopus arrhizus*. Carbon hydroxylation and sulfoxidation reactions were observed, but in neither case did opening of the cyclopropyl ring occur. Both these reactions were subject to inhibition by carbon monoxide but not by cyanide ion, properties characteristic of cytochrome P-450 dependent mono-oxygenase enzymes. Hydroxylation at a cyclopropyl C—H bond has been studied by the use of phenylcyclopropane and phenylthiirane as substrates for the mono-oxygenase of *M. isabellina*. The former was not oxidized, but the latter was converted to phenyl glyoxylic acid in moderate yield.

Key words: biotransformation, cyclopropanes, fungi, metabolism.

HERBERT L. HOLLAND, MICHAEL J. CHERNISHENKO, MORGAN CONN, ANTHONY MUNOZ, T. SAMUEL MANOHARAN et MICHAEL A. ZAWADSKI. Can. J. Chem. **68**, 696 (1990).

On a préparé une série de composés contenant un noyau cyclopropyle adjacent de la position qui subit l'oxydation lors de la biotransformation à l'aide de champignons et on a soumis ces composés à une oxydation enzymatique à l'aide de *Mortierella isabellina* ou de *Rhizopus arrhizus*. On a observé des réactions d'hydroxylation du carbone et de sulfoxydation; toutefois, aucune de ces réactions n'a provoqué d'ouverture du noyau cyclopropyle. Les deux réactions sont sujettes à une inhibition par le monoxyde de carbone, mais non par l'ion cyanure; ces propriétés sont caractéristiques d'enzymes mono-oxydases dépendant du cytochrome P-450. On a étudié l'hydroxylation d'une liaison C—H du cyclopropyle en utilisant le phénylcyclopropane et le phénylthiirane comme substrats pour le mono-oxygénase de la *M. isabellina*. Le premier de ces composés n'est pas oxydé, mais le second est transformé en acide phénylglyoxylique avec un rendement moyen.

Mots clés : biotransformation, cyclopropanes, champignons, métabolisme.

[Traduit par la revue]

Introduction

Biotransformation of an organic compound by a growing or resting fungal culture has been used to perform a variety of reactions, the most remarkable of which are the direct introduction of the hydroxyl group in an asymmetric fashion, particularly into the steroid nucleus (1), and the asymmetric oxidation of sulfides to sulfoxides (2). The enzymes responsible for these reactions have yet to be fully purified and characterized from fungal sources, but are thought to be cytochrome P-450 dependent mono-oxygenases (1, 2), whose mode of action involves the radical abstraction/rebound recombination process outlined in Fig. 1 for the hydroxylation reaction (3).

A possible limitation on the synthetic utility of such bio-oxidations is posed by the presence in the substrate of a functionality that may be incompatible with the requirements of Fig. 1. In particular, the presence of groups close to the reactive site whose structure or integrity can be compromised may be contraindicated. Such radical sensitive groups may include alkenes susceptible to rearrangement or cyclopropyl units that may undergo cyclopropyl–allyl or cyclopropylcarbinyl–homoallyl conversions.

Migration of double bonds adjacent to the reactive centre has been observed during enzymic hydroxylation of terpenes (4) and steroids (5), and attributed to allylic rearrangement of a carbon radical intermediate. Fungal hydroxylation or sulfoxidation adjacent to a cyclopropyl ring has not been reported, however; the cyclopropyl-containing steroids that have been used as substrates for fungal biotransformation are hydroxylated at sites remote from the cyclopropyl functionality (6).

Cyclopropyl compounds have nevertheless been used as probes for the presence of free radical intermediates in enzymic

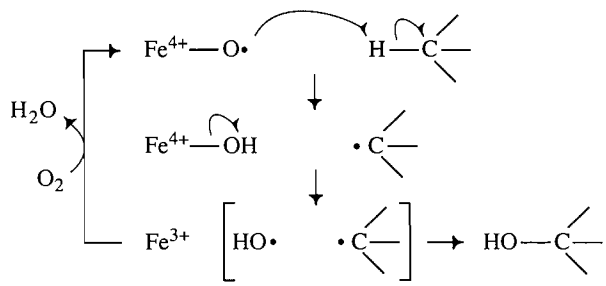

FIG. 1 Catalytic cycle of cytochrome P-450 dependent mono-oxygenases.

hydroxylation reactions (7). Dopamine β-hydroxylase, a copper-containing enzyme that catalyses the hydroxylation of dopamine at the benzylic position, is inactivated by benzylcyclopropanes analogous to **1** by a mechanism thought to involve cyclopropylcarbinyl–homoallyl rearrangement (8).

While oxidation at nitrogen (9, 10) and hydroxylation of highly strained cyclopropyl-containing substrates such as bicyclo[2.1.0]pentane (11) by cyt. P-450 dependent enzymes can involve opening of an adjacent cyclopropyl ring, other reactions such as the 7α hydroxylation of 5,6α-methanocholesterol (12) and the hydroxylation of methylcyclopropane (13) proceed without involvement of the cyclopropyl unit. These data have been rationalized by the assumption that, under normal circumstances, the rate of radical recombination of Fig. 1 (estimated as $\geq 10^9\ s^{-1}$) exceeds the rate of ring opening of a cyclopropyl methyl radical (ca. $1 \times 10^8\ s^{-1}$) (14).

Ring opening of cyclopropylbenzyl radicals, such as might be formed from **1** and **3** during benzylic oxidation by mono-

Can. J. Chem. Downloaded from www.nrcresearchpress.com by 91.144.44.67 on 09/07/12
For personal use only.

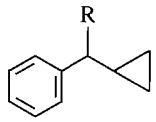

1: R = H
2: R = OH

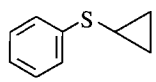

3
4:**3**: sulfoxide
5:**3**: sulfone

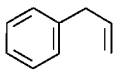

6

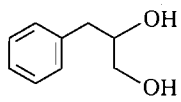

7

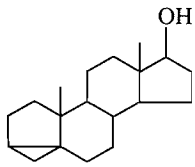

8

oxygenase enzymes, is slower than the opening of cyclopropyl methyl radicals by several orders of magnitude (15), so that no rearrangement is to be expected. To confirm this prediction, and the suitability of cyclopropyl compounds in general as substrates for biotransformation, we have used **1** and **3** as substrates for benzylic oxidation and sulfoxidation respectively by the fungus *Mortierella isabellina*, an efficient benzylic hydroxylating (16) and sulfoxidizing (17) microorganism; the cyclopropyl steroids **8** and **11**, with cyclopropyl functionality adjacent to C-6, as substrates for the steroid 6β hydroxylating fungus *Rhizopus arrhizus* (18); and finally, in view of the report that phenylcyclopropane (**13**) can act as a mechanistic probe[1] and inhibitor (20) of benzylic hydroxylating enzymes, we have undertaken a study of the biotransformation of this compound, and the corresponding thiirane **14**, by *M. isabellina*.

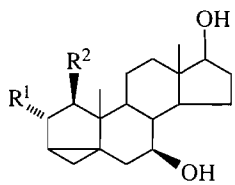

9: R^1 = H, R^2 = OH
10: R^1 = OH, R^2 = H

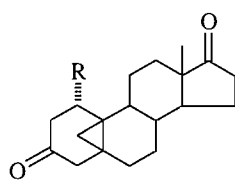

11: R = H
12: R = OH

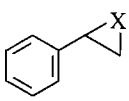

13: X = CH_2
14: X = S

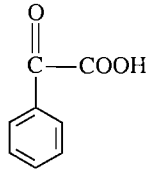

15

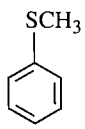

16

[1]P. Riley and R. P. Hanzlik. Personal communication.

TABLE 1. Summary of biotransformations

Substrate	Fungus	Products (%)
1	*M. isabellina*	**2** (15)
3	*M. isabellina*	**4** (58), **5** (2)
6	*M. isabellina*	**7** (4)
8	*R. arrhizus*	**9** (2), **10** (6)
11	*R. arrhizus*	**12** (38)
13	*M. isabellina*	None
13 + **16**	*M. isabellina*	**16**-sulfoxide (55)
14	*M. isabellina*	**15** (31)

Results and discussion

The results of the incubations discussed below are summarized in Table 1. The hydroxylation of **1** at the benzylic position by *M. isabellina*, giving the alcohol **2** in low yield and moderate enantiomeric enrichment, proceeded without any detectable involvement of the cyclopropyl ring. This was also the case for the sulfoxidation of phenyl cyclopropyl sulfide **3**, where the sulfoxide **4** was accompanied only by a minor amount of the sulfone **5**. In a similar vein, allyl benzene (**6**) was metabolized to give only 3-phenylpropane-1,2-diol (**7**) in low yield. This product is presumably formed by hydrolysis of an intermediate epoxide; hydroxylase enzymes are known to be capable of epoxidation of olefins located at or close to their normal site of hydroxylation (21).

The steroid substrates **8** and **11** were incubated with *R. arrhizus*. In neither case was the expected 6-hydroxy product obtained, but both substrates were hydroxylated at positions adjacent to the cyclopropyl ring (at C-2 of product **10** and C-1 of product **12**, respectively) without involvement of this functionality in the reaction. The structures of all the products formed from **8** and **11** were based on spectral analysis (see Experimental), with ^{13}C nmr being particularly diagnostic. The ^{13}C nmr data for substrates and products **8**–**12**, together with data for the product acetates, are listed in Table 2.

The ^{13}C nmr spectrum of substrate **8** in $CDCl_3$ was assigned in rings A and B by comparison with the published data for 3,5α-cyclocholestanes (22), and in rings C and D by comparison with data for 17β-hydroxyandrostanes (23). Using this spectrum of **8**, the assignments in DMSO-d_6 were then deduced and used as a basis for the determination of the sites of hydroxylation in the products **9** and **10**, which were soluble only in the latter solvent. Both products showed downfield shifts of the signals assigned to C-6 and C-8 with respect to their positions in **8**, indicating the presence of hydroxyl at C-7. The stereochemistry of substitution at C-7 (β) follows from the absence of γ *gauche* upfield effects at C-9 and C-14 present in the spectra of C-7α hydroxy steroids when compared to the unsubstituted analogues (23).

The location of the third hydroxyl group in product **9** as C-1β was apparent from its characteristic effect on the resonance position of C-19 (23), while the third hydroxyl group of product **10** is assigned to the C-2α position on the basis of the downfield shifts of C-1 and C-3, which locate the substituent at C-2, and the upfield shift at C-4, which confirms the α stereochemistry. A similar effect is caused by the C-6α hydroxy group of 6-hydroxy-3,5α-cyclocholestanes (22). The acetates of both **9** and **10** show chemical shifts that are consistent with the proposed structures.

Product **12** was assigned the 1α-hydroxy-5β,19-cycloandrostane-3,17-dione structure shown, on the basis of a comparison

Can. J. Chem. Downloaded from www.nrcresearchpress.com by 91.144.44.67 on 09/07/12
For personal use only.

TABLE 2. The ^{13}C nmr spectra of steroids **8–12**

Carbon	**8**		**9**[a]	**9**-OAc[b]	**10**[a]	**10**-OAc[b]	**11**[b]	**12**[b]
1	32.6[b]	30.6[a]	73.8	79.0	39.0	37.4	31.8	67.0
2	22.5	20.6	34.1	*33.9	68.5	75.0	36.2	44.9
3	23.5	*21.5	20.4	22.2	27.2	25.9	212.1	209.0
4	12.4	10.6	13.0	14.6	7.9	10.6	46.9	47.1
5	34.9	33.0	32.1	*33.7	32.0	33.7	18.8	18.7
6	*30.6	*28.3	38.3	35.1	36.9	34.3	26.6	*24.4
7	*29.4	27.4	70.8	76.0	71.3	75.6	26.2	*25.7
8	36.2	34.2	41.2	39.9	41.4	39.8	35.5	35.1
9	48.0	46.1	45.7	47.6	46.5	48.3	48.3	41.4
10	43.0	41.1	45.5	47.9	40.0	42.0	25.3	30.5
11	25.3	23.4	24.5	25.5	24.8	25.6	24.7	*31.0
12	37.0	35.4	35.2	36.7	35.3	36.7	31.7	*31.4
13	43.0	41.0	41.6	43.5	41.7	43.5	46.9	48.1
14	51.2	49.2	48.8	49.8	48.8	49.6	50.3	50.2
15	23.5	*21.4	21.0	22.9	20.7	22.4	21.7	21.6
16	30.2	*28.4	28.5	27.8	28.7	27.7	35.8	35.7
17	82.0	78.8	78.0	82.1	78.3	82.2	220.7	220.8
18	11.1	9.6	9.8	12.0	9.8	12.1	14.1	14.0
19	17.5	15.7	10.6	12.3	15.3	16.8	18.1	18.9
Other				21.1		21.1		
				21.2		21.2		
				21.7		21.7		
				170.4		170.4		
				170.5		171.0		
				171.0		171.2		

[a]Entries in this column obtained in DMSO-d_6/$CDCl_3$ solution.
[b]Entries in this column obtained in $CDCl_3$ solution.
*Similar chemical shifts in vertical columns may be interchanged.

of its ^{13}C nmr spectrum with that of substrate **11** (24). A downfield shift of the resonance assigned to C-10 locates the hydroxyl group at C-1 or C-9, and the observation of the shift for the latter carbon at a position 6.9 ppm upfield from its position in **11** is indicative of a *trans* diaxial substitution, suggesting the location of hydroxyl as C-1α. This is supported by the ^1H nmr spectrum, in which the signal for the hydrogen geminal to hydroxyl is located at 4.40 ppm, shifted downfield by the adjacent cyclopropyl ring current.

The final substrates used in this study were phenyl cyclopropane **13** and the thiirane **14**. As the rationale for their use was predicated on the assumption that the benzylic hydroxylating and sulfoxidizing enzyme of *M. isabellina* is a cytochrome P-450 dependent mono-oxygenase, it was first necessary to address the nature of the enzyme. Fungal hydroxylase enzymes are notoriously difficult to isolate, very few having been obtained even in crude cell-free form (25), so our experiments were perforce carried out with whole cell cultures.

We have previously demonstrated that the enzyme in *M. isabellina* responsible for sulfoxidation of thioanisole (**16**) utilizes molecular oxygen as the source of the oxygen atom (26), a feature of cytochrome P-450 dependent mono-oxygenases. We now report that this reaction, and the benzylic hydroxylation of ethylbenzene, shows the inhibition characteristics associated with P-450 catalysed reactions, namely, a susceptibility to inhibition by carbon monoxide and an insensitivity to inhibition by cyanide. For these reasons, we use as a working hypothesis the assumption that these reactions are indeed catalysed by cytochrome P-450 dependent mono-oxygenases, although in the absence of a purified enzyme preparation this cannot be definitively stated.

We were unable to isolate any products following the incubation of phenylcyclopropane (**13**) with *M. isabellina*. Cytochrome P-450 of rat liver origin is reported to convert **13** to benzoic acid in a multiple oxidation sequence in which the substrate does not leave the enzyme's active site (20, 27), but no benzoic acid was detected in the extracts following our incubations of **13**. Control extractions in which benzoic acid was added to the aqueous medium prior to treatment with methylene chloride gave excellent recoveries of the acid, confirming that the failure to isolate benzoic acid following incubations of **13** cannot be attributed to the extraction procedures employed.

To test the proposal that **13** was deactivating the enzyme following radical formation and subsequent alkylation of the haem of the enzyme's active site, one route for which is presented in Fig. 2 (20), experiments were carried out in which *M. isabellina* was incubated with **13**, followed by the addition of thioanisole as a second substrate. In this case, sulfoxidation of thioanisole proceeded in the usual manner, indicating that pre-incubation with phenylcyclopropane did not incapacitate the sulfoxidizing enzyme.

The oxidation of phenylthiirane (**14**) by *M. isabellina* proceeded to give a single product, phenylglyoxylic acid (**15**), in moderate yield. The formation of this product parallels the reported mammalian oxidation of phenylcyclopropane in that multiple oxidations have apparently taken place (20, 27). Incubations of potential intermediates such as 1-phenylethane-1,2-diol and phenyl acetic acid resulted only in recovered starting material in near-quantitative amount,[2] suggesting that, as proposed for the oxidation of phenylcyclopropane to benzoic acid (20), all the oxidative steps occur in the active site without

[2]H. L. Holland and M. A. Zawadski. Unpublished data.

Can. J. Chem. Downloaded from www.nrcresearchpress.com by 91.144.44.67 on 09/07/12
For personal use only.

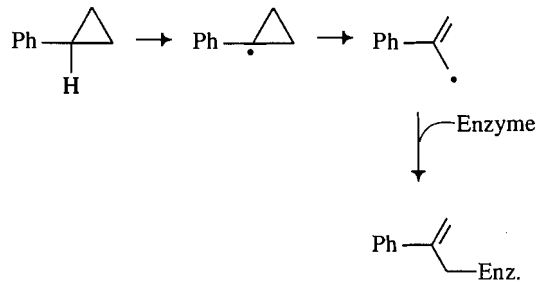

FIG. 2. Phenylcyclopropane as an irreversible inhibitor of cytochrome P-450 dependent mono-oxygenases.

dissociation of partially oxidized intermediates, but, without further information, proposal of a reaction scheme is premature.

Thiiranes may thus prove to be poor substrates for biotransformation, but from the above data it is apparent that, in spite of concerns based on mechanistic considerations, fungal oxidative biotransformation of compounds containing cyclopropyl groups can proceed with this functionality intact, even in cases where oxidation occurs adjacent to the three-membered ring.

Experimental

Melting points (uncorrected) were determined on a Kofler heating stage. Infrared spectra were recorded with an Analect 6260FX spectrometer. Proton nmr spectra were recorded at 200 MHz, and carbon nmr at 50.3 MHz (J MOD mode) with a Bruker AC200 spectrometer, using $CDCl_3$ as solvent and $CHCl_3$ as internal standard unless otherwise stated. Enantiomeric ratios were determined in CCl_4 in the presence of tris[3-(heptafluoropropylhydroxymethylene)-*d*-camphorato], europium(III). Electron impact mass spectra (eims) were obtained with an AEI MS30/Kratos DS55 system, and fast atom bombardment mass spectra (fabms) with the same machine fitted with an Ion Tech saddle field gun operating at 7 eV using a glycerol matrix. Thin-layer chromatography was performed on Merck silica gel 60F-254 and flash column chromatography on silica gel (230–400 mesh). Optical rotations were determined in 95% ethanol solution with a Rudolph Autopol III instrument, operating at 20°C. *Mortierella isabellina* NRRL 1757 (26) and *Rhizopus arrhizus* ATCC 11145 (29) were grown and maintained as previously described by us. Incubations with *M. isabellina* (26) and *R. arrhizus* (29) were also carried out as described. The incubation periods were 24 h for sulfoxidation or 72 h for hydroxylation by *M. isabellina*, and 48 h for hydroxylation by *R. arrhizus*. Products were identified following extraction, chromatography, and purification by crystallization (in the case of solid samples) or Kugelrohr distillation in the case of liquids. Microanalysis was performed by Guelph Analytical Laboratories.

Preparation of substrates

Compounds **3**, **6**, and **13** were commercial samples. The following were prepared by the published procedures and gave satisfactory spectral and analytical data: **1** (30), **8** (31), **11** (32), and **14** (33). Where relevant to product analysis, ^{13}C nmr data for substrates are presented in the tables.

Incubation of substrates

Benzylcyclopropane (1)

Incubation of **1** (1 g) with *M. isabellina* afforded (−)-cyclopropyl phenyl methanol (**2**, 0.17 g, oil), bp 140–145°C/18 Torr (1 Torr = 133.3 Pa) (lit. (30) bp 121°C/12 Torr); $[\alpha]_D$ −11.2°, ee 62% by nmr; ir (thin film) ν_{max}: 3366 cm^{-1}; ^1H nmr δ: 0.3–0.6 (4H, m, cyclopropyl CH_2's), 1.1–1.3 (1H, cyclopropyl CH), 4.0 (1H, d, J = 8.3 Hz, C*H*OH), and 7.25–7.45 (5H, m, aromatic H's) ppm; ^{13}C nmr δ: 2.8, 3.5 (cyclopropyl CH_2's), 19.2 (cyclopropyl CH), 78.5 (*C*HOH), 126.0 (2C), 127.5, 128.3 (2C), and 143.6 (aromatic C's) ppm; eims m/z (%): 148 (2), 129 (14), 120 (100), 104 (39), 91 (56), 77 (41).

Cyclopropyl phenyl sulfide (3)

Incubation of **3** (1 g) with *M. isabellina* gave the corresponding (+)-sulfoxide (**4**, 0.65 g, oil), bp 150–155°C/5 Torr (lit. (34) bp 137–138°C/1 Torr); $[\alpha]_D$ +99.2°, ee 66% by nmr, 69% by rotation (37); ^1H nmr and ir as reported (35, 36); ^{13}C nmr δ: 2.5, 3.3 (cyclopropyl CH_2's), 33.6 (cyclopropyl CH), 123.9 (2C), 129.0 (2C), 130.8 and 144.9 (aromatic C's) ppm; fabms m/z (%): 167 (M + H, 61), 150 (10), 125 (32) relative to 39 (100). Also obtained was the sulfone **5** (0.03 g), mp 34–36°C (lit. (38) mp 35–36°C); ir ν_{max}: 1148, 1291, 1315 cm^{-1}; ^1H nmr δ: 0.9–1.5 (4H, m, cyclopropyl CH_2's), 2.4–2.5 (1H, m, cyclopropyl CH), 7.5–7.7 (3H, m, aromatic *m*- and *p*-H's), 7.8–8.0 (2H, m, aromatic *o*-H's) ppm; ^{13}C nmr δ: 5.9 (cyclopropyl CH_2's), 32.9 (cyclopropyl CH), 127.5 (2C), 129.2 (2C), 133.3, and 141.5 ppm; fabms m/z (%): 183 (M + H, 10), 125 (16), 91 (8), 77 (19) relative to 39 (100).

Allyl benzene (6)

Incubation of **6** with *M. isabellina* gave, in addition to recovered starting material, *R*-(+)-3-phenylpropane-1,2-diol (**7**, 0.05 g), $[\alpha]_D$ +13.4°, ee 38% by comparison with $[\alpha]_D$ −36° reported for the *S*-(−) isomer (19), identified by comparison of spectral data with those reported for racemic material (28).

3α,5-Cyclo-5α-androstan-17β-ol (8)

Incubation of **8** (2 g) with *R. arrhizus* gave, in addition to recovered substrate, 3α,5-cyclo-5α-androstane-1β,7β,17β-triol (**9**, 35 mg), mp 254–256°C from ethyl acetate; ir ν_{max}: 3350 cm^{-1}; ^1H nmr (DMSO-d_6/$CDCl_3$) included signals at δ: −0.09 (1H, m, C-4 H), 0.65 (3H, s, C-18 CH_3), 0.84 (3H, s, C-19 CH_3), 3.06 (1H, d of t, J = 4.6, 8.9 Hz, C-7α H), 3.36 (1H, t, C-17α H), and 3.68 (1H, d, J = 6.3 Hz, C-1α H) ppm; ^{13}C nmr, see Table 2; fabms, m/z (%): 306 (M^+, 10), 305 (13), 289 (32), 271 (33), 253 (16) relative to 55 (100). Anal. calcd. for $C_{19}H_{30}O_3$: C 74.47, H 9.87%; found: C 74.56, H 9.51%; converted (pyridine/acetic anhydride) to the triacetate, oil; ir ν_{max}: 1245, 1739 cm^{-1}; ^1H nmr included signals at δ: 0.14 (1H, m) and 0.68 (1H, t), both cyclopropyl H's, 0.82 (3H, s, C-18 CH_3), 0.88 (3H, s, C-19 CH_3), 1.99, 2.01, and 2.06 (each 3H, s, $COCH_3$), 4.46–4.56 (2H, m, including t and 4.51, C-7α and -17α H's), and 5.05 (1H, d, J = 4.3 Hz, C-1α H) ppm; ^{13}C nmr, see Table 2; fabms m/z (%): 433 (M + H, 2), 373 (4), 313 (18) relative to 43 (100). Also obtained was 3α,5-cyclo-5α-androstane-2α,7β,17β-triol (**10**, 0.12 g), mp 212–215°C from ethyl acetate; ir ν_{max}: 3310 cm^{-1}; ^1H nmr (DMSO-d_6/$CDCl_3$) included signals at δ: 0.05 (1H, m, C-4 H), 0.62 (3H, s, C-18 CH_3), 0.81 (3H, s, C-19 CH_3), 3.09 (1H, d of t, J = 3.8, 8.5 Hz, C-7α H), 3.37 (1H, t, C-17α H), and 4.15–4.33 (1H, m, C-2β H) ppm; ^{13}C nmr, see Table 2; fabms m/z (%): 305 (M − H, 18), 287 (18), 271 (24), 253 (12) relative to 55 (100). Anal. calcd. for $C_{19}H_{30}O_3$: C 74.47, H 9.87%; found: C 74.72, H 9.58%; converted (pyridine/acetic anhydride) to the triacetate, oil; ir ν_{max}: 1245, 1739 cm^{-1}; ^1H nmr included signals at δ: 0.20 (d of d, J = 2.1, 5.4 Hz, C-4 H), 0.79 (3H, s, C-18 CH_3), 0.92 (3H, s, C-19 CH_3), 1.97, 2.0, and 2.03 (each 3H, s, $COCH_3$), 4.4–4.7 (2H, m, C-7α and C-17α H's), and 5.20 (d of t, J = 3.8, 7.6 Hz, C-2β H) ppm; ^{13}C nmr, see Table 2; eims m/z (%): 373 (M − acetic acid, 8), 312 (100), 297 (18).

5β,19-Cycloandrostane-3,17-dione (11)

Incubation of **11** (0.17 g) with *R. arrhizus* gave as the only detectable product 1α-hydroxy-5β,19-cycloandrostane-3,17-dione (**12**, 65 mg), mp 153–155°C from ethyl acetate; ir ν_{max}: 1705, 1738, 3340 cm^{-1}; ^1H nmr included signals at δ: 0.45 (2H, s, C-19 H's), 0.75 (3H, s, C-18 CH_3), 2.55 (2H, s, C-4 H's), and 4.40 (1H, d of d, J = 4, 3.8 Hz, C-1β H); ^{13}C nmr, see Table 2; eims m/z (%): 302 (M^+, 20), 284 (37), 269 (5), 258 (70), 241 (16), 230 (16) relative to 55 (100). Anal. calcd. for $C_{19}H_{26}O_3$: C 75.47, H 8.66%; found: C 75.27, H 8.51%.

Phenylcyclopropane (13)

Incubation of phenylcyclopropane with *M. isabellina* at substrate concentrations of 0.1–0.5 mg/mL produced no detectable products following methylene chloride extraction. Incubation of *M. isabellina* with phenylcyclopropane (0.2 mg/mL) for a period of 12 h, followed by the addition of thioanisole (0.4 mg/mL), and incubation for a further period of 24 h, produced thioanisole sulfoxide with yield and enantiomeric excess as reported (17).

Can. J. Chem. Downloaded from www.nrcresearchpress.com by 91.144.44.67 on 09/07/12
For personal use only.

Phenylthiirane (14)

Incubation of **14** (1 g) with *M. isabellina* gave an extract from which phenyl glyoxylic acid (**15**) was recovered in 31% yield. The product was identified by comparison of spectral data with those of commercial material.

Inhibitor experiments

Experiments with *M. isabellina* as fungus and thioanisole and ethylbenzene as substrates were performed as follows. Carbon monoxide inhibition was carried out in closed 1 L vessels under an atmosphere of 15% CO/85% air. No oxidation products were observed. Experiments with cyanide were carried out in aqueous medium containing 5×10^{-4} M KCN. In this case, normal yields and stereochemistries of product were obtained (16, 17).

Acknowledgements

Financial support was provided by the Natural Sciences and Engineering Research Council of Canada. We are grateful to Mr. T. Jones and to Mrs. D. Vukmanic for their assistance in obtaining spectral data.

1. H. L. HOLLAND. Chem. Soc. Rev. **11**, 371 (1982).
2. H. L. HOLLAND. Chem. Rev. **88**, 473 (1988).
3. J. D. FOURNERON, A. ARCHELAS, and R. FURSTOSS. J. Org. Chem. **54**, 2478 (1989).
4. R. H. MCCLANAHAN, A. C. HUITRIC, P. G. PEARSON, J. C. DESPER, and S. D. NELSON. J. Am. Chem. Soc. **110**, 1979 (1988).
5. H. L. HOLLAND and E. REIMLAND. Can. J. Chem. **63**, 1121 (1985).
6. H. K. THOA, Z. PROCHAZKA, M. BUDESINSKY, and P. KOCOVSKY. Collect. Czech. Chem. Commun. **43**, 2305 (1978).
7. C. J. SUCKLING. Angew. Chem. Int. Ed. Engl. **27**, 537 (1988).
8. P. F. FITZPATRICK and J. J. VILLAFRANCA. J. Am. Chem. Soc. **107**, 5022 (1985).
9. A. BONDON, T. L. MACDONALD, T. M. HARRIS, and F. P. GUENGERICH. J. Biol. Chem. **264**, 1988 (1989).
10. T. L. MACDONALD, K. ZIRVI, L. T. BURKA, P. PEYMAN, and F. P. GUENGERICH. J. Am. Chem. Soc. **104**, 2050 (1982).
11. P. R. ORTIZ DE MONTELLANO and P. R. STEARNS. J. Am. Chem. Soc. **109**, 3415 (1987).
12. L. BROWN, W. J. S. LYALL, C. J. SUCKLING, and K. E. SUCKLING. J. Chem. Soc. Perkin Trans. 1, 595 (1987).
13. H. DALTON, B. T. GOLDING, B. W. WATERS, R. HIGGINS, and J. A. TAYLOR. J. Chem. Soc. Chem. Commun. 482 (1981).
14. P. R. ORTIZ DE MONTELLANO. Acc. Chem. Res. **20**, 289 (1987).
15. J. MASNOVI, E. G. SAMSEL, and R. M. BULLOCK. J. Chem. Soc. Chem. Commun. 1044 (1989).
16. H. L. HOLLAND, E. J. BERGEN, P. C. CHENCHAIAH, S. H. KHAN, B. MUNOZ, R. W. NINNISS, and D. RICHARDS. Can. J. Chem. **65**, 502 (1987).
17. H. L. HOLLAND, H. PÖPPERL, R. W. NINNISS, and P. C. CHENCHAIAH. Can. J. Chem. **63**, 1118 (1985).
18. H. L. HOLLAND. Acc. Chem. Res. **17**, 398 (1984).
19. W. BARGSTEIN, A. KLEEMAN, and J. MARTENS. Synthesis, 76 (1981).
20. C. J. SUCKLING, D. C. NONHEBEL, L. BROWN, K. E. SUCKLING, and S. SEILMAN. Biochem. J. **232**, 199 (1985).
21. B. M. BLOOM and G. M. SHULL. J. Am. Chem. Soc. **77**, 5767 (1955).
22. W. B. SMITH, D. L. DEAVENPORT, J. A. SWANZY, and G. A. PATE. J. Magn. Reson. **12**, 15 (1973).
23. J. W. BLUNT and J. B. STOTHERS. Org. Magn. Reson. **9**, 439 (1977).
24. H. L. HOLLAND, P. R. P. DIAKOW, and G. J. TAYLOR. Can. J. Chem. **56**, 3121 (1978).
25. K. BRESKVAR and T. HUDNIK-PLEVNIK. Biochem. Biophys. Res. Commun. **74**, 1192 (1977).
26. H. L. HOLLAND and I. M. CARTER. Can. J. Chem. **60**, 2420 (1982).
27. K. E. SUCKLING, C. D. SMELLIE, I. E. S. IBRAHIM, D. C. NONHEBEL, and C. J. SUCKLING. FEBS Lett. **145**, 179 (1982).
28. A. MEDLIK-BALAN and J. KLEIN. Tetrahedron, **36**, 299 (1980).
29. H. L. HOLLAND and B. J. AURET. Can. J. Chem. **53**, 2041 (1975).
30. W. J. CLOSE. J. Am. Chem. Soc. **79**, 1455 (1957).
31. A. KASAL, V. CERNY, and F. SÔRM. Collect. Czech. Chem. Commun. **30**, 472 (1965).
32. S. RAKHIT and M. GUT. J. Am. Chem. Soc. **86**, 1432 (1964).
33. T. H. CHAN and J. R. FINKENBINE. J. Am. Chem. Soc. **94**, 2880 (1972).
34. N. FURUKAWA, T. MASUDA, M. YAKUSHIJI, and S. OAE. Bull. Chem. Soc. Jpn. **49**, 2247 (1974).
35. C. R. JOHNSON and E. R. JANIGA. J. Am. Chem. Soc. **95**, 7692 (1973).
36. T. MASUDA, T. NUMATA, N. FURUKAWA, and S. OAE. J. Chem. Soc. Perkin Trans. 2, 1302 (1978).
37. E. DUNACH and H. B. KAGAN. Nouv. J. Chim. **9**, 1 (1985).
38. H. E. ZIMMERMAN and B. S. THYAGARAJAN. J. Am. Chem. Soc. **82**, 2505 (1960).

Can. J. Chem. Downloaded from www.nrcresearchpress.com by 91.144.44.67 on 09/07/12
For personal use only.

1,1-Dichlorocyclopropane derivatives of α and β ionones. Structure determination of 3*R*,3′*S*-bis[3-methyl-5-(1′,3′,3′-trimethylcyclohex-1′-en-2′-yl)-2(1*H*)-furanone]

E. Díaz and R. A. Toscano
Instituto de Química, Universidad Nacional Autónoma de México, Circuito Exterior, Ciudad Universitaria, Coyoacán 04510 México, D.F.

A. Alvarez
Facultad de Química, Universidad Autónoma del Estado de México, Toluca, Edo. de México

J. N. Shoolery
Varian Association, Palo Alto, CA 94303, U.S.A.

and

K. Jankowski[1]
Université de Moncton, Faculté des études supérieures et de la recherche, Moncton, N.B., Canada E1A 3E9

Received June 23, 1989[2]

E. Díaz, R. A. Toscano, A. Alvarez, J. N. Shoolery, and K. Jankowski. Can. J. Chem. **68**, 701 (1990).

1,1-Dihalocyclopropane derivatives and furanones were synthesized from ±α- and β-ionones using $CHCl_3$, NaOH, and triethylbenzyl ammonium chloride (TEBAC). 2D NMR and single-crystal X-ray analyses of the products are reported.

Key words: addition of 1,1-dihalocarbenes to ionones, phase transfer addition of 1,1-dihalo systems, formation of cyclopropanes.

E. Díaz, R. A. Toscano, A. Alvarez, J. N. Shoolery et K. Jankowski. Can. J. Chem. **68**, 701 (1990).

Utilisant des ± α- et β-ionones comme produits de départ et du $CHCl_3$, du NaOH et du chlorure de triéthylbenzylammonium (CTEBA) comme réactifs, on a préparé des dérivés dihalo-1,1 cyclopropanes et des furanones. On a déterminé les spectres de résonance magnétique nucléaire en 2D et les spectres de diffraction des rayons-X des produits.

Mots clés : addition de dihalo-1,1 carbènes aux ionones, addition par transfert de phase des systèmes dihalo-1,1, formation des cyclopropanes.

[Traduit par la revue]

Discussion

A large number of C_{13} compounds formed by oxidative cleavage of carotenoids isolated from *Tobacco* (1) and marine sponges (2) or their derivatives originate from the α and β ionones (**1** and **3**) (3, 4). The synthesis of several damascones (5) and abscisic acids (6, 7), using readily available and inexpensive ionones as raw materials, encourages us to perform a new reaction leading to some new, more functionalized and useful, unsaturated compounds.

We describe here the products obtained when ionones **1** and **3** were treated with $CHCl_3$, NaOH, and triethylbenzyl ammonium chloride (TEBAC) under a phase transfer condition.

It has been reported that, in phase transfer dihalocarbene addition, stereochemistry and regioselectivity can be controlled by varying the catalyst (8–11). Accordingly ±**1** affords the expected dichlorocarbene bicycloheptane adduct **2**. Characterization of its structure and configuration were supported by NMR and X-ray analysis (Fig. 1, Table 1).

On the other hand when β-ionone (**3**) was treated under the same conditions, two new furenones (**4** and **5**) were isolated. The IR spectrum of **4** showed a signal at 1743 cm^{-1}, which clearly indicates an α,β-unsaturated γ-lactone group.

The proton NMR spectrum showed a one-proton quintet and a one-proton multiplet at 7.05 and 5.55 ppm respectively. The latter was converted to a quartet (J = 1 Hz) when the vinylic proton at 7.05 was decoupled.

A vinylic methyl group appeared at 2.0 ppm as a triplet (J = 1 Hz) instead of the methyl ketone group singlet recorded at 2.31 ppm in the spectrum of the starting ionone **3**. This triplet collapsed to a doublet (J = 1 Hz) when the proton at 5.55 ppm was decoupled. These findings suggest that a partial structure for compound **4** must contain an α,β-unsaturated γ-lactone moiety.

The mass spectrum of compound **4** shows the molecular ion at m/z 220 corresponding to the molecular formula of $C_{14}H_{20}O_2$.

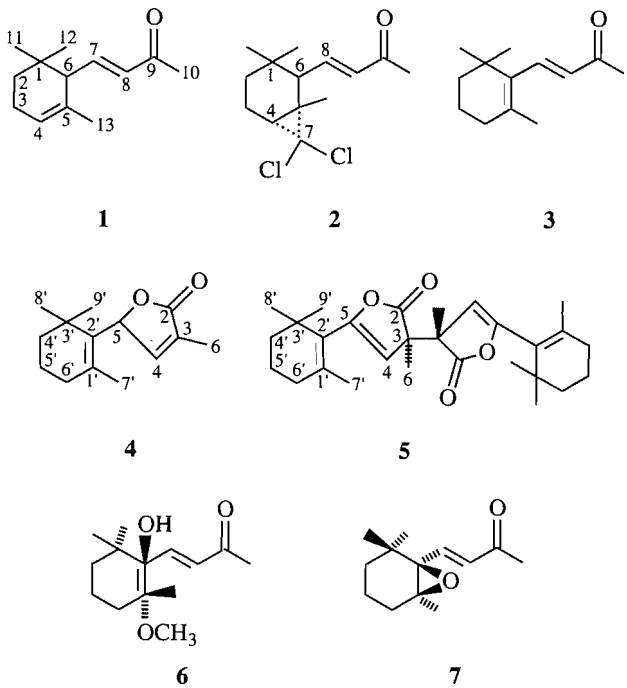

[1]Author to whom correspondence may be addressed.
[2]Revision received January 8, 1990.

Can. J. Chem. Downloaded from www.nrcresearchpress.com by 88.85.125.76 on 09/07/12
For personal use only.

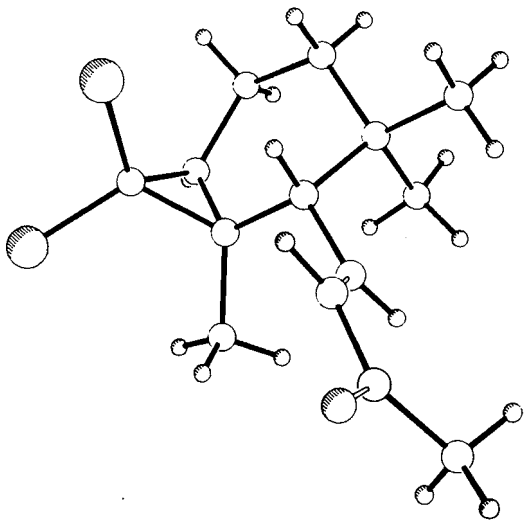

FIG. 1. X-ray structure of **2** (ORTEP plot).

TABLE 1. ^{1}H NMR spectrum of compound **2**

Proton	H	Multiplicity	(No. of protons)	J(Hz)
8	6.85	dd	(1H)	10.6, 16.5
9	6.17	dd	(1H)	1.0, 15.6
6	2.31	dd	(1H)	1.0, 10.6
11	2.28	s	(3H)	
3 ax	1.93	m	(1H)	7.92, 10.0, 14.0, 7.0
3 eq	1.83	m	(1H)	3.0, 1.0, 14.0
4	1.37	dd	(1H)	7.92, 1.0
13	1.28	s	(3H)	
2	1.18	m	(2H)	
11	0.91	s	(3H)	
12	0.74	s	(3H)	

It suggests an increase in the molecular weight of the starting ionone **3** by 28 atomic mass units.

The second compound, **5**, was identified as 3*R*,3′*S*-bis[3-methyl-5-(1′,3′,3′-trimethylcyclohex-1′-en-2′-yl)-2(1*H*)-furanone] with a molecular weight of 438 corresponding to the formula $C_{28}H_{38}O_4$. The structure was fully confirmed by 2D NMR and X-ray crystallography data.

The 400 MHz ^{1}H NMR of **5** showed methyl signals at 1.06, 1.39, and 1.71 ppm. A very well defined triplet at 2.04 ppm and a one-proton singlet at 5.59 ppm suggest the presence of one olefinic proton. The strong IR band at 1778 cm^{-1} and the ^{13}C NMR signal at 179.1 both indicate the presence of an enol lactone carbonyl.

COSY data enable us to establish the key proton vicinities. There exists a strong correlation between the methylene at δ = 2.04 and a signal at 1.68, and a weaker one between methylenes at 2.04 and the methyl at 1.71 ppm. The latter also displays a correlation with a methylene moiety at δ = 1.51 ppm.

The 1D and DEPT edited (12) spectra allowed the partial assignment of the carbon atoms (protonated carbons) and the ^{13}C spectrum enables us to assign the non-protonated carbons. The $^1J_{C-H}$ heterocorrelated spectra (13) enabled us to establish connectivities between proton-bearing carbons, and the results are shown in Table 2.

To confirm this dimeric structure we carried out an X-ray crystallographic study on compound **5** (Fig. 2).

TABLE 2. ^{1}H and ^{13}C chemical shifts for compound **5**

Carbon	n_H[b]	δ_H[a]	δ_C[a]
2	0		179.0
5	0		152.6
2′	0		138.2
1′	0		129.5
4	1	5.59	110.3
3	0		53.0
4′	2	1.51	38.7
3′	0		33.8
6′	2	2.05	32.1
8′	3	1.06	28.8
9′	3	1.06	28.8
7′	3	1.71	21.8
6	3	1.39	20.9
5′	2	1.68	18.9

[a]Chemical shifts relative to internal TMS.
[b]Number of attached protons as determined from normal and DEPT-edited ^{13}C spectra.

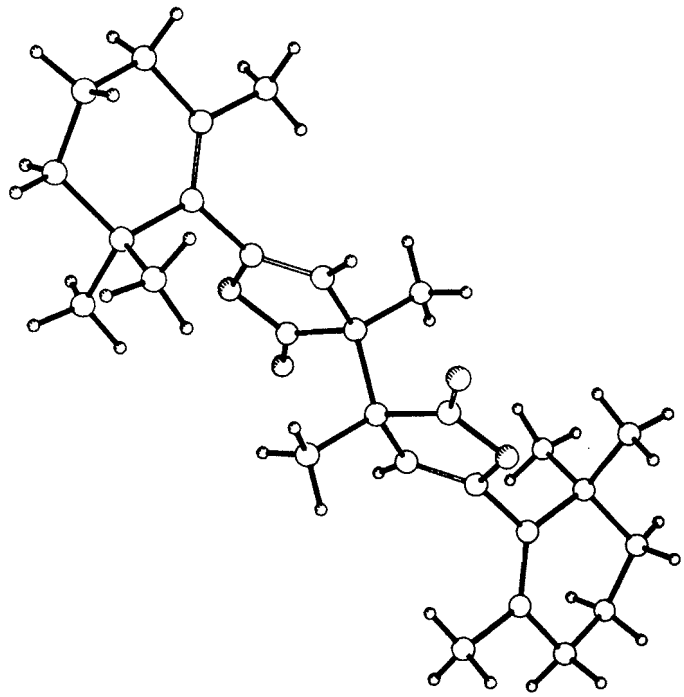

FIG. 2. X-ray structure of **5** (ORTEP plot).

The mechanism of formation of compounds is proposed in Scheme 1. For the lactone **4** one can assume an initial chemoselective adduct formation on the dienone **3** to generate the epoxide, which is rapidly transformed to an intermediate dichloroether that is hydrolysed to the γ-lactone **4**.

For the transformation of **4** into **5** we can assume that the presence of atmospheric oxygen during the reaction induces a free radical dimerization. It is supported by the fact that when the reaction was performed under a N_2 atmosphere the yield of **5** decreased dramatically and the yield of compound **4** increased. The unsaturated lactone **4** produces first a biradical that reacts with molecular oxygen, forms a tertiary radical, and finally dimerizes to compound **5**.

Finally, the sample of pure lactone **4** treated under similar conditions produced compound **5** under the N_2 oxygen-containing

Can. J. Chem. Downloaded from www.nrcresearchpress.com by 88.85.125.76 on 09/07/12
For personal use only.

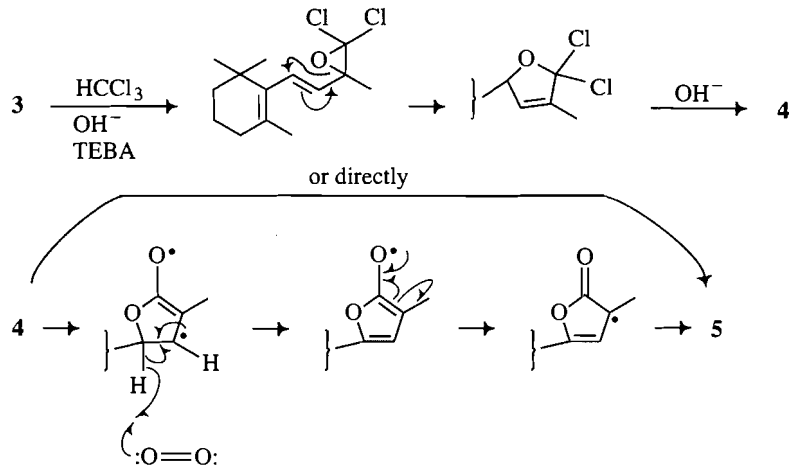

SCHEME 1

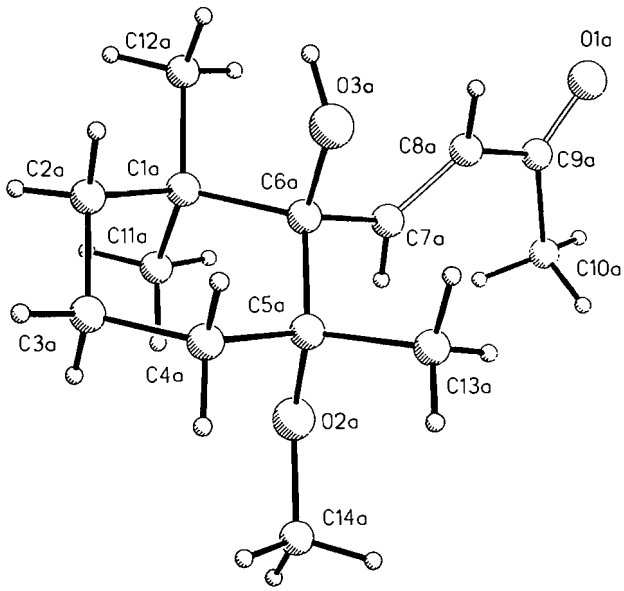

FIG. 3. X-ray structure of **6** (ORTEP plot).

atmosphere (there is no meaningful yield of **5** under the N_2 oxygen-free atmosphere).

Compound **6** was isolated in only trace amounts. The molecular weight as identified from the MS was 240 ($C_{14}H_{24}O_3$). The proton NMR presents an AX pattern (δ_A = 7.50 (H-7) and δ_x = 6.21 (H-8), J = 16 Hz), three proton singlets at 3.09 (OMe) and 2.24 (COMe), signals at 1.11, 0.92, and 0.72 for the methyls C-11, C-13, and C-12, and unresolved signals for six protons of C-2, C-3, and C-4 methylenes. The structure and configuration of compound **6** was confirmed by an X-ray crystallographic study (Fig. 3) showing the apparent diastereoselective formation of **6**.

One possible explanation for the formation of product **6** is the "normal" opening of the epoxide **7** obtained in a small quantity under phase transfer conditions with methanol (recrystallization). Similar oxidation has been observed for some sesquiterpene lactones (14).

Experimental

Infrared spectra were obtained on a Nicolet FT5X spectrometer (liquid films) and mass spectra (EI, PI) on a Hewlett–Packard 5985 A or on a VG703 high-resolution instrument. NMR spectra were recorded on Varian FT-80 (80 MHz), Varian VXR-400 (400 MHz), and Bruker 500 spectrometers. ^1H and ^{13}C spectra were run in $CDCl_3$.

X-Ray analysis

Crystals were mounted on top of a glass fiber. Intensities were collected on a Nicolet R3m automated diffractometer using graphite-monochromatized MoKα radiation. The crystal structure was solved by direct methods using the SHELXTL program package (15).

7,7-Dichloro-1,1-dimethyl-6-(3-oxo-1-butenyl)bicyclo[4,1,0]^{4,5} heptane (2)

± α-Ionone (Merck) (1) (1.92 g, 0.01 mol), 30 mL $CHCl_3$, TEBA (50 mg), and 10 mL aqueous sodium hydroxide (50%) were mixed slowly and stirred at room temperature for 24 h. The reaction product was extracted with $CHCl_3$, the organic extract was dried (Na_2SO_4), and the product was recrystallized from MeOH; mp 56–57°C; yield 52%; ^1H NMR δ: 0.74 (s, 3H), 0.91 (s, 3H), 1.37 (3H), 2.28 (s, 3H), 6.17 (d, J = 15.6, 1H), 6.85 (dd, J = 10.6, 15.6, 1H). MS m/z: 274 $M^{+\cdot}$ ($C_{14}H_{20}OCl_2$), $M^+ + 2$ 276, $M^+ + 4$ 278, 239, 241, 259, 261, 263, 109 (100%).

X-rays

Crystal size 0.2 × 0.3 × 0.4 mm. Monoclinic, spatial group $P_{2\,1/a}$. λ = 0.7071 Å (MoKα), ρ_{calc} = 1.186 g/cm^3, a = 1176(8) Å, b = 7.950(4) Å, c = 16.720(12) Å, β = 93.94(6)°, V = 1483.08 ± 1.72 Å^3, Z = 4.

Preparation of 4, 5, and 6

β-Ionone **3** (Merck) (1.92 g) in 30 mL $CHCl_3$ was added slowly to 50 mg of TEBA in 10 mL aqueous sodium hydroxide (50%) and stirred together at room temperature for 4 h. The reaction products were extracted with $CHCl_3$ and the organic extract was dried (Na_2SO_4). The solvent was removed *in vacuo* and a resulting oil showed two major spots on TLC. The oil underwent partial crystallization on addition of MeOH.

Products **4**, **5**, and **6** were separated by preparative TLC with 22, 17, and 0.1% yields. Product **4**: 3-methyl-5-(1′,3′,3′-trimethylcyclohex-1′-en-2′-yl)2(1*H*)-furanone; mp 106–107°C. IR ν_{max}: 3070, 2995, 2990, 2860, 1743, 1645, 1450, 1378 cm^{-1}; ^1H NMR δ: 1.1 (s, 3H), 1.2 (s, 3H), 1.5 (bs, 3H), 2.0 (t, J = 1.0, 3H), 5.55 (multiplet, J = 1.0), 7.0 (quintet, J = 1.0, 1H). MS m/z: M^+ 220.1490 ($C_{14}H_{20}O_2$), 105, 159, 123, 91, 97 (100%).

Product **5**: 3*R*,3′*S*-bis[3-methyl-5-(1′,3′,3′-trimethylcyclohex-1′-en-2′-yl)-2(1*H*)-furanone] was recrystallized from MeOH; mp 177–178°C; IR ν_{max}: 3010, 2960, 2925, 1778, 1665, 1450, 1380, 1200 cm^{-1}; ^1H NMR δ: 1.06 (s, 3H), 1.39 (s, 3H), 1.51 (m, 2H), 1.68 (m, 2H), 1.707 (s, 3H), 2.045 (t, 2H), 5.59 (s, 1H); also see Fig. 3. ^{13}C NMR, see Table 2. MS m/z: M^+ 438, 220, 218 (100%), 192.

Crystal data: Crystal size 0.20 × 0.28 × 0.32 mm, monoclinic crystals, spatial group P_2 13*a*; λ = 0.7071 Å (MoKα), ρ_{calc} = 1.152 g/cm^3, a = 10.297(9) Å, b = 8.163(4) Å, c = 15.069(11) Å, β = 94.60(7)°, V = 1262.39 Å^3, F(0,0,0) = 476, Z = 2.

Can. J. Chem. Downloaded from www.nrcresearchpress.com by 88.85.125.76 on 09/07/12
For personal use only.

Product **6**: 6-hydroxy-5-methoxy β-ionone was recrystallized from MeOH, mp 140–141°C; ^{1}H NMR δ: 0.72 (s, 3H), 0.92 (s, 3H), 1.11 (s, 3H), 2.24 (s, 3H), 6.21 (d, J = 16 Hz, 1H), 7.50 (d, 1H). MS m/z: M^+ 240, 208, 142, 125, 109, 98, 87, 85, 55, 43 (100%).

Crystal data: Crystal size 0.6 × 0.2 × 0.36 mm. λ = 1.54178 Å (CuKα), ρ_{calc} = 1.1368 g/cm^3, a = 6.214(1) Å, b = 17.077(6) Å, c = 26.422(7) Å, β = 90°(0), V = 2803.49 Å^3, F(0,0,0) = 1055, 89, Z = 8.

Acknowledgements

One of us (A.A.) thanks the Coordinacion de la Investigación Científica for partial support from U.A.E.M. grant.

1. A. J. Aasen, B. Kimland, S. O. Almquist, and C. R. Enzell. Acta Chem. Scand. **26**, 2573 (1972); I. Wahlberg and C. R. Enzell. Nat. Prod. Rep. **4**, 237 (1987).
2. M. R. Kernan, D. J. Faulkner, and R. S. Jacobs. J. Org. Chem. **52**, 3081 (1987).
3. E. Demole, P. Enggist, M. Winter, A. Furrer, K. H. Schulte-Elte, B. Egger, and G. Ohloff. Helv. Chim. Acta, **62**, 67 (1979).
4. D. Behr, I. Wahlberg, T. Nishida, and C. R. Enzell. Acta Chem. Scand. Ser. B: **B31**, 609 (1977).
5. (*a*) G. Buchi and J. C. Vederas. J. Am. Chem. Soc. **94**, 9128 (1972); (*b*) E. Demole and D. Berthet. Helv. Chim. Acta, **54**, 681 (1981); (*c*) R. L. Snowden, S. M. Linder, B. L. Muller, and K. H. Schulte-Elte. Helv. Chim. Acta, **70**, 1858 (1987).
6. J. A. Findlay and W. D. MacKay. Can. J. Chem. **49**, 2369 (1971).
7. (*a*) D. L. Roberts, R. A. Heckman, B. P. Hege, and S. A. Bellin. J. Org. Chem. **33**, 3566 (1968); (*b*) T. Oritani and K. Yamashita. Tetrahedron Lett. 2521 (1972).
8. E. V. Demlow and M. Prashad. J. Chem. Res. 354 (1982).
9. M. S. Baird, A. G. W. Baxter, B. R. J. Devlin, and R. J. G. Searle. J. Chem. Soc. Chem. Commun. 210 (1979).
10. L. K. Sydnes. Acta Chem. Scand. Ser. B: **B31**, 823 (1977).
11. L. K. Sydnes and L. Skattebal. Tetrahedron Lett. 4603 (1975).
12. D. M. Doddrell, D. T. Pegg, and M. R. Bendall. J. Magn. Reson. **48**, 323 (1982).
13. A. Bax and G. A. Morris. J. Magn. Reson. **42**, 501 (1981).
14. D. Mannino. M.Sc. Thesis, UAEM, Toluca, Mexico. 1981. p. 62.
15. G. M. Sheldrick. SHELXTL 81. An integrated system for crystal structure determination. Revision 3. Univ. of Göttingen, Federal Republic of Germany. 1981.

Can. J. Chem. Downloaded from www.nrcresearchpress.com by 88.85.125.76 on 09/07/12
For personal use only.

Substituted ferrocenecarboxylic acids and esters

W. R. CULLEN AND E. B. WICKENHEISER
Chemistry Department, University of British Columbia, Vancouver, B.C., Canada V6T 1Y6

Received August 28, 1989

W. R. CULLEN and E. B. WICKENHEISER. Can. J. Chem. **68**, 705 (1990).

The synthesis of Fe(η-C_5H_5)(η-C_5H_3(CHMeNMe$_2$)(COOH)-1,2), **3***a*, and its methyl and ethyl esters is described. Esterification of **3***a* by using RI in DMA affords Fe(η-C_5H_5)(η-C_5H_3(CHMeOH)(COOR)-1,2), R = Me, Et, with retention of configuration at the chiral center. The variable temperature ^{1}H NMR spectrum of **3***a* reveals H-bonding between the two functional groups.

Key words: ferrocenecarboxylic acids and esters, NMR spectra, synthesis, hydrogen bonding.

W. R. CULLEN et E. B. WICKENHEISER. Can. J. Chem. **68**, 705 (1990).

On décrit la synthèse de l'acide Fe(η-C_5H_5)(η-C_5H_3(CHMeNMe$_2$)(COOH)-1,2), **3***a*, et de ses esters méthylique et éthylique. L'estérification du composé **3***a* à l'aide de RI dans le DMA conduit aux Fe(η-C_5H_5)(η-C_5H_3(CHMeOH)(COOR)-1,2), R = Me et Et, avec rétention de configuration au centre chiral. Les spectres de RMN du ^{1}H du produit **3***a*, mesurés en fonction de la température, révèlent l'existence de liaisons hydrogènes entre les deux groupements fonctionnels.

Mots clés : acides et esters ferrocènecarboxyliques, spectres de RMN, synthèse, liaisons hydrogènes.

[Traduit par la revue]

Can. J. Chem. Downloaded from www.nrcresearchpress.com by 91.144.44.67 on 09/07/12
For personal use only.

We have shown that rhodium(I) derivatives of β-diketonate ligands such as **1** are active catalysts for the hydrogenation of olefins (1) and the hydrosilylation of ketones (2). Moreover rhodium(I) derivatives of the enantiomers of **2***b* are efficient catalysts for the asymmetric hydrogenation of selected olefins (3–6). Therefore it was of interest to combine these observations and establish whether metal complexes of **2***c* would be of use as catalysts.

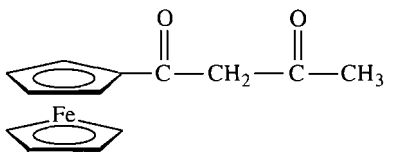

1

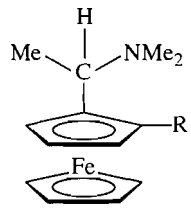

2*a* R = H
b R = PPh_2
c R = $C(O)CH_2C(O)CH_3$

The present paper outlines some unsuccessful attempts to prepare **2***c*: the properties of some esters of ferrocenecarboxylic acids, prepared as intermediates for the synthesis of **2***c*, are described.

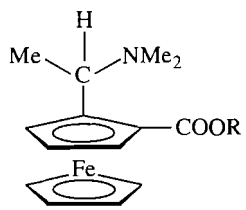

3*a* R = H
b R = CH_3
c R = C_2H_5

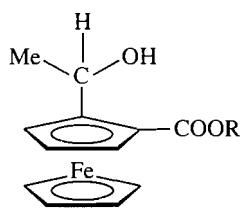

4*a* R = CH_3
b R = C_2H_5

Experimental

All equipment and techniques used in this study have been described previously (2). α-*N*,*N*-Dimethylaminoethylferrocene, **2***a*, was prepared by literature methods (7).

*Preparation of 2'-(*N,N*-dimethylaminoethylferrocene)carboxylic acid, 3*a

Butyllithium (12.1 mL of 1.6 M solution in hexanes, 19.4 mmol) was added to a solution of α-*N*,*N*-dimethylaminoethylferrocene (5.00 g, 19.4 mmol) in diethyl ether (100 mL). The solution was stirred overnight, and then cooled to −78°C. Solid carbon dioxide (5 g, 100 mmol) was then added in small portions, affording a light yellow precipitate. The mixture was stirred at −78°C for 2 h and allowed to warm to room temperature. The mixture was filtered under a nitrogen atmosphere and the precipitate was washed with several portions of ether. The precipitate was dissolved in methanol and chromatographed on a silica column using methanol as eluant. The product band was collected and the solvent removed under reduced pressure. The product was dissolved in dichloromethane and dried over magnesium sulfate. Removal of the solvent at reduced pressure afforded 5.15 g of a yellow glassy solid (88% yield). ^{1}H NMR spectrum ($CDCl_3$, 300 MHz) δ: 1.40 (d (J = 6.5 Hz), 3, C(CH_3)), 2.03 (s, 3, N(CH_3)), 2.54 (s, 3, N(CH_3)), 4.10 (s, 5, C_5H_5), 4.28 (m, 2, C*H*), 4.53 (q (J = 6.5 Hz), 1, C*H*(CH_3)), 5.01 (m, 1, C*H*), 17.7 (s, 1, OH). Mass spectrum *m/e* (relative intensity): 301 (36), 286 (21), 256 (100), 242 (37), 230 (20), 212 (61), 186 (12). Anal. calcd. for $C_{15}H_{19}FeNO_2 \cdot 0.5H_2O$: C 58.08, H 6.50, N 4.52; found: C 58.31, H 6.89, N 4.58.

*Preparation of 2-(*N,N*-dimethylaminoethylferrocene)carboxylic acid methyl ester, 3*b

This was prepared in a manner similar to that described by Grundy *et al.* (8) for the esterification of hindered carboxylic acids. A solution of **3***a* (0.38 g, 1.2 mmol) and potassium carbonate (0.19 g, 1.4 mmol) in 10 mL dry acetone was prepared and stirred for 30 min. Dimethyl sulfate (0.159 g, 1.26 mmol) was then added and the mixture was refluxed for 3 h. The solution was filtered, concentrated to 1 mL under reduced pressure, and chromatographed on silica. A mixture of acetone, ethyl acetate, and triethylamine (75:175:6) was used as the eluant and gave adequate separation. The major band was collected and the solvent removed at reduced pressure giving 0.195 g (50% yield) of analytically pure product. ^{1}H NMR spectrum ($CDCl_3$, 300 MHz) δ: 1.49 (d (J = 7.0 Hz), 3, C(CH_3)), 2.06 (s, 6, N(CH_3)$_2$), 3.79 (s, 3, OCH_3), 4.18 (s, 5, C_5H_5), 4.35 (m, 2, C*H*), 4.43 (q (J = 7.0 Hz), 1, C*H*(CH_3)), 4.75 (m, 1, C*H*). Mass spectrum *m/e* (relative intensity): 315 (1), 300 (2), 270 (2), 239 (1), 59 (100). Anal. calcd. for $C_{16}H_{21}FeNO_2$: C 60.96, H 6.72, N 4.44; found: C 61.13, H 6.81, N 4.61.

*Preparation of 2-(*N,N*-dimethylaminoethylferrocene)carboxylic acid ethyl ester, 3*c

The ester was also prepared using the method of Grundy *et al.* (8). A solution of **3***a* (0.96 g, 3.1 mmol) and potassium carbonate (0.48 g, 3.5 mmol) in 45 mL of dry acetone was prepared and stirred for 1 h. Diethyl sulfate (0.49 g, 3.2 mmol) was added and the mixture was

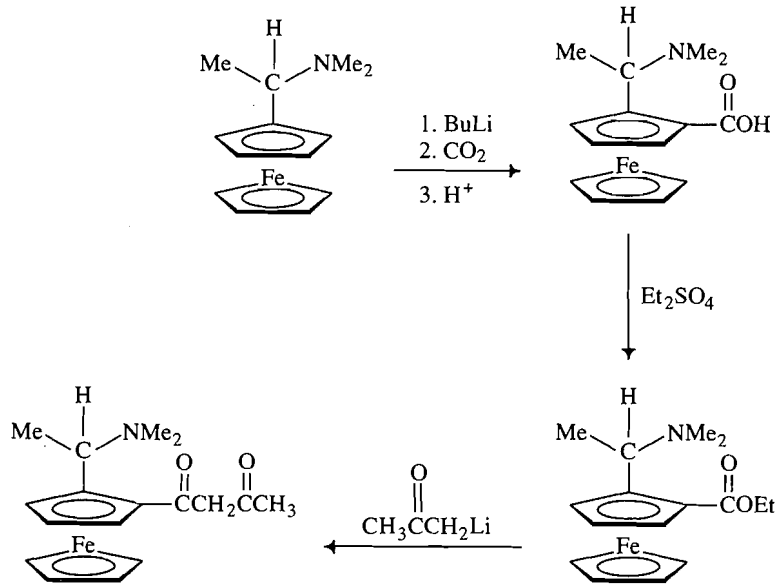

SCHEME 1

refluxed for 4 h. The mixture was filtered and the solvent removed at reduced pressure. The product was dissolved in 2 mL of methylene chloride, loaded onto a silica column, and eluted with a mixture of ethyl acetate/triethylamine (97:3). The major band was collected and the solvent removed at reduced pressure yielding 0.625 g (61% yield) of the pure ester. ^{1}H NMR spectrum ($CDCl_3$, 300 MHz) δ: 1.34 (t (J = 6.9 Hz), 3, $CH_2(CH_3)$), 1.49 (d (J = 6.9 Hz), 3, $CH(CH_3)$), 2.07 (s, 6, $N(CH_3)_2$), 4.13 (s, 5, C_5H_5), 4.08–4.36 (m, 4, CH, CH_2CH_3), 4.46 (q, 1, $CH(CH_3)$), 4.78 (m, 1, CH). Mass spectrum m/e (relative intensity): 329 (34), 314 (100), 285 (16), 263 (21), 256 (12), 239 (7), 211 (11). Anal. calcd. for $C_{17}H_{23}FeNO_2$: C 62.02, H 7.04, N 4.25; found: C 61.73, H 7.00, N 4.06.

Preparation of 2-(α-hydroxyethylferrocene)carboxylic acid methyl ester, **4**a

This was prepared using the method of esterification described by Alvarez and Watt (9); the reaction also effected replacement of the dimethylamino group with a hydroxyl group. A solution of **3***a* (213 mg, 0.687 mmol), sodium bicarbonate (131 mg, 1.56 mmol), and methyl iodide (402 mg, 283 mmol) in 1.5 mL of dimethylacetamide was prepared and stirred in the dark for 48 h. The mixture was then hydrolyzed by the addition of 30 mL of 10% aqueous sodium chloride. The product was extracted from the aqueous phase with ether and the combined extracts were dried over magnesium sulfate. The extract solution was filtered and the volume reduced to 2 mL at reduced pressure. The mixture was then chromatographed on silica using petroleum ether and triethylamine (97:3) as the eluant. The major band was collected and the solvent removed yielding 88.3 mg (44.6% yield) of the pure ester. ^{1}H NMR ($CDCl_3$, 300 MHz) δ: 1.45 (d (J = 6.7 Hz), 3, CCH_3), 3.78 (s, 3, OCH_3), 4.12 (s, 5, C_5H_5), 4.27 (m, 1, CH), 4.36 (d (J = 6.7 Hz), 1, COH), 4.40 (m, 1, CH), 4.70 (m, 1, CH), 5.00 (dq (J = 6.7 Hz), 1, $C(OH)H$). Mass spectrum m/e (relative intensity): 288 (50), 270 (26), 256 (23), 223 (16), 212 (33), 152 (16), 138 (16), 119 (100). Anal. calcd. for $C_{14}H_{16}FeO_3$: C 58.36, H 5.60, O 16.66; found: C 58.07, H 5.86, O 16.69.

Preparation of 2-(α-hydroxyethylferrocene)carboxylic acid ethyl ester, **4**b

A solution of **3***a* (0.23 g, 0.74 mmol), sodium bicarbonate (0.14 g, 1.7 mmol), and ethyl iodide (0.48 g, 3.1 mmol) in 1.5 mL of dimethylacetamide was stirred in the dark for 100 h. The reaction mixture was hydrolyzed with 30 mL of 10% aqueous sodium chloride solution. The product was then extracted from the aqueous layer with several portions of ether, and the extracts combined and dried over magnesium sulfate. The solution was filtered, concentrated to 2 mL at reduced pressure, and chromatographed on silica using ether, petroleum ether, and triethylamine (50:50:3) as the eluant. The major band was collected and the solvent removed to give 0.13 g (58% yield) of the pure ester. ^{1}H NMR ($CDCl_3$, 300 MHz) δ: 1.36 (t (J = 6.3 Hz), 3, CH_2CH_3), 1.48 (d (J = 6.3 Hz), 3, CCH_3), 4.17 (s, 5, C_5H_5), 4.43 (m, 4, CH, CH_2), 4.52 (d (J = 7.2 Hz), 1, COH), 4.76 (m, 1, CH), 4.97 (dq, 1, $CHCH_3$). Mass spectrum m/e (relative intensity): 302 (49), 284 (39), 256 (40), 237 (20), 219 (14), 212 (19), 119 (100). Anal. calcd. for $C_{15}H_{19}FeO_3$: C 59.63, H 6.00, O 15.88; found: C 59.62, H 5.95, O 16.00.

Results and discussion

Our chosen synthetic route to **2***c* is shown in Scheme 1 and is based on the stereospecific lithiation of **2***a* (7, 10). The carboxylic acid, **3***a*, was prepared by the addition of solid carbon dioxide to a solution of the lithio derivative of **2***a* and was isolated as the lithium salt (88% yield). The salt was dissolved in MeOH and subsequent chromatography on silica was used to isolate the deliquescent acid. The reaction is analogous to that used for the preparation of mono- and 1,1′-ferrocenedicarboxylic acids (11, 12). Esters of **3***a* were prepared by the reaction of the acid with dialkyl sulfates with yields of 50% (methyl **3***b*) and 61% (ethyl **3***c*). A condensation reaction between the esters and deprotonated ketones was then attempted. This reaction is similar to the one used to prepare the **1** and related ligands (1, 2). Unfortunately, no indication of any reaction (TLC monitoring) was seen after treating **3***b* and **3***c* with the lithium salts of acetophenone, acetone, and acetylferrocene in a variety of solvents and over a range of temperatures, e.g., refluxing toluene.

The analytical and spectroscopic results for **3***a* support the formulation. The mass spectrum shows a parent ion (m/e 301) and peaks associated with the loss of CH_3 (m/e 286), COOH (m/e 256), and $CHMeNMe_2$ (m/e 230). The ^{1}H NMR spectrum of **3***a* at ambient temperature shows some resonances that are broader than usual, indicating that some fluxionality is present. Part of the spectrum is shown in Fig. 1. Two broad singlets at 2.54 and 2.03 ppm are assigned to the *N*-methyl protons. These resonances coalesce at −38°C. This effect appears to be due to hindrance of the inversion at nitrogen, which otherwise would make the methyl groups equivalent. The probable cause is

Can. J. Chem. Downloaded from www.nrcresearchpress.com by 91.144.44.67 on 09/07/12
For personal use only.

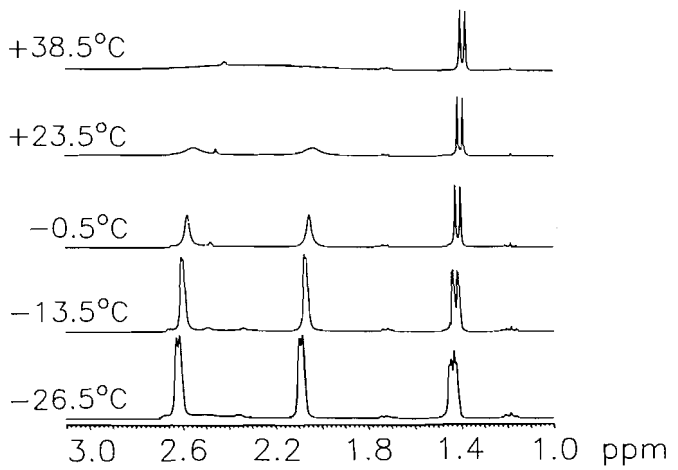

FIG. 1. The variable temperature ^{1}H NMR spectrum of **3***a* in the *N*-methyl region.

hydrogen bond formation between the COOH and the $N(CH_3)_2$ moieties. A similar effect has been noted in the NMR spectra of rhodium complexes of ligands related to **2***b* (5). The "extra" splitting seen in the resonances in the figure may be due to some long-range coupling or to the presence of frozen conformers: the latter possibility seems to be more likely. Conformers can be identified in solutions of rhodium complexes of ligands such as **2***b* (4).

The ^{1}H NMR spectra of the esters **3***b* and **3***c* show the NMe_2 groups as singlets, and the rest of the spectra are as expected and are not temperature dependent. The mass spectra show parent ions at *m/e* 315 (**3***b*) and *m/e* 329 (**3***c*).

Attempts to esterify **3***a* by using a method developed for sterically hindered carboxylic acids (9) resulted in esterification *and* replacement of the NMe_2 group by OH, eq. [1], and the

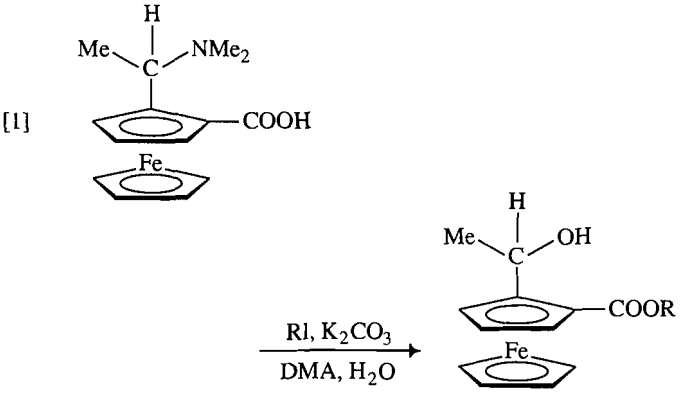

formation of **4***a* and **4***b*. (Replacement of the NMe_2 group of **2***a* can be accomplished by first replacing it with an acetate group, by reaction with acetic anhydride, followed by base hydrolysis (13).)

The analytical and spectroscopic data for **4***a* and **4***b* are consistent with the proposed structures. A doublet at 4.36 ppm in the ^{1}H NMR spectrum of **3***a* is assigned to the O*H* proton: this is coupled to the $C(CH_3)H$ proton as confirmed by shaking the samples with D_2O, which "decouples" the $C(CH_3)H$ resonance from the O*H*, converting it into the usual quartet.

Because the lithiation of **2***a* is stereospecific (7), derivatives are isolated as a pair of enantiomers of either (*R*,*R*) or (*S*,*S*) configuration due to the presence of the chiral carbon atom and the planar chirality of the disubstituted ferrocene ring. The products **4***a* and **4***b* are not mixtures of diastereomers as judged

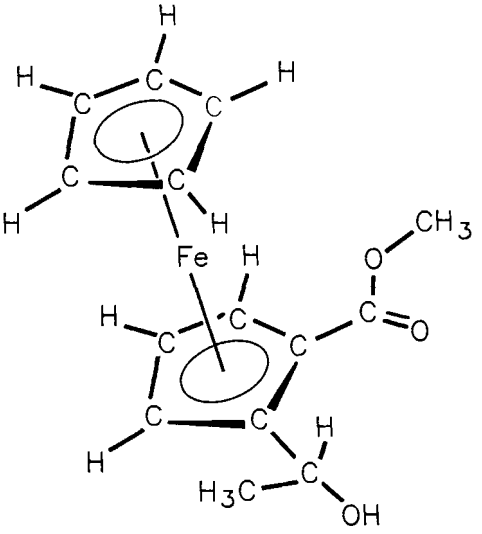

FIG. 2. The structure of **4***a*.

by their ^{1}H NMR spectra, and hence the substitution of the NMe_2 group must proceed either with complete retention of configuration, most likely (7, 14), or with complete inversion. The structure of **4***a* is shown in Fig. 2.[1] If the OH group is rotated such that it is adjacent to the substituted carbon on the cyclopentadiene ring, the CMe group is outside the rings and the CH group is between the rings. This is the conformation that would result in lithiation at the same substituted cyclopentadiene carbon atom if the OH group were replaced by NMe_2 (10). Thus the reaction of eq. [1] proceeds with overall retention of the configuration at the chiral carbon atom.

Acknowledgements

We thank the Natural Sciences and Engineering Research Council of Canada for financial support, and Dr. R. Barton, University of Regina, for details of the crystal structure of **4***a* shown in Fig. 2.

1. W. R. CULLEN and E. B. WICKENHEISER. Inorg. Chem. In press.
2. W. R. CULLEN and E. B. WICKENHEISER. J. Organomet. Chem. **370**, 141 (1989).
3. W. R. CULLEN, T.-J. KIM, F. W. B. EINSTEIN, and T. JONES. Organometallics, **4**, 346 (1985).
4. T. D. APPLETON, W. R. CULLEN, S. V. EVANS, T.-J. KIM, and J. TROTTER. J. Organomet. Chem. **279**, 5 (1985).
5. W. R. CULLEN and J. D. WOOLLINS. Can. J. Chem. **60**, 1793 (1982).
6. W. R. CULLEN, F. W. B. EINSTEIN, A. C. WILLIS, and E.-S. YEH. J. Am. Chem. Soc. **102**, 988 (1980).
7. D. MARQUARDING, H. KLUSACEK, G. GOKEL, P. HOFFMANN, and I. UGI. J. Am. Chem. Soc. **92**, 5389 (1970).
8. J. GRUNDY, B. G. JAMES, and G. PATTENDEN. Tetrahedron Lett. **9**, 757 (1972).
9. F. S. ALVAREZ and A. N. WATT. J. Org. Chem. **33**, 2143 (1968).
10. I. R. BUTLER, W. R. CULLEN, F. G. HERRING, and N. R. JAGANNATHAN. Can. J. Chem. **64**, 667 (1986).
11. W. REEVE and E. F. GROUP, JR. J. Org. Chem. **32**, 122 (1967).
12. C. MOISE, J. TIROUFLET, and H. SINGER. Bull. Soc. Chim. Fr. **4**, 1182 (1969).
13. T. HAYASHI, K. YAMAMOTO, and M. KUMADA. Tetrahedron Lett. **49**, 4405 (1974).
14. M. L. H. GREEN. Organometallic compounds. Vol. 2. The transition metals. 3rd ed. Methuen, London. 1968. p. 142.

[1]R. Barton, unpublished results.

Can. J. Chem. Downloaded from www.nrcresearchpress.com by 91.144.44.67 on 09/07/12
For personal use only.

Antineoplastic agents. 193. Isolation and structure of the cyclic peptide hymenistatin 1

GEORGE R. PETTIT,[1] PAUL J. CLEWLOW, CLAUDE DUFRESNE, AND DENNIS L. DOUBEK
Cancer Research Institute and Department of Chemistry, Arizona State University, Tempe, AZ 85287-1604, U.S.A.
RONALD L. CERNY
Midwest Center for Mass Spectrometry, The University of Nebraska, Lincoln, NE 68588-0362, U.S.A.
AND
KLAUS RÜTZLER
National Museum of Natural History, Smithsonian Institution, Washington, DC 20560, U.S.A.

Received June 27, 1989

GEORGE R. PETTIT, PAUL J. CLEWLOW, CLAUDE DUFRESNE, DENNIS L. DOUBEK, RONALD L. CERNY, and KLAUS RÜTZLER. Can. J. Chem. **68**, 708 (1990).

The Western Pacific Ocean sponge *Hymeniacidon* sp. was found to contain a cyclo-octapeptide designated hymenistatin 1 (**1**) active against the P388 leukemia cell line (ED_{50} 3.5 μg/mL). Structural determination was accomplished utilizing high field NMR (400 MHz) and mass spectral techniques (FAB MS/MS) followed by chiral gas chromatographic analysis to establish the absolute configuration (all *S*-amino acids).

Key words: cytostatic, *Hymeniacidon*, hymenistatin, cyclo-octapeptide, P388 leukemia.

GEORGE R. PETTIT, PAUL J. CLEWLOW, CLAUDE DUFRESNE, DENNIS L. DOUBEK, RONALD L. CERNY et KLAUS RÜTZLER. Can. J. Chem. **68**, 708 (1990).

On a trouvé que l'éponge *Hymeniacidon* sp., trouvée dans l'ouest de l'océan Pacifique, contient un cyclo-octapeptide appelé hymenistatine 1 (**1**) qui est actif contre la ligne des cellules P388 de la leucémie (ED_{50} 3,5 μg/mL). On déterminé la structure à l'aide des techniques de la RMN à 400 MHz et de la spectrométrie de masse (FAB MS/MS) et, en se basant sur une analyse par chromatographie en phase gazeuse chirale, on a pu établir que tous les acides aminés sont de configuration *S*.

Mots clés : cytostatique, *Hymeniacidon*, hymenistatine, cyclo-octapeptide, P388 de la leucémie.

[Traduit par la revue]

Early (2) investigations directed at isolation of marine sponge antineoplastic constituents led us initially to the geodiastatin proteins (3) and later to a series of pyrrolactams (4). Meanwhile, we have been pursuing other more promising leads in the Porifera phylum, including antineoplastic peptides. While a number of amino acids (5) have been isolated from marine sponges, only a small number of peptides (6) and antineoplastic sub- ances (7) have been isolated from these organisms. One of the *Hymeniacidon* sp. (Demospongiae Class) we collected in Palau in 1979 gave aqueous 2-propanol – methylene chloride extracts that led to a 30% life extension against the U.S. National Cancer Institute's murine P388 lymhocytic leukemia (PS system). Bioassay directed isolation using the PS leukemia led to isolation of a new cytostatic peptide designated hymenistatin (1).

After extraction and a preliminary solvent partition separation, a 1985 recollection (~ 250 kg wet wt.) of the sponge gave a PS active methylene chloride extract that was successively partitioned between 9:1 methanol–water and hexane, then diluted to 3:2 methanol–water and extracted with methylene chloride. Upon evaporation of the chlorocarbon an orange-colored solid was obtained, which significantly (PS ED_{50} 0.26 μg/mL) inhibited the PS leukemia. Initial gel-permeation chromatographic separation of the methylene chloride soluble fraction on Sephadex LH-20 and elution with 3:2 methylene chloride – methanol led to a further concentration of activity. A much better separation was achieved employing partition chromatography on Sephadex LH-20 with 3:1:1 hexane–toluene–methanol. The two principal active fractions from this chromatogram were combined and separated on a column of

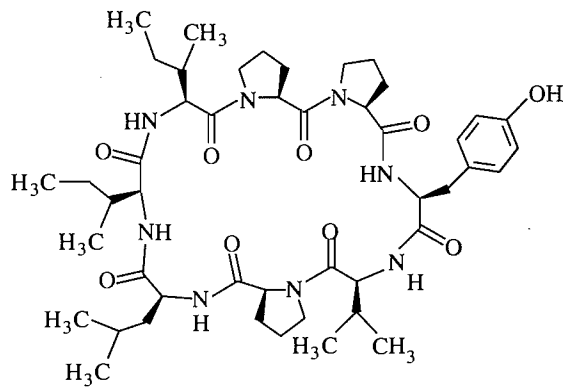

Hymenistatin 1

(**1**)

Sephadex LH-20 in methanol. The nearly pure cytostatic constituent obtained by this means was chromatographed using a silica gel Lobar column. Elution with 97.5:2.5 methylene chloride – methanol afforded the cell growth inhibitory (PS ED_{50} 3.5 μg/mL) biosynthetic product we designated as hymenistatin 1 (**1**).

Mass spectral measurements of hymenistatin indicated the presence of eight nitrogen atoms, and that information combined with the eight amide carbonyls observed in the ^{13}C NMR spectrum pointed to an octapeptide. The relatively high intensity of the molecular ion (base peak) observed in the FAB-MS spectrum suggested that the presumed octapeptide might be cyclic. Extensive application of 2D NMR techniques was next used to determine the identity of the eight amino acid units. The 400 MHz ^1H NMR spectrum clearly showed the presence of only five amide protons. By following the spin systems of these protons using $^1H,^1H$-COSY, and $^1H,^1H$-relayed COSY (8),

[1]Author to whom correspondence may be addressed. For antineoplastic agents, Part 192, please refer to ref. 1.

Can. J. Chem. Downloaded from www.nrcresearchpress.com by 91.144.44.67 on 09/07/12
For personal use only.

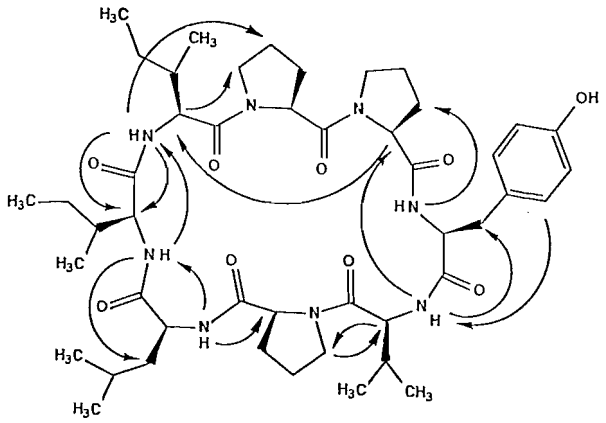

FIG. 1. Selected NOE's for hymenistatin **1** in deuteriochloroform.

cyclo [Pro^a-Pro^b-Tyr-Val-Pro^c-Leu-Ile-Ile]

Observed mass spectral fragmentation resulting from protonation at proline (indicated by a, b, or c):

a,	ProH$^+$---Pro---Tyr---Val---Pro---Leu---Ile---Ile		
m/z	195 358 457 554 667 780		from ms of *m/z* 780
b,	ProH$^+$---Tyr---Val---Pro---Leu---Ile---Ile---Pro		
m/z	261 360 457 570 683 796		from ms of *m/z* 796
c,	ProH$^+$---Leu---Ile---Ile---Pro---Pro---Tyr---Val		
m/z	211 324 437 534 794		from ms of *m/z* 794

FIG. 2. Hymenistatin 1 peptide sequence determination by FAB MS/MS.

these amino acids were determined to be valine, leucine, tyrosine, and two isoleucine units. Utilization of $^1H,^{13}C$-COSY, and $^1H,^1H,^{13}C$-RELAY (9) showed that the remaining NMR signals consisted of three independent spin systems of the type X-CH-CH_2-CH_2-CH_2-X typical of proline (10). The eight amino acid units accounted for the observed accurate-mass molecular weight. Actual sequence of the amino acids was ascertained from 1D-NOE experiments as summarized in Fig. 1.

To further corroborate the proposed structure, positive ion FAB MS/MS was pursued. As shown in Fig. 2, protonation at each proline nitrogen afforded three different linear peptide ions in the mass spectrum noted as A, B, and C. All but one of the ions predicted from their fragmentation was also observed, thereby confirming the structure assigned hymenistatin (**1**).

The absolute configuration of each chiral center was assigned using chiral GC analysis (Chirasil-Val III column) of the peptide hydrolysate following preparation of the *N*-pentafluoropropionyl/isopropyl ester derivatives (11). All of the amino acid units were found to bear the L configuration. Discovery of hymenistatin 1 (**1**), a seemingly unexceptional (12) cyclic peptide, that has cell growth inhibitory properties provides a new insight into structure requirements for such biological activity. Further biological evaluations and total synthesis are in progress.

Experimental

General methods

Solvents used for chromatographic procedures were redistilled. The Sephadex LH-20 (25-100 μm) employed for gel permeation and partition chromatography was obtained from Pharmacia Fine Chemicals AB, Uppsala, Sweden. Gilson FC-220 race track and F-80 microfractionators connected to Gilson HM UV–VIS Holochrome detectors were used for chromatographic fractionation experiments. Column chromatographic procedures with silica gel utilized the silica gel 60 prepacked "Lobar" columns supplied by E. Merck, Darmstadt, West Germany. The silica gel GF Uniplates for TLC were from Analtech Inc., Newark, Delaware. All TLC plates were viewed with UV light and (or) developed with a ceric sulphate – sulfuric acid spray (heating to approximately 150°C for 10 min).

The uncorrected melting points were observed using a Kofler-type melting point apparatus. The UV spectrum was recorded using a Hewlett–Packard 8450A UV–VIS spectrophotometer equipped with a HP7225A plotter. Optical rotation and IR spectral data were obtained using a Perkin–Elmer 241 polarimeter and a Nicolet MX-1 FTIR spectrophotometer, respectively. Mass spectra (70 eV and FAB) were recorded employing a Kratos MS-50 spectrometer. The NMR experiments were conducted with a Bruker WH-400 instrument and deuteriochloroform as solvent (TMS internal standard).

Animal collection and preliminary experiments

In early 1979, approximately 2 kg (wet wt) of the sponge *Hymeniacidon* sp. (Hymeniacidonidae family, Halichondrida Order, Ceratinomorpha Subclass, Demospongiae Class) was collected by scuba near Long Island (south side) in the Palau Archipelago, Western Caroline Islands. Taxonomic identification was conducted in the Smithsonian Institution where reference specimens are on file. The initial sample of Hymeniacidon sp. was preserved in 2-propanol. Removal of solvent gave an extract that reached a confirmed level of activity against the U.S. National Cancer Institute's murine P388 lymphocytic leukemia (PS system) with 30% life extension at 5.5 mg/kg.

Animal extraction and solvent partitioning

In March 1985, 250 kg (wet wt) of the *Hymeniacidon* sp. was recollected from the same area in Palau near the south side of Long Island and preserved in 2-propanol. The 2-propanol solution was decanted and the sponge was reextracted with the same alcohol. The extract was evaporated (*in vacuo*) to a 50 L water concentrate and found to contain a considerable amount (1.2 kg) of a pale brown suspension (PS T/C toxic at ≥ 50 mg/kg), which was removed by centrifugation (1000 *g*) and decantation. The cream-colored aqueous phase was successively partitioned between methylene chloride (90 L) and *n*-butanol (90 L). Evaporation of solvent from the chlorocarbon and *n*-butanol extracts gave, respectively, a very dark, brown, gel-like solid (180 g, PS ED_{50} 1.8 μg/mL and T/C 105 at 50 mg/kg) and a pale brown amorphous solid (300 g PS ED_{50} 6.1 μg/mL and T/C toxic at ≥ 50 mg/kg). The remaining aqueous extract was found to be PS inactive and was discarded. A solution of the methylene chloride fraction (180 g) in 9:1 methanol–water (1 L) was extracted with hexane (3 × 1 L). The methanol–water phase was diluted to 3:2 and extracted with methylene chloride. The resulting hexane (146 g), methylene chloride (20 g), and 3:2 methanol–water (14 g) fractions were concentrated and aliquots submitted for bioassay. Significant PS cytostatic activity (PS ED_{50} 0.26 μg/mL) was found to reside in the methylene chloride extract.

Isolation of hymenistatin 1 (1)

The 20 g sample of the PS active methylene chloride fraction in 3:2 methylene chloride – methanol was chromatographed on a column of Sephadex LH-20 (2.5 kg; 9 × 130 cm). While no pronounced separation of components was observed, further concentration to an active fraction designated A (elution volume 3.9 L, 18 g, PS ED_{50} 1.6 μg/mL) was realized. Further partition chromatography on Sephadex LH-20 (2.5 kg; 9 × 130 cm) and elution with 3:1:1 hexane–toluene–methanol gave active fractions B (elution vol. 500 mL, 0.50 g, PS ED_{50} 2.6 μg/mL) and C (elution vol. 480 mL, 1.64 g, PS ED_{50} 1.7 μg/mL)

Can. J. Chem. Downloaded from www.nrcresearchpress.com by 91.144.44.67 on 09/07/12
For personal use only.

Can. J. Chem. Downloaded from www.nrcresearchpress.com by 91.144.44.67 on 09/07/12
For personal use only.

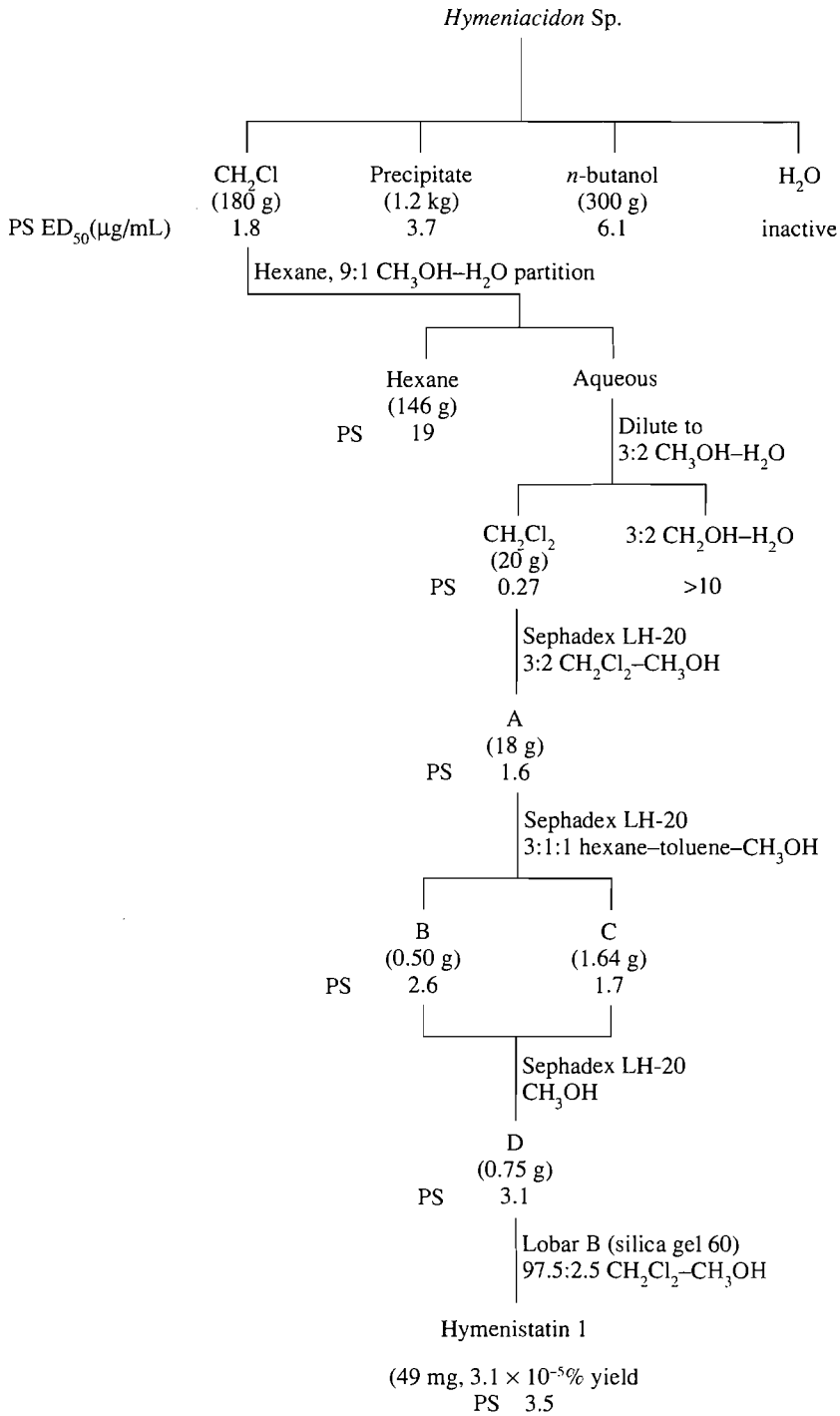

SCHEME 1

among 11 distinct composite fractions. Fractions B and C were combined and further separated in methanol on a Sephadex LH-20 column (500 g, 3.5 × 120 cm). Among the ten fraction groups obtained, a fraction labeled D (at elution vol. 60 mL, 0.75 g, PS ED_{50} 3.1 μg/mL) showed an almost single spot on tlc. Final purification was achieved utilizing a medium pressure (to 50 psi; 1 psi = 6.9 kPa) liquid chromatograhy unit with a prepacked silica gel 60 column (2.5 × 30 cm) and elution with 97.5:2.5 methylene chloride – methanol. Hymenistatin 1 was isolated as a colorless, amorphous solid (49 mg, 3.1×10^{-5} % yield) melting at 180–182°C: $[\alpha]_D$ −8.6° (*c* 1, $CHCl_3$); UV (CH_3OH) λ_{max} (log ε): 222 (3.82), 278 (3.16) nm; IR (NaCl plate): 3320, 2960, 2920, 1680, 1617, 1517 cm^{-1}; MS (HR-FAB): 893.5505 $[M + H]^+$ for $C_{47}H_{73}N_8O_9$; calcd. 893.5510; NMR ($CDCl_3$), δ, **Proline-a** unit, ^1H: 4.20 (H-2), 3.72 (H-5a), 3.38 (H-5b), 2.15 (H-3a), 2.11 (H-4a), 1.95 (H-4b), 1.93 (H-3b); ^{13}C: 60.89 (C-2), 47.35 (C-5), 31.87 (C-3), 25.06 (C-4); **Proline-b** unit, ^1H: 4.10 (dd, *J* = 9.4, 3.5; H-2), 3.28 (H-5a), 3.21 (H-5b), 2.16 (H-3a), 1.77 (H-3b), 1.60 (H-4a), 0.85 (H-4b); ^{13}C: 59.19 (C-2), 46.94 (C-5), 28.52 (C-3), 21.11 (C-4); **Proline c** unit, ^1H: 3.92 (H-5a), 3.79 (t, *J* = 7.8; H-2), 3.68 (H-5b), 2.31 (H-3a), 2.08 (H-4a), 2.06 (H-4b), 1.91 (H-3b), ^{13}C: 63.11 (C-2), 48.55 (C-5), 30.00 (C-3), 24.75 (C-4); **Tyrosine** unit, ^1H: 8.70 (br s, OH), 7.03 (d, *J* = 8.1; H-5), 6.84 (d, *J* = 8.0; H-6), 4.22 (H-2), 3.29 (H-3a), 2.90 (t, *J* = 13.0, H-3b); ^{13}C: 156.56 (C-7), 129.67 (C-5, C-9), 127.00 (C-4), 115.94 (C-6, C-8), 58.13 (C-2),

36.67 (C-3); **Valine** unit, ^{1}H: 7.58 (d, J = 8.8; NH), 4.56 (t, J = 5.9, H-2), 1.95 (H-3), 0.98 (6H; H-4, H-5); ^{13}C: 56.29 (C-2), 31.67 (C-3), 19.29 (C-4), 18.19 (C-5); **Leucine** unit, ^{1}H: 6.25 (br s, NH), 3.98 (H-2), 1.96 (H-3a), 1.82 (H-3b), 1.55 (H-4), 0.93 (3H; d, J = 6.3, H-6), 0.88 (3H, H-5); ^{13}C: 55.79 (C-2), 39.27 (C-3), 25.31 (C-4), 22.95 (C-6), 21.27 (C-5); **Isoleucine-a** unit, ^{1}H: 7.70 (d, J = 8.5, NH), 4.40 (t, J = 8.5, H-2), 1.57 (H-3), 1.50 (H-4a), 1.15 (H-4b), 0.96, (3H; H-6), 0.87 (3H; H-5); ^{13}C: 60.52 (C-2), 38.26 (C-3), 24.95 (C-4), 15.47 (C-6), 10.64 (C-5); and **Isoleucine-b** unit, ^{1}H: 7.40 (d, J = 8.5, NH), 4.69 (t, J = 9.0, H-2), 1.76 (H-3), 1.53 (H-4a), 1.05 (H-4b), 0.82 (3H; H-6), 0.80 (3H; H-5); ^{13}C: 55.01 (C-2), 36.94 (C-3), 24.79 (C-4), 16.20 (C-6), 11.87 (C-5). Eight carbonyl ^{13}C resonances appear at 172.72, 172.29, 172.10, 171.49, 171.95, 171.18, 170.41, 170.35. Where no multiplicity is indicated it could not be determined due to overlapping signals.

Assigment of the hymenistatin (1) chiral centers

The cyclo-octapeptide was hydrolyzed with 1:1 propionic acid – 12 N hydrochloric acid at 160°C for 15 min (13). The corresponding amino acids were converted to *N*-pentafluoropropionyl/isopropyl ester derivatives and configurations established by chiral capillary chromatography as reported by Shaw and Cotter (11) using a Chirasil Val III column. Each amino acid component was found to belong to the *S*(L) series.

Acknowledgments

The funds for this research were provided and received with appreciation from the Fannie E. Rippel Foundation, Grant CA-16049-05-12, and Outstanding Investigator Grant CA 44344-01A1 awarded by the Division of Cancer Treatment, NCI, DHHS, the Robert B. Dalton Endowment, the Arizona Disease Control Research Commission, Virginia G. Piper, Eleanor W. Libby, the Donald Ware Waddell Foundation, Herbert and Dianne Cummings, the Nathan Cummings Foundation, Lotte Flugel, and Polly J. Trautman. We are pleased to thank for other assistance the Government of Palau (Dr. T. Paulis and K. B. Batcheller), Drs. C. L. Herald, J. M. Schmidt, and M. Suffness, Messrs. P. J. Daschner, L. P. Tackett, L. Williams, and Mrs. D. N. Tackett, the National Science Foundation for equipment Grant CHE-8409644, and the NSF Regional Instrumentation Facility in Nebraska (Grant CHE-8620177).

1. G. R. Pettit, D. Sengupta, C. L. Herald, and P. M. Blumberg. J. Med. Chem. Submitted.
2. G. R. Pettit, J. F. Day, J. L. Hartwell, and H. B. Wood. Nature, **227**, 962 (1970); G. R. Pettit. Biosynthetic products for cancer chemotherapy. Vol. 1. Plenum Press, New York. 1977.
3. G. R. Pettit, J. A. Rideout, and J. A. Hasler. J. Nat. Prod. **44**, 588 (1981).
4. G. R. Pettit, C. L. Herald, R. Gupta, J. E. Leet, D. E. Schaufelberger, R. B. Bates, P. J. Clewlow, D. L. Doubek, K. P. Manfredi, K. Rutzler, J. M. Schmidt, L. P. Tackett, F. B. Ward, M. Bruck, and F. Camou. Can. J. Chem. In press.
5. M. Adamczeski, E. Quiñoã, and P. Crews. J. Org. Chem. **55**, 240 (1990); A. D. Rodriguez, R. K. Akee, and P. J. Scheuer. Tetrahedron Lett. **28**, 4989 (1987).
6. S. Omar, L. Tenenbaum, L. V. Manes, and P. Crews. Tetrahedron Lett. **29**, 5489 (1988); P. A. Grieco, Y. S. Hon, and A. Perez-Medrano. J. Am. Chem. Soc. **110**, 1630 (1988); I. Kitagawa, N. K. Lee, M. Kobayashi, and H. Shibuya. Chem. Pharm. Bull. **35**, 2129 (1987); P. Crews, L. V. Manes, and M. Boehler. Tetrahedron Lett. **27**, 2797 (1986); I. Kitagawa, M. Kobayashi, N. K. Lee, H. Shibuya, Y. Kawata, and F. Sakiyama. Chem. Pharm. Bull. **34**, 2664 (1986).
7. G. P. Gunawardana, S. Kohmoto, S. P. Genasekera, O. J. McConnell, and F. E. Koehn. J. Am. Chem. Soc. **110**, 4856 (1988); S. Sakemi, T. Ichiba, S. Kohmoto, and G. Saucy. J. Am. Chem. Soc. **110**, 4851 (1988); M. Ishibashi, Y. Ohizumi, J. F. Cheng, H. Nakamura, Y. Hirata, T. Sasaki, and J. Kobayashi. J. Org. Chem. **53**, 2855 (1988); T. F. Molinski and C. M. Ireland. J. Org. Chem. **53**, 2103 (1988); J. Kobayashi, J. F. Cheng, M. R. Walchli, H. Nakamura, Y. Hirata, T. Sasaki, and Y. Ohizumi. J. Org. Chem. **53**, 1800 (1988); D. Gouiffes, S. Moreau, N. Helbecque, J. L. Bernier, J. P. Henichart, Y. Barbin, D. Laurent, and J. F Verbist. Tetrahedron, **44**, 451 (1988); T. Ishida, M. Inoue, Y. Hamada, S. Kato, and T. Shioiri. J. Chem. Soc. Chem. Commun. 370 (1987); Y. Kato, N. Fusetani, S. Matsunaga, K. Hashimoto, R. Sakai, T. Higa, and Y. Kashman. Tetrahedron Lett. **28**, 6225 (1987); J. Kobayashi, J. F. Cheng, M. Ishibashi, H. Nakamura, Y. Ohizumi, Y. Hirata, T. Sasaki, H. Lu, and J. Clardy. Tetrahedron Lett. **28**, 4939 (1987).
8. A. J. Bax and G. Drobny. J. Magn. Reson. **61**, 306 (1985).
9. P. H. Bolton. J. Magn. Reson. **48**, 336 (1982); A. J. Bax. J. Magn. Reson. **53**, 149 (1983).
10. G. R. Pettit, Y. Kamano, C. L. Herald, A. A. Tuinman, F. E. Boetner, H. Kizu, J. M. Schmidt, L. Baczynskyj, K. B. Tomer, and R. J. Bontems. J. Am. Chem. Soc. **109**, 6883 (1987).
11. C. J. Shaw and M. L. Cotter. Chromatographia, **21**, 197 (1986).
12. A. V. Schally. Cancer Res. **48**, 6977 (1988).
13. F. Westall and H. Hesser. Anal. Biochem. **61**, 610 (1974).

Can. J. Chem. Downloaded from www.nrcresearchpress.com by 91.144.44.67 on 09/07/12
For personal use only.

g-Values for γ-irradiated water as a function of temperature

A. JOHN ELLIOT,[1] MONIQUE P. CHENIER, AND DENIS C. OUELLETTE

System Chemistry and Corrosion Branch, Chalk River Nuclear Laboratories, Atomic Energy of Canada Limited, Chalk River, Ont., Canada K0J 1J0

Received August 14, 1989

A. JOHN ELLIOT, MONIQUE P. CHENIER, and DENIS C. OUELLETTE. Can. J. Chem. **68**, 712 (1990).

The *g*-values of primary species formed in the γ-radiolysis of water have been estimated for the temperature range 25–300°C. The *g*-values for the hydrated electron, the hydroxyl radical, and molecular hydrogen all increase approximately 50% over this temperature range. The *g*-values for the minor products, hydrogen peroxide and atomic hydrogen, probably also increase with temperature; however, there is evidence from some of the experimental data which suggests that these *g*-values may slightly decrease with increasing temperature.

Key words: radiolysis, *g*-values, temperature dependence.

A. JOHN ELLIOT, MONIQUE P. CHENIER et DENIS C. OUELLETTE. Can. J. Chem. **68**, 712 (1990).

On a évalué les valeurs-*g* des espèces primaires qui se forment lors de la radiolyse-γ de l'eau à des températures allant de 25 à 300°C. Pour cet écart de température, les valeurs-*g* de l'électron hydraté, du radical hydroxyle et de l'hydrogène moléculaire augmentent toutes d'environ 50%. Il est probable que les valeurs-*g* des produits mineurs comme le peroxyde d'hydrogène et l'hydrogène moléculaire subissent aussi des augmentations avec la température; toutefois, certaines données expérimentales suggèrent que ces valeurs-*g* diminuent légèrement avec une augmentation de la température.

Mots clés : radiolyse, valeurs-*g*, relation avec la température.

[Traduit par la revue]

Can. J. Chem. Downloaded from www.nrcresearchpress.com by 91.144.44.67 on 09/07/12
For personal use only.

Introduction

The primary heat transport systems in both pressurized and boiling water nuclear power reactors generally operate in the 250–310°C temperature range with a 25°C pH of 7–11 (1). To computer model the water radiolysis under these conditions, the yields of the primary species (eq. [1]) are required for both the γ and the fast neutron radiation. The term "primary species" refers to the species formed by the action of the radiation as opposed to those formed by chemical reactions afterwards. The yields in radiation chemistry are generally measured in terms of *G* (or *g*)-values, which, in this paper, are defined as the number of species formed or destroyed per 100 eV of energy absorbed (2, 3). The symbol "*g*" will be used for the yield of primary species while "*G*" will be used for all other yields.

$$[1] \qquad H_2O \xrightarrow{\text{radn.}} e_{aq}^-, OH, H, H_2O_2, H_2, HO_2$$

Experimental data are available for the *g*-values up to 250–300°C for both fast neutrons (4) and γ-radiation (5–7) in 0.4 mol dm^{-3} sulphuric acid. However, for water of near-neutral pH, there are only pulse radiolysis data up to 200–250°C (8–11) and some contradictory steady-state radiolysis results (12–14) in the 250–300°C temperature range. For fast neutrons, there are only estimates for the *g*-values at room temperature (15, 16) based on the *g*-values measured using radiation with different linear energy transfer characteristics.

In this report, the literature data are combined with our recent steady-state radiolysis results to predict the *g*-values for the γ-radiolysis of water up to 300°C.

Experimental

The chemicals that were used in these experiments were AR quality or better and were used as supplied. The solutions were prepared in water that had been distilled, passed through a Millipore purification system, and then redistilled from alkaline permanganate. The solutions were degassed on a vacuum line and then transferred to and sealed in 1.5×10^{-2} dm^3 cylindrical Pyrex cells. Unless otherwise stated, for solutions to be irradiated at 300°C, the amount of solution added to the sample cell was such that, at temperature, the cell was essentially filled with liquid to minimize the proportion of water in the vapour phase. (The density of water at 300°C is 0.71 kg dm^{-3}.) At lower temperatures, there was sufficient solution in the ampoules to ensure more than 98% of the water was in the liquid phase.

The samples were heated in an autoclave and irradiated in an AECL Gamma-Cell. The dose rate as measured by Fricke dosimetry (3) was near 7.25×10^{18} eV kg^{-1} s^{-1}. Hydrogen was the only product analyzed and its yield was measured using a gas burette coupled to a gas chromatograph. At room temperature and at the highest temperature studied, the *G*-value for hydrogen was always calculated from yield–dose plots, while at intermediate temperatures it was normally calculated from the hydrogen yield from duplicate samples measured at only one dose. As the yield–dose plots were always linear within experimental error and passed through the origin, this indicated that hydrogen formed through thermal decomposition of the solutions was insignificant. This was confirmed by heating some of the solutions at 300°C without irradiation.

Two sets of experiments were carried out in ca. 8.5×10^{-2} mol kg^{-1} KOH. The concentration of KOH was determined by titration with HCl. The loss of OH^- after irradiations at 200 and 300°C was found to be only ca. 6 and 15%, respectively.

Results

(A) Estimation of $g(H_2)$

At room temperature, the hydrogen yield measured in degassed dilute solutions containing either KBr (17) or KNO_2 (18) is a good estimate of $g(H_2)$. This is because both Br^- and NO_2^- scavenge the hydroxyl radical to prevent reaction [2], which would destroy the molecular hydrogen formed in the radiolysis (eq. [1]) (2).

$$[2] \qquad OH + H_2 \rightarrow H + H_2O$$

For this study, we have irradiated both solutions over the 25–300°C temperature range.

(i) Radiolysis of 2×10^{-3} *mol* kg^{-1} *KBr solutions*

Figures 1 and 2 summarize the results obtained for γ-irradiated degassed 2×10^{-3} mol kg^{-1} KBr solutions. Also shown in Fig. 2 are the results reported by Kabakchi and Lebedeva (14), who irradiated (possibly aerated) 10^{-3} mol kg^{-1} KBr solutions in open Pyrex ampoules in an autoclave, and

[1]Author to whom correspondence may be addressed.

Can. J. Chem. Downloaded from www.nrcresearchpress.com by 91.144.44.67 on 09/07/12
For personal use only.

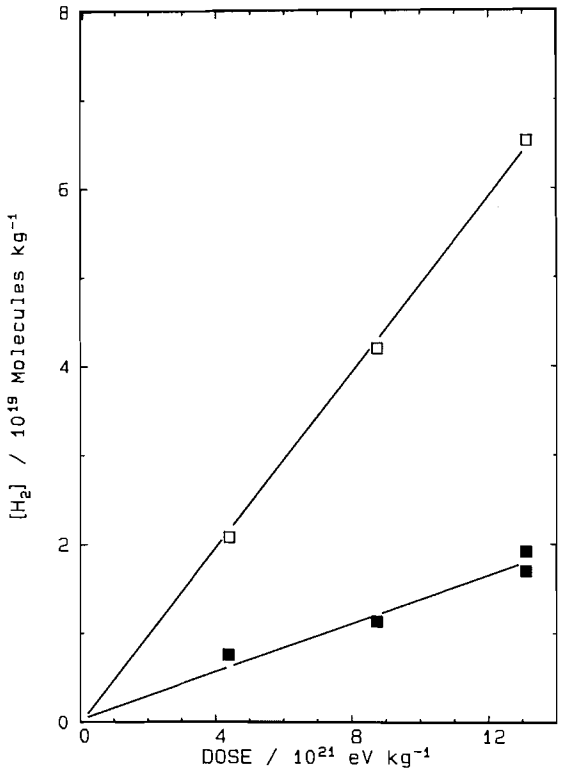

FIG. 1. The hydrogen yield from degassed 2×10^{-3} mol kg^{-1} KBr solutions irradiated at 25°C (□) and 300°C (■).

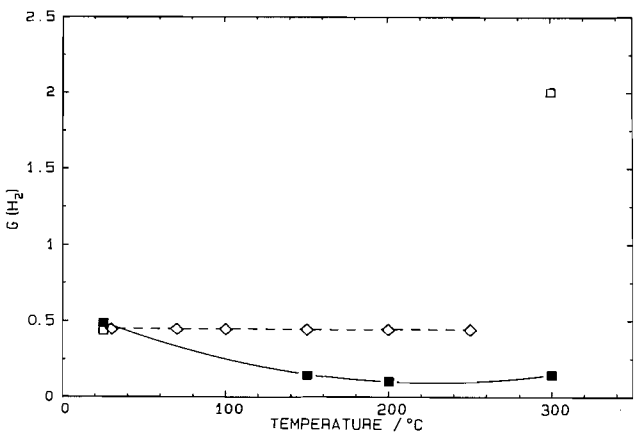

FIG. 2. $G(H_2)$ measured from (1–2) $\times 10^{-3}$ mol kg^{-1} KBr solutions as a function of temperature: this work (■), Burns and Marsh (13) (□), and Kabakchi and Lebedeva (14) (◇).

the results reported by Burns and Marsh (13), who irradiated deaerated 2×10^{-3} mol kg^{-1} KBr solutions in a stainless steel loop. While these data agree well with each other and the literature data (17) at room temperature, there is no agreement at higher temperatures.

Figure 3 shows the $G(H_2)$ obtained for a series of experiments conducted at 300°C with different proportions of water in the vapour phase. The proportion of water in the vapour phase at 300°C was calculated from the mass of the sample, the volume of the cell, and the densities of liquid water and steam (19). The line in Fig. 3 was fitted to the data using eq. [3]:

$$[3] \quad G(H_2) = (M_{gas}/M_{total})G(H_2)_{gas} + (M_{liq}/M_{total})G(H_2)_{liq}$$

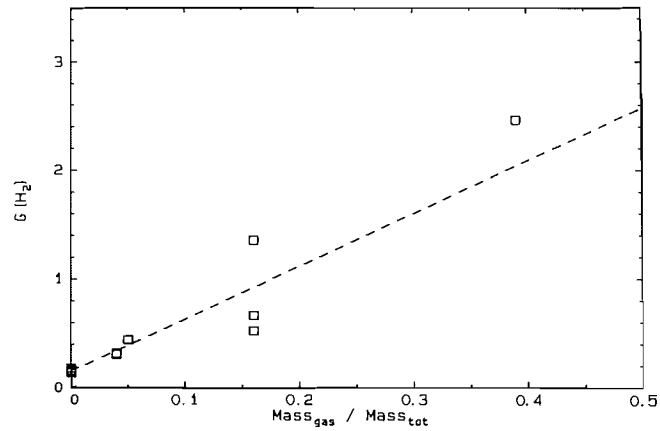

FIG. 3. $G(H_2)$ measured from degassed 2×10^{-3} mol kg^{-1} KBr solutions irradiated at 300°C as a function of the proportion of water in the gas phase.

where M is the mass of water, and $G(H_2)_{liq}$ and $G(H_2)_{gas}$ are the G-values for hydrogen formed in the liquid and steam phase, respectively. The values for $G(H_2)_{liq}$ of 0.15 and for $G(H_2)_{gas}$ of 5 were used. This $G(H_2)_{gas}$ is consistent with measurements of hydrogen yields in irradiated steam. We have measured a value of $G(H_2)$ of 4.1 at 300°C for steam under similar conditions to the above experiments. Two other groups of workers (ref. 20 and footnote 2) who have measured $G(H_2)$ in steam (at 0.5–1 atm pressure; 1 atm = 101.3 kPa) as a function of temperature have reported values of 2 at 100°C rising sigmoidally to 8 at >400°C. At 300°C, a value for $G(H_2)$ near 7 was found (ref. 20 and footnote 2). These results indicate that, depending on the proportion of water in the vapour phase, radiolysis of water vapour can contribute significantly to the measured hydrogen yield. To minimize the radiolysis of water vapour at high temperatures, the ratio of the gas to liquid volume in the sample should be minimized.

This may explain why the G-values observed by Kabakchi and Lebedeva (14) are higher than the values measured in this study. They irradiated open ampoules in an autoclave and calculated $G(H_2)$ from the gas pressure increase in the autoclave and the gas composition. Under this arrangement a large portion of the water must have been present as steam at the higher temperatures.

In the experiments by Burns and Marsh (13), corrosion of the stainless steel loop was ruled out as a source for the high $G(H_2)$ value measured at 300°C. However, in the irradiation vessel, a steam layer may have developed where the excess hydrogen could be formed by steam radiolysis, perhaps enhanced by wall effects (22).

(ii) Radiolysis of 10^{-3} mol kg^{-1} KNO_2 solutions

Figures 4 and 5 summarize the results obtained when the degassed 10^{-3} mol kg^{-1} KNO_2 solutions were irradiated. The yield–dose curves were linear at 25 and 300°C and the room temperature value of 0.42 ± 0.04 is in agreement with the literature value (18). The $G(H_2)$ of 0.62 ± 0.03 measured at 300°C is much higher than the $G(H_2)$ of 0.15 ± 0.02 measured at the same temperature from the KBr solution.

(B) Estimation of g(H_2) + g(H)

To estimate $g(H_2) + g(H)$, solutes were chosen that not only scavenged the hydrogen atoms to form hydrogen, but were also good hydroxyl radical scavengers to protect the hydrogen

[2]D. A. Armstrong and R. Ahmad. Unpublished data.

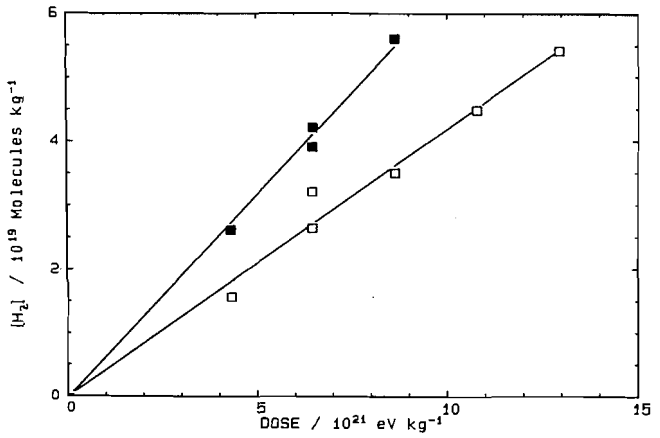

FIG. 4. The hydrogen yield from degassed 10^{-3} mol kg^{-1} KNO_2 solutions irradiated at 25°C (□) and 300°C (■).

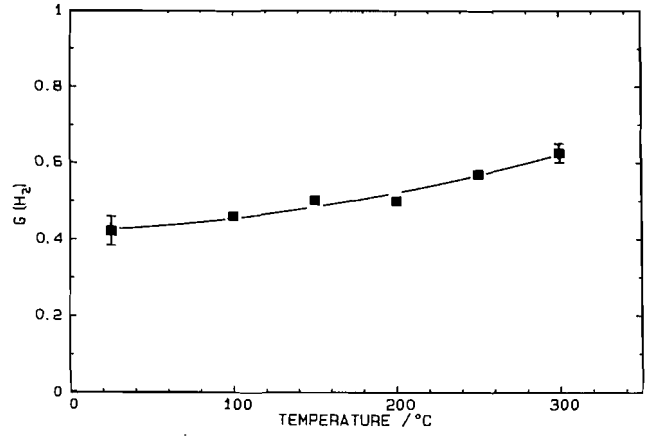

FIG. 5. $G(H_2)$ measured from degassed 10^{-3} mol kg^{-1} KNO_2 solutions as a function of temperature.

formed. The hydrated electron scavengers were selected on the basis that they were either relatively ineffective hydrogen atom scavengers or, if they did react with the hydrogen atom, molecular hydrogen was formed.

[4] $CH_3OH + OH, H \rightarrow \cdot CH_2OH + H_2O, H_2$

[5] $(CH_3)_2CHOH + OH, H \rightarrow (CH_3)_2COH + H_2O, H_2$

[6] $e_{aq}^- + Cd^{2+} \rightarrow Cd^+$

[7] $e_{aq}^- + (CH_3)_2C{=}O \xrightarrow{H^+} (CH_3)_2COH$

Three systems were studied over the 25–300°C temperature range: (a) degassed 10^{-3} mol kg^{-1} $CdSO_4$, 10^{-2} mol kg^{-1} methanol; (b) degassed 10^{-3} mol kg^{-1} acetone, 10^{-2} mol kg^{-1} methanol; and (c) degassed 10^{-3} mol kg^{-1} acetone, 10^{-2} mol kg^{-1} 2-propanol. The results are summarized in Figs. 6 and 7. At room temperature, a $G(H_2)$ of 1 was found for these systems, which is in good agreement with previously published data (23–25). Up to 200°C, all three solutions had essentially the same $G(H_2)$; above 200°C, there is a dramatic, but different, increase in $G(H_2)$ for each solution. As the yield–dose plot for each solution at 300°C was linear and passed through the origin (Fig. 6), this indicates that the hydrogen yield arose from radiation-induced processes and not thermal decomposition of the starting solution. Thermal decomposition of the stable end products of the radiolysis is also unlikely to be the source of the excess hydrogen because a $G(H_2)$ of near 1 was still found for

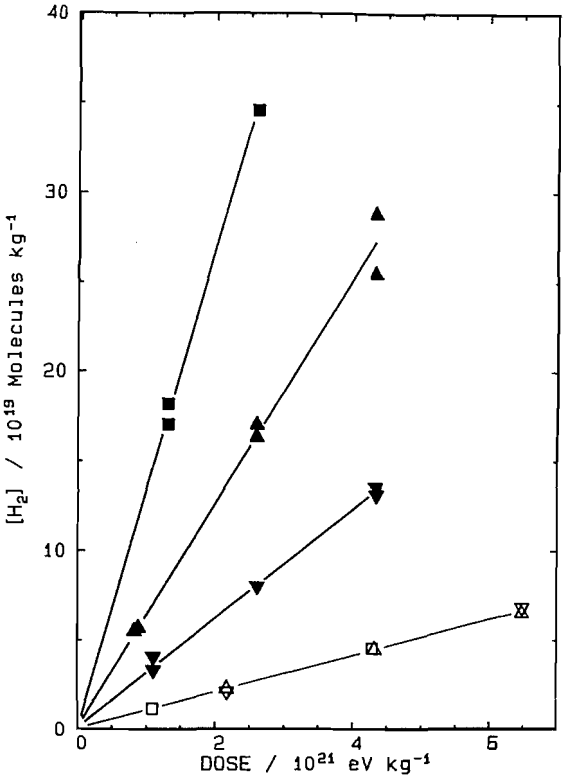

FIG. 6. The hydrogen yield from degassed solutions containing: 10^{-3} mol kg^{-1} $CdSO_4$, 10^{-2} mol kg^{-1} methanol (△, ▲); 10^{-3} mol kg^{-1} acetone, 10^{-2} mol kg^{-1} methanol (▽, ▼); and 10^{-3} mol kg^{-1} acetone, 10^{-2} mol kg^{-1} 2-propanol (□, ■). The open and solid points are solutions irradiated at 25 and 300°C, respectively.

solution (c) when it was irradiated at room temperature and then heated to 300°C.

(C) Estimation of $g(e_{aq}^-) + g(H_2) + g(H)$

Degassed solutions containing 10^{-3} mol kg^{-1} perchloric acid and 10^{-2} mol kg^{-1} methanol were irradiated to estimate $g(e_{aq}^-) + g(H_2) + g(H)$. In these solutions, the hydrated electron is converted into a hydrogen atom (reaction [8])

[8] $e_{aq}^- + H^+ \rightarrow H$

which in turn reacts with the methanol to form hydrogen (reaction [4]). The total molecular hydrogen yield is then a measure of $g(e_{aq}^-) + g(H_2) + g(H)$. Unfortunately, this system could only be studied over the 25–200°C range because at higher temperatures the acid solution reacted with the Pyrex ampoule and the pH increased. (After heating to 300°C, the room temperature pH rose from 3 to 7.) These results are given in Fig. 8. The room temperature G-value is consistent with the results of Baxendale and Dixon (25).

Increasing the acid concentration to minimize the loss of protons reacting with the Pyrex ampoule would also lead to excessive scavenging of the hydrated electron in the spur (2). To circumvent this, degassed 10^{-2} mol kg^{-1} methanol solutions containing 0.1 mol kg^{-1} KH_2PO_4 were used. The room temperature pH was adjusted to 2.4 with perchloric acid, which, at 200 and 300°C, represents pH values of 3.4 and 4.3, respectively (26). In these solutions the hydrated electron can be converted to hydrogen atoms by reactions [8] and [9] (27).

[9] $e_{aq}^- + H_3PO_4(H_2PO_4^-) \rightarrow H + H_2PO_4^-(HPO_4^{2-})$

The hydrogen atoms formed in these reactions either react with

Can. J. Chem. Downloaded from www.nrcresearchpress.com by 91.144.44.67 on 09/07/12
For personal use only.

Can. J. Chem. Downloaded from www.nrcresearchpress.com by 91.144.44.67 on 09/07/12
For personal use only.

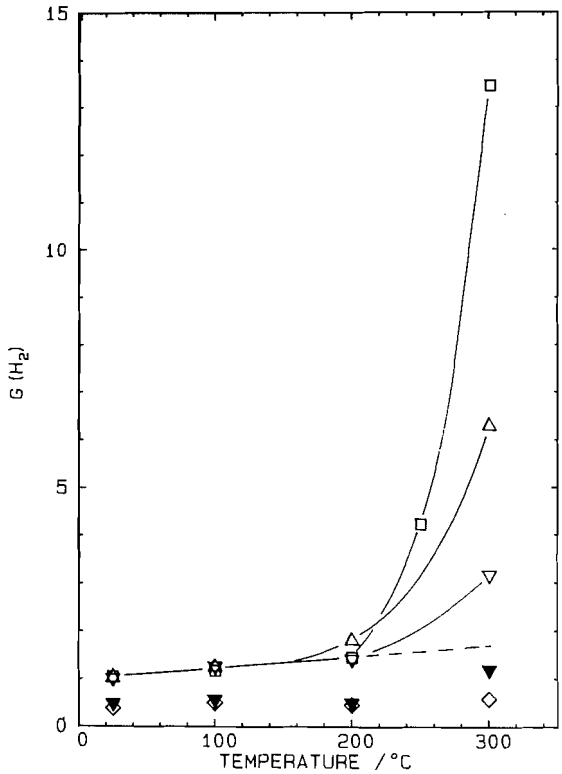

FIG. 7. $G(H_2)$ as a function of temperature as measured from degassed solutions containing: 10^{-3} mol kg^{-1} $CdSO_4$, 10^{-2} mol kg^{-1} methanol (△); 10^{-3} mol kg^{-1} acetone, 10^{-2} mol kg^{-1} methanol (▽); 10^{-3} mol kg^{-1} acetone, 10^{-2} mol kg^{-1} 2-propanol (□); 10^{-3} mol kg^{-1} acetone, 10^{-2} mol kg^{-1} methanol, 8.5×10^{-2} mol kg^{-1} KOH (▼); and 10^{-3} mol kg^{-1} KNO_2, 8.5×10^{-2} mol kg^{-1} KOH (◇).

the methanol (reaction [4]) or by reaction [10] (27).

[10] $H + H_3PO_4(H_2PO_4^-) \rightarrow H_2 + H_2PO_4(HPO_4^-)$

The $G(H_2)$ that are shown in Fig. 8 steadily increase in value with temperature over the whole temperature range but are consistently 0.92 of the $G(H_2)$ obtained from the 10^{-3} mol kg^{-1} perchloric acid and 10^{-2} mol kg^{-1} methanol solutions. The important point is that the yield smoothly increases between 200 and 300°C, which suggests that no abrupt change in yields occurred in this temperature range. The room temperature pH of the solution did not change after an irradiation at 300°C.

(D) Estimation of g(H_2) and g(H) in alkaline solutions

Because of the conflicting results for $g(H_2)$ in section (A) above, the hydrogen yields were measured from irradiated degassed 8.5×10^{-3} mol kg^{-1} KOH solutions containing either 10^{-3} mol kg^{-1} KNO_2 or 10^{-3} mol kg^{-1} acetone and 10^{-2} mol kg^{-1} methanol. In the latter solution, because of the high OH^- concentration, most of the atomic hydrogen will react by eq. [11] to form the hydrated electron (17) rather than by reaction [4] to form hydrogen.

[11] $H + OH^- \rightarrow e_{aq}^- + H_2O$

The results are summarized in Fig. 7. Up to 200°C, the hydrogen yields for the acetone–methanol solution were slightly higher than that from the nitrite solution. At 25 and 200°C, $G(H_2)$ for the nitrite solution were 0.38 and 0.45, respectively, and $G(H_2)$ for the acetone–methanol solution were 0.48 and 0.50, respectively. At 300°C, in the acetone–methanol solution, the $G(H_2)$ was 1.19, which is considerably greater than

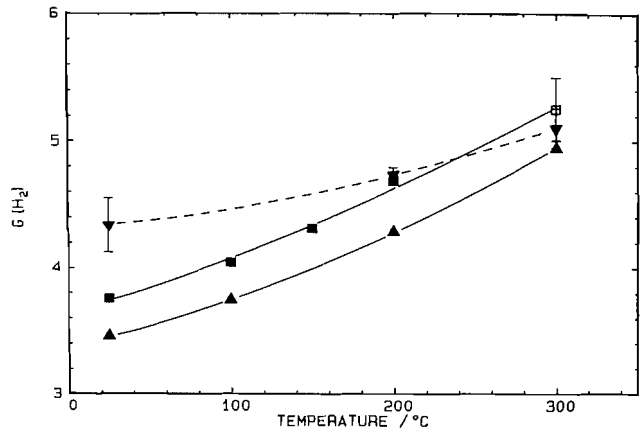

FIG. 8. $G(H_2)$ as a function of temperature as measured from degassed solutions containing: 10^{-2} mol kg^{-1} methanol, 10^{-3} mol kg^{-1} $HClO_4$ (■); value estimated at 300°C (□); 10^{-2} mol kg^{-1} methanol, 10^{-1} mol kg^{-1} KH_2PO_4, pH adjusted to 2.4 at 25°C (▲); 10^{-1} mol kg^{-1} methanol, 0.4 mol kg^{-1} H_2SO_4 (▼) (5).

the 0.57 observed in the nitrite solution. The excess hydrogen production in the acetone–methanol solution probably arises through the same process operating in this solution at neutral pH (see section D above).

The $G(H_2)$ of 0.38 for the alkaline nitrite solution at 25°C is slightly lower than the neutral pH value of 0.41 and is consistent with the hydrogen atom precursor of the molecular hydrogen reacting by eq. [11] in the spur.

The difference between $G(H_2)$ for the acetone–methanol solution at neutral pH and $G(H_2)$ from one containing 8.5×10^{-2} mol kg^{-1} KOH provides an alternative estimate of $g(H)$.

Discussion

(A) Estimation of g(H_2)

While the values of $G(H_2)$ from Br^- solutions (Fig. 2) are quite different from those obtained from NO_2^- solutions (Fig. 5), we consider the latter to best represent $g(H_2)$. At room temperature, Br^- protects the molecular hydrogen by scavenging the hydroxyl radical as shown in the following sequence of equilibria [12]–[14] (28, 29):

[12] $OH + Br^- \rightleftarrows HOBr^-$

[13] $HOBr^- \rightleftarrows Br + OH^-$

[14] $Br + Br^- \rightleftarrows Br_2^-$

At room temperature, equilibrium [14] lies well to the right ($K_{14} = 2 \times 10^5$ M^{-1} (30)). By analogy with the corresponding equilibria involving I^- and SCN^- (31, 32), as the temperature increases, K_{14} will decrease to allow intermediate species like bromine atoms and $HOBr^-$ to react with the molecular hydrogen to lower the hydrogen yield. Similar reactions involving $Br/HOBr^-$ and $SCN/HOSCN^-$ have also been observed when studying reactions of Br_2^- (33) and $(SCN)_2^-$ (34).

Further support for the assignment of $g(H_2)$ to $G(H_2)$ from the nitrite solution comes from the alkaline solution study (Fig. 7) where $G(H_2)$ was similar for both the nitrite and acetone–methanol solutions up to 200°C. As mentioned earlier, the hydrogen yield from the latter solution should represent $g(H_2)$ only as the atomic hydrogen that escaped the spur would undergo reaction [11] rather than reaction [4].

(B) Estimation of $g(H_2) + g(H)$

Up to 200°C, there is reasonable agreement between the three systems studied for the temperature dependence of $g(H_2) + g(H)$ (see Fig. 7). Above this temperature, the observed increase in $G(H_2)$ can be explained in terms of thermal reactions of the intermediates formed during the radiolyses.

In solutions containing Cd^{2+} and methanol, the principal reactions involving the primary species are given by reactions [4], [6], and [15] (2, 24, 35). From earlier studies (5) of the radiolysis of 0.4 mol kg^{-1} sulphuric acid solutions containing methanol, the hydrogen yield did not increase abruptly above 200°C (summarized in Fig. 8), which indicates that the $\cdot CH_2OH$ does not thermally decompose to form hydrogen in the 200–300°C range. It is most likely that the hydrolysis of either Cd^+, Cd_2^{2+}, or Cd^0 (reactions [6] and [15] (35))

[15] $Cd^+ + Cd^+ \rightarrow Cd_2^{2+} \rightleftarrows Cd^0 + Cd^{2+}$

gives rise to the excess hydrogen (reactions [16] or [17] followed by [4]).

[16] Cd^0 (or Cd_2^{2+}) $+ 2H_2O \rightarrow Cd^{2+}$ (or $2Cd^{2+}$) $+ H_2 + 2OH^-$

[17] $Cd^+ + H_2O \rightarrow H + Cd^{2+} + OH^-$

In the two solutions where acetone was used as the hydrated electron scavenger, the radical, $(CH_3)_2COH$, formed in reactions [5] and [7] appears to be responsible for the increase in the hydrogen yield above 200°C.

Again, it is obvious that the $\cdot CH_2OH$ radical is not the origin of the excess hydrogen. At 300°C, a $G(H_2)$ of 3.2 ± 0.3 is observed in the solutions containing acetone and methanol; here approximately equal amounts of $\cdot CH_2OH$ and $(CH_3)_2COH$ were formed. In solutions containing acetone and 2-propanol where essentially all the organic radicals were $(CH_3)_2COH$, a $G(H_2)$ of 13.5 ± 0.3 was measured. Based on the estimated g-values for water at 300°C (see later), the maximum possible G-value for $(CH_3)_2COH$ is 10.7 and this assumes that all the hydrogen peroxide thermally decomposes to form two hydroxyl radicals (reaction [18]) (36).

[18] $H_2O_2 \rightarrow 2OH$

This suggests a chain reaction must be occurring, but, unfortunately, under the present experimental arrangement the dose rate cannot be varied to screen for a chain reaction. One possible mechanism is the thermally induced reaction [19] to form atomic hydrogen

[19] $(CH_3)_2COH \xrightarrow{\text{heat}} (CH_3)_2C{=}O + H$

followed by reaction [5] to form the excess molecular hydrogen and another $(CH_3)_2COH$ radical to propagate the chain. When methanol is present, reaction [4] produces some extra molecular hydrogen but, as $\cdot CH_2OH$ does not thermally decompose at these temperatures, the chain reaction cannot occur.

Also consistent with the above mechanism is the much lower increase in hydrogen yield observed at 300°C in the acetone–methanol solution containing 8.5×10^{-2} mol kg^{-1} KOH compared to the same solution at neutral pH (Fig. 7). In this alkaline solution at 300°C, $(CH_3)_2COH$ will probably exist largely as the acetone radical anion (equilibrium [20]) based on the measured pK_a of 12.2 at 25°C and 11.7 at 64°C (41).

[20] $(CH_3)_2COH + OH^- \rightleftarrows (CH_3)_2C{-}O^- + H_2O$

The radical anion, $(CH_3)_2C{-}O^-$, is unlikely to undergo a reaction similar to [19].

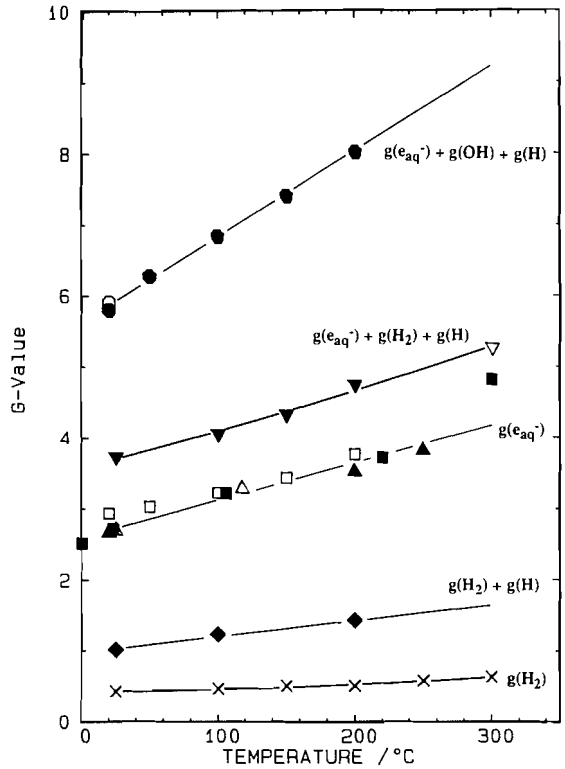

FIG. 9. The data used to calculate the g-values for the primary species as a function of temperature. $g(H)$ (X), $g(H_2) + g(H)$ (◆); $g(e_{aq}^-) + g(H_2) + g(H)$ (▼, ▽) (this work). $g(e_{aq}^-)$: (■) (12), (▲) (11), (□) (10), and (△) (40). $g(e_{aq}^-) + g(OH) + g(H)$: (●) (see text, 9, 10) and (○) (8). The values used in the calculations are given by the solid lines.

Since the marked increase in $G(H_2)$ above 200°C appears to arise from thermally initiated processes involving the intermediates and not the primary species, the data up to 200°C were extended to 300°C in a linear fashion, as shown in Fig. 7.

(C) Estimation of $g(e_{aq}^-) + g(H_2) + g(H)$

The values of $G(H_2)$ from solutions containing 10^{-2} mol kg^{-1} methanol and 0.1 mol kg^{-1} KH_2PO_4 increase smoothly over the 25–300°C temperature range. Although these data are 8% lower than the $G(H_2)$ from the solutions containing 10^{-3} mol kg^{-1} perchloric acid and 10^{-2} mol kg^{-1} methanol, we have used this temperature dependence to extrapolate the G-values for the perchloric acid – methanol solution from 200 to 300°C (Fig. 8).

Also shown in Fig. 8 is the $G(H_2)$ obtained in an earlier study of 0.1 mol kg^{-1} methanol in 0.4 mol kg^{-1} sulphuric acid (5). The increase of $G(H_2)$ with temperature for the 0.4 mol kg^{-1} sulphuric acid solution is less than with the 10^{-3} mol kg^{-1} perchloric acid. In general, it appears that the increase in G-value with temperature is less, the more acidic the solution. Further evidence of this comes from pulse radiolysis studies: Elliot (37) has observed at pH 2 that $g(e_{aq}^-) + g(H)$ was constant over the temperature range 20–80°C; and studies where G(radical) was measured at different pH's using HO_2/O_2^- yields in solutions containing formate ions (8) or saturated with hydrogen (38) also showed the same effect.

(D) g*-Values for the primary species as function of temperature*

The data used to estimate the g-values for the primary species in γ-irradiated near-neutral water are shown in Fig. 9. The yields for $g(e_{aq}^-) + g(OH) + g(H)$ were taken from Fig. 6 in ref. 9 and corrected by the recently published (10) extinction

Can. J. Chem. Downloaded from www.nrcresearchpress.com by 91.144.44.67 on 09/07/12
For personal use only.

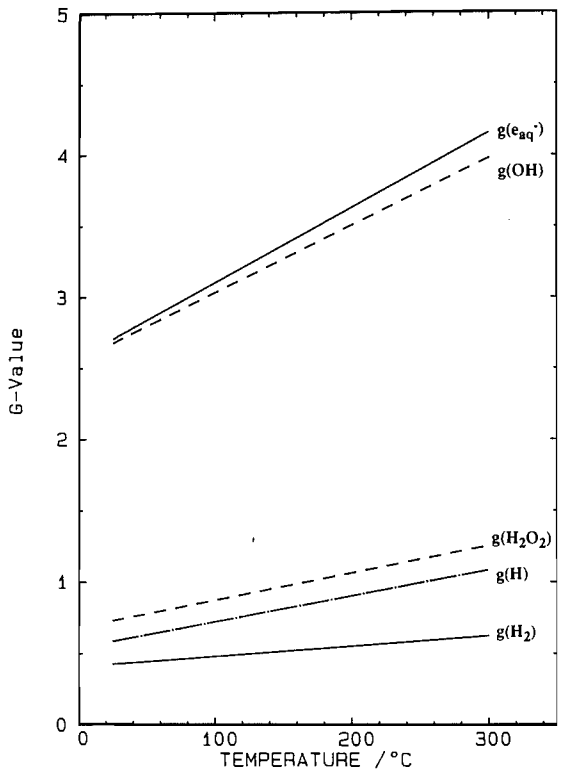

FIG. 10. The temperature dependence of the g-values for the primary species based on $g(H_2) + g(H)$ data (see text).

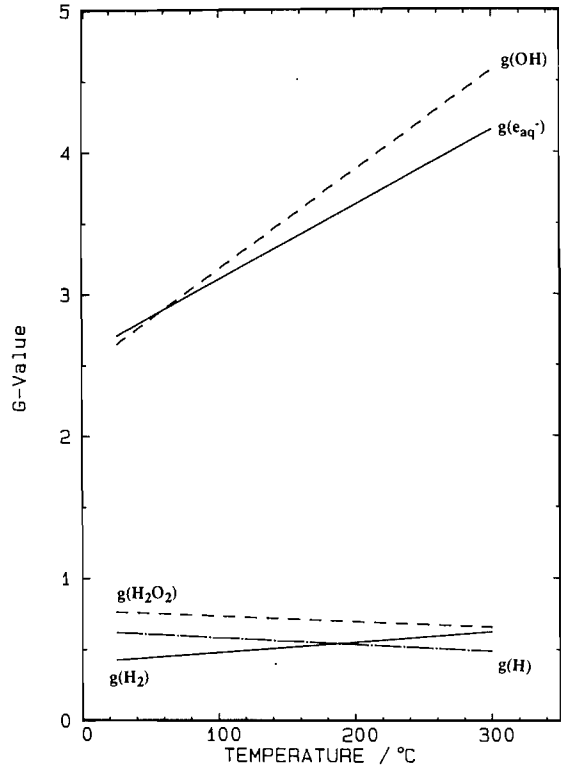

FIG. 11. The temperature dependence of the g-values for the primary species based on $g(e_{aq}^-) + g(H_2) + g(H)$ data (see text).

coefficients for the mono-cation, MV^+, formed by the one-electron reduction of the methyl viologen (1,1′-dimethyl-4,4′-bipyridylium) di-cation. In general, the data selected from the literature were chosen because there was little ambiguity associated with the value. There are pulse radiolysis experiments where the absorptions of e_{aq}^-, O_2^-, and HO_2 were followed as a function of temperature but, because their extinction coefficients at different temperatures are not known, the results were not used (8, 38, 39). The lines in Fig. 9 represent the actual values used in the calculations. In choosing the line for $g(e_{aq}^-)$, data obtained with the least spur scavenging were used.

The data in Fig. 9, as they stand, are not altogether self-consistent. Different values for $g(H)$ are calculated from $g(H_2) + g(H)$ and from $g(e_{aq}^-) + g(H_2) + g(H)$ using $g(H_2)$ and $g(e_{aq}^-)$. This can be seen in Fig. 10, where the primary g-values based on $g(H_2) + g(H)$ are given, and in Fig. 11, where the primary g-values based on $g(e_{aq}^-) + g(H_2) + g(H)$ are shown.

For both figures, the g-values for hydrogen peroxide were calculated using the mass balance eq. [21]:

$$[21] \quad g(H_2O_2) = (g(H) + g(e_{aq}^-) + 2g(H_2) - g(OH))/2$$

The g-values at 25°C in Figs. 10 and 11 are essentially the same and agree with the accepted values for the γ-radiolysis of water (2, 3). However, as the temperature increases, the $g(H)$ difference becomes apparent and, as a consequence of this, $g(H_2O_2)$ (eq. [21]) also differs. Figure 10 probably best represents the g-values for γ-irradiated water of near-neutral pH for a number of reasons. Firstly, the values of $g(H_2) + g(H)$ were derived from *three* experimental systems at near-neutral pH whereas the values of $g(e_{aq}^-) + g(H_2) + g(H)$ were measured from one acidic solution, and G-values from acidic solutions do appear to have a lower temperature dependence than in near-neutral solutions. Secondly, the $g(H)$ calculated from the difference in the $G(H_2)$ value for the acetone–methanol solution at neutral pH and 8.5×10^{-2} mol kg^{-1} KOH is consistent with the $g(H)$ in Fig. 10 over the 25–200°C range. Thirdly, an independent estimate of $g(H)$ over the temperature range 20–200°C, from pulse radiolytic estimates of $G(CO_3^-)$ (which equals $g(e_{aq}^-) + g(OH)$) from N_2O-saturated 9.2×10^{-2} mol kg^{-1} sodium bicarbonate solutions (42) and from the $g(e_{aq}^-) + g(OH) + g(H)$ data given in Fig. 9, gave values of $g(H)$ equal, within experimental error, to those shown in Fig. 10.

At the present time there are probably not enough experimental data available to say whether the g-values reported here for 300°C conform with the currently accepted views of water radiolysis. However, certain observations can be made.

At 25°C the radiation chemistry of water at 1 ps, before any of the spur reactions occur, can be written as (43):

$$[22] \quad 5.70H_2O \xrightarrow{100\ eV} 4.78e_{aq}^- + 4.78H^+ + 0.62H + 5.7OH + 0.15H_2 + 0.0H_2O_2$$

At 300°C, the radiation chemistry, after all the spur reactions are complete, can be written, based on Fig. 10, as:

$$[23a] \quad 6.47H_2O \xrightarrow{100\ eV} 4.15e_{aq}^- + 4.15H^+ + 1.08H + 3.97OH + 0.62H_2 + 1.25H_2O_2$$

or, based on Fig. 11, as:

$$[23b] \quad 5.87H_2O \xrightarrow{100\ eV} 4.15e_{aq}^- + 4.15H^+ + 0.48H + 4.57OH + 0.62H_2 + 0.65H_2O_2$$

For both reactions [23*a*] and [23*b*], the amount of water

Can. J. Chem. Downloaded from www.nrcresearchpress.com by 91.144.44.67 on 09/07/12
For personal use only.

decomposed at the end of the spur reactions at 300°C is equal to or greater than the 1 ps 25°C value (reaction [22]). However, the $g(-H_2O)$ at 1 ps for 300°C water radiolysis will be greater than that at the end of the spur reactions. We have some evidence for this from ongoing work on the effect of scavenger concentration on g-values at 300°C where, at nitrite concentrations of 0.05 and 0.5 mol kg^{-1}, $g(H_2)$ was 0.52 and 0.37, respectively. The fact that nitrite, a hydrated electron and hydroxyl radical scavenger, lowers the molecular hydrogen yield implies it is being formed, at least in part, by free radical processes (reaction [24]),

[24] $e_{aq}^-, H \rightarrow H_2$

which, in turn, implies that some recombination (reaction [25]) to reform water must also have occurred (2).

[25] $H, e_{aq}^- + OH \rightarrow H_2O, OH^-$

While the overall decomposition of water is higher at 300°C, this could be due in part to increases in the yield of excitation rather than ionization processes (43).

Recently it was found that the temperature dependence of rate constants of a number of reactions that were near-diffusion-controlled at 25°C was less than that of diffusion in water (44). As most of the important spur reactions are near-diffusion-controlled at 25°C (2), this means that, as the temperature is raised, more free radical species will diffuse out of the spur than will react in the spur to form water, molecular hydrogen, and hydrogen peroxide, i.e., the yield of free radicals relative to molecular products should increase with temperature. Furthermore, as the density of the solution decreases with increased temperature, this should lead to an expanded spur, which also should facilitate the escape of the radicals from the spur.

The fast neutron radiolysis of 0.4 mol dm^{-3} sulphuric acid is consistent with this model as the g-values for radicals do show a marked increase with temperature while the molecular product yields decrease (4). However, the γ-radiolysis g-values do not follow the above prediction. In Fig. 10, the yield of all the primary species increases, while in Fig. 11 all the yields increase except that for the free radical, H, and the molecular product, hydrogen peroxide.

Focusing on Fig. 10, the increase in the molecular products, hydrogen and hydrogen peroxide, might be accounted for by an increase in the yield arising from excitation processes alluded to above (reaction [26]) (43).

[26] $H_2O^* \rightarrow H_2O + O$

The oxygen atom can lead to peroxide formation through recombination of hydroxyl radicals formed in reactions [22] and [27] or the dismutation of the hydroperoxy radical formed in reaction [28].

[27] $O + H_2O \rightarrow 2OH$

[28] $O + OH \rightarrow HO_2$

Obviously more experimental data are required before any comprehensive mechanism for the radiolysis of water at 300°C can be given. In particular, scavenger studies are needed, both steady state and pulse radiolysis. Other systems that are thermally stable at 300°C need to be found with which to determine both yields and kinetics. The role of reactions that occur in steam but not in liquid water at lower temperatures needs to be assessed.

Conclusions

The g-values for the primary species formed in the γ-radiolysis of water at 250–300°C in near-neutral pH are similar in distribution to, but 50% greater than, those observed at room temperature. Furthermore, these g-values are quite different from those used recently in computer simulations (45–47) based on the 300–400°C results reported by Burns and Marsh (13). However, because the present results are derived from a broad spectrum of experimental data from different sources, it is felt that the g-values reported here are a more realistic set.

Acknowledgements

The authors thank Dr. G. V. Buxton for many discussions and for access to his experimental results prior to their publication. This work was cofunded by the CANDU's Owners Group.

1. P. Cohen. Water coolant technology of power reactors. American Nuclear Society, 1980.
2. I. G. Draganic and Z. D. Draganic. The radiation chemistry of water. Academic Press, New York. 1971.
3. J. W. T. Spinks and R. J. Woods. An introduction to radiation chemistry. John Wiley, New York. 1976.
4. Y. Katsumura, Y. Takeuchi, D. Hiroishi, and K. Ishigure. Radiat. Phys. Chem. **33**, 299 (1989).
5. A. J. Elliot, D. C. Ouellette, D. Reid, and D. R. McCracken. Radiat. Phys. Chem. **34**, 747 (1989).
6. Y. Katsumura, Y. Takeuchi, and K. Ishigure. Radiat. Phys. Chem. **32**, 259 (1988).
7. S. A. Kabakchi and I. E. Lebedeva. High Energy Chem. **21**, 261 (1987).
8. G. V. Buxton, N. D. Wood, and S. Dyster. J. Chem. Soc. Faraday Trans. 1, **84**, 1113 (1988).
9. G. V. Buxton and N. D. Wood. Radiat. Phys. Chem. **34**, 699 (1989).
10. H. Shiraishi, G. V. Buxton, and N. D. Wood. Radiat. Phys. Chem. **33**, 519 (1989).
11. H. Shiraishi, Y. Katsumura, D. Hiroishi, K. Ishigure, and M. Washio. J. Phys. Chem. **92**, 3011 (1988).
12. K. N. Jha, T. G. Ryan, and G. R. Freeman. J. Phys. Chem. **79**, 868 (1975).
13. W. G. Burns and W. R. Marsh. J. Chem. Soc. Faraday Sci. **77**, 197 (1981).
14. S. A. Kabakchi and I. E. Lebedeva. High Energy Chem. **16**, 248 (1982).
15. S. Gordon, K. H. Schmidt, and J. R. Honekamp. Radiat. Phys. Chem. **21**, 247 (1983).
16. W. G. Burns and P. B. Moore. Radiat. Eff. **30**, 233 (1976).
17. K. Sehested, E. Bjergbakke, and H. Fricke. Radn. Res. **56**, 385 (1973).
18. H. A. Schwarz, J. M. Caffrey, and G. Scholes. J. Am. Chem. Soc. **81**, 1801 (1959).
19. T. F. Irvine and J. P. Hartnett. Steam and air tables in SI units. McGraw–Hill, New York. 1976.
20. B. G. Dzantiev, A. N. Ermakov, and V. N. Popov. Sov. At. Energy (Engl. Transl.), **46**, 414 (1979).
21. S. A. Lukac. Radiat. Phys. Chem. **33**, 223 (1989).
22. D. Dautzenberg. Radiat. Phys. Chem. **33**, 61 (1989).
23. J. Rabani and G. Stein. J. Phys. Chem. **37**, 1865 (1962).
24. M. Freiberg and D. Meyerstein. J. Chem. Soc. Faraday Trans. 1, **73**, 622 (1977).
25. J. H. Baxendale and R. S. Dixon. Z. Phys. Chem. Neue Folge, **43**, 161 (1964).
26. R. E. Messmer and C. F. Baes. J. Solution Chem. **3**, 307 (1974).
27. G. V. Buxton, C. L. Greenstock, W. P. Helman, and A. B. Ross. J. Phys. Chem. Ref. Data, **17**, 513 (1988).
28. U. K. Klaning. Ber. Bunsen-Ges. Phys. Chem. **89**, 243 (1985).
29. M. D'Angelantonio, M. Venturi, and Q. Mulazzani. Radiat. Phys. Chem. **32**, 319 (1988).
30. B. Cercek, M. Ebert, C. W. Gilbert, and A. J. Swallow. Pulse radiolysis. *Edited by* M. Ebert, J. P. Keene, A. J. Swallow, and J. H. Baxendale. Academic Press, New York. 1965. p. 83.

Can. J. Chem. Downloaded from www.nrcresearchpress.com by 91.144.44.67 on 09/07/12
For personal use only.

31. A. J. ELLIOT and F. C. SOPCHYSHYN. Int. J. Chem. Kinet. **16**, 1247 (1984).
32. J. H. BAXENDALE, P. L. T. BEVEN, and D. A. STOTT. Trans. Faraday Soc. **64**, 2389 (1968).
33. G. E. ADAMS, J. W. BOAG, and B. D. MICHAEL. Trans. Faraday Soc. **61**, 1417 (1965).
34. A. J. ELLIOT and A. S. SIMSONS. Radiat. Phys. Chem. **24**, 229 (1984).
35. M. KELM, J. LILIE, and A. HENGLEIN. J. Chem. Soc. Faraday Trans. 1, **71**, 1132 (1975).
36. J. TAKAGI and K. ISHIGURE. Nucl. Sci. Eng. **89**, 177 (1985).
37. A. J. ELLIOT. Radiat. Phys. Chem. **34**, 753 (1989).
38. H. CHRISTENSEN and K. SEHESTED. J. Phys. Chem. **92**, 3007 (1988).
39. H. CHRISTENSEN and K. SEHESTED. J. Phys. Chem. **90**, 186 (1986).
40. A. J. ELLIOT and F. C. SOPCHYSCHYN. Can. J. Chem. **61**, 1578 (1983).
41. P. TOFFEL and A. HENGLEIN. Ber. Bunsen-Ges. Phys. Chem. **80**, 525 (1976).
42. N. D. WOOD. Ph.D. Thesis, Univ. of Leeds, U.K. 1989.
43. N. V. KLASSEN. Radiation chemistry. *Edited by* Farhataziz and M. A. J. Rodgers. VCH Publishers, New York. 1987. p. 29.
44. A. J. ELLIOT, D. R. MCCRACKEN, G. V. BUXTON, and N. D. WOOD. J. C. S. Faraday Trans. 1. In press.
45. W. G. BURNS. UKAEA Report Harwell AERE-R-10216. 1982.
46. K. ISHIGURE, J. TAKAGI, and H. SHIRAISHI. Radiat. Phys. Chem. **29**, 195 (1987).

Can. J. Chem. Downloaded from www.nrcresearchpress.com by 91.144.44.67 on 09/07/12
For personal use only.

Selective reduction of less reactive carbonyl groups in the presence of diborane and sodium bisulfite on silica gel

TEIJI CHIHARA
The Institute of Physical and Chemical Research (RIKEN), Wako-shi, Saitama 351-01, Japan

AND

TAMIE WAKABAYASI, KAZUO TAYA, AND HARUO OGAWA[1]
Department of Chemistry, Tokyo Gakugei University, Koganei-shi, Tokyo 184, Japan

Received August 30, 1989

TEIJI CHIHARA, TAMIE WAKABAYASI, KAZUO TAYA, and HARUO OGAWA. Can. J. Chem. **68**, 720 (1990).

The less reactive carbonyl group of a mixture of reducible groups of carbonyl compounds was preferentially reduced with diborane on silica gel by first forming an adduct of the more reactive carbonyl group with sodium bisulfite. For example, 4-acetylbenzaldehyde could be converted to 4-(1-hydroxylethyl)benzaldehyde in 93% selectivity; in a mixture of 4-phenylacetophenone and 4-phenylbenzaldehyde, biphenylethanol was preferentially formed in 95% yield with 16% yield of 4-phenylbenzyl alcohol. Silica gel and sodium bisulfite were essential for this selective reaction. Aliphatic and aromatic aldehydes and unhindered cyclohexanones could be selectively protected by this method.

Key words: sodium bisulfite, silica gel, carbonyl compound, selective reduction, diborane.

TEIJI CHIHARA, TAMIE WAKABAYASI, KAZUO TAYA et HARUO OGAWA. Can. J. Chem. **68**, 720 (1990).

Lorsqu'un mélange de divers groupements carbonyles pouvant être réduits est soumis à l'action du diborane déposé sur du gel de silice, il est possible de ne réduire que le groupement carbonyle le moins réactif en procédant à la formation préalable d'un adduit bisulfitique avec le groupement carbonyle le plus réactif. Par exemple, le 4-acétylbenzaldéhyde peut être transformé en 4-(1-hydroxyéthyl)benzaldéhyde avec 93% de sélectivité; dans un mélange de 4-phénylacétophénone et de 4-phénylbenzaldéhyde, le biphényléthanol se forme préférentiellement avec un rendement de 95% alors que le rendement d'alcool 4-phénylbenzilique n'est que de 16%. Le gel de silice et le bisulfite de sodium sont tous les deux essentiels pour réaliser cette réaction sélective. Les aldéhydes aliphatiques et aromatiques ainsi que les cyclohexanones qui ne sont pas encombrées peuvent être protégées d'une façon sélective par cette méthode.

Mots clés : bisulfite de sodium, gel de silice, composés carbonylés, réduction sélective, diborane.

[Traduit par la revue]

Can. J. Chem. Downloaded from www.nrcresearchpress.com by 88.85.125.76 on 09/07/12
For personal use only.

It is known that sodium bisulfite (SBS) gives adducts, α-hydroxysulfonic acids, with some carbonyl compounds (1), especially with aliphatic and aromatic aldehydes. With ketones, SBS gives adducts with acetone, cyclohexanone, and cycloheptanone, but not with diethyl ketone, 2-methylcyclohexanone, or cyclooctanone (2). Thus SBS exhibits specific adduct formation with carbonyl compounds; however, it has never been used for the purpose of protecting carbonyl groups. Selective reductions of ketones in the presence of aldehydes by cerium trichloride with $NaBH_4$ (3) and selective carbonylalkylation of ketones in the presence of aldehydes by methylaluminium bis(2,6-di-*tert*-butyl-4-methylphenoxide) (4) have been reported. In addition to the specific differentiation between aldehyde and ketone, SBS makes it possible to get specific selectivity among ketones.

Because of the limited stability of the adduct with SBS, it has been used only to isolate or purify carbonyl compounds. Usually the adducts are produced in aqueous natural solution and are stable as crystalline solids. In aqueous solution, a small quantity of unreacted carbonyl compound still exists in equilibrium with the adduct (eq. [1]). When a reaction

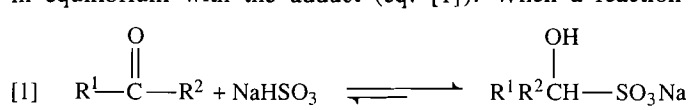

[1] $R^1R^2C{=}O + NaHSO_3 \rightleftharpoons R^1R^2CH{-}SO_3Na$

consuming the carbonyl compound proceeds under these conditions, the successional regeneration of the carbonyl compound by dissociation of the adduct will occur readily.

Solid adsorbents such as silica gel and alumina have been used as media for controlling organic reactions (5). Examples include terminal ozonation and chlorination of a methyl or methylene group remote from the adsorbed amino, carbonyl, or carboxyl group (6, 7), ozonation of olefin to normal ozonide with the suppression of complete dissociation of the intermediate (8), regioselective photocycloaddition of alkenes or allene to steroidal enones (9), and monomethyl esterification of dicarboxylic acids (10, 11).

The solid adsorbents have a large surface area and the solvent can be easily removed by evacuation (12). The well-dispersed and supported adduct of SBS is a good candidate for protection of the carbonyl groups. This is because the equilibrium expressed by eq. [1] is quenched by lack of solvent, and water-sensitive reagents can be used. We have reported briefly on the selective reduction of 4-acetylbenzaldehyde to 4-(1-hydroxyethyl)benzaldehyde (**2**) in an earlier paper (13). This paper presents details of this reaction and its application to a mixture of carbonyl compounds.

Results and discussion

Selective reduction of 4-acetylbenzaldehyde (1)

Compound **1** (100 mg) and SBS (145 mg) were allowed to react in a dioxane–water solvent (3.2 mL). To the resulting solution was added silica gel (2.5 g) and the solvent evaporated under reduced pressure. The supported sample contained 76–78% of the amount of **1** added, accompanying the formation of the adduct with SBS. Reduction of the supported sample with diborane (30 molar excess), followed by hydrolysis, afforded 4-(1-hydroxyethyl)benzaldehyde (**2**) selectively: the selectivity for **2** showed 87% at 65% conversion of **1**.

The reaction profile is illustrated in Fig. 1. This shows that **2**, produced by the reduction of the acetyl group of **1**, was formed

[1]Author to whom correspondence may be addressed.

TABLE 1. The effect of sodium bisulfite (SBS) and solid supports on the selective formation of 4-(1-hydroxymethyl)benzaldehyde (**2**) from 4-acetylbenzaldehyde (**1**)

Entry	Amount of SBS[a]	Adsorbent	Amount of adsorbent[b]	Selectivity for **2** (%)[c]	Amount of diborane[d]
1	0.5	SiO_2	10	66	15
2	1.0	SiO_2	10	80	25
3	2.0	SiO_2	10	87	30
4	5.0	SiO_2	5	93	30
5	5.0	SiO_2	10	86	40
6	5.0	SiO_2	50	70	50
7	5.0	Al_2O_3	10	77	30

[a]Molar ratio to **1**.
[b]Weight ratio to the combined amount of **1** and SBS.
[c]{**2**/(**2** + **3** + **4**)} × 100, at about 60% conversion. **3**: 4-acetylbenzyl alcohol. **4**: 1-{4-(hydroxymethyl)phenyl}ethanol.
[d]Molar ratio to **1** to achieve about 60% conversion.

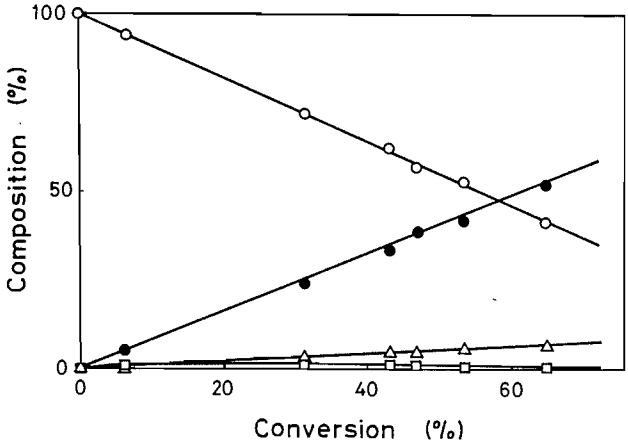

FIG. 1. Selective reduction of carbonyl group of 4-acetylbenzaldehyde (**1**) with sodium bisulfite (SBS) on silica gel. SBS:**1** = 2:1 (mol/mol), (SBS + **1**):SiO_2 = 1:10 (w/w), at 0°C; **1** (○); 4-(1-hydroxyethyl)benzaldehyde (**2**) (●); 4-acetylbenzyl alcohol (**3**) (□); 1-{4-(hydroxymethyl)phenyl}ethanol (**4**) (△).

predominantly with decrease in **1**. In contrast, 4-acetylbenzyl alcohol (**3**), produced by the reduction of the formyl group of **1**, was formed at early stages of the reaction with the maximum 0.9% selectivity; it disappeared and was converted to 1-[4-(hydroxymethyl)phenyl]ethanol (**4**) as the reaction progressed. Compound **4** was produced in a maximum 13% selectivity.

The necessity for both sodium bisulfite (SBS) and silica gel

Figure 2(a) shows the reduction profile of **1** in bis(2-methoxyethyl) ether with diborane in the absence of both SBS and silica gel. The formyl group was more reactive than the acetyl group: only after almost quantitative reduction of the formyl group was the acetyl group reduced.

The reduction profile of **1** on silica gel with diborane in the absence of SBS is represented in Fig. 2(b). Compound **3** was the main product in the first half of the reaction and **4** in the latter half. Compound **2** was not detected in this reduction. The profile was similar to that of the reduction in bis(2-methoxyethyl) ether solution (Fig. 2(a)). The preferential reduction of the acetyl group of **1** was not achieved unless SBS was used.

The adduct was then reduced with sodium borohydride (SBH) in an aqueous solution without silica gel. The reduction profile is illustrated in Fig. 2(c). The selective reduction of the acetyl group of **1** did not proceed: the amount of **2** produced was only half as much as that of **3**. The maximum yield of **2** was only 16%, and **4** was the main product of the reaction.

In the presence of water the equilibrium expressed by eq. [1] is established. The non-selective reduction in an aqueous system appears to be a consequence of the equilibrium. Thus both SBS and silica gel were essential for the selective reduction.

Dependence of amounts of SBS and silica gel on selectivity

The effect of the amount of SBS on the formation of **2** was examined (Table 1). The selectivity increased with increasing amounts of SBS (entries 1–3 and 5), but decreased with increasing the amount of available silica gel (entries 4–6).

The maximum selectivity (93%) for the formation of **2** was obtained with a 5:1 ratio of silica gel to the combined amount of **1** and SBS (entry 4), but the reduction did not proceed further than 60% conversion in spite of the addition of a large excess of diborane. On the other hand, when large quantities of silica gel were used (entry 6), the reduction proceeded in 84% conversion and afforded **2** in 70% selectivity. Multilayer deposition of the adduct with small quantities of the silica gel probably prevented complete reduction. Alumina was also an effective solid support for this reaction (entry 7), but the selectivity is lower than that using the silica gel. Interestingly, the same tendency appeared in the former study of Girard's reagent for the protection of carbonyl groups (12).

*The preferential reduction of 4-phenylacetophenone (**5**) in the presence of 4-phenylbenzaldehyde (**6**)*

Upon adding a 40 molar excess of diborane, 95% of the acetyl group of **5** was reduced; in contrast, only 16% of the formyl group of **6** was reduced. Further addition of diborane (120 molar excess) led to reduction of 99% of the acetyl group of **5** and 22% of the formyl group of **6**, before the reaction ceased. The formyl group of **6** (Fig. 3) was effectively protected with SBS, while the acetyl group of **5** was thoroughly reduced.

On the other hand, in a THF solution in the absence of SBS and silica gel the more reactive formyl group in **6** was reduced first followed by the acetyl group in **5** (open circles, Fig. 3). On silica gel in the absence of SBS both carbonyl groups were evenly and completely reduced. These results clearly demonstrate that SBS functions as a protecting agent to the more highly reactive carbonyl group.

In the presence of SBS in aqueous ethanol, the mixture of **6**

Can. J. Chem. Downloaded from www.nrcresearchpress.com by 88.85.125.76 on 09/07/12
For personal use only.

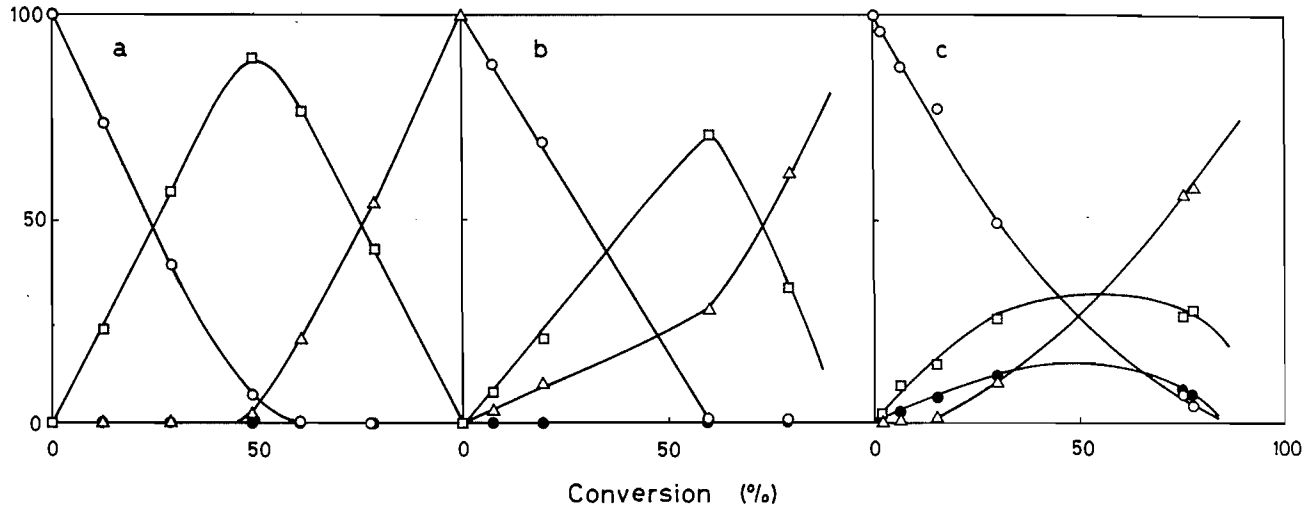

FIG. 2. Reduction profiles of 4-acetylbenzaldehyde (**1**); **1** (○); 4-(1-hydroxyethyl)benzaldehyde (**2**) (●); 4-acetylbenzyl alcohol (**3**) (□); 1-{4-(hydroxymethyl)phenyl}ethanol (**4**) (△) at 0°C. (a) With diborane in 2,2′-dimethoxydiethyl ester in the absence of both sodium bisulfite (SBS) and silica gel. (b) With diborane on silica gel in the absence of SBS, **1**:SiO_2 = 1:10 (w/w). (c) With sodium borohydride (SBH) in aqueous solution in the presence of SBS, SBS:**1** = 1:5 (mol/mol), water:ethanol = 1:1 (w/w).

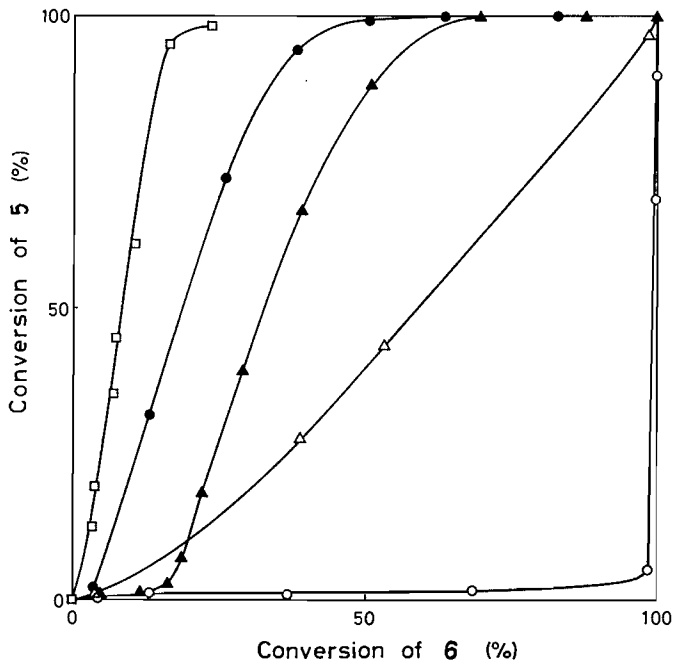

FIG. 3. Competitive reduction of 4-phenylbenzaldehyde (**6**) and 4-phenylacetophenone (**5**). Equal moles of **6** and **5** were used, at 0°C. □: With diborane on SiO_2 in the presence of sodium bisulfite (SBS), SBS:**6** = 1:2 (mol/mol), **6**:SiO_2 = 1:20 (w/w). ○: With diborane in THF solution in the absence of both silica gel and SBS. △: With diborane on silica gel in the absence of SBS, **6**:SiO_2 = 1:20 (w/w). ▲: With sodium borohydride (SBH) in aqueous solution in the presence of SBS, SBS:**6** = 2:1 (mol/mol), water:ethanol = 1:1 (v/v). ●: With SBH in aqueous solution in the presence of SBS, SBS:**6** = 5:1 (mol/mol), water:ethanol = 1:1 (v/v).

and **5** was allowed to react with SBH (Fig. 3). The formyl group of **6** was predominantly reduced to give 4-phenylbenzyl alcohol in up to about 20% yield, with only 5% yield of 1-(4-phenylphenyl)ethanol at the initial stages of the reduction, when using a twofold molar excess of SBS. The acetyl group of **5** was reduced at about twice the rate of the formyl group. After the complete reduction of the acetyl group, the remaining formyl group was reduced. When a fivefold molar excess of SBS was used, a little improvement was observed (Fig. 3). However, the protection of the formyl group was inadequate. Thus, combination of SBS and silica gel was necessary for preferential reduction in a mixture of the carbonyl compounds.

Selectivity in protection by SBS

The selective reduction of pairs of different kinds of carbonyl compounds was examined, and the results are listed in Table 2. Less than 16% of undecanal (**7**) or of **6** was reduced, so both aliphatic aldehyde **7** and aromatic aldehyde **6** were sufficiently protected (entries 1–5); the counter pairs **5**, 2-undecanone (**8**), and 3-undecanone (**9**) were readily reduced to the corresponding alcohols.

On the other hand, methyl ketone **8** was largely unprotected by using a twofold molar excess of SBS (entry 4). A mixture of **8** and **9** gave nearly as effective selectivity, if a twofold molar excess of SBS was used (entry 6), but the selectivity was raised to 1.9 with a tenfold molar excess of SBS (entry 7). On the whole, aldehydes were selectively protected in the presence of ketone but only a low selectivity could be observed in the competitive reduction of methyl ketone and ethyl ketone (Table 2).

4-Phenylcyclohexanone (**10**), an unhindered derivative of cyclohexanone (**11**), was effectively protected in competitive reduction with 2-methyl-4-phenylcyclohexanone (**12**) (entries 8–10).

The selective protection of the carbonyl groups of alicyclic ketones was also studied (Table 2). The selectivity in protection was high in the competition between **11** and cyclooctanone (**13**) or cycloheptanone (**14**) (entries 12, 13). In contrast, the selectivity was low in the competition between **11** and cyclopentanone (**15**) (entry 11). A similar tendency in the reactivity of the ketones was reported in liquid phase hydrogenation with metal catalysts in which **11** was shown to be the most reactive alicyclic ketone (14).

Carbonyl compounds contained in the adsorbed sample could be recovered before reduction. In a few cases, the recovery was lower than 80% because of evaporation of the unprotected

Can. J. Chem. Downloaded from www.nrcresearchpress.com by 88.85.125.76 on 09/07/12
For personal use only.

TABLE 2. Selectivity for protection of carbonyl groups with sodium bisulfite (SBS)

Entry	Carbonyl compounds[a] A	Carbonyl compounds[a] B	Amount of SBS[b]	Reduction yield (%)[c] A	Reduction yield (%)[c] B	Selectivity[d]	Recovery (%)[e] A	Recovery (%)[e] B
1	4-Phenylbenzaldehyde (**6**)	4-Phenylacetophenone (**5**)	2	16	95	5.94	97	96
2	4-Phenylbenzaldehyde (**6**)	4-Phenylacetophenone (**5**)	5	12	70	5.83	91	84
3	Undecanal (**7**)	2-Undecanone (**8**)	1	14	99	7.07	95	85
4	Undecanal (**7**)	2-Undecanone (**8**)	2	12	88	7.33	89	89
5	Undecanal (**7**)	3-Undecanone (**9**)	2	16	99	6.19	90	95
6	2-Undecanone (**8**)	3-Undecanone (**9**)	2	80	93	1.16	91	84
7	2-Undecanone (**8**)	3-Undecanone (**9**)	10	36	70	1.94	90	84
8	4-Phenylcyclohexanone (**10**)	2-Methyl-4-phenylcyclohexanone (**12**)	1	29	99	3.41	93	80
9	4-Phenylcyclohexanone (**10**)	2-Methyl-4-phenylcyclohexanone (**12**)	1.6	18	91	5.06	94	87
10	4-Phenylcyclohexanone (**10**)	2-Methyl-4-phenylcyclohexanone (**12**)	2	15	86	5.73	94	97
11	Cyclohexanone (**11**)	Cyclopentanone (**15**)	2	24	39	1.63	92	56
12	Cyclohexanone (**11**)	Cycloheptanone (**14**)	2	19	97	5.11	99	77
13	Cyclohexanone (**11**)	Cyclooctanone (**13**)	2	19	97	5.11	96	81
14	Cyclopentanone (**15**)	Cycloheptanone (**14**)	2	67	97	1.45	69	71
15	Cyclopentanone (**15**)	Cycloheptanone (**14**)	5	51	88	1.73	62	67
16	Cyclopentanone (**15**)	Cyclooctanone (**13**)	2	73	99	1.36	69	79
17	Cyclopentanone (**15**)	Cyclooctanone (**13**)	5	50	99	1.98	64	70
18	Cycloheptanone (**14**)	Cyclooctanone (**13**)	2	95	98	1.03	83	86
19	Cycloheptanone (**14**)	Cyclooctanone (**13**)	5	87	97	1.11	68	68

[a]Equimolar quantities (0.34 mmol) of A and B were used.
[b]Molar ratio of SBS to A.
[c]Large excess (about 40 molar excess) of diborane was used.
[d](Reduction yield for B)/(reduction yield for A).
[e]The percentage of carbonyl compound that could be recovered from the adsorbed sample before the reduction.

Can. J. Chem. Downloaded from www.nrcresearchpress.com by 88.85.125.76 on 09/07/12
For personal use only.

carbonyl compounds. For example, in the case of alicyclic ketones, the values of recovery of **13**, **14**, and **15** were low and decreased in the order of entries 11–18. Interestingly, the order was the reverse of their vapor pressure. On the other hand, the recovery of **11** shown was as high as that of **10**, in spite of the high vapor pressure of **11**. These results implied that those three ketones, not forming the adducts, were lost from the system, probably because of their high vapor pressure. High mass compounds, which generally have low vapor pressure, are suitable for this method.

Selective reduction with other reagents

A supported sample was prepared by using the mixture of **6** and **5**, which was then allowed to react with a THF solution containing a 100 molar excess of each reducing agent. Sodium hydrotrimethoxyborate, lithium aluminum hydride, and SBH were used for the reduction. More than 96% of **5** was reduced to the corresponding alcohol in every run. On the contrary, the reactivity of the counter component **6** was suppressed and only 29% of **6** was reduced by sodium hydrotrimethoxyborate, while about 70% of **6** was reduced by lithium aluminum hydride or SBH. Sodium hydrotrimethoxyborate was the most effective reagent, but less selective results were observed with this reducing agent than with diborane in the absence of solvent. Trace amounts of water, which could not be removed completely from the supported sample, may have caused the dissociation of the adduct.

We conclude that aliphatic and aromatic aldehydes are selectively protected in the presence of ketones by SBS in combination with silica gel, and that unhindered cyclohexanones are also selectively protected. This selectivity has not been achieved by any other method. The selectivity for protection by SBS differs from that of Girard's reagent, which protected relatively reactive carbonyl groups in spite of the nature of these carbonyl groups (12).

Experimental

Materials

4-Acetylbenzaldehyde (**1**, bp 155°C/15 Torr; 1 Torr = 133.3 Pa) (15), 4-phenylacetophenone (**5**, mp 121–122°C) (16), 4-phenylcyclohexanone (**10**, mp 78°C) (17), 2-methyl-4-phenylcyclohexanone (**12**, mp 139°C) (18), diborane (19), and sodium hydrotrimethoxyborate (20) were obtained according to the literature procedures. Silica gel and alumina were Wakogel C-200 and activated alumina, 200 mesh, respectively (Wako Pure Chemical Industries, Ltd.), and were used as received; it is certified that Merck Silica Gel 60 for column chromatography gives substantially the same results. Other materials were also commercial products. Solvents were dried over synthetic zeolite 3A or calcium hydride.

Methods

Typically, 100 mg (0.67 mmol) of **1** and 145 mg (1.38 mmol) of sodium bisulfite (SBS) were added to 3.2 mL of a dioxane–water mixture (1:2 (v/v)). The resulting solution was stirred well for 1 h at 30°C to produce the adduct and then 2.5 g of silica gel was added. The solvent was evaporated under reduced pressure (10 Torr) for 40 min at 40°C and then for 30 min at 70°C. About 76–78% of **1** could be recovered from this supported sample. Compound **1** was partially lost through the evaporation procedure. The supported sample contained less than 10% solvent by weight.

The supported sample (500–1000 mg) was packed into a glass column (5 mm i.d.) maintained at 0°C by iced water, and a 30 molar excess of diborane was introduced from the bottom of the column in a stream of dry nitrogen for 15 min. The reaction column was allowed to stand for 20 min, then the hydroborated adduct was decomposed by the addition of an aqueous solution of sodium hydroxide. The resulting mixture was then extracted with benzene. After concentration of the extract under reduced pressure, the residue was analyzed by gas–liquid chromatography (GLC). The unreacted **1** and the products 4-(1-

hydroxyethyl)benzaldehyde (**2**) (51.9%), 4-acetylbenzyl alcohol (**3**) (0.5%), and 1-[4-(hydroxymethyl)phenyl]ethanol (**4**) (5.0%) were recovered in high mass balance: the loss was less than 2% based on the initial quantity of **1** on the supported sample.

A mixture of water and 2-propanol or water alone could be used as alternative solvents for the preparation of the supported sample. The quantity of solvent was adjusted to the minimum volume necessary to wet the silica gel.

In competitive reactions, equimolar quantities (0.34 mmol) of two carbonyl compounds were used.

Analysis

The recovery of the substrates from the supported samples before the reduction was determined by means of GLC and (or) UV spectroscopy. For example, the supported sample of **1** was decomposed by the addition of an aqueous solution of sodium hydroxide and then the mixture was extracted with ether followed by evaporation of the solvent. The amount of **1** extracted was determined by Shimazu model GC-7A GLC equipped with a polyethylene glycol 20 000 column, using 1,2-diphenylbenzene as an internal standard. The amount of **1** recovered was also determined by dissolving the extract with 1,4-dioxane followed by UV absorption measurement at 254 nm (ε 2.22 $\times$ 10^4). A Hitachi model 124 spectrophotometer with 1 cm quartz cells was used. The results obtained from the measurements by these two methods agreed with a difference of less than 2%.

The progress of reaction was followed by GLC analysis of aliquot samples. Shimazu model GC-7A and GC-4BPTF gas chromatographs with columns of polyethylene glycol 20 000, bis(2,3-dihydroxypropyl) ether, and Apiezone Grease L were used. Naphthalene, 1-methylnaphthalene, anthracene, 1,2-diphenylbenzene, or *trans*-stilbene was used as internal standard. All the products were identified by comparison of authentic samples obtained independently.

Acknowledgment

We are grateful to Professor Marye Ann Fox, University of Texas, U.S.A., for linguistic comments and for helpful suggestions.

1. L. F. Fieser and M. Fieser. *In* Reagents for organic chemistry. *Edited by* John Wiley and Sons, New York. 1967. pp. 1047–1049.
2. E. Mosetting and A. Burger. J. Am. Chem. Soc. **52**, 3456 (1930).
3. J.-L. Luche and A. L. Gemal. J. Am. Chem. Soc. **101**, 5848 (1979).
4. K. Maruoka, Y. Arai, and H. Yamamoto. Tetrahedron Lett. **29**, 3101 (1988).
5. A. McKillop and D. W. Young. Synthesis, 401 (1979); G. H. Posner. Angew. Chem. Int. Ed. Engl. **17**, 487 (1978); P. de Mayo. Pure Appl. Chem. **54**, 1623 (1982); A. Cornelis and P. Laszlo. Synthesis, 909 (1985).
6. E. Keinan and Y. Mazur. J. Org. Chem. **42**, 844 (1977); A. L. J. Beckwith and T. Duong. J. Chem. Soc. Chem. Commun. 690 (1979).
7. N. C. Deno, R. Fishbein, and C. Pierson. J. Am. Chem. Soc. **92**, 1451 (1970).
8. I. E. D. Besten and T. H. Kinstle. J. Am. Chem. Soc. **102**, 5968 (1980).
9. R. Farwaha, P. de Mayo, J. H. Schauble, and Y. C. Toong. J. Org. Chem. **50**, 245 (1985); V. Dave, R. Farwaha, P. de Mayo, and J. B. Stothers. Can. J. Chem. **63**, 2401 (1985).
10. H. Ogawa, T. Chihara, and K. Taya. J. Am. Chem. Soc. **107**, 1365 (1985).
11. H. Ogawa, T. Chihara, S. Teratani, and K. Taya. J. Chem. Soc. Chem. Commun. 1337 (1986); H. Ogawa, N. Hiraga, T. Chihara, S. Teratani, and K. Taya. Bull. Chem. Soc. Jpn. **61**, 2383 (1988).
12. T. Chihara, E. Waniguchi, T. Wakabayashi, and K. Taya. Bull. Chem. Soc. Jpn. **57**, 2479 (1984).
13. T. Chihara, T. Wakabayashi, and K. Taya. Chem. Lett. 1657 (1981).
14. P. Geneste, M. Bonnet, and M. Rodriguez. J. Catal. **57**, 147 (1979).
15. P. Tinappe and E. Moltgen. Arch. Pharm. (Weinheim, Ger.), **309**, 766 (1976); L. Friedman and H. Shechter. J. Org. Chem. **26**, 2522 (1961).
16. J. Luche and A. L. Gemal. J. Am. Chem. Soc. **101**, 5848 (1979).
17. L. M. Long and H. R. Henze. J. Am. Chem. Soc. **63**, 1939 (1941).
18. A. G. Cook. *In* Enamines. Marcel Dekker, New York. 1969. pp. 2 and 346.
19. G. Zweifel and H. C. Brown. *In* Organic reaction. Vol. 13. *Edited by* R. Adams. John Wiley and Sons, New York. 1963. p. 31.
20. H. C. Brown, H. I. Schlesinger, I. Sheft, and D. M. Ritter. J. Am. Chem. Soc. **75**, 192 (1953); H. C. Brown and E. J. Mead. J. Am. Chem. Soc. **75**, 6263 (1953).

Can. J. Chem. Downloaded from www.nrcresearchpress.com by 88.85.125.76 on 09/07/12
For personal use only.

Partial molar volumes of some dipolar ions in water at 35°C

M. IQBAL[1] AND M. MATEEULLAH
Department of Chemistry, Bahauddin Zakariya University, Multan, Pakistan 60800

Received May 24, 1989[2]

M. IQBAL and M. MATEEULLAH. Can. J. Chem. **68**, 725 (1990).

This work reports partial molar volumes, V^0, of eight peptides and three other dipolar ions (glycine, diglycine, triglycine, *dl*-alanyl-*dl*-valine, glycyl-*dl*-alanine, glycyl-*dl*-leucine, glycyl-tyrosine dihydrate, *dl*-alanyl-glycyl-glycine, *l*-valyl-glycyl-glycine, *l*-lysine-*l*-aspartate, *l*-lysine-*l*-glutamate) in water, calculated from density data obtained at 35°C. V^0 data are interpreted in terms of solute–solvent interactions. In some cases where V^0 data at 25°C were available from the literature, a comparison indicates that partial molar volumes of these solutes at 35°C are higher than their respective volumes at 25°C by about 2–3 $cm^3\ mol^{-1}$. Partial molar expansibilities, E^0, were also estimated in such cases. Expansibility data appear to show a trend indicating dependence of E^0 values on the chain length of the solute molecules. Some plausible modes of solute–solute interactions are also discussed.

Key words: hydration of dipolar ions, partial molar volumes of peptides, solute–solvent interactions, electrostriction, solute–solute interactions.

M. IQBAL et M. MATEEULLAH. Can. J. Chem. **68**, 725 (1990).

Utilisant des données de densités obtenues à 35°C, on a calculé les volumes molaires partiels, V^0, de huit peptides et des trois autres ions dipolaires (glycine, diglycine, triglycine, *dl*-alanyl-*dl*-valine, glycyl-*dl*-alanine, glycyl-*dl*-leucine, dihydrate de glycyl-tyrosine, *dl*-alanyl-glycyl-glycine, *l*-valyl-glycyl-glycine, *l*-lysine-*l*-aspartate, *l*-lysine-*l*-glutamate) en solution dans l'eau. On interprète les données de V^0 en fonction d'interactions soluté–solvant. Dans quelques cas pour lesquels les valeurs de V^0 à 25°C sont disponibles dans la littérature, une comparaison indique que les volumes molaires partiels des solutés à 35°C sont plus élevés que les volumes respectifs à 25°C et que la différence est d'environ 2 à 3 $cm^3\ mol^{-1}$. On a aussi évalué les dilatabilités molaires partielles, E^0, et les données relatives à cette propriété présentent une tendance qui semble indiquer que les valeurs de E^0 varient avec la longueur de la chaîne des molécules de soluté. On discute aussi des quelques modes plausibles pour les interactions soluté–soluté.

Mots clés : hydratation d'ions dipolaires, volumes molaires partiels de peptides, interactions, soluté–solvant, électrostriction, interactions soluté–soluté.

[Traduit par la revue]

Introduction

Hydration of dipolar ions is a concept of particular significance in chemistry and biology. Among the dipolar ions frequently studied, amino acids, peptides, proteins, certain types of hormones, and antibiotics are common. In physiological media such as blood, membranes, cellular fluids, etc., where water happens to be involved in an important manner, the dipolar character of these compounds has an important bearing on their biological function. The study of zwitterions in aqueous solutions, therefore, offers an opportunity for investigating the molecular phenomenon occurring in physiological media.

The study of some of the thermodynamic properties of proteins can be facilitated by investigating the behaviour of their constituents, viz., amino acids and peptides. Some of these properties are found to be implicated in several biochemical processes, such as protein hydration (1, 2), aggregation (3, 4), denaturation (5, 6), antigen–antibody reactions (7), etc. The property of partial specific volume of proteins is believed to be implicated in the phenomenon of anaesthesia. According to the concept of "critical volume of anaesthesia" (8, 9), the reversal of anaesthesia under applied pressure has been viewed as important evidence in favor of this concept (8). Expansion of membrane proteins is believed to be the key factor in the mechanism (9). Experimental evidence for the concept, however, remains sketchy and highlights the importance of data concerning volumetric behaviour of proteins, particularly those found in the membranes.

Several important works on volumetric investigations of amino acids and peptides have been reported in the past, at normal laboratory temperature (25°C) (10–19). These studies have contributed significantly toward an understanding of water – dipolar ion interactions. Volume contributions of the glycyl residue and of various side groups are now known with a greater degree of accuracy, and have been used in additivity schemes for computing improved volumetric data for proteins (20).

This work focusses on the determination of partial molar volumes of 11 dipolar ions in water at 35°C. The choice of temperature (35°C) was made to (a) obtain greater relevance of the present data for macromolecules in certain biological systems (such as mammals), operating near physiological temperatures, and (b) to assist in estimating expansibility behaviour of selected compounds by comparing present and previous data (reported at 25°C). The expansibility data for biological macromolecules are believed to be beneficial for the study of living systems under different physiological conditions such as fever or hypothermia.

Experimental

The compounds studied in this work were of reasonably good purity. Glycine (Merck lot no. 721K 118690), diglycine (Sigma lot no. 102F-5037), triglycine (Sigma lot no. 87C-0417), *dl*-alanyl-*dl*-valine (Sigma lot no. 73F-0078), glycyl-*dl*-alanine (Sigma lot no. 20F-0103), glycyl-*dl*-leucine (Sigma lot no. 111F-0297), glycyl-tyrosine dihydrate (Sigma lot no. 41F-0130), *dl*-alanyl-glycyl-glycine (Sigma lot no. 114C-0163), *l*-valyl-glycyl-glycine (Sigma lot no. 119C-0187), *l*-lysine-*l*-aspartate (Sigma lot no. 98B-06801), *l*-lysine-*l*-glutamate (Sigma lot no. 59B-1270) were further purified by recrystallizing from ethanol–water mixtures. After recrystallization, compounds were dried under vacuum at room temperature. Water used in the experiments was doubly distilled, deionized, and degassed.

Density measurements were carried out at 35°C using 20-mL

[1]Author to whom correspondence may be addressed.
[2]Revision received December 4, 1989.

Can. J. Chem. Downloaded from www.nrcresearchpress.com by 91.144.44.67 on 09/07/12
For personal use only.

TABLE 1. Volumetric data for the compounds studied

Compound	V_{35}^0 ($cm^3\ mol^{-1}$)	S_v ($cm^3\ mol^{-2}\ kg$)	V_{25}^0 ($cm^3\ mol^{-1}$)	E^0 ($cm^3\ mol^{-1}\ K^{-1}$)
Glycine	44.9_5 ±0.03	0.80 ±0.05	43.19[a]	0.18
Diglycine	78.7_1 ±0.05	1.33 ±0.17	76.23[a]	0.25
Triglycine	114.9_3 ±0.34	5.95 ±3.78	112.11[a]	0.28
dl-Alanyl-*dl*-valine	145.9_4 ±0.07	0.99 ±0.68	—	—
Glycyl-*dl*-alanine	94.2_9 ±0.10	1.84 ±0.38	92.30[a]	0.20
Glycyl-*dl*-leucine	141.3_1 ±0.16	0.16 ±0.97	139.70[a]	0.16
Glycyl-tyrosine dihydrate	171.1_8 ±0.10	−2.08 ±1.22	—	—
dl-Alanyl-glycyl-glycine	133.9_3 ±0.16	2.41 ±1.07	130.16[b]	0.38
l-Valyl-glycyl-glycine	167.8_2 ±0.10	2.55 ±1.25	—	—
l-Lysine-*l*-aspartate	174.5_1 ±0.09	1.11 ±0.55	—	—
l-Lysine-*l*-glutamate	202.0_6 ±0.07	2.21 ±0.41	—	—

[a]From ref. 17.
[b]From ref. 19.

Can. J. Chem. Downloaded from www.nrcresearchpress.com by 91.144.44.67 on 09/07/12
For personal use only.

pyknometer flasks (Pyrex) and a Lauda RC3 thermostat bath providing a temperature control accurate within better than ±0.01°C. Calibration of pyknometers was done using water (21) and NaCl (Merck Art 6400) (22, 23). All weighings were carried out on a Sartorious 2434 balance (±0.01 mg). Reproducible Δd values were obtained through careful and refined experimentation providing an accuracy of $\pm 0.5 \times 10^{-4}\ g\ cm^{-3}$ in the density data.

Results and discussion

Apparent molal volumes (ϕ_v, $cm^3\ mol^{-1}$) were calculated using the following equation

$$[1] \quad \phi_v = 1000/mdd_0(d_0 - d) + M/d$$

where d and d_0 are the densities of solution and solvent respectively, m the solution molality, and M is the relative molar mass of the solute.[3] ϕ_v data obtained from eq. [1] were fitted to the following equation using a weighted least-squares fit program.

$$[2] \quad \phi_v = \phi_v^0 + S_v m$$

Values of ϕ_v^0, i.e., the apparent molal volume at infinite dilution, were taken as the partial molar volumes at 35°C, V_{35}^0, and are shown in Table 1, along with the values of coefficient S_v, the pair interaction parameter, indicative of solute–solute interactions. Table 1 also shows values of partial molar volumes at 25°C, V_{25}^0, for six of these compounds (glycine, diglycine, triglycine, glycyl-alanine, glycyl-leucine, alanyl-glycyl-glycine), reported by previous workers, for comparison.

Due to the limited accuracy of density data obtained in this work ($\pm 0.5 \times 10^{-4}$ g cm^{-3}), the errors associated with parameters V^0 and S_v are larger than those achieved from current state-of-the-art techniques such as vibrating-tube electronic densimetry (24), where the level of accuracy is higher by at least an order of magnitude. Errors in the apparent molal volumes ($\Delta\phi_v$) were computed using a differentiated form of eq. [1] (with respect to density and molality), and were employed as weighting parameters in the least-squares fit computations of V^0 and S_v.

Solute–solvent interactions

Previous studies on dipolar ions have shown that, in aqueous systems, these types of solutes represent unique hydration characteristics, which can be described briefly as follows.

(i) In amino acids and peptides, NH_3^+ and CO_2^- terminals, being charged ends, are hydrated in an electrostrictive manner while the intervening backbone is hydrated in accordance with its character, which may be hydrophilic, hydrophobic, amphiphilic, or that involving hydrogen bonding, etc. (10–18).

(ii) The electrostriction of the NH_3^+ group is known to be greater than that of the CO_2^- group by about a factor of 10 (25).

(iii) The change in volume occurring from the overlapping of hydration shells (of the terminals and of the groups adjacent to them) is believed to be due to the net result of two opposing effects (26): (a) an increase in V^0 due to the reduction in electrostriction at the terminal; (b) a decrease in V^0 due to the disruption of side-group hydration by that of the charged end.

[3]Tables of molality and density data for the compounds studied, at 35°C, have been deposited, and may be purchased from the Depository of Unpublished Data, CISTI, National Research Council of Canada, Ottawa, Ont., Canada K1A 0S2.

Can. J. Chem. Downloaded from www.nrcresearchpress.com by 91.144.44.67 on 09/07/12
For personal use only.

(iv) As a consequence of (ii), a side group falling near the N-terminal effects a relatively larger volume release from the electrostricted region than is produced in the case of a C-adjacent group. Present V^0 data, obtained at 35°C, appear to support these observations.

For instance, a comparison between the V^0 values of two isomeric peptides, viz., *dl*-alanyl-*dl*-valine and glycyl-*dl*-leucine, both having a relative molar mass of 188.2 g mol^{-1}, indicates a higher V^0 value for the former (145.94 cm^3 mol^{-1}) than for the latter (141.31 cm^3 mol^{-1}). A glance at the molecular structure of these peptides (shown below) reveals that a relatively freer N-terminal in glycyl-leucine appears to contribute toward greater volume contraction than an obstructed N-terminal in alanyl-valine.

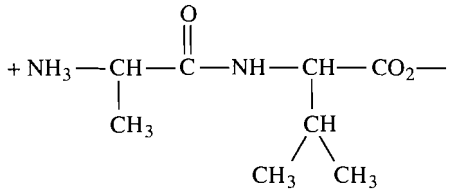

Alanyl-valine

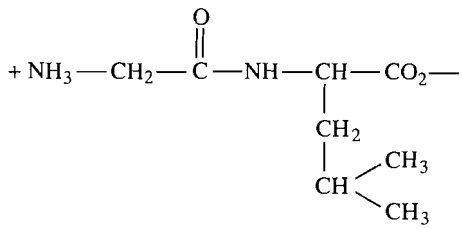

Glycyl-leucine

Comparison of these two compounds with triglycine highlights this effect rather more conspicuously. Triglycine, despite having a slightly greater relative molar mass (189.2), shows a smaller V^0 value (114.93 cm^3 mol^{-1}) than those of the above named isomers, which can be ascribed to a more independent $-NH_3^+$ group.

Partial molar expansibilities

Comparison between V_{35}^0 and V_{25}^0 values for six of the above compounds shows that V_{35}^0 values are greater than the respective V_{25}^0 values by about 2–3 cm^3 mol^{-1}. Assuming that a linear variation of V^0 occurs within this temperature range, partial molar expansibility, E^0 $(= (\partial V^0/\partial T)_p)$, of these compounds can be calculated by taking ∂V as $(V_{35}^0 - V_{25}^0)$ and $\partial T = 10$°C. E^0 values obtained in this manner are included in Table 1. Given the magnitude of errors associated with the V^0 data, values of expansibilities do not appear to be very significant. Nevertheless, these may be regarded as indicative of a trend showing correlation between E^0 and the chain length of a solute molecule. Further studies involving high precision data are needed to test the trend.

Solute–solute interactions

S_v values shown in Table 1 represent quantitative estimates of solute–solute (pairwise) interactions for the compounds studied. It is seen that all S_v values are positive except that for glycyl-tyrosine, where this value is found to be negative (-2.08 ± 1.21 cm^3 mol^{-2} kg). Studies conducted on a variety of hydrophilic, hydrophobic, and amphiphilic solutes in the past have shown that positive S_v values are generally associated with solutes showing an overall hydrophilic character while negative values are found to be associated with hydrophobic solutes. Amphiphilic solutes are found to show little or no concentration dependence of V^0 data.

In the context of solute–solute interactions, the Cosphere overlap model proposed by Gurney (27) is also a frequent reference used and is often employed in interpreting S_v data. Using this model and the generalizations obtained from the study of a variety of model compounds, it appears that all of the present compounds exhibit hydrophilic character in aqueous environments except glycyl-tyrosine, which shows an overall hydrophobic character. This may be due to the nonpolar tyrosyle residue whose presence appears to affect the dipolar character of this molecule. Gurney's model describes the overlapping of hydrated solutes using spherical shapes for hydrated species. In the case of solutes having nonspherical shapes (oblong, cylindrical, rod shaped, etc.), e.g., the peptides under study, the overlapping of hydrated entities may not be exactly in the spherical manner. Instead, the overlaps may preferably be direction oriented such that the N-terminal of one hydrated peptide may prefer to align with the C-terminal of the other, particularly in cases where side chains are smaller and do not offer any hindrance to these anisotropic overlaps. In cases where side chains happen to be larger in size, this kind of alignment, however, may not be possible due to obstruction caused by the side group.

1. G. Ling. *In* Water and aqueous solutions. *Edited by* R. A. Horn. Wiley Interscience, New York. 1972. Chap. 16.
2. H. B. Bull and K. Breese. J. Phys. Chem. **72**, 1817 (1968).
3. J. M. Cassell and R. G. Christensen. Biopolymers, **5**, 431 (1967).
4. W. Kauzmann. Adv. Protein Chem. **14**, 1 (1959).
5. R. B. Simpson and W. Kauzmann. J. Am. Chem. Soc. **75**, 5139 (1953).
6. P. I. Bendzko, W. A. Pfeil, P. L. Privalov, and E. I. Tiktopulo. Biophys. Chem. **29**, 301 (1988).
7. M. A. Lauffer. Entropy driven processes in biology. Springer-Verlag, W. Berlin. 1975.
8. S. Roth. Ann. Rev. Pharmacol. Toxicol. **19**, 1959 (1979).
9. N. P. Frank and W. R. Leib. Nature, **292**, 248 (1981).
10. E. J. Cohn and T. J. Edsall. Proteins, amino acids and peptides. Hafner, New York. 1965. Chaps. 7, 16.
11. A. A. Yayanos. J. Phys. Chem. **76**, 1783 (1972).
12. F. J. Millero, A. L. Surdo, and C. Shin. J. Phys. Chem. **82**, 784 (1978).
13. C. Jolicoeur and J. Boilieu. Can. J. Chem. **56**, 2707 (1978).
14. F. Shahidi and P. G. Farrell. J. Chem. Soc. Faraday Trans. 1, **77**, 963 (1981).
15. S. Cabani, G. Conti, E. Matteoli, and M. R. Tine. J. Chem. Soc. Faraday Trans. 1, **77**, 2377 (1981).
16. S. Cabani, G. Conti, E. Matteoli, and M. R. Tine. J. Chem. Soc. Faraday Trans. 1, **77**, 2385 (1981).
17. A. K. Mishra and J. C. Ahluwalia. J. Phys. Chem. **88**, 86 (1984).
18. M. Iqbal and R. E. Verrall. J. Phys. Chem. **91**, 967 (1987).
19. G. R. Hedwig. J. Solution Chem. **17**, 383 (1988).
20. M. Iqbal and R. E. Verrall. J. Biol. Chem. **263**, 4159 (1988).
21. G. S. Kell. J. Chem. Eng. Data, **20**, 97 (1975).
22. F. Vaslow. J. Phys. Chem. **70**, 2286 (1966).
23. F. J. Millero. Chem. Rev. **71**, 147 (1971).
24. O. Kratky, H. Leopold, and H. Stabinger. Angew. Phys. **27**, 273 (1969).
25. F. Shahidi and P. G. Farrell. J. Chem. Soc. Faraday Trans. 1, **74**, 858 (1978).
26. R. Zana. J. Phys. Chem. **81**, 1817 (1977).
27. R. W. Gurney. Ionic processes in solutions. McGraw–Hill, New York. 1954.

Photodissolution of iron oxides II: The lack of efficiency of thiocyanate

MARTA I. LITTER AND MIGUEL A. BLESA[1]

Departamento de Química de Reactores, Comisión Nacional de Energía Atómica, Avenida del Libertador 8250, 1429 Buenos Aires, Argentina

Received August 3, 1989

MARTA I. LITTER and MIGUEL A. BLESA. Can. J. Chem. **68**, 728 (1990).

Thiocyanate does not enhance, and even inhibits, the photochemical dissolution of iron oxides at 254 nm. At low SCN^- concentrations, surface complexes $\rangle Fe^{III}—SCN^-$ are formed only to a small extent due to the low affinity for the surface by the monovalent anion, and electron-hole pairs essentially recombine. At higher ligand concentrations, only the homogeneous photolysis of SCN^- is observed. At 450 nm, there is no appreciable light absorption by the oxide but homogeneous photolysis of $Fe^{III}—SCN^-$ complexes produces Fe^{II}, which dissolves the oxide by a reductive mechanism.

Key words: iron oxides photodissolution, thiocyanate heterogeneous photochemistry, metal oxides surface complexation.

MARTA I. LITTER et MIGUEL A. BLESA. Can. J. Chem. **68**, 728 (1990).

Le thiocyanate loin d'augmenter, inhibe plutôt, la dissolution photochimique des oxydes de fer, à 254 nm. À des concentrations faibles de SCN^-, la quantité de complexes superficiels de $\rangle Fe^{III}—SCN^-$ qui se forme est faible à cause de la faible affinité de l'anion monovalent pour la surface et du fait que les paires de trous électroniques ne font essentiellement que se recombiner. À des concentrations plus élevées de ligand, on n'observe que la photolyse homogène du SCN^-. À 450 nm, l'oxyde n'absorbe pas beaucoup la lumière; toutefois, la photolyse homogène des complexes $Fe^{III}—SCN^-$ conduit à la formation de Fe^{II} qui dissout l'oxyde par un mécanisme réducteur.

Mots clés : photodissolution d'oxydes de fer, photochimie hétérogène du thiocyanate, complexation superficielle d'oxydes métalliques.

[Traduit par la revue]

Introduction

Reductive dissolution of iron oxides in the presence of a variety of complexing agents has been the subject of a number of papers (1–7). The proposed mechanisms involve an interfacial electron transfer, and it is therefore not surprising that light absorption by the oxide may substitute for the reducing agent in thermal dissolutions, in the presence of adequate complexants and hole scavengers (8–14). In fact, organic carboxylate anions may play the role of both complexing agents and hole scavengers, and it is only because of kinetic factors that the implicit reducing power does not give rise to fast thermal dissolution at room temperature. Reductive thermal dissolution does, however, take place at higher temperatures (4, 5). In this view there is a close parallel between the thermal and photochemical behaviour of aqueous and surface $\rangle Fe^{III}—L$ complexes (15). Electron transfer, either thermal or photochemical, may take place, generating $Fe^{II} + L^\bullet$ pairs that may either revert to $Fe^{III} + L^-$, or further evolve to Fe_{aq}^{2+} + oxidation products of L.

In this context, thiocyanate appears almost as a paradigmatic case. It is a very simple species, which forms well-characterized complexes with iron(III) (16–19), and these complexes are known to exhibit both the thermal (20) and photochemical (21) reactivity mentioned above. Furthermore, another study from our laboratory[2] showed its ability to promote thermal dissolution of iron oxides through a reductive mechanism.

In this paper, the photochemical behaviour of γ-Fe_2O_3 suspended in thiocyanate solutions is described, and shown not to correspond to the expectations mentioned above.

The photochemistry of thiocyanate ion in aqueous solutions has been explored in several papers. Ultraviolet irradiation of SCN^- solutions results in the production of cyanide, sulfur, and lesser amounts of sulfate. Two main reaction paths have been proposed (23–25):

[1] $SCN^- \rightarrow SCN^\bullet + e_{aq}^-$

[2] $SCN^- \rightarrow S + CN^-$

followed by complex reactions in which cage recombination and further reaction with SCN^- are central:

[3] $SCN^\bullet + SCN^- \rightleftharpoons (SCN)_2^{\dot{-}}$

[4] $2(SCN)_2^{\dot{-}} \rightarrow (SCN)_2 + 2SCN^-$

[5] $3(SCN)_2 + 4H_2O \rightarrow 7H^+ + 5SCN^- + HCN + SO_4^{2-}$

[6] $S + SCN^- \rightarrow S_2 + CN^-$

The photochemistry and thermal decomposition of iron(III)–thiocyanate complexes has also been much studied (20, 21). At 436 nm, absorption of light in the charge-transfer band of the complex produces Fe^{2+} and $SCN^\bullet$, which then reacts with SCN^- according to eq. [3] (21). The same intermediate $(SCN)_2^{\dot{-}}$ was proposed in the thermal dark reaction (20).

The photooxidation of thiocyanate by semiconducting oxides has also been described (26–28). In the case of colloidal titanium dioxide, band-gap excitation by a laser leads to electron-hole pair formation (26); the hole migrates to the semiconductor interface and is transferred to SCN^-, producing $SCN^\bullet$. In this system, Kamat (28) was able to observe directly the association of SCN^- with the TiO_2 surface from an absorption band at 295 nm. SCN^- anions complex with TiO_2 with an association constant of 350 $mol^{-1}\,dm^3$.

In the case of iron oxides, Schumacher *et al.* (27) report an increase in the photocurrent of thin film electrodes after boiling in 0.5 mol dm^{-3} KSCN. They suggest that the complexing agent stabilizes surface Fe^{2+} ions on the oxide surface, thereby enhancing the charge-transfer step at the interface.

[1]Author to whom correspondence may be addressed.

[2]A. E. Regazzoni and M. Blesa. Unpublished results.

Can. J. Chem. Downloaded from www.nrcresearchpress.com by 91.144.44.67 on 09/07/12
For personal use only.

Can. J. Chem. Downloaded from www.nrcresearchpress.com by 91.144.44.67 on 09/07/12
For personal use only.

Experimental

Materials and instrumentation

Potassium thiocyanate (analytical grade) from Mallinckrodt was dried at reduced pressure and 50°C and used without further purification. Maghemite (γ-Fe_2O_3) was a commercial sample (Hercules HHO), and was characterized by X-ray diffractometry, chemical analyses, scanning electronic microscopy (SEM), and surface area measurements. It was composed of acicular particles, of average length 0.5 μm, aspect ratio 7:1, and specific surface area 25 $m^2\ g^{-1}$. All other reagents were analytical grade, and used without further purification. Water was bidistilled in a quartz apparatus.

pH adjustments were made with 0.05 mol dm^{-3} H_2SO_4 or NaOH.

The reaction cell was a 10-mm path-length quartz tube of rectangular section fitted with a PTFE stopcock. The cell was thermostatted by a water circulating holder connected to a thermostatic bath.

The sources of light were a low-pressure mercury germicidal lamp for 254 nm and a 200-W tungsten filament lamp with an interference filter for 450 nm.

Procedures

The suspensions were irradiated in the closed cell at the chosen wavelength during different periods of time, with magnetic stirring. After the irradiation, the cell content was transferred to a beaker containing 20 cm^3 0.25% Na_2CO_3 (to prevent HCN loss) by inverting the cell, immersing the outlet in the beaker solution, and opening the stopcock. The iron oxide was filtered off through a 0.45-μm pore-size membrane. Cyanide was analyzed colorimetrically in the filtrate with sodium picrate (29), and iron by the thioglycolate method (30). Actinometry was performed at 254 nm by the ferrioxalate method (31); the Reineckate salt method was used at 450 nm (32). The reported quantum yields are apparent, calculated on the assumption of total absorption of incident light.

Results and discussion

The results obtained in this study can be essentially described as negative: not only is photodissolution not observed, but in some cases the oxide protects thiocyanate from homogeneous photodecomposition. In spite of being negative, the results are of interest because they shed light on the conditions favouring the photocorrosion of iron oxides.

Tables 1 and 2 compare the quantum yield at 254 nm for cyanide, ϕ_{CN^-}, with and without maghemite for various photolysis times. In homogeneous solutions (Table 1), there is a steady decrease in ϕ_{CN^-} with irradiation time, in agreement with previous reports (23, 24). This effect is due to precipitated sulfur (observed visually), which filters incident radiation and (or) back-reacts with cyanide.

In the presence of maghemite, ϕ_{CN^-} drops (see Table 2), becoming essentially zero when the mass concentration of particles is ca. 10 g dm^{-3}. This effect is obviously due also to a filter effect that reduces absorption of light by dissolved SCN^- (ε = 14 $mol^{-1}\ dm^3\ cm^{-1}$). In the more concentrated dispersions, at least 0.9 I_0 is therefore absorbed by the oxide. Under these conditions, no detectable photochemistry is observed, indicating that electron-hole recombination is far more efficient than any other reaction. The two conditions that favor the photodissolution of iron oxides are (*i*) that surface states corresponding to electron traps within the band gap are created by surface complexation of iron(III) centers with dissolved ligands; (*ii*) that adequate hole scavengers are available. In the case of thiocyanate solutions, neither condition is fulfilled under accessible experimental conditions. Surface complexation is characterized by a low affinity constant: we have found K_s = 0.87 $mol^{-1}\ dm^3$ at pH 2 and 80°C;[2] appreciable complexation takes place therefore only when thiocyanate concentration is 1 mol dm^{-3} or higher. At these high concentrations, light is essentially absorbed by dissolved SCN^-, and the observed photochemistry is that of homogeneous solutions. Even the best set of conditions ([SCN^-] = 5×10^{-2} mol dm^{-3}, 10 g dm^{-3} dispersed solid) is insufficient: although light is absorbed by the solid, the density of surface states is too low to produce noticeable photocorrosion.

Thiocyanate is also a poor hole scavenger both because of the low affinity for the surface and the reversibility of its oxidation process; a very likely fate of SCN$^\bullet$ or $(SCN)_2^{\dot{-}}$ is to recombine with electrons, without any net photochemical transformation. Only at very high light intensities (i.e., laser flash photolysis experiments) and in the presence of oxygen to scavenge electrons has it been possible to observe the heterogeneous photooxidation of thiocyanate (26, 28), proceeding through the dismutation of $(SCN)_2^{\dot{-}}$ (eq. [4]).

The crux of the very low quantum yields of thiocyanate-assisted dissolution resides therefore in its low surface affinity. By now, several pieces of evidence indicate that chemisorption of simple mononegative anions on iron oxides is low, even if the corresponding solution complexes are well known. This assertion is especially true for the case of anions of strong (or moderately strong) acids, such as SCN^-.

This behavior is appreciably different from that of TiO_2, on which an appreciable chemisorption and photooxidation of SCN^- have been reported (26, 28). The reasons for the

TABLE 1. Quantum yields of cyanide production at 254 nm. Influence of the irradiation time

c_{KSCN} (mol dm^{-3})	pH	λ (nm)	T (°C)	Irradiation time (min)	ϕ_{CN^-}
5×10^{-2}	2	254	20	10	0.25
5×10^{-2}	2	254	20	30	0.21
5×10^{-2}	2	254	20	60	0.17
5×10^{-2}	2	254	20	120	0.16
5×10^{-2}	2	254	20	240	0.12
2	7	254	30	10	0.29
2	7	254	20	15	0.27
2	7	254	30	30	0.26
2	2	254	30	60	0.24

TABLE 2. Quantum yields of cyanide production by KSCN photolysis at 254 nm. Influence of the addition of maghemite. R is the ratio of cyanide quantum yields in the presence and in the absence of maghemite

c_{KSCN} (mol dm^{-3})	$c_{\gamma\text{-}Fe_2O_3}$ (g dm^{-3})	pH	T (°C)	Irradiation time (min)	ϕ_{CN^-}	R
5×10^{-2}	0	2	20	10	0.25	0.00
5×10^{-2}	10	2	20	6	0.00	
5×10^{-2}	0	2	20	30	0.21	0.00
5×10^{-2}	10	2	20	30	0.00	
5×10^{-2}	0	2	20	60	0.17	0.12
5×10^{-2}	10	2	20	60	0.02	
5×10^{-2}	0	2	20	120	0.16	0.13
5×10^{-2}	10	2	20	120	0.02	
5×10^{-2}	0	2	20	240	0.12	0.25
5×10^{-2}	10	2	20	240	0.03	
2	0	7	30	10	0.29	0.93
2	1	7	30	10	0.27	
2	0	2	30	60	0.24	0.54
2	5	2	30	60	0.13	

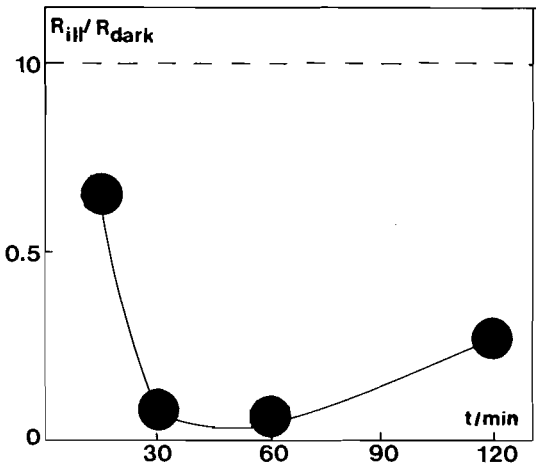

FIG. 1. Photolysis of KSCN at 254 nm. Ratio of iron dissolution rate under illumination to rate in the dark, R_{ill}/R_{dark}, vs. irradiation time (c_{KSCN} = 2 mol dm^{-3}; $c_{\gamma\text{-}Fe_2O_3}$ = 1 g/L; pH 2).

difference are not clear, although they may be related to a higher affinity of Ti^{IV} for SCN^- in homogeneous solution. Also, it is possible that chemisorption may not always be a reversible process; the findings of Schumacher *et al.* (27) may reflect the presence of irreversibly bound SCN^-.

Figure 1 shows that the ratio of the rate of iron dissolution under illumination to the rate in the dark, R_{ill}/R_{dark}, varies with irradiation time, showing a minimum at ca. 60 min. The initial decrease can be assigned to the filter effect already described; the rise in the ratio at longer times is a simple consequence of the thermal reaction between Fe^{II} (formed by homogeneous photolysis of dissolved Fe^{III}—SCN^-) and the oxide. This type of thermal reaction is well known in iron oxides (22). At 450 nm, only photochemistry associated with light absorption by Fe^{III}—SCN^- complexes is possible. It is, however, impossible to demonstrate any effect associated with surface complexes because there is always a modest leach of iron(III) to solution prior to irradiation, and observed effects may be simply attributed to photolysis of aqueous Fe^{III}—SCN^-: at short irradiation times R_{ill}/R_{dark} is, within experimental error, close to one. At longer times, however, the ratio grows (e.g., 1.36 at 120 min) because Fe^{II} species build up in solution and promote the thermal dissolution of the oxide.

Acknowledgements

The authors are members of CONICET, which also partially supported this work through PID 3910704.

1. M. A. BLESA, E. B. BORGHI, A. J. G. MAROTO, and A. E. REGAZZONI. J. Colloid Interface Sci. **98**, 295 (1984).
2. E. B. BORGHI, A. E. REGAZZONI, A. J. G. MAROTO, and M. A. BLESA. J. Colloid Interface Sci. In press.
3. G. V. BUXTON, T. RHODES, and R. M. SELLERS. Nature (London), **295**, 538 (1982).
4. R. N. TORRES, M. A. BLESA, and E. MATIJEVIĆ. J. Colloid Interface Sci. **134**, 475 (1990).
5. R. M. SELLERS and W. J. WILLIAMS. Faraday Discuss. Chem. Soc. **77**, 265 (1984).
6. M. A. BLESA and A. J. G. MAROTO. J. Chim. Phys. **83**, 757 (1986).
7. M. A. BLESA, A. J. G. MAROTO, and P. J. MORANDO. J. Chem. Soc. Faraday Trans. 1, **82**, 2345 (1986).
8. K. M. CUNNINGHAM, M. C. GOLDBERG, and E. R. WEINER. Photochem. Photobiol. **41**, 409 (1985).
9. T. D. WAITE and F. M. M. MOREL. J. Colloid Interface Sci. **102**, 121 (1984).
10. T. D. WAITE, A. TORIKOV, and J. D. SMITH. J. Colloid Interface Sci. **112**, 412 (1986).
11. B. C. FAUST and M. R. HOFFMAN. Environ. Sci. Technol. **20**, 943 (1986).
12. M. GRÄTZEL, J. KIWI, and C. L. MORRISON. J. Chem. Soc. Faraday Trans. 1, **81**, 1883 (1985).
13. T. D. WAITE and A. TORIKOV. J. Colloid Interface Sci. **119**, 228 (1987).
14. M. I. LITTER and M. A. BLESA. J. Colloid Interface Sci. **125**, 679 (1988).
15. M. A. BLESA, V. I. E. BRUYÈRE, A. J. G. MAROTO, and A. E. REGAZZONI. An. Asoc. Quím. Argent. **73**, 39 (1985).
16. S. M. EDMONDS and N. BIRNBAUM. J. Am. Chem. Soc. **63**, 1471 (1941).
17. R. K. GOULD and W. C. VOSBURGH. J. Am. Chem. Soc. **64**, 1630 (1942).
18. S. E. POLCHLOPEK and J. H. SMITH. J. Am. Chem. Soc. **71**, 3280 (1949).
19. H. S. FRANCK and R. L. OSTWALT. J. Am. Chem. Soc. **69**, 1321 (1947).
20. R. H. BETTS and F. S. DAINTON. J. Am. Chem. Soc. **75**, 5721 (1963).
21. K. J. ELLIS and G. S. LAURENCE. Trans. Faraday Soc. **63**, 91 (1967).
22. M. A. BLESA, A. E. REGAZZONI, and A. J. G. MAROTO. *In* External and internal surfaces of metal oxides. Mat. Sci. Forum. Vol. 29. *Edited by* L. C. Dufour and J. Nowotny. Trans. Tech. Publications, Aedermannsdorf, Switzerland. 1988. pp. 31–98.
23. M. LURIA and A. TREININ. J. Phys. Chem. **72**, 305 (1968).
24. L. DOGLIOTTI and E. HAYON. J. Phys. Chem. **72**, 1800 (1968).
25. R. C. RUMFELDT. Can. J. Chem. **49**, 1262 (1971).
26. D. DUONGHONG, J. RAMSDEN, and M. GRÄTZEL. J. Am. Chem. Soc. **104**, 2977 (1982).
27. L. C. SCHUMACHER, S. MAMICHE-AFARA, M. F. WEBER, and M. J. DIGNAM. J. Electrochem. Soc. **132**, 2945 (1985).
28. P. V. KAMAT. Langmuir, **1**, 608 (1985).
29. F. B. FISHER and J. S. BROWN. Anal. Chem. **24**, 1440 (1952).
30. (*a*) D. L. LEUSSING and I. M. KOLTHOFF. J. Am. Chem. Soc. **75**, 390 (1953); (*b*) D. L. LEUSSING and L. NEWMAN. J. Am. Chem. Soc. **78**, 552 (1956).
31. C. G. HATCHARD and C. A. PARKER. Proc. R. Soc. Ser. A, **235**, 518 (1956).
32. E. E. WEGNER and A. W. ADAMSON. J. Am. Chem. Soc. **88**, 394 (1966).

Can. J. Chem. Downloaded from www.nrcresearchpress.com by 91.144.44.67 on 09/07/12
For personal use only.

Energetics of intra- and intermolecular bonds in ω-alkanediols. III. Thermochemical study of 1,6-hexanediol, 1,7-heptanediol, 1,8-octanediol, 1,9-nonanediol, and 1,10-decanediol at 298.15 K

P. KNAUTH AND R. SABBAH[1]

Centre de thermodynamique et de microcalorimétrie du Centre national de la recherche scientifique 26, rue du 141è R.I.A., 13003 Marseille, France

Received November 21, 1989

P. KNAUTH and R. SABBAH. Can. J. Chem. **68**, 731 (1990).

The enthalpies of combustion and sublimation or vaporization of the title compounds were determined on milligram samples and used to derive, at 298.15 K, the enthalpies of formation in the gaseous phase and the enthalpies of atomization. The previous conclusions drawn from the investigation of the lower ω-alkanediols were confirmed: the enthalpy of a hydrogen bond in solid ω-alkanediols amounts to 27 kJ mol^{-1} and the intramolecular C—C and C—OH bond enthalpies to 343.2 and 819.5 kJ mol^{-1}, respectively. The enthalpies of fusion and the triple point temperatures of the ω-alkanediols ($2 \leqslant n \leqslant 10$) are reported and discussed.

Key words: ω-alkanediols, enthalpies of formation, triple point temperatures, differential thermal analysis, calorimetry.

P. KNAUTH et R. SABBAH. Can. J. Chem. **68**, 731 (1990).

Ce travail concerne l'étude thermochimique à 298,15 K des ω-alcanediols de formule générale HO—$(CH)_n$—OH pour lesquels $6 \leqslant n \leqslant 10$. Elle a été réalisée principalement par calorimétrie de combustion et de sublimation sur de faibles quantités de substance (quelques milligrammes par essai), ce qui a permis la détermination des fonctions thermodynamiques correspondantes à partir desquelles ont été calculées d'abord les enthalpies de formation à l'état gazeux puis d'atomisation. Les résultats acquis montrent l'existence de liaison hydrogène dans les alcanediols solides dont l'énergie aurait pour valeur 27 kJ mol^{-1}. À partir de l'enthalpie d'atomisation ont pu être déterminées les valeurs des enthalpies des liaisons intramoléculaires C—C (343, 2 kJ mol^{-1}), et C—OH (819,5 kJ mol^{-1}). Toutes ces valeurs sont en bon accord avec celles qui ont précédemment été obtenues à partir de l'étude des premiers membres de cette série ($2 \leqslant n \leqslant 5$). Sont aussi consignées et discutées dans ce mémoire, les températures du point triple ainsi que les enthalpies de fusion des ω-alcanediols ($2 \leqslant n \leqslant 10$) obtenues expérimentalement.

Mots clés: ω-alcanediols, enthalpies de formation, températures du point triple, analyse thermique différentielle, calorimétrie.

1. Introduction

The ω-alkanediols are compounds with important technical applications, especially as intermediates for polyester resins. Their thermodynamic properties have been only partly investigated. We previously reported the thermochemical properties of the lower ω-alkanediols HO—$(CH_2)_n$—OH ($2 \leqslant n \leqslant 5$) and discussed the inter- and intramolecular bond enthalpies (1–3). The same type of investigation remains to be done for the higher homologues, for which only sparse information is available: Gardner and Hussain (4) reported the enthalpies of combustion, sublimation, and formation of 1,6-hexanediol; Parks and Mosher (5) determined the enthalpy of combustion of 1,10-decanediol. In the present work, we have studied the higher homologues ($6 \leqslant n \leqslant 10$) by combustion and vaporization or sublimation calorimetry and tested the validity of the previously derived equations for the whole series. Furthermore, the triple point temperatures and the enthalpies of fusion of the ω-alkanediols ($2 \leqslant n \leqslant 10$) have been determined.

2. Experimental

2.1. Substances

The pure commercial products 1,8-octanediol (>98%, Fluka), 1,9-nonanediol (97%, Fluka), 1,10-decanediol (99%, Aldrich) were purified by sublimation at 313 K under a residual pressure of 10^{-2} Torr (1 Torr = 133.322 Pa). 1,6-Hexanediol (99+%, "Gold Label", Aldrich) was used without further purification. The liquid 1,7-heptanediol (purum, Fluka) was purified by rectification over a rotating band column (Büchi, type Dr. Abegg). The purified hygroscopic samples were then stored in a glove box over diphosphorus pentoxide.

[1]Author to whom correspondence may be addressed.

2.2 Differential thermal analysis

The purities of the investigated samples were determined by differential thermal analysis using the freezing-point method (6). The mean-temperature version of our differential thermal analyzer used for the investigation of 1,8-octanediol and 1,10-decanediol has been described previously (6). The low-temperature version used for the other compounds is described elsewhere (7). The mole fraction purities of the investigated samples were as follows: 1,6-hexanediol, 0.9938 ± 0.0002; 1,7-heptanediol, 0.9920 ± 0.0003; 1,8-octanediol, 0.9991 ± 0.0001; 1,9-nonanediol, 0.9981 ± 0.0001; and 1,10-decanediol, 0.9933 ± 0.0003. The triple point temperatures and the enthalpies of fusion of the ω-alkanediols ($2 \leqslant n \leqslant 10$) were determined after calibration of the apparatuses with standard reference substances (7).

2.3. Vaporization and sublimation calorimetry

A Tian–Calvet calorimeter equipped with a Knudsen effusion cell was used to determine the enthalpies of sublimation or vaporization of the investigated substances. The method of operation has been described in detail elsewhere (8). The calorimeter was calibrated electrically. The temperature T of the calorimeter and the diameter of the effusion cell orifice were adapted to the volatility of the compounds. The substance with the highest saturated vapour pressure, 1,6-hexanediol, was investigated at 298 K with an effusion cell orifice diameter of 3 mm. The enthalpies of sublimation of 1,8-octanediol and 1,10-decanediol were determined respectively at 323 K (effusion cell orifice: 1 mm) and 342 K (effusion cell orifice: 0.5 mm). The enthalpies of vaporization at 323 K of 1,7-heptanediol and 1,9-nonanediol, both liquid at this temperature, were measured with an effusion cell orifice of 0.5 mm. The correction to the standard temperature of 298.15 K required knowledge of the molar heat capacities of the substances in the condensed and the gaseous phases. The molar heat capacities in the gas phase at 298.15 K and T K were calculated from the group increments tabulated by Benson (9). The enthalpy differences $H(T) - H$

Printed in Canada / Imprimé au Canada

Can. J. Chem. Downloaded from www.nrcresearchpress.com by 88.85.125.76 on 09/07/12
For personal use only.

Can. J. Chem. Downloaded from www.nrcresearchpress.com by 88.85.125.76 on 09/07/12
For personal use only.

TABLE 1. Triple point temperatures T_{tp} and molar enthalpies of fusion $\Delta_{fus}H_m$ of ω-alkanediols HO—$(CH_2)_n$—OH (mean of 6 experiments)

n	T_{tp} (K)	$\Delta_{fus}H_m$/(kJ mol^{-1})
2	256.6±0.2	9.5±0.2
3	245.5±0.1	7.1±0.3
4	289.9±0.1	12.0±0.3
5	254.4±0.1	9.7±0.2
6	314.6±0.2	22.2±0.3
7	295.0±0.2	21.3±0.3
8	332.7±0.1	36.1±0.2
9	319.5±0.1	36.4±0.2
10	345.4±0.1	41.7±0.3

(298.15 K) of the condensed phase were measured with a Tian–Calvet calorimeter using the drop method. The calorimeter was calibrated with standard α-alumina samples from the National Bureau of Standards, and the accuracy of the results was checked with naphthalene, the enthalpy difference $H(342\text{ K}) - H(298.15\text{ K})$ of which is well known (10).

The saturated vapour pressures P of the ω-alkanediols can be calculated according to eq. [1], if Knudsen effusion conditions are fulfilled during the experiment.

$$[1] \quad P \approx \Delta P = \mathrm{d}m/\mathrm{d}t\,(1/aF)\,(2\pi RT/M)^{1/2}$$

ΔP is the difference of pressure between the inside and the outside of the effusion cell, $\mathrm{d}m/\mathrm{d}t$ the effusion rate, a the surface of the effusion cell orifice, F the Clausing factor, R the ideal gas constant, T the absolute temperature, and M the molar mass of the substance (11).

2.4. Combustion calorimetry

The enthalpies of combustion were determined on milligram samples with a CRMT calorimeter equipped with a stainless-steel microbomb. The apparatus and the method of operation for liquid ω-alkanediols have been described elsewhere (2). The solid samples were investigated with an original container technique using polythene foil of 0.05 mm thickness (12). The calorimeter was calibrated using benzoic acid standard reference sample 39i of the National Bureau of Standards. The Washburn and buoyancy corrections to the weighings were performed with computer programs.

3. Results

The triple point temperatures and the molar enthalpies of fusion of the ω-alkanediols studied ($2 \leqslant n \leqslant 10$) are summarized in Table 1. In Table 2, the experimental molar enthalpies of vaporization or sublimation of the title compounds and their saturated vapour pressures are reported. Since the saturated vapour pressures of the ω-alkanediols are relatively low, the identity $\Delta_{vap\text{ or }sub}H_m(T) \equiv \Delta_{vap\text{ or }sub}H^0_m(T)$ is assumed.

In Table 3, the enthalpy differences $H(T) - H(298.15\text{ K})$ for ω-alkanediols in condensed and gaseous phases are tabulated. For 1,9-nonanediol, which was studied at 323 K, the main part of the enthalpy difference for the condensed phase is due to the melting of the substance ($T_{tp} = 319.5$ K). The uncertainties of the enthalpy differences for the gas phase are estimated from the last digit given by Benson. The values are used to determine the molar enthalpies of sublimation and vaporization at 298.125 K (Table 4).

The standard molar enthalpies of combustion and formation in the condensed phase at 298.15 K of the ω-alkanediols have been reported in detail elsewhere (12). Using the standard molar enthalpies of vaporization (1,7-heptanediol) or sublimation (other compounds) at 298.15 K, the standard molar enthalpies of formation in the gaseous phase were calculated (Table 4). The standard molar enthalpies of the dissociation reaction of the molecules in the ideal gas phase into the atoms in the ideal gas phase, the so-called enthalpies of atomization, were then calculated using the standard molar enthalpies of formation of the gaseous ω-alkanediols and gaseous carbon, hydrogen, and oxygen atoms taken from the literature (13) (Table 4). The accompanying experimental uncertainties are standard deviations of the mean.

TABLE 2. Molar enthalpies of sublimation and vaporization of the ω-alkanediols ($6 \leqslant n \leqslant 10$)

Substance	No.	$m\times10^6$ (kg)	$\Delta_{vap\text{ or }sub}H^0_m(T)$ (kJ mol^{-1})	ΔP (T) (Torr)
1,6-Hexanediol	1	11.1603	111.6	—
	2	6.1385	111.2	3.3×10^{-5}
	3	10.9996	111.1	3.3
	4	4.2380	112.2	3.5
	5	12.3180	113.2	4.0
	6	13.7358	112.7	—
Mean values and standard deviations of the means: $\Delta_{sub}H^0_m(298.15\text{ K}) = 112.0 \pm 0.4$ kJ mol^{-1}; ΔP (298.15 K) $= 4 \times 10^{-5}$ Torr				
1,7-Heptanediol	1	11.3895	93.1	—
	2	7.6274	94.1	—
	3	9.3417	94.5	2.9×10^{-3}
	4	16.1047	95.7	3.2
	5	14.1515	93.1	4.4
	6	27.2675	92.4	3.2
Mean values and standard deviations of the means: $\Delta_{vap}H^0_m(323\text{ K}) = 93.8 \pm 0.5$ kJ mol^{-1}; ΔP (323 K) $= 3.5 \times 10^{-3}$ Torr				
1,8-Octanediol	1	13.7147	139.1	1.1×10^{-3}
	2	7.8213	139.6	1.0
	3	7.4189	137.0	0.9
	4	7.2799	139.9	1.2
	5	5.5424	134.9	1.1
	6	6.9037	139.5	1.1
Mean values and standard deviations of the means: $\Delta_{sub}H^0_m(323\text{ K}) = 138.3 \pm 0.8$ kJ mol^{-1}; ΔP (323 K) $= 1 \times 10^{-3}$ Torr				
1,9-Nonanediol	1	8.9387	112.4	9.5×10^{-4}
	2	5.8271	108.9	—
	3	9.2417	113.6	8.2
	4	17.9295	107.3	8.3
	5	15.8837	109.5	8.7
	6	11.0492	108.5	7.9
Mean values and standard deviations of the means: $\Delta_{vap}H^0_m(323\text{ K}) = 110.0 \pm 1.0$ kJ mol^{-1}; ΔP (323 K) $= 8.5 \times 10^{-4}$ Torr				
1,10-Decanediol	1	5.8117	148.9	2.8×10^{-3}
	2	6.4203	148.3	2.2
	3	7.9762	151.9	2.3
	4	5.3630	149.7	2.7
	5	11.1200	149.0	2.8
	6	7.9569	151.0	2.2
Mean values and standard deviations of the means: $\Delta_{sub}H^0_m(342\text{ K}) = 149.8 \pm 0.6$ kJ mol^{-1}; ΔP (342 K) $= 2.5 \times 10^{-3}$ Torr				

TABLE 3. Enthalpy differences for ω-alkanediols in condensed and gas phases.

	$H(T) - H(298.15\ K)$ (kJ mol^{-1})			
	$T = 323K$		$T = 342\ K$	
Substance	Gas	Cond.	Gas	Cond.
1,7-Heptanediol	4.9±0.3	7.66±0.03	—	—
1,8-Octanediol	5.5±0.3	6.48±0.05	—	—
1,9-Nonanediol	6.1±0.3	44.82±0.03	—	—
1,10-Decanediol	—	—	12.1±0.3	18.1±0.6

4. Discussion

4.1. Triple point temperatures, enthalpies and entropies of fusion

The triple point temperatures of the even-membered chain alkanediols are always higher than those of the next higher odd-membered. Within the class of the odd- and the even-membered compounds, the triple point temperatures and the molar enthalpies of fusion increase regularly. The molar entropy of fusion can be calculated by dividing the molar enthalpy of fusion by the temperature of fusion (or by the triple point temperature, which is nearly identical). The molar entropy of fusion is particularly sensitive to the existence of ordering phenomena in the liquid state, reducing free rotation of the molecules. The most consistent effects are due to hydrogen bonds. Bondi (14) pointed out that the presence of hydrogen bonds in liquid *n*-alkanols resulted in a decrease of $\Delta_{fus} S_m/R$ of about 1.1, compared with isoelectronic *n*-alkanes. In the case of ω-alkanediols, the difference (Table 5) amounts to about 3.4, reflecting a high order in the liquid state due to the existence of two hydrogen bonds per diol molecule. This is in agreement with earlier conclusions drawn from a discussion of the enthalpies of vaporization (1). On the other hand, intramolecular hydrogen bonds, which permit free rotation in the liquid state and therefore enhance the entropy of fusion (14), can be excluded, with the exception of 1,2-ethanediol. In the case of 1,2-ethanediol, the molar entropy of fusion is nearly identical to that of *n*-butane; this result indicates the possibility of an intramolecular hydrogen bond in 1,2-ethanediol.

4.2. Enthalpies of sublimation

In a previous paper (1), we showed that the contributions of London-type interactions, dipolar interactions, and hydrogen bonds to the enthalpies of vaporization can be separated and calculated by comparison with the enthalpies of vaporization of isoelectronic *n*-alkanes and ethers. In the same manner, we compared the molar enthalpies of sublimation at 298.15 K of the ω-alkanediols with the sum of the molar enthalpy of vaporization at 298.15 K (15) and the molar enthalpy of fusion at the melting temperature (16) of isoelectronic *n*-alkanes (Table 6). In a first approximation, the temperature variation of the enthalpy of melting is neglected. The comparison with ω-alkanediols reveals that the mean difference amounts to about 56 kJ mol^{-1}, which corresponds to the contributions of dipolar interactions and of hydrogen bonds to the enthalpy of sublimation. The contribution of dipolar interactions is rather small and should amount, as shown previously (1), to only about 1 kJ

TABLE 4. Thermodynamic properties of ω-alkanediols ($6 \leq n \leq 10$) at 298.15K

Substance	$-\Delta_c H_m^0$ (cd, 298.15K) (kJ mol^{-1})	$-\Delta_f H_m^0$ (cd, 298.15K) (kJ mol^{-1})	$\Delta_{vap\ or\ sub} H_m^0$ (298.15K) (kJ mol^{-1})	$-\Delta_f H_m^0$ (g, 298.15K) (kJ mol^{-1})	$\Delta_{a,\ exp} H_m^0$ (298.15K) (kJ mol^{-1})
1,6-Hexanediol	3787.7±4.4	574.1±4.4	112.0±0.4	462.0±4.4	8312.3±4.6
1,7-Heptanediol	4467.0±9.3	574.2±9.3	96.6±0.6	477.6±9.3	9480.6±9.4
1,8-Octanediol	5094.0±4.8	626.6±4.8	139.3±0.9	487.3±4.9	10 642.9±5.2
1,9-Nonanediol	5742.3±7.0	657.6±7.0	148.7±1.1	508.9±7.1	11 817.2±7.4
1,10-Decanediol	6400.3±2.2	678.9±2.3	155.8±0.9	523.1±2.5	12 984.1±3.3

TABLE 5. Comparison of $\Delta_{fus} S_m/R$ for isoelectronic ω-alkanediols and *n*-alkanes

	n								
	2	3	4	5	6	7	8	9	10
HO—$(CH_2)_n$—OH	4.5	3.5	5.0	4.6	8.5	8.7	13.1	13.7	14.5
H_3C—$(CH_2)_n$—CH_3	4.2	7.0	8.8	9.2	11.5	16.8	14.2	10.8	16.8
Difference	−0.3	3.5	3.8	4.6	3.0	8.1	1.1	−2.9	2.3

TABLE 6. Comparison of the molar enthalpies of sublimation $\Delta_{sub}H_m^0$ (298.15K) of the ω-alkanediols with $H = \Delta_{vap}H_m^0$ (298.15 K) + $\Delta_{fus}H_m$ (T_f) of the *n*-alkanes

		n			
		6	8	9	10
HO—$(CH_2)_n$—OH	$\Delta_{sub}H_m^0$ (kJ mol^{-1}):	112.0	139.3	148.7	155.8
H_3C—$(CH_2)_n$—CH_3	H (kJ mol^{-1}):	62.2	80.1	(78.6)	98.1
Difference		49.8	59.2	—	57.7

Can. J. Chem. Downloaded from www.nrcresearchpress.com by 88.85.125.76 on 09/07/12
For personal use only.

mol^{-1}. A structural study of 1,6-hexanediol (17) showed that two hydrogen bonds are formed by each molecule; the enthalpy of a hydrogen bond is thus about 27 kJ mol^{-1}. This value is slightly higher than the value previously found in liquid ω-alkanediols (23 kJ mol^{-1} (1)), in accordance with the lower intermolecular distance in the solid state.

4. 3. Enthalpies of combustion, formation, and atomization

The standard molar enthalpies of combustion and formation at 298.15 K of the solid ω-alkanediols can, as was previously reported, be expressed as a linear function of the number n of methylene groups.

$$\Delta_c H^0_m \text{ (s, 298.15 K) / (kJ mol}^{-1}) = 129.0 - 652.7n$$

$$\Delta_f H^0_m \text{ (s, 298.15 K) / (kJ mol}^{-1}) = -414.7 - 26.6n$$

The standard molar enthalpies of formation in the gaseous phase at 298.15 K (Table 4) can be used together with the previously reported values (3) to derive an equation valid for all members of the compound family.

$$\Delta_f H^0_m \text{ (g, 298.15 K) / (kJ mol}^{-1}) = -361.4 - 16.2n$$

Furthermore, we can express the standard molar enthalpies of atomization of the ω-alkanediols ($2 \leqslant n \leqslant 10$) as a linear relation of n.

$$\Delta_{a,\,exp} H^0_m \text{ (298.15 K) / (kJ mol}^{-1}) = 1295.8 + 1168.9n$$

Both equations are in excellent agreement with the equations previously derived for the lower ω-alkanediols ($2 \leqslant n \leqslant 5$). The conclusions drawn in ref. 3 are thus reinforced: the enthalpy of the C—OH bond amounts to 819.5 kJ mol^{-1}, the mean enthalpy of the C—C bonds to 343.2 kJ mol^{-1}. The mean C—C bond enthalpy is lower than in other aliphatic compounds, because the bond is weakened by the electron-attracting effect of the hydroxyl groups. The low CH_2-group contribution to the enthalpy of formation in the gaseous phase can thus be explained.

Acknowledgement

P. K. gratefully acknowledges a postdoctoral fellowship grant from the Deutscher Akademischer Austauschdienst (DAAD).

1. P. KNAUTH and R. SABBAH. Bull. Soc. Chim. Fr. **5**, 834 (1988).
2. P. KNAUTH and R. SABBAH. J. Chem. Thermodyn. **21**, 203 (1989).
3. P. KNAUTH and R. SABBAH. Struct. Chem. **1**, 43 (1990).
4. P. J. GARDNER and K. S. HUSSAIN. J. Chem. Thermodyn. **4**, 819 (1972).
5. G. S. PARKS and H. P. MOSHER. J. Chem. Phys. **37**, 919 (1962).
6. R. SABBAH and I. ANTIPINE. J. Thermal Anal. **32**, 1929 (1987).
7. P. KNAUTH and R. SABBAH. J. Thermal Anal. In press.
8. R. SABBAH, I. ANTIPINE, M. COTEN, and L. DAVY. Thermochim. Acta, **115**, 153 (1987).
9. S. W. BENSON. Thermochemical kinetics. 2nd ed. Wiley, New York. 1976.
10. A. J. HEAD and R. SABBAH. *In* Recommended reference materials for the realization of physicochemical properties. *Edited by* K. N. Marsh. Blackwell, Oxford. 1987. Chap. 9.
11. Atomic masses of the elements 1987. Pure and Appl. Chem. **60**, 841 (1988).
12. P. KNAUTH and R. SABBAH. J. Chem. Thermodyn. **21**, 779 (1989).
13. CODATA recommended key values for thermodynamics 1977. J. Chem. Thermodyn. **10**, 903 (1978).
14. A. BONDI. Physical properties of molecular crystals, liquids, and glasses. John Wiley, New York. 1968.
15. V. MAJER, V. SVOBODA, and H. V. KEHIAIAN. Enthalpies of vaporization of organic compounds: a critical review and data compilation. IUPAC Chemical Data Series No. 32. Blackwell, Oxford. 1985.
16. D. R. STULL, E. F. WESTRUM, JR., and G. C. SINKE. The chemical thermodynamics of organic compounds. Wiley, New York. 1969.
17. M. LINDGREN, T. GUSTAFSSON, J. WESTERLING, and A. LUND. Chem. Phys. **106**, 441 (1986).

Can. J. Chem. Downloaded from www.nrcresearchpress.com by 88.85.125.76 on 09/07/12
For personal use only.

Elemental analysis of the marine biological reference material LUTS-1 by instrumental neutron activation, graphite furnace atomic absorption spectroscopy, and anodic stripping voltammetry

NORINE MOTKOSKY, ANGELO RANSIRIMAL FERNANDO, AND BYRON KRATOCHVIL
Department of Chemistry, University of Alberta, Edmonton, Alta., Canada T6G 2G2

Received October 27, 1989

NORINE MOTKOSKY, ANGELO RANSIRIMAL FERNANDO, and BYRON KRATOCHVIL. Can. J. Chem. **68**, 735 (1990).

Marine biological reference material LUTS-1, lobster heptopancreas, was analyzed for elemental homogeneity using graphite furnace atomic absorption, anodic stripping voltammetry, and neutron activation analysis. Analysis of samples taken from 12 bottles of LUTS-1 bottled on two different days showed no statistical differences at the 95% confidence level for within-bottle variance for a large number of elements. Differences were observed for between-day variances for aluminum, iron, cobalt, sodium, chlorine, bromine, and iodine, but not at a level sufficient to affect utility as a reference material.

Key words: neutron activation analysis, graphite furnace atomic absorportion spectroscopy, anodic stripping voltammetry, elemental analysis, marine biological reference material.

NORINE MOTKOSKY, ANGELO RANSIRIMAL FERNANDO et BYRON KRATOCHVIL. Can. J. Chem. **68**, 735 (1990).

Afiin de déterminer l'homogénéité élémentaire de l'hepatopancréas de homard, le produit de référence de biologie marine LUTS-1, on a fait appel à l'absorption atomique avec fournaise de graphite, à la voltamétrie anodique et à des analyses par activation neutronique. Des analyses d'échantillons provenant de 12 bouteilles de LUTS-1 embouteillées à deux jours différents démontrent qu'il n'y a pas de différences statistiques, au niveau de confiance de 95%, pour des variations d'un grand nombre d'éléments à l'intérieur d'une même bouteille. On a toutefois observé des variations entre échantillons provenant de jours différents pour l'aluminium, le fer, le cobalt, le sodium, le chore, le brome et l'iode; ces différences sont suffisamment faibles pour qu'elles n'affectent pas l'utilité de ces échantillons comme produits de référence.

Mots clés : analyse par activation neutronique, spectroscopie d'absorption atomique avec fournaise de graphite, voltamétrie anodique, analyse élémentaire, produit de référence de biologie marine.

[Traduit par la revue]

Introduction

The marine biological reference material LUTS-1 has recently been prepared under the Canadian Marine Analytical Standards program. Unlike most other materials developed for monitoring and evaluating analytical procedures, LUTS-1 is a slurry obtained through mechanical homogenization of lobster heptopancreas tissue. Since no pretreatment such as acetone extraction of fatty matter has been carried out, this material is closer in nature and properties to the original matrix, thereby allowing more realistic scrutiny of analytical procedures.

As in any reference material, establishing homogeneity is of prime importance. In view of the trend toward smaller and smaller analytical test portions to satisfy instrumental requirements such as direct solid insertion for atomic or mass spectroscopic techniques, and to assess localized distribution of elements within substances such as biological tissues, homogeneity of reference samples can be expected to become more important in the future.

This study was undertaken to assess the homogeneity of LUTS-1. Three different analytical techniques were used: atomic absorption spectroscopy using graphite furnace atomization for lead, cadmium, and aluminum; anodic stripping voltammetry employing mercury electrodes with differential pulse stripping for lead, and instrumental neutron activation analysis using the SLOWPOKE II reactor facility of the University of Alberta for 17 additional elements.

Experimental

Apparatus

Atomic absorption measurements were made on a Perkin Elmer model 5000 spectrophotometer with background correction, an HGA 2200 furnace, and an AS-1 autosampler. Injected volumes were 20 μL. Pyrolytic graphite tubes with platforms were used. Operating conditions are given in Table 1. The argon purge gas flow was stopped during atomization of lead but was continued using the normal (40 mL/min) setting for the first 3 s for cadmium and 6 s for aluminum. Peak areas were recorded on a Perkin Elmer PRS-10 printer sequencer.

Differential pulse anodic stripping analyses were done using a Princeton Applied Research (PAR) model 174 polarographic analyzer coupled to a PAR model 315 automated electroanalysis controller and a PAR model 303 stationary mercury drop electrode. A Hewlett Packard 7045A *xy* recorder was used for data recording. Some of the solutions were analyzed with a PAR model 303 operating in the hanging mercury drop mode (HMDE). Others were analyzed using a thin mercury film deposited on a glassy carbon electrode (PAR model GO197) mounted on the PAR 303 electrode assembly (MTFE). All solutions were deaerated for 5 min by bubbling nitrogen. All analyses were done using differential pulse stripping. Typical parameters for a run are listed in Table 2. When the MTFE was used, each deposition/stripping operation was preceded by a conditioning step (−0.3 V for 1.5 min). Mercury deposition was carried out from a 500 ppm Hg^{2+} solution, with a −0.1 V applied potential for 50 s.

Instrumental neutron activation analyses studies were carried out at the SLOWPOKE II reactor facility of the University of Alberta. For those elements producing useful short-lived radioisotopes upon irradiation, two irradiation–decay–count schemes were used. The first was 120 s irradiation, 10 s decay, and 180 s count, which gave satisfactory counting statistics for radioisotopes of Al and V. This set was irradiated in site 5 of the reactor at a flux of 1×10^{12} n cm^{-2} s^{-1} and was counted at a sample-to-detector distance of 10 cm. The second was 120 s irradiation, 45 s decay, and 600 s counting, which gave satisfactory results for Na, Cl, Mn, Ca, Br, I, Mg, and Cu. These irradiations were carried out in site 1 of the reactor at the same flux but were counted at a sample-to-detector distance of 6 cm within a 10-cm lead cave with graded shield to reduce natural background. For those elements that only produce longer-lived ($T_{1/2} > 1$ day) radioisotopes, irradiation for 4 h at a flux of 1×10^{12} n cm^{-2} s^{-1} was carried out. Following a 6-day decay period the samples and standards were counted for 2.5 h at a distance of 1 cm from the detector to determine As, La, Sb, Na, Br, Co, Zn, and Fe. The

Can. J. Chem. Downloaded from www.nrcresearchpress.com by 91.144.44.67 on 09/07/12
For personal use only.

TABLE 1. Parameters for graphite furnace atomic absorption spectrophotometry

Parameter	Value		
	Al	Cd	Pb
Wavelength	308.2	228.8	283.3
Integration time	6 s	5 s	6 s
Spectral slit width	0.7 nm	0.7 nm	0.7 nm
Drying temperature and time	120°C, 30 s	120°C, 30 s	120°C, 50 s
Ashing temperature and time	1400°C, 45 s	350°C, 40 s	550°C, 30 s
Atomization temperature and time	2550°C, 6 s	2100°C, 5 s	2200°C, 7 s
HCL current	12 mA	6 mA	6 mA

TABLE 2. Typical parameters used for anodic stripping analysis

Operation	Parameter	Value
Deposition	Potential	−0.6 V (vs. Ag/AgCl)
	Time	300 or 500 s
Equilibration	Time	15 s
Stripping	Mode	Differential pulse
	Scan rate	2 or 5 mV/s
	Modulation	50 mV
	Clock	0.5 s
	Final potential	−0.3 V (vs. Ag/AgCl)

samples were then counted again after about 21 days for 10 h to determine Ag, Co, Fe, Sb, and Zn. The long counts were performed 1 cm from the detector in a 10-cm lead cave.

Counting was carried out on three different systems. For the 180-s counts an Ortec 86 cm^3 active volume WIN-15 coaxial Ge (Li) detector with an Ortec 472A amplifier and a Nuclear Data (ND) 575 ADC was used. Detector specifications include a relative efficiency of 18.5%, a measured FWHM of 2.1 keV, and a peak-to-Compton ratio of 53:1 for the 1332-keV photopeak of ^{60}Co. For the 600-s counts a GEM 20180 hyperpure Ge detector coupled to a ND 660 multichannel analyzer with an Ortec 572 amplifier and ND 575 ADC was used. Detector specifications include a relative efficiency of 22.4%, a measured FWHM of 1.7 keV, and a peak-to-Compton ratio of 59:1. For the 2.5- and 10-h counts a GEM 18180 hyperpure Ge detector coupled to a Canberra Series 80 multichannel analyzer with a Canberra 8622 amplifier and ADC was used. Detector specifications include a relative efficiency of 19.7%, a FWHM of 1.68 keV, and a peak-to-Compton ratio of 58:1. Signals were stored on floppy discs for later analysis.

The specific activities (counts/microgram for each radionuclide) were determined for each counting period, and the masses of the elements in the NRC standards were determined via an adaptation of the comparator (semi-absolute) method for INAA (1), that is, by dividing the photopeak areas of the unknowns by the specific activities of the relevant radionuclides. Deadtime corrections (2) for the decay of short-lived radioisotopes in the presence of active, long-lived isotopes such as ^{14}Na and ^{38}Cl were applied to each peak. In addition, a correction factor for random summing effects was calculated and applied following the procedure of Wyttenbach (3).

Measurements of photopeak areas and associated computations were carried out using standard Nuclear Data software (with modifications made by personnel at the SLOWPOKE Facility) and the University of Alberta Amdahl mainframe computer or an IBM personal computer. Statistical analysis procedures were performed on an Apple Macintosh computer using the statistical package StatWorks by Data Metrics, Inc.

Reagents

Distilled deionized water was obtained either from a modified Barnsted Bantam still or from a column of mixed-bed strong acid–strong base ion exchange resins (Amberlite MB-3, Rohm and Haas). Nitric and perchloric acids of ultra pure grade produced via subboiling distillation were used (Seastar Chemicals, Sidney, B.C., Canada). All other chemicals were reagent grade. Certified standard metal ion solutions (Fisher Scientific) were used as stock solutions for calibrations and standard additions, except in DPASV analysis where a 1000 ppm stock solution prepared by dissolving analytical grade $Pb(NO_3)_2$ was used to prepare working standards. For checking purposes, certified reference materials TORT-1 from the National Research Council of Canada and NBS 1566 Oyster Tissue from the U.S. National Institute for Standards and Technology were also analyzed.

Sample preparation

Atomic absorption analyses

Twelve bottles of LUTS-1, six labelled Day 1 and six labelled Day 2, were obtained from the Marine Standards Analytical Program, Division of Chemistry, National Research Council of Canada, Ottawa, Canada. The bottles were sonicated for 30 min prior to opening and before removal of subsequent samples. Appropriate amounts were pipetted directly from the bottles and weighed to ±0.01 mg on a Mettler H-51 semimicro balance into Savillex 60-mL Teflon PFA digestion vessels (Savillex Corp., Minnetonka, Minn.). After adding acids in amounts listed below the vessels were closed and placed on a turntable in a Sears Kenmore microwave oven and heated for 2 min at 100% power, followed by 10 min at 15% power.

For aluminum analysis 500-μL portions of LUTS-1 were treated with 2 mL of concentrated HNO_3 and 0.25 mL of concentrated HF in the above manner. After cooling, the samples were transferred to 30-mL Teflon bottles containing 0.232 g of H_3BO_3 dissolved in 5 mL of water and were diluted to about 15 g by weight. The final volume of solution was obtained by dividing the weight by the density, the density being determined by weighing a 1-mL portion. For the standard additions procedure 2 mL of the above solution, 1 mL of 0.547 M $Mg(NO_3)_2$, and from 0 to 600 μL of 1 μg/mL Al standard were added to 60-mL pothyethylene bottles and diluted to about 10 g. The volume of solution was again determined by dividing the weight of the solution by its density. The value of the Al concentration was determined by least-squares calculations on the standard additions plots.

For cadmium, approximately 100-μL portions were weighed and digested with about 2.5 mL of concentrated nitric acid as described above. After cooling, the samples were transferred to 10-mL volumetric flasks and diluted to volume with deionized water. For the standard additions, 200 μL of this solution and 0–60 μL of a solution containing 1 μg Cd per mL were added to 2-mL volumetric flasks and diluted to volume with deionized water. The value of the Cd concentration was determined by a least-squares calculation on the standard additions plot as for aluminum.

Can. J. Chem. Downloaded from www.nrcresearchpress.com by 91.144.44.67 on 09/07/12
For personal use only.

TABLE 3. Results of LUTS-1 analyses by GFAAS and DPASV (all concentrations in μg/g). Uncertainties for results found are ±1 standard deviation; uncertainties for certified values are 95% tolerance levels

	Element determined			
	Al	Cd	Pb (GFAAS)	Pb (DPASV)
NRC LUTS-1				
Found	3.2±0.4	2.43±0.2	0.049±0.013	0.052±0.018
NRC value	na[a]	2.12±0.15	0.010±0.002	0.010±0.002
SRM 1566 (Oyster Tissue)				
Found	—	3.32±0.36	—	—
NBS value	—	3.5±0.4	—	—
NRC TORT-1				
Found	44±4	26.69±1.71	9.4±0.7	9.82±1.03
NRC value	na[a]	26.3±2.1	10.4±2.0	10.4±2.0
NRC DOLT-1				
Found	—	—	1.5±0.5	—
NRC value	—	—	1.36±0.29	—
NRC DORM-1				
Found	—	—	0.54±0.04	—
NRC value	—	—	0.40±0.12	—

[a]Not available. Value obtained earlier in this laboratory by INAA and GFAAS on 300-mg portions of TORT-1 was 43±3 μg/g (5).

For lead, approximately 1-mL portions were weighed and digested as above using about 3 mL of concentrated nitric acid. After cooling, the samples were transferred to 10-mL volumetric flasks and diluted to volume with water. For analysis, 0.36 mL of sample and 0.06 mL of 2% $NH_4H_2PO_4$ were placed in sample cups and mixed before being injected by the auto sampler. Each solution was run at least four times.

Anodic stripping voltammetry

LUTS-1 solutions obtained by digestion with nitric acid for the analysis of lead by graphite furnace atomic absorption spectrophotometry were further treated according to the following procedure.

A 1-mL portion of HNO_3 digested solution was placed in a Teflon PFA voltammetric cell (Princeton Applied Research GO 174) with 1 mL of $HClO_4$ and heated under cover (Teflon TFE cover plates) for about 2 h at approximately 200°C. The covers were then removed and the solution was allowed to evaporate to dryness (2–3 h) at a temperature near 240°C. Heating was done on a sandbath covered with aluminum foil to prevent contamination and adherence of sand particles to the hot Teflon. The evaporation procedure was carried out in a stainless steel fumehood designed to handle perchloric fumes. (**Caution**: The usual precautions must be taken when working with hot, concentrated $HClO_4$.)

Residue from the above procedure was dissolved in 5 mL of 0.01 M HNO_3 pipetted directly into the cell. After addition of a Teflon-coated stirbar the cell was placed in the electrode assembly for subsequent anodic stripping analysis.

All solutions were analyzed at least three times with and without added standard. The addition was of standard Pb solution with a micropipet in volumes corresponding either to a 2 or a 2.5 ppb increase in Pb content. For samples where interferences from residual organics were suspected, as indicated by the appearance of foreign peaks, five or six measurements were made on each solution. In one or two cases a second standard addition was used.

Measured peak heights were evaluated by least squares after a Q test on each set to reject outliers. The resulting estimates for the lead concentrations, along with corresponding standard deviations, were used with the sample weight and dilution factors to estimate the lead levels in the sample. These evaluations were performed using a standard addition data treatment program (4).

Instrumental neutron activation analysis

Samples were taken from each of 12 bottles of LUTS-1 provided by the National Research Council of Canada. The bottles were sonicated for 30 min before opening and before removal of subsequent samples. One-millilitre portions were pipetted into small, acid-washed polyethylene irradiation vials. The vials were heat sealed and enclosed in large irradiation vials that were also heat sealed.

Standards were prepared from commercial atomic absorption standard solutions (Spex, Fisher, Custom Std., and NBS) and from standard compounds (Fisher, Anachemia, and Aldrich). For both long and short irradiations multielement standards were prepared by pipetting 100 μL of a multielement standard solution onto Whatman no. 2 filter paper cut to fit the inside walls of a small irradiation vial. The multielement standard solution was prepared by micropipetting aliquots of individual standard solutions into a 10-mL volumetric flask and diluting to volume. The treated filter papers, except for those containing arsenic, were dried slowly under an infrared lamp. All vials were then heat sealed.

For the short irradiations certified reference materials were irradiated as a slurry by combining solid material with water and mixing by sonication. For the 4-h irradiations the reference materials were irradiated as solids because of possible problems with leakage from the vials.

Results and discussion

Results of the atomic absorption and anodic stripping determinations are listed in Table 3. The procedure for aluminum used here was checked by analysis of TORT-1, for which a value had been determined earlier in our laboratories (5). The graphite furnace AA technique described here allows convenient quantification of aluminum in these materials, although sample contamination must be guarded against. Because of lack of agreement among various laboratories and methods neither LUTS-1 nor TORT-1 have been certified for aluminum. This is also the situation for a number of other reference materials.

In the GFAAS work done here the absolute standard

Can. J. Chem. Downloaded from www.nrcresearchpress.com by 91.144.44.67 on 09/07/12
For personal use only.

TABLE 4. Results of analyses of NRC and NBS reference materials for major elements by INAA (all concentrations in percent). Uncertainties for results of this work are ±1 standard deviation; those from NBS and NRC are 95% tolerance levels

	Element determined				
	Na	Cl	K	Ca	Mg
NRC LUTS-1					
Found	0.123±0.002	0.208±0.002	0.090±0.017	0.020±0.002	0.0083±0.002
NRC value	na[a]	na[a]	0.0948±0.0072	0.0203±0.0033	0.0090±0.004
SRM 1566 (Oyster Tissue)					
Found	0.535±0.023	0.946±0.010	0.987±0.115	0.15±0.016	0.131±0.020
NBS value	0.51±0.03	(1.0)[b]	0.969±0.005	0.15±0.02	0.128±0.009
SRM 1577 (Bovine Liver)					
Found	0.244±0.003	0.28±0.001	0.949±0.026	(0.0096)[c]	0.076±0.002
NBS value	0.243±0.013	0.28±0.01	0.996±0.007	0.0124±0.0006	0.060±0.001
NRC TORT-1					
Found	3.72±0.10	5.61±0.17	0.853±0.205	(0.906)[c]	0.196±0.039
NRC value	3.67±0.20	5.58±0.10	1.041±0.040	0.895±0.058	0.255±0.025
NRC DOLT-1					
Found	0.726±0.003	0.714±0.008	1.05±0.001	—	0.105±0.003
NRC value	0.726±0.073	0.688±0.022	1.01±0.10	—	0.111±0.015
NRC DORM-1					
Found	0.789±0.006	1.16±0.01	1.77±0.09	—	0.123±0.020
NRC value	0.800±0.060	1.13±0.03	1.59±0.10	—	0.121±0.013

[a]Not available.
[b]Uncertified value from original certificate of analysis.
[c]Based on a single data point.

Can. J. Chem. Downloaded from www.nrcresearchpress.com by 91.144.44.67 on 09/07/12
For personal use only.

deviations of the determinations were found to depend largely on the amount of analyte injected into the furnace. This amount in turn depends on the material being analysed as well as on the sample preparation technique, and should be given consideration during data interpretation.

An analysis of variance procedure was used to check the homogeneity of the material. No significant bottle-to-bottle variations were observed for aluminum within either the Day 1 or Day 2 sets of bottles. Between-day variations appeared to be high enough to reject the null hypothesis of no significant difference between Day 1 and 2 at the 95% confidence level; the null hypothesis is not rejected, however, at the 99% confidence level. Average values for the two sets of samples were 3.4 ± 0.4 μg/g for Day 1 and 3.1 ± 0.4 μg/g for Day 2. Thus the homogeneity between these two sets of samples with respect to aluminum is borderline in a statistical sense at the 0.5-mL test portion level. In view of this, a practical value for the aluminum content reported in Table 3 was established by calculating the overall average for all samples.

An analysis of variance of the data for LUTS-1 did not indicate any between-bottle variability for cadmium content at the 95% confidence level for 0.1-mL test portions. No difference was observed in cadmium levels at the 95% confidence level for the bottles labeled Day 1 and Day 2. Therefore this material can be considered homogeneous with respect to cadmium for subsampling at the 0.1-g level. Our best estimate for the cadmium level, reported in Table 3, was obtained by calculating the overall average.

Relative standard deviations associated with individual values for lead in LUTS-1 samples by atomic absorption covered a wide range: 2–19% with an average of 7%. Ranges for the other certified reference materials were narrower. On the other hand, as mentioned before, a correlation was observed between the relative standard deviation and the amount of lead injected into the graphite furnace. For LUTS-1 the amount of lead injected was roughly 83 pg, with an observed relative standard deviation of 7%. For Dogfish Muscle the amount of lead was approximately 116 pg, giving a relative standard deviation of 4%, for TORT-1 about 134 pg of lead gave a relative standard deviation of 2.4%, and for Dogfish Liver about 321 pg of lead gave a relative standard deviation of 1.6%. Considering the differences in the composition of these four materials, the results cannot be considered as evidence for deterioration of the quality of the analyses. Rather, the lower precision observed may be related to the lower lead level in the sample.

An analysis of variance for the LUTS-1 lead data does not reject the homogeneity assumption for between-bottle variation or between-day variation. The lower precision of the analytical procedures for lead, however, makes the degree of homogeneity less certain than for more precise measurements for other elements. It should be noted, though, that the relative standard deviations for the individual measurements of lead in LUTS-1 by DPASV averaged 7.6% and for TORT-1 8.3%. These values agree well with each other and with literature values for comparable analytical systems (4, 6, 7).

Most of the imprecision in the DPASV analyses can be traced to errors in Hg drop reproducibility and to poor reproducibility of flow conditions during the deposition step. Data points with very high relative standard deviations were associated with the analyses done using the hanging mercury drop electrode. Considering the low lead level and the organic matrix of the samples, precision and analytical control of the analysis can be viewed as satisfactory for the equipment used. Anodic stripping data does not offer any significant improvement in precision for the determination of lead relative to graphite furnace atomic absorption analysis, and homogenity conclusions based on

Can. J. Chem. Downloaded from www.nrcresearchpress.com by 91.144.44.67 on 09/07/12
For personal use only.

TABLE 5. Results of analyses of NRC and NBS reference materials for trace elements by INAA (all concentrations in μg/g). Uncertainties for results of this work are ±1 standard deviation; those from NBS and NRC are 95% tolerance levels

	Element determined									
	Br	Cu	I	Mn	Fe	Ag	As	Co	V	Zn
NRC LUTS-1										
Found	13.6±0.9	17.6±1.1	15.9±0.3	1.19±0.28	11.7±2.5	0.61±0.04	2.88±0.12	0.056±0.15	0.25±0.03	12.4±0.9
NRC value	na[a]	15.9±1.2	na[a]	1.20±0.13	11.6±0.9	0.580±0.049	2.83±0.13	0.051±0.006	na[a]	12.4±0.8
SRM 1566 (Oyster Tissue)										
Found	54.5±3.1	65.9±5.1	4.34±0.37	17.2±1.6	222±24	1.04±0.11	13.1±0.2	0.33±0.02	—	924±16
NBS value	(55)[b]	63.0±3.5	(2.8)[b]	17.5±1.2	195±34	0.89±0.09	13.4±1.9	(0.4)[b]	—	852±14
SRM 1577 (Bovine Liver)										
Found	10.5±1.1	176±4	—	9.45±0.09	—					
NBS value	9.1±0.9	193±10	(0.180)[c]	10.3±1.0	268±8					
NRC TORT-1										
Found	371±10	410±8	24.1±10.1	23.8±4.5	155±16	11.0±1.4	25.0±0.6	0.45±0.03	1.6±0.7	167±2
NRC value	(372±12)[c]	439±22	(26±9)[c]	23.4±1.0	86±11	13.4±0.5	24.6±2.2	0.42±0.05	1.4±0.3	177±10
NRC DOLT-1										
Found	24.7±3.2	19.6±2.7	—	10.6±0.80	616±31	1.08±0.10	(10.2)[d]	0.182±0.006	0.98±0.12	(90.2)[d]
NRC value	(24±10)[c]	20.8±1.2	—	8.72±0.53	712±48	(1.07±0.05)[b]	10.1±1.4	0.157±0.037	—	92.5±2.3

[a]Not available.
[b]Uncertified value from original certificate of analysis.
[c]Uncertified value from previous work done by this laboratory.
[d]Based on a single data point.

GFAAS work were not, as expected, affected by the DPASV data.

Correlation diagrams for the graphite furnace and anodic stripping data indicated random scatter. Since both analyses were done on the same sample solutions, any differences during the subsampling stage can be ruled out as the origin of high uncertainty. This puts the burden on instrumental performance, allowing one to accept sufficient homogeneity of LUTS-1 for the analysis of lead using 1-g subsamples.

The overall average estimate for lead by anodic stripping for LUTS-1 is 0.052 ± 0.018 μg/g, the uncertainty being one standard deviation. On the basis of a *t*-test assuming unequal and unknown variances (8), this value is not significantly different from the value obtained from graphite furnace atomic absorption (0.049 ± 0.013). Therefore the mean of these two values, 0.050 μg/g, is proposed as our best estimate for the lead content in LUTS-1, with a standard deviation calculated by combining the variances for the two data sets of ± 0.011 μg/g. This lead value is approximately 0.04 μg/g higher than the certified value. The reason for this discrepancy is unknown; the most likely explanation is contamination in some way of the original sample bottles.

A summary of the analytical results obtained by instrumental neutron activation analysis on 1-g samples of LUTS-1 is given for the major elements in Table 4 and for the trace elements in Table 5. The NRC certified reference materials TORT-1 and DOLT-1 and the NBS standard reference materials SRM 1566 (Oyster Tissue) and SRM 1577 (Bovine Liver) were run as controls. The results for these materials, along with the accepted values, are included in Tables 4 and 5.

The INAA data were tested for differences in within- vs. between-bottle and for within- vs. between-day homogeneity for each element by a one-way analysis of variance. Prior to running of the ANOVA program the data were tested for outliers by the Dean and Dixon *Q* test (9) and values falling outside the Dean and Dixon criteria at the 90% confidence level (Q_{90}) were deleted.

An ANOVA study of the data from 2.5- and 10-h counts for between- vs. within-bottle variability did not indicate significant heterogeneity at the 95% confidence level except for silver (658 keV) and zinc on Day 1. The silver and zinc data are affected by two relatively high values coming from the same bottle, which markedly increase the average of that bottle. On the other hand, data for 3- and 10-min counts did not allow rejection of the homogeneity assumption for any of the elements determined. Therefore we conclude that within-bottle homogeneity is satisfactory for all elements listed in Tables 4 and 5 at the 95% confidence level for 1-mL test portions.

When tested in a between- vs. within-day format, the 2.5- and 10-h count data did not show significant differences for any of the elements except iron (1099 and 1291 keV) and cobalt (1173 keV). The iron counts at both energies were consistently higher in the Day 1 samples than in those from Day 2. The cobalt data were affected by two high values occurring in the Day 2 data.

When tested in the same format, data for the 3- and 10-min counts indicate significant between-day differences for sodium (1368 and 2754 keV), chlorine (1643 and 2167 keV), bromine (617 and 666 keV), and iodine at the 95% confidence level. For these elements Day 1 values were consistently higher than Day 2 values.

Aluminum count data were also obtained by INAA, but could not be corrected for either phosphorus or silicon interferences because concentration values for these elements were not determined. As P and Si data become available our results can be corrected and an aluminum value obtained.

In summary, the results obtained in this work agree well with certified values except for magnesium and copper, both of which are low. Other elements for which further investigation might be warranted are iron and possibly cobalt. Lower values of Na, Cl, Br, and I were found for material bottled on Day 2, which may indicate either loss of soluble salts from the solution phase between days, or an increase in water content between days. The variation is not sufficiently large, however, to cause a discrepancy in the overall values reported at the tolerance levels established by the NRC.

Acknowledgements

We thank W. George, Environmental Engineering Group, University of Alberta, for the use of the atomic absorption spectrophotometer and furnace. Assistance from M. J. M. Duke, Peter Ford, and Gordon Haverland of the University of Alberta SLOWPOKE II Reactor Facility is greatly appreciated. Financial support of the National Research Council of Canada and the University of Alberta is gratefully acknowledged.

1. C. Bergerioux, G. Kennedy, and L. Zikovsky. J. Radioanal. Chem. **50**, 229 (1979).
2. T. Takeuchi, S. Uehara, and T. Hayashi. J. Radioanal. Chem. **56**, 25 (1980).
3. A. Wyttenbach. J. Radioanal. Chem. **8**, 335 (1971).
4. A. R. Fernando. PhD. Thesis, University of Alberta, Edmonton, Alberta, Canada. 1988.
5. B. Kratochvil, N. Motkosky, M. J. M. Duke, and D. Ng. Can, J. Chem. **65**, 1047 (1987).
6. K. W. Pratt and W. F. Koch. Anal. Chim. Acta, **215**, 21 (1988).
7. P. Valenta, H. Rutzel, and H. W. Nurnberg. Z. Anal. Chem. **285**, 25 (1977).
8. C. Liteanu and I. Rica. Statistical theory and methodology of trace analysis, Ellis Horwood, Chichester. 1980.
9. R. B. Dean and W. J. Dixon. Anal. Chem. **23**, 636 (1951).

Can. J. Chem. Downloaded from www.nrcresearchpress.com by 91.144.44.67 on 09/07/12
For personal use only.

Photochromic systems. Part 1. Structural and spectroscopic study of photochromically active products of Stobbe condensation. 2,3-Dibenzylidenesuccinic acid and its anhydride

P. ADRIAAN DAVIDSE, JAN L. M. DILLEN, ANTON M. HEYNS, TOMASZ A. MODRO,[1] AND PETRUS H. VAN ROOYEN
Department of Chemistry, University of Pretoria, Pretoria 0002, South Africa

Received December 19, 1988[2]

P. ADRIAAN DAVIDSE, JAN L. M. DILLEN, ANTON M. HEYNS, TOMASZ A. MODRO, and PETRUS H. VAN ROOYEN. Can. J. Chem. **68**, 741 (1990).

E,E-2,3-Dibenzylidenesuccinic acid (**2**) and its anhydride (**1**) were synthesized, their crystal structures and ^1H and ^{13}C nuclear magnetic resonance spectra were determined, and electron charge densities of carbon atoms were calculated. These results were related to the corresponding data available for *E*-cinnamic acid (**3**) in order to evaluate the effect of structural changes in a series **3** → **2** → **1** on the molecular parameters and spectroscopic properties of the cinnamic system. In the molecule of **2** most of the steric strain is released by the rotation about the C(α)—C(α′) bond giving rise to a structure consisting of two, approximately independent, cinnamic acid moieties. In **1**, severe steric strain is introduced, as demonstrated by the unusually large values of the CCC bond angles exocyclic with respect to the anhydride ring, as well as by significant deviations from the plane of the cinnamic skeleton. The geometry of **1** results in an intramolecular shielding of the aromatic hydrogen atoms due to the proximity of the two benzene rings; this shielding effect for the *ortho*, *meta*, and *para* hydrogen atoms correlates well with the intramolecular distances between the corresponding positions of both rings. The common linear relationship between ^{13}C chemical shifts and the electron charge densities on the given carbon atom has been obtained for compounds **1**, **2**, and **3**.

Crystal data. Anhydride (**1**): space group $P2_1/c$ with a = 13.536(3), b = 14.391(3), c = 7.159(1) Å; β = 98.69(1)°; R_w = 0.029 and R = 0.055. Succinic acid (**2**): space group $P\bar{1}$ with a = 8.881(3), b = 9.786(1), c = 11.355(3) Å; α = 85.56(1), β = 88.76(2), γ = 69.46(2)°; R_w = 0.048 and R = 0.081. This compound cocrystallizes with one molecule of the solvent (acetic acid).

Key words: photochromic, cinnamic, succinic.

P. ADRIAAN DAVIDSE, JAN L. M. DILLEN, ANTON M. HEYNS, TOMASZ A. MODRO et PETRUS H. VAN ROOYEN. Can. J. Chem. **68**, 741 (1990).

On a synthétisé l'acide *E,E*-2,3-dibenzylidènesuccinique (**2**) et son anhydride (**1**), on a déterminé leurs structures cristallines et leurs spectres de résonance magnétique nucléaire du ^1H et du ^{13}C et on a calculé les densités des charges électroniques des atomes de carbone. En comparant ces données avec les données correspondantes disponibles pour l'acide *E*-cinnamique, on a évalué l'effet des changements structuraux reliés à la série **3** → **2** → **1** sur les paramètres moléculaires et sur les propriétés spectroscopiques du système cinnamique. Dans la molécule **2**, on peut éliminer complètement les contraintes stériques en effectuant une rotation autour de la liaison C(α)—C(α′) pour obtenir une structure comportant deux portions pratiquement indépendantes d'acide cinnamique. Dans le cas de la molécule **1**, des contraintes stériques importantes sont introduites; elles sont mises en évidence par des valeurs exceptionnellement élevées pour les angles des liaisons CCC exocycliques par rapport aux valeurs correspondantes du cycle anhydride ainsi que par des déviations importantes par rapport au plan du squelette cinnamique. Le géométrie de la molécule **1** est le résultat d'un blindage intramoléculaire des atomes d'hydrogène aromatiques provenant de la proximité des deux noyaux benzéniques; il existe une corrélation entre cet effet de blindage sur les atomes d'hydrogène en *ortho*, en *meta* et en *para* et les distances intramoléculaires entre les positions correspondantes des deux cycles. Pour les composés **1**, **2** et **3**, on a obtenu le relation linéaire habituelle entre les déplacements chimiques du ^{13}C et les densités des charges électroniques sur les atomes de carbones donnés.

Données cristallographiques. Anhydride (**1**) : groupe d'espace $P2_1/c$, avec a = 13,536(3), b = 14,391(3) et c = 7,159(1) Å, β = 98,69(1)°; R_w = 0,029 et R = 0,055. Acide succinique (**2**) : groupe d'espace $P\bar{1}$, avec a = 8,881(3), b = 9,786(1) et c = 11,355(3) Å; α = 85,56(1), β = 88,76(2) et γ = 69,46(2)°; R_w = 0,048 et R = 0,081. Ce composé co-cristallise avec une molécule de solvant (acide acétique).

Mots clés : photochromique, cinnamique, succinique.

[Traduit par la revue]

Introduction

Fulgides (**1**) represent a well-known photochromic system investigated since the early 1900's (1), and their photochemical and thermal transformations still attract considerable attention (2). Anhydrides (**1**), prepared by the Stobbe condensation (3) of aromatic aldehydes with succinic acid derivatives, are formed almost exclusively as *E,E* isomers (4), i.e., compounds with the maximum steric interactions between the aromatic groups.

This stereoselectivity was explained by Johnson *et al.* (5), as well as by Heller and co-workers (6), who proposed the mechanism involving "overlap control", according to which the maximum overlap of the developing *p*-orbitals is achieved in the transition state with no eclipsing effects between the aryl and ester groups. The *E,E*-diacid (**2**) is thus formed in two successive condensations, and suffers no serious steric congestion because of the free rotation about the α,α′ carbon–carbon bond. It is only when the diacid **2** is converted into the anhydride **1** that severe steric interactions between aromatic rings are introduced (9). Systems **2** and **1** are formally derived from *E*-cinnamic acid (**3**) by α,α′ coupling and then closure to the anhydride ring.

The first (and only) structural study on fulgides (**1**) was carried out by Cohen *et al.* (7), who demonstrated, using X-ray diffraction and ^1H nmr spectroscopy, the *E,E* configuration of the di-*p*-anisylidenesuccinic anhydride prepared from *p*-methoxybenzaldehyde via Stobbe condensation. In this paper, which is the first of a series aimed at the comprehensive study of

[1]Author to whom correspondence may be addressed.
[2]Revision received November 17, 1989.

Printed in Canada / Imprimé au Canada

Can. J. Chem. Downloaded from www.nrcresearchpress.com by 88.85.125.76 on 09/07/12
For personal use only.

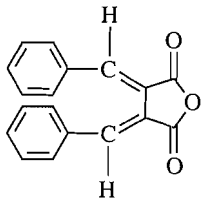

1

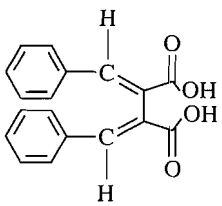

2

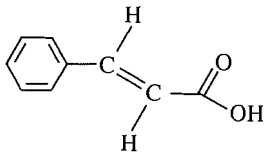

3

the structural and chemical properties of **1**, we focussed our attention on the effect of the sequence of the structural changes **3** → **2** → **1** on the molecular parameters and spectroscopic properties of these compounds. We report here the crystal and molecular structures of **1** and **2** (Ar = Ph) together with the detailed interpretation of their nmr (^{1}H, ^{13}C) spectra, and relate these data to the corresponding characteristics available for *E*-cinnamic acid. Whenever possible, our results are related to the literature data (7) for the *p*-anisyl system in order to reaffirm the structural assignments. MNDO calculations were also performed (8) on all three compounds and the electron densities determined for each atom are correlated with the ^{13}C chemical shift data.

Results and discussion

Molecular structures

Selected molecular parameters relevant for the discussion of the structural relationship of compounds **1**, **2**, and **3** are listed in Table 1, and the projections of molecules of **1** and **2** are given in Figs. 1 and 2.

Compound **2** incorporates, in the solid state, a molecule of solvent (acetic acid). Each molecule of **2** is involved in four hydrogen bonds forming a cluster of two acid **2** and two solvent molecules. The conformation of the succinic acid part of the molecule is, however, similar to that found in the *Z*,*E* isomer of **2**, recently synthesized in this laboratory, and which crystallizes without solvent molecules.

It is clear that coupling of two molecules of cinnamic acid, which yields diacid **2**, as well as dehydrating the latter to form **1**, has a profound effect on the geometry of the system. The compound of reference (**3**), can be considered as an unhindered, fully conjugated system as indicated by almost identical C(2)—C(3) and C(8)—C(9) distances, as well as by the almost ideal planarity of the molecule (the values of the torsion angles of **3** based on the numbering of **2** are as follows: C(2)—C(3)—C(8)—C(9) −178.2°, O(1)—C(2)—C(3)—C(8) −1.5°, O(7)—C(2)—C(3)—C(8) 178.1°, C(3)—C(8)—C(9)—C(10) 0.9°, and C(3)—C(8)—C(9)—C(14) 179.6°). (*Note*: for the numbering of atoms in **3** see numbering of atoms O(1A)—C(14) in **2**, Fig. 2.) This structure gives rise to an extensive chromophore, characterized by the λ_{max} value of 287.5 nm and by the molar extinction coefficient, ε, of 19 500 (10). Fusion of two molecules of **3** through the C(α)—C(α′) bond to yield **2** introduces significant intramolecular steric interactions. Most of this strain can be released by the rotation about the C(α)—C(α′) bond, as can be seen by the value (104.2° (7)) of

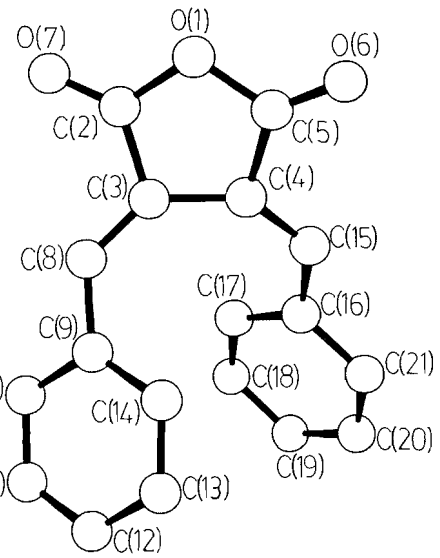

FIG. 1. A perspective view of **1** with atomic numbering.

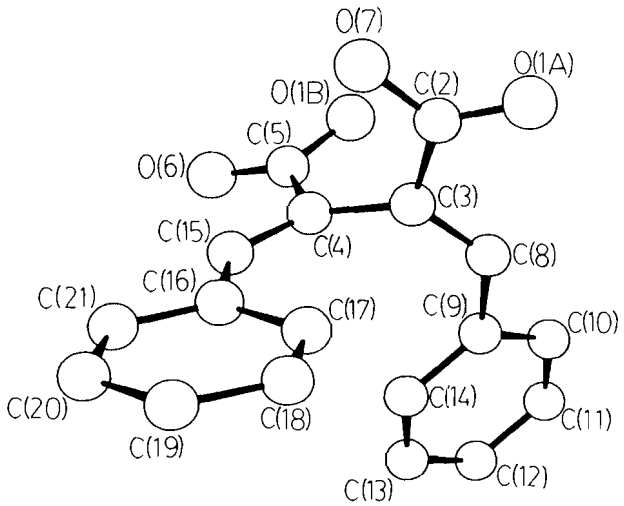

FIG. 2. A perspective view of **2** with atomic numbering.

the C(8)—C(3)—C(4)—C(15) torsion angle. As a result of this rotation, the molecule of **2** should be considered as consisting of two independent cinnamic acid moieties, without any electronic feature of the 1,4-diphenyl-1,3-butadiene molecule (**2** is a colorless substance). Moreover, the close proximity of two skeletons of **3** in the molecules of **2** results in the deviation of the individual halves of the system from the cinnamic acid geometry. The C(2)—C(3) (and C(4)—C(5)) bond distances are different from C(8)—C(9) (and C(15)—C(16)) distances, and both phenyl rings deviate significantly (22° and 39°) from the plane of the olefinic group. This deviation, aiming to minimize intramolecular interactions between two aromatic rings, is paralleled by the hypsochromic effect and the decrease of intensity in the electronic spectrum. Compound **2** exhibits the absorption maximum at 272.5 nm with an ε value of 27 000, i.e., of 13 500 per single cinnamic acid unit.

In the molecule of **1**, the anhydride ring imposes severe steric strain upon the whole cinnamic system. In this case, however, any rotation about the C(3)—C(4) bond is prohibited, so the relief of the strain can be achieved via changes of the bond angles at these two carbon atoms. This is demonstrated by the dramatic *increase* of the exocyclic bond angles C(3)—C(4)—

Can. J. Chem. Downloaded from www.nrcresearchpress.com by 88.85.125.76 on 09/07/12
For personal use only.

TABLE 1. Selected molecular parameters of **1**, **2**, and **3** determined by X-ray diffraction; standard deviation in parentheses. For atom numbering, see Figs. 1 and 2

	1		**2**		**3**[a]	
Bond(s)	Distance (Å)	Order[b]	Distance (Å)	Order[b]	Distance (Å)	Order[b]
C(2)—C(3)	1.490(3)	0.919	1.471(6)	0.938	1.470(4)	0.950
C(4)—C(5)	1.486(3)	0.921	1.479(6)	0.940		
C(3)—C(8)	1.338(3)	1.802	1.357(6)	1.845	1.332(4)	1.856
C(4)—C(15)	1.339(3)	1.801	1.336(5)	1.824		
C(8)—C(9)	1.453(3)	1.028	1.459(6)	1.010	1.467(4)	1.021
C(15)—C(16)	1.456(3)	1.028	1.471(6)	1.028		
C(3)—C(4)	1.452(3)	1.021	1.484(5)	0.978		
	Angle (deg)		Angle (deg)		Angle (deg)	
C(2)—C(3)—C(8)	116.8(2)		116.8(4)		122.3(3)	
C(5)—C(4)—C(15)	118.0(2)		117.5(4)			
C(3)—C(8)—C(9)	130.7(2)		130.6(5)		126.2(3)	
C(4)—C(15)—C(16)	129.1(2)		126.6(4)			
C(2)—C(3)—C(4)	105.9(2)		115.5(4)			
C(3)—C(4)—C(5)	105.7(2)		116.0(4)			
C(3)—C(4)—C(15)	135.7(2)		125.9(4)			
C(4)—C(3)—C(8)	136.9(2)		127.4(5)			
	Torsion angle (deg)[c]		Torsion angle (deg)		Torsion angle (deg)	
O(1)—C(2)—C(3)—C(8)	161.5(2)		−12.5(7)		178.3	
O(7)—C(2)—C(3)—C(8)	−17.1(4)		165.1(5)		−2.9	
O(7)—C(2)—C(3)—C(4)	169.2(3)		−8.7(1)			
O(1)—C(2)—C(3)—C(4)	−12.3(3)		173.7(5)			
O(6)—C(5)—C(4)—C(3)	169.9(2)		−174.6(4)			
O(1)—C(5)—C(4)—C(3)	−12.4(3)		5.6(7)			
O(1)—C(5)—C(4)—C(15)	160.1(2)		177.6(5)			
O(6)—C(5)—C(4)—C(15)	−17.7(4)		−2.6(7)			
C(2)—C(3)—C(8)—C(9)	−167.2(2)		−172.6(5)		−179.2	
C(5)—C(4)—C(15)—C(16)	−164.4(2)		−177.4(5)			
C(3)—C(8)—C(9)—C(10)	−159.2(3)		169.8(6)		174.8	
C(3)—C(8)—C(9)—C(14)	24.7(4)		−9.0(9)		−4.5	
C(4)—C(15)—C(16)—C(17)	28.3(4)		−39.2(8)			
C(4)—C(15)—C(16)—C(21)	−154.6(3)		144.3(5)			
C(2)—C(3)—C(4)—C(5)	14.7(3)		88.8(6)			
C(15)—C(4)—C(3)—C(8)	32.4(5)		104.5(7)			
C(15)—C(4)—C(3)—C(2)	−155.8(3)		−82.5(7)			
C(8)—C(3)—C(4)—C(5)	−157.1(3)		−84.3(6)			
C(3)—C(4)—C(15)—C(16)	5.2(5)		−6.3(9)			
C(4)—C(3)—C(8)—C(9)	4.0(5)		0.3(9)			

[a]Taken from ref. 9.
[b]Calculated (8).
[c]In all cases the phenyl rings together with atoms C(8), C(15) form planes with all torsion angles of ca. 180°.

C(15) (in **1** 135.5(2)° and **2** 127.4(5)°) and C(4)—C(3)—C(8) (in **1** 137.0(2)° and **2** 126.0(5)°) and a *decrease* of the endocyclic angles C(2)—C(3)—C(4) (in **1** 105.6(2)° and **2** 115.8(4)°) and C(3)—C(4)—C(5) (in **1** 105.5(2)° and **2** 116.9(4)°). The corresponding exo- and endocyclic bond angles in the bis-*p*-anisyl analogue (**1***a*) are very similar (7) (average 137.8° and average 106.2° respectively), but since the molecular structure of the corresponding diacid has not been determined, no direct effect of structural change on molecular parameters could be assessed for this system. For (*Z*)-veratrylidene succinic acid (11) the corresponding exo- and endocyclic bond angles are 129.0° and 107.7°. This trend indicates that the increase in exocyclic bond angles results from the steric interactions experienced by the phenyl groups. In addition, individual atoms in **1** deviate more from the plane of the cinnamic acid system than corresponding atoms in **2**. Consideration of two planes in **1**, each determined by ten atoms (O(6)—C(5)—C(4)—C(15)—[C(16) to C(21)], and O(7)—C(2)—C(3)—C(8)—[C(9) to C(14)]), reveals that both carbonyl oxygens (O(6) and O(7)) deviate by −0.4(2) and 0.4(2) Å respectively from these planes, and both α carbons (C(4) and C(3)) deviate by 0.5(2) and −0.5(2) Å respectively from these planes. Similar deviations from planarity have been reported (7) for the bis-*p*-anisyl compound. The deviation of the phenyl rings from the plane of the olefinic groups is 21° and 25° in **1** and approximately 30° for di-*p*-anisylidenesuccinic anhydride (7).

Can. J. Chem. Downloaded from www.nrcresearchpress.com by 88.85.125.76 on 09/07/12
For personal use only.

TABLE 2. Chemical shifts, δ, and shielding effects, Δδ[a], (in ppm) of olefinic and aromatic hydrogen atoms in cinnamic acid (**3**) and its derivatives; $CDCl_3$, 18°C

Compound	H(α)	H(β)	H(*ortho*)	H(*meta*)	H(*para*)
1	—	7.89(s)	6.81(m)	6.81(m)	7.12(t)
2	—	7.94(s)	7.55(d of d)	7.30(m)	7.30(m)
3	6.50(d)	7.80(d)	7.55(d of d)	7.41(m)	7.41(m)
4	6.54(d)	7.87(d)	7.55(d of d)	7.40(m)	7.40(m)
Δδ(**2**/**3**)	—	+0.14	0.00	−0.11	−0.11
Δδ(**1**/**4**)	—	+0.02	−0.74	−0.59	−0.28

[a]Δδ(**i**/**j**) corresponds to the chemical shift for **i** relative to that for **j**; positive values of Δδ indicate deshielding.

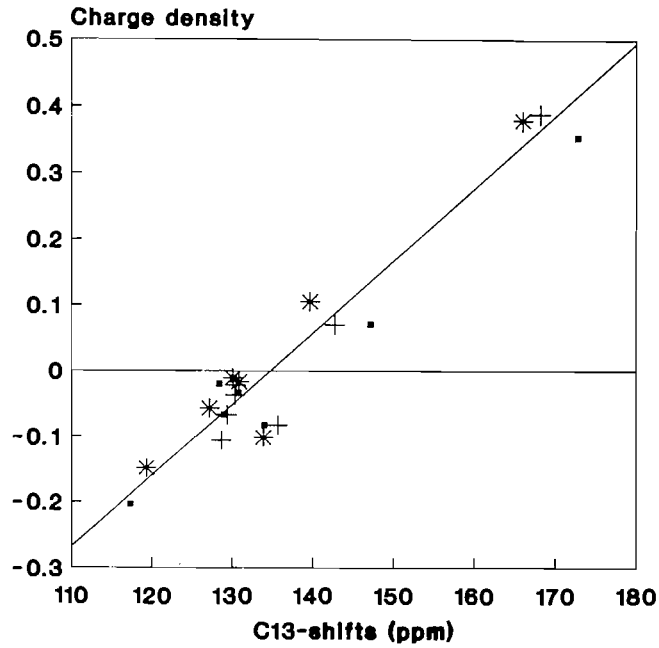

FIG. 3. The correlation between observed ^{13}C shifts and calculated electron charge densities. The points marked * are the values for **1**; +, values for **2**; and ■, values for **3**.

In contrast, the alignment of the phenyl ring in (*Z*)-veratrylidene succinic acid is virtually parallel (6°) to the enone π-system (11). The structure of **1** does not affect significantly the spectroscopic properties of the cinnamic moiety, as shown by the similarity of the section of the uv spectrum of **1** (λ_{max} 290 nm; ε, 34 000) to the spectrum of cinnamic anhydride, (λ_{max} 290 nm; ε, 49 000) (12). In addition to the π electron system of the cinnamic acid derivative, **1** is also a derivative of 1,4-diphenyl-1,3-butadiene, as indicated by the shift of the electronic spectrum of **1** to the visible region (yellow substance, λ_{max} 360 nm; ε, 12 600). The most obvious structural feature of **1**, illustrated in Fig. 1, is the tendency of the aromatic rings to maximize their mutual intramolecular distance. As will be seen from the analysis of the ^1H nmr spectrum of **1**, the intramolecular relation of the phenyl groups has a strong effect on the shielding of aromatic hydrogen atoms. The angle between the vectors normal to the phenyl rings is −76° in **2**, 35° in **1**, and 19° in the bis-*p*-anisyl compound.

^1H nuclear magnetic resonance spectra

Table 2 lists chemical shift values, as well as relative chemical shifts, for all hydrogen atoms in compounds **1**, **2**, and **3**.

The diacid **2** can be viewed as consisting of two independent cinnamic acid moieties linked through the C(α)—C(α′) bond. At the temperature of the measurements the rotation about this bond seems to be completely free, as the two olefinic protons in **2** are magnetically equivalent and give rise to a sharp singlet at δ 7.94 (the corresponding olefinic protons in the diacid derived from **1***a* also give rise to a singlet (7)). Slight deshielding of H(β) in **2** relative to **3** can be easily attributed to the effect of the 2-cinnamyl group substituted for the hydrogen atom at carbon α. The aromatic hydrogen atoms in **2** have chemical shifts similar to those in **3**, except for a weak shielding of *meta* and *para* positions, suggesting some long-distance mutual interactions between two aromatic rings. Much more significant changes in the shielding of the individual hydrogen atoms are, however, observed upon closing the diacid **2** into the anhydride **1**. Olefinic hydrogens, H(β), H(β′), which belong to the planar, rigid bis-methylenesuccinic anhydride system, have an almost identical chemical shift to that of the equivalent hydrogen atoms in **2**. For the aromatic rings, on the other hand, steric constraint of the *E,E* geometry of system **1** requires significant rotation around the C(8)—C(9) and C(15)—C(16) bonds. However, this effect locates the benzene rings in the near-parallel planes, hence results in repulsive interactions between the two sets of aromatic π electrons. As a result of this, aromatic rings increase their intramolecular distance. In consequence of this geometry, aromatic hydrogen atoms of one ring are located in the shielding section of the magnetic field induced by the second ring. The shielding effects decrease in the order *ortho* > *meta* > *para*, as the distances between the corresponding positions in the rings increase. This correlation can be easily demonstrated by comparing chemical shifts of aromatic hydrogen atoms in **1** with the corresponding values for the strain-free *E*-cinnamic anhydride **4**, whose ^1H nmr data have been also included in Table 2. The relative shielding of ring hydrogens in **1**, as compared with **4**, decreases from −0.74 to −0.59 to −0.28 ppm for the *ortho*, *meta*, and *para* hydrogen atoms, respectively.

^{13}C nuclear magnetic resonance spectra

Chemical shift data, together with the net atomic charges (calculated by the MNDO method (8)) for individual carbon atoms in compounds **1**–**3** are given in Table 3. Assignment of ^{13}C resonances was based on the comparison of chemical shifts with the literature data for similar derivatives, on the relative peak intensities, and on the INEPT experiments, which allowed the identification of all CH carbon atoms. In *E*-cinnamic acid the C(β) atom is strongly deshielded relative to the C(α) atom, the difference being Δδ = 30.1 ppm. This difference indicates strong polarization of the olefinic bond, which effectively transmits the conjugation between the (donor) phenyl and the

Can. J. Chem. Downloaded from www.nrcresearchpress.com by 88.85.125.76 on 09/07/12
For personal use only.

TABLE 3. The ^{13}C nmr chemical shifts[a] and (in parentheses) net atomic charges[b] for carbon atoms of substrates **1–3**

Carbon	Compound		
	3[c]	**2**[d]	**1**[c]
$C_{carbonyl}$	172.8 (0.355)	168.2 (0.390)	166.0 (0.380)
C_{α}	117.3 (−0.204)	128.6 (−0.106)	119.3 (−0.149)
C_{α}	147.1 (0.071)	142.7 (0.070)	139.6 (0.105)
C_{ipso}	133.9 (−0.083)	135.6 (−0.083)	133.8 (−0.102)
C_{ortho}	128.3 (−0.020)	130.4 (−0.022)	130.0 (−0.011)
C_{meta}	128.9 (−0.067)	129.3 (−0.067)	127.1 (−0.057)
C_{para}	130.7 (−0.034)	130.3 (−0.037)	130.8 (−0.017)

[a]In ppm, relative to TMS.
[b]Calculated by MNDO method (8).
[c]In $CDCl_3$.
[d]In acetone-d_6.

(acceptor) carboxylic group. The presence of the β-phenyl group is necessary for such polarization to occur since the chemical shifts for olefinic carbons in a molecule of ethyl acrylate are almost identical ($\Delta\delta$ = 0.7 ppm) (13). The transmission of the conjugative effects is, for steric reasons, diminished in the diacid **2**. Consequently, the relative deshielding of C(β) vs. C(α) decreases in compound **2** ($\Delta\delta$ = 14.1 ppm), paralleling the effects of the deviation of **2** from planarity on its uv spectrum (*vide supra*). In agreement with the known fact that shieldings of vinyl carbons are more sensitive to polar effects than those of aromatic carbons (14), the only significant changes in chemical shifts for a series **1**, **2**, **3** are observed for the C(carbonyl), C(α), and C(β) atoms. The strongest effects operate at C(α); attachment of a second moiety of cinnamic acid results in strong deshielding of this atom (for **3** → **2**, $\Delta\delta$ = 11.3 ppm), as expected from the electronic effects of the 2-cinnamyl substituent relative to the hydrogen atom. Interestingly, this deshielding effect is almost completely lost upon the closure of the diacid **2** into the anhydride **1**, the deshielding of C(α) in **1** relative to that in **3** being only $\Delta\delta$ = 2.0 ppm. This loss could possibly be a compensation effect brought about by the delocalization in the more planar diphenylbutadiene system in **1**.

The most common assumption made in the interpretation of ^{13}C nmr chemical shifts is that there is a linear correlation between shifts and the electron density on the given carbon atom (15). Although this assumption has been frequently questioned, the chemical shift – charge density linear correlation has been used for the determination of unknown compounds (16). We have tested this assumption by plotting the observed ^{13}C chemical shifts for compounds **1**, **2**, and **3** vs. net atomic charges calculated by the MNDO method (Fig. 3). The plot, involving 21 carbon atoms, is reasonably linear (r = 0.955) and the carbon atoms of all three substrates follow the same relationship. This common dependance of the chemical shifts on the electron densities for these three configurationally different structures suggests that shielding parameters of a given carbon atom are mainly determined by the electronic state of an atom (a diamagnetic and a paramagnetic shielding term) with negligible contribution from anisotropy effects of neighbouring atoms and groups.

Experimental

Melting points are uncorrected. The nmr spectra were recorded on a superconducting FT Bruker AC 300 spectrometer with TMS as internal standard. The uv spectra were recorded on a Beckman Acta MIV spectrophotometer. All solvents and reagents were purified by conventional methods immediately before use. *E*-cinnamic acid (**3**) (Aldrich, Gold Label, mp 133–134°C) was used as supplied. Anhydride (**1**) was prepared directly from crude acid (**2**), which was synthesized following the procedure given in the literature (3). Crude **2** was added to acetyl chloride (20 mL per 1 g of **2**) and the mixture was heated under reflux for 2 h. After evaporation of the excess of acetyl chloride under reduced pressure, crude **1** was first crystallized from ethyl acetate, and then from benzene. Yield 22%; yellow crystals, mp 210–211°C (from benzene; lit. (17) mp 203°C); ^1H and ^{13}C nmr spectra are given in Tables 2 and 3. Diacid **2** was prepared from **1** in the following manner: **1** (0.5 g, 1.8 mmol) was dissolved in dioxane (20 mL), water (1 mL, 55 mmol) and concentrated hydrochloric acid (ca. 5 drops) were added, and the solution was heated under reflux until it became colourless. Solvent was removed under reduced pressure and crude **2** was recrystallized from glacial acetic acid. Yield 0.51 g (95%); colourless prisms; mp ca. 217°C (varies with the rate of heating); ^1H and ^{13}C nmr spectra are given in Tables 2 and 3.

Crystal structure determination

Diffraction quality crystals of **1** (0.21 × 0.23 × 0.29 mm) and **2** (0.32 × 0.25 × 0.27 mm) were obtained by crystallization from benzene and glacial acetic acid respectively. Crystals of $C_{18}H_{12}O_3$ (**1**) are monoclinic, space group $P2_1/c$, a = 13.536(3), b = 14.391(3), c = 7.159(1) Å, β = 98.69(1)°, Z = 4, V = 1378.5 Å^3, μ = 0.52 cm^{-1}, $F(000)$ = 576, MW = 276.1 g mol^{-1}, D_c = 1.33 g cm^{-3}, D_{obs} = 1.32 g cm^{-3}.

Crystals of $C_{18}H_{14}O_4$ (**2**) cocrystallize with one acetic acid molecule and are triclinic, space group $P\bar{1}$, a = 8.881(3), b = 9.786(1), c = 11.355(3) Å, α = 85.56(1), β = 88.76(2), γ = 69.46(2)°, Z = 2, V = 921.4 Å^3, μ = 0.57 cm^{-1}, $F(000)$ = 372, MW = 354.4 g mol^{-1}, D_c = 1.28 g cm^{-3}, D_{obs} = 1.27 g cm^{-3}.

Diffraction data were collected at room temperature with an Enraf Nonius CAD4 diffractometer using graphite monochromated MoKα (λ = 0.71073 Å) radiation. For both crystals an ω:2θ scan method was employed, where the ω angle changed as (0.60 + 0.34 tan θ)° for **1** and (0.65 + 0.34 tan θ)° for **2**. For **1**, 4154 reflections with h(0:19), k(0:20), l(0:10) and 3 ≤ θ ≤ 30° were measured, and for **2** 4022 reflections with h(0:11), k(−12:12), l(−14:14) and 3 ≤ θ ≤ 27°. The horizontal aperture was fixed at 1.3 mm and the vertical slit at 4 mm. Variable scan speed was used, with a maximum of 5.49° min^{-1} and a minimum corresponding to 50 s reflection^{-1}. Data were corrected for Lorentz and polarization effects, and for decay (13%) in the case of **2**. Both structures were determined by direct methods (MULTAN80) (18) and the non-hydrogen atoms were refined with anisotropic thermal parameters (SHELX76) (19). Compound **2** cocrystallizes with one acetic acid solvent molecule. All hydrogen atoms for **1** were refined in experimentally determined positions with a common isotropic thermal parameter that refined to U = 0.071(2) Å^2. The hydrogen atoms of the methyl group of the solvent molecule in **2** were placed in calculated positions (C—H = 1.08 Å, H—C—H = 109.5°) and refined as a rigid group. Distance constraints (r(O—H) = 0.9 Å, r(CO..H) = 2.4 Å, σ_r = 0.05 Å) were applied to HIB and HS. The common isotropic temperature factor refined to U = 0.126(6) Å. All other hydrogen atoms in (**2**) were refined in experimentally determined positions.[3]

The final residuals were R_w = 0.029 and R = 0.055 using $\sigma^{-2}(F)$ weights and 1981 reflections ($I > 2\sigma(I)$) for 227 parameters for **1**,

[3]Tables of fractional atomic coordinates, bond lengths, bond angles, anisotropic temperature parameters, and structure factors have been deposited as supplementary material, and may be purchased from the Depository of Unpublished Data, CISTI, National Research Council of Canada, Ottawa, Ont., Canada K1A 0S2.

The tables of atomic coordinates, bond lengths, and bond angles have also been deposited with the Cambridge Crystallographic Data Centre, and can be obtained on request from The Director, Cambridge Crystallographic Data Centre, University Chemical Laboratory, Lensfield Road, Cambridge CB2 1EW, UK.

Can. J. Chem. Downloaded from www.nrcresearchpress.com by 88.85.125.76 on 09/07/12
For personal use only.

and $R_w = 0.048$, $R = 0.081$ for 2222 reflections ($I > \sigma(I)$) and 284 variables for **2**, using $\sigma^{-2}(F)$ weights (19). The maximum shift/esd for **1** was <0.2 Å and <0.34 Å for **2**, and the residual electron density ranges are (−0.24, 0.18) and (−0.26, 0.28) e Å^{-3} for **1** and **2**, respectively.

Each molecule of **2** is involved in four hydrogen bonds to molecules at $(-x, -y, 2 - z)$ acting as both a donor (O1A...OS1 = 2.620 Å and O1B...O6 = 2.606 Å) and an acceptor (O6...O1B = 2.606 Å and O7...OS2 = 2.672 Å).

1. H. Stobbe. Ann. **380**, 1 (1911).
2. V. Ramamurthy and K. Venkatesan. Chem. Rev. **87**, 433 (1987).
3. J. Andersson. Acta Chem. Scand. **B31**, 340 (1977).
4. A. S. R. Anjaneyum, P. Raghu, K. U. Ramakrishna Rao, Ch. V. M. Sastry, O. Umasundari, and P. Satyanarayana. Curr. Sci. **53**, 239 (1984).
5. W. S. Johnson, A. L. McCloskey, and D. A. Dunnigan. J. Am. Chem. Soc. **72**, 514 (1950).
6. R. J. Hart and H. G. Heller. J. Chem. Soc. Perkin Trans. 1, 1321 (1972); H. G. Heller, S. Oliver, and M. Shawe. J. Chem. Soc. Perkin Trans. 1, 154 (1979).
7. M. D. Cohen, H. W. Kaufman, D. Sinnreich, and G. M. J. Schmidt. J. Chem. Soc. (B), 1035 (1970).
8. M. J. S. Dewar and J. J. P. Stewart. Quantum Chemistry Program Exchange, **506** (1986).
9. R. F. Bryan and D. P. Freyberg. J. Chem. Soc. Perkin Trans. 2, 1835 (1975).
10. J. Méndez and M. I. Lojo. Microchem. J. **13**, 232 (1968).
11. J. C. A. Boeyens, L. Denner, and G. W. Perold. S. Afr. J. Chem. **40**, 44 (1987).
12. R. C. Weast (*Editor*). Handbook of chemistry and physics. 53rd ed. CRC Press Inc., Boca Raton, FL. 1972. C-243.
13. G. C. Levy, R. L. Lichter, and G. L. Nelson. Carbon-13 nuclear magnetic resonance spectroscopy. Wiley–Interscience, New York, NY. 1980. p. 83.
14. J. B. Stothers. Carbon-13 NMR spectroscopy. Academic Press, New York, NY. 1972. p. 185.
15. G. E. Maciel. *In* Topics in carbon-13 NMR spectroscopy. *Edited by* G. C. Levy. Wiley–Interscience, New York, NY. 1974. p. 61.
16. I. Bangov. Izv. Khim. **17**, 459 (1984); Chem. Abstr. **104**, 88029 (1986).
17. O. Crescente, H. G. Heller, and S. Oliver. J. Chem. Soc. Perkin Trans. 2, 150 (1979).
18. P. Main, S. J. Fiske, S. E. Hull, L. Lessinger, G. Germain, J. P. Declercq, and M. M. Woolfson. MULTAN80, a system of computer programs for the automatic solution of structures from X-ray diffraction data. Universities of York, England, and Louvain, Belgium. 1980.
19. G. M. Sheldrick. SHELX76, a program for crystal structure determination. University of Cambridge, England. 1976.

Can. J. Chem. Downloaded from www.nrcresearchpress.com by 88.85.125.76 on 09/07/12
For personal use only.

The photoelectron spectra and electronic structure of 2-carbonyl furans

DIETER KLAPSTEIN,[1] CHARLES D. MACPHERSON, AND ROBERT T. O'BRIEN
Department of Chemistry, St. Francis Xavier University, Antigonish, N.S., Canada B2G 1C0

Received November 23, 1989

DIETER KLAPSTEIN, CHARLES D. MACPHERSON, and ROBERT T. O'BRIEN. Can. J. Chem. **68**, 747 (1990).

The He(I), $\lambda = 58.4$ nm, photoelectron spectra of a series of six 2-carbonyl furans and 2-furonitrile have been measured in the gas phase. The low ionization energy bands are assigned to photoionizations from π orbitals of the furan ring, orbitals localized on the carbonyl group, and orbitals of the carbonyl substituents. Changes in ionization energies within the series can be rationalized in terms of the relative conjugative and inductive effects of the substituents. Substituent inductive effects were found to be dominant. The relatively broad vibrational fine structure on the low IE bands of the carbonyl furans could result from the presence of rotational isomers of the species.

Key words: photoelectron spectra, 2-carbonyl furans, molecular orbitals.

DIETER KLAPSTEIN, CHARLES D. MACPHERSON et ROBERT T. O'BRIEN. Can. J. Chem. **68**, 747 (1990).

Opérant en phase gazeuse, on a mesuré les spectres photo-électroniques (He(I), $\lambda = 58{,}4$ nm) d'une série de six 2-carbonyl furanes et de 2-furonitrile. On a attribué les bandes aux basses énergies d'ionisation aux photo-ionisations des orbitales-π du noyau furane, des orbitales localisées sur le groupement carbonyle et des orbitales des substituants du groupement carbonyle. On peut rationaliser les changements observés dans les énergies d'ionisation des composés formant la série en fonction des effets relatifs de conjugaison et d'induction des substituants. On a trouvé que les effets inductifs des substituants prédominent. On a observé une structure fine vibrationnelle relativement importante dans les bandes de basse énergie d'ionisation des carbonyl furanes; ces observations pourraient être attribuées à la presence d'isomères de rotation des espèces.

Mots clés : spectres photo-électroniques, 2-carbonyl furanes, orbitales moléculaires.

[Traduit par la revue]

Introduction

The five-membered furan ring is an important building block in organic and natural product chemistry. As well, furan itself is a model compound of heteroaromatic systems. In contrast to benzene, the π-electron distribution over the furan ring is not homogeneous due to the presence of the oxygen atom. The higher nuclear charge of the heteroatom and the concomitant higher electron density results in the appreciable dipole moment of furan and the inequality of the 2- and 3-positions towards electrophilic substitution (for a review, see ref. 1).

A method for obtaining information on the electronic structure of molecules is photoelectron spectroscopy (PES), wherein monochromatic photons are used to photoeject electrons from the occupied molecular orbitals, followed by kinetic energy analysis. Within the approximation of Koopmans' Theorem, equating the experimental vertical ionization energy (IE) with the negative of the orbital eigenvalue, the PE spectrum then gives an energy mapping of the occupied molecular orbitals. While the electronic structure of furan itself has been the subject of several PES investigations (2–7), very little has been done on substituted furans (8). Extending our earlier work on the electronic structure of carbonyl ethynes (9), propynes (10), and ethenes (11), this work presents the photoelectron spectra of a series of substituted 2-carbonyl furans **1** with X = H, F, Cl, Br, OH, and CH_3, and 2-furonitrile, and their interpretation to yield information on the electronic structures of the species.

1

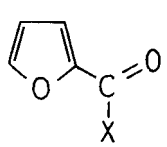

Experimental

The gas-phase photoelectron spectra were obtained with an instrument incorporating a high-voltage helium discharge lamp and a 127° cylindrical sector electrostatic deflection analyzer. Data acquisition and spectral scanning were handled by a Nicolet 1170 signal averager/Apple IIe microcomputer data system. The spectral ionization energies were calibrated with nitrogen, argon, or iodomethane as internal calibrants; the ionization energies for well-resolved bands have an uncertainty of ± 0.02 eV while for broad maxima it is ± 0.1 eV.

Commercially available (Aldrich) samples of 2-furaldehyde, 2-furoic acid, and 2-furonitrile were used. 2-Furoyl chloride (Aldrich) was used following vacuum distillation. 2-Furoyl fluoride was prepared by reacting the corresponding chloride with spray-dried potassium fluoride (12), distilling off the resulting acid fluoride, and purifying by fractional distillation. 2-Furoyl bromide was prepared by reacting the acid with thionyl bromide and hexamethylphosphoramide (13) (HMPA) at −40°C, followed by vacuum distillation. In all cases the samples were checked by infrared and ^{13}C NMR spectroscopies.

Semi-empirical MO calculations were carried out using the MNDO method (14) adapted for use on a PC, and by the HAM/3 method (15) on a VAX 11/780 minicomputer. As few structural parameters are available for this series of molecules, the full geometry optimization of the MNDO program was used. The derived geometries were then used for the HAM/3 calculation. The MNDO program is not parameterized for Br, while the HAM/3 program is not parameterized for Cl or Br.

Results and discussion

The He(I) photoelectron spectra are shown on a common energy scale in Figs. 1 and 2. Also included in Fig. 1 is the spectrum of furan, which is important to the assignment of the spectra of this work. The experimental ionization energies (IEs) and observed vibrational structure are summarized in Tables 1–7. The spectrum of 2-furaldehyde has been presented elsewhere (16) but without discussion; the ring π-orbital ionization energies of 2-furoic acid and 2-furonitrile have also been reported previously (8). The results of this work are in agreement with these earlier reports.

The C_s symmetry of these planar species allows orbital classifications of only in-plane (a') or out-of-plane (a''). However, in this analysis a composite molecule approach will be taken: the occupied molecular orbitals will be assumed to be localized to a large degree on specific atoms or functional groups and will be described as such. This will allow trends in

[1]Author to whom correspondence may be addressed.

Can. J. Chem. Downloaded from www.nrcresearchpress.com by 91.144.44.67 on 09/07/12
For personal use only.

Can. J. Chem. Downloaded from www.nrcresearchpress.com by 91.144.44.67 on 09/07/12
For personal use only.

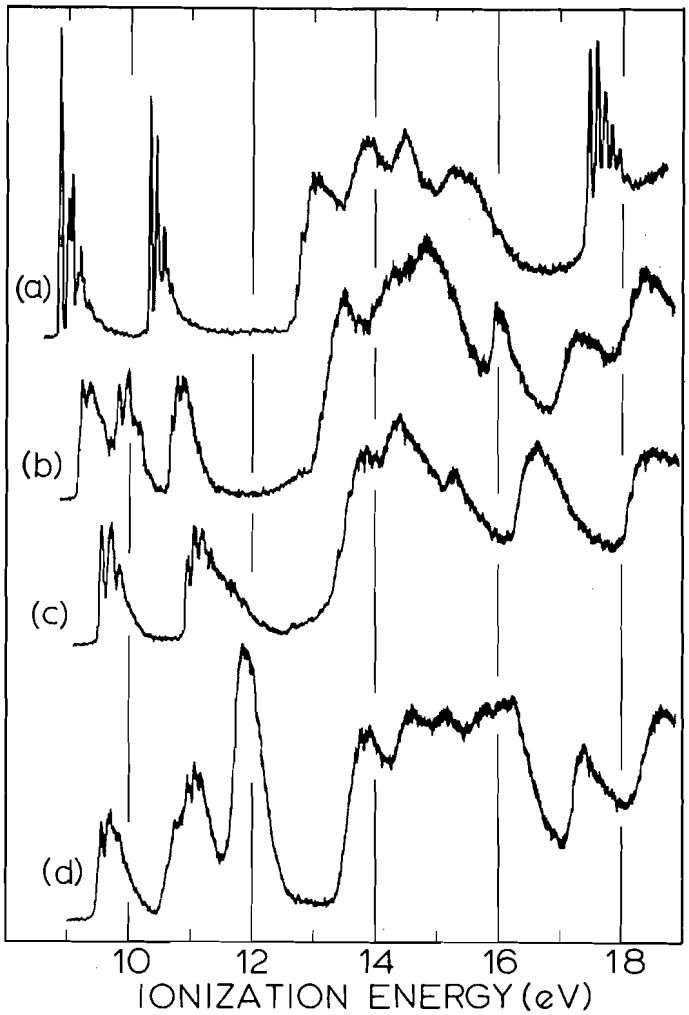

FIG. 1. The He(I) photoelectron spectra of (a) furan, (b) 2-furaldehyde, (c) 2-furoyl fluoride, and (d) 2-furoyl chloride.

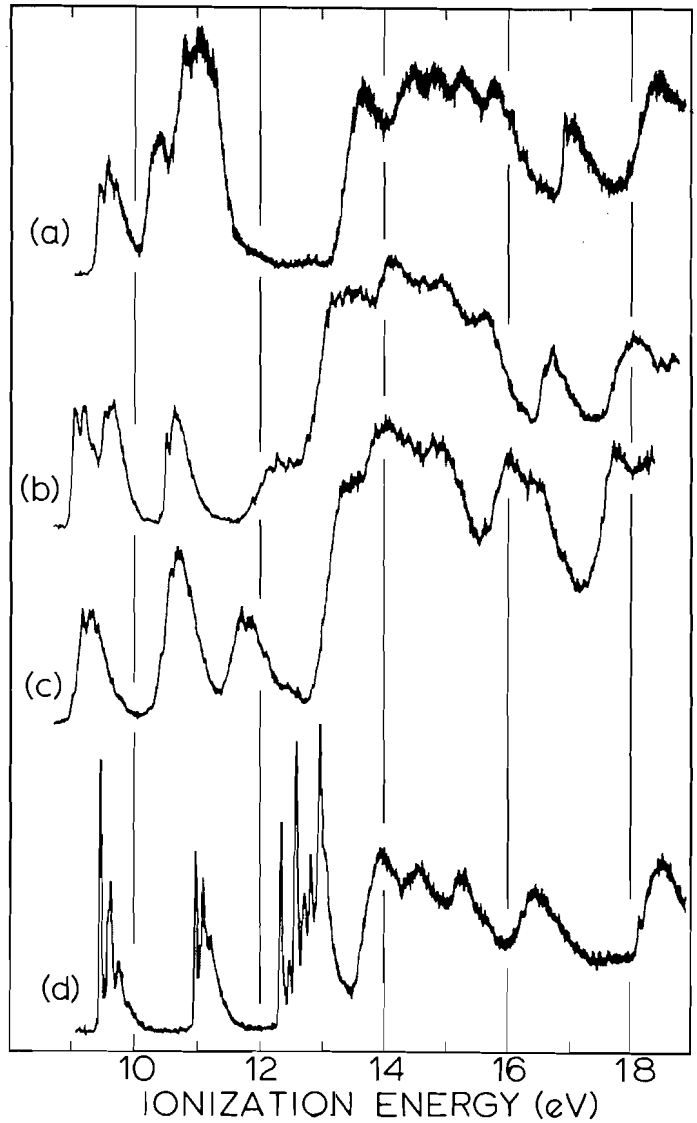

FIG. 2. The He(I) photoelectron spectra of (a) 2-furoyl bromide, (b) 2-acetyl furan, (c) 2-furoic acid, and (d) 2-furonitrile.

localized orbital energy changes within the series to be discussed and also allow comparison with the appropriate (π) orbital energies of furan itself.

Furan

Furan has been the subject of many studies with regards to its electronic structure. Of special interest have been the relative energies of the three occupied π molecular orbitals of the aromatic ring. These molecular orbitals (17) can be depicted by the appropriate linear combinations of atomic orbitals, the symmetries in the point group C_{2v} being given in parentheses:

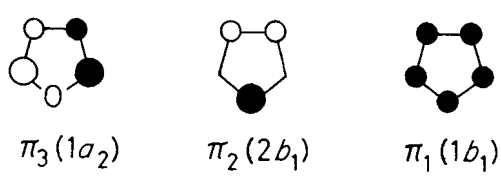

The photoelectron spectrum shows that the first two ionization events give rise to sharply structured bands at 8.87 and 10.38 eV ionization energy. These are undoubtedly due to electron photoejection from the highest two occupied orbitals π_3 and π_2, respectively (2, 3). The assignment of the π_1 band is, however, less certain. Early workers (2–4) assigned the well-structured band at 17.77 eV to ionization from π_1, but subsequent molecular orbital calculations (5, 18) seem to indicate it should be found in a congested part of the spectrum at about 15.5 eV. This seems to be confirmed by a comparison of band intensity ratios of the spectra taken with He(I), 21.22 eV, and He(II), 40.8 eV, photon sources (7).

2-Furaldehyde

Substitution of an aldehyde functional group at the 2-position of the ring gives 2-furaldehyde, the PE spectrum of which is shown in Fig. 1. The aldehyde functionality has, in general, two characteristic photoelectron bands (19): ionization from the carbonyl oxygen in-plane lone-pair orbital n'_O in the region 9.5–11 eV, while the π_{CO} band is found in the region 14–15 eV. Thus for the spectrum of 2-furaldehyde, the low ionization energy region shows three distinct bands corresponding to ionization from π_3 and π_2, still mainly ring orbitals, and n'_O.

The ordering of the first three bands can be rationalized by considering the photoelectron results for similar systems. The doubly degenerate HOMO of benzene, $1e_{1g}$, has its degeneracy lifted and the two orbitals are stabilized by about 0.45 eV in benzaldehyde (20), relative to benzene. Applying this same magnitude of stabilization to the 8.87 and 10.38 eV bands of

TABLE 1. Photoelectron and MO calculation data for 2-furaldehyde

IE[a] (eV)	Vibrational structure (cm^{-1})	Assignment	MNDO	HAM/3
9.22	830, 1430	π_3	9.56	9.62
9.94(9.80)	1120	n'_O	11.08	9.36
10.76(10.67)	770	π_2	10.73	10.85
				12.96 $a''(\pi_{CO})$
13.5			13.89	13.29
			14.08 $a''(\pi_{CO})$	
14.3			14.45	14.24
14.8			14.73	14.67
				14.83
15.97			16.08 $a''(\pi_1)$	15.76 $a''(\pi_1)$
			16.42	15.82
17.2			16.57	16.82
				17.86
18.4			18.27	

[a]Vertical values, adiabatic values in parentheses.

furan leads to the prediction that the ring π orbitals of furaldehyde should give rise to bands at about 9.3 and 10.8 eV. This is in good agreement with the observed positions of the first and third bands in the furaldehyde spectrum, 9.22 and 10.76 eV, which are thus assigned to ionizations from the ring orbitals π_3 and π_2, respectively. The stabilization of these orbitals, relative to furan, reflects the inductive effect of the carbonyl group. The second band of the spectrum, 9.94 eV, is assigned to ionization from the in-plane orbital centered mainly on the carbonyl oxygen ("lone pair", n'_O). The corresponding band of acetaldehyde is found at 10.26 eV (19), that of propenal at 10.11 eV (11), that of propynal at 10.70 eV (9), and that of benzaldehyde at 9.69 eV (20).

An alternative scheme would have the band assignments, in order of increasing ionization energy, $n'_O < \pi_3 < \pi_2$. This ordering is not favoured for several reasons. Firstly, it would give the n'_O orbital an anomalously low ionization energy relative to benzaldehyde and other substituted carbonyl compounds. Secondly, substitution at the carbonyl carbon by halides and hydroxyl produces much greater IE shifts for the second band than for the first and third (*vide infra*); the n'_O orbital IE should be much more sensitive to these electronegative substituents than the more delocalized ring π orbitals. Thirdly, if the second and third bands were both assigned as ring π-orbital bands, the small energy separation, 0.8 eV, does not compare favourably with that of other monosubstituted furans (8) where the separation is ca. 1.5 eV. The preferred assignment order is $\pi_3 < n'_O < \pi_2$. This ordering, at first glance, is at odds with the results from the ultraviolet absorption spectrum of 2-furaldehyde (21), in which the singlet–singlet $\pi^* \leftarrow n$ absorption band is at lower energy than the $\pi^* \leftarrow \pi$ band. This would imply $n'_O < \pi_3$ in terms of ionization energy. However, a CNDO MO treatment (22) has shown that the relative energies of the $\pi^* \leftarrow n$ and $\pi^* \leftarrow \pi$ transitions are a result of configuration interaction in the excited state. As well, the CNDO calculation (22) of the neutral ground state gave the ordering of the orbital eigenvalues as $\pi_3 < n'_O < \pi_2$, in agreement with this work.

The carbonyl π orbital is expected to give rise to a band at about 13–14 eV, a heavily congested part of the spectrum. However, that the ring π orbitals π_3 and π_2 are both shifted to higher ionization energy by about the same amount, relative to furan, implies that any conjugation between π_{CO} and π_3 and π_2 (all of a'' symmetry in C_s) is quite small on this energy scale.

The MO calculation results are listed in Table 1. Both the HAM/3 and MNDO methods predict IEs in good agreement with the experimental vertical IEs for the out-of-plane orbitals. The calculations predict very little interaction between the ring π orbitals and the carbonyl π system. The atomic orbital coefficients also show that π_3, π_2, and π_1 of substituted furans correlate well with the $1a_2$, $2b_1$, and $1b_1$ orbitals, respectively, of furan itself. The MO calculations do not predict the carbonyl oxygen lone pair (n'_O) IE very well: the MNDO value is about 1 eV too high, while the HAM/3 value is 0.6 eV too low.

2-Furoyl fluoride

Substitution of fluorine for hydrogen at the carbonyl position introduces a heteroatom that is able to cause significant changes in the orbital energies, on account of both its high electronegativity and the favourable overlap of the fluorine orbitals with other orbitals. The low IE region of the spectrum shows only two distinct bands, but the second is probably due to two separate bands overlapping. The first band, at 9.72 eV, and the maximum of the second, at 11.10 eV, are assigned to ionizations from π_3 and π_2, respectively. This energy separation is again characteristic of substituted furans (8). The shift towards higher IEs relative to furan is indicative of the strong influence of the electronegative fluorine atom. This influence is shown even better by the shift of the n'_O band, assigned as the broad maximum at about 11.6 eV, a shift of 1.7 eV from its position in the spectrum of 2-furaldehyde. Although heavily overlapped by the π_2 band, the n'_O band probably has quite a broad profile; for acyl fluorides the n'_O description of this orbital loses some of its meaning since the MO calculations show that the in-plane carbonyl oxygen and fluorine orbitals mix to a considerable extent. This mixing in of some fluorine AO character also tends to stabilize the MO and gives the band a broader shape (more bonding character). The MO calculations, Table 2, again predict IEs in agreement with the experimental values for π_3 and π_2 but not for n'_O, although the inductive effect of fluorine, relative to the aldehyde, is clearly predicted.

2-Furoyl chloride

The spectrum is dominated by the intense band at 11.70 eV

Can. J. Chem. Downloaded from www.nrcresearchpress.com by 91.144.44.67 on 09/07/12
For personal use only.

TABLE 2. Photoelectron and MO calculation data for 2-furoyl fluoride

IE[a] (eV)	Vibrational structure (cm^{-1})	Assignment	MNDO	HAM/3
9.72(9.56)	1290	π_3	9.99	9.83
11.10	970	π_2	11.10	11.03
11.6		n'_O	12.21	10.31
13.8			13.60 $a''(\pi_{CO})$	12.65(π_{CO})
				13.52
14.3			14.30	14.14
			14.81	14.95
15.3			15.67	15.08
			16.26 $a''(\pi_1)$	15.79(π_1)
16.6			17.47	15.83(n'_F)
			17.62 $a''(\pi_{COF})$	16.67
18.5			17.90	16.86(n''_F)
				17.44
				18.86

[a]Vertical values, adiabatic values in parentheses.

TABLE 3. Photoelectron and MO calculation data for 2-furoyl chloride

IE[a] (eV)	Vibrational structure (cm^{-1})	Assignment	MNDO
9.56(9.44)	1100	π_3	10.00
10.66		n'_O	11.86
10.93(10.82)	880	π_2	11.09
11.70		n'_{Cl}, n''_{Cl}	12.87 $a''(n_{Cl})$
			12.78 $a''(n_{Cl})$
13.7			
14.4			14.30
			14.80
15.0			15.19
15.6			15.34 $a''(\pi_{CO})$
16.2			16.64 $a''(\pi_1)$
17.2			17.06
			17.30
18.3			18.77

[a]Vertical values, adiabatic values in parentheses.

TABLE 4. Photoelectron data for 2-furoyl bromide

IE[a] (eV)	Vibrational structure (cm^{-1})	Assignment
9.56(9.42)	1080	π_3
10.36		n'_O
10.78		π_2
11.04		n'_{Br}, n''_{Br}
11.26		
13.7		
14.4		
14.8		
15.7		
17.0		
18.4		

[a]Vertical values, adiabatic values in parentheses.

due to ionization from the in- and out-of-plane chlorine lone-pair orbitals. These orbitals are not degenerate by symmetry but their energies are rather similar in this case, interaction of the n''_{Cl} orbital with the other out-of-plane orbitals being small. The broadness of the band is due to the slight inequivalency of the orbitals.

Ionization from the ring orbitals π_3 and π_2 gives rise to the bands at 9.56 and 10.93 eV, respectively. These are intermediate to the corresponding values for the aldehyde and the acyl fluoride, reflecting the relative electronegativities of the carbonyl substituents. The n'_O IE is much more sensitive to the carbonyl substituent than π_3 and π_2, the n'_O band shifting to lower IE by about 0.9 eV whereas π_3 and π_2 shift by less than 0.2 eV on going to the chloride from the fluoride.

2-Furoyl bromide

The lowest IE band of the spectrum is clearly due to ionization from the π_3 ring orbital. The IE is essentially unchanged relative to that of the chloride, any change in heteroatom electronegativity having a negligible effect on the ring π electrons. With this in mind the π_2-orbital band is assigned to the maximum at 10.78 eV (cf. 10.93 eV for the chloride). There is a slight destabilization which might result from interaction of π_2 with n''_{Br}, which is energetically very close. Such an interaction would also tend to stabilize n''_{Br} relative to n'_{Br}; the former is assigned to the band at 11.26 eV while the 11.04 eV maximum is assigned as n'_{Br}. The remaining band in the low IE region, at 10.36 eV, is assigned to the carbonyl n'_O orbital.

2-Acetyl furan

With reference to the molecules discussed thus far, 2-acetyl furan represents a furoyl unit with an electron-donating group attached at the carbonyl site. This results in the photoelectron bands being generally shifted to lower IEs relative to the aldehyde and the furoyl halides.

The π_3 and π_2 ring orbital bands are found at 9.02 and 10.61 eV, respectively, a modest shift of 0.2 eV or less from the corresponding values for the aldehyde. However, the carbonyl oxygen lone-pair band is more strongly affected, the n'_O band at 9.64 eV being 0.3 eV lower ionization energy than for the aldehyde. These shifts are also predicted by the MO calculations, Table 5, although the absolute value of the n'_O ionization energy does not agree well with either calculation. The broad band observed at 12.27 eV is associated with an out-of-plane

Can. J. Chem. Downloaded from www.nrcresearchpress.com by 91.144.44.67 on 09/07/12
For personal use only.

TABLE 5. Photoelectron and MO calculation data for 2-acetyl furan

IE[a] (eV)	Vibrational structure (cm^{-1})	Assignment	MNDO	HAM/3
9.02	1210	π_3	9.50	9.27
9.64(9.50)	1130	n'_O	10.94	8.79
10.61(10.49)	850	π_2	10.67	10.59
12.27		π_{CH_3}	13.27 $a''(\pi_{CH_3} - \pi_{CO})$	11.46 a''
				12.48
13.4			13.82	13.09
			13.96	13.46
14.1				14.19 a''
			14.39	14.39
14.9			14.80	14.69
15.6			15.08 $a''(\pi_{CO} + \pi_{CH_3})$	14.89
			15.77	15.54 a''
16.7			16.09 $a''(\pi_1)$	16.49
			16.63	17.17
18.0			18.06	

[a]Vertical values, adiabatic values in parentheses.

TABLE 6. Photoelectron and MO calculation data for 2-furoic acid

IE[a] (eV)	Vibrational structure (cm^{-1})	Assignment	MNDO	HAM/3
9.32(9.17)	1300, 900	π_3	9.66	9.47 a''
10.74(10.57)	1020	n'_O, π_2	10.78 $a''(\pi_2)$	10.68 a''
			(11.61 $a'(n'_O)$	9.99 $a'(n'_O)$
11.90(11.67)	1700	n''_O	12.27 $a''(n''_O)$	11.22 $a''(n''_O)$
13.5				13.07
			13.93	13.38
14.0			14.37	14.49 a''
14.4			14.48	14.62
				14.71
14.9			15.30 $a''(\pi_{CO} - \pi_1)$	15.16
			15.37	15.77 a''
16.0			16.36 $a''(\pi_1 + \pi_{CO})$	16.12
				16.90
17.8			17.99	18.04

[a]Vertical values, adiabatic values in parentheses.

MO, which the calculations predict to be a combination of the π''_{CH_3} and π''_{CO} orbitals.

2-Furoic acid

The carboxylic acid is predicted to have four bands with IEs less than 13 eV, π_3, π_2, n'_O, and n''_O, the last one being centered on the hydroxyl oxygen. The spectrum shows three distinct bands in this region but the intensity of the second band leads to the conclusion that it is composed of two overlapping bands. The first band, at 9.32 eV, is due to ionization from the ring π_3 orbital. The second, intense, band at 10.74 eV is due to overlap of the ring π_2-orbital band (again a $\pi_2 - \pi_3$ band separation of about 1.5 eV) and the n'_O band of the carbonyl group. The latter band is shifted to higher IE relative to the aldehyde and methyl ketone, but not as much as for the acyl fluoride. This trend nicely reflects the relative electron-withdrawing abilities of the carbonyl substituents. The out-of-plane lone-pair orbital on the hydroxyl oxygen, n''_O, gives rise to the band at 11.70 eV. Conjugation of this a'' orbital with the other a'' orbitals on the furan ring (π_3, π_2) appears to be small since (i) the π_3, π_2 band separation is not noticeably different than for the other members of this series, and (ii) the n''_O band position is not substantially changed from that of (unconjugated) carboxylic acids (ref. 19, pp. 164–165): the n''_O band of acetic acid is found at 12.05 eV and for propionic acid at 12.04 eV. The MO calculations, Table 6, predict the a'' orbital IEs quite well and reinforce the preceding arguments. The IE of the in-plane n'_O orbital of the carbonyl group is again distinctly different from the predicted values: the MNDO value is 0.9 eV too high while the HAM/3 result is 0.7 eV too low.

2-Furonitrile

The nitrile substituent on the furan ring provides an interesting contrast to the carbonyl substituent in terms of the photoelectron spectra. The -CN group has both in- and out-of-plane π orbitals, as well as an in-plane lone pair centered on the nitrogen atom. The nitrogen lone pair has a substantially higher IE than the carbonyl lone pair, usually rationalized in terms of the larger *s*-atomic character of the nitrogen pair (*sp* "hybridization" versus sp^2). Thus the two lowest IE bands, at

Can. J. Chem. Downloaded from www.nrcresearchpress.com by 91.144.44.67 on 09/07/12
For personal use only.

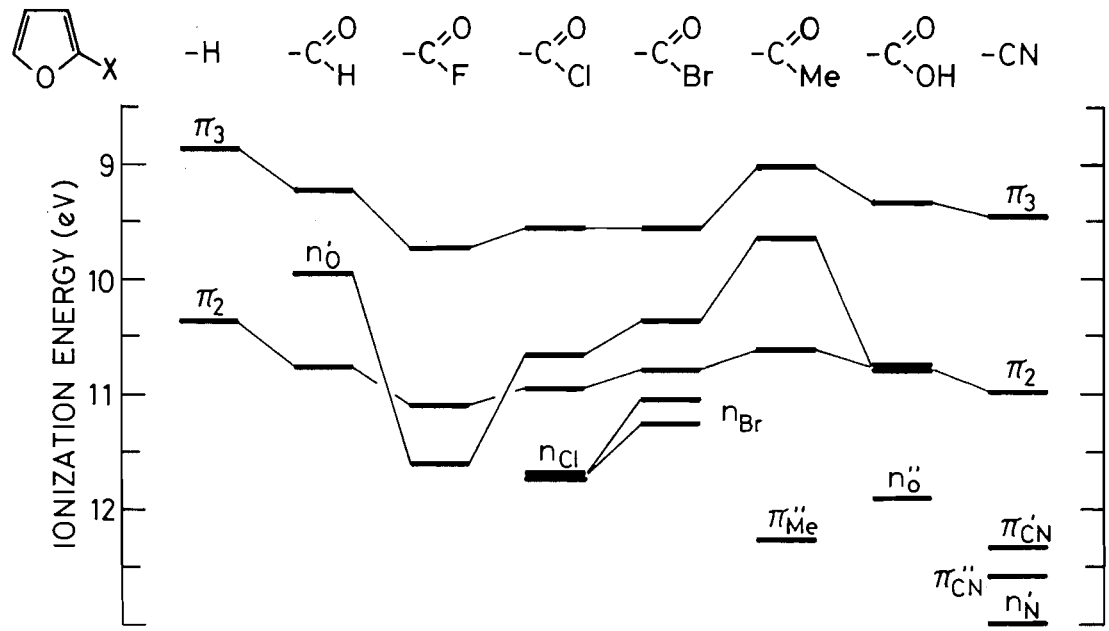

FIG. 3. Orbital ionization energy correlation diagram.

TABLE 7. Photoelectron and MO calculation data for 2-furonitrile

IE[a] (eV)	Vibrational structure (cm^{-1})	Assignment	MNDO	HAM/3
9.45	1170, 1440	π_3	9.64	9.51
10.98	990, 580	π_2	10.88	10.84
12.35	1050	π'_{CN}	13.16	12.27
12.58	1290	π''_{CN}	13.69	12.46
12.98		n'_{CN}	14.19	12.65
				13.48
13.9				
14.6			14.36	14.80
			14.61	14.89
15.3			15.48	
16.5			16.30 $a''(\pi_1)$	15.86 (π_1)
				16.50
18.5			17.42	17.33

[a]Vertical values.

9.45 and 10.98 eV, are assigned as the ring π_3- and π_2-orbital bands, respectively. The π_3 and π_2 IEs are predicted well by the MO calculations, Table 7. The group of bands in the region of 12–14 eV ionization energy belong to the nitrile orbitals. For simple alkyl nitriles (ref. 19, pp. 178–182) the ordering of the band IEs is π'_{CN}, $\pi''_{CN} < n'_N$; thus the high IE band in this group, at 12.98 eV, is assigned as n'_N. The corresponding bands for acetonitrile and propionitrile are found at 13.14 and 12.83 eV, respectively (ref. 19, pp. 178–182). The nitrile π-orbital bands here are found at 12.35 eV (π'_{CN}) and 12.58 eV (π''_{CN}). The splitting of 0.23 eV is due to the stabilization of π''_{CN} by interaction with the lower IE π_3 ad π_2 orbitals and (or) destabilization of π'_{CN} by interaction with the higher IE, in-plane, σ-type orbitals. The ordering and energies of the nitrile group orbitals are confirmed by the MO calculations.

General trends

Comparison of the spectra and band assignments to ionizations from specific orbitals brings out several trends. Figure 3 shows the experimental ionization energies of the lower IE bands. Within the approximation of Koopmans' Theorem (23), equating the experimental vertical IE with the negative of the orbital eigenvalue, the correlation diagram shows how the energies of the higher, occupied, orbitals change as a function of ring or carbonyl substituent.

For all members of this series the HOMO is a furan ring π orbital correlating with the π_3 orbital of furan. The ionization energy of the HOMO varies slightly with the electron-withdrawing ability of the substituent. The penultimate occupied out-of-plane orbital has also been identified for all species and correlates with the π_2 orbital of furan. The energy separation of π_3 and π_2 of furan has been conserved in the substituted compounds. This implies that interactions between any a'' orbitals centered on the substituents and the ring a'' orbitals are rather small, on the photoelectron energy scale; otherwise one might expect the π_3, π_2 separation to vary as a result of unequal interactions with π_3 and π_2 due to energy or proximity considerations. This is borne out by the MNDO and HAM/3 MO calculations, which predict the π_3 and π_2 orbital ionization energies quite well and also show, by way of the atomic orbital coefficients, that the source orbitals are essentially the same as those of furan itself in terms of nodal characteristics. However, this does not imply that conjugation of the out-of-plane orbitals is negligible, only that the observed π_3, π_2 band separation does not seem to reflect them. This could be due to the delocalization of the ring electrons. That conjugation of the out-of-plane orbitals can be measured by PES is shown by the splitting of the π_{CN} bands of 2-furonitrile. Unfortunately, such an indicator is not available for the carbonyl compounds.

The substituent inductive effect arguments are further exemplified by the energies of the n'_O orbitals of the carbonyl compounds, which show large variations in accord with the electronegativities of the carbonyl substituents, e.g., F versus H. The magnitudes of the n'_O band shifts parallel those found for other substituted carbonyls (9–11).

For carbonyl substituents with loosely bound lone pairs, the low IE regions of the spectra show the corresponding bands. Interaction of the lone-pair orbitals with the ring π orbitals

Can. J. Chem. Downloaded from www.nrcresearchpress.com by 91.144.44.67 on 09/07/12
For personal use only.

Can. J. Chem. Downloaded from www.nrcresearchpress.com by 91.144.44.67 on 09/07/12
For personal use only.

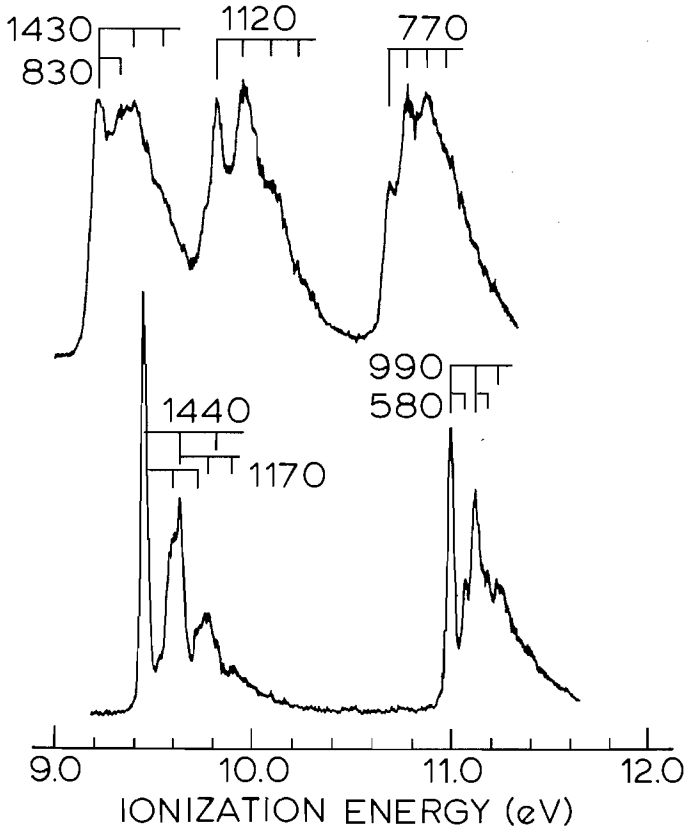

FIG. 4. Vibrational structure on the low ionization energy bands of 2-furaldehyde (top) and 2-furonitrile (bottom). Vibrational intervals are in wavenumbers.

is small. For similarly substituted acetylenic and ethylenic carbonyl compounds (9–11) the strongest interaction of the substituent lone-pair orbitals was found to be with the carbonyl π system. Unfortunately in this series the carbonyl π-orbital bands are found in the heavily congested part of the spectra and could not be identified. However, comparison of the spectra of the furan carbonyl species with that of furonitrile suggests that for the carbonyl species the π_{CO} band is one of the bands in the region of 13–14 eV ionization energy.

The semiempirical MO calculations predict ionization energies that, in general, agree well with the experimental values where the PES bands are resolvable. Within the series of compounds the calculations confirm that the effect of the carbonyl group and its substituents on the ring π orbitals is mainly of an inductive nature, and justify our interpretation of the photoelectron spectra in terms of orbitals localized on the ring and on the carbonyl group. However, neither MO method satisfactorily predicts the ionization energies of the in-plane lone-pair orbital (n'_O) of the carbonyl oxygen or the lone-pair orbitals of other heteroatom substituents. The cause is undoubtedly the choice of initial atomic parameters used in the calculations. This series of molecules could be treated by more rigorous MO methods to investigate these problems. Nevertheless, the calculations do correctly predict the relative changes in the n'_O IE as a function of carbonyl substituent changes. It is also of interest that the MO calculations predict the most tightly bound π orbital of the furan ring, π_1, to have IEs in the range 15.5–16.5 eV, in agreement with previous arguments for furan itself (5, 7, 18).

The experimental ionization energies give directly the energies of the doublet ground and excited states of the molecular radical cations. These, along with the observed vibrational structure, may be used in identifying and characterizing the electronic states of the molecular ions.

The lower IE bands of all species show some vibrational fine structure (Tables 1–7). The π_3 bands exhibit cationic vibrational intervals in the range 1000–1400 cm^{-1}, probably excitation of the cationic ring $\nu_{C=C}$ mode (1486 cm^{-1} in the neutral ground state of furan). The π_2 bands usually exhibit a smaller vibrational interval and a broader Franck–Condon envelope, both in accord with the increased bonding character of π_2 relative to π_3. The vibrational structure of the furan bands has already been discussed elsewhere (2, 3). The structures of the 2-furaldehyde and 2-furonitrile bands are shown in Fig. 4. Assignment of the vibrational intervals to specific cationic modes is difficult due to the large number of vibrational modes possible and the lack of specific experimental vibrational data. The π_3 band shows a progression of 1440 cm^{-1}, probably the ring C=C stretch corresponding to the 1486 cm^{-1} mode of furan. The π_2 band shows progressions of 1000 cm^{-1} and 570 cm^{-1}. Possible vibrational progressions are indicated for the π_{CN} bands but they are only tentative due to the considerable overlap of the bands. Clearly evident from a comparison of the spectra is that the π_3 and π_2 bands of all the carbonyl compounds are considerably less resolved than the corresponding bands of furan itself and 2-furonitrile, all spectra being run with the same instrumental resolution.

The cause of the broadness of the vibrational fine structure of the carbonyl furans could be the rotational isomerism of the species, two planar conformations being possible:

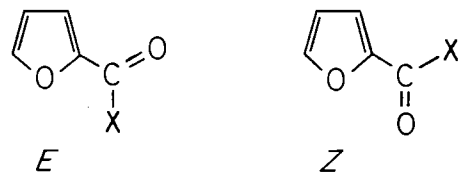

The notation *E* and *Z* indicates the relative orientations of the oxygen atoms. Existence of two rotamers has been known for some time from other spectroscopic measurements. Interpretation of the data has been hampered by the strong dependence of the rotational equilibrium on the medium and the low energy barrier to interconversion.

From IR and variable-temperature NMR studies it appears that the *Z* isomer of 2-furaldehyde is the more stable in the gas phase and in nonpolar solvents (24, 25), with the *E* isomer being about 4 kJ/mol higher in energy (26). Thus appreciable quantities of both rotamers should exist in the gas phase at room temperature. Similar rotational isomerism has been observed for 2-furoyl fluoride (25, 27) and chloride (28), and 2-acetyl furan (29). As well, MO calculations on the relative stabilities of the rotamers of 2-furaldehyde (30) and other substituted carbonyl furans (31) have been reported. Both experimental and theoretical results indicate that for all species the energy difference between the two planar configurations is small, with a low barrier to interconversion. Even though the total electronic energies of the two rotamers are similar, the energies of individual orbitals might vary slightly between the two forms, superimposition leading to the observed broad structure of the photoelectron bands. To investigate this possibility MNDO MO calculations were carried out for 2-furaldehyde and 2-furoyl fluoride, in which the carbonyl group orientation relative to the plane of the five-membered ring was varied. For the aldehyde, Fig. 5 shows the variation of the orbital eigenvalues as a function of the angle of rotation ϕ. It can be seen that the

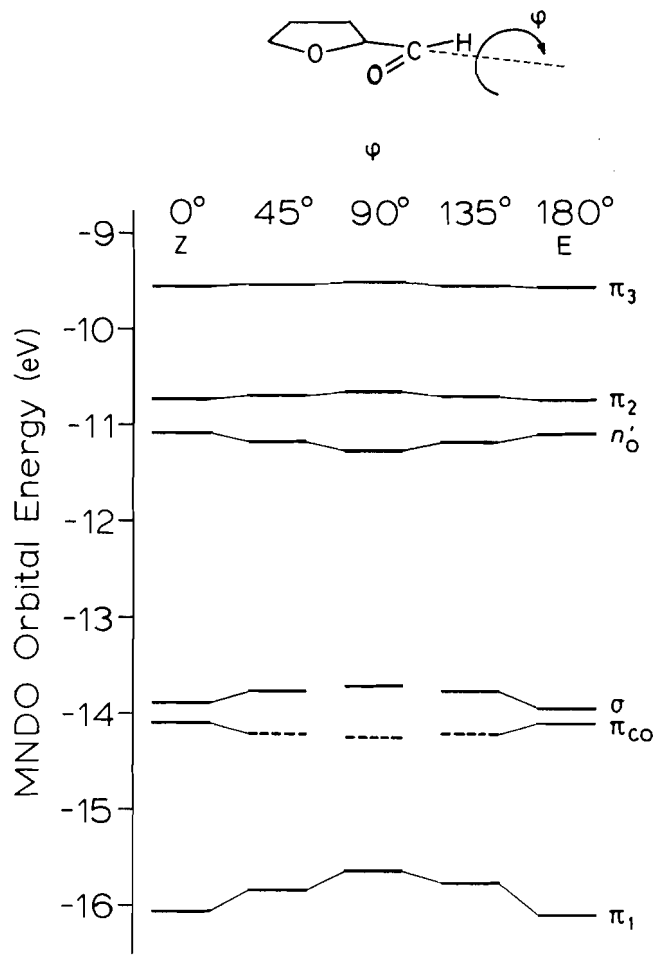

FIG. 5. MNDO calculated orbital eigenvalues for conformations of 2-furaldehyde as a function of the angle of rotation. The calculated heats of formation are -178.955 kJ mol^{-1} for the Z isomer and -178.603 kJ mol^{-1} for the E isomer.

presence of the two conformers, and their free interconversion, could lead to broadening of the associated photoelectron bands and their vibrational fine structure. Furthermore, the calculation results again predict very little delocalization energy between the ring π orbitals and the carbonyl π system since the eigenvalues of the planar configurations differ only slightly from those of the nonplanar configurations. The conclusions from the 2-furoyl fluoride calculations are similar.

Conclusions

The 58.4 nm photoelectron spectra of 2-furaldehyde and a series of substituted carbonyl furans, as well as 2-furonitrile, have been interpreted by comparison within the series and by reference to the relative inductive effects of the substituents. Assignments were made for the low ionization energy bands, which result from ionization out of the ring π orbitals and lone-pair orbitals centered on the substituents. Interaction between the furan ring π orbitals and the carbonyl and substituent groups is mainly of an inductive nature. The qualitative trends of ionization energy changes within the series are supported by the semiempirical HAM/3 and MNDO molecular orbital calculations. As well, the calculations show that rotational isomerism could result in the broad vibrational fine structure observed in the photoelectron spectra of the 2-carbonyl furan compounds.

Acknowledgments

The authors wish to thank Prof. B.M. Lynch for recording the ^{13}C NMR spectra for checking sample purity. Financial support of the Natural Sciences and Engineering Research Council of Canada and the St. Francis Xavier University Council for Research is gratefully acknowledged.

1. G. MARINO. Adv. Heterocycl. Chem. **13**, 235 (1971).
2. A. D. BAKER, C. R. BRUNDLE, and D. W. TURNER. Int. J. Mass Spectrom. Ion Phys. **1**, 443 (1968).
3. J. H. D. ELAND. Int. J. Mass Spectrom. Ion Phys. **2**, 471 (1969).
4. P. J. DERRICK, L. ÅSBRINK, O. EDQVIST, B. O. JONSSON, and E. LINDHOLM. Int. J. Mass Spectrom. Ion Phys. **6**, 161 (1971).
5. L. ÅSBRINK, C. FRIDH, and E. LINDHOLM. J. Electron Spectrosc. Relat. Phenom. **16**, 65 (1979).
6. J. A. SELL and A. KUPPERMANN. Chem. Phys. Lett. **61**, 355 (1979).
7. L. KLASINC, A. SABLJIC, G. KLUGE, J. RIEGER, and M. SCHOLZ. J. Chem. Soc. Perkin Trans. 2, 539 (1982).
8. F. FRINGUELLI, G. MARINO, A. TITICCHI, G. DISTEFANO, F. P. COLONNA, and S. PIGNATARO. J. Chem. Soc. Perkin Trans. 2, 276 (1976).
9. D. KLAPSTEIN. J. Electron Spectrosc. Relat. Phenom. **42**, 149 (1987).
10. D. KLAPSTEIN and R. T. O'BRIEN. Can. J. Chem. **66**: 143 (1988).
11. D. KLAPSTEIN and R. T. O'BRIEN. Can. J. Chem. **65**, 683 (1987).
12. N. ISHIKAWA, T. KITAZUME, T. YAMAZAKI, Y. MOCHIDA, and T. TATSUNO. Chem. Lett. 761 (1981).
13. J. F. NORMANT, J. P. FOULON, and H. DESHAYES. C. R. Acad. Sci. Paris, Ser. C, **269**, 1325 (1969).
14. W. THIEL. Quantum Chemistry Program Exchange, QCMP002.
15. L. ÅSBRINK, C. FRIDH, and E. LINDHOLM. Quantum Chemistry Program Exchange, **13**, 393 (1981).
16. H. BOCK and O. BREUER. Angew. Chem. Int. Ed. Engl. **26**, 461 (1987).
17. W. L. JORGENSEN and L. SALEM. The organic chemist's book of orbitals. Academic Press, New York. 1973. p. 235.
18. W. VON NIESSEN, W. P. KRAEMER, and L. S. CEDERBAUM. J. Electron Spectrosc. Relat. Phenom. **8**, 179 (1976).
19. K. KIMURA, S. KATSUMATA, Y. ACHIBA, T. YAMAZAKI, and S. IWATA. Handbook of He I photoelectron spectra of fundamental organic molecules. Halsted Press, New York. 1981. pp. 144–147.
20. J. W. RABALAIS and R. J. COLTON. J. Electron Spectrosc. Relat. Phenom. **1**, 83 (1972/73).
21. R. ZWARICH and I. RABINOWITZ. J. Chem. Phys. **63**, 4565 (1975); A. GANDINI, P. A. HACKETT, and R. A. BACK. Can. J. Chem. **54**, 3089 (1976).
22. J. DEL BENE and H. H. JAFFÉ. J. Chem. Phys. **48**, 4050 (1968).
23. T. KOOPMANS. Physica, **1**, 104 (1933).
24. B. R. LARSEN, F. NICOLAISEN, and J. T. NIELSEN. Acta Chem. Scand. **26**, 1736 (1972).
25. D. J. CHADWICK and I. A. CLIFFE. Khim. Geterotsikl. Soedin. **5**, 579 (1984); Engl. Transl. p. 461, and references therein.
26. F. MÖNNIG, H. DREIZLER, and H. O. RUDOLPH. Z. Naturforsch. A: Astrophys. Phys. Phys. Chem. **20**, 1323 (1965).
27. D. J. CHADWICK. Tetrahedron Lett. 679 (1975).
28. G. CASSANAS-FABRE and L. BARDET. J. Mol. Struct. **25**, 281 (1975).
29. L. ARLINGER, K. DOHLQVIST, and S. FORSEN. Acta Chem. Scand. **24**, 662 (1970).
30. I. JUCHNOVSKI and J. KANETI. Tetrahedron, **27**, 4269 (1971).
31. I. G. JOHN and L. RADOM. J. Am. Chem. Soc. **100**, 3981 (1978).

Can. J. Chem. Downloaded from www.nrcresearchpress.com by 91.144.44.67 on 09/07/12
For personal use only.

The hemiacetal–*cis*-chalcone equilibrium of malvin, a natural anthocyanin

RAYMOND BROUILLARD

Laboratoire de chimie des pigments des plantes, associé au Centre national de la recherche scientifique, Université Louis Pasteur, Institut de chimie, 1, rue Blaise Pascal, 67008 Strasbourg, France

AND

JACQUES LANG

Institut Charles Sadron (Centre de recherche des macromolécules – École d'application des hauts-polymères), Centre national de la recherche scientifique – Université Louis Pasteur Strasbourg, 6, rue Boussingault, 67000 Strasbourg, France

Received June 1, 1989[1]

RAYMOND BROUILLARD and JACQUES LANG. Can. J. Chem. **68**, 755 (1990).

In slightly acidic aqueous solutions, malvin essentially exists, in a stable form, as a fast equilibrating reaction between a ring structure, the hemiacetal B, and a chain structure, the *cis*-chalcone C_E. The temperature-jump technique has been used for the determination of the relaxation time τ characterizing this equilibrium. At 20°C τ-values were found to be in the range 1s (for the more acidic solutions) to 2×10^{-4} s (for the neutral solutions). Both buffered and unbuffered solutions were investigated. It was found that τ is largely dependent upon pH and upon the concentration of the buffer. For instance, at constant pH, a plot of the observed first-order rate constant τ^{-1} versus the acetic acid – sodium acetate buffer concentration shows a nonlinear variation that can only be interpreted as a change in the proton transfer rate-limiting step with the buffer concentration. At 20°C, the constant $K = [C_E]/[B]$ is 0.25 (±0.05) and the enthalpy change ΔH associated with this equilibrium is 20.7 (±2) kJ mol^{-1}. Therefore, increasing the temperature greatly enhances the stability of the open *cis*-chalcone isomer. Possible implications arising from the existence of a fast chemical ring-closure reaction, in the case of natural anthocyanins, for the biosynthesis of flavonoids are discussed. In particular, it is suggested that, along with the main biosynthetic pathway to flavonoids, a minor pathway involving the anthocyanin *cis*-chalcone C_E could also occur under favorable circumstances. Physico-chemical conditions in the plant organelles containing flavonoids (vacuoles) make this alternative plausible.

Key words: flavonoids, malvin, chalcone, catalysis, temperature jump.

RAYMOND BROUILLARD et JACQUES LANG. Can. J. Chem. **68**, 755 (1990).

En solution aqueuse légèrement acide, la malvine existe essentiellement, et de manière stable, sous forme d'un équilibre rapide entre la forme cyclique hémiacétal B et la forme ouverte *cis*-chalcone C_E. En utilisant la technique de saut de température par effet Joule, nous avons mesuré pour cet équilibre des temps de relaxation d'environ 1s (milieux les plus acides proches de pH 1) à environ 2×10^{-4} s (milieux proches de la neutralité), à 20°C. Les mesures ont été réalisées avec des solutions tamponnées (acide acétique – acétate de sodium ou acide phosphorique – acétate de sodium) et des solutions sans tampon. Le temps de relaxation est influencé par le pH et aussi par la concentration du tampon. On trouve par exemple, qu'à pH constant, la relation entre l'inverse du temps de relaxation (constante cinétique d'ordre 1), et la concentration du tampon n'est pas linéaire. Ce phénomène peut être interprété par un changement de l'étape de transfert de proton limitant la vitesse de la réaction avec l'augmentation de la concentration du tampon. La constante $K = [C_E]/[B]$, vaut, à 20°C, 0,25 (±0,05) et la variation d'enthalpie ΔH de l'équilibre est égale à 20,7 (±2) kJ mol^{-1}. Une élévation de température favorise donc la formation de l'isomère *cis*-chalcone C_E. On discute aussi de la possibilité de l'existence, chez les flavonoïdes, d'une voie mineure de biosynthèse basée sur la formation chimique rapide de l'hétérocycle oxygéné central à partir de la fermeture de la *cis*-chalcone C_E. Cette forme est probablement abondante dans les milieux vacuolaires contenant des anthocyanes.

Mots clés : flavonoïdes, malvine, chalcone, catalyse, saut de température.

Introduction

Ten years ago, one of us published a series of articles essentially devoted to the structural transformations that occur when a natural anthocyanin is dissolved in an aqueous medium (1). The existence, in the case of these natural molecules, of a ring–chain isomeric equilibrium leading to an open chalcone structure, previously unknown, was demonstrated (eq. [1]). The stereostructure of the chalcone, however, could not be established, and it is now believed that it is the *trans*-chalcone C_Z. In particular, relaxation times for the interconversion between the ring form (hemiacetal B), and the chain form (*trans*-chalcone C_Z), were found to be larger than 1 h at room temperature.

More recently, McClelland and co-workers (2) convincingly

[1]

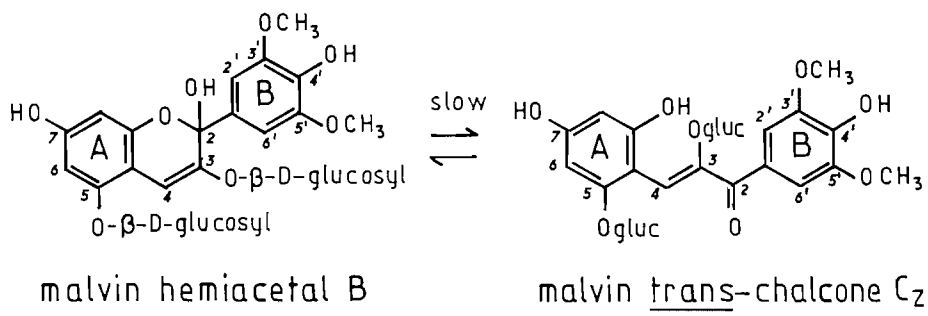

[1]Revision received January 2, 1990.

Can. J. Chem. Downloaded from www.nrcresearchpress.com by 91.144.44.67 on 09/07/12
For personal use only.

[2] 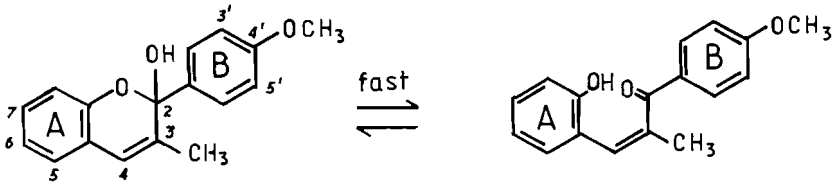

demonstrated that, in the case of some synthetic, non-natural flavylium cations, the ring-opening – ring-closure equilibrium is fast and is characterized by a relaxation time, in slightly acidic buffered aqueous solutions, lower than 1 s. They attributed this relaxation process to a rapid, base-catalyzed reaction between the hemiacetal ring structure and the *cis*-chalcone chain structure (eq. [2]). This interesting finding prompted us to check whether such a reaction also occurs for natural anthocyanins. As will be seen in the following, the existence of such a fast reaction has indeed been evidenced from temperature-jump (T-jump) experiments, in the case of malvin. The reaction between the hemiacetal form and the *cis*-chalcone form of malvin has been found to occur over a large pH range in aqueous solution at room temperature. Malvin is an anthocyanin frequently found in colored organs of higher plants (3). Moreover, our kinetic results completely agree with the proposed mechanism given in ref. 2*d* for the interconversion shown in eq. [2]. Thus, the originality of our work essentially lies in the extension to natural anthocyanins of the existence of this fast ring–chain isomeric equilibrium, as well as in a detailed treatment of the temperature-jump spectroscopic relaxation amplitudes. Finally, since anthocyanins belong to a large group of the biosynthetically related flavonoids, it may be worth asking whether the fast spontaneous chemical ring-closure reaction is of some biological importance.

Experimental

Materials

Solutions were prepared using distilled water. The purity of malvin chloride (Roth) was checked both by HPLC and by recording its ^{1}H NMR and UV–visible absorption spectra according to published procedures (4). Acetic acid, sodium acetate, potassium chloride, hydrochloric acid, sodium hydroxide, and phosphoric acid were all purchased from Merck (Suprapur). Aqueous solutions, most frequently with a 0.20 M ionic strength adjusted by means of KCl, were prepared in the following way: 1.50 mg of malvin chloride was added, at room temperature, to 5 mL of a buffer (acetic acid – sodium acetate or phosphoric acid – sodium acetate) with a known amount of KCl. After vigorous stirring or sonication, the solution was allowed to stand for about half an hour, in order for it to reach equilibrium before running the temperature-jump experiment. A given aliquot (3.0 mL) of the solution was then transferred to the T-jump cell and the pH was recorded, before and after the T-jump run, by means of a Metrohm 654 pH-meter fitted with a small combined glass electrode (EA 125). Experiments where pH values had shifted by more than 0.05 were discarded. Malvin solutions without buffer were also investigated.

Temperature-jump relaxation measurements

Absorbance changes, induced by small temperature jumps, were recorded using a Joule-heating double beam spectrometer described previously (5). Most of the relaxation transient signals were obtained for temperature jumps going from 16.5 to 20°C and were detected at a wavelength of 325 nm, which corresponds to the best signal-to-noise ratio obtainable with our system. The initial temperature was controlled within ±0.1°C, using a Haake thermo-cryostat, in the temperature range 2–20°C. The bandwidth of the spectrometer was set to a value close to 2.5 nm. For each solution investigated, several runs (usually 3–6) were undertaken. For each run, the resulting data (absorbance changes versus time) were stored on a transient recorder (Datalab). The 3–6 runs were added using a computer (Computer Automation Inc.) and the relaxation amplitude Amp as well as the relaxation time τ were obtained by fitting the equation: Amp $\times$ exp $(-t/\tau)$, where t is time, to the data, with Amp and τ as adjustable parameters, using a nonlinear least-squares procedure (6). Relaxation amplitudes (Amp) reported in the following are expressed in arbitrary absorbance units. No attempt was made to calibrate the temperature-jump spectrometer in absorbance units.

Equilibrium measurements

Ultraviolet–visible absorption spectra of malvin chloride solutions, at different temperatures and different pH values, were recorded with a Perkin Elmer Lambda 5 spectrophotometer equipped with a thermostated quartz cuvette. Stopped-flow equilibrium measurements were run using a commercial apparatus (Durrum–Gibson D-110).

Results and discussion

When an acidic malvin chloride solution, previously equilibrated, is submitted to a fast transient temperature jump from 16.5 to 20°C, a fast change in the absorbance of the solution is observed in the spectral range 250–400 nm. Figure 1 shows that the change in the amplitude of the relaxation process obtained from the T-jump experiment, as a function of wavelength, parallels the change in the absorbance obtained when the solution is submitted to the same temperature variation and the absorbance recorded with a conventional spectrometer. UV–visible absorption spectra, at two different temperatures for a pH 3.46 malvin solution, are shown in Fig. 2. It is usually admitted that the strong absorption band close to 275 nm is characteristic of the hemiacetal cyclic B structure, whereas the shoulder, visible in the neighbourhood of 330 nm, is likely to correspond to a chalcone structure (1). Another structure, resulting from the addition of water to the C-4 position of the malvin flavylium cation (see Scheme 1), may well contribute slightly to the absorption in the 275 nm region. However, this species is only a minor one, and its presence does not actually affect the relaxation process investigated in this study. As long as the pH is not too low (pH > 3), the very small amounts of the colored flavylium cation AH^+ and the colored neutral bases A (Scheme 1) produce some absorption, not only in the visible, but also in the UV range. As will be shown later, they have no effect on the kinetics of the hemiacetal B – *cis*-chalcone C_E reaction (Scheme 1); it is only the relaxation amplitude which diminishes when the flavylium cation becomes stable, that is, in the more acidic solutions (pH < 3). At room temperature and below, the *trans*-chalcone C_Z (Scheme 1) only appears in negligible quantity (1). Inspection of Figs. 1 and 2 shows that increasing the temperature favors the C_E open form at the expense of the B ring form. Increasing the temperature well above room temperature would significantly increase the quantity of the malvin *trans*-chalcone C_Z (1).

In the pioneering chemical relaxation work on anthocyanins (1), no evidence for the existence of a fast ring–chain hemiacetal B – *cis*-chalcone C_E equilibrium was reported for the following reasons: (i) experiments were made in the visible

Can. J. Chem. Downloaded from www.nrcresearchpress.com by 91.144.44.67 on 09/07/12
For personal use only.

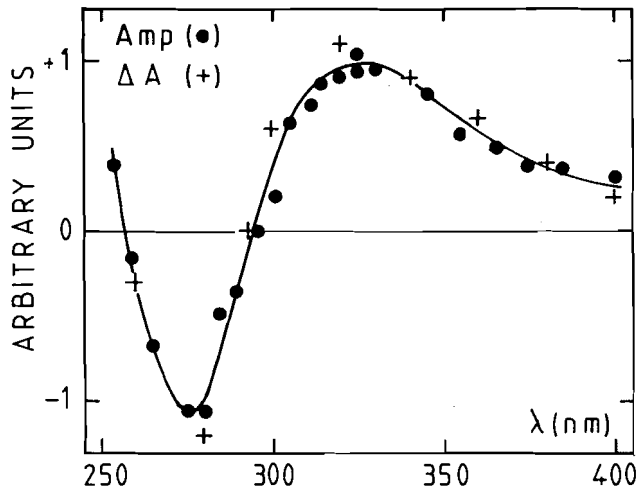

FIG. 1. (●): Plot of the hemiacetal–*cis*-chalcone relaxation amplitude, Amp, of malvin (1.50×10^{-4} M) versus wavelength. T_i = 16.5°C; T_f = 20°C; pH = 4.57; I = 0.20 M. (+): Difference in the absorbance, ΔA, of a pH 4.57 malvin solution (1.50×10^{-4} M), initially at 16.5°C and finally at 20°C, as a function of wavelength.

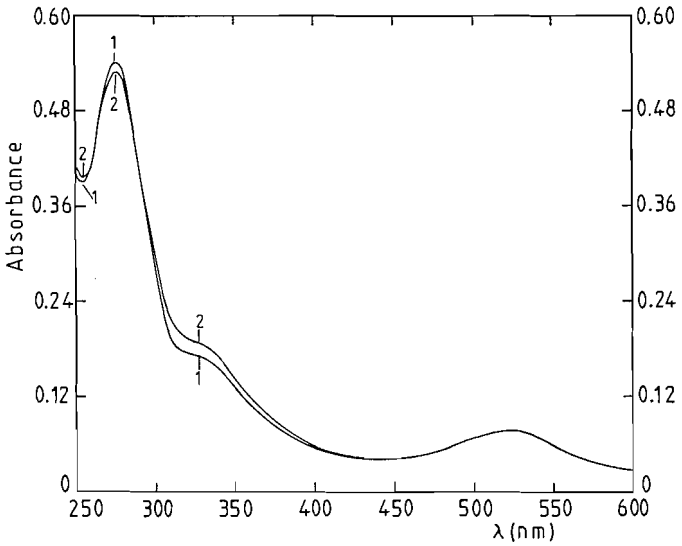

FIG. 2. Ultraviolet–visible absorption spectra of malvin (5.40×10^{-4} M) in aqueous solution at pH 3.46 and 0.20 M ionic strength; l = 1 mm. (1): T = 6.2°C; (2): T = 20.5°C.

range where the flavylium cation AH^+ and the neutral bases A are the only absorbing species (Fig. 2); (ii) at pH > 1, the $B \rightleftharpoons C_E$ equilibrium is much faster than the $AH^+ \rightleftharpoons B + H^+$ equilibrium and therefore optical detection, in the visible range, is only sensitive to the second equilibrium. This also means that the hydration equilibrium constant K_h, previously written as $([B] \times a_{H^+})/[AH^+]$, corresponds in fact to the expression $([B] + [C_E]) \times a_{H^+}/[AH^+]$, where [B], $[C_E]$, and $[AH^+]$ are the equilibrium concentrations of species B, C_E, and AH^+, respectively, and a_{H^+} is the activity of the hydronium ion (7).

From a kinetic viewpoint, the situation encountered in Scheme 1 is interesting and rather unusual. Since the equilibrium between the hemiacetal B and the *cis*-chalcone C_E is coupled to two equilibria ($AH^+ \rightleftharpoons B + H^+$ and $C_E \rightleftharpoons C_Z$), which are slow compared to the $B \rightleftharpoons C_E$ equilibrium, the observed first-order rate constant $k_{obs} = \tau^{-1}$ associated with this equilibrium is unaffected by their presence. Such a result is illustrated by the great similarity between our kinetic results on malvin and the results reported in ref. 2*d* in the case of the 4′-methoxy-3-methylflavylium cation (eq. [2]), which had been precisely selected for the absence of a quinonoidal base A and a *trans*-chalcone C_Z. One can conclude that, whatever the structural complexity of the anthocyanin or the synthetic flavylium salt under study, the hemiacetal–*cis*-chalcone equilibrium will be characterized by a kinetic first-order relaxation law identical to the one that would be obtained in the absence of all or any one of the other structures drawn in Scheme 1. However, as will be seen in the following, the variation of k_{obs}, as a function of $[H^+]$ or of the concentration of the buffer, does not conform to any simple rate law but can be understood using the model established by McClelland *et al.* (2*d*) for the 4′-methoxy-3-methyl flavylium cation.

Relaxation amplitudes

The relaxation amplitude Amp associated with the $B \rightleftharpoons C_E$ equilibrium can be affected by the presence of the other species shown in Scheme 1. For instance, when B and C_E become minor species, the relaxation signal disappears. This occurs at both low and high pH values. The lower limit is in the pH range 1–2 (Fig. 3), and the upper limit is close to neutrality. In fact, for pH values above 7, a new absorption band, with a maximum of absorption close to 400 nm, appears. We attribute this spectral feature to the presence of the ionized C_E^- chalcone form. Therefore, at pH > 7, our system transforms into a new one. In this work, investigations were limited to the acidic pH range where no ionized chalcone form could be found to occur in measurable amount. It is remarkable that the hemiacetal–*cis*-chalcone relaxation exists in the pH range usually found in vacuoles. Vacuoles are the organelles where flavonoids are stored if not synthesized. Effectively, in the case of the vacuoles of epidermal cells of many flowers, pH values have been demonstrated to range from 2.5 to 7.5 (8).

The amplitude for the relaxation process of a two-species equilibrium, as monitored by absorption spectroscopy, was previously derived for the case of the tautomerism of adenine and cytosine (9). The relaxation amplitude for the $B \rightleftharpoons C_E$ equilibrium is given therefore by eq. [3],

$$[3] \quad \text{Amp} = \frac{\Delta H}{RT^2} \times \Delta T \times \frac{K}{(1+K)^2} \times l \times (\varepsilon_{C_E} - \varepsilon_B)([B] + [C_E])$$

where ΔH is the molar enthalpy, K the equilibrium constant, l the optical pathlength, ΔT the magnitude of the temperature jump, ε_{C_E} and ε_B are the molar absorption coefficients, and $[C_E]$ and [B] are the equilibrium concentrations of C_E and B at temperature T, respectively. If one neglects the small amounts of the ionized quinonoidal base A^-, of the C-4 hydration product as well as of the *trans*-chalcone C_Z, eq. [3] transforms into eq. [4],

$$[4] \quad \text{Amp} = \frac{\Delta H}{RT^2} \times \Delta T \times \frac{K}{(1+K)^2} \times l \times (\varepsilon_{C_E} - \varepsilon_B) \times \frac{K_h(1+K)C_0}{K_a + K_h(1+K) + a_{H^+}}$$

where K_h is the hydration constant, K_a the acid–base constant defined as $[A] \times a_{H^+}/[AH^+]$, a_{H^+} the activity of the hydronium ion, and C_0 the concentration of malvin. At pH 4.55 and λ = 325 nm with T_i = 16.5°C and T_f = 20°C, we have observed that a plot of the relaxation amplitude, as a function of the

Can. J. Chem. Downloaded from www.nrcresearchpress.com by 91.144.44.67 on 09/07/12
For personal use only.

Can. J. Chem. Downloaded from www.nrcresearchpress.com by 91.144.44.67 on 09/07/12
For personal use only.

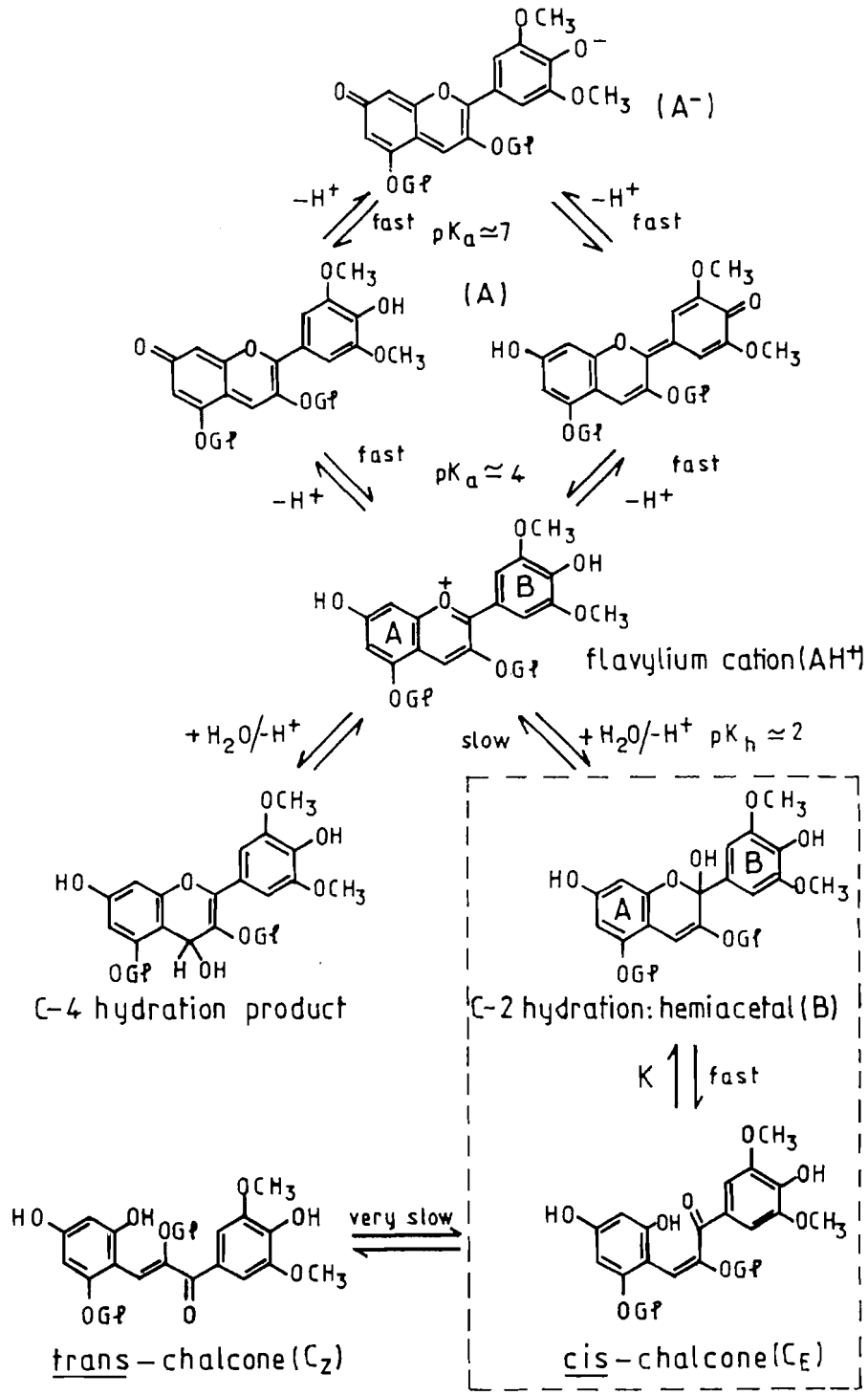

SCHEME 1

concentration of malvin (up to $C_0 = 7.2 \times 10^{-4}$ M), gives a straight line passing through the origin. The change in the amplitude versus the wavelength of observation is reported in Fig. 1. Due to so many interchanging malvin forms, it was not possible to seriously determine either the separate values of ε_{C_E} and ε_B or their difference. The results in Fig. 1 only permit us to conclude that, at a wavelength larger than 295 nm, $\varepsilon_{C_E} > \varepsilon_B$, and that at wavelengths between 255 and 295 nm the reverse is true. Equation [4] shows that Amp should increase as a_{H^+} decreases, i.e., as the pH increases, and should level off for $a_{H^+} \ll K_a + K_h(1 + K)$. This has indeed been found, as shown in Fig. 3, the levelling off of Amp (Amp_{max}) occurring at pH > 3.5, approximately. Equation [4] also predicts that, for sufficiently acidified solutions (pH < 1), the relaxation amplitude should become vanishingly small and this is indeed seen in Fig. 3. This can be understood on the basis of the formation of large quantities of the flavylium cation AH^+, which is the only stable species in the lowest pH range (Scheme 1). Another interesting feature appears in Fig. 3. Since $K_a/K_h \cong 10^{-2}$ (1), the a_{H^+} value at $Amp_{max}/2$ equals $K_h(1 + K) = 7 \times 10^{-3}$ M at 20°C. This gives $p(K_h(1 + K)) = 2.15$, a value in good agreement with previous estimates of

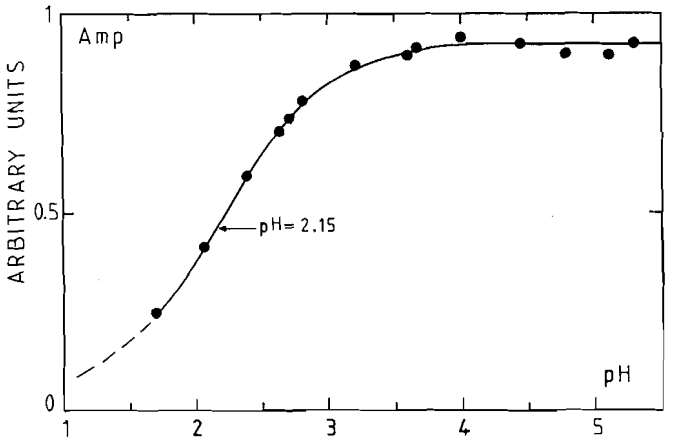

FIG. 3. Plot of the hemiacetal–*cis*-chalcone spectroscopic relaxation amplitude as a function of pH. Concentration of malvin chloride: 4.4×10^{-4} M; T_i = 16.5°C; T_f = 20°C; λ = 325 nm; I = 0.20 M (KCl).

the equilibrium constant for the hydration reaction of malvin chloride (10).

The value of K was obtained by performing a suitable stopped-flow experiment according to a procedure described previously (2). A slightly acidic aqueous solution containing malvin is mixed, at 20°C, with an equal volume of a strongly acidic aqueous solution of perchloric acid (0.58 M). After complete rapid mixing of the two solutions, the decrease in the transmittance is recorded at 540 nm, a value close to the maximum of absorption of the flavylium form AH^+. One observes that the flavylium cation is regenerated according to a two-step mechanism. This time the fastest step corresponds to the acid-catalyzed dehydration reaction of the hemiacetal B, whereas the slower step is now characteristic of the base-catalyzed ring closure of the *cis*-chalcone to the hemiacetal. Indeed, for pH values lower than 1, the first-order rate constant for the ring closure becomes smaller than the pseudo-first-order rate constant for the dehydration process. It is demonstrated that the ratio of the amplitude of the slow step to the amplitude of the fast step gives K = 0.25 (±0.05) at 20°C. It should be noticed that this value is very similar to the one measured, at 25°C, in the case of the 4′-methoxy-3-methylflavylium cation (K = 0.25) (2*d*). In eq. [4], K is defined as the ratio of the concentration of the minor isomer (C_E) to the concentration of the major isomer (B). In ref. 2*d* the reverse definition has been adopted. Since $K_h(1 + K)$ is 7×10^{-3} M and K = 0.25, a rough estimate of K_h gives 5.6×10^{-3} M (pK_h = 2.25).

Assuming that ΔH and $(\varepsilon_{C_E} - \varepsilon_B)$ do not vary with temperature and also that ln $(1 + K)$ can be approximated by K, one obtains eq. [5] (9).

$$[5] \qquad \frac{d[\ln (\text{Amp} \times T^2)]}{dT} = (1 - 2K)\frac{d \ln K}{dT}$$

A plot of ln (Amp × T^2) as a function of the reciprocal of the temperature should therefore be linear with a slope equal to $-(\Delta H/R)(1 - 2K)$. Such a linear relationship has indeed been found and it is expressed by $\ln (\text{Amp} \times T^2) = 20.6 - 1243/T$ (r = −0.996). ΔH is found to be 20.7 (±2) kJ mol^{-1}. The ring-opening reaction is endothermic and raising the temperature will greatly favor the open isomer. The somewhat large value for ΔH can, at least, partly explain the excellent signal-to-noise ratios that were obtained for the relaxation curves.

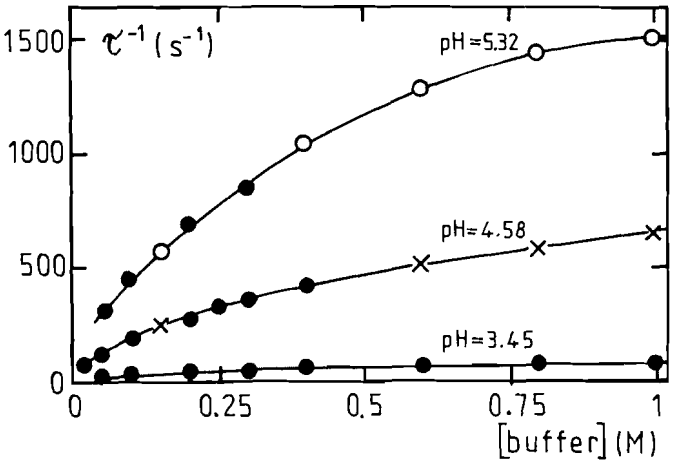

FIG. 4. Plot of the reciprocal of the relaxation time as a function of the acetic acid – sodium acetate buffer concentration at different pH values. (●): I = 0.20 M; (×): I = 0.50 M; and (○): I = 1.00 M. λ = 325 nm. Concentration of malvin chloride: 4.3×10^{-4} M. T_i = 16.5°C. T_f = 20°C.

Relaxation kinetics

From pH 1 to 7, relaxation times were found to range, approximately, between 1s and 2×10^{-4} s at 20°C. In the absence of buffer, relaxation times were observed to decrease as the pH increased. At constant pH, relaxation times became smaller as the concentration of the buffer increased. Typical results are shown in Fig. 4. The reciprocal of the relaxation time τ^{-1} is the first-order rate constant usually measured for acid- and base-catalyzed reactions. One can see that τ^{-1} is not affected by the ionic strength of the medium (Fig. 4). However, the most striking feature of Fig. 4 is the curvature exhibited by the change in τ^{-1} as a function of the concentration of the buffer. Such a result seems to indicate a reduction in the strength of the catalyst as its concentration increases. It is, however, difficult to admit this hypothesis since no change in the molecular structure (as, for example, self-association) of either acetic acid or sodium acetate occurs in the concentration range used in the present work (Fig. 4). A variation of τ^{-1} with the acid form of the buffer concentration, analogous to that shown in Fig. 4, was previously observed by McClelland *et al.* (2*d*), in the case of the hemiacetal–*cis*-chalcone system of the artificial 4′-methoxy-3-methylflavylium cation (eq. [2]). It was assumed to be related to a change in the rate-limiting step with the increase in the concentration of the buffer. The same conclusion probably applies to our own results. The mechanism given in ref. 2*d* is shown in eq. [6]. In dilute buffer, the rate-limiting step

$$[6] \qquad B \underset{k_3^0 + k_3^H[H^+] + k_3^{HA}[HA]}{\overset{k_{-3}^{OH}[OH^-] + k_{-3}^0 + k_{-3}^A[A^-]}{\rightleftharpoons}} B^- + H^+ \overset{k_{-2}}{\underset{k_2}{\rightleftharpoons}} C_E^- + H^+ \underset{k_1^{OH}[OH^-] + k_1^0 + k_1^A[A^-]}{\overset{k_{-1}^0 + k_{-1}^H[H^+] + k_{-1}^{HA}[HA]}{\rightleftharpoons}} C_E$$

is the proton transfer of the third step, and in more concentrated buffer it is the proton transfer of the first step, whereas in fairly concentrated buffer it is the ring-closure and ring-opening equilibrium occurring between the two anions which limits the rate. A detailed kinetic analysis of eq. [6] has been given (2*d*). It takes into account all the base and acid catalytic effects brought about by the species present in the aqueous medium. Rate constants in eq. [6] are those defined by McClelland *et al.* (2*d*). They have been shown (2*d*) to be related according to

Can. J. Chem. Downloaded from www.nrcresearchpress.com by 91.144.44.67 on 09/07/12
For personal use only.

TABLE 1. Rate constants for the hemiacetal–chalcone isomerization in the case of malvin

Constant	Expression	Value[a]
$k_1^0(s^{-1})$	$k_{-1}^{H}K_C$	32
$k_{-1}^0(s^{-1})$	$k_1^{OH}K_W/K_C$	2.6×10^4
$k_{-3}^0(s^{-1})$	$k_3^{H}K_B$	5×10^{-3}
$k_3^0(s^{-1})$	$k_{-3}^{OH}K_W/K_B$	1.6×10^8
$k_1^A(M^{-1}\,s^{-1})$	$k_{-1}^{HA}K_C/K_{HA}$	1×10^6
$k_{-3}^A(M^{-1}\,s^{-1})$	$k_3^{HA}K_B/K_{HA}$	1.6×10^2
$k_1^{OH} = k_{-3}^{OH}(M^{-1}\,s^{-1})$	Measured	1.3×10^{10}
A	$k_1^{OH}K_W$	$1.6\times10^{-4}(2\times10^{-4})$
B	$k_1^{A}K_{HA}$	32(32)
C	$K_{HA}k_1^Ak_3^{HA}/k_3^0$	$10^3(1.3\times10^3)$
D	$(K^{-1}/(1+K^{-1}))K_{HA}k_1^A/K_CK^-k_3^0$	$3.8\times10^4(1.6\times10^4)$
E	$(K^{-1}/(1+K^{-1}))K_{HA}k_1^Ak_3^{HA}/K_Ck_2k_3^0$	$2.1\times10^4(2.8\times10^4)$

[a]Values in parentheses are those obtained from the solid line in Fig. 5 using eq. [9]. K^- is 6.3×10^{-4} and k_2 has been taken from ref. 2*d* ($6\times10^6\ s^{-1}$).

eqs. [7] and [8], where K_C, K_B, K_W, and K_{HA} are the acidity constant of the *cis*-chalcone C_E, the acidity constant of the hemiacetal B, the dissociation constant of water, and the acidity constant of the buffer, respectively.

$$[7]\quad K_C = \frac{k_1^0}{k_{-1}^H} = \frac{k_1^{OH}K_W}{k_{-1}^0} = \frac{k_1^AK_{HA}}{k_{-1}^{HA}}$$

$$[8]\quad K_B = \frac{k_{-3}^0}{k_3^H} = \frac{k_{-3}^{OH}K_W}{k_3^0} = \frac{k_{-3}^AK_{HA}}{k_3^{HA}}$$

k_1^{OH}, k_{-3}^{OH}, k_{-1}^H, k_3^H, k_{-1}^{HA}, and k_3^{HA} are diffusion-controlled rate constants whose values are close to $5\times10^9\,M^{-1}\,s^{-1}$. At 20°C and I = 0.20 M, K_W and K_{HA} are $10^{-13.9}$ and $10^{-4.50}$, respectively. At the same temperature and ionic strength, K_C has been measured by us and found to be $10^{-8.20}$. K_B could not be measured and its value (10^{-12}) has been taken from ref. 2*d*. Values of the rate constants k_1^0, k_{-1}^0, k_1^A, k_3^0, k_{-3}^0, and k_{-3}^A are reported in Table 1. Strong experimental support was given to the mechanism in eq. [6] by the existence of a curved relationship between the product $\tau^{-1}\times[H^+]$ and the HA concentration (2*d*). It was also shown that this relationship does not depend on the free acidity of the medium. A similar plot is found in the case of the hemiacetal–*cis*-chalcone equilibrium of malvin (Fig. 5). Therefore the assumption made by McClelland and co-workers (2*d*) to interpret their results can basically also be used in our case. Since B^- and C_E^- are highly unstable species under our experimental conditions (acidic pH range), only one relaxation process is observable in the case of eq. [6]. The reciprocal of the relaxation time has been derived by McClelland *et al.* (2*d*) and demonstrated to correspond to eq. [9], where A, B, C, D, and E are composite constants

$$[9]\quad \tau^{-1} = \frac{1}{[H^+]}\frac{A + B[HA] + C[HA]^2}{1 + D[HA] + E[HA]^2}$$

obtained in the relaxation treatment. Values of these constants according to their expressions in ref. 2*d* are reported in Table 1 as well as the values of the same constants based on the best fit of eq. [9] to the experimental data as shown in Fig. 5. Agreement between the two series of values is interpreted as good evidence for the validity of the mechanism shown in eq. [6]. However, only one change in the slope is apparent in Fig. 5, whereas two slope changes were observed in the $\tau^{-1}\times[H^+]$ versus [HA] plot for the 4′-methoxy-3-methylflavylium cation. Two explanations can be put forward for this difference: (i) Our work has been performed at pH values lower than those used for the study of the 4′-methoxy-3-methylflavylium compound, and it could happen that the base catalysis of the proton transfer between B and B^- is not efficient enough so that the ring-closure – ring-opening equilibrium would become rate determining. Or (ii) due to the existence of a better nucleophilic leaving group (ring A of malvin, eq. [1]), as compared to the less substituted A ring of the compound in eq. [2], the B^- species cannot form and eq. [6] reduces to a two-step system (11). It can also be admitted that B^- and C_E^- are non-classical resonant anions. In this case, the interconversion between B^- and C_E^- will always be referred to as extremely fast.

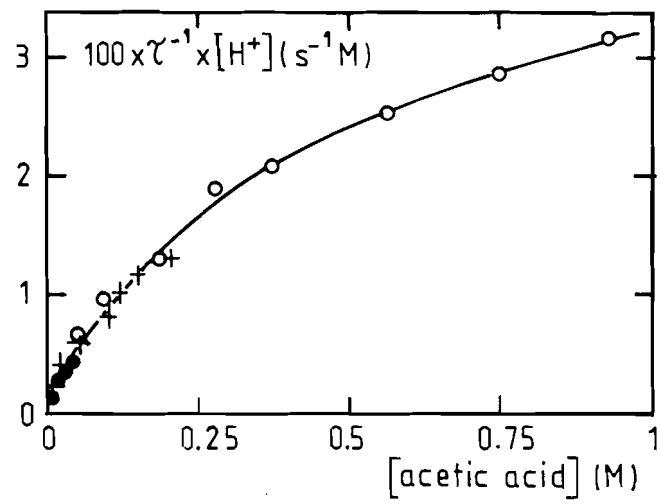

FIG. 5. Reciprocal of the relaxation time multiplied by the proton concentration as a function of the concentration of acetic acid. T_i = 16.5°C; T_f = 20°C; I = 0.20 M; (○): pH = 3.45; (+): pH = 4.58; (●): pH = 5.32. The solid line corresponds to eq. [9] using parameters A, B, C, D, and E shown in parentheses in Table 1.

Chalcones previously detected in the case of malvin and malvidin 3-glucoside (1) are *trans*-chalcones (see eq. [1]). In the acidification experiments reported elsewhere (1), what was observed is their slow conversion, via the *cis*-chalcone, to the flavylium cation, the rate-limiting step being the isomerization process. Therefore, previously reported chalcone contents in anthocyanins relate to the ratio $[C_Z]/([B] + [C_E])$, since B

Can. J. Chem. Downloaded from www.nrcresearchpress.com by 91.144.44.67 on 09/07/12
For personal use only.

[10]

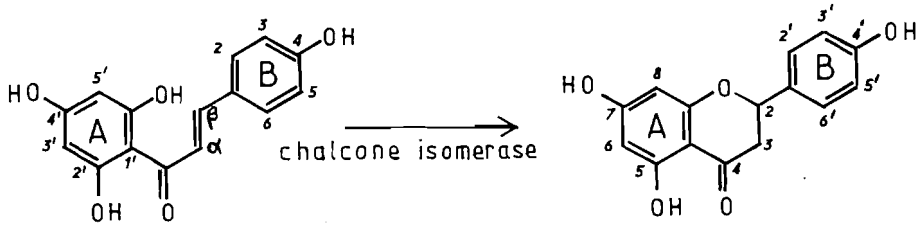

a regular chalcone (special numbering of the carbon atoms)

a flavanone (usual numbering of the carbon atoms)

and C_E rapidly revert to the flavylium ion and not to the ratio $[C_Z]/[B]$ as estimated in ref. 1. This remark also applies to the work done on the preparation of natural anthocyanin chalcones using high performance liquid chromatography (12).

Biological implication

Now that we have demonstrated the existence, for a natural anthocyanin, of a fast ring-closure reaction, the question is whether this feature is important in the biosynthesis of flavonoids. The key step in the biosynthesis of flavonoids is the formation of a regular chalcone whose isomerization to a cyclic flavanone is catalyzed by a chalcone isomerase (13). This type of chalcone, however, differs from the anthocyanin type of chalcone (retrochalcone) by the location of the carbonyl group and the ethylenic double bond with respect to the A and B phenolic rings as exemplified in eq. [10]. The flavanones thus formed are at the origin of many of the flavonoids, i.e., flavones, isoflavones, proanthocyanidins, anthocyanins, etc. (14). Since the chalcones formed from anthocyanins (retrochalcones) transform so easily into hemiacetals, it is worth asking whether there is a possibility of a second, minor, biosynthetic pathway to flavonoids, avoiding the chalcone isomerase catalyzed ring-closure step. Moreover, and as far as anthocyanins are concerned, generation of the strongly colored A^-, A, and AH^+ forms (Scheme 1), starting from the *cis*-chalcone C_E, only proceeds through fast, acid- or base-catalyzed steps. Natural physico-chemical conditions in vacuoles do provide such acid and base catalysts in good amounts.

Evidence has been given for the existence of a few rare natural regular chalcones with the structural requirement necessary to a fast chemical ring-closure reaction (15). Such rarely identified regular chalcones possess a 2-hydroxyl group in the B ring and, therefore, fast chemical ring closure takes place by the attack of the 2-hydroxyl on the carbonyl group leading to a hemiacetal form (16). This corresponds to an exchange of the roles played by the A and B rings with respect to the ring-closure process. Until now, such molecules were not shown to play an important role in the biosynthesis of flavonoids. It should also be mentioned that only a very limited number of natural retrochalcones (the anthocyanin type of chalcone) have previously been identified (17). To this group one could now add the anthocyanin retrochalcones. Their number is probably as large as the number of the anthocyanins themselves. However, one should not forget that the retrochalcones are difficult to detect, not only in their natural environment but also in model solutions.

1. R. BROUILLARD and B. DELAPORTE. J. Am. Chem. Soc. **99**, 8461 (1977); R. BROUILLARD, B. DELAPORTE, and J. E. DUBOIS. J. Am. Chem. Soc. **100**, 6202 (1978); R. BROUILLARD and J. M. EL HAGE CHAHINE. J. Am. Chem. Soc. **102**, 5375 (1980).
2. (*a*) R. A. MCCLELLAND and S. GEDGE. J. Am. Chem. Soc. **102**, 5838 (1980); (*b*) R. A. MCCLELLAND and G. H. MCGALL. J. Org. Chem. **47**, 3730 (1982); (*c*) D. B. DEVINE and R. A. MCCLELLAND. J. Org. Chem. **50**, 5656 (1985); (*d*) R. A. MCCLELLAND, D. B. DEVINE, and P. E. SORENSEN. J. Am. Chem. Soc. **107**, 5459 (1985).
3. J. B. HARBORNE. 1967. Comparative biochemistry of the flavonoids. Academic Press, New York.
4. A. CHEMINAT and R. BROUILLARD. Tetrahedron Lett. 4457 (1986); T. GOTO. *In* Progress in the chemistry of organic natural products. *Edited by* W. Herz, H. Grisebach, G. W. Kirby, and Ch. Tamm. Springer Verlag, Vienna. 1987. p. 113.
5. J. STURM. D. Sc. Thesis, Université Louis Pasteur, Strasbourg, France, 1974; K. KUSTIN (*Editor*). Methods in enzymology. Vol. 16. Academic Press, New York. 1969.
6. K. HYUNYONG. J. Chem. Educ. **47**, 120 (1970).
7. R. BROUILLARD, G. MAZZA, Z. SAAD, A. M. ALBRECHT-GARY, and A. CHEMINAT. J. Am. Chem. Soc. **111**, 2604 (1989).
8. R. N. STEWART, K. H. NORRIS, and S. ASEN. Phytochemistry, **14**, 937 (1975).
9. M. DREYFUS, G. DODIN, O. BENSAUDE, and J. E. DUBOIS. J. Am. Chem. Soc. **97**, 2369 (1975); M. DREYFUS, O. BENSAUDE, G. DODIN, and J. E. DUBOIS. J. Am. Chem. Soc. **98**, 6338 (1976).
10. C. F. TIMBERLAKE and P. BRIDLE. J. Sci. Food Agric. **18**, 473 (1967); R. BROUILLARD and J. E. DUBOIS. J. Am. Chem. Soc. **99**, 1359 (1977); E. S. SADLOWSKI. Ph.D. Thesis, Colorado State University, Fort Collins, CO. 1985.
11. W. P. JENCKS. Acc. Chem. Res. **13**, 161 (1980).
12. N. W. PRESTON and C. F. TIMBERLAKE. J. Chromatogr. **214**, 222 (1981); K. BRONNUM-HANSEN and S. H. HANSEN. J. Chromatogr. **262**, 385 (1983).
13. W. HELLER and G. FORKMANN. *In* The flavonoids. Advances in research since 1980. *Edited by* J. B. Harborne. Chapman and Hall, London. 1988. p. 399.
14. H. GRISEBACH. *In* Anthocyanins as food colors. *Edited by* P. Markakis. Academic Press, New York. 1982. p. 69.
15. B. A. BOHM. *In* The flavonoids. Advances in research since 1980. *Edited by* J. B. Harborne. Chapman and Hall, London. 1988. p. 329.
16. D. L. DREYER, K. P. MUNDERLOH, and W. E. THEISSEN. Tetrahedron, **31**, 287 (1975); C. D. HUFFORD, B. O. OGUNTIMEIN, and J. K. BAKER. J. Org. Chem. **46**, 3073 (1981).
17. P. M. DEWICK. *In* The flavonoids. Advances in research since 1980. *Edited by* J. B. Harborne. Chapman and Hall, London. 1988. p. 125.

Can. J. Chem. Downloaded from www.nrcresearchpress.com by 91.144.44.67 on 09/07/12
For personal use only.

Conformations and charge distributions in fluoronitrosoethylenes and nitrosoethylene[1,2]

CECILIA SARASOLA, FERNANDO P. COSSÍO, AND JESUS M. UGALDE[2]
Kimika Fakultatea, Euskal Herriko Unibertsitatea, Posta Kutxa 1072, 20080 Donostia, Spain

Received August 2, 1989[3]

CECILIA SARASOLA, FERNANDO P. COSSÍO, and JESUS M. UGALDE. Can. J. Chem. **68**, 762 (1990).

The optimized structures, bond orders, and electrostatic potentials for both transoid and cisoid fluoronitrosoethylenes and nitrosoethylene have been calculated by *ab initio* self-consistent-field molecular orbital procedure. The transoid structures are found to be of lower energy than the cisoids. Analyses of the calculated bond orders show that the C—C bond energy compares well with that of ethylene and the C—N bond energy with that of ethylamine, and therefore the contributions from ionic resonance structures are predicted to be small. The calculated electrostatic potential contour maps show that the presence of the nitroso group completely eliminates the negative potential region associated with the C—C double bond, thus rendering it less susceptible to electrophilic attack. Analyses of the values and relative locations of positive electrostatic potentials correctly predict that the nucleophilic addition to β-carbon is favoured when in the transoid conformation.

Key words: conformation, charge distribution, fluoronitrosoethylenes, nitrosoethylenes.

CECILIA SARASOLA, FERNANDO P. COSSÍO et JESUS M. UGALDE. Can. J. Chem. **68**, 762 (1990).

Utilisant une procédure *ab initio* d'orbitales moléculaires en champ auto-cohérent, on a calculé les structures optimisées, les ordres des liaisons ainsi que les potentiels électrostatiques des formes tant transoïdes que cisoïdes des fluoronitrosoéthylènes et nitrosoéthylène. On a évalué que l'énergie des structures transoïdes est plus faible que celle des formes cisoïdes. Une analyse des ordres de liaison calculées montre que l'énergie de la liaison C—C se compare bien à celle de l'éthylène alors que l'énergie de la liaison C—N se compare bien à celle de l'éthylamine; on en conclut que les contributions des structures ioniques de résonance doivent être faibles. Les cartes des contours des potentiels électrostatiques calculés montrent que la présence du groupement nitroso élimine complètement la région de potentiel négatif associée à la double liaison C—C; cette liaison est donc moins susceptible à une attaque nucléophile. Une analyse des valeurs et des positions relatives des potentiels électrostatiques positifs permet de prédire correctement que, lorsque la conformation est transoïde, l'addition nucléophile sur le carbone β est favorisée.

Mots clés : conformation, distribution de charge, fluoronitrosoéthylènes, nitrosoéthylènes.

[Traduit par la revue]

1. Introduction

Interest in the chemistry of conjugated nitroso compounds has been renewed in recent years. Although the nitroso group has been recognized for many years as a powerful activating group for nucleophilic substitution in benzenoid aromatics (1), and nitrosocarbonyl compounds (RCONO) have been generated and shown to participate, through the nitroso group, in Diels–Alder and ene reactions (2), it is only recently that the chemistry of conjugated nitrosoalkenes has been reviewed (3). Only a few conjugated nitrosoalkenes have been isolated so far. The first of such compound, the trifluoronitrosoethylene, was reported in 1960 (4). Since then a few others, usually with bulky alkyl or halo substituents at the β-carbon atom, have been described (3). There is, however, substantial evidence for the existence of a wide range of conjugated nitrosoalkenes in solution as transient intermediates (5).

Conjugated nitrosoalkenes are potentially very useful synthetic intermediates because of the presence of a double bond in conjugation with a powerful inductive electronic charge withdrawer such as the nitroso group (6). Thus the β-carbon should be expected to be highly electrophilic, and indeed reactions with nucleophiles are the best-known features of their chemistry (3).

This paper reports the results of a study using *ab initio* molecular orbital theory of the fluoronitrosoethylenes and nitrosoethylene. We have completely optimized all the transoid (**I**) and cisoid (**II**) structures, for R_1, R_2, R_3 = F or H; and then carried out an analysis of the conformations and electronic charge distributions by means of the relative bond strengths and molecular electrostatic potentials.

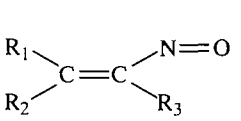

I

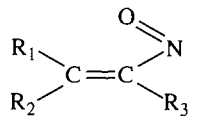

II

2. Methods

All results presented in this paper are based upon *ab initio* self-consistent-field molecular orbital theory, using the GAUSSIAN-86 (7) series of programs. Complete geometry optimizations were carried out at the 4-21G* level of theory. This particular basis set has been selected because earlier calculations (8) on molecules containing the nitroso group have shown that the inclusion of *d*-type polarization functions has a substantial effect on the optimimzed geometries. On the other hand, larger basis sets such as 6-31G* has been shown to have little effect on the optimized geometries. For instance, the optimized HF/6-31G* and the HF/4-21G* geometries of the *cis*-1,2-dinitrosoethylene never differ more than 0.6% (9). To improve energies, MP2/4-21G* single point calculations were carried out on the previously 4-21G* optimized structures. The size of the molecules involved in the calculation prevented us to go further in the perturbation expansion. Along with the geometrical characteristics we have focused attention upon relative bond orders (10), calculated as

$$[1] \quad \text{Bond order} = 0.55747\,(k/R_e)^{1/2}$$

where R_e is the 4-21G* equilibrium bond length (in Å) and k is the force constant of the bond under study. Politzer *et al.* have shown (10) that experimentally measured bond dissociation

[1]This paper is dedicated to Professor G. M. Guzman on the occasion of his nomination to Professor Emeritus.

[2]To whom correspondence should be addressed.

[3]Revision received April 4, 1990.

Printed in Canada / Imprimé au Canada

Can. J. Chem. Downloaded from www.nrcresearchpress.com by 91.144.44.67 on 09/07/12
For personal use only.

Can. J. Chem. Downloaded from www.nrcresearchpress.com by 91.144.44.67 on 09/07/12
For personal use only.

energies correlate well with bond orders calculated using eq. [1]. Hence it represents a practical means for predicting the relative strengths of chemical bonds, particularly when it is a given type of bond in different environments.

We have also studied the electrostatic potential $V(\boldsymbol{r})$ on the previously 4-31G* optimized geometries as

[2] $V(\boldsymbol{r}) = \Sigma_A Z_A |\boldsymbol{r} - \boldsymbol{R}_A|^{-1} - \mathrm{tr}(\boldsymbol{P}\cdot\boldsymbol{V})$

$V(\boldsymbol{r})$ was computed using eq. [2] with the STO-5G basis set, which has been shown to be generally reliable for determining this property (11–13). In particular, it has been shown to be superior to the standard STO-3G minimal basis set (13), while keeping the computational cost still affordable. In eq. [2], Z_A is the charge on nucleus A, located at $\boldsymbol{R}_A$, $\mathbf{P}$ is the total density matrix and $V_{\mu\nu} = \langle\mu||\boldsymbol{r} - \boldsymbol{r}'|^{-1}|\nu\rangle$ is the matrix element of the coulombic potential operator $|\boldsymbol{r} - \boldsymbol{r}'|^{-1}$ and $\{\phi_\mu|\mu = 1, 2,\ldots\}$ is the basis functions set. The electrostatic potential is a real physical property, which can be determined experimentally as well as computationally, and is related to the electronic charge distribution. Therefore it can be used to study the approaching channels of molecules, and since at this stage the interactions are weak, the frozen charge distribution approximation is valid. For instance, electrostatic calculations are in substantial agreement with SCF calculations performed by keeping the internal geometries of the partners unaltered. The latter approximation allows for mutual polarization effects, the non-classical exchange contributions to the energy, and to some extent the charge transfer effects. The accord between the two approximations is of course better at larger distances, but it is also present at intermediate values of the approach coordinate (11), in such a way that the electrostatic potential has proven to be an effective means for interpreting and predicting the initial reactive sites of molecules (12, 13). Other methods, such as the Bader type of analysis of molecular electron density distribution (14), have also proven to be useful for predictions of reactivity patterns. In particular, we would like to mention that reactivities of a series of molecules in a Michael addition reaction have been analyzed on the basis of properties expressed in terms of the Laplacian of charge density distribution (15). However, since electrostatic potentials are directly available from the GAUSSIAN-86 program package, we will focus on the $V(\boldsymbol{r})$ function.

Our calculated 4-21G* optimized structures for all the fluoronitrosoethylenes and the nitrosoethylene are shown in Table 1. Figures in square brackets belong to the transoid conformer and those in parentheses belong to the cisoid. Using the same notation, the HF/4-21G* and the MP2/4-21G*//HF/4-21G* energies have been collected in Table 2, and the bond orders in Table 3. Finally in Table 4 are reported the magnitudes and locations of the planar electrostatic potential maxima that are associated with each molecule.

3. Discussion

3.1 Structures

All HF/4-21G* optimized structures were found to be planar. Subsequent harmonic vibrational frequencies, calculated at the same level of theory, confirm that all but the monofluoronitrosoethylenes were true minima. We were unable to find true minima structures for the monofluoronitrosoethylenes for all attempts converged to the geometries given in Table 1. These structures were found to have three imaginary frequencies at the HF/4-21G* level of theory. Table 1 shows that the N—O bond lengths remain almost constant around a value of 1.18 Å all through the series of molecules under study. Changes affect at most the third decimal figure. The differences between the corresponding transoid and cisoid conformers are kept within a maximum value of 0.001 Å. Earlier calculations on related molecules like nitrosoacetylene (16), and nitrosomethanol (17, 18), with basis sets including no polarization functions report N—O bond lengths of 1.208 Å for nitrosoacetylene (6-31G basis set was employed) and 1.21 Å for nitrosomethanol (standard DZ (17), and 3-21G (18) basis sets). The discrepancy between these data and our calculated N—O bond lengths should be attributed to the electron donation from the $2p$ orbitals of the nitroso oxygen into d-type orbitals on nitroso nitrogen (19). For instance, we have found that the 4-31G* bond length has been reduced by 0.041 Å in the transoid nitrosoethylene with respect to the corresponding 4-31G optimized bond length (see Table 1 in ref. 8). Clearly basis sets including polarization functions are needed to take into account the effect of the back donation into the d-type orbitals on nitrogen, which bring about this N—O bond length reduction.

The differences found for the carbon–carbon optimized bond lengths are worthy of mention. Inspection of Table 1 reveals that the C—C bond distances are always slightly larger for the cisoid than for the corresponding transoid structure. The calculated mean bond distance of 1.31 Å appears to be underestimated with respect to the experimental average carbon–carbon double bond length of 1.34 Å (20). The latter is typical of SCF calculations, with extended sets (19). The C—N bond lengths are slightly larger in the cisoid conformers than in their corresponding transoid ones. The carbon–nitrogen HF/4-21G* equilibrium distance decreases as the number of fluorine substituents increases.

The C—F bond lengths vary slightly around a value of 1.31 Å, which compares well with the experimental bond lengths of 1.325 Å in 1-chloro-1-fluoroethylene (21) and 1.323 Å in 1,1-difluoroethylene (22). A remarkable point from Table 1 is that the C—F bond lengths appear to be slightly larger in the transoids than in the cisoids.

3.2 Energies

For all the molecules under study the transoid conformations are calculated to be more stable than their corresponding cisoid conformations, at both HF/4-21G* and MP2/4-21G* levels of theory, see Table 2. However, as the energy differences are less than 5 kcal/mol, a word of caution should be put on whether larger basis sets and more particularly higher level correlation energy treatments will not reverse the calculated MP2/4-21G* stability order. We would also like to point out that the average relative transoid/cisoid stability increase, due to the inclusion of electron correlation via Moller–Plesset perturbation theory up to the second order at the 4-21G* level of theory, is approximately 1 kcal/mol, in favour of the transoid conformation.

3.3 Bond orders

As discussed earlier the bond orders in Table 3, calculated using eq. [1], will be taken as measures of relative bond strengths of bonds of a given type. Thus we can see that the C—H bond orders, and therefore the bond energy, appears to be larger when the hydrogen atom is attached to the α-carbon than when it is attached to the β-carbon. The β-C—H bond energies are very similar. However, we would like to point out that all C—H bonds of molecules studied are stronger than the more typical methyl C—H bonds (4), because of the well-known strengthening effect that strong inductive withdrawers of electronic charge have on adjacent single bonds (23, 24). The behavior of the C—F bond energies parallels that of the C—H

Can. J. Chem. Downloaded from www.nrcresearchpress.com by 91.144.44.67 on 09/07/12
For personal use only.

TABLE 1. 4-31G* Optimized geometries[a]

Parameter	Value							
	$R_1 = R_2 = R_3 = F$	$R_1 = H$ $R_2 = R_3 = F$	$R_2 = H$ $R_1 = R_3 = F$	$R_3 = H$ $R_1 = R_2 = F$	$R_1 = R_2 = H$ $R_3 = F$	$R_1 = R_3 = H$ $R_2 = F$	$R_2 = R_3 = H$ $R_1 = F$	$R_1 = R_2 = R_3 = H$
C—C	[1.316] (1.317)	[1.314] (1.316)	[1.315] (1.314)	[1.318] (1.320)	[1.298] (1.300)	[1.315] (1.316)	[1.316] (1.318)	[1.316] (1.314)
C—R_1	[1.291] (1.293)	[1.072] (1.070)	[1.316] (1.312)	[1.229] (1.284)	[1.074] (1.072)	[1.075] (1.073)	[1.314] (1.309)	[1.077] (1.075)
C—R_2	[1.291] (1.286)	[1.311] (1.316)	[1.073] (1.072)	[1.315] (1.321)	[1.076] (1.073)	[1.311] (1.310)	[1.075] (1.074)	[1.079] (1.075)
C—R_3	[1.317] (1.323)	[1.311] (1.316)	[1.315] (1.321)	[1.073] (1.071)	[1.311] (1.310)	[1.076] (1.073)	[1.075] (1.074)	[1.078] (1.075)
C—N	[1.412] (1.419)	[1.419] (1.431)	[1.425] (1.432)	[1.425] (1.435)	[1.436] (1.450)	[1.428] (1.445)	[1.434] (1.446)	[1.441] (1.462)
N—O	[1.184] (1.184)	[1.182] (1.183)	[1.182] (1.182)	[1.185] (1.184)	[1.180] (1.179)	[1.184] (1.184)	[1.184] (1.183)	[1.184] (1.181)
R_1CC	[123.2] (124.8)	[121.1] (121.5)	[121.2] (123.4)	[124.7] (126.5)	[118.7] (118.9)	[122.6] (123.0)	[122.9] (124.9)	[120.2] (120.0)
R_2CC	[123.9] (122.6)	[122.9] (122.3)	[123.1] (121.3)	[123.8] (122.4)	[121.6] (121.0)	[123.0] (122.5)	[123.4] (121.7)	[121.9] (121.6)
R_3CC	[121.8] (119.8)	[125.2] (124.1)	[121.8] (119.9)	[122.4] (119.2)	[125.2] (124.7)	[125.3] (123.0)	[122.6] (119.4)	[125.7] (124.1)
NCC	[121.8] (119.8)	[125.2] (124.1)	[121.8] (119.9)	[122.8] (119.2)	[125.2] (124.7)	[125.3] (123.0)	[122.6] (119.4)	[125.7] (124.1)
ONC	[113.0] (114.5)	[113.2] (113.9)	[112.4] (113.5)	[112.7] (114.9)	[112.6] (113.2)	[112.9] (114.4)	[112.3] (114.2)	[112.3] (113.7)

[a]Figures in square brackets belong to the transoids and those in parentheses belong to the cisoids.

TABLE 2. Energies[a]

Parameter	Value				
	$R_1 = R_2 = R_3 = F$	$R_1 = H$ $R_2 = R_3 = F$	$R_2 = H$ $R_1 = R_3 = F$	$R_3 = H$ $R_1 = R_2 = F$	$R_1 = R_2 = R_3 = H$
HF/4-21G* (au)	[−502.2732] (−502.2669)	[−403.6159] (−403.6110)	[−403.6137] (−403.6079)	[−403.6352] (−403.6265)	[−206.3239] (−206.3187)
Δ(T − C) (kcal/mol)	−4.329	−3.076	−3.640	−3.577	−3.263
MP2/4-21G* (au)	[−503.0093] (−503.0002)	[−404.3493] (−404.3565)	[−404.3571] (−404.3650)	[−404.5464] (−404.5531)	[−207.0597] (−207.0532)
Δ(T − C) (kcal/mol)	−5.710	−4.518	−4.957	−4.204	−4.078

[a]Figures in square brackets belong to the transoids and those in parentheses belong to the cisoids.

TABLE 3. Calculated bond orders[a]

Parameter	$R_1 = R_2 = R_3 = F$	$R_1 = H$ $R_2 = R_3 = F$	$R_2 = H$ $R_1 = R_3 = F$	$R_3 = H$ $R_1 = R_2 = F$	$R_1 = R_2 = R_3 = H$
C—C	[1.652] (1.640)	[1.658] (1.647)	[1.670] (1.650)	[1.636] (1.609)	[1.648] (1.639)
C—R_1	[1.517] (1.527)	[1.403] (1.382)	[1.415] (1.438)	[1.521] (1.528)	[1.348] (1.355)
C—R_2	[1.511] (1.502)	[1.425] (1.429)	[1.352] (1.358)	[1.535] (1.493)	[1.352] (1.351)
C—R_3	[1.438] (1.433)	[1.453] (1.442)	[1.462] (1.430)	[1.321] (1.371)	[1.339] (1.350)
C—N	[1.094] (1.079)	[1.093] (1.066)	[1.082] (1.051)	[1.093] (1.046)	[1.036] (1.007)
N—O	[2.057] (2.046)	[2.050] (2.048)	[2.065] (2.062)	[2.036] (2.037)	[2.062] (2.063)

[a]Figures in square brackets correspond to the transoids and those in parentheses to the cisoids.

bonds. From Table 3 one may observe that the C—F bonds are stronger on the α-carbon than on the β-carbon, and do not vary significantly between the *cis* and *trans* dispositions of the fluorine atom on the β-carbon, with respect to the nitroso group. Also the data in Table 3 reveal that both C—H and C—F bonds are a little stronger for the cisoid than for the transoid conformers. This is fully consistent with the optimized C—H bond lengths, which appear to be shorter for the cisoid conformers than for their corresponding transoids.

The C—C bond orders of the transoid conformers fluctuate between 1.67 and 1.609. These values compare well with the 4-21G* C—C bond order of 1.637 in ethylamine (24). Therefore one should expect no significant contribution from ionic resibabce structures like **III**.

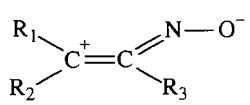

III

The calculated C—N bond orders further confirm this point. The values for the transoid structures go from a maximum value of 1.334 to a minimum of 1.285, and those of the cisoids from 1.094 to 1.007. These figures compare well with the 4-31G* bond order of 1.266 in ethylamine (24), where the C—N bond is a single bond, and differ markedly from the 4-31G* C—N bond order of 1.952 in methylenamine (24), and 1.730 in 1,2-dinitrosoethylene (25), where the C—N bond has a significant double bond character. These values suggest that there is little conjugation of the electrons in C=C and N=O.

3.4 Electrostatic potentials

Figures 1 to 3 show the electrostatic potential contour maps for some of the molecules under study, at the conventional (13) 1.75 Å above the molecular plane. To save space we do not present the plots of the other molecules, though they are available upon request.

Figures 1 to 3 clearly show that the strong inductive electron withdrawing power of the nitroso group completely eliminates the large negative electrostatic potential region associated with the carbon–carbon double bond (26). As a consequence of this effect one should expect a less nucleophilic olefinic double bond. For instance, the trifluoronitrosoethylene has been reported to react smoothly with chlorine in the dark to give 1,2-dichlorotrifluoro-1-nitrosoethene (4). Major negative electrostatic potentials are now associated with the nitroso nitrogen,

Can. J. Chem. Downloaded from www.nrcresearchpress.com by 91.144.44.67 on 09/07/12
For personal use only.

Can. J. Chem. Downloaded from www.nrcresearchpress.com by 91.144.44.67 on 09/07/12
For personal use only.

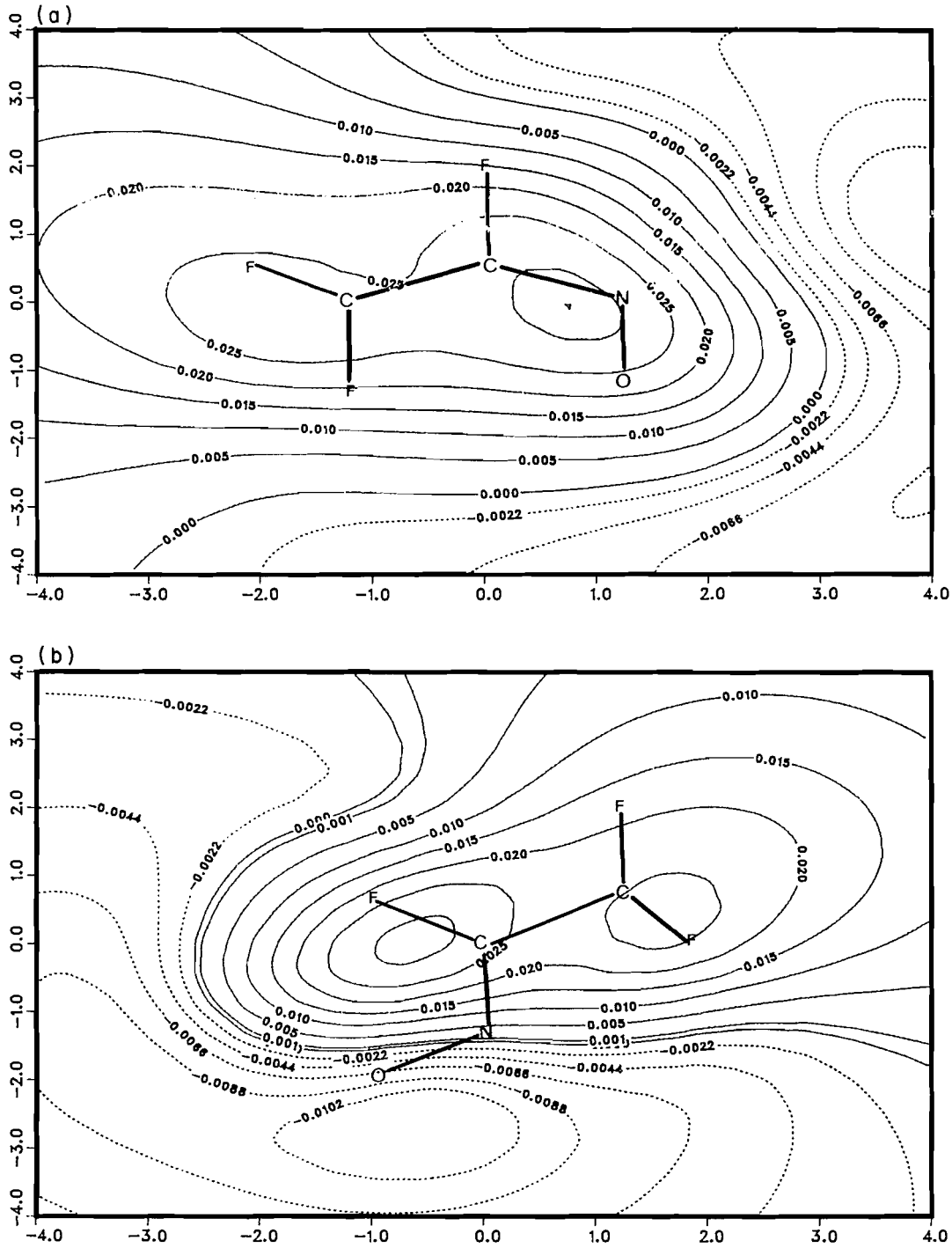

FIG. 1. Calculated electrostatic potential of (*A*) cisoid, (*B*) transoid trifluoronitrosoethylene 1.75 Å above the molecular plane. The positions of the nuclei are indicated. Dashed contours represent negative potential; all values are in kcal/mol.

which has a relatively localized lone pair and corresponding strong negative potential. It can be regarded as a likely initial reaction site for nucleophilic attack.

The positive electrostatic potential regions of these molecules are also of considerable interest for they determine the initial reaction stages for nucleophilic attack, which are the best-known reactions for compounds of this type.[4] Inspection of Figs. 1 to 3 indicates the existence of a number of positive buildups of electrostatic potential. As pointed out by Politzer and Bar-Adon (16), positive buildups of electrostatic potential are generally associated with nuclei, and it is rather unusual, and noteworthy, to find them elsewhere, especially above bonds. The magnitudes and approximate locations of these maxima are given in Table 4. Thus we see that the cisoid trifluoronitrosoethylene has a unique positive buildup on the C—N—O angle (see Fig. 1*a*), but the transoid conformer has two positive buildups, one above the C—N—O angle and the other, which

[4]For a recent review about nucleophilic addition to conjugated nitrosoalkenes, see ref. 3 section 4B.

Can. J. Chem. Downloaded from www.nrcresearchpress.com by 91.144.44.67 on 09/07/12
For personal use only.

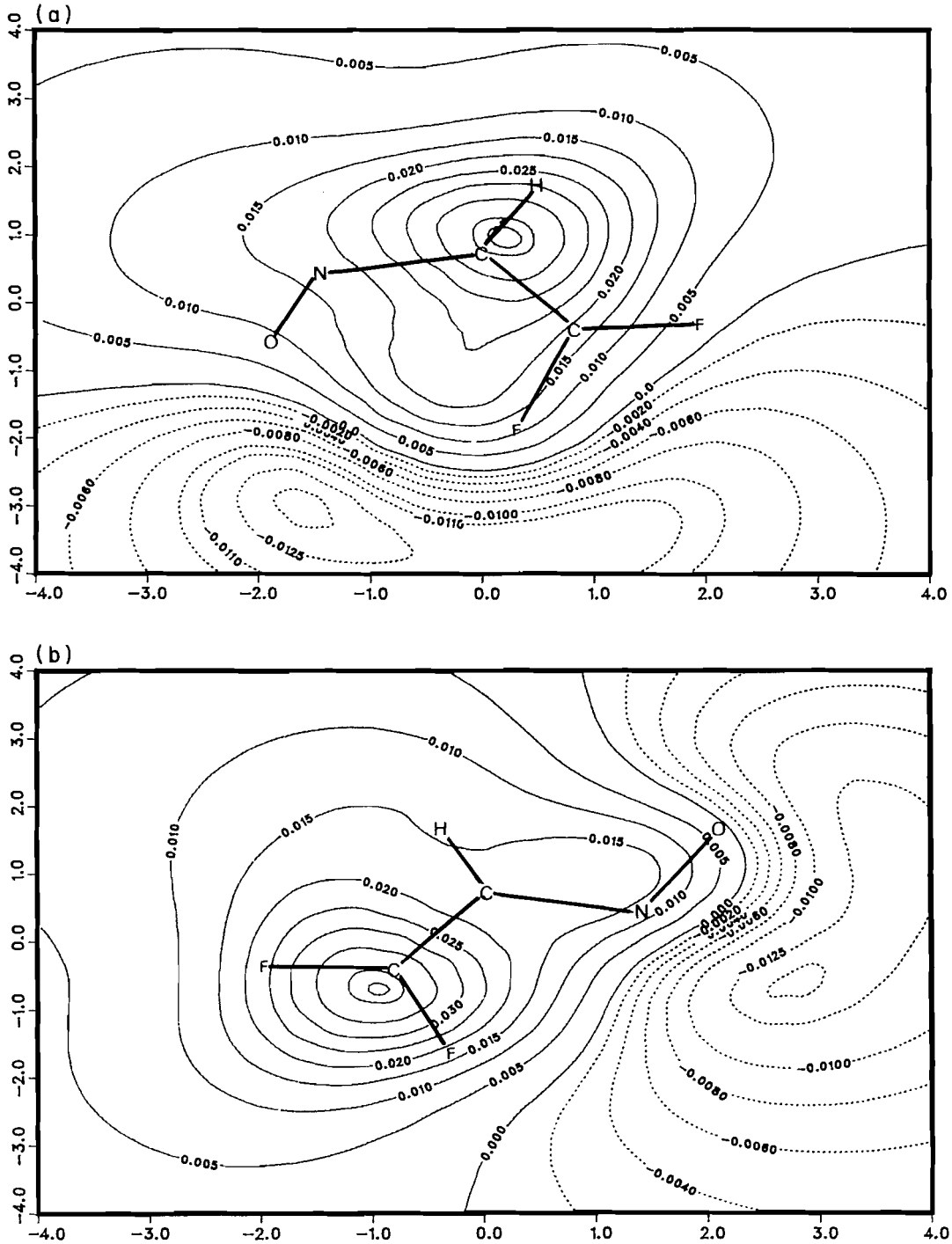

FIG. 2. Calculated electrostatic potential of (*A*) cisoid, (*B*) transoid β-difluoronitrosoethylene 1.75 Å above the molecular plane. The positions of the nuclei are indicated. Dashed contours represent negative potential; all values are in kcal/mol.

turns out to be the largest one, above the F—β-C—F angle. Figures 2*a* and 2*b* show that major positive values of the electrostatic potential in the cisoid β-difluoronitrosoethylene are located above the α-C—H bond. This positive buildup disappears and a new larger one arises above the F—β-C—F angle in the transoid conformer. Consistent with this, it has been reported that conjugated nitroso-alkenes preferentially add nucleophiles to the β-carbon atom when in the transoid conformation (27). Two positive electrostatic potential buildups in the transoid conformer have been found for all the molecules except for the nitrosoethylene (see Table 4). These molecules present positive electrostatic potential regions above the C—N—O angle irrespective of whether their conformation is cisoid or transoid (see Fig. 3, Table 4). Similar buildups of positive potential have been found on other molecules like nitro- and nitrosoacetylene (16), and related to the tendencies of these species to undergo nucleophilic attack upon the C—NO_2 and C—NO bonds (28).

Can. J. Chem. Downloaded from www.nrcresearchpress.com by 91.144.44.67 on 09/07/12
For personal use only.

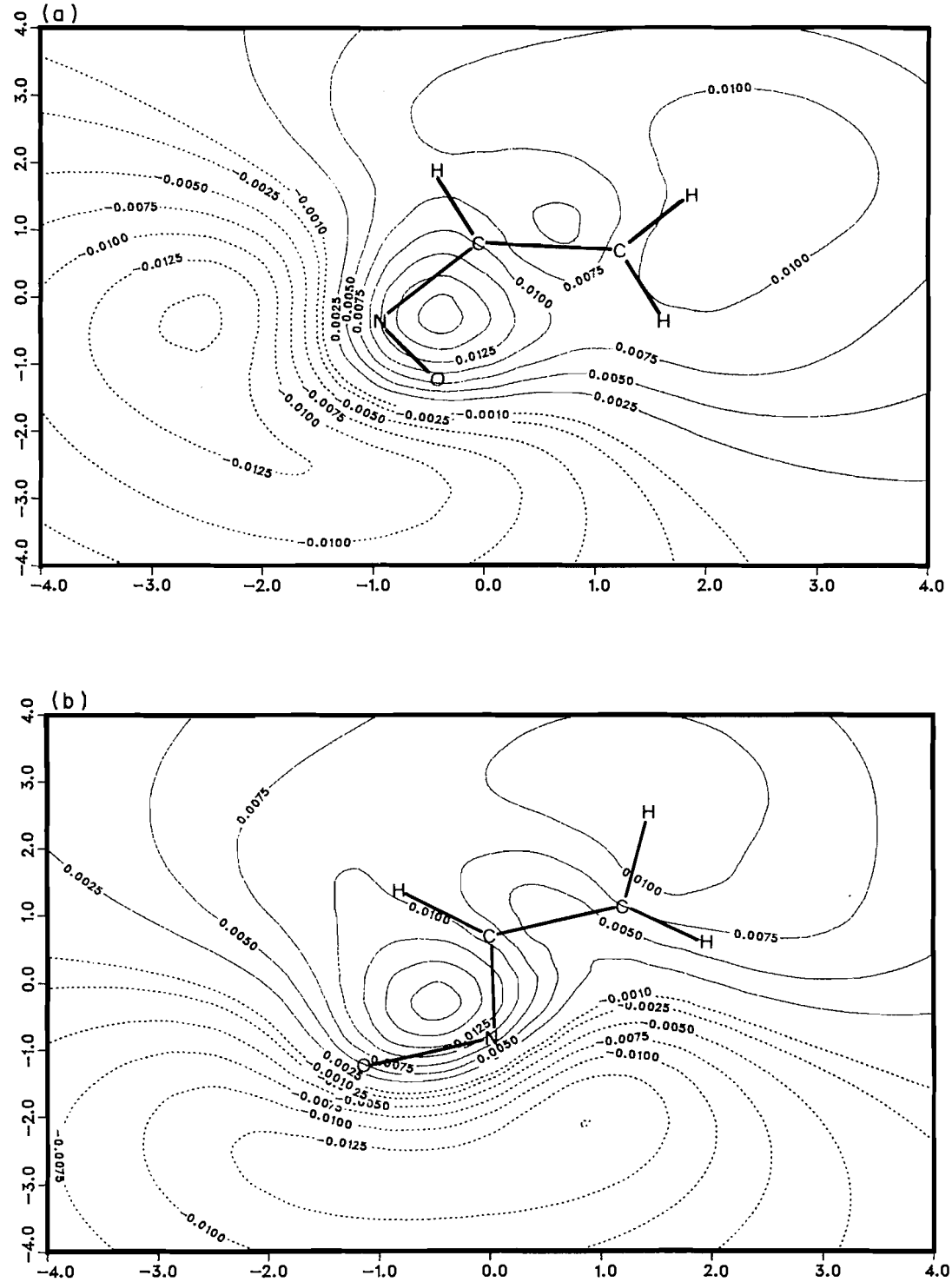

FIG. 3. Calculated electrostatic potential of (*A*) cisoid, (*B*) transoid α-fluoronitrosoethylene 1.75 Å above the molecular plane. The positions of the nuclei are indicated. Dashed contours represent negative potential; all values are in kcal/mol.

4. Summary

We have computed the optimized geometries, bond orders, and the electrostatic potentials for both transoid and cisoid fluoronitrosoethylenes and nitrosoethylene, with an objective of gaining insight into the nature of intramolecular interactions of the nitroso group with the carbon—carbon double bond, and determining the initial reactive interaction sites of these molecules. Calculations at the single determinant Hartree–Fock level of theory demonstrate that the transoid conformers are more stable than the cisoids. Inclusion of electron correlation via Moller–Plesset theory up to the second order does not vary this trend. Analyses of the bond orders show that all the C—H bonds are found to be stronger than more typical aliphatic C—H bonds, due to the strong inductive withdrawing effect by the nitroso group. It is also of interest to note that the C—C bond and C—N bond orders, and consequently their bond

TABLE 4. Summary of calculated electrostatic potentials

Molecule	Approximate location of planar maxima	Values of maxima (kcal/mol)
$R_1 = R_2 = R_3 = F$	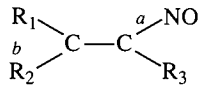	Cisoid *a*:19.56 Transoid *a*:13.04 *b*:20.22
$R_1 = H$ $R_2 = R_3 = F$	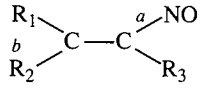	Cisoid *a*:15.00 Transoid *a*:12.39 *b*:16.30
$R_2 = H$ $R_1 = R_3 = F$	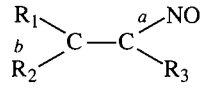	Cisoid *a*:16.00 Transoid *a*:13.10 *b*:15.93
$R_3 = H$ $R_1 = R_2 = F$	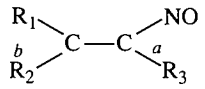	Cisoid *a*:18.36 Transoid *b*:20.31
$R_1 = R_2 = R_3 = H$	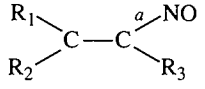	Cisoid *a*:8.34 Transoid *a*:8.37

energies, compare well with those of ethylene and ethylamine, respectively, and therefore contributions from ionic resonance structures should be small.

Examining the electrostatic potential contour maps we have observed that introduction of the nitroso group completely eliminates the negative potential region associated with the C—C double bond. Consequently, the carbon–carbon double bond should be regarded to be less nucleophilic than olefinic double bonds, in agreement with earlier experimental studies (4). The values and relative locations of the positive electrostatic potential maxima clearly show that nucleophilic addition to the β-carbon occurs preferentially when the molecule is in the transoid conformation.

Finally positive potential buildups that are found above the C—N—O angle and in some of the molecules also above the α-C—H bond are other remarkable features of these molecules.

Acknowledgments

This work has been supported by the Basque Country University (Euskal Herriko Unibertsitatea), Grant UPV 203.215-76/88. The authors gratefully acknowledge the Computing Center of the Basque Country University (Euskal Herriko Unibertsitatearen Donostiako Kalkulu-Zentroa) for providing us with the necessary computer facilities.

1. J. MILLER and A. J. PARKER. Aust. J. Chem. **11**, 302 (1958).
2. G. W. KIRBY. Chem. Soc. Rev. **6**, 1 (1977).
3. T. L. GILCHRIST. Chem. Soc. Rev. **12**, 53 (1983).
4. C. E. GRIFFIN and R. N. HASZELDINE. J. Chem. Soc. 1398 (1960).
5. F. B. MALLORY and A. CAMMARATA. J. Am. Chem. Soc. **88**, 61 (1966).
6. J. MARCH. Advanced organic chemistry. 3rd ed. Wiley-Interscience, New York. 1985. p. 1103.
7. M. J. FRISH, J. S. BINKLEY, H. B. SCHLEGEL, K. RAGHAVACHARI, C. F. MELIUS, R. L. MARTIN, J. J. P. STEWART, F. W. BOBROWICZ, C. M. ROHLFING, L. R. KHAN, D. J. DEFRESS, R. SEEGER, R. A. WHITESIDE, D. J. FOX, E. M. FLEUDER, and A. J. POPLE. GAUSSIAN86. Carnegie-Mellon Quantum Chemistry Publishing Unit, Pittsburgh, PA. 1984.
8. E. SEDANO, C. SARASOLA, J. M. UGALDE, I. IRAZABALBEITIA, and A. GONZALEZ. J. Phys. Chem. **92**, 5094 (1988).
9. C. SARASOLA, S. C. CHOI, J. M. UGALDE, and R. J. BOYD. J. Phys. Org. Chem. In press.
10. P. POLITZER and S. RANGANATHAM. Chem. Phys. Lett. **124**, 527 (1986).
11. G. ALGONA, E. SCROCCO, and J. TOMASI. J. Am. Chem. Soc. **97**, 6976 (1975).
12. E. SCROCCO and J. TOMASI. Adv. Quant. Chem. **11**, 115 (1978).
13. P. POLITZER and D. G. TRUHLAR (*Editors*). Chemical applications of atomic and molecular electrostatic potentials. Plenum, New York. 1981.
14. R. F. W. BADER. Acc. Chem. Res. **18**, 9 (1985).
15. M. T. CARROLL, J. R. CHEESEMAN, R. OSMAN, and H. WEINSTEIN. J. Phys. Chem. **93**, 5120 (1989).
16. P. POLITZER and R. BAR-ADON. J. Am. Chem. Soc. **109**, 3534 (1987).
17. M. PAGE. THEOCHEM, **34**, 267 (1987).
18. J.-G. YU and R.-Z. LUI. THEOCHEM, **50**, 55 (1988).
19. W. J. HEHRE, L. RADOM, P. V. R. SCHLEYER, and J. A. POPLE. Ab initio molecular orbital theory. Wiley-Interscience, New York. 1986.
20. K. KUTSITSU, T. FUKUYAMA, and Y. MORINO. J. Mol. Struct. **1**, 463 (1967).
21. R. G. STONE and W. H. FLYGARE. J. Mol. Spectrosc. **32**, 233 (1969).
22. V. W. LAURIE and D. T. PENCE. J. Chem. Phys. **38**, 2693 (1963).
23. E. B. WILSON, JR. Tetrahedron, **17**, 191 (1962).
24. C. SARASOLA and J. M. UGALDE. Unpublished results.
25. E. SEDANO, C. SARASOLA, and J. M. UGALDE. Tetrahedron. In press.
26. P. POLITZER and W. L. HEDGES. Int. J. Quant. Chem. Quant. Biol. Symp. **9**, 307 (1982).
27. J. H. SMITH, J. H. HEIDEMA, and E. J. KAISER. J. Am. Chem. Soc. **94**, 9276 (1972).
28. P. POLITZER, P. A. LAURENCE, ABRAHMSEN, and B. A. ZILLES. Chem. Phys. Lett. **111**, 75 (1984).

Can. J. Chem. Downloaded from www.nrcresearchpress.com by 91.144.44.67 on 09/07/12
For personal use only.

The audio frequency conductances of magnesium, manganese II, and barium malonates in aqueous medium at 25°C

ANIS A. AL-NAJAR AND AWATIF M. IBRAHIM
Department of Chemistry, College of Science, University of Basrah, Basrah, Iraq

Received April 10, 1989[1]

ANIS A. AL-NAJAR and AWATIF M. IBRAHIM. Can. J. Chem. **68**, 770 (1990).

The conductance of aqueous solutions of magnesium, manganese II, and barium malonates has been measured at 1.59 kHz, using a conventional audio frequency bridge. Conductance data were evaluated using different modern theoretical conductance equations, each a three-parameter equation in K_A, Λ_0, and a. These are the complete and expanded forms of both the Fuoss–Hsia (F/H) and Pitts (P) equations and the Lee–Wheaton (L/W) equation. Our results show that the Lee–Wheaton equation is the most satisfactory.

Key words: conductance, aqueous medium, magnesium malonate, manganese malonate, barium malonate.

ANIS A. AL-NAJAR et AWATIF M. IBRAHIM. Can. J. Chem. **68**, 770 (1990).

Utilisant un pont à fréquence audio conventionnel et opérant à 1,59 kHz, on a mesuré les conductivités de solutions aqueuses de malonates de magnésium, de manganèse(II) et de baryum. On a évalué les données de conductivité à l'aide de diverses équations théoriques modernes de la conductivité; chacune de ces équations implique trois paramètres, soit le K_A, le Λ_0 et le a. Les équations utilisées sont : les formes complètes et étendues de l'équation de Fuoss–Hsia (F/H), celle de Pitts (P) ainsi que celle de Lee–Wheaton (L/W). Les paramètres de conductivité obtenus à l'aide d'une analyse faisant appel à ces théories indique que l'équation de L/W reproduit les données mieux que les autres équations.

Mots clés : conductivité, milieu aqueux, malonate de magnésium, malonate de manganèse, malonate de baryum.

[Traduit par la revue]

Introduction

Within experimental uncertainty, Onsager's limiting equation (1) agrees with the data for numerous uni–univalent salts in water up to 0.001 M. Agreement with experiment is also found for most uni–bivalent and uni–tervalent salts, but when the valency product increases to four the equation no longer holds. A much steeper slope of the experimental points than the theoretical Onsager value is usually obtained when the equivalent conductance of a bi–bivalent is plotted against the square root of the concentration. The increase in divergence with increasing concentration of the experimental data from the theoretical conductance data in these cases can be attributed to ion-pair formation of an essentially electrostatic and non-specific kind, described by K_A. K_A may be derived if it is assumed that the free ions obey the limiting equation, that the ion-pair is non-conducting, and that its activity coefficient in dilute solution is unity (2). Under these conditions, the conductance equation chosen for representing the phoreogram of a given salt in a particular solvent is a function of the three parameters K_A, Λ_0, and a.

On the other hand, the conductance behaviour of 2:2 electrolytes has received relatively little attention. This is largely due to the difficulty encountered in analysing such data since the usual methods require an arbitrary choice for some of the parameters needed in the analysis. In this paper we report conductance measurements of magnesium, manganese II, and barium malonates in aqueous medium. Five currently used conductance equations, the complete and expanded forms of both the Fuoss–Hsia (3, 4) and the Pitts (5, 6) equations and a recent equation Lee–Wheaton (7) describing charge transport in electrolyte solutions, based on a new and specifically chemical model for ions in solution (7, 8) have been used to analyse conductance data for these malonate salts.

Experimental

Measurements were made at 25°C with Wayne–Kerr B331 audio frequency bridge of admittance in all four quadrants of complex plane. It combines speed and simplicity of operation with 0.01% accuracy.

The cell used for measuring conductances has been described elsewhere (9).

The cell constant (as determined by standard solutions (10) of potassium chloride) was 0.20261 ± 0.00002 cm^{-1}. The method used for measuring conductances has been described (11).

Materials

The KCl used in this work was purified and used according to the literature (9).

Magnesium malonate was prepared by the addition of clean and dried magnesium metal to a solution of malonic acid. The pH of the solution was continuously tested until the solution became neutral. The mixture was then filtered to remove excess added metal, after which the solvent was evaporated on a water bath. The product was recrystallised twice from conductivity water and air-dried at room temperature. The final product was a white crystalline material, a dihydrate. Manganese malonate was prepared as described by Vogel (12) for calcium malonate but with some modification. AnalaR grade manganese chloride solution was added to a solution of sodium malonate. The mixture was heated on a water bath for a few minutes with continuous stirring. The light pink precipitate formed was allowed to cool to room temperature. The mixture was filtered off and the filtrate tested for chloride ions. The product was washed with cold conductivity water until chloride-ion free, after that the final product, a dihydrate was air-dried at room temperature. Barium malonate was prepared the same way as manganese malonate. The product was a white crystalline salt in the form of a dihydrate. The magnesium and manganese malonates were analysed for Mg and Mn contents by titration with EDTA, while the analysis for barium content was carried out using the method described by Vogel (13). The compositions of the three salts were determined by thermogravimetric analysis for hydration.

All stock solutions were prepared by weight, and all measurements were done using the weight dilution technique.

Results and discussion

The measured molar conductances Λ_{exp} and the corresponding concentrations C in moles per liter at 298 K are given in Table 1. These data were analyzed using the complete and modified forms of both F/H and P equations as well as using the L/W equation. For the interpretation of the characteristic parameters of an electrolyte solution from conductance data, a

[1]Revision received November 21, 1989.

Can. J. Chem. Downloaded from www.nrcresearchpress.com by 91.144.44.67 on 09/07/12
For personal use only.

TABLE 1. Experimental conductance data of malonate salts at $T = 298$ K

	$MgC_3H_2O_4.2H_2O$		$MnC_3H_2O_4.2H_2O$		$BaC_3H_2O_4.2H_2O$	
No.	$C \times 10^4$*	Λ_{exp}†	$C \times 10^4$*	Λ_{exp}†	$C \times 10^4$	Λ_{exp}†
1	3.6111	186.432	2.0523	179.110	1.4047	256.267
2	4.4813	180.736	2.6983	170.540	2.5321	249.565
3	4.9907	177.715	3.4776	162.053	3.6312	244.245
4	5.7731	173.489	4.7326	151.520	4.8669	239.115
5	6.7708	168.611	4.8847	150.466	6.0441	234.822
6	7.9597	163.692	5.3112	147.325	7.2922	230.725
7	9.0915	159.429	6.8041	138.552	8.3528	227.543
8	9.8520	156.792	8.6760	129.668	9.4159	224.578
9	10.5836	154.467	9.5270	126.388	10.5033	221.747
10	11.6307	151.354	10.2952	123.555	11.4726	219.365
11	12.7410	148.217	10.9975	121.169	12.4631	217.065
12	14.0206	144.895	11.9497	118.221	13.5206	214.732
13	15.6259	141.412	12.7742	115.850	14.4631	212.749
14	16.6838	139.069	13.7778	113.197	15.422	210.822
15	17.9943	136.525	14.7049	110.961	16.3292	209.068
16	18.6999	135.279	16.2020	107.631	17.1978	207.455
17	19.9076	132.944			18.9180	204.425

*Concentration in mol dm^{-3}.
†Λ_{exp} in Ω^{-1} cm^2 mol^{-1}.

TABLE 2. The best fit parameters for malonate salts found in the present work at $T = 298$ K

Electrolyte	Λ_0 (Ω^{-1} cm^2 mol)	K_A (l mol^{-1})	a (Å)	σ	Conductance equation
$MgC_3H_2O_4$	231.74	613	3.05	0.029	F/H complete
	231.76	637	5.15	0.029	F/H modified
	230.02	592	7.45	0.077	Pitts complete
	231.94	639	2.45	0.029	Pitts modified
	231.76	620	6.2	0.008	Lee/Wheaton
$MnC_3H_2O_4$	232.38	1663	2.55	0.025	F/H complete
	232.36	1688	4.85	0.025	F/H modified
	231.60	1658	8.45	0.041	Pitts complete
	232.32	1674	1.75	0.026	Pitts modified
	232.38	1780	5.3	0.008	Lee/Wheaton
$BaC_3H_2O_4$	272.58	90	3.1	0.011	F/H complete
	272.58	96	3.7	0.014	F/H modified
	271.74	87	5.75	0.033	Pitts complete
	272.58	98	1.95	0.011	Pitts modified
	272.58	93	5.4	0.009	Lee/Wheaton

minimisation technique has been used (14) in terms of K_A, Λ_0, and a. For analysis of each set of data points C_j, Λ_j ($j = 1, \ldots, N$), an Algol computer program has been written. All calculations were performed on an ICL. 1905 F computer using Λ_0, a, and K_A which produce a theoretical curve giving the best fit to the measured conductance. The results of the minimisation technique for the best fit values of the three parameters Λ_0, K_A, and a are listed in Table 2 together with the corresponding values of the standard deviation σ, given by

$$[1] \quad \sigma = (S^2/N)^{1/2}$$

where S^2 is defined by

$$[2] \quad S^2 = \sum_{j=1}^{N} (\Lambda_{calc} - \Lambda_j)^2$$

The results from other workers are listed in Table 3.

From the association constants given in Table 2, it can be

TABLE 3. The association constants of malonate salts taken from the literature

Electrolyte	K_A (l mol^{-1})	Method
$MgC_3H_2O_4$	714	Colorimetry (16)
	724	Colorimetry (17)
	632	Conductometry (15)
	728	Colorimetry (18)
	694	Potentiometry (19)
$MnC_3H_2O_4$	1961	Colorimetry (16)
	1950	Colorimetry (17)
$BaC_3H_2O_4$	135	Colorimetry (16)
	80	Conductometry (20)
	71	Colorimetry (17)
	189	Colorimetry (18)

Can. J. Chem. Downloaded from www.nrcresearchpress.com by 91.144.44.67 on 09/07/12
For personal use only.

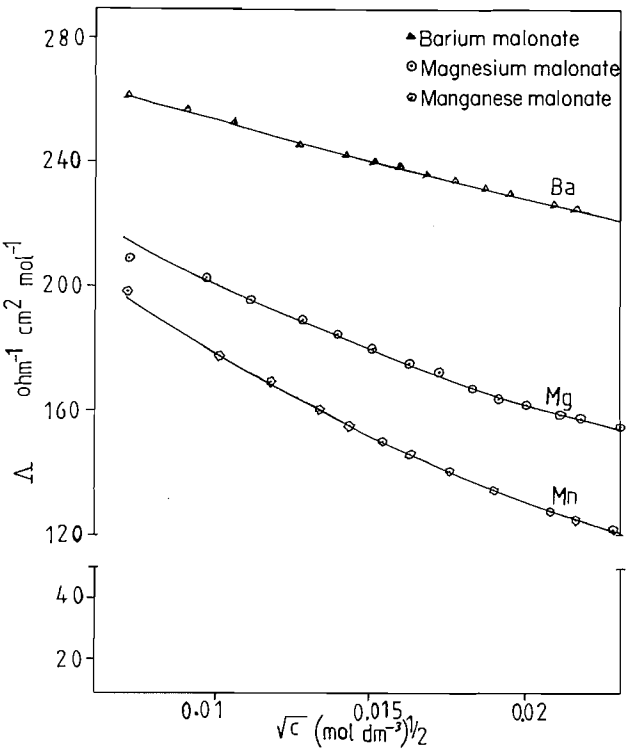

FIG. 1. Experimental molar conductances versus square root of concentration.

deduced that these salts do not behave as "strong" electrolytes, and their dissociations are far from complete. It can also be seen that manganese malonate undergoes more ion-pair formation according to the quantitative conductance data. The same conclusion was given by Riley and Fisher (15) who predicted that the degree of dissociation fluctuates significantly from one to another.

The malonate ion is less of a donor compared to the oxalate ion (15), thus it can also be emphasized that magnesium and manganese malonates are more highly dissociated than the oxalates (21).

The values obtained in this work for K_A, Λ_0, and a are satisfactory, providing a particularly good example of typical incompletely dissociated electrolyte the thermodynamic association constants of which conform to the law of mass action. The abnormally low conductances of these electrolytes (Fig. 1) are not due to the presence of electrically neutral molecules but to the ion-pair formation. This was indicated by measurements at high frequency (22).

It is of interest to note from Table 2 that the values of parameter a are small for all salts studied. This agrees with the previous results obtained by Stock and Davies (16) that a = 2.9 Å for magnesium malonate, a = 2.4 Å for manganese malonate, but a = 10 Å for barium malonate. Their explanation for these results is that the small a values indicate that the linkage is largely covalent (16, 17) and not merely due to "coulomb" ion association. The large a value for barium malonate was explained (16) by the fact that the assumption of spherical symmetry and a central charge is far from the truth for the malonate ion. The idea of ionic radii from Gane and Ingold (23) was used by Jones and Stock (17), who suggested that the molecules of the malonate salts acquire a coiled configuration as an explanation for the small a values they have obtained for the malonate salts.

Later (18), it was found that the hydrated radii for Mg^{2+} and Ba^{2+} ions are 4.1 Å and 4.2 Å respectively as calculated from the dissociation constants.

The small a values obtained in the present work agree with Prue's (24) point of view, Justice's suggestion (25) and Beronius' results (26).

Unfortunately, no recent determinations of Λ_0 at 298 K for magnesium, manganese, and barium malonates have been found. Moreover, Λ_0 was only found (15) to be 223.72 $ohm^{-1}\,cm^2\,mol^{-1}$ for magnesium malonate. Thus in comparison with ionic mobilities at infinite dilution at 298 K taken from ref. 27: $\lambda_0(Mg^{2+})$ = 106.12, $\lambda_0(Mn^{2+})$ = 106.20 and $\lambda_0(Ba^{2+})$ = 127.28 together with the value of 129.4 for malonate ion (20), good agreement has been shown in Table 2 for both magnesium and manganese malonates. The value obtained in this work for barium malonate is much higher than that given by direct combination of λ_0 values of ionic mobilities.

It was noted that the minimisation Λ_0 values for the complete and modified F/H equation were always greater than those values obtained using the complete form of the Pitts equation. The reason for this has been discussed briefly by Fernandez Prini and Prue (4, 6) and in detail by Pitts *et al.* (28). The Brownian terms in the velocity of the ion was neglected by Pitts. Also, Pitts equation does not allow for the kinetic (osmotic) terms which contributed to the increase in velocity of the ion. Another feature of the minimisation results is that the modified Pitts equation yields values of a lower than those given by other equations.

It was obvious from the minimisation techniques that the parameter Λ_0 had the greatest effect on the values of S^2 during the variation of the three parameters K_A, Λ_0, and a. This is to be expected, in so far as Λ_0 is the leading term in all the conductance equations. However, Λ_0 was relatively insensitive to the values of K_A and a at the corresponding minima of S^2.

However, it was shown that the L/W equation, relative to the other four equations, is preferable for the analysis of conductance data (as indicated by σ) for our present system. This may be due to the inclusion of third order terms (7, 8) in the plasma parameter (ϵK) of their equation. The same behaviour was found in another system (29).

1. L. ONSAGER. Z. Physik. Z. **27**, 388 (1926), **28**, 277 (1927).
2. R. M. FUOSS and F. ACCASINA. Electrolytic conductance. 1st ed. Interscience Publishers Inc., New York. 1959. p. 196.
3. R. M. FUOSS and K. L. HSIA. Proc. Nat. Acad. Sci. **57**, 1550 (1967); **58**, 1818 (1967).
4. R. FERNANDEZ PRINI. Trans. Faraday Soc. **65**, 3311 (1969).
5. E. PITTS. Proc. R. Soc. A, **217**, 43 (1953).
6. R. FERNANDEZ PRINI and J. E. PRUE. Z. Phys. Chem. **228**, 373 (1965).
7. W. H. LEE and R. J. WHEATON. J. Chem. Soc. Faraday II, **74**, 743 (1978); **74**, 1456 (1978).
8. R. J. WHEATON. Ph.D. Thesis. University of Surrey. 1978.
9. W. H. LEE, R. W. PENGILLY, and R. W. RANCE. Z. Phys. Chem. Leipzig. **257**, No. 3, 433 (1976).
10. J. E. LIND, J. J. ZWOLENIK, and R. M. FUOSS. J. Am. Chem. Soc. **81**, 1557 (1959).
11. A. M. IBRAHIM. M.Sc. Thesis. University of Basrah. 1978.
12. A. I. VOGEL. Practical organic chemistry. 3rd ed. Longmans Green and Co. Ltd. 1966.
13. A. I. VOGEL. Quantitative inorganic analysis. 3rd ed. Longmans, Green and Co., Ltd., London. 1964. p. 275.
14. A. A. AL-NAJAR. Iraqi J. Sci. **21**, 491 (1980).
15. H. L. RILEY and N. I. FISHER. J. Chem. Soc. 2006 (1929).
16. D. I. STOCK and C. W. DAVIES. J. Chem. Soc. 1371 (1949).

Can. J. Chem. Downloaded from www.nrcresearchpress.com by 91.144.44.67 on 09/07/12
For personal use only.

17. R. H. JONES and D. I. STOCK. J. Chem. Soc. 306 (1962).
18. U. K. KLANING, and O. OSTERBY. J. Chem. Soc. Faraday I, **72**, 513 (1976).
19. J. I. EVANS and C. B. MONK. Trans. Faraday Soc. **48**, 934 (1952).
20. J. M. PEACOCK and J. C. JAMES. J. Chem. Soc. 2233 (1951).
21. A. A. AL-NAJAR. Ph.D. Thesis, University of Surrey. 1974.
22. A. A. AL-NAJAR and A. M. IBRAHIM. To be published.
23. N. G. GANE and C. K. INGOLD. J. Chem. Soc. 1594 (1928); 2153 (1931).
24. E. M. HANNA, A. D. PETHYBRIDGE, and J. E. PRUE. Electrochem. Acta, **16**, 677 (1971).
25. J. BARTHEL, J. C. JUSTICE, and R. WACHTER. Z. Phys. Chem. **84**, 100 (1973).
26. P. BERONIUS. Acta Chem. Scand. **30**, 115 (1976).
27. C. B. MONK. Electrolytic dissociation. 1st ed. Academic Press, London. 1961. p. 271.
28. E. PITTS, B. E. TABOR, and J. DALY. Trans. Faraday Soc. **65**, 849 (1969); **66**, 693 (1970).
29. A. A. AL-NAJAR and A. M. IBRAHIM. Iraqi J. Sci. **22**, 466 (1981).

Can. J. Chem. Downloaded from www.nrcresearchpress.com by 91.144.44.67 on 09/07/12
For personal use only.

Studies on complexes of VO(II), Mn(II), Cu(II), Ni(II), Co(II), Zn(II), Fe(III), and UO_2(II) with hydrazone β-diketone ligands[1]

MOHAMED S. ABDEL-MOEZ, SHAKER L. STEFAN,[2] MOSTAFA M. EL-BEHAIRY, MOHAMED M. MASHELY, AND BASHEIR A. EL-SHETARY

Chemistry Department, Faculty of Education, Ain Shams University, Roxy, Cairo, Egypt

Received February 14, 1989[3]

MOHAMED S. ABDEL-MOEZ, SHAKER L. STEFAN, MOSTAFA M. EL-BEHAIRY, MOHAMED M. MASHELY, and BASHEIR A. EL-SHETARY. Can. J. Chem. **68**, 774 (1990).

The stepwise stability constants of VO(II), Mn(II), Cu(II), Ni(II), Co(II), Zn(II), Fe(III), and UO_2(II) metal ions with 2-(2-acetylphenylhydrazone)-5,5-dimethyl-1,3-cyclohexane dione (2-APHDm), 3-(2-acetylphenylhydrazone)pentane-2,4-dione (2-APHA), 2-(2-acetylphenylhydrazone)-1-phenyl-1,3-butane dione (2-APHB), 2-(2-acetylphenylhydrazone)-1,3-diphenyl-1,3-propane dione (2-APHDB), and 3-(2-acetylphenylhydrazone)-1,1,1-trifluoropentane-2,4-dione (2-APHTA) were determined at 30°C by pH titrations in 75% (v/v) dioxane–water solvent. In addition, metal complexes of three related β-diketones, 2-APHA, 2-APHB, and 2-APHDB have been synthesized and characterized by elemental analysis, uv–visible, ir spectra, and conductance in DMF and magnetic susceptibility measurements. The structure of the complexes have been proposed.

Key words: transition metal complexes of hydrazone-β-diketone ligands.

MOHAMED S. ABDEL-MOEZ, SHAKER L. STEFAN, MOSTAFA M. EL-BEHAIRY, MOHAMED M. MASHELY et BASHEIR A. EL-SHETARY. Can. J. Chem. **68**, 774 (1990).

Opérant à 30°C, dans un mélange à 75% (v/v) de dioxane–eau et faisant appel à des titrations par pH, on a déterminé les constantes de stabilité des ions VO(II), Mn(II), Cu(II), Ni(II), Co(II), Zn(II), Fe(III) et UO_2(II) avec la 2-(2-acétylphényl-hydrazone)-5,5-diméthylcyclohexane-1,3-dione (2-APHDm), 3-(2-acétylphénylhydrazone)-pentane-2,4-dione (2-APHA), 2-(2-acétylphénylhydrazone)-1-phényl-butane-1,3-dione (2-APHB), 2-(2-acétylphénylhydrazone)-1,3-diphényl-propane-1,3-dione (2-APHDB) et 3-(2-acétylphénylhydrazone)-1,1,1-trifluoropentane-2,4-dione (2-APHTA). On a aussi synthétisé des complexes métalliques de trois β-dicétones apparentées et on les a caractérisés par analyse élémentaire, par spectroscopie uv et ir et par des mesures de susceptibilité magnétique et de conductivité dans le DMF. On propose des structures pour les complexes.

Mots clés : complexes de métaux de transitions avec des ligands d'hydrazones β-cétoniques.

[Traduit par la revue]

Introduction

β-Diketone as well as hydrazone compounds have been used widely as chelating agents with transition elements (1, 2). However, the combination products of the two classes of chelating agents form new interesting compounds which act as very good bi- or tridentate ligands (3). The present study investigates the physicochemical properties of the complexes of chelating agents with transition metals in both solution and solid states. The structure and basicity effects of the ligands on the stability of the formed complexes are discussed and some correlations attempted.

The hydrazone structure of the five related ligands **I** to **V** is given in Scheme 1.

Experimental

(i) Materials and methods

Solutions of Cu(II), Co(II), Ni(II), Fe(III), Zn(II) and UO_2(II) were prepared from their nitrate salts. Solutions of Mn(II) and VO(II) were prepared from the sulphates. The exact concentration was determined by titration with EDTA in the presence of a suitable indicator (4). The concentration of UO_2(II) was determined gravimetrically as uranium oxide U_3O_8 (4).

(ii) Preparation of solid complexes

The organic ligands were prepared by coupling the diazonium salt of 2-aminoacetophenone with the following diketones: **1**, pentane-2,4-dione (2-APHA); **II**, 1-phenyl-1,3-butane dione (2-APHB); **III**, 1,3-diphenyl-1,3-propane dione (2-APHDB); **IV**, 1,1,1-trifluoropentane-2,4-dione 2-APHTA; and **V**, dimedone (2-APHDm) in sodium acetate medium.

The solid complexes were prepared by adding equimolar amounts of aqueous solutions of the metal salts and ethanolic solution of the respective ligands in 1:1 molar ratio. The pH of the mixture was adjusted between 3.5–4.0 by addition of KOH with continuous stirring. The mixture was refluxed for about 4.0 h. The solid complexes were separated on cooling, then filtered, washed with water and alcohol, and dried under vacuum. The purity of the ligands (5) and their solid complexes was checked by elemental analysis, melting points, uv–visible and ir spectra.

3-(2-Acetylphenylhydrazone)pentane-2,4-dione (2-APHA)

This compound was obtained as yellow crystals from acetic acid, mp 159.0–159.5°C; λ_{max} (nm) in DMF: 365 1st band, 255 2nd band; ir (KBr) ν: 3050–3020(NH) (mb), 1663(C=O) (s), 1563(C=N) (s) cm. *Anal.* calcd. for $C_{13}H_{14}N_2O_3$: C 63.41, H 5.69, N 11.38; found: C 63.60, H 5.80, N 10.67.

[Mn(2-APHA)] complex

This compound was obtained as yellowish green crystals, decomposed at 182–182.5°C; λ_{max} (nm) in DMF: 362 1st band, 252 2nd band; ir (KBr) ν: 1660(C=O) (s), 1565(C=N) (s), 550(M—N) (m), 470(M—O) (w) cm^{-1}. *Anal.* calcd. for $[Mn(C_{13}H_{13}N_2O_3)_2]$: C 57.24, H 4.77, N 10.27; found: C 57.30, H 5.20, N 10.00.

[Fe(2-APHA)] complex

This compound was obtained as orange crystals, decomposed at 178–175.5°C; λ_{max} (nm) in DMF: 375 1st band, 250 2nd band; ir (KBr) ν: 1660(C=O) (s), 1565(C=N) (s), 550(M—N) (w), 450(M—O) (m) cm^{-1}. *Anal.* calcd. for $[Fe(C_{13}H_{13}N_2O_3)_3]$: C 59.16, H 4.93, N 10.61; found: C 60.09, H 4.90, N 10.89.

[Co(2-APHA)] complex

This compound was obtained as deep yellow crystals, decomposed

[1]This paper is published without authors' reading of the proofs.

[2]Author to whom correspondence should be addressed.

[3]Revision received October 19, 1989.

Can. J. Chem. Downloaded from www.nrcresearchpress.com by 88.85.125.76 on 09/07/12
For personal use only.

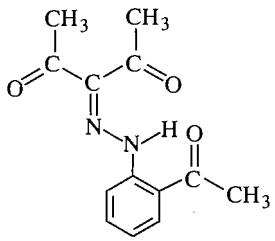

(I)
3-(2-Acetylphenylhydrazone)-pentane-2,4-dione (2-APHA)

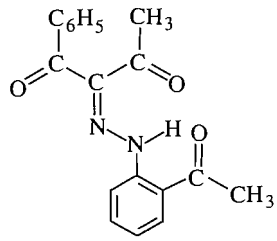

(II)
3-(2-Acetylphenylhydrazone)-1-phenyl-1,3-butanedione (2-APHB)

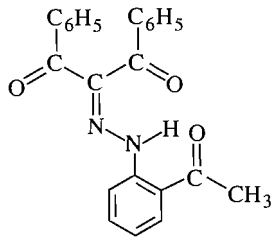

(III)
3-(2-Acetylphyenylhydrazone)-1,3-diphenyl-1,3-propane dione (2-APHDB)

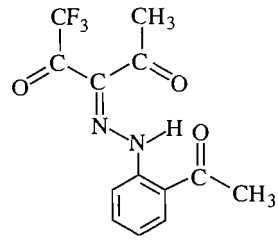

(IV)
3-(2-Acetylphyenylhydrazone)-1,1,1-trifluoro-2,4-pentane dione (2-APHTA)

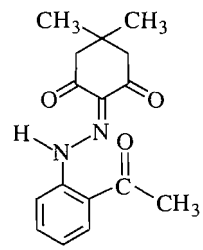

(V)
2-(2-Acetylphenylhydrazone)-5,5-dimethyl-1,3-cyclohexane dione (2-APHDm)

SCHEME 1. The structure of the hydrazone-β-diketone ligands (I to V)

at 196–196.5°C: λ_{max} (nm) in DMF: 362 1st band, 250 2nd band; ir (KBr) ν: 1660(C=O) (s), 1565(C=N) (s), 550(M—N) (w), 455(M—O) (w) cm^{-1}. *Anal.* calcd. for $[Co(C_{13}H_{13}N_2O_3)_2]$: C 56.83, H 4.73, N 10.20; found: C 57.16, H 4.99, N 10.25.

[Ni(2-APHA)] complex

This compound was obtained as yellow crystals, decomposed at 191–191.5°C; λ_{max} (nm) in DMF: 370 1st band, 252 2nd band; ir (KBr) ν: 1660(C=O) (s), 1565(C=N) (s), 550(M—N) (w), 460(M—O) (w) cm^{-1}. *Anal.* calcd. for $[Ni(C_{13}H_{13}N_2O_3)_2]$: C 56.83, H 4.73, N 10.20; found: C 56.60, H 5.01, N 10.50.

[Cu(2-APHA)] complex

This compound was obtained as yellowish green crystals, decomposed at 181–181.5°C, λ_{max} (nm) in DMF: 360 1st band, 250 2nd band; ir (KBr) ν: 3515–3400(OH) (b), 1660(C=O) (s), 1565(C=N) (s), 810 (m) coordinated H_2O, 550(M—N) (w), 460(M—O) (m) cm^{-1}. *Anal.* calcd. for $[Cu(C_{13}H_{13}N_2O_3)(H_2O)(OH)]$: C 45.41, H 4.66, N 8.15; found: C 44.91, H 4.77, N 8.40.

2-(2-Acetylphenylhydrazone)-1-phenyl-1,3-butane dione (2-APHB)

This compound was obtained as yellow crystals from acetic acid, mp 114.0–114.5°C; λ_{max} (nm) in DMF: 370 1st band, 256 2nd band; ir (KBr) ν: 3060(NH) (mb), 1642(C=O) (s), 1570(C=N) (s) cm^{-1}. *Anal.* calcd. for $C_{18}H_{16}N_2O_3$: C 70.12, H 5.19, N 9.09; found: C 69.96, H 5.42, N 8.89.

[Mn(2-APHB)] complex

This compound was obtained as yellowish green crystals, decomposed at 178–178.5°C; λ_{max} (nm) in DMF: 368 1st band, 253 2nd band; ir (KBr) ν: 1645(C=O) (s), 1575(C=N) (s), 565(M—N) (m), 430(M—O) (m) cm^{-1}. *Anal.* calcd. for $[Mn(C_{18}H_{15}N_2O_3)_2]$: C 64.57, H 4.48, N 8.37; found: C 64.31, H 4.72, N 8.30.

[Fe(2-APHB)] complex

This compound was obtained as deep orange crystals, decomposed at 180–180.5°C; λ_{max} (nm) in DMF: 367 1st band, 252 2nd band; ir (KBr) ν: 1645(C=O) (s), 1575(C=N) (s), 565(M—N) (m), 468, 430(M—O) (w) cm^{-1}. *Anal.* calcd. for $[Fe(C_{18}H_{15}N_2O_3)_2NO_3]$: C 59.0, H 4.09, N 9.56; found: C 58.75, H 4.30, N 9.30.

[Co(2-APHB)] complex

This compound was obtained as reddish brown crystals, decomposed at 194–194.5°C; λ_{max} (nm) in DMF: 365 1st band, 250 2nd band; ir (KBr) ν: 1645(C=O) (s), 1575(C=N) (s), 565(M—N) (m), 430(M—O) (w) cm^{-1}. *Anal.* calcd. for $[Co(C_{18}H_{15}N_2O_3)_2]$: C 64.19, H 4.46, N 8.32; found: C 64.70, H 5.00, N 7.93.

Can. J. Chem. Downloaded from www.nrcresearchpress.com by 88.85.125.76 on 09/07/12
For personal use only.

Can. J. Chem. Downloaded from www.nrcresearchpress.com by 88.85.125.76 on 09/07/12
For personal use only.

TABLE 1. Formation constants of 1:1 and 1:2 complexes of

Metal ion	2-APHDm, pK = 13.13				2-APHB, pK = 13.99			
	log K_1	ΔG_1	log β	log K_1 − log K_2	log K_1	ΔG_1	log β	log K_1 − log K_2
VO^{2+}	12.80	73.22	23.20	2.40	12.85	71.96	23.58	2.12
Mn^{3+}	6.80	38.89	10.77	2.83	7.60	43.47	11.52	3.68
Fe^{3+}	13.07	74.76	24.77	1.37	14.00	80.08	26.70	1.30
Co^{2+}	8.80	50.34	16.63	0.97	9.58	54.80	18.58	0.58
Ni^{2+}	9.45	54.05	17.85	1.05	9.70	53.31	17.99	1.41
Cu^{2+}	12.20	69.79	20.98	3.42	11.72	67.04	19.87	3.57
Zn^{2+}	9.28	53.08	17.90	0.66	10.25	58.63	19.67	0.83
UO_2^{2+}	11.92	68.18	22.87	0.97	12.72	72.76	24.37	1.07

*ΔG_1 in kJ/mol. The values of log K_1 − log K_2 ranged between 0.52 and 3.57. The uncertainty in the stability

[Ni(2-APHB)] complex

This compound was obtained as orange crystals, decomposed at 187–187.5°C; λ_{max} (nm) in DMF: 368 1st band, 252 2nd band; ir (KBr) ν: 1645(C=O) (s), 1575(C=N) (s), 565(M—N) (m), 435(M—O) (w) cm^{-1}. *Anal.* calcd. for $[Ni(C_{18}H_{15}N_2O_3)_2]$: C 64.19, H 4.46, N 8.33; found: C 64.70, H 4.60, N 8.43.

[Cu(2-APHB)] complex

This compound was obtained as yellowish green crystals, decomposed at 165–165.5°C; λ_{max} (nm) in DMF: 365 1st band, 252 2nd band; ir (KBr) ν: 1645(C=O) (s), 1575(C=N) (s), 560(M—N) (w), 430(M—O) (w) cm^{-1}. *Anal.* calcd. for $[Cu(C_{18}H_{15}N_2O_3)_2]$: C 63.76, H 4.43, N 8.26; found: C 63.38, H 4.50, N 8.28.

2-(2-acetylphenylhydrazone)-1,3-phenyl-1,3-propane dione (2-APHDB)

This compound was obtained as yellow crystals from acetic acid, mp 78.0–78.5°C; λ_{max} (nm) in DMF: 368 1st band, 252 2nd band; ir (KBr) ν: 3130(NH) (mb), 1625(C=O) (s), 1567(C=N) (s) cm^{-1}. *Anal.* calcd. for $C_{23}H_{18}N_2O_3$: C 74.59, H 4.86, N 7.56; found: C 74.52, H 5.17, N 7.58.

[Mn(2-APHDB)] complex

This compound was obtained as yellowish green crystals, decomposed at 179–179.5°C; λ_{max} (nm) in DMF: 355 1st band, 250 2nd band; ir (KBr) ν: 1630(C=O) (s), 1570(C=N) (s), 590(M—N) (m), 515(M—O) (m) cm^{-1}. *Anal.* calcd. for $[Mn(C_{23}H_{17}N_2O_3)_2]$: C 69.60, H 4.28, N 7.06; found: C 69.20, H 4.10, N 6.80.

[Fe(2-APHDB)] complex

This compound was obtained as red crystals, decomposed at 182–182.5°C; λ_{max} (nm) in DMF: 380 1st band, 254 2nd band; ir (KBr) ν: 1634(C=O) (s), 1576(C=N) (s), 550(M—N) (m), 490, 440(M—O) (w) cm^{-1}. *Anal.* calcd. for $[Fe(C_{23}H_{17}N_2O_3)_2NO_3]$: C 64.48, H 3.97, N 8.17; found: C 64.50, H 3.90, N 8.23.

[Co(2-APHDB)] complex

This compound was obtained as deep yellow crystals, decomposed at 198–198.5°C; λ_{max} (nm) in DMF: 370 1st band, 250 2nd band; ir (KBr) ν: 1629(C=O) (s), 1570(C=N) (s), 560(M—N) (m), 510, 435(M—O) (w) cm^{-1}. *Anal.* calcd. for $[Co(C_{23}H_{17}N_2O_3)_2]$: C 69.28, H 4.26, N 7.20; found: C 69.33, H 4.70, N 7.17.

[Ni(2-APHDB)] complex

This compound was obtained as yellowish green crystals, melted above 234°C; λ_{max} (nm) in DMF: 352 1st band, 250 2nd band; ir (KBr) ν: 1629(C=O) (s), 1570(C=N) (s), 565(M—N) (m), 440(M—O) (m) cm^{-1}. *Anal.* calcd. for $[Ni(C_{23}H_{17}N_2O_3)_2]$: C 69.28, H 4.27, N 7.03; found: C 69.81, H 4.50, N 7.09.

[Cu(2-APHDB)] complex

This compound was obtained as yellowish green crystals, melted above 235°C; λ_{max} (nm) in DMF: 340 1st band, 250 2nd band; ir (KBr) ν: 1635(C=O) (s), 1575(C=N) (s), 570(M—N) (m), 510, 440(M—O) (m) cm^{-1}. *Anal.* calcd. for $[Cu(C_{23}H_{17}N_2O_3)_2]$: C 68.87, H 4.24, N 6.98; found: C 68.70, H 4.20, N 6.78.

(iii) Measurements

Titrations of 5×10^{-3} M free ligand as well as mixtures of the free ligand with 1×10^{-3} M metal ion were carried out against standard KOH in 75% dioxane–water (v/v) to avoid precipitation. Dilute solutions (10^{-3} M) were used to reduce the possibility of formation of polynuclear species. pH titrations were carried out using a WTW 520 digital pH meter fitted with a combination electrode at 30°C and ionic strength of 0.1 M in 75% (v/v) dioxane–water solvent in an inert atmosphere (nitrogen).

The dissociation constants pK_H as well as the stability constants were calculated as mentioned before (5). The method of Irving and Rossotti was employed to determine the parameters $\bar{n}$ and pL (6), where $\bar{n}$ is the average number of molecules of ligand bound by one metal atom and L is the concentration of the free ligand.

Infrared spectra were obtained using a Perkin-Elmer 598 spectrophotometer in the range of 200–4000 cm^{-1}, using the KBr disk technique. Ultraviolet and visible spectra in pure DMF solvent were obtained using a recording Perkin-Elmer 550 S spectrophotometer.

The conductance of 1×10^{-3} M solutions of the solid complexes in purified DMF were measured using a WTW, D-812 Weilheim conductivity meter, Model LBR, fitted with a cell model LTA 100.

Magnetic measurements were carried out at 28.5°C using the Gouy method.

(iv) Organic solvent

Dioxane was purified by refluxing with sodium metal, lithium aluminium hydride and pure dioxane was collected between 100.5 to 101°C (7). Dimethyl formamide was purified as mentioned by Verlag (8). The DMF fraction was collected under vacuum at about 53°C in a dark bottle (9).

Results and discussion

1. pH-metric studies

Titration curves of metal ion and organic ligand mixtures of ratio 1:5 at 30°C ± 0.5 were greatly different from those of the free ligands (Fig. 1) as a result of complex formation.

The titration curve of 2-APHDm ligand in the presence of Cu^{2+} ion showed distinct inflections at m = 1 and m = 2, where m = moles of base per mole of ligand, which indicated the stepwise formation of ML and ML_2 species. The same behaviour was obtained for the VO^{2+}–2-APHDm mixture whereas in the case of the Mn^{2+}–2-APHDm mixture, the titration curve showed an inflection at m = 1, which suggested the formation of 1:1 (ML) species. Titration curves obtained in the presence of the bivalent metal ions (Co^{2+}, Ni^{2+}, Zn^{2+}, UO^{2+}) and the trivalent Fe^{3+} ion showed an inflection at m = 2 corresponding to the formation of the bischelate represented by the equilibrium

$$M^{2+} + 2HL \rightleftharpoons ML_2 + 2H^+$$

transition metal ions with hydrazone-β-diketone ligands in 75% dioxane–water*

2-APHA, pK = 14.43				2-APHDB, pK = 12.54				2-APHTA, pK = 12.50			
log K_1	ΔG_1	log β	log K_1 − log K_2	log K_1	ΔG_1	log β	log K_1 − log K_2	log K_1	ΔG_1	log β	log K_1 − log K_2
12.75	72.93	24.22	1.28	11.42	65.32	20.60	2.24	10.68	61.09	18.68	2.68
7.75	44.33	12.75	2.75	7.18	41.07	11.58	2.78	6.10	34.89	10.90	1.30
14.50	82.94	28.15	0.85	12.42	71.04	23.69	1.15	12.50	71.50	24.18	0.82
9.82	56.17	19.02	0.62	9.50	55.08	17.40	1.60	8.00	46.90	15.10	0.90
9.85	56.34	19.00	0.70	9.65	57.20	17.60	1.70	8.20	45.76	15.73	0.67
12.33	70.53	21.46	3.20	11.08	69.10	19.50	2.66	10.42	59.60	19.25	1.59
10.60	60.63	20.12	1.08	9.32	53.31	16.87	1.77	8.77	50.16	17.02	0.52
13.16	75.39	25.29	1.03	12.28	70.24	23.51	1.05	10.75	61.49	20.60	0.90

constants ranged between 0.01 to 0.05 and the correlation coefficient (r) ranged between 0.95 to 0.98.

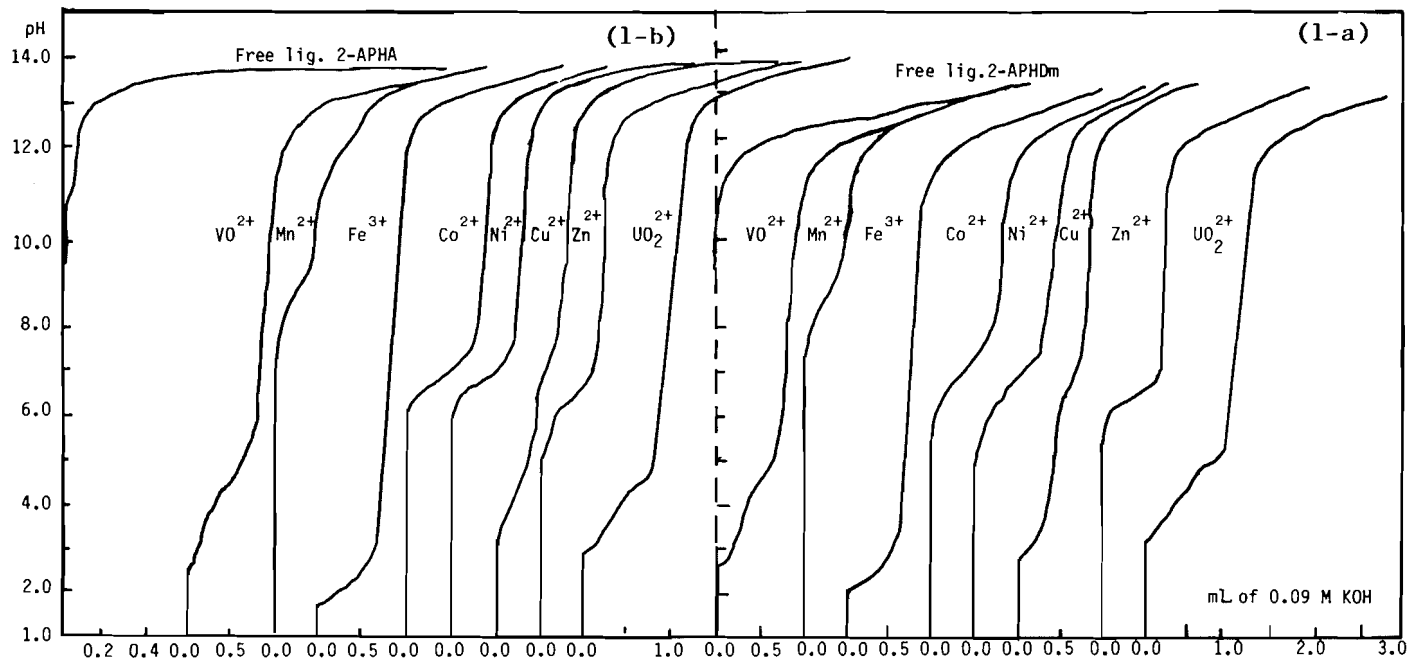

FIG. 1. pH-metric titration curves for 5 × 10^{-3} M ligand and 1 × 10^{-3} M metal ion at 30°C in 75% (v/v) dioxane–water and V_0 = 40 mL.

Titration curves of the 2-APHTA and 2-APHDB ligands obtained in the presence of the divalent VO^{2+}, Co^{2+}, Ni^{2+}, Cu^{2+}, Zn^{2+}, and UO_2^{2+} ions and the trivalent Fe^{3+} ion showed an inflection at m = 2 corresponding to the formation of bischelates. In the case of the Mn^{2+} ion, an additional weak inflection was observed at m = 1, corresponding to the formation of an ML species as well as ML_2 chelate compounds. Titration curves of metal–2-APHTA mixtures were characterized by the appearance of a weak inflection at pH values higher than eleven which may be attributed to the neutralization of the excess ligand present in the mixture by the alkali or due to the formation of hydroxo complexes. Titration curves of 2-APHB and 2-APHA ligands obtained in the presence of VO^{2+}, Co^{2+}, Ni^{2+}, Zn^{2+}, and Fe^{3+} metal ions showed an inflection at m = 2, indicating the formation of bischelates. Titration curves obtained in the presence of both Cu^{2+} and Mn^{2+} ions showed a distinct inflection at m = 1 in addition to that at m = 2 which accounted for the stepwise formation of ML and ML_2. The stepwise formation constants log K_1 and log K_2 were evaluated as given in Table 1. The formation constants of Fe^{3+} complexes had higher observed values than the other metal complexes which may be attributed to increased covalency of the bond. The stability of the complex formed generally increased with increasing oxidation number of the metal ion (9).

The formation constants of the divalent oxygenated cation complexes (VO^{2+} and UO_2^{2+}) had higher values than the other divalent cations. This may be attributed to the bonded oxygen atoms which may increase the electrostatic attraction between the metal ion and the coordinated ligands and overcome any steric hindrance offered by the oxygen of the oxygenated cation. Moreover, high chelate stability values of oxygenated cations were observed for the complexes of β-diketones themselves (10–12).

The order of increasing formation constants of metal complexes for a series of similar divalent metal ions with the different complexing agents under investigation were as follows

$$Mn < Co < Ni < Cu > Zn$$

This order is in good agreement with that of formation constants reported by Irving and Williams (13).

Can. J. Chem. Downloaded from www.nrcresearchpress.com by 88.85.125.76 on 09/07/12
For personal use only.

Can. J. Chem. Downloaded from www.nrcresearchpress.com by 88.85.125.76 on 09/07/12
For personal use only.

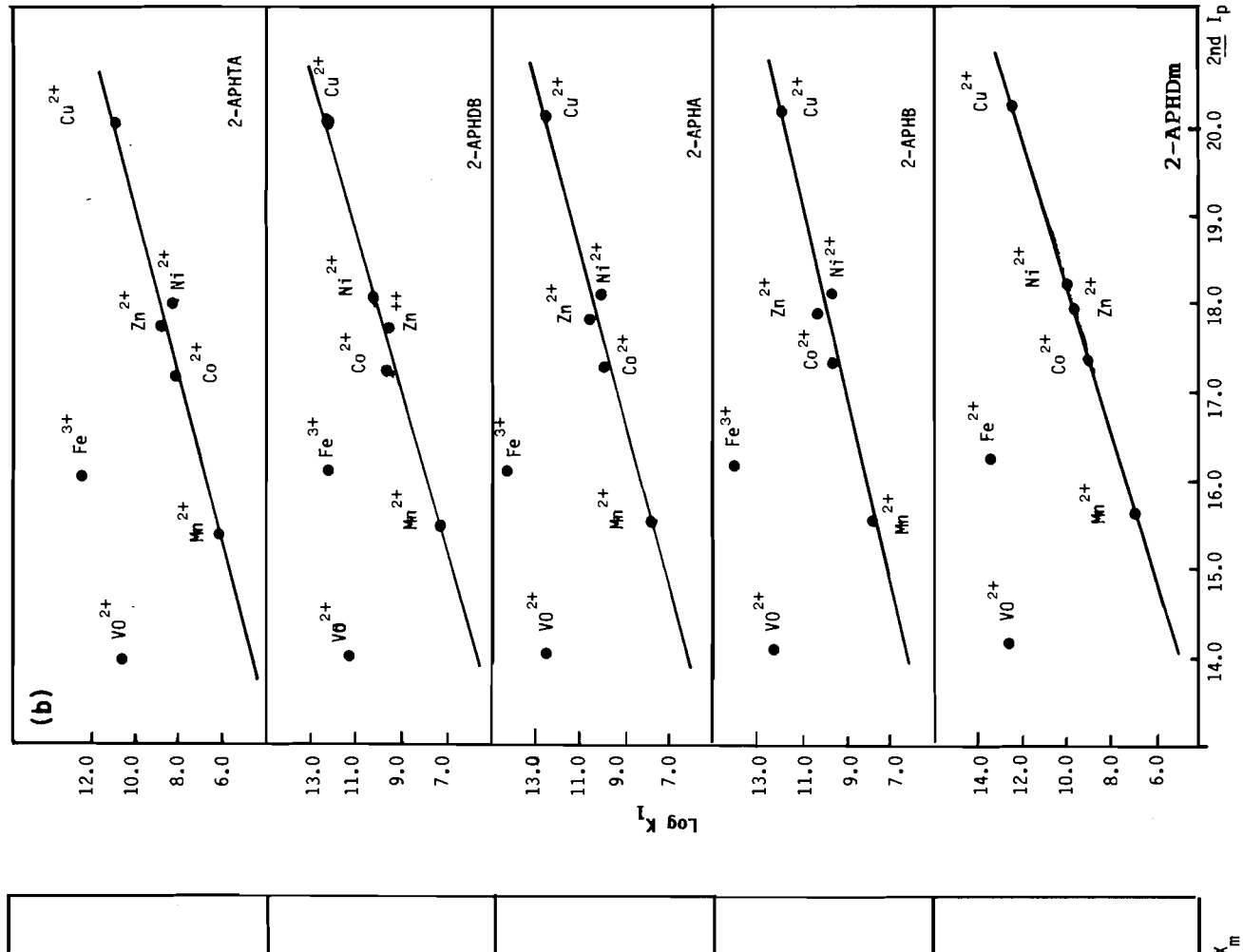

FIG. 2. (*a*) Plot of log K_1 for the different metal ions with different chelating agents vs. the electronegativity (X_m) of the respective metal ion. (*b*) Plot of log K_1 for the different metal ions with different chelating agents vs. the second ionization potential (2nd I_p) of the respective metal ion.

TABLE 2. Physicochemical studies of the organic ligands and their metal-complexes

Compound	Molar conductance $\Delta_2 m$ in $ohm^{-1}\ cm^2\ mol^{-1}$ in 1×10^{-3} M DMF solution at 30°C	μ_{eff} in BM (at 301.5 K)	λ_{max} (nm) in DMF	
			1st band	2nd band
$C_{13}H_{14}N_2O_3$ (2APHA)			365	255
$[Mn(C_{13}H_{13}N_2O_3)_2]$	1.22	—	362	252
$[Fe(C_{13}H_{13}N_2O_3)_3]$	16.82	—	375	250
$[Co(C_{13}H_{13}N_2O_3)_2]$	—	—	362	250
$[Ni(C_{13}H_{13}N_2O_3)_2]$	0.60	2.719	370	252
$[Cu(C_{13}H_{13}N_2O_3)(H_2O)OH]$	8.20	1.468	360	250
$C_{18}H_{16}N_2O_3$ (2APHB)	—	—	370	256
$[Mn(C_{18}H_{15}N_2O_3)_2]$	3.52	—	368	253
$[Fe(C_{18}H_{15}N_2O_3)_2NO_3]$	6.52	—	367	252
$[Co(C_{18}H_{15}N_2O_3)_2]$	1.52	—	365	250
$[Ni(C_{18}H_{15}N_2O_3)_2]$	—	—	368	252
$[Cu(C_{18}H_{15}N_2O_3)_2]$	3.72	—	365	252
$C_{23}H_{18}N_2O_3$ (2APHDB)	—	—	338	252
$[Mn(C_{23}H_{17}N_2O_3)_2]$	—	—	355	250
$[Fe(C_{23}H_{17}N_2O_3)_2NO_3]$	10.50	5.423	380	254
$[Co(C_{23}H_{17}N_2O_3)_2]$	—	—	370	250
$[Ni(C_{23}H_{17}N_2O_3)_2]$	4.55	2.963	352	250
$[Cu(C_{23}H_{17}N_2O_3)_2]$	5.00	1.731	340	250

The order largely reflects the change in heat of complex formation across the series, and arises from a combination of the influence of both polarising ability of metal ion, which varies in the sequence Mn < Fe < Co < Ni ~ Co > Zn (14) and crystal-field stabilization energies which vary in the oder (15)

Mn < Fe < Co < Ni > Zn

More bulky entering ligands will obviously suppress the stability constant, whereas less bulky ligands will enhance the stability constant (14). Accordingly, metal ions that are susceptible to large crystal-field stabilization effects form stronger complexes with less bulky ligands (16, 17).

In the selected series of the complexing agents two important factors were considered, i.e., steric and basicity effects. Considering the substitution effects, the ligands were arranged according to decreasing basicity in the following order:

2-APHDm < 2-APHA > 2-APHB > 2-APHDB > 2-APHTA

The pK values (see Table 1) of these ligands appear to be high, but this can be explained by the higher pK's in 75% dioxane and also the effect of hydrogen bonding with acetyl-carbonyl which retards deprotonation of hydrazo hydrogen. Thus orthohydroxyacetophenone has a very high pK (14.0) compared to phenol (12.0) (18).

The most basic ligands form the most stable complexes. In addition, the role of the steric effect due to the bulky phenyl group is quite clear in the stability order of complexes for the three ligands 2-APHA, 2-APHB, and 2-APHDB. The two factors, i.e., basicity and steric effects of ligands together influence the order in the same direction (Table 1).

2-APHA > 2-APHB > 2-APHDB

Chelating agents may be classified according to whether the skeleton of the molecule is flexible or rigid. In the present study, 2-APHA represents the most flexible molecule and 2-APHDm represents the most rigid one. Rigid chelating agents exhibit less loss of configurational entropy on complex formation. Therefore the complex stability values of the complexing agent 2-APHA are found to be higher than that of the rigid complexing agent 2-APHDm.

The ratio of successive stability constants is affected by ligand and metal ion. The effect of ligands can be subdivided into their electrostatic and steric effects. The electrostatic effect accounts for the charges on the ligand and the metal ion. The effect of steric size on the ratio of successive constants depends on whether the entering ligand is more bulky or less bulky than the ligand it is replacing.

Table 1 shows that for all systems studied here, log K_1 − log K_2 is positive. The different log K values of the complexes of the studied compounds (**I–V**) may be explained by the difference in the basicity of these ligands. Calculated values show that they depend on the nature of the substituent on the hydrazone moiety, indicating that the complexation of the studied ligands is increased by increasing electron density at the reaction site, thus explaining the higher stability in electron-repeling substituents. The lower stability of ligand **V** compared to ligand **I** complexes may be attributed to both the cyclic structure and the distant location of the methyl groups from the hydrazone moiety.

In Fig. 2 both the electronegativity (19) (X_m) and second ionisation potentials (2nd I_p) of metal ions were plotted against log K_1 (first formation constant) for the ligands under investigation. Straight lines were obtained for all the divalent metal ions indicating that the stability constants decrease in the following order for different metal ligand complexes:

Zn < Cu > Ni > Co > Mn

This trend indicates that the stability of chelate compounds increases with increase of both electronegativity (X_m) and second ionization potential (2nd I_p) of the metal ion.

2. Solid complexes studies

The ultraviolet spectra of the organic ligands were recorded in pure DMF. Two maxima were observed in all of the ligands investigated. These bands may be assigned to $\pi-\pi^*$ transitions

Can. J. Chem. Downloaded from www.nrcresearchpress.com by 88.85.125.76 on 09/07/12
For personal use only.

Can. J. Chem. Downloaded from www.nrcresearchpress.com by 88.85.125.76 on 09/07/12
For personal use only.

of the hydrazone and carbonyl groups. The electronic absorption spectra of the free ligands compared to the spectra of their complexes in DMF reveals a shift of maxima (Table 2) which, produces evidence for sharing of both hydrazone and carbonyl groups in the complexation process.

The comparison of ir spectra of the solid organic ligands and their solid metal complexes may be helpful in identifying the structure of the solid complexes.

The studied ligands exhibit a stretching vibration band due to >NH at 3050, 3060, and 3130 cm^{-1} for 2-APHA, 2-APHB, and 2-APHDB ligands, respectively. Disappearance of the >NH stretching frequency was observed on chelate formation, which may be caused by coordination of hydrazone nitrogen to the metal atom upon complexation.

The only exception observed was the appearance of new medium intensity composite broad bands at 3515 and 3400 cm^{-1} in the spectrum of Cu(II)–2-APHA complex. These bands may be attributed to the ν_{H_2O} vibration of a coordinated water molecule. The appearance of a new medium intensity band at 810 cm^{-1} in the spectrum may be attributed to π_{H_2O} modes of coordinated water (20, 21). Elemental analysis is also consistent with the presence of coordinated water. Furthermore, the nonelectrolytic nature indicated by the molar conductance of the solid complex suggests that the complex has a 1:1 composition with the formula $[CuLH_2O(OH)]$.

A very interesting feature in the infrared spectra is the appearance of new bands at lower frequencies due to metal–nitrogen and metal–oxygen interactions. The interaction is closely related to the stability of the chelates and provides information about the ligand–metal bond. In the metal complexes, there are new medium to weak intensity bands at lower frequencies (590–530 cm^{-1}) which may be assigned to ν_{M-N} modes of vibration (22–24). The metal–oxygen (22) interaction is observed at frequencies of 515–435 cm^{-1} for different metal complexes of 2-APHA, 2-APHB, and 2-APHDB ligands, depending upon both the metal ion and organic ligand.

The observed values for molar conductance of the complexes in DMF solution are shown in Table 2. All the measured complexes have molar conductance values which are indicative of a nonelectrolytic nature. In the case of Fe(III) nitrate complexes for both 2-APHB and 2-APHDB ligands, the molar conductance values indicate that the nitrate ion is not affected by DMF and is still present in the inner coordination sphere (Table 2).

The magnetic moment values for Cu^{2+}–2-APHA and Cu^{2+}–2-APHDB are 1.468 and 1.731 BM, respectively, indicating one unpaired electron. The complex may be square-planar and it is possible to propose the following structures for the Cu^{2+} complexes:

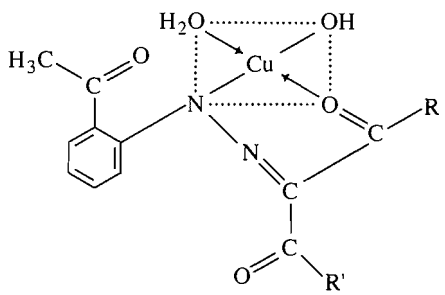

$[CuL\,H_2O(OH)]$, 1:1 complex

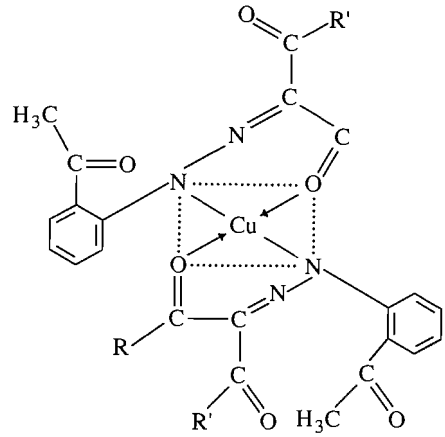

$[CuL_2]$, 1:2 complex

The magnetic moment for Fe(III)–2-APHDB complexes is 5.423 BM, indicating a spin-free configuration which may have octahedral structure.

The magnetic moment for Ni^{2+}–2-APHA and Ni^{2+}–2-APHDB complexes are 2.719 and 2.963 BM, respectively, indicating spin-free configurations. These magnetic moments are consistent with the assignment of octahedral configurations (25, 26). Consequently, the proposed structure of the octahedral M^{2+} complexes is as follows:

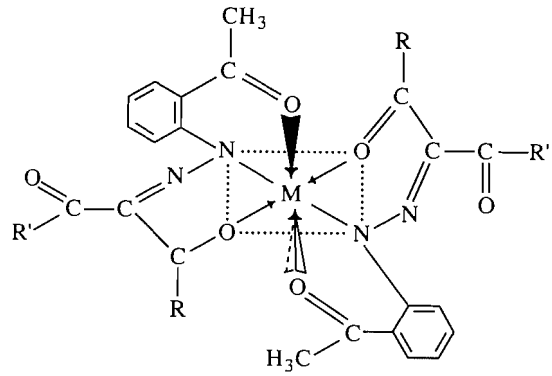

$[M^{2+}:L_2]$, 1:2 complex

1. F. R. Clarke, J. F. Steinbach, and W. F. Wanger. J. Inorg. Nucl. Chem. **26**, 1311 (1964).
2. F. A. Snavely, B. D. Krecker, and C. C. Clark. J. Am. Chem. Soc. **81**, 2337 (1959).
3. (*a*) A. M. El-Atrash, G. A. El-Inany, A. El-Hilali, M. Ebeid, and B. El-Shetary. J. Electroanal. Chem. Interfac. Electrochem. **79**, 375 (1977); (*b*) A. G. Evans, J. C. Evans, B. A. El-Shetary, C. C. Rowlands, and P. H. Morgans. J. Coord. Chem. **2**, 19 (1979); (*c*) G. A. El-Inany, B. A. El-Shetary, and F. Zidan. Egypt. J. Chem. **25**, 301 (1982).
4. A. I. Vogel. Text book of practical inorganic chemistry. 3rd ed. Longman, London.
5. B. A. El-Shetary, S. L. Stefan, M. S. Abdel-Moez, and M. M. Mashaly. Can. J. Chem. **66**, 2362 (1988).
6. H. M. Irving and H. S. Rossotti. J. Chem. Soc. 3397 (1953); 2904 (1954).
7. B. A. El-Shetary, M. S. Abdel-Moez, and H. S. Sleem. Thermochim. Acta, **113**, 21 (1987).
8. Der Dentschet Verlag. Der Wissenschaften "Organikum". Berlin. 1977. p. 794.

9. J. JNCZEDY. Analytical applications of complex equilibria. Ellis Horwood Limited. Chichester, 1976. p. 70.
10. B. E. BRYANT. Phys. Chem. **58**, 573 (1954).
11. R. BRITO and R. TRYJILLO. Anal. Real Soc. Espan. Fis Quim. **52**B, 407 (1956).
12. E. H. HOLST. Doctor Diss, Pennsylvania State Univ. 1955.
13. H. IRVING and R. J. P. WILLIAMS. J. Chem. Soc. 3192 (1953).
14. F. R. HARLLY, C. BURGESS, and R. M. ALCOCK. Solution equilibria. 1st ed. Ellis Horwood Limited, Chichester. 1980. p. 257.
15. C. S. G. PHILLIPS and R. J. P. WILLIAMS. Inorganic chemistry, Vol. 2. Oxford. 1966. p. 268.
16. C. K. JORGENSEN. Absorption spectra and chemical bonding in complexes. Pergamon, London. 1962.
17. G. ATKENSON and J. E. BAUMAN. Inorg. Chem. **2**, 64 (1963).
18. RATNAKAR, O. DESHPANDE, and D. V. JAHAGIRDAR. J. Inorg. Nucl. Chem. **39**, 1385 (1977).
19. J. D. LEE. A new concise inorganic chemistry. 3rd ed. 1977. p. 101.
20. G. BRINK and M. FALK. Can. J. Chem. **48**, 1096 (1970).
21. P. B. CHAKRWARTI and P. KHANNA. J. Indian Chem. Soc. **61**, 2 (1984).
22. K. NAKAMOTO. Infrared spectra of inorganic and coordination compounds. 2nd ed. Wiley Interscience. 1969. pp. 167, 236.
23. E. POWELL and N. SHEPPARD. (*a*) Spectrochim. Acta, **25**, 301 (1962); (*b*) J. Chem. Soc. 1112 (1961).
24. G. G. PERCY and D. A. THORNTON. J. Inorg. Nucl. Chem. **34**, 3357 (1972).
25. B. N. FIGGIS and J. LEWIS. Prog. Inorg. Chem. **6**, 37 (1964).
26. P. SINGH, V. SINGH, G. P. POKHARIYAL, and K. B. S. CHANHAN. J. Indian Chem. Soc. **57**, 1025 (1980).

Can. J. Chem. Downloaded from www.nrcresearchpress.com by 88.85.125.76 on 09/07/12
For personal use only.

Synthesis of a biologically active isomer of frontalin and some new products from acylative decarboxylation of 3-methyltricarballylic acid

GEORGE M. STRUNZ,[1] CHAO-MEI YU, AND LI YA
Forestry Canada — Maritimes Region, P.O. Box 4000, Fredericton, N.B., Canada E3B 5P7

PETER S. WHITE
Department of Chemistry, University of New Brunswick, Fredericton, N.B., Canada E3B 6E2

AND

E. A. DIXON
Department of Chemistry, University of Calgary, Calgary, Alta., Canada T2N 1N4

Received August 22, 1989

This paper is dedicated to Professor G. B. Marini-Bettòlo on the occasion of his 75th birthday

GEORGE M. STRUNZ, CHAO-MEI YU, LI YA, PETER S. WHITE, and E. A. DIXON. Can. J. Chem. **68**, 782 (1990).

2-Acetonyl-2-methylsuccinic anhydride, **3**, the major product from base-catalysed reaction of 3-methyltricarballylic acid with acetic anhydride, was converted by simple manipulation of functional groups into 1,5-dimethyl-2,7-dioxabicyclo[3.2.1]octane. This bicyclic ketal (**6**) is isomeric with frontalin, **7**, an aggregation pheromone for *Dendroctonus* bark beetles. It elicited electroantennogram responses in *D. ponderosae* and *D. rufipennis*. Besides **3** and the known compounds, **4** and **5**, two new minor products, **8** and **9**, were identified from base-catalysed acylative decarboxylation of 3-methyltricarballylic acid.

Key words: pheromone analogue, *Dendroctonus*, bark beetles.

GEORGE M. STRUNZ, CHAO-MEI YU, LI YA, PETER S. WHITE et E. A. DIXON. Can. J. Chem. **68**, 782 (1990).

L'anhydride 2-acétonyl-2-méthyl succinique, **3**, le produit majeur provenant de la réaction de l'acide 3-méthyl tricarballylique avec l'anhydride acétique sous catalyse basique, a été transformé en 1,5-diméthyl-2,7-dioxobicyclo[3.2.1]octane. Cet acétal bicyclique (**6**) est isomère avec la frontaline, **7**, une phéromone d'agrégation des *Dendroctonus*. L'électroantennogramme indique une réaction de *D. ponderosae* et *D. rufipennis* à ce composé. De plus **3** et les composés connus **4** et **5**, on a identifié deux nouveaux produits mineurs, **8** et **9**, provenant de la décarboxylation acylative de l'acide 3-méthyl tricarballylique.

Mots clés : analogue de phéromone, *Dendroctonus*, scolytes.

Acylative decarboxylation of tricarballylic acid (3-carboxyglutaric acid) by the action of acid anhydrides under basic catalysis produces the Fittig bislactones **1** (1). These compounds have been found to be convenient precursors for the synthesis of certain 1,4-diketones, hence of substituted cyclopentenones (2, cf. 3). Tricarballylic acids that are fully substituted at C-3 undergo acylation at one or both of the methylene carbons, and decarboxylation of the resulting β-keto acids results in a different array of products (4, 5). Thus, when 3-methyltricarballylic acid, **2**, was heated under reflux with an excess of acetic anhydride in the presence of 4-dimethylamino pyridine (6), the keto-anhydride **3** and the bridged bislactone **4** were isolated in yields of 42 and 7.4% respectively (4, cf. 5). A minor product (~1%) was identified as the enol-lactone **5** (4).

We recognized that **3** and **4** offered ready access to the bicyclic ketal **6**, which has an interesting structural relationship to frontalin **7** (7, cf. 8), an aggregation pheromone for several species of *Dendroctonus* bark beetles. Frontalin has been detected in various *Dendroctonus* species, including *D. adjunctus* (9), *D. brevicomis* (10, 11), *D. frontalis* (7, 12), *D. pseudotsugae* (13), *D. rufipennis* (14), and *D. vitei* (15). It was detected in male *D. ponderosae* fed on Ponderosa pine but, somewhat surprisingly, not in the females (16). Structure–activity relationships of frontalin isomers and analogues may shed some light on the interaction between the pheromone and its receptors (8).

In this paper we report the conversion of **3** to **6** by straightforward manipulation of functional groups, and the results of some preliminary electrophysiological bioassays[2] of **6** using two *Dendroctonus* species. The characterization of two novel minor products, **8** and **9**, from the base-catalysed reaction of **2** with acetic anhydride is also recorded.

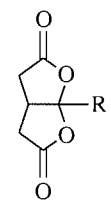

1

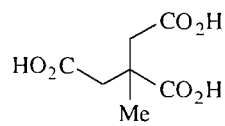

2

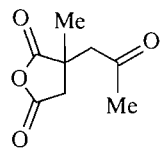

3

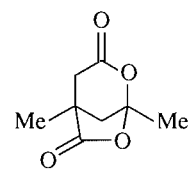

4

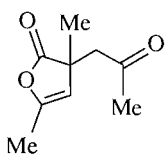

5

[1]Author to whom correspondence may be addressed.

[2]Electroantennogram responses signal the interaction of a substance with receptors on the insects' antennae: behavioral studies are necessary to establish whether the compound actually displays pheromone activity.

Can. J. Chem. Downloaded from www.nrcresearchpress.com by 91.144.44.67 on 09/07/12
For personal use only.

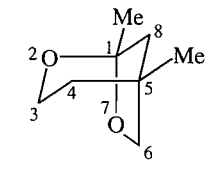

6

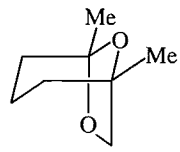

7

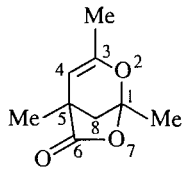

8

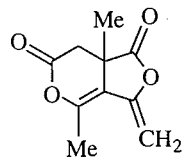

9

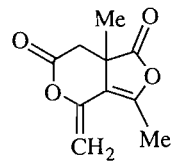

10

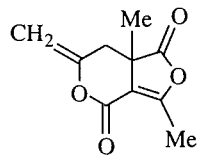

11

Both the keto-anhydride **3** and the bridged bislactone **4**, which are interconvertible via the corresponding keto-diacid (4), are suitable precursors of the frontalin isomer **6**. Acid-catalysed methanolysis of **3**, selected because of its greater abundance, afforded dimethyl 2-acetonyl-2-methylsuccinate in excellent yield. The ketone functionality was then protected as its ethylene ketal to allow the selective reduction of the ester groups using an excess of sodium bis(2-methoxyethoxy) aluminum hydride (19). Work-up of the latter reaction under acidic conditions resulted in removal of the protecting group, and the bicyclic ketal **6** was obtained in an overall yield of 48% from **3**.

Bioassays of the frontalin isomer **6**, which has a characteristic "camphor-like" odour, involved measuring the electroantennogram (EAG) responses which it elicited in *D. rufipennis*, the spruce bark beetle, and *D. ponderosae*, the mountain pine beetle. Frontalin is an aggregation pheromone for *D. rufipennis* (14), but has not been proven to play the same role for *D. ponderosae* (16, cf. 13). Racemic frontalin was used as a standard for comparison. It was observed that the shapes of the dose–response curves for **6** and (±) frontalin are quite similar. They differ in the threshold concentration that elicits an EAG signal: with both *Dendroctonus* species tested, the threshold concentration is 10–100 times higher than **6** than for racemic frontalin. At the 10 μg level (see Experimental) the response to **6** was 75% that produced by frontalin for *D. rufipennis*, and 67% for *D. ponderosae*. There were no significant differences in the relative responses of male and female insects.

To provide starting materials **3** and **4**, for the synthesis of **6** in sufficient quantity for field studies, the reaction of 3-methyltricarballylic acid with acetic anhydride was conducted on a larger scale than in the exploratory study (4). From the scaled-up process, which required a longer reaction time, besides **3** (42% yield), **4** (3.4%), and **5** (3.1%), two new minor products were obtained. The more abundant of these (4.5% yield) was a crystalline solid, $C_9H_{12}O_3$, identified as **8** on the basis of its spectroscopic characteristics and mechanistic considerations. Infrared absorption at 1787 cm^{-1} is consistent with the presence of a strained lactone system, and the mass spectrum shows loss of carbon dioxide as a prominent feature. In the ^1H nmr spectrum, singlets at δ 1.33 and 1.71, each corresponding to three protons, are assigned to the methyl groups on C-5 and C-1 respectively. A three-proton doublet (J 1.2 Hz) at δ 1.78 represents the allylic methyl hydrogens that are coupled with the C-4 olefinic proton. The latter is manifested as a narrow multiplet at δ 4.62. The olefinic hydrogen also exhibits long-range W-coupling (1.7 Hz) (17, cf. 4) with the low-field component of an AB quartet at δ 1.97 (J_{AB} 11.2 Hz, $\Delta\nu_{AB}$ 25.5 Hz) assigned to the geminal hydrogens on C-8. The bridged lactone **8** is isomeric with **5**, and may similarly be derived from the double acylation–decarboxylation product 4-carboxy-4-methylheptane-2,6-dione or an acid anhydride thereof.

The other new product, $C_{10}H_{10}O_4$, also a crystalline solid, was isolated in about 1% yield. Its structure, **9**, was deduced from spectroscopic evidence and confirmed by a single crystal X-ray analysis. A notable feature of its ^1H nmr spectrum is an AB quartet at δ 4.83 (J_{AB} 3.4 Hz, $\Delta\nu_{AB}$ 85.3 Hz) that clearly signals the presence of a terminal methylene group. A singlet at δ 2.16 indicates an allylic methyl group. The spectrum also includes an AB quartet at δ 2.80 (J_{AB} 15.7 Hz, $\Delta\nu_{AB}$ 48.3 Hz) whose upfield component displays long-range coupling with a methyl group (three-proton doublet at δ 1.42, J 0.6 Hz). Enol-lactone functionality is suggested by the infrared absorption at 1804 cm^{-1}, with shoulders at 1795 and 1787 cm^{-1}. Considering the origins of the product, these data are best accommodated by structures **9** or **10**. Formulations such as **11**, which are mechanistically plausible, can be excluded by the absence of any sign of allylic coupling of the terminal methylene protons. Of the proposed alternative representations, **9** or **10**, the former was favored on the basis of its ultraviolet chromophore. Thus, absorption at 252 nm (ε 8600) is consistent with a system containing two double bonds in conjugation and exocyclic to a five-membered ring (18) as in **9**.

Since this evidence was considered less than totally compelling, the product was subjected to a single crystal X-ray analysis that has provided rigorous proof for structure **9**. An ORTEP representation of **9** is shown in Fig. 1, and atomic coordinates, bond lengths, and bond angles are presented in Tables 1–3.

Experimental

Melting points were determined on a hot-stage apparatus and are uncorrected. Infrared spectra were recorded on a Philips Pye Unicam PU 9516 infrared spectrophotometer, and ultraviolet spectra on a Philips PU 8800 uv/vis spectrophotometer. Proton and carbon magnetic resonance spectra were run on a Varian XL-200 instrument. The gc/ms analysis was performed on a Finnigan 3200F-100 coupled with a 6110 data system (35 eV, SP 1000 capillary column, split, 220°C). Accurate mass measurements were provided through the courtesy of Dr. A. Hogg, University of Alberta. Microanalysis was performed by Spang Microanalytical Laboratory, Eagle Harbor, MI.

Reaction of 3-methyltricarballylic acid with acetic anhydride (cf. ref. 4)

A solution of 3-methyltricarballylic acid (4.0 g; 21.0 mmol) and 4-dimethylaminopyridine (337 mg; 2.76 mmol) in freshly distilled acetic anhydride (50 mL) was heated under reflux. After 16 h, evolution of CO_2 had almost ceased, and the mixture was evaporated to dryness on a rotary vacuum evaporator.

The major (and most polar) product **3** was isolated by flash chromatography (20) on silica gel using chloroform – ethyl acetate (9:1, then 4:1) as eluent. The yield of **3**, after crystallization from ethyl acetate, was 1.49 g (42%). Physical and spectroscopic characteristics are described in ref. 4.

Can. J. Chem. Downloaded from www.nrcresearchpress.com by 91.144.44.67 on 09/07/12
For personal use only.

Can. J. Chem. Downloaded from www.nrcresearchpress.com by 91.144.44.67 on 09/07/12
For personal use only.

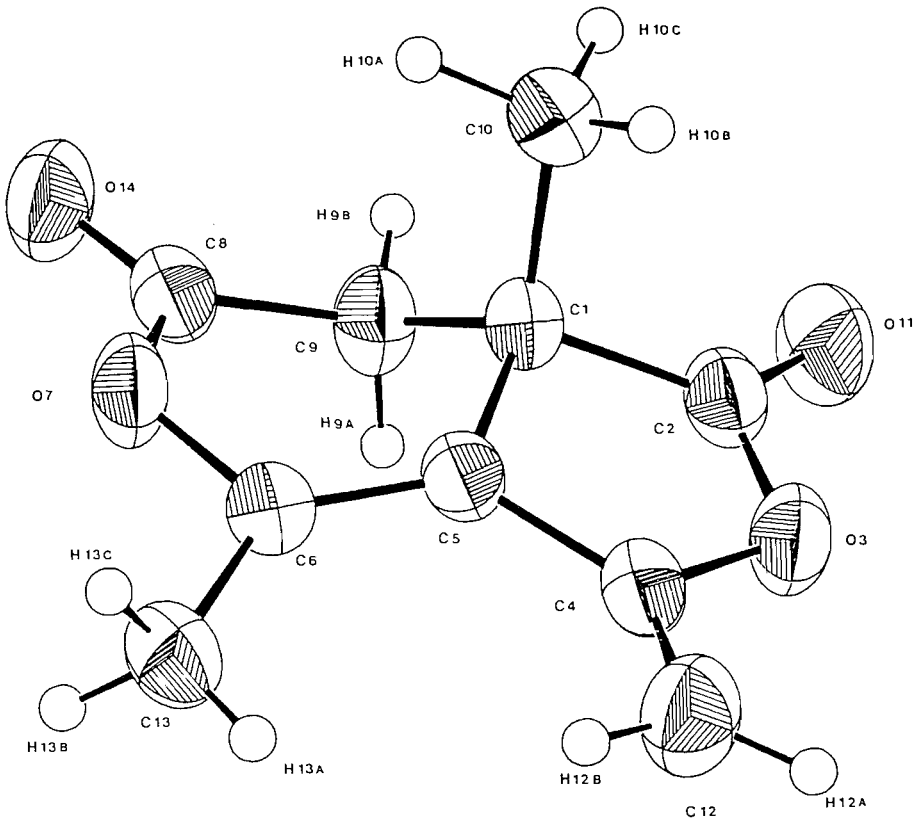

FIG. 1. ORTEP representation of compound **9**.

The less polar fractions were combined and separated by flash chromatography on silica gel employing hexane – ethyl acetate (9:1, then 3:1) as eluent. In order of decreasing chromatographic mobility the products isolated were **8**, **9**, **5**, and **4**.

The yield of bislactone **4** (4) after crystallization from ethyl acetate – hexane was 3.4%, and **5** (4) was obtained in 3.1% yield as an oil.

The bridged lactone **8**, after crystallization from ethyl acetate – hexane, was obtained as colorless crystals (160 mg, 4.5%), mp 75–78°C; ir ($CHCl_3$), *inter alia*: 1787, 1662, 1450, 1395, 1385, 1320, 1165, 1142, 1080, 1000, 910, and 880 cm^{-1}; ^1H nmr ($CDCl_3$, 200 MHz), see text; mass spectrum (*inter alia*), *m/e* (relative intensity) (ion): 168.0784(28) $(C_9H_{12}O_3)^{\ddagger}$ $(M^{\ddagger})$, 125.0603(47) $(C_7H_9O_2)^+$, 124.0886(36) $(C_8H_{12}O)^{\ddagger}$ $(M - CO_2)^{\ddagger}$, 123.0813(50) $(C_8H_{11}O)^+$ $(M - CO_2 - H)^+$, 111.0455(29) $(C_6H_7O_2)^+$, 83.0505(100) $(C_5H_7O)^+$.

The bis enol-lactone **9**, following crystallization from ethyl acetate – hexane, was obtained in 1% yield (40 mg) as colorless crystals, mp 123–124°C; ir ($CHCl_3$), *inter alia*: 1804, 1795 (sh), 1787 (sh), 1702, 1655, 1148, 1120, 1040, and 975 cm^{-1}; ^1H nmr ($CDCl_3$, 200 MHz), see text; mass spectrum (*inter alia*), *m/e* (relative intensity) (ion): 194.0573 (100) $(C_{10}H_{10}O_4)^{\ddagger}$ $(M^{\ddagger})$, 179.0329(2) $(C_9H_7O_4)^+$ $(M - CH_3)^+$, 166.0627(9) $(C_9H_{10}O_3)^{\ddagger}$ $(M - CO)^{\ddagger}$, 152.0470(68) $(C_8H_8O_3)^{\ddagger}$, 149.0236(24) $(C_8H_5O_3)^+$, 138.0680(20) $(C_8H_{10}O_2)^{\ddagger}$ $(M - CO - CO)^{\ddagger}$, 124.0523 (78) $(C_7H_8O_2)^{\ddagger}$ $(M - CO - CO - CH_2)^{\ddagger}$, 123.0447(24) $(C_7H_7O_2)^+$, 109.0305(56) $(C_6H_5O_2)^+$, 96.0573(31) $(C_6H_8O)^+$, 81.0342(24) (C_5H_5O). X-ray crystallography, see below.

Dimethyl 2-acetonyl-2-methylsuccinate

A solution of keto-anhydride **3** (400 mg; 2.35 mmol) in dry methanol (15 mL) containing concentrated sulfuric acid (10 drops) was heated at reflux under anhydrous conditions. After 12 h, the solution was concentrated to near dryness on a rotary vacuum evaporator. The residue was redissolved in chloroform and the solution was washed successively with saturated $NaHCO_3$ and water before being dried over anhydrous $MgSO_4$. Removal of solvent under reduced pressure afforded dimethyl 2-acetonyl-2-methylsuccinate as a colorless oil (480 mg, 94%) that was sufficiently pure to be used directly in the next step without further purification; ir ($CHCl_3$): 1730 cm^{-1}; ^1H nmr ($CDCl_3$, 200 MHz) δ: 1.32 (3H, s), 2.13 (3H, s), 2.78 (2H, s), 2.98 (2H, AB_q, J_{AB} 18.0 Hz, $\Delta\nu_{AB}$ 29.5 Hz), 3.65 (3H, s), 3.69 (3H, s); mass spectrum (*inter alia*), *m/e* (relative intensity) (ion): 216.1000(18) $(C_{10}H_{16}O_5)^{\ddagger}$ $(M^{\ddagger})$, 201.0767(6) $(C_9H_{13}O_5)^+$ $(M - CH_3)^+$, 185.0816(55) $(C_9H_{13}O_4)^+$ $(M - OCH_3)^+$, 159.0661(44) $(C_7H_{11}O_4)^+$ $(M - CH_2COCH_3)^+$, 157.0867(19) $(C_8H_{13}O_3)^+$ $(M - COOCH_3)^+$, 143.0705(13) $(C_7H_{11}O_3)^+$ $(M - CH_2COOCH_3)^+$, 141.0555(45) $(C_7H_9O_3)^+$, 127.0398(39) $(C_6H_7O_3)^+$, 125.0605(100) $(C_7H_9O_2)^+$ $(M - COOCH_3, OCH_3,$ and $H)^+$, 114.0682(51) $(C_6H_{10}O_2)^{\ddagger}$ $(M - COCH_3$ and $COOCH_3)^{\ddagger}$, 111.0447(31) $(C_6H_7O_2)^+$, 73.0657(40) $(C_4H_9O)^+$, 55.0566(34) $(C_4H_7)^+$.

Ethylene ketal of dimethyl 2-acetonyl-2-methylsuccinate

A solution of dimethyl 2-acetonyl-2-methylsuccinate (477 mg; 2.21 mmol) in dry benzene (25 mL) containing ethylene glycol (2.1 g, 33.8 mmol) and *p*-toluenesulfonic acid (50 mg) was heated under reflux for 10 h. The apparatus was then fitted with a Dean–Stark water separator containing molecular sieves and reflux was continued for an additional 2 h. When cool, the solution was diluted by addition of benzene (25 mL), washed successively with saturated $NaHCO_3$ solution and brine, and dried over $MgSO_4$. Removal of solvent *in vacuo* then afforded the ethylene ketal of dimethyl 2-acetonyl-2-methylsuccinate (555 mg, 96%) as a colorless oil, sufficiently pure to be used directly in the next step without further purification; ir ($CHCl_3$): 1730 cm^{-1}; ^1H nmr ($CDCl_3$, 200 MHz) δ: 1.26 (3H, s), 1.37 (3H, s), 2.21 (2H, AB_q, J_{AB} 14.9 Hz, $\Delta\nu_{AB}$ 36.9 Hz), 2.68 (2H, AB_q, J_{AB} 16.4 Hz, $\Delta\nu_{AB}$ 36.5 Hz), 3.65 (3H, s), 3.68 (3H, s), 3.89 (4H, narrow m); mass spectrum (*inter alia*), *m/e* (relative intensity) (ion): 260.1258(2) $(C_{12}H_{20}O_6)^{\ddagger}$ $(M^{\ddagger})$, 245.1029(7) $(C_{11}H_{17}O_6)^+$ $(M - CH_3)^+$, 229.1074(7) $(C_{11}H_{17}O_5)^+$ $(M - OCH_3)^+$, 216.0995(10) $(C_{10}H_{16}O_5)^{\ddagger}$, 215.0921(12) $(C_{10}H_{15}O_5)^+$, 189.0765(9) $(C_8H_{13}O_5)^{\ddagger}$, 185.0816(45) $(C_9H_{13}O_4)^+$, 171.0658(13) $(C_8H_{11}O_4)^+$, 159.0662(12)

Can. J. Chem. Downloaded from www.nrcresearchpress.com by 91.144.44.67 on 09/07/12
For personal use only.

TABLE 1. Atomic parameters x, y, z and B_{iso} for compound **9**. (Estimated standard deviations in parentheses)

Atom	x	y	z	B_{iso}*
C1	0.4302(4)	0.2797 (3)	0.2644 (3)	3.13(12)
C2	0.6105(4)	0.3181 (4)	0.1507 (3)	3.59(13)
O3	0.7328(3)	0.16209(24)	0.09512(19)	4.10(10)
C4	0.6443(4)	0.0207 (4)	0.1503 (3)	3.37(12)
C5	0.4368(4)	0.1020 (3)	0.23806(25)	2.97(12)
C6	0.2628(4)	0.0526 (3)	0.2793 (3)	3.29(12)
O7	0.0749(3)	0.16690(24)	0.35218(20)	4.10(10)
C8	0.0355(4)	0.3521 (4)	0.3429 (3)	3.80(14)
C9	0.2028(4)	0.4277 (4)	0.2491 (3)	3.84(14)
C10	0.4975(5)	0.2528 (4)	0.4090 (3)	4.09(15)
O11	0.6576(3)	0.4544 (3)	0.11340(21)	4.97(11)
C12	0.7544(5)	−0.1445 (4)	0.1168 (3)	4.72(16)
C13	0.2332(5)	−0.1138 (4)	0.2644 (3)	4.28(15)
O14	−0.1278(3)	0.4403 (3)	0.40762(23)	5.31(12)
H9A	0.183 (5)	0.453 (4)	0.149 (3)	5.2 (7)
H9B	0.176 (5)	0.545 (4)	0.278 (3)	6.0 (7)
H10A	0.380 (4)	0.225 (4)	0.489 (3)	4.4 (6)
H10B	0.641 (4)	0.152 (3)	0.413 (3)	4.3 (6)
H10C	0.497 (5)	0.373 (4)	0.416 (3)	5.0 (6)
H12A	0.878 (5)	−0.161 (4)	0.058 (3)	4.9 (6)
H12B	0.693 (5)	−0.237 (4)	0.159 (3)	6.5 (8)
H13A	0.338 (5)	−0.183 (4)	0.216 (3)	6.0 (7)
H13B	0.099 (5)	−0.084 (4)	0.242 (3)	7.3 (9)
H13C	0.224 (6)	−0.202 (5)	0.355 (4)	7.7 (9)

*B_{iso} is the mean of the principal axes of the thermal ellipsoid.

TABLE 2. Bond lengths (Å) for compound **9**

Bond	Length (Å)
C(1)—C(2)	1.518(3)
C(1)—C(5)	1.496(3)
C(1)—C(9)	1.518(4)
C(1)—C(10)	1.531(4)
C(2)—O(3)	1.364(3)
C(2)—O(11)	1.196(3)
O(3)—C(4)	1.411(3)
C(4)—C(5)	1.459(3)
C(4)—C(12)	1.314(4)
C(5)—C(6)	1.331(3)
C(6)—O(7)	1.395(3)
C(6)—C(13)	1.474(4)
O(7)—C(8)	1.373(3)
C(8)—C(9)	1.502(4)
C(8)—O(14)	1.184(3)

$(C_7H_{22}O_4)^+$, 141.0555(23) $(C_7H_9O_3)^+$, 127.0399(36) $(C_6H_7O_3)^+$, 125.0607(90) $(C_7H_9O_2)^+$, 114.0684(35) $(C_6H_{10}O_2)^{+\cdot}$, 111.0451(30) $(C_6H_7O_2)^+$, 87.0451(100) $(C_4H_7O_2)^+$.

Frontalin isomer: 1,5-dimethyl-2,7-dioxabicyclo[3.2.1]octane

To a stirred solution of sodium bis(2-methoxyethoxy) aluminum hydride (2.3 g of 60% solution, 6.83 mmol) (Red-Al^R) in dry benzene (11 mL) under nitrogen was added by syringe the ketal diester prepared above (700 mg, 2.69 mmol) in dry benzene (7 mL). The mixture was heated under reflux for 3 h, and was then cooled in an ice bath. Excess reagent was decomposed by cautious addition of water (8 mL), then the mixture was poured into cold aqueous sulfuric acid solution (25 mL of 20% solution) in a 125-mL Erlenmeyer flask. The mixture was stirred with ice-cooling for 30 min, then extracted with 4 × 50 mL ether.

TABLE 3. Bond angles (deg) for compound **9**

Bonds	Angle (deg)
C(2)—C(1)—C(5)	101.71(19)
C(2)—C(1)—C(9)	114.66(21)
C(2)—C(1)—C(10)	107.03(20)
C(5)—C(1)—C(9)	108.54(19)
C(5)—C(1)—C(10)	112.52(20)
C(9)—C(1)—C(10)	112.02(21)
C(1)—C(2)—O(3)	109.33(20)
C(1)—C(2)—O(11)	129.62(24)
O(3)—C(2)—O(11)	120.95(23)
C(2)—O(3)—C(4)	111.55(18)
O(3)—C(4)—C(5)	106.67(20)
O(3)—C(4)—C(12)	118.80(23)
C(5)—C(4)—C(12)	134.53(25)
C(1)—C(5)—C(4)	107.98(19)
C(1)—C(5)—C(6)	121.08(21)
C(4)—C(5)—C(6)	130.52(22)
C(5)—C(6)—O(7)	118.74(21)
C(5)—C(6)—C(13)	130.12(23)
O(7)—C(6)—C(13)	111.12(21)
C(6)—O(7)—C(8)	121.79(19)
O(7)—C(8)—C(9)	117.03(21)
O(7)—C(8)—O(14)	117.92(24)
C(9)—C(8)—O(14)	125.05(25)

The combined extracts were washed successively with saturated $NaHCO_3$ solution and brine, and then dried over $MgSO_4$. The solvent was removed *in vacuo*, and the residue distilled. A fraction, bp 82°C/30 Torr (1 Torr = 133.3 Pa), was characterized as the frontalin isomer **6** (201 mg, 53%); ir ($CHCl_3$) (*inter alia*): 2970, 2940, 2880, 1455, 1390, 1330, 1325, 1170, 1125, 1075, 1050, 1015, and 980 cm^{-1}; ^{1}H nmr ($CDCl_3$, 200 MHz) δ: 1.07 (3H, s, C(5)Me), 1.29 (3H, s, C(1)Me), 1.3 (1H, m, C(4)H_{eq}), 1.52 (2H, s, C(8)H_2), 1.6 (1H, m, C(4)H_{ax}), 3.44 (1H, dd, J 7.6, 2.3 Hz (W coupling), C(6)H_{exo}), 3.6–3.85 (3H, m, C(3)H_2, C(6)H_{endo}); ^{13}C nmr ($CDCl_3$) δ: 22.1 (Me on C(5)), 23.9 (Me on C(1)), 36.4 (C(4)), 39.8 (C(5)), 48.9 (C(8)), 60.7 (C(3)), 77.9 (C(6)), 106.2 (C(1)); gc/ms (*inter alia*): 142 (28) $(C_8H_{14}O_2)^{+\cdot}$ ($M^{+\cdot}$), 98 (100).

X-ray crystallography

The crystal data and X-ray diffraction conditions were as follows:

$C_{10}H_{10}O_4$ Formula weight 194.12

Triclinic, $P\bar{1}$, a = 6.7661(9) Å, b = 7.9960(5) Å, c = 9.8676(12) Å, α = 73.808(8)°, β = 76.237(12)°, γ = 65.748(8)°, V = 462.8 Å^3, Z = 2, ρ_{calc} = 1.394 Mg m^{-3}, $F(000)$ = 204e, MoKα radiation (λ = 0.71073 Å), μ = 0.10 mm^{-1}, $2\theta_{max}$ = 50°, crystal dimensions 0.74 × 0.30 × 0.15 mm, temperature 293 K.

Intensity data were collected on an Enraf–Nonius CAD-4 diffractometer equipped with graphite-monochromated MoKα radiation, using the NRCCAD control routines (21). The cell dimensions were obtained by a least-squares fit to the coordinates of 25 reflections, in the range 30° < 2θ < 35°, which were obtained by centering each reflection at four equivalent positions. An ω/2θ scan with profile analysis was used for the intensity data, 1623 reflections were measured of which 1197 had $I_{net} > 2.5\sigma(I)$ and were included in subsequent calculations. Three standard reflections measured every hour during data collection showed no significant deviation from their mean values. No correction was made for absorption.

The structure was solved by direct methods using the MULTAN-80 suite of programs (22). All subsequent computations were performed using the PC version of NRCVAX (23). Hydrogen atom positions were located from a difference synthesis. The structure was refined using least squares and minimizing $\Sigma\omega(|F_o| - |F_c|)^2$, with weights derived from counter statistics. In the final cycles all non-hydrogen atoms were

assigned anisotropic thermal parameters; the hydrogen atoms were permitted to refine with isotropic thermal parameters. Scattering factors were taken from ref. 24 and corrected for anomalous dispersion. The final agreement factors were $R = 0.051$ and $R_w = 0.071$ (0.071 and 0.077 for all reflections). The number of parameters refined was 167 and the largest shift/error was 0.10. A final difference synthesis showed no recognizable features and varied from -0.18 to 0.23 e $Å^{-3}$.[3]

An ORTEP (25) representation of the molecule is shown in Fig. 1, and final atomic coordinates are given in Table 1.

Bioassay

Electroantennograms (EAG's) indicating the response of the entire olfactory antennal club of the bark beetles to the stimulant vapor were recorded. The details of the technique have been described previously (26) and are based on the procedure reported by Dickens *et al.* (27). EAG's were recorded with Ag/AgCl capillary electrodes filled with insect saline. The recording electrode was placed in the distal end of the antennal club following prepuncture with an electrolytically sharpened tungsten needle. The indifferent electrode was placed in the beetle's head in the mouth region. The response signals were amplified by a Grass P-16 amplifier and plotted. The magnitude of the EAG response was measured as a percentage of the mean of two bracketing standards, 10 μg racemic frontalin.

The test compounds were diluted in *n*-pentane in decade steps. A 10-μL sample on a 20 × 6 mm filter-paper strip in a 80 × 5 mm glass chamber held about 1 cm away from the insect preparation was puffed towards the beetle by passing air at 1.7 L/min through the chamber for 1 s. Samples were presented from lowest to highest concentration for six different dilutions. Five replicates with different beetles and for both sexes were made at each concentration. A minimum interval of 4 min was allowed between stimuli, except at higher concentrations when 6 min was allowed. Racemic frontalin (10 μg on filter paper) was used as the standard for comparison, and this stimulus was presented between every set of two stimulations. Responses for *n*-pentane, but not for air, were subtracted from all responses. Generally, the response to air was either minor or absent.

Acknowledgements

We thank Mr. See-Hua Tan, Research and Productivity Council, for the gc/ms study. The EAG bioassays were conducted in the laboratory of Dr. A. T. Whitehead, Brigham Young University, and we thank him for his hospitality and assistance.

[3]Tables of anisotropic temperature factors and $10F_o$, $10F_c$ values may be purchased from the Depository of Unpublished Data, CISTI, National Research Council of Canada, Ottawa, Ont., Canada K1A 0S2.

1. R. FITTIG. Justus Liebigs Ann. Chem. **314**, 1 (1901).
2. G. M. STRUNZ and G. S. LAL. Can. J. Chem. **60**, 2528 (1982).
3. G. M. STRUNZ, P. GIGUÈRE, and M. EBACHER. Synth. Commun. **13**, 823 (1983).
4. G. M. STRUNZ, G. BRISARD, and P. GIGUÈRE. Can. J. Chem. **63**, 2123 (1985).
5. G. M. STRUNZ and P. GIGUÈRE. Can. J. Chem. **64**, 204 (1986).
6. W. STEGLICH and G. HÖFLE. Angew. Chem. Int. Ed. Engl. **8**, 981 (1969).
7. G. W. KINZER, A. F. FENTIMAN, JR., T. F. PAGE, JR., R. L. FOLTZ, J. P. VITÉ, and G. B. PITMAN. Nature, **221**, 477 (1969).
8. H. WIESER, E. A. DIXON, N. IBRAHIM, and C. CASTRO. Abstr. Sixth International Congress of Pesticide Chemistry. IUPAC. Ottawa, Canada. 1986. 2C-O4.
9. P. R. HUGHES. Z. Angew. Entomol. **80**, 280 (1976).
10. J. P. VITÉ and G. B. PITMAN. J. Insect Physiol. **15**, 1617 (1969).
11. D. L. WOOD, L. E. BROWNE, B. EWING, K. LINDAHL, W. D. BEDARD, P. E. TILDEN, K. MORI, G. B. PITMAN, and P. R. HUGHES. Science, **192**, 896 (1976).
12. T. E. STEWART, E. L. PLUMMER, L. L. MCCANDLESS, J. R. WEST, and R. M. SILVERSTEIN. J. Chem. Ecol. **3**, 27 (1977).
13. G. B. PITMAN and J. P. VITÉ. Ann. Entomol. Soc. Am. **63**, 661 (1970).
14. E. D. A. DYER. Can. Entomol. **107**, 979 (1975).
15. J. A. A. RENWICK, P. R. HUGHES, and J. P. VITÉ. J. Insect Physiol. **21**, 1097 (1975).
16. H. D. PIERCE, J. E. CONN, A. C. OEHLSCHLAGER, and J. H. BORDEN. J. Chem. Ecol. **13**, 1455 (1987).
17. L. M. JACKMAN and S. STERNHELL. Applications of nuclear magnetic resonance spectroscopy in organic chemistry. Pergamon Press, New York. 1969.
18. A. I. SCOTT. Interpretation of the ultraviolet spectra of natural products. Pergamon Press, New York. 1964.
19. J. MÁLEK and M. CERNÝ. Synthesis, 217 (1972).
20. W. C. STILL, M. KAHN, and A. MITRA. J. Org. Chem. **43**, 2923 (1978).
21. Y. LE PAGE, P. S. WHITE, and E. J. GABE. NRCCAD, an enhanced CAD-4 control program. Annual meeting of the American Crystallographic Association. Hamilton, Ontario. 1986.
22. P. MAIN. MULTAN-80. University of York. 1980.
23. E. J. GABE, Y. LE PAGE, J.-P. CHARLAND, F. L. LEE, and P. S. WHITE. J. Appl. Crystallogr. In press.
24. International tables for X-ray crystallography. Vol. IV. Kynoch Press, Birmingham, England. 1974.
25. C. K. JOHNSON. ORTEP-II. Technical Report ORNL-5138, Oak Ridge National Laboratory, Oak Ridge, TN. 1976.
26. A. T. WHITEHEAD. J. Chem. Ecol. **12**, 1603 (1986).
27. J. C. DICKENS, A. GUTMANN, T. L. PAYNE, L. C. RYKER, and J. A. RUDINSKY. J. Chem. Ecol. **10**, 583 (1983).

Can. J. Chem. Downloaded from www.nrcresearchpress.com by 91.144.44.67 on 09/07/12
For personal use only.

Raman spectroscopy and electrochemistry of water-soluble porphyrins at a silver electrode

HIDEO ORITA,[1] MASAO SHIMIZU, CHIZUKO NISHIHARA, TAKASHI HAYAKAWA, AND KATSUOMI TAKEHIRA
National Chemical Laboratory for Industry, Tsukuba, Ibaraki 305, Japan

Received February 21, 1989[2]

HIDEO ORITA, MASAO SHIMIZU, CHIZUKO NISHIHARA, TAKASHI HAYAKAWA, and KATSUOMI TAKEHIRA. Can. J. Chem. **68**, 787 (1990).

Cyclic voltammetry and laser Raman spectroscopy were applied to investigate *in situ* the properties and structures of metal *meso*-tetrakis (*p*-sulfonatophenyl)porphyrins (MeTPPS, Me = Co, Fe, Mn, Cu, Ni) adsorbed on a silver electrode in 0.05 M H_2SO_4 aqueous solution. The cyclic voltammograms for O_2 reduction were investigated by changing the metal cations in the porphyrin ring. Among the porphyrins examined, only CoTPPS shows catalytic behavior for O_2 electrochemical reduction. The Raman spectra of MeTPPS in aqueous solution are very similar to those of metal tetraphenylporphyrins (MeTPP), and the band assignments were carried out on the basis of the results for $[FeTPP]_2O$. The Raman spectra of MeTPPS on a silver electrode were measured under a N_2 or O_2 atmosphere, changing the applied potentials and the metal cations in the porphyrin ring. Their spectra are very sensitive to metal cations, but not so to applied potential.

Key words: porphyrin, SERS, electrochemistry, dioxygen, silver electrode.

HIDEO ORITA, MASAO SHIMIZU, CHIZUKO NISHIHARA, TAKASHI HAYAKAWA et KATSUOMI TAKEHIRA. Can. J. Chem. **68**, 787 (1990).

On a fait appel à la voltamétrie cyclique et à la spectroscopie Raman au laser pour étudier *in situ* les propriétés et les structures de *méso*-tétrakis(*p*-sulfonatophényl)porphyrines métalliques (MeTPPS, Me=Co, Fe, Mn, Cu, Ni) adsorbées sur une électrode d'argent, dans une solution aqueuse de H_2SO_4, à 0,05 M. On a examiné les voltamogrammes cycliques de la réduction de O_2 par des porphyrines contenant divers cations métalliques. Parmi les porphyrines étudiées, seule la CoTPPS présente un comportement catalytique pour la réduction électrochimique de O_2. Les spectres Raman des MeTPPS en solutions aqueuses sont très semblables à ceux des tétraphénylporphyrines (MeTPP) et l'on a procédé à l'attribution des bandes en se basant sur les résultats obtenus avec le $[FeTPP]_2O$. On a déterminé les spectres Raman des MeTPPS déposées sur une électrode d'argent sous des atmosphères de N_2 et de O_2, en faisant varier les potentiels appliqués ainsi que les cations métalliques du cycle de la porphyrine. Ces spectres sont très sensibles à la nature des cations métalliques, mais non au potentiel appliqué.

Mots clés : porphyrine, SERS, électrochimie, dioxygène, électrode d'argent.

[Traduit par la revue]

Introduction

Transition metal porphyrins and phthalocyanines catalyze the electrochemical reduction of O_2 when they are present either in solution or on electrode surfaces (1–10). Recently, water-soluble porphyrins and phthalocyanines have been introduced in order to identify the chemical species and understand the mechanism of O_2 electroreduction in aqueous solution (1–9).

In situ Raman spectroscopy is a very useful technique in studying electrochemical reactions in aqueous solutions because it provides a large amount of information about structures of adsorbates from their vibrational spectra. On the other hand, infrared spectroscopy usually cannot be applied to these systems, since strong absorption of infrared radiation of water makes it difficult to observe weak band intensities of adsorbates. Furthermore, surface enhanced Raman scattering (SERS) provides a means for detecting small amounts of adsorbates because of its large enhancement of the Raman signal.

The SERS spectra of water-soluble *meso*-tetrakis(*p*-sulfonatophenyl)porphyrin (TPPS) have already been reported by Cotton *et al.* (11) and Itabashi *et al.* (12). They studied the dependence of the spectra upon potential and found that the adsorbed porphyrins undergo partial incorporation of Ag from the electrode during the anodization step. However, neither of the two research groups investigated the effect of metal cations other than Ag, in a porphyrin ring, on the SERS spectra. In the present work, we selected MeTPPS (Me=Co, Fe, Mn, Cu, Ni) as a catalyst of O_2 reduction, and silver as electrode. We investigated the effect of metal cations on properties of water-soluble porphyrins during electrochemical reduction of O_2 in aqueous solution by the use of cyclic voltammetry and laser Raman spectroscopy and found that the cyclic voltammograms for O_2 reduction and the SERS spectra are very sensitive to metal cations.

Experimental

A silver rod (Furu-Uchi Chemicals, 99.99%, 5 mm in diameter, its side walls covered by a heat-shrinkable tube) was polished to a mirror finish with a suspension of alumina (Baikalox, 0.05 μm) and used as a working electrode after ultrasonic cleaning. A saturated calomel electrode (SCE) and a platinum wire were used as reference electrode and counter electrode, respectively. The potential of the electrode was controlled by the combination of a potentiogalvanostat (Hokuto Denko HA-501 or PAR M273) and a function generator (Hokuto Denko HB-105) or a personal computer (NEC PC-9801 VX2). The rotating ring-disk electrode (RRDE) apparatus used has been described before (13). An Au(ring)–Ag(disk) electrode was employed after the final polishing with alumina suspension. The measurements of Raman spectra using the 488.0 nm line of an argon ion laser (Coherent Radiation CR-8, ca. 50 mW) and a double dispersion Raman spectrometer (JASCO R-800) were carried out during electrochemical reduction of O_2 at a given potential. The incident angle was about 60° and the scattered light was collected in the perpendicular direction.

meso-Tetrakis(*p*-sulfonatophenyl)porphyrin was synthesized (14) and its metallation was carried out (15) by the published procedure. The sample solutions were prepared by dissolving porphyrins (10^{-2}–10^{-5} M) and H_2SO_4 (0.05 M) in distilled water.

Results and discussion

Cyclic voltammograms for O_2 reduction in 0.05 M H_2SO_4 aqueous solution are given in Fig. 1. Before the oxidation–reduction cycle (ORC) was applied, between −0.4 and +0.6 V

[1]Author to whom correspondence may be addressed.
[2]Revision received January 5, 1990.

Printed in Canada / Imprimé au Canada

Can. J. Chem. Downloaded from www.nrcresearchpress.com by 91.144.44.67 on 09/07/12
For personal use only.

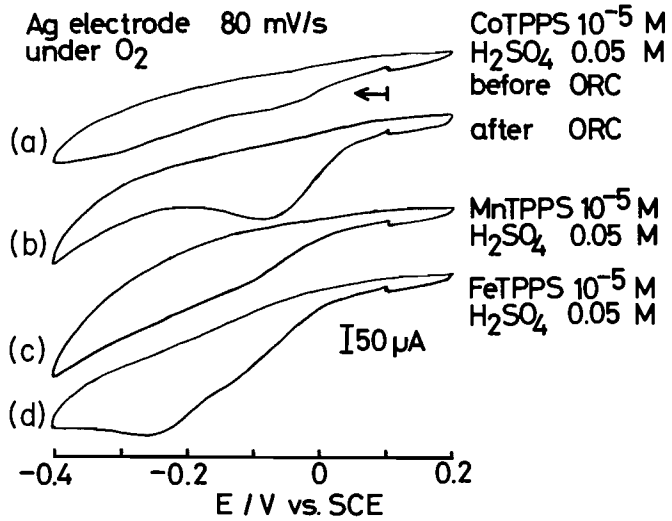

FIG. 1. Cyclic voltammograms for O_2 reduction in 0.05 M H_2SO_4 aqueous solution on a silver electrode at 80 mV/s: (a) CoTPPS 10^{-5} M, before oxidation–reduction cycles (ORC) between −0.4 and +0.6 V; (b) CoTPPS 10^{-5} M, after ORC; (c) MnTPPS 10^{-5} M, after ORC; (d) FeTPPS 10^{-5} M, after ORC.

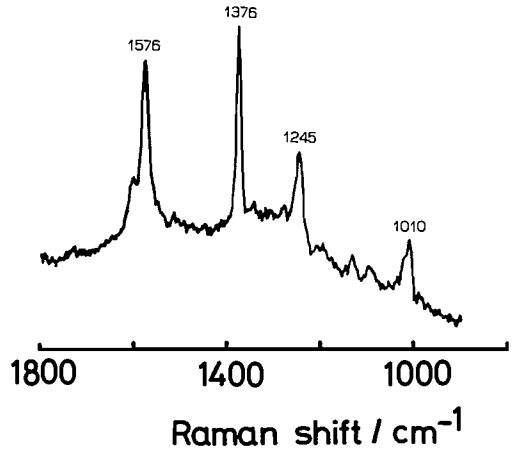

FIG. 2. Raman spectrum of CoTPPS in aqueous solution (10^{-2} M) with 488.0 nm excitation.

vs. SCE, the peak of the O_2 reduction wave was not clearly observed between −0.4 and +0.2 V in any of the cases investigated in this work (e.g., Fig. 1a). After ORC (usually ORC was applied in aqueous acidic solutions of MeTPPS), the peak of the O_2 reduction wave was distinctly observed at ca. −0.1 V in the presence of CoTPPS (Fig. 1b), suggesting that special sites involving an interaction of CoTPPS with the Ag electrode were created by ORC. When the same experiment was carried out for aqueous acidic solutions of MnTPPS, FeTPPS, CuTPPS, or NiTPPS, the peak of the reduction wave at −0.1 V did not appear (e.g., Figs. 1c and d). There was some increase in current for MnTPPS and a peak at ca. −0.25 V for FeTPPS. For CuTPPS, NiTPPS, or in absence of MeTPPS, only a small increase in the O_2 reduction current was observed at ca. −0.3 V after ORC. The electrode that was used after ORC in the solutions of MeTPPS other than CoTPPS was washed with water, and when the solution was changed to that of CoTPPS, the peak of the O_2 reduction wave at −0.1 V appeared clearly as is the case in Fig. 1b. Therefore, the cyclic voltammograms for O_2 reduction are very sensitive to metal cations, and CoTPPS clearly shows catalytic behavior for O_2 reduction. In neutral or alkaline solution, the effect of porphyrins on O_2 reduction was not observed. To check the presence of H_2O_2 as a product of O_2 reduction, RRDE experiments were carried out (Ag disk, 6 mm diameter, 0.2 mm gap width; Au ring, 1 mm ring width, calculated collection efficiency=0.4, 1000 rpm, 80 mV/s, ring potential=0.6 or 1.0 V). The formation of H_2O_2 generated by two-electron reduction of O_2 was not observed by RRDE in the present work. Consequently, it is considered that O_2 reduction mainly proceeds through a four-electron pathway (O_2 to H_2O). Ozer *et al.* (6) have studied the electrochemical reduction of O_2 by using cobalt tetra(4-N,N′,N″-trimethylanilinium) porphyrin and a glassy carbon electrode. They reported that dioxygen reduction proceeds mostly through a four-electron reduction in acidic solutions in the presence of adsorbed (or dissolved) porphyrin. Collman *et al.* (10) have also reported that cobalt derivatives of particular cofacial porphyrin dimers catalyze the overall four-electron reduction of O_2 while adsorbed on graphite electrodes in acidic solution, and that a Lewis-acid center facilitates the four-electron path.

Surface enhanced Raman scattering was applied to the present electrochemical system in order to obtain information about structures of MeTPPS at the electrode–solution interface and to investigate the effect of metal cations on O_2 electroreduction. At first, the spectra of MeTPPS in aqueous solution were measured; a typical result for CoTPPS is shown in Fig. 2. As the 488.0 nm line of the argon ion laser was not in resonance with the absorption bands of CoTPPS, spectra could be measured only when the concentration of CoTPPS was higher than 10^{-3} M. The spectrum in Fig. 2 is very similar to the spectrum of cobalt tetraphenylporphyrin (CoTPP) (16) or $[FeTPP]_2O$ (17). Therefore we have the following assignments based on the results obtained for $[FeTPP]_2O$, assuming D_{4h} symmetry: 1576, $\nu(C_\beta–C_\beta) + \delta(C_\beta–H)$; 1376, $\nu(C_\alpha–N) + \delta(C_\beta–H)$; 1245, $\nu(C_m–Ph)$; 1010, $\nu(C_\alpha–C_m)$. Here, ν and δ denote the stretching and in-plane bending mode, respectively, and all the numbers are given in cm^{-1}. All the bands that appeared strongly are assigned to the totally symmetric (A_{1g}) modes.

Figure 3a shows the Raman spectrum of CoTPPS on a silver electrode at −0.3 V under a N_2 atmosphere after ORC. In spite of low concentration (10^{-5} M), a spectrum of CoTPPS was obtained with a good S/N ratio. Compared with the solution-phase spectrum in Fig. 2, the bands were shifted to the lower wavenumber, and the relative intensity of bands at 1572 and 1193 cm^{-1} increased. These facts indicate that the observed Raman spectrum with the silver electrode is associated with adsorbed CoTPPS rather than with the solution-phase species. The solution-phase concentration during these experiments was too low to detect Raman signals under the conditions of the present work. The dependence upon potential of the Raman spectrum was examined by changing the electrode potential between −0.5 and +0.2 V. No significant shifts of bands were observed, within experimental accuracy. At potentials more positive than −0.1 V, all the peaks rapidly decreased in intensity as the potential was increased, suggesting that this phenomenon could be due to the desorption of CoTPPS from the electrode.

No change in the Raman spectrum of the adsorbed CoTPPS was observed with introduction of O_2, compared to N_2 saturation in the O_2 reduction region between −0.1 and −0.4 V, in spite of the effect of CoTPPS on the O_2 reduction wave for

Can. J. Chem. Downloaded from www.nrcresearchpress.com by 91.144.44.67 on 09/07/12
For personal use only.

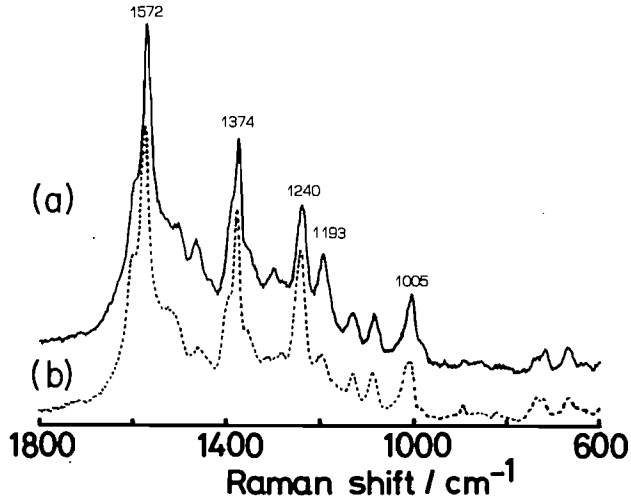

FIG. 3. Raman spectrum of MeTPPS on a Ag electrode with 488.0 nm excitation (10^{-5}, 0.05 M H_2SO_4, −0.3 V vs. SCE): (a) CoTPPS, N_2 atmosphere; (b) NiTPPS, O_2 atmosphere.

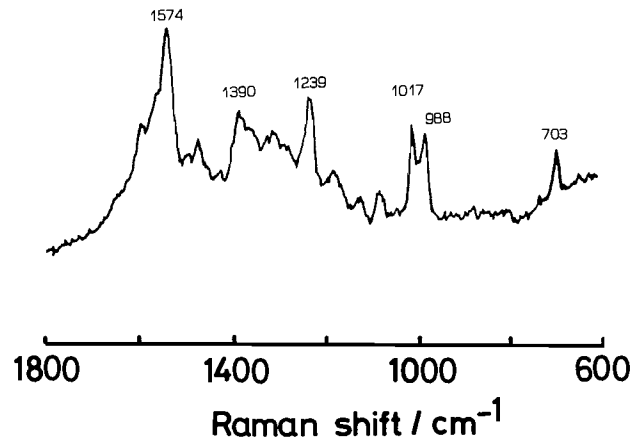

FIG. 4. Raman spectrum of MnTPPS on a Ag electrode with 488.0 nm excitation (10^{-5} M, 0.05 M H_2SO_4, −0.3 V vs. SCE, N_2 atmosphere).

the cyclic voltammogram. On the other hand, it is well known that cobalt porphyrins can form 1:1 O_2/Co adducts, and Bajdor *et al.* (18) reported that the O_2 stretching vibration ($\nu(O_2)$) of the dioxygen adduct of CoTPP with proper ligands and higher pressures of O_2 (ca. 4 atm; 1 atm = 101.3 kPa) was observed at 1144 cm^{-1} by the use of resonance Raman spectroscopy. Two possible explanations for no change in the Raman spectrum with introduction of O_2 can be considered. One is that at the quite negative potential used in the present study (at potentials more positive than −0.1 V, the Raman signal decreased rapidly and a spectrum with a good S/N ratio was not obtained), the O_2 was reduced easily and the concentration of O_2 in solution at the electrode surface, as well as the surface concentration of any O_2 adduct, was reduced effectively to zero. The other is that the residual O_2 in solution, even after prolonged N_2 bubbling, was sufficient to saturate the surface completely with respect to the formation of O_2 adduct (at a rough estimation, only ca. 10^{-9} moles per cm^2 of Ag surface were required to cover the Ag electrode as a monolayer). For CuTPPS and NiTPPS, which did not show any effect on O_2 reduction, similar spectra were obtained except that the band intensity at 1193 cm^{-1} was much weaker (Fig. 3b). The second explanation suggests that the band at 1193 cm^{-1} might arise from the interaction between CoTPPS and O_2, but the precise assignment of this band cannot be done at the present stage. More detailed and careful experiments by the use of isotopes (deuterated TPPS, $^{18}O_2$) and various laser lines (resonance Raman effect) will be necessary.

The Raman spectrum of MnTPPS on a silver electrode is shown in Fig. 4. The spectrum of MnTPPS is somewhat different from that of CoTPPS: the band at ca. 1000 cm^{-1} is split into two bands; the band at ca. 1200 cm^{-1} was very weak; the band at 1390 cm^{-1} broadened, shifted to higher wavenumber, and decreased in intensity, indicating that the adsorbed state of MnTPPS is a little different from that of CoTPPS. The spectrum of FeTPPS could not be measured because FeTPPS was decomposed to unknown compounds by laser radiation. No spectrum of MeTPPS on Ag could be obtained in alkaline solution. As no effects of MeTPPS on O_2 reduction were observed in alkaline solution, the adsorption of MeTPPS on a Ag electrode in alkaline solution may be hindered. Although the above-mentioned SERS measurements did not give definitive evidence with respect to the mechanism of O_2 reduction for CoTPPS because of experimental restrictions, they have revealed that Raman spectra of MeTPPS adsorbed on a Ag electrode are very sensitive to metal cations, but not so to applied potential.

Conclusions

The Raman spectra of MeTPPS were obtained on a Ag electrode and in aqueous solution. The spectra are similar to that of MeTPP, and the band assignments were carried out on the basis of the results for $[FeTPP]_2O$. All the bands that appeared strongly are assigned to totally symmetric modes. The cyclic voltammograms for O_2 reduction and SERS spectra are sensitive to the metal cations of MeTPPS. The band at 1193 cm^{-1} was clearly observed only when the electrochemical reaction was carried out using CoTPPS, which showed the highest activity of O_2 reduction among the porphyrins examined.

Acknowledgments

The authors wish to thank Dr. H. Shindo for use of the Raman apparatus and for advice on surface enhanced Raman scattering. The authors also thank the reviewers, whose valuable advice greatly helped to improve the discussion in this paper.

1. T. KUWANA, M. FUJIHIRA, K. SUNAKAWA, and T. OSA. J. Electroanal. Chem. **88**, 299 (1978).
2. N. KOBAYASHI, M. FUJIHIRA, K. SUNAKAWA, and T. OSA. J. Electroanal. Chem. **101**, 269 (1979).
3. R. KOTZ and E. YEAGER. J. Electroanal. Chem. **113**, 113 (1980).
4. K. OKABAYASHI, O. IKEDA, and H. TAMURA. J. Chem. Soc. Chem. Commun. 684 (1983).
5. N. KOBAYASHI and T. OSA. J. Electroanal. Chem. **157**, 269 (1983).
6. D. OZER, R. PARASH, F. BROITMAN, U. MOR, and A. BETTELHEIM. J. Chem. Soc. Faraday Trans. 1, **80**, 1139 (1984).
7. O. IKEDA, K. OKABAYASHI, N. YOSHIDA, and H. TAMURA. J. Electroanal. Chem. **191**, 157 (1985).
8. J. J. MCMAHON, S. BAER, and C. A. MELENDRES. J. Phys. Chem. **90**, 1572 (1986).
9. T. OSAKA, K. NAOI, T. HIRABAYASHI, and S. NAKAMURA. Bull. Chem. Soc. Jpn. **59**, 2717 (1986).
10. J. P. COLLMAN, N. H. HENDRICKS, K. KIM, and C. S. BENCOSME. J. Chem. Soc. Chem. Commun. 1537 (1987).

Can. J. Chem. Downloaded from www.nrcresearchpress.com by 91.144.44.67 on 09/07/12
For personal use only.

11. T. M. COTTON, S. G. SCHULTZ, and R. P. VAN DUYNE. J. Am. Chem. Soc. **104**, 6528 (1982).
12. M. ITABASHI, C. KATO, and K. ITO. Chem. Phys. Lett. **97**, 528 (1983).
13. C. NISHIHARA and H. SHINDO. J. Electroanal. Chem. **202**, 231 (1986).
14. T. S. SRIVASTAVA and M. TSUTSUI. J. Org. Chem. **38**, 2103 (1973).
15. E. B. FLEISCHER, J. M. PALMER, T. S. SRIVASTAVA, and A. CHATTERJEE. J. Am. Chem. Soc. **93**, 3162 (1971).
16. M. KOZUKA, and N. NAKAMOTO. J. Am. Chem. Soc. **103**, 2162 (1981).
17. J. M. BURKE, J. R. KINCAID, and T. G. SPIRO. J. Am. Chem. Soc. **100**, 2162 (1978).
18. K. BAJDOR, K. NAKAMOTO, and J. KINCAID. J. Am. Chem. Soc. **105**, 678 (1983); K. BAJDOR, J. R. KINCAID, and K. NAKAMOTO. J. Am. Chem. Soc. **106**, 7741 (1984).

Can. J. Chem. Downloaded from www.nrcresearchpress.com by 91.144.44.67 on 09/07/12
For personal use only.

Vilsmeier–Haack reaction with succinamidals. A convenient synthesis of 5-chloropyrrole-2-carboxaldehydes and 5-chloropyrrole-2,4-dicarboxaldehydes[1]

ANGEL GUZMÁN AND MOISES ROMERO[2]
Syntex, S.A., División de Investigación, Apartado Postal 10-820, Mexico 10, D.F., Mexico

AND

JOSEPH M. MUCHOWSKI[3]
Syntex Research, Institute of Organic Chemistry, 3401 Hillview Avenue, Palo Alto, CA 94304, U.S.A.

Received October 10, 1989

ANGEL GUZMÁN, MOISES ROMERO, and JOSEPH M. MUCHOWSKI. Can. J. Chem. **68**, 791 (1990).

It is shown that the reaction of *N*-alkylsuccinamidals (**2**) with the Vilsmeier–Haack reagent derived from DMF and phosphorus oxychloride can be controlled to preferentially produce either 5-chloropyrrole-2-carboxaldehydes (**8**) or 5-chloropyrrole-2,4-dicarboxaldehydes (**9**). The corresponding *N*-unsubstituted aldehydes are obtained when *N*-*tert*-butoxycarbonylsuccinamidal (**11**) is the substrate in the above reactions.

Key words: Vilsmeier–Haack reaction, succinamidals, 5-chloropyrrole-2-carboxaldehydes, 5-chloropyrrole-2,4-dicarboxaldehydes.

ANGEL GUZMÁN, MOISES ROMERO et JOSEPH M. MUCHOWSKI. Can. J. Chem. **68**, 791 (1990).

On a démontré que la réaction des *N*-alkylsuccinamidals (**2**) avec le réactif de Vilsmeier–Haack, obtenu à partir du DMF et de l'oxychlorure de phosphore, peut être contrôlée afin qu'elle produise préférentiellement soit des 5-chloropyrolle-2-carboxyaldéhydes (**8**) ou des 5-chloropyrolle-2,4-dicarboxyaldéhydes (**9**). Lorsque le substrat des réactions mentionnées plus haut est le *N*-*tert*-butoxycarbonylsuccinamidal (**11**), on obtient les aldéhydes correspondants qui ne sont pas substitués sur l'azote.

Mots clés : réaction de Vilsmeier–Haack, succinamidals, 5-chloropyrolle-2-carboxaldéhydes, 5-chloropyrolle-2,4-dicarboxaldéhydes.

[Traduit par la revue]

In connection with other studies in progress in these laboratories, it became necessary to develop a synthesis of 5-chloropyrrole-2-carboxaldehydes that was more convenient than those in existence. Such compounds have been prepared by the action of Vilsmeier–Haack reagents on 2-chloropyrrole derivatives (1) or 3-pyrroline-2-ones (2, 3). The first method does provide the aldehydes in good yields but the notorious instability of 2-chloropyrroles (1) makes this process distinctly unattractive. The second method possesses some degree of generality but 3-pyrrolin-2-ones are often not trivial to prepare (4–11).

It has been known for some time that succinimides are reduced to succinamidals by sodium borohydride (12). Dehydration of these reduction products under acidic conditions leads to 3-pyrrolin-2-ones but because of competing side reactions the process is usually not a useful one. It occurred to us that succinamidals might undergo dehydration under the conditions of the Vilsmeier–Haack reaction. The *in situ* generated 3-pyrrolin-2-ones would be expected to react rapidly with the Vilsmeier–Haack reagent, thus reducing potential competing acid-promoted side reactions. This paper describes results that demonstrate that this does indeed constitute a viable route to 5-chloropyrrole-2-carboxaldehyde derivatives.

Reaction of *N*-methylsuccinamidal (**2***a*, Scheme 1) with dimethylformamide (DMF) and phosphorus oxychloride (1:3:6 molar ratio)[4] in dichloromethane, at room temperature, gave the known (1) 5-chloro-1-methylpyrrole-2-carboxaldehyde (**8***a*, 33% yield, Table 1), after hydrolysis with aqueous sodium carbonate solution. Application of these conditions to other *N*-substituted succinamidals produced the expected 5-chloropyrrole-2-carboxaldehyde derivatives in modest yields (Table 1), but only a small amount (2%) of 5-chloropyrrole-2-carboxaldehyde (**8***d*) was obtained from succinamidal itself. In addition, in every case, except when succinamidal was the starting material, trace amounts of a second product, subsequently shown to be the 5-chloropyrrole-2,4-dicarboxaldehyde derivative **9**, were formed. This material doubtless stemmed from further reaction of the primary product **6** with the Vilsmeier–Haack reagent. The dialdehyde could be made the major or exclusive product by effecting the reaction at 50°C in the presence of 5 molar equivalents of the Vilsmeier–Haack reagent though, under these conditions, 5-chloropyrrole-2,4-dicarboxaldehyde (**9***d*) was isolated in only 2% yield from succinamidal.

The synthesis of 5-chloropyrrole-2-carboxaldehyde (**8***d*) was

TABLE 1. Synthesis of 5-chloropyrrole-2-carboxaldehydes and 5-chloropyrrole-2,4-dicarboxaldehydes from succinamidals under Vilsmeier–Haack conditions

Starting material	$DMF/POCl_3$ molar ratios	T (°C)	Products (% yield)
2*a*	3/6	25	**8***a* (33), **9***a* (trace)
2*a*	5/10	50	**8***a* (5), **9***a* (62)
2*b*	3/6	25	**8***b* (35), **9***b* (trace)
2*b*	5/10	50	**8***b* (4), **9***b* (56)
2*c*	3/6	25	**8***c* (57), **9***c* (trace)
2*c*	5/10	50	**9***c* (87)
2*d*	3/6	25	**8***d* (2)
2*d*	5/10	50	**9***d* (2)
11	3/3	25	**8***d* (46), **9***d* (trace)
11	5/5	25	**8***d* (25), **9***d* (9)

[1]Contribution no. 791 from the Syntex Institute of Organic Chemistry.

[2]Research completed in partial fulfillment for the degree of "Maestria en Ciencias" at the Departamento de Química, División de Estudios Superiores, Universidad Nacional Autónoma de México, México, D.F.

[3]Author to whom correspondence may be addressed.

[4]Only 3 molar equivalents of $POCl_3$ are required in theory.

Can. J. Chem. Downloaded from www.nrcresearchpress.com by 88.85.125.76 on 09/07/12
For personal use only.

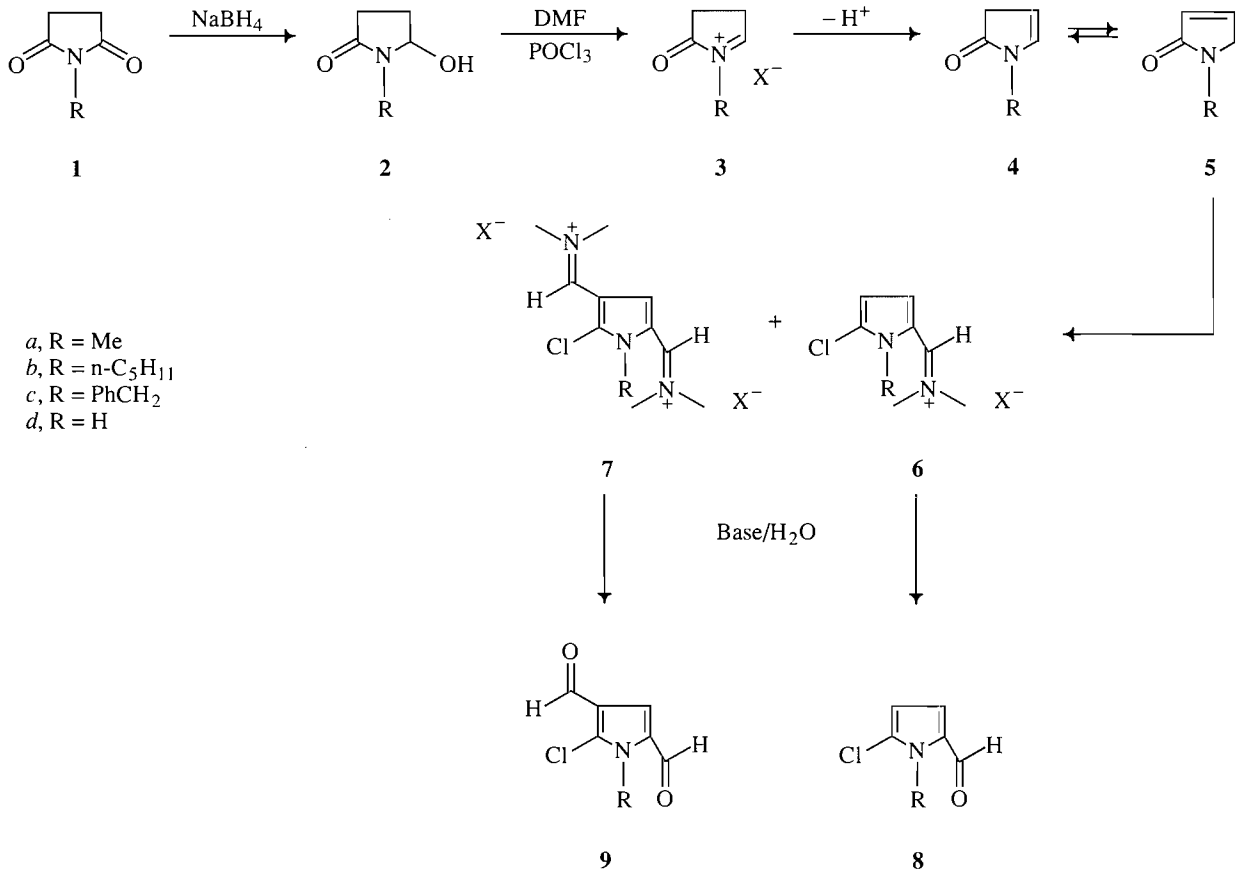

1 2 3 4 5 7 6 9 8

SCHEME 1

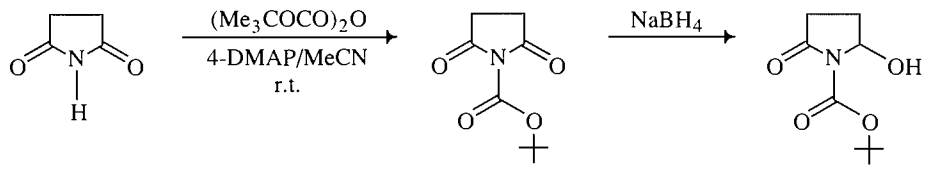

2*d* 10 11

SCHEME 2

dramatically improved by utilization of *N-tert*-butoxycarbonylsuccinamidal (**11**, Scheme 2) in the Vilsmeier–Haack reaction. This compound, upon reaction with 3 equivalents of the Vilsmeier–Haack reagent, gave rise to **8***d* in 46% yield, after hydrolysis with aqueous sodium acetate.[5,6] The loss of the protecting group must have occurred during the course of the reaction[7] since *N-tert*-butoxycarbonyl-5-chloropyrrole-2-carboxaldehyde (**12**) was stable to the hydrolysis conditions. The *N*-protected succinamidal **11** was prepared in the usual manner from *N-tert*-butoxycarbonylsuccinimide (**10**), which in turn was synthesized by the 4-dimethylaminopyridine-catalysed reaction of di-*tert*-butyldicarbonate with succinimide (14).

In conclusion, 5-chloropyrrole-2-carboxaldehydes or 5-chloropyrrole-2,4-dicarboxaldehydes are readily synthesized by reaction of the Vilsmeier–Haack reagent with succinamidals. Although the aldehyde yields, in most cases, are modest, the simplicity and brevity of the process as well as the low cost of the starting material(s) make this a particularly attractive route to such pyrrole derivatives.

In view of the observations of von Dobeneck and co-workers (2, 3), it is highly probable that the methodology described herein will be applicable to the synthesis of 5-brominated pyrrole mono- or dicarboxaldehyde derivatives and to 5-halo-2-acetylpyrroles (15).

Experimental

The melting points were determined in a Mel-Temp melting point apparatus and are not corrected. The infrared spectra were measured in chloroform solution, unless stated otherwise, with a Perkin–Elmer model 1420 infrared spectrophotometer or a Nicolet 5 PC FT infrared spectrophotometer. The ^{1}H nmr spectra were obtained in deuteriochloroform with a Varian EM-390 or a Bruker WM 300 nmr spectrometer and are expressed as parts per million (δ) from internal tetramethylsilane. When exchangeable protons were present, the data are given for deuterium oxide exchanged spectra.

[5]Much lower product yields resulted when the hydrolysis of the reaction products of **11** was effected with aqueous sodium carbonate.

[6]The chlorination of pyrrole-2-carboxaldehyde with sulfuryl chloride or *tert*-butyl hypochlorite is known (13) to produce a mixture of 4-chloropyrrole-2-carboxaldehyde, compound **8***d*, and 4,5-dichloropyrrole-2-carboxaldehyde.

[7]This is not unreasonable since 3 equiv. of hydrogen chloride are produced in the reaction.

Can. J. Chem. Downloaded from www.nrcresearchpress.com by 88.85.125.76 on 09/07/12
For personal use only.

Can. J. Chem. Downloaded from www.nrcresearchpress.com by 88.85.125.76 on 09/07/12
For personal use only.

The terms "worked up in the usual manner" or "the usual work-up" signify that the extract was dried over sodium sulfate and evaporated *in vacuo*.

Succinimide and the *N*-alkyl congeners thereof were obtained from commercial sources or synthesized by literature methods.

N-tert-*Butoxycarbonylsuccinimide (**10**)*

Di-*tert*-butyldicarbonate (13.1 g, 60 mmol) and 4-dimethylaminopyridine (0.610 g, 5 mmol) were added to a magnetically stirred solution of succinimide (5.0 g, 50 mmol) in reagent grade acetonitrile (100 mL). Carbon dioxide evolution began immediately. After 3 h, the solvent was removed *in vacuo* and the residue was subjected to column chromatography on silica gel (80 g). The product (8.8 g, 88%), eluted with hexane – ethyl acetate (4:1), was obtained as a solid that, after crystallization from hexane–dichloromethane, had mp 86°C; ir: 1806, 1767, 1709 cm^{-1}; nmr δ: 1.58 (s, 9H, *t*-Bu), 2.77 (s, 4H, CH_2CH_2). Anal. calcd. for $C_9H_{13}NO_4$: C 54.26, H 6.57, N 7.03; found: C 53.98, H 6.61, N 7.01.

Synthesis of the succinamidals

Succinamidal and *N*-methylsuccinamidal were prepared by the method of Speckamp and co-workers (12) in 60–65% yields.

(a) N-n-*Pentylsuccinamidal (**2**b)*

Powdered sodium borohydride (4.0 g, 106 mmol) was added in portions to a stirred, cooled (−20°C) solution of *N*-*n*-pentylsuccinimide (12.0 g, 71 mmol) in methanol (50 mL). After 2 h, a saturated aqueous solution of ammonium chloride (50 mL) was added and the reaction mixture was stirred for 1 h at ambient temperature. The mixture was filtered, the solids were washed well with ethyl acetate, and the washings and filtrate were evaporated *in vacuo*. The residue was extracted with dichloromethane and, after the usual work-up, the crude product was purified by column chromatography on silica gel (150 g). The product was eluted from the column with 1:1 hexane – ethyl acetate and was obtained as an oil (7.0 g, 60%); ir: 3350, 1685, 1680 cm^{-1}; nmr δ: 0.90 (t, 3H, J = 6.0 Hz, Me), 1.20 (m, 6H, $(CH_2)_3$), 1.86–2.69 (m, 4H, CH_2CH_2), 2.96–3.72 (m, 2H, NCH_2), 4.92–5.30 (m, 1H, CH). Anal. calcd. for $C_9H_{17}NO_2$: C 60.15, H 7.06, N 7.01; found: C 60.40, H 7.18, N 6.96.

(b) N-*Benzylsuccinamidal (**2**c)*

Powdered sodium borohydride (2.0 g, 43 mmol) was added portionwise to a stirred solution of *N*-benzylsuccinimide (4.0 g, 20 mmol) in 1:1 tetrahydrofuran (THF) – 95% ethanol (60 mL) at 0°C. After 3 h, the reaction was quenched by the addition of 10% aqueous hydrochloric acid (10 mL) and the mixture was worked up as described above for **2***b*. The crude product was diluted with water, extracted with ethyl acetate, and, after the usual work-up, the material obtained was purified as described for **2***b*. A solid (2.6 g, 50% yield) was obtained, which had mp 105–107°C after crystallization from ethyl acetate; ir: 3355, 1685 cm^{-1}; nmr δ: 1.74–2.72 (m, 4H, CH_2CH_2), 4.15 (d, 1H, J_{AB} = 15.1 Hz, H_A of NCH_2), 4.84 (d, 1H, J_{AB} = 15.1 Hz, H_B of NCH_2), 5.07 (dd, 1H, J_{AX} = 2.1 Hz, J_{BX} = 4.2 Hz, CH), 7.30 (s, 5H, C_6H_5). Anal. calcd. for $C_{11}H_{13}NO_2$: C 69.09, H 6.85, N 7.32; found: C 69.12, H 6.78, N 7.17.

(c) N-tert-*Butoxycarbonylsuccinamidal (**11**)*

This compound was synthesized in the same manner as **2***c* except that the reduction was effected at −50°C for 5 h. The reaction was quenched with 5% hydrochloric acid, the mixture was filtered, the solids were washed well with ethyl acetate, and the washings and filtrate were evaporated *in vacuo*. After the usual work-up, the crude product was purified by column chromatography on silica gel (350 g for a 47 mmol reaciton). Elution of the column with hexane – ethyl acetate (3:7) gave a solid (70% yield), which on crystallization from hexane – ethyl acetate had mp 78–79°C; ir: 3510, 1767, 1709 cm^{-1}; nmr δ: 1.57 (s, 9H, *t*-Bu), 1.93–2.97 (m, 4H, CH_2CH_2), 5.71 (dd, 1H, J_{AX} = 2.1 Hz, J_{BX} = 4.2 Hz, CH). Anal. calcd. for $C_9H_{15}NO_2$: C 53.72, H 7.51, N 6.86; found: C 53.88, H 7.73, N 6.85.

*Synthesis of 5-chloropyrrole-2-carboxaldehydes (**8**)*

*(a) 1-Methyl-5-chloropyrrole-2-carboxaldehyde (**8**a)*

The Vilsmeier–Haack reagent was prepared by slow addition of anhydrous DMF (1 mL, 0.94 g, 13 mmol) to phosphorus oxychloride (2.4 mL, 4.0 g, 26 mmol) with stirring at 0°C in a nitrogen atmosphere. The reaction mixture was left at room temperature for 3 h and then a solution of *N*-methylsuccinamidal (0.500 g, 4.34 mmol) in anhydrous 1,2-dichloroethane (10 mL) was added and the reaction mixture was stirred for 15 h at room temperature. A solution of sodium carbonate (4.6 g, 43 mmol) in water (20 mL) was added and the mixture was stirred for 2–3 h at room temperature. The products were extracted into dichloromethane and, after the usual work-up and purification by column chromatography on silica gel (60 g), using hexane – ethyl acetate (7:3) as the eluting solvent, the aldehyde **8***a* was obtained as an oil (0.205 g, 33% yield), which had spectroscopic properties identical to those reported (1).

*(b) 1-*n*-Pentyl-5-chloropyrrole-2-carboxaldehyde (**8**b)*

This compound was synthesized in the same manner as described for **8***a* except that hexane – ethyl acetate (95:5) was used in the column chromatographic purification. The product was obtained as an oil; ir: 1678 cm^{-1}; nmr δ: 0.87 (t, 3H, J = 6.1 Hz, Me), 1.23–1.47 (m, 4H, CH_2CH_2), 1.55–1.86 (m, 2H, CH_2), 4.37 (t, 2H, J = 7.3 Hz, NCH_2), 6.21 (d, 1H, J = 4.3 Hz, H-4), 6.90 (d, 1H, J = 4.3 Hz, H-3), 9.44 (s, 1H, CHO). Anal. calcd. for $C_{10}H_{14}ClNO$: C 60.15, H 7.06, N 7.01; found: C 60.40, H 7.18, N 6.96.

*(c) 1-Benzyl-5-chloropyrrole-2-carboxaldehyde (**8**c)*

Prepared in the same way as described for **8***a* except that hexane – ethyl acetate (9:1) was used for the column chromatographic purification. Compound **8***c* was obtained as an oil; ir: 2715, 1695 cm^{-1}; nmr δ: 5.66 (s, 2H, CH_2), 6.25 (d, 1H, J = 4.1 Hz, H-4), 6.93 (d, 1H, J = 4.1 Hz, H-3), 7.04–7.40 (m, 5H, C_6H_5), 9.46 (s, 1H, CHO). Anal. calcd. for $C_{12}H_{10}ClNO$: C 65.61, H 4.58, N 6.37; found: C 66.00, H 4.71, N 6.13.

*(d) 5-Chloropyrrole-2-carboxaldehyde (**8**d)*

This compound was prepared from compound **11** as described for **8***a* except that 3 molar equivalents of DMF and of phosphorus oxychloride were used. At the end of 15 h, sodium acetate (6 g for a 2.5 mmol scale reaction) in water (10 mL) was added to the reaction mixture and, after stirring for 3 h at room temperature, the reaction mixture was processed exactly as described for **8***a*. After crystallization from dichloromethane–hexane, compound **8***d* had mp 110°C (lit. (1) mp 110–111°C).

*Synthesis of 5-chloropyrrole-2,4-dicarboxaldehydes (**9**)*

*(a) 1-Methyl-5-chloropyrrole-2,4-dicarboxaldehyde (**9**a)*

The Vilsmeier–Haack reagent was prepared as described for **8***a* except that 5 molar equivalents of DMF and 10 molar equivalents of phosphorus oxychloride were used. The amidal was added in 1,2-dichloroethane solution (10 mL for a 4.34 mmol reaction) and the reaction mixture was maintained at 50°C for 15 h. The reaction mixture was cooled to 0°C, sodium carbonate (9.4 g for a 4.34 mmol reaction) in water (45 mL) was added, and the mixture was stirred for 2–3 h at room temperature. The reaction mixture was processed in the same manner as described for **8***a*, to give the desired product as well as a small amount (5%) of **8***a*. After crystallization from hexane–dichloromethane, the dialdehyde **9***a* had mp 153–154°C; ir: 2810, 1676 cm^{-1}; nmr δ: 4.00 (s, 3H, Me), 7.39 (s, 1H, H-3), 9.62 (s, 1H, CHO), 9.97 (s, 1H, CHO). Anal. calcd. for $C_7H_6ClNO_2$: C 49.00, H 3.52, N 8.16; found: C 48.83, H 3.50, N 8.03.

*(b) 1-*n*-Pentyl-5-chloropyrrole-2,4-dicarboxaldehyde (**9**b)*

Prepared in the same manner as described for **9***a* except that hexane – ethyl acetate (9:1) was used in the column chromatographic purification. The dialdehyde **9***b* and a small amount (4%) of **8***b* were obtained. After crystallization from hexane–dichloromethane, compound **9***b* had mp 70°C; ir: 1674, 1663 cm^{-1}; nmr δ: 0.91 (t, 3H, J = 7.0 Hz, Me), 1.35 (m, 4H, CH_2CH_2), 1.73 (m, 2H, CH_2), 4.44 (t, 2H, J = 7.6 Hz, NCH_2), 9.53 (s, 1H, CHO), 9.90 (s, 1H, CHO). Anal. calcd. for $C_{11}H_{14}ClNO_2$: C 58.02, H 6.14, N 6.15; found: C 57.94, H 6.17, N 5.83.

*(c) 1-Benzyl-5-chloropyrrole-2,4-dicarboxaldehyde (**9**c)*

Prepared in the same way as described for **9***a* except that hexane –

ethyl acetate (4:1) was used in the column chromatographic purification. After crystallization from hexane–dichloromethane, the dialdehyde **9***c* had mp 103–104°C; ir: 2720, 1680 cm^{-1}; nmr δ: 5.73 (s, 2H, CH_2), 7.17 (m, 2H), 7.33 (m, 3H), 7.42 (s, 1H, H-3), 9.54 (s, 1H, CHO), 9.92 (s, 1H, CHO). Anal. calcd. for $C_{13}H_{10}ClNO_2$: C 63.04, H 4.06, N 5.65; found: C 63.08, H 4.11, N 5.68.

*(d) 5-Chloropyrrole-2,4-dicarboxaldehyde (***9**d*)

Prepared in the same manner as described for **8***d* except that 5 molar equivalents each of DMF and $POCl_3$ were used and the reaction was left at room temperature for 40 h. The dialdehyde **9***d* was obtained in 9% yield together with the monoaldehyde **8***d*. After crystallization from methanol, **9***d* had mp 180°C; ir (KBr): 3440, 2722, 1650 cm^{-1}; nmr δ: 7.30 (s, 1H, H-3), 9.55 (s, 1H, CHO), 9.93 (s, 1H, CHO). Anal. calcd. for $C_6H_4ClNO_2$: C 45.93, H 2.50, N 8.88; found: C 46.10, H 2.72, N 8.70.

*1-*tert*-Butoxycarbonyl-5-chloropyrrole-2-carboxaldehyde (**12**)*

Di-*tert*-butyldicarbonate (0.335 g, 1.54 mmol) was added to a solution of 5-chloropyrrole-2-carboxaldehyde (0.100 g, 0.57 mmol) and 4-dimethylaminopyridine (0.010 g, 0.07 mmol) in reagent grade acetonitrile (5 mL). The solution was stirred at room temperature for 2 h, the solvent was then removed *in vacuo*, and the residue was purified by column chromatography on silica gel (15 g) using hexane – ethyl acetate (3:1) as the eluting solvent. The product (0.124 g, 70%) was obtained as a pale yellow oil; ir: 1767, 1678 cm^{-1}; nmr δ: 1.50 (s, 9H, *t*-Bu), 6.25 (d, 1H, J = 4.1 Hz, H-4), 6.95 (d, 1H, J = 4.1 Hz, H-3), 9.60 (s, 1H, CHO). Anal. calcd. for $C_{10}H_{12}ClNO_3$: C 52.29, H 5.27, N 6.10; found: C 52.37, H 5.28, N 5.99.

1. G. A. CORDELL. J. Org. Chem. **40**, 3161 (1975).
2. F. SCHNIERLE, H. REINHARD, N. DIETER, E. LIPPACHER, and H. VON DOBENECK. Liebigs Ann. Chem. **715**, 90 (1968).
3. H. VON DOBENECK and T. MESSERSCHMITT. Liebigs Ann. Chem. **751**, 32 (1971).
4. G. STORK and R. MATTHEWS. Chem. Commun. 445 (1970).
5. H. PLIENINGER and A. MÜLLER. Synthesis, 586 (1970).
6. P. ZORETIC and P. SOJA. J. Org. Chem. **41**, 3587 (1976); J. Heterocycl. Chem. **14**, 681 (1977).
7. A. GUZMÁN, J. M. MUCHOWSKI, and J. SALDAÑA. Chem. Ind. 357 (1977).
8. A. GUZMÁN, J. M. MUCHOWSKI, A. M. STROSBERG, and J. M. SIMS. Can. J. Chem. **59**, 3241 (1981).
9. R. J. P. CORRIU, J. J. E. MOREAU, and C. VERNHET. Tetrahedron Lett. **28**, 2963 (1987).
10. R. J. P. CORRIU, V. HUYNH, J. IQBAL, and J. J. E. MOREAU. J. Organomet. Chem. **276**, C61 (1984).
11. F. HENIN, J. MUZART, and J.-P. PETE. Tetrahedron Lett. **27**, 6339 (1986).
12. J. C. HUBERT, J. B. P. A. WIJNBERG, and N. SPECKAMP. Tetrahedron, **31**, 1437 (1975).
13. M. FARNIER and P. FOURNARI. Bull. Soc. Chim. Fr. 351 (1973).
14. L. GREHN and V. RAGNARSSON. Angew. Chem. Int. Ed. Engl. **23**, 296 (1984).
15. T. MESSERSCHMITT, U. VON SPECHT, and H. VON DOBENECK. Liebigs Ann. Chem. **751**, 50 (1971).

Can. J. Chem. Downloaded from www.nrcresearchpress.com by 88.85.125.76 on 09/07/12
For personal use only.

Michael W. Majchrzak and John Warkentin. Thermolysis of 2-acyloxy-Δ^3-1,3,4-oxadiazolines. Evidence for a preferred sense of cycloreversion to carbonyl ylides and for fast 1,4-sigmatropic ylide rearrangement. Can. J. Chem. **67**, 1753 (1989).

Page 1753. Scheme 1 should be

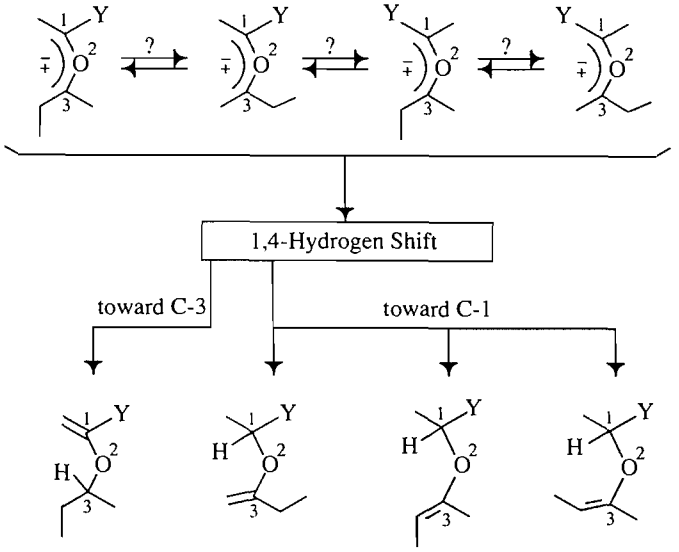

SCHEME 1

Can. J. Chem. Downloaded from www.nrcresearchpress.com by 91.144.44.67 on 09/07/12
For personal use only.

The crystal and molecular structures of two isostructural complexes: $[(H_3O \cdot 18\text{-crown-}6)_2(ZnCl_4)]$ and $[(H_3O \cdot 18\text{-crown-}6)_2(MnCl_4)]$

ROBERT CHÊNEVERT[1] AND DANIEL CHAMBERLAND

Département de chimie, Faculté des sciences et de génie, Université Laval, Québec (Québec), Canada G1K 7P4

AND

MICHEL SIMARD AND FRANÇOIS BRISSE[1]

Département de chimie, Université de Montréal, C.P. 6128, Succ. A, Montréal (Québec), Canada H3C 3J7

Received September 25, 1989

ROBERT CHÊNEVERT, DANIEL CHAMBERLAND, MICHEL SIMARD, and FRANÇOIS BRISSE. Can. J. Chem. **68**, 797 (1990).

New macrocycle polyether 18-crown-6 complexes of stoichiometry $[(H_3O^+ \cdot 18\text{-crown-}6)_2(MCl_4^{2-})]$ have been synthesized for M = Zn and Mn. The two complexes are isostructural and crystallize in the monoclinic system, space group $C2/c$. The unit cell dimensions are as follows: a = 16.229(9), b = 11.535(3), c = 20.134(8) Å, β = 97.55(4)° and a = 16.255(6), b = 11.625(3), c = 20.122(8) Å, β = 96.54(3)° for the Zn and Mn complexes respectively. In both crystal structures (final R_w = 0.048 with 1817 reflections for Zn and R_w = 0.074 with 728 reflections for Mn), the crown ether molecule and the H_3O^+ cation to which it is hydrogen-bonded are disordered over two sites. The MCl_4^{2-} anions, which have tetrahedral coordination, are on crystallographic twofold axes of rotation. The Mn—Cl and Zn—Cl distances average 2.270 and 2.361 Å respectively. The hydronium cation, H_3O^+, has pyramidal coordination. Of the two disordered crown ether molecules in the Zn and the Mn complexes, one has a slightly deformed $(ttg)_6$ conformation while the other one may be described as having the distorted $(ttg)_5(ttc)$ conformation. These observations are in agreement with the infrared analyses of the complexes.

Key words: 18-crown-6 complexes, hydronium ion, $ZnCl_4^{2-}$, $MnCl_4^{2-}$, crystal structure.

ROBERT CHÊNEVERT, DANIEL CHAMBERLAND, MICHEL SIMARD et FRANÇOIS BRISSE. Can. J. Chem. **68**, 797 (1990).

On a synthétisé de nouveaux complexes de polyéthers macrocycliques 18-couronne-6 de stoechiométrie $(H_3O^+ \cdot 18\text{-couronne-}6)_2(MCl_4^{2-})$ dans lesquels M = Zn et Mn. Les deux complexes sont isostructuraux et ils cristallisent dans le système monoclinique, groupe d'espace $C2/c$ avec a = 16,229(9), b = 11,535(3) et c = 20,134(8) Å, β = 97,55(4)° et a = 16,255(6), b = 11,625(3) et c = 20,122(8) Å, β = 96,54(3)° respectivement pour les complexes du Zn et du Mn. Dans chacune des structures cristallines (valeurs finales de R_w = 0,048 avec 1817 réflexions pour le Zn et R_w = 0,074 avec 728 réflexion pour Mn), la molécule d'éther couronne et le cation H_3O^+ auquel elle est attachée par liaisons hydrogène est désordonnée sur les deux sites. Les anions MCl_4^{2-} qui possèdent une coordination tétraédrique se retrouvent sur des axes cristallographiques binaires. Les distances moyennes Mn—Cl et Zn—Cl sont respectivement 2,270 et 2,361 Å. La coordination du cation hydronium, H_3O^+, est pyramidale. Des deux molécules d'éthers couronnes désordonnées qui sont présentes dans les complexes du Zn et du Mn, l'une possède une conformation légèrement déformée $(ttg)_6$ alors que l'on peut décrire la conformation déformée de l'autre par $(ttg)_5(ttc)$. Ces observations sont en accord avec les analyses infrarouges de ces complexes.

Mots clés : complexes 18-couronne-6, ion hydronium, $ZnCl_4^{2-}$, $MnCl_4^{2-}$, structure cristalline.

[Traduit par la revue]

Introduction

The macrocyclic polyether 18-crown-6 readily forms complexes with hydrates of strong acids (pK_a of the acid $< pK_a$ of H_3O^+ at −1.7), which exist as hydronium salts. In 1972, Izatt *et al.* (1) reported the formation of 1:1 complexes between *cis-syn-cis*-dicyclohexano-18-crown-6 and $H_3O^+ClO_4^-$ or $H_3O^+PF_6^-$. These stable complexes were characterized by elemental analysis and infrared spectroscopy. In recent years, it has been shown that 18-crown-6 and derivatives are good complexing agents for the hydronium ion, and complexes have been obtained with several strong acids (2–9). X-ray diffraction studies have shown that the H_3O^+ ion in the adduct is anchored at the center of the macrocyclic cavity by three OH---O hydrogen bonds (5–9). One aim of these X-ray studies was the determination of the geometry (planar or pyramidal) of the hydronium ion, i.e., the position of the central oxygen relative to the plane of the three attached hydrogen atoms. Several structures lend strong support for the pyramidal H_3O^+ but two have been interpreted in terms of planar H_3O^+. Recently, Reinhoudt and co-workers (9) reported that 2-sulfo-1,3-xylyl crown ethers are good receptor molecules not only for H_3O^+ but also for higher hydrated species, $H_3O^+(H_2O)_n$ where n = 1, 2.

In the present study we report the preparation and characterization of new complexes of 18-crown-6 with hydronium ions derived from transition metal (Mn and Zn) chlorides and hydrochloric acid.

Experimental

Preparation of the complexes (general procedure)

The transition metal chloride (2 mmol) is dissolved in tetrahydrofuran (25 mL) and concentrated hydrochloric acid (2 mL). This solution is added to a solution of 18-crown-6 (2 mmol) in tetrahydrofuran (15 mL). The complex crystallizes immediately at room temperature. The solid complex is filtered and dried under vacuum. The complex is recrystallized in tetrahydrofuran and dried under vacuum until a constant melting point is obtained. Physical data pertaining to the individual complexes are given below.

*$[(H_3O^+ \cdot 18\text{-crown-}6)_2(ZnCl_4^{2-})]$ **1***

Yield: 90%; mp 142–143°C (colorless). IR (Nujol): 2950, 2180, 1685, 1350, 1285, 1245, 1140, 1090, 960, 935, 830, 805 cm^{-1}. ^1H NMR (CD_2Cl_2) δ: 3.74 (24H, s, crown), 10.57 (3H, br s, H_3O^+). ^{13}C NMR (CD_2Cl_2) δ: 70.34. Anal. calcd. for $C_{24}H_{54}O_{14}ZnCl_4$: C 37.25, H 7.03, Zn 8.45, Cl 18.33; found: C 37.63, H 7.22, Zn 8.32, Cl 18.41.

*$[(H_3O^+ \cdot 18\text{-crown-}6)_2(MnCl_4^{2-})]$ **2***

Yield: 84%; mp 135–137°C (colorless). IR (Nujol): 2950, 2180, 1670, 1350, 1290, 1245, 1140, 1090, 960, 935, 830, 805 cm^{-1}. ^1H NMR: useless because of extreme line broadening. ^{13}C NMR

[1]Authors to whom correspondence may be addressed.

Can. J. Chem. Downloaded from www.nrcresearchpress.com by 88.85.125.76 on 09/07/12
For personal use only.

TABLE 1. Crystal data for the Zn and Mn complexes

Parameter	Zn	Mn
Composition	$[(H_3O^+ \cdot 18\text{-crown-}6)_2(ZnCl_4^{2-})]$ $C_{24}H_{54}O_{14}ZnCl_4$	$[(H_3O^+ \cdot 18\text{-crown-}6)_2(MnCl_4^{2-})]$ $C_{24}H_{54}O_{14}MnCl_4$
MW	773.88	763.43
$F(000)$	1632	1624
Crystal system	Monoclinic	Monoclinic
Space group	$C2/c$	$C2/c$
a, Å	16.229(9)	16.255(6)
b, Å	11.535(3)	11.625(3)
c, Å	20.134(8)	20.122(8)
β, deg	97.55(4)	96.54(3)
V, Å^3	3736.4	3777.6
d_c, g cm^{-3}	1.376	1.342
Z	4	4
μ, cm^{-1} (radiation)	41.0 (Cu)	6.7 (Mo)
λ, Kᾱ, Å	1.54178	0.71069
Crystal size, mm	0.20 × 0.36 × 0.41	0.10 × 0.42 × 0.76
T, °C	22	22

(CD_2Cl_2) δ: 72.07. Anal. calcd. for $C_{24}H_{54}O_{14}MnCl_4$: C 37.76, H 7.13, Mn 7.20, Cl 18.58; found: C 37.44, H 7.15, Mn 6.76, Cl 18.80.

The NMR spectra were taken on a Varian XL-200 multinuclear spectrometer. The infrared spectra, obtained from Nujol mulls contained between Irtran-2 (ZnS) windows, were recorded on a Beckman-4250 spectrometer. The microanalyses were performed by Dr. C. Daessle, Organic Microanalysis, Montreal, or by ourselves on a Carlo Erba Strumentazione-1106 elemental analyser.

Crystallographic characterization of the $[(H_3O^+ \cdot 18\text{-crown-}6)_2(MCl_4^{2-})]$ complexes

Single crystals suitable for X-ray diffraction analysis were obtained after a slow recrystallization of the complex in tetrahydrofuran. The unit cell dimensions were computed from the angular settings of 25 well-centered reflections in the range $40 \leq 2\theta \leq 50°$ (Zn) or $18 \leq 2\theta \leq 22°$ (Mn). The final parameters and other crystal data of interest are presented in Table 1. The data collection for the Zn complex was done over 4 octants, by the ω scan technique, with graphite monochromatized copper radiation. The intensities of six standard reflections were monitored every hour. The largest fluctuation of the intensities of the standard reflections was 3.5%, revealing a slight decomposition of the crystal under radiation. The averaging (R averaging = 0.08) of the 7182 measured reflections to the $2/m$ Laue symmetry yielded 3587 reflections of which 1817 were considered observed ($I/\sigma(I) \geq 3.0$). In the data reduction,[2] all the reflections were placed on a common scale, thus taking care of the small decay of the crystal. The final σ was computed as $\sigma = [\sigma_1^2 + \sigma_2^2]^{1/2}$. In this relation σ_1 and σ_2 are the individual σ's associated with the intensities of the reflections being averaged. Lorentz, polarization, and absorption corrections (10 × 10 × 10 grid, extreme values of the transmission factor: 0.23–0.52) were applied to the data.

In the case of the Mn complex, the intensities of only two octants were measured by the ω scan technique using graphite monochromatized molybdenum radiation. The intensities of seven reference reflections were evaluated every hour. They did not fluctuate by more than 4.9% over the duration of the data collection. Of the 3314 measured reflections only 728 were retained for the structure determination ($I/\sigma(I) \geq 3.0$). The reflections were placed on a common scale to compensate for the decomposition of the crystal. Lorentz and polarization corrections were applied, but due to the small value of the absorption coefficient for the Mo radiation the data were not corrected for absorption. The small proportion of observed reflections is attributed to the disorder present in the structure.

Both structures were solved using the Patterson method combined with difference Fourier syntheses (SHELX). The (MCl_4^{2-}) anions are located on a crystallographic twofold axis of rotation. The crown ether molecule and H_3O^+ are disordered over two sites. Initially the refinement of the crown ether was conducted with a constrained model. In this model, the C—C and C—O distances were allowed to vary within ±0.05 Å from the corresponding quantities as found in other 18C6 macrocycles (8, 19, 20). This was relaxed in the last refinement cycles. The occupancy factor, which was also refined, converged to a 50/50 occupation for the Zn complex. The refinements, based on F's, minimized the quantity $\Sigma w \Delta F^2$ using the block-diagonal approximation. All non-hydrogen atoms were refined anisotropically. The H-atom coordinates were calculated at idealized positions, (d_{C-H} = 0.95 Å, B_{iso} = 15.0 Å^2 (crown), B_{iso} = 12.0 Å^2 (H_3O^+)), riding on the atom to which they are bonded. The H atoms of the hydronium ion were placed at 0.85 Å from OW along the OW...O line and were not refined. The procedure was very much the same in the case of the Mn complex. However, since the number of observed reflections was small the refinement was always constrained. The refinement converged to a situation where the crown ether is also disordered over two orientations but with a 60/40 occupancy. The refinements were concluded when the indicators given in Table 2 reached their minimum values.[3] In both cases, the weights used in the least-squares refinement were derived from the counting statistics. The scattering curves for the non-hydrogen atoms were taken from ref. 13 and those for the H-atoms from ref. 14.

Results and discussion

Hydronium ion – crown ether complexes are prepared in 80–90% yield by mixing the transition metal chloride, aqueous hydrochloric acid, and 18-crown-6 in tetrahydrofuran. The

[2]The programs used here are modifications of NRC-2, data reduction; NRC-3, absorption correction; NRC-10, bond distances and angles; FORDAP, Fourier and Patterson maps (A. Zalkin); SHELX, program for structure determination; and ORTEP, stereodrawings (10–12).

[3]Tables of the bond distances, angles, and torsion angles of the 18-crown-6 molecules, of the anisotropic thermal parameters, the calculated H-atom coordinates, and the structure factor amplitudes may be purchased from the Depository of Unpublished Data, CISTI, National Research Council of Canada, Ottawa, Ont., Canada K1A 0S2.

Tables of bond distances and angles and of the calculated H-atom coordinates have also been deposited with the Cambridge Crystallographic Data Centre, and can be obtained on request from The Director, Cambridge Crystallographic Data Centre, University Chemical Laboratory, Lensfield Road, Cambridge CBE 1EW, U.K.

Can. J. Chem. Downloaded from www.nrcresearchpress.com by 88.85.125.76 on 09/07/12
For personal use only.

TABLE 2. Data collection and refinement

Parameter	Zn	Mn
Radiation	CuK$\bar{\alpha}$	MoK$\bar{\alpha}$
$2\theta_{max}$, deg	140.0	50.0
Scan	ω	ω
Scan width, deg	$(1.00 + 0.14 \tan\theta)$	$(1.00 + 0.35 \tan\theta)$
Width of aperture, mm	4.00	4.00
Vertical size of the slit, mm	4.00	4.00
Octants measured	$-19 \leq h \leq 19$	$0 \leq h \leq 19$
	$-14 \leq k \leq 0$	$0 \leq k \leq 13$
	$-24 \leq l \leq 24$	$-23 \leq l \leq 23$
Number of measured reflections	7182	3314
Acceptance level $I/\sigma(I) \geq$	3.0	3.0
Number of unique observed reflections	1817	728
Extreme values of the transmission factor	0.23, 0.52	—
$R = \Sigma\|\|F_o\| - \|F_c\|\|/\Sigma\|F_o\|$	0.053	0.076
$R_w = [\Sigma w(\|F_o\| - \|F_c\|)^2/\Sigma wF_o^2]^{1/2}$	0.048	0.074
$S = [\Sigma w(\|F_o\| - \|F_c\|)^2/(m - n)]^{1/2}$	1.81	2.33
Residual fluctuations in electron density map, e Å^{-3}	−0.42; 0.08	−0.23; 0.38
Shift-to-σ ratio at the end of the refinement,		
maximum	0.50	0.24
average	0.12	0.02

complexes are stable solids with sharp melting points. The stoichiometry of the compounds was determined by elemental analysis (hydrogen, carbon, chlorine) and by atomic absorption spectroscopy (zinc, manganese). The analyses are in agreement with the stoichiometry defined by eqs. [1] and with that observed in the X-ray determinations.

[1] $2(18\text{–crown–}6) + 2H_2O + 2HCl + MCl_2 \rightarrow$

M = Zn, **1**
M = Mn, **2**
$(18\text{–crown–}6 \cdot H_3O^+)_2 \cdot MCl_4^{2-}$

Spectroscopy

The infrared spectra are clearly indicative of the presence of the H_3O^+ ion in both complexes. The bands are readily assigned by comparison to literature (15, 16) values for hydronium salts: 2780–3250 cm^{-1} (ν_1, symmetric stretching), 2500–3100 cm^{-1} (ν_3 asymmetric stretching), 1480–1705 cm^{-1} (ν_4, asymmetric bending), and 1050–1180 cm^{-1} (ν_2, symmetric bending). The stretching modes of H_3O^+ (ν_1, ν_3) are responsible for the strong and broad band at ~2950 cm^{-1}, which overlaps with the sharper maximum arising from the C–H stretching of the crown in the 2925 cm^{-1} region. The exact position of the ν_2 mode is difficult to determine as it occurs in a region of strong absorption by the C—O stretching of the crown ether. However, the first harmonic of ν_2 is always present at ~2190 cm^{-1}. The asymmetric bending mode (ν_4) gives a characteristic band at ~1650 cm^{-1}. Infrared spectra also indicate some departure from the D_{3d} symmetry for the crown. IR spectra of symmetric complexes such as $M^+ \cdot 18\text{-crown-}6 \cdot Br^-$ contain two singlets in the 800–1000 cm^{-1} region: CH_2 rocking at 960 cm^{-1} and C–C stretching at 835 cm^{-1} (17, 18). The crown is distorted to a lower symmetry and two doublets are observed at ~805,830 and ~930,960 cm^{-1} in the spectra of hydronium complexes **1** and **2**. This distortion of the ring is confirmed by the X-ray diffraction study.

The ^{1}H NMR signal of the crown ether protons in complex **1** is shifted downfield (3.74 ppm) compared to free 18-crown-6 (3.60 ppm) in the same solvent (CD_2Cl_2) and a new signal characteristic of the hydronium ion protons appears in the 10–11 ppm range. The chemical shift for the hydronium ion protons is concentration-dependent. The ^{1}H NMR spectrum of complex **2** shows extreme line broadening and chemical shifts cannot be evaluated. In ^{13}C NMR, the chemical shift of the crown carbons in the zinc and manganese adducts (70.34 and 72.07 ppm) are close to the shift of the free crown carbons in the same solvent (70.67 ppm).

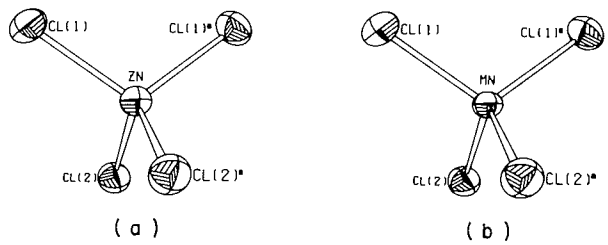

FIG. 1. Views and atomic numbering of the individual anions. (a) $ZnCl_4^{2-}$; (b) $MnCl_4^{2-}$.

Crystal structure

The unit cell dimensions, the space group (Table 1), and the refinement confirm that the two compounds are isostructural. The atomic numbering adopted for the anions and for the crown ether are shown in Figs. 1 and 2 respectively. Those figures also show the structural units with their thermal ellipsoids at the end of the refinement. The bond distances and angles calculated from the final atomic coordinates (Tables 3 and 4) are compared in Tables 5 and 6 for the anions and the 18-crown-6 molecules respectively. The structural units (18-crown-6, H_3O^+, MCl_4^{2-}) that are the constituents of the complexes are shown in their relative environment by the stereopair of Fig. 4.

The 18-crown-6 macrocycle

In both complexes the crown ether macrocycles are disordered over two orientations. It was thought that the space group might be $P2/c$ rather than $C2/c$. Then there would be two independent molecules per asymmetric unit rather than two molecules related by centering. This possibility has been

Can. J. Chem. Downloaded from www.nrcresearchpress.com by 88.85.125.76 on 09/07/12
For personal use only.

Can. J. Chem. Downloaded from www.nrcresearchpress.com by 88.85.125.76 on 09/07/12
For personal use only.

TABLE 3. Fractional atomic coordinates and their esd's ($\times 10^5$ for Zn and Cl, $\times 10^4$ for O and C), and U_{eq} ($\times 10^3$ for Zn and Cl, $\times 10^2$ for O and C) for the $[(18\text{-crown-6}\cdot H_3O)_2(ZnCl_4)]$ complex

Atom	x/a	y/b	z/c	U_{eq}*
Zn	0	477(8)	25000	78
Cl(1)	7029(9)	−10918(12)	32998(7)	106
Cl(2)	9536(9)	11789(11)	20782(7)	97
OW(1)	3889(5)	985(5)	4674(3)	10
OW(2)	3410(4)	1038(5)	4728(3)	9
O(11)	3721(7)	−988(6)	5424(3)	17
O(41)	3445(5)	−996(5)	4070(3)	10
O(71)	3494(6)	847(6)	3258(4)	17
O(101)	3617(6)	2872(6)	3967(4)	14
O(131)	3935(7)	3013(6)	5294(3)	16
O(161)	3983(5)	1058(5)	5973(3)	11
O(12)	4045(9)	−133(9)	5971(6)	24
O(42)	3439(7)	−1293(7)	4869(6)	20
O(72)	3367(6)	−232(9)	3576(5)	20
O(102)	3273(6)	2240(8)	3605(4)	18
O(132)	3708(6)	3596(9)	4784(4)	19
O(162)	3931(7)	2174(9)	5886(4)	20
C(21)	3933(10)	−1944(10)	5048(6)	15
C(31)	3537(7)	−2071(9)	4451(6)	12
C(51)	3109(8)	−1038(9)	3363(6)	12
C(61)	3063(10)	−67(11)	3054(5)	16
C(81)	3568(11)	1883(14)	2922(6)	19
C(91)	3500(9)	2819(9)	3260(5)	13
C(111)	3857(8)	3897(10)	4268(6)	14
C(121)	4174(11)	3838(13)	4925(12)	26
C(141)	4090(8)	3087(10)	5953(6)	16
C(151)	4025(7)	2122(11)	6306(5)	13
C(171)	4265(8)	108(11)	6334(5)	14
C(181)	4332(10)	−933(13)	6005(7)	18
C(22)	3666(11)	−1098(11)	6026(7)	19
C(32)	3843(10)	−1710(13)	5398(7)	18
C(52)	3352(11)	−1799(13)	4262(6)	19
C(62)	2987(8)	−1331(11)	3700(6)	14
C(82)	2922(7)	466(13)	3107(6)	16
C(92)	3164(8)	1669(12)	2993(5)	13
C(112)	3498(8)	3314(11)	3613(6)	14
C(122)	3386(9)	3937(10)	4175(8)	17
C(142)	3660(11)	3916(13)	5269(10)	23
C(152)	3761(10)	3276(12)	5847(9)	20
C(172)	4338(8)	1648(13)	6412(6)	17
C(182)	4035(11)	514(15)	6447(7)	21

*$U_{eq} = \frac{1}{3}\sum_i\sum_j U_{ij}a_i^*a_j^*a_i\cdot a_j$.

TABLE 4. Fractional atomic coordinates and their esd's ($\times 10^4$ for Mn and Cl, $\times 10^3$ for O and C), and U_{eq} ($\times 10^3$ for Mn and Cl, $\times 10^2$ for O and C) for the $[(18\text{-crown-6}\cdot H_3O)_2(MnCl_4)]$ complex

Atom	x/a	y/b	z/c	U_{eq}*
Mn	0	41(3)	2500	73
Cl(1)	712(3)	−1129(4)	3330(2)	112
Cl(2)	1008(3)	1210(4)	2067(2)	105
OW(1)	342(1)	106(2)	473(1)	9
OW(2)	391(2)	102(2)	466(1)	6
O(11)	379(2)	−107(3)	541(2)	19
O(41)	345(1)	−104(2)	407(1)	12
O(71)	351(2)	80(3)	321(1)	18
O(101)	358(2)	295(2)	393(1)	15
O(131)	394(2)	313(3)	531(2)	20
O(161)	401(2)	111(3)	602(1)	16
O(12)	424(3)	−17(3)	598(2)	24
O(42)	330(3)	−123(4)	489(2)	22
O(72)	335(3)	−20(3)	362(2)	23
O(102)	317(3)	223(3)	366(2)	21
O(132)	369(2)	363(3)	479(2)	15
O(162)	376(3)	221(4)	596(2)	23
C(21)	395(2)	−190(3)	508(2)	15
C(31)	360(3)	−192(4)	450(2)	14
C(51)	309(2)	−97(3)	343(2)	11
C(61)	306(3)	−4(4)	306(2)	15
C(81)	343(3)	196(4)	297(2)	17
C(91)	343(3)	284(4)	333(2)	17
C(111)	385(3)	393(4)	430(2)	16
C(121)	407(4)	392(5)	498(3)	26
C(141)	410(3)	298(4)	593(2)	16
C(151)	410(3)	203(4)	635(2)	14
C(171)	398(2)	8(4)	632(2)	15
C(181)	432(4)	−88(4)	599(3)	24
C(22)	356(3)	−94(5)	605(2)	21
C(32)	358(5)	−176(4)	548(2)	24
C(52)	328(4)	−189(4)	429(2)	15
C(62)	291(4)	−128(4)	373(2)	16
C(82)	281(3)	48(3)	318(3)	17
C(92)	311(4)	160(3)	310(2)	15
C(112)	341(5)	340(4)	362(2)	25
C(122)	322(3)	396(3)	419(2)	9
C(142)	335(4)	386(5)	537(2)	26
C(152)	384(4)	342(4)	595(2)	23
C(172)	454(3)	172(4)	619(4)	26
C(182)	441(3)	60(4)	648(3)	20

*$U_{eq} = \frac{1}{3}\sum_i\sum_j U_{ij}a_i^*a_j^*a_i\cdot a_j$.

explored in the case of the Zn complex. However, upon refinement and Fourier difference syntheses, it was found that the disorder remained. Thus the space group is $C2/c$ and there are indeed two disordered molecules in the asymmetric unit. The only difference between the Zn and Mn complexes is that the two molecules are in equal proportion for the former and 60/40 for the latter.

The disorder of the crown ether molecules, which is responsible for the small number of observed reflections, is detrimental to the obtention of accurate bond distances and angles in this part of the structure. With this in mind, the bond distances and angles of the two molecules in the two complexes are within the ranges reported for the 18-crown-6 macrocycles (8, 19, 20). There are, however, some large fluctuations in the bond distances, bond angles, and in the torsion angles. For the Zn complex the conformation of molecule A is $(ttg)_6$, the *t* torsion angle (*t* = *trans*) has values in the range 170–179° while the values of the *g* torsion angle (*g* = *gauche*) vary between 14 and 44°. In the second molecule B of the Zn complex, the conformation is more regular, $(ttg)_5ttc$. Here *t* is in the range 170–180°, while *g* varies from 51 to 72° and *c* has the value of 12°.

In the case of the Mn complex, for which fewer reflections were observed, one notes the same disparities. In molecule A the fluctuations of the non-*trans* torsion angles are in the range 9–69°, while molecule B has the nearly perfect $(ttg)_6$ conformation. It is not possible to establish with certainty whether these differences are real or are effects associated with the disorder. This latter possibility is the most likely.

The hydronium cation

Each H_3O^+ ion forms three hydrogen bonds to the oxygen atoms of the 18-crown-6 molecule (see Figs. 2 and 3). The

TABLE 5. Comparison of the bond distances (Å) and angles (deg) in the $ZnCl_4^{2-}$ and $MnCl_4^{2-}$ anions

Bond	Distances (esd's), Å	Bonds	Angles (esd's), deg
$ZnCl_4^{2-}$			
Zn—Cl(1)	2.264(2)	Cl(1)—Zn—Cl(2)	107.2(1)
Zn—Cl(2)	2.275(2)	Cl(1)—Zn—Cl(1)*	109.1(1)
		Cl(1)—Zn—Cl(2)*	111.7(1)
		Cl(2)—Zn—Cl(2)*	110.0(1)
$MnCl_4^{2-}$			
Mn—Cl(1)	2.353(5)	Cl(1)—Mn—Cl(2)	106.7(2)
Mn—Cl(2)	2.370(5)	Cl(1)—Mn—Cl(1)*	109.4(2)
		Cl(1)—Mn—Cl(2)*	112.0(2)
		Cl(2)—Mn—Cl(2)*	110.0(2)

*$-x, y, \frac{1}{2} - z$.

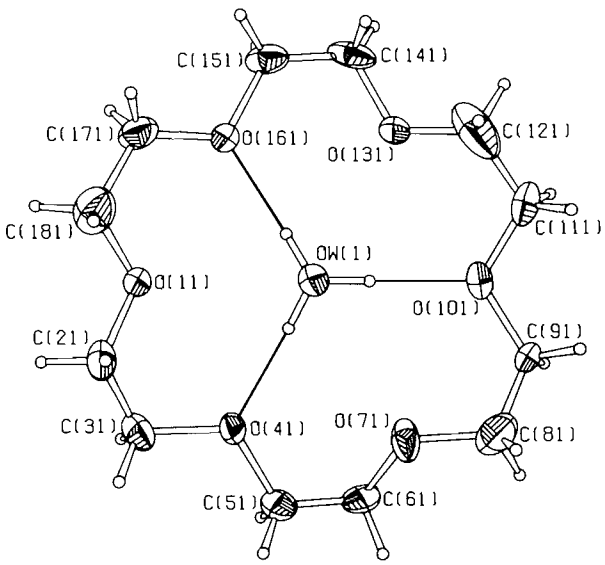

FIG. 2. Numbering scheme adopted for the 18-crown-6·H_3O^+ cation.

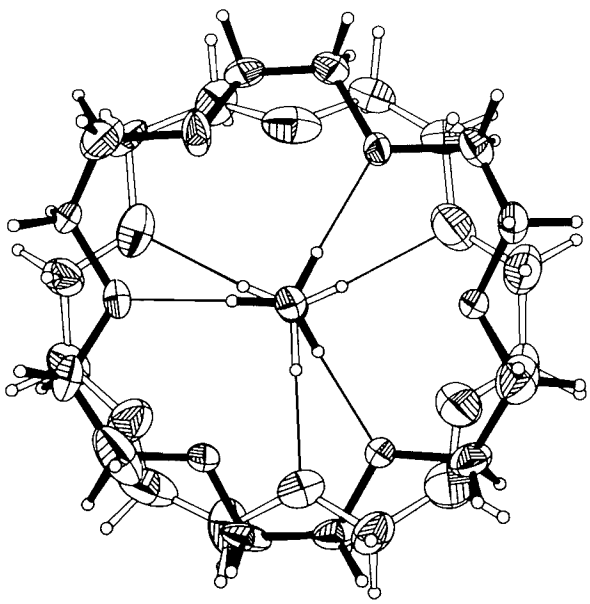

FIG. 3. View of the two overimposed orientations of the 18-crown-6·H_3O^+ cations found in the $ZnCl_4^{2-}$ complex. Darkened bonds are used to distinguish one of the two disordered cations. The disorder in the $MnCl_4^{2-}$ complex is similar.

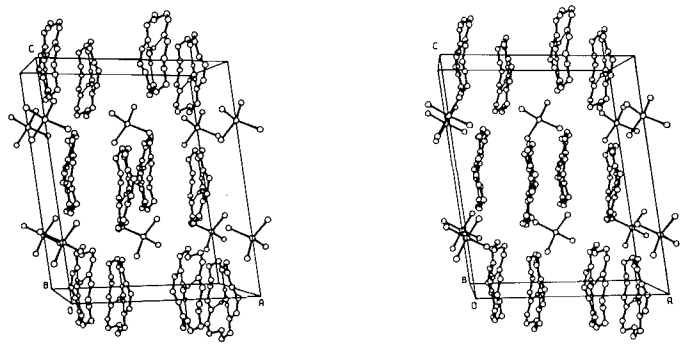

FIG. 4. Stereoview of the unit cell content of the (18-crown-6·H_3O)$_2$(MCl_4) complex. For clarity, only one orientation of the crown ether is shown and its hydrogen atoms have been omitted.

O(hydronium)...O(crown) distances are in the range 2.603(9)–2.710(11) Å (Zn complex) and 2.66(3)–2.99(5) Å for the Mn complex. The H_3O^+ ion in the Zn complex is more strongly bonded to the macrocycle than in the Mn analog. Although the H atoms were not located on Fourier difference syntheses, the position of the OW atoms above the plane of the three oxygen atoms of the 18-crown-6 molecule is clearly indicative of a pyramidal geometry. Thus, in the Zn complex, the water molecules are at 0.333(7) and −0.194(7) Å from the plane formed by the three oxygen atoms of the corresponding disordered crown ether molecules. These distances are −0.45(2) and 0.88(2) Å respectively in the Mn complex.

The MCl_4^{2-} anion, M = Zn, Mn

As indicated earlier, the MCl_4^{2-} anions occupy a crystallographic twofold axis of symmetry. Each anion is tetrahedral. The Cl—M—Cl angles vary between 107.2(1) and 111.7(1)° and between 106.7(2) and 112.0(2)° for the Zn and Mn complexes respectively. The M—Cl bond distances average 2.270 and 2.361 Å for the Zn and Mn complexes respectively. Such distances are in good agreement with values reported for other Zn and Mn complexes. For example, in pyridinium tetrachloromanganate(II), the four Mn—Cl distances are in the range 2.350(4)–2.376(4) Å (21) while the four Zn—Cl distances vary between 2.263(2) and 2.273(2) in monomethylammonium tetrachlorozincate(II) (22) and between 2.241(2) and 2.272(2) in 1,3-propanediammonium tetrachlorozincate(II) (23).

Packing of the structural units

There are only two structurally distinct units, the MCl_4^{2-}

Can. J. Chem. Downloaded from www.nrcresearchpress.com by 88.85.125.76 on 09/07/12
For personal use only.

TABLE 6. Bond distances (Å) and angles (deg) related to the hydrogen bonding in the Zn and Mn complexes

Bond	Distances (esd's), Å	Bonds	Angles (esd's), deg
		$(18\text{-crown-6}\cdot H_3O)_2(ZnCl_4)$	
Molecule A			
O(W1)—O(41)	2.641(9)	O(41)—O(W1)—O(101)	117.0(3)
O(W1)—O(101)	2.605(9)	O(41)—O(W1)—O(161)	117.8(3)
O(W1)—O(161)	2.603(9)	O(101)—O(W1)—O(161)	120.4(3)
		O(W1)—O(41)—C(31)	119.4(6)
		O(W1)—O(41)—C(51)	121.5(6)
		O(W1)—O(101)—C(91)	120.3(7)
		O(W1)—O(101)—C(111)	117.6(7)
		O(W1)—O(161)—C(151)	120.3(6)
		O(W1)—O(161)—C(171)	118.8(7)
Molecule B			
O(W2)—O(42)	2.701(10)	O(42)—O(W2)—O(102)	127.7(4)
O(W2)—O(102)	2.637(11)	O(42)—O(W2)—O(162)	113.0(4)
O(W2)—O(162)	2.710(11)	O(102)—O(W2)—O(162)	117.8(4)
		O(W2)—O(42)—C(32)	117.7(9)
		O(W2)—O(42)—C(52)	109.7(9)
		O(W2)—O(102)—C(92)	120.0(9)
		O(W2)—O(102)—C(112)	120.2(9)
		O(W2)—O(162)—C(152)	112.4(9)
		O(W2)—O(162)—C(172)	122.3(9)
		$(18\text{-crown-6}\cdot H_3O)_2(MnCl_4)$	
Molecule A			
O(W1)—O(41)	2.78(3)	O(41)—O(W1)—O(101)	114.4(10)
O(W1)—O(101)	2.75(3)	O(41)—O(W1)—O(161)	117.4(10)
O(W1)—O(161)	2.66(3)	O(101)—O(W1)—O(161)	120.3(10)
		O(W1)—O(41)—C(31)	112(2)
		O(W1)—O(41)—C(51)	112(2)
		O(W1)—O(101)—C(91)	118(3)
		O(W1)—O(101)—C(111)	112(2)
		O(W1)—O(161)—C(151)	123(2)
		O(W1)—O(161)—C(171)	113(2)
Molecule B			
O(W2)—O(42)	2.85(5)	O(42)—O(W2)—O(102)	118.5(15)
O(W2)—O(102)	2.63(4)	O(42)—O(W2)—O(162)	102.6(14)
O(W2)—O(162)	2.99(5)	O(102)—O(W2)—O(162)	110.2(14)
		O(W2)—O(42)—C(32)	118(2)
		O(W2)—O(42)—C(52)	109(3)
		O(W2)—O(102)—C(92)	110(3)
		O(W2)—O(102)—C(112)	117(3)
		O(W2)—O(162)—C(152)	115(3)
		O(W2)—O(162)—C(172)	87(3)

anion and the $H_3O^+\cdot$18-crown-6 cation, the hydronium anion and the crown ether being hydrogen-bonded together. As may be clearly appreciated in Fig. 4, the structure consists of alternating layers of MCl_4^{2-} anions and $H_3O^+\cdot$8-crown-6 cations. The MCl_4^{2-} units are in planes parallel to *ab*, at $c/4$ and $3c/4$. The mean plane of the 18-crown-6 macrocycle is parallel to the *bc* plane of the unit cell. These molecules form layers, also parallel to *ab*, at $c = 0, 1/2, 1$, etc. Thus the macrocycles are perpendicular to the layer. There are no short contacts between atoms in consecutive layers. The packing of the structural units in the Zn and Mn complexes is comparable to that observed in $(18\text{-crown-6}\cdot H_3O^+)_2(Pd_2Cl_6^{2-})$ (8).

Acknowledgements

We acknowledge the financial support of this work by the Natural Sciences and Engineering Research Council of Canada and the Ministère de l'Éducation du Québec.

1. R. M. IZATT, B. L. HAYMORE, and J. J. CHRISTENSEN. J. Chem. Soc. Chem. Commun. 1308 (1972).
2. R. CHÊNEVERT, A. RODRIGUE, M. PIGEON-GOSSELIN, and R. SAVOIE. Can. J. Chem. **60**, 853 (1982).
3. R. CHÊNEVERT, A. RODRIGUE, P. BEAUCHESNE, and R. SAVOIE. Can. J. Chem. **62**, 2293 (1984).
4. G. S. HEO and R. A. BARTCH. J. Org. Chem. **47**, 3557 (1982).
5. J. P. BEHR, P. DUMAS, and D. MORAS. J. Am. Chem. Soc. **104**, 4540 (1982).
6. C. B. SHOEMAKER, L. V. MCAFEE, D. P. SHOEMAKER, and C. W. DEKOCK. Acta Crystallogr. Sect. C: Cryst. Struct. Commun. **42**, 1310 (1986).
7. J. L. ATWOOD, S. G. BOTT, A. W. COLEMAN, K. D. ROBINSON, S. B. WHETSTONE, and C. M. MEANS. J. Am. Chem. Soc. **109**, 8100 (1987).
8. R. CHÊNEVERT, D. CHAMBERLAND, M. SIMARD, and F. BRISSE. Can. J. Chem. **67**, 32 (1989).
9. J. VAN EERDEN, M. SKOWRONSKA-PTASINSKA, P. D. J. GROOT-

Can. J. Chem. Downloaded from www.nrcresearchpress.com by 88.85.125.76 on 09/07/12
For personal use only.

ENHUIS, S. HARKEMA, and D. N. REINHOUDT. J. Am. Chem. Soc. **111**, 700 (1989).
10. F. R. AHMED, S. R. HALL, M. E. PIPPY, and C. P. HUBER. The NRC system of crystallographic computer programs for the IBM/360. Accession nos. 133–147. *In* J. Appl. Crystallogr. **6**, 309 (1973).
11. G. SHELDRICK. SHELX 76. A crystallographic computation system for crystal structure determination. Univ. of Cambridge, England. 1976.
12. C. K. JOHNSON. ORTEP. Report ORNL-3794. Oak Ridge National Laboratory, Oak Ridge, TN. 1965.
13. D. T. CROMER and J. T. WABER. Acta Crystallogr. **18**, 104 (1965).
14. R. F. STEWART, E. R. DAVIDSON, and W. T. SIMPSON. J. Chem. Phys. **42**, 3175 (1965).
15. R. D. GILLARD and G. WILKINSON. J. Chem. Soc. 1640 (1964).
16. R. SAVOIE and P. A. GIGUÈRE. J. Chem. Phys. **41**, 2698 (1967).
17. M. FOUASSIER and J. C. LASSEGUES. J. Chem. Phys. **75**, 865 (1978).
18. J. DALE and P. O. KRISTIANSEN. Acta Chem. Scand. **26**, 1471 (1972).
19. S. DEGUIRE, F. BRISSE, J. OUELLET, and R. SAVOIE. Can. J. Chem. **64**, 142 (1986).
20. L. PARENTEAU and F. BRISSE. Can. J. Chem. **67**, 1293 (1989).
21. C. BRASSY, R. ROBERT, B. BACHET, and R. CHEVALIER. Acta Crystallogr. Sect. B: Struct. Crystallogr. Cryst. Chem. **32**, 1371 (1976).
22. B. MOROSIN and K. EMERSON. Acta Crystallogr. Sect. B: Struct. Crystallogr. Cryst. Chem. **32**, 294 (1976).
23. A. KALLEL, J. FAIL, H. FUESS, and A. DAOUD. Acta Crystallogr. Sect. B: Struct. Crystallogr. Cryst. Chem. **36**, 2788 (1980).

Can. J. Chem. Downloaded from www.nrcresearchpress.com by 88.85.125.76 on 09/07/12
For personal use only.

A spiro-annulation approach to the zizaane sesquiterpenes

D. Jean Burnell[1] and Yong-Jin Wu

Department of Chemistry, Memorial University of Newfoundland, St. John's, Nfld., Canada A1B 3X7

Received December 20, 1989

D. Jean Burnell and Yong-Jin Wu. Can. J. Chem. **68**, 804 (1990).

4,4-Dimethyl-2-oxabicyclo[3.2.1]octan-3-one (**10**), obtained in two steps from norcamphor, was converted to 3-(1,1-dimethyl-2-oxopropyl)cyclopentanone (**14**), then selectively ketalized. The ketal function underwent Lewis acid catalysed spiro-annulation with 1,2-bis)trimethylsiloxy)cyclobutene (**4**) yielding 7-(1,1-dimethyl-2-oxopropyl)spiro[4.4]nonane-1,4-dione (**21**), and intramolecular titanium-induced ketone–ketone coupling and oxidation afforded (±)-isokhusimone (**3**) in an overall yield of 35% from norcamphor. In an alternative approach, the ethylene ketal of methyl 2-methyl-2-(3-oxocyclopentyl)propanoate (**27**) was prepared from **10**. Spiro-annulation proceeded in good yield, but subsequent titanium-induced ketone–ester coupling failed to provide the desired tricyclic product, 7,7-dimethyltricyclo[6.2.1.0^{1,5}]undecane-2,6-dione (**30**).

Key words: annulation, carbonyl coupling, isokhusimone, terpene.

D. Jean Burnell et Yong-Jin Wu. Can. J. Chem. **68**, 804 (1990).

Le 4,4-diméthyl-2-oxabicyclo[3.2.1]octane-3-one (**10**), que l'on obtient en deux étapes à partir du norcamphre, peut être transformée en 3-(1,1-diméthyl-2-oxopropyl)cyclopentanone (**14**) dont on forme ensuite le cétal. Avec le 1,2-bis(triméthylsiloxy)cyclobutène (**4**), cette fonction subit une spiro-annelation, catalysée par les acides de Lewis, qui conduit à la 7-(1,1-diméthyl-2-oxopropyl)spiro[4.4]nonane-1,4-dione (**21**) et éventuellement, par un couplage cétone–cétone intramoléculaire induit par le titane et une oxydation, à la (±)-isokhusimone (**3**) avec un rendement global de 35% à partir du norcamphre. Dans une approche alternative, on a préparé le cétal éthylénique du 2-méthyl-2-(3-oxocyclopentyl)propanoate de méthyle (**27**) à partir du composé **10**. Sa spiro-annellation s'est produite avec un bon rendement; toutefois, le couplage subséquent cétone–ester, induit par le titane, n'a pas fourni le produit tricyclique désiré, soit la 7,7-diméthyltricyclo[6.2.1.0^{1,5}]undécane-2,6-dione (**30**).

Mots clés : annelation, couplage carbonyl, khusimone, terpène.

[Traduit par la revue]

Introduction

Vetiver oil is a rich source of sesquiterpenoids including many with a tricyclo[6.2.1.0^{1,5}]undecane ring system, characteristic of a group of sesquiterpenes termed the zizaanes. These include the fragrant norsesquiterpenoid (−)-khusimone (**1**) (1). Khusimone is a natural insect repellent (2), which, nevertheless, has been used as a flavoring material (3). Maurer produced **1** by degradation of natural zizanoic acid (**2**), and he showed that **1** isomerizes to isokhusimone (**3**) on treatment with warm

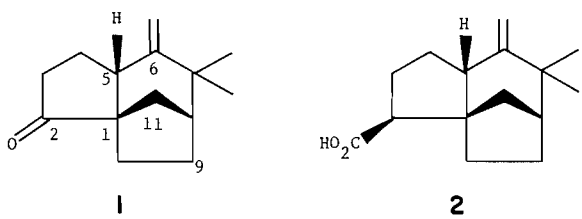

1 **2**

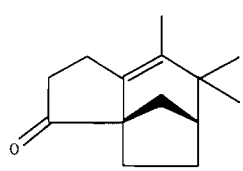

3

formic acid (3). The first total synthesis of (racemic) khusimone (**1**) was by Büchi *et al.* (4). Their route proceeded via **3** by rearrangement of the minor product of an intramolecular Diels–Alder reaction. Other syntheses of racemic and of (−)-khusimone have involved as key steps a photochemical [2 + 2] cycloaddition (5), the intramolecular magnesium–ene reaction (6), and an intermolecular Diels–Alder reaction (7). Furthermore, Liu and Chan (5) have converted **1** into zizanoic acid (**2**) and its C-2 epimer.[2] In this paper we describe an efficient, alternative strategy for the synthesis of isokhusimone (**3**) and hence, in a formal sense, of the zizaane sesquiterpenes.[3]

Results and discussion

Retrosynthetic scission of the six-membered ring of the zizaane skeleton leads to a system with spiro-linked five-membered rings, of which one could be a symmetrical, 1,3-cyclopentanedione moiety. *C*-Alkylation of cyclic β-diketones can be a poor reaction (10), but Kuwajima and co-workers (11) demonstrated that the Lewis acid catalysed reaction of a dimethyl, a diethyl, or a dibenzyl ketal (but not a ketone) with 1,2-bis(tri-

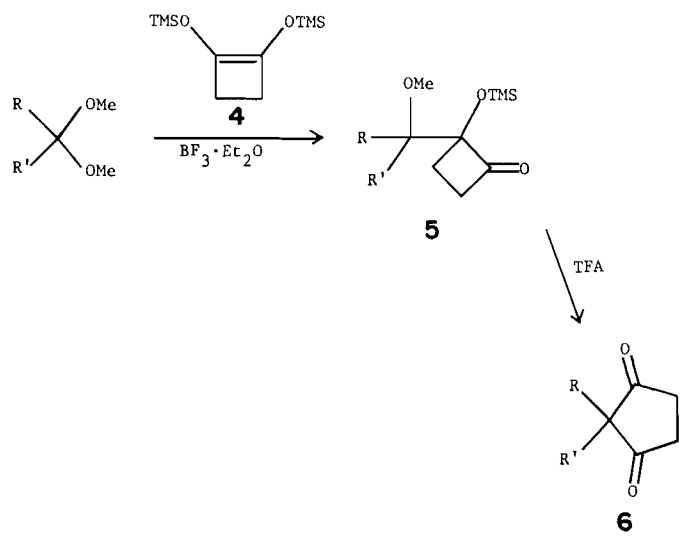

4 **5** **6**

[1]Author to whom correspondence may be addressed.

[2]Some other routes to the tricyclo[6.2.1.0^{1,5}]undecane ring system and the various zizaane sesquiterpenes are given in ref. 8.

[3]A preliminary account of some of this work was reported in ref. 9.

Can. J. Chem. Downloaded from www.nrcresearchpress.com by 88.85.125.76 on 09/07/12
For personal use only.

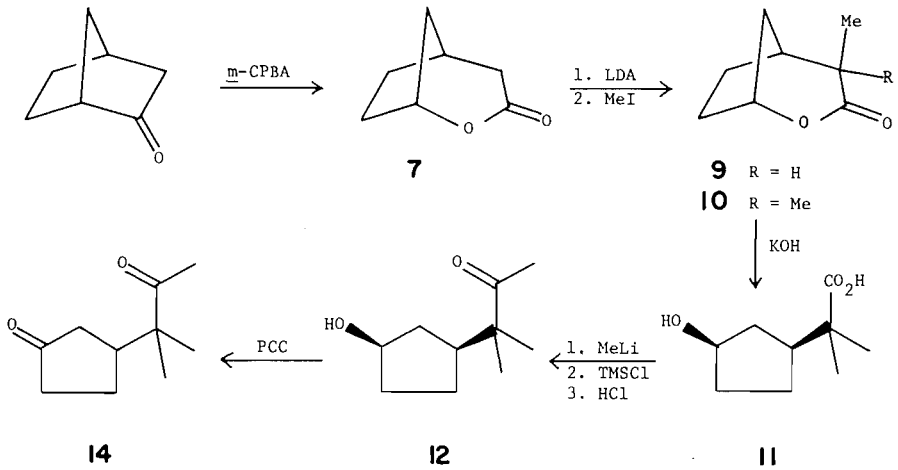

methylsiloxy)cyclobutene (**4**) followed by rearrangement of the resulting cyclobutanone **5** with trifluoroacetic acid (TFA) can give a 2,2-disubstituted 1,3-cyclopentanedione **6** in a reasonable yield.[4] Thus, our plan was to obtain an appropriately functionalized cyclopentanone, to ketalize it, to spiro-annulate using **4**, and lastly to cyclize the six-membered ring.

The first cyclopentanone moiety was derived from norcamphor. Baeyer–Villiger oxidation with *m*-chloroperoxybenzoic acid at room temperature gave lactone **7** in a yield of 86% following vacuum distillation. An older preparation (using peroxyacetic acid) advocated strongly acidic conditions for the formation of **7** (14). We found that a strongly acidic medium gave mainly **8**. Methylation of the lithium enolate of **7** with one equivalent of iodomethane provided **9**, and a second methylation to give **10** followed cleanly. Base hydrolysis of the lactone yielded the solid hydroxy-acid **11** almost quantitatively and, without purification, this could be treated with 15 equivalents of methyl lithium, then quenched with 20 equivalents of chlorotrimethylsilane, after the method of Rubottom and Kim (15). Aqueous work-up afforded mainly the desired hydroxy-ketone **12** (in a yield of 85% from the lactone **10**) and only a little (6%) of the diol **13**.[5] Direct conversion of the lactone **10** to the

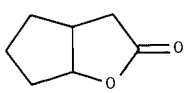

8

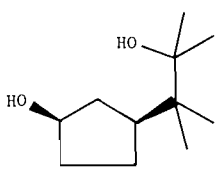

13

hydroxy-ketone **12** with methylmagnesium chloride in HMPA (17) proved to be of much lower yield than the two-step procedure via the acid. Oxidation of **12** with pyridinium chlorochromate (PCC) yielded the diketone **14**.

Diketals were formed easily from **14**. Consequently, we were unable to monoketalize the ring ketone of **14** selectively as a dimethyl or diethyl ketal, and formation of the monoketal with ethylene glycol produced both **15***a* and **16***a* under a variety of conditions. Nevertheless, the reaction of **14** with 2,2-dimethylpropanediol catalysed by pyridinium *p*-toluenesulfonate (PPTS) under carefully controlled conditions yielded, after chromatography, 89% of the monoketal **15***b* and only 4% of the diketal **16***b*. The methylene signals of the 1,3-dioxane rings in the 300 MHz ^{1}H nmr spectrum of the diketal **16***b* appeared as a four-proton singlet at δ 3.45 ppm flanked by two two-proton doublets. The spectrum of the monoketal **15***b* showed only the singlet at δ 3.45 ppm, which was consistent with conformational mobility of the dioxane ring. As expected, the side-chain dioxane of **16***b* was predominantly in one conformation, its axial and equatorial methylene protons giving rise to the two doublets.

Kuwajima and co-workers (11) had used neither a 1,3-dioxolane nor a 1,3-dioxane with **4** in a geminal acylation reaction leading to a spiro-annulated product. Regarding a related reaction leading to a keto-ester, they commented that unlike the dimethyl, diethyl, and dibenzyl ketals the (cyclic) trimethylene ketal of 4-methyl-3-cyclohexen-1-one "posed considerable problems." Therefore, we were apprehensive about trying the spiro-annulation reaction with **15***a*/*b* or **16***a*/*b*. First we chose to examine the reactions of **4** with simpler cyclic ketals, and we wondered if conditions might be found that might effect the acid-catalysed rearrangement (**5** → **6**) in the same operation. Cyclic ketals of both types reacted with **4**. Furthermore, in the presence of a much larger excess of BF_3 etherate than in the Kuwajima procedure, 1,3-cyclopentanediones (**17**–**20**) were obtained *directly*, obviating the isolation of the cyclobutanones **5** and their treatment with TFA, and our yields of the 2,2-disubstituted 1,3-cyclopentanediones were generally higher than by the original two-step procedure. (Unsubstituted 1,3-cyclopentanedione was not produced from either 5,5-dimethyl-1,3-dioxane or *s*-trioxane, even after the addition of TFA.)

The monoketal **15***b* was treated with three equivalents of **4** and 15 equivalents of BF_3 etherate at −78°C. We were gratified that the gc–ms of the crude product indicated only one component. After column chromatography to remove a trace amount of some stubborn colored material, we were left with an 86% yield of a pure compound that was clearly the desired triketone **21**. (The ^{13}C nmr spectrum of this product showed signals at δ 213.0, 215.3, and 215.7 ppm for three ketone carbonyls, and the ^{1}H nmr spectrum included a complex four-proton multiplet around δ 2.778 ppm for the adjacent methylenes of the 1,3-cyclopentanedione moiety.) The same triketone could also be obtained from the diketals. We expected steric hindrance to render the side-chain ketal in **16***a* and **16***b* less reactive than the other ketal. Indeed, the diketal **16***a* with **4** gave, after aqueous

[4]Other syntheses employing this reaction are given in refs. 12 and 13.

[5]In contrast, without the chlorotrimethylsilane quench, following the procedure of House and Bare (16), we obtained 22% of **13**, 37% of **14**, and 31% recovered **12**.

Can. J. Chem. Downloaded from www.nrcresearchpress.com by 88.85.125.76 on 09/07/12
For personal use only.

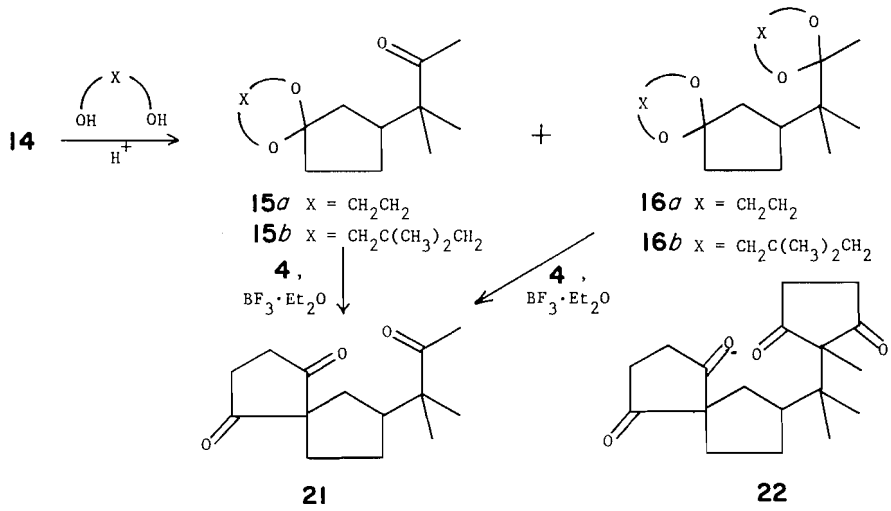

work-up, a good yield of the desired triketone **21**, a little **14** (by hydrolysis), and none of the tetraketone **22**. Reaction of **16***b* with **4** provided **21**, but the product was accompanied by an equal amount of the hydrolysis product **14**, and one small-scale reaction with **16***b* produced a small amount of a compound tentatively identified as the tetraketone **22**. Thus, the reaction of the monoketal **15***b* presented a route to **21** that was marginally cleaner than via either diketal.

McMurry (18) has reported many intramolecular carbonyl coupling reactions involving low-valent titanium, but for our synthesis it was necessary to effect an intramolecular coupling of two ketones while suppressing the reduction and intermolecular coupling of a third ketone. This required considerable experimentation. One of our first attempts followed McMurry's "representative procedure" with $TiCl_3$ and the Zn–Cu couple (19). Chromatography of the product provided only 8% isokhusimone (**3**) along with 29% of a 1:1 mixture of the epimeric alcohols **23***a* and **23***b*, 28% recovered triketone **21**, and a significant amount of very nonpolar, heterogeneous material. The ^{13}C nmr spectrum of this material displayed many signals in the region of δ 140 ppm, which suggested a mixture of the overreduced and intermolecularly coupled hydrocarbons, **24**, and molecules with gross structure **25**. Similar results were obtained with $TiCl_3$ and other reducing agents: $LiAlH_4$, potassium metal, or Zn–Ag (20). However, when the triketone **21** was added *very slowly* by syringe pump to the slurry produced by $TiCl_3$ and freshly prepared Zn–Cu couple in a relatively large volume of boiling DME, the product we obtained repeatably was over 50% **3** with another (approximately) 20% of the alcohols **23***a*/*b* and very little hydrocarbon.

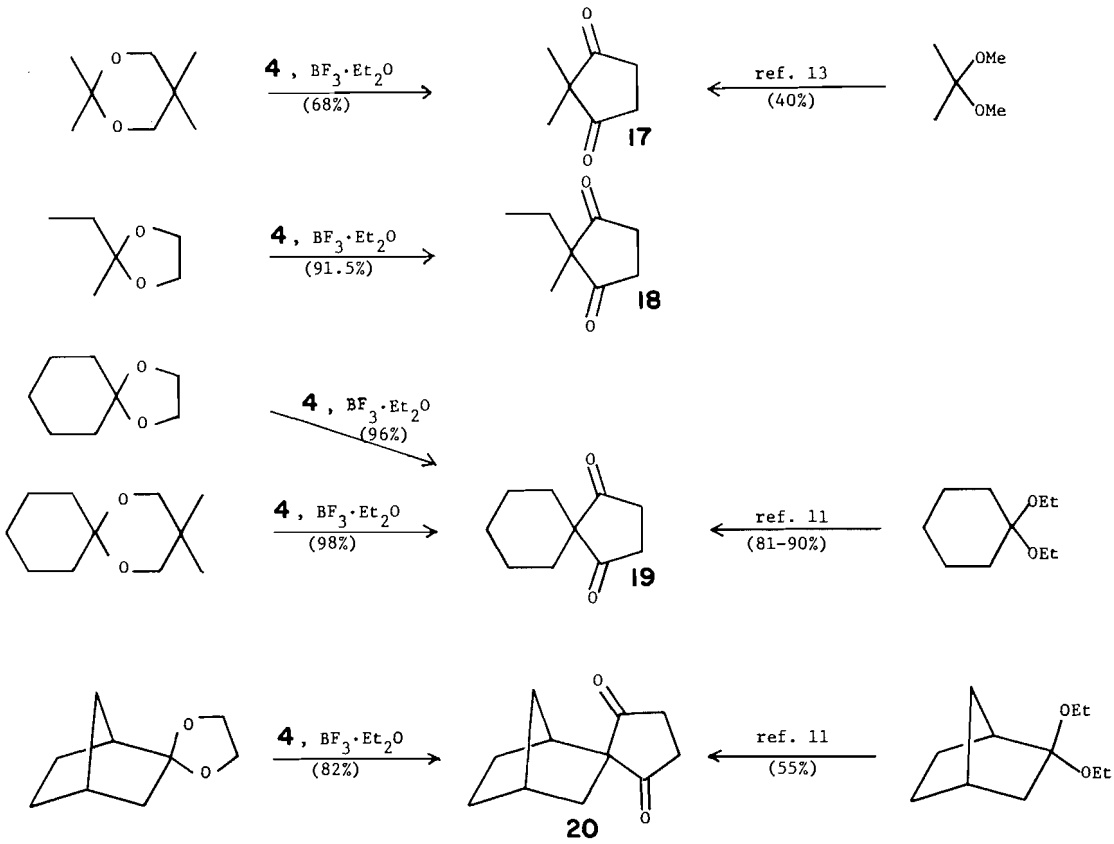

Can. J. Chem. Downloaded from www.nrcresearchpress.com by 88.85.125.76 on 09/07/12
For personal use only.

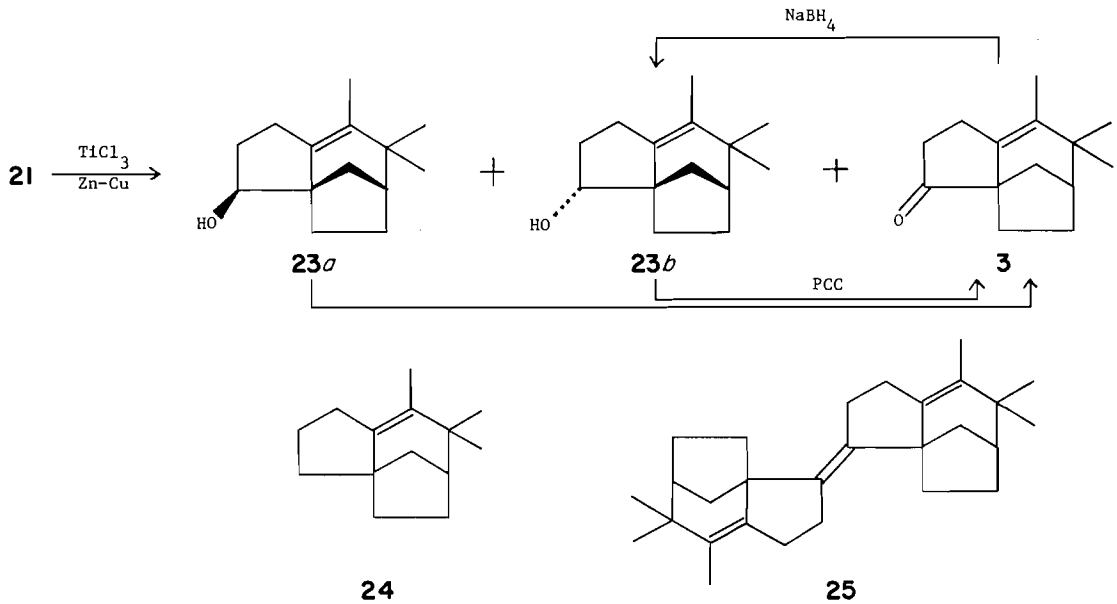

Oxidation of **23***a*/*b* to **3** with PCC was essentially quantitative,[6] so it was more efficient to oxidize the mixture of reaction products without separation of **3** from **23***a*/*b*. Our best yield of **3** over the two steps from **21** was 78%, and overall our yield of isokhusimone (**3**) was 35% from norcamphor. The ir, ^{1}H nmr, and mass spectra of our product were completely in accord with spectra of isokhusimone kindly provided by Professor G. Büchi. Büchi's group (4) has converted isokhusimone (**3**) to khusimone (**1**) in two steps, and Liu and Chan (5) have derived **2** and its epimer from **1** in a straightforward fashion.

As a sideline to our synthesis of **3**, we attempted a variation on our approach to the tricyclic skeleton that involved intramolecular carbonyl-coupling of a ketone with an ester (18). Methanolysis of the dimethyl-lactone **10** gave the methyl ester **26**, which in turn was oxidized with PCC to the keto-ester **27** and ketalized with ethylene glycol to give the ketal **28** in a yield of 83% from **10**. Addition of **28** to a solution of three equivalents of **4** and 15 equivalents of BF_3 etherate at −78°C provided the spiro-annulated compound **29** in a yield of 80% after chromatography. However, all our attempts to modify McMurry's con-

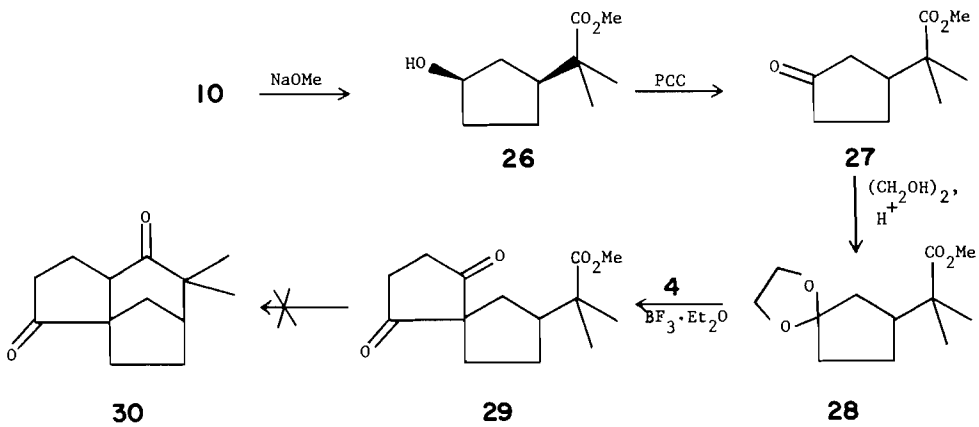

ditions to effect ketone–ester coupling to a tricyclic product **30** resulted in complex mixtures of many unidentified products and significant amounts of recovered **29**.

Although this second approach was ultimately unsuccessful, both routes demonstrated the synthetic utility of spiro-annulation with **4**, particularly via the simple one-pot procedure described here. Indeed, our first route was a considerable improvement over others for the construction of the zizaane system in its racemic form, and it should be amenable to chiral syntheses of zizaane sesquiterpenoids by starting from readily available (+)- or (−)-norcamphor (21).

Experimental

Melting points were determined on a Fisher–Johns apparatus and are uncorrected. Infrared (ir) spectra were recorded on a Perkin Elmer 283 spectrophotometer. Nuclear magnetic resonance (nmr) spectra were obtained in $CDCl_3$ solution, unless otherwise noted, on a General Electric GE 300-NB (300 MHz) instrument; chemical shifts were measured relative to internal standards: tetramethylsilane for ^{1}H and $CDCl_3$ (δ 77.0 ppm) for ^{13}C. Multiplicities are described by standard abbreviations. The nmr assignments were aided by APT, COSY, and HET-CORR 2-D spectra. Except where noted, both the low and the

[6]Reduction of **3** back to the alcohol with sodium borohydride resulted in the formation of *only one* of the epimeric alcohols. Molecular models suggest that formation of **23***b* might be favored because of somewhat less steric hindrance to the approach of the reducing agent from the face *syn* to the methano bridge.

Can. J. Chem. Downloaded from www.nrcresearchpress.com by 88.85.125.76 on 09/07/12
For personal use only.

Can. J. Chem. Downloaded from www.nrcresearchpress.com by 88.85.125.76 on 09/07/12
For personal use only.

high resolution mass spectral (ms) data were obtained on a V.G. Micromass 7070HS instrument. A Hewlett–Packard system (model 5890 gas chromatograph coupled to a model 5970 mass selective detector) equipped with a Hewlett–Packard 12.5-m fused silica capillary column with cross-linked dimethylsilicone as the liquid phase was used for gc–ms analyses. Microanalyses were by the Canadian Microanalytical Service Ltd., New Westminster, B.C. All reactions were run under an atmosphere of dry N_2. Solvents and reagents were purified by distillation; tetrahydrofuran (THF) and dimethoxyethane (DME) were distilled from sodium. "Ether" refers to diethyl ether. Silica gel (230–400 mesh) was used for flash column chromatography.

2-Oxabicyclo[3.2.1]octan-3-one (7)

Norcamphor (6.00 g, 52.5 mmol) and 85% *m*-chloroperoxybenzoic acid (14.10 g, 69.4 mmol) were stirred in $CHCl_3$ for 2 days at room temperature. The solution was washed with 10% NaOH (×5) and H_2O (×4), dried ($MgSO_4$), and concentrated. Vacuum distillation of the residue provided pure lactone **7** (5.70 g, 86%); ir (film) ν_{max}: 1730 cm^{-1}; ^1H nmr δ: 1.62–2.05 (5H, mm), 2.171 (1H, dt, J = 2.3, 9.5 Hz), 2.491 (1H, dt, J = 1.9, 18.4 Hz), 2.554 (1H, br d, J = 4.6 Hz), 2.727 (1H, ddd, J = 1.8, 5.0, 18.4 Hz), and 4.866 (1H, br s); ^{13}C nmr δ (attached H's): 28.5 (2), 31.1 (1), 31.8 (2), 35.0 (2), 39.9 (2), 80.4 (1), and 170.2 (0); ms from gc–ms m/z (%): 126 (5.5, M^+), 98 (14), 97 (11), 83 (39), 82 (66), 69 (42), 67 (99), 55 (48), 54 (51), 42 (54), and 41 (100). Exact mass calcd. for $C_7H_{10}O_2$: 126.0680; found: 126.0677.

2-Oxabicyclo[3.3.0]octan-3-one (8)[7]

Repeating the above on a small scale, but with the addition of concentrated H_2SO_4, gave a dark solution that was mainly **8** (98% by gc–ms analysis) with a small amount of **7**. For **8**: ir (film) ν_{max}: 1765 cm^{-1}; ^1H nmr δ: 1.50–2.08 (6H, mm), 2.290 (1H, dd, J = 1.6, 17.1 Hz), 2.78–2.94 (2H, mm), and 5.008 (1H, t, J = 5.1 Hz); ^{13}C nmr δ (attached H's): 23.2 (2), 33.3 (2), 33.4 (2), 35.9 (2, C-3), 37.7 (1), 86.2 (1), and 178.6 (0); ms from gc–ms m/z (%): 126 (6, M^+), 98 (31), 97 (29), 83 (17), 82 (12), 80 (22), 67 (100), 55 (56), 54 (54), and 41 (79).

4,4-Dimethyl-2-oxabicyclo[3.2.1]octan-3-one (10)

Lactone **7** (938 mg, 7.44 mmol) in dry THF was added slowly to 2.0 equivalents of LDA in THF at −78°C. The solution was stirred for 1 h before a solution of CH_3I (3.17 g, 22.3 mmol) and HMPA (22) (2.59 mL, 14.9 mmol) in THF was added over 10 min. The mixture was allowed to warm to −40°C, and was stirred for 1 h. The reaction was quenched with saturated NH_4Cl and extracted with ether (×4). The combined organic layers were washed with saturated NaCl (×2), dried ($MgSO_4$), and concentrated to provide the crude monomethyl-lactone **9**: ir (film) ν_{max}: 1720 cm^{-1}; ^1H nmr δ: 1.326 (3H, d, J = 7.5 Hz), 1.55 (1H, m), 1.71 (1H, m), 1.83–2.15 (4H, mm), 2.267 (1H, br t), 2.524 (1H, tq, J = 1.2, 7.5 Hz), and 4.817 (1H, br s); ^{13}C nmr δ: 18.9, 29.5, 31.9, 32.0, 38.3, 45.2, 80.7, and 174.4; ms m/z (%): 140 (4, M^+), 112 (4), 111 (3), 97 (50), 96 (21), 83 (26), 81 (56), 68 (30), 67 (67), 56 (33), and 55 (100). Exact mass calcd. for $C_8H_{12}O_2$: 140.0836; found: 140.0833. Repetition of this procedure with **9** as the starting material gave the crude dimethyl-lactone **10**. Chromatography (4% acetone in petroleum ether) yielded pure **10** (936 mg, 82% from **7**): mp 64–65°C; ir (Nujol) ν_{max}: 1740 cm^{-1}; ^1H nmr δ: 1.247 (3H, s), 1.328 (3H, s), 1.55–1.78 (2H, m), 1.90–2.10 (3H, mm), 2.110 (1H, t, J = 5.5 Hz, methine), 2.269 (1H, br d, J = 13.0 Hz), and 4.772 (1H, br s, methine); ^{13}C nmr δ (attached H's): 24.0 (2), 24.4 (3), 28.4 (3), 31.2 (2), 33.5 (2), 43.1 (0), 43.4 (1), 80.5 (1), and 177.1 (0); ms from gc–ms m/z (%): 154 (2, M^+), 111 (14), 110 (16), 95 (20), 69 (100), 67 (68), and 41 (75). Anal. calcd. for $C_9H_{14}O_2$: C 70.10, H 9.15; found: C 69.87, H 9.01.

cis-*2-(3-Hydroxycyclopentyl)-2-methylpropanoic acid (11)*

A solution of the dimethyl-lactone **10** (261 mg, 1.69 mmol) in ethanol, to which 10 mL of 10% KOH was added, was heated at reflux for 15 h. Once the solution had cooled, H_2O and 5% HCl were added until pH 4.5. Extraction with EtOAc (×5) followed by washing with saturated NaCl (×2), drying ($MgSO_4$) of the organic layer, and evaporation of the solvent yielded **11** as a colorless solid (289 mg, 99%): mp 105–106°C; ir (film) ν_{max}: 3600–2500 (very br) and 1700 cm^{-1}; ^1H nmr (CD_3SOCD_3) δ: 1.026 (3H, s), 1.035 (3H, s), 1.16 (1H, m), 1.35–1.48 (3H, m), 1.61 (1H, m), 1.80 (1H, m), 2.03 (1H, m), 4.01 (1H, m), 4.45 (1H, O*H*), and 12.01 (1H, CO_2H); ^{13}C nmr (CD_3SOCD_3) δ: 22.4, 22.5, 24.4, 34.9, 36.8, 43.1, 45.3, 71.3, and 178.8; ms m/z (%): no M^+, 155 (0.9), 154 (0.8), 128 (2), 111 (9), 109 (22), 88 (90), 69 (67), 67 (100), and 41 (68). Anal. calcd. for $C_9H_{16}O_3$: C 62.77, H 9.36; found: C 62.30, H 9.24.

cis-*3-(3-Hydroxycyclopentyl)-3-methyl-2-butanone (12)*

To an ice-bath-cooled solution of **11** (4.661 g, 27.06 mmol) in THF was added 228 mL (319 mmol) of 1.4 M CH_3Li in hexanes. The solution was stirred for 47 h, then at ice-bath temperature $(CH_3)_3SiCl$ (75 mL) was added all at once (solution became cloudy), followed by 5% HCl (solution cleared again). After stirring for 0.5 h, the mixture was extracted with ether (×3), and the combined organic layers were washed with H_2O, saturated $NaHCO_3$, and saturated NaCl. The solution was dried ($MgSO_4$) and concentrated. Chromatography (5% acetone in petroleum ether) yielded the hydroxy-ketone **12** (3.936 g, 85%) and a very small amount of the diol **13**. For **12**: ir (film) ν_{max}: 3420 (br) and 1700 cm^{-1}; ^1H nmr δ: 1.111 (3H, s), 1.119 (3H, s), 1.22–2.02 (6H, mm), 2.131 (3H, s), 2.168 (1H, apparent quintet, J = 8.7 Hz, methine), 2.45 (1H, v br, O*H*), and 4.265 (1H, apparent quintet, J = 4.8 Hz); ^{13}C nmr δ (attached H's): 21.8 (3), 22.0 (3), 24.8 (2), 25.6 (3), 35.4 (2), 36.8 (2), 45.0 (1), 49.3 (0), 73.1 (1), and 214.1 (0); ms m/z (%): 170 (0.4, M^+), 152 (3), 127 (14), 109 (100), 86 (44), 67 (78), 55 (35), and 43 (82). Exact mass calcd. for $C_{10}H_{18}O_2$: 170.1307; found: 170.1294; and calcd. for $C_{10}H_{16}O$ ($M^+ - H_2O$): 152.1201; found: 152.1213. For cis-*3-(2-hydroxy-1,1,2-trimethylpropane)-1-cyclopentanol* (**13**): ir (film) ν_{max}: 3380 (br), 1470, and 1380 cm^{-1}; ^1H nmr (OH signals first removed by exchange) δ: 0.880 (3H, s), 0.893 (3H, s), 1.191 (6H, s), 1.383 (1H, m), 1.45–1.76 (4H, mm), 1.94–2.11 (2H, mm), and 4.220 (1H, m); ^{13}C nmr δ (attached H's): 19.7 (3), 20.4 (3), 26.2 (3), 26.5 (2), 34.8 (2), 38.9 (2), 41.3 (0), 43.8 (1), 72.7 (1), and 76.2 (0); ms from gc–ms m/z (%): no M^+, 153 (2), 150 (4), 135 (9), 110 (20), 109 (24), 84 (60), 83 (91), 69 (78), 67 (77), 59 (59), 55 (93), 43 (55), and 41 (100).

3-(1,1-Dimethyl-2-oxopropyl)cyclopentanone (14)

A solution of the hydroxy-ketone **12** (3.6642 g, 21.52 mmol) in CH_2Cl_2 (30 mL) was added to PCC (23) (6.97 g, 32.3 mmol) in CH_2Cl_2. The solution was stirred at room temperature for 26 h. Filtration through a Florisil pad removed a black precipitate. Five volumes of anhydrous ether were passed through the pad, and concentration of the combined organic solutions provided the diketone **14** (3.5937 g, 99%): ir (film) ν_{max}: 1740 and 1700 cm^{-1}; ^1H nmr δ: 1.144 (3H, s), 1.167 (3H, s), 1.54–2.40 (6H, mm), 2.175 (3H, s), and 2.537 (1H, m, methine); ^{13}C nmr δ (attached H's): 21.1 (3), 21.5 (3), 24.0 (2), 25.5 (2), 38.6 (2), 40.0 (2), 43.4 (1), 48.7 (0), 212.6 (0), and 218.0 (0); ms m/z (%): 168 (0.5, M^+), 140 (18), 125 (19), 97 (16), 86 (57), 83 (55), 82 (18), 69 (44), 55 (100), 43 (74), and 41 (47). Exact mass calcd. for $C_{10}H_{16}O_2$: 168.1149; found: 168.1149.

Ketalization of 14 with ethylene glycol: 15a and 16a

A solution of the diketone **14** (37.5 mg, 0.223 mmol), ethylene glycol (13.7 μL, 0.25 mmol), and a very small amount of *p*-toluenesulfonic acid (*p*-TSA) in benzene was heated under reflux for 8 h with a Barrett water-separator filled with 4 Å molecular sieves. The cooled solution was washed with saturated $NaHCO_3$ and saturated NaCl. The aqueous layers were reextracted with ether (×4). The combined organic extracts were dried ($MgSO_4$) and concentrated. Column chromatography (4% acetone in petroleum ether) of the residue provided 15.0 mg of starting ketone and 22.2 mg (49%) of the monoketal **15***a*: ^1H nmr δ: 1.072 (3H, s), 1.083 (3H, s), 1.35–1.95 (6H, mm), 2.128 (3H, s), 2.363 (1H, m), and 3.84–394 (4H, mm); ms from gc–ms m/z (%): no M^+, 169 (2, $M^+ - COCH_3$), 141 (6), 127 (100), 99 (31), 86 (17), 83 (19), 55 (38), 43 (40), and 41 (28). In a similar reaction a benzene solution of **14** was heated overnight in the presence of a large excess of ethylene glycol and a catalytic amount of PPTS.

[7]We thank Mr. Paul F. Walsh for performing this experiment.

Can. J. Chem. Downloaded from www.nrcresearchpress.com by 88.85.125.76 on 09/07/12
For personal use only.

The product consisted of **15***a* and the diketal **16***a* (1:2, respectively, by gc–ms). For **16***a*: ir (film) ν_{max}: 2975, 2880, 1475, 1370, and 1330 cm^{-1}; ^1H nmr δ: 0.876 (3H, s), 0.912 (3H, s), 1.235 (3H, s), 1.41–1.56 (1H, m), 1.62–1.94 (5H, mm), 2.09–2.22 (1H, m, methine), and 3.83–3.97 (8H, mm); ^{13}C nmr δ (attached H's): 19.2 (3), 19.4 (3), 20.1 (3), 25.9 (2), 35.8 (2), 38.9 (2), 42.9 (0), 43.3 (1), 64.0 (2), 64.1 (2), 64.5 (2), 64.6 (2), 114.3 (0), and 117.4 (0); ms from gc–ms *m/z* (%): no M^+, 241 (3.5), 141 (2), 127 (40), 99 (19), 87 (100), 55 (14), and 43 (32).

*Ketalization of **14** with 2,2-dimethyl-1,3-propanediol: **15**b and **16**b*

A solution of the diketone **14** (435.3 mg, 2.587 mmol), 2,2-dimethyl-1,3-propanediol (700 mg, 6.72 mmol), and PPTS (approximately 120 mg) in benzene was heated under reflux for 40 min. After cooling, ether was added to the solution, which was washed with saturated $NaHCO_3$, H_2O, and saturated NaCl, then dried ($MgSO_4$). Evaporation of the solvent under reduced pressure followed by chromatography (8% acetone in petroleum ether) provided 577.0 mg (88%) of the monoketal **15***b* and 37.6 mg (4%) of the diketal **16***b*. For **15***b*: ir (film) ν_{max}: 1710 and 1120 cm^{-1}; ^1H nmr δ: 0.948 (3H, s), 0.965 (3H, s), 1.067 (3H, s), 1.078 (3H, s), 1.3–1.7 (3H, mm), 1.80–2.03 (3H, mm), 2.128 (3H, s), 2.340 (1H, m, methine), and 3.455 (4H, m); ^{13}C nmr δ (attached H's): 21.1 (2C, 3), 22.3 (3), 22.4 (3), 24.5 (2), 25.3 (3), 30.0 (0), 34.8 (2), 36.1 (2), 43.6 (1), 49.1 (0), 71.7 (2), 72.0 (2), 108.3 (0), and 213.4 (0); ms *m/z* (%): no M^+, 239 (0.4, $M^+ - CH_3$), 211 (2, $M^+ - COCH_3$), 183 (2), 169 (94), 141 (18), 128 (14), 83 (100), 69 (86), 55 (64), 43 (52), and 41 (56). Anal. calcd. for $C_{15}H_{26}O_3$: 70.83, H 10.30; found: C 70.86, H 10.20. Similarly, heating a benzene solution of **14** (81.4 mg, 0.484 mmol) and a catalytic amount of PPTS with a large excess of the diol for 19 h yielded, after chromatography, 20.1 mg (16%) of the monoketal **15***b* and 129.4 mg (79%) of the diketal **16***b*: ir (film) ν_{max}: 2945, 2865, 1470, and 1120 cm^{-1}; ^1H nmr δ: 0.704 (3H, s), 0.917 (6H, s), 0.937 (3H, s), 0.981 (3H, s), 1.143 (3H, s), 1.314 (3H, s), 1.460 (1H, m), 1.53–1.78 (3H, m), 1.981 (1H, dd, J = 8.9, 10.5 Hz), 2.112 (1H, dd, J = 7.4, 13.4 Hz), 2.273 (1H, m, methine), 3.298 (1H, d, J = 11.5 Hz), 3.469 (4H, s), and 3.652 (2H, d, J = 11.5 Hz); ^{13}C nmr δ (attached H's): 11.8 (3), 18.9 (3), 19.7 (3), 22.38 (2C, 3), 22.42 (3), 23.3 (3), 26.4 (2), 29.7 (0), 30.0 (0), 34.2 (2), 38.8 (2), 42.3 (1), 43.6 (0), 69.9 (2C, 2), 71.6 (2), 71.9 (2), 102.4 (0), and 108.7 (0); ms *m/z* (%): no M^+, 325 (0.6), 205 (3), 169 (10), 141 (5), 129 (7), 115 (18), 88 (10), 86 (63), 84 (100), 69 (24), 56 (46), 47 (22), and 41 (44).

*Typical procedure for reaction of 1,2-bis(trimethylsiloxy)cyclobutene (**4**) with a ketal: 2-ethyl-2-methylcyclopentane-1,3-dione (**18**)*

Compound **4** was prepared by the method of Bloomfield and Nelke (24). A solution of 2-ethyl-2-methyl-1,3-dioxolane (280.5 mg, 2.42 mmol) in CH_2Cl_2 was stirred at −78°C as freshly distilled BF_3 etherate (2.98 mL, 24.2 mmol) was added, followed over a period of 5 min by a solution of **4** (1.61 mL, 6.05 mmol) in CH_2Cl_2. The mixture was allowed to attain room temperature while stirring overnight. The solution was washed with H_2O, saturated $NaHCO_3$, and saturated NaCl. The aqueous layers were reextracted with CH_2Cl_2 (×3), then the combined organic extracts were dried ($MgSO_4$) and concentrated to provide a yellow oil that showed only one component on gc–ms. The oil was chromatographed to yield colorless **18** (309.3 mg, 91.5%): ir (film) ν_{max}: 1750 (shoulder) and 1720 cm^{-1}; ^1H nmr δ: 0.808 (3H, t, J = 7.4 Hz), 1.095 (3H, s), 1.668 (2H, q, J = 7.4 Hz), and 2.785 (4H, s); ^{13}C nmr δ (attached H's): 8.7 (3), 17.8 (3), 28.6 (2), 35.0 (2), 56.9 (0), and 216.4 (0); ms *m/z* (%): 140 (51, M^+), 125 (92), 97 (31), 84 (12), 83 (13), 69 (100), 56 (36), 55 (29), and 41 (83). Exact mass calcd. for $C_8H_{12}O_2$: 140.0837; found: 140.0843.

Similarly, the 5,5-dimethyl-1,3-dioxane derived from acetone gave **17** (crude product 92.6% by gc–ms, 68% after chromatography): ir (film) ν_{max}: 1725 cm^{-1}; ^1H nmr δ: 1.153 (6H, s) and 2.810 (4H, s); ^{13}C nmr δ (attached H's): 20.2 (3), 34.5 (2), 52.6 (0), and 216.3 (0); ms *m/z* (%): 126 (54, M^+), 111 (19), 83 (18), 70 (100), 56 (23), 55 (21), and 42 (83). Exact mass calcd. for $C_7H_{10}O_2$: 126.0680; found: 126.0678.

The 1,3-dioxolane and the 5,5-dimethyl-1,3-dioxane derived from cyclohexanone gave **19** (96% and 98%, respectively, crystallized from EtOAc): mp 60–61°C (lit.(11) mp 61–62°C); ir (film) ν_{max}: 1755 (weak) and 1720 cm^{-1}; ^1H nmr δ: 1.4–1.7 (10H, mm) and 2.677 (4H, s); ^{13}C nmr δ (attached H's): 20.4 (2), 24.9 (2), 29.2 (2), 34.3 (2), 55.9 (0), and 215.8 (0); ms *m/z* (%): 166 (100, M^+), 137 (25), 124 (32), 112 (61), 111 (46), 85 (46), 81 (37), 67 (74), and 56 (44). Exact mass calcd. for $C_{10}H_{14}O_2$: 166.0993; found: 166.0985.

The 1,3-dioxolane derived from norcamphor gave **20** (82%, crystallized from ether): mp 108–109°C (lit. (11) mp 109.5–110.5°C); ir (film) ν_{max}: 1760 (weak) and 1715 cm^{-1}; ^1H nmr δ: 1.18–1.57 (6H, mm), 1.76–1.89 (2H, mm), 2.372 (1H, br t, bridgehead H), 2.480 (1H, br d, bridgehead H), and 2.51–3.07 (4H, mm); ^{13}C nmr δ (attached H's): 24.5 (2), 28.0 (2), 32.9 (2), 34.4 (2), 35.3 (2), 37.0 (1), 37.2 (2), 48.9 (1), 66.6 (0), 213.1 (0), and 213.4 (0); ms *m/z* (%): 178 (19, M^+), 149 (46), 112 (100), 93 (15), 79 (13), 67 (19), 66 (12), and 65 (13). Exact mass calcd. for $C_{11}H_{14}O_2$: 178.0993; found: 178.1002.

*7-(1,1-Dimethyl-2-oxopropyl)spiro[4.4]nonane-1,4-dione (**21**)*

*From the monoketal **15**b*

A solution of **15***b* (611.0 mg, 2.402 mmol) in CH_2Cl_2 was cooled to −78°C. Freshly distilled BF_3 etherate (4.44 mL, 36.1 mmol) was added followed, dropwise, by a solution of **4** (1.60 mL, 6.05 mmol) in CH_2Cl_2. The mixture was stirred overnight, over which time the solution was allowed to attain room temperature. The black solution was washed with H_2O, saturated $NaHCO_3$, and saturated NaCl. The aqueous layers were reextracted with CH_2Cl_2 (×3), and the combined organic extracts were dried ($MgSO_4$). Concentration of the solvent left a yellow oil (716.5 mg) that was chromatographed (5% acetone in petroleum ether) to provide pure **21** (491.2 mg, 87%): ir (film) ν_{max}: 1760 (shoulder), 1725, and 1705 cm^{-1}; ^1H nmr δ: 1.100 (3H, s), 1.136 (3H, s), 1.44–1.96 (6H, mm), 2.141 (3H, s), 2.491 (1H, m, methine), and 2.778 (4H, m); ^{13}C nmr δ (attached H's): 21.2 (3), 21.6 (3), 25.3 (3), 27.6 (2), 34.1 (2), 34.7 (2), 34.9 (2), 35.2 (2), 46.7 (1), 48.9 (0), 62.3 (0), 213.0 (0), 215.3 (0), and 215.7 (0); ms from gc–ms *m/z* (%): 236 (0.1, M^+), 221 (0.4), 193 (96), 176 (12), 175 (15), 151 (66), 137 (17), 133 (25), 125 (30), 111 (29), 109 (22), 86 (56), 55 (30), 43 (100), and 41 (56). Exact mass calcd. for $C_{12}H_{17}O_2$ ($M^+ - COCH_3$): 193.1227; found: 193.1215.

*From the diketal **16**a*

A CH_2Cl_2 solution of the diketal **16***a* (91.9 mg, 0.359 mmol) was treated as above with BF_3 etherate (0.89 mL, 7.2 mmol) and **4** (0.58 mL, 2.2 mmol). The gc–ms analysis of the crude product showed **21** as the almost exclusive component along with ca. 3% **14**. Chromatography (5% acetone in petroleum ether) provided 72.9 mg (86%) of pure **21**.

*From the diketal **16**b*

A CH_2Cl_2 solution of the diketal **16***b* (129.4 mg, 0.380 mmol) was treated as above with BF_3 etherate (0.94 mL, 7.6 mmol) and **4** (0.61 mL, 2.3 mmol). The gc–ms analysis of the crude product showed a mixture of mainly **21** and **14** (1 : 1). Chromatography provided 42.3 mg (47%) of pure **21** and 27.6 mg (43%) of recovered **14**. The following is the mass spectrum of a compound tentatively identified as **22** from the gc–ms of the crude product of one very small-scale reaction of **16***b* with **4**: *m/z* (%): 304 (2, M^+), 239 (5), 221 (2), 219 (2), 207 (24), 153 (25, complete side chain), 137 (23), 123 (100), 81 (33), 79 (24), 73 (15), 69 (18), 55 (18), and 41 (26).

*Intramolecular titanium-induced ketone–ketone coupling in **21**: isokhusimone (**3**)*

Zn–Cu couple was made by the procedure of McMurry *et al.* (19). The couple (556 mg, 8.56 mmol) was added to $TiCl_3$ (516 mg, 3.35 mmol) in 150 mL of dry DME, and this was heated under reflux for 4 h. A solution of the triketone **21** (96.6 mg, 0.409 mmol) in DME (20 mL) was added to the hot slurry over a period of 50.5 h using a syringe pump, then the reaction mixture was heated for another 84 h. After cooling, the solution was passed through a pad of Florisil. The residue from concentration of the solvent was chromatographed (2% acetone in petroleum ether) to afford, in order of elution, isokhusimone (**3**) (47.4 mg, 57%), a 1:1 mixture of the epimeric alcohols **23***a* and **23***b* (17.8 mg, 21%), and 8.1 mg of recovered triketone **21**. For **3**: ir (film) ν_{max}:

Can. J. Chem. Downloaded from www.nrcresearchpress.com by 88.85.125.76 on 09/07/12
For personal use only.

1740 and 1675 (weak) cm^{-1}; ^1H nmr δ: 1.020 (3H, s), 1.039 (3H, s), 1.534 (3H, s), 1.64–1.88 (7H, mm), 2.025 (1H, m, methine), and 2.28–2.71 (3H, mm); ^{13}C nmr δ (attached H's): 12.2 (3), 23.1 (2), 24.7 (2), 25.1 (3), 28.2 (3), 35.7 (2), 38.0 (2), 38.3 (2), 40.5 (0), 48.6 (1), 55.9 (0), 130.6 (0), 136.3 (0), and 222.6 (0); ms *m/z* (%): 204 (15, M^+), 189 (36), 161 (23), 133 (30), 119 (100), 105 (12), 91 (22), 77 (15), and 41 (29). Exact mass calcd. for $C_{14}H_{20}O$: 204.1513; found: 204.1531. For **23***a* (tentative assignment of relative stereochemistry at C-2): ^1H nmr (from the spectrum of the mixture of epimers) δ: 0.990 (3H, s), 1.037 (3H, s), 1.479 (3H, s), and 4.031 (1H, m); ^{13}C nmr (from the spectrum of the mixture of epimers) δ: 13.4, 25.0, 25.1, 25.8, 32.6, 33.3, 36.6, 40.4, 47.7, 56.3, 79.7, 128.9, and 139.5; ms nearly identical with **23***b*. For **23***b*: see below. Oxidation of **23***a*/*b* with PCC yielded **3** essentially quantitatively.

Reduction of **3**

Isokhusimone (38.2 mg, 0.187 mmol) was dissolved in methanol (8 mL) and cooled in an ice-bath as $NaBH_4$ was added in small portions. Thin-layer chromatography indicated a complete reaction within 30 min. Some H_2O was added and much of the methanol was removed by evaporation under reduced pressure. The product was extracted into ether, which was washed with saturated NaCl, dried ($MgSO_4$), and concentrated. Although the crude oily residue (39.1 mg) was homogeneous by tlc and gc–ms, column chromatography (10% acetone in petroleum ether) was used to remove some yellow color. This afforded the alcohol tentatively assigned as epimer **23***b* as a colorless powder, mp 102–103°C; ir (film) ν_{max}: 3370 (very br) cm^{-1}; ^1H nmr δ: 0.989 (3H, s), 1.006 (3H, s), 1.20–2.35 (mm), 1.421 (3H, s), and 4.002 (1H, dd, J = 6.0, 11.2 Hz); ^{13}C nmr δ (attached H's): 12.5 (3), 24.1 (2C, 2), 24.9 (3), 28.3 (3), 28.4 (2), 32.1 (2), 36.2 (2), 40.4 (0), 47.2 (1), 53.0 (0), 76.3 (1), 129.7 (0), and 138.8 (0); ms from gc–ms *m/z* (%): 206 (29, M^+), 191 (75), 173 (10), 163 (24), 145 (48), 119 (100), 105 (17), and 91 (25). Exact mass calcd. for $C_{13}H_{19}O$ ($M^+ - CH_3$): 191.1435; found: 191.1435.

Methyl cis*-2-(3-hydroxycyclopentyl)-2-methylpropanoate (***26***)*

Sodium (800 mg) was added to dry methanol (160 mL) followed by **10** (1.1665 g, 7.564 mmol), and the solution was heated at reflux for 22 h. Much of the solvent was removed by evaporation under reduced pressure, then H_2O was added followed by concentrated HCl to pH 4.5. This was extracted with EtOAc (×4). The organic solution was washed with saturated $NaHCO_3$ and saturated NaCl, dried ($MgSO_4$), and concentrated to give a yellow oil (1.5048 g) containing mainly **26** and a little **10**. Only a small portion was purified; for **26**: ir (film) ν_{max}: 3430 (br) and 1730 cm^{-1}; ^1H nmr δ: 1.170 (3H, s), 1.175 (3H, s), 1.376 (1H, m), 1.55–1.77 (3H, mm), 1.95–2.20 (2H, mm), 2.21 (1H, v br, O*H*), 3.660 (3H, s), and 4.258 (1H, m); ^{13}C nmr δ (attached H's): 23.0 (3), 23.2 (3), 24.9 (2), 35.4 (2), 37.0 (2), 44.1 (0), 46.3 (1), 51.6 (3), 73.1 (1), and 178.3 (0); ms *m/z* (%): no M^+, 169 (0.4), 155 (1.3), 111 (11), 110 (10), 109 (63), 102 (100), 87 (20), 83 (16), 69 (92), 67 (87), 55 (31), and 41 (68).

*Methyl 2-methyl-2-(3-oxocyclopentyl)propanoate (***27***)*

A CH_2Cl_2 solution of the crude **26** from the above reaction was stirred overnight in the presence of PCC (2.45 g, 11.37 mmol). The mixture was filtered through a Florisil pad, which was washed with ether (×4), and the combined organic solutions were concentrated to give a colorless liquid (1.239 g). A small portion was purified; for **27**: ir (film) ν_{max}: 1740 and 1730 cm^{-1}; ^1H nmr δ: 1.205 (3H, s), 1.214 (3H, s), 1.646 (1H, m), 1.98–2.53 (6H, mm), and 3.687 (3H, s); ^{13}C nmr δ (attached H's): 22.5 (3), 22.6 (3), 24.4 (2), 38.8 (2), 40.4 (2), 43.7 (0), 45.0 (1), 51.8 (3), 177.2 (0), and 218.2 (0); ms *m/z* (%): 184 (1, M^+), 156 (3), 125 (17), 102 (100), 87 (14), 83 (57), 82 (19), 70 (13), 69 (28), 55 (65), and 41 (36). Anal. calcd. for $C_{10}H_{16}O_3$: C 65.18, H 8.76; found: C 65.03, H 8.80.

*7-(1-Carbomethoxy-1-methylethyl)-1,4-dioxaspiro[4.4]nonane (***28***)*

To benzene solution of the crude **27** from the above reaction was added ethylene glycol (4.3 mL, 75.8 mmol) and a small amount of *p*-TSA. The mixture was heated under reflux with a Barrett water separator for 21 h. The solution was washed with saturated $NaHCO_3$, H_2O, and saturated NaCl. The aqueous layers were reextracted with ether (×2), and the combined organic extracts were dried ($MgSO_4$) and concentrated to give a yellow oil (1.5405 g). Chromatography (2% acetone in petroleum ether) of this material provided pure **28** (1.2429 g, 72% from **10**): ir (film) ν_{max}: 1730 and 1130 cm^{-1}; ^1H nmr δ: 1.141 (3H, s), 1.144 (3H, s), 1.40–1.91 (6H, mm), 2.313 (1H, m, methine), 3.653 (3H, s), and 3.890 (4H, m); ^{13}C nmr δ (attached H's): 22.2 (3), 22.4 (3), 24.7 (2), 35.7 (2), 37.4 (2), 43.7 (0), 45.1 (1), 51.4 (3), 63.9 (2), 64.0 (2), 117.2 (0), and 117.5 (0); ms *m/z* (%): no M^+, 199 (1), 169 (9), 127 (100), 99 (78), 83 (22), 55 (30), and 41 (18). Anal. calcd. for $C_{12}H_{20}O_4$: C 63.14, H 8.83; found: C 63.42, H 8.82.

*7-(1-Carbomethoxy-1-methylethyl)spiro[4.4]nonane-1,4-dione (***29***)*

A solution of **28** (52.2 mg, 0.229 mmol) in CH_2Cl_2 was cooled to −78°C and BF_3 etherate (0.43 mL, 3.45 mmol) was added, followed dropwise by a CH_2Cl_2 solution of **4** (0.25 mL, approximately 0.92 mmol). The mixture was stirred for 28 h during which time the reaction was allowed to attain room temperature. The solution was washed with H_2O, saturated $NaHCO_3$, and saturated NaCl, then dried ($MgSO_4$) and concentrated. The residue was chromatographed to provide pure **29** (46.1 mg, 80%): mp 32–33°C; ir (film) ν_{max}: 1715 (br) cm^{-1}; ^1H nmr ($CDCl_3$) δ: 1.174 (3H, s), 1.182 (3H, s), 1.53–1.95 (6H, mm), 2.435 (1H, m, methine), 2.777 (4H, br s), and 3.668 (3H, s); ^1H nmr (C_6D_6) δ: 1.123 (6H, s), 1.55–1.80 (6H, s), 2.050 (4H, br s), 2.444 (1H, m), and 3.381 (3H, s); ^{13}C nmr ($CDCl_3$) δ (attached H's): 22.7 (3), 22.9 (3), 27.8 (2), 34.1 (2), 34.6 (2), 34.8 (2), 35.2 (2), 43.5 (0), 48.2 (1), 51.6 (3), 62.4 (0), 177 (0), 215.3 (0), and 215.6 (0); ^{13}C nmr (C_6D_6) δ: 23.0, 23.4, 28.2, 34.6 (2C), 34.7, 35.4, 43.8, 48.9, 51.3, 62.3, 176.9, 214.3, and 214.5; ms *m/z* (%): 252 (0.4, M^+), 250 (1), 193 (10), 191 (10), 190 (15), 151 (16), 150 (22), 149 (36), 102 (100), 87 (16), 55 (15), and 41 (26). Anal. calcd. for $C_{14}H_{20}O_4$: C 66.65, H 7.99; found: 66.62, H 7.99.

Attempted intramolecular titanium-induced ketone–ester coupling in **29**

Reaction media based on $TiCl_3$/Zn–Cu couple (19) and on $TiCl_3$/$LiAlH_4$ (25) gave complex mixtures along with significant amounts of recovered starting material. (Oxidation of the crude product with PCC did not appear to lead to a simpler mixture.)

Acknowledgements

We thank Dr. C. R. Jablonski and Messrs. A. Earle and R. Sammynaiken for 300 MHz nmr spectra, and Dr. B. Gregory and Miss M. Baggs for mass spectra. We are grateful to Drs. Ž. Stojanac and A. G. Fallis for helpful discussions, and we thank Professor G. Büchi for spectra of authentic isokhusimone. The Natural Sciences and Engineering Research Council of Canada and the Memorial University of Newfoundland provided financial support for this work.

1. D. C. Umrani, R. Seshadri, K. G. Gore, and K. K. Chakravarti. Flavour Ind. **1**, 623 (1970); B. Maurer, M. Fracheboud, A. Grieder, and G. Ohloff. Helv. Chim. Acta, **55**, 2371 (1972).
2. S. C. Jain, S. Nowicki, T. Eisner, and J. Meinwald. Tetrahedron Lett. **23**, 4639 (1982).
3. B. Maurer. Ger. Offen. 2,350,388; Chem. Abstr. **81**, 25216k (1974).
4. G. Büchi, A. Hauser, and J. Limacher. J. Org. Chem. **42**, 3323 (1977).
5. H.-J. Liu and W. H. Chan. Can. J. Chem. **60**, 1081 (1982).
6. W. Oppolzer and R. Pitteloud. J. Am. Chem. Soc. **104**, 6478 (1982); W. Oppolzer, R. Pitteloud, G. Bernardinelli, and K. Baettig. Tetrahedron Lett. **24**, 4975 (1983).
7. K. Sakurai, T. Kitahara, and K. Mori. Tetrahedron, **44**, 6581 (1988).
8. D. F. MacSweeney and R. Ramage. Tetrahedron, **27**, 1481 (1971); A. Deljac, W. D. MacKay, C. S. J. Pan, K. J. Wiesner, and K. Wiesner. Can. J. Chem. **50**, 726 (1972); F.

KIDO, H. UDA, and A. YOSHIKOSHI. J. Chem. Soc. Perkin Trans. 1, 1755 (1972); R. M. COATES and R. L. SOWERBY. J. Am. Chem. Soc. **94**, 5386 (1972); A. ALEXAKIS, M. J. CHAPDELAINE, and G. H. POSNER. Tetrahedron Lett. 4209 (1978); W. OPPOLZER and S. C. BURFORD. Helv. Chim. Acta, **63**, 788 (1980); A. J. BARKER and G. PATTENDEN. Tetrahedron Lett. **22**, 2599 (1981); E. PIERS, J. BANVILLE, C. K. LAU, and I. NAGAKURA. Can. J. Chem. **60**, 2965 (1982); H. M. R. HOFFMANN, R. HENNING, and O. R. LALKO. Angew. Chem. Int. Ed. Engl. **21**, 442 (1982); K. PRAMOD and G. S. R. SUBBA RAO. J. Chem. Soc. Chem. Commun. 762 (1982); H. M. R. HOFFMANN and R. HENNING. Helv. Chim. Acta, **66**, 828 (1983); H. M. R. HOFFMANN, U. EGGERT, U. GIBBELS, K. GIESEL, O. KOCH, R. LIES, and J. RABE. Tetrahedron, **44**, 3899 (1988).

9. Y.-J. WU and D. J. BURNELL. Tetrahedron Lett. **29**, 4369 (1988).
10. H. O. HOUSE. Modern synthetic reactions. 2nd ed. W. A. Benjamin, Menlo Park, CA. 1972. pp. 518–525; M. E. GARST and B. J. MCBRIDE. J. Org. Chem. **48**, 1362 (1983), and references therein.
11. J. SHIMADA, K. HASHIMOTO, B. H. KIM, E. NAKAMURA, and I. KUWAJIMA. J. Am. Chem. Soc. **106**, 1759 (1984); E. NAKAMURA and I. KUWAJIMA. Org. Synth. **65**, 17 (1987).
12. W. K. ANDERSON and G. E. LEE. J. Org. Chem. **45**, 501 (1980); W. K. ANDERSON and G. E. LEE. Synth. Commun. **10**, 351 (1980); W. OPPOLZER and R. D. WYLIE. Helv. Chim. Acta, **63**, 1198 (1980); J. C. EVANS, R. C. KLIX, and R. D. BACH. J. Org. Chem. **53**, 5519 (1988); D. J. BURNELL and Y.-J. WU. Can. J. Chem. **67**, 816 (1989).
13. K. A. PARKER, K. A. KOZISKI, and G. BREAULT. Tetrahedron Lett. **26**, 2181 (1985).
14. J. MEINWALD and E. FRAUENGLASS. J. Am. Chem. Soc. **82**, 5235 (1960).
15. G. M. RUBOTTOM and C. KIM. J. Org. Chem. **48**, 1550 (1983).
16. H. O. HOUSE and T. M. BARE. J. Org. Chem. **33**, 943 (1968).
17. F. HUET, G. EMPTOZ, and A. JUBIER. Tetrahedron, **29**, 479 (1973).
18. J. E. MCMURRY. Acc. Chem. Res. **16**, 405 (1983); J. E. MCMURRY. Chem. Rev. **89**, 1513 (1989).
19. J. E. MCMURRY, M. P. FLEMING, K. L. KEES, and L. R. KREPSKI. J. Org. Chem. **43**, 3255 (1978).
20. A. L. BAUMSTARK, E. J. H. BECHARA, and M. J. SEMIGIAN. Tetrahedron Lett. 3265 (1976); J. E. PAUW and A. C. WEEDON. Tetrahedron Lett. **23**, 5485 (1982); F. E. ZIEGLER and H. LIM. J. Org. Chem. **47**, 5229 (1982).
21. C. LE DRIAN and A. E. GREENE. J. Am. Chem. Soc. **104**, 5473 (1982), and references therein; D. BORDEAUX and G. GAGNAIRE. Tetrahedron Lett. **23**, 3353 (1982); C. MAIGNAN and R. A. RAPHAEL. Tetrahedron, **39**, 3245 (1983); C. R. JOHNSON and J. R. ZELLER. Tetrahedron, **40**, 1225 (1984).
22. J. L. HERRMANN and R. H. SCHLESSINGER. J. Chem. Soc. Chem. Commun. 711 (1973).
23. E. J. COREY and J. W. SUGGS. Tetrahedron Lett. 2647 (1975).
24. J. J. BLOOMFIELD and J. M. NELKE. Org. Synth. **57**, 1 (1977).
25. J. E. MCMURRY and D. D. MILLER. J. Am. Chem. Soc. **105**, 1660 (1983).

Can. J. Chem. Downloaded from www.nrcresearchpress.com by 88.85.125.76 on 09/07/12
For personal use only.

Intrazeolite photochemistry. VI. Diffuse reflectance laser flash photolysis and product studies of diphenylmethyl radicals on solid supports[1]

GRAEME KELLY, C. J. WILLSHER, AND F. WILKINSON[2]
Department of Chemistry, University of Technology, Loughborough, Leicestershire, LE11 3TU, U.K.

AND

J. C. NETTO-FERREIRA, A. OLEA, D. WEIR, L. J. JOHNSTON,[2] AND J. C. SCAIANO[2]
Division of Chemistry, National Research Council of Canada, Ottawa, Ont., Canada K1A 0R6

Received December 13, 1989

GRAEME KELLY, C. J. WILLSHER, F. WILKINSON, J. C. NETTO-FERREIRA, A. OLEA, D. WEIR, L. J. JOHNSTON, and J. C. SCAIANO. Can. J. Chem. **68**, 812 (1990).

Diphenylmethyl radicals have been generated by 266 nm laser excitation of 1,1,3,3-tetraphenylacetone adsorbed on silica gel and included in NaX and Silicalite zeolites and have been studied using diffuse reflectance laser flash photolysis techniques. The spectrum for the radical shows λ_{max} at ~335 nm in all three supports and is similar to that in solution. The radicals decay over time scales that vary from hundreds of nanoseconds to minutes and there are indications that some radicals may be decaying on shorter time scales than we can monitor. The efficiency of oxygen quenching increases in going from Silicalite to NaX to silica gel, consistent with the greater accessibility of oxygen to silica gel pores as compared to the narrow channels in Silicalite. Laser dose and ketone loading effects were also examined for the various supports. Potential applications of a kinetic treatment of the data based on dispersive reaction kinetics are also discussed as a means of dealing with the problem of decay kinetics that occur over a wide range of time scales.

Key words: zeolites, kinetics, diphenylmethyl radicals, laser photolysis.

GRAEME KELLY, C. J. WILLSHER, F. WILKINSON, J. C. NETTO-FERREIRA, A. OLEA, D. WEIR, L. J. JOHNSTON et J. C. SCAIANO. Can. J. Chem. **68**, 812 (1990).

On a produit des radicaux diphénylméthyles en excitant, à l'aide d'un laser opérant à 266 nm, de la 1,1,3,3-tétraphénylacétone adsorbée sur du gel de silice ou incluse dans des zéolithes de NaX et de Silicalite et on les a étudiés en faisant appel aux techniques de photolyse «flash» à l'aide de laser à réflectance diffuse. Le spectre du radical présente un λ_{max} à environ 335 nm dans chacun des trois supports et il est semblable à celui observé en solution. Les radicaux se décomposent à des vitesses qui varient de quelques centièmes de nanosecondes à des minutes; certaines indications nous laissent croire que certains radicaux pourraient se décomposer à des vitesses plus rapides que celles que l'on peut mesurer. L'efficacité du piégeage par l'oxygène augmente lorsqu'on passe de la Silicalite au NaX au gel de silice; cet ordre est en accord avec la plus grande disponibilité de l'oxygène sur les pores du gel de silice par comparaison avec les canaux étroits qui existent sur la Silicalite. Pour divers supports, on a aussi examiné les effets de la dose du laser ainsi que de la quantité de cétone utilisée. On discute aussi des applications potentielles d'un traitement cinétique des données basé sur la cinétique de réactions dispersives comme moyen de résoudre le problème de la cinétique de décompositions qui se produisent à des vitesses très différentes.

Mots clés : zéolithes, cinétique, radicaux diphénylméthyles, photolyse de laser.

[Traduit par la revue]

There is considerable current interest in the study of photochemical reactions on solid supports (1–3). In many cases it has been demonstrated that adsorption on solids such as silica and alumina and inclusion in zeolites can often modify the normal solution photochemistry of a given species. In particular, a variety of benzyl radical pairs have been used to examine the effects of zeolites and silicas on the pathways available to organic molecules adsorbed on the various surfaces (1, 2, 4). These studies have investigated the effects of the additives, temperature, and modifications of the silica or zeolite properties upon the observed chemistry of the radicals. In several cases, novel reactions have been observed as a result of the restrictions imposed upon radical pairs or biradicals by their environment within the zeolite (1).

Recent developments in diffuse reflectance laser flash photolysis have made it possible to study transients in a variety of opaque samples (5–10). For example, there are several reports of time-resolved investigations of triplet states of organic molecules adsorbed on or included in solids (5, 6, 11–13), as well as a recent study of radical cations on surfaces (14). These have demonstrated that restrictions on the mobility may often enhance the transient lifetimes with respect to those observed in solution, and have provided evidence for multiple absorption and inclusion sites. We report herein the first example of the application of diffuse reflectance laser photolysis to the study of radicals in opaque samples. Diphenylmethyl radicals supported on silica gel and NaX and Silicalite zeolites have been examined using both diffuse reflectance transient techniques and product studies.

Experimental

Silica gel (Aldrich, Davisil grade 633, 60 Å), NaX (BDH), and Silicalite (Union Carbide) were heated at 500°C for ~12 h before use. 1,1,3,3-Tetraphenylacetone (TPA) was synthesized according to a previously described modification (15) of a literature procedure (16) and purified by either recrystallization or chromatography.

Sample preparation

Samples of tetraphenylacetone on silica gel and NaX were prepared by stirring solutions of the ketone in hexane with the support (~2 mL solvent/g solid) for 2 h and then slowly removing the solvent on a rotary evaporator. The material was then vacuum dried at room temperature for at least 2 h. Silicalite samples were prepared by stirring the solid with isooctane solutions of the ketone for 12 h, filtering the sample, and washing the solid twice with 2 mL isooctane. The solid was then vacuum dried. The amount of ketone remaining in the isooctane was determined by gas chromatography in order to calculate

[1]Issued as NRCC No. 30998.

[2]Authors to whom correspondence may be addressed.

Printed in Canada / Imprimé au Canada

Can. J. Chem. Downloaded from www.nrcresearchpress.com by 88.85.125.76 on 09/07/12
For personal use only.

Can. J. Chem. Downloaded from www.nrcresearchpress.com by 88.85.125.76 on 09/07/12
For personal use only.

the sample loading. It should be noted that in earlier work we observed some problems with color formation during sample preparation for certain batches of Silicalite (17). However, this was not a problem for any of the samples used in the present experiments.

Diffuse reflectance laser flash photolysis

The frequency quadrupled line (266 nm) from a Lumonics HY400 Nd/Yag laser was used for the transient experiments. The experimental setup for diffuse reflectance laser flash photolysis was the same as that which has been described except for the use of the laser indicated above and an IBM-PC compatible computer for experiment control and data acquisition (8). The samples were contained in 3×7 mm^2 quartz cells and were deaerated by passing a stream of nitrogen or oxygen through the cell.

The kinetic analysis is based on the fraction of reflected light absorbed by the intermediate ($\Delta J/J_0$) where J_0 is the signal before laser excitation and ΔJ is the difference between J_0 and J_t, the signal at time t after excitation. Laser dose experiments (see later) show that increasing the laser intensity leads to an increase in the intensity of the transient absorption, demonstrating that a saturated plug of totally converted ground state to transient is not produced and, therefore, a Kubelka–Munk treatment is not appropriate (18).

Product studies

The samples were prepared as outlined above using 8:2 isooctane/dichloromethane, and removing the solvent on a rotary evaporator. The samples for the nitrogen vs. oxygen effects were evacuated at room temperature on a vacuum line (0.01 Torr; 1 Torr = 133.3 Pa) and then placed under a positive pressure of nitrogen or oxygen and sealed. In the case of a sample equilibrated with $H_2{}^{18}O$, a sample of silica gel was dried as usual and then stored under nitrogen in a dry box. The sample (2 g) was placed in a round-bottom flask, which was attached to a second flask containing 1 g $H_2{}^{18}O$, and the entire system was evacuated and closed. After 24 h all the water had been adsorbed by the silica and the ketone was adsorbed as usual, except that the entire procedure was done in a dry box and the solvent was removed using an Air-Cadet pump.

The samples were irradiated using 300-nm Rayonet lamps and were rotated constantly during the irradiation to provide for adequate sample mixing. After irradiation each sample was extracted in a Soxhlet apparatus for ~12 h using benzene as solvent. This was found to be the best solvent for quantitatively removing ketone from the support. The extract was concentrated and analyzed by GC (Perkin Elmer 8320 gas chromatograph; DB-1 on fused silica capillary column; 15 m × 0.242 mm) using biphenyl as an internal standard and solutions of TPA, benzophenone, and 1,1,2,2-tetraphenylethane for calibration purposes.

Results and discussion

The α-cleavage of 1,1,3,3-tetraphenylacetone (reaction [1]) was used as a source of diphenylmethyl radicals in our experiments. The production of the second diphenylmethyl radical via decarbonylation of the initial diphenylacetyl radical occurs rapidly ($k = 1.3 \times 10^8$ s^{-1} (19)) and reaction [1] is thus an efficient and practically instantaneous source of two diphenylmethyl radicals per ketone molecule (15).

[1] $Ph_2CHC(O)CHPh_2 \rightarrow Ph_2CH\dot{C}O + Ph_2\dot{C}H \rightarrow 2Ph_2\dot{C}H$

The three solid supports used in these experiments differ considerably in their properties. Silica gel is a porous solid with, in our case, an average pore size of 60 Å and a surface area of 480 m^2/g. Silicalite has a channel system consisting of near-circular zigzag channels (diameter of 5.4 Å), cross-linked by elliptical straight channels with a cross-section of 5.75 × 5.15 Å (20). Both silica gel and Silicalite contain primarily silicon and oxygen although the latter is hydrophobic whereas in the former the surface is rich in SiOH groups and has a large amount of physically adsorbed water. The structure of the aluminosilicate NaX zeolite is composed of a three-dimensional network of relatively large cavities or supercages (~12 Å) connected by 7–8 Å pores or channels (21). The Si/Al ratio of approximately 1.5 results in a large proportion of exchangeable cations (in our case Na) and a strongly hydrophilic zeolite. It should be noted that TPA can easily fit within the pore structure of silica gel and the channel system of NaX. However, the relatively small channels of Silicalite result in adsorption of TPA only on the external surface, although the diphenylmethyl radicals may migrate into the channels. For all three supports the external surface is a small fraction of the internal pore or channel surfaces. Ground-state spectra for tetraphenylacetone on the three solids were similar to that in methanol and showed a clearly defined n,π^* band at ~300 nm, which was only slightly broader than that in solution.

The transient experiments for diphenylmethyl radicals on each of the solid supports are discussed separately below. In each case the radicals were generated by 266 nm pulsed laser irradiation of TPA contained at 1–3% (w/w) on the various supports. Unless otherwise stated, all experiments were carried out under a nitrogen atmosphere.

Silica gel

Figure 1 illustrates two time-resolved diffuse reflectance traces obtained from a sample of TPA (1% w/w) on silica gel under nitrogen. The acquisition conditions for these two traces differ only in the time scale monitored, i.e., 0.1 and 1.6 μs per point (tpp) for decay traces of 250 points. It is apparent that the first half-life, as obtained from $\Delta J/J_0$, is much shorter than the second half-life, which is shorter than the third half-life, etc. Also, when the acquisition rate is decreased and the values are averaged over a much longer time, very rapid information may be lost, yielding an artificially low initial value of $\Delta J/J_0$. Thus, the first half-life measured for trace A for this particular tpp is 2.2 μs while both the initial value of $\Delta J/J_0$ and the first half-life measured from trace B change. Trace B gives a half-life of 7 μs (tpp = 1.6 μs). Even longer lifetimes can be obtained if the starting point of the calculation is delayed in time. Throughout the entire time range monitored the transient spectra retain the characteristic features of the diphenylmethyl radicals expected from the photocleavage of TPA, with $\lambda_{max} \sim 330$ nm and no significant absorptions above 400 nm.[3] Figure 2 (bottom) shows a spectrum obtained at 5 μs following the laser pulse for a 5% sample.

It is rather remarkable that, after the laser experiment, the steady-state diffuse reflectance spectrum of samples exposed to a few tens to a hundred laser shots also reveals the presence of diphenylmethyl radicals. This is illustrated in Fig. 3, which shows difference spectra obtained at various times following the laser exposure; these clearly reveal the presence of the same intermediate produced in the transient experiment, i.e., $Ph_2\dot{C}H$. The half-life under these conditions was approximately 30 min (see insert in Fig. 3), although all indications are that with improved spectral sensitivity and longer recording times, even longer values could be obtained. Even the limited data of Fig. 3 indicate that the long-time data show positive deviations. Similar results were observed for other plots of the same type for the other supports employed in our work. It should be noted that while both Figs. 2 and 3 show difference spectra, the parameter

[3]The absence of absorptions in this region rules out the possible involvement of species such as benzophenone triplets, which show $\lambda_{max} \sim 530$ nm (28).

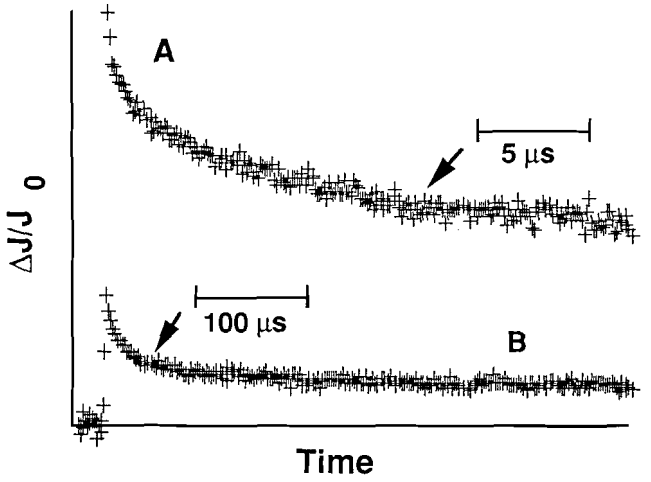

FIG. 1. Transient decay traces monitored at 340 nm on two time scales following 266 nm excitation of a 1% sample of TPA on silica gel.

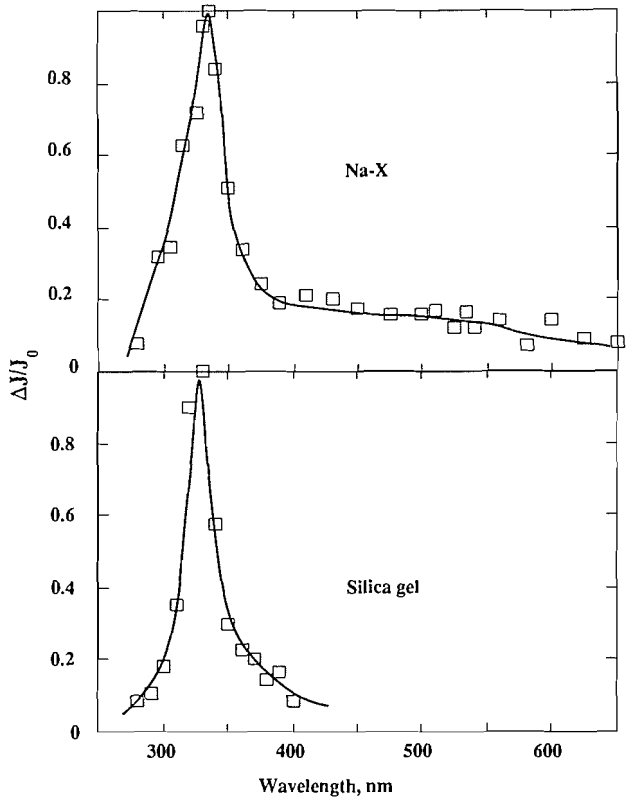

FIG. 2. Transient spectra for diphenylmethyl radicals produced by 266 nm excitation of samples of 5% TPA on NaX (top) and 3% TPA on silica gel. Spectra were recorded 5 and 2 μs after the laser for the silica gel and NaX spectra, respectively.

is not strictly the same for the transient and steady-state spectra. The former reflect spectral differences after and before laser excitation. For the latter (i.e., the steady-state measurements) the difference was calculated between the spectrum at a given time, and at a time arbitrarily defined as "infinite" time. For example, this measurement for Fig. 3 was taken 270 min after the end of the laser irradiation. The two types of measurement would be equivalent if the laser experiment did not induce permanent absorption changes in the spectral region of interest; while this is not strictly the case for any of the supports used, the changes are sufficiently small that the approximation does not invalidate our conclusions.

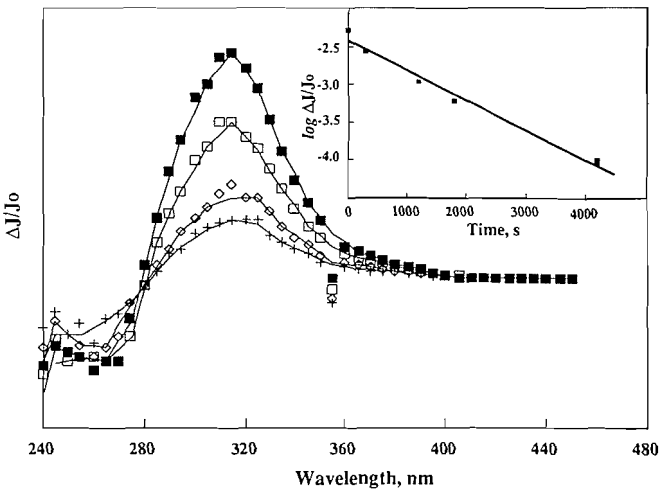

FIG. 3. Difference spectra measured using a UV spectrometer 0 (■), 300 (□), 1200 (◇), and 1800 (+) s after exposure of a 3% TPA on silica gel sample to ~100 laser shots. Insert: plot of log $(\Delta J/J_0)$ as a function of time for the same sample.

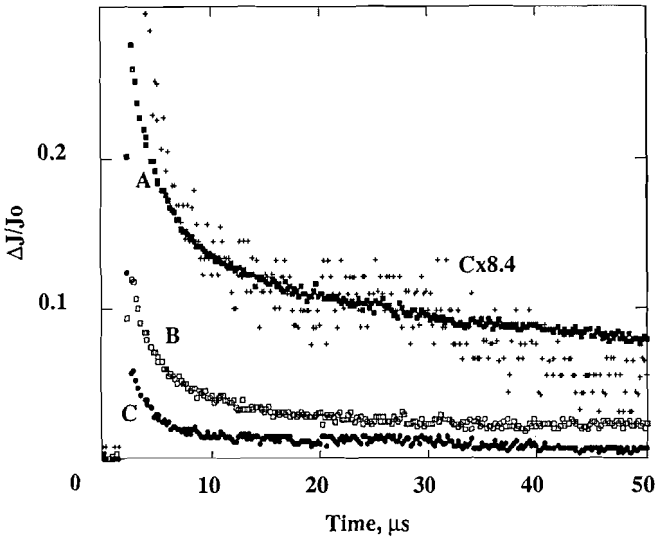

FIG. 4. Transient decay traces monitored at 340 nm following 266 nm excitation of 1% TPA on silica gel using 100% (A,■), 37% (B,□), and 11% (C, • and +) of the full laser intensity.

Studies of the dose dependence of the absorption signals and their decay kinetics were carried out by varying the laser intensity by a factor of ~8. Figure 4 shows representative traces recorded at a tpp of 200 ns for a 1% sample of TPA on silica gel deaerated with nitrogen. Two features of the data are worth noting: the changes in the decay kinetics are minor in comparison with the extensive changes in excitation dose, and the initial absorbance does not fully reflect the changes in laser intensity. The insensitivity of the decay kinetics to the laser intensity indicates that the complex behaviour observed is dominated by pseudo-first-order processes in the time domain examined. However, the fact that the total signal does not fully reflect the laser dose suggests that rapid geminate processes may take place at shorter time scales. It is also possible that light absorption by $Ph_2\dot{C}H$ radicals produced during the early part of the laser pulse also contributes to the attenuation effect mentioned above due to a UV screening effect.

The transient decay traces such as that shown in Fig. 1A can frequently be fitted with a biexponential expression; however,

Can. J. Chem. Downloaded from www.nrcresearchpress.com by 88.85.125.76 on 09/07/12
For personal use only.

Can. J. Chem. Downloaded from www.nrcresearchpress.com by 88.85.125.76 on 09/07/12
For personal use only.

such a treatment is probably of little significance (*vide infra*) and should be regarded simply as a convenient form of analysis that may only be useful in some cases (e.g., when comparing the effects of scavengers within a selected time scale). The results in Figs. 1 and 3 demonstrate that the time domain selected for monitoring plays a key role in determining the observed dynamics. In experiments similar to those in Fig. 1, we recorded half-lives of 0.8 ms and 0.2 s for tpps of 0.9 μs and 100 μs, respectively. The initial signals on the longer time scale were typically about 10% of those recorded in the traces measured at 50–100 ns tpp. This clearly indicates that ~80% of the radicals decay during the first millisecond.

Studies of surface coverage illustrate some of the interesting features of radical decay on surfaces. For example, a comparison of 1 and 3% w/w samples of TPA on a tpp of 0.1 μs show that the initial absorbance is only about 25% higher for the higher coverage. The decay kinetics are similar for the two samples over a range of time scales (0.1–1.0 μs tpp) and in both cases the amount of residual absorption is the same within experimental error. It is possible that at the higher coverage there may be a higher proportion of fast decay processes, which are not observable on our shortest time scale and which tend to deplete a higher fraction of the initial radical concentration for the 3% sample.

Oxygen has a dramatic effect on the transient decay traces for diphenylmethyl radical on silica gel. The initial optical absorption decreases between 20 and 50% with respect to that observed under nitrogen for both short (tpp = 50 ns) and intermediate (tpp = 5 μs) time scales. The effect on the dynamics of radical decay is even more dramatic. Figure 5 shows decay traces under oxygen and nitrogen; these were recorded on time scales that differ by approximately a factor of three in order to adequately capture the two decay processes. Under oxygen the decay fits reasonably a monoexponential process with a lifetime of 280 ns, although there is some residual absorption (~20%). This residual and the fact that some radicals persist for very long times (*vide supra*) suggest the presence of a limited number of highly protected sites. In addition, the variations in amplitude in the presence of nitrogen, air, and oxygen suggest that even faster processes than those monitored for tpp < 20 ns may account for some of the loss of signal in the presence of oxygen. Note, for example, that the amplitude is higher under nitrogen despite the longer acquisition times.

Our results also indicate that sequential two-photon processes may play a role in the very early phenomena observed upon laser excitation. Specifically, in the 530 nm region we detect a short-lived emission that is readily characterized as due to excited $Ph_2\dot{C}H$ produced by photoexcitation of $Ph_2\dot{C}H$ formed during the early part of the laser pulse. The lifetimes for this emission ranged from 130 to 170 ns in various samples, corresponding to about one half the lifetime in homogeneous solution (236 ns in methanol) (15). Figure 6 illustrates a typical decay trace and the emission spectrum obtained for a sample containing 5% w/w TPA. The excited radicals probably represent only a small fraction of the radicals present; in solution the decay of excited diphenylmethyl radicals occurs without chemical change. It is not clear if their fate is the same on silica surfaces.

NaX zeolite

In some respects the data obtained for diphenylmethyl radicals in this zeolite are similar to those observed on silica gel. The transient produced upon excitation of TPA on NaX may be readily identified as the diphenylmethyl radical on the basis of its spectrum (Fig. 2). Just as in the case of silica gel, there are no absorption maxima above 400 nm. However, the decay of the radicals occurs less rapidly than on silica gel. For example, Fig. 7 shows decay traces monitored on both 0.1 and 2 μs tpp for a 1% w/w sample; the trace on the longer time scale still shows extensive residual absorption even after 500 μs. When this residual is compared to the maximum signal obtained on the shorter time scale, one can estimate that the residual accounts

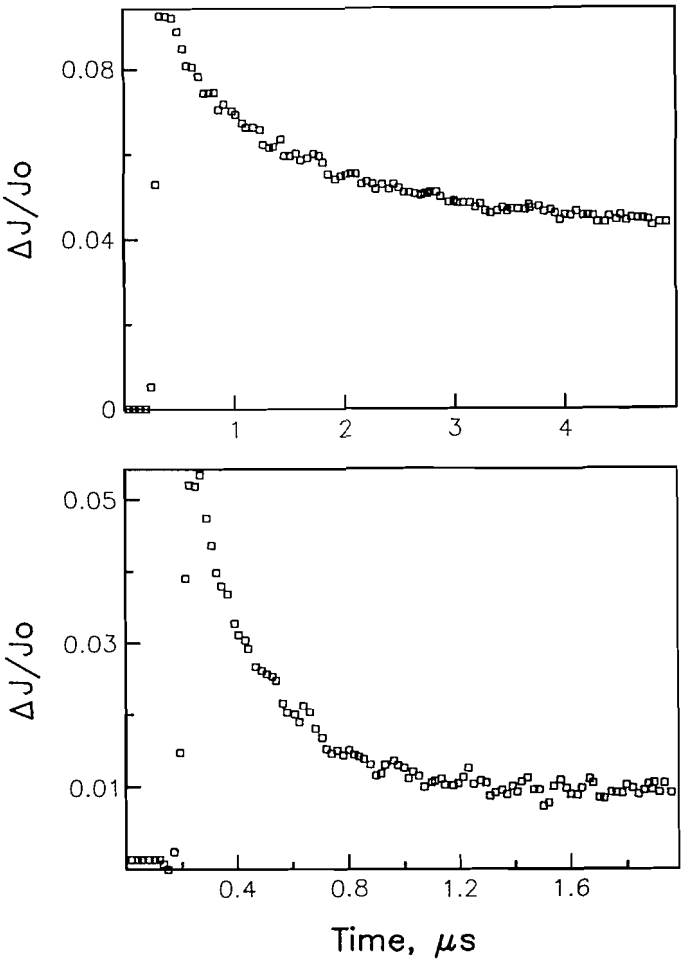

FIG. 5. Transient decay traces monitored at 340 nm for a 3% sample of TPA on silica gel in the presence of nitrogen (top) and oxygen (bottom).

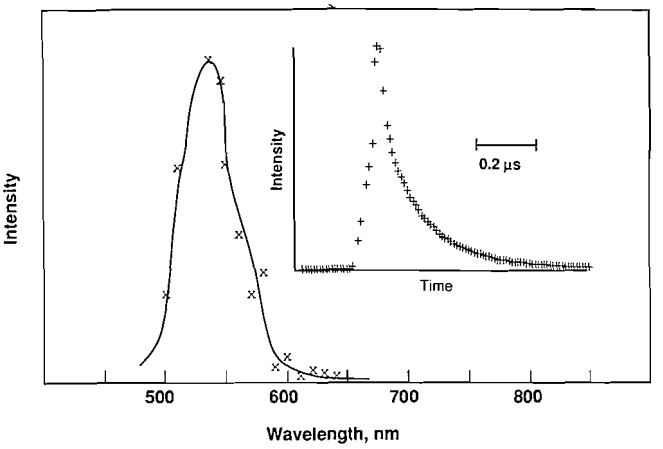

FIG. 6. Emission spectrum for the diphenylmethyl radical obtained by 266 nm excitation of 5% TPA on silica gel. Insert: emission decay trace monitored at 530 nm for the same sample.

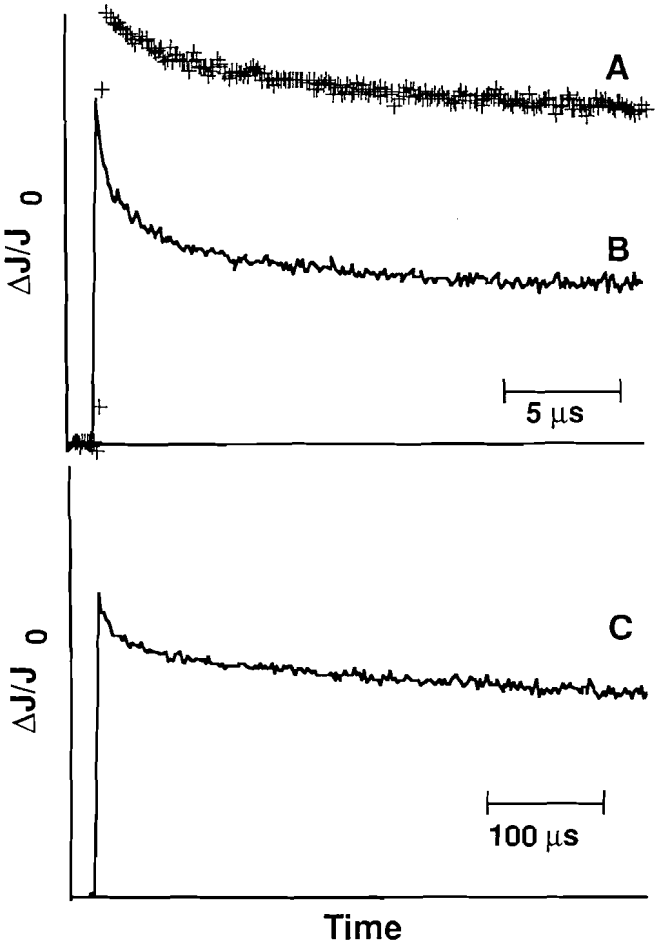

FIG. 7. Transient decay traces monitored at 340 nm following 266 nm excitation of 1% TPA on NaX in the presence of nitrogen (A, C) and oxygen (B). The vertical scale is the same for all three traces.

for 40% of the original signal, i.e., ~3% times that obtained on silica gel. The somewhat higher initial signals for the NaX samples and the slower decays suggest that in this case there are probably fewer radicals decaying on shorter time scales than those we can conveniently monitor.

Ground-state diffuse reflectance studies similar to those already described for silica gel show that the residual absorption also corresponds to the diphenylmethyl radical. These experiments lead to lifetimes of over 30 min, which may be compared to the fact that transient decay traces such as those in the insert of Fig. 6 show that a significant fraction of the initial radicals decay in ~20 μs. This corresponds to a range of time scales of over seven orders of magnitude. As far as we can tell, any time scale within this range will show that a significant fraction of the remaining radicals will decay over the time frame monitored.

The reactivity towards oxygen is considerably lower for diphenylmethyl radicals on NaX as compared to silica gel. Figure 7 shows decay traces recorded on a tpp of 0.1 μs for a sample of 1% TPA on NaX in the presence of nitrogen and oxygen. In the presence of oxygen approximately half of the detectable radicals decay within ~4 μs and the observed decrease in the maximum signal indicates that there are some which decay even more rapidly. Qualitatively similar results are observed for a 3% w/w sample. Despite the fact that some of the radicals react reasonably efficiently with oxygen, the residual absorption indicates that there are others which are very well protected from the quencher. This is further confirmed by

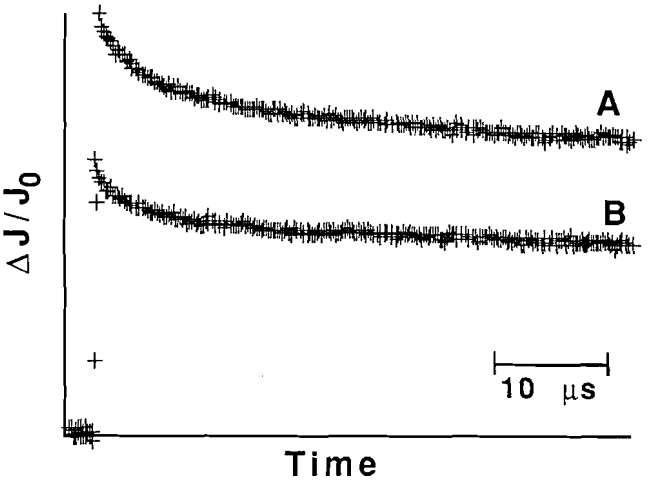

FIG. 8. Transient decay traces monitored at 340 nm following 266 nm excitation of 3% TPA (A) and 1% TPA (B) on NaX.

examining the radical decay under oxygen on longer time scales (1–2 μs tpp). In this case the amount of residual absorption is decreased to approximately one third of what it was under nitrogen but the decay kinetics for the two are very similar. These results suggest that there is a very wide variation in the accessibility of the radicals to oxygen for the NaX samples.

Changes in the load of TPA (1% vs. 3% w/w) show a more pronounced enhancement in the initial signals for the higher load than do those on silica gel. For example, for samples under nitrogen at a tpp of 0.2 μs the ratio of initial signals was ~1.7 for the high/low load. This may be a reflection of the fact that the radicals are longer lived on NaX and there is, therefore, a smaller fraction of radicals that decay on shorter time scales than we can monitor. There may also be contributions due to differences in the light penetration depth for the various supports. As shown in Fig. 8, the two samples showed very similar decay kinetics. The residual absorption was larger for the higher load, although the residuals accounted for similar fractions of the initial signals for both samples.

The effect of laser power on the signals was examined for a 1% w/w sample under nitrogen. Attenuation of the laser by a factor of eight decreased the signal intensity to 34% of its initial value as measured on a tpp of 0.2 μs and there was essentially no change in the decay kinetics or the relative amounts of residual absorption. Very similar results were also obtained on a longer time scale (2 μs tpp).

Silicalite

The transient spectrum for TPA on Silicalite agrees well with that expected for diphenylmethyl radical. In general, the radicals decayed considerably more rapidly on Silicalite than on NaX and there was less residual absorption. This is illustrated in the decay trace for a 3% w/w sample on 0.1 μs tpp shown in Fig. 9. In this system approximately 80% of the radicals decayed within 10–15 μs and the traces gave reasonable fits to a monoexponential decay.

Ground-state diffuse reflectance experiments similar to those described for both silica gel and NaX samples were attempted for Silicalite samples. Although there were certainly changes in the ground-state spectra recorded at increasing delays after the laser irradiation, these were not sufficiently large or reproducible to allow us to positively conclude that we were looking at long-lived diphenylmethyl radicals. The problems with this particular system arise partly from the fact that the lower absorption for these samples results in lower initial radical

Can. J. Chem. Downloaded from www.nrcresearchpress.com by 88.85.125.76 on 09/07/12
For personal use only.

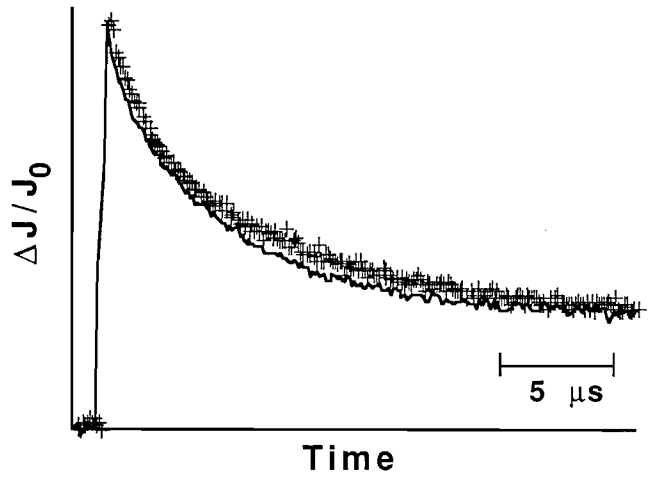

FIG. 9. Transient decay traces monitored at 340 nm following 266 nm excitation of 3% TPA on Silicalite in the presence of nitrogen (+) and oxygen (−).

concentrations and partly from the more rapid deterioration of the samples at high laser doses.

Loading effects were also examined for Silicalite samples. The ratio of initial signals on a tpp of 0.1 μs was ~2.5 for 2.5%/0.6% samples. However, the decay kinetics were identical for the two samples. Similarly, there was very little effect of oxygen on the decay of the radicals on a tpp of 0.1 μs (Fig. 9), although for some samples there were small changes in the amounts of initial signals. These results are in sharp contrast to the oxygen effects on silica gel where very efficient quenching was observed, and suggest that the diphenylmethyl radicals move into the Silicalite channels where they are well protected from oxygen.

Attenuation of the laser dose leads to results similar to those already discussed for silica gel and NaX. That is, there was no change in the decay of the radicals and the maximum signal decreased to 38% of its initial value for an eightfold decrease in laser dose.

Product studies

Laser excitation (266 nm) of TPA on silica gel gave 1,1,2,2-tetraphenylethane as the main product along with trace amounts of benzophenone. The high yield of the radical dimer is the anticipated result based on the solution behavior of diphenylmethyl radicals. To carry out experiments at higher conversions under relatively simple irradiation conditions, we carried out a series of lamp irradiations for TPA on all three supports. To our surprise, the products extracted from a photolysed sample on silica gel showed approximately equal amounts of benzophenone and tetraphenylethane, whereas on NaX the benzophenone accounted for only 20–30% of the isolated products.[4] In contrast, photolysis of TPA on Silicalite yielded very little benzophenone.

Several experiments were carried out to test for the involvement of water and oxygen in the production of benzophenone in the lamp irradiations. Firstly, matched samples of TPA (1%) on each of the three supports were degassed and then had either nitrogen or oxygen added. The product mixtures extracted after irradiation showed similar amounts of benzophenone and tetraphenylethane for the two samples under nitrogen and oxygen for each of the supports. Secondly, a sample of the ketone on silica gel was prepared using silica gel that had been dried and then stored under dry conditions. The sample was then equilibrated with water-^{18}O as described in the experimental section and irradiated. Based on GC/MS analysis of the extracted products, there was no evidence for the incorporation of ^{18}O in the recovered benzophenone. These experiments indicate that neither oxygen or water present in the sample during the photolysis is responsible for the isolation of benzophenone from the irradiated samples. At this point the only other possibilities which come to mind are the incorporation of oxygen from the surface itself or during the extraction procedure. The former seems very unlikely; the latter possibility would require the presence of a stable intermediate, which reacts during the extraction procedure but is not sensitive to water or oxygen present during the photolysis. Additional experiments are obviously necessary to identify the source of this unexpected formation of benzophenone. However, the products in the laser irradiation give us confidence that this unusual reaction of diphenylmethyl radicals is of minor importance under the conditions of our transient experiments.

Conclusions and suggestions for improved kinetic analysis

The above results demonstrate that diphenylmethyl radicals may be readily generated on silica gel, and on the zeolites NaX and Silicalite. Table 1 summarizes the data obtained for the three supports under a variety of conditions of loading, degassing, and laser intensity. The diphenylmethyl radicals show a very wide range of lifetimes on all three supports, as evidenced by the fact that one can obtain lifetimes of anywhere from several microseconds to minutes. Furthermore, for some of the samples there are probably radicals that are decaying on shorter time scales than we can monitor. These results suggest that there are a wide range of possible sites or environments for the radicals. It should be noted that these may reflect largely the distribution of the radicals with respect to each other and the starting ketone rather than particular surface sites on which the radicals are particularly stable. For the surface loadings that have been examined in these experiments, we do not see any evidence for preferential filling of particular sites at low loadings. Neither do we see attenuation effects that can be attributed to the dominance of second-order components in the decay of the radicals. A lengthening of the transient lifetimes would have been expected if radical–radical coupling involving diffusion of both partners was determining the transient lifetime. However, we note that the product studies indicate that the radical dimer accounts for most of the products for the laser irradiations. It is likely that a large fraction of the radicals decay very rapidly via dimerization and are invisible in our transient experiments.

Our results for the three supports indicate that diphenylmethyl radicals have substantially longer lifetimes on NaX than on silica gel or Silicalite. Even more striking differences are observed between the three supports in the oxygen quenching experiments. The radicals are very well protected from oxygen within the channel structure of Silicalite but are rapidly quenched by oxygen on silica gel. This is consistent with the much larger pores in the silica gel structure, which should allow ready access of oxygen to most of the available surface area. The intermediate size of the cages and channels in NaX results in behavior that is intermediate between that of silica gel and Silicalite.

It is clear from the preceding discussion that at the present time we lack a good model that would allow us to interpret the kinetic behavior of free radicals on nonreactive surfaces.

[4]We emphasize that benzophenone is an important product *only* under lamp irradiation. Under laser excitation only traces of benzophenone are detected.

Can. J. Chem. Downloaded from www.nrcresearchpress.com by 88.85.125.76 on 09/07/12
For personal use only.

Can. J. Chem. Downloaded from www.nrcresearchpress.com by 88.85.125.76 on 09/07/12
For personal use only.

TABLE 1. Summary of results

Effect	Silica gel	NaX	Silicalite
Absorption sites	Surface/pores (60 Å)	Cavities ca. 12 Å Channels ca. 8 Å	Surface for TPA, surface + channels for radicals
Initial (100 ns) signal ($\Delta J/J_0$)	High	Highest	Low
Decay fraction 0.2 μs ⇒ 100 μs	~85%	≤50%	>80%
Long-lived radicals (minutes) detected	Yes	Yes	Possibly
Decrease of laser dose of 8:1	Load 1%; tpp 0.2 μs	Load 1%; tpp 0.2 μs	Load 0.6%; tpp 0.2 μs
on ($\Delta J/J_0$)	1:0.2	1:0.34	1:0.38
on kinetics	Minor	Minor	Minor
Reduce load by 3			
on ($\Delta J/J_0$)	1.3:1	1.7:1	2.5:1
on kinetics	Similar	Very similar	Identical
Oxygen effect			
on ($\Delta J/J_0$)	20–50% decrease	<20%	Small decrease
on kinetics	1st order with τ of 280 ns and 20% residual	50% decay in 4 μs, the rest well protected; decay complex	no effect for tpp 0.1 μs, decay as under nitrogen
Excited radical detected?	Yes		

First- and second-order kinetic analyses, as well as various combinations of these, fail to provide a good versatile model suitable for the interpretation of data obtained over a wide range of time scales. This situation is neither new, nor specific to free radicals; for example, in the case of xanthone triplets on Silicalite (13), we obtained traces on time scales differing by a factor of 1000, which in spite of this look remarkably similar. While the simple approach of earlier sections is useful in comparing specific effects (oxygen, loading, laser dose), it cannot offer a detailed understanding of the system. Quite clearly, our data emphasize the need for a better model.

In the last few years dispersive kinetic analysis has provided a solid basis for understanding some complex kinetic problems in solid systems (22–27), notably, the decay kinetics of methyl radicals in methanol glasses (23–27). This analysis assumes a distribution of rate constants for decay; detailed models are available for a Gaussian distribution of exponential decays. This analysis leads to the conclusion that a plot of (signal) vs. log (time) should give a smooth sigmoid curve, from which it is possible to determine the *most probable rate constant* (at the peak of the distribution) as well as the width of the distribution; the former is obtained directly from the inflection point of the plot mentioned above. While keeping in mind the mechanistic differences between our system and that for which the model was developed, we tried a similar representation. This is illustrated in Fig. 10 for TPA on silica gel under nitrogen (top) and TPA on NaX (bottom) in the absence and presence of oxygen.[5] A polynomial fit of these curves indicates inflection

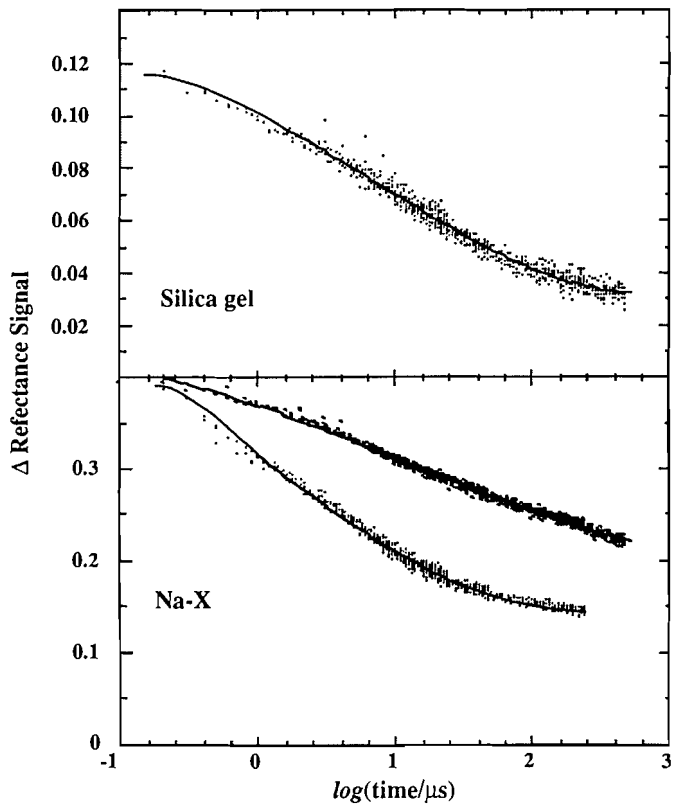

FIG. 10. Decay of diphenylmethyl radicals on silica gel under nitrogen (top) and in NaX under nitrogen (bottom, upper trace) and oxygen (bottom, lower trace), plotted following the format employed for dispersive kinetics analysis (see text). Four or five traces on different time scales were combined in each case by normalizing in the time range where they overlap.

[5]To obtain the data in Fig. 10 it is necessary to combine traces obtained in different, but overlapping, time scales. To do this the traces were normalized in the overlap region, since variations of the laser dose from shot to shot tend to cause some vertical displacements. This normalization required multipliers in the 0.86–1.26 range.

points at 7.3, 10.5, and 0.97 μs for silica gel (N_2), NaX (N_2), and NaX (O_2), respectively. Clearly, oxygen reduces dramatically the most probable value of the lifetime; in addition, the corresponding curve shows a clear break after the first 60% of the decay is complete. This suggests that under oxygen there are at least two distributions of lifetimes, indicating that some radicals are better protected than others.

In summary, it would appear that a model based on dispersive kinetics can probably be adapted to the understanding of radical self-reactions on solid supports. At this point, three advances are needed before a proper quantitative analysis can be performed: (i) an adequate mathematical model; (ii) an improvement in the time resolution of the experiment, so that the early part of the decay can be monitored in more detail; and (iii) temperature dependence capabilities in the diffuse reflectance measurements. These problems are currently being addressed.

Acknowledgements

The travel required to carry out the experiments reported herein was funded by NATO grant 372/84 and this support is gratefully acknowledged.

1. N. J. TURRO. Pure Appl. Chem. **58**, 1219 (1986).
2. N. J. TURRO. Tetrahedron, **43**, 1589 (1987).
3. P. DE MAYO. Pure Appl. Chem. **54**, 1623 (1982).
4. B. FREDERICK, L. J. JOHNSTON, P. DE MAYO, and S. K. WONG. Can. J. Chem. **62**, 403 (1984).
5. R. W. KESSLER and F. WILKINSON. J. Chem. Soc. Faraday Trans. I, **77**, 309 (1981).
6. R. W. KESSLER, G. KRABICHLER, S. UHL, D. OELKRUG, W. P. HAGAN, J. HYSLOP, and F. WILKINSON. Opt. Acta, **30**, 1099 (1983).
7. F. WILKINSON and C. J. WILLSHER. Tetrahedron, **43**, 1197 (1987).
8. F. WILKINSON and G. KELLY. Handbook of organic photochemistry. Vol. I. *Edited by* J. C. Scaiano. CRC Press, Boca Raton, FL. 1989. Chap. 12.
9. F. WILKINSON and C. J. WILLSHER. Chem. Phys. Lett. **104**, 272 (1984).
10. F. WILKINSON and C. J. WILLSHER. Appl. Spectrosc. **38**, 897 (1984).
11. N. J. TURRO, M. B. ZIMMT, and I. R. GOULD. J. Am. Chem. Soc. **107**, 5826 (1985).
12. N. J. TURRO, I. R. GOULD, M. B. ZIMMT, and C.-C. CHENG. Chem. Phys. Lett. **119**, 484 (1985).
13. F. WILKINSON, C. J. WILLSHER, H. L. CASAL, L. J. JOHNSTON, and J. C. SCAIANO. Can. J. Chem. **64**, 539 (1986).
14. D. OELKRUG, G. KRABICHLER, W. HONNEN, F. WILKINSON, and C. J. WILLSHER. J. Phys. Chem. **92**, 3589 (1988).
15. J. C. SCAIANO, M. TANNER, and D. WEIR. J. Am. Chem. Soc. **107**, 4396 (1985).
16. D. O. DEAN, W. B. DICKINSON, O. R. QUAYLE, and C. T. LESTER. J. Am. Chem. Soc. **72**, 1740 (1950).
17. F. GESSNER, A. OLEA, J. H. LOBAUGH, L. J. JOHNSTON, and J. C. SCAIANO. J. Org. Chem. **54**, 259 (1989).
18. D. OELKRUG, W. HONNEN, F. WILKINSON, and C. J. WILLSHER. J. Chem. Soc. Faraday Trans. 2, **83**, 2081 (1987).
19. I. R. GOULD, B. H. BARETZ, and N. J. TURRO. J. Phys. Chem. **91**, 925 (1987).
20. E. M. FLANIGEN, J. M. BENNETT, R. W. GROSE, J. P. COHEN, R. L. PATTON, R. M. KIRCHENER, and J. V. SMITH. Nature, **271**, 512 (1978).
21. W. J. LEIGH and L. J. JOHNSTON. Handbook of organic photochemistry. Vol. II. *Edited by* J. C. Scaiano. CRC Press, Boca Raton, FL. 1989. Chap. 22.
22. W. J. ALBERRY, P. N. BARTLETT, C. P. WILDE, and J. R. DARWENT. J. Am. Chem. Soc. **107**, 1854 (1985).
23. T. DOBA, K. U. INGOLD, W. SIEBRAND, and T. A. WILDMAN. Faraday Discuss. Chem. Soc. **78**, 175 (1984).
24. T. DOBA, K. U. INGOLD, W. SIEBRAND, and T. A. WILDMAN. J. Phys. Chem. **88**, 3165 (1984).
25. T. DOBA, K. U. INGOLD, and W. SIEBRAND. Chem. Phys. Lett. **103**, 339 (1984).
26. T. DOBA, K. U. INGOLD, W. SIEBRAND, and T. A. WILDMAN. Chem. Phys. Lett. **115**, 51 (1985).
27. W. SIEBRAND and T. A. WILDMAN. Acc. Chem. Res. **19**, 238 (1986).
28. I. CARMICHAEL and G. L. HUG. J. Phys. Chem. Ref. Data, **15**, 1 (1986).

Can. J. Chem. Downloaded from www.nrcresearchpress.com by 88.85.125.76 on 09/07/12
For personal use only.

Computer simulation studies of the solvation of oligosaccharides

HELMUT BEIERBECK[1] AND RAYMOND U. LEMIEUX[2]
Department of Chemistry, University of Alberta, Edmonton, Alta., Canada T6G 2G2

Received August 30, 1989

HELMUT BEIERBECK and RAYMOND U. LEMIEUX. Can. J. Chem. **68**, 820 (1990).

Computer simulations of the hydration of the tetrasaccharide αLFuc(1→2)βDGal(1→3)[αLFuc(1→4)]βDGlcNAc-OMe and one of its deoxy derivatives were carried out as a first step toward an understanding of the role of water in the recognition of oligosaccharides by proteins. The model consisted of one solute molecule in one of its low-energy conformations, surrounded by 250 water molecules. The solute–water and water–water interaction energies were evaluated with Clementi's potentials. Ensemble states for the derivation of average properties were generated by Monte Carlo methods. As expected, the strength of interaction between water and the amphiphilic solute was found to be considerably greater at hydrophilic than at hydrophobic sites. Furthermore, the average distance between the solvation shell and the solute surface was about 1 Å greater near hydrophobic than around hydrophilic groups. There is also a definitive alignment of the water dipole around the hydroxyl groups of the saccharide, which is not evident over the hydrophobic regions. Finally, in a parallel investigation the tetrasaccharides were solvated by adding water to the solute at sites of minimum energy of association, in order to explore less-CPU-time-consuming alternatives to Monte Carlo simulations. While the patterns of interaction energies, distances, and dipole orientations were found to be similar to Monte Carlo results, the time savings were not as significant as hoped.

Key words: Monte Carlo simulations, numerical solvation studies, solvation simulations of oligosaccharides, molecular recognition, carbohydrate solvation.

HELMUT BEIERBECK et RAYMOND U. LEMIEUX. Can. J. Chem. **68**, 820 (1990).

Comme première étape vers une compréhension du rôle de l'eau dans la reconnaissance des oligosaccharides par les protéines, on a effectué des simulations par ordinateurs de l'hydratation du tétrasaccharide αLFuc(1→2)βDGal(1→3)[αLFuc(1→4)]βDGlcNAc-OMe ainsi que celle d'un de ses dérivés désoxylés. Le modèle comporte une molécule de soluté, dans l'une de ses conformations de basse énergie et entourée par 250 molécules d'eau. Utilisant des potentiels de Clementi, on a évalué les énergies d'interaction soluté–eau et eau–eau. On a fait appel à des méthodes de Monte Carlo pour générer les états d'ensemble nécessaires pour dériver les propriétés moyennes. Comme on pouvait s'y attendre, on a trouvé que la force de l'interaction entre l'eau et les solutés amphiliques est beaucoup plus importante aux sites hydrophiles plutôt qu'aux sites hydrophobes. De plus, la distance moyenne entre la couche de solvatation et la surface du soluté est environ 1 Å plus grande près des groupes hydrophobes qu'autour des groupes hydrophiles. Il existe aussi un alignement certain du dipôle de l'eau autour des groupements hydroxyles du saccharide; on n'observe pas ce phénomène dans les régions hydrophobes. Enfin, dans le cadre d'une étude parallèle destinée à évaluer des méthodes de calcul alternatives demandant moins de temps de CPU que les simulations de Monte Carlo, on a solvaté des tétrasaccharides par l'addition d'eau au soluté à des sites d'énergie minimale d'association. Alors que les résultats pour les énergies d'interactions, les distances et les orientations dipolaires sont très semblables à celles obtenues à l'aide de simulations de Monte Carlo, le temps de calcul qui est sauvé n'est pas aussi important qu'on l'avait espéré.

Mots clés : simulations de Monte Carlo, études numériques de solvatation, solvatation simulations des oligosaccharides, reconnaissance moléculaire, solvatation du hydrate de carbone.

[Traduit par la revue]

Introduction

The formation in aqueous solution of a complex between an oligosaccharide and a protein is expected to be enthalpy driven as the result of an energetically favorable exchange in molecular partnerships. The changes in intermolecular polar and nonpolar interactions occur not only between the complementary surfaces presented by the oligosaccharide and the protein, but also between the solute surfaces and the solvation shell. Therefore the driving force for molecular association cannot be properly understood without a consideration of the role played by water.

To better appreciate the energetics of molecular recognition we initiated computer simulations of intermolecular interactions, particularly interactions with the solvation shell. We chose for these solvation studies the tetrasaccharide αLFuc (1→2)βDGal(1→3)[αLFuc(1→4)]βDGlcNAc-OMe, or Le^b-OMe (Fig. 1), a carbohydrate related to the determinant of the human Lewis b blood group. Le^b-OMe is one of a number of oligosaccharides whose recognition by lectins and antibodies we have studied (1–8). It is conformationally well defined in aqueous solution and strongly bound ($\Delta G^\circ = -6.3$ kcal/mol at 305 K) by GS4, the readily accessible fourth lectin derived from the African plant *Griffonia simplicifolia*. We were able to identify the key functionalities of Le^b-OMe from the relative potencies of its derivatives, and to propose models for its recognition by the protein receptors. The conclusions from the immunological work on the Le^b-OMe–GS4 system are supported by the strong binding between GS4 and the Y-tetrasaccharide, another human blood group determinant which differs from Le^b-OMe only by the interchange of the substituents at C-3a and C-4a. In aqueous solution these two oligosaccharides have precisely those surface features in common that, according to the immunological data, are recognized by GS4. Another reason for the choice of Le^b-OMe in the computer simulations was the successful crystallization of complexes of Le^b-OMe and derivatives with GS4 (9). The crystal structure of the Le^b-OMe–GS4 complex has recently been established to 2.8 Å resolution (10).

The main approach to the computer analysis of Le^b-OMe solvation consisted of Monte Carlo simulations and ensemble averaging. However, in a second series of calculations low-energy solvation clusters were generated by adding water molecules to the emerging shell at geometries of minimum energy. This was done mainly to see whether information comparable to Monte Carlo results could be obtained at lower

[1]University of Alberta Research Associate, 1987–present.
[2]Author to whom correspondence should be addressed.

Can. J. Chem. Downloaded from www.nrcresearchpress.com by 88.85.125.76 on 09/07/12
For personal use only.

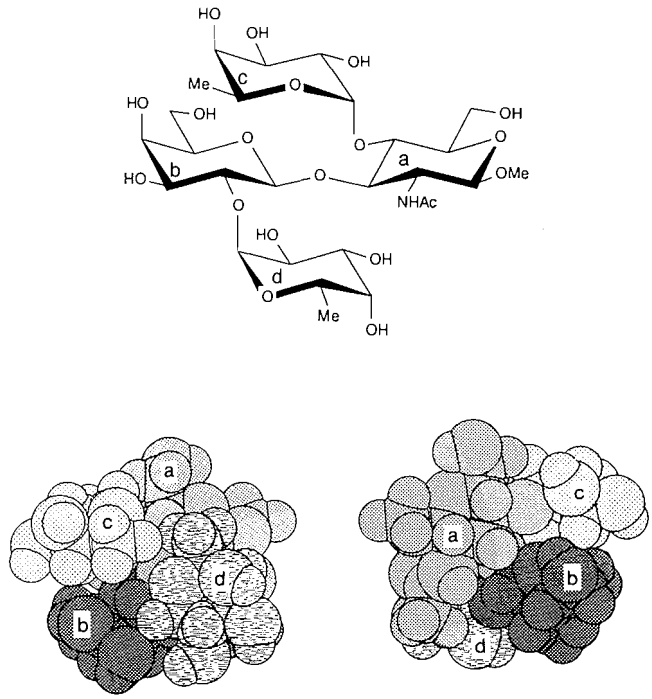

FIG. 1. Structure of the Le^b-OMe tetrasaccharide related to the human Lewis-b blood group determinant, and views of opposite sides of a CPK model of Le^b-OMe.

computing costs. In all cases Clementi's additive potentials for solute–water (11, 12) and water–water (13) interactions were used.

The work described here represents the first stage in an investigation aimed at an appreciation of the differential changes in enthalpy that occur in the binding of Le^b-OMe and its derivatives by GS4.

Methods

The Le^b-OMe coordinates were generated in the usual way from X-ray data for the monosaccharides (14), using the torsion angles about the intersugar glycosidic bonds for the predominant conformation, as determined by ^{1}H NMR interunit deshielding effects and nuclear Overhauser enhancements (8). This same conformation also proved to be an energy minimum in hard sphere *exo*-anomeric (HSEA) calculations (15) and was found to be compatible with the electron density map determined by X-ray diffraction (10). The glycosidic C—O—C valency angles were set to 117° (14).

ϕ^H	ψ^H
H—C-1b—O—C-3a = 55°	C-1b—O—C-3a—H = 10°
H—C-1c—O—C-4a = 55°	C-1c—O—C-4a—H = 25°
H—C-1d—O—C-2b = 45°	C-1d—O—C-2b—H = 15°

Free rotation about all ten hydroxyl groups of Le^b-OMe would give rise to 3^{10} staggered conformations. Based on our immunological results the hydroxyl group orientations on the CPK model shown in Fig. 1 are considered the most likely arrangement in the GS4–Le^b-OMe complex. This will therefore be the reference conformation throughout this presentation, although other Le^b-OMe conformers were also used in the solvation simulations. The bond lengths, 0.9572 Å, and valency angle, 104.5°, for the water molecule were taken from the paper by Benedict *et al.* (16).

The energy of interaction between atom i of the organic solute and atom j of water was calculated with Clementi's three-term expression (11, 12):

$$[1] \quad E_{ij} = -A_{ij}/r_{ij}^6 + B_{ij}/r_{ij}^{12} + C_{ij}q_iq_j/r_{ij}$$

where r_{ij} is the internuclear distance, q_i and q_j are effective nuclear charges, and A_{ij}, B_{ij}, and C_{ij} are constants (see Tables V and VII in ref. 12). There are two sets of constants A, B, and C for every class of solute atoms, i.e., every substitution pattern, one for the interaction with water oxygen atoms and one for hydrogen. The q_i and q_j are the average class charges computed by Fraga (17) from Clementi's quantum-mechanically obtained effective nuclear charges for amino acids (11) and DNA bases (12). These class charges were scaled (17) according to eq. [2]:

$$[2] \quad q_i^{\text{corr}} = q_i\,(1 + cq_i/|q_i|)$$

where

$$c = (q^m - \sum_i q_i)/\sum_i |q_i|$$

in order to arrive at the correct (neutral) molecular charge for Le^b-OMe, $q^m = 0$. The water charges were $q^H = 0.3321$ and $q^O = -0.6642$ esu (18). The average and corrected charges are shown in Table 1, and the class assignments are given in Table 2.

The energy of interaction between two water molecules was calculated with Clementi's expression (13):

$$\begin{aligned}[3] \quad E_{WW} = {} & q^2[(1/r_{13} + 1/r_{23} + 1/r_{14} + 1/r_{24}) + 4/r_{78} \\ & -2(1/r_{18} + 1/r_{28} + 1/r_{37} + 1/r_{47})] + a_1\exp(-b_1r_{56}) \\ & + a_2[\exp(-b_2r_{13}) + \exp(-b_2r_{14}) + \exp(-b_2r_{23}) \\ & \qquad + \exp(-b_2r_{24})] \\ & + a_3[\exp(-b_3r_{16}) + \exp(-b_3r_{26}) + \exp(-b_3r_{35}) \\ & \qquad + \exp(-b_3r_{45})] \\ & - a_4[\exp(-b_4r_{16}) + \exp(-b_4r_{26}) + \exp(-b_4r_{35}) \\ & \qquad + \exp(-b_4r_{45})].\end{aligned}$$

where q^2, a_1–a_4, and b_1–b_4 are constants (see Table VIII, column ϵ_{inter} in ref. 13), the r_{ij} are distances between H, O, and M, and M is a point along the C_{2v} axis of water, 0.26765 Å from oxygen.

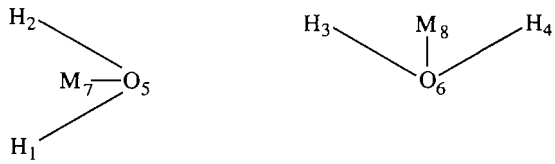

The charges and coefficients for eq. [1] are the result of quantum-mechanical calculations for amino acids and DNA bases. While the assignment for most of the Le^b-OMe atoms presented no problem, no parameters were available for the anomeric carbons. These atoms were therefore assigned to class 18, together with all other oxygenated carbons (Table 2), which is undoubtedly the most questionable of all class assignments. For example, the effective nuclear charges for the anomeric carbons in DNA fragments were calculated to be 0.13–0.14 esu (19), i.e., considerably more positive than 0.008, the net charge for class 18.

Low-energy solvation shells were constructed by adding one water molecule at a time to the growing cluster, at a geometry of minimum energy, i.e., a hydrogen-bonding site. A set of r^2

Can. J. Chem. Downloaded from www.nrcresearchpress.com by 88.85.125.76 on 09/07/12
For personal use only.

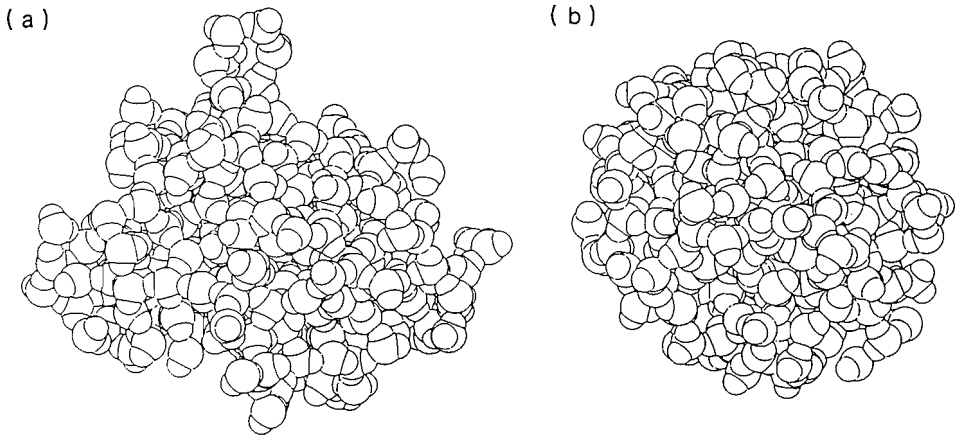

FIG. 2. Solvation cluster consisting of one Le^b-OMe molecule and 250 water molecules, built by adding water at geometries of minimum energy. (a) Cluster generation by water addition at minima of lowest energy led to the formation of local water droplets and arbitrarily shaped hydration shells. (b) Cluster generation by water addition at the innermost energy minima gave uniform coverage of Le^b-OMe.

TABLE 1. Effective charges q and q^{corr}, in esu, for Clementi's atomic classes represented in Le^b-OMe and in 4d-deoxy-Le^b-OMe

Atom type	Class	q	q^{corr} Le^b-OMe	q^{corr} 4d-Deoxy-Le^b-OMe
>N—**H**	1	0.266	0.2697	0.2703
CH, **CH$_2$**	2	0.204	0.2069	0.2073
—C—**H$_3$**	3	0.205	0.2079	0.2083
—O—**H**	4	0.404	0.4097	0.4106
N—**C**=O	5	0.511	0.5182	0.5193
H$_3$C—C	6	−0.608	−0.5995	−0.5981
>**CH$_2$**	7	−0.383	—	−0.3767
>**C**—N	8	−0.135	−0.1331	−0.1328
—**O**—H	9	−0.539	−0.5314	−0.5302
>**C**=**O**	10	−0.409	−0.4033	−0.4023
>**N**—	13	−0.630	−0.6212	−0.6197
>C-**OH**	18	0.008	0.0081	0.0081

random water coordinates (probe locations) was generated, restricted only by the requirement that the oxygen atoms lay on a sphere of radius $r + 3$ from the center of mass of the solute. The radius r was initially the largest distance of any atom from the solute center and was subsequently replaced by the largest distance of any water oxygen atom from the center. A water molecule, the probe, was then placed at each probe location in turn, and that probe was rotated and translated until a probe geometry of minimum energy was reached. The search for the energy minima was carried out by the method of steepest descent (20). When all probe locations were optimized, one of the minima was occupied and that probe geometry was replaced in the probe coordinate set by new random coordinates. If r increased, a corresponding number of new random coordinates was added to the set of probe locations, and the next search cycle was started. Occupation of the geometry of lowest energy resulted in poor coverage, since existing water molecules were solvated in preference to hydrophobic regions of the solute to form clusters of water molecules, as shown in Fig. 2a. A uniform coverage was achieved by picking that geometry instead, which put the water oxygen atom closest to the center of Le^b-OMe, as shown in Fig. 2b. The addition of 250 water molecules gave reasonable coverage of Le^b-OMe (about three water layers, see Fig. 3a) at acceptable computing costs (about one hour on a Cyber 205 computer).

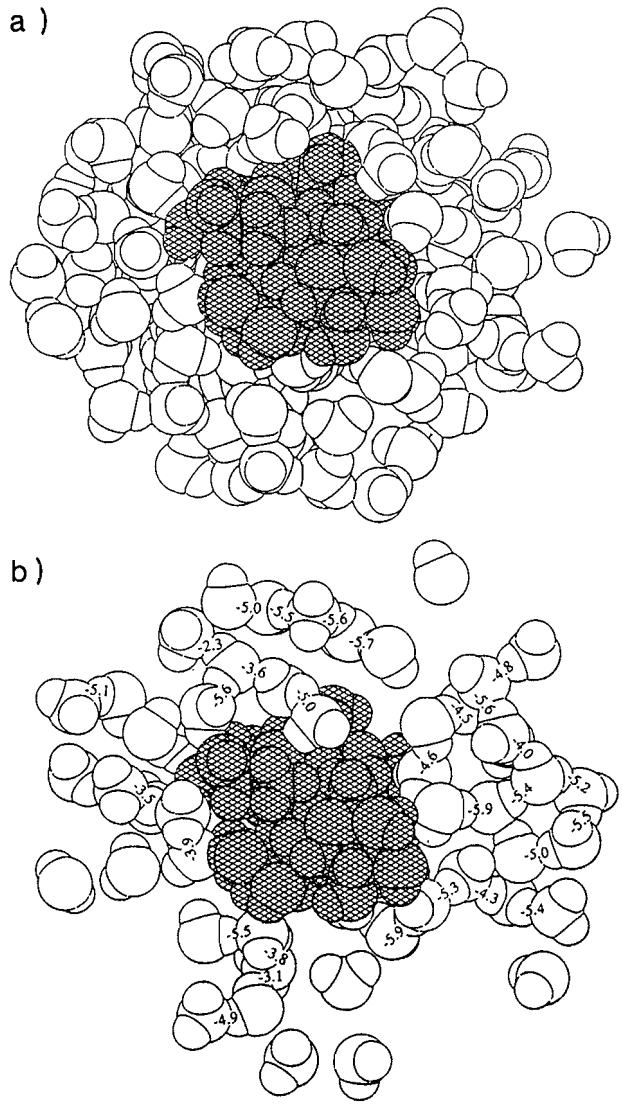

FIG. 3. Cuts through the hydration shell of Fig. 2b. (a) All water molecules in front of the plane through the center of mass of Le^b-OMe were removed to show the thickness of the solvation shell. (b) Hydrogen-bonding networks and energies inside a slice through the shell; the cross section is defined by two planes ±0.5Å to either side of the center of Le^b-OMe. The seemingly isolated molecules are hydrogen bonded to water outside this slice.

Can. J. Chem. Downloaded from www.nrcresearchpress.com by 88.85.125.76 on 09/07/12
For personal use only.

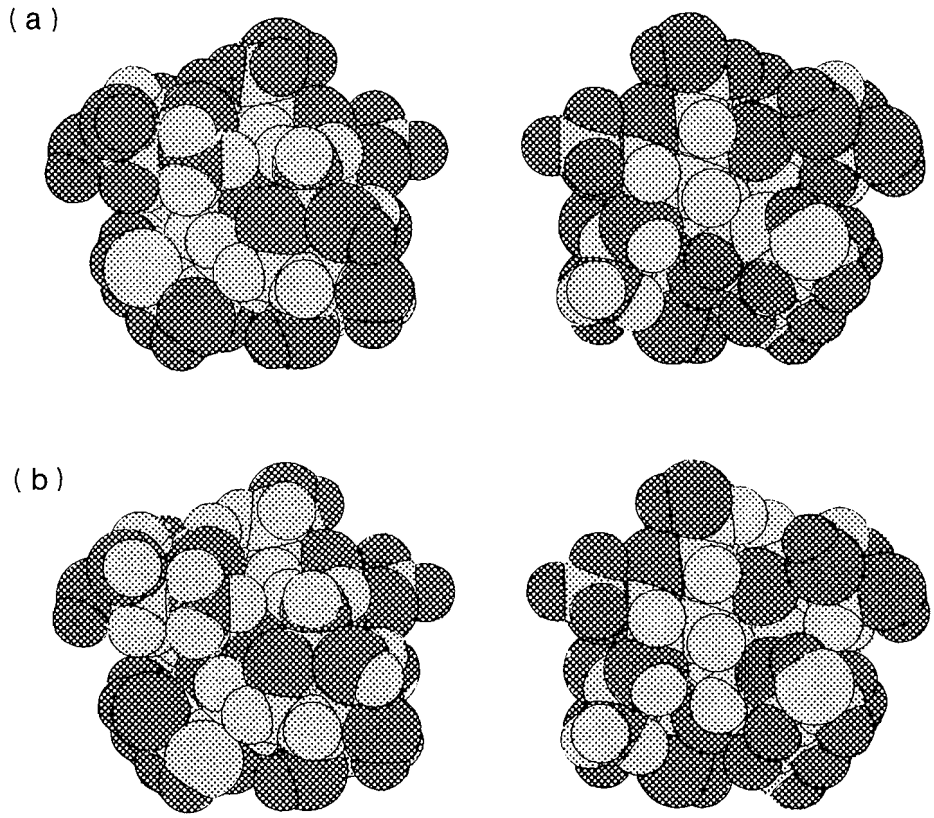

FIG. 4. Energies of interaction between Le^b-OMe atoms and the solvation shell. Atoms with negative interaction energies are darker. (a) Interaction energies for the hydration cluster of Fig. 2b built by the addition of water at innermost minima. (b) Averages over 3000 Monte Carlo sampling cycles. In each cycle every water molecule is moved once.

TABLE 2. Assignment of Le^b-OMe and 4d-deoxy-Le^b-OMe atoms to Clementi's classes[a]

C-1a 18	C-1b 18	C-1c 18	C-1d 18
C-2a 8	C-2b 18	C-2c 18	C-2d 18
C-3a 18	C-3b 18	C-3c 18	C-3d 18
C-4a 18	C-4b 18	C-4c 18	C-4d[b] 18
C-5a 18	C-5b 18	C-5c 18	C-5d 18
C-6a 18	C-6b 18	C-6c 6	C-6d 6
C-7a 5	O-2b 9	O-2c 9	O-2d 9
C-8a 6	O-3b 9	O-3c 9	O-3d 9
C-9a 18	O-4b 9	O-4c 9	O-4d 9
N-2a 13	O-5b 9	O-5c 9	O-5d 9
O-1a 9	O-6b 9		
O-3a 9			
O-4a 9			
O-5a 9			
O-6a 9			
O-7a 10			

[a]Hydrogen class assignments: H—N = 1, CH_3 = 3, HO = 4, all others = 2.
[b]C-4d in 4d-deoxy-Le^b-OMe assigned to class 7.

The Monte Carlo simulations (21, 22) were carried out on solvation clusters consisting of one solute molecule and 250 water molecules, enclosed in a sphere, at unit density and 300 K. The procedure was started either from the low-energy cluster or by randomly adding water molecules to the solute in the spherical enclosure, subject to the constraint that no two atoms approach each other more closely than 90% of the sum of the van der Waals radii. The solute was kept immobile and the water molecules were moved in cycles; in each cycle every water molecule was moved once, in a random sequence. Each move consisted of random translations along, and random rotations about, all three axes by maximally ±0.1 Å and ±0.1 radians, respectively. A move was accepted, i.e., the old water coordinates were replaced, if $\exp(-\Delta E/RT)$ exceeded a random number between 0 and 1, and if the molecule did not penetrate the restraining sphere. If the simulation started from a low-energy cluster, in which case some water molecules usually penetrated the containing sphere, an acceptable move had to fulfil the additional condition that any exterior atom move closer to the sphere. These conditions resulted in the acceptance of about 80% of all moves. The ensemble properties of interest were updated after every move, using either the properties of the new configuration or, if the move was rejected, by using again the old configuration.

Typical Monte Carlo simulations consisted of 500 equilibration and 3000 sampling cycles, i.e., 3000 × 250 different cluster geometries, and required about two hours of Cyber 205 CPU time. Interaction energies between solute atoms and the solvation shell, radial distribution functions for water oxygen, and orientational water correlation functions were calculated.

The radial distribution and orientational correlation functions (23) for water were generated as follows. The space around each solute atom was divided by concentric spheres into intervals of 0.1 Å thickness. Furthermore, a water molecule was considered to be near a given solute atom only if its oxygen atom fell inside a cone of 45° containing the van der Waals sphere of that solute atom and with the cone apex either (X—*H*) on the bond axis or (R—*O*—R′) on the bisector of the valency angle. The radial distribution functions were then constructed by determining the average numbers of water oxygen atoms at the various 0.1 Å intervals from the solute atom. The orientational correlation functions were derived by calculating the average values, for

Can. J. Chem. Downloaded from www.nrcresearchpress.com by 88.85.125.76 on 09/07/12
For personal use only.

Can. J. Chem. Downloaded from www.nrcresearchpress.com by 88.85.125.76 on 09/07/12
For personal use only.

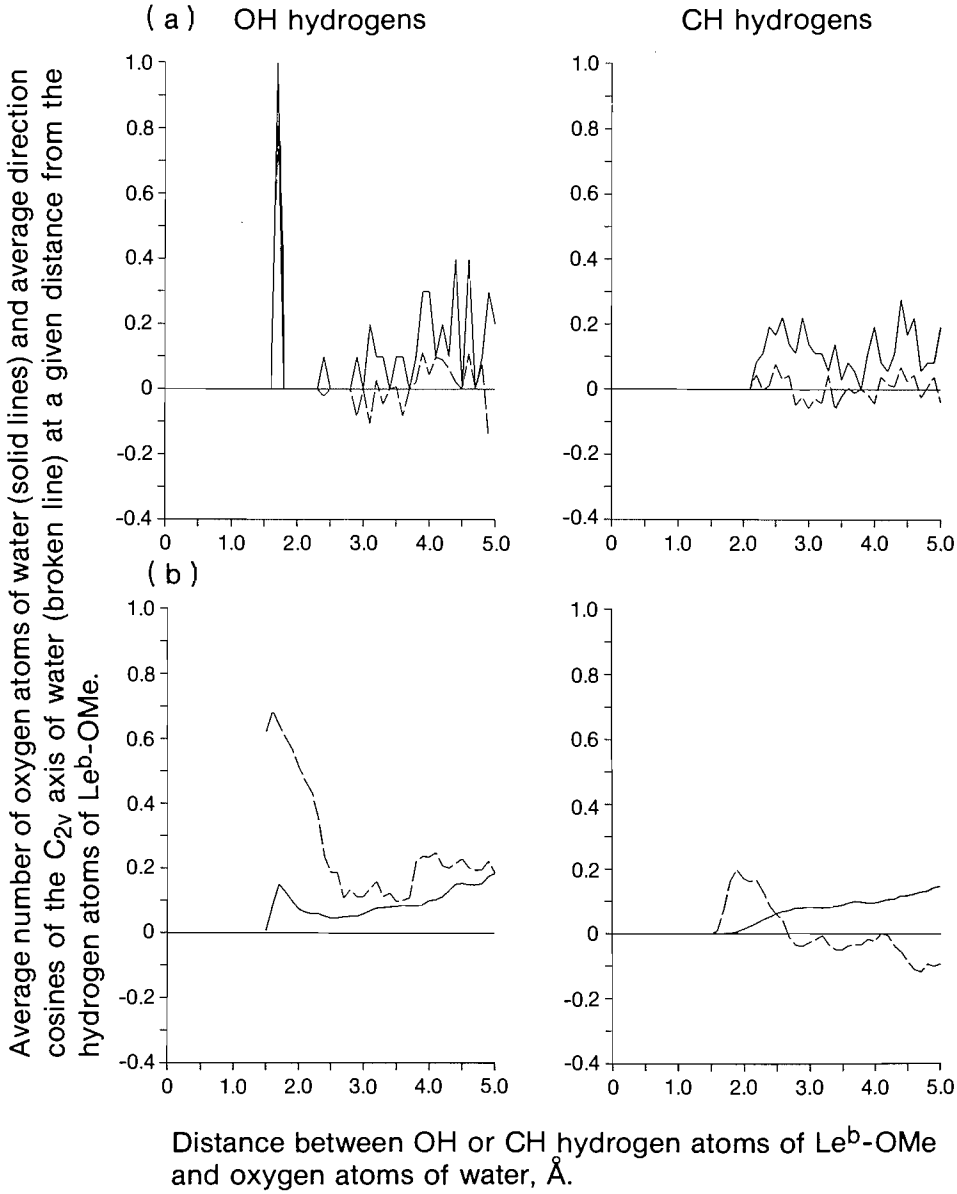

FIG. 5. Average radial distribution functions (solid lines) and orientational correlation functions (broken lines) for the 10 OH and 36 CH hydrogen atoms of Le^b-OMe. The average hydrogen bond distance and angles are H...O ~1.98 Å and ∠O—H...O ~157 (24). (a) The solvation cluster in Fig. 2b. (b) Averages over 3000 Monte Carlo sampling cycles.

each 0.1 Å interval, of the cosines of the angles between the C_{2v} axes of the water molecules and the vectors pointing from the solute atoms to the oxygen atoms of the water molecules.

All programs were written in FORTRAN 77, and the calculations were carried out on the Cyber 205 computer at the University of Calgary.[3]

Results and discussion

The stepwise buildup of a solvation shell by energy minimization was mainly undertaken to see if information comparable to Monte Carlo results could be obtained at significantly lower computing costs. This comparison was one of the reasons for enclosing the solvation cluster in a sphere during the Monte Carlo simulation, rather than using a box with periodic boundary conditions (21, 22). The main reason for choosing a spherical enclosure was the need to eventually apply the procedure to the receptor–Le^b-OMe complex, where periodic boundary conditions are inapplicable. The solvation of Le^b-OMe was, in fact, repeated with the usual boundary conditions and found to give essentially the same interaction energies, water–solute distances, and average water orientations near the solute surface.

The addition of 250 water molecules to Le^b-OMe at geometries of minimum energy resulted in a uniform solvation shell, which provided a complete coverage of the solute (Fig. 2b). As the cut solvent shell in Fig. 3a shows, the cluster consists of about three water layers. The hydrogen-bonding network is evident in a slice through the solvation shell (Fig. 3b). Only those water molecules are shown whose oxygen nuclei are within ±0.5 Å of a plane through the center of mass of Le^b-OMe. Some of the energies of hydrogen bonding within the cross section are indicated in the figure. The bonding energies to water molecules outside this slice are of the same magnitude. Solute–solvent interaction energies, radial distribution functions, and orientational correlation functions for low-energy and

[3]A copy of the computer programs may be purchased from the Depository of Unpublished Data, CISTI, National Research Council of Canada, Ottawa, Ont., Canada K1A 0S2.

Can. J. Chem. Downloaded from www.nrcresearchpress.com by 88.85.125.76 on 09/07/12
For personal use only.

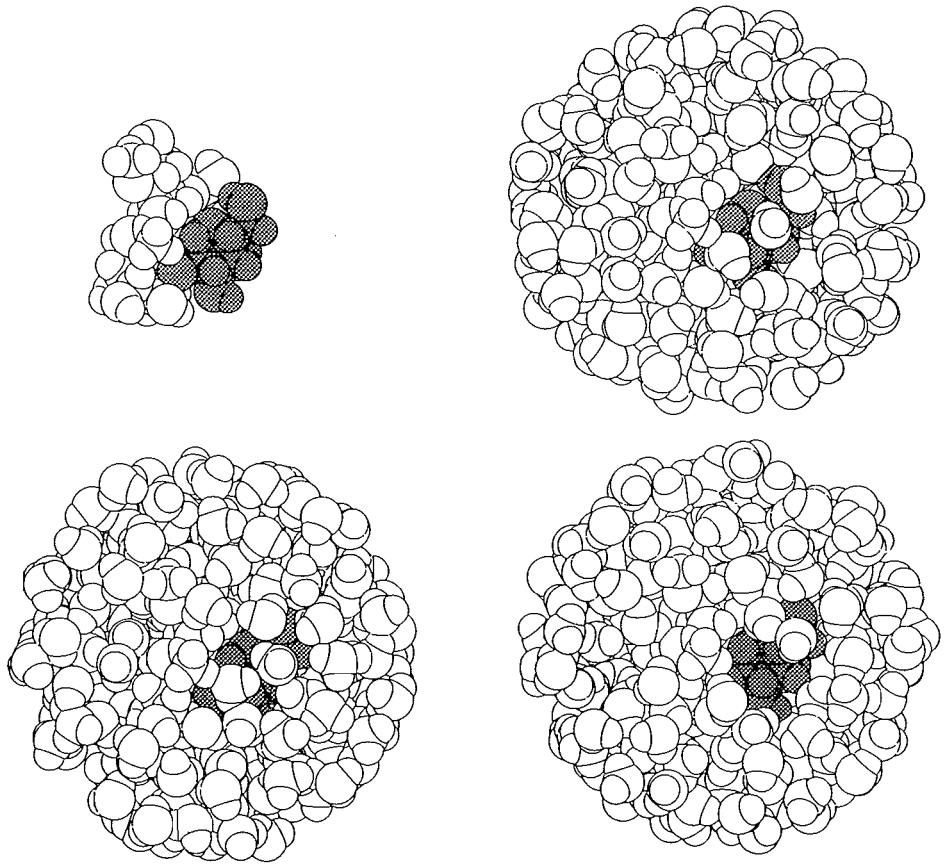

FIG. 6. CPK models of Le^b-OMe and the solvation cluster after 1000 (top right), 2000 (bottom left), and 3000 Monte Carlo sampling cycles, cut to show the extent of hydration of the hydrophobic region of the galactose. H-1b, H-3b, and H-5b are in the plane of the paper, and water molecules entirely in front of a plane 3 Å from these hydrogen nuclei are removed.

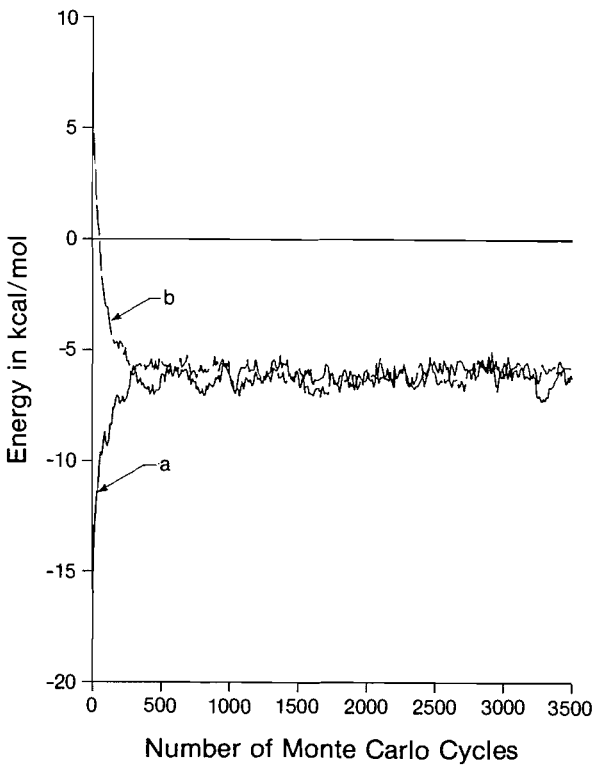

FIG. 7. Convergence of the average energy of interaction between a water molecule and the rest of the Le^b-OMe solvation cluster to the ensemble average, starting from (a) low-energy and (b) random configurations, respectively.

Monte Carlo clusters are compared in Figs. 4 and 5. Figure 4 shows CPK models of Le^b-OMe in which negative energies of interaction between individual solute atoms and the complete solvation shell are identified by dark shading, and positive interaction energies are indicated by light shading. These patterns map out the hydrophilic and hydrophobic surface areas of Le^b-OMe and, as a comparison of Figs. 4a and 4b shows, the distribution of attractive and repulsive interactions is quite similar for the low-energy cluster and the Monte Carlo averages.

Figure 5 shows radial distribution functions (RDFs) and orientational correlation functions (OCFs) for the low-energy (5a) and Monte Carlo (5b) solvation clusters of Le^b-OMe. The hydrophilic and hydrophobic RDFs and OCFs for the low-energy cluster are averages for all O-H and C-H protons in Le^b-OMe, respectively, whereas the corresponding functions for the Monte Carlo cluster are additionally averaged over all sampled states of the solvation shell. In the case of the low-energy cluster, the functions for the hydrophilic protons show sharp peaks at the hydrogen bonding distance (ca. 1.7–1.8 Å), with indistinct features at distances corresponding to second and higher solvation shells. The water molecules are tightly held by the hydroxyl groups of Le^b-OMe and are aligned such that oxygen points toward the solute and the hydrogens into water. The average hydrogen-bonding distances and angles are H...O ~1.98 Å and ∠ O—H... ~157°, from neutron diffraction data for crystalline hydrates (24). The first maximum of the RDF for the hydrophobic hydrogens is not nearly as well defined. The interactions are weaker and often repulsive (Fig. 4), and consequently there is no strongly preferred internuclear distance or water dipole orientation.

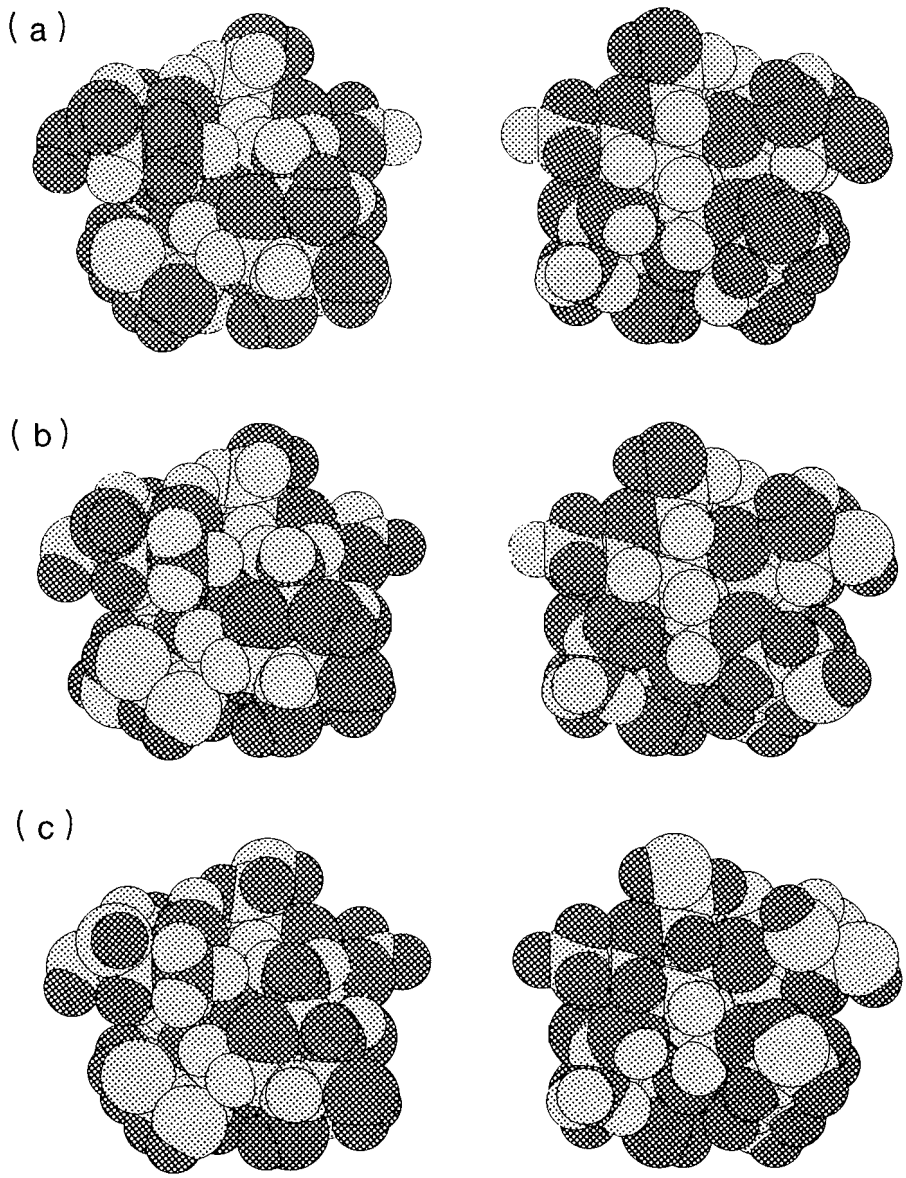

FIG. 8. Energies of interaction between solute atoms and the solvation shell. Atoms with negative interaction energies are darker. (a) Le^b-OMe, differing from the reference conformation in Fig. 1 by rotation about the C-4d—O-4d bond. (b) Le^b-OMe after rotation about bonds C-5b—C-6b and C-6b—O-6b. (c) 4d-Deoxy-Le^b-OMe in the Le^b-OMe reference conformation of Fig. 1.

The RDFs and OCFs from the Monte Carlo simulation show the same trends. For hydrophilic hydrogens the optimal hydrogen-bond length is again the preferred solute–solvent distance, with strongly aligned water dipoles. Near hydrophobic hydrogens, on the other hand, the distance and orientation of the first solvation shell are much less critical. On average, water is about 1 Å further from hydrophobic surface areas than from hydrophilic groups.

That there are voids between the solvation shell and the hydrophobic regions of Le^b-OMe may also be demonstrated by stripping away the solvation shell. For example, if after 1000, 2000, and 3000 Monte Carlo sampling cycles the solvation shell was cut 3 Å from the plane defined by H1b, H3b, and H5b, these three hydrogens were all visible to varying degrees (Fig. 6).

While the results from the low-energy solvation clusters agree satisfactorily with the Monte Carlo simulations, the savings in computing cost were not as significant as hoped, and the stepwise addition of water at minimum energy was abandoned. The low-energy cluster served, however, as a useful test for the convergence of the Monte Carlo simulation to equilibrium (Fig. 7).

Figure 8 shows the patterns of attractive (dark shading) and repulsive (light shading) energies of interaction between solute atoms and the solvation shell, for two slightly different conformers and the 4d-deoxy derivative of Le^b-OMe. The only qualitative change of significance occurs at C-4d of 4d-deoxy-Le^b-OMe, which now falls into a different atomic class. The changes in interaction energies with water on bond rotation are quantitative and essentially restricted to the hydroxyl group closest to the site of conformational change. On rotation about C-4d—O-4d the energy of interaction with the solvation shell increases for O-4d and decreases for HO-4d, without significantly altering the radial distribution functions or orientational correlation function for that hydroxyl group. On rotation about C-5b—C-6b and C-6b—O-6b the same quantitative shift is observed at the hydroxyl group on C-6b.

Can. J. Chem. Downloaded from www.nrcresearchpress.com by 88.85.125.76 on 09/07/12
For personal use only.

In summary, the solvation of a tetrasaccharide was computer simulated in two ways, first by building a hydration cluster by water addition at sites of minimum energy, and then by Monte Carlo determinations of ensemble averages over time. The static and dynamic procedures generated essentially the same picture of the distribution and extent of hydrophilic and hydrophobic surface areas. Both methods also showed that there is a strong alignment of the water dipoles around hydrogen-bonding substituents on the oligosaccharide. Finally, the solvation shell was found to be on average about 1 Å further from the lipophilic than from the hydrophilic surface portions, regardless of the orientations of the H—O bonds of Le^b-OMe. This finding supports the earlier expectation (25) that an important contribution to the driving force for complexation is the filling of these voids through the association of complementary surfaces, and, indeed, was the main reason for initiating these studies. Consequently, similar studies of the solvation of the receptor on the protein are planned, once the X-ray structure determination of the GS4—Le^b-OMe complex is completed at the highest resolution that can be achieved. Together these results should afford a much improved appreciation of the role of water in the recognition of oligosaccharides by proteins.

Acknowledgments

This research was supported by an operational grant for research to R.U.L. by the Natural Sciences and Engineering Research Council of Canada (A170). We thank the Supercomputer Allocation Committee of the University of Alberta for generous access to the Cyber 205 computer at the University of Calgary. We are deeply grateful for the opportunity thus granted to explore this approach to the understanding of molecular recognition. We also wish to acknowledge helpful discussions with Professor S. Fraga.

1. R. U. Lemieux, T. C. Wong, J. Liao, and E. A. Kabat. Mol. Immunol. **21**, 751 (1984).
2. U. Spohr, O. Hindsgaul, and R. U. Lemieux. Can. J. Chem. **63**, 2644 (1985).
3. O. Hindsgaul, D. P. Khare, M. Bach, and R. U. Lemieux. Can. J. Chem. **63**, 2653 (1985).
4. U. Spohr, N. Morishima, O. Hindsgaul, and R. U. Lemieux. Can. J. Chem. **63**, 2659 (1985).
5. R. U. Lemieux, A. P. Venot, U. Spohr, P. Bird, G. Mandal, N. Morishima, O. Hindsgaul, and D. R. Bundle. Can. J. Chem. **63**, 2664 (1985).
6. R. U. Lemieux, O. Hindsgaul, P. Bird, S. Narashiman, and W. W. Young, Jr. Carbohydr. Res. **178**, 293 (1988).
7. U. Spohr and R. U. Lemieux. Carbohydr. Res. **174**, 211 (1988).
8. R. U. Lemieux, R. Cromer, and U. Spohr. Can. J. Chem. **66**, 3083 (1988).
9. M. Vandonselaar, L. T. J. Delbaere, U. Spohr, and R. U. Lemieux. J. Biol. Chem. **262**, 10848 (1987).
10. L. T. J. Delbaere, M. Vandonselaar, L. Prasad, J. W. Quail, U. Spohr, and R. U. Lemieux. American Crystallographic Association, Abstract of Papers, **17**, V5 (1989).
11. E. Clementi, F. Cavallone, and R. Scordamaglia. J. Am. Chem. Soc. **99**, 5531 (1977).
12. R. Scordamaglia, R. Cavallone, and E. Clementi. J. Am. Chem. Soc. **99**, 5545 (1977).
13. O. Matsuoka, E. Clementi, and M. Yoshimine. J. Chem. Phys. **64**, 1351 (1976).
14. R. U. Lemieux, K. Bock, L. T. J. Delbaere, S. Koto, and V. S. Rao. Can. J. Chem. **58**, 631 (1980).
15. H. Thørgersen, R. U. Lemieux, K. Bock, and B. Mayer. Can. J. Chem. **60**, 44 (1982).
16. W. S. Benedict, N. Gailar, and E. K. Plyler. J. Chem. Phys. **24**, 1139 (1956).
17. S. Fraga. J. Comput. Chem. **3**, 329 (1982).
18. S. Romano and E. Clementi. Int. J. Quantum Chem. **14**, 839 (1978).
19. E. Clementi and G. Corongiu. IBM Research Report Pok-09, 1982.
20. R. Fletcher and M. J. D. Powell. Comput. J. **6**, 163 (1963).
21. N. Metropolis, A. W. Rosenbluth, M. N. Rosenbluth, A. H. Teller, and E. Teller. J. Chem. Phys. **21**, 1087 (1953).
22. J. A. Barker and D. Henderson. Rev. Mod. Phys. **48**, 587 (1976).
23. E. Clementi. Lecture notes in chemistry. Vol. 19. Springer Verlag, Berlin. 1980.
24. G. Chiari and G. Ferraris. Acta Crystallogr. Sect. B: Struct. Crystallogr. Cryst. Chem. **B38**, 2331 (1982).
25. R. U. Lemieux. Med. Chem. Proc. 8th Int. Symp. August 27–31, 1984, Uppsala, Sweden. Vol. 1. p. 329.

Can. J. Chem. Downloaded from www.nrcresearchpress.com by 88.85.125.76 on 09/07/12
For personal use only.

Synthesis of glycan fragments of glycoproteins using peracetylated *N*-allyloxycarbonyl-β-D-glucosamine and 1,6-anhydro-β-D-mannopyranose derivatives

DOMINIQUE LAFONT,[1] PAUL BOULLANGER, JOSEPH BANOUB,[2] AND GERARD DESCOTES

Laboratoire de chimie organique 2, Université Claude Bernard, Lyon 1 (Centre national de la recherche scientifique, Unité de recherche associée n° 463), École superieure de chimie industrielle de Lyon, 43, Bd. du 11 Novembre 1918 – 69622, Villeurbanne CEDEX, France

Received November 24, 1989

DOMINIQUE LAFONT, PAUL BOULLANGER, JOSEPH BANOUB, and GERARD DESCOTES. Can. J. Chem. **68**, 828 (1990).

The disaccharides β-D-GlcNAOC-(1→2)-D-Man, β-D-GlcNAOC-(1→4)-D-Man, the trisaccharide β-D-GlcNAOC-(1→2)-[β-D-GlcNAOC-(1→4)]-D-Man, and the tetrasaccharide β-D-GlcNAOC-(1→2)-[β-D-GlcNAOC-(1→3)]-[β-D-GlcNAOC-(1→4)]-D-Man have been synthesized in their peracetylated form, using the Lewis acid catalyzed condensations of 1,3,4,6-tetra-*O*-acetyl-2-*N*-allyloxycarbonylamino-2-deoxy-β-D-glucopyranose **1** with properly substituted 1,6-anhydro-β-D-mannopyranose derivatives. The anhydro glycosylation products obtained were then easily transformed into the $^4C_1$ peracetylated derivatives by acetolysis. The *N*-allyloxycarbonyl groups could be converted into *N*-acetyl groups in the presence of Pd(0) complexes, followed by reacetylation of the free amino function in high yields.

Key words: *N*-allyloxycarbonyl, glycosylation, glucosamine, glycan fragments.

DOMINIQUE LAFONT, PAUL BOULLANGER, JOSEPH BANOUB et GERARD DESCOTES. Can. J. Chem. **68**, 828 (1990).

Les disaccharides β-D-GlcNAOC-(1→2)-D-Man, β-D-GlcNAOC-(1→4)-D-Man, le trisaccharide β-D-GlcNAOC-(1→2)-[β-D-GlcNAOC-(1→4)]-D-Man et le tétrasaccharide β-D-GlcNAOC-(1→2)-[β-D-GlcNAOC-(1→3)]-[β-D-GlcNAOC-(1→4)]-D-Man ont été synthétisés sous forme acétylée, en condensant, en présence d'un acide de Lewis, le tétra-*O*-acétyl-1,3,4,6-*N*-allyloxycarbonylamino-2-désoxy-2-β-D-glucopyranose **1** avec des dérivés de l'anhydro-1,6-β-D-mannopyranose convenablement protégés. Les produits de glycosylation de type anhydro ont ensuite été transformés, par acétolyse, en composés peracétylés de configuration $^4C_1$. Le passage du groupe protecteur *N*-allyloxycarbonyle au groupe *N*-acétyle a été réalisé par coupure en présence de complexes du Pd(0), suivie d'une réacétylation de la fonction amine libre avec des rendements élevés.

Mots clés : *N*-allyloxycarbonyl, glycosylation, glucosamine, glycan fragments.

Introduction

The chemistry and biochemistry of glycoproteins have acquired a tremendous importance during the past decade (1–3). The glycan chains of glycoproteins have highly complex structures and are abundant at the cell surfaces. Because of these characteristics, they are assumed to play a key role in recognition phenomena and in immunochemical events.

Amongst *N*-glycoproteins, the immunologically important *N*-acetyl-lactosaminic type (1) is composed of a pentasaccharide inner core formed of a trisaccharide of mannose attached by a β-glycosidic linkage to a di-*N*-acetylchitobiose-asparagine-*N*-glycoside. The two terminal non-reducing mannose residues of the pentasaccharide inner core are substituted by a variable number of residues of *N*-acetyl-lactosamine [β-D-Gal-(1→4)-D-GlcNAc]. The linkages between the *N*-acetyl glucosamine and these mannose residues constitute the branched points of the antenna structure.

Previous work in our laboratories (4) established the efficiency of the *N*-allyloxycarbonyl derivatives of D-glucosamine as potent promoters of 1,2-*trans*-glycosylation. Using the *N*-allyloxycarbonyl approach, a variety of disaccharides and immunologically important heptopyranose-disaccharides were synthesized in a stereospecific and regioselective manner. The *N*-allyloxycarbonyl protective group was easily removed with Pd(0) complexes, thus affording the free amino group, which could then be smoothly acetylated.

To broaden the scope of applications of the *N*-allyloxycarbonyl procedure and before attempting to extend this method to the lactosamine-type structures, we devoted our efforts towards the glycosylation of the different positions of D-mannose in order to obtain the different di-, tri-, and tetrasaccharides containing one, two, or three glucosaminyl residues respectively.

We describe in this paper the stereocontrolled syntheses of the fragments β-D-GlcNAc-(1→2)-Man, β-D-GlcNAc-(1→4)-Man, β-D-GlcNAc-(1→2)-[β-D-GlcNAc-(1→4)]-Man, and related precursor oligosaccharides, in their peracetylated forms. These syntheses were realised by the trimethylsilyl triflate glycosylation of the suitably protected 1,6-anhydro-β-D-mannopyranose glycosyl acceptor with 1,3,4,6-tetra-*O*-acetyl-2-*N*-allyloxycarbonylamino-2-deoxy-β-D-glucopyranose as glycosyl donor (4).

Results and discussion

The syntheses of fragments related to compounds **3**, **9**, and **15** have already been reported (5–8) in the literature, using the *N*-phthaloyl derivatives of D-glucosamine or D-lactosamine as donors and various mannopyranosides as acceptors. To our knowledge there have been only a few examples of glycosylations involving 1,6-anhydro-β-D-mannopyranoses as acceptors (8–11). Therefore, because of the bidentate simultaneous protection of the very reactive OH-1 and OH-6 positions, and the ease of opening the anhydro-ring structure, the 1,6-anhydro-β-D-mannopyranoses were chosen as acceptors in this work.

1,6-Anhydro-2,3-*O*-isopropylidene-β-D-mannopyranose **2** (12) was prepared by the Zemplen deacetylation of 2,3,4-tri-*O*-acetyl-1,6-anhydro-β-D-mannopyranose (12, 13) followed by acetalization. Condensation of 1,3,4,6-tetra-*O*-acetyl-2-*N*-allyloxycarbonylamino-2-deoxy-β-D-glucopyranose **1** (4) with one equivalent of the acceptor **2**, promoted by trimethylsilyl trifluoromethanesulfonate (1 equiv.) at low temperature, afforded

[1]Author to whom correspondence may be addressed.

[2]On leave from Fisheries and Oceans Canada, Science Branch, P.O. Box 5667, St John's, Nfld., Canada A1C 5X1.

Printed in Canada / Imprimé au Canada

Can. J. Chem. Downloaded from www.nrcresearchpress.com by 88.85.125.76 on 09/07/12
For personal use only.

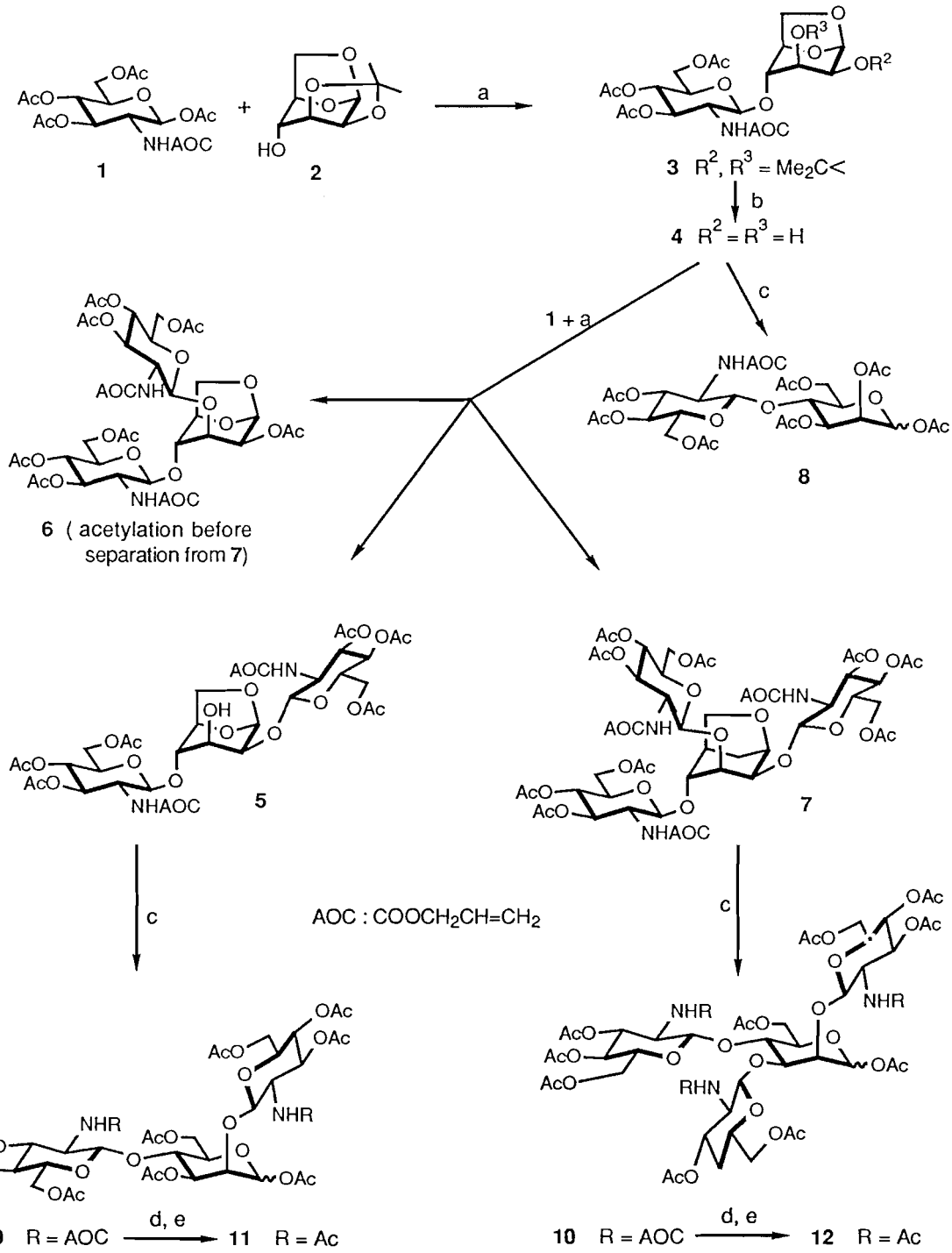

SCHEME 1

the expected β-linked disaccharide in 77% yield. The disaccharide **3** was easily converted into the diol **4** (85%) followed by treatment with 10% trifluoroacetic acid in acetic anhydride to afford an α/β (3:1) mixture of 1,2,3,6-tetra-*O*-acetyl-4-*O*-(3,4,6-tri-*O*-acetyl-2-*N*-allyloxycarbonylamino-2-deoxy-β-D-glucopyranosyl)-D-mannopyranose **8** in 91% yield (Scheme 1). The β configurations of the glucosidic linkages were ascertained by ^1H and ^{13}C nmr (Table 1).

Disaccharide **4** was in turn glycosylated with one equivalent of the donor **1**; the trisaccharide **5** was obtained in a 36% yield together with other compounds, which, after acetylation, were separated and identified as the trisaccharide **6** (6%) and the tetrasaccharide **7** (37%). When two equivalents of the donor and the Lewis acid were used, the yields were brought respectively to 17, 4, and 63%. From these results, it can be mentioned that an increase in nucleophilicity of OH-3 is observed when OH-2 has been glycosylated, despite the higher steric hindrance created. Such an observation has already been indicated in the

Can. J. Chem. Downloaded from www.nrcresearchpress.com by 88.85.125.76 on 09/07/12
For personal use only.

TABLE 1. The ^{13}C nmr spectra of compounds **2–23**[a]

Compound	D-Glucosamine moiety						D-Mannose moiety					
	C-1	C-2	C-3	C-4	C-5	C-6	C-1	C-2	C-3	C-4	C-5	C-6
2							100.04	73.16	76.81	70.18	77.39	65.04
3	100.87	56.89	73.45	69.86	72.62	62.80	99.90	73.10	75.71	77.30	74.09	65.06
4	102.67	56.98	73.50	69.98	72.52	62.98	101.03	67.27	70.48	80.26	74.26	65.14
5	101.51	56.78	73.49	69.79	72.47	62.79	100.25	76.71	70.55	79.41	74.44	65.17
	101.00	56.78	73.30	69.72	72.47	62.67						
6	103.42	57.10	73.50	69.62[b]	72.59	62.66	99.98	69.92[b]	77.27	78.61	74.94	65.34
	101.23	56.72	73.38	69.62	72.47	62.41						
7	102.87	56.92	73.93	69.83	72.64	62.68	100.70	76.76	76.76	79.57	74.44	65.25
	102.50	56.74	73.66	69.60	72.53	62.42						
	101.38	56.63	73.20	69.41	72.15	62.34						
8α	101.56	57.26	73.67[b]	69.50	72.24	62.95[c]	91.09	69.18	70.17	73.26[b]	71.70	62.86[c]
9α	102.06	57.27	73.65	69.62	72.42	63.22	91.69	74.82	71.34[b]	73.65[c]	71.74[b]	63.22[d]
	101.69	56.40	73.54[c]	69.62	72.22	62.92[d]						
10α	100.55	56.99	73.38	69.91	72.18	63.89	90.90	74.45[b]	74.21[b]	74.21[b]	71.77	63.09
	99.18	56.46	73.27	69.50	72.18	62.51						
	97.40	56.27	72.96	69.14	72.18	61.93						
11[e]	101.54	54.34	72.90	68.69	71.79[b]	62.15[c]	90.69	73.48	70.52	73.42	71.47[b]	62.23[c]
	101.38	53.54	72.14	68.32	71.67[b]	62.06[c]						
12	102.38	54.70	73.10	69.79	72.54[b]	63.64[c]	90.90	73.82[d]	74.00[d]	73.36[d]	72.29[b]	62.88[c]
	101.35	54.40	72.85	69.79	72.54[b]	62.64[c]						
	101.35	54.08	72.85	69.28	72.29	62.25[c]						
13							99.92	72.83	73.60	76.20	74.13	65.00
14							102.04	67.05	69.00	79.02	73.97	65.28
15	101.68	56.72	73.39	69.84	72.64	62.86	100.53	75.99	69.43	78.51	74.22	65.37
16	104.82	57.09	73.62	69.78	72.74	62.73	102.57	67.27	79.05	76.73	72.88	65.34
17	102.75	56.86	73.77	70.10	72.76	62.78	101.01	75.55	78.42	76.03	73.77[b]	65.45
	102.46	56.43	73.21[b]	69.64	72.21	62.78						
18	101.67	56.74	73.25	69.79	72.50[b]	62.83	100.08	76.40	72.51[b]	72.23[b]	77.27	65.40
19	103.02	56.90	74.02	70.24	72.70[b]	62.88	100.96	76.82	78.00	72.02[b]	77.10	65.44
	102.16	56.59	73.10	69.73	72.50[b]	62.83						
20	101.04	56.39	73.35	69.75	72.54	62.93[b]	91.67	74.49	70.58	66.05	71.26	63.09[b]
21	100.14	56.69	73.33	69.85	72.37	62.83[b]	90.77	74.42[c]	74.69[c]	67.92	71.73	63.24[b]
	98.00	56.57	73.15	69.42	72.37	62.20[b]						
22	101.66	56.72	73.57	69.52	72.28	62.72	100.55	74.58	71.28	72.28	77.13	65.58
23	101.86	56.84	73.62	69.69	72.62	62.58	100.30	74.55[b]	70.11	79.51	74.94[b]	65.52
	101.50	58.84	73.55	69.46	72.32	62.58						

[a]Spectra recorded in CD_3COCD_3 unless otherwise stated.
[b,c,d]Assignments could be reversed in the same compound.
[e]Spectrum recorded in $CDCl_3$.

glycosylation of 4,6-diols of the *gluco* and *manno* series, using the same glycosylation procedure (14). The precise sites of glycosylation in compounds **5** and **6** were determined by two-dimensional heteronuclear (^1H–^{13}C) shift correlation. In compound **5**, the connectivity between H-2 (δ 3.69 ppm) and C-2 (δ 76.71 ppm) was clearly established. Furthermore, an important upfield chemical shift of C-2 (+9.5 ppm from **4** to **5**) was observed, while in compound **6** the H-2 chemical shift (δ 4.66 ppm) was characteristic of an acetylated OH-2 position of the anhydro ring. The β-glucosidic linkages were also confirmed by both ^1H and ^{13}C nmr.

The openings of the anhydro ring in compounds **5** and **7** were realized to afford respectively **9α** (71%) – **9β** (27%) and **10α** (77%) – **10β** (18%). The deprotection of the *N*-allyloxycarbonyl group for compounds **9α** and **10α** was realized as already reported (4), with catalytic amounts of tetrakis(triphenylphosphine) palladium in the presence of an excess of dimethyl malonate as allyl acceptor. The free amino groups were then reacetylated respectively to afford compounds **11** and **12** with overall yields of 86 and 84%. The ^1H and ^{13}C nmr spectra of these products were in complete agreement with the assigned structures.

An alternative route to the trisaccharide **9** is the stereoselective glycosylation of a OH-4 protected 1,6-anhydro-β-D-mannopyranose. In this route, compound **2** was reacted with trichloroethylchloroformate (15) to afford compound **13** in 90% yield. After hydrolysis of the 2,3-isopropylidene protective group from **13**, the compound **14** obtained was glycosylated with one equivalent of the glycosyl donor **1**, as already described for the disaccharide **4**. Two disaccharides (**15** and **16**) and one trisaccharide (**17**) were separated from the reaction mixtures in the respective yields of 56, 10, and 16%. The regioselectivity of this reaction was due to a lack of reactivity of the C-3 position and could be attributed to the deactivating effect of the strongly electronegative trichloroethoxycarbonyl protective group on OH-4 (Scheme 2).

The regio- and stereochemistry of glycosylation at the anomeric centers of disaccharides **15** and **16** were determined by ^1H and ^{13}C nmr. The chemical resonances of glycosylated carbon atoms were shifted upfield from their values in the diol

Can. J. Chem. Downloaded from www.nrcresearchpress.com by 88.85.125.76 on 09/07/12
For personal use only.

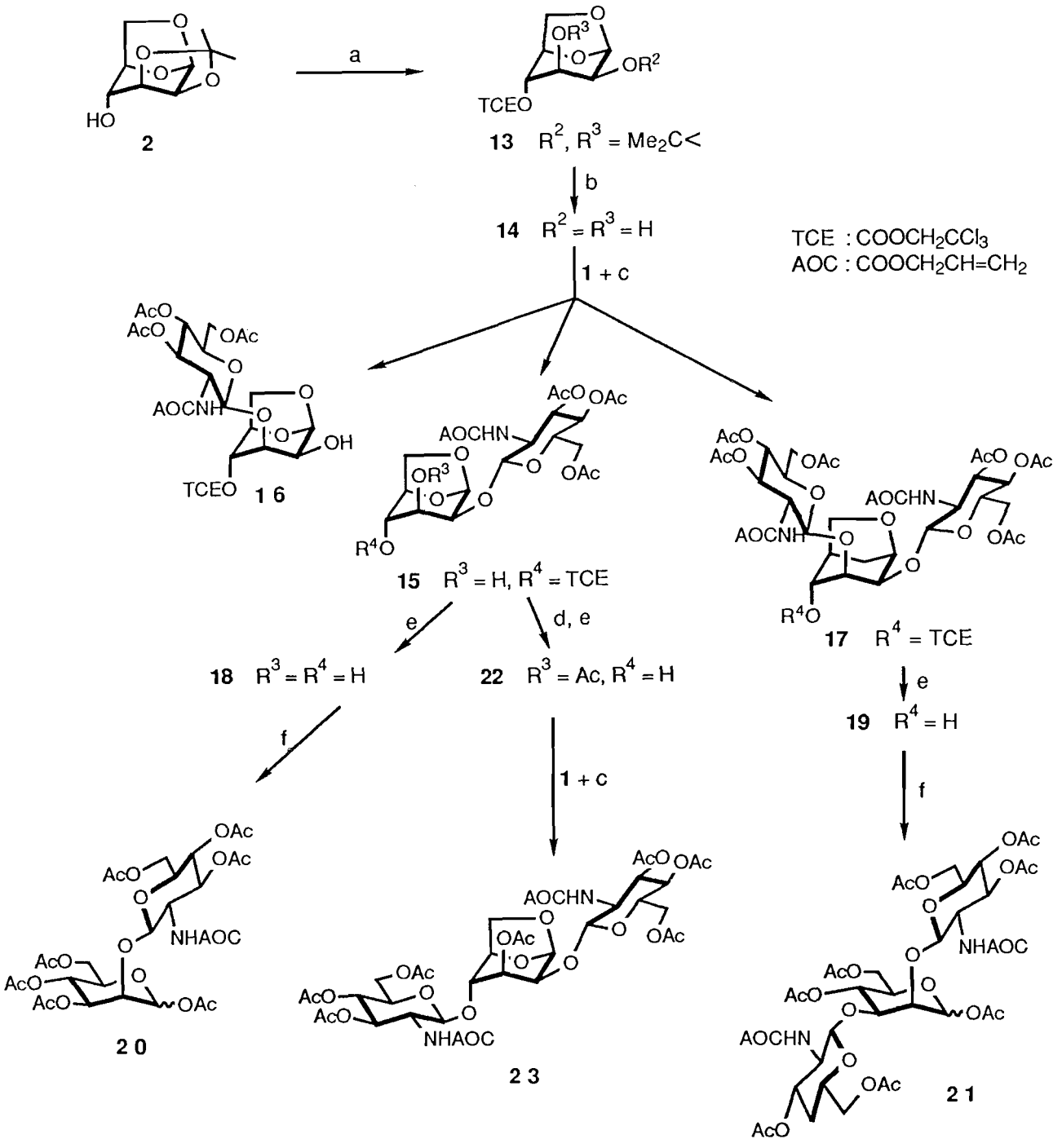

a.TCECl, pyr. b. AcOH, H_2O, 100°C. c. TMSOTf, -30°C, CH_2Cl_2. d. Ac_2O, DMAP, pyr.
e. Zn / Cu, AcOH. f. 10% CF_3COOH, Ac_2O.

SCHEME 2

14 (respectively 8.9 and 10.0 ppm for C-2 in **15** and C-3 in **16**) while the non-glycosylated positions remained unchanged. The 1,2-*trans*-glycosylation was confirmed by the ^{13}C-1 chemical shifts (Table 1) and ^{1}H-1 chemical shifts (5.11 and 4.92 ppm in **15** and **16** respectively) and J_{12} coupling constants (8.5 Hz in **15** and **16**).

The trichloroethoxycarbonyl protective group in compound **15** was then removed by treatment with a Zn/Cu couple in acetic acid (16) to afford compound **18** recovered in 93% yield. The anhydro ring of diol **18** was then opened with 10% trifluoroacetic acid in acetic anhydride to afford disaccharide **20** (95% yield) as an anomeric mixture (α/β, 7:1). The ^{1}H and ^{13}C nmr spectra of compound **20** were in complete agreement with the expected structure and, moreover, confirmed the structure of compound **15**.

The same treatment as previously described was applied to trisaccharide **17**, which afforded compound **21** (83% overall yield) as an anomeric mixture (α/β, 9:1).

On the other hand, the free OH-3 group of disaccharide **15** was acetylated, and the compound obtained was deprotected

Can. J. Chem. Downloaded from www.nrcresearchpress.com by 88.85.125.76 on 09/07/12
For personal use only.

Can. J. Chem. Downloaded from www.nrcresearchpress.com by 88.85.125.76 on 09/07/12
For personal use only.

by treatment with a Zn/Cu couple to afford disaccharide **22** containing the free OH-4 group, which in turn was glycosylated with donor **1** (under the usual conditions) to give the trisaccharide **23** in 69% yield. The structure of compound **23** was assigned by ^1H and ^{13}C nmr and confirmed by acetylation of the already obtained trisaccharide **5**, which yielded to the same derivative.

Conclusion

The strategy of the syntheses presented in this paper for the preparation of the various glycan fragments broadens the scope of applications of the methods previously reported (17).

The 1,6-anhydro-β-D-mannopyranose intermediates, structurally protected on OH-1 and OH-6, are good acceptors for the Lewis acid catalyzed glycosylation reactions, allowing several protective group variations and subsequent possibilities of opening the anhydro ring for further elongation.

The *N*-allyloxycarbonyl glycosylation procedure allowed the preparation of different glycan fragments in high yields and high stereoselectivities on all of the mannose positions, depending on the structure of the selected glycosyl acceptor. It is worthwhile to mention that the steric hindrance in a polysubstituted mannose oligosaccharide does not seem to represent a limitation to this method. As can be judged from the results presented in this paper, the yields of glycosylation are quite comparable with those previously reported in the literature for similar derivatives. For example, van Boom and co-workers (8) reported the coupling of 1,3,4,6-tetra-*O*-acetyl-2-deoxy-2-phthalimido-β-D-glucopyranose with 1,6-anhydro-2,3-*O*-(4-methoxybenzylidene)-β-D-mannopyranose in 71% yield (to be compared with the glycosylation of **2** on OH-4 in 77% yield). Glycosylation on OH-2 of $^4C_1$ mannose acceptors with stoichiometric amounts of D-glucosaminyl donors are usually realized in 65–75% yield (see for examples refs. 5, 7, 18, and 19), which is of the same order as the results described in this paper (the synthesis of **15** + **17** from **14** represents a 72% yield of glycosylation on OH-2).

Beside the glycosylation yields, the most important improvement of the *N*-allyloxycarbonyl approach lies in the high chemioselectivity and the very smooth conditions required for the cleavage of the amino protective group. Most of the functionalities are stable in presence of Pd(0) complexes and the use of *O*- and *N*-allyloxycarbonyl protective groups has been well documented in the fields of carbohydrates (20), nucleotides (21), and peptides (22).

Experimental

Melting points were determined on a Büchi apparatus and were uncorrected. Optical rotations were measured on a Perkin–Elmer 241 polarimeter in a 1-dm cell. The ^1H and ^{13}C nmr spectra were recorded on a Bruker AM 300 spectrometer working respectively at 300 and 75.5 MHz with tetramethylsilane as internal reference; interpretations are tentative since no distinction was made between the different glucosamine moieties in oligosaccharides; all the spectra contain additional signals corresponding to the acetyl protons. Elemental analyses were realized by the "Laboratoire Central d'Analyses du CNRS" (Solaize, France). Silica gel columns were realized on silica gel Amicon (230–400 mesh). Dry alcohol-free dichloromethane was obtained by washing with water, drying over calcium chloride, distillation on phosphorus pentoxide, and storage over 4 Å molecular sieves before use in the glycosylation steps.

4-O-(3,4,6-Tri-O-acetyl-2-N-allylcarbonylamino-2-deoxy-β-D-glucopyranosyl)-1,6-anhydro-2,3-O-isopropylidene-β-D-mannopyranose (3)

1,3,4,6-Tetra-*O*-acetyl-2-*N*-allyloxycarbonylamino-2-deoxy-β-D-glucopyranose **1** (4) (0.906 g, 2.10 mmol) and the alcohol **2** (0.404 g, 2.0 mmol) (12) were dissolved in dichloromethane (30 mL). The mixture was flushed with dry nitrogen while cooling to −30°C. Trimethylsilyl triflate (382 μL, 2.10 mmol) was then introduced through a syringe and the mixture stirred at −30°C for 16 h. The reaction was then quenched with triethylamine (620 μL, 4.5 mmol), the mixture allowed to reach 0°C, and then poured into a cold, dilute aqueous solution of sodium carbonate. The aqueous layer was extracted with dichloromethane (3 × 30 mL); the organic phase was washed with water (5 mL), dried over calcium chloride, and evaporated to afford a mixture, which was chromatographed on silica gel (eluent: ethyl acetate/hexane, 3:1). The title compound was recovered as a white crystalline material (77%); mp 184–185°C (ethanol); $[\alpha]_D^{20}$ −18.5° (*c* 1.5, $CHCl_3$); ^1H nmr (CD_3COCD_3) δ: 6.61 (d, 1H, $J_{2',NH}$ = 8.3 Hz, N*H*), 5.91 (m, 1H, -C*H*=CH_2), 5.32 (dd, 1H, $J_{2',3'}$ = 9.7 Hz, $J_{3',4'}$ = 9.8 Hz, H-3'), 5.26 (m, 1H, 0.5 × C*H*$_2$=CH-), 5.22 (d, 1H, $J_{1,2}$ = 2.9 Hz, H-1), 5.16–5.12 (m, 2H, H-1', 0.5 × C*H*$_2$=CH-), 5.00 (dd, 1H, $J_{4',5'}$ = 9.6 Hz, H-4'), 4.64 (m, 1H, $J_{4,5}$ = 1.5 Hz, $J_{5,6a}$ = 1.2 Hz, $J_{5,6b}$ = 6.3 Hz, H-5), 4.60–4.56 (m, 2H, allyl C*H*$_2$), 4.28 (m, 1H, H-3), 4.27 (dd, 1H, $J_{5',6'a}$ = 5.2 Hz, $J_{6'a,6'b}$ = 12.0 Hz, H-6'a), 4.11 (dd, 1H, $J_{5',6'b}$ = 2.4 Hz, H-6'b), 4.10 (m, 1H, H-4), 3.96 (dd, 1H, $J_{2,3}$ = 6.2 Hz, H-2), 3.88 (dd, 1H, $J_{6a,6b}$ = 7.2 Hz, H-6a), 3.87 (m, 1H, H-5'), 3.64 (dd, 1H, H-6b), 3.63 (m, 1H, H-2'), 1.46, 1.28 (2s, 6H, C*H*$_3$ isopropylidene). Anal. calcd. for $C_{25}H_{35}NO_{14}$ (Mol. Wt. 573.54): C 52.35, H 6.15, N 2.44; found: C 52.29, H 5.95, N 2.42.

4-O-(3,4,6-Tri-O-acetyl-2-N-allyloxycarbonylamino-2-deoxy-β-D-glucopyranosyl)-1,6-anhydro-β-D-mannopyranose (4)

Compound **3** (0.860 g, 1.5 mmol) was heated for 0.7 h at 100°C in 40% aqueous acetic acid (25 mL). The solution was then evaporated to dryness and the syrup redissolved in and reevaporated from toluene to provide a solid, which was recrystallized from ethanol (75%). Column chromatography of the mother liquor (eluent: ethyl acetate/acetone, 7:1) gave an additional amount of compound **4** (0.080 g, 10%); mp 179–180°C (ethanol); $[\alpha]_D^{20}$ −43.1° (*c* 1.0, $CHCl_3$); ^1H nmr (CD_3COCD_3) δ: 6.54 (d, 1H, $J_{2',NH}$ = 8.2 Hz, N*H*), 5.91 (m, 1H, -C*H*=CH_2), 5.30 (dd, 1H, $J_{2',3'}$ = 10.2 Hz, $J_{3',4'}$ = 9.4 Hz, H-3'), 5.26 and 5.14 (m, 2H, C*H*$_2$=CH-), 5.19 (br s, 1H, $J_{1,2}$ = 2.0 Hz, H-1), 5.06 (d, 1H, $J_{1',2'}$ = 8.3 Hz, H-1'), 4.98 (dd, 1H, $J_{4',5'}$ = 10.0 Hz, H-4'), 4.57 (m, 1H, $J_{3,5}$ = $J_{4,5}$ = 1.5 Hz, $J_{5,6a}$ = 0.9 Hz, $J_{5,6b}$ = 6.0 Hz, H-5), 4.51 (m, 2H, allyl C*H*$_2$), 4.29 (dd, 1H, $J_{5',6'a}$ = 5.2 Hz, $J_{6'a,6'b}$ = 12.2 Hz, H-6'a), 4.14 (dd, 1H, $J_{6a,6b}$ = 7.0 Hz, H-6a), 4.13–4.12 (m, 2H, OH), 4.07 (dd, 1H, $J_{5',6'b}$ = 2.5 Hz, H-6'b), 4.04 (m, 1H, H-3), 3.95 (dd, 1H, $J_{3,4}$ = 1.5 Hz, H-4), 3.86 (m, 1H, H-5'), 3.63 (m, 1H, H-2'), 3.59 (dd, 1H, H-6b), 3.55 (m, 1H, $J_{2,3}$ = 5.3 Hz, $J_{2,OH}$ = 8.0 Hz, H-2). Anal. calcd. for $C_{22}H_{31}NO_{14}$ (Mol. Wt. 533.48): C 49.53, H 5.86, N 2.63; found: C 49.54, H 5.99, N 2.53.

Glycosylation of compound 4

Disaccharide **4** (0.468 g, 0.88 mmol) was glycosylated with the donor **1** (0.380 g, 0.88 mmol) and trimethylsilyl triflate (320 μL, 1.76 mmol) for 24 h under the same conditions and work-up procedure as described for compound **3**. The recovered mixture was purified by column chromatography on silica gel (eluent: ethyl acetate). The first fraction (0.280 g) was acetylated (pyridine, 2 mL/acetic anhydride, 1 mL/DMAP, catalytic) for 4 h at 0°C and, after the usual work-up, chromatographed again (eluent: dichloromethane/acetone, 3:1) to afford compounds **6** (6%) and **7** (37%). The second fraction from the first chromatographic separation was compound **5**, recovered directly as a crystalline material (36%).

2,4-Di-O-(3,4,6-tri-O-acetyl-2-N-allyloxycarbonylamino-2-deoxy-β-D-glucopyranosyl)-1,6-anhydro-β-D-mannopyranose (5)

White crystalline material: mp 208–210°C (ethanol); $[\alpha]_D^{20}$ −21.5° (*c* 1.0, $CHCl_3$); ^1H nmr (CD_3COCD_3) δ: 6.56 (d, 2H, N*H*), 5.90 (m, 2H, C*H*=CH_2), 5.30 (br s, 1H, $J_{1,2}$ = 1.6 Hz, H-1), 5.29–5.28 (m, 2H, H-3', H-3"), 5.26 and 5.13 (m, 4H, C*H*$_2$=CH-), 5.03 (d, 2H, $J_{1',2'}$ = $J_{1",2"}$ = 8.5 Hz, H-1', H-1"), 5.00 (dd, 1H, $J_{3',4'}$ = $J_{4',5'}$ = 9.5 Hz, H-4'), 4.99 (dd, 1H, $J_{3",4"}$ = $J_{4",5"}$ = 9.5 Hz, H-4"), 4.60 (m, 1H, $J_{3,5}$ = $J_{4,5}$ = 1.5 Hz, $J_{5,6a}$ = 1.0 Hz, $J_{5,6b}$ = 6.0 Hz,

Can. J. Chem. Downloaded from www.nrcresearchpress.com by 88.85.125.76 on 09/07/12
For personal use only.

H-5), 4.59–4.49 (m, 4H, allyl CH_2), 4.31 (dd, 1H, $J_{5',6'a}$ = 4.7 Hz, $J_{6'a,6'b}$ = 12.0 Hz, H-6'a), 4.30 (dd, 1H, $J_{5'',6''a}$ = 5.8 Hz, $J_{6''a,6''b}$ = 12.2 Hz, H-6''a), 4.15 (m, 1H, H-3), 4.14 (dd, 1H, $J_{6a,6b}$ = 7.0 Hz, H-6a), 4.11 (dd, 1H, $J_{5',6'b}$ = 2.2 Hz, H-6'b), 4.10 (dd, 1H, $J_{5'',6''b}$ = 2.5 Hz, H-6''b), 3.99 (m, 1H, H-5''), 3.97 (br s, 1H, H-4), 3.88 (m, 1H, H-5'), 3.72 (m, 1H, H-2'), 3.69 (dd, 1H, $J_{2,3}$ = 5.0 Hz, H-2), 3.67 (m, 1H, H-2''), 3.60 (dd, 1H, H-6b). Anal. calcd. for $C_{38}H_{52}N_2O_{23}$ (Mol. Wt. 904.81): C 50.44, H 5.79, N 3.10; found: C 50.15, H 5.89, N 3.08.

2-O-Acetyl-3,4-di-O-(3,4,6-tri-O-acetyl-2-N-allyloxycarbonylamino-2-deoxy-β-D-glucopyranosyl)-1,6-anhydro-β-D-mannopyranose (6)

White crystalline material; mp 207–208°C (ethanol); $[\alpha]_D^{20}$ −5.0° (*c* 1.0, $CHCl_3$); ^{1}H nmr (CD_3COCD_3) δ: 6.56 and 6.40 (2d, 2H, *J* = 8.7 and 9.1 Hz, N*H*), 5.93 (m, 2H, -C*H*=CH_2), 5.32–5.22 (m, 4H, CH_2=CH-, H-3', H-3''), 5.28 (d, 1H, $J_{1,2}$ = 1.5 Hz, H-1), 5.15 (m, 2H, CH_2=CH-), 5.10 (d, 1H, $J_{1',2'}$ = 8.5 Hz, H-1'), 5.04 (dd, 1H, $J_{3',4'}$ = 9.5 Hz, $J_{4',5'}$ = 9.9 Hz, H-4'), 5.02 (dd, 1H, $J_{3'',4''}$ = 9.4 Hz, $J_{4'',5''}$ = 10.0 Hz, H-4''), 4.88 (d, 1H, $J_{1'',2''}$ = 8.5 Hz, H-1''), 4.66 (dd, 1H, $J_{2,3}$ = 5.2 Hz, H-2), 4.57 (m, 1H, H-5), 4.55–4.48 (m, 4H, allyl CH_2), 4.40–4.24 (m, 7H, H-6a, H-6'a, H-6''a, H-6'b, H-6''b, H-3, H-4), 3.90 (m, 2H, H-5', H-5''), 3.68 (m, 1H, $J_{2',3'}$ = 9.5 Hz, H-2'), 3.67 (m, 1H, H-2''), 3.62 (dd, 1H, $J_{5,6b}$ = 6.1 Hz, $J_{6a,6b}$ = 7.0 Hz, H-6b). Anal. calcd. for $C_{40}H_{54}N_2O_{24}$ (Mol. Wt. 946.85): C 50.73, H 5.75, N 2.96; found: C 50.40, H 5.92, N 2.82.

2,3,4-Tri-O-(3,4,6-tri-O-acetyl-2-N-allyloxycarbonylamino-2-deoxy-β-D-glucopyranosyl)-1,6-anhydro-β-D-mannopyranose (7)

White crystalline material; mp 107–109°C (ether/hexane); $[\alpha]_D^{20}$ −22.3° (*c* 1.0, $CHCl_3$). Anal. calcd. for $C_{54}H_{73}N_3O_{32}$ (Mol. Wt. 1276.15): C 50.82, H 5.77, N 4.20; found: C 50.87, H 5.93, N 3.93.

1,2,3,6-Tetra-O-acetyl-4-O-(3,4,6-tri-O-acetyl-2-N-allyloxycarbonylamino-2-deoxy-β-D-glucopyranosyl)-α-D-mannopyranose (8α)

Trifluoroacetic acid (0.6 mL) was added to a cold solution of compound **4** (0.267 g, 0.5 mmol) in acetic anhydride (6 mL) with stirring. After 4 h, the solution was evaporated to dryness and the syrup redissolved in and reevaporated twice from toluene. Column chromatography (eluent: ethyl acetate/hexane, 3:1) afforded an anomeric mixture (91%) of **8α** and **8β** (3:1); the pure α anomer was obtained after four successive recrystallizations in ethanol; mp 192°C (ethanol); $[\alpha]_D^{20}$ +42.0° (*c* 1.0, $CHCl_3$); ^{1}H nmr (CD_3COCD_3) δ: 6.53 (d, 1H, *J* = 9.0 Hz, N*H*), 5.97 (d, 1H, $J_{1,2}$ = 1.8 Hz, H-1), 5.92 (m, 1H, -C*H*=CH_2), 5.30 (dd, 1H, $J_{2,3}$ = 3.6 Hz, $J_{3,4}$ = 9.6 Hz, H-3), 5.29 (m, 1H, H-3'), 5.24 and 5.15 (m, 2H, CH_2=CH-), 5.20 (dd, 1H, H-2), 4.98 (dd, 1H, $J_{3',4'}$ = 9.5 Hz, $J_{4',5'}$ = 10.0 Hz, H-4'), 4.95 (d, 1H, $J_{1',2'}$ = 8.5 Hz, H-1'), 4.56–4.43 (m, 2H, allyl CH_2), 4.39 (dd, 1H, $J_{5,6a}$ = 1.5 Hz, $J_{6a,6b}$ = 12.1 Hz, H-6a), 4.30 (dd, 1H, $J_{5',6'a}$ = 4.9 Hz, $J_{6'a,6'b}$ = 12.2 Hz, H-6'a), 4.19 (dd, 1H, H-4), 4.17 (dd, 1H, $J_{5,6b}$ = 4.9 Hz, H-6b), 4.06 (m, 1H, H-5), 4.02 (dd, 1H, $J_{5',6'b}$ = 2.2 Hz, H-6'b), 3.87 (m, 1H, H-5'), 3.59 (m, 1H, H-2'). Anal. calcd. for $C_{30}H_{41}NO_{19}$ (Mol. Wt. 719.64): C 50.07, H 5.74, N 1.95; found: C 49.98, H 5.83, N 1.91.

For compound **8β**: 6.00 (d, 1H, $J_{1,2}$ = 0.8 Hz, H-1), 5.44 (dd, 1H, $J_{2,3}$ = 3.5 Hz, H-2).

1,3,6-Tri-O-acetyl-2,4-di-O-(3,4,6-tri-O-acetyl-2-N-allyloxycarbonylamino-2-deoxy-β-D-glucopyranosyl)-α-D-mannopyranose (9α)

The same treatment and work-up procedure as in the case of compound **4** were applied to compound **5** (0.230 g, 0.254 mmol). The recovered cristalline material was purified by column chromatography (eluent: ethyl acetate/hexane, 3:1). The α anomer was eluted first (0.195 g, 71%). White crystalline material; mp 184–185°C (2-propanol); $[\alpha]_D^{20}$ +2.8° (*c* 1.0, $CHCl_3$); ^{1}H nmr (CD_3COCD_3) δ: 6.63 and 6.52 (2d, 2H, *J* = 9.6 Hz, N*H*), 6.00 (d, 1H, $J_{1,2}$ = 1.7 Hz, H-1), 5.89 (m, 2H, -C*H*=CH_2), 5.28–5.09 (m, 6H, CH_2=CH-, H-3', H-3''), 5.07 (dd, 1H, $J_{2,3}$ = 3.7 Hz, $J_{3,4}$ = 9.7 Hz, H-3), 5.00 (dd, 1H, $J_{3',4'}$ = $J_{4',5'}$ = 9.7 Hz, H-4'), 4.97 (dd, 1H, $J_{3'',4''}$ = $J_{4'',5''}$ = 9.7 Hz, H-4''), 4.95 (d, 1H, $J_{1',2'}$ = 8.5 Hz, H-1'), 4.80 (d, 1H, $J_{1'',2''}$ = 8.5 Hz, H-1''), 4.60–4.25 (m, 7H, allyl CH_2, H-6a, H-6'a, H-6''a), 4.21 (dd, 1H, H-2), 4.12 (dd, 1H, $J_{4,5}$ = 9.6 Hz, H-4), 4.07–3.80 (m, 6H, H-5, H-5', H-5'', H-6b, H-6'b, H-6''b), 3.76 (m, 1H, $J_{2',3'}$ = 10.2 Hz, H-2'), 3.64 (m, 1H, $J_{2'',3''}$ = 10.5 Hz, H-2''). Anal. calcd. for $C_{44}H_{60}N_2O_{27}$ (Mol. Wt. 1048.93): C 50.38, H 5.77, N 2.67; found: C 50.26, H 5.73, N 2.58.

Compound **9β** (27%) was obtained as a mixture with **9α** and had the following ^{1}H nmr characteristics: 5.84 (br s, 1H, H-1), 4.85 (d, 1H, $J_{1',2'}$ = 8.5 Hz, H-1').

1,6-Di-O-acetyl-2,3,4-tri-O-(3,4,6-tri-O-acetyl-2-N-allyloxycarbonylamino-2-deoxy-β-D-glucopyranosyl)-α-D-mannopyranose (10α)

The same treatment and work-up procedure as in the case of compounds **4** and **5** were applied to compound **7** (0.180 g, 0.14 mmol). The recovered crystalline material was purified by column chromatography (eluent: ethyl acetate). The α anomer was eluted first (0.151 g, 77%). Syrup; $[\alpha]_D^{20}$ −10.8° (*c* 1.0, $CHCl_3$); ^{1}H nmr (CD_3COCD_3) δ: 6.09 (d, 1H, $J_{1,2}$ = 2.2 Hz, H-1). Anal. calcd. for $C_{58}H_{79}N_3O_{35}$ (Mol. Wt. 1378.23): C 50.54, H 5.78, N 3.05; found: C 50.17, H 5.89, N 2.93.

Compound **10β** had $[\alpha]_D^{20}$ +27.0° (*c* 1.0, $CHCl_3$); ^{1}H nmr (CD_3COCD_3) δ: 5.71 (d, 1H, $J_{1,2}$ = 0.8 Hz, H-1).

1,3,6-Tri-O-acetyl-2,4-di-O-(2-acetamido-3,4,6-tri-O-acetyl-2-deoxy-β-D-glucopyranosyl)-α-D-mannopyranose (11)

Palladium bis(dibenzylidene acetone) (0.014 g, 0.024 mmol) was reacted with triphenylphosphine (0.035 g, 0.134 mmol) in dry, oxygen-free oxolane (2 mL) at room temperature for 10 min. Compound **9α** (0.240 g, 0.228 mmol) dissolved in oxygen-free oxolane (5 mL) and dimethylmalonate (0.42 mL, 4.9 mmol) was then added to the above solution and the mixture was stirred for 24 h at room temperature. After concentration to 1 mL, the mixture was applied to the top of a small silica gel column and eluted first with ethyl acetate, to remove the triphenylphosphine by-products, and then with ethyl acetate/methanol (2:1), to recover the expected amino-free derivative, which was acetylated overnight and extracted as usual. After column chromatography (eluent: ethyl acetate/acetone, 4:1), the pure compound **11** (86%) was recovered as a white foam; $[\alpha]_D^{20}$ −17.9° (*c* 1.0, $CHCl_3$); ^{1}H nmr ($CDCl_3$) δ: 6.81 and 6.65 (2d, 2H, *J* = 7.2 and 8.7 Hz, N*H*), 6.02 (br s, 1H, H-1), 5.31–5.07 (m, 5H, H-3, H-3', H-3'', H-4', H-4''), 4.62 (d, 1H, $J_{1',2'}$ = 8.0 Hz, H-1'), 4.58 (d, 1H, $J_{1'',2''}$ = 8.2 Hz, H-1''), 4.40–3.70 (m, 13H, H-2, H-2', H-2'', H-4, H-5, H-5', H-5'', H-6a, H-6'a, H-6''a, H-6b, H-6'b, H-6''b). Anal. calcd. for $C_{40}H_{56}N_2O_{25}$ (Mol. Wt. 964.86): C 49.79, H 5.85, N 2.90; found: C 49.32, H 5.91, N 2.69.

1,6-Di-O-acetyl-2,3,4-tri-O-(2-acetamido-3,4,6-tri-O-acetyl-2-deoxy-β-D-glucopyranosyl)-α-D-mannopyranose (12)

The same treatment and work-up procedure as described for compound **9α** were applied to compound **10α**. The recovered material was purified by column chromatography (eluent: ethyl acetate/methanol, 8:1) to afford compound **12** (84%) as a white foam; $[\alpha]_D^{20}$ −10.8° (*c* 1.0, $CHCl_3$); ^{1}H nmr (CD_3COCD_3) δ: 7.39 and 7.26 (2d, 2H, *J* = 9.4 and 9.6 Hz, N*H*), 6.70 (m, 1H, N*H*), 6.02 (d, 1H, $J_{1,2}$ = 3.4 Hz, H-1), 5.27, 5.17, 5.14 (3t, 3H, *J* = 9.8 and 9.9 Hz, H-3', H-3'', H-3'''), 5.03, 5.02, 5.02 (3t, 3H, H-4', H-4'', H-4'''), 4.94 (d, 1H, 5.17, $J_{1',2'}$ = 8.5 Hz, H-1'), 4.91 (d, 2H, *J* = 8.6 Hz, H-1'', H-1'''), 4.60–3.88 (m, 18H, H-2, H-2', H-2'', H-2''', H-3, H-4, H-5, H-5', H-5'', H-5''', H-6a, H-6'a, H-6''a, H-6'''a, H-6b, H-6'b, H-6''b, H-6'''b). Anal. calcd. for $C_{52}H_{73}N_3O_{32}$ (Mol. Wt. 1252.13): C 49.87, H 5.88, N 3.36; found: C 49.46, H 5.63, N 3.01.

1,6-Anhydro-2,3-O-isopropylidene-4-O-(2,2,2-trichloroethoxycarbonyl)-β-D-mannopyranose (13)

Trichloroethylchloroformate (0.76 mL, 5.5 mmol) was added dropwise to a cold (−5°C) solution of compound **2** (1.010 g, 5.0 mmol) in dry pyridine (20 mL). The mixture was stirred overnight and the solvent then evaporated under vacuum. The mixture obtained was redissolved in and reevaporated from toluene (2 × 10 mL) and chromatographed on silica gel (eluent: ethyl acetate/hexane, 1:3) to afford compound **13** as a white crystalline material (90%); mp 142–

Can. J. Chem. Downloaded from www.nrcresearchpress.com by 88.85.125.76 on 09/07/12
For personal use only.

143°C (ethanol); $[\alpha]_D^{20}$ −56.3° (*c* 1.0, $CHCl_3$); ^1H nmr (CD_3COCD_3) δ: 5.32 (br s, 1H, $J_{1,2}$ = 3.0 Hz, H-1), 4.98, 4.93 (2d, 2H, *J* = 12.3 Hz, CH_2CCl_3), 4.97 (m, 1H, H-4), 4.73 (m, 1H, $J_{3,5} = J_{4,5} = J_{5,6a}$ = 1.5 Hz, $J_{5,6b}$ = 6.4 Hz, H-5), 4.30 (m, 1H, $J_{1,3}$ = 0.9 Hz, $J_{2,3}$ = 6.3 Hz, $J_{3,4}$ = 1.5 Hz, H-3), 4.09 (dd, 1H, H-2), 4.04 (dd, 1H, $J_{6a,6b}$ = 7.6 Hz, H-6a), 3.76 (dd, 1H, H-6b), 1.49, 1.29 (2s, 6H, CH_3 isopropylidene). Anal. calcd. for $C_{12}H_{15}Cl_3O_7$ (Mol. Wt. 377.60): C 38.17, H 4.00; found: C 38.18, H 4.00.

*1,6-Anhydro-4-*O*-(2,2,2-trichloroethoxycarbonyl)-β-D-mannopyranose (**14**)*

Prepared from **13** as described for compound **4**. White crystalline material (85%); mp 128–130°C (ethanol); $[\alpha]_D^{20}$ −82.0° (*c* 0.5, CH_3COCH_3); ^1H nmr (CD_3COCD_3) δ: 5.29 (br s, 1H, H-1), 4.99 (s, 2H, CH_2CCl_3), 4.85 (m, 1H, H-4), 4.68 (m, 1H, H-5), 4.50, 4.29 (m, 2H, O*H*), 4.27 (dd, 1H, $J_{5,6a}$ = 1.0 Hz, $J_{6a,6b}$ = 7.5 Hz, H-6a), 4.00 (m, 1H, $J_{2,3}$ = 5.1 Hz, H-3), 3.71 (dd, 1H, $J_{5,6b}$ = 3.5 Hz, H-6b), 3.63 (m, 1H, H-2). Anal. calcd. for $C_9H_{11}Cl_3O_7$ (Mol. Wt. 337.54): C 32.02, H 3.28; found: C 31.93, H 3.52.

*Glycosylation of compound **14***

Compound **14** (0.608 g, 1.8 mmol) was glycosylated with the donor **1** (0.777 g, 1.8 mmol) and trimethylsilyl triflate (327 μL, 1.8 mmol) for 24 h under the same conditions and work-up procedure as described for the synthesis of compound **3**. The recovered mixture crystallized spontaneously and was recrystallized twice from ethanol to afford the pure disaccharide **15** (53%). The mother liquor was concentrated and chromatographed on silica gel (eluent: dichloromethane/acetone, 6:1). The disaccharide **16** (10%) was first eluted, the trisaccharide **17** (16%) and remaining **15** (3%) were then obtained by further elution.

*2-*O*-(3,4,6-Tri-*O*-acetyl-2-*N*-allyloxycarbonylamino-2-deoxy-β-D-glucopyranosyl)-1,6-anhydro-4-*O*-(2,2,2-trichloroethoxycarbonyl)-β-D-mannopyranose (**15**)*

White crystalline material; mp 178°C (ethanol); $[\alpha]_D^{20}$ −44.0° (*c* 1.0, $CHCl_3$); ^1H nmr (CD_3COCD_3) δ: 6.57 (d, 1H, $J_{2',NH}$ = 7.5 Hz, N*H*), 5.92 (m, 1H, -C*H*=CH_2), 5.40 (br s, 1H, H-1), 5.33 (m, 2H, 0.5 × CH_2=CH-, H-3′), 5.18–5.13 (m, 1H, 0.5 × CH_2=CH-), 5.11 (d, 1H, $J_{1',2'}$ = 8.5 Hz, H-1′), 5.00 (dd, 1H, $J_{3',4'} = J_{4',5'}$ = 9.7 Hz, H-4′), 4.96 (m, 2H, CH_2CCl_3), 4.83 (br s, 1H, H-4), 4.71 (m, 1H, H-5), 4.58–4.47 (m, 2H, allyl CH_2), 4.29 (dd, 1H, $J_{5,6a}$ = 1.0 Hz, $J_{6a,6b}$ = 7.2 Hz, H-6a), 4.24 (dd, 1H, $J_{5',6'a}$ = 5.8 Hz, $J_{6'a,6'b}$ = 12.2 Hz, H-6′a), 4.16 (m, 1H, H-3), 4.13 (dd, 1H, $J_{5',6'b}$ = 2.6 Hz, H-6′b), 3.95 (m, 1H, H-5′), 3.82 (dd, 1H, $J_{2,3}$ = 5.1 Hz, $J_{1,2}$ = 1.9 Hz, H-2), 3.72 (m, 1H, H-2′), 3.71 (dd, 1H, $J_{5,6b}$ = 6.2 Hz, H-6b), 3.56 (s, 1H, O*H*). Anal. calcd. for $C_{25}H_{32}Cl_3NO_{16}$ (Mol. Wt. 708.87): C 42.36, H 4.55, Cl 15.00, N 1.98; found: C 42.40, H 4.55, Cl 14.88, N 1.90.

*3-*O*-(3,4,6-Tri-*O*-acetyl-2-*N*-allyloxycarbonylamino-2-deoxy-β-D-glucopyranosyl)-1,6-anhydro-4-*O*-(2,2,2-trichloroethoxycarbonyl)-β-D-mannopyranose (**16**)*

White crystalline material; mp 145–146°C (2-propanol); $[\alpha]_D^{20}$ −25.4° (*c* 1.0, $CHCl_3$); ^1H nmr (CD_3COCD_3) δ: 6.58 (d, 1H, $J_{2',NH}$ = 8.2 Hz, N*H*), 5.93 (m, 1H, -C*H*=CH_2), 5.30 (m, 2H, H-1, H-3′), 5.24 (m, 2H, 0.5 × CH_2=CH-, H-4), 5.15 (m, 1H, 0.5 × CH_2=CH-), 5.01 (dd, 1H, $J_{3',4'}$ = 9.5 Hz, $J_{4',5'}$ = 10.1 Hz, H-4′), 5.00, 4.93 (2d, 2H, CH_2CCl_3), 4.92 (d, 1H, $J_{1',2'}$ = 8.5 Hz, H-1′), 4.68 (m, 1H, H-5), 4.59–4.45 (m, 2H, allyl CH_2), 4.27 (dd, 1H, $J_{5,6a}$ = 0.9 Hz, $J_{6a,6b}$ = 7.5 Hz, H-6a), 4.24 (dd, 1H, $J_{5',6'a}$ = 5.2 Hz, $J_{6'a,6'b}$ = 12.2 Hz, H-6′a), 4.18 (dd, 1H, $J_{5',6'b}$ = 2.7 Hz, H-6′b), 4.07 (m, 1H, H-3), 3.88 (m, 1H, H-5′), 3.75 (m, 1H, $J_{2',3'}$ = 9.9 Hz, H-2′), 3.71 (dd, 1H, $J_{5,6b}$ = 6.0 Hz, H-6b), 3.59 (m, 1H, $J_{1,2}$ = 1.8 Hz, $J_{2,3}$ = 5.7 Hz, $J_{2,OH}$ = 12.1 Hz, H-2), 3.26 (d, 1H, O*H*). Anal. calcd. for $C_{25}H_{32}Cl_3NO_{16}$ (Mol. Wt. 708.87): C 42.36, H 4.55, Cl 15.00, N 1.98; found: C 42.13, H 4.49, Cl 14.86, N 1.93.

*2,3-Di-*O*-(3,4,6-tri-*O*-acetyl-2-*N*-allyloxycarbonylamino-2-deoxy-β-D-glucopyranosyl)-1,6-anhydro-4-*O*-(2,2,2-trichloroethoxycarbonyl)-β-D-mannopyranose (**17**)*

White crystalline material; mp 99–102°C (2-propanol/hexane); $[\alpha]_D^{20}$ −42.9° (*c* 1.3, $CHCl_3$); ^1H nmr (CD_3COCD_3) δ: 6.59, 6.28 (2m, 2H, N*H*), 5.96 (m, 1H, -C*H*=CH_2), 5.32 (br s, 1H, H-1), 5.30–4.90 (m, 13H, CH_2=CH-, H-1′, H-1″, H-3′, H-3″, H-4, H-4′, H-4″, CH_2CCl_3), 4.68 (m, 1H, H-5), 4.66–4.50 (m, 4H, allyl CH_2), 4.47 (dd, 1H, $J_{5',6'a}$ = 5.9 Hz, $J_{6'a,6'b}$ = 12.2 Hz, H-6′a), 4.31–4.26 (m, 3H, H-3, H-6a, H-6″a), 4.11 (dd, 1H, $J_{5',6'b}$ = 2.4 Hz, H-6′b), 4.08 (dd, 1H, $J_{5'',6''b}$ = 2.0 Hz, H-6″b), 3.94–3.89 (m, 3H, H-2′, H-5′, H-5″), 3.85 (dd, 1H, $J_{1,2}$ = 1.7 Hz, $J_{2,3}$ = 5.0 Hz, H-2), 3.75 (m, 1H, H-2″), 3.68 (dd, 1H, $J_{5,6b}$ = 6.2 Hz, $J_{6a,6b}$ = 7.2 Hz, H-6b). Anal. calcd. for $C_{41}H_{53}Cl_3N_2O_{25}$ (Mol. Wt. 1080.21): C 45.58, H 4.95, N 2.59; found: C 45.29, H 5.04, N 2.52.

*2-*O*-(3,4,6-Tri-*O*-acetyl-2-*N*-allyloxycarbonylamino-2-deoxy-β-D-glucopyranosyl)-1,6-anhydro-β-D-mannopyranose (**18**)*

Compound **15** (0.500 g, 0.705 mmol) in acetic acid (10 mL) was treated for 3 h at room temperature with an excess of zinc/copper couple (15). After filtration on Celite, the solution was evaporated to dryness and the recovered product was purified by column chromatography (eluent: ethyl acetate/acetone, 4:1). The disaccharide **18** (93%) was recovered as a white foam; $[\alpha]_D^{20}$ −32.9° (*c* 1.0, $CHCl_3$); ^1H nmr (CD_3COCD_3) δ: 6.59 (d, 1H, $J_{2',NH}$ = 9.2 Hz, N*H*), 5.90 (m, 1H, -C*H*=CH_2), 5.32 (br s, 1H, H-1), 5.27 (dd, 1H, $J_{2',3'}$ = 10.1 Hz, $J_{3',4'}$ = 9.3 Hz, H-3′), 5.25–5.13 (m, 2H, CH_2=CH-), 5.04 (d, 1H, $J_{1',2'}$ = 8.8 Hz, H-1′), 4.98 (dd, 1H, $J_{4',5'}$ = 10.2 Hz, H-4′), 4.62–4.47 (m, 2H, allyl CH_2), 4.46 (m, 1H, H-5), 4.34 (d, 1H, O*H*), 4.26 (dd, 1H, $J_{5',6'a}$ = 5.5 Hz, $J_{6'a,6'b}$ = 12.2 Hz, H-6′a), 4.17 (dd, 1H, $J_{5,6a}$ = 0.5 Hz, $J_{6a,6b}$ = 6.9 Hz, H-6a), 4.09 (dd, 1H, $J_{5',6'b}$ = 2.5 Hz, H-6′b), 4.04 (m, 1H, $J_{2,3}$ = 5.0 Hz, $J_{1,3} = J_{3,4} = J_{3,5}$ = 1.5 Hz, H-3), 3.96 (m, 1H, H-5), 3.85 (dd, 1H, $J_{1,2}$ = 1.8 Hz, H-2), 3.83 (m, 1H, H-4), 3.74 (m, 1H, H-2′), 3.62 (dd, 1H, $J_{5,6b}$ = 5.9 Hz, H-6b), 3.29 (s, 1H, O*H*). Anal. calcd. for $C_{22}H_{31}NO_{14}$ (Mol. Wt. 533.47): C 49.53, H 5.86, N 2.63; found: C 49.58, H 5.82, N 2.33.

*2,3-Di-*O*-(3,4,6-tri-*O*-acetyl-2-*N*-allyloxycarbonylamino-2-deoxy-β-D-glucopyranosyl)-1,6-anhydro-β-D-mannopyranose (**19**)*

Compound **19** was prepared from trisaccharide **17** (0.200 g, 0.185 mmol) as in the case of compound **15**. After chromatographic purification (eluent: ethyl acetate), the expected derivative was recovered as a white foam (90%); $[\alpha]_D^{20}$ −41.0° (*c* 1.0, $CHCl_3$); ^1H nmr (CD_3COCD_3) δ: 6.55, 6.21 (2d, 2H, $J_{2,NH}$ = 9.0 Hz, N*H*), 5.98, 5.93 (2m, 2H, -C*H*=CH_2), 5.23 (d, 1H, $J_{1,2}$ = 1.8 Hz, H-1), 5.32–5.12 (m, 6H, CH_2=CH-, H-3′, H-3″), 5.03 (dd, 1H, $J_{3',4'}$ = 9.8 Hz, $J_{4',5'}$ = 9.4 Hz, H-4′), 4.97 (dd, 1H, $J_{3'',4''}$ = 9.8 Hz, $J_{4'',5''}$ = 9.4 Hz, H-4″), 4.96 (d, 1H, $J_{1',2'}$ = 8.5 Hz, H-1′), 4.93 (d, 1H, $J_{1'',2''}$ = 8.5 Hz, H-1″), 4.62–4.51 (m, 4H, allyl CH_2), 4.49 (dd, 1H, $J_{5',6'a}$ = 5.7 Hz, $J_{6'a,6'b}$ = 12.3 Hz, H-6′a), 4.41 (m, 1H, H-5), 4.37 (d, 1H, *J* = 6.4 Hz, O*H*), 4.33 (dd, 1H, $J_{5'',6''a}$ = 4.9 Hz, $J_{6''a,6''b}$ = 12.2 Hz, H-6″a), 4.18 (dd, 1H, $J_{5,6a}$ = 1.0 Hz, $J_{6a,6b}$ = 7.1 Hz, H-6a), 4.16 (m, 1H, H-4), 4.09 (dd, 1H, $J_{5',6'b}$ = 2.4 Hz, H-6′b), 4.07 (dd, 1H, $J_{5'',6''b}$ = 2.1 Hz, H-6″b), 3.97–3.94 (m, 4H, H-2′, H-3, H-5′, H-5″), 3.86 (dd, 1H, $J_{2,3}$ = 4.8 Hz, H-2), 3.74 (m, 1H, $J_{2'',3''}$ = 9.9 Hz, H-2″), 3.54 (dd, 1H, $J_{5,6b}$ = 6.0 Hz, H-6b). Anal. calcd. for $C_{38}H_{52}N_2O_{23}$ (Mol. Wt. 904.81): C 50.44, H 5.79, N 3.10; found: C 50.00, H 5.75, N 3.03.

*1,3,4,6-Tetra-*O*-acetyl-2-*O*-(3,4,6-tri-*O*-acetyl-2-*N*-allyloxycarbonylamino-2-deoxy-β-D-glucopyranosyl)-α-D-mannopyranose (**20α**)*

Compound **18** (0.243 g, 0.455 mmol) was treated as in the case of compound **4**, affording **8**. The recovered α/β mixture (7:1) was purified by column chromatography (eluent: ethyl acetate/hexane, 3:1). The pure α derivative (72%) was recovered first as a white crystalline material; a second fraction contained an unseparated α/β mixture (1:1, 23%); mp 149–150°C (2-propanol); $[\alpha]_D^{20}$ −2.8° (*c* 1.0, CH_2Cl_2); ^1H nmr (CD_3COCD_3) δ: 6.64 (d, 1H, $J_{2',NH}$ = 9.3 Hz, N*H*), 6.07 (d, 1H, $J_{1,2}$ = 1.9 Hz, H-1), 5.89 (m, 1H, -C*H*=CH_2), 5.37–5.12 (m, 4H, H-3′, H-4, CH_2=CH-), 5.06 (dd, 1H, $J_{2,3}$ = 2.5 Hz, $J_{3,4}$ = 10.4 Hz, H-3), 5.01 (dd, 1H, $J_{3',4'} = J_{4',5'}$ = 9.7 Hz, H-4′), 4.89 (d, 1H, $J_{1',2'}$ = 8.5 Hz, H-1′), 4.56–4.47 (m, 2H, allyl CH_2), 4.30 (dd, 1H, H-2), 4.26 (dd, 1H, $J_{5',6'a}$ = 5.4 Hz, $J_{6'a,6'b}$ = 11.8 Hz, H-6′a), 4.15–3.98 (m, 4H, H-5, H-6a, H-6b, H-6′b), 3.82 (m, 1H, $J_{5',6'b}$ = 2.3 Hz, H-5′), 3.74 (m, 1H, $J_{2',3'}$ = 10.1 Hz, H-2′).

Anal. calcd. for $C_{30}H_{41}NO_{19}$ (Mol. Wt. 719.64): C 50.07, H 5.74, N 1.95; found: C 49.80, H 5.83, N 1.94.

Compound **20**β was characterized by an anomeric proton at 5.88 (d, 1H, $J_{1,2}$ = 0.8 Hz, H-1).

1,4,6-Tri-O-acetyl-2,3-di-O-(3,4,6-tri-O-acetyl-2-N-allyloxycarbonylamino-2-deoxy-β-D-glucopyranosyl)-D-mannopyranose (21)

This derivative was prepared as compound **8** from compound **4**, to afford, after chromatographic purification (eluent: ethyl acetate), an anomeric mixture (87%, α/β, 9:1) that was difficult to separate; ^{1}H nmr (CD_3COCD_3) δ: 6.73, 6.18 (2m, 2H, N*H*), 6.13 (d, 0.9H, $J_{1,2}$ = 2.7 Hz, H-1α), 6.08, 5.92 (2m, 2H, -C*H*=CH_2), 5.83 (d, 0.1H, $J_{1,2}$ = 0.8 Hz, H-1β). Anal. calcd. for $C_{44}H_{60}N_2O_{27}$ (Mol. Wt. 1048.94): C 50.38, H 5.77, N 2.67; found: C 50.37, H 5.89, N 2.52.

3-O-Acetyl-2-O-(3,4,6-tri-O-acetyl-2-N-allyloxycarbonylamino-2-deoxy-β-D-glucopyranosyl)-1,6-anhydro-β-D-mannopyranose (22)

The disaccharide **15** (0.690 g, 0.974 mmol) was acetylated as usual and then treated with the Zn/Cu couple as already described for the synthesis of compound **18**. After column chromatography (eluent: ethyl acetate/acetone, 7:1), **22** was recovered as a white foam (91%); $[\alpha]_D^{20}$ −44.7° (*c* 1.0, $CHCl_3$); ^{1}H nmr (CD_3COCD_3) δ: 6.54 (d, 1H, $J_{2',NH}$ = 8.6 Hz, N*H*), 5.94 (m, 1H, -C*H*=CH_2), 5.30 (m, 1H, 0.5 × CH_2=CH-), 5.25 (dd, 1H, $J_{2',3'} = J_{3',4'}$ = 9.7 Hz, H-3′), 5.20 (m, 1H, $J_{2,3}$ = 5.6 Hz, $J_{3,4}$ = 1.5 Hz, H-3), 5.17 (m, 1H, 0.5 × CH_2=CH-), 4.98 (dd, 1H, $J_{4',5'}$ = 10.0 Hz, H-4′), 4.96 (d, 1H, $J_{1',2'}$ = 8.5 Hz, H-1′), 4.64 (d, 1H, *J* = 6.0 Hz, O*H*), 4.60–4.49 (m, 3H, H-5, allyl CH_2), 4.23 (dd, 1H, $J_{5',6'a}$ = 4.6 Hz, $J_{6'a,6'b}$ = 12.2 Hz, H-6′a), 4.11 (dd, 1H, $J_{5,6a}$ = 1.0 Hz, $J_{6a,6b}$ = 7.1 Hz, H-6a), 4.02 (dd, 1H, $J_{5',6'b}$ = 2.2 Hz, H-6′b), 3.99 (dd, 1H, H-2), 3.86 (m, 1H, H-5′), 3.75 (m, 1H, $J_{4,5}$ = 1.5 Hz, H-4), 3.69 (dd, 1H, $J_{5,6b}$ = 6.0 Hz, H-6b), 3.65 (m, 1H, H-2′). Anal. calcd. for $C_{24}H_{33}NO_{15}$ (Mol. Wt. 575.51): C 50.08, H 5.78, N 2.43; found: C 50.10, H 5.74, N 2.53.

3-O-Acetyl-2,4-di-O-(3,4,6-tri-O-acetyl-2-N-allyloxycarbonylamino-2-deoxy-β-D-glucopyranosyl)-1,6-anhydro-β-D-mannopyranose (23)

The disaccharide **22** (0.460 g, 0.80 mmol) was glycosylated as usual with the donor **1** (0.360 g, 0.83 mmol) and trimethylsilyl triflate (0.218 mL, 1.2 mmol). After the usual work-up procedure and column chromatography (eluent: ethyl acetate), compound **23** was obtained as a white crystalline material (68%); mp 216°C (ether); $[\alpha]_D^{20}$ −4.5° (*c* 1.0, $CHCl_3$); ^{1}H nmr (CD_3COCD_3) δ: 6.51 (2m, 2H, N*H*), 5.97–5.87 (m, 2H, C*H*=CH_2), 5.51 (m, 1H, H-3), 5.37 (br s, 1H, H-1), 5.31–5.13 (m, 6H, CH_2=CH-, H-3′, H-3″), 5.03 (d, 1H, $J_{1',2'}$ = 8.0 Hz, H-1′), 5.02 (dd, 1H, $J_{3',4'}$ = 9.8 Hz, $J_{4',5'}$ = 10.0 Hz, H-4′), 4.98 (dd, 1H, $J_{3'',4''}$ = 9.5 Hz, $J_{4'',5''}$ = 10.0 Hz, H-4″), 4.95 (d, 1H, $J_{1'',2''}$ = 8.0 Hz, H-1″), 4.58–4.52 (m, 5H, allyl CH_2, H-5), 4.28–4.26 (m, 2H, H-6′a, H-6″a), 4.18 (dd, 1H, $J_{5',6'b}$ = 2.5 Hz, $J_{6'a,6'b}$ = 12.2 Hz, H-6′b), 4.08 (dd, 1H, $J_{5,6a}$ = 1.0 Hz, $J_{6a,6b}$ = 7.2 Hz, H-6a), 3.99 (dd, 1H, $J_{5'',6''b}$ = 2.1 Hz, $J_{6''a,6''b}$ = 12.2 Hz, H-6″b), 3.89–3.81 (m, 4H, H-2, H-4, H-5′, H-5″), 3.69 (dd, 1H, $J_{5,6b}$ = 6.0 Hz, H-6b), 3.65 (m, 1H, H-2′), 3.62 (m, 1H, H-2″). Anal. calcd. for $C_{40}H_{54}N_2O_{24}$ (Mol. Wt. 946.85): C 50.74, H 5.75, N 2.96; found: C 50.94, H 5.86, N 2.98.

1. J. MONTREUIL. Adv. Carbohydr. Chem. Biochem. **37**, 157 (1980).
2. J. MONTREUIL. Pure Appl. Chem. **56**, 859 (1984).
3. R. KORNFELD and S. KORNFELD. *In* The biochemistry of glycoproteins and proteoglycans. *Edited by* W. J. Lennarz. Plenum Press, New York. 1980. p. 1.
4. P. BOULLANGER, J. BANOUB, and G. DESCOTES. Can. J. Chem. **65**, 1343 (1987).
5. J. ARNARP and J. LÖNNGREN. J. Chem. Soc. Perkin Trans. 1, 2070 (1981).
6. J. ARNARP, M. HARALDSSON, and J. LÖNNGREN. Carbohydr. Res. **97**, 307 (1981).
7. V. HINDSGAUL, O. HINDSGAUL, and J. U. BAENZIGER. Can. J. Chem. **65**, 1645 (1987).
8. M. KLOOSTERMAN, P. WESTERDUIN, and J. H. VAN BOOM. Recl. Trav. Chim. Pays-Bas, **105**, 136 (1986).
9. K. K. SADOZAI, T. NUKADA, Y. ITO, Y. NAKAHARA, T. OGAWA, and A. KOBATA. Carbohydr. Res. **157**, 101 (1986).
10. P. L. DURETTE and T. Y. SHEN. Carbohydr. Res. **65**, 314 (1978).
11. K. BOCK and M. MELDAL. Acta Chem. Scand. Ser. B: 775 (1983).
12. A. E. KNAUF, R. M. HANN, and C. S. HUDSON. J. Am. Chem. Soc. **63**, 1447 (1941).
13. D. LAFONT, P. BOULLANGER, O. CADAS, and G. DESCOTES. Synthesis, 191 (1989).
14. P. BOULLANGER, D. LAFONT, J. BANOUB, and G. DESCOTES. J. Carbohydr. Chem. **8**, 343 (1989).
15. T. B. WINDHOLZ and D. B. R. JOHNSTON. Tetrahedron Lett. 2555 (1967).
16. A. F. COOK. J. Org. Chem. **33**, 3589 (1968).
17. R. U. LEMIEUX, M. T. TAKEDA, and B. Y. CHUNG. Am. Chem. Soc. Symp. Ser. **39**, 90 (1976).
18. H. LÖNN. Carbohydr. Res. **139**, 105 (1985).
19. T. OGAWA, M. SUGIMOTO, T. KITAJIMA, K. K. SADOZAI, and T. NUKADA. Tetrahedron Lett. **27**, 5739 (1986).
20. P. BOULLANGER, P. CHATELARD, G. DESCOTES, M. KLOOSTERMAN, and J. H. VAN BOOM. J. Carbohydr. Chem. **5**, 541 (1986).
21. Y. HAYAKAWA, H. KATO, M. UCHIYAMA, H. KAJINO, and R. NOYORI. J. Org. Chem. **51**, 2400 (1986).
22. O. DANGLES, F. GUIBE, G. BALAVOINE, S. LAVIELLE, and A. MARQUET. J. Org. Chem. **52**, 4984 (1987).

Can. J. Chem. Downloaded from www.nrcresearchpress.com by 88.85.125.76 on 09/07/12
For personal use only.

Structure and conformation of 5-methoxymethyl-2′-deoxycytidine

ZONGCHAO JIA AND GUY TOURIGNY
Department of Chemistry, University of Saskatchewan, Saskatoon, Sask., Canada S7N 0W0
LOUIS T. J. DELBAERE
Department of Biochemistry, University of Saskatchewan, Saskatoon, Sask., Canada S7N 0W0
AND
ALLAN L. STUART AND SAGAR V. GUPTA[1]
Department of Veterinary Physiological Sciences, University of Saskatchewan, Saskatoon, Sask., Canada S7N 0W0

Received November 28, 1989

ZONGCHAO JIA, GUY TOURIGNY, LOUIS T. J. DELBAERE, ALLAN L. STUART, and SAGAR V. GUPTA. Can. J. Chem. **68**, 836 (1990).

The three-dimensional structure of the antiviral agent 5-methoxymethyl-2′-deoxycytidine (MMdCyd) was deduced by X-ray crystallographic analysis. MMdCyd crystallized in space group $P2_1$ with $a = 7.9255(6)$ Å; $b = 16.1505(15)$ Å, $c = 10.1861(5)$ Å, $\beta = 103.801(5)°$, and $Z = 4$ (2 molecules per asymmetric unit); $R = 0.044$ ($R_w = 0.046$) for 2560 observed reflections with net $I > 3\sigma(I)$. The furanose ring adopts the C(3′)-*exo* envelope conformation ($_3E$) in molecule A and the C(2′)-*endo* envelope conformation (^2E) in molecule B. In the sugar ring of both crystallographically independent molecules A and B, the side chain at C(5′) has the g^+ conformation. This appears to be a preferred geometry required for antiherpes activity in 2′-deoxyribonucleosides. The glycosyl linkage is *anti* with $\chi = 213.7°$ for the A molecule and 222.2° for the B molecule. With respect to this *anti* conformation, the methoxy group at C(5) in molecules A and B exhibits different conformations; it is on the same side of the pyrimidine plane as the deoxyribofuranose ring oxygen (O4′) in molecule B and on the opposite side in molecule A.

Key words: antiherpes agent, conformation, 5-methoxymethyl-2′-deoxycytidine, crystal structure.

ZONGCHAO JIA, GUY TOURIGNY, LOUIS T. J. DELBAERE, ALLAN L. STUART et SAGAR V. GUPTA. Can. J. Chem. **68**, 836 (1990).

On a déduit la structure tridimensionnelle de l'agent antiviral, 5-méthoxyméthyl-2′-désoxycytidine (MMdCyd), d'une analyse par diffraction des rayons-X. Le MMdCyd crystallise dans le groupe d'espace $P2_1$, avec $a = 7{,}9255(6)$, $b = 16{,}1505(15)$ et $c = 10{,}1861(5)$ Å, $\beta = 1030{,}801(5)°$ et $Z = 2$ (2 molécules par unité asymétrique); $R = 0{,}044$ ($R_w = 0{,}046$) pour 2560 réflexions observées avec $I > 3\sigma(I)$. Le cycle furanose adopte la conformation enveloppe C(3′)-*exo* ($_3E$) dans la molécule A et la conformation enveloppe C(2′)-*endo* (^2E) dans la molécule B. Dans le sucre cyclique de chacune des molécules A et B qui sont indépendantes d'un point de vue cristallographique, la chaîne latérale en C(5′) possède une conformation g^+. Cette conformation semble possédée la géométrie préférée pour détenir une activité antiherpès dans les 2′-désoxyribonucléosides. La liaison glycosyle est *anti* avec $\chi = 213{,}7°$ pour la molécule A et 222,2° pour la molécule B. Par rapport à cette conformation *anti*, les groupements méthoxyles présents dans les positions C(5) des molécules A et B présentent des conformations différentes; ils se trouvent sur le même côté du plan pyrimidine sous la forme de l'oxygène O4′ du cycle du désoxyribofuranose de la molécule B et sur des côtés opposés dans la molécule A.

Mots clés : agent antiherpès, conformation, 5-méthoxyméthyl-2′-désoxycytidine, structure cristalline.

[Traduit par la revue]

Introduction

The discovery of 5-substituted-2′-deoxyuridines with selective activity against Herpes simplex virus was a major development in the area of viral chemotherapy (for reviews see refs. 1–3). The basis for selective antiherpes activity of 5-alkyl-2′-deoxyuridines is primarily due to the specific interaction with two virus-induced enzymes, the deoxythymidine-deoxycytidine (dThd/dCyd) kinase (viral-K) and the DNA polymerase. Cleavage of the *N*-glycosidic bond of many of these 5-substituted-2′-deoxyuridines by nucleoside phosphorylases rapidly leads to loss of biological activity (4–6). Thymidine phosphorylase (EC 2.4.2.4) is specific for the 2′-deoxyribosyl moiety of the nucleosides whereas uridine phosphorylase (EC 2.4.2.3) has broader substrate specificity (7–10). One possible approach to overcome this limitation is to use deoxycytidine analogs. The rationale for this hypothesis is (i) dCyd analogs are not substrates for thymidine and (or) uridine phosphorylase and (ii) in HSV-infected cells, dCyd analogs will be metabolized primarily by the virus-induced dCyd kinase – deoxycytidylate kinase pathway. Our findings on the biological activity of (*E*)-5-(2-bromovinyl)-2′-deoxycytidine (BrVdCyd) and 5-methoxymethyl-2′-deoxycytidine (MMdCyd) are consistent with the proposed hypothesis. When deamination is prevented, BrVdCyd and MMdCyd are potent and selective inhibitors of HSV replication (11, 12).[2] MMdCyd is selectively phosphorylated by the viral-K and the substrate specificity is related to the chain length of the substituent at the C(5) position of the pyrimidine ring. MMdCyd triphosphate is utilized preferentially by HSV-induced DNA polymerase and is also a potent inhibitor of viral DNA polymerase (11).[3]

As a part of our program to determine the steric conformation required for the substrate specificity towards viral-K and mammalian phosphorylases (15–19), we have determined the crystal structure of MMdCyd and the results are discussed in this paper. Impetus for continuing these investigations is that understanding molecular conformation requirements for biological activity would aid in the design of better drugs for the treatment of viral infections.

[1]Author to whom correspondence may be addressed.

[2]Also, P. J. Aduma, V. S. Gupta, A. L. Stuart, and G. Tourigny. Submitted to Antiviral Chem. Chemother.

[3]Also., P. J. Aduma, V. S. Gupta, H. S. Allaudeen, A. L. Stuart, and G. Tourigny. Submitted to J. Biol. Chem.

Can. J. Chem. Downloaded from www.nrcresearchpress.com by 88.85.125.76 on 09/07/12
For personal use only.

TABLE 1. Bond distances (Å, estimated standard deviation of the last digit is given in parentheses)

Bond*	Distance (Å)	Bond†	Distance (Å)
N(1A)—C(2A)	1.396(4)	N(1B)—C(2B)	1.390(4)
N(1A)—C(6A)	1.359(4)	N(1B)—C(6B)	1.365(4)
N(1A)—C(1′A)	1.492(3)	N(1B)—C(1′B)	1.477(3)
C(2A)—O(2A)	1.227(4)	C(2B)—O(2B)	1.239(4)
C(2A)—N(3A)	1.354(3)	C(2B)–N(3B)	1.355(3)
N(3A)—C(4A)	1.337(4)	N(3B)—C(4B)	1.336(4)
C(4A)—N(4A)	1.327(3)	C(4B)—N(4B)	1.328(3)
C(4A)—C(5A)	1.442(4)	C(4B)—C(5B)	1.440(4)
C(5A)—C(5, 1A)	1.494(4)	C(5B)—C(5, 1B)	1.495(4)
C(5A)—C(6A)	1.344(3)	C(5B)—C(6B)	1.346(3)
C(5, 1A)—O(5, 2A)	1.411(4)	C(5, 1B)—O(5, 2B)	1.417(5)
O(5, 2A)—C(5, 3A)	1.414(4)	O(5, 2B)—C(5, 3B)	1.418(5)
C(1′A)—C(2′A)	1.508(5)	C(1′B)—C(2′B)	1.516(4)
C(1′A)—O(4′A)	1.410(4)	C(1′B)—O(4′B)	1.416(5)
C(2′A)—C(3′A)	1.518(4)	C(2′B)—C(3′B)	1.520(4)
C(3′A)—O(3′A)	1.429(4)	C(3′B)—O(3′B)	1.433(3)
C(3′A)—C(4′A)	1.517(5)	C(3′B)—C(4′B)	1.530(5)
C(4′A)—O(4′A)	1.449(4)	C(4′B)—O(4′B)	1.447(3)
C(4′A)—C(5′A)	1.510(6)	C(4′B)—C(4′B)	1.514(5)
C(5′A)—O(5′A)	1.412(5)	C(5′B)—O(5′B)	1.410(5)

*MMdCyd, molecule A.
†MMdCyd, molecule B.

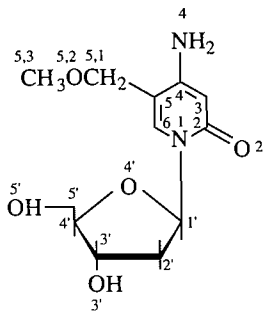

FIG. 1. Structure and atomic numbering of MMdCyd.

Results and discussion

The synthesis of MMdCyd **5** was accomplished from MMdUrd (1) in four steps. Protection of the 3′- and 5′-OH groups by acetylation was followed by conversion to the 4-triazolyl derivative which was treated with a saturated solution of ammonia in dioxane. Deacetylation with methanolic ammonia gave the desired product, **5**, in 44% yield. The structural formula with atomic numbering for MMdCyd is shown in Fig. 1.

X-Ray analysis

The bond lengths and angles determined for MMdCyd are given in Tables 1 and 2 respectively. The stereoscopic view of the molecules A and B of MMdCyd are shown in Fig. 2. The two crystallographically independent molecules are very similar to each other. Bond lengths and angles for MMdCyd molecules are similar to those reported for 5-methoxymethyl-2′-deoxyuridine (MMdUrd) and are in the range reported for 2′-deoxycytidine nucleosides (15, 20–25). Selected torsion angles for molecules A and B of MMdCyd compared to the corresponding angles in MMdUrd are shown in Table 3. The conformation of the glycosidic bond is *anti* with the torsion angle O(4′)-C(1′)-N(1)-C(2), χ, having values of 213.7° and 222.2° for molecules A and B, respectively. These values are lower than the χ value of MMdUrd (233.3°) but are in the range reported for cytidine and deoxycytidine nucleosides (200–222°). The exocyclic 5′CH_2OH side chain has the g^+ conformation in both molecules A and B of MMdCyd and also in MMdUrd; this seems to be a preferred conformation for antiherpes activity in 2′-deoxyribonucleosides. The g^+ conformation is the most common found in cytidine and deoxycytidine compounds. However, it is interesting to note that 5-methyl-2′-deoxycytidine displays the t conformation (21).

In addition to the slightly different conformation of the deoxyribofuranose ring, the orientation of the methoxymethyl group at C(5) of the cytosine moiety is different in molecules A and B of MMdCyd. With respect to the *anti* conformation of the glycosidic bond, the C(5) substituent is on the same side of the pyrimidine ring plane as O(4′) in molecule B and on the opposite side in molecule A as demonstrated by torsion angles, C(6)—C(5)—C(5,1)—O(5,2), 129.5(4)°(A), −115.8(4)°(B) (Fig. 2.). It is interesting to note that for HMdUrd, the only other case where different steric orientation of the C(5) substituent has previously been reported, the two possible orientations were attributed to disorder, with little difference in energy between them (26). In the case of MMdCyd, the two different orientations of the C(5) substituent are not the result of statistic disorder but are probably due to packing forces in the unit cell.

The deoxyribose ring has an envelope conformation in both molecules A and B of MMdCyd. The conformations and the corresponding displacements from the mean plane through the other four ring atoms are as follows: C(3′)-*exo* ($_3E$), 0.49 Å (planar within 0.04 Å) for molecule A and C(2′)-*endo* (^2E), 0.52 Å (planar within 0.05 Å) for molecule B. The values calculated for the two pseudo-rotational parameters of the furanose ring torsion angles in terms of the two degrees of freedom for ring puckering (27) are phase angles P = 185.5° and 174.5° and puckering amplitude τ_m = 32.3° and 36.3° for

Can. J. Chem. Downloaded from www.nrcresearchpress.com by 88.85.125.76 on 09/07/12
For personal use only.

Can. J. Chem. Downloaded from www.nrcresearchpress.com by 88.85.125.76 on 09/07/12
For personal use only.

TABLE 2. Bond angles (degrees, estimated standard deviation of the last digit is given in parentheses)

Bonds*	Angle	Bonds†	Angle
C(2A)—N(1A)—C(6A)	120.9(2)	C(2B)—N(1B)—C(6B)	120.6(2)
C(2A)—N(1A)—C(1′A)	117.5(2)	C(2B)—N(1B)—C(1′B)	119.6(2)
C(6A)—N(1A)—C(1′A)	121.4(2)	C(6B)—N(1B)—C(1′B)	119.8(2)
N(1A)—C(2A)—O(2A)	118.5(2)	N(1B)—C(2B)—O(2B)	119.7(2)
N(1A)—C(2A)—N(3A)	118.6(2)	N(1B)—C(2B)—N(3B)	118.5(2)
O(2A)—C(2A)—N(3A)	122.9(3)	O(2B)—C(2B)—N(3B)	121.8(2)
C(2A)—N(3A)—C(4A)	120.5(2)	C(2B)—N(3B)—C(4B)	120.8(2)
N(3A)—C(4A)—N(4A)	117.5(2)	N(3B)—C(4B)—N(4B)	117.8(2)
N(3A)—C(4A)—C(5A)	122.0(2)	N(3B)—C(4B)—C(5B)	121.8(2)
N(4A)—C(4A)—C(5A)	120.4(2)	N(4B)—C(4B)—C(5B)	120.3(2)
C(4A)—C(5A)—C(5, 1A)	121.6(2)	C(4B)—C(5B)—C(5, 1B)	122.0(2)
C(4A)—C(5A)—C(6A)	116.0(2)	C(4B)—C(5B)—C(6B)	115.9(2)
C(5, 1B)—C(5A)—C(6A)	122.0(2)	C(5, 1B)—C(5B)—C(6B)	122.1(2)
C(5A)—C(5, 1A)—O(5, 2A)	109.3(2)	C(5B)—C(5, 1B)—O(5, 2B)	109.6(2)
C(5, 1A)—O(5, 2A)—C(5, 3A)	111.9(2)	C(5, 1B)—O(5, 2B)—C(5, 3B)	111.4(3)
N(1A)—C(6A)—C(5A)	121.9(2)	N(1B)—C(6B)—C(5B)	122.1(2)
N(1A)—C(1′A)—C(′2A)	114.9(2)	N(1B)—C(1′B)—C(2′B)	113.3(2)
N(1A)—C(1′A)—O(4′A)	107.4(2)	N(1B)—C(1′B)—O(4′B)	108.3(2)
C(2′A)—C(1′A)—O(4′A)	107.4(2)	C(2′B)—C(1′B)—O(4′B)	106.5(2)
C(1′A)—C(2′A)—C(3′A)	103.4(2)	C(1′B)—C(2′B)—C(3′B)	102.1(2)
C(2′A)—C(3′A)—O(3′A)	113.1(3)	C(2′B)—C(3′B)—O(3′B)	112.4(2)
C(2′A)—C(3′A)—C(4′A)	102.5(2)	C(2′B)—C(3′B)—C(4′B)	102.0(2)
O(3′A)—C(3′A)—C(4′A)	110.8(3)	O(3′B)—C(3′B)—C(4′B)	108.2(2)
C(3′A)—C(4′A)—O(4′A)	105.9(2)	C(3′B)—C(4′B)—O(4′B)	105.9(2)
C(3′A)—C(4′A)—C(5′A)	115.6(3)	C(3′B)—C(4′B)—C(5′B)	116.1(3)
O(4′A)—C(4′A)—C(5′A)	111.0(2)	O(4′B)—C(4′B)—C(5′B)	109.8(2)
C(1′A)—O(4′A)—C(4′A)	110.1(2)	C(1′B)—O(4′B)—C(4′B)	109.9(2)
C(4′A)—C(5′A)—O(5′A)	110.5(3)	C(4′B)—C(5′B)—O(5′B)	113.2(3)

*MMdCyd, molecule A.
†MMdCyd, molecule B.

TABLE 3. Comparison of selected torsion angles (degrees, estimated standard deviation of the last digit is given in parentheses) of MMdCyd and MMdUrd

Torsion angle	A*	B†	MMdUrd‡
C(1′)—C(2′)—C(3′)—C(4′)	−32.2(4)	−36.1(3)	−36.0
C(2′)—C(3′)—C(4′)—O(4′)	28.5(4)	28.2(3)	22.4
C(3′)—C(4′)—O(4′)—C(1′)	−13.6(4)	−8.6(3)	1.4
C(4′)—O(4′)—C(1′)—C(2′)	−7.4(4)	−15.1(3)	−24.8
O(4′)—C(1′)—C(2′)—C(3′)	25.2(4)	32.4(3)	38.0
O(5′)—C(5′)—C(4′)—O(3′)	−69.4(4)	−58.8(4)	−63.1
O(5′)—C(5′)—C(4′)—C(3′)	51.1(4)	61.3(4)	55.9
H(C1′)—C(1′)—C(2′)—H(1C2′)	48	49	36
H(C1′)—C(1′)—C(2′)—H(2C2′)	169	168	162
H(1C2′)—C(2′)—C(3′)—H(C3′)	84	78	82
H(2C2′)—C(2′)—C(3′)—H(C3′)	−35	−41	−41
H(C3′)—C(3′)—C(4′)—H(C4′)	−87	−89	−97
H(C4′)—C(4′)—C(5′)—H(1C5′)	−72	−63	−62
H(C4′)—C(4′)—C(5′)—H(2C5′)	49	60	60
O(4′)—C(1′)—N(1)—C(2)§	213.7(4)	222.2(3)	233.3
C(5)—C(5, 1)—O(5, 2)—C(5, 3)	166.9(3)	168.6(3)	−114.2
C(6)—C(5)—C(5, 1)—O(5, 2)	129.5(4)	−115.8(4)	−99.2

*MMdCyd, molecule A.
†MMdCyd, molecule B.
‡The data for 5-methoxymethyl-2′-deoxyuridine (MMdUrd) were included for comparison (15).
§The convention (14), based on accepted IUPAC nomenclature, differs from χ_{CN}, which was defined by O(4′)—C(1′)—N(1)—C(6). $\chi = \chi_{CN} \pm 180$, viz. *syn* = 0 ± 90 and *anti* = 180 ± 90.

Can. J. Chem. Downloaded from www.nrcresearchpress.com by 88.85.125.76 on 09/07/12
For personal use only.

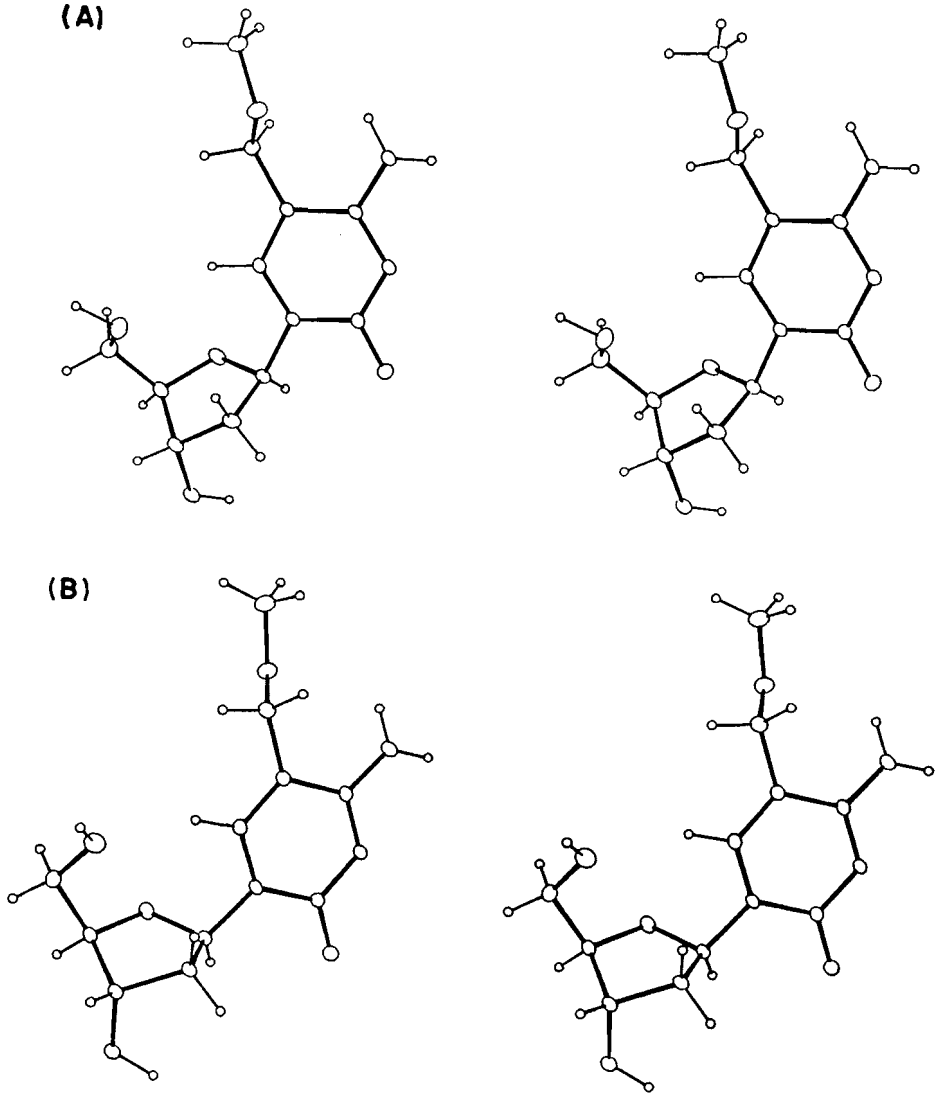

FIG. 2. Stereoscopic ORTEP view of MMdCyd. Top: molecule A. Bottom: molecule B.

TABLE 4. Intermolecular hydrogen-bond (Å) in MMdCyd

D—H...E	H...E	D—H...E	Symmetry operation on atom*
O(5'B)—H(O5'B)*...O(3'B)	1.80	2.86	$-x, y+1/2, -z$
N(4A)—H(1N4A)...O(3'B)*	2.23	2.86	$x-1, y, z+1$
O(3'B)—H(O3'B)...O(2A)*	1.74	2.70	$x, y, z+1$
O(3'A)—H(O3'A)*...O(2B)	1.97	2.80	$x, y, z+1$
N(4B)—H(2N4B)...N(3A)*	2.08	2.98	$x+1, y, z$
N(4A)—H(N4A)*...N(3B)	2.21	3.06	$x+1, y, z$
O(5'B)—H(O5'B)*...N(3B)	2.14	2.99	$x-1, y, z$

molecules A and B, respectively. The values calculated for the two pseudorotational parameters for MMdUrd were $P = 159.3°$ and $\tau_m = 39.6°$. These results indicate that the deoxyribose moiety in both molecules A and B of MMdCyd has a typical *S* conformation. Most deoxycytidine derivatives have either ^2E or $_3E$ puckering of the sugar ring.

The crystal structure has several intermolecular hydrogen bonds, which are summarized in Table 4.

Experimental

Chemistry

5-Methoxymethyl-3',5'-di-O-acetyl-2'-deoxyuridine, 2

Acetic anhydride (22 mL, 240 mmol) was added to a solution of 5-methoxymethyl-2'-deoxyuridine, **1**, (5.00 g, 18.4 mmol) in 75 mL of anhydrous pyridine and the solution was stirred at room temperature for 18 h. The reaction mixture, concentrated to 25 mL, was added slowly to 250 mL of cold water. The aqueous solution was extracted with $CHCl_3$ and the organic layer was washed with 0.1 M HCl, 5% $NaHCO_3$, and H_2O. Residual pyridine was removed by coevaporation with toluene. The solution was dried and the solvent was removed on a rotary evaporator. Recrystallization from ethyl acetate – petroleum ether gave *5-methoxymethyl-3',5'-di-O-acetyl-2'-deoxyuridine*, **2**, (6.0 g, 70%), mp 110–112°C; UV (MeOH), λ_{max}: 264 nm (ϵ, 9300), λ_{min}: 232 nm (ϵ, 2100); ^{1}H NMR (DMSO-d_6), δ: 11.46 (s, 1, 3-NH), 7.61 (s, 1, 6-H), 6.17 (m, 1, 1'-H), 5.18 (m, 1, 3'-H), 4.22 (m, 2, 5'-H, 5''-H), 4.18 (m, 1, 4'-H), 4.06 (s, 2, 5-CH_2O), 3.24 (s, 5-OCH_3), 2.35 (m, 2, 2'-H, 2''-H), 2.06 (s, 6, CH_3COO). Anal. calcd. for $C_{15}H_{20}N_2O_8$: C 50.56, H 5.66, N 7.86; found: C 50.86, H 5.63, N 7.60.

5-Methoxymethyl-3',5'-di-O-acetyl-2'-deoxycytidine, 4

1,2,4-Triazole (11.2 g, 162 mmol), redistilled $POCl_3$ (3.4 mL, 36 mmol), and triethylamine (22 mL, 160 mmol) were added dropwise

Can. J. Chem. Downloaded from www.nrcresearchpress.com by 88.85.125.76 on 09/07/12
For personal use only.

TABLE 5. Fractional coordinates and average thermal parameters for MMdCyd molecule A and molecule B (estimated standard deviation of the last digit is given in parentheses; non-hydrogen atoms × 10^4; $U_{eq} = (U_{11} + U_{22} + U_{33})/3$)

Atom	x/a	y/b	z/c	$10^3\ U_{eq}$ (Å^2)
C(2A)	1654(4)	8562(3)	4702(3)	34
O(2A)	1859(3)	8844(3)	5771(2)	53
N(3A)	2898(3)	8594(2)	3533(2)	35
C(4A)	2616(3)	8263(2)	2401(3)	29
N(4A)	3890(3)	8311(3)	1290(3)	39
C(5A)	0985(3)	7879(2)	2363(3)	28
C(5, 1A)	0601(4)	7606(3)	1063(3)	34
O(5, 2A)	1882(3)	7038(2)	0415(2)	42
C(5, 3A)	1819(5)	6896(3)	0943(3)	47
C(6A)	0225(4)	7861(2)	3538(3)	29
C(1′A)	1343(4)	8241(3)	5955(3)	31
C(2′A)	1461(4)	7506(3)	6887(3)	39
C(3′A)	3399(4)	7415(3)	7482(3)	35
O(3′A)	4015(3)	7911(2)	8662(2)	47
C(4′A)	4169(4)	7707(3)	6335(3)	36
O(4′A)	2936(3)	8296(2)	5572(2)	37
C(5′A)	4573(5)	7035(3)	5426(4)	53
O(5′A)	3115(3)	6517(3)	4971(3)	56
N(1B)	0177(3)	9890(2)	0045(2)	28
C(2B)	1758(3)	9529(3)	0007(3)	31
O(2B)	2030(3)	9314(2)	1092(2)	48
N(3B)	2976(3)	94385	1183(2)	34
C(4B)	2648(4)	9668(3)	2358(3)	30
N(4B)	3915(3)	9587(3)	3469(3)	44
C(5B)	0981(3)	9991(2)	2437(3)	29
C(5, 1B)	0574(4)	10199(3)	3757(3)	35
O(5, 2B)	1652(3)	10859(2)	4381(2)	44
C(5, 3B)	1552(6)	10969(4)	5741(4)	60
C(6B)	0188(3)	10089(2)	1249(3)	29
C(1′B)	1116(3)	10059(2)	1233(3)	27
C(2′B)	2616(4)	9450(2)	1516(3)	27
C(3′B)	4088(3)	9970(2)	2344(3)	29
O(3′B)	4003(3)	10042(2)	3729(2)	36
C(4′B)	3707(4)	10821(3)	1679(3)	32
O(4′B)	1847(3)	10850(2)	1134(2)	32
C(5′B)	4635(5)	11022(3)	0580(4)	47
O(5′B)	4209(3)	10475(3)	0530(2)	53

with stirring to 49 mL of acetonitrile at 4°C. **2** (2.14 g, 6.05 mmol), dissolved in 24 mL of acetonitrile, was added to the suspension and the mixture was stirred at room temperature for 1.5 h. The solvent was evaporated and the residue was dissolved in $CHCl_3$, washed with saturated $NaHCO_3$, then with water, and dried over $MgSO_4$. TLC on silica gel G with EtOAc indicated one UV sensitive spot (R_f 0.29). The ratio of the UV absorption maxima in MeOH, λ250: λ322, was 1.45. The crude 4-triazolyl-5-methoxymethyl-3′,5′-di-*O*-acetyl-2′-deoxyuridine, **3**, was dissolved in 50 mL of dried, peroxide-free 1,4-dioxane. The solution was chilled, saturated with ammonia, and stored in a Wheaton pressure bottle at room temperature for 18 h. The solvent was evaporated and the gummy residue was eluted with 90:10 $CHCl_3$–MeOH on a silica gel column (2.7 cm × 100 cm). Recrystallization from EtOAc gave *5-methoxymethyl-3′,5′-di-*O*-acetyl-2′-deoxycytidine*, **4** (1.81 g, 84%), mp 124–125°C; UV (0.1 M HCl), λ_{max}: 283 nm (ε, 11 800), λ_{min}: 244 nm (ε, 1600); UV (0.1 M NaOH), λ_{max}: 274 nm (ε, 7800), λ_{min}: 252 nm (ε, 5500); ^{1}H NMR (DMSO-d_6), δ: 7.61 (s, 1, 6-H), 7.46, 6.75 (broad peaks, 4-NH_2), 6.18 (m, 1′-H), 5.17 (m, 1, 3′-H), 4.23 (m, 2, 5′-H, 5″-H), 4.16 (m, 1, 4′-H), 4.11 (s, 2, 5-CH_2O), 3.22 (s, 3, OCH_3), 2.29 (m, 2, 2′-H, 2″-H), 2.06 (s, 3, CH_3COO), 2.04 (s, 3, CH_3COO). Anal. calcd. for $C_{15}H_{21}N_3O_7$: C 50.70, H 5.96, N 11.83; found: C 50.65, H 5.58, N 11.64.

5-Methoxymethyl-2′-deoxycytidine, 5

The diacetyl (**4**, 4.80 g, 13.5 mmol) was dissolved in 240 mL of MeOH, cooled to 4°C, saturated with ammonia, and stored at room temperature for 4 h. Removal of solvent gave *5-methoxymethyl-2′-deoxycytidine*, **5**, as a white amorphous solid, which was recrystallized from MeOH–EtOAc (2.7 g, 74%), mp 171–172°C; UV (0.1 M HCl), λ_{max}: 284 nm (ε, 12 500), λ_{min}: 244 nm (ε, 1300); UV (0.1 M NaOH), λ_{max}: 274 nm (ε, 8300), λ_{min}: 252 nm (ε, 5500); ^{1}H NMR (DMSO-d_6), δ: 7.85 (s, 1, 6-H), 7.35, 6.62 (broad peaks, 4-NH_2), 6.13 (m, 1, 1′-H), 5.17 (d, 1, 3′-OH), 4.98 (t, 1, 5′-OH), 4.20 (m, 1, 3′-H), 4.10, 4.07 (pair d, 2, 5-CH_2O), 3.75 (m, 1, 4′-H), 3.56 (m, 2, 5′-H, 5″-H), 3.20 (s, 3, OCH_3), 2.12 (m, 2″-H), 1.94 (m, 1, 2′-H). Anal. calcd. for $C_{11}H_{17}N_3O_5$: C 48.70, H 6.32, N 15.49; found: C 48.84, H 6.11, N 15.44.

X-ray crystallography

Suitable crystals were obtained from a solution of MMdCyd in ethyl ether – methanol. The colorless crystal of MMdCyd, empirical formula $C_{11}H_{17}N_3O_5$, size 0.60 × 0.28 × 0.19 mm, has the space group $P2_1$ with a = 7.9255(6) Å, b = 16.1505(15) Å, c = 10.1861(5) Å, β = 103.801(5)°, V = 1266.19 Å^3, Z = 4 (2 molecules per asymmetric unit), μ = 1.31 cm^{-1}, calculated density = 1.44 g cm^{-3} (density was not determined). The estimated standard deviations of the unit cell dimensions represent the values obtained after least-squares refinement using 25 reflections with $25.52 < \theta < 38.53°$; these esd's are smaller than usually quoted because the diffractometer had the long detector arm configuration (368 mm from crystal to detector) with a helium-filled tube located between the crystal and the detector. The diffractometer room is maintained at 14 ± 1°C. Quantitative data collection was done on an Enraf–Nonius CAD4F diffractometer with an ω/2θ scan and Ni-filtered copper radiation (λ = 1.5418 Å). Three standard reflections were checked every 10 000 s for intensity variations and every 200 reflections for orientation. There was no significant decay of the crystal over the entire data collection. A total of 2950 reflections were collected out to $\theta = 75°$, $-9 \le h \le 9$, $0 \le k \le 20$, $0 \le l \le 12$; of 2682 unique reflections, 2560 had net $I > 3\sigma(I)$. No absorption or extinction corrections were applied. Merging R based on intensities was 2.16% for 397 replicate reflections. X-ray data were processed and the structure was solved by direct methods using XTAL 2.4 (28).

All non-hydrogen atoms were found on the E map and H atoms were located by using a difference Fourier map. Finally, refinement was carried out by full-matrix least-squares refinement of positions and anisotropic temperature factors for non-H atoms; hydrogen atom parameters were not refined (with U_{iso} assigned as U_{equiv} of the attached atom).

The anisotropic refinement for non-hydrogen atoms converged to an R index[4] of 0.044. R_w was 0.046 and S was 2.955 for 2560 observed reflections. A total of 342 parameters were refined and structure factor amplitudes were used in least-squares refinement. Final $(\Delta/\sigma)_{ave}$ = 0.032, $(\Delta/\sigma)_{max}$ = 0.23. Δρ in the final difference map were +0.26 and −0.28 e Å^{-3}. Atomic scattering factors were from International tables for X-ray crystallography (1974) (13). The final coordinates of non-hydrogen atoms are given in Table 5.[5] All calculations were performed on a VAX8650 computer at the University of Saskatchewan.

[4] $R = \Sigma||F_o| - |F_c||/\Sigma|F_o|$
$R_w = [\Sigma w(|F_o| - |F_c|)^2/\Sigma w|F_o|^2]^{1/2}$
$S = [\Sigma w\Delta F^2/(m - n)]^{1/2}$

[5] Tables of structure amplitudes, thermal parameters, and H-atom coordinates may be purchased from the Depository of Unpublished Data, CISTI, National Research Council of Canada, Ottawa, Ont., Canada K1A 0S2.

The table of H-atom coordinates has also been deposited with the Cambridge Crystallographic Data Centre, and can be obtained on request from The Director, Cambridge Crystallographic Data Centre, University Chemical Laboratory, Lensfield Road, Cambridge CB2 1EW, UK.

Acknowledgements

This research was funded by grants from the Medical Research Council. We thank Mr. Ted Mazurek, Plant Biotechnology Institute, for the NMR spectra, Mr. Ken Toms, Department of Chemistry, for the CHN analyses, and Dr. L. Prasad, Department of Biochemistry, for valuable suggestions. Mr. Z. Jia is the recipient of a Graduate Scholarship from the University of Saskatchewan.

1. R. A. SMITH, R. W. SIDWELL, and R. K. ROBINS. Annu. Rev. Pharmacol. Toxicol. **20**, 259 (1980).
2. E. DECLERCQ. Acta Microbiol. Acad. Sci. Hung. **28**, 289 (1981).
3. E. DECLERCQ. Trends Pharmacol. Sci. **3**, 492 (1982).
4. C. DESGRANGES, G. FAZAKA, M. RABOUD, H. BRICAUD, H. BALZARINI, and E. DECLERCQ. Biochem. Pharmacol. **32**, 3583 (1983).
5. N. K. AYISI, R. A. WALL, R. J. WANKLIN, H. MACHIDA, E. DECLERCQ, and S. L. SACKS. Mol. Pharmacol. **31**, 422 (1987).
6. Z. VERES, A. SZABOLES, I. SZINAI, G. DENES, and A. JENEY. Biochem. Pharmacol. **35**, 1057 (1986).
7. T. A. KRENITSKY, J. W. MELLORS, and R. K. BARCLAY. J. Biol. Chem. **240**, 1281 (1965).
8. H. ISHITSUKA, M. MIWA, K. TAKEMOTO, K. FUKUOKA, A. ITOGA, and H. B. MARUYAMA. Gann, **71**, 112 (1980).
9. P. W. WOODMAN, A. M. SARRIF, and C. HEIDELBERGER. Cancer Res. **40**, 507 (1980).
10. C. NAKAYAMA, Y. WATAYA, R. B. MEYER, JR., D. V. SANTI, M. SANEYOSHI, and T. UEDA. J. Med. Chem. **23**, 962 (1980).
11. V. S. GUPTA, G. TOURIGNY, P. J. ADUMA, and A. L. STUART. U.S. and Canadian Patent. Application filed.
12. P. J. ADUMA, V. S. GUPTA, and E. DECLERCQ. Antiviral Res. In press.
13. International tables for X-ray crystallography. Vol. IV. Kynoch Press, Birmingham (Present distributor D. Reidel, Dordrecht, The Netherlands). 1974.
14. D. B. DAVIES. Prog. Nucl. Magn. Reson. Spectrosc. **12**, 136 (1978).
15. O. A. L. EL-KABBANI, I. EKIEL, L. T. J. DELBAERE, G. TOURIGNY, A. L. STUART, and V. S. GUPTA. Nucleosides & Nucleotides, **5**, 95 (1986).
16. V. S. GUPTA, G. TOURIGNY, A. L. STUART, E. DECLERCQ, J. W. QUAIL, I. EKIEL, O. A. L. EL-KABBANI, and L. T. J. DELBAERE. Antiviral Res. **7**, 69 (1987).
17. J. W. QUAIL, I. EKIEL, O. A. L. EL-KABBANI, G. TOURIGNY, L. T. J. DELBAERE, A. L. STUART, and V. S. GUPTA. Can. J. Chem. **64**, 1355 (1986).
18. J. W. QUAIL, G. TOURIGNY, L. T. J. DELBAERE, O. A. L. EL-KABBANI, A. L. STUART, and V. S. GUPTA. Acta Crystallogr. Sect. C: Cryst. Struct. Commun. **C44**, 150 (1988).
19. G. TOURIGNY, A. L. STUART, I. EKIEL, P. J. ADUMA, and V. S. GUPTA. Nucleosides Nucleotides **8**, 1189 (1989).
20. S. FURBERG, C. S. PETERSEN and C. ROMMING. Aata Crystallogr. **18**, 313 (1965).
21. D. W. YOUNG and H. R. WILSON. Acta Crystallogr. Sect. B: Struct. Crystallogr. Cryst. Chem. **B31**, 961 (1975).
22. T. SATO. Acta Crystallogr. Sect. C: Cryst. Struct. Commun. **C44**, 870 (1988).
23. J. N. LOW, P. TOLLIN, R. A. HOWIE, and H. R. WILSON. Acta Crystallogr. Sect. C: Cryst. Struct. Commun. **C44**, 2109 (1988).
24. S. KASCHINO, K. NEGISHI, and H. HAYATSU. Acta Crystallogr. Sect. C: Cryst. Struct. Commun. **C44**, 1454 (1988).
25. J. V. SILVERTON, F. R. QUIN, and R. D. HAUGWITZ. Acta Crystallogr. Sect. C: Cryst. Struct. Commun. **C44**, 321 (1988).
26. G. I. BIRNBAUM, R. DESLAURIERS, T. S. LIN, G. T. SHIAU, and W. H. PRUSOFF. J. Am. Chem. Soc. **102**, 4236 (1980).
27. C. ALTONA and M. SUNDARALINGAM. J. Am. Chem. Soc. **94**, 8205 (1972).
28. S. R. HALL and J. M. STEWART (*Editors*). XTAL 2.4. The XTAL system of crystallographic programs. Universities of Western Australia and Maryland, 1988.

Can. J. Chem. Downloaded from www.nrcresearchpress.com by 88.85.125.76 on 09/07/12
For personal use only.

Nouvelle voie de synthèse d'isoindolones et d'isoquinoléines par condensation d'iminophosphoranes avec l'*ortho*-phtalaldéhyde : réactions, mécanismes et étude structurale

THIERRY AUBERT, MICHEL FARNIER ET ROGER GUILARD[1]

Laboratoire de synthèse et d'électrosynthèse organométallique associé au Centre national de la recherche scientifique (Unité associée 33), Faculté des sciences Gabriel, 6, Boulevard Gabriel, 21100 Dijon, France

Reçu le 13 mai 1989

THIERRY AUBERT, MICHEL FARNIER et ROGER GUILARD. Can. J. Chem. **68**, 842 (1990).

Des isoindoline-ones-1 *N*-substituées et des isoquinoléines 3-acylées ont été synthétisées en une étape par condensation de l'*ortho*-phtalaldéhyde sur divers iminophosphoranes. Trois types de schémas réactionnels sont proposés, en fonction de la nature de l'iminophosphorane et des conditions opératoires. Tous les composés obtenus ont été pleinement caractérisés, en particulier par spectroscopie de résonance magnétique nucléaire mono- et bi-dimensionnelle.

Mots clés : isoindolones, isoquinoléines, iminophosphoranes.

THIERRY AUBERT, MICHEL FARNIER, and ROGER GUILARD. Can. J. Chem. **68**, 842 (1990).

The condensation of various iminophosphoranes with *o*-phthalaldehyde led directly to *N*-substituted isoindoline-1-ones and 3-acylisoquinolines. Three different mechanisms, depending on the nature of the iminophosphorane and reaction conditions, are proposed. All the compounds have been fully characterized, particularly by one- and two-dimensional nuclear magnetic resonance spectroscopy.

Key words: isoindolones, isoquinolines, iminophosphoranes.

Introduction

Les iminophosphoranes, obtenus généralement par action d'un azide sur un composé trisubstitué du phosphore selon la réaction de Staudinger (pour une revue, voir réf. 1), sont connus pour réagir avec la plupart des composés monocarbonylés selon la réaction d'aza-Wittig 1 (2–6).

En revanche, la réactivité d'iminophosphoranes vis-à-vis de composés dicarbonylés n'a jusqu'alors pas été explorée systématiquement. Ainsi, mis à part quelques réactions de condensation où l'une des deux fonctions du dérivé dicarbonylé n'a qu'un rôle secondaire et reste inchangée après réaction (7, 8), seules sont décrites dans la littérature dès condensations de composés dicarbonylés avec des bis-iminophosphoranes (9, 10). Ce type de réaction ne fait donc pas apparaître une réactivité nouvelle puisque chacune des fonctions iminophosphoranes réagit selon le schéma 1. En revanche, Garcia *et al.* (11) a signalé récemment la condensation de monoiminophosphoranes avec l'anhydride phtalique qui conduit directement à des phtalimides. Ceci permettait d'envisager une réaction de cyclisation analogue au départ d'autres composés dicarbonylés.

Dans le cadre des travaux réalisés au laboratoire sur l'intérêt des iminophosphoranes en synthèse hétérocyclique (12, 13), nous avons donc entrepris l'étude de la réactivité de synthons porteurs d'une seule fonction iminophosphorane vis à vis de divers composés dicarbonylés. Dans une communication préliminaire (14), nous avons décrit les résultats obtenus lors de la condensation sur l'*ortho*-phtalaldéhyde (OPTA) d'iminophosphoranes comportant un groupe méthylène en α d'une fonction cétone. Afin de proposer un schéma réactionnel général en fonction de la nature du synthon mis en jeu et des conditions opératoires, l'OPTA a été opposé à une série beaucoup plus large d'iminophosphoranes et nous reportons dans ce mémoire l'ensemble de nos résultats.

Résultats et discussion

Comme la réaction de Staudinger (1) est quantitative, nous avons réalisé toutes les condensations au départ des azides en générant *in situ* les iminophosphoranes correspondants. Outre la rapidité de la méthode, ce procédé présente l'avantage de ne pas avoir à isoler les iminophosphoranes, composés souvent sensibles aux traces d'humidité ou susceptibles de réactions d'autocondensation (15). Ainsi l'addition à température ambiante d'une solution d'iminophosphorane dans le dichlorométhane à une solution d'OPTA dans le même solvant conduit, avec les rendements indiqués dans le tableau 1, à un mélange des isoindolones **1** et **2** ou uniquement aux isoquinoléines **3** selon la nature de l'iminophosphorane (schéma 1). Dans le premier cas, les isoindolones **1** sont obtenues majoritairement quand l'OPTA et l'iminophosphorane sont utilisés dans les proportions stoechiométriques. Les proportions peuvent être inversées en opérant avec un excès d'OPTA. À titre d'exemple, en utilisant 1,5 moles d'OPTA par mole d'iminophosphorane Ph-NPPh$_3$, nous avons isolé les isoindolones **1***a* et **2***a* avec des rendements respectifs de 10 et 44%. Contrairement à nos prévisions, en opérant avec un plus large excès d'OPTA (2 équiv.), le

TABLEAU 1. Rendements des condensations d'iminophosphoranes sur l'OPTA

R	Isoindolone **1**	Isoindolone **2**	Isoquinoléine **3**
Ph	22	17	
	10[a]	44[a]	
CH_2Ph	45	5	
CH_2(Th-2)[b]	35	4	
CH_2(Th-3)[b]	40	5	
CH_2CO_2Et	16[c]	17[c]	
	30[d]		6[d]
CH_2CN	31	0	
CH_2COPh			30
CH_2CO(Th-2)[b]			35
CH_2CO(Th-3)[b]			30
CH_2COMe			30

[a]En opérant avec 1,5 moles d'OPTA par mole d'iminophosphorane.
[b]Th = thiényl.
[c]Réaction à température ambiante.
[d]Réaction à −20°C.

1. Auteur à qui adresser toute correspondance.

Printed in Canada / Imprimé au Canada

Can. J. Chem. Downloaded from www.nrcresearchpress.com by 88.85.125.76 on 09/07/12
For personal use only.

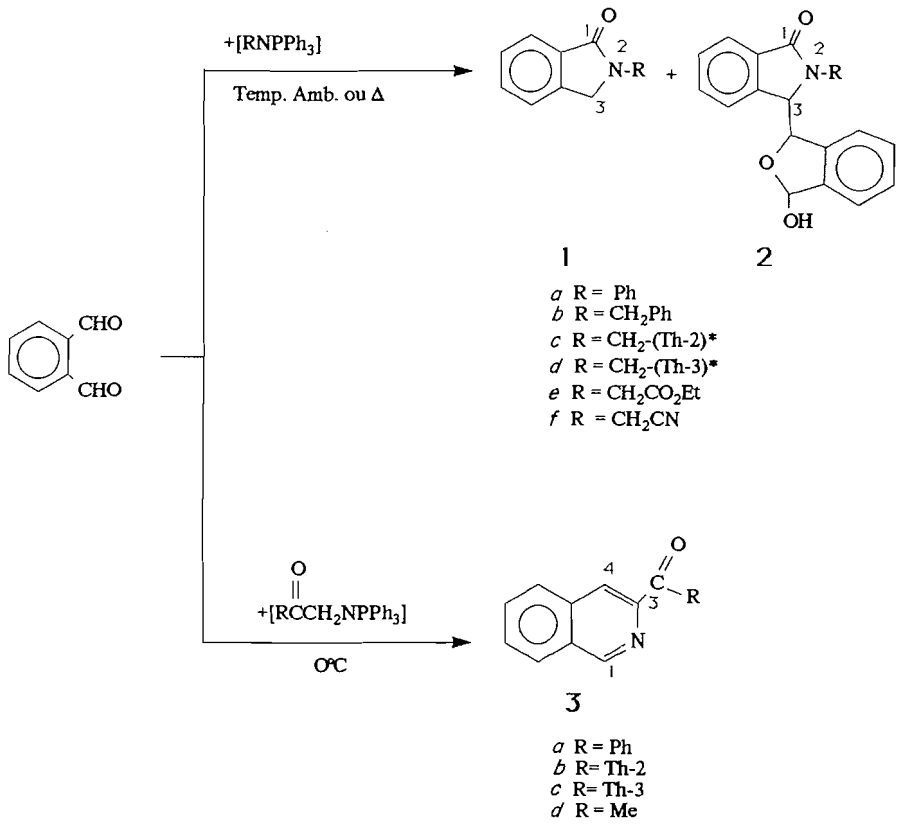

SCHÉMA 1

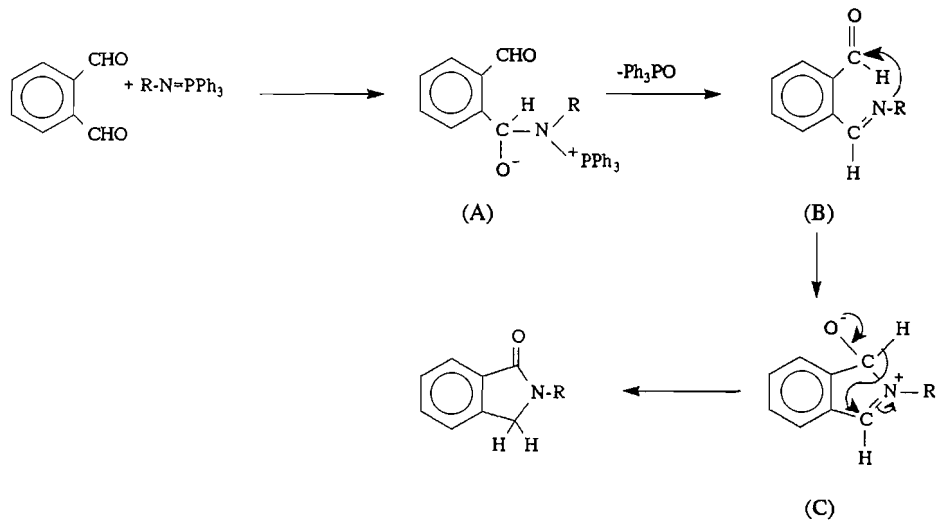

SCHÉMA 2

rendement en **2***a* est sensiblement le même. De plus, il est alors difficile d'isoler l'isoindolone **1***a* en raison de la présence d'OPTA qui n'a pas réagi car ces deux composés sont de polarité voisine. D'autre part, lorsqu'on inverse l'addition de réactifs (OPTA en défaut), le rendement en isoindolone **2***a* diminue (10%) comme attendu, mais le rendement en **1***a* reste voisin de 20%. Par ailleurs, sauf dans le cas où deux équivalents d'OPTA sont mis en jeu, ce réactif est consommé entièrement lors de la formation des isoindolones. Le bilan (isoindolone **1** + isoindolone **2**) fait donc apparaître une perte de masse de 35–70% selon les cas. Cette donnée expérimentale résulte pour l'essentiel de la grande polarité des iminophosphoranes et des dérivés qui peuvent éventuellement se former lors de la réaction. En effet, l'iminophosphorane inaltéré ou les intermédiaires iminiques ne peuvent pas être séparés de l'oxyde de triphénylphosphine lui-même très polaire.

Le mécanisme que nous proposons pour expliquer la formation des isoindolones **1** est représenté sur le schéma 2. Après élimination d'oxyde de triphénylphosphine, une attaque nucléophile de l'atome d'azote sur la deuxième fonction aldéhyde suivie d'une migration d'un ion hydrure conduit aux isoindolones **1**. Il faut souligner que des migrations d'ions hydrure sur des carbones de type iminique ont déjà été proposées par plusieurs auteurs (16, 17) et en particulier quelques exemples

Can. J. Chem. Downloaded from www.nrcresearchpress.com by 88.85.125.76 on 09/07/12
For personal use only.

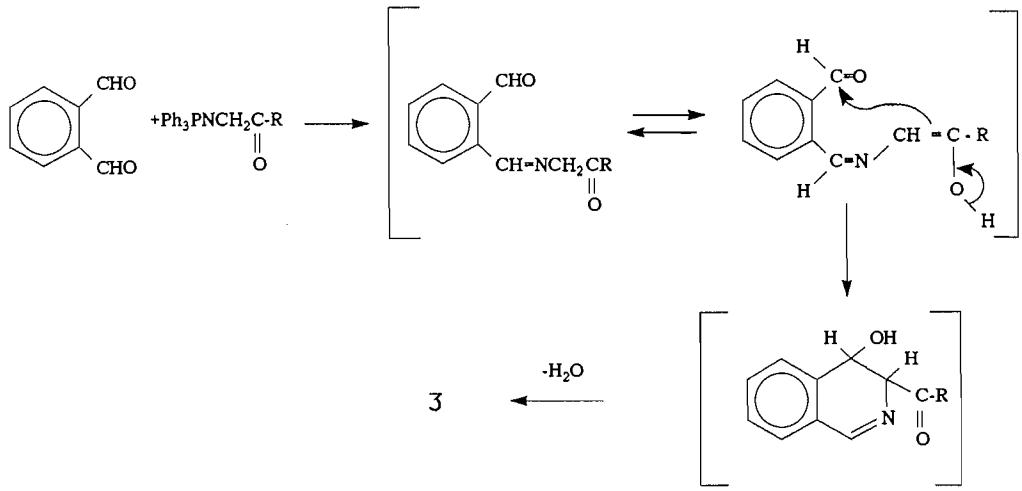

SCHÉMA 3

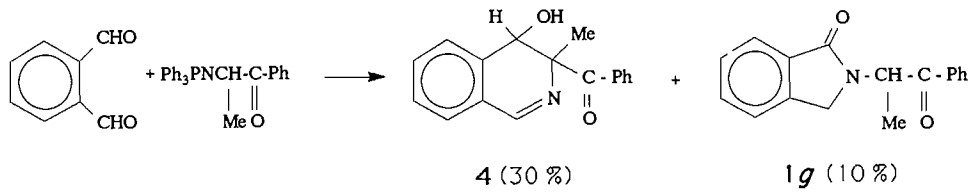

SCHÉMA 4

de migration 1–3 ont été signalés pour des systèmes cycliques à cinq chaînons (17–19). De plus, l'hypothèse d'une intervention d'un intermédiaire iminique est fortement supportée par l'obtention, au départ des iminophosphoranes cétoniques $RCOCH_2NPPh_3$, de systèmes cycliques présentant le motif iminique.

La formation des isoindolones **2** implique de plus la condensation d'une deuxième molécule d'OPTA qui s'effectue probablement sur l'intermédiaire (C) (schéma 2) selon un mécanisme que nous n'avons pas élucidé. En effet, il est peu probable que cette condensation intervienne au niveau des intermédiaires (A) ou (B) car l'élimination d'oxyde de triphénylphosphine et la formation de la liaison C—N par attaque nucléophile de l'atome d'azote sont a priori des réactions plus rapides. Enfin, et de manière inattendue, nous n'avons pas observé la formation de l'isoindolone **2***a* par chauffage à reflux prolongé de l'isoindolone **1***a* et de l'OPTA en excès (2 équiv.) dans le dichlorométhane.

Dans le cas de la formation des isoquinoléïnes **3**, en raison de l'équilibre céto-énolique représenté sur le schéma 3, la cyclisation conduit à un système hydroxylé à six chaînons qui subit ensuite une réaction de déshydratation. Nous avons mis en évidence l'intervention d'un dérivé hydroxylé comme entité intermédiaire en opérant au départ d'un iminophosphorane porteur d'un seul hydrogène méthylénique (schéma 4). Nous avons alors obtenu majoritairement l'isoquinoléine **4**, l'étape finale du mécanisme décrit dans le schéma 3 étant bloquée. Conjointement au dérivé **4**, nous avons également isolé une faible proportion de l'isoindolone **1***g*. Dans ce cas, il y a donc compétition entre les deux centres nucléophiles, l'atome de carbone α-énolique et l'atome d'azote iminique. Celle-ci résulte vraisemblablement de la présence du groupe méthyle qui induit une diminution de la mobilité de l'atome d'hydrogène méthylénique et défavorise donc la forme énolique.

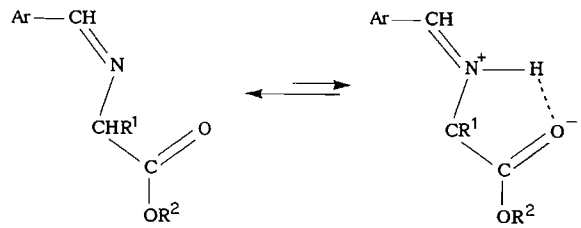

SCHÉMA 5

Ajoutons que la condensation sur l'OPTA de l'iminophosphorane $EtO_2CCH_2NPPh_3$ a conduit uniquement aux isoindolones **1***e* et **2***e* bien que cet iminophosphorane présente également un groupe méthylène en α d'une fonction carbonyle. Ce résultat est en bon accord avec le mécanisme proposé pour les iminophosphoranes cétoniques (schéma 3). En effet, les équilibres céto-énoliques n'interviennent que rarement dans le cas des fonctions ester et la cyclisation en isoquinoléines n'est donc pas favorisée pour l'iminophosphorane $EtO_2CCH_2NPPh_3$. Grigg *et al.* (20) a cependant montré récemment que des imines comportant une fonction ester en α de l'atome d'azote sont en équilibre avec une forme dipolaire grâce à l'existence d'une liaison hydrogène intramoléculaire selon le schéma 5. Or, après la condensation de l'iminophosphorane $EtO_2CCH_2NPPh_3$ sur l'une des fonctions aldéhydes de l'OPTA, un équilibre de ce type était envisageable. La présence d'un carbanion en α de l'atome d'azote suggérait alors la possibilité d'orientation de la cyclisation vers la formation d'une isoquinoléine. Pour vérifier cette hypothèse, nous avons opéré à basse température (−20°C) de manière à favoriser la forme pour laquelle interviendrait une liaison hydrogène : nous avons alors isolé l'isoquinoléine **3***e* (**3**, R = OEt) attendue mais le produit de cyclisation majoritaire reste cependant l'isoindolone **1***e*.

En résumé, le schéma 6 représente les trois types de méca-

Can. J. Chem. Downloaded from www.nrcresearchpress.com by 88.85.125.76 on 09/07/12
For personal use only.

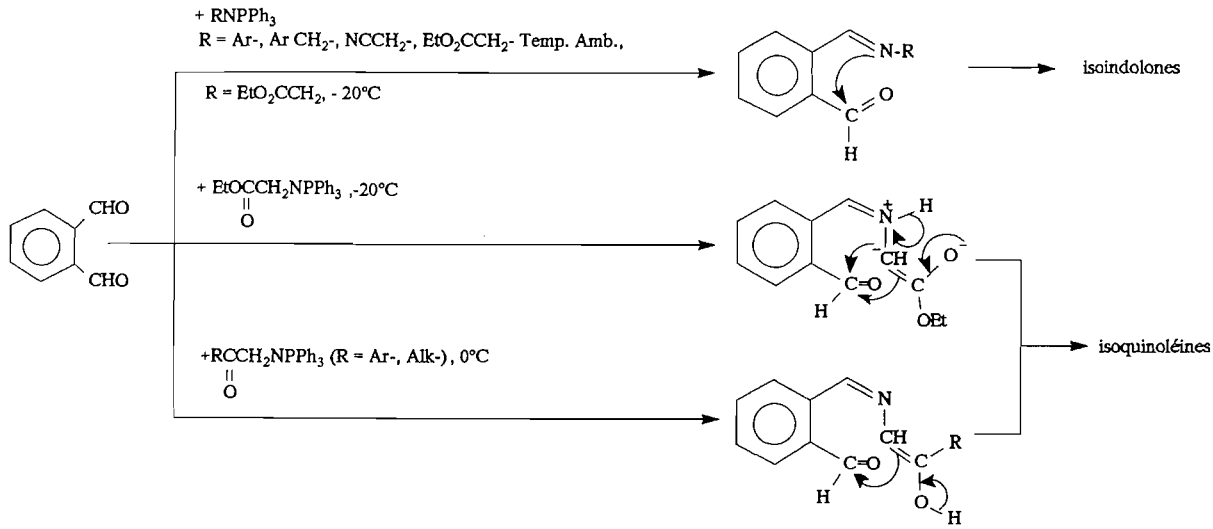

SCHÉMA 6

nisme que nous avons proposés pour expliquer la cyclisation en isoindolones et en isoquinoléines, en fonction de la nature de l'iminophosphorane et des conditions opératoires. Nous pensons que la condensation d'iminophosphoranes sur des composés dicarbonylés est une nouvelle voie de synthèse très prometteuse d'hétérocycles azotés puisque, comme nous l'avons montré en utilisant l'OPTA, la cyclisation peut s'effectuer en une seule étape à partir d'azides organiques très aisément accessibles. Ainsi, à l'exception des isoindolones de type **1**, notre méthode se révèle supérieure, quant aux rendements, à celles décrites dans la littérature. En effet, dans le cas des isoindolones de type **2** qui n'ont été signalées antérieurement que par DoMinh *et al.* (21), l'isoindolone **2***a* a été obtenue par cet auteur avec un rendement de 39% en produit brut alors que dans les mêmes conditions de stoechiométrie, nous avons isolé la même isoindolone avec un rendement de 44% après recristallisation. Enfin, les quatre synthèses d'isoquinoléines acylées en position 3 reportées dans la littérature comportent de nombreuses étapes et la préparation préalable d'isoquinoléines substituées en position 3 par un reste de type halogène (22, 23), méthyle (24) ou carboxylate d'éthyle (25). Enfin les multiples possibilités synthétiques au départ des cétones rendent notre méthode particulièrement intéressante pour accéder à la famille des isoquinoléines substituées en position 3, composés qui ont été étudiés en tant qu'inhibiteurs d'enzymes (26), intermédiaires de synthèse (27), ou modèles biologiques (25). Ajoutons également que certains métabolites fongiques appartiennent à cette classe d'hétérocycles (28).

Étude structurale

Les isoindolones **1***a,b*, **2***a* et isoquinoléines **3***a,d,e*, décrites dans la littérature, ont été identifiées en comparant leurs caractéristiques physicochimiques à celles déjà reportées ou à celles des composés de la même série (voir partie expérimentale). La structure des nouvelles isoindolones **1***c–g*, **2***b–e* et isoquinoléines **3***b,c* a été établie en particulier par analyse des spectres de rmn protonique dont les caractéristiques sont rassemblées dans les tableaux 2, 3 et 4. Il faut noter que l'isoindolone **1***e* a déjà été signalée, mais seulement sous forme de mélange et donc sans précision sur ses caractéristiques (voir partie expérimentale).

L'attribution des signaux singulets correspondants aux méthylènes intra- et extracycliques des isoindolones **1***c–f* a été effectuée sans ambiguïté par enregistrement des spectres COSY LR (Long Range) pour **1***c*, **1***e* et **1***f* et par comparaison avec **1***c* pour **1***d*. À titre d'exemple, le spectre COSY LR de l'isoindolone **1***c* présente deux taches de corrélation entre le singulet le plus déblindé et les signaux des protons thiophéniques $H_{3'}$ (^4J) et $H_{4'}$ (^5J) respectivement, ce qui permet d'attribuer ce singulet au méthylène extracyclique. De même, le singulet le plus blindé présente deux taches de corrélation avec deux des multiplets correspondant aux protons H_4–H_6.

Concernant la série des isoindolones **2**, seul le composé **2***a* (R = Ph) a été décrit par DoMinh *et al.* (21). Celui-ci n'a cependant fourni aucune preuve formelle pour confirmer la structure proposée et en particulier éliminer une structure de type isoquinoléine. Les deux structures (I) et (II) (schéma 7) étaient en effet envisageables d'après les données spectroscopiques et nous avons cherché à confirmer, par voie chimique, la structure des composés **2** obtenus. Pour cela, nous avons réalisé successivement, au départ du dérivé **2***a* (schéma 8), une réaction de déshydratation dans l'acide acétique et une réaction d'ozonolyse dans le dichlorométhane du dérivé **5** obtenu. Nous avons ainsi isolé le phtalimide **6**, identifié par comparaison avec un échantillon de référence, ce qui permet de proposer une structure de type isoindolone pour le produit de déshydratation **5**. À l'exception du singulet à 5,59 ppm correspondant au méthylène en position 3', les signaux du spectre de rmn protonique unidimensionnel du dérivé **5** se situent de manière inattendue entre 6 et 8,4 ppm. Nous avons donc confirmé la structure proposée par l'enregistrement du spectre COSY de ce composé (figures 1 et 2). En supposant que le signal le plus déblindé correspond au proton H_7, comme c'est le cas dans toute la série des isoindolones **1** et **2**, on peut attribuer aisément les trois signaux qui sont corrélés à H_7 aux protons du cycle A. Par suite, le deuxième système de quatre signaux corrélés correspond au cycle B. Enfin, le dernier système de trois signaux corrélés est attribué au cycle C (figure 2). Ainsi, bien que le mécanisme de la réaction de déshydratation conduisant au produit **5** soit encore mal compris, l'obtention d'une isoindolone permet sans ambiguïté d'écarter l'hypothèse d'une structure de type isoquinoléine (II) pour les composés **2**.

L'examen des spectres de rmn protonique des isoindolones **2**, dont les caractéristiques sont rassemblées dans le tableau 4, montre qu'il se forme toujours un mélange de deux diastéréoisomères dont les proportions relatives dépendent de la nature du

Can. J. Chem. Downloaded from www.nrcresearchpress.com by 88.85.125.76 on 09/07/12
For personal use only.

TABLEAU 2. Caractéristiques RMN des isoindolones **1** (400 MHz, $CDCl_3$)

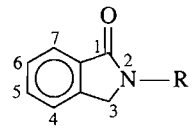

Composé	R	Déplacement chimique des protons en ppm				Constantes de couplage J (Hz)
		$(CH_2)_3$	H_7	CH_2 extracyclique	Autres protons	
1*a*		4,87 (s/2H)	7,93 (m/1H)		$H_{2'}$ et $H_{6'}$: 7,88, m/2H Aromatiques : 7,16 à 7,62, m/6H	
1*b*	$-CH_2C_6H_5$	4,26 (s/2H)	7,89 (m/1H)	4,81 (s/2H)	Aromatiques : 7,26 à 7,53, m/8H	
1*c*	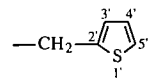	4,35 (s/2H)	7,87 (m/1H)	4,97 (s/2H)	H_4–H_6 : 7,38 à 7,54, m/3H $H_{3'}$: 7,04, m/1H $H_{4'}$: 6,96, dd/1H $H_{5'}$: 7,23, dd/1H	$J_{2'-3'}$ = 3,46 $J_{3'-4'}$ = 5,01 $J_{2'-4'}$ = 1,28
1*d*	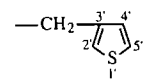	4,29 (s/2H)	7,88 (m/1H)	4,81 (s/2H)	H_4–H_6 : 7,38 à 7,53, m/3H $H_{2'}$: 7,20, m/1H $H_{4'}$: 7,05, dd/1H $H_{5'}$: 7,29, dd/1H	$J_{4'-5'}$ = 4,99 $J_{2'-5'}$ = 2,97 $J_{2'-4'}$ = 1,30
1*e*	$-CH_2CO_2Et$	4,53 (s/2H)	7,88 (m/1H)	4,40 (s/2H)	H_4–H_6 : 7,45 à 7,58, m/3H CH_2–CH_3 : 4,22, q/2H CH_2–CH_3 : 1,28, t/3H	$J_{CH_2-CH_3}$ = 7,11
1*f*	$-CH_2CN$	4,55 (s/2H)	7,88 (m/1H)	4,61 (s/2H)	H_4–H_6 : 7,49 à 7,64, m/3H	
1*g*	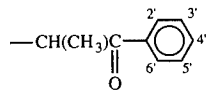	4,44 4,32 (système AB)	7,86 m/1H		$H_{2'}$ et $H_{6'}$: 8,10, m/2H Aromatiques : 7,39 à 7,57, m/6H $CHCH_3$: 6,12, q/1H $CHCH_3$: 1,55, d/3H	J_{AB} = 16,91 J_{CH-CH_3} = 7,00

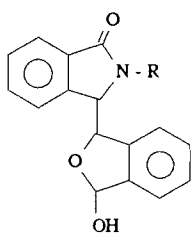

(I)

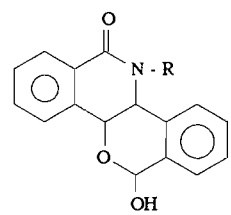

(II)

SCHÉMA 7

reste lié à l'atome d'azote. La comparaison des déplacements chimiques des protons de l'isoindolone **2***a* reportés par DoMinh *et al.* (21) et nous-mêmes tend à indiquer qu'il s'agit du même diastéréoisomère (majoritaire). Toutefois, nous proposons une attribution différente de celle de cet auteur pour les signaux situés à 5,78 et 6,11 ppm. En effet, le signal à 6,11 ppm apparaît sous forme de doublet, inchangé après deutériation, et ne peut donc être attribué qu'au proton H_3 et non $H_{1'}$. Le signal à 5,78 ppm est quant à lui attribuable à $H_{1'}$ et non à $H_{3'}$, puisqu'il apparaît sous forme de pseudo-triplet par couplage avec H_3 et $H_{3'}$ avec des valeurs de constante de couplage voisines.

Enfin, les signaux des protons H_1 et H_4 des isoquinoléines **3** résonnent sous forme de multiplets en raison de la présence de couplages ^4J et ^5J de l'ordre de 0,8–1 Hz. Leur attribution a été réalisée par comparaison des valeurs des glissements chimiques avec les valeurs données dans la littérature pour des isoquinoléines non substituées en position 1,3 et 4 (29) ou pour des thiénopyridines (30, 31), dont l'attribution des signaux du cycle azoté est non ambigüe.

Partie expérimentale

Les points de fusion ont été déterminés sur un banc de Kofler et ne sont pas corrigés. Les spectres ir ont été enregistrés sur un spectrophotomètre Perkin Elmer 580 B à partir de dispersions à 1% dans l'iodure de césium ou le bromure de potassium. Les spectres de masse ont été obtenus sur appareil Finnigan 3300 (70 eV, 0,4 mA). Les spectres de rmn ont été relevés à 400 MHz sur un appareil Bruker WM 400 du CEREMA («Centre de Résonance Magnétique» de l'Université de Bourgogne). Les valeurs de δ sont exprimées en ppm, le tétraméthylsilane étant pris comme référence (s : singulet, d : doublet, dd : double doublet, t : triplet, q : quadruplet, m : multiplet). Les analyses ont été effectuées par le Laboratoire central de microanalyses du C.N.R.S.

Matériel de départ

Les azides ont été préparés par les méthodes citées en référence : PhN_3 (32), Ph- et Th-CH_2N_3 (33), $RCOCH_2N_3$ (R = Me ou EtO) (34), $PhCOCHRN_3$ (R = H ou Me) (35), $ThCOCH_2N_3$ (36).

*Méthode générale de synthèse des isoindolones **1** et **2***

À une solution d'azide (0,01 mol) dans le dichlorométhane anhydre (ou le benzène dans le cas de l'azidoacétate d'éthyle) (10 mL), est ajoutée à température ambiante et goutte à goutte une solution de triphénylphosphine (2,62 g, 0,01 mol) dans 20 mL du même solvant. À la fin de l'addition, l'agitation est maintenue 2–4 h à température

Can. J. Chem. Downloaded from www.nrcresearchpress.com by 88.85.125.76 on 09/07/12
For personal use only.

Can. J. Chem. Downloaded from www.nrcresearchpress.com by 88.85.125.76 on 09/07/12
For personal use only.

TABLEAU 3. Caractéristiques RMN des isoindolones **5** (400 MHz, DMSO-d_6)

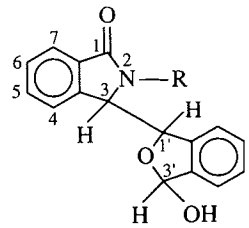

Composé	R	% diaster. major. % diaster. minor.	H_3 (d)	H_4 (m)	H_7 (m)	$H_{1'}$ (t)	$H_{3'}$ (dd)	OH (d)	Méthylène extracycl. (d)	(d)	Aromat. ou autres (diaster. major.)	Constantes de couplage N-CH_2	 J (Hz) Autres
2a	Ph	91	6,11	6,61	7,82	5,78	5,25	6,72			7,14–7,83		$J_{1'-3}$ = 2,00 $J_{1'-3'}$ = 2,28
		9	5,46	6,14	7,86	6,11	6,18	6,36					$J_{3'-OH}$ = 7,51
2b	CH_2Ph	79	5,00	Dans le massif des aromatiques		6,01	6,38	6,91	4,07	5,08	7,03–7,67	J = 15,29	$J_{1'-3}$ = 3,08 $J_{1'-3'}$ = 2,36
		21	4,95			6,41	5,77		3,77	5,12			$J_{3'-OH}$ = 6,97
2b	—CH_2— (3"-thiophène-2",5")	75	5,07	6,63	7,76	6,14	5,94	6,92	4,66	5,18	7,31–7,65 + 6,80 (ArH)	J = 15,55	$J_{1'-3}$ = 2,33 $J_{3''-4''}$ = 3,45
		25			7,79				5,03	5,10	$H_{3''}$ = 7,16, dd/1H $H_{4''}$ = 7,03, dd/1H $H_{5''}$ = 7,47, dd/1H		$J_{4''-5''}$ = 5,09 $J_{3''-5''}$ = 1,09
2d	—CH_2— (3"-thiophène-2",5")	82	5,04	6,71	7,75	6,09	5,86	6,87	4,49	5,02	7,32–7,55 + 6,72 (ArH)	J = 15,35	$J_{1'-3}$ = 1,42 $J_{1'-3'}$ = 2,08
		18							4,83	4,91	$H_{2''}$: dans massif aromatiques $H_{4''}$ = 7,07, dd/1H $H_{5''}$ = 7,52, dd/1H		$J_{3'-OH}$ = 7,02 $J_{2''-4''}$ = 1,22 $J_{4''-5''}$ = 4,88 $J_{2''-5''}$ = 2,75
2e	CH_2CO_2Et	53	5,24	6,66	Dans le massif des aromatiques	6,08	5,91	6,89	Dans le massif à 4,18	4,54	7,10–7,80 CH_2CH_3 : 4,18	J = 17,65	$J_{1'-3}$ = 2,29 $J_{1'-3'}$ = 1,82
		47	5,30	5,83		5,87	6,44	Dans le massif des aromatiques	4,37	4,72	CH_2CH_3 : 1,79		$J_{3'-OH}$ = 5,08 $J_{CH_2-CH_3}$ = 7,11

Can. J. Chem. Downloaded from www.nrcresearchpress.com by 88.85.125.76 on 09/07/12
For personal use only.

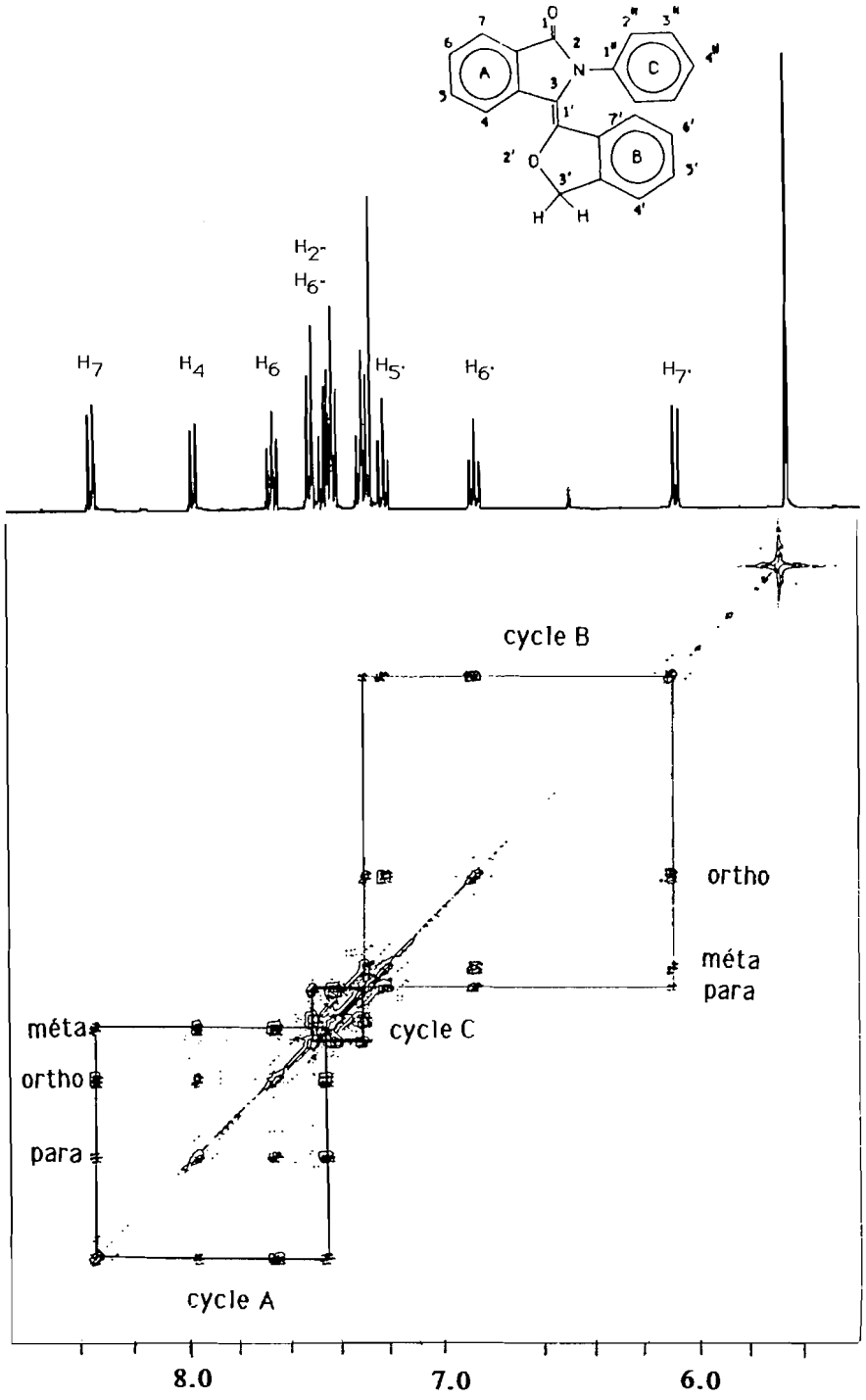

FIG. 1. Spectre COSY (400 MHz, $CDCl_3$) de l'isoindolone **5** (voir agrandissement du cycle C sur la figure 2).

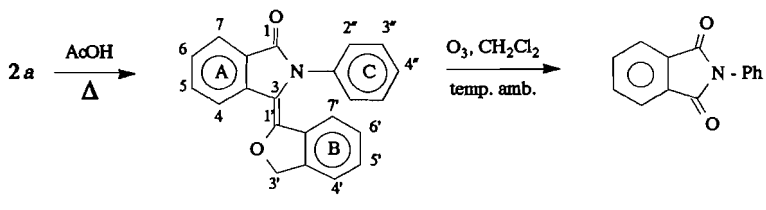

5 **6**

SCHÉMA 8

Can. J. Chem. Downloaded from www.nrcresearchpress.com by 88.85.125.76 on 09/07/12
For personal use only.

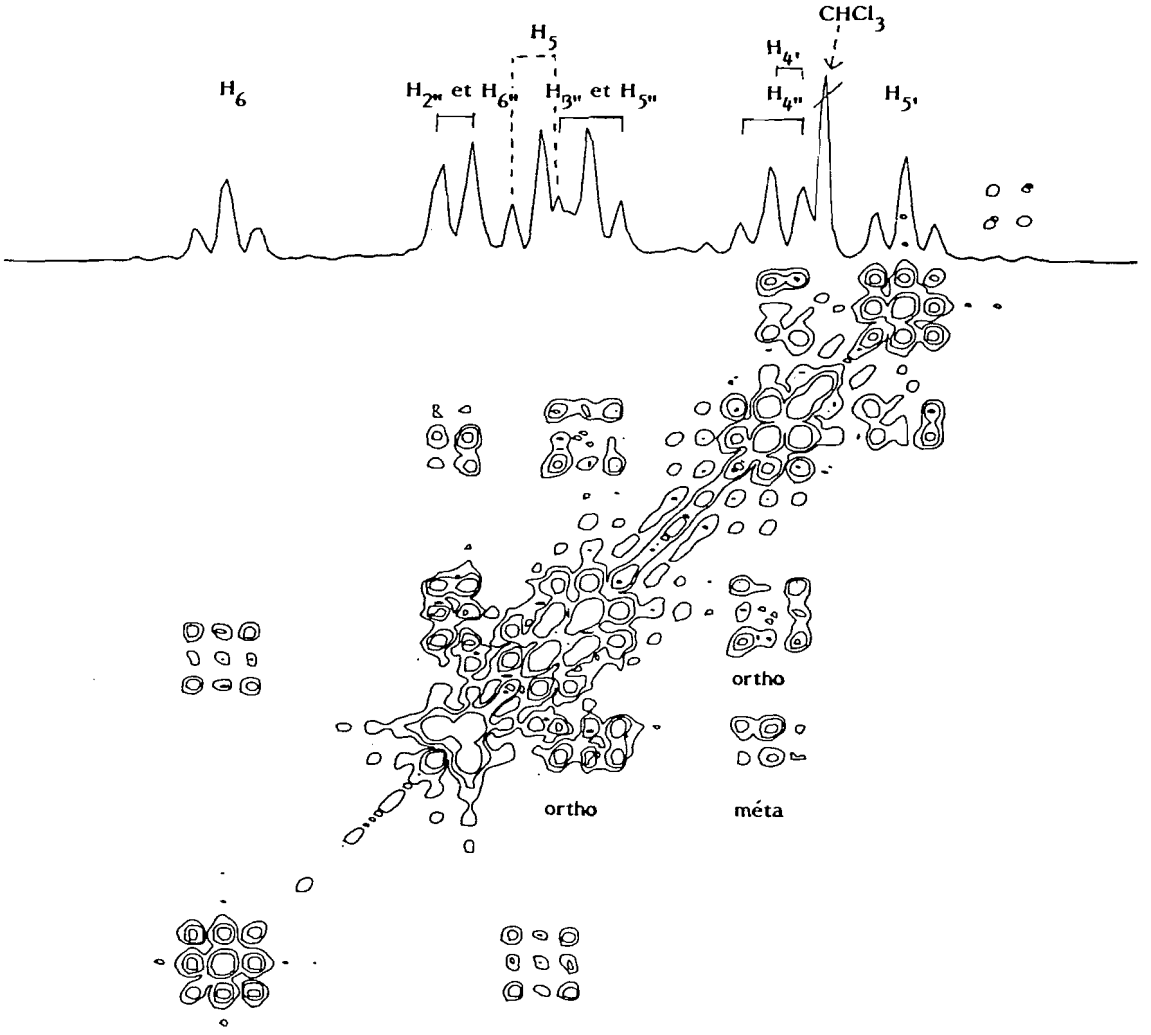

FIG. 2. Agrandissement du spectre COSY (400 MHz, $CDCl_3$) de l'isoindolone **5**.

TABLEAU 4. Caractéristiques RMN des isoquinoléines **3** (400 MHz, $CDCl_3$)

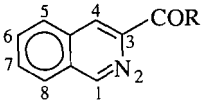

Composé	R	H_1	H_4	H_5, H_8	H_6, H_7	R	J (Hz)
3*a*		9,34 (m/1H)	8,48 (m/1H)	8,08 (m/1H) 8,01 (m/1H)	7,78 (m/2H)	$H_{2'}$ et $H_{6'}$: 8,08, m/2H $H_{3'}$ et $H_{5'}$: 7,51, m/2H $H_{4'}$: 7,61, m/1H	
3*b*		9,36 (m/1H)	8,64 (m/1H)	8,08 (m/1H) 8,03 (m/1H)	7,77 (m/2H)	$H_{3'}$: 8,48, dd/1H $H_{4'}$: 7,22, dd/1H $H_{5'}$ dans le massif avec H_6, H_7	$J_{3'-4'}$ = 3,95 $J_{3'-5'}$ = 1,32 $J_{4'-5'}$ = 5,05
3*c*		9,36 (m/1H)	8,58 (m/1H)	8,09 (m/1H) 8,03 (m/1H)	7,78 (m/2H)	$H_{2'}$: 8,90, dd/1H $H_{4'}$: 7,92, dd/1H $H_{5'}$: 7,37, dd/1H	$J_{2'-4'}$ = 1,14 $J_{2'-5'}$ = 2,85 $J_{4'-5'}$ = 5,13
3*d*	—CH_3	9,29 (m/1H)	8,48 (m/1H)	8,06 (m/1H) 8,00 (m/1H)	7,76 (m/2H)	CH_3 : 2,84, s/3H	
3*e*	—OCH_2CH_3	9,33 (m/1H)	8,58 (m/1H)	8,04 (m/1H) 7,96 (m/1H)	7,75 (m/2H)	CH_2 : 4,52, q/2H CH_3 : 1,47, t/3H	$J_{CH_2-CH_3}$ = 7,22

Can. J. Chem. Downloaded from www.nrcresearchpress.com by 88.85.125.76 on 09/07/12
For personal use only.

ambiante. Cette solution est ensuite ajoutée goutte à goutte à une solution d'*ortho*-phtalaldéhyde dans le dichlorométhane anhydre (50 mL). Après 2–4 h d'agitation à température ambiante, évaporation du solvant, élution du résidu sur gel de silice par le mélange dichlorométhane–acétone (30 : 1) et recristallisation, on isole les isoindolones **1** et **2**.

*Phényl-2 isoindoline one-1 (**1**a)* : Rdt 22% (0,46 g); F = 164°C (dichlorométhane–hexane) (litt. (37) F = 162–163°C).

*Phénylméthyl-2 isoindoline one-1 (**1**b)* : Rdt 45% (1,00 g); F = 90–92°C (éther éthylique – hexane) (litt. (38) F = 90–91°C).

*(Thiényl-2 méthyl)-2 isoindoline one-1 (**1**c)* : Rdt 35% (0,80 g); F = 92–94°C (éther éthylique); ir ν_{max} (CsI) : 1674 (CO), 1468, 1301, 733, 710 cm^{-1}; sm m/z : 229 (M^+, 100), 228 (51), 196 (19), 146 (10), 145 (15), 132 (18), 119 (82), 97 (78), 91 (47). Anal. calc. pour $C_{13}H_{11}NOS$: C 68,10, H 4,84, N 6,11, S 13,98; tr. : C 67,91, H 4,83, N 6,11, S 13,67.

*(Thiényl-3 méthyl)-2 isoindoline one-1 (**1**d)* : Rdt 40% (0,92 g); F = 65–66°C (éther éthylique – hexane); ir ν_{max} (KBr) : 1685 (CO), 1454, 1297, 743 cm^{-1}; sm m/z : 229 (M^+, 88), 228 (21), 196 (9), 146 (11), 145 (10), 132 (36), 119 (51), 97 (100), 91 (43). Anal. calc. pour $C_{13}H_{11}NOS$: C 68,10, H 4,84, N 6,11, S 13,98; tr. : C 68,25, H 4,94, N 6,13, S 14,17.

*Ethoxycarbonylméthyl-2 isoindoline one-1 (**1**e)* : Rdt 16% (0,35 g); (ce composé a été signalé (39) mais n'a jamais été isolé à l'état de pureté analytique); F = 78–80°C (éther éthylique – hexane); ir ν_{max} (KBr) : 1738 (CO_2Et), 1681 (*CO*N), 1207, 740 cm^{-1}; sm m/z : 219 (M^+, 15), 146 (100), 145 (57), 132 (6), 118 (9), 91 (28). Anal. calc. pour $C_{12}H_{13}NO_3$: C 65,74, H 5,98, N 6,39; tr. : C 65,57, H 5,83, N 6,39.

*Cyanométhyl-2 isoindoline one-1 (**1**f)* : Rdt 31% (0,53 g); F = 119–120°C (éther éthylique – heptane); ir ν_{max} (CsI) : 2244 (CN), 1698 (CO) cm^{-1}; sm m/z : 172 (M^+, 100), 171 (42), 143 (41), 118 (29), 104 (29), 89 (24), 77 (24). Anal. calc. pour $C_{10}H_8N_2O$: C 69,76, H 4,68, N 16,27; tr. : C 69,84, H 4,71, N 16,29.

*Hydroxy-3 dihydro-1,3 isobenzofurannyl-1)-3 phényl-2 isoindoline one-1 (**2**a)* : Rdt 17% (0,58 g); F = 200–201°C (litt. (21) F = 196–198°C).

À noter que lorsqu'on opère avec 1,5 moles d'*ortho*-phtalaldéhyde par mole de $PhNPPh_3$, les rendements respectifs en isoindolones **1***a* et **2***a* sont de 10 et 44%.

*(Hydroxy-3 dihydro-1,3 isobenzofurannyl-1)-3 phénylméthyl-2 isoindoline one-1 (**2**b)* : Rdt 5% (0,18 g); F = 204°C (dichlorométhane); ir ν_{max} (KBr) : 3312 (OH), 1665 (CO), 1414, 1000 cm^{-1}; sm m/z : 358 (0,2), 357 (M^+, 0,1), 340 (0,1), 223 (100), 132 (28), 91 (73). Anal. calc. pour $C_{23}H_{19}NO_3$: C 77,29, H 5,36, N 3,92; tr. : C 76,76, H 5,41, N 3,92.

*(Hydroxy-3 dihydro-1,3 isobenzofurannyl-1)-3 (thiényl-2 méthyl)-2 isoindoline one-1 (**2**c)* : Rdt 4% (0,15 g); F = 202°C (dichlorométhane–hexane); ir ν_{max} (KBr) : 3346 (OH), 1674 (CO), 1427, 1040, 693 cm^{-1}; sm m/z : 345 ([M − 18]$^+$, 0,2), 229 (55), 145 (60), 135 (19), 132 (12), 97 (100). Anal. calc. pour $C_{21}H_{17}NO_3S$: C 69,40, H 4,72, N 3,85, S 8,82; tr. : C 69,50, H 4,75, N 3,77, S 8,88.

*(Hydroxy-3 dihydro-1,3 isobenzofurannyl-1)-3 (thiényl-3 méthyl)-2 isoindoline one-1 (**2**d)* : Rdt 5% (0,18 g); F = 214°C (dichlorométhane–hexane); ir ν_{max} (KBr) : 3352 (OH), 1668 (CO), 1434 cm^{-1}; sm m/z : 363 (M^+, 0,2), 345 (0,2), 229 (100), 145 (7), 132 (20), 97 (38). Anal. calc. pour $C_{21}H_{17}NO_3S$: C 69,40, H 4,72, N 3,85, S 8,82; tr. : C 70,00, H 4,66, N 3,81, S 8,59.

*(Hydroxy-3 dihydro-1,3 isobenzofurannyl-1)-3 éthoxycarbonylméthyl-2 isoindoline one-1 (**2**e)* : Rdt 17% (0,60 g); F = 174–175°C (dichlorométhane–hexane); ir ν_{max} (KBr) : 3379 (OH), 2925 (CO), 1732 (CO_2Et), 1688 (*CO*N), 1215 cm^{-1}; sm m/z : 353 (M^+, 4), 336 (20), 335 (11), 308 (65), 280 (100), 262 (46), 248 (20), 232 (51). Anal. calc. pour $C_{20}H_{19}NO_5$: C 67,98, H 5,41, N 3,96; tr. : C 67,98, H 5,19, N 3,92.

*Méthode générale de synthèse des isoquinoléines **3***

À une solution d'azidocétone (2,5 mmol) dans 50 mL de dichlorométhane anhydre est ajoutée à 0°C et goutte à goutte une solution de triphénylphosphine (0,66 g, 2,5 mmol) dans le même solvant. La solution est maintenue à 0°C jusqu'à disparition des produits de départ (suivie en chromatographie sur couches minces) puis ajoutée à la même température, à une solution d'*ortho*-phtalaldéhyde (0,34 g, 2,5 mmol) dans 20 mL de dichlorométhane anhydre. À la fin de l'addition, la solution est maintenue 30 min à 0°C et on laisse ensuite remonter la température lentement jusqu'à l'ambiante. Après évaporation du solvant, élution du résidu sur gel de silice par le mélange dichlorométhane–acétone (40 : 1) et recristallisation on isole les isoquinoléines **3**.

*Phényl isoquinolyl-3 cétone (**3**c)* : Rdt 30% (0,17 g); F = 82°C (éther éthylique – hexane) (litt. (22) F = 79–81°C).

*Thiényl-2 isoquinolyl-3 cétone (**3**b)* : Rdt 35% (0,21 g); F = 124°C (éther éthylique – hexane); ir ν_{max} (KBr) : 1641 (CO), 1614, 1498, 1404 cm^{-1}; sm m/z : 239 (M^+, 25), 211 (100), 128 (16), 128 (16), 111 (67). Anal. calc. pour $C_{14}H_9NOS$: C 70,27, H 3,79, N 5,85, S 13,40; tr. : C 70,49, H 3,69, N 5,81, S 13,43.

*Thiényl-3 isoquinolyl-3 cétone (**3**c)* : Rdt 30% (0,18 g); F = 89–90°C (éther éthylique – hexane); ir ν_{max} (KBr) : 1661 (CO), 1618, 1508, 1391 cm^{-1}; sm m/z : 239 (M^+, 56), 211 (60), 210 (53), 128 (23), 111 (100). Anal. calc. pour $C_{14}H_9NOS$: C 70,27, H 3,79, N 5,85, S 13,40; tr. : C 69,95, H 3,74, N 5,88, S 13,30.

*Méthyl isoquinolyl-3 cétone (**3**d)* : Rdt 30% (0,13 g); F = 90–92°C (éther éthylique – hexane) (litt. (40) F = 92–92,8°C).

Condensation de l'iminophosphorane dérivé de l'azide $PhCOCH(Me)N_3$ sur l'OPTA

Le mode opératoire décrit pour la synthèse des isoquinoléines **3** conduit, après chromatographie sur gel de silice par le mélange dichlorométhane–acétone (40 : 1), à l'isoindolone **1***g* et à l'isoquinoléine **4**.

*(Méthyl-1 phénacyl)-2 isoindoline one-1 (**1**g)* : Rdt 10% (0,53 g); F = 80–82°C (éther éthylique – hexane); ir ν_{max} (KBr) : 1690 (CO extracyclique), 1678 (CO intracyclique), 1220, 740 cm^{-1}; sm m/z : 265 (M^+, 1), 174 (7), 160 (100), 132 (8), 119 (4), 105 (5), 91 (14), 77 (10). Anal. calc. pour $C_{17}H_{15}NO_2$: C 76,96, H 5,70, N 5,28; tr. : C 76,83, H 5,71, N 5,06.

*Benzoyl-3 hydroxy-4 méthyl-3 dihydro-3,4 isoquinoléine (**4**)* : Rdt 30% (1,59 g); F = 137–138°C (éther éthylique – hexane); ir ν_{max} (KBr) : 3132 (OH), 1680 (CO), 1672 (CN) cm^{-1}; rmn ^1H (DMSO-d_6) δ : 1,12 (3H, s, CH_3), 4,79 (1H, d, J = 5,23 Hz, singulet après deutériation, C*H*OH), 5,74 (1H, d, J = 5,23 Hz, s'échange avec D_2O, OH), 7,43–7,61 (7H, m, ArH), 7,86 (2H, m, $H_{2'}$ et $H_{6'}$), 8,49 (1H, s, H_1) ppm; sm m/z : 265 (M^+, 3), 248 (27), 143 (60), 118 (38), 105 (100), 77 (51). Anal. calc. pour $C_{17}H_{15}NO_2$: C 76,96, H 5,70, N 5,28; tr. : C 76,74, H 5,56, N 5,10.

Condensation à basse température de l'iminophosphorane dérivé de l'azidoacétate d'éthyle sur l'OPTA

À une solution de l'azidoacétate d'éthyle (2,58 g, 20 mmol) dans le dichlorométhane anhydre (25 mL) est ajoutée à température ambiante et goutte à goutte une solution de triphénylphosphine (5,24 g, 20 mmol) dans 60 mL du même solvant. À la fin de l'addition, l'agitation est maintenue 4 h à température ambiante puis la solution est refroidie à −20°C et ajoutée, à cette température et goutte à goutte, à une solution d'*ortho*-phtalaldéhyde dans le dichlorométhane anhydre (200 mL). À la fin de l'addition, on laisse la température revenir très progressivement à l'ambiante puis on maintient l'agitation à cette température pendant 3 h. Après évaporation du solvant et élution du résidu sur gel de silice par le mélange dichlorométhane–acétone (50 : 1), on isole l'isoindolone **1***e* et l'isoquinoléine **3***e*.

*Ethoxycarbonyl-2 isoindoline one-1 (**1**e)* : Rdt 30% (1,31 g).

*Ethoxycarbonyl-3 isoquinoléine (**3**e)* : Rdt 6% (0,24 g); identifiée par spectroscopie rmn (voir tableau 4).

*(Dihydro-1,3 isobenzofurannylidène-1)-3 phényl-2 isoindoline one-1 (**5**)*

Une solution de l'isoindolone (**2***a*) (0,86 g, 2,5 mmol) dans 100 mL

d'acide acétique est chauffée à reflux pendant 10 min. La solution est diluée à l'eau et extraite au dichlorométhane. Les phases organiques sont lavées par une solution de bicarbonate de sodium, puis à l'eau jusqu'à neutralité. Après séchage des phases organiques sur sulfate de magnésium, évaporation du solvant et élution du résidu sur gel de silice par le mélange dichlorométhane–acétone (25 : 1), on isole 0,28 g d'isoindolone **5**; Rdt 35%; F = 230°C (acétone–eau); ir ν_{max} (KBr) : 1688 (CO), 1628, 1334, 1144 cm^{-1}; rmn ^1H ($CDCl_3$) δ : 5,59 (2H, s, $(CH_2)_{3'}$), 6,04 (1H, m, $H_{7'}$), 6,84 (1H, m, $H_{6'}$), 7,20 (1H, m, $H_{5'}$), 7,27–7,32 (2H, m, $H_{4'}$ et $H_{4''}$), 7,39–7,46 (3H, m, $H_{3''}$, $H_{5''}$ et H_5), 7,50 (2H, m, $H_{2''}$ et $H_{6''}$), 7,65 (1H, m, H_6), 7,96 (1H, m, H_4), 8,37 (1H, m, H_7); sm m/z : 325 (M^+, 100), 296 (57), 268 (54), 165 (19). Anal. calc. pour $C_{22}H_{15}NO_2$: C 81,22, H 4,64, N 4,31; tr. : C 81,11, H 4,66, N 4,17.

Ozonolyse du dérivé **5**

Une solution de l'isoindolone **5** (32,5 mg, 0,1 mmol) dans le dichlorométhane (40 mL) est soumise au passage d'un courant d'ozone (O_3 + O_2) à température ambiante pendant 1 h. L'excès d'ozone est éliminé par un courant d'azote puis on ajoute au milieu réactionnel 1 mL d'une solution d'hydrogénosulfite de sodium (d = 1,32). La phase organique est lavée à l'eau puis séchée sur sulfate de magnésium. Après évaporation du solvant, on isole 19 mg de phtalimide **6**; Rdt 87%; F = 208°C (dichlorométhane); identifiée par comparaison avec un échantillon de référence.

1. Yu. G. Gololobov, I. N. Zhmurova et L. F. Kasukhin. Tetrahedron, **37**, 437 (1981).
2. S. C. K. Wong et A. W. Johnson. J. Org. Chem. **37**, 1850 (1972).
3. D. M. B. Hickey, A. R. MacKenzie, C. J. Moody et C. W. Rees. J. Chem. Soc. Perkin Trans. 1, 921 (1987).
4. E. Zbiral et E. Bauer. Phosphorus, **2**, 35 (1972).
5. M. Kennedy, C. J. Moody, C. W. Rees et J. J. Vaquero. J. Chem. Soc. Perkin Trans. 1, 1395 (1987).
6. G. Askner et P. Froyen. Acta Chem. Scand. **23**, 2697 (1969).
7. J. A. Kloek and K. L. Leschinsky. J. Org. Chem. **43**, 1460 (1978).
8. M. E. Jung, K. Shishido, L. Light et L. Davis. Tetrahedron Lett. **22**, 4607 (1981).
9. R. Appel et P. Volz. Chem. Ber. **108**, 623 (1975).
10. R. Appel et G. Siegmund. Z. Anorg. Allg. Chem. **363**, 183 (1968).
11. J. Garcia, J. Vilarrasa, X. Bordas et A. Banaszek. Tetrahedron Lett. **27**, 639 (1986).
12. B. Tabyaoui, T. Aubert, M. Farnier et R. Guilard. Synth. Commun. **18**, 1475 (1988).
13. T. Aubert, B. Tabyaoui, M. Farnier et R. Guilard. Synthesis, 742 (1988).
14. T. Aubert, M. Farnier, B. Hanquet et R. Guilard. Synth. Commun. **17**, 1831 (1987).
15. E. Zbiral, E. Bauer et J. Stroh. Monatsh. Chem. **102**, 168 (1971).
16. A. W. Lochead, G. R. Proctor et M. P. L. Caton. J. Chem. Soc. Perkin Trans. 1, 2477 (1984).
17. I. Yamamoto, Y. Tabo et H. Gotoh. Tetrahedron Lett. 2295 (1971).
18. F. Benachenhou, M. A. Mesli, M. El Borai, B. Hanquet et R. Guilard. J. Heterocycl. Chem. **25**, 1531 (1988).
19. R. Grigg, H. Q. N. Gunaratne et V. Sridharan. J. Chem. Soc. Chem. Commun. 1183 (1985).
20. (*a*) R. Grigg, H. Q. N. Gunaratne et J. Kemp. J. Chem. Soc. Perkin Trans. 1, 41 (1984); (*b*) R. Grigg. Bull. Soc. Chim. Belg. **93**, 593 (1984).
21. T. DoMinh, A. L. Johnson, J. E. Jones et P. P. Senise. J. Org. Chem. **42**, 4217 (1977).
22. Y. Yamamoto et A. Yanagi. Chem. Pharm. Bull. **30**, 2003 (1982).
23. T. Sakamoto, Y. Kondo, M. Shiraiwa et H. Yamanaka. Synthesis, 245 (1984).
24. F. R. Crowne et J. G. Breckenridge. Can. J. Chem. **32**, 641 (1954).
25. G. R. Clemo et S. P. Popli. J. Chem. Soc. 1406 (1951).
26. S. Klutchko, C. J. Blankley, R. W. Fleming, J. M. Hinkley, A. E. Werner, I. Nordin, A. Holmes, M. L. Hoefle, D. M. Cohen, A. D. Essenburg et H. R. Kaplan. J. Med. Chem. **29**, 1953 (1986).
27. G. A. Swan. J. Chem. Soc. 2038 (1958).
28. G. R. Birchall, M. N. Galbraith et W. B. Whalley. J. Chem. Soc. Chem. Commun. 474 (1966).
29. D. L. Boger, C. E. Brotherton et M. D. Kelley. Tetrahedron, **37**, 3977 (1981).
30. M. Farnier, S. Soth et P. Fournari. Can. J. Chem. **54**, 1066 (1976).
31. M. Farnier, S. Soth et P. Fournari. Can. J. Chem. **54**, 1074 (1976).
32. R. O. Lindsay et C. F. H. Allen. Org. Synth. Collect. Vol. 3, 710 (1955).
33. Fr. Moulin. Helv. Chim. Acta, **35**, 167 (1952).
34. O. Forster et H. E. Fierz. J. Chem. Soc. **93**, 72 (1908).
35. D. Knittel, H. Hemetsberger et H. Weidmann. Monatsh. Chem. **101**, 157 (1970).
36. G. Kumar, K. Rajagopalan et S. Swaminathan. Indian J. Chem. Sect. B, **20**, 271 (1981).
37. R. E. Ludt et C. R. Hauser. J. Org. Chem. **36**, 1607 (1971).
38. M. Mori, K. Chiba et Y. Ban. J. Org. Chem. **43**, 1684 (1978).
39. J. S. New et J. P. Yevich. J. Heterocycl. Chem. **21**, 1355 (1984).
40. K. Kigasawa, M. Huragi, H. Ishimaru, S. Haga et K. Shirayama. J. Heterocycl. Chem. **15**, 369 (1978).

Can. J. Chem. Downloaded from www.nrcresearchpress.com by 88.85.125.76 on 09/07/12
For personal use only.

Cycloaddition reactions of dichlorodithionitronium hexafluoroarsenate(V) with alkynes and alkenes; the preparation and X-ray crystal structure of 1,3-dichloro-1,3,2-dithiazolidinium hexafluoroarsenate(V)

SIMON PARSONS, JACK PASSMORE,[1] MELBOURNE J. SCHRIVER, AND PETER S. WHITE[1]
Department of Chemistry, University of New Brunswick, Fredericton, N.B., Canada E3B 6E2

Received September 18, 1989

SIMON PARSONS, JACK PASSMORE, MELBOURNE J. SCHRIVER, and PETER S. WHITE. Can. J. Chem. **68**, 852 (1990).

The dichlorodithionitronium cation, $ClSNSCl^+$, undergoes symmetry-allowed, concerted, cycloaddition reactions with alkynes and alkenes in liquid sulphur dioxide. With ethyne and propyne it gives corresponding 1,3,2-dithiazolium salts in quantitative yield. Cycloaddition with alkenes yields (hitherto unknown) 1,3-dichloro-1,3,2-dithiazolidinium cations. The reactions are sensitive to substituents, and only the cycloaddition with ethene occurs quantitatively on a preparative scale. Cycloadditions with propyne and *E*- and *Z*-2-butene have been observed in solution. The preparation, characterization, and X-ray crystal structure of the product of the reaction of $ClSNSCl^+$ with ethene, 1,3-dichloro-1,3,2-dithiazolidinium hexafluoroarsenate(V), are reported. Crystals of 1,3-dichloro-1,3,2-dithiazolidinium hexafluoroarsenate(V) are monoclinic, of space group $P2_1/c$, $a = 6.3161(6)$ Å, $b = 17.1724(23)$ Å, $c = 19.1558(18)$ Å, and $\beta = 98.143(8)°$; $Z = 4$ and $R = 0.061$. The 1,3-dichloro-1,3,2-dithiazolidinium cation consists of a five-membered $\overline{CSNSC}^+$ ring, axially substituted at the sulphurs by chlorine (average bond lengths: S—N 1.603(8) Å, S—Cl 2.025(4) Å, S—C 1.822(10) Å, and C—C 1.504(13) Å). Two crystallographically unique cations are linked by weak S..N contacts into pseudo-dimers. These data are used, together with structural comparisons with related SNS-containing cations and the sulphoxides and the ^{14}N chemical shift, to show that the bonding in the SNS region of the cation is best represented by the valence canonicals $\rangle S^+—N^-—S^+\langle$ and $\rangle S{=}N—S^+\langle$, such that the sulphur and nitrogen atoms respectively carry absolute positive and negative charges. This picture is also supported by the fluoride contacts to the cation from the AsF_6^- anion, which are exclusively to sulphur. Nuclear magnetic resonance data were consistent with the retention of the solid state structure of $H_2\overline{C(Cl)N(Cl)CH_2}^+$ in solution.

Key words: sulphur-nitrogen chloride, sulphur-nitrogen cations, 1,3-dichloro-1,3,2-dithiazolidinium, cycloaddition reactions, X-ray crystallography.

SIMON PARSONS, JACK PASSMORE, MELBOURNE J. SCHRIVER et PETER S. WHITE. Can. J. Chem. **68**, 852 (1990).

Dans le bioxyde de soufre, le cation dichlorodithionitronium, $ClSNSCl^+$, réagit avec les alcynes et les alcènes pour donner des produits de cycloadditions concertées permises par la symétrie. Avec l'éthyne et le propyne, il y a formation des sels 1,3,2-dithiazolium correspondants, avec des rendements quantitatifs. Les cycloadditions avec les alcènes conduisent aux cations 1,3-dichloro-1,3,2-dithiazolidinium inconnus jusqu'à maintenant. Les réactions sont très sensibles à la présence de substituants et seule la cycloaddition avec l'éthène se produit d'une façon quantitative sur une base préparative. En solution, on a observé des cycloadditions avec le propyne et les *E*- et *Z*-but-2-ènes. On rapporte la préparation, la caractérisation ainsi que la détermination de la structure cristalline du produit de la réaction du $ClSNSCl^+$ avec l'éthène, l'hexafluoroarsénate du 1,3-dichloro-1,3,2-dithiazolidinium. Les cristaux de l'hexafluoroarsénate du 1,3-dichloro-1,3,2-dithiazolidinium sont monocliniques, groupe d'espace $P2_1/c$ avec $a = 6{,}3161(6)$, $b = 17{,}1724(23)$ et $c = 19{,}1558(18)$ Å, $\beta = 98{,}143(8)°$, $Z = 4$ et $R = 0{,}061$. Le cation 1,3-dichloro-1,3,2-dithiazolidinium comporte un cycle $\overline{CSNSC}^+$ dont les soufres sont substitués par des chlores axiaux (longueurs moyennes des liaisons : S—N, 1,603(8) Å; S—Cl, 2,025(4) Å; S—C, 1,822(10) Å et C—C, 1,504(13) Å). Deux cations qui sont distincts d'un point de vue cristallographique sont liés par de faibles contacts S..N pour former des pseudo-dimères. On a comparé ces données ainsi que les valeurs des déplacements chimiques en RMN du ^{14}N avec celles obtenues pour des structures de sulfoxydes et de cations apparentés contenant du SNS et on en conclut que la meilleure façon de représenter les liaisons dans la région du cation est d'utiliser les valences canoniques $\rangle S^+—N^-—S^+\langle$ et $\rangle S{=}N—S^+\langle$; de cette façon, les atomes de soufre et de carbone portent respectivement des charges absolues positive et négative. Cette représentation est en accord avec les contacts des ions fluorures avec le cation de l'anion AsF_6^- qui se font uniquement avec le soufre. Les données de la RMN sont aussi en accord avec le fait que la structure du cation $H_2\overline{C(Cl)N(Cl)CH_2}^+$ à l'état solide est maintenue en solution.

Mots clés : chlorure de soufre et d'azote, cations de soufre et d'azote, 1,3-dichloro-1,3,2-dithiazolidinium, réactions de cycloaddition, cristallographie à l'aide de rayons-X.

[Traduit par la revue]

Introduction

The cycloaddition reactions of sulphur-nitrogen compounds have been the subject of recent interest (1). S_4N_4 undergoes cycloaddition reactions only with some strained alkenes (2). In contrast, SNS^+ undergoes a series of general, symmetry-allowed, quantitative cycloadditions with a variety of unsaturated species (3, 4). Not only do the symmetries of the frontier orbitals of SNS^+ match those of many unsaturated species, but its cationic charge lowers its molecular orbital energies relative to those in neutral sulphur-nitrogen compounds, and thermodynamically and kinetically facilitates reverse electron demand cycloadditions (4). This is illustrated in Fig. 1.

The π-manifold of SNS^+ contains two perpendicular 3 centre/4 electron π bonds (Fig. 1). We have recently shown that the 1:1 cycloadduct of SNS^+ and ethene, $\overline{CH_2SNSCH_2}^+$, which contains a similar 3 centre/4 electron π bond in one plane

[1]Authors to whom correspondence may be addressed.

Can. J. Chem. Downloaded from www.nrcresearchpress.com by 88.85.125.76 on 09/07/12
For personal use only.

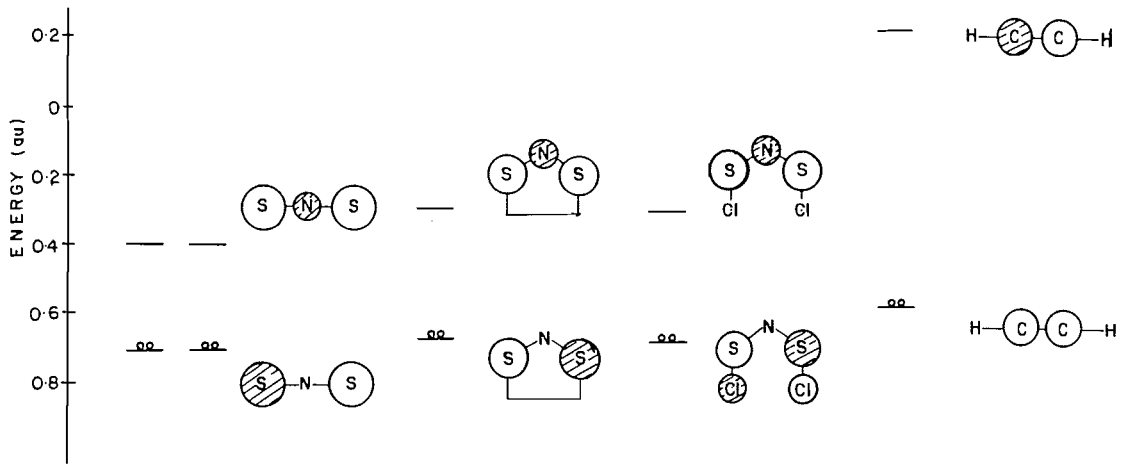

FIG. 1. The frontier molecular orbital energies of SNS^+, $\overline{CH_2SNSCH_2}^+$, $ClSNSCl^+$, and ethyne. Calculated by CNDO/2. Geometries: $ClSNSCl^+$ experimental (27); SNS^+ experimental for AsF_6^- salt corrected for thermal effects (31); $\overline{CH_2SNSCH_2}^+$ extrapolated from the observed structure of **5** (4): bond lengths: S—N 1.65 Å, S—C 1.81 Å, C—C 1.51 Å, C—H 1.0 Å; bond angles at: N 112°, S 102°, C 112°).

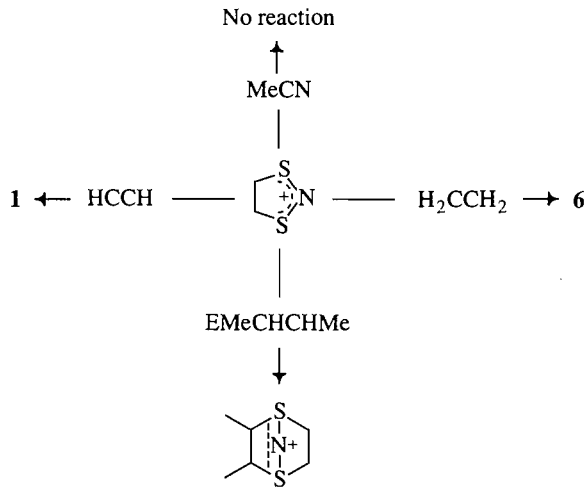

SCHEME 1. Reactions of $\overline{CH_2SNSCH_2}^+$ (all as the AsF_6^- salt in SO_2 solvent (4, 5)).

(Fig. 1), undergoes cycloadditions analogous to those of SNS^+ (Scheme 1) (4, 5). The allowedness of these reactions is enhanced by the positive charge on $\overline{CH_2SNSCH_2}^+$, although it is less reactive than SNS^+ (for example, it does not react with acetonitrile).

We predicted that any $XSNSX^+$ fragment with similar frontier molecular orbitals would undergo similar cycloaddition reactions with unsaturated centres. In this paper we describe experiments carried out to confirm this hypothesis with $ClSNSCl^+$, and the synthesis and characterization of the first 1,3-dichloro-1,3,2-dithiazolidinium salt, prepared by the reaction of $ClSNSClAsF_6$ and ethene. A preliminary abstract of this work has been published (6*a*).

Various $ClSNSCl^+$ salts have been prepared in good yield (6*b*; see also ref. 12), but apart from a recent report of its quantitative reduction to SNS^+ (6*c*), very little is known of its chemistry. In this paper we describe a systematic investigation of its cycloaddition chemistry, and compare its reactivity with that of SNS^+ and $\overline{CH_2SNSCH_2}^+$.

Experimental

Apparatus, techniques, and chemicals, unless specified, have been described (7–11). $ClSNSClAsF_6$ was prepared as in ref. 12. Ethyne, ethene (Canadian Liquid Air), propene, *E*-2-butene (Matheson), *Z*-2-butene (Aldrich), perfluoroethene (Columbia), perfluoro-2-butyne (PCR), propyne (Farchan), and triphenyl antimony (Lancaster Synthesis) were used as received.

All nmr spectra were recorded on a Varian Associates XL-200 spectrometer and accumulated in 4K (^{14}N), 16K (^1H), or 32K (^{13}C and ^{19}F) of memory, and obtained unlocked at room temperature. ^1H spectra were run at 200 MHz in 32–200 scans with a spectral width of 2.6 kHz (0.3 Hz/data point, acquisition time 2.991 s, pulse width 6.1 μs). ^{19}F spectra were obtained at 188.15 MHz in 100–200 scans with a spectral width of 56.5 kHz (3.8 Hz/data point, acquisition time 0.266 s, pulse width 4 μs). ^{13}C spectra were run at 50.29 MHz with a spectral width of 15.0 kHz (1 Hz/data point, acquisition time 1.001 s, pulse width 4 μs) with broad band "waltz" decoupling. ^{14}N spectra were run at 14.45 MHz in 2000–10000 scans with a spectral width of 15.0 kHz (10.2 Hz/data point, acquisition time 0.098 s, pulse width 38 μs). The pulse widths quoted correspond to tip angles of 90° (^{14}N), 60° (^1H), 30° (^{19}F), and 22.5° (^{13}C). Samples for ^1H and ^{19}F nmr spectroscopy were contained in sealed thick-walled 5-mm precision nmr tubes, and those for ^{13}C and ^{14}N nmr in thick-walled 10-mm (or occasionally 16-mm for ^{14}N) nmr tubes fitted with J. Young "O Ringette" type valves. Spectra were referenced externally to a solution of TMS and Freon-11 in SO_2 (^1H and ^{19}F), TMS in SO_2 (^{13}C), or neat nitromethane (^{14}N).

Reaction of $ClSNSClAsF_6$ with unsaturated bonds

SO_2 (0.842 g, 13.14 mmol) and ethyne (0.004 g, 0.14 mmol) were successively condensed onto $ClSNSClAsF_6$ (0.048 g, 0.14 mmol) in a 5-mm nmr tube, which was then flame sealed. The mixture was kept at −196°C until the ^1H nmr was acquired. This showed only a singlet at 11.0 ppm ($\overline{HCSNSCH}^+$, **1***a* (5)). The results of this and other experiments, performed according to a similar procedure, are given in Table 1.

Reaction of substituted alkenes (propene, *E* and *Z* but-2-enes) with $ClSNSCl^+$ according to this procedure led to the formation of mixtures containing mostly RCH(Cl)CHR(Cl) and $\overline{RCHSNSCHR}^+$ (R = Me or H). In an attempt to obtain clean cycloaddition, experiments were carried out in which solutions of alkenes were poured directly onto solid $ClSNSClAsF_6$. The results are shown in Table 2. Experiments in which solutions of alkenes and $ClSNSClAsF_6$ were mixed gave essentially the same results as those carried out in nmr tubes.

The preparation of $HCSNSCHAsF_6$ by the reaction of $ClSNSClAsF_6$ with ethyne

The ^{14}N nmr spectrum of a yellow solution of $ClSNSClAsF_6$ (0.338 g, 1.00 mmol) in SO_2 (3.70 g) in a 16-mm nmr tube showed only one resonance at 19 ppm ($\Delta\nu$ = 450 Hz) due to $ClSNSCl^+$ (13).

Can. J. Chem. Downloaded from www.nrcresearchpress.com by 88.85.125.76 on 09/07/12
For personal use only.

TABLE 1. Reactions of $ClSNSClAsF_6$ carried out in 5-mm nmr tubes

Reaction and stoichiometry Weights No. of mmols Colour changes	^1H NMR spectrum δ (ppm) (multiplicity, relative intensity (%))	Assignments (5)
$ClSNSClAsF_6 + HCCH \xrightarrow{SO_2}{}^{a}$	11.0 (s, 100)	$\overline{HCSNSCH}^+$ (**1***a*)
0.048 g 0.004 g 0.842 g		
0.14 0.14		
Little change		
$ClSNSClAsF_6 + MeCCH \xrightarrow{SO_2}{}^{a,c}$	10.7 (s, 16)	$Me\overline{CSNSCH}^+$ (**1***b*)
0.039 g 0.004 g 0.763 g	3.4 (s, 58)	**1***b*
0.11 0.11	2.6 (s, 6)	Unassigned
Yellow → pale orange	2.5 (d, J = 4.3 Hz, 4)	Unassigned
	1.0 (d, J = 6.6 Hz, 15)	Allene (impurity in MeCCH)
$ClSNSClAsF_6 + H_2CCH_2 \xrightarrow{SO_2}{}^{b}$	5.3 (m, 100)	$H_2\overline{C(SCl)N(SCl)CH_2}^+$ (**2**)
0.033 g 0.002 g 1.370 g		
0.10 0.07		
Yellow → pale yellow		
$ClSNSClAsF_6 + 2H_2CCH_2 \xrightarrow{SO_2}{}^{b}$	5.3 (s, 31)	**2**
0.032 g 0.006 g 1.290 g	4.9 (s, 36)	$H_2\overline{CSNSCH_2}^+$
0.10 0.21	4.0 (s, 6)	$CH_2Cl—CH_2Cl$
Yellow → little change	3.7 (m) 3.2 (m) } (25)	$S_2N(C_2H_4)_2^+$ (**6**)
	1.6 (m, 1)	Unassigned
$ClSNSClAsF_6 + xsMeCN \xrightarrow{SO_2}{}^{d}$	1.92 (s, 100)	MeCN
0.089 g 0.206 g 0.502 g		
0.27 5.02		
Yellow → no change		
	^{19}F NMR spectrum δ (ppm) (multiplicity)	
$ClSNSClAsF_6 + xsCF_3CCCF_3 \xrightarrow{SO_2}{}^{d}$	−53 (s)	CF_3CCCF_3
0.036 g 0.075 g 0.722 g	−58 (q, J = 930 Hz)	AsF_6^-
0.15 0.47		
Yellow → little change		
$ClSNSClAsF_6 + F_2CCF_2 \xrightarrow{SO_2}{}^{a}$	−132 (s)	F_2CCF_2
0.051 g 0.018 g 0.872 g	−58 (q, J = 930 Hz)	AsF_6^-
0.15 0.18		
Yellow → little change		

[a]Experiments carried out in 5-mm nmr tube according to procedure described in text.
[b]A less concentrated solution was used here. More concentrated solutions led to a less well resolved multiplet.
[c]See Table 2 for comparison.
[d]Procedure as described in text, and in addition the sample was heated to 70°C for 14 h before recording nmr spectrum.

HCCH (0.086 g, 3.30 mmol, 2.3-fold excess with respect to eq. [2] (see below)) was added, giving a clear yellow solution that became colourless after 20 h, and one resonance in the ^{14}N nmr spectrum at −5 ppm ($\Delta\nu$ = 350 Hz), **1***a* (13). The volatile products contained SO_2, SO_2Cl_2, HCCH, and H(Cl)CC(Cl)H (ir). The white-brown solid product was $\overline{HCSNSCH}AsF_6$ (ir) (0.283 g, 0.97 mmol, 97% yield) (3).

Synthesis of $\overline{CH_2(SCl)N(SCl)CH_2}AsF_6$ (2)

SO_2 (8.140 g) and ethene (0.160 g, 5.72 mmol) were condensed onto $ClSNSClAsF_6$ (1.936 g, 5.73 mmol) in a two-bulbed vessel incorporating a sintered glass frit. The solution turned from bright yellow to pale yellow within a minute of thawing, but the reaction mixture was stirred at room temperature for 20 min to ensure complete reaction. The volatiles (SO_2, ir) were removed, leaving pure **2** (2.087 g, 5.71 mmol, 99% yield, according to eq. [1]).

[1] $ClSNSClAsF_6 + H_2CCH_2 \rightarrow \overline{CH_2(SCl)N(SCl)CH_2}AsF_6$

Characterization of 2

Melting point 161–164°C (dec.). Infrared spectrum (Nujol mull

Can. J. Chem. Downloaded from www.nrcresearchpress.com by 88.85.125.76 on 09/07/12
For personal use only.

TABLE 2. Reactions of $ClSNSClAsF_6$ with substituted alkenes carried out by pouring a solution of the alkene in SO_2 onto solid $ClSNSClAsF_6$

Reaction and stoichiometry Weights No. of mmols Colour changes	^{1}H NMR spectrum δ (ppm) (multiplicity, relative intensity (%))	Assignments (5)
$ClSNSClAsF_6$ + $MeCHCH_2$ $\xrightarrow{SO_2}$[a]		
0.133 g 0.014 g 1.968 g	5.9 (m, 6)	**3***a*,[b] methine
0.392 0.340	5.6 (m, 8)	**3***b*,[b] methylene
Yellow → pale yellow	5.3 (m, 8)	**3***a*, methylene
	5.0 (m, 15)	**3***a*, methylene, **3***b*, methine
	4.7 (m, 11)	**3***b*, methylene
	2.3 (d, J = 6.2 Hz, 34)	**3***b*, methyl
	2.0 (d, J = 7.3 Hz, 17)	**3***a*, methyl
	1.8 (d, J = 7.3 Hz, 1)	$MeCHSNSCH_2^+$
$ClSNSClAsF_6$ + *E*-MeCHCHMe $\xrightarrow{SO_2}$[a,c]		
	5.7 (d, J = 10.4 Hz of q, J = 7.2 Hz, 8)	*anti*-$MeCH(SCl)N(SCl)CHMe^+$[d]
0.128 g 0.018 g 2.506 g	5.25 (m, <1)	$MeCHSNSCHMe^+$
0.377 0.320	4.9 (br, 5)	Unassigned
Yellow → yellow-orange	4.73 (d, J = 10.4 Hz of q, J = 6.2 Hz, 7)	*anti*-$MeCH(SCl)N(SCl)CHMe^+$
	4.34 (m, <1)	MeCHCl—CHClMe
	2.23 (d, J = 7.2 Hz) } 72%	*anti*-$MeCH(SCl)N(SCl)CHMe^+$
	2.18 (d, J = 6.4 Hz) } 72%	*anti*-$MeCH(SCl)N(SCl)CHMe^+$
	1.72 (m, 7)	$MeCHSNSCHMe^+$ MeCHClCHClMe
$ClSNSClAsF_6$ + *Z*-MeCHCHMe $\xrightarrow{SO_2}$[a,e]		
	5.8 (m, 7)	*syn-endo*-$MeCH(SCl)N(SCl)CHMe^+$[f]
0.125 g 0.018 g 2.347 g	5.25 (2 overlapping resonances, 6)	*syn-exo*-$MeCH(SCl)N(SCl)CHMe^+$ / $MeCHSNSCHMe^+$
0.369 0.326	4.9 (m, 2)	Unassigned
No change	4.6 (br, 5)	Unassigned
	4.4 (m, 2)	MeCHCl—CHClMe
	2.2 (d, J = 6.0 Hz, 16)	*syn-exo*-$MeCH(SCl)N(SCl)CHMe^+$
	2.0 (d, J = 6.7 Hz, 27)	*syn-endo*-$MeCH(SCl)N(SCl)CHMe^+$
	1.9 (m, overlapping resonances, 8)	$MeCHSNSCHMe^+$ and unassigned
	1.7 (m, 26)	MeCHClCHClMe and unassigned

[a] Solution of alkene poured onto solid $ClSNSClAsF_6$; procedure described in text.

[b] $MeCH(SCl)N(SCl)CH_2^+$ can exist in either diastereomeric form **3***a* or **3***b*. **3***b* is expected to be more abundant because this isomer will experience less steric hindrance between the methyl group and the chlorines than **3***a*. The assignment of individual resonances was made using 2D-COSY ^{1}H nmr and confirmed using a series of low power ^{1}H decoupling experiments. The ^{13}C spectrum of a 0.6 M solution prepared by pouring $MeCHCH_2$ (0.063 g, 1.50 mmol) in SO_2 (3.432 g) onto solid $ClSNSClAsF_6$ (0.527 g, 1.56 mmol) showed resonances at 78.7, 73.3, 68.6, 66.0, 18.6, and 13.0 ppm (**3***a*,*b*); 67.1, 62.4, and 15.7 ppm ($MeCHSNSCH_2^+$); and 57.7, 50.5, and 22.3 ppm ($MeCHClCH_2Cl$).

[c] ^{13}C spectrum of a solution prepared by pouring *E*-MeCHCHMe (0.044 g, 0.78 mmol) in SO_2 (3.883 g) onto solid $ClSNSClAsF_6$ (0.305 g, 0.902 mmol): 82.1, 76.1, 12.1, and 11.4 ppm (*anti*-$MeCH(SCl)N(SCl)CH_2^+$); 74.1 and 14.2 ppm ($MeCHSNSCH_2^+$); 62.0 and 21.1 ppm ($MeCHClCH_2Cl$); and 70.4, 58.6, 17.3, and 9.9 ppm (unassigned).

[d] The connectivities implied by these assignments were deduced from a 2D-COSY ^{1}H nmr experiment. This also showed that the broad resonance at 4.9 ppm was linked to another broad resonance beneath the two doublets at 2.2 ppm. This accounts for the anomalously large integration of this set of resonances.

[e] ^{13}C spectrum of a solution prepared by pouring *Z*-MeCHCHMe (0.052 g, 0.93 mmol) in SO_2 (2.146 g) onto $ClSNSClAsF_6$ (0.330 g, 0.98 mmol): 80.8, 71.6, 12.7, and 10.5 ppm (*syn*-$MeCH(SCl)N(SCl)CH_2^+$; two isomers, *exo* and *endo*); 70.8 and 8.4 ppm (*syn*-$MeCHSNSCHMe^+$); 62.5 and 21.1 ppm (MeCHClCHClMe); and 67.6, 67.3, 65.6, 13.4, and 13.0 (unassigned).

[f] *syn*-$MeCH(SCl)N(SCl)CHMe^+$ can exist in *exo* and *endo* forms. By similar reasoning to that given in footnote *b*, the *endo* form is likely to be more abundant. The connectivities implied by these assignments were confirmed by a series of low power decoupling experiments.

Can. J. Chem. Downloaded from www.nrcresearchpress.com by 88.85.125.76 on 09/07/12
For personal use only.

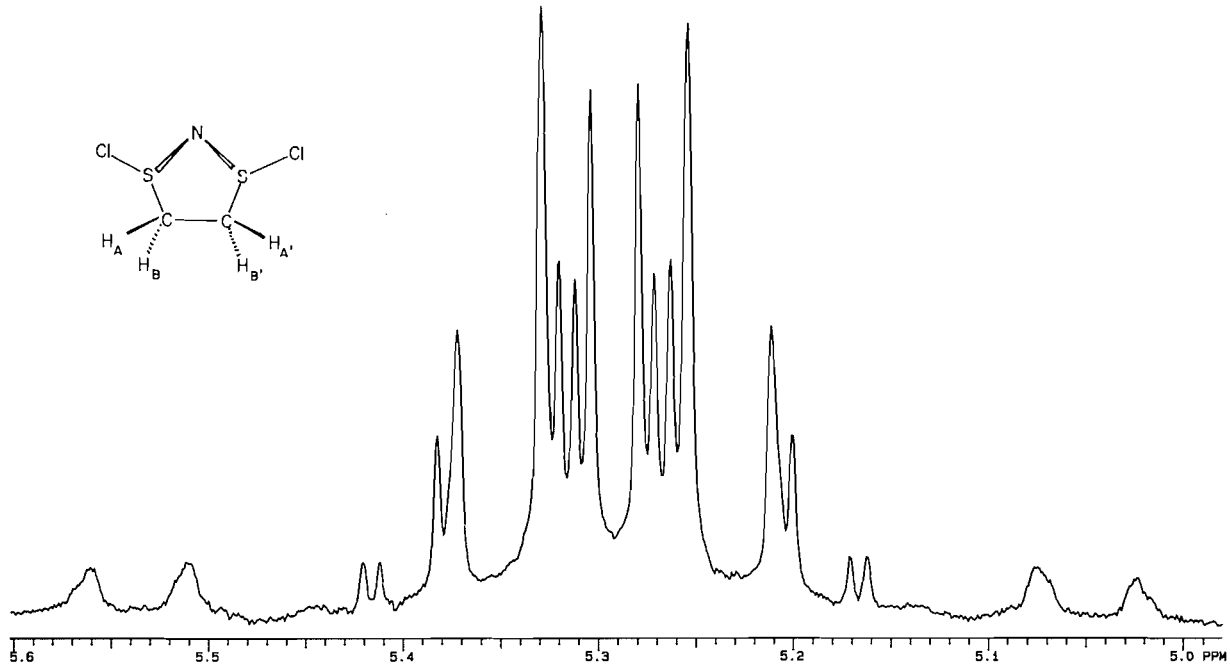

FIG. 2. The ^1H nmr spectrum (at 200 MHz) of $\overline{CH_2(SCl)N(SCl)CH_2}AsF_6$ in SO_2 at room temperature. (A line narrowing function has been applied.)

1*a* R = H
b R = Me

2

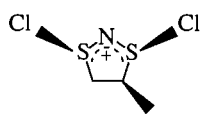

3*a*

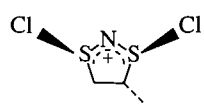

3*b*

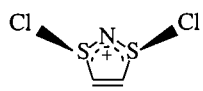

4

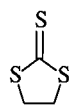

5

between KBr plates): 3027 (m), 3002 (m, ν(CH)), 1417 (m), 1402 (m, $\beta(CH_2)$), 1149, 1101 (mw, $\nu_{asym}(S_2N)$), 906 (s, $\beta(CH_2)$), 738 (s), 690 (vs, $\nu_3(AsF_6^+)$), 659 (sh), 651 (sh), 617 (m), 551 (mw), 521 (s, ν_{asym}(S-Cl)), 476 (s), 455 (s, ν_{sym}(S-Cl)), 396 (s, $\nu_4(AsF_6^-)$) cm^{-1}. A copy of the spectrum has been deposited.[2] The ^1H nmr spectrum: AA′BB′ pattern about 5.3 ppm (Fig. 2) (due to **2**). An additional peak at 4.9 ppm (ca. 3% of total integrated intensity) was observed in solutions of isolated **2** redissolved in SO_2. This is due to $H_2\overline{CSNSCH_2}^+$ arising from dechlorination of **2**; ^{13}C nmr: δ = 62.5 ppm. A much weaker resonance at 55.2 ppm was also observed and assigned to the dechlorinated product (5); ^{14}N nmr: δ = −243 ppm ($\Delta\nu$ = 415 Hz). Anal. calcd. for $C_2H_4S_2NCl_2AsF_6$: S 17.52, N 3.83, Cl 19.37, C 6.56, H 1.10%; found: S 17.78, N 3.91, Cl 19.54, C 6.79, H 1.13%.

Dechlorination of 2

The appearance of the resonances at 4.9 ppm (^1H) and 55.2 ppm (^{13}C) in the nmr spectra of isolated **2** redissolved in SO_2 indicated that it is unstable with respect to dechlorination. Solutions of **2** prepared *in situ* in SO_2 only showed slight dechlorination (2%) after standing at room temperature for over four hours (^1H nmr). In the presence of a large excess of chlorine the ^1H nmr of a solution of **2** in SO_2 showed only a broadish singlet at 5.2 ppm ($\Delta\nu$ = 9 Hz).

Dechlorination of **2** becomes quantitative in the presence of a stronger chlorine acceptor. The ^1H nmr of a mixture of **2** (0.047 g, 0.13 mmol) and $SbPh_3$ (0.044 g, 0.14 mmol) in SO_2 exhibited resonances only at 8.3 ppm, 7.7 ppm ($SbPh_3Cl_2$), and 4.9 ppm ($H_2\overline{CSNSCH_2}^+$).

Single crystal X-ray diffraction study

Crystals of **2** (0.148 g) suitable for X-ray crystallography were grown from a mixture of SO_2 (3.419 g) and Freon-11 (1.938 g) by slow evaporation of the solvent over 12 h, and mounted under dry nitrogen in rigorously dried Pyrex capillaries as described elsewhere (14).

After a preliminary photographic investigation a suitable crystal was mounted on an Enraf–Nonius CAD4 diffractometer equipped with graphite monochromated Mo Kα radiation and under the control of the NRCCAD (15) program system. Full details of the data collection and other crystallographic information are given in Table 3.

The structure was solved by direct methods. After refinement with isotropic thermal parameters and empirical absorption correction was applied using the DIFABS routine (16). In the final cycles of least-squares refinement all non-hydrogen atoms were permitted to refine with anisotropic thermal parameters. Hydrogen atoms were placed at calculated positions (with C—H bond length 0.96 Å) and assigned isotropic thermal parameters based on the carbon atom to which they are attached. Scattering factors were taken from ref. 17 and corrected for anomalous dispersion. Final atomic coordinates are given in Table 4.[2] All computations were performed using the PC version of the NRCVAX suite of programs (18).

Discussion

Concerted, symmetry-allowed cycloaddition reactions of $ClSNSCl^+$ are observed in dilute solution for a number of

[2]Tables of anisotropic thermal parameters and observed and calculated structure factors, calculated hydrogen atomic parameters, a stereo view of the unit cell of $CH_2(SCl)N(SCl)CH_2AsF_6$, and its ir as a Nujol mull between KBr plates have been deposited and may be purchased from the Depository of Unpublished Data, CISTI, National Research Council of Canada, Ottawa, Ont., Canada K1A 0S2.

Can. J. Chem. Downloaded from www.nrcresearchpress.com by 88.85.125.76 on 09/07/12
For personal use only.

TABLE 3. Crystal data for $\overline{CH_2(SCl)N(SCl)CH_2}AsF_6$ (**2**)

System	Monoclinic
Space group	$P2_1/c$
a (Å)	6.3161(6)
b (Å)	17.1724(23)
c (Å)	19.1558(18)
β (°)	98.143(8)
V (Å^3)	2056.7
Z	4
Crystal size (mm)	0.52 × 0.33 × 0.15
μ (mm^{-1})	4.26
D_{calc} (mg m^{-3})	2.36
$F(000)$	1408
Diffractometer	Nonius CAD4
Scan type	θ–2θ
Scan width (deg 2θ corrected for dispersion)	1.8
Scan speed (deg 2θ min^{-1})	2
$2\theta_{max}$	50
Number of standards per interval per hour	3
Number of measured reflections	7214
Number of observed reflections ($I > 2.5\sigma(I)$)	2662
Number of unique reflections	3607
Octants collected	$\pm h, \pm k, l$, with h(max) = 7, k(max) = 19, l(max) = 22
λ – Mo K_α (Å)	0.70930
Temperature (K)	293
Relative transmission factors	0.70–1.73
Weighing scheme	$w = 1/(\sigma(F) + 0.001F^2)$
R (= $\Sigma\|\Delta F\|/\Sigma\|F\|$) observed data	0.061
all data	0.089
R (= $\Sigma w\|\Delta F\|^2/\Sigma wF_o^2$) observed data	0.078
all data	0.085
Number of refined parameters	257
Final difference synthesis maximum (e/Å^3)	1.23
Final difference synthesis minimum (e/Å^3)	−0.99

non-electrophilic alkenes and alkynes. A summary of results is given in Scheme 2. The cycloaddition reactions are less general than those of SNS^+, and more resemble those of $\overline{CH_2SNSCH_2}^+$ (see Scheme 1 and below) (4). The higher reactivity of SNS^+ relative to $ClSNSCl^+$ is likely a kinetic effect, arising in part from the smaller energy differences between its LUMO and the HOMOs of alkenes and alkynes (see Fig. 1) (19).

The reaction of $ClSNSCl^+$ with ethyne on a preparative scale gave **1***a* quantitatively, and it is likely that this reaction is a general preparative route to a variety of derivatives of **1**. In contrast, only ethene gave the corresponding dichloro cycloadduct (**2**) in high yield on a preparative scale.

Reactions with alkynes

$ClSNSClAsF_6$ was reacted with HCCH, MeCCH, and CF_3CCCF_3. Cycloaddition with chlorine elimination occurred in the case of ethyne and propyne (eq. [2]), but no reaction was observed with CF_3CCCF_3, even in the presence of an excess of alkyne with heating to 70°C for 14 h.

[2] $HCCH + ClSNSClAsF_6 \rightarrow \overline{HCSNSCH}AsF_6 + Cl_2$

The reactions were followed by ^1H or ^{19}F nmr, and the nmr results were confirmed on a prepative scale in the reaction with ethyne.

The cycloaddition of alkynes with the $ClSNSCl^+$ cation likely proceeds via an intermediate of type **4**, which then loses Cl_2 under the driving force of the aromaticity of the final product (here **1***a* and *b*), and the formation of SO_2Cl_2:

[3] $Cl_2 + SO_2 \rightarrow SO_2Cl_2$

Although these heterocycles can also be obtained by the reaction of SNS^+ or $\overline{CH_2SNSCH_2}^+$ with an alkyne (3), their synthesis from more readily available $ClSNSCl^+$ salts potentially represents a more convenient route.

MeCN did not react with $ClSNSCl^+$, in contrast to its facile cycloaddition with SNS^+. This is consistent with the known reluctance of nitriles to behave as dienophiles (20): for example, Diels–Alder cycloaddition to a nitrilic function often requires very high temperatures or even gas phase conditions.

The reaction of SNS^+ with CF_3CCCF_3 is slower than with alkyl analogues (5), and it is not surprising that it does not react at all with $ClSNSCl^+$. CF_3CCCF_3 is a poorer electron donor than R_HCCR_H, and would therefore be expected to be less reactive towards acceptors. In addition, SNS^+ is a better acceptor than $ClSNSCl^+$, by virtue of its lower energy LUMO (see Fig. 1). This observation is an illustration of the general requirement that components of cycloaddition reactions have "complimentary electronic character" (20).

Reactions with alkenes

$ClSNSClAsF_6$ was reacted with ethene, propene, *E*- and *Z*-2-butene, and perfluoroethene in SO_2 at room temperature (Scheme 2). The predicted cycloaddition was observed in solution to some extent in all cases except the last. These findings constitute the first observation of 1,3-dichloro-1,3,2-dithiazolidinium cations, which are potentially useful prepara-

Can. J. Chem. Downloaded from www.nrcresearchpress.com by 88.85.125.76 on 09/07/12
For personal use only.

TABLE 4. Atomic parameters x,y,z, and B_{iso}. ESDs refer to the last digit printed

Atom	x	y	z	B_{iso}[a]
S1	0.5551 (4)	0.18463(14)	0.01930(11)	2.54(9)
Cl1	0.3785 (5)	0.26031(20)	0.06865(16)	5.62(15)
N1	0.4620 (13)	0.1837 (4)	−0.0626 (4)	3.0 (3)
S2	0.5686 (5)	0.24555(13)	−0.11031(12)	3.28(12)
Cl2	0.4496 (6)	0.35168(16)	−0.09265(18)	6.20(16)
C1	0.8278 (16)	0.2528 (6)	−0.0569 (5)	3.3 (4)
C2	0.7975 (14)	0.2411 (6)	0.0183 (5)	3.0 (4)
S3	0.4303 (4)	0.47686(14)	0.34174(12)	3.01(11)
Cl3	0.5611 (4)	0.57826(14)	0.31538(16)	4.35(12)
N2	0.5203 (12)	0.4075 (4)	0.2981 (4)	2.7 (3)
S4	0.4174 (4)	0.40178(12)	0.21674(12)	2.36(9)
Cl4	0.6049 (4)	0.46167(18)	0.15784(15)	4.65(13)
C3	0.1936 (14)	0.4706 (5)	0.2145 (5)	2.8 (4)
C4	0.1676 (14)	0.4868 (5)	0.2907 (5)	2.9 (4)
As1	0.96622(14)	0.23627(5)	0.23631(4)	1.96(4)
F11	1.0053 (14)	0.3054 (4)	0.1751 (4)	7.3 (4)
F12	0.9216 (15)	0.1694 (4)	0.2954 (3)	7.8 (5)
F13	0.7072 (12)	0.2612 (5)	0.2274 (5)	9.5 (5)
F14	0.9040 (12)	0.1715 (3)	0.1699 (3)	5.3 (3)
F15	1.2275 (12)	0.2172 (6)	0.2428 (6)	9.6 (6)
F16	1.0312 (14)	0.3015 (4)	0.3033 (4)	7.8 (4)
As2	0	1	0	1.87(5)
F21	0.1092 (13)	0.9445 (4)	0.0691 (4)	7.2 (4)
F22	0.1891 (16)	1.0655 (7)	0.0166 (5)	12.6 (7)
F23	−0.1322 (20)	1.0468 (6)	0.0573 (5)	12.1 (7)
As3	1	1	1/2	2.02(5)
F31	0.9480 (19)	0.9213 (4)	0.4485 (4)	10.5 (7)
F32	0.9897 (14)	1.0575 (4)	0.4278 (3)	7.5 (5)
F33	1.2577 (16)	0.9888 (9)	0.4985 (8)	15.7 (10)
H1A	0.890	0.303	−0.063	3.5
H1B	0.924	0.214	−0.071	3.5
H2A	0.918	0.214	0.044	3.2
H2B	0.786	0.290	0.042	3.2
H3A	0.067	0.448	0.189	3.1
H3B	0.223	0.518	0.191	3.1
H4A	0.103	0.537	0.293	3.7
H4B	0.068	0.449	0.303	3.7

[a] B_{iso} is the mean of the principal axes of the thermal ellipsoid.

tive intermediates because they contain synthetically versatile S—Cl bonds.

^1H and ^{13}C nuclear magnetic resonance were used to characterize the products of these reactions. $ClSNSCl^+$ reacts quantitatively with ethene to give **2**, the 200-MHz ^1H nmr spectrum of which shows an AA′BB′ resonance that is consistent with **2** containing a CH_2CH_2 moiety with no plane of symmetry through the carbon atoms, as also shown by X-ray diffraction (see below), which confirms that the structure in solution is the same as in the solid state. The ^1H nmr spectra of reaction mixtures involving substituted alkenes were complicated by second-order effects and the overlap of peaks. However, selective low power decoupling and ^1H-COSY experiments largely enabled these spectra to be completely assigned, although small amounts (5%) of unidentified species were present in the reactions with *E* and *Z* butenes.

The nature of the products obtained in these reactions depended on experimental conditions. Strict 1:1 stoichiometry was necessary because dechlorination occurred in the presence of excess alkene. Reaction of substituted alkenes with $ClSNSCl^+$ in nmr tubes led to the formation of mixtures. The highest yields of cycloadducts with substituted alkenes were observed when a solution of the alkene was poured onto solid $ClSNSClAsF_6$, and reaction mixtures were 0.2–0.3 M in the reactants. Under these conditions the cycloaddition of $ClSNSCl^+$ with propene proceeded quantitatively, but those with *E* and *Z* butenes only in 56 and 70% yields respectively (as calculated from nmr integrations).

All the cycloadditions with alkenes were observed in solution by nmr on a small scale, but only the ethene cycloadduct was isolated and fully characterized. The only substituted species to be obtained pure in solution (**3***a*,*b*) gave an involatile reddish oil on removal of the solvent. Given these findings, it is unlikely that the procedures described here will constitute viable general syntheses of 1,3-dichloro-1,3,2-dithiazolidinium salts. (N.B. Reaction of $\overline{CH_2SNSCH_2}AsF_6$ with Cl_2 leads to a mixture of products not including **2** (5).)

The side products of the reactions of substituted alkenes with $ClSNSCl^+$ were usually chlorinated alkene and $R\overline{CHSNSCHR}^+$. It is likely that these arise via two alternative routes, one mediated by SO_2:

[4] $R\overline{CH(SCl)N(SCl)CHR}^+ + SO_2 \rightarrow R\overline{CHSNSCHR}^+ + SO_2Cl_2$

[5] $RCH{=}CHR + SO_2Cl_2 \rightarrow RCH(Cl)CH(Cl)R + SO_2$

and another by alkene:

[6] $R\overline{CH(SCl)N(SCl)CHR}^+ + RCH{=}CHR \rightarrow R\overline{CHSNSCHR}^+ + RCH(Cl)CH(Cl)R$

The sensitivity to substituents of the cycloadditions of alkenes with $ClSNSCl^+$ is seen to a limited extent in their related cycloadditions with SNS^+. Although *E*- and *Z*-2-butene cycloadd cleanly to SNS^+, the fully substituted alkene 2,3-dimethyl-2-butene (Me_2CCMe_2) produces a variety of products, which have so far not been identified. It is possible that these effects are a result of steric factors.

F_2CCF_2, a very poor electron donor, did not react with $ClSNSCl^+$. Neither have we observed it to react with SNS^+ (5).

The preparation of **2**

The symmetry-allowed cycloaddition of ethene and $ClSNSCl^+$ proceeds quantitatively according to eq. [1] to produce **2**, the first example of a 1,3-dichloro-1,3,2-dichlorodithiazolidinium salt. Figure 1 illustrates the dominant frontier orbital interactions.

Although **2** is unstable with respect to dechlorination in sulphur dioxide, the process is slow, and the product is obtained pure provided reaction times are kept short. The dechlorination reaction:

[7] $\mathbf{2} \rightarrow H_2\overline{CSNSCH_2}AsF_6 + Cl_2$

is likely displaced to the right by the formation of SO_2Cl_2 (eq. [3]).

Addition of excess chlorine to a solution of **2** in SO_2 inhibits dechlorination, but also causes the collapse of the AA′BB′ multiplet to a broadish singlet at 5.2 ppm ($\Delta\nu$ = 9 Hz), conceivably due to rapid chlorine exchange causing equilibration of the A and B protons.

Dechlorination of **2** becomes quantitative in the presence of a stronger chlorine acceptor. **2** reacts with $SbPh_3$ according to eq. [8]:

[8] $\mathbf{2} + SbPh_3 \rightarrow H_2\overline{CSNSCH_2}AsF_6 + SbPh_3Cl_2$

Acetonitrile dissolves $ClSNSClAsF_6$ without reaction, and it was hoped that dechlorination would be lessened in this solvent.

Can. J. Chem. Downloaded from www.nrcresearchpress.com by 88.85.125.76 on 09/07/12
For personal use only.

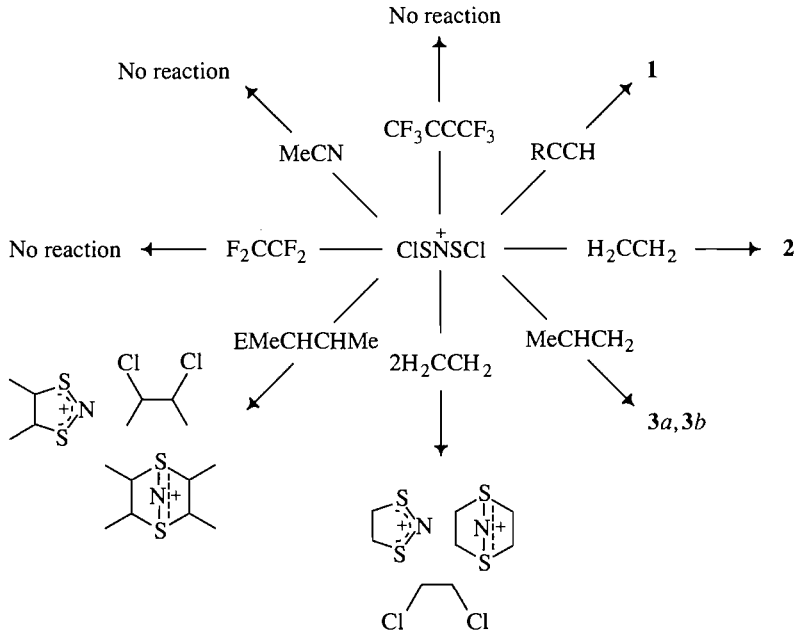

SCHEME 2. Reactions of $ClSNSCl^+$ (all as the AsF_6^- salt in SO_2).

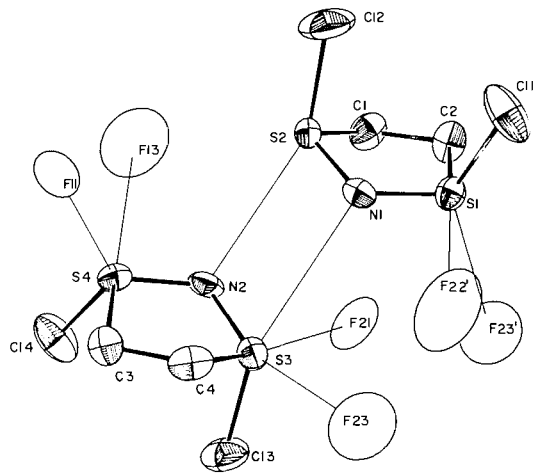

FIG. 3. The two crystallographically different cations in $\overline{CH_2(SCl)N(SCl)CH_2}AsF_6$ (**2**), showing fluorine contacts to the rings.

However, the ^1H nmr spectra of reactions of alkenes with $ClSNSClAsF_6$ in CD_3CN showed complex mixtures of products, which included the same dechlorinated sulphur-nitrogen heterocycles as observed in the reactions carried out in SO_2.

The X-ray crystal structure of **2**

2 consists of discrete $\overline{CH_2(SCl)N(SCl)CH_2}^+$ cations and AsF_6^- anions, which are packed in the unit cell in alternate layers.[3] Two structurally identical (see below), but crystallographically distinct, $\overline{CH_2(SCl)N(SCl)CH_2}$ cations are observed, with weak cation–cation and cation–anion contacts (Fig. 3). Bond distances and angles are presented in Tables 5 and 6. The two crystallographically different heterocyclic cations both have half-chair conformations (Fig. 3), with torsional S—C—C—S angles of 24.8° along C1—C2 and 29.9° along C3—C4,

[3]A stereoview of the unit cell of **2** has also been deposited (see footnote 2).

TABLE 5. Cationic and anionic bond and contact distances in $\overline{CH_2(SCl)N(SCl)CH_2}AsF_6$

Cation 1:		Cation 2:	
S1...Cl1	2.031(4)	S3...Cl3	2.022(4)
C2	1.815(9)	C4	1.811(10)
N1	1.595(8)	N2	1.605(7)
S2...Cl2	2.018(4)	S4...Cl4	2.028(3)
C1	1.808(11)	C3	1.838(9)
N1	1.609(8)	N2	1.604(8)
C1...C2	1.492(13)	C3...C4	1.518(13)
Inter-cationic distances:			
S2...N2	3.150(7)	S3...N1	3.301(7)
Cation–anion contact distances:			
Cation 1:		Cation 2:	
S1...F22′	3.080(8)	S3...F21	3.200(8)
F23′	3.103(8)	F23	3.120(10)
		S4...F11	3.092(8)
		F13	3.019(9)
Anion:			
As1...F11*	1.711(6)	As2...F21*	1.697(6)
F12	1.664(6)	F22*	1.638(5)
F13*	1.676(8)	F23*	1.675(8)
F14*	1.694(6)	As3...F31*	1.677(7)
F15	1.670(8)	F32*	1.693(6)
F16*	1.709(7)	F33	1.643(10)

NOTE: Sums of van der Waals radii: S—F (3.27 Å), S—N (3.35 Å), and (21). The fluorine atoms marked * make significant contacts to the cations.

similar to that observed in the structure of $S{=}\overline{CSCH_2CH_2}S$ (**5**) (21). Chlorine atoms are situated axially on the sulphur atoms with equatorially directed lone pairs. This overall geometry is consistent with the cycloaddition of an ethene molecule to planar $ClSNSCl^+$.

The average cationic bond lengths (S—N 1.603 Å, S—Cl

Can. J. Chem. Downloaded from www.nrcresearchpress.com by 88.85.125.76 on 09/07/12
For personal use only.

TABLE 6. Cationic and anionic bond and contact angles in $\overline{CH_2(SCl)N(SCl)CH_2}AsF_6$ (**2**)

Cation 1:		Cation 2:	
C2...S1...Cl1	100.6(3)	C4...S3...Cl3	99.2(3)
C2...S1...N1	100.9(4)	C4...S3...N2	98.9(4)
Cl1...S1...N1	108.3(3)	Cl3...S3...N2	108.8(3)
C1...S2...Cl2	99.9(3)	C3...S4...Cl4	99.7(3)
C1...S2...N1	98.1(4)	Cl4...S4...N2	100.8(4)
Cl2...S2...N1	107.8(3)	Cl4...S4...N2	108.7(3)
S1...N1...S2	115.3(5)	S3...N2...S4	115.3(4)
S2...C1...C2	107.9(6)	S4...C3...C4	106.4(6)
S1...C2...C1	107.8(6)	S3...C4...C3	106.6(6)
Inter-cationic contact angles:			
N2...S2...Cl2	99.9(3)	N1...S3...Cl3	149.7(2)
N2...S2...C1	112.4(4)	N1...S3...C4	110.9(3)
N2...S2...N1	75.6(3)	N1...S3...N2	70.8(3)
Cation–anion contact angles:			
Cation 1:		Cation 2:	
F22...S1...Cl1	88.4(3)	F21...S3...Cl3	84.9(2)
F22...S1...N1	78.8(3)	F21...S3...N2	77.7(3)
F22...S1...C2	84.3(4)	F21...S3...C4	175.4(3)
F23...S1...C11	138.8(2)	F23'...S3...Cl3	97.3(2)
F23...S1...N1	136.4(3)	F23'...S3...N2	153.7(3)
F23...S1...C2	170.6(4)	F23'...S3...C4	73.2(4)
		F11...S4...Cl4	131.7(2)
		F11...S4...N2	119.6(3)
		F11...S4...C3	73.8(3)
		F13...S4...Cl4	92.7(2)
		F13...S4...N2	79.3(3)
		F13...S4...C3	166.5(4)
Anion angles			
F11...As1...F12	178.5(4)	F21...As2...F21'	180.0(0)
F11...As1...F13	89.2(5)	F21...As2...F22	91.7(4)
F11...As1...F14	89.0(3)	F21...As2...F23	86.8(5)
F11...As1...F15	87.1(5)	F22...As2...F22'	180.0(0)
F11...As1...F16	90.9(4)	F22...As2...F23	87.7(6)
F21...As2...F23'	93.3(5)	F23...As2...F23'	180.0(0)
F12...As1...F13	89.3(5)	F31...As3...F31'	180.0(0)
F12...As1...F14	90.8(3)	F31...As3...F32	90.5(3)
F12...As1...F15	176.2(5)	F31...As3...F33	90.4(7)
F12...As1...F16	89.3(4)	F32...As3...F32'	180.0(0)
F13...As1...F14	88.4(4)	F32...As3...F33	88.7(6)
F13...As1...F15	176.2(5)	F33...As3...F33'	180.0(0)
F13...As1...F16	92.1(4)		
F14...As1...F15	92.8(4)		
F14...As1...F16	179.5(4)		
F15...As1...F16	86.7(5)		

2.025 Å, S—C 1.822 Å, and C—C 1.504 Å) may be used to calculate average bond orders (S—N 1.6, S—Cl 1.0, S—C 1.0, C—C 1.1).[4] These imply that π bonding (of $p\pi$–$d\pi$ type according to one model described in ref. 23) is only significant in the SNS region.

The cations are loosely associated as head-to-head pseudo-dimers with contacts between S2—N2 and S3—N1 just below the sum of the van der Waals radii of N and S (Table 5, Fig. 3) (24). Equivalent bond distances and angles in the two cations

[4]For SN bonds in which the N possesses a nonparticipating lone pair, bond order (bo) is related to length (22*a*) (Å) by the equation: $bo(NS) = 0.429 + 6.850d(NS) - 3.825d(NS)^2$. For other systems: $D_n = D_1 - 0.71 \log(bo)$, where D_1 is the length of a formal single bond (22*b*).

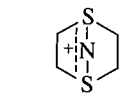

6

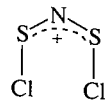

7

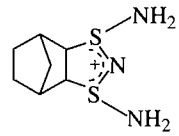

8

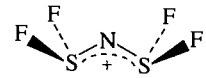

9

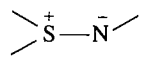

10*a*

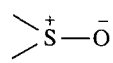

10*b*

are not significantly different. Cation–fluorine contacts are exclusively to sulphur, and weak (averaging 5% less than the sum of the van der Waals radii of S and F (3.27 Å)). Fluorine contacts are on average weaker to those sulphurs (S2 and S3) contacted by nitrogen, with no fluorine contacts to S2[5] (which has the stronger N contact). The sulphur atoms adopt pseudo-octahedral or -trigonal bipyramidal geometries in the second coordination sphere (see Table 6): AX_3Y_2E (S1, S3, S4) or AX_3YE (S2) (26).

Table 7 compares the average bond distances observed in **2** with those in the related systems **6** (4), **7** (27), **8** (28), and **9** (12). The S—N bond length in **2** is shorter than that in **6**, and this is consistent with the formal replacement of Cl in **2** by the less electronegative hydrocarbon fragment in **6**. Conversely, replacement of Cl and CH_2 in **2** with more electronegative fluorine (**9**) results in a shorter S—N distance.

Similar effects are observed in the sulphoxides (**10***a* and **10***b* are isoelectronic, cf. ref. 29). In fact, the ratio of the SO distances in F_2SO and Me_2SO (0.953) (30) is essentially the same as the ratio of the SN distances in **9** and **5** (0.949). The charge on the S and O atoms in sulphoxides and the S and N atoms in $\rangle SNS\langle$ species reflect, to a first approximation, the relative lengths of the SO and SN bonds (ref. 22*b*, Chap. 9). The larger the charge, the longer the corresponding bond. The trend in SN bond length in the series **6**, **2**, and **9** relates to the contribution of the forms $\rangle S^+—N^-—S^+\langle$ and $\rangle S{=}N—S^+\langle$, both being significant in bonding in **2**.

The average bond angle at nitrogen in **2** is 115.3°. Banister *et al.* (32) have shown that in cationic SNS moieties the S—N bond length (pm) is related to the SNS bond angle (°) by the equation:

$$[9] \quad d(SN) = 187.03 - 0.2263\angle N$$

A sulphur–nitrogen distance of 1.603 Å corresponds to an ideal bond angle of 118°, which is in reasonable agreement with that observed and implies that ring strain does not affect the ring

[5]Nyburg (25) has shown that the van der Waals radii of atoms are generally not spherical, but spheroidal, with the longest effective radii being perpendicular to bond vectors. This will very likely increase the significance of S..N contacts, and decrease the importance of most S..F contacts. Nyburg's treatment, however, is limited to S(II) bonded to carbon in R_2CS compounds, and is not quantitatively applicable in this form to this cation, which contains tricoordinate S(IV) bonded to Cl and N.

Can. J. Chem. Downloaded from www.nrcresearchpress.com by 88.85.125.76 on 09/07/12
For personal use only.

TABLE 7. Comparison of the geometry of $\overline{CH_2(SCl)N(SCl)CH_2}^+$ with similar species

Cation	Average d(SN) (Å)	Average d(SCl) (Å)	∠SNS (°)	∠NSCl (°)
$H_2C(SCl)N(SCl)CH_2^+$ (**2**)	1.603(8)	2.025(4)	115.3(5)	108.4(4)
$ClSNSCl^+$ (**7**)	1.528(2)	1.992(1)	151.0(2)	110.7(1)
$S_2N(C_2H_4)_2^+$ (**5**)	1.634(4)		102.4(2)	
$C_7H_{14}SN_3S_2^+$ (**8**)	1.622(2)		115.9(2)	
$F_2SNSF_2^+$ (**9**)	1.551(10)		121.1(6)	

angles in this system. The bond angles around the sulphur atoms in **2** (NSCl 108.4°, NSC 99.7°, CSCl 99.9°) show them to be pseudo-tetrahedral (AX_3E) in the first coordination sphere. This too implies that the sulphur atoms carry significant positive charge (cf. isoelectronic tri-coordinate phosphorus(III) compounds). The NSCl angle in **2** (108.4°) is greater than the CSCl angle (99.9°), contrary to predictions based purely on atomic electronegativity arguments, but consistent with the π contribution to the SN bond (24). The presence of cation–cation S..N contacts implies that the nitrogen atom of one cation is at least as effective an electron donor towards another cation as the AsF_6^- anion. This is consistent with a negative charge of some absolute fractional value residing on the nitrogen atom. A similar situation is observed in the Sb(III) fluorocations, in which fluoroantimony(III) cations are better donors than the SbF_6^- counteranions, leading to cationic polymers (33).

It is clear from the data presented that in **2** significant absolute positive and negative charges reside on the sulphur and nitrogen atoms respectively. Valence canonical **11** therefore contributes significantly to bonding in **2**. This is supported by the ^{14}N nmr chemical shift (−243 ppm), which suggests a strongly shielded nitrogen atom, the cation–anion contacts being only to sulphur and the head-to-head alignment of the cations in the unit cell. However, the empirical S—N bond order of 1.6 (see above) implies that canonical form **12** must also contribute to overall bonding, and therefore **2** is best represented as a resonance hybrid of **11** and **12**.

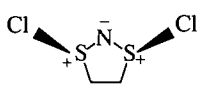

11

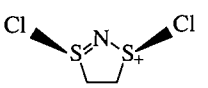

12

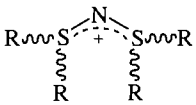

13

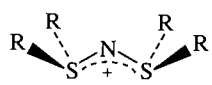

14

2 is a member of the series of cations $R^1R^2SNSR^3R^{4+}$, **13**, the geometries of which depend on whether they are a-, mono-, or bi-cyclic. The acyclic members **9** (12) and **14** (34, R = Me) have the same geometry as $(PF_2)_2N$ in $P_3N_3F_6$ (35). It is not geometrically possible for the monocyclic cations to adopt this conformation, and **2** and **15** have sulphur substituents (Cl and NH_2 respectively) in the 1,3-diaxial positions, and the more sterically demanding lone pair in the equatorial position. The nitrogen atoms in **2** and **15** are slightly displaced from the plane containing the two sulphur atoms and the mid-point of the C—C bond (by 0.3 Å in the case of **2**). In the bicyclic cation **6** (4) the nitrogen lies in the middle of the two C_2S_2 planes, significantly displaced from both.

The average As—F distance (1.676(8) Å) in the independent AsF_6^- anions is shorter than that observed in an ionic AsF_6^- salt (1.69 Å) (36). This reflects the fact that cation–anion contacts are weak in this structure, in part because of the presence of cation–cation interactions. In addition, the average As—F bond length is longer (1.686 Å) when the fluorines are involved in contacts to the cation than when they are not (1.659 Å) (see Table 5).

Acknowledgements

We thank NSERC (Canada) for financial support and a graduate scholarship (M.J.S.), and the Canadian Commonwealth Scholarship and Fellowship Committee for a graduate scholarship (S.P.). We are also grateful to Dr. A. J. Banister (University of Durham, UK) for useful discussions and Mr. E. G. Awere (UNB) for technical assistance.

1. R. T. OAKLEY. Prog. Inorg. Chem. **36**, 299 (1988).
2. M. R. BRINKMAN and C. W. ALLEN. J. Am. Chem. Soc. **94**, 2550 (1972); W. L. MOCK and L. MEHROTU. J. Chem. Soc. Chem. Commun. 123 (1976); V. G. ERTL and J. WEISS. Z. Anorg. Allg. Chem. **420**, 155 (1976).
3. G. K. MACLEAN, J. PASSMORE, M. N. S. RAO, M. J. SCHRIVER, P. S. WHITE, D. BETHALL, R. S. PILKINGTON, and L. H. SUTCLIFFE. J. Chem. Soc. Dalton Trans. 1405 (1985).
4. N. BURFORD, J. P. JOHNSON, J. PASSMORE, M. J. SCHRIVER, and P. S. WHITE. J. Chem. Soc. Chem. Commun. 966 (1986).
5. M. J. SCHRIVER. Ph.D. Thesis. University of New Brunswick, Fredericton. 1988.
6. (*a*) S. PARSONS, J. PASSMORE, and M. J. SCHRIVER. Phosphorus, Sulfur Silicon Relat. Elem. **41**, 463 (1989); (*b*) R. MEWS. Angew. Chem. Int. Ed. Engl. **15**, 691 (1976); G. G. ALANGE, A. J. BANISTER, and P. J. DAINTY. Inorg. Nucl. Chem. Lett. **15**, 175 (1979); (*c*) A. J. BANISTER and J. M. RAWSON. J. Chem. Soc. Dalton Trans. In press.
7. J. PASSMORE and P. TAYLOR. J. Chem. Soc. Dalton Trans. 804 (1976).
8. J. PASSMORE, E. K. RICHARDSON, and P. TAYLOR. Inorg. Chem. **17**, 1681 (1978).
9. C. D. DESJARDINS and J. PASSMORE. J. Fluorine Chem. **6**, 379 (1975).
10. C. LAU and J. PASSMORE. J. Chem. Soc. Dalton Trans. 2528 (1973).
11. M. MURCHIE and J. PASSMORE. Inorg. Synth. **24**, 76 (1986).
12. W. V. F. BROOKS, G. K. MACLEAN, J. PASSMORE, P. S. WHITE, and C. M. WONG. J. Chem. Soc. Dalton Trans. 1961 (1983).
13. J. PASSMORE and M. J. SCHRIVER. Inorg. Chem. **27**, 2749 (1988).
14. A. APBLETT, F. GREIN, J. P. JOHNSON, J. PASSMORE, and P. S. WHITE. Inorg. Chem. **25**, 422 (1986).
15. Y. LE PAGE, P. S. WHITE, and E. J. GABE. NRCCAD, An enhanced CAD-4 control program. Annual meeting of the American Crystallographic Association, Hamilton, Ontario. 1986.
16. N. WALKER and D. STUART. Acta Crystallogr. Sect. A: Found Crystallogr. **A39**, 158 (1983).

Can. J. Chem. Downloaded from www.nrcresearchpress.com by 88.85.125.76 on 09/07/12
For personal use only.

17. International tables for X-ray crystallography. Vol. IV. Kynoch Press, Birmingham. 1974.
18. E. J. GABE, Y. LE PAGE, J.-P. CHARLAND, F. L. LEE, and P. S. WHITE. J. Appl. Crystallogr. **22**, 384 (1989).
19. S. W. LIBLONG, R. T. OAKLEY, A. W. CORDES, and M. C. NOBLE. Can. J. Chem. **61**, 2062 (1983).
20. W. CARRUTHERS. Some modern methods of organic synthesis. Cambridge University Press, Cambridge. 1980. p. 170.
21. B. KLEWE and H. M. SEIP. Acta. Chem. Scand. **26**, 1860 (1972).
22. (*a*) S. C. NYBERG. J. Cryst. Mol. Struct. **3**, 331 (1973); (*b*) L. PAULING. The nature of the chemical bond. 3rd ed. Cornell University Press, Ithaca, NY. 1960. p. 239.
23. J. E. HUHEEY. Inorganic chemistry. 3rd ed. Harper and Row, New York, NY. 1983. Chap. 17.
24. A. BONDI. J. Phys. Chem. **68**, 441 (1964).
25. S. C. NYBERG. Acta Crystallogr. Sect. B: Struct. Sci. **B41**, 274 (1985).
26. R. J. GILLESPIE. Molecular geometry. Van Nostrand Reinhold, London. 1972.
27. O. GLEMSER, E. KINDLER, B. KREBS, R. MEWS, F. M. SCHNEPEL, and J. WEGENER. Z. Naturforsch. B: Anorg. Chem. Org. Chem. **35B**, 657 (1980).
28. A. C. HAZEL, R. G. HAZEL, A. J. BANISTER, and A. J. FIELDER. Acta Crystallogr. Sect. B: Struct. Crystallogr. Cryst. Chem. **B37**, 177 (1975).
29. H. OBERHAMMER, R. C. KUMAR, G. D. KNERR, and J. M. SHREEVE. Inorg. Chem. **20**, 3871 (1981).
30. I. HARGITTAI. The structure of volatile sulphur compounds. D. Reidel, Dordrecht. 1985.
31. J. P. JOHNSON, J. PASSMORE, P. S. WHITE, A. J. BANISTER, and A. G. KENDRICK. Acta Crystallogr. Sect. C: Cryst. Struct. Commun. **C43**, 1651 (1987).
32. A. J. BANISTER, I. B. GORRELL, and R. S. ROBERTS. J. Chem. Soc. Faraday Trans. 2, **81**, 1783 (1985).
33. W. A. S. NANDANA, J. PASSMORE, P. S. WHITE, and C. M. WONG. J. Chem. Soc. Dalton Trans. 1989 (1987).
34. A. M. GRIFFIN and G. M. SHELDRICK. Acta Crystallogr. Sect. B: Struct. Crystallogr. Cryst. Chem. **B31**, 893 (1975).
35. H. ALCOCK. Phosphorus nitrogen compounds. Academic Press, New York, NY. 1972.
36. A. F. WELLS. Structural inorganic chemistry. 5th ed. Oxford University Press, Oxford. 1984.

Can. J. Chem. Downloaded from www.nrcresearchpress.com by 88.85.125.76 on 09/07/12
For personal use only.

Réaction du fluoroborate de 2-benzoyl-1,2-dihydro isoquinaldonitrile avec les esters α,β-éthyléniques. II. Cas des esters oléfiniques *gem*-disubstitués. Stéréochimie des produits de condensation–réarrangement, dérivés du 4,5-dihydro-3*H*-pyrrole

GÉRARD SCHMITT, BOUBKER NASSER, NGUYEN DINH AN, BERNARD LAUDE[1] ET MAXIME ROCHE

Laboratoire de chimie organique, Université de Franche-Comté Besançon, La Bouloie, 16 route de Gray, 25030 Besançon CEDEX, France

Reçu le 26 octobre 1989

GÉRARD SCHMITT, BOUBKER NASSER, NGUYEN DINH AN, BERNARD LAUDE et MAXIME ROCHE. Can. J. Chem. **68**, 863 (1990).

La réaction du fluoroborate d'un composé de Reissert avec divers esters α,β-éthyléniques *gem*-disubstitués est effectuée en présence de triéthylamine. La structure des produits de condensation–réarrangement **8** confirme un mécanisme suggéré par d'autres auteurs. Les paramètres de résonance magnétique nucléaire protonique de ces composés permettent de déterminer leur stéréochimie et de mettre en évidence un phénomène d'isomérisation pour deux d'entre eux.

Mots clés : fluoroborate d'un compose de Reissert, cycloaddition [4 + 2], stéréochimie.

GÉRARD SCHMITT, BOUBKER NASSER, NGUYEN DINH AN, BERNARD LAUDE, and MAXIME ROCHE. Can. J. Chem. **68**, 863 (1990).

The previously suggested mechanism of the condensation–rearrangement reaction of a Reissert compound hydrofluoroborate salt with reactive olefins was reexamined in the case of methyl methacrylate, itaconate, citraconate, and mesaconate. Addition of triethylamine to the reaction medium leads to the isolation of a presumed intermediate **8**. Spectrometric (proton magnetic resonance) data of the compounds **8** allow us to specify their stereochemistry and in two cases to point out an isomerization equilibrium.

Key words : Reissert compound fluoroborate salt, [4 + 2] cycloaddition, stereochemistry.

Introduction

Des études antérieures (1, 2) de solutions de fluoroborates de 2-acyl-1,2-dihydroisoquinaldonitriles (composés de Reissert **1**) ont mis en évidence l'existence d'un équilibre entre diverses structures, l'espèce **2** étant généralement majoritaire (figure 1).

Dans un précédent article (3) nous avons décrit la compétition entre les réactions de cycloaddition dipolaire-1,3 et de cycloaddition de Diels–Alder du fluoroborate d'un composé de Reissert **1** (R = Ph) avec trois dipolarophiles-diénophiles : les esters acrylique, fumarique et maléïque. Cette compétition intervient en présence de triéthylamine dans le mélange réactionnel. Dans les mêmes conditions, mais avec d'autres esters éthyléniques dont la double liaison est plus encombrée, nous n'avons pas observé la formation d'un cycloadduit [3+2], mais seulement une cycloaddition de type Diels–Alder, faisant intervenir l'espèce **2** (R = Ph). C'était d'ailleurs la seule réaction décrite par McEwen *et al.* (4, 5) avec toutes les oléfines mises en oeuvre. Ces auteurs rendent compte de la structure du produit **7** obtenu en suggérant le mécanisme réactionnel représenté sur la figure 2 (partie gauche) : dans le mélange initial, l'entité majeure **2** est un hétérodiène et la séquence débute par une cycloaddition de Diels–Alder. Si l'oléfine est monosubstituée à chaque extrêmité de la double liaison (R^2 = H), le cycloadduit **4** évolue ensuite vers le composé **7** totalement aromatisé. Dans tous les travaux décrits jusqu'à présent, hormis notre note préliminaire (6), aucun intermédiaire n'a été isolé ou décrit. Cette évolution qui implique, à partir de l'intermédiaire **6**, la perte d'un proton (R^2 = H) sur le sommet 3 du cycle pyrrolinique et une déshydratation acido-catalysée par HBF_4, peut être empêchée si le sommet 3 du cycle est disubstitué et si le milieu réactionnel n'est pas suffisamment acide. C'est ce que nous avons observé en mettant en oeuvre quatre esters α,β-éthyléniques *gem*-disubstitués en présence de triéthylamine.

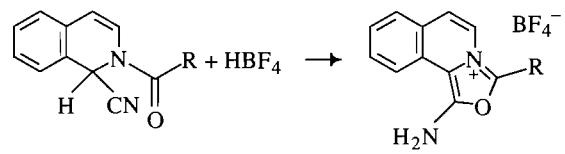

1 **2**

FIGURE 1

Résultats

À partir des diénophiles **3***a–d*, en présence de triéthylamine, nous avons isolé les produits de structure **8** dérivés du 2-(1-isoquinoléïnyl)-5-hydroxy-5-phényl-4,5-dihydro-3*H*-pyrrole (partie droite de la figure 2). Si les rendements sont convenables pour **8***a* et **8***b*, ils diminuent considérablement pour **8***c* et **8***d* par suite des contraintes stériques. Les réactions de cycloaddition conduites sur ces mêmes diénophiles sans adjonction de triéthylamine donnent directement les 3*H*-pyrroles **9** et le traitement des composés **8** à l'ébullition dans l'éthanol, acidifié par l'acide sulfurique, conduit quantitativement aux mêmes produits **9**.

Ces résultats apportent déjà un argument en faveur de la régiospécificité de la réaction de cycloaddition initiale. Le seul produit **8** obtenu ne peut donner une réaction de déshydratation que si hydrogène et hydroxyle sont situés sur deux atomes de carbone vicinaux et c'est le même sens de cycloaddition de Diels–Alder que celui observé dans le cas de l'acrylate d'éthyle (**7**, $R^1 = CO_2Et$, R^3 = H) et déjà décrit par McEwen *et al.* (5).

Les transformations chimiques représentées dans la figure 3 confirment les structures **8** et **9** et par suite la régiochimie de la réaction. Ainsi le produit **9***a* (issu du méthacrylate de méthyle) saponifié et décarboxylé donne un produit **7***a*. Ce même produit a pu être obtenu en plusieurs étapes à partir du composé **9***c* issu du mésaconate et du citraconate de méthyle et également à partir du composé **9***b* provenant de l'itaconate de méthyle.

1. Auteur à qui adresser toute correspondance.

Printed in Canada / Imprimé au Canada

Can. J. Chem. Downloaded from www.nrcresearchpress.com by 88.85.125.76 on 09/07/12
For personal use only.

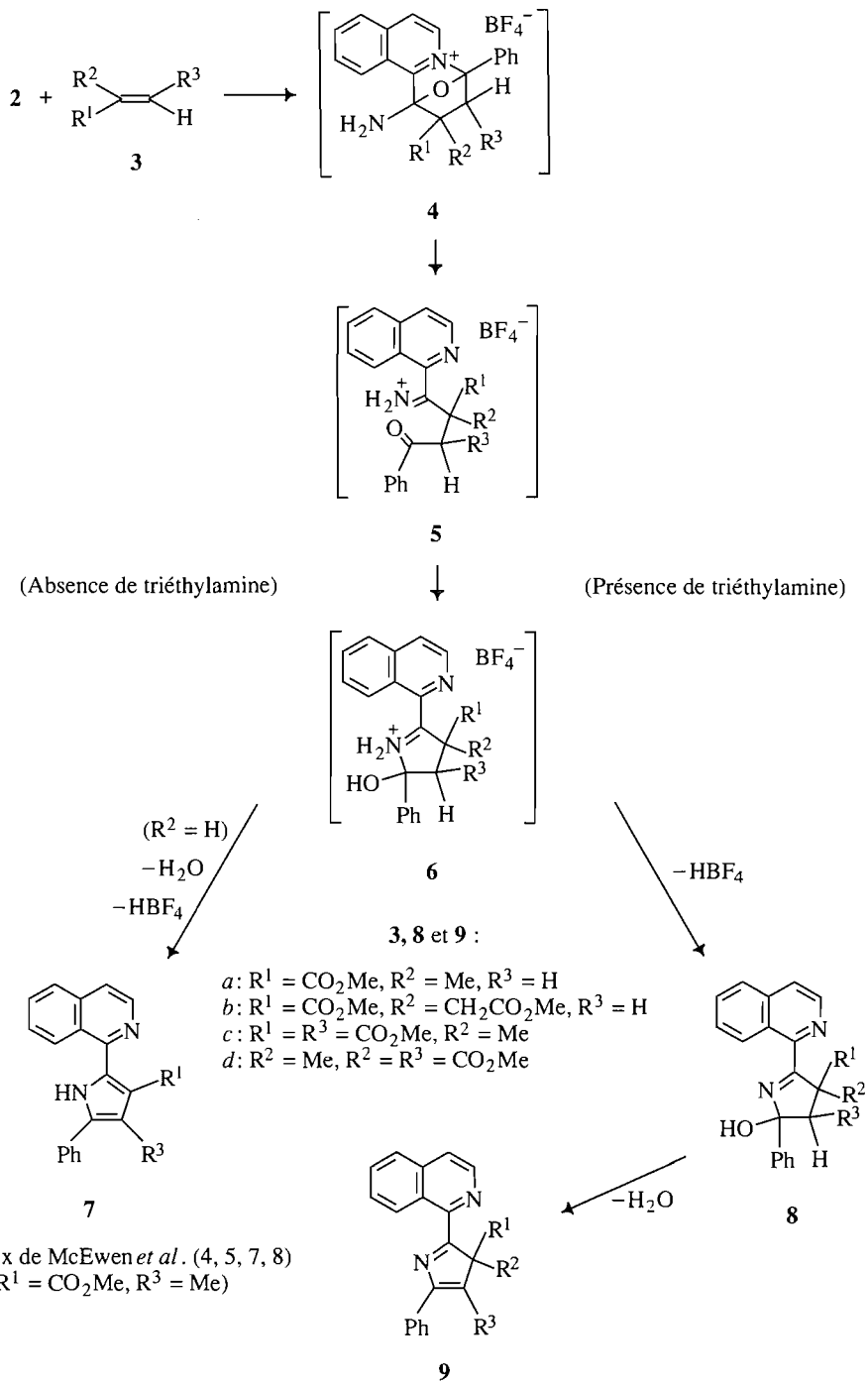

FIGURE 2

Pour confirmer cette régiochimie, nous avons fait réagir le fluoroborate **2** avec le crotonate de méthyle en l'absence de triéthylamine. La réaction conduit alors au produit **7***e* sans qu'il soit possible d'isoler un intermédiaire. La saponification suivie d'une décarboxylation du produit **7***e* conduit au composé **7***f* qui diffère du composé **7***a* par la position du groupe méthyle qui se trouve en 3 dans le produit **7***a* et en 4 dans l'isomère **7***f* (figure 4).

L'ensemble de ces réactions confirme sans ambiguïté l'hypothèse mécanistique suggérée par Evanguelidou et McEwen (8) pour expliquer la formation des composés **7** à partir d'un cycloadduit de type Diels–Alder (non isolé), obtenu par action du fluoroborate d'un composé de Reissert **1** sur une oléfine. L'addition de triéthylamine au milieu réactionnel nous a permis d'obtenir, dans certains cas, le précurseur de **7** qui n'avait jamais été isolé. Les résultats d'analyse et les paramètres spectroscopiques sont en bon accord avec la structure proposée pour les composés **7**, **8** et **9**.

Ces paramètres spectroscopiques nous ont d'ailleurs permis de mener une étude de la stéréochimie des composés **8**.

Étude spectrométrique de la stéréochimie des composés 8

Puisque la séquence réactionnelle débute par une cycloaddition de Diels–Alder, la stéréochimie relative autour de la liaison

Can. J. Chem. Downloaded from www.nrcresearchpress.com by 88.85.125.76 on 09/07/12
For personal use only.

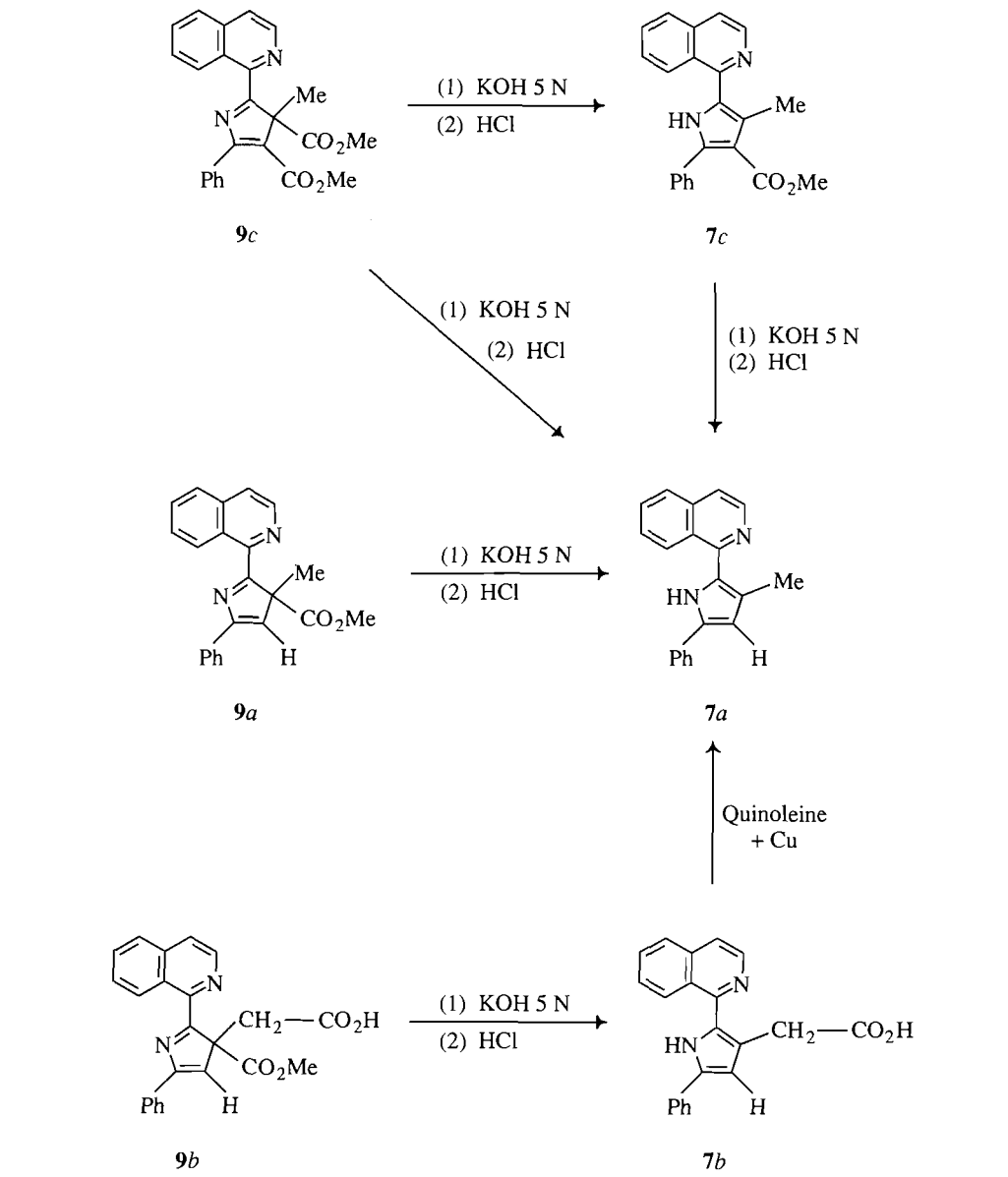

FIGURE 3

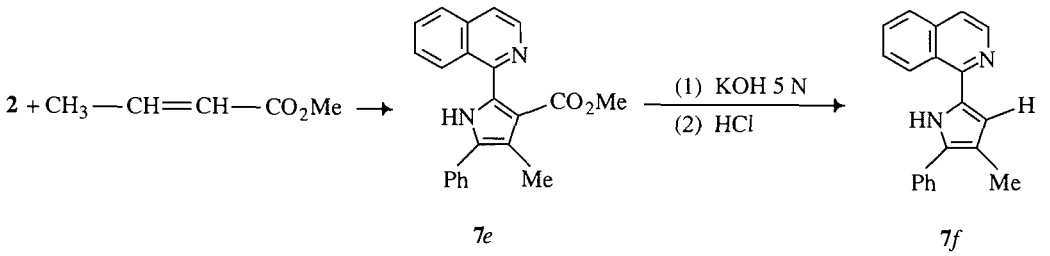

FIGURE 4

C3—C4 reste celle des oléfines de départ et le seul problème à résoudre est celui de la disposition des groupes phényle et hydroxyle situés sur le carbone 5, par rapport à la disposition des groupements R^1, R^2, H et R^3 fixés sur les sommets 3 et 4 (figure 5).

Les spectres des produits uniques **8***c* et **8***d* obtenus à partir du mésaconate et du citraconate de méthyle sont les plus aisés à analyser. Le tableau 1 rassemble leurs paramètres spectrométriques. L'existence d'une bande assez fine vers 3410–3420 cm^{-1}, dont la position ne varie pas avec la concentration d'une solution dans CCl_4 rend compte de l'existence d'une liaison hydrogène intramoléculaire entre le groupe OH en position 5 et le groupe méthoxycarbonyle en position 4. Ceci est confirmé par l'existence d'une bande νCO = 1690 cm^{-1} (**8***d*) et 1700 cm^{-1} (**8***c*) dont la fréquence est abaissée par liaison hydrogène et par la valeur élevée du déplacement chimique du proton du

Can. J. Chem. Downloaded from www.nrcresearchpress.com by 88.85.125.76 on 09/07/12
For personal use only.

TABLEAU 1. Paramètres spectroscopiques (ir et rmn ^1H) des composés **8***c* et **8***d*

Composés	ir cm^{-1}	rmn ^1H, C_6D_6, δ ppm/TMS					
	ν(OH) = 3410	$R^1 = CO_2CH_3$	$R^2 = CH_3$	$R^3 = CO_2CH_3$	H^b	OH	H aromatiques
8*c*	ν(CO) = 1700, 1745	3,14 (s, 3H)	2,02 (s, 3H)	3,48 (s, 3H)	4,20 (s, 1H)	6,57 (s, 1H)	7,00–10,20 (m, 11H)
	ν(OH) = 3420	$R^1 = CH_3$	$R^2 = CO_2CH_3$	$R^3 = CO_2CH_3$	H^b	OH	H aromatiques
8*d*	ν(CO) = 1690, 1740	1,72 (s, 3H)	3,30 (s, 3H)	3,72 (s, 3H)	3,62 (s, 1H)	6,20 (s, 1H)	7,00–9,60 (m, 11H)

TABLEAU 2. Paramètres de rmn ^1H des épimères **8***a* et **8**′*a* (C_6D_6, δ ppm/TMS, *J* en Hz)

Composés	$R^2 = CH_3$	$R^3 = H^a$	H^b	OH	$R^1 = CO_2CH_3$	H aromatiques
8*a*	2,08 (s, 3H)	2,52 (d, 1H) J = 13,5	2,75 (d, 1H) J = 13,5	2,70 (sl, 1H)	3,30 (s, 3H)	7,00–10,10 (m, 11H)
8′*a*	1,58 (s, 3H)	2,30 (d, 1H) J = 13,5	2,85 (d, 1H) J = 13,5	4,25 (sl, 1H)	3,40 (s, 3H)	7,00–9,90 (m, 11H)

TABLEAU 3. Paramètres de rmn ^1H des épimères **8***b* et **8**′*b* (C_6D_6, δ ppm/TMS, *J* en Hz)

Composés	$R^3 = H^a$	H^b	OCH_3	$R^1 = CO_2CH_3$	Hα et Hβ	OH	H aromatiques
8*b*	2,80 (d, 1H) J = 14,5	2,95 (d, 1H) J = 14,5	2,93 (s, 3H)	3,28 (s, 3H)	3,38 (d, 1H) 3,77 (d, 1H) J = 18	5,18 (s, 1H)	7,00–10,10 (m, 11 H)
8′*b*	2,75 (d, 1H) J = 15	2,87 (d, 1H) J = 5	2,98 (s, 3H)	3,35 (s, 3H)	3,24 (d, 1H) 3,37 (d, 1H) J = 17	4,98 (sl, H)	7,00–9.90 (m, 11H)

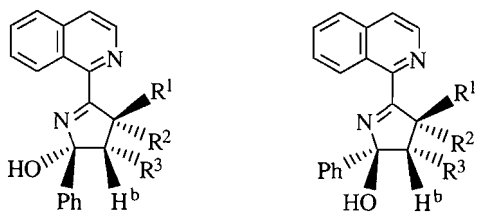

8 **8'**

a: $R^1 = CO_2Me$, $R^2 = Me$, $R^3 = H^a$
b: $R^1 = CO_2Me$, $R^2 = CH^{\alpha}H^{\beta}CO_2Me$, $R^3 = H^a$
c: $R^1 = R^3 = CO_2Me$, $R^2 = Me$
d: $R^2 = R^3 = CO_2Me$, $R^1 = Me$

Les composés **8** et **8**′ sont des racémiques et la représentation employée ici pour différencier les configurations relatives n'implique pas l'indication d'une configuration absolue

FIGURE 5

groupe hydroxyle (δ = 6,20 ppm et 6,57 ppm). Une telle disposition *cis* pour deux groupes OH et ester situés sur deux carbones vicinaux au cours d'une addition nucléophile intramoléculaire conduisant à un cycle pentagonal a déjà été décrite par d'auteurs (9, 10).

Cette stéréochimie est confirmée par le relatif blindage du groupe méthyle en position 3 dans le cas du composé **8***d* (δ = 1,72 ppm), blindage dû à l'effet du phényle-5 en *cis* par rapport à ce méthyle, alors que le groupe méthyle en 3 qui, dans le produit **8***c*, ne subit pas l'effet de ce phényle présente un déplacement chimique de 2,02 ppm.

Les produits **8** issus du méthacrylate et de l'itaconate de méthyle présentent un centre de chiralité de moins que ceux discutés plus haut. On peut toutefois encore envisager l'existence de deux diastéréoisomères **8** et **8**′ selon la disposition relative des substituants sur les sommets 3 et 5. Le spectre de rmn ^1H d'une solution du **8***a* préparée extemporanément dans le benzène hexadeutéré permet de relever un ensemble de signaux dont les paramètres sont rassemblés dans le tableau 2.

La valeur du déplacement chimique du groupe méthyle en 3 (δ = 2,08 ppm) est proche de celle observée pour le groupe méthyle du produit **8***c* issu du mésaconate (δ = 2,02 ppm) et permet d'envisager une disposition *trans* pour les groupes méthyle en 3 et phényle en 5 (structure **8***a*). Mais cette solution, laissée à température ambiante pendant plusieurs heures, donne alors un spectre de rmn protonique où apparaissent des signaux supplémentaires. Ces nouvelles transitions sont également répertoriées dans le tableau 2 pour le produit **8**′*a*. Nous rejetons l'hypothèse de l'existence de deux conformères, puisque ces deux ensembles de signaux apparaissant rapidement par chauffage, persistent après retour à température ordinaire. Il s'agit donc des deux isomères **8***a* et **8**′*a*. Cette isomérisation peut s'expliquer par une réaction d'ouverture–fermeture de l'« hémiaminoacétal » **8** en solution qui conduit aux deux isomères **8** et **8**′. Cette hypothèse est confortée par le fait que le produit **8***a* mis en solution dans $CDCl_3$ présente immédiatement un spectre de rmn ^1H comportant les signaux des deux isomères. Cette rapidité d'isomérisation peut s'expliquer par une catalyse dûe à la légère acidité résiduelle du chloroforme deutéré. Le deuxième isomère **8**′*a*, comportant les deux groupes phényle en 5 et méthyle en 3 dans une disposition *cis*, présente une

Can. J. Chem. Downloaded from www.nrcresearchpress.com by 88.85.125.76 on 09/07/12
For personal use only.

Can. J. Chem. Downloaded from www.nrcresearchpress.com by 88.85.125.76 on 09/07/12
For personal use only.

déplacement chimique plus faible pour le groupe méthyle mais aussi pour le proton $R^3 = H^a$ qui est soumis à l'influence simultanée des blindages par les groupes méthyle et phényle.

Le produit **8***b* issu du l'itaconate a un comportement analogue à celui du composé **8***a*. Une solution dans C_6D_6 fraîchement préparée conduit à un spectre de rmn ^1H comportant uniquement les signaux de l'isomère **8***b*. Avec le temps, les signaux de l'autre isomère **8′***b* apparaissent. Ces paramètres sont rassemblés dans le tableau 3.

Il n'est pas impossible que la réaction de cyclisation par addition nucléophile intramoléculaire lors du passage de l'intermédiaire **5** au composé **8** conduise au mélange de deux isomères **8** et **8′**, mais par cristallisation nous n'avons jamais réussi à isoler que l'isomère **8** même à partir d'une solution contenant les deux produits **8** et **8′**.

Le phénomène d'isomérisation n'apparaît pas dans le cas des composés **8***c* et **8***d* issus du mésaconate et du citraconate et nous pensons que ceci s'explique parce qu'ils sont plus stables que leurs éventuels isomères **8′**. Cette plus grande stabilité est dûe à la fois à une moindre interaction stérique dans le cas d'une disposition *trans* des groupes phényle en 5 et méthoxycarbonyle en 4 et par l'existence d'une liaison hydrogène intramoléculaire entre les groupes hydroxyle en 5 et méthoxycarbonyle en 4. L'absence de ce dernier groupe en 4 dans le cas des composés **8***a* et **8***b* rend possible une isomérisation partielle en composés **8′**.

Conclusion

La réaction du fluoroborate de 2-benzoyl-1,2-dihydroisoquinaldonitrile **1** (R = Ph) effectuée en présence de triéthylamine sur les esters éthyléniques étudiés dans le présent travail permet de confirmer le mécanisme envisagé par McEwen puisque nous avons réussi à isoler les intermédiaires supposés de structure **8**.

L'étude stéréochimique de ces derniers nous a permis de montrer que certains d'entre eux pouvaient s'épimériser par une réaction d'ouverture–fermeture et ce phénomène conforte l'existence de l'intermédiaire ouvert de structure **5**.

Partie expérimentale

Les points de fusion déterminés sur banc Kofler ne sont pas corrigés. Les spectres d'absorption ir ont été obtenus avec un spectrophotomètre Beckman IR 33, les produits étant pastillés dans KBr. Les spectres de rmn protonique ont été obtenus avec un spectromètre Bruker AC 200, les échantillons étant dissous dans C_6D_6 ou $CDCl_3$ avec le tétraméthylsilane comme référence interne. Les chromatographies sur colonne ouverte ont été effectuées avec la silice Merck (70–230 mesh) comme support. Les microanalyses ont été assurées par le Service d'Analyses du CNRS à Vernaison. Le fluoroborate de 2-benzoyl-1,2-dihydro isoquinaldonitrile **2** (R = Ph) est obtenu selon le mode opératoire de McEwen *et al.* (4). Les esters **3** sont des produits du commerce exceptés **3***c* et **3***d* qui ont été préparés par réaction du méthanol avec les chlorures d'acide correspondants.

1. Condensations en présence de triéthylamine

Mode opératoire général : À une solution de 3 g de fluoroborate **2** (R = Ph) dans 25 mL de DMF, on ajoute 3 mL d'ester **3**. Le mélange est refroidi à 0°C au bain de glace et on additionne lentement et sous agitation magnétique une solution de 2 mL de triéthylamine dans 15 mL de DMF (l'addition dure environ une demi-heure). Après 4 h d'agitation à 0°C, on verse le mélange réactionnel dans 200 mL d'eau froide. L'huile qui se sépare est extraite à l'éther. La solution éthérée est lavée à l'eau, séchée et concentrée. L'huile résiduelle est alors soit reprise par l'éthanol (**8***a*, **8***b*), soit chromatographiée (**8***c*, **8***d*).

*2-(1-Isoquinoléïnyl)-3-méthyl-5-hydroxy-5-phényl-4,5-dihydro-3*H*-pyrrole-3-carboxylate de méthyle* **8***a* : F = 146°C (éthanol), Rdt : 50%. Anal. calc. pour $C_{22}H_{20}N_2O_3$: C 73,31; H 5,59; N 7,77; trouvé : C 73,52; H 5,32; N 7,63.

*2-(1-Isoquinoléïnyl)-3-méthoxycarbonylméthyl-5-hydroxy-5-phényl-4,5-dihydro-3*H*-pyrrole-3-carboxylate de méthyle* **8***b* : F = 140°C (éthanol), Rdt : 42%. Anal. calc. pour $C_{24}H_{22}N_2O_5$: C 68,88; H 5,30; N 6,69; trouvé : C 68,72; H 5,47; N 6,80.

2-(1-Isoquinoléïnyl)-3-*méthyl-5-hydroxy-5-phényl-4,5-dihydro-*3H*-pyrrole*-trans*-3,4-dicarboxylate de diméthyle* **8***c* : la chromatographie du brut réactionnel (éluant $CHCl_3$) permet de séparer d'abord l'excès d'ester et de composé de Reissert **1** (R = Ph). Elle livre ensuite le produit **8***c*, F = 138,5°C (éthanol), Rdt : 18%. Anal. calc. pour $C_{24}H_{22}N_2O_5$: C 68,88; H 5,30; N 6,69; trouvé : C 69,03; H 5,18; N 6,48.

*2(1-Isoquinoléïnyl)-3-méthyl-5-hydroxy-5-phényl-4,5-dihydro-3*H*-pyrrole*-cis*-3,4-dicarboxylate de diméthyle* **8***d* : la chromatographie du brut réactionnel (éluant $CHCl_3$) livre le produit **8***d* après élution des excès d'ester de départ et de composé de Reissert **1** (R = Ph), F = 160°C (éthanol), Rdt : 12%. Anal. calc. pour $C_{24}H_{22}N_2O_5$: C 68,88; H 5,30; N 6,69; trouvé : C 68,67; H 5,42; N 6,57.

Les paramètres spectrométriques de ces composés ont été donnés en partie théorique.

II. Condensations effectuées sans addition de triéthylamine

1. *2-(1-Isoquinoléïnyl)-3-méthyl-5-phényl-3*H*-pyrrole-3,4-dicarboxylate de diméthyle* **9***c* à partir du mésaconate ou du citraconate de méthyle.

Une solution de 3 g de fluoroborate et 3 mL de citraconate ou de mésaconate de méthyle dans 50 mL de DMF est abandonnée 48 h à température ambiante puis 12 h à l'étuve à 60°C. On verse alors dans l'eau. L'huile ainsi formée est extraite à l'éther et cette solution lavée 4 fois à l'eau. Après séchage et évaporation du solvant, le résidu est repris à l'éthanol et filtré. Le solide est recristallisé dans l'éthanol. F = 110°C, Rdt : 58%; ir : ν(C=O) = 1710, 1730 cm^{-1}; rmn ^1H ($CDCl_3$) : δ = 1,75 ppm (s, 3H, CH_3 en -3); δ = 3,50 ppm (s, 3H, OCH_3); δ = 3,70 ppm (s, 3H, OCH_3); δ = 7,00–9,00 ppm (m, 11H arom.). Anal. calc. pour $C_{24}H_{20}N_2O_4$: C 71,98; H 5,03; N 6,99; trouvé : C 72,13; H 4,97; N 6,82.

2. *2-(1-Isoquinoléïnyl)-4-méthyl-5-phényl pyrrole-3-carboxylate de méthyle* **7***e* à partir du crotonate de méthyle.

Une solution de 3 g de fluoroborate et 4 mL de crotonate de méthyle dans 20 mL de DMF est abandonnée 24 h à température ambiante. On dissout le tout dans 150 cm^3 d'éther et lave 3 fois avec une solution aqueuse saturée de chlorure de sodium. La phase éthérée est séchée puis évaporée. Le résidu violet est trituré avec de l'éthanol et le solide obtenu est recristallisé dans l'éthanol. F = 216°C, Rdt = 68%; ir : ν(C=O) = 1700 cm^{-1}, ν(NH) = 3060 cm^{-1}; rmn ^1H ($CDCl_3$) : δ = 2,5 ppm (s, 3H, CH_3 en -4); δ = 3,80 ppm (s, 3H, OCH_3); δ = 12,10 ppm (s, NH); δ = 7,00–9,30 ppm (m, 11H arom.). Anal. calc. pour $C_{22}H_{18}N_2O_2$: C 77,17; H 5,30; N 8,18; trouvé : C 76,92; H 5,47; N 7,97.

III. Deshydratation des composés 8

Mode opératoire général : Chaque composé **8** (10 mmol) est dissout dans 30 mL d'éthanol additionnés de 4 gouttes d'acide sulfurique concentré. Le mélange est ensuite porté à reflux durant 1 h puis versé dans l'eau froide. Le précipité est filtré, lavé et recristallisé. Les rendements sont quantitatifs. Les composés **8***c* et **8***d* conduisent au produit **9***c*.

*2-(1-Isoquinoleïnyl)-3-méthyl-5-phényl-3*H*-pyrrole-3-carboxylate de méthyle* **9***a* obtenu à partir du composé **8***a*, F = 139°C (recristallisé de CH_3COOH); ir : ν(=O) = 1690 cm^{-1}; rmn ^1H ($CDCl_3$) : δ = 1,80 ppm (s, 3H, CH_3 en -3); δ = 3,60 ppm (s, 3H, OCH_3); δ = 6,60 ppm (s, 1H, H-4); δ = 7,00–9,60 ppm (m, 11H arom.). Anal. calc. pour $C_{22}H_{18}N_2O_2$: C 77,17; H 5,30; N 8,18; trouvé : C 77,26; H 5,18; N 8,32.

*2-(1-Isoquinoleïnyl)-3-méthoxycarbonylméthyl-2-phényl-3*H*-pyrrole-3-carboxylate de méthyle* **9***b*, F = 144°C (éthanol); ir : ν(C=O) = 1690 cm^{-1}; rmn ^1H ($CDCl_3$) : δ = 2,90 ppm (d, 1H) et δ = 3,50 ppm (d, 1H); J = 15 Hz -CH_2- CO_2Me; δ = 3,50 ppm (s, 3H, OCH_3); δ = 7,00 ppm (s, 1H, H-4); δ = 7,05–9,60 ppm (m, 11H arom.). Anal. calc. pour $C_{24}H_{20}N_2O_4$: C71,98; H 5,03; N 6,99; trouvé : C 72,07; H 5,12; N 6,77.

IV. Réactions de saponification et decarboxylation des esters **9**

1. Saponification par la potasse méthanolique 2 N

Mode opératoire général : 5 mmol de chaque ester étudié sont dissoutes dans 20 mL de potasse méthanolique 2 N. On porte à ébullition durant 2 h. On verse alors dans l'eau froide et neutralise par action de HCl 2 N. Le précipité qui se forme est extrait à l'éther, lavé, séché et le solvant évaporé. Le résidu est repris par un solvant de cristallisation.

2-(1-Isoquinoléïnyl)-3-méthyl-5-phényl pyrrole **7***a* à partir du composé **9***a*, F = 203°C (isopropanol), Rdt : 95%; ir : ν(NH) = 3100 cm^{-1}; rmn ^1H ($CDCl_3$) : δ = 2,25 ppm (s, 3H, CH_3 en -3); δ = 6,60 ppm (s, 1H, H-4); δ = 7,10–9,10 ppm (m, 11H arom.); δ = 9,90 ppm (s, 1H, NH). Anal. calc. pour $C_{20}H_{16}N_2$: C 84,47; H 5,67; N 9,85; trouvé : C 84,62; H 5,54; N 10,05.

Acide 2-(1-isoquinoléïnyl)-5-phényl pyrrole-3-acétique **7***b* à partir du composé **9***b*, F = 250°C (du *n*-propanol), Rdt : 70%; ir : ν(C═O) = 1700 cm^{-1}, ν(OH) et (νNH) bande élargie entre 2600 et 3400 cm^{-1}; rmn ^1H ($CDCl_3$) : δ = 3,70 ppm (s, 2H, CH_2-COOH); δ = 6,70 ppm (s, 1H, H-4); δ = 7,10–9,10 ppm (m, 11H arom.); δ = 9,20 ppm (s, 1H, OH); δ = 11,80 ppm (s, 1H, NH). Anal. calc. pour $C_{21}H_{16}N_2O_2$: C 76,80; H 4,91; N 8,53; trouvé : C 76,67; H 5,07; N 8,75.

2-(1-Isoquinoléïnyl)-3-méthyl-5-phényl pyrrole-4-carboxylate de méthyle **7***c* à partir du composé **9***c*, F = 194°C de l'éthanol, Rdt : 44%; ir : ν(C═O) = 1680 cm^{-1}, ν(NH) = 3060 cm^{-1}; rmn ^1H ($CDCl_3$) : δ = 2,20 ppm (s, 3H, CH_3 en -3); δ = 3,80 ppm (s, 3H, OCH_3); δ = 7,10–9,20 ppm (m, 11H arom.); δ = 12,30 ppm (s, 1H, NH). Anal. calc. pour $C_{22}H_{18}N_2O_2$: C 77,17; H 5,30; N 8,18; trouvé : C 77,32; H 5,17; N 8,02.

2. Saponification par la potasse méthanolique 5 N

Le mode opératoire est le même que le précédent excepté que l'on utilise de la potasse 5 N au lieu de 2 N.

(a) Obtention du produit **7***a* (déjà décrit) à partir du composé **9***c*, Rdt : 81%.

(b) *2-(1-Isoquinoléïnyl)-4-méthyl-5-phényl pyrrole* **7***f* à partir de **7***e*, F = 137°C (éthanol), Rdt = 49%; ir : ν(NH) = 3100 cm^{-1}; rmn ^1H ($CDCl_3$) : δ = 2,30 ppm (s, 3H, CH_3 en -4); δ = 6,90 ppm (s, 1H, H-3); δ = 7,10–9,30 ppm (m, 11H arom.); δ = 10,20 ppm (s, 1H, NH). Anal. calc. pour $C_{20}H_{16}N_2$: C 84,47; H 5,67; N 9,85; trouvé : C 84,28; H 5,79; N 10,02.

3. Produit **7**a *par décarboxylation du composé* **7**b

De l'acide **7***b* (1 g) et 0,1 g de cuivre en poudre sont chauffés à reflux 4 h dans 30 cm^3 de quinoléine. Le mélange est refroidi, versé dans l'eau et acidifié. On extrait à l'éther, sèche la solution et évapore le solvant. Le résidu très noir est filtré sur colonne de silice en éluant par du chloroforme. On récupère une très faible quantité de produit jaune, identifié au produit **7***a* (ir, rmn ^1H et point de fusion de mélange).

1. W. E. McEwen, M. A. Calabro, I. C. Mineo et I. C. Wang. J. Am. Chem. Soc. **95**, 2392 (1973).
2. M. J. Cook, A. R. Katritzky et A. D. Page. J. Am. Chem. Soc. **99**, 165 (1977).
3. G. Schmitt, B. Laude, J. Vebrel, N. Rodier et F. Theobald. Bull. Soc. Chim. Belg. **98**, 113 (1989).
4. W. E. McEwen, C. C. Cabello, M. A. Calabro, A. M. Ortega, P. E. Scott, A. F. Zapata, C. M. Zepp et J. J. Lubinkowski. J. Org. Chem. **44**, 111 (1979).
5. W. E. McEwen, M. A. Hernandez, Chei-Fei Ling, E. Marmugi, R. M. Padronaggio, C. M. Zepp et J. J. Lubinkowski. J. Org. Chem. **46**, 1656 (1981).
6. G. Schmitt, T. Fathi, E. Cerutti et B. Laude. Bull. Soc. Chim. Belg. **96**, 531 (1987).
7. W. E. McEwen, I. C. Wang Huang, C. P. Cartaya Marin, F. McCarty, E. M. Segnini, C. M. Zepp et J. J. Lubinkowski. J. Org. Chem. **47**, 3098 (1982).
8. E. K. Evanguelidou et M. E. McEwen. J. Org. Chem. **31**, 4110 (1966).
9. A. Xicluna, J. F. Robert, J. F. Ombetta, J. J. Panouse, B. Baude, L. Pizalla et H. Bodot. Spectrochim. Acta, **41A**, 877 (1985).
10. P. Varin, J. Vebrel, B. Laude, A. Xicluna et J. F. Robert. Spectrochim. Acta, **43A**, 1397 (1987).

Can. J. Chem. Downloaded from www.nrcresearchpress.com by 88.85.125.76 on 09/07/12
For personal use only.

Dihydride formation versus H_2-elimination in the protonation of the heterobimetallic FePt complex $(CO)_3Fe(\mu\text{-}H)(\mu\text{-}PCy_2)Pt(PEt_3)_2$

HILARY A. JENKINS AND STEPHEN J. LOEB[1]
Department of Chemistry, University of Winnipeg, Winnipeg, Man., Canada R3B 2E9
AND
DAVID G. DICK AND DOUGLAS W. STEPHAN
Department of Chemistry and Biochemistry, University of Windsor, Windsor, Ont., Canada N9B 3P4

Received August 23, 1989

HILARY A. JENKINS, STEPHEN J. LOEB, DAVID G. DICK and DOUGLAS W. STEPHAN. Can. J. Chem. **68**, 869 (1990).

The reaction of $Li[Fe(CO)_4(PCy_2)]$ with *trans*-$PtCl(H)(PEt_3)_2$ results in the formation of the hydride complex $(CO)_3Fe(\mu\text{-}H)(\mu\text{-}PCy_2)Pt(PEt_3)_2$, **1.** This heterobimetallic, phosphido-bridged complex reacts with one equivalent of $HBF_4 \cdot Et_2O$ to give the complex $[(CO)_3Fe(\mu\text{-}H)_2(\mu\text{-}PCy_2)Pt(PEt_3)_2][BF_4]$, **2,** which contains two bridging hydride ligands. This species is isolated and fully characterized by $^{31}P\{^1H\}$ and ^1H NMR and infrared spectroscopy. In contrast, **1** reacts with one equivalent of HCl·DMA (DMA = dimethylacetamide) to give the complex $(CO)_3ClFe(\mu\text{-}PCy_2)Pt(PEt_3)_2$, **3.** This species is the result of oxidative addition of HCl with subsequent reductive elimination of H_2(g). This complex is fully characterized by $^{31}P\{^1H\}$ and ^1H NMR, infrared spectroscopy and an X-ray crystal structure determination. **3** crystallizes in the space group $P\bar{1}$ with $a = 10.037(4)$ Å, $b = 10.644(3)$ Å, $c = 17.137(9)$ Å, $\alpha = 102.80(3)°$, $\beta = 76.74(3)°$, $\gamma = 103.99(3)°$, $V = 1702(1)$ Å^3, and $Z = 2$. The structure was refined to $R = 2.54\%$ and $R_w = 2.73\%$ for 4056 reflections with $F_o^2 > 3\sigma(F_o^2)$.

Key words: heterobimetallic, hydride, phosphide, protonation.

HILARY A. JENKINS, STEPHEN J. LOEB, DAVID G. DICK et DOUGLAS W. STEPHAN. Can. J. Chem. **68**, 869 (1990).

La réaction du $Li[Fe(CO)_4(PCy_2)]$ avec le *trans*-$PtCl(H)(PEt_3)_2$ conduit à la formation de l'hydrure complexe $(CO)_3Fe(\mu\text{-}H)(\mu\text{-}PCy_2)Pt(PEt_3)_2$, **1.** Ce complexe hétérobimétallique comportant une pont phosphido réagit avec un équivalent de $HBF_4 \cdot Et_2O$ pour fournir le complexe $[(CO)_3Fe(\mu\text{-}H)_2(\mu\text{-}PCy_2)Pt(PEt_3)_2][BF_4]$, **2** qui contient deux ligands hydrures agissant comme ponts. On a isolé cette espèce et on l'a caractérisée complètement par rmn du $^{31}P\{^1H\}$ et du ^1H ainsi que par spectroscopie infrarouge. Par opposition, le composé **1** réagit avec un équivalent de HCl·DMA (DMA = diméthylacétamide) pour donner le complexe $(CO)_3ClFe(\mu\text{-}PCy_2)Pt(PEt_3)_2$, **3.** Cette espèce est le résultat d'une addition oxydante du HCl avec une élimination réductrice subséquente de H_2(g). On a caractérisé complètement ce complexe par rmn du $^{31}P(^1H)$ et du ^1H, par spectroscopie infrarouge ainsi que par une détermination de sa structure par diffraction des rayons-X. Le composé **3** cristallise dans le groupe d'espace $P\bar{1}$ avec $a = 10{,}037(4)$, $b = 10{,}644(3)$ et $c = 17{,}137(9)$ Å, $\alpha = 102{,}80(3)$, $\beta = 76{,}74(3)$ et $\gamma = 103{,}99(3)°$, $V = 1702(1)$ Å^3, et $Z = 2$; on a affiné la structure jusqu'à des valeurs respectives de $R = 0{,}0254$ et $R_w = 0{,}0273$ pour 4056 réflexions avec $F_o^2 > 3\sigma(F_o^2)$.

Mots clés : hétérobimétallique, hydrure, phosphure, protonation.

[Traduit par la revue]

Introduction

The protonation of transition metal hydride complexes is a fundamental process in organometallic and catalytic chemistry. In general, the reactions of transition metal hydrido complexes with protonic acids can be divided into three types (1): (*i*) strong acids with weakly coordinating conjugate bases which form salts of the dihydride complex, (*ii*) weak acids with strongly coordinating conjugate bases which form oxidative addition products, and (*iii*) strong acids with non-coordinating conjugate bases which form salts of the molecular hydrogen (η^2-H_2) complex. These reactions are often followed by the rapid evolution of H_2(g) via a reductive elimination reaction or direct labilization of an η^2-H_2 ligand. The analogous reactions of a heterobimetallic hydrido complex are complicated by the fact that protonation may occur at either of the two metal sites or at the metal—metal bond if one exists (2). It is thus of interest to investigate the protonation reactions of heterobimetallic hydride complexes to determine the basic reactivity differences between these and monometallic species. To this end, we describe herein a comparison of the reactivity of the phosphido-bridged complex $(CO)_3Fe(\mu\text{-}H)(\mu\text{-}PCy_2)Pt(PEt_3)_2$, **1,** with the protonic acids HCl and HBF_4.

[1]Author to whom correspondence should be addressed. Present address: Department of Chemistry and Biochemistry, University of Windsor, Windsor, Ont., Canada N9B 3P4.

Experimental section

General

$Fe(CO)_4(PCy_2H)$, *trans*-$PtCl(H)(PEt_3)_2$, and DMA·HCl (DMA = dimethylacetamide) were prepared by the literature methods (3–5). $Fe_2(CO)_9$, PCy_2H (Strem), K_2PtCl_4, PEt_3, $HBF_4 \cdot Et_2O$ (Aldrich) were purchased and used as received. THF (tetrahydrofuran), toluene, and *n*-hexane were dried by distillation from Na–benzophenone ketyl under N_2. All other solvents were dried on molecular sieves and degassed prior to use. All reactions were conducted under an atmosphere of dry N_2 using standard Schlenk techniques.

$^{31}P\{^1H\}$ and ^1H NMR spectra were recorded at 121.5 and 300.1 MHz, respectively, on a Bruker AM300 spectrometer using deuterated solvents as lock. Phosphorus chemical shifts were measured relative to external H_3PO_4 with positive shifts downfield. Infrared spectra were recorded on a Perkin-Elmer 781 grating spectrometer. Elemental analyses were performed by Canadian Microanalytical Services Ltd., New Westminster, British Columbia.

Preparation of $(CO)_3Fe(\mu\text{-}H)(\mu\text{-}PCy_2)Pt(PEt_3)_2$, 1

n-Butyllithium (1.27 mL, 2.03 mmol of 1.6 M solution in hexanes) was added dropwise via syringe to a brown solution of $Fe(CO)_4(PCy_2H)$ (0.742 g, 2.03 mmol) in THF (10 mL). This solution was stirred for 30 min and then added dropwise, over 20 min, to a solution of *trans*-$PtCl(H)(PEt_3)_2$ (0.948 g, 2.03 mmol) in THF (15 mL). The resulting orange–red solution was stirred at room temperature for 18 h, and the solvent removed *in vacuo*. The orange residue was extracted with acetone (5 × 10 mL), the volume reduced to 15 mL, and the solution cooled to −20°C for 18 h. This yielded orange microcrystals of

Can. J. Chem. Downloaded from www.nrcresearchpress.com by 88.85.125.76 on 09/07/12
For personal use only.

Can. J. Chem. Downloaded from www.nrcresearchpress.com by 88.85.125.76 on 09/07/12
For personal use only.

1; yield 1.56 g (71%). Infrared: ν(CO) (CH_2Cl_2) 1945 (s), 1862 (s), 1851 (s). *Anal.* calcd. for $C_{27}H_{53}FeO_3P_3Pt$: C 42.13, H, 6.96; found: C 42.96, H 6.55.

Preparation of [(CO)$_3$Fe(μ-H)$_2$(μ-PCy$_2$)Pt(PEt$_3$)$_2$][BF$_4$], 2

1 (0.254 g, 0.330 mmol) was dissolved in CH_2Cl_2 (5 mL) and $HBF_4 \cdot Et_2O$ (0.18 mL) added via microsyringe. The orange–red solution immediately turned a very pale yellow colour. The solution was filtered to remove a small amount of white solid and diethylether (3 mL) added. The resulting solution was cooled to −20°C for 15 h to give colourless microcrystals of **2**; yield 0.218 g (77%). Infrared: ν(CO) (CH_2Cl_2) 1998 (m), 1862 (m, br). *Anal.* calcd. for $C_{27}H_{94}BF_4FeO_3P_3Pt$: C 37.82, H, 6.36; found: C 37.33, H 6.18.

Preparation of (CO)$_3$ClFe(μ-PCy$_2$)Pt(PEt$_3$)$_2$, 3

1 (0.288 g, 0.374 mmol) was dissolved in CH_2Cl_2 (5 mL) and HCl·DMA (0.048 g, 0.390 mmol) added with stirring. The solution slowly changed colour from orange-red to orange-brown over 30 min. The solution was stirred for a further 12 h, the solvent removed *in vacuo*, and the brownish residue taken up in acetone (10 mL). Cooling to −20°C for 48 h yielded orange-brown crystals of **3** suitable for X-ray diffraction studies. A second crop of solid product was obtained by reduction of the solution volume to 5 mL and further cooling for 24 h. This gave a total of 0.198 g of **3**; (66%). Infrared: ν(CO) (CH_2Cl_2) 2009 (m), 1938 (s,br). *Anal.* calcd. for $C_{27}H_{92}ClFeO_3P_3Pt$: C 40.33, H, 6.53; found: C 39.77, H 6.44.

X-ray crystallographic analysis of (CO)$_3$ClFe(μ-PCy$_2$)Pt(PEt$_3$)$_2$, 3

Orange-brown crystals of **3** were grown from acetone at −20°C. Diffraction experiments were performed on a four-circle Syntex $P2_1$ diffractometer with graphite monochromatized MoKα radiation. The initial orientation matrix was obtained from 15 machine-centered reflections selected from rotation photographs. Partial rotation photographs around each axis were consistent with a triclinic crystal system. Ultimately, 40 high-angle reflections ($22° < 2\theta < 25°$) were used to obtain the final lattice parameters and orientation matrix. Machine parameters, crystal data, and data collection parameters are summarized in Table 1. Intensity data ($\pm h$, $\pm k$, $+l$) were collected in two shells ($4.5° < 2\theta < 40°$, $40° < 2\theta < 45°$) and three standard reflections were recorded every 197 reflections. The intensities of these standard reflections showed an 8% decay in intensity over the duration of the data collection. Therefore, a decay correction was applied to the data. The data were processed using the SHELX-76 program package on the computing facilities at the University of Windsor. A total of 4682 reflections were collected and 4056 unique reflections with $F_o^2 > 3\sigma(F_o^2)$ were used in the refinement. An empirical absorption correction (μ = 45.71 cm^{-1}) was applied to the data based on three ψ-scans.

The Pt atom position was determined using the Patterson method, ($P\bar{1}$), and the remaining non-hydrogen atoms located from successive difference Fourier map calculations. Refinement was carried out using full-matrix least-squares techniques on F minimizing the function $\Sigma w(|F_o| - F_c|)^2$, where $w = 4F_o^2/\sigma^2(F_o^2)$ and F_o and F_c are the observed and calculated structure factors. Atomic scattering factors (6) and anomalous dispersion (7, 8) terms were taken from the usual sources. The space group $P\bar{1}$ was confirmed by a successful structure solution and refinement. In the final cycles of refinement, all the non-hydrogen atoms were assigned anisotropic thermal parameters. Fixed H atom contributions were included with C—H bond distances of 0.95 Å and thermal parameters equal to 1.1 times the isotropoic thermal parameters of the bonded C atoms. No H atoms were refined, but all values were updated as refinement continued. This resulted in $R = \Sigma||F_o| - |F_c||/\Sigma|F_o| = 2.54\%$ and $R_w = (\Sigma w(|F_o| - |F_o|)^2/\Sigma wF_o^2)^{1/2} = 2.73\%$ at final convergence.

The Δ/σ values for any parameter in the final cycles were less than 0.002. A final difference Fourier map calculation showed no peaks of chemical significance; the largest was 1.30 electrons /Å^3 and associated with the Pt atom. Selected bond distances and angles are summarized in Table 2 and atomic positional parameters in Table 3. Anisotropic thermal parameters (Table S-1), hydrogen atom parame-

TABLE 1. Summary of crystal data, intensity collection, and structure refinement for (CO)$_3$ClFe(μ-PCy$_2$)Pt(PEt$_3$)$_2$, **3**

Formula	$C_{27}H_{52}ClFeP_3PtO_3$
Crystal colour, form	Red–orange blocks
a (Å)	10.037(4)
b (Å)	10.644(3)
c (Å)	17.137(9)
α (deg)	102.80(3)
β (deg)	76.74(3)
γ (deg)	103.99(3)
Crystal system	Triclinic
Space group	$P\bar{1}$
Volume (Å^3)	1702(1)
Density (g cm^{-3}), calcd.	1.57
Z	2
Crystal dimension (mm)	0.51 × 0.30 × 0.33
Absorption coefficient, μ (cm^{-1})	45.71
Radiation, λ (Å)	MoKα (0.71069)
Temperature (°C)	24
Scan speed (deg min^{-1})	2.0–5.0 (θ-2θ scan)
Scan range (deg)	1.0 below Kα_1, 1.0 above Kα_2
Background/scan time ratio	0.5
Data collected	4682; 2θ of 4.5 to 45° ($\pm h$, $\pm k$, $+l$)
Unique data, $F_o^2 > 3\sigma F_o^2$	4056
Number of variables	325 (2 blocks)
R (%)	2.54
R_w (%)	2.73

TABLE 2. Selected bond distances and angles

Bond	Distance (Å)	Bond	Distance (Å)
Pt—Fe	2.675(1)	Pt—P1	2.276(1)
Pt—P2	2.276(2)	Pt—P3	2.330(1)
Fe—P1	2.199(2)	Fe—CL	2.376(2)
Fe—C1	1.774(6)	Fe—C2	1.801(7)
Fe—C3	1.806(6)	P1—C11	1.871(5)
P1—C21	1.863(5)	P2—C31	1.836(6)
P2—C33	1.836(6)	P2—C35	1.829(5)
P3—C41	1.817(5)	P3—C43	1.837(6)
P3—C45	1.826(6)	C1—01	1.145(7)
C2—02	1.156(8)	C3—03	1.149(7)

Bonds	Angle (deg)	Bonds	Angle (deg)
Fe—Pt—P1	52.0(1)	Fe—Pt—P2	157.1(1)
Fe—Pt—P3	99.9(1)	P1—Pt—P2	107.0(1)
P1—Pt—P3	150.0(1)	P2—Pt—P3	102.3(1)
Pt—Fe—P1	54.6(1)	Pt—Fe—CL	112.4(1)
Pt—Fe—C1	150.6(2)	Pt—Fe—C2	93.0(2)
Pt—Fe—C3	70.4(2)	P1—Fe—CL	167.1(1)
P1—Fe—C1	97.9(2)	P1—Fe—C2	94.6(2)
P1—Fe—C3	92.0(2)	CL—Fe—C1	94.9(2)
CL—Fe—C2	85.1(2)	CL—Fe—C3	82.9(2)
C1—Fe—C2	100.1(3)	C1—Fe—C3	104.0(3)
C2—Fe—C3	153.8(2)	Pt—P1—Fe	73.4(1)
Pt—P1—C11	122.5(2)	Pt—P1—C21	117.8(2)
Fe—P1—C11	120.7(2)	Fe—P1—C21	120.2(2)
C11—P1—C22	102.0(2)	Pt—P2—C31	115.4(2)
Pt—Pt2—C33	112.1(2)	Pt—Pt2—C35	119.3(2)
Pt—P3—C41	116.6(2)	Pt—P3—C43	118.4(2)
Pt—P3—C45	109.7(2)	Fe—C1—01	178.0(6)
Fe—C2—02	173.9(6)	Fe—C3—03	172.6(6)

TABLE 3. Positional parameters[a]

Atom	x	y	z	Atom	x	y	z
Pt	1981(1)	882(1)	2440(1)	Fe	718(1)	2798(1)	2389(1)
CL	−1449(2)	1968(2)	1938(1)	P1	2747(1)	3094(1)	2756(1)
P2	3413(1)	−92(1)	2859(1)	P3	601(1)	−911(1)	1750(1)
O1	322(5)	5504(4)	2930(3)	O2	1808(5)	2830(5)	638(3)
O3	−893(4)	1490(4)	3762(3)	C1	455(6)	4437(6)	2713(4)
C2	1455(6)	2824(6)	1329(4)	C3	−187(5)	1995(5)	3242(4)
C11	3002(5)	3941(5)	3807(3)	C12	3150(8)	5427(5)	3939(4)
C13	3438(9)	6079(7)	4793(4)	C14	2337(9)	5487(7)	5450(4)
C15	2212(8)	3995(7)	5316(4)	C16	1903(6)	3378(5)	4471(3)
C21	4377(5)	3857(5)	2116(3)	C22	4259(7)	5048(6)	1791(4)
C23	5703(8)	5676(6)	1329(5)	C24	6331(8)	4708(7)	672(5)
C25	6474(8)	3560(8)	985(5)	C26	5008(7)	2883(6)	1426(4)
C31	4734(6)	1036(5)	3403(4)	C32	5601(7)	438(7)	3797(5)
C33	2441(6)	−1198(6)	3574(3)	C34	1602(8)	−536(8)	4343(4)
C35	4422(5)	−1189(5)	2111(3)	C36	5239(7)	−654(6)	1361(4)
C41	−1240(5)	−1290(5)	2205(4)	C42	−1526(6)	−1849(6)	2983(4)
C43	1132(6)	−2509(5)	1510(4)	C44	251(8)	−3639(6)	1003(5)
C45	576(6)	−593(5)	750(3)	C46	2014(7)	−317(7)	228(4)

[a]Multiplied by 10^4.

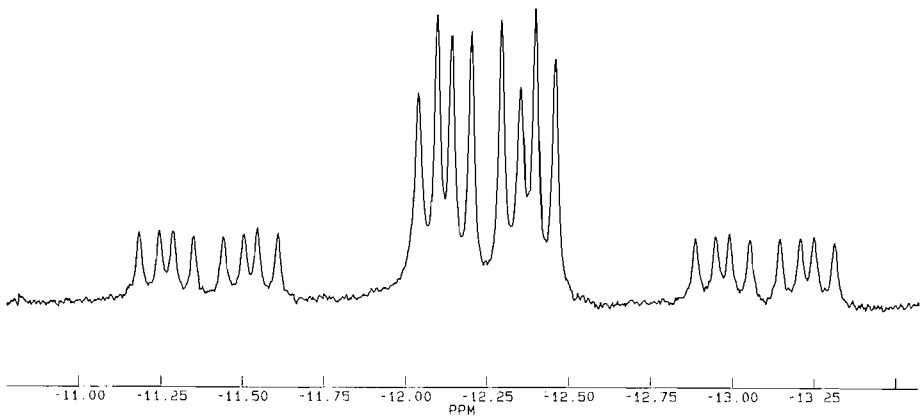

FIG. 1. The ^{1}H NMR spectrum of $(CO)_3Fe(\mu\text{-}H)(\mu\text{-}PCy_2)Pt(PEt_3)_2$, **1**, at 300 K, showing the hydride resonance only.

ters (Table S-2), bond distances and angles associated with the cyclohexyl groups (Table S-3), and values of $10|F_o|$ and $10|F_c|$ (Table S-4) are deposited as supplementary material.[2]

Results

Synthesis and reactions

The complex $(CO)_3Fe(\mu\text{-}H)(\mu\text{-}PCy_2)Pt(PEt_3)_2$, **1**, containing both a bridging dicyclohexylphosphido group and a bridging hydride ligand, can be easily prepared by the bridge-assisted synthetic method (3, 9–11). This involves the nucleophilic displacement of chloride from *trans*-$PtCl(H)(PEt_3)_2$ by the phosphido group of $Li[Fe(CO)_4(PCy_2)]$ in THF. The $^{31}P\{^1H\}$ NMR shows a downfield resonance (δ 220.6 (ddt)) due to the bridging PCy_2 ligand coupled to two different PEt_3 groups ($^2J_{PP}$ (μ-*trans*) = 205.7 Hz and $^2J_{PP}$ (μ-*cis*) = 12.7 Hz) and the ^{195}Pt centre ($^1J_{PtP}$ = 1822 Hz).[3] The two PEt_3 ligands are both coordinated to the Pt atom and are designated as being either *trans* (δ 10.4 (ddt); $^1J_{PtP}$ = 3596 Hz) or *cis* (δ 10.3 (ddt); $^2J_{PP}$ (*cis–trans*) = 18.2 Hz; $^1J_{PtP}$ = 2348 Hz) to the μ-PCy_2 group. The ^{1}H NMR exhibits a single downfield resonance (Fig. 1) indicative of the hydride ligand (δ − 12.25 (dddt)) coupled to the μ-PCy_2 ligand ($^2J_{PH}(\mu)$ = 17.7 Hz), the PEt_3 ligands ($^2J_{PH}$ = 30.9 Hz and $^2J_{PH}$ = 76.5 Hz), and the Pt centre ($^1J_{PtH}$ = 511.7 Hz). The bridging nature of the hydride ligand is indicated by the relatively small value of $^1J_{PtH}$ (2, 12–16). The infrared spectrum (CH_2Cl_2) shows three ν(CO) absorptions at 1945 (s), 1862 (s), and 1851 (s) cm^{-1} confirming the presence of three terminal CO groups bonded to Fe. The spectroscopic and X-ray characterization of this complex were recently communicated in the literature and our spectroscopic data agree well with those reported (12).

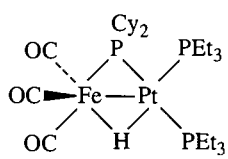

1

[2]Supplementary Tables S-1, S-2, S-3, and S-4 may be purchased from the Depository of Unpublished Data, CISTI, National Research Council of Canada, Ottawa, Ont., Canada K1A 0S2.

[3]The triplets associated with ^{195}Pt satellites are non-binomial.

Can. J. Chem. Downloaded from www.nrcresearchpress.com by 88.85.125.76 on 09/07/12
For personal use only.

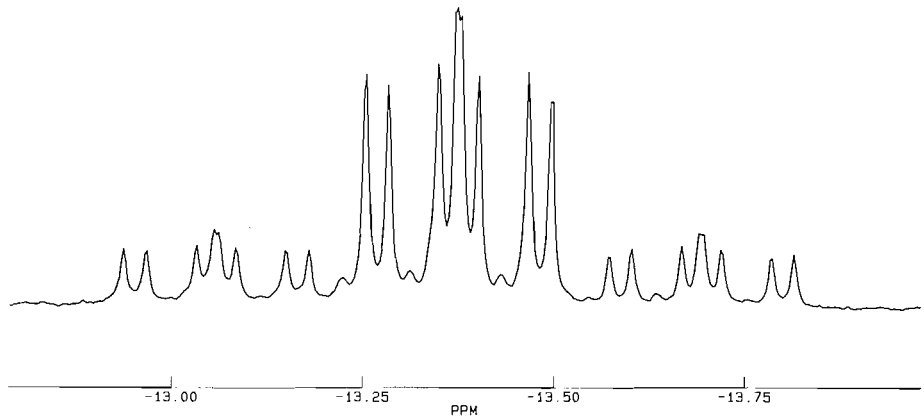

FIG. 2. The ^1H NMR spectrum of $[(CO)_3Fe(\mu\text{-}H)_2(\mu\text{-}PCy_2)Pt(PEt_3)_2][BF_4]$, **2**, at 300 K, showing the hydride resonances only.

The addition of one equivalent of $HBF_4 \cdot Et_2O$ to **1** results in the rapid protonation of this species to give a single product as evidenced by $^{31}P\{^1H\}$ and ^1H NMR monitoring. This compound is identified as the dihydride complex $[(CO)_3Fe(\mu\text{-}H)_2(\mu\text{-}PCy_2)Pt(PEt_3)_2][BF_4]$, **2**. The $^{31}P\{^1H\}$ NMR spectrum shows the same pattern as **1** with resonances due to the μ-PCy_2 group (δ 222.6) and the two PEt_3 ligands (δ 12.3 (*cis*); 9.0 (*trans*)). The phosphorus–phosphorus coupling constants ($^2J_{PP}$ (μ-*trans*) = 217.0 Hz, $^2J_{PP}$ (μ-*cis*) < 3 Hz, and $^2J_{PP}$ (*cis-trans*) = 21.1 Hz) indicate no major change has occurred in the relative geometry of these ligands. However, the platinum–phosphorus coupling constant for the μ-PCy_2 group ($^1J_{PtP}$ (μ) = 1290 Hz) is reduced considerably. These results suggest that protonation has occurred at the bridging site and this is supported by the ^1H NMR spectrum of **2** which is very different from **1** (Fig. 2). There is a single resonance in the hydride region (δ −13.38), which integrates as two protons, establishing the equivalence of the two hydride ligands. The coupling constants ($^2J_{PH}(\mu)$ = 9.0 Hz, $^2J_{PH}$(*trans*) = 35.7 Hz, $^2J_{PH}$(*cis*) = 28.5 Hz and $^1J_{PtH}$ = 190.9 Hz) reflect the change in geometry from a singly bridging hydride to a doubly bridging hydride complex. The infrared spectrum (CH_2Cl_2) of **2** shows ν(CO) absorptions at 1998(m) and 1973 (s,br).

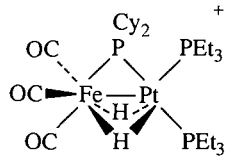

2

The reaction of **1** with HCl, as the DMA adduct, also results in the relatively rapid production of only one complex, **3**, as shown by the $^{31}P\{^1H\}$ NMR spectrum of the reaction solution. This species also displays the same type of $^{31}P\{^1H\}$ NMR resonance pattern as **1**, but with significant chemical shift differences. Upon conversion of **1** to **3**, the resonance due to μ-PCy_2, bridging the FePt bond, shifts to higher field (δ 183.8) while the resonances due to the PEt_3 groups shift to lower field (δ(*trans*) 16.5; (*cis*) 20.5). This infers that the basic geometry of the phosphorus ligands has remained the same, but some change in the structural or electronic nature of the coordination sphere has occurred. This notion is supported by the infrared spectrum (CH_2Cl_2) of **3** which shows two ν(CO) absorptions at 2009 (m), and 1938 (s, br): a significant blue shift compared to **1**. The major difference however, is that the ^1H NMR spectrum

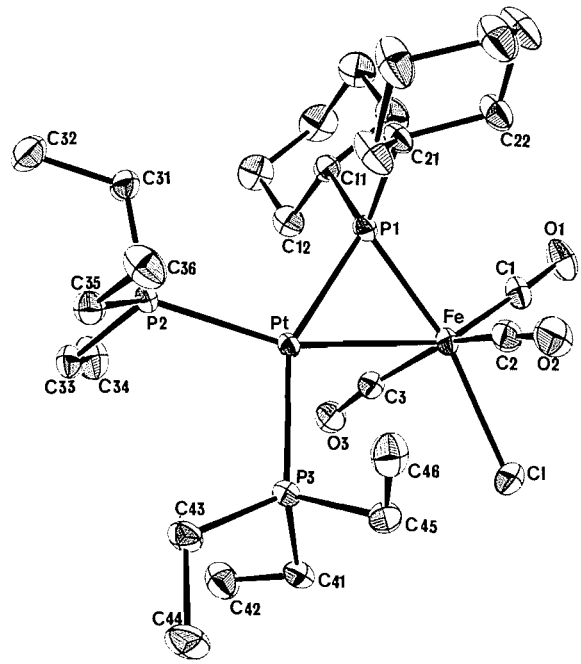

FIG. 3. Perspective ORTEP drawing of $(CO)_3ClFe(\mu\text{-}PCy_2)Pt(PEt_3)_2$, **3**, showing the numbering scheme. The numbering of cyclohexyl ring carbon atoms starts at the atom bound to phosphorus: 20% thermal ellipsoids are shown.

shows no evidence of a resonance due to a hydride ligand. It was therefore assumed that **3** was the product of oxidative addition of HCl to **1** followed by reductive elimination of H_2 and incorporation of the conjugate base, the chloride ligand, into the coordination sphere. The identification of **3** as $(CO)_3ClFe(\mu\text{-}PCy_2)Pt(PEt_3)_2$ required an X-ray crystallographic study which verified the presence of a terminal chloride ligand bound to the Fe centre.

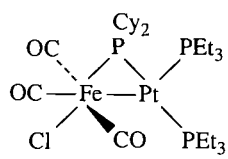

3

X-ray Structure of $(CO)_3ClFe(\mu\text{-}PCy_2)Pt(PEt_3)_2$, *3*

The unit cell contains two discrete molecules of **3**. A perspective ORTEP drawing of the molecule is shown in Fig. 3.

Can. J. Chem. Downloaded from www.nrcresearchpress.com by 88.85.125.76 on 09/07/12
For personal use only.

TABLE 4. $^{31}P\{^1H\}$ and ^1H nmr spectral data [a]

(*a*) $^{31}P\{^1H\}$ chemical shifts

Complex[b]	δ(μ-PCy_2)	δ(PEt_3)$_c$	δ(PEt_3)$_t$
$(CO)_3Fe(\mu\text{-}PCy_2)(\mu\text{-}H)Pt(PEt_3)_2$, (**1**)[c]	220.6 (ddt)[d]	10.3 (ddt)	10.4 (ddt)
$[(CO)_3Fe(\mu\text{-}PCy_2)(\mu\text{-}H)_2Pt(PEt_3)_2][BF_4]$, (**2**)	222.6 (ddt)	12.3 (ddt)	9.0 (ddt)
$(CO)_3ClFe(\mu\text{-}PCy_2)Pt(PEt_3)_2$, (**3**)	183.8 (ddt)	20.5 (ddt)	16.5 (ddt)

(*b*) $^{31}P\{^1H\}$ coupling constants

Complex	$^2J_{PP}(\mu\text{—}c)$	$^2J_{PP}(\mu\text{—}t)$	$^2J_{PP}(c\text{—}t)$	$^1J_{PPT}(\mu)$	$^1J_{PPt}(c)$	$^1J_{PPt}(t)$
$(CO)_3Fe(\mu\text{-}PCy_2)(\mu\text{-}H)Pt(PEt_3)_2$, (**1**)	12.7	205.7	18.2	1822	2348	3596
$[(CO)_3Fe(\mu\text{-}PCy_2)(\mu\text{-}H)_2Pt(PEt_3)_2][BF_4]$, (**2**)	<3	217.0	21.1	1290	2348	3673
$(CO)_3ClFe(\mu\text{-}PCy_2)Pt(PEt_3)_2$, (**3**)	20.7	241.8	<3	2002	2715	3385

(*c*) ^1H hydride resonance

Complex	δ (μ—H)	$^2J_{PH}(\mu)$	$^2J_{PH}(c)$	$^2J_{PH}(t)$	$^1J_{PtH}$
$(CO)_3Fe(\mu\text{-}PCy_2)(\mu\text{-}H)_2Pt(PEt_3)_2$, (**1**)	−12.25	17.7	76.5	30.9	511.7
$[(CO)_3Fe(\mu\text{-}H)_2(\mu\text{-}PCy_2)Pt(PEt_3)_2][BF_4]$, (**2**)[e]	−13.38	9.0	28.5	35.7	190.9

[a]Recorded in CD_2Cl_2 unless otherwise noted.
[b]μ = PCy_2 group, *c* = PEt_3 group *cis* to PCy_2 group, *t* = PEt_3 group *trans* to PCy_2 group.
[c]Recorded in benzene-d_6.
[d]d = doublet, t = triplet.
[e]Recorded in acetone-d_6.

The closest intermolecular nonbonded contact is 2.3 Å between H25A and H46B. Complete listings of the interatomic bond distances and angles can be found in Tables 2 and S-3.

The geometry at the Fe centre is distorted octahedral with bonds to the μ-PCy_2 group, the chloride ligand, three CO groups, and the Pt atom. The chloride ligand is *trans* to the μ-PCy_2 group with a CL—Fe—P1 angle of 167.1(1)°. The three CO groups and the Pt atom are in a distorted square plane such that the angles within the plane are 100.1(3)° (C1—Fe—C2), 104.0(3)° (C1—Fe—C3), 93.0(2)° (Pt—Fe—C2), and 70.4(2)° (Pt—Fe—C3). The major distortion from octahedral geometry at Fe is due to the geometric restrictions imposed by a μ-PCy_2 ligand bridging a metal–metal bond. This causes the Pt atom to be pulled out of the square plane towards P1 and results in a Pt—Fe—P1 angle of 54.6(1)° and a Pt—Fe—CL angle of 112.4(1)°. The geometry at the Pt centre is best described as severely distorted square planar with P1 *trans* to P3 and P2 *trans* to Fe with angles of 150.0(1)° and 157.0(1)°, respectively. Again, the square plane is distorted in order to allow for the bridging phosphido ligand and the presence of a metal–metal bond. We therefore observe a small Fe—Pt—P1 angle (52.0(1)°) offset by increases in the other *cis* angles to give P1—Pt—P2 (107.0(1)°), P2—Pt—P3 (102.3(1)°), and Fe—Pt—P3 (99.9(1)°). The Fe—Pt bond distance of 2.675(1)Å is consistent with a single bond between these centres. This compares well to the value of 2.698(2) Å found for $(CO)_3(H)Fe(\mu\text{-}PPh_2)Pt(PPh_3)_2$ but is significantly shorter than that measured for **1**; 2.800(4) Å (12).

Discussion

In a preliminary report on complex **1** and some related FePt hydride complexes, Powell *et al.* demonstrated that these types of molecules may undergo an equilibration between bridging and terminal hydride coordination modes (12).

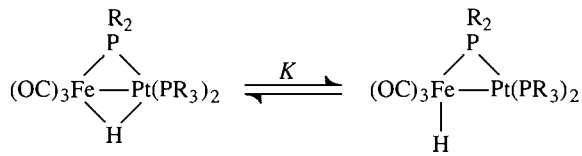

For **1**, the equilibrium was shifted completely to the bridging hydride and the X-ray crystal structure was determined. The observed geometries at the two metal atoms suggested that this complex is best described as having Fe(0) and Pt(II) centres.

The geometry of **3** is very different from that observed for **1**. The presence of an anionic chloride ligand at Fe, a shorter FePt bond distance (2.675(1) Å for **3** compared to 2.800(4) Å for **1**) and the distorted octahedral geometry at Fe are the major differences. This geometry is also what was observed by Powell *et al.* for the FePt hydride complex $(CO)_3HFe(\mu\text{-}PPh_2)Pt(PPh_3)_2$, except that for **3** the chloride ligand is *trans* to the μ-PCy_2 group while the hydride ligand for $(CO)_3HFe(\mu\text{-}PPh_2)Pt(PPh_3)_2$ is *trans* to a carbonyl group with the FeH bond perpendicular to the Fe(μ-PPh_2)Pt plane (12). The pseudo-octahedral geometry at Fe and the considerable blue shift of the ν(CO) absorptions are consistent with the formulation of **3** as a complex which now contains Fe(II) and Pt(0) centres. The downfield shift in the ^{31}P resonance due to the μ-PR_2 group and the upfield shift in the ^{31}P resonances of the Pt bound PR_3 groups may also be an indication of the reduction to Pt(0). However, this may simply be indicative of structural changes at the Fe(μ-PCy_2)Pt bridging fragment, since Carty has shown that ^{31}P NMR shifts in μ-PR_2 complexes can be very dependent on the nature of the M—M bonding, the M—M separation and the M—P—M angle (17).

A number of bonding descriptions are possible for **2**, but the lack of structural data makes a detailed discussion difficult. Observations of a small blue shift in the infrared ν(CO) absorptions and a very pale colour are not inconsistent with the

Can. J. Chem. Downloaded from www.nrcresearchpress.com by 88.85.125.76 on 09/07/12
For personal use only.

description of **2** as an Fe(II)—Pt(II) complex. This is also consistent with the idea that these protonation reactions involve oxidation addition to the Fe(0)—Pt(II) complex **1** to give Fe(II)—Pt(II) species such as **2**, which can be stabilized in the presence of a non-coordinating anion (BF_4^-). This would then be followed by hydride transfer and reductive elimination of H_2 from the Pt(II) centre to give an Fe(II)—Pt(0) complex such as **3**.

In conclusion, we observed that the heterobimetallic FePt complex **1** reacted with protic acids HCl and HBF_4 in a way that was reminiscent of monometallic species (1). When the conjugate base was a non-coordinating anion (BF_4^-) the dihydride complex **2** was stabilized. However, when the conjugate base could occupy a coordination site (Cl^-) reductive elimination of H_2 was favoured. Thus the resulting product and the ease of H_2 reductive elimination was dependent on the ability of the conjugate base to act as a coordinating anion to the transition metal. The major difference between these FePt complexes and simple monometallic species is the ability of the heterobimetallic complexes to transfer ligands or electrons between metal centres as part of the overall reaction scheme. This may result in an intramolecular redox isomerization between bridging and terminal hydride modes (12) or changes in individual metal oxidation states in the stepwise oxidative addition, reductive elimination sequence, as was observed in the conversion of **1** to **3**. This cooperativity between metal centres is therefore an important factor in the protonation of heterobimetallic hydride complexes.

Acknowledgements

We thank the Natural Science and Engineering Research Council of Canada for financial support of this work. The Chemistry Department of the University of Manitoba is gratefully acknowledged for use of their NMR facilities and as the home department of graduate student H.A.J. D.G.D, is grateful for the award of an NSERC of Canada Postgraduate Scholarship.

1. D. S. Moore and S. D. Robinson. Chem. Soc. Rev. 415 (1984).
2. J. Powell, J. F. Sawyer, and S. J. Smith. J. Chem. Soc. Chem. Commun. 1312 (1985).
3. H. A. Jenkins, S. J. Loeb, and D. W. Stephan. Inorg. Chem. **28**, 1998 (1989).
4. G. W. Parshall. Inorg. Synth. **12**, 26 (1970).
5. M. Cowie, S. J. Loeb, and I. R. McKeer. Organometallics, **5**, 854 (1986).
6. D. T. Cromer and J. T. Waber. International tables for crystallography. Vol. IV. Kynoch Press, Birmingham, England. 1974.
7. D. T. Cromer and J. B. Mann. Acta Crystallogr. Sect. A: Cryst. Phys. Diffr. Theor. Gen. Crystallogr. **A24**, 321 (1968).
8. D. T. Cromer and J. B. Mann. Acta Crystallogr. Sect. A: Cryst. Phys. Diffr. Theor. Gen. Crystallogr. **A24**, 390 (1968).
9. D. A. Roberts and G. L. Geoffroy, In Comprehensive organometallic chemistry. *Edited by* G. Wilkinson, F. G. A. Stone, and E. Abel. Pergamon Press, Oxford, England. 1982. Chap. 40.
10. S. J. Loeb, H. A. Taylor, and D. W. Stephan. Inorg. Chem. **25**, 1977 (1986).
11. H. A. Jenkins and S. J. Loeb. Can. J. Chem. **67**, 1230 (1989).
12. J. Powell, M. R. Gregg, and J. F. Sawyer. J. Chem. Soc. Chem. Commun. 1029 (1987).
13. P. M. Triechel, W. K. Dean, and W. M. Douglas. J. Organomet. Chem. **42**, 145 (1972).
14. J. Powell, M. R. Gregg, and J. F. Sawyer. J. Chem. Soc. Chem. Commun. 1149 (1984).
15. P. Braunstein, G. L. Geoffroy, and B. Metz. Nouv. J. Chem. **9**, 221 (1985).
16. J. Powell, J. F. Sawyer, and M. V. R. Stainer. J. Chem. Soc. Chem. Commun. 1314 (1985).
17. A. J. Carty, S. A. MacLaughlin, and D. Nuccarione. *In* Phosphorus-31 NMR spectroscopy in stereochemical analysis. *Edited by* J. G. Verkade and L. D. Quin. 1987. Chap. 16 and references therein.

Can. J. Chem. Downloaded from www.nrcresearchpress.com by 88.85.125.76 on 09/07/12
For personal use only.

The orientational ordering of solute molecules in nematic solvents: cyanobenzenes, bromobenzenes, and *p*-benzoquinone in EBBA and 1132

C. T. YIM

Department of Chemistry, Dawson College, 3040 Sherbrooke St. W., Westmount, P.Q., Canada H3Z 1A4

AND

D. F. R. GILSON

Department of Chemistry, McGill University, 801 Sherbrooke St. W., Montreal, P.Q., Canada H3A 2K6

Received September 15, 1989

C. T. YIM and D. F. R. GILSON. Can. J. Chem. **68**, 875 (1990).

The orientational order parameters of benzonitrile and *o*-, *m*-, and *p*-dicyanobenzene, monobromo- and *p*-dibromobenzene, and *p*-benzoquinone, dissolved in two nematic solvents, 1132 and EBBA, have been measured as functions of temperature, and used to determine the potential energy parameters for each solute–solvent pair. These parameters have been correlated with a short-range interaction based upon a shape and size function of the solute molecule and a long-range contribution due to the interaction between the solute molecular quadrupole moment and the average electric field gradient.

Key words: nematic liquid crystals, orientational ordering of solutes.

C. T. YIM et D. F. R. GILSON. Can. J. Chem. **68**, 875 (1990).

On a mesuré les paramètres d'ordre d'orientation du benzonitrile, des *o*-, *m*- et *p*-dicyanobenzènes, des monobromo- et *p*-dibromobenzènes ainsi que de la benzoquinone dissous dans deux solvants nématiques, le 1132 et l'EBBA, en fonction de la température et on a utilisé ces données pour déterminer les paramètres d'énergie potentielle pour chacune des paires soluté–solvant. On a établi une corrélation entre ces paramètres et une interaction à courte distance évaluée en se basant sur une fonction de la forme et de la grosseur des molécules de solutés ainsi que sur a contribution à longue distance qui serait due à l'interaction entre le moment quadripolaire moléculaire du soluté et le gradient moyen du champ électrique.

Mots clés : cristaix liquides nématiques, ordre orientationnel des solutés.

[Traduit par la revue]

Introduction

When solutes are dissolved in nematic liquid crystal solvents, the interaction between solute and solvent molecules results in an orientational ordering of the solute. An understanding of solvent–solute interactions in these anisotropic systems is desirable in view of their importance, for instance, as analogues of biological membranes and in various technological applications. Recently, the orientational behaviour of mono- and dichlorobenzenes in two nematic solvents, EBBA (a Schiff-base) and 1132 (a mixed phenylcyclohexylcyanide solvent), was studied as a function of temperature and of concentration (1, 2). The results showed that chlorobenzene molecules were more highly oriented in 1132 than in EBBA. This difference was attributed to a change in sign of the electric field gradient in the two solvents and the resulting effect upon the interaction between the molecular quadrupole moment of the solute and the average electric field gradient from the solvent. The importance of this interaction in determining the solute orientation was first demonstrated in studies of D_2 and HD dissolved in nematic solvents by Burnell and co-workers (3–6), who also showed that a mixture of the two solvents in which the field gradient is zero could be used to eliminate the long-range interaction and limit the potential to a short-range interaction. This latter contribution was interpreted using a Hooke's law force constant for the displacement of the solvent molecules with the molecular circumference of the solute defining this displacement (6). Diehl and co-workers (7) have studied a series of eleven chlorobenzenes and interpreted the orientation using a bond interaction model. They concluded that a molecular shape function must be included and adopted the force constant – molecular circumference model. In our earlier studies on chlorobenzene and the dichlorobenzenes dissolved in EBBA and 1132 (1, 2), the short range term was shown to depend on the shape and size of the solute molecule, and, to further probe the solute–solvent interaction in these two solvent systems, we have extended our investigation to include other substituted benzenes. In particular, the cyano-derivatives were chosen, as this substituent group is common to the phenylcyanocyclohexyl class of liquid crystals, and *p*-benzoquinone, which is often a component part of dye molecules used as guests in display devices.

The solute orientation parameters are entirely determined by the orientation-dependent part of the intermolecular interaction potential. Since all the molecules studied in the present work possess at least C_{2v} symmetry, a two-parameter function is required to describe the orientation potential $U(\Theta, \Phi)$:

$$[1] \qquad U(\Theta, \Phi) = -AS^{(1)}(\cos^2\Theta + B\sin^2\Theta\cos 2\Phi)$$

where Θ and Φ are the polar and azimuthal angles, and $S^{(1)}$ is the solvent order parameter. The solvent molecules are assumed to be rigid cylinders. For the solute molecules, the three-axis is taken to be the long molecular axis, and the two-axis to be perpendicular to the ring plane, as shown in Fig. 1. The parameter A corresponds to a potential energy difference between two solute orientations when axis-3 is parallel and perpendicular to the liquid crystal director, while (AB) represents the difference between orientations with axis-1 and axis-2 parallel to the director. The parameters A and (AB) are divided into a long-range contribution, due to the field gradient – molecular quadrupole moment interaction, and a size–shape dependent short-range term. Thus, $A = A_{LR} + A_{SR}$, and $(AB) = (AB)_{LR} + (AB)_{SR}$.

For the short-range term, we employ a function of the type commonly used to describe anisotropic properties, in this case based on molecular dimensions:

$$[2] \qquad A_{SR} = A_L(L_3 - (1/2)(L_1 + L_2)) = A_L A[\mathrm{vdW}]$$

$$[3] \qquad (AB)_{SR} = (1/2)A_L(L_1 - L_2)$$

Can. J. Chem. Downloaded from www.nrcresearchpress.com by 88.85.125.76 on 09/07/12
For personal use only.

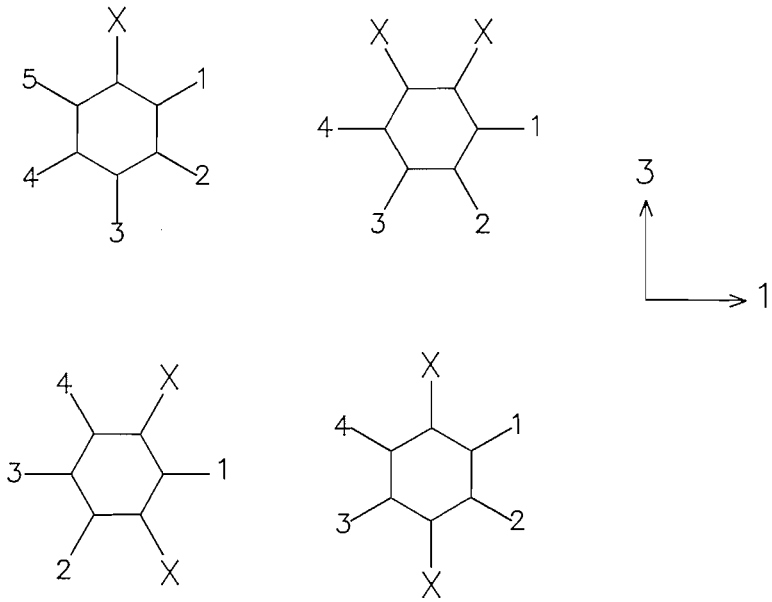

FIG. 1. Coordinate system and atomic labelling for mono- and disubstituted benzenes.

[4] $B_{SR} = (L_1 - L_2)/(2L_3 - L_1 - L_2) = B[\text{vdW}]$

where L_i is the molecular dimension, including the van der Waals radii, along the ith axis, and A_L is a constant which is assumed to depend only on the properties of the solvent. The long-range terms, A_{LR} and $(AB)_{LR}$, are given by similar functions based, in this case, upon the molecular quadrupole moments:

[5] $A_{LR} = (1/2)(Q_{33} - (1/2)(Q_{11} + Q_{22}))F_{ZZ}^0$

[6] $(AB)_{LR} = (1/4)(Q_{11} - Q_{22})F_{ZZ}^0$

where Q_{ii} are the components of the molecular quadrupole moment tensor, and $F_{ZZ}^0 = F_{ZZ}/S^{(1)}$, with F_{ZZ} being the average electric field gradient along the liquid crystal director as the z-axis. For both the short- and long-range interactions, the B parameters should depend only on the solute properties.

In analyzing the orientational potential function, the A_L value for each solvent can be obtained from our earlier studies (1, 2, 8), and, for the molecules studied in the present work, the molecular quadrupole moments will be treated as unknown parameters to be fitted. In eqs. [2]–[6], it is assumed that A_L is constant and that the electric field gradient is invariant over all the local environments that a solute molecule might prefer, so that the potential can be factorized into solvent-dependent and solute-dependent terms. This type of factorization is usually considered valid for dispersion forces (9, 10), but has also been suggested for repulsion forces (11).

Experimental

Spectra were recorded on either Varian XL-200 or XL-300 spectrometers and the solute order parameters were determined by analyzing the proton nmr spectra to give the direct dipole–dipole coupling constants. The molecular geometry was optimized by fitting to the dipolar coupling constants obtained from the room temperature spectra, and the same geometry was used for analyzing the spectra recorded at other temperatures. The solutes were obtained from commercial sources. Bromobenzene, *p*-dibromobenzene, *p*-dicyanobenzene, and benzoquinone were purified before use. The remaining chemicals were of high purity grade and used without further purification. Dilute solutions were used, with concentrations between 0.6 and 1.8 mol%.

Results and discussion

The calculated proton–proton distance ratios are given in Table 1, where they are compared with values reported in the literature. There were no significant differences between the present results and the previously published data, and minor differences can be attributed to the use of different nematic solvents. Corrections for the effects of molecular vibrations were not included in the analysis.

The values of experimental parameters A and B at each temperature were calculated by computer fits to the experimentally determined order parameters, S_{33} and $(S_{11} - S_{22})$, via the following equations:

[7] $$S_{33} = (3/2Z)(\int\int \cos^2\Theta \exp\{-U(\Theta, \Phi)/kT\} \sin\Theta \, d\Theta \, d\Phi) - 1/2$$

[8] $$(S_{11} - S_{22}) = (3/2Z) \int\int (\sin^2\Theta \cos 2\Phi \exp\{-U(\Theta, \Phi)/kT\} \sin\Theta \, d\Theta \, d\Phi)$$

where

$$Z = \int\int \exp\{-U(\Theta, \Phi)/kT\} \sin\Theta \, d\Theta \, d\Phi$$

The order parameters of the pure solvents were taken from the literature (refs. 12, 13 and our unpublished results for EBBA), and the computation of A and B used the reduced temperature dependence, since the solvent order parameter is a function of reduced temperature only, and is independent of the solute and its concentration (14). The parameter A should include the variation of the molar volume with temperature and its effect on the intermolecular forces, but, in the study of the chlorobenzenes (1, 2), it was found that including this volume dependence neither led to a significant improvement in the fit, nor had a marked effect on the relative magnitudes of the parameters A for the two solvent systems. Since the available data do not permit us to take full account of the small temperature effect on the energy parameters, only the averaged values of A and B were

Can. J. Chem. Downloaded from www.nrcresearchpress.com by 88.85.125.76 on 09/07/12
For personal use only.

Can. J. Chem. Downloaded from www.nrcresearchpress.com by 88.85.125.76 on 09/07/12
For personal use only.

TABLE 1. Interproton distance ratios

	1132	EBBA	Lit.
Bromobenzene			
r_{13}/r_{12}	1.740	1.735	1.731[a], 1.737[b]
r_{14}/r_{12}	1.994	2.002	1.998[a], 1.997[b]
r_{15}/r_{12}	1.696	1.733	1.731[a], 1.719[b]
r_{23}/r_{12}	1.020	1.003	0.998[a], 1.007[b]
r_{24}/r_{12}	1.755	1.735	1.730[a], 1.737[b]
p-Dibromobenzene			
r_{13}/r_{12}	1.997	2.000	2.000[c]
r_{14}/r_{12}	1.729	1.732	1.733[c]
Benzonitrile			
r_{13}/r_{12}	1.719	1.732	1.731[d], 1.724[e]
r_{14}/r_{12}	1.998	2.002	2.001[d], 1.999[e]
r_{15}/r_{12}	1.732	1.737	1.732[d], 1.728[e]
r_{23}/r_{12}	0.991	0.999	1.000[d], 0.997[e]
r_{24}/r_{12}	1.727	1.732	1.733[d], 1.735[e]
o-Dicyanobenzene			
r_{12}/r_{23}	1.010	1.001	1.003[f]
r_{13}/r_{23}	1.729	1.735	1.732[f]
r_{14}/r_{23}	1.972	2.008	1.995[f]
m-Dicyanobenzene			
r_{12}/r_{23}	1.733	1.735	1.73[f]
r_{13}/r_{23}	2.006	2.003	2.00[f]
r_{24}/r_{23}	1.728	1.732	1.73[f]
p-Dicyanobenzene			
r_{13}/r_{12}	1.998	2.002	1.999[f]
r_{14}/r_{12}	1.730	1.734	1.731[f]
1,4-Benzoquinone			
r_{13}/r_{12}	1.977	2.005	2.003[g]
r_{14}/r_{12}	1.706	1.737	1.736[g]

[a]Reference 19.
[b]Reference 20.
[c]Reference 21.
[d]Reference 22.
[e]Reference 23.
[f]Reference 24.
[g]Reference 25.

used, and these are listed in Table 2 for each of the systems studied. The values of B showed a small variation with temperature, with rms deviations from the mean value ranging from 1.3 to 9.3%. The largest value was for *p*-dibromobenzene in EBBA. It has been suggested that the temperature dependence of B can be attributed to the neglect of higher rank terms in the order potential, or to the biaxiality of the solvent molecules (9, 10). The short- and long-range interactions in the ordering potential may have different temperature coefficients (15), which could also contribute to the observed temperature dependence of B.

The average field gradient, F_{ZZ}, decreases with increasing temperature, and it seems reasonable to assume that it is proportional to the solvent order parameter, $S^{(1)}$. This assumption can be avoided if the data are compared at the same reduced temperatures used by Burnell and co-workers (16) to measure the field gradients, which would limit the fit to only two temperatures. In the study on dichlorobenzenes (2), it was shown that the conclusions were unchanged. The average electric field gradient in the host solvent is also assumed to be independent of the size of the solute molecule. Therefore, F_{ZZ}^0 in eqs. [5] and [6] can be taken to be constant for a given solvent. Based on the reported data on the two solvents (16), the F_{ZZ}^0 values were found to be 2.41×10^{18} and -2.62×10^{18} V m^{-2} for 1132 and EBBA, respectively. The direct calculation of A_{LR} and $(AB)_{LR}$, using eqs. [5] and [6], requires values for the molecular quadrupole moments, which, unfortunately, are not available for the compounds studied here. However, since A_L is a constant for a given solvent, the ratio $(A_L)^{1132}/(A_L)^{EBBA}$ is independent of the solute and the long-range interaction can be written as

$$[9] \qquad A_{LR}{}^{1132} = (A^{1132} - wA^{EBBA})/(1-wx)$$

where $w = A_L{}^{1132}/A_L{}^{EBBA}$, and the x is the ratio of the electric field gradients, $F_{ZZ}{}^{0,EBBA}/F_{ZZ}{}^{0,1132}$. Similar equations can be obtained for $A_{LR}{}^{EBBA}$ and the $(AB)_{LR}$ terms. The value of w can be derived in the cases where the molecular quadrupole moments of the solute molecules are known, and, using the results for benzene, trichlorobenzene, and tribromobenzene (8), an average value of 1.13 was obtained. The short-range contributions A_{SR} and $(AB)_{SR}$ can then be obtained by subtracting the corresponding long-range term from the experimental values. The values of A_{LR}, $(AB)_{LR}$, A_{SR}, and $(AB)_{SR}$ calculated in this way are listed in Table 2. The same short-range contributions can also be calculated directly by using eqs. [2]–[4], with the molecular dimensions and van der Waals radii (17). The required A_L values in the two solvents, 1132 and EBBA, are taken to be 3.40 and 3.02×10^{-11} J m^{-1} molecule^{-1}, respectively, from the dependence of A_{SR} on A[vdW], obtained from the results on benzene, tribromobenzene, and five chlorobenzenes (1, 2, 8). The A[vdW] values were calculated using eq. [2] and the values of $A_L A$[vdW] and B[vdW] were then combined with the long-range contributions, listed in Table 2, to yield A^{calc} $(=A_L A[\text{vdW}] + A_{LR})$, $(AB)^{calc}$ $(=A_L A[\text{vdW}]B[\text{vdW}] + (AB)_{LR})$, and B^{calc}, Table 3. These values were then used to calculate the order parameters S_{33} and S_{22}. The results are compared with the experimental values in Fig. 2 for the four cyanobenzenes. The average percent rms errors between the calculated and observed order parameters for each solvent–solute pair are also given in Table 3. It can be seen that, for the substituted benzenes in either solvent, an orientation potential based on the proposed short-and long-range interactions yields order parameters in reasonable agreement with the experimental values, the worst case being a total disagreement of 15% summed over all the experimental points.

The molecular quadrupole moments, which, by necessity, have become fitted parameters, are listed in Table 4. For all molecules described in these studies, except *p*-benzoquinone, the contribution of A_{LR} is less than 20% and, therefore, a 50% variation in the term $(Q_{33} - (Q_{11} + Q_{22})/2)$ would not change A^{cal} by more than 10%. On the other hand, $(AB)^{cal}$ would be more strongly affected by the uncertainty in the term $(Q_{11} - Q_{22})$. Therefore the values of the individual tensor components may not be very significant.

In our analysis of orientational potentials we have shown that the short-range interaction in solvent 1132 is stronger by about 10%, as reflected in the corresponding A_L values. However, the average orientation along the long molecular axis, S_{33}, under similar conditions, also depends upon the contributions from the long-range interactions. To illustrate this, the order parameters at room temperature for benzene, benzoquinone, and other mono- and disubstituted compounds are given in Table 5. The interaction between the electric field gradient and the molecular quadrupole moment makes its most important contribution not

TABLE 2. Experimental AND calculated potential energy parameters: Units are $\times 10^{-20}$ J molecule^{-1} for A, A_{LR}, $(AB)_{LR}$, A_{SR}, and $(AB)_{SR}$

Solvent/solute	A	B	A_{LR}	$(AB)_{LR}$	A_{SR}	$(AB)_{SR}$	B_{SR}
1132							
Benzonitrile	1.511	0.438	0.158	0.208	1.353	0.454	0.336
o-Dicyano	1.105	0.796	−0.073	0.124	1.178	0.756	0.642
m-Dicyano	1.537	0.511	0.088	0.149	1.449	0.636	0.439
p-Dicyano	2.145	0.271	−0.206	0.163	2.351	0.418	0.178
Bromobenzene	1.314	0.553	0.170	0.222	1.144	0.505	0.441
p-Dibromo	1.764	0.381	−0.007	0.228	1.771	0.444	0.251
p-Benzoquinone	0.844	0.780	−0.278	0.121	1.122	0.537	0.479
EBBA							
Benzonitrile	1.031	0.173	−0.172	−0.226	1.203	0.404	0.336
o-Dicyano	1.127	0.477	0.080	−0.134	1.047	0.672	0.642
m-Dicyano	1.193	0.340	−0.095	−0.162	1.288	0.566	0.439
p-Dicyano	2.314	0.084	0.224	−0.177	2.090	0.371	0.178
Bromobenzene	0.832	0.249	−0.185	−0.242	1.017	0.449	0.441
p-Dibromo	1.581	0.093	0.007	−0.248	1.574	0.394	0.251
p-Benzoquinone	1.299	0.280	0.302	−0.131	0.977	0.477	0.479

TABLE 3. Calculated potential energy parameters using molecular simensions and Van der Waals radii: Units are $\times 10^{-20}$ J molecule^{-1} for A^{cal}, and $(AB)^{cal}$, and $\times 10^{-10}$m for A[vdW]

						% rms error	
Solvent/solute	A[vdW]	B[vdW]	A^{cal}	$(AB)^{cal}$	B^{cal}	S_{33}	S_{22}
1132							
Benzonitrile	4.16	0.379	1.571	0.743	0.473	3.1	5.3
o-Dicyano	2.96	0.645	0.932	0.772	0.828	14.7	9.2
m-Dicyano	4.67	0.409	1.674	0.797	0.476	10.6	3.9
p-Dicyano	6.07	0.260	1.856	0.699	0.377	15.7	2.6
Bromobenzene	3.59	0.417	1.389	0.731	0.526	7.3	3.2
p-Dibromo	5.05	0.296	1.709	0.736	0.431	5.4	2.6
p-Benzoquinone	3.14	0.514	0.789	0.669	0.848	9.0	2.7
EBBA							
Benzonitrile	4.16	0.379	1.084	0.250	0.231	5.0	13.5
o-Dicyano	2.96	0.645	0.973	0.442	0.454	13.5	12.7
m-Dicyano	4.67	0.409	1.315	0.415	0.316	10.6	6.2
p-Dicyano	6.07	0.260	2.057	0.299	0.145	10.5	3.9
Bromobenzene	3.59	0.417	0.899	0.210	0.234	9.1	6.6
p-Dibromo	5.05	0.296	1.532	0.203	0.133	3.7	1.9
p-Benzoquinone	3.14	0.514	1.250	0.356	0.285	4.8	3.9

Can. J. Chem. Downloaded from www.nrcresearchpress.com by 88.85.125.76 on 09/07/12
For personal use only.

through the term A_{LR}, but through $(AB)_{LR}$, which has a positive value in 1132 but a negative value in EBBA for all the biaxial solutes studied so far (1, 2, 8). This explains the experimental result that higher B values, and, correspondingly, a larger difference in the order parameters along the molecular axes 1 and 2, i.e. $(S_{11} - S_{22})$, are always observed for 1132 and, therefore, the ring plane (see Fig. 1) is much better oriented along the liquid crystal director in this solvent than in EBBA. This may be an important factor in the choice of solvent when the anisotropic property of interest is more associated with the ring structure than with a particular substitution group, or vice versa (18).

Liquid crystal display devices may incorporate a pleochroic dye as a solute in order to improve the contrast properties of the display, or to add colours. Apart from the photochemical stability, absorption wavelength, etc., the "guest" molecule must have a high dichroic ratio, since the contrast between the on-and-off states of the display depends upon the difference between the absorption of light polarized parallel and perpendicular to the liquid crystal director. Two different types of guest molecule can be considered, either a long cylindrical

TABLE 4. Calculated molecular quadrupole moments, $\times 10^{-40}$ C m^2

Species	Q_{11}	Q_{22}	Q_{33}
Benzonitrile	12.87	−21.61	8.74
o-Dicyano	12.28	−8.23	−4.05
m-Dicyano	9.91	−14.76	4.85
p-Dicyano	19.24	−7.84	−11.40
Bromobenzene	13.74	−23.15	9.41
p-Dibromo	19.14	−18.77	−0.36
p-Benzoquinone	17.72	−2.35	−15.36

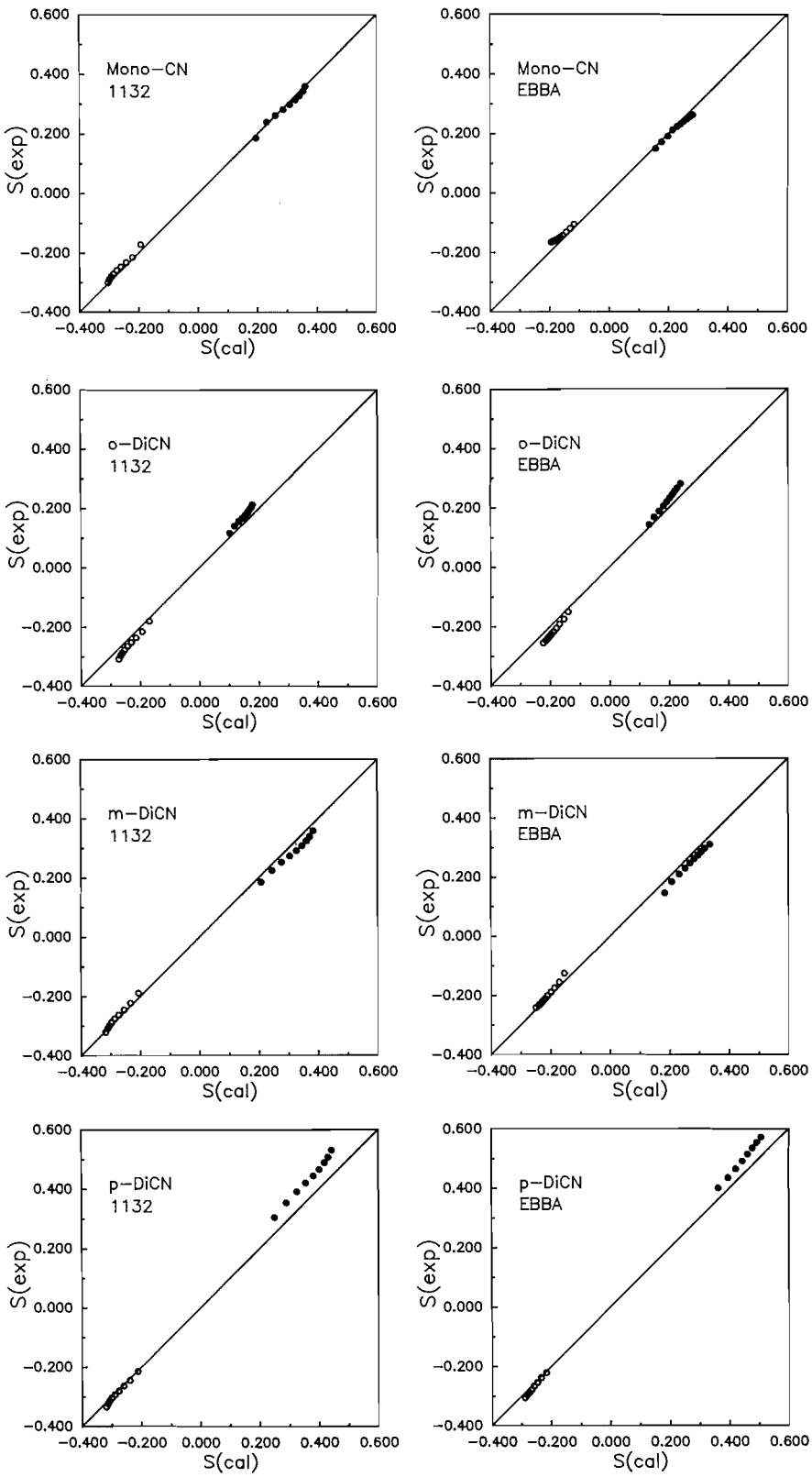

FIG. 2. Experimental versus calculated order parameters for cyanobenzenes. Filled circles are for S_{33} and empty circles for S_{22}.

shape (approximately) or a planar molecule, and two different electronic transitions, $\pi \rightarrow \pi^*$ or $n \rightarrow \pi^*$. Ideally, the transition moment should lie along, or very close to, the axis of highest orientation, but, for molecules with less than C_{2v} symmetry, the direction of the transition moment and the axis of principal orientation are not necessarily coincident.

The term A represents the difference in potential energy between orientations with the long molecular axis parallel and perpendicular to the liquid crystal axis, and, in order to achieve the highest orientation along this axis, A_{SR} and A_{LR} should be large. This requires that L_3 should be much greater than $(L_1 + L_2)$, that Q_{33} should be large and have the same sign as

Can. J. Chem. Downloaded from www.nrcresearchpress.com by 88.85.125.76 on 09/07/12
For personal use only.

TABLE 5. Order parameters of benzene, benzoquinone, and several chloro-, bromo-, and cyano-benzenes at room temperature

Solute	1132		EBBA	
	S_{33}	$S_{11} - S_{22}$	S_{33}	$S_{11} - S_{22}$
Benzene	0.132	0.397	0.059	0.176
p-Benzoquinone	0.166	0.350	0.337	0.146
Monochloro	0.265	0.319	0.208	0.099
o-Dichloro	0.217	0.401	0.159	0.191
m-Dichloro	0.243	0.364	0.221	0.143
p-Dichloro	0.369	0.265	0.419	0.053
Monobromo	0.299	0.294	0.210	0.095
p-Dibromo	0.434	0.212	0.425	0.040
Benzonitrile	0.359	0.243	0.262	0.069
o-Dicyano	0.214	0.402	0.281	0.228
m-Dicyano	0.359	0.283	0.310	0.175
p-Dicyano	0.531	0.138	0.572	0.040

the electric field gradient, and that either Q_{11} or Q_{22} should have the opposite sign. (AB) describes the potential energy difference between the alignment of axis-1 and axis-2 parallel to the liquid crystal director and in planar molecules, this term should be large in order to orient the plane of the molecule (rather than the longest axis) parallel to the liquid crystal axis. In this case L_1 should be greater than L_2, which is normal for planar aromatics, since L_2 is always the shortest dimension and is approximately constant at the thickness of the ring. To maximize the long-range term in the potential, Q_{11} should have the same sign as F_{zz} and be greater than Q_{22}. The component of the quadrupole moment perpendicular to the ring, Q_{22}, is usually negative, while Q_{11} is positive, and, therefore, $(Q_{11} - Q_{22})$ is always positive. In a solvent with a field gradient of opposite sign, as in EBBA, the $(AB)_{LR}$ term would have a negative sign resulting in a diminished orientational potential.

In designing suitable guest molecules it is unfortunate that the molecular quadrupole moment data are not easily available. It is clear, however, that the choice of solvent is important since the orientation of the molecular plane can, in some cases, be enhanced at the expense of the longer molecular axis by choosing a solvent with an electric field gradient of opposite sign to the A_{LR} parameter, leading to improved contrast for displays based on $n \rightarrow \pi^*$ transitions.

Acknowledgements

This work was supported by grants from F.C.A.R. (Quebec) (C.T.Y.) and from N.S.E.R.C. (D.F.R.G.). We are grateful to Professor E. E. Burnell for communicating his results prior to publication.

1. C. T. YIM AND D. F. R. Gilson. Can. J. Chem. **65**, 2513 (1987).
2. C. T. YIM AND D. F. R. Gilson. Can. J. Chem. **67**, 54 (1989).
3. E. E. BURNELL, C. A. DE LANGE, AND J. G. Snijders. Phys. Rev. A. **25**, 2339 (1982).
4. E. E. BURNELL, A. J. VAN DER EST, G. N. PATEY, C. A. DE LANGE, AND J. G. Snijders. Bull. Magn. Res. **9**, 4 (1987).
5. C. A. DE LANGE, J. G. SNIJDERS, AND E. E. Burnell. *In* Nuclear magnetic resonance of liquid crystals. *Edited by* J. W. Emsley. Reidel Publishing Co., Dordrecht. 1985. Chap. 8.
6. A. J. VAN DER EST, M. Y. KOK, AND E. E. Burnell. Mol. Phys. **60**, 397 (1987).
7. M. KELLERHALS AND P. Diehl. Mol. Cryst. Liq. Cryst. **174**, 127 (1989).
8. C. T. YIM AND D. F. R. Gilson. Can. J. Chem. **66**, 1749 (1988).
9. J. W. EMSLEY, R. HASHIM, G. R. LUCKHURST, AND G. N. Shilstone. Liq. Cryst. **1**, 437 (1986).
10. J. W. EMSLEY, G. R. LUCKHURST, G. N. SHILSTONE, AND I. Sage. J. Chem. Soc. Faraday Trans. 2, **83**, 371 (1987).
11. B. W. VAN DER MEER AND G. Vertogen. Phys. Lett. A. **59**, 279 (1976).
12. B. BAHADUR AND S. Chandra. J. Phys. C: Solid State Phys. **9**, 5 (1976).
13. B. BAHADUR, R. K. SARNA, AND V. G. Bhide. Mol. Cryst. Liq. Cryst. **72**, 139 (1982); B. BAHADUR, R. K. SARNA, AND V. G. Bhide. Mol. Cryst. Liq. Cryst. **82**, 183 (1982).
14. B. KRONBERG, D. F. R. GILSON, AND D. D. Patterson. J. Chem. Soc. Faraday Trans. 2, **72**, 1673 (1976).
15. A. WEAVER, A. J. VAN DER EST, J. C. T. RENDELL, G. L. HOATSON, G. S. BATES, AND E. E. Burnell. Liq. Cryst. **2**, 633 (1987).
16. G. N. PATEY, E. E. BURNELL, J. G. SNIJDERS, AND C. A. de Lange. Chem. Phys. Lett. **99**, 271 (1983).
17. A. BONDI. J. Phys. Chem. **68**, 441 (1964).
18. M. A. OSMAN, L. PIETRONERO, T. J. SCHEFFER, AND H. R. Zeller. J. Chem. Phys. **74**, 5377 (1981).
19. J. P. JACOBSEN AND K. Schaumburg. J. Mag. Reson. **28**, 1 (1977).
20. J. JOKISAARI AND T. Vaananen. J. Mag. Reson. **45**, 379 (1981).
21. E. E. BURNELL AND M. A. J. Sweeney. Can. J. Chem. **52**, 3565 (1974).
22. J. P. JACOBSEN AND K. Schaumburg. Mol. Phys. **28**, 1505 (1974).
23. P. DIEHL, J. AMREIN, AND C. A. Veracini. Org. Mag. Reson. **20**, 276 (1982).
24. W. DE KIEVIET AND C. A. de Lange. Chem. Phys. Lett. **22**, 378 (1973).
25. T. C. WONG AND E. E. Burnell. J. Mol. Struct. **33**, 217 (1976).

Can. J. Chem. Downloaded from www.nrcresearchpress.com by 88.85.125.76 on 09/07/12
For personal use only.

A chemiluminescence study of the kinetics of reactions of Cr(III) with carboxylate ligands: oxalate, salicylate, and humic acid

DOUGLAS L. HUIZENGA[1] AND HOWARD H. PATTERSON
Department of Chemistry, University of Maine, Orono, ME 04469, USA
Received April 7, 1989[2]

DOUGLAS L. HUIZENGA and HOWARD H. PATTERSON. Can. J. Chem. **68**, 881 (1990).

The reaction of Cr(III) with chelate-forming carboxylate ligands can be monitored at the low ligand concentrations typical of natural waters by chemiluminescence analysis of unreacted Cr(III). This technique is utilized here for the measurement of Cr(III) reaction kinetics with oxalate, salicylate, and humic acid over a wider ligand concentration range than previously reported. Variation of the pH and ligand concentrations allowd the determination of rates of reaction by three pathways with different pH dependencies. The magnitude of rate constants of these pathways for Cr(III) with inorganic (Cl^-, SCN^-) and carboxylate ligands gives insight into the reaction pathways for the environmentally important ligand humic acid.

Key words: Cr(III), oxalate, salicylate, humic acid.

DOUGLAS L. HUIZENGA et HOWARD H. PATTERSON. Can. J. Chem. **68**, 881 (1990).

Faisant appel à des analyses de chimiluminescence du Cr(III) qui n'a pas réagi, on peut suivre l'évolution de la réaction du Cr(III) avec des ligands carboxylates pouvant former des chélates à de faibles concentrations de ligand types de celles qui existent dans les eaux naturelles. On a utilisé cette technique pour la mesure de cinétriques de réactions du Cr(III) avec les acides oxalique, salicylique et humique, sur des écarts de concentration beaucoup plus grands que ceux rapportés antérieurement. En faisant varier le pH et les concentrations de ligand, on a pu déterminer que, suivant le pH, il existe trois voies réactionnelles différentes. L'amplitude des constantes de vitesse des réactions du Cr(III) avec des ligands inorganiques (Cl^-, SCN^-) et carboxyliques permet de comprendre les voies réactionnelles du ligand, acide humique, qui est important d'un point de vue environnemental.

Mot clés : Cr(III), oxalate, salicylate, acide humique.

[Traduit par la revue]

Introduction

Knowledge of both the rate of conversion of aquated Cr(III) to bound forms and the ultimate equilibrium speciation of Cr(III) are important in predicting its biogeochemical behavior in natural waters. In general, the reaction kinetics of Cr(III) are dominated by the slow exchange of water molecules from the inner coordination sphere. The rates of reaction of Cr(III) with inorganic ligands such as Cl^- and SCN^- have been extensively studied either directly or indirectly by combination of aquation rate and equilibrium measurements and the results have been systematically compared (1). In contrast, the rates of reaction of Cr(III) with carboxylate ligands and humic materials have been little studied. The few studies available for carboxylate ligands have been conducted under acid conditions and at high ligand concentrations (2).

The rates of reaction of Cr(III) with carboxylate ligands at the low concentrations typical of dissolved organic matter in natural waters (about 10^{-5} M) have not been reported. At such low concentrations, the rate of reaction should become dependent upon the ligand concentration. We have used chemiluminescence analysis to monitor rates of reaction of Cr(III) with the carboxylate ligands oxalate, salicylate, and humic acid over a wide range of ligand concentrations (10^{-2} to 10^{-5} M). The technique involves the oxidation of luminol by hydrogen peroxide in the presence of unbound Cr(III) to yield a product which luminesces (3). The intensity of luminescence is proportional to the unreacted Cr(III) concentration. Because of its high sensitivity, chemiluminescence analysis is well suited to kinetic studies of Cr(III) reacting with carboxylate and humic ligands at low concentrations.

Methods

Monitoring of Cr(III) reaction rates was performed by the technique of chemiluminescence analysis as described in Huizenga and Patterson (3). Reagent grade chemicals were used for this work except for the humic acid. The water was distilled and passed through an organic absorbent followed by a mixed bed chelating resin. The ionic strength of test solutions was maintained at 0.10 by mixing of 0.1 M KNO_3 with 0.1 ionic strength ligand stock solutions. The 0.1 M KNO_3 medium was acidified to pH 3.5 by addition of nitric acid and purged with nitrogen prior to preparation of samples in order to remove traces of carbon dioxide.

The salicylate stock solution was prepared by neutralization of salicylic acid with KOH. The solution was adjusted to pH 4 and purged with nitrogen. The oxalate stock was prepared from $Na_2C_2O_4$ to be 0.0333 M. The humic acid stock solution was prepared from the sodium salt of humic acid (Aldrich) at 20 g/L. Samples prepared with humic acid were adjusted to pH 3.5 and purged with nitrogen prior to adjustment to the test pH. The chromium(III) stock solution was prepared from $Cr(NO_3)_3 \cdot 9H_2O$ to give 0.01 M Cr(III). Nitric acid (0.01 M) was added to the Cr(III) stock to suppress formation of polymeric species.

A temperature of 25.0°C was maintained with a circulating water bath for all reactions and pH measurements. The measurement of pH was performed with a combination pH electrode and digital pH meter. Dilute NBS pH buffers were prepared according to Bates (4). The electrodes were standardized several times a day with a single buffer, the 0.05 molal phthalate buffer (pH_{NBS} = 4.008 at 25.0°C). Care was taken to prevent transfer of phthalate into sample solutions. Periodically a second buffer was used, the 1:3.5 phosphate buffer (pH_{NBS} = 7.413 at 25.0°C). Titrations of standardized 0.1 M HNO_3 into 0.1 M KNO_3 were performed in order to calibrate the electrodes in terms of hydrogen ion concentration. Comparison of these two hydrogen ion scales yielded the relationship:

$$[1] \quad -\log [H^+] = pH_{NBS} - 0.114$$

This relationship is dependent upon the specific electrodes used for the measurements. All results are reported here on the hydrogen ion

[1]Present address: Department of Physical Sciences, Rhode Island College, Providence, RI 02908 (USA)

[2]Revision received October 10, 1989.

Printed in Canada / Imprimé au Canada

Can. J. Chem. Downloaded from www.nrcresearchpress.com by 88.85.125.76 on 09/07/12
For personal use only.

TABLE 1. Equilibrium constants used for calculations (7, 8)

β_1^*	$= [CrOH^{2+}][H^+] / [Cr^{3+}]$	9.55×10^{-5}
β_2^*	$= [Cr(OH)_2^+][H^+] / [Cr^{3+}]$	4.79×10^{-11}
ox^{K_2}	$= [H^+][C_2O_2^{2-}] / [C_2O_2H^-]$	1.55×10^{-4}
sa^{K_1}	$= [H^+][C_6H_4(OH)CO_2^-] / [C_6H_4(OH)CO_2H]$	1.55×10^{-3}

concentration scale. Conversion between the hydrogen ion concentration and NBS activity scales can be made with the above relationship.

Reactions were initiated by addition of Cr(III) solution into the reaction medium containing ligand to give 10^{-6} M Cr(III). The reacting solutions were maintained at 25.0°C and pH measurements were performed just after the Cr(III) addition and after the final analysis of the sample. The pH was continuously monitored during rapid reactions (high pH reactions). A single standard for the chemiluminescence measurements was prepared just prior to use to be 10^{-6} M Cr(III) in 0.1 M KNO_3 acidified with 1.6×10^{-4} M KNO_3. The standard was run after every four to five samples. Rapid reactions were followed continuously with the standard run before and after the reaction. Rapid reactions were run in 500 mL polyethylene bottles and inserted into a jacketed beaker temperature controlled by a circulating water bath. Slower reactions were run in 250 mL polyethylene bottles which were suspended in the thermostated water bath between measurements.

The ionic strength was maintained at 0.10 M and the temperature at 25.0°C for the reaction of chromium with the various ligands. Only data with the degree of reaction less than 50% were used for the calculation of the pseudo-first order rate constants for oxalate and salicylate reactions. The pseudo-first order rate constants were calculated from the slope of the plot of log [unreacted Cr(III)] versus time.

Results and discussion

Rate of reaction of Cr(III) with oxalate

The pseudo-first order rate constants for reaction of 10^{-6} M Cr(III) with oxalate at concentrations between 4×10^{-5} and 1×10^{-2} M were determined over the pH range 3.5 to 7. The rate of disappearance of unreacted Cr(III) in terms of the pseudo-first order rate constant, k_{obs}, is given by:

$$[2] \quad \text{Rate} = k_{obs}[\text{unreacted Cr(III)}]$$

The observed pseudo-first order rate constant varies with pH and oxalate concentration (see Fig. 1). At low oxalate concentration and a fixed pH, the k_{obs} is proportional to the ligand concentration, so second order kinetics are observed. At low pH and high oxalate concentration, the k_{obs} approaches a limiting value, indicating limiting first order kinetics. At high pH and oxalate concentrations up to 0.01 M, limiting kinetics are not observed. At low pH, the slope of log k_{obs} against pH for any given oxalate concentrations approaches one. This indicates the importance of a reaction path through an activated complex containing a hydroxide ion.

The rate of disappearance of total Cr(III) by pathways with different hydrogen ion dependencies under conditions where second order kinetics are observed is given by:

$$[3] \quad \text{Rate} = (k_0 + k_1[H^+]^{-1} + k_2[H^+]^{-2})[Cr^{3+}][L]$$

where L represents the fully dissociated ligand, the k_n values represent the reaction rate constants for the various reaction pathways. The term in parentheses is the observed second-order rate constant, k, and the three terms describe its pH variation for the following reactions in which outer-sphere complexes react to give inner-sphere complexes:

$$[4a] \quad Cr(H_2O)_6,L \xrightarrow{k_0} Cr(H_2O)_5L + H_2O$$

$$[4b] \quad Cr(OH)(H_2O)_5,L \xrightarrow{k_1} Cr(OH)(H_2O)_4L + H_2O$$

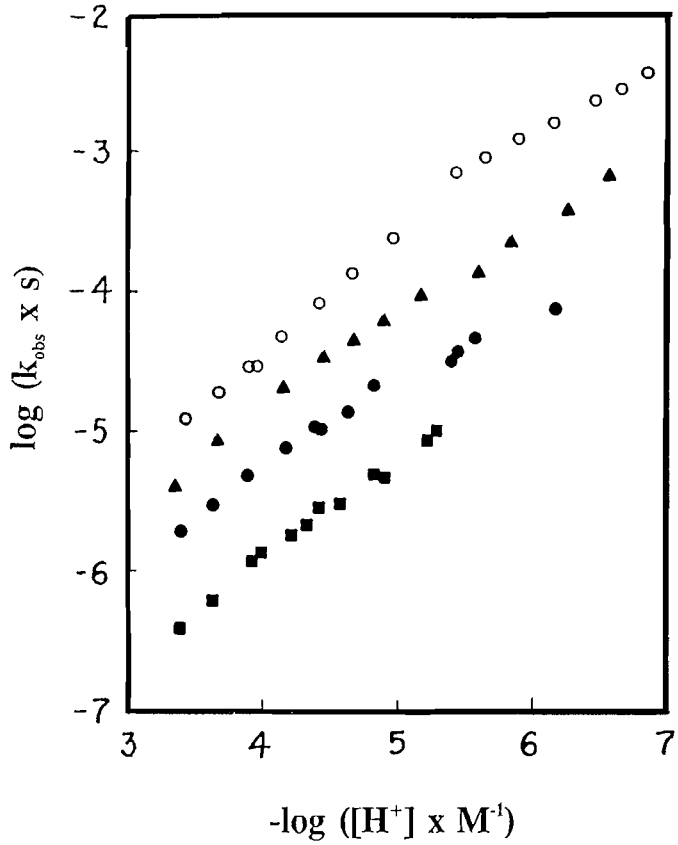

FIG. 1. Variation in the log of the observed pseudo-first order rate constant k_{obs} with pH for the reaction of 10^{-6} M Cr(III) with varying concentrations of oxalate: ■ 4×10^{-5} M oxalate; ● 1.7×10^{-4} M oxalate; ▲ 10^{-3} M oxalate; and ○ 10^{-2} M oxalate.

$$[4c] \quad Cr(OH)_2(H_2O)_4,L \xrightarrow{k_2} Cr(OH)_2(H_2O)_3L + H_2O$$

The inner-sphere complexes shown would be the initial reaction products. Addition of the ligand into the inner-sphere will render the Cr(III) more labile toward further reaction to form multi-ligand species. The observed pseudo-first order rate constant, k_{obs}, can be converted into the second order rate constant, k, as follows:

$$[5] \quad k = k_{obs}(1 + \beta_1^*[H^+]^{-1} + \beta_2^*[H^+]^{-2})/[L]$$

where the stability constants β_1^* and β_2^* describe the hydrolysis equilibria of Cr(III) and are defined in Table 1.

The second-order rate constant, k, was calculated from eq. [5] for the rate data obtained at low oxalate concentrations (see Fig. 2). The concentration of the fully dissociated oxalate was used for the ligand concentration. The value used for the second acid dissociation constant of oxalate for these calculations is listed in Table 1. Toward pH 7 the slope of the curve was two indicating that the predominant reaction has an activated complex containing two hydroxide ions. At pH 4.2 the slope was one, indicating reaction predominantly by a pathway with an activated complex that contains one hydroxide ion. The slope of the line at pH 3.5 was less than one, indicating the presence of an acid independent pathway. These data were modeled with the following equation:

$$[6] \quad k = k_0 + k_1[H^+]^{-1} + k_2[H^+]^{-2}$$

and the results are reported in Table 2.

Can. J. Chem. Downloaded from www.nrcresearchpress.com by 88.85.125.76 on 09/07/12
For personal use only.

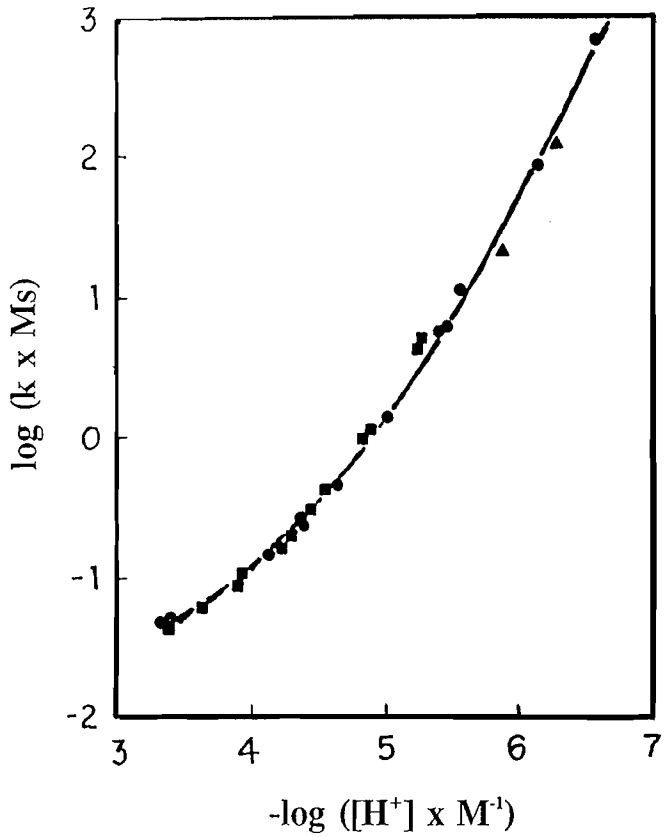

FIG. 2. Variation in the log of the second order rate constant k as a function of pH for the reaction between Cr(III) and oxalate: ■ 4×10^{-5} M oxalate; ● 1.7×10^{-4} M oxalate; and ▲ 10^{-3} M oxalate (pH > 5.8). The solid line represents the model fit with log $k_0 = -1.60$, log $k_1 = -5.05$, and log $k_2 = -10.35$.

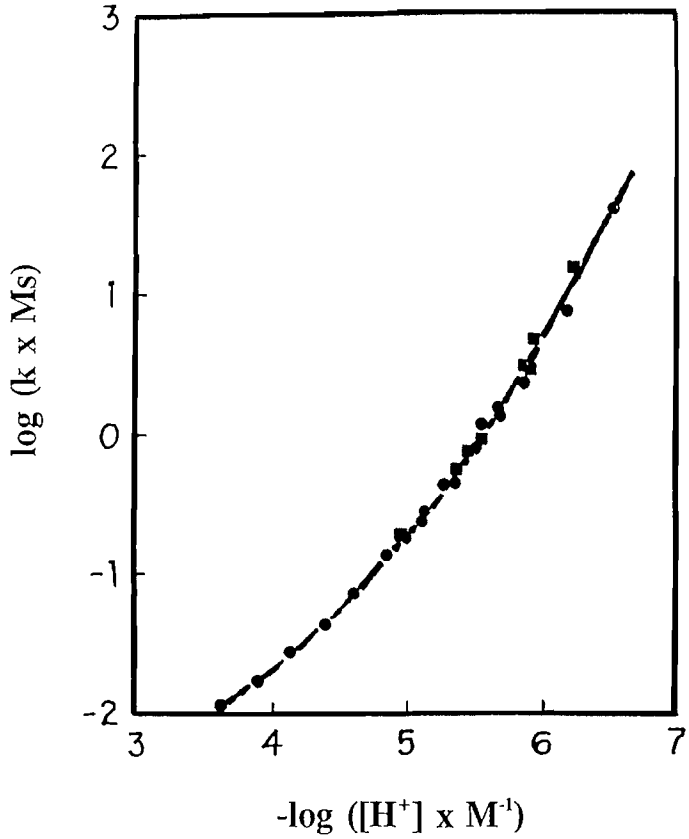

FIG. 3. Variation in the log of the second order rate constant k as a function of pH for the reaction between Cr(III) and salicylate: ● 5×10^{-4} M salicylate; and ■ 10^{-3} M salicylate. The solid line represents the model fit with log $k_0 = -2.32$, log $k_1 = -5.82$, and log $k_2 = -11.48$.

TABLE 2. Second order rate constants for reaction of Cr(III) with various ligands at an ionic strength of 0.1

Ligand	log k_0	log k_1	log k_2	Source
Oxalate	−1.60	−5.04	−10.35	This work
Salicylate	−2.32	−5.82	−11.48	This work
Humic acid	—	−5.15	−9.03	This work
Cl^-	−7.52[a]	−8.66[a]	—	Reference 1
SCN^-[6]	−5.50	−7.88	−11.38[a]	Reference 9

[a]Rate corrected to I = 0.1 according to ref. 5, p. 106.

Rate of reaction of Cr(III) with salicylate

The pseudo-first order rate constants for the reaction of 10^{-6} M Cr(III) with salicylate was measured at concentrations of 5×10^{-4} to 1×10^{-2} over the pH range 3.5 to 7. All other experimental conditions were the same as for the oxalate reactions. The variation in the observed pseudo-first order rate constant is qualitatively similar to that observed for oxalate. For a given pH and ligand concentration, however, the rate of reaction is higher for oxalate than for salicylate, especially at lower ligand concentrations. The variation in the second order rate constant k with pH is shown in Fig. 3. The data were modeled and the resulting k_i values reported in Table 2.

Limiting behavior for reaction of Cr(III)

At higher concentrations of oxalate and salicylate, the rate of reaction of Cr(III) with a ligand approaches a limiting rate. There are two general models for describing this limiting behavior. In the first model, formation of an outer-sphere complex between Cr(III) and the ligand precedes the reaction to give the inner-sphere complex. In this case, the limiting behavior would result from nearly total association of the Cr(III) with ligand and movement of the ligand into the inner-sphere upon loss of a water molecule from the inner-sphere. The second model assumes that one water molecule has been lost from the inner-coordination sphere of the Cr(III) and that water and ligand molecules compete for the open inner-sphere position. With this model, as the concentration of ligand is increased, a concentration will be reached where the ligand out competes water molecules for the vacancy in the inner-sphere and the maximum rate of reaction will be obtained. The two models are generally experimentally indistinguishable and lead to the same functional relationship (5):

$$[7] \quad k_{obs}^{-1} = a[L]^{-1} + b$$

where [L] represents the concentration of fully dissociated ligand. The mechanistic significance of the constants a and b differ for the two models. For a fixed pH, the fraction of the ligand that is not protonated is constant and the total ligand concentration may be substituted without altering the form of the equation.

The oxalate data were plotted to examine the limiting behavior of the reaction between Cr(III) and oxalate for two fixed pH values (Fig. 4). The relationship is not linear; the highest concentration data point (lowest [salicylate]$^{-1}$) at both pHs falls below the line fitting the rest of the data. This more

Can. J. Chem. Downloaded from www.nrcresearchpress.com by 88.85.125.76 on 09/07/12
For personal use only.

Can. J. Chem. Downloaded from www.nrcresearchpress.com by 88.85.125.76 on 09/07/12
For personal use only.

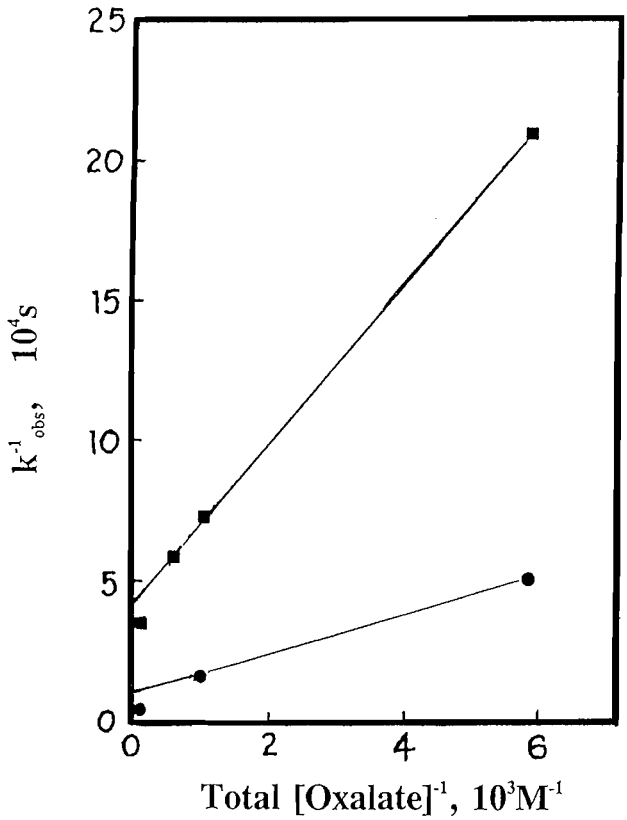

FIG. 4. Limiting behavior of k_{obs} for the reaction of 10^{-6} M Cr(III) with varying concentrations of oxalate for pH 3.9 (■) and pH 4.9 (●).

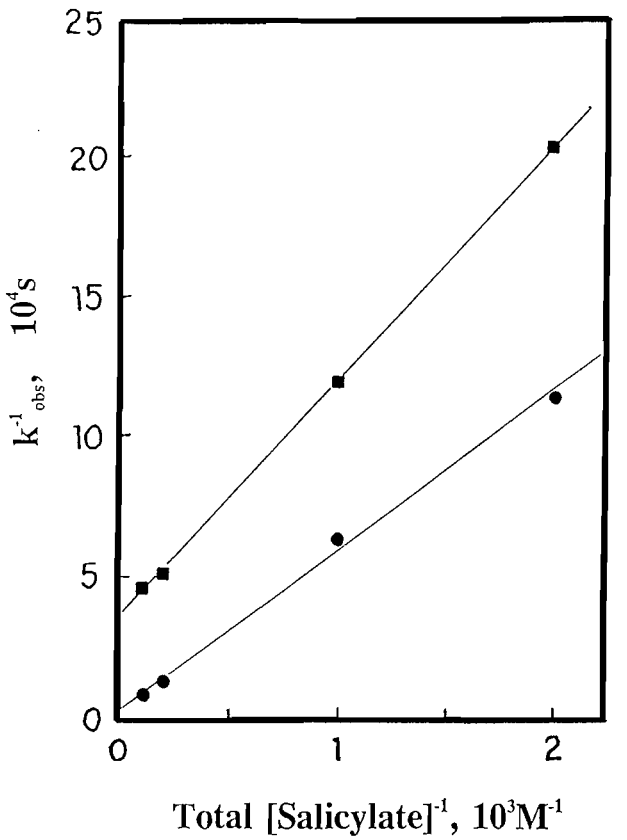

FIG. 5. Limiting behavior of k_{obs} for the reaction of 10^{-6} M Cr(III) with varying concentrations of salicylate for pH 4.0 (■) and pH 5.0 (●).

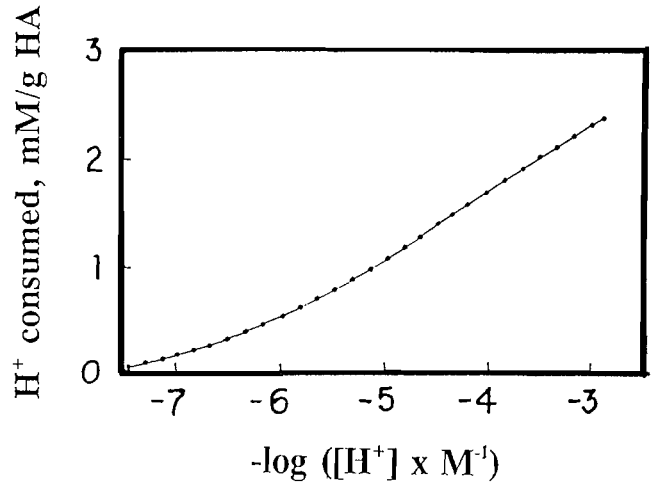

FIG. 6. Consumption of protons during acid titration of 240 mg/L humic acid. The solid line represents the modified Henderson-Hasselbach model of the data.

complicated relationship could be due to association between Cr(III) ion and more than one oxalate molecule at the same time.

A similar examination of the salicylate data for the simple limiting model does show a linear relationship (Fig. 5). The stronger electrostatic interaction between oxalate and Cr(III) may lead to more complicated limiting behavior near 0.01 M oxalate where oxalate makes up a significant portion of the total ionic strength of the test solutions. It is possible that salicylate would show the same type of behavior at higher concentrations (>0.01 M), especially considering that the final limiting rates for the two ligands are expected to be the same (6).

Rates of reaction of Cr(III) with humic acid

The pseudo-first order rate constant for reaction of Cr(III) with humic acid was determined for concentrations of 1, 5, and 25 mg/L humic acid in 0.1 M KNO_3 over the pH range 3.5 to 7. Because of non-linearity of plots of log [Cr(III)] versus time for the reaction of Cr(III) with humic acid, initial reaction rates were utilized. We have previously shown that the non-linearity is not related to the relative concentrations of different reaction sites on the humic acid (3). However, the non-linear first order behavior could be accounted for by the simultaneous formation of chelated and non-chelated bound Cr(III). Non-chelated bound Cr(III) gives the same response with the chemiluminescence technique as unbound Cr(III) (3). The initial rate method will provide the best estimate of the rate of reaction of Cr(III) with humic acid to form chelated complexes.

The observed first-order rate constant varies with humic acid concentration and pH. The k_{obs} at a fixed pH is proportional to the concentration of humic acid. No tendency toward limiting first-order kinetics is observed for humic acid concentrations up to 25 mg/L.

In order to compare the reaction rate data for humic acid with that observed for oxalate and salicylate, the protonation behavior of the humic acid must be known. The acid titration curve of 240 mg/L humic acid in 0.1 M KNO_3 is shown in Fig. 6. The data can be modeled with the modified Henderson–Hasselbach equation:

$$[8] \quad pH = pK_a + n \log ([A]/[HA])$$

Simple acid dissociation has an n value of 1 in this equation. Because of its polymeric nature and chemical differences in the functional group environments, humic acid generally shows n

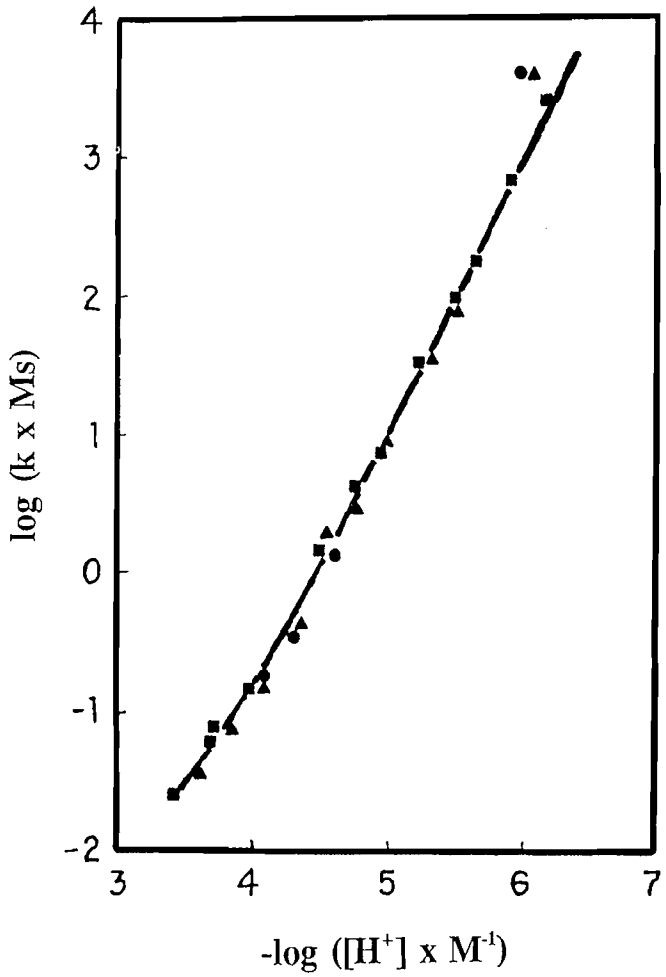

FIG. 7. Variation in the log of the second order rate constant k with pH for the reaction of Cr(III) with humic acid: ● 1 mg/L humic acid; ▲ 5 mg/L humic acid; and ■ 25 mg/L humic acid.

values of about 2.5. Non-linear least-squares modeling of the titration data yielded $pK_a = 4.30 \pm 0.02$ (standard error), $n = 3.22 \pm 0.03$, and 3.71 ± 0.03 millimolar carboxylate/(g humic acid).

The protonation model (eq. 6) was used to calculate the concentration of dissociated carboxylic functional groups as a function of pH. The rate data for reaction of Cr(III) with humic acid were plotted as the calculated second-order rate constant against pH (see Fig. 7). These data were then modeled with eq. [6] and the k_i values for the different pathways are presented in Table 2. The slope of the curve near pH 3.5 is not less than one as was observed for oxalate and salicylate. Consequently, the pathway which is zero order in $[H^+]$ does not appear to be important in the experimental pH range and has been omitted from the model.

The second-order rate constant for humic acid is similar to that for oxalate at low pH values; the k_1 of the humic acid is similar to the k_1 for oxalate. At higher pH where an inverse second order dependency on hydrogen ion is observed, the k_2 for humic acid is much greater than that of either oxalate or salicylate. Calculation of the second order rate constant for humic acid simply on the basis of its dissociated carboxylate functional groups does not adequately describe its reactivity with Cr(III).

The absence of limiting first-order kinetics for the reaction of Cr(III) with humic acid is due to the low concentration of functional groups. At the highest concentration of humic acid studied, 25 mg/L, the total concentration of carboxylate groups is only 9×10^{-5} M. Oxalate and salicylate both show simple second-order kinetics at such low concentrations.

Comparison of reaction rates for carboxylate and inorganic ligands

The nature of the reaction of Cr(III) with carboxylate ligands differs greatly from that with simple inorganic ligands. Carboxylate ligands show limiting first-order behavior while the inorganic ligands do not. The electrostatic interactions that would lead to formation of outer-sphere ion pairs for both types of ligands should be approximately the same. Comparison of k_1 values for Cr(III) with two inorganic ligands of the same charge type, CL^- and SCN^-, shows large differences for the various reaction pathways. The k_0 values for the inorganic ligands are 3 to 5 orders of magnitude lower than for salicylate. The k_1 values for the inorganic ligands are 2 to 3 orders of magnitude lower than for salicylate. The k_2 values, however, are similar. The differences in the kinetic behavior between the two types of ligands decreases as the number of hydroxide ions in the activated complex increases. This correlates with a decrease in electrostatic interaction between the ligand and the chromium species.

The two simple carboxylate ligands differ from each other due to charge differences. For all three pathways, oxalate (charge −2) reacts almost one order of magnitude faster than salicylate (charge −1).

Conclusion

The carboxylate ligands, oxalate, salicylate, and humic acid, showed second-order rate laws at low ligand concentrations ($<10^{-3}$ M). These data can be used to predict the rate of conversion of Cr(III) to chelate bound forms under environmental conditions. Conversion of Cr(III) to bound forms may affect its biogeochemical behavior in natural waters. The initial product formed with a single ligand per metal ion will likely react further with other ligands as the system moves toward equilibrium.

Acknowledgements

This research was financed in part by the United States Department of the Interior as authorized by the Water Research and Development Act of 1978 (P.L. 95–467). A fellowship from the INRS-Eau of the Université du Québec aided D.L.H. in the completion of this manuscript.

1. J. H. ESPENSON. Inorg. Chem. **8**, 1554 (1969).
2. R. E. HAMM and R. E. DAVIS. J. Am. Chem. Soc. **75**, 3085 (1953).
3. D. L. HUIZENGA and H. H. PATTERSON. Anal. Chim. Acta, **206**, 263 (1988).
4. R. G. BATES. The determination of pH. Wiley, New York, NY. 1973.
5. R. G. WILKINS. The study of kinetics and mechanisms of reaction of transition metal complexes. Allyn and Bacon, Boston, MA. 1974.
6. R. E. HAMM, R. L. JOHNSON, R. H. PERKINS, and R. E. DAVIS. J. Am. Chem. Soc. **80**, 4469 (1958).
7. A. E. MARTELL and R. M. SMITH. Critical stability constants. Vol. 4. Plenum, New York, NY. 1976.
8. MARTELL and R. M. SMITH. Critical stability constants. Vol. 5. Plenum, New York, NY. 1982.
9. C. POSTMUS and E. L. KING. J. Phys. Chem. **59**, 1216 (1955).

Can. J. Chem. Downloaded from www.nrcresearchpress.com by 88.85.125.76 on 09/07/12
For personal use only.

Enzymatically catalysed decarboxylation of β-carboxyaspartic acid (Asa)

ROBERT G. ANNETT,[1] VANITA M. HASSAMAL, ANNETTE M. FISHPOOL, PANADDA KOSAKARN, ALLEN CASSAMALLI, AND E. TRACEY ALLINSON

Department of Chemistry, Trent University, Peterborough, Ont., Canada K9J 7B8

Received December 7, 1989

ROBERT G. ANNETT, VANITA M. HASSAMAL, ANNETTE M. FISHPOOL, PANADDA KOSAKARN, ALLEN CASSAMALLI, and E. TRACEY ALLINSON. Can. J. Chem. **68**, 886 (1990).

A better synthetic route to β-carboxyaspartic acid (Asa) was achieved through condensation of sodium dibenzyl malonate and benzyl 2-bromoacetate as an alternative to two steps in the method of Koch *et al.* Catalytic hydrogenation at 5 atm pressure in a shaken stainless steel vessel removed protecting carbobenzyloxy groups. Asa was purified on a cation exchange column. An extract of *E. coli* was found to catalyse the decarboxylation of Asa in a doubly coupled assay designed to be specific for produced aspartic acid. Evidence for enzymatic decarboxylation includes complete loss of activity on boiling and progressive loss of activity on repeated freeze–thawing of the extract.

Key words: decarboxylation, β-carboxyaspartic acid, Asa decarboxylase.

ROBERT G. ANNETT, VANITA M. HASSAMAL, ANNETTE M. FISHPOOL, PANADDA KOSAKARN, ALLEN CASSAMALLI et E. TRACEY ALLINSON. Can. J. Chem. **68**, 886 (1990).

On a développé une meilleure méthode de synthèse de l'acide β-carboxyaspartique (Asa) qui fait appel à une condensation du sel de sodium du malonate de dibenzyle avec le 2-bromoacétate de benzyle, à la place de deux étapes de la méthode de Koch et ses collaborateurs. Pour éliminer les groupements protecteurs carbobenzyloxy, on a effectué une hydrogénation catalytique, à une pression de 5 atmosphères, dans des contenants en acier inoxydable qui étaient agités. On a purifié l'Asa par un échange cationique sur colonne. Lors d'essais doublement couplés effectués dans le but spécifique d'évaluer l'acide aspartique produit, on a trouvé qu'un extrait d'*E. coli* catalyse la décarboxylation de l'Asa. Parmi les données suggérant l'existence du décarboxylation enzymatique, on doit mentionner la perte totale d'activité qui est observée lorsqu'on fait bouillir l'extrait ainsi que la perte progressive de son activité lorsqu'on le soumet d'une façon répétée à des congélations suivies de périodes de réchauffement.

Mots clés : décarboxylation, l'acide β-carboxyaspartique, Asa-décarboxylase.

[Traduit par la revue]

Can. J. Chem. Downloaded from www.nrcresearchpress.com by 88.85.125.76 on 09/07/12
For personal use only.

Introduction

Discovery of the carboxylated amino acids, aminomalonic acid (Ama),[2] γ-carboxyglutamic acid (Gla), and Asa in various tissues including atherosclerotic plaque (1), osteocalcin (2), and *E. coli* ribosomal proteins (3) has generated considerable interest in their synthesis and properties. Several methods for racemic Asa (3–5) and one for D-β-Asa (6) have been reported. All prescribe millimolar quantities, with suggestions for scaling up offered in one procedure (4).

Carboxylations of the amino acids are thought to take place post-translationally and, in the case of Gla, a Vitamin K-dependent carboxylase has been characterized (7). The kinetics of thermal decarboxylation of the three synthetically prepared carboxy amino acids have been compared (8). Enzymes catalysing the decarboxylation of Ama have been described (9, 10). We wish to report the demonstration of Asa decarboxylase activity in an extract of *E. coli*.

Experimental

Asa was prepared essentially by the scaled-up method of Koch *et al.* (4) with the following modifications. The first two steps involving the nucleophilic substitution of sodium diethylmalonate with methyl chloroacetate to produce 1,1,2-tris(carbomethoxy)ethane followed by transesterification to 1,1,2-tris(carbobenzyloxy)ethane were replaced by a single reaction. The consideration of equimolar amounts of sodium dibenzyl malonate and benzyl 2-bromoacetate result in a larger yield (84% overall) of product.

$$BnO_2CCH_2Br + NaCH(CO_2Bn)_2 \rightarrow BnO_2CCH_2CH(CO_2Bn)_2 + NaBr$$

In a typical experiment 1.65 g of Na was added in small pieces to 20.36 g of dibenzyl malonate in 163 mL of dry methanol at 0°C and stirred for 1 h. After addition of 16.41 g of benzyl 2-bromoacetate, stirring was continued at room temperature overnight. Following rotary evaporation of the methanol an orange oil was obtained; this oil was placed in a separatory funnel with 100 mL of ether, 200 mL of deionized water, and 7.5 mL of 6 M HCl. After extraction and separation of the ether layer the water layer was back-extracted twice with 100-mL portions of ether. The ether layers were combined, dried over anhydrous $MgSO_4$, and rotary evaporated. The residue was a light yellow oil weighing 25.98 g.

The catalytic hydrogenation of the azide, tribenzyl 1-azidoethane-1,2,2-tricarboxylate, to reduce the protective carbobenzyloxy groups to toluene and yield Asa was carried out by placing 0.70 g of azide, 0.35 g of $PdCl_2$, and 150 mL of dry methanol in a stainless steel vessel (inner diameter 54 mm, height 78 mm), purging, then pressurizing to 5 atm with H_2 (1 atm = 101.3 kPa). After shaking mechanically for 48 h the reaction mixture was filtered and rotary evaporated. Three additions of benzene were followed by rotary evaporation to remove traces of toluene. The yellow solid remaining was washed five times with ether, then dissolved in 4 mL of deionized water, pH 7.0. A small amount of insoluble material was removed by centrifugation at 10 000 g for 15 min. The supernatant was passed through a 5-cm column of Amberlite IRC-50 cation exchange resin. After freeze-drying of the clear eluate, there remained 0.112 g of a white crystalline powder (yield 43%), which was shown to be chromatographically pure and was identified as Asa monohydrate by NMR, IR, and MS.

For the enzyme assay an *E. coli* extract was prepared by suspending late log phase cells harvested from 30 mL of nutrient broth in 5 mL of H_2O. After ultrasonic disruption at 5°C, cellular debris was removed centrifugally. Commercial preparations of GOT (1667 units/mL) and MDH (10 000 units/mL) were dialysed against deionized water and diluted to working solutions with a 0.1 M potassium phosphate

[1]Author to whom correspondence may be addressed.

[2]The abbreviations used are Asa, β-carboxyaspartic acid; Ama, aminomalonic acid; Gla, γ-carboxyglutamic acid; L-Asp, L-aspartic acid; GOT, glutamate–oxalacetate transaminase; OAA, oxalacetic acid; MDH, malate dehydrogenase; NADH, nicotinamide adenine dinucleotide.

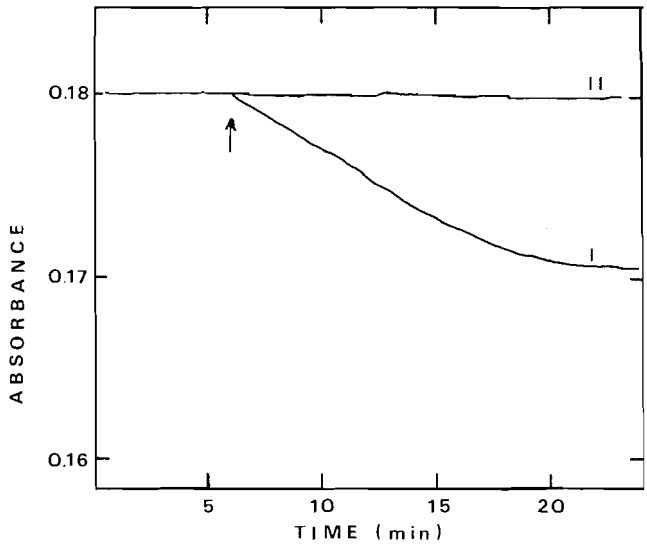

FIG. 1. Assay of Asa decarboxylase activity in an extract of *E. coli*. (I) Complete assay mixture. (II) Boiled extract. (↑) Point of addition of extract.

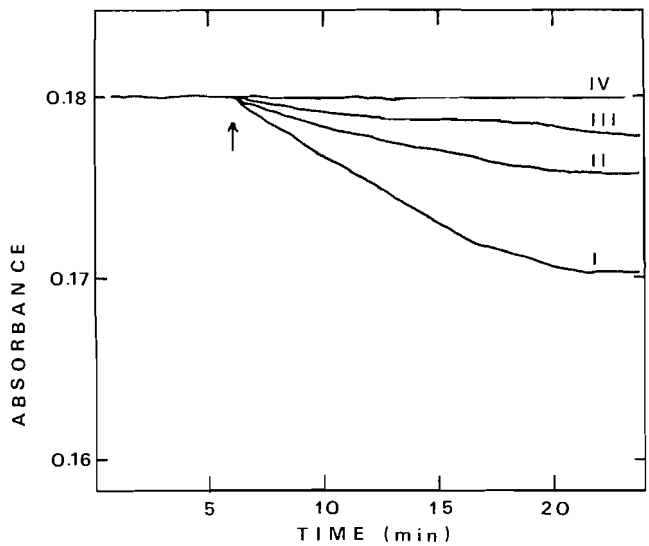

FIG. 2. Effect of freeze-thawing on Asa decarboxylase activity. (I) Complete assay mixture. (II), (III), (IV) Subsequent freezings and thawings of extract. (↑) Point of addition of extract.

buffer solution, pH 7.6, containing 1 mg bovine serum albumin per mL.

The assay mixture was as follows: 0.1 mL 10^{-2} M α-ketoglutarate, 0.1 mL 1/10 diluted GOT, 0.1 mL 5/1000 diluted MDH, 0.1 mL 10^{-3} M NADH, 0.3 mL 0.1 M potassium phosphate buffer pH 7.6, 1.6 mL H_2O, 0.1 mL 10^{-2} M Asa, and 0.1 mL *E. coli* extract.

Results

The assay procedure is a doubly coupled one, with the first appearance of L-aspartic acid (L-Asp) being scavenged by the glutamate–oxalacetate transaminase (GOT) reaction, using a suitable excess of α-ketoglutarate and GOT. The oxalacetate (OAA) produced is coupled to the malate dehydrogenase (MDH) reaction. The disappearance of coenzyme NADH is followed spectrophotometrically at 340 nm, and is a direct measure of the rate-limiting decarboxylase step:

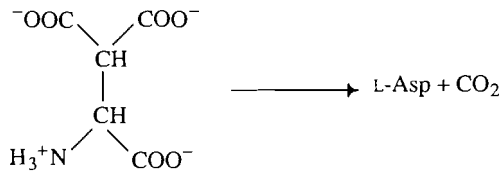

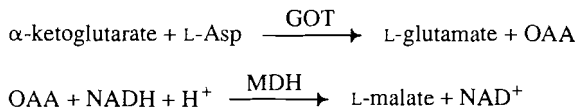

Evidence for enzymatic decarboxylation of Asa is shown in Fig. 1. When GOT is left out of the assay mixture no absorbance decrease is observed, suggesting the effective absence of any interfering levels of dehydrogenases. MDH is known to be highly specific for OAA, making the doubly coupled assay a true indicator of Asa decarboxylation. Boiling the *E. coli* extract for 5 min results in a total loss of enzyme activity. Further evidence of enzyme character (Fig. 2) is the progressive loss of activity due to repeated freezing and thawing of the extract.

Acknowledgements

We thank the Trent University Committee on Research for support of this work, and Miss Joanne Gooley for her valuable technical assistance.

1. J. J. VAN BUSKIRK, W. M. KIRSCH, D. L. KLEYER, R. M. BARKLEY, and T. H. KOCH. Proc. Natl. Acad. Sci. U.S.A. **81**, 722 (1984).
2. P. V. HAUSCHKA, J. B. LIAN, and P. M. GALLOP. Proc. Natl. Acad. Sci. U.S.A. **72**, 3925 (1975).
3. M. R. CHRISTY, R. M. BARKLEY, T. M. KOCH, J. J. VAN BUSKIRK, and W. M. KIRSCH. J. Am. Chem. Soc. **103**, 3935 (1981).
4. T. H. KOCH, M. R. CHRISTY, R. M. BARKLEY, R. SLUSKI, D. BOHEMIER, J. J. VAN BUSKIRK, and W. M. KIRSCH. Methods Enzymol. **107**, 563 (1984).
5. E. B. HENSON, P. M. GALLOP, and P. V. HAUSCHKA. Tetrahedron, **37**, 2561 (1981).
6. R. M. WILLIAMS, P. J. SINCLAIR, and W. ZHAI. J. Am. Chem. Soc. **110**, 482 (1988).
7. G. M. WOOD and J. W. SUTTIE. J. Biol. Chem. **263**, 3234 (1988).
8. P. V. HAUSCHKA, E. B. HENSON, and P. M. GALLOP. Anal. Biochem. **108**, 57 (1980).
9. K. SHIMURA, H. NAGAYAMA, and A. KIKUCHI. Nature (London), **177**, 935 (1956).
10. A. G. PALEKAR, S. S. TATE, and A. MEISTER. J. Biol. Chem. **248**, 1158 (1973).

Can. J. Chem. Downloaded from www.nrcresearchpress.com by 88.85.125.76 on 09/07/12
For personal use only.

Intrinsic gramicidin fluorescence lifetimes in bilayer lipid membranes and in vesicles

JOSE-MIGUEL CAMALEÑO-DELGADO, XIAO KANG ZHAO, AND JANOS H. FENDLER[1]

Département de chimie, Université de Montréal, C.P. 6128, succursale A, Montréal (Québec), Canada H3C 3J7

Received October 28, 1989

JOSE-MIGUEL CAMALEÑO-DELGADO, XIAO KANG ZHAO, and JANOS H. FENDLER. Can. J. Chem. **68**, 888 (1990).

Intrinsic Gramicidin A′ tryptophan steady-state fluorescence anisotropies and fluorescence lifetimes have been determined in bilayer lipid membranes (BLMs) prepared from glyceryl monooleate (GMO). In GMO BLMs, fluorescence anisotropy, the r value, was found to be 0.05 ± 0.02. Decays of Gramicidin A′ fluorescence intensities were fitted to the sum of three exponentials (τ_1, τ_2, and τ_3) and appropriate pre-exponentials (A_1, A_2, and A_3). These values allowed for the assessment of average fluorescence lifetimes, $\langle\tau\rangle$. These values related to those determined in vesicles prepared from dipalmitoylphosphatidylcholine (DPPC), dioleoylphosphatidylcholine (DOPC), distearoylphosphatidylcholine (DSPC), and diphytanoylphosphatidylcholine (DPhPC). In BLMs, $\langle\tau\rangle$ = 1.9 ns, 3.6 ns, and 2.3 ns were determined for vertically, horizontally, and unpolarized average fluorescence lifetimes, respectively. Increasing the applied potential across the BLM from 0 to 80 mV increased $\langle\tau\rangle$ from 2.2 ns to 4.9 ns and τ_1 from 0.43 ± 0.05 to 0.73 ± 0.06 ns, as well as the contributions and lifetimes of the longer lived fluorescence (A_2 and A_3, τ_2 and τ_3). The emission maximum of Gramicidin A′ (334 nm in DPPC) and the absence of quenching by iodide ions indicated complete incorporation of the polypeptide into vesicles. The r values were of the order of 0.10 in vesicles prepared from DPPC and DSPC, both in the absence and in the presence of added 1.2×10^{-4} M CsCl. In vesicles prepared from DOPC and DPhPC, r values increased to 0.13 and 0.14 in water and to 0.15 and 0.20 in 1.2×10^{-4} M CsCl, respectively. At 25.0°C, the temperature of the measurements, DPPC and DSPC are in their "solid" states, but DOPC and DPhPC are in their "liquid" states. $\langle\tau\rangle$ values for Gramicidin A′ in vesicles prepared from DPPC, DOPC, and DSPC were all in the 3.0 ± 0.3 ns range. In DPhPC vesicles, $\langle\tau\rangle$ = 2.2 ns was determined. Time-dependent anisotropies became observable in DOPC and DPhPC vesicles, particularly in the presence of 1.2×10^{-4} M CsCl.

Key words: gramicidin, fluorescence lifetimes, vesicles, bilayer lipid membranes, time-dependent anisotropies.

JOSE-MIGUEL CAMALEÑO-DELGADO, XIAO KANG ZHAO et JANOS H. FENDLER. Can. J. Chem. **68**, 888 (1990).

On a déterminé les anisotropies intrinsèques de fluorescence et les temps de vie de fluorescence de l'état stationnaire de la Gramicidine A′ et du tryptophane dans des membranes lipidiques en bicouches (MLB) préparées à partir de monooléate de glycéryle (MOG). On a trouvé que dans des MLB de MOG, l'anisotropie de fluorescence, la valeur r, est égale à 0,05 ± 0,02. On a ajusté les intensités de la dégénérescence de la fluorescence de la Gramicidine A′ avec la somme des trois exponentielles (τ_1, τ_2 et τ_3) et des pré-exponentielles appropriées (A_1, A_2 et A_3). On a utilisé ces valeurs pour évaluer les temps de vie moyens de la fluorescence $\langle\tau\rangle$. Il existe une corrélation entre ces valeurs et celles déterminées dans des vésicules préparées à partir de dipalmitoylphosphatidylcholine (DPPC), de dioléoylphosphatidylcholine (DOPC), de distéaroylphosphatidylcholine (DSPC) et de diphytanoylphosphatidylcholine (DPhPC). Dans les MLB, on a déterminé des valeurs de $\langle\tau\rangle$ de 1,9, 3,6 et 2,3 ns respectivement pour les temps de vie moyens verticaux, horizontaux ainsi que non polarisés. Une augmentation du potentiel appliqué sur les MLB de 0 à 80 mV provoque une augmentation de la valeur de $\langle\tau\rangle$ de 2,2 à 4,9 ns et de la valeur de τ_1 de 0,43 ± 0,05 à 0,73 ± 0,06 ns ainsi que des augmentations des contributions et des temps de vie de la fluorescence (A_2 et A_3, τ et τ_3). L'émission maximale de la Gramicidine A′ (334 nm dans le DPPC) ainsi que l'absence de piégeage par les ions iodures indique que le polypeptide est complètement incorporé dans les vésicules. Les valeurs de r sont de l'ordre de 0,10 dans les vésicules préparées à l'aide de DPPC et de DSPC soit en l'absence ou en présence de CsCl ajouté à la concentration de $1,2 \times 10^{-4}$ M. Dans les vésicules préparées à l'aide de DOPC et de DPhPC, les valeurs de r augmentent respectivement jusqu'à 0,13 et 0,14 dans l'eau et jusqu'à 0,15 et 0,20 dans une solution à $1,2 \times 10^{-4}$ M de CsCl. À 25,0°C, la température à laquelle les mesures ont été faites, les DPPC et DSPC sont dans leur état «solide» alors que les DOPC et DPhPC sont dans leur état liquide. Toutes les valeurs de $\langle\tau\rangle$ pour la Gramicidine A′ dans des vésicules préparées à l'aide de DPPC, de DOPC et de DSPC sont dans l'ordre de 3,0 ± 0,3 ns. Dans les vésicules de DPhPC, on a établi la valeur de $\langle\tau\rangle$ à 2,2 ns. Avec les vésicules de DOPC et de DPhPC, on a commencé à observer des anisotropies variant en fonction du temps, particulièrement en présence d'une solution à $1,2 \times 10^{-4}$ M de CsCl.

Mots clés : gramicidine, temps de vie de fluorescence, vésicules, membranes lipidiques en bicouches, anisotropies variant en fonction du temps.

[Traduit par la revue]

Introduction

The importance of transmembrane ion transport and the comparative simplicity of gramicidin have prompted extensive investigations of this channel-forming ionophore (1–4). The primary structure of Gramicidin A has been determined to be HCO-Val[1]-Gly[2]-Ala[3]-D-Leu[4]-Ala[5]-D-Val[6]-L-Val[7]-D-Val[8]-L-Trp[9]-D-Leu[10]-L-Trp[11]-D-Leu[12]-L-Trp[13]-D-Leu[14]-L-Trp[15]-$NHCH_2CH_2OH$ (5). The membrane channel, a left-handed, 26 Å long, β helix with 6.3 residues per turn, is formed from two gramicidins that are linked together at their amino terminals (6). This organization exposes the hydrophobic parts to the membrane while the carbonyl moieties of the peptide form an internal pore of about 4 Å diameter, which can accommodate monovalent cations. The four tryptophans, located close to the entry and exit ports of the channel, have been shown to play an essential role in ion transport (7–11).

Gramicidin conformation and association are dynamic and media-dependent (12, 13). In ethanol, several conformers coexist with the antiparallel β double helix dimer being predominant. In dimethyl sulfoxide, monomers prevail. In anhydrous lipids, X-ray crystallography established that gramicidin forms a cylindrical, intertwined, antiparallel double helix (14, 15). Introduction of gramicidin into phospholipid dispersion results not only in head-to-head (amino terminal to

[1]Author to whom correspondence may be addressed.

Can. J. Chem. Downloaded from www.nrcresearchpress.com by 88.85.125.76 on 09/07/12
For personal use only.

Can. J. Chem. Downloaded from www.nrcresearchpress.com by 88.85.125.76 on 09/07/12
For personal use only.

amino terminal) dimer formation, but also in a concomitant reorganization of the bilayer structure (16, 17). The dynamics of this reorganization have been monitored by examining the deuterium magnetic resonance of gramicidin, deuterated in its tryptophan residues, in different phospholipid dispersions (18). In 1-palmitoyl-*sn*-glycero-3-phosphocholine/gramicidin = 4:1 dispersion, the peptide was found to be rigid in the fluid lipid over a large temperature range. Conversely, in 1,2-dioleoyl-*sn*-glycero-3-phosphocholine or 1,2-dimyristoyl-*sn*-glycero-3-phosphocholine dispersions, gramicidin was mobile above, but rigid below, the phase transition of the lipid (18). Clearly, different membrane models elicit different behavior in a less-than-straightforward way.

Similar conclusions were drawn from observing gramicidin tryptophan rotational amplitudes by phase modulation fluorometry in different phospholipid dispersions (19). To the best of our knowledge, there are only two additional reports on tryptophan fluorescence measurements on lipid-aggregate-incorporated gramicidin. Steady-state (20) and time-resolved (21) intrinsic gramicidin fluorescence were measured in lysolipid dispersions. The data obtained were fitted to three exponentials with decay times in the 6–8 ns, 1.8–3.0 ns, and 0.3–0.8 ns ranges (21). The low emission efficiency of tryptophan has to date precluded intrinsic fluorescence measurements of the tiny amounts of gramicidin present in a bilayer lipid membrane (BLM). Measurements of extrinsic dansyl fluorescence simultaneously with ion conductances have provided, of course, an early and crucial substantiation for dimeric (dansyl) gramicidin as the active channel in BLMs (22–24).

Our ability to observe intrinsic gramicidin fluorescence lifetimes in GMO BLMs is the most significant result of the present work. Fluorescence lifetime parameters have been shown to be substantially affected by the angle of observation and by the application of a potential across the BLM.

Intrinsic fluorescence lifetime parameters of gramicidin tryptophans have also been determined in unilamellar dipalmitoylphosphatidylcholine (DPPC), dioleoylphosphatidylcholine (DOPC), diphytanoylphosphatidylcholine (DPhPC), and distearoylphosphatidylcholine (DSPC) surfactant vesicles. Addition of KI or CsCl as quenchers did not affect the fluorescence lifetime parameters in vesicles at a constant gramicidin concentration. Steady-state and time-dependent gramicidin fluorescence anisotropies have also been determined in vesicles prepared from DPPC, DSPC, DOPC, and DPPC in the absence and in the presence of CsCl.

Materials and methods

Gramicidin A′ is a mixture of Gramicidin A/Gramicidin B/Gramicidin C = 80:5:15. These gramicidins are identical in all respects, with the exception that Trp^{11} in Gramicidin A (see structure in the Introduction) is replaced by Tyr^{11} or Phe^{11} in Gramicidin B or Gramicidin C, respectively (22–25). Some measurements were carried out on authentic Gramicidin A. Emission spectra and lifetimes (see Tables 4 and 5) determined on this sample were identical, within the experimental error, with those obtained on the commercial sample. DPPC (Sigma), DOPC (Sigma), DPhPC (Sigma), DSPC (Sigma), GMO (Nucheck), NaOH, and HCl (Baker analyzed reagents) were used as received. No fluorescences of the solvents were detected by single photon counting. Decane, chloroform, or ethanol (Aldrich spectroscopic grade) were used, therefore, as received. Water was purified with a Millipore Milli-Q system provided with a 0.4 μm Millistack filter at the outlet.

Vesicles were prepared by dispersing the appropriate lipid (0.5–5.0 mg/mL) in water, or in aqueous 10 mM Tris HCl buffer at pH 7.5, by sonication for 15 min at 70°C using the microtip of a Braunsonic 1510 sonicator. Ethanolic solutions of Gramicidin A′ were added to vesicles to yield the appropriate gramicidin/lipid ratios. Gramicidin-containing vesicles were incubated at 70°C for 9 h prior to the removal of titanium particles by centrifugation (26). These preparations gave predominantly unilamellar unidispersed vesicles of 600–800 Å in diameter (27).

BLMs were formed on a Teflon pinhole separating two aqueous, electrically isolated compartments. A thin (100–150 μm) Teflon film containing a 0.10 cm diameter hole was sandwiched between two triangular pathlength quartz cells by silicon rubber adhesive. The hypotenuse faces of the two cells, in contact with the Teflon film, contained 0.6 cm × 1.5 cm windows through which the 0.1 cm diameter hole and some surrounding area of the Teflon film remained exposed. The cells were filled with 4 mL of water or 2 M KCl solutions at ambient temperature. The BLMs were made by brushing a small amount of the BLM-forming solution (4×10^{-4} M Gramicidin A′ in hexadecane) on the 0.1 cm diameter hole. Thinning of the initially formed thick film to a black bilayer lipid membrane was monitored by observing the reflected light from a 200-W mercury–xenon lamp through a microscope and by capacitance measurements (28, 29). The accuracy of capacitance measurements was found to be within 1.0%. GMO BLMs typically lasted for 4–6 h, after which time they broke. This lack of long-term stability did not allow extensive gramicidin incubation into the BLMs. Electrical measurements indicated, however, the presence of well-functioning channels prior to commencing the fluorescence lifetime measurements. Fluorescence measurements were limited to the bilayer (i.e., excluding the Plateau–Gibbs borders) by focusing the laser to a 0.05 cm diameter spot in the middle of the BLM.

Excitation of gramicidin at 280 nm has been shown to result in channel inactivation (30–32). Conductance measurements subsequent to the accumulation of lifetime data indicated conductances identical to those measured prior to fluorescence measurements. Under our experimental conditions (294 nm excitation by nanojoule/pulse laser energies), therefore, gramicidin does not suffer appreciable photodamage.

Absorption spectra were taken on a Hewlett–Packard 8450 diode-array spectrophotometer.

Fluorescence lifetimes were determined on a time-correlated, single-photon counting system, which uses a synchronously pumped, cavity-dumped, Rhodamine 6G dye laser (Spectra-Physics 375) pumped by a mode-locked argon ion laser (Spectra-Physics 2020) as an excitation source. Vertical polarization of the excitation is assured by a Glan air space prism. The laser beam is attenuated by suitable neutral density filters to ensure that the fluorescence count rate is always less than 1% of the cavity-dumper frequency (generally 819 kHz). For ultraviolet operation, the dye laser beam is frequency doubled by using a temperature-tuned, ammonium dihydrogen arsenate crystal (Inrad) and is rotated to vertical polarization by a Babinet–Soliel compensator (Karl Lambrecht). Single fluorescence photons are detected by a Hamamatsu 1564 microchannel plate photomultiplier tube (MCPPMT). The quartz collection optics are matched to those of the 0.25-m Jarrel–Ash monochromator that is used for wavelength resolution. The output of the MCPPMT is amplified by a Hewlett–Packard 8447 F preamplifier power amplifier and conditioned by one of the four channels of a Tennelec TC 455 quad constant fraction discriminator (CFD) whose output serves as the start signal for an Ortec 457 biased, time-to-pulse-height converter (TAC). The stop signal comes from a TIED 56 photodiode, which monitors the output of the dye laser and is conditioned by another section of the CFD. This signal is delayed (Ortec 425) such that the signal appears on the screen of a Tracor Northern 7200/4NP multichannel analyzer. The 1024-point histogram is accumulated to at least 10 000 counts at its maximum and is transferred to a Zenith ZW118 microcomputer, which is equipped with 768K memory and an 8087 coprocessor. The time per channel of the TAC–MCA combination was calibrated by slightly detuning the cavity dumper to allow two consecutive pulses to be dumped. The known spacing between the pulses was used as the time standard for ranges where both pulses appear on the MCA screen. For the shorter time ranges, a previously measured length of cable was inserted and used

Can. J. Chem. Downloaded from www.nrcresearchpress.com by 88.85.125.76 on 09/07/12
For personal use only.

as the standard. The instrument response function of the system, measured by using a dilute scattering solution (either non-dairy coffee creamer or Ludox), was found to be 130 ps full-width at half-maximum and 250 ps full-width at tenth-maximum and is independent of wavelength. The decays were analyzed in terms of sums of exponentials:

$$[1] \quad I(t) = \sum_i A_i e^{-t/\tau_i}$$

where τ_i's are the fluorescence lifetimes and A_i's measure the contribution of the different lifetimes to the total fluorescence decay. The fluorescence parameters were determined from

$$[2] \quad S(t) = I(t)_r I(t) = \int_0^t I_r(t')I(t - t')dt$$

where $S(t)$ is the convolution of the fluorescence due to the sample measured, $I(t)$, and the instrument response, $I_r(t)$. Decays were analyzed by a reiterative, nonlinear least-squares routine using the Marquardt algorithm (33). In this procedure, the weighted sum of squared residuals, WSSR, is minimized according to

$$[3] \quad \text{WSSR} = \sum_{k=1}^{n} w_k[S(t_k) - S_c(t_k)]^2$$

where $S_c(t)$ is the calculated fit of $S(t)$, w_k is the weight factor of the data points $S(t_k)$, and n is the total number of data points. Goodness of an individual fit was judged by the magnitude of the reduced χ^2 and the randomness of the weighted residuals. Each method also employs a time-shift parameter that is minimized in the fitting routines. In our case, this time-shift parameter arises from the long-term stability of the electronics rather than from any wavelength dependence of the detector. This small but measurable shift is rarely greater than 30 ps and seems to arise from small, ambient temperature changes. We do not correct for background signal (dark noise) since it never exceeds 5×10^{-4} counts per second per channel. The procedure involves the measurement of the instrument response function by detection of the excitation pulse scattered from a dilute colloidal solution. One then measures the fluorescent intensity of the sample at the selected wavelength and polarization(s). Next one calculates the intensity on the basis of the instrument response function and an assumed photophysical model using initial parameter guesses. The weighted square differences between the experimental and calculated intensities are minimized with respect to the parameters until convergence is attained. Any combination of the parameters may be held constant while the others vary, though most often all parameters are allowed to vary freely. Lack of any instrumental artifact was demonstrated by reproducing the published fluorescence lifetimes of *N*-acetyltryptophan in water (2.82 ± 0.04 ns) using a single exponential decay function (34).

Steady-state fluorescence anisotropies were determined by integrating the total emission intensities recorded on the MCA by sequentially placing HNB polaroid polarizers (Polaroid Corporation, Cambridge, Massachusetts) vertically and horizontally into the emission signal generated in the excitation of the samples by vertically polarized laser pulses (*vide supra*). The steady-state anisotropy, r, of the fluorescence signal was measured at 340 nm as

$$[4] \quad r = \frac{I_{VV} - GI_{VH}}{I_{VV} + 2GI_{VH}}$$

where I_{VV} and I_{VH} are the vertical (parallel to vertical excitation, 90°) and horizontal (vertical to vertical excitation, 0°) components of the emitted light when excited by vertically polarized light. The factor G corrects for emission monochromator polarization effects and is equal to I_{HH}/I_{HV} (where I_{HH} and I_{HV} are the horizontal and vertical components of emission from horizontally polarized exciting light). The value of G at 340 nm was determined to be 0.80. Correction for light scattering by the vesicles was made by subtracting the emission signal due to vesicles that did not contain gramicidin. This correction was found to be negligible.

BLM resistances and capacitances were measured by an RLC Digibridge (model 1689 M, Genrad).

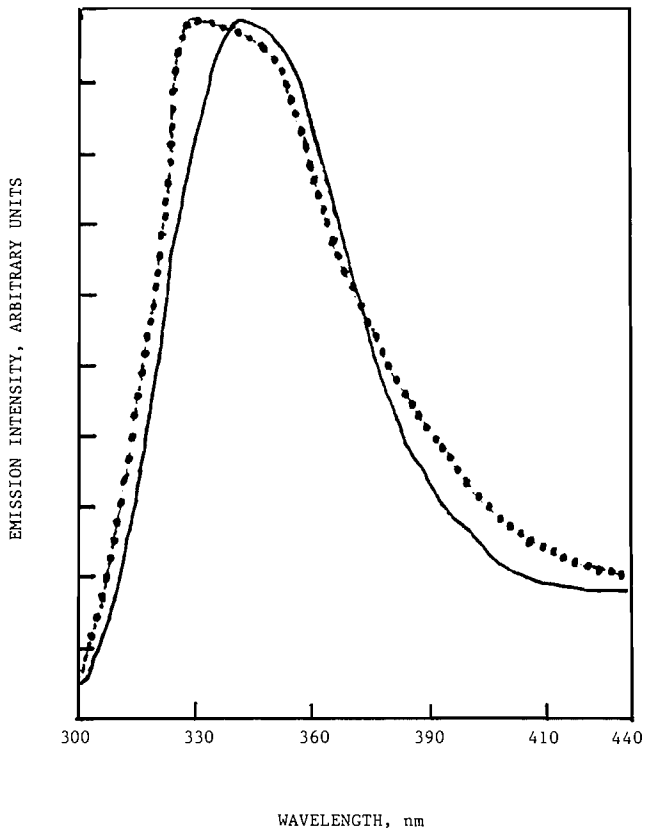

FIG. 1. Normalized emission spectra of Gramicidin A′ in DPPC vesicles (solid line) and in GMO BLMs (dotted line). λ_{ex} = 294 nm. Spectra were taken by the time-correlated single-photon counting system using the MCA to record emission intensities at different wavelengths.

Results and discussion

Gramicidin A′ in bilayer lipid membranes

Intrinsic gramicidin fluorescence spectra, anisotropy, and lifetimes have been determined in a 50 Å thick BLM in the present work. Introduction of Gramicidin A′ into the BLM-forming solution ensures its incorporation into the bilayer in the form of functioning channels. The observed emission spectra of Gramicidin A′ in GMO BLMs (Fig. 1), as well as conductivity measurements, substantiate this interpretation. It should be pointed out, however, that the GMO BLM is fluid (T_{PT} = 16°C) at the temperature of the measurements. GMO, hexadecane, and gramicidin molecules are distributed between the bilayer and the surrounding Plateau–Gibbs border, which serves as a reservoir. While thermodynamically the fluidity should favor dimeric channel formation, this process is kinetically controlled. Under the experimental conditions, a considerably greater number of dimeric channels are likely to prevail in vesicles than in BLMs.

Gramicidin A′ steady-state fluorescence anisotropy, the r value, in GMO BLMs (0.050 ± 0.02; Table 1) is somewhat higher than that in alcohols (ca. 0.03), indicating the decreased rotational freedom of the tryptophan moieties in the bilayers. Tryptophans at the 9th, 11th, 13th, and 15th positions in gramicidin are located at the outside turns of the left-hand helices and are thus exposed to relatively hydrophobic environments (35). The r values for Gramicidin A′ in DPPC and DSPC vesicles (ca. 0.1, Table 1) are similar to those reported for lysolecithin dispersions (0.1; ref. 20) and are unaffected by

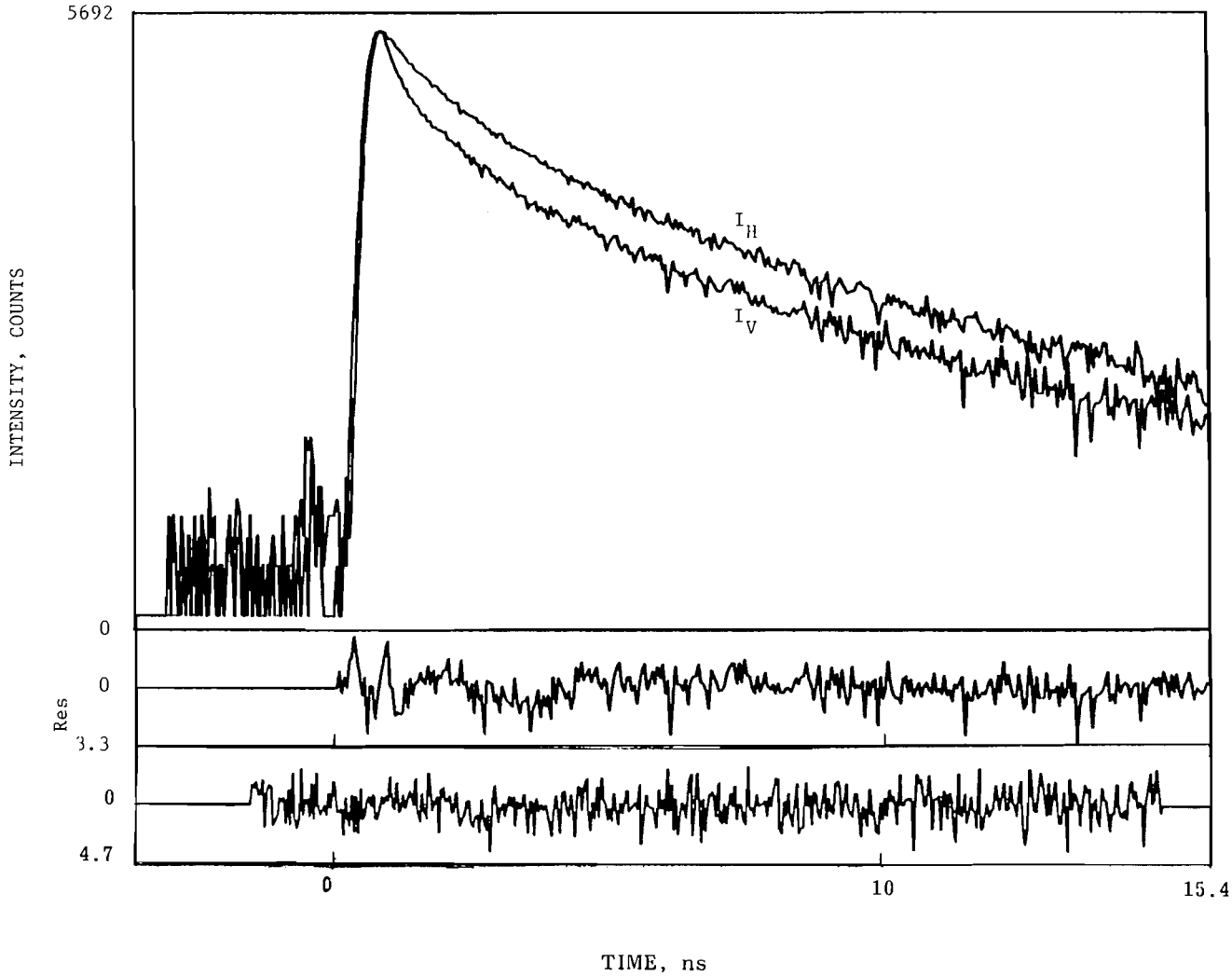

FIG. 2. Fluorescence decay of Gramicidin A′ in GMO BLMs. GMO BLMs were prepared by brushing a hexadecane solution of Gramicidin A′ across the Teflon pinhole separating the two compartments. Gramicidin A′/lipid ratios were kept at 1:50. λ_{ex} = 294 nm (vertically polarized), λ_{em} = 340 nm. V = vertical (90°) and H = horizontal (0°) observation of the emission. The solid lines are the best fits of the experimental data fitted to three exponential decays. Weighted sums of squared residuals are below the curves.

TABLE 1. Steady-state fluorescence polarization of Gramicidin A′ in vesicles and BLMS[a]

Vesicle	Solvent	T_{PT}, °C	Anisotropy, r^b
GMO BLM	2.0 M KCl	16	0.050±0.02
DPPC	H_2O	41	0.109±0.012
DPPC	1.2×10^{-4} M CsCl		0.097±0.015
DPPC[c]	H_2O		0.118±0.010
DPPC	1.2×10^{-4} M CsCl		0.107±0.012
DSPC	H_2O	55	0.094±0.005
DSPC	1.2×10^{-4} M CsCl		0.089±0.02
DOPC	H_2O	−22	0.132±0.09
DOPC	1.2×10^{-4} M CsCl		0.153±0.03
DPhPC	H_2O	<15	0.140±0.08
DPhPC	1.2×10^{-4} M CsCl		0.199±0.05

[a]All r values were measured at 25°C and represent the mean of four determinations, with the exception of GMO BLMs. Vesicles were prepared by sonication (0.5 mg lipid/1.0 mL H_2O). Gramicidin A′/lipid ratios were kept at 1:50, unless stated otherwise. λ_{ex} = 294 nm, λ_{em} = 340 nm.
[b]See eq. [4] and Materials and methods for details.
[c]Gramicidin A′/lipid = 1:1000.

the addition of 1.2×10^{-4} M CsCl (Table 1). Gramicidin fluorescence anisotropy in GMO BLMs was found to be considerably smaller than that in vesicles (Table 1). Although GMO is fluid at the temperature of the experiment, insufficient incubation precluded extensive dimer formation. Apparently, it is the hindered rotation of dimeric channels rather than the tryptophan moieties that determines gramicidin anisotropies.

Typical Gramicidin A′ intensity decays in GMO BLMs, observed at 0° and 90°, are shown in Fig. 2. Attempts to fit the intensity to one and two exponential decays gave poor results (long time convergence of the iterations, $\chi^2 > 3$, and non-random fits of the residuals). Good fits were obtained, however, in terms of three exponential decays. Sums of the three exponentials provide, of course, a better fit for intensity decays than the simpler one or two exponentials. This has been observed for tryptophan decays in proteins (36, 37). The three exponential fluorescence decays of gramicidin in lysolecithin dispersions have been attributed to three different sets of tryptophans in the polypeptide ionophore (21). The short (ca. 0.3 ns) lifetime component was suggested to originate in

Can. J. Chem. Downloaded from www.nrcresearchpress.com by 88.85.125.76 on 09/07/12
For personal use only.

TABLE 2. Fluorescence decay parameters of Gramicidin A′ in GMO BLMS[a]

Solvent	Polarization[b]	A_1	τ_1, ns	A_2	τ_2, ns	A_3	τ_3, ns	$\langle\tau\rangle$, ns[c]	χ^2
H_2O	0	0.69±0.07	0.43±0.08	0.29±0.03	1.76±0.08	0.02±0.01	6.78±0.08	2.2	1.146
H_2O[d]	0	0.69±0.08	0.41±0.09	0.29±0.04	1.72±0.03	0.02±0.01	6.65±0.09	2.1	1.109
2.0 M KCl	0	0.56±0.07	0.28±0.07	0.39±0.05	1.45±0.09	0.06±0.02	5.08±0.08	2.3	1.349
2.0 M KCl	V	0.51±0.06	0.15±0.08	0.38±0.02	1.10±0.08	0.11±0.02	3.33±0.07	1.9	1.288
2.0 M KCl	M	0.57±0.07	0.28±0.08	0.37±0.03	1.57±0.09	0.06±0.02	5.07±0.08	2.3	1.206
2.0 M KCl	H	0.47±0.05	0.79±0.09	0.20±0.03	1.80±0.08	0.33±0.01	4.68±0.06	3.6	1.105

[a]All determinations were carried out at 25°C. GMO BLMs were prepared by brushing a hexadecane solution of Gramicidin A′ and GMO across the Teflon pinhole separating the two compartments. Gramicidin A′/GMO ratios were kept at 1:50. λ_{ex} = 294 nm (vertical polarization), λ_{em} = 340 nm.
[b]O = no polarizer, V = vertical (90°C), H = horizontal (0°), and M = magic angle (54.9°) polarizations.
[c]Average lifetimes were calculated as $\langle\tau\rangle = \sum_i A_i\tau_i^2 / \sum_i A_i\tau_i$.
[d]Using authentic Gramicidin A.

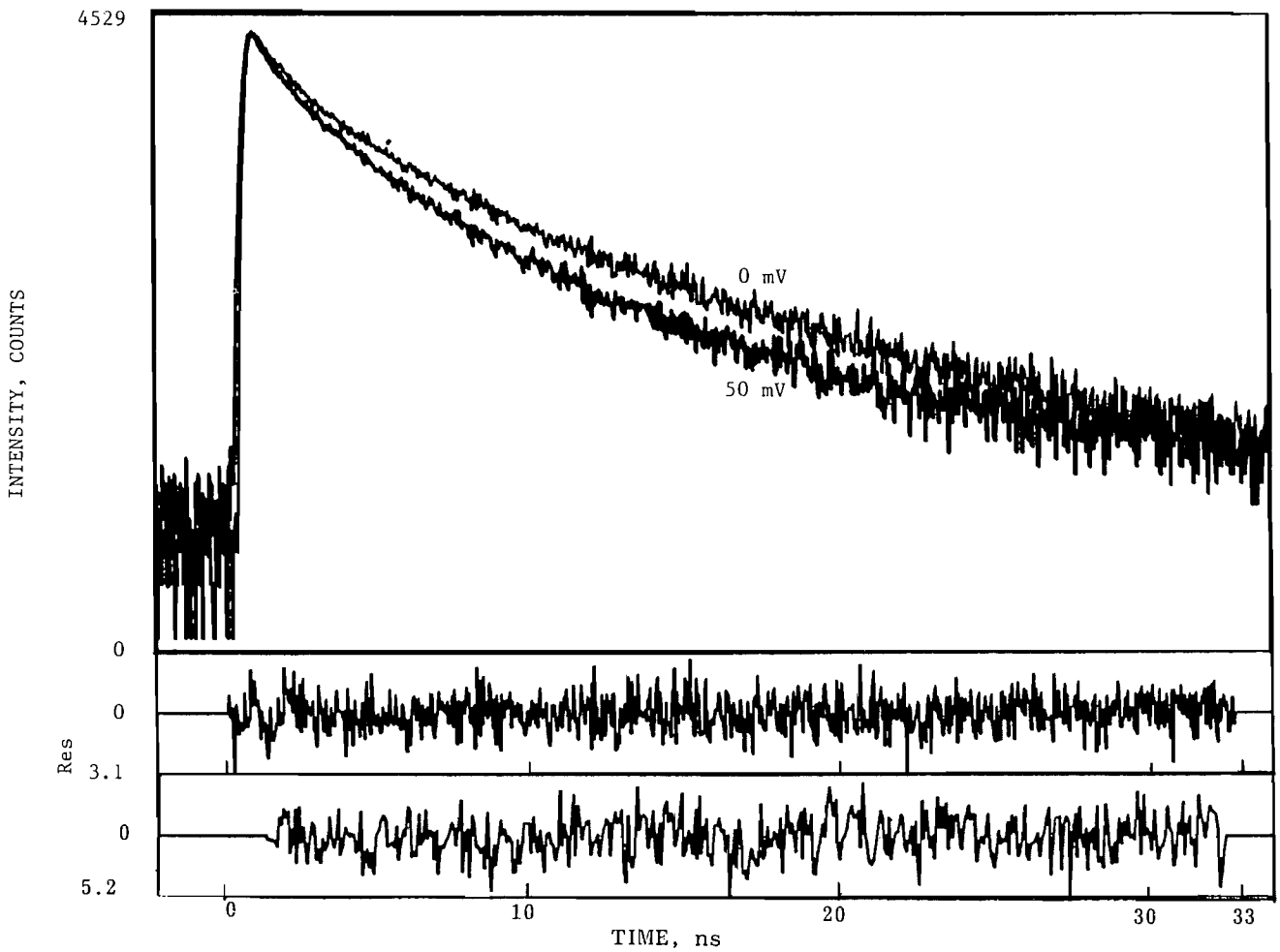

FIG. 3. Fluorescence decay of Gramicidin A′ in GMO BLMs in the absence and in the presence of 50-mV transmembrane potential. GMO BLMs were prepared by brushing a hexadecane solution of Gramicidin A′ across the Teflon pinhole separating the two compartments. Gramicidin A′/lipid ratios were kept at 1:50. λ_{ex} = 294 nm (vertically polarized), λ_{em} = 340 nm (no polarizer). The solid lines are the best fits of the experimental data fitted to three exponential decays. Weighted sums of squared residuals are below the curves.

exciton interactions between the indole groups in neighboring tryptophan moieties, 9 and 15. The long (6–8 ns) lifetime component was ascribed to tryptophans that are "deeply buried" in the bilayer, 11 and 13, while the medium lifetime was attributed to tryptophans that are located close to the membrane surface, 13 and 15. Although appealing, these assignments are likely to be gross oversimplifications since the A values determined in the present work in a variety of different vesicles do not correspond to the ratios of the different tryptophans in gramicidin. Different fluorescence decay components could also be ascribed to different gramicidins (monomers, dimers, and higher aggregates), different conformations of gramicidin channels, or indeed to different conformation states of the tryptophan. Even though no unambiguous assignment can be given to the three-component gramicidin decays, fluorescence lifetimes of the different systems can be fruitfully compared. The determined gramicidin fluorescence lifetimes (τ_1, τ_2, and τ_3 values), mean lifetimes ($\langle\tau\rangle$ values), pre-exponentials (A_1,

Can. J. Chem. Downloaded from www.nrcresearchpress.com by 88.85.125.76 on 09/07/12
For personal use only.

TABLE 3. Effect of potential applied across GMO BLMS on the fluorescence decay parameters of Gramicidin A′ [a]

Applied potential, MV	A_1	τ_1, ns	A_2	τ_2, ns	A_3	τ_3, ns	$\langle\tau\rangle$, ns[b]	χ^2
0	0.69±0.07	0.43±0.08	0.29±0.03	1.76±0.08	0.02±0.01	6.78±0.08	2.2	1.146
50	0.47±0.05	0.80±0.08	0.41±0.04	2.50±0.05	0.12±0.02	6.38±0.09	3.5	1.140
80	0.38±0.06	0.73±0.06	0.42±0.05	2.84±0.09	0.20±0.04	7.40±0.09	4.9	1.047

[a]All determinations were carried out at 25°C in the presence of 2.0 M KCl. GMO BLMs were prepared by brushing a hexadecane solution of Gramicidin A′ and GMO across the Teflon pinhole separating the two compartments. Gramicidin A′/GMO ratios were kept at 1:50. λ_{ex} = 294 nm, λ_{em} = 340 nm. No polarizer was placed in the emission beam.
[b]Average lifetimes were calculated as $\langle\tau\rangle = \sum_i A_i\tau_i^2/\sum_i A_i\tau_i$.

TABLE 4. Fluorescence decay parameters of Gramicidin A′ in vesicles[a]

Vesicle	A_1	τ_1, ns	A_2	τ_2, ns	A_3	τ_3, ns	$\langle\tau\rangle$, ns[b]	χ^2
DPPC	0.48±0.07	0.65±0.06	0.44±0.05	2.30±0.09	0.070±0.004	5.82±0.01	2.9	1.32
DPPC[c]	0.48±0.03	0.64±0.06	0.40±0.05	2.22±0.10	0.11 ±0.05	5.35±0.10	2.9	1.05
DSPC	0.50±0.06	0.68±0.02	0.44±0.05	2.42±0.04	0.07 ±0.01	6.10±0.01	2.9	1.65
DOPC	0.52±0.03	0.73±0.02	0.39±0.01	2.37±0.04	0.09 ±0.02	5.96±0.04	3.2	1.29
DPhPC	0.63±0.03	0.44±0.12	0.32±0.03	1.76±0.19	0.05 ±0.01	5.10±0.27	2.2	1.62
LL[d]	0.50	0.70	0.32	2.30	0.17	7.8	3.4	
DOPC[e]							2.5	
DMPC[e]							3.5	
EggPC[e]							2.4	

[a]Decay parameters were measured at 25°C and represent the means of five (DPPC and DOPC) and four (DSPC and DPhPC) determinations. Vesicles were prepared by sonication (0.5 mg/1.0 mL H_2O). Gramicidin A′/lipid ratios were kept at 1:50. λ_{ex} = 294 nm, λ_{em} = 340 nm. Fluorescence intensities were observed at the magic angle (54.9°).
[b]Average lifetimes were calculated as $\langle\tau\rangle = \sum_i A_i\tau_i^2/\sum_i A_i\tau_i$.
[c]Using an authentic Gramicidin A sample.
[d]Data interpolated for the published (21) figure to 24 h incubation time and λ_{em} = 340 nm. LL = lysolecithin dispersion.
[e]Taken from ref. 19. DMPC = dimyristoylphosphatidylcholine. EggPC = egg phosphatidylcholine.

A_2, and A_3 values), and χ^2 in GMO BLMs are collected in Table 2. There are marked differences between the behavior of the ionophore in BLMs and vesicles. Thus, the average Gramicidin A′ fluorescence lifetimes (determined without polarizers) in GMO BLMs (ca. 2.0 ns) are shorter than those found in vesicles (ca. 3.0 ns, Table 4). There are more pronounced differences in A and τ values. In particular, A_1 values are greater and A_3 values are smaller in BLMs than in vesicles. Differences between GMO and the lipids used for vesicle preparations, as well as the presence of hexadecane molecules and the Plateau–Gibbs border in the BLM, are responsible for the observed fluorescences in these two matrices. The complexity of the system does not warrant, however, more detailed interpretation. Pronounced differences between horizontal and vertical Gramicidin A′ fluorescence decays in GMO BLMs (Fig. 2 and Table 2) underscore the disparate behavior of the two bilayer systems. The average lifetime of the vertically observed Gramicidin A′ fluorescence (1.9 ns) is shorter than that observed horizontally (3.6 ns), while the $\langle\tau\rangle$ value in the absence of polarization (i.e., at magic angle) falls between these two extremes (2.3 ns). The A_3 value is markedly higher and the A_1 value is somewhat smaller for horizontally than for vertically observed Gramicidin A′ fluorescence in GMO BLMs.

Effects of potential applied across GMO BLMs on the fluorescence decay are illustrated in Fig. 3 and the data are collected in Table 3. Increasing the applied potential increased the average Gramicidin A′ fluorescence lifetimes (τ_1, τ_2, and τ_3) and the contributions of the longer lived fluorescences (A_2 and A_3) at the expense of the short component (A_1). This paralleled the observed increase of conductance with increasing transmembrane potential. The significant increase of τ_1 with increasing transmembrane potential (from 0.43 ns at 0 mV to 0.74 ns at 80 mV applied potential, Table 3) suggests the increased importance of stacking interaction. Increasing the transmembrane potential is likely to decrease the thickness of the solvent therein. This, in turn, may lead to increased gramicidin dimerization. Increasing the gramicidin dimer population results in decreased mobilities and, hence, in increased fluorescence lifetimes. It is interesting to note that applying a transmembrane potential across the GMO BLM has the same effect as changing the angle of observation of gramicidin fluorescence from 0° to 90°.

Gramicidin A′ in vesicles

Steady-state emission spectra, fluorescence quenching, and anisotropy measurements have been used to establish the incorporation of Gramicidin A′ into vesicles prepared from DPPC, DSPC, DOPC, and DPhPC. Addition of iodide ions in Gramicidin A′-containing vesicle solutions did not result in fluorescence quenching. Since iodide ions cannot penetrate into bilayers, their inability to quench gramicidin fluorescence has been taken as evidence for the incorporation of this polypeptide into the vesicle matrix (19). The shift of the gramicidin emission maximum to a wavelength shorter than 340 nm was used as an additional criterion for gramicidin incorporation into apolar medium of vesicles (21). Fluorescence spectra of Gramicidin A′ in all vesicles used in the present work had emission maxima

Can. J. Chem. Downloaded from www.nrcresearchpress.com by 88.85.125.76 on 09/07/12
For personal use only.

Can. J. Chem. Downloaded from www.nrcresearchpress.com by 88.85.125.76 on 09/07/12
For personal use only.

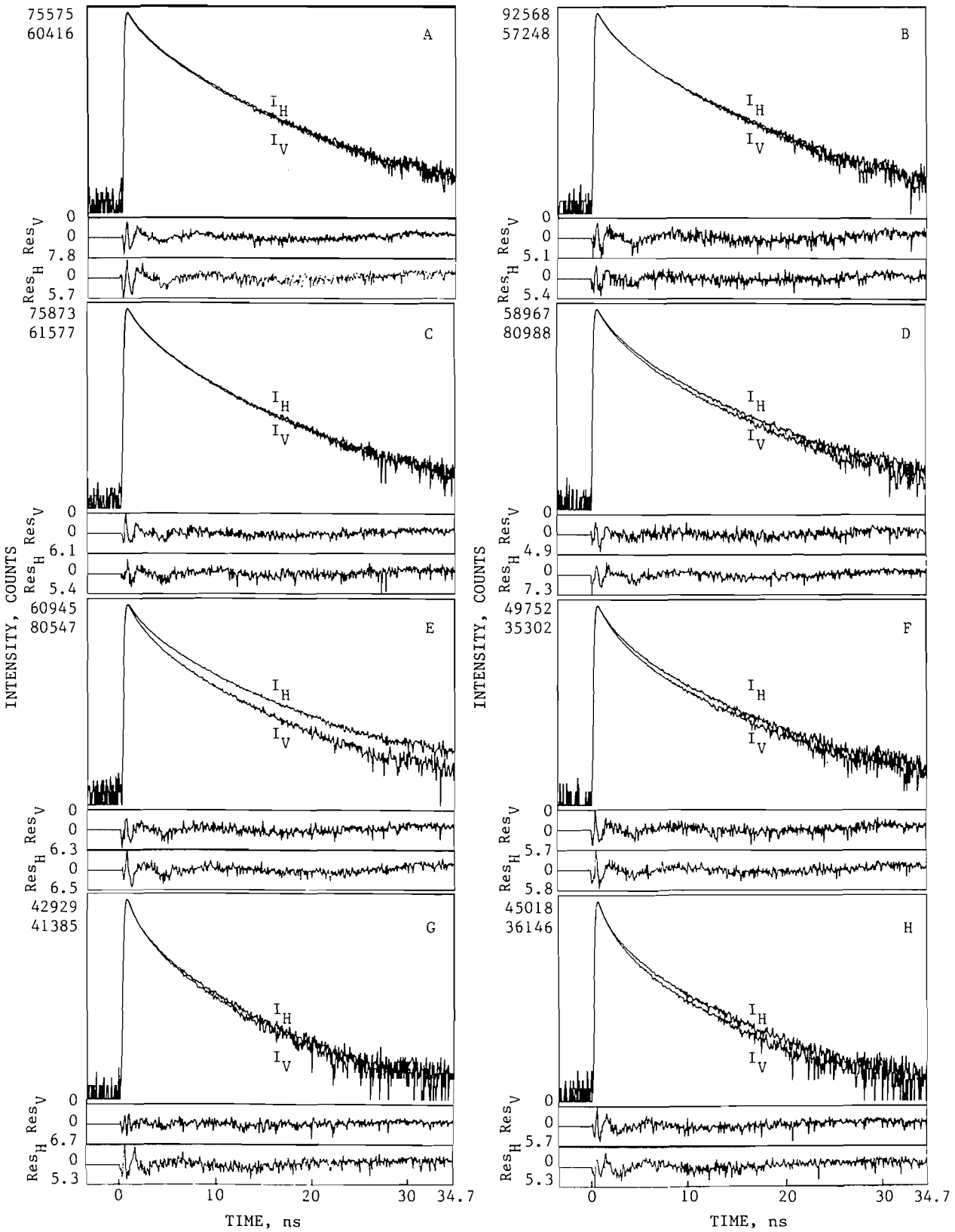

FIG. 4. Fluorescence decay of Gramicidin A′ in DPPC vesicles in the absence (A) and in the presence of 1.2×10^{-4} M CsCl (B); in DSPC vesicles in the absence (C) and in the presence of 1.2×10^{-4} M CsCl (D); in DOPC vesicles in the absence (E) and in the presence of 1.2×10^{-4} M CsCl (F); and in DPhPC vesicles in the absence (G) and in the presence of 1.2×10^{-4} M CsCl (H). Vesicles were prepared by sonication (0.5 mg lipid/1.0 mL H_2O). Gramicidin A′/lipid ratios were kept at 1:50. λ_{ex} = 294 nm (vertically polarized), λ_{em} = 340 nm. V = vertical (90°) and H = horizontal (0°) observation of the emission. The solid lines are the best fits of the experimental data fited to three exponential decays. Weighted sums of squared residuals are below the curves.

TABLE 5. Fluorescence decay parameters of Gramicidin A′ in vesicles at different polarizations[a]

		Polarization[b]	A_1	τ_1, ns	A_2	τ_2, ns	A_3	τ_3, ns	$\langle\tau\rangle$, ns[c]	χ^2
DPPC	H_2O	H	0.51±0.06	0.63±0.06	0.43±0.30	2.38±0.10	0.06±0.02	5.96±0.02	2.8	2.33
	H_2O	V	0.49±0.06	0.63±0.08	0.44±0.40	2.42±0.09	0.07±0.03	6.03±0.03	3.0	2.14
	1.2×10^{-4} M CsCl	H	0.52±0.06	0.69±0.07	0.42±0.03	2.45±0.08	0.06±0.01	6.09±0.02	2.8	1.78
	1.2×10^{-4} M CsCl	V	0.46±0.06	0.59±0.08	0.46±0.04	2.03±0.07	0.08±0.03	5.68±0.03	2.9	1.73
DSPC	H_2O	H	0.50±0.06	0.68±0.07	0.43±0.04	2.40±0.06	0.07±0.02	6.06±0.02	2.9	1.71
	H_2O	V	0.49±0.07	0.69±0.08	0.44±0.05	2.46±0.08	0.07±0.03	6.17±0.03	3.0	1.53
	1.2×10^{-4} M CsCl	H	0.50±0.06	0.68±0.07	0.44±0.03	2.37±0.09	0.06±0.03	5.98±0.04	2.9	1.45
	1.2×10^{-4} M CsCl	V	0.49±0.07	0.65±0.08	0.44±0.04	2.44±0.09	0.07±0.04	6.20±0.03	3.0	1.19
DOPC	H_2O	H	0.59±0.07	0.76±0.09	0.36±0.04	2.41±0.10	0.05±0.02	6.37±0.05	2.7	1.89
	H_2O	V	0.49±0.07	0.69±0.08	0.44±0.05	2.46±0.08	0.07±0.03	6.17±0.03	3.0	1.53
	1.2×10^{-4} M CsCl	H	0.59±0.07	0.76±0.08	0.37±0.05	2.36±0.07	0.04±0.02	6.34±0.05	2.7	1.84
	1.2×10^{-4} M CsCl	V	0.56±0.06	0.73±0.08	0.39±0.04	2.62±0.06	0.05±0.02	6.81±0.05	3.0	1.78
DPhPC	H_2O	H	0.60±0.04	0.37±0.05	0.35±0.05	1.66±0.05	0.05±0.02	4.80±0.05	2.0	1.85
	H_2O	V	0.60±0.06	0.36±0.05	0.35±0.04	1.65±0.09	0.05±0.02	4.98±0.06	2.2	1.75
	1.2×10^{-4} M CsCl	H	0.61±0.07	0.39±0.06	0.34±0.05	1.66±0.07	0.05±0.02	4.81±0.05	2.0	1.68
	1.2×10^{-4} M CsCl	V	0.61±0.06	0.35±0.07	0.33±0.04	1.68±0.06	0.06±0.01	5.21±0.04	2.4	1.70

[a]Decay parameters were measured at 25°C. Vesicles were prepared by sonication (0.5 mg lipid/1.0 mL H_2O). Gramicidin A′/lipid ratios were kept at 1:50. λ_{ex} = 294 nm, λ_{em} = 340 nm.
[b]V = vertical (90°) and H = horizontal (0°).
[c]Average lifetimes were calculated as $\langle\tau\rangle = \sum_i A_i\tau_i^2/\sum_i A_i\tau_i$.

below 340 nm. As an example, the emission spectrum of Gramicidin A′ in DPPC vesicles is shown in Fig. 1.

Gramicidin A′ steady-state fluorescence anisotropy, r values, in DPPC, DSPC, DOPC, and DPhPC vesicles in the absence and in the presence of added 1.2×10^{-4} M CsCl are collected in Table 1. Rotation of the tryptophans in DPPC was not affected by diluting the gramicidin. The r values, within the experimental error, remained the same for 1:50 and 1:1000 gramicidin/lipid ratios. These ratios correspond to having 25 and 1 gramicidin channels per vesicle, respectively. Phase transition temperatures of DPPC and DSPC (Table 1) are higher than the temperature of fluorescence measurements (25°C). Thus, Gramicidin A′ is spanning "solid" phases of vesicles prepared from DPPC and DSPC and the presence of ions in the channels is unlikely to influence the mobility of tryptophans. Since DOPC and DPhPC have low temperature phase transitions (Table 1), gramicidin anisotropies were determined in the fluid phases of vesicles prepared from these lipids. Addition of CsCl resulted in marked increases in the anisotropy and, hence, in appreciable decreases in tryptophan mobilities. This is attributed to shifting the gramicidin monomer ↔ gramicidin dimer equilibrium in favor of the latter (38, 39).

Typical Gramicidin A′ intensity decays, observed at 0° and 90°, in the absence and in the presence of added 1.2×10^{-4} M CsCl in vesicles prepared from DPPC, DSPC, DOPC, and DPhPC are shown in Fig. 4. Fluorescence decay components were not influenced by the sample used (Gramicidin A′, which is a mixture of Gramicidin A/Gramicidin B/Gramicidin C = 80:5:15) since identical lifetimes were obtained on using an authentic sample of Gramicidin A (see Tables 4 and 5).

Values of $\langle\tau\rangle$ for Gramicidin A′ in vesicles prepared from DPPC, DOPC, and DSPC are all in the 3.0 ± 0.3 ns range (Table 4). The average gramicidin fluorescence lifetimes in vesicles prepared from DOPC (2.5 ns), DMPC (3.5 ns), and EggPC (2.4 ns) reported previously by Scarlata (19) agree with values obtained in DPPC, DOPC, and DSPC vesicles in the present work (Table 4). Gramicidin in lysolecithin dispersions has a similar $\langle\tau\rangle$ value (3.4 ns; ref. 21). There is a notable deviation: the average gramicidin fluorescence lifetime in DPhPC vesicles is much shorter ($\langle\tau\rangle$ = 2.2 ns) than those determined in other vesicles in the present work (Table 4). Decrease in the average gramicidin fluorescence lifetime cannot be ascribed to the fluidity of DPhPC since DOPC is also fluid, but DPPC and DSPC are solid at the temperature of the experiments.

Conclusion

Advantage has been taken, in the present work, of intrinsic gramicidin fluorescence to obtain information on the behavior of this ionophore in GMO BLMs and vesicles. Although the emission spectrum of gramicidin in GMO BLMs was quite similar to that in vesicles, considerable differences were found in steady-state anisotropies and fluorescence lifetime parameters. In general, in BLMs, gramicidin anisotropy values were lower and fluorescence lifetimes were shorter than those in vesicles. The necessity of treating fluorescence lifetimes in terms of three exponential decays did not allow unambiguous assignments or warrant undue mechanistic interpretation. Nevertheless, the observed increase in the average gramicidin fluorescence lifetimes, paralleling the increased contribution of

Can. J. Chem. Downloaded from www.nrcresearchpress.com by 88.85.125.76 on 09/07/12
For personal use only.

the longer lived components with increasing applied potential across the GMO BLM, is highly significant and is likely to be the consequence of increased gramicidin dimerization.

Acknowledgments

Support of this work by a grant from the Natural Sciences and Engineering Research Council (NSERC) is gratefully acknowledged. We also express our sincere appreciation to Dr. Ranieri Rolandi for providing an authentic Gramicidin A sample.

1. D. W. URRY. Proc. Natl. Acad. Sci. U.S.A. **68**, 672 (1971).
2. D. W. URRY. *In* Membranes and transport. Vol. 2. *Edited by* A. Martonosi. Plenum Press, New York. 1982. p. 285.
3. D. W. URRY. *In* Modern physical methods in biochemistry. Part A. *Edited by* H. Neuberger and J. Van Deenan. Elsevier, New York. 1985. p. 266.
4. O. S. ANDERSON. Annu. Rev. Physiol. **46**, 531 (1984).
5. R. SARGES and B. WITKOP. J. Am. Chem. Soc. **86**, 1862 (1964).
6. B. A. WALLACE. Biophys. J. **49**, 295 (1986).
7. D. W. URRY, C. M. VENKATACHALAM, A. SPISNI, P. LAUGER, and M. A. KHALED. Proc. Natl. Acad. Sci. U.S.A. **77**, 2028 (1980).
8. D. W. URRY, J. T. WALKER, and T. L. TRAPANE. J. Membr. Biol. **69**, 225 (1982).
9. D. D. BUSATH and R. C. WALDBILLIG. Biochim. Biophys. Acta, **736**, 28 (1983).
10. J. A. KILLIAN and B. DE KRUIJFF. Chem. Phys. Lipids, **40**, 259 (1986).
11. J. A. KILLIAN, J. W. TIMMERMANS, S. KEUR, and B. DE KRUIJFF. Biochim. Biophys. Acta, **820**, 154 (1985).
12. E. HEITZ, A. HEITZ, and Y. TRUDELLE. Biophys. Chem. **24**, 149 (1986).
13. B. A. WALLACE. Biopolymers, **22**, 397 (1983).
14. D. A. LANGS. Science,**241**, 188 (1988).
15. B. A. WALLACE and K. RAVIKUMAR. Science, **241**, 182 (1988).
16. I. PASQUALI-RONCHETTI, A. SPISNI, E. CASALI, L. MASOTTI, and D. W. URRY. Biosci. Rep. **3**, 127 (1983).
17. C. S. A. VAN ECHTELD, B. DE KRUIJFF, A. J. VERKLEIJ, J. LEUNISSEN-BIJVELT, and J. DE GIER. Biochim. Biophys. Acta, **692**, 126 (1982).
18. P. M. MACDONALD and J. SEELIG. Biochemistry, **27**, 2357 (1988).
19. S. F. SCARLATA. Biophys. J. **54**, 1149 (1988).
20. P. CAVATORTA, A. SPISNI, E. CASALI, L. LINDNER, L. MASOTTI, and D. URRY. Biochim. Biophys. Acta, **689**, 113 (1982).
21. L. MASOTTI, P. CAVATORTA, G. SARTOR, E. CASALI, and A. G. SZABO. Biochim. Biophys. Acta, **862**, 265 (1986).
22. W. R. VEATCH, R. MATHIES, M. EISENBERG, and L. STRYER. J. Mol. Biol. **99**, 75 (1975).
23. W. VEATCH and L. STRYER. J. Mol. Biol. **113**, 89 (1977).
24. R. SARGES and B. WITKOP. Biochemistry, **4**, 2491 (1965).
25. E. GROSS and B. WITKOP. Biochemistry, **4**, 2495 (1965).
26. P. V. LOGRASSO, F. MOLL III, and T. A. CROSS. Biophys. J. **54**, 259 (1988).
27. J. H. FENDLER. Membrane mimetic chemistry. John Wiley, New York. 1982.
28. X. K. ZHAO, S. BARAL, R. ROLANDI, and J. H. FENDLER. J. Am. Chem. Soc. **110**, 1012 (1988).
29. S. BARAL and J. H. FENDLER. J. Am. Chem. Soc. **111**, 1604 (1989).
30. P. JONES, E. HAYON, and D. BUSATH. Biochim. Biophys. Acta, **861**, 62 (1986).
31. D. D. BUSATH and R. C. WALDBILLIG. Biochim. Biophys. Acta, **944**, 73 (1988).
32. M. STRÄSSLE, G. STARK, M. WILHELM, P. DAUMAS, F. HEITZ, and R. LAZARO. Biochim. Biophys. Acta, **980**, 305 (1989).
33. S. R. FLOM and J. H. FENDLER. J. Phys. Chem. **92**, 5908 (1988).
34. C. D. TRAN, G. S. BEDDARD, R. MCCONNELL, C. F. HOYNG, and J. H. FENDLER. J. Am. Chem. Soc. **104**, 3002 (1982).
35. C. D. BUSTER, J. F. HINTON, F. S. MILLET, and D. C. SHUNGU. Biophys. J. **53**, 145 (1988).
36. K. VOS, A. VAN HOEK, and A. J. W. G. VISSER. Eur. J. Biochem. **165**, 55 (1987).
37. E. JOHN and F. JÄHNIG. Biophys. J. **54**, 817 (1988).
38. A. RING and J. SANDBLOM. Biophys. J. **53**, 541 (1988).
39. A. RING and J. SANDBLOM. Biophys. J. **53**, 549 (1988).

Can. J. Chem. Downloaded from www.nrcresearchpress.com by 88.85.125.76 on 09/07/12
For personal use only.

Dialkyl and diaryl boron halides: reductive opening of benzylidene acetals

YVAN GUINDON,[1] YVES GIRARD,[2] SYLVIE BERTHIAUME, VIDA GORYS, RENÉ LEMIEUX, AND CHRISTIANE YOAKIM[1]
Bio-Méga Inc., 2100 Cunard, Laval (Québec), Canada H7S 2G5

Received December 4, 1989

YVAN GUINDON, YVES GIRARD, SYLVIE BERTHIAUME, VIDA GORYS, RENÉ LEMIEUX, and CHRISTIANE YOAKIM. Can. J. Chem. **68**, 897 (1990).

Dimethylboron bromide or diphenylboron bromide can be used in combination with borane to achieve the regiocontrolled conversion of benzylidene acetals to their corresponding hydroxy benzyl ethers with moderate to high yields.

Key words: dimethylboron bromide, diphenylboron bromide, reductive opening, benzylidene, acetals.

YVAN GUINDON, YVES GIRARD, SYLVIE BERTHIAUME, VIDA GORYS, RENÉ LEMIEUX et CHRISTIANE YOAKIM. Can. J. Chem. **68**, 897 (1990).

Le bromure de diméthylbore ou le bromure de diphénylbore peuvent être utilisés en présence de complexe borane–THF pour transformer de façon régiosélective un acétal de type benzylidène en un dérivé diol mono benzylé avec de bons à excellents rendements.

Mots clés : bromure de diméthylbore, bromure de diphénylbore, ouverture réductive, benzylidène, acétals.

Can. J. Chem. Downloaded from www.nrcresearchpress.com by 88.85.125.76 on 09/07/12
For personal use only.

Introduction

We have recently included benzylidene acetals in an ongoing study to better understand the reactivity and chemoselectivity (1) of dialkyl and diaryl boron halides. Moreover, during the course of this work, it was found that the application of these boron reagents to benzylidene acetals incorporating 1,3-dioxolane or 1,3-dioxane systems (2) offers, after a two-step sequence, a means of selective protection of the secondary hydroxyl in the presence of a primary hydroxyl group in 1,2- and 1,3-diol systems. This two-step sequence would involve initial protection of the primary and secondary hydroxyls as a benzylidene acetal, followed by Lewis acid induced reductive cleavage of the acetal to give the protected secondary alcohol.

The rearrangement of benzylidene acetals has been well documented. For instance, Hanessian and Pleassas (3), as well as Hullar and Siskin (4), have independently reported the cleavage of *O*-benzylidene protected sugars with *N*-bromosuccinimide (NBS) to afford the corresponding bromo benzoates. A modification of this reaction employing NBS and photochemical initiation was used by Binkley *et al.* (5) to give the corresponding hydroxy benzoates, which can also be produced via oxidative cleavage of benzylidene acetals with ozone (6).

Reductive ring cleavage of benzylidene acetals can be achieved using different reducing reagents under acidic conditions. For example, reagents such as sodium cyanoborohydride combined with acetic acid or trifluoroacetic acid (7), lithium aluminum hydride with aluminum chloride (8) or diisobutylaluminum hydride (9), and sodium cyanoborohydride with hydrogen chloride (10) have been utilized. Although some of these reactions have proven useful, those that employ strong reducing agents are restricted in their use, particularly in the presence of sensitive functionalities. Moreover, in some cases, protection of the less substituted alcohol occurs preferentially when an unsymmetrical benzylidene acetal is cleaved (10).

We would like to report herein the tandem use of dimethyl (or diphenyl) boron bromide and borane for the regiocontrolled conversion of benzylidene acetals to their corresponding hydroxy benzyl ethers. The scope and limitations of this method will also be discussed.

1 $R^1 = R^2 = Me$ **2** $R^1 = R^2 = H$

3 $R^1 = H$, $R^2 = Ph$ **4** $R^1 = BMe_2$, $R^2 = CH(Br)Ph$

5 $R^1 = H$, $R^2 = CH(SPh)Ph$

SCHEME 1

Results and discussion

Reactivity of benzylidene acetals to Me_2BBr

Our preliminary work showed that various acetals and ketals react with dimethylboron bromide at −78°C to afford within 1 h the corresponding α-bromo ethers, which serve as useful intermediates for the synthesis of thioglycosides, cyanomethyl ethers, and hemithioacetals (11). Under these conditions, for example, the acetonide **1** (Scheme 1) afforded the diol **2** in 86% yield. However, treatment of the benzylidene acetal **3** under similar conditions gave only starting material. The apparent lack of reactivity of the benzylidene acetal in the latter case was rather surprising in light of our previous results. It was possible that the benzylidene acetal had indeed reacted with Me_2BBr to give the intermediate bromo ether **4**, which subsequently recyclized to give the starting material **3** after hydrolysis of the borinate ester and intramolecular displacement of bromide. To test this hypothesis, a nucleophile was added after treatment with Me_2BBr in an attempt to trap the presumed ring-opened intermediate. Indeed treatment of **3** at −78°C with Me_2BBr followed by the addition of 3 equivalents of thiophenol in the presence of triethylamine gave the corresponding hydroxy *O*,*S*-acetal **5** in 85% yield.

The reaction of a number of polyfunctional benzylidene acetals incorporating substituted 1,3-dioxolane or 1,3-dioxane systems illustrates the scope of this process. As shown in

[1]Authors to whom correspondence may be addressed.

[2]Merck Frosst Canada Inc., P.O. Box 1005, Pointe-Claire (Quebec), Canada H9R 4P7.

TABLE 1. Reductive cleavage of symmetrical benzylidenes using Me_2BBr[a]

ENTRY	SUBSTRATE	REAGENT	PRODUCT	YIELD (%)[b]
1	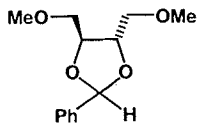 **6**	PhSH[c]	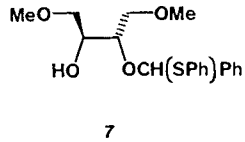 **7**	88
2	**6**	Super Hydride[d]	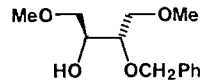 **8**	62
3	**6**	DIBAL-H[d]	**8**	80
4	**6**	BH_3•THF[e]	**8**	96
5	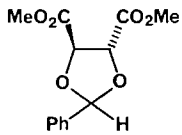 **9**	PhSH[c]	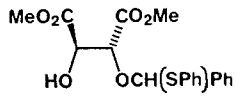 **10**	92
6	**9**	BH_3•THF[e]	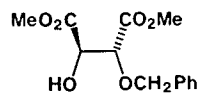 **11**	75
7	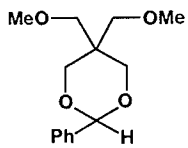 **12**	PhSH[c]	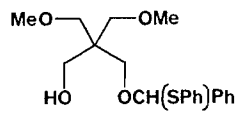 **13**	70
8	**12**	BH_3•THF[e]	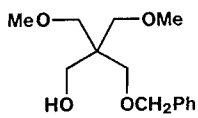 **14**	91

[a] *All reactions were carried out at a concentration of 0.2M in CH_2Cl_2 using 0.1 equiv of Et_3N and 2.2 equiv of Me_2BBr at -78°C for 45 min.*

[b] *Yields of isolated products.*

[c] *PhSH (3.0 equiv) and Et_3N (3.5 equiv) were added and the reaction mixture was stirred at -78°C for 1 h.*

[d] *DIBAL or Super Hydride (2.0 equiv) was added and the reaction mixture was stirred at -78°C for 1 h.*

[e] *BH_3•THF (2.0 equiv) was added at -78°C and the reaction mixture was warmed to -20°C for 1 h.*

Table 1, both five- and six-membered analogs were converted to the corresponding monoprotectd diols in excellent yields. Notably, methyl ethers **6** and **12** and methyl ester **9** are stable under the reaction conditions. To generate a monobenzylated diol as the product of benzylidene ring cleavage, a hydride source was used as the nucleophile. Both Super-Hydride (entry 2) and diisobutylaluminum hydride (entry 3) were found to react rapidly with the intermediate arising from **6** at −78°C to give **8** in good yields. Borane–tetrahydrofuran (BH_3·THF) complex reacted cleanly (entries 4, 6, 8), although it was necessary to warm the reaction mixture to −20°C. The advantage of these latter conditions is the chemoselective conversion of a benzylidene acetal to a monobenzylated diol in the presence of an ester.

Reductive cleavage of unsymmetrical benzylidene acetals

To investigate the regioselectivity of the reductive cleavage of benzylidene acetals upon reaction with Me_2BBr/borane,

Can. J. Chem. Downloaded from www.nrcresearchpress.com by 88.85.125.76 on 09/07/12
For personal use only.

TABLE 2. Reductive cleavage of unsymmetrical benzylidene acetals[a]

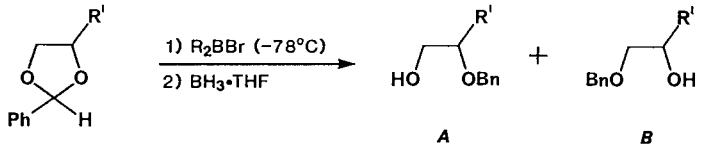

ENTRY	SUBSTRATE	R	RATIO A/B[b]	YIELD (%)[c]
1	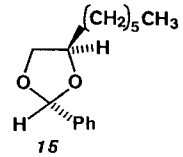 15	Me	14:1	83
2	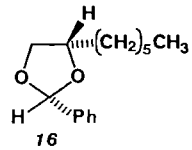 16	Me	6:1	93
3	16	Ph	10:1	90
4	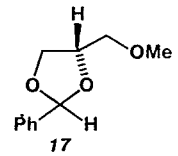 17	Me	2:1	80
5	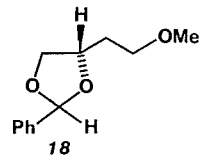 18	Me	4:1	98
6	18	Ph	8:1	97

[a] *All reactions were carried out at a concentration of 0.2M in CH_2Cl_2 using 0.1 equiv of Et_3N and 2.2 equiv of Me_2BBr or Ph_2BBr at -78°C for 45 min. BH_3•THF (2.0 equiv) was then added and the reaction mixture was warmed to -20°C during 1 h.*

[b] *The ratio was determined by ^1H NMR spectral analysis of the reaction mixture.*

[c] *Isolated yield of isomeric mixture.*

unsymmetrically substituted acetals were used. As shown in Table 2, it is possible to generate predominately the primary alcohol **A** rather than the secondary alcohol **B**. This regioselectivity is attributed to the preferential complexation of the less hindered oxygen with the boron reagent, followed by reductive ring cleavage to give the secondary alcohol protected as a benzyl ether. It is noteworthy that greater regioselectivity for the primary alcohol **A** is observed for the *trans*-disubstituted dioxolane (entry 1) than for the corresponding *cis*-disubstituted dioxolane (entry 2). For the *trans* isomer the complexation of the boron reagent to the oxygen corresponding to the secondary alcohol would be less favoured owing to the steric congestion of a substituent on both α and β faces.

Such regioselectivity might also be enhanced by the use of bulkier ligands on the boron reagent. Indeed, this hypothesis was confirmed by the use of diphenylboron bromide, which exhibited a greater preference for the formation of **A** over **B** (entries 3 and 6 compared with 2 and 5, respectively).

The regioselectivity may be altered by the presence of neighboring functionalities capable of coordinating with the boron halide, a similar effect observed in the boron bromide mediated ring opening of tetrahydrofuran systems (1*b*). For example, in the presence of a methyl ether (as in **17**) proximal to the reactive acetal it is possible to form a bidentate complex (see Scheme 2),[3] which would favor the formation of the secondary alcohol **B** more than the analogous systems in which functionalities capable of chelation are absent. Poorer regioselectivity was observed in those examples (entries 4 and 5) where anchimeric participation competes with steric factors.

[3]As suggested by one referee, complexation of the borane to the exocyclic methoxy group could explain the loss in regiocontrol based on the principal of least chemical distance argument (i.e., monodentate vs. bidentate explanation). It is reasonable to suggest, based on our previous results, that an ester could replace the ether functionality as a coordinating species (1*b*).

Can. J. Chem. Downloaded from www.nrcresearchpress.com by 88.85.125.76 on 09/07/12
For personal use only.

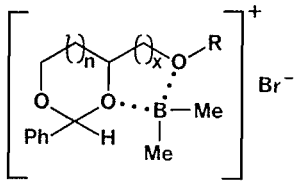

SCHEME 2

Such bidentate complexation is destabilized by the use of the bulkier diphenylboron bromide reagent, thus improving selectivity for **A**, as illustrated by the comparison between entries 5 and 6.

Although more complex, the 1,3-dioxane benzylidene acetal derivatives of methyl pyranosides (see Table 3), upon treatment with boron bromides, were found to rearrange in the same fashion as the simpler acetal system described above. That is, complexation of the boron bromide reagent with the least hindered oxygen of the acetal is followed by ring cleavage and formation of the putative acyclic bromo acetal intermediate, which is subsequently trapped in excellent yields with nucleophiles such as thiolate (entry 1). The results obtained for the simpler unsymmetrical benzylidene acetals (as above) would lead one to predict that the regioselectivity arising from the coordination of the boron bromide to the *O*-6 of the pyranoside would increase as bulkier boron reagents are used (i.e., dimethylboron bromide < diphenylboron bromide = 9-borobicyclo[3.3.1]nonanyl bromide (9-BBN-Br)). Indeed, when dimethylboron bromide was reacted with **19** (entry 1) and the reaction was quenched with thiophenol, the primary alcohol **20** was obtained as the major isomer in a 4:1 ratio. In contrast, the use of the bulkier diphenylboron and 9-BBN bromides (entries 2 and 3, respectively) gave **20** as the sole product detected.

High regioselectivity was observed as well when BH_3·THF complex served as the trapping agent (entry 4). The reagent combination of dialkylboron bromide/BH_3·THF offers a significant advantage over reagents such as $LiAlH_4$–$AlCl_3$ (12), the use of which requires the presence of a large protective group such as a benzyl ether at *O*-3 in order to obtain practical yields of the primary alcohol. In other words, it is necessary to increase the steric factor at *O*-3 to decrease the coordination of *O*-4 with $AlCl_3$ prior to ring cleavage and hydride delivery by $LiAlH_4$. However, when diphenyl boron bromide/BH_3·THF was used, a methyl ether at *O*-3 sufficed to afford exclusively the 4-*O*-benzyl ether **22** in excellent yield. Moreover, a comparison of entries 4 and 5 demonstrates that the regioselectivity in favor of the primary alcohol is unaffected by the anomeric configuration.

A potential limitation of the described protocol for cleavage of the benzylidene acetals is the necessity to work with protected hydroxyl groups in order to avoid the hydrolysis of the boron halides to Brønsted acids, which could affect the product ratio (13). It has been reported that the treatment of benzylidene acetal pyranosides with such acids leads to the formation of 6-*O*-benzyl derivatives, the regioselectivity of which has been attributed to the relative acidities of *O*-4 versus *O*-6 (7, 10). A more plausible explanation might be the existence of an equilibrium between the primary (*O*-6) and secondary (*O*-4) oxonium species (or corresponding halo ethers) arising from the parent acetal and the faster rate of hydride delivery to the former species. Another limitation of the described reductive cleavage employing the tandem addition of dialkyl (diaryl) boron bromide – borane reagents is the reactivity of these Lewis acids with other functionalities (14) besides benzylidene acetals. For example, we have reported the Me_2BBr-induced endocyclic and exocyclic carbon–oxygen bond cleavage at the glycosidic centers of carbohydrate derivatives (14*b*). Since the anomeric centres of the 2-deoxy series were found to be particularly reactive with dimethylboron bromides, it is not surprising that a complex mixture was obtained when the 2-deoxy benzylidene acetal **25** was subjected to the tandem addition of dimethylboron bromide and thiophenol (entry 6 of Table 3).

Conclusion

Dimethylboron and diphenylboron bromides are versatile reagents for the cleavage of benzylidene acetals under mild conditions. Under such conditions, these boron-based Lewis acids exhibit good chemoselectivity and therefore predictable reactivity. Bromo ether – borinate esters resulting from the ring cleavage can be quenched with thiophenol to yield hydroxy *O*,*S*-acetals, or can be reduced with different hydride sources to give monobenzylated diols. The regioselectivity of these reactions can be predicted on the basis of steric and anchimeric considerations.

Experimental

General

Infrared (ir) spectra were recorded on a Perkin–Elmer model 681 or 781 spectrophotometer. Proton nuclear magnetic resonance (^{1}H nmr) spectra were recorded on a Bruker AM250 or a Bruker AC200, using in all instances tetramethylsilane as a reference. Mass spectrometric measurements were performed by Morgan Schaffer, Montreal, Quebec, using a Hitachi Perkin–Elmer RMV-6D mass spectrometer. Elemental analyses were performed by Guelph Chemical Laboratories Ltd., Guelph, Ontario. Flash chromatography was accomplished using 230–400 mesh silica gel (E. Merck).

All reactions were carried out under inert atmosphere of nitrogen. Glassware and syringes were dried in an oven (120°C) prior to use. Chlorinated solvents as well as triethylamine were distilled from CaH_2 and stored over 4 Å molecular sieves.

Dimethylboron bromide was purchased from the Alfa Division of Ventron Corp. or from Aldrich Chemical Co. or prepared from tetrabutyltin and boron tribromide (1*d*). Diphenylboron bromide was purchased from Alfa. Solutions of these reagents were prepared in dry CH_2Cl_2 (1.5–2.0 M) and could be stored at −5°C for several months without noticeable decomposition. Solutions of β-bromo-9-BBN in CH_2Cl_2 were used as purchased (Aldrich Chemical Co.). Starting materials were obtained from Aldrich Chemical Co. or prepared under standard conditions (2).

Representative procedure A for the rearrangement of benzylidene acetals using thiophenol as nucleophile. Preparation of O,S-*acetal* **7**

To a cold (−78°C), stirred solution of the benzylidene **6** (76 mg, 0.32 mmol) in 1.5 mL of dry CH_2Cl_2 were added successively Et_3N (9 μL, 0.064 mmol) and a solution of Me_2BBr (2.1 M, 335 μL) in CH_2Cl_2. The reaction mixture was stirred at −78°C for 45 min and then treated with Et_3N (1.12 mmol) and a solution of thiophenol in CH_2Cl_2 (1 M, 960 μL). After 1 h at −78°C the mixture was cannulated into a saturated aqueous solution of $NaHCO_3$ (5 mL). Ether (20 mL) was then added. The layers were separated and the organic layer was successively washed with saturated aqueous $NaHCO_3$, water, and brine, and dried over anhydrous $MgSO_4$. Removal of solvent and purification by flash chromatography gave the hydroxy compound **7** in 88% yield: ir (neat): 3450 (OH) cm^{-1}; ^{1}H nmr ($CDCl_3$) δ: 2.70 (br s, 1H, OH, D_2O exchangeable), 3.35 (s, 3H, OCH_3), 3.36 (s, 3H, OCH_3), 3.40–3.70 (m, 5H, $2CH_2OMe$, CHO), 4.87 (m, 1H, CHOH), 6.10 (2s, 1H, CHAr), 7.20–7.55 (m, 10H, 2Ar). Mass spectrum, *m/e*: 239 (M^+ − SPh). Anal. calcd. for $C_{19}H_{24}O_4S$: C 65.43, H 6.94, S 9.20; found: C 65.43, H 6.68, S 9.38.

Can. J. Chem. Downloaded from www.nrcresearchpress.com by 88.85.125.76 on 09/07/12
For personal use only.

TABLE 3. Reductive cleavage of benzylidene acetals of pyranosides

ENTRY	SUBSTRATE	REAGENTS[a]	PRODUCTS	YIELD (%)[b]
1	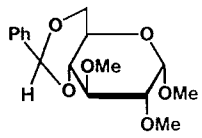 **19**	1) Me_2BBr 2) PhSH	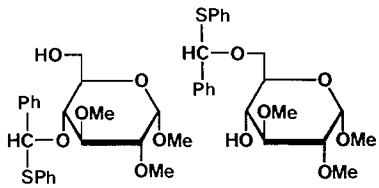 **20** **21**	85 (RATIO[c] 4 : 1)
2	**19**	1) Ph_2BBr 2) PhSH	**20**	96
3	**19**	1) 9-BBN-Br 2) PhSH	**20**	90
4	**19**	1) Ph_2BBr 2) BH_3•THF	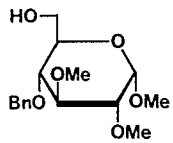 **22**	88
5	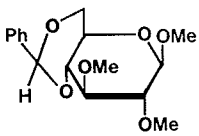 **23**	1) Ph_2BBr 2) BH_3•THF	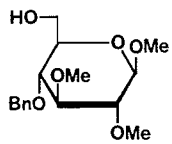 **24**	90
6	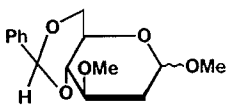 **25**	1) Me_2BBr 2) PhSH	COMPLEX MIXTURE	—

[a] All reactions were carried out at a concentration of 0.2 M in CH_2Cl_2 using 0.1 equiv of Et_3N and 2.2 equiv of Me_2BBr or Ph_2BBr at -78°C for 45 min. PhSH (3.0 equiv) and Et_3N (3.5 equiv) were then added and stirred at -78°C for 1 h., or BH_3•THF (2.0 equiv) was added and the reaction mixture was warmed to -20°C during 1 h.

[b] Yields of isolated products.

[c] The ratio was determined by ^1H NMR spectral analysis of the reaction mixture.

Representative procedure B for the formation of benzyl ethers using Super Hydride or diisobutylaluminium hydride. The preparation of benzyl ether 8

To a cold (−78°C) solution of benzylidene **6** (1.0 mmol) in 3.8 mL of dry CH_2Cl_2, under nitrogen, were added successively Et_3N (0.2 mmol) and a solution of Me_2BBr (2.1 M, 2.2 mmol). After 45 min at −78°C the reaction mixture was treated with Super Hydride or DIBAL-H (2.0 equiv.) and stirred at −78°C for 1 h. Saturated aqueous $NaHCO_3$ (10 mL) and Et_2O (40 mL) were then added. The organic layer was washed with H_2O, then with brine, and dried over anhydrous $MgSO_4$. Concentration and purification by flash chromatography gave pure benzyl ether **8** in 62 and 80% yield respectively; ir (neat): 3425 (OH) cm^{-1}; ^1H nmr ($CDCl_3$) δ: 2.60 (br s, 1H, OH, D_2O exchangeable), 3.35 (s, 3H, OCH_3), 3.36 (s, 3H, OCH_3), 3.40–3.70 (m, 5H, $2CH_2OMe$, CHOBn), 4.60, 4.80 (2d, 2H, CH_2Ar), 4.87 (m, 1H, CHOH), 7.20–7.40 (m, 5H, Ar). Mass spectrum, *m/e*: 240 (M^+). Anal. calcd. for $C_{13}H_{20}O_4$: C 64.98, H 8.39; found: C 64.89, H 8.30.

Representative procedure C for the formation of benzyl ethers using BH_3·THF. The preparation of benzyl ether 8

Following the same procedure as described in B with the exception that BH_3·THF complex (2.0 equiv.) was added (instead of Super Hydride or DIBAL-H) at −78°C and the reaction mixture was allowed to warm to −20°C for 1 h. The solution was then diluted with Et_2O (40 mL) and H_2O (10 mL) and treated as described above to afford benzyl ether **8** in 96% yield.

Compound 5 was obtained as a diastereoisomeric mixture using procedure A: ir (neat): 3470 (OH) cm^{-1}; ^1H nmr ($CDCl_3$) δ: 1.10–1.95 (m, 10H), 2.25, 2.50 (2s, 1H, OH), 3.30–3.40, 3.50–3.65 (2m, 2H, 2CHO), 7.20–7.55 (m, 10H, 2Ar). Mass spectrum, *m/e*: 219 (M^+ −

Can. J. Chem. Downloaded from www.nrcresearchpress.com by 88.85.125.76 on 09/07/12
For personal use only.

Can. J. Chem. Downloaded from www.nrcresearchpress.com by 88.85.125.76 on 09/07/12
For personal use only.

SPh). Anal. calcd. for $C_{20}H_{24}O_2S$: C 73.13, H 7.36, S 9.76; found: C 72.89, H 7.55, S 9.70.

Compound ***10*** was obtained as a diastereoisomeric mixture using procedure A: ir (neat): 3500 (OH), 1700 (CO) cm^{-1}; ^1H nmr ($CDCl_3$) δ: 3.10 (d, 1H, OH), 3.65, 3.66, 3.72, 3.79 (4s, 6H, $2CO_2Me$), 4.30, 5.15 (2d, 1H, CHO), 4.65 (dd, 1H, CHOH), 6.03, 6.21 (2s, 1H, CH-Ar), 7.25–7.50 (m, 10H, 2Ar). Mass spectrum, *m/e*: 267 (M^+ − SPh).

Compound ***11*** was obtained as an oil using procedure C; ^1H nmr ($CDCl_3$) δ: 3.46 (dd, 1H, OH), 3.66, 3.84 (2s, 6H, $2CO_2Me$), 4.33, 4.60 (2d, 2H, 2CHO), 4.42, 4.87 (2d, 2H, CH_2-Ar), 7.25–7.36 (m, 5H, Ar). Mass spectrum, *m/e*: 269 (M^+ + 1). Anal. calcd. for $C_{13}H_{16}O_6$: C 58.20, H 6.01; found: C 58.41, H 6.07.

Compound ***13*** was obtained as a diastereoisomeric mixture using procedure A; ir (neat): 3450 (OH) cm^{-1}; ^1H nmr ($CDCl_3$) δ: 2.80 (br s, 1H, OH), 3.29 (s, 6H, $2OCH_3$), 3.40, 3.41 (2s, 4H, $2CH_2OMe$), 3.65–3.70 (m, 2H, CH_2OH), 3.45–3.47, 3.82–3.86 (2m, 2H, CH_2O), 5.42, 5.75 (2s, 1H, CH-Ar), 7.20–7.50 (m, 10H, 2Ar). Mass spectrum, *m/e*: 253 (M^+ − SPh). Anal. calcd. for $C_{20}H_{26}O_4S$: C 66.27, H 7.23, S 8.85; found: C 66.55, H 6.90, S 8.95.

Compound ***14*** was obtained as an oil using procedure C; ir (neat): 3425 (OH) cm^{-1}; ^1H nmr ($CDCl_3$) δ: 2.90 (br s, OH, D_2O exchangeable), 3.32 (s, 6H, 2OMe), 3.44 (s, 4H, $2CH_2OMe$), 3.50 (s, 2H, CH_2OBn), 3.71 (s, 2H, CH_2OH), 4.50 (s, 2H, CH_2-Ar), 7.27–7.38 (m, 5H, Ar). Mass spectrum, *m/e*: 254 (M^+). Anal. calcd. for $C_{14}H_{22}O_4$: C 66.12, H 8.72; found: C 66.09, H 8.60.

Compound ***15A*** was obtained as an oil using procedure C; ir (neat): 3430 (OH) cm^{-1}; ^1H nmr ($CDCl_3$) δ: 0.90 (t, 3H, CH_3), 1.20–1.60 (m, 10H, $5CH_2$), 2.00 (t, 1H, OH, D_2O exchangeable), 3.45–3.75 (m, 3H, CH_2OH, CHOBn), 4.65 (2d, 2H, CH_2-Ar), 7.30–7.45 (m, 5H, Ar). Anal. calcd. for $C_{15}H_{24}O_2$: C 76.23, H 10.23; found: C 76.16, H 10.10.

Compound ***15B*** was obtained as an oil using procedure C; ir (neat): 3400 (OH) cm^{-1}; ^1H nmr ($CDCl_3$) δ: 0.88 (t, 3H, CH_3), 1.18–1.50 (m, 10H, $5CH_2$), 2.35 (d, 1H, OH, D_2O exchangeable), 3.28–3.35, 3.48–3.55 (2m, 2H, CH_2OBn), 3.75–3.90 (m, 1H, CHOH), 4.58 (s, 2H, CH_2-Ar), 7.30–7.45 (m, 5H, Ar). Mass spectrum, *m/e*: 236 (M^+). Anal. calcd. for $C_{15}H_{24}O_2$: C 76.23, H 10.23; found: C 76.16, H 10.10.

Compound ***17A + 17B*** was obtained as an oil using procedure C; ir: 3430 (OH) cm^{-1}; ^1H nmr ($CDCl_3$) δ: 3.35 (s, 3H, OCH_3), 3.50–3.70 (m, 5H, CH_2OMe, CHO, CH_2O), 4.54 (s, 2H, CH_2-Ar, **17B**); 4.55 (2d, CH_2-Ar, **17A**), 7.25–7.40 (m, 5H, Ar). Mass spectrum, *m/e*: 196 (M^+).

Compound ***18A*** was obtained as an oil using procedure C; ir (neat): 3450 (OH) cm^{-1}; ^1H nmr ($CDCl_3$) δ: 1.75–2.00 (m, 2H, CH_2), 2.20 (br s, 1H, OH, D_2O exchangeable), 3.35 (s, 3H, OCH_3), 3.42–3.52 (m, 2H, CH_2OMe), 3.53–3.78 (m, 3H, CH_2OH, CHOBn), 4.60 (s, 2H, CH_2-Ar), 7.30–7.43 (m, 5H, Ar). Mass spectrum, *m/e*: 179 (M^+ − OMe). Anal. calcd. for $C_{12}H_{18}O_3$: C 68.55, H 8.63; found: C 68.15, H 8.59.

Compound ***18B*** was obtained as an oil using procedure C; ir (neat): 3500 (OH) cm^{-1}; ^1H nmr ($CDCl_3$) δ: 1.65–1.80 (m, 2H, CH_2), 2.05 (br s, OH, D_2O exchangeable), 3.35 (s, 3H, OCH_3), 3.20–3.40 (m, 2H, CH_2OMe), 3.70 (t, 2H, CH_2OBn), 3.93–4.05 (m, 1H, CHOH), 4.56 (s, 2H, CH_2-Ar), 7.28–7.40 (m, 5H, Ar). Mass spectrum, *m/e*: 179 (M^+ − OMe). Anal. calcd. for $C_{12}H_{18}O_3$: C 68.55, H 8.63; found: C 68.15, H 8.59.

Compound ***20*** was obtained as a diastereoisomeric mixture using procedure A; ^1H nmr ($CDCl_3$) δ: 3.10–3.25 (m, 1H, H-2), 3.28, 3.38, 3.45 (3s, 9H, OMe), 4.75, 4.85 (2d, 1H, H-1), 6.18, 6.42 (2s, 1H, CH-Ar), 7.19–7.57 (m, 10H, 2Ar). Mass spectrum, *m/e*: 419 (M^+ − 1). Anal. calcd. for $C_{22}H_{28}O_6S$: C 62.83, H 6.71, S 7.62; found: C 62.25, H 6.95, S 7.18.

Compound ***21*** was obtained as a diastereoisomeric mixture using procedure A; ^1H nmr ($CDCl_3$) δ: 1.56, 2.40 (2 br s, 1H, OH), 3.10–3.37 (m, 1H, H-2), 3.39, 3.49, 3.63 (3s, 9H, 3OMe), 3.40–3.55 (m, 2H, H-3, H-5), 3.70–3.85 (m, 2H, H-6), 4.02–4.20 (m, 1H, H-4); 4.78–4.85 (m, 1H, H-1), 5.86–6.18 (2s, 1H, CH-Ar), 7.15–7.55 (m, 10H, 2Ar). Mass spectrum, *m/e*: 419 (M^+ − 1). Anal. calcd. for $C_{22}H_{28}O_6S$: C 62.83, H 6.71, S 7.62; found: C 62.15, H 6.98, S 7.14.

Compound ***22*** was obtained using procedure C; ^1H nmr ($CDCl_3$) δ: 1.45 (br s, 1H, OH), 3.22 (dd, 1H, H-2), 3.41 (s, 3H, OMe), 3.48 (m, 1H, H-4), 3.55 (s, 3H, OMe), 3.68 (s, 3H, OMe), 3.55–3.70 (m, 2H, H-3, H-5), 3.72–3.85 (m, 2H, H-6), 4.65, 4.90 (2d, 2H, CH_2-Ar), 4.84 (d, 1H, H-1), 7.30–7.43 (m, 5H, Ar). Mass spectrum, *m/e*: 312 (M^+). Anal. calcd. for $C_{16}H_{24}O_6$: C 61.52, H 7.74; found: C 61.20, H 7.62.

Compound ***24*** was obtained using procedure C; ^1H nmr ($CDCl_3$) δ: 1.85 (t, 1H, OH); 3.00 (dd, 1H, H-2), 3.27–3.54 (m, 3H, H-3, H-4, H-5), 3.55, 3.59, 3.65 (3s, 9H, OMe), 3.60–3.90 (m, 2H, H-6), 4.22 (d, 1H, H-1), 4.64, 4.86 (2d, 2H, CH_2-Ar), 7.30–7.40 (m, 5H, Ar). Mass spectrum, *m/e*: 312 (M^+). Anal. calcd. for $C_{16}H_{24}O_6$: C 61.52, H 7.74; found: C 61.44, H 7.70.

Acknowledgements

To the Natural Sciences and Engineering Research Council of Canada for an Industrial COOP Fellowship (R. Lemieux). The authors would like to thank Dr. J. Manson and Dr. G. Jung for their assistance during the preparation of this manuscript.

1. (*a*) Y. Guindon, P. C. Anderson, C. Yoakim, Y. Girard, S. Berthiaume, and H. E. Morton. Pure Appl. Chem. **60**, 1705 (1988); (*b*) Y. Guindon, M. Therien, Y. Girard, and C. Yoakim. J. Org. Chem. **52**, 1680 (1987); (*c*) Y. Guindon, J. G. Atkinson, and H. E. Morton. J. Org. Chem. **49**, 4538 (1984).
2. T. W. Greene. Protective groups in organic synthesis, Wiley–Interscience, New York. 1981.
3. S. Hanessian and N. R. Pleassas. J. Org. Chem. **34**, 1035 (1969); **34**, 1045 (1969); **34**, 1053 (1969).
4. T. L. Hullar and S. B. Siskin. J. Org. Chem. **35**, 225 (1970).
5. R. W. Binkley, G. S. Goewey, and J. C. Johnston. J. Org. Chem. **49**, 992 (1984).
6. P. Deslongchamps, C. Moreau, D. Fredel, and R. Chênevert. Can. J. Chem. **53**, 1204 (1975).
7. R. Johannson and B. Samuelsson. J. Chem. Soc. Perkin Trans. 1, 2371 (1984).
8. (*a*) E. L. Eliel, V. G. Badding, and M. N. Rerick. J. Am. Chem. Soc. **84**, 2371 (1962); (*b*) E. L. Eliel, L. Pilato, and V. G. Badding. J. Am. Chem. Soc. **84**, 23377 (1962).
9. S. Takano, M. Akiyama, S. Sato, and K. Ogagawara. Chem. Lett. 1593 (1983).
10. P. J. Garegg, H. Hultberg, and S. Wallin. Carbohydr. Res. **108**, 97 (1982).
11. H. E. Morton and Y. Guindon. J. Org. Chem. **50**, 5379 (1985).
12. A. Liptak, I. Jodal, and P. Nanasi. Carbohydr. Res. **44**, 1 (1975).
13. S. S. Bhattacharjee and P. A. J. Gorin. Can. J. Chem. **47**, 1195 (1969).
14. (*a*) Y. Guindon, M. A. Bernstein, and P. C. Anderson. Tetrahedron Lett. **28**, 2225 (1987); (*b*) Y. Guindon and P. C. Anderson. Tetrahedron Lett. **28**, 2485 (1987).

A novel electrochemical method for benzoylation of aminoalcohols with methyl benzoates at room temperature

KENJI ARAI, SHOHEI TAMURA, TATSUYA MASUMIZU, KEN-ICHI KAWAI, AND SHOICHI NAKAJIMA[1]
Faculty of Pharmaceutical Sciences, Hoshi University, Ebara 2-4-41, Shinagawa-ku, Tokyo, Japan 142
AND
AKIRA UEDA
Central Research Inst., Mitsubishi Metal Corporation, Kitafukuro 1-297, Oomiya, Saitama-ken, Japan 330
Received March 30, 1989[2]

KENJI ARAI, SHOHEI TAMURA, TATSUYA MASUMIZU, KEN-ICHI KAWAI, SHOICHI NAKAJIMA, and AKIRA UEDA. Can. J. Chem. **68**, 903 (1990).

A novel electrochemical method of benzoylating aminoalcohols **2** by use of methyl benzoates **1** at room temperature was developed. 2-Aminoethanols **2** ($n = 0$, $R^3 = H$) and 3-aminopropanols **2** ($n = 1$, $R^3 = H$) gave the corresponding benzamides **4**, as a result of electrochemical transesterification followed by *O,N*-actyl migration. In contrast, *o*- and *m*-aminobenzylalcohols (**7***a* and **7***b*) and *trans*-4-(aminomethyl)cyclohexanemethanol (**8***a*) afforded the corresponding benzoic esters, since their acyl migration is hindered. A local anesthetic, procaine, was prepared by using this electrochemical reaction. A mechanism for electrochemical transesterification, which involves a formation of alcoholate anion by a one-electron reduction of alcohol, is presented.

Key words: amides, aminoalcohols, benzoylation, electrochemical, esters.

KENJI ARAI, SHOHEI TAMURA, TATSUYA MASUMIZU, KEN-ICHI KAWAI SHOICHI NAKAJIMA et AKIRA UEDA. Can. J. Chem. **68**, 903 (1990).

On a mis au point une nouvelle méthode électrochimique permettant de benzoyler des aminoalcools de type **2** à l'aide de benzoates de méthyle de type **1**, à la température ambiante. Les 2-aminoéthanols **2** ($n = 0$, $R^3 = H$) et 3-aminopropanols **2** ($n = 1$, $R^3 = H$) fournissent les benzamides **4** correspondants qui sont le résultat d'une transestérification électrochimique suivie d'une migration acyle-*N,O*. Par opposition, les *o*- et *m*-aminobenzylalcools (**7***a* et **7***b*) ainsi que le *trans*-4-(aminométhyl)cyclohexaneméthanol (**8***a*) conduisent aux esters benzoïques correspondants parce que, dans ces cas, la migration acyle est empêchée. Faisant appel à cette réaction électrochimique, on a préparé un anesthésique local, la procaïne. On propose un mécanisme pour la transestérification électrochimique; celui-ci implique la formation de l'anion alcoolate par la réduction de l'alcool par un électron.

Mots clés : amides, aminoalcools, benzoylation, électrochimique, esters.

[Traduit par la revue]

Can. J. Chem. Downloaded from www.nrcresearchpress.com by 88.85.125.76 on 09/07/12
For personal use only.

Introduction

The principal advantage of electrochemical reactions lies in the fact that they do not require thermal energy to overcome activation barriers, and hence are applicable to thermally sensitive compounds. We recently (1) published a versatile electrochemical procedure for the transesterification of phenylacetic, cinnamic, and phenylglyoxylic esters in acetonitrile on a glassy carbon electrode. This method of transesterification does not require high temperature nor specific reagents such as metal alcoholate (2), aluminum oxide (3), sulfuric acid (4), *p*-toluenesulfonic acid (5), and so on. As a continuation of this work, we report an electrochemical method for either *N*- or *O*-benzoylation of aminoalcohols **2**, by methyl benzoates **1**, on a Pt electrode. All the electrochemical reactions (Scheme 1 or Table 1) proceeded smoothly at room temperature merely by passing electric current under the conditions specified below. In contrast, it was shown that even after heating the contents of each cathodic solution at the boiling point of the solvent for 3 h, no reaction products were formed. An earlier preparation of aminoalkyl benzoates was by reaction of benzoyl chloride with aminoalcohols either by heating for 4–24 h, or by leaving at room temperature for 5 days (6). In the present method, we can use such mild reagents as esters, in place of acid chlorides.

Method, results, and discussion

The electrochemical reaction of aminoalcohols **2** with methyl benzoates **1***a–f* was performed in the cathodic compartment of a divided cell on Pt electrodes at a controlled potential of either −1.2 or −1.7 V vs. SCE. As shown in entry 3 or 6 of Table 1, electrolysis at the potential −1.2 V vs. SCE of **1***a* in the presence of **2***a* ($n = 0$, $R^1 = Me$, $R^2 = R^3 = H$) or **2***a* ($n = 1$, $R^1 = R^2 = R^3 = H$) provided the corresponding benzamide **4***a* in 49 and 73% yield, but at the more negative potential of −1.7 V vs. SCE, the yields were better (86 and 92%) (entries 4 and 7). Alteration of the molar ratio (aminoalcohol to benzoate) from 1.5 to 5.0 led to an improvement of the amide yields: 32% (entry 2) to 86% (entry 4); 36% (entry 5) to 92% (entry 7). Thus all other reactions were carried out at the potential −1.7 V vs. SCE and the molar ratio five, as shown in Table 1.

Interestingly, although 2-aminoethanol (**2**; $n = 0$, $R^1 = R^2 = R^3 = H$) reacted with methyl benzoate **1***a* affording amide **4***a* ($n = 0$, $R^1 = R^2 = H$) in 73% yield (entry 1), 2-methoxyethylamine, whose hydroxyl group is protected, did not react with **1***a*. This fact suggests that the electrochemical reaction is not actually an amidation but a transesterification, which is followed non-electrochemically by *O,N*-acyl migration (7) to give an amide as the product. This hypothesis was clearly substantiated by monitoring the product distribution in the catholyte solution during the course of the electrolytic reaction of **1***a* with 3-aminopropanol (**2**; $n = 1$, $R^1 = R^2 = R^3 = H$) (see

[1]Author to whom correspondence may be addressed.
[2]Revision received January 31, 1990.

Printed in Canada / Imprimé au Canada

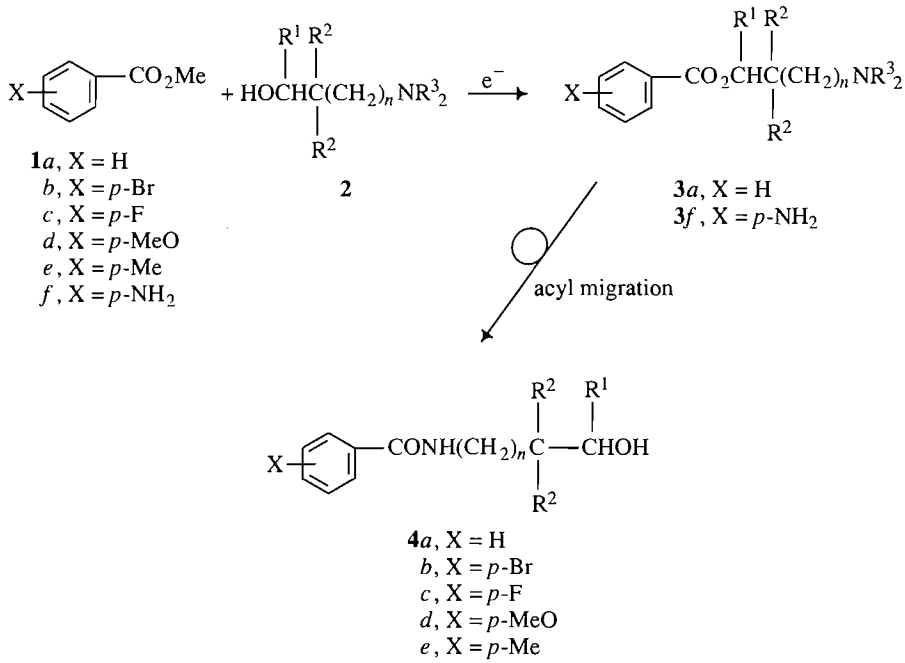

SCHEME 1

TABLE 1. Cathodic *O*- or *N*-benzoylation of aminoalcohols with methyl benzoates[a]

Entry	Benzoate	Aminoalcohol				Molar ratio aminoalcohol/ benzoate	Potential (V vs. SCE)	Product (yield.%)[b]
		n	R^1	R^2	R^3			
1	**1***a*	0	H	H	H	5	−1.7	**4***a*(73)
2	**1***a*	0	Me	H	H	1.5	−1.7	**4***a*(32)
3	**1***a*	0	Me	H	H	5	−1.2	**4***a*(49)
4	**1***a*	0	Me	H	H	5	−1.7	**4***a*(86)
5	**1***a*	1	H	H	H	1.5	−1.7	**4***a*(36)
6	**1***a*	1	H	H	H	5	−1.2	**4***a*(73)
7	**1***a*	1	H	H	H	5	−1.7	**4***a*(92)
8	**1***a*	1	H	Me	H	5	−1.7	**4***a*(70)
9	**1***b*	0	H	H	H	5	−1.7	**4***b*(79)
10	**1***c*	0	H	H	H	5	−1.7	**4***c*(80)
11	**1***d*	0	H	H	H	5	−1.7	**4***d*(70)
12	**1***e*	0	H	H	H	5	−1.7	**4***e*(69)
13	**1***f*	0	H	H	Et	5	−1.7	**3***f*(58)

[a]Electrolyses were carried out in the cathodic compartment of a divided cell with Pt electrodes (4 cm^2), by passing 1.2 F/mol (on the basis of benzoate) of electricity into the acetonitrile solution containing 0.15 M TEAP.
[b]Based on isolated products.

Fig. 1). The amount of substrate **1***a* (○) decreases as the amount of the intermediate ester **3***a* (n = 1, R^1 = R^2 = R^3 = H) increases (quantitized as its acetate **5**, △). Further, the amount of this intermediate decreases with increase in the amount of the product amide **4***a* (n = 1, R^1 = R^2 = H) (quantitized as its acetate **6**, ●). At the end of the electrolysis (1.2 F/mol of benzoate), the product is totally changed into the amide.[3]

[3]It can be considered from Fig. 1 that the necessary amount of current passed would be ca. 0.25 F/mol. Since this value is less than one, it is likely that the methanolate anion liberated by the reaction deprotonates the aminoalcohol to furnish the aminoalkyl anion for further reaction. The current efficiency, on the basis of pathway B of Scheme 2, thus reaches about 400%.

Furthermore, the electrolyic reaction of **1***a* was tried with *o*- and *m*-aminobenzyl alcohols (**7***a* and **7***b*), whose ester intermediates are not expected to rearrange due to the low nucleophilicity of the amino group (it is attached directly to the benzene nucleus), and also with *trans*-4-(aminomethyl)cyclohexanemethanol **8***a*, whose intermediate ester is unlikely to rearrange due to steric

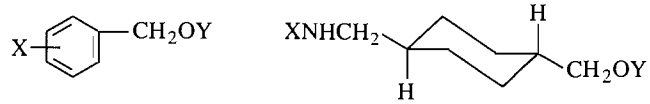

7*a*, X = *o*-NH_2, Y = H
b, X = *m*-NH_2, Y = H
c, X = *o*-NHAc, Y = PhCO
d, X = *m*-NHAc, Y = PhCO

8*a*, X = H, Y = H
b, X = H, Y = PhCO
c, X = Ac, Y = PhCO

Can. J. Chem. Downloaded from www.nrcresearchpress.com by 88.85.125.76 on 09/07/12
For personal use only.

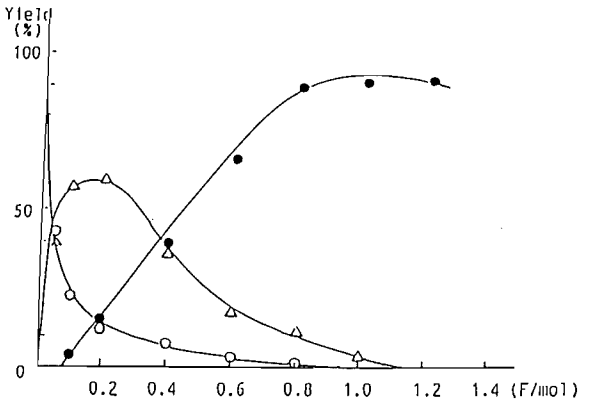

FIG. 1. plots of product distribution of the cathodic reaction of **1***a* and **2** (n = 1, $R^1 = R^2 = R^3$ = H) with electricity passed (F/mol). ○: **1***a*. △: 3-Acetylaminopropyl benzoate (*N*-acetate **5** of **3***a*: n = 1, $R^1 = R^2 = R^3$ = H). ●: 3-Benzoylaminopropyl acetate (*O*-acetate **6** of **4***a*: n = 1, $R^1 = R^2 = R^3$ = H). NOTE: Percent yield was calculated on the basis of the acetylated products.

hindrance. As expected, we obtained the transesterification product **7***d* or, after treatment with Ac_2O-pyridine, the acetylated transesterification products (**7***c* and **8***c*) exclusively, but not the amides nor the acetylated amides.

As an example of the application of this electrochemical reaction, the widely used local anesthetic procaine (**3***f*; n = 0, $R^1 = R^2$ = H, R^3 = Et) was prepared from methyl *p*-aminobenzoate **1***f* and *N,N*-diethylaminoethanol (**2**; n = 0, $R^1 = R^2$ = H, R^3 = Et) as shown in entry 13 of Table 1. We can anticipate that this electrochemical method will find wide application not only for benzoylation but for other acylations on various amino-alcohols.

The mechanistic aspects of this electrochemical transesterification were examined as follows. When benzyl alcohol was mixed and stirred for 30 min at room temperature with a pre-electrolyzed (−1.7 V vs. SCE, 0.5 F/mol of ester) solution of a mixture of methyl cinnamate and tetraethylammonium perchlorate (TEAP) in acetonitrile, no transesterification product was formed. In contrast, when methyl cinnamate was stirred similarly with the pre-electrolyzed acetonitrile solution of a mixture of benzyl alcohol and TEAP, the transesterification occurred in fairly good yield (71%). In a similar way, methyl phenylglyoxylate was prepared in 66% yield by mixing (−)-menthyl phenylglyoxylate with the pre-electrolyzed acetonitrile solution of methanol and TEAP. Thus it is certain that the intermediary active species produced by the cathodic reduction at the Pt electrode does not come from the esters but from the alcohol, solvent, or supporting electrolyte. It is very likely that an alcoholate anion is formed in the cathodic compartment and serves as an initiator for this electrochemical transesterification (see below).

The formation of an alcoholate anion by cathodic reduction has previously been suggested (8). In particular, Islam *et al.* (8*b*)[4] recently indicated that their electrochemical transesterification, conducted not on Pt but on a mercury electrode, was a base-catalyzed reaction (pathway A of Scheme 2). Their reaction mixture contained the oxalic ester, which is known to electro-reduce particularly easily to give an anion radical as an electrogenerated base (8*b*), but our mixture does not contain such an easily electro-reducible ester, as demonstrated by the

[4]This paper followed our first communication on electrochemical transesterification (1).

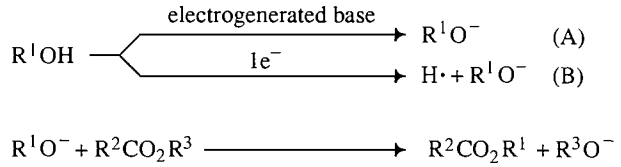

SCHEME 2

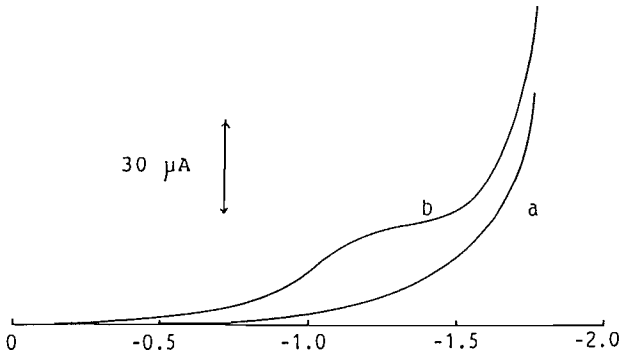

FIG. 2. Linear sweep voltammograms of (a) methanol and (b) 1-amino-2-propanol on platinum electode substrate, ca. 2 mM; acetonitrile-0.3 M TEAP; scan rate, 50 mV/s^{-1}.

pre-electrolysis experiments described above.[5] In addition, we used Pt, as electrode of low hydrogen overvoltage, instead of mercury, and it is probable that the alcoholate anion, the initiator of this reaction, was formed by direct cathodic reduction as shown in pathway B of Scheme 2. Supporting this speculation, the linear voltammograms of methanol and 1-amino-2-propanol (see Fig. 2) showed curves bending upward slightly at the potential near −1.0 V, and steeply at −1.7 V vs. SCE. Furthermore, hydrogen evolution is clearly observed in this potential range. This postulation is also applicable to the reaction of Shono *et al.* (8*a*), who prepared ether from aliphatic alcohol and alkyl chloride by cathodic reaction, since their reaction was conducted on a Pt electrode.[6] It is possible that this electrochemical reaction is supported by the tetraalkylammonium ion as the counter cation to the alcoholate anion (9).

Experimental

EI-MS spectra were measured on a JEOL JMS-D 300 spectrometer. IR spectra were taken with a Hitachi model 215 grating spectrophotometer. ^1H NMR spectra were obtained on a JEOL JNM FX-100 spectrometer at 99.60 MHz, using tetramethylsilane as an internal standard. High-pressure liquid chromatography (HPLC) was performed with a Jasco 880-PU apparatus equipped with a Soma S-310A model II ultraviolet (UV) detector (Soma Kogaku Co., Ltd.), and a Senshu Pak. ODS-1251-S No. 3331 (Senshu Kagaku Co., Ltd.) (4.8 × 250 mm).

Electrolysis apparatus

Electrolyses were conducted by use of a Hokuto Denko HA-105 potentio-galvanostat connected with a Hokuto Denko HF-201 coulom-

[5]Voltammetric work showed no occurrence of the reduction of methyl benzoate at −1.7 V vs. SCE.

[6]Partial translation, referring to tabulated results in ref. 8*a*: "As shown in Table 1, not only primary or secondary alcohols, but also tertiary alcohol(s) (run 6) or diols (run 7, 8) afford the corresponding ether in good yield. From this result, we consider that the alcoholate anion, probably generated electrochemically, has a higher reactivity than the same anion non-electrochemically produced."

Can. J. Chem. Downloaded from www.nrcresearchpress.com by 88.85.125.76 on 09/07/12
For personal use only.

Can. J. Chem. Downloaded from www.nrcresearchpress.com by 88.85.125.76 on 09/07/12
For personal use only.

eter. An ordinary H-type cell divided into two compartments with a glass frit, equipped with Pt plate (4 cm^2) electrodes and a saturated calomel electrode as a reference, was used. The temperature of the catholyte solution was kept at 23 ± 2°C by external cooling with water and stirring by use of a magnetic stirrer.

Reagents

The aminoalcohols **7***a*, **7***b*, **8***a* were prepared by reduction of the corresponding esters with $LiAlH_4$ (10). Acetonitrile was dried by distillation from P_2O_5, then CaH_2. Benzyl alcohol was dried by distillation from $LiAlH_4$. Commercially available anhydrous methanol with water content not exceeding 0.05% (Wako Junyaku Kogyo Co., Ltd.) was used. Other materials used were commercially available reagents dried over P_2O_5.

*General procedure for the electrochemical benzoylation of aminoalcohols (**2**, **7**a, **7**b, and **8**a)*

The benzoylation was carried out by passing 1.2 F/mol of electricity (based on the consumption of the benzoate) under potential control (at −1.7 V vs. SCE unless otherwise designated) through the anhydrous acetonitrile solution (20 mL) containing benzoate **1** (2 mmol), aminoalcohol **2**, **7***a*, **7***b*, or **8***a* (10 mmol except when designated otherwise), and tetraethylammonium perchlorate (TEAP) (3 mmol). After the electrolysis, the solvent was removed *in vacuo*. The product amide **4** or alcoholysis product procaine (**3***f*; $n = 0$, $R^1 = R^2 = H$, $R^3 = Et$), **7***d* or **8***b*, as well as any recovered benzoate, were separated either by chromatography on silica gel (procaine, **4**, **7***d*) or by chromatography on silica gel after acetylation by treatment with Ac_2O-pyridine (**7***c*, **8***c*). The solvent compositions for the elutions as follows: $CHCl_3$ – EtOH (25:1) for **4**; CH_2Cl_2–hexane (5:1) for procaine and **7***b*; benzene–acetone (25:1) for **7***c*; benzene–acetonitrile–$CHCl_3$ (1:0.5:2) for **8***c*.

The procaine prepared by this procedure was identified by mixture melting point and comparison of the IR spectrum with that for the commercially available authentic sample. The products **4***a* ($n = 0$, $R^1 = R^2 = H$), **4***a* ($n = 0$, $R^1 = Me$, $R^2 = H$), **4***a* ($n = 1$, $R^1 = H$, $R^2 = Me$), **4***b–e*, and **7***c* obtained by this procedure were identified by mixture melting point and by the comparison of the spectral data listed below with those for each authentic sample, synthesized from the corresponding aminoalcohols either by reaction with benzoyl chloride and NaOH at room temperature (**4***a*; $n = 0$, $R^1 = Me$, $R^2 = H$, and **4***a*; $n = 1$, $R^1 = H$, $R^2 = Me$), by refluxing for 3 h with each benzoate (**4***b–e* and **4***a*; $n = 0$, $R^1 = R^2 = H$) (11), or by the method of Raiford *et al.* (**7***c*) (12), respectively. The product **4***a* ($n = 1$, $R^1 = R^2 = H$), which is an oil, was identified by comparing the spectral data with those for the sample synthesized by the reaction with benzoyl chloride and NaOH at room temperature. The product **7***d* was identified by comparing the mp and the spectral data with those described in literature (13).

The yields of procaine and **4** are listed in Table 1. The yields of **7***c*, **7***d*, and **8***c* were 52, 54, and 65% respectively.

The physical properties and spectral data of the electrolysis products **4**, **7***c*, **7***d*, and **8***c* are as follows.

N-*(2-Hydroxyethyl)benzamide (**4**a; n = 0, $R^1 = R^2 = H$)*

Colorless needles, mp 60°C (lit. (11) mp 61°C). IR (KBr, cm^{-1}): 3325 (OH), 1637 and 1540 (amide).

N-*(2-Hydroxypropyl)benzamide (**4**a; n = 0, $R^1 = Me$, $R^2 = H$)*

Colorless needles, mp 94°C (lit. (14) mp 93–94°C). IR (KBr, cm^{-1}): 3325 (OH), 1640 and 1560 (amide). ^1H NMR ($CDCl_3$, δ): 1.25 (3H, d, $J = 6$ Hz, Me), 2.67 (1H, d, $J = 5$ Hz, OH), 3.16–3.79 (2H, m, CH_2), 4.00 (1H, brm, CH), 6.66 (1H, br, NH), 7.35–7.83 (5H, m, Ar). MS *m/z*: 161 ($M^+ - H_2O$).

N-*(3-Hydroxypropyl)benzamide (**4**a; n = 1, $R^1 = R^2 = H$) (ref. 15)*

Colorless oil. IR (film, cm^{-1}): 3350 (OH), 1640 (amide). ^1H NMR ($CDCl_3$, δ): 1.80 (2H, m, C-CH_2-C), 2.68 (1H, OH), 3.66 (4H, m, NCH_2, OCH_2), 6.73 (1H, br, NH), 7.50–7.82 (5H, m, Ar). MS *m/z*: 179 (M^+).

N-*(2,2-Dimethyl-3-hydroxypropyl)benzamide (**4**a; n = 1, $R^1 = H$, $R^2 = Me$)*

Colorless crystals, mp 111°C. IR (KBr, cm^{-1}): 3300 (OH), 1640 (amide). ^1H NMR ($CDCl_3$, δ) 0.95 (6H, s, Me), 3.29 (4H, t, $J = 7$ Hz, CH_2), 3.93 (1H, t, $J = 7$ Hz, OH), 6.69 (1H, br, NH), 7.33–7.83 (5H, m, Ar). MS *m/z*: 207 (M^+). Anal. calcd. for $C_{12}H_{17}NO_2$: C 69.54, H 8.27, N 6.76; found: C 69.44, H 8.35, N 6.71.

N-*(2-Hydroxyethyl)-*p*-bromobenzamide (**4**b; n = 0, $R^1 = R^2 = H$) (ref. 16)*

Colorless crystals, mp 120–121°C. IR (KBr, cm^{-1}): 3300 (OH), 1635 (amide). ^1H NMR ($CDCl_3$, δ) 2.36 (1H, brm, OH), 3.58 (2H, m, CH_2), 3.71 (2H, m, CH_2), 6.96 (1H, br, NH), 7.15 (2H, d, $J = 6.3$ Hz, Ar), 7.65 (2H, d, $J = 6.3$ Hz, Ar). MS *m/z*: 243 (M^+), 245 (M^+).

N-*(2-Hydroxyethyl)-*p*-fluorobenzamide (**4**c; n = 0, $R^1 = R^2 = H$)*

Colorless crystals, mp 101°C. IR (KBr, cm^{-1}): 3325 (OH), 1640 (amide). ^1H NMR ($CDCl_3$, δ): 2.59 (1H, brm, OH), 3.60 (2H, m, CH_2), 3.81 (2H, m, CH_2), 6.59 (1H, br, NH), 7.41 (2H, m, Ar), 7.79 (2H, m, Ar). MS *m/z*: 183 (M^+).

N-*(2-Hydroxyethyl)-*p*-methoxybenzamide (**4**d; n = 0, $R^1 = R^2 = H$)*

Colorless crystals, mp 104°C (lit. (17) mp 101.1–104.2°C). IR (KBr, cm^{-1}): 3320 (OH), 1625 (amide). MS *m/z*: 195 (M^+).

N-*(2-Hydroxyethyl)-*p*-methylbenzamide (**4**e; $R^1 = R^2 = H$) (ref. 18)*

Colorless crystals, mp 90°C. IR (KBr, cm^{-1}): 3340 (OH), 1638 and 1565 (amide). MS *m/z*: 179 (M^+).

o-*Acetylaminobenzyl benzoate (**7**c)*

Colorless crystals, mp 111–112°C (lit. (12) mp 110°C). IR (KBr, cm^{-1}): 1720 (ester), 1658 (amide). MS *m/z*: 269 (M^+).

m-*Aminobenzyl benzoate (**7**d)*

Colorless crystals of mp 65–66°C (lit. (13) mp 67–69°C):. IR (KBr, cm^{-1}): 1710 (ester). ^1H NMR ($CDCl_3$, δ) 3.69 (2H, br, NH_2), 5.28 (2H, s, CH_2), 6.64–8.10 (9H, m, Ar). MS *m/z*: 227 ($M^+ - H_2O$).

trans-*4-(Acetylaminomethyl)cyclohexylmethyl benzoate (**8**c)*

Colorless crystals, mp 94–96°C. IR (KBr, cm^{-1}): 1720 (ester), 1640 (amide). ($CDCl_3$, δ): 0.52–2.44 (10H, br, CH_2 and CH), 1.99 (3H, s, COMe), 3.12 (2H, t, $J = 6$ Hz, NCH_2), 4.14 (2H, d, $J = 6$ Hz, OCH_2), 5.48 (1H, br, NH), 7.34–8.08 (5H, m, Ar). MS *m/z*: 289 (M^+). Anal. calcd. for $C_{17}H_{23}NO_3$: C 70.56, H 8.01, N 4.84; found: C 70.42, H 8.20, N 4.82.

*Analysis of product distribution (Fig. 1) of 3-acetylaminopropyl benzoate **5** and 3-benzoylaminopropyl acetate **6** during the course of electrolysis*

All the conditions for the electrolysis are the same as those described above for the preparative scale experiments. After passing each faraday of electricity (at −1.7 V vs. SCE), 1.0 mL each of catholyte and anolyte was removed and combined. The resulting solution was mixed with Ac_2O–pyridine (1:1, 2 mL) and stirred overnight at room temperature. Then the mixture was treated with ice-water, extracted with $CHCl_3$, dried over Na_2SO_4, and the $CHCl_3$ was removed *in vacuo*. The residual substance was dissolved in MeOH (50 mL) and used for separation and quantitation of **5** and **6** as well as the recovered **1***a*, by HPLC with the solvent AcOH–MeOH–H_2O (1:500:500).

The physical and spectral data of the products obtained are as follows.

*3-Acetylaminopropyl benzoate (**5**)*

Colorless prisms, mp 59–60°C. IR (KBr, cm^{-1}): 1720 (ester), 1635 (amide). ^1H NMR ($CDCl_3$, δ): 1.98 (2H, m, C-CH_2-C), 1.98 (3H, s, COMe), 3.39 (2H, q, $J = 6$ Hz, NCH_2), 4.41 (2H, t, $J = 6$ Hz, OCH_2), 5.84 (1H, br, NH), 7.35–8.08 (5H, m, Ar). MS *m/z*: 221 (M^+). Anal. calcd. for $C_{12}H_{15}NO_3$: C 65.14, H 6.83, N 6.33; found: C 65.03, H 6.93, N 6.31.

*3-Benzoylaminopropyl acetate (**6**)*

Colorless needles, mp 55–57°C. IR (KBr, cm^{-1}): 1720 (ester), 1630 (amide). ^1H NMR ($CDCl_3$, δ): 1.98 (2H, m, C-CH_2-C), 2.08 (3H, s, COMe), 3.51 (2H, q, $J = 6$ Hz, NCH_2), 4.23 (2H, t, $J = 6$ Hz, OCH_2), 6.60 (1H, br, NH), 7.40–7.84 (5H, m, Ar). MS *m/z*: 221 (M^+). Anal. calcd. for $C_{12}H_{15}NO_3$: C 65.14, H 6.83, N 6.33; found: C 65.11, H 6.93, N 6.32.

Reaction of methyl cinnamate (or (−)-menthyl phenylglyoxylate) with the pre-electrolyzed solution of benzylalcohol (or methanol)

An anhydrous solution of benzyl alcohol (or methanol) (80 mmol),

TEAP (4 mmol), and acetonitrile (70 ml) was electrolysed at −1.7 V vs. SCE until 2 mF of electricity was passed. The catholyte was then mixed with methyl cinnamate (or (−)-menthyl phenylglyoxylate, 4 mmol) and stirred for 30 min at room temperature. The residue, obtained after evaporation of solvent at room temperature *in vacuo*, washing with water, and drying, was purified by column chromatography on silica gel with benzene–hexane (1:5), affording pure benzyl cinnamate in 71% yield (or methyl phenylglyoxylate, 66% yield). Each product was identified by comparison of the thin-layer chromatography, MS, and IR spectra with those of authentic samples.

When benzyl alcohol (or (−)-menthol) was stirred with the pre-electrolyzed anhydrous acetonitrile solution of methyl cinnamate (or methyl phenylglyoxylate) and TEAP, no reaction occurred.

Linear sweep voltammetry

Linear sweep voltammograms of methanol and 1-amino-2-propanol were obtained in acetonitrile solution containing TEAP as supporting electrolyte. A three-electrode system consisting of a Pt indicator electrode (0.38 mm^2), a Pt counter electrode, and a saturated calomel electrode was used. To protect the solution from moisture, a compartment (a glass tube of 15 mm. diameter with one sharp end outlet) of 0.3 M acetonitrile solution of TEAP was placed between the catholyte and the KCl agar salt bridge. Measurements were made at 22°C with a substrate concentration of ca. 2 mM and with a scanning rate of 50 mV s^{-1}. The concentration of supporting electrolute was 0.3 M.

1. T. Masumizu, K. Nozawa, K. Kawai, and S. Nakajima. Tetrahedron Lett. **27**, 55 (1986).
2. A. Said. Chimia, **28**, 234 (1974).
3. G. H. Posner and M. Oda. Tetrahedron Lett. **22**, 5003 (1981).
4. R. L. Adelman. J. Org. Chem. **14**, 1057 (1949).
5. C. E. Rehberg. Org. Synth. Coll. Vol. **3**, 146 (1955).
6. T. Y. Luh and Y. H. Chong. Synth. Commun. **8**, 327 (1978).
7. (*a*) L. H. Welsh. J. Am. Chem. Soc. **71**, 3500 (1949); (*b*) J. Wein. Acta Chim. Akad. Sci. Hung. **17**, 189 (1958).
8. (*a*) T. Shono, S. Kawashima, and H. Mori. 49th National Meeting of the Chemical Society of Japan, Tokyo, March 1984. Abstr. No. 4F28; (*b*) N. Islam, D. W. Sopher, and J. H. P. Utley. Tetrahedron, **43**, 989 (1987).
9. J. H. Wagenknecht and M. M. Baizer. Synth. Commun. **2**, 215 (1972).
10. L. H. Conover and D. S. Tarbell. J. Am. Chem. Soc. **72**, 3586 (1950).
11. B. Elpern. U.S. Patent No. 3,125,573 (1964).
12. L. C. Raiford and E. P. Clark. J. Am. Chem. Soc. **48**, 483 (1926).
13. G. Barnikow, E. Fritsche, and S. Pfeifer. Pharmazie, **37**, 76 (1982).
14. D. C. Dejongh, D. C. K. Lin, P. Leclair-Lanteigne, and D. Gravel. Can. J. Chem. **53**, 3175 (1975).
15. W. R. Vaughan and R. S. J. Klonowski. J. Org. Chem. **26**, 145 (1961).
16. J. Taboada, A. Pavon, and R. Cetina. Rev. Soc. Quim. Mex. **19**, 10 (1975).
17. B. Elpern. U.S. Patent No. 3,125,573 (1964).
18. D. Arlt. Ger. Offen. 2,155,492 (1973).

Can. J. Chem. Downloaded from www.nrcresearchpress.com by 88.85.125.76 on 09/07/12
For personal use only.

Synthesis, electronic spectroscopy, and evaluation of photoconducting oligomers with pendant bichromophores. Part 1. Influence of donor–acceptor orbital overlap on aggregate emission and photoactivity

D. GRAVEL,[1] S. GAUTHIER, F. BRISSE,[1] S. RAYMOND, M. D'AMBOISE, P. MESSIER, B. ZELENT, AND G. DUROCHER[1]

Département de chimie, Université de Montréal, C.P. 6128, Succ. A, Montréal (Québec), Canada H3C 3J7

Received June 12, 1989[2]

D. GRAVEL, S. GAUTHIER, F. BRISSE, S. RAYMOND, M. D'AMBOISE, P. MESSIER, B. ZELENT, and G. DUROCHER. Can. J. Chem. **68**, 908 (1990).

The synthesis, electronic spectroscopy, and photoactivity of two polysebacate oligomers with pendant donor–acceptor bichromophores of the alkylcarbazole–dinitrofluorene type ($\mathbf{P_1}$) and the alkylcarbazole–trinitrofluorenone carboxylic acid ester type ($\mathbf{P_2}$) are reported. The crystal structure of the basic acceptor chromophore $\mathbf{A_2}$ and donor–acceptor bichromophore $\mathbf{B_2}$ of oligomer $\mathbf{P_2}$ are also reported. In bichromophore $\mathbf{B_2}$, the amount of overlap is evaluated at 50% while the distance between the donor and the acceptor is 3.42 Å. It is shown that while no ground state intramolecular charge-transfer interaction takes place in the bichromophore $\mathbf{B_1}$ of oligomer $\mathbf{P_1}$ itself (in solution or the solid state), aggregates (acceptor–acceptor) are present in 3MP and in the solid state. The spectrum of oligomer $\mathbf{P_1}$ in low temperature 3MP matrices indicates a small aggregation effect while aggregate fluorescence of bichromophore $\mathbf{B_1}$ and oligomer $\mathbf{P_1}$ is observed in the solid state. Absorption spectra show that bichromophores $\mathbf{B_2}$ and $\mathbf{B_{2a}}$ and oligomer $\mathbf{P_2}$ give rise to charge-transfer bands with maxima at around 550 and 450 nm in CH_3CN and 590 and 470 nm in the solid state. The fluorescence and the phosphorescence of the carbazolyl chromophore and the phosphorescence of the 2,4,7-trinitro-9-fluorenone chromophore are quenched for $\mathbf{B_2}$, $\mathbf{B_{2a}}$, and $\mathbf{P_2}$ in EPA but a structureless emission is observed between 500 and 680 nm in the solid state that can be assigned to aggregate fluorescence. The negative values of ΔG_{ET} indicate that intramolecular electron transfer in bichromophores $\mathbf{B_1}$, $\mathbf{B_2}$, and $\mathbf{B_{2a}}$ should be highly probable on thermodynamic grounds if optimal orbital overlap is available. The spectroscopic properties of the bichromophoric compounds studied are discussed on the basis of conformational effects. The photoactivity evaluation of oligomers $\mathbf{P_1}$ and $\mathbf{P_2}$ shows that $\mathbf{P_2}$ is more photoactive than $\mathbf{P_1}$ due, mainly, to better orbital overlap between the donor and the acceptor moieties in oligomer $\mathbf{P_2}$ as compared to oligomer $\mathbf{P_1}$. Furthermore, a comparison of $\mathbf{P_1}$ and $\mathbf{P_2}$ to a standard PVK–TNF system reveals that the latter is much more photoactive due, again, mainly to better orbital overlap. Finally, the relative efficiencies of these systems as hole or electron conductors is discussed.

Key words: photoconducting polymers, donor–acceptor bichromophores, bichromophores, substituted carbazoles, polynitrofluorene derivatives.

D. GRAVEL, S. GAUTHIER, F. BRISSE, S. RAYMOND, M. D'AMBOISE, P. MESSIER, B. ZELENT et G. DUROCHER. Can. J. Chem. **68**, 908 (1990).

On a réalisé la synthèse et on a examiné les spectres électroniques ainsi que la photoactivité de deux oligomères polysébacates portant des bichromophores donneur–accepteur de type alkylcarbazole-dinitrofluorène ($\mathbf{P_1}$) et de type alkylcarbazole–ester de l'acide trinitrofluorénonecarboxylique ($\mathbf{P_2}$). On a aussi déterminé la structure cristalline du chromophore accepteur de base $\mathbf{A_2}$ ainsi que celle du bichromophore donneur–accepteur $\mathbf{B_2}$. Dans le bichromophore $\mathbf{B_2}$, on a évalué que le recouvrement est d'environ 50% alors que la distance entre le donneur et l'accepteur est de 3,42 Å. On démontre que, même s'il ne se produit pas d'interaction intramoléculaire de transfert de charge dans l'état fondamental du bichromophore $\mathbf{B_1}$ de l'oligomère $\mathbf{P_1}$ lui-même (tant en solution qu'à l'état solide), il existe des agrégats (accepteur–accepteur) dans le 3MP ainsi qu'à l'état solide. Les spectres de l'oligomère $\mathbf{P_1}$ obtenus à basse température dans des matrices de 3MP suggèrent la présence d'un faible effet d'agrégation alors que, à l'état solide, on observe de la fluorescence d'agrégats du bichromophore $\mathbf{B_1}$ et de l'oligomère $\mathbf{P_1}$. Les spectres d'absorption des bichromophores $\mathbf{B_2}$, $\mathbf{B_{2a}}$ et de l'oligomère $\mathbf{P_2}$ donnent lieu à des bandes de transfert de charge avec des maxima autour de 550 et de 450 nm dans le CH_3CN et de 590 et 470 nm à l'état solide. La fluorescence et la phosphorescence du chromophore carbazolyle et la phosphorescence du chromophore 2,4,7-trinitrofluorèn-9-one des composés $\mathbf{B_2}$, $\mathbf{B_{2a}}$ et $\mathbf{P_2}$ dans l'EPA sont piégées; toutefois, à l'état solide, on n'observe qu'une émission sans structure entre 500 et 680 nm et on l'attribue à de la fluorescence d'agrégats. Les valeurs négatives de ΔG_{ET} indiquent que, sur une base thermodynamique, le transfert intramoléculaire d'électrons dans les bichromophores $\mathbf{B_1}$, $\mathbf{B_2}$ et $\mathbf{B_{2a}}$ devrait être très probable si le recouvrement des orbitales est optimal. On utilise des arguments basés sur les effets conformationnels pour discuter des propriétés spectroscopiques des composés bichromophoriques étudiés. L'évaluation de la photoactivité des oligomères $\mathbf{P_1}$ et $\mathbf{P_2}$ permet de démontrer que $\mathbf{P_2}$ est plus photoréactif que $\mathbf{P_1}$ principalement à cause d'un meilleur recouvrement d'orbitales entre les portions donneur et accepteur de l'oligomère $\mathbf{P_2}$ par opposition à ce qui existe dans l'oligomère $\mathbf{P_1}$. De plus, une comparaison de $\mathbf{P_1}$ et de $\mathbf{P_2}$ avec le système standard PVK–TNF révèle que ce dernier est beaucoup plus photoréactif principalement à cause d'un meilleur recouvrement d'orbitales. Enfin, on discute des efficacités relatives de ces systèmes comme conducteurs de trous ou d'électrons.

Mots clés: polymères photoconducteurs, bichromophores donneur–accepteur, bichromophores, carbazoles substitués, dérivés polynitrofluorènes.

[Traduit par la revue]

Introduction

The continued widespread interest in the synthesis, evaluation, and physical characterization of organic based photoconducting polymers attests to their importance both from the economic and academic point of view (1). On the one hand, the industrial competitiveness of the electrophotographic and reprographic industry relies on the development of new, better performing, and cheaper photoactive materials and, on the other, the fundamental description of the morphology and intimate mechanism of action of these systems remains an area of great scientific challenge.

[1]Authors to whom correspondence may be addressed.

[2]Revision received January 5, 1990.

Can. J. Chem. Downloaded from www.nrcresearchpress.com by 88.85.125.76 on 09/07/12
For personal use only.

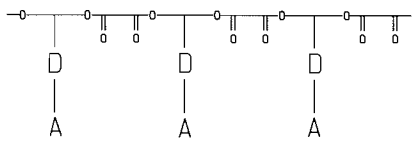

FIG. 1. Polyester with pendant D–A bichromophores.

One system that continues to attract much attention is the carbazole based family of polymers (2, 3) where charge is generated by an organic acceptor chromophore or an inorganic acceptor. This, no doubt, is a result of the fact that poly-*N*-vinylcarbazole (PVK) molecularly doped with 2,4,7-trinitrofluorenone (TNF) had yielded the best performing system in the early days (4). Although this performance has today been superseded by new industrial materials, the interest around the carbazole system remains high because of the wealth of information accumulated in the literature and the opportunity it may provide for the rational design and optimization of high performance organic based photoactive polymers.

Our approach to the study of this basic system has been to generate polyesters bearing carbazole based donor–acceptor bichromophores as pendant groups (Fig. 1). These should yield information on the influence, on the photoactivity of these polymers, of the relative distance between D–A pairs, of the relative distance between the donor and the acceptor chromophores, of the free energy changes in electron transfer, and of the eventual formation of chromophore aggregates, ground state charge transfer complexes, excimers, or exciplexes. The main difference between this system and the well-studied molecularly doped PVK is the possibility of varying the interbichromophore distance along the chain and of better controlling the distance between donors and acceptors, which was impossible, by design, in the doped PVK systems where phase separation between dopant and polymer could occur.

In earlier papers, we reported on the synthesis, crystal structure, and absorption spectroscopy of a carbazole–dinitrofluorene bichromophore (5) and on the intramolecular photoprocesses of the same bichromophore and a polysebacate containing it as pendant bichromophore (6). In the present paper, we report on the synthesis and a comparison of the electronic spectroscopy and photoactivity of two polysebacate oligomers with pendant D–A bichromophores where the nature (electron affinity) of the acceptor is varied.

Results and discussion

1. Synthesis of the D-A oligomers, the model chromophores, and bichromophores

For the sake of simplicity, the key substrates referred to in this study are identified as oligomers $\mathbf{P_1}$ and $\mathbf{P_2}$, the model acceptors $\mathbf{A_1}$ and $\mathbf{A_2}$, the model donors $\mathbf{D_1}$ and $\mathbf{D_2}$, and the model bichromophores $\mathbf{B_1}$, $\mathbf{B_2}$, and $\mathbf{B_{2a}}$. Scheme 1 outlines first the synthesis of the D–A oligomer $\mathbf{P_1}$ starting from *N*-benzylcarbazole (**1**). Formylation of the starting material **1** under the usual conditions yields 92% of the desired *N*-benzylcarbazole-3-carboxaldehyde (**2**), which is condensed with diethyl malonate under Knoevenagel conditions to give 90% of the expected malonylidene derivative **3**. Although the next operation pertains to three different reductions, namely reduction of the conjugated double bond, reduction of the malonyl moiety, and reductive cleavage of the *N*-benzyl group, it has unfortunately not been possible to carry out the three stages of reduction in one single step with good yield. In a first stage, catalytic reduction of the olefin is achieved in quantitative yield to give the malonate derivative **4**, which in turn is reduced with LAH to the corresponding 1,3-diol **5** in an 89% yield; then, reductive debenzylation is carried out in the presence of sodium in liquid ammonia to give a mixture of the desired debenzylated compound **6** contaminated with some overreduced material. Treatment of the crude product for 3 h with 10% palladium over charcoal in refluxing 1,3,5-trimethylbenzene, however, affords the desired 1,3-diol **6** in a 68% yield or better, depending on the reaction scale. In preparation for the attachment of the acceptor chromophore, diol **6** is first protected in the form of an acetonide acetal **7** in 83% yield; coupling to the 9-(3-bromopropyl)-9-methyl-2,7-dinitrofluorenyl acceptor chromophore **8** then takes place in the presence of sodium hydride in THF, in the presence of HMPA, and the desired diol monomer **9** is obtained directly by acid hydrolysis of the reaction mixture. An overall yield of 77% is obtained for the two steps. The final reaction in the sequence is the preparation of the oligomer by condensation of diol **9** with sebacoyl chloride in the presence of triethylamine. The desired D–A oligomer $\mathbf{P_1}$ is obtained as a low molecular weight orange solid in a 93% yield, after precipation from hexanes. On the other hand, the synthesis of model $\mathbf{D_2}$, which is patterned on the same scheme following the sequence: **10**, **11**, **12**, **13**, $\mathbf{D_2}$, will not be discussed here and the reader is referred to the experimental section for details.

Scheme 2 outlines the synthesis of D–A oligomer $\mathbf{P_2}$ along with those of models $\mathbf{A_2}$, $\mathbf{B_2}$, and $\mathbf{B_{2a}}$. The first sequence leading to model $\mathbf{B_2}$ and oligomer $\mathbf{P_2}$ is based on compound **7** from the previous scheme. In a first step, the β-hydroxethyl spacer group is introduced on the carbazole derivative **7** by reaction with ethylene oxide in the presence of powdered KOH in anhydrous butanone. The desired intermediate **14** is obtained in a 68% yield along with a small amount of the double condensation product, i.e., the *N*-β-hydroxyethyloxyethyl derivative **14***a* (see Experimental). Precursor **14** is then attached to the acceptor chromophore by reaction with the trinitrofluorenonecarboxylic acid chloride **15** in the presence of triethylamine to yield the bichromophoric monomer model $\mathbf{B_2}$ in a 97% yield. Finally, the bichromophore monomer is liberated in 83% yield by 10%HCl in THF and the resulting diol **16** oligomerized by reaction with sebacoyl chloride at 170–180°C. The desired oligomer $\mathbf{P_2}$ is obtained in a 45% yield as a low molecular weight grey solid. Again, as in the previous case, the synthesis of model $\mathbf{B_{2a}}$, which is patterned on the same scheme following the sequence: **17**, **18**, $\mathbf{B_{2a}}$, will not be discussed here and the reader is referred to the experimental section for details.

2. Crystallographic investigation of the acceptor chromophore A_2 and the bichromophore B_2

The atomic numbering for the description of the acceptor chromophore and the donor–acceptor bichromophore, whose crystal structures have been established, is shown in Fig. 2.

2.1. Acceptor A_2

The bond distances and angles of the two independent molecules in the unit cell have been deposited.[3] Corresponding values are in good agreement with one another. The point of

[3]Atomic coordinates, anisotropic thermal parameters, bond distances and angles (12 pages), and tables of observed and calculated structure factors (48 pages) may be purchased from the Depository of Unpublished Data, CISTI, National Research Council of Canada, Ottawa, Ont., Canada K1A 0S2.

Tables of atomic coordinates, bond lengths, and bond angles have also been deposited with the Cambridge Crystallographic Data Centre. They may be obtained on request from The Director, Cambridge Crystallographic Data Centre, University Chemical Laboratory, Lensfield Road, Cambridge CB2 1EW, U.K.

Can. J. Chem. Downloaded from www.nrcresearchpress.com by 88.85.125.76 on 09/07/12
For personal use only.

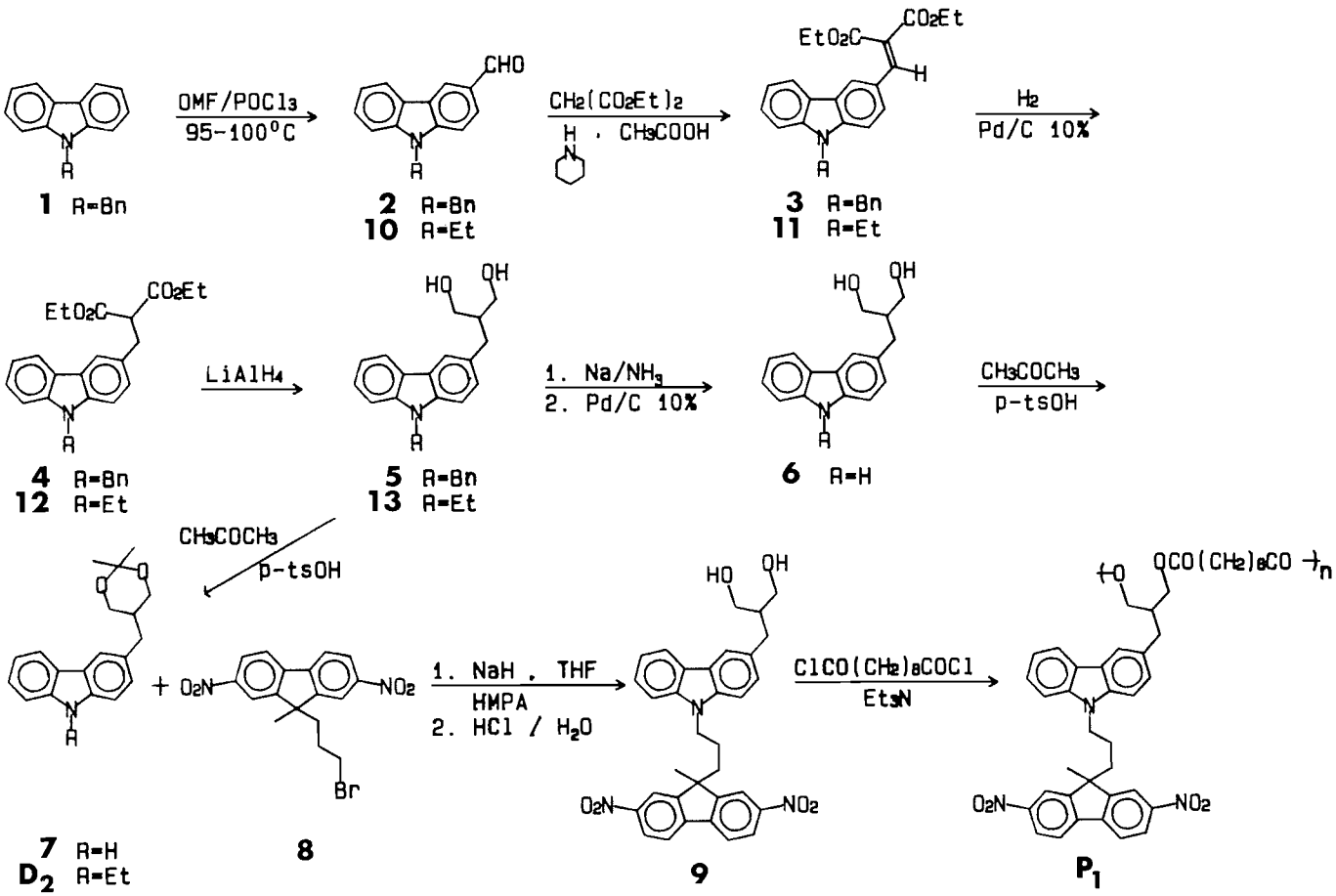

SCHEME 1

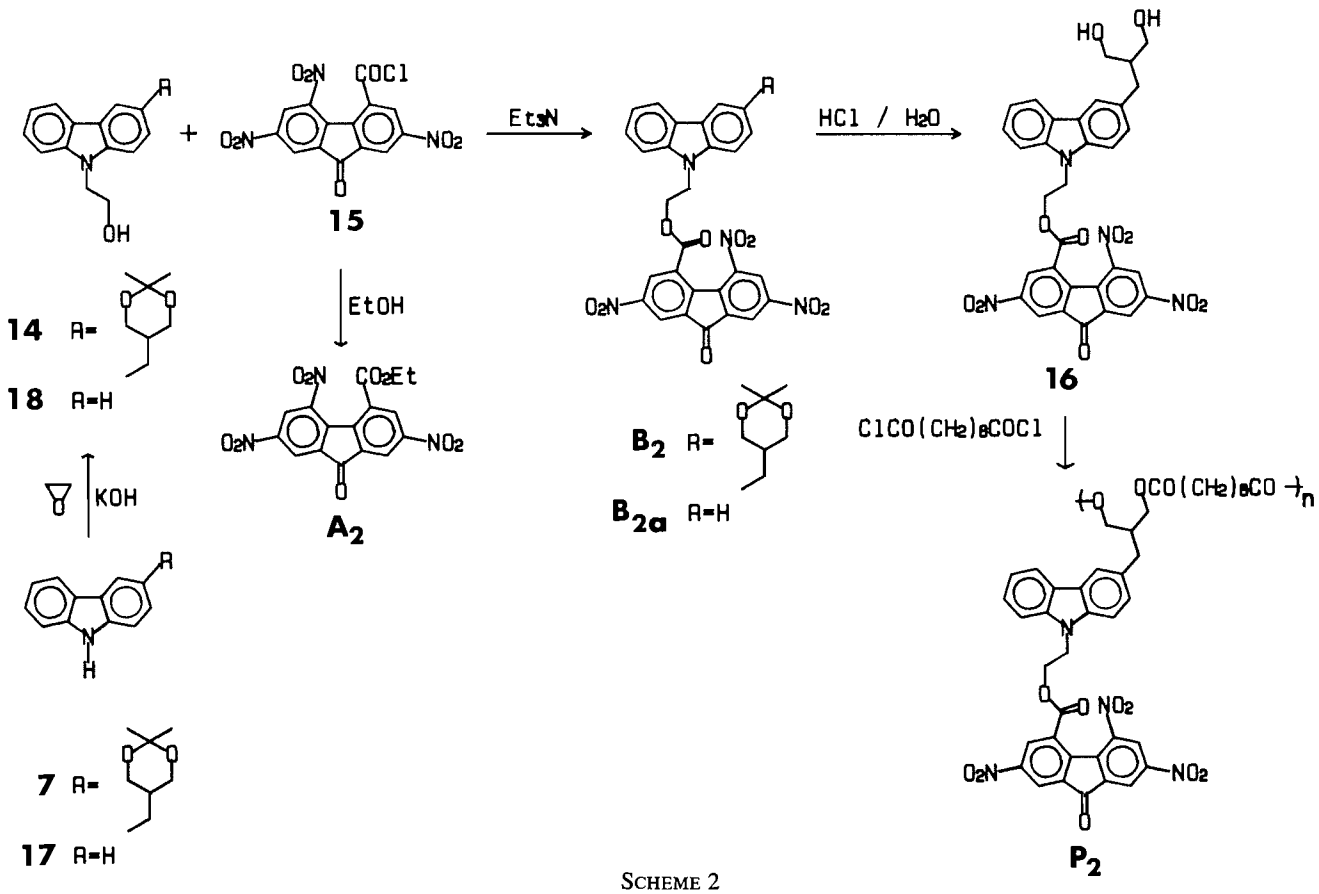

SCHEME 2

Can. J. Chem. Downloaded from www.nrcresearchpress.com by 88.85.125.76 on 09/07/12
For personal use only.

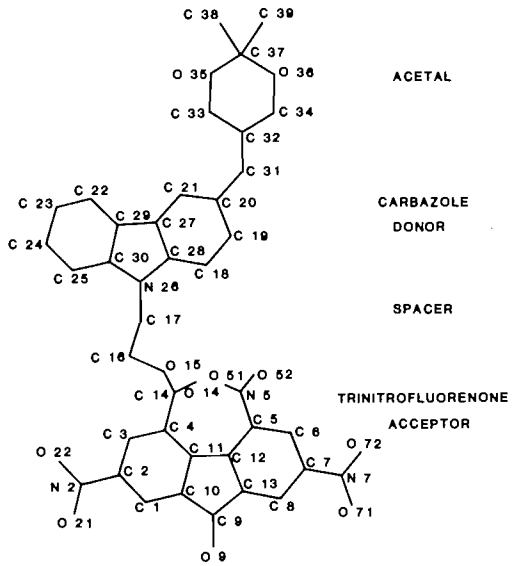

FIG. 2. Atomic numbering for $\mathbf{B_2}$.

TABLE 1. Dihedral angles of the carboxylate or the nitro groups with respect to the fluorenone mean plane

		Dihedral angle (deg)			
		Nitro at		Carboxylate at	
		C(2)	C(7)	C(5)	C(4)
Trinitrofluorenone $\mathbf{A_2}$	a	1.4	6.5	39.6	30.6
	b	2.1	1.1	35.7	37.1
Bichromophore $\mathbf{B_2}$		8.1	5.8	37.0	44.8

interest, however, lies with the nitro groups. As one may appreciate from the data of Table 1, the carboxylate group and each nitro group are planar but none is coplanar with the fluorenone ring system. The tilt of some of the nitro groups with respect to the fluorenone system is in the range of 2°–8°. However, the carboxylate group at C(4) and the nitro group at C(5) are inclined by as much as 35° with respect to the fluorenone mean plane. This of course is to minimize the interactions between oxygen atoms of the two neighbouring groups. It is worth noting that in this arrangement, although strongly tilted, the NO_2 and CO_2 groups remain nearly parallel to one another.

2.2. Bichromophore B_2

The bichromophore molecule is represented by the stereopair in Fig. 3. The bond distances and angles of the fluorenyl moiety of the bichromophore $\mathbf{B_2}$ compare very well with the corresponding quantities in the trinitrofluorenone molecule $\mathbf{A_2}$. All the effects described for the latter are observed here as well. The geometrical characteristics of the carbazole part have been deposited.

2.3 Flatness of the fluorenyl ring system

This is a major concern when studying the potentiality of a close approach between fluorenyl groups. In a systematic survey of fluorene and substituted fluorene ring systems Raymond (7) has recognized three types of distortions of such systems. A V-type distortion occurs when the outer atoms of the six-membered rings deviate on the same side of the fluorenyl mean plane. When the deviation from the same mean plane is positive on one side and negative on the other, this is referred to as an S-type distortion. The third distortion is of the propeller-type. This type of deviation from "planarity", as observed here for both molecules within the asymmetric unit, is to be associated with substitution at both C(4) and C(5). Here, the two bulky nitro and carboxylate groups cannot remain in the fluorenyl plane and tend to move apart from one another. This repulsion also affects atoms C(4) and C(5), which are thus displaced in opposite directions.

The intracyclic angles at the NO_2-substituted carbons, C(2), C(5), and C(7), are systematically larger than 120°. The average angle has a value of 122.0° and the spread between extreme values is only 1.4°. The corresponding bond angle and spread are 118.6° and 0.5° at the carboxylate-substituted C(4) atom. However, more importantly, it is the values of the exocyclic bond angles that are the most revealing. The 12 exocyclic bond angles at C(2) and C(7) are nearly all equal; they average 118.8° with a spread of 1.1°. In the case of the C(5) atom, also NO_2 substituted, three of the angles average 115.4° (spread 1.7°) while the other three average 122.6° (spread 0.7°). At C(4), the carboxylate-substituted atom, the dissymmetry is just as marked, since the two exocyclic angles have values of 114.3(5)° and 126.7(5)°. Thus the proximity of substituents causes major deviations from planarity of the fluorenyl ring system and its substituents.

2.4 The conformation of the spacer and molecular packing

The conformation of the spacer in the bichromophore $\mathbf{B_2}$ is given by the sequence of torsion angles in Table 2. From C(4) to N(26), the torsion angles of interest are successively *trans* and *gauche*. Bearing in mind that the carboxylate group is tilted by about 45° away from the trinitrofluorenone mean plane, this puts the two planar groups of the same bichromophore molecule parallel to one another. These are the carbazole (a) and trinitrofluorenone (b) groups in Fig. 4a. The amount of overlap is evaluated at 50% while the distance between the donor and the acceptor is 3.42 Å (Fig. 4b). All the acceptor and donor moieties are parallel to one another and nearly equidistant. There is no contact between semi-heavy atoms shorter than 3.4 Å.

There are two crystallographically distinct molecules of trinitrofluorenone $\mathbf{A_2}$ in a unit cell, molecules (a) and (b). The dihedral angle between these two planar molecules, (a) and (b), is 50°. However, each molecule is in turn centrosymmetrically related to another one, respectively (a′) and (b′). Because of the centers of symmetry, the overlaps are of the head-to-tail type. The amount of overlap and the interplanar distance are 60% and 3.34 Å for the (a,a′) pair and 65% and 3.47 Å for the (b,b′) pair. The disposition of the molecules in the crystal may be visualized in the projections of Fig. 5.

3. Spectroscopic properties of the D–A oligomers as compared to those of the bichromophores

3.1. Absorption spectra of P_1 and B_1

The electronic absorption spectra of bichromophore $\mathbf{B_1}$ and polysebacate $\mathbf{P_1}$, containing $\mathbf{B_1}$ as a pendant bichromophore in 3MP, EPA, and acetonitrile solutions at room temperature, are presented in Fig. 6. As can be seen in the figure, the second and third electronic transitions in the absorption spectra of the oligomer $\mathbf{P_1}$ as compared to the spectra of the bichromophoric molecule $\mathbf{B_1}$ are shifted to lower energies. Such a shift in the spectra is due to the substituent effect at position 3 of the carbazolyl chromophore in $\mathbf{P_1}$ since the second and third bands in the spectra of the bichromophore have been assigned to the carbazole moiety (5). This substitutional effect also explains the

Can. J. Chem. Downloaded from www.nrcresearchpress.com by 88.85.125.76 on 09/07/12
For personal use only.

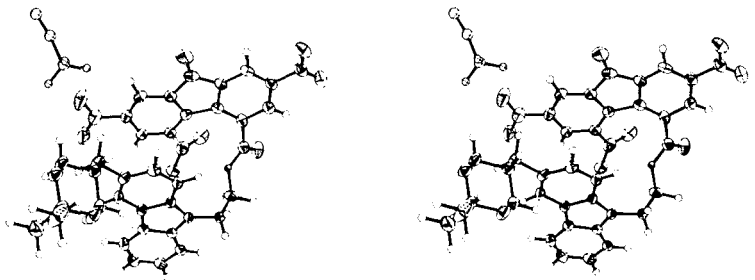

FIG. 3. Stereopair showing the bichromophore $\mathbf{B_2}$ and the solvent molecule.

TABLE 2. Torsion angles describing the conformation of the spacer in the bichromophore $\mathbf{B_2}$ and of the carboethoxyethyl fragment in the trinitrofluorenone molecules

	Torsion angle (deg)		
	Trinitrofluorenone $\mathbf{A_2}$		
Bonds	a	b	Bichromophore $\mathbf{B_2}$
C(3)—C(4)—C(14)—O(14)	−141.7(3)	−137.5(4)	−45.6(7)
C(3)—C(4)—C(14)—O(15)	33.9(4)	40.4(4)	130.9(5)
C(4)—C(14)—O(15)—C(16)	−170.8(3)	−171.6(3)	−171.2(4)
C(14)—O(15)—C(16)—C(17)	−80.9(4)	−87.6(4)	163.8(4)
O(15)—C(16)—C(17)—N(26)	—	—	73.2(5)
C(16)—C(17)—N(26)—C(28)	—	—	−91.9(6)

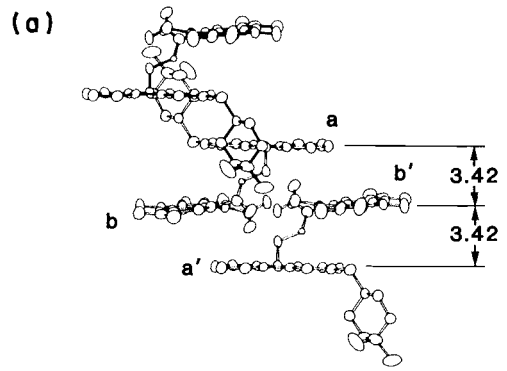

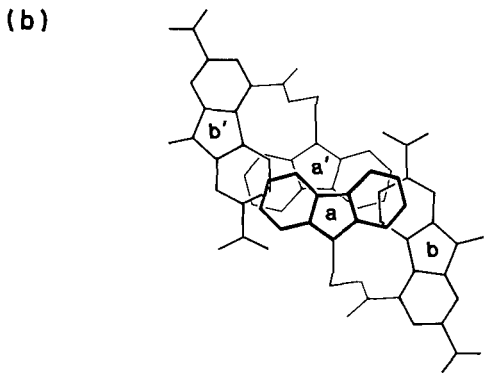

FIG. 4. (a) Side view of the packing of the bichromophore $\mathbf{B_2}$ in the unit cell. (b) Overlap of the various units of the bichromophore $\mathbf{B_2}$. The primed and unprimed molecules are centrosymmetrically related.

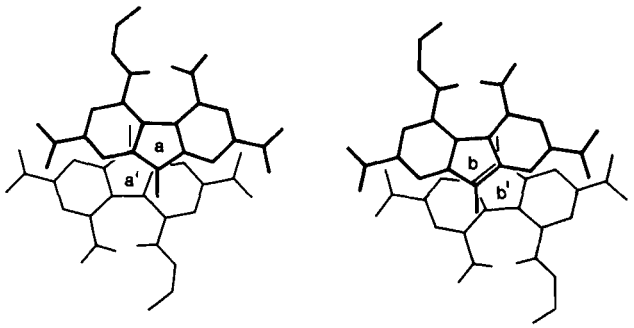

FIG. 5. The two kinds of overlap between molecules (a) and (b) of trinitrofluorenone $\mathbf{A_2}$. The primed and unprimed molecules are centrosymmetrically related.

observed shifts between the absorption spectra of $\mathbf{P_1}$ and $\mathbf{B_1}$ in the solid state (see Table 3 and Fig. 7). Figure 6 clearly shows that no ground state intramolecular charge-transfer interaction exists between the carbazolyl chromophore as the electron donor and the 2,7-dinitrifluorene chromophore as the electron acceptor in the oligomer $\mathbf{P_1}$, as already shown (5, 6). On the other hand, the absorption spectra presented in Fig. 6 also show that no aggregation takes place between two 2,7-dinitrofluorene chromophores in polar solutions at these concentrations.

In 3MP, even at 10^{-6} M, the aggregate is present (band at 365 nm). For the bichromophoric molecule $\mathbf{B_1}$ in 3MP such absorption, assigned as the absorption of the aggregates (acceptor–acceptor interactions), appears and increases in intensity (5) when the temperature of the solution decreases from 296 to 148 K. The aggregation effect observed in 3MP strongly depends on the concentration of $\mathbf{B_1}$ in the solution, and at low temperature is clearly detectable even in the concentration range of 10^{-6}–10^{-5} M. Since the edge-to-edge distance between the bichromophoric segments in the stretched conformation of oligomer $\mathbf{P_1}$ is 23.75 Å (according to Dreiding models), the observed aggregation effect for $\mathbf{P_1}$ in 3MP would be due to the interchain chromophore–chromophore interactions rather than intrachain interactions only if the oligomer adopts the rigid rod structure in 3 MP. But the very fact that the aggregates appear at much lower concentrations in the oligomer than in the bichromophore (Fig. 6) tends to show that the former rather

Can. J. Chem. Downloaded from www.nrcresearchpress.com by 88.85.125.76 on 09/07/12
For personal use only.

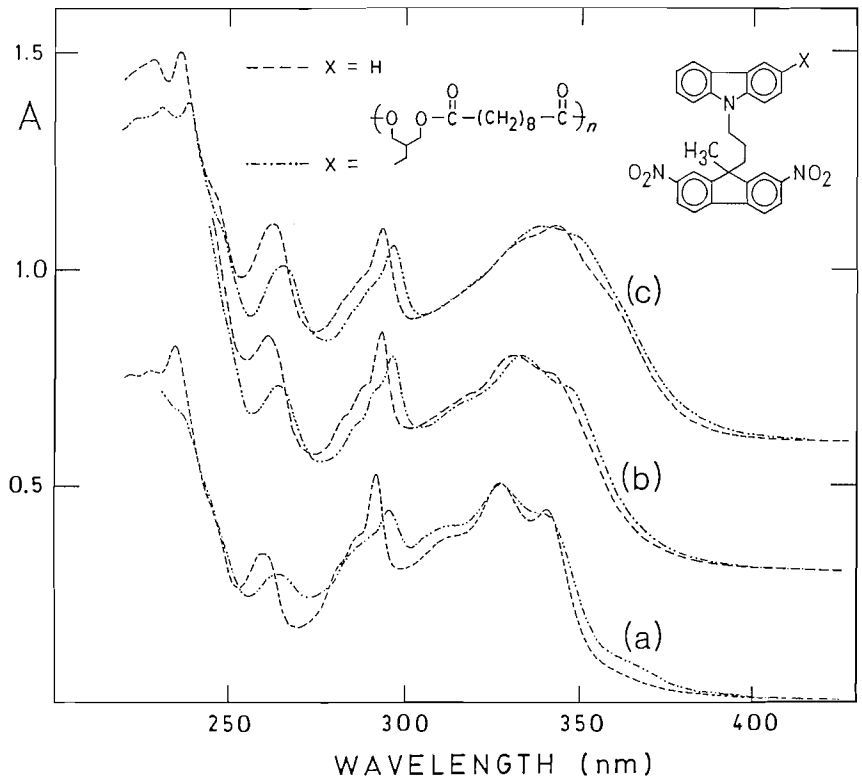

FIG. 6. Electronic absorption spectra of polysebacate $\mathbf{P_1}$ (–··–··–) (a) in 3MP ($C = 1 \times 10^{-6}$ M, $l = 5$ cm, $A \times 15$), (b) in EPA ($C \approx 5 \times 10^{-5}$ M, $l = 1$ cm, $A \times 1.5$), and (c) in acetonitrile ($C = 4.3 \times 10^{-5}$ M, $l = 1$ cm, $A \times 2.0$) as compared to the absorption spectra of bichromophore $\mathbf{B_1}$ (––––) (a) in 3MP ($C = 3.8 \times 10^{-6}$ M, $L = 5$ cm, $A \times 10$), (b) in EPA ($C = 1 \times 10^{-5}$ M $l = 1$ cm, $A \times 1.8$), and (c) in acetonitrile ($C = 1 \times 10^{-5}$ M, $l = 1$ cm, $A \times 2$). All spectra have been measured at 296 K.

adopts a flexible random coil in 3MP, giving rise to intrachain interactions between two 2,7-dinitrofluorene moieties in different segments. Since 3MP is a poor solvent for the bichromophore, it will surely tend to make the macromolecular coil contract below the normal value expected in better solvents. This might explain quite well the fact that at the lowest concentration available, in order to see something in the absorption spectra of the oligomer (10^{-7} M), the "aggregation band" is always present (there is not much difference between the 10^{-6} or 10^{-7} M spectra) because, obviously, the isolated random coils in 3MP are always present.

On the other hand one can see in Fig. 7 that the aggregation effect for $\mathbf{B_1}$ and $\mathbf{P_1}$ in the solid state is about the same. The solid state absorption spectra of $\mathbf{P_1}$ and $\mathbf{B_1}$, with the characteristic new absorption band at 370 nm assigned to aggregates (5), are similar.

Apart from the substituent effect already discussed, Fig. 6 also shows the solvent effect on the absorption spectra of the bichromophoric molecule $\mathbf{B_1}$ and the oligomer $\mathbf{P_1}$. This normal spectral shift, which increases with the solvent polarity, is due to the solute–solvent dipole–dipole interactions in which the 2,7-dinitrofluorene and the carbazolyl chromophores in $\mathbf{B_1}$ and $\mathbf{P_1}$ are involved (see Table 3). The long-wavelength absorption bands of $\mathbf{P_1}$ and $\mathbf{B_1}$ are modified and strongly shifted to lower energy when the temperature of the solution decreases from 296 to 77 K (Fig. 8). This is mainly due to the changes in the absorption spectrum of the 2,7-dinitrofluorene chromophore. For instance, the $^1L_b \leftarrow {}^1A$ transition in model $\mathbf{D_2}$ in EPA going from room temperature to 77 K decreases in energy only by 160 cm^{-1} (see Table 3). But the absorption band of acceptor model $\mathbf{A_1}$ clearly shifts to lower energy by 860 cm^{-1} at 77K.

Figure 8 also shows the phosphorescence excitation spectrum of $\mathbf{A_1}$ and the absorption spectrum of $\mathbf{P_1}$ in EPA at 77 K. These spectra are all identical to the $\mathbf{A_1}$ absorption spectra at 77 K in the region of the first electronic transition, indicating that the phosphorescence of $\mathbf{A_1}$ and the absorption of the oligomer in this electronic region of the spectrum are due to the free $\mathbf{A_1}$ chromophore.

3.2 Luminescence properties of B_1 and P_1

The fluoresence and phosphorescence emissions of the carbazole molecule in EPA solution are well known to have a good quantum yield (8–11). Nevertheless, the electronic excitation of the carbazolyl chromophore ($\lambda_{exc} = 295$ nm) in $\mathbf{B_1}$ in EPA solution does not lead to the appearance of any fluorescence at room temperature or fluorescence and phosphorescence at 77 K. This indicates that the singlet state of the carbazolyl chromophore in $\mathbf{B_1}$ is completely quenched by the 2,7-dinitrofluorene moiety. On the other hand, no fluorescence emission has been detected at room temperature ($\lambda_{exc} = 345$ nm) or at 77 K ($\lambda_{exc} = 362$ nm) for the 2,7-dinitrofluorene chromophore in $\mathbf{B_1}$ or in $\mathbf{A_1}$. But molecule $\mathbf{A_1}$ is characterized by a phosphorescence emission in the range 490–650 nm in EPA at 77 K. This phosphorescence remains unchanged in the bichromophoric molecule (6) $\mathbf{B_1}$ ($\phi_p = 0.06$). The same luminescence properties as described for the bichromophoric molecule $\mathbf{B_1}$ in EPA solution have also been observed for the oligomer $\mathbf{P_1}$ ($\phi_p = 0.06$).

The phosphorescence spectra of $\mathbf{A_1}$ and $\mathbf{B_1}$ in a nonpolar solvent like 3MP at the concentration of 1×10^{-6} M (Fig. 9) are the same as in EPA solutions (spectrum 1). It is well known that the phosphorescence spectra are not much affected by the polarity of the solvent. On the other hand the emission spectrum of $\mathbf{B_1}$ in 3MP changes drastically when the concentration increases from 1×10^{-6} to 5×10^{-6} M (curves 1–4). The phosphorescence of the 2,7-dinitrofluorene monochromophore

Can. J. Chem. Downloaded from www.nrcresearchpress.com by 88.85.125.76 on 09/07/12
For personal use only.

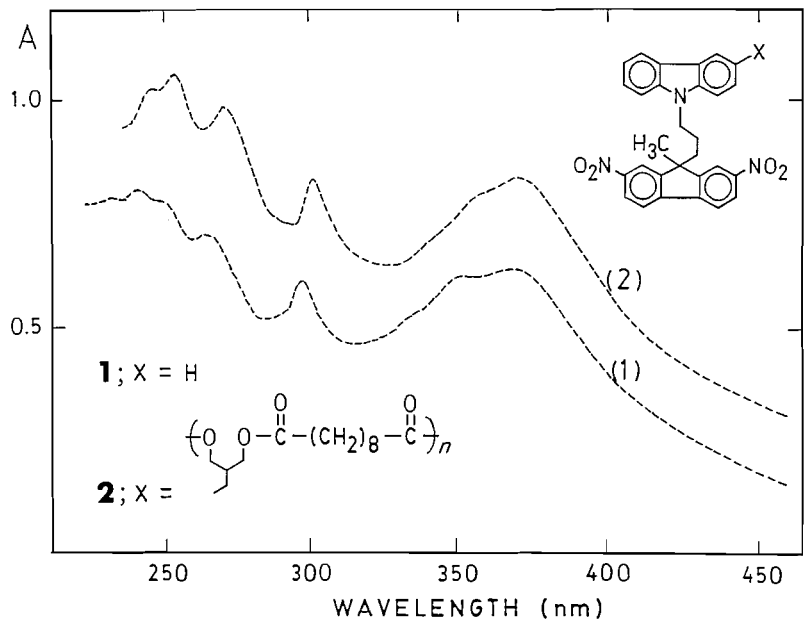

FIG. 7. Electronic absorption spectra of (1) bichromophore $\mathbf{B_1}$ and (2) polysebacate $\mathbf{P_1}$ in the solid state.

TABLE 3. Energies of the first three electronic transitions of the carbazolyl chromophore in different compounds

Compound	Experimental conditions	$\tilde{\nu}(0,0)$ (cm^{-1}) (±60)		
		$^1L_b \leftarrow {}^1A$	$^1L_A \leftarrow {}^1A$	$^1B_a \leftarrow {}^1A$
N-Ethylcarbazole ($\mathbf{D_1}$)	3 MP, 296 K	29 110	34 130	38 170
	EPA, 296 K	28 990	34 010	38 170
Donor model $\mathbf{D_2}$	3 MP, 296 K	28 650	33 730	37 880
	EPA, 296 K	28 530	33 730	37 880
	EPA, 77 K	28 370	33 610	37 880
Bichromophore $\mathbf{B_1}$	3 MP, 296 K	—	34 250	38 460
	EPA, 296 K	—	34 130	38 310
	CH_3CN, 296 K	—	34 070	38 170
	Solid state, 296 K	—	33 560	37 740
Polysebacate $\mathbf{P_1}$	3 MP, 296 K	—	33 960	38 100
	EPA, 296 K	—	33 780	37 880
	CH_3CN, 296 K	—	33 730	37 740
	Solid state, 296 K	—	33 110	36 970

in $\mathbf{B_1}$ decreases in intensity while a new broad structureless emission, at $\lambda_{max} = 575$ nm, increases in intensity. The limit of these changes can be visualized in the emission spectrum of $\mathbf{B_1}$ in the solid state (curve 5), which is the same at room temperature and at 77 K. This new emission can be assigned to aggregate fluorescence of $\mathbf{B_1}$ in 3MP. Such a conclusion is supported by the absorption spectroscopy of $\mathbf{B_1}$ in 3MP (Fig. 6) as previously reported (5) and in the solid state (Fig. 7) for both $\mathbf{B_1}$ and $\mathbf{P_1}$. Secondly, this new emission is short lived compared to the long-lived phosphorescence emission of $\mathbf{B_1}$ ($\tau_p = 0.12$ s) (6). Moreover, the emission excitation spectrum ($\lambda_{em} = 575$ nm) of the oligomer in the solid state at room temperature perfectly superimposes over the corresponding absorption spectrum in Fig. 7. The phosphorescence spectra of the polysebacate $\mathbf{P_1}$ in a 3MP clear glassy solution (77 K) (saturated solution: $C < 1 \times 10^{-6}$ M) (Fig. 9, curve 8) indicate a small aggregation in the solution even at this very low concentration since the ratio I_{540}/I_{500} increases in the oligomer spectrum (curve 8 vs. 7). The spectra (curve 5) in the solid state can also be shifted depending upon the film thicknesses. Indeed, the solid state fluorescence spectrum of $\mathbf{P_1}$ has the same shape as the spectrum of $\mathbf{B_1}$ (curves 6 and 5) but, as stated above, the bichromophore aggregate spectrum gives rise to different maxima depending upon the thickness of the film used.

3.3 Absorption and luminescence properties of B_2, B_{2a}, and P_2

2,4,7-Trinitro-9-fluorenone (TNF) is known as a strong organic electron acceptor that forms charge transfer (CT) complexes with various carbazolyl donor molecules (12–14). These CT complexes can be characterized by new asymmetric absorption bands in the visible region of the spectrum. The asymmetry of these new CT bands is due to the presence of two electronic CT transitions involving two closely lying higher occupied molecular π-orbitals of the carbazolyl chromophore

Can. J. Chem. Downloaded from www.nrcresearchpress.com by 88.85.125.76 on 09/07/12
For personal use only.

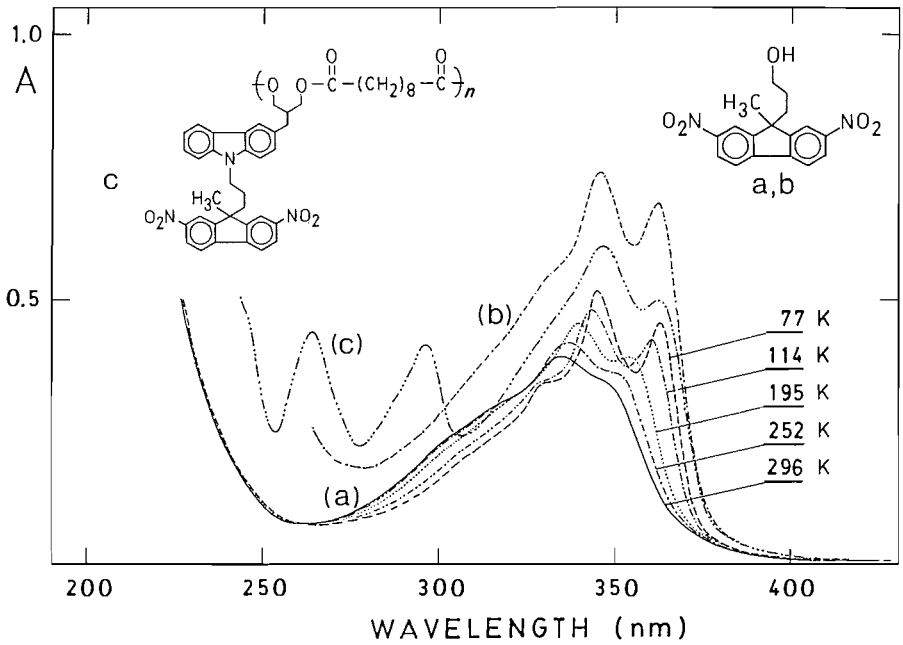

FIG. 8. (a) Changes in the absorption spectrum of acceptor model $\mathbf{A_1}$ ($C = 1 \times 10^{-5}$ M, $l = 1.3$ cm) in EPA solution when temperature decreases and (b) phosphorescence excitation spectrum of $\mathbf{A_1}$ in EPA at 77 K ($C = 1 \times 10^{-5}$ M) at $\lambda_{em} = 499$ nm as compared to (c) the absorption spectrum of polysebacate $\mathbf{P_1}$ ($C = 1 \times 10^{-6}$ M, $l = 1.3$ cm, $A \times 8$) in EPA at 77 K.

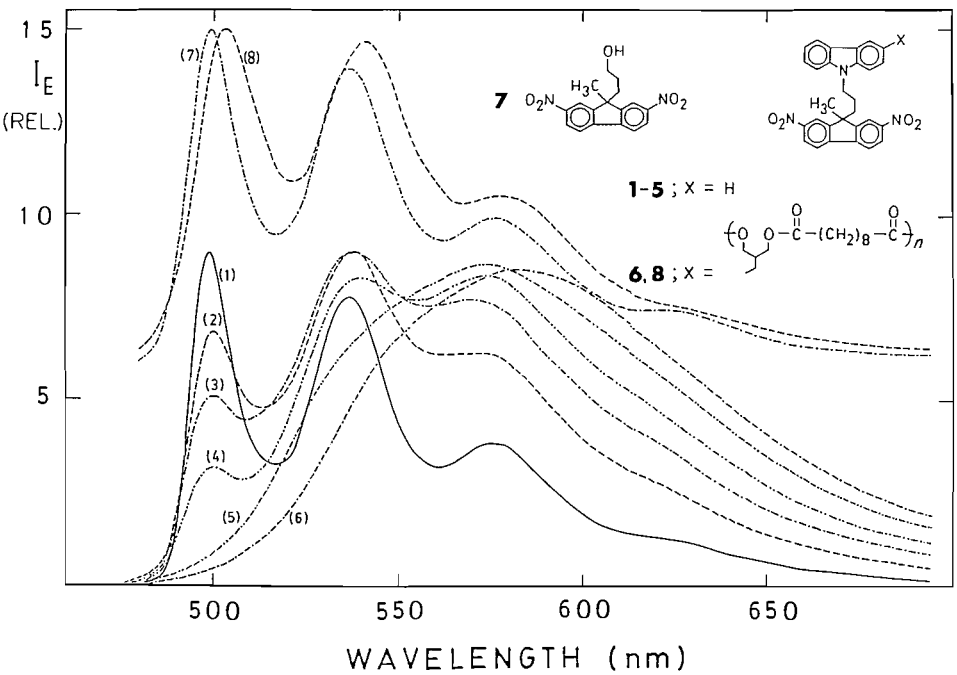

FIG. 9. Changes in the phosphorescence spectrum of bichromophore $\mathbf{B_1}$ in 3MP when concentration increases: (1) 1×10^{-6} M; (2) 1.66×10^{-6} M; (3) 2×10^{-6} M; and (4) 5×10^{-6} M; along with the solid state fluorescence spectra of (5) $\mathbf{B_1}$ and (6) polysebacate $\mathbf{P_1}$. Curves (7) and (8) refer to phosphorescence spectra of acceptor model $\mathbf{A_1}$ (1×10^{-6} M) and $\mathbf{P_1}$ (saturated solution) in 3MP at 77 K ($\lambda_{exc} = 360$ nm).

and the lowest vacant π-orbital of TNF. For *N*-ethylcarbazole ($\mathbf{D_1}$) the first two ionization potentials taken from the photoelectron spectra are $IP_1 = 7.41$ eV and $IP_2 = 7.96$ eV (15). In the absorption spectra of the TNF-D_1 system, the CT bands are at $\lambda_1 = 557$ nm and $\lambda_2 = 429$ nm in CH_2Cl_2 (14) and at $\lambda_1 = 550$ nm and $\lambda_2 = 470$ nm in tetrahydrofuran (14). These CT interactions are also observed in the bichromophoric compounds $\mathbf{B_2}$, $\mathbf{B_{2a}}$ and the polysebacate $\mathbf{P_2}$ dissolved in CH_3CN even if they are much weaker than in the intermolecular systems. Figure 10 shows the long-wavelength absorption bands of the electronic absorption spectra $\mathbf{B_2}$, $\mathbf{B_{2a}}$, and $\mathbf{P_2}$ along with the spectrum of the model electron-acceptor molecule $\mathbf{A_2}$ in an acetonitrile solution. These spectra indicate that $\mathbf{B_2}$, $\mathbf{B_{2a}}$, and $\mathbf{P_2}$ possess similar CT absorption bands with maxima at around 550 nm and 450 nm. $\mathbf{B_2}$ and $\mathbf{B_{2a}}$ show the same CT bands in the solid state. In these transparent films the CT electronic absorption spectra (Fig. 11) are shifted to lower energy and the corresponding maxima are at 590 nm and 470 nm respectively. Similar CT interactions in the

Can. J. Chem. Downloaded from www.nrcresearchpress.com by 88.85.125.76 on 09/07/12
For personal use only.

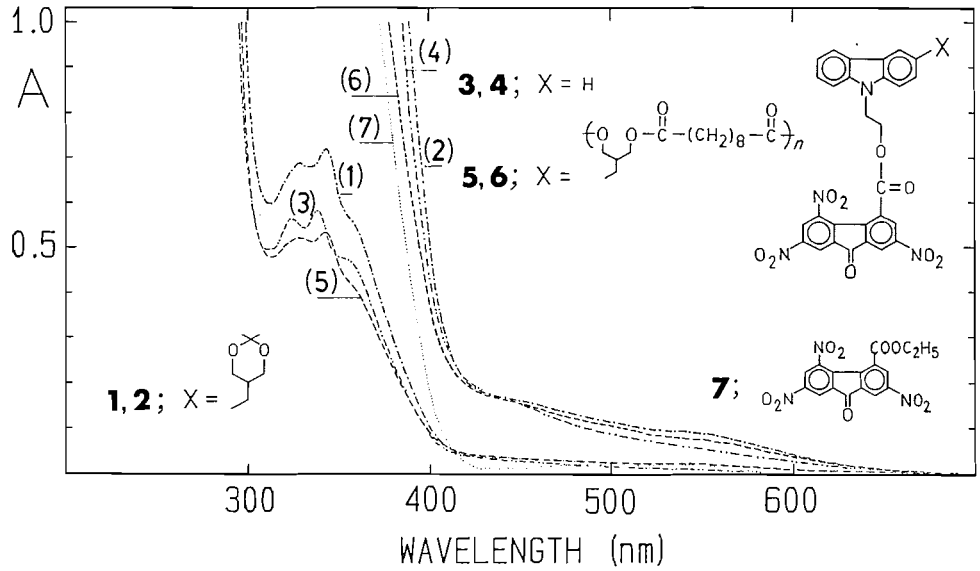

FIG. 10. Electronic absorption spectra of $\mathbf{B_2}$: (1) $C = 4.2 \times 10^{-5}$ M, $l = 1$ cm, $A \times 2$; (2) $C = 4.2 \times 10^{-5}$ M, $l = 1$ cm, $A \times 10$; $\mathbf{B2_a}$: (3) $C = 3.3 \times 10^{-5}$ M. $l = 1$ cm, $A \times 2$; (4) $C = 3.3 \times 10^{-5}$ M, $l = 1$ cm, $A \times 10$; $\mathbf{P_2}$: (5) $C = 1.1 \times 10^{-5}$ M, $l = 1$ cm, $A \times 5$; (6) $C = 1.1 \times 10^{-5}$ M, $l = 1$ cm, $A \times 20$; and $\mathbf{A_2}$: (7) $C = 4.3 \times 10^{-5}$ M, $l = 1$ cm, $A \times 5$; in acetonitrile.

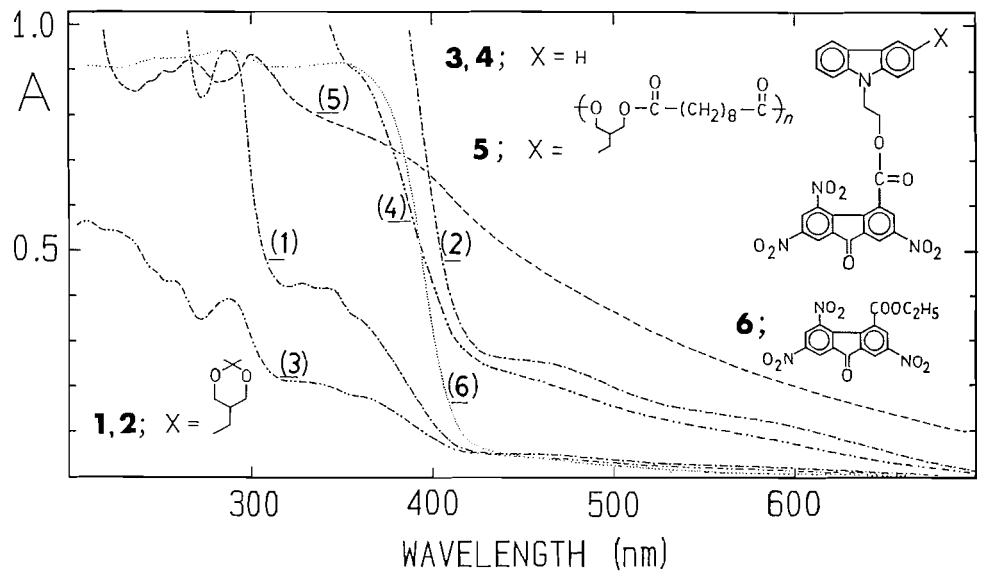

FIG. 11. Solid state electronic absorption spectra of $\mathbf{B_2}$: (1) at A and (2) at $A \times 5$; $\mathbf{B_{2a}}$: (3) at $A \times 2$ and (4) at $A \times 10$; as well as $\mathbf{P_2}$: (5) at $A \times 10$ and $\mathbf{A_2}$: (6) at $A \times 2$.

solid state would also be expected for the polysebacate $\mathbf{P_2}$ but it seems that the CT bands of $\mathbf{P_2}$ are hidden due to light scattering by the oligomer samples.

These absorption spectra (Figs. 10 and 11) strongly suggest the existence of molecular orbital overlap between the donor (carbazolyl) and the acceptor (2,4,7-trinitro-9-fluorenonyl) chromophores in the ground electronic states of the bichromophoric units in acetonitrile and also in the solid state. It is worth noting that these CT bands were never observed in the $\mathbf{B_1}$ and $\mathbf{P_1}$ electronic absorption spectra in acetonitrile or in the solid state.

Similarly as in $\mathbf{B_1}$ and $\mathbf{P_1}$, the fluorescence and the phosphorescence of the carbazolyl chromophore when excited are not observed in the bichromophoric compounds $\mathbf{B_2}$ and $\mathbf{B_{2a}}$ or in the polysebacate $\mathbf{P_2}$ in EPA or acetonitrile solutions. This indicates the strong intramolecular quenching effect of the singlet excited electronic state of the carbazolyl chromophore by the 2,4,7-trinitro-9-fluorenone chromophore. Considering the electron affinity of $\mathbf{A_2}$ as well as the singlet and the triplet energy levels of $\mathbf{A_2}$, which are of lower energy than the singlet and the triplet energy levels of $\mathbf{D_1}$ (see Table 4), we can expect two photoprocesses as quenching mechanisms in the bichromophoric systems when the donor is excited: the electron and (or) the energy transfer. However, this discussion would be irrelevant to the photoactivity experiment, where visible light is used and can only excite the acceptor moiety of the bichromophore. In such cases, no fluorescence of the 2,4,7-trinitro-9-fluorenone chromophore in $\mathbf{A_2}$ or in $\mathbf{B_2}$, $\mathbf{B_{2a}}$, and $\mathbf{P_2}$ has been observed. A weak phosphorescence emission of $\mathbf{A_2}$ in EPA at 77 K was detected with a quantum yield of 0.005. But this phosphorescence emission is completely quenched in $\mathbf{B_2}$, $\mathbf{B_{2a}}$, and $\mathbf{P_2}$. This quenching effect of the excited triplet state of the 2,4,7-trinitro-9-fluorenone chromophore might only be due to

Can. J. Chem. Downloaded from www.nrcresearchpress.com by 88.85.125.76 on 09/07/12
For personal use only.

TABLE 4. Ionization potential (IP), electron affinity (EA), half-wave polarographic oxidation and reduction potentials, and first singlet and triplet energy levels for electron-donor and electron-acceptor molecules (solvent: acetonitrile)

Compound	IP (eV)	EA[b] (eV)	$E^{ox}_{1/2}(D/D^+)$ [V]	$E^{red}_{1/2}(A^-/A)$ [V]	E_s (D) (eV)	E_T (D) (eV)	E_s (A) (eV)	E_T (A) (eV)
D_1	7.41[a]	—	+1.28	—	3.58	3.02[c]	—	—
D_2		—	+1.24	—	3.51	2.99[c]	—	—
A_1	—	1.27	—	−1.02	—	—	3.49	2.46[c]
A_2	—	1.83	—	−0.33	—	—	3.43	2.46[d]

[a]Value taken from ref. 8.
[b]EA in the gas phase calculated from EA = 0.81 $E_{1/2}$ + 2.10 (eV); $E_{1/2}$ is the half-wave reduction potential vs. the SCE in methylene chloride; see ref. 16.
[c]In acetontirile at 77 K.
[d]In EPA at 77 K.

the intramolecular electron transfer process in the singlet or in the triplet states of the acceptor moiety. Furthermore, $\mathbf{A_2}$ as well as $\mathbf{B_2}$, $\mathbf{B_{2a}}$, and $\mathbf{P_2}$ in the solid state also show very low structureless emissions between 500 nm and 680 nm with λ_{max} = 590 nm at λ_{exc} = 370 nm. Such emissions, which are about of the same intensity at room temperature and at 77 K, can be assigned as fluorescence from aggregates of the acceptor moieties. But these emissions are much lower (by a factor of about ten) for $\mathbf{B_2}$, $\mathbf{B_{2a}}$, and $\mathbf{P_2}$ than those for $\mathbf{B_1}$ and $\mathbf{P_1}$ (Fig. 9). This shows that the overlap between two acceptor moieties is much weaker in $\mathbf{B_2}$, $\mathbf{B_{2a}}$, and $\mathbf{P_2}$.

The above spectroscopic results on the polysebacates $\mathbf{P_1}$ and $\mathbf{P_2}$ clearly show that the spectroscopic properties in solution of the oligomers in the ground and in the excited electronic states are rather similar to those of the corresponding bichromophoric molecules $\mathbf{B_1}$, $\mathbf{B_2}$, or $\mathbf{B_{2a}}$. On the other hand it has been shown that, in the solid state, the oligomers and the bichromophores show some spectral properties that are assigned to aggregate formation between the acceptor moieties. This is another example where the effect of phase on the oligomer spectroscopy is important (17).

4. Electron transfer in the bichromophoric donor–acceptor system

The electrochemical measurements of the half-wave potentials of the oxidation of $\mathbf{D_1}$ and $\mathbf{D_2}$ and the reduction of $\mathbf{A_1}$ and $\mathbf{A_2}$ molecules in the ground electronic states, along with their lowest singlet and triplet excitation energy considering acetonitrile as a solvent, are presented in Table 4. These data were used to obtain the ΔG_{ET} values for the $\mathbf{D_1A_1}$, $\mathbf{D_2A_2}$, and $\mathbf{D_1A_2}$ system pairs from the Rehm–Weller equation (6, 18, 20) (see Table 5). As can be seen in the table the free-energy changes for the photoinduced electron transfer in all systems considered would be negative for perfect overlapping between the donor and the acceptors. In such donor–acceptor molecular systems, the electron transfer can then be represented by the following equation when the acceptor moiety alone is excited in its first electronic singlet and (or) triplet state:

$$\mathbf{D} + {}^{1,3}\mathbf{A}^* \rightarrow \mathbf{D}^{\cdot +} + \mathbf{A}^{\cdot -} \quad (\Delta G_{ET} < 0)$$

Table 5 also shows that the ΔG_{ET} values for the $\mathbf{D_2A_2}$ and $\mathbf{D_1A_2}$ systems are about the same and they are ~0.7 eV more negative than the corresponding ΔG_{ET} values for the $\mathbf{D_1A_1}$ system. Such a difference in the ΔG_{ET} is mainly due to the higher EA value of the $\mathbf{A_2}$ molecule as compared to that of the $\mathbf{A_1}$ molecule (see Table 4). The effect of intermolecular distances on the ΔG_{ET} values plays a minor role. The negative values of ΔG_{ET} in Table 5 indicate that intramolecular electron transfer in the bichromophoric compounds $\mathbf{B_1}$, $\mathbf{B_2}$, and $\mathbf{B_{2a}}$, which correspond to the $\mathbf{D_1A_1}$, $\mathbf{D_2D_2}$, and $\mathbf{D_1A_2}$ systems, is highly probable on the basis of thermodynamic grounds alone (19). When the acceptor chromophore is excited in its singlet state, the electron transfer photoprocess can then compete with the intersystem crossing process ($S_1 \rightsquigarrow T_1$) which is strongly allowed by the nitro substituents in the fluorene chromophore (21).

5. Conformational effect in B_1 and B_2

We previously reported (6) that, for the bichromophoric compound $\mathbf{B_1}$ in EPA solution, no intramolecular charge transfer or electron transfer interactions exist in the ground or in the excited electronic states even if $\Delta G_{ET} < 0$. $\mathbf{B_1}$ also behaves the same way in acetonitrile solutions. This might be explained by steric and conformational effects since the sp^3-hybridized carbon-9 in the fluorene chromophore is connected to the nitrogen atom in the carbazolyl chromophore through the propylene bridge, which prevents appropriate overlap of the chromophores (5).

Because of the sp^3-hybridization of the fluorene carbon-9, the sandwich conformation of the two chromophores in $\mathbf{B_1}$ (vertical distance of ~3.75 Å estimated from Dreiding models) should be unstable. We have shown (5) from crystalline structure that such a conformation of the bichromophoric molecule can easily change to the low-energy conformation with a center-to-center donor–acceptor distance of 6.1 Å with no ring orbital overlap.

The same sandwich conformation between the two carbazolyl chromophores in 1,3-bis(carbazolyl)-propane (22–26) is the low energy conformation with a distance of 2.5 Å between the chromophores (according to Dreiding models). The propylene bridge between the two *N*-carbazolyl groups in the 1,3-bis-(carbazolyl)propane creates convenient conditions for intramolecular charge-transfer interactions when one of the chromophores of the molecule is in the excited electronic state. For 1,3-bis(carbazolyl)propane, the low-energy sandwich excimers have been detected through the well-known structureless emission band at 420 nm. Such sandwich excimers can be formed directly or by reorientation of the high-energy excimers (λ_{max} = 375 nm) in which only one pair of phenyl rings from the two carbazolyl chromophores overlaps.

For the 1,3-bis(*N*-carbazolyl)propane molecule, the excimer emissions have been observed even if the carbazolyl chromophore is a poorer electron acceptor than 2,7-dinitrofluorene. Considering the sandwich conformation between the two chromophores in the bichromophoric molecule $\mathbf{B_1}$ as the proper conformation for intramolecular CT or ET interactions, this would mean that in the low energy conformation the center-to-center distance (6.1 Å in the crystal), along with the restricted mutual orientation between the chromophores, does not allow any electron transfer to take place.

Can. J. Chem. Downloaded from www.nrcresearchpress.com by 88.85.125.76 on 09/07/12
For personal use only.

TABLE 5. Free energy for the electron-transfer process (ΔG_{ET}) and calculated rate constant (k_q) of quenching of the excited singlet and triplet states in the donor–acceptor systems

Ground and excited electronic states of donor and acceptor molecules		ΔG_{ET} (eV)		ΔG_s^* (eV)	ΔG_t^* (eV)	k_q ($M^{-1}s^{-1}$) 296 K
		$R_{sandwich}$	R_{max}			
		3.75 Å	7.1 Å			
$\mathbf{D_1}$	A_1	2.20	2.25	—	—	—
$\mathbf{D_1}$	$^1A_1$*	−1.29	−1.24	8.66×10^{-3}	—	1.48×10^{10}
$\mathbf{D_1}$	$^3A_1$*	−0.26	−0.21	—	1.12×10^{-1}	9.44×10^{8}
		2.7 Å	9.4 Å			
$\mathbf{D_2}$	A_2	1.43	1.53	—	—	—
$\mathbf{D_2}$	$^1A_2$*	−2.00	−1.90	5.68×10^{-3}	—	1.52×10^{10}
$\mathbf{D_2}$	$^3A_2$*	−1.03	−0.93	—	2.85×10^{-2}	1.13×10^{10}
		2.7 Å	9.4 Å			
$\mathbf{D_1}$	A_2	1.47	1.57	—	—	—
$\mathbf{D_1}$	$^1A_2$*	−1.96	−1.86	5.80×10^{-3}	—	1.52×10^{10}
$\mathbf{D_1}$	$^3A_2$*	−0.99	−0.89	—	2.98×10^{-2}	1.11×10^{10}

The conformational effect of the chromophores in the bichromophoric molecule $\mathbf{B_2}$ is quite different than that in $\mathbf{B_1}$. The four-atom UV-transparent spacer in $\mathbf{B_2}$ connects the carbazolyl chromophore with the trinitrofluorenone chromophore at position 5 of the fluorenone aromatic ring. Such a connection between the chromophores in $\mathbf{B_2}$ allows for the existence of numerous conformers for the bichromophore. The highest available center-to-center chromophore–chromophore distance in a linear conformer of $\mathbf{B_2}$ is 9.4 Å. On the other hand, for the sandwich conformer of $\mathbf{B_2}$, assuming 100% of donor–acceptor molecular orbital overlap, the vertical distance between the chromophores would be 2.7 Å. These two conformers of $\mathbf{B_2}$, even sterically highly probable, seem to be the limiting cases in the spatial arrangements of the chromophores in the molecule. Indeed, from crystallographic studies of the solid state of $\mathbf{B_2}$, the lowest energy conformer of the bichromophoric molecule possesses about 50% of molecular orbital overlap between the donor and the acceptor chromophores separated by 3.42 Å. The center-to-center chromophore–chromophore distance in $\mathbf{B_2}$ has been measured as 5.75 Å.

From the crystallographic data alone, it is clear that the low energy conformer of $\mathbf{B_2}$ allows for intramolecular CT interactions between the chromophores. This is evidenced by the weak ground state CT electronic transitions observed in $\mathbf{B_2}$ in the solid state as well as in acetonitrile solutions. The acetal substituent at position 3 of the carbazolyl chromophore in $\mathbf{B_2}$ seems to play a minor role in the mutual orientation of the chromophores since the electronic absorption spectra of $\mathbf{B_{2a}}$ in the solid state and in acetonitrile solutions are similar to those for $\mathbf{B_2}$. Two other spectroscopic results might also be correlated to the conformational effect in the bichromophoric systems studied, and these are the phosphorescence quantum yields and the fluorescence spectra of the aggregates. As far as the phosphorescence quantum yield is concerned, it is the same for $\mathbf{B_1}$ and $\mathbf{A_1}$, whereas the phosphorescence of $\mathbf{A_2}$ is completely quenched in $\mathbf{B_2}$ or $\mathbf{B_{2a}}$ when exciting in the acceptor moiety alone. Since the energy transfer is forbidden from the acceptor to the donor, the electron transfer from the donor D to the excited singlet or triplet

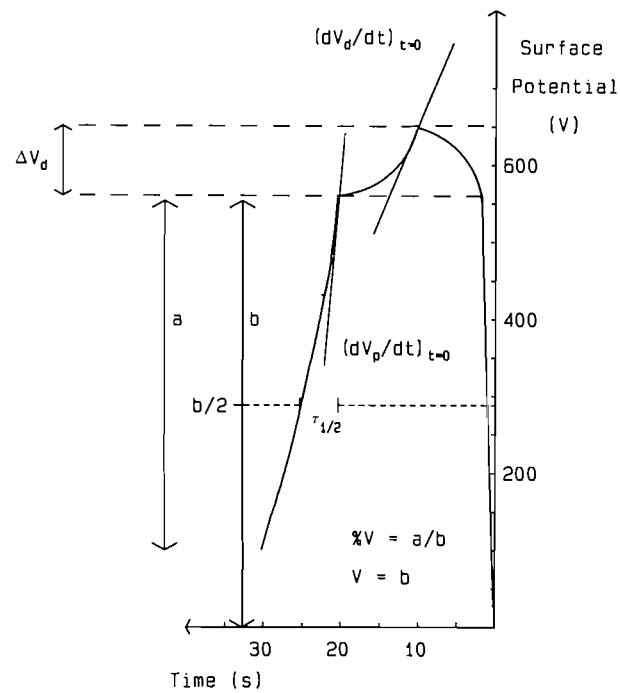

FIG. 12. Typical xerographic pattern and important quantities derivable from it.

of the acceptor A appears to be the only mechanism responsible for the phosphorescence quenching in $\mathbf{B_2}$ and $\mathbf{B_{2a}}$. On the other hand the fluorescence spectra of the aggregates in $\mathbf{B_1}$ are much stronger than in $\mathbf{B_2}$ or $\mathbf{B_{2a}}$, probably because the acceptor moiety in $\mathbf{B_1}$ is entirely free to interact with the other acceptors on other bichromophore units since practically no CT interactions (no orbital overlap) can occur between the donor and the acceptor in the same unit. All these spectroscopic results can be explained by the conformational effect discussed above.

6. Evaluation of photoactivity

The photoactivity of oligomers $\mathbf{P_1}$ and $\mathbf{P_2}$ was evaluated by

Can. J. Chem. Downloaded from www.nrcresearchpress.com by 88.85.125.76 on 09/07/12
For personal use only.

TABLE 6. Photoactivity characteristics of polymers $\mathbf{P_1}$ and $\mathbf{P_2}$ relative to PVK–TNF

Entry	Material	d^a (μm)	V^b (V)	$(dV_p/dt)_{t=0}$ (V/s)	%V	$\tau_{1/2}$ (s)	$(dV_d/dt)_{t=0}$ (V/s)	ΔV_d (V)
				Negative charging				
1	Polymer $\mathbf{P_1}$	12.0	345	1.3	2.9	≫10	8.2	15
2			940[c]	24	18	≫10	43	65
3	Polymer $\mathbf{P_2}$	4.6	132	8.1	43	>10	0.1	1
4			295	36	56	7.5	2.1	15
5			430[c]	50	63	5.3	16	35
6	PVK–TNF[d]	10	175	267	100	0.25	2.1	10
7			285[c]	286	100	0.25	32	60
				Positive charging				
8	Polymer $\mathbf{P_1}$	12.0	340	1.4	2.9	≫10	0.0	0
9			860[c]	18	16	≫10	31	120
10	Polymer $\mathbf{P_2}$	4.6	131	7.4	35	>10	0.0	0
11			305[c]	29	48	>10	4.0	25
12	PVK–TNF[d]	10	165[c]	222	100	0.38	24	75

[a]Polymer film thickness.
[b]Residual surface potential, after dark decay.
[c]Maximum surface potential.
[d]Molar ratio 1:1.

the xerographic technique using a static charge analyzer (27). This apparatus allows the measurement of the surface potential decay as a function of time. The surface charge, either positive or negative, which is applied to the surface by a corona, is allowed to decay in the dark and its rate recorded; then, illumination with visible light gives rise to photosensitized decay, which is also recorded.

Since photoactivity is related to photoconductivity, which is a function of carrier generation efficiency and carrier mobility (27), it follows that, although the present xerographic evaluation of oligomers $\mathbf{P_1}$ and $\mathbf{P_2}$ cannot provide any separate information on the number of charge carriers and their mobility, an analysis of the shape of the xerographic decay curves and other quantities derived with respect to the other physical measurements already described above, and a comparison with an appropriate sample of the classic PVK–TNF system, should provide useful information that may be used in the design or optimization of future photoactive materials in this series.

Figure 12 represents a typical xerographic pattern, which can be analyzed in terms of its charge decay profile. The important quantities derivable are defined as follows:

$(dV_d/dt)_{t=0}$: the initial rate of surface potential decay in the dark.

$(dV_p/dt)_{t=0}$: the initial rate of surface potential decay under irradiation, after a period of dark decay.

$\tau_{1/2}$: the time required to reduce the initial surface potential to half its value.

$\%V$: the percentage of surface potential neutralized upon illumination for a time t.

ΔV_d: the surface potential lost (in volts) by dark decay after a time t.

A priori, favorable conditions for a good photoconductor are (a) a high initial surface potential, (b) a slow dark decay, (c) a fast initial rate of photosensitized decay, (d) a small $\tau_{1/2}$ value, (e) a short tailing of the decay curve, and (f) a large percentage of neutralized surface potential after illumination.

Evaluation of the first oligomer $\mathbf{P_1}$ reveals (Table 6) that, although it has excellent film forming properties and takes up negative charge very well, the material is nevertheless a very poor photoconductor relative to the standard PVK–TNF system. Indeed, for equivalent electric field charging ($d_{p2} \cdot V_{p1} = d_{p1} \cdot V_{p2}$, where d = film thickness), it has an initial rate of photosensitized surface potential decay 220 times slower than that of the reference (entries 1 and 7), a long half-life of the surface potential (≫ 10 s versus 0.25 s), and an almost negligibly small percentage (2.9%) of neutralized surface potential after illumination. As expected, maximum charging of the film (entry 2) improves performance markedly but, nevertheless, the material remains a relatively poor performer.

The main explanation for this behavior derives directly from the spectroscopic study, which showed an absence of charge transfer interaction in the pendant bichromophores of the oligomer $\mathbf{P_1}$ in the ground state. This then leaves only the long-wavelength absorption of the dinitrofluorenyl group, which tails in the visible, to serve as the only absorbing chromophore for the photosensitizing source used in the xerographic technique. These results are corroborated by the X-ray and spectroscopic study, which showed that in the single crystal and the aggregates of the oligomer, close interaction takes place between the acceptor chromophores but not between the donor and acceptor chromophores, most probably because of the sp^3 hybridized carbon at C-9 of the dinitrofluorenyl spacer and the three-carbon chain, which prevents good overlap between the donor and the acceptor. This morphology could perhaps be favorable to good electron mobility but not to electron transfer required for charge generation, in spite of the fact that the estimated ΔG_{ET} is less than zero for this donor–acceptor pair in close contact.

Evaluation of the second oligomer $\mathbf{P_2}$ reveals (Table 6) that the material is superior to $\mathbf{P_1}$ (compare, as above, entries 1 and 3) but still not a good photoconductor relative to PVK–TNF (see below). On the other hand, when the oligomeric film $\mathbf{P_2}$ is charged to its maximum, one again observes an enhanced performance (compare entries 3 and 5) but, relative to the

Can. J. Chem. Downloaded from www.nrcresearchpress.com by 88.85.125.76 on 09/07/12
For personal use only.

Can. J. Chem. Downloaded from www.nrcresearchpress.com by 88.85.125.76 on 09/07/12
For personal use only.

standard PVK–TNF system, oligomer $\mathbf{P_2}$ remains a relatively poor photoconductor (compare entries 3 and 7). If the comparison was made at maximum charging (entries 5 and 7), it is evident that oligomer $\mathbf{P_2}$ would compare more favorably because of its greater electric field capacity. Comments regarding the general difference between $\mathbf{P_1}$, $\mathbf{P_2}$, and the PVK–TNF system will be deferred until the end of the present discussion.

In view of the above considerations it is concluded that the photoactivity results observed for oligomers $\mathbf{P_1}$ and $\mathbf{P_2}$ are largely explainable on the basis of the spectroscopic and X-ray crystallographic results reported herein. Indeed, the marked enhancement of photoactivity of oligomer $\mathbf{P_2}$ over $\mathbf{P_1}$ is most logically attributable to the charge transfer complex formation between the donor and acceptor chromophores observed in $\mathbf{P_2}$, which absorb in the visible. Also, the measured photoactivity correlates well with the observed complete quenching of the phosphorescence of the acceptor chromophore in $\mathbf{P_2}$ by an electron transfer mechanism (since energy transfer is not possible in this case), which generates the charge carriers for photoconduction. Finally, although the experiments performed do not give direct information on the nature of the charge carrier(s) and its (their) mobility, it is interesting to note that the structureless emission observed for $\mathbf{P_1}$ and $\mathbf{P_2}$ is due to aggregate fluorescence of the acceptor moieties, as could be anticipated from the X-ray data, which suggests the possibility that these oligomers could function preferentially as electron rather than hole conductors because of the propensity of the acceptor groups to associate and therefore favor the electron hopping process. This effect has been discussed previously (28, 29) and it appears that the formation of large aggregates is detrimental to good mobility because of phase separation, which causes deep traps at the amorphous–crystalline interface (30) and, of course, reduces the concentration of potential sites for charge migration.

An experimental test of the possibility that $\mathbf{P_1}$ and $\mathbf{P_2}$ may function better as electron rather than hole conductors is to compare the photoactivity characteristics of the systems upon positive charging of the films with those observed for negative charging (31) (see Table 6). It is apparent from the table that for equivalent electric field charging there is no significant difference in the case of oligomer $\mathbf{P_1}$ (entries 1 and 8). However, if the comparison was made at maximum charging (entries 2 and 9), positive charging gives a lower photoactivity, which is certainly attributable to the lower electric field capacity under positive polarity. In the case of oligomer $\mathbf{P_2}$, positive charging gives values approximately 10–20% lower for the initial rate of surface potential decay under irradition and percentage of surface potential neutralized (entries 3 and 10 or 4 and 11). The fact that $\mathbf{P_1}$ shows no difference depending on the sign of the surface charge, whereas $\mathbf{P_2}$ shows a slight decrease upon positive charging, suggests that oligomer $\mathbf{P_2}$ may, in fact, be a slightly better electron than hole conductor, not because of the propensity of its acceptor groups to associate as aggregates as in $\mathbf{P_1}$ (which shows no voltage polarity effect) but because of the formation of charge-transfer complexes (with the donor chromophores), which prevents their aggregation as crystallites as remarked by Loufty and Ong (29). This, in turn, should keep them relately free to participate in the hopping process for electron transport, whereas the donor chromophores, which are bound to both an acceptor and the backbone of the oligomer and which participate, in many cases, in charge transfer complexing, should be relatively more hindered in their donor–donor interactions for hole transport. It is important to recall here that, at least for PVK–TNF, hole transport appears to involve only noncomplexed carbazole groups, whereas electron transport occurs via both free and complexed TNF molecules (1*a*).

Finally, examination of the standard PVK–TNF system under negative and positive charging shows that photoactivity is lower, as seen by the initial rate of surface potential decay under irradiation, for positive charging than for negative charging (entries 6 and 12). As in the case of oligomer $\mathbf{P_2}$, this value is approximately 20% lower for positive charging. This phenomenon has been discussed by Pearson (1*a*) and appears to be due to the fact that "electron transport involves the LUMO orbitals of the acceptor chromophores which are more spatially delocalized than the bonding orbitals involved in hole transport in PVK and therefore can tolerate larger separation/perturbations without impacting the local electron transfer reactions". On the other hand, "hole transport is dependent on the overlap between the HOMO orbitals of the donor chromophores and all the results from the vinylcarbazole polymers and copolymers plus the PVK–TNF systems indicate that this overlap is very sensitive to perturbation, either morphological or from other chemical species, e.g. comonomers, end groups, dopants". As indicated above, hole transport appears to involve only noncomplexed carbazole groups whereas electron transport occurs via both free and complexed TNF molecules.

Now that the standard PVK–TNF system has been compared under negative and positive charging and pertinent literature discussion has been recalled, a comment regarding the great difference between the photoactivity of oligomers $\mathbf{P_1}$ and $\mathbf{P_2}$ and that of PVK–TNF would be in order. A priori, it would appear that four major factors could be at the origin of the difference observed: (1) a greater absorbance in the visible because of better donor–acceptor overlap due to the freedom of the acceptor chromophore, which would lead to more efficient charge-carrier generation; (2) a greater concentration of chromophores versus polymer backbone (one chromophore unit every third backbone atom in PVK compared to one chromophore unit every 16 backbone atoms in $\mathbf{P_2}$ or $\mathbf{P_1}$), which translates into a 95% chromophore loading for PVK–TNF compared to 78% for $\mathbf{P_2}$ and 75% for $\mathbf{P_1}$, and which should affect charge mobility through the bulk and also possibly charge-carrier generation; (3) a greater freedom of both chromophores to interact with chromophores of the same nature in the charge transport process; and (4) a greater charge mobility due to the much larger molecular weight of PVK, which means fewer chain ends that can act as traps. Although all of these factors most certainly contribute to various extents to the observed difference, a comparison of the absorption constants α (cm^{-1}) at 450 nm, where only the D,A charge transfer complexes absorb, reveals for films of the $\mathbf{P_2}$ oligomer and the 1:1 PVK–TNF system reported in the literature (32) that the absorption constant for the latter is about 10–20% greater than that for $\mathbf{P_2}$. This in itself should certainly make the first factor mentioned above the major contributor to the observed difference.

Further systematic work is in progress to better probe these and other new oligoesters with pendant donor–acceptor bichromophores, and will be reported in due course.

Experimental

Synthetic investigation

Melting points were determined on a Büchi apparatus and are uncorrected. Infrared spectra were taken in KBr pellets (unless otherwise specified) on a Perkin–Elmer apparatus, model 710-B or 783, using the 1601 cm^{-1} band of polystyrene as reference. High resolution mass spectra (EI) were recorded on an AEI MS-902 apparatus. The ^1H

TABLE 7. Crystal data of interest and data collection summary for the acceptor $\mathbf{A_2}$ and the bichromophore $\mathbf{B_2}$

Crystal data	Acceptor $\mathbf{A_2}$	Bichromophore $\mathbf{B_2}$
Formula	$C_{16}H_9N_3O_9$	$C_{35}H_{28}N_4O_{11}\cdot C_2H_3N$
M_r	387.26	721.69
Melting point, °C	157.5–159	256–257
Unit cell	Triclinic	Triclinic
Space group	$P\bar{1}$	$P\bar{1}$
a, Å	11.789(2)	10.588(2)
b, Å	12.308(1)	13.034(4)
c, Å	12.336(2)	13.041(4)
α, deg	84.59(1)	106.52(2)
β, deg	69.11(1)	91.23(2)
γ, deg	74.44(1)	95.00(2)
V, Å^3	1611.0(4)	1716.7(4)
d, g cm^{-3}	1.597	1.396
Z	4	2
μ(CuKα), cm^{-1}	11.14	8.37
$F(000)$	792	752
Crystal size, mm	0.15 × 0.15 × 0.30	0.04 × 0.10 × 0.33
Data collection		
$2\theta_{max}$, deg	140.0	140.0
Octants measured	$0 \leq h \leq 14$ $-15 \leq k \leq 15$ $-15 \leq l \leq 15$	$0 \leq h \leq 12$ $-15 \leq k \leq 15$ $-15 \leq l \leq 15$
Largest intensity fluctuation	1.9%	1.2%
Number of measured reflections	6103	6517
Number of observed reflections	3903	4190
Acceptance level	1.96	1.96
Temperature, K	293	143

NMR spectra were determined in deuterochloroform ($CDCl_3$) (unless otherwise indicated) using a Bruker WH-90 (90 MHz) spectrometer; the chemical shifts are expressed in ppm, downfield from tetramethylsilane (TMS), used as internal standard. The symbols s, d, dd, t, q, and m were respectively used for singlet, doublet, doublet of doublets, triplet, quartet, and multiplet. Number-average molecular weights, $\bar{M}_n$, and weight-average molecular weights, $\bar{M}_p$, were determined by GPC on a Waters model 510 apparatus using three Ultrastyragel columns in series, THF as eluant, and a Waters 410 differential refractometer; the calibration curve used was that of polystyrene. Glass temperatures (T_g) were measured on a Perkin– Elmer model DSC-4 apparatus equipped with a System 4 thermal analyser from Perkin–Elmer. Thin-layer chromatography (TLC) analyses were done on Merck, 0.2 mm, silica gel 60 F_{254} aluminum sheets and were visualized with UV light. Flash column chromatography was carried out on Merck 60 silica gel, 230–400 mesh. Microanalytical data were obtained from Guelph Chemical Laboratories Ltd., Guelph, Ont.

X-Ray investigation

Acceptor A_2

Crystals of the acceptor $\mathbf{A_2}$ were obtained from dichloromethane–methanol. They are tabular yellow-orange crystals. The unit-cell dimensions, given in Table 7 with other crystallographic data of interest, were obtained by least-squares fit to the angular settings of 25 well-centered reflections in the range $40 \leq 2\theta \leq 50°$. Intensity data were collected on a Nonius CAD4 diffractometer using copper (λCuK$\bar{\alpha}$ = 1.54178 Å), graphite-monochromatized radiation. The $\omega/2\theta$ scan mode was used with a scan range calculated by $\Delta\omega = (1.00 + 0.14 \tan\theta)°$. The intensities of seven reference reflections were monitored every hour while the orientation of the crystal was verified every 100 measurements, and readjustment was made when needed. The details of the data collections are placed in Table 7. Data reduction, i.e., scaling and Lorentz and polarization corrections, was performed, but no absorption correction was applied since the crystal is small and the absorption coefficient has a low value.

Bichromophore B_2

Crystals of the bichromophore $\mathbf{B_2}$ obtained from an acetonitrile solution are dark red. They are in the shape of very thin platelets. The unit-cell dimensions were obtained by least squares from angular data measured in the range $40 \leq 2\theta \leq 50°$. These and other crystal data are presented in Table 7. The data collection and reduction were obtained as for the acceptor $\mathbf{A_2}$. The bichromophore $\mathbf{B_2}$ crystallized with a molecule of solvent. Because of this, the data collection was done at 143 K. The structures were solved by direct methods using the multi-solution program MULTAN80 (33).

For the acceptor $\mathbf{A_2}$ the E-map computed for the set of phases corresponding to the highest figure of merit revealed all the non-hydrogen atoms. In the case of the bichromophore $\mathbf{B_2}$, it turned out that the crystal contains one molecule of acetonitrile, the crystallization solvent, for every molecule of bichromophore $\mathbf{B_2}$. This was only revealed near the end of the structure determination. The atomic coordinates and the anisotropic temperature of the non-hydrogen atoms were refined by least squares using the block-diagonal approximation (SHELX program (34)). For the acceptor $\mathbf{A_2}$ the coordinates and the isotropic temperature factors of the H atoms were refined except for those on C(16) and C(17), which were kept at a fixed position and given a U_{iso} value 0.125. In the case of the bichromophore $\mathbf{B_2}$, the coordinates of the solvent molecule were not refined. All the H atoms except those on C(38) and C(39) were refined.

The quantity minimized was $\Sigma w\Delta F^2$, where each reflection was assigned a weight $w = 1/\sigma^2(F_o)$. The final agreement indices[4] were $R_w = 0.047$ and $S = 2.052$ for the acceptor $\mathbf{A_2}$ and $R_w = 0.071$ and $S = 2.904$ for the bichromophore $\mathbf{B_2}$. The average and largest para-

[4] $R_w = [\Sigma w\Delta F^2/\Sigma wF_0]^{1/2}$; $S = [\Sigma w\Delta F^2/(m - n)]^{1/2}$.

Can. J. Chem. Downloaded from www.nrcresearchpress.com by 88.85.125.76 on 09/07/12
For personal use only.

meter shifts of the atomic coordinates and temperature factors were 0.04, 0.33, and 0.03, 0.09 for the acceptor $\mathbf{A_2}$ and the bichromophore $\mathbf{B_2}$ respectively. The final difference Fourier syntheses showed no significant residual electron density, the extreme fluctuations being in the range ± 0.25 e $Å^{-3}$ (acceptor $\mathbf{A_2}$) – ± 0.36 e $Å^{-3}$ (bichromophore $\mathbf{B_2}$). The X-ray scattering factors were taken from ref. 35 for O, N, and C atoms and from ref. 36 for H atoms.

Spectroscopic investigation

Materials

N-Ethylcarbazole ($\mathbf{D_1}$), γ-hydroxypropylmethyldinitrofluorene $\mathbf{A_1}$, and bichromophore $\mathbf{B_1}$ were synthesized and purified as described previously (5). Donor model $\mathbf{D_2}$, acceptor model $\mathbf{A_2}$, bichromophores $\mathbf{B_2}$ and $\mathbf{B_{2a}}$, and polysebacates $\mathbf{P_1}$ and $\mathbf{P_2}$ were synthesized, purified, and characterized as reported herein.

Acetonitrile, 99%, spectrophotometric grade, was obtained from Aldrich Chemical Co. and was distilled before use. 3-Methylpentane (3MP), pure grade (99%) from Phillips Petroleum Co., was further purified as described previously (5). Isopentane, of pure grade quality from Phillips Petroleum Co., and ethyl ether are analyzed reagents from Baker and were purified in the same way as 3MP. Ethanol was purified by refluxing with concentrated sulfuric acid (4 mL H_2SO_4/1000 mL solvent) for 24 h and then distilled twice before use. The EPA solvent mixture was made from ethyl ether, isopentane, and ethanol in the volume ratio 5:5:2 respectively.

Apparatus

The absorption spectra were recorded by means of a Cary-17 spectrophotometer and a PU 8800 UV/VIS spectrophotomer (Phillips) using 1.0, 1.3, and 5 cm quartz cells. Quartz plates were used to measure the absorption spectra of solids. The low temperature Dewar, including a 1.3 cm quartz cell, was designed and built in our laboratory. Liquid nitrogen and also a mixture of propionitrile–*n*-butyronitrile (1.1 v/v) cooled by liquid nitrogen were used to stabilize the temperature in the range 296–77 K for the solutions studied. The temperatures of the solutions and the solvent were measured in the cell with a calibrated copper–constantan thermocouple with an accuracy of ±0.5 K.

Phosphorescence spectra along with phosphorescence excitation spectra were recorded on a Spex Fluorolog fluorometer model 1902 using a cylindrical Dewar assembly.

Relative fluorescence and phosphorescence quantum yields were measured and calculated by means of the Spex Fluorolog – Nova 3/12 minicomputer couple system using a FORTRAN program called SURFREND. Carbazole (**17**) was used as the fluorescence quantum yield standard. To check the system, the fluorescence quantum yields of carbazole (**17**) and *N*-ethylcarbazole ($\mathbf{D_1}$) in ethanol glasses were reproduced (8).

Electrochemical investigation

Electrochemical measurements were made using an EG&G Princeton Applied Research model 264 polarographic analyzer/stripping voltammeter. Linear sweep voltammograms (LSV) were recorded on a 7005 B *X–Y* recorder (Hewlett–Packard); the current varied between 1 and 50 μA. Voltage sweep rate was 5 mV/s. Oxidations were measured using a platinum disk electrode rotated at 20 rpm. Reduction potentials were measured using a dropping mercury working electrode (EG&P PARC model 303 static mercury drop electrode assembly); droptime was 0.5 s. LSV and polarograms were measured in the differential pulse mode; pulse amplitude was 20–50 mV. Potentials were measured against an Ag/AgCl reference electrode; a platinum wire was used as auxiliary electrode. Tetraethylammonium perchlorate (TEAP) (0.05 M) in acetonitrile was the supporting electrolyte. Solutions of the electron donor (10^{-4} M) to which the supporting electrolyte had been added were deaerated using dry nitrogen gas; purge time was 4 min. A nitrogen blanket was maintained above the solutions during electrometric measurements.

Photoactivity investigation

Photoconducting films were prepared by the following method. Under reduced light, the polymer was weighed in a brown bottle and appropriate solvent was added (dichloromethane for polymer $\mathbf{P_1}$ and dioxane for polymer $\mathbf{P_2}$). The solution contained 15% by weight of the solids for polymer $\mathbf{P_1}$ and 10% by weight for polymer $\mathbf{P_2}$. The solution was stirred overnight, then manually cast over an aluminum sheet (3-1/3 in. × 8 in., Western DP plates, brush grained) with a multiple-clearance film applicator (2 in. × 2 in.). The film obtained was dried in air overnight in the dark and in an oven at 125°C for 20 min and punched to give disks (diameter of 1 in.). The thickness of the film was measured with a coating thickness tester (Dermitron D-9).

Film photoactivity was evaluated by using a static charge analyzer (Monroe no. 276A), which has a tungsten lamp (GE no. 1076) as light source. Xerographic patterns were obtained and the quantities $(dV_d/dt)_{t=0}$, $(dV_p/dt)_{t=0}$, $\tau½$, $\%V$, and ΔV_d derived from them (Table 6).

N-*Benzylcarbazole-3-carboxaldehyde (2) (ref. 37)*

In a preliminary step, the imidoyl halide is prepared by treating, under argon and at 0°C, *N*,*N*-dimethylformamide (1.50 g, 0.0205 mol) with phosphorus oxychloride (4.0 mL, 0.043 mol) and stirring for 1 h. The mixture is then heated on an oil bath at 45°C and treated, over a 1 h period, with *N*-benzylcarbazole (**1**) (38) (5.00 g, 0.0194 mol); towards the end of the addition, the reaction mixture, which becomes solid, is heated at 95–100°C overnight.

The reaction mixture is treated with 10 mL of water, then transferred to a beaker and the volume increased to approximately 100 mL with water. The mixture is stirred overnight at about 40°C. The precipitate is filtered, washed generously with water, and dried in air to give 5.9 g of crude product. Recrystallization from 95% ethanol yields the desired formyl derivative **2** (5.08 g, 92%) in the form of a slightly beige solid; R_f 0.66 (30% ethyl acetate – 70% hexane); mp 131.5–132.5°C; IR:710, 740, 810, 1130, 1330, 1590, 1680, 2725, and 2800 cm^{-1}; NMR δ: 5.28 (s, 2H), 6.94–7.39 (m, 9H), 7.83 (dd, 1H), 8.04 (dd, 1H), 8.46 (d, 1H), and 9.96 (s, 1H). Exact mass calcd. for $C_{20}H_{15}NO$: 285.1153; found: 285.1158.

*Ethyl 2-carbethoxy-3-(*N*-benzyl-3-carbazolyl)propenoate (3)*

A solution of *N*-benzylcarbazole-3-carboxaldehyde (**2**) (4.28 g, 0.0150 mol), diethyl malonate (2.40 g, 0.0150 mol), acetic acid (0.30 mL), and piperidine (0.09 mL) in 10 mL anhydrous benzene is heated to reflux for 20 h in a Dean-Stark apparatus where the water separator tube is filled with benzene and 3Å molecular sieves.

The mixture is cooled and transferred to a separatory funnel with 30 mL of benzene. The organic phase is washed twice with 40 mL of saturated aqueous sodium bicarbonate solution, twice with 40 mL of brine, and then dried over magnesium sulfate. Evaporation of the solvent *in vacuo* gives a crude solid. Recrystallization in 95% ethanol yields a yellow solid (5.79 g, 90%); R_f 0.64 (30% ethyl acetate – 70% hexane); mp 126.5–127.5°C; IR: 810, 1150, 1160, 1180, 1210, 1230, 1260, 1480, 1500, 1600, 1620, and 1720 cm^{-1}; NMR δ: 1.34 (t, 6H), 4.32 (q, 2H), 4.41 (q, 2H), 5.50 (s, 2H), 7.12–7.61 (m, 10H), 7.93 (s, 1H), 8.08 (dd, 1H), and 8.26 (d, 1H). Exact mass calcd. for $C_{27}H_{25}NO_4$: 427.1783; found: 427.1777.

*Ethyl 2-carbethoxy-3-(*N*-benzyl-3-carbazolyl)propionate (4)*

A suspension of ethyl 2-carbethoxy-3-(*N*-benzyl-3-carbazolyl) propenoate (**3**) (5.50 g, 0.0129 mol) and 10% palladium on charcoal (280 mg) in ethyl acetate (75 mL) is stirred overnight while hydrogen is bubbled gently through the solution. Argon is then bubbled through the solution to displace the remaining hydrogen and the suspension is filtered over Celite. The precipitate is washed generously with ethyl acetate and the solvent evaporated *in vacuo* to yield a white solid (5.60 g, quantitative yield); R_f 0.58 (30% ethyl acetate – 70% hexane); mp 58–60°C; IR: 1150, 1220, 1290, and 1730 cm^{-1}; NMR δ: 1.18 (t, 6H), 3.40 (d, 2H) 3.66–3.83 (m, 1H), 4.15 (q, 4H), 5.47 (s, 2H), 7.03–7.43 (m, 10H), 7.96 (s, 1H), and 8.08 (d, 1H). Exact mass calcd. for $C_{27}H_{27}NO_4$: 429.1940; found: 429.1887.

*2-Hydroxymethyl-3-(*N*-benzyl-3-carbazolyl)propanol (5)*

Under inert atmosphere, a suspension of lithium aluminum hydride (0.76 g, 0.020 mol) in anhydrous THF (10 mL) is prepared and cooled to 0°C. The latter is treated at 0°C, over a period of 30 min, with a solution of ethyl 2-carbethoxy-3-(*N*-benzyl-3-carbazolyl) propionate (**4**) (4.29 g, 0.0100 mol) in dry THF (12 mL) and the reaction mixture

Can. J. Chem. Downloaded from www.nrcresearchpress.com by 88.85.125.76 on 09/07/12
For personal use only.

heated to reflux for 3 h. The mixture is cooled to 0°C and treated dropwise in sequence with cooled distilled water (0.75 mL), 10% aqueous sodium hydroxide (0.75 mL), and distilled water (2.25 mL). The salts are filtered over fritted glass and the solids washed repeatedly with THF. The combined organic solutions are dried over anhydrous sodium sulfate, filtered, and evaporated *in vacuo*. The residue obtained is recrystallized from 95% ethanol–ether to yield a white solid (3.08 g, 89%); R_f 0.52 (ethyl acetate); mp 121.5–122°C; IR: 740. 1040, 1330, 1450, 1460, 1490, and 3300 cm^{-1}; NMR δ: 2.14 (m, 1H), 2.34 (br s, 2H), 2.78 (d, 2H), 3.75 (br d, 4H), 5.47 (s, 2H), 7.05–7.43 (m, 10H), 7.92 (s, 1H), and 8.09 (d, 1H). Exact mass calcd. for $C_{23}H_{23}NO_2$: 345.1729; found: 345.1740.

*2-Hydroxymethyl-3-(3-carbazolyl)propanol (**6**)*

Under inert atmosphere, a solution of 2-hydroxymethyl-3-(*N*-benzyl-3-carbazolyl) propanol (**5**) (0.450 g, 0.00130 mol) is prepared in dry THF (7 mL) and added at −78°C to distilled liquid ammonia (25 mL) contained in a three-necked flask equipped with a Dry Ice – acetone condenser. The mixture is treated with tiny, hexane-rinsed, pieces of metallic sodium (0.120 g, 0.0052 mol) and the cooling bath removed to accelerate the discharge of the blue color. After 15 min, the reaction mixture is again cooled to −78°C and again treated with metallic sodium (0.060 mg, 0.0026 mol); once again the cooling bath is removed and, after 2 h, TLC analysis shows that the reaction is complete. After an additional hour, the mixture is cooled to −78°C and treated with ammonium chloride. The ammonia is allowed to evaporate overnight, the residual mixture treated with distilled water (20 mL), and most of the THF contained in the mixture evaporated *in vacuo*. The remaining reaction mixture is saturated with sodium chloride and extracted with ethyl acetate (3 × 25 mL). The organic phase is dried over anhydrous magnesium sulfate, filtered, and evaporated *in vacuo* to yield a yellowish solid (0.315 g), which is a mixture of the desired debenzylated carbazole derivative **6** and some debenzylated material where the carbazole ring system is partially reduced.

To minimize loss of material, the crude product (0.315 g) is treated for 3 h under inert atmosphere with 10% palladium on charcoal (60 mg) in 0.6 mL of anhydrous refluxing 1,3,5-trimethylbenzene. The catalyst is filtered on Celite and washed generously with THF. The organic phase is evaporated *in vacuo* and the residue (0.288 g) recrystallized from ethanol–water to yield a white solid (0.225 g, 68%) (yields are generally higher on larger scales); R_f 0.43 (ethyl acetate); mp 147–149°C; IR: 750, 1030, 1240, 1450, 1470, 3350, and 3400 cm^{-1}; NMR (acetone-d_6) δ: 2.02 (m, 1H, visible only in CD_3OD), 2.81 (d, 2H), 3.67 (d, 4H), 7.05–7.55 (m, 5H), 7.96 (s, 1H), 8.09 (d, 1H), and 10.22 (m, 1H). Exact mass calcd. for $C_{16}H_{17}NO_2$: 255.1259; found: 255.1216.

*5-(3-Carbazolylmethyl)-2,2-dimethyl-1,3-dioxane (**7**)*

A mixture of 2-hydroxymethyl-3-(3-carbazolyl) propanol (**6**) (0.201 g, 0.787 mmol), *p*-toluenesulfonic acid monohydrate (19 mg, 0.10 mmol), 3 Å (a dozen granules) molecular sieves, and Spectrograde acetone (10 mL) is prepared and stirred under inert atmosphere for 24 h. Triethylamine (3 drops) is added and the mixture stirred for an additional hour. The reaction mixture is filtered over Celite and the solvent evaporated *in vacuo*. Flash chromatography (20% ethyl acetate – 80% hexane; for large scale preparation, a solvent gradient of dichloromethane to 10% ethyl acetate – 90% dichloromethane is used) of the crude product gives a white solid (0.194 g, 83%); R_f 0.22 (20% ethyl acetate – 80% hexane); mp 135.5–136.5°C; IR: 750, 810, 830, 1070, 1130, 1150, 1200, 1250, 1260, 1380, 1390, and 3400 cm^{-1}; NMR δ: 1.43 and 1.48 (2s, 6H), 2.16 (m,1H), 2.77 (d, 2H), 3.58–4.00 (m, 4H), 7.12–7.42 (m, 5H), 7.85 (s, 1H), and 8.04 (d, 1H). Exact mass calcd. for $C_{19}H_{21}NO_2$: 295.1572; found: 295.1547.

*Bichromophore **9***

Under inert atmosphere, freshly washed (pentane) 60% sodium hydride (0.500 g, 0.0125 mol) is treated with a solution of 5-(3-carbazolylmethyl)-2,2-dimethyl-1,3-dioxane (**7**) (1.22 g, 0.00413 mol) in dry THF (25 mL). Vigorous liberation of hydrogen takes place at first, then the mixture is stirred for 15 min and heated to reflux for 30 min. The pink solution is cooled to room temperature and treated over a 30 min period with a solution of 9-(3-bromopropyl)-9-methyl-2,7-dinitrofluorene (**8**) (1.70 g, 0.00435 mol) in dry THF (25 mL). The reaction mixture, which goes from pink to green to brown during the addition, is treated with a solution of HMPA (0.70 mL, 0.0038 mol) in dry THF (15 mL) and left stirring for 20 h. A solution of cold 3.3% hydrochloric acid (45 mL) is carefully added and the mixture stirred for 1.5 h, after which time it is neutralized with 10% aqueous sodium bicarbonate and stirred again for 1 h. Evaporation *in vacuo* of the THF leaves an aqueous mixture, which is diluted with 50 mL distilled water and extracted with dichloromethane (3 × 100 mL). The organic phase is washed with brine (2 × 200 mL), dried over anhydrous magnesium sulfate, and evaporated *in vacuo*, to yield a crude product (2.9 g), which is flash chromatographed (solvent gradient: dichloromethane to 3% methanol – 97% dichloromethane) to yield a yellow solid (1.79 g, 77%); R_f 0.34 (ethyl acetate); mp 118–122°C; IR: 740, 1020, 1340, 1470, 1480, 1520, and 3400 cm^{-1}; NMR δ: 1.10–1.34 (m, 2H), 1.46 (s, 3H), 2.04–2.32 (m, 5H), 2.79 (d, 2H), 3.72–3.92 (m, 4H), 4.06 (t, 2H), 6.85–7.40 (m, 5H), and 7.80–8.30 (m, 8H). Exact mass calcd. for $C_{33}H_{31}N_3O_6$: 565.2212; found: 565.2189. Anal. calcd. for $C_{33}H_{31}N_3O_6$: C 70.08, H 5.52, N 7.43; found: C 69.76, H 5.42, N 7.40.

Oligomer P_1

A solution of bichromophore **9** (1.00 g, 0.00177 mol) in dry 1,2-dichloroethane (5.0 mL) and dry triethylamine (0.50 mL, 0.0036 mol) is treated, at 0°C under inert atmosphere and over a 45 min period, with a cooled solution of sebacoyl chloride (0.43 g, 0.0018 mol) in dry 1,2-dichloroethane (7.0 mL). The ice bath is removed and the reaction mixture stirred for 90 min, after which time it is taken up in 1,2-dichloroethane (approximately 20 mL) and washed with distilled water (20 mL). The organic phase is dried over anhydrous magnesium sulfate and concentrated *in vacuo* to approximately one half its volume, after which it is precipitated by dropwise addition, over a 1 h period, to a large volume of hexanes (200 mL). The precipitated oligomer is then stirred overnight in the solvent mixture and the latter decanted. The oligomer is taken up in 1,2-dichloroethane and placed in a round-bottom flask where the solvent is evaporated *in vacuo* to yield an orange solid (1.20 g, 93%); $\overline{M}_n$ 4964; $\overline{M}_w$ 13584; $\overline{DP}_w$ 18.6; T_m 99°C; T_g 85.5°C; IR: 740, 1170, 1350, 1520, 1730, 2850, and 2925 cm^{-1}; NMR δ: 1.20 (m, 2H), 1.30 and 1.40 (2s, 8H), 1.44 (s, 3H), 1.62 (m, 4H), 1.90–2.65 (m, t, 7H), 2.85 (d, 2H), 4.09 (d, deformed, 6H), 6.87–7.37 (m, 5H), and 7.76–8.26 (m, 8H). Anal. calcd. for $C_{43}H_{45}N_3O_8$: C 70.57, H 6.20, N 5.74; found: C 70.12, H 6.52, N 5.50.

*Ethyl-2-carbethoxy-3-(N-ethylcarbazolyl)propenoate (**11**)*

The title compound **11** is prepared by the same method as described for compound **3**. The following amounts were used: *N*-ethylcarbazole-3-carboxaldehyde (**10**) (6.70 g, 0.0300 mol) (obtained from Aldrich Chemical Co. and recrystallized in 95% ethanol), diethyl malonate (4.81 g, 0.0300 mol), acetic acid (0.60 mL), and piperidine (0.18 mL) in 8 mL of anhydrous benzene. Recrystallization in 95% ethanol yields a yellow solid (9.35 g, 85%); R_f 0.37 (30% ethyl acetate – 70% hexane); mp 98–99°C; IR: 820, 1130, 1170, 1180, 1220, 1240, 1260, 1480, 1600, 1620, and 1720 cm^{-1}; NMR δ: 1.35 (t, 6H), 1.39 (t, 3H), 4.29 (q, 2H), 4.32 (q, 2H), 4.43 (q, 2H), 7.15–7.63 (m, 5H), 7.93 (s, 1H), 8.03 (d, 1H), and 8.20 (d, 1H). Exact mass calcd. for $C_{22}H_{23}NO_4$: 365.1627; found: 365.1634.

*Ethyl-2-carbethoxy-3-(N-ethyl-3-carbazolyl)propionate (**12**)*

The title compound (**12**) is prepared by the same method as described for compound **4**. The following amounts were used: ethyl 2-carbethoxy-3-(*N*-ethyl-3-carbazolyl)propenoate (**11**) (9.00 g, 0.0246 mol) and 10% palladium on charcoal (450 mg) in 100 mL of ethyl acetate. Evaporation of solvent yields a white solid (9.10 g, quantitative yield; R_f 0.46 (30% ethyl acetate – 70% hexane); mp 47–49°C; IR: 1150, 1230, and 1740 cm^{-1}; NMR δ: 1.19 (t, 6H), 1.39 (t, 3H), 3.42 (d, 2H), 3.67–3.84 (m, 1H), 4.16 (q, 4H), 4.32 (q, 2H), 7.05–7.55 (m, 5H), 7.93 (s, 1H), and 8.06 (d, 1H). Exact mass calcd. for $C_{22}H_{25}NO_4$: 367.1783; found: 367.1887.

Can. J. Chem. Downloaded from www.nrcresearchpress.com by 88.85.125.76 on 09/07/12
For personal use only.

Can. J. Chem. Downloaded from www.nrcresearchpress.com by 88.85.125.76 on 09/07/12
For personal use only.

2-Hydroxymethyl-3-(N-ethyl-3-carbazolyl)propanol (13)

The title compound (**13**) is prepared by the same method as described for compound **5**. After destruction of the excess of hydride, the salts are filtered over fritted glass and the solids washed once with THF. The organic phase is evaporated *in vacuo* and the residue recrystallized from ethanol–water to yield a white solid (2.47 g, 87%); R_f 0.28 (ethyl acetate); mp 117.5–119°C; IR: 750, 1040, 1240, 1480, 1490, and 3300 cm^{-1}; NMR δ: 1.42 (t, 3H), 2.24 (m, 3H), 2.80 (d, 2H), 3.61–3.96 (m, 4H), 4.34 (q, 2H), 7.11–7.48 (m, 5H), 7.90 (s, 1H), and 8.07 (d, 1H). Exact mass calcd. for $C_{18}H_{21}NO_2$: 283.1572; found: 283.1572.

5-(N-Ethyl-3-carbazolylmethyl)-2,2-dimethyl-1,3-dioxane (D_2)

The title compound $\mathbf{D_2}$ is prepared by the same method as described for compound **7** using 2-hydroxymethyl-3-(*N*-ethyl-3-carbazolyl)propanol (**13**) as starting material. Flash chromatography (25% ethyl acetate – 75% hexane) of the crude product yields a white solid (0.512 g, 90%); R_f 0.33 (25% ethyl acetate – 75% hexane); mp 77.5–80.5°C; IR ($CHCl_3$): 1070, 1150, 1200, 1230, 1370, 1380, 1470, and 1490 cm^{-1}; NMR δ: 1.20 (t, 3H), 1.42 and 1.47 (2s, 6H), 2.23 (m, 1H), 2.78 (d, 2H), 3.57–3.99 (m, 4H), 4.32 (q, 2H), 7.13–7.45 (m, 5H), 7.87 (s, 1H), and 8.07 (d, 1H). Exact mass calcd. for $C_{21}H_{25}NO_2$: 323.1885; found: 323.1879.

5-(N-β-Hydroxyethyl-3-carbazolylmethyl)-2,2-dimethyl-1,3-dioxane (14)

At 0°C, a solution of 5-(3-carbazolylmethyl)-2,2-dimethyl-1,3-dioxane (**7**) (3.63 g, 0.0123 mol) and potassium hydroxide powder (0.69 g, 0.0123 mol) in 8.0 mL anhydrous butanone is treated with cold ethylene oxide (0.62 mL, 0.0123 mol). The reaction mixture is stirred for 15 min, heated at 55°C for 3 h, then treated again with potassium hydroxide powder (0.070 g, 0.0012 mol) and cold ethylene oxide (0.05 mL, 0.001 mol) and stirred at the same temperature for 1 h. The red solution is cooled, treated with water (10 mL), and evaporated *in vacuo*. The aqueous phase is extracted with ether (6 × 15 mL). The organic phase is washed with brine (2 × 35 mL), dried over sodium sulfate, and evaporated *in vacuo*. The crude oil is flash chromatographed (solvent gradient: 60% ethyl acetate – 40% hexane to ethyl acetate) to yield the starting material (0.54 g, 15%), the desired product (compound **14**) as a white solid (2.84 g, 68%), and a yellowish oil (0.51 g, 11%) (identified as 5-(*N*-β-hydroxyethyloxyethyl-3-carbazolylmethyl)-2,2-dimethyl-1,3-dioxane (**14***a*)). (a) Compound **14**: R_f 0.39 (60% ethyl acetate – 40% hexane); mp 49–51°C; IR: 745, 825, 1070, 1200, 1470, 1490, and 3440 cm^{-1}; NMR δ: 1.35–1.41 (2s, 6H), 2.08 (m, 1H), 2.31 (s, 1H), 2.70 (d, 2H), 3.57–3.91 (m, 6H), 4.29 (t, 2H), 7.11–7.40 (m, 5H), 7.81 (s, 1H), and 8.01 (d, 1H). Exact mass calcd. for $C_{21}H_{25}NO_3$: 339.1834; found: 339.1823. (b) Compound **14***a*: R_f 0.24 (60% ethyl acetate – 40% hexane); IR (film): 730, 745, 825, 1075, 1130, 1200, 1470, 1490, and 3440 cm^{-1}; NMR δ: 1.42 and 1.48 (2s, 6H), 1.61 (s, 1H), 2.17 (m, 1H), 2.78 (d, 2H), 3.43–3.93 (m, 10H), 4.49 (t, 2H), 7.12–7.65 (m, 5H), 7.87 (s, 1H), and 8.06 (d, 1H). Exact mass calcd. for $C_{23}H_{29}NO_4$: 383.2097; found: 383.1996.

2,5,7-Trinitrofluorenonecarboxylic acid chloride (15)

A solution of 2,5,7-trinitrofluorenonecarboxylic acid (39) (2.70 g, 0.00752 mol) in 35 mL thionyl chloride is heated to reflux overnight. The black solution is distilled *in vacuo* and the crude solid obtained recrystallized from toluene, then dried in an Abder–Alden apparatus (P_2O_5, 5×10^{-2} Torr (1 Torr = 133.3 Pa), water) to yield a yellow solid (2.52 g, 89%); mp 193.5–196°C; IR: 690, 730, 760, 790, 835, 1345, 1535, 1590, 1615, and 1740 cm^{-1}; NMR (acetone-d_6) δ: 8.84 (d, 2H), 9.04 (d, 1H), and 9.11 (d, 1H).

Bichromophore B_2

Under inert atmosphere, a suspension of 5-(3-carbazolylmethyl)-2,2-dimethyl-1,3-dioxane (**7**) (0.90 g, 0.00265 mol) and 2,5,7-trinitrofluorenonecarboxylic acid chloride (**15**) (1.05 g, 0.00278 mol) in anhydrous dichloromethane (25 mL) is prepared and cooled to 0°C. The latter is treated at 0°C, over a 10 min period, with anhydrous triethylamine (0.41 mL, 0.00295 mol). The red-brown solution is stirred and allowed to warm up to room temperature over a period of 2.5 h, during which time a brown solid precipitates. The reaction mixture is then transferred to a separatory funnel with 40 mL of saturated aqueous sodium bicarbonate solution, extracted once, decanted, and concentrated *in vacuo*. The resulting suspension is filtered and the crude solid washed with water and dried in air to yield a brown solid (1.75 g, 97%). A sample is recrystallized from acetonitrile; R_f 0.59 (15% ethyl acetate – 85% dichloromethane); mp 256–257°C; IR: 1070, 1090, 1155, 1175, 1200, 1280, 1345, 1545, and 1740 cm^{-1}; NMR (benzene-d_6) δ: 1.45 and 1.47 (2s, 6H), 2.00 (m, 1H), 2.61 (d, 2H), 3.43–3.87 (m, 6H), 4.30 (t, 2H), 6.89–7.27 (m, 5H), 7.71 (s, 1H), 7.78 (d, 1H), 7.84 (br s, 1H), 7.94 (d, 1H), 8.07 (d, 1H), and 8.13 (d, 1H). Exact mass calcd. for $C_{35}H_{28}N_4O_{11}$: 680.1754; found: 680.1574. Anal. calcd. for $C_{37}H_{31}N_5O_{11}$: C 61.58, H 4.33, N 9.70; found: C 61.51, H 4.42, N 9.51.

Bichromophore 16

A solution of bichromophore $\mathbf{B_2}$ (1.75 g, 0.00257 mol) in 45 mL of 2:1 (v/v) THF – 10% HCl solution is heated to reflux for 15 min and cooled to room temperature. The THF is evaporated *in vacuo* and the resulting suspension filtered; the brown solid is then washed with water, dried in air, and stirred with Spectrograde methanol (60 mL) for 3 days. The suspension is filtered and the crude solid washed with methanol and dried in air to yield a brown solid (1.37 g, 83%); R_f 0.33 (ethyl acetate); mp 236.5–237.5°C; IR: 1025, 1345, 1470, 1540, 1595, 1620, 1740, and 3430 cm^{-1}; NMR (DMSO-d_6) δ: 1.78 (m, 1H), 2.66 (d, 2H), 3.40 (d, 4H), 4.40 (t, 2H), 4.65 (br s, 4H), and 6.97–7.94 (m, 11H). Anal. calcd. for $C_{32}H_{24}N_4O_{11}$: C 60.00, H 3.78, N 8.75; found: C 60.44, H 4.27, N 9.28.

Oligomer P_2

Under inert atmosphere, bichromophore **16** (0.213 g, 0.333 mmol) and sebacoyl chloride (0.081 g, 0.34 mmol) are heated gradually on an oil bath to 180°C for 90 min. Then the reaction mixture is evacuated to 0.01 Torr for 2 h, cooled to room temperature, treated once more with sebacoyl chloride (0.020 g, 0.084 mmol), heated to 170°C for 1 h, and again cooled to room temperature. The crude oligomer is dissolved in dioxane (5 mL) and the resulting solution filtered over cotton wool and precipitated by dropwise addition to a large volume of methanol (100 mL). The purified oligomer, isolated by centrifugation, is then dried in air to yield a grey solid (0.120 g, 45%); $\overline{M}_n$ 2934; $\overline{M}_w$ 6150; $\overline{DP}_w$ 7.6; T_m 78°C; T_g 54.5°C; IR: 1090, 1155, 1175, 1345, 1470, 1540, 1545, 1595, 1615, and 1740 cm^{-1}; NMR (pyridine-d_5) δ: 1.28 (br s, 8H), 1.71 (m, 4H), 2.45 (br t, 5H), 3.05 (m, 2H), 4.41 (br d, 4H), 4.76 (m, 2H), 4.91 (m, 2H), 7.0–7.6 (m, 5H), 8.06 (br s, 2H), and 8.45–8.95 (m, 4H). Anal. calcd. for $C_{42}H_{38}N_4O_{13}$: C 62.53, H 4.75, N 6.94; found: C 62.49, H 5.00, N 6.51.

Bichromophore B_{2a}

The title compound $\mathbf{B_{2a}}$ is prepared by the same method as described for bichromophore $\mathbf{B_2}$. The following amounts were used: *N*-β-hydroxyethylcarbazole (40) (**18**) (0.317 g, 0.00150 mol) and 2,5,7-trinitrofluorenonecarboxylic acid chloride (**15**) (0.595 g, 0.00158 mol) in anhydrous dichloromethane (25 mL) and anhydrous triethylamine (0.83 mL, 0.0060 mol). The crude solid obtained is recrystallized from dimethyl sulfoxide to yield a black solid (0.400 g, 48%); R_f 0.02 (15% ethyl acetate – 85% dichloromethane); mp 310°C; IR: 725, 740, 755, 1090, 1150, 1280, 1310, 1340, 1460, 1485, 1535, 1595, 1620, and 1740 cm^{-1}; NMR (DMSO-d_6) δ: 4.65 (br s, 4H) and 6.99–7.99 (m, 12H).

Ethyl 2,5,7-trinitrofluorenonecarboxylate (A_2)

Under inert atmosphere, a solution of 2,5,7-trinitrofluorenonecarboxylic acid chloride (**15**) (0.190 g, 0.500 mol) in 4.0 mL anhydrous ethanol is heated to reflux for 1 h. After dissolution of the starting material, the desired product precipitates. The suspension is cooled and filtered. The crude solid is washed with cold ethanol, dried in air, then taken up in 85% dichloromethane – 15% benzene, filtered over silica gel, and recrystallized from dichloromethane–methanol to yield a yellow solid (0.130 g, 69%); R_f 0.25 (20% ethyl acetate – 80% hexane); mp 157.5–159°C; IR: 710, 740, 835, 1090, 1185, 1235, 1290, 1315, 1345, 1545, 1595, 1620, 1720, and 1740 cm^{-1}; NMR δ: 1.47 (t, 3H), 4.46 (q, 2H), 8.76 (d, 1H), 8.82 (d, 1H), 8.87 (d, 1H), and 8.96 (d, 1H). Exact mass calcd. for $C_{16}H_9N_3O_9$: 387.0339; found: 387.0345.

Acknowledgments

We gratefully acknowledge the financial assistance of the Natural Sciences and Engineering Research Council of Canada and the Fonds FCAR (Québec), in the form of grants and fellowships. We are also indebted to Professor J. Prud'homme and Alain Vallée for their expert assistance.

1. (*a*) J. M. Pearson. Pure Appl. Chem. **49**, 463 (1977); (*b*) M. Stolka and D. M. Pai. Adv. Polym. Sci. **29**, 1 (1978); (*c*) D. A. Seanor, (*Editor*). Electrical properties of polymers. Academic Press, New York. 1982
2. M. Biswas and S. K. Das. Polymer, **23**, 1713 (1982).
3. M. Biswas and T. Uryu. Macromol. Chem. Phys. **26**, 249 (1986).
4. R. M. Schaffert. IBM J. Res. Dev. **15**, 75 (1971).
5. F. Brisse, G. Durocher, S. Gauthier, D. Gravel, R. Marquès, C. Vergelati, and B. Zelent. J. Am. Chem. Soc. **108**, 6579 (1986).
6. B. Zelent, P. Messier, D. Gravel, S. Gauthier, and G. Durocher. J. Photochem. Photobiol. **A40**, 145 (1987).
7. S. Raymond. M.Sc. Thesis, Department of Chemistry, Université de Montréal. 1988.
8. P. D. Harvet and G. Durocher. J. Luminesc. **33**, 175 (1985).
9. E. C. Lim and M. Kedzierski. Chem. Phys. Lett. **20**, 242 (1973).
10. J. Adams, W. W. Mantulin, and J. R. Huber. J. Am. Chem. Soc. **95**, 5477 (1973).
11. H. J. Hainkm and J. R. Huber. Chem. Phys. Lett. **44**, 117 (1976).
12. J. H. Sharp. J. Phys. Chem. **70**, 584 (1966).
13. E. E. Sirotkina, I. L. Gaibel', V. I. Malkowa, and V. D. Filimonov. Zh. Obshch. Khim. **50**, 1589 (1980).
14. K. H. Brown and J. P. Montillier. Photogr. Sci. Eng. **22**, 22 (1978).
15. P. D. Harvey, B. Zelent, and G. Durocher. Spectrosc. Int. J. **2**, 128 (1983).
16. R. O. Loutfy, C. K. Hsiao, B. S. Ong, and B. Keoschkerian. Can. J. Chem. **62**, 1877 (1984).
17. S. C. Weber. *In* Polymer photophysics. *Edited by* D. Phillips. Chapman and Hall, London. 1985. Chap. 2. p. 41.
18. D. Rehm and A. Weller. Ber. Bunsen-ges. Phys. Chem. **73**, 834 (1969); Isr. J. Chem. **8**, 259 (1970).
19. A. K. Chibisov. Usp. Khim. **50**, 1169 (1981); Prog. React. Kinet. **13**, 1 (1984).
20. S.-I. Tamura, K. Kikuchi, H. Kokubun, and Y. Usui. Z. Phys. Chem. N. F. **111**, 7 (1978).
21. S. P. McGlynn, T. Azumi, and M. Kinoshita. Molecular spectroscopy of the triplet state. Prentice–Hall, Englewood Cliffs, NJ. 1969. p. 251.
22. G. E. Johnson. J. Chem. Phys. **61**, 3002 (1974); **62**, 4697 (1975); **63**, 4047 (1975).
23. C. E. Hoyle, T. L. Nemzek, A. Mar, and J. E. Guillet. Marcromolecules, **11**, 429 (1978); D. Ng and J. E. Guillet. Macromolecules, **14**, 405 (1981).
24. J. Vandendriessche, P. Palmans, S. Toppet, N. Boens, F. C. De Schryver, and H. Masuhara. J. Am. Chem. Soc. **106**, 8057 (1984); J. Vandendriessche and F. C. De Schryver. Polym. Photochem. **7**, 153 (1986).
25. F. C. De Schryver, J. Vandendriessche, S. Toppet, K. Demeyer, and N. Boens. Macromolecules, **15**, 406 (1982); H. Masuhara, J. Vandendriessche, J. Demeyer, and F. C. De Schryver. Macromolecules, **15** 1471 (1982).
26. F. Evers, K. Kobs, R. Memming, and D. R. Terrel. J. Am. Chem. Soc. **105**, 5988 (1983).
27. S. Tazuke, T. Inoue, and H. Kokado. Polym. Photochem. **6**, 385 (1985).
28. S. Tazuke. Kagaku (Kyoto), **33**, 696 (1978).
29. R. O. Loutfy and B. S. Ong. Can J. Chem. **62**, 2546 (1984).
30. D. A. Seanor. *In* Electrical properties of polymers. *Edited by* D. A. Seanor. Academic Press, New York. 1982. pp. 1–58.
31. J. Mort and R. L. Emerald. J. Appl. Phys. **45**, 175 (1974).
32. G. Weiser. J. Appl. Phys. **43**, 5028 (1972).
33. P. Main, S. J. Fiske, S. E. Hull, L. Lessinger, G. Germain, J. Declercq, and M. M. Woolfson. MULTAN80. A system of computer programs for automatic solution of crystal structures from X-ray diffraction data. Universities of York, England, and Louvain, Belgium. 1980.
34. G. M. Sheldrick. SHELX. X-ray system report. University Chemical Laboratory, Lensfield Road, Cambridge, England. 1976.
35. D. T. Cromer and J. T. Waber. Acta Crystallogr. **18**, 104 (1965).
36. R. F. Stewart, E. R. Davidson, and W. T. Simpston. J. Chem. Phys. **42**, 3175 (1965).
37. E. E. Renfrew. Chem. Abstr. **82**, P74464u (1975); Chem. Abstr. **85**, P7283h (1976); P. Burri. Chem. Abstr. **89**, P138384x (1978); H. Okazaki, H. Imagome, S. Suzuka, and K. Sakai. Chem. Abstr. **99**, P244037n (1983).
38. H. Nishi, H. Kohno, and T. Kano. Bull. Chem. Soc. Jpn. **54**, 1897 (1981).
39. G. I. Migachev, N. G. Grekhova, and N. S. Dokunikhin. Zh. Org. Khim. **14**, 2380 (1978) (Russian); **14**, 2193 (1978) (English).
40. V. P. Lopatinskii, E. E. Sirotkina, and I. P. Zherebtsov. Chem. Abstr. **64**, 19542e (1966).

Can. J. Chem. Downloaded from www.nrcresearchpress.com by 88.85.125.76 on 09/07/12
For personal use only.

Medium effect on reactions between anions carrying different charges

AMALIA RODRIGUEZ AND FRANCISCO SÁNCHEZ BURGOS
Departamento de Quimica Fisica, Universidad de Sevilla, 41012 Sevilla, Spain
JOHN BURGESS
Department of Chemistry, University of Leicester, Leicester, U.K.
AND
CARMEN CARMONA[1]
Departamento de Quimica Fisica, Universidad de Sevilla, 41012 Sevilla, Spain

Received October 27, 1989

AMALIA RODRIGUEZ, FRANCISCO SÁNCHEZ BURGOS, JOHN BURGESS, and CARMEN CARMONA. Can. J. Chem. **68**, 926 (1990).

The reactions between hexacyanoferrate(II)–peroxodisulphate, hexacyanoferrate(III)–sulphite, hexacyanoferrate(III)–iodide and peroxodisulphate–iodide have been studied in methanol–water mixtures at different methanol concentrations. The results have been analyzed using different approaches, namely electrostatic theory, the $\delta\mu^{\theta}$ initial state – transition state analysis, the decomposition of free energy of activation into enthalpic and entropic terms and, finally, correlation between reactivity and the Grunwald–Winstein parameter, Y. The four reactions show similar behaviour and a correlation between reactivity and the charge of the reactants apparently does not exist. The effect of solvent polarity on the encounter formation processes seems to be an important factor in determining reactivity. However, the influence of solvent on electron transfer process within the encounter complexes cannot be discarded.

Key words: Solvent effects, kinetics, methanol, activation parameters, thermodynamic functions of transfer.

AMALIA RODRIGUEZ, FRANCISCO SÁNCHEZ BURGOS, JOHN BURGESS et CARMEN CARMONA. Can. J. Chem. **68**, 926 (1990).

Opérant à diverses concentrations de méthanol, dans des mélanges de méthanol-eau, on a étudié les réactions entre les ions hexacyanoferrate(II) et peroxodisulfate, hexacyanoferrate(III) et sulfite, hexacyanoferrate(III) et iodure et peroxodisulfate et iodure. On a analysé les résultats à l'aide de diverses approches, soit la théorie électrostatique, l'analyse de l'état initial $\delta\mu^{\theta}$ et de l'état de transition, la décomposition de l'énergie libre d'activation en termes enthalpique et entropique et finalement la corrélation entre la réactivité et le paramètre Y de Grunwald–Winstein. Les quatre réactions présentent des corportements semblables, mais il ne semble pas exister de corrélation entre la réactivité et la charge des réactifs. Il semble que la réactivité soit fortement influencée par l'effet de la polarité du solvant sur les processus de formation des rencontres. Toutefois, on ne peut pas éliminer l'influence du solvant sur le processus de transfert d'électron à l'intérieur des complexes de rencontre.

Mots clés : effets de solvant, cinétique, méthanol, paramètres d'activation, fonctions thermodynamiques de transfert.

[Traduit par la revue]

Introduction

Over the years different approaches have been used to examine solvent effects on reaction rates. Rate constants may be correlated with a physical parameter characteristic of the solvent or with an empirical parameter (1, 2). Recently this type of analysis has been extended to multiple linear correlations to assess the relative importance of the different variables (3, 4). Also, the solvent effect on log k or $\Delta G^{\neq}$ can be dissected into contributions from the initial state and the transition state using the thermodynamic functions of transfer (5–7). This study allows an analysis of the importance of the solvation changes of both states on reactivity. Finally, the variation of the enthalpy and entropy of activation with solvent composition has been utilized to discuss the influence of solvent structure on reactivity (8, 9).

Although the above methods have been used extensively in discussions on solvent effects, they are not usually utilized simultaneously. For this reason and because of our interest on the influence of medium effects on reaction rates (9–13), we were interested in analyzing reactivity trends in binary aqueous mixtures using the above methods simultaneously. To start with, methanol–water mixtures have been chosen. Also for purposes of comparison and to make the study more general, we have selected four reactions: iodide–peroxodisulphate, iodide–hexacyanoferrate(III), sulphite–hexacyanoferrate(III), and peroxodisulphate–hexacyanoferrate(II) reactions. The choice has been made because firstly there is already some information on medium effects on these reactions (9–15) and secondly they are reactions between anions of different charges. As a result the influence of changing the charge of the reactants can also be analyzed.

Experimental

Reagents

All reagents were AnalaR grade chemicals. The water used had a resistivity $> 6\ M\Omega\ cm^{-1}$. Sodium hexacyanoferrate(III) was obtained by passing potassium hexacyanoferrate(III) through a mixed bed cation-exchange column "Lawatit S 100 (cationic)".

The pH of the sulphite solutions was maintained at a value of nine and these solutions were always titrated before used.

Kinetic data

Kinetic runs were carried out in 1-cm silica cells in the thermostated cell compartment of a Perkin-Elmer 554 spectrophotometer. The temperature in the cell was fixed at 20.0, 25.0, 30.0, 35.0, and 40.0 ± 0.1°C. Mixtures water–methanol were prepared by weight. The dielectric constant data at 25.0°C are from ref. 16. In each case the cosolvent was found to be inert in relation to the reactants and products. The solution also contained K_2H_2edta to prevent catalysis of any metal ions that might be present as impurities ($[K_2H_2edta] = 5 \times 10^{-4}$ mol dm^{-3}). Duplicate and triplicate runs were made under all the experimental conditions. The rate constant error was estimated to be less than 2%.

The activation energy was obtained in water + methanol mixtures prepared to have the same dielectric constant at 25.0°C.

The reaction between sulphite and hexacyanoferrate(III) ions was made in solutions containing an excess of sulphite ions by following the change in absorbance at 420 nm at fixed time intervals (at this

[1]Author to whom correspondence should be addressed.

Printed in Canada / Imprimé au Canada

Can. J. Chem. Downloaded from www.nrcresearchpress.com by 88.85.125.76 on 09/07/12
For personal use only.

Can. J. Chem. Downloaded from www.nrcresearchpress.com by 88.85.125.76 on 09/07/12
For personal use only.

wavelength only hexacyanoferrate(III) absorbs). The concentrations of reactants were $[Na_3Fe(CN)_6] = 1 \times 10^{-3}$ mol dm^{-3} and $[Na_2SO_3] = 1 \times 10^{-2}$ mol dm^{-3}, respectively. The rate constants were evaluated by Guggenheim's method (17).

The peroxodisulphate–hexacyanoferrate(II) reaction was carried out in solutions containing an excess of hexacyanoferrate(II) ions by following the change in absorbance at 420 nm. The concentrations of reactants were $[K_4Fe(CN)_6] = 3 \times 10^{-2}$ and $[K_2S_2O_8] = 7.5 \times 10^{-4}$ mol dm^{-3}, respectively. The rate constants were evaluated from linear plots of the function $-\ln(A_\infty - A_t)$ versus time. A_∞ and A_t are the absorbances at equilibrium time and time t, respectively.

The reaction between hexacyanoferrate(III) and iodide ions was followed by monitoring the changes in absorbance at 400 nm at fixed time intervals. At this wavelength both hexacyanoferrate(III) and tri-iodide ions absorb. Thus, under these conditions, relation [1] is maintained where A is the total absorbance of the solutions,

$$[1] \quad A = \epsilon(a - x) + \epsilon'(x/2)$$

ϵ and ϵ' are the molar absorption coefficients of hexacyanoferrate(III) and tri-iodide ions respectively, a is the initial concentration of hexacyanoferrate(III), and $(a - x)$ its concentration at the time of measurement. The concentrations of reactants were $[KI] = 4 \times 10^{-1}$ mol dm^{-3} and $[K_3Fe(CN)_6] = 8 \times 10^{-4}$ mol dm^{-3}.

Solubilities

The values of the standard transfer chemical potentials were calculated from solubilities, at 298.2 K, in water and in water–methanol mixtures, respectively. The solubilities were determined after achieving an equilibrium between the solid phase and its solution. Due to sulphite instability, we have made the assumption that the general trends on solubilities of this ion and sulphate ion should be kept. Thus, solubilities of the sulphate ion instead of the sulphite ion have been measured. The concentrations of the salts in different methanol–water mixtures and in water were estimated iodometrically ($(K_2S_2O_8)$ (18)), turbidimetrically ((K_2SO_4) (19)), and spectrophotometrically (for $K_4Fe(CN)_6$ $\epsilon = 1810$ at 270 nm (20), for Ph_4AsI $\epsilon = 3200$ at 266 nm, for $Co(NH_3)_6Fe(CN)_6$ $\epsilon = 1030$ at 420 nm (21)). The solubilities of $Co(NH_3)_6Pi_3$, KPi, KPh_4B, and Ph_4AsPi were also measured. The preparation and characterization of these compounds was made using literature sources (22–25).

Results

The values of the rate constants for the four reactions at different methanol concentrations and different temperatures are recorded in Table 1. The only comparable literature values (i.e. those obtained at the same ionic strength) are in parentheses in this table. As can be seen, the general pattern of rate constants for all reactions is remarkably similar: there is a decrease in k values with increasing methanol concentration. At this point, it should be noted that because of experimental requirements, the four reactions have been studied at different ionic strengths. Since ionic strength increase gives rise to a rate constant increase for reactions between ions of the same sign, if we wish to compare the results of the four reactions, the k values should be corrected. Thus we will examine the results after extracting a standard allowance for the long-range Debye–Hückel interactions (26) according to:

$$[2] \quad \log k = \log k_0' + 2\frac{1.814 \times 10^6}{(DT)^{3/2}} Z_A Z_B \frac{I^{1/2}}{1 + I^{1/2}}$$

where k is the actual rate constant, D is the macroscopic dielectric constant and the other symbols have their usual meaning. The values of k_0' have been tabulated in Table 2 as $\delta\Delta G^{\neq}_{I=0}$ where

$$\delta\Delta G^{\neq}_{I=0} = \Delta G^{\neq}_{I=0}(\text{methanol–water}) - \Delta G^{\neq}_{I=0}(\text{water})$$

The activation parameters obtained from the k_0' values at different temperatures are plotted against organic solvent mole fraction in Figs. 1–4.

The solubilities for all reactants in water and in methanol–water mixtures are recorded in Table 3. Our data look reasonable in relation to published solubilities in water of KPi

TABLE 1. Observed rate constants (k) and dielectric constants (D), in water and in methanol–water mixtures, for the four reactions

(*a*) Hexacyanoferrate(II)–peroxodisulphate

Percentage of organic component	$10^3 \times k$/dm^{-3} mol^{-1} s^{-1}				
	20°C	25°C	30°C	35°C	40°C
Water	3.90	5.15	6.95	8.90	11.7
5.68	5.15	6.62	8.60	11.1	14.4
10.20	6.28	8.17	10.4	13.4	17.0
18.37	9.48	11.8	14.7	18.7	22.7
26.53	15.3	19.5	24.2	29.5	35.7

(*b*) Hexacyanoferrate(III)–sulphite

Percentage of organic component	$10^3 \times k$/dm^{-3} mol^{-1} s^{-1}				
	20°C	25°C	30°C	35°C	40°C
Water	11.7	16.8	24.0	34.2	45.9
5.68	8.37	12.5	17.8	26.0	35.5
10.20	6.33	9.33	13.7	19.9	26.9
18.37	4.00	6.17	9.10	13.7	19.2
26.53	2.79	4.30	6.65	10.0	14.2
30.64	2.43	3.89	5.82	8.74	12.8
39.15	1.71	2.88	4.54	6.98	11.1

(*c*) Hexacyanoferrate(III)–iodide

Percentage of organic component	$10^3 \times k$/dm^{-3} mol^{-1} s^{-1}				
	20°C	25°C	30°C	35°C	40°C
Water	5.56	6.82 (6.81)[a]	8.49	10.5	12.6
5.68	4.14	5.15	6.54	8.24	10.4
10.20	3.03	3.77 (3.69)[a]	4.84	6.10	7.68
18.37	2.05	2.89	4.05	5.57	7.60
26.53	1.39	2.12	3.13	4.41	6.74
30.64	0.989	1.55	2.48	3.77	5.69
39.15	0.818	1.29	2.01	3.13	4.71

(*d*) Peroxodisulphate–iodide[b]

Percentage of organic component	$10^4 \times k$/dm^{-3} mol^{-1} s^{-1}				
	20°C	25°C	30°C	35°C	40°C
Water	29.08	41.17	56.40	78.62	107.3
5.68	22.48	31.75	44.50	60.47	83.00
10.20	18.77	26.60	36.95	51.35	70.10
18.37	14.55	20.50	28.43	39.82	55.25
26.53	10.87	15.27	21.30	29.52	40.82
30.64	9,62	13.72	19.28	26.62	37.07
39.15	8.00	11.52	16.27	23.03	31.92

[a]Values taken from ref. 10.
[b]Values taken from ref. 9.

TABLE 2. Values of $\delta\Delta G^{\neq}_{I=0}$ at 298.2 K for the four reactions in methanol–water mixtures

	$\delta\Delta G^{\neq}_{I=0}$/kJ mol^{-1}			
D	$Fe(CN)_6^{4-}$–$S_2O_8^{2-}$	$Fe(CN)_6^{3-}$–SO_3^{2-}	$Fe(CN)_6^{3-}$–I^-	$S_2O_8^{2-}$–I^-
76	0.20	1.00	1.04	0.79
74	0.38	1.97	2.10	1.35
70	1.02	3.52	3.41	2.25
66	1.59	5.12	4.91	3.29
64		5.70	6.09	3.73
60		7.12	7.48	4.54

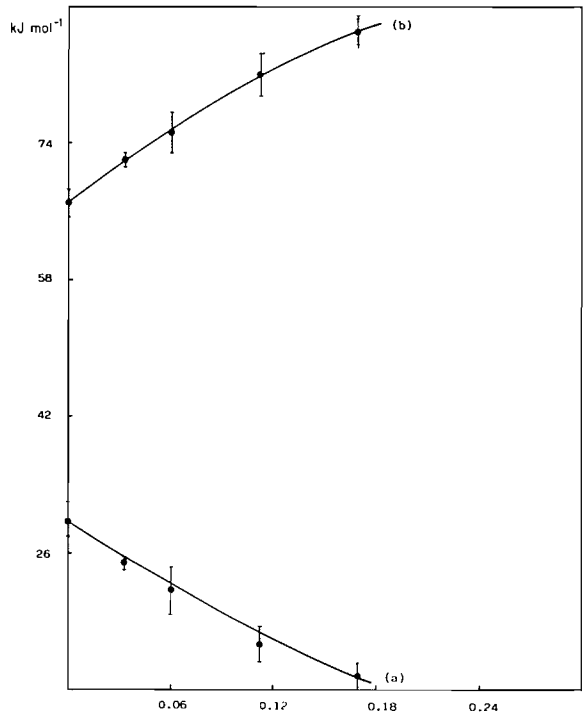

FIG. 1. Plot of (*a*) $\Delta H^{\neq}_{I=0}$ and (*b*) $-T\Delta S^{\neq}_{I=0}$ vs. mole fraction of methanol at 298.2 K for the reaction between hexacyanoferrate(II) and peroxodisulphate ions.

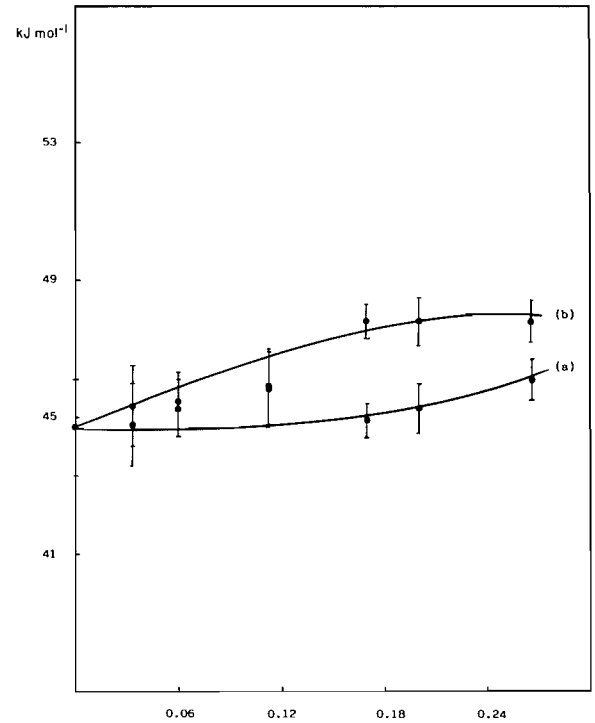

FIG. 2. Plot of (*a*) $\Delta H^{\neq}_{I=0}$ and (*b*) $-T\Delta S^{\neq}_{I=0}$ vs. mole fraction of methanol at 298.2 K for the reaction between peroxodisulphate and iodide ions.

$(2.42 \times 10^{-2} - 1.97 \times 10^{-2}$ mol dm$^{-3})$ (22, 24, 27), KPh_4B $(1.72 \times 10^{-4} - 3.00 \times 10^{-4}$ mol dm$^{-3})$ (22, 24, 27), and $K_2S_2O_8$ $(1.92 \times 10^{-1}$ mol dm$^{-3})$ (18).

The standard transfer chemical potentials for all the salts were calculated using eq. [2]

$$[2] \quad \delta_m\mu^\theta(\text{salt}) = nRT \ln \frac{s(\text{w})\gamma_\pm(\text{w})}{s(\text{x})\gamma_\pm(\text{x})}$$

where s(w) and s(x) are the solubilities in water and in the solvent mixtures, respectively. Usually, $\delta_m\mu^\theta$(salt) values are calculated on the assumption that the ratio of the mean activity coefficients in water and in the aqueous solvent mixtures is in all cases a unity (28, 29). However, we have calculated these ratios by means of eq. [3] and their values have been considered in eq. [2]

$$[3] \quad \log \gamma_\pm = 1.826 \times 10^6 (DT)^{-3/2} \frac{Z_+ Z_- I^{1/2}}{1 + I^{1/2}}$$

Although the absolute values of $\delta_m\mu^\theta$(salt) differ from those obtained assuming $\gamma_\pm(\text{w})/\gamma_\pm(\text{x})$ ca. 1, the trends observed on changing solvent composition are completely similar.

The estimation of transfer chemical potentials for ions has been made using the extrathermodynamic assumption $\delta_m\mu^\theta(Ph_4As^+) = \delta_m\mu^\theta(BPh_4^-)$ (30, 31). Finally, with the individual values, the transfer functions of the initial states for the four reactions in every methanol composition have been obtained. Also from the kinetic data, the values for the transition states have been calculated. These values together with $\delta\Delta G^{\neq}_{I=0}$ values are plotted against solvent composition in Fig. 5 for the peroxodisulphate–iodide rection.

Discussion

As expected, the general trends of k'_0 on changing methanol composition are the same as those observed before the ionic strength correction. There is always a decrease of reactivity on decreasing the macroscopic dielectric constant of the medium. Although this decrease of reactivity is in agreement with the electrostatic theory predictions (32), the results of the present experiments cannot be unequivocally explained by application of this theory. The $\delta\Delta G^{\neq}_{I=0}$ vs. D^{-1} dependence is nonlinear in all cases. As an example, $\delta\Delta G^{\neq}_{I=0}$ vs. D^{-1} has been plotted for the hexacyanoferrate(III)–sulphite reaction in Fig. 6.

Can. J. Chem. Downloaded from www.nrcresearchpress.com by 88.85.125.76 on 09/07/12
For personal use only.

TABLE 3. Solubilities of different compounds in methanol–water mixtures at 298.2 K

Compound	$S \times 10^3$/mol dm^{-3}						
	78.5	76	74	70	66	64	60
KPi	24.8	20.5	19.2	17.1	16.2	15.1	14.1
$Pi_3Co(NH_3)_6$	0.481	0.463	0.442	0.401	0.370	0.361	0.352
$Fe(CN)_6Co(NH_3)_6$	4.8	3.1	1.8	1.1	0.71	0.50	0.20
$KBPh_4$	0.179	0.215	0.231	0.314	0.398	0.428	0.689
Ph_4AsPi	0.0342	0.0482	0.0580	0.0950	0.130	0.172	0.237
Ph_4AsI	2.45	3.09	3.47	4.13	4.86	5.24	5.66
$K_2S_2O_8$	190	141	92	63	41	32	26
$K_4Fe(CN)_6$	1120	600	480	96	37	26	9
K_2SO_4	700	570	490	350	290	190	130

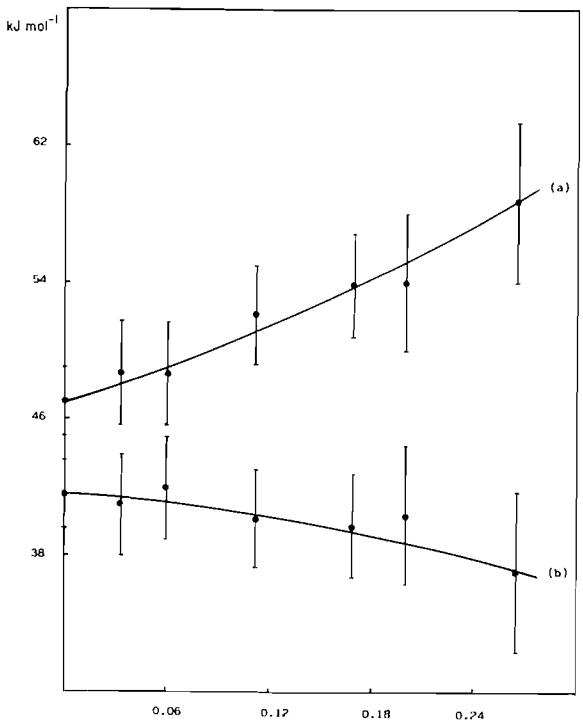

FIG. 3. Plot of (*a*) $\Delta H^{\neq}_{I=0}$ and (*b*) $-T\Delta S^{\neq}_{I=0}$ vs. mole fraction of methanol at 298.2 K for the reaction betweeen sulphite and hexacyanoferrate(III) ions.

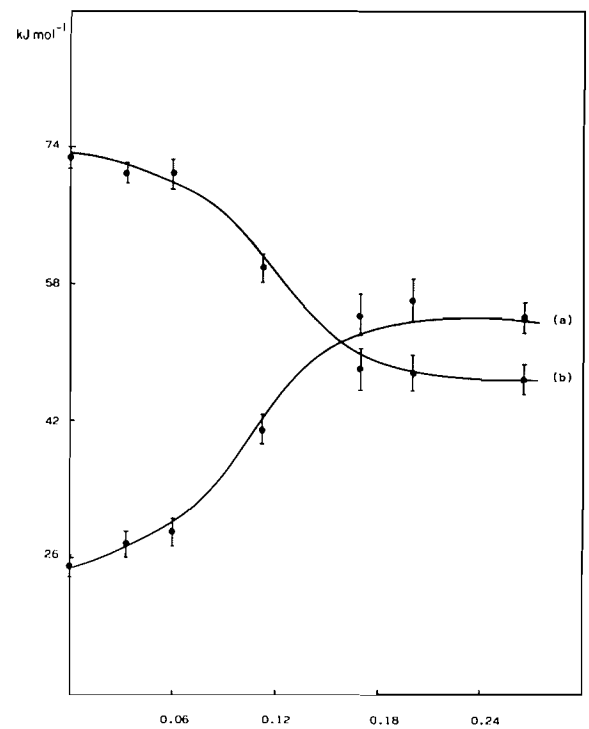

FIG. 4. Plot of (*a*) $\Delta H^{\neq}_{I=0}$ and (*b*) $-T\Delta S^{\neq}_{I=0}$ vs. mole fraction of methanol at 298.2 K for the reaction between iodide and hexacyanoferrate(III) ions.

The nonlinearity of $\delta\Delta G^{\neq}_{I=0}$ vs. D^{-1} plots has sometimes been associated with the differential effect of solvent structure between the initial and transition states (8). This effect is not necessarily apparent in $\delta\Delta G^{\neq}_{I=0}$ behaviour, but it could be evident in the changes of $\delta\Delta H^{\neq}_{I=0}$ and $\delta\Delta S^{\neq}_{I=0}$ with organic solvent composition (8). In spite of the fact that methanol, when mixed with water, does not produce very pronounced extrema in the variation of physical properties with solvent composition (33), which have been imputed to structural effects, the changes of $\delta\Delta H^{\neq}_{I=0}$ and $\delta\Delta S^{\neq}_{I=0}$ on changing solvent composition have been analyzed. As can be seen in Figs. 1–4 a smooth and monotonic variation of these parameters is always observed except for the iodide–hexacyanoferrate(III) reaction. However, even in this case no clear extrema are observed.

Figures 1–4 also show that although $\delta\Delta G^{\neq}_{I=0}$ always increases with methanol concentration, this increase is sometimes due to the dominance of the entropic term and sometimes due to the dominance of the enthalpic term. There is even a changeover in the dominant parameter for the iodide–hexacyanoferrate(III) reaction. These effects cannot be related to charge increase in the transition state but rather to the characteristics of the substrates and reactions.

On the other hand, the variation in the thermodynamic parameters of activation as a function of methanol composition is composed of initial and transition state contributions. In order to separate them, $\delta_m\mu^\theta$ of transfer from water to the binary mixtures has been determined for all the solutes studied in the present work. The initial state – transition state analysis for peroxodisulphate–iodide reaction in the methanol–water mixtures is shown in Fig. 5. The destabilization of the initial state reflects a marked destabilization of both reactants on increasing methanol content.

A perusal of Fig. 5 shows that great changes of transfer chemical potentials of the initial and transition states give rise to minor variations of $\delta\Delta G^{\neq}_{I=0}$, with methanol composition. In all cases, the small increase in $\delta\Delta G^{\neq}_{I=0}$ with increasing mole fraction of methanol is due to a somewhat more pronounced

Can. J. Chem. Downloaded from www.nrcresearchpress.com by 88.85.125.76 on 09/07/12
For personal use only.

Can. J. Chem. Downloaded from www.nrcresearchpress.com by 88.85.125.76 on 09/07/12
For personal use only.

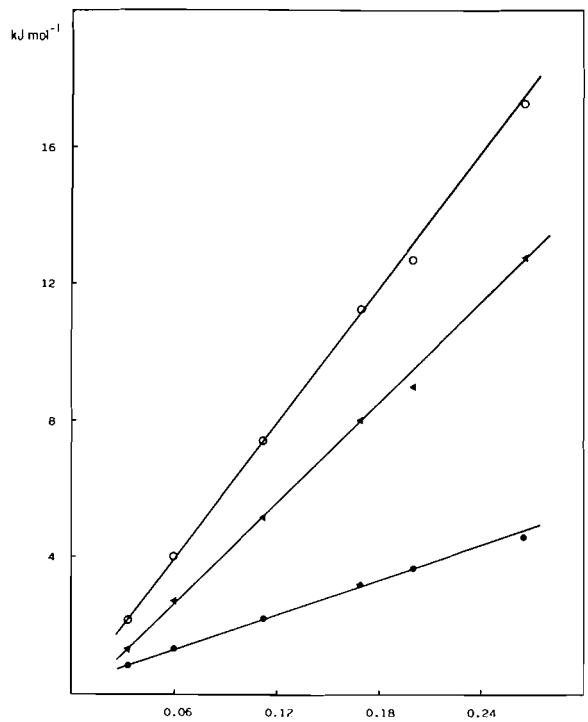

FIG. 5. Plots of Gibbs free energy of activation, (●), and Gibbs free energy of transfer of initial state, (△), and transition state (○) vs. mole fraction of methanol for peroxodisulphate–iodide reaction in methanol–water mixtures at 298.2 K.

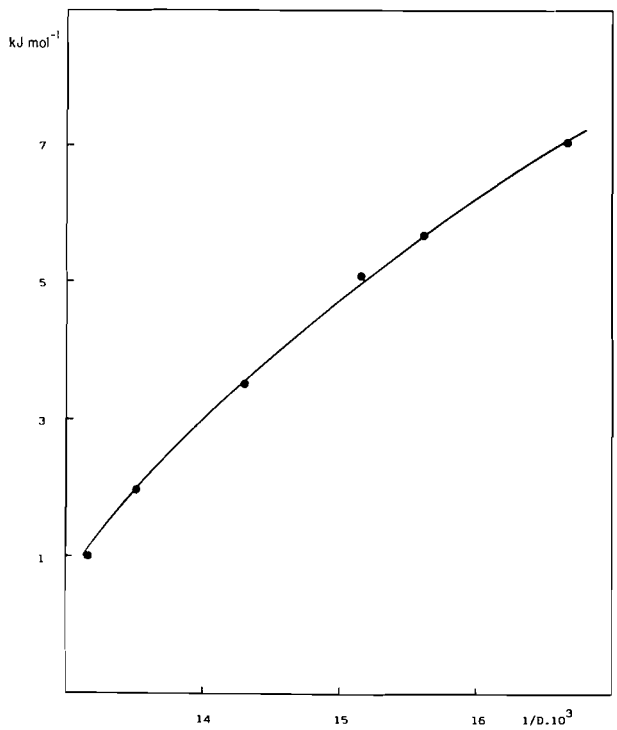

FIG. 6. Plot of Gibbs free energy of activation, (●), vs. D^{-1} for hexacyanoferrate(III) and sulphite ion reaction in methanol–water mixtures at 298.2 K.

destabilization of the transition state in comparison with the destabilization of the initial state. This behaviour is in agreement with the charge increase upon transferring the substrates into the transition states. In fact, $\delta\mu^{\theta}_{TS}$ decreases linearly on increasing the polarity of the media as measured by the

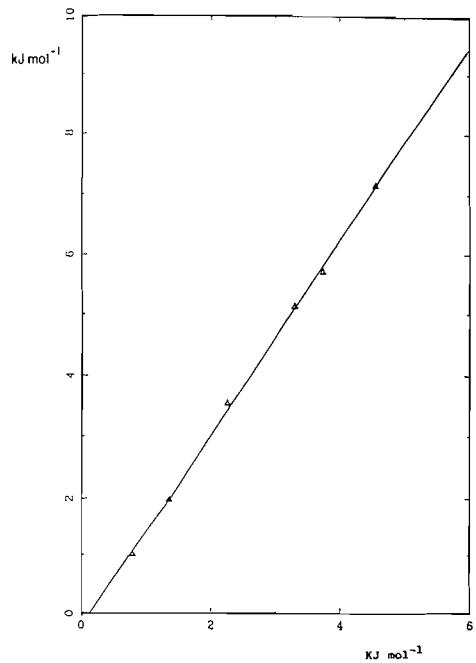

FIG. 7. Plot of $\delta\Delta G^{\neq}_{I=0}$ for peroxodisulphate–iodide reaction vs. $\delta\Delta G^{\neq}_{I=0}$ for sulphite–hexacyanoferrate(III) reaction in methanol–water mixtures at 298.2 K.

TABLE 4. Gibbs free energy of transfer, $\delta_m\mu^{\theta}$, for $Fe(CN)_6^{3-}$, I^-, $S_2O_8^{2-}$, $Fe(CN)_6^{4-}$, SO_4^{2-} ions from water to water–cosolvent mixture at 298.2 K

Percentage of organic component	$\delta_m\mu^{\theta}$/kJ mol^{-1}				
	$S_2O_8^{2-}$	I^-	$Fe(CN)_6^{4-}$	$Fe(CN)_6^{3-}$	SO_4^{2-}
5.68	0.667	0.650	3.780	1.750	2.130
10.20	1.824	0.913	4.100	3.420	3.770
18.37	2.830	2.370	11.60	4.230	6.750
26.53	4.770	3.210	16.00	5.170	9.930
30.64	5.100	3.840	16.00	5.690	11.70
39.15	7.090	5.670	23.30	11.40	16.20

Grunwald–Winstein parameter (34), $\delta y = y_{H_2O} - y_{MetOH-water}$. Moreover, the negative slopes of these plots decrease as the charge of the transition states increases.

On the other hand, if $\delta\Delta G^{\neq}_{I=0}$ for one of the reactions is plotted against $\delta\Delta G^{\neq}_{I=0}$ for another, good linear correlations are observed. As an example, $\delta\Delta G^{\neq}_{I=0}$ values for sulphite–hexacyanoferrate(III) reaction have been plotted against $\delta\Delta G^{\neq}_{I=0}$ for iodide–peroxodisulphate reaction in Fig. 7. The existence of such linear plots is noteworthy, taking into account that the reactions have been carried out in the presence of different cations at different concentrations. Therefore, under the present conditions, specific cation effects do not seem to be important. At this point, it is apparent that whatever the solvent properties important in determining reactivity are, they are similar for all reactions studied in the present work. Thus, if log k'_0 for one reaction is linearly related to log k'_0 for another, the existence of a solvent parameter that could be linearly related to both sets of log k'_0 values could be suggested (35). As $\delta\mu^{\theta}_{TS}$ values vary linearly with δY parameter, we have tried to correlate $\delta\Delta G^{\neq}_{I=0}$ with the same solvent parameter. These plots are depicted in

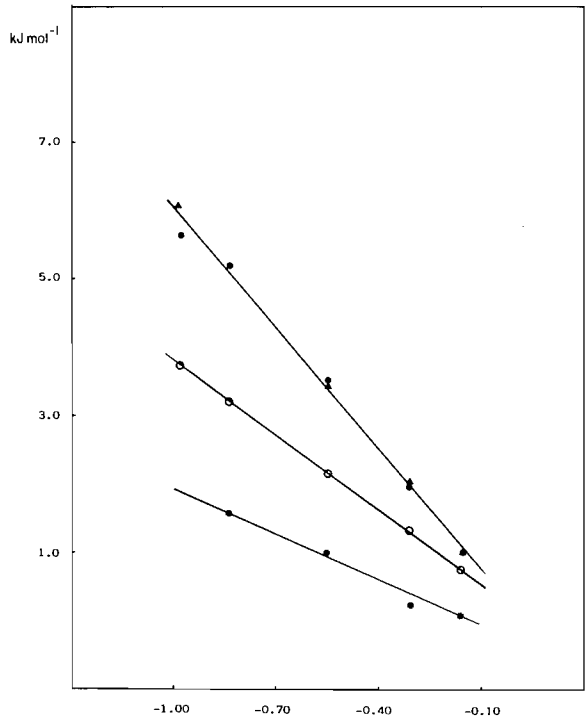

FIG. 8. Plots of Gibbs free energies of activation $\delta\Delta G^{\neq}_{I=0}$ vs. the Grunwald–Winstein parameter δY at 298.2 K. (△)hexacyanoferrate(III)–iodide reaction; (●) hexacyanoferrate(III)–sulphite reaction; (○) peroxodisulphate–iodide reaction; (*) peroxodisulphate–hexacyanoferrate(II) reaction.

Fig. 8 for all reactions. As can be seen in this figure linear correlations are always observed; there is no relation between the slopes of the plots and the charge of the reactants. However, these relations should not be expected because free energy activation parameter is composed of initial and transition state contributions.

The observed linearity between $\delta\Delta G^{\neq}_{I=0}$ and δY parameter suggests a plausible explanation of the experimental results. As is known (36), the rate constant for a bimolecular electron transfer reaction can be expressed as a product of an equilibrium constant for the formation of the precursor complex and the first order rate constant for electron tranfer within the precursor complex. The diffusing together of the similarly charged reactants to form the precursor complex will be favoured on increasing polarity of the media (37), while the energy required to reorganize the solvent decreases as the polarity decreases (37). Finally, the standard free energy change for the overall reactions can make a positive or negative contribution depending on the reactants. Thus it appears that the formation of the precursor complex is, if not the only, an important factor on determining reactivity for the reactions studied. However, it should be realized that if the formation of the precursor complexes was the dominant factor, the correlation of $\delta\Delta G^{\neq}_{I=0}$ against δY should have the same slopes in different solvent systems. Therefore the study of these reactions in mixtures of water with organic solvents, different from methanol, could help in the analysis of the relative importance of other terms; for example, the reorganization free energy of the solvent. Further work is in progress on this theme.

Can. J. Chem. Downloaded from www.nrcresearchpress.com by 88.85.125.76 on 09/07/12
For personal use only.

Acknowledgements

The authors acknowledge the financial support of the CICYT and Consejeria de Educacion y Ciencia de la Junta de Andalucia.

1. C. REICHARDT. Angew Chem. Int. Ed. **4**, 29 (1965).
2. M. H. ABRAHAM. Prog. Phys. Org. Chem. **11**, 1 (1974).
3. W. ORLAND and J. KOLLING. Phys. Chem. **90**, 4664 (1986).
4. D. MATHER and J. SHORTER. J. Chem. Soc. Perkin Trans. **2**, 1179 (1983).
5. M. J. BLANDAMER and J. BURGESS. Coord. Chem. Rev. **31**, 93 (1980).
6. V. HOLBA, J. BENKO, O. GRANČIČOV'A, and O. VOLL'AROV'A. Transition Met. Chem. **10**, 84 (1985).
7. M. J. BLANDAMER, J. BURGESS, J. B. F. N. ENGBERTS, and F. SÁNCHEZ. Faraday Discuss. Chem. Soc. **85**, 1 (1988).
8. A. E. EID and C. F. WELLS. J. Chem. Soc. Faraday Trans. **1, 79**, 253 (1983).
9. M. C. CARMONA GUZMÁN, J. RODRIGUEZ VELASCO, and F. SÁNCHEZ BURGOS. J. Chem. Soc. Faraday Trans. 1, **80**, 3429 (1984).
10. P. PEREZ TEJEDA, J. RODRIGUEZ VELASCO, and F. SÁNCHEZ BURGOS. J. Chem. Soc. Dalton Trans. 2679 (1983).
11. M. C. CARMONA GUZMÁN, J. RODRIGUEZ VELASCO, F. SÁNCHEZ BURGOS, and J. HILDALGO TOLEDO. J. Chem. Soc. Dalton Trans. 31 (1985).
12. J. BAÑOS, F. SÁNCHEZ BURGOS, and M. C. CARMONA GUZMÁN. J. Chem. Soc. Dalton, 1975 (1985).
13. A. RODRIGUEZ, S. LÓPEZ, M. C. CARMONA GUZMÁN, F. SÁNCHEZ BURGOS, and C. PIAZZA. J. Chem. Soc. Dalton Trans. 1265 (1986).
14. W. J. HOWELLS. J. Chem. Soc. 5844 (1964).
15. J. BURGESS. J. Chem. Soc. A, 2351 (1970).
16. G. J. TANZ and R. P. T. TONKINS. Nonaqueous Electrolyte Handbook. vol. I. Academic Press, New York. 1972.
17. G. A. GUGGENHEIM. Phil. Mag. **2**, 538 (1926).
18. O. VOLL'AROV'A and J. BENKO. J. Chem. Soc. Dalton Trans. 2359 (1983).
19. Z. MARCZENKO. Spectrophotometric determination of elements. 505 (1976).
20. P. L. DOMINGO, B. GARCIA, and J. M. LEAL. Can J. Chem. **65**, 583 (1987).
21. P. PEREZ. Tesis, Sevilla. 1982.
22. O. POPOVYCH and R. M. FRIEDMAN. J. Phys. Chem. **70**, 1671 (1966).
23. P. SALOMAA and M. MATTSON. Acta Chem. Scand. **25**, 361 (1971).
24. K. K. KUNDU and K. A. DAS. J. Solution Chem. **8**, 295 (1979).
25. J. BJERRUM and J. P. MC REYNOLDS. Inorg. Synth. **2**, 217 (1963).
26. A. D. PETHYBRIDGE and J. E. PRUE. Prog. Inorg. Chem. **17**, 327 (1972).
27. J. BURGESS and M. J. BLANDAMER. Chem. Soc. Rev. (1985).
28. M. J. BLANDAMER, J. BURGESS, and E. A. ABU-GHARIB. Transition Met. Chem. **9**, 193 (1984).
29. V. HOLBA, J. BENKO, O. GRANČIČOVA, and O. VOLL'AROV'A. Transition Met. Chem. **10**, 84 (1985).
30. B. G. COX, G. R. HEDWIG, A. J. PARKER, and D. W. WATTS. Austr. J. Chem. **27**, 477 (1974).
31. B. G. COX. Ann. Rep. Chem. Soc. **70** A, 249 (1973).
32. E. A. MOELWYN-HUGHES. Chemical statics and kinetics of solutions. Academic Press, London. 1971. p. 178.
33. F. FRANKS and D. J. G. IVES. Q. Rev. **1**, 20 (1966).
34. E. GRUNDWALD and S. WINSTEIN. J. Am. Chem. Soc. **70**, 846 (1948).
35. M. H. ABRAHAM. Pure Appl. Chem. **57**, 1055 (1985).
36. R. A. MARCUS. J. Chem. Phys. **26**, 867 (1957); **26**, 872 (1957).
37. N. SUTIN. Prog. Inorg. Chem. **30**, 441 (1983).

An electrostatic approach to negatively charged substrate reactions with hydroxide ion in cationic CTAB micelles

C. DOLCET AND E. RODENAS[1]

Departamento de Química Física, Universidad de Alcalá, Alcalá de Henares, Madrid, Spain

Received August 1, 1989[2]

C. DOLCET and E. RODENAS. Can. J. Chem. **68**, 932 (1990).

An electrostatic treatment is presented to explain the experimental kinetic data we obtained for the basic hydrolysis of the negatively charged substrates acetylsalicylic acid and 3-acetoxy-2-naphthoic acid. This treatment, based on the non-linearized Poisson–Boltzmann equation, considers specific interactions between the counterions and the micellar surface and explains the displacement of these substrates from the micellar to the aqueous phase through bromide counterion addition.

Key words: electrostatic approach, cationic CTAB micelles.

C. DOLCET et E. RODENAS. Can. J. Chem. **68**, 932 (1990).

On présente un traitement électrostatique qui permet d'expliquer les données cinétiques expérimentales que nous avons obtenues lors de l'hydrolyse basique de substrats chargés d'une façon négative et obtenus à partir des acides acétylsalicylique et 3-acétoxy-2-naphtoïque. Ce traitement, qui est basé sur une équation de Poisson–Boltzmann non-linéarisée, considère les interactions spécifiques entre les contre-ions et la surface micellaire et il explique le déplacement de ces substrats de la phase micellaire vers la phase aqueuse par le biais de l'addition du brome comme contre-ion.

Mots clés : traitement électrostatique, cationique CTAB micelles.

[Traduit par la revue]

Can. J. Chem. Downloaded from www.nrcresearchpress.com by 88.85.125.76 on 09/07/12
For personal use only.

Introduction

In earlier papers we have reported our results in the basic hydrolysis of some aromatic esters in cationic micelles (CTAB, CTACl, CTAOH), hexadecyltrimethilammonium bromide, chloride, and hydroxide respectively (1, 2). These results were accounted for with the pseudophase ion-exchange (3, 4) and the mass-action models (5). To explain the results for negatively charged substrates like acetylsalicylic acid (2-acetoxybenzoic acid) and 3-acetoxy-2-naphthoic acid the micellar counterion effect had to be taken into account. For reactions in CTAB micelles the addition of an additional Br^- counterion to the CTAB micelles displaces these substrates from the micellar to the aqueous phase (6). The opposite effect has been found with positively charged substrates for which Br^- counterion addition produces a sharp increase in substrate to micelle binding (7–9). It is also known that the pseudophase ion-exchange model fails at high reactive ion concentrations according to some experimental evidence in literature (10) so that it becomes necessary to consider an increase in the fraction of neutralized micellar head groups (11, 12) or to consider an additional reaction pathway in which the reactive ion in the aqueous phase reacts with the micelle bound substrate (13).

From all of this evidence, it becomes necessary to develop a new theoretical treatment. For these negatively charged substrates, in an early paper, we assumed that the substrate distribution between aqueous and micellar phases was the same as that for ions in solution as did other authors in literature (14). This treatment neglects the micellar surface potential and is not able to explain our kinetic results (15).

In trying to fit all our kinetic results we developed an electrostatic treatment that treats the ion distribution around micelles by the Poisson–Boltzmann non-linearized equation (NLPB). The Poisson–Boltzmann ion distribution around micelles has been successfully used to explain the thermodynamic behavior of ionic colloids with monovalent ions (16, 17) although it fails to describe the distribution of multivalent ions adequately (18). This treatment explains kinetic results in reactive-ion counterion micelles (19).

In the case of CTAB micelles, the bromide ion distribution around micelles according to the Poisson–Boltzmann equation does not explain the experimental value for the fraction of neutralized micellar head groups. To explain this value it is necessary to consider specific interactions between the Br^- ion and the micellar surface. Some authors in the literature consider the amount of bromide ions specifically adsorbed to be independent of surface potential (20, 21) but this treatment does not fit our kinetic data either.

We have developed a new approach which relates the number of ions that is adsorbed depending on the micellar surface potential. This treatment explains the basic hydrolysis kinetic results for positively charged substrates such as crystal violet (22). In this paper we discuss the validity of this approach to explain kinetic data for the basic hydrolysis of negatively charged substrates such as acetylsalicylic acid and 3-acetoxy-2-naphthoic acid. The experimental data have been reported in earlier papers (1, 2, 6).

Theoretical description of this electrostatic approach

According to the non-linearized Poisson–Boltzmann equation the ion distribution around CTAB micelles can be obtained on the basis of the cell model. Under our experimental conditions, CTAB micelles and cells are considered spherical (23), and the ions are distributed in the region $r_m < r < r_c$ according to the non-linearized Poisson–Boltzmann equation which, for spherical symmetry and if only monovalent ions are present in solution, is expressed as

$$[1] \quad \epsilon_r\epsilon_0(1/r^2)\mathrm{d}/\mathrm{d}r(r^2\mathrm{d}\phi/\mathrm{d}r) = -F\{c_{+0}\exp(-e\phi/kT) - c_{-0}\exp(e\phi/kT)\}$$

Here r_m is the micelle radius, r_c the cell radius, ϵ_r the relative permittivity assumed to be constant in the cell with a value of 78.54, ϵ_0 the vacuum permittivity, T the absolute temperature, k the Boltzmann constant, ϕ the electrostatic potential, e the electron charge, and c_{+0} and c_{-0} are the concentrations

[1]Author to whom all correspondence should be addressed.

[2]Revision received February 21, 1990.

Printed in Canada / Imprimé au Canada

Can. J. Chem. Downloaded from www.nrcresearchpress.com by 88.85.125.76 on 09/07/12
For personal use only.

(mol m^{-3}) of positive and negative ions, respectively, at a point on the solution where $\phi = 0$.

The parameters c_{+0} and c_{-0} are related to the total number of positive and negative ions in the cell, n_+ and n_-, by the normalization conditions

$$[2] \quad n_+ = c_{+0}N_A\int_{r_m}^{r_c} \exp(-e\phi/kT)(4\pi r^2)dr$$

$$[3] \quad n_- = c_{-0}N_A\int_{r_m}^{r_c} \exp(e\phi/kT)(4\pi r^2)dr$$

where N_A is Avogadro's number.

Equation [1] can be solved with the fourth order Runge–Kutta method using the boundary conditions

$$[4] \quad \phi(r = r_c) = 0$$

$$[5] \quad (d\phi/dr)_{(r=r_c)} = \phi'(r = r_c) = 0$$

and with the electroneutrality condition

$$[6] \quad (d\phi/dr)_{(r=r_m)} = \phi'(r = r_m) = -\sigma/\epsilon_0\epsilon_r$$

where σ is micellar surface charge per m^2.

Solution of the Poisson–Boltzmann equation gives the average concentration of bromide ions in a layer of thickness Δr around the micelle. The fraction of micellar head groups neutralized with statistically distributed bromide ions that can be considered part of the micellar aggregate is expressed as

$$[7] \quad m_{BrNCA} = (N_A/N)\int_{r_m}^{r_m+\Delta r} c_{-0}\exp(e\phi_0/kT)4\pi r^2dr$$

where N is the micellar aggregation number and ϕ_0 is the micellar surface potential.

The values of β, $\beta = m_{BrNCA}$, obtained from eq. [7] do not agree with experiments (22). For CTAB micelles, β values have been determined by different methods such as emf (24) and conductivity (25, 26); β is essentially independent of surfactant concentration (27) ($\beta = 0.8$), although some experimental evidence shows a slight increase with surfactant concentration and with added salt (28). To explain the β values for CTAB micelles in solution, we assume that the Br^- ion specifically adsorbs on charged surfaces, in agreement with experimental evidence. The number of ions specifically adsorbed, [Br^-_{CA}], depends on surface charge, solvent, environment, etc. (29). For this study we have considered the following equilibrium accounting for Br^- ion contact adsorption according to Butler–Volmer

$$Br^-_{NCA} + Dn \underset{\overleftarrow{k}}{\overrightarrow{k}} Br^-_{CA}$$

with an equilibrium condition given by

$$[8] \quad \frac{m_{BrCA}}{[Br^-_{NCA}](1 - m_{BrCA})} = K_{BrCA}\exp(e\phi_0/kT)$$

where [Br^-_{NCA}] is the non-specifically adsorbed bromide ion concentration, m_{BrCA} the fraction of micellar surface neutralized by the specifically adsorbed bromide ions, $(1 - m_{BrCA})$ represents the fraction of free micellar surface, and K_{BrCA} is the bromide ion specific adsorption constant.

We solved eq. [1] using an iterative method with the fourth order Runge–Kutta method, starting from chosen initial values of ϕ_0, c_{+0}, and c_{-0} and optimizing to a complete solution using the boundary conditions (4, 5) and normalization conditions (2, 3) and then checked the calculated results using eq. [6] where $\sigma = Ne(1 - m_{BrCA})/4\pi r_m^2$. The numerical values for the integral in eqs. [2] and [3] were obtained by Simpson's rules.

In this case, the total fraction of neutralized micellar head groups is given by

$$[9] \quad \beta = m_{BrCA} + m_{BrNCA}$$

where m_{BrNCA} is given by eq. [7].

As reported (22), a K_{BrCA} value of 30 M^{-1} best explains the observed value of β for CTAB.

Since the experimental results in this paper were obtained with an added quantity of acetonitrile in the reaction mixture, we have considered the additional ionization of CTAB micelles produced by acetonitrile. According to the results of our conductivity measurements, the fraction of neutralized micellar head groups is 0.74 independent of surfactant concentration (30). The bromide ion specific adsorption constant, K_{BrCA} in eq. [8] that best fits this result is 25 M^{-1} which means that the added acetonitrile slightly decreases the bromide ion specific adsorption on to the CTA^+ micelles.

The acetonitrile in the concentration used also produces a slight decrease in the micellar aggregation number (31). The micellar aggregation numbers used in the calculations were determined by fluorescence quenching measurements (31–33) with pyrene as probe and cetylpiridinium chloride as static quencher (34). Our experimental results, given in Table 2, are smaller than the CTAB aggregation numbers reported (35). Acetonitrile does not affect the peak intensity ratio I_1/I_{III} in the pyrene spectra, which means that acetonitrile does not appreciably affect the dielectric constant micellar surface (31).

Hydroxide ions can be considered non-specifically adsorbed on the micellar surface and once the Poisson–Boltzmann equation has been solved, the average concentration of bromide and hydroxide ions in a layer of thickness Δr can be calculated by eq. [10].

$$[10] \quad m_{OH} + m_{BrNCA} = (N_A/N)\int_{r_m}^{r_m+\Delta r} c_{-0}\exp(e\phi_0/kT)4\pi r^2dr$$

m_{OH} and m_{BrNCA} are the fraction of micellar head groups neutralized with hydroxide and bromide ions statistically distributed in the layer $r_m + \Delta r$.

The total fraction of micellar head groups neutralized is given by

$$[11] \quad \beta = m_{OH} + m_{BrCA} + m_{BrNCA}$$

and m_{OH}

$$[12] \quad m_{OH} = \frac{(m_{BrNCA} + m_{OH})[OH^-]}{[Br^-_{NCA}] + [OH^-]}$$

At the total concentration of hydroxide ions used in this study the fraction of micellar head groups neutralized with statistically distributed bromide and hydroxide ions (given by eq. [10]) cannot be neglected relative to m_{BrCA}, the fraction of neutralized micellar head groups with specifically adsorbed bromide ion, given by eq. [8], as one can see from Table 1. We therefore improved our calculation using the following equilibrium condition to give the amount of bromide ion specifically adsorbed

Can. J. Chem. Downloaded from www.nrcresearchpress.com by 88.85.125.76 on 09/07/12
For personal use only.

TABLE 1. Calculated values for the micellar surface potential, ϕ_0 and $\phi_{4\text{Å}}$, fraction of micellar head groups neutralized with the adsorbed hydroxide ions, m_{OH}, non-specifically adsorbed bromide ions, m_{BrNCA}, specifically adsorbed bromide ions, m_{BrCA}, and total fraction of micellar head groups neutralized, β (m_{BrCA} values were obtained from eq. [8])

[CTAB] (M)	N	$\phi_{4\text{Å}}$ (mV)	ϕ_0 (mV)	$m_{OH} \times 100$	$m_{BrNCA} \times 100$	m_{BrCA}	β
			[NaOH] = 0.050 M				
0.004	40	45.8	81.5	13.4	0.5	0.544	0.683
0.006	43	43.8	77.2	11.4	0.6	0.578	0.699
0.010	50	42.7	74.2	9.8	0.8	0.635	0.740
0.020	60	39.7	68.1	7.5	1.0	0.693	0.777
0.040	64	35.4	60.4	5.6	1.2	0.738	0.806
0.060	64	32.4	55.8	4.8	1.4	0.761	0.823
[(KBr)] (M)	N	$\phi_{4\text{Å}}$ (mV)	ϕ_0 (mV)	$m_{OH} \times 100$	$m_{BrNCA} \times 100$	m_{BrCA}	β
			[D] = 0.010 M, [NaOH] = 0.030 M				
0.010	60	36.1	58.9	3.7	1.5	0.758	0.810
0.030	60	25.1	43.0	2.2	2.4	0.811	0.856
0.050	60	19.5	34.8	1.7	2.9	0.834	0.881
9.100	60	12.8	25.2	1.3	4.2	0.871	0.926
0.300	60	4.0	10.4	0.8	8.0	0.919	1.007
0.500	60	2.1	6.5	0.7	11.9	0.942	1.068

TABLE 2. Calculated values for the micellar surface potential, ϕ_0 and $\phi_{4\text{Å}}$, fraction of micellar head groups neutralized with the adsorbed hydroxide ions, m_{OH}, non-specifically adsorbed bromide ions, m_{BrNCA}, specifically adsorbed bromide ions, m_{BrCA}, and total fraction of micellar head groups neutralized, β (m_{BrCA} values were obtained from eq. [13])

[CTAB] (M)	N	$\phi_{4\text{Å}}$ (mV)	ϕ_0 (mV)	$m_{OH} \times 100$	$m_{BrNCA} \times 100$	m_{BrCA}	β
			[NaOH] = 0.010 M				
0.004	40	64.6	96.6	5.1	0.9	0.620	0.680
0.006	43	62.3	92.6	4.2	1.0	0.651	0.703
0.010	50	60.2	88.4	3.4	1.1	0.693	0.738
0.020	60	55.6	81.4	2.4	1.3	0.739	0.776
0.040	64	48.8	72.1	1.6	1.5	0.772	0.803
0.060	64	43.7	65.9	1.3	1.7	0.786	0.816
			[NaOH] = 0.030 M				
0.004	40	53.7	89.5	10.9	0.7	0.548	0.664
0.006	43	52.0	85.9	9.4	0.8	0.588	0.690
0.010	50	50.0	81.4	7.6	1.0	0.637	0.723
0.020	60	46.9	75.6	5.8	1.2	0.697	0.767
0.040	64	41.8	67.2	4.2	1.5	0.740	0.796
0.060	64	38.1	61.8	3.4	1.7	0.761	0.813
			[NaOH] = 0.050 M				
0.004	40	47.2	84.3	14.4	0.6	0.500	0.651
0.006	43	46.0	81.6	12.9	0.7	0.547	0.684
0.010	50	44.4	77.5	10.7	0.9	0.602	0.718
0.020	60	41.5	71.5	8.2	1.1	0.666	0.760
0.040	64	37.2	63.9	6.2	1.4	0.717	0.793
0.060	64	34.2	59.0	5.2	1.6	0.742	0.810
[KBr] (M)	N	$\phi_{4\text{Å}}$ (mV)	ϕ_0 (mV)	$m_{OH} \times 100$	$m_{BrNCA} \times 100$	m_{BrCA}	β
			[D] = 0.010 M, [NaOH] = 0.030 M				
0.010	60	38.4	62.9	4.1	1.8	0.742	0.800
0.030	60	26.9	46.2	2.4	2.6	0.788	0.839
0.050	60	22.0	39.4	1.9	3.4	0.812	0.866
0.100	60	15.1	29.8	1.4	4.8	0.835	0.897
0.300	60	8.2	21.1	1.0	10.5	0.836	0.951
0.500	60	5.9	18.6	0.9	15.8	0.831	0.998

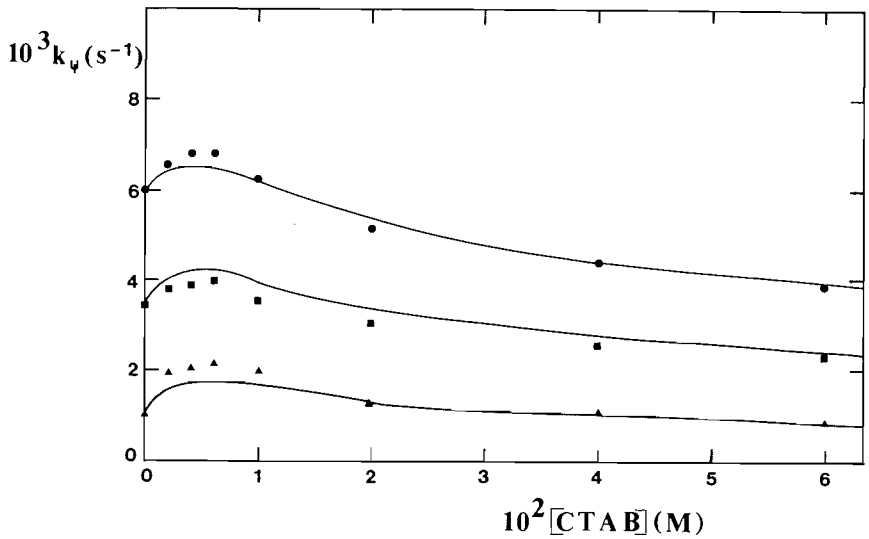

FIG. 1. Pseudo-first order rate constant for the basic hydrolysis of acetylsalicylic acid in CTAB micelles at different surfactant and ion concentrations. Solid lines are the calculated values (▲ [NaOH] = 0.010 M; ■ [NaOH] = 0.030 M; ● [NaOH] = 0.050 M).

$$[13]\quad \frac{m_{BrCA}}{[Br^-_{NCA}](1 - m_{BrCA} - m_{BrNCA} - m_{OH})} = K_{BrCA} \exp(e\phi_0/kT)$$

In the iterative calculation method used to solve the Poisson–Boltzmann equation, initial values were assigned ($m_{OH} + m_{BrNCA}$), c_{-0}, and c_{+0}, which were then optimized until a satisfactory solution of the equation was obtained.

In the calculation, cells have been considered spherical with a radius, r_c, given by

$$[14]\quad 4\pi r_c^3/3 = N/10^3 N_A([D] - \text{cmc})$$

where [D] is the surfactant concentration and cmc is the critical micelle concentration with added salt, calculated using the empirical equation (36)

$$[15]\quad \log \text{cmc} = -3.7671 - 0.2133 \log (c_m + [NaOH] + [KBr])$$

c_m is the critical micellar concentration for simple CTAB micelles, $c_m = 9 \times 10^{-4}$ M.

The Stern layer thickness has been assumed to be constant, $\Delta r = 4$ Å as we used in ref. 22. The micellar radius, r_m, has been calculated from Tanford's expression (37)

$$[16]\quad (4/3)\pi r_m^3 = N(27.4 + 26.9 n_c)$$

where $n_c = 15$ for CTAB, so that the volume of micellar phase per mol of micellized surfactant, $\bar{V}$, is constant with a surfactant concentration, the value is 0.259 L mol^{-1}.

Above the cmc, the substrate distributes between the aqueous and micellar phases. The binding of these negatively charged substrates to cationic micelles has been described by assuming an ideal behavior of the micellar pseudophase. In this way the electrochemical substrate potential in the micellar and aqueous phases would be equal at equilibrium:

$$[17]\quad \mu^0_{SM} + RT \ln [\overline{S_M}] + z_s F \phi_M = \mu^0_{SW} + RT \ln [\overline{S_W}] + z_S F \phi_W$$

Here μ^0_{SM} and μ^0_{SW} denote the substrate standard chemical potential in the micellar and in the aqueous phase, respectively, and $[\overline{S_M}]$ and $[\overline{S_W}]$ are the effective substrate concentrations in the micellar and the aqueous phases. These quantities are related to the analytical concentrations by

$$[18]\quad [\overline{S_M}] = \frac{[S_M]}{[Dn]\bar{V}} \qquad [\overline{S_W}] = \frac{[S_W]}{1 - [Dn]\bar{V}}$$

under our experimental conditions $1 - [Dn]\bar{V} \simeq 1$.

The substrate partition coefficient, P_S, between both phases is given by

$$[19]\quad P_S = \frac{[\overline{S_M}]}{[\overline{S_W}]} = P^0_S \exp\{-ez_S(\phi_M - \phi_W)/kT\}$$

where $P^0_S = \exp(\mu^0_{SW} - \mu^0_{SM})/RT$ and $(\phi_M - \phi_W)$ denotes the electrostatic attractive potential that contributes to the binding of these negatively charged substrates to cationic micelles.

The partition coefficient P_S is related to the substrate to micelle binding constant, K_S, by $P_S = K_S/\bar{V}$ as

$$[20]\quad K_S = \frac{[S_M]}{[S_W][Dn]}$$

This electrostatic approach shows that substrate binding to cationic micelles increases with micellar surface potential.

The reaction rate defined in terms of effective concentration in the micellar and the aqueous phase is given by

$$[21]\quad v = k_m[\overline{S_M}][\overline{OH^-_M}][Dn]\bar{V} + k_W[\overline{S_W}][\overline{OH^-_W}](1 - [Dn]\bar{V})$$

where $\bar{V}$ is the micellar phase molar volume, k_m is the second order rate constant for the reaction in the micellar phase. The pseudo-first order rate constant is easily deduced in terms of the substrate partition coefficient as

$$[22]\quad k_\psi = \frac{k_W[OH^-] + (k_m P_S - k_W) m_{OH}[Dn]}{1 + P_S[Dn]\bar{V}}$$

Results and discussion

The pseudo-first order rate constant for the basic hydrolysis of acetylsalicylic acid and 3-acetoxy-2-naphthoic acid at different hydroxide ion and surfactant concentrations are represented by

Can. J. Chem. Downloaded from www.nrcresearchpress.com by 88.85.125.76 on 09/07/12
For personal use only.

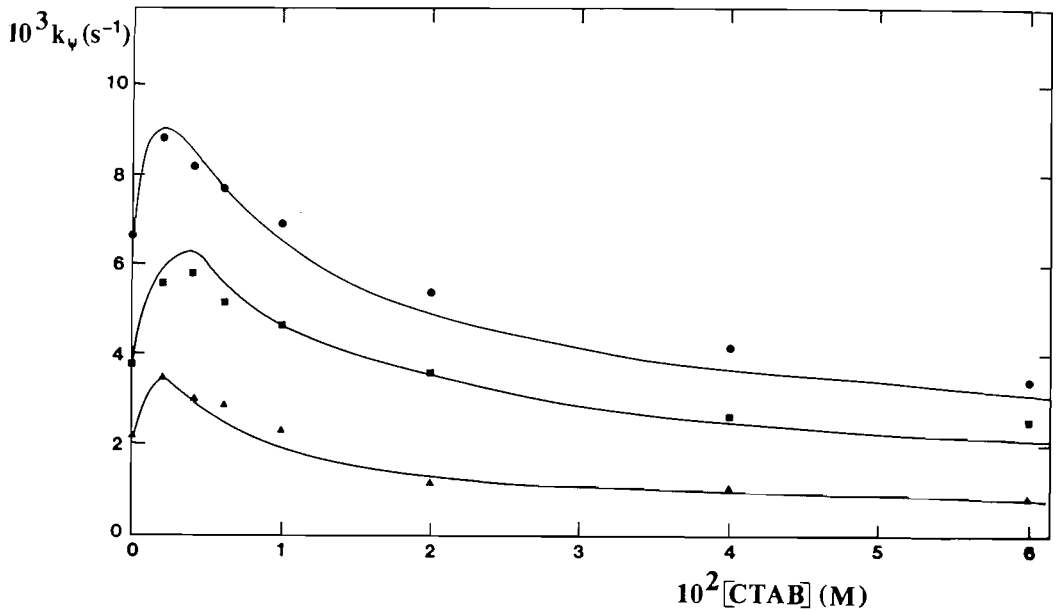

FIG. 2. Pseudo-first order rate constant for the basic hydrolysis of 3-acetoxy-2-naphthoic acid in CTAB micelles at different surfactant and ion concentrations (see legend of Fig. 1).

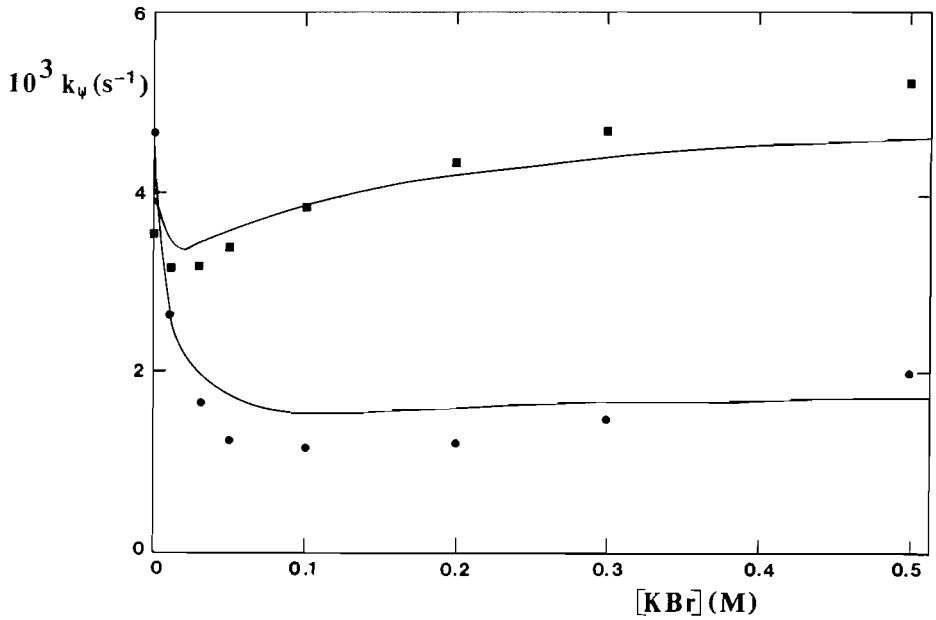

FIG. 3. Pseudo-first order rate constant for the basic hydrolysis of acetylsalicylic acid (■) and 3-acetoxy-2-naphthoic acid (●) in CTAB micelles at different KBr concentrations for [D] = 0.010 M and [NaOH] = 0.030 M. Solid lines are the calculated values.

dots in Figs. 1 and 2 from refs. 1 and 2. The effect of an additional amount of KBr is shown in Fig. 3 from ref. 6. These results have been obtained using acetonitrile substrate stock solution. The amount of acetonitrile in the reaction mixture is 3% as previously reported (1, 2, 6).

Second order rate constants of both substrate for the reaction in water are 0.124 M^{-1} s^{-1} and 0.160 M^{-1} s^{-1} for acetylsalicylic acid and 3-acetoxy-2-naphthoic acid, respectively. These second order rate constants are strongly affected for by the following empirical variations according to the results given in ref. 6.

$$[23] \quad \log k_W = (-0.896 + 0.5581[KBr] - 0.6229[KBr]^2)$$

$$[24] \quad \log k_W = (-0.799 + 0.3556[KBr] - 0.3296[KBr]^2)$$

The kinetic results in micelles have been explained with the pseudophase ion-exchange model by considering a displacement of these negatively charged substrates from the micellar to the aqueous phase with Br^- ion addition (6).

To fit the experimental results, m_{OH} and $\phi_{4Å}$ have been calculated by the electrostatic treatment given before and P^0_S and k_m have been taken as adjustable parameters. The values that best fit these results are $P^0_S = 36.7$ and $k_m = 0.015\ M^{-1}\ s^{-1}$ for acetylsalicylic acid and $P^0_S = 1083.0$ and $k_m = 0.0155\ M^{-1}\ s^{-1}$ for 3-acetoxy-2-naphthoic acid. The pseudo-first order rate constant calculated is represented by the solid lines in Figs. 1, 2, and 3. The calculated values for ϕ_0, $\phi_{4Å}$, the fraction of neutralized micellar head groups with bromide ions specifically adsorbed (m_{BrCA}), the fraction of neutralized micellar head

Can. J. Chem. Downloaded from www.nrcresearchpress.com by 88.85.125.76 on 09/07/12
For personal use only.

TABLE 3

(*a*) Ion exchange equilibrium constant, K^{OH}_{Br}, and substrate to micelle binding constant, K_S, of acetylsalicylic acid in CTAB micelles

			[NaOH] = 0.010 M			
[D] (M)	0.004	0.006	0.010	0.020	0.040	0.060
K^{OH}_{Br}	69	66	62	57	51	47
K_S (M^{-1})	117	107	99	83	63	52
			[NaOH] = 0.030 M			
[D] (M)	0.004	0.006	0.010	0.020	0.040	0.060
K^{OH}_{Br}	76	71	66	58	51	47
K_S (M^{-1})	77	72	67	59	48	42
			[NaOH] = 0.050 M			
[D] (M)	0.004	0.006	0.010	0.020	0.040	0.060
K^{OH}_{Br}	81	74	68	60	52	46
K_S (M^{-1})	60	57	53	48	40	36
			[NaOH] = 0.30 M, [D] = 0.010 M			
[KBr] (M)	0.010	0.030	0.050	0.100	0.300	0.500
K^{OH}	43	31	25	18	9	6
K_S (M^{-1})	42	27	22	17	13	12

(*b*) Ion exchange equilibrium constant, K^{OH}_{Br}, and substrate to micelle binding constant, K_S, of 3-acetoxy-2-naphthoic acid in CTAB micelles

			[NaOH] = 0.010 M			
[D] (M)	0.004	0.006	0.010	0.020	0.040	0.060
K^{OH}_{Br}	69	66	62	57	51	47
K_S (M^{-1})	3467	3171	2917	2443	1873	1539
			[NaOH] = 0.030 M			
[D] (M)	0.004	0.006	0.010	0.020	0.040	0.060
K^{OH}_{Br}	76	71	66	58	51	47
K_S (M^{-1})	2268	2121	1965	1743	1425	1234
			[NaOH] = 0.050 M			
[D] (M)	0.004	0.006	0.010	0.020	0.040	0.060
K^{OH}_{Br}	81	74	68	60	52	46
K_S (M^{-1})	1758	1681	1579	1410	1194	1060
			[NaOH] = 0.030 M, [D] = 0.010 M			
[KBr] (M)	0.010	0.030	0.050	0.100	0.300	0.500
K^{OH}_{Br}	43	31	25	18	9	6
K_S (M^{-1})	1248	800	660	505	385	353

groups with OH^- and Br^- ions non-specifically adsorbed (m_{OH} and m_{BrNCA}) and the total fraction of neutralized micellar head groups (β) are given in Table 2.

This calculation predicts that the micellar surface potential decreases with surfactant concentration and with the amount of additional KBr in solution, in agreement with our experimental results (6) and with results in the literature (38). The drop in the micellar surface potential is related to the decreased binding of these negatively charged substrates to the micelle according to eq. [19].

Second order rate constants for both substrate reactions in the micellar phase are nearly one hundred times smaller than the second order rate constant for the reaction in the aqueous phase. Clearly, micelles produce a strong inhibition effect on these reactions. The same effect is predicted by the pseudophase ion-exchange and mass-action models (1, 2, 6).

The P^0_S obtained for 3-acetoxy-2-naphthoic acid is higher than P^0_S for acetylsalicylic acid, as would be expected for a more hydrophobic substrate.

To compare these results with those obtained with the pseudophase ion-exchange kinetic model we have calculated values of substrate to micelle binding constant, K_S, given by eq. [20], and the exchange equilibrium constant given by equation

$$[25] \quad K^{OH}_{Br} = \frac{[OH^-_W][Br^-_M]}{[OH^-_M][Br^-_W]}$$

and predicted by this electrostatic treatment. The results are shown in Table 3.

As one can see this treatment predicts that the substrate-to-micelle binding constant given by eq. [20] decreases with surfactant concentration and hydroxide ion concentration in solution. The opposite effect is found for positively charged substrates (7–9, 11, 39, 40). The ion-exchange equilibrium constant from eq. [25] decreases with surfactant concentration and with the addition of KBr. This exchange equilibrium constant increases with the concentration of hydroxide ions in solution. However, the average value is much larger than the values, $K^{OH}_{Br} = 2$ and 5 obtained by using the ion-exchange equilibrium treatment for acetylsalicylic acid and 3-acetoxy-

Can. J. Chem. Downloaded from www.nrcresearchpress.com by 88.85.125.76 on 09/07/12
For personal use only.

2-naphthoic acid, respectively. Note that some larger values are also reported in the literature (41).

We conclude that the non-linearized Poisson–Boltzmann equation, which treats the ion distribution around micelles, can explain our experimental results for reactions with negatively-charged substrates in cationic CTAB micelles. This treatment predicts the decrease in substrate binding to micelle with added ions, based on the decrease in the micellar surface potential. This effect can not be explained by the pseudophase ion-exchange model.

Considering the results we have obtained with this electrostatic treatment we have come to the conclusion that it explains our kinetic data for positively or negatively charged substrates such as crystal violet, acetylsalicylic acid, or 2-acetoxy-2-naphthoic acid, which are supposed to be solubilized near the micellar Stern layer. However, this treatment fails for very hydrophobic charged or neutral substrates like tris(4,7-diphenyl-1,10-phenantroline)Fe(II) ion or DDT, perhaps because they are solubilized within the micellar core and thereby changing the micellar structure. This agrees with our initial conclusion in ref. 42 but still needs experimental verification.

1. S. VERA and E. RODENAS. An. Real. Acad. Farm. **50**, 73 (1984); S. VERA and E. RODENAS. Tetrahedron, **42**, 143 (1986); S. VERA, E. RODENAS, F. ORTEGA, and C. OTERO. J. Chim. Phys. **80**, 543 (1983).
2. E. RODENAS and S. VERA. J. Phys. Chem. **89**, 513 (1985).
3. C. A. BUNTON. Catal. Rev. Sci. **20**, 1 (1979).
4. L. S. ROMSTED. *In* Micellization solubilization and microemulsions. Vol. 2. *Edited by* K. L. Mittal. Plenum, New York. 1977. p. 509.
5. H. AL-LOHEDAN, C. A. BUNTON, and L. S. ROMSTED. J. Phys. Chem. **87**, 332 (1983).
6. S. VERA and E. RODENAS. J. Phys. Chem. **90**, 3414 (1986).
7. H. AL-LOHEDAN, C. A. BUNTON, and L. S. ROMSTED. J. Phys. Chem. **85**, 2123 (1981).
8. C. A. BUNTON, L. H. GAN, J. R. MOFFATT, L. S. ROMSTED, and G. SAVELLI. J. Phys. Chem. **85**, 4118 (1981).
9. L. MIOLA, R. A. ABAKERLI, M. F. GINANI, P. B. FILHO, V. G. TOSCANO, and F. H. QUINA. J. Phys. Chem. **87**, 4417 (1983).
10. F. NOME, A. F. RUBIRA, C. FRANCO, and L. G. IONESCU. J. Phys. Chem. **86**, 1881 (1982).
11. F. ORTEGA and E. RODENAS. J. Phys. Chem. **90**, 2408 (1986).
12. C. OTERO and E. RODENAS. Can. J. Chem. **63**, 2892 (1985).
13. C. A. BUNTON, L. S. ROMSTED, and F. SAVELLI. J. Am. Chem. Soc. **101**, 1253 (1979); E. STADLER, M. ZANETTE, M. C. REZENDE, and F. NOME. J. Phys. Chem. **88**, 1892 (1984).
14. L. S. ROMSTED. J. Phys. Chem. **89**, 5107 (1985); **89**, 5113 (1985).
15. S. VERA and E. RODENAS. An. Quim. **84**, 174 (1988).
16. D. STIGTER. J. Phys. Chem. **79**, 1008 (1975); **79**, 1015 (1975).
17. M. MILLE and G. VANDERKOOI. J. Colloid Interface Sci. **59**, 211 (1977); G. GUNNARSSON, B. JÖNSSON, and H. WENNERSTRÖM. J. Phys. Chem. **84**, 3114 (1980).
18. B. JÖNSSON, P. LINZE, T. AKESSON, and H. WENNERSTRÖM. *In* Surfactants in solution. Vol. 3. *Edited by* K. L. Mittal and B. Lindman. Plenum Press, New York. 1984. p. 2023.
19. F. ORTEGA and E. RODENAS. J. Phys. Chem. **91**, 837 (1987).
20. C. A. BUNTON and J. R. MOFFAT. J. Phys. Chem. **90**, 538 (1986); **89**, 4166 (1985).
21. M. ALMGREN and R. RYDHOLM. J. Phys. Chem. **83**, 360 (1979).
22. E. RODENAS, C. DOLCET, and M. VALIENTE. J. Phys. Chem. **94**, 1472 (1990).
23. C. Y. YOUNG, P. J. MISSEL, N. A. MAZER, and G. B. BENEDEK. J. Phys. Chem. **82**, 1375 (1978).
24. R. ZANA, S. YIV, C. STRAZIELLE, and P. LIANOS. J. Colloid Interface Sci. **80**, 208 (1981).
25. H. C. EVANS. J. Chem. Soc. 579 (1956).
26. H. HOFFMANN and W. ULBRICHT. Z. Phys. Chem. N. F. **106**, 167 (1977); H. HOFFMANN and B. TAGESSON. Z. Phys. Chem. N. F. **110**, 8 (1978).
27. L. SEPÚLVEDA and J. CORTÉS. J. Phys. Chem. **89**, 5322 (1985).
28. A. RHODE and E. SACKMANN. J. Colloid Interface Sci. **70**, 494 (1979); J. Phys. Chem. **84**, 1598 (1980).
29. J. O'M. BOCKRIS and A. K. N. REDDY. Modern electrochemistry. Plenum Press, New York. 1970.
30. M. VALIENTE and E. RODENAS. An. Quim. **85**, 192 (1989).
31. E. PEREZ and E. RODENAS. An. Quim. In press.
32. N. J. TURRO and A. YEKTA. J. Am. Chem. Soc. **100**, 5951 (1978).
33. K. KALYANASUNDARAM. Photochemistry in microheterogeneous systems. Academic Press, New York. 1987.
34. A. MALLIARIS, J. LANG, and R. ZANA. J. Chem. Soc. Faraday Trans. I, **82**, 109 (1986).
35. P. LIANOS and R. ZANA. J. Colloid Interface Sci. **84**, 100 (1981).
36. C. A. BUNTON and L. ROBINSON. J. Am. Chem. Soc. **90**, 5972 (1968).
37. C. TANFORD. J. Phys. Chem. **78**, 2469 (1974).
38. M. S. FERNÁNDEZ and P. FROMHERZ. J. Phys. Chem. **81**, 1755 (1977).
39. M. VALIENTE and E. RODENAS. J. Colloid Interface Sci. **127**, 522 (1989).
40. F. ORTEGA and E. RODENAS. Can. J. Chem. **67**, 305 (1989).
41. L. S. ROMSTED. Surfactants in solution. Vol. 2. *Edited by* K. L. Mittal and B. Lindman. Plenum, New York. 1984. p. 1015.
42. E. RODENAS, F. ORTEGA, S. VERA, C. OTERO, and S. MAESTRO. VI International Symposium on Surfactants in Solution, New Delhi. 1986.

Can. J. Chem. Downloaded from www.nrcresearchpress.com by 88.85.125.76 on 09/07/12
For personal use only.

On the possibilities of π-ylides

RICHARD FRANCIS LANGLER[1] AND LAURA PRECEDO
Department of Chemistry, Florida Institute of Technology, Melbourne, FL 32901-6988, U.S.A.

Received November 24, 1989

RICHARD FRANCIS LANGLER and LAURA PRECEDO. Can. J. Chem. **68**, 939 (1990).

A systematic survey of substituted annulenes, using zeroth order Hückel theory, has uncovered a subclass of such structures which are predicted to have very substantial charge separation. An examination of selected structures by MNDO semi-empirical molecular orbital computations provided support for the Hückel descriptions. Such compounds may be of immediate interest to those pursuing synthetic or mechanistic problems which involve cycloaddition reactions.

Key words: π-ylides.

RICHARD FRANCIS LANGLER et LAURA PRECEDO. Can. J. Chem. **68**, 939 (1990).

Un examen systématique d'annulénes substitués, faisant appel à la théorie d'ordre zéro de Hückel, a permis de déceler des sous-classes de ces structures pour lesquelles on prédit qu'il existera de trés importantes séparations de charges. Des calculs semi-empiriques d'orbitales moléculaires MNDO effectués sur des structures choisies ont fourni un support pour les descriptions de Hückel. De tels composés peuvent présenter un intérét immédiat pour ceux qui examinent les problèmes de synthèse ou mécanistiques impliquant des réactions de cyclo-additions.

Mots clés : π-ylides.

[Traduit par la revue]

Introduction

Recently, our interest in Hückel theory (1) has prompted us to begin an examination of substituted even annulenes. We outline here our conclusions regarding those species for which fully π-bonded Lewis structures cannot be drawn,[2] e.g. **1**, **2***a*, and **3**.

In graph theoretical terms,[3] any hydrocarbon with a π system can be assigned a characteristic polynomial (2, 3) of the general form:

$$[1] \quad a_0x^j + a_1x^{j-1} + a_2x^{j-2} + \ldots\ldots + a_j = 0$$

The roots of the polynomial r_1, $r_2 \ldots . r_j$ are related to the eigenvalues of the Hückel eigenfunctions as shown in eq. [2].

$$[2] \quad E_i = \alpha + r_i\beta$$

The coefficients a_0, a_1, a_2 ..... a_j may be determined (in conjunction with the Sachs' formula (2, 3) by counting Sachs' graphs(s) containing the appropriate number of carbon atoms, e.g., j carbon atoms/graph (s_j) to determine a_j. For "diradical" substituted even annulenes, e.g. **1**, **2**, and **3**, no Sachs' graphs, s_j, can be drawn. Therefore a_j must be zero. All such "diradicals" must have a non-bonding molecular orbital ($E = \alpha$).

These systems can be subdivided (4) into alternant hydrocarbons **1** and non-alternant hydrocarbons **2***a* and **3**. For all even alternant hydrocarbons a_{j-1} must be zero. As is the case for **1**, all even alternant "diradicals"[4] must have a pair of non-bonding molecular orbitals (NBMO's) and are expected to be ground state triplets in accord with their simple Lewis structures. Consistent with that picture, each carbon in **1** has a Hückel π-electron population-derived partial charge of zero.

The following conclusions are most easily reached from even non-alternant "diradical" structures[4] in which one electron is endocyclic and the other is exocyclic as shown for **2***a* and **3**. For Lewis structures of that type, in which one or more of the ring carbons are involved in exocyclic π bonds e.g. **2***a*, it is not possible to draw any Sachs' graphs: s_{j-1}. Therefore, (*i*) a_{j-1} is zero, (*ii*) there is a second NBMO, and (*iii*) they too must be ground state triplets. Consistent with that picture, the ring in **2***a* only develops a small positive charge as shown in **2***b*. The total π-electron-based charge developed in the ring for **2***a*, **2***b* is substantially less than that of other non-alternant systems e.g. **4**.

For even non-alternant "diradical" structures[4] (one endocyclic and one exocyclic electron) which have no exocyclic π bonds, e.g., **3**, it is always possible to draw at least one Sachs' graph:[5] s_{j-1}.

Therefore, (*i*) a_{j-1} cannot be zero, (*ii*) there is only one NBMO, and (*iii*) *unlike* **1** *and* **2***a*, **3** *is expected to be a ground state singlet*.

Since **3** has a spin-pair of non-bonding electrons, why not write the Lewis structure with a lone pair as shown in **5***a*? We choose the charge separated structure **5***a* which has the aromatic cyclopropenyl ring.

Related arguments have permitted earlier workers to deduce that **5***a* and **7***a* have one NBMO each (5). Both earlier reports raise the question of ground state multiplicity for such compounds and both conclude that they are likely to be ground state singlets. Our next article will examine the question of ground state multiplicity for **5***a* and **7***a* using, *inter alia, ab initio* computations at the STO 3-21G level. Further discussion, here, will focus exclusively on singlet states.

The present report is a theoretical study of non-alternant structures like **3**, **5***a* with a view to the exploration of (*i*) the likelihood that such structures will be strongly polarized, (*ii*) the possibility that these structures may be accessible in the laboratory, and (*iii*) the synthetic potential structural analogues might have for the construction of carbocycles and heterocycles.

Method

Simple Hückel calculations, assuming the orthogonality of adjacent p orbitals, were carried out in the usual way (4).

Full molecular orbital computations were done using the

[1]Author to whom correspondence should be addressed. Present address: Department of Chemistry, Mount Allison University, Sackville, N.B., Canada E0A 3C0.

[2]The present report is limited to a consideration of structures which have two non-bonding electrons in their Lewis structures.

[3]Zeroth order Hückel theory and graph spectral theory are fully equivalent (2).

[4]Generalizations apply only to substituted monocycles.

[5]All Sachs' graphs s_{j-1} for such structures must contain the ring as a component.

Printed in Canada / Imprimé au Canada

Can. J. Chem. Downloaded from www.nrcresearchpress.com by 88.85.125.76 on 09/07/12
For personal use only.

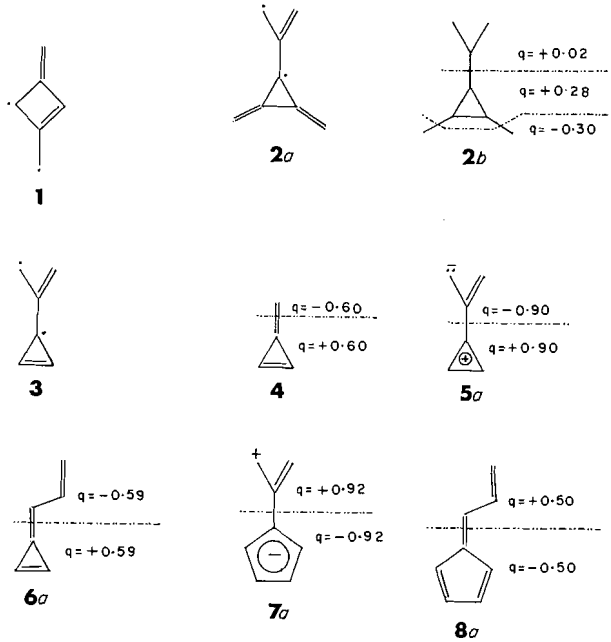

Fig. 1. Structures and partial group charges (q) derived from Hückel π-electron population numbers.

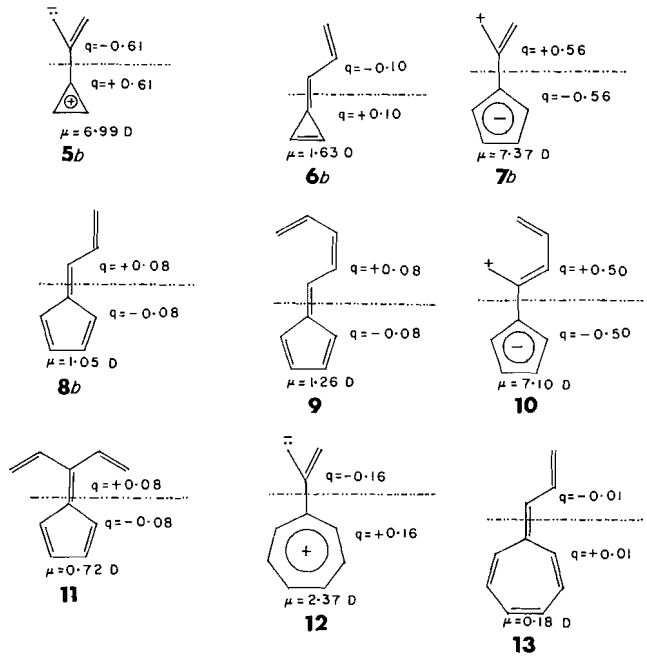

Fig. 2. Structures, MNDO calculated dipole moments (μ) and partial group charges (q) obtained from MNDO π-electron population numbers.

MNDO (Modified Neglect of Differential Overlap) semiempirical method (6).

The isopropyl substituted systems were constrained to have C_{2v} symmetry but were otherwise fully optimized. All other structures were fully optimized.

Results

Figure 1 presents the results of simple Hückel calculations on an assortment of non-alternant hydrocarbons. They ascribe very strongly polarized π systems to the representative "π-ylides" **5***a* and **7***a*. Their close structural relatives **4**, **6***a*, and **8***a* have more weakly polarized π systems at the Hückel level.

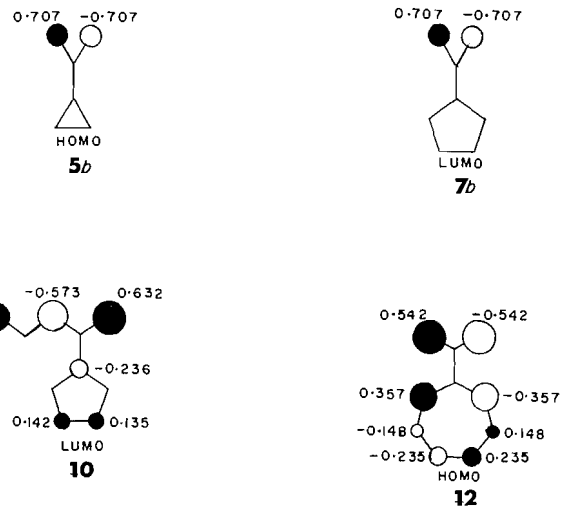

Fig. 3. MNDO frontier orbitals for "π-ylides."

Figure 2 presents the results of our MNDO computations on an assortment of "π-ylides" and some close structural relatives. The MNDO results suggest systematically weaker polarization for non-alternant hydrocarbons than do the Hückel results. However, the MNDO computations suggest a much more dramatic difference in the degree of polarization in the π systems of the "π-ylides" **5***b*, **7***b*, **10**, and **12** and their close structural relatives **6***b*, **8***b*, **9**, **11**, and **13**.

Furthermore, the calculated dipole moments are as much as an order of magnitude larger for the "π-ylides" than for their structural isomers. We note that the calculated dipole moments for **5***b*, **7***b*, and **10** (*ca.* 7 D) are comparable to the experimental gas phase dipole moment of LiBr (7. 27 D) (7).

Discussion

Our calculations, both simple Hückel and MNDO, fully support the strongly polarized π systems we first proposed for structures like **5***a* when we deduced that each had a single NBMO at the Hückel level. In each case, the side chain would be expected to have high reactivity while the aromatic ring would be expected to be relatively unreactive. In accord with these expectations, the appropriate MNDO frontier molecular orbital, i.e. that which corresponds to the Hückel NBMO, indicates significantly higher reactivity (8) in the side chain as shown in Fig. 3.

The chemistry expected for "π-ylides" with electron-rich side-chains may have much in common with that of conventional ylides. Those with electron-deficient side chains offer the novel possibility of *umpolung* ylide reactivity.

Cycloaddition reactions between appropriately selected "π-ylides" should be unusually facile since they may proceed through symmetry-allowed transition states which would enjoy very favorable coulombic interactions, e.g. reaction [3]. Reactions [3]–[5] illustrate potential applications of "π-ylides" to the construction of some carbocycles.

Attempts to develop "π-ylide" reagents for synthetic purposes must presuppose that such structures may be sufficiently stable to permit their preparation. The very substantial charge development in the rings of the "π-ylide" structures **5***a* and **7***a* compares favorably with the total charge in their annulene counterparts, the cyclopropenyl cation and the cyclopentadienyl anion. To obtain further support for the highly developed aromatic character of the "π-ylides," we have calculated the

Can. J. Chem. Downloaded from www.nrcresearchpress.com by 88.85.125.76 on 09/07/12
For personal use only.

TABLE 1. Topological resonance energies of substituted annulenes

Compound	Topological resonance energy[a] (per electron)	Status[b]
1	−0.041	AA
2	0.002	NA
$C_3H_3^+$][c]	0.268	A
4	0.017	A
5	0.078	A
6	0.016	A
$C_5H_5^-$][c]	0.053	A
7	0.036	A
8	0.005	NA
9	0.005	NA
10	0.028	A
11	0.005	NA
$C_7H_7^+$][c]	0.038	A
12	0.021	A
13	0.001	NA

[a]The unit for topological resonance energy is the Hückel β.
[b]A = aromatic, NA = nonaromatic, AA = antiaromatic.
[c]Selected annulenes are included for comparative purposes.

topological resonance energies[6] for the substitited annulenes shown in Figs. 1 and 2 (see Table 1). The topological resonance energies clearly indicate pronounced aromatic character for the "π-ylides" **5**, **7**, **10**, and **12**. Consequently, there is some reason to hope that such structures may be successfully prepared.

[3] 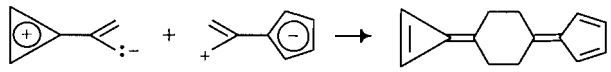

5 **7**

[4] 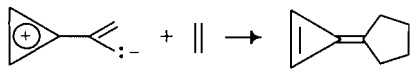

5

[5] 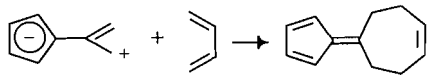

7

The development of synthetic methodology using such reagents would be severely limited in scope if products had to contain pendant carbocyclic rings. It would be advantageous should such reagents be constructed with heterocyclic rings instead of carbocyclic rings. This would open up the possibility that the heterocyclic ring might be transformed into useful functionality after formation of the desired carbocycle. The design of such heterocycles would be facilitated by application of the rule of *topological charge stabilization* (9). Simply stated, one should introduce ring heteroatoms which best support the excess charge indicated by *Hückel calculations on the hydrocarbon system*.

The result might well be a reagent with satisfactory initial stability and a product amenable to removal of the polarizing ring. As an example, **7** might be replaced (in reaction [3]) by a nitrogen heterocycle which would be more amenable to hydrolysis. One could easily envision a sequence of the sort shown in reaction [6].

[6] 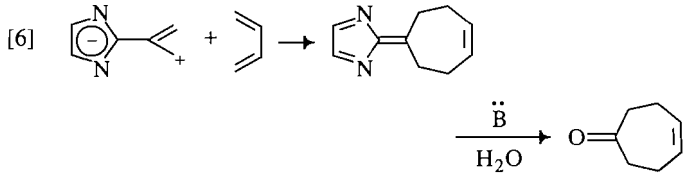

We note that the foregoing discussion could be applied to the side chain of the "π-ylide." In the event that heteroatoms were incorporated into the side chain, the newly constructed ring in the product would be heterocyclic. Synthetic strategies based on π-ylides might well facilitate access to new heterocyclic systems.

Summary

A highly polar group of non-alternant hydrocarbons have been recognized viz: "π-ylides."

Both simple Hückel calculations and MNDO computations suggest a very high degree of charge separation in "π-ylide" structures.

Topological resonance energies indicate a pronounced aromatic character for "π-ylides," suggesting that these novel structures may be accessible in the laboratory.

"π-ylides" offer tantalizing potential for new synthetic methodology vis-à-vis the preparations of carbocycles and heterocycles.

Acknowledgment

Financial support from the Florida Institute of Technology is gratefully acknowledged.

1. K. A. DURKIN and R. F. LANGLER. J. Phys. Chem. **91**, 2422 (1987).
2. N. TRINAJSTIC. Chemical graph theory. Vol. 1. CRC Press, Boca Raton. pp. 64–67.
3. J. R. DIAS. J. Chem. Educ. **64**, 213 (1987).
4. (*a*) K. HIGASI, H. BABA, and A. REMBAUM, Quantum organic chemistry. Interscience, New York. 1965. pp. 112–135; (*b*) K. YATES. Hückel molecular orbital theory. Academic Press, New York. 1978. pp. 78–85.
5. (*a*) W. C. HERNDON and M. L. ELLZEY, JR. Tetrahedron Lett. 1399 (1974); (*b*) J. V. KNOP, D. PLAVSIC, M. RANDIC, and N. TRINAJSTIC. Croat. Chem. Acta, **56**, 411 (1983).
6. (*a*) M. J. S. DEWAR and W. THIEL. J. Am. Chem. Soc. **99**, 4899 (1977); (*b*) M. J. S. DEWAR and W. THIEL. J. Am. Chem. Soc. **99**, 4907 (1977); (*c*) M. J. S. DEWAR, M. L. MCKEE and H. S. REPZA. J. Am. Chem. Soc. **100**, 3607 (1978).
7. R. C. WEAST (*Editor*) Handbook of chemistry and physics. 50th ed. CRC Press, Cleveland, OH. 1969. p. E-69.
8. I. FLEMING. Frontier orbitals and organic chemical reactions. Wiley, New York. 1976. pp. 121–142.
9. B. M. GIMARC. J. Am. Chem. Soc. **105**, 1979 (1983).

[6]Topological resonance energies were selected for this purpose because of the enhanced precision they offer in assessing aromaticity in complex molecules. See ref. 2, Vol. 2, pp. 1–4.

Can. J. Chem. Downloaded from www.nrcresearchpress.com by 88.85.125.76 on 09/07/12
For personal use only.

Syntheses of model oligosaccharides of biological significance. X. Syntheses and NMR and mass spectral analysis of trideuteriomethyl di-3,6-*O*-(4-*O*-β-D-galactopyranosyl-2-acetamido-2-deoxy-β-D-glucopyranosyl)-β-D-galactopyranoside: the I antigen branchpoint penta- and tetrasaccharides and a related trisaccharide[1]

DENNIS M. WHITFIELD[2]

Department of Medical Genetics, University of Toronto, Toronto, Ont., Canada M5S 1A8

AND

HENRIANNA PANG, JEREMY P. CARVER, AND JIRI J. KREPINSKY[3]

Departments of Medical Genetics and Medical Biophysics, University of Toronto, and Carbohydrate Research Center, Faculty of Medicine, University of Toronto, Toronto, Ont., Canada M5S 1A8

Received September 12, 1989

DENNIS M. WHITFIELD, HENRIANNA PANG, JEREMY P. CARVER, and JIRI J. KREPINSKY. Can. J. Chem. **68**, 942 (1990).

As part of our studies of complex oligosaccharides, in particular their three-dimensional structure, we have synthesized the antigen I branchpoint penta- and tetrasaccharides. The unbranched trisaccharide **3***D* was also synthesized, and its derivative **3***B* served as the intermediate for the synthesis of higher oligosaccharides. NMR spectra of major intermediates as well as of the final oligosaccharides were completely assigned. Mass spectra of the synthetic intermediates and the final oligosaccharides were analyzed and compared with those of a similar group of oligosaccharides containing L-fucose, *N*-acetyl-D-glucosamine, and D-galactose. Certain observations were made that could be utilized in the interpretation of mass spectra for the structural determination of protected oligosaccharides during the synthesis.

Key words: oligosaccharide synthesis, I antigen, carbohydrate mass spectrometry, carbohydrate NMR spectrometry, Gal-GlcNAc oligomers.

DENNIS M. WHITFIELD, HENRIANNA PANG, JEREMY P. CARVER et JIRI J. KREPINSKY. Can. J. Chem. **68**, 942 (1990).

Dans le cadre de nos travaux sur les oligosaccharides complexes, en particulier en ce qui a trait à leur structure tridimensionnelle, on a synthétisé les penta- et tétra-saccharides des ramifications de l'antigène I. On a aussi synthétisé le trisaccharide linéaire **3***D* et on utilisé son dérivé **3***B* comme intermédiaire dans la synthèse d'oligosaccharides plus importants. On a attribué toutes les bandes des spectres RMN des intermédiaires principaux ainsi que des oligosaccharides finaux. On a analysé les spectres de masse des intermédiaires de synthèse ainsi que des oligosaccharides finaux et on les a comparés avec ceux d'un groupe similaire d'oligosaccharides contenant du L-fucose, de la *N*-acétyl-D-glucosamine et du D-galactose. On a fait certaines observations qui pourraient être utilisées durant les synthèses pour interpréter les spectres de masse et pour déterminer les structures d'oligosaccharides.

Mots clés : synthèse d'oligosaccharides, l'antigène I, spectrométrie de masse des hydrates de carbone, spectrométrie RMN des hydrates de carbone, oligomères Gal-GlcNAc.

[Traduit par la revue]

Introduction

Biological functions of the oligosaccharide moieties of glycoproteins depend on their three-dimensional structures, and of particular interest are the branching points, since these are areas of potential interactions between different chains (1). The more highly branched oligosaccharides have been consistently reported in both O-linked and N-linked oligosaccharides from glycoproteins obtained from tumour tissues and transformed or cancer cell lines (2). One such branching, resulting from the glycosylation of O-6 of the galactose residue of an "i" disaccharide fragment by another GlcNAc residue is responsible for the oncofetal differentiation from "i" to "I" structures (3). We have investigated by NMR spectroscopy and potential energy calculations the conformations of "minimal" structure of the "I" antigen class of compounds, GlcNAc(β1-3)[GlcNAc(β1-6)]-Galβ-, and in order to assess the influence of elongation of the oligosaccharide chains on the spatial arrangements of the chains, we have now synthesized tetra- and pentaoligosaccharides (the results of our conformational studies will be reported later).[4]

Synthesis

For our conformational analysis we required an NMR "silent" glycoside in order to avoid the overlap of OCH_n of an aglycon with ring hydrogens on the chemical shift scale and the ambiguity of anomerization (in the case of a free reducing sugar), and to reduce the number of relaxation pathways. Consequently, all our compounds are trideuteriomethyl glycosides.

Several groups have investigated methods for the formation of oligosaccharides at this branchpoint. Previously, Veyrières and co-workers prepared reducing oligosaccharides similar to **3***D* and **6***C* (5). They used an acid catalyzed oxazoline approach to prepare the GlcNAc(β1-3)Gal linkage in approximately 50% yield, and a similar yield is reported using silver promoted glycosylation with halides (6). These yields are comparable to those reported by Abbas and Matta (7) and Tejima and co-workers (8) for this linkage. Reports from both the Veyrières (6) and Ogawa (9) laboratories indicate yields in the 70–80% range using Lewis acid catalyzed glycosylation with fluorides or trichloroacetimidates. Enzymic synthesis also has been applied

[1]For part 9, see ref. 16.

[2]Present address: Department of Biochemistry, Hospital for Sick Children Research Institute, 500 University Avenue, Toronto, Ont., Canada M5G 1X8.

[3]Author to whom correspondence may be addressed.

[4]D. M. Whitfield, J. G. Shelling, J. J. Krepinsky, and J. P. Carver. Manuscript in preparation.

Can. J. Chem. Downloaded from www.nrcresearchpress.com by 88.85.125.76 on 09/07/12
For personal use only.

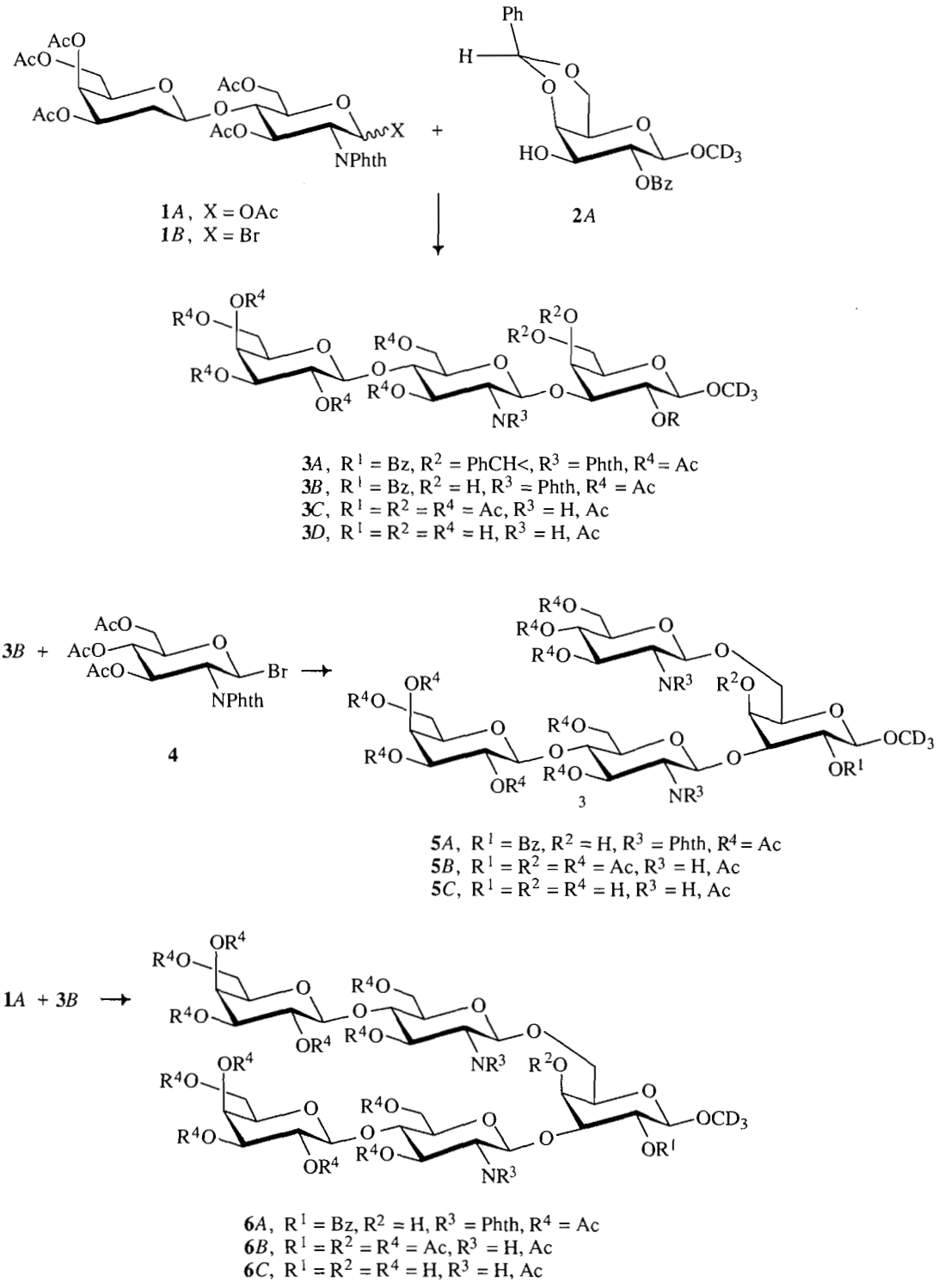

SCHEME 1

to syntheses of oligosaccharides in this area (10). The approach described in this communication utilizes the non-nucleophilic base 2,6-di-*tert*-butyl-4-methylpyridine (DTBMP) to provide easily reproducible 72% yields. This base (DTBMP) was crucial to success of the silver triflate coupling, as the more often used bases such as sym-collidine (11) produced intractable mixtures from which only traces of the desired product **3***A* could be isolated after extensive purification by HPLC (16).

The lactosamine unit protected as **1***A* was transformed into the bromide **1***B* (11) with which the galactosyl derivative **2***A* (8, 12) was glycosylated to give the protected trisaccharide **3***A* (previously the chloride (13) had also been used as a glycosylating agent). Both bromides **1***B* and **4** have been used for syntheses of larger oligosaccharides; e.g., refs. 9 and 11. The compound **3***A* was first subjected to hydrogenolysis to remove the benzylidine protection at the galactose, yielding **3***B* (it

Can. J. Chem. Downloaded from www.nrcresearchpress.com by 88.85.125.76 on 09/07/12
For personal use only.

TABLE 1. ^{1}H NMR spectra of synthetic intermediates: trisaccharides

Sugar	H1 (J_{12})	H2 (J_{23})	H3 (J_{34})	H4 (J_{45})	H5 (J_{56})	H6 ($J_{66'}$)	H6′ ($J_{56'}$)
				3A			
Gal-β OCD_3	4.431 d (8.0)	5.403 dd (10.1)	3.888 dd (3.5)	4.447 brd (<0.5)	3.443 brs (<0.5)	4.006 brd (6.8)	3.807 brdd —
GlcNPhth	5.591 d (8.4)	4.239 dd (10.4)	5.605 dd (8.8)	3.873 dd (9.9)	3.743 brdt (2.1)	4.855 dd (−12.0)	4.019 dd (3.6)
Gal-β-1,4-	4.559 d (7.9)	5.112 dd (10.5)	4.957 dd (3.4)	5.303 brd (<0.5)	3.840 brs (1.4)	4.340 dd (−12.2)	4.131 dd (1.0)
Acetates	2.117, 2.058, 2.048, 1.999, 1.961, 1.801 6× s(3)						
Aromatics	7.607 Bz_o dd(2), 7.454 Bz_p brt (1), 7.233 Bz_m brt(2) (8.0, 1.4) (7.4)						
	7.548 $Phth_o$ dd(2), 7.3–7.4 m Benz + $Phth_m$ m(7) (7.6, 1.9)						
Benzylidene	$PhCHO_2$ 5.588 s(1)						
				3B			
Gal-β OCD_3	4.381 d (8.0)	5.317 dd (9.8)	3.790 dd (3.3)	4.270 brd (<0.5)	3.628 brt (6.1)	3.95[1] m —	3.8[2] m —
GlcNPhth	5.608 d (8.5)	4.293 dd (10.6)	5.568 dd (8.7)	3.95[1] m —	3.8[2] m (1.8)	4.749 dd (−11.8)	4.08[3] m —
Gal-β-1,4-	4.650 d (7.8)	5.112 dd (10.3)	5.019 dd (3.4)	5.302 dd (0.5)	3.95[1] —	3.95[1] —	4.08[3] m —
Acetates	2.195, 2.118, 2.071, 2.008, 1.960, 1.813 6× s(3)						
Aromatics	7.570 Bz_o dd(2), 7.383 Bz_p brt(1), 7.139 Bz_m brt(2) (7.1, 1.2) (7.4) 7.43–7.36 Phth brm(4)						
Hydroxyls	3.269 OH_4 brs(1), 2.945 OH_6 dd(1) — (7.8, 5.6)						
				3C			
Gal-β OCD_3	4.295 d (8.0)	5.092 dd (9.9)	3.8[4] m —	5.35 brd[5] —	3.875 brt (7.2)	4.12[6] m —	4.12[6] m —
GlcNAc	4.782 d (7.6)	3.43[7] m (10.1)	5.227 dd (8.8)	3.8[4] m —	3.43[7] m (2.6)	4.725 dd (−12.0)	3.990 dd (3.6)
Gal-β-1,4-	4.533 d (7.9)	5.111 dd (10.4)	4.975 dd (3.4)	5.35 brd[5]	3.8[4] m	4.12[6] m	4.12[6] m
Acetates	2.155, 2.148, 2.121, 2.096, 2.087, 2.066, 2.062, 2.046, 1.970, 1.905 10× s(3)						
N-H	5.418 brd (8.6)						

should be noted that an attempted removal with acetic acid led to splitting off of the complete galactose unit). Hydrazinolysis with hydrazine hydrate in ethanol effected the removal of the phthalimido protection in good yield and after acetylation gave **3***C*. Peracetylated oligosaccharides are usually more suitable for purification by chromatography than completely deprotected compounds; consequently **3***C* was subjected to chromatography and the acetyls were then removed by KCN-catalyzed methanolysis to give **3***D*. Potassium cyanide was superior to sodium methoxide (Zemplen reagent) in this situation since the latter afforded partially decomposed products only.

Protected tetrasaccharide **5***A* and pentasaccharide **6***A* were prepared by taking advantage of the differential reactivity in **3***B* of the primary (O*H*; δ = 2.945 ppm, dd, J = 7.8 and 5.6 Hz) and the secondary (O*H*; δ = 3.269 ppm, broad singlet) hydroxyls (cf. Table 1). After glycosylation only the secondary hydroxyls at δ = 2.863 ppm in **5***A* (cf. Table 2) and at δ = 2.866 ppm in **6***A* (cf. Table 3) were present in the spectra of the respective compounds.

Thus, glycosylation of **3***B* with the bromide **4**, using silver zeolite promoter (13), gave tetrasaccharide **5***A*, which was subjected to hydrazinolysis to remove both phthalimido protecting groups and the benzoyl group. Acetyls were lost during the hydrazinolysis as well. Complete reacetylation yielded **5***B*, from which *O*-acetyl groups were removed smoothly during KCN-catalyzed methanolysis to give the desired oligosaccharide **5***C*.

Protected pentasaccharide **6***A* was again prepared from the intermediate **3***B* using the bromide **1***B*. As in the case of the protected tetrasaccharide **5***A*, the hydroxyl on C-6 was substantially more reactive than the hydroxy group on C-4 and the pentasaccharide derivative **6***A* was obtained exclusively. Depro-

Can. J. Chem. Downloaded from www.nrcresearchpress.com by 88.85.125.76 on 09/07/12
For personal use only.

TABLE 2. ^{1}H NMR spectra of synthetic intermediates: tetrasaccharides

Sugar	H1 (J_{12})	H2 (J_{23})	H3 (J_{34})	H4 (J_{45})	H5 (J_{56})	H6 ($J_{66'}$)	H6′ ($J_{56'}$)
				5A			
Gal-β OCD_3	4.263 d (8.1)	5.223 dd (9.8)	3.92 m[1] —	4.02 m[2] —	3.6 m[3] —	4.2 m[4] —	3.85 m[5] —
GlcNAc-1,3	5.141 d (8.1)	4.100 dd (10.7)	5.386 dd (8.8)	3.6 m[3] —	3.9 m[1] (2.2)	4.193 dd (−12.3)	3.85 m[5] —
Gal-β-1,4	4.456 d (7.9)	5.126 dd (10.4)	4.964 dd (3.4)	5.327 dd (0.8)	3.6 m[3] —	3.85 m[5] —	3.85 m[5] —
GlcNAc-1,6	5.539 d (8.5)	4.348 dd (9.7)	5.730 dd (9.1)	5.206 dd (9.7)	3.006 ddd (1.8)	4.351 m[2] (−12.3)	4.0 m[2] (6.9)
Acetates	2.150, 2.145, 2.131, 2.114, 2.044, 2.016, 1.974, 1.870, 1.782, 9 × s(3)						
Aromatics	Phth 7.78 brm (4), Phth 7.42 brm (4) Bz_o 7.534 dd(2), Bz_p 7.313 brt(1), Bz_m 7.065 brt(2) (7.5, 1.3) (7.5)						
Hydroxyl	Gal_4 2.863 brd						
				5B			
Gal-β OCD_3	4.263 d (8.1)	5.081 dd (9.9)	3.7 m[6] (3.5)	5.328 brd —	3.7 m[6] —	4.1 m[7] —	3.8 m —
GlcNAc-1,3	4.735 d (7.8)	3.52 m[8] (10.3)	5.219 dd (8.9)	3.75 m[6] —	3.55 m[8] (2.2)	4.791 dd (−12.0)	3.971 dd (3.1)
N-H	5.540 (9.4)						
Gal-β-1,4	4.350 d (7.9)	5.109 dd (10.4)	4.980 dd (3.4)	5.348 brd —	3.75 m[6] —	4.1 m[7] —	4.1 m[7] —
GlcNAc-1,6	4.882 d (8.2)	3.48 m[8] (9.5)	5.537 dd (9.5)	5.025 dd (8.2)	3.55 m[8] (2.0)	4.261 dd (−12.0)	4.1 m[7] —
N-H	6.375 (8.6)						
Acetates	2.186, 2.147, 2.096, 2.091, 2.081, 2.044, 1.970, 1.936, 1.901, 9 × s(3) 2.066, 2.023 2 × s(6)						

tection of **6*A*** by hydrazinolysis and KCN-catalyzed methanolysis subsequently gave **6*B*** and **6*C***.

NMR spectrometry

The ^{1}H NMR data of the synthetic intermediates are listed in the tables: the trisaccharide, Table 1, tetrasaccharide, Table 2, and pentasaccharide, Table 3. In most cases it was possible to assign also ^{1}H resonances by conventional decoupling and (or) ^{1}H–^{1}H COSY techniques. All coupling constants and chemical shifts are based on peak separations. Overlapping resonances are marked with the same superscript numbers. All spectra are consistent with the proposed structures. The ^{13}C and ^{1}H resonances of the unprotected oligosaccharides were assigned through heteronuclear ^{1}H–^{13}C COSY (cf. Tables 4 and 5).

The only ambiguity is in the assignment of the terminal galactose residues of the pentasaccharide derivatives. The appropriate connectivities were readily established within the respective arms, but which arm (6 or 3) remained ambiguous. The proposed assignments are based on a comparison with tetrasaccharides **5*A*–5*C*** where the terminal galactose is definitively on the 3 arm.

Several of these compounds contain a single benzoate group. Since its aromatic (*o, m, p*) resonances are very distinct, they provided a reliable marker allowing the assessment of the purity of individual preparations. All ^{1}H and ^{13}C phthalimido resonances were broad, and in the cases where these resonances overlapped with other aromatic resonances, their presence could only be ascertained by integration values. Fortunately, characteristic fragments for the phthalimido group were found in the mass spectra of the same samples (cf. below).

One surprising observation was made in connection with the upfield shift of the GlcNAcβ1,6 H-5 proton in compounds **5*A*** (3.006) and **6*A*** (2.823). The origin of this effect is not immediately apparent but it is suggestive of a juxtaposition of this hydrogen and an aromatic ring (such as the phthalimide).

Mass spectrometry

Fast atom bombardment mass spectrometry (FAB/MS) in positive ion mode was utilized to confirm the structures of the target substances and synthetic intermediates. In addition, a number of compounds previously synthesized in this laboratory (12, 16) (cf. formulae listed in Table 6) were also investigated by FAB/MS. We have often noted that, particularly in the case of more complicated protected oligosaccharides, it is difficult to interpret unequivocally their unidimensional NMR spectra because of the complexity and overlapping of their signals. In some such cases mass spectrometry can give a quick and definitive proof of the presence of certain structural elements

Can. J. Chem. Downloaded from www.nrcresearchpress.com by 88.85.125.76 on 09/07/12
For personal use only.

Can. J. Chem. Downloaded from www.nrcresearchpress.com by 88.85.125.76 on 09/07/12
For personal use only.

TABLE 3. ^{1}H NMR spectra of synthetic intermediates: pentasaccharides

Sugar	H1 (J_{12})	H2 (J_{23})	H3 (J_{34})	H4 (J_{45})	H5 (J_{56})	H6 ($J_{66'}$)	H6' ($J_{56'}$)
				6A			
Gal-β OCD_3	4.289 d (8.0)	5.230 dd (9.7)	3.604 dd (3.2)	3.85 m[1] —	3.85 m[1] —	4.05 m[2] —	3.85 m[1] —
GlcNAc-1,3	5.531 d (8.5)	4.195 dd (10.5)	5.681 dd (8.3)	3.903 dd (9.8)	3.85 m[1] (1.2)	4.307 dd (−11.8)	3.950 (7.3)
Gal-β-1,4	4.442 d (7.9)	5.128 dd (10.4)	4.966 m[3] (3.4)	5.325 m[4] (0.8)	3.6 m[5] —	4.05 m[2] —	4.05 m[1] —
GlcNAc-1,6	5.077 d (8.5)	4.066 dd (10.6)	5.350 dd (8.8)	3.85 m[1] (9.8)	2.823 ddd (1.4)	4.534 dd (−12.0)	4.185 dd (5.0)
Gal-β-1,4	4.551 d (8.1)	5.134 dd (10.4)	4.966 m[3] (3.4)	5.348 m[4] (0.8)	3.6 m[5] —	4.05 m[2] —	4.05 m[2] —
Acetates	2.179, 2.152, 2.139, 2.133, 2.091, 2.079, 2.045, 2.011, 1.975, 1.971, 1.914, 1.777 12 × s(3)						
Aromatics	Phth 8.147 brd (1), 7.909 m(1), 7.776 m(2), Phth 7.48 m(2), 7.38 m(2) Bz_o 7.541 dd(2), Bz_p 7.317 tt (1), Bz_m 7.059 brt(2)						
Hydroxyl	Gal_4 2.866 dd (2.6, 1.1)						
				6B			
Gal-β OCD_3	4.264 d (8.0)	5.057 dd (9.8)	3.775 dd (3.3)	5.308 brd (<0.5)	3.53 m[6] —	4.00 m[7] —	3.64 m[8] —
GlcNAc-1,3	4.683 d (7.7)	3.85 m[9] (10.1)	5.165 dd (8.3)	3.75 m[10] —	3.55 m[6] (1.9)	4.660 dd (−12.2)	3.998 dd (4.3)
N-H	6.161 (9.0)						
Gal-β-1,4	4.522 d (7.6)	5.109 dd (10.4)	4.979 dd (3.3)	5.356 brd (<0.5)	3.88 m[9] —	4.1 m[7] —	4.1 m[7] —
GlcNAc-1,6	4.681 d (7.6)	3.65 m[8] (10.1)	5.165 dd (8.3)	3.75 m[10] —	3.62 m[8] (1.2)	4.508 dd (−12.0)	4.08 m[7]
N-H	5.711 (8.7)						
Gal-β-1,4	4.516 d (7.6)	5.097 dd (10.4)	4.962 dd (3.4)	5.347 brd (<0.5)	3.88 m[9] —	4.1 m[7] —	4.1 m[7] —
Acetates	2.154, 2.152, 2.145, 2.122, 2.072, 2.063, 2.047, 1.972, 1.970, 1.932, 1.903 11 × s(3), 2.097 s(6), 2.057 s(9)						

TABLE 4. ^{13}C NMR spectra of free unprotected oligosaccharides

Sugar	C1	C2	C3	C4	C5	C6	C=O	CH_3
Gal(β1-4)GlcNAc(β1-3)Gal(β-OCD_3) ***3D***								
Gal-OCD_3	104.64	70.53	83.11	68.52	75.51	61.74		
GlcNAc	103.49	56.08	73.04	78.95	75.41	60.67	175.76	23.02
Gal-1,4	103.67	71.79	73.32	67.51	76.60	61.86		
Gal(β1-4)GlcNAc(β1-3)[GlcNAc(β1-6)]Gal(β-OCD_3) ***5C***								
Gal-OCD_3	104.48	71.79	82.95	69.34	74.22	70.14		
GlcNAc-1,3	103.45	56.08	73.03	78.92	75.40	60.68	175.77	23.01
Gal-1,4	103.68	70.45	73.32	69.34	76.17	61.85		
GlcNAc-1,6	102.31	56.30	74.56	70.72	76.64	61.52	175.28	23.01
Gal(β1-4)GlcNAc(β1-3)[Gal(β1-4)GlcNAc(β1-6)]Gal(β-OCD_3) ***6C***								
Gal-OCD_3	104.71	70.68	83.17	69.58	74.46	70.36		
GlcNAc-1,3	103.67	56.30	73.26	79.13	75.62	60.89	175.99	23.25
Gal-1,4(3)	103.90	72.01	73.32	69.59	76.41	62.08		
GlcNAc-1,6	102.46	56.06	73.40	79.44	75.76	61.05	175.46	23.25
Gal-1,4(6)	103.93	72.01	73.32	65.59	76.41	62.08		

TABLE 5. ^{1}H NMR spectra of synthetic unprotected oligosaccharides

Sugar	H1 (J_{12})	H2 (J_{23})	H3 (J_{34})	H4 (J_{45})	H5 (J_{56r})	H6r (J_{6r6s})	H6s' (J_{56s})
			Gal(β1-4)GlcNAc(β1-3)Gal(β-OCD_3) **3***D*				
Gal-OCD_3	4.299 d (8.0)	3.544 dd (9.9)	3.709 dd (3.2)	4.142 brd (<0.5)	3.684 m[7] —	3.772 m[8] —	3.754 m[8] —
GlcNAc	4.715 d (8.0)	3.789 dd (9.8)	3.731 m[8] —	3.736 m[8] —	3.578 m (2.2)	3.956 dd (−12.3)	3.844 dd (4.6)
$NHCOCH_3$	2.028						
Gal-1,4	4.475 d (7.8)	3.537 dd (10.0)	3.688 dd (3.3)	3.924 brd (<0.5)	3.719 m (3.6)	3.795 dd (−12.2)	3.75[8] m —
			Gal(β1-4)GlcNAc(β1-3)[GlcNAc(β1-6)]Gal(β-OCD_3) **5***C*				
Gal-OCD_3	4.273 d (8.0)	3.530 dd (9.9)	3.668 dd (3.4)	4.115 brd (<0.5)	3.765 m (7.0)	3.768 m (−12.0)	4.033 m (5.0)
GlcNAc-1,3	4.704 d (8.0)	3.790 dd (10.2)	3.715 m —	3.737 m —	3.582 ddd (2.2)	3.954 dd (−12.3)	3.845 dd (4.4)
$NHCOCH_3$	2.028						
GlcNAc-1,6	4.535 d (8.5)	3.710 dd (10.4)	3.541 dd (8.8)	3.443 dd —	3.450 m (1.40)	3.934 dd (−12.4)	3.735 m —
$NHCOCH_3$	2.024						
Gal-1,4	4.475 d (7.8)	3.536 dd (10.1)	3.694 dd (3.3)	3.923 brd (<0.5)	3.715 m (3.6)	3.744 m (−12.2)	3.744 m —
			Gal(β1-4)GlcNAc(β1-3)[Gal(β1-4)GlcNAc(β1-6)]Gal(β-OCD_3) **6***C*				
Gal-OCD_3	4.275 d (8.0)	3.536 dd (9.9)	3.676 dd (3.4)	4.115 brd (<0.5)	3.755 m (7.0)	3.750 (−12.0)	4.033 m (5.0)
GlcNAc-1,3	4.706 d (8.0)	3.771 dd (10.2)	3.708 —	3.715 —	3.597 ddd (2.2)	3.961 dd (−12.3)	3.835 dd (4.4)
Gal-1,4	4.472 d (7.8)	3.517 dd (10.1)	3.644 dd (3.3)	3.924 brd (<0.5)	3.708 m (3.6)	3.75 m (−12.2)	3.75 m —
GlcNAc-1,6	4.559 d (8.5)	3.755 dd (10.4)	3.700 m —	3.708 m —	3.515 m (1.40)	3.996 dd (−12.4)	3.827 m —
Gal-1,4	4.476 d (7.8)	3.517 dd (10.1)	3.644 dd (3.3)	3.924 brd (<0.5)	3.708 m (3.6)	3.75 m (−12.2)	3.75 m —
Acetate	2.026 s(6)						

in the molecule, in addition to the molecular mass of the compounds.

The mass spectra of the compounds investigated can be exemplified by that of compounds **6***A*, **6***C*, **8***A*, and **8***B* (shown in Figs. 1 and 2). Other mass spectrometric data are listed in Table 7. Relatively weak $[M+H]^+$ ions and $[M+Na]^+$ and $[M+NH_4]^+$ ions are observed in all the spectra. In compounds containing several benzyl and sometimes benzylidine protecting groups, $[M-H]^+$ ions become more dominant than $[M+H]^+$ ions; cf. for example, the more abundant m/z 804 $[M-H]^+$ ion than m/z 806 $[M+H]^+$ ion in Fig. 2a. Completely deprotected oligosaccharides usually display the $[M+H]^+$ ion with fair intensity: often it is one of the most abundant ions in the spectrum (with the exception of ions at very low m/z).

Fragmentation in the FAB mass spectra of peracetylated and permethylated oligosaccharides (4, 14, 17) occurs at the glycosidic bonds between the anomeric carbon and the charge-carrying oxygen (fragmentation pathway (a)). This fragmentation pathway gives rise to a series of fragment ions, for example, m/z 331, 706, and 1677 of compound **6***A* (Fig. 1a). The cleavage of the aglycon (loss of OCD_3 or OC_3D_7), however, is difficult in deprotected larger oligosaccharides and they consequently display very few $[M-OCD_3]^+$ or $[M-OC_3D_7]^+$ ions.

Gal- |-O-GN- |-O-Gal-| -O-Agl

(a)

In unprotected oligosaccharides (**14**, **3***D*, **5***C*, **6***C*), *N*-acetyllactosamine consistently gives rise to an abundant ion (m/z 366, fragmentation pathway (a), Fig. 1b). Terminal 2-acetamido-2-deoxyhexose (such as *N*-acetylglucosamine) gives rise to an ion at m/z 204 (**13***C*).

After the initial loss of the aglycon moiety through fragmentation pathway (a), further cleavage between the anomeric carbon and the oxygen, accompanied by hydrogen transfer to the oxygen and charge retention at the "reducing" end of the oligosaccharides, gives rise to m/z 972 in compound **6***A* (Fig. 1a), m/z 351 in compound **8***B* (Fig. 2b), and m/z 355 in compound **8***A* (Fig. 2a; cf. formula **15**, Table 6). The ion **15** (m/z 355, Table 6) indicates the presence of 2-*O*-benzoyl-4,6-*O*-benzylidene hexose in the molecule (e.g., monosaccharides **2***A* or **2***C*, or oligosaccharides **3***A*, **8***A*, **10**α, **10**β**A**). Transfer of

Can. J. Chem. Downloaded from www.nrcresearchpress.com by 88.85.125.76 on 09/07/12
For personal use only.

Can. J. Chem. Downloaded from www.nrcresearchpress.com by 88.85.125.76 on 09/07/12
For personal use only.

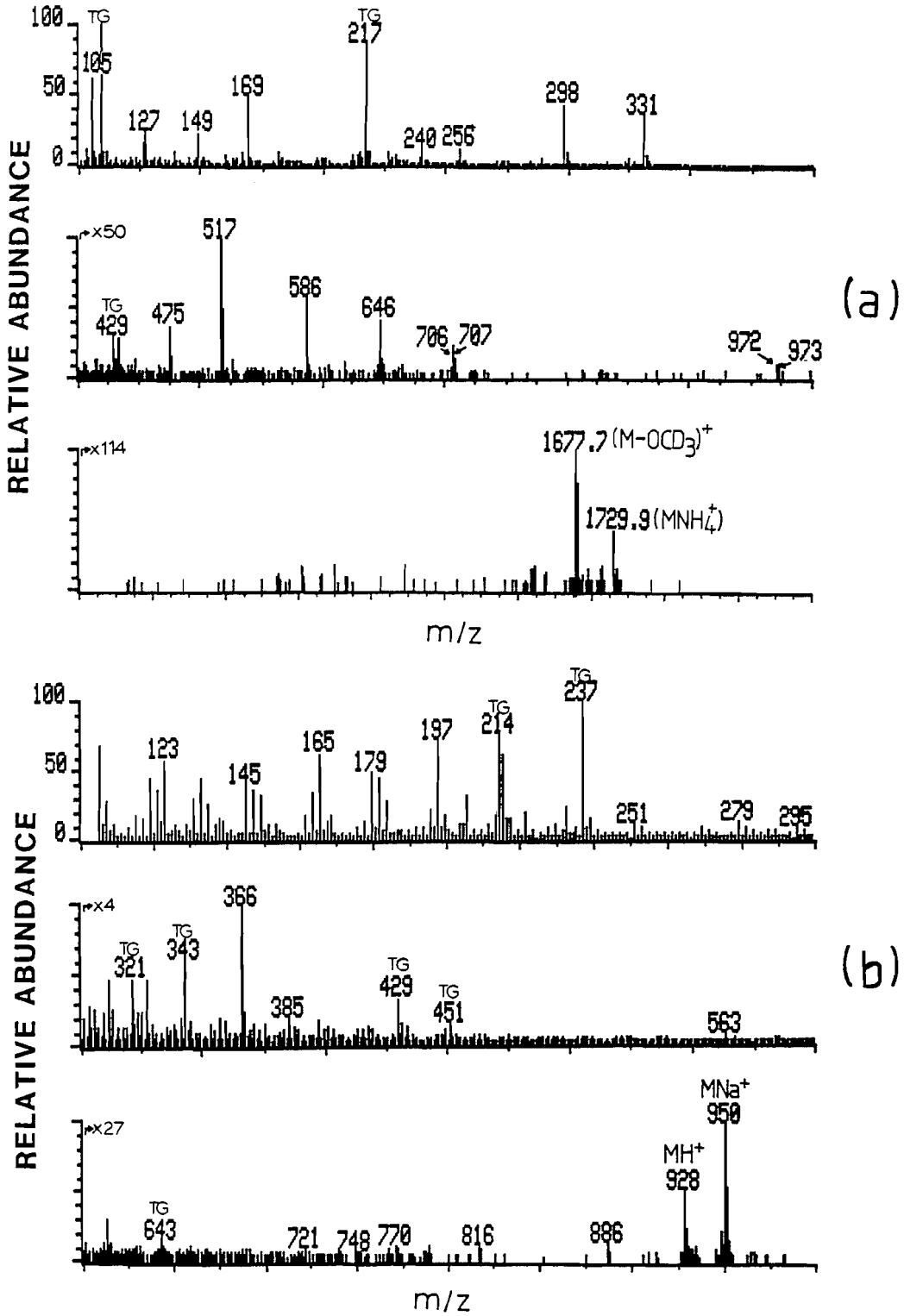

FIG. 1. FAB mass spectra of (a) compound **6***A*, and (b) compound **6***C*. TG indicates ions originating from thioglycerol matrix.

groups other than hydrogen, such as benzyl or acetyl, to the oxygen has occasionally been observed.

Certain protecting groups also can be identified. For instance, benzoyls give rise to an ion at m/z 105 in every compound studied (**7***A*–**7***C*, **8***A*, **8***B*; cf. spectra of **8***A* and **8***B*, Fig. 2). Benzyl groups can be identified through the loss of 90 mass units (benzyl group and hydrogen transfer). The phthalimido group used frequently for the protection of the NH_2 functionality reveals itself by the presence of an ion at m/z 418 (2-deoxy-2-phthalimido-3,4,6-tri-*O*-acetylhexose, at a non-reducing terminus), which subsequently loses two acetyl groups to give an abundant m/z 298 ion. The m/z 298 ion is also formed from an internal unit bearing an *N*-phthalimido group (**3***A*, **3***B*, **9***A*, **10**α, **10**β*A*, **10**β*B*, **11***A*, **13***A*).

As an example of a quick analysis utilizing the above principles, the mass spectrum of **6***A* (Fig. 1) reveals the presence of benzoyl (m/z 105), peracetylated *N*-phthalimido-lactosamine (m/z 706, 331, 298), and the remaining portion of the molecule after the loss of one arm from $[M-OCD_3]^+$ at m/z 1677. The spectrum of **6***B* confirms that the phthalimido group

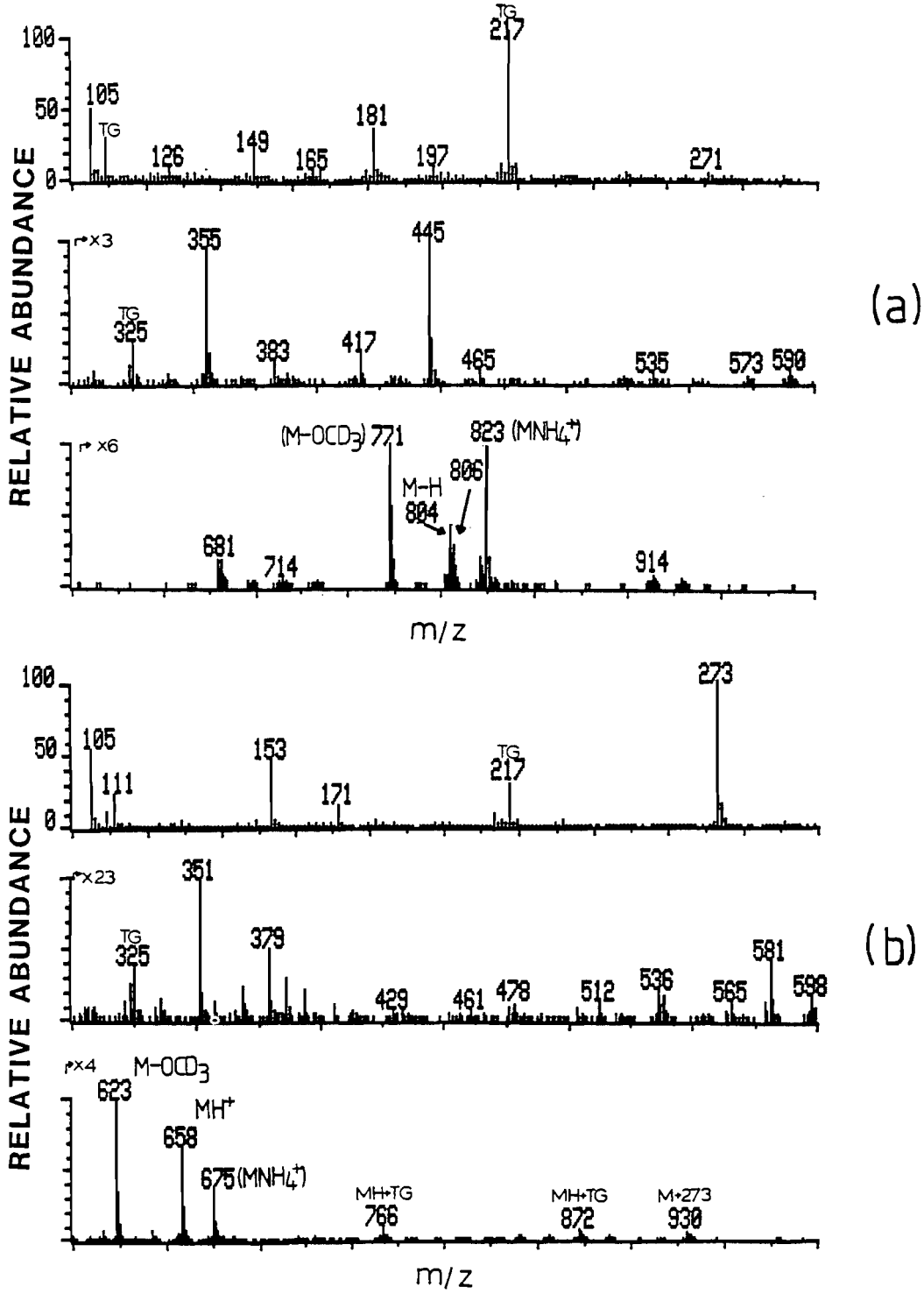

FIG. 2. FAB mass spectra of (a) compound **8***A*, and (b) compound **8***B*. TG indicates ions originating from thioglycerol matrix.

was completely replaced by *N*-acetyl (ions at m/z 618, 331; the other part of the molecule after the loss of one arm from $[M+H]^+$ gives rise to an ion at m/z 899).

Experimental

General methods

Melting points were determined on a Reichert Thermovar melting point apparatus and are uncorrected. Optical rotations were measured with a Perkin–Elmer polarimeter (model 243B) at 26 ± 1°C. Microanalyses were performed by the Micro Analytical Laboratory Ltd., Markham, Ontario. IR spectra were recorded on a Perkin–Elmer (model 1430) spectrometer using thin film on NaCl plates.

^{1}H NMR spectra were recoreded at 360.06 MHz with a Nicolet spectrometer at the NMR Spectroscopy Laboratory of the Carbohydrate Research Centre, University of Toronto. ^{13}C NMR spectra were recorded at 100.566 MHz with a Varian XL-400 spectrometer at the Chemistry Department, University of Toronto. Spectra were obtained at 19 ± 2°C either in $CDCl_3$ containing a trace of TMS (0 ppm, ^{1}H and ^{13}C) as the internal standard or in D_2O (99.98%, Aldrich) containing a trace of acetone (2.225 ppm relative to internal DSS, ^{1}H) as the internal standard. ^{13}C spectra in D_2O were referenced to external dioxane (67.4 ppm relative to TMS). Samples for NMR analyses in D_2O were passed through a Chelex 100 (Bio-Rad) ion-exchange resin in doubly distilled H_2O to remove paramagnetic impurities, lyophilized, and then lyophilized three times with D_2O. In the ^{1}H NMR tables, overlapping

Can. J. Chem. Downloaded from www.nrcresearchpress.com by 88.85.125.76 on 09/07/12
For personal use only.

TABLE 6. Structures of compounds used for mass spectrometric studies

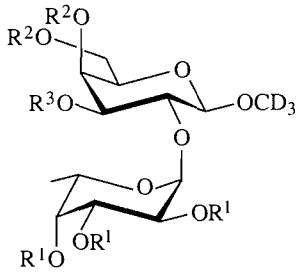

7*A*, R^1 = Bn, R^2 = PhCH<, R^3 = Bz
7*B*, $R^1 = R^2$ = Ac, R^3 = Bz
7*C*, $R^1 = R^2 = R^3$ = H

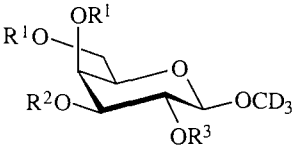

2*A*, R^1 = PhCH<, R^2 = H, R^3 = Bz
2*B*, R^1 = PhCH<, $R^2 = R_3$ = Bz
2*C*, R^1 = PhCH<, R^2 = Bz, R^3 = H
2*D*, R^1 = H, $R^2 = R^3$ = Bz

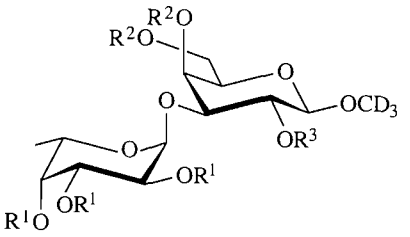

8*A*, R^1 = Bn, R^2 = PhCH<, R^3 = Bz
8*B*, $R^1 = R^2$ = Ac, R^3 = Bz
8*C*, $R^1 = R^2 = R^3$ = H

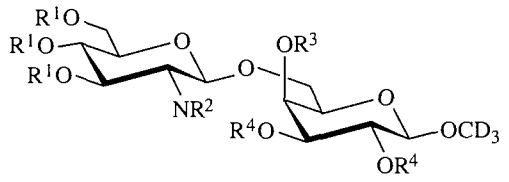

9*A*, R^1 = Ac, R^2 = Phth, R^3 = H, R^4 = Bz
9*B*, $R^1 = R^3 = R^4$ = Ac, R^2 = H, Ac
9*C*, $R^1 = R^3 = R^4$ = H, R^2 = H, Ac

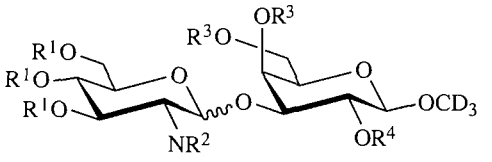

10α, R^1 = Ac, R^2 = Phth, R^3 = PhCH<, R^4 = Bz
10β*A*, R^1 = Ac, R^2 = Phth, R^3 = PhCH<, R^4 = Bz
10β*B*, R^1 = Ac, R^2 = Phth, R^3 = H, R^4 = Bz
10β*C*, $R^1 = R^3 = R^4$ = Ac, R^2 = H, Ac

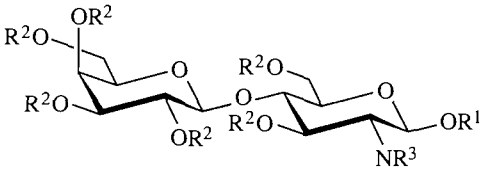

10*A*, $R^1 = C_3D_7$, R^2 = Ac, R^3 = Phth
10*B*, $R^1 = C_3D_7$, R^2 = H, R^3 = H, Ac
10*C*, $R^1 = CD_3$, R^2 = Ac, R^3 = H, Ac
10*D*, $R^1 = CD_3$, R^2 = H, R^3 = H, Ac

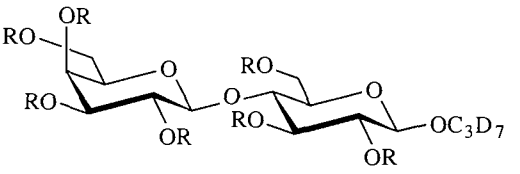

12*A*, R = Ac
13*B*, R = H

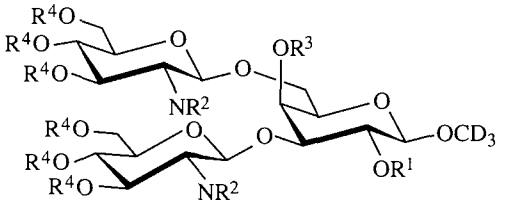

13*A*, R^1 = Bz, R^2 = Phth, R^3 = H, R^4 = Ac
13*B*, $R^1 = R^3 = R^4$ = Ac, R^2 = H, Ac
13*C*, $R^1 = R^3 = R^4$ = H, R^2 = H, Ac

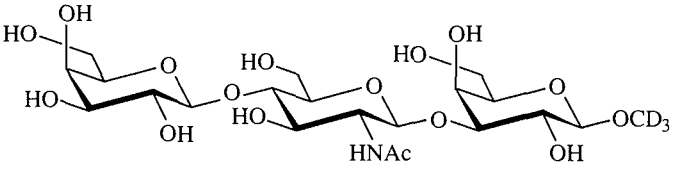

14

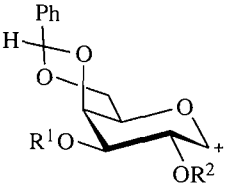

15

R^1 = H, R^2 = Bz
R^1 = Bz, R^2 = H

Can. J. Chem. Downloaded from www.nrcresearchpress.com by 88.85.125.76 on 09/07/12
For personal use only.

Can. J. Chem. Downloaded from www.nrcresearchpress.com by 88.85.125.76 on 09/07/12
For personal use only.

TABLE 7. Mass spectrometric data of unprotected oligosaccharides and synthetic intermediates

Compounds	*M*	*M*−aglycon	Diagnostic fragment(s)
2*A*	389	355	105
2*B*	493	459	105
2*C*	389	355	—
2*D*	405	371	105
3*A*	1094	1060	298, 331, 355, 706
3*B*	1006	972	105, 298, 331, 706
3*C*	940	—	331, 618
3*D*	562	—	366
5*A*	1423	1389	298, 331, 706, 684, 972
5*B*	1227	—	330, 331, 618
5*C*	765	—	366
6*B*	1515	—	331, 618
6*C*	927	—	366
7*A*	805	771	105, 355, 417, 445
7*B*	657	623	105, 273
7*C*	343	309	147
9*A*	822	788	105, 298
9*B*	652	618	330
9*C*	400	366	—
10α	806	772	105, 298, 355, 418
10β*A*	806	772	105, 298, 355, 418
10β*B*	718	684	105, 298, 418
10β*C*	652	618	330
11*A*	772	706	331
11*B*	432	366	—
11*D*	400	366	—
12*A*	685	619	331
12*B*	391	—	163
13*A*	1135	1101	105, 298, 418, 684
13*B*	939	—	330
13*C*	603	—	204
14	562	—	366

resonances are marked with the same superscript numbers. Throughout the experimental section, ^{13}C NMR resonances whose resonances may be interchanged are marked with the same superscript numbers.

Fast Atom Bombardment mass spectras (FAB-MS) were recorded with a VG Analytical ZAB-SE mass spectrometer at the Mass Spectrometry Laboratory of the Carbohydrate Research Centre, University of Toronto. The samples in thioglycerol were bombarded by neutral xenon atoms (8 keV and 1 mA anode current) generated by Ion-Tech Saddle Field Ion Gun.

Thin-layer chromatography (TLC) was performed on silica gel $^{60}F_{254}$ (Merck) plastic plates and visualized by spraying with 50% sulfuric acid and (or) 1% orcinol acidic ferric chloride (15) and heating at 200°C. Silica gel (230–400 mesh; Toronto Research Chemicals) was used for flash chromatography. All starting materials were dried overnight under vacuum (10^{-3} Torr; 1 Torr = 133.3 Pa) prior to use and the solvents were distilled from appropriate drying agents. Solutions were concentrated at water aspirator pressure.

Trideuteriomethyl 2-O-*benzoyl-4,6-*O-*benzylidene-3-*O-*(2,3,4,6-tetra-*O-*acetyl-4-*O-β-D-*galactopyranosyl-3,6-di-*O-*acetyl-2-deoxy-2-phthalimido-β-D-glucopyranosyl)-β-D-galactopyranoside (3*A*)*

The crude bromide **1***B* was prepared by saturating a mixture of dichloromethane (30 mL) and acetic anhydride (2 mL) with HBr gas at 5°C, adding acetate **1***A* (1.86 g; 2.4 mmol) as a solid, and rinsing the residue into the flask with dichloromethane (10 mL). HBr was bubbled through this mixture for 45 min and then the flask was tightly stoppered and the temperature allowed to rise for 1.5 h. Excess HBr was removed by flushing the flask with argon gas for 20 min. The remaining solvents were removed by evaporation on a rotary evaporator at high vacuum without heating. Dry dichloromethane (5 mL) and toluene (10 mL) were added to the residue and evaporated at high vacuum (twice), to remove residual acetic anhydride. The residue was dried under vacuum overnight, then dissolved in dry dichloromethane (15 mL) and added to a stirred mixture of alcohol **2***A* (0.46 g; 1.2 mmol), silver trifluoromethanesulphonate (0.6 g; 2.4 mmol), 2,6-di-*tert*-butyl-4-methylpyridine (0.48 g; 2.4 mmol), flame dried molecular sieves 3 Å (5 g), and dry dichloromethane (20 mL) at 0–5°C under an atmosphere of argon. The stirring was continued for 16 h and the temperature was allowed to rise to room temperature. The solids were removed by filtration through a Celite bed, washed with dichloromethane, and the combined filtrates evaporated to dryness. The residue was purified by flash chromatography on silica gel (ethyl acetate:toluene:hexane 60:30:10) to yield **3***A* as a mixture (1.1 g; 85:15; 72%) with an unidentified impurity. A small sample of this mixture was purified to homogeneity by preparative HPLC (μ Porasil, hexane:dichloromethane:ethyl acetate 40:20:40); mp 268–272°C; $[\alpha]_D$ +29.9° (*c* 0.68, $CHCl_3$); IR (neat): 1780 sh, 1750, 1725 (CO) cm^{-1}; ^{13}C NMR ($CDCl_3$) δ: 169.1–170.3 (6 × CH_3CO), 167.5 (br, CONCO), 167.3 (PhCO), 101.7[1] (Cl-Gal-β-OCD_3), 101.0[1] (Cl-Gal-β-1,4-), 100.8[1] ($PhCO_2$), 99.5 (Cl-Glc). Anal. calcd. for $C_{53}H_{54}D_3NO_{24}$ (1095.002): C 58.14, H 4.97, N 1.28; found: C 57.92, H 4.91, N 1.28.

Trideuteriomethyl 2-O-*benzoyl-3-*O-*(2,3,4,6-tetra-*O-*acetyl-4-*O-β-D-*galactopyranosyl-3,6-di-*O-*acetyl-2-deoxy-2-phthalimido-β-D-glucopyranosyl)-β-D-galactopyranoside (3*B*)*

Compound **3***A* (1.0 g, 0.78 mmol), prepared as described above and without purification, was dissolved in acetic acid (40 mL) and hydrogenated at room temperature and atmospheric pressure for 16 h with Palladium black (Strem, 700 mg) as catalyst. The solids were removed by filtration through acetic acid wetted Celite, rinsed with 95% ethanol, and the solvents were evaporated at high vacuum. The residual acetic acid and water were removed by azeotropic distillation with toluene (2 × 50 mL). The residue was purified by flash chromatography on silica gel (isopropanol:dichloromethane 8:92) to yield pure **3***B* (0.68 g, 87%); mp 153–154°C; $[\alpha]_D$ +36.7° (*c* 1.8, $CHCl_3$); IR (neat):3250 (br OH), 1780 sh, 1750, 1725 (CO) cm^{-1}; ^{13}C NMR ($CDCl_3$) δ: 169.2–171.0 (6 × CH_3CO), 167.8 (br, CONCO), 164.7 (PhCO), 101.9[2] (Cl-Gal-β-OCD_3, $^2J_{C-H}$ 160), 101.1[2] (Cl-Gal-β-1,4-, $^2J_{C-H}$ 162), 98.5 (Cl-Glc, $^2J_{C-H}$ 160). Anal. calcd, for $C_{46}H_{50}D_3NO_{24}$ (1006.893): C 54.87, H 5.00, N 1.39; found: C 55.45, H 5.03, N 1.36

*Trideuteriomethyl 2,4,6-tri-*O-*acetyl-3-*O-*(2,3,4,6-tetra-*O-*acetyl-4-*O-β-D-*galactopyranosyl-2-acetamido-3,6-di-*O-*acetyl-2-deoxy-β-D-glucopyranosyl)-β-D-galactopyranoside (3*C*)*

Diol (**3***B*) (0.35 g, 0.35 mmol) was dissolved in ethanol (6 mL), hydrazine hydrate (Aldrich 85%, 3 mL) was added, and the mixture heated at 70°C for 30 min. The liquids were removed by evaporation at high vacuum and the residual water removed by coevaporation with toluene (2 × 25 mL). The residue was cooled in an ice bath under an atmosphere of argon, then dry pyridine (8 mL) and dry acetic anhydride (5 mL) were added. The stirring was continued for 60 h and the temperature allowed to rise to room temperature. The liquids were removed by evaporation at high vacuum followed by coevaporation with toluene (3 × 20 mL). The residue was purified by chromatography on silica gel (isopropanol:dichloromethane 6:94) to yield **3***C* (0.28 g, 85%); mp 124–127°C; $[\alpha]_D$ +7.8° (*c* 1.04, $CHCl_3$); IR (neat): 3365 br (OH), 1750 (COO), 1680, 1550 (CON) cm^{-1}. Anal. calcd. for $C_{39}H_{52}D_3NO_{25}$ (940.8315): C 49.79, H 5.57, N 1.49; found: C 50.10, H 5.61, N 1.53.

*Trideuteriomethyl 3-*O-*(2-acetamido-2-deoxy-4-*O-β-D-*galactopyranosyl-β-D-glucopyranosyl)-β-D-galactopyranoside (3*D*)*

Peracetate (**3***C*) (0.15 g, 0.16 mmol) was dissolved in methanol (6 mL) and KCN (70 mg) was added under argon; the mixture was left to stir for 16 h under an argon atmosphere. To this mixture was added methanol (10 mL), water (5 mL), and mixed bed resin Ag 501-X8 (5 g). After 30 min of stirring, the solids were removed by filtration, washed with methanol:water (1:1, 50 mL), and methanol (50 mL). The filtrate was concentrated at high vacuum and taken up in a small volume of water, filtered through a disposable millipore filter, and lyophilized to yield pure **3***D* (0.82 g, 91%); mp 181–186°C; $[\alpha]_D$ −8.3° (*c* 1.21,

Can. J. Chem. Downloaded from www.nrcresearchpress.com by 88.85.125.76 on 09/07/12
For personal use only.

$CH_3OH:H_2O$ 4:1); IR (neat): 3350 (br, OH, NH), 1665, 1550 (CON), cm^{-1}. Anal. calcd. for $C_{21}H_{34}D_3NO_{16}$ (562.4967): C 44.84, H 6.09, N 2.49; found: C 45.16, H 5.83, N 2.43.

Trideuteriomethyl 2-O-benzoyl-3-O-(2,3,4,6-tetra-O-acetyl-4-O-β-D-galactopyranosyl-3,6-di-O-acetyl-2-deoxy-2-phthalimido-β-D-glucopyranosyl)-6-O-(3,4,6-tri-O-acetyl-2-deoxy-2-phthalimido-β-D-glucopyranosyl)-β-D-galactopyranoside (5A)

Bromide **4** (Toronto Research Chemicals, 85 mg; 0.17 mmol) dissolved in dichloromethane (1 mL) was added to a stirred mixture of diol **3*B*** (115 mg; 0.11 mmol), silver zeolite 13X (2 g), and dichloromethane (6 mL) under an atmosphere of argon. The stirring was continued for 2.5 h and the solids removed by filtration through Celite and rinsed with dichloromethane. The filtrates were evaporated to dryness and the residue was purified by flash chromatography (silica gel, dichloromethane:isopropanol 25:1) to yield tetrasaccharide **5*A*** (112 mg; 69%; mp 170–173°C; $[\alpha]_D$ +32.7° (*c* 0.97, $CHCl_3$); IR (neat): 3400 (OH), 1780 sh, 1750, 1720 (CO) cm^{-1}; ^{13}C NMR ($CDCl_3$) δ: 169.4–170.8 (9 × CH_3CO), 167.5 (br, CONCO), 164.4 (PhCO), 101.4[3] (Cl-Gal-β-OCD_3), 101.3[3], (Cl-Gal-β-1,4-) 97.7[4], (Cl, 3-Glc), 97.6[4], (Cl, 6-Glc). Anal. calcd. for $C_{66}H_{69}D_3N_2O_{33}$ (1424.265): C 55.66, H 4.88, N 1.97; found: C 55.82, H 5.03, N 1.92.

Trideuteriomethyl 2,4-di-O-acetyl-3-O-(2,3,4,6-tetra-O-acetyl-4-O-β-D-galactopyranosyl-2-acetamido-3,6-di-O-acetyl-2-deoxy-β-D-glucopyranosyl)-6-O-(2-acetamido-3,4,6-tri-O-acetyl-2-deoxy-β-D-glucopyranosyl-β-D-galactopyranoside (5B)

Tetrasaccharide **5*A*** (112 mg; 0.079 mmol) was treated with the same procedure described for the peracetate **3*C***. The product was purified by flash chromatography (silica gel, isopropanol:dichloromethane 1:10) to yield **5*B*** (77 mg; 80%); mp 269–273°C; $[\alpha]_D$ −19.3° (*c* 0.23, $CHCl_3$); IR (neat): 3300 (br, NH), 1750 (COO), 1660, 1550 (CON) cm^{-1}; ^{13}C NMR ($CDCl_3$) δ: 169.0–171.2 (13 × CH_3CO), 101.7[5] (Cl-Gal-β-OCD_3, $^2J_{C-H}$ 160), 101.0[5] (Cl-Gal-β-1,4-, $^2J_{C-H}$ 160), 100.3[6] (Cl, 3-Glc; $^2J_{C-H}$ 160), 99.9[6] (Cl, 6-Glc, $^2J_{C-H}$ 160. Anal. calcd. for $C_{51}H_{69}D_3N_2O_{32}$ (1228.10): C 49.88, H 5.66, N 2.28; found: C 49.98, H 5.62, N 2.26

Trideuteriomethyl 3-O-(4-O-β-D-galactopyranosyl-2-acetamido-2-deoxy-β-D-glucopyranosyl)-6-O-(2-acetamido-2-deoxy-β-D-glucopyranosyl)-β-D-galactopyranoside (5C)

The acetyls of **5*B*** (20 mg; 0.016 mmol) were removed following the procedure used for compound **3*D*** to yield pure tetrasaccharide **5*C*** (8 mg; 65% (**5*C***)); mp 238–243°C; $[\alpha]_D$ −17.4° (*c* 0.47, $CH_3OH:H_2O$ 5:1); IR (neat): 3320 (br, OH, NH), 1650, 1550 (CON) cm^{-1}. Anal. calcd. for $C_{29}H_{47}D_3N_2O_{21}$ (765.6911): C 45.49, H 6.19, N 3.66; found: C 45.42, H 6.28, N 3.76.

Trideuteriomethyl 2-O-benzoyl-3,6-di-O-(2,3,4,6-tetra-O-acetyl-4-O-β-D-galactopyranosyl-3,6-di-O-acetyl-2-deoxy-2-phthalimido-β-D-glucopyranosyl-β-D-galactopyranoside (6A)

Compound **6*A*** was prepared as described for tetrasaccharide **5*A*** from diol **3*B*** (464 mg; 0.46 mmol) except that bromide **1*B*** generated from acetate **1*A*** (545 mg; 0.69 mmol), as described above, was used as the donor. The pentasaccharide **6*A*** was purified by flash chromatography (silica gel, dichloromethane:isopropanol 25:1) to yield pure **6*A*** (361 mg; 46%); mp 169–173°C; $[\alpha]_D$ +25.4 (*c* 1.7, $CHCl_3$); IR (neat): 3560 (OH), 1780 sh, 1750, 1720 (CO) cm^{-1}; ^{13}C NMR ($CDCl_3$) δ: 169.1–170.8 (12 × CH_3CO), 168, 167.5 (br, CONCO), 164.4 (PhCO), 101.4[7], (Cl-Gal-β-OCD_3, $^2J_{C-H}$ 160), 101.4[7] (Cl-Gal-β-1,4 (6), $^2J_{C-H}$ 160), 101.2[7] (Cl-Gal-β,4 (3), $^2J_{C-H}$ 160), 97.6[8] (Cl,3-Glc, $^2J_{C-H}$ 160), 97.3[8] (Cl,6-Glc, $^2J_{C-H}$ 160). Anal. calcd. for $C_{78}H_{85}D_3N_2O_{41}$ (1712.518); C 54.71, H 5.00, N 1.64; found: C 54.71, H 4.84, N 1.42.

Trideuteriomethyl 2,4-di-O-acetyl-3,6-di-O-(2,3,4,6-tetra-O-acetyl-4-O-β-D-galactopyranosyl-2-acetamido-3,6-di-O-acetyl-2-deoxy-β-D-glucopyranosyl)-β-D-galactopyranoside (6B)

Pentasaccharide **6*A*** (279 mg; 0.16 mmol) was treated with the same procedure described for the peracetate **3*C***. The product was purified by flash chromatography (silica gel, isopropanol:dichloromethane 1:10) to yield pure **6*B*** (173 mg; 70%); mp 135–142°C; $[\alpha]_D$ −3.5° (*c* 1.5, $CHCl_3$); IR (neat): 3340, 3220 (NH), 1750 (COO), 1660, 1545 (CON) cm^{-1}. Anal. calcd. for $C_{63}H_{85}D_3N_2O_{40}$ (1516. 354): C 49.90, H 5.65, N 1.85; found: C 50.06, H 5.62, N 1.83.

Trideuteriomethyl 3,6-di-O-(4-O-β-D-galactopyranosyl-2-acetamido-2-deoxy-β-D-glucopyranosyl)-β-D-galactopyranoside (6C)

The acetates of **6*B*** (112 mg; 0.074 mmol) were removed, following the procedure used for compound **3*D***, to yield pure pentasaccharide **6*C*** (50 mg; 73%); mp 204–207°C; $[\alpha]_D$ −7.67° (*c* 0.30, $CH_3OH:H_2O$ 1:1); IR (neat): 3300 (br, OH, NH), 1650, 1550 (CON) cm^{-1}. Anal. calcd. for $C_{35}H_{57}D_3N_2O_{26}$ (927.8331): C 45.31, H 6.19, N 3.02; found: C 45.41, H 6.18, N 2.92.

Acknowledgements

This work was supported by the Ludwig Institute for Cancer Research and the Medical Research Council of Canada (by a grant to J.J.K.). D.M.W. is grateful to NSERC for a postdoctoral fellowship. We thank Dr. D. W. Hughes for running the ^{13}C NMR spectra and Mr. J. Baptista for the HPLC separations as well as the optical rotation measurements.

1. J. P. Carver, S. W. Michnik, A. Imberty, and D. A. Cumming. Glycoproteins in biological recognition. *Edited by* G. Bock and S. Harnett. CIBA Foundation, Wiley, Chichester 1989. pp. 6–18.
2. J. W. Dennis, S. Laferte, C. Waghorne, M. L. Breitman, and R. S. Kerbel. Science, **236**, 582 (1987).
3. T. Feizi. Trends Biochem. Sci. **6**, 333 (1981).
4. H. Egge, A. Dell, and H. U. Nicolai. Arch. Biochem. Biophys. **224**, 235 (1983).
5. C. Auge, S. David, and A. Veyrières. Nouv. J. Chim. **3**, 491 (1979); M. A. Nashed, M. Kisco, C. W. Slife, and L. Anderson. Carbohydr. Res. **90**, 71 (1981).
6. A. Maranduba and S. Veyrières. Carbohydr. Res. **151**, 105 (1986).
7. S. A. Abbas and K. L. Matta. Carbohydr. Res. **123**, 53 (1983); **124**, 115 (1983).
8. T. Takamura, T. Chiba, and S. Tejima. Chem. Pharm. Bull. **29**, 1027 (1981).
9. Y. Ito, S. Sato, M. Mori, and T. Ogawa. J. Carbohydr. Chem. **7**, 359 (1988).
10. C. Augé, C. Mathieu, and C. Merienne. Carbohydr. Res. **151**, 147 (1986); C. Augé, S. David, C. Mathieu, and C. Gautheron. Tetrahedron Lett. **25**, 1467 (1984).
11. R. U. Lemieux, T. Takeda, and B. Y. Chung. *In* Synthetic methods for carbohydrates. *Edited by* H. S. El Khadem. ACS Symposium Series 39, Am. Chem. Soc., Washington, DC, 1976; J. Arnarp, M. Haraldsson, and J. Longgren. J. Chem. Soc. Perkin Trans. 1, 535 (1985); H. Baumann, H. Lönn, and J. Lönggren. Carbohydr. Res. **114**, 317 (1983).
12. D. M. Whitfield, J. P. Carver, and J. J. Krepinsky. J. Carbohydr. Chem. **4**, 369 (1985); A. Stoffyn and P. Stoffyn. J. Org. Chem. **32**, 4001 (1967).
13. R. U. Lemieux, S. Z. Abbas, B. Y. Chung. Can. J. Chem. **60**, 58 (1981); **60**, 68 (1981); R. U. Lemieux, S. Z. Abbas, M. H. Burczynska, and R. M. Ratcliffe. Can. J. Chem. **60**, 63 (1981); J. Alais and A. Veyrières. Tetrahedron Lett. **24**, 5223 (1983).
14. H. Egge and J. Peter-Katalinic. Mass Spectrom. Rev. **6**, 331 (1987).
15. J. C. Touchstone and M. F. Dobbins. Practice of thin layer chromatography. Wiley, New York. 1983.
16. D. M. Whitfield, C. J. Ruzicka, J. P. Carver, and J. J. Krepinsky. Can. J. Chem. **65**, 693 (1987).
17. A. Dell and M. Panico. *In* Mass spectrometry in biomedical research. *Edited by* S. Gaskel. Wiley, New York. 1986. pp. 149–180.

Syntheses of model oligosaccharides of biological significance. XI. A short synthesis of fucosylated chitobiosides, also bound to asparagine in a synthon (as in *N*-linked glycoproteins)[1,2]

HO HUAT LEE[3] AND JOSE A. B. BAPTISTA[4]

Ludwig Institute for Cancer Research, Toronto Branch, Toronto, Ont., Canada M4Y 1M4

AND

JIRI J. KREPINSKY[5]

Ludwig Institute for Cancer Research, Toronto Branch, Toronto, Ont., and Departments of Medical Genetics and Medical Biophysics, University of Toronto, Toronto, Ont., Canada M5S 1A8

Received September 12, 1989

HO HUAT LEE, JOSE A. B. BAPTISTA, and JIRI J. KREPINSKY. Can. J. Chem. **68**, 953 (1990).

We describe a simple and efficient method for the preparation of the trisaccharide GlcNAc(β1-4)-[Fuc(α1-6)-]GlcNAc(β1-) (**1**) and of the protected form of GlcNAc(β1-4)-[Fuc(α1-6)-]GlcNAc(β1-Asn) (**2**). The key intermediate is benzyl 4,6-benzylidene chitobioside **5** giving the desired trisaccharide by *in situ* anomerization–glycosylation reaction with 2,3,4-tribenzylfucosyl bromide. The benzyl glycoside in the trisaccharide **6** has been replaced by acetate and then bromine; this glycosylating agent was used to prepare methyl and 8-methoxycarbonyloctyl glycosides as well as isothiocyanate **12**, in a series of reactions. The latter compound gave, on reaction with 1-benzyl *N*-benzyloxycarbonyl-L-asparate, compound **13** (a protected derivative of **2**), which should serve as a synthon for syntheses of glycopeptides.

Key words: glycopeptide, synthesis; oligosaccharide, synthesis; chitobiosides; fucosylated chitobiosides; *N*-linked oligosaccharides.

HO HUAT LEE, JOSE A. B. BAPTISTA et JIRI J. KREPINSKY. Can. J. Chem. **68**, 953 (1990).

On décrit une méthode simple et efficace de préparer le trisaccharide GlcNAc(β1-4)-[Fuc(α1-6)-]GlcNAc(β1-) (**1**) ainsi que la forme protégée du GlcNAc(β1-4)-[Fuc(α1-6)-]GlcNAc(β1-Asn) (**2**). L'intermédiaire clé est le 4,6-benzylidène chitobioside de benzyle (**5**) qui fournit le trisaccharide désiré grâce à une réaction d'anomérisation et de glycosylation *in situ* à l'aide du bromure de 2,3,4-tribenzylfucosyle. On a remplacé le glucoside de benzyle du trisaccharide **6** par l'acétate et finalement le bromure; dans une série de réactions, on a utilisé cet agent de glycosylation pour préparer les glucosides de méthyle ou de 8-méthoxycarbonyloctyle ainsi que l'isothiocyanate **12**. Ce dernier composé, par réaction avec le *N*-benzyloxycarbonyl-L-aspartate de benzyle, conduit au composé **13** (une forme protégée du composé **2**) qui devrait s'avérer être un synthon utile pour la synthèse de glycopeptides.

Mots clés: glucoside, synthèse; oligosaccharide, synthèse; chitobiosides; chitobiosides fucosylés; oligosaccharides liés à l'azote.

[Traduit par la revue]

As part of our studies of unusual carbohydrate epitopes appearing in neoplasia and cancer (cf. also ref. 1), we are investigating synthetic approaches to complex oligosaccharides and building blocks for syntheses of glycopeptides. The carbohydrate structures in an appropriate form are usually immunogenic and consequently can be used for the preparation of antibodies, which in turn can recognize the original carbohydrate structure. Suitably modified or as such, the antibodies can serve as diagnostic reagents. Glycosylasparagine derivatives also can be used for the construction of glycosylpeptides required as models for immunological and conformational studies. The very common trisaccharide GlcNAc(β1-4)-[Fuc(α1-6)-]GlcNAc(β1-) (**1**) occurs in the core portion of the structure of N-linked oligosaccharides in glycoproteins. The procedures that we previously described for syntheses of trisaccharide glycosides **10** and **11** were lengthy (1, 3). Consequently, we have attempted to synthesize **1** from peracetylated chitobiose (which can be obtained in quantity (2) by acetolysis of chitin). We also wanted to ascertain whether a bromide derived from **1** could be obtained without disturbing the linkage of L-fucose to one of the *N*-acetylglucosamines.[6] We anticipated that such a bromide could be utilized for a synthesis of the synthon GlcNAc(β1-4)-[Fuc(α1-6)-]GlcNAc(β1-Asn) (**2**), which could in turn be used for the preparation of glycopeptides by an extension of the peptide chain.

A major problem connected with the formation of such a synthetic intermediate is the acid lability of α-L-fucosides. To achieve glycosylation with a glycosylating agent based on fucose, fucose has to be protected by benzyl groups. Otherwise the glycosylating agent would not be sufficiently reactive (5). For instance, glycosylation of benzylidene chitobioside **5** with 2,3,4-triacetylfucosyl halogenides does not give any identifiable product. Benzyl protection on the other hand renders fucose sensitive to acid conditions. Therefore, to effect transformation of the 1-*O*-acetyl of trisaccharide **1** into a bromide for eventual use as a glycosylating agent, all hydroxy groups of **1** have to be protected as their acetyls. Thus it can be expected that the peracetylated bromide of **1** should be sufficiently stable to act as a glycosylating agent.

[1]For part 10, see D. M. Whitfield *et al.*, preceding paper.

[2]Presented in part at the UCLA Symposium on Altered Glycosylation in Tumor Cells, Keystone, CO, April 1987.

[3]Present address: Cancer Research Laboratory, School of Medicine, Auckland University, Auckland, New Zealand.

[4]Present address: Department of Medical Genetics and Carbohydrate Research Centre, Faculty of Medicine, University of Toronto, Toronto, Ont., Canada, M5S 1A8.

[5]Author to whom correspondence may be addressed at the Department of Medical Genetics, University of Toronto, Toronto, Ont., Canada M5S 1A8.

[6]After completion of the experimental work and during the preparation of this manuscript, a publication by Kunz and Unverzagt appeared (4), in which this problem was studied using a different approach.

Can. J. Chem. Downloaded from www.nrcresearchpress.com by 88.85.125.76 on 09/07/12
For personal use only.

Can. J. Chem. Downloaded from www.nrcresearchpress.com by 88.85.125.76 on 09/07/12
For personal use only.

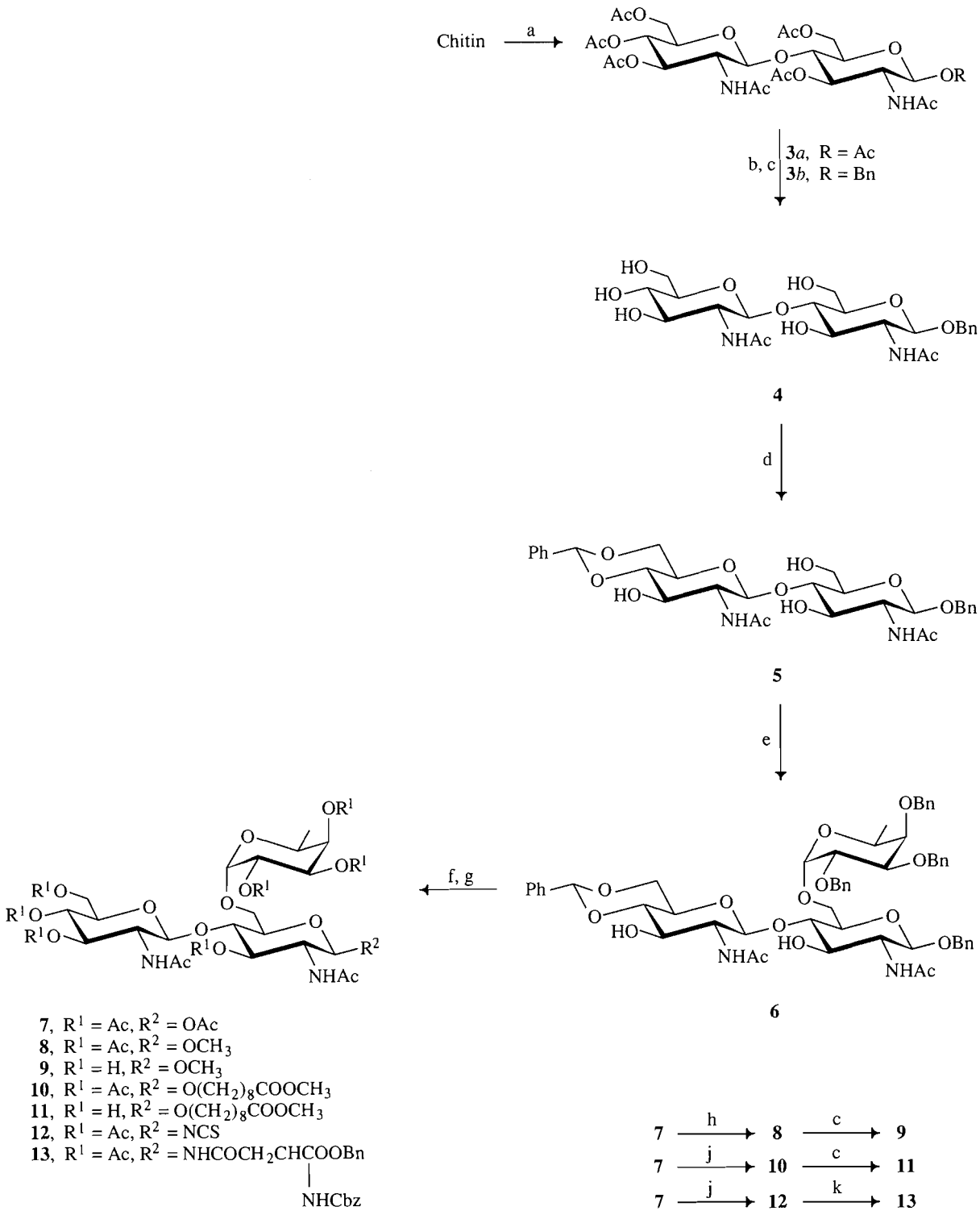

a, H_2SO_4, Ac_2O; b, $TiBr_4/CH_2Cl_2$; BnOH, *p*-tosyl acid/CH_2Cl_2 or HCl/Ac_2O–AcOH; BnOH, Ag_2CO_3, anh. $CuSO_4$; c, NaOMe/MeOH, RT; d, $PhCH(OMe)_2$, *p*-tosyl acid/CH_3CN–DMF; e, Et_4NBr/DMF+2,3,4–tri-*O*-benzyl-α-L-fucopyranosyl bromide/CH_2Cl_2; f, Pd/C–H_2/AcOH–MeOH; g, Ac_2O/C_5H_5N, RT, h, $TiBr_4/CH_2Cl_2$; *p*-tosyl acid/ anh. MeOH; i, $TiBr_4/CH_2Cl_2$; 8-methoxycarbonyl octanol, *p*-tosyl acid/CH_2Cl_2; j, $TiBr_4/CH_2Cl_2$; KNS, *p*-tosyl acid/CH_3CN; k, 1-Benzyl *N*-(benzyloxy)carbonyl-L-aspartate, Et_3N, toluene

SCHEME 1

The formation of *N*-glycosidic linkages between glucose (6–8), 2-acetamido-2-deoxy glucose (or chitobiose) (9–13) or derivatives (16), and asparagine has been previously reported. Most often glycosylamides (4, 6–16) were used in reaction with 1-benzyl *N*-(benzyloxycarbonyl)-L-aspartate. However, in alternate approaches glycosylamines were reacted with *N*-(benzyloxycarbonyl)-L-aspartic anhydride (14), with 1-benzyl *N*-[2-(-triphenylphosphonio)ethoxycarbonyl]aspartate (15), or 1-*tert*-butyl *N*-allyloxycarbonylaspartate (4). The glycosylamines were prepared either by reduction of azides (4, 6–16, 20) or by reaction of reducing aldoses with ammonium hydrogen carbonate (19). These procedures are all relatively time-consum-

Can. J. Chem. Downloaded from www.nrcresearchpress.com by 88.85.125.76 on 09/07/12
For personal use only.

ing, and thus our objective has been to reduce the complexity and shorten time requirements for the synthesis. Glycosylisothiocyanate (17) was successfully reacted with 1-benzyl *N*-benzyloxycarbonyl-L-aspartate (18), which served as precedent for our final coupling to give **13**.

Octaacetylchitobiose (**3***a*) obtained by acetolysis of chitin (2) can be transformed efficiently into either heptaacetylchitobiosyl chloride by treatment with anhydrous HCl or heptaacetylchitobiosyl bromide by treatment with titanium tetrabromide. Both of these halogenides yield benzyl glycosides on reaction with benzyl alcohol. The 4- and 6-hydroxy groups on the "nonreducing" terminal monosaccharide unit of this benzyl glycoside are protected as their benzylidene derivative, rendering the other 6-hydroxy group (residing on the "reducing" monosaccharide unit) as the only available primary hydroxyl for the reaction with 2,3,4-tri-*O*-benzyl-L-fucosyl bromide (1, 3). The secondary OH-3 groups do not react with the fucosyl residue to any appreciable extent under these conditions.

The protected trisaccharide **6**, made in just four steps, is then debenzylated and acetylated. The acetylated intermediates are suitable for chromatography, assuring that the starting material for the preparation of the bromide, by a reaction with titanium tetrabromide (21), is indeed pure. The bromide was then used without purification as the glycosylating synthon to prepare methyl glycoside **8** and 8-methoxycarbonyloctyl glycoside **10** by reaction with appropriate alcohols, and isothiocyanate **12** by reaction with potassium thiocyanate. The two former compounds were identical to samples synthesized previously by a substantially more tedious procedure (the acetyl protecting groups were smoothly removed using Zemplen's conditions) (1, 3). The isothiocyanate served as one of the starting materials for the simple and efficient synthesis of the protected derivative **13** of GlcNAc(β1-4)-[Fuc(α1-6)-]GlcNAc(β1-Asn). The anomericity of 2-acetamido-2-deoxy D-glucosides in both **12** and **13** is β, as can be seen from the diaxial coupling constants of H-1 and H-1′: J = 8.3 Hz (**12**), and 9.0 and 9.7 Hz (**13**), cf. Experimental. The synthetic design is portrayed in Scheme 1.

The choice of the isothiocyanate reaction for the introduction of the amino function into the anomeric position at the trisaccharide reducing end deserves a comment. Most importantly, it was chosen because of the mild reaction conditions required. An alternate pathway via glycosyl azides (22) (in this case the azide derived from **7** (R^1 = Ac, R^2 = N_3)) involves the reduction of the N_3 group to an amino group. The resulting amine (R^1 = Ac, R^2 = NH_2) is unstable because of the complex pattern of acetyl migrations to the amino group (cf. ref. 22). Considering the overall requirements of the azide route (cf. ref. 22 for an excellent discussion of the azide procedure), we believed that, although it gives moderate yields, the isothiocyanate approach is preferable since it is experimentally simple and easily reproducible.

After appropriate deprotection, compound **13** can be used in oligopeptide synthesis or, alternatively, the glycosylated asparagine can be obtained. The use of **13** and its variations in glycopeptide synthesis will be described in a future communication.

Experimental

General methods

Melting points were determined with a Reichert Thermovar melting point apparatus and are uncorrected. Optical rotations were measured with a Perkin–Elmer polarimeter (model 243B) at 26 ±1°C. Microanalyses were performed by the Microanalytical Laboratory Ltd., Markham, Ontario. ^{1}H NMR spectra were recorded at 360.06 MHz with a Nicolet spectrometer or at 500 MHz with a Bruker AM spectrometer at the NMR spectroscopy laboratory of the Carbohydrate Research Centre, University of Toronto. Spectra were obtained at 23 ±2°C; chemical shifts are cited in δ (ppm) scale relative to TMS (0 ppm) and coupling constants are reported in hertz (Hz). The IR spectra were recorded on a Perkin–Elmer (model 1430) spectrometer using thin film or NaCl plates. Fast Atom Bombardment mass spectra (FAB-MS) were performed with a VG Analytical ZAB-SE high-mass high-resolution mass spectrometer at the mass spectrometry laboratory of the Carbohydrate Research Centre, University of Toronto.

Thin-layer chromatography (TLC) was performed on silica gel $60F_{254}$ (Merck) plastic plates, which were developed using 30% sulfuric acid followed by heating at 150°C. Silica gel (230–400 mesh; Toronto Research Chemicals) was used for flash chromatography. All starting materials were dried under high vacuum over P_2O_5 or KOH overnight prior to use. Solvents were distilled under argon from appropriate drying agents onto anhydrous 3 Å molecular sieves and were transferred via syringe. Solvents were removed at reduced pressures using a rotary evaporator at temperatures not exceeding 40°C.

Benzyl 2-acetamido-4-O-(2′-acetamido-2′-deoxy-3′, 4′, 6′-tri-O-acetyl-β-D-glucopyranosyl)-2-deoxy-3,6-di-O-acetyl-β-D-glucopyranoside (3b)

Method A

To solid titanium(IV) bromide (12.2 g) stirring at 0°C was added a solution of chitobiosyl octaacetate (2) (3.00 g, 4.23 mmol) in dry dichloromethane (120 mL), followed by ethyl acetate (30 mL) (21). The resulting homogeneous reddish brown mixture was further stirred at room temperature for 6 h. It was diluted with dry dichloromethane (50 mL) and anhydrous sodium acetate (12 g) was added. After stirring for 15 min the reaction mixture was poured onto ice-water (100 mL) and the product was extracted into dichloromethane (300 mL), dried over $MgSO_4$, and evaporated and coevaporated with toluene (2 × 30 mL) to give a colourless solid residue (3.08 g). This was dissolved in dichloromethane (300 mL) and treated with benzyl alcohol (14.4 mL, 141 mmol) and *p*-toluenesulfonic acid monohydrate (160 mg, 0.85 mmol) at room temperature for 69 h. The reaction mixture was washed with ice-water (150 mL), dried over $MgSO_4$, and evaporated to dryness giving a light orange liquid residue. It was subjected to chromatography on a silica gel column ($CHCl_3$–acetone, 2:1), giving pure **3***b* (1.11 g, 36%) as a colourless solid, mp 277–280°C (dichloromethane–acetone); $[\alpha]_D$ −63.0° (*c* 0.60, $CHCl_3$); R_f 0.58 (threefold development in chloroform–acetone, 2:1); IR (neat); 3295 (NH), 3075 (aromatic CH), 1750 (COOR), and 1665 (CONH) cm^{-1}; ^{1}H NMR (δ): 7.32 (m, 5, $C_6H_5CH_2$), 6.02 (d, 1H, J = 9.0 Hz, N*H*′), 5.62 (d, 1H, J = 9.3 Hz, N*H*′), 5.18 (t, 1H, J= 9.3 Hz, H-3′), 5.04 (t, 2H, J = ca. 9.02 Hz, overlapping H-3 and H-4′), 4.86 and 4.57 (2d, 2H, J = 12.2 Hz, $C_6H_5CH_2$), 4.56 (d, 1H, J = 8.6 Hz, H-1′), 4.44 (d, 1H, J = 7.9 Hz, H-1), 4.09 (td, 1H, J = 9.3 and 7.9 Hz, H-2), 3.87 (br q, 1H, J = 9.0 Hz, H-2′), 3.74 (t, 1H, J = 8.6 Hz, H-4), 3.59–3.67 (m, 2H, H-5, H-5′), 2.16, 2.07, 2.03, 2.01, and 1.96 (5s, 21H, CH_3CO). Anal. calcd. for $C_{33}H_{44}N_2O_{16}$: C 54.69, H 6.12, N 3.87; found: C 54.60, H 6.23, N 3.72.

Method B

To a solution (14 mL) of acetic acid and acetic anhydride (1:1, v/v) saturated with anhydrous HCl at 0°C was added chitobiosyloctaacetate (1.1 g) and the reaction mixture was slowly stirred for 60 h at room temperature. Then the reaction mixture was diluted with ice-cold $CHCl_3$ (50 mL), ice was added, and the solution was washed successively with ice-cold water, saturated aqueous $NaHCO_3$, and water, dried over Na_2SO_4, and evaporated to dryness at temperatures <35°C. The residue was triturated with dry diethyl ether and recrystallized from chloroform–acetone mixture, giving a white crystalline chloride, mp 212–214°C, 420 mg (11, 23). The chloride (0.2 g) was dissolved in benzylalcohol (12 mL; dried over 4 Å molecular sieve), anhydrous Ag_2CO_3 (65 mg) and anhydrous $CaSO_4$ (680 mg) were added, and the mixture was slowly stirred for 48 h at room temperature. After filtering the reaction mixture through a bed of Celite that was subsequently washed with $CHCl_3$, the combined washings were evaporated to dryness *in vacuo*, and the residue was

Can. J. Chem. Downloaded from www.nrcresearchpress.com by 88.85.125.76 on 09/07/12
For personal use only.

subjected to chromatography on a silica gel column as described in Method A (cf. above).

Benzyl 2-acetamido-4-O-(2'-acetamido-4,6-O-benzylidene-2'-deoxy-β-D-glucopyranosyl)-2-deoxy-β-D-glucopyranoside (5)

Compound **3***b* (300 mg) in CH_3OH (25 mL) was stirred with 0.1 N sodium methoxide at room temperature for 4 h. Methanol was evaporated at <30°C, water (60 mL) was added to the residue, and the resulting solution was washed with diethyl ether (3×). The combined ether washings were washed with water, and all aqueous fractions were combined, neutralized with 1 M aqueous HCl, treated with mixed bed resin AG 501 X-8 for 45 min, filtered, and evaporated to dryness to give **4**. To a clear solution of compound **4** (537 mg, 1.04 mmol) and *p*-toluenesulfonic acid monohydrate (145 mg) in acetonitrile–DMF (1:4, 25 mL) was added benzaldehyde dimethyl acetal (0.50 mL) (24) and the reaction mixture was stirred in the dark at room temperature. After 22 h additional acetal (0.30 mL) was added and the reaction mixture was stirred for another 74 h. Triethylamine (1 mL) was added and the solution was stirred for 5 min, evaporated to dryness, and the light brown residue was taken up into DMF (1.5 mL) and applied to a silica gel column (chloroform–methanol, 10:1) to give compound **5** (457 mg, 73%) as a colourless solid; mp 287–290°C (chloroform–methanol; dec.); $[\alpha]_D$ −81.7° (*c* 0.59, MeOH–H_2O, 2:1); R_f 0.30 (chloroform–methanol, 8:1); ^1H NMR (δ): 7.20–8.00 (m, 10, H, C_6H_5), 5.60 (s, 1H, PhC*H*(-O)$_2$), 4.77 (d, 1H, *J* = 12.5 Hz, PhC*H*H), 4.59 (d, 1H, *J* = 7.6 Hz, H-1'), 4.51 (d, 1H, *J* = 12.5 Hz, PhCH*H*), 4.38 (d, 1H, *J* = 8.4 Hz, H-1), 1.84 and 1.81 (2s, 6H, CH_3CO). Anal. calcd. for $C_{30}H_{38}N_2O_{11}$: C 59.79, H 6.36, N 4.65; found: C 59.82, H 6.38, N 4.71.

Benzyl 2-acetamido-4-O-(2'-acetamido-4,6-O-benzylidene-2'-deoxy-β-D-glucopyranosyl)-2-deoxy-6-O-(2'',3'',4''-tri-O-benzyl-α-L-fucopyranosyl)-β-D-glucopyranoside (6)

Dry dichloromethane (9 mL) and powdered 4 Å molecular sieve (1.12 g) were added to a mixture of compound **5** (570 mg, 0.943 mmol) and tetraethylammonium bromide (1.12 g) in DMF (9 mL) and the resulting suspension was stirred for 0.5 h. Then a solution of 2,3,4-tri-*O*-benzyl-α-L-fucopyranosyl bromide (0.562 g, 1.13 mmol) in dichloromethane (2 mL) was added. The residue of bromide in the flask was rinsed into the reaction vessel with additional dichloromethane (2 × 1 mL). To this reaction mixture, after being slowly stirred for 19 h, triethylamine (2 mL) was added and the mixture was stirred for an additional few minutes. The solids were filtered off and washed with dichloromethane (3 × 50 mL). The combined filtrate and washings were washed with water (2 × 50 mL) and the aqueous portions back-extracted with chloroform (2 × 30 mL). The combined organic extracts were dried over $MgSO_4$, then evaporated to dryness to give a light brown syrup (1.40 g), which was purified by chromatography on a silica gel column (ethyl acetate eluted nonpolar impurities, and chloroform–methanol, 20:1, eluted the required product) to yield compound **6** (474 mg, 49%) as a colorless solid, mp 256–260°C (dec.) (methanol – ethyl acetate); $[\alpha]_D$ −88.3° (*c* 0.53, $CHCl_3$); R_f 0.36 (chloroform–methanol, 10:1); ^1H NMR (δ): 7.20–7.60 (m, 25H, C_6H_5), 6.53 (d, 1H, *J* = 8.7 Hz, exchangeable with D_2O, N*H*), 5.47 (s, 1H, PhC*H*(-O$_2$), 5.46 (d, 1H, partly overlapped with the signal at 5.47, *J* approx. 6 Hz, exchangeable with D_2O, N*H*), 4.87 (d, 1H, *J* = 3.5 Hz, H-1''), 4.47 (d, 1H, *J* = 8.4 Hz, H-1'), 4.29 (d, 1H, *J* = 8.2 Hz, H-1), 4.15 (q, 1H, *J* = 6.5 Hz, H-5''), 2.02 and 1.80 (2s, 6H, CH_3CO), 1.17 (d, 3H, *J* = 6.5 Hz, H-6''). Anal. calcd. for $C_{57}H_{66}N_2O_{15}$: C 67.18, H 6.53, N 2.75; found: C 67.21, H 6.60, N 2.68.

2-Acetamido-4-O-(2'-acetamido-2'-deoxy-3',4'-6'-tri-O-acetyl-β-D-glucopyranosyl)-2-deoxy-1,3-di-O-acetyl-6-O-(2'',3'',4''-tri-O-acetyl-α-L-fucopyranosyl)-α-D-glucopyranose (7)

Compound **6** (97 mg, 0.095 mmol) in acetic acid – methanol (10 mL, 3:2) was hydrogenolysed on Pd–C (10%). After the reaction was completed (monitored by TLC), the catalyst was filtered off using a Celite bed, the bed was washed with methanol–water (1:1, 5 × 20 mL), and the combined filtrates were evaporated to dryness. The residue was treated with acetic anhydride (3 mL) and pyridine (3 mL) at room temperature. The white precipitate formed was brought into solution by warming up the reaction mixture to 40°C. The homogeneous mixture was then stirred at room temperature for 16 h. It was diluted with ethyl acetate (100 mL) and washed with cold (0°C) water (3 × 30 mL). The organic layer was dried over $MgSO_4$ and evaporated to give compound **7** as a colourless solid (67 mg, 78%), homogeneous by TLC (ethyl acetate – methanol, 9:1, R_f 0.47); mp 262–265°C (from ethyl acetate – hexane); $[\alpha]_D$ −25.1° (*c* 0.55, $CHCl_3$). ^1H NMR (δ): 6.11 (d, 1H, *J* = 3.9 Hz, H-1), 5.64 (d, 1H, *J* = 8.4 Hz, N*H*), 5.52 (d, 1H, *J* = 9.0 Hz, N*H*), 5.11 (d, 1H, *J* = 3.6 Hz, H-1''), 4.89 (d, 1H, *J* = 8.2 Hz, H-1'), 2.18, 2.17, 2.16, 2.09, 2.08, 2.02, 2.01, 2.00, 1.94, and 1.93 (10s, 30H, CH_3CO), 1.15, (d, 3H, *J* = 6.5 Hz, H-6''). Anal. calcd. for $C_{38}H_{54}N_2O_{23}$: C 50.33, H 6.00, N 3.09; found: C 50.52, H 6.12, N 3.15.

Methyl 2-acetamido-4-O-(2'-acetamido-2'-deoxy-β-D-glucopyranosyl)-2-deoxy-6-O-(α-L-fucopyranosyl)-α-D-glucopyranoside (9)

To solid titanium(IV) bromide (1.29 g) was added a solution of α-1-*O*-acetyl trisaccharide **7** (204 mg, 0.225 mmol) in dry dichloromethane (9 mL) stirring at 0°C, followed by addition of ethyl acetate (2.5 mL) (21). The resulting homogeneous reddish brown mixture was stirred at room temperature for 4.5 h. Then it was diluted with dry dichloromethane (10 mL), anhydrous sodium acetate (4 g) was added, and the mixture was stirred for 5 min, poured onto ice-water (50 mL), and the product extracted into dichloromethane (200 mL). It was then dried over $MgSO_4$, and evaporated and coevaporated with toluene (2 × 50 mL) to give a pure yellow solid (159 mg), which was treated with dry methanol (0.564 mL of 1 mmol per mL CH_2Cl_2 solution, 0.564 mmol) and *p*-toluenesulfonic acid monohydrate (4 mg, 0.019 mmol) in dichloromethane (2 mL) at room temperature for 18 h. It was diluted with dichloromethane (30 mL), poured into ice-water (20 mL), separated, dried over $MgSO_4$, and evaporated to give a pale yellow solid (129 mg), which was purified on a silica gel column ($CHCl_3$–acetone, 1:1), yielding peracetylated compound **8** (67 mg, 35%); R_f 0.47 (twofold development in $CHCl_3$–acetone, 1:1; identical with an authentic sample prepared by acetylation of compound **8** prepared by another method (3); ^1H NMR (δ): 5.74 (d, 1H, *J* = 8.3 Hz, exchangeable with D_2O, N*H*), 5.67 (d, 1H, *J* = 9.4 Hz, exchangeable with D_2O, N*H*), 5.09 (d, 1H, *J* = 3.6 Hz, H-1''), 4.93 (d, 1H, *J* = 8.3 Hz, H-1'), 4.41 (d, 1H, *J* = 7.6 Hz, H-1), 4.30 (br, 1, 1H, *J* approx. 6.8 Hz, H-5''), 3.45 (s, 3H, OCH_3), 2.18, 2.15, 2.07, 2.01, 2.00, 1.98, and 1.92 (7s, 27H, CH_3CO), 1.15 (d, 3H, *J* = 6.5 Hz, H-6'').

Compound **8** was dried and treated with 1% sodium methoxide (1 mL) in dry methanol (92 mL) at room temperature for 20 min. Then the reaction mixture was neutralized with acidic resin (0.5 mL), filtered, washed with MeOH–H_2O (1:1, 3 × 10 mL), and evaporated to give compound **9** (45 mg, 34%) as a colourless solid; mp 300–302°C (from ethanol–water); $[\alpha]_D$ −67.9° (*c* 0.67, H_2O) (lit. (3) mp 298–300°C (dec.); $[\alpha]_D$ −65.8° (*c* 0.53, H_2O). The ^1H NMR spectrum of **9** was identical with that of the authentic sample (3).

8-Methoxycarbonyloctyl 2-acetamido-4-O-(2'-acetamido-2'-deoxy-3',4'-6'-tri-O-acetyl-β-D-glucopyranosyl)-3-O-acetyl-2-deoxy-6-O-(2'',3'',4''-tri-O-acetyl-α-L-fucopyranosyl)-β-D-glucopyranoside (10)

To solid titanium(IV) bromide (0.79 g) was added a solution of α-1-*O*-acetyl trisaccharide **7** (124 mg, 0.137 mmol) in dry dichloromethane (4 mL) stirring at 0°C, followed by an addition of ethyl acetate (1 mL) (21). The reaction mixture was stirred at room temperature for 17 h. Then it was diluted with dry dichloromethane (15 mL), anhydrous sodium acetate (1.5 g) was added, and after stirring for 15 min it was shaken with ice-water (25 mL). The product was then extracted into dichloromethane (70 mL), dried over $MgSO_4$, and the solvents were evaporated and coevaporated with toluene (100 mL) to give pale yellow solid bromide (96 mg). It was treated with 8-methoxycarbonyl-octanol (25) (400 mg, 2.12 mmol) and *p*-toluenesulfonic acid (3 mg) in dichloromethane (2 mL) at room temperature for 26 h. The reaction mixture was then diluted with dichloromethane (70 mL) and poured into ice-water (20 mL). The usual work-up gave a crude product, which after chromatography on a silica gel column (ethyl acetate) yielded pure

10 (38 mg, 27%); $[\alpha]_D$ −68.5° (*c* 0.99, $CHCl_3$) (lit. (1) $[\alpha]_D$ −69.2° (*c* 1.0, $CHCl_3$)); R_f and ^1H NMR were identical with those of an authentic sample (1).

*8-Methoxycarbonyloctyl 2-acetamido-4-*O*-(2′-acetamido-2′-deoxy-β-*D*-glucopyranosyl)-2-deoxy-6-*O*-α-fucopyranosyl-p-*D*-glycopyranoside (**11**)*

Zemplen deacetylation of **10** (52 mg, 0.050 mmol) in dry methanol (2 mL) was done as described previously (1), using 1% sodium methoxide (1 mL) and neutralizing acidic resin (0.5 mL). The trisaccharide **11** (37 mg, 100%) was obtained as a colourless solid, mp 282–286°C (aqueous ethanol); $[\alpha]_D$ −60.6° (*c* 0.31, 50% aqueous ethanol); (lit. (1) mp 283–286°C; $[\alpha]_D$ −63.5° (*c* 0.42, 50% aqueous ethanol). The ^1H NMR was identical with that of the authentic sample (1).

*2-Acetamido-4-*O*-(2′-acetamido-2′-deoxy-3′,4′-6′-tri-*O*-acetyl-β-*D*-glucopyranosyl)-3-*O*-acetyl-2-deoxy-6-*O*-(2″,3″,4″-tri-*O*-acetyl-α-*L*-fucopyranosyl)-β-*D*-glucopyranosyl isothiocyanate (**12**)*

Trisaccharide **7** (308 mg, 0.340 mmol) was treated with titanium(IV) bromide (1.68 g) in dichloromethane (15 mL) and ethyl acetate (4 mL) as described for compound **10**. The reaction mixture was diluted after 4.5 h with dry dichloromethane (50 mL) and after the usual work-up (using anhydrous sodium acetate (5 g), ice-water (100 mL), dichloromethane (220 mL), and toluene (2 × 50 mL)) a pale yellow solid bromide (229 mg) was obtained. It was treated (26) with potassium thiocyanate (0.5 g) and *p*-toluenesulfonic acid monohydrate (50 mg) in acetonitrile (10 mL) at 70°C (bath temperature) for 15 min. Then the reaction mixture was cooled, diluted with dichloromethane (100 mL), washed with water (50 mL), and the organic layer was dried over $MgSO_4$ and evaporated to give a light yellow solid (220 mg). By chromatography on a silica gel column using chloroform–acetone, 37:13 (followed by solvent ratio 2:1), pure **12** (161 mg, 53%) was obtained as a colourless solid; mp 155–157°C (ethyl acetane – hexane); $[\alpha]_D$ −74.2° (*c* 0.67, $CHCl_3$); R_f 0.34 (twofold development in chloroform–acetone, 2:1); IR (neat). 3320 (NH), 2022(-NCS), 1750 (COOR), 1670 (CONH) cm^{-1}; ^1H NMR (δ): 6.03 (br, d, 1H *J* = 8.6 Hz, exchangeable with D_2O, N*H*), 5.81 (d, 1H, *J* = 7.9 Hz exchangeable with D_2O, N*H*′), 5.39 (dd, 1H, *J* = 10.8 and 3.2 Hz, H-3″), 5.32 (br d, 1H, *J* = 3.2 Hz, H-4″), 5.18 (dd, 1H, *J* = 10.8 and 3.6 Hz, H-2″), 5.09 (d, 1H, *J* = 3.6 Hz, H-1″), 5.06 (d, 1H, *J* = 8.3 Hz, H-1), 4.92 (d, 1H, *J* = 8.3 Hz, H-1′), 4.27 (br q, 1H, *J* = 6.5 Hz, H-5″), 3.57 (m, 1H, became dd after exchange with D_2O, *J* = 10.4 and 8.3 Hz, H-2′), 2.18, 2.16, 2.10, 2.08, 2.02, 2.01, and 1.92 (7s, 27H, C*H*$_3$CO), 1.17 (d, 3H, *J* = 6.5 Hz, H-6″). Anal. calcd. for $C_{37}H_{51}N_3SO_{21}$: C 49.06, H 5.68, N 4.64, S 3.54; found: C 49.26, H 5.56, N 4.81, S 3.62.

*2-Acetamido-4-*O*-(2′-acetamido-2′-deoxy-3′,4′-6′-tri-*O*-acetyl-β-*D*-glucopyranosyl)-3-*O*-acetyl-2-deoxy-6-*O*-(2″,3″,4″-tri-*O*-acetyl-α-*L*-fucopyranosyl)-1-*N*-[1-benzyl *N*-(benzyloxy)carbonyl-*L*-aspart-4-oyl]-β-*D*-glucopyranosylamine (**13**)*

A mixture of isothiocyanate **12** (114 mg, 0.126 mmol), 1-benzyl *N*-(benzyloxy)carbonyl-L-aspartate (134 mg, 0.378 mmol), and triethylamine (0.03, 0.192 mmol) in dry toluene (2.5 mL) was stirred (18) at room temperature for 71 h. Then it was diluted with chloroform (70 mL), and the chloroform solution was washed successively with cold (0°C) aqueous sodium bicarbonate (20 mL) and water (20 mL). The chloroform solution was dried over $MgSO_4$ and evaporated to give a pale yellow syrup (185 mg), which after chromatography on a silica gel column (chloroform–acetone, 37:13) yielded pure **13** (49 mg, 32%) as a colourless solid, mp 185°C (with sintering at 128°C; recrystallized from hexane – methanol); $[\alpha]_D$ −43.7° (*c* 0.51, $CHCl_3$); R_f 0.35 (fivefold development in $CHCl_3$–acetone, 37:13); IR (neat):3360 (NH), 3062 and 3036 (aromatic C—H), 1750 (COOR), 1678 (CONH) cm^{-1}; ^1H NMR (δ): 7.30 (m, 10H, $C_6H_5CH_2$), 5.50 (t, 1H, *J* = 9.7 Hz, H-3′), 5.36 (dd, 1H, *J* = 10.8 and 3.2 Hz, H-3″), 5.29 (br d, 1H, *J* = 3.0 Hz, H-4″), 5.21 (d, 1H, *J* approx. 9.0 Hz, H-1′), 5.06 (d, 1H, *J* = 3.6 Hz, H-1″), 5.01 (t, 1H, *J* = 9.7 Hz, H-4′), 4.73 (br t, 1H, *J* approx. 8.6 Hz; became d after exchange with D_2O, *J* = 9.7 Hz, H-1) 4.64 (m, 1H, became t after exchange with D_2O, *J* = 3.6 Hz, H-2 (asparagine)), 4.29 (br q, 1H, *J* = 6.5 Hz, H-5″), 4.02 (br q, 1H, became t after exchange with D_2O, *J* = 10.0 Hz, H-2), 3.90 (t, 1H, *J* = 9.4 Hz, H-4), 3.54 (br d, 1H, *J* = 9.4 Hz, H-5), 3.20 (m, 1H, became br t after exchange with D_2O, *J* approx. 9.3 Hz, H-2′), 2.85 (dd, 1H, *J* = 16.2 and 4.0 Hz, H-3 (asparagine)), 2.68 (dd, 1H, *J* = 16.2 and 4.0 Hz, H-3) (asparagine)), 2.15, 2.13, 2.05, 2.00, 1.99, 1.91, and 1.86 (7s, 27H, C*H*$_3$CO), 1.03 (d, 3H, *J* = 6.5 Hz, H-6″). Anal. calcd. for $C_{55}H_{70}N_4O_{26}$: C 54.91, H 5.87, N 4.66; found: C 54.72, H 5.71, N 4.83.

Acknowledgements

This work was supported by the Ludwig Institute for Cancer Research. We thank Mrs. L. N. Congson for technical assistance and Mr. J. McGoey for recording the NMR spectra.

1. H. H. Lee, D. A. Schwartz, J. F. Harris, J. P. Carver, and J. J. Krepinsky. Can. J. Chem. **64**, 1912 (1986).
2. M. Bergmann, L. Zervas, and E. Silberkweit. Ber. Dtsch. Chem. Ges. **64**, 2436 (1931).
3. D. A. Schwartz, H. H. Lee, J. P. Carver, and J. J. Krepinsky. Can. J. Chem. **63**, 1073 (1985).
4. H. Kunz and C. Unverzagt. Angew. Chem. Int. Ed. Engl. **27**, 1697 (1988).
5. H. Paulsen. Angew. Chem. Int. Ed. Engl. **21**, 155 (1982).
6. T. Ogawa, S. Nakabayashi, and S. Shibata. Carbohydr. Res. **86**, C7 (1980).
7. T. Takeda, Y. Sugiura, C. Hamada, R. Fujii, K. Suzuki, Y. Ogihara, and S. Shibata. Chem. Pharm. Bull. **29**, 3196 (1981).
8. H. G. Garg and R. W. Jeanloz. Carbohydr. Res. **43**, 371 (1975).
9. D. E. Cowley, L. Hough, and C. M. Peach. Carbohydr. Res. **19**, 231 (1971).
10. M. Kiyozumi, K. Kato, T. Komori, A. Yamamoto, and H. Tsukamoto. Carbohydr. Res. **14**, 355 (1970).
11. M. Spinola and R. W. Jeanloz. J. Biol. Chem. **245**, 4158 (1970).
12. M. Shaban and R. W. Jeanloz. Carbohydr. Res. **21**, 347 (1972).
13. C. H. Bolton, L. Hough, and M. Y. Khan. Biochem. J. **101**, 184 (1966).
14. M. Tamura, H. Nishizaki, C. Miyazaki, and H. Okai. Bull. Chem. Soc. Jpn. **37**, 3167 (1984).
15. H. Kunz and H. Kauth. Liebigs Ann. Chem. 337 (1983).
16. D. Dunstan and L. Hough. Carbohydr. Res. **23**, 17 (1972).
17. M. J. Camarasa, P. Fernandez-Resa, M. T. Garcia-Lopez, F. G. de las Heras, P. P. Mendez-Castrillon, and A. San Felix. Synthesis, 509 (1984).
18. A. Y. Khorlin, S. E. Zurabyan, and R. G. Macharadze. Carbohydr. Res. **85**, 201 (1980).
19. L. M. Likhosherstov, O. S. Novikova, V. A. Derevitskaja, and N. A. Kochetkov. Carbohydr. Res. **146**, C1 (1986).
20. O. L. Galmarini and I. O. Mastronardi. Carbohydr. Res. **21**, 476 (1972).
21. H. Paulsen and H. Bunsch. Chem. Ber. **114**, 3126 (1981).
22. S. Nakabayashi, C. D. Warren and R. W. Jeanloz. Carbohydr. Res. **174**, 279 (1988).
23. T. Osawa. Carbohydr. Res. **1**, 435 (1966).
24. K. I. Takeo and K. Shinmitsu. Carbohydr. Res. **133**, 135 (1984).
25. R. U. Lemieux, D. R. Bundle, and D. A. Baker. J. Am. Chem. Soc. **97**, 4076 (1975).
26. F. Micheel, H. Peterson, and H. Kochling. Chem. Ber. **93**, 1 (1960).

Can. J. Chem. Downloaded from www.nrcresearchpress.com by 88.85.125.76 on 09/07/12
For personal use only.

On the relationship between thermodynamic pK_a's of azoles and the oxidation potentials of their pentacyanoferrate(II) complexes

VICENTA LOPEZ AND JAVIER CATALAN

Departamento de Química, Facultad de Ciencias, Universidad Autónoma de Madrid, Cantoblanco, 28049 Madrid, Spain

AND

ROSA M^A CLARAMUNT, CONCEPCION LOPEZ, EDUARDO CAYON,[1] AND JOSE ELGUERO

Departamento de Química Orgánica and Instituto de Química Médica, UNED and CSIC, Ciudad Universitaria, 28040 Madrid, Spain

Received August 20, 1989

VICENTA LOPEZ, JAVIER CATALAN, ROSA M^A CLARAMUNT, CONCEPCION LOPEZ, EDUARDO CAYON, and JOSE ELGUERO. Can. J. Chem. **68**, 958 (1990).

The comparison between thermodynamic pK_a values and oxidation potentials of the pentacyanoferrate(II) complexes of a series of azoles shows the existence of two parallel lines: one for pyrazoles and another one for benzazoles. Using the equation corresponding to the second one, the pK_a value of 1-methylbenzotriazole (2.49) can be estimated from the $E_{1/2}$ value of its complex.

Key words: azole basicity, oxidation potentials, pyrazoles, benzotriazoles.

VICENTA LOPEZ, JAVIER CATALAN, ROSA M^A CLARAMUNT, CONCEPCION LOPEZ, EDUARDO CAYON et JOSE ELGUERO. Can. J. Chem. **68**, 958 (1990).

La comparaison entre les pK_a thermodynamiques d'une série d'azoles et les potentiels d'oxydation de leurs complexes avec l'anion pentacyanoferrate(II) montre l'existence de deux relations linéaires, une pour les pyrazoles et l'autre pour les benzazoles. La seconde permet d'estimer le pK_a du méthyl-1 benzotriazole (2,49) à partir de la valeur de $E_{1/2}$ de son complexe.

Mots clés : basicité des azoles, potentiels d'oxydation, pyrazoles, benzotriazoles.

[Traduit par la revue]

Can. J. Chem. Downloaded from www.nrcresearchpress.com by 88.85.125.76 on 09/07/12
For personal use only.

Introduction

Our interest in the acid–base properties of azoles (1) prompted us to study Brisset and Ilimby's method (2) of indirect determination of the basicity of pyrazoles and indazoles. This method has the advantage that it can be used to determine the pK_a of very weak bases. Since $E_{1/2}$ is constant for a wide range of pH values, it is possible to determine the pK_a value without reaching the pH zone corresponding to the pK_a. Following previous studies on pyridines, these authors determined the oxidation potentials $E_{1/2}$ (in mV) of the pentacyanoferrate(II) complexes of five pyrazoles (pyrazole itself, 3(5)-methylpyrazole, 3,5-dimethylpyrazole, 4-chloropyrazole, and 1-methylpyrazole) and of indazole, and postulated the existence of a linear relationship between $E_{1/2}$ and the corresponding pK_a (proton gain) of the free ligands:

[1] $$E_{1/2} = 309.43 - 41.65\, p\mathrm{K_a} \qquad n = 6,\ r^2 = 0.98$$

With this equation and the experimental $E_{1/2}$ values of other pyrazoles and indazoles they predicted the pK_a of the following compounds: 1-acetylpyrazole (2.99, reported in ref. 1), 4-nitroindazole (0.25, reported in ref. 1), 5-nitroindazole (−0.04), 6-nitroindazole (0.49), 7-nitroindazole (−1.00, reported in ref. 1), and 5,6-dinitroindazole (−0.90, reported in ref. 1). The values for 5- and 6-nitroindazoles were not reported in ref. 1 since we had previously determined (3) their thermodynamic pK_a's (−0.96 and −0.97, respectively).

Due to the discrepancies involving the last two compounds, we decided to test the method of Brisset and Ilimby (2) using a larger and better-balanced set of azoles.

TABLE 1. Half-wave potentials (mV) of the complexes and pK_a values (proton gain) of the azole ligand

No.	Ligand	E^a1/2	pK_a^b
1	Pyrazole	192 R	2.48
2	3(5)-Methyl	152 R	3.27
3	3,5-Dimethyl	136 R	4.06
4	1,3,5-Trimethyl	160.5 QR	3.74
5	4-Phenyl	203.5 QR	1.64
6	3,5-Diphenyl	198.5 NR	1.75
7	4-Bromo	240 R	0.63
8	1-Nitro	180.5 NR	−4.15
9	3(5)-Nitro	332.5 NR	−4.66
10	4-Nitro	301 R	−2.0
11	3,5-Dimethyl-4-nitro	263 NR	−0.45
12	1,2,4-Triazole	233.5 QR	2.45
13	Benzimidazole	140 QR	5.56
14	2-Methyl	127.5 QR	6.19
15	1-Ethyl-2-methyl	128 QR	6.30
16	Indazole	265.5 QR	1.04
17	5-Nitro	317.5 NR	−0.96
18	6-Nitro	323.5 QR	−0.97
19	Benzotriazole	243.5 QR	1.6
20	1-Methyl	226 R	[c]

[a] R: reversible, QR: quasi-reversible, NR: not reversible.
[b] All values from ref. 1 save that of compound **15** taken from ref. 5.
[c] Unknown.

Experimental

All the compounds are commercially available or were prepared by conventional methods (4). The complexes were prepared *in situ* by dissolving solid $Na_3Fe(CN)_5NH_3$ (2) and the corresponding azole or benzazole in a ratio close to 1:10 in a 0.5 M electrolytic solution of $NaClO_4$. The pH was varied by small additions of strong acid ($HClO_4$) or base (NaOH). The electrochemical method used was identical to that described by Brisset and Ilimby (2).

[1] On leave from the Universidad Autónoma de Barcelona, Spain.

Printed in Canada / Imprimé au Canada

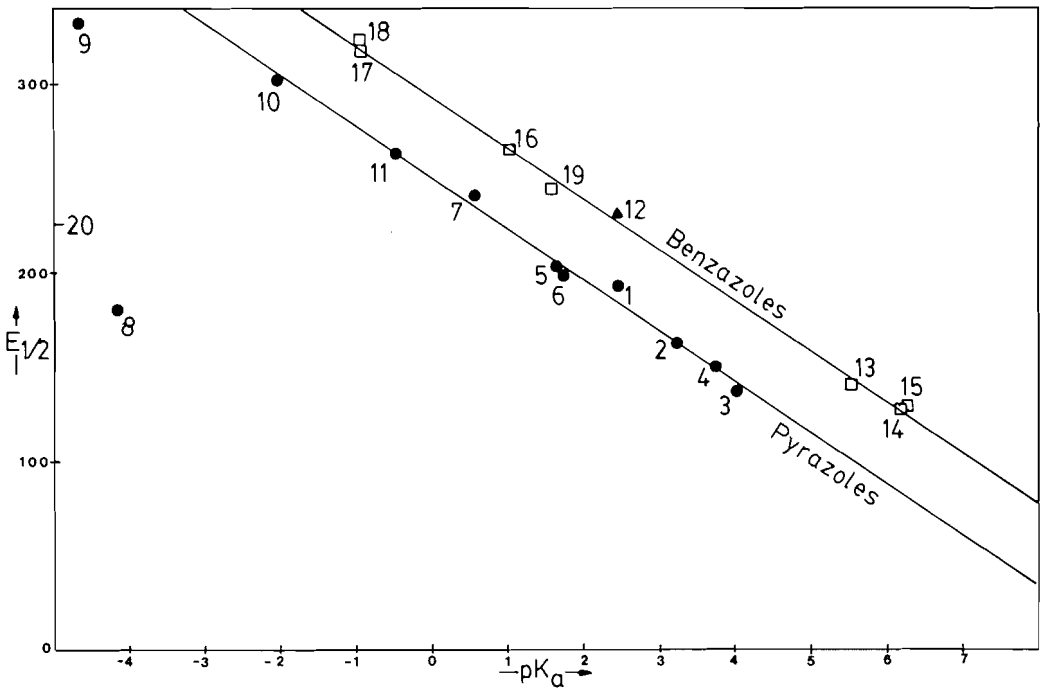

FIG. 1. Representation of the half-wave potentials vs. the pK_a's. Pyrazoles (●); benzazoles (□); 1,2,4-triazole (▲).

Results and discussion

Table 1 contains the $E_{1/2}$ values determined here together with the thermodynamic pK_a values; the corresponding bi-dimensional plot is that represented in Fig. 1.

The following conclusions can be drawn:

(i) Two *parallel* lines are observed, pyrazoles having a special behaviour as in other studies dealing with their basicity or acidity (6, 7).

(ii) *All* benzazoles have been included in the linear regression, which yields eq. [2].

[2] $E_{1/2} = 292.7 - 26.8\,p\mathrm{K_a}$ $\quad n = 7,\ r^2 = 0.998$

(iii) Nitropyrazoles **8** and **9** have been excluded from the regression leading to eq. [3].

[3] $E_{1/2} = 250.2 - 26.8\,p\mathrm{K_a}$ $\quad n = 9,\ r^2 = 0.98$

(iv) 1,2,4-Triazole **12** is near the line for the benzazoles. From eq. [2']

[2'] $p\mathrm{K_a} = 10.9 - 0.037\ \mathrm{E_{1/2}}$

and from the $E_{1/2}$ value of 1-methylbenzotriazole **20**, its pK_a can be estimated (2.49). The pyrazoles that behave abnormally, **8** and **9**, both have a nitro group near the basic center:

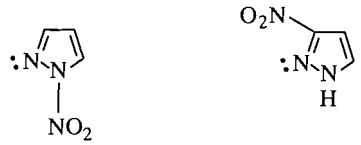

8

9

This situation could interfere with the complex formation.

The fact that the value of the slope in eq. [1] is twice those of eqs. [2] and [3] results from the fact that it was calculated using points belonging to both lines, pyrazoles **1**, **2**, **3**, and 4-chloropyrazole, and benzazoles, indazole **16**. With our values for compounds **1**, **2**, **3**, and **16**, the following equation is found: $E_{1/2} = 306.6 - 44.3\ p\mathrm{K_a}$, $n = 4$, $r^2 = 0.98$, which is close to eq. [1].

It is not possible to use the $E_{1/2}$ values of ref. 2 and our equations [2] and [3] to calculate the pK_a of the compounds studied by Brisset and Ilimby, since for common derivatives the $E_{1/2}$ values differ. However, with their $E_{1/2}$ value for 4-chloropyrazole (225), eq. [3] yields pK_a = 0.88, which is much closer to the thermodynamic value (0.59 (1)) than the value calculated with eq. [1] (1.86 (2)).

Acknowledgements

We thank the Comité Conjunto Hispano–Norteamericano para la Cooperación Científica y Tecnológica for financial support (CCB 86/04/009). One of us (C.L.) is indebted to the Consejería de Educación y Juventud de la Comunidad de Madrid of Spain for a grant.

1. J. CATALAN, J. L. M. ABBOUD, and J. ELGUERO. Adv. Heterocycl. Chem. **41**, 187 (1987).
2. J. L. BRISSET and V. ILIMBI. Can. J. Chem. **58**, 1250 (1980), and references therein.
3. J. ELGUERO, A. FRUCHIER, and R. JACQUIER. Bull. Soc. Chim. Fr. 2619 (1967).
4. A. R. KATRITZKY and C. W. REES. Comprehensive heterocyclic chemistry. Pergamon Press, Oxford. 1984.
5. M. KRISHNAMURTHY, P. PHANIRAJ, and S. K. DOGRA. J. Chem. Soc. Perkin Trans. 2, 1917 (1986).
6. J. CATALAN and J. ELGUERO. J. Chem. Soc. Perkin Trans. 2, 1869 (1983).
7. J. CATALAN, O. MO, J. L. G. DE PAZ, P. PEREZ, M. YAÑEZ, and J. ELGUERO. J. Org. Chem. **49**, 4379 (1984).

Can. J. Chem. Downloaded from www.nrcresearchpress.com by 88.85.125.76 on 09/07/12
For personal use only.

Resolution of β-hydroxy-α-amino acids by the action of proteases on their *N*-acyl methyl esters

ROBERT CHÊNEVERT,[1] MARTIN LÉTOURNEAU, AND SONIA THIBOUTOT

Département de chimie, Faculté des sciences et de génie, Université Laval, Québec (Québec), Canada G1K 7P4

Received May 18, 1989[2]

ROBERT CHÊNEVERT, MARTIN LÉTOURNEAU, and SONIA THIBOUTOT. Can. J. Chem. **68**, 960 (1990).

Methyl *N*-acetyl phenylserinates (**1**, **2**), methyl *N*-acetyl nitrophenylserinates (**3**, **4**), and methyl *N*-benzoyl threoninates (**5**, **6**) were resolved conveniently into the enantiomers with high optical purities by enzymatic hydrolysis in the presence of α-chymotrypsin, subtilisin, or bromelain. The *threo* and *erythro* forms were treated separately and the latter form was usually more reactive. Chymotrypsin and subtilisin are highly specific for the enantiomer having the same configuration on carbon-2 (*S*) as the natural standard amino acids. In contrast, bromelain shows the reverse specificity on phenylserine derivatives. This is a notable exception to the usual *S*-stereospecificity pattern of proteases.

Key words: enzymatic hydrolysis, resolution of amino acids.

ROBERT CHÊNEVERT, MARTIN LÉTOURNEAU et SONIA THIBOUTOT. Can. J. Chem. **68**, 960 (1990).

Nous décrivons la résolution des *N*-acétyl phénylsérinates de méthyle (**1**, **2**), des *N*-acétyl *p*-nitrophénylsérinates de méthyle (**3**, **4**) et des *N*-benzoyl thréoninates de méthyle (**5**, **6**) par hydrolyse enzymatique en présence de l'α-chymotrypsine, de la subtilisine ou de la bromélaine. Les formes *thréo* et *erythro* ont été traitées séparément et la forme *érythro* est habituellement plus réactive. La chymotrypsine et la substilisine sont spécifiques pour l'énantiomère ayant la même configuration (*S*) que les acides aminés standards. Au contraire, la bromélaine montre une stéréospécificité inverse sur les dérivés de la phénylsérine. Il s'agit d'une exception notable à la stéréospécificité usuelle des protéases.

Mots clés : hydrolyse enzymatique, résolution des acides aminés.

Introduction

Hydrolytic enzymes are useful catalysts in asymmetric synthesis (1, 2). In recent years, several hydrolases have been used for the resolution of racemates (3–6) or the enantiotopic group differentiation in meso compounds (7–10). Hydrolases have proved particularly useful for the resolution of amino acids (11–13). Past studies on the enzymatic resolution of amino acids have been confined mostly to substrates with only one asymmetric center. We report here a study on the enzymatic resolution of β-hydroxy-α-amino acids by the action of proteases on their *N*-acyl methyl esters (14). These compounds exist in four stereoisomeric forms and enzymes can exhibit diastereoselectivity as well as enantioselectivity. β-Hydroxy-α-amino acids are frequently encountered as part structures of many biologically active compounds (11). *S*-Threonine is an essential amino acid. Derivatives of phenylserine are intermediates in the synthesis of natural compounds such as chloramphenicol (15), resolving reagents (16), chiral auxiliaries, and precursors to chiral 2-oxazolines (17).

Results and discussion

Methyl β-hydroxyl-*N*-acylamino esters **1**–**6** were obtained in their pure (±)-*threo* and (±)-*erythro* forms by literature methods. Methyl esters were selected because proteases usually show a higher rate of hydrolysis and a better enantioselectivity when the alcohol component of the ester is a methyl or a small group. Acylation of the amino group was necessary to meet the requirements of endopeptidases used in this study. The benzoyl group was preferred over the more usual acetyl group in the case of threonine because these derivatives are easier to purify and the corresponding *N*-benzoyl amino acids are easier to extract from the aqueous medium after the hydrolysis.

Preparative-scale (2–6 mmol) enzyme-catalyzed hydrolyses were performed in buffered aqueous solutions at pH 7–8. The enzymatic reaction was indicated by the decrease of pH, which was maintained at its initial value by the addition of a dilute sodium hydroxide solution. The reactions were monitored by the consumption of base and terminated when 50% of the ester was hydrolyzed. The unreacted esters were recovered from the reaction mixtures by extraction with ethyl acetate at pH 8. The product acids that are present in the aqueous phase as sodium salts were isolated by acidification to pH 2 and extraction with ethyl acetate. Samples of the acids were converted to their methyl esters before determining their optical purity. Enantiomeric excess (ee) values were determined by ^{1}H nmr analysis using tris[3-(heptafluoropropylhydroxymethylene)-*d*-camphorato]europium(III) as a chiral shift reagent. In every case, well-resolved signals were obtained for the ester methyl protons. Absolute configurations were assigned by chemical hydrolyses of the *N*-acylamino acids obtained from the enzymatic reactions and comparison with the optical rotation signs reported in the literature for these free amino acids. The results are summarized in Table 1.

Subtilisin exhibits wide substrate specificity and catalyzes the hydrolyses of all esters **1**–**6** with very high enantioselectivity. Chymotrypsin is also highly enantioselective but its substrate specificity is somewhat narrower and *threo-p*-nitrophenylserinate **3** is not a substrate. Both enzymes that are serine proteases catalyze the hydrolysis of the enantiomer having the same configuration on carbon-2 (*S*) as the natural standard amino acids.

Bromelain, a sulfhydryl protease, has a much narrower substrate specificity and only phenylserines **1** and **2** are hydrolyzed by this enzyme. The enantioselectivity is low for the *threo* form but very high for the *erythro* form. It is noteworthy that bromelain has the opposite enantioselectivity to chymotrypsin and subtilisin. Bromelain selectively hydrolyzes compounds with the *R* configuration on carbon-2. This is a notable exception to the usual *S*-stereoselectivity pattern of proteases.

Based on the time required to hydrolyze 50% of the racemic mixture under the same experimental conditions, the *erythro*

[1]Author to whom correspondence may be addressed.

[2]Revision received January 22, 1990.

Can. J. Chem. Downloaded from www.nrcresearchpress.com by 88.85.125.76 on 09/07/12
For personal use only.

TABLE 1. Protease-catalysed hydrolysis of compounds **1–6**[a,b]

Enzyme	Substrate	Time (h)	Recovered ester			Acid product		
			% Yield	% ee	Abs. conf.	% Yield	% ee	Abs. conf.
α-Chymotrypsin	1	3,5	96	89	2*R*3*S*	83	92	2*S*3*R*
	2	1	98	≥98	2*R*3*R*	67	≥98	2*S*3*S*
	3	—	—	—	—	—	—	—
	4	11	99	≥98	2*R*3*R*	88	≥98	2*S*3*S*
	5	5	98	92	2*R*3*S*	88	93	2*S*3*R*
	6	9	90	96	2*R*3*R*	92	96	2*S*3*S*
Subtilisin	1	10,5	100	≥98	2*R*3*S*	68	≥98	2*S*3*R*
	2	2	94	≥98	2*R*3*R*	64	≥98	2*S*3*S*
	3	23	94	≥98	2*R*3*S*	84	≥98	2*S*3*R*
	4	6,5	84	≥98	2*R*3*R*	96	≥98	2*S*3*S*
	5	15	96	≥98	2*R*3*S*	93	≥98	2*S*3*R*
	6	20	86	≥98	2*R*3*R*	88	≥98	2*S*3*S*
Bromelain	1	70	94	22	2*S*3*R*	64	17	2*R*3*S*
	2	48	96	≥98	2*S*3*S*	68	≥98	2*R*3*R*

[a]Average values of three runs.
[b]The ee values were determined by ^{1}H nmr (200 MHz) using the chiral shift reagent Eu(hfc)$_3$; the accuracy of this method is ±2%.

forms are more reactive than the *threo* forms for phenylserine and *p*-nitrophenylserine. In the threonine series, the difference of reactivity between the *threo* and *erythro* forms is small in favor of the *threo* form. Chymotrypsin is highly enantioselective and diastereoselective for *p*-nitrophenylserines. Similarly, Shiba and co-workers reported the enantio- and diastereoselective hydrolysis of β-hydroxyornithine by acylase (18). Esterase (pig liver), acetylesterase, and lipase (porcine pancreatic) are not active on compounds **1–6**. Also, these compounds are not substrates for other sulfhydryl proteases like papain, chymopapain, and ficin.

In previous studies (11–13), the resolutions of *RS*-threonine and *RS-allo*-threonine were achieved via asymmetric hydrolytic action of acylase on their *N*-chloroacetyl derivatives. Threonine has also been resolved by papain-catalyzed amidation of its *N*-capryloyl derivative with aniline. Acylase I and carboxypeptidase A were found ineffective toward either *N*-acetyl or *N*-chloroacetyl derivatives of β-phenylserines. However (±)-*threo* and (±)-*erythro* phenylserines have been resolved as the reactive *N*-trifluoroacetyl derivatives by carboxypeptidase.

The stereospecificity exhibited by chymotrypsin towards compounds **1–6** can be rationalized in terms of Cohen's active-site model (12). Figure 1 shows schematic representations of the binding of the good substrate *N*-acetyl-*S*-phenylalanine methyl ester (a), and *erythro* isomers of compounds **1–6** (b). The *ar*-site is a hydrophobic pocket large enough to accommodate aromatic or aliphatic groups. The *am*-site binds *N*-acyl groups by means of hydrogen bonding. The nucleophilic attack occurs at the *n*-site where the ester group is bonded. The hydrogen on carbon-2 fits into the volume restricted *h*-site. The stereochemical consequence of this topography is that only amino acids with the 2*S* configuration are hydrolyzed rapidly. This is what we observed with substrates **1–6**. For the preferred *erythro* stereoisomers, the 3*R*-OH group must occupy the position at the junction of *ar* and *h* sites (equivalent to the H_S position of the *N*-acetyl-*S*-phenylalanine methyl ester.

Subtilisin and chymotrypsin are both serine protease. They have a similar active site and often have the same stereoselectivity. However the substrate specificity of subtilisin is broader than that of chymotrypsin (12). Data in Table 1 confirm this statement.

Bromelain, a thiol protease, has not been exploited so far for resolution. Papain is the best documented member of the group and available data show that its enantioselectivity is not wholly predictable. Although an *S*-enantioselectivity is usual, several examples of reactions for which the *R* enantiomers are substrates have been reported (12).

Our results constitute a valuable alternative to the enzymatic resolution of threonines and phenylserines and provide the first enzymatic resolution of *p*-nitrophenylserines.

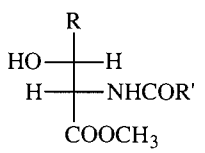

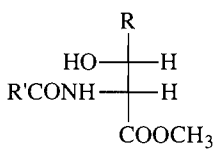

1: R = , R' = CH_3

2: R = 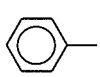 , R' = CH_3

3: R = NO_2 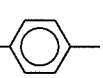 , R' = CH_3

4: R = NO_2 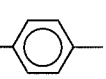 , R' = CH_3

5: R = CH_3, R' =

6: R = CH_3, R' = 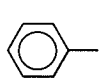

Can. J. Chem. Downloaded from www.nrcresearchpress.com by 88.85.125.76 on 09/07/12
For personal use only.

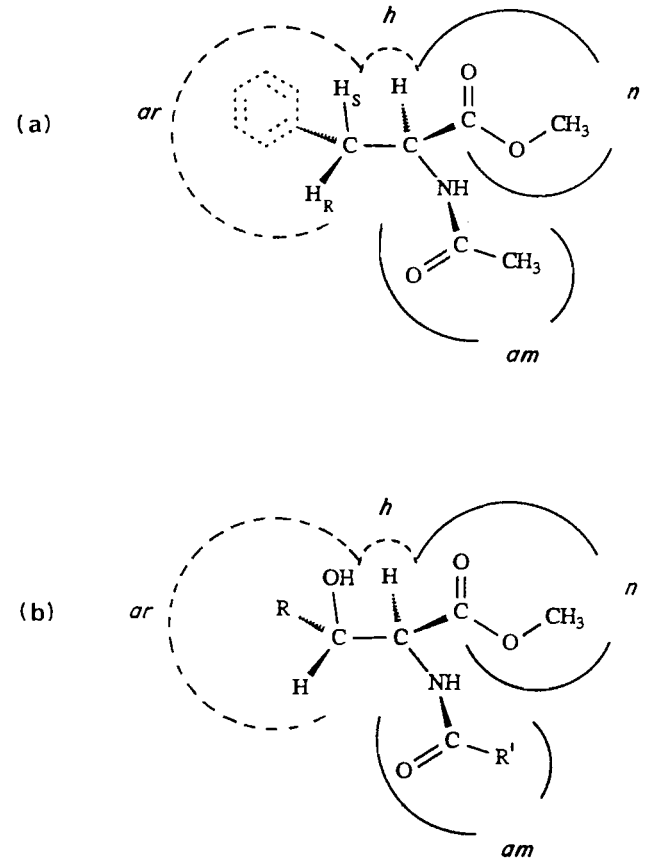

FIG. 1. The active site of α-chymotrypsin according to Cohen's model. (a) The binding of the good specific substrate *N*-acetyl-*S*-phenylalanine methyl ester, and (b) binding of *erythro* isomers of compounds **1–6**.

Experimental

Melting points were determined on a Thomas–Hoover capillary apparatus and are uncorrected. IR spectra were recorded on a Beckman 4250 spectrometer. NMR spectra were recorded on a Varian XL-200 multinuclear instrument. Optical rotations were measured with a Jasco DIP-360 digital polarimeter. α-Chymotrypsin (EC 3.4.21.1, type II), subtilisin (EC 3.4.21.14, Carlsberg, protease type VIII), and bromelain (EC 3.4.22.4) were purchased from Sigma.

Methyl (±)-threo-N-*acetyl-β-phenylserinate (1)*

Acetic anhydride (2.6 mL, 27 mmol) was added dropwise to a cold solution (5°C) of commercially available methyl (±)-*threo* β-phenylserinate hydrochloride (2.09 g, 9 mmol) and sodium acetate (2.96 g, 36 mmol) in 45 mL of water. The reaction mixture was stirred overnight at room temperature. The product was collected by filtration and recrystallized from water. Yield 87%; mp 182–183°C (lit. (19) mp 174–180°C); IR (KBr): 3410, 3205, 1750, 1540, 1305, 1220, 1150, 1100, 1070, 725 cm^{-1}; ^1H NMR (DMSO) δ: 1.76 (3H, s), 3.59 (3H, s), 4.53 (1H, dd, $J_1 = 7$ H, $J_2 = 3$ Hz), 5.08 (1H, dd, $J_1 = 3$ Hz, $J_2 = 5$ Hz), 5.83 (1H, d, $J = 5$ Hz), 7.29 (5H, m), 8.12 (1H, d, $J = 7$ Hz).

Methyl (±)-erythro-N-*acetyl-β-phenylserinate (2)*

Methyl (±)-*erythro*-β-phenylserinate was first prepared from methyl benzoylacetate (20) and then *N*-acetylated as described for the *threo* isomer. Yield 83%; mp 118–119°C (lit. (21) mp 120–122°C); IR (KBr): 3400, 3320, 1720, 1670, 1540, 1305, 1240, 1200, 1060, 730 cm^{-1}; ^1H NMR (DMSO) δ: 1.70 (3H, s), 3.59 (3H, s), 4.47 (1H, d, $J = 7$ Hz), 4.69 (1H, d, $J = 7$ Hz), 5.82 (1H, d, $J = 3$ Hz), 7.31 (5H, m), 8.26 (1H, d, $J = 8$ Hz).

Methyl (±)-threo-N-*acetyl*-p-*nitrophenylserinate (3)*

Methyl (±)-*threo-p*-nitrophenylserinate was first obtained by condensation of *p*-nitrobenzaldehyde with methyl glycinate according to the procedure of Ehrhart *et al.* (15) and then *N*-acetylated. The product was recrystallized in water/methanol. Yield 97%; mp 195–197°C (lit. (21) mp 198–200°C); IR (KBr): 3360, 3500–3100, 1745, 1650, 1520, 1340, 1215 cm^{-1}. ^1H NMR (DMSO) δ: 1.74 (3H, s), 3.65 (3H, s), 4.73 (1H, dd, $J_1 = 3.5$ Hz, $J_2 = 9$ Hz), 5.29 (1H, dd, $J_1 = 3.5$ Hz, $J_2 = 5$ Hz), 6.21 (1H, d, $J = 5$ Hz), 7.70 (2H, d, $J = 9$ Hz), 8.16 (2H, d, $J = 9$ Hz), 8.27 (1H, d, $J = 9$ Hz).

Methyl (±)-erythro-N-*acetyl*-p-*nitrophenylserinate (4)*

This compound was prepared according to the procedure of Bergmann *et al.* (22). Yield 91%; mp 179–181°C (lit. (21) mp 181–184°C); IR (KBr): 3300, 1735, 1635, 1500, 1330, 1200 cm^{-1}. ^1H NMR δ: 1.73 (3H, s), 3.59 (3H, s), 4.52 (1H, dd, $J_1 = J_2 = 8.5$ Hz), 4.85 (1H, dd, $J_1 = 8.5$ Hz, $J_2 = 7$ Hz), 6.14 (1H, d, $J = 7$ Hz), 7.62 (2H, d, $J = 8.5$ Hz), 8.18 (2H, d, $J = 8.5$ Hz), 8.43 (1H, d, $J = 8.5$ Hz).

Methyl N-*benzoyl (±)-threoninate (5)*

Commercially available (±)-threonine methyl ester hydrochloride (11.5 g, 68 mmol) was dissolved in 100 mL of water/dioxane (2:1). Benzoyl chloride (6.20 mL, 68 mmol) was added dropwise over a period of 1 h. The pH of the solution was maintained at 8.5–9.0 by addition of 4 M aqueous NaOH and the temperature was kept below 30°C. Dioxane was removed under reduced pressure and the aqueous phase was extracted with ethyl acetate. The organic phase was dried ($MgSO_4$) and evaporated under vacuum to give an oil that crystallized on standing. The crude product was recrystallized from chloroform. Yield 64%; mp 94–95.5°C (lit. (23) mp 92–94°C); IR (KBr): 3415, 3320, 1745, 1640, 1520, 1260, 1110, 1020, 780, 710 cm^{-1}; ^1H NMR (DMSO) δ: 1.16 (3H, d, $J = 4$ Hz), 3.65 (3H, s), 4.18 (1H, m), 4.51 (1H, dd, $J_1 = 5$ Hz, $J_2 = 2$ Hz), 4.95 (1H, d, $J = 4$ Hz), 7.52 (3H, m), 7.88 (2H, dd, $J_o = 5$ Hz, $J_m = 1$ Hz), 8.20 (1H, d, $J = 5$ Hz).

Methyl N-*benzoyl (±)*-allo-*threoninate (6)*

Prepared by esterification and benzoylation of commercial (±)-*allo*-threonine. Yield 57%; mp 95–96°C (lit. (24) mp 110–111°C); IR (KBr): 3415, 3320, 1745, 1640, 1520, 1260, 1110, 1020, 710 cm^{-1}; ^1H NMR (DMSO) δ: 1.25 (3H, d, $J = 4$ Hz), 3.72 (1H, m), 3.83 (3H, s), 4.31 (1H, m) 4.89 (1H, dd, $J_1 = 4$ Hz, $J_2 = 2$ Hz), 7.19 (1H, d, $J = 4$ Hz), 7.49 (3H, m), 7.82 (2H, dd, $J_o = 4$ Hz, $J_m = 0.5$ Hz).

Enzyme-catalyzed hydrolyses of methyl β-hydroxy-N-*acyl-α-amino-esters. General procedure*

The ester (2 mmol) was suspended in a buffered aqueous solution (50 mL) at room temperature. The enzyme was added and the pH of the solution was maintained at its initial value by addition of 0.1 M aqueous NaOH. The reaction was stopped at the 50%-of-hydrolysis point (reaction times are reported in Table 1). The reaction mixture was first extracted at initial pH with ethyl acetate (3 × 250 mL) to remove the unchanged ester. The aqueous mixture was then acidified to pH 2.0 with cold 2 M aqueous HCl and was extracted with ethyl acetate (3 × 250 mL) again to remove the product acid. Organic extracts were dried ($MgSO_4$) and evaporated under vacuum. Details pertaining to each enzyme are the following. α-Chymotrypsin: enzyme (20 mg, 800 units), solvent (phosphate buffer, pH 7.70). Subtilisin: enzyme (60 mg, 800 units), solvent (phosphate buffer, pH 7.70). Bromelain: enzyme (1300 mg, 800 units), solvent (phosphate buffer, pH 6.00), catalytically essential sulfhydryl groups of the enzyme were activated by cysteine (200 mg).

Properties of recovered esters

The physical and spectral properties of recovered esters were identical with those reported above, except for the magnitudes of their rotations. The $[\alpha]_D^{25}$ values observed for recovered esters were as follows:

Substrate **1**: (2*R*, 3*S*), [α] = −27.6° (*c* 2.0, acetic acid).
Substrate **2**: (2*R*, 3*R*), [α] = −62.8° (*c* 2.0, acetic acid); (2*S*, 3*S*), [α] = +62.6° (*c* 2, acetic acid).
Substrate **3**: (2*R*, 3*S*), [α] = −36.6° (*c* 1.0, methanol).
Substrate **4**: (2*R*, 3*R*), [α] = −48.0° (*c* 1.0, methanol).
Substrate **5**: (2*R*, 3*S*), [α] = −22.8° (*c* 1.0, ethanol).
Substrate **6**: (2*R*, 3*R*), [α] = −5.8° (*c* 1.0, methanol).

Can. J. Chem. Downloaded from www.nrcresearchpress.com by 88.85.125.76 on 09/07/12
For personal use only.

Properties of acid products

threo-N-*Acetyl-β-phenylserine*: mp 163–164°C. IR (KBr): 3505, 3320, 3080, 3025, 2980, 1695, 1615, 1555, 1495, 1365, 1250, 1115, 1040, 760, 695 cm^{-1}. ^1H NMR (DMSO) δ: 1.74 (3H, s), 4.46 (1H, dd, J_1 = 5 Hz, J_2 = 1 Hz), 5.12 (1H, d, J = 1 Hz), 5.80 (2H, m), 7.35 (5H, m), 7.97 (1H, d, J = 5 Hz). [α] for the 2*S*,3*R* isomer, +29.7° (*c* 2.0, acetic acid).

erythro-N-*Acetyl-β-phenylserine:* mp 177–178°C. IR (KBr): 3540, 3320, 3080, 3025, 2980, 1695, 1615, 1555, 1495, 1365, 1250, 1115, 1040, 760, 695 cm^{-1}. ^1H NMR (DMSO) δ: 1.7 (3H, s), 4.42 (1H, dd, J_1 = 5 Hz, J_2 = 8 Hz), 4.69 (1H, d, J = 8 Hz), 7.34 (5H, m), 8.11 (1H, d, J = 5 Hz). [α] for the 2*S*,3*S* isomer, +64.9° (*c* 2.0, acetic acid); 2*S*,3*S* isomer, −63.9° (*c* 2.0, acetic acid).

threo-N-*Acetyl*-p-*nitrophenylserine:* mp 160–172°C. IR (KBr): 3585, 3400, 3090, 3035, 2985, 1710, 1660, 1610, 1550, 1530, 1500, 1345, 1250, 1190, 1140, 1065, 855, 710 cm^{-1}. ^1H NMR (DMSO) δ: 1.79 (3H, s), 4.75 (1H, dd, J_1 = 5 Hz, J_2 = 1 Hz), 5.41 (1H, d, J = 1 Hz), 7.76 (2H, d, J = 4 Hz), 7.84 (1H, d, J = 5 Hz), 8.18 (2H, d, J = 4 Hz). [α] for the 2*S*,3*R* isomer, +27.4 (*c* 1.0, methanol).

erythro-N-*Acetyl*-p-*nitrophenylserine*: mp 147–148°C. IR (KBr): 3440, 3380, 3090, 3030, 2985, 1705, 1660, 1610, 1550, 1530, 1500, 1345, 1250, 1190, 1140, 1065, 855, 710 cm^{-1}. ^1H NMR (DMSO) δ: 1.76 (3H, s), 4.50 (1H, dd, J_1 = 5 Hz, J_2 = 4 Hz), 4.88 (1H, d, J = 4 Hz), 7.66 (2H, d, J = 4 Hz), 8.22 (2H, d, J = 4 Hz), 8.28 (1H, d, J = 5 Hz). [α] for the 2*S*,3*S* isomer, +65.2° (*c* 1.0, methanol).

threo-N-*Benzoyl-threonine*: mp 137–138°C. IR (KBr): 3405, 3106, 3015, 2975, 1760, 1700, 1530, 1340, 1210, 1110, 710 cm^{-1}. ^1H NMR (DMSO) δ: 1.13 (3H, d, J = 6 Hz), 4.19 (1H, m), 4.44 (1H, dd, J_1 = 4 Hz, J_2 = 2 Hz), 4.51 (1H, m), 7.52 (3H, m), 7.87 (2H, dd, J_1 = 5 Hz, J_2 = 1 Hz), 8.05 (1H, d, J = 4 Hz), 12.32 (1H, m). [α] for the 2*S*,3*R* isomer, +33.4° (*c* 1.0, methanol).

erythro-N-*Benzoyl-threonine*: mp 132–133°C. IR (KBr): 3425, 3200, 3015, 2975, 1765, 1705, 1530, 1340, 1210, 1110, 1095, 710 cm^{-1}. ^1H NMR (DMSO) δ: 1.21 (3H, d, J = 6 Hz), 4.06 (1H, m), 4.39 (1H, dd, J_1 = 8 Hz, J_2 = 4 Hz), 7.52 (3H, m) 7.87 (2H, dd, J_1 = 6 Hz, J_2 = 1 Hz), 8.38 (1H, d, J = 8 Hz), 12.14 (1H, m). [α] for the 2*S*,3*S* isomer, +23.9° (*c* 1.0, methanol).

Absolute configuration

For substrates **1** and **2**, absolute configurations were assigned by chemical hydrolyses of the *N*-acylamino acids obtained from the enzymatic reactions and comparison with the optical rotation signs reported in the literature for these free amino acids. 2*S*,3*R*, [α] = −29.2 (*c* 0.5, H_2O) (lit. (25) α = −31.1° (*c* 1.0, H_2O)); 2*S*,3*S*, [α] = +7.9° (*c* 0.5, H_2O) (lit. (25) [α] = +8.2° (*c* 1.0, H_2O)). For substrates **3–6**, absolute configurations were assigned by comparison of optical rotation signs of recovered esters or acid products, or both, with signs reported in the literature for these compounds.

Substrate **3**: 2*R*,3*S* ester, [α] = −36.6° (*c* 1.0, methanol) (lit. (26) [α] = −37.6° (*c* 1, methanol)). 2*S*,3*R* acid, [α] = +27.4° (*c* 1.0 methanol) (lit. (26) [α] = +27.4° (*c* 1.0, methanol)).

Substrate **4**: 2*R*,3*R* ester, [α] = −40.6° (*c* 4.0, methanol) (lit. (26) [α] = −40.0° (*c* 4.0, methanol)).

Substrate **5**: 2*R*,3*S* recovered ester, [α] = −22.3° (*c* 1.0, ethanol) (lit. (23) [α] = −22.0 (*c* 6.0, ethanol)).

Substrate **6**: 2*S*,3*S* acid, [α] = +22.9° (*c* 0.5, methanol) (lit. (24) [α] = +23.7° (*c* 1.0, methanol)).

Acknowledgments

Financial support of this work by the Natural Sciences and Engineering Research Council of Canada and the Ministère de l'Education du Québec is gratefully acknowledged.

1. J. B. Jones. Tetrahedron, **42**, 3351 (1986).
2. G. M. Whitesides and C. H. Wong. Angew. Chem. Int. Ed. Engl. **24**, 617 (1985).
3. K. Laumen and M. P. Schneider. J. Chem. Soc. Chem. Commun. 598 (1988).
4. P. E. Sonnet. J. Org. Chem. **52**, 3477 (1987).
5. G. Kirchner, M. P. Scollar, and A. M. Klibanov. J. Am. Chem. Soc. **107**, 7072 (1985).
6. M. Schneider, N. Engel, and M. Boensmann. Angew. Chem. Int. Ed. Engl. **23**, 64 (1984).
7. J. Zemlicka, L. E. Craine, M. J. Heeg, and J. P. Olivier. J. Org. Chem. **53**, 937 (1988).
8. G. Sabbioni and J. B. Jones. J. Org. Chem. **52**, 4565 (1987).
9. R. Roy and A. W. Rey. Tetrahedron Lett. **28**, 4935 (1987).
10. M. Luyten, S. Muller, B. Herzog, and R. Keese. Helv. Chim. Acta, **70**, 1250 (1987).
11. G. C. Barrett. *In* Chemistry and biochemistry of the amino acids. Chapman and Hall, New York. 1984. Chap. 10. pp. 338–353.
12. J. B. Jones and J. F. Beck. *In* Applications of biochemical systems in organic chemistry. Part I. *Edited by* J. B. Jones, C. J. Sih, and D. Perlman. Wiley, New York. 1976. Chap. 4. pp. 107–401.
13. J. P. Greenstein and M. Winitz. *In* Chemistry of the amino acids. Vol. 1. Wiley, New York. 1961. Chap. 9. pp. 728–750.
14. R. Chênevert and M. Létourneau. Chem. Lett. 1151 (1986).
15. G. Ehrhart, W. Siedel, and H. Nahm. Chem. Ber. **90**, 2088 (1957).
16. J. Jacques., A. Collet, and S. H. Wilen. *In* Enantiomers, racemates, and resolutions. Wiley, New York. 1981. Chap. 5.
17. K. A. Lutomski and A. I. Meyers. *In* Asymmetric syntheses. Vol. 3. *Edited by* J. D. Morrison. Academic Press, New York. 1984. Chap. 3.
18. T. Teshima, K. Konishi, and T. Shiba. Bull. Chem. Soc. Jpn. **53**, 508 (1980).
19. D. O. Holland, P. A. Jenkins, and J. H. C. Nayler. J. Chem. Soc. 273 (1953).
20. K. Vogler. Helv. Chim. Acta, **33**, 2111 (1950).
21. S. H. Pines, M. A. Kozlowski, S. Karady. J. Org. Chem. **34**, 1621 (1969).
22. E. D. Bergmann, H. Bendas, and N. Taub. J. Chem. Soc. 2763 (1951).
23. J. L. Morrell, P. Fleckeinstein, and E. Gross. J. Org. Chem. **42**, 355 (1977).
24. J. P. Greenstein and M. Winitz. *In* Chemistry of the amino acids. Vol. 3. Wiley, New York. 1961. Chap. 37. p. 2238.
25. W. S. Fones. J. Biol. Chem. **204**, 323 (1953).
26. N. Yoshida and Y. Nakamura. Takamine Kenkyusho Nempo, **12**, 22 (1960); Chem. Abstr. **55**, 6394c (1961).

Can. J. Chem. Downloaded from www.nrcresearchpress.com by 88.85.125.76 on 09/07/12
For personal use only.

New total synthesis of phenanthrene alkaloids

JUAN C. ESTÉVEZ, M. CARMEN VILLAVERDE, RAMÓN J. ESTÉVEZ, JULIO A. SEIJAS, AND LUIS CASTEDO[1]

Departamento de Química Orgánica, Facultad de Química y Sección de Alcaloides del C.S.I.C., Universidad de Santiago de Compostela, Spain

Received October 4, 1989

JUAN C. ESTÉVEZ, M. CARMEN VILLAVERDE, RAMÓN J. ESTÉVEZ, JULIO A. SEIJAS, and LUIS CASTEDO. Can J. Chem. **68**, 964 (1990).

We describe a new synthesis of phenanthrene alkaloids based on the photocyclization of stilbene compounds prepared by a simple, efficient new method. It allows the preparation of phenanthrene compounds with a primary amine group in their side chain.

Key words: alkaloid, phenanthrene, stilbene, photocyclization.

JUAN C. ESTÉVEZ, M. CARMEN VILLAVERDE, RAMÓN J. ESTÉVEZ, JULIO A. SEIJAS et LUIS CASTEDO. Can. J. Chem. **68**, 964 (1990).

On décrit une nouvelle méthode de synthèse d'alcaloïdes dérivés du phénanthrène qui est basée sur une photocyclisation de composés du stilbène qui ont été préparés par une nouvelle méthode simple et efficace. Cette nouvelle méthode permet de préparer des composés du phénanthrène qui contiennent des groupements amines sur leur chaîne latérale.

Mots clés : alcaloïdes, phénanthrène, stilbène, photocyclisation.

[Traduit par la revue]

Can. J. Chem. Downloaded from www.nrcresearchpress.com by 88.85.125.76 on 09/07/12
For personal use only.

Introduction

The phenanthrene alkaloids are a minor group of isoquinoline bases biogenetically related to the aporphines, from which they can be obtained by degradative procedures (1). The first total synthesis of a member of this family of natural compounds involved the photochemical electrocyclization of a stilbene compound (2) prepared by mixed dicarbonyl coupling of aldehydes with low valent titanium (3). We now wish to describe the total synthesis of the phenanthrene alkaloids secoglaucine **9***a*, *N*-methylsecoglaucine **9***b*, and atherosperminine **9***c* using a modified approach that seems to be a suitable alternative to the titanium method when the aldehydes required fr coupling are not easily available. This modified method, which requires the preparation of the stilbene compounds from type-**1** ketoacids, constitutes yet another example of the usefulness of these ketoacids in the synthesis of isoquinoline alkaloids (4).

Results and discussion

As indicated in Scheme 1, when ketoacid **1***a* (obtained by self-condensation of 3,4-dimethoxyphenylacetic acid) was treated with $NaBH_4$ in methanol and the resulting mixture acidified and then heated gently, the lactone **2***a* was obtained in almost quantitative yield. Subsequent treatment of this lactone with methanol saturated with hydrogen chloride gave, also in high yield, the *E* isomer of the stilbene compound **3***a* as indicated by the ^1H nmr spectrum.

Photochemical irradiation of compound **3***a* for 3 h with a 450-W Hanovia medium-pressure mercury lamp equipped with a Pyrex filter gave, in moderate yield, the phenanthrene ester **5***a*, which was transformed in good yield into the corresponding amide **6***a* by treatment with aqueous ammonia. Alternatively, the phenanthreneacetamide **6***a* was also prepared, in lower yield, by photocyclization of the stilbene compound **4***a* previously obtained by treatment of **3***a* with aqueous ammonia.

Finally, LAH reduction of amide **6***a* afforded the desired phenanthreneamine **7***a*, which was then transformed into the phenanthrene alkaloids **9***a* and **9***b* as follows (Scheme 2). Treatment of **7***a* with ethyl chloroformate furnished the phenanthrene urethane **8***a*, which was converted into its *N*-methyl analogue **8***b*. Basic hydrolysis of the *N*-carbethoxy group yielded the phenanthrene alkaloid secoglaucine **9***a*. Alternatively, compound **8***b* was easily transformed into the phenanthrene alkaloid *N*-methylsecoglaucine **9***b* by treatment with LAH.

A parallel synthetic approach allowed atherosperminine **9***c* to be obtained from the ketoacid **1***c* via the lactone **2***b*. Ketoacid **1***c* itself could not be prepared in the same way as **1***a* because it has different substituents in the aromatic rings. Instead, it was prepared by Friedel–Crafts acylation of methyl 3,4-dimethoxyphenylacetate (5) with phenylacetyl chloride and subsequent hydrolysis of the ester group.

The approach to phenanthrene alkaloids described here allows the preparation of phenanthrene alkaloid analogues with a primary amine group in the side chain.

Experimental

Melting points were determined on a Kofler Thermogeräte apparatus and are uncorrected. Infrared spectra were determined in potassium bromide on a Perkin Elmer 1420 spectrophotometer. Ultraviolet spectra were recorded in ethanol on a Pye Unicam SP-1700 spectrophotometer. The nuclear magnetic resonance spectra were determined on a Bruker WM-250 apparatus in deuteriochloroform solution containing tetramethylsilane as the internal standard. Mass spectra were obtained on a Kratos MS 50 TC mass spectrometer. Elemental analyses were performed at Instituto de Química Orgánica General del C.S.I.C. (Madrid). Photolyses were carried out with medium-pressure mercury vapor arc lamps (Hanovia, 450 W) using Pyrex-filtered light and cooling by water. Thin-layer chromatography (tlc) was performed using Merck GF-254 type 60 silica gel and methylene chloride – methanol mixtures as eluent; the tlc spots were visualized with ultraviolet light or iodine vapour. Column chromatography was carried out using Merck type 9385 silica gel. Solvents were purified as in ref. 6.

*Methyl 2-phenylacetyl-4,5-dimethoxyphenylacetate (**1**b)*

A mixture of commercial phenylacetic acid (1.5 g, 11 mmol) and thionyl chloride (5 mL, 70 mmol) was refluxed under a dry atmosphere (calcium chloride tube) for 1 h. The excess thionyl chloride was evaporated *in vacuo* and the residue was dissolved in dry methylene chloride (3 mL). This solution was added dropwise to a stirred suspension of aluminium trichloride (1.74 g, 13 mmol) in dry methylene chloride (4 mL). To this mixture, cooled at 0°C in an ice/water bath, a solution of methyl 3,4-dimethoxyphenylacetate (1.89

[1]Author to whom correspondence may be addressed.

Printed in Canada / Imprimé au Canada

Can. J. Chem. Downloaded from www.nrcresearchpress.com by 88.85.125.76 on 09/07/12
For personal use only.

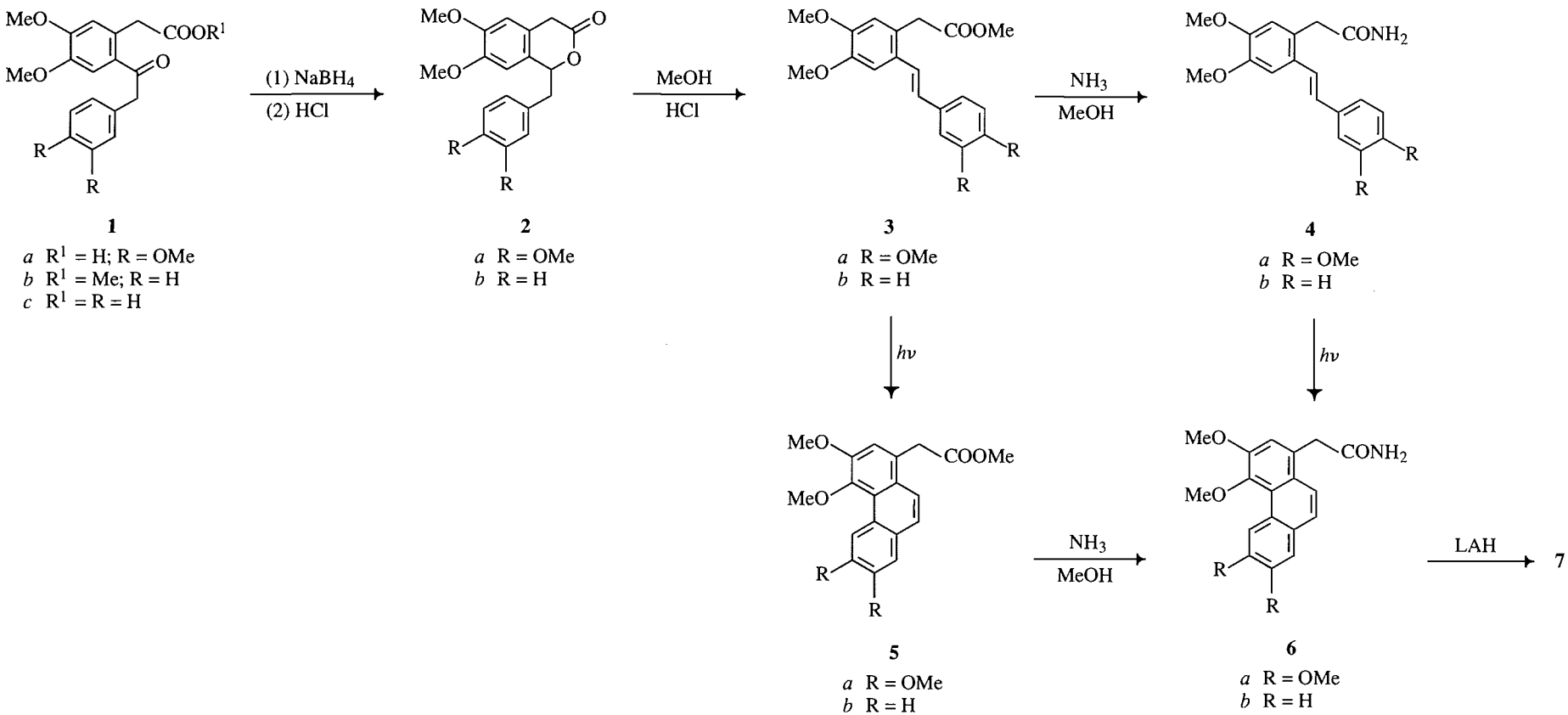

1

a R^1 = H; R = OMe
b R^1 = Me; R = H
c R^1 = R = H

2

a R = OMe
b R = H

3

a R = OMe
b R = H

4

a R = OMe
b R = H

5

a R = OMe
b R = H

6

a R = OMe
b R = H

SCHEME 1

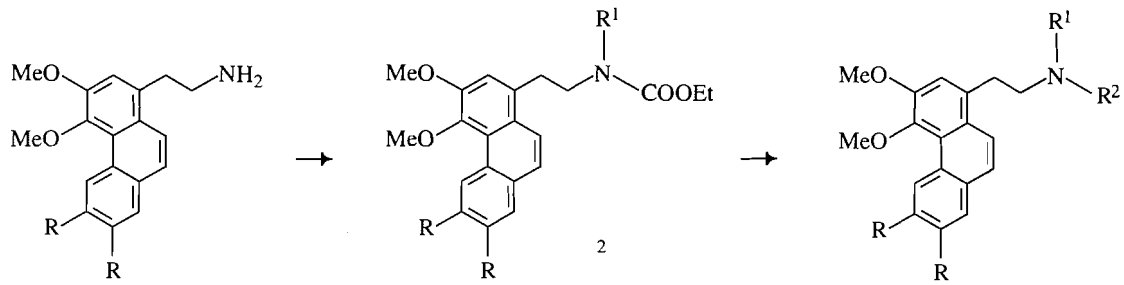

7
a R = OMe
b R = H

8
a R^1 = H; R = OMe
b R^1 = Me; R = OMe
c R^1 = R = H
d R^1 = Me; R = H

9
a R^1 = H; R^2 = Me; R = OMe
b R^1 = R^2 = Me; R = OMe
c R^1 = R^2 = Me; R = H

SCHEME 2

g, 9 mmol) in dry methylene chloride (3 mL) was added dropwise over 15 min. The mixture was stirred for 2 h at room temperature and was then added to an ice/concentrated hydrochloric acid solution. The mixture was extracted with dichloromethane (3 × 50 mL) and the organic layers were washed with saturated sodium bicarbonate solution followed by water, dried with anhydrous sodium sulphate, and concentrated *in vacuo* to give 2.6 g (88% yield) of white crystals, mp 119°C (MeOH); ir (ν,cm^{-1}): 1735, 1670, 1600, 1270; nmr (δ): 3.68 (s, 3H, -$COOCH_3$), 3.86 (s, 3H, Ar-OCH_3), 3.88 (s, 2H, -CH_2-COO), 3.92 (s, 3H, Ar-OCH_3), 4.22 (s, 2H, -CH_2-CO), 6.71 (s, 1H, Ar-H), 7.26–7.32 (m, 5H, 5 × Ar-H), 7.38 (s, 1H, Ar-H); ms (*m/z*): 237 (25), 235 (18), 210 (21), 209 (100), 181 (14), 179 (21), 178 (12), 169 (16), 151 (49), 150 (26). Anal. calcd. for $C_{19}H_{20}O_5$: c 69.51, H 6.10; found: C 69.45, H 6.08.

*2-Phenylacetyl-4,5-dimethoxphenylacetic acid (**1**c)*

A mixture of methyl 2-phenylacetyl-4,5-dimethoxyphenylacetate (**1***b*) (3 g, 9.1 mmol) and a 5:1 solution of dioxane/20% aqueous sulphuric acid (30 mL) was refluxed for 2 h. The mixture was concentrated *in vacuo* and then diluted in water and extracted with dichloromethane (3 × 25 mL). The organic layers were washed with water, dried with anhydrous sodium sulphate, and evaporated *in vacuo* to afford **1***c* (2.28 g, 79% yield), mp 164–165°C (MeOH); nmr (δ): 3.79 (s, 2H, -CH_2-COO), 3.87 (s, 3H, Ar-OCH_3), 3.92 (s, 3H, Ar-OCH_3), 4.26 (s, 2H, -CH_2-CO), 6.80 (s, 1H, Ar-H), 7.22–7.33 (m, 5H, 5 × Ar-H), 7.35 (s, 1H, Ar-H); ms (*m/z*): 195 (17), 92 (15), 91 (100), 89 (10).

*1-Benzyl-6,7-dimethoxy-3-isocromanone (**2**b)*

To a stirred solution of **1***c* (2 g, 6.4 mmol) in 200 mL of methanol, sodium borohydride (2.3 g, 60.1 mmol) was added in small portions for 3 h. Then 300 mL of water was added and the solution acidified to pH 3 with 20% hydrochloric acid, and heated at 60°C for 30 min with stirring. The organic solvent was evaporated off, and the remaining aqueous solution was extracted with dichloromethane. Work-up provided **2***b*, 1.8 g (95% yield), mp 109–111°C (MeOH); ir (ν, cm^{-1}): 1740, 1610, 1515; nmr (δ): 2.83 and 3.36 (AB, *J* = 19.7 Hz, 2H, -CH_2-CO), 3.21 (m, 2H, -CH_2-CO), 3.76 (s, 3H, Ar-OCH_3), 3.84 (s, 3H, Ar-OCH_3) 5.59 (t, *J* = 5.6 Hz, 1H, -CH-O), 6.44 (s, 1H, Ar-H), 6.49 (s, 1H, Ar-H) 6.96 (m, 2H, 2 × Ar-H), 7.21 (m, 3H, 3 × Ar-H); ms (*m/z*): 298 (M^+, 2), 207 (44), 179 (100), 151 (20). Anal. calcd. for $C_{18}H_{18}O_4$: C 72.48, H 6.04; found: C 72.62, H 6.09.

*Methyl (E)-4,5-dimethoxy-2-(3′,4′-dimethoxystyryl)phenylacetate (**3**a)*

A mixture of 1-(3′,4′-dimethoxybenzyl)-6,7-dimethoxy-3-isocromanone (**2***a*) (7) (1 g, 2.8 mmol) and 50 mL of methanol saturated with hydrogen chloride was refluxed for 5 h. Work-up supplied 1 g (96% yield) of **3***a*, mp 121–122°C (MeOH); uv (λ,nm): 224, 295(sh), 332; ir (ν, cm^{-1}): 1735, 1600, 1515; nmr (δ): 3.68 (s, 3H, -$COOCH_3$), 3.72 (s, 2H, -CH_2-CO), 3.89 (s, 6H, 2 × Ar-OCH_3), 3.94 (s, 6H, 2 × Ar-OCH_3), 6.75 (s, 1H, Ar-H), 6.85 (d, *J* = 15.9 Hz, 1H, CH=C), 6.86 (d, *J* = 8.5 Hz, 1H, Ar-H), 7.05 (s, 1H, Ar-H), 7.06 (d, *J* = 8.5 Hz, 1H, Ar-H), 7.11 (s, 1H, Ar-H), 7.17 (d, *J* = 15.9 Hz, 1H, -C=CH-); ms (*m/z*): 372 (M^+, 100), 357 (15), 313 (16), 297 (11), 284 (10), 282 (18). Anal. calcd. for $C_{21}H_{24}O_6$: C 67.74, H 6.45; found: C 67.55, H 6.72.

*Methyl (E)-2-styryl-4,5-dimethoxyphenylacetate (**3**b)*

Compound **3***b* was obtained in 94% yield from **2***b* using the same procedure as above; mp 78–80°C (MeOH); uv (λ, nm): 215, 230, 296 (sh), 308, 326; ir(ν, cm^{-1}): 1735, 1600, 1515; nmr (δ): 3.69 (s, 3H, -$COOCH_3$), 3.73 (s, 2H, -CH_2-CO), 3.91 (s, 3H, Ar-OCH_3), 3.95 (s, 3H, Ar-OCH_3), 6.76 (s, 1H, Ar-H), 6.91 (d, *J* = 16.0 Hz, 1H, -CH=C), 7.13 (s, 1H, Ar-H), 7.20–7.60 (m, 6H, 5 × Ar-H and -C=CH-); ms (*m/z*): 312 (M^+, 100), 253 (41), 222 (33), 221 (27).

*(E)-4,5-Dimethoxy-2-(3′,4′-dimethoxystyryl)phenylacetamide (**4**a)*

A mixture of methyl (*E*)-4,5-dimethoxy-2(3′, 4′-dimethoxystyryl)-phenylacetate (**3***a*) (1 g, 2.7 mmol), methanol (100 mL), and concentrated aqueous ammonia solution (100 mL) was stirred at room temperature for 48 h. Work-up provided (*E*)-4,5-dimethoxy-2(3′,4′-dimethoxystyryl)phenylacetamide (**4***a*) (0.92 g, 96% yield), mp 149–150°C (MeOH); ir (ν, cm^{-1}): 3325, 1665, 1600, 1515; nmr (δ): 3.69 (s, 2H, -CH_2-CO), 3.90 (s, 6H, 2 × Ar-OCH_3), 3.94 (s, 3H, Ar-OCH_3), 3.95 (s, 3H, Ar-OCH_3), 5.45 (bs, 1H, -NH_2), 5.75 (bs, 1H, -NH_2), 6.73 (s, 1H, Ar-H), 6.85 (d, *J* = 8.3 Hz, 1H, Ar-H), 6.88 (d, *J* = 16.0 Hz, 1H, -CH=C-), 7.05 (s, 1H, Ar-H), 7.05 (d, *J* = 8.3 Hz, 1H, Ar-H), 7.05 (d, *J* = 16.0 Hz, 1H, -C=CH-), 7.15 (s, 1H, Ar-H); ms (*m/z*): 357 (M^+, 100); hrms: 357.1566 (M^+, 100); calcd. for $C_{20}H_{23}NO_5$: 357.1576.

*(E)-4,5-Dimethoxy-2-styrylphenylacetamide (**4**b)*

Compound **4***b* was prepared in 90% yield from methyl (*E*)-2-styryl-4,5-dimethoxyphenylacetate (**3***b*) by the same procedure as above; mp 198–199°C (MeOH); ir (ν, cm^{-1}): 3410, 1660, 1605, 1520; nmr (δ): 3.69 (s, 2H, -CH_2-CO), 3.90 (s, 3H, Ar-OCH_3), 3.96 (s, 3H, Ar-OCH_3), 5.43 (bs, 1H, NH_2), 5.63 (bs, 1H, NH_2), 6.74 (s, 1H, Ar-H), 6.93 (d, *J* = 16.0 Hz, 1H, -CH=C-), 7.15–7.55 (m, 7H, 6 × Ar-H and -C=CH-); ms (*m/z*): 297 (M^+, 96), 253 (100), 222 (70), 207 (36).

*Methyl (3,4,6,7-tetramethoxy-1-phenanthryl)acetate (**5**a)*

A stirred mixture of stilbene **3***a* (200 mg, 0.54 mmol), 200 mL of ethyl ether, and a catalytic amount of iodine (12 mg, 0.03 mmol) was oxygenated by passing air for 15 min and was then irradiated at room temperature for 3 h. The ether solution was washed with saturated sodium thiosulphate and water, dried with anhydrous sodium sulphate, and evaporated *in vacuo* to give a mixture that was separated by preparative tlc (methylene chloride) to afford methyl (3,4,6,7-tetramethoxy-1-phenanthryl)acetate (**5***a*) (107 mg, 54% yield), mp 145–146°C (MeOH); ir (ν, cm^{-1}): 1740, 1600, 1520; nmr (δ): 3.70 (s, 3H,

Can. J. Chem. Downloaded from www.nrcresearchpress.com by 88.85.125.76 on 09/07/12
For personal use only.

Can. J. Chem. Downloaded from www.nrcresearchpress.com by 88.85.125.76 on 09/07/12
For personal use only.

-$COOCH_3$), 3.94 (s, 3H, Ar-OCH_3), 4.04 (s, 6H, 2 × Ar-OCH_3), 4.07 (s, 5H, Ar-OCH_3 and -CH_2-CO), 7.20 (s, 1H, Ar-H), 7.23 (s,1H, Ar-H), 7.56 and 7.69 (AB, J = 9.1 Hz, 2H, -CH=CH-), 9.27 (s, 1H, Ar-H); ms (m/z): 370 (M^+, 100), 355 (42), 311 (39). Anal. calcd. for $C_{21}H_{22}O_6$: C 68.11, H 5.95; found: C 67.75, H 6.12.

*Methyl (3,4-dimethoxy-1-phenanthryl)acetate (**5**b)*

Photochemical irradiation of **3***b* (168 mg, 0.54 mmol) in the same conditions as above gave compound **5***b* (58 mg, 35% yield), mp 125–126°C (MeOH); ir (ν, cm^{-1}): 1735, 1595, 1270; nmr (δ): 3.70 (s, 3H, -$COOCH_3$), 3.93 (s, 3H, Ar-OCH_3), 4.04 (s, 3H, Ar-OCH_3), 4.09 (s, 2H, -CH_2-CO), 7.28 (s, 1H, Ar-H), 7.50–7.70 (m, 2H, Ar-H), 7.63 and 7.78 (AB, J = 9.2 Hz, 2H, -CH=CH-), 7.84 (m, 1H, Ar-H), 9.65 (d, J = 8.5 Hz, 1H, Ar-H); ms (m/z): 310 (M^+, 100), 295 (35), 267 (22), 251 (82), 235 (64), 225 (26), 208 (44), 207 (35). Anal. calcd. for $C_{19}H_{18}O_4$: C 73.55, H 5.81; found: C 73.39, H 6.02.

*3,4,6,7-Tetramethoxy-1-phenanthrylacetamide (**6**a)*

Procedure a

Photochemical irradiation of styrene **4***a* (193 mg, 0.54 mmol) following the same procedure as above gave 3,4,6,7-tetramethoxy-1-phenanthrylacetamide (**6***a*) (77 mg, 40% yield), mp 162–163°C (MeOH); ir (ν, cm^{-1}): 3430, 1670, 1600, 1520; nmr (δ): 3.96 (s, 3H, Ar-OCH_3), 4.05 (s, 8H, 2 × Ar-OCH_3 and -CH_2-CO-), 4.08 (s, 3H, Ar-OCH_3), 5.34 (bs, 1H, -NH_2), 5.43 (bs, 1H, -NH_2), 7.23 (s, 1H, Ar-H), 7.25 (s, 1H, Ar-H), 7.59 and 7.67 (AB, J = 9.1 Hz, 2H, -CH=CH-), 9.27 (s, 1H, Ar-H); ms (m/z): 355 (M^+, 16), 312 (16), 311 (18), 208 (18), 193 (33), 181 (55), 165 (42), 69 (100). Anal. calcd. for $C_{20}H_{21}NO_5$: C 67.61, H 5.92, N 3.94; found: C 67.21, H 6.09, N 3.61.

Procedure b

A mixture of methyl (3,4,6,7-tetramethoxy-1-phenanthryl)acetate (**5***a*) (250 mg, 0.67 mmol), methanol (50 mL), and a concentrated aqueous ammonia solution (50 mL) was stirred at room temperature for 24 h. Work-up provided a mixture that was separated by preparative tlc (Cl_2CH_2/methanol 95:5) to afford phenanthrylamide **6***a* (167 mg, 70% yield), which was crystallized from methanol.

*3,4-Dimethoxy-1-phenanthrylacetamide (**6**b)*

Procedure a

Photochemical irradiation of **4***b* (160 mg, 0.54 mmol) using the general procedure gave compound **6***b* (47.6 mg, 30% yield), mp 147–148°C (MeOH); ir (ν, cm^{-1}): 3360, 1660, 1595, 1270; nmr (δ): 3.95 (s, 3H, Ar-OCH_3), 4.04 (bs, 5H, Ar-OCH_3 and -CH_2-CO), 5.34 (bs, 1H, -NH_2), 5.56 (bs, 1H, -NH_2), 7.25 (s, 1H, Ar-H), 7.61 (m, 2H, 2 × Ar-H), 7.64 and 7.74 (AB, J = 9.1 Hz, 2H, -CH=CH-), 7.85 (m, 1H, Ar-H), 9.65 (d, J = 8.5 Hz,1H, Ar-H); ms (m/z): 295 (M^+, 74), 252 (19), 251 (100), 237 (19), 165 (20).

Procedure b

Compound **6***b* was prepared in 65% yield from **5***b* by the procedure described above.

*2-(3′,4′,6′,7′-Tetramethoxy-1′-phenanthryl)ethylamine (**7**a)*

A solution of 3,4,6,7-tetramethoxy-1-phenanthrylacetamide (**6***a*) (250 mg, 0.7 mmol) in dry THF (20 mL) was added dropwise to a vigorously stirred suspension of LAH (100 mg) in dry THF (25 mL). The mixture was refluxed for 5 h and was then left at room temperature overnight. A 15% aqueous solution of sodium hydroxide (4 mL) was added dropwise, followed by water (12 mL); the suspension was filtered and the THF of the filtrate evaporated off *in vacuo*. The residue was extracted with methylene chloride (3 × 25 mL) and the combined organic extracts treated with a 10% aqueous solution of hydrochloric acid (3 × 25 mL); the aqueous extracts were basified with a 10% aqueous solution of sodium hydroxide and extracted with methylene chloride (3 × 25 mL). The extracts were dried with anhydrous sodium sulphate and concentrated *in vacuo* to afford crude amine **7***a* as an oil that was used without further purification; nmr (δ): 3.12 (t, J = 6.0 Hz, 2H, -CH_2-), 3.24 (t, J = 6.0 Hz, 2H, -CH_2-), 3.92 (s, 3H, Ar-OCH_3), 4.03 (s, 3H, Ar-OCH_3), 4.04 (s, 3H, Ar-OCH_3), 4.07 (s, 3H, Ar-OCH_3), 7.19 (s, 1H, Ar-H), 7.20 (s, 1H, Ar-H), 7.53 and 7.77 (AB, J = 9.1 Hz, 2H, -CH=CH-), 9.28 (s, 1H, Ar-H); ms (m/z): 341 (M^+, 43), 312 (72), 311 (100), 297 (22).

*2-(3′,4′-Dimethoxy-1′-phenanthryl)ethylamine (**7**b)*

Amide **6***b* (200 mg, 0.68 mmol) was treated as above to afford compound **7***b* as an oil that was used without further purification; nmr (δ): 3.15 (t, J = 6.3 Hz, 2H, -CH_2-), 3.30 (t, J = 6.3 Hz, 2H, -CH_2-), 3.92 (s, 3H, Ar-OCH_3), 4.03 (s, 3H, Ar-OCH_3), 7.24 (s, 1H, Ar-H), 7.50–7.70 (m, 3H, 2 × Ar-H and -CH=C-), 7.82 (m, 1H, Ar-H), 7.86 (d, J = 9.2 Hz, 1H, -C=CH-), 9.65 (d, J = 8.3 Hz, 1H, Ar-H); ms (m/z): 281 (M^+, 36), 252 (90), 251 (100), 237 (23).

N-*Carbethoxy-2-(3′,4′,6′,7′-tetramethoxy-1′-phenanthryl)ethylamine (**8**a)*

A solution of crude 2-(3′,4′,6′,7′-tetramethoxy-1′-phenanthryl)-ethylamine (**7***a)* (225 mg) in methylene chloride (10 mL) was treated with an excess of ethyl chloroformate (1 mL) and stirred at room temperature for 30 min. Then water (10 mL) was added and the organic layers separated, dried with anhydrous sodium sulphate, and concentrated. The residue was purified by preparative tlc to afford 218 mg (75% from **6***a*) of urethane **8***a*; ir (ν, cm^{-1}): 1370, 1715, 1520; nmr (δ): 1.26 (t, J = 7.1 Hz, 3H, -CH_2-*CH_3*), 3.30 (t, J = 7.6 Hz, 2H, -CH_2-), 3.57 (m, 2H, -CH_2-), 3.93 (s, 3H, Ar-OCH_3), 4.03 (s, 3H, Ar-OCH_3), 4.05 (s, 3H, Ar-OCH_3), 4.07 (s, 3H, Ar-OCH_3), 4.15 (q, J = 7.1 Hz, 2H, -O-*CH_2*-CH_3) 4.75 (bs, 1H, -NH-), 7.16 (s, 1H, Ar-H), 7.21 (s,1H, Ar-H), 7.56 and 7.81 (AB, J = 9.1 Hz, 2H, -CH=CH-), 9.28 (s, 1H, Ar-H); ms (m/z): 413 (M^+, 45), 367 (23), 311 (100), 297 (14), 265 (13).

N-*Carbethoxy-2-(3′,4′-dimethoxy-1′-phenanthryl)ethylamine (**8**c)*

Crude amine **7***b* (160 mg) was treated as above to afford 168 mg (70% from **6***b*) of *N*-carbethoxyamine **8***c*, nmr (δ): 0.88 (t, J = 7.3 Hz, 3H, -CH_2-*CH_3*), 3.32 (t, J = 7.1 Hz, 2H, -CH_2-), 3.55 (m, 2H, -CH_2-), 3.93 (s, 3H, Ar-OCH_3), 4.03 (s, 3H, Ar-OCH_3), 4.16 (q, J = 7.3 Hz, 2H, -O-*CH_2*-CH_3), 7.20 (s, 1H, Ar-H), 7.50–7.70 (m, 3H, 3 × Ar-H), 7.80–8.00 (m, 2H, 2 × Ar-H), 9.67 (d, J = 7.7 Hz, 1H, Ar-H); ms (m/z): 353 (M^+, 50), 251 (100).

N-*Carbethoxy*-N-*methyl-2-(3′,4′,6′,7′-tetramethoxy-1′-phenanthryl)-ethylamine (**8**b)*

A solution of urethane **8***a* (200 mg, 0.48 mmol) in dry THF (5 mL) was added dropwise to a stirred mixture of sodium hydride (100 mg) in dry THF (5 mL). This suspension was stirred at room temperature for 30 min, then an excess of methyl iodide (1 mL) was added and the mixture stirred at room temperature for 2 h. Water (25 mL) was added and the THF was eliminated *in vacuo*. The aqueous mixture was extracted with methylene chloride, dried with anhydrous sodium sulphate, and concentrated *in vacuo* to give quantitatively the urethane **8***b*, mp 110–111°C (EtOH): ir (ν, cm^{-1}): 1690, 1590, 1480, 1200, 1110; nmr (δ): 1.22–1.32 (m, 3H, -CH_2-*CH_3*), 2.85 and 2.95 (2s, 3H, -N-CH_3), 3.24–3.38 (m, 2H -CH_2-), 3.55–3.65 (m, 2H, -CH_2-), 3.92 (s, 3H, Ar-OCH_3), 4.03 (s, 3H, Ar-OCH_3), 4.04 (s, 3H, Ar-OCH_3), 4.07 (s, 3H, Ar-OCH_3), 4.04–4.10 (m, 2H, -O-*CH_2*-CH_3), 7.11 and 7.19 (2s, 1H, Ar-H), 7.21 (s, 1H, Ar-H), 7.56 (d, J = 8.9 Hz, 1H, -CH=C-), 7.84 and 7.90 (2d, J = 9.2 Hz, 1H, -C=CH-), 9.28 (s, 1H, Ar-H); ms (m/z): 427 (M^+, 35), 311 (100), 116 (28), 44 (93). Anal. calcd. for $C_{24}H_{29}NO_6$: C 67.43, H 6.83, N 3.28; found: C 67.90, H 7.10, N 3.60.

N-*Carbethoxy*-N-*methyl-2-(3′,4′-dimethoxy-1′phenanthryl)-ethylamine (**8**d)*

Starting with **8***c* (100 mg, 0.28 mmol), the same procedure as above gave compound **8***d* in quantitative yield; ir (ν, cm^{-1}): 1700, 1590, 1510, 1200; nmr (δ): 1.25–1.29 (m, 3H, -CH_2-*CH_3*), 2.84 and 2.95 (2s, 3H, N-CH_3), 3.25–3.40 (m, 2H, -CH_2-N), 3.54 (m, 2H, Ar-CH_2), 3.91 (s, 3H, Ar-OCH_3), 4.03 (s, 3H, Ar-OCH_3), 4.01–4.13 (m, 2H, -O-*CH_2*-CH_3), 7.16–7.36 (m, 2H, Ar-H), 7.55–7.66 (m, 2H, Ar-H), 7.83–8.01 (m, 2H, Ar-H), 9.67 (m,1H, Ar-H); ms (m/z): 367 (M^+, 30), 251 (80), 44 (100).

*Secoglaucine (**9**a)*

A mixture of potassium hydroxide (2 g) and absolute ethanol (10

mL) was refluxed under argon until total dissolution. This solution, under an argon atmosphere, was added to 100 mg (0.23 mmol) of urethane **8***b* and the mixture refluxed for 15 h. Then a solution of citric acid (2 g) in water (15 mL) was added dropwise and the mixture stirred at room temperature for 15 min. The ethanol was evaporated and the residue extracted with methylene chloride; work-up provided 62 mg (75%) of secoglaucine **9***a*, which was identified by direct comparison with an authentical sample (8).

N-*Methyl secoglaucine (***9**b*)*

A solution of urethane **8***b* (100 mg, 0.23 mmol) in dry THF (5 mL) was added dropwise to a stirred suspension of LAH (50 mg, 1.31 mmol) and $AlCl_3$ (100 mg, 0.75 mmol) in dry THF (10 mL). This mixture was refluxed for 1.5 h and then water (1 mL), 10% aqueous sodium hydroxide solution (1 mL), and water (4 mL) were successively added dropwise. The mixture was filtered, the THF evaporated off, and the residue extracted with methylene chloride (3 × 25 mL). The mixed organic extracts were treated with 10% hydrochloric acid (3 × 25 mL). The combined aqueous extracts were brought to pH 9 with 10% aqueous sodium hydroxide solution and then extracted again with methylene chloride (3 × 25 mL), dried with anhydrous sodium sulphate, and concentrated *in vacuo* to give 61 mg (70%) of *N*-methylsecoglaucine **9***b*, which was compared with an authentic sample (9).

*Atherosperminine (***9**c*)*

Urethane **8***d* (100 mg, 0.27 mmol) was transformed into atherosperminine (**9***c*) (57 mg, 68%) by the same procedure as above. Compound **9***c* was compared with an authentic sample (2).

Acknowledgements

We thank the Xunta de Galicia for financial support and for a grant to Juan C. Estévez.

1. M. SHAMMA. The isoquinoline alkaloids. Academic Press, New York.1972; M. SHAMMA and J. L. MONIOT. Isoquinoline alkaloids research 1972–77. Plenum Press, New York. 1978.
2. J. A. SEIJAS, A. R. DE LERA, M. C. VILLAVERDE, and L. CASTEDO. J. Chem. Soc. Chem. Commun. 839 (1985).
3. L. CASTEDO, J. M. SAÁ, R. SUAU, and G. TOJO. J. Org. Chem. **46**, 4292 (1981).
4. L. CASTEDO, R. J. ESTÉVEZ, J. M. SAÁ, and R. SUAU. J. Heterocycl. Chem. **19**, 1319 (1982).
5. L. CASTEDO, J. M. SAÁ, R. SUAU, and R. J. ESTÉVEZ. An. Quím. Ser. C, **79**, 329 (1983).
6. D. D. PERRIN and W. L. F. ARMAREGO. Purification of laboratory chemicals. Pergamon Press, New York. 1988.
7. I. W. ELLIOT. J. Org. Chem. **42**, 1090 (1977).
8. J. A. SEIJAS, A. R. DE LERA, C. VILLAVERDE, and L. CASTEDO. Heterocycles, **23**, 3079 (1985).
9. O. BLANCO, L. CASTEDO, M. M. CID, J. A. SEIJAS, and M. C. VILLAVERDE. Heterocycles. In press.

Can. J. Chem. Downloaded from www.nrcresearchpress.com by 88.85.125.76 on 09/07/12
For personal use only.

Electron transfer reactions. Reaction of nitrogen heterocycles with potassium[1]

MOHAMMED MUNEER
Photochemistry Research Unit, Regional Research Laboratory, Trivandrum 695019, India, and Department of Chemistry, Indian Institute of Technology, Kanpur 208016, India

PRASHANT V. KAMAT[2]
Radiation Laboratory, University of Notre Dame, Notre Dame, IN 46556, U.S.A.

AND

MANAPURATHU V. GEORGE[2]
Photochemistry Research Unit, Regional Research Laboratory, Trivandrum 695019, India, and Radiation Laboratory and Department of Chemistry and Biochemistry, University of Notre Dame, Notre Dame, IN 46556, U.S.A.

Received August 9, 1988[3]

MOHAMMED MUNEER, PRASHANT V. KAMAT, and MANAPURATHU V. GEORGE. Can. J. Chem. **68**, 969 (1990).

The results of our studies on potassium-induced transformations of some selected nitrogen heterocycles are presented. The substrates under investigation include 2,3-diphenylindole (**1***a*), 2,3-diphenyl-1-methylindole (**1***b*), 1,2,3-triphenylindole (**1***c*), 2,3,4,5-tetraphenylpyrrole (**5***a*), 1,2,3,5-tetraphenylpyrrole (**5***b*), 1-benzyl-2,3,5-triphenylpyrrole (**5***c*), 2,4,5-triphenyloxazole (**15***a*), 4,5-diphenyl-2-methyloxazole (**15***b*), 2,4-diphenyl-5-methyloxazole (**15***c*), and 2,4,5-triphenylimidazole (**19**). Treatment of **1***a* with potassium in THF gave 9*H*-dibenzo[*a*,*c*]carbazole (**3***a*), whereas **1***c* gave a mixture of 9-phenyl-9*H*-dibenzo-[*a*,*c*]carbazole (**3***c*) and 2,3-diphenylindole (**1***a*). Under identical conditions, **1***b* gave only the cleavage product **1***a*. In contrast, when the reactions of **1***a*,*c* were carried out with potassium in THF saturated with oxygen, and with potassium superoxide in benzene containing 18-crown-6, a mixture of 2-benzamidobenzophenone (**4***a*), the carbazoles **3***a*,*c*, and **1***a* was formed. Although no product was isolated on treatment of **5***a* with potassium in THF, the reaction of **5***a* with potassium in THF saturated with oxygen gave a mixture of tetraphenylpyrazine (**7***a*), the benzoylaminostilbene **8***a*, the lactam **12***a*, benzamide (**11***a*), and benzoic acid (**14**). Similar results were obtained in the reaction of **5***a* with potassium superoxide. The reaction of N-substituted pyrroles such as **5***b*,*c* with potassium gave the NH pyrrole **9***b* in each case, whereas the reaction of **5***b*,*c* with potassium in THF, saturated with oxygen, gave a mixture of **9***b*, the butanone **10***b*, the 1,4-dione **13***b*, the lactam **12***b*, the amides **11***a*–*c*, and benzoic acid (**14**). Attempted reactions of **5***b*,*c* with potassium superoxide did not give any isolable product; most of the starting material could be recovered unchanged in each case. A mixture of *N*-(1,2-diphenylethyl)benzamide (**18***a*) and benzoic acid (**14**) was formed in the reaction of the oxazole **15***a* with potassium, whereas **15***b*,*c*, under analogous conditions, gave the *N*-vinylamides **17***b*,*c* and benzoic acid (**14**). In contrast, treatment of the imidazole **19** with potassium in THF did not give any product; however, when the reaction of **19** was carried out with potassium in THF saturated with oxygen, and with potassium superoxide, dibenzamide (**21**) was isolated, in each case.

Radical ions have been invoked as intermediates in the transformation of the different substrates to the observed products. Cyclic voltammetric studies have been carried out to measure the reduction potentials of these radical anion intermediates. These radical anions have also been generated by pulse radiolysis in methanol, and their absorption spectra recorded.

Key words: nitrogen heterocycles, radical ions, potassium-induced transformations, pulse radiolysis, cyclic voltammetry.

MOHAMMED MUNEER, PRASHANT V. KAMAT, et MANAPURATHU V. GEORGE. Can. J. Chem. **68**, 969 (1990).

On rapporte les résultats obtenus lors de notre étude sur les réactions du potassium avec quelques hétérocycles azotés choisis. On a étudié le 2,3-diphénylindole (**1***a*), le 2,3-diphényl-1-méthylindole (**1***b*), le 1,2,3-triphénylindole (**1***c*), le 2,3,4,5-tétraphénylpyrrole (**5***a*), le 1,2,3,5-tétraphénylpyrrole (**5***b*), le 1-benzyl-2,3,5-triphénylpyrrole (**5***c*), le 2,4,5-triphényl-oxazole (**15***a*), le 4,5-diphényl-2-méthyloxazole (**15***b*), le 2,4-diphényl-5-méthyloxazole (**15***c*) et le 2,4,5-triphénylimidazole (**19**). La réaction du produit **1***a* avec le potassium dans le THF donne le 9*H*-dibenzo[*a*,*c*]carbazole (**3***a*), tandis que le **1***c* conduit à un mélange de 9-phényl-9*H*-dibenzo[*a*,*c*]carbazole (**3***c*) et de 2,3-diphénylindole (**1***a*). Dans des conditions semblables, le produit **1***b* ne donne que le produit de clivage **1***a*. Par ailleurs, lorsqu'on a soumis les produits **1***a* et **1***c* à l'action du potassium dans du THF saturé avec de l'oxygène ou à l'action du superoxyde de potasium dans du benzéne contenant de l'éther 18-couronne-6, on isole un mélange formé de 2-benzamidobenzophénone (**4***a*), des carbazoles **3***a* et **3***c* et du composé **1***a*. Même si la réaction du composé **5***a* avec le potassium dans le THF ne permet pas d'isoler de produit, la réaction du produit **5***a* avec du potassium dans du THF saturé d'oxygène fournit un mélange de tétraphénylpyrazine (**7***a*), de benzoylaminostilbène (**8***a*), de lactame **12***a*, de benzamide **11***a* et d'acide benzoïque (**14**). On a obtenu des résultats semblables lors de la réaction du composé **5***a* avec le superoxyde de potassium. La réaction de pyrroles N-substitués, comme les produits **5***b et* **5***c*, avec du potassium dans le THF saturé d'oxygène fournit un mélange formé du composés **9***b*, de la butanone **10***b*, de la 1,4-dione **13***b*, de la lactame **12***b*, des amides **11***a*–*c* et de l'acide benzoïque (**14**). Lorsqu'on a essayé de faire réagir les composés **5***b* et **5***c* avec du superoxyde de potassium, aucun produit n'a pu être isolé; dans chaque cas, on a récupéré pratiquement tout le produit de départ. La réaction de l'oxazole **15***a* avec du potassium fournit un mélange de *N*-(1,2-diphényléthyl)benzamide (**18***a*) et d'acide benzoïque (**14**); mis dans les mêmes conditions, les produits **15***b* et **15***c* fournissent les *N*-vinylamides (**17***b* et **17***c*) et de l'acide benzoïque (**14**). Par ailleurs, la réaction de l'imidazole **19** avec du potassium dans le THF ne fournit aucun produit; toutefois, lorsqu'on traite le

---

[1]Document No. NDRL-3018 from the Notre Dame Radiation Laboratory and No. RRLT-PRU-4 from the Regional Research Laboratory, Trivandrum.

[2]Authors to whom correspondence may be addressed.

[3]Revision received January 31, 1990.

Printed in Canada / Imprimé au Canada

Can. J. Chem. Downloaded from www.nrcresearchpress.com by 88.85.125.76 on 09/07/12
For personal use only.

composé **19** soit avec du potassium dans le THF saturé d'oxygène soit avec du superoxyde de potassium, on isole dans chaque cas du dibenzamide (**21**).

Pour expliquer la formation des divers produits observés, on suggère l'existence d'intérmédiaires de types ions radicaux. On a réalisé des études de voltamétrie cyclique pour mesurer les potentiels de réduction de ces intermédiaires anions radicalaires. On a aussi généré ces anions radicaux en faisant intervenir des radiations pulsées dans le méthanol et on a enregistré leurs spectres d'absorption.

Mots clés: hétérocycles azotés, ions radicaux, réactions du potassium avec hétérocycles, radiations pulsées, voltamétrie cyclique.

[Traduit par la revue]

Can. J. Chem. Downloaded from www.nrcresearchpress.com by 88.85.125.76 on 09/07/12
For personal use only.

Introduction

Very few examples of the reaction of nitrogen heterocycles with alkali metals are reported in the literature (1–5). It has been reported that pyrrole is not reduced by potassium in liquid ammonia, whereas indoles are reduced to the corresponding dihydroindoles, on treatment with sodium in ammonia (2). However, when indole is reduced by a large excess of lithium and methanol, a mixture of 4,7-dihydroindole and 4,5,6,7-tetrahydroindole, in equal amounts, is reported to be formed (3). Subsequent studies by Remers *et al.* (4) have shown that ring selectivity in the reduction of indoles and quinolines by sodium in liquid ammonia could be controlled, depending on whether or not the reduction is carried out in the presence of methanol. The sodium–ethanol reduction of 2,4,5-triphenyloxazole has been reported to give *N*-(2-oxy-1,2-diphenylethyl)-benzylamine, whereas the reduction of 4,5-diphenyl-2-methyloxazole gives *N*-(1,2-diphenylethyl)acetamide (5).

In a recent study (6), we showed that several Δ^2-oxazoline-5-ones react with potassium in THF to give a variety of products, arising through radical anion and dianion intermediates. The object of the present investigation has been to examine the reactions of some selected heterocyclic substrates such as indoles, pyrroles, oxazoles, and imidazoles with potassium in THF, to study the nature of the products formed in these reactions.

Results and discussion

In the present studies, we have examined the reactions of 2,3-diphenylindole (**1***a*), 2,3-diphenyl-1-methylindole (**1***b*), 1,2,3-triphenylindole (**1***c*), 2,3,4,5-tetraphenylpyrrole (**5***a*), 1,2,3,5-tetraphenylpyrrole (**5***b*), and 1-benzyl-2,3,5-triphenylpyrrole (**5***c*) with potassium in THF. In addition, the reactions of a few oxazoles such as 2,4,5-triphenyloxazole (**15***a*), 4,5-diphenyl-2-methyloxazole (**15***b*), and 2,4-diphenyl-5-methyloxazole (**15***c*) and an imidazole such as 2,4,5-triphenylimidazole (**19**) with potassium have been examined. The reaction of **1***a* with potassium in THF, for example, gave 9*H*-dibenzo[*a*,*c*]carbazole (**3***a*, 49%), whereas **1***c*, under analogous conditions, gave a mixture of 9-phenyl-9*H*-dibenzo[*a*,*c*]carbazole (**3***c*, 20%) and 2,3-diphenylindole (**1***a*, 19%). The reaction of **1***b* with potassium gave **1***a* (68%) as the only isolable product. In contrast, the reactions of **1***a*,*c* with potassium in THF saturated with oxygen, and with potassium superoxide, gave a mixture of 2-benzamidobenzophenone (**4***a*, 20–34%), the carbazoles **3***a*,*c* (10–13%), and 2,3-diphenylindole (**1***a*, 7–9%), in each case.

The formation of the different products in the reaction of **1***a–c* with potassium in THF may involve the radical anion intermediates **2***a–c*, which can undergo subsequent transformations (Scheme 1). The radical anion intermediates **2***a–c*, for example, can undergo a radical type of cyclization to give the corresponding dihydrocarbazoles and ultimately the carbazoles **3***a*,*c*, under the work-up conditions. The formation of **1***a* from both **1***b* and **1***c*, on the other hand, may be through the cleavage reactions of the corresponding radical anion intermediates **2***b* and **2***c*, respectively. The different oxygenated products and ring cleavage products formed when the reactions were carried out under oxygen saturation, and also in presence of potassium superoxide, may arise through complex reaction pathways. It may be mentioned, in this connection, that ring cleavage products such as **4***a* have been observed in the reaction of several indole derivatives with potassium superoxide, and dioxetane intermediates have been invoked in these reactions (7).

An attempted reaction of a pyrrole such as 2,3,4,5-tetraphenylpyrrole (**5***a*) with potassium in THF did not give any product; most of the starting material could be recovered unchanged. However, when the reaction of **5***a* was carried out with potassium in THF saturated with oxygen, a mixture of tetraphenylpyrazine (**7***a*, 13%), α-benzoylamino-α′-benzoylstilbene (**8***a*), 2,3,4,4-tetraphenyl-2-pyrrolin-5-one (**12***a*, 19%), benzamide (**11***a*, 15%), benzoic acid (**14**, 10%), and some unchanged starting material (**5***a*, 30%) was obtained (Scheme 2). The reaction of the N-substituted pyrroles **5***b*,*c* with potassium gave the pyrrole **9***b* (30–33%) in each case, whereas the reaction of **5***b*,*c* with potassium in THF saturated with oxygen gave a mixture of **9***b* (7–8%), 1,3,4-triphenylbutan-1-one (**10***b*, 12–14%), 1,2,4-triphenylbutan-1,4-dione (**13***b*, 11–13%), 2,4,4-triphenyl-2-pyrrolin-5-one (**12***b*, 10–12%), the amides **11***a–c* (9–17%), and benzoic acid (**14**, 14–15%).

The reaction of an oxazole such as 2,4,5-triphenyloxazole (**15***a*) with potassium in THF gave a mixture of *N*-(1,2-diphenylethyl)benzamide (**18***a*, 27%) and benzoic acid (**14**, 5%), whereas the oxazoles **15***b*,*c*, under analogous conditions, gave a mixture of the *N*-vinylamides **17***b*,*c* (30–37%) and benzoic acid (**14**, 4%) (Scheme 3). In contrast, the reaction of the imidazole **19** under similar conditions did not give any product; however, treatment of **19** with potassium in THF saturated with oxygen gave dibenzamide (**21**, 21%) as the only isolable product.

The formation of the different products in the reactions of **5***a–c*, **15***a–c*, and **19** with potassium in THF may involve the initially formed radical anion intermediates **6***a–c*, **16***a–c*, and **20**, respectively, which can undergo further transformations.

To examine whether any of the oxygenated products formed in the reaction of **1***a–c*, **5***a–c*, **15***a–c*, and **19** with potassium in THF arises through the involvement of superoxide in these reactions, we have carried out the reaction of these substrates with potassium superoxide in benzene containing 18-crown-6. It is interesting to note that the products formed in most of these cases closely resemble those formed in the reaction of these substrates with potassium in THF, saturated with oxygen. In the case of the N-substituted pyrroles **5***b–c*, however, the reaction with potassium superoxide did not give any product under our conditions and it is likely that, in these cases, the radical anion intermediates **6***b*,*c* are not formed through electron transfer from potassium superoxide. The fact that oxygenated products were observed in the case of **5***a*, on the other hand, would suggest that potassium superoxide may be abstracting the NH

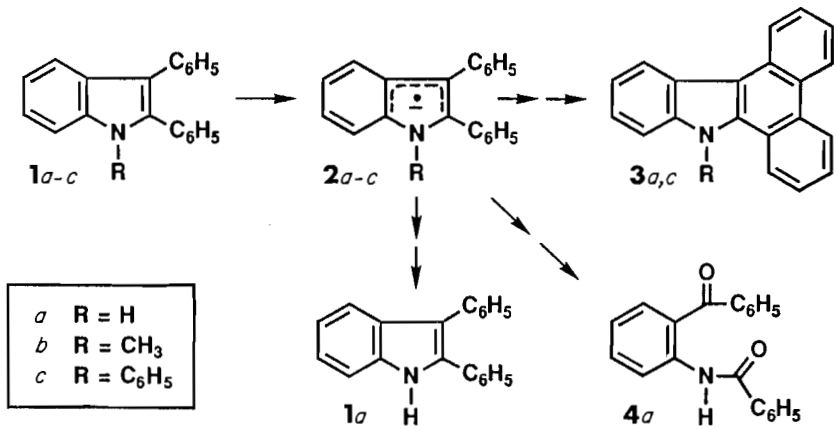

SCHEME 1

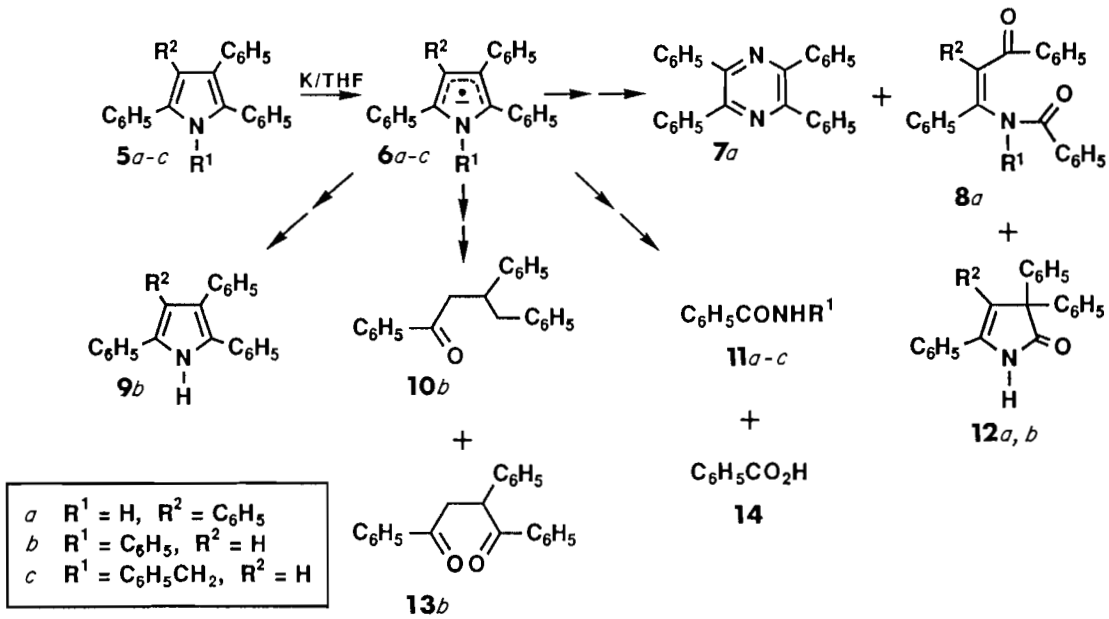

SCHEME 2

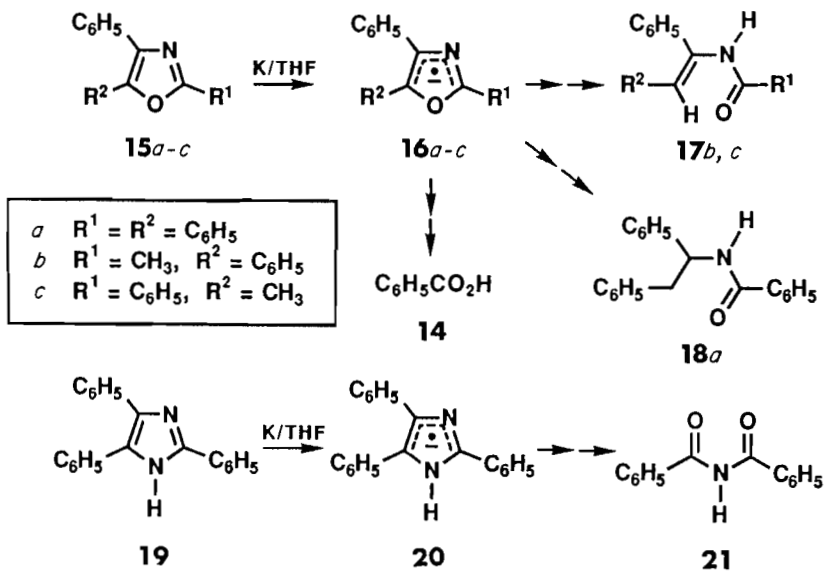

SCHEME 3

Can. J. Chem. Downloaded from www.nrcresearchpress.com by 88.85.125.76 on 09/07/12
For personal use only.

TABLE 1. Electrochemical, spectral, and kinetic data of indoles (**1***a–c*), pyrroles (**5***a–c*), oxazoles (**15***a–c*), and imidazole (**19**)

Substrate	Reduction potential[a] $E_{p/2}$ (V vs. SSCE)	Absorption maxima[c] of radical anion (nm)	k[d] ($10^9\ M^{-1}\ s^{-1}$)	$\tau_{1/2}$[e] (μs)
1*a*	−2.35	365	3.3	8
1*b*	−2.6	365	5.4	275
1*c*	−2.25	367 (~460)	5.1	9
5*a*	−1.88	370 (440)	6.7	12
5*b*	−2.35	365 (440)	7.8	19
5*c*	−2.10	346, 365 (450)	4.7	33
15*a*	−2.21 (−2.23)[b]	345, 380	14.9	4
15*b*	−2.36 (−2.38)[b]	330 (~550)	10.6	10
15*c*	−2.46 (−2.49)[b]	350	10.8	2
19	−2.42	375	5.1	2

[a]In acetonitrile containing 0.1 M tetrabutylammonium perchlorate.
[b]The values in parentheses are the standard reduction potentials as obtained from the reversible cyclic voltammograms.
[c]In methanol.
[d]Rate constant for the reaction of the substrate with solvated electron (e^-_{sol}) in methanol.
[e]Half-life of the radical anion in methanol.

proton from **5***a* to give initially the corresponding anionic species, which may then undergo further transformations to give the observed products.

The structures of all the products formed in the reaction of **1***a–c*, **5***a–c*, **15***a–c*, and **19** with potassium were established on the basis of analytical results, spectral data, and comparison with authentic samples, wherever possible.

Cyclic voltammetric studies

In earlier studies (6, 8–10), we highlighted the importance of electrochemical investigations in the generation and characterization of radical anions, the primary intermediates involved in the reaction of several unsaturated organic substrates with potassium in THF. In the present study, we have generated electrochemically the radical anions of **1***a–c*, **5***a–c*, **15***a–c*, and **19**, the substrates under investigation, and the reduction potentials are summarized in Table 1. The substrates **1***a–c*, **5***a–c*, and **19** exhibited irreversible reduction peaks with the reduction potentials in the region of −1.88 to −2.6 V versus SSCE. Because of the irreversible nature of the reduction peaks, it was not possible to elaborate further the electrochemical investigations of these compounds. The substrates **15***a–c* underwent reversible reduction with half-peak potentials in the range of −2.21 to −2.46 V versus SSCE.

Pulse radiolysis studies

As reported earlier (6, 9–13), the radical anions of unsaturated organic compounds can be generated through their reaction with solvated electron (e^-_{sol}) in polar solvents such as methanol under pulse radiolytic conditions. In the present investigation, the radical anions of **1***a–c*, **5***a–c*, **15***a–c*, and **19** were generated in methanol. These radical anions were characterized by strong absorption maxima in the region of 300–500 nm (Table 1). The lifetimes of these radical anions in methanol varied from 2 to 275 μs. It is evident from Table 1 that these radical anions are formed from their appropriate precurcors through the reaction with solvated electrons under diffusion controlled rates.

Experimental

All melting points are uncorrected and were determined on a Mel-Temp apparatus. The petroleum ether used was the fraction with bp 60–80°C. THF used was dried over sodium and was distilled before use. Gold Label (Aldrich) acetonitrile was used for cyclic voltammetric studies and spectral grade methanol (Fisher Scientific) was used for pulse radiolysis.

Starting materials

2,3-Diphenylindole (**1***a*) (14), mp 123–124°C; 2,3-diphenyl-1-methylindole (**1***b*) (14), mp 129–130°C; 1,2,3-triphenylindole (**1***c*) (15), mp 186–187°C; 2,3,4,5-tetraphenylpyrrole (**5***a*) (16), mp 212–213°C; 1,2,3,5-tetraphenylpyrrole (**5***b*) (17), mp 199–200°C; 1-benzyl-2,3,5-triphenylpyrrole (**5***c*), (17), mp 166–167°C; 2,4,5-triphenyloxazole (**15***a*) (18), mp 116–117°C; 4,5-diphenyl-2-methyloxazole (**15***b*) (18), bp 210–212°C (18 Torr; 1 Torr = 133.3 Pa); 2,4-diphenyl-5-methyloxazole (**15***c*) (19), mp 74–75°C; and 2,4,5-triphenylimidazole (**19**) (18, 20), mp 274–275°C, were prepared by reported procedures.

Reaction of **1**a–c, **5**a–c, **15**a–c, *and* **19** *with potassium in THF under nitrogen and oxygen*

A general procedure was to shake the appropriate substrate with finely cut potassium metal in THF under nitrogen, for several hours in a stoppered Schlenk tube. A few clean, broken glass pieces were added to the mixture to ensure a fresh surface of the metal throughout the reaction. The reaction mixture underwent pronounced color changes, in each case, indicative of the formation of radical anion intermediates. On completion of the reaction, the mixture was drained into moist THF (10 mL) to destroy any unchanged potassium and the solvent was removed under reduced pressure. The residual solid was treated with water (10 mL) and extracted with methylene chloride. The aqueous layer was acidified with dilute hydrochloric acid and worked up in the usual manner to give acidic products, which were purified by recrystallization from suitable solvents. Work-up of the organic layer by removal of the solvent under vacuum and fractional crystallization from suitable solvents or chromatography over neutral alumina gave the non-acidic products, which were further purified by recrystallization from suitable solvents.

In cases where the reactions were carried out under oxygen saturation, the same experimental procedure was adopted in each case, except that the starting substrates were shaken initially with potassium in THF for several hours, under oxygen saturation.

The details of reaction conditions and products are shown in Table 2.

Reaction of **1**a–c, **5**a–c, **15**a–c, *and* **19** *with potassium superoxide*

A general procedure was to stir the appropriate substrate (2 mmol) with potassium superoxide (4 mmol) and 18-crown-6 (2 mmol) in

Can. J. Chem. Downloaded from www.nrcresearchpress.com by 88.85.125.76 on 09/07/12
For personal use only.

TABLE 2. Reaction of **1***a–c*, **5***a–c*, **15***a–c*, and **19** with potassium in THF under nitrogen and oxygen

No.	Reactants and conditions	Products
1	**1***a* (0.81 g, 3 mmol) + K (0.23 g, 6 mmol)+ THF (125 mL) (nitrogen, 8 h)	**1***a* (recovered, 240 mg, 30%),[a,b,c] mp 123–124°C (mixture mp) + **3***a* (390 mg, 49%),[a,b,c] mp 192–193°C (mixture mp) (22)
2	**1***a* (0.81 g, 3 mmol) + K (0.23 g, 6 mmol) + THF (125 mL) (oxygen, 7 h)	**1***a* (recovered, 490 mg, 60%),[a,b,c] + **3***a* (80 mg, 10%),[a,b,c] + **4***a* (180 mg, 20%),[a,d] mp 89–90°C (mixture mp) (22)
3	**1***b* (0.57 g, 2 mmol) + K (0.16 g, 4 mmol) + THF (125 mL) (nitrogen, 15 h)	**1***b* (recovered, 110 mg, 19%),[a,b,c] mp 129–130°C (mixture mp) + **1***a* (366 mg, 68%)[a,b,c]
4	**1***b* (0.57 g, 2 mmol) + K (0.16 g, 4 mmol)+ THF (125 mL) (oxygen, 4 h)	**1***b* (recovered, 470 mg, 83%)[a,b,c] + **1***a* (40 mg, 7%)[a,b,c]
5	**1***c* (1.0 g, 3 mmol) + K (0.23 g, 6 mmol) + THF (125 mL) (nitrogen, 15 h)	**1***c* (recovered, 380 mg, 38%),[a,b] mp 186–187°C (mixture mp) + **1***a* (150 mg, 19%)[a,b] + **3***c* (200 mg, 20%),[a,b,c] mp 197–198°C (mixture mp) (22)
6	**1***c* (1.0 g, 3 mmol) + K (0.23 g, 6 mmol) + THF (125 mL) (oxygen, 7 h)	**1***a* (70 mg, 9%)[a,b] + **3***c* (80 mg, 8%)[a,b] +**4***a* (250 mg, 29%),[a,b,d] mp 89–90°C (mixture mp)
7	**5***a* (1.1 g, 3 mmol) + K (0.23 g, 6 mmol) + THF (125 mL) (nitrogen, 10 h)	**5***a* (recovered, 640 mg, 59%),[a,b] mp 212–213°C (mixture mp)
8	**5***a* (1.1 g, 3 mmol) + K (0.23 g, 6 mmol) + THF (125 mL) (oxygen, 6 h)	**14** (36 mg, 10%),[e] mp 120–121°C (mixture mp) + **5***a* (recovered, 330 mg, 30%)[a,b] + **8***a* (80 mg, 7%),[a,h,g] mp 190–191°C (mixture mp) (23) + **12***a* (220 mg, 19%),[a,h,g] mp 213–214°C (mixture mp) (24,25) + **7***a* (150 mg, 13%),[a,f,g] mp 249–250°C (mixture mp) (25) + **11***a* (53 mg, 15%),[a,i,j] mp 128–129°C (mixture mp) (26)
9	**5***b* (1.1 g, 3 mmol) + K (0.23 g, 6 mmol) + THF (125 mL) (nitrogen, 10 h)	**5***b* (recovered, 540 mg, 49%),[a,b] mp 199–200°C (mixture mp) + **9***b* (260 mg, 30%),[a,b] mp 140–141°C (mixture mp) (17)
10	**5***b* (1.1 g, 3 mmol) + K (0.23 g, 6 mmol) + THF (125 mL) (oxygen, 10 h)	**14** (50 mg, 14%)[e] + **5***b* (99 mg, 9%)[a,b] + **9***b* (60 mg, 7%)[a,b] + **10***b* (88 mg, 12%),[a,h,g] mp 112–113°C (mixture mp) (27) + **11***b* (85 mg, 16%),[a,h,g] mp 163–164°C (mixture mp) (ref. 26, p. 683) + **11***a* (30 mg, 9%),[a,i,j] mp 128–129°C (mixture mp) + **13***b* (120 mg, 13%),[a,b] mp 125–126°C (mixture mp) (17) + **12***b* (90 mg, 10%),[a,d,f] mp 224–225°C (mixture mp) (29)
11	**5***c* (1.2 g, 3 mmol) + K (0.23 g, 6 mmol) + THF (125 mL) (nitrogen, 10 h)	**5***c* (recovered, 540 mg, 45%),[a,b] mp 166–167°C (mixture mp) + **9***b* (300 mg, 33%)[a,b,g]
12	**5***c* (1.2 g, 3 mmol) + K (0.23 g, 6 mmol) + THF (125 mL) (oxygen, 10 h)	**14** (57 mg, 15%)[e] + **5***c* (recovered, 165 mg, 14%),[a,b] mp 166–167°C (mixture mp) + **9***b* (72 mg, 8%),[a,b] mp 140–141°C (mixture mp) + **10***b* (130 mg, 14%),[a,f] mp 112–113°C (mixture mp) + **11***c* (110 mg, 17%),[a,h] mp 105–106°C (mixture mp) (30) + **11***a* (33 mg, 9%),[a,i] + **13***b* (106 mg, 11%),[a,k] + **12***b* (115 mg, 12%)[a,d]
13	**15***a* (0.6 g, 2 mmol) + K (0.16 g, 4 mmol) + THF (125 mL) (nitrogen, 10 h)	**14** (10 mg, 5%)[e] + **15***a* (recovered, 280 mg, 47%),[a,b] mp 116–117°C (mixture mp) + **18***a* (160 mg, 27%),[a,b,g] mp 177–178°C (mixture mp) (31)
14	**15***a* (0.6 g, 2 mmol) + K (0.16 g, 4 mmol) + THF (125 mL) (oxygen, 20 h)	**14** (20 mg, 10%)[e] + **15***a* (recovered, 400 mg, 23%)[a,b] + **18***a* (90 mg, 15%)[a,b]
15	**15***b* (0.47 g, 2 mmol) + K (0.16 g, 4 mmol) + THF (125 mL) (nitrogen, 10 h)	**14** (10 mg, 4%)[e] + **15***b* (recovered, 230 mg, 45%),[a,b] bp 210–212°C (18) + **17***b* (190 mg, 37%),[a,b] mp 175–176°C (mixture mp) (32)
16	**15***b* (0.47 g, 2 mmol) + K (0.16 g, 4 mmol) + THF (125 mL) (oxygen, 10 h)	**14** (30 mg, 11%)[e] + **15***b* (recovered, 300 mg, 59%)[a,b] + **17***b* (70 mg, 14%)[a,b]
17	**15***c* (0.47 g, 2 mmol) + K (0.16 g, 4 mmol) + THF (125 mL) (nitrogen, 10 h)	**14** (10 mg, 4%)[e] + **15***c* (recovered, 260 mg, 52%)[a,b] + **17***c* (150 mg, 30%),[a,b,g] mp 164–165°C (mixture mp) (33)
18	**15***c* (0.47 g, 2 mmol) + K (0.16 g, 4 mmol) + THF (125 mL) (oxygen, 10 h)	**15***c* (recovered, 310 mg, 62%)[a,b] + **17***c* (80 mg, 16%)[a,b]
19	**19** (0.6 g, 2 mmol) + K (0.16 g, 4 mmol) + THF (125 mL) (nitrogen, 12 h)	**19** (recovered, 500 mg, 83%),[a,h,l] mp 274–275°C (mixture mp)
20	**19** (0.6 g, 2 mmol) + K (0.16 g, 4 mmol) + THF (125 mL) (oxygen, 10 h)	**19** (recovered, 400 mg, 67%)[a,h,l] + **21** (110 mg, 21%),[a,k,g] mp 144–145°C (mixture mp) (28)

[a]From the non-aqueous fraction.
[b]Elution with petroleum ether.
[c]Recrystallization from a mixture (1:9) of benzene and petroleum ether.
[d]Elution with a mixture (4:1) of benzene and petroleum ether.
[e]From the aqueous fraction.
[f]Elution with a mixture (1:4) of benzene and petroleum ether.
[g]Recrystallization from ethanol.
[h]Elution with a mixture (2:3) of benzene and petroleum ether.
[i]Elution with a mixture (1:1) of benzene and petroleum ether.
[j]Recrystallization from hot water.
[k]Elution with a mixture (3:2) of benzene and petroleum ether.
[l]Recrystallization from a mixture (1:1) of ethanol and water.

Can. J. Chem. Downloaded from www.nrcresearchpress.com by 88.85.125.76 on 09/07/12
For personal use only.

TABLE 3. Reaction of **1***a–c*, **5***a–c*, **15***a–c*, and **19** with potassium superoxide

No.	Reactants and conditions	Products
1	**1***a* (0.54 g, 2 mmol) + potassium superoxide (0.29 g, 4 mmol) + 18-crown-6 (0.53 g, 2 mmol) + benzene (100 mL) (24 h)	**1***a* (recovered, 250 mg, 47%)[a] + **4***a* (160 mg, 27%),[a,b] mp 89–90°C (mixture mp) + **3***a* (70 mg, 13%)[a,c]
2	**1***b* (0.57 g, 2 mmol) + potassium superoxide (0.29 g, 4 mmol) + 18-crown-6 (0.53 g, 2 mmol) + benzene (100 mL) (24 h)	**1***a* (30 mg, 5%)[a,b] + **1***b* (recovered, 510 mg, 89%),[a,b] mp 129–130°C (mixture mp)
3	**1***c* (0.69 g, 2 mmol) + potassium superoxide (0.29 g, 4 mmol) + 18-crown-6 (0.53 g, 2 mmol) + benzene (100 mL) (24 h)	**1***a* (40 mg, 7%)[a,b] + **1***c* (recovered, 200 mg, 29%),[a,b] mp 186–187°C (mixture mp) + **4***a* (200 mg, 34%),[a,b,d] mp 89–90°C (mixture mp) + **3***c* (80 mg, 11%)[a,c] mp 196–197°C (mixture mp).
4	**5***a* (1.1 g, 3 mmol) + potassium superoxide (0.43 g, 6 mmol) + 18-crown-6 (0.79 g, 3 mmol) + benzene (100 mL) (24 h)	**14** (47 mg, 13%),[e] mp 120–121°C (mixture mp) + **5***a* (recovered, 220 mg, 20%),[a,b] mp 212–213°C (mixture mp) + **7***a* (170 mg, 15%),[a,f] mp 249–250°C (mixture mp) + **8***a* (270 mg, 23%),[a,g] mp 190–191°C (mixture mp) + **11***a* (50 mg, 14%),[a,h] mp 128–129°C (mixture mp) + **12***a* (125 mg, 11%),[a,i] mp 213–214°C (mixture mp)
5	**5***b* (1.1 g, 3 mmol) + potassium superoxide (0.43 g, 6 mmol) + 18-crown-6 (0.79 g, 3 mmol) + benzene (100 mL) (24 h)	**5***b* (recovered, 990 mg, 90%),[a,b,j] mp 199–200°C (mixture mp)
6	**5***c* (1.2 g, 3 mmol) + potassium superoxide (0.43 g, 6 mmol) + 18-crown-6 (0.79 g, 3 mmol) + benzene (100 mL) (24 h)	**5***c* (recovered, 1.0 g, 84%),[a,b,j] mp 166–167° (mixture mp)
7	**15***a* (0.6 g, 2 mmol) + potassium superoxide (0.29 g, 4 mmol) + 18-crown-6 (0.53 g, 2 mmol) + benzene (100 mL) (24 h)	**14** (20 mg, 10%)[e] + **15***a* (recovered, 410 mg, 68%),[a,b] mp 116–117°C (mixture mp) + **18***a* (110 mg, 19%),[a,b,j] mp 177–178°C (mixture mp)
8	**15***b* (0.94 g, 4 mmol) + potassium superoxide (0.58 g, 8 mmol) + 18-crown-6 (1.06 g, 4 mmol) + benzene (100 mL) (24 h)	**14** (60 mg, 13%)[e] + **15***b* (recovered, 500 mg, 53%)[a,b] + **17***b* (160 mg, 17%),[a,b] mp 175–176°C (mixture mp)
9	**15***c* (0.47 g, 2 mmol) + potassium superoxide (0.29 g, 4 mmol) + 18-crown-6 (0.53 g, 2 mmol) + benzene (100 mL) (24 h)	**14** (20 mg, 9%)[e] + **15***c* (320 mg, 64%),[a,b] mp 74–75°C (mixture mp) + **17***c* (90 mg, 18%),[a,b] mp 164–165°C (mixture mp)
10	**19** (0.6 g, 2 mmol) + potassium superoxide (0.14 g, 2 mmol) + 18-crown-6 (0.53 g, 2 mmol), + benzene (100 mL) (24 h)	**19** (recovered, 310 mg, 52%),[a,g] mp 274–275°C (mixture mp) + **21** (120 mg, 27%)[a,i,j]

[a]From the non-aqueous fraction.
[b]Elution with petroleum ether.
[c]Recrystallization from a mixture (1:9) of benzene and petroleum ether.
[d]Elution with a mixture (3:7) of benzene and petroleum ether.
[e]From the aqueous fraction.
[f]Elution with a mixture (1:4) of benzene and petroleum ether.
[g]Elution with a mixture (2:3) of benzene and petroleum ether.
[h]Elution with a mixture (1:1) of benzene and petroleum ether.
[i]Elution with a mixture (3:2) of benzene and petroleum ether.
[j]Recrystallization from ethanol.

benzene (100 mL) for 24 h. On completion of the reaction, the mixture was treated with water (20 mL) and extracted with an aqueous solution of sodium chloride. The organic layer was dried over sodium sulfate and the solvent was removed under vacuum. The residual solid was chromatographed over neutral alumina and recrystallized from suitable solvents to give the non-acidic products. The aqueous layer, on acidification with dilute hydrochloric acid, gave the acidic products, which were purified by recrystallization from suitable solvents.

The details of reaction conditions and products are indicated in Table 3.

Cyclic voltammetry

Measurements were made with a Princeton Applied Research (PAR) model 173 potentiostat/galvanostat, a PAR model 175 universal programmer, and a Kipp and Zonen X–Y recorder. Experiments were performed in a standard three-compartment cell, equipped with a Pt-disc working electrode, a Pt-wire counter electrode, and a saturated sodium chloride – calomel electrode (SSCE). Cyclic voltammograms were recorded in deaerated acetonitrile containing 0.1 M tetrabutylammonium perchlorate (TBAP).

Pulse radiolysis

The pulse radiolysis experiments were carried out using a computer controlled apparatus (21) and the irradiation was carried out with 5-ns electron pulses from the Notre Dame 7 MeV ARCO LP-7 linear accelerator, using a dose rate of $\sim 2 \times 10^{16}$ eV/g per pulse. The solutions (0.2–0.5 mM) of the substrates were taken in graduated 250-mL cylindrical reservoirs and deaerated by bubbling nitrogen for at least 30 min prior to irradiation. Nitrogen bubbling was continued in the reservoir from which the solution was allowed to flow continuously through the cell (1 cm pathlength). The rate constants for the reactions with solvated electrons (e^-_{sol}) were determined from the kinetic analysis of the enhanced rate of decay of e^-_{sol} in the presence of the substrate or from the growth rate of the radical anion.

Acknowledgements

The authors thank the Department of Science and Technology and Council of Scientific and Industrial Research, Government of India, Regional Research Laboratory Trivandrum, Indian Institute of Technology, Kanpur, and the Office of Basic Energy

Can. J. Chem. Downloaded from www.nrcresearchpress.com by 88.85.125.76 on 09/07/12
For personal use only.

Sciences of the U.S. Department of Energy for financial support of this work.

1. E. C. FRANKLIN. J. Phys. Chem. **24**, 81 (1920).
2. G. W. WATT. Chem. Rev. **46**, 317 (1950).
3. (*a*) S. O'BRIAN and D. C. C. SMITH. J. Chem. Soc. 4609 (1960); (*b*) H. SMITH. Chemistry in nonaqueous ionizing solvents. Vol. I, Part 2. *Edited by* G. Jander, H. Spandau, and C. C. Addison. Wiley–Interscience, New York. 1963.
4. W. A. REMERS, G. J. GIBS, C. PIDACKS, and M. J. WEISS. J. Org. Chem. **36**, 279 (1971).
5. A. DORNOW and H. EICHHOLTZ. Chem. Ber. **86**, 384 (1953).
6. M. MUNEER, R. K. TIKARE, P. V. KAMAT, and M. V. GEORGE. Can. J. Chem. **65**, 1624 (1987).
7. E. B. HERGOVICH and G. SPEIER. Tetrahedron Lett. **23**, 4473 (1982).
8. B. PANDEY, R. K. TIKARE, M. MUNEER, P. V. KAMAT, and M. V. GEORGE. Chem. Ber. **119**, 917 (1986).
9. K. ASHOK, P. M. SCARIA, P. V. KAMAT, and M. V. GEORGE. Can. J. Chem. **65**, 2039 (1987).
10. M. MUNEER, R. K. TIKARE, P. V. KAMAT, and M. V. GEORGE. New J. Chem. **13**, 215 (1989).
11. K. B. PATEL and R. L. WILSON. J. Chem. Soc. Faraday Trans. 1, **69**, 814 (1973).
12. J. H. BAXENDALE and P. WARDMAN. Natl. Stand. Ref. Data Ser. (U.S. Natl. Bur. Stand.), **54**, 1 (1975).
13. N. V. RAGHAVEN, P. K. DAS, and K. BOBROWSKI. J. Am. Chem. Soc. **103**, 4569 (1981).
14. E. E. BARONI and K. A. KOVYRZINA. Zh. Obsch. Khim. **29**, 3815 (1959); Chem. Abstr. **54**, 19643h (1960).
15. M. B. RICHARDS. J. Chem. Soc. **97**, 977 (1910).
16. D. DAVIDSON. J. Org. Chem. **3**, 361 (1938).
17. A. LESPAGNOL, J. M. DUMONT, J. MERCIER, and M. ETZENSPERGER. Bull. Soc. Pharm. Lille, **1**, 87 (1955); Chem. Abstr. **50**, 3399b (1956).
18. D. DAVIDSON, M. WEISS, and M. JELLING. J. Org. Chem. **2**, 328 (1937).
19. D. L. ALDOUS, J. L. RIEBSOMER, and R. N. CASTLE. J. Org. Chem. **25**, 1151 (1960).
20. W. B. LESLIE and G. W. WATT. J. Org. Chem. **7**, 73 (1942).
21. L. K. PATTERSON and J. LILLIE. Int. J. Radiat. Phys. Chem. **6**, 129 (1974).
22. C. A. MUDRY and A. R. FRASCA. Tetrahedron, **30**, 2983 (1974).
23. E. P. KOHLER and N. K. RICHTMYER. J. Am. Chem. Soc. **50**, 3092 (1928).
24. F. KLINGEMANN and W. F. LAYCOCK. Chem. Ber. **24**, 510 (1891).
25. F. R. JAPP and W. D. DAVIDSON. J. Chem. Soc. **67**, 32 (1895).
26. A. I. VOGEL. A text book of practical organic chemistry. English Language Book Society and Longman Group Ltd., London. 1978. p. 517.
27. P. J. HAMRICK and C. R. HAUSER. J. Am. Chem. Soc. **81**, 493 (1959).
28. A. W. TITHERLEY. J. Chem. Soc. **85**, 1673 (1904).
29. F. R. JAPP and F. KLINGEMANN. J. Chem. Soc. **57**, 662 (1890).
30. O. C. DERMER and J. KING. J. Org. Chem. **8**, 168 (1943).
31. M. MOUSSERON, H. CHRISTOL, and A. LAURENT. C. R. Hebd. Seances Acad. Sci. **248**, 1904 (1959); Chem. Abstr. **53**, 17934e (1959).
32. W. KRABBE, A. SEHER, and E. POLZIN. Chem. Ber. **74B**, 1892 (1941).
33. A. N. TISCHLER and M. H. TISCHLER. Tetrahedron Lett. 3407 (1978).

Can. J. Chem. Downloaded from www.nrcresearchpress.com by 88.85.125.76 on 09/07/12
For personal use only.

COMMUNICATION

Biomimetic ion transport: on the mechanism of ion transport by an artificial ion channel mimic

THOMAS M. FYLES,[1] TONY D. JAMES, AND KATHARINE C. KAYE
Department of Chemistry, University of Victoria, Victoria, B.C., Canada V8W 2Y2

Received December 4, 1989

THOMAS M. FYLES, TONY D. JAMES, and KATHARINE C. KAYE. Can. J. Chem. **68**, 976 (1990).

The influx of cations into vesicles mediated by a synthetic transporter is coupled to proton efflux and may be quantified by a pH-stat technique. The dependence of the transport upon cation type and concentration, upon transporter concentration, and upon temperature has been examined. The synthetic transporter is closely similar to the natural channel forming compound gramicidin, and significantly different from the carrier valinomycin, with respect to the variables examined.

Key words: ion transport, vesicle membrane, channel, gramicidin, transport mechanism.

THOMAS M. FYLES, TONY D. JAMES et KATHARINE C. KAYE. Can. J. Chem. **68**, 976 (1990).

On a couplé l'influx de cations dans des vésicules qui est assisté par un transporteur de synthèse avec un efflux de proton et on l'a quantifié à l'aide d'une technique de pH. On a examiné la relation qui existe entre le transport et le type et la concentration du cation, la concentration du transporteur et la température. Par rapport aux variables qui ont été examinées, le transporteur de synthèse est très semblable à la gramicidine, le composé naturel formant des canaux, mais il diffère de la valinomycine.

Mots clés : transport ionique, membranes vésiculaires, canaux, gramicidine, mécanismes de transport.

[Traduit par la revue]

Introduction

Biomimetic model systems of ion transport processes seek to illuminate the fundamental features of natural transport systems (1). Two main molecular mechanisms can be discerned: transport mediated by carriers, and transport mediated by pores or channels. Recent emphasis from synthesis has been on the former (2), despite the fact that the latter mechanism appears to be more general among natural systems (3). A few notable exceptions are the synthetic channels of Tabushi *et al.* and Nolte and co-workers (4*a*)[2] and systems involving amphiphile association for the creation of pores (5). We recently reported the synthesis and ion transport activity of a type of ion channel designed to mimic channels such as gramicidin (6). An example is sketched in Fig. 1. The speculative structure illustrated served initially as a guide to target selection and synthesis. This report addresses the question of the implied mechanism embedded in the design: does the mimic transport cations by a channel mechanism?

The transport of cations across vesicle bilayer membranes was determined by a pH-stat method (7).[3] Vesicles were prepared and purified in a choline sulfate/Bis-Tris buffer at pH 6.60, diluted in unbuffered choline sulfate, and brought to pH 7.5 with choline base. Addition of the proton carrier FCCP and the transporter has little effect on the slow rate of proton efflux due to the collapse of the pH gradient. Upon addition of metal ion, a trans-membrane cation gradient is established, which collapses via electroneutral cation/proton antiport (7). The proton efflux can then be determined by addition of choline base to maintain the external pH. Proton efflux occurs rapidly, but decreases in a monotonic fashion to a steady-state rate equal to the slow efflux of the background in the absence of transporter. Addition of Triton X100 provokes complete vesicle lysis and releases any remaining internal buffer. Figure 2 illustrates the experimental result provoked by the transporter, at a concentration of 7×10^{-10} M (about 1 per vesicle), for variation in the metal ion added.

The principal feature of all experiments is that the synthetic transporter fails to empty all the vesicles. By electron microscopy,[3] the vesicle preparations are predominantly unilamellar (LUV, 125 nm diameter) but contain some larger multilamellar structures (MLV), accounting for 10–15% of the entrapped proton titer. Gary-Bobo and co-workers (7) previously noted that carriers such as valinomycin can empty the LUV fraction irrespective of the amount of carrier added, but that channel forming compounds (gramicidin, amphotericin) exhibit a concentration-dependent plateau, lower than the total LUV fraction. The results given in Fig. 2 for the synthetic transporter are

[1]Author to whom correspondence may be addressed.

[2]Non-functional channels have also been described (4*b*).

[3]Egg phosphatidyl choline, cholesterol, and phosphatidic acid (8:1:1) in ether was mixed with 0.2 M Bis-Tris/sulfate buffer (pH 6.60) containing 0.054 M D-mannitol. The mixture was sonicated, the organic solvent removed at reduced pressure, and the vesicle solution diluted with more buffer solution and successively filtered through 3- and 0.4 μm cellulose acetate filters. The sized vesicles were isolated by chromatography on Sephadex G10 (10 mL) using 0.11 M choline sulfate containing 0.093 M D-mannitol as eluent and then aged for 16 h at ambient temperature. The lipid content was determined (11); 3.3 mg/mL was a typical value. The pH-stat method described in the text utilized 0.00491 M choline base in 0.35 M D-mannitol as titrant. A vesicle sample (0.5 mL, 2.4 μmol lipid) was diluted with 3.5 mL of the choline sulfate/ D-mannitol solution and brought to pH 7.5 (about 1 mL of titrant added). FCCP (carbonyl cyanide (4-trifluoromethoxy) phenyl hydrazone, 80 pmol) followed by the transporter (**6***b* of ref. 6, prepared and purified as previously, 3.4 pmol) were added as solutions in methanol. Transport was initiated by addition of metal sulfates. The electron microscopy samples were prepared by dipping Formvar-coated copper grids into the vesicle solution, air drying, and staining with phosphotungstic acid at pH 7.2. A Phillips EM360 transmission electron microscope was used. Controls establish the following: no transport without the addition of transporter, no effect of methanol alone, no detergent effect of the transporter on the vesicles, and vesicles are intact at the end of the pH-stat experiment.

Can. J. Chem. Downloaded from www.nrcresearchpress.com by 88.85.125.76 on 09/07/12
For personal use only.

Can. J. Chem. Downloaded from www.nrcresearchpress.com by 88.85.125.76 on 09/07/12
For personal use only.

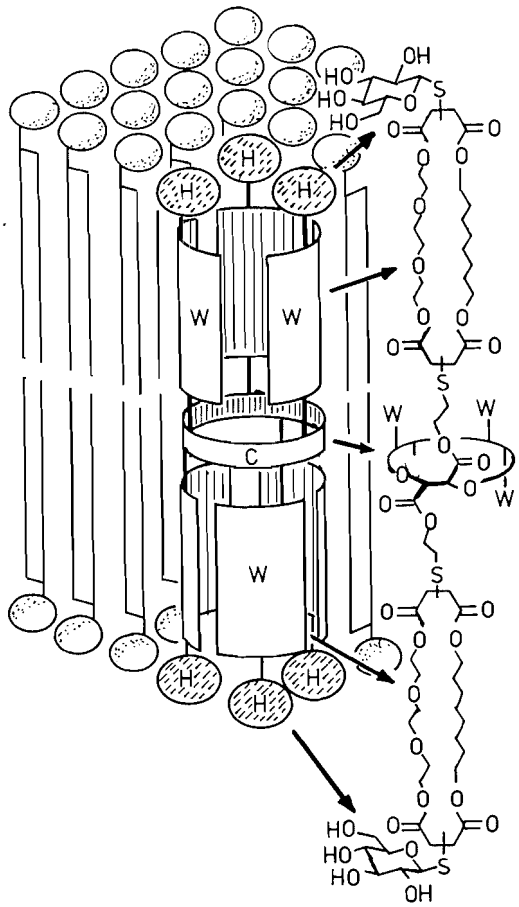
OH
HO
HO
HO
S
O
O
O

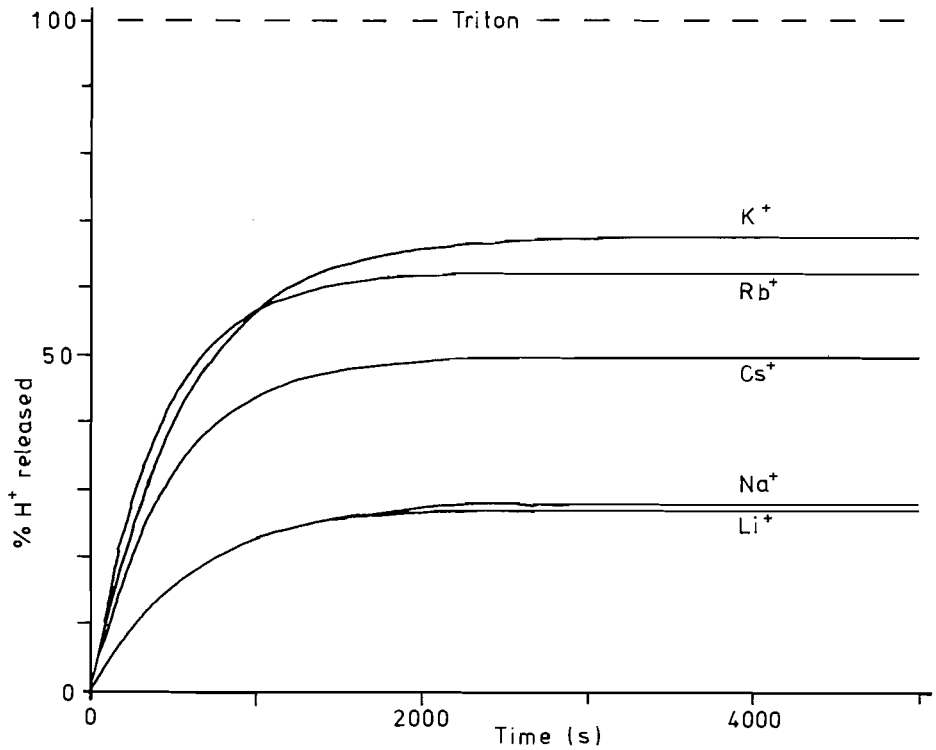

FIG. 2. Extent of proton efflux as a function of time, expressed as the percentage of the total entrapped titer released by Triton X100 lysis. See Table 1 for conditions, data of entries 5–8 and 11.

gramicidin is 32 ± 8 kJ/mol, while for the carrier valinomycin the value is 43 ± 16 kJ/mol. The extent of transport is not temperature dependent in the latter two cases.

Taken together, the available data are most consistent with the synthetic transporter acting via a channel mechanism: the observation of the plateau behaviour, the inability of the transporter to move between vesicles, the low kinetic order in transported cation, and the temperature dependence and activation energy all argue for this view. The unit order in transporter, the observation of a saturable process, and the observation of ion selectivity are consistent with either a carrier or a channel mechanism. The selectivity of the gramicidin pore can be directly determined under conditions where the anion symport (or cation antiport) is not rate limiting (10). The use of FCCP is intended to achieve this condition (7), thus the selectivities determined here could also derive from a channel mechanism. In total, the synthetic transporter is more similar to a known channel-forming compound, gramicidin, than to a known carrier such as valinomycin. The sketch of Fig. 1 thus represents a likely mode of action of this synthetic channel in a bilayer.

Acknowledgements

This work was supported by grants from the University of Victoria and the Natural Sciences and Engineering Research Council of Canada. The services of the Electron Microscope Facility of the Department of Biology at the University of Victoria are gratefully acknowledged.

1. D. W. URRY. Top. Curr. Chem. **128**, 175 (1985); P. LAUGER. Angew. Chem. Int. Ed. Engl. **24**, 905 (1985).
2. M. OKAHARA and Y. NAKATSUJI. Top. Curr. Chem. **128**, 37 (1985); R. M. IZATT, G. C. LINDH, R. L. BRUENING, J. S. BRADSHAW, J. D. LAMB, and J. J. CHRISTENSEN. Pure Appl. Chem. **58**, 1453 (1986).
3. M. D. HOUSLAY and K. K. STANLEY. Dynamics of biological membranes. J. Wiley and Sons, New York. 1982.
4. (*a*). I. TABUSHI, Y. KURODA, and K. YOKOTA. Tetrahedron Lett. **23**, 4601 (1982); R. J. M. NOLTE, A. J. M. VAN BEIJNEN, J. G. NEEVEL, J. W. ZWIKKER, A. J. VERKLEY, and W. DRENTH. Isr. J. Chem. **24**, 297 (1984); U. F. KRAGTEN, M. F. ROKS, and R. J. M. NOLTE. J. Chem. Soc. Chem. Commun. 1275 (1985); (*b*) J. P. BEHR, J. M. LEHN, A. C. DOCK, and D. MORAS. NATURE, **295**, 295 (1982); L. JULIEN and J. M. LEHN. Tetrahedron Lett. **29**, 3803 (1988).
5. T. KUNITAKE. Ann. N. Y. Acad. Sci. **471**,(1986); J. H. FURHOP, H. H. DAVID, J. MATHIEU, U. LIMAN, M. J. WINTER, and E. BOEKEMA. J. Am. Chem. Soc. **108**, 1785 (1986); J. H. FURHOP and D. FRITSCH. Acc. Chem. Res. **19**, 130 (1986).
6. V. E. CARMICHAEL, P. J. DUTTON, T. M. FYLES, T. D. JAMES, J. A. SWAN, and M. ZOJAJI. J. Am. Chem. Soc. **111**, 767 (1989).
7. B. CYBULSKA, T. ZIMINSKI, E. BOROWSKI, and C. M. GARY-BOBO. Mol. Pharmacol. **24**, 270 (1983); C. THOMAS, C. SAUTEREY, M. CASTAING, C. M. GARY-BOBO, J. M. LEHN, and P. PLUMERE. Biochem. Biophys. Res. Commun., **116**, 981 (1983); M. HERVE, B. CYBULSKA, and C. M. GARY-BOBO. Eur. J. Biochem. **12**, 1212 (1985); B. CYBULSKA, M. HERVE, E. BOROWSKI, and C. M. GARY-BOBO. Mol. Pharmacol. **29**,293 (1986).
8. L. M. DULYEA, T. M. FYLES, and D. M. WHITFIELD. Can. J. Chem. **62**, 498 (1984); T. M. FYLES. J. Chem. Soc. Faraday Trans. 617 (1986).
9. R. M. IZATT, J. S. BRADSHAW, S. A. NIELSEN, J. D. LAMB, J. J. CHRISTENSEN, and D. SEN. Chem. Rev. **85**, 271 (1985).
10. B. E. COHEN. J. Membr. Biol. **68**, 79(1982).
11. R. K. RAHEDJA, C. KAUR, A. SINGH, and I. S. BAHTIA. J. Lipid Res. **14**, 695 (1973).

Can. J. Chem. Downloaded from www.nrcresearchpress.com by 88.85.125.76 on 09/07/12
For personal use only.

Conformational analysis of key disaccharide components of *Brucella* A and M antigens[1]

THOMAS PETERS,[2] JEAN-ROBERT BRISSON, AND DAVID R. BUNDLE
Division of Biological Sciences, National Research Council of Canada, Ottawa, Ont., Canada K1A 0R6

Received December 19, 1989

This paper is dedicated to Professor Arthur S. Perlin on the occasion of his 67th birthday

THOMAS PETERS, JEAN-ROBERT BRISSON, and DAVID R. BUNDLE. Can. J. Chem. **68**, 979 (1990).

The synthetic α1,2 and α1,3 disaccharide methyl glycosides of 4-amino-4,6-dideoxy-D-mannose **1–6** that constitute key structural elements of *Brucella* A and M antigens were analyzed by ^1H and ^{13}C nuclear magnetic resonance spectroscopy. A detailed conformational analysis was performed for the *N*-acetylated derivatives **1** and **4** as well as for the amino derivatives **2** and **5**. Potential energy calculations using the GESA program established the global minima for the disaccharides **1**, **2**, **4**, and **5**, and mapped the energy surface as a function of the glycosidic torsion angles ϕ and ψ. Ensemble averaged nuclear Overhauser enhancements, weighted according to the Boltzmann distribution function, were derived for each of the four disaccharides. This procedure improved the fit between experimentally and theoretically derived nOe values, when compared to interpretations based on a single conformer model. The *Brucella* A and M antigens are homopolymers of 4-formamido-4,6-dideoxy-D-mannose and, as *N*-formyl groups (saccharides **3**, **6**, and **8**) are essential for the binding of these antigens to their respective antibodies, amide conformation was analyzed by examination of the vicinal proton–proton and proton–carbon coupling constants of the model monosaccharide **8**. The conformational properties of the model compounds **1–8** were used to model the *Brucella* A and M polysaccharide antigens.

Key words: conformational analysis, disaccharide conformation, nuclear Overhauser measurements, molecular modeling, *Brucella* antigen.

THOMAS PETERS, JEAN-ROBERT BRISSON et DAVID R. BUNDLE. Can. J. Chem. **68**, 979 (1990).

Faisant appel à la spectroscopie en résonance magnétique nucléaire du ^1H et du ^{13}C, on a analysé les α1,2 et α1,3 disaccharide glucosides de méthyle (**1–6**) du 4-amino-4,6-didésoxy-D-mannose qui constituent les éléments clés de la structure des antigènes de la *Brucella* A et M. On a réalisé une analyse conformationnelle détaillée des dérivés *N*-acétylés **1** et **4** ainsi que des dérivés aminés **2** et **5**. Des calculs d'énergie potentielle effectués à l'aide du programme GESA ont permis d'établir les minima globaux des disaccharides **1**, **2**, **4** et **5** ainsi qu'une carte de l'énergie superficielle en fonction des angles de torsion ϕ et ψ de la liaison glycosidique. Pour chacun des quatre disaccharides, on a déterminé les valeurs moyennes de nOe des ensembles, pondérés à l'aide d'une fonction de distribution de Boltzmann. Cette procédure a permis d'améliorer la corrélation entre les valeurs expérimentales des nOe et les valeurs calculées d'une façon théorique à l'aide d'un modèle conformère unique. Les antigènes de la *Brucella* A et M sont des homopolymères du 4-formamido-4,6-didésoxy-D-mannose dont les groupements *N*-formyles (saccharides **3**, **6** et **8**) sont essentiels pour la liaison de ces antigènes avec leurs anticorps respectifs; on a donc analysé la conformation de l'amide grâce à un examen des constantes de couplage proton–proton et proton–carbone vicinaux du monosaccharide modèle, **8**. On a utilisé les propriétés conformationnelles des composés modèles **1–8** pour déduire un modèle des polysaccharides des antigènes de la *Brucella* A et M.

Mots clés: analyse conformationnelle, conformation du disaccharide, mesures de nOe, modèle moléculaire, antigène de la *Brucella*.

[Traduit par la revue]

Introduction

Brucella polysaccharide antigens are homopolymers of the rare sugar 4,6-dideoxy-4-formamido-D-mannopyranose (D-Rha4NFo). The A polysaccharide is α1,2 linked and hence may be regarded as having a monomeric repeating unit (1, 2), while the M antigen has a pentameric repeating sequence due to the replacement of one α1,2 linkage in every five by an α1,3 linkage (2, 3).

A antigen: [→2)-α-D-Rha4NFo-(1-]

M antigen: [→2)-α-D-Rha4NFo-(1→2)-α-D-Rha4NFo-(1→2)-α-D-Rha4NFo-(1→2)-α-D-Rha4NFo-(1→3)-α-D-Rha4NFo-(1-]

Monoclonal antibodies that bind these antigens have been crystallized in the form of Fab fragments and as complexes with a synthetic pentasaccharide (4). One of these crystal structures has been solved at 2.7 Å resolution (4), and separate work on binding site modeling based upon sequence homology with solved structures has also yielded a model of the protein site (5).

In order that the bound ligand may be realistically modeled in the combining site it is desirable to understand the conformational properties of short oligomeric di-, tri-, tetra-, and pentasaccharide sequences of the *Brucella* antigens, which have also been used to immunochemically map the binding site (6). To accomplish this, key α1,2- and α1,3-linked disaccharides in the form of acetamido-deoxy derivatives **1** and **4**, amino-deoxy derivatives **2** and **5**, and deoxy-formamido derivatives **3** and **6** were synthesized in addition to tri-, tetra-, and pentasaccharides (7–9). The structural variation at the 4-amino group was considered to be a necessity in the conformational analysis of antigen fragments because 4,6-dideoxy-4-formamido-D-mannose exists in solution as both *E* and *Z* isomers (2, 10, 11), a complication that prevents a practical analysis of conformation at the level of trisaccharide or higher homologues. Consequently, *N*-acetyl derivatives **1** and **4** as well as the amino derivatives **2** and **5** were synthesized together with the *N*-acetylated and *N*-formylated monosaccharides **7** and **8** so that a detailed conformational analysis by nmr spectroscopy could be performed on the basic element of the antigen structure.

In this paper we describe the detailed conformational analysis of the disaccharides **1**, **2**, **4**, and **5** by nmr spectroscopy and

[1]NRCC No. 31332.

[2]Present address: University of Frankfurt, Institute of Biophysical Chemistry, Theodor-Stern-Kai 7-15, 6000 Frankfurt/M. 70, F.R.G.

Can. J. Chem. Downloaded from www.nrcresearchpress.com by 88.85.125.76 on 09/07/12
For personal use only.

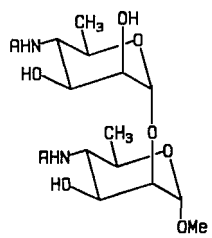

1 R = Ac
2 R = H
3 R = CHO

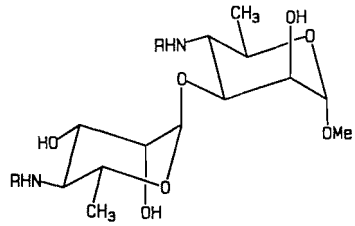

4 R = Ac
5 R = H
6 R = CHO

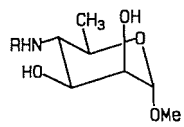

7 R = Ac
8 R = CHO

potential energy calculations. The approach adopted utilized the HSEA force field (12, 13) to map the energy surface defined by the glycosidic torsion angles, but rather than rely upon a single-state model to interpret the nmr data (12–19), the method of Cummings and Carver (20, 21) was used to predict ensemble averaged nOe values. Finally, a three-dimensional model for the *Brucella* A and M polysaccharide chains is proposed by combining the results of the potential energy calculations with vicinal proton–proton and proton–carbon coupling constant data for the *N*-formylated monosaccharide **8**, data that defines the orientation of the *N*-formyl group.

Results

Calculations

Potential energy calculations were performed using the GESA program (17).[3] This program embodies the rigid body HSEA (Hard Sphere Exo Anomeric) approach of Lemieux (11, 12), which assumes that van der Waals interactions and the *exo*-anomeric (23) effect are the main forces determining conformational equilibria of carbohydrates in aqueous solution. Treatment of hydroxyl group orientation is deliberately avoided by omitting hydrogen atoms attached to oxygen. The torsional degrees of freedom defining a certain conformation ϕ^H (H1—C1—O1—CX) and ψ^H (C1—O1—CX—HX) at the glycosidic linkages and the torsional angle ω (O5—C5—C6—O6) describing the orientation of the hydroxymethyl group (not used here) are minimized simultaneously using the Davidon–Fletcher–Powell algorithm (24) from a chosen set of starting angles. The initial parameter settings may be varied to ensure that the global minimum is reached. Consequently, it is important to know the shape of the energy surface prior to minimization. For the disaccharides to be discussed, this surface is a function of only two variable angles and Fig. 1 shows the energy surfaces of the *N*-acetyl derivatives of the α1,2- and α1,3-linked disaccharide methyl glycosides **1** and **4**. These two surfaces are very similar despite the difference of linkage position. For both linkages the global minima are found to exhibit ϕ and ψ angles between $-40°$ and $-50°$ and between $-10°$ and $-20°$ respectively. The shapes of the energy surfaces indicate that not only the ψ but also the ϕ angle exhibits flexibility, although the latter in general is more restricted because of the *exo*-anomeric effect (23). Varying ϕ and ψ to positive values yields local minima about 16 kJ above the respective global minima for the two disaccharides (Fig. 1). The global and local minima have been refined for the disaccharides **1**–**6** and are summarized in Table 1.

These results suggest that in solution the disaccharides can sample a relatively wide range of energetically accessible ϕ,ψ values and cannot be adequately represented by a single fixed conformer. In this study we use nOe's to probe conformational behaviour. Calculation of nOe's based upon a multi-state model requires averaging over all energetically accessible conformational microstates (cf. Fig. 1). If the internal motion responsible for the interconversion of different conformational microstates is slow relative to the overall molecular tumbling, and the correlation time τ_i for the internal motion is greater than the molecular tumbling time τ_c, two cases (a and b) can be distinguished (20, 25).[4] If the internal motion is faster than the overall molecular tumbling, cases c and d have to be considered.

(a) $T_1 \ll \tau_i$: interconversion of conformers is very slow and each single conformer can separately reach a steady state during the nOe experiment. The average nOe's are simply calculated by weighting the nOe's for the different conformers using the Boltzmann distribution function.

(b) $\tau_c < \tau_i < T_1$: fast interconversion of conformers takes place and ensemble averaged nOe's, denoted ⟨nOe⟩, are calculated by first weighting the r^{-6} term for the different conformers, again using the Boltzmann distribution function, then taking the average giving rise to ensemble averaged values, denoted $\langle r^{-6}\rangle$. The relaxation matrix constructed from these $\langle r^{-6}\rangle$ values is finally used to calculate the ⟨nOe's⟩.

(c) $\tau_i < \tau_c$: under these conditions it can be shown that the effective nOe is determined by $\langle r^{-3}\rangle^2$ (26, 27).

(d) the C-6 methyl groups of 4-amino-4,6-dideoxy-D-mannose undergo fast internal rotation, which is also taken into account for the calculation of ⟨nOe's⟩ from the ensemble average relaxation matrix (for details see the experimental section).

Case b has been applied to conformational equilibria at glycosidic linkages (20) and thus one treatment here considers ⟨nOe's⟩ calculated on the basis of $\langle r^{-6}\rangle$ values. On the other hand, molecular dynamics calculations for peptides and proteins reveal internal motions to occur on the picosecond time scale, and for this reason a second approach calculates nOe's on the basis of $\langle r^{-3}\rangle^2$ values. The results of these calculations will be discussed together with the experimentally determined values (Table 5).

Nuclear magnetic resonance spectroscopic experiments

A complete assignment of the ^1H and ^{13}C nmr signals of all disaccharides was achieved by applying standard homonuclear,

[3]Also, B. Meyer. Manuscript in preparation.

[4]After submission of this manuscript two papers by Lipkind *et al.* (22) appeared, which deal with ensemble averaged nOe, but use an algorithm that assumes slow exchange of conformers on the nmr time scale (case a, this manuscript). It is important to emphasize that interconversion occurs on a fast time scale (case b, above).

Can. J. Chem. Downloaded from www.nrcresearchpress.com by 88.85.125.76 on 09/07/12
For personal use only.

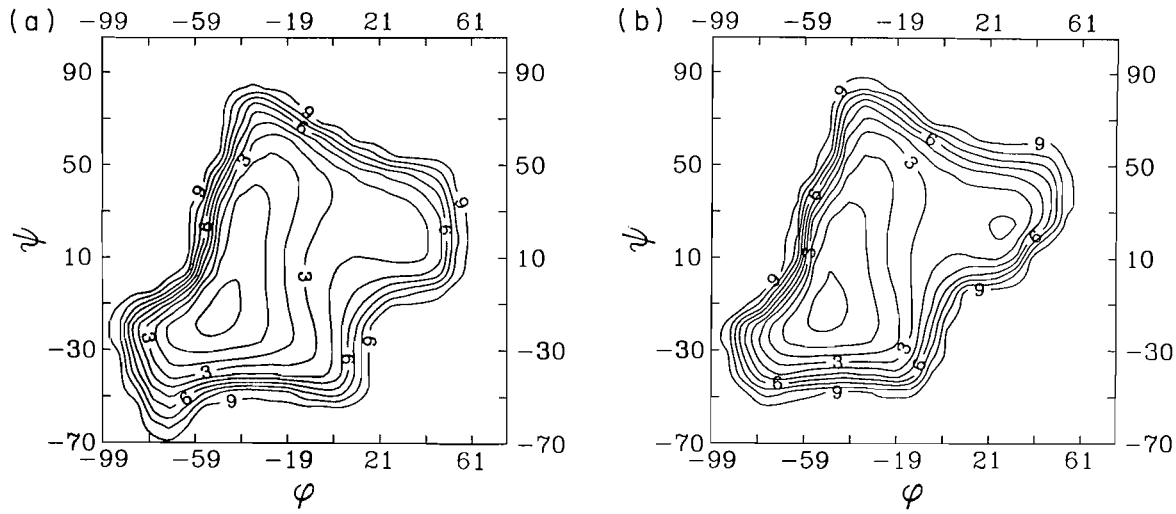

FIG. 1. Potential energy surfaces as a function of ϕ and ψ for the α1,2- and α1,3-linked disaccharides **1** and **4**. Isoenergy contours are scaled at 0.5 kcal intervals above the global minimum energy; (a)α-D-Rha4NAc-(1→2)-α-D-Rha4NAc; (b)α-D-Rha4NAc-(1→3)-α-D-Rha4NAc.

TABLE 1. Dihedral angles ϕ, ψ (deg) and relative energies E (kJ/mol) for the refined minima of the disaccharides **1–6**

	Global minimum[a]		Local minimum		
Disaccharide	ϕ	ψ	ϕ	ψ	ΔE
1	−48	−19	29	20	15.9
2	−49	−14	31	22	15.7
3	−48	−20	30	19	15.7
4	−50	−13	27	23	13.4
5	−48	−7	25	29	16.0
6	−49	−10	27	25	14.9

[a]The relative energy of the global minimum is 0.0 kJ/mol in all cases.

COSY (28), and heteronuclear shift correlated experiments (29). In the case of the *N*-formylated saccharides **3**, **6**, and **8**, spectral interpretation is complicated by the E/Z isomerism of the *N*-formyl groups (2, 10, 11). The two isomeric forms of each *N*-formyl group interconvert slowly on the nmr time scale thus giving rise to 2^n different isomers for an oligosaccharide consisting of n monosaccharide residues. Therefore, each proton in the disaccharides **3** and **6** should theoretically split into four different signals corresponding to $2^n = 4$ isomers. As might be expected, this splitting cannot be observed for each proton even at 500 MHz, a field strength at which most protons are affected only by the orientation of the *N*-formyl group within the same monosaccharide residue. Protons directly attached to the carbonyl carbon of the *N*-formyl groups give eight separate lines between δ 8.0 and 8.3 ppm confirming the presence of four equilibrating isomers. Integration of these signals reveals a $Z{:}E$ ratio of 3.5:1 in deuterium oxide. The most pronounced effect of the rotational isomerism is found for the protons attached to C-4. When the *N*-formyl group adopts the E orientation the chemical shift of H-4 is found at high field around δ 3.4 ppm, whilst in the Z form eclipsing of H-4 by the carbonyl group results in substantial deshielding that moves the resonance to roughly δ 3.9 ppm. The same complications arise for ^{13}C nmr spectra. Again inspection of chemical shift differences caused by E/Z isomerism of the *N*-formyl groups reveals that their orientation has only a minor influence on the chemical shifts of the adjacent sugar ring. Only for the α1,3-linked disaccharide **6** are the signals for the two carbon atoms, C-3′ and C-5′, split into the theoretical four lines (Table 3). Major differences occur in the chemical shifts of the carbon atoms C4, C4′ and the carbonyl carbons. Those signals arising from the E isomers are shifted downfield several ppm. Additionally, the adjacent carbon atoms C5 and C5′ show small upfield shifts in the range of 0.5 ppm. The resonances of the carbon atoms involved in the glycosidic linkage are unaffected by the E/Z isomerism. All ^1H and ^{13}C nmr data (chemical shifts and coupling constants) are summarized in Tables 2 and 3.

Isotropic reorientation with correlation times in the extreme narrowing limit, $\tau_c \simeq 10^{-10}$ s, allows a simplified protocol for the calculation of nOe's or proton spin lattice relaxation times from geometry parameters, provided longitudinal relaxation is dominated by dipole–dipole interactions. Similar ^{13}C T_1 values for the pyranose ring carbon atoms provided supporting evidence for isotropic tumbling of the disaccharides **1** and **4**, although fluctuations in the T_1's of carbon atoms involved in the glycosidic linkage suggested the emergence of a preferred axis of motion (Table 4). The same T_1 measurements also revealed internal motion about the C5—C6 bond, since NT_1 values (N = number of protons attached to a particular carbon) are not constant when T_1's of C-6 atoms are compared with those of the ring carbon atoms. It is clear that an adequate model, such as the three-state jump model (30), must take internal motion for the methyl group rotation about the C5—C6 bonds into account when nOe's are calculated (cf. experimental section, calculations).

Steady-state, one-dimensional nOe difference experiments were performed for the *N*-acetylated disaccharides **1** and **4**, and the amino derivatives **2** and **5**. The quantitative data were compared with the nOe predicted by calculation of ensemble averaged values as well as those predicted by the global minimum conformation (Table 5). Selective irradiation of single resonances (31, 32) and, hence, quantitative nOe measurements could only be accomplished in those instances where anomeric or other ring protons were well resolved and free of overlap. Those experiments which allowed precise quantitation are compared with theoretical predictions (Table 5). One of these experiments performed on disaccharide **1** is representative

Can. J. Chem. Downloaded from www.nrcresearchpress.com by 88.85.125.76 on 09/07/12
For personal use only.

TABLE 2. The ^{1}H nmr chemical shifts[a] and coupling constants,[b] compounds **1**–**8**

Compound	H-1	H-2	H-3	H-4	H-5	H-6	OMe	NR
1	4.82	3.92	3.89	3.89	3.74	1.21	3.40	2.05
R = Ac	(1.6)	(3.2)				(6.3)		
	5.02	4.10	3.96	3.85	3.85	1.19		2.04
	(2.0)	(3.2)	(10.4)			(6.2)		
2	4.79	3.90	3.85	2.99	3.77	1.30	3.40	
R = H	(1.8)	(3.0)	(10.2)	(10.0)		(6.2)		
	5.01	4.02	3.85	2.97	3.90	1.28		
	(1.8)	(3.0)	(10.1)	(10.0)		(6.3)		
3	4.84	3.96	3.96	3.94	3.79	1.23	3.40	8.21
R = CHO	(1.8)					(6.3)		
Z Isomer	5.04	4.13, 4.17	3.98	3.95	3.90	1.22		8.20
	(2.10)	(3.2, 3.3)	(10.0)			(6.0)		
E Isomer	4.82	3.96	3.96	3.39	3.83	1.29	3.40	8.04
	(2.0)					(6.4)		
Z:*E* 3.8:1	5.05	4.09	3.98	3.39	3.93	1.27		8.03
	(2.0)	(3.0)	(10.0)			(6.4)		
4	4.71	3.98	3.83	3.94	3.81	1.22	3.40	2.04
R = Ac	(1.9)	(3.1)	(10.6)	(10.0)		(6.1)		
	4.90	3.82	3.80		3.92	1.18		2.03
	(1.7)					(5.8)		
5	4.67	3.96	3.65	2.83	3.68	1.27	3.39	
R = H	(1.8)	(3.2)	(10.0)	(10.1)		(6.4)		
	4.96	4.02	3.72	2.78	3.81	1.26		
	(1.5)	(3.2)	(10.0)	(10.2)		(6.4)		
6	4.72	3.99	3.89	4.01	3.85	1.24	3.47	8.21
R = CHO	(2.0)	(3.4)		(10.0)		(6.3)		
Z Isomer	4.93	3.89	3.91	3.91	3.91	1.21		8.19
	(1.7)					(6.0)		
E Isomer	4.72	4.02, 4.01, 400	3.83	3.46	3.88	1.29, 126	3.41	8.03
	(2.0)	(3.2–3.4)		(10.4)		(6.2, 6.5)		
Z:*E* 3.4:1	4.90	3.91	3.91	3.35	3.95	1.25		8.03
	(1.6)			(10.0)		(6.3)		
7	4.72	3.91	3.78	3.84	3.71	1.20	3.39	2.03
R = Ac	(1.8)	(3.2)	(10.2)	(10.1)		(6.2)		
8								
Z Isomer	3.91	3.81	3.89	3.77	3.38	1.11	8.20	
R = CHO	(1.7)	(3.1)	(10.2)	(10.0)		(6.5)		
E Isomer	4.72	3.93	3.79	3.34	3.77	1.17	3.38	8.03
	(1.7)	(3.1)	(10.0)	(10.5)		(6.5)		

[a]First-order chemical shifts were measured for solutions in D_2O at 37°C, referenced to internal 1% (v/v) acetone (δ 2.225 ppm).

[b]Coupling constants are first-order values.

of the quality of these measurements (Fig. 2). For the *N*-formylated disaccharides **3** and **6** selective irradiation was not possible because of severe overlap of the signals belonging to the different isomers. Thus NOESY spectra (33) were recorded to qualitatively detect nOe's (data not presented). Those results are in good agreement with the one-dimensional nOe data for disaccharides **1**, **2**, **4**, and **5**.

Discussion

Conformational analysis of glycosidic linkages

Measurement of experiment nOe's for biomolecules represents one of the most important tools by which their solution tertiary structure may be elucidated. In the case of proteins nOe values can provide sufficient conformational constraints to define a unique solution structure (34). With few exceptions comparable nOe experiments performed on oligosaccharides fail to deliver enough distance or torsional constraints to define a unique solution conformation. It has been proposed recently that the hydroxyl functions can be used as so-called "long range sensors" to obtain additional conformational constraints (35) but this method requires nOe experiments to be performed in dimethyl sulfoxide. The problem remains that under physio-

Can. J. Chem. Downloaded from www.nrcresearchpress.com by 88.85.125.76 on 09/07/12
For personal use only.

TABLE 3. ^{13}C chemical shifts[a] δ (ppm) of the disaccharides **1**–**6**, and monosaccharide **8**

Compound	C-1	C-2	C-3	C-4	C-5	C-6	OMe	CO	NAc
1	99.83	77.98	68.24	53.46	68.02	17.12	55.29	174.98	22.48
	102.31	69.38	68.44	53.22	68.55	17.12		174.98	22.48
2	100.42	77.85	69.28	54.15	68.54	17.12	55.31		
	102.98	69.56	69.55	54.35	68.75	17.12			
3	99.75	77.82	67.90	52.09	67.68	17.10	55.23	165.11	
Z-Isomer	102.24	69.24	68.13	52.20	68.22	17.10		165.11	
3	99.75	77.66	67.83	56.92	67.13	16.93	55.23	168.04	
E-Isomer	102.34	69.24	68.13	57.13	67.75	16.93		168.04	
4	100.98	69.15	77.12	52.11	67.55	17.01	55.09	174.83	22.43
	102.45	69.74	68.43	53.12	68.40	17.01		174.59	22.33
5	101.33	69.08	80.52	52.83	69.55	17.33	54.97		
	103.36	69.50	70.41	53.81	69.94	17.17			
6	100.95	69.08	76.88	50.84	67.34	17.03	55.09	165.06	
Z-Isomer	102.44	69.52	68.16	51.92	68.07	17.06		164.92	
6	100.98	68.95	76.88	55.71	66.88	16.91	55.14	168.12	
E-Isomer			68.13		67.81				
			67.95		67.68			169.01	
8	101.72	69.89	69.00	52.70	68.04	17.73	55.61	163.84	
Z-Isomer									
8	101.72	69.89	68.81	57.56	67.54	17.59	55.61	166.81	
E-Isomer									

[a]Chemical shifts were measured for solutions in D_2O at 37°C and are expressed relative to 1% (v/v) internal acetone (δ 30.50 ppm).

TABLE 4. ^{13}C T_1 values [a] (s) for disaccharides **1** and **4**

Disaccharide		C-1	C-2	C-3	C-4	C-5	C-6
1	Reducing	0.51	0.59	0.51	0.52	0.52	0.72
	Nonreducing	0.61	0.59	0.57	0.54	0.57	0.72
4	Reducing	0.57	0.53	0.57	0.57	0.57	0.72
	Nonreducing	0.53	0.56	0.55	0.53	0.54	0.72

[a]The values are the mean of two values determined at 37°C and the standard deviation was ±0.03 s.

logical conditions in aqueous solutions the conformational behaviour of oligosaccharides cannot be assessed solely on the basis of nOe experiments. Thus additional nmr experimental data such as ^1H chemical shifts (14) or ^{13}C chemical shifts (36) have to be invoked in the discussion of carbohydrate solution conformation. Most often, inferences of tertiary structure from these data have been based upon further correlations with potential energy calculations, and a large body of literature has accumulated on this topic (12–19).

Flexibility about glycosidic linkages poses an additional problem for conformational analysis (20, 21). In general, and in particular for the disaccharides under investigation, the energy minima as a function of the torsional angles ϕ and ψ at the glycosidic linkages are seen to be rather shallow and even exhibit local minima (Fig. 1). In the following discussion experimentally derived nOe's are compared with data calculated on the basis of models that take into account motional averaging according to methods described by Cumming and Carver (20, 21) or Kessler *et al.* and Torda *et al.* (26, 27). Data calculated for the global and local minima are presented as well. The results of this comparison are summarized in Table 5 (details of the computational procedures are described in the experimental section). Two points are immediately obvious:

1. The nOe values calculated for the local minima cannot account for the observed data.
2. The single-state model based only on the calculated global minima predicts reasonable nOe values but in four cases the relative order of magnitude of the observed nOe's is opposite to that calculated.

The nOe experiments carried out on compounds **1**, **2**, and **5** lead to the following observations:

Irradiation of H-1′ (**5**) causes an interglycosidic nOe to H-3 that is more than twice as large as the intra-residue nOe experienced by H-2′, the opposite magnitude to that predicted by the single-state model. For the same compound irradiation of H-2 produces a similar result, a larger nOe to H-3 than to H-5′, opposite to the relative ordering predicted by the global minimum conformation. When compounds **1** and **2** were used for nOe measurements, irradiation of H-1′ in either compound **1** or **2** produced an inter-glycosidic nOe to H-2 that is observed to be larger than the intra-glycosidic nOe of H-2′. None of these results is consistent with or predicted by the calculations based upon the global minimum conformer.

The fit between experimentally available data and theoretical values can be significantly improved by calculating ensemble averaged nOe's as described in the experimental section. It is seen (Table 5) that where incorrect relative ordering of the nOe magnitude is predicted by the single-state model, the statistical mechanical model (20, 21) based upon averaging either r^{-6} or r^{-3} terms predicts the correct order or at least significantly improves the situation, as exemplified by the irradiation of H-2 in disaccharide **5**: the nOe calculated for H-1 shows good agreement with the observed value, and nOe's for H-3 and H-5′ now converge toward the experimental values, although the

Can. J. Chem. Downloaded from www.nrcresearchpress.com by 88.85.125.76 on 09/07/12
For personal use only.

Can. J. Chem. Downloaded from www.nrcresearchpress.com by 88.85.125.76 on 09/07/12
For personal use only.

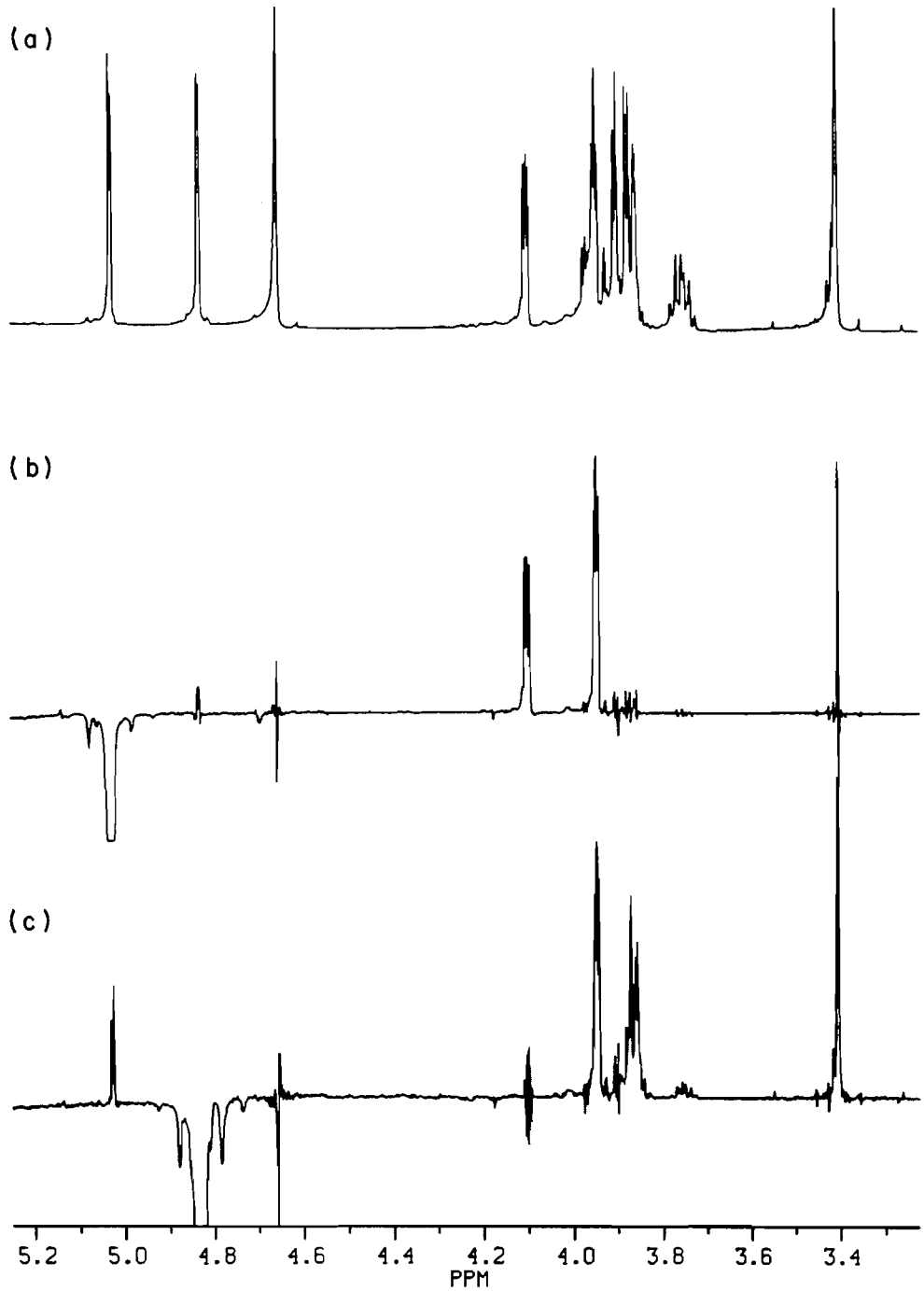

FIG. 2. The nOe difference spectra for disaccharide **1**; (a) reference spectrum; (b) irradiation of H-1′; (c) irradiation of H-1.

nOe for H-5′ remains larger than that at H-3. This might indicate that the calculated energy surface is too crude to allow the prediction of nOe's that are generally sensitive to conformational preferences.

As pointed out above, for the *N*-formylated disaccharides **3** and **6** only qualitative nOe data from NOESY experiments are available. These values are consistent with the results discussed above and there is no indication that the *N*-formyl groups alter the glycosidic linkage conformation.

To evaluate the effect of glycosylation on the ^{1}H chemical shifts, Table 2 also contains the ^{1}H chemical shifts of the monosaccharide building blocks **7** and **8**. A comparison of the chemical shift data of the disaccharides carrying the *N*-formyl and the *N*-acetyl group with the corresponding monosaccharides reveals several points of interest and these should be compared with the short H····O distances. Major changes in chemical shifts are observed for the protons H-1′ and H-2′ of disaccharide **1**; H-1′ is 0.30 ppm downfield shifted in comparison to H-1 in the monosaccharide compound **7**. This is explained by a close proximity of H-1′ to O-3 across the glycosidic linkage (for the minimum energy molecule a H-1····O-3 distance of about 2.6 Å is calculated). A downfield shift of 0.19 ppm for H-2′ due to the formation of the glycosidic linkage cannot readily be explained by the single-state conformer in terms of short H-2′ to oxygen distances. The local minimum provides a short distance between H-2′ and O-3 (2.7 Å), indicating the necessity

TABLE 5. Comparison of experimentally and theoretically derived nOe's

Compound	Proton sat	Proton obsd.	n^a	Experimental nOe's[b] Mean	s.d.	Calculated nOe's[b] Global	Local min	⟨nOe⟩[c] ($\langle r^{-6}\rangle$)	⟨nOe⟩[d] ($\langle r^{-3}\rangle^2$)
1	H-1′	H-2′	10	0.39	0.02	0.52	0.27	0.45	0.47
		H-1		0.00	0.0	−0.02	0.28	−0.01	−0.02
		H-2		0.61	0.02	0.50	0.45	0.56	0.55
	H-1	H-2		0.42	0.02	0.36	0.34	0.34	0.37
		H-5	4	0.01	0.02	0.04	0.02	0.04	0.04
		H-1′		0.05	0.03	−0.06	0.58	−0.03	−0.04
		H-5′		0.52	0.02	0.66	0.06	0.63	0.63
2	H-1′	H-2′	1	0.41		0.56	0.30	0.49	0.51
		H-1		0.00		0.00	0.26	−0.01	−0.02
		H-2		0.59		0.44	0.44	0.52	0.51
4	H-1′	H-2		0.02		−0.05	0.32	−0.04	−0.05
		H-4	1	0.09		0.04	−0.01	0.03	0.03
		H-3, H-2′		0.89		1.01	0.69	1.01	1.02
5	H-1′	H-2′		0.32	0.02	0.56	0.30	0.51	0.52
		H-3	5	0.68	0.02	0.48	0.36	0.51	0.51
		H-2		0.00	0.00	−0.04	0.34	−0.02	0.03
	H-2	H-1		0.44	0.04	0.39	0.41	0.42	0.44
		H-3	5	0.34	0.01	0.29	0.26	0.28	0.30
		H-5′		0.22	0.03	0.37	0.00	0.32	0.30
		H-1′		0.00	0.00	−0.05	0.33	−0.03	−0.04

[a] n = number of experiments.
[b] For details see experimental section.
[c] ⟨nOe⟩ = ensemble average $\langle r^{-6}\rangle$ nOe's.
[d] ⟨nOe⟩ = ensemble average $\langle r^{-3}\rangle^2$ nOe's.

for motional averaging. Equivalent observations can be made for the *N*-formylated disaccharide **3**. For the α1,3-linked disaccharides **4** and **6** no such large shift differences can be observed. The most interesting but not the largest shift is observed for H-2′, which is upfield shifted by 0.10 ppm. This effect is found to be even more pronounced in the naturally occurring M polysaccharide (2) and can be explained by the relative orientation of H-2′ towards the *N*-acetyl or the *N*-formyl group in the reducing unit. The molecular model for the global minimum conformation, which is shown in Fig. 3, indicates that H-2′ is in a region of the anisotropy cone of the amide carbonyl where shielding is caused. Another significant shift is that of H-1′ in **4** which is shifted 0.22 ppm downfield compared to monosaccharide **7**. The same is observed for the corresponding *N*-formylated derivative **6**. In this case the shift must be due to a close proximity to the *N*-acetyl group in the case of **4** and to the *N*-formyl group in the case of **6**.

The ^{13}C nmr chemical shift data also reveal several points of interest. It is known that the chemical shift of the anomeric carbon atom as well as the aglyconic carbon atom can be used to qualitatively access the glycosidic linkage conformation (36). Inspection of the chemical shifts of the anomeric carbons of the disaccharides **1** and **6** (Table 3) indicates that neither the *E*/*Z* isomerism nor the nature of the substituent at the nitrogen atom greatly influences the glycosidic linkage conformation. This is in agreement with the results of the HSEA calculations, which predict that the conformations of the glycosidic linkage are closely related for compounds **1**–**6**.

Conformation of the N*-formyl groups*

The carbonyl carbon – nitrogen bond in methyl 4,6-dideoxy-4-formamido-α-D-mannopyranoside **8** exhibits considerable double bond character, in accordance with the energy barrier to rotation of ca. 87 kJ/mol measured by dynamic nmr studies in dimethyl sulfoxide (11). Interconversion between isomers *Z* (**8***a*) and *E* (**8***c*) is slow on the nmr chemical shift time scale, with a half-life for each isomer of ~30 s (11). Proton–proton as well as heteronuclear vicinal coupling constants, $^3J_{CH}$, were used to determine the conformation of the *N*-formyl group in monosaccharide **8** and to exclude other possible isomers **8***b* and **8***d* (11).

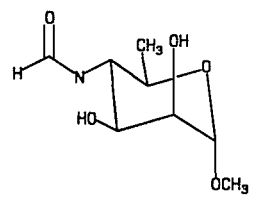

8*a*

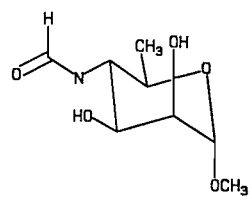

8*c*

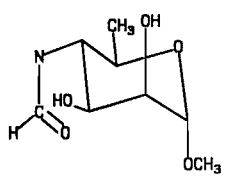

8*b*

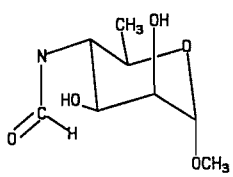

8*d*

Can. J. Chem. Downloaded from www.nrcresearchpress.com by 88.85.125.76 on 09/07/12
For personal use only.

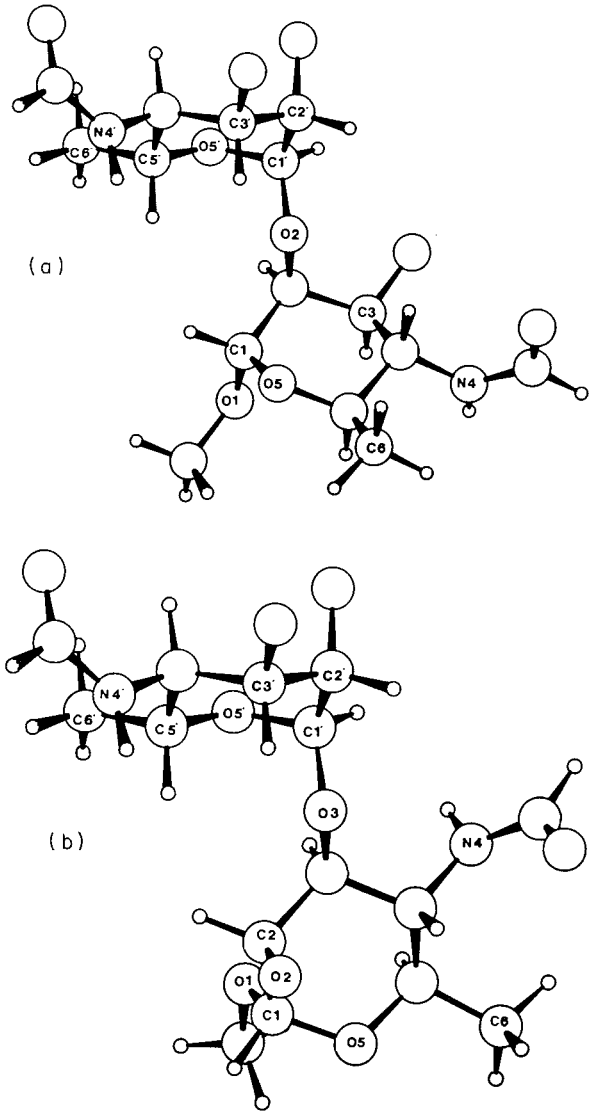

FIG. 3. Molecular models for the global minimum energy conformations of the disaccharides **3** and **6**; (a) global minimum for **3**, α-D-Rha4NFo-(1→2)-α-D-Rha4NFo-1-OMe; (b) global minimum for **6**, α-D-Rha4NFo-(1→3)-α-D-Rha4NFo-1-OMe.

Amide coupling constants measured for **8** in water were 10.0 Hz for both *Z* and *E* isomers, which is in agreement with the usual in-plane, anti-periplanar arrangement for the fragment H—N—C—H. Vicinal coupling constants observed for the *Z* isomer (^3J = 2.2 Hz, *HCONH*; $^3J_{C,H}$ = 2.6 Hz, *CONCH*) could be interpreted as suggesting an orientation for the *N*-formyl fragment in which a hydrogen bond is formed between CO and HO-3. A similar hydrogen bond was suggested by other authors (10) on the basis of ^{13}C T_1 data for *N*-formyl neuraminic acid. However, attempts to titrate this putative hydrogen bond with monosaccharide **8** dissolved in dimethyl sulfoxide as done for sucrose (37) were unsucccessful. In fact it is unnecessary to assume a hydrogen bond to explain these coupling constants, nor does it require a "W" arrangement between the formyl proton and H-4 in the *Z* conformer to explain the long-range coupling between these two protons. The long-range coupling can be understood as an allylic type coupling and the vicinal coupling constants are governed by the amount of double bond character of the carbonyl carbon – nitrogen bond, a feature which invalidates the Karplus relationship. In support of this interpretation a comparison with values for the model compounds *N*-cyclohexylformamide and *N*-formanilide clearly indicates that electronic factors satisfactorily explain the observed vicinal coupling constants (*N*-cyclohexylformamide, *Z* isomer: ^3J = 2.1 Hz, *HCONH*; ^3J = 2.8 Hz (*Z*), *CONCH*; formanilide, *Z* isomer: ^3J = 2.1 Hz *HCONH*). In these cases no hydrogen bond is possible.

It is concluded that the *N*-formyl groups in both the *Z* and *E* isomers have an "in-plane arrangement" of all bonds, with the NH bond antiperiplanar to the C4—H4 bond. No evidence was found in the nmr measurements performed on methyl 4,6-dideoxy-4-formamido-α-D-mannopyranoside **8** that would support the existence in water of the two isomers **8***b* or **8***d*, one of which, **8***d*, was postulated to exist in DMSO solution (11).

Conclusions

Advances in the molecular modeling of the conformational behaviour of biomolecules in solution have increased due to progress in fields such as nmr spectroscopy and computer technology. A relatively simple, computationally fast and inexpensive method, HSEA potential energy calculations (12–19), has been remarkably successful for carbohydrates, a class of molecules that have not responded well to generalized force fields, such as MM2, without additional parameterization (38). Recent improvement to the HSEA method includes explicit treatment of populated conformational states other than the global minimum (20, 21). This motional averaging has been shown to be of practical importance for the calculation of nOe's and T_1's. In the present paper we applied this approach to a series of disaccharide molecules that represent the key elements of *Brucella* A and M antigens. The comparison of observed nOe's with values calculated on the basis of the "classical" single-state model and the more realistic statistical mechanical model indicates that ensemble average values provide an improved fit with the experimental data. This fit depends on the quality of the calculated energy surface and it may be expected that in the future more sophisticated energy calculations can be performed on even faster computers to model more accurately such energy surfaces and, possibly even more importantly, the contribution and influence of solvent water. For the present, the described approach appears to provide agreement with experimental data better than or as good as the more sophisticated MM2 (38), MNDO (39), or PCILO calculations (40), because incorporation of motional averaging with these models becomes demanding in terms of computational time and costs. The calculation of ensemble averaged nOe's represents a more realistic treatment of oligosaccharide conformational properties, which is supported by the improved fit between experimental and calculated nmr parameters for those compounds studied here and elsewhere (20, 21), but the general validation of this approach by examination of a wider range of oligosaccharides is highly desirable.

The models for the α1,2- and the α1,3-linked disaccharides **3** and **6** can be best represented by depicting the global minimum energy conformations for an impression of the proximities between atoms in the molecules (Fig. 3). This should be used in combination with the energy surfaces for these linkages (Fig. 1) to appreciate the degree of oligosaccharide mobility. One major finding of this work concerns the relative orientation of the *N*-acyl substituents in the two disaccharide types. Whereas these groups are at an angle of 144° in the α1,2-linked disaccharides **1** and **3**, they are disposed almost at a right angle in the case of the α1,3-linked disaccharides **4** and **6**. This has

Can. J. Chem. Downloaded from www.nrcresearchpress.com by 88.85.125.76 on 09/07/12
For personal use only.

Can. J. Chem. Downloaded from www.nrcresearchpress.com by 88.85.125.76 on 09/07/12
For personal use only.

important consequences for the conformation of the polysaccharide incorporating these features. When glycosidic torsion angles close to those of the minimum energy conformation are adopted, a helical structure results that contains five α1,2-linked residues per turn of the *Brucella* A polysaccharide. This is consistent with immunochemical findings that monoclonal antibodies specific for the A antigen require a pentasaccharide fragment for optimum binding (6), and with molecular modeling studies of the binding of the antigenic determinant in the combining site, which suggests that residues one and five of a pentasaccharide effectively interact with amino acid residues at either end of the combining site (5). The occurrence of an α1,3 linkage at every fifth residue in the *Brucella* M polysaccharide alters the direction of chain propagation, resulting in a much wider helix. The surface topology of this antigen cannot interact with the complementary surfaces of antibodies that bind the A antigen, even though the M polysaccharide also has a pentasaccharide repeating unit. Other antibodies that require only an α1,2-linked tetrasaccharide to fill the binding site are able to bind either the A or M antigens with equal affinity (6).

Experimental

Computational methods

Calculation of the global minima was performed using the GESA (17, 22) program. The torsional angles at the glycosidic linkages and the C5—C6 axes are defined as follows, ϕ^H = H1—C1—O1—CX, ψ^H = C1—O1—CX—HX, and ω = O5—C5—C6—O6, where X is the aglyconic linkage site. Clockwise rotations are always positive (14).

Energy surfaces for the disaccharides **1**, **2**, **4**, and **5** were calculated covering a φ/ψ range from −90° to +90° in 5° steps thus giving rise to 36^2 conformational microstates. On the basis of these energies, ensemble average values for the r^{-6} (r = distance between two protons) were calculated, which are denoted as $\langle r^{-6}\rangle$: r^{-6} values for each microstate j are weighted according to the Boltzmann distribution function and subsequently these values are summed over the whole conformational space,

$$[1] \quad \langle r^{-6}\rangle = \sum_j P_j r_j^{-6}$$

where r = distance between any two protons, j = index of the microstate, P = relative population (probability) of the jth microstate.

The relative population is given by expression [2]

$$[2] \quad P_j = e^{(-\Delta E_j/RT)} \Big/ \left[\sum_j e^{(-\Delta E_j/RT)}\right]$$

where ΔE_j = the energy difference between the microstate j and the global minimum, R = gas constant, and T = temperature (in the calculations, 310 K); values greater than 20 kcal above the global minimum were not considered.

From $\langle r^{-6}\rangle$ values an ensemble average cross relaxation matrix $\langle R\rangle$ was constructed, eq. [3]. This matrix was subsequently used to calculate ensemble average nOe's, ⟨nOe⟩;

$$[3] \quad \langle R\rangle = \sum_j P_j R_j$$

with j and P defined as above.

In the same way $\langle r^{-3}\rangle$ values are obtained, which then can be used to construct an ensemble average relaxation matrix $\langle R\rangle$ from the $\langle r^{-3}\rangle^2$ values.

The internal motions of *C*-methyl groups were treated according to Heatley *et al.* (41) and Brisson and Carver (15), who based their calculations on expressions given by Rowan *et al.* (42). For the calculation of the relaxation matrix $\langle R\rangle$, the overall molecular correlation time τ_c and the internal correlation time τ_i for the methyl group reorientation have to be known, which may be calculated from the ^{13}C T_1 data (Table 4) using eq. [4] (10, 43, 44):

$$[4] \quad \tau = r^6/(N\gamma_H^2\gamma_C^2 h^2 T_1)$$

where $\tau = \tau_c$ or $\tau = (\tau_c^{-1} + \tau_i^{-1})^{-1}$ for a methyl group, r = C—H bond distance (1.10 Å), N = number of protons attached to the particular carbon atom, γ_H, γ_C = gyromagnetic ratio for ^1H and ^{13}C respectively, T_1 = spin-lattice relaxation time of the particular carbon atom. Utilising eq. [4], the measured ^{13}C T_1 values (Table 4) give a mean value of 2.3×10^{-11} s for τ_i and 0.9×10^{-10} s for τ_c.

For steady-state conditions the ensemble average nOe's, ⟨nOe's⟩, can be calculated by solving the series of simultaneous eqs. [5] given by Heatley *et al.* (41):

$$[5] \quad \sum_{j\neq k} \langle R_{ij}\rangle\langle \mathrm{nOe}(j,k)\rangle = \langle R_{ik}\rangle (i \neq k)$$

where $\langle R_{ij}\rangle$, $\langle R_{ik}\rangle$ = elements of the ensemble average cross relaxation matrix $\langle R\rangle$, ⟨nOe(j, k)⟩ = ensemble average nuclear Overhauser enhancement factor of proton j upon irradiation of proton k. Single-state nOe's are calculated using the same series of eqs. [5] but instead utilize a single-state relaxation matrix.

The Fortran listing of the GESA program and subroutines that have been specifically written or modified from the original GESA program (22) to accomplish the task of ensemble averaging and nOe calculation will be deposited with the journal, and copies of the programs will be supplied on request to the authors. Coordinates for the minimum energy molecules will also be supplied.

Nuclear magnetic resonance experiments

The model compounds **1–8** were of synthetic origin (7–9). Samples were dissolved in 0.5 mL D_2O (99.996 at.% D, Aldrich) after repeated lyophilization from D_2O (99.96 at.% D, Aldrich). The samples were not degassed and were prepared at concentrations of 20–30 mM for ^1H nmr and 50–100 mM for ^{13}C nmr measurements. Acetone was used as internal reference (^1H δ 2.225 ppm, ^{13}C δ 30.50 ppm).

^1H and ^{13}C nmr spectroscopy

The nmr experiments were performed at 37°C, unless stated otherwise, using Bruker AM500 and AM200 spectrometers. Coupling constants for the exchangeable amide protons in monosaccharide **8** were measured in 98% H_2O/2% D_2O solution at 500 MHz. Suppression of the water signal was achieved by presaturation of the H_2O resonance. Spectral width and size of the data sets were chosen to give digital resolutions of 0.2 Hz/pt in the case of the ^1H nmr spectra. The coupling constants reported are first-order values.

Amide coupling constants

Compound **8** dissolved in 98% H_2O/2% D_2O solution gave the following three-bond coupling constants. Heteronuclear couplings were measured for the ^{13}C label *N*-formyl derivative that was prepared in separate work (Peters and Bundle, unpublished work).

Z isomer: ^3J = 10.0 Hz, N*H*C*H*; ^3J = 2.2 Hz, *H*CON*H*; $^3J_{C,H}$ = 2.6 Hz, CONC*H*

E isomer: ^3J = 10.0 Hz, N*H*C*H*; ^3J = 11.8 Hz, *H*CON*H*; $^3J_{C,H}$ = 5.5 Hz, CONC*H*

Solutions of *N*-cyclohexylformamide and formanilide in deuteriochloroform were used to measure both homonuclear and heteronuclear coupling constants.

N-cyclohexylformamide:

Z isomer: ^3J = 2.1 Hz, *H*CON*H*; $^3J_{C,H}$ = 2.8 Hz, CONC*H*

E isomer: ^3J = 12.0 Hz, *H*CON*H*; $^3J_{C,H}$ = 5.6 Hz, CONC*H*

Formanilide:

Z isomer: ^3J = 2.1 Hz, *H*CON*H*

E isomer: ^3J = 11.3 Hz, *H*CON*H*

Nuclear Overhauser enhancement difference spectroscopy

The nOe experiments were performed in the difference mode (31). Steady-state experiments were performed with irradiation times and relaxation delays that were at least five times the largest T_1 values in the sample. Saturation of signals was accomplished by single line irradiation (32).

^{13}C T_1 measurements

^{13}C spin-lattice relaxation times were measured by the fast inversion–recovery method (45, 46) utilizing a composite 180° pulse (47). Calculation of T_1 values was achieved by employing an exponential three-parameter fit with standard Bruker software.

Two-dimensional nmr spectroscopy

Phase sensitive COSY experiments (28) used 512 increments in $t1$ and 2K data points in $t2$. The data matrix was multiplied by sine bell window functions and Fourier transformed to a 2K × 2K spectral matrix. H/C heteronuclear shift correlation experiments were performed with decoupling in both frequency dimensions (29). Carbon spectra, 256 experiments each collected over 4K data points, were recorded, and the data matrix was multiplied in both dimensions by $\pi/4$ shifted sine bell squared window functions, followed by Fourier transformation to give a power spectrum.

Acknowledgements

We wish to thank Professor H. Rüterjans, Institute of Biophysics, University of Frankfurt, for access to a Bruker AM500 that was used for water suppression experiments. The final stages of the modification of the GESA program were facilitated by NATO research grant RG 85/0021 to D.R.B., together with access to the computer facilities of the Carlsberg Laboratory, Copenhagen, kindly made available by Professor Klaus Bock.

1. M. Caroff, D. R. Bundle, M. B. Perry, J. W. Cherwonogrodzky, and J. R. Duncan. Infect. Immun. **46**, 384 (1984).
2. D. R. Bundle, J. W. Cherwonogrodzky, and M.B. Perry. Biochemistry, **26**, 8717 (1987).
3. P. J. Meikle, M. B. Perry, J. C. Cherwonogrodzky, and D. R. Bundle. Infect. Immun. **57**, 2820 (1989).
4. D. Rose, M. Przybylska, E. Vorberg, and D. R. Bundle. J. Mol. Biol. In press.
5. R. Oomen, N. M. Young, and D. R. Bundle. ICSU Short Rep. **10**, 56 (1990).
6. D. R. Bundle. Pure Appl. Chem. **61**, 1171 (1989).
7. T. Peters and D. R. Bundle. J. Chem. Soc. Chem. Commun. 1648 (1987).
8. T. Peters and D. R. Bundle. Can. J. Chem. **67**, 491 (1989).
9. T. Peters and D. R. Bundle. Can. J. Chem. **67**, 497 (1989).
10. M. F. Czarniecki and E. R. Thornton. J. Am. Chem. Soc. **99**, 8273 (1977).
11. L. Kenne, P. Unger, and T. Wehler. J. Chem. Soc. Perkin Trans. 1, 1183 (1988).
12. R. U. Lemieux, K. Bock, L. T. J. Delbaere, S. Koto, and V. S. Rao. Can. J. Chem. **58**, 631 (1980).
13. H. Thøgersen, R. U. Lemieux, K. Bock, and B. Meyer. Can. J. Chem. **60**, 44 (1981).
14. K. Bock. Pure Appl. Chem. **55**, 605 (1983).
15. J.-R. Brisson and J. P. Carver. Biochemistry, **22**, 1362 (1983); **22**, 3671 (1983).
16. K. Bock, M. Meldal, D. R. Bundle, T. Iversen, B. M. Pinto, P. J. Garegg, I. Kvanström, T. Norberg, A. A. Lindberg, and S. B. Svenson. Carbohydr. Res. **130**, 35 (1984).
17. H. Paulsen, T. Peters, V. Sinnwell, R. Lebuhn, and B. Meyer. Liebigs Ann. Chem. 951 (1984).
18. C. A. Bush, Z.-Y. Yan, and B. N. N. Ras. J. Am. Chem. Soc. **108**, 6168 (1986).
19. J. N. Scarsdale, R. K. Yu, and J. H. Pestegaard. J. Am. Chem. Soc. **108**, 6778 (1986).
20. D. A. Cumming and J.P. Carver. Biochemistry, **26**, 6664 (1987).
21. D. A. Cumming and J.P. Carver. Biochemistry, **26**, 6676 (1987).
22. G. M. Lipkind, A. S. Shashkov, O. A. Nechaev, V. I. Torgov, V. N. Shibaev, and N. K. Kochetkov. Carbohydr. Res. **195**, 11 (1989); **195**, 27 (1989).
23. R. U. Lemieux, A. A. Pavia, J. C. Martin, and K. A. Watanabe. Can. J. Chem. **47**, 4427 (1969); J. P. Praly and R. U. Lemieux. Can. J. Chem. **65**, 213 (1987).
24. R. Fletcher and M. J. D. Powell. Comput. J. **6**, 163 (1963).
25. J. H. Noggle and R. E. Schirmer. The nuclear Overhauser effect. Academic Press, New York. 1971.
26. H. Kessler, C. Griesinger, J. Lautz, A. Müller, W. F. van Gunsteren, and H. J. C. Berendsen. J. Am. Chem. Soc. **110**, 3393 (1988).
27. A. E. Torda, R. M. Scheek, and W. F. van Gunsteren. Chem. Phys. Lett. **157**, 289 (1989).
28. D. Marion and K. Wüthrich. Biochem. Biophys. Res. Commun. **113**, 9676 (1983).
29. A. Bax. J. Magn. Reson. **53**, 517 (1983).
30. D. E. Woessner, B. S. Snowden, and G. H. Meyer. J. Chem. Phys. **59**, 719 (1989).
31. R. Richart and K. Wüthrich. J. Magn. Reson. **30**, 147 (1978).
32. M. Kinns and J. K. M. Sanders. J. Magn. Reson. **56**, 518 (1984).
33. A. Kumar, R. R. Ernst, and K. Wüthrich. Biochem. Biophys. Res. Commun. **95**, 1 (1980).
34. K. Wüthrich. Science, **243**, 45 (1989); NMR of proteins and nucleic acids. Wiley, New York. 1986.
35. J. Dabrowski and L. Poppe. J. Am. Chem. Soc. **111**, 1510 (1989).
36. K. Bock, A. Brignole, and B. W. Sigurskjold. J. Chem. Soc. Perkin Trans. 2, 1711 (1986).
37. R. U. Lemieux and K. Bock. Carbohydr. Res. **100**, 63 (1982).
38. I. Tvaroska and S. Pérez. Carbohydr. Res. **149**, 389 (1986); V. Tran, A. Buleon, A. Imberty, and S. Pérez. Biopolymers, **28**, 679 (1989).
39. S. W. Homans, R. A. Dwek, and T. W. Rademacher. Biochemistry, **26**, 6571 (1987).
40. J. S. Yadav and P. Luger. Carbohydr. Res. **119**, 57 (1983); I. Tvaroska and T. Kozar. J. Am. Chem. Soc. **102**, 6929 (1980).
41. F. Heatley, L. Akhter, and R. T. Brown. J. Chem. Soc. Perkin Trans. 2, 919 (1980).
42. R. Rowan, J. A. McCammon, and B. D. Sykes. J. Am. Chem. Soc. **96**, 4773 (1974).
43. A. Allerhand, D. Doddrell, and R. Komoroshi. J. Chem. Phys. **55**, 189 (1971).
44. D. Doddrell, A. V. Glushko, and A. Allerhand. J. Chem. Phys. **56**, 3683 (1972).
45. R. L. Vold and R. R. Vold. Prog. Nucl. Magn. Reson. Spectrosc. **12**, 79 (1978).
46. D. J. Craik and G. C. Levy. Topics in carbon-13 nmr spectroscopy. Vol. 4. Wiley, New York. 1984; G. C. Levy and J. R. Peat. J. Magn. Reson. **18**, 199 (1975).
47. S. Wimperis and R. Freeman. J. Magn. Reson. **58**, 348 (1984).

Can. J. Chem. Downloaded from www.nrcresearchpress.com by 88.85.125.76 on 09/07/12
For personal use only.

Ionization potentials of multiply charged ions from generalized exchange local-spin-density functional theory

YUFEI GUO[1] AND M. A. WHITEHEAD
Theoretical Chemistry Group, Department of Chemistry, McGill University, 801 Sherbrooke Street West, Montreal, P.Q., Canada H3A 2K6

Received October 30, 1989

This paper is dedicated to Professor Arthur S. Perlin on the occasion of his 67th birthday

YUFEI GUO and M. A. WHITEHEAD. Can. J. Chem. **68**, 989 (1990).

The self-interaction-corrected generalized exchange local-spin-density functional theory (LSD-GX-SIC) with Gopinathan, Whitehead, and Bogdanovic (GWB) Fermi-hole exchange parameters is used to calculate the ionization potentials of the multiply charged ions for the elements C, Al, Cl, Ar, Ca, Fe, and Br. The effect of the correlation correction on the ionization potentials is considered. The calculated ionization potentials are compared with Hartree–Fock, recent Xα, and experiment. The correlation correction is important in the calculations. The results in the LSD-GX-SIC theory with GWB Fermi-hole exchange parameters and the Vosko, Wilk, and Nusair correlation correction are in excellent agreement with experiment. The LSD-GX-SIC theory can predict unknown ionization potentials for the multiply charged ions with acceptable computational time, since there is no need to optimize the exchange parameters.

Key words: ionization potentials, multiply charged ions, density functional theory.

YUFEI GUO et M. A. WHITEHEAD. Can. J. Chem. **68**, 989 (1990).

Pour calculer les potentials d'ionisation des ions à charges multiples du C, du Al, du Cl, du Ar, du Ca, du Fe et du Br, on a utilisé la théorie fonctionnelle de la densité locale de spin, avec échange généralisé et correction par auto-interaction (LSD-GX-SIC) ainsi que des paramètres d'échange des trous de Fermi de Gopinathan, Whitehead et Bogdanovic (GWB). On a considéré l'effet de la correction de corrélation sur les potentials d'ionisation. On a comparé les potentials d'ionisation avec ceux de Hartree–Fock, avec de récents Xα et avec des données expérimentales. La correction de la corrélation est importante dans les calculs. Les résultats obtenus à l'aide de la théorie LSD-GX-SIC et les paramètres GWB d'échange de trous de Fermi et la correction de corrélation de Vosko, Wilk et Nusair sont en excellent accord avec les résultats expérimentaux. Puisqu'il n'y a pas besoin d'optimiser les paramètres d'échange, la théorie LSD-GX-SIC peut prédire les potentials d'ionisation inconnus d'ions portant de multiples charges en ne requérant que des temps de calcul acceptables.

Mots clés : potentials d'ionisation, ions à charges multiples, théorie fonctionnelle de la densité.

[Traduit par la revue]

Introduction

Investigation of ionization potentials for multiply charged ions has attracted attention (1, 2) because of the interest in these ionization potentials for interpreting stellar spectra. Other properties of multiply charged ions, e.g., ionization cross section, have also attracted some attention (3, 4) experimentally. Theoretical calculations for them might be interesting.

Few publications dealing with the ionization potentials of ions using the local-spin-density functional (LSD) theory (5) can be found in the literature, even for the multiply charged ions (2), although the LSD theory has been widely used in the calculations for atoms, molecules, and the solid state. The reason might be that the values of the exchange parameters, e.g., α in the Xα theory (6) and *a* in the Ξ*a* theory (7), have been missing in the literature for ions. Also it is time consuming to search for the optimal exchange parameters for all multiply charged ions of all atoms in the periodic table.

In 1987, Gáspár and Nagy (2) published the ionization potentials for some multiply charged ions evaluated by means of the Xα method in which the value of α was self-consistently determined by the electron charge density; their results are comparable with those from the Hartree–Fock method and agree with experiment. The advantage in Gáspár and Nagy's Xα method is that the exchange parameter α can be optimized in each iteration according to the electron density during the self-consistent field process, unlike the traditional Xα method in which α was determined by fitting the total Xα energy to the Hartree–Fock total energy, or by fitting the total energy to satisfy the virial theorem.

The generalized exchange local-spin-density functional (LSD-GX) theory derived by Manoli (8) and Manoli and Whitehead (9) is somewhat analogous to Gáspár and Nagy's Xα method in determining the optimal exchange parameters for atoms and ions. However, obtaining the exchange parameters is much easier and simpler in the LSD-GX theory than in Gáspár and Nagy's Xα method. The exchange parameters in the LSD-GX theory are fixed once the Fermi-hole shape is chosen (5, 9–11). Therefore one set of parameters applies for all atoms and ions. In addition, the LSD-GX theory with self-interaction correction (LSD-GX-SIC) and correlation correction has proved successful in calculating atomic properties, especially the first ionization potentials and electron affinities of atoms (12–15), and in predicting the negative-ion structure of the alkaline-earth elements and noble gases (16, 17).

The present paper tests the reliability of the LSD-GX theory in predicting ionization potentials of multiply charged ions. If it works, it can be used to calculate the ionization potentials for the multiply charged ions that have not been experimentally measured. The LSD-GX theory is much easier to use than Hartree–Fock theory because the local exchange potential is used in the LSD-GX theory, and is even easier to use than Xα theory because there is a unique set of parameters for all atoms once the Fermi hole is selected.

Therefore the LSD-GX-SIC theory is used to calculate the ionization potentials of multiply charged ions for C, Al, Ca, Fe, and Br, to compare the results with those from Xα calculations,

[1]Permanent address: Department of Applied Physics, National University of Defense Technology, Changsha, Hunan, People's Republic of China.

Can. J. Chem. Downloaded from www.nrcresearchpress.com by 88.85.125.76 on 09/07/12
For personal use only.

TABLE 1. Ionization potentials (in Ry) for the multiply charged ions of carbon, compared with other calculations and experiment

Degree of ionization	LSD-GX-SIC		HF			
	No correl.[a]	With correl.[b]	Rel.[c]	Unrel.[d]	Xα[e]	Expt.[f]
0	0.801	0.827	0.793	0.867	0.809	0.828
1	1.772	1.814	1.767	1.808	1.817	1.792
2	3.316	3.411	3.365	3.388	3.617	3.518
3	4.689	4.699	4.730	4.733	4.630	4.739
Avg.%[g]	(2.8)	(1.3)	(2.5)	(2.4)	(2.2)	

[a]The difference of the statistical total energies for the ith and $(i+1)$th ions in the two separate calculations, Δ_{SCF}.
[b]Δ_{SCF} plus VWN correlation correction.
[c]Δ_{SCF} in HF theory (25).
[d]Orbital energy in HF theory (25).
[e]Transition-state calculation in Xα method with theoretically determined parameter α (2).
[f]Reference 29.
[g]$\text{Avg.}\% = \left[\sum_{i=1}^{N} |(I_i^{\text{theor}} - I_i^{\text{exp}})|/I_i^{\text{exp}} \times 100\right]/N.$

and for Cl and Ar, which are interesting to chemists and astrophysicists. The effect on the ionization potential of the correlation correction proposed by Vosko *et al.* (18) is considered.

Method

Details of the LSD-GX theory were given by Manoli (8), and Manoli and Whitehead (9); a short summary is provided.

The one-electron Schrödinger equation, in Rydberg atomic units is

$$[1] \qquad [\hat{f} + V_c(\mathbf{r}) + V_{X_j}^{GX}(\mathbf{r})]u_j(\mathbf{r}) = \varepsilon_j u_j(\mathbf{r})$$

where the kinetic and nuclear attraction energy operator is

$$[2] \qquad \hat{f} = -\nabla^2 - \frac{2Z}{r}$$

and $V_c(\mathbf{r})$ and $V_{X_j}^{GX}(\mathbf{r})$ are the Coulomb and generalized statistical exchange potentials, respectively,

$$[3] \qquad V_c(\mathbf{r}) = \int n(\mathbf{r}')(2/|\mathbf{r}-\mathbf{r}'|)d\mathbf{r}'$$

and

$$[4] \qquad V_{X_j}^{GX}(\mathbf{r}) = -\frac{9}{2}c\,\alpha^{\lim}\left\{\sum_i^s [n_s(\mathbf{r}) + B_2\, n_i(\mathbf{r})]^{-2/3}\, n_i(\mathbf{r}) - \frac{2}{3}\sum_i^s [n_s(\mathbf{r}) + B_1 n_i(\mathbf{r})][n_s(\mathbf{r}) + B_2 n_i(\mathbf{r})]^{-5/3}\, n_i(\mathbf{r}) + [n_s(\mathbf{r}) + 2B_1 n_j(\mathbf{r})][n_s(\mathbf{r}) + B_2 n_j(\mathbf{r})]^{-2/3} - \frac{2}{3}B_2[n_s(\mathbf{r}) + B_1 n_j(\mathbf{r})][n_s(\mathbf{r}) + B_2 n_j(\mathbf{r})]^{-5/3}\, n_j(\mathbf{r})\right\}$$

where $n(\mathbf{r})$ is the total density of the electrons, $n_s(\mathbf{r})$ the total density of electrons with spin s, and $n_i(\mathbf{r})$ the ith electron density; c is a constant equal to $(3/4\pi)^{1/3}$. The exchange parameters B_1, B_2, and $\alpha^{\lim}$ are constants depending on the Fermi-hole shape. Several Fermi holes can be found in the literature (5, 9–11). The parameters B_1, B_2 and $\alpha^{\lim}$ for these Fermi holes have been given by Manoli and Whitehead (9).

Because the self-interactions in the Coulomb and exchange terms do not cancel exactly in the LSD theory, the statistical total energy in the LSD-GX theory (9) differs from that in Hartree–Fock theory in which this cancellation is exact. Perdew and Zunger (19) proposed a self-interaction correction (SIC) by explicity removing the Coulomb self-interaction and the approximate exchange self-interaction. For atomic systems (neutral), this self-interaction correction approach leads to a potential that exhibits the correct asymptotic $1/r$ behaviour. If the SIC is used in the LSD-GX theory, eq. [1] becomes

$$[5] \qquad [\hat{f} + V_{c_j}(\mathbf{r}) + V_{X_j}^{GX}(\mathbf{r}) + V_{s_j}(\mathbf{r})u_j(\mathbf{r}) = \varepsilon_j u_j(\mathbf{r})$$

where $V_{c_j}(\mathbf{r})$ is the pure Coulomb potential without self-interaction and $V_{s_j}(\mathbf{r})$ is the self-exchange potential for electron j,

$$[6] \qquad V_{c_j}(\mathbf{r}) = \int [n(\mathbf{r}') - n_j(\mathbf{r}')](2/|\mathbf{r}-\mathbf{r}'|)d\mathbf{r}'$$

and

$$V_{s_j}(\mathbf{r}) = 6\,c\,\alpha^{SI} n_j^{1/3}(\mathbf{r})$$

Using the Perdew and Zunger procedure, it is easy to relate exchange parameters α^{SI} and $\alpha^{\lim}$(20, 21).

The statistical total energy of an atom or ion in the LSD-GX-SIC theory can be written as

$$[7] \qquad E_{tot} = \sum_i f_i \langle u_i(\mathbf{r})|f|u_i(\mathbf{r})\rangle + \sum_{i>j} f_i f_j \langle u_i(\mathbf{r})u_j(\mathbf{r}') \parallel u_i(\mathbf{r})u_j(\mathbf{r}')\rangle + \frac{1}{2}\sum_i f_i \langle u_i(\mathbf{r})|U_{+_i}^{GX\text{-}SIC}(\mathbf{r})|u_i(\mathbf{r})\rangle + \frac{1}{2}\sum_i f_i \langle u_i(\mathbf{r})|U_{-_i}^{GX\text{-}SIC}(\mathbf{r})|u_i(\mathbf{r})\rangle$$

where f_i is the occupation number of orbital i. The energy density functional of the generalized exchange with self-exchange interaction correction, per electron, is

$$[8] \qquad U_{s_i}^{GX\text{-}SIC}(\mathbf{r}) = -9c\,\alpha^{\lim}\{n_s(\mathbf{r}) + B_1 n_i(\mathbf{r}\}\{n_s(\mathbf{r}) + B_2 n_i(\mathbf{r})\}^{-2/3} + 9c\,\alpha^{SI}\, n_i^{1/3}(\mathbf{r})$$

The statistical exchange approximation is treated in the LSD-

Can. J. Chem. Downloaded from www.nrcresearchpress.com by 88.85.125.76 on 09/07/12
For personal use only.

TABLE 2. Ionization potentials (in Ry) for the multiply charged ions of aluminum, compared with other calculations and experiment

Degree of ionization	LSD-GX-SIC		HF			
	No correl.[a]	With correl.[b]	Rel.[c]	Unrel.[d]	Xα[e]	Expt.[f]
0	0.386	0.412	0.404	0.419	0.378	0.440
1	1.316	1.386	1.288	1.308	1.364	1.384
2	2.093	2.108	2.060	2.065	2.043	2.090
3	8.734	8.822	8.715	8.967	9.019	8.817
4	11.195	11.304	11.191	11.539	11.704	11.302
5	13.707	13.854	13.858	14.479	14.607	13.996
6	17.892	17.932	17.776	17.860	17.716	17.782
7	20.891	20.942	20.921	21.020	21.018	20.958
8	24.102	24.171	24.252	24.328	24.488	24.263
9	29.007	29.144	28.915	28.885	29.250	29.291
Avg.%[g]	(2.4)	(1.0)	(2.1)	(2.1)	(3.0)	

[a]The difference of the statistical total energies for the ith and $(i + 1)$th ions in the two separate calculations, Δ_{SCF}.
[b]Δ_{SCF} plus VWN correlation correction.
[c]Δ_{SCF} in HF theory (25).
[d]Orbital energy in HF theory (25).
[e]Transition-state calculation in Xα method with theoretically determined parameter α (2).
[f]Reference 29.
[g]$\text{Avg.}\% = \left[\sum_{i=1}^{N} |(I_i^{\text{theor}} - I_i^{\text{exp}})|/I_i^{\text{exp}} \times 100\right]/N.$

TABLE 3. Ionization potentials (in Ry) for the multiply charged ions of chlorine, compared with other calculations and experiment

Degree of ionization	LSD-GX-SIC		HF		
	No correl.[a]	With correl.[b]	Rel.[c]	Unrel.[d]	Expt.[e]
0	0.874	0.942	0.867	1.013	0.956
1	1.633	1.728	1.645	1.878	1.749
2	2.842	2.868	2.875	2.917	2.933
3	3.830	3.865	3.854	3.885	3.932
4	4.870	4.918	4.904	4.922	4.983
5	7.009	7.100	6.958	6.972	7.108
6	8.383	8.406	8.332	8.334	8.399
7	25.503	25.606	25.517	25.741	25.601
8	29.315	29.440	29.336	29.801	29.452
9	33.218	33.382	33.338	34.207	33.466
10	38.957	39.003	39.011	39.120	
11	43.430	43.487	43.480	43.560	
12	47.980	48.057	48.132	48.181	
Avg.%[f]	(2.6)	(0.8)	(2.5)	(2.3)	

[a]The difference of the statistical total energies for the ith and $(i + 1)$th ions in the two separate calculations, Δ_{SCF}.
[b]Δ_{SCF} plus VWN correlation correction.
[c]Δ_{SCF} in HF theory (25).
[d]Orbital energy in HF theory (25).
[e]Reference 29.
[f]$\text{Avg.}\% = \left[\sum_{i=1}^{N} |(I_i^{\text{theor}} - I_i^{\text{exp}})|/I_i^{\text{exp}} \times 100\right]/N.$

GX theory but not the Coulomb correlation. Wigner (22) proposed the Coulomb hole to correct the electron correlation; many other methods for correlation correction have been proposed (see, for example, San-Fabián and Moscardó (23)), but one derived by Vosko, Wilk, and Nusair (18) (VWN) has been widely used in calculating atoms and molecules. In the VWN procedure, the correlation correction energy is

$$[9] \qquad E_c = \int [n_+(\mathbf{r}) + n_-(\mathbf{r})] + \psi(n_+(\mathbf{r}), n_-(\mathbf{r}))\, d\mathbf{r}$$

The function $\varepsilon_c(n_+(\boldsymbol{r}), n_-(\boldsymbol{r}))$ is the correlation energy per

Can. J. Chem. Downloaded from www.nrcresearchpress.com by 88.85.125.76 on 09/07/12
For personal use only.

TABLE 4. Ionization potentials (in Ry) for the multiply charged ions of argon, compared with other calculations and experiment

Degree of ionization	LSD-GX-SIC		HF		
	No correl.[a]	With correl.[b]	Rel.[c]	Unrel.[d]	Expt.[e]
0	1.085	1.192	1.086	1.181	1.158
1	1.938	2.064	1.940	2.093	2.031
2	2.861	3.013	2.879	3.135	2.995
3	4.269	4.359	4.311	4.352	4.396
4	5.406	5.504	5.433	5.463	5.514
5	6.589	6.699	6.624	6.643	6.689
6	9.010	9.159	8.956	8.969	9.138
7	10.526	10.606	10.470	10.473	10.544
8	30.955	31.151	30.977	31.201	31.050
Avg.%[f]	(−2.6)	(0.6)	(−2.4)	(0.6)	

[a]The difference of the statistical total energies for the ith and $(i + 1)$th ions in the two separate calculations, Δ_{SCF}.
[b]Δ_{SCF} plus VWN correlation correction.
[c]Δ_{SCF} in HF theory (25).
[d]Orbital energy in HF theory (25).
[e]Reference 29.
[f]$\text{Avg.}\% = \left[\sum_{i=1}^{N} |(I_i^{\text{theor}} - I_i^{\text{exp}})|/I_i^{\text{exp}} \times 100\right]/N.$

TABLE 5. Ionization potentials (in Ry) for the multiply charged ions of calcium, compared with other calculations and experiment

Degree of ionization	LSD-GX-SIC		HF			
	No correl.[a]	With correl.[b]	Rel.[c]	Unrel.[d]	Xα[e]	Expt.[f]
0	0.401	0.452	0.376	0.389	0.417	0.45
1	0.867	0.881	0.833	0.830	0.825	0.87
2	3.645	3.714	3.668	3.748	3.726	3.74
3	4.820	4.905	4.833	4.998	4.997	4.93
4	6.043	6.155	6.068	6.372	6.341	6.20
5	7.830	7.864	7.883	7.923	7.761	8.00
6	9.254	9.296	9.284	9.312	9.246	9.39
7	10.714	10.770	10.751	10.767	10.789	10.82
8	13.685	13.786	13.630	13.641	13.860	13.84
9	15.477	15.504	15.422	15.435	15.432	15.53
10	43.624	43.734	43.403	43.658	43.961	43.46
11	47.574	47.708	48.218	48.729	49.150	48.24
12	53.428	53.602	53.214	54.241	54.535	53.36
13	59.658	59.707	60.197	60.268	60.105	60.02
14	66.407	66.468	65.656	65.707	65.842	65.79
15	71.491	71.573	71.295	71.366	71.714	71.59
16	77.980	78.139	78.984	78.937	79.547	79.75
Avg.%[g]	(1.8)	(0.8)	(2.0)	(1.9)	(1.6)	

[a]The difference of the statistical total energies for the ith and $(i + 1)$th ions in the two separate calculations, Δ_{SCF}.
[b]Δ_{SCF} plus VWN correlation correction.
[c]Δ_{SCF} in HF theory (25).
[d]Orbital energy in HF theory (25).
[e]Transition-state calculation in Xα method with theoretically determined parameter α (2).
[f]Reference 29.
[g]$\text{Avg.}\% = \left[\sum_{i=1}^{N} |(I_i^{\text{theor}} - I_i^{\text{exp}})|/I_i^{\text{exp}} \times 100\right]/N.$

Can. J. Chem. Downloaded from www.nrcresearchpress.com by 88.85.125.76 on 09/07/12
For personal use only.

TABLE 6. Ionization potentials (in Ry) for the multiply charged ions of iron, compared with other calculations and experiment

Degree of ionization	LSD-GX-SIC		HF			
	No correl.[a]	With correl.[b]	Rel.[c]	Unrel.[d]	Xα[e]	Expt.[f]
0	0.512	0.579		0.514	0.588	0.58[f]
1	1.205	1.217			1.134	1.19
2	2.221	2.321	2.084	2.631	2.488	2.25
3	4.071	4.112	3.979	4.145	3.888	4.03
4	5.632	5.681	5.483	5.689	5.469	5.51
5	7.336	7.393	7.249	7.423	7.211	7.28
6	8.896	8.961	9.156	9.261	9.100	9.19
7	11.393	11.468	11.052	11.172	11.127	11.10[g]
8	17.036	17.123	17.104	17.198	17.221	17.20
9	19.070	19.174	19.104	19.330	19.389	19.26
10	21.125	21.257	21.165	21.608	21.622	21.31
11	23.982	24.026	22.069	24.107	23.912	24.33
12	26.232	26.285	28.278	26.312	25.257	26.53
13	28.499	28.567	28.546	28.591	28.644	28.81
14	33.123	33.239	33.040	33.074	33.431	33.59
15	35.733	35.765	35.649	35.646	35.682	35.94
16	92.629	92.751	92.711	92.901	93.492	93.05
17	99.437	99.583	99.508	100.173	100.801	99.81
18	106.263	106.452	106.484	107.821	108.295	107.00
19	115.960	116.014	116.080	116.200	115.961	116.30
20	123.569	123.636	123.513	123.550	123.775	124.10
21	130.914	131.003	131.127	131.194	131.700	132.20
22	141.417	141.590	141.403	141.440	142.926	143.30
Avg.%[h]	(1.6)	(1.2)	(1.6)	(2.2)	(1.6)	

[a]The difference of the statistical total energies for the ith and $(i+1)$th ions in the two separate calculations, Δ_{SCF}.
[b]Δ_{SCF} plus VWN correlation correction.
[c]Δ_{SCF} in HF theory (25).
[d]Orbital energy in HF theory (25).
[e]Transition-state calculation in Xα method with theoretically determined parameter α (2).
[f]Reference 29.
[g]References 28 and 30.
[h]$\text{Avg.}\% = \left[\sum_{i=1}^{N} |(I_i^{\text{theor}} - I_i^{\text{exp}})|/I_i^{\text{exp}} \times 100\right]/N.$

particle of the homogeneous electron gas with partial densities $n_+(\mathbf{r})$ and $n_-(\mathbf{r})$ for spin-up and spin-down electrons. In eq. [9], the correlation self-interaction is included. If a self-interaction correction of the correlation (SICC) is introduced into E_c by using the definition of Stoll, Pavlidou, and Preuss (24), expression [9] becomes

$$[10] \quad E_c = \int [n_+(\mathbf{r}) + n_-(\mathbf{r})]\, \varepsilon_c(n_+(\mathbf{r}), n_-(\mathbf{r}))\, d\mathbf{r} - \int n_+(\mathbf{r})\, \varepsilon_c(n_+(\mathbf{r}), 0)\, d\mathbf{r} - \int n_-(\mathbf{r})\, \varepsilon_c(0, n_-(\mathbf{r}))\, d\mathbf{r}$$

The explicit expression for $\varepsilon_c(n_+, n_-)$ is given by Vosko, Wilk, and Nusair (18).

Consequently, the ionization potential for the k^{th} ion, including the SIC contribution and the SICC correction, is

$$[11] \quad I^k = [E_{\text{tot}}(f_k - 1) - E_{\text{tot}}(f_k)] + [E_c(f_k - 1) - E_c(f_k)]$$

The first term in eq. [11] is the contribution of the kinetic, Coulomb, and exchange energies, and the second term is the correlation energy. The energies E_{tot} and E_c are obtained from separate self-consistent wavefunctions of the k^{th} and $(k+1)^{\text{th}}$ ions.

Results and discussion

The one-electron Schrödinger equation, [5], combined with eq. [2], [4], and [6] is solved numerically (9). As is usual in LSD calculations, the electron densities, $n_i(\mathbf{r})$, were spherically averaged before calculating the potential and the total energy for atoms. This "central-field" approximation is perhaps most severe for the $2p$ orbital, which makes a sizable contribution to the total self-interaction correction. However, according to Perdew and Zunger (19), the self-Coulomb energy for a hydrogenic $2p$ orbital (with $m_l = 0$) is only 4% larger than it would be for the spherically averaged density.

Of the four Fermi-hole shapes in the literature (5, 9–11), the statistical total energies of atoms (atomic number $Z \leq 36$) in the LSD-GX-SIC theory with the exchange parameters of Gopinathan, Whitehead, and Bogdanovic's Fermi-hole shape (GWB) are in excellent agreement with the total energies in the Hartree–Fock theory (25). The percentage differences between the statistical total energies and Hartree–Fock energies for all these atoms are less than 0.08. Furthermore, the differences decrease with increasing atomic number. Thus the LSD-GX-SIC theory with GWB should give the best ionization potentials.

The ionization potential is (i) approximately the negative of

Can. J. Chem. Downloaded from www.nrcresearchpress.com by 88.85.125.76 on 09/07/12
For personal use only.

TABLE 7. Ionization potentials (in Ry) for the multiply charged ions of bromine, compared with other calculations and experiment

Degree of ionization	LSD-GX-SIC No correl.[a]	LSD-GX-SIC With correl.[b]	HF Unrel.[c]	Xα[d]	Expt.[e]
0	0.802	0.867	0.911	0.859	0.87
1	1.480	1.570	1.676	1.608	1.60
2	2.522	2.549	2.580	2.433	2.65
3	3.379	3.414	3.410	3.322	3.48
4	4.276	4.323	4.292	4.261	4.39
5	6.318	6.397	6.196	6.370	6.51
6	7.521	7.557	7.350	7.457	7.57
7	14.237	24.327	14.040	14.255	14.41
Avg.%[f]	(3.8)	(1.5)	(3.3)	(2.8)	

[a]The difference of the statistical total energies for the ith and $(i+1)$th ions in the two separate calculations, Δ_{SCF}.

[b]Δ_{SCF} plus VWN correlation correction.

[c]Orbital energy in HF theory (25).

[d]Transition-state calculation in Xα method with theoretically determined parameter α (2).

[e]Reference 29.

[f]$$\text{Avg.}\% = \left[\sum_{i=1}^{N} |(I_i^{\text{theor}} - I_i^{\text{exp}})|/I_i^{\text{exp}} \times 100\right]/N.$$

the one-electron eigenvalue in the LSD-GX-SIC theory under the frozen orbital approximation (26), and equals (ii) the negative of the one-electron eigenvalue generated by removing a half-electron from the corresponding orbital to infinity in the LSD-GX theory (Slater transition state theory (27)). Finally, the ionization potential is (iii) the difference between two statistical total energies, one for the k^{th} ion and another for the $(k+1)^{th}$ ion obtained by two separated self-consistent field (SCF) calculations. Although (i) and (ii) are computationally easier than (iii), there is not much difference in the computational time, when all the ionization potentials of the successive multiply charged ions for an atom are needed. The orbital relaxation in the ionization process is neglected totally in (i) and partly in (ii), but is included completely in (iii). Therefore the ionization potentials of the multiply charged ions are calculated by (iii).

The LSD-GX-SIC theory with GWB Fermi-hole parameters was used to calculate the wavefunctions of some neutral atoms (atomic numbers 6, 13, 17, 18, 20, 26, and 35) together with the wavefunctions of the corresponding multiply charged ions. These numerical wavefunctions were then used to calculate the corresponding statistical total energies (eq. [7]) and VWN correlation energies (eq. [10]) for the atoms and ions. The VWN correlation potential (28) has not been treated self-consistently, because it is not important in calculating ionization potentials (13–15, 29), although it is essential in predicting electron affinities for the alkaline-earth elements, noble gases, and actinides (16, 17, 30). The ionization potentials were obtained from the differences of the statistical total energies, which included the VWN correlation energies for the k^{th} and $(k+1)^{th}$ ions (eq. [11]). Results in Tables 1–7 are compared to the Hartree-Fock results (25) and with experiment (31–33).

Relaxation lowers the total energy but decreases as the number of the electrons increases. The Hartree–Fock results in columns 4 and 5 of Tables 1–6 show the ionization potentials of the multiply charged ions without relaxation to be usually larger. In addition, correlation lowers the total energy but increases as the number of electrons increases and, therefore, the correlation correction increases the ionization potential; all the values in column 3 are larger than those in column 2.

The Coulomb correlation correction plays an important role in the first ionization potentials, and electron affinities (13, 14, 16), because the contribution of the correlation correction to the electron affinity is comparable to that of the kinetic, Coulomb, and exchange interaction energies. Comparing the results of the LSD-GX-SIC theory with GWB Fermi-hole parameters and the VWN correlation correction in column 3 of Tables 1–7 with those excluding VWN in column 2 shows that the correlation energy correction also plays a role in the ionization potentials of the multiply charged ions.

In Tables 1, 2, and 5–7, the recent calculations of the multiply charged ions obtained by using a Slater transition state calculation in the Xα method with the theoretically determined parameter α(2) are also presented. The data show that the results in LSD-GX-SIC theory with GWB Fermi-hole parameters and transition state of the Xα theory with the theoretically determined parameter α are comparable with the results from Hartree–Fock theory. But ionization potentials of the multiply charged ions in LSD-GX-SIC theory with GWB Fermi-hole parameters and correlation corrections are much better than all others. Their agreement with experiment is excellent.

The deviation of each calculated ionization potential, Tables 1–7, from the experimental value is expressed as a percentage. These percentages are averaged for all multiply charged ions of the same element to give the average percentage deviation from the experiment. The last lines in Tables 1–7 list the average percentage deviations for the theories discussed in this work, the relaxed and the unrelaxed Hartree–Fock, and the recent Xα transition state results. The results using LSD-GX-SIC theory with GWB Fermi-hole parameters and VWN correlation correction are the best. The average percentage deviations for all these elements in this theory are less than 1.5%. Furthermore, the percentage deviation for each value is around one.

One might expect to calculate the ionization potentials of the multiply charged ions by using the traditional Xα theory with the corresponding optimal α values of the neutral atoms. To compare the LSD-GX-SIC results with those in the traditional Xα theory, the relaxed Xα calculations for the ionization potentials of these multiply charges ions were carried out using Schwarz's α values(34) for neutral atoms and the corresponding α values of the atoms that are of the same electrons as the multiply charged ions. The results (not listed here because of the limited length of the paper) are much worse, in the agreement with experiment, than those in Hartree–Fock and LSD-GX-SIC theories. The averge percentage deviations are around 3.5.

Conclusion

The ionization potentials of multiply charged ions calculated by means of the difference between two statistical total energies in the LSD-GX-SIC theory with GWB Fermi-hole exchange parameters are comparable with those in Hartree–Fock theory. The LSD-GX-SIC theory is much easier and cheaper to use than Hartree–Fock theory. The correlation energy correction of the electrons with different spin is important, so that the LSD-GX-SIC theory with GWB Fermi-hole exchange parameters and with VWN correlation correction gives excellent ionization potentials for the multiply charged ions, in agreement with experiment. One can expect that the quasi-relativistic (35, 36) LSD-GX-SIC theory with GWB and VWN should give very

Can. J. Chem. Downloaded from www.nrcresearchpress.com by 88.85.125.76 on 09/07/12
For personal use only.

good ionization potentials of the multiply charged ions for the high-Z elements, even for the actinides, with acceptable computational time, because there is no need to search for optimal exchange parameters for each atom or ion. Based on the excellent agreement between the calculated and experimental values, the LSD-GX-SIC theory with GWB exchange parameters and VWN correlation correction can be used to predict ionization potentials of multiply charged ions that are unknown experimentally.

Acknowledgments

Dr. Perlin by his vision, humour, gentleness, kindness, and openness has always appreciated and encouraged research in fields other than his own. The authors also wish to thank Mr. M. Wrinn for interesting discussions. The research was supported by the Natural Sciences and Engineering Research Council of Canada.

1. T. A. Carlson, C. W. Nestor, N. Wasserman, Jr., and J. D. McDowell. At. Date, **2**, 63 (1970)
2. R. Gáspár and Á. Nagy. J. Phys. B: At. Mol. Phys. **20**, 3631 (1987).
3. J. Binder, H. R. Kaslowski, B. A. Huber, and K. Wiesemann. 10th International Conference on Atomic Physics. *Edited by* H. Narumi and I. Shimamura. Tokyo. 1986
4. M. A. Chaudhry, A. J. Duncan, R. Hippler, and H. Kleinpoppen. 10th International Conference on Atomic Physics. *Edited by* H. Narumi and I. Shimamura. Tokyo. 1986.
5. J. C. Slater. Quantum theory of molecules and solids, Vol. 4, McGraw–Hill, New York. 1974.
6. J. C. Slater. Phys. Rev. **81**, 385 (1951).
7. M. S. Gopinathan. Phys. Rev. A, **15**, 2135 (1977).
8. S. Manoli. Ph.D. Thesis, McGill University, Montreal. 1986.
9. S. Manoli and M. A. Whitehead. Phys. Rev. A, **34**, 4629 (1986).
10. M. S. Gopinathan, M. A. Whitehead, and R. Bogdanovic. Phys. Rev. A, **14**, 1 (1976).
11. J. L. Gázquez and J. Keller. Phys. Rev. A, **16**, 1358 (1977).
12. Y. Guo, S. Manoli, and M. A. Whitehead. Phys. Rev. A, **38**, 1120 (1988).
13. Y. Guo and M. A. Whitehead. Phys. Rev. A, **38**, 3166 (1988).
14. Y. Guo and M. A. Whitehead. Phys. Rev. A, **39**, 28 (1989).
15. Y. Guo and M. A. Whitehead. Phys. Rev. A, **39**, 2317 (1989).
16. Y. Guo and M. A. Whitehead. Phys. Rev. A, **40**, 28 (1989).
17. Y. Guo, M. C. Wrinn, and M. A. Whitehead. Phys. Rev. A, **40**, 6685 (1989).
18. S. H. Vosko, L. Wilk, and M. Nusair. Can. J. Phys. **58**, 1200 (1980).
19. J. P. Perdew and A. Zunger. Phys. Rev. B, **23**, 5048 (1981).
20. S. Manoli and M. A. Whitehead. Phys. Rev. A, **38**, 630 (1988).
21. S. Manoli and M. A. Whitehead. Collect. Czech. Chem. Commun. **53**, 2279 (1988).
22. E. P. Wigner. Phys. Rev. **46**, 1002 (1934).
23. E. San-Fabián and F. Moscardó. J. Chem. Phys. **81**, 4008 (1984).
24. H. Stoll, C. M. Pavlidou, and H. Preuss. Theoret. Chim. Acta, **49**, 143 (1978).
25. E. Clementi. IBM J. Res. Dev. **9**, 2 (1965).
26. T. A. Koopmans. Physica, **1**, 104 (1933).
27. J. C. Slater. In Computational methods in band theory. *Edited by* P. M. Marcus, J. F. Janak, and A. R. Williams. Plenum, New York. 1971.
28. G. S. Painter. Phys. Rev. B, **24**, 4264 (1981).
29. E. Clementi, S. J. Chakravorty, G. Coronigiu, and V. Carravetta. Modern techniques in computational chemistry. To be published.
30. S. H. Vosko, J. B. Lagowski, and I. L. Mayer. Phys. Rev. A, **39**, 446 (1989).
31. S. Bashkin and J. O. Stoner, Jr. Atomic energy levels and Grotian diagrams. North-Holland, Amsterdam. 1975.
32. C. E. Moore. Ionization potentials and ionization limits derived from the analyses of optical spectra. NBS Report No. 34. U.S. Govt. Printing Office, Washington, DC. 1974.
33. K. Mori and T. Kato. At. Data Nucl. Data Tables, **23**, 196 (1979).
34. K. Schwarz. Phys. Rev. B, **5**, 2466 (1972).
35. R. D. Cowan and D. C. Griffin. J. Opt. Soc. Am. **66**, 1010 (1976).
36. J. D. Wood and A. M. Boring. Phys. Rev. B, **18**, 2701 (1978).

Can. J. Chem. Downloaded from www.nrcresearchpress.com by 88.85.125.76 on 09/07/12
For personal use only.

The conformational equilibria of 3-methoxybenzaldehyde in polar and nonpolar solutions. ^{1}H NMR and MO calculations

TED SCHAEFER, RUDY SEBASTIAN, HUA YAN LI,[1] AND TINH QUACH[1]
Department of Chemistry, University of Manitoba, Winnipeg, Man., Canada R3T 2N2

Received August 31, 1989

This paper is dedicated to Professor Arthur S. Perlin on the occasion of his 67th birthday

TED SCHAEFER, RUDY SEBASTIAN, HUA YAN LI, and TINH QUACH. Can. J. Chem. **68**, 996 (1990).

Analyses of the ^{1}H nuclear magnetic resonance spectra of 3-methoxybenzaldehyde in CS_2/C_6D_{12} and in acetone-d_6 solutions at 300 K yield the values of stereospecific long-range spin–spin coupling constants for the aldehydic and methyl protons. These coupling constants are used to deduce the conformational bias for both substituents. The conformers in which the carbonyl group lies *trans* to the methoxy group have a population P_t, which is $0.63(2)P_c$ for the CS_2/C_6D_{12} solution, P_c being the population of the conformers in which the carbonyl group lies *cis* to the methoxy substituent; in acetone-d_6 solution, $P_t = 0.80(2)P_c$. Both of these numbers are substantially larger than that deduced from nuclear Overhauser enhancements for a $CDCl_3$ solution. If P_t is the fractional population of the conformers in which the methoxy is oriented *trans* to the aldehyde substituent, then $P_t = 0.53(1)P_c$ in CS_2/C_6D_{12} and $P_t = 0.67(1)P_c$ in acetone-d_6, both numbers again being rather larger than that deduced from polarization experiments. STO-3G and 4-21G MO computations of the conformer stabilities agree qualitatively with the relative stabilities of the four planar conformers. Extrapolation of the populational data in solution yields vapor phase estimates midway between the two theoretical estimates. Limits can be placed on the fractional population of each of the conformers in the vapor and in the solutions. The relative stabilities of the free conformers can be rationalized in terms of electrostatics and of preferences of the carbonyl and methoxy groups for certain orientations with respect to the ring C—C bonds of highest double bond character.

Key words: 3-methoxybenzaldehyde, NMR; 3-methoxybenzaldehyde, conformations for solutions and vapor; 3-methoxybenzaldehyde, MO calculations.

TED SCHAEFER, RUDY SEBASTIAN, HUA YAN LI et TINH QUACH. Can. J. Chem. **68**, 996 (1990).

Une analyse des spectres RMN du ^{1}H du 3-méthoxybenzaldéhyde mesurés à 300 K, en solutions dans le CS_2/C_6D_{12} ainsi que dans l'acétone-d_6, fournit les valeurs des constantes de couplage spin–spin à longue distance qui sont spécifiques aux protons de l'aldéhyde et des méthyles. On a utilisé ces constantes de couplage pour déduire les tendances conformationnelles des deux substituants. Pour la solution dans le CS_2/C_6D_{12}, la population P_t des conformères dans lesquels le groupement carbonyle se trouve en position *trans* par rapport au groupement méthoxy est égale à $0,63(2)P_c$ et P_c correspond à la population des conformères dans lesquels le groupement carbonyle est *cis* par rapport au groupement méthoxy; pour la solution dans l'acétone-d_6, $P_t = 0,80(2)P_c$. Ces deux valeurs sont beaucoup plus élevées que celles obtenues en faisant appel à des mesures de rehaussement de l'effet Overhauser pour des solutions dans le $CDCl_3$. Si la valeur P_t est égale à la fraction de la population des conformères dans lesquels le groupement méthoxy est orienté *trans* par rapport au substituant aldéhydique, alors $P_t = 0,53(1)P_c$ pour la solution dans le CS_2/C_6D_{12} et $P_t = 0,67(1)P_c$ pour la solution dans l'acétone-d_6 et ces deux valeurs sont encore une fois plus élevées que celles obtenues à partir d'expériences de polarisation. Des calculs d'OM aux niveaux STO-3G et 4-21G conduisent à des stabilités des conformères qui correspondent qualitativement avec les stabilités relatives des quatre conformères plans. Une extrapolation des données relatives aux populations en solution fournit une évaluation des valeurs en phase gazeuse qui est intermédiaire entre les deux évaluations théoriques. On peut placer des limites sur les fractions de population de chacun des conformères en phase vapeur et en solutions. On peut rationaliser les stabilités relatives des conformères libres en fonction de facteurs électrostatiques et des préférences des groupements carbonyle et méthoxy pour certaines orientations par rapport aux liaisons C—C du cycle dont le caractère de double liaison est le plus élevé.

Mots clés : 3-méthoxybenzaldéhyde, RMN; 3-méthoxybenzaldéhyde, conformations en phase vapeur et en solutions; 3-méthoxybenzaldéhyde, calculs d'OM.

[Traduit par la revue]

Introduction

In the vapor phase, low-resolution microwave spectroscopy provides evidence for the existence of three of the four possible planar conformers of 3-methoxybenzaldehyde (1). The spectrum of **1** is not seen but, noting the broadness and weakness of the spectra of **2–4**, the probable low dipole moment of **1** may account for its apparent absence. The relative populations of the conformers are difficult to extract from these spectra (1).

In solution, the barriers to rotation about the C_{sp^2}—C_{sp^2} and C_{sp^2}—O bonds for the aldehyde (2) and methoxy (3) groups are large enough to allow a discussion of the conformational behaviour of 3-methoxybenzaldehyde at ambient temperatures in terms of the planar conformers, **1–4**. In acetone-d_6 solution (4), ^5J(H-5,CHO) is 0.375(13) Hz; as a stereospecific spin–spin coupling constant, it indicates the population of **1** + **2**

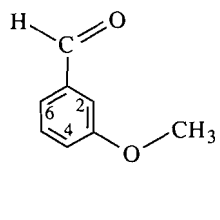

1

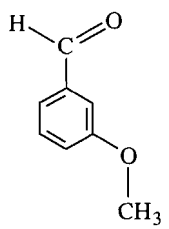

2

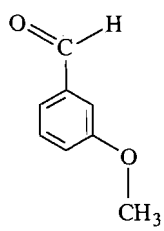

3

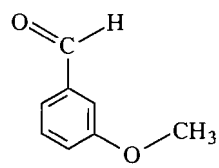

4

[1]Undergraduate research participant, 1987–1988.

Can. J. Chem. Downloaded from www.nrcresearchpress.com by 88.85.125.76 on 09/07/12
For personal use only.

Can. J. Chem. Downloaded from www.nrcresearchpress.com by 88.85.125.76 on 09/07/12
For personal use only.

relative to that of **3** + **4**, although this population was not deduced. Decoupling experiments show that the methoxy protons are coupled to H-2 and H-4 but the coupling constants are not resolved (4). On the basis of PCILO computations (4), it is suggested that electrostatic interactions between *meta* substituents make an important contribution to the relative stability of the conformers of 2,5-dimethoxybenzaldehyde and, by inference, of 3-methoxybenzaldehyde. In other words, the roughly antiparallel electric dipoles in **1** presumably favour this conformation. No populations are deduced (4).

An alternative interpretation of the conformational preferences of the aldehyde and methoxy groups in aromatic systems (5–7) is that the former is preferentially arranged so that the carbonyl lies *trans* to the *ortho* position of highest double bond character, as in **5** (valence-bond picture), or of highest

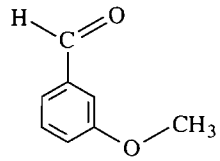

5

π-electron density (molecular orbital picture); the latter, however, prefers to lie *cis* to the bond of the highest double character, as in vinyl ether. It is not clear to us whether it is the methoxy group or the aldehyde group which causes the lower energy of the resonance form indicated in **5**. In any event, the nuclear Overhauser effect for the protons *ortho* to the aldehyde functionality (irradiation of the aldehyde proton peaks) is interpreted to mean that $K = (P_1 + P_2)/(P_3 + P_4)$ is roughly 1.8 for $CDCl_3$ or benzene-d_6 solutions (7). There exist (6, 8) various complications in the interpretation of these polarization experiments. Nevertheless, from measurements of the polarizations (enhancements) and of spin-lattice relaxation times of ^{13}C and ^1H nuclei of 3-methoxyacetophenone in $CDCl_3$ solutions (6), it is concluded that the acetyl group displays the same conformational behaviour as the aldehyde group in 3-methoxybenzaldehyde and, furthermore, that the methoxy group has $K = (P_1 + P_4)/(P_2 + P_4)$ as 2.2. In other words, the methoxy group is strongly oriented towards the aldehyde site.

Now, both $^5J(H,CHO)$ and $^5J(H,OCH_3)$ are stereospecific (9–17). Thus, ^5J(H-5,CHO) in **1** and **2** are expected to vanish (9, 12), whereas they will be as large as 0.9 Hz in **3** and **4**. Again, ^5J(H-4,OCH_3) in **2** and **3** will be near −0.3 Hz but negligible in **1** and **4**; corresponding statements (13–17) hold for ^5J(H-2,OCH_3). $^5J(H,OCH_3)$ is a proximate coupling (14) and, as such, is sizeable only when the methoxy protons lie very near the ring proton. Therefore, a precise analysis of the ^1H NMR spectrum of 3-methoxybenzaldehyde should yield precise values of ^5J(H-5,CHO) and $^5J(H,OCH_3)$, from which $K = (P_1 + P_2)/(P_3 + P_4)$ and $K = (P_1 + P_4)/(P_2 + P_3)$, respectively, can be deduced for solutions. Molecular orbital calculations may give an indication of the conformational behaviour of the free molecule, including relative populations of each of **1**–**4**. Such measurements and calculations are reported below.

Experimental

Solutions of 3-methoxybenzaldehyde in CS_2/C_6D_{12} and in acetone-d_6 (see Table 1) were transferred to 5 mm od NMR sample tubes, were degassed by the freeze–pump–thaw procedure, and were then flame-sealed under vacuum. ^1H NMR spectra were acquired at a probe temperature of 300 K on a Bruker AM300 spectrometer under conditions previously described (18). A wide sweepwidth survey spectrum was obtained in order to reference the spectrum with respect to TMS, and to obtain the locations of the aromatic and side-chain regions. Each region was examined in detail, with sweepwidth and data region adjusted to give acquisition times of approximately 40 s. Four to 16 scans were acquired. Zero filling to twice the original data region was done before transforming the FIDs using a small amount of Gaussian multiplication. Linewidths at half height were approximately 0.04 Hz after this resolution enhancement. Because of the many long-range coupling constants between the four ring protons and the four on the side chains, spectra were obtained by decoupling, successively, the aldehydic proton and then the methoxy protons. The ensuing spectra, corresponding to seven and five spin 1/2 systems, were amenable to reasonably precise analyses.

Molecular orbital computations utilized the computer program GAUSSIAN 86 (19). The geometry optimization procedures contained the constraint that the carbon and hydrogen atoms of the aromatic nucleus remain in a plane; all other bond angles and lengths were allowed to change.

Results and discussion

The ^1H NMR spectra were analyzed with the computer program NUMARIT (20), as modified by R. Sebastian in this laboratory. The spectral parameters of 3-methoxybenzaldehyde appear in Table 1. The decoupling procedures during spectral acquisition caused Bloch–Siegert shifts, apparent in Table 1. For the CS_2/C_6D_{12} solvent mixture, the existence of large correlations (footnotes to Table 1) between certain coupling constants within the ring, and between them and some chemical shifts, causes a relatively large imprecision in these parameters. Fortunately, those long-range coupling constants of immediate interest to the following discussion do not suffer from such imprecision. Figure 1 shows the ^1H NMR spectrum of H-2 in CS_2 solution.

The conformational behaviour of the aldehydic group

In benzaldehyde, $^5J(H,CHO)$ is 0.431(2) Hz for a CS_2/C_6D_{12} solution and is 0.430(1) Hz for an acetone-d_6 solution (21). The available evidence (9–12) on benzaldehyde derivatives implies that $^5J(H,CHO)$ vanishes in **1** and **2**, thereby implying that $^5J(H,CHO)$ is 0.861(4) in **3** and **4**; the methoxy group is distant from the coupling path for this σ electron coupling (21) and will therefore minimally perturb the magnitude of the coupling constant.

Accordingly, because $^5J(H,CHO)$ is 0.332(6) Hz in CS_2/C_6D_{12} solution and is 0.382(4) Hz in acetone-d_6, $K(CHO) = (P_3 + P_4)/(P_1 + P_2) = 0.332(6)/(0.861(4) - 0.332(6)) = 0.63(2)$ for the former and is $0.382(4)/(0.861(4) - 0.382(4)) = 0.80(2)$ for the latter solution at 300 K. The nuclear Overhauser enhancements measured for $CDCl_3$ and (or) C_6D_6 solutions of 3-methoxybenzaldehyde (7) imply a K(CHO) of 0.56 (temperature not stated). It is unlikely that the *meta* substituent perturbs $^5J(H,CHO)$ enough to reduce the value of K(CHO) to 0.56. Thus, for 4-fluorobenzaldehyde in acetone-d_6 solution, in which the substituent is now rather closer to the coupling path, $^5J(H,CHO)$ is 0.439(1) Hz (unpublished work in this laboratory). If this number were to apply, then K(CHO) would become 0.77(2) for 3-methoxybenzaldehyde in acetone-d_6 solution.

The present results show that the conformational bias of the aldehydic group in 3-methoxybenzaldehyde is solvent dependent.

Conformational behaviour of the methoxy group

Precise analyses of the ^1H NMR spectra of anisole yield $^5J(H,OCH_3)$ as −0.152(0) and −0.155(0) Hz in CS_2/C_6D_{12}

TABLE 1. ^{1}H NMR spectral parameters for 3-methoxybenzaldehyde at 300 K

Parameter	CS_2/C_6D_{12}[a]		Acetone-d_6[b]	
ν(CHO)[c]	2957.62[d]	—[e]	3003.57[d]	—[e]
$\nu(OCH_3)$	—	1136.096(1)	—	1164.868(1)
ν_2	2175.934(2)	2176.279(1)	2231.567(1)	2231.932(1)
ν_4	2112.848(2)	2113.206(1)	2175.458(1)	2175.826(1)
ν_5	2198.511(10)	2198.825(7)	2254.361(2)	2254.722(1)
ν_6	2195.099(10)	2195.484(7)	2254.389(2)	2254.756(1)
$^3J_{45}$	8.172(20)[f]	8.248(14)[f]	8.285(4)[g]	8.294(2)
$^3J_{56}$	7.421(4)	7.417(2)	7.479(2)	7.481(1)
$^4J_{26}$	1.415(4)	1.417(3)	1.428(3)	1.427(2)
$^4J_{24}$	2.706(3)	2.702(2)	2.721(2)	2.721(1)
$^4J_{46}$	1.095(20)[f]	1.019(14)[f]	0.979(4)[g]	0.972(2)
$^5J_{25}$	0.431(4)	0.430(3)	0.443(3)	0.455(2)
^4J(2,CHO)	−0.073(5)	—	−0.089(3)	—
^4J(6,CHO)	−0.151(6)	—	−0.153(4)	—
^5J(5,CHO)	0.332(6)	—	0.382(4)	—
^6J(4,CHO)	0.047(4)	—	0.039(2)	—
$^5J(2,OCH_3)$	—	−0.195(1)	—	−0.180(1)
$^5J(4,OCH_3)$	—	−0.103(1)	—	−0.121(1)
$^6J(5,OCH_3)$	—	0.008(2)	—	0.014(2)[h]
$^7J(6,OCH_3)$	—	−0.008(2)	—	−0.013(2)[h]
Transitions assigned	63	247	72	205
Root-mean-square deviation	0.009	0.009	0.006	0.005
Largest difference	0.026	0.027	0.014	0.014

[a]4.0 mol% in CS_2, containing also 10 mol% C_6D_{12} and 0.5 mol% TMS.
[b]4.0 mol%, containing also 0.5 mol% TMS.
[c]In Hz at 300.135_2 MHz to high frequency of internal TMS.
[d]For a spectrum in which the methoxy protons are decoupled.
[e]For a spectrum in which the aldehyde proton is decoupled; consequently, Bloch–Siegert shifts are present for all chemical shifts, accounting for the different values in a given solvent.
[f]$^3J_{45}$ and $^4J_{46}$ are correlated with each other and with ν_5 and ν_6 by 0.95 or more, accounting for their imprecision.
[g]$^3J_{45}$ and $^4J_{46}$ correlate by 0.69.
[h]$^6J(5,OCH_3)$ and $^7J(6,OCH_3)$ correlate by 0.704.

TABLE 2. Theoretical and experimental data for the conformers of 3-methoxybenzaldehyde

Property		Conformer[a] 1	2	3	4
Energy (STO-3G)[b]		0.000	1.78_9	1.10_0	1.40_1
Energy (4-21G)[c]		0.000	7.45_9	6.09_6	6.78_9
μ (STO-3G)[d]		0.73_5	3.02	2.58	1.89
μ (4-21G)[d]		1.69	4.88	4.48	3.42
μ (group)[e]		1.74	4.18	3.04	3.95
Population (STO-3G)[f]		0.37	0.18	0.24	0.21
Population (4-21G)[f]		0.83	0.04_3	0.07_2	0.05_5
	STO-3G	4-21G	Vapor[h]	CS_2	Acetone-d_6
K(CHO)[g]	0.81_5	0.14_5	0.46_5	0.63(2)	0.80(2)
$K(OCH_3)$[g]	0.72	0.13	0.39(1)	0.53(1)	0.67(1)
$P_1 + P_2$	0.55	0.87	0.68(2)	0.61(1)	0.55(1)
$P_1 + P_4$	0.58	0.88_5	0.72(2)	0.65(1)	0.60(1)
$P_2 + P_3$	0.42	0.11_5	0.28(2)	0.35(1)	0.40(1)
$P_4 - P_2$	0.03	0.01	0.03_5	0.04(1)	0.04(1)
$P_1 - P_3$	0.13	0.76	0.40(2)	0.27(1)	0.15(1)
P_1	0.37	0.83	>0.40(2)	>0.27(2)	>0.15(2)
			<0.68(2)	<0.61(2)	<0.60(2)

[a]See text for structures **1**–**4**.
[b]In kJ/mol, the total energy of conformer **1** being −451.541 394 au.
[c]In kJ/mol, the total energy of conformer **1** being −456.309 997 au.
[d]In units of debyes.
[e]Based on group moments (27).
[f]At 300 K, assuming a simple Boltzmann distribution based on the relative energies above.
[g]$K(CHO) = (P_3 + P_4)/(P_1 + P_2)$; $K(OCH_3) = (P_2 + P_3)/(P_1 + P_4)$.
[h]Obtained from the data in solution, as elaborated in the text.

Can. J. Chem. Downloaded from www.nrcresearchpress.com by 88.85.125.76 on 09/07/12
For personal use only.

Can. J. Chem. Downloaded from www.nrcresearchpress.com by 88.85.125.76 on 09/07/12
For personal use only.

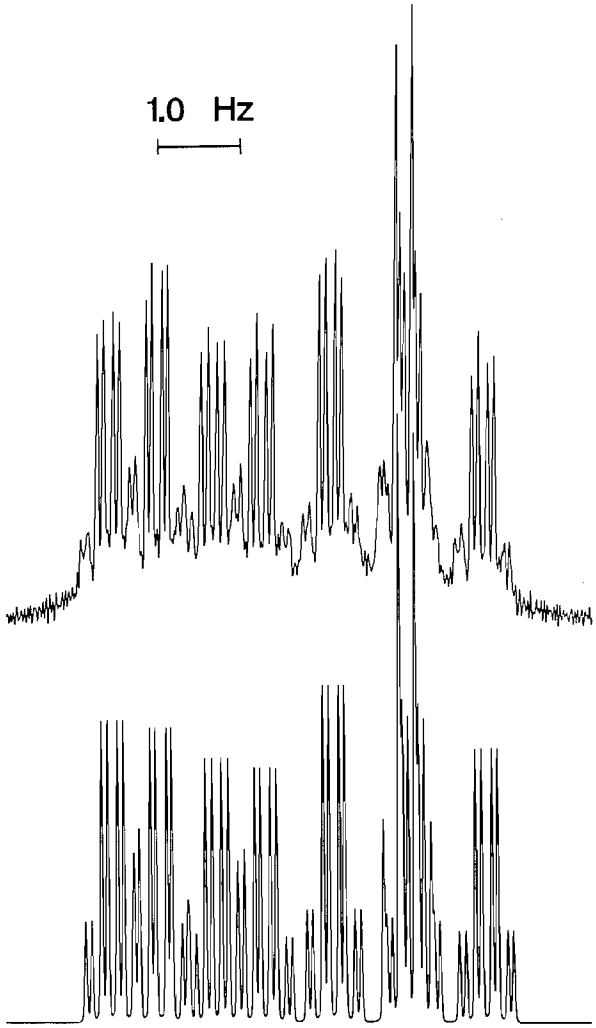

FIG. 1. The ^{1}H NMR spectrum of H-2 in 3-methoxybenzaldehyde, as a dilute solution in CS_2/C_6D_{12}/TMS (Table 1), is displayed. The linewidth at half-height is about 0.04 Hz and the small splittings (quartets of doublets) are very near 0.07 Hz in magnitude. The theoretical spectrum uses the coupling constants in Table 1, but the chemical shifts lie midway between those given in Table 1. Bloch–Siegert shifts, caused by the decoupling fields, render the true chemical shifts in the fully coupled spectrum somewhat uncertain; this uncertainty probably accounts for the quite small incongruence between the measured and theoretical spectra above.

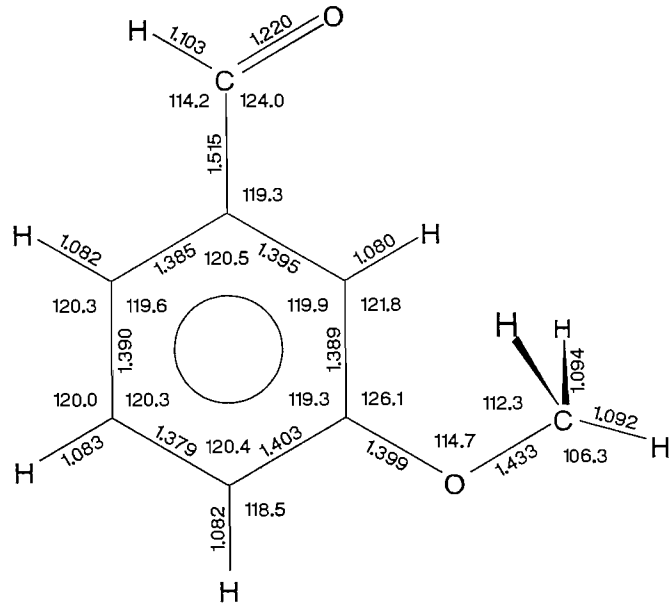

FIG. 2. The STO-3G MO structure of 3-methoxybenzaldehyde is shown for the planar conformer, **1**, which is most stable. Bond angles are in degrees and lengths in angstrom units. The bond lengths within the benzene moiety show some degree of alternation, of some interest to literature interpretations of the conformational bias of the substituents (see text), but appear to be controlled by the orientation of the methoxy group (see Figs. 3–5).

and acetone-d_6 solutions, respectively (16). The evidence is again (13–17) that ^5J(H,OCH$_3$) is vanishingly small if the methoxy group lies *trans* to the *ortho* C—H bond containing the coupled proton. If so, then ^5J(H,OCH$_3$) is -0.304 and -0.310 Hz for the CS_2/C_6D_{12} and acetone-d_6 solutions when the methoxy group lies *cis* to the *ortho* C—H bond. The sums of ^5J(H-2,OCH$_3$) and ^5J(H-4,OCH$_3$) in Table 1 are $-0.298(2)$ Hz for the CS_2 solution and $-0.301(2)$ Hz for the acetone-d_6 solution. It appears that the perturbation of this coupling interaction by the aldehyde substituent is rather small.

Based on this appearance, it follows that $K(OCH_3) = (P_2 + P_3)/(P_1 + P_4) = 0.103(1)/0.195(1) = 0.53(1)$ for the nonpolar solvent and is $0.121(1)/0.180(1) = 0.67(1)$ for the acetone-d_6 solution. For a 0.1M solution of 3-methoxyacetophenone in $CDCl_3$ (temperature not given) the nuclear Overhauser enhancements yield a $K(OCH_3)$ of 0.45 if they are corrected for the spin-lattice relaxation times and for the correlation times of the protons *ortho* to the methoxy group. Without these corrections, $K(OCH_3)$ would be 0.53. Again, the long-range coupling constants imply a lower conformational bias for the methoxy group than do the combined polarization and relaxation measurements. The spin coupling data also yield a solvent dependence of $K(OCH_3)$, the equilibrium constant being nearer unity for the polar solvent.

Of course, both types of measurements give the conformational bias, relative to the other substituent, of each substituent individually. They cannot give the populations of each of **1**–**4**. At this juncture, molecular orbital computations become of some value.

STO-3G MO computations

Previous experience with minimal basis set calculations on benzaldehyde (22, 23) shows that the torsional potential for the exocyclic C—C bond is better reproduced than with split-valence bases, even those containing polarization functions. For anisole, a 6-31G* basis yields a potential for torsion about the C_{sp^2}—O bond very similar to that obtained from the minimal basis, STO-3G (24, 25). It appears, therefore, that computations of the conformational properties of 3-methoxybenzaldehyde with the minimal basis set may well be sensible.

Table 2 displays the computed energies of the four planar conformers, as well as their dipole moments. The most stable conformer is computed to be **1**, in which the group dipole moments are arranged in such a way as to lead to a small dipole moment and lending some support to the electrostatic arguments (4) discussed above. Figure 2 displays the STO-3G structure of **1** and, judging by the C—C bond lengths within the ring, some apparent support exists for the importance (7) of valence-bond structure **5**, as also discussed in the introduction. However, the alternation in bond lengths is not striking and, in Figs. 3–5, showing the computed geometries of the other conformers, it appears that the bond lengths in the benzene nucleus are

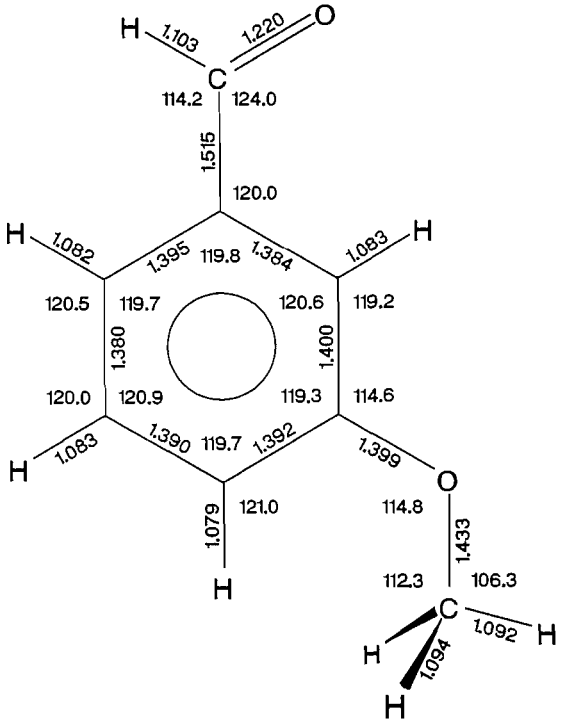

FIG. 3. Comparison of this STO-3G structure of 3-methoxybenzaldehyde with that in Fig. 2 implies that the orientation of the methoxy group determines the bond length variations within the ring.

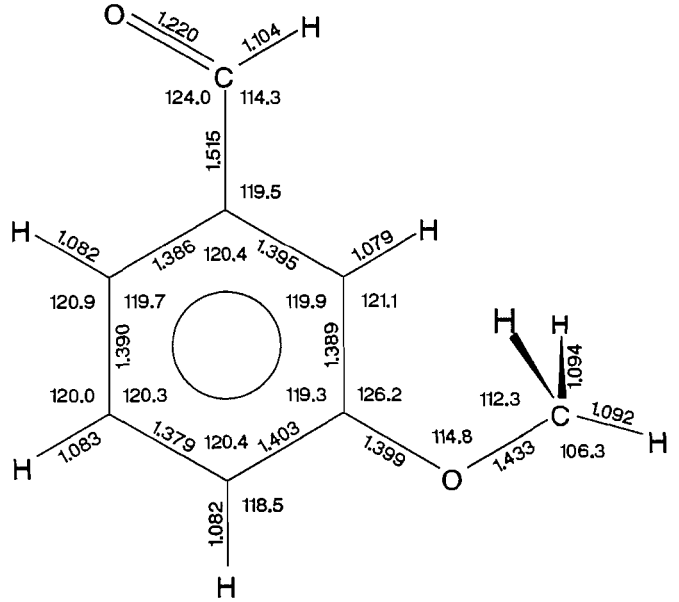

FIG. 4. Comparison of this STO-3G structure with that in Fig. 2 implies that the orientation of the aldehyde substituent does not change the computed bond lengths within the benzene moiety.

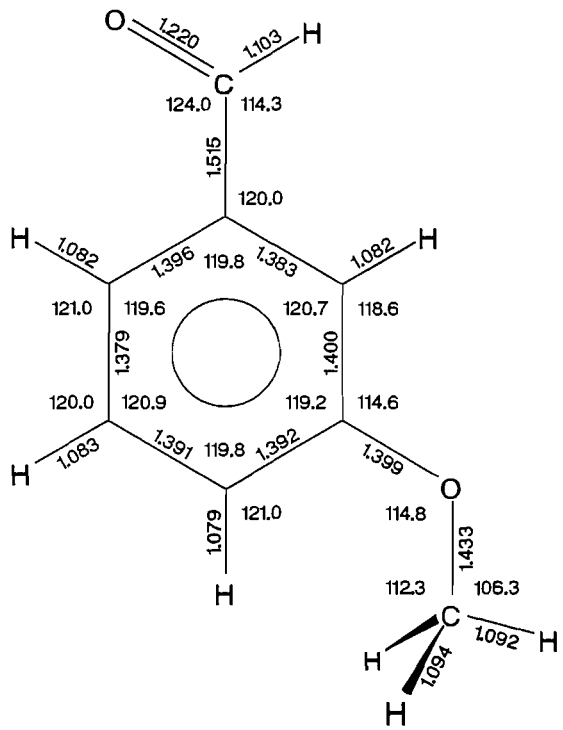

FIG. 5. Again, comparison of this STO-3G structure with that in Fig. 3 bears out the independence of the ring geometry on the aldehyde orientation.

determined by the conformation of the methoxy group and not by that of the aldehyde substituent. At this level of MO theory, therefore, a combined interpretation of the stability of **1** postulates that electrostatic interactions determine the preponderance of **1**. This, in turn, leads to the apparent preference of the methoxy group for that *ortho* ring C—C bond of larger double character and, thereby, also to the apparent preference of the C=O bond to lie *trans* to a similar C—C bond of the ring. The flaw in this description is that, while the STO-3G dipole moment of anisole is within 5% of the experimental value (26), the computed dipole moment of benzaldehyde, at 1.92 D (22), is much less than the experimental value of 2.96 D (27). Clearly, the charge redistribution[2] caused by the aldehydic substituent is incorrectly given by the minimal basis set (it does *not* follow that conformational energies and internal rotational barriers are badly estimated (28)).

Suppose that 1.0 D is added to each of the computed dipole moments of **1**–**4**; this seems reasonable in that, for example, the dipole moment of **1** becomes 1.73_5 D, as compared to 1.74 D assumed on the basis of group moments in a study (27) of the dipole moment of 3-methoxybenzaldehyde. Such an adjustment of the dipole moments in Table 2, combined with the STO-3G MO populations, yields a computed dipole moment of 2.98 D at 300 K. The experimental value, in benzene solution, is 2.94 D at 298 K. This agreement is coincidental, of course.

Thus (Table 2), the populations of **1**–**4** must alter in passing from CS_2 to acetone-d_6 solution, according to the long-range coupling constants. No doubt coincidentally, the values of K(CHO) and $K(OCH_3)$ obtained from the coupling constants in acetone-d_6 solution agree rather closely with those computed for the free molecule from the minimal basis set. In fact, the populations given by the latter at 300 K, combined with the coupling constants expected for each of the conformers (see above) yield ^5J(H,CHO) as 0.386 Hz (the measured value in acetone-d_6 is 0.382(4) Hz) and $^5J(\text{H-2,OCH}_3)$ and $^5J(\text{H-4,OCH}_3)$ as −0.174 and −0.126 Hz, respectively (the measured values are −0.180(1) and −0.121(1) Hz), reflecting the difference of 0.05 between the STO-3G and experimental $K(OCH_3)$ values in Table 2. These comparisons, taken with the clear solvent dependence of the populational distribution,

[2]The computed dipole moment depends on the way in which overlap populations are divided among the atoms in question, the standard Mulliken population analysis being used in this paper.

Can. J. Chem. Downloaded from www.nrcresearchpress.com by 88.85.125.76 on 09/07/12
For personal use only.

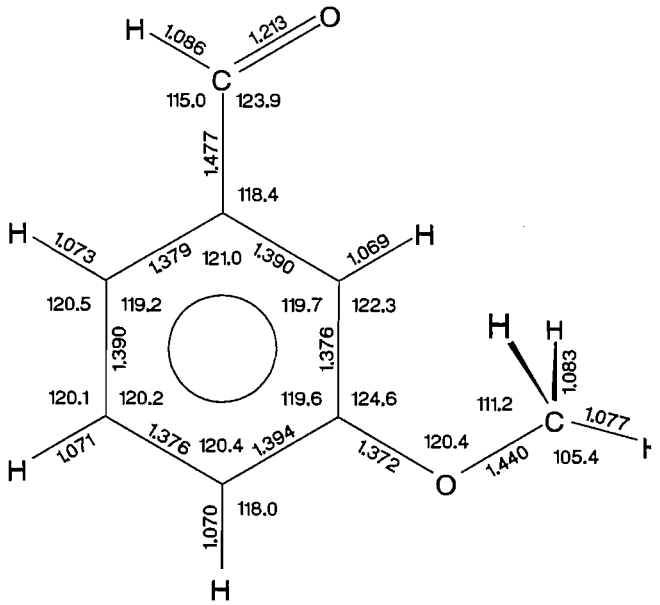

FIG. 6. The 4-21G structure of the most stable conformer of 3-methoxybenzaldehyde is displayed. The bond lengths are rather smaller than those from the minimal basis (Fig. 2). The carbonyl bond and the methoxy group are situated *trans* and *cis*, respectively, to the shorter of the two possible C—C bonds in the ring (see the text for a discussion).

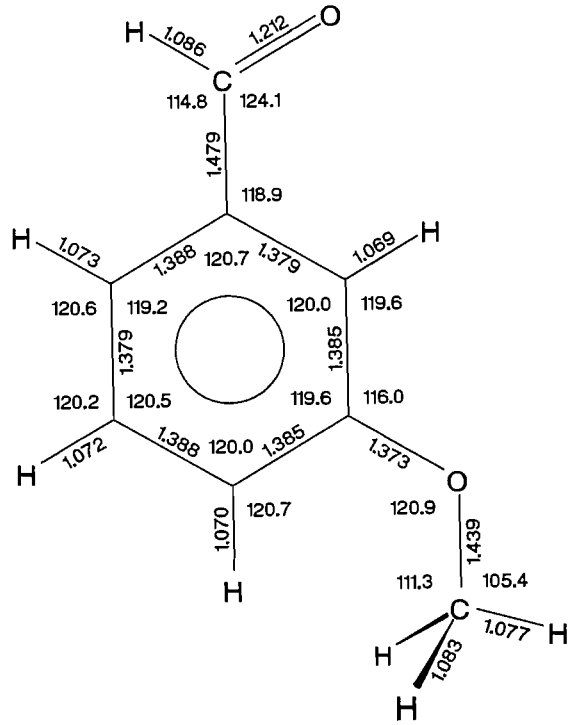

FIG. 7. The 4-21G structure of conformer **2**, the least stable, of 3-methoxybenzaldehyde is shown. The C=O bond is now *trans* to the longer of the two neighbouring C—C bonds and both C—C bonds next to the methoxy group have the same length. In addition, the group dipoles now repel one another (27). The three unfavorable interactions rationalize the instability of this conformer.

demonstrate that the STO-3G MO populations for the free molecule are probably incorrect.

4-21 G MO computations

From unpublished calculations in this laboratory, using various split-valence bases and including polarization functions, it appears that the 4-21G basis, with a dipole moment of 3.37D for benzaldehyde, comes closest to experiment. Accordingly, 4-21G MO computations were performed for the planar conformers, **1**–**4**. The relative energies and dipole moments of the four planar forms are found in Table 2. Comparison of the dipole moments with those from STO-3G computations (note discussion above) and from group moments suggests that the dipole moment of **1** may indeed be very near 1.7 D; the dipole moments of the other conformers are not reproduced by the 4-21G basis, judging by those deduced from group moments in Table 2.

Furthermore, the relative energies of the various conformers, as given by the two bases, agree that $P_1 >> P_3 + P_4 + P_2$ at 300 K (Table 2) but imply strikingly different values for the values of P_1–P_4 and, of course, for K(CHO) and $K(OCH_3)$. Consequently, a semiempirical approach, outlined in the next section, is adopted.

Prior to that, however, note that the 4-21G structures of **1**–**4**, as given in Figs. 6–9, tend to bear out the relative C—C bond lengths in the ring obtained with the minimal basis set. Again, the relative bond lengths appear to be controlled by the orientation of the methoxy group. The methoxy group lies *cis* to the shorter C—C bond (in **2** the two C—C bonds are equal in length), but the C=O bond does not always lie *trans* to the shorter of the two C—C bonds in the ring. In fact, the two structures in which the C=O bond is *trans* to the longer of the two C—C bonds, **2** and **4**, also have the highest computed energies. Furthermore, **2** is of higher energy than **4** and has equal C—C bonds next to the methoxy substituent. In this sense, the relative stabilities of **2**–**4** can be understood in terms of the valence-bond approach (5, 6), given that **1** is the most stable because of electrostatic attraction between the group dipoles (4).

Extrapolation from solution data

An estimate of K(CHO) and $K(OCH_3)$ can be had from a plot of ln K versus $(\epsilon - 1)/(2\epsilon + 1)$ and extrapolation to a value of unity for the dielectric constant, ϵ, of the solution. This approach is based on the reaction field model (30), noting (31, 32) that this model yields free energy differences between conformers (examine eq. 13.18 and p. 562 of ref. 30). Various corrections ignored in such a plot, and the uncertainties in the actual dielectric constants of the CS_2 and acetone-d_6 solutions in Table 1, at first imply that large errors could be involved even within the assumptions of the model. Yet, because of the logarithm and because of the relatively large difference in the dielectric functions for the two solutions, the error in extrapolation is rather small.

The extrapolation yields K(CHO) and $K(OCH_3)$ as 0.46_5 and 0.39(1) in the vapor at 300 K, very nearly midway between the two theoretical estimates (Table 2). From the expressions for K(CHO) and $K(OCH_3)$, together with the normalization condition for the four fractional populations, sums and differences of populations can be had and are presented in Table 2. It follows that the fractional population of **1**, P_1, is greater than 0.40(2) and less than 0.68(2) in the vapor phase. It also follows that $P_4 - P_2 = 0.03_5$. Suppose that $P_1 = 0.54(4)$, the mean of the limiting values; then $P_2 = 0.14(4)$, $P_3 = 0.14(4)$, and $P_4 = 0.18(4)$. Qualitatively, but by no means quantitatively, one has agreement with the theoretical estimates of the *relative* proportions of the conformers in the vapor.

Can. J. Chem. Downloaded from www.nrcresearchpress.com by 88.85.125.76 on 09/07/12
For personal use only.

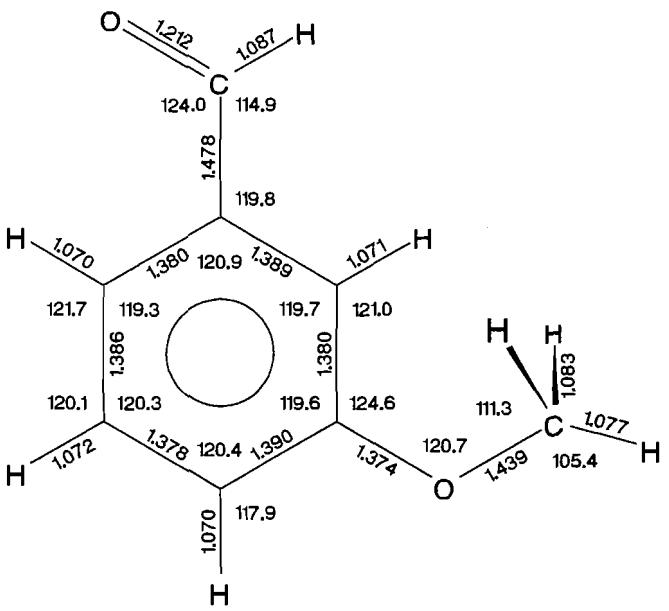

FIG. 8. The 4-21G structure of conformer **4** is displayed. The C=O bond is again *trans* to the longer of the ring C—C bonds but the methoxy group lies *cis* to the shorter of the two C—C bonds. Qualitatively, as discussed in the text, it is therefore sensible that this conformer is somewhat more stable than **2** (Fig. 7).

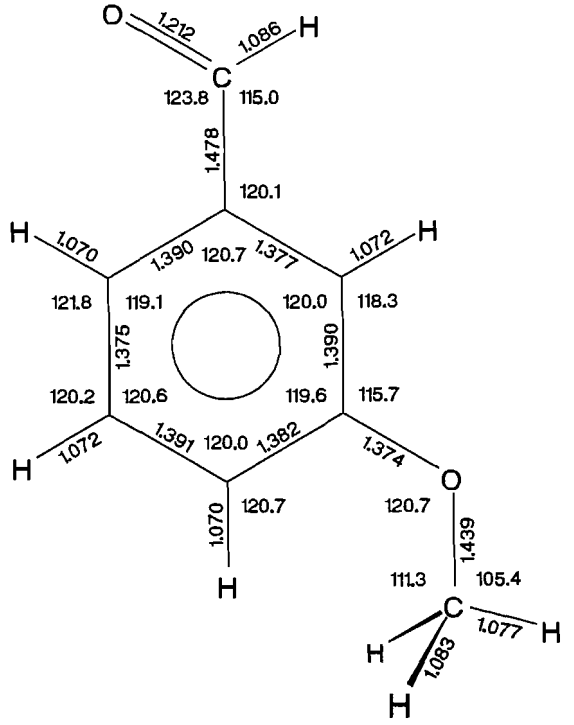

FIG. 9. The 4-21G structure of conformer **3** has the C=O bond *trans* to the shorter C—C in the ring and the methoxy group *cis* to such a bond. Presumably this conformer is of higher energy than **1** because in the latter the group dipoles are roughly antiparallel.

In the solutions, $P_4 - P_2$ remains at 0.04(1) and P_1 apparently decreases, as is sensible for the conformer with the lowest dipole moment. In the CS_2 solvent mixture, take P_1 as 0.44(4), again the means of its limits. Then P_2 is 0.18(4), P_3 is 0.17(4), and P_4 0.21(4). In the acetone-d_6 solution, the mean of the limits for P_1 is 0.37(4).

Of course, if a stereospecific coupling constant involving nuclei within the two substituents were to exist, then the individual populations could be derived. The existence of such a coupling constant, for instance, that over six bonds between the aldehydic proton and the ^{13}C nucleus in the methoxy group, is rather unlikely. Thus, ^5J(H,CHO) in planar benzaldehyde is apparently a pure σ electron coupling interaction because in 3,5-dimethylbenzaldehyde (21) there is no evidence for a finite coupling constant $^6J(H,CH_3)$, involving the aldehydic and methyl protons. It happens (33) that CNDO/2 FPT (34) computations of ^5J(H,CHO) reproduce its magnitude and stereospecificity. Therefore such computations (35) were done for **1**–**4** employing the 4-21 G geometries. $^6J(CHO,OCH_3)$ was computed as less than 0.01 Hz for **1**, **3**, and **4** and as only 0.06 Hz for **2**, implying that this parameter cannot be used as a measure of the population of one of these conformers. $^5J(CHO,OCH_3)$ was calculated as 0.11 Hz for **2** and **3** and as <0.01 Hz for **1** and **4**, again suggesting that an individual population is unavailable from this coupling constant.

Internal rotational barriers

The STO-3G energies were also computed for conformations in which one substituent lay in-plane while the other rotated about the exocyclic bond in steps of 15°. These results are not presented here in detail, but are available from the authors.

Rotation of the aldehyde group by 90° for conformer **1** raises the energy by 24.64 kJ/mol, whereas it costs 23.24 kJ/mol to do so for **4**. These numbers are very similar to the 24.28 kJ/mol computed with the same basis set for benzaldehyde (23) and that measured as 22.7 ± 1.4 kJ/mol from vibronic fluorescence spectra (29). A substantial substituent effect on the C_{sp^2}—C_{sp^2} barrier is not apparent.

Again, rotation about the C_{sp^2}—O bond by 90° in **1** is calculated to raise the energy by 8.25 kJ/mol but, while the aldehydic rotational potential is predominantly twofold, both for 3-methoxybenzaldehyde and benzaldehyde, that for the methoxy group is now rather complex. In fact, for rotation in conformer **1**, the 13 energies in ϕ, the angle of twist about the C_{sp^2}—O bond, are fit by eq. [1], the standard error in

$$[1]\quad V(\phi)/\text{kJ mol}^{-1} = 1.98\sin^2(\phi/2) + 7.43\sin^2\phi - 0.06\sin^2(3\phi/2) + 2.48\sin^2 2\phi - 0.15\sin^2 3\phi - 0.29\sin^2 4\phi$$

the coefficients being 0.10 kJ/mol. Thus, there are significant twofold, in $\sin^2\phi$, and fourfold, in $\sin^2 2\phi$, components. A very similar equation holds for rotation in ϕ for **4**. For anisole, the minimal basis set gives the twofold and fourfold components as 5.6(4) and 2.1(4) kJ/mol, respectively (24). It appears that the aldehyde substituent has increased the twofold component by 1.8(5) kJ/mol in 3-methoxybenzaldehyde, whereas in 4-methoxybenzaldehyde this increase is calculated as 1.7(9) kJ/mol (24). The usual explanation for the latter molecule is that the aldehyde group accepts π electron density from the methoxy group, thereby increasing the double-bond character of the C_{sp^2}—O bond and hence the twofold component of the ϕ barrier. The barrier in the gas phase of anisole itself has not been determined.

Acknowledgments

We thank the Natural Sciences and Engineering Research Council of Canada for financial support.

Can. J. Chem. Downloaded from www.nrcresearchpress.com by 88.85.125.76 on 09/07/12
For personal use only.

1. W. E. STEINMETZ. J. Am. Chem. Soc. **96**, 685 (1974).
2. F. A. L. ANET and M. AHMAD. J. Am. Chem. Soc. **86**, 119 (1964).
3. T. SCHAEFER and R. SEBASTIAN. Can. J. Chem. **67**, 1148 (1989).
4. M. A. NATIELLO, R. H. CONTRERAS, J. C. FACELLI, and D. G. DE KOWALEWSKI. J. Phys. Chem. **87**, 2603 (1983).
5. L. I. KRUSE and J. K. CHA. J. Chem. Soc. Chem. Commun. 1329 (1982).
6. L. I. KRUSE, C. W. DEBROSSE, and C. H. KRUSE. J. Am. Chem. Soc. **107**, 5435 (1985).
7. L. I. KRUSE and J. K. CHA. Tetrahedron Lett. **24**, 2367 (1983).
8. J. KEELER, D. NEUHAUS, and M. P. WILLIAMSON. J. Magn. Reson. **73**, 45 (1987).
9. G. J. KARABATSOS and F. M. VANE. J. Am. Chem. Soc. **85**, 3887 (1963).
10. R. WASYLISHEN and T. SCHAEFER. Can. J. Chem. **49**, 3216 (1971).
11. D. G. DEKOWALEWSKI and S. CASTELLANO. Mol. Phys. **16**, 567 (1969).
12. T. SCHAEFER, G. H. PENNER, K. J. DAVIE, and R. SEBASTIAN. Can. J. Chem. **63**, 777 (1985).
13. H. A. GAUER, J. VRIEND, and W. G. B. HUYMANS. Tetrahedron Lett. 1999 (1969).
14. T. SCHAEFER and R. LAATIKAINEN. Can. J. Chem. **61**, 224 (1983).
15. T. SCHAEFER and T. A. WILDMAN. Can. J. Chem. **57**, 450 (1979).
16. T. SCHAEFER and R. SEBASTIAN. J. Magn. Reson. **73**, 541 (1987).
17. T. SCHAEFER, S. R. SALMAN, T. A. WILDMAN, and G. H. PENNER. Can. J. Chem. **63**, 782 (1985).
18. T. SCHAEFER, R. SEBASTIAN, and G. H. PENNER. Can. J. Chem. **63**, 2597 (1985).
19. M. J. FRISCH, J. S. BINKLEY, H. B. SCHLEGEL, K. RAGHAVACHARI, C. F. MELIUS, R. L. MARTIN, J. J. P. STEWART, F. W. BOBROWICZ, C. F. ROHLFING, L. R. KAHN, D. J. DEFREES, R. SEEGER, R. A. WHITESIDE, D. J. FOX, E. M. FLUDER, and J. A. POPLE. Carnegie–Mellon Quantum Publishing Unit, Pittsburgh, PA. 1984.
20. J. S. MARTIN, A. R. QUIRT, and K. E. WORVILL. The NMR program library, Daresbury Laboratory, Daresbury, U.K.
21. T. SCHAEFER and C. S. TAKEUCHI. Can. J. Chem. **67**, 827 (1989).
22. T. SCHAEFER, T. A. WILDMAN, and R. SEBASTIAN. J. Mol. Struct. (Theochem), **89**, 93 (1982).
23. G. H. PENNER, P. GEORGE, and C. W. BOCK. J. Mol. Struct. (Theochem), **152**, 201 (1987).
24. T. SCHAEFER and G. H. PENNER. J. Mol. Struct. (Theochem), **152**, 179 (1987).
25. T. SCHAEFER and R. SEBASTIAN. Can. J. Chem. **67**, 2965 (1989).
26. T. A. WILDMAN. Ph.D. Thesis, University of Manitoba, Winnipeg, Manitoba. 1982.
27. H. LUMBROSO and C. G. ANDRIEU. Bull. Soc. Chim. Fr. 1575 (1973).
28. T. SCHAEFER, G. H. PENNER, R. SEBASTIAN, and C. S. TAKEUCHI. Can. J. Chem. **64**, 158 (1986).
29. L. A. GLEBOVA, Y. A. PENTIN, and V. I. TYULIN. Vestn. Mosk. Univ., Khim., Ser. 2, 21 (1980).
30. R. J. ABRAHAM and E. BRETSCHNEIDER. *In* Internal rotation in molecules. *Edited by* W. J. Orville-Thomas. J. Wiley and Sons, New York. 1974. Chap. 13.
31. J. J. MOURA RAMOS, L. DUMONT, M. L. STIEN, and J. REISSE. J. Am. Chem. Soc. **102**, 4150 (1980).
32. A. Y. MEYER. J. Mol. Struct. **195**, 147 (1989).
33. R. WASYLISHEN and T. SCHAEFER. Can. J. Chem. **49**, 3216 (1971).
34. J. A. POPLE, J. W. MCIVER, and N. S. OSTLUND. J. Chem. Phys. **49**, 2965 (1968).
35. P. A. DOBOSH. Quantum Chemistry Program Exchange, **11**, 142 (1979).

Can. J. Chem. Downloaded from www.nrcresearchpress.com by 88.85.125.76 on 09/07/12
For personal use only.

The acetolysis of reduced *Acacia saligna* (syn. *cyanophylla*) gum exudate

ALEXANDER J. CHARLSON
School of Chemistry, Macquarie University, North Ryde, N.S.W., 2109, Australia
AND
ALISTAIR M. STEPHEN AND NEIL RAVENSCROFT
Department of Chemistry, University of Cape Town, Rondebosch 7700, Republic of South Africa

Received November 6, 1989

This paper is dedicated to Professor Arthur S. Perlin on the occasion of his 67th birthday

ALEXANDER J. CHARLSON, ALISTAIR M. STEPHEN, and NEIL RAVENSCROFT. Can. J. Chem. **68**, 1004 (1990).

Carboxyl groups in *Acacia saligna* (syn. *cyanophylla*) gum were reduced by reacting the gum propionate with diborane. Acetolysis of the reduced gum afforded a mixture of oligosaccharide acetates. After de-*O*-acetylation, 3-*O*-(α-D-galactopyranosyl)-L-arabinose, 3-*O*-(β-D-galactopyranosyl)-D-galactose, and 4-*O*-(α-L-rhamnopyranosyl)-D-glucose were isolated from the mixture.

Key words: acetolysis, *Acacia* gums.

ALEXANDER J. CHARLSON, ALISTAIR M. STEPHEN et NEIL RAVENSCROFT. Can. J. Chem. **68**, 1004 (1990).

On a réduit les groupements carboxyles de gommes de l'*Acacia saligna* (syn. *cyanophylla*) en soumettant le propionate de la gomme à l'action du diborane. Une acétolyse de la gomme réduite fournit un mélange d'acétates d'oligosaccharides. Après une de-*O*-acétylation du mélange, on a pu isoler du 3-*O*-(α-D-galactopyranosyl)-L-arabinose, du 3-*O*-(β-D-galactopyranosyl)-D-galactose et 4-*O*-(α-L-rhamnopyranosyl)-D-glucose.

Mots clés : acétolyse, gommes de l'*Acacia*.

[Traduit par la revue]

Introduction

We reported (1) that *A. saligna* (syn. *cyanophylla*) gum yielded D-galactose, L-arabinose, L-rhamnose, and D-glucuronic acid on acid hydrolysis. It was known that these monosaccharides were also produced on acid hydrolysis of *A. senegal* gum (gum arabic) (2), *A. mollissima* (now *mearnsii*) gum (3), and *A. pycnantha* gum (4). The proportions of the monomers were different in each of the four polysaccharides, as shown subsequently for *Acacia* gums in general, notably by Anderson and his co-workers (5, 6). Glucuronic acid often occurs as its 4-methyl ether (7). Since the molar ratio of L-rhamnose to D-glucuronic acid was nearly unity for *A. saligna* gum, for *A. mollissima* (now *mearnsii*) gum, and for gum arabic, we postulated (1) that L-rhamnose may be glycosidically linked to D-glucuronic acid in the three gums. Smith and Montgomery had also suggested (8) that L-rhamnose might be glycosidically linked to D-glucuronic acid in gum arabic. Aspinall *et al.* (9, 10) isolated 4-*O*-(α-L-rhamnopyramosyl)-D-glucose from the de-*O*-acetylated mixture produced on acetolysis of reduced gum arabic. This result provided definite evidence that some of the L-rhamnose residues are glycosidically linked to D-glucuronic acid in gum arabic. On the basis of more recent investigations of gum arabic structure employing base degradation of methylated gums, Aspinall and Rosell reported (11) that all the L-rhamnose residues are linked to D-glucuronic acid, and such linkages have been demonstrated in a similar manner for other *Acacia* gums (12).

In this investigation the reduced *A. saligna* gum was prepared by reacting the gum propionate with diborane, and acetolysis was performed on the *O*-acetylated reduced gum. The product from the acetolysis was de-*O*-acetylated and the oligosaccharide mixture produced was fractionated using cellulose column chromatography. Crystalline samples of 3-*O*-(β-D-galactopyranosyl)-D-galactose and 3-*O*-(α-D-galactopyranosyl)-L-arabinose were obtained, and shown to be identical with authentic material. Smith reported (2) that 3-*O*-(α-D-galactopyranosyl)-L-arabinose was present in the autohydrolysis mixture from gum arabic, and we found (1) that the same disaccharide was cleaved in a similar manner from *A. saligna* gum; the disaccharide (obtained from *Watsonia* corm-sacs, ref. 13) has been fully characterized by nmr spectroscopy using COSY, HETCOR, and APT to assign all ^1H and ^{13}C signals for the α and β forms in D_2O solution (14). Hirst and Perlin (4) obtained 3-*O*-(β-D-galactopyranosyl)-D-galactose using graded acid hydrolysis of *A. pycnantha* gum.

In addition to the two crystalline disaccharides, a syrupy disaccharide consisting of rhamnose and glucose was isolated. The results from lead tetraacetate and periodate oxidations suggested that rhamnose was joined to glucose by a 1→4 linkage. Aspinall *et al.* (9, 10) described similar experiments. Further evidence for the 1→4 linkage was obtained by examination of the methanolysis products from the methylated disaccharide using gas–liquid chromatography. The specific rotation of the disaccharide, $[\alpha]_D$ −5°, is close to the value, $[\alpha]_D$ −6°, recorded by Aspinall *et al.* (9, 10). Recently, Fügedi (16) reported $[\alpha]_D$ −10.5° for synthetic 4-*O*-(α-L-rhamnopyranosyl)-D-glucose. The nmr characteristics of this disaccharide produced from *A. saligna* gum have been described (17), a combination of the ^1H spectrum (at 200 MHz), the COSY experiment, the ^{13}C spectrum (at 50.3 MHz), HETCOR, and long-range HETCOR leading to a complete assignment of the proton and carbon signals and a listing of glycosylation shifts relative to α-Glc-OH, β-Glc-OH, and α-RhapOMe. The solvent was D_2O. Anomeric signals were assigned for α-Rhap ($\delta_{H\text{-}1}$ 4.85 ppm; δ_{C-1} 101.46), for α-Glc-OH (δ_{H-1} 5.21, J 3.5 Hz; δ_{C-1} 92.42), and for β-Glcp-OH (δ_{H-1} 4.62, J 8 Hz; δ_{C-1} 96.37). The H-5 (δ 4.01) and H-6 (δ 1.28) resonances established the α-Rha configuration in the disaccharide, supporting a deduction made on the basis of $[\alpha]_D$, found and calculated from Hudson's rules (18). The site of glucosylation at O-4 of Glc was deduced from positive glycosylation shifts (ppm) for H-4 (+0.25α, +0.24β) and C-4 (+7.4α, +7.2β) and the negative shifts for C-3 (−1.8α, −1.0β) and C-5 (−1.2α, −1.8β). The ^{13}C data were in conformity with the absolute configurations of Rha and Glc as L and D respectively (19).

Printed in Canada / Imprimé au Canada

Can. J. Chem. Downloaded from www.nrcresearchpress.com by 88.85.125.76 on 09/07/12
For personal use only.

Can. J. Chem. Downloaded from www.nrcresearchpress.com by 88.85.125.76 on 09/07/12
For personal use only.

Long-range HETCOR (setting of $^3J_{C,H} = 6$ Hz) established connectivities as follows: (i) H-1 and C-5 of α-Glc; (ii) H-5 and C-3 of α-Rhap; (iii) H-1 with C-3 and C-5 of α-Rhap; and, importantly, (iv) H-1 of α-Rha with C-4 of Glc (across the glycosidic bond).

The isolation of 4-*O*-(α-L-rhamnopyranosyl)-D-glucose provides definite evidence that some of the rhamnose residues are glycosidically linked to glucuronic acid in *A. saligna* gum. Our postulate that rhamnose may be glycosidically linked to glucuronic acid in three different *Acacia* gums (1) has been shown in this way to be correct for gum arabic and *A. saligna* gum. Lindberg and co-workers reported (20) that rhamnose is glycosidically linked to glucuronic acid in a bacterial polysaccharide. Since then it has been demonstrated that rhamnose is linked to glucuronic acid in several bacterial polysaccharides (21–25). In all these cases the linkages are 1→4. The fact that this identical structural feature occurs in a number of different bacterial polysaccharides and also in *Acacia* gums is of interest. It is possible that the biosynthesis of *Acacia* gums involves a step where rhamnose is transferred from bacterial nucleotide diphosphate rhamnose to the plant polysaccharide utilizing a bacterial glycosyl transferase.

Experimental

Unless otherwise stated, concentration of solutions was carried out at 40°C/20 Torr (1 Torr = 133.3 Pa), melting points are uncorrected, and specific rotations were measured in aqueous solution. Paper chromatography was performed on Whatman No. 1 filter papers with the following solvent systems (V/V): (A) ethyl acetate – acetic acid – formic acid – water (18:3:1:4); (B) ethyl acetate – pyridine–water (10:4:3); (C) 2-butanone – acetic acid – water, saturated with boric acid (9:1:1). The nmr spectra were determined on a Varian VXR-200 instrument, the sample being D-exchanged thrice before analysis.

Carboxyl reduced A. saligna *gum acid*

Crude *A. saligna* gum was precipitated once from slightly acid solution with ethanol. *Acacia saligna* gum acid was then precipitated from aqueous solution with ethanol. The gum acid (11.5 g), equivalent mass 750 and $[\alpha]_D$ −23° (*c* 1.0), was acetylated with acetic anhydride and pyridine in formamide according to the method of Carson and Maclay (26) to yield 15.6 g of the acetate $[\alpha]_D$ −41° (*c* 1.0, chloroform). An attempt was made to reduce the gum acetate (15 g) in 1,2-dimethoxyethane (300 mL) with boron trifluoride – ether complex (6 g) and sodium borohydride (7.1 g) by the *in situ* method (27) as described by Aspinall *et al.* (9, 10). The yield of the partially reduced product was 9.8 g: a sample of this material in water was deionized with Amberlite IR-120 (H^+) and Amberlite IR-4B (OH^-), then deionized again with IR-120 (H^+) and freeze-dried. An acid equivalent mass of 1570, obtained on the freeze-dried product, corresponds to 52% reduction of carboxyl groups. The gum acid (31 g) was reacted with propionic anhydride and pyridine (26) to yield 43 g of the propionate $[\alpha]_D$ −43° (*c* 2, chloroform). The gum propionate (21 g) was reduced with diborane using the *in situ* method to yield 11.5 g of carboxyl-reduced *A. saligna* gum $[\alpha]_D$ −13° (*c* 1.1) A sample was deionized and freeze-dried as described above: the product had an acid equivalent mass of 4500 corresponding to 83% reduction. In a second preparation the propionate (21 g) was reduced with diborane to yield reduced *A. saligna* gum (11.4 g) $[\alpha]_D$ −20° (*c* 0.96); acid equivalent mass 4000 or 81% reduction. Galactose, arabinose, rhamnose, and glucose were detected on a paper chromatogram run in solvent (B) after acid hydrolysis of the reduced gum. The spot on paper corresponding to the aldobiouronic acid was very faint.

Acetolysis of acetylated reduced A. saligna *gum*

The reduced gum (12 g) was converted (26) into the acetate (16.2 g) $[\alpha]_D$ −19° (*c* 1.3, chloroform). The acetate (14 g) was added with stirring to a solution of concentrated sulphuric acid (4.5 mL) in acetic anhydride (150 mL) at 0°C. Stirring was continued 0.5 h at 0°C and then 4 h at ambient temperature. After standing at room temperature overnight, the reaction mixture was decomposed with ice water and the acetates produced were extracted with chloroform (5 × 100 mL). The chloroform extract was washed successively with water, sodium hydrogen carbonate solution, and water, and then dried over anhydrous sodium sulphate. Removal of the chloroform in vacuum left a viscous syrup (17.5 g); this was de-*O*-acetylated at 3°C in 0.2 M sodium methoxide (100 mL). After acidifying with a few drops of acetic acid and distilling off the methanol, the residue was dissolved in water, deionized, and concentrated to a syrup (8.1 g). The syrup was fractionated on a cellulose column (40 × 6.4 cm) by eluting with half-saturated aqueous butanol, then three-quarter-saturated aqueous butanol, and finally acetone. Earlier fractions contained monosaccharides (rhamnose, arabinose, galactose, and glucose) and some material with chromatographic mobility faster than rhamnose (possibly saccharides that had not been completely deacetylated). Later five oligosaccharide fractions were collected. Fraction 2 (a mixture of fractions 1 and 3) and fraction 4 (a mixture of fractions 3 and 5) were not investigated further.

Fraction 1: 4-O-*(α-L-rhamnopyranosyl)-D-glucose*

The syrup (0.73 g) had $[\alpha]_D$ −5° (*c* 2.0): chromatographic mobilities were R_{gal} 0.82 in solvent (A) and R_{gal} 1.0 in solvent (B), and the material afforded glucose and rhamnose on acid hydrolysis (paper chromatographic identification using solvent (B)). Lead tetraacetate oxidation of the syrup (12 mg) was carried out for 2.5 h in 98% acetic acid at room temperature (15). Excess lead tetraacetate was destroyed and lead (II) ions were precipitated by addition of oxalic acid in acetic acid. Hydrolysis of the oxidation product afforded rhamnose and erythrose (paper chromatographic identification using solvent (C)). Periodate oxidation and formation of a formaldehyde dimedone derivative was performed according to Reeves (28). The syrup (15 mg) yielded the dimedone derivative (11 mg), mp 172–174°C; after recrystallization from aqueous methanol it had mp 187–188°C undepressed on admixture with an authentic sample. Methylation of the syrup (145 mg) was conducted in dimethyl sulphoxide (10 mL) with potassium tertiary butoxide (370 mg) and methyl iodide (1 mL) by the method of Hakomori (29). After methanolysis of this material, peaks having the retention times of the methyl glycosides of 2,3,4-tri-*O*-methylrhamnose and 2,3,6-tri-*O*-methylglucose were detected using gas–liquid chromatography.

Fraction 3: 3-O-*(α-D-galactopyranosyl)-L-arabinose*

The syrup (0.42 g) showed mobilities on paper identical to an authentic sample of 3-*O*-(α-D-galactopyranosyl)-L-arabinose using solvent (A) and solvent (B), and on acid hydrolysis afforded galactose and arabinose (paper chromatographic identification using solvent (B)). A solution of the syrup in methanol deposited crystals, $[\alpha]_D$ +197° (*c* 1.0), and mp and mixture mp 156°C after seeding with the authentic disaccharide.

Fraction 5: 3-O-*(β-D-galactopyranosyl)-D-galactose*

A solution of the syrup (0.24 g) in methanol slowly deposited crystals, $[\alpha]_D$ +60° (*c* 0.4), which on hydrolysis gave only galactose (identified on paper using solvent (B)). The crystals were shown to be 3-*O*-(β-D-galactopyranosyl)-D-galactose, by comparison with the authentic disaccharide using paper chromatography, by mp and mixture mp 161°C, and by production of galactose and lyxose (paper chromatography using solvent (B)) on hydrolysis of the lead tetraacetate oxidation product (15).

Acknowledgements

We are indebted to the C.S.I.R. (South Africa) and the Council of the University of Cape Town for financial support, and we thank Assoc. Prof. G. E. Jackson for helpful discussions on the nmr data.

1. A. J. CHARLSON, J. R. NUNN, and A. M. STEPHEN. J. Chem. Soc. 269 (1955).

2. F. SMITH. J. Chem. Soc. 744 (1939).
3. A. M. STEPHEN. J. Chem. Soc. 646 (1951).
4. E. L. HIRST and A. S. PERLIN. J. Chem. Soc. 2622 (1954).
5. D. M. W. ANDERSON. Kew Bull. **32**, 529 (1978).
6. A. M. STEPHEN. *In* The polysaccharides. Vol. 2. *Edited by* G. O. Aspinall. Academic Press, New York, NY. 1983. pp. 97–193.
7. D. M. W. ANDERSON and G. M. CREE. Carbohydr. Res. **6**, 214 (1968).
8. F. SMITH and R. MONTGOMERY. Chemistry of plant gums and mucilages. Van Nostrand – Reinhold, Princeton, NJ. 1959.
9. G. O. ASPINALL, A. J. CHARLSON, E. L. HIRST, and R. YOUNG. J. Chem. Soc. 1696 (1963).
10. G. O. ASPINALL and R. YOUNG. J. Chem. Soc. 3003 (1965).
11. G. O. ASPINALL and K.-G. ROSELL. Can. J. Chem. **56**, 680 (1978).
12. S. C. CHURMS, E. H. MERRIFIELD, and A. M. STEPHEN. S. Afr. J. Chem. **33**, 39 (1980).
13. D. H. SHAW, A. M. STEPHEN, and (in part) A. O. FULLER. J. Chem Soc. 2287 (1965).
14. H. I. JOÃO, G. E. JACKSON, N. RAVENSCROFT, and A. M. STEPHEN. Carbohydr. Res. **176**, 300 (1988).
15. A. J. CHARLSON and A. S. PERLIN. Can. J. Chem. **34**, 1200 (1956).
16. P. FÜGEDI. J. Carbohydr. Chem. **6**, 377 (1987).
17. N. RAVENSCROFT. PhD Thesis, University of Cape Town (1988).
18. C. S. HUDSON. J. Am. Chem. Soc. **31**, 66 (1909).
19. N. K. KOCHETKOV, O. S. CHIZHOV, and A. S. SHASHKOV. Carbohydr. Res. **133**, 173 (1984).
20. H. BJÖRNDAL, B. LINDBERG, J. LÖNNGREN, W. NIMMICH, and K. -G. ROSELL. Carbohydr. Res. **27**, 373 (1973).
21. M. CURVALL, B. LINDBERG, J. LÖNNGREN, and W. NIMMICH. Carbohydr. Res. **42**, 73 (1975).
22. G. G. S. DUTTON and K. L. MACKIE. Carbohydr. Res. **62**, 321 (1978).
23. G. G. S. DUTTON and T. E. FOLKMAN. Carbohydr. Res **80**, 147 (1980).
24. P.-E. JANSSON, B. LINDBERG, H. LINDQUIST, and D. J. CARLO. Carbohydr. Res. **118**, 157 (1983).
25. G. G. S. DUTTON and D. N. KARUNARATNE. Carbohydr. Res. **119**, 157 (1983).
26. J. F. CARSON and W. D. MACLAY. J. Am. Chem. Soc. **68**, 1015 (1946).
27. F. SMITH and A. M. STEPHEN. Tetrahedron Lett. No. 7, 17 (1960).
28. R. E. REEVES. J. Am. Chem. Soc. **63**, 1476 (1941).
29. S. HAKOMORI. J. Biochem. (Toyko), **55**, 205 (1964).

Can. J. Chem. Downloaded from www.nrcresearchpress.com by 88.85.125.76 on 09/07/12
For personal use only.

The structures and reactions of stannylene acetals from carbohydrate-derived *trans*-diols. Part I. In the absence of added nucleophiles

T. Bruce Grindley and Rasiah Thangarasa
Department of Chemistry, Dalhousie University, Halifax, N.S., Canada B3H 4J3

Received September 12, 1989

This paper is dedicated to Professor Arthur S. Perlin on the occasion of his 67th birthday

T. Bruce Grindley and Rasiah Thangarasa. Can. J. Chem. **68**, 1007 (1990).

Di-*n*-butylstannylene acetals of benzyl 4,6-*O*-benzylidene-α- and -β-D-glucopyranoside and galactopyranoside have been prepared and studied in solution by ^{1}H, ^{13}C, and ^{119}Sn nuclear magnetic resonance spectroscopy. The species present in solution have been identified from the ^{119}Sn nmr spectral data, by comparison of the ^{13}C nmr chemical shifts of the stannylene acetals and their precursor diols and also by analysis of the products of reactions performed without added nucleophiles. The orientations of the two substituents on the carbons in the pyranose ring attached to the carbons in the stannylene ring determine the structures adopted by the stannylene acetal in solution. If one substituent is axial and the other equatorial, the stannylene acetal exists as a single symmetrical dimer in which the two oxygen atoms in the two 1,3,2-dioxastannolane rings adjacent to the axial substituents are dicoordinate. A stannylene acetal with two adjacent equatorial substituents exists as a non-interconverting mixture of dimers; one with two adjacent axial substituents is present as a rapidly interconverting mixture of dimers, trimers, and tetramers. Benzoylation and benzylation of the latter two types of stannylene acetals have been performed and have been shown to be only slightly regioselective in contrast to the known highly regioselective reactions of the first type. Only when single dimers are present are regiospecific or highly regioselective reactions obtained. The causes of the variation in the species present and of the reaction regioselectivity for different stannylene acetals are discussed.

Key words: stannylene acetals, 1,3,2-dioxastannolanes, ^{119}Sn NMR spectroscopy, regioselective reactions, carbohydrates.

T. Bruce Grindley et Rasiah Thangarasa. Can. J. Chem. **68**, 1007 (1990).

On a préparé les di-*n*-butylstannylène acétals des 4,6-*O*-benzylidène-α- et -β-glucopyranosides et galactopyranosides de benzyle et on les a étudiés, en solution, en faisant appel à la résonance magnétique nucléaire du ^{1}H, du ^{13}C et du ^{119}Sn. On a identifié les espèces présentes en solution à partir des données de la rmn du ^{119}Sn, par comparaison des déplacements chimiques en rmn du ^{13}C des stannylène acétals et des diols qui leur ont donné naissance ainsi que par une analyse des produits des réactions réalisées en l'absence de nucléophiles. Les orientations des deux substituants attachés aux carbones du cycle pyranosique qui font partie du cycle stannylène déterminent les structures adoptées par le stannylène acétal en solution. Si l'un des substituants est axial alors que l'autre est équatorial, le stannylène acétal existe sous la forme d'un dimère symétrique unique dans lequel les deux atomes d'oxygène des deux cycles 1,3,2-dioxastannolanes adjacents aux substituants axiaux sont doublement coordonnés. Un stannylène acétal comportant deux substituants équatoriaux adjacents existe sous la forme d'un mélange de dimères qui ne se convertissent pas l'un dans l'autre; l'un des deux substituants axiaux adjacents est présent sous la forme d'un mélange de dimères, de trimères et de tétramères qui se convertissent les uns dans les autres. On a effectué la benzoylation et la benzylation des deux derniers types de stannylène acétals et on a montré que ces réactions ne sont que légèrement régiosélectives; ce comportement diffère grandement des réactions hautement régiosélectives observées avec le premier type. On n'obtient des réactions régiospécifiques ou hautement régiosélectives qu'avec des dimères isolés. On discute des causes qui affectent la variation dans les espèces présentes et la régiosélectivité des réactions des divers stannylène acétals.

Mots clés : stannylène acétals, 1,3,2-dioxastannolanes, spectroscopie RMN du ^{119}Sn, réactions régiosélectives, hydrates de carbone.

[Traduit par la revue]

Introduction

A continuing goal of synthetic organic chemists, particularly those working with carbohydrates, has been to develop reactions that occur at only one of two or more hydroxyl groups in similar environments. Dialkylstannylene acetals are easily formed from diols and serve as intermediates in reactions that have shown considerable promise towards achieving this goal. Since their initial use by Moffat and co-workers and by David (1), di-*n*-butylstannylene acetals derived from many different carbohydrates have been observed to react with several types of electrophiles to give predominantly monosubstitution products (2). Alkylation, esterification, and oxidation of stannylene acetals are the most common reactions and the monosubstitution products are often obtained in a regiospecific or highly regioselective manner (2). Sometimes, even enzyme-like selectivity has been achieved, where one hydroxyl group of many reacts (3). In addition, stannylene acetals react much faster with electrophiles than do free diols (2). However, the stannylene acetals of many carbohydrate diols do not undergo regioselective reactions (2) and neither the types of structures of substrates for which selective reactions can be anticipated, nor the cause of the selectivity, have been fully defined. The marked effects of additional nucleophiles on the rates (4) and regioselectivity (5) of reactions with di-*n*-butylstannylene acetals will be analysed later (6).

A number of suggestions have been made as to the causes of both the regioselectivity and of the rate enhancement (2). Evidence will be presented here that supports the idea that the regioselectivity obtained in a reaction is related to the particular oligomeric structure or structures assumed by the stannylene acetal in solution (7). In the solid state, the simplest stannylene acetal, 2,2-di-*n*-butyl-1,3,2-dioxastannolane, exists as an infinite ribbon polymer (8). Of the two carbohydrate stannylene acetals whose X-ray structures have been determined, one exists as a dimer (9) while the other is a pentamer (10). We have shown that di-*n*-butylstannylene acetals derived from simple symmetrical primary or secondary diols exist in solution in nonpolar solvents as complex mixtures containing dimers, trimers, tetramers, pentamers, and possibly higher oligomers. The composition of the mixture present is extremely tempera-

Can. J. Chem. Downloaded from www.nrcresearchpress.com by 88.85.125.76 on 09/07/12
For personal use only.

ture and concentration dependent, with dimers being minor constituents at −50°C but becoming increasingly favoured as the temperature is increased from 0 to 100°C (11).

We now report a study of the ^1H, ^{13}C, and ^{119}Sn nmr spectra of a series of di-*n*-butylstannylene acetals derived from carbohydrates that contained isolated *trans*-1,2-diols on pyranose rings with the four possible combinations of different stereochemistries at the adjacent centres. Some reactions have been performed on those stannylene derivatives for which there were insufficient data about reaction selectivity. The aims of the study are to define the solution structures, to relate them to reactivity and selectivity, and to identify the causes of the selectivity in the absence of added nucleophiles.

Results

The compounds examined were the 2,2-di-*n*-butylstannylene derivatives (**1***b*–**5***b*, respectively) of methyl 4,6-*O*-benzylidene-α-D-glucopyranoside (**1***a*), benzyl 4,6-*O*-benzylidene-α- and -β-D-glucopyranoside (**2***a* and **3***a*, respectively), and benzyl 4,6-*O*-benzylidene-β- and -α-D-galactopyranoside (**4***a* and **5***a*, respectively). Carbohydrates **1***a*–**4***a* were made by standard methods. **5***a* was prepared by the method used to make **2***a* (12). The di-*n*-butylstannylene derivatives were prepared by refluxing the diols with di-*n*-butyltin oxide in benzene for 12 h with azeotropic distillation of water.

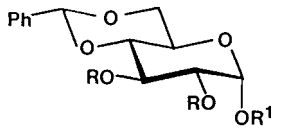

1 R^1 = Me
2 R^1 = Bn

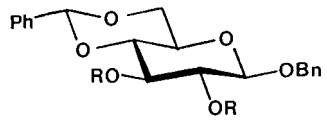

3

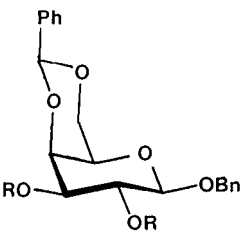

4

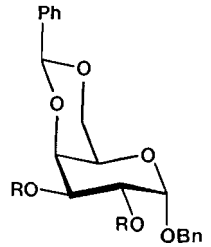

5

a R = H

b 2 R = $Sn(Bu)_2$

The best method currently available for identifying the nature of the tin species present in solution is ^{119}Sn nmr spectroscopy. The ^{119}Sn nmr chemical shift is closely related to the coordination status of the tin atom; in 2,2-di-*n*-butyl-1,3,2-dioxastannolanes and related acyclic tin derivatives, tetracoordinate, pentacoordinate, and hexacoordinate tin nuclei absorb in the ranges −20 to −40 ppm, −100 to −170 ppm, and −230 to −300 ppm, respectively, relative to tetramethyl tin (11, 14, 15).[1]

The ^{119}Sn nmr chemical shifts observed are listed in Table 1. As has been previously noted, two of the compounds (**1***b* and **4***b* in chloroform-*d* (7, 9) and **1***b* in toluene-d_8 (16)) gave spectra containing a single sharp line in the region of the spectrum where pentacoordinate tin is expected to absorb, consistent with a dimeric structure. In each monomer unit in a dimer, one oxygen atom is dicoordinate, while the other is tricoordinate. A particular dimer structure will be named here by using the number of the two tricoordinate oxygen atoms, illustrated for compound **3***b* in Fig. 1. For the compounds studied, three dimers are possible, the 2,2, the 2,3, and the 3,3 dimers. An X-ray crystal structure determination showed that **1***b* is present in the solid state as a 3,3 dimer (9).

To confirm that the same structure is present in solution as in the solid state for **1***b*, the ^{119}Sn and ^{13}C solid state nmr spectra have been recorded. The chemical shifts observed are listed in Tables 1 and 2. The solid-state spectra of both nuclei contained two sets of equal intensity lines with values of the chemical shifts close to those observed in solution. In the X-ray crystal structure, the two halves of the dimer had slightly different geometries (9) and these differences presumably account for the line doubling. The ^{119}Sn nmr chemical shift values observed for **3***b* (see later) demonstrate that different dimer structures give different ^{119}Sn nmr chemical shifts and considerable differences would also be expected in the ^{13}C nmr spectra if a different dimer was present in solution. Hence, it can be concluded that **1***b* is present in solution predominantly as a 3,3 dimer.

Tables 2 and 3 contain the ^{13}C and ^1H nmr chemical shifts of the di-*n*-butylstannylene acetals and their percursors, and the differences between them. In all cases, assignments were made initially for the ^1H nmr spectra by single frequency homonuclear decoupling, then for the ^{13}C nmr spectra by correlation with the ^1H nmr spectra through single frequency heteronuclear decoupling or by 2-D correlation experiments. The ^{13}C nmr spectrum of only one stannylene acetal, **1***b*, had been examined previously and the assignments for C-2 and C-3 considered less likely (16) were found to be correct.

Compound **2***b*, the benzyl analog of the methyl glycoside **1***b*, has almost the same ^{13}C nmr chemical shifts as **1***b*. The ^1H nmr chemical shifts of the skeletal protons, except for H-1, are also very similar. In addition, the pattern of differences between the ^1H and ^{13}C nmr chemical shifts of **1***b* and **1***a* and of **2***b* and **2***a* are similar. Thus, **2***b* is present as the same 3,3 dimer as **1***b* in solution. The ^{119}Sn nmr spectra of both **1***b* and **2***b* in chloroform-*d* contain a single sharp line from −55 to +55°C, consistent with the 3,3 dimer being the predominant species present over this temperature range.

An outline of the reactions performed on di-*n*-butylstannylene derivatives of carbohydrates containing *trans*-diols on pyranose rings is given in Table 4. As for **1***b*, **2***b* reacts almost exclusively at O-2. Comparison of the ^{13}C nmr chemical shifts of the stannylene derivatives **1***b* and **2***b* with those of their precursor diols (Table 2) shows that the signals of the C-2's, the carbons bearing the reactive oxygens, are shifted downfield by 4.3 and 4.4 ppm, respectively, on stannylene acetal formation. The signals of the C-1's are also shifted downfield, by 2.6 and 3.3 ppm, but changes in shifts of the other carbons are small.

The ^{119}Sn nmr spectra of solutions of **3***b* in chloroform-*d* (0.25 M), benzene-d_6 (0.10 M), or toluene-d_8 (0.19 M) are more complex (Fig. 1). Each contains one major signal, plus two smaller identical intensity signals, all close together in the pentacoordinate tin region of the spectrum. Thus, only dimers are present. Spectra recorded over a temperature range of −60 to +50°C in chloroform-*d* or −60 to +100°C in toluene-d_8 all contain the same three signals with about the same intensities, although the relative chemical shifts vary considerably. The benzal proton region of the ^1H nmr spectrum in chloroform-*d*

[1]Also, T. B. Grindley, M. D. Lumsden, and R. Thangarasa, unpublished results.

Can. J. Chem. Downloaded from www.nrcresearchpress.com by 88.85.125.76 on 09/07/12
For personal use only.

TABLE 1. ^{119}Sn chemical shifts

Compound	Chemical shifts (ppm)[a]		
	In chloroform-*d*	In toluene-d_8	In benzene-d_6
1*b*	−124.9 (−125.4)[b] (−126.8 and −128.6)[c]	−131.6[d]	
2*b*	−135.4	−131.7	−130.7
3*b*	−132.6, −132.8,[e] −133.0[e]	−133.0, −132.0,[e] −136.2[e]	−128.7, −127.9,[e] −131.5[e]
4*b*	−143.8[f] (−145.1)[b]	−138.4, −143.4,[g] −154.8,[g] −122.0, −133.6, −287.1	
5*b*[h]	−119.1, −121.8, −123.7[i] −125.4,[i] −126.3,[j] −255.0,[i] −262.6[i]		

[a]At 25°C unless otherwise specified referenced to external tetramethyltin.
[b]Reference 7.
[c]Solid-state values, referred to tetracyclohexyltin at −97.35 ppm.
[d]Reference 16.
[e]Minor but equally intense.
[f]$^2J_{Sn\text{-}119,Sn\text{-}117}$ = 110 Hz.
[g]Impurity peaks.
[h]At −55°C.
[i]About half the intensity of peaks at −119.1 and −121.8 ppm.
[j]Somewhat less intense than the peak at −125.4 ppm.

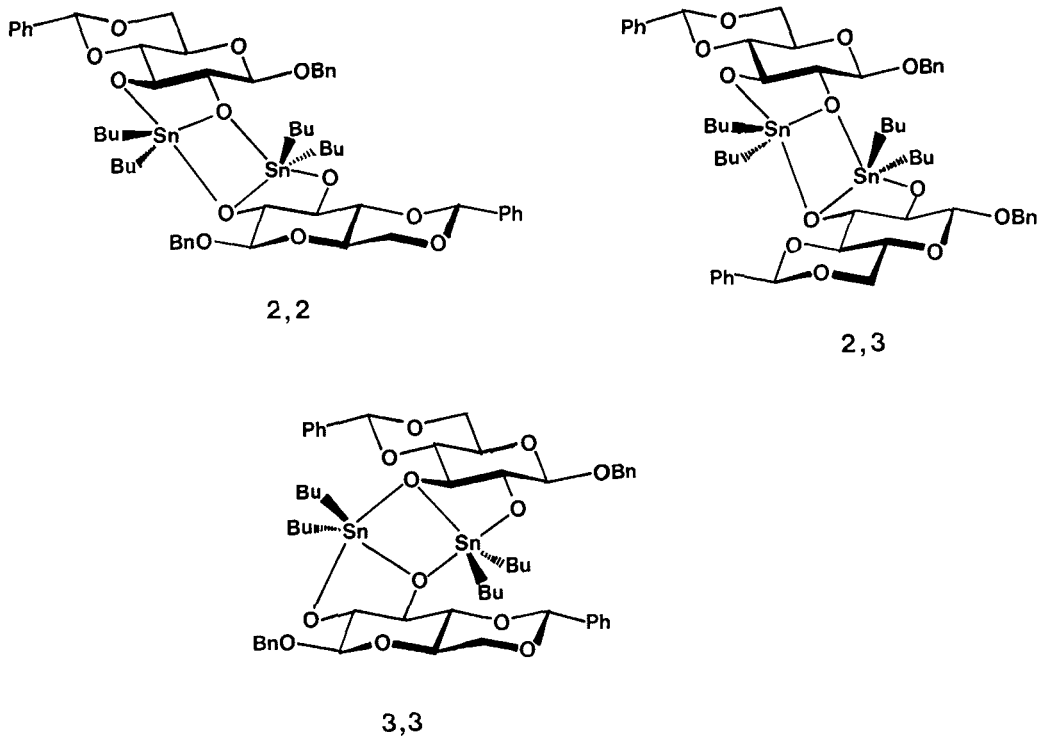

FIG. 1. The structures of dimers possible for compound **3***b*.

contains one large peak at 5.389 ppm, plus two smaller equal intensity peaks at 5.525 and 5.375 ppm, and a much smaller peak at 5.56 ppm. The peaks at 5.525 and 5.375 ppm continued to have identical intensities when the sample was diluted to 0.025 M. In the benzyl region, there was one intense AB quartet (*J* 12.3 Hz) (Table 3), plus two smaller AB quartets, with chemical shifts 5.054 and 4.506 ppm (*J* 10.6 Hz) and 4.884 and 4.807 (*J* 12.3 Hz), plus a much smaller AB quartet at 4.96 and 4.65 ppm (*J* 12 Hz). The other signals were more complex but single frequency decoupling experiments starting with H-1 and H-6_{eq} allowed assignment of the shifts of the signals arising from the major species present. The ^{13}C nmr spectrum in chloroform-*d* contains one major set of peaks (eight peaks between 60 and 110 ppm), assigned by correlation with the ^{1}H nmr spectrum, plus a number of smaller peaks. The observation of one set of intense peaks containing the number

Can. J. Chem. Downloaded from www.nrcresearchpress.com by 88.85.125.76 on 09/07/12
For personal use only.

TABLE 2. Comparison of ^{13}C nmr chemical shifts of the stannylene acetals with those of their precursors

	Chemical shifts[a]							
Compound	C-1	C-2	C-3	C-4	C-5	C-6	C-7[b]	Me or CH_2Ph
1*b*	102.5	76.7[c]	72.2[c]	82.5	63.6	69.2	102.5	55.6
1*a*	99.9	72.4	71.1	80.9	62.3	68.8	101.5	55.3
Diff.[d]	+2.6	+4.3	+1.1	+1.6	+1.3	+0.4	+1.0	+0.3
1*b*[e]	103.0, 104.0	75.7, 77.8	73.6	83.5	64.7, 65.3	69.5	104.0	55.1, 56.3
Diff.[f]	+1.0	0.0	+1.4	+1.0	+1.4	+0.3	+1.5	−0.1
2*b*	101.6	77.2	72.1	82.5	64.0	69.2	102.5	70.3
2*a*	98.3	72.8	71.5	81.0	62.8	68.9	101.8	70.1
Diff.[d]	+3.3	+4.4	+0.6	+1.5	+1.2	+0.3	+0.7	+0.2
3*b*	104.0	77.9	75.9	81.2	67.5	68.8	102.4	70.4
3*a*	102.0	74.4	73.0	80.4	66.3	68.5	101.7	71.3
Diff.[d]	+2.0	+3.5	+2.9	+0.8	+1.2	+0.3	+0.7	−0.9
3*b*[g]	105.2	78.9	77.1	81.9	67.5	69.1	102.7	70.2
3*a*[g]	102.7	75.3	73.9	81.0	66.7	68.9	101.8	71.1
Diff.[d]	+2.5	+3.6	+3.2	+0.9	+0.8	+0.2	+0.9	−0.9
4*b*	103.3	72.7	76.8	76.9	67.8	69.7	100.4	71.2
4*a*	101.6	71.8	72.7	75.3	66.7	69.1	101.4	70.9
Diff.[d]	+1.7	+0.9	+4.2	+1.6	+1.1	+0.6	−1.0	+0.4

[a]In chloroform-*d* referred to TMS or to the central line of chloroform-*d* unless otherwise noted. Each pair has the same reference.
[b]Benzylidene acetal carbon.
[c]"Most likely" assignments reversed (16).
[d]Differences are from non-rounded chemical shifts.
[e]Solid-state values. Note that two signals were observed for some carbons.
[f]Difference between solution values for **1***b* and average solid-state values (where two signals were observed).
[g]In toluene-d_8.

TABLE 3. Comparison of ^1H nmr chemical shifts of stannylene acetals with those of their precursors

	Chemical shifts (ppm)[a]								
Compound	H-1	H-2	H-3	H-4	H-5	H-6	H-6′	H-7[b]	Me or CH_2Ph
1*b*	4.846	3.316	3.652	3.396	3.804	3.758	4.256	5.416	3.423
1*a*	4.689	3.545	3.877	3.424	3.754	3.683	4.244	5.480	3.386
Diff	+0.157	−0.229	−0.225	−0.028	+0.050	+0.075	+0.012	−0.064	+0.037
2*b*	5.087	3.410	3.728	3.417	3.870	3.736	4.195	5.403	4.597, 4.757
2*a*	4.902	3.556	3.887	3.422	3.794	3.658	4.175	5.458	4.501, 4.700
Diff	+0.185	−0.146	−0.159	−0.005	+0.076	+0.078	+0.020	−0.055	+0.096, +0.057
3*b*	4.49	3.23	3.24	3.47	3.46	3.79	4.30	5.389	4.780, 4.867
3*a*	4.396	3.484	3.687	3.475	3.319	3.720	4.289	5.445	4.860, 4.572
Diff	+0.09	−0.25	−0.45	−0.1	+0.14	+0.07	+0.01	−0.056	+0.007, +0.208
4*b*	4.380	3.728	3.407	4.229	3.490	4.133	4.334	5.571	4.181, 5.147
4*a*	4.383	3.816	3.678	4.203	3.463	4.100	4.379	5.557	4.626, 5.000
Diff	−0.003	−0.088	−0.271	−0.026	+0.027	+0.033	−0.065	+0.014	+0.147, −0.445

[a]From TMS in chloroform-*d*.
[b]Proton on benzylidene acetal carbon.

Can. J. Chem. Downloaded from www.nrcresearchpress.com by 88.85.125.76 on 09/07/12
For personal use only.

TABLE 4. Reactivity of di-*n*-butylstannylene derivatives of carbohydrates having *trans*-1,2-diols on pyranose rings

Compound	Reaction	Solvent	Concentration	Temperature (°C)	Reaction selectivity % at C-2	% at C-3	% at C-4	Ref.
1*b*	Benzoylation	Dioxane[a]	0.5 M	20	86	—	[b]	17
		Benzene	0.1 M	20	93	—	[b]	18
		Benzene	0.07 M	20	100	—	[b]	5
		Benzene[c]	0.07 M	20	100	—	[b]	5
	Benzylation	DMF, BnBr	0.3 M	100	70	20	[b]	19
	Methylation	DMF	[d]	45	57	30	[b]	18
	Oxidation	CH_2Cl_2	0.17 M	20	60	—	[b]	18
	Tosylation	Dioxane[a]	0.1 M	20	70	—	[b]	17
2*b*	Benzylation	DMF, BnBr	0.3 M	110	77	—	[b]	19
6	Oxidation	CH_3CN[f]	0.063 M	25	33	17	[b]	20
3*b*	Benzoylation	Benzene[f]	0.013 M	25	53	37	[b]	Here
	Benzylation	Benzene[e]	0.04 M	80	21	55	[b]	Here
7	Allylation	Benzene[e]	[d]	80	33	60	[b]	21
	Benzoylation	Benzene[f]	[d]	20	49	39	[b]	21
	Benzylation	Benzene[e]	[d]	80	29	61	[b]	21
	Methylation	DMF	[d]	45	22	66	[b]	21
	Tosylation	Benzene[e]	[d]	20	21	63	[b]	21
8	Oxidation	CH_3CN[f]	0.063 M	25	—	50	[b]	20
9	Benzoylation	Benzene[f]	0.22 M	20	[b]	59	22	18
	Oxidation	Benzene, CH_2Cl_2	0.22 M	20	[b]	—	72	18
4*b*	Benzoylation	Benzene[f]	0.22 M	20	—	95	[b]	18
	Benzylation	Benzene[e]	0.04 M	80	10	55	[b]	4
	Oxidation	CH_2Cl_2	0.17 M	23	—	72	[b]	18
5*b*	Benzoylation	Benzene[f]	0.013 M	25	38	46	[b]	Here
	Benzoylation	DME[a,g]	0.013 M	25	51	49	[b]	Here
	Benzylation	Benzene[e]	0.04 M	80	43	49	[b]	Here
10	Tosylation	Dioxane[a]	[d]	25	64	—	[b]	17
11	Benzoylation	Toluene[a]	0.04 M	−45	[b]	70	—	22
	Benzylation	Benzene[e]	0.04 M	80	[b]	70	—	22
	Methylation	Benzene[e]	0.04 M	80	[b]	52	18	22
	Tosylation	Benzene[e]	0.04 M	20	[b]	75	—	22
12	Benzylation	Toluene[e]	0.1 M	70	50[h]	39[i]	[b]	23
13	Benzylation	Toluene[e]	0.1 M	70	[b]	46	43	23

[a]Added triethylamine.
[b]Site not available.
[c]Added *N*-methylimidazole.
[d]Concentration not reported.
[e]Added tetrabutylammonium bromide or iodide.
[f]Molecular sieves added.
[g]1,2-Dimethoxyethane.
[h]Position 5.
[i]Position 6.

of peaks expected for a monomer in the spectra of all nuclei indicates that the major species present is a symmetrical dimer. For **1***b*, **2***b*, and **4***b* (*vide infra*), comparison of the ^{13}C nmr chemical shifts of the carbons involved in stannylene acetal formation in the spectra of the stannylene acetals with those from their precursors allowed assignment of the carbon bearing the dicoordinate oxygen atom from its markedly larger chemical shift change. The signals for both C-2 and C-3 had larger chemical shifts in the spectra of the major species of **3***b* than in those of **3***a* (by 3.5 and 2.9 ppm in chloroform-*d* and 3.6 and 3.2 ppm in toluene-d_8, respectively). Thus, the structure of the major dimer cannot be determined from these shift differences. Also present in the ^1H and ^{119}Sn nmr spectra of **3***b* were two other sets of signals having identical intensities under all conditions. The equality of the intensities indicates that these lines are caused by a single species, the nonsymmetrical 2,3 dimer. The observation of some very minor signals suggests that the third dimer is present to a very limited extent. Integration of the ^{119}Sn nmr signals allowed evaluation of the relative proportions of the major and minor dimers; at 26°C, these were 57:38, 75:25, and 72:28 for solutions in chloroform-*d* (0.25 M), in toluene-d_8 (0.19 M), and in benzene-d_6 (0.10 M), respectively.

Reactions with electrophiles performed on **7**, the methyl analogue of **3***b*, gave mixtures of products with selectivity that varied with the reaction type and conditions (21). Benzylation of **3***b* was performed in benzene with added tetra-*n*-butylammonium bromide at reflux. The structures of the benzyl derivatives (**3***c* and **3***d*) were assigned by analysis of the ^1H nmr spectra of their acetates; the key observation was the size of the coupling constants for the most downfield signal of a skeletal proton. $J_{1,2}$ is noticeably smaller than $J_{2,3}$ or $J_{3,4}$. Benzoylation was performed in benzene without added base. The structures of the benzoates were assigned directly from their ^1H nmr spectra.

Can. J. Chem. Downloaded from www.nrcresearchpress.com by 88.85.125.76 on 09/07/12
For personal use only.

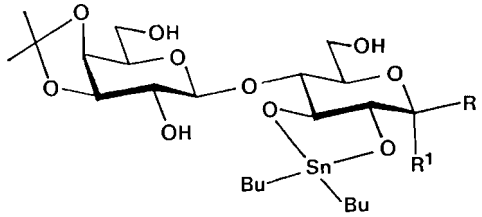

6 R = H, R^1 = OMe

8 R = OMe, R^1 = H

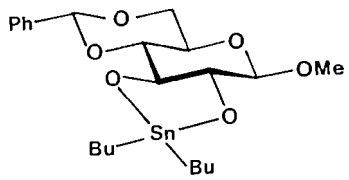

7

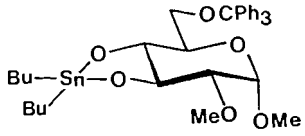

9

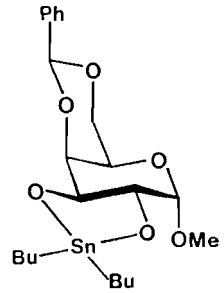

10

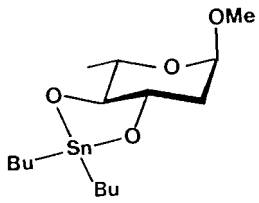

11

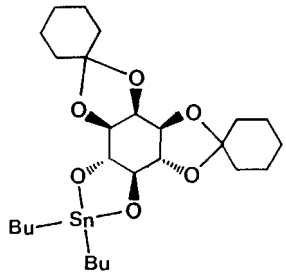

12

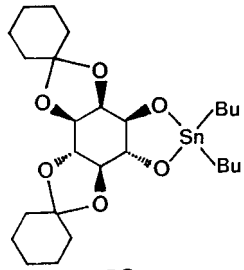

13

Benzylation gave more of the 3-*O*-benzyl derivative (55:21) but benzoylation yielded more of the 2-*O*-benzoate (53:37). All reactions with **7** except for benzoylation gave about a 2:1 to 3:1 preference for reaction at O-3 (21). Benzoylation here and in ref. 21 was conducted at room temperature in the absence of additional nucleophiles whereas the other reactions were conducted in the presence of added nucleophiles often at elevated temperatures. The products of benzoylation are, therefore, most likely to be related to the structures of the major species present in solution in the solvent alone. We conclude that the major symmetrical dimer present for **3***b* and **7** is the 3,3 dimer.

As previously noted (7), the ^{119}Sn nmr spectrum of **4***b* in chloroform-*d* contains a single sharp line at temperatures ranging from −55 to +50°C, consistent with a single symmetrical dimer. The ^{1}H and ^{13}C nmr spectra contain a single set of lines, indicating that the dimer present is symmetrical. The downfield shift (4.2 ppm) observed for C-3 on conversion of **4***a* to **4***b* indicates that the dimer present is the 2,2 dimer. In agreement with this conclusion, **4***b* reacts almost exclusively at O-3 (Table 4).

Confirmation of the structures of the dimers present in chloroform-*d* for **2***b* and **4***b* can be obtained by consideration of the differences in the chemical shifts of the methylene protons in the benzyl groups when the ^{1}H nmr spectra of the diols are compared with those of the stannylene acetals (Table 3). In the assignment of these signals, it was assumed that there was no reversal of chemical shift order for the signals from the benzyl groups on stannylene acetal formation. For **2***b*, where O-2 is dicoordinate, the large substituents attached to tin are held away from the benzyl group and the chemical shift changes observed are small. For **4***b*, the major dimer has O-2 tricoordinate. The two *n*-butyl groups are close to the glycosidic benzyls and presumably influence the mixtures of conformations present. Large changes in chemical shift are observed when the chemical shifts of the benzyl protons of **4***b* are compared with those of **4***a*. For **3***b*, the differences in chemical shift differences (ΔΔδ 0.20) were much smaller than for **4***b* (ΔΔδ 0.59), but were larger than for **2***b* (ΔΔδ 0.04). This result is in agreement with the evidence presented earlier that the major dimer for **3***b* was the 3,3 dimer.

The spectra of solutions of **4***b* in toluene-d_8 were rather complicated and very temperature dependent (see Fig. 2). At all temperatures, the ^{119}Sn nmr spectra contained one main signal (at −136.0 ppm at −40°C), presumably that of the 2,2 dimer. At −40°C and below, the ^{119}Sn nmr spectrum contained eight other signals including three in the hexacoordinate region of the spectrum, at −248.0, −294.7, and at −298.9 ppm. If signals for hexacoordinate tin are observed, higher oligomers than the dimer must be present. The most likely species are trimers and

Can. J. Chem. Downloaded from www.nrcresearchpress.com by 88.85.125.76 on 09/07/12
For personal use only.

Can. J. Chem. Downloaded from www.nrcresearchpress.com by 88.85.125.76 on 09/07/12
For personal use only.

tetramers (11). There are four possible trimer structures, none of which have any symmetry, and ten possible tetramer structures, of which four have C_2 symmetry. We believe that two trimers, one tetramer, and possibly the 2,3 dimer are also present. The two trimers, termed A and B, were assigned as trimers on the basis of the chemical shifts of the high field signals and of changes in intensities with temperature. In the spectra of a number of di-*n*-butylstannylene acetals derived from ethylene glycol and simple di-secondary diols, the chemical shifts of hexacoordinate tin signals of trimers were 15–20 ppm more negative than those of tetramers, falling in the range of −280 to −295 ppm (11). In spectra recorded at −60°C, the signal assigned to the tetramer, at −251.4 ppm, was about the same size as the other two signals arising from hexacoordinate tin; at −40°C, it was much smaller than the other two; by −20°C, the signal had almost disappeared and it was not present in spectra recorded at 0°C and above. Lower temperatures favour higher oligomers (11, 15). Similarly, the signals assigned to trimers were larger in comparison to those assigned to dimers at low temperatures than they were at higher temperatures; the ratios of mole fractions of dimers to trimers changed from 0.51 to 1.5 to 6.8 at −60, −20, and 30°C, respectively. The ^{119}Sn nmr spectra of trimers should contain three signals, two in the pentacoordinate region. Two signals at −294.7 and −119.6 ppm with identical intensities are assigned to trimer A. A second set of two signals at −298.9 and −121.3 ppm with intensities identical to each other but lower than those assigned to trimer A is assigned to trimer B. A signal at −132.2 ppm had an intensity about equal to the sum of the intensities at −294.7 and −298.9 ppm or −119.6 and −121.3 ppm and probably was due to a coincidence of the third signal of both trimers.

The trimer structures are named here from the numbers of the positions of the bonded tricoordinate oxygen atoms in the sequence present in the structure. The four possibilities are the 2,3,2,2, 2,2,3,3, 2,3,2,3, and 3,3,2,3 trimers, shown in Fig. 3. We believe that the two trimers present are the 2,2,3,3 and the 2,3,2,3 structures, for reasons that will be discussed later.

At 50°C and above, the only sharp signal visible to the high frequency side of the main signal was a small signal with a chemical shift of −132.9 ppm at 70°C. At low temperatures, a slight shoulder was observed on the high frequency side of the main peak at chemical shifts close to this value. This signal may have been caused by the 2,3 dimer; if it was, and if it is assumed that the nonsymmetrical 2,3 dimer gave rise to a second signal coincident with the main signal, the 2,3 dimer contributed about 12% of the mixture present at these temperatures.

The line widths and intensities of the remaining two signals, at −140.3 and +151.6 ppm, were much less sensitive to changes in temperature. They were therefore assigned to an impurity or impurities arising from reaction of **4***b* with a slight amount of water present in the system. Compounds with similar chemical shifts were obtained when model compounds were exposed to water (11).

There was considerable evidence in these spectra of **4***b* in toluene-d_8 that exchange processes were becoming more rapid as the temperature increased. The signals assigned to hexacoordinate tin in trimers were very broad at 30°C and were too broad to be observed at higher temperatures. The two highest frequency trimer signals broadened and merged at 0°C and continued to broaden as the temperature increased so that at 70°C they formed part of the shoulder on the envelope of the main dimer peak. The other trimer peak also broadened so that it

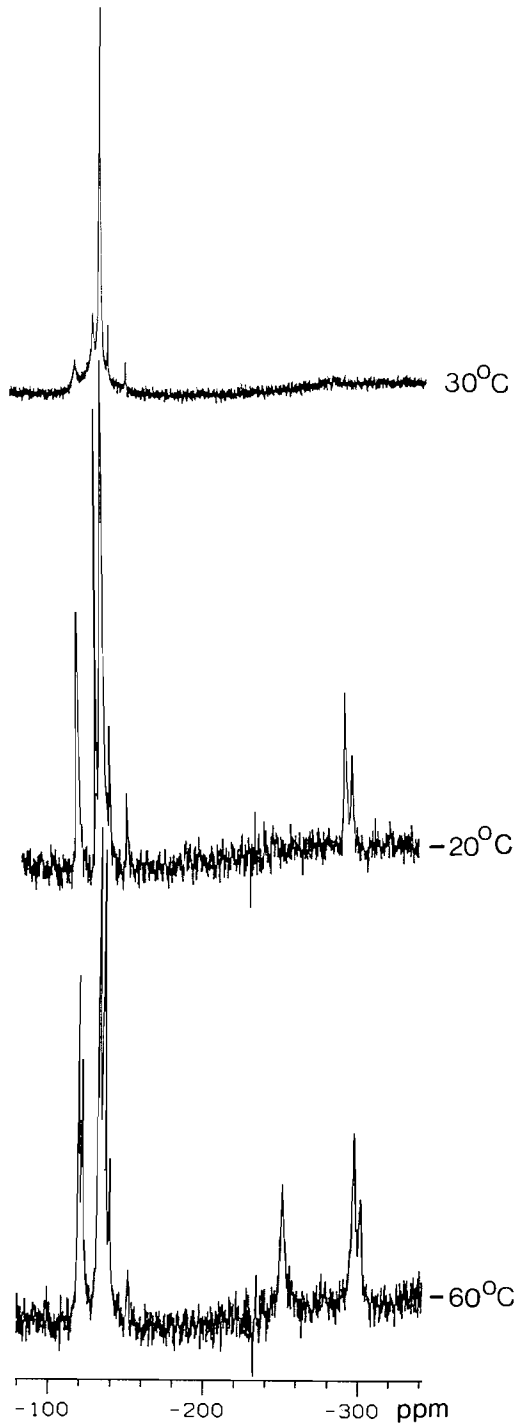

FIG. 2. 134.6 MHz ^{119}Sn nmr spectra of a 0.19 M solution of compound **4***b* in toluene-d_8 at various temperatures.

was part of the shoulder of the main peak by 50°C. The minor peak tentatively assigned to the 2,3 dimer broadened as the temperature was raised but was still distinct at the highest temperature recorded, 90°C. The peaks assigned to hydrolysis products were much sharper than the other two peaks at 70 and 90°C.

The nmr spectra of compound **5***b* are very different. At room temperature, the ^{119}Sn nmr spectrum of **5***b* in chloroform-*d* contains a number of very broad lines that sharpen as the temperature is lowered. At −55°C, there are two intense lines plus three lines of about half their intensity between −119 and

Can. J. Chem. Downloaded from www.nrcresearchpress.com by 88.85.125.76 on 09/07/12
For personal use only.

−127 ppm, plus two lines of about half the intensity of the most intense lines at −255.0 and −262.6 ppm. The latter two lines are from hexacoordinate tin. In addition, there were low intensity lines between −138 and −144 ppm and between −233 and −243 ppm. It is probable that the more intense hexacoordinate tin signals arise from trimers and the very weak penta- and hexa-coordinate signals come from tetramers. Trimers and (or) tetramers alone could not account for all of the signals observed. One or more dimers must be present and cause at least part of the most intense signals.

The behaviour of the ^{13}C nmr spectra of **5***b* is also complex. At 50°C in chloroform-*d*, the spectrum contains the number of lines anticipated for a monomeric structure but all lines are broad. As the temperature is lowered the lines broaden, split, then sharpen to give very complex patterns. For instance, the signal for C-5 divides into at least two major peaks, plus two peaks of about half the intensity of the major peaks. The coalescence point for the two major peaks for C-5 was about 28°C, giving a rough estimate of $\Delta G^{\ddagger}$ of 14.7 kcal mol^{-1}.

No reactions had previously been performed for **5***b*. Benzylation and benzoylation were performed here. The structures of the benzyl derivatives were assigned by analysis of the ^1H nmr spectra. In each case, the spectra of the dry crystalline sample in dry chloroform-*d* contained a sharp one-hydrogen doublet near 2 ppm due to the OH proton, which could be assigned by decoupling experiments. Analysis of the remainder of the spectra, confirmed by decoupling experiments, yielded the positions of the benzyl groups. The 2-*O*-benzyl derivative (**5***e*) was a known compound (24). Benzoylation was performed in benzene in the presence and absence of triethylamine. Structures of products were determined as for the benzyl derivatives. Little selectivity was observed in these reactions (see Table 4). These results are in contrast to the excellent selectivity claimed for tosylation of **10**, the methyl analog of **5***b* (17).

Discussion

Structures of species present in solution

The spectral results described above have allowed assignment of the species present in solution. Compounds **1***b* and **2***b* are present as single species, the 3,3 dimers. In chloroform-*d*, **4***b* is also present as a single dimer, but now a different one, the 2,2 dimer. Although solutions of **4***b* in toluene-d_8 are more complex, the 2,2 dimer was the major species present at temperatures above −50°C and constituted more than 80% of the species present on a molar basis at 30°C and above, for a 0.19 M solution. Presumably, the more dilute solutions used for reactions would contain even more of the 2,2 dimer and less of the trimers, as was observed for model compounds (11). **3***b* exists as a mixture of dimers in all solvents; the 3,3 dimer, to a lesser extent the 2,3 dimer, and perhaps a small amount of the 2,2 dimer are present. Interconversion of these species is slow on the nmr time-scale, at 50°C in chloroform-*d* and at 100°C in toluene-d_8. **5***b* exists as a rapidly interconverting mixture of dimers and trimers at room temperature.

Steric factors are clearly most important in determining which species is present in solution for a particular stannylene acetal. The compound without adjacent axial substituents (**3***b*) exists as a mixture of dimers; those with one adjacent axial oxygen (**1***b*, **2***b*, and **4***b*) exist in chloroform-*d* as single dimers, the ones with the tricoordinate oxygens not adjacent to the axial groups; two adjacent axial substituents (**5***b*) make all possible dimers less stable. Evidently an adjacent axial substituent destabilizes the dimer that has the closest oxygen atom of the stannylene acetal tricoordinate. Examination of models and of the available crystal structures (9, 10) indicates that the largest destabilizing interaction in a dimer with a tricoordinate oxygen adjacent to an axial substituent is between the axial group and one of the butyl groups on pentacoordinate tin. The interaction between an equatorial substituent and the other butyl group is much less destabilizing. In the crystal structure of **1***b*, the two substituents on the two O-4's in the dimer are each almost equally distant from their adjacent pair of butyl groups; the distances from each of the two O-4's to the closest two α-methylene carbons of the butyl groups calculated from the crystal coordinates (9) are 3.40 and 3.37 Å and 3.65 and 3.48 Å.

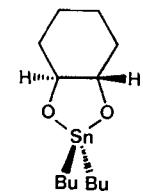

14

The behaviour of **3***b* and that of the di-*n*-butylstannylene acetal derived from (*S*,*S*)-1,2-cyclohexanediol (**14**) provide an instructive contrast. Neither compound has axial substituents on carbons adjacent to those bearing the stannylene acetal. In chloroform solutions, **3***b* contains at least two dimers that do not interconvert on the nmr time-scale even at the highest temperature studied, 100°C, and there is no evidence of higher oligomers at any temperature. Compound **14** is present at room temperature as a complex, rapidly interconverting mixture containing dimers, trimers, tetramers, and, to a small extent, pentamers (11). For **14**, interconversion becomes slow on the nmr time-scale only when the temperature is below −30°C. The positions of the complex equilibria are highly dependent on temperature and, to a lesser extent, dependent on concentration. For a 0.43 M solution, the mole fraction of dimer present is 0.15 at −73°C but 0.75 at 27°C. The routes available for equilibration of oligomers were shown to be the reversible association of dimer molecules to tetramers, of dimer and trimer molecules to pentamers, of trimer molecules to hexamers, and of dimer and tetramer molecules to hexamers (11). **3***b* interconverts much more slowly because trimers and still higher oligomers are sterically disfavoured.

The relatively lower stability of higher oligomers for stannylene acetals from carbohydrates with *trans*-diequatorial-1,2-diols probably arises from interactions between alternate monomer units in the higher oligomer, for instance, between the terminal units of a trimer. The distorted octahedral arrangement about a hexacoordinate tin atom in a higher oligomer holds the two four-membered Sn_2O_2 rings attached to that tin atom close to coplanar, and the three attached 1,3,2-dioxastannolane rings are also close to coplanar. Hence, the alternate carbohydrate rings are nearly coplanar, but the shortest distance between coordinated oxygen atoms on these rings is about 4.8 Å due to the two long Sn--O bonds (2.50 Å) and the large O--Sn--O angle (142–151°) (8, 10). The distance between alternate rings is slightly increased because the bonds from the coordinated oxygens to the rings are inclined slightly away from each other. However, the ends of the two rings decrease the separation by about 2.5 Å so that the distance between C-1 on one ring and C-4 on the other is in the order of 2–4 Å. Therefore, equatorial substituents on those two carbons, particularly large substituents, will cause severe nonbonded interactions between

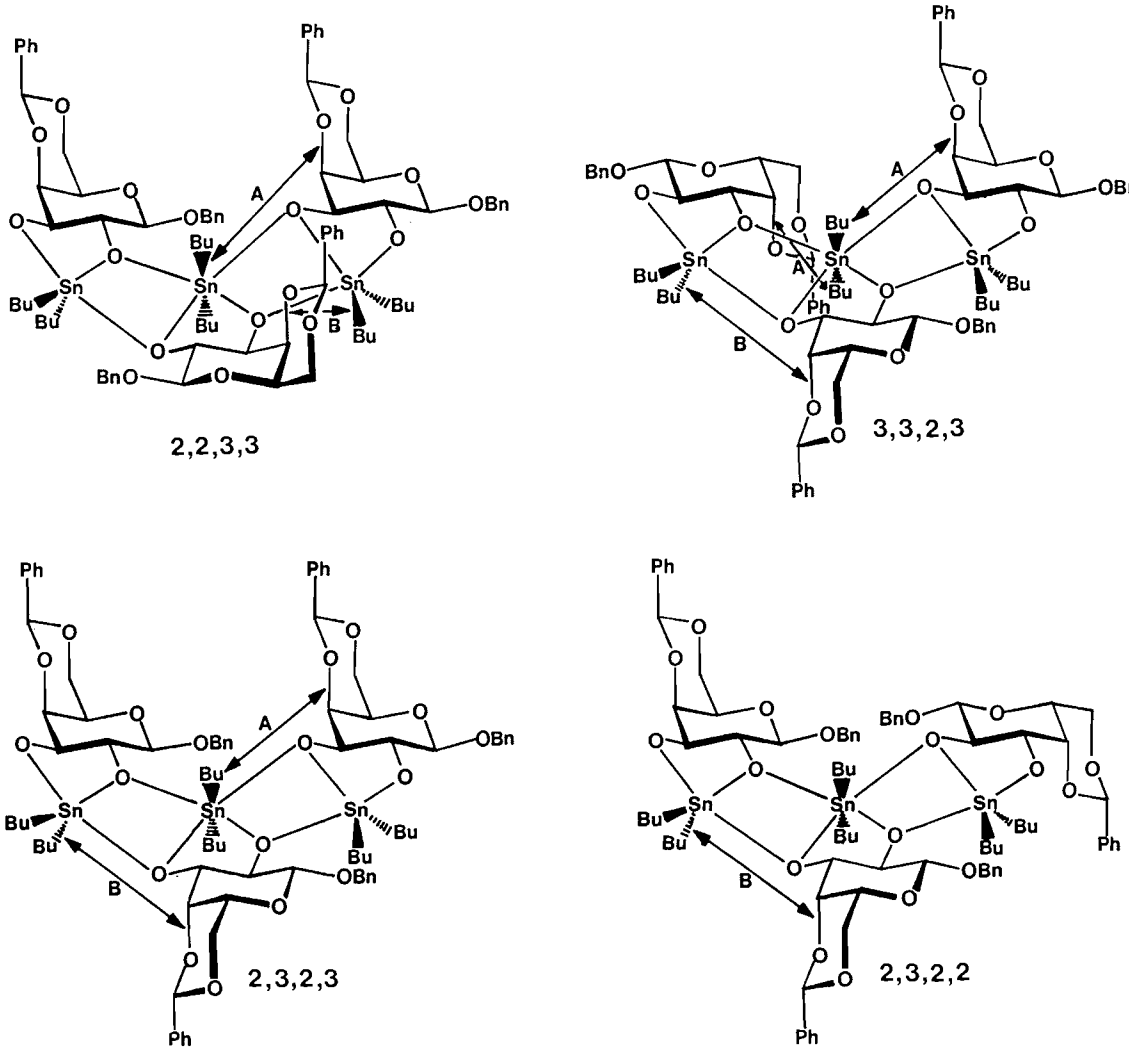

FIG. 3. Possible trimer structures for compound **4***b*. Steric interactions between axial substituents and butyl groups on hexacoordinate and pentacoordinate tin are indicated by arrows labelled by the letters A and B, respectively.

alternate monomer units in the higher oligomers. A single large rigid equatorial substituent, like a 4,6-*O*-benzylidene ring with a length of about 8 Å, as in **1***b* or **2***b*, is quite sufficient to inhibit higher oligomer formation. The equatorial *O*-benzyl group, as in **4***b*, is less effective. In chloroform-*d* no higher oligomers were observed, but in toluene-d_8 the signals of higher oligomers were prominent, particularly at low temperatures. Presumably, in higher oligomers of **4***b*, the rotamer about the C1—O1 bond favoured by the *exo*-anomeric effect and the rotamers about the O1—CH_2 bond that take the phenyl group away from the stannylene side of the molecule are populated. The formation of higher oligomers for **3***b* is very unfavourable. Interconversion of dimers for **3***b*, which occurs via higher oligomers for **14**, is observed to be very slow, in agreement with the conclusion drawn above and earlier (11) that the normal lowest energy mechanism for interconversion of dimers involves higher oligomers. Consideration of the formation and cleavage of various higher oligomers shows that oligomers with odd numbers of monomer units must be involved to interconvert 3,3 dimers and 2,3 dimers. **5***b*, with axial substituents at both C-1 and C-4, avoids the severe interannular steric interactions in the higher oligomers. Hence, it is present as trimers and tetramers as well as dimers, and the various species interconvert rapidly at room temperature.

The slight preferences for **3***b* to assume a 3,3 dimer rather than a 2,3 dimer are calculated to be 0.24 and 0.65 kcal mol^{-1} in chloroform-*d* and toluene-d_8, respectively, at 299 K. If it is assumed that this difference reflects the difference in energy for O-3 rather than O-2 to be tricoordinate, the relative stability of the 2,2 dimer can be calculated. Evaluation of the equilibrium constants indicates that the 2,2 dimer should be present at 21% and 8% levels in chloroform-*d* and toluene-d_8, respectively. No signals assignable to the 2,2 dimer were observed in toluene-d_8. In chloroform-*d*, it may have been present at the 5% level. Obviously, the 2,2 dimer is less stable than was anticipated on the basis of the relative stabilities of the 3,3 and 2,3 dimers. The small difference in stability between the 3,3 and 2,3 dimers may simply be due to the effects associated with the greater freedom of movement of the glycosidic benzyl group than the almost identically sized but sterically restricted 4,6-*O*-benzylidene group.

The considerations discussed above can be used to assign the structures of the trimers present in toluene-d_8 solutions of **4***b*. The four possible structures and the destabilizing interactions contained in each are illustrated in Fig. 3. The 2,3,2,2 structure can be ruled out because it has two equatorial *O*-benzyl groups opposing each other from the inside ends of the two terminal units of the trimer. Support for this contention can be drawn

Can. J. Chem. Downloaded from www.nrcresearchpress.com by 88.85.125.76 on 09/07/12
For personal use only.

Can. J. Chem. Downloaded from www.nrcresearchpress.com by 88.85.125.76 on 09/07/12
For personal use only.

from the equilibrium mixture present for **3***b*; no trimers were observed although its 2,3,2,2 trimer would be destabilized only by this interaction. The 3,3,2,3 trimer has no interactions between equatorial substituents on the terminal units but has the maximum number of intermonomer interactions between axial *O*-4 benzylidene groups and butyl groups on tin atoms: two interactions involving butyl groups on a hexacoordinate tin atom (A type) and one involving a butyl group on a pentacoordinate tin atom (B type). The 2,2,3,3 and 2,3,2,3 trimers should have similar stabilities because each has two different intermonomer interactions (types A and B). These two isomers should also have similar chemical shifts because they differ only by changing the bonding order of the central unit. Because two dimers of similar stabilities having small chemical shift differences between each of the pairs of tin signals were observed, it is considered most likely that the species present are these two latter structures.

The presence of higher oligomers in solutions of **4***b* in toluene-d_8 in contrast to their absence in chloroform-*d* can be ascribed to the lower polarity of the former solvent. Less polar solvents should favour association of the relatively polar stannylene acetals. Similar results have been observed for other carbohydrate-derived stannylene acetals.[1]

The cause of the selectivity and the reaction mechanism

David *et al.* suggested that the structure of the dimer present determines the product obtained in these reactions (7). For the first time, the exact structures present in solution have been determined here. For some compounds, the products obtained are directly related to the nature of the major species present. When a stannylene acetal exists predominantly as a single dimer (**1***b*, **2***b*, **4***b*), reaction normally occurs at the dicoordinate oxygen although products of attack at the other oxygen are sometimes observed. These other products are only found when the reaction is conducted in the presence of added nucleophiles or polar solvents at higher than room temperature.

Compound **3***b* contains a mixture of the 3,3 dimer (major) and the 2,3 dimer (minor). The amounts of the two dimers present determine the extent to which the individual oxygen atoms are dicoordinate. For a 0.2 M solution in benzene-d_6 at 26°C, 86% of the O-2's in the two types of dimer are dicoordinate. Benzoylation of **3***b* in benzene at room temperature in the absence of additional nucleophiles yields a mixture of products containing more of the 2-benzoate (53:37) but the product composition does not match the amount of dicoordinate oxygen. Additional factors need to be considered. Possibly the different dicoordinate oxygen atoms have different reactivities. Another explanation could be that the chloride released from benzoyl chloride affects the product composition, as do added nucleophiles. In the presence of added nucleophiles, a preference for addition at O-3 is observed.

Compound **5***b* is present as a complex, rapidly interconverting mixture and little selectivity is obtained. The tosylation of the methyl analogue **7** reported by Munavu and Szmant (17) is anomalous in this regard.

The cause of the enhanced reactivity towards electrophiles of the oxygens in stannylene acetals has been the subject of considerable discussion (2). One suggestion was that electron density was transferred from the electropositive tin atom to the dicoordinate oxygen, making it more nucleophilic. If considerable electron density had been transferred to the dicoordinate oxygen, upfield chemical shifts would be observed for the attached carbon. Similarly, Lewis structures of these species suggest that the tricoordinate oxygen is electron deficient and a significant downfield shift for the attached carbon is anticipated. For instance, protonation or methylation of ethereal or alcoholic oxygens results in downfield shifts of 10–19 ppm for α-carbons (25). Comparison of the ^{13}C nmr shifts of starting diols and stannylene acetals (Table 3) demonstrates that the chemical shift of the carbon that becomes attached to the dicoordinate oxygen moves downfield by 3–5 ppm, while the carbon that becomes attached to the tricoordinate oxygen moves downfield by 1–3 ppm, similar to the effects observed for most of the other carbons in the diols. The magnitudes and directions of these changes in shift are similar to the values observed when normal acetals are formed (26). Surprisingly, the observed chemical shift changes are not consistent with significant transfers of electron density to or from oxygen on formation of the stannylene acetal. Similar results were obtained when the effects of complexation with tin (27) were compared with the effects of protonation (28) on ^1H and ^{13}C nmr chemical shifts of pyridines.

A possible explanation for the rate enhancement observed for the stannylene acetals is that significant electron transfer towards the dicoordinate oxygen only occurs in the transition state for reaction, when there is greatly increased electron demand.

Of the literature studies, the results of oxidation of the 2,3-*O*-dibutylstannylene acetals of methyl 3′,4′-*O*-isopropylidene-α- and -β-lactoside are contrary to the general trend observed for simple glucose derivatives **1***b*, **2***b*, **3***b*, and **7** (Table 4), since the α-derivative (**6**) gives a mixture while the β-derivative (**8**) gives one product (20). However, these particular glucose derivatives (**6** and **8**) have a very large equatorial substituent on O-4, a 3,4-*O*-isopropylidene-β-D-galactose unit. Presumably the butyl groups on tin in the 3,3 dimer are sufficiently close to this large group for this particular dimer to be sterically destabilized. Thus compound **6** probably exists as a rapidly interconverting mixture of species, like compound **5***b*, while **8** is present as a single species, like **1***b* and **2***b*. Oxidation of stannylene acetals with bromine is the reaction most likely to give products with structures directly related to the species present in solution because the reaction occurs instantaneously.

The oxidation of the dibutylstannylene acetal of methyl 2-*O*-methyl-6-*O*-triphenylmethyl-α-D-glucopyranoside (**9**) gives a single product, in accord with the results on **6** and **8** (18). Here the stannylene acetal oxygen atoms are flanked by two equatorial groups, as for **3***b*, but one is much larger, a triphenylmethoxymethyl group, as compared with a methoxy group. Thus the dimer having the dicoordinate oxygen atom close to the large group, the 3,3 dimer, should be favoured, and reaction should take place at position 4, as observed. The benzoylation reaction on **9** did not give results in accord with this suggestion but the long time required for the reaction to go to completion, 48 h, may allow the inherently greater reactivity of position 3 (18) to influence the results.

The results obtained on compounds **6**, **8**, and **9** indicate that the proper choice of groups on centres adjacent to diol units used to form stannylene acetals may allow direction of electrophiles to one of the two diol oxygens.

The results of benzylation of the dibutylstannylene acetal of 1,2:5,6-*O*-cyclohexylidene-*myo*-inositol (**13**) (23) also appear to be contrary to the predictions made here because the two oxygen atoms in the acetal are equatorial and flanked by equatorial and axial groups if the inositol ring is present in a

Can. J. Chem. Downloaded from www.nrcresearchpress.com by 88.85.125.76 on 09/07/12
For personal use only.

chair conformation. However, the vicinal coupling constants in the ^{1}H nmr spectrum of **13** (23) show that it is not present in a chair conformation, making predictions unreliable. The results of benzylation of compound **12** (23) are similar to those with similar adjacent stereochemistry, **3***b* and **7**, as expected.

Conclusions

The regioselectivity of reactions of dibutylstannylene acetals derived from *trans*-1,2-diols on six-membered rings with electrophiles in the absence of added nucleophiles is determined by the structure of the dimer and (or) oligomers present in solution. In a dimer, two of the oxygen atoms are dicoordinate and two are tricoordinate. If only a single dimer is present, reaction occurs on the two dicoordinate oxygen atoms. The structures of the dimers or oligomers formed are determined by the stereochemistry of the substituents on carbons adjacent to the diol oxygens. Axial substituents destabilize species that have the adjacent oxygen atom tricoordinate, probably because of repulsive steric interactions between the axial substituent and one of the butyl groups on tin. As a result, compounds with one adjacent substituent axial and the other equatorial exist mainly as single dimers and give virtually regiospecific reactions on the oxygen atom adjacent to the axial substituent. Compounds having other stereochemistries for adjacent substituents do not give highly regioselective reactions and exist as mixtures of dimers and (or) higher oligomers.

Experimental

Melting points were determined using a Fisher–Johns melting point apparatus and are uncorrected. Rotations were measured with a Perkin–Elmer model 141 polarimeter. Elemental analyses were performed by Canadian Microanalytical Service Ltd., Vancouver, B.C. Thin-layer chromatography (tlc) was performed on 0.20 mm thick Merck silica gel 60F-254 aluminum sheets cut to be approximately 7 cm long. Components were located by spraying with 2% ceric sulfate in 2 N sulfuric acid and heating on a hot plate for a few minutes at 150°C. Column chromatography was performed on 60–200 mesh silica gel. The ^{1}H, ^{13}C, and ^{119}Sn nmr spectra at 361.04, 90.79, and 134.62 MHz respectively were recorded on a Nicolet NT-360 NB spectrometer. The ^{119}Sn nmr spectra were recorded with gated broad-band decoupling on only during acquisition and pulse intervals of 0.85–3 s. The short pulse intervals were used because ^{119}Sn atoms in dialkyldialkoxytin compounds, where the tin atom is pentacoordinate or hexacoordinate, have T_1 values in the 10–200 ms range (29). Under these conditions, signal intensity will be directly related to the amount of ^{119}Sn present. The ^{119}Sn nmr chemical shifts were referenced to external tetramethyltin. The ^{1}H nmr spectra at 60 MHz and ^{13}C nmr spectra at 20 MHz were measured on Varian EM-360L and Varian CFT-20 spectrometers respectively. Solutions for ^{1}H and ^{13}C nmr spectra were prepared in chloroform-*d* with tetramethylsilane (TMS) as internal reference, unless stated otherwise. Chemical shifts are reported in ppm downfield from TMS. The ^{1}H nmr spectra were analysed on a first-order basis. The appearance of ^{13}C nmr signals in off-resonance decoupled or in coupled spectra are indicated in the experimental using the designations s, d, t, and q. Solid-state ^{13}C and ^{119}Sn nmr spectra were recorded on a Bruker MSL 200 nmr spectrometer at 50.32 and 74.54 MHz respectively. In the work-up of reactions, the final organic solutions were dried with anhydrous magnesium sulfate, then filtered. Acetylation reactions were performed by stirring the compound in dried pyridine and acetic anhydride at room temperature. Pyridine was dried by distilling from barium oxide after refluxing for 4 h, and it was maintained over anhydrous calcium sulfate. The term "pet ether" refers to petroleum ether 30–60°C.

Methyl 4,6-*O*-benzylidene-α-D-glucopyranoside (**1***a*) (30), benzyl 4,6-*O*-benzylidene-α-D-glucopyranoside (**2***a*) (12), benzyl 4,6-*O*-benzylidene-β-D-glucopyranoside (**3***a*) (31), and benzyl 4,6-*O*-benzylidene-β-D-galactopyranoside (**4***a*) (32) were prepared by standard methods and had physical constants in agreement with literature values. For most ^{13}C chemical shifts, see Table 2. The other values are δ: **1***a*, 137.1, 129.1, 128.2, 126.3 (Ph C); **1***b*, 136.9, 128.3, 129.4, 126.4 (Ph C), 27.0, 26.8 (β- and γ-Bu C), 23.5, 22.0 (α-Bu C), 13.6, 13.4 (δ-Bu C); **1***b* (solid state), 138.8, 138.5, 131.7, 131.3, 129.4, 128.9, 127.4 (Ph C), 28.5, 27.9, 27.0, 25.7 (β- and γ-Bu C), 23.1, 22.2 (α-Bu C), 15.9, 15.3, 14.3, 13.9 (δ-Bu C); **2***b*, 27.2, 27.0, 26.9, 26.7 (β- and γ-Bu C), 23.6, 21.9 (α-Bu C), 13.7, 13.6 (δ-Bu C); **3***b*, 27.2, 26.9, 26.7 (β- and γ-Bu C), 23.7, 22.1 (α-Bu C), 13.6, 13.5 (δ-Bu C), lower intensity signals, 23.8, 23.7, 13.7, 13.5; **4***a*, 137.4, 137.0, 129.2, 128.5, 128.2, 128.0, 126.4 (Ph C); **4***b* (chloroform-*d*), 138.0, 136.5, 128.7, 128.4, 128.3, 128.1, 127.8 (Ph C), 27.2, 27.0, 26.7 (β- and γ-Bu C), 23.7 ($^1J_{Sn,C}$ 586, 612 Hz), 22.6 ($^1J_{Sn,C}$ 580, 603 Hz) (α-Bu C), 13.7, 13.6 (δ-Bu C).

Sample preparation for nuclear magnetic resonance

Most solutions for ^{119}Sn nmr spectroscopy were prepared by refluxing equimolar amounts of the diol and di-*n*-butyltin oxide for 12 h in benzene in an apparatus for the azeotropic removal of water. The clear solutions in benzene were attached to a vacuum system, then concentrated to a solid. Previously dried and degassed nmr solvents, stored under vacuum over molecular sieves, were distilled under vacuum onto the solid. The resulting solutions were transferred through a sintered glass frit under vacuum to the nmr tube, which was then sealed. A few samples were prepared under argon but not sealed.

*Benzyl 4,6-O-benzylidene-α-D-galactopyranoside (**5**a)*

A solution of D-galactose (100 g) and *p*-toluenesulfonic acid (5 g) in benzyl alcohol (188 mL) was kept at 70–80°C for 3 days, cooled, and then poured into an excess of ether. The ether solution was stirred for 15 min and stored overnight at room temperature. The supernatant was decanted from a syrupy residue that contained both benzyl pyranosides. A mixture of this residue and zinc chloride (62.5 g) in benzaldehyde (188 mL) was stirred vigorously at room temperature for 3 h, then poured into a mixture of water (375 mL) and pet ether (375 mL). The solution was stirred for 30 min. The oily product was separated using a separatory funnel, then dissolved in the minimum volume of hot ethanol (containing ammonia). The ethanolic solution was poured into excess water. The oily product was again separated, then fractionated into α and β anomers by column chromatography on silica gel using 4:1 chloroform–THF as eluent (R_f's 0.42, 0.24). The title compound (**5***a*) was recrystallized from ethanol as fine needles, mp 109–110°C, $[\alpha]_D^{22.5}$ +109.4° (*c* 1.2, chloroform) (lit. (33) mp 108–109°C, $[\alpha]_D^{20}$ +117°); ^{1}H nmr δ: 3.60 (1H, br s, H-5), 3.92 (2H, m, H-2 and H-3), 3.98 (1H, dd, $J_{6,6'}$ = 12.53 Hz, $J_{5,6}$ = 1.49 Hz, H-6), 4.17 (1H, m, H-4), 4.18 (1H, dd, $J_{5,6'}$ = 1.27 Hz, H-6'), 4.60 and 4.72 (2H, 2d, J = 11.92 Hz, $PhCH_2$), 5.11 (1H, d, $J_{1,2}$ = 1.91 Hz, H-1), 5.50 (1H, s, benzal H), 7.26–7.50 (10H, m, Ph H), ^{13}C nmr δ: 63.0 (d, C-5), 69.1 (dd, C-6), 69.4, 69.5 (2 d, C-2 and C-3), 70.0 (t, $PhCH_2$), 76.0 (d, C-4), 98.7 (d, C-1), 101.0 (d, benzal C), 126.0–137.5 (Ph C).

General procedure for preparation of di-n-butylstannylene derivatives of monosaccharides

An equimolar mixture of monosaccharide and di-*n*-butyltin oxide in benzene was refluxed 12 h in an apparatus equipped for the azeotropic removal of water. Evaporation of solvent under reduced pressure gave the crude stannylene derivative, which was used for acylation and alkylation reactions without further purification.

*Benzylation of **3**a*

To a solution of stannylene derivative of **3***a* (1 mmol) in benzene (25 mL) was added powdered molecular sieves (type 4A, 1 g), tetra-*n*-butylammonium iodide (0.37 g, 1 mmol), and benzyl bromide (520 μL, 4.4 mmol). The mixture was refluxed for 24 h, then cooled and filtered. The filtrate was diluted with dichloromethane (50 mL). The resulting solution was washed with a 1 M sodium thiosulfate solution (20 mL) and with water (2 × 20 mL), then dried and concentrated. The syrup was dissolved in chloroform and filtered through a short column of silica gel to give a mixture of **3***c* and

Can. J. Chem. Downloaded from www.nrcresearchpress.com by 88.85.125.76 on 09/07/12
For personal use only.

3*d* (340 mg). The major component was benzyl 3-*O*-benzyl-4,6-*O*-benzylidene-β-D-glucopyranoside (**3***d*); ^{1}H nmr δ: 2.43 (1H, d, $J_{H,H}$ = 1.96 Hz, HO-2), 3.40–3.48 (1H, m, H-5), 3.6 (1H, dd, H-2), 4.38 (1H, dd, H-6$_{eq}$), 4.50 (1H, d, $J_{1,2}$ = 7.45 Hz, H-1), 4.63–5.00 (CH_2Ph), 5.58 (1H, s, benzal H), 7.25–7.50 (m, Ph); ^{13}C nmr δ: 66.6 (d, C-5), 68.8 (dd, C-6), 71.4 (t, $PhCH_2$-O C-1), 74.4 (d, C-2), 74.6 (t, $PhCH_2$-O C-3), 80.3 (d, C-4), 81.4 (d, C-3), 101.3 (d, benzal C), 102.3 (d, C-1). The minor component was benzyl 2-*O*-benzyl-4,6-*O*-benzylidene-β-D-glucopyranoside (**3***c*); ^{1}H nmr δ: 2.48 (1H, d, J = 2.0 Hz, HO-3), 3.40–3.48 (1H, m, H-5), 4.63–5.00 (CH_2Ph), 4.65 (1H, d, H-1), 5.53 (1H, s, benzal H); ^{13}C nmr δ: 66.2 (d, C-5), 68.8 (dd, C-6), 71.6 (t, $PhCH_2$-O C-1), 73.3 (d, C-3), 74.9 (t, $PhCH_2$-O C-2), 80.5 (d, C-4), 81.9 (d, C-2), 101.8 (d, benzal C), 102.8 (d, C-1). The mixture was acetylated and the components in the mixture of the acetates were identified by assignment of signals of skeletal protons with shifts greater than 5 ppm by means of single frequency homonuclear decoupling experiments starting with the doublet of H-1 from the major isomer. The major isomer was benzyl 2-*O*-acetyl-3-*O*-benzyl-4,6-*O*-benzylidene-β-D-glucopyranoside (**3***f*); ^{1}H nmr δ: 1.95 (3H, s, $COCH_3$), 3.43 (1H, dt, H-5), 3.69 (1H, t, J = 9.10 Hz, H-3), 3.801 (1H, t, J = 9.4 Hz, H-4), 3.83 (1H, t, J = 10.3 Hz, H-6$_{ax}$), 4.38 (1H, dd, $J_{6eq,6ax}$ = 10.46 Hz, $J_{5,6eq}$ = 4.96 Hz, H-6$_{eq}$), 4.52 (1H, d, $J_{1,2}$ = 7.94 Hz, H-1), 4.589, 4.879 (2H, 2d, J = 12.35 Hz, CH_2Ph), 4.659, 4.864 (2H, 2d, J = 12.12 Hz, CH_2Ph), 5.10 (1H, dd, $J_{1,2}$ = 7.98 Hz, $J_{2,3}$ = 9.00 Hz, H-2), 5.58 (1H, s, benzal H), 7.30–7.50 (m, Ph H). The minor isomer was benzyl 3-*O*-acetyl-2-*O*-benzyl-4,6-*O*-benzylidene-β-D-glucopyranoside (**3***e*); ^{1}H nmr δ: 2.08 (3H, s, $COCH_3$), 3.494 (1H, dd, $J_{1,2}$ = 7.79 Hz, $J_{2,3}$ = 9.14 Hz, H-2), 3.50 (1H, m, H-5), 3.595 (1H, t, J = 9.5 Hz, H-4), 3.785 (1H, t, J = 10.1 Hz, H-6$_{ax}$), 4.64, 4.66, 4.86, 4.96 (4H, 4d, J = 11.8, 12.3 Hz, 2 CH_2Ph), 4.72 (1H, d, $J_{1,2}$ = 7.7 Hz, H-1), 5.31 (1H, t, J = 9.3 Hz, H-3), 5.46 (1H, s, benzal H), 7.30–7.50 (15H, m, Ph H).

The ratios of **3***c* to **3***d* obtained from the peak heights of H-1 in the spectra of the mixture and of the acetylated mixture were 28:72. Thus, the overall yields for **3***c* and **3***d* were 21 and 55% respectively.

Benzoylation of **3**a

A solution of benzoyl chloride (130 μL, 1.1 mmol) in benzene (25 mL) was added dropwise over 30 min to a vigorously stirred mixture of **3***b* (1 mmol) and powdered molecular sieves (type 4A, 1 g) in benzene (50 mL). After being stirred for 2 h, the mixture was filtered. The filtrate was diluted with dichloromethane (100 mL) and the solution was washed with water (2 × 25 mL), dried, and concentrated. The resulting solid was separated by column chromatography on silica gel using chloroform–hexane – ethyl acetate (6:3:1) as eluent. The first fraction (102 mg, 22%) was recrystallized from ethyl acetate and pet ether to give fine needles of benzyl 3-*O*-benzoyl-4,6-*O*-benzylidene-β-D-glucopyranoside (**3***g*); mp 168–169°C, $[\alpha]_D^{25}$ −105.5° (*c* 0.77, chloroform) (lit. (13) mp 167–169°C, $[\alpha]_D$ −103.5°); ^{1}H nmr δ: 2.62 (1H, d, $J_{2,OH}$ = 3.14 Hz, OH-2), 3.60 (1H, dt, $J_{4,5}$ = $J_{5,6ax}$ = 9.5 Hz, $J_{5,6eq}$ = 4.82 Hz, H-5), 3.80 (1H, ddd, $J_{1,2}$ = 7.68 Hz, $J_{2,3}$ = 9.7 Hz, H-2), 3.84 (1H, t, $J_{3,4}$ = $J_{4,5}$ = 9.6 Hz, H-4), 3.86 (1H, t, H-6$_{ax}$), 4.42 (1H, dd, $J_{6eq,6ax}$ = 10.51 Hz, H-6$_{eq}$), 4.65 (1H, d, H-1), 4.69, 4.97 (2H, 2d, J = 11.65 Hz, $PhCH_2$), 5.48 (1H, t, $J_{3,4}$ = $J_{2,3}$ = 9.7 Hz, H-3), 5.54 (1H, s, benzal H), 7.20–8.10 (15H, m, Ph H); ^{13}C nmr δ: 66.6 (C-5), 68.7 (C-6), 71.6 (CH_2Ph), 73.6 (C-2), 74.2 (C-3), 78.6 (C-4), 101.5 (C-7), 102.5 (C-1), 126.1–136.8 (Ph C), 166.4 (C=O). A mixed fraction (152 mg) was followed by another solid (164 mg, 35%), which was recrystallized from the same solvent mixture to give fine needles of benzyl 2-*O*-benzoyl-4,6-*O*-benzylidene-β-D-glucopyranoside (**3***h*); mp 154–155.5°C; $[\alpha]_D^{25}$ −78.6° (*c* 0.91, chloroform) (lit. (13) mp 154–156°C; $[\alpha]_D$ −96.4° (*c* 0.44, chloroform)); ^{1}H nmr δ: 2.72 (1H, d, $J_{3,OH}$ = 3.14 Hz, OH-3), 3.51 (1H, dt, $J_{5,6eq}$ = 4.89 Hz, $J_{4,5}$ = $J_{5,6ax}$ = 9.8 Hz, H-5), 3.70 (1H, t, $J_{3,4}$ = $J_{4,5}$ = 9.2 Hz, H-4), 3.86 (1H, t, $J_{5,6ax}$ = $J_{6eq,6ax}$ = 10.4 Hz, H-6$_{ax}$), 4.01 (1H, dt, $J_{2,3}$ = $J_{3,4}$ = 9.2 Hz, H-3), 4.42 (1H, dd, H-6$_{eq}$), 4.65, 4.88 (2H, 2d, J = 12.52 Hz, $PhCH_2$), 4.71 (1H, d, $J_{1,2}$ = 7.91 Hz, H-1), 5.26 (1H, dd, $J_{2,3}$ = 9.17 Hz, H-2), 5.58 (1H, s, benzal H), 7.20–8.02 (15H, m, Ph H); ^{13}C nmr δ: 66.2 (C-5), 68.6 (C-6), 70.6 (CH_2Ph), 72.5 (C-3), 74.8 (C-2), 80.9 (C-4), 99.7 (C-1), 101.9 (C-7), 126.3–136.9 (Ph C), 165.9 (C=O). The mixed fraction consisted of **3***h* and **3***g* in the ratio of 23:27 as measured by ^{1}H nmr peak heights, giving overall yields of **3***h* and **3***g* of 53 and 37%, respectively.

Benzylation of **5**a

To a solution of stannylene derivative of **5***a* (0.5 mmol) in benzene (20 mL) was added powdered molecular sieves (type 4A, 0.5 g), tetra-*n*-butylammonium bromide (161 mg, 0.5 mmol), and benzyl bromide (65 μL, 0.55 mmol). The mixture was refluxed for 48 h, then cooled and filtered. The filtrate was diluted with dichloromethane (50 mL) and the solution was washed with water (2 × 20 mL), dried, and concentrated to a syrup that was separated by column chromatography on silica gel using 9:1 chloroform – ethyl acetate as eluent. The first fraction, a solid (80 mg, 36%), was crystallized from ethyl acetate and pet ether to give fine needles containing benzyl 3-*O*-benzyl-4,6-*O*-benzylidene-α-D-galactopyranoside (**5***f*) and one equivalent of water of crystallization; mp 134–136°C, $[\alpha]_D^{22.5}$ +128.3° (*c* 0.71, chloroform); ^{1}H nmr δ: 1.580 (2H, s, H_2O of crystallization), 2.194 (1H, d, $J_{2,OH}$ = 7.05 Hz, OH), 3.59 (1H, br s, H-5), 3.842 (1H, dd, $J_{2,3}$ = 10.01 Hz, $J_{3,4}$ = 3.40 Hz, H-3), 3.976 (1H, dd, $J_{5,6}$ = 1.64 Hz, $J_{6,6'}$ = 12.55 Hz, H-6), 4.188 (1H, dd, $J_{5,6'}$ = 1.49 Hz, H-6′), 4.21 (1H, narrow m, H-4), 4.24 (1H, ddd, H-2), 4.75 (2H, s, $PhCH_2$-O C-3), 4.74 and 4.66 (2H, 2d, $J_{H,H}$ = 11.97 Hz, $PhCH_2$-O C-1), 5.20 (1H, d, $J_{1,2}$ = 3.79 Hz, H-1), 5.45 (1H, s, benzal H), 7.27–7.93 (15H, m, Ph H). Anal. calcd. for $C_{27}H_{28}O_6 \cdot H_2O$: C 69.51, H 6.48; found: C 69.52, H 6.45. A mixed fraction (75 mg) was followed by a solid (50 mg, 22%), which was also recrystallized from ethyl acetate and petroleum ether to give fine needles of benzyl 2-*O*-benzyl-4,6-*O*-benzylidene-α-D-galactopyranoside (**5***e*); mp 131.5–133.5°C, $[\alpha]_D^{22.5}$ +88.7° (*c* 0.62, chloroform) (lit. (24) mp 131.5–133°C, $[\alpha]_D$ +103°); ^{1}H nmr δ: 2.422 (1H, d, $J_{3,OH}$ = 7.43 Hz, OH), 3.69 (1H, br s, H-5), 3.85 (1H, dd, $J_{1,2}$ = 3.47 Hz, $J_{2,3}$ = 9.95 Hz, H-2), 4.03 (1H, dd, $J_{6,6'}$ = 12.55 Hz, $J_{5,6}$ = 1.62 Hz, H-6), 4.20 (1H, dd, $J_{5,6'}$ = 1.19 Hz, H-6$_{eq}$), 4.22 (1H, ddd, H-3), 4.30 (1H, br d, $J_{3,4}$ = 3.7 Hz, H-4), 4.552, 4.575, 4.694, 4.694 (4H, 4d, J = 11.26, 11.52 Hz, 2 CH_2Ph), 5.06 (1H, d, $J_{1,2}$ = 3.42 Hz, H-1), 5.56 (1H, s, benzal H), 7.09–7.52 (15H, m, Ph H). Anal. calcd. for $C_{27}H_{28}O_6$: C 72.31, H 6.29; found: C 72.07, H 6.29.

The mixed fraction consisted of **5***e* and **5***f* in the ratio of 3:2 as measured by ^{1}H nmr spectroscopy. Thus, the overall yields for **5***e* and **5***f* were 43 and 49%.

Benzoylation of **5**a

5*b* (1 mmol) was benzoylated exactly as for **3***b*. The resulting syrup was separated by column chromatography on silica gel using chloroform – ethyl acetate (99:1) as eluent. The first fraction, a solid (84 mg, 18%), was recrystallized from ethyl acetate and pet ether to give fine colorless needles of benzyl 3-*O*-benzoyl-4,6-*O*-benzylidene-α-D-galactopyranoside (**5***h*); mp 148–149°C, $[\alpha]_D^{25}$ +218.9° (*c* 1.14, chloroform); ^{1}H nmr δ: 2.02 (1H, d, $J_{2,OH}$ = 10.71 Hz, OH-2), 3.77 (1H, br s, H-5), 4.04 (1H, dd, $J_{5,6}$ = 1.34 Hz, $J_{6,6'}$ = 10.50 Hz, H-6), 4.24 (1H, dd, $J_{5,6'}$ = 1.30 Hz, H-6′), 4.35 (1H, dt, $J_{1,2}$ = 3.75 Hz, $J_{2,3}$ = $J_{2,OH}$ = 10.7 Hz, H-2), 4.49 (1H, d, $J_{3,4}$ = 3.39 Hz, H-4), 4.66, 4.80 (2H, 2d, J = 11.79 Hz, $PhCH_2$), 5.24 (1H, d, H-1), 5.43 (1H, dd, H-3), 5.52 (1H, s, benzal H), 7.25–8.08 (15H, m, Ph H). Anal. calcd. for $C_{27}H_{26}O_7$: C 70.12, H 5.67; found: C 70.10, H 5.51. A mixed fraction (234 mg) was followed by a syrup (75 mg, 16%), which was crystallized from the same solvent mixture to give fine colorless needles of benzyl 2-*O*-benzoyl-4,6-*O*-benzylidene-α-D-galactopyranoside (**5***g*); mp 118–119°C; $[\alpha]_D^{25}$ +144.6° (*c* 0.88, chloroform); ^{1}H nmr δ: 2.43 (1H, d, $J_{3,OH}$ = 10.43 Hz, OH-3), 3.82 (1H, br s, H-5), 4.08 (1H, dd, $J_{5,6}$ = 1.60 Hz, $J_{6,6'}$ = 12.51 Hz, H-6), 4.29 (1H, dd, $J_{5,6'}$ = 1.00 Hz, H-6′), 4.36 (1H, br s, H-4), 4.38 (1H, m, H-3), 4.62, 4.76 (2H, 2d, J = 12.38 Hz, $PhCH_2$), 5.30 (1H, d, $J_{1,2}$ = 3.53 Hz, H-1), 5.40 (1H, dd, $J_{2,3}$ = 9.82 Hz, H-2), 5.59 (1H, s, benzal H), 7.23–8.09 (15H, m, Ph H). Anal. calcd. for $C_{27}H_{26}O_7$: C 70.12, H 5.67; found: C 69.99, H 5.67. The mixed

fraction consisted of **5***g* and **5***h* in the ratio of 11:14 as measured from the average of several ^{1}H nmr peak heights, to give overall yields of **5***g* and **5***h* of 38 and 46%, respectively.

A reaction conducted exactly as above, but with 1,2-dimethoxyethane as solvent and with triethylamine (154 μL, 1 mmol) present, gave a mixture of **5***g* and **5***h* in the ratio of 51:49 as measured from ^{1}H nmr peak heights from a sample of the crude product.

Acknowledgements

We thank Drs. R. Wasylishen and M. McKinnon for recording the solid-state nmr spectra and Dr. N. Burford for help with preparing nmr samples under vacuum. We are grateful to the Atlantic Research Laboratories of NRC for use of their polarimeter. The financial support of the Natural Sciences and Engineering Research Council of Canada is gratefully acknowledged.

1. D. WAGNER, J. VERHEYDEN, and J. G. MOFFATT. J. Org. Chem. **39**, 24 (1974); S. DAVID. C.R. Acad. Sci. Ser. C, **278**, 1051 (1974).
2. S. DAVID and S. HANESSIAN. Tetrahedron, **41**, 643 (1985); M. PEREYRE, J.-P. QUINTARD, and A. RAHM. Tin in organic synthesis. Butterworths, London. 1987. Chap. 11; S. J. BLUNDEN, P. A. CUSAK, and P. J. SMITH. J. Organomet. Chem. **325**, 141 (1987).
3. J. ALAIS, A. MARANDUBA, and A. VEYRIERES. Tetrahedron Lett. **23**, 2383 (1983).
4. S. DAVID, A. THIEFFRY, and A. VEYRIERES. J. Chem. Soc. Perkin Trans. 1, 1796 (1981).
5. C. W. HOLZAPFEL, J. M. KOEKEMOER, and C. F. MARAIS. S. Afr. J. Chem. **37**, 19 (1984).
6. T. B. GRINDLEY and R. THANGARASA. Can. J. Chem. In preparation.
7. S. DAVID, A. THIEFFRY, and A. FORCHIONI. Tetrahedron Lett. **22**, 2647 (1981).
8. A. G. DAVIES, A. J. PRICE, H. M. DAWES, and M. B. HURSTHOUSE. J. Chem. Soc. Dalton Trans. 297 (1986).
9. S. DAVID, C. PASCARD, and M. CESARIO. Nouv. J. Chim. **3**, 63 (1979).
10. C. W. HOLZAPFEL, J. M. KOEKEMOER, C. F. MARAIS, G. J. KRUGER, and J. A. PRETORIUS. S. Afr. J. Chem. **35**, 81 (1982).
11. T. B. GRINDLEY and R. THANGARASA. J. Am. Chem. Soc. **112**, 1364 (1990).
12. T. D. INCH and G. J. LEWIS. Carbohydr. Res. **22**, 91 (1972).
13. A. LIPTAK, E. CSIK, and P. NANASI. Acta Chim. Acad. Sci. Hung. **94**, 267 (1977).
14. P. J. SMITH, R. F. M. WHITE, and L. SMITH. J. Organomet. Chem. **40**, 341 (1972); J. D. KENNEDY. J. Chem. Soc. Perkin Trans. 2, 242 (1977).
15. S. ROELENS and M. TADDEI. J. Chem. Soc. Perkin Trans. 2, 799 (1985).
16. S. J. BLUNDEN, P. J. SMITH, P. J. BEYNON, and D. G. GILLIES. Carbohydr. Res. **88**, 9 (1981).
17. R. M. MUNAVU and H. H. SZMANT. J. Org. Chem. **41**, 1832 (1976).
18. S. DAVID and A. THIEFFRY. J. Chem. Soc. Perkin Trans. 1, 1568 (1979).
19. T. OGAWA and T. KABURAGI. Carbohydr. Res. **103**, 53 (1982).
20. A. FERNANDEZ-MAYORALAS, M. BERNABE, and M. MARTIN-LOMAS. Tetrahedron, **15**, 4877 (1988).
21. K. TAKEO and K. SHIBATA. Carbohydr. Res. **133**, 147 (1984).
22. C. MONNERET, R. GAGNET, and J.-C. FLORENT. J. Carbohydr. Chem. **6**, 221 (1987).
23. P. J. GAREGG, B. LINDBERG, I. KVARNSTROM, and S. C. T. SVENSSON. Carbohydr. Res. **173**, 205 (1988).
24. P. A. GENT and R. GIGG. J. Chem. Soc. Perkin Trans. 1, 1446 (1974).
25. G. A. OLAH, H. DOGGWEILER, J. D. FELBERG, and S. FROHLICH. J. Org. Chem. **50**, 4847 (1985).
26. T. B. GRINDLEY and C. WICKRAMAGE. J. Carbohydr. Chem. **4**, 171 (1985); T. B. GRINDLEY, C. J. P. COTE, and C. WICKRAMAGE. Carbohydr. Res. **140**, 215 (1985); T. B. GRINDLEY and C. WICKRAMAGE. Carbohydr. Res. **167**, 105 (1987).
27. C. PICARD, P. TISNES, and L. CAZAUX. J. Organomet. Chem. **315**, 277 (1986).
28. D. K. LAVALLEE, M. D. BAUGHMAN, and M. P. PHILLIPS. J. Am. Chem. Soc. **99**, 718 (1977).
29. T. B. GRINDLEY, R. D. CURTIS, R. THANGARASA, and R. E. WASYLISHEN. Can. J. Chem. Submitted.
30. D. M. HALL. Carbohydr. Res. **86**, 158 (1980).
31. A. KLEMER. Chem. Ber. **92**, 218 (1959).
32. J. R. TURVEY and T. P. WILLIAMS. J. Chem. Soc. 2119 (1962).
33. A. LIPTAK, I. JODAL, and P. NANASI. Carbohydr. Res. **44**, 1 (1975).

Can. J. Chem. Downloaded from www.nrcresearchpress.com by 88.85.125.76 on 09/07/12
For personal use only.

Structure and stereochemistry of a 7-phosphabicyclo[2.2.1]hept-2-ene-7-oxide from X-ray, multinuclear NMR, and 2D-*J* resolved NMR studies[1]

MARTIN B. HOCKING[2] AND GORDON W. BUSHNELL
Department of Chemistry, University of Victoria, Victoria, B.C., Canada V8N 2Y2

Received November 20, 1989

This paper is dedicated to Professor Arthur S. Perlin on the occasion of his 67th birthday

MARTIN B. HOCKING and GORDON W. BUSHNELL. Can. J. Chem. **68**, 1020 (1990).

Preparations of a 7-phosphanorbornene, from the reaction of 1,2,5-triphenylphosphole-1-oxide with inhibited acrylonitrile in benzene, were repeated under various conditions to determine if one, or more than one, stereoisomer was formed. Adduct formation failed to occur when the reaction was attempted in ethanol, or when the precursor 1,2,5-triphenylphosphole was substituted for the phosphole oxide. Elemental analysis and spectroscopic measurements confirmed that a 1:1 adduct had been obtained, and an X-ray structure determination of the ethanol complex established that this was 5-cyano-1,4,7-triphenyl-7-phosphabicyclo[2.2.1]hept-2-ene-7-oxide, **3***a*. Details of the ^{1}H, ^{13}C, and ^{31}P NMR assignments, of potential value in the structural assignment of other similar adducts, are related to previous results. The results of a brief mass spectrometric analysis of the changes in the thermal fragmentation pattern of the adduct with temperature are discussed in relation to the synthetic reaction.

Key words: phosphole adduct, phosphanorbornene, phosphabicycloheptene, acrylonitrile.

MARTIN B. HOCKING et GORDON W. BUSHNELL. Can. J. Chem. **68**, 1020 (1990).

Dans le but de déterminer s'il se forme un ou plusieurs stéréoisomères, on a fait varier les conditions expérimentales utilisées lors de préparations d'un 7-phosphanorbornène par réaction du 1,2,5-triphénylphosphole-1-oxyde avec de l'acrylonitrile inhibé, dans le benzène. Il n'y a pas de formation d'adduit lorsqu'on essaye de réaliser la réaction dans l'éthanol ou lorsqu'on essaye de substituer l'oxyde par le 1,2,5-triphénylphosphole. Des analyses élémentaires et des données spectroscopiques ont permis de confirmer qu'un adduit 1:1 est obtenu et la diffraction des rayons-X du complexe avec l'éthanol a permis d'établir sa structure, le 5-cyano-1,4,7-triphényl-7-phosphabicyclo[2.2.1]hept-2-ène-7-oxyde, **3***a*. On a établi une corrélation entre les attributions détaillées de ses spectres RMN du ^{1}H, du ^{13}C et du ^{31}P et ceux obtenus antérieurement; ces données peuvent s'avérer utiles pour déterminer les structures d'adduits semblables. On a déterminé la variation des patrons de fragmentation des spectres de masse de l'adduit en fonction de la température; on discute de ces variations en relation avec la réaction de synthèse.

Mots clés : adduit de phosphole, phosphanorbornène, phosphabicycloheptène, acrylonitrile.

[Traduit par la revue]

Introduction

1,2,5-Triphenylphosphole-1-oxide was known to form a 1:1 adduct with acrylonitrile from elemental analysis data (1), and subsequent NMR studies enabled an assignment of its stereochemistry (2). As part of a current, more comprehensive study of the behaviour of the phosphole ring under Diels–Alder reaction conditions, this preparation was repeated several times to provide further samples for more detailed study. Careful work-ups, followed by an X-ray crystal structure determination, were used to confirm the original adduct ratio and the previously assigned stereochemistry (2), and to determine whether a single or several stereoisomers were formed. Stereochemical details of the adduct were found to be in accord with those predictable from Woodward–Hoffman theory. Finally, it was anticipated that application of unequivocally determined proton, phosphorus, and carbon NMR parameters for this adduct would be valuable aids to the establishment of the structure and stereochemistry of other adducts in the series.

Experimental

Melting points were determined on an Electrothermal model A/FBM/AJB apparatus using a calibrated thermometer, and are uncorrected. Infrared spectra were recorded on a Perkin Elmer 1320 instrument using Nujol mulls between sodium chloride plates. Chemical ionization mass spectra were obtained from a Finnigan model 3300 quadrupole GC/MS system. Electron impact spectra were obtained using the Finnigan, using an LKB 9000 instrument equipped with a Varian data processing unit, and for the accurate mass determinations a Kratos (AEI) MS 50 instrument operated in 10 000 resolution mode, in all cases using a heated solid inlet probe. Ion source conditions for all electron impact spectra were as follows: energy, 70 eV; temperature, 290°C; current, 60 mA.

*Preparation of 1,2,5-triphenylphosphole **1**, and its 1-oxide **2***

The phosphole was prepared by heating (*E,E*)-1,4-diphenyl-1,3-butadiene with dichlorophenylphosphine at 215°C using the original procedure (3). The crude product was recrystallized from chloroform, mp 186–188°C (lit. (3) mp 186.5–187.5°C). ^{31}P NMR ($CDCl_3$): proton decoupled, +3.28 ppm (lit. (4) +3 ppm); coupled, an apparent quintet, low to high field: peak number, relative intensity, (separation, Hz, to next peak) 1, 1.0, (9.1); 2, 3.2, (9.2); 3, 4.5, (9.1); 4, 3.1, (9.8); 5. 0.95.

The phosphole oxide **2** was obtained from a solution of 1,2,5-triphenylphosphole (15.00 g; 48.0 mmol) dissolved in 1.3 L of a warm 1.7:1 (by volume) mixture of ethyl acetate and ethanol, by oxidation with 13 mL (114 mmol) of 30% aqueous hydrogen peroxide. Concentration and cooling gave two crops of yellow prisms (9.94 g; 63%). Recrystallization from ethyl acetate gave material that melted at 239–240°C (lit. (1, 3) mp 237.5–238°C).

*Preparation of phosphole oxide – acrylonitrile adduct, **3***

1,2,5-Triphenylphoshole-1-oxide (1.40 g, 4.26 mmol) was dissolved in hot benzene (100 mL) that had just been azeotropically dried. Acrylonitrile (BDH, 3.0 mL, 45 mmol) was then added, with retention of the *p*-methoxyphenol (50 ppm) inhibitor, and then boiled under reflux, protected from atmospheric moisture, for 6 h. The benzene was then evaporated from the now pale yellow solution under reduced pressure using a 50°C water bath, and the residual amorphous pale

[1]Presented at the 72nd Canadian Chemical Conference, Victoria, B.C., Canada, June 4–8, 1989; and at the Second International Conference of Heteroatom Chemistry, Albany, New York, July 17–21, 1989.

[2]Performed partly during this author's tenure as a Research Fellow, Department of Chemistry, University College London, 1987–1988.

Can. J. Chem. Downloaded from www.nrcresearchpress.com by 88.85.125.76 on 09/07/12
For personal use only.

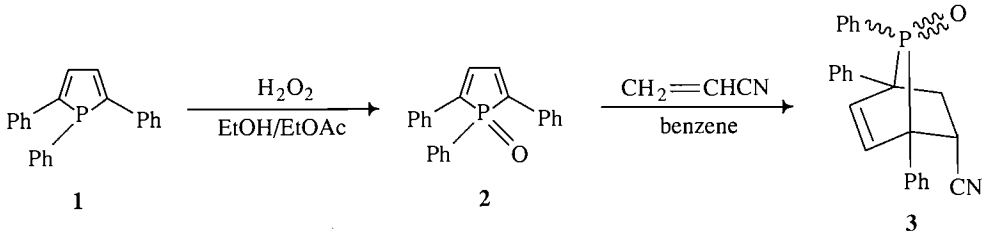

SCHEME 1

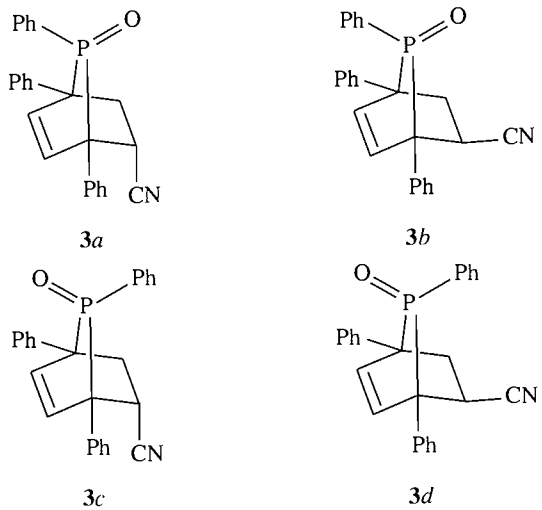

yellow powder (1.45 g) recrystallized twice from 100% ethanol. Colourless prisms of pure 5-cyano-1,4,7-triphenyl-7-phosphabicyclo [2.2.1]hept-2-ene-7-oxide, **3**, 0.80 g, mp 183–186°C (lit. (1) mp 180°C; (2) mp 174.6–176.6°C) were obtained. Anal. calcd. for $C_{25}H_{20}NOP$: C 78.73, H 5.29, N 3.67, P 8.12; found: C 78.96, H 5.43, N 3.55, P 7.65. Accurate mass determination calcd. for $C_{25}H_{20}NOP$: 381.1282; found: 381.1277. A second crop of a further 0.23 g was also obtained; purified yield on phosphole oxide, 63%. Crystals of this pure material were used for the spectroscopic data below and the NMR experiments.

Spectroscopic details: IR (Nujol mull); 2245s (CN), 1450m (P—Ph), 1190s (P=O), 760s, 700s (C—Ph arom.), 750m, 690m (P—Ph arom.) cm^{-1}; NMR, see Tables 1–3. Low resolution electron impact ms, probe temperature 63°C: no molecular ion, m/z (relative intensity): 328(3), 327(2), 259(2), 258(21), 257(100), 256(10), 255(3), 254(2), 251(2), 242(1), 241(1), 240(1). Lower masses >3% of base: 215(3), 202(4), 180(5), 179(3), 153(2), 152(3), 128(3), 115(4), 102(3), 91(17), 77(6.5), 51(3). Low resolution methane chemical ionization ms, probe temperature 250°C: $M+1$, 382 (100); $M+29$, 410 (15); $M+41$, 422 (6), established molecular weight as 381.

Selected accurate mass data, Kratos (AE) MS 50, inlet probe temperature 150°C; measured mass found, fragment formula, mass deviation from calculated (millimass units): 381.1277, $C_{25}H_{20}NOP$, (−0.5), parent ion; 328.1010, $C_{22}H_{17}OP$, (−0.7), phosphole oxide **2**; 257.1204, $C_{19}H_{15}N$, (0.0), parent ion less PhPO; 256.1120, $C_{19}H_{14}N$, (−0.7), parent ion less PhPO(H); 251.0664, $C_{16}H_{12}OP$, (3.9), acrylonitrile plus phenyl loss; 230.1094, $C_{18}H_{14}$, (−0.2), terphenyl; 180.0822, $C_{13}H_{10}N$, (0.8), PhPO plus phenyl loss; 124.0043, C_6H_5OP, (−3.5), PhPO bridge; 91.0550, C_7H_7, (0.2), tropylium; 77.0406, C_6H_5, (1.5), phenyl.

Crystals for X-ray diffraction measurements were successfully obtained from a hot filtered solution of 250 mg of pure adduct in 5 mL of 100% ethanol diluted with a further 3 mL of ethanol at ambient temperature. Slow initial solvent evaporation plus use of a seed crystal eventually yielded suitable crystals.

X-ray structure

The colourless crystal of compound **3** gave a well-defined optical extinction between crossed polars. It was mounted on the a-axis in a Lindemann tube and subjected to Weissenberg and precision photography using CuK_α radiation. The compound was found to be monoclinic, space group $P2_1/c$ (No. 14), and approximate unit cell dimensions were established. The crystal was then transferred to a Picker 4-circle diffractometer automated with a PDP 11/10 computer and, using Zr filtered MoK_α radiation ($\lambda = 0.71069$ Å), the cell and matrix were refined using 20 2θ measurements in the range 20–44°, each measured in both the positive and negative directions. The crystal data are given in Table 4. Intensity measurements were made in the 2θ range 2–50° from $hkl = -12,0,0-+12,23,12$. The scanning was in 200 steps of 0.01° in 2θ counting for 0.5 s per step with background counting for 50 s at each end of the scan. Three standard reflections 4,0,0; 0,12,0; and 0,0,4 were measured before each batch of 50 reflections. 4037 reflections were measured. The measurements were corrected for absorption using a numerical integration method (5) and a Gaussian grid of 16 × 8 × 8 points. The crystal shape was defined by the following crystal face indices and perpendicular distances to the origin in mm: ±(100), 0.4795; ±(010), 0.1748; ±(001), 0.2944. The transmission range was 0.471–0.637. The intensities were corrected for Lorentz and polarisation effects, and reflections for which $I < 2.5\,\sigma(I)$ were omitted from the subsequent refinement. 2415 reflections were retained using this criterion. The SHELX-76 set of programs were used to solve and refine the structure. The phase problem yielded to direct methods. The structure was completed by successive Fourier maps, and was refined by least squares minimizing $\Sigma w\Delta^2$ where $\Delta = \| F_o| - |F_c \|$ and $w = 1/(\sigma^2(F) + 0.001\ F^2)$. The f-curves used were those built into the SHELX program, and anomalous dispersion corrections were done. All atoms, including H, were found. During the final stages of refinement, six of the H atoms were put in calculated positions at a C—H separation of 1.02 Å. The refinement converged with a maximum shift/esd (non-H) of 0.06. The final difference map had a maximum of 0.43 e $Å^{-3}$ and a minimum of 0.12 e $Å^{-3}$, and indicated that nothing had been missed. The final residuals were $R = 0.0695$, $R_w = 0.0839$, for 360 parameters and 2415 independent observations. Supplementary tables S1–S4, including observed and calculated structure factors, have been deposited.[3]

NMR data

Preliminary 60 MHz proton magnetic resonance spectra were recorded from deuteriochloroform solutions using tetramethylsilane as reference, on a JEOL JNM-PMX 60 spectrometer. Detailed interpretation was from proton NMR spectra obtained on a Bruker WM 250 (250 MHz) spectrometer, and from proton, phosphorus, and carbon NMR spectra obtained on a Varian VXR-400 (at 400, 161.92, and 100.59 MHz, respectively) spectrometer. Tetramethylsilane (TMS) or solvent deuterium was used for the lock signal on the high frequency spectrometers. Proton and carbon shifts are referenced to internal

[3]Supplementary tables S1–S4 may be purchased from the Depository of Unpublished Data, CISTI, National Research Council of Canada, Ottawa, Ont., Canada K1A 0S2.

Tables of atomic coordinates, interatomic distances, and bond angles for the hydrogen atoms have also been deposited with the Cambridge Crystallographic Data Centre, and can be obtained on request from The Director, Cambridge Crystallographic Data Centre, University Chemical Laboratory, Lensfield Road, Cambridge CB2 1EW, U.K.

Can. J. Chem. Downloaded from www.nrcresearchpress.com by 88.85.125.76 on 09/07/12
For personal use only.

Can. J. Chem. Downloaded from www.nrcresearchpress.com by 88.85.125.76 on 09/07/12
For personal use only.

TABLE 1. 400 MHz proton NMR data for nitrile adduct **3***a* in deuteriochloroform at room temperature

Proton assignment	Chemical shift (ppm)	Multiplicity	Coupling constants (Hz) Atom pair	|J|
H(2)[a]	7.03	d of d	H(2), H(3)	7.6
			H(2), P	11.1
H(3)[a]	6.92	d of d	H(3), H(2)	7.6
			H(3), P	9.6
H(5x)[b]	4.22	d of d (with structure)	H(5x), H(6x)	10.0
			H(5x), H(6n)	4.4
			H(5x), P	0.7
H(6n)	2.27	d of d of d	H(6n), H(6x)	12.3
			H(6n), H(5x)	4.4
			H(6n), P	24.5
H(6x)[b]	3.52	Complex triplet	H(6x), H(6n)	12.3
			H(6x), H(5x)	10.0
			H(6x), P	1.6
ortho H's[c] Ph on C(1)	7.51	d of multiplets (d of quartets)	H *ortho*, H *meta*	ca. 7.1
ortho H's[c] Ph on C(4)	7.64	d of multiplets (d of quartets)	H *ortho*, H *meta*	ca. 7.2
ortho H's[d] Ph on P(?)	7.19	t of doublets	J_t	7.7
			J_d	3.4

[a]Assignments determined by olefinic shift, correct matches of multiplicity and coupling constants, and two-stage NOE experiments (see Discussion).
[b]Assignments based on shift, multiplicity, decoupling experiments, and similar phosphorus couplings.
[c]Assignments based on NOE experiments to H(5x) and H(6x).
[d]Assignments tentatively based on influence of P coupling on apparent multiplicity.

TABLE 2. 161.92 MHz coupled phosphorus NMR data for nitrile adduct **3***a* in deuteriochloroform at room temperature[a]

Assignment	|J| (Hz)	P, H Torsion angle, (degrees)[b]
P,H(2)	11.1	144(2)
P,H(3)	9.6	144(3)
P,H(5x)	0.7	77(4)
P,H(6n)	24.5	160(3)
P,H(6x)	1.6	73(2)

[a]Proton-decoupled shift was +75.47 ppm (lit.(2), +75.5 ppm) from 85% phosphoric acid. Superimposed on the proton-coupled, apparent quintet was a fine structure of about 1 Hz presumably arising from couplings to H(5x) and H(6x) (see Table 1, and Discussion).
[b]Torsion angles were calculated from respective carbon, hydrogen, and phosphorus atomic coordinates. Estimated error (one standard deviation) given in parentheses.

TMS. Phosphorus shifts are referenced to external 85% phosphoric acid, positive values being downfield from the reference. Assignments were determined from decoupling experiments, measurement of nuclear Overhauser effects, connectivity experiments, and homonuclear and hetero-correlated 2D-*J* resolved experiments confirmed where necessary with the use of computer simulations.

Homonuclear 2D-*J* resolved experiments on protons were carried out at 399.95 MHz, spectral width 5000 Hz, 2D spectral width 50.0 Hz, acquisition time 0.41 s, pulse width 90°, first pulse 180°, FT size 4K × 256 using pseudo echo weighting and double precision acquisition. The proton–carbon heterocorrelated 2D-*J* resolved experiment was run at 100.6 MHz in the carbon domain, using sweep width 11376.6 Hz, acquisition time 0.090 s, with a delay of 1.500 s (recycle time 1.59 s) for 2048 data points, 128 transients per spectrum with decoupling during detection for C spectra; and in the proton domain using 4599.8 Hz sweep width for 256 experiments, again processed with a pseudo weighting function in both domains.

Results and discussion

Synthetic background

An isolated yield of 63% of a single stereoisomer of the phosphabicycloheptene was obtained from a 4 mmolar preparation, suggested by the relatively easy purification with high recovery, and a sharp melting point of the purified adduct. When the scale was raised to 50 mmolar the yield of purified product was raised to 82% (both based on starting phosphole oxide).

If the phosphole **1** was substituted for the phosphole oxide **2**, otherwise using the same conditions, the starting phosphole was recovered unchanged (6). Similarly, if the benzene solvent used in the reported preparation was replaced by ethanol under otherwise the same conditions, no reaction was obtained (6). This evidence strongly suggests that a polar transition state is involved in the cycloaddition.

The infrared spectrum established that nitrile, phosphoryl, and monosubstituted aromatic chromophores were all still present in the product, and combustion analysis confirmed that it was a 1:1 adduct.

Stereochemical predictions

The stereochemistry of the anticipated product of the Diels–Alder reaction of 1,2,5-triphenylphosphole-1-oxide with acrylonitrile can be predicted, based on the principles of Woodward and Hoffman (ref. 7, Fig. 1). Electron withdrawal as a consequence of the charged, zwitterionic resonance form

TABLE 3. 100.59 MHz ^{13}C NMR assignments for nitrile adduct **3***a* in deuteriochloroform at room temperature

Carbon[a]	Chemical shifts (ppm) Experimental	Calculated[b]	Coupling constants (Hz) J(C,P)[c]	C,H[a]	J(C,H)	Assignment basis[d]
C(1) or C(4)	55.99	48.1±3.8	63.1	—	None	Quat. C, large J(C,P)
C(2)	135.91	132.4±8	11.8	H(2)	7.0	Alkene, not C(3) via connectivity, heteronuclear
C(3)	131.14	132.4±8	11.9	H(3)	6.9	Alkene, not C(2) via connectivity etc., as C(2)
C(4) or C(1)	58.44	48.1±3.8	66.0	—	None	Quat. C, large J(C,P)
C(5)	35.91	33.9±13.0	22.2	H(5x)	4.3	Connectivity to H(5) via heteronuclear
C(6)	39.42	38.9±5.2	10.1	H(6x)	3.55	Connectivity to H(6x) via heteronuclear
C(7)	119.83	121.0±0.6	14.4	—	None	Nitrile shift, no H, smaller J(C,P)
C(21) or C(31)	133.77	144.4±12	7.1	—	None	Quat. C, C(1) phenyl shift and J(C,P) progression, elimination
C(22) and C(26)	126.85	128.8±1.2	18.3	H(22), H(25)	7.5	*o*-C's, C(1) phenyl, via proton NOE, multiplicity
C(23), C(25), C(33), and C(35)	129.08	127.8±1.0	12.9	H(23), H(25), H(33), H(35)	7.37	*m*-C's, C(1) and C(4) phenyls, J(C,P) progression, proton shift and multiplicity, large C peak
C(24) and C(34)	132.27	127.3±1.0	2.8	H(24), H(34)	7.36	*p*-C's, C(1) and C(4) phenyls, connectivity via heteronuclear, shift progression, small J(C,P)
C(31) or C(21)	134.45	144±12.0	4.4	—	None	As C(21), plus influence of nitrile
C(32) and C(36)	126.91	128.8±1.2	17.7	H(32), H(36)	7.6	*o*-C's, C(4) phenyl, using proton NOE, and connectivity via heteronuclear
C(11)	123.68	132.4±1.0	(88.5)	—	None	Quat. C, P phenyl, via large J(C,P), elimination
C(12), C(16)	127.93	131.2±0.6	(37.6)	H(12), H(16)	7.2	*o*-C's, P phenyl, via shift progression, J(C,P) progression, heteronuclear proton connectivity
C(13) and C(15)	127.87	128.4±0.2	(28.1)	H(13), H(24)	7.3	*m*-C's, P phenyl, via heteronuclear for proton connectivity, proton shift and multiplicity
C(14)	128.13	132.0±0.4	(24.4)	H(23)	7.35	*p*-C's P phenyl, via proton and C shift progression, largest *para* J(C,P), small C peak

[a]X-ray crystal structure numbering system (Fig. 2) is used for carbon and hydrogen assignments here.
[b]Calculated carbon shifts for comparison obtained via on-line computer link, via ^{13}C NMR Spectrum Estimation Program, STN, Karlesruhe.
[d]Confirmatory NMR experiments listed in abbreviated form, e.g., heteronuclear – heteronuclear 2D – *J* resolved experiments, carbon and proton, details given in experimental section.

TABLE 4. Crystal data

Parameter	Value
Crystal system	Monoclinic
Space group	$P2_1/c$ (No. 14)
a	10.435(3) Å
b	20.091(5) Å
c	11.600(3) Å
β	109.39(2)°
V_{cell}	2294 Å^3
Z	4 molecules
D (meas.)	1.22 g cm^{-3}
D (calcd.)	1.24 g cm^{-3}
Crystal size	0.96 × 0.35 × 0.59 mm
Temperature	20°C
μ	13.58 cm^{-1}

P^+—O^- of the phosphoryl group in the phosphole makes it probable that the LUMO of the phosphole would be the most likely to react. Likewise the electron-withdrawing effect of the nitrile on acrylonitrile makes it likely that the HOMO of this dienophile would be the form involved in an electrocyclic reaction. A LUMO plus HOMO concerted $4\pi + 2\pi$ electrocyclic reaction is thermally allowed, to obtain conservation of orbital symmetry.

Frontier orbital considerations, however, do not permit a clear prediction of product stereochemistry without further information. Consideration of the Alder rule, which dictates that the transition state that maximizes the accumulation of unsaturation will lead to the preferred product (Fig. 1a), would predict formation of the *endo* adduct. On the other hand, the opposite orientation of the nitrile confers a strongly stabilizing interaction with the phosphoryl oxygen favouring a transition state that would lead to the formation of the *exo* adduct (Fig. 1b). The *exo* transition state would also dictate phosphoryl orientation over the saturated, nitrile side rather than over the

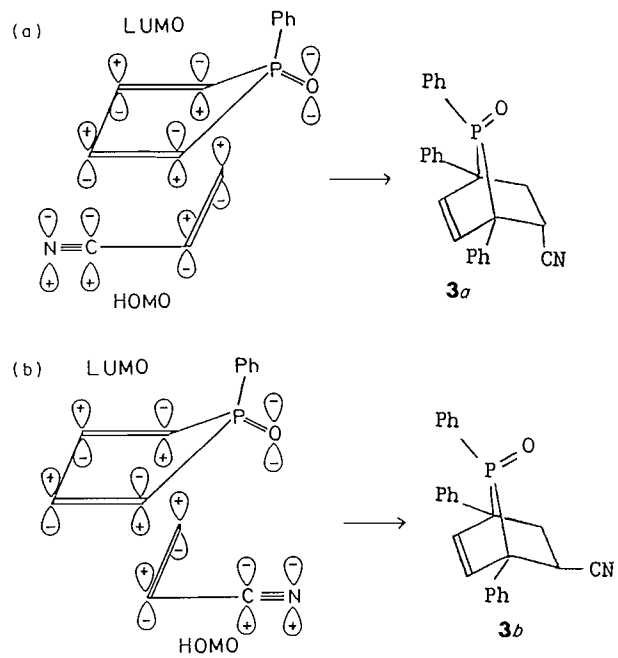

FIG. 1. Frontier orbital interactions for adduct formation.

Can. J. Chem. Downloaded from www.nrcresearchpress.com by 88.85.125.76 on 09/07/12
For personal use only.

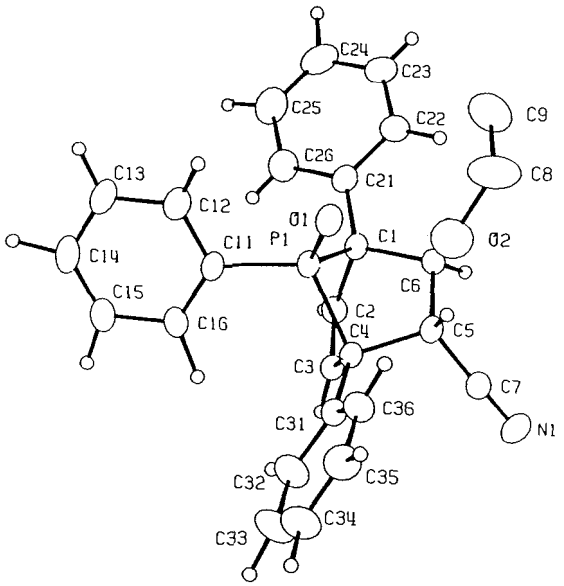

FIG. 2. X-ray crystal structure of ethanol complex of nitrile adduct **3***a*.

TABLE 5. Fractional atomic coordinates and temperature parameters

Atom	*x/a*	*y/b*	*z/c*	U_{eq}
P(1)	−36249(12)	33135(6)	29252(11)	479(4)
O(1)	−3543(3)	3539(2)	1737(3)	62(1)
O(2)	−1445(4)	4185(3)	1334(5)	104(2)
N(1)	480(4)	4280(2)	6172(5)	78(2)
C(1)	−4024(4)	3959(2)	3916(4)	48(2)
C(2)	−3643(5)	3557(2)	5076(4)	51(2)
C(3)	−2540(5)	3183(2)	5247(4)	49(2)
C(4)	−1983(4)	3237(2)	4207(4)	45(2)
C(5)	−1521(4)	3988(2)	4196(5)	47(2)
C(6)	−2792(5)	4434(2)	4026(5)	49(2)
C(7)	−399(5)	4146(2)	5315(5)	55(2)
C(8)	−1780(8)	4739(5)	540(8)	144(5)
C(9)	−2972(9)	5101(4)	437(8)	115(4)
C(11)	−4687(4)	2581(2)	2738(4)	51(2)
C(12)	−5751(5)	2551(3)	1649(5)	65(2)
C(13)	−6663(6)	2022(3)	1390(6)	76(3)
C(14)	−6449(6)	1513(3)	2237(7)	80(3)
C(15)	−5402(7)	1537(3)	3317(7)	85(3)
C(16)	−4498(6)	2072(3)	3577(6)	73(2)
C(21)	−5407(5)	4268(3)	3505(4)	54(2)
C(22)	−5635(5)	4925(3)	3129(5)	66(2)
C(23)	−6923(7)	5191(4)	2768(6)	79(3)
C(24)	−8001(6)	4806(4)	2757(6)	87(3)
C(25)	−7812(7)	4166(4)	3128(8)	100(4)
C(26)	−6514(6)	3899(4)	3488(6)	78(3)
C(31)	−968(4)	2730(2)	4082(4)	51(2)
C(32)	−677(7)	2165(3)	4789(6)	75(3)
C(33)	252(8)	1696(3)	4664(7)	95(3)
C(34)	897(7)	1794(3)	3823(7)	87(3)
C(35)	603(6)	2343(3)	3111(6)	78(3)
C(36)	−366(5)	2811(3)	3233(5)	60(2)

Estimated standard deviations are given in parentheses.
Coordinates × 10^n where n = 5,4,4,4 for P,O,N,C.
Temperature parameters × 10^n where n = 4,3,3,3 for P,O,N,C.
U_{eq} = the equivalent isotropic temperature parameter.
$U_{eq} = 1/3\Sigma_i\Sigma_j U_i ja_i^* aj^* (a_i.aj)$.
Primed values indicate that U_{iso} is given.
$T = \exp - (8\pi^2 U_{iso} \sin^2\theta/\lambda^2)$.

TABLE 6. Interatomic distances (Å)

Atoms	Distance	Atoms	Distance
O(1)—P(1)	1.480(3)	C(16)—C(11)	1.380(7)
C(1)—P(1)	1.868(5)	C(13)—C(12)	1.392(8)
C(4)—P(1)	1.865(4)	C(14)—C(13)	1.385(9)
C(11)—P(1)	1.811(5)	C(15)—C(14)	1.362(9)
C(8)—O(2)	1.413(8)	C(16)—C(15)	1.396(7)
C(7)—N(1)	1.138(6)	C(22)—C(21)	1.385(7)
C(2)—C(1)	1.505(6)	C(26)—C(21)	1.367(7)
C(6)—C(1)	1.573(6)	C(23)—C(22)	1.376(8)
C(21)—C(1)	1.496(6)	C(24)—C(23)	1.362(10)
C(3)—C(2)	1.333(6)	C(25)—C(24)	1.349(10)
C(4)—C(3)	1.507(6)	C(26)—C(25)	1.387(9)
C(5)—C(4)	1.585(6)	C(32)—C(31)	1.375(7)
C(31)—C(4)	1.510(6)	C(36)—C(31)	1.376(7)
C(6)—C(5)	1.558(7)	C(33)—C(32)	1.394(8)
C(7)—C(5)	1.466(7)	C(34)—C(33)	1.371(9)
C(9)—C(8)	1.410(11)	C(35)—C(34)	1.351(9)
C(12)—C(11)	1.379(7)	C(36)—C(35)	1.387(8)

Estimated standard deviations are given in parentheses.

olefinic, phosphole side of the adduct. Secondary orbital interactions in the *endo* transition state would also favour this as a likely outcome for phosphoryl orientation. In the absence of any more quantitative information to support the favouring of one transition state over the other it is not possible to unequivocally predict an *endo* or *exo* result for this process. However, this analysis does predict that the phosphoryl group would be expected to be oriented in the direction of the newly reacting dienophile in either case.

X-ray structure

The X-ray crystal structure determination of the 1:1 ethanol complex served to unequivocally establish the *endo* orientation of the nitrile group and that the orientations of the phosphoryl group and P-phenyl were over the newly formed saturated carbon–carbon bond of the original acrylonitrile and the olefinic bond of the adduct, respectively (Fig. 2, Tables 5–8). Thus, structure **3***a* was known for the adduct prior to the NMR analysis, which permitted a number of assignments that would otherwise have been difficult or inconclusive. Oxygen–oxygen atom spacing in the ethanol complex was 2.715 Å, midway between the normal 2.4–3.0 range and good evidence of an H-bonded interaction.

The olefinic bond of the adduct at 1.333(6) Å is 0.016 Å shorter than the 1.349 Å average of the two olefinic bonds of the non-oxidized precursor phosphole, **1**. The single bonds adjacent to the olefinic bond in the adduct have an average length of 1.506(6) Å, 0.066 Å longer than the 1.440 Å of the comparable C—C bond in the phosphole. These bond length differences are all in the correct direction to suggest some small degree of electron delocalization in the phosphole as compared to the necessarily fully localized bonds in the adduct. However, this change is also evidently partly the consequence of the presence of tetracovalent phosphoryl phosphorus in the adduct as compared to the trivalent phosphorus in the non-oxidized phosphole, from an examination of the close agreement of the C—C single bond distance of the adduct with the former (Table 9).

In the adduct, the phosphorus–carbon bridgehead bond length average, 1.867(5) Å, and the phosphorus to phenyl carbon bond length of 1.811(5) Å, both come close to the 1.822

Can. J. Chem. Downloaded from www.nrcresearchpress.com by 88.85.125.76 on 09/07/12
For personal use only.

TABLE 7. Bond angles (deg)

Atoms	Angle	Atoms	Angle
C(1)—P(1)—O(1)	117.0(2)	C(9)—C(8)—O(2)	118.8(7)
C(4)—P(1)—O(1)	116.5(2)	C(12)—C(11)—P(1)	114.8(4)
C(4)—P(1)—C(1)	84.3(2)	C(16)—C(11)—P(1)	125.3(4)
C(11)—P(1)—O(1)	111.1(2)	C(16)—C(11)—C(12)	119.8(5)
C(11)—P(1)—C(1)	112.6(2)	C(13)—C(12)—C(11)	121.0(6)
C(11)—P(1)—C(4)	113.1(2)	C(14)—C(13)—C(12)	118.3(6)
C(2)—C(1)—P(1)	97.5(3)	C(15)—C(14)—C(13)	121.2(6)
C(6)—C(1)—P(1)	97.4(3)	C(16)—C(15)—C(14)	120.3(6)
C(6)—C(1)—C(2)	106.7(4)	C(15)—C(16)—C(11)	119.4(6)
C(21)—C(1)—P(1)	118.7(3)	C(22)—C(21)—C(1)	122.9(5)
C(21)—C(1)—C(2)	116.6(4)	C(26)—C(21)—C(1)	120.0(5)
C(21)—C(1)—C(6)	116.7(4)	C(26)—C(21)—C(22)	117.1(5)
C(3)—C(2)—C(1)	113.2(4)	C(23)—C(22)—C(21)	121.0(6)
C(4)—C(3)—C(2)	112.6(4)	C(24)—C(23)—C(22)	120.1(7)
C(3)—C(4)—P(1)	98.5(3)	C(25)—C(24)—C(23)	120.4(6)
C(5)—C(4)—P(1)	96.7(3)	C(26)—C(25)—C(24)	119.3(7)
C(5)—C(4)—C(3)	106.0(4)	C(25)—C(26)—C(21)	122.1(7)
C(31)—C(4)—P(1)	117.8(3)	C(32)—C(31)—C(4)	121.6(5)
C(31)—C(4)—C(3)	119.8(4)	C(36)—C(31)—C(4)	121.0(4)
C(31)—C(4)—C(5)	114.6(4)	C(36)—C(31)—C(32)	117.4(5)
C(6)—C(5)—C(4)	107.4(3)	C(33)—C(32)—C(31)	121.3(6)
C(7)—C(5)—C(4)	110.8(4)	C(34)—C(33)—C(32)	119.9(6)
C(7)—C(5)—C(6)	112.5(4)	C(35)—C(34)—C(33)	119.2(6)
C(5)—C(6)—C(1)	107.4(4)	C(36)—C(35)—C(34)	121.0(6)
C(5)—C(7)—N(1)	178.5(6)	C(35)—C(36)—C(31)	121.1(6)

Estimated standard deviations are given in parentheses.

TABLE 8. Selected intermolecular distances (Å)

Atoms		Distance	Sym	T_x	T_y	T_z
O(1)	. O(2)	2.715	1	0	0	0
C(32)	.. O(2)	3.487	−2	0	1	1
C(33)	.. O(2)	3.507	−2	0	1	1
C(6)	.. N(1)	3.594	−1	0	1	1
C(7)	.. N(1)	3.591	−1	0	1	1
C(14)	.. N(1)	3.421	−2	−1	1	0
C(23)	.. C(2)	3.457	−1	−1	1	1
C(7)	.. C(7)	3.662	−1	0	1	1
C(23)	.. C(8)	3.624	−1	−1	1	0

The symmetry positions are for the second atom. They are defined: 1 = x,y,z; $z = -x$, 0.5 + y, 0.5 − Z. A negative symmetry position denotes inversion. The translations (T) are applied finally.

Å average given for all P—C bond distances in the phosphole (8) and to the equivalent 1.831(5) Å P—C bond in triphenylphosphine (11). The 1.810(3) and 1.796(3) Å bond lengths seen for the bonds to ring carbon and to phenyl carbon in 1,2,3,4,5-pentaphenylphosphole-1-oxide (9) are each somewhat shorter than the analogous bonds in the adduct, possibly because of some delocalization in the phosphole oxide.

Ring bonds for the saturated, non-bridgehead carbons are near the expected tetrahedral angles at 107.4 (4) and 107.4 (3)°. However, the bridged ring distorts the ring bonds to carbon from the olefinic carbons from normal sp^2 angles to bond angles of 113.2(4)° for C(2) and 112.6(4)° for C(3). This bridged ring distortion even more severely strains the angle at phosphorus, which has a value of only 84.3(2)° in the adduct as compared to a near tetrahedral angle of 107.2° in triphenylphosphine oxide (Table 10). Mean plane calculations show that the plane including phosphorus and the two bridgehead carbons is nearly evenly displaced between the olefin and the saturated sides of the carbocyclic ring with an angle to the olefin side of 125.9(5)° and 117.2(5)°, respectively (15). The dihedral angle of the 6-membered carbocyclic ring is 116.9(5)°, with bond angles of 106.0(4)° and 106.7(4)° at the carbons on the intersection of the planes.

Proton NMR

Preliminary proton spectra were obtained at 60 and 90 MHz followed by 250 and 400 MHz results, which assisted differentiation of shifts from coupling constants in the more complex multiplets. Analysis of spectra at different frequencies was particularly valuable in this system because of the prevalent variable dihedral angles, which affected through-bond coupling of protons and carbon to phosphorus (Table 1). Together with the X-ray data, these enabled assignment of many previously unreported shifts and coupling constants.

At high NMR frequencies the resonances due to the olefinic protons, H(2) and H(3), could be readily differentiated from the mass of aromatic multiplets. There is a slightly smaller coupling to phosphorus for H(2) than for H(3), 9.6 versus 11.1 Hz. Other factors than torsion angle must be operating to produce this coupling difference since the torsion angles calculated from the X-ray atomic coordinates were an identical 144° (Table 2).

Two-stage nuclear Overhauser effect (NOE) experiments were conducted to enable unequivocal assignment of the olefinic protons. Irradiation at $\delta = 3.5$ and 4.3 ppm enhanced the 7.5 and 7.6 ppm aromatic doublets, which established that these resonances originated from the *ortho* protons of the phenyls at C(1) and C(4), respectively. Irradiation at 7.5 and 7.6 ppm enhanced the multiplets at 7.03 and 6.92 ppm respec-

Can. J. Chem. Downloaded from www.nrcresearchpress.com by 88.85.125.76 on 09/07/12
For personal use only.

TABLE 9. Comparison of bond lengths (Å) of the phosphorus-containing ring

	C—C	C=C	C—P	P—Ph	P=P	Reference
Nitrile adduct **3***a*	1.506(6)[b]	1.333(6)	1.867(5)[b]	1.811(5)	1.480(3)	This work
1,2,5-Triphenylphosphole	1.440	1.349	1.822	1.822	—	8
1,2,3,4,5-pentaphenyl-phosphole-1-oxide	1.505(4)	1.355(4)	1.810(3)	1.796(3)	1.479(3)	9
1,8-diphenyl-1,3,5,7-octatetraene	1.453[b]	1.350[b]	—	—	—	10
Triphenylphosphine	—	—	1.831(5)	1.831(5)	—	11
Triphenylphosphine oxide						
orthorhombic	—	—	1.75(1)	1.77(1)[c]	1.46(1)	12
monoclinic	—	—	1.787(3)[c]	1.796(3)[c]	1.483(2)	13
monoclinic	—	—	1.79(1)[c]	1.86(1)[c]	1.49(1)	14

[a]Standard deviations given when available.
[b]Average values.
[c]Lengths quoted represent the extremes of the three P—Ph bond distances quoted by each reference.

TABLE 10. Comparison of heteroatom to carbon, and carbon only bond angles[a]

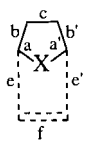

Compound	X	Bond angles (deg) a–a′	a–b	b–c	Reference
Cyclopentane	C—*C*H$_2$—C	102.8	109.3	109.4	16
Tetra-*H*-pyrrole	C—*N*H—C	109.8	107.7	107.4	17
Ph_3P	Ph—*P*—Ph	103.3(0.2)[b]	—	—	11
Ph_3PO	Ph—*P*—Ph	107.2(0.7)[b]	—	—	12
Ph_3PO	Ph—*P*=O	110.7(0.5)[b]	—	—	12
Ph_3phosphole	C—*P*—C	105.3	—	—	8
Ph_5phosphole-	C—*P*—C	93.3(0.1)	108.6(0.2)	114.7(0.2)	9
P-oxide	Ring C—*P*=O	116.5(0.1)	—	—	
P-oxide	Ring C—*P*=O	117.5(0.1)	—	—	
P-oxide	*exo* C—*P*=O	111.6(0.1)	—	—	
1-Benzylphosphole	C—*P*—O	90.7(0.2)	109.9(0.3)	114.1(0.4)	18, 19
Nitrile adduct **3***a*	C—*P*—C	84.3(0.2)	113.2(0.4)	112.6(0.4)	This work
	Ring C—*P*=O	116.5(0.2)	—	—	
	Ring C—*P*=O	117(0.2)	—	—	
	exo C—*P*=O	111.1(0.2)	—	—	

[a]Standard deviations given in parentheses, when available.
[b]Intermediate value of three selected for entry.

tively, which established in turn that these resonances arose from H(2) and H(3), in accord with the previous assignment (2). The *ortho* aromatic proton assignments that this procedure established are listed for the first time.

The *exo* orientation of aliphatic H(5) decreases the phosphorus coupling to an almost negligible 0.7 Hz, in keeping with its torsion angle of 77(4)° and not previously determined. This is part of the evidence used to assign the *exo* H(6x), since this coupling to phosphorus is also a small 1.6 Hz, relative to H(6n), which has a relatively large coupling of 24.5 Hz. This assignment of shifts and coupling constants is also confirmed by the geminal coupling constant for the methylenes of 12.3 Hz, which is close in absolute value to the methine, eclipsed methylene proton coupling of 10.0 Hz. Both the geminal and the eclipsed proton couplings are much larger than the methine, staggered methylene proton coupling value of 4.4 Hz.

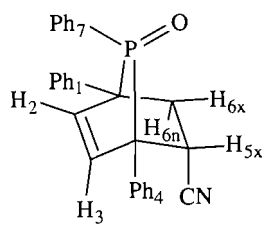

3*a*, for NMR assignments

Phosphorus NMR

The 161.92 MHz decoupled ^{31}P NMR of nitrile adduct **3***a* in deuteriochloroform at room temperature gave a single sharp peak at +75.47 ppm from 85% phosphoric acid, in agreement with the previously determined value of +75.5 ppm (2). This

Can. J. Chem. Downloaded from www.nrcresearchpress.com by 88.85.125.76 on 09/07/12
For personal use only.

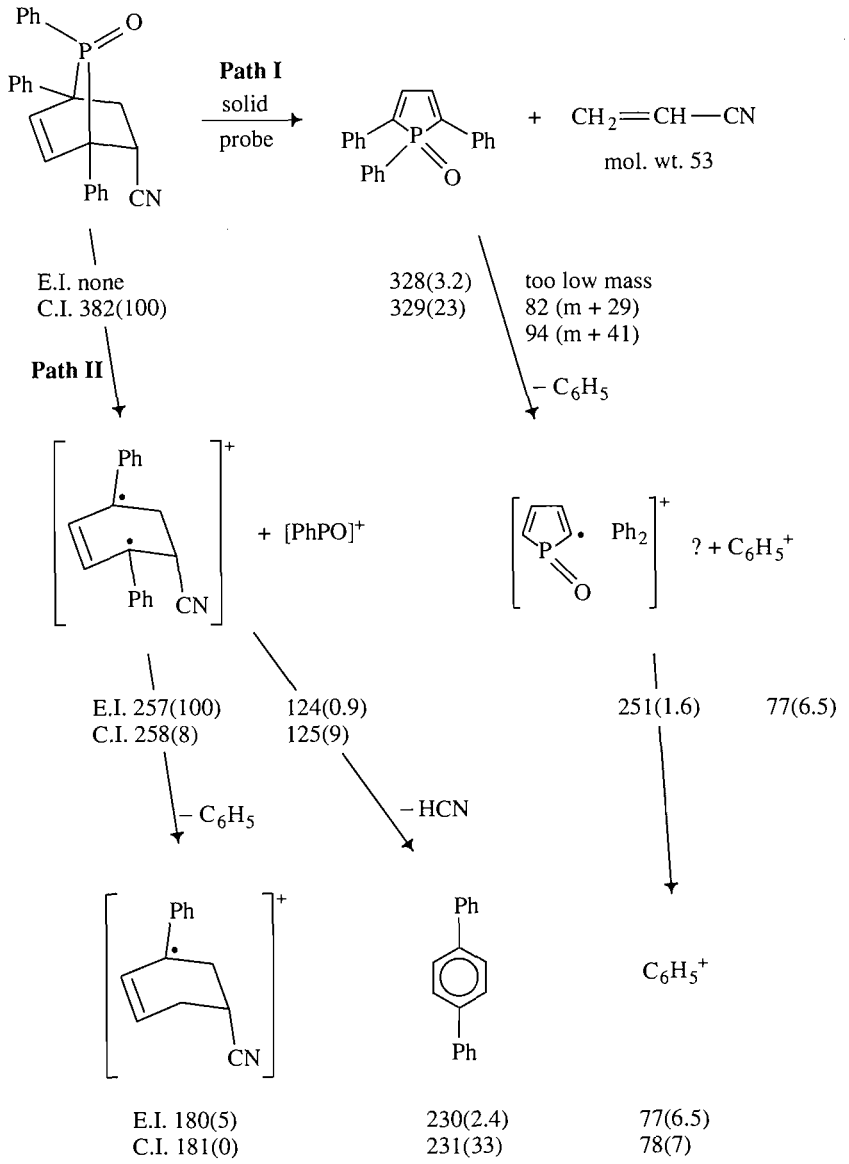

FIG. 3. Thermal decomposition pathways of adduct **3***a*.

value also compares quite closely to the +70.5 ppm (*trans*) and +77.1 ppm (*cis*) phosphorus shifts recorded by Quin and Symmes (20) for an analogous hexahydrophosphoindole oxide **4**. Proton-decoupled phosphorus shifts for the 1,2,5-triphenylphosphole-1-oxide **2**, and for its precursor phosphole **1** in the same solvent, were found to be +40.69 and +3.28 ppm respectively, the latter quite close to the experimental value previously recorded by Waite and Tebby of +3 ppm (4). These are both significantly downfield of the adduct **3***a*. Apparently the change in the electronic structure of the adduct is the key feature reflected in the strong downfield shift change since alternative aryl substitution patterns or heteroatom insertion as represented by 3,5-diphenyl-1-phenoxyphosphole-1-oxide still gave a phosphorus shift of only +46.6 ppm (21).

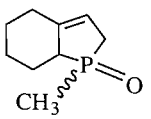

4

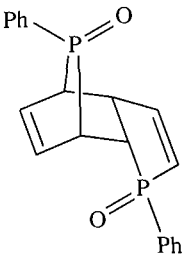

5

The proton-coupled phosphorus spectrum of the nitrile adduct gave an apparent broad quintet, specified low to high field as follows: peak number, relative intensity, (spacing, Hz, to next) 1. 1.0, (10.2); 2. 1.7, (11.5); 3. 1.9, (11.5); 4. 1.8, (9.0); 5. 1.2 Superimposed on this "quintet" was a fine structure of about 1Hz. The quintet evidently arose from four overlapping doublets, because of the close coincidence of the large phosphorus to H(6n) coupling of 24.5 Hz, to the sum of the couplings of the two olefinic protons, H(2) 9.6 and H(3) 11.1 Hz (Table 2). In agreement with this assignment are the measured experimental multiplet width at half height of 49.5 Hz as compared to a calculated requirement of 47.5 Hz, the relative intensities of 1.0:1.7:1.9:1.8:1.2, as compared to a required 1:2:2:2:1, and the full confirmation of phosphorus couplings from proton and 2D-*J* resolved spectra, with simulations of these. Evidently the approximately 1Hz couplings to H(5x) and H(6x) are the consequence of the operation of a Karplus-type relationship with the near 80° torsion angles between the bonds

Can. J. Chem. Downloaded from www.nrcresearchpress.com by 88.85.125.76 on 09/07/12
For personal use only.

involved. The large 24.5 Hz coupling is observed for the 160(3)° torsion angle, near 180° when it would be expected to be at a maximum.

The coupled phosphorus NMR for the trivalent phosphorus in the phosphole precursor **1** also gave an apparent quintet, although much better resolved. From the closer match of the relative intensity pattern to the 1:4:6:4:1 pattern expected for a true quintet, this appeared to be a likely interpretation, and from a comparison with the proton couplings it is probable that this coupling is to the four chemically equivalent *ortho* hydrogens of the two phenyl groups bonded to carbon.

The immediate precursor of the adduct, the phosphole oxide **2**, gave a well-resolved proton-coupled phosphorus spectrum of a triplet of triplets with intensity ratios of 1:2:1:2:4:2:1:2:1 in complete agreement with theory. Couplings of 37.3 Hz to the olefinic protons on the phosphole ring and 12.3 Hz to the *ortho* phenyl protons on phosphorus were confirmed from proton spectra at 400 MHz where the olefinic resonances could be clearly differentiated, and from low frequency spectra.

Carbon-13 NMR

Assignment of ^{13}C NMR shift data, using the numbering given on the X-ray structure, was based on information obtained from normal, proton-decoupled ^{13}C and coupled ^{13}C spectra as well as heteronuclear 2D-*J* resolved NMR experiments to obtain $^{13}C-^{1}H$ connectivity, and hence shift information (Table 3). Carbon–^{1}H coupling constants were also assignable with confidence from this information. Quaternary carbons were determined by DEPT experiments. Shifts and coupling constants of the bridgehead carbons of the nitrile adduct, δ's 55.99 and 58.44 ($J_{C,P}$'s 63.1 and 66.0 Hz), are in good agreement with those measured for the phosphorus bridge in the analogous phosphole dimer **5**, δ's 41.9 and 44 ($J_{C,P}$'s 61.7 and 62.9 Hz) (23).

Mass spectrometry

It was not possible to detect a molecular ion from low resolution electron impact mass spectrometry, but from a base peak at m/z 257 it is likely that loss of the PhPO bridge unit (mass 124), either as a concerted process or in stages, represents the major fragmentation path. An m/z of 381 was established for the adduct using low resolution chemical ionization (CI) mass spectrometry from a base peak at 382 ($M + 1$) plus $M + 29$ and $M + 41$ peaks. More interesting though, under these milder ionization conditions, was the observance of a peak at m/z of 329 ($M + 1$) of intensity nearly 70% of base, which corresponds to the molar mass (M) of the phosphole oxide **2**. Since the ratio of these peak intensities varied with the temperature of the direct heated probe used for sample entry to the spectrometer, this result prompted a series of adduct thermal fragmentation studies.

Thermal decomposition pathways

Two dominant routes for the thermal fragmentation of adduct **3***a* were detected by electron impact (EI) mass spectrometry. By EI the reverse Diels–Alder process (Path I, Fig. 3) was always dominant over loss of the PhPO bridge (Path II, Fig. 3). However, the ratio of these processes changed from about 100:5, Path I to Path II, at a solid ms probe temperature of 63°C, to about 100:40 at 200°C. In a separate EI test with the precursor phosphole oxide **2** the base peak was the molecular ion at m/z 328, and carried 20% of the total ion current (22). This test established the reliability of using the 328 mass ion as a measure of the proportion of adduct **3***a* that thermally fragmented via the reverse Diels–Alder path. The phenyl phosphoryl (PhPO) moiety of Path II presumably left primarily as a neutral fragment from the observed low intensity of the m/z 124 ion.

Accurate mass determinations confirmed the elemental composition of all the molecular fragments of Fig. 3 (see Experimental) and enabled likely structures to be assigned. They also verified, from the presence of only a 0.2% abundance ion at 124.0043 m/z (for $PhPO^+$) as the only ion below mass 251 to contain C,H,O, and P, that very little fragmentation of the ionized phosphole oxide **2** occurs. Since chemical ionization (CI) mass spectrometry enabled observation of $M + 1$, $M + 29$, and $M + 41$ peaks for all major fragments ions, CI established that the major ions observed via EI mass spectrometry were ionized, thermally induced fragments of the initial adduct **3***a*, and were not formed from subsequent ion fragmentation reactions.

Acknowldegements

The authors thank O. Mamer of the Biomedical Mass Spectrometry Unit, McGill University, for the LKB-9000 mass spectrum. R. A. Jacobson, Iowa State University, is thanked for a copy of the atomic coordinates from the X-ray structure determination of 1,2,5-triphenylphosphole, from which mean plane calculations were performed for comparison purposes

1. I. G. M. Campbell, R. C. Cookson, M. B. Hocking, and A. N. Hughes. J. Chem. Soc. 2184 (1965).
2. L. D. Quin, K. C. Caster, J. C. Kisalus, and K. A. Mesch. J. Am. Chem. Soc. **106**, 7021 (1984).
3. I. G. M. Campbell, R. C. Cookson, and M. B. Hocking. Chem. Ind. (London), 359 (1962).
4. N. E. Waite and J. C. Tebby. J. Chem. Soc. (C), 386 (1970).
5. P. Coppens, L. Leiserowitz, and D. Rabinovitch. Original absorption routines for the CDC 1604 (Rehovoth, Israel) modified for the University of Victoria Picker Diffractometer.
6. M. B. Hocking, K. Bhandari, and R. W. Day. To be published.
7. R. B. Woodward and R. Hoffman. Angew. Chem. Int. Ed. Engl. **8**, 781 (1969), and earlier references.
8. W. P. Ozbirn, R. A. Jacobsen, and J. C. Clardy. Chem. Commun. 1062 (1971).
9. M. Draeger and K. G. Walter. Chem. Ber. **109**, 877 (1976).
10. W. Drenth and E. H. Wiebenga. Acta Crystallogr. **8**, 755 (1955).
11. J. J. Daly. J. Chem. Soc. 3799 (1964).
12. G. Bandoli, G. Bortolozzo, D. A. Clemente, U. Croatto, and C. Pannatoni. J. Chem. Soc. (A), 1778 (1970).
13. G. Ruban and V. Zabel. Cryst. Struct. Commun. **5**, 671 (1976).
14. A. I. Gusev, N. G. Bokii, N. N. Afonina, T. V. Timofeeva, A. E. Kalinin, and Yu. T. Struchkov. Zh, Strukt. Khim. **14**, 115 (1973); J. Struct. Chem. **14**, 101 (1973) (Engl. translation).
15. F. R. Ahmed and M. E. Pippy. Program for the calculation of weighted mean planes through atom groups. N.R.C. of Canada. (1967).
16. L. H. Sharpen and V. W. Laurie. J. Chem. Phys. **43**, 2765 (1965).
17. L. Nygaard, J. Tormod Neilsen, J. Kirchenheimer, G. Maltesen, J. Rastrup-Andersen, and G. O. Sorensen. J. Mol. Struct. **3**, 491 (1969).
18. P. Coggon, J. R. Engel, A. T. McPail, and L. D. Quin. J. Am. Chem. Soc. **92**, 5779 (1970).
19. P. Coggon and A. T. McPhail. J. Chem. Soc. Dalton Trans. 1888 (1973).
20. L. D. Quin and C. Symmes. J. Org. Chem. **41**, 238 (1976).
21. F. B. Clark III and F. H. Westheimer. J. Am. Chem. Soc. **93**, 4541 (1971).
22. M. B. Hocking. To be published.
23. L. D. Quin, K. A. Mesch, R. Bodalski, and K. M. Pietrusiewicz. Org. Magn. Reson. **20**, 83 (1982).

Can. J. Chem. Downloaded from www.nrcresearchpress.com by 88.85.125.76 on 09/07/12
For personal use only.

Structure of the L1 and L6 core oligosaccharide epitopes of *Neisseria meningitidis*[1]

JOSE L. DI FABIO,[2] FRANCIS MICHON,[2] JEAN-ROBERT BRISSON, AND HAROLD J. JENNINGS[3]
Division of Biological Sciences, National Research Council of Canada, Ottawa, Ont., Canada K1A 0R6

Received November 23, 1989

This paper is dedicated to Professor Arthur S. Perlin on the occasion of his 67th birthday

JOSE L. DI FABIO, FRANCIS MICHON, JEAN-ROBERT BRISSON, and HAROLD J. JENNINGS. Can. J. Chem. **68**, 1029 (1990).

The core oligosaccharides obtained from the lipopolysaccharides of *Neisseria meningitidis* serotypes 1 and 6 were isolated by mild acid hydrolysis, and their structures elucidated by combined chemical, biochemical, and physical techniques. Use was made of 500 MHz ^{1}H nuclear magnetic resonance measurements in both one-dimensional and two-dimensional modes as well as of nuclear Overhauser enhancement experiments. To assist in the structural assignments, the purified oligosaccharides were also degraded by chemical and enzymatic procedures to smaller fragments. The L1 oligosaccharide is a biantennary partially *O*-acetylated heptasaccharide in which the larger antenna terminates in a α-D-Gal*p* 1→4β-D-Gal*p* 1→4β-D-Glc*p* unit, whereas the smallest disaccharide antenna carries phosphorylethanolamine groups at *O*-3 of its heptosyl moiety. The L6 oligosaccharide is also a biantennary partially *O*-acetylated heptasaccharide but, unlike the L1 core, is terminated by a β-D-Glc*p*NAc1→3β-D-Gal*p* 1→4β-D-Glc*p* unit in its larger antenna. The heptosyl moiety in the small disaccharide antenna bears a phosphorylethanolamine group at *O*-7, unlike *O*-3 for the L1 determinant.

Key words: lipopolysaccharides, *Neisseria meningitidis*, oligosaccharide epitopes, structure, NMR spectroscopy.

JOSE L. DI FABIO, FRANCIS MICHON, JEAN-ROBERT BRISSON et HAROLD J. JENNINGS. Can. J. Chem. **68**, 1029 (1990).

On a procédé à une hydrolyse douce en milieu acide pour isoler les oligosaccharides de base des lipopolysaccharides du *Neisseria meningitidis* des sérotypes 1 et 6; on a aussi élucidé leurs structures en combinant des techniques chimiques, biochimiques et physiques. On a utilisé la résonance magnétique nucléaire du ^{1}H dans les modes mono- et bi-dimensionnels ainsi que des expériences d'effet Overhauser nucléaire. Afin de faciliter les attributions de structure, on a aussi utilisé des méthodes chimiques ainsi qu'enzymatiques pour dégrader les oligosaccharides en fragments plus petits. L'oligosaccharide L1, un heptasaccharide partiellement *O*-acétylé, portant deux antennes, dans lequel l'antenne la plus importante est une unité α-D-Gal*p* 1→4β-D-Gal*p* 1→4β-D-Glc*p* alors que la plus petite antenne est un disaccharide portant des groupements phosphoryléthanolamine en position *O*-3 de sa portion heptosyle. L'oligosaccharide L6 est aussi un heptasaccharide partiellement *O*-acétylé portant deux antennes; toutefois, par opposition au produit L1, il se termine avec antenne portant une unité β-D-Glc*p*NAc1→3β-D-Gal*p* 1→4β-D-Glc*p*. La portion heptosyle du disaccharide de la petite antenne porte un groupement phosphoryléthanolamine qui se trouve en position *O*-7 plutôt qu'en *O*-3 comme dans le déterminant L1.

Mots clés : lipopolysaccharides, *Neisseria meningitidis*, épitopes d'oligosaccharide, structure, spectroscopie RMN.
[Traduit par la revue]

Can. J. Chem. Downloaded from www.nrcresearchpress.com by 88.85.125.76 on 09/07/12
For personal use only.

Introduction

The meningococcal lipopolysaccharides (LPS) have been implicated in the immune response to natural infection (1) and at least 11 serotypes (L1–L11) have been identified (2, 3). There is no apparent correlation between meningococcal serogroup, designated by meningococci having a common capsular polysaccharide, and LPS serotype, except that the L10 and L11 serotypes are exclusively associated with serogroup A organisms (4). The LPS serotype epitopes are located in the glycose moieties of the LPS (5), the latter having been identified as low molecular weight oligosaccharides of the R-type (6, 7). By injecting rabbits with protein conjugates of the above oligosaccharides it has also been demonstrated (5) that they contain bactericidal epitopes. Structural studies (7, 8) on the largest of the oligosaccharides obtained from some individual meningococcal serotypes have identified regions of structural similarity and structural difference in them that are probably responsible for both the serotype specificity and cross reactivity exhibited by meningococci (3, 5).

However, the above structural studies did not address the phenomenon of heterogeneity among the LPS oligosaccharides associated with individual meningococcal serotypes (9, 10), which is probably the basis of even further immunologic diversity. This heterogeneity is generated either by structurally similar oligosaccharides having phosphoethanolamine groups in differing locations (8) or by glycose deletions from the oligosaccharides (11). These phenomena were first hypothesized to explain the molecular size heterogeneity exhibited by the LPS of individual meningococcal serotypes when run in SDS gels (12, 13), and this heterogeneity has since been established by column chromatographic procedures on the isolated oligosaccharides (8, 14). It was also hypothesized that the oligosaccharides obtained from each meningococcal serotype would be structurally related, the smaller being biological precursors of the larger. This latter hypothesis has also been recently confirmed by the isolation and structural determination of three different sized but structurally related oligosaccharides from the meningococcal L5 serotype (11). This paper describes the structural determination of the oligosaccharides of the L1 and L6 serotypes, both of which exhibit heterogeneity, which is due only to *O*-acetyl substituents. *O*-Acetyl substituents have been previously reported (11) in the oligosaccharides of the L5 serotype.

Experimental

Materials

Group B *Neisseria meningitidis* strain M992 (serotype L6) and group C *Neisseria meningitidis* strain 126E (serotype L1) were grown in *Neisseria* chemically defined medium (General Biochemical Inc., Chagrin Falls, Ohio) as described previously (7), as has also isolation of the LPS.

Analytical methods

Quantitative colorimetric methods used were the phenol – sulfuric acid assay for neutral glycoses (15), the periodate – thiobarbituric acid

[1]This is NRCC No. 31386 and was presented at the Xth International Symposium on Glycoconjugates, Jerusalem, Israel, September 10–15, 1989.

[2]Supported by IAF Biochem. International Inc., Laval, Quebec.

[3]Author to whom correspondence may be addressed.

assay for 3-deoxy-octulosonate (16), and the method of Chen for phosphate (17).

Glycoses were determined essentially as previously described (6); following hydrolysis, deamination, and conversion into alditol acetates, the sugars were identified and quantified by glc. Methylation analyses were performed by the method of Hakomori (18), the products purified with C_{18} Sep-Pak cartridges (Waters Associates). Methylated products were hydrolyzed with 0.5 N H_2SO_4 in 95% acetic acid for 18 h at 80°C and, following a twofold dilution with water, samples were hydrolyzed for an additional 5 h at 80°C (19). The individual methylated components were identified and quantified by glc–ms after conversion into alditol acetates. The absolute configuration of the glycoses was established by capillary glc of their silylated (−)-2-butyl glycosides according to the method of Leontein *et al.* (20).

Gel filtrations were done at room temperature on columns (1.6 × 90 cm) of Bio-Gel P4 (Bio-Rad Laboratories, minus 400 mesh) using pyridinium acetate buffer (0.02 M, pH 5.4). Individual fractions were monitored using a Waters R 403 differential refractometer.

Instrumental methods

Gas–liquid chromatography (glc) was performed on a Hewlett–Packard 5830A instrument equipped with a flame ionization detector and a model 3380A electronic integrator. The following conditions were used with a capillary column (0.32 mm × 25 m) of 007 bonded-phase, fused silica OV-17 (Quadrex Corp.). Program A for alditol acetates: from 180°C to 240°C at 4°C/min, and program B for methylated alditol acetates: from 200°C to 240°C at 1°C/min. Combined gas–liquid chromatography – mass spectrometry (glc–ms) was carried out on a Hewlett–Packard 5985B instrument using the above capillary column and employing programs A and B as described above and an ionization potential of 70 eV.

The ^{1}H nmr spectra were recorded at 500 MHz at 300 and 343 K with a Bruker AM500 spectrometer, in the pulsed Fourier transform mode. The chemical shifts (δ) are quoted relative to internal acetone (0.1%, v/v); δ = 2.225 ppm downfield from sodium 4,4-dimethyl-4-silapentane-1-sulfonate (DSS). Proton homonuclear shift-correlated 2D nmr experiments COSY (21) and relayed COSY (22) were performed using the standard pulse sequences provided by Bruker (DISB87). Quadrature detection in both dimensions was employed. The initial (t_1,t_2) matrices of 256 × 1024 data points provided 1.6 Hz/point digital resolution in the second domain. Resolution enhancement in both dimensions was done by the unshifted sine bell window function prior to Fourier transformation. Magnitude spectra symmetrized about the diagonal were used to represent data. The nuclear Overhauser enhancement (nOe) experiments were performed in the difference mode with sequential irradiation of each line in a multiplet (23, 24). Total irradiation time per multiplet was 1 s.

Isolation of oligosaccharides

The core oligosaccharides were obtained by heating the LPS (10 mg/mL) in 1% acetic acid for 2 h at 100°C. The insoluble lipid A was eliminated from the hydrolysis mixture by centrifugation at 10 000 rpm. The cores were then purified by gel filtration on Bio-Gel P4 using pyridinium acetate buffer as eluant. A main oligosaccharide fraction was identified for each individual serotype L1 and L6 LPS. A portion of the core oligosaccharide was de-*O*-acetylated in 0.1 N NH_4OH at room temperature for 16 h and purified by gel filtration on Bio-Gel P4. Dephosphorylation of the core fractions was performed with 48% aqueous HF at 4°C for 72 h. After removal of HF under vacuum, over NaOH pellets, the purification was done by gel filtration on Bio-Gel P4.

Enzymatic deglycosylations

Treatment with α-galactosidase: oligosaccharide (5–15 mg) was dissolved in 0.1 M potassium phosphate buffer pH 6.5 (0.5–1.0 mL), and to this solution was added 5 U of α-galactosidase (Boehringer Mannheim GmBH) (EC 3.2.1.22) from green coffee beans. A few drops of toluene were added to the solution and incubation was carried out at 37°C for 48 h.

Treatment with β-*N*-acetylglucosaminidase: oligosaccharide (10–15 mg) was dissolved in 0.05 M sodium citrate buffer, pH 4.5 (0.5–1.0 mL), and to this solution was added 2 U of β-*N*-acetylglucosaminidase (Sigma Laboratories) from *Aspergillus niger* (EC 3.2.1.30). A few drops of toluene were added and incubation was carried out at 37°C for 48 h.

Digestion products were purified by gel filtration on Bio-Gel P4 using conditions described above and thereafter analyzed by methylation and ^{1}H nmr.

Results

Structure of the L1 core oligosaccharide

The L1 oligosaccharide was obtained by mild 1% acetic acid hydrolysis with subsequent elution of the hydrolyzate from a Bio-Gel P4 column. The column afforded a single fraction, which eluted from the column as a broad peak. Sugar analysis of the fraction indicated that it was composed of D-galactose, D-glucose, 2-acetamido-2-deoxy-D-glucose, L-*glycero*-D-*manno*heptose, and 3-deoxy-D-*manno*-octulosonic acid (KDO) in the ratios 2:1:1:2:1. In addition it contained one mole of phosphorus and one mole of ethanolamine, suggesting the presence of one mole of phosphoethanolamine. Examination of this fraction by ^{1}H nmr indicated that it was heterogeneous, as reflected by the complexity of the anomeric region of its spectrum between δ 5.50 and 4.30. The spectrum also suggested that *O*-acetyl groups (signal at δ 2.19), which were present in the molar ratio of ≈0.4, were a contributing factor to this heterogeneity. This was confirmed when removal of *O*-acetyl by mild base produced pure **1**, which eluted as a narrow peak (K_{av} 0.49) from a Bio-Gel P4 column and which did not exhibit the complexity of anomeric signals associated with the ^{1}H nmr spectrum of its precursor. The ^{1}H nmr spectrum of **1** (Table 2) was still in agreement with the sugar analysis, i.e., six signals in the anomeric region integrating for six protons indicating that **1** contained at least six sugar residues. Four of these anomeric signals at δ 5.516, 5.163, 5.075, and 4.951 with small vicinal coupling constant values ($^3J_{1,2}$ = 1–3 Hz) were assigned to residues with α-anomeric configuration; the last two at δ 4.554 and 4.538 having large vicinal coupling constants ($^3J_{1,2}$ = 7–8 Hz) were assigned the β-anomeric configuration. In addition, the spectrum had one signal at δ 2.050 associated with one *N*-acetyl group, indicating that the 2-amino-2-deoxy-D-glucosyl units are *N*-acetylated.

The ^{13}C nmr of **1** is complex, but it exhibited intense signals at δ 103.70, 103.07, 101.59, 101.09, 100.39, and 100.05 associated with six anomeric carbon atoms. A less intense signal at δ 96.6 could be associated with C-2 of one of the anomeric forms of the reducing KDO. A doublet at δ 40.95 ($^3J_{C,P}$ = 8.0 Hz) is characteristic of a phosphoethanolamine substituent (7), in agreement with the composition analysis described above. Other signals at δ 54.82, 38.41, and 23.09 are assigned to the carbons linked to acetamido groups, to C-3 of the reducing KDO, and to the methyl of the *N*-acetyl groups, respectively.

Methylation analysis of **1** (Table 1) indicated that it contained terminal non-reducing galactose and 2-acetamido-2-deoxy-glucose residues, one galactose, and one glucose linked at *O*-4; both heptoses were branch points, one of them substituted at *O*-3 and *O*-4 and the other at *O*-2 and *O*-3. KDO was linked at *O*-5 (Table 1), as it is in the L3 and L5 oligosaccharide (7, 11). When **1** was dephosphorylated with aqueous HF to afford **2**, its methylation analysis (Table 1) indicated that the 4,6,7-trimethyl-heptopyranosyl residue present in the methylation analysis of **1** was now replaced by a 3,4,6,7-tetramethyl-heptopyranosyl residue, indicating that the phosphoethanolamine groups were located at *O*-3 of the *O*-2 linked heptose

Can. J. Chem. Downloaded from www.nrcresearchpress.com by 88.85.125.76 on 09/07/12
For personal use only.

Can. J. Chem. Downloaded from www.nrcresearchpress.com by 88.85.125.76 on 09/07/12
For personal use only.

TABLE 1. Methylation analysis of oligosaccharides derived from the L1 lipopolysaccharide cores

	Molar ratios[a]		
Methylated sugars[b,c]	1	2	3
2,3,4,6-Me_4 Gal	1.00	1.00	1.00
2,3,6-Me_3 Gal	1.05	1.00	—
2,3,6-Me_3 Glc	1.05	0.95	1.05
3,4,6,7-Me_4 Hep	—	0.80	0.80
3,4,6-Me_3 GlcNMeAc	0.60	0.75	0.80
2,6,7-Me_3 Hep	0.85	0.85	0.85
4,6,7-Me_3 Hep	0.55	—	—

[a]1: de-*O*-acetylated core; 2: de-*O*-acetylated and dephosphorylated core; 3: de-*O*-acetylated, dephosphorylated, and α-galactosidase treated core.
[b]Upon hydrolysis, removal of PEA located at *O*-3 of the heptosyl residue occurred.
[c]KDO was detected in 1 as its 1,2,4,6,7,8-hexamethyl-3-deoxy-5-OAc derivative as described in Jennings *et al.* (6).

TABLE 2. Proton nmr chemical shift data at 300 K and 500 MHz for de-*O*-acetylated oligosaccharides derived from the L1 lipopolysaccharide cores

Proton[a]	1	2	3
1-a	5.516	5.535	5.542
1-b	5.163	5.077	5.079
1-c	5.075	5.067	5.071
1-d	4.951	4.951	—
1-e	4.554	4.554	4.555
1-f	4.538	4.530	4.476

[a]a–f letters to residues a–f of compounds **1–3** reported in Fig. 1.

TABLE 3. Proton chemical shifts[a] of some of the signals of dephosphorylated L1 core oligosaccharide **2**

	Proton				
Residue	H-1	H-2	H-3	H-4	H-5
a	5.54	4.12	3.96	3.64	—
b	5.08	3.89	3.80	3.53	—
c	5.07	4.12	4.13	4.24	—
d	4.95	3.84	3.91	4.04	—
e	4.55	3.44	3.64	3.47	3.73
f	4.53	3.57	3.78	4.05	3.63

[a]Measured at 300 K and 500 MHz, assignments made from data obtained by homonuclear 2D shift-correlated (H,H) COSY and two-step relayed COSY.

residue. Thus, this would indicate that a phosphoethanolamine group located at position *O*-3 of a L,D-heptose is very labile under the hydrolysis conditions used for permethylated **1**.

To obtain evidence for the sequence of the sugar residues in the L1 core, **2** was treated with α-galactosidase and, following purification by gel filtration on Bio-Gel P4, the product of hydrolysis was identified as **3** following methylation (Table 1) and ^{1}H nmr analysis (Table 2). The disappearance of a 2,3,6-trimethyl-galactopyranosyl residue (*O*-4 linked), in the methylation analysis of **3** with respect to that of **2**, indicated that a terminal α-D-galactopyranosyl residue had been removed from the oligosaccharide by the enzyme and that this residue was previously linked to *O*-4 of another galactopyranosyl unit. Thus, the sequence α-D-Gal*p*1→4Gal was ascertained. This evidence was supported by ^{1}H nmr data obtained from **3** (Table 2), where the anomeric signal (H-1d) at δ 4.951 present in **2** was no longer present in the spectrum of **3**.

TABLE 4. Nuclear Overhauser enhancements for dephosphorylated L1 core oligosaccharide **2**

	Observed nOe	
Saturated signal[a]	Intra-residue	Inter-residue
1-a	2-a	3-c
1-b	2-b	2-a
1-c	2-c	NA
1-d	2-d	4-f
1-e	2-e,3-e,5-e	4-c
1-f	2-f,3-f,4-f,5-f	4-e

[a]Letters a–f refer to residues a–f as depicted in Fig. 1. NA: not assigned.

The complete sequence and anomeric configurations of the individual residues of dephosphorylated L1 core (**2**) were ascertained from ^{1}H nmr (nOe) data. First, the chemical shifts of some of the protons associated with the individual residues of **2** were assigned by 2D (H,H) COSY using one-step (21) and two-step relayed coherent transfer (22) (Table 3). Following assignments, the individual anomeric signals of each of the residues a, b, c, d, e, and f in **2** (Fig. 1) were selectively irradiated, and the observed nOe's are listed in Table 4. Irradiation of H-1a gave enhancements on both vicinal H-2a and on H-3c, which indicated that the L-*glycero*-D-*manno*-heptopyranosyl residue **2**a is in the α-D-*manno* configuration since no enhancements are observed on its own H-3a and H-5a, and is also linked to *O*-3 of the branch L-*glycero*-D-*manno*-heptopyranosyl residue **2**c. Irradiation of H-1b gave enhancements on vicinal H-2b as well as on H-2a, indicating that the 2-acetamido-2-deoxy-D-glucopyranosyl residue **2**b is in the α-D-*gluco* configuration and in addition is linked to *O*-2 of the L-*glycero*-α-D-*manno*-heptopyranosyl residue a. When H-1c was irradiated, enhancement was observed for H-2c but not for H-3c or H-5c, indicating that the branch L-*glycero*-D-*manno*-heptopyranosyl residue c is in the α-D-*manno* configuration; other not-assigned resonances, which could belong to the *O*-5 linked KDO residue g, were enhanced. Irradiation of H-1d gave clear enhancements on both H-2d and H-4f, indicating that the D-galactopyranosyl residue is in the α-D-*galacto* configuration and is linked to *O*-4 of the adjacent galactosyl residue **2**f. Irradiation of H-1e gave enhancements on H-2, H-3, and H-5 of the same residue as well as on H-4 of the branch L-*glycero*-D-*manno*-heptopyranosyl residue (**2**c), indicating that the D-glucopyranosyl residue **2**e has the β-D-*gluco* configuration and furthermore is linked to *O*-4 of residue **2**c. At this point, the following sequences (i) β-D-Glc*p*1→4[α-D-Glc*p*NAc1→2-α-LD-Hep*p*1→3]-α-LD-Hep*p*1→5KDO and also (ii) α-D-Gal*p*1→4-β-D-Gal*p*1→ can be written. How (i) and (ii) are linked together can be decided from enhancements observed following irradiation of H-1f. In effect, besides expected nOe's for H-2, H-3, H-4, and H-5 of the β-galactosyl residue **2**f, enhancement was also observed for H-4 of the β-D-glucopyranosyl residue e, indicating that **2**f was linked to *O*-4 of **2**e.

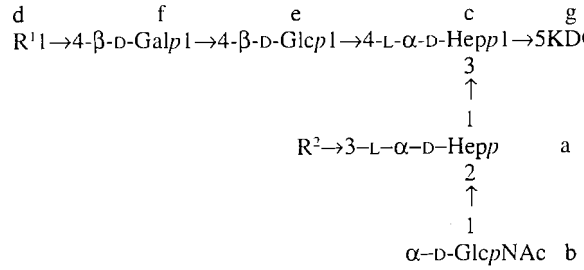

1 R^1 = α-D-Gal*p*; R^2 = PEA
2 R^1 = α-D-Gal*p*; R^2 = H
3 $R^1 = R^2$ = H

FIG. 1. Structure of the *O*-deacetylated L1 core oligosaccharide and derived products.

TABLE 5. Methylation analysis of oligosaccharides derived from the L6 lipopolysaccharide cores

Methylated sugars[b]	Molar ratios[a] 4	5	6
2,3,4,6-Me_4 Gal	—	—	1.00
2,3,6-Me_3 Glc	1.00	1.00	1.05
2,4,6-Me_3 Gal	0.95	1.00	—
3,4,6,7-Me_4 Hep	—	0.80	0.85
3,4,6-Me_3 GlcNMeAc	1.75	1.75	0.80
2,6,7-Me_3 Hep	0.90	0.90	0.85
3,4,6-Me_3 Hep[c]	0.65	—	—

[a]4: de-*O*-acetylated core; 5: de-*O*-acetylated and dephosphorylated core; 6: de-*O*-acetylated, dephosphorylated, and β-*N*-acetylglucosaminidase treated core.
[b]KDO was detected in **4** as its 1,2,4,6,7,8-hexamethyl-3-deoxy-5-OAc derivative as described in Jennings *et al.* (6).
[c]Obtained after methylation and treatment with 48% HF.

Thus the disaccharide sequence (ii) is linked to the pentasaccharide (i) via *O*-4 of residue **2**e, and the final sequence for the L1 oligosaccharide (**1**) is therefore as reported in Fig. 1. It is a phosphorylated core as opposed to the L5 determinant (11), the phosphoethanolamine groups being located at *O*-3 of the L-*glycero*-D-*manno*-heptopyranosyl moiety (**2**a).

Structure of the L6 core oligosaccharide

The L6 oligosaccharide was obtained as described for L1 by mild hydrolysis of the serotype L6 LPS and gel filtration on Bio-Gel P4. It afforded a single fraction that eluted as a broad peak. Sugar analysis of this fraction indicated that it contained D-galactose, D-glucose, 2-acetamido-2-deoxy-D-glucose, L-*glycero*-D-*manno*-heptose, and KDO in the ratios of 1:1:2:2:1. In addition, it contained one mole of phosphoethanolamine. Examination of this fraction by ^{1}H nmr indicated that it had extensive microheterogeneity as reflected by the complexity of the anomeric region of its spectrum between δ 5.50 and 4.30 and also by the presence of three signals at δ 2.18, 2.12, and 2.10 associated with multiple *O*-acetyl groups. Upon mild treatment of the above fraction with base, the generated de-*O*-acetylated product referred to as **4** eluted as a very narrow peak (K_{av} 0.47) on Bio-Gel P4. The ^{1}H nmr analysis of **4** showed in its spectrum absence of *O*-acetyl signals, indicating complete *O*-deacetylation. The anomeric region (Table 6) with five signals integrating for six anomeric protons indicated that **4** contained at least six sugar residues. Two of these signals at δ 5.645 (1H), 5.077 (2H)

TABLE 6. Proton nmr data at 300 K and 500 MHz for de-*O*-acetylated oligosaccharides derived from the L6 lipopolysaccharide cores

Proton[a]	4	5	6
1-a	5.645	5.552	5.542
1-b	5.077	5.081	5.079
1-c	5.077	5.073	5.071
1-d	4.700	4.697	—
1-e	4.555	4.547	4.555
1-f	4.470	4.464	4.476

[a]a–f letters refer to residues a–f of compounds **4–6** reported in Fig. 2.

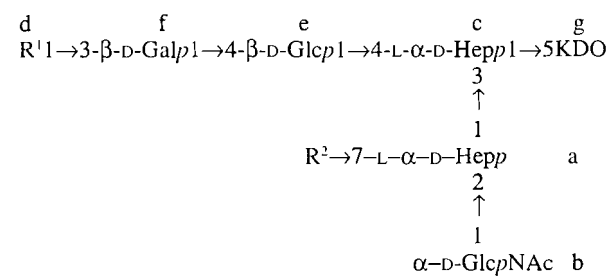

4 R^1 = β-D-Glc*p*NAc; R^2 = PEA
5 R^1 = β-D-Glc*p*NAc; R^2 = H
6 $R^1 = R^2$ = H

FIG. 2. Structure of the *O*-deacetylated L6 core oligosaccharide and derived products.

with small vicinal coupling constants ($^3J_{1,2}$ = 1–3 Hz) were assigned to residues with α-anomeric configuration; the other three at δ 4.700 (1H), 4.555 (1H), and 4.470 (1H) having large coupling constant values ($^3J_{1,2}$ = 7–8 Hz) were assigned the β-anomeric configuration. In addition, the spectrum had one signal at δ 2.050 integrating for six protons associated with two *N*-acetyl groups.

Methylation analysis of **4** (Table 5) indicated that it contained two terminal non-reducing 2-acetamido-2-deoxy-glucose residues, glucose linked through *O*-4, galactose linked at *O*-3, KDO linked at *O*-5, and one heptose branch point substituted at *O*-3 and *O*-4. No other heptose was detected, suggesting that this residue was phosphorylated. Indeed, when permethylated **4** was treated with aqueous HF and then subjected to acid hydrolysis and glc–ms analysis, a 3,4,6-trimethyl heptose appeared in the methylation analysis, indicating that the missing heptose was also a branch point substituted at *O*-2 and *O*-7. Thus the phosphoethanolamine substituent must be located at either *O*-2 or *O*-7 of this sugar residue. To conclusively decide, **4** was treated with aqueous HF to afford **5**. Methylation analysis of **5** (Table 5) gave the same methylated products found in that of **4** except for the appearance of a 3,4,6,7-tetramethyl heptose and disappearance of the 3,4,6-trimethyl heptose, indicating that this heptose residue is *O*-2 linked and therefore carries the phosphoethanolamine groups at *O*-7 in the native core. The chemical shifts associated with the anomeric protons of **5** are not significantly different from those associated with phosphorylated **4** except for the anomeric proton (H1-a).

As for the L1 core, the sequence of the sugar residues of L6 had to be established. Firstly, dephosphorylated **5** was treated

Can. J. Chem. Downloaded from www.nrcresearchpress.com by 88.85.125.76 on 09/07/12
For personal use only.

Can. J. Chem. Downloaded from www.nrcresearchpress.com by 88.85.125.76 on 09/07/12
For personal use only.

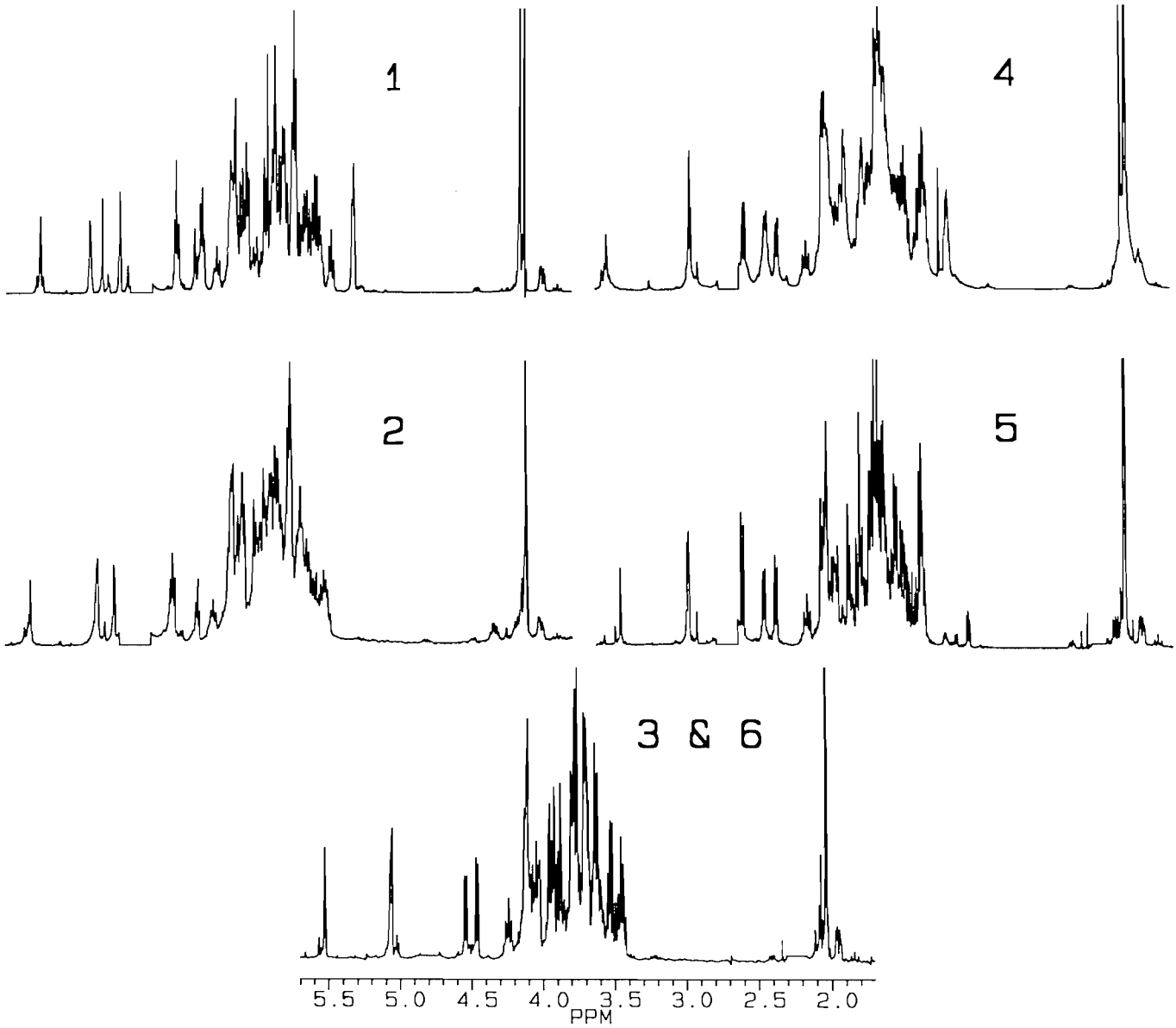

FIG. 3. The ^{1}H nmr spectra (500 MHz, 300 K) of *O*-deacetylated L1 (**1**) and L6 (**4**) core oligosaccharides, their respective derived dephosphorylated products (**2** and **5**), and their respective products following treatment with glycosidases (**3** and **6**). The chemical shift scale shown applies to all spectra in the figure.

with β-*N*-acetylglucosaminidase from *Aspergillus niger*. The digestion products were purified by gel filtration on Bio-Gel P4, and a major oligosaccharide product **6** was identified by methylation and ^{1}H nmr analysis. By comparison with the methylation analysis of **5**, that of **6** has an additional 2,3,4,6-tetramethyl galactopyranosyl residue corresponding to the 2,4,6-trimethyl galactopyranosyl residue present in the methylation of **5**. In addition, one of the two 2,3,4,6-tetramethyl-2-acetamido-2-deoxy-glucopyranosyl residues is missing, indicating the enzyme had removed the terminal 2-acetamido-2-deoxy-β-D-glucopyranosyl residue (**5**d) from **5** and that **5**d was linked to *O*-3 of the adjacent galactopyranosyl residue **5**f (Fig. 2).

Interestingly, the methylation analysis of **6** yielded the same methylated components and in the same ratios as were found for the dephosphorylated and degalactosylated L1 core (**3**), suggesting identical structure for **3** and **6**. Indeed, this was confirmed upon examination of the ^{1}H nmr spectrum of **6** (Table 6 and Fig. 3), which is identical to that of **3** (Table 2 and Fig. 3). Therefore we can conclusively say that **3** and **6** are identical and that the structure of the *O*-deacetylated L6 core is as reported in Fig. 2. It is also a phosphorylated core, with the phosphoethanolamine groups located at *O*-7 (instead of *O*-3 for L1) of the L-*glycero*-D-*manno*-heptopyranosyl residue (**4**a), and its glycose sequence is identical to that of the L1 core except for the fact that L6 has a non-reducing terminal 2-acetamido-2-deoxy-β-D-glucopyranosyl linked to *O*-3 of an adjacent β-D-galactopyranosyl residue (Fig. 2), whereas L1 has a non-reducing terminal α-D-galactopyranosyl residue linked to *O*-4 of the same adjacent β-D-galactopyranosyl residue (Fig. 1).

Both the L1 and L6 oligosaccharides contain *O*-acetyl groups previously identified as substituents of the L5 serotype oligosaccharides (11). The sharpening of the peaks in the elution profiles (Bio-Gel P4) of both the *O*-deacetylated L1 (**1**) and L6 (**4**), when compared to those of peaks in the elution profiles (Bio-Gel P4) of the original oligosaccharides, would suggest

that the heterogeneity exhibited in the latter, unlike that exhibited by the L5 oligosaccharides (11), is due only to the presence of *O*-acetyl substituents. However, it cannot be stated with certainty that this heterogeneity also extends to the LPS-associated oligosaccharide epitopes, because it is a distinct possibility that *O*-acetyl groups could be partially removed under the mild hydrolytic conditions used to obtain the oligosaccharides from the LPS.

Acknowledgements

We thank Fred Cooper for the glc–ms analyses.

1. I. GOLDSCHNEIDER, E. C. GOTSCHLICH, and M. S. ARTENSTEIN. J. Exp. Med. **129**, 1327 (1969).
2. R. E. MANDRELL and W. D. ZOLLINGER. Infect. Immun. **16**, 471 (1977).
3. W. D. ZOLLINGER and R. E. MANDRELL. Infect. Immun. **18**, 424 (1977).
4. W. D. ZOLLINGER and R. E. MANDRELL. Infect. Immun. **28**, 451 (1980).
5. H. J. JENNINGS, C. LUGOWSKI, and F. E. ASHTON. Infect. Immun. **43**, 407 (1984).
6. H. J. JENNINGS, A. K. BHATTACHARJEE, L. KENNE, C. P. KENNY, and G. CALVER. Can. J. Biochem. **58**, 128 (1980).
7. H. J. JENNINGS, K. G. JOHNSON, and L. KENNE. Carbohydr. Res. **121**, 233 (1983).
8. H. J. JENNINGS, M. BEURRET, A. GAMIAN, and F. MICHON. Antonie van Leeuwenhoek, **53**, 519 (1987).
9. C. M. TSAI, R. BOYKINS, and C. E. FRASCH. J. Bacteriol. **155**, 498 (1983).
10. J. M. GRIFFISS, J. P. O'BRIEN, R. YAMASAKI, G. D. WILLIAMS, P. A. RICE, and H. SCHNEIDER. J. Bacteriol. **155**, 498 (1987).
11. F. MICHON, M. BEURRET, A. GAMIAN, J.-R. BRISSON, and H. J. JENNINGS. J. Biol. Chem. In press.
12. J. T. POOLMAN, C. T. P. HOPMAN, and H. C. ZANEN. FEMS Microbiol. Lett. **13**, 339 (1982).
13. H. SCHNEIDER, T. L. HALE, W. D. ZOLLINGER, R. C. SEID, JR., C. A. HAMMACK, and J. M. GRIFFISS. Infect. Immun. **45**, 544 (1984).
14. B. W. GIBSON, J. W. WEBB, R. YAMASAKI, S. J. FISHER, A. L. BURLINGAME, R. E. MANDRELL, H. SCHNEIDER, and J. MCLEOD GRIFFISS. Proc. Natl. Acad. Sci. U.S.A. **86**, 17 (1989).
15. H. DUBOIS, K. A. GILLES, P. A. REBERS, and F. SMITH. Anal. Chem. **28**, 350 (1956).
16. D. AMINOFF. Biochem. J. **81**, 384 (1961).
17. P. S. CHEN, T. Y. TORIBARA, and H. WARNER. Anal. Chem. **28**, 1756 (1956).
18. S. HAKOMORI. J. Biochem. (Tokyo), **55**, 205 (1964).
19. K. STELLNER, H. SAITO, and S. HAKOMORI. Arch. Biochem. Biophys. **155**, 464 (1973).
20. K. LEONTEIN, B. LINDBERG, and J. LONNGREN. Carbohydr. Res. **62**, 359 (1978).
21. A. BAX and R. FREEMAN. J. Magn. Reson. **44**, 542 (1981).
22. A. BAX and G. DROBNY. J. Magn. Reson. **61**, 306 (1985).
23. M. KINNS and J. K. M. SANDERS. J. Magn. Reson. **56**, 518 (1984).
24. D. NEUHAUS. J. Magn. Reson. **53**, 109 (1983).

Can. J. Chem. Downloaded from www.nrcresearchpress.com by 88.85.125.76 on 09/07/12
For personal use only.

Enantiospecific synthesis of (6*R*, 7*S*)-diastereoisomer of asperlin

TONY K. M. SHING[1] AND MAHMOUD ALOUI
Department of Chemistry, The Victoria University of Manchester, Manchester M13 9PL, U.K.

Received November 14, 1989

This paper is dedicated to Professor Arthur S. Perlin on the occasion of his 67th birthday

TONY K. M. SHING and MAHMOUD ALOUI. Can. J. Chem. **68**, 1035 (1990).

An unambiguous synthesis of the (6*R*,7*S*)-diastereoisomer of asperlin from D-glucose involving a tandem epoxide formation/intramolecular Wadsworth–Emmons–Horner olefination has established the absolute configuration of the oxirane moiety in natural asperlin as (6*S*,7*R*).

Key words: asperlin, synthesis; Wadsworth–Emmons–Horner olefination; epoxide formation.

TONY K. M. SHING et MAHMOUD ALOUI. Can. J. Chem. **68**, 1035 (1990).

Grâce à une synthèse non ambiguë du diastéréoisomère (6*R*,7*S*) de l'asperline, à partir du D-glucose et faisant appel à un tandem de réactions impliquant la formation d'un époxyde et une oléfination intramoléculaire de Wadsworth–Emmons–Horner, on a pu établir que la configuration absolue de la portion oxirane de l'asperline naturelle est (6*S*,7*R*).

Mots clés : asperline, synthèse; oléfination Wadsworth–Emmons–Horner; formation d'un époxyde.

[Traduit par la revue]

Introduction

Asperlin, a fungal metabolite isolated (1) from cultures of *Aspergillus nidulans*, has been shown (2) to exhibit antibiotic and antitumour activity. Earlier nmr spectroscopic (3, 4) and synthetic studies (4, 5) of asperlin have demonstrated that the 4,5-substituents[2] of the lactone ring had the L-*threo* configuration and the exocyclic epoxypropyl moiety was *trans*; the absolute stereochemisty of the oxirane remained unsolved. These data have reduced the possible constitutions of asperlin to absolute configuration **1** or its 6,7-diastereoisomer **2.** Recently,

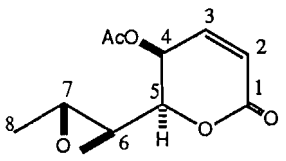

1

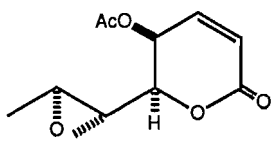

2

spin-lattice relaxation and nuclear Overhauser enhancement experiments were used to assign the (6*R*,7*S*)-diastereoisomer **2** to asperlin (6). However, a very recent synthesis (7) of D-asperlin indicated that natural asperlin was the (6*S*,7*R*)-diastereoisomer, i.e., **1.** This paper describes an unambiguous synthesis of **2**, which is diastereoisomeric to asperlin, thereby confirming by exclusion that the absolute configuration of the natural material is **1**. A preliminary account of this work has appeared (8).

Results and discussion

The strategy for the enantiospecific fabrication of **2**, illustrated in Scheme 1, involves a tandem oxirane formation/intramolecular Wadsworth–Emmons–Horner (9) olefination (this would guarantee the *Z*-geometry of the double bond) of the lactol **3**, which is readily derived from D-glucose.

3-*O*-Benzyl-1,2:5,6-di-*O*-isopropylidene-D-glucose **4** (10), readily affordable from D-glucose in two steps, was converted into the epoxy-lactone **2** in eight steps with an overall yield of 14%. Thus selective hydrolysis of the terminal isopropylidene group in **4** followed by esterification of the resultant diol with methanesulphonyl chloride as described previously (11) gave the dimethanesulphonate **5** in 73% overall yield. The primary methanesulphonate in **5** was displaced with lithium aluminium hydride (LAH) to provide the deoxy derivative **6** (91%), which then was debenzylated by palladium hydroxide catalysed hydrogenolysis to give the alcohol **7** in 94% yield. Esterification of **7** with dimethylphosphonoacetic acid in the presence of dicyclohexylcarbodiimide (DCCI) afforded the phosphonate **8** in 92% yield. Acetolysis of **8** with acetic anhydride mediated by boron trifluoride etherate gave smoothly the diacetate **9** (a mixture of anomers) in 97% yield. The anomeric acetoxy group in **9** was selectively (12) hydrolyzed ($SnCl_4$/MeCN followed by aqueous $HCONMe_2$) to the lactol **3** in 52% yield. The β-D-configuration of the anomeric hydroxy group in **3** was evident from the nmr spectrum ($J_{1,2} \approx 0.0$Hz). Transformation of the base labile **3** into the target epoxy-lactone **2** proved eventful. After considerable experimentation, treatment of **3** with mild base (13) (LiCl, 1,8-diazabicyclo[5.4.0]undec-7-ene (DBU)) gratifyingly produced the desired pyrone **2** in 47% yield. The epoxy-lactone **2** had mp 55–57°C, $[\alpha]_D$ +172° (*c* 1, EtOH), R_f 0.45 (silica gel tlc, diethyl ether), and spectroscopic data (mass, ir, ^{1}H nmr) similar to those of an authentic sample of asperlin. Since natural asperlin had mp 71–73°C, $[\alpha]_D$ +345° (*c* 0.5, EtOH) (1), R_f 0.50 (diethyl ether), **2** must be its diastereoisomer. The absolute configuration **1** is therefore assigned to asperlin.

Experimental

Melting points were recorded on a Kofler block. ^{1}H nuclear magnetic resonance (nmr) spectra were recorded on a Varian SC300 spectrometer at 300 MHz using deuteriochloroform as solvent unless otherwise stated. Mass spectra were recorded on a Kratos MS25 instrument. Infrared (ir) spectra were recorded on a Perkin–Elmer FT-IR 1710 spectrometer with samples as thin films; selected absorptions are reported in wave numbers (cm^{-1}). Optical rotations were measured on an AA-100 polarimeter using acetone as solvent unless otherwise stated. Thin-layer chromatography (tlc) was performed on glass plates precoated with Merck silica $60F_{254}$, and compounds were visualized with a spray of 5% v/v sulphuric acid in ethanol and subsequent heating. Tetrahydrofuran (THF) was distilled from sodium and benzophenone under dry nitrogen. Dichloromethane and acetonitrile were distilled from P_2O_5.

[1]Author to whom correspondence may be addressed.

[2]The numbering is indicated on structure **1**.

Printed in Canada / Imprimé au Canada

Can. J. Chem. Downloaded from www.nrcresearchpress.com by 88.85.125.76 on 09/07/12
For personal use only.

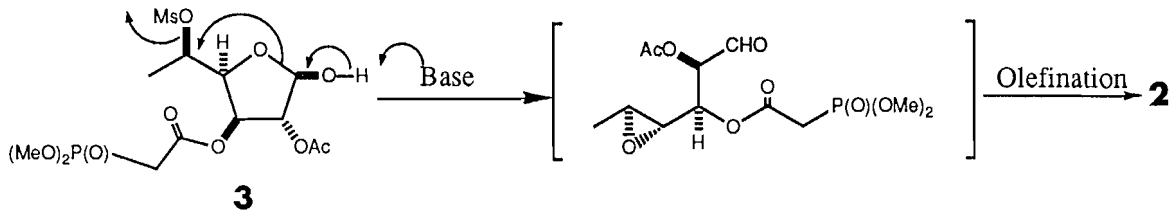

Ms = $MeSO_2$; Ac = MeCO

SCHEME 1

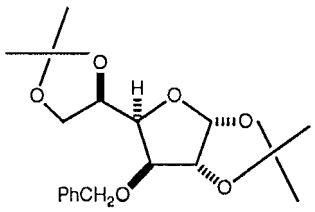

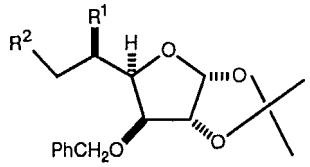

5 $R^1 = R^2 = MsO$

6 $R^1 = MsO$; $R^2 = H$

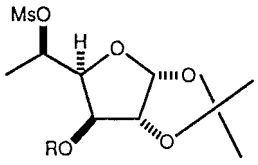

7 R = H

8 R = $(OMe)_2P(O)CH_2CO$

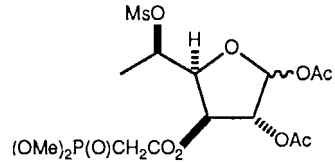

3-O-Benzyl-6-deoxy-1,2-O-isopropylidene-5-O-methanesulphonyl-α-D-glucofuranose **6**

To a stirred solution of the dimesylate **5** (11) (3.12 g, 6.69 mmol) in dry THF (95 mL) was added LAH (0.509 g, 13.39 mmol). The resultant solution was then heated at reflux under argon for 5 h. The reaction was quenched cautiously with water (3 mL), followed by the addition of aqueous ammonium chloride (15 mL), and extracted into chloroform (3 × 50 mL). The combined extracts were washed with water and aqueous ammonium chloride, dried (NA_2SO_4), and filtered. The filtrate was concentrated and the residue was chromatographed (ethyl acetate – hexane (1:2 v/v)) to give the 6-deoxy derivative **6** (2.25 g, 91%) as a colourless syrup that crystallized slowly. Recrystallization from diethyl ether – light petroleum (bp 40–60°C) afforded white crystals, mp 82–84°C; $[\alpha]_D^{20}$ −25.3° (*c* 4.4); R_f 0.50 (tlc, ethyl acetate – hexane (4:1 v/v)); ^{1}H nmr δ: 1.30 and 1.49 (2s, 6H, 2Me), 1.55 (d, 3H, $J_{6,5}$ 6.4 Hz, Me-6), 2.92 (s, 3H, CH_3SO_2), 4.05 (d, 1H, $J_{3,4}$ 2.9 Hz, H-3), 4.15 (d, 1H, $J_{4,5}$ 8.0 Hz, H-4), 4.61 (obscured by $PhCH_2$, 1H, H-2), 4.60 and 4.64 (2d, 2H J_{gem} 11.2 Hz, $PhCH_2$), 5.14 (m, 1H, H-5), 5.89 (d, 1H, $J_{1,2}$ 4.0 Hz, H-1), 7.35 (br s, 5H, pH); ms *m/z* (CI, NH_3): 390 (92%, MNH_4^+). Anal. calcd. for $C_{17}H_{24}O_7S$: C 54.8, H 6.5, S 8.6; found: C54.4, H 6.6, S 8.8.

6-Deoxy-1,2-O-isopropylidene-5-O-methanesulphonyl-α-D-glucofuranose **7**

A solution of **6** (3.03 g, 8.1 mmol) in ethanol (40 mL) was hydrogenated over $Pd(OH)_2$ (1.2 g) at room temperature and atmospheric pressure for 15 h. The catalyst was removed by filtration and the filtrate concentrated to give the alcohol **7** (2.18 g, 94%) as a white solid, which was recrystallized from diethyl ether–light petroleum (bp 40 – 60°C), mp 56–58°C; $[\alpha]_D^{20}$ −22.0° (*c* 2.9); R_f 0.24 (tlc, ethyl acetate – hexane (1:1 v/v)); ir: 3500 (OH); ^{1}H nmr δ: 1.30 and 1.49 (2s, 6H, 2Me), 155 (d, 3H, $J_{6,5}$ 6.5 Hz, Me-6), 3.07 (s, 3H, CH_3SO_2), 3.10 (d, 1H, $J_{OH,3}$ 4.2 Hz, OH-3), 4.02 (dd, 1H, $J_{4,3}$ 2.2, $J_{4,5}$ 9 Hz, H-4), 4.29 (dd, 1H, H-3), 4.55 (d, 1H, $J_{2,1}$ 3.7 Hz, H-2), 4.97 (dq, 1H, H-5), 5.89 (d, 1H, H-1); ms *m/z* (CI, NH_3): 300 (100%, MNH_4^+). Anal. calcd. for $C_{10}H_{18}O_6S$: C 42.5, H 6.4, S 11.3; found: C 42.5, H 6.4, S 11.4.

6-Deoxy-3-O-dimethylphosphonoacetyl-1,2-O-isopropylidene-5-O-methanesulphonyl-α-D-glucofuranose **8**

Dicyclohexylcarbodiimide (3.60 g, 17.4 mmol) was added in one portion to a stirred solution of the alcohol **7** (3.07 g, 10.88 mmol) and dimethylphosphonoacetic acid (2.2 g, 13.06 mmol) in dry dichloromethane (60 mL) at 0°C. After 2 h, the reaction was quenched with ethanol (5 mL) and acetic acid (1 mL), and filtered. The filtrate was concentrated and the residue chromatographed (ethyl acetate) to give **8** (4.31 g, 92%) as a colourless syrup; $[\alpha]_D^{20}$ −8.3° (*c* 3.4); R_f 0.18 (tlc, ethyl acetate); ir: 1747 (ester C=O); ^{1}H nmr δ: 1.23 and 1.48 (2s, 6H, 2Me), 1.54 (d, 3H, $J_{6,5}$ 6.5 Hz, Me-6), 2.97 (s, 3H, CH_3SO_2), 3.02 (dd, 1H, $^2J_{PH'}$ 21.0, J_{gem} 15.0 Hz, PCH'), 3.12 (dd, 1H, $^2J_{PH}$ 21.0 Hz, PCH), 3.76 and 3.80 (2d, 6H, $^3J_{PH}$ 11.5 Hz, 2 MeO), 4.17 (dd, 1H, $J_{4,3}$ 2.8, $J_{4,5}$ 8.6 Hz, H-4), 4.52 (d, 1H, $J_{2,1}$ 3.5 Hz, H-2), 4.96 (dq, 1H, H-5), 5.32 (d, 1H, H-3), 5.89 (d, 1H, H-1); ms *m/z* (CI, NH_3): 433 (57%, MH^+). Exact mass calcd. for $C_{14}H_{26}O_{11}PS$ (MH^+): 433.0931; found: 433.0933.

1,2-Di-O-acetyl-6-deoxy-3-O-dimethylphosphonoacetyl-5-O-methanesulphonyl-D-glucofuranose **9**

The acetonide **8** (5.7 g, 13.2 mmol) was dissolved in acetic anhydride (40 mL) and $BF_3 \cdot OEt_2$ (4 mL, 32.5 mmol) was introduced at 0°C with stirring. After 1 h, the reaction mixture was quenched with ice-water and extracted into ethyl acetate (3 × 120 mL). The combined extracts were washed successively with brine (2 × 80 mL), aqueous $NaHCO_3$ (2 × 70 mL), and brine (2 × 70 mL), dried (Na_2SO_4), and filtered. The filtrate was concentrated and the residue chromatographed to give **9** (6.1 g, 97%) as a pale yellow syrup; $[\alpha]_D^{22}$ +17.4° (*c* 9.3 ethanol); R_f 0.39 (tlc, chloroform–methanol (9:1 v/v)); ir: 1751 (ester C=O); ^{1}H nmr δ: inter alia 6.05 (s, 0.4H, αH-1), 6.40 (d, 0.6H, $J_{1,2}$ 4.4 Hz, βH-1); ms *m/z* (CI, NH_3): 494 (43% MNH_4^+). Exact mass calcd. for $C_{15}H_{21}NO_{13}PS$ (MH_4^+): 494.10951; found: 494.11429.

2-O-Acetyl-6-deoxy-3-O-dimethylphosphonoacetyl-5-O-methanesulphonyl-β-D-glucofuranose **3**

Stannic chloride (0.869 mL, 7.41 mmol) was added to a solution of the diacetate **9** (1.17 g, 2.47 mmol) in acetonitrile (15 mL) with stirring at 0°C. After 2 h at room temperature, the reaction mixture was treated with acetonitrile (5 mL) containing water (4 M) and $HCONMe_2$ (0.4 M). After a further 20 h, the reaction was quenched with aqueous $NaHCO_3$ (3 mL) and extracted with chloroform (40 mL). The extract was dried (Na_2SO_4), filtered, and the filtrate concentrated. The residue was chromatographed to give the lactol **3** (0.407 g, 55% based on recovered starting material (0.35 g)) as a colourless syrup; $[\alpha]_D^{20}$ +13.26° (*c* 1.9); R_f 0.25 (tlc, chloroform–methanol (9:1 v/v)); ir: 3450 (OH), 1747 (ester C=O); ^{1}H nmr δ: 1.58 (d, 3H, $J_{6,5}$ 6.2 Hz, Me-6), 2.93 (s, 3H, CH_3SO_2), 3.24 (dd, 1H, $^2J_{PH'}$ 21.0, J_{gem} 14.5 Hz, PCH'), 3.32 (dd, 1H, $^2J_{PH}$ 21.0 Hz, PCH), 3.82 (d, 6H, $^3J_{PH}$ 11.5 Hz, 2 MeO), 4.12 (dd, 1H, $J_{4,3}$ 3.5, $J_{4,5}$ 8.7 Hz, H-4), 5.02 (s, 1H, H-1), 5.11 (dq, 1H, H-5), 5.21 (s, 1H, H-2), 5.28 (d, 1H, H-3); ms *m/z* (CI,

Can. J. Chem. Downloaded from www.nrcresearchpress.com by 88.85.125.76 on 09/07/12
For personal use only.

NH_3): 452 (11%, MH_4^+). Exact mass calcd. for $C_{13}H_{27}NO_{12}PS$ (MH_4^+): 452.0989; found: 452.0992.

(*6R,7S*)-*Diastereoisomer of asperlin* **2**

1,8-Diazabicyclo[5.4.0]undec-7-ene (0.158 mL, 1.06 mmol) was added to a stirred solution of the lactol **3** (0.23 g, 0.53 mmol) in dry acetonitrile containing LiCl (0.024 g, 0.58 mmol) under nitrogen at room temperature. After 1 h, the reaction was quenched with aqueous NH_4Cl (1 mL) and extracted into chloroform (2 × 10 mL). The combined extracts were washed with water (2 × 5 mL), aqueous NH_4Cl (2 × 5 mL), dried (Na_2SO_4), and filtered. Solvent removal afforded a syrup that was chromatographed to give the epoxy-lactone **2** (0.058 g, 47%) as a colourless syrup, which crystallized with time, mp 56–57°C; $[\alpha]_D^{22}$ +172.0° (*c* 1, ethanol); R_f 0.45 (diethyl ether); ir: 1735 (ester C=O); ^{1}H nmr δ: 1.34 (d, 3H, $J_{8,7}$ 5.1 Hz, Me-8), 2.15 (s, 3H, CH_3CO), 3.00 (dd, 1H, $J_{6,7}$ 2.2, $J_{6,5}$ 4.9 Hz, H-6), 3.04 (dq, 1H, H-7), 4.35 (dd, 1H, $J_{5,4}$ 3.6 Hz, H-5), 5.50 (dd, 1H, $J_{4,3}$ 5.2 Hz, H-4), 6.22 (d, 1H, $J_{2,3}$ 9.8 Hz, H-2), 6.86 (d, 1H, H-3); ms *m/z* (CI, NH_3): 230 (100%, MH_4^+). Exact mass calcd. for $C_{10}H_{16}NO_5$ (MH_4^+): 230.10276; found: 230.10274.

For an authentic sample of asperlin, ^{1}H nmr data δ: 1.39 (d, 3H, $J_{8,7}$ 5.0 Hz, Me-8), 2.14 (s, 3H, CH_3CO), 3.04–3.10 (m, 2H, H-6,7), 4.10 (dd, 1H, $J_{5,6}$ 6.9, $J_{5,4}$ 2.8 Hz, H-5), 5.31 (dd, 1H, $J_{4,3}$ 5.7 Hz, H-4), 6.22 (d, 1H, $J_{2,3}$ 9.7 Hz, H-2), 7.07 (d, 1H, H-3).

Acknowledgments

We thank Professor A. S. Perlin for an authentic sample of asperlin, Professor J. K. Sutherland for discussion, and the Algerian government for a scholarship (to M. A.).

1. A. D. Argoudelis and J. F. Zieserl. Tetrahedron Lett. 1969 (1966).
2. A. D. Argoudelis, J. H. Coats, and R. R. Herr. Antimicrob. Agents Chemother. 801 (1965); S. P. Owen and B. K. Bhuynan. Antimicrob. Agents Chemother. 804 (1965).
3. S. Lesage and A. S. Perlin. Can. J. Chem. **56**, 3117 (1978).
4. S. Lesage and A. S. Perlin. Can. J. Chem. **56**, 2889 (1978).
5. H. Hiraoka, K. Furata, N. Ikeda, and H. Yamamoto. Bull. Chem. Soc. Jpn. **57**, 2777 (1984).
6. P. Davis and A. S. Perlin. Can. J. Chem. **63**, 1009 (1985).
7. S. Valverde, B. Herradon, R. M. Rabanal, and M. Martin-Lomas. Can. J. Chem. **65**, 339 (1987).
8. T. K. M. Shing and M. Aloui. J. Chem. Soc. Chem. Commun. 1525 (1988).
9. G. W. J. Fleet and T. K. M. Shing. J. Chem. Soc. Chem. Commun. 849 (1983); I. Gosney and A. G. Rowley. *In* Organophosphorus reagents in organic synthesis. *Edited by* J. I. G. Cadogan. Academic Press, New York. 1979.
10. G. W. J. Fleet and T. K. M. Shing. J. Chem. Soc. Chem. Commun. 835 (1984).
11. J. S. Brimacombe and O. A. Ching. Carbohydr. Res. **8**, 82 (1968).
12. A. Banaszek, X. B. Cornet, and A. Zamojski. Carbohydr. Res. **144**, 342 (1985).
13. M. A. Blanchette, W. Choy, J. T. Davis, A. P. Essenfeld, S. Masamune, W. R. Roush, and T. Sakai. Tetrahedron Lett. 2183 (1984).

Can. J. Chem. Downloaded from www.nrcresearchpress.com by 88.85.125.76 on 09/07/12
For personal use only.

Thermal fragmentation analysis of neutral polysaccharides and the presence of 1,6-anhydrooligosaccharides

R. J. HELLEUR AND P. JACKMAN

Department of Chemistry, Memorial University of Newfoundland, St. John's, Nfld., Canada A1B 3X7

Received December 7, 1989

This paper is dedicated to Professor Arthur S. Perlin on the occasion of his 67th birthday

R. J. HELLEUR and P. JACKMAN. Can. J. Chem. **68**, 1038 (1990).

Small quantities of pyrolysates were obtained from micro-scale off-line pyrolysis of the neutral polysaccharides: cellulose, amylose, laminaran, nigeran, and a mannan from ivory nut. The pyrolytic fragments were analyzed by desorption chemical ionization – mass spectrometry, trimethylsilyl derivatization – capillary gas chromatography (– ammonia chemical ionization mass spectrometry) and benzoyl derivatization – high pressure liquid chromatography. Intact 1,6-anhydrohexosemonosaccharide, and -disaccharide fragments were identified as major products. By using off-line analytical pyrolysis information on saccharide composition can be obtained from the formation of anhydromonosaccharide products while linkage information is obtainable from distinctive anhydrodisaccharide products.

Key words: pyrolysis, polysaccharides, 1,6-anhydrooligosaccharides, desorption chemical ionization, mass spectrometry, gas chromatography, high pressure liquid chromatography.

R. J. HELLEUR et P. JACKMAN. Can. J. Chem. **68**, 1038 (1990).

La pyrolyse périphérique à l'échelle microscopique de polysaccharides neutres, comme la cellulose, l'amylose, la laminarane, le nigerane et un mannane tiré de la noix d'ivoire, permet d'isoler de faibles quantités de produits de pyrolyse. On a analysé les fragments de la pyrolyse en faisant appel à la spectroscopie de masse par désorption et ionisation chimique, par chromatographie capillaire en phase gazeuse après formation de dérivés triméthylsilyles (spectroscopie de masse par ionisation chimique à l'aide de l'ammoniac) et par chromatographie liquide à haute performance sur des dérivés benzoyles. Les produits majeurs sont des fragments de 1,6-anhydrohexosemonosaccharides et -disaccharides. Faisant appel à la pyrolyse analytique et en se basant sur la nature des anhydro-monosaccharides, on peut obtenir de l'information sur la composition des saccharides alors que la nature des anhydro-disaccharides fournit de l'information sur la nature des liaisons qui les relient.

Mots clés: pyrolyse, polysaccharides, 1,6-anhydrooligosaccharides, désorption et ionization chimique, spectroscopie de masse, chromatographie en phase gazense, chromatographie liquide à haute performance.

[Traduit par la revue]

Can. J. Chem. Downloaded from www.nrcresearchpress.com by 88.85.125.76 on 09/07/12
For personal use only.

Introduction

Structural elucidation of polysaccharides has been a particularly formidable biochemical problem to which solid sample analyses such as fast atom bombardment mass spectrometry has begun to make important contributions. To date, most of the work has been in the structural confirmation of saccharides resolved by gas chromatography. The importance of the structural identification problem is such that a more extensive and diverse contribution by other methods of analysis such as analytical pyrolysis (more appropriately called thermal fragmentation analysis) should be expected.

Numerous studies involving rapid pyrolysis of carbohydrates have shown that anhydrosugars are primary products (1–4). Rapid removal of pyrolysis products from the heated zone is important and this can be accomplished either by vacuum conditions or with the aid of a carrier gas flow. Recently, Helleur *et al.* (5–7) have used the thermal formation of anhydrosugars as a means of developing a new and rapid, solid sample technique of polysaccharide analysis. A heterolytic mechanism has been proposed for the glycosidic bond cleavage which involves a nucleophilic displacement of the glycosidic group by one of the ring hydroxyl groups to form an anhydrosugar (8). Another mechanism proposed by Essig *et al.* (9) suggests that anhydrosugar products from polysaccharides arise by a pyrolytic scission of glycosidic linkages to generate a resonance-stabilized glycose cation, which then adds an oxygen-nucleophile from within the same glycose cation to generate the anhydrosugar.

Pyrolysis in combination with gas chromatography (py-g.c.) has been used successfully in the identification of the saccharide composition of oligosaccharides and polysaccharides (6) and of more complex heterosaccharides (7). Each saccharide residue (e.g., gluco, arabino) produces its characteristic anhydrosugar (i.e., 1,6-anhydroglucopyranose, 1,4-anhydroarabinopyranose) which are then separated and identified using a polar phase – capillary gas chromatography column.

Past studies have reported or speculated on the existence of anhydrooligosaccharides in the pyrolytic sirups obtained from cellulose pyrolysis (10, 11). Recently, Radlein *et al.* (12) have identified cellobiosan, or, 4-O-(β-D-glucopyranosyl)-1,6-anhydro-β-D-glucopyranose, as the major anhydrodisaccharide product from rapid cellulose pyrolysis using a large fluid bed unit. the observation of intact anhydrooligomers of pyrolysis has also been claimed by Helleur *et al.* (13) and by others (14, 15) using the technique of pyrolysis – direct chemical ionization – mass spectrometry. In the present study, the optimization of "off-line" pyrolysis and the isolation and characterization of intact anhydrooligosaccharides is reported as a novel means of generating oligomer fragments from which linkage information can be obtained.

Experimental

Materials

Amylose, cellulose, laminaran, nigeran, sodium hydride, DMSO, methyl iodide, benzoic anhydride, 1,6-anhydro-β-D-glucopyranose, and 4-dimethylaminopyridine were purchased from Sigma Chemicals. HPLC Spectro-grade acetonitrile was obtained from Canlab. Silyl-grade pyridine and Tri-Sil Z were from Pierce Chemicals. Sephadex LH 20 was obtained from Pharmacia Fine Chemicals while Sep-Pak

Can. J. Chem. Downloaded from www.nrcresearchpress.com by 88.85.125.76 on 09/07/12
For personal use only.

C-18 cartridges were purchased from Waters. The mannan gum of ivory nut was a gift from Dr. G. Hay, Queen's University. 1,6-Anhydromannopyranose was a gift of Dr. A. S. Perlin, McGill University. Cellobiosan, maltosan, and 4-*O*-(6-*O*-β-D-galactopyranosyl-β-D-galactopyranosyl)-1,6-anhydro-β-D-glucopyranose were kindly donated by Dr. Taku Chiba, Nagoya City University.

Benzoylation

The samples (0.01–0.2 mg) were benzoylated by a procedure similar to that of Daniel *et al.* (16) using a dry pyridine solution (1.5 mL) containing 10% (w/v) benzoic anhydride and 5% (w/v) 4-dimethylaminopyridine. Reaction product mixtures were purified by chromatography using Sep-Pak C-18 cartridges.

Methylation

Dried pyrolysate oils were dissolved in DMSO (0.2 mL) under a nitrogen atmosphere and methylated with methyl sulfinyl anion and methyl iodide according to Hakomori's procedure (17). The methylated products were isolated from methylating agents by passage through a small column of Sephadex LH-20 suspended in chloroform followed by elution with the same solvent. Eluting fractions at 1 mL intervals were tested by TLC for products and, later, the fractions were combined and the chloroform evaporated off. The products were fully methylated as determined by IR.

Trimethylsilylation

Trimethylsilyl (TMS) derivatives were prepared using Tri-Sil Z reagent (*N*-trimethylsilylimidazole in dry pyridine) (TMS derivatization procedure as given in ref. 18). Samples were heated in 0.5 mL Reacti-Vials at 90°C for 20 min. In some cases the reaction mixture was diluted with water and the TMS-derivatized products were isolated by extraction with hexane.

Off-line pyrolysis

The off-line pyrolysis apparatus, illustrated in Fig. 1, was constructed using the water condenser part of a micro-sublimator (Kontes Glassware, $24/25 joint, #306500-000) and a Ace-Thred thermometer adapter (Aldrich Chemicals, $24/40 joint, #Z17,501-3). The adapter was modified by the addition of a gas purge side arm. The end of the condenser was drawn out to a fine tip so as to fit just inside the pyrolysis tube (about 0.25 cm from the pyrolysis zone).

The polysaccharide (50–200 μg) was placed between two porous plugs of silanized quartz wool in the quartz tube. The tube was positioned inside the coil of a Pyroprobe 1/4 inch probe (Chemical Data Systems) as shown in Fig. 1. The nitrogen flow of 5 mL/min and a vacuum of 2 mm Hg was normally applied during pyrolysis. Pyrolysis was usually carried out at 600°C for 10 s. The condensed pyrolysate was washed off with small amounts of the solvent used during derivatization.

Chromatographic methods

Gas chromatography was performed using a Varian 3700 gas chromatograph equipped with a flame ionization detector. A non-polar fused silica capillary column (J&W Scientific, DB-5, 1.0 μm thickness, 30 m × 0.322 mm id) operated at a colum flow rate of 2.5 mL of He/min and a split ratio of 10:1 was used for high resolution separation of TMS derivatives. Temperature program settings were as follows: initial temperature, 120°C, hold 2 min; increase 5°C/min until 270°C, hold for 15 min. The injection port and detector were heated at 280°C. TMS derivatives were also analyzed using an on-column injector (J&W Scientific) and a non-polar capillary column (J&W DB-5, 1.0 μm thickness, 10 m × 0.25 mm id) with a column flow rate of 2 mL He/min. Temperature program settings were initial temperature, 80°C, hold 2 min; increase 8°C/min until 340°C, hold 10 min. The detector was heated at 350°C. One μL samples were injected in each case.

High pressure liquid chromatography (HPLC) of benzoylated derivatives were analyzed using a Varian 5000 HPLC equipped with a Varian Model UV-10, variable wavelength UV detector. The detector wavelength was set at 230 nm. Reversed phase chromatography was performed on a 5 μm Sperisorb ODS-2, 250 × 4.6 mm column

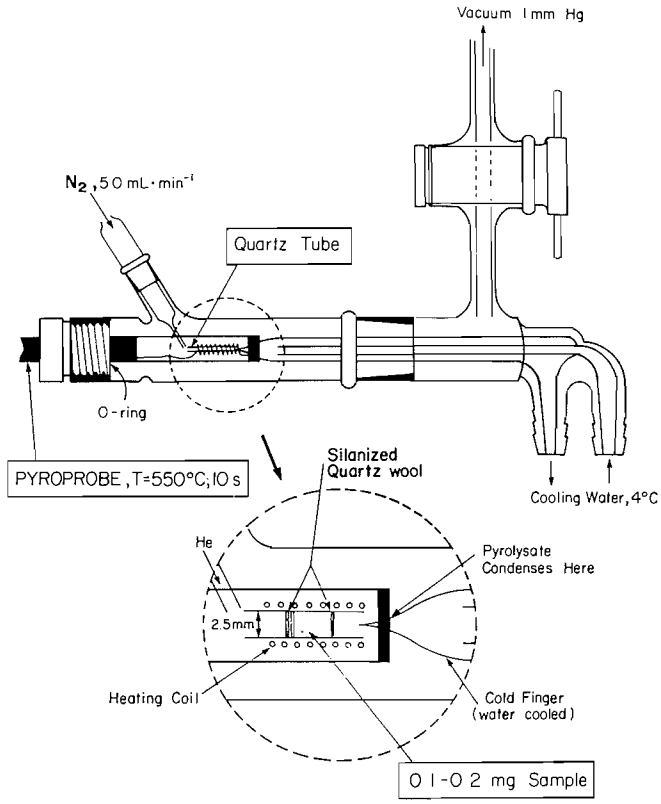

FIG. 1. Off-line pyroprobe pyrolysis apparatus.

(Alltech), sample loop 10 μL. Gradient elution from 65% CH_3CN/35% H_2O to 100% CH_3CN in 20 min, at a flow rate of 1 mL/min, was used.

Gas chromatography – mass spectrometry

The conditions of chromatography were identical to those used for high resolution separation, i.e., 30 m column, but with a reduced column flow rate. The column outlet was led directly into the ion source of a VG 7070HS double focusing mass spectrometer equipped with a DS 2035 data system. Mass spectrometric detection was carried out under chemical ionization conditions using ammonia as reagent gas and with a combinaion EI-CI source in the CI mode (CI slit). The ammonia gas was admitted into the ion source until the pressure above the diffusion pump was 6×10^{-5} mbar. The electron impact ionization energy was set at 100 eV, the source temperature at 140°C and the column inlet temperature at 270°C. The resulting ion abundance ratio of adducts of ammonia, m/z 18 and 35 were observed to be approximately 5 to 1.

Desorption chemical ionization – mass spectrometry

Mass spectra were acquired with a VG analytical ZAB-EQ hybrid instrument fitted with a VG 11-250J data system. Samples were evaporated onto a DCI platinum filament probe and inserted into a combination EI-CI source in the CI mode (CI slit). The source was operated at 160°C. Ammonia gas was admitted into the source until the pressure above the diffusion pump was 7×10^{-5} mbar. Electrons with 100 eV energy were used to ionize the ammonia reagent gas. A reasonably high ammonia gas pressure was obtained in this source where the ion abundance ratios of the ammonia adducts m/z 18, 35, and 52 were measured at 2:8:5. The samples were desorbed by heating the platinum filament for approximately 120 s, the final temperature of the filament being close to 350°C. The mass spectra were time-integrated.

Results and discussion

"Off-line" pyrolysis conditions

The important considerations in the design of the pyrolysis apparatus, as shown in Fig. 1, were that it should bear the

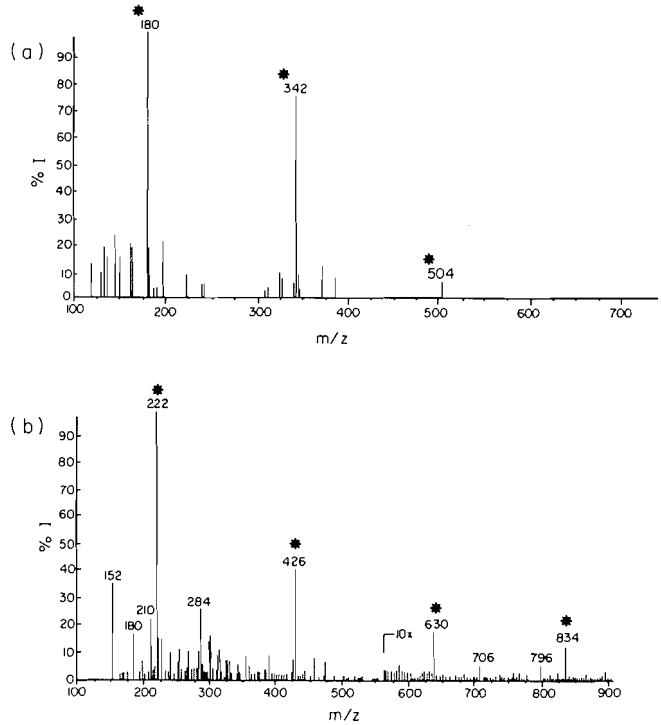

FIG. 2. Desorption ammonia chemical ionization – mass spectra of (*a*) underivatized amylose pyrolysate and (*b*) permethylated derivative of amylose pyrolysate.

following features: of simple construction, using commercially available parts; afford a means for observing the pyrolysis; and use of the CDS pyroprobe, an ultra-rapid pyrolysis unit widely used in research. Three major parameters were found to affect the generation and isolation of anhydrosugars: the pyrolysis temperature, the vacuum, and the location of the cold finger. Conditions were optimized to obtain the lowest anhydro monomer-to-dimer ratio using amylose (100 μg) as the standard. A pyrolysis temperature of 600°C was selected. It was found that temperatures outside the range 600 ± 100°C resulted in change in product distribution and poor reproducibility. A temperature of 600°C was found to be suitable for many other polysaccharides studied. The heat transfer from the heating coil to the quartz tube was retarded if the pressure was much less than 1 mm Hg. The positioning of the cold finger condensor was important because if it were too close to the pyrolysis tube partial blockage of the flow of gases occurred, whereas if it were too far from the tube higher molecular weight products were not trapped and the ratio of dimeric products to monomeric decreased.

Once the pyrolysis conditions were set up replicate analyses of amylose showed only small variations (approximately 10%) in reproducibility of the anhydro monomer-to-dimer ratio. Average yields of total anhydrosugars ranged from 10 to 20%. A study of yields among the glucans having different linkage and anomeric configuration was not carried out with off-line pyrolysis but preliminary studies using py–g.c. indicate a substantial difference in anhydro glucose yields among three different glucan samples (samples had been washed free of trace metals before pyrolysis).

Desorption ammonia chemical ionization mass spectra isolated pyrolysates

Preliminary evidence of the presence of oligomeric products in the condensate from our "off-line" pyrolysis was obtained by direct probe mass spectrometry. The mass spectrum of the underivatized mixture of pyrolysis products of amylose (Fig. 2*a*) shows important pseudo-molecular ions, i.e., m/z 180, 342, and 504. These fragment ions most likely correspond to the ammonium adducts of an anhydrohexose, an anhydrohexose disaccharide, and an anhydrohexose trisaccharide, respectively. The ammoniated anhydrooligosaccharide ion series can be described as $[(162)_n + 18]$ in which "n" represents the number of saccharide units and 18 represents the NH_4^+-adduct. Additional information pertaining to the structure of the anhydrosaccharides was obtained by the mass spectrum (Fig. 2*b*) of the per-*O*-methylate pyrolysate of amylose. The spectrum reveals ions corresponding to the ammonia ion adducts of the per-*O*-methylated anhydrooligosaccharides. This homologous series of per-*O*-methylated products can be described as $[(204)_n + 18]$ in which n represents the number of methylated saccharide units.

High temperature gas chromatographic analysis of TMS derivatives and identification of anhydrosugar products

Sample analysis by on-column injection short-column gas chromatography coupled with high temperature programming insures, first, that labile compounds do not degrade when injected, and, second, that high mass products such as a TMS anhydrotrimer compound will elute from the chromatographic column. The chromatogram of the TMS derivatives of an amylose pyrolysate is given in Fig. 3. The frontal peaks correspond to large amounts of remaining TMS reagent and decomposition products. (It was found that no loss of product was observed if the TMS reaction mixture was extracted with hexane.) Two large chromatographic peaks are observed, peak A and peak B, the retention times which corresponds to those of the standards 1,6-anhydro-2,3,4-tri-*O*-(trimethylsilyl)β-D-glucopyranose and 4-*O*-(2,3,4,6-tetra-*O*-(trimethylsilyl)α-D-glucopyranosyl)-1,6-anhydro-2,3-di-*O*-(trimethylsilyl)-βD-glucopyranose, respectively. Confirmation of the molar mass of these anhydrosugars was obtained by gas chromatography – ammonia chemical ionization mass spectrometry. Their ammonia chemical ionization mass spectra are shown in Fig. 3. Note that extensive fragmentation is observed even under ammonia chemical ionization conditions. Parent ions of carbohydrates are usually not observed unless very soft ionization is used.

No TMS anhydrotrimer product was observed in the chromatogram even though an anhydrotrimer ion was observed by desorption – mass spectrometry as shown above. The TMS derivative of our anhydrotrisaccharide standard eluted with a retention time of 33.1 min.

Separation of benzoylated derivatives of amylose pyrolysate by HPLC

The technique of HPLC was used in this study to obtain chromatographic evidence of an anhydrotrisaccharide product and to be able, in future studies, to isolate small quantities of fractionated products for structural characterization. The HPLC chromatogram of the benzoylated products of an amylose pyrolysate, Fig. 4, shows a large solvent and reagent peak along with a number of small molecular weight products of pyrolysis. There are also three later-eluting peaks whose elution times are 12.9, 20.5, and 23.7 min. Under the conditions employed the benzoylated derivatives of 1,6-anhydro-β-D-glucopyranose and 4-*O*-(α-D-glucopyranosyl)-β-D-glucopyranose standards had retention times of 12.9 and 20.5 min. The compound eluting at 23.7 has not been identified.

Can. J. Chem. Downloaded from www.nrcresearchpress.com by 88.85.125.76 on 09/07/12
For personal use only.

Can. J. Chem. Downloaded from www.nrcresearchpress.com by 88.85.125.76 on 09/07/12
For personal use only.

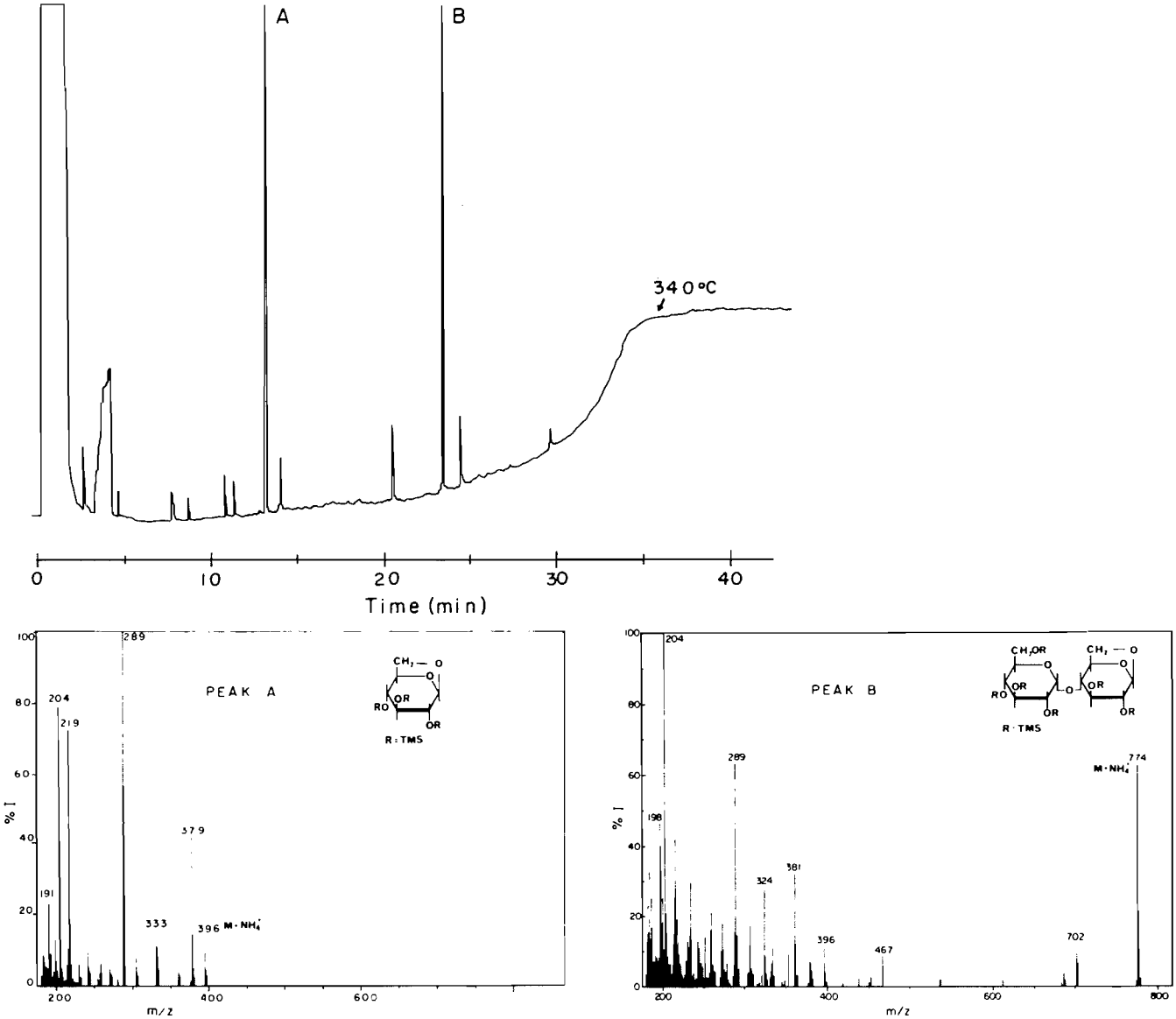

FIG. 3. On-column injected – short column – gas chromatogram of TMS derivative of amylose pyrolysate and ammonia chemical ionization mass spectra representing those of the compounds of peak A and Peak B whose spectra closely resemble the standards, 1,6-anhydro-2,3,4-tri-*O*-(trimethylsilyl)-β-D-glucopyranose and 4-*O*-(2,3,4,6-tetra-*O*-(trimethylsilyl)-α-D-glucopyranosyl)-1,6-anhydro-2,3-di-*O*-(trimethylsilyl)-β-D-glucopyranose, respectively.

Structural analysis of polysaccharides by off-line pyrolysis – TMS derivatization – high resolution g.c.

One of the objectives of this study is to develop a rapid analysis for polysaccharides to obtain both saccharide and structural information. Five different polysaccharides were analyzed: four glucans, i.e., amylose (-α-D-(1→4)-linked), cellulose (-β-D-(1 → 4)-), laminaran (-β-D-(1→3)-), and nigeran (alternating -α-D-(1→4)- and -α-D(1→3)-linked), and, a ivory nut mannan. Current evidence (19) indicates that ivory nut mannans are principally linear β-D-(1→4)-linked D-mannans. The gas chromatograms of all five TMS-pyrolysate samples are given in Fig. 5. The identity of the minor peaks, which are not labelled, has not been confirmed. Based on previous pyrolysis work (20) and comparison with the retention times of other standards, the minor peaks eluted before the M-labelled one have been tentatively assigned to 5-(hydroxymethyl)-2-furaldehyde, and 1,5-anhydro-4-deoxyD-*glycero*-hex-1-en-3-ulose. The minor peaks in the high mass region, around the

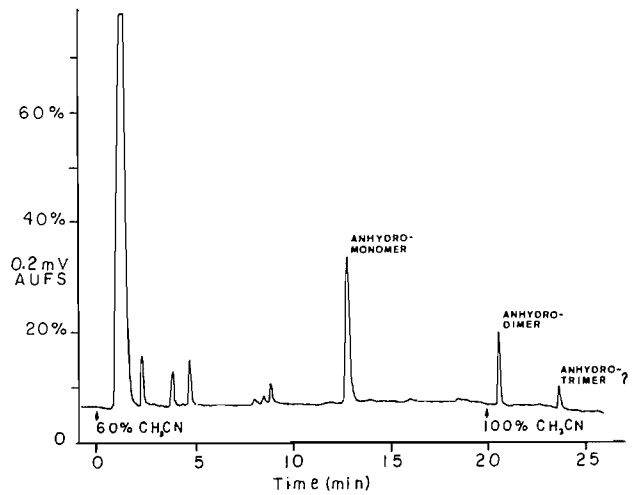

FIG. 4. Separation of benzoylated derivative of amylose pyrolysate by HPLC.

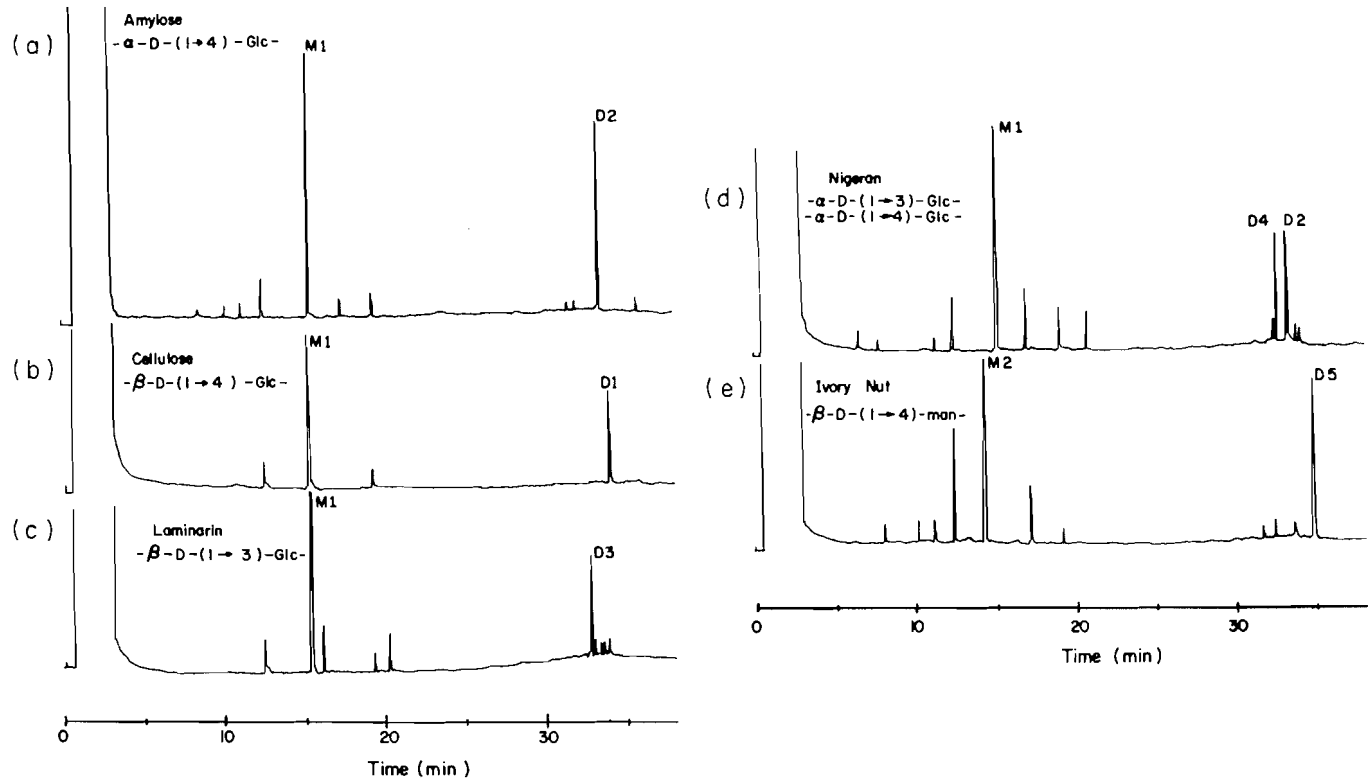

FIG. 5. High resolution gas chromatographic analysis of TMS derivatives of pyrolysates of (*a*) amylose, (*b*) cellulose, (*c*) laminaran, (*d*) nigeran, and (*e*) a mannan from ivory nut. Identity (* = tentative) of labelled peaks: *peak M1*, 15.4 min, 1,6-anhydro-2,3,4-tri-*O*-(trimethylsilyl)-β-D-glucopyranose; *peak M2*, 14.2 min, 1,6-anhydro-2,3,4-tri-*O*-(trimethylsilyl)-β-D-mannopyranose; *peak D1*, 33.8 min, 4-*O*-(2,3,4,6-tetra-*O*-(trimethylsilyl)-β-D-glucopyranosyl)-1,6-anhydro-2,3-di-*O*-(trimethylsilyl)-β-D-glucopyranose; *peak D2*, 33.4 min, 4-*O*-(2,3,4,6-tetra-*O*-(trimethylsilyl)-α-D-glucopyranosyl)-1,6-anhydro-2,3-di-*O*-(trimethylsilyl)-β-D-glucopyranose; *peak D3*, 32.7 min, 3-*O*-(2,3,4,6-tetra-*O*-(trimethylsilyl)-β-D-glucopyranosyl)-1,6-anhydro-2,3-di-*O*-(trimethylsilyl)-β-D-glucopyranose*; *peak D4*, 32.8 min, 3-*O*-(2,3,4,6-tetra-*O*-(trimethylsilyl)-α-D-glucopyranosyl)-1,6-anhydro-2,3-di-*O*-(trimethylsilyl)-β-D-glucopyranose*; *peak D5*, 34.7 min, 4-*O*-(2,3,4,6-tetra-*O*-(trimethylsilyl)-β-D-mannopyranosyl)-1,6-anhydro-2,3-di-*O*-(trimethylsilyl-β-D-mannopyranose*.

retention time of the D-labelled peaks, are believed to be various anhydrodisaccharides having different glucosidic linkages as the result of polymerization of levoglucosan in the melt and re-pyrolysis (21, 22). It is noteworthy that laminaran (Fig. 5*c*), by giving the highest amount of levoglucosan, generated a large number of minor anhydrodisaccharide products.

Each polysaccharide sample produced major quantities of anhydromonomeric and -dimeric fragments characteristic of their saccharide composition and structural linkage. A remarkable feature of these products is that each has its distinctive retention time as listed in the legend of Fig. 5.

In summary, this study has described a relatively simple pyrolysis apparatus for the isolation of intact 1,6-anhydrooligosaccharides from thermal fragmentation of neutral polysaccharides. With TMS derivatization followed by g.c. analysis, information on saccharide composition can be obtained from anhydromonosaccharide products while linkage information can be obtained from distinctive anhydrodisaccharide products. Future studies will be conducted to obtain higher mass fragments and HPLC will be used more extensively. In addition to neutral saccharides, analysis of thermal fragments from uronic acid- and amino-containing polysaccharides will improve our understanding of the complex pyrolysis mechanisms of these important polymeric units.

Acknowledgements

The work was funded by the Natural Sciences and Engineering Research Council of Canada. The authors are grateful to Dr. B. Gregory, Department of Chemistry, Memorial University of Newfoundland, and, to Dr. R. Guevremont, National Research Council of Canada, Ottawa, for aiding in mass spectral work.

1. F. SHAFIZADEH, R. H. FURNEAUX, T. G. COCHRAN, J. P. SCHOLL, and Y. SAKAI. J. Appl. Polym. Sci. **23**, 3525 (1979).
2. J. S. SAWARDECKER, J. H. SLONEKKER, and R. J. DIMLER. J. Chromatogr. **20**, 260 (1965).
3. J. PISKORZ, D. ST. A. G. RADLEIN, D. S. SCOTT, and S. CZERNIK. J. Anal. Appl. Pyrol. **16**, 127 (1989).
4. M. G. ESSIG and G. N. RICHARDS. Carbohydr. Res. **181**, 189 (1988).
5. D. R. BUDGELL, E. R. HAYES, and R. J. HELLEUR. Anal. Chim. Acta, **192**, 243 (1987).
6. R. J. HELLEUR, D. R. BUDGELL, and E. R. HAYES. Anal. Chim. Acta, **192**, 367 (1987).
7. R. J. HEULEUR. J. Anal. Appl. Pyrol. **11**, 297 (1987).
8. F. SHAFIZADEH. Adv. Carbohydr. Chem. **26**, 297 (1971).
9. M. ESSIG, G. N. RICHARDS, and E. SCHENCK. *In* Cellulose and wood, chemistry and technology. *Edited by* C. Schuerch. Wiley Interscience. 1989. p. 841.
10. M. J. ANTAL, JR. Adv. Solar Energy, **1**, 61 (1982).
11. F. SHAFIZADEH and Y. L. FU. Carbohydr. Res. **29**, 113 (1973).
12. D. ST. A. G. RADLEIN, A. GRINSHPUN, J. PISKORZ, and D. S. SCOTT. J. Anal. Appl. Pyrol. **12**, 39 (1987).
13. R. J. HELLEUR and R. GUEVREMONT. J. Anal. Appl. Pyrol. **15**, 85 (1989).
14. A. D. POUWELS, G. B. EIJKEL, P. W. ARISZ, and J. J. BOON. J. Anal. Appl. Pyrol. **15**, 71 (1989).

Can. J. Chem. Downloaded from www.nrcresearchpress.com by 88.85.125.76 on 09/07/12
For personal use only.

15. A. C. TAS, A. KERKENAAR, G. F. LAVOS, and J. VAN DER GREEF. J. Anal. Appl. Pyrol. **15**, 55 (1989).
16. P. F. DANIEL. Methods Enzymol. **138**, 94 1987).
17. S. HAKOMORI. J. Biochem. Jpn. **55**, 205 (1964).
18. 1989 Pierce Catalogue, Rockford, Il.
19. D. A. REES. MTP Int. Rev. Sci.: Org. Chem., Ser. One **7**, 251 (1973).
20. R. J. HELLEUR, E. R. HAYES, W. D. JAMIESON, and J. S. CRAIGIE. J. Anal. Appl. Pyrol. **8**, 333 (1985).
21. M. L. WOLFROM, A. THOMPSON, R. B. WARD, D. HORTON, and R. H. MOORE. J. Org. Chem. **26**, 4617 (1961).
22. M. L. WOLFROM, A. THOMPSON, and R. B. WARD. J. Am. Chem. Soc. **81**, 4623 (1959).

Can. J. Chem. Downloaded from www.nrcresearchpress.com by 88.85.125.76 on 09/07/12
For personal use only.

Structural characterization, by two-dimensional NMR spectroscopy and fast-atom-bombardment mass spectrometry, of a highly acylated trirhamnoside from *Mezzettia leptopoda (Annonaceae)*

DONALD A. POWELL, WILLIAM S. YORK, AND HERMAN VAN HALBEEK[1]

Complex Carbohydrate Research Center and Department of Biochemistry, University of Georgia, 220 Riverbend Road, Athens, GA 30602, U.S.A.

JOSEPH T. ETSE

School of Pharmacy, University of Georgia, Athens, GA 30602, U.S.A., and Phytochemistry Research Laboratories, Department of Pharmacy, University of Strathclyde, 204 George Street, Glasgow G1 1XW, U.K.

AND

ALEXANDER I. GRAY AND PETER G. WATERMAN

Phytochemistry Research Laboratories, Department of Pharmacy, University of Strathclyde, 204 George Street, Glasgow G1 1XW, U.K.

Received December 4, 1989

This paper is dedicated to Professor Arthur S. Perlin on the occasion of his 67th birthday

DONALD A. POWELL, WILLIAM S. YORK, HERMAN VAN HALBEEK, JOSEPH T. ETSE, ALEXANDER I. GRAY, and PETER G. WATERMAN. Can. J. Chem. **68**, 1044 (1990).

The structure of Mezzettiaside 3, a highly acylated trisaccharide obtained from the stem bark of *Mezzettia leptopoda*, was determined by a combination of double-quantum-filtered $\{^1H,^1H\}$ correlation spectroscopy, two-dimensional homonuclear Hartmann–Hahn, and ^1H-detected $\{^1H,^{13}C\}$ one-bond and multiple-bond shift correlation nuclear magnetic resonance experiments, in conjunction with fast-atom-bombardment mass spectrometry. Mezzettiaside 3 was found to be the α-(*n*-octyl)glycoside of 3,4-di-*O*-acetyl-L-rhamnopyranosyl-α(1→3)-2,4-di-*O*-acetyl-L-rhamnopyranosyl-α(1→3)-4-*O*-hexanoyl-L-rhamnopyranose. The heteronuclear multiple-bond correlation NMR technique proved to be invaluable in establishing the location of the *O*-acyl groups in this complex carbohydrate.

Key words: oligosaccharide, HMBC, HMQC, HOHAHA, FAB-MS.

DONALD A. POWELL, WILLIAM S. YORK, HERMAN VAN HALBEEK, JOSEPH T. ETSE, ALEXANDER I. GRAY et PETER G. WATERMAN. Can. J. Chem. **68**, 1044 (1990).

La structure du Mezzettiaside 3, un trisaccharide très acylé, obtenu à partir de l'écorce du tronc de *Mezzettia leptopoda*, a été elucidée en faisant appel à la spectrométrie de masse par bombardement avec des atomes rapides (SM-FAB) en combinaison avec les methodes de résonance magnétique nucléaire (RMN) suivantes : spectroscopie de corrélation $\{^1H,^1H\}$ doublement filtré d'un point de vue quantique, spectroscopie Hartmann-Hahn homonucléaire bidimensionelle et spectroscopie de corrélation des déplacements $\{^1H,^{13}C\}$ par liaisons simples et multiples avec détection de ^1H. On a trouvé que la Mezzettiaside 3 est l'α-(*n*-octyl)glycoside du 3,4-di-*O*-acétyl-L-rhamnopyranosyl-α(1→3)-2,4-di-*O*-acétyl-L-rhamnopyranosyl-α(1→3)-4-*O*-hexanoyl-L-rhamnopyranose. La technique de corrélation hétéronucléaire des liaisons multiples par RMN s'est avérée très utile pour déterminer la position des groupements *O*-acylés de ce carbohydrate complexe.

Mots clés : oligosaccharide, HMBC, HMQC, HOHAHA, FAB-MS.

Can. J. Chem. Downloaded from www.nrcresearchpress.com by 88.85.125.76 on 09/07/12
For personal use only.

Introduction

Mezzettiaside 3 (ML-3) is the third of seven oligorhamnosides whose isolation and purification from the stem bark of *Mezzettia leptopoda* Oliv. *ex* King (*Annonaceae*) has been described (1). Here we report the characterization of the primary structure of ML-3 by utilizing results from three different techniques: (i) gas chromatography (GC) of *S*(+)-2-butylglycosides generated from ML-3; (ii) fast-atom-bombardment mass spectrometry (FAB-MS) of the native ML-3, of deuterio-acetylated ML-3, and of de-acylated ML-3; and (iii) a combination of one-dimensional (1-D) and two-dimensional (2-D) NMR spectroscopy, including homonuclear Hartmann–Hahn (HOHAHA) spectroscopy, and heteronuclear multiple quantum coherence (HMQC and HMBC) experiments.

Experimental

Isolation and purification of Mezzettiaside 3 (ML-3)

Highly acylated oligorhamnosides were isolated (1) in a mixture from the stem bark of *Mezzettia leptopoda* by extraction with petroleum ether (bp 60–80°C). Seven components were separated by silica gel chromatography utilizing stepwise elution with toluene, toluene containing 10–40% ethyl acetate, and finally with pure methanol. The third fraction, designated ML-3, eluted with toluene containing 15% ethyl acetate, in a yield of 0.1% (w/w of powdered stem bark). Further purification of ML-3 was performed by circular preparative thin-layer chromatography on silica gel using chloroform/methanol (95:5, v/v). The optical rotation $[\alpha]_D$ of ML-3 was −49° (*c* 0.38, chloroform, 20°C) (1).

Butanolysis and gas chromatography

For glycosyl composition analysis, ML-3 was subjected to butanolysis followed by trimethylsilylation and gas chromatography. The chemicals used in this analysis were acetyl chloride and L-rhamnose (purchased from Sigma), *S*(+)-2-butanol and *R*/*S*(−/+)-2-butanol (from Aldrich), and Trisil (from Pierce). The *S*(+)- and *R*(−)-2-butylglycosides of L-rhamnose, and the *S*(+)-2-butylglycosides from ML-3 were prepared according to the butanolysis method of Gerwig *et al.* (2, 3). Gas chromatography of these derivatives was performed on a Hewlett Packard 5890 instrument with a Supelco SP2330 capillary column (30 m × 0.25 mm i.d.). Cochromatography of the ML-3

[1]Author to whom correspondence may be addressed.

Printed in Canada / Imprimé au Canada

derived butylglycosides with the appropriate standards, namely, *S*(+)-2-butyl-L-rhamnoside and *R*(−)-2-butyl-L-rhamnoside (which behaves the same on the column as its enantiomer *S*(+)-2-butyl-D-rhamnoside) was applied for identification of the ML-3 glycosyl residues.

Fast-atom-bombardment mass spectrometry

FAB mass spectra were recorded on a VG Analytical ZAB-SE mass spectrometer (4). ML-3 samples (5 μg/μL methanol) were prepared in several ways for different FAB-MS experiments. Approximately 1 mg of ML-3 was deuterio-acetylated as described by Dell and Tiller (5). Also, 0.5 mg of ML-3 was de-acylated in 0.4 mL methanol with 0.1 mL of 0.5 M NaOH at 30°C. After 16 h, water (0.3 mL) was added and the solution was desalted over a Dowex-50 cation exchange column at 4°C and dried with filtered air.

FAB mass spectra of the native ML-3 and its de-acylated derivative were recorded in the negative-ion mode using an aminoglycerol matrix (4). The FAB mass spectrum of deuterio-acetylated ML-3 was recorded in the positive-ion mode using a thioglycerol matrix. Sodium acetate was added to the deuterio-acetylated derivative to give a strong parent ion (6).

NMR spectroscopy

NMR experiments were performed on a Bruker AM-500 instrument interfaced with an Aspect 3000 computer using the DISR88 software package. The ML-3 sample (20 mg) was dissolved in 0.4 mL of benzene-d_6/methanol-d_4 (Aldrich) (4:1, v/v), in a 5-mm Wilmad 535-PP NMR tube. ^{1}H and ^{13}C chemical shifts are expressed in ppm downfield from internal tetramethylsilane (TMS, Aldrich). 1-D nuclear Overhauser effect (NOE) difference experiments were performed by the selective presaturation method of Wagner and Wüthrich (7).

A double-quantum-filtered {^{1}H,^{1}H} COSY spectrum was recorded in the phase-sensitive mode, with quadrature detection in t_1 according to the TPPI method (8, 9). The spectral width was 2500 Hz, and the relaxation delay 4.5 s; 512 FIDs each having 1k data points were acquired with a t_1 increment of 200 μs. Unshifted sine bell window functions were used in processing the data both in the t_1 and t_2 dimensions. The data matrix was expanded to a 2k × 2k data file before Fourier transformation, giving rise to a digital resolution in F2 of 2.441 Hz/pt.

2-D HOHAHA spectroscopy was performed in the phase-sensitive mode (TPPI) using the MLEV-17 sequence for mixing (10–13). The spectral width was 2500 Hz; 512 experiments of 48 scans and 2k data points each (relaxation delay 1 s; t_1 increment 200 μs; mixing time 100 ms) were acquired. The total time for data collection of the HOHAHA experiment was 11.5 h. For processing, a sine bell window shifted by $\pi/10$ was applied in both dimensions, followed by expansion of the data matrix to 2k × 2k data points and transformation. The resulting digital resolution in F2 was 2.441 Hz/pt.

Heteronuclear 2-D *J*-resolved NMR spectroscopy was carried out using the spin–flip method (14). The spectral width was 31 250 Hz in F2 and 556 Hz in F1. 128 experiments of 96 scans each were acquired in 8k data points (relaxation delay 3 s; t_1 increment 900 μs). After applying a 10 Hz Gaussian linebroadening in the t_2 dimension only, the data matrix was expanded to a 16k × 512 w file (F2 digital resolution: 3.81 Hz/pt; F1 digital resolution: 2.17 Hz/pt) and then transformed.

The ^{1}H-detected {^{1}H,^{13}C} shift correlation experiments utilized a 5-mm broadband probe with reversed geometry. The decoupler transmitter was used for ^{1}H pulses (reverse mode) and the sample was not spun.

^{1}H-Detected heteronuclear multiple quantum coherence (HMQC) experiments were performed according to Bax and co-workers (12, 15), preceded by a BIRD pulse to suppress ^{1}H resonances not coupled to ^{13}C (12, 16) and with GARP1 ^{13}C decoupling during ^{1}H data acquisition (17). The spectral width in the ^{1}H dimension was 2500 Hz and in the ^{13}C dimension 12 500 Hz; 250 experiments of 200 scans each (relaxation delay 1 s; t_1 increment 400 μs; delay after BIRD pulse 300 ms) were acquired in 1k data points each; the total time for data collection in the HMQC experiment conducted under these conditions was 18.5 h. An unshifted sine bell window function was applied in the t_2 dimension and a Gaussian window (line broadening 100 Hz) in the t_1 dimension; then the data matrix was expanded to 1k × 512w before Fourier transformation. The resulting digital resolutions were 4.883 Hz/pt in F2 (^{1}H) and 24.415 Hz/pt in F1 (^{13}C dimension).

Heteronuclear multiple bond correlation (HMBC) spectroscopy was performed according to Bax and co-workers (11, 12, 18). The spectral width in the ^{1}H dimension was 2500 Hz, and in the ^{13}C dimension 25 000 Hz; 200 FIDs of 192 scans in 2k data points each (relaxation delay 1 s; t_1 increment 200 μs) were collected during a total time of 17 h. An unshifted sine bell window function was applied in the t_2 dimension, and a Gaussian window (line broadening 100 Hz) in the t_1 dimension. The data matrix was then expanded to 2k × 512w and transformed. The final resolution in F2 was 2.441 Hz/pt, in F1 48.82 Hz/pt.

Results

Composition and sequence analysis by GC and FAB-MS

The glycosyl composition of ML-3, including the absolute configuration of the constituent monosaccharide residues, was determined by butanolysis followed by gas chromatography of the TMS derivatives of the butylglycosides. GC of the *S*(+)-2-butylglycosides generated from ML-3 showed exclusively *S*(+)-2-butyl-L-rhamnoside; therefore, ML-3 was found to consist of L-rhamnose residues.

Negative-ion FAB-MS of native ML-3 gave a molecular ion $[M-H]^-$ at *m/z* 833 but the intensity of fragment ion peaks was weak. To enhance fragment ion information, the free hydroxyl groups in ML-3 were deuterio-acetylated. Use of acetic acid-d_3 in the derivatization procedure allowed the endogenous *O*-acetyl groups to be distinguished from those introduced chemically (5). From the $[M+Na]^+$ ion (*m/z* 947) and the fragment ions (*m/z* 795, 506, and 276) observed in the positive-ion FAB mass spectrum of the deuterio-acetylated sample (see Fig. 1a), ML-3 was deduced to be the octyl glycoside of a linear trirhamnoside which has a number of endogenous acyl substituents, as follows. Comparison of *m/z* 947 for the $[M+Na]^+$ peak of the deuterio-acetylated ML-3 and *m/z* 833 for $[M-H]^-$ of native ML-3 (see above) indicates that only two deuterio-acetyl (Ac*) groups were introduced chemically. One of these occurs at the non-reducing-end Rha residue denoted Rha-C, as was inferred from the *m/z* value of fragment ion 276 $[Rha(Ac^*)Ac_2]^+$; the other one is at Rha-A, since a type A fragment ion (5, 6) was observed at *m/z* 795 $[Rha_3(Ac^*)_2Ac_4R]^+$, while another type A fragment at *m/z* 506 $[Rha_2(Ac^*)Ac_4]^+$ indicates that Rha-B does not become deuterio-acetylated. From the mass of the fragment ion at *m/z* 795 it was determined that R is a hexanoyl group. The aglycone R′ of ML-3 was deduced to be an octyl group, by virtue of the mass of OR′ being 129, i.e., the difference between M and the A fragment at *m/z* 795. This implies that the Rha residue at the non-reducing end (Rha-C) has two endogenous *O*-acetyl groups attached; the adjacent residue Rha-B also has two endogenous *O*-acetyl groups, and the third residue, Rha-A at the potentially reducing end, has an *O*-hexanoyl substituent and an *O*-octyl aglycone.

To confirm the nature of the aglycone, an aliquot of ML-3 was de-acylated. Under the mild alkali conditions used to remove the *O*-acyl groups, the base-stable glycoside was not cleaved. The FAB mass spectrum of de-acylated ML-3 recorded in the negative-ion mode (see Fig. 1b) showed the $[M-H]^-$ ion at *m/z* 567 that represents $[Rha_3$-*O*-octyl$]^-$; this interpretation is supported by the presence of ions at *m/z* 421 and 275 that arise by consecutive losses of rhamnosyl residues from the nonreducing end. Each of these fragment ions still contains the octyl aglycone.

Can. J. Chem. Downloaded from www.nrcresearchpress.com by 88.85.125.76 on 09/07/12
For personal use only.

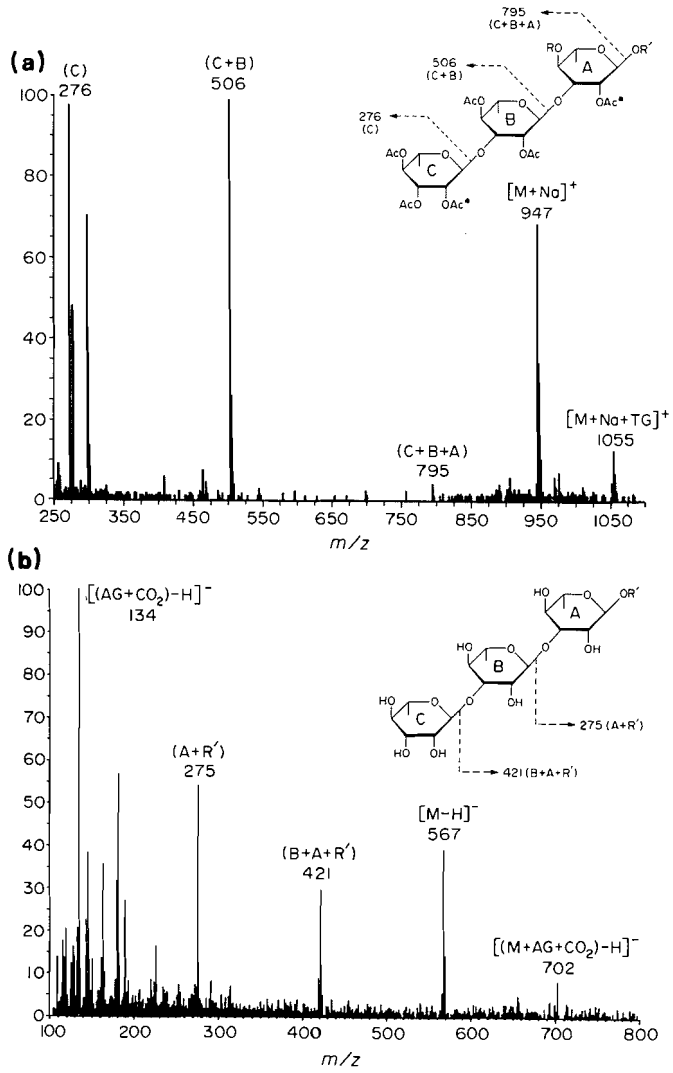

FIG. 1. (a) FAB mass spectrum of deuterio-acetylated ML-3 in the positive-ion mode; (b) FAB mass spectrum of deacylated ML-3 in the negative-ion mode. Insets illustrate the observed fragmentation patterns; R = $CO(CH_2)_4CH_3$; R′ = $-(CH_2)_7CH_3$; Ac* = trideuterioacetyl group. In spectrum (a), a matrix adduct ion $[M+Na+TG]^+$ is observed at m/z 1055, where TG stands for thioglycerol. In spectrum (b), a characteristic matrix ion $[AG+CO_2-H]^-$ occurs at m/z 134; it is formed when the aminoglycerol (AG) matrix is exposed to CO_2 (W.S. York; unpublished observations). This process also gives rise to an adduct ion at m/z 702 $[(M+AG+CO_2)-H]^-$.

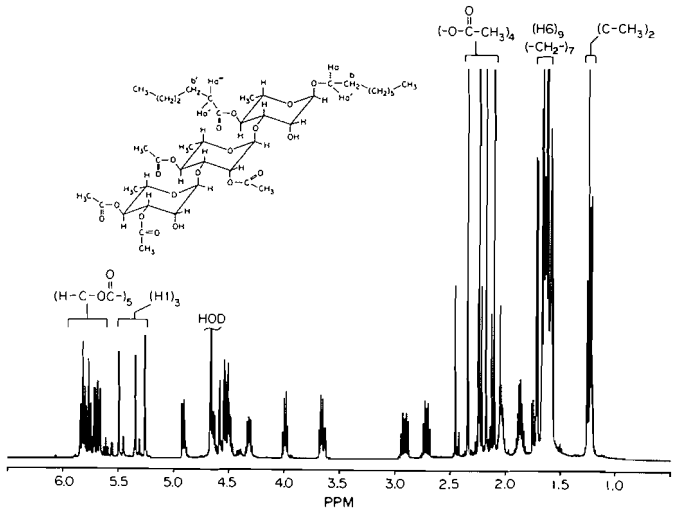

FIG. 2. 500-MHz ^1H NMR spectrum of ML-3 at 27°C in benzene-d_6/methanol-d_4 (4:1, v/v) with an inset of its structure. $(H1)_3$ refers to the anomeric protons of the three Rha residues and HOD refers to residual water in the solvent. Between δ 5.65 and 5.85 ppm, five non-anomeric rhamnosyl ring proton resonances are observed, indicating the presence of five acyl substituents in ML-3. In the upfield region of the spectrum, four acetyl methyl singlets are observed between δ 2.1 and 2.4 ppm; seven methylene multiplets and the doublets of three Rha C6 methyl groups are overlapping at δ ≈ 1.6 ppm, whereas two aliphatic methyl groups show intertwined triplets at δ ≈ 1.25 ppm. Chemical shifts are referenced to TMS.

Determination of glycosyl linkage positions and configurations, and locations of appended groups by NMR

To complete the determination of the primary structure of ML-3, various 1-D and 2-D, ^1H and ^{13}C NMR spectra of the compound were recorded. Their assignments allowed the determination of the linkage positions between the L-rhamnose residues and the positions of attachment of the acetyl and hexanoyl groups.

The ^1H NMR spectrum of ML-3 (Fig. 2) was virtually completely assigned by the combination of double-quantum-filtered (DQF) COSY (Fig. 3a) and 2-D HOHAHA experiments (Fig. 3b). The ^1H chemical shifts and coupling constants are listed in Table 1; in the methylene proton region ($1.55 < \delta < 1.68$) severe signal overlap prevented more detailed assignments. The three resonances observed at δ 5.49, 5.34, and 5.25 ppm were assigned to the anomeric protons by virtue of their being doublets. The signals, at this point, were designated H1X, H1Y, and H1Z, respectively, since the identity of the spin systems to which each belonged, i.e., Rha-A, -B, or -C, was yet to be determined. Downfield of the anomeric proton signals, between δ 5.85 and 5.65 ppm, a group of five non-anomeric ring proton signals was found, reflecting the presence of five acyl substituents. Other signals of interest, at δ 3.99, 3.66, 2.91, and 2.71 ppm, are due to methylene protons that are adjacent to the glycosidic oxygen in the aglycone or the carbonyl group in the hexanoyl substituent (denoted as Ha, Ha′, Ha″, and Ha‴, respectively, in the inset of Fig. 2). In addition, there are four acetyl singlets (at δ 2.34, 2.24, 2.18, and 2.10 ppm) and three methyl doublets arising from the H6 protons of the rhamnosyl residues (at δ 1.71, 1.66, and 1.62 ppm). The DQF-COSY experiment allowed the sequential assignment of several resonances for each rhamnosyl ring system, starting from the anomeric resonances. This is illustrated for Rha-Y (later identified as Rha-B; see below) in Fig. 3a. Not all of the Rha proton resonances could successfully be assigned from the COSY spectrum, since some of the crosspeaks were overlapping, e.g., those for proton pairs H4X/H5X and H3Z/H4Z. To complete the assignments, a 2-D HOHAHA spectrum was recorded (Fig. 3b). From this experiment, subspectra were obtained for each isolated spin system, in this case rhamnosyl residue (see Fig. 3b). All of the Rha proton resonances were assigned by the combination of HOHAHA and COSY results (see Table 1), except for the H4X and H4Z protons. The latter two signals, although resolved in the 1-D spectrum by 0.004 ppm (2 Hz) (Fig. 2), were not discernible in the 2-D (COSY and HOHAHA) spectra, because of the limitations in digital resolution (2.441 Hz/pt). In addition to the Rha proton signals, some key resonances for protons in the octyl aglycone (Ha, Ha′, and Hb) and hexanoyl group (Ha″, Ha‴, and Hb′) spin systems were identified (see Table 1). However, since the protons across the

Can. J. Chem. Downloaded from www.nrcresearchpress.com by 88.85.125.76 on 09/07/12
For personal use only.

TABLE 1. ^{1}H nuclear magnetic resonance data[a] for Mezzettiaside ML-3

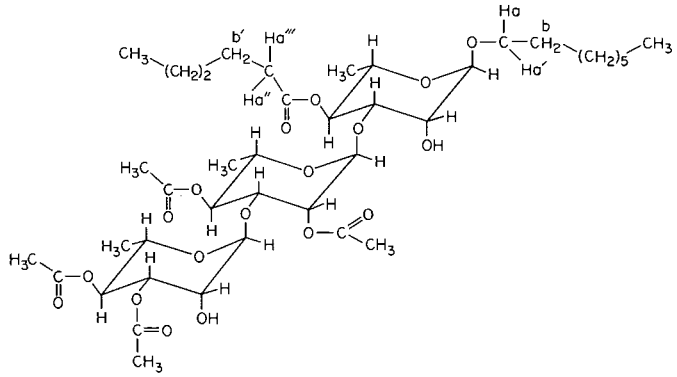

H-atom[c]	Chemical shifts[b] (ppm) Rha-A	Rha-B	Rha-C	J_{H-H}	Coupling constants (Hz) Rha-A	Rha-B	Rha-C
1	5.259	5.344	5.493	1–2	1.4	1.7	2.1
2	4.541	5.714	4.581	2–3	3.3	3.5	3.2
3	4.514	4.912	5.678	3–4	9.7	9.9	9.9
4	5.824[d]	5.769	5.820[d]	4–5	9.8	9.9	9.8
5	4.315	4.639	4.492	5–6	6.2	6.3	6.2
6	1.658	1.616	1.710				
R′ a	3.99	—	—	R′ a–a′	−9.7	—	—
R′ a′	3.66	—	—	R′ a–b	6.7	—	—
R′ b (2)	1.857	—	—	R′ a′–b	6.7	—	—
R′ c–g (5 × 2)	1.55–1.68[e]	—	—				
R′ h (3)	1.253	—	—	R′ g–h	6.9	—	—
R a″	2.91	—	—	R a″–a‴	−16.2	—	—
R a‴	2.71	—	—	R a″–b′	7.5	—	—
R b′ (2)	1.857	—	—	R a‴–b′	7.5	—	—
R c–d (2 × 2)	1.55–1.68[e]	—	—				
R e (3)	1.253	—	—	R d–e	6.9	—	—
Ac (3)	—	2.340[f]	2.176[f]				
Ac (3)	—	2.237[f]	2.104[f]				

[a]Measured at 27°C in benzene-d_6/methanol-d_4 (4:1, v/v).

[b]First-order data.

[c]For designations Rha A–C, for numbering of H atoms in the rhamnosyl rings, and for lettering of the H atoms in the substituent groups, see the structure of ML-3. R′ = octyl aglycone (at A1); R = hexanoyl (at A4); Ac = acetyl (at B2, B4, C3 and C4). The number of equivalent protons is given in parentheses.

[d]The triplets of H4A and H4C are resolved in the resolution-enhanced 1-D spectrum (see the ^{1}H projection in Fig. 4B), but not in the 2-D COSY and HOHAHA experiments (see Fig. 3). The lack of resolution in the 2-D {^{1}H,^{1}H} spectra prevented conclusive assignment of these signals by NMR alone. The combination of the FAB-MS and HMBC results enabled us to assign the signal at δ 5.824 ppm to H4A (see text and Fig. 4B).

[e]Individual chemical shifts and coupling constants could not be deduced for any signal within this range.

[f]Assignments of these signals are inconclusive with respect to the location of the acetyl groups, essentially due to lack of resolution of the corresponding carbonyl signals in the ^{13}C spectrum (see Fig. 4B).

glycosidic linkages are four bonds apart and therefore do not show any scalar coupling, no correlations between individual spin systems are observed in COSY or HOHAHA spectra; in other words, no sequence information was obtained from these experiments.

To establish the sequence of the three rhamnosyl spin systems X, Y, and Z (i.e., to determine how they match residues A, B, and C) and to determine the glycosyl linkage positions, a series of 1-D NOE experiments was carried out. The NOE difference spectrum upon presaturation of the H1Z at δ 5.25 ppm showed an NOE across the glycosidic linkage to Ha and Ha′ (at 3.99 and 3.66 ppm) of the aglycone and thereby identified spin system Z as Rha-A. The NOE difference spectrum obtained upon presaturation of the H1Y resonance at 5.34 ppm showed an interglycosidic NOE to H3Z (identified as H3A) at 4.51 ppm. This established spin system Y as being Rha-B, and also indicated the linkage between Rha-B and Rha-A to be (1→3). The interglycosidic NOE from H1X at 5.49 ppm to H3B (i.e., H3Y) at 4.91 ppm confirmed that spin system X is Rha-C, and indicated the linkage between Rha-C and Rha-B to be (1→3).

Presaturation of each of the H1 resonances showed, in addition to the aforementioned interresidue NOE, only one intraresidue NOE, namely, to H2. It is interesting to note the absence of intraresidue NOEs between the H1 atoms and the (axial) H3 and H5 atoms within the same residue. This implies that each H1 is in equatorial orientation, which strongly suggests the α configuration for both L-Rha*p*-(1→3)-L-Rha*p* linkages.

To determine conclusively the anomeric configuration of the glycosyl linkages, a 2-D J_{CH}-resolved experiment was performed. From the completely resolved multiplets for the three anomeric ^{13}C atoms, at δ 102.0, 100.4, and 99.8 ppm, all three of the $^1J_{C1H1}$ coupling constants were found to be >169 Hz. Such values for $^1J_{C1H1}$ establish the α configuration for each L-Rha*p*-(1→3)-L-Rha*p* linkage (19, 20). In addition, long-

Can. J. Chem. Downloaded from www.nrcresearchpress.com by 88.85.125.76 on 09/07/12
For personal use only.

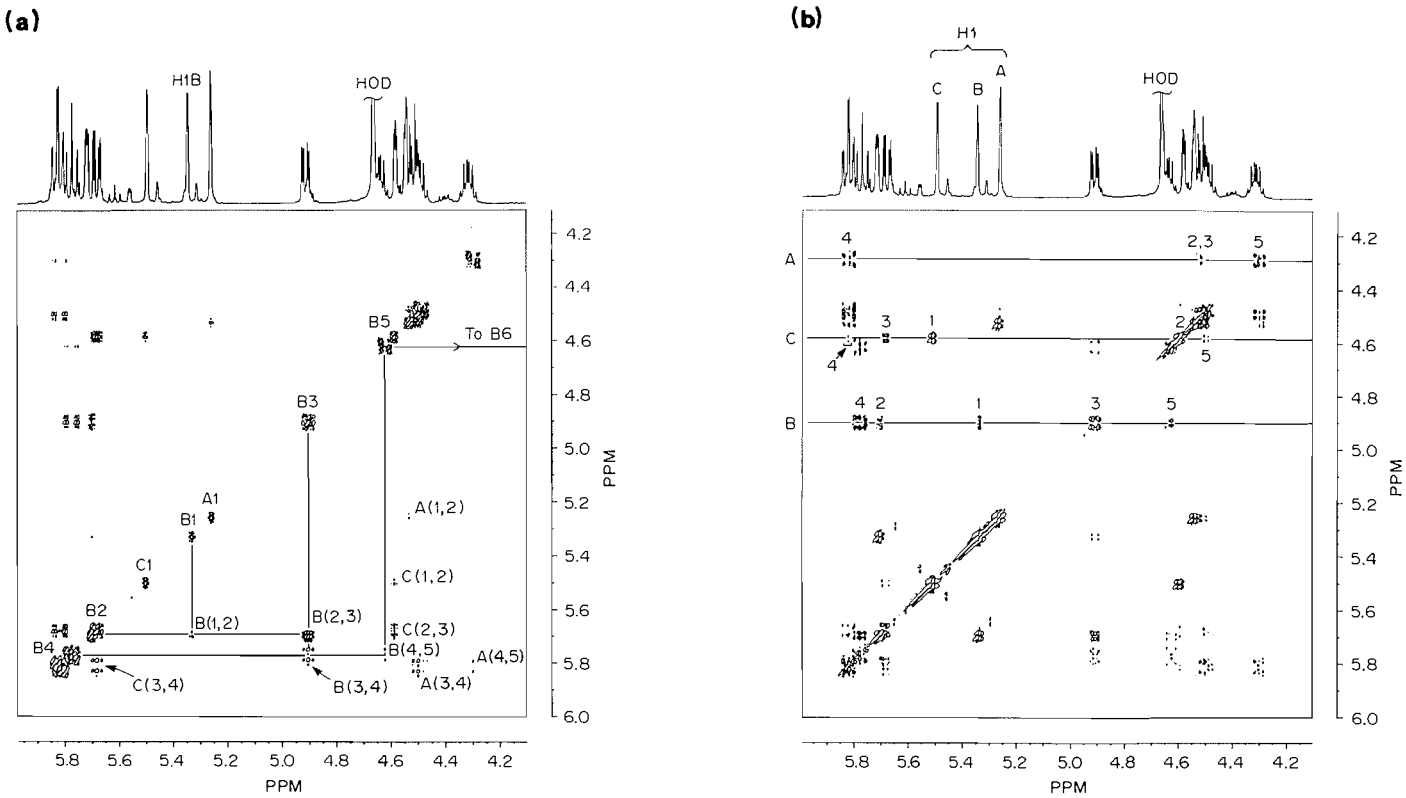

FIG. 3. Two-dimensional $\{^1H,^1H\}$ correlation NMR spectra of ML-3, recorded at 27°C in benzene-d_6/methanol-d_4 (4:1, v/v). (a) Expanded region of phase-sensitive DQF-COSY spectrum with high resolution 1-D projection. Selected region shows intraring crosspeaks for H1–H5 of each ring. Tracing of the *J*-connectivity trail is indicated for Rha-B residue. (b) Expanded region of HOHAHA spectrum with high resolution 1-D projection. Selected region shows each intraring H1–H5 subspectrum; those in the F2 cross sections through H5A, H3B, and H2C on the diagonal are indicated. Note that the H4A and H4C crosspeaks show no apparent difference in their chemical shifts (see Results).

range ($^2J_{CH}$ and (or) $^3J_{CH}$) couplings of 7–8 Hz were seen for the Rha-B and Rha-C anomeric carbons. The ^{13}C chemical shifts and the one-bond and long-range coupling constants observed are listed in Table 2.

To locate the positions of the substituents, i.e., the four acetyl groups and the hexanoyl group, the pertinent resonances in the ^{13}C spectrum were assigned. By utilizing the assignments from the ^1H spectrum (see above), this was accomplished via a ^1H-detected $\{^1H,^{13}C\}$ one-bond correlation experiment (HMQC). As suggested by Bax and Subramanian (16) for molecules in the extreme narrowing limit, such as ML-3, a BIRD pulse was used to suppress signals arising from protons linked to ^{12}C. The GARP1 composite pulse sequence was used for ^{13}C decoupling during ^1H data acquisition. Almost all carbon signals between 10 and 110 ppm were assigned from this experiment. Unfortunately, due to limited resolution in the ^{13}C domain, three of the four acetyl methyl carbon signals (two carbons at δ 20.11 and one carbon at 20.02 ppm) did not have well-resolved cross peaks in the HMQC experiment, thus preventing their definitive assignments. Only two other methyl carbon resonances were identified in the ^{13}C spectrum, namely, at δ 14.28 and δ 14.08 ppm (their proton multiplicity was verified by a 1-D DEPT experiment (21)). This implies that the alkyl chains in the hexanoyl (R) and octyl (R′) groups are both linear since only one terminal CH_3 group per chain occurs.

With the ^{13}C assignments summarized in Table 2, the locations of the various substituents were established by means of a ^1H-detected multiple-bond correlation (HMBC) spectrum optimized for long-range couplings ($^2J_{CH}$ and $^3J_{CH} \approx 7$ Hz). The results of this experiment first of all enabled us to assign the carbonyl carbon signals via $^2J_{CH}$ crosspeaks between the hexanoyl ester carbonyl (δ 173.5 ppm) and each of the atoms Ha″ (δ 2.91 ppm) and Ha‴ (δ 2.71 ppm) on one hand, and between the acetyl methyl protons (δ 2.34, 2.24, 2.18, and 2.10 ppm) and the acetyl carbonyls (δ 170.7 ppm) on the other (not shown in Fig. 4). The interglycosidic $^3J_{CH}$ crosspeaks between H1C and C3B, and also between H1B and C3A (Fig. 4a), confirmed the positions of the linkages to be (1→3), as suggested by the 1-D NOE experiments. The acetyl carbonyl resonances showed $^3J_{CH}$ connectivities to the ring protons H2B, H3C, H4B, and either H4C or H4A (Fig. 4b), thus indicating that the acetyl groups are attached to C2B, C3C, C4B, and either C4C or C4A. The connectivity of the hexanoyl carbonyl signal to either H4A or H4C indicated that this acyl group is attached to either C4A or C4C. The ambiguity is due to the inconclusive ^1H NMR assignments of H4A and H4C mentioned previously. However, the FAB-MS studies had already located the hexanoyl group on Rha-A (see above). Therefore, the combination of the results from NMR and mass spectral analyses identifies C4A as the location of the hexanoyl group, leaving C4C as the site of attachment for the fourth acetyl group.

In conclusion, the primary structure of ML-3 was determined to be

{3,4-OAc$_2$-L-Rha*p*}-α(1→3)-{2,4-OAc$_2$-L-Rha*p*}-
α(1→3)-{4-O-*n*-hexanoyl-L-Rha*p*}-α(1→*n*-octyl)

Can. J. Chem. Downloaded from www.nrcresearchpress.com by 88.85.125.76 on 09/07/12
For personal use only.

TABLE 2. ^{13}C nuclear magnetic resonance data[a] for Mezzettiaside ML-3

	Chemical shifts (ppm)			Coupling constants[b] (Hz)			
C-atom[c]	Rha-A	Rha-B	Rha-C	$^1J_{C-H}$	Rha-A	Rha-B	Rha-C
1	100.39	99.82	102.05	1[d]	169.38	173.95 (7)	170.90 (7)
2	71.66	71.12	69.15	2	149	154	150
3	78.88	74.66	72.20	3	145	141	153
4	72.59	73.07	71.43	4	154	154	156
5	66.94	67.35	67.61	5	145 (7)	145 (7)	145 (7)
6	17.44	17.23	17.23	6	126 (7)	129	129
R′ CH_2a	68.02	—	—	a	140 (7)	—	—
R′ CH_2b	29.90	—	—	b	125	—	—
R′ $(CH_2)_5$c–g	⇐26.33, 29.49, 29.40, 31.98, 22.75[e]⇒			c–g	125–126	—	—
R′ CH_3h	14.28[f]	—	—	h	125	—	—
R CH_2a	34.26	—	—	a	127.5	—	—
R CH_2b	29.90	—	—	b	125	—	—
R $(CH_2)_2$c–d	⇐31.77, 22.42[e]⇒		—	c–d	125–126	—	—
R CH_3e	14.08[f]	—	—	e	125	—	—
R C=O	173.54	—	—				
Ac CH_3	—	20.20[g]	20.11[g]		—	129	129
Ac CH_3	—	20.11[g]	20.02[g]		—	129	129
Ac C=O	—	170.79[h]	170.76[h]				
Ac C=O	—	170.70[h]	170.67[h]				

[a]Measured at 27°C in benzene-d_6/methanol-d_4 (4:1, v/v).

[b]One-bond $^{13}C-^1H$ coupling constants. The two- and three-bond (long-range) $^{13}C-^1H$ coupling constants, as measured via heteronuclear *J*-resolved spectroscopy, are given in parentheses.

[c]For designations Rha A–C, for numbering of carbon atoms in the rhamnosyl rings, and for lettering of the carbon atoms in the substituent groups, see the structure of ML-3 (Table 1). R′ = octyl aglycone (at A1); R = hexanoyl (at A4); Ac = acetyl (at B2, B4, C3 and C4).

[d]These values were measured both via heteronuclear *J*-resolved spectroscopy and via a 1-D ^1H-coupled ^{13}C spectrum with high digital resolution.

[e]Assignments of these signals are inconclusive with respect to number of the carbon atom in the chain, or even with respect to the octyl or the hexanoyl chain, because of lack of resolution of the corresponding CH_2 signals in the ^1H spectrum. Tentative assignments are based on ^{13}C chemical shifts for 1-octanol and hexanoate (27).

[f]Assignments may be interchanged.

[g]Assignments may be interchanged.

[h]Assignments may be interchanged.

Discussion

The primary structure elucidation of the highly acylated trisaccharide ML-3 required the application of a combination of techniques, among which FAB-MS and NMR spectroscopy were the most powerful. Given that ML-3 consists of L-Rha residues, as determined by GC analysis of *S*(+)-2-butylglycosides, FAB-MS revealed the size of the compound, the size of each of the appended groups, and their distribution to the residue level. Thus, it was deduced from the FAB-MS results that ML-3 is a trisaccharide with sequence C–B–A, with two *O*-acetyl groups attached to each of the Rha residues B and C, and an *O*-hexanoyl acyl and an octyl aglycone group to Rha-A. The mass spectra did not contain information on the positions and configurations of the glycosyl linkages, on the precise location of the appended groups on the Rha rings, or on the branching pattern of the hexanoyl and octyl groups. However, NMR spectroscopy did yield each of these structural parameters. To accomplish this, the virtually complete assignment of the ^1H and ^{13}C spectra of ML-3 was necessary.

Since L-Rha*p* occurs in the $^1C_4$ conformation, with H2 in equatorial orientation, neither the H1 and C1 chemical shifts nor the coupling constants $^3J_{H1H2}$ were useful in determining the configuration of the linkages (19, 20, 22). Evidence for the α configurations was obtained from the $^1J_{C1H1}$ values; this was consistent with the absence of intraresidue H1–H3 and H1–H5 NOEs.

Once the ^1H and ^{13}C spectra of ML-3 had been assigned, by the combination of COSY, HOHAHA, and HMQC experiments, the key experiment to determine the linkage positions and the positions of the attached acyl groups was the HMBC experiment. Long-range, $^3J_{CH}$ couplings between anomeric protons and substituted carbon atoms across the glycosidic linkages allowed the linkage positions to be determined as (1→3), whereas the $^3J_{CH}$ couplings between the acyl carbonyl carbons and the Rha ring protons permitted the localization of the acyl groups at C3C, C4C, C2B, C4B, and C4A. In the particular case of ML-3, because of the ambiguity in the assignment of H4A and H4C from the COSY and HOHAHA spectra, the determination of the exact position of the hexanoyl group required the combination of the FAB-MS results (indicating that it was linked to Rha-A), and the NMR HMBC results (indicating its attachment to either C4C or C4A). Once the structure of ML-3 had been elucidated, the unequivocal assignment of the proton signals at δ 5.824 ppm and δ 5.820 ppm to H4A and H4C, respectively, could be made (see Table 1 and Fig. 4b).

It is noteworthy that the results of 1-D NOE difference spectroscopy suggested that the two Rha→Rha linkages in ML-3 were (1→3); however, care must be taken in assigning linkage positions based solely on NOE data as several instances are documented where the strongest interresidue NOE upon saturation of the anomeric proton did not arise from the proton at the linkage position of the adjacent residue (22–24).

Can. J. Chem. Downloaded from www.nrcresearchpress.com by 88.85.125.76 on 09/07/12
For personal use only.

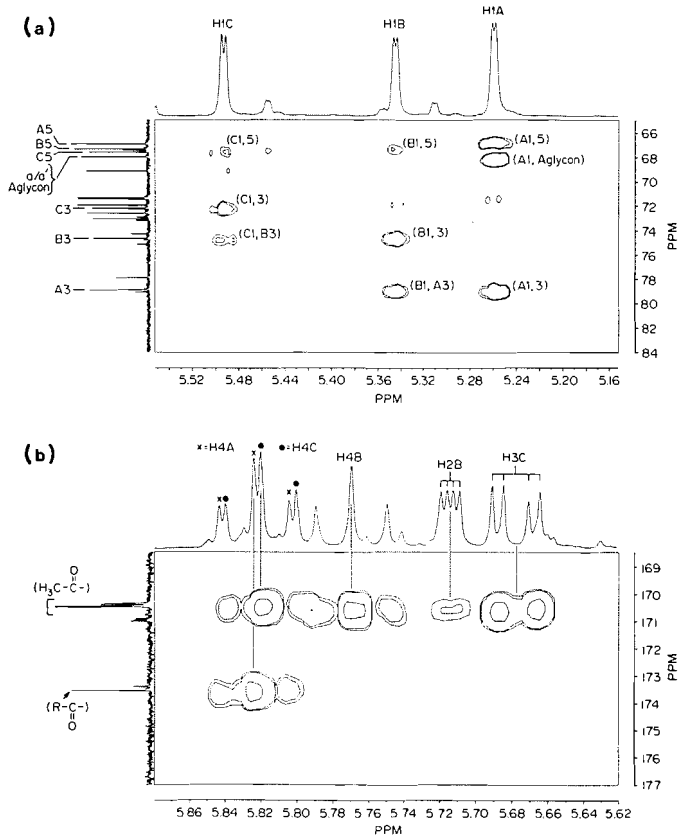

FIG. 4. ^{1}H-Detected heteronuclear multiple-bond correlation (HMBC) spectrum of ML-3 with high resolution 1-D ^{1}H and ^{13}C projections. (a) Expanded region showing the connectivities of the anomeric protons across the glycosidic linkages, as well as intraring connectivities. (b) Expanded region showing the connectivities of the ^{13}C carbonyl signals with the downfield rhamnosyl ring proton signals. Note that H4A and H4C are nearly coresonant in the high resolution ^{1}H projection. The carbonyl signal at 173.54 ppm was assigned to the hexanoyl group by virtue of its $^2J_{CH}$ correlation to Ha″ and Ha‴ in the HMBC spectrum (not shown).

The characterization of Mezzettiaside 3 (ML-3) is an elegant illustration of the combination of FAB-MS and NMR spectroscopy to structural analysis of complex carbohydrates (compare, e.g., refs. 25 and 26). To the best of our knowledge, this study represents the first example of the complete characterization, by these techniques, of a carbohydrate that is so highly acylated, including the exact identification of the nature and location of its acyl substituents.

Acknowledgements

This research was supported in part by U.S. Department of Energy grant no. DE-FG09-85ER13810 as part of the USDA/DOE/NSF Plant Science Centers Program, and by U.S. Department of Energy grant DE-FG09-85ER13424. The Association of Commonwealth Universities is thanked for the award of a scholarship (to J.T.E.). We acknowledge, with gratitude, the supply of plant material by Dr. G. Davison, Department of Zoology, Universiti Kebangsaan Malaysia, and the continuous technical support from Mr. D. L. Warrenfeltz (CCRC Instrumentation Manager).

1. J. T. ETSE. Ph.D. Thesis, Univ. Strathclyde, Glasgow, U.K. 1986. pp. 335–381 and 427–430.
2. G. J. GERWIG, J. P. KAMERLING, and J. F. G. VLIEGENTHART. Carbohydr. Res. **62**, 349 (1978).
3. G. J. GERWIG, J. P. KAMERLING, and J. F. G. VLIEGENTHART. Carbohydr. Res. **77**, 1 (1979).
4. W. S. YORK, H. VAN HALBEEK, A. G. DARVILL, and P. ALBERSHEIM. Carbohydr. Res. In press.
5. A. DELL and P. R. TILLER. Biochem. Biophys. Res. Commun. **135**, 1126 (1986).
6. A. DELL. Adv. Carbohydr. Chem. Biochem. **45**, 19 (1987).
7. G. WAGNER and K. WÜTHRICH. J. Magn. Reson. **33**, 675 (1979).
8. D. MARION and K. WÜTHRICH. Biochem. Biophys. Res. Commun. **113**, 967 (1983).
9. M. RANCE, O. W. SØRENSEN, G. BODENHAUSEN, G. WAGNER, R. R. ERNST, and K. WÜTHRICH. Biochem. Biophys. Res. Commun. **117**, 479 (1983).
10. A. BAX and D. G. DAVIS. J. Magn. Reson. **65**, 355 (1985).
11. M. F. SUMMERS, L. G. MARZILLI, and A. BAX. J. Am. Chem. Soc. **108**, 4285 (1986).
12. L. LERNER and A. BAX. Carbohydr. Res. **166**, 35 (1987).
13. S. W. HOMANS, R. A. DWEK, J. BOYD, N. SOFFE, and T. W. RADEMACHER. Proc. Natl. Acad. Sci. U.S.A. **84**, 1202 (1987).
14. G. BODENHAUSEN, R. FREEMAN, R. NIEDERMEYER, and D. L. TURNER. J. Magn. Reson. **26**, 133 (1977).
15. A. BAX, R. H. GRIFFEY, and B. L. HAWKINS. J. Magn. Reson. **55**, 301 (1983).
16. A. BAX and S. SUBRAMANIAN. J. Magn. Reson. **67**, 565 (1986).
17. A. J. SHAKA, P. B. BARKER, and R. FREEMAN. J. Magn. Reson. **64**, 547 (1985).
18. A. BAX and M. F. SUMMERS. J. Am. Chem. Soc. **108**, 2093 (1986).
19. K. BOCK and H. THØGERSEN. Annu. Rep. NMR Spectrosc. **13**, 1 (1983).
20. K. BOCK, C. PEDERSEN, and H. PEDERSEN. Adv. Carbohydr. Chem. Biochem. **42**, 193 (1984).
21. D. M. DODDRELL, D. T. PEGG, and M. R. BENDALL. J. Magn. Reson. **48**, 323 (1982).
22. D. R. BUNDLE, J. W. CHERWONOGRODZKY, and M. B. PERRY. Biochemistry, **26**, 8717 (1987).
23. V. K. DUA, B. N. N. RAO, S. S. WU, V. E. DUBE, and C. A. BUSH. J. Biol. Chem. **261**, 1599 (1986).
24. V. POZSGAY, J. R. BRISSON, and H. J. JENNINGS. Can. J. Chem. **65**, 2764 (1987).
25. C. A. BUSH. Bull. Magn. Reson. **10**, 73 (1988).
26. H. VAN HALBEEK. *In* Frontiers of NMR in molecular biology. *Edited by* D. Live, I. Armitage, and D. Patel. Alan R. Liss Inc., New York, NY. 1990. pp. 195–213.
27. E. BREITMAIER AND V. VOELTER. *In* Carbon-13 NMR spectroscopy. 3rd ed. VCH Publishers, New York, NY. 1987. pp. 208 and 228.

Can. J. Chem. Downloaded from www.nrcresearchpress.com by 88.85.125.76 on 09/07/12
For personal use only.

The Perlin Effect: bond lengths, bond strengths, and the origins of stereoelectronic effects upon one-bond C–H coupling constants

SAUL WOLFE
Department of Chemistry, Queen's University, Kingston, Ont., Canada K7L 3N6

AND

B. MARIO PINTO, VIKRAM VARMA, AND RONALD Y. N. LEUNG
Department of Chemistry, Simon Fraser University, Burnaby, B.C., Canada V5A 1S6

Received December 14, 1989

This paper is dedicated to Professor Arthur Perlin on the occasion of his 67th birthday

SAUL WOLFE, B. MARIO PINTO, VIKRAM VARMA, and RONALD Y. N. LEUNG. Can. J. Chem. **68**, 1051 (1990).

The magnitude of a one-bond C–H coupling constant depends upon the chemical environment of the hydrogen atom and, especially, upon its stereochemical relationship to vicinal lone electron pairs. However, a lone electron pair is not essential for the observation of a stereoelectronic effect, since even cyclohexane exhibits different axial and equatorial C–H coupling constants. We propose the name "Perlin Effect" to describe such observations. An analysis of the extensive experimental data regarding the Perlin Effect reveals that, in cyclohexane and in six-membered rings having one or more heteroatoms of the first row attached to the carbon of interest, $^1J_{C-H}$ is always larger for an equatorial hydrogen than for an axial hydrogen. The magnitude of the Perlin Effect is reduced when the carbon carrying the hydrogen of interest is attached to first row and second row atoms or heteroatoms, and it reverses when the carbon atom carries two heteroatoms from below the first row.

The existence of the Perlin Effect in nuclear magnetic resonance spectra is reminiscent of an infrared effect known as the Bohlmann bands, whose origin has previously been explained by quantitative perturbational molecular orbital (PMO) theory in terms of the effects of lone electron pairs upon the lengths and strengths and, therefore, the chemical reactivities of vicinal C—H bonds. Since the magnitude of a one-bond C–H coupling constant is expected to vary inversely with bond length, the origins of the Perlin Effect and of the Bohlmann bands would seem to be the same, i.e., the longer (weaker) C—H bond has the smaller one-bond coupling constant. This expectation has now been confirmed: for 25 molecules, representing a total of 35 different kinds of C—H bonds, the bond lengths, stretching force constants, and charge distributions have been determined from fully optimized 6-31G* molecular orbital calculations. In nine of ten cases for which experimental data exist for pairs of diastereomeric or diastereotopic hydrogens, the shorter C—H bond of the pair has the larger coupling constant; in the tenth case, the experimental difference is only 1–2 Hz. Moreover, a global analysis of the data in terms of the equation $J = A + Bq_Cq_H + C/r$, where J is an experimental coupling constant, q is a total atomic charge, and r is a C—H bond length, correlates 23 different types of C—H bonds linearly with a correlation coefficient of 0.915. The C parameter is the leading term of the correlation. Among the systems studied theoretically are eight molecules of the type CH_3CHXY (Y = OH, SH; X = F, Cl, OH, SH), which are representative of systems containing both endocyclic and exocyclic first row and second row anomeric effects. The exocyclic effect is found to be very similar for first row and second row substituents, but the endocyclic effect is larger for the first row substituent. Both findings agree with experimental data in solution. Finally, quantitative PMO analysis has been employed to analyse the origins of the different C—H bond lengths in the various molecules of the study.

Key words: anomeric effect, PMO analysis, NMR, stereochemistry, molecular orbital calculations.

SAUL WOLFE, B. MARIO PINTO, VIKRAM VARMA et RONALD Y. N. LEUNG. Can. J. Chem. **68**, 1051 (1990).

L'amplitude de la constante de couplage d'un C–H à travers une liaison dépend de l'environnement chimique de l'atome d'hydrogène et spécialement de sa relation stéréochimique avec les paires d'électrons non partagées vicinales. Toutefois, la présence d'une paire d'électrons non partagée n'est pas essentielle pour observer un effet stéréoélectronique puisque même le cyclohexane présente des contantes de couplage différentes pour les C–H axiaux et équatoriaux. On propose d'appeler de telles observations l'«effet Perlin». Une analyse d'un large ensemble de données expérimentales relatives à l'effet Perlin révèle que, dans le cyclohexane et dans les cycles à six chaînons dans lesquels un ou plusieurs hétéroatomes de la première rangée sont attachés au carbone examiné, la valeur de $^1J_{C-H}$ est toujours plus grande pour un hydrogène équatorial que pour un hydrogène axial. L'amplitude de l'effet Perlin est réduite lorsque le carbone qui porte l'hydrogène examiné est attaché à des atomes ou des hétéroatomes des deux premières rangées et elle est inversée lorsque l'atome de carbone porte deux hétéroatomes des rangées autres que la première.

L'existence de l'effet Perlin dans les spectres de résonance magnétique nucléaire rappelle les bandes de Bohlmann observées dans les spectres infra-rouges dont les origines ont été expliquées antérieurement, en se basant sur la théorie des orbitales moléculaires perturbationnelles quantitatives (OMP), en fonction d'effets de paires d'électrons non partagées sur les longueurs et sur les forces et, donc, sur les réactivités chimiques des liaisons C—H vicinales. Puisqu'on peut s'attendre à ce que l'amplitude d'une constante de couplage d'une liaison C—H varie d'une façon inverse de la longueur de la liaison, il peut apparaître que les origines de l'effet Perlin et des bandes de Bohlmann sont les mêmes, à savoir que la liaison C—H la plus longue (la plus faible) possède la constante de couplage la plus faible. Cette attente est confirmée : utilisant des calculs d'orbitales moléculaires 6-31G* complètement optimisés, on a déterminé les longueurs de liaison, les constantes de force d'élongation et les distributions de charge pour 25 molécules représentant un total de 35 sortes différentes de liaisons C—H. Dans neuf des dix cas pour lesquels il existe des données expérimentales pour des paires diastéréomères ou diastéréotopes d'hydrogènes, la liaison C—H la plus courte de la paire est associée à la constante de couplage la plus grande; dans le dixième cas, la différence expérimentale n'est que de 1–2 Hz. De plus, un analyse globale des données en fonction de l'équation $J = A + Bq_Cq_M + C/r$, dans laquelle J est une constante de couplage expérimentale, q est une charge atomique totale et r est une longueur de liaison C—H, permet d'établir une corrélation

Can. J. Chem. Downloaded from www.nrcresearchpress.com by 88.85.125.76 on 09/07/12
For personal use only.

linéaire de 23 types différents de liaisons C—H avec un coefficient de corrélation de 0,915. Le paramètre *C* est le terme principal de la corrélation. Les systèmes étudiés d'une façon théorique comprennent huit molécules du type CH_3CHXY (Y = OH, SH; X = F, Cl, OH, SH) qui sont représentatives des systèmes donnant lieu à des effets anomériques endocycliques ainsi qu'exocycliques avec des éléments des deux premières rangées. On a trouvé que l'effet exocyclique est très semblable pour les substituants issus des deux premières rangées; toutefois, l'effet endocyclique est plus important avec les substituants de la première rangée. Ces deux observations sont en accord avec les données expérimentales obtenues en solution. Enfin, on a utilisé une analyse OMP quantitative pour analyser les origines des longueurs des diverses liaisons C—H contenues dans les diverses molécules examinées dans ce travail.

Mots clés : effet anomérique, analyse OMP, RMN, stéréochimie, calculs d'orbitales moléculaires.

[Traduit par la revue]

Introduction

The methyl hydrogens of methylamine (**1**) are diasterotopic. One, H_a, is antiperiplanar to the nitrogen lone pair; the other two, H_g, are *gauche* to the lone pair. The diastereotopic relationship is reflected in structural, spectroscopic, and chemical differences between C—H_a and C—H_g; C—H_a is longer (1) and weaker (2), and a 6–7 kcal/mol difference in the bond dissociation energies has been estimated (3).

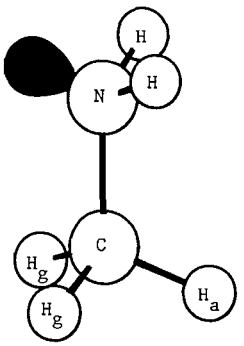

1

These stereoelectronic effects are also encountered in more complex amines when at least one α-hydrogen is antiperiplanar to the nitrogen lone pair (4). Their existence was discovered by Bohlmann (5), in studies of infrared stretching frequencies of quinolizidine alkaloids, and the presence or absence of "Bohlmann bands" in infrared spectra is commonly employed in the assignment of configuration and (or) conformation. Methylamine itself also exhibits Bohlmann bands (2).

The rate constants for the reactions of *tert*-butoxyl and *tert*-butylhydroperoxyl radicals and the benzophenone triplet with amines have been determined (6). There is a pronounced preference for attack upon a C—H bond that is eclipsed with the axis of the nitrogen lone pair.

Methanol (**2**), like methylamine, contains diastereotopic methyl hydrogens. One, H_a, is antiperiplanar to the O—H *bond*; the other two, H_g, are *gauche* to this bond. Unlike methylamine, methanol contains two *energetically nonequivalent* lone pairs

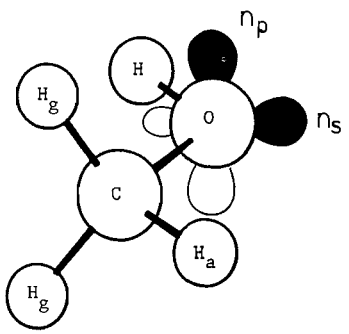

2

(7). One, n_p, is derived mainly from the 2*p* atomic orbital of oxygen that is perpendicular to the H—O—C plane; the other, n_s, is a hybrid orbital containing contributions from the 2*p* atomic orbital of oxygen that lies in the H—O—C plane, and from the 1*s* atomic orbital of hydrogen and 2*s* or 2*p* atomic orbitals of carbon (8). The experimental energy difference between n_p and n_s is 35.5 kcal/mol (7).

Methanol, like methylamine, exhibits Bohlmann bands in its infrared spectrum (9). In this case, it is H_g that is longer (10) and weaker (2), and a 5 kcal/mol difference in bond dissociation energies has been estimated (3). When the skeleton of methanol is incorporated into a 6-membered ring (e.g., **3**), it can be seen

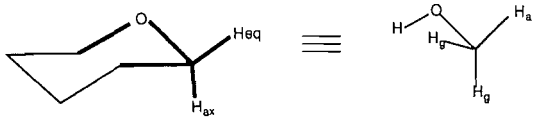

3

that H_g becomes H_{ax} and H_a becomes H_{eq}. All known examples of radical abstraction adjacent to the ether oxygens of such cyclic structures exhibit a kinetic preference for H_{ax} (11).

Clearly the Bohlmann band phenomenon and the relative radical reactivities of diastereotopic hydrogens α to nitrogen or α to oxygen can be traced to the differences in the C—H bond lengths and bond strengths associated with these hydrogens.

It seems natural to seek an interpretation of these differences in terms of "lone pair" effects. The problem, however, is that the lone pair of methylamine and the energetically nonequivalent lone pairs of methanol are not localized entities as depicted in **1** and **2**, but are major contributors to specific molecular orbitals that are delocalized over the molecules. In methylamine, the HOMO is mainly the nitrogen "lone pair", delocalized over all three of the methyl hydrogens (12). In methanol, the HOMO is mainly n_p, delocalized over H_g but not H_a (12); the subjacent orbital is mainly n_s, delocalized over all three methyl hydrogens.

These delocalization effects can be understood in terms of the symmetry properties of atomic orbitals and the concept of orbital interactions (13). Just as the Hückel molceular orbitals of butadiene can be seen to consist of in-phase and out-of-phase combinations of the Hückel molecular orbitals of two ethylene fragments (14), the molecular orbitals of methylamine can be written in terms of symmetry-allowed linear combinations of the orbitals of CH_3 and NH_2 fragments (15). Likewise, the molecular orbitals of methanol can be written in terms of symmetry-allowed linear combinations of the orbitals of CH_3 and OH fragments. Structure **4** depicts the linear combinations (orbital interactions) that lead to the frontier molecular orbitals of methylamine. The HOMO results from the out-of-phase combination of n_{NH_2} with π_{CH_3} and the in-phase combination of n_{NH_2} with $\pi^*_{CH_3}$ (16). The n–π interaction is two-orbital four-

Can. J. Chem. Downloaded from www.nrcresearchpress.com by 88.85.125.76 on 09/07/12
For personal use only.

Can. J. Chem. Downloaded from www.nrcresearchpress.com by 88.85.125.76 on 09/07/12
For personal use only.

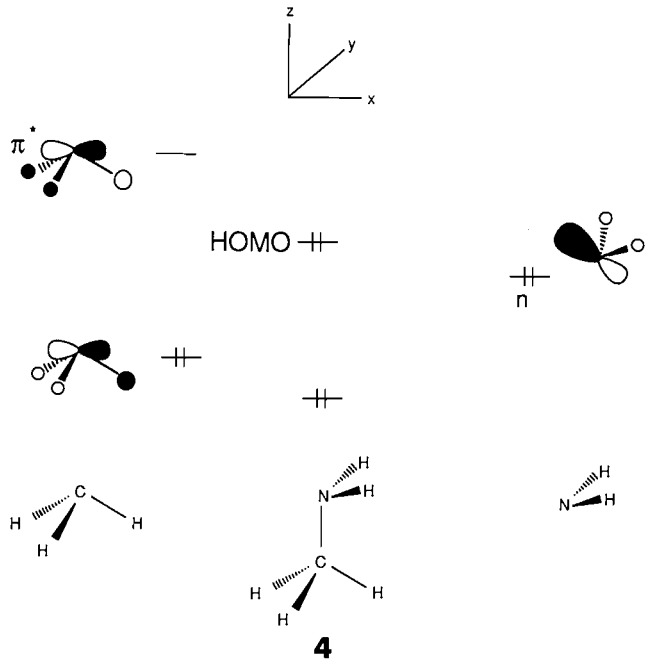

4

electrons in nature, and is destabilizing. The n–π^* interaction is two-orbital two-electrons in nature, and is stabilizing; a consequence of this latter interaction is a partial population of the π^* orbital. Since all three C—H regions of this orbital are antibonding, the result of the "charge transfer" is a weakening of all three C—H bonds. However, in the coordinate system shown in **4**, the *yz*-plane is a nodal plane. Therefore, in both π and π^*, the *s*-atomic orbital coefficient at H_a is twice that of H_g. This causes *the C—H_a bond to be weakened preferentially*. This preferential weakening is the origin of all of the stereoelectronic effects in amines discussed earlier.

The corresponding treatment of methanol (**5**) is slightly more complicated, because orbital interactions associated with both n_p and n_s should be taken into account. The left-hand side of **5** shows the degenerate π and π^* methyl group orbitals; the right-hand side shows n_p, n_s, and also σ^*_{O-H}, which has a symmetry-allowed interaction with π'. The centre of **5** shows the approximate positions of the occupied frontier molecular orbitals of the molecule. The HOMO is mainly n_p, but now contains contributions from π and π^*; the subjacent orbital is mainly n_s, but now contains contributions from π', $\pi^{*\prime}$, and σ^*_{O-H} (13).

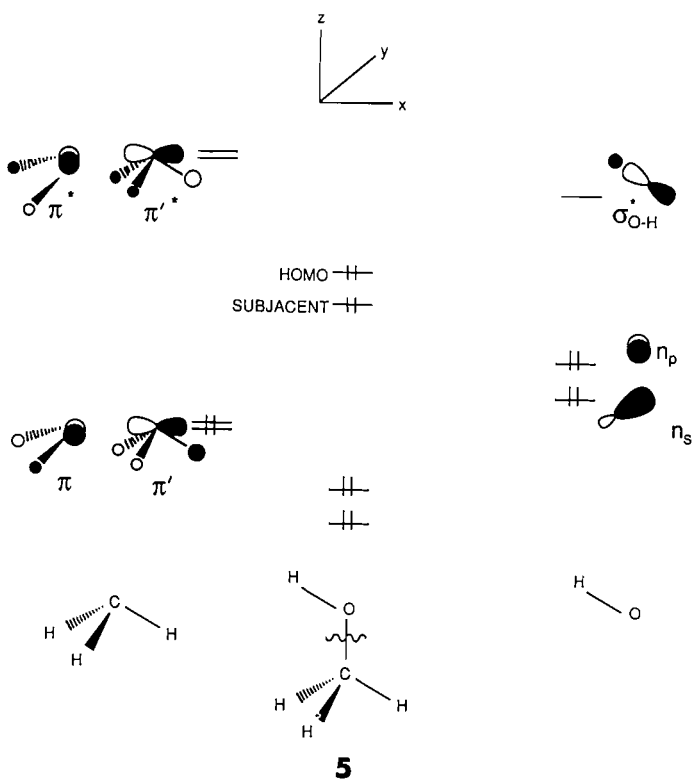

5

Symmetry-allowed charge transfer is possible (a) between n_p and π^*, (b) between n_s and $\pi^{*\prime}$, and (c) between π' and σ^*_{O-H}. Interaction (a) leads to a weakening of C—H_g, because H_a lies in the *xz*-nodal plane and its atomic orbital coefficient is zero in both π and π^*; interactions (b) and (c) lead to a preferential weakening of C—H_a, because the H_a atomic orbital coefficient is larger than that of H_g in both π' and $\pi^{*\prime}$. Since the magnitude of a stabilizing orbital interaction (and of charge transfer) is inversely proportional to the energy difference between the donor and acceptor orbitals (15, 16), interaction (a) is expected to dominate, *causing C—H_g of methanol to be weaker than C—H_a*. This preferential weakening is the origin of the stereoelectronic effects in ethers discussed earlier.

The Perlin Effect

In 1969, Perlin and Casu discovered that there is an approximately 10 Hz difference in $^1J_{C-H}$ coupling constants at the anomeric centres of anomeric pairs of glycosides (17). In the case of D-glucose (**6**), the α anomer, which contains an equatorial hydrogen at C1, had the larger coupling constant. As we have seen, an equatorial C1—H bond in a pyranose ring is shorter and stronger than an axial C1—H bond. Since the Fermi contact term makes the principal contribution to coupling between directly bonded nuclei (18), it is not surprising that the magnitude of the coupling should vary inversely with the C—H bond length.

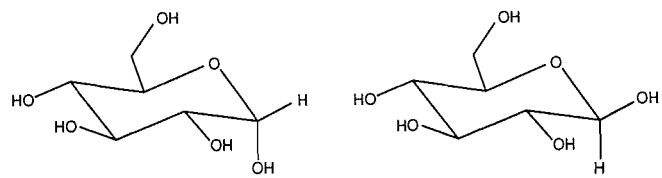

6*a* **6***b*

The original observations of Perlin and Casu were rapidly extended by Perlin and his co-workers, and subsequently by many others (19). It seems proper to honour Professor Perlin at this time with the proposal that stereoelectronic effects upon one-bond C—H coupling constants be termed "Perlin Effects".

Table 1 summarizes some of the extensive experimental information related to the Perlin Effect (19) in cyclic and acyclic structures RCHXY. Even a cursory study of these data suggests that ΔJ for epimeric pairs of compounds is largest when both X and Y are atoms of the first row, somewhat smaller when one of X or Y is an atom below the first row, *and reverses* when both X and Y are atoms below the first row.

The factors that determine the magnitudes of one-bond C–H coupling constants have been the subject of much discussion (18, 20). The earliest work (20*a*, *b*) was greatly influenced by the finding that the trend of increasing coupling constant in the series C_2H_6, C_2H_4, C_2H_2 correlated linearly with the extent of *sp* hybridization on the carbon atom. This approach has been

TABLE 1. ^1J(C–H) data in RCHXY molecules

Compound	Substituents X/Y	Orientation of H[a]	^1J(C–H) (Hz)	Reference
Pyranose derivatives (26 examples)	O/O	H_{eq}	168–173	19*a–c*
Pyranose derivatives (16 examples)	O/O	H_{ax}	160–163	19*a–c*
1,3-Dioxane	O/O	H_{eq}	166	19*d*
		H_{ax}	158	19*d*
4,6-Dimethyl-1,3-dioxane	O/O	H_{eq}	167.5	19*e*
		H_{ax}	157.4	19*d*
trans-2-Methoxy-4-methyl-1,3-dioxane	O_2/O	H_{eq}	192.2	19*f*
cis-2-Methoxy-4-methyl-1,3-dioxane	O_2/O	H_{ax}	182.2	19*f*
	O/C	H_{eq}[b]	147	19*f*
		H_{ax}[b]	138	19*f*
Methyl 4,6-*O*-benzylidene α-D-glucopyranoside	O/C	H_{eq}[b]	151	19*g*
		H_{ax}[b]	141	19*g*
Tetra-*O*-acetyl-α-D-glucopyranosyl fluoride	O/F	H_{eq}	186	19*b*
Tetra-*O*-acetyl-β-D-glucopyranosyl fluoride	O/F	H_{ax}	178	19*b*
Tetra-*O*-acetyl-α-D-glucopyranosyl chloride	O/Cl	H_{eq}	184	19*b*
Tetra-*O*-acetyl-β-D-glucopyranosyl chloride	O/Cl	H_{ax}	171	19*b*
Ethyl 1-thio-α-D-glucopyranoside	O/S	H_{eq}	163	19*g*
Ethyl 1-thio-β-D-glucopyranoside	O/S	H_{ax}	154	19*g*
Methyl 5-thio-α-D-glucopyranoside	S/O	H_{eq}	161	19*g*
Methyl 5-thio-β-D-glucopyranoside	S/O	H_{ax}	159	19*g*
Methyl 5-thio-α-D-galactopyranoside	S/O	H_{eq}	160	19*h*
Methyl 5-thio-β-D-galactopyranoside	S/O	H_{ax}	159	19*h*
4,6-Dimethyl-1,3-dithiane	S/S	H_{eq}	144.9	19*e*
		H_{ax}	154.1	19*e*
r-2, *cis*-4-*trans*-6-Trimethyl-1,3-dithiane	S/C	H_{eq}[b]	139.9	19*g*
		H_{ax}[b]	143.2	19*g*
2-Carboethoxy-5-methyl-5-aza-1,3-dithiacyclohexane	$(S)_2/CO_2Et$	H_{eq}	150	19*i*
		H_{ax}	152	19*i*
2-Carbophenoxy-5-methyl-5-aza-1,3-dithiacyclohexane	$(S)_2/CO_2Ph$	H_{eq}	151	19*i*
		H_{ax}	155	19*i*
r-2-(4-Methoxyphenylseleno)-*trans*-4-*trans*-6-dimethyl-1,3-dithiane	$(S)_2$/SeAr	H_{eq}	160	19*j*
r-2-(4-Methoxyphenylseleno)-*cis*-4-*cis*-6-dimethyl-1,3-dithiane	$(S)_2$/SeAr	H_{ax}	167	19*j*
5-Methyl-1,3-diselenane	Se/Se	H_{eq}	150	19*k*
		H_{ax}	157	19*k*
Cyclohexyl fluoride	C/F	H_{eq}	161	19*l*
		H_{ax}	148	19*l*
Cyclohexyl chloride	C/Cl	H_{eq}	160	19*l*
		H_{ax}	149	19*l*
Cyclohexyl bromide	C/Br	H_{eq}	159	19*l*
		H_{ax}	151	19*l*
Cyclohexyl iodide	C/I	H_{eq}	157	19*l*
		H_{ax}	149	19*l*
Cyclohexane	C/C	H_{eq}	126.4	19*m*
		H_{ax}	122.4	19*m*
$CH_3CH_2CH{=}N{-}OH$	$=N{-}OH$	H_{syn}[c]	173	19*n*
		H_{anti}[c]	160	19*n*
$CH_3CH_2CH{=}N{-}N(CH_3)_2$	$=N{-}N(CH_3)_2$	H_{syn}	174	19*n*
		H_{anti}	155	19*n*
$(CH_3)_2CHCH{=}N{-}N(CH_3)_2$	$=N{-}N(CH_3)_2$	H_{syn}	170	19*n*
		H_{anti}	154	19*n*
$CH_3CH_2CH{=}N{-}N(CH_2)_2Ph$	$=N{-}N(CH_2)_2Ph$	H_{syn}	170	19*n*
		H_{anti}	153	19*n*
$(CH_3)_2CHCH{=}N(CH_2)_2Ph$	$=N{-}(CH_2)_2Ph$	H_{syn}	171	19*n*
		H_{anti}	154	19*n*
$CH_3CH_2CH{=}N{-}CH(CH_3)_2$	$=N{-}CH(CH_3)_2$	H_{syn}	170	19*n*
		H_{anti}	151	19*n*
$(CH_3)_2CHCH{=}N{-}CH(CH_3)_2$	$=N{-}CH(CH_3)_2$	H_{syn}	170	19*n*
		H_{anti}	152	19*n*
$CH_2{=}N{-}H$	$=N{-}H$	H_{syn}	172.9	19*o*
		H_{anti}	163.7	19*o*
$CH_3CH{=}N{-}OH$	$=N{-}OH$	H_{syn}	177	19*p*
		H_{anti}	163	19*p*

[a]Denotes anomeric hydrogen unless otherwise specified.
[b]Denotes hydrogens on C-4 or C-6 of the heterocyclic ring.
[c]Denotes H_{syn} or H_{anti} to the N lone pair.

Can. J. Chem. Downloaded from www.nrcresearchpress.com by 88.85.125.76 on 09/07/12
For personal use only.

Can. J. Chem. Downloaded from www.nrcresearchpress.com by 88.85.125.76 on 09/07/12
For personal use only.

criticized (20*c*, *d*) because of problems with the specification of the hybridization at carbon in systems more complex than the simple hydrocarbons. Although the problem would seem to be even more severe when the different hybridizations at carbon in a pair of stereoisomers have to be explained, in principle, molecular orbital theory (21) contains the required information in the bond order matrix element between the carbon 2*s* and hydrogen 1*s* orbitals, $P_{s_C s_H}$. The coupling constant is expected to be proportional to the square of this quantity. This approach forms the basis of the many semi-empirical (INDO, CNDO) calculations of $^1J_{C-H}$ (18), which give qualitatively reasonable results. Unfortunately, INDO and CNDO are not reliable for calculations of stereoelectronic effects on $^1J_{C-H}$, because the different bond lengths of diastereotopic hydrogens are not reproduced reliably by such methods.

Other correlations dealing with hybridization have been proposed, in which a leading term is the inverse of S^2_{CH}, the square of the overlap integral between the carbon hybrid and the hydrogen 1*s* orbital (20*e*).

Both *P* and S^2 depend upon bond length. Since, as we have seen, the consequences of the different bond lengths (bond strengths) of diastereotopic hydrogens are well established, and the origins of these trends can be explained, the principal initial objective of the present work was to determine, for pairs of epimers, whether the magnitude of $^1J_{C-H}$ varies inversely with the C—H bond length. As will be seen, this trend has been found to exist, *regardless of the nature of X and Y*. In the second phase of the work, we were, therefore, encouraged to seek an additional property, which varies as X and Y are varied, that would allow all of the compounds of the study to be included in a single correlation. As will be seen, the suggested property is $q_C q_H$, the product of the charges on carbon and hydrogen. Finally, using the appropriate modification of the orbital interaction diagram **5**, we are able to suggest an explanation for the reversal in $^1J_{C-H}$ (and in C—H bond lengths) when X and Y are atoms below the first row.

Methods

Bond lengths are taken from fully optimized geometries computed at the 6-31G* level (22), using GAUSSIAN 86 (23). Several of the systems were also examined at lower (3-21G, 3-21G* (24)) and higher (6-31+G* (25), 6-31++G* (26)) computational levels to check that 6-31G* is the appropriate basis set for the computation of C—H bond lengths. A one-point FORCE calculation was performed following optimization of each structure, to obtain diagonal stretching force constants. Total atomic charges were taken from the Mulliken population analysis (27). Quantitative PMO analyses were performed by the method of Whangbo, Schlegel, and Wolfe (16). Since this procedure is not yet available in GAUSSIAN 86, but has been incorporated into MONSTERGAUSS (28), the calculations were performed by Dr. M. R. Peterson at the University of Toronto, whose assistance is greatly appreciated. Initial study of the quantitative PMO data revealed very extensive charge transfer involving d-type functions, because of the use of the 6-31G* basis set. Therefore, to simplify the orbital analysis, this was performed at STO-3G. As will be seen, this strategy appears to identify the principal differences between first and second row X and Y.

Results and discussion

Data base

Figure 1 summarizes the C—H bond lengths (Å), C–H stretching force constants (in parentheses; units are mdyn/Å), and the total atomic charges on carbon and on hydrogen in the 6-31G* optimized structures of 22 molecules examined theoretically in the present work. Ethane, ethylene, and acetylene were also calculated.[1] The experimental value of $^1J_{C-H}$, shown beside each structure, is taken from the appropriate entry of Table 1. Except for the imines (entries 1–4) the calculations refer to model structures containing the C—H bond(s) of interest. For example, entry 5, methanediol in the conformation shown, is the model for a 1,3-dioxane ring in the chair conformation; entry 7 is the model for an α-D-glycopyranosyl fluoride; entry 8 is the model of a β-D-glycopyranosyl fluoride, etc.

To simulate more closely the cyclic structures from which the experimental data are taken, wherever appropriate a methyl group was attached to the carbon atom bearing the hydrogen of interest, and included in the complete geometry optimization. In the case of entries 7–16, this allows an updating of the theoretical anomeric effects of pyranosyl-X (X = F, Cl, OH, SH) and thiopyranosyl-X (X = OH) (29). The *exo*-anomeric effect (30) was taken into account for X = OH, SH, as can be seen upon inspection of these entries. In the case of entry 17, gauche butane, the model predicts that the axial C—H bond of cyclohexane is longer and weaker than the equatorial C—H bond; this is consistent with the 3-21G (31), 4-21G (32), and 4-31G (33) optimized structures of this molecule. In the calculations of Wiberg *et al.* (33), the axial and equatorial C—H bond lengths of cyclohexane are 1.088 and 1.086 Å, respectively. Our values for gauche butane are 1.0883 and 1.0874; the effect of the added methyl group can be seen in the structure found for propane (entry 18), in which the bond lengths are 1.0865 Å ("axial") and 1.0857 Å ("equatorial").

Several entries (1, 2, 5, 6, 17–22) contain diastereotopic C—H bonds, leading to a theoretical data base of 35 C—H bonds (including ethane, ethylene, and acetylene) for inclusion in a global analysis. However, experimental data appropriate to entires 2 and 19–22 are not available, leading to an experimental data base of 23 $^1J_{C-H}$ values.

The longer C—H bond has the lower one-bond C–H coupling constant

Of the ten pairs of diastereomers or molecules containing pairs of diastereotopic C—H bonds, in only one (entries 15 and 16) does the isomer having the longer C—H bond exhibit the larger $^1J_{C-H}$. In this pair, corresponding to the α and β anomers of a thiopyranoside, the isomer having the equatorial C—H bond has the larger coupling constant, *and also the longer bond*. It is noteworthy that this pair exhibits the smallest experimental difference in $^1J_{C-H}$, 1–2 Hz.

It is also noteworthy that the relative axial and equatorial C—H bond lengths of entries 15 and 16 are paralleled only in the 1,3-dithiane analog (entry 6), i.e., these are the only anomeric type systems in which *the equatorial C—H bond is longer than the axial C—H bond*. In the case of entry 6, however, the reversal of the usual trend in the bond lengths is accompanied by a reversal of the usual trend in the coupling constants, and *the shorter bond is characterized by the larger* $^1J_{C-H}$.

We conclude that the observations of Bailey *et al.* (19*e*) regarding the reversal of the relative magnitudes of the coupling constants at C2 in dioxanes and dithianes are not anomalous. The anomaly resides instead in the reversal of the relative magnitudes of *the bond lengths*. This point will be examined in a later section, but it is already clear that the Perlin Effect, like the Bohlmann band phenomenon, originates in the lengths and strengths of C—H bonds. It should therefore be possible to

[1]Full details of these structures have been deposited and may be purchased from the Depository of Unpublished Data, CISTI, National Research Council of Canada, Ottawa, Ont., Canada K1A 0S2.

Can. J. Chem. Downloaded from www.nrcresearchpress.com by 88.85.125.76 on 09/07/12
For personal use only.

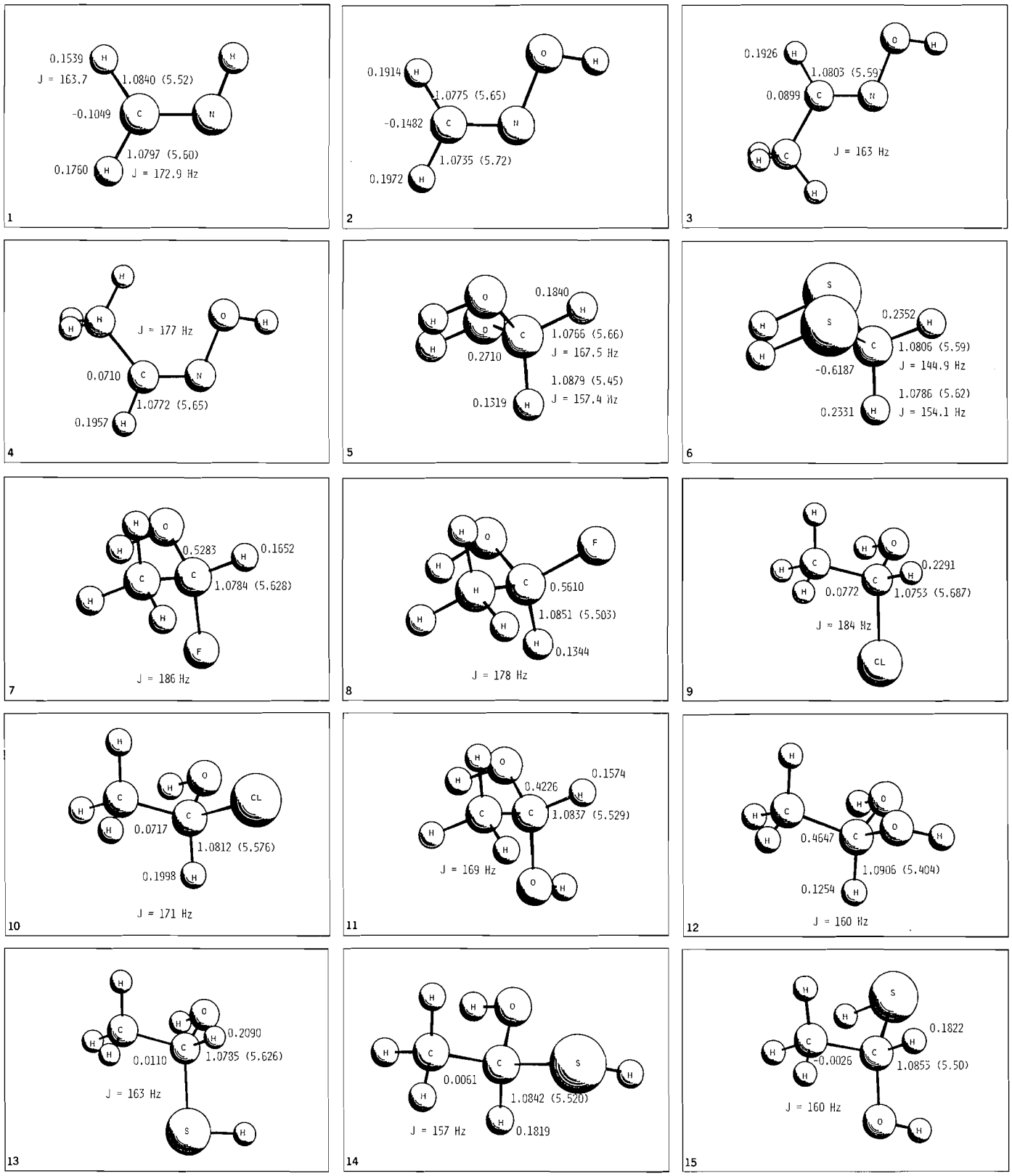

FIG. 1. Structures of the molecules computed in the present work. Entry numbers are at the lower left.

analyze the Perlin Effects in different classes of compounds in the manner described in the Introduction.

Propane, gauche butane, and cyclohexane

As noted above, propane (entry 18 of Fig. 1) exhibits the same trend in its "axial" and "equatorial" C—H bond lengths as gauche butane (entry 17) and cyclohexane. In the latter case Cieplak has suggested (34) that the longer and weaker (3*b*) axial C—H bond is the result of σ,σ^* hyperconjugation between antiperiplanar CH bonds. An examination of the 6-31G* HOMO of propane suggests a slightly different explanation of the effect. This HOMO is found to be π-type, resembling allyl. The orbital

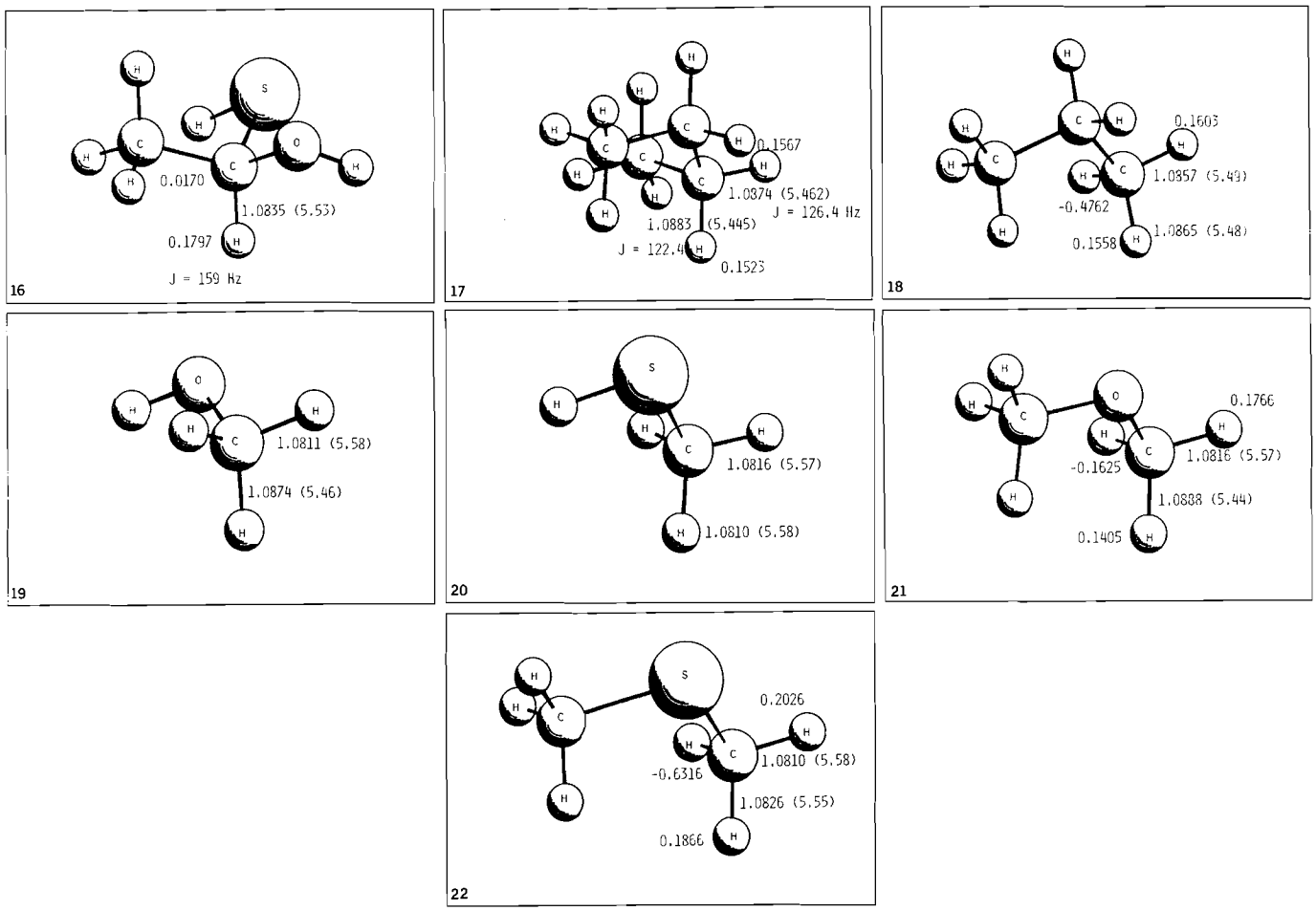

FIG. 1 (*concluded*)

interaction analysis of propane, based on the fragmentation $CH_3\cdots CH_2CH_3$, will therefore resemble the orbital interaction analysis of methanol, based on the fragmentation $CH_3\cdots OH$ (see **5**). The counterpart of n_p of methanol is the out-of-phase combination of π_{CH_2} and π_{CH_3} of the CH_2CH_3 moiety. As in **5**, charge transfer from this highest occupied fragment orbital of CH_2CH_3 to $\pi^*_{CH_3}$ weakens the methyl C—H bonds *gauche* to C—C. The quantitative PMO analysis reveals that this direction of charge transfer dominates over the alternative, i.e., π_{CH_3} to $\pi^*_{CH_2CH_3}$, which will also weaken the *gauche* C—H bonds of the methyl group.

Methanol and methanethiol

Inspection of entries 19 and 20 of Fig. 1 reveals that, at the 6-31G* level, *there is a reversal in the relative bond lengths of the "axial" and "equatorial" hydrogens*. The n_p,π^* interaction that accounts for the relative strengths and lengths of the C—H bonds of methanol (see **5**) must, in methanethiol, be overcome by an interaction that leads to preferential weakening of the C—H bond antiperiplanar to S—H. This interaction must be one of (b) or (c), discussed earlier in the qualitative analysis of methanol.

Figure 2 shows the orbital energies found in the quantitative PMO analyses of methanol and methanethiol. Preferential weakening of a C—H bond antiperiplanar to X—H can be caused by the combined effects of the (n_s,π^*_2), and (π_2,σ^*_{XH}) interactions outweighing the (n_p,π^*_1) interaction. It will be noted that the nonbonding n_p and n_s orbitals of sulfur lie higher, and the antibonding σ^*_{SH} orbital lies lower than the corresponding orbitals of oxygen. This is a well-known first row – second row effect (35). Neglecting overlap, charge transfer from the n_s orbital of sulfur is, therefore, greater than from the n_s orbital of oxygen but, of course, so is charge transfer from n_p of sulfur, which operates in the opposite direction. This argument leads to the conclusion that the first row – second row difference in the C—H bond length trends in methanol and methanethiol can be attributed to the effect of the lower lying σ^*_{SH} acceptor orbital. For the data shown in Fig. 2, this lies 102 kcal/mol lower than σ^*_{OH}, the corresponding acceptor orbital in methanol. In the language employed by Cieplak (34), this would correspond to $(\sigma_{CH},\sigma^*_{SH})$ hyperconjugation as the origin of the reversal.

Dimethyl ether and dimethyl sulfide

These are entries 21 and 22 of Fig. 1. With the 6-31G* basis set, attachment of the methyl group causes both C—H bond lengths of the ether to lengthen slightly. In the sulfide, the "equatorial" C—H bond shortens slightly and the "axial" C—H bond lengthens slightly, so that the trend in the bond lengths is the same in both compounds. On the other hand, the data from the PMO analysis, shown in Fig. 3, suggest that the small effect in the opposite direction seen in methanethiol should have been slightly enhanced in the sulfide, because the energy difference between the σ^*_{S-Me} and σ^*_{O-Me} acceptor orbitals is now 114 kcal/mol. The difference between CH_3OH/CH_3SH and CH_3OCH_3/CH_3SCH_3 may be too small to be found by the theoretical methods employed here. It might be noted that, in the work of McKean (*3b*), $\Delta\Delta D^\circ_{298}$, the difference in the bond dissociation energies of the diastereotopic hydrogens of metha-

Can. J. Chem. Downloaded from www.nrcresearchpress.com by 88.85.125.76 on 09/07/12
For personal use only.

Can. J. Chem. Downloaded from www.nrcresearchpress.com by 88.85.125.76 on 09/07/12
For personal use only.

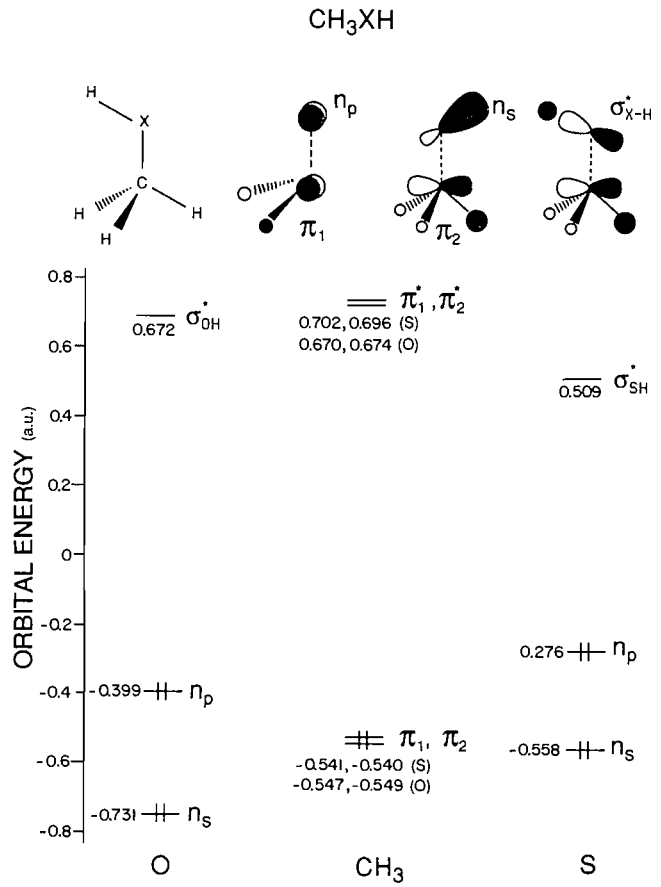

FIG. 2. Quantitative PMO analyses of methanol and methanethiol (orbital energies only).

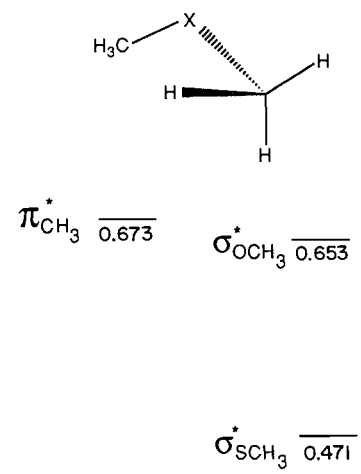

FIG. 3. Quantitative PMO analyses of dimethyl ether and dimethyl sulfide, showing the positions of the acceptor orbitals.

nol compared to that of methanethiol, is 5.1 kcal/mol, and for dimethyl ether and dimethyl sulfide $\Delta\Delta D^{\circ}_{298}$ is 5.8 kcal/mol.

Methanediol and methanedithiol

These are entries 5 and 6 of Fig. 1. Both 1,3-dioxane and 1,3-dithiane exhibit axial–equatorial differences in $^1J_{C-H}$ of 10 Hz, but in opposite directions. The "axial"–"equatorial" C—H bond lengths also show opposite trends. Relevant data from the quantitative PMO analysis are found in Fig. 4. Not shown are the π_{CH_2} donor orbitals of the two molecules. The magnitudes of

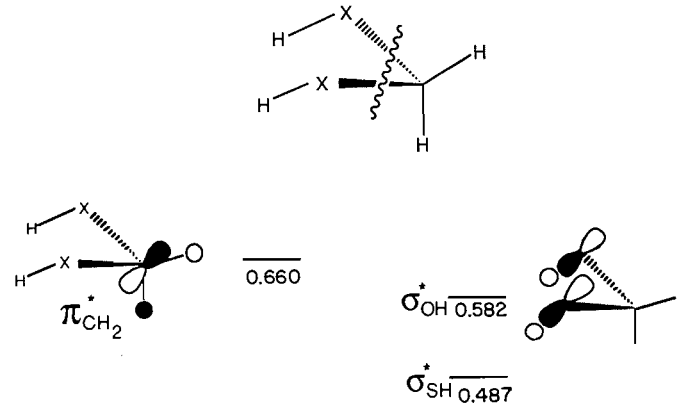

FIG. 4. Quantitative PMO analyses of methanediol and methanedithiol, showing the positions of the acceptor orbitals for the fragmentation $CH_2\cdots(XH)_2$.

the atomic orbital coefficients of the "axial" and "equatorial" C2 hydrogens are different in these donor orbitals; in the oxygen compound, the "axial" hydrogen has the larger coefficient but, in the sulfur compound, the "equatorial" hydrogen has the larger coefficient. The same differences in atomic orbital coefficients are found in the $\pi^*_{CH_2}$ acceptor orbitals. Thus, a (π,σ^*_{S-H}) charge transfer will weaken the equatorial C2—H bond preferentially, but a (π,σ^*_{O-H}) charge transfer will weaken the axial C2—H bond preferentially. The same trends will result from charge transfer in the opposite direction, i.e., (σ_{S-H},π^*) or (σ_{O-H},π^*). Interestingly, the magnitudes of charge transfer computed at STO-3G suggest that the former effect dominates in the oxygen compound, and the latter effect dominates in the sulfur compound. Using the language of Cieplak (34), the reversal in the C—H bond lengths can be said to be the result of $\sigma_{S-H},\sigma^*_{C-H}$ hyperconjugation. It will be noted that the direction of the hyperconjugation is the reverse of that found in methanethiol.

The "anomeric effects" in CH_3CHXY molecules

We define the "anomeric stabilization" in the molecules of the present study as the energy difference between the *gauche* and *anti* conformations, e.g., entries 7 versus 8 of Fig. 1, or the energy difference between the *gauche,gauche* and *anti,gauche* conformations, e.g., entries 11 versus 12. An alternative definition has been proposed by Schleyer *et al.* (35), in terms of the stabilization energies derived from the isodesmic reaction $XCH_2Y + CH_4 \rightarrow CH_3X + CH_3Y$ (36). The latter studies, carried out mainly at the 3-21G* level, suggest that the stabilization is greater than 10 kcal/mol for all combinations of first row X and Y (X,Y = F, OH, NH_2), but insignificant for all combinations of the second row substituents X,Y = Cl, SH, PH_2. However, significant anomeric interactions involving second row elements have been observed experimentally (19*i*, and references cited therein; also, unpublished results by Juaristi *et al.*).[2]

Tables 2 and 3 summarize the theoretical anomeric effects calculated for the relevant molecules of the present study, i.e., entries 7–16 of Fig. 1. Entries 7–14 refer to systems containing an endocyclic oxygen and an exocyclic X at the anomeric centre; entries 15 and 16 refer to molecules containing an endocyclic

[2]A more recent reexamination of $CH_2(SH)_2$ at a higher level of computation (MP4SDTQ/6-31G*//6-31G*)[3] now indicates that this system has greater stabilization than had been thought (35, 37).

[3]P.v.R. Schleyer and U. Salzner. Personal communication.

TABLE 2. Bond lengths (Å), bond angles, C–H force constants (mdyn/Å), and anomeric effects (6-31G*, kcal/mol) in $CH_3CH(OH)$—X compounds

X	Conformation	E(rel) (kcal/mol)	C—O (Å)	C—X (Å)	C–H (FC) (Å) (mdyn/Å)	O—C—X (deg)	O—C—C (deg)
F	Axial	0.00	1.3694	1.3688	1.0784 (5.628)	109.4	113.6
F	Equatorial	4.35	1.3820	1.3522	1.0851 (5.503)	105.4	112.9
Cl	Axial	0.00	1.3693	1.8233	1.0753 (5.687)	110.4	113.4
Cl	Equatorial	4.48	1.3868	1.7890	1.0812 (5.576)	106.4	110.2
OH	Axial	0.00	1.3915	1.3912	1.0837 (5.529)	110.9	112.7
OH	Equatorial	3.34	1.4005	1.3795	1.0906 (5.404)	107.2	112.4
SH	Axial	0.00	1.3903	1.8340	1.0785 (5.626)	112.1	112.3
SH	Equatorial	3.12	1.3995	1.8171	1.0842 (5.520)	108.1	111.9

TABLE 3. Bond lengths, bond angles, C–H force constants, and anomeric effects in $CH_3CH(SH)$—X

X	Conformation	E(rel) (kcal/mol)	C—S (Å)	C—X (Å)	C–H (FC) (Å) (mdyn/Å)	S—C—X (deg)	S—C—C (deg)
OH	Axial	0.00	1.8333	1.3916	1.0853 (5.50)	112.0	113.4
OH	Equatorial	2.18	1.8443	1.3903	1.0835 (5.53)	107.4	113.0

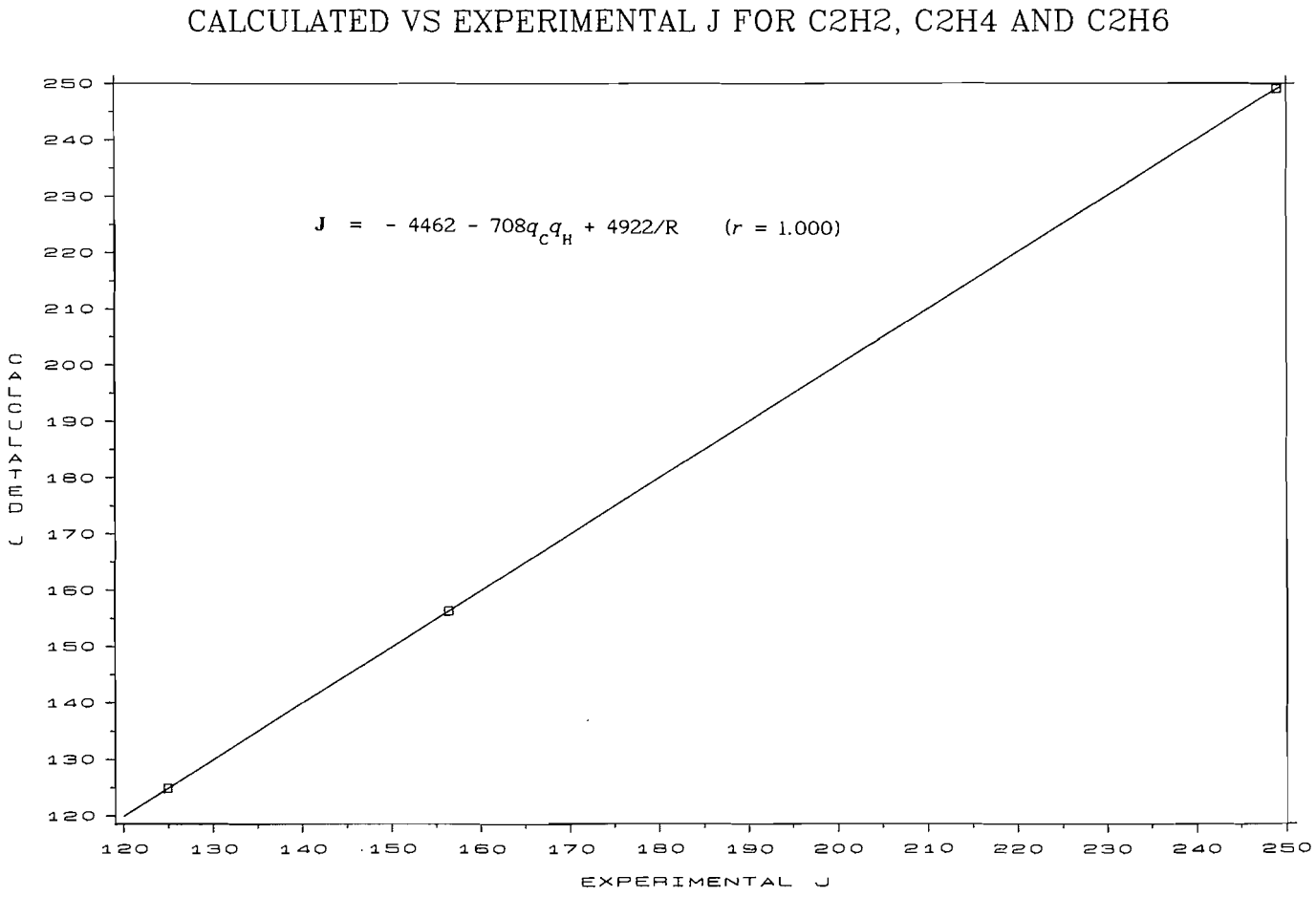

FIG. 5. Correlation of the experimental C–H coupling constants of ethane, ethylene, and acetylene against the inverse of the bond lengths and the product of the atomic charges on carbon and hydrogen.

Can. J. Chem. Downloaded from www.nrcresearchpress.com by 88.85.125.76 on 09/07/12
For personal use only.

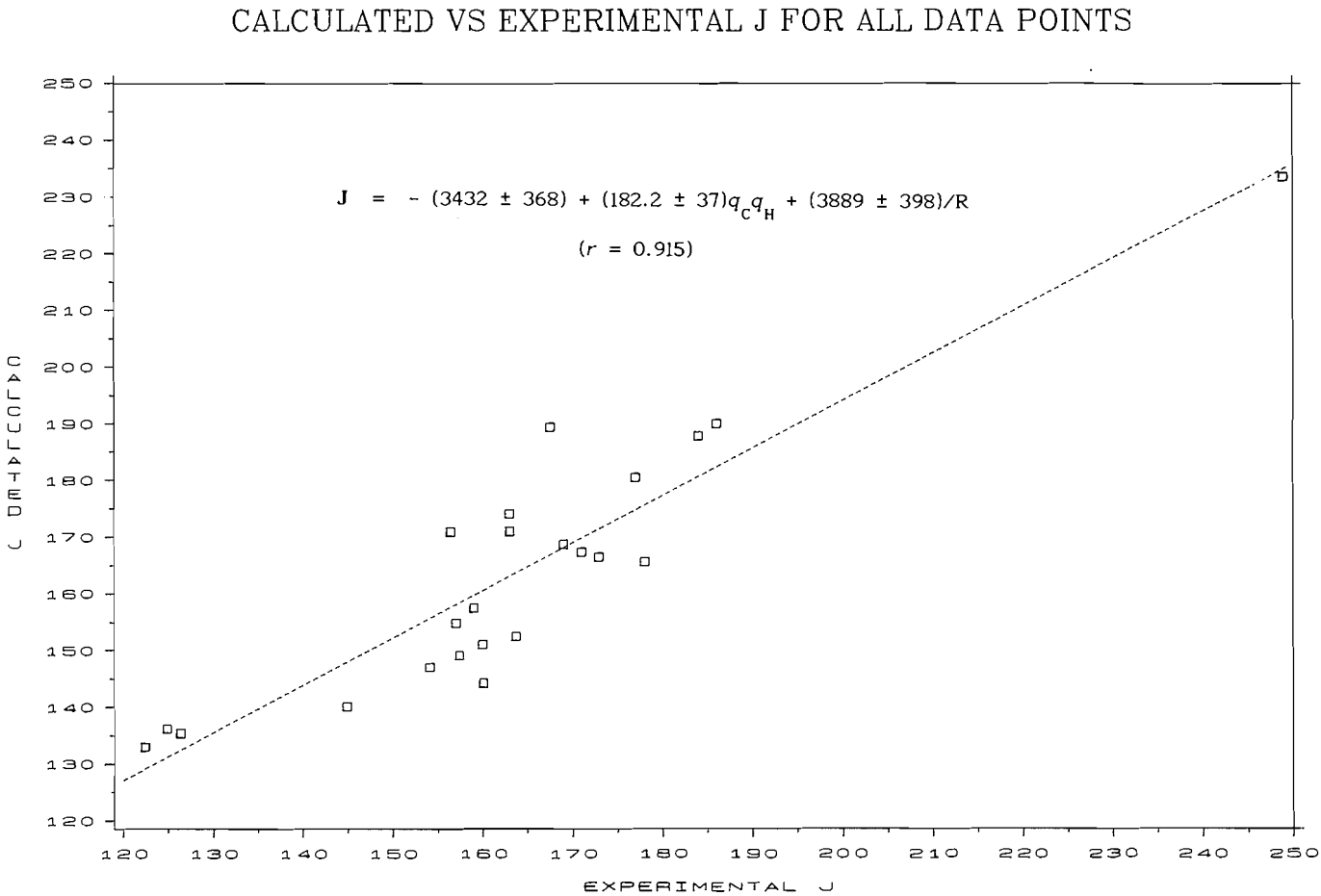

FIG. 6. Same as Fig. 5, for the set of data summarized in Table 4.

sulfur and an exocyclic hydroxyl group at the anomeric centre. The relative energies are given in kcal/mol. The tables include the calculated C—X and C—Y bond lengths, and the Y—C—X and Y—C—C bond angles in the two isomers. As expected from the geometrical consequences of the anomeric effect (29, 38), in all cases the C—Y bond is shorter, the C—X bond is longer, and the Y—C—X angle is larger in the "axial" isomers.

Interestingly, for "pyranosyl"-X, there is very little difference between the computed gas phase "anomeric effects" of first row and second row X. A value of 1.35 kcal/mol has been estimated for the anomeric effect in 2-MeS-tetrahydropyran, from the reported $\Delta G°$ value (0.35 in CCl_4 (39)), and the A value of MeS (1.0 kcal/mol (40)). A corresponding value of 1.29 kcal/mol in $CFCl_3/CDCl_3$ solvent can be estimated for 2-MeO-tetrahydropyran from the thermodynamic data for this compound and methoxycyclohexane (41). However, taking into account the conformational free energies for the axial–equatorial equilibria in 2-Me-tetrahydropyran (2.86 kcal/mol (42)) and methylcyclohexane (1.74 kcal/mol (43)) leads to experimental free energy anomeric effects of 1.67 and 1.99 kcal/mol, respectively, in 2-MeO- and 2-MeS-tetrahydropyran.

On the other hand, for a common X, there is an approximately 1 kcal/mol difference in the theoretical gas phase "anomeric effects" of "pyranosyl"-X and "thiapyranosyl"-X. Based on the available data (41–44) and the axial–equatorial equilibrium in 2-Me-tetrahydrothiapyran (1.40 kcal/mol (45)), we estimate experimental free energy anomeric effects of 3.07 and 2.19 kcal/mol, respectively, in 2-Cl-tetrahydropyran and 2-Cl-tetrahydrothiapyran.

Global analysis of the relationship between C—H bond lengths and one-bond coupling constants

As we have seen, for every diastereomeric or diastereotopic pair of C—H bonds, there is an inverse relationship between the C—H bond length and the magnitude of $^1J_{C-H}$. This is consistent with the simple notion that an interaction between two directly bonded atoms, in this case Fermi contact, will vary inversely with the distance between these atoms. Not surprisingly, however, when the 20 experimental C—H coupling constants listed in Fig. 1 are plotted against $1/R_{CH}$, the inverse of the C—H bond length, no statistically significant global correlation can be seen. Because of the different electronegativities of X and Y, the charges on the central carbon and on hydrogen vary throughout the series. One way to take these into account might involve a correlation such as $J = A + Bq_Cq_H + C/R$, where the q's are the total atomic charges on carbon and hydrogen, from the Mulliken population analysis. Figure 5 shows the result thus obtained for ethane, ethylene, and acetylene; in this case, taking the "electronegativity" contribution into account leads to a perfect correlation (r = 1.000). The inverse bond length term makes the dominant contribution to the correlation.

Accordingly, using the data of Table 4, a regression analysis of the type just described was performed on the 20 C—H bonds of the present study, to which ethane, ethylene, and acetylene were added. The result is shown in Fig. 6. As seen, the standard errors of the parameters of the equation are ca. 10%, and the correlation coefficient r = 0.915. Although an improved correlation might be achieved by taking additional geometrical and electronic effects into account, this is unlikely to alter our principal conclusions, namely, (1) the length of the C—H bond

Can. J. Chem. Downloaded from www.nrcresearchpress.com by 88.85.125.76 on 09/07/12
For personal use only.

TABLE 4. Data employed for the regression analysis of Fig. 6

Entry[a]	$1/r^b$	$q_C q_H$	$^1J_{C-H}$[c]
1 *app*	0.9225	−0.0161	163.7
syn	0.9262	−0.0185	172.9
3 *app*	0.9257	0.0173	163.0
4 *syn*	0.9283	0.0139	177.0
5 *ax*	0.9192	0.0357	157.4
eq	0.9289	0.0499	167.5
6 *ax*	0.9271	−0.1442	154.1
eq	0.9254	−0.1455	144.9
7	0.9273	0.0873	186.0
8	0.9216	0.0754	178.0
9	0.9300	0.0177	184.0
10	0.9249	0.0143	171.0
11	0.9228	0.0665	169.0
12	0.9169	0.0583	160.0
13	0.9272	0.0023	163.0
14	0.9223	0.0011	157.0
15	0.9214	−0.0005	160.0
16	0.9229	0.0031	159.0
17 *ax*	0.9189	−0.0461	122.4
eq	0.9196	−0.0475	126.4
C_2H_2	0.9462	−0.0762	249.0
C_2H_4	0.9274	−0.0622	156.4
C_2H_6	0.9211	−0.0754	124.9

[a]Refers to the appropriate entry of Fig. 1.
[b]The inverse of the 6-31G* bond length.
[c]Experimental value from Table 1.

is the dominant factor that determines the magnitude of $^1J_{C-H}$; (2) the two quantities are inversely related; (3) the Perlin Effect is the NMR counterpart of the Bohlmann bands.

Implications and predictions

The calculations on entry 6 of Fig. 1 predict that the relative reactivities towards radical abstraction of the C2-equatorial and C2-axial hydrogens of a 1,3-dithiane will be the opposite of that observed in a 1,3-dioxane (11). This prediction is currently under experimental investigation, but it is important to note that the analysis of the Perlin Effect presented herein would have allowed this prediction on the basis of the experimental $^1J_{C-H}$ coupling constants. Since a reversal of the relative magnitudes of the coupling constants at C2 is also observed in the third row analog 1,3-diselenane (19*k*, and unpublished results by Pinto *et al.*), this system is expected to resemble a 1,3-dithiane in the relative radical reactivities of its C2 hydrogens.

Acknowledgements

The authors thank the Natural Sciences and Engineering Research Council of Canada for financial support, Queen's University for generous allocation of computing time and resources, Dr. M. R. Peterson for assistance with the quantitative PMO calculations, and Dr. C.-K. Kim for advice and assistance regarding the regression analyses.

1. W. J. HEHRE, L. RADOM. P. V. R. SCHLEYER, and J. A. POPLE. Ab initio molecular orbital theory. Wiley–Interscience, New York. 1986. p. 148.
2. J. SKOLIK, P. J. KRUEGER, and M. WIEWOROWSKI. Tetrahedron, **24**, 5439 (1968), and references cited therein; P. J. KRUEGER, J. JAN, and H. WIESER. J. Mol. Struct. **5**, 375 (1970).
3. (*a*) F. BERNARDI, H. B. SCHLEGEL, and S. WOLFE. J. Mol. Struct. **35**, 149 (1976); (*b*) D. C. MCKEAN. Chem. Soc. Rev. **7**, 399 (1978); Int. J. Chem. Kinet. **21**, 445 (1989).
4. M. GOLFIER. *In* Stereochemistry, fundamentals and methods. Vol. 1. *Edited by* H. B. Kagan. Georg Thieme Verlag, Stuttgart. 1977. p. 7.
5. F. BOHLMANN. Angew. Chem. **69**, 641 (1957); Chem. Ber. **91**, 2157 (1958).
6. D. GRILLER, J. A. HOWARD, P. R. MARRIOTT, and J. C. SCAIANO. J. Am. Chem. Soc. **103**, 619 (1981).
7. M. J. S. DEWAR and S. D. WORLEY. J. Chem. Phys. **50**, 654 (1969).
8. W. L. JORGENSEN and L. SALEM. The organic chemist's book of orbitals. Academic Press, New York. 1973; B. M. GIMARC. Molecular structure and bonding. The qualitative molecular approach. Academic Press, New York. 1979.
9. R. M. LEES and J. G. BAKER. J. Chem. Phys. **48**, 5299 (1968).
10. J. S. BINKLEY, J. A. POPLE, and W. J. HEHRE. J. Am. Chem. Soc. **102**, 939 (1980).
11. V. MALATESTA and K. U. INGOLD. J. Am. Chem. Soc. **103**, 609 (1981); A. J. L. BECKWITH and C. J. EASTON. J. Am. Chem. Soc. **103**, 615 (1981).
12. R. F. HOUT, JR., W. J. PIETRO, and W. J. HEHRE. A pictorial approach to molecular structure and reactivity. Wiley–Interscience, New York. 1984.
13. T. A. ALBRIGHT, J. K. BURDETT, and M. H. WHANGBO. Orbital interactions in chemistry. John Wiley, New York. 1985.
14. A. STREITWIESER, JR. Molecular orbital theory for organic chemists. John Wiley, New York. 1962.
15. S. WOLFE, H. B. SCHLEGEL, M. H. WHANGBO, and F. BERNARDI. Can. J. Chem. **52**, 3787 (1974); D. KOST, H. B. SCHLEGEL, D. J. MITCHELL, and S. WOLFE. Can. J. Chem. **57**, 729 (1979).
16. M. H. WHANGBO, H. B. SCHLEGEL, and S. WOLFE. J. Am. Chem. Soc. **99**, 1296 (1977).
17. A. S. PERLIN and B. CASU. Tetrahedron Lett. 292 (1969).
18. J. KOWALEWSKI. Prog. Nucl. Magn. Reson. Spectrosc. **11**, 1 (1977); G. E. MACIEL, J. W. MCIVER, JR., N. S. OSTLUND, and J. A. POPLE. J. Am. Chem. Soc. **92**, 1 (1970); G. E. MACIEL, J. W. MCIVER, JR., N. S. OSTLUND, and J. A. POPLE. J. Am. Chem. Soc. **92**, 11 (1970).
19. (a) K. BOCK, I. LUNDT, and C. PEDERSEN. Tetrahedron Lett. 1037 (1973); (b) K. BOCK and C. PEDERSEN. J. Chem. Soc. Perkin Trans. 2, 293 (1974); (c) K. BOCK and C. PEDERSEN. Acta Chem. Scand. **B29**, 258 (1975); (d) K. BOCK and L. WIEBE. Acta Chem. Scand. **27**, 2676 (1973); (e) W. F. BAILEY, A. D. RIVERA, and K. ROSSI. Tetrahedron Lett. **29**, 5621 (1988); (f) V. S. RAO. Can. J. Chem. **60**, 1067 (1982); (g) V. S. RAO and A. S. PERLIN. Carbohydr. Res. **92**, 141 (1981); (h) J. E. N. SHIN and A. S. PERLIN. Carbohydr. Res. **76**, 165 (1979); (i) E. JUARISTI, E. A. GONZALEZ, B. M. PINTO, B. D. JOHNSTON, and R. NAGELKERKE. J. Am. Chem. Soc. **111**, 6745 (1989); (j) B. M. PINTO, J. SANDOVAL-RAMIREZ, R. D. SHARMA, A. C. WILLIS, and F. W. B. EINSTEIN. Can. J. Chem. **64**, 732 (1986); (k) B. M. PINTO, B. D. JOHNSTON, and R. NAGELKERKE. Heterocycles, **28**, 389 (1989); (l) D. E. BUGAY, C. H. BUSHWELLER, C. T. DANEHEY, JR., S. HOOGASIAN, J. A. BLERSCH, and W. L. LEENSTRA. J. Phys. Chem. **93**, 3908 (1989); (*m*) H.-O. KALINOWSKI. *In* Carbon-13 nmr spectroscopy. *Edited by* S. Berger and S. Braun. John Wiley, New York. 1988. p. 495; (*n*) R. R. FRASER and M. BRESSE. Can. J. Chem. **61**, 576 (1983); (*o*) B. BRAILLON, M. C. LASNE, J. L. RIPOLLI, and J. M. DENIS. Nouv. J. Chim. **6**, 121 (1982); (*p*) T. YONEZAWA and I. MORISHIMA. J. Mol. Spectrosc. **27**, 210 (1968); (*q*) J. AUGE and S. DAVID. Nouv. J. Chim. **1**, 57 (1977); (*r*) J. A. SCHWARCZ and A. S. PERLIN. Can. J. Chem. **50**, 3667 (1972); (*s*) A. S. PERLIN. Pure Appl. Chem. **50**, 1401 (1978); (*t*) F. R. TARAVEL and P. J. A. VOTTERO. Tetrahedron Lett. **28**, 2341 (1975); (*u*) N. S. CUSSANS and T. N. HUCKERBY. Tetrahedron, **31**, 2719 (1975); (*v*) S. BRAUN and D. J. KINKELDEI. Tetrahedron, **33**, 3127 (1977); (*w*) G. R. WEISMAN, V. JOHNSON, and R. E. FIALA. Tetrahedron Lett. **21**, 3635 (1980); G. R. WEISMAN, V. B. JOHNSON, and M. B. COLLIDGE. Tetrahedron Lett. **22**, 4365 (1981); (*x*) Y. TAKEUCHI,

Can. J. Chem. Downloaded from www.nrcresearchpress.com by 88.85.125.76 on 09/07/12
For personal use only.

P. J. CHIVERS, and T. A. CRABB. J. Chem. Soc. Chem. Commun. 210 (1974); (*y*) P. E. HANSEN. Progr. NMR Spectrosc. **14**, 175 (1981); (*z*) V. M. S. GIL and W. V. PHILIPSBORN. Magn. Reson. Chem. **27**, 409 (1989).

20. (*a*) N. MULLER and D. E. PRITCHARD. J. Chem. Phys. **31**, 768 (1959); (*b*) J. N. SHOOLERY. J. Chem. Phys. **31**, 1427 (1959); (*c*) F. B. DUIJNEVELDT, V. M. S. GIL, and J. N. MURRELL. Theor. Chim. Acta, **4**, 85 (1966); (*d*) D. M. GRANT and W. M. LITCHMAN. J. Am. Chem. Soc. **87**, 3394 (1965); (*e*) Z. B. MAKSIC, M. E. ECKERT-MAKSIC, and M. RANDIC. Theor. Chim. Acta, **22**, 70 (1971); M. RANDIC, Z. MEIC, and A. RUBCIC. Tetrahedron, **28**, 565 (1972).
21. H. M. MCCONNELL. J. Chem. Phys. **24**, 460 (1956).
22. P. C. HARIHARAN and J. A. POPLE. Theor. Chim. Acta, **28**, 213 (1973).
23. M. J. FRISCH, J. S. BINKLEY, H. B. SCHLEGEL, K. RAGHAVACHARI, C. F. MELIUS, R. L. MARTIN, J. J. P. STEWART, F. W. BOBROWICZ, C. M. ROHLFING, L. R. KAHN, D. J. DEFREES, R. SEEGER, R. A. WHITESIDE, D. J. FOX, E. M. FLUDER, and J. A. POPLE. GAUSSIAN 86. Gaussian, Inc., Pittsburgh, PA 15213, U.S.A.
24. W. J. PIETRO, M. M. FRANCL, W. J. HEHRE, D. J. DEFREES, J. A. POPLE, and J. S. BINKLEY. J. Am. Chem. Soc. **104**, 5039 (1982).
25. M. J. FRISCH, J. A. POPLE, and J. S. BINKLEY. J. Chem. Phys. **80**, 3265 (1984).
26. M. M. FRANCL, W. J. PIETRO, W. J. HEHRE, J. S. BINKLEY, M. S. GORDON, D. J. DEFREES, and J. A. POPLE. J. Chem. Phys. **77**, 3654 (1982).
27. R. S. MULLIKEN. J. Chem. Phys. **23**, 1833 (1955); **23**, 1841 (1955); **23**, 2338 (1955); **23**, 2343 (1955).
28. M. R. PETERSON and R. A. POIRIER. MONSTERGAUSS. University of Toronto, Toronto, Ont. 1981.
29. S. WOLFE, M. H. WHANGBO, and D. J. MITCHELL. Carbohydr. Res. **69**, 1 (1979); K. B. WIBERG and M. A. MURCKO. J. Am. Chem. Soc. **111**, 4821 (1989), and references cited therein.
30. R. U. LEMIEUX, A. A. PAVIA, J. C. MARTIN, and K. A. WATANABE. Can. J. Chem. **47**, 4427 (1969).
31. I. H. WILLIAMS. J. Chem. Soc. Chem. Commun. 627 (1986).
32. N. S. CHIU, J. D. EWBANK, and L. SCHAFER. J. Mol. Struct. (THEOCHEM). **86**, 397 (1982).
33. K. B. WIBERG, V. A. WALTERS, and W. P. DAILEY. J. Am. Chem. Soc. **107**, 4860 (1985).
34. A. S. CIEPLAK. J. Am. Chem. Soc. **103**, 4540 (1981).; A. S. CIEPLAK, B. D. TAIT, and C. R. JOHNSON. J. Am. Chem. Soc. **111**, 8447 (1989).
35. P. V. R. SCHLEYER, E. D. JEMMIS, and G. W. SPITZNAGEL. J. Am. Chem. Soc. **107**, 6393 (1985).
36. W. J. HEHRE, R. DITCHFIELD, L. RADOM, and J. A. POPLE. J. Am. Chem. soc. **92**, 4796 (1970).
37. A. E. REED and P. V. R. SCHLEYER. Inorg. Chem. **27**, 3969 (1988).
38. B. M. PINTO, H. B. SCHLEGEL, and S. WOLFE. Can. J. Chem. **65**, 1658 (1987).
39. E. L. ELIEL and C. A. GIZA. J. Org. Chem. **33**, 3754 (1968).
40. F. R. JENSEN, C. H. BUSHWELLER, and B. H. BECK. J. Am. Chem. Soc. **91**, 344 (1969).
41. H. BOOTH and K. A. KHEDHAIR. J. Chem. Soc. Chem. Commun. 467 (1985); H. BOOTH, T. B. GRINDLEY, and K. A. KHEDHAIR. J. Chem. Soc. Chem. Commun. 1047 (1982).
42. E. L. ELIEL, K. D. HARGRAVE, K. M. PIETRUSIEWICZ, and M. MANOHARAN. J. Am. Chem. Soc. **104**, 3635 (1982).
43. H. BOOTH and J. R. EVERETT. J. Chem. Soc. Chem. Commun. 278 (1976).
44. A. J. DE HOOG. Ph.D. Thesis, University of Leiden, The Netherlands. 1971.
45. R. L. WILLER and E. L. ELIEL. J. Am. Chem. soc. **99**, 1925 (1977).

Can. J. Chem. Downloaded from www.nrcresearchpress.com by 88.85.125.76 on 09/07/12
For personal use only.

Chemical synthesis of GDP-fucose analogs and their utilization by the Lewis α(1→4) fucosyltransferase

UDAY B. GOKHALE AND OLE HINDSGAUL[1]
Department of Chemistry, University of Alberta, Edmonton, Alta., Canada T6G 2G2
AND
MONICA M. PALCIC
Department of Food Science, University of Alberta, Edmonton, Alta. Canada T6G 2P5

Received December 11, 1989

This paper is dedicated to Professor Arthur S. Perlin on the occasion of his 67th birthday

UDAY B. GOKHALE, OLE HINDSGAUL, and MONICA M. PALCIC. Can. J. Chem. **68**, 1063 (1990).

Chemical syntheses are reported for GDP-fucose (**5**), GDP-3-deoxy-fucose (**6**), and GDP-arabinose (**7**), the demethyl analog of **5**. All three sugar nucleotides were found to act as donor substrates for an α(1→4) fucosyltransferase isolated from human milk when βDGal(1→3)βDGlcNAc-O(CH_2)$_8$COOMe (**1**) was used as the acceptor. The rate of transfer of sugar residues to **1** was measured using a coupled spectrophotometric assay and was found to be 100% (**5**), 2.3% (**6**), and 5.9% (**7**). The product Le^a-active oligosaccharide analogs were identified by both an enzyme-linked immunosorbent assay (ELISA) and by ^1H NMR spectroscopy.

Key words: glycosyltransferase, oligosaccharide synthesis, sugar-nucleotide analog, ELISA assay, fucosyltransferase.

UDAY B. GOKHALE, OLE HINDSGAUL et MONICA M. PALCIC. Can. J. Chem. **68**, 1063 (1990).

On a réalisé la synthèse du GDP-fucose (**5**), du GDP-3-désoxy-fuxose (**6**) et du GDP-arabinose (**7**), l'analogue déméthylé du produit **5**. On a trouvé que, lorsque le βDGal(1→3)βDGlcNAc-O(CH_2)$_8$COOMe (**1**) est utilisé comme accepteur, ces trois nucléotides de sucre peuvent agir comme des substrats donneurs pour une α(1→4) fucosyltransférase isolée du lait humain. Utilisant une méthode spectrophotométrique couplée, on a mesuré les vitesses de transfert des résidus de sucre vers le produit **1** et on a trouvé que ces vitesses sont respectivement de 100% (**5**), de 2,3% (**6**) et de 5,9% (**7**). Faisant appel à la RMN du ^1H et à une méthode d'immunosorbance liée à un enzyme, on a identifié les analogues d'oligosaccharides actifs vis-à-vis de Le^a.

Mots clés : glycosyltransférase, synthèse d'oligosaccharides, analogue des nucléotides de sucre, méthode d'immunosorbance liée à un enzyme, fucosyltransférase.

[Traduit par la revue]

Can. J. Chem. Downloaded from www.nrcresearchpress.com by 88.85.125.76 on 09/07/12
For personal use only.

Introduction

The use of enzyme assisted oligosaccharide synthesis is gaining wide popularity since it allows the rapid and specific homologation of relatively small, readily chemically synthesized mono- and disaccharides into larger and more complex structures (1). This homologation is most frequently accomplished using specific glycosyltransferases that transfer sugars from the appropriate sugar-nucleotide donors, all of which are commercially available, to suitable oligosaccharide acceptors. Accessibility to the required mammalian glycosyltransferases, most of which must still be isolated from natural sources, has been the single major impediment to the general applicability of this combined chemical–enzymatic approach to oligosaccharide synthesis. The availability of the required enzymes is, however, rapidly increasing as three of these enzymes are now commercially available and at least six have recently been cloned (2).

Analogs of the naturally occurring oligosaccharides, particularly deoxygenated oligosaccharides, are invaluable probes in studies on the molecular recognition of complex carbohydrates by protein combining sites (3, 4). The effect of specifically deoxygenating individual hydroxyl groups of oligosaccharide ligands, for example, provides direct evidence for the involvement of those hydroxyl groups in hydrogen bonding with the protein. While the utility of oligosaccharide analogs is generally recognized, the difficulty of preparing the required structures by multistep chemical synthesis remains a major obstacle to their broad use in the study of carbohydrate binding by antibodies, lectins, enzymes, and other receptors.

In anticipation of a wider availability of glycosyltransferases as "routine reagents" for the combined chemical–enzymatic synthesis of oligosaccharides, we have begun an evaluation of the scope of these enzymes in the production of oligosaccharide analogs. We present here an investigation using a readily isolated Lewis blood-group associated α(1→4) fucosyltransferase, a glycosyltransferase that has previously been used in the combined chemical–enzymatic synthesis of oligosaccharides terminating in the Lewis-a (Le^a) blood-group determinant (5). The Lewis fucosyltransferase (Le-Fuc-T), which has also recently been cloned (2), transfers an L-fucopyranosyl residue from guanosine-5′-diphospho-fucose (GDP-fucose, **5**) to the 4-hydroxyl group of oligosaccharides terminating in the Type 1 sequence βDGal(1→3)βDGlcNAc-OR (**1**), to produce the Le^a-active terminus βDGal(1→3)[αLFuc(1→4)]βDGlcNAc-OR (**2**) (5). This reaction has been kinetically characterized in vitro where R in the synthetic oligosaccharides **1** and **2** was the 8-methoxycarbonyloctyl aglycone (5). We report here a simple chemical synthesis of the parent GDP-fucose (**5**), as well as the preparation of GDP-3-deoxy-L-fucose (**6**, GDP-3-deoxy-β-L-*xylo*-hexose, GDP-colitose) and GDP-D-arabinose (**7**, GDP-β-D-*arabino*-pentose), its 5-demethyl analog. Both of these analogs were found to be sufficiently reactive as donors to allow the production of the Le^a-active trisaccharide analogs **3** and **4**. Formation of **3** and **4** could be detected in an enzyme-linked immunosorbent assay (ELISA) using a monoclonal anti-Le^a antibody that had previously been shown to recognize these modified structures (6, 7). The initial rates of transfer of fucose analogs was further

[1]Author to whom correspondence may be addressed. Part of this work is from a Ph.D. thesis submitted by U.B.G. to the Department of Chemistry.

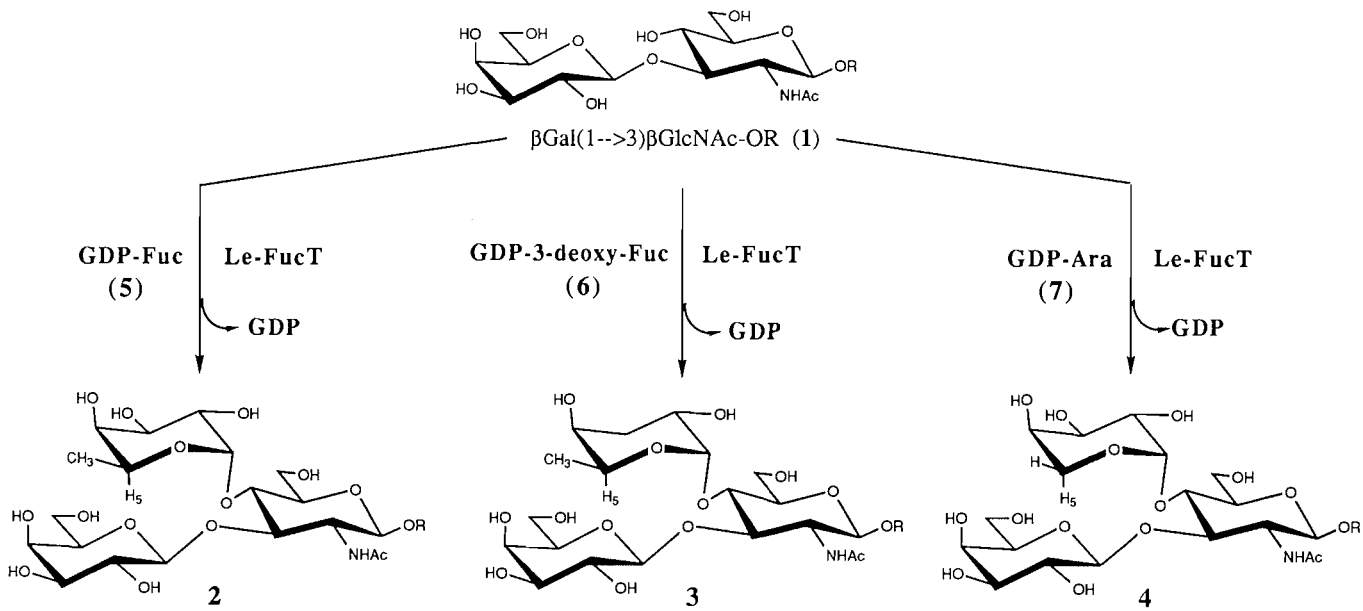

SCHEME 1

estimated using a novel spectrophotometric coupled enzyme assay. The structures of the enzymatically produced trisaccharides **2–4** were verified by ^{1}H NMR spectroscopy.

Chemical synthesis of GDP-fucose (5) and its analogs 6 and 7

Previous chemical syntheses of GDP-fucose required the stereospecific hydrolysis of acetobromofucose (**8**) to produce the β-reducing sugar **9** as the kinetic product (8). Compound **9** was then purified by fractional crystallization and phosphorylated using the highly reactive *o*-phenylene phosphorochloridate under conditions where isomerization to the more stable α-anomer **10** was minimized. Deprotection over three steps then provided the β-phosphate **14**, which could be converted to **5** (8). We found it very difficult to reproducibly obtain even 20% yields of **14** using this procedure. Since it was furthermore not assured that the required analogs of β-L-fucopyranose could be isolated by fractional crystallization of their glycosyl-bromide hydrolysis products, we elected instead to develop a simpler and potentially more general synthesis of β-pyranosyl phosphates.

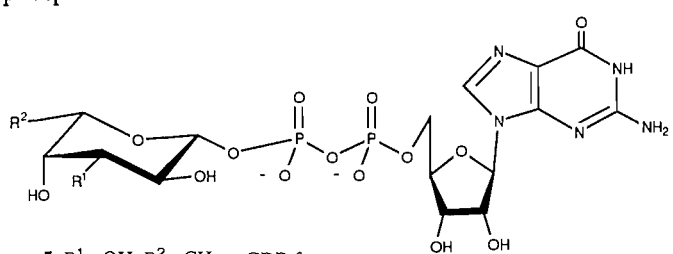

5: R^1= OH, R^2= CH_3, GDP-fucose
6: R^1= H, R^2= CH_3, GDP-3-deoxy-fucose
7: R^1= OH, R^2=H, GDP-arabinose

Reaction of **8** with tetra-*n*-butylammonium dibenzylphosphate (**11**) in DMF was found to proceed within 5 min at room temperature to produce a labile β-linked phosphotriester **12**. Compound **12** could be partially purified by rapid (< 10 min) chromatography on silica gel. The β-anomer of **12** proved to be unstable to extended contact with the silica gel and was completely destroyed by contact times as short as 2 h. Hydrogenolysis of the benzyl protecting groups in **12** gave the stable glycosyl phosphate **13**, which was treated with aqueous NaOH to provide **14**. Compound **14** was reproducibly obtained in 50% yield from **8** following ion-exchange chromatography and desalting. The ^{1}H NMR of **14** showed it to be a β/α mixture in the ratio 12:1. Similar reaction of 2,3,4-tri-*O*-acetyl-α-D-arabinopyranosyl bromide (**15**) gave phosphate **16** (β/α = 10:1) in 47% overall yield.

The synthesis of 3,6-dideoxy-L-*xylo*-hexopyranosyl phosphate (**27**) required several steps. Reaction of benzyl β-L-fucopyranoside (**17**) with dimethoxypropane gave acetal **18**, which was benzolated to provide **19** (60% from **17**). Removal of the isopropylidene group in **19** gave diol **20**, which was selectively 3-*O*-phenylthionocarbonylated (9) to provide **21** (68%). Reduction of **21** (Bu_3SnH, 51%) furnished the 3-deoxy derivative **22**, which was *O*-acetylated to give **23** (80%). Hydrogenolysis of the benzyl aglycon in **23** then gave the reducing sugar **24** (98%). Reaction of **24** with oxalyl bromide/DMF gave the unstable α-bromide **25**, which was immediately treated with **11**, followed by hydrogenation and saponification, to provide **26** (β/α = 5.4:1, 14%). The low yield of **26** is attributed at least partially to side reactions of the dideoxyglycosyl bromide **25**. Phosphates **14, 16**, and **26** were prepared at least four times following the above procedures and the isolated yields varied by less than 10%.

Two procedures were examined for conversion of **14, 16**, and **26** to the required GDP derivatives **5–7.** In our hands, coupling of these phosphates using either GMP-morpholidate (**27**) (8) or the phosphinothioic anhydride **28** (8) gave similar yields, which varied from experiment to experiment but always remained in the range of 25–50%. Similar observations were made in connection with a recent synthesis of CDP-quinovose (10). Representative procedures are reported in the experimental section. The product GDP derivatives could be purified by chromatography on Dowex anion-exchange resins using a LiCl gradient elution, which separated the faster eluting α-anomers. After desalting by passage through Bio-Gel P-2, the β-linked sugar nucleotides were isolated as their sodium salts following ion exchange. We wish to *explicitly* point out that the GDP derivatives **5–7** are unstable to either mildly acidic conditions

Can. J. Chem. Downloaded from www.nrcresearchpress.com by 88.85.125.76 on 09/07/12
For personal use only.

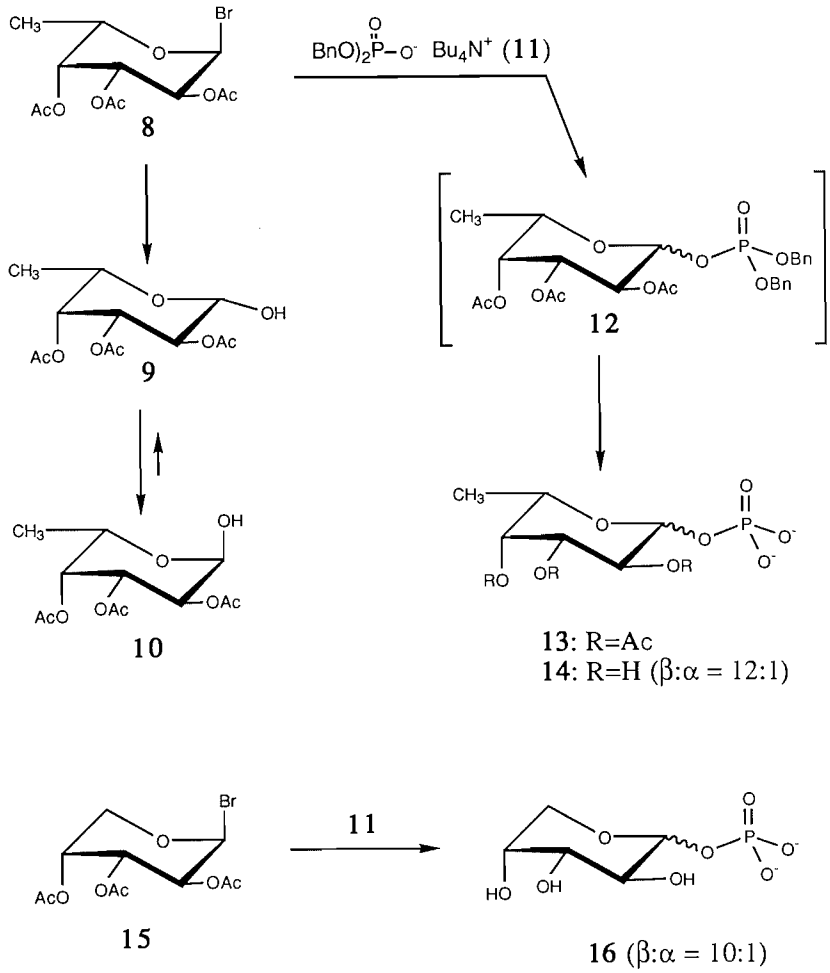

or even in neutral solution of high ionic strength. For example, attempted removal of water from a frozen aqueous LiCl solution of GDP-fucose by lyophilization resulted in its complete destruction, to produce fucose and GDP. The analogs **6** and **7** are expected to be even less stable.

Enzymatic synthesis of trisaccharides 2–4

The Le-FucT from human milk has previously been shown to transfer fucosyl residues from GDP-fucose to the Type 1 disaccharide acceptor βDGal(1→3)βDGlcNAc-O(CH_2)$_8$$COOCH_3$ (**1**) to yield the Le^a-active trisaccharide **2** (5). Compound **2** had earlier been prepared by total chemical synthesis (11). It was considered important to establish early in this investigation whether the GDP-fucose analogs **6** and **7** would also be utilized by the Le-FucT. All of the quantitative fucosyltransferase assays published to date involve the measurement of the rate of transfer of radiolabelled (^3H or ^{14}C) fucose from radiolabelled GDP-fucose to acceptor oligosaccharides (12). Since the chemically synthesized GDP-fucose analogs described here were not radiolabelled, alternate fucosyltransferase assays had to be devised.

We recently described an enzyme-linked immunosorbent assay (ELISA) for the Le-FucT that utilizes a monoclonal antibody, directed against **2**, to detect the conversion of **1** to **2** using unlabelled GDP-fucose, when these are immobilized on microtiter plates as their bovine serum albumin (BSA) conjugates (6). The combining site of the antibody used in these studies, clone CF4-C4, has been thoroughly probed by Lemieux *et al.* (7) using chemically synthesized derivatives of the Le^a-trisaccharide **2** as the methyl glycoside (R = Me). These studies showed that CF4-C4 not only bound to the Le^a trisaccharide (**2**), *but also* to the corresponding chemically synthesized 3-deoxy-fucose and arabinose analogs. Incubation of microtiter plates coated with the BSA-conjugate of acceptor **1** with the purified human milk Le-FucT in the presence of the GDP-fucose analogs **6** and **7** did indeed produce an immobilized product that was recognized by CF4-C4 as evidenced by the ELISA. No attempt was made to quantitate the rate of production of Le^a-active trisaccharides in these solid-phase reactions but this evidence for the utilization of **6** and **7** by the enzyme was nevertheless considered unequivocal.

A concentrated solution of the affinity-purified Le-FucT was prepared and added to acceptor **1** and to each of **5–7**. The initial rate of glycosylation of **1**, using **5–7** as the donors, was estimated by monitoring the reaction spectrophotometrically using a coupled-enzyme assay previously applied to the detection of galactosyltransferase activity (13) and described here for the first time for a fucosyltransferase. Since the glycosylation of **1** would result in the formation of one equivalent of GDP in all 3 cases (see Scheme 1), the rate of formation of GDP in these reaction mixtures would reflect the rate of glycosylation. This rate could be estimated by coupling the GDP formation to NADH oxidation employing pyruvate kinase and lactate dehydrogenase. Reaction progess could therefore be monitored spectrophotometrically by observing the decrease in absorbance at 340 nm. Incubation of the Le-FucT with acceptor **1** and GDP donors **5–7** in the presence of the enzyme coupling system thus gave the initial reaction rates listed in Table 1. These data

Can. J. Chem. Downloaded from www.nrcresearchpress.com by 88.85.125.76 on 09/07/12
For personal use only.

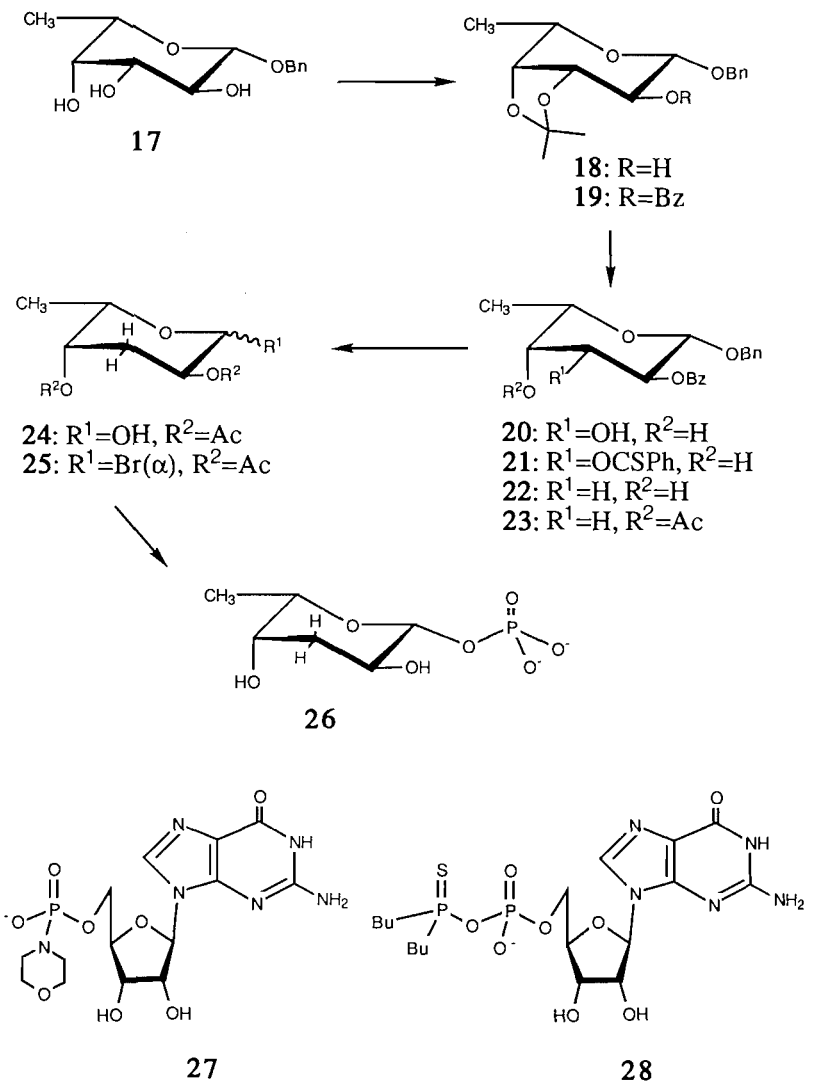

TABLE 1. Comparisons of GDP-fucose (**5**), GDP-3-deoxy-fucose (**6**), and GDP-arabinose (**7**) as donor substrates for the Lewis α(1→4) fucosyltransferase using βGal(1→3)βGlcNAc-O(CH_2)$_8$COOMe as the acceptor

Donor	ΔA_{340}(min)[a]	Relative rate (ΔA_{340})
GDP-fucose (**5**)	−0.064	100
GDP-3-deoxy-fucose (**6**)	−0.0015	2.3
GDP-arabinose (**7**)	−0.0038	5.9

[a]Rates are expressed as decrease in absorbance/0.87 mL for 11 milliunits of enzyme; details are given in the experimental section. The background in these experiments (i.e., the change in absorbance in the absence of acceptor **1**) was 0.0023 and has been subtracted from the values listed.

provide an estimate of the relative rate of transfer of glycosyl residues from the GDP-fucose analogs to be 100% (**5**), 2.3% (**6**), and 5.9% (**7**).

The data obtained using the above spectrophotometric assay (Table 1), coupled with a positive product identification by antibody CF44-C4 in the ELISA, provided strong evidence that trisaccharides **2–4** had been produced by the enzyme. It was nevertheless considered essential to provide definitive structural proof for the products formed in these enzymatic syntheses and the reactions were therefore carried out on a scale that would permit product characterization by ^{1}H NMR. The product of the reaction of **1** and GDP-fucose (**5**), catalyzed by the Le-FucT, has previously been characterized by ^{1}H NMR spectroscopy and shown to be identical with the Le^a-trisaccharide **2** prepared by total chemical synthesis (11). The characteristically deshielded signal for H-5 of the fucosyl residue in **2** (δ = 4.874 ppm) (5, 11) is considered diagnostic for βDGal(1→3)βDGlcNAc structures that have been α-fucosylated at the 4-position of the GlcNAc residue. This unusual deshielding has been attributed (11, 14) to the van der Waals contact of H-5 to both the ring and aglyconic oxygens of the βDGal residue in **2** as a result of its rigid solution conformation. Trisaccharides **3** and **4** would be expected to adopt solution conformations similar to that of **2** and the signals for H-5 (axial) in these structures would therefore be predicted to be correspondingly deshielded. Incubations designed to provide products in quantities sufficient for detection by ^{1}H NMR spectroscopy were therefore carried out. The extent of conversion of **1** to the Le^a -analogs **2–4** was estimated by integration of the appropriate proton resonances to be 100, 30, and 65%, respectively. The Le^a trisaccharide analogs **3** and **4** were not purified away from unreacted **1** since their structures could be deduced from the ^{1}H NMR spectra of the crude reaction mixtures (Fig. 1). As expected, the signal for H-5 in the 3-deoxy Le^a analog **3** was characteristically deshielded and resonated at 4.79 ppm where it was partially obscured by the residual DOH

Can. J. Chem. Downloaded from www.nrcresearchpress.com by 88.85.125.76 on 09/07/12
For personal use only.

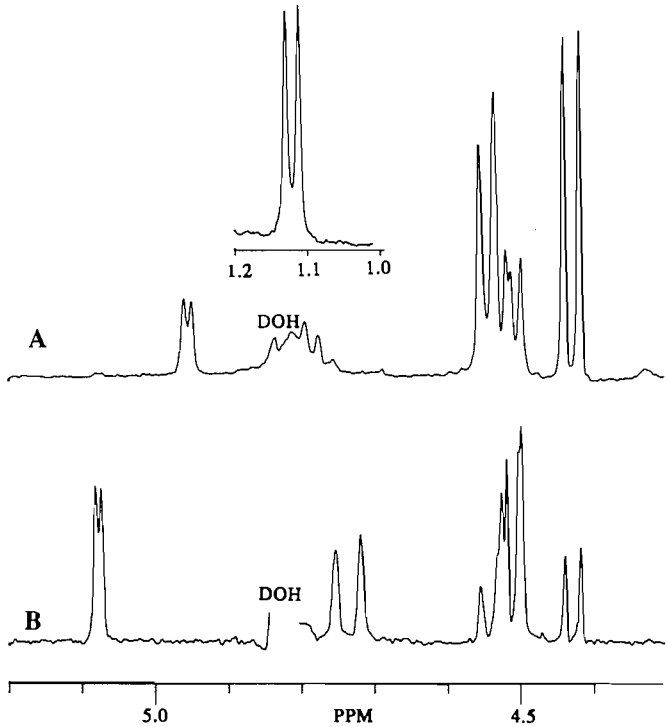

FIG. 1. Partial 360-MHz ^{1}H NMR spectra of the crude reaction products obtained on glycosylation of disaccharide **1** using GDP-3-deoxy-fucose **6** (A) and GDP-arabinose **7** (B) in D_2O. The spectral artifacts appearing near δ 4.82 ppm result from suppression of the residual DOH signal by presaturation.

signal (Fig. 1A). Irradiation at 4.79 ppm collapsed the methyl group doublet appearing at 1.120 ppm (inset, Fig. 1A) to a singlet, thereby confirming the signal assignments. The signal from the H-5 (axial) proton in the arabino-Le^a analog **4** was similarly deshielded (Fig. 1B), appearing at 4.736 ppm (J_{gem} = −12.5 Hz). The signals for the anomeric protons of the α-linked glycosyl residues in **3** and **4** are seen at 4.955 and 5.078 ppm, respectively, with vicinal coupling constants near 3 Hz. Both the ELISA and spectrophotometric assays are therefore concluded to be reliable assays for monitoring the synthesis of the Le^a-related structures described in this study.

In summary, straightforward syntheses of GDP-fucose and two of its analogs have been described. All three GDP-fucose derivatives were found to act as donors for an Le-FucT, as assayed by both ELISA and spectrophotometric methods, and the structures of the products were confirmed by ^{1}H NMR spectroscopy. The objective of this study was to demonstrate that glycosyltransferases could be used to synthesize analogs of the structures that they assemble in nature and thereby provide an attractive alternative to laborious total chemical syntheses for the provision of such oligosaccharide analogs. It remains to be determined whether other fucosyltransferases will also utilize the GDP-fucose analogs described here, thereby expanding the scope of the enzyme-assisted synthesis of oligosaccharide analogs. These studies with both fucosyltransferases and *N*-acetylglucosaminyltransferases (21) are currently in progress.

Experimental

General procedures

All solvents and reagents used were reagent grade, and in cases where further purification was required, standard procedures (15) were followed. All solid reactants for glycosylation and for moisture sensitive reactions were dried overnight over phosphorus pentoxide in high vacuum prior to use. Solution transfers where anhydrous conditions were required were done under dry nitrogen or argon using hypodermic syringes. Molecular sieves were purchased from BDH chemicals.

Thin-layer chromatograms (TLC) were performed on precoated silica gel 60-F254 plates (E. Merck, Darmstadt) and visualized by quenching of fluorescence and (or) by charring after spraying with 5% sulfuric acid in ethanol. For "silica gel chromatography" 40–63 μm (400–230 mesh) silica gel 60 (E. Merck No. 9385) and distilled solvents were used, and the ratio of silica gel to compound was in the range 50:1–100:1. Water was evaporated under the vacuum of an oil pump using a rotary evaporator equipped with a condenser containing acetone and Dry Ice. Organic solvents were removed on a rotary evaporator under the vacuum of a water aspirator with bath temperatures of 40°C or lower. For gel filtration, Bio-Gel P-2 (200–400 mesh) (Bio-Rad Laboratories, Richmond, California, U.S.A.) was used. Elemental analyses were performed by the Analytical Service Laboratory of the Chemistry Department. Proton nuclear magnetic resonance (^{1}H NMR) spectra were recorded at either 300 or 360 MHz (Bruker AM-300 or WM-360) with tetramethylsilane (δ 0 in $CDCl_3$) or acetone (δ 2.225 in D_2O) or TSP-d4 (δ 0 in D_2O) or acetonitrile (δ 2.049 in D_2O) as the internal standard at ambient temperature. Carbon-13 nuclear magnetic resonance (^{13}C NMR) spectra were recorded at 75 mHz (Bruker AM-300) with either external tetramethylsilane (δ 0 in $CDCl_3$) or external 1,4-dioxane (δ 67.4 in D_2O) as the reference standard. Phosphorus-31 nuclear magnetic resonance (^{31}P NMR) spectra were recorded at 161.97 MHz (Bruker AM-300) with external H_3PO_4 (85%) (δ 0 in D_2O) as the reference standard. The chemical shifts at lower field, relative to external H_3PO_4, are expressed as positive numbers while those at higher field are expressed as negative numbers. For some compounds, consideration of the water of hydration was necessary in order to obtain a match between the combustion analysis results and the expected elemental composition. Optical rotations were determined on a Perkin–Elmer 241 polarimeter in a 1 dm cell at ambient temperature (23 +/− 1°C). The melting points are uncorrected. High performance liquid chromatography (HPLC) was performed on a Waters Delta Prep 3000 preparative chromatography system.

Chemical synthesis

*Benzyl 2-O-benzoyl-3,4-di-O-isopropylidene-β-L-fucopyranoside (**19**)*

To a clear solution of **17** (16) (5.32 g, 20.9 mmol) in dichloromethane (80 mL) containing *p*-toluenesulfonic acid (50 mg) was added 2,2-dimethoxypropane (7.7 mL, 3 equiv.). The resulting solution was protected from moisture and stirred at 23°C for 6 h. Evaporation of the solvent gave **18** as a brown oil (R_f 0.68, ethyl acetate:hexane:EtOH, 10:10:1), which was dissolved in dichloromethane (15 mL) containing *N*,*N*-dimethylaminopyridine (100 mg). To this solution were then added pyridine (5 mL, 60 mmol) and benzoyl chloride (6.1 mL, 2.5 equiv.). After stirring for 10 h the solvent was evaporated and the residue was partitioned between dichloromethane (40 mL) and water (20 mL). The organic layer was successively washed with saturated $NaHCO_3$ (20 mL), water (20 mL), dried ($MgSO_4$) and evaporated. Purification of the residue by silica gel chromatography (ethyl acetate:hexane, 1:1) gave **19** (R_f 0.50) as a crystalline solid (4.96 g, 60% for two steps); mp 100–103°C; $[\alpha]_D$ −6.2° (*c* 0.28, $CHCl_3$); R_f 0.64 (toluene:ether, 2:1); ^{1}H NMR ($CDCl_3$) δ: 7.120–8.060 (arom, 10H), 5.306 (dd, 1H, $J_{1,2}$ = 8.5 Hz, $J_{2,3}$ = 7.5 Hz, H-2), 4.873 and 4.635 (2 × d, 2H, J_{gem} = 12.0 Hz, $C_6H_5CH_2$), 4.458 (d, 1H, H-1), 4.251 (dd, 1H, $J_{3,4}$ = 5.0 Hz, H-3), 4.058 (dd, 1H, $J_{4,5}$ = 2.0 Hz, H-4), 3.894 (dq, 1H, $J_{5,6}$ = 6.5 Hz, H-5), 1.646 and 1.357 (2 × s, 6H, isopropylidene methyls), 1.498 (d, 3H, H-6); ^{13}C NMR ($CDCl_3$ δ: 110.5 (quaternary carbon of isopropylidene), 28.1, 26.6 (isopropylidene methyls. Anal. calcd. for $C_{23}H_{26}O_6$: C 69.33, H 6.58; found: C 69.27, H 6.77.

*Benzyl 2-O-benzoyl-β-L-fucopyranoside (**20**)*

A solution of **19** (4.96 g, 12.45 mmol) in 60% aqueous AcOH (160 mL) was stirred for 2 h at 60°C. The solvent was evaporated and the residue was coevaporated with toluene (3 × 50 mL) to afford the

Can. J. Chem. Downloaded from www.nrcresearchpress.com by 88.85.125.76 on 09/07/12
For personal use only.

Can. J. Chem. Downloaded from www.nrcresearchpress.com by 88.85.125.76 on 09/07/12
For personal use only.

title compound as a colourless solid (4.34 mg, 97%); mp 151–152°C; $[\alpha]_D$ +64° (*c* 0.2, $CHCl_3$); R_f 0.20 (ethyl acetate:hexane, 1:1); ^1H NMR ($CDCl_3$ D_2O exchanged) δ: 7.12–8.06 (arom, 10H), 5.238 (dd, 1H, $J_{1,2}$ = 8.0 Hz, $J_{2,3}$ = 8.9 Hz, H-2). Anal. calcd. for $C_{20}H_{22}O_6$: C 67.03, H 6.19; found: C 66.47, H 6.18.

Benzyl 2-O-benzoyl-3-O-phenoxythionocarbonyl-β-L-fucopyranoside (21)

To a stirred solution of **20** (1.09 g, 2.98 mmol) in dichloromethane (50 mL) at −78°C were added pyridine (1 mL) and phenoxychlorothionocarbonate (9) (0.48 mL, 1.2 equiv.). Stirring of the reaction mixture at −10°C for 0.5 h resulted in a slow formation of the title compound (R_f 0.6, ethyl acetate:hexane, 1:1) at the expense of the starting material **20** (R_f 0.2). Finally, stirring at 0°C for 0.5 h resulted in a >95% conversion of **20** into the desired compound. The reaction mixture was partitioned between dichloromethane (40 mL) and cold water (20 mL). The organic layer was then dried ($MgSO_4$) and concentrated to a thick brown syrup. For the isolation of the product, a silica column (3 × 20 cm) was prepared in ethyl acetate:hexane (1:1) solvent mixture. The syrup was adsorbed on to the silica column and the material was eluted quickly (silica contact time, 10 min) with the same solvent mixture to provide the product. Evaporation of the appropriate fractions left **21** as a pale brown solid (960 mg, 68%); mp 145–146°C; $[\alpha]_D$ +27.8° (*c* 0.21, dichloromethane), R_f 0.6 (ethyl acetate: hexane, 1:1); ^1H NMR ($CDCl_3$) δ: 8.037–6.854 (arom, 15H), 5.741 (dd, $J_{1,2}$ = 7.5 Hz, $J_{2,3}$ = 10.0 Hz, H-2), 5.646 (dd, $J_{3,4}$ = 3.0 Hz, H-3), 4.911 (d, 1H, J_{gem} = 13.0 Hz, C_6H_5CHH), 4.676 (d, 1H, C_6H_5CHH), 4.657 (d, 1H, H-1), 4.187 (ddd, $J_{4,5}$ = 1.0 Hz, $J_{4,OH}$ = 7.0 Hz, H-4), 3.807 (dq, 1H, H-5), 2.309 (d, 1H, 4-OH), 1.446 (d, 3H, $J_{5,6}$ = 6.5 Hz, H-6). Anal. calcd. for $C_{27}H_{26}O_7S \cdot H_2O$: C 63.30, H 5.51, S 6.26; found: C 64.64, H 5.31, S 6.88.

Benzyl 2-O-benzoyl-3,6-dideoxy-β-L-xylohexopyranoside (22)

Compound **21** (960 mg, 1.94 mmol) was subjected to the radical deoxygenation exactly as described by Robins and Wilson (9). Evaporation of the solvent left a residue, which was dissolved in acetonitrile and extracted with hexane until the smell of tin residues was absent. Evaporation of the acetonitrile afforded a syrup (R_f 0.45, ethyl acetate:hexane, 1:1), which solidified under vacuum. The resulting solid was purified by silica gel chromatography (ethyl acetate:hexane, 2:3) to provide the title compound as colourless needles (340 mg, 51%); mp 128°C; $[\alpha]_D$ +98° (*c* 0.93, dichloromethane); ^1H NMR ($CDCl_3$) δ: 8.10–7.20 (arom, 10H), 5.292 (ddd, 1H, H-2), 4.619 (d, 1H, $J_{1,2}$ = 7.5 Hz), 3.746 (m, 2H, H-4 and H-5), 2.523 (ddd, 1H, J_{gem} = 13.0 Hz, $J_{2,3eq}$ = 5.0 Hz, $J_{3eq,4}$ = 3.0 Hz, H-3eq), 2.269 (d, 1H, $J_{4,OH}$ = 8.0 Hz, HO-4), 1.736 (ddd, $J_{2,3ax}$ = 12.0 Hz, $J_{3ax,4}$ = 3.0 Hz, H-3ax), 1.343 (d, 3H, $J_{5,6}$ = 6.5 Hz, H-6). Anal. calcd. for $C_{20}H_{22}O_5$: C 70.16, H 6.48; found: C 69.74, H 6.33.

Benzyl 4-O-acetyl-2-O-benzoyl-3,6-dideoxy-β-L-xylohexopyranoside (23)

Compound **22** (1.45 g, 4.24 mmol) was dissolved in pyridine (20 mL) and acetic anhydride (10 mL). After 24 h at room temperature, the reaction mixture was poured onto crushed ice and water (50 mL). The resulting sticky solid was taken up in dichloromethane (40 mL). The organic layer was washed with water (20 mL) and saturated $NaHCO_3$ (2 × 30 mL). Drying ($MgSO_4$) and evaporation of the solvent left a syrup, which was purified by silica gel chromatography in ethyl acetate: hexane (1:2) to afford the title compound as a colourless solid (1.3 g, 80%); mp 68°C; $[\alpha]_D$ +89° (*c* 0.36, dichloromethane); ^1H NMR ($CDCl_3$) δ: 7.83–7.18 (arom, 10H), 5.276 (ddd, 1H, H-2), 5.066 (m, 1H, H-4), 4.656 (d, 1H, $J_{1,2}$ = 8.0 Hz, H-1), 3.822 (dq, 1H, $J_{4,5}$ = 1.0 Hz, $J_{5,6}$ = 6.5 Hz, H-5), 2.475 (ddd, 1H, J_{gem} = 13.0 Hz, $J_{2,3eq}$ = 5.0 Hz, $J_{3eq,4}$ = 3.0 Hz, H-3eq), 2.177 (s, 3H, OAc), 1.800 (ddd, $J_{2,3ax}$ = 12.0 Hz, $J_{3ax,4}$ = 3.0 Hz, H-3ax), 1.267 (d, 3H, H-6). Anal. calcd. for $C_{22}H_{24}O_6$: C 68.73, H 6.29; found: C 68.79, H 6.27.

4-O-Acetyl-2-O-benzoyl-3,6-dideoxy-L-xylohexopyranose (24)

Compound **23** (930 mg, 2.42 mmol) was dissolved in ethanol (20 mL) containing Pd/C (5%, 650 mg) and stirred under H_2 (1 atm (= 101.3 kPa), for 24 h. The catalyst was filtered and washed with ethanol (2 × 40 mL). The combined filtrate was evaporated to dryness to afford the syrupy title compound as an α/β (1:1) mixture (710 mg, 98%); $[\alpha]_D$ −1.6° (*c* 1.4, methanol, 24 h); ^1H NMR ($CDCl_3$) δ: 5.519 (dd, $J_{1,2}$ = $J_{1,OH}$ = 3.0 Hz, H-1: α anomer), 4.793 (dd, $J_{1,2}$ = $J_{1,OH}$ = 8.0 Hz, H-1: β anomer). Anal. calcd. for $C_{15}H_{18}O_6 \cdot H_2O$: C 57.69, H 6.46; found: C 57.33, H 5.73.

4-O-Acetyl-2-O-benzoyl-3,6-dideoxy-α-L-xylopyranosyl bromide (25)

Compound **24** (568 mg, 1.9 mmol) was dissolved in dichloromethane (10 mL) containing DMF (2 mL) and the resulting solution was stirred at −10°C. Oxalyl bromide (1.5 equiv.) was then added at the same temperature. Stirring at 23°C for 1 h resulted in near-complete conversion of **24** into the title compound (R_f 0.78, ethyl acetate: hexane, 1:1), along with products of lower mobility, presumably hydrolysis products. This solution was used directly in the preparation of glycosyl phosphate **26** without any work-up.

Tetra-n-butylammonium dibenzyl phosphate (11)

(Procedure for the preparation of 16.2 mmol of **11**)

A suspension of dibenzyl hydrogen phosphate (4.37 g, 15.7 mmol) in water (50 mL) was stirred at room temperature. Tetra-*n*-butylammonium hydroxide (approx. 40% aq. w/w, 8.42 g) was added dropwise to the suspension to obtain a clear solution. At this stage some undissolved solid must remain to indicate that the reaction was not too basic. Filtration through Whatman filter paper gave a clear filtrate (pH 8–9). To this was added dibenzyl hydrogen phosphate in small portions until the pH decreased to 7. The resulting clear solution was lyophilized to afford **11** as a colourless syrup.

L-Fucose-1-phosphate (14)

To a clear solution of fucosyl bromide **8** (freshly prepared (8) from 1.2 g, 3.6 mmol of L-fucose tetraacetate) in dry DMF (3 mL) was added **11** (6 equiv.) in dry DMF (4 mL) to yield a pale yellow solution. After 10 min at 23°C the reaction mixture was partitioned between dichloromethane (30 mL) and cold water (10 mL). The organic layer was washed once more with cold water (10 mL), dried ($MgSO_4$), and evaporated to a syrup. A silica gel column (2.5 × 20 cm) packed in dichloromethane:ethyl acetate (1:1) was prepared and the syrup was placed on top of it. Rapid elution (10 min) using the same solvent afforded a material with R_f 0.80, presumably the intermediate triester (**12**). This material was concentrated to afford a syrup that was not characterized but was stirred in ethanol (40 mL) containing aqueous $NaHCO_3$ (1 N, 10 mL) and Pd/C (5%, 300 mg) under an atmosphere of hydrogen. After 2 h at room temperature, the material with R_f 0.8 (dichloromethane:ethyl acetate, 1:1) and which was UV absorbing had disappeared to give a baseline carbohydrate material. The solids were removed by filtration and the filtrate was concentrated to a syrup, which was partitioned between dichloromethane (20 mL) and water (20 mL). The aqueous layer was separated and aqueous NaOH (1 M, 20 mL) was added. After 0.5 h at 23°C the pH was carefully adjusted to 7 with cold AcOH (1 N). The resulting solution was diluted to about 200 mL with water and slowly adsorbed onto a resin bed of Dowex 2 (2.5 × 10 cm, Cl^-). The column was washed with water (100 mL) and then developed with a linear gradient (8) of LiCl. The mixing chamber contained 250 mL of water and the reservoir contained 250 mL of 0.45 M LiCl. The column was run at 23°C at a flow rate of about 120 mL/h and fractions (4 mL) were collected automatically. The eluate was monitored for the presence of acid-labile phosphate (H_2SO_4 spraying was used for the detection of the *carbohydrate material* and ammonium molybdate spray was used to detect the *phosphate*) (17). The appropriate fractions containing L-fucose-1-phosphates were pooled and lyophilized to provide a white solid. This solid was then transferred to screw-cap centrifuge tubes and shaken (exothermic!) with diethyl ether:95% ethanol, 2:1. Centrifugation of the resulting suspension afforded clear supernatants, which were discarded. The residues were extracted several times with the same solvent system (the presence of

Can. J. Chem. Downloaded from www.nrcresearchpress.com by 88.85.125.76 on 09/07/12
For personal use only.

Cl^- ions in the supernatants could be detected with aqueous $AgNO_3$). After all the LiCl had been extracted by this procedure, residual solids were dried over P_2O_5 and the L-fucose-1-phosphate content was assessed by ^1H NMR using trimethylsilyl propionate as the internal standard (**14**, 1.8 mmol, 50%, eq./ax.ratio = 12.5:1). The ^1H and ^{13}C NMR spectral characteristics of **14** were in accord with those in the literature (8). ^1H NMR (D_2O) δ: 4.830 (dd, $J_{1,2} = J_{1,P} = 8.0$ Hz, H-1), 3.8190 (dq, H-5), 3.759 (dd, $J_{3,4} = 3.5$ Hz, $J_{4,5} = 1.0$ Hz, H-4), 3.700 (dd, $J_{2,3} = 10.0$ Hz, H-3), 3.501 (dd, H-2), 1.253 (d, $J_{5,6} = 6.5$ Hz); ^{31}P NMR (D_2O) δ: −0.86 (s). This dilithium salt was dissolved in water and passed through a bed of Dowex 50-X8 (NEt_3H^+) resin. The water was then evaporated to afford the monotriethyl ammonium salt, which was dried over P_2O_5 prior to its use in the pyrophosphate coupling reaction for the synthesis of GDP-fucose (**5**).

D-Arabinose-1-phosphate (16)

Freshly prepared (18) crystalline 2,3,4-tri-*O*-acetyl-β-D-arabinopyranosyl bromide (**15**, 1.0 g, 2.9 mmol, δ ($CDCl_3$): 6.710 (d, $J_{1,2} = 3.7$ Hz, H-1)) was treated with **11** (6 equiv.) in dry DMF (7 mL). After 10 min at 23°C, all of the bromosugar (R_f 0.7, ethyl acetate:hexane, 1:1) had been converted into slower moving UV-absorbing phosphotriester (R_f 0.30, (major), 0.32 (minor)). The reaction mixture was partitioned between dichloromethane (40 mL) and cold water (20 mL). The organic layer was dried ($MgSO_4$) and evaporated to a syrup, which was purified by rapid elution through a silica gel column (2 × 20 cm, ethyl acetate:hexane, 3:2) to yield a material with R_f 0.30 (ethyl acetate:hexane, 1:1). The sample was then processed as described for the preparation of **14** to provide **16** as the dilithium salt (1.35 mmol, 47%, eq. (α)/ax. (β) = 10.7:1); $[\alpha]_D$ −31.9° (*c* 0.14, H_2O) (lit. (18) −39.1°); ^1H NMR (D_2O) δ: 5.456 (dd, $J_{1,2} = 3.6$ Hz, $J_{1,P} = 7.0$ Hz, H-1: axial (β)anomer), 4.800 (dd, $J_{1,2} = J_{1,P} = 7.5$ Hz, H-1:equatorial (α) anomer), 3.973–3.636 (m, H-3, H-4, H-5s), 3.586 (dd, H2, $J_{2,3} = 9.0$ Hz); ^{13}C NMR (D_2O) δ: 97.69 (d, $J_{C,1P} = 4.2$ Hz, C-1), 72.26 (C-3), 72.01 (d, $J_{C\text{-}2,P} = 5.8$ Hz, C-2), 68.19 (C-4), 66.15 (C-5).

3,6-Dideoxy-L-xylohexopyranose-1-phosphate (3-deoxy-L-fucose phosphate (26)

The bromosugar **25** (from 1.9 mmol of **24**) was treated with **11** (6 equiv.) in dry DMF (10 mL). Stirring at room temperature for 4 h resulted in a reaction mixture that, on TLC examination, showed the presence of a new spot (presumably the phosphotriester, R_f 0.47, ethyl acetate:hexane, 1:1). A spot corresponding to the bromosugar (**25**) still persisted. The reaction was terminated at this stage by partitioning the mixture between dichloromethane (40 mL) and water (20 mL). The organic layer was dried ($MgSO_4$) and evaporated to a syrup, which was purified by rapid passage through a short silica gel column (2 × 20 cm, ethyl acetate:hexane, 13:10). The fractions containing material with R_f 0.47 (ethyl acetate:hexane, 1:1) were pooled and concentrated to a syrup, which was then dissolved in ethanol (40 mL) containing aqueous $NaHCO_3$ (1 N, 20 mL) and Pd/C (5%, 1.2 g). Hydrogenation, saponification, and ion-exchange chromatography (as described for the preparation of **14**) afforded the title compound as the dilithium salt (0.266 mmol, 14%, eq. (α)/ax.(β) ratio = 5.4:1); ^1H NMR (D_2O, β anomer) δ: 4.833 (dd, $J_{1,2} = J_{1,P} = 7.5$ Hz, H-1), 3.863 (dq, $J_{4,5} = 1$ Hz, $J_{5,6} = 6.5$ Hz, H-5), 3.484 (m, H-4), 3.690 (ddd, H-2), 2.190 (ddd, $J_{gem} = 13.0$ Hz, $J_{2,3eq} = 5.0$ Hz, $J_{3eq,4} = 4.0$ Hz, H-3eq), 1.737 (ddd, $J_{2,3ax} = 12.0$ Hz, $J_{3ax,4} = 3.0$ Hz, H-3ax), 1.223 (d, H-6); ^{13}C NMR (D_2O) δ: 100.17 (d, $J_{C\text{-}1,P} = 3.5$ Hz, C-1), 75.23, 69.02 (C-5, C-4), 67.74 (d, $J_{C\text{-}2,P} = 3.5$ Hz, C-2), 37.37 (C-3), 16.53 (C-6); ^{31}P NMR (D_2O) δ: +2.5.

Guanosine 5′-(β-L-fucopyranosyl)-diphosphate (GDP-fucose, 5)

L-Fucose-1-phosphate **14** (triethylammonium salt, 0.89 mmol) and guanosine-5′-monophosphate morpholidate **27** (8) (800 mg, 1.2 equiv.) were combined in dry pyridine (10 mL). The heterogenous reaction was stirred at 23°C for 4 days. Evaporation of the solvent gave a syrup, which was diluted to 200 mL volume with water. It was then slowly passed through Dowex 2-X8 (2.5 × 30 cm, Cl^-). The column was washed with water (300 mL) and then eluted with a linear gradient of LiCl. The mixing vessel contained 1800 mL water. The reservoir contained 1800 mL of 0.8 M LiCl in water. The column was operated at 23°C at a flow rate of 3 mL/min and 15-mL fractions were collected and monitored at 262 nm. GDP-fucose eluted at 0.52 M and these fractions were pooled and concentrated (23°C) to a 5 mL volume and passed through a Bio-Gel P2 column (2 × 60 cm) in 10% EtOH in water. Fractions containing the product were pooled, concentrated to 5 mL, and repassed through the column until chloride ion could no longer be detected in the eluate. Four columns were required. The material obtained after this desalting was dissolved in water (10 mL) and passed through a column of AG-50 (Na^+, 1 × 20 cm). Lyophilization of the resulting solution furnished GDP-fucose as a white fluffy solid (155 mg, 27%); $[\alpha]_D$ −34° (*c* 0.18, H_2O); R_f 0.54 (NH_4OH:*i*PrOH:H_2O, 3:5:2), 0.76 (*i*PrOH:NH_4OAc 0.3 M, 1:1); ^1H NMR (D_2O) δ: 8.125 (s, 1H, H-8 base), 5.950 (d, 1H, $J_{1,2} = 6$ Hz H-1 ribose), 4.928 (dd, 1H, $J_{1,2} = J_{1,P} = 8.0$ Hz, H-1 fucose), 4.80 (H-2 ribose), 4.545 (m, 1H, H-3 ribose), 4.360 (m, 1H, H-4 ribose), 4.220 (m, 2H, H-5 ribose), 3.780 (q, 1H, H-5 fucose), 3.720 (dd, 1H, $J_{4,5} = 1.0$ Hz, H-4 fucose), 3.668 (dd, 1H, $J_{3,4} = 4.0$ Hz, $J_{2,3} = 10.0$ Hz, H-3 fucose), 3.565 (dd, 1H, H-2, fucose), 3.565 (dd, 1H, H-2, fucose), 1.225 (d, $J_{5,6} = 6.5$ Hz, H-6, fucose); ^{13}C NMR (D_2O) δ: 159.85 (C-6 base), 154.8 (C-2 base), 152.69 (C-4 base), 117.13 (C-5 base), 99.23 (d, $J_{C\text{-}1,P} = 5.7$ Hz, C-1 fucose), 57.60 (C-1 ribose), 84.68 (d, $J_{C\text{-}4,P} = 9.1$ Hz, C-4 ribose), 73.32 (C-3 fucose), 74.35, 72.25, 72.00, 71.84 (C-2, C-3, C-4, C-5, fucose; $J_{C\text{-}2,P}$ = approx. 8 Hz, GDP-3-deoxy-fucose), 71.32 (C-3 ribose), 66.18 (d, $J_{C\text{-}5,P} = 5.7$ Hz, C-5 ribose), 16.24 (C-6 fucose); ^{31}P NMR (D_2O) δ: −10.8 (d, $J_{P,P} = 20.8$ Hz, P attached to guanosine), −12.7 (d, P attached to fucose).

Guanosine 5′-(3,6-dideoxy-β-L-xylohexopyranosyl)-diphosphate (GDP-3-deoxy-fucose, 6)

The 3-deoxy-L-fucose-1-phosphate (mono triethylammonium salt, 0.2 mmol) and the phosphinothioc anhydride (8, 19) **28** (tetra-*n*-butylammonium salt, monohydrate, 211 mg, 0.29 mmol) were dried over P_2O_5. Dry pyridine (10 mL) was then added and evaporated *in vacuo*. This process was repeated three times using dry pyridine (10 mL). Dry pyridine (5 mL), followed by dry AgOAc (195 mg, 5.9 equiv.), was then added to the flask and the contents were vigorously stirred at 23°C, protected from light and moisture.

After 20 h at 23°C, H_2O (0.5 mL) was added to hydrolyze any unreacted **28**. After an additional 0.5 h the contents were transferred to screw-capped centrifuge tubes and a slow stream of H_2S was bubbled through the mixture for 5 min to precipate silver sulfide. Centrifugations afforded clear supernatants, which were removed. The residues were extracted with pyridine:water, 1:1. The combined supernatants were evaporated *in vacuo* to a syrup, which was partitioned between water (30 mL) and diethyl ether (30 mL). The aqueous layer was separated, diluted to 100 mL with water, and then adsorbed slowly onto a column of Dowex 1-X2 (2.5 × 15 cm, Cl^-). The column was washed with water (200 mL) and then eluted with a linear gradient of LiCl. The mixing vessel contained 200 mL water. The reservoir contained 200 mL of 0.8 M LiCl in water. The column was operated at 23°C at a rate of 0.5 mL/min. Fractions (4.5 mL) were collected and monitored by UV absorption at 262 nm. The desired nucleotide eluted near the end of the gradient in fractions 75–89 and these were desalted on Bio-Gel P-2 as described for the preparation of **5**. After conversion to the sodium form by passage through AG-50(Na^+) resin (1 × 10 cm), the product was lyophilized to furnish **6** as a white fluffy solid (58.6 mg, 47%); $[\alpha]_D$ −10.0° (*c* 0.12, H_2O); ^1H NMR (D_2O) δ: 8.100 (s, 1H, H-8 base), 5.999 (d, 1H, $J_{1,2} = 6.0$ Hz, H-1 ribose), 4.999 (dd, 1H, $J_{1,2} = J_{1,P} = 8.0$ Hz, H-1 fucose), 4.789 (m, 1H, H-2 ribose), 4.523 (m, 1H, H-3 ribose), 4.336 (m, 1H, H-4 ribose), 4.200 (m, 2H, H-5,5 ribose), 3.819–3.643 (m, 3H, H-2, H-4, H-5, fucose), 2.186 (ddd, 1H, $J_{gem} = 13.0$ Hz, $J_{2,3eq} = 5.0$ Hz, $J_{3eq,4} = 4.0$ Hz, H-3eq fucose), 1.689 (ddd, 1H, $J_{2,3ax} = 12.0$ Hz, $J_{3ax,4} = 3.0$ Hz, H-3ax fucose), 1.166 (d, 3H, $J_{5,6} = 6.5$ Hz, H-6 fucose methyl); ^{13}C NMR (D_2O) δ: 159.80 (C-6 base), 154.76 (C-2 base), 152.66 (C-4 base), 138.52 (C-8 base), 117.13 (C-5 base), 101.19 (d, $^2J_{C\text{-}1,P} = 6.0$ Hz, C-1 fucose), 87.65 (C-1 ribose), 84.64 (d, $J_{C\text{-}4,P} = 9.1$ Hz, C-4 ribose), 75.58 (C-2 ribose),

Can. J. Chem. Downloaded from www.nrcresearchpress.com by 88.85.125.76 on 09/07/12
For personal use only.

74.36 and 68.82 (C-4 and C-5 fucose), 71.29 (C-3 ribose), 66.62 (d, $J_{C\text{-}2,P}$ = 8.3 Hz, C-2 fucose), 66.10 (d, $J_{C\text{-}5,P} \leq 6$ Hz, C-5 ribose), 37.16 (C-3 fucose), 16.45 (C-6 fucose); ^{31}P NMR (D_2O) δ: −10.8 (d, $J_{P,P}$ = 20.9 Hz, P attached to guanosine), −12.7 (d, P attached to fucose).

Guanosine 5′-(α-D-arabinopyranosyl)-diphosphate (GDP-arabinose, 7)

The D-arabinosyl-1-phosphate **16** (triethylammonium salt, 0.83 mmol), **28** (900 mg, 1.5 equiv.), and AgOAc (550 mg, 4 equiv.) were engaged in the pyrophosphate coupling reaction as described for the preparation of **6**. The contents were vigorously stirred at 23°C, protected from moisture.

After 10 h at 23°C, H_2O (0.5 mL) was added to hydrolyze any unreacted **28**. After 0.5 h the contents were transferred to screw-capped centrifuge tubes and a slow stream of H_2S was bubbled (5 min) to precipitate silver sulfide. Centrifugations afforded clear supernatants, which were removed. The residues were extracted with pyridine:water, 1:1. The combined supernatants were evaporated *in vacuo* to a syrup, which was partitioned between water (30 mL) and diethyl ether (30 mL). The aqueous layer was separated, diluted to 100 mL with water, and then adsorbed slowly onto a column of Dowex 1-X2 (2.5 × 30 cm, Cl^-). The column was washed with water (200 mL) and then eluted with a linear gradient of LiCl. The mixing vessel contained 1700 mL water. The reservoir contained 1700 mL of 0.8 M LiCl in water. Fractions (28 mL) were collected at a flow rate of 0.5 mL/min and monitored by UV absorption at 262 nm. The sugar nucleotide eluted at 0.45 M LiCl. The product was desalted, lyophilized, and converted to the sodium form, as described for **6**, to provide **7** as a white solid (145 mg, 28%); $[\alpha]_D$ −39° (*c* 0.6, H_2O); R_f 0.53 (NH_4OH:*i*PrOH: H_2O, 3:5:2), ^{1}H NMR (D_2O) δ: 7.925 (s, 1H, H-8 base), 5.736 (d, 1H, $J_{1,2}$ = 6.0 Hz, H-1 ribose), 4.723 (dd, $J_{1,2} = J_{1,P}$ = 7.5 Hz, H-1 arabinose), 4.583 (m, 1H, H-2 ribose), 4.349 (m, 1H, H-3 ribose), 4.173 (m, 1H, H-4 ribose), 4.033 (m, 1H, H-5, 5′ ribose), 3.790–3.707 (m, 2H), and 3.559–3.419 (m, 3H, H-2, 3, 4, 5, 5′, arabinose); ^{13}C NMR (D_2O) δ: 159.56 (C-6 base), 154.62 (C-2 base), 152.42 (C-4 base), 138.22 (C-8 base), 116.89 (C-5 base), 99.45 (d, $^2J_{C\text{-}1,P}$ = 5.8 Hz, C-1 arabinose), 87.67 (C-1 ribose), 84.46 (d, $^3J_{C\text{-}4,P}$ = 9.2 Hz, C-4 ribose), 74.66 (d, C-2, ribose), 72.69 (C-3 arabinose), 71.17 (d, $^3J_{C\text{-}2,P}$ = 8.2 Hz, C-2 arabinose), 71.17 (C-3 ribose), 68.79 (C-4 arabinose), 67.25 (C-5 arabinose), 66.10 (d, $J_{C\text{-}5,P}$ = 5.6 Hz, C-5 ribose); ^{31}P NMR (D_2O) δ: −10.4 (d, $J_{P,P}$ = 20.8 Hz, P attached to guanosine), −12.3 (d, attached to fucose).

ELISA assays

ELISA assays were carried out in triplicate with minor modifications of a previously described method (6). Microtiter plates coated with synthetic BSA-glycoconjugate of **1** (6) were incubated with 25 μunits of affinity-purified Lewis fucosyltransferase (**5**), and 50 μM GDP-fucose (**5**) or 50 μM analog **6** or **7** in 110 μL of 50 mM sodium cacodylate buffer pH 6.5 containing 5 mM $MnCl_2$. After reaction at ambient temperature for 15 h, solutions were removed from the microtiter plates by aspiration, and the wells washed with 200 μL H_2O and 200 μL phosphate-buffered saline containing 0.05% Tween 20 (PBST) (6). Antibody CF4-C4 (0.78 μg/mL in 100 μL PBST with 1% bovine serum albumin) was added to each well and the plate was kept at ambient temperature for 2 h. This solution was aspirated, the wells were washed, incubated with alkaline phosphatase conjugated IgG, washed, and incubated with *p*-nitrophenyl phosphate solution (6). The formation of *p*-nitrophenoxide was monitored at 405 nm. The absorbance in the control wells containing enzyme without nucleotide donor was 0.10 after 40 min and 0.26 after 80 min. The absorbance in wells containing only nucleotide donor without enzyme was 0.08 after 40 min and 0.18 after 80 min. With both fucosyltransferase and sugar nucleotide the absorbances at 40 min were 1.01 (**5**), 0.38 (**6**), and 0.29 (**7**). For 80-min readings, values of 1.86 (**5**), 0.80 (**6**), and 0.67 (**7**) were obtained.

Spectrophotometric assay for fucosyltransferase activity

Fucosyltransferase activity was estimated spectrophotometrically using a modification (20) of a method described for galactosyltransferase (13). Plastic cuvettes containing 1.4 mM **6** or **7**, 0.9 mM phosphoenolpyruvate, 0.45 mM NADH, 50 mM KCl, 5 mM $MnCl_2$, 50 units of pyruvate kinase, 50 units of lactate dehydrogenase, and 11 milliunits of purified Lewis α(1→4) fucosyltransferase (6) in 0.77 mL sodium cacodylate buffer pH 6.5 were equilibrated to 37°C in a Beckman DU-8 spectrophotometer. Background rates (0.0023 ΔOD/min) were estimated by monitoring the decrease in absorbance at 340 nm. Reaction was initiated by the addition of 590 μg **1** in 100 μL water, and the initial rate of GDP formation estimated using a millimolar extinction of 6.2 mM^{-1} cm^{-1} for NADH absorbance. After 8 h reaction at 37°C, an additional 750 μg of **6** or **7** was added to the mixtures. After 30 h reaction, samples were diluted to 10 mL with water and applied to reverse-phase C-18 cartridges, which were washed with 30 mL water. Products **3** and **4** were eluted in 15 mL methanol, evaporated to dryness, redissolved in water (5 mL), filtered through 0.22 μm Millex-GV filters, and lyophilized. The relative intensities of the characteristic ^{1}H NMR signals for unreacted **1** and the products **3** and **4** showed the extent of trisaccharide formation to be 30 and 65%, respectively. These yields are in good agreement with those extrapolated from the relative initial rates estimated spectrophotometrically (Table 1). The products were not isolated but the following ^{1}H NMR parameters could be determined on the mixtures. Trisaccharide **3**: δ 4.955 (d, H-1″, $J_{1'',2''}$ = 3.5 Hz), 4.79 (obscured by DO*H*, H-5″), 4.523 and 4.508 (each d, *J* = 7.8 Hz, H-1 and H-1′), 3.687 (OCH_3), 2.391 (CH_2COO), 2.034 ($COCH_3$), and 1.120 (d, *J* = 6.5 Hz, H-6″). Trisaccharide **4**: δ 5.078 (d, H-1″, $J_{1'',2''}$ = 2.9 Hz), 4.736 (d, $J_{5''a,5''e}$ = 12.5 Hz, H-5″a), 4.513 and 4.508 (each d, *J* = 7.5 Hz, H-1 and H-1′), 3.687(OCH_3), 2.389 (CH_2COO), and 2.033 (COCH3). Compound **5** was assayed similarly with 3 milliunits of fucosyltransferase, in a total volume of 1.2 mL. In this case, reaction was complete after 12 h at 37°C, as judged by ^{1}H NMR. The initial rates listed in Table 1 are corrected to account for the difference in fucosyltransferase concentration and volume.

Acknowledgements

The authors gratefully acknowledge the ongoing support of the Natural Sciences and Engineering Research Council of Canada through both operating and strategic grants.

1. E. J. Toone, E. S. Simon, M. D. Bednarski, and G. M. Whitesides. Tetrahedron, **45**, 5365 (1989).
2. J. C. Paulson and K. J. Colley. J. Biol. Chem. **264**, 17615 (1989).
3. R. U. Lemieux. Chem. Soc. Rev. **18**, 347 (1989).
4. J. Kihlberg, S. J. Hultgren, S. Normark, and G. Magnusson. J. Am. Chem. Soc. **111**, 6364 (1989).
5. M. M. Palcic, A. P. Venot, R. M. Ratcliffe, and O. Hindsgaul. Carbohydr. Res. **190**, 1 (1989).
6. M. M. Palcic, R. M. Ratcliffe, L. R. Lamontagne, A. H. Good, G. Alton, and O. Hindsgaul. Carbohydr. Res. **196**, 133 (1990).
7. R. U. Lemieux, O. Hindsgaul, P. Bird, S. Narasimhan, and W. W. Young, Jr. Carbohydr. Res. **178**, 293 (1988).
8. H. A. Nunez, J. V. O'Conner, P. R. Rosevear, and R. Barker. Can. J. Chem. **59**, 2086 (1981).
9. M. J. Robins and J. S. Wilson. J. Am. Chem. Soc. **103**, 932 (1981).
10. L. D. Liu and H. W. Liu. Tetrahedron Lett. **30**, 35 (1989).
11. R. U. Lemieux, D. R. Bundle, and D. A. Baker. J. Am. Chem. Soc. **97**, 4076 (1975).
12. M. Basu, T. De, K. K. Das, J. W. Kyle, H. -C. Chon, R. J. Schaeper, and S. Basu. Methods Enzymol. **138**, 575 (1987).
13. D. K. Fitzgerald, B. Colvin, R. Mawal, and K. E. Ebner. Anal. Biochem. **36**, 43 (1970).
14. R. U. Lemieux, K. Bock, L. T. J. Delbaere, S. Koto, and V. S. Rao. Can. J. Chem. **58**, 631 (1980).
15. D. D. Perrin, W. L. Armarego, and D. R. Perrin. Purification

of laboratory compounds. 2nd ed. Pergamon Press, London. 1980.
16. H. M. FLOWERS, A. LEVY, and N. SHARON. Carbohydr. Res. **4**, 189 (1967).
17. F. SEELA and S. WALDEK. Nucleic Acids Res. **2**, 2343 (1975).
18. R. W. WRIGHT and H. G. KHORANA. J. Am. Chem. Soc. **80**, 1994 (1958).
19. K. FURUSAWA, M. SEKINE, and T. HATA. J. Chem. Soc. Perkin Trans. 1, 1711 (1976).
20. M. M. PALCIC, L. D. HEERZE, M. PIERCE, and O. HINDSGAUL. Glycoconjugate J. **5**, 49 (1988).
21. G. SINGH, G. ALTON, and O. HINDSGAUL. Carbohydr. Res. In press.

Can. J. Chem. Downloaded from www.nrcresearchpress.com by 88.85.125.76 on 09/07/12
For personal use only.

A novel method of inversion for a class of matrices: application to calculation of two-component plasma viscosities in a magnetic field

BYUNG CHAN EU[1]

Department of Chemistry, McGill University, 801 Sherbrooke Street West, Montreal, P.Q., Canada H3A 2K6

Received October 24, 1989

This paper is dedicated to Professor Arthur S. Perlin on the occasion of his 67th birthday

BYUNG CHAN EU. Can. J. Chem. **68**, 1072 (1990).

To calculate transport coefficients for a plasma in a magnetic field in a linear approximation it is necessary to invert matrices of fairly high dimensions. In this paper we present a novel method of inverting matrices involved in such problems. The method requires a solution of an inhomogeneous matrix integral equation in the Neumann series and a resummation of the series obtained. It involves inversions of lower order matrices, which can be achieved easily. We then apply the method to calculate viscosities of a two-component plasma subject to a homogeneous magnetic field. The structure of the viscosity matrix (tensor) calculated thereby is shown to be the same as that of a neutral system with an axial symmetry; namely, it can be decomposed into a scalar, a 2×2 matrix, and a 3×3 matrix. The method developed here can be applied to calculate other transport coefficients of the two-component plasma.

Key words: mathematical method, viscosity, plasmas, transport coefficients, kinetic theory.

BYUNG CHAN EU. Can. J. Chem. **68**, 1072 (1990).

Lorsqu'on veut calculer les coefficients de transport d'un plasma dans un champ magnétique à l'aide d'une approximation linéaire, il est nécessaire d'inverser des matrices de dimensions hautes. Dans ce travail, on présente une nouvelle méthode pour inverser les matrices impliquées dans des tels problèmes. La méthode fait appel à une solution d'une équation intégrale matricielle inhomogène à l'aide de séries de Neumann et à une resommation des séries obtenues. Elle implique des inversions de matrices d'ordres moins élevés que l'on peut réaliser facilement. On a alors appliqué la méthode pour calculer les viscosités d'un plasma à deux composantes soumis à un champ magnétique homogène. On a démontré que la structure de la matrice de viscosité (tenseur) calculée ainsi est la même que celle d'un système neutre possédant une symétrie axiale, à savoir que l'on peut la décomposer en une matrice scalaire, une matrice 2×2 et une matrice 3×3. La méthode que l'on a développée ici peut être appliquée pour le calcul d'autres coefficients de transport de plasmas à deux composantes.

Mots clés : méthode mathématique, viscosité, plasmas, coefficients de transport, théorie cinétique.

[Traduit par la revue]

I. Introduction

Transport processes in plasmas subject to an external magnetic field are of considerable interest technologically (1–3) and also from the basic kinetic theory viewpoint (4–6) since they provide a good model for theoretical studies in kinetic theory and irreversible thermodynamics. The theoretical result presented in this article is an outcome of our efforts to develop kinetic theory methods (6) to handle dilute plasmas subject to steep thermodynamic gradients or a strong external magnetic field; these kinds of conditions call for special techniques that the conventional Chapman–Enskog method of solution for the Boltzmann equation fails to provide. The constitutive equations taken for shear stresses in this article are derived from the Boltzmann equation for a two-component plasma by using the modified moment method (7). This is a method that is proven to be applicable in the regime where the Chapman–Enskog method is inadequate.

If a fluid is a plasma or a paramagnetic substance that interacts with an external magnetic field, then the system is no longer isotropic and as a consequence the viscosity is not scalar. If the system has an axial symmetry around the external magnetic field, there are five independent phenomenological coefficients (8), i.e., viscosities. To demonstrate this feature, we will assume a two-component plasma subject to a homogeneous magnetic field applied in a direction, say, the x direction of the Cartesian coordinate system. These assumptions simplify the analysis. We would like to find such viscosities in terms of molecular parameters and the magnetic field strength. To that end we need to solve 12 coupled algebraic equations for shear stresses; these equations are in principle possible to solve, but their solutions are very cumbersome to obtain unless a numerical method is used. The aim of this paper is twofold: We would like to present a method to handle the aforementioned problem with much reduced algebraic labor, and then apply the method to calculate the viscosity formulas for a two-component plasma in terms of inverses of one-, two-, and three-dimensional matrices. The viscosity matrix thus calculated has the same structure as for a single component anisotropic system. The method used here can be applied to other problems involving a class of matrices similar to the one appearing in the present problem.

The present paper is organized as follows: In Sect. II constitutive equations are presented for shear stresses under the assumption that there is no heat flow in the system. The constitutive equations naturally define the problem in question, since it is now necessary to invert the relation between the shear stresses and the shear rate tensors. In Sect. III the matrix inversion method is developed to solve the problem and in Sect. IV various shear viscosities are given in terms of inverse matrices of one-, two-, and three-dimensional matrices.

II. Constitutive equations for shear stresses

It is convenient to define various symbols appearing in the constitutive equations before the latter are presented. The vector potential $\boldsymbol{A}$ of magnetic field $\boldsymbol{B}$ is defined by the relation

$$[1] \qquad \boldsymbol{B} = \nabla \times \boldsymbol{A}$$

We will find it convenient to work with an antisymmetric tensor $\vec{\omega}_A$ associated with the vector potential $\boldsymbol{A}$

[1]Also at the Department of Physics, McGill University.

Can. J. Chem. Downloaded from www.nrcresearchpress.com by 88.85.125.76 on 09/07/12
For personal use only.

[2] $\overleftrightarrow{\omega}_A = \nabla A - (\nabla A)^t$

and the commutator of $\overleftrightarrow{\omega}_A$ with the traceless symmetric stress tensor $\overleftrightarrow{\Pi}$:

[3] $[\overleftrightarrow{\Pi},\overleftrightarrow{\omega}_A] = \overleftrightarrow{\Pi}\cdot\overleftrightarrow{\omega}_A - \overleftrightarrow{\omega}_A\cdot\overleftrightarrow{\Pi}$

These tensors generally have six components, which will be assigned a numerical subscript in the following manner:

$$a \equiv (1,2,3,4,5,6) \Leftrightarrow b \equiv (xx,yy,zz,yz,zx,xy)$$

Thus, for example, component xx is assigned subscript 1, component yz is assigned subscript 4, etc. Under this convention we denote various tensor components by the symbols below:

[4] $$\Pi_a^{(i)} = \Pi_{ib} \qquad (a = 1,2,3;\ b = xx,yy,zz \text{ or } 1,2,3)$$
$$\Pi_a^{(i)} = 2\Pi_{ib} \qquad (a = 4,5,6;\ b = yz,zx,xy \text{ or } 4,5,6)$$

For example,

$$\Pi_1^{(i)} = \Pi_{ixx}, \qquad \Pi_4^{(i)} = 2\Pi_{iyz}, \text{ etc.}$$

where index i refers to the species. In the case of a two-component plasma the index i runs over 1 and 2. The same subscript convention holds for the antisymmetric tensor $\overleftrightarrow{\omega}_A$ and the rate-of-strain (shear rate) tensor $\overleftrightarrow{\gamma} = -[\nabla u + (\nabla u)^t]/2 + \overleftrightarrow{U}\nabla\cdot u/3$ where u is the fluid velocity and $\overleftrightarrow{U}$ is the unit second rank tensor. We also define the following symbols:

[5] $$\Omega_a^{(i)} = (Z_i/2cp_ik_BT)g\omega_{Ab} \qquad (a = 4,5,6;\ b = yz,zx,xy \text{ or } 4,5,6)$$

[6] $$g = (m_r/2k_BT)^{1/2}/n^2d^2$$

where $Z_i = e_i/m_i$, e_i = charge on species i, m_r = reduced mass, n = number density, d = mean size parameter of the particles, c = speed of light, p_i = pressure of component i, T = temperature, and k_B = Boltzmann constant. The factor $Z_i\omega_{Ab}/c$ appearing in $\Omega_a^{(i)}$ is the cyclotron (Larmor) frequency of charged particle i precessing around the external magnetic field.

The constitutive equations for stress tensor $\overleftrightarrow{\Pi}_i$ can be shown to be given by the equation (7b)

[7] $$-2p_i\overleftrightarrow{\gamma} + [\overleftrightarrow{\Pi}_i,\overleftrightarrow{\omega}_A]Z_i/c - (2p_ik_BT/g)\sum_{j=1}^{2}\theta R_{ij}\overleftrightarrow{\Pi}_j = 0, \qquad (i = 1,2)$$

where θ is a parameter defined such that

$$\theta = \begin{cases} 1 \text{ for diagonal components of tensor } \overleftrightarrow{\Pi}_i \\ 2 \text{ for off-diagonal components of tensor } \overleftrightarrow{\Pi}_i \end{cases}$$

This parameter may be absorbed into R_{ij}, but it is made explicit in deference to the kinetic theory result from which eq. [7] is derived. The coefficients R_{ij} may be given in terms of bracket integrals in the Boltzmann kinetic theory, but in this paper will be regarded as phenomenological coefficients since their statistical representation is not our concern here. By using the subscript convention, eq. [4], adopted in this paper we can cast eq. [7] in matrix form

[8] $$\mathcal{M}\Pi = -(g/k_BT)\gamma$$

where

[9a] $$\Pi = (\Pi_1^{(1)},\ldots,\Pi_6^{(1)},\Pi_1^{(2)},\ldots,\Pi_6^{(2)}) \equiv (\Pi^{(1)},\Pi^{(2)})$$

[9b] $$\gamma = (\gamma_1,\ldots,\gamma_6,\gamma_1,\ldots,\gamma_6) \equiv (\hat{\gamma},\hat{\gamma})$$

[10] $$\mathcal{M} = \begin{bmatrix} \boldsymbol{M}^{(11)} & \boldsymbol{M}^{(12)} \\ \boldsymbol{M}^{(21)} & \boldsymbol{M}^{(22)} \end{bmatrix}$$

[11] $$\boldsymbol{M}^{(ij)} = \begin{bmatrix} R_{ij} & 0 & 0 & 0 & -\delta_{ij}\Omega_5^{(j)} & \delta_{ij}\Omega_6^{(j)} \\ 0 & R_{ij} & 0 & \delta_{ij}\Omega_4^{(j)} & 0 & -\delta_{ij}\Omega_6^{(j)} \\ 0 & 0 & R_{ij} & -\delta_{ij}\Omega_4^{(j)} & \delta_{ij}\Omega_5^{(j)} & 0 \\ 0 & -\delta_{ij}\Omega_4^{(j)} & \delta_{ij}\Omega_4^{(j)} & R_{ij} & -\tfrac{1}{2}\delta_{ij}\Omega_6^{(j)} & \tfrac{1}{2}\delta_{ij}\Omega_5^{(j)} \\ \delta_{ij}\Omega_5^{(j)} & 0 & -\delta_{ij}\Omega_5^{(j)} & \tfrac{1}{2}\delta_{ij}\Omega_6^{(j)} & R_{ij} & -\tfrac{1}{2}\delta_{ij}\Omega_4^{(j)} \\ -\delta_{ij}\Omega_6^{(j)} & \delta_{ij}\Omega_6^{(j)} & 0 & -\tfrac{1}{2}\delta_{ij}\Omega_5^{(j)} & \tfrac{1}{2}\delta_{ij}\Omega_4^{(j)} & R_{ij} \end{bmatrix}$$

with $i,j = 1,2$. Here δ_{ij} are Kronecker's deltas. Since $\Omega_a^{(j)}$ all vanish except for $\Omega_4^{(j)}$ in the case of a magnetic field parallel to the x axis, we in fact obtain $\boldsymbol{M}^{(ij)}$ in the form

[12] $$\boldsymbol{M}^{(ij)} = \begin{bmatrix} R_{ij} & 0 & 0 & 0 & 0 & 0 \\ 0 & R_{ij} & 0 & \delta_{ij}\Omega_4^{(j)} & 0 & 0 \\ 0 & 0 & R_{ij} & -\delta_{ij}\Omega_4^{(j)} & 0 & 0 \\ 0 & -\delta_{ij}\Omega_4^{(j)} & \delta_{ij}\Omega_4^{(j)} & R_{ij} & 0 & 0 \\ 0 & 0 & 0 & 0 & R_{ij} & -\tfrac{1}{2}\delta_{ij}\Omega_4^{(j)} \\ 0 & 0 & 0 & 0 & \tfrac{1}{2}\delta_{ij}\Omega_4^{(j)} & R_{ij} \end{bmatrix}$$

The phenomenological matrix $\boldsymbol{R}$ is symmetric: $R_{ij} = R_{ji}$ in accordance with the Onsager reciprocity relation (8). Therefore, $\boldsymbol{M}^{(ij)}$ is symmetric in the following sense:

[13] $$\boldsymbol{M}^{(ij)}(\overleftrightarrow{\omega}_A) = \boldsymbol{M}^{(ji)}(-\overleftrightarrow{\omega}_A)$$

in accordance with the Onsager reciprocal theorem (8) for the case of an external magnetic field.

Inverting matrix $\mathcal{M}$, we obtain from eq. [8] the equation for Π

Can. J. Chem. Downloaded from www.nrcresearchpress.com by 88.85.125.76 on 09/07/12
For personal use only.

[14] $\Pi = -2\eta\gamma$

which defines the viscosity tensor

[15] $\eta = (g/2k_BT)\mathcal{M}^{-1}$

Our aim here is to find $\mathcal{M}^{-1}$ in terms of R_{ij} and $\Omega_a^{(i)}$. Note that the matrix $\mathcal{M}$ is 12×12. Before discussing the inversion of $\mathcal{M}$ it is useful to note that

[16] $$M^{(ii)-1} = \beta\begin{bmatrix} \bar{\eta}_1^{(i)} & 0 & 0 & 0 & 0 & 0 \\ 0 & \bar{\eta}_2^{(i)} & (\bar{\eta}_1^{(i)} - \bar{\eta}_2^{(i)}) & -\bar{\eta}_4^{(i)} & 0 & 0 \\ 0 & -(\bar{\eta}_1^{(i)} - \bar{\eta}_2^{(i)}) & \bar{\eta}_2^{(i)} & \bar{\eta}_4^{(i)} & 0 & 0 \\ 0 & \bar{\eta}_4^{(i)} & -\bar{\eta}_4^{(i)} & (2\bar{\eta}_2^{(i)} - \bar{\eta}_1^{(i)}) & 0 & 0 \\ 0 & 0 & 0 & 0 & \bar{\eta}_3^{(i)} & \bar{\eta}_5^{(i)} \\ 0 & 0 & 0 & 0 & -\bar{\eta}_5^{(i)} & \bar{\eta}_3^{(i)} \end{bmatrix}$$

where

$$\beta = (2k_BT/g)$$

[17] $\tau_i = (g/2p_ik_BT)R_{ii}^{-1}$

[18] $\Omega_i = \Omega_4^{(i)}(2p_ik_BT/g) = (Z_i/c)\omega_{Ayz} = (Z_i/c)B_x$

[19] $\bar{\eta}_1^{(i)} = p_i\tau_i$

[20] $\bar{\eta}_2^{(i)} = p_i\tau_i[1 + (\tau_i\Omega_i)^2]/[1 + 2(\tau_i\Omega_i)^2]$

[21] $\bar{\eta}_3^{(i)} = p_i\tau_i/[1 + \frac{1}{4}(\tau_i\Omega_i)^2]$

[22] $\bar{\eta}_4^{(i)} = p_i\tau_i\tau_i\Omega_i/[1 + 2(\tau_i\Omega_i)^2]$

[23] $\bar{\eta}_5^{(i)} = \frac{1}{2}p_i\tau_i\tau_i\Omega_i/[1 + \frac{1}{4}(\tau_i\Omega_i)^2]$

These formulas eventually give the magnetic field dependence for viscosities; in fact, there are five viscosities in the case of a system consisting of species i only. Note that in the limit of $\tau_i\Omega_i \to 0$, that is, as the magnetic field vanishes, the inverse matrix $M^{(ii)-1}$ tends to a diagonal matrix and

[24] $\bar{\eta}_1^{(i)} = \bar{\eta}_2^{(i)} = \bar{\eta}_3^{(i)}, \quad \bar{\eta}_4^{(i)} = \bar{\eta}_5^{(i)} = 0$

In this limit we obtain a diagonal viscosity tensor

[25] $$\eta = \begin{bmatrix} p_1\tau_1\boldsymbol{I} & \mathbf{0} \\ \mathbf{0} & p_2\tau_2\boldsymbol{I} \end{bmatrix} \qquad (\boldsymbol{I} = \text{unit matrix})$$

if the off-diagonal matrices $M^{(12)}$ and $M^{(21)}$ are neglected. This neglect of the off-diagonal matrices is equivalent to the assumption that the transport processes of the two components are not coupled with each other. It must be emphasized that this assumption is not made in this work except for the approximate equation [40] below.

III. A novel method for inverting $\mathcal{M}$

Although it is in principle possible to invert the matrix $\mathcal{M}$, which is 12×12, it is rather cumbersome in practice to invert it without resorting to a numerical method. We present a new method of inverting a class of matrices to which the matrix $\mathcal{M}$ belongs. This method requires inversions of 6×6 block-diagonal matrices, which are much simpler than the inversion of a 12×12 matrix, and it eventually reduces the problem to inversions of two- and three-dimensional matrices. To illustrate the method we write

[26] $\mathcal{M} = \mathcal{M}_0 + \mathcal{M}_1$

where

$$\mathcal{M}_0 = \begin{bmatrix} M^{(11)} & \mathbf{0} \\ \mathbf{0} & M^{(22)} \end{bmatrix}$$

[27]

$$\mathcal{M}_1 = R_{12}\begin{bmatrix} \mathbf{0} & \mathbf{I} \\ \mathbf{I} & \mathbf{0} \end{bmatrix}$$

$\boldsymbol{I}$ being the unit matrix of dimension 6. Note that R_{12} plays the role of coupling constant in this problem. Then the inverse $\mathcal{M}^{-1}$ of the matrix $\mathcal{M}$ may be formally written in the form

[28] $\mathcal{M}^{-1} = \mathcal{M}_0^{-1} - \mathcal{M}_0^{-1}\mathcal{M}_1\mathcal{M}^{-1}$

This is easy to obtain by using the matrix identity

$$\boldsymbol{A}^{-1} - \boldsymbol{B}^{-1} = -\boldsymbol{B}^{-1}(\boldsymbol{A} - \boldsymbol{B})\boldsymbol{A}^{-1}$$

Written in the form of eq. [28], the inverse $\mathcal{M}^{-1}$ obeys a linear integral equation similar to the Lippmann–Schwinger equation in quantum scattering theory (9), and the latter may be solved by iteration. The result of iteration is the Neumann series

[29] $$\mathcal{M}^{-1} = \mathcal{M}_0^{-1} - \mathcal{M}_0^{-1}\mathcal{M}_1\mathcal{M}_0^{-1} + \mathcal{M}_0^{-1}\mathcal{M}_1\mathcal{M}_0^{-1}\mathcal{M}_1\mathcal{M}_0^{-1} - \ldots$$

This series converges provided that $\|\mathcal{M}_0^{-1}\mathcal{M}_1\| < 1$, and thus is exact. However, it is not very useful for computing $\mathcal{M}^{-1}$ in its present form. Fortunately, this Neumann series is amenable to a block-by-block resummation, and since such resummations involve only lower order matrices as will be shown, the labor of inversion is very much reduced, making it possible to obtain the matrix elements easily.

Since

$$\mathcal{M}_0^{-1} = \begin{bmatrix} M^{(11)-1} & \mathbf{0} \\ \mathbf{0} & M^{(22)-1} \end{bmatrix}$$

and

$$\mathcal{M}_0^{-1}\mathcal{M}_1\mathcal{M}_0^{-1} = R_{12}\begin{bmatrix} \mathbf{0} & M^{(11)-1}M^{(22)-1} \\ M^{(22)-1}M^{(11)-1} & \mathbf{0} \end{bmatrix}$$

$$\mathcal{M}_0^{-1}\mathcal{M}_1\mathcal{M}_0^{-1}\mathcal{M}_1\mathcal{M}_0^{-1} = R_{12}^2\begin{bmatrix} M^{(11)-1}M^{(22)-1}M^{(11)-1} & \mathbf{0} \\ \mathbf{0} & M^{(22)-1}M^{(11)-1}M^{(22)-1} \end{bmatrix}$$

Can. J. Chem. Downloaded from www.nrcresearchpress.com by 88.85.125.76 on 09/07/12
For personal use only.

etc., so that, if we put $\boldsymbol{L} \equiv \boldsymbol{M}^{(11)-1}$ and $\boldsymbol{L}' \equiv \boldsymbol{M}^{(22)-1}$, we obtain

$$\boldsymbol{\mathcal{M}}^{-1} = \begin{bmatrix} \boldsymbol{L}(1 + R_{12}^2\boldsymbol{L}'\boldsymbol{L} + R_{12}^4\boldsymbol{L}'\boldsymbol{L}\boldsymbol{L}'\boldsymbol{L} + \ldots) & -R_{12}\boldsymbol{L}\boldsymbol{L}'(1 + R_{12}^2\boldsymbol{L}\boldsymbol{L}' + \ldots) \\ -R_{12}\boldsymbol{L}'\boldsymbol{L}(1 + R_{12}^2\boldsymbol{L}'\boldsymbol{L} + \ldots) & \boldsymbol{L}'(1 + R_{12}^2\boldsymbol{L}\boldsymbol{L}' + R_{12}^4\boldsymbol{L}\boldsymbol{L}'\boldsymbol{L}\boldsymbol{L}' + \ldots) \end{bmatrix}$$

Therefore the iterative series for $\boldsymbol{\mathcal{M}}^{-1}$ may be resummed block by block to yield the following form:

[30] $$\boldsymbol{\mathcal{M}}^{-1} = \begin{bmatrix} \boldsymbol{W}_{11} & \boldsymbol{W}_{12} \\ \boldsymbol{W}_{21} & \boldsymbol{W}_{22} \end{bmatrix}$$

where the submatrices are given by

[31]
$$\begin{aligned} \boldsymbol{W}_{11} &= \boldsymbol{M}^{(11)-1}[1 - R_{12}^2(\boldsymbol{M}^{(11)}\boldsymbol{M}^{(22)})^{-1}]^{-1} \\ \boldsymbol{W}_{22} &= \boldsymbol{M}^{(22)-1}[1 - R_{12}^2(\boldsymbol{M}^{(22)}\boldsymbol{M}^{(11)})^{-1}]^{-1} \\ \boldsymbol{W}_{12} &= -R_{12}(\boldsymbol{M}^{(22)}\boldsymbol{M}^{(11)})^{-1}[1 - R_{12}^2(\boldsymbol{M}^{(22)}\boldsymbol{M}^{(11)})^{-1}]^{-1} \\ \boldsymbol{W}_{21} &= -R_{12}(\boldsymbol{M}^{(11)}\boldsymbol{M}^{(22)})^{-1}[1 - R_{12}^2(\boldsymbol{M}^{(11)}\boldsymbol{M}^{(22)})^{-1}]^{-1} \end{aligned}$$

Equations [30] and [31] represent the result of the inversion method we set out to describe. This result holds for the class of matrices given in eq. [27]. It is important to recognize that although eq. [29] is basically a perturbation series the final results presented in eqs. [30] and [31] above are not, since the perturbation series in eq. [30] has been resummed block by block. The matrices in eq. [31] are exact.

IV. Viscosities of a binary plasma in a magnetic field

As is clear from eq. [31], since each submatrix in eq. [30] is 6×6 and the inverses of $\boldsymbol{M}^{(11)}$ and $\boldsymbol{M}^{(22)}$ are block-diagonal, it is rather simple to compute explicitly the elements of the inverse matrix $\boldsymbol{\mathcal{M}}^{-1}$. If we write $\boldsymbol{M}^{(ii)-1}$ in the form

[32] $$\boldsymbol{M}^{(ii)-1} = \beta \begin{bmatrix} \boldsymbol{V}_{1i} & \boldsymbol{0} & \boldsymbol{0} \\ \boldsymbol{0} & \boldsymbol{V}_{2i} & \boldsymbol{0} \\ \boldsymbol{0} & \boldsymbol{0} & \boldsymbol{V}_{3i} \end{bmatrix}$$

where

[33a] $$\boldsymbol{V}_{1i} = \bar{\eta}_1^{(i)}$$

[33b] $$\boldsymbol{V}_{2i} = \begin{bmatrix} \bar{\eta}_2^{(i)} & (\bar{\eta}_1^{(i)} - \bar{\eta}_2^{(i)}) & -\bar{\eta}_4^{(i)} \\ -(\bar{\eta}_1^{(i)} - \bar{\eta}_2^{(i)}) & \bar{\eta}_2^{(i)} & \bar{\eta}_4^{(i)} \\ \bar{\eta}_4^{(i)} & -\bar{\eta}_4^{(i)} & (2\bar{\eta}_2^{(i)} - \bar{\eta}_1^{(i)}) \end{bmatrix}$$

[33c] $$\boldsymbol{V}_{3i} = \begin{bmatrix} \bar{\eta}_3^{(i)} & \bar{\eta}_5^{(i)} \\ -\bar{\eta}_5^{(i)} & \bar{\eta}_3^{(i)} \end{bmatrix}$$

then with the definition

$$\alpha = (2R_{12}k_BT/g)^2$$

the submatrices $\boldsymbol{W}_{ij}$ $(i,j = 1,2)$ can be written as

[34a] $$\begin{aligned} \boldsymbol{W}_{11} &= \beta \begin{bmatrix} \boldsymbol{V}_{11}(1-\alpha\boldsymbol{V}_{12}\boldsymbol{V}_{11})^{-1} & \boldsymbol{0} & \boldsymbol{0} \\ \boldsymbol{0} & \boldsymbol{V}_{21}(1-\alpha\boldsymbol{V}_{22}\boldsymbol{V}_{21})^{-1} & \boldsymbol{0} \\ \boldsymbol{0} & \boldsymbol{0} & \boldsymbol{V}_{31}(1-\alpha\boldsymbol{V}_{32}\boldsymbol{V}_{31})^{-1} \end{bmatrix} \\ &\equiv \beta\boldsymbol{H}_1 \end{aligned}$$

[34b] $$\begin{aligned} \boldsymbol{W}_{22} &= \beta \begin{bmatrix} \boldsymbol{V}_{12}(1-\alpha\boldsymbol{V}_{11}\boldsymbol{V}_{12})^{-1} & \boldsymbol{0} & \boldsymbol{0} \\ \boldsymbol{0} & \boldsymbol{V}_{22}(1-\alpha\boldsymbol{V}_{21}\boldsymbol{V}_{22})^{-1} & \boldsymbol{0} \\ \boldsymbol{0} & \boldsymbol{0} & \boldsymbol{V}_{32}(1-\alpha\boldsymbol{V}_{31}\boldsymbol{V}_{32})^{-1} \end{bmatrix} \\ &\equiv \beta\boldsymbol{H}_2 \end{aligned}$$

[34c] $$\begin{aligned} \boldsymbol{W}_{12} &= (\alpha/R_{12}) \begin{bmatrix} \boldsymbol{V}_{11}\boldsymbol{V}_{12}(1-\alpha\boldsymbol{V}_{11}\boldsymbol{V}_{12})^{-1} & \boldsymbol{0} & \boldsymbol{0} \\ \boldsymbol{0} & \boldsymbol{V}_{21}\boldsymbol{V}_{22}(1-\alpha\boldsymbol{V}_{21}\boldsymbol{V}_{22})^{-1} & \boldsymbol{0} \\ \boldsymbol{0} & \boldsymbol{0} & \boldsymbol{V}_{31}\boldsymbol{V}_{32}(1-\alpha\boldsymbol{V}_{31}\boldsymbol{V}_{32})^{-1} \end{bmatrix} \\ &\equiv (\alpha/R_{12})\boldsymbol{H}_3 \end{aligned}$$

Can. J. Chem. Downloaded from www.nrcresearchpress.com by 88.85.125.76 on 09/07/12
For personal use only.

$$[34d]\quad \boldsymbol{W_{21}} = (\alpha/R_{12})\begin{bmatrix} V_{12}V_{11}(1-\alpha V_{12}V_{11})^{-1} & 0 & 0 \\ 0 & V_{22}V_{21}(1-\alpha V_{22}V_{21})^{-1} & 0 \\ 0 & 0 & V_{32}V_{31}(1-\alpha V_{32}V_{31})^{-1} \end{bmatrix} \equiv (\alpha/R_{12})\boldsymbol{H_4}$$

Here the first elements on the diagonals are one-dimensional, the second are three-dimensional, and the third are two-dimensional. Therefore the matrix $\boldsymbol{W}$ is a tri-block diagonal with one-, three-, and two-dimensional matrices on the main diagonals of the four submatrices. Note that these submatrices have exactly the same structure as the matrices $\boldsymbol{M}^{(ii)-1}$, $i = 1,2$; see eq. [16].

Since $\boldsymbol{\Pi} = -2\boldsymbol{\eta\gamma}$, we find

$$[35a]\quad \boldsymbol{\Pi}^{(1)} = -2(\boldsymbol{\eta}_{11} + \boldsymbol{\eta}_{12})\hat{\boldsymbol{\gamma}}$$

$$[35b]\quad \boldsymbol{\Pi}^{(2)} = -2(\boldsymbol{\eta}_{21} + \boldsymbol{\eta}_{22})\hat{\boldsymbol{\gamma}}$$

where

$$[36]\quad \boldsymbol{\eta}_{ij} = (R_{12}/\alpha)^{1/2}\boldsymbol{W}_{ij}$$

In view of the fact that the stresses on different charged species are not measured separately in practice, it is necessary to add the stresses together and obtain the total shear stress

$$[37]\quad \boldsymbol{\Pi}_t = \boldsymbol{\Pi}^{(1)} + \boldsymbol{\Pi}^{(2)} = -2(\boldsymbol{\eta}_{11} + \boldsymbol{\eta}_{22} + \boldsymbol{\eta}_{21} + \boldsymbol{\eta}_{12})\hat{\boldsymbol{\gamma}} = -2\boldsymbol{\eta}_t\hat{\boldsymbol{\gamma}}$$

Since $\boldsymbol{\eta}_{ij}$ have the same structure as eq. [16], so does the viscosity matrix $\boldsymbol{\eta}_t$. We note that

$$[38]\quad \boldsymbol{\eta}_t = (\boldsymbol{H_1} + \boldsymbol{H_2}) + (\alpha/R_{12})^{1/2}(\boldsymbol{H_3} + \boldsymbol{H_4})$$

This is clearly a block-diagonal matrix with a structure the same as eq. [16]. That is,

$$[39]\quad \boldsymbol{\eta}_t = \begin{bmatrix} \eta_{11} & 0 & 0 & 0 & 0 & 0 \\ 0 & \eta_{22} & \eta_{23} & \eta_{24} & 0 & 0 \\ 0 & \eta_{32} & \eta_{33} & \eta_{34} & 0 & 0 \\ 0 & \eta_{42} & \eta_{43} & \eta_{44} & 0 & 0 \\ 0 & 0 & 0 & 0 & \eta_{55} & \eta_{56} \\ 0 & 0 & 0 & 0 & \eta_{65} & \eta_{66} \end{bmatrix}$$

where the matrix elements are defined by eqs. [34], [36], and [38]. The total viscosity can be easily calculated from these formulas, although the exact expressions for the components can be quite complicated. To the approximation neglecting the terms of $O(\alpha)$ or $O(R_{12})$ $\boldsymbol{\eta}_t$ is given by the formula

$$[40]\quad \boldsymbol{\eta}_t \approx \boldsymbol{H_1}(\alpha = 0) + \boldsymbol{H_2}(\alpha = 0) = (\boldsymbol{M}^{(11)-1} + \boldsymbol{M}^{(22)-1})/\beta$$

In this approximation matrices $\boldsymbol{W_{12}}$ and $\boldsymbol{W_{21}}$ in eq. [30] are neglected and the viscosity is then given by the sum of those for independent charged species 1 and 2:

$$\eta_{11} \approx \bar{\eta}_1^{(1)} + \bar{\eta}_1^{(2)}$$

$$\eta_{22} = \eta_{33} \approx \bar{\eta}_2^{(1)} + \bar{\eta}_2^{(2)}$$

$$\eta_{23} = \eta_{32} \approx \bar{\eta}_1^{(1)} + \bar{\eta}_1^{(2)} - (\bar{\eta}_2^{(1)} + \bar{\eta}_2^{(2)})$$

$$\eta_{24} = -\eta_{42} \approx -(\bar{\eta}_4^{(1)} + \bar{\eta}_4^{(2)})$$

$$\eta_{34} = -\eta_{43} \approx \bar{\eta}_4^{(1)} + \bar{\eta}_4^{(2)}$$

$$\eta_{44} \approx 2(\bar{\eta}_2^{(1)} + \bar{\eta}_2^{(2)}) - (\bar{\eta}_1^{(1)} + \bar{\eta}_1^{(2)})$$

$$\eta_{55} = \eta_{66} \approx \bar{\eta}_3^{(1)} + \bar{\eta}_3^{(2)}$$

$$\eta_{56} = -\eta_{65} \approx \bar{\eta}_5^{(1)} + \bar{\eta}_5^{(2)}$$

where $\bar{\eta}_k^{(i)}$ are defined in eqs. [19]–[23]. Inclusion of off-diagonal submatrices $\boldsymbol{W}_{12}$ and $\boldsymbol{W}_{21}$ is straightforward but results in complicated formulas. The next order approximation would be

$$[41]\quad \boldsymbol{\eta}_t \approx \boldsymbol{H_1}(\alpha = 0) + \boldsymbol{H_2}(\alpha = 0) + (\alpha/R_{12})^{1/2}[\boldsymbol{H_3}(\alpha = 0) + \boldsymbol{H_4}(\alpha = 0)]$$

where $\boldsymbol{H_3}(\alpha = 0)$ and $\boldsymbol{H_4}(\alpha = 0)$ can be easily computed from eqs. [34*c*] and [34*d*]. In this approximation the coupling is taken into account to $O(R_{12}^{1/2})$. It must be noted that the second term in eq. [41] is proportional to $R_{12}^{1/2}$, which differs from the perturbation theory prediction of R_{12} for the factor. This qualitative difference originates from the resummation performed in eq. [30] to obtain the exact result, eq. [31], in the present method.

Acknowledgments

This work is supported in part by the Natural Sciences and Engineering Research Council of Canada and Fonds FCAR of Quebec.

1. J. P. Freidberg. Rev. Mod. Phys. **54**, 801 (1982).
2. C. E. Max, C. F. McKee, and W. C. Mead. Phys. Fluids, **23**, 1620 (1980).
3. W. L. Kruer. Commun. Plasma Phys. **5**, 69 (1979).
4. S. I. Braginskii. Rev. Plasma Phys. **1**, 205 (1965).
5. J. H. Ferziger and H. Kaper. Mathematical theory of transport processes in gases. North-Holland, Amsterdam. 1972.
6. B. C. Eu. Phys. Fluids, **28**, 222 (1985).
7. B. C. Eu. J. Chem. Phys. (*a*) **73**, 2958 (1980); (*b*) **82**, 4283 (1985).
8. S. R. de Groot and P. Mazur. Nonequilibrium thermodynamics. North-Holland, Amsterdam. 1962.
9. E. Merzbacher. Quantum mechanics. Wiley, New York. 1970.

Can. J. Chem. Downloaded from www.nrcresearchpress.com by 88.85.125.76 on 09/07/12
For personal use only.

W-shape C_p^E and solution non-randomness: hydrocarbons + tetraalkoxysilanes

LINA ANDREOLI-BALL AND DONALD PATTERSON

Chemistry Department, McGill University, 801 Sherbrooke St. W., Montreal, P.Q., Canada H3A 2K6

Received January 2, 1990

This paper is dedicated to Professor Arthur S. Perlin on the occasion of his 67th birthday

LINA ANDREOLI-BALL and DONALD PATTERSON. Can. J. Chem. **68**, 1077 (1990).

The excess heat capacity, C_p^E, has been measured through the concentration range at 25°C for cyclohexane + $Si(OR)_4$ where R = methyl (Me), ethyl (Et), propyl (Pr), and butyl (Bu). C_p^E is negative and concave upward for the last three oxysilanes. For R = Me C_p^E has a region of zero curvature, which, on reducing T to 2°C, becomes concave downward, i.e., its concentration dependence becomes *W*-shaped. C_p^E has also been obtained at 15°C for $Si(OMe)_4$ mixed with the following hydrocarbons of increasing molecular size: cyclooctane, *cis*-decalin, dicyclohexyl, n-hexadecane, 2,2,4,4,6,8,8-heptamethylnonane, 2,6,10,14-tetramethylpentadecane, and 2,6,10,15,19,23-heptamethyltetracosane (at 25°C). All C_p^E values for these systems present a *W*-shape, which, with increasing hydrocarbon size becomes increasingly pronounced and moves to lower hydrocarbon concentration. C_p^E behaviour correlates with degrees of non-randomness in the systems as quantified by the concentration–concentration correlation function S_{cc} which is predicted using the Flory–Huggins theory with a group-interaction model and assuming interaction between molecular surfaces. Differences between C_p^E for n-C_{16} and highly branched C_{16} isomer, 2,2,4,4,6,8,8-heptamethylnonane, are attributed to liquid state orientational order and higher molecular surface/volume ratio for the normal isomer.

Key words: excess heat capacity, W-shape, non-randomness, hydrocarbons, tetraalkylsiloxanes.

LINA ANDREOLI-BALL et DONALD PATTERSON. Can. J. Chem. **68**, 1077 (1990).

Opérant à 25°C et à des concentrations couvrant l'ensemble des possibilités, on a mesuré la capacité calorifique en excès, C_p^E, du système cyclohexane + $Si(OR)_4$ dans lequel R = méthyle (Me), éthyle (Et), propyle (Pr) et butyle (Bu). Pour les trois derniers oxysilanes, la valeur de C_p^E est négative et concave vers le haut; par ailleurs, lorsque R = Me, la valeur de C_p^E possède une région dont la courbure est nulle et qui, lorsqu'on réduit la température à 2°C, devient concave vers le bas, c'est'à-dire que sa dépendance sur la concentration prend la forme d'un *W*. On a aussi obtenu la valeur de C_p^E à 15°C pour le $Si(OMe)_4$ mélangé avec les hydrocarbures suivants, de grosseurs moléculaires croissantes: cyclooctane, cis-décaline, dicyclohexyle, n-hexadécane, 2,2,4,4,6,8,8-heptaméthylnonane, 2,6,10,14-tétraméthylpentadécane et 2,6,10,15,19,23-heptaméthyltétracosane (à 25°C). Les C_p^E de tous ces systèmes présentent une forme en W qui, par augmentation de la grosseur de l'hydrocarbure, devient plus prononcée et qui se déplace vers les concentrations plus faibles d'hydrocarbure. Il existe une corrélation entre le comportement du C_p^E et le manque de hasard des systèmes, tel que quantifié par la fonction de corrélation concentration–concentration S_{cc} qui est prédite lorsqu'on utilise la théorie de Flory–Huggins de concert avec un modèle d'interaction de groupe et en faisant l'hypothèse qu'il existe des interactions entre les surfaces moléculaires. La différence qui est observée entre les valeurs de C_p^E des hydrocarbures en C_{16} normal et hautement ramifié, 2,2,4,4,6,8,8-heptaméthylnonane, est attribuée à un ordre d'orientation de l'état liquide et à un rapport surface moléculaire/volume qui est plus grand pour l'isomère normal.

Mots clés : capacité calorifique d'excès, dépendance en W sur la concentration, solution non-aléatoire, hydrocarbures, tetraalkylsiloxanes.

[Traduit par la revue]

Introduction

An unusual *W*-shape concentration dependence of the excess heat capacity, C_p^E, of a non-electrolyte mixture has been found (1) and extensively studied (2) by Grolier and collaborators (examples in Fig. 3). The *W*-shape is considered (3) to arise from a combination of a negative C_p^E of normal parabolic shape with a positive contribution manifesting itself toward the middle of the concentration range. The second contribution is due to non-randomness in solution where molecular antipathy between the components causes the equimolar H^E and G^E values to exceed, respectively, ~1200 and ~800 J mol^{-1}. Non-randomness may be better quantified through (4, 5) the concentration –concentration correlation function, S_{cc} or the concentration fluctuations:

$$[1] \quad S_{cc} = N\langle\overline{\Delta x^2}\rangle = [\partial^2(G/RT)/\partial x^2]^{-1}$$

Rayleigh light scattering gives values of S_{cc} through

$$[2] \quad S_{cc} = x_1 x_2 R_c / R_{id}$$

where R_c is the concentration fluctuation Rayleigh ratio and R_{id} is its ideal value obtainable through calculation. A correlation has been found to exist between S_{cc} and the magnitude of the *W*-shape, a value of 0.7 in S_{cc} being suggested as the threshold for the occurrence of the *W*-shape, rather than the normal parabolic, C_p^E. S_{cc} is also obtainable from the concentration dependence of G^E for the system and a simple Flory–Huggins expression (4, 5) for G and G^E relates S_{cc} to molecular size of the components and their interaction. It predicts that S_{cc} and hence the *W*-shaped C_p^E should be enhanced by reduction of T and increase of molecular size of the components.

The excess thermodynamic quantities, e.g., H^E and V^E have been extensively studied (6) at 25°C for cyclohexane mixed with a series of tetraalkoxysilanes $Si(OR)_4$ where R is varied from methyl (Me) to butyl (Bu). Excess enthalpies (7) and excess free energies (8) are also available when R = 2-ethylbutyl (br–Hex). With increase of alkyl chain size, i.e., with decreasing exposure of the oxygen atom to the cyclohexane component, the equimolar H^E values decrease rapidly as Me 1351, Et 716, Pr 371, Bu 343, and 2-ethylbutyl 167 J mol^{-1}. H^E per volume decreases even more dramatically through the series, by a factor of 10. Furthermore, light scattering measurements at 25°C have been made (9) on cyclohexane + $Si(OMe)_4$ giving R_c values which, through eq. [2] give S_{cc} with a maximum value of 0.75

Can. J. Chem. Downloaded from www.nrcresearchpress.com by 88.85.125.76 on 09/07/12
For personal use only.

at $x_1 \sim 0.45$. Integration of R_c through the concentration range gave G^E with an equimolar value of 817 J mol^{-1}. Thus values of the quantities H^E, G^E, and S_{cc} for cyclohexane + Si(OMe)$_4$ all fall near the threshold for appearance of the *W*-shape while other Si(OR)$_4$ give H^E below threshold. It was therefore of interest to obtain C_p^E for the cyclohexane + Si(OR)$_4$ series and to test Flory–Huggins S_{cc} predictions by varying T and by mixing Si(OMe)$_4$ with hydrocarbons larger than cyclohexane. These were taken to be three cycloalkanes, cyclooctane, *cis*-decalin, and dicyclohexyl, and three branched alkanes, 2,2,4,4,6,8,8-heptamethylnonane (br–C_{16}), a branched C_{19}, 2,6,10,14-tetramethylpentadecane (pristane), and a branched C_{30}, 2,6,10,15,19,23-hexamethyltetracosane (squalane). n-C_{16} was also used for comparison with the isomer, br-C_{16}.

Flory–Huggins treatment of S_{cc}

Reference 6 showed that the excess quantities for the c-C_6 + Si(OR)$_4$ systems could be treated using a model (10) based on a Flory–Huggins (FH) combinatorial term and interactions between surfaces of groups in the component molecules. Using this model, the following expression is found for S_{cc}:

$$[3] \quad S_{cc}^{-1} = (x_1x_2)^{-1} + \left(\frac{r_1 - r_2}{x_1r_1 + x_2r_2}\right)^2 - \frac{2\,q_1^2q_2^2\,\frac{g_{12}}{RT}}{(x_1q_1 + x_2q_2)^3}$$

In the equation which is analogous to eq. [21] of ref. 4. r_i and q_i are numbers of segments in the component molecules which are proportional to, respectively, molecular volume and surface area, normalized by the volume and surface area of the methane molecule. g_{12} is the average interaction free energy per segment of the components analogous to $z\Delta w_{12}$ in the regular solution theory. In eq. [3], the three terms on the right hand side are, respectively, ideal, non-ideal combinatorial and interactional. The first two terms decrease S_{cc}, i.e., randomizing, while the third term increases non-randomness. It indicates that S_{cc} and *W*-shape character are enhanced by lowering T and by increasing the molecular surface area of either component, i.e. q_1 or q_2. Furthermore, it is clearly largest at low concentration of the component having the larger value of q, hence presumably larger molecular size.

Quantitative application of eq. [3] requires q values for the components mostly taken from refs. 6 and 10 where they were derived using Bondi group surface contributions (11). Ratios of r values may be obtained as the ratios V_2^*/V_1^* of hard-core volumes for the components obtained in the usual way from the thermal expansion coefficients and molar volumes. g_{12} is related to α_o, the fraction of molecular surface of an Si(OR)$_4$ molecule which is of oxygen character using the general eq. [80] of ref. 10 or, more specifically, eq. [7] of ref. 12. For the cycloalkanes + Si(OR)$_4$ we have

$$[4] \quad g_{12} = g_{oa}\alpha_o^2 - (g_{ac} + g_{oa} - g_{oc})\alpha_o + g_{ac}$$

Values of α_o are found in Table 1 of ref. 6, related to the surface areas of the oxygen atom and of the Si(OR)$_4$ molecule by $\alpha_o = q_0/q_1$. The g_{ij} are parameters for interaction between oxygen (o), aliphatic (a), and cyclohexyl (c) surfaces of the molecules. g_{ac}/RT is given in Table 1 of ref. 10 to be 0.0512 at 25°C and following ref. 6 we tentatively assume $g_{oa} = g_{oc}$. On the other hand, for the alkanes + Si(OR)$_4$, we have

$$[5] \quad g_{12} = g_{oa}\alpha_o^2$$

The only undetermined parameter in eqs. [4] and [5] is therefore g_{oa} which must be fitted to experiment. One possibility is to fit to G^E for c-C_6 + Si(OMe)$_4$ or to the corresponding value of S_{cc}, i.e. 0.75. When this is done, eqs. [3] and [4] predict that S_{cc} will have attained infinite values at 57 and 87°C for the pristane and squalane + Si(OMe)$_4$ systems. In fact, the UCST for these systems are much lower, that for the squalane system being measured to be 17°C. This incorrect prediction prompted an alternative procedure to obtain g_{oa}, i.e. fitting so that $S_{cc} \rightarrow \infty$ at 17°C for the squalane system. Using an equimolar H^E value of (6) 1571 J mol^{-1} for cyclohexane + Si(OMe)$_4$ to give the temperature dependence of g_{oa}, and the temperature dependence of g_{ac} from ref. 10, we have for cycloalkanes + Si(OR)$_4$,

$$[6] \quad g_{12}/RT = (3620T^{-1} - 6.29)\alpha_o^2 + (45.7T^{-1} - 0.102)(1 - \alpha_o)$$

and for alkanes + Si(OR)$_4$

$$[7] \quad g_{12}/RT = (3620T^{-1} - 6.29)\alpha_o^2$$

Experimental

Excess heat capacities were obtained using the Picker flow microcalorimeter and methods found in the literature (13, 14). The components were from Aldrich Chemical Co. and of 99% stated purity. The instrument measures the difference $\Delta C_p/V$ in volumetric heat capacity between liquid A in the working cell and liquid B in the reference cell. However, as in previous work (5) with systems with large values of H^E a "boundary effect" leads to a different $\Delta C_p/V$ value. If liquids A and B are interchanged then the "correct" value is the average of the two. Data in ref. 13 allow an estimate of the error incurred. Correspondingly, C_p^E depends on $\Delta C_p/V$ values between successive solutions (14). the C_p^E given here are based on average $\Delta C_p/V$ found through interchanging the two solutions, except in the case of squalane + Si(OMe)$_4$ where measurements in one direction were difficult due to the high viscosity of squalane. We estimate the accuracy of C_p^E to be ±0.03 J K^{-1} mol^{-1} toward the middle of the concentration range, and perhaps ±0.1 J K^{-1} mol^{-1} for the squalane system.

Results and discussion

Cyclohexane systems

The lower part of Fig. 1 shows S_{cc} values at 25°C for the series of cyclohexane + Si(OR)$_4$ systems with R from Me to br-Hex calculated using eq. [3] with eq. [6] for g_{12}/RT and with values of α_o, q, and r for the components from Table 1 of ref. 6. The upper part of Fig. 1 shows C_p^E values at 25°C for the same series of systems. C_p^E for all systems are negative with minima at high cyclohexane mole fraction reflecting the difference in molecular size of the components. However, for c-C_6 + Si(OMe)$_4$ the curvature of C_p^E is much less, suggesting an incipient *W*-shape at $x_1 \sim 0.6$ where the non-randomness indicator S_{cc} reaches its maximum. The special character of the c-C_6 + Si(OMe)$_4$ system is consistent with the S_{cc} values, S_{cc} being larger for this system than for others. Nevertheless, the calculated S_{cc} value of ~0.5 is lower than the threshold value of 0.7 found previously. This low value is due to fitting the theory by requiring $\partial^2(G/RT)/\partial x^2 = 0$ at the Upper Critical Solution Temperature or UCST for squalane + Si(OMe)$_4$. In fact, it is not surprising that a mean-field theory ignoring non-randomness does not give a good value of this curvature for the cyclohexane system far from its UCST. As the temperature rises above the UCST, the rate of increase of $\partial^2(G/RT)/\partial x^2$ away from zero is too large in a mean-field theory. This corresponds to $\partial^2H^E/\partial x^2$ remaining finite at the UCST instead of falling to zero as found (15) experimentally and theoretically, the classical critical exponent γ having a value of 1 instead of 1.24.

In Fig. 1, in order of increasingly negative C_p^E at the minima, the systems are Me < Pr < ET < Bu < br-Hex, the Pr system

Can. J. Chem. Downloaded from www.nrcresearchpress.com by 88.85.125.76 on 09/07/12
For personal use only.

Can. J. Chem. Downloaded from www.nrcresearchpress.com by 88.85.125.76 on 09/07/12
For personal use only.

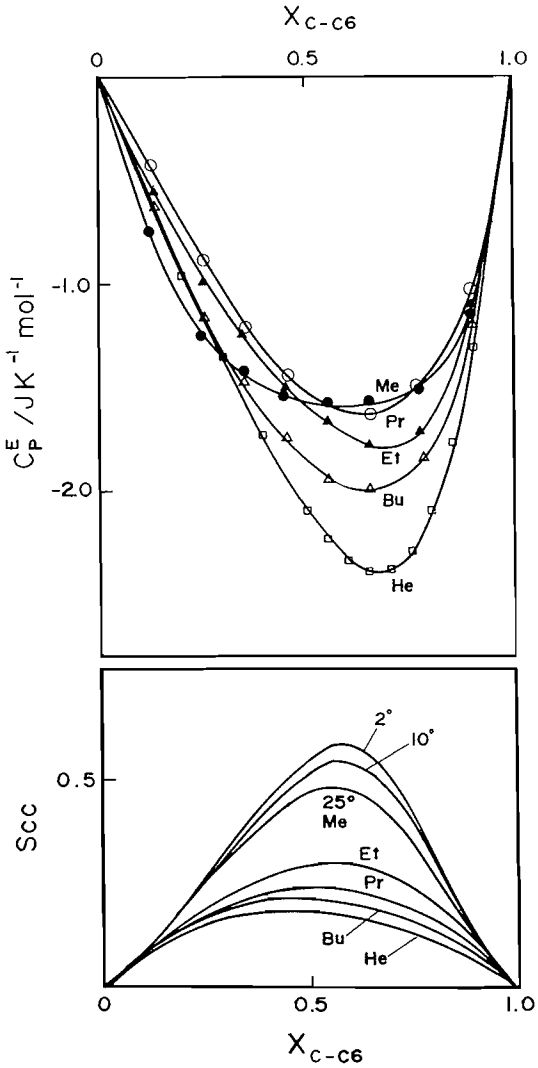

FIG. 1. (Upper part) C_p^E at 25°C for cyclohexane + Si(OR)$_4$, R = Me, Et, Pr, Bu, and branched-hexyl (at 30°C from $H^E(T)$ data (7)), against cyclohexane mole function. (Lower part) S_{cc} at 25°C for the same systems at 25°C and for cyclohexane + Me at 10 and 2°C.

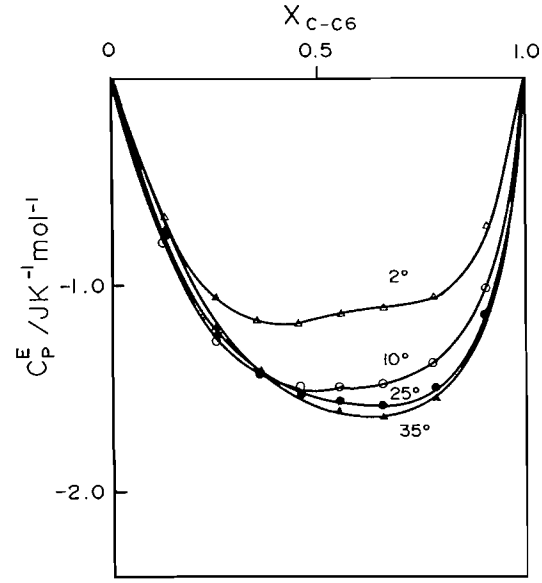

FIG. 2. C_p^E for cyclohexane + Si(OMe)$_4$ at various temperatures (for 2°C see text).

appearing out of place. We can only suggest tentatively that this anomaly may be due to an interplay of the positive non-randomness contribution with the two negative contributions which explain the overall negative sign of C_p^E. These are due to (*1*) destruction on mixing of polar order in the pure alkoxysilanes arising from dipole moments (6) which range from 1.83 D for Me to 1.61 D for Bu. This relatively important effect should increase with decreasing alkoxy group size which exposes the dipole and increases polar order, (*2*) free volume effects which should increase in magnitude as the alkoxy group becomes larger. We suggest that in the absence of the non-randomness contribution the polar effect would dictate the order of systems to be Pr < Et < Me as seen at low cyclohexane concentration and that non-randomness in the Me system at $x_1 \sim 0.6$ changes the order to Me < Pr < Et. The Bu and br-Hex positions are perhaps due to the increas higher temperature, 35°C. In the case of 2°C which lies below the melting point of pure cyclohexane at 6°C, the apparent molar heat capacity ϕ_c could be obtained for Si(OMe)$_4$ as a function of x_1 up to $x_1 = 0.95$. The curve was then extrapolated to $x_1 = 1$. Data at 10 and 25°C show that ϕ_c in the $0.95 < x_1 < 1.0$ region is a smooth extrapolation of data at lower x_1. Thus, C_p^U of the supercooled cyclohexane at 2°C was obtained and C_p^E calculated. Figure 2 shows the results and indeed at 2°C the *W*-shape is more apparent while at 35°C the curvature of C_p^E has increased. Figure 1 shows S_{cc} values for this system at 10 and 2°C calculated using eq. [6] for g_{12}/RT at those temperatures and eq. [3] for S_{cc}. There is clearly an increase of non-randomness with decrease of temperature with a maximum at $x_1 \sim 0.6$, an observation that is consistent with the C_p^E data.

The effect of temperature was also investigated for cyclohexane + Et, Pr, and Bu by measuring C_p^E at 10°C and using $H^E(T)$ data (7) for br-Hex. The effect of temperature is small, barely outside experimental error, with a maximum at $x_1 = 0.65$ where the magnitudes of dC_p^E/dT are $\sim 10^{-2}$ J K^{-2} mol^{-1} but the signs of the quantity vary as follows: Et −, Pr +, Bu ~0 and br-Hex +. C_p^E for Et may reflect some non-randomness while C_p^E for the other alkoxysilanes may be dominated by the dipolar term which undoubtedly would give $dC_p^E/dT > 0$.

Other hydrocarbon systems

Figure 3 shows C_p^E for Me mixed with a series of cycloalkanes of increasing molecular size: cyclooctane, *cis*-decalin, and dicyclohexyl and with a series of branched alkanes, br-C_{16}, pristane, and squalane. The temperature for all systems except squalane was 15°C. The squalane + Me system phase separates at a UCST of 17°C and the C_p^E measurements were made at 25°C. In Fig. 3, the *W*-shape is strongly enhanced with increase of the size of the hydrocarbon whether cycloalkane or branched alkane, finally reaching a strong positive peak with a value of ~4 J K^{-1} mol^{-1} for squalane + Si(OMe)$_4$. Correspondingly, as expected from the non-randomness concept, the central maximum or region of negative curvature moves to lower hydrocarbon concentration, finally to $x_1 \sim 0.15$ for the squalane system. Figure 3 also shows C_p^E for the largest cyclic, dicyclohexyl mixed with the next tetraalkylsilane, Et. The pronounced *W*-shape has now disappeared leaving only a flat region at $x_1 \sim 0.55$.

Figure 4 gives S_{cc} for the same systems and it is clear that there is at least a qualitative similarity between the evolution of S_{cc} and C_p^E with increasing molecular size of the hydrocarbons

Can. J. Chem. Downloaded from www.nrcresearchpress.com by 88.85.125.76 on 09/07/12
For personal use only.

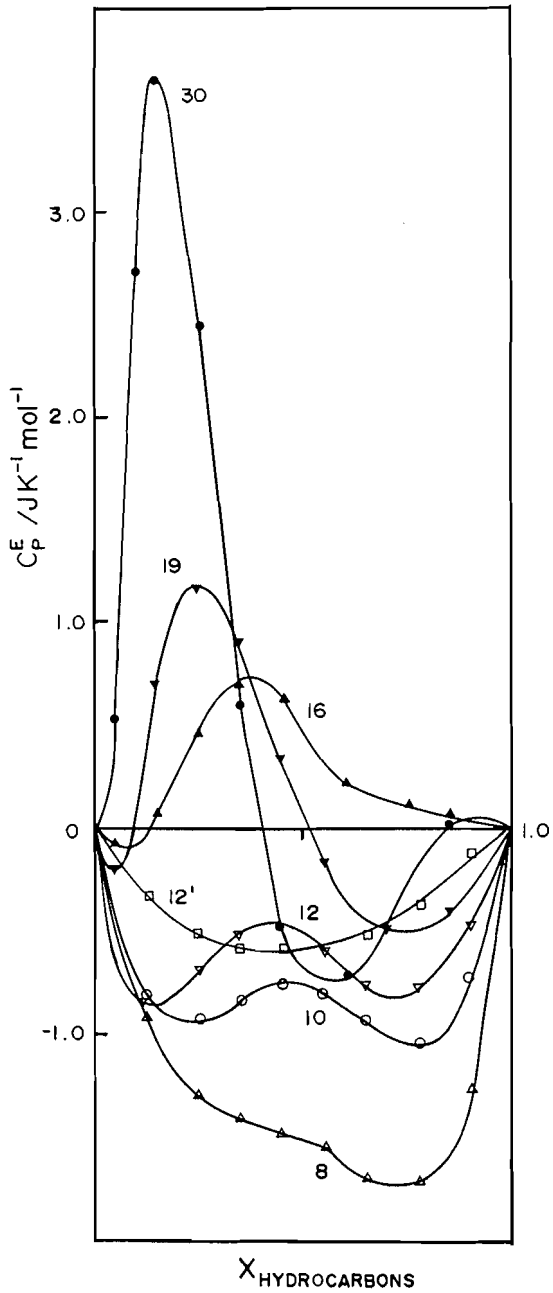

FIG. 3. C_p^E at 15°C for the following hydrocarbons, designated by their carbon numbers + $Si(OMe)_4$: cyclooctane, *cis*-decalin, dicyclohexyl, heptamethylnonane, tetramethylpentadecane (pristane), and hexamethyltetracosane (squalane, at 25°C). 12′ indicates dicyclohexyl + $Si(OEt)_4$.

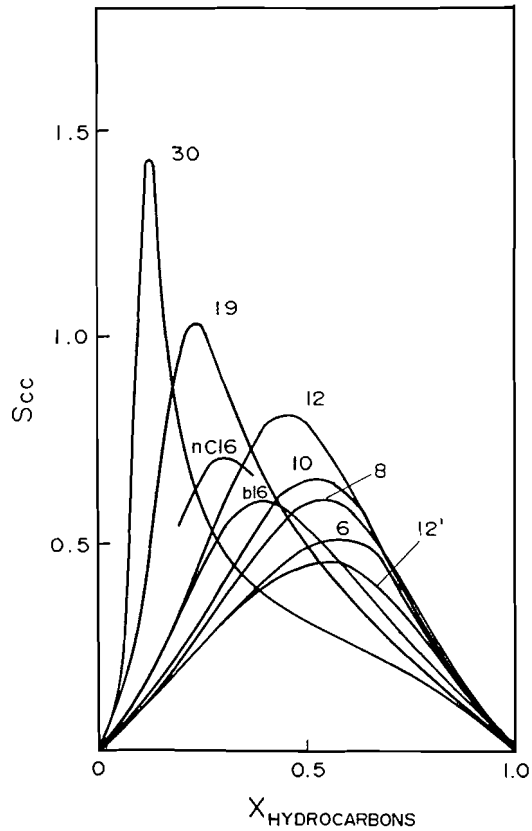

FIG. 4. S_{cc} at 15°C for the systems of Fig. 3, i.e., hydrocarbons, designated by their carbon numbers, + $Si(OMe)_4$: The squalane + $Si(OMe)_4$ system is at 25°C and 12′ indicates the dicyclohexyl + $Si(OEt)_4$ system. N16 and b16 indicate n-C_{16} (at 25°C) and br-C_{16} (at 15°C) + $Si(OMe)_4$.

mixed with $Si(OMe)_4$. The S_{cc} for dicyclohexyl + $Si(OEt)_4$ is small, similar to S_{cc} for cyclohexane + $Si(OMe)_4$ at 25°C, and consistent with the presence of only an incipient *W*-shape for this system. In general, the consistency between S_{cc} in Fig. 4 and C_p^E in Fig. 3 confirms the non-randomness origin for the *W*-shape.

The S_{cc} values were calculated using eqs. [3] and [6] for the cyclic hydrocarbons. All these cycloalkanes are of similar chemical character as suggested by the very small values of H^E, from 0 to 20 J mol^{-1} for a number of their mixtures (17). Equations [3] and [7] were used for the branched alkanes. Equation [3] requires molecular surface areas or q_1 values. Consistent with refs. 6 and 10 these may be computed using Bondi surface area contributions for CH and CH_2 groups (Table 14.16) and surface decrements (Table 14.17) required by intramolecular crowding which decreases the surface area in the cyclics. *cis*-Decalin is found to have a q_1 value smaller than for cyclooctane in spite of its substantially larger volume. This anomaly arises from the *cis*-decalin molecule being given a particularly large surface area decrement due to its "folded" shape. Corresponding to this, the maximum S_{cc} value for *cis*-decalin calculated through eq. [3] will be less than that for cylcooctane. In contrast to this prediction, the *cis*-decalin *W*-shape in Fig. 3 is in fact pronounced and that for cyclooctane hardly apparent. We therefore believe that the *cis*-decalin decrement is overestimated, and have turned to an alternative method of q_1 estimation from core volume V^* values assuming the cyclohexane, cyclooctane, and *cis*-decalin molecules to be spheres. Dicyclohexyl and br-C_{16} were assumed to be right cylinders with radii equal to, respectively, that of cyclohexane, 3.22 Å, and that of the polyisobutylene chain, 3.48 Å. This procedure to find the molecular surface of br-C_{16} has been used earlier (18). In each case, the q value was reduced by an almost trivial factor of 1.042 in order to bring the cyclohexane q_1 value into coincidence with that from Bondi given in ref. 6. The final values of q_1 are cyclooctane 3.07, *cis*-decalin 3.42, dicyclohexyl 4.49, and br-C_{16} 6.04. Bondi contributions were used, however, for the lightly branched pristane and squalane molecules, leading to q values of, respectively, 7.98 and 14.48. Figure 4 shows that S_{cc} and non-randomness in the br-C_{16} + $Si(OMe)_4$ system is less than for dicyclohexyl + $Si(OMe)_4$, predicting a less pronounced *W*-shape for C_p^E. This is not borne

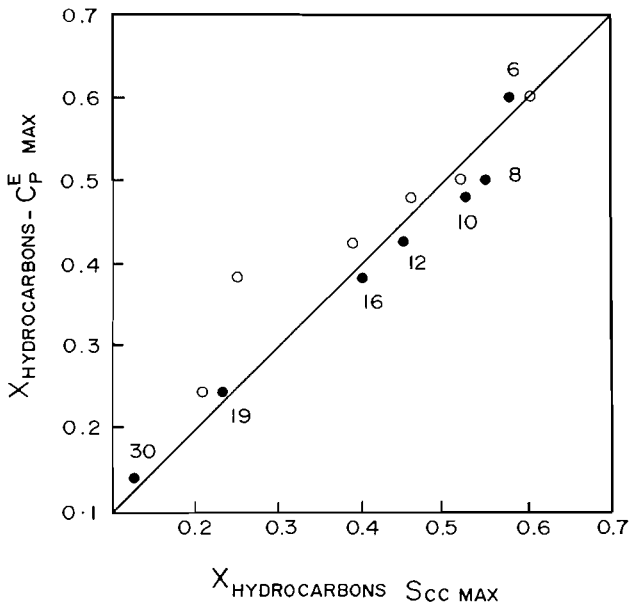

FIG. 5. Hydrocarbon mole fraction for maximum in C_p^E W-shape against mole fraction for maximum of predicted S_{cc}. Full points from eq. [3], i.e. using q; open points from eq. [3] setting $q = r$, i.e. molecular surfaces replaced by volumes in interactional term. Only the br-C_{16} isomer is shown.

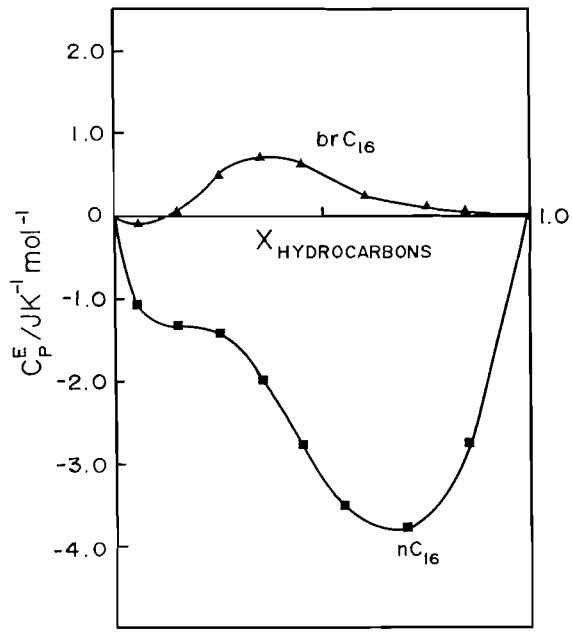

FIG. 6. C_p^E for n-C_{16} + Si(OMe)$_4$ (at 25°C) compared with C_p^E for br-C_{16} + Si(OMe)$_4$ (at 15°C).

out in the experimental results in Fig. 3 where the maximum of C_p^E is clearly much higher than for dicylcohexyl. However, it should be noted that it is difficult to assess the size of the non-randomness contribution in the br-C_{16} case relative to dicyclohexyl since, unlike the curves for other systems, C_p^E is positive throughout the concentration range, the normal random C_p^E apparently being positive instead of negative.

Figure 5 shows a plot of the hydrocarbon concentration at which C_p^E reaches a maximum or has maximum negative curvature against the concentration of maximum S_{cc}. An excellent correlation appears which becomes less good when q is replaced by r, i.e. using the original Flory–Huggins expression with molecular volumes in the interaction term, eq. [21] of ref. 4. Thus the maximum C_p^E for br-C_{16} occurs at a concentration which corresponds to the low surface/volume ratio of this compact molecule which is reflected in the q value but not the r value. As a test, C_p^E has been obtained for n-C_{16} + Si(OMe)$_4$.

The C_p^E results, as shown in Fig. 6, are strikingly different from those with the branched isomer, br-C_{16} which, for comparison, are repeated in Fig. 6. First, C_p^E is now negative at all concentrations, and, second, the mole fraction of C_{16} where the W-shape is most prominent has shifted to a lower value. The negative C_p^E is clearly due to the presence of orientational order or correlations of molecular orientation in the pure n-C_{16}, but not present in the pure br-C_{16}. This order is destroyed on mixing with the second component leading (19) to a negative "random" contribution to C_p^E. The size of this contribution in Fig. 6 makes it difficult to evaluate the "non-random" contribution, but it seems clear that its maximum value will occur at a lower C_{16} concentration than in the case of br-C_{16}. This is in accord with S_{cc} which is shown in Fig. 4 (at 25°C) and which is shifted with respect to br-C_{16}. Consistent with the extended molecular shape of n-C_{16} the Bondi group contribution method has been used to calculate the q parameter. This gives $q = 7.98$ for n-C_{16} comparing with the smaller value of 6.04 found for the more compact isomer, br-C_{16}. The increased surface area of n-C_{16} increases the interactional term in eq. [3] for S_{cc}, increasing S_{cc} and displacing its maximum to lower hydrocarbon concentration. The q parameters in eq. [3] may again be replaced by r, corresponding to the simple Flory–Huggins theory. However, the r values reflecting molar volumes are almost identical for normal and branched C_{16} as are the calculated S_{cc} values. We believe therefore that the displacement of the W-shape C_p^E found for n-C_{16} provides evidence for molecular interaction taking place between surfaces as provided for in the solution thermodynamics of ref. 10.

Acknowledgements

We are grateful for the support of the Natural Sciences and Engineering Research Council of Canada and of the Ministère de l'Education du Québec.

1. A. INGLESE, J. P. E. GROLIER, and E. WILHELM. J. Chem. Thermodyn. **16**, 67 (1984).
2. M. PINTOS, R. BRAVO BALUJA, M. I. PAZ ANDRADE, G. ROUS-DESGRANGES, and J. P. E. GROLIER. Can. J. Chem. **66**, 1179 (1988) and references therein.
3. M. E. ST. VICTOR and D. PATTERSON. Fluid Phase Equilibria, **35**, 237 (1987).
4. R. G. RUBIO, M. CACERES, R. M. MASEGOSA, L. ANDREOLI-BALL, M. COSTAS, and D. PATTERSON. Ber. Bunseges. Phys. Chem. **93**, 48 (1989).
5. L. ANDREOLI-BALL, M. COSTAS, D. PATTERSON, R. G. RUBIO, M. CACERES, and R. M. MASEGOSA. Ber. Bunseges. Phys. Chem. **93**, 882 (1989).
6. P. NKINAMUBUANZI, G. CHARLET, and G. DELMAS. Fluid Phase Equilibria, **20**, 57 (1985).
7. R. P. TOMLINS and M. ADAMSON. J. Chem. Thermodyn. **6**, 757 (1974).
8. R. P. TOMLINS. J. Chem. Thermodyn. **6**, 1195 (1976).
9. P. NKINAMBUANZI. M.Sc. thesis, Université du Québec à Montréal. 1984.
10. H. V. KEHIAIAN, J. P. E. GROLIER, and G. C. BENSON. J. Chim. Phys. **75**, 1031 (1975).

Can. J. Chem. Downloaded from www.nrcresearchpress.com by 88.85.125.76 on 09/07/12
For personal use only.

11. A BONDI. Physical properties of molecular crystals, liquids and glasses. John Wiley and Sons, New York. 1968. Chap. 14.
12. R. J. MEYER, J. V. MEYER, C. KEHIAIAN, and H. V. KEHIAIAN. Thermochim. Acta, **38**, 197 (1940).
13. J. L. FORTIER, G. C. BENSON, and P. PICKER. J. Chem. Thermodyn. **8**, 289 (1976).
14. J. L. FORTIER and G. C. BENSON. J. Chem. Thermodyn. **8**, 411 (1976).
15. E. DRABER and D. WOERMANN. Fluid Phase Equilibria, **49**, 211 (1989).
16. M. E. ST. VICTOR and D. PATTERSON. Thermochim. Acta. **159**, 177 (1990).
17. P. DE ST. ROMAIN, H. V. TRA, and D. PATTERSON. J. Chem. Soc. Faraday 1, **75**, 1708 (1979).
18. V. T. LAM, P. PICKER, D. PATTERSON, and P. TANCREDE. J. Chem. Soc. Faraday, 2, **70**, 1465 (1974).
19. S. N. BHATTACHARYYA and D. PATTERSON. J. Phys. Chem. **83**, 2979 (1979).

Can. J. Chem. Downloaded from www.nrcresearchpress.com by 88.85.125.76 on 09/07/12
For personal use only.

The solution conformation of the luteinizing hormone-releasing hormone (LHRH) anti-sense and reversed anti-sense peptides

ALBIN OTTER
Department of Chemistry, University of Alberta, Edmonton, Alta., Canada T6G 2G2

PAUL G. SCOTT
Department of Oral Biology, University of Alberta, Edmonton, Alta., Canada T6G 2E9

JOHN M. STEWART
Department of Biochemistry, University of Colorado, Health Sciences Centre, Denver, CO, 80262, U.S.A.

AND

GEORGE KOTOVYCH[1]
Department of Chemistry, University of Alberta, Edmonton, Alta., Canada T6G 2G2

Received October 30, 1989

This paper is dedicated to Professor Arthur S. Perlin on the occasion of his 67th birthday

ALBIN OTTER, PAUL G. SCOTT, JOHN M. STEWART, and GEORGE KOTOVYCH. Can. J. Chem. **68**, 1083 (1990).

The LHRH anti-sense peptide (Ser[1]-Arg[2]-Ala[3]-Gln[4]-Ser[5]-Ile[6]-Gly[7]-Pro[8]-Val[9]-Leu[10]) and the inversed sequence, the LHRH inversed anti-sense peptide, have been studied by ^1H and ^{13}C NMR in one and two dimensions. The spectroscopic evidence, obtained in CD_3OH/H_2O (60/40) solution at pH 3.6, indicates that the first four amino acids of the anti-sense peptide form one complete 3_{10}-helical turn followed by an extended conformation for the rest of the peptide. On the time-averaged NMR scale the molecules in the 3_{10}-helical conformation are in fast exchange with the molecules that are extended throughout (major conformer). The reversed anti-sense peptide exhibits less discernible features. It appears likely that a small percentage of the molecules form a β-turn in the C-terminal four residues. Another β-turn might be located in the Val[2]-Ile[5] fragment. Both turns occur in very minor concentrations only, and therefore it is impossible to define what kind of β-turns are present.

Key words: LHRH anti-sense, inversed anti-sense, conformation, NMR.

ALBIN OTTER, PAUL G. SCOTT, JOHN M. STEWART et GEORGE KOTOVYCH. Can. J. Chem. **68**, 1083 (1990).

Faisant appel à la rmn du ^1H et du ^{13}C en une et en deux dimensions, on a étudié le peptide LHRH anti-sens (Ser[1]-Arg[2]-Ala[3]-Gln[4]-Ser[5]-Ile[6]-Gly[7]-Pro[8]-Val[9]-Leu[10]) ainsi que la séquence inversée, le peptide LHRH anti-sens inversé. Les données spectroscopiques, obtenues en solution dans le CD_3OH/H_2O (60/40), à un Ph de 3,6, indiquent que les quatre premiers acides aminés du peptide anti-sens forment une hélice 3_{10} complète alors que le reste de la molécule existe dans une conformation allongée. A l'échelle de temps de la rmn, les molécules de la conformation hélicoïdale 3_{10} s'échangent rapidement avec les molécules qui sont dans la conformation complètement allongée (conformère principal). Les caractéristiques du peptide anti-sens inversé sont moins bien définies. Il semble probable que les quatre résidues du terminal C donnent lieu à une faible proportion de molécules possédant une hélice β. Il est possible qu'une autre hélice β puisse exister dans le fragment Val[2]-Ile[5]. Les concentrations de ces deux hélices sont très faibles et il est donc impossible de définir quels sont les types d'hélice β qui sont présents.

Mots clés : LHRH anti-sens, anti-sens inversé, conformation, rmn.

[Traduit par la revue]

Introduction

The luteinizing hormone releasing hormone (LHRH) is a decapeptide that has been studied in detail by various techniques, including nuclear magnetic resonance (NMR) (1). The complementary decapeptide, Ser[1]-Arg[2]-Ala[3]-Gln[4]-Ser[5]-Ile[6]-Gly[7]-Pro[8]-Val[9]-Leu[10] (LHRH anti-sense peptide), specified by the RNA sequence complementary to the mRNA for human LHRH (2), was prepared as described in ref. 3. This sequence results from the fact that in cells, the sequence of amino acids along peptide chains is determined by the sequence of triplet nucleotides along genes coding for the proteins. It has been suggested that the LHRH and its anti-sense peptide may be interacting (3). Furthermore, antibodies directed against a peptide complementary to a particular hormone also bind to that hormone's receptor binding site (4). Since such interactions are almost certainly conformation-dependent, we studied the LHRH anti-sense peptide by ^1H and ^{13}C NMR. Included in our study is the conformational analysis of the LHRH reversed anti-sense peptide with the sequence Leu[1]-Val[2]-Pro[3]-Gly[4]-Ile[5]-Ser[6]-Gln[7]-Ala[8]-Arg[9]-Ser[10]. This decapeptide has been studied to find out to what extent the conformation is changed by a simple reversal of the orignal sequence. Our efforts are to be seen in light of ongoing interest in the formation and stabilization of secondary structures in small linear peptides (5–7). The results are based on several one and two-dimensional NMR techniques (8) for both proton and ^{13}C.

[1]To whom correspondence should be addressed.

Materials and methods

The two decapeptides were synthesized and purified according to standard procedures (9). The NMR samples were prepared by dissolving 5 mg each of the solid materials in 0.2 mL H_2O/D_2O (1:1). The pH was adjusted to 3.6 (meter readings without adjustment for deuterium) by adding small aliquots of 0.2 N NaOH. CD_3OH (0.3 mL) (Merck, Sharp and Dohme, MD-67, 99.9% D) was added, the samples were bubbled with argon for approximately 15 min and then sealed. The final concentrations were 8 mM for both decapeptides.

The NMR experiments were essentially the same for both peptides under investigation and were carried out on Bruker AM 600 and AM 400 NMR spectrometers at ambient (295 ± 1° K) temperature. The temperature coefficients of the amide protons were calculated by comparing spectra recording at 286, 290, and 294° K. Data collection and

Can. J. Chem. Downloaded from www.nrcresearchpress.com by 88.85.125.76 on 09/07/12
For personal use only.

Can. J. Chem. Downloaded from www.nrcresearchpress.com by 88.85.125.76 on 09/07/12
For personal use only.

data processing were controlled by an Aspect 3000 computer using 1987 DISMR software. Chemical shifts were measured relative to CD_3OH at 3.30 ppm (^1H) and 49.0 ppm (^{13}C), respectively.

The 600 MHz one-dimensional proton spectra were recorded with a sweep width of 6400 Hz and 16K (zero-filled to 32K) data points. A total of 168 scans were accumulated and the spectra were resolution enhanced by means of a Gaussian multiplication (line-broadening factor −5 Hz). The solvent signals originating from H_2O and OH of CD_3OH at ca. 4.72 ppm and the undeuterated fraction of CD_3OH at 3.30 ppm were both presaturated during a 2.4 s relaxation delay. The frequency of the decoupler was switched every 0.2 s between the two solvent peaks and the water signal was presaturated twice as long as the methyl group to account for the difference in intensity of the two signals. The possibility of saturation transfer to the amide protons was carefully monitored. With the exception of NH(Arg^2) no loss of intensity was observed. The experimental conditions at 400 MHz were essentially the same as at 600 MHz except for a shorter sweep width and, accordingly, a reduced number of data points.

The ^{13}C spectra were recorded at 100.6 MHz (AM 400) using the DEPT (distortionless enhancement by polarization transfer) pulse sequence (10). The sweep width was 20 kHz divided into 32K (zero-filled to 64K) data points. To obtain a very good S/N ratio more than 40 000 scans were acquired. The total relaxation delay including the acquisition time was 1.8 s and the evolution time for the polarization transfer was 8.3 ms. The final ^1H detection pulse was 135°, resulting in positive signals for CH and CH_3 groups and negative signals for CH_2. Proton broadband decoupling was achieved by a WALTZ (11) composite pulse train. The FID was multiplied by a Gaussian function (line broadening factor −3.0 Hz, Gaussian multiplication factor 0.075) providing good resolution without too much loss in signal-to-noise. This procedure proved to be superior to the more commonly used exponential multiplication.

The parameters of the various two-dimensional NMR techniques are summarized in Table 1. The COSY (12), ROESY (13, 14), and the $^{13}C/^1H$ correlation experiments using DEPT for the polarization transfer (15) were carried out in the phase-sensitive mode using TPPI (time-proportional phase increments) (16), hence the denomination "PH" in Table 1.

Solvent suppression in the COSY and ROESY experiments was achieved as outlined for the one-dimensional spectra. In addition, continuous irradiation was applied at all times aside from the data acquisition (18). The ROESY spectra suffered somewhat from baseline distortions around intense diagonal peaks. This problem could be eliminated in both dimensions by fitting a polynomial function of fifth degree to the baseline (Bruker ABS baseline correction). Due to the non-negligible offset dependence of the ROE cross-peaks (19) it is often difficult to observe ROE interactions at the edge of the spectrum, such as between amide protons, irrespective of the internuclear distance involved. Therefore, the ROESY experiment was also recorded with the transmitter placed in the middle of the NH absorption range (approximately 8.3 ppm). The spin-lock conditions were achieved by a series of hard pulses of small flip angle (20) with a spin-locking time of 150 ms (at 600 MHz) and 125 ms (at 400 MHz, transmitter in the low-field region), respectively. The spin-locking field strength was 5.7 kHz at 600 MHz and 4.0 kHz at 400 MHz.

The samples for circular dichroism spectroscopy were prepared in water or in water/methanol (40/60) and spectra were recorded in a 0.0994 cm pathlength cell at ambient temperature in a Jasco J-20A spectropolarimeter that had been previousy calibrated with *d*-10-camphorsulfonic acid (21). Samples were 0.3 mg/mL for recordings in the range 245 nm to 205 nm and 0.1 mg/mL for recordings between 205 nm and 195 nm. The 32 scans under each set of conditions were averaged and combined to cover the full wavelength range.

TABLE 1. Experimental parameters in the two-dimensional NMR experiments[a,b]

Parameters	Value		
	COSYPH	ROESYPH[c]	XHDEPTPH
Sweep width F2 (Hz)	6410	6410	5500
Sweep width F1 (Hz)	3205	3205	400[d]
Matrix size (F1 × F2) before zero-filling	512 × 4K	512 × 4K	30 × 4K[d]
Matrix size (F1 × F2) after zero-filling	1K × 8K	1K × 4K	128 × 4K
Evolution time			
initial value (μs)	1	1	1
increment (μs)	78	78	312
Number of scans (dummy scans)	16(2)	32(2)	1464(2)
Acquisition time (s)	0.32	0.32	0.37
Relaxation delay (s)	1.80	1.80	1.45
Other delays (ms)	—	150[e]	4.17[f]
Window functions for 2D FT (F1/F2)[g]	S/S	S/S	E/E
Shifts of window functions in fractions of π (F1/F2)	6/8	3/4	5/5[h]

[a]Abbreviations of the techniques are explained in the text.
[b]The parameter sets, referred to the ^1H work at 600 MHz, were the same for both decapeptides. The concentration was 8 mM at pH 3.6 in CD_3OH/H_2O (60/40, v/v) in both cases. The temperature was ambient (295 ± 1K).
[c]The ROESY experiment was performed twice with different transmitter frequencies (see Materials and Methods).
[d]Due to the low concentration of the samples only a limited number of t_1-increments was feasible. Therefore, the sweep width in the proton domain was reduced and soft pulses (90°(^1H) pulse = 600 μs) with an approximate excitation range of 400 Hz were applied (17).
[e]Spin locking time, average field strength 5.6 kHz.
[f]$(2J_{^{13}C-^1H})^{-1}$.
[g]S: sine bell; E: exponential function.
[h]Line broadening factors.

Results and discussion

The spectral analysis of both decapeptides is based on the results of two-dimensional, phase-sensitive NMR experiments such as COSY (16), ROESY (13, 14), and $^{13}C/^1H$ shift correlation (15). Since most amino acids are unique in the sequence under study, assignments are fairly straightforward. The "fingerprint" region of the contour plots of the LHRH anti-sense peptide are shown in Fig. 1, those of the inversed anti-sense peptide in Fig. 2. The ROESY experiments depicted in these figures have been recorded with the transmitter approximately in the middle of the entire spectral range (ca. 4.8 ppm). It is noteworthy that all ROESY spectra obtained in this study were basically free from often reported artifacts (14, 19, 20, 22) which can be identified by their phase relative to the diagonal peaks. Only the ABM spin systems of the Serine moieties showed some, albeit not detrimental, Hartmann-Hahn magnetization transfer. This observation is quite typical for strongly coupled protons absorbing in a narrow range (23). The proton NMR assignments are summarized in Tables 2 and 3 together with the NH—H_α coupling constants and the NH temperature coefficients obtained from spectra recorded at 286, 290, and 294° K.

The NMR data (NH—H_α coupling constants, ROE distance constraints, amide temperature coefficients) provide the necessary information to estimate the torsion angles ϕ, Ψ, and ω (24) of the peptide backbone. Due to conformational averaging,

Can. J. Chem. Downloaded from www.nrcresearchpress.com by 88.85.125.76 on 09/07/12
For personal use only.

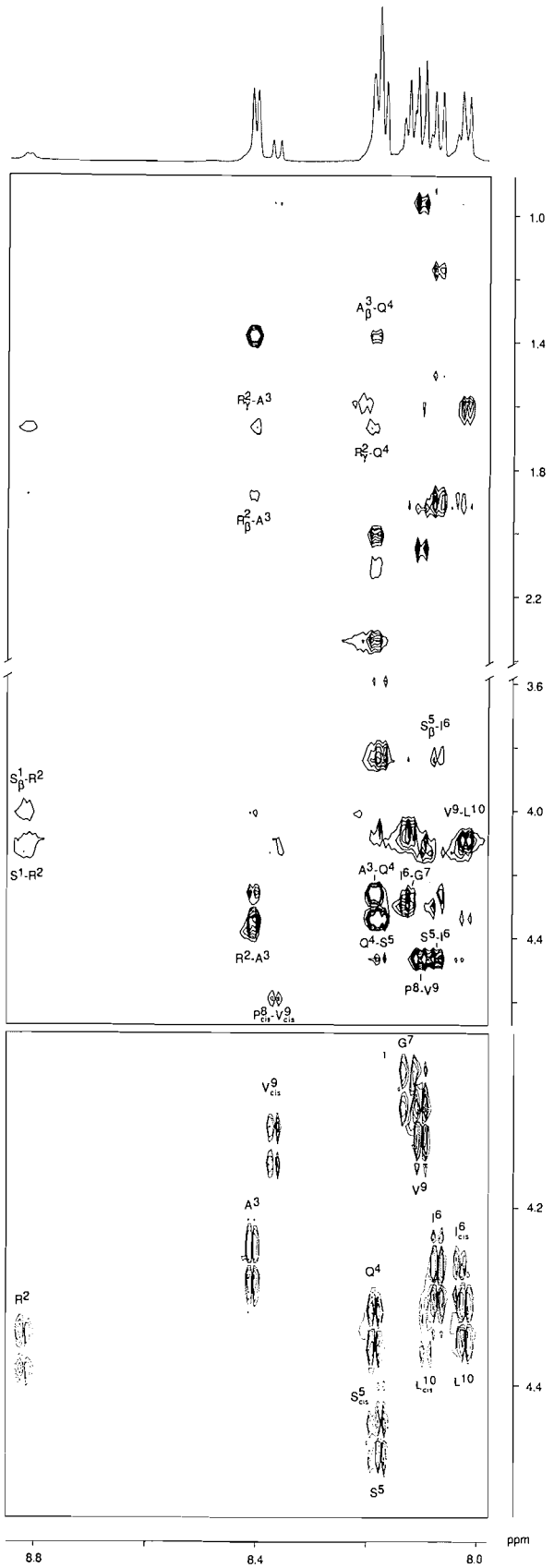

FIG. 1. 600 MHz two-dimensional contour plot of a phase-sensitive COSY (bottom) and phase-sensitive ROESY (top) experiment of the LHRH anti-sense peptide recorded at ambient temperature in CD_3OH/H_2O (60/40). The concentration was 8 mM, the pH 3.60. Positive and negative contours are plotted without distinction. In the ROESY spectrum the contours are equidistant and of opposite sign with respect to the diagonal. The ROE cross-peaks are labeled only when of sequential nature. The first number refers to $H_\alpha(i)$, the second to NH(i + 1) unless otherwise indicated.

which is always present in peptides of this size, the measured effects are the weighted average over two or more conformations making a numerically precise interpretation of, for example, the coupling constants impossible. Nevertheless, certain characteristics of the NMR parameters are diagnostic for the detection of non-extended conformers (5, 25). (*i*) Small NH—H_α coupling constants of one or more residues, (*ii*) NH(i)—NH(i + 1) nuclear Overhauser effect(s) due to short interproton distance(s), and (*iii*) reduced temperature coefficient of one or more of the amide protons. In addition, some of the amide protons might be shifted considerably to lower field (7, 26). This low-field shift together with a reduced NH temperature coefficient is clearly indicative of the formation of a hydrogen bond, whereas the coupling constants and the NOEs reflect altered torsion angles ϕ and Ψ. Depending on what kind of non-extended secondary structure is present and to what extent it coexists with different types of extended conformers, the magnitude of the effects might be small and therefore easily overlooked.

The ^{13}C assignments, based on $^{13}C/^1H$ shift correlation experiments, are listed in Table 4 for both peptides and the DEPT spectrum of the anti-sense peptide is depicted in Fig. 3.

Conformation of the LHRH anti-sense peptide

A review of the NMR data summarized in Table 2 reveals that this decapeptide is a typical representative of short linear peptides with *some* secondary structure. Most of the coupling constants and temperature coefficients as well as the ROEs (Fig. 4) are indicative of an extended conformation. However, the small NH—H_α coupling constants measured in Arg^2 and Ala^3 together with a reduced NH temperature coefficient of Gln^4 clearly show that the N-terminal end is not completely extended. This conclusion is further corroborated by the observation of weak NH(i)—NH(i + 1) ROEs between the residues Arg^2/Ala^3 and Ala^3/Gln^4 (only visible in cross-sections of the two-dimensional ROESY spectrum, not shown) and to a lesser extent by $H_\beta(i)$—NH(i + 1) ROEs (see Fig. 4). Moreover, the low-field shift and broad appearance of the NH(Arg^2) strongly suggests that C=O(Ser^1) takes part in a hydrogen bond (7, 26). In view of all these data, we conclude that the first four residues of the LHRH anti-sense peptide (Ser^1-Arg^2-Ala^3-Gln^4) form a 3_{10}-helical turn (25) stabilized by a C=O(Ser^1)—NH(Gln^4) hydrogen bond, followed by an extended conformation for the remaining residues 5 to 10. The magnitude of the effects discussed above and the observation of ROEs which are only consistent with an extended conformation, for example $H_\alpha(i)$—NH(i + 1) and the complementary $H_\alpha(i)$—$H_{\delta\delta'}(i + 1)$ throughout the peptide chain, entail that only a minor fraction of the molecules adopts the partially helical structure whereas the majority is extended throughout. Because of rapid interchange of the conformers on the NMR time scale, it is not possible to assess the relative populations of the molecules in the two conformations in a numerically precise way. Nevertheless, in comparison to values typically found in fully extended peptides, the reduced coupling constants and the NH(Gln^4) temperature coefficient indicate a time-averaged conformational ratio of approximately 3:1 (fully extended vs. 3_{10}-helical) as the upper limit for the 3_{10}-helical population.

Can. J. Chem. Downloaded from www.nrcresearchpress.com by 88.85.125.76 on 09/07/12
For personal use only.

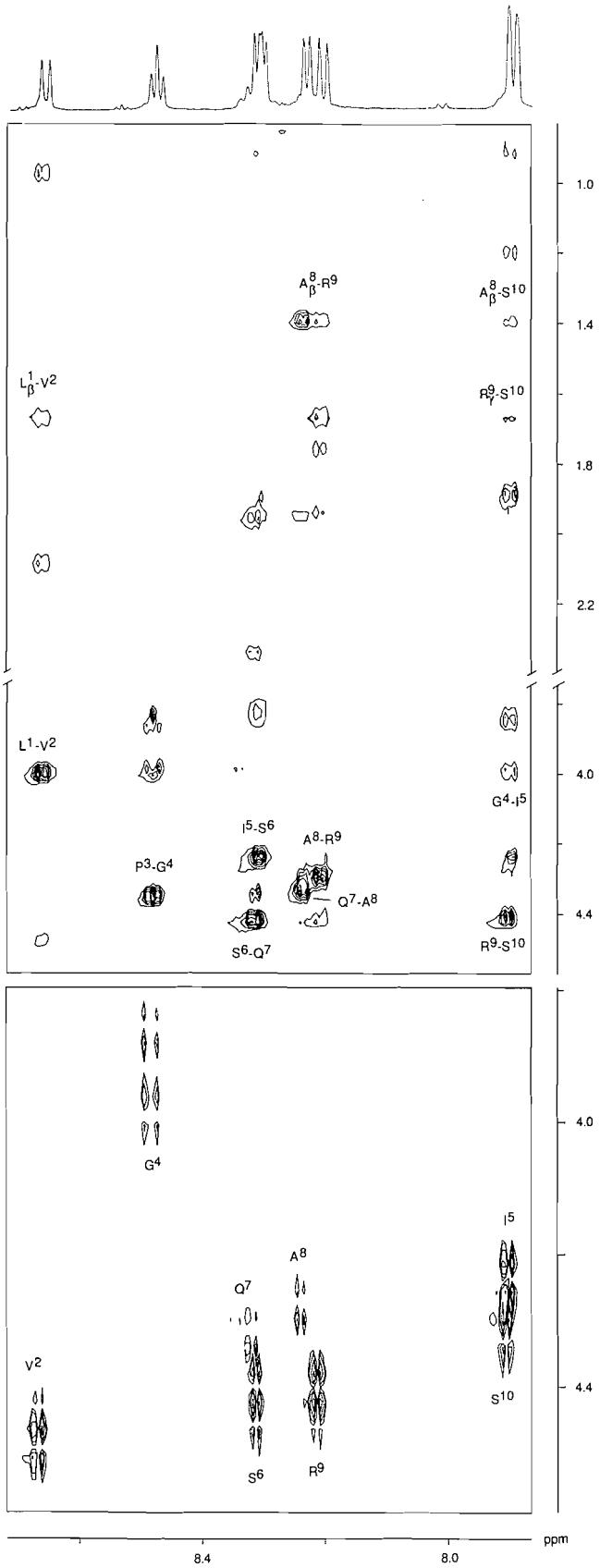

FIG. 2. The same data set as outlined in Fig. 1 recorded from the LHRH inversed anti-sense peptide. The conditions were equivalent to those reported in Fig. 1.

The observation of two ^{13}C resonance lines for most C_α-resonances (Fig. 3) is not conformation-related but due to an H/D isotope effect (27, 28). The ratio of 62:38 reflects the relative proportion of protons and deuterons in the mixed solvent. In the same, but completely deuterated solvent mixture, all C_α-resonances appear as single lines.

Having identified the first four residues to form a non-linear secondary structure, other conformations than the 3_{10}-helical turn have to be considered as well. In particular, the possibility of a β-turn has to be studied. Of the classical β-turn types, the type I turn is two to three times more common than the type II, while the mirror images (types I′ and II′) are very rare (29). The main difference in terms of NMR observables between a 3_{10}-helical turn and a type I β-turn is the observation of two consecutive small NH—H_α coupling constants in the former one whereas in the latter a small coupling constant is followed by a fairly large one (25). Using torsion angles of "ideal" turns (3_{10}: $\phi_2 = -60°$, $\Psi_2 = -26°$, $\phi_3 = -60°$, $\Psi_3 = -26°$, type I β-turn: $\phi_2 = -60°$, $\Psi_2 = -30°$, $\phi_3 = -90°$, $\Psi_3 = 0°$) and the well-known Karplus equation (30) with Karplus constants found in BPTI (basic pancreatic trypsin inhibitor) (31), the corresponding J-values are 4.2 Hz twice (3_{10}) and 4.2, 8.0 Hz (βI). The coupling constant data recorded for the LHRH anti-sense peptide (Table 2) are clearly not consistent with a type I β-turn structure and hence the conclusions as outlined before.

The weighted average distance between two consecutive amide protons in the Ser^1-Gln^4 region is approximately 3.9 Å for an estimated 3:1 ratio of extended versus 3_{10} conformation, instead of 2.6 Å as found in an ideal 3_{10}-helical turn. This result, based on molecular modeling (32) of the 3_{10} and fully extended conformation, explains why the NH—NH ROEs are of very weak nature, since the maximum obtainable nuclear Overhauser effect is reduced by ca. 90% relative to an ideal, 100% populated 3_{10}-helix.

As can be expected in view of the Gly^7-Pro^8 subunit, the peptide bond angles ω are not uniformly *trans* (ω = 180°). Evidence for *cis*/*trans* isomerism (33, 34) about the Gly^7-Pro^8 peptide bond is found in the ^{13}C as well as in the proton spectra. The *cis* isomer is present to the extent of 25% which is very close to the ratio found recently in another Gly-Pro case (26). Besides the doubling of ^1H resonances close to the isomerization site, a $H_\alpha(Gly^7)$—$H_\alpha(Pro^8)$ ROE was observed which is very diagnostic for the existence of a *cis* isomer. The chemical shifts related to the minor isomer are included in Tables 2 and 4 (footnote *d*).

The circular dichroism spectra of the LHRH anti-sense peptide (Fig. 5) show increased negative ellipticity around 215–230 nm in the presence of methanol, suggesting that a conformational change is induced by this organic cosolvent. These spectra do not lend themselves to quantitative analysis but visual comparison with reference spectra for peptides (35) and proteins (36) suggests that a small proportion of ordered secondary structure is present in 60% methanol. The dominant conformer, however, is a random coil.

Conformation of the inversed anti-sense peptide

The spectroscopic data are listed in Table 3 (^1H) and Table 4 (^{13}C) and the ^1H spectra are shown in Fig. 2. An overview of the proton data shows clearly that, in comparison to the previously studied anti-sense peptide, there are less discernible characteristics leading to the conclusion that a large majority of the peptide adopts an extended conformation. The only indications in the ^1H domain for possibly some non-linear conformation are the somewhat reduced temperature coefficients of NH(Ile^5) and NH(Ser^{10}) and the Ala^8 coupling constant of 6.0 Hz. However,

TABLE 2. ^{1}H chemical shifts,[a] coupling constants,[b] and NH temperature coefficients[c] of the LHRH anti-sense peptide[d]

Peptide	NH	H_α	H_β[e]	H_γ[e]	Others	J_{NH-H_α}	ΔT_{NH}
Ser^1[f]	N/A	4.11	4.00 3.97	—	—	N/A	N/A
Arg^2	8.82	4.36	1.87 1.76	1.67	$H_{\delta\delta'}$: 3.20 NH: 7.40	5.5	4.5
Ala^3	8.40	4.26	1.36	—	—	5.6	4.9
Gln^4	8.18	4.34	2.10 2.00	2.33	NH_2: 7.62 6.87	7.1	3.5
Ser^5[f]	8.17 (8.19)	4.46 (4.46)	3.84 3.80	—	—	7.2	4.1
Ile^6	8.07 (8.03)	4.28 (4.28)	1.90 — (1.91)	CH_2: 1.48 1.15 CH_3: 0.91	H_δ: 0.85	8.5	4.4
Gly^7	8.12	4.07 (4.06)	—	—	—	5.6/5.6	4.8
Pro^8[g]	—	4.46 (4.59)	2.20 1.94 (2.37)	2.00	H_δ: 3.63 $H_{\delta'}$: 3.57 (3.52)	—	—
Val^9	8.10 (8.36)	4.10 (4.14)	2.05 — (2.08)	0.95 0.94 (0.96)	—	8.7 (8.2)	5.2 (5.5)
Leu^{10}	8.02 (8.09)	4.33 (4.35)	1.59	1.61 — (1.60)	H_δ: 0.90 $H_{\delta'}$: 0.86	8.2 (8.0)	6.4 (6.4)

[a]Chemical shifts in ppm relative to the undeuterated fraction of the CD_3OH methyl group (3.30 ppm downfield from TMS).
[b]Coupling constants in Hz.
[c]The effect of temperature change on the chemical shifts of the NH protons is measured in ppb/K.
[d]The spectra were measured at 8 mM concentration in CD_3OH/H_2O (60/40), pH 3.60. The temperature was 295 K.
[e]Pairs of protons x (x = β, γ, δ) could not be assigned stereospecifically. In an arbitrary manner, the larger chemical shift was assigned to proton x, the smaller one to x′.
[f]The hydroxyl protons of the two Ser moieties were observed at lower temperature (260 K): 7.25 and 6.75 ppm (not individually assigned).
[g]Values in brackets refer to the *cis* isomer (*cis* Gly^7-Pro^8 peptide bond), which is present to the extent of 25%. Entries into the table are only made where the minor isomer peak could be assigned without ambiguity.

TABLE 3. ^{1}H chemical shifts,[a] coupling constants,[b] and temperature coefficients[c] of the LHRH reversed anti-sense peptide[d]

Peptide	NH	H_α	H_β[e]	H_γ[e]	Others	J_{NH-H_α}	ΔT_{NH}
Leu^1	N/A	3.99	1.67	1.63 —	H_δ: 0.94 $H_{\delta'}$: 0.94	N/A	N/A
Val^2	8.67	4.47	2.08 —	1.00 0.97	—	8.2	8.4
Pro^3[f]	—	4.34	2.26 1.94	2.10 1.95	H_δ: 3.89 (3.63) $H_{\delta'}$: 3.71 (3.50)	—	—
Gly^4	8.48 (8.55)	4.00 3.85	—	—	—	5.9/5.9 (5.8/5.8)	7.6
Ile^5	7.90 (8.02)	4.23 (4.21)	1.88 —	CH_2: 1.45 1.19 CH_3: 0.92	H_δ: 0.86	7.9 (7.5)	5.5
Ser^6	8.31	4.41	3.85 3.81	—	—	6.3	7.6
Gln^7	8.32	4.33	2.13 1.94	2.34	NH_2: 7.60 6.85	7.0	7.0
Ala^8	8.24	4.29	1.39	—	—	6.0	6.4
Arg^9	8.21	4.40	1.93 1.75	1.66	$H_{\delta\delta'}$: 3.20 NH: 7.39	7.5	7.9
Ser^{10}	7.91	4.29	3.84	—	—	8.0	5.5

[a–e]See footnotes Table 2.
[f]The Val^2-Pro^3 peptide bond undergoes *cis/trans* isomerization. Values in parentheses refer to the *cis* isomer which is present to the extent of approximately 6%. Due to the low population of the minor isomer only very few signals were observed and assigned.

Can. J. Chem. Downloaded from www.nrcresearchpress.com by 88.85.125.76 on 09/07/12
For personal use only.

Can. J. Chem. Downloaded from www.nrcresearchpress.com by 88.85.125.76 on 09/07/12
For personal use only.

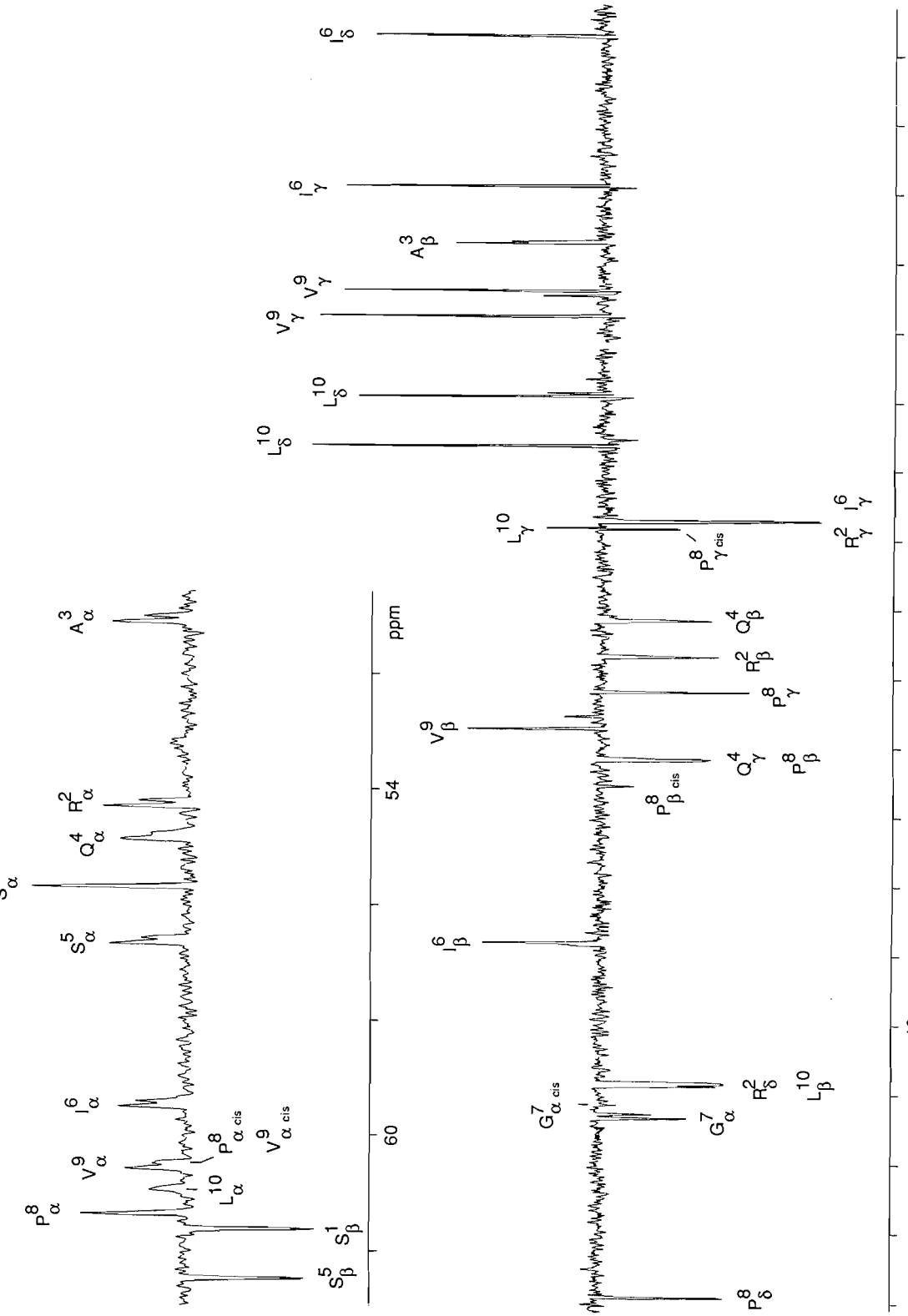

FIG. 3. The 100.6 MHz ^{13}C spectrum of the LHRH anti-sense peptide using the DEPT sequence for polarization transfer. The concentration of the decapeptide was 8 mM at pH 3.60 in CD_3OH/H_2O (60/40), ambient temperature. Positive peaks are due to CH and CH_3 multiplicities, negative signals are observed for CH_2.

TABLE 4. ^{13}C chemical shifts[a] of the LHRH anti-sense peptide and the LHRH reversed anti-sense peptide[b]

LHRH anti-sense peptide[c]					LHRH reversed anti-sense peptide[c]				
Peptide	C_α	C_β	C_γ	C_δ	Peptide	C_α	C_β	C_γ	C_δ
Ser^1	55.70	61.60	—	—	Leu^1	52.88	41.26	25.02	22.89/22.12
Arg^2	54.32	29.38	25.46	41.79	Val^2	58.23	31.34	19.38/18.70	—
Ala^3	51.10	17.41	—	—	Pro^3	61.83	30.47	25.83	49.28
Gln^4	54.88	28.34	32.35	—	Gly^4	43.63	—	—	—
Ser^5	56.69	62.46	—	—	Ile^5	59.59	37.31	25.66/15.71	11.02
Ile^6	59.52	37.63	25.46/15.77	11.45	Ser^6	56.93	62.32	—	—
Gly^7	42.71	—	—	—	Gln^7	54.13	28.22	32.32	—
Pro^{8d}	61.36	32.36	30.40	47.84	Ala^8	50.89	17.61	—	—
Val^9	60.59	31.46	19.56/18.81	—	Arg^9	54.13	29.66	25.50	41.75
Leu^{10}	60.95	41.73	25.65	23.30/21.84	Ser^{10}	57.94	63.36	—	—

[a]Chemical shifts in ppm relative to CD_3OH at 49.0 ppm downfield from TMS.

[b]The spectra of both peptides were measured at 8 mM concentration in CD_3OH/H_2O (60/40), pH 3.60. The temperature was 295 K.

[c]Most α-carbons and C_β (Ala) were observed as two lines at a ratio of 62:38 (anti-sense) and 75:25 (reversed anti-sense), respectively. The reason for this effect is discussed in the text. Only the chemical shifts of the main signals are listed.

[d]The Gly^7—Pro^8 peptide bond consists of 75% *trans* and 25% *cis* isomer. The chemical shifts of the *cis* isomer are $C_\beta(I^6)$: 37.71, $C_\alpha(Gly^7)$: 42.32, $C_\alpha(Pro^8)$: 60.51, $C_\beta(Pro^8)$: 33.12, $C_\gamma(Pro^8)$: 25.68, $C_\alpha(Val^9)$: 60.51, $C_\beta(Val^9)$: 31.11, $C_{\gamma'}(Val^9)$: 18.95, $C_{\delta'}(Leu^{10})$: 21.75.

[e]The Val^2-Pro^3 peptide bond is predominantly *trans* (~94%). Due to the low population of the *cis* isomer only very few signals can be observed and assigned unambiguously: $C_{\delta'}(Leu^1)$: 21.95, $C_\gamma(Val^2)$: 19.10, $C_{\gamma'}(Val^2)$: 18.55, $C_\delta(Ile^5)$: 11.40.

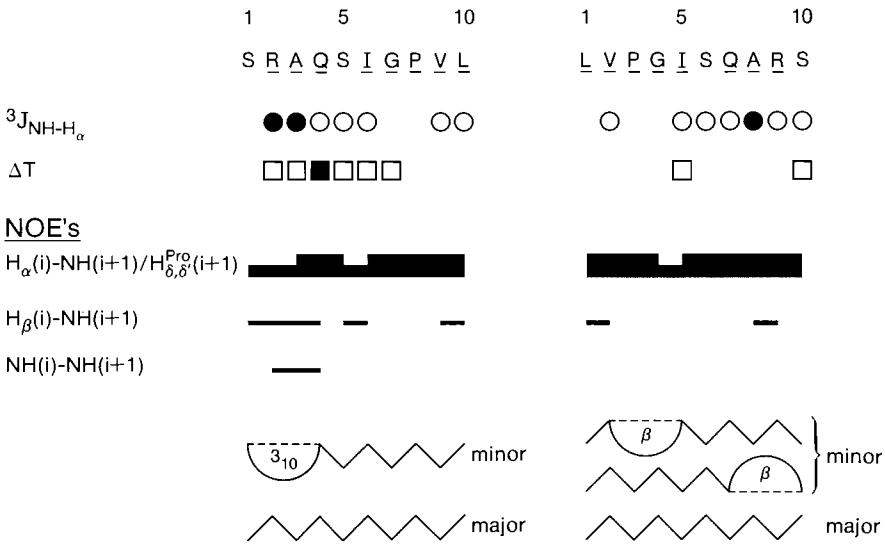

FIG. 4. A summary of NMR data obtained from the two peptides under study. The amino acid sequences are shown for the LHRH anti-sense peptide (left) and its reversed sequence, the LHRH inversed anti-sense peptide (right). Unique amino acids are underlined. The ^3J coupling constants (NH—H_α) are represented by the following symbols: filled circles for values ≤6.0 Hz, open circles for J above 6.0 Hz but below 9.0 Hz. A filled square stands for a NH temperature coefficient of 3.5 ppb/K, open squares are used for values between 4 and 5 ppb/K (left) and 5.5 ppb/K on the right. The ROEs are indicated by bars, the height of which depicts the strength of the effects separated into strong, medium and weak. The secondary structure is depicted schematically at the bottom together with an estimation of the relative population. β-turns and 3_{10}-helical turns are shown by half circles and dashed lines representing NH(i + 3)—C═O(i) hydrogen bonds. An extended chain is drawn as a zig-zag line.

all these effects are small and do not permit very firm conclusions. The absence of any measurable NH—NH ROEs further aggravates the situation. Based on the proton data, we exclude the possibility of a single non-linear conformation in coexistence with an extended conformer. Nevertheless, the presence of two minor conformers in rapid exchange with the molecules in an extended form appears to be a possible explanation. First, the combination of the reduced NH(Ser^{10}) temperature coefficient with the small NH—H_α(Ala^8) coupling constant suggests that a small amount (5 to 10%) of a β-turn could be present in the C-terminal part of the molecule. The sequence Gln-Ala-Arg-Ser shows an above average occurrence in type I β-turn form (29) which can be considered as further evidence although not as proof for our conclusion. It should be emphasized that our data do not permit defining what kind of β-turn is present but a type I β-turn in small proportion certainly does not violate our data set. Second, an additional turn could be located in the Val^2-Pro^3-Gly^4-Ile^5 part of the molecule with NH(Ile^5) taking part in a hydrogen bond and hence the somewhat reduced temperature dependence of its amide proton. Again, not more than 5 to 10% of the molecules are expected to adopt this conformation. In this sequence, the potentially small coupling constant of the second amino acid can, of course, not be observed, since this is a proline moiety. Therefore, our conclusion has to be considered

Can. J. Chem. Downloaded from www.nrcresearchpress.com by 88.85.125.76 on 09/07/12
For personal use only.

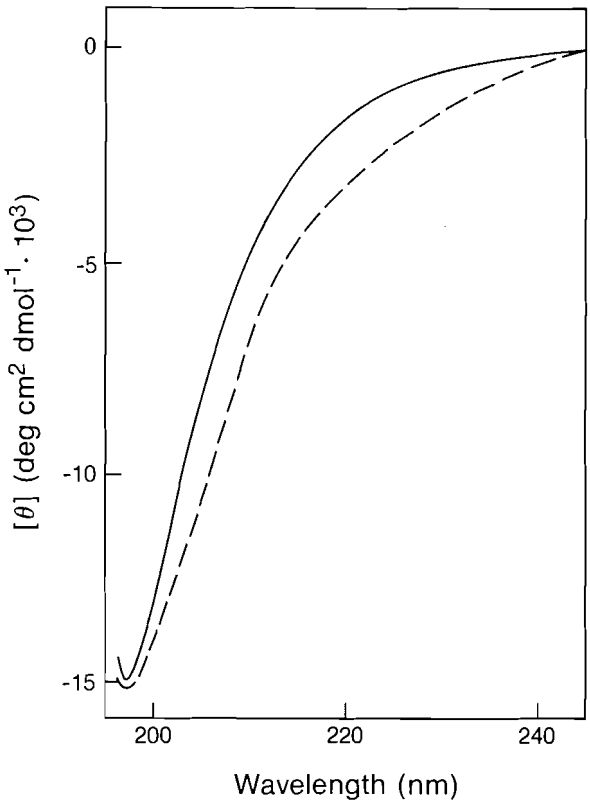

FIG. 5. Circular dichroism spectra of the LHRH anti-sense peptide in water (—) and in water/methanol (40/60) (---).

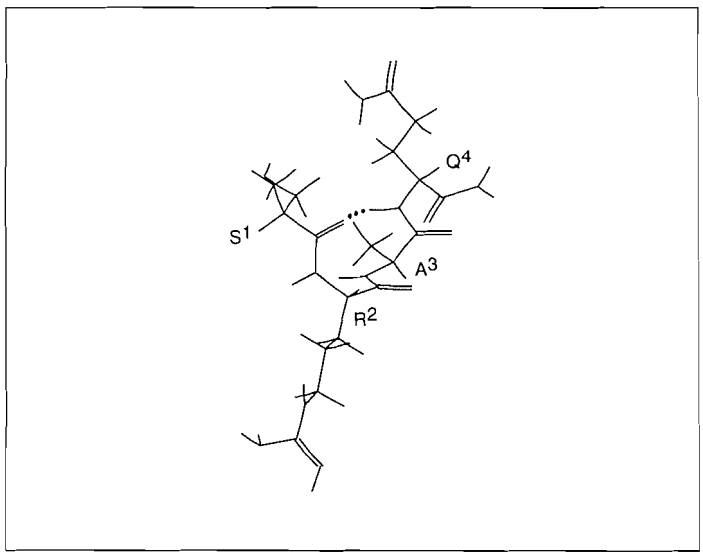

FIG. 6. A molecular model of the first four amino acids of the LHRH anti-sense peptide, forming one 3_{10}-helical turn stabilized by a hydrogen bond (dotted line) between NH(Gln^4) and C=O(Ser^1). The model depicted does not represent the only conformation of all the molecules, and it has been drawn by using torsion angles as described in the text.

somewhat speculative, but again, a statistical analysis (29) shows a high occurrence of a β-turn (type II in this case) in the tetrapeptide under question. It is noteworthy that the results of our attempt to understand an only partly conclusive data set coincide with the statistically clearly highest occurrence of β-turns anywhere in the decapeptide (29). The two possible β-turns do not necessarily have to coexist in the same molecules simultaneously. In view of the NMR evidence, showing that only a very minor percentage of the conformers are non-extended, we refrained from recording circular dichroism spectra of the reversed anti-sense peptide.

A final remark is directed towards the aforementioned *cis/trans* isomerism. Not surprisingly, this effect is much smaller compared to the anti-sense peptide. The Val^2-Pro^3 peptide bond exhibits a *cis*-isomer content of only 6%. The drastic decline from 25% in the Gly-Pro case demonstrates that in the absence of any additional stabilizing effects such as charge interactions (37) the *cis* isomer is rare when bulky amino acids precede proline. Due to the low percentage of *cis* isomer only few resonances were observed. They are included in Tables 3 and 4 (footnote *e*).

Conclusion

The ^{1}H and ^{13}C spectra of the LHRH anti-sense peptide as well as the LHRH inversed anti-sense peptide were analyzed by various two-dimensional NMR techniques in CD_3OH/H_2O (60/40) solutions. A summary of the spectroscopic data obtained from both decapeptides is presented in Fig. 4. There is very strong evidence that the N-terminal end of the anti-sense peptide forms one complete 3_{10}-helical turn stabilized by a NH(Gln^4)/C=O(Ser^1) hydrogen bond, followed by an extended conformation for the rest of the peptide. These conclusions are based on proton NMR results such as NH—NH ROEs (Ser^1/Arg^2 and Arg^2/Ala^3), reduced NH—H_α coupling constants (Arg^2, Ala^3), a low-field shift of NH(Arg^2) and a reduced temperature coefficient of NH(Gln^4). However, the magnitudes of these effects demonstrate clearly that on the time-averaged NMR scale the molecules with the 3_{10}-helical turn are in fast exchange with molecules that are extended throughout and hence the ratio between the two conformers can only be estimated. In comparison to linear peptides that are fully extended, we conclude that the 3_{10}-helix conformation is only present to a maximum of 25% of the time. Figure 6 depicts the first four amino acids of the anti-sense peptide in a 3_{10}-helical conformation. This was produced by molecular modeling (32) using torsion angles of an ideal 3_{10}-helical turn, followed by energy minimization (32) and checking for consistency with the NMR data set. The torsion angles used in Fig. 6 are (in the order Ser, Arg, Ala, Gln): ϕ = —, −72°, −50°, −71°; Ψ = 142°, −33°, −43°, 138°; ω = 173°, 174°, 177°, —; χ_1 = −63°, +63°, —, 180°, remaining χ's 180°. The distance O(Ser^1)—N(Gln^4) is 3.1 Å which is well within the 3.5 Å considered as the upper limit for hydrogen bonds.

The conformational data of the LHRH anti-sense peptide resemble those of LHRH (ref. 4 and references therein) in the sense that both peptides exist in solution as mixtures of several conformers in fast exchange. On the other hand, and not surprisingly in view of the different peptide sequences, the non-extended features are quite different.

The data obtained from the LHRH inversed anti-sense peptide are less conclusive. It appears likely that a small percentage of the molecules form a β-turn (probably type I) located in the C-terminal end. Another β-turn (possibly type II) could be located in the Val^2-Ile^5 fragment. In view of the somewhat incomplete evidence, we refrain from presenting a molecular model of the LHRH inversed anti-sense peptide. While both decapeptides exist in predominantly extended conformations, the minor, non-extended conformers are significantly different from each other both in terms of their nature and their percentage.

Can. J. Chem. Downloaded from www.nrcresearchpress.com by 88.85.125.76 on 09/07/12
For personal use only.

Acknowledgements

We wish to thank Bruker-Spectrospin in Switzerland and, in particular, Dr. Hans-Peter Kellerhals and Dr. Gerhard Wider for providing access to and technical assistance on the AM 600 system. The Natural Sciences and Engineering Research Council of Canada and the University of Alberta are acknowledged for generous financial support.

1. E. L. Baniak, J. E. Rivier, R. S. Struthers, A. T. Hagler, and L. M. Gierasch. Biochemistry, **26**, 2642 (1987).
2. P. H. Seeburg and J. P. Adelman. Nature (London), **311**, 666 (1984).
3. J. J. Mulchahey, J. D. Neill, L. D. Dion, K. L. Bost, and J. E. Blalock. Proc. Natl. Sci. USA, **83**, 9714 (1986).
4. P. M. Conn. Methods Enzymol. **168**, 697 (1989).
5. H. J. Dyson, M. Rance, R. A. Houghten, R. A. Lerner, and P. E. Wright. J. Mol. Biol. **201**, 161 (1988).
6. H. J. Dyson, M. Rance, R. A. Houghten, P. E. Wright, and R. A. Lerner. J. Mol. Biol. **201**, 201 (1988).
7. A. Otter, P. G. Scott, X. Liu, and G. Kotovych. J. Biomol. Struct. Dyn. **7**, 455 (1989).
8. R. R. Ernst, G. Bodenhausen, and A. Wokaun. Principles of nuclear magnetic resonance in one and two dimensions. Clarendon Press, Oxford, 1987.
9. J. M. Stewart and J. D. Young. Solid phase peptide synthesis. Pierce Chemical Co., Rochford, Il. 1985.
10. D. M. Doddrell, D. T. Pegg, and M. R. Bendall. J. Magn. Reson. **48**, 323 (1982).
11. A. J. Shaka, J. Keeler, and R. J. Freeman. J. Magn. Reson. **53**, 313 (1983).
12. W. P. Aue, E. Bartholdi, and R. R. Ernst. J. Chem. Phys. **64**, 2229 (1976).
13. A. A. Bothner-By, R. L. Stephens, J. Lee, C. D. Warren, and R. W. Jeanloz. J. Am. Chem. Soc. **106**, 811 (1984).
14. A. Bax and D. G. Davis. J. Magn. Reson. **63**, 207 (1985).
15. M. R. Bendall and D. T. Pegg. J. Magn. Reson. **53**, 144 (1983).
16. D. Marion and K. Wüthrich. Biochem. Biophys. Res. Commun. **113**, 967 (1983).
17. R. Brüschweiler, J. C. Madsen, Ch. Griesinger, O. W. Sorensen, and R. R. Ernst. J. Magn. Reson. **73**, 380 (1987).
18. G. Wider, R. V. Hosur, and K. Wüthrich. J. Magn. Reson. **52**, 130 (1983).
19. Ch. Griesinger and R. R. Ernst. J. Magn. Reson. **75**, 261 (1987).
20. H. Kessler, Ch. Griesinger, R. Kerssebaum, R. Wagner, and R. R. Ernst. J. Am. Chem. Soc. **109**, 607 (1987).
21. Del. F. DeTar. Anal. Chem. **41**, 1406 (1969).
22. D. Neuhaus and J. Keeler. J. Magn. Reson. **68**, 568 (1986).
23. A. Bax. J. Magn. Reson. **77**, 134 (1988).
24. IUPAC-IUB Commission on Biochemical Nomenclature. Biochemistry, **9**, 3471 (1970).
25. K. Wüthrich. NMR in proteins and nucleic acids. Wiley-Interscience, New York, 1986.
26. A. Otter, G. Kotovych, and P. G. Scott. Biochemistry, **28**, 8003 (1989).
27. A. Otter, X. Liu, and G. Kotovych. J. Magn. Reson. **86**, 657 (1990).
28. P. E. Hansen. Prog. NMR Spectrosc. **20**, 207 (1988).
29. C. M. Wilmot and J. M. Thornton. J. Mol. Biol. **203**, 221 (1988).
30. M. J. Karplus. J. Am. Chem. Soc. **85**, 2870 (1963).
31. A. Pardi, M. Billeter, and K. Wüthrich. J. Mol. Biol. **180**, 741 (1984).
32. Alchemy II, Tripos Associates Inc., St. Louis, MO 63144, USA.
33. R. Deslauriers and I. C. P. Smith. Topics in carbon-13 NMR spectroscopy. *Edited by* G. C. Levy. Wiley-Interscience, New York. 1976. pp. 2–66.
34. A. Otter and G. Kotovych. J. Magn. Reson. **74**, 293 (1987).
35. N. J. Greenfield and G. D. Fasman. Biochemistry, **8**, 4108 (1969).
36. C. T. Chang, C.-S.C. Wu, and J. T. Yang. Anal. Biochem. **91**, 13 (1978).
37. A. Szollosy, A. Otter, J. M. Stewart, and G. Kotovych. J. Biomol. Struct. Dyn. **4**, 501 (1986).

Can. J. Chem. Downloaded from www.nrcresearchpress.com by 88.85.125.76 on 09/07/12
For personal use only.

Characterization of asphaltenes from Cold Lake heavy oil: variations in chemical structure and composition with molecular size

KATHLEEN M. SEMPLE
Department of Microbiology, University of Alberta, Edmonton, Alta., Canada T6G 2E9
NATSUKO CYR
Alberta Research Council, PO Box 8330, Postal Station F, Edmonton, Alta., Canada T6H 5X2
AND
PHILLIP M. FEDORAK AND DONALD W. S. WESTLAKE
Department of Microbiology, University of Alberta, Edmonton, Alta., Canada T6G 2E9

Received November 22, 1989

This paper is dedicated to Professor Arthur S. Perlin on the occasion of his 67th birthday

KATHLEEN M. SEMPLE, NATSUKO CYR, PHILLIP M. FEDORAK, and DONALD W. S. WESTLAKE. Can. J. Chem. **68**, 1092 (1990).

Asphaltenes from Cold Lake oil were separated into fractions by size exclusion chromatography to study the molecular size dependence of chemical structural characteristics. Each fraction was analyzed by proton NMR and UV–visible spectroscopy and by elemental analyses for C, H, N, S, Ni, and V. The results indicated that the nature of the average chemical structures in Cold Lake asphaltenes were not uniform throughout the total range of molecular sizes but varied significantly; some changed gradually and some changed quite abruptly. Especially in the very low molecular-weight fraction, the size of aromatic moieties seems to be much smaller, the contents of both aromatic carbon and aromatic hydrogen are higher, the C/H ratio is higher, and the porphyrin and vanadium concentrations are much higher than in heavier fractions.

Key words: Cold Lake asphaltenes, size fractionation, vanadium, proton NMR, porphyrin, chemical structural analysis.

KATHLEEN M. SEMPLE, NATSUKO CYR, PHILLIP M. FEDORAK, et DONALD W. S. WESTLAKE. Can. J. Chem. **68**, 1092 (1990).

Dans le but d'étudier la relation entre les caractéristiques chimiques et la grosseur des molécules et faisant appel à la chromatographie par perméation, on a séparé des asphaltènes provenant de l'huile de Cold Lake en plusieurs fractions. Chaque fraction a été analysée par run du ^1H, par spectroscopie UV–visible et par analyse élémentaire du C, H, N, S, Ni et V. Les résultats indiquent que les structures chimiques moyennes des asphaltènes provenant de l'huile de Cold Lake n'ont pas une nature uniforme et que les structures varient beaucoup en fonction des grosseurs des molécules; quelques-unes varient graduellement alors que d'autres changent brusquement. Dans la fraction de très bas poids moléculaire, on note en particulier que la grosseur des portions aromatiques est beaucoup plus petite, que les quantités de carbones et d'hydrogènes aromatiques sont plus élevées, que le rapport C/H est plus élevé et que les concentrations de porphyrine et de vanadium sont beaucoup plus élevées que dans les fractions de poids moléculaires plus élevées.

Mots clés : asphaltene de Cold Lake, fraction par taille, vanadium, RMP, porphyrin, analyse chimique structurale.
[Traduit par la revue]

Introduction

Asphaltenes, the pentane-insoluble fraction of oil, consist of very high molecular-weight compounds of both aromatic and aliphatic nature (1). They are rich in heteroatoms (N, S, O) and metals (2, 3). There have been a number of studies which indicated that asphaltenes consist of condensed polynuclear aromatic rings bearing alkyl side chains (4–6) aggregated to different degrees through stacking of large aromatic sheets (5–8).

For a given oil, the asphaltene fraction is generally thought to consist of structurally similar molecules varying mainly in molecular weight (6, 9). However, there is evidence that the chemical charcateristics and "average" molecular structures may vary considerably with their sizes. For example, heavy metals are not uniformly distributed in asphaltenes (10) with vanadium concentrations being higher in lower molecular-weight fractions (11, 12). Similarly, petroporphyins (3, 11, 12) were found to be most abundant in low-molecular weight fractions. In addition, Ignasiak *et al.* (13) observed that the very high molecular-weight fraction of Athabasca asphaltenes was more prone to forming methylene chloride-insoluble polymers on heating than the low molecular-weight fractions which even seem to act as inhibitor of polymerization. These differences in chemical reactivity suggested that some molecular size fractions of asphaltenes may be more susceptible to enzymatic or microbial attack than other fractions.

Microorganisms have been shown to associate with bitumens. For example, Wyndham and Costerton (14) observed bacterial colonization of bitumen particles suspended in the Athabasca river and reported that these isolates reduced the maltene content of bitumen but were unable to grow on the asphaltene fraction. In addition, bacterial rods have been observed in freeze-fractured samples of Athabasca bitumen examined by transmission electron microscopy (15).

Although there have been numerous reports demonstrating that microorganisms can degrade *n*-alkanes, isoprenoids (16), aromatic hydrocarbons (17), and sulfur heterocycles (18), there is no chemical or physical evidence that microorganism can modify asphaltenes. The data reported in this paper are the results of the separation (by gel permeation chromatography) and chemical and physical characterization of various size fractions of Cold Lake asphaltenes which will be used in biotransformation studies. The analyses focus on variations in C/H ratio, aromatic characteristics, and the distributions of petroporphyrins, vanadium, and nickel among the fractions. Where possible, the results of our work with the Cold Lake

Can. J. Chem. Downloaded from www.nrcresearchpress.com by 88.85.125.76 on 09/07/12
For personal use only.

TABLE 1. Characterization of the five major fractions and the unfractionated Cold Lake asphaltenes

Fraction No.	Eluted volume (mL)	Solid yield (wt%)[a]	MW at peak maxima[b]	Elemental analysis (wt%) C	H	N	S	C/100 H
1	10	14±3	5 000	81.2	7.8	1.3	7.8	87.4
2	10	33±5	4 000	80.9	7.8	1.2	7.4	86.7
3	10	25±5	3 000	80.8	7.8	1.5	7.3	86.2
4	30	16±6	1 800	81.0	8.1	1.3	7.3	83.4
5	170	12±2	800	80.6	7.2	1.4	6.3	92.9
Unfractionated	—	—	2 000	79.9	7.5	1.3	7.6	88.9

[a]Yield average of 12 separations.
[b]Based on polystyrene standards.

asphaltenes were compared to those obtained from Athabasca asphaltenes that had been fractionated using the same GPC method.

Experimental

Preparation of asphaltenes

Cold Lake bitumen (i.e. asphalt-like hydrocarbons found in oil sands) is an oil (API gravity of 11) with approximately 15% asphaltene content. It was recovered by steam injection by ESSO Resources and provided through the Alberta Research Council sample bank. Asphaltenes were prepared from fresh Cold Lake bitumen using *n*-pentane precipitation. Oil was dissolved overnight in one volume of toluene (19), thereby decreasing viscosity. Water and solids were sedimented by centrifugation (15 min in an IEC Clinical Centrifuge). The layer of oil/toluene was removed and the asphaltenes were precipitated by adding 40 volumes of *n*-pentane (pentane:toluene:oil = 40:1:1) and stirring at room temperature for 2 h. Asphaltenes were collected by vacuum filtration through a 10–15 μm scintered glass funnel. They were washed repeatedly with pentane. Asphaltenes were redissolved in a minimum amount of toluene and precipitated with 40 volumes of pentane and collected by filtration. This procedure was repeated three more times to remove any occluded resins and aromatics (20). Asphaltenes isolated in this manner were stored under a nitrogen atmosphere to minimize oxidation.

Fractionation of asphaltenes

Fractionation of asphaltenes was done using the gel permeation chromatography (GPC) method used by Ignasiak *et al.* (13). All solvents were reagent grade and used as provided by the manufacturer (Mallinckordt). Asphaltenes were fractionated on 2.5 × 100 cm Biobeads S-X1 columns using chloroform as eluent. Fraction collection was started when the first color was eluted (average void volume = 110 mL). Five major fractions (designated 1 to 5) corresponding to the fractions obtained by Ignasiak *et al.* (13) were collected (see Table 1). Fraction 5 was comprised of the last 170 mL collected from the GPC column. This volume was collected in five subfractions designated 5-1 to 5-5 (see Table 2). These subfractions were either characterized separately or pooled to give fraction 5. The solvent was removed using a rotary evaporator, then the samples were transferred in methylene chloride to preweighted vials and the solvent was evaporated overnight at room temperature. The samples were weighed and stored under a nitrogen atmosphere with Teflon-lined caps. The disappearance of solvent in samples was confirmed during NMR analyses.

Analytical GPC

The fractions from the Biobeads S-X1 columns were analyzed by GPC using three 30 cm × 7.8 mm i.d. Waters μ-Styragel columns (1000, 500, and 100 Å) in series with methylene chloride as eluent (21). The instrument used was a Milton-Roy HPLC system with a UV detector at 254 nm. Asphaltenes were dissolved in methylene chloride to a concentration of 5 mg/mL. The injection volume was 20 μL and the solvent flow rate was 1.5 mL/min. The relationship between the elution time and the apparent molecular weight was calibrated using monodispersed polystyrene standards (Perkin-Elmer) and toluene. The elution time of the peak mode for an asphaltene fraction was compared to the calibration curve and this value was taken as the apparent molecular weight.

TABLE 2. Yields and apparent molecular weights of Cold Lake asphaltenes in subfractions of fraction 5

Fraction	Eluted volume (mL)[a]	Solid yield (wt%)[b]	MW peak maxima[c]
5-1	30	6	1 200
5-2	30	3	700
5-3	30	2	450
5-4	30	1	200
5-5	50	0.5	100

[a]After fraction 4.
[b]Based on total weight of asphaltenes applied to GPC column.
[c]Based on polystyrene standards.

Nuclear magnetic resonance (NMR)

Proton NMR spectra were measured on a Bruker WP-80 spectrometer at 80 MHz in $CDCl_3$ solutions using TMS as internal standard. Each spectrum was integrated to determine the relative abundance of different types of protons in the sample.

Cross polarization/magic angle spinning (CP/MAS) C-13 NMR spectra of solid samples were recorded on a Bruker CXP-200 spectrometer operating at 50.3 MHz. The contact time was 1 ms, the recycle delay was 1 s, and the proton 90 degree pulse width was 6 μs (22). Cylindrical $A1_20_3$ rotors were used in a Doty Scientific probe and samples were spun at ~4.5 kHz. The apparent aromaticity, f_a, was calculated assuming that spinning sidebands on both sides of aromatic carbons were of equal size.

Electron spin resonance (ESR)

Electron spin resonance measurements were done on a Bruker ESR model ER-200 SRC spectrometer. Details of the experimental conditions and the method of calculation of spin numbers have been described elsewhere (23).

Ultraviolet–visible spectrophotometry and calculation of porphyrin concentration

A Pye-Unicam 8740 spectrophotometer was used to obtain UV–visible scans (200 to 600 nm) of asphaltene fractions dissolved in methylene chloride. The presence of petroporphyrins was detected by the prominent absorbance peak at ~410 nm (Soret peak) and a weaker absorbance at 573 nm (α peak) (24). Semi-quantitative analysis of porphyrins in asphaltenes was done in the concentration ranges where

Can. J. Chem. Downloaded from www.nrcresearchpress.com by 88.85.125.76 on 09/07/12
For personal use only.

the relationship between the absorption and the concentration was linear. Peak heights were measured using the baseline extrapolated from the minimum on each side of the peak (25, 26). For samples which showed a slight shoulder at 590 nm, the baseline for the 573 nm peak was measured back to 600 nm (27, 28). Peak heights were converted to absorbance values and the absorbance per mg of the original sample was calculated. The amount of porphyrin (μmol/g) in each fraction was estimated using the previously reported values for the molar extinction coefficients for pure and petroporphyrins in chloroform. Molar extinction coefficient $\epsilon = 45.0 \times 10^4$ was used for calculations at 410 nm (28, 29). Various molar extinction coefficients ranging from 2.15 to 3.7×10^4 (3, 28–33) were used for the peak at 573 nm. The concentration, in parts per million (μg/g) was estimated using an approximated molecular weight for porphyrins of 600 (vanadium octaethylporphyrin (30)).

Elemental analysis

Elemental analysis for C, H, and N was done in duplicate or quadruplicate at the microanalytical laboratory of the Chemistry Department, University of Alberta using a Perkin-Elmer 240B CHN analyzer. The Schoeniger combustion method was used for sulfur analysis (34).

Nickel and vanadium analyses were done on an Inductively Coupled Plasma (ICP) simultaneous spectrometer (Model 34000, Applied Research Laboratory). Samples of asphaltene fractions were dissolved in 10 mL xylene/mineral oil mixture.

Method of calculation

To obtain information on the molecular composition of the asphaltenes in each fraction, the total signal intensity from each NMR spectrum was taken as 100 and each spectrum was divided into four chemical shift regions, as is often done (5, 6, 35, 36): H1, methyl protons at the end of aliphatic chains (0.2–1.0 ppm); H2, methylene protons on aliphatetic chains (1.0–2.1 ppm); Ha, α protons to aromatic carbon (2.1–5.0 ppm); and Har, aromatic protons (7.0–9.0 ppm).

Chemical shift values separating regions were chosen at the minima of the spectra so that the errors in integrals are minimized. Naphthenic protons may appear in the region 1.5–2.1 ppm but this region was combined with the other types of methylene and methyne protons since there was no spectral minimum to separate this region.

For every 100 hydrogens detected by proton NMR, the following values were calculated to determine similarities and differences in chemical structures among asphaltene fractions. Figure 1 illustrates the different types of H atoms and C atoms considered in those calculations.

(i) Average number of aliphatic chains and their length

If we assume that all the aliphatic chains were composed of methylene groups (35) and these were longer than two-carbon length, the number of aliphatic chains ending with methyl groups can be calculated from the number of end methyl protons, H1 (0.2–1.0 ppm):

[1] The number of end methyl groups = H1/3

There should be an equal number of α carbons for each end methyl group. Therefore, the excess α carbons must belong to aliphatic chains not ending with methyl groups. These aliphatic chains would connect aromatic carbons or acyclic rings attached to aromatic rings. Heteroatoms, such as O or S, may be included in these aliphatic chains.

The number of α carbons can be obtained from Ha divided by 2, because of the assumption that only methylene groups were present:

[2] The number of α carbons = Ha/2

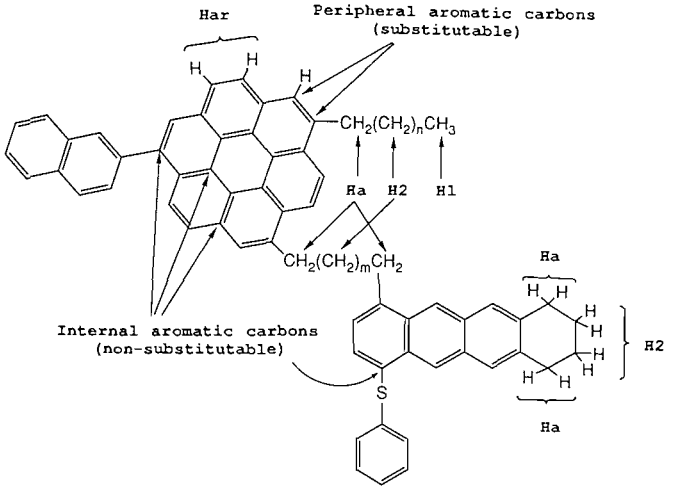

FIG. 1. Illustration of the types of hydrogen and carbon atoms considered for NMR analysis.

Because two methylene carbons are involved in connecting aromatic carbons, the number of such aliphatic chains is

[3] The number of chains connecting aromatic carbons
$= (1/2) \times [(Ha/2) - (H1/3)]$

The total number of aliphatic chains are the sum of [1] and [3]:

[4] The total aliphatic chains $= (1/2) \times (Ha/2 + H1/3)$

The average number of middle methylene carbons in the aliphatic chains can be calculated by dividing the total number of methylene carbons, H2/2, by the number of chains:

[5] The number of CH_2 in a chain $= (H2/2)/[(1/2) \times (Ha/2 + H1/3)]$

(ii) Average degree of alkyl substitution in aromatic rings

Assuming that no heteroatoms were directly bonded to aromatic carbons, but only methylene carbons were bonded to aromatic carbons, the total peripheral aromatic carbons can be obtained from the sum of the number of aromatic hydrogens, Har, and the number of α carbons, Ha:

[6] The peripheral aromatic carbons = Har + Ha/2

The degree of substitution on peripheral aromatic carbons can be obtained from the ratio of the total number of α carbons to the number of peripheral aromatic carbons calculated in [6]:

[7] The degree of substitution in peripheral aromatic carbons
$= (Ha/2)/(Ha/2 + Har)$

(iii) The total number of substitutable carbons

Although the number of quarternary carbons (other than methylene substituted aromatic carbons) was not obtainable from the analysis of the proton NMR, the total number of substitutable carbons can be calculated from the sum of the total end methyl carbons (H1/3), the total methylene carbons (H2/2), the total α carbons (Ha2/2), and the total peripheral aromatic carbon (Ha/2 + Har):

[8] The total number of substitutable carbons
$= H1/3 + H2/2 + Ha + Har$

(iv) Carbon aromaticity

The carbon aromaticity values based on proton NMR are the ratios of the peripheral aromatic carbons in [6] to the total

Can. J. Chem. Downloaded from www.nrcresearchpress.com by 88.85.125.76 on 09/07/12
For personal use only.

number of substitutable carbons in [8]. Types of carbons not included in this calculation are the inner aromatic carbons in condensed aromatic rings, those aromatic carbons directly connecting two aromatic moieties (such as found in biphenyl), aromatic carbons directly bonded to heteroatoms and quarternary aliphatic carbons.

The number of carbons for every 100 hydrogens calculated from the results of elemental analysis is larger than that obtained by eq. [8] because non-substitutable carbons are not included in the latter. The difference between those two numbers should be the number of non-substitutable carbons (see Fig. 1). If we assume that all the non-substitutable carbons are aromatic, the "true" carbon aromaticity can be calculated by adding this difference to the number of peripheral aromatic carbons in [6] and dividing by the total number of carbons:

[9] The "true" carbon aromaticity

$$= (D + \mathrm{Ha}/2 + \mathrm{Har})/(C/100\mathrm{H})$$

where $D = C/100\mathrm{H} - (\mathrm{H1}/3 + \mathrm{H2}/2 + \mathrm{Ha} + \mathrm{Har})$ and $C/100\mathrm{H}$ is the number of carbon for 100 hydrogen obtained from the elemental analysis.

Results and discussion

Yields and characteristics of fractionated Cold Lake asphaltenes

The volumes of chloroform solutions collected after the Biobeads S-X1 column separation and the yields of solid asphaltenes are shown in Tables 1 and 2. Figure 2 shows the analyses of these fractions by analytical GPC chromatography used to assign the apparent molecular weights. Although polymer molecular weight standards are known to have limited applications (11, 37–39), polystyrene molecular weight standards were chosen for use with the analytical GPC method because of simplicity and the need for apparent molecular weight markers in subsequent biotransformation studies.

The possible effect of adsorption of asphaltenes on the GPC columns was previously investigated by adding a polar solvent, methanol, to the eluent (40). This did not decrease the retention volume of the asphaltene indicating that there was no significant adsorption effect during the size separation process. Based on the results of 12 fractionations of the Cold Lake asphaltenes on Biobeads S-X1, 103 ± 3% of the asphaltenes applied to the column were recovered.

Table 1 also shows the elemental analyses of each of the major fractions of the Cold Lake asphaltenes. According to the result of the Duncan's multiple range test (41), there were no differences among the $C/100\mathrm{H}$ ratios of fractions 1 to 4, but this ratio was significantly higher in fraction 5 ($P < 0.05$). Similarly, there were no differences among the sulfur contents of fractions 1 to 4, but the sulfur content of fraction 5 was significantly lower than those in the other fractions.

The preparative-scale column chromatography procedure used in this study was the same as used in earlier work with Athabasca asphaltenes (13). The results of these two studies are summarized in Table 3. The yields of each fraction were somewhat different and these may be due to the differences in the nature of the asphaltenes in the two oils, in the method of asphaltenes preparation or in the void volumes of the chromatography columns. However, in both studies, the first two fractions contained approximately half of the asphaltenes. For each fraction, the value of $C/100\mathrm{H}$ of the Cold Lake asphaltenes is higher than that of the Athabasca asphaltenes suggesting that the former has a higher degree of aromaticity.

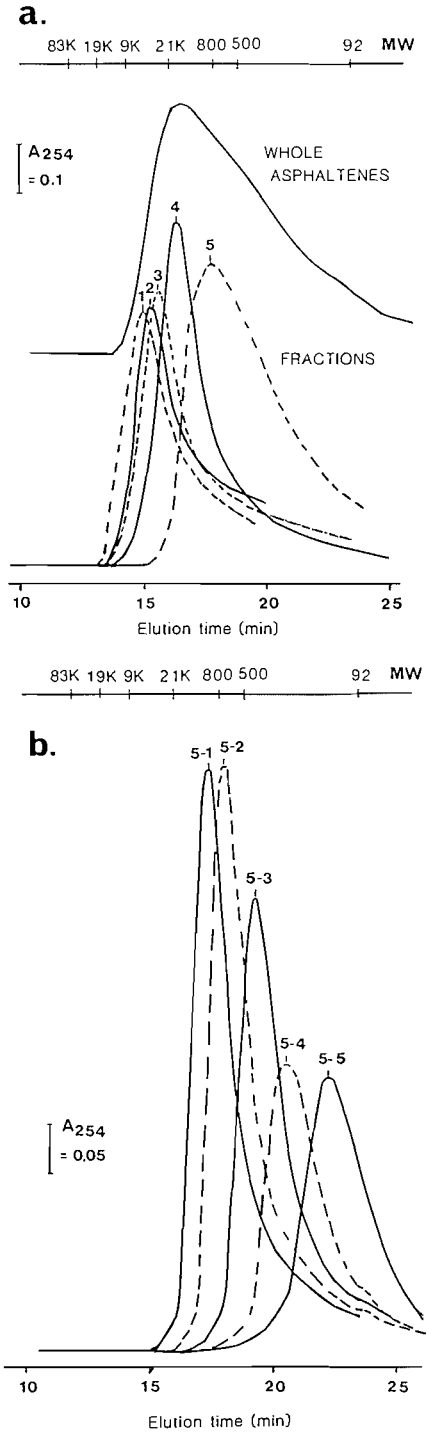

FIG. 2. Analytical gel permeation chromatograms of (*a*) the five major fractions and (*b*) the subfractions of fraction 5. For each fraction and subfraction, a solution of ~5 mg/mL was prepared and a 20 μL portion of these was analyzed. The areas under the curve do not reflect the fraction yields. The elution times of various polystyrene MW standards and toluene (MW = 92) are shown above the chromatograms.

NMR analyses

Proton NMR spectra have been used to character bitumes and their fractions (6, 36, 42–44). A stack plot of the proton NMR spectra is shown in Fig. 3. The general appearance of the spectra for fractions 1 to 4 was very similar. The spectrum of fraction 5 showed a much higher proportion of aromatic protons (Har) as well as of α protons (Ha) than those of other fractions. This may

Can. J. Chem. Downloaded from www.nrcresearchpress.com by 88.85.125.76 on 09/07/12
For personal use only.

TABLE 3. Comparisons for Cold Lake and Athabasca asphaltenes obtained by the same preparative GPC method

	Yield (wt%)		C/100H	
Fraction No.	Cold Lake	Athabasca	Cold Lake	Athabasca[a]
1	14	22.5	87.4	82.6
2	33	30.5	86.7	81.3
3	25	13.6	86.2	80.0
4	16	11.1	83.4	77.5
5	12	20.8	92.9	81.3
Unfractionated			88.9	80.6[b]

[a]Calculated from data given by Ignasiak *et al.* (13).
[b]Calculated from data given by Cyr *et al.* (39).

be due to the presence of more peripheral aromatic carbons in low molecular-weight fractions than in high molecular-weight fractions. The spectra of the major fractions (Fig. 3a) showed no detectable signals between 4 and 6 ppm, the region which is characteristic of olefin protons. Nor were there detectable signals between 8.5 and 9.0 ppm where protons on condensed aromatic rings normally appear. Signals in this latter region became more apparent in the low molecular-weight subfractions of fraction 5 (Fig. 3b).

The integrated values of the various designated regions are shown in Table 4 as percent of the total intensity. Similarly, the proportion of aromatic protons measured in the various fractions of Athabasca asphaltenes (13) are also summarized in Table 4. For both asphaltene samples, the proportions of aromatic protons increased as the molecular weight of the fractions decreased. The lowest molecular-weight subfractions of the Cold Lake asphaltenes (5-4 and 5-5) had the highest proportion of aromatic hydrogen atoms. The proportions of aromatic hydrogen atoms in each major fraction of Cold Lake asphaltenes were higher than the corresponding fractions of the Athabasca asphaltenes. These results are consistent with the predicted higher aromaticity of the former asphaltenes based on the C/100H ratios.

The data in Table 5 summarizes the estimates of the average molecular composition in fractions of Cold Lake asphaltenes. Based on the NMR data it is seen that as the molecular weight decreases there is a decreasing trend in the number of aliphatic chains ending with methyl groups and an increasing trend in those connecting aromatic carbons. The average number of CH_2 groups in aliphatic chains seems to be fairly constant over the whole molecular-weight range with a slight tendency to decrease in the subfractions of fraction 5. The average aliphatic chain lengths are somewhat different from those of Athabasca asphaltenes which were determined from C-13 NMR spectra (45). The fractionated Athabasca asphaltenes had larger variations in chain lengths ranging from 7 to 12 carbon atoms (including α carbons and end methyl carbons). Results of ruthenium(VIII) catalyzed oxidation of Athabasca asphaltenes also had indicated the methylene chain length distribution to range between 4 and 13 (46, 47). The discrepancy could be attributed to the assumptions made for calculations based on NMR spectra.

From Table 5, the degree of substitution on peripheral aromatic carbons decreased as the molecular weights decreased and the C (substitutable) to H ratio increased with decreasing molecular weight. The carbon aromaticity, calculated using

TABLE 4. Proton NMR spectral data from the analyses of the unfractionated and fractionated Cold Lake asphaltenes. Total signal intensity was taken as 100[a]

	Aliphatic				
Fraction No.	H1	H2	Ha	Aromatic Har	Aromatic Athabasca[b]
Unfractionated	17	52	21	10	—
1	18	54	20	8	6.8
2	19	53	20	8	7.5
3	16	54	21	9	7.7
4	16	52	21	11	8.5
5	14	43	25	18	10.5
5-1	14	44	29	13	—
5-2	14	45	26	15	—
5-3	11	38	31	20	—
5-4	7	21	27	42	—
5-5	4	20	36	40	—

[a]H1 (0.2–1.0 ppm), H2 (1.0–2.1 ppm), Ha (2.1–5.0 ppm), Har (7.0–9.0 ppm)
[b]From Ignasiuk *et al.* (13).

only substitutable aromatic carbons, increased as the molecular weight decreased. The value for fraction 5 (44%) is much higher than those of the other fractions. This does not necessarily mean that the number of aromatic carbons in low molecular-weight fractions is larger. High molecular-weight fractions may contain more non-substitutable aromatic carbons such as condensed aromatic rings and/or biphenyl type of structures which contain very few aromatic protons.

The "true" carbon aromaticities (from [9]) as well as the apparent carbon aromaticities, f_a, obtained by solid-state CP/MAS NMR spectra are shown in Table 5. Because the apparent aromaticity values vary with spectral conditions such as contact time (22), they are not absolute measures. Nonetheless, the f_a value for fraction 5 is much larger than those for other fractions where the variation is small. This trend agrees well with the calculated aromaticity values.

Petroporphyrin, V, and Ni contents

Ultraviolet–visible analysis directly detected the presence of petroporphyrins in all fractions of Cold Lake asphaltenes without extraction. The total porphyrin content of each fraction, estimated from the prominent absorbance peak at ~410 nm (Soret peak), is shown in Table 6. Although it was preferable to use the absorbance at 573 nm (α peak) for quantitative analysis

Can. J. Chem. Downloaded from www.nrcresearchpress.com by 88.85.125.76 on 09/07/12
For personal use only.

TABLE 5. Estimates of the average molecular composition of the unfractionated and fractionated Cold Lake asphaltenes based on proton NMR spectral data

Fraction No.	No. chains ending in CH_3 Eq. [1]	No. chains connecting aromatic C Eq. [3]	No. CH_2 in chain[a] Eq. [5]	Degree of substitution[b] Eq. [7]	Total No. substitutable carbons/100H Eq. [8]	Carbon aromaticity (%)		
						Eq. [6]/[8]	Eq. [9][c]	CP/MAS[d]
Unfractionated	6	2	3	0.51	63	33	(52)	—
1	6	2	3	0.56	61	30	(51)	43
2	6	2	3	0.56	61	30	(52)	42
3	5	3	3	0.54	62	31	(50)	43
4	5	5	3	0.49	63	34	(50)	40
5	5	4	3	0.41	69	44	(58)	56
5-1	5	5	2	0.53	69	40		—
5-2	5	4	3	0.46	68	41		—
5-3	4	6	2	0.44	74	48		—
5-4	2	6	2	0.24	67	83		—
5-5	1	8	1	0.31	66	87		—

[a]α carbons to aromatics not included.
[b]Only the substitutable peripheral aromatic carbons are considered.
[c]Numbers in parentheses were calculated including non-substitutable carbons.
[d]Solid state NMR data.

Can. J. Chem. Downloaded from www.nrcresearchpress.com by 88.85.125.76 on 09/07/12
For personal use only.

of porphyrins because high background can flatten the Soret peak at 410 nm (38), this weaker peak was not measurable in fractions with very low porphyrin content (fractions 1 to 4). However, for fraction 5 and its subfractions, the 573 nm peak was easily measured over a series of dilutions. The porphyrin concentrations determined using the absorbance readings at 410 nm ($\epsilon = 45 \times 10^4$) and at 573 nm (average $\epsilon = 2.5 \times 10^4$) were in close agreement. The ratio of the two extinction coefficients at 410 nm and at 573 nm is 18:1. From the measurements, the average ratio of the absorbance readings at 410 nm and at 573 nm (A_{410}:A_{573}) was also found to be approximately 18:1. Therefore, the petroporphyrin content of the various fractions of Cold Lake asphaltenes was determined from the absorbance at 410 nm (Table 6). Approximately 80% of all the petroporphyrins detected were contained in fraction 5. Other studies (3, 11, 12, 38, 39, 48) using extracted petroporphyrin fractions have also reported that vanadium petroporphyrins occurred in a narrow, low molecular-weight band corresponding to the 800 molecuar weight polystyrene standard. The fact that low porphyrin concentrations were found in the high molecular-weight fractions suggests that porphyrins are not involved in geothermal chemical reactions such as polymerization or aromatization. Although the distribution of porphyrin structures was concentrated in fraction 5, they were minor components in these fractions. For example, the actual concentration of petroporphyrins was only about 2% (by weight) in subfraction 5-4, which contained the largest proportion (29%) of petroporphyrins (Table 6).

Vanadium and nickel were the main metallic elements found in bitumen (49, 50). Their contents in each of the fractions are listed in Table 7. Nickel was distributed fairly evenly through all fractions, except in the two lightest fractions where the concentration was approximately double of others. The vanadium concentration in fraction 5 was twice as high as that in the heavier fractions. By ESR measurements, only paramagnetic vanadium cations (V(II) and V(IV)) were detected. The order of magnitude found by ESR was the same as the amount detected by ICP. Therefore, the results suggest that most of V in asphaltenes exist in paramagnetic forms such as VO^{2+}.

TABLE 6. Petroporphyrin content of Cold Lake asphaltenes based on Soret peak (A_{410}) measurements

Fraction	A_{410}/mg	Porphyrin content		Distribution in asphaltene (%)[b]
		μmol/g	μg/g[a]	
Unfractionated	0.88	2.0	1 200	100
1	0.15	0.33	200	3
2	0.10	0.22	130	4
3	0.19	0.42	250	5
4	0.44	0.98	590	8
5	5.28	12.0	7 000	80
5-1	1.59	3.5	2 100	11
5-2	4.22	9.4	5 600	18
5-3	11.1	25.0	15 000	29
5-4	16.6	37.0	22 000	22
5-5	ND[c]	—	—	—

[a]Molecular weight of 600 used for porphyrin.
[b]Calculation based on fraction yield.
[c]ND, not detected.

The vanadium content seemed to vary together with the porphyrin concentrations. Because petroporphyrins are known to be associated with vanadium (49, 50), the percent of vanadium associated with petroporphyrins have been estimated assuming all porphyrins were vanadium complexes. The data are also shown in Table 7. In the fraction with the highest porphyrin concentration, fraction 5-4, about 58% of vanadium was found to be associated with porphyrins. Smaller portions were associated in the heavier fractions. Non-porphyrin metal (V and Ni) complexes seem to be distributed over the whole range of molecular weights and constitute a majority of the metal containing compounds. These results agree with studies

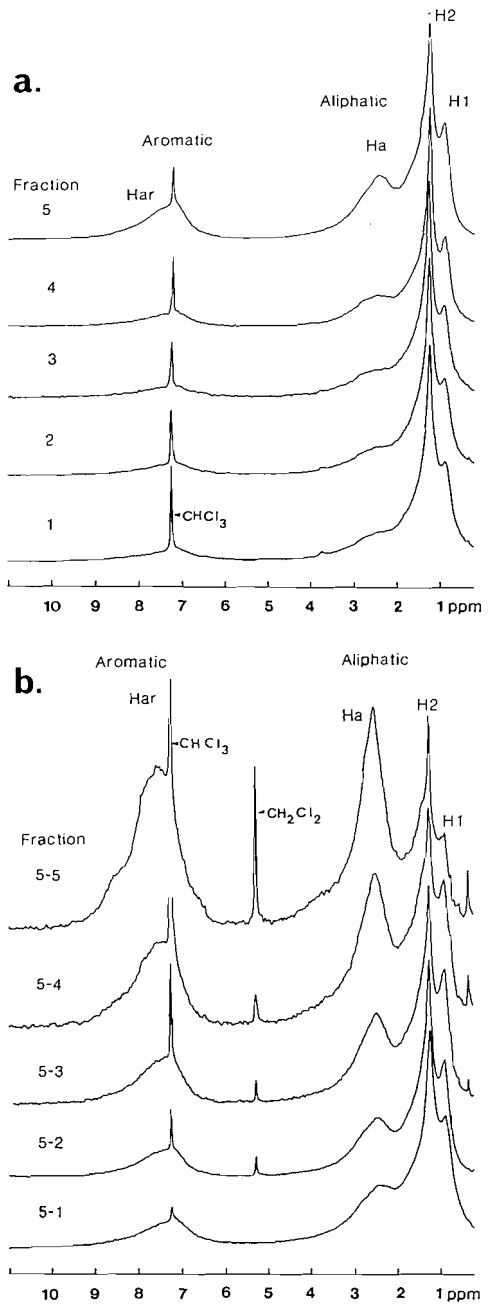

FIG. 3. Proton NMR spectra of (*a*) the five major asphaltene fractions and (*b*) the five subfractions of fraction 5. Designations for aromatic and aliphatic protons are shown: Har = aromatic protons; H1 = methyl protons at the end of aliphatic chains; H2 = methylene protons; Ha = protons α to aromatic carbons. Internal TMS was used as a chemical shift reference.

on the size distribution and characterization of porphyrin and non-porphyrin metal complexes in asphaltenes from Athabasca and Cold Lake bitumen (51, 52) and other oils (11, 12, 38, 39, 48, 49, 51–55).

In summary, the nature of the average chemical structures is not uniform in asphaltenes throughout their molecular weight range. The very low molecular-weight fractions have very different chemical characteristics from heavy fractions. From the estimated number of inner non-substitutable carbons, the size of aromatic moieties decreased with the molecular weight except for fraction 5, where the size abruptly increases. The $C/100H$ ratio for fraction 5 was higher than the other fractions indicating fewer protons in the low molecular-weight fractions. Inspite of this, the degree of substitution on available aromatic carbons decreased with decreasing molecular weight. This implies the presence of fewer aliphatic carbons and agrees with the high aromaticity in low molecular-weight fractions. In addition, the porphyrin-type structure and vanadium were not uniform throughout the fractions. Based on these analyses, the various fractions of Cold Lake asphaltenes have different chemical moieties. These will likely have different susceptibilities to enzymatic or microbiol attack.

TABLE 7. Vanadium and nickel content per g ashphaltenes and their relationships to porphyrins[a]

	Metal conc. (μg/g)		V in porphyrins concentration	
Fraction No.	V	Ni	In μg/g[b]	In %
Unfractionated	820	320	100	12
1	740	330	17	2
2	740	320	11	1
3	710	310	21	3
4	660	270	50	8
5	1 500 (1 800)	310	600	41
5-1	870 (920)	250	180	20
5-2	1 400	290	480	35
5-3	2 800 (1 700)	330	1 300	45
5-4	3 200 (2 200)	550	1 900	58
5-5	180	420	~0	0

[a]Values in parentheses were determined by ESR.
[b]Determined from μmol/g porphyrin assuming 1 mol V complexed per mol porphyrin.

Acknowledgments

One of us (N.C.) would like to thank Professor A. S. Perlin for showing her how fascinating and rewarding research in chemistry is. We thank Dr. K. F. Schulz for ESR analysis and Drs. M. L. Selucky and R. G. S. Ritchie and Mr. J. Laidler for helpful discussions. This work was funded by a grant from Alberta Oil Sands Technology and Research Authority (D.W.S.W. and P.M.F.).

1. J. G. SPEIGHT and S. E. MOSCHOPEDIS. *In* Chemistry of asphaltenes. *Edited by* W. Bunger and N. C. Li. Advances in Chemistry 195, 1 (1981) and references cited therein.
2. M. L. BOYD and D. S. MONTGOMERY. Fuel, **41**, 335 (1962).
3. Z. FRAKMAN, T. M. IGNASIAK, D. S. MONTGOMERY, and O. P. STRAUSZ. AOSTRA J. Res. **4**, 171 (1988).
4. R. S. WINNIFORD. J. Inst. Petrol. **49**, 215 (1963).
5. Y. TAKEGAMI, Y. WATANABE, T. SUZUKI, T. MITSUDO, and M. ITO. Nenroyo Kyokai Shi, **58**, 350 (1979).
6. T. F. YEN, W. H. WU, and G. V. CHILINGAR. Energy Sources, **7**, 275 (1984).
7. T. F. YEN, J. G. ERDMAN, and S. S. POLLACK. Anal. Chem. **33**, 1587 (1961).
8. T. F. YEN. Energy Sources, **1**, 447 (1974).
9. R. PELET, F. BEHAR, and J. C. MONIN. Org. Geochem. **10**, 481 (1986).
10. G. HALL and S. P. HERRON. *In* Chemistry of asphaltenes. *Edited by* J. W. Bunger and N. C. Li. Advances in Chemistry 195, 137 (1981).

Can. J. Chem. Downloaded from www.nrcresearchpress.com by 88.85.125.76 on 09/07/12
For personal use only.

11. J. G. REYNOLDS and W. R. BIGGS. Acc. Chem. Res. **21**, 319 (1988).
12. J. G. REYNOLDS and W. R. BIGGS. Fuel Sci. Technol. Int. **4**, 593 (1986).
13. T. M. IGNASIAK, L. KOTLYAR, N. SAMMAN, D. S. MONTGOMERY, and O. P. STRAUSZ. Fuel, **62**, 363 (1983).
14. C. WYNDHAM and W. B. COSTERTON. Appl. Environ. Microbiol. **41**, 791 (1981).
15. J. E. ZAJIC, D. G. COOPER, J. A. MARSHALL, and D. F. GERSON. Fuel, **60**, 619 (1981).
16. L. N. BRITTON. *In* Microbial degradation of organic compounds. *Edited by* D. T. Gibson. Marcel Dekker Inc., New York. 1984. p. 89.
17. D. T. GIBSON and V. SUBRAMANIAN. *In* Microbial degradation of organic compounds. *Edited by* D. T. Gibson. Marcel Dekker Inc., New York. 1984. p. 181.
18. P. M. FEDORAK and D. W. S. WESTLAKE. Can. J. Microbiol. **29**, 291 (1983).
19. D. WALLACE, D. HENRY, K. PONGER, and D. ZIMMERMAN. Fuel, **66**, 44 (1987).
20. W. L. ORR. Org. Geochem. **10**, 499 (1986).
21. M. L. Selucky, D. Bizzotto, and T. MANSKE. Prepr. Am. Chem. Soc. Div. Petrol. Chem. **34**, 214 (1989).
22. N. CYR and M. L. SELUCKY. Liq. Fuels Tech. **3**, 377 (1985).
23. K. F. SCHULZ and M. L. SELUCKY. Fuel, **60**, 951 (1981).
24. E. W. BAKER. *In* Organic geochemistry. *Edited by* G. Eglinton and M. T. J. Murphy. Springer-Verlag, Berlin. 1969. p. 464.
25. J. M. SUGIHARA and R. M. BEAN. J. Chem. Eng. Data,**7**, 269 (1962).
26. J. G. ERDMAN and P. H. HARJU. J. Chem. Eng. Data, **8**, 252 (1963).
27. E. W. BAKER, T. F. YEN, J. P. DICKIE, R. E. RHODES, and L. F. CLARK. Prepr. Am. Chem. Soc. Div. Petrol. Chem. **12**, A59 (1967).
28. R. J. ROSSCUP and H. P. POHLMANN. Prepr. Am. Chem. Soc. Div. Petrol. Chem. **12**, A103 (1967).
29. G. B. VAUGHN, E. C. TYNAN, and T. F. YEN. Chem. Geol. **6**, 203 (1970).
30. K. M. SMITH. Porphyrins and metalloporphyrins. Elsevier, New York. 1975. pp. 884–886.
31. H. N. DUNNING and N. A. RABON. 1951. Ind. Eng. Chem. **48**, 951 (1951).
32. J. B. F. CHAMPLIN and H. N. DUNNING. Economic Geol. **55**, 797 (1960).
33. M. F. MILLSON, D. S. MONTGOMERY, and S. R. BROWN. Geochim. Cosmochim. Acta, **30**, 207 (1966).
34. N. H. FURMAN. Standard methods of chemical analysis. Van Norstrand Co., Princeton, N.J. 1962. p. 1014.
35. J. K. BROWN and W. R. LADNER. Fuel, **39**, 87 (1960).
36. I. SCHWAGER, J. T. KWAN, W. C. LEE, S. MENG, and T. F. YEN. Anal. Chem. **51**, 1803 (1979).
37. J. W. LARSEN and Y.-C. WEI. Energy Fuels. **2**, 344 (1982).
38. W. A. SPENCER, J. F. GALOBARDES, M. A. CURTIS, and L. B. ROGERS. Separation Sci. Technol. **17**, 797 (1982).
39. R. H. FISH, J. J. KOMLENIC, and B. K. WINES. Anal. Chem. **56**, 2452 (1984).
40. M. L. SELUCKY. Unpublished results.
41. R. G. D. STEEL and I. H. TORRIE. *In* Principles and procedures of statistics. A biometrical approach. 2nd ed. McGraw-Hill, New York. 1980. p. 187.
42. T. SUZUKI, M. ITOH, Y. TAKAGAMI, and Y. WATANABE. Fuel, **61**, 402 (1982).
43. J. G. SPEIGHT. Fuel, **49**, 76 (1970).
44. J. G. SPEIGHT. Fuel, **50**, 102 (1971).
45. N. CYR, D. D. MCINTRYE, G. TOTH, and O. P. STAUSZ. Fuel, **66**, 1709 (1987).
46. O. P. STRAUSZ. Prepr. Am. Chem. Soc. Div. Petrol. Chem. **33**, 264 (1988).
47. O. P. STRAUSZ. Prepr. Am. Chem. Soc. Div. Petrol. Chem. **34**, 395 (1989).
48. W. R. BIGGS, J. C. FETZER, R. J. BROWN, and J. G. REYNOLDS. Liq. Fuel Technol. **3**, 397 (1985).
49. T. F. YEN. The role of trace metals in petroleum. Ann Arbour Science, Ann Arbour. 1975. Chapt. 1.
50. V. VALKOVIC. Trace metals in petroleum. Petroleum Pub. Co. Tulsa, OK. 1978. Chapt. 2.
51. D. STRONG and R. H. FILBY. *In* Metal complexes in fossil fuels. *Edited by* R. H. Filby and J. F. Branthaver. Am. Chem. Soc. Washington, D.C. 1987. p. 154.
52. S. N. NGUYEN and R. H. FILBY. *In* Metal complexes in fossil fuels. *Edited by* R. H. Filby and J. F. Branthaver. Am. Chem. Soc. Washington, D.C. 1987. p. 384.
53. R. H. FILBY and G. J. VAN BERKEL. *In* Metal complexes in fossil fuels. *Edited by* R. H. Filby and J. F. Branthaver. Am. Chem. Soc. Washington, D.C. 1987. p. 2.
54. R. H. FISH and J. J. KOMLENIC. Anal. Chem. **56**, 510 (1984).
55. R. H. FISH, J. G. REYNOLDS, and E. J. GALLEGOS. *In* Metal complexes in fossil fuels. *Edited by* R. H. Filby and J. F. Branthaver. Am. Chem. Soc. Washington, D.C. 1987. p. 332.

Can. J. Chem. Downloaded from www.nrcresearchpress.com by 88.85.125.76 on 09/07/12
For personal use only.

Copper(I) chloride catalyzed cross-dehydrocoupling reactions between silanes and ethynyl compounds. A new method for the copolymerization of silanes and alkynes

HUA QIN LIU AND JOHN F. HARROD
Chemistry Department, McGill University, Montreal, P.Q., Canada H3A 2K6

Received November 27, 1989

This paper is dedicated to Professor Arthur S. Perlin on the occasion of his 67th birthday

HUA QIN LIU and JOHN F. HARROD. Can. J. Chem. **68**, 1100 (1990).

In the presence of an amine, copper(I) chloride is an effective catalyst for the cross-dehycrocoupling of silanes with alkynes. The reactions proceed at useful rates above 100°C, but rates drop dramatically on going from 1° to 2° to 3° organosilanes. Primary silanes, $RSiH_3$ (R = Ph, *n*-hexyl), react in a stepwise fashion with phenylacetylene to give the products $RSiH_{3-x}(CCPh)_x$ ($x = 1-3$), each of which has been isolated and characterized. The secondary silanes $RR'SiH_2$ (R = R′ = Ph; R = Ph, R′ = Me; R = *n*-Bu, R′ = Me) also give mono- and diphenylethynyl products. The dehydrocoupling reaction has been applied to the synthesis of new polymers containing both acetylene units and silicon atoms in the backbone. 1,3-Diethynylbenzene gives polymers of relatively high molecular weight ($\overline{M}_w \approx 10^4-10^5$) with phenylsilane and phenylmethylsilane, but reactions of phenylmethyldiethynylsilane are too slow to give anything beyond low molecular weight oligomers.

Key words: organosilanes, alkynes, dehydrocoupling, copper(I) chloride, polymers, catalysis.

HUA QIN LIU et JOHN F. HARROD. Can. J. Chem. **68**, 1100 (1990).

En présence d'une amine, le chlorure de cuivre(I) est un catalyseur efficace pour le déhydro-couplage croisé des silanes avec les alcynes. Les réactions se produisent à des vitesses raisonnables lorsqu'on opère au-dessus de 100°C; toutefois, les vitesses diminuent d'une façon dramatique lorsqu'on passe des organosilanes 1° aux 2° et aux 3°. La réaction des silanes primaires, $RSiH_3$ (R = Ph, *n*-hexyle), avec le phénylacétylène se produit par étape pour donner les produits $RSiH_{3-x}(CCPh)_x$ ($x = 1-3$); chacun de ces produits a été isolé et caractérisé. Les silanes secondaires $RR'SiH_2$ (R = R′ = Ph; R = Ph, R′ = Me; R = *n*Bu, R′ = Me) donnent aussi des produits mono- et di-phényléthynyles. On a appliqué la réaction de déhydro-couplage à la synthèse de nouveaux polymères dont la chaîne fondamentale contient à la fois des unités acétylènes et des atomes de silicium. Avec le phénylsilane et le phénylméthylsilane, le 1,3-diéthynylbenzène fournit des polymères de poids moléculaires relativement élevés ($\overline{M}_w \approx 10^4-10^5$); toutefois, les réactions du phénylméthyldiéthynylsilane sont tellement lentes que les seuls produits isolés sont des oligomères de bas poids moléculaires.

Mots clés : organosilanes, alcynes, déhydro-couplage, chlorure de cuivre(I), polymères, catalyse.

[Traduit par la revue]

Introduction

The unusual electronic properties of polyenes, polyynes, and polysilanes have attracted a great deal of attention in recent years (1, 2). A number of workers have drawn attention to the similarity that exists between the delocalized π-bonding systems of the carbon chains in polyenes and the delocalized σ-bonding systems of the silicon chains in polysilanes (3). It is obvious that mixed chains of unsaturated carbons and of silicons are of a similar interest. However, synthetic routes to such chains are presently very limited.

In this paper, we present the results of a preliminary study of a promising new methodology for the production of copolymers of silanes and acetylenic compounds based on dehydrogenative coupling. Primary silanes have already been polymerized by catalytic dehydrocoupling with some success (4). The initial experiments in the present work were performed in an attempt to use hydrosilylation of acetylenic groups as a means of cross-linking low molecular weight polysilanes bearing Si—H groups on the backbone. Since attempts using the conventional group 8, 9, and 10 catalysts, such as complexes of platinum or rhodium (5), were all unsuccessful we turned to the catalyst developed by Bluestein (6) for the hydrosilylation of acrylonitrile and its derivatives. To our surprise, this copper(I) chloride/amine catalyst led to the highly selective cross-dehydrocoupling of the reactants, with no evidence of hydrosilation.

To our knowledge there is only one case in the literature of such a reaction occurring cleanly and in high yield (7). In this case, the coupling was achieved with an iodine-modified chloroplatinic acid catalyst and, despite the normally high catalytic activity of platinum towards hydrosilation, the reaction is highly selective for dehydrocoupling at room temperatures. In two other cases, dehydrocoupling in low yield was found to accompany hydrosilation (8) and hydrogen transfer (9) reactions. In addition, acetylenes have been successfully coupled by copper(I) catalyzed oxidative coupling (10), but there was no evidence that the coupling can be carried out in the absence of oxygen.

We describe herein some coupling experiments using di- and trifunctional silanes with monofunctional acetylenes, followed by some studies on the formation of polymers using di- and trifunctional silanes with difunctional acetylenes.

Results and discussion

Cross-dehydrocoupling reactions between silanes and phenylacetylene

Copper(I) chloride is an active catalyst for the dehydrocoupling reaction between phenylsilane (PS) and phenylacetylene (PA). In the presence of CuCl and N,N,N′,N′-tetramethylethylenediamine (TMED), or tributylamine, PS and PA react cleanly and rapidly under inert atmosphere, at temperatures around 100°C, to give the cross-dehydrocoupling products: $PhSiH_2CCPh$, **1**, $PhSiH(CCPh)_2$, **2**, and $PhSi(CCPh)_3$, **3**, depending on the initial ratio of the two monomers, and on the reaction time (eqs.[1]–[3]).

[1] $PhSiH_3 + PhCCH \rightarrow PhSiH_2(CCPh) + H_2$ **1**

[2] $PhSiH_2(CCPh) + PhCCH \rightarrow PhSiH(CCPh)_2 + H_2$ **2**

[3] $PhSiH(CCPh)_2 + PhCCH \rightarrow PhSi(CCPh)_3 + H_2$ **3**

Can. J. Chem. Downloaded from www.nrcresearchpress.com by 88.85.125.76 on 09/07/12
For personal use only.

TABLE 1. Dehydrocoupling reaction of phenylsilane and phenylacetylene under different reaction conditions

$[PhSiH_3]$ (M)	[PhCCH] (M)	[CuCl][a] (M)	T (°C)	t (h)	Conversion[b] (mol%)	Composition of products (mol%) 1	2	3
4	4	0.27	100	18	60	67	33	0
2.8	5.6	0.19	100	18	70	4	61	35
1.8	5.4	1	90	3.5	80	0	0	100

[a]CuCl:TMED molar ratio is 1:1.1.
[b]Conversion based on phenylsilane.

The reaction leads to the successive formation of **1, 2**, and **3** when carried out with an excess of phenylacetylene. The conversion of **2** to **3** requires much longer reaction times than the two first additions, but in the presence of high concentrations of catalyst and a sufficient amount of phenylacetylene, this reaction can be pushed essentially to completion (see Table 1).

Traces of styrene and 1,4-diphenylbutenyne (*cis* and *trans*), formed by Straus reaction (11), were detected in the reaction products. No trace of homocoupling product was found and the catalyst was found to be completely ineffective for the dehydrocoupling of the silane alone. The hydrogen evolved from the reaction was identified by ^1H NMR at 4.6 ppm in $CDCl_3$. The structures of compounds **1, 2**, and **3** were confirmed by ^1H and ^{13}C NMR and $^1H/^{13}C$ heterocoupling NMR, mass spectroscopy, and, for compounds **1** and **2**, elemental analysis. These data are summarized in Table 7 and in the experimental section.

The presence of amine is essential for the catalytic activity of CuCl but, on the basis of a comparison of tributylamine and TMED (Table 2), it appears that the nature of the amine has little effect on the reaction rate or the final products.

The influence of temperature on the reaction rate is large. At a 1:1 molar ratio of phenylsilane:phenylacetylene and a 15:1 ratio of monomer:CuCl, the rate of reaction was negligible at room temperature. The initial rate of consumption of phenylsilane increased from 7.3×10^{-5} M s^{-1} at 57°C to 1.1×10^{-3} M s^{-1} at 110°C, a factor of ca. 15 for the increase of ca. 50°C, or an Arrhenius coefficient of ca. 57 kJ/mol.

The initial rate of reaction increases with increasing catalyst concentration, but not in simple proportion. For example, increasing the CuCl concentration by a factor of 6 (from 0.047 to 0.27 M) increased the initial reaction rate by a factor of 10 (from 1.1×10^{-4} to 1.1×10^{-3} M s^{-1}).

A number of other silanes were studied to evaluate their reactivity with phenylacetylene. Diphenylsilane (DPS), phenylmethylsilane (PMS), and *n*-hexylsilane react with phenylacetylene in the same manner as phenylsilane to give mono-, di-, and (for *n*-hexylsilane) triphenylethynyl products. Some typical results for these reactions are summarized in Table 3.

The structures of the coupling products were assigned on the basis of their mass, ^1H, and ^{13}C NMR spectra. The MS results and the ^{13}C NMR chemical shifts of the phenylethynyl products are given in Table 8.

A study of the rates of coupling for different silanes indicates that the reactivity of the silanes decreases in the following order (Table 4):

$$PhSiH_3 >> n\text{-}C_6H_{13}SiH_3 > Ph_2SiH_2 > PhMeSiH_2$$

Although a number of possible mechanisms can be invoked on the basis of the foregoing results, one based on the initial formation of the cuprous acetylide seems most likely to us. It is well known that terminal alkynes react with CuCl to form acetylides (12, 13), thus:

TABLE 2. The influence of the amine on the rate of reaction of phenylsilane with phenylacetylene ($PhSiH_3$:PhCCH = 1:1)

$[PhSiH_3]_0$ (M)	[TMED] (M)	$[Bu_3N]$ (M)	[CuCl] (M)	$V_i \times 10^4$ (M s^{-1})
4	0.29	0	0.27	5.7
3.7	0.16	0.41	0.24	4.4
3.8	0	0.49	0.25	4.2

[4] RCC—H + CuCl → RCC—Cu + HCl

This reaction has been widely applied in organic synthesis (13). Hence, it is very likely that the first step of the dehydrocoupling involves such a reaction. In the second, rate-determining step, the cuprous acetylide probably reacts with the silane to form phenylethynyl substituted product and copper(I) hydride, thus:

[5] PhCC—Cu + $R^1R^2R^3$Si—H → PhCCSi$R^1R^2R^3$ + CuH

The catalytic cycle would then be completed by reaction of CuH with another phenylacetylene molecule to regenerate the cuprous phenylacetylide and evolve hydrogen, as shown in eq. [6].

[6] CuH + PhCC—H → PhCC—Cu + H_2

Reaction [5] most likely takes place through a four-center intermediate (eq.[7]), similar to that proposed for the "heterolytic" activation of H_2 by copper(I) complexes (14). In such a process, the nucleophilic acetylide displaces a hydride from the Si to the Cu. Thus, the more electrophilic the Si, the more easily the reaction will proceed. Lucovsky (15) and Sahn *et al.* (16) found that the infrared stretching frequency for Si–H in a series of silanes was proportional to the sum of the electronegativities of the substituents. Application of this correlation to the silanes used in the phenylacetylene dehydrocoupling experiments (see IR frequencies in Table 5) leads to the following ordering in terms of increasing electronegativity sum for the substituents

[7] 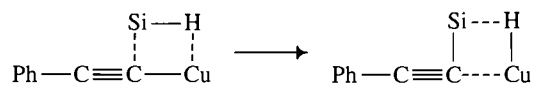

$$PhMeSiH_2 \cong Ph_2SiH_2 < n\text{-}C_6H_{13}SiH_3 < PhSiH_3$$

This sequence corresponds to the observed rate sequence. However, the small range of the IR frequencies renders the correlation rather tenuous and it is almost certainly the case that steric effects also play a role in determining the reactivity of the silane. The relatively modest differences in rate for the

Can. J. Chem. Downloaded from www.nrcresearchpress.com by 88.85.125.76 on 09/07/12
For personal use only.

TABLE 3. Dehydrocoupling reaction between R^1 R^2 SiH_2 and PhCCH

R^1, R^2	[Silane]/[PhCCH]/[CuCl]/[TMED]	T (°C)	t (h)	Conversion[a] (%)	Main product	Isolated yield (%)
Ph,H	1.8/5.6/1/1.1	90	3	100	$PhSi(CCPh)_3$	80
Ph,Ph	2.15/4.3[b]/0.76/0.85	90	40	100	$Ph_2Si(CCPh)_2$	44
	3.27/3.27/0.22/0.24	97	17	80	$Ph_2SiH(CCPh)$[d]	54
Ph,Me	2.3/5.0[c]/0.82/0.9	90	18	80	$PhMeSi(CCPh)_2$	40
	3.9/3.9/0.26/0.28	97	19	100	PhMeSiH(CCPh)	34
n-Hexyl,H	1.7/5.2/0.92/1	90	17	100	*n*-$HexylSi(CCPh)_3$[d]	51
	3.5/3.5/0.24/0.26	97	18	95	*n*-$HexylSiH_2(CCPh)$[d]	31
n-Bu,Me	3.7/3.7/0.25/0.27	105	31	47	*n*-BuMeSiH(CCPh)	[e]
	2.3/4.6/0.82/0.95	105	15	86	*n*-$BuMeSi(CCPh)_2$	57
Ph_2,Me[f]	2.9/2.9/0.18/0.19	110	19	0	—	—
	2.7/2.7/0.57/0.61	108	17	12	$Ph_2MeSi(CCPh)$	

[a]The conversions are based on the consumption of silane from ^1H NMR spectra.
[b]An additional 0.9 mL (90% of the initial amount) of phenylacetylene was added gradually after 8 h of reaction to compensate for consumption in side reactions leading to the formation of styrene and 1,4-diphenylbutenyne.
[c]An additional 0.5 mL (30% of the initial amount) of phenylacetylene was added 6 h after the start of the reaction.
[d]$Ph_2SiH(CCPh)$: white solid (mp 48°C) after recrystallization from hexane; PhMeSiH(CCPh): colourless liquid, bp 95°C at 0.1 Torr; *n*-$hexylSi(CCPh)_3$: white solid (mp 81.5°C) after recrystallization from hexane; *n*-$hexylSiH_2(CCPh)$: colourless liquid, bp 145°C at 0.1 Torr.
[e]After 3 days of reaction, the conversion was 94% and the yield was 34%.
[f]The silane in this case is Ph_2MeSiH.

TABLE 4. Rate study of the coupling reaction of phenylacetylene with different silanes (T = 97°C)

Silanes	[Silane][a] (M)	[CuCl] (M)	[TMED] (M)	v_i/[SiH] $\times 10^6$ (s^{-1})
$PhSiH_3$	4.00	0.27	0.29	47.5
n-$HexylSiH_3$	3.54	0.23	0.26	8.5
Ph_2SiH_2	3.27	0.22	0.24	6.0
$PhMeSiH_2$	3.87	0.25	0.28	3.6
n-$BuMeSiH_2$[b]	3.70	0.25	0.27	2.1

[a][Silane]:[PhCCH] = 1:1.
[b]Reaction temperature 105°C.

TABLE 5. IR and ^1H NMR data of silanes carrying a Si—H bond

Compound	ν_{Si-H} (cm^{-1})	δ_{Si-H} (ppm)[a] (solvent:$CDCl_3$)	J_{Si-H} (Hz)
$PhSiH_3$	2157	—	—
n-$HexylSiH_3$	2150	—	—
Ph_2SiH_2	2139	—	—
$PhMeSiH_2$	2139	—	—
$BuMeSiH_2$	2133	—	—
Ph_2MeSiH	2122	—	—
$PhSiH_2(CCPh)$	2159	4.81(s)	215.0
$PhSiH(CCPh)_2$	2161	5.14(s)	229.5
$Ph_2SiH(CCPh)$	2156	5.30(s)	213.6
PhMeSiH(CCPh)	2159	4.80(q)	208.2
n-$HexylSiH_2(CCPh)$	2153	4.08(t)	206.6

[a]s: singlet; t: triplet; q: quartet.

production of the mono-, di-, and triethynyl products from primary silanes (see Table 1) strongly suggest that the greater electron-withdrawing power of the ethynyl group compensates for its greater size relative to the H atom. On the other hand, the lower electronegativity and larger steric requirements of alkyl groups are in accord with the low activity of dialkylsilanes and the extremely low reactivity of trialkylsilanes.

TABLE 6. Evolution of SiH_n species (n = 1, 2, or 3) in the reaction of phenylsilane with DEB[a]

Reaction time (h)	SiH_3 (mol %)	SiH_2 (mol %)	SiH (mol %)
0	100	—	—
17	11	64	25
24	6	57	37
41[b]	0	47	53
72	0	20	80

[a][Monomer]$_0$: 3.4 M; [CuCl]: 0.26 M; [TMED]: 0.18 M; [Bu_3N]: 0.45 M; T: 100°C.
[b]At this time, the temperature was brought to 125°C.

Dehydrocoupling polymerization of PS and PMS with m-*diethynylbenzene (DEB) and phenylmethyldiethynylsilane (PMDS)*

m-Diethynylbenzene reacts with phenylsilane in the same manner as phenylacetylene and leads to the formation of polymers. Depending on the molar ratio between the monomers and cuprous chloride, the reaction temperature, and the reaction time, the reaction products may be low molecular weight oligomers or relatively high molecular weight polymers. The evolution of the various SiH_n groups in the course of a dehydrocoupling reaction of DEB and phenylsilene in a typical reaction is given in Table 6.

These data show that the reaction proceeds in two stages. The first is a coupling reaction between the initial reactants to form a new cross-coupled monomer, **4**:

[8] $PhSiH_3 + HC{\equiv}C$–C$_6$H$_4$–$C{\equiv}CH \longrightarrow$

$H_2Si(Ph)C{\equiv}CC_6H_4C{\equiv}CH + H_2$

4

Can. J. Chem. Downloaded from www.nrcresearchpress.com by 88.85.125.76 on 09/07/12
For personal use only.

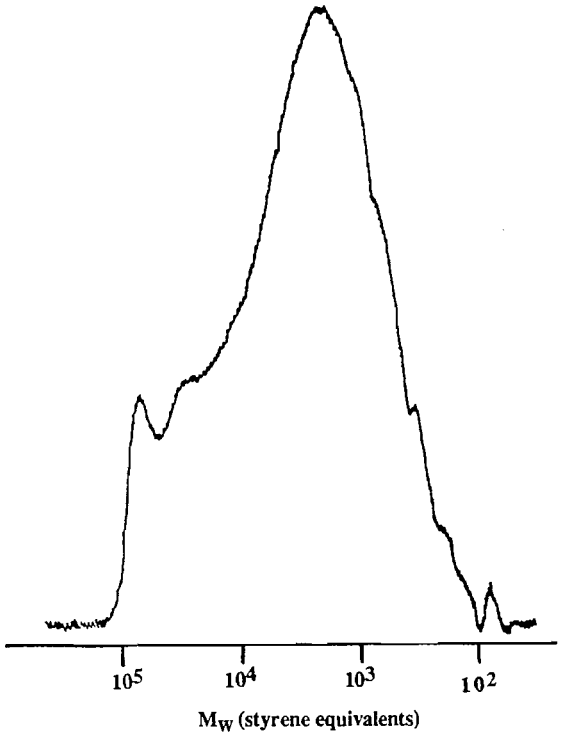

FIG. 1. Gel permeation chromatogram of a phenylsilane/DEB polymer.

In the second stage, this cross-coupled species reacts with either the small amounts of initial monomers remaining, or with other cross-coupled monomers to give higher oligomers, e.g.,

[9] $2\ H(SiHPhC{\equiv}CC_6H_4C{\equiv}C)_n\ H \rightarrow$

$$H(SiHPhC{\equiv}CC_6H_4C{\equiv}C)_{2n}\ H + H_2$$

At a molar ratio of monomer:CuCl of ca. 13:1, very high reaction temperatures are required to yield high molecular weight material. However, such reaction conditions are likely to induce cross-linking reactions. For example, after reacting at 100°C for 41 h, the degree of polymerization (DP) of the product is only about 4 for the conditions listed in Table 6. The same reaction performed at 90°C for 20 h, followed by a further 20 h at 120°C, gives a much higher molecular weight product with a DP ranging from 30 up to about 500 (see Fig. 1). These polymers remain soluble in common organic solvents.

Analysis of the polymers by ^1H NMR confirmed the presence of the tertiary Si-H at 5.2 ppm, the secondary Si-H at 4.75 ppm, and the ethynyl hydrogen at 3.1 ppm. The presence of C≡C was also confirmed by ^{13}C NMR (107.2 and 86.6 ppm.). The presence of these functional groups was also detected by infrared spectroscopy, ($\nu_{Si\text{-}H}$ at 2156 cm^{-1}, $\nu_{C{\equiv}C\text{—}H}$ at 3295 cm^{-1}, $\nu_{Si\text{—}H}$ at 473 and 492 cm^{-1}).

The high polydispersity of the high molecular weight material is most likely due to side reactions of the triple bonds, leading to branching and cross-linking. Increasing the ratio of CuCl:monomers from 1:14 to 1:4 results in the formation of insoluble polymer after 20 h at 90°C. Using a secondary silane such as phenylmethylsilane eliminates the cross-linking problem but the reaction rate is much slower and it is more difficult to achieve high molecular weight, even at very high catalyst concentrations. For a molar ratio of CuCl:monomer of 1:3 and at 100°C for 3 days, a polymer of $\overline{M}_w$ = 18 000 was obtained. It should be noted that, given the level of purity of the monomers

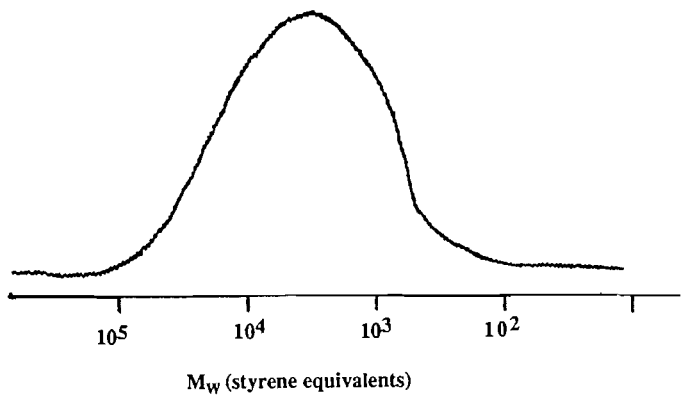

FIG. 2. Gel permeation chromatogram of a phenylsilane/phenylmethyldiethynylsilane polymer.

TABLE 7. ^{13}C NMR chemical shifts for **1**, **2**, and **3** (ppm) in $CDCl_3$ at room temperature

Position[a]	1	2	3
a	129.22	130.53	132.00
b	135.19	134.82	134.52
c	128.19	128.22	128.20
d	130.20	130.47	130.63
1	122.31	122.18	122.11
2	132.09	132.26	132.36
3	128.29	128.27	128.22
4	129.17	129.29	129.17
5	84.77	85.63	86.79
6	109.36	108.52	107.68

[a]Position labelling scheme:

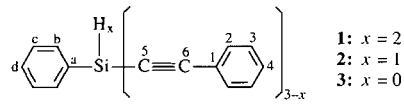

and the existence of side reactions, higher molecular weights than those observed would not be expected.

The cross-coupling of phenylsilane with phenylmethyldiethynylsilane also requires more forcing reaction conditions, because of the lower reactivity of the acetylene. For example, with a molar ratio of CuCl:monomer of 1:14 at 115°C for 22 h, most of the product consisted of the dimer **5**, by ^1H NMR analysis.

$$H_2Si(Ph)C{\equiv}CSi(PhMe)C{\equiv}CH$$

5

The highest molecular weight product obtained after 9 h at 130°C was only tetramer. Higher molecular weight material was formed by using CuCl equimolar with the two reactants. The $\overline{M}_w$, by GPC analysis, was 8000 (see Fig. 2). The freshly prepared polymer is soluble in common organic solvents but becomes insoluble after several days even under inert atmosphere. As would be expected from the reactivity patterns described above, cross-coupling of phenylmethylsilane with PMDES is extremely slow. For a molar ratio of CuCl:monomer of 1:2 after 18 h at 110°C, the reaction only leads to oligomers with $\overline{M}_w$ 1500, by GPC analysis.

Conclusion

The surprising reactivities of mono- and disubstituted silanes

Can. J. Chem. Downloaded from www.nrcresearchpress.com by 88.85.125.76 on 09/07/12
For personal use only.

TABLE 8. ^{13}C NMR chemical shifts (ppm) in $CDCl_3$ at room temperature for the products of coupling DPS, PMS, *n*-hexylsilane, and butylmethylsilane with PhCCH

	Ph_2SiH_x $(CCPh)_{2-x}$		$PhMeSiH_x$ $(CCPh)_{2-x}$		*n*-HexylSiH_x $(CCPh)_{3-x}$		$BuMeSiH_x$ $(CCPh)_{2-x}$	
Position[a]	$x = 1$	$x = 0$	$x = 1$	$x = 0$	$x = 2$	$x = 0$	$x = 1$	$x = 0$
1	122.44	122.37	122.62	122.45	122.64	122.36	122.90	122.67
2	132.18	132.31	132.08	132.18	132.01	132.30	131.98	132.05
3	128.28	128.24	128.26	128.20	128.26	128.20	128.21	128.15
4	129.13	129.20	128.93	129.02	128.90	129.13	128.65	128.77
5	87.14	87.61	88.92	88.98	86.19	87.30	90.39	88.98
6	109.55	108.77	108.03	107.37	108.09	106.68	106.76	106.21
a	132.11	132.99	133.63	134.12	9.88	16.77	13.19	13.78
b	135.19	134.89	134.42	134.12	24.82	23.22	25.89	25.77
c	128.13	128.08	128.05	128.04	32.22	32.35	26.36	25.94
d	130.12	130.24	129.85	130.04	31.49	31.49	13.78	15.90
e					22.55	22.58	4.69	−1.21
f					14.09	14.13		

[a]Position labelling scheme.

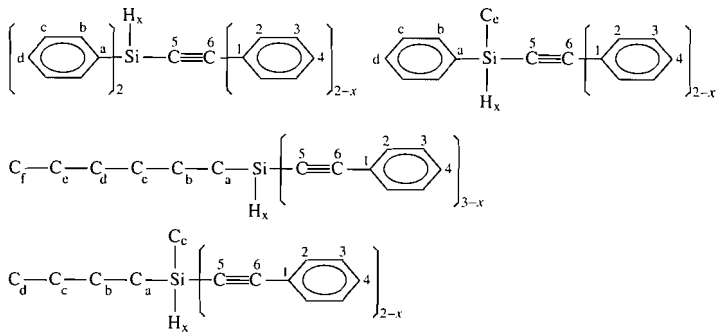

TABLE 9. Experimental conditions for some polymerization reactions at 110°C

Silane (mL)	Alkyne (mL)	TMED (mL)	CuCl (mg)	Toluene (mL)	Time (h)	Yield (g)
PS (1.0)	DEB (1.0)	0.01	60	—	20	0.94
PMS (1.0)	DEB (0.95)	0.43	256	2.0	72	1.40
PS (0.35)	PMD (0.5)	0.42	275	0.5	17	0.66
PMS (0.38)	PMDS (0.5)	0.84	550	1.0	18	0.33

with acetylenic monomers by cross-dehydrocoupling opens up an attractive new route to the synthesis of new simple and polymeric compounds containing both Si atoms and C≡C bonds in the same molecule. Such compounds could be useful in organic synthesis, or as novel electronic materials. The first generation of catalysts leaves much to be desired in terms of activity and it is hoped that they can be improved upon in the future. Although more work needs to be done to increase the molecular weights of the polymers, the simplicity and the effectiveness of the catalytic system together with the highly functionalized nature of the polymers already make this reaction very attractive in terms of practical application.

Experimental

Phenylsilane, phenylmethylsilane, diphenylsilane, and *n*-hexylsilane were prepared using a previously described method (17). Phenylacetylene, TMED, and tributylamine (Aldrich Chemical Co.) were distilled once immediately prior to use. CuCl (Anachemia) was used as received. *m*-Diethynylbenzene, kindly furnished by Dr. A. S. Hay of this department, was distilled, trap-to-trap, under vacuum immediately prior to use. Phenylmethyldiethynylsilane was synthesized according to the literature (18).

^1H NMR spectra were recorded on a Varian XL-200FT spectrometer and ^{13}C NMR spectra on a Varian XL-300FT spectrometer. The assignments of the chemical shifts of the dehydrocoupling products were made using 2D NMR methods (COSY and $^1H/^{13}C$ HETECOR).

Mass spectra were measured on a Dupont 21-492B spectrometer at a potential of 70 eV, and on a ZAB-HS mass spectrometer using FAB with an atomic energy of 8 kV at 1 mA.

The molecular weights of polymers were measured on a Varian 5000 gel permeation chromatograph, equipped with a Waters Ultrastyragel 1000 Å column at 35°C, and with tetrahydrofuran as solvent. Polystyrene standards were used for calibration.

Infrared spectra were measured on an Analect AQS-18 FTIR spectrometer.

Synthesis of $PhSiH_2(CCPh)$ and $PhSiH(CCPh)_2$

Reactions were carried out in carefully dried standard glassware under nitrogen. The following is a typical reaction. A mixture of phenylsilane (1.7 mL; 13.6 mmol), phenylacetylene (1.5 mL; 13.6 mmol), TMED (0.14 mL; 1.1 mmol), and CuCl (90 mg; 0.9 mmol) was

Can. J. Chem. Downloaded from www.nrcresearchpress.com by 88.85.125.76 on 09/07/12
For personal use only.

heated at 100°C with stirring for 18 h. Initially, the reaction proceeded rapidly with visible evolution of hydrogen. After a few hours, gas evolution was no longer evident. On completion of the reaction, the product was triturated with a few millilitres of toluene and the catalyst was removed by filtration. Removal of the toluene under vacuum gave 1.95 g of crude product. Vacuum distillation (100°C, 10^{-3} Torr; 1 Torr = 133.3 Pa), gave 1.12 g of **1**. (Anal. calcd. for $C_{14}H_{12}Si$: C 80.71, H 5.81, Si 13.48; found: C 80.41, H 5.61, Si 13.39). The residue (0.83 g) was shown by ^1H NMR to be **2** (>95%). The viscous yellow oil was further purified by distillation under vacuum (160°C, 10^{-3} Torr). (Anal. calcd. for $C_{22}H_{16}Si$: C 85.67, H 5.23, Si 9.10; found: C 85.74, H 5.28, Si 8.98).

The molecular weights of compounds **1**, **2** and **3** were confirmed by the observation of molecular ions in their mass spectra at 208, 308, and 408 respectively. The ^{13}C NMR chemical shifts of these compounds are listed in Table 7.

The coupling reactions of phenylacetylene with phenylmethylsilane, diphenylsilane, and *n*-hexylsilane were performed using essentially the same procedure. The results of these reactions are summarized in Table 3. The ^{13}C NMR data for the products are listed in Table 8.

Polymerization reactions

The polymerization reactions were carried out using the same techniques described in the previous section. The following specific example provides a general picture of the methodology.

Reaction of phenylsilane with m*-diethynylbenzene*

Oxygen-free phenylsilane (1.0 mL; 8 mmol), DEB (1.0 mL; 8 mmol), TMED (0.10 mL; 0.067 mmol), and CuCl (60 mg; 0.6 mmol) were introduced into a stirred nitrogen-filled reactor. The mixture was heated to 110°C and the colour changed from yellow to red and then to dark green. After 20 h, the initially mobile mixture had become very viscous. The product was dissolved in a few millilitres of toluene and the catalyst was removed by filtration. The solvent was removed under vacuum and the polymer was dried under high vacuum. Yield: 0.94 g; 80%.

The experimental conditions for the other polymerization reactions are given in Table 9.

Acknowledgments

Financial support from the National Research Council of Canada and from Fonds FCAR du Québec is gratefully acknowledged.

1. T. A. SKOTHEIM (*Editor*). The handbook of conducting polymers. Vols. 1 and 2. Marcel Dekker, New York and Basel. 1986.
2. M. ZELDIN, K. J. WYNNE, and H. R. ALLCOCK (*Editors*). Inorganic and organometallic polymers. ACS Symp. Ser. No. 360. American Chemical Society, Washington, DC. 1988. Chaps. 2, 4, 6, 8, and 9.
3. J. MICHL, J. W. DOWNING, T. KARATSU, K. A. KLINGENSMITH, G. M. WALLRAFF, and R. D. MILLER. *In* Inorganic and organometallic polymers. *Edited by* M. Zeldin, K. J. Wynne, and H. R. Allcock. ACS Symp. Ser. No. 360. American Chemical Society, Washington, DC. 1988. Chap. 5.
4. C. T. AITKEN, J. F. HARROD, and E. SAMUEL. J. Organomet. Chem. **279**, C11 (1985); J. Am. Chem. Soc. **108**, 4059 (1986); C. T. AITKEN, E. SAMUEL, J. F. HARROD. Can. J. Chem. **64**, 1677 (1986); J. F. HARROD and S. S. YUN. Organometallics, **6**, 1381 (1987); J. F. HARROD. *In* Inorganic and organometallic polymers. *Edited by* M. Zeldin, K. J. Wynne, and H. R. Allcock. ACS Symp. Ser. No. 360. American Chemical Society, Washington, DC. 1988. Chap 7.; J. F. HARROD. *In* The design, activation and transformation of organometallics into common and exotic materials. *Edited by* R. M. Laine. NATO ASI Series E, 141. Martinus Nijhoff, Amsterdam. 1988. p. 103.
5. J. L. SPEIER. Adv. Organomet. Chem. **17**, 407 (1979); J. F. HARROD and A. J. CHALK. *In* Organic syntheses via metal carbonyls. *Edited by* P. Pino and I. Wender. John Wiley & Sons, New York. 1977. p. 673.
6. B. A. BLUESTEIN. U.S. Patent No. 2971970, Feb. 14, 1961.
7. M. G. VORONKOV, N. L. USHAKOVA, I. I. TSYKHANSKAYA, and V. B. PUKHNARAVICH. J. Organomet. Chem. **264**, 39 (1984); M. G. VORONKOV, V. B. PUKHNARAVICH, N. L. USHAKOVA, I. I. TYSKHANSKAYA, A. L. ALBANOV, and V. YU. VIKOVSKII. J. Gen. Chem. USSR, **55**, 80 (1985).
8. E. LUKEVICS, O. PUDOVA, R. STURKOVICH, and A. GAUKHAM. J. Organomet. Chem. **346**, 297 (1988).
9. L. A. ORO, M. J. FERNANDEZ, M. A. ESTERUELAS, and M. S. JIMENEZ. J. Mol. Catal. **37**, 151 (1986).
10. A. S. HAY. J. Polym. Sci. Part A-1, **7**, 1625 (1969).
11. F. STRAUS. Ann. **190**, 342 (1905).
12. C. GLASER. Ann. **137**, 154 (1869).
13. G. EGLINTON and W. MCCRAE. Adv. Org. Chem. **4**, 225 (1963).
14. J. HALPERN. Q. Rev. **10**, 463 (1956).
15. G. LUCOVSKY. Solid State Commun. **29**, 571 (1979).
16. S. N. SAHN, T. S. SHI, P. W. GE, and J. W. CORBETT. J. Chem. Phys. **77**, 4330 (1982).
17. R. A. BENKESER, H. LANDESMAN, and D. J. FOSTER. J. Am. Chem. Soc. **74**, 648 (1965).
18. C. S. KRAIHANZEL and M. L. LOSEE. J. Organmet. Chem. **10**, 427 (1967).

Can. J. Chem. Downloaded from www.nrcresearchpress.com by 88.85.125.76 on 09/07/12
For personal use only.

^{13}C magnetic resonance studies. 142.[1] The fate of highly substituted acyclic ketones in strong base: β-enolization, Haller–Bauer cleavage, and an alkyl to aryl acyl shift

RAINER A. DYLLICK-BRENZINGER, VIJAY PATEL,[2] MOLLIN B. RAMPERSAD, J. B. STOTHERS, AND SHIRLEY E. THOMAS

Department of Chemistry, The University of Western Ontario, London, Ont., Canada N6A 5B7

Received December 1, 1989

This paper is dedicated to Professor Arthur S. Perlin on the occasion of his 67th birthday

RAINER A. DYLLICK-BRENZINGER, VIJAY PATEL, MOLLIN B. RAMPERSAD, J. B. STOTHERS, and SHIRLEY E. THOMAS. Can. J. Chem. **68**, 1106 (1990).

Di-*tert*-butyl ketone (**2***a*), 5,5,7,7-tetramethyl-6-undecanone (**2***b*), and 2,4-dimethyl-2,4-diphenyl-3-pentanone (**2***d*) have been found to undergo slow rearrangement by β-proton abstraction from the α-methyl groups upon treatment with *t*-BuO$^-$/*t*-BuOH/≥185°C. This is in contrast to the absence of such rearrangement in cyclic systems. It is the only significant process observed for **2***a* and **2***b*, whereas with **2***d* and its monomethyl analog **22** Haller–Bauer type cleavage and an unprecedented 1,3-acyl shift from sp^3 to sp^2 carbon accompany the β-enolate rearrangement. The rates of $^1H/^2H$ exchange of the methyl protons in **2***a*, *b* were found to be similar to those reported for a variety of cyclic systems but this exchange does not occur in **2***d*, where only aryl proton exchange was observed.

Key words: β-enolization, acyclic ketones, acyl shift.

RAINER A. DYLLICK-BRENZINGER, VIJAY PATEL, MOLLIN B. RAMPERSAD, J. B. STOTHERS et SHIRLEY E. THOMAS. Can. J. Chem. **68**, 1106 (1990).

On a trouvé que, si on soumet la di-*tert*-butyl-cétone (**2***a*), la 5,5,7,7-tétraméthyl-undécan-6-one (**2***b*) ainsi que la 2,4-diméthyl-1,4-diphényl-pentan-3-one (**2***d*) à un traitement par le *tert*-BuO$^-$/*tert*-BuOH/≥185°C, il se produit une transposition lente impliquant un enlèvement du proton-β des groupements méthyles en α. Ce résultat est en opposition avec le fait que l'on n'observe pas de telles transpositions dans les systèmes cycliques. Cette transportation est le seul processus qui est observé à partir des composés **2***a* et **2***b* alors que, avec le produit **2***d* ainsi que son analogue monométhylé **22**, on observe un clivage de Haller–Bauer et un déplacement acyle-1,3 sans précédent du carbone sp^3 vers le carbone sp^2 qui accompagne la transposition de l'énolate β. On a trouvé que les taux d'échange $^1H/^2H$ des protons des groupements méthyles des composés **2***a* et **2***b* sont semblables à ceux rapportés antérieurement pour une variété de systèmes cycliques; toutefois, cet échange ne se produit pas avec le produit **2***d* alors que l'on n'observe que l'échange des protons aromatiques.

Mots clés : β-énolisation, cétones acycliques, déplacement acyle.

[Traduit par la revue]

Introduction

Over the past several years since the original discovery of the homoenolization process (1), the rearrangements of many cyclic monoketones have been found to occur through proton abstraction from carbons remote from the carbonyl group (2), generally from β-methylene carbons via β-enolates but with a few examples of γ-enolization leading to rearrangement (3). In most cases α-enolization was precluded as a competitive process, through α-methyl substitution or structurally with an α-proton at a bridgehead such that only an anti-Bredt α-enolate could be formed. Generally the investigations of these processes of remote proton abstraction have included examination of $^1H/^2H$ exchange to establish the regio- and stereoselectivity of proton abstraction. Invariably, exchange has been found to occur at the α-methyl sites but no ring-expanded products have been observed corresponding to those expected through ketonization of the putative cyclopropoxide intermediate **1**, i.e., cleavage *b* in Scheme 1. Evidence has been presented (4) in support of cyclopropoxide species as reasonable intermediates for α-methyl exchange in cyclic systems, and one example of rearrangement through an α-methyl carbon in a bicyclic diketone has been described (5). In contrast to the cyclic systems, however, some acyclic monoketones do undergo skeletal isomerization through β-enolizable methyl groups as was first observed with di-*tert*-butyl ketone and 5,5,7,7-tetramethylundecan-6-one (6). While this rearrangement is a very slow process for these aliphatic systems, a marked increase in the rate of rearrangement was observed for 2,4-dimethyl-2,4-diphenyl-3-pentanone (7). In addition, products from the competitive rearrangement involving an acyl shift from alkyl to aryl carbon were found, together with significant amounts of acidic components arising from Haller–Bauer type cleavage. While the results of these studies have been described in preliminary form, we wish to present the full details of our examination of these and some closely related ketones.

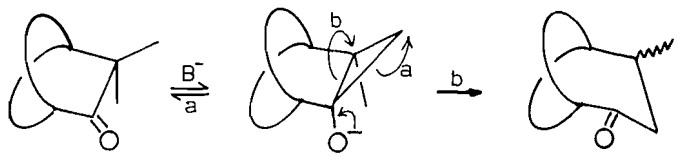

1

SCHEME 1

Results and discussion

Homoenolization experiments

(*a*) *Saturated ketones*

As the first model compound for our examination of acyclic ketones, commercially available di-*tert*-butyl ketone (**2***a*) was selected and dried over 4Å molecular sieves. Following our usual procedures (8), **2***a* was dissolved in anhydrous *t*-BuO$^-$/*t*-BuOH to provide a solution 0.2 M in **2***a* and 0.7 M in base. Aliquots of this solution were transferred to glass tubes under nitrogen, sealed under vacuum, and heated at 195°C for various times. The products were recovered by extraction with pentane

[1]For Part 141, see ref. 24.

[2]Present address: 3M Canada Inc., London, Ont., Canada.

Can. J. Chem. Downloaded from www.nrcresearchpress.com by 88.85.125.76 on 09/07/12
For personal use only.

TABLE 1. Composition[a] of the neutral product from treatment of **2***a* and **2***b* with *t*-BuO$^-$/*t*-BuOH at 195°C and ^{2}H incorporation in the *tert*-butyl groups of **2***a* and **3***a* at 195°C.

	Neutral products[b]				^{2}H assay[c]	
Time (h)	**2***a*	**3***a*	**2***b*	**3***b*	**2***a*-d_x	**3***a*-d_x
25	96	4			0.26	0.34
50	92	8	94	6	0.47	0.58
75	88	12	90	10		0.69
100	84	16	88	12	0.70	
125	82	18			0.80	
150	81	19	84	16	0.88	
225	76	24	80	20		
350	74	26				

[a]Determined by glc analysis (15% DEGS) of the total neutral product.
[b]Neutral products recovered in >90% yields.
[c]Total atoms ^{2}H/molecule by mass spectrometry.

(>90% yields) and analyzed by gas–liquid chromatography (glc) to reveal the presence of small amounts of a new component, in addition to the starting material, slowly increasing with increased reaction times (Table 1). After 75 h at 195°C, the new compound constituted 12% of the product and the amount doubled after 225 h; the data in Table 1 indicate that the pseudo first-order rate constant for rearrangement is $\sim 5 \times 10^{-7}$ s^{-1}. Longer reaction times gave only slightly greater amounts (26%, 350 h), as expected, since it has been shown that slow dehydration of *tert*-butyl alcohol occurs at elevated temperatures, leading to deterioration of the basic medium over reaction times >100 h (9), and some of the base is destroyed by reaction with the glass. In evidence of this, the product mixture, obtained after 200 h containing 22% of the new component, was treated with fresh base and found to contain 36% of the new ketone after 90 h at 195°C. Samples of the new ketone (1720 cm^{-1}, δ_C 215.3) were isolated by preparative glc and found to be identical to 2,2,5-trimethyl-3-hexanone (**3***a*) by ir and ^{1}H and ^{13}Cmr spectra. Samples of **3***a* in *t*-BuO$^-$/*t*-BuOH were heated at 195°C for up to 200 h and, in each case, **3***a* was recovered as the sole product in good yield (>80). Two samples were heated for >500 h; the recovered product contained very small amounts (<1%, by glc) of a second component having the same retention time as that of 2,6-dimethyl-4-heptanone (**4***a*) on three different glc columns. Two other tubes were heated at 210°C for 14 days and the neutral products also contained ~1% of the minor component, which was shown to be **4***a* by gc–ms.

The isomerization of **2***a* → **3***a* must involve proton abstraction leading to an intermediate β-enolate **5***a*, or its equivalent, which can suffer cleavage in two ways: path *a*, to regenerate **2***a*, or through cleavage of the original C-2, -3 bond, path *b*, to form **3***a*. Since no **2***a* was detected in the product obtained by the treatment of **3***a* with base, the cleavage of **5***a* → **3***a* is unidirectional. Trace quantities of **4***a* indicated that β-enolate **6***a* is generated, presumably reversibly, from **3***a*. Evidence confirming the sequence **2***a* ⇌ **5***a* → **3***a* ⇌ **6***a* → **4***a* was provided by the examination of ^{1}H/^{2}H exchange of the *tert*-butyl hydrogens in each of **2***a* and **3***a* under these strongly basic conditions. While **4** could undergo condensation, no such products were detected. Exchange in **2***a* was observed at 230°C in *t*-BuO$^-$/*t*-BuOD several years ago but no quantitative data were provided and the product mixture was not examined (10*a*).

Upon treatment of **2***a*, with anhydrous *t*-BuOD as solvent, the recovered samples of **2***a*-d_x were analyzed by mass

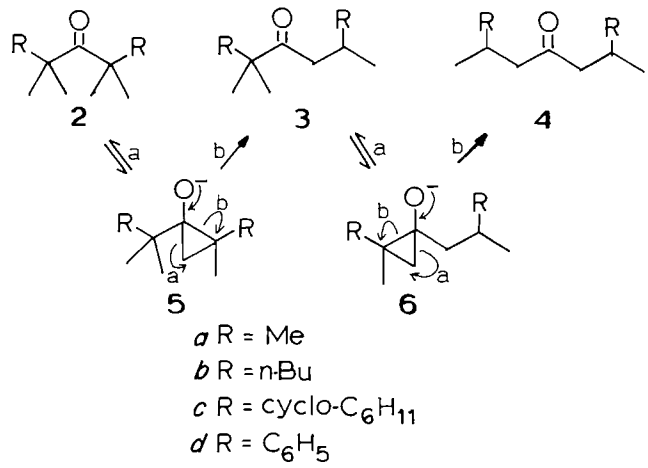

spectrometry to determine the extent of ^{2}H incorporation as a function of time. From the ^{2}H content in samples heated for 25, 50, 100, 125, and 150 h (Table 1), the rate constant for ^{2}H exchange was found to be $\sim 35 \times 10^{-7}$ s^{-1}, or approximately 7 times the rate of rearrangement. Clearly, the formation of **5***a* from **2***a* is reversible. Similar experiments with **3***a* for 25, 50, and 75 h revealed that slow exchange of the *tert*-butyl hydrogens (Table 1) accompanies rapid exchange of the α-methylene hydrogens, showing that the formation of **6***a* from **3***a* is also reversible. For each **3***a*-d_x sample, the ^{2}H content was determined by mass spectrometry and the proportions at the two sites of exchange were measured by integration of the ^{2}Hmr spectra. The rapid equilibration of the deuterium pool through α-exchange, however, may render the observed rate for β-exchange, $\sim 45 \times 10^{-7}$ s^{-1}, as a lower limit. In any event, β-exchange in **3***a* is twice as fast as that in **2***a*, on a per hydrogen basis, perhaps because of reduced steric strain, from nonbonded interactions, in **6***a* relative to that in **5***a*.

The second system chosen for examination was 5,5,7,7-tetramethylundecan-6-one (**2***b*) which, in principle, could undergo rearrangement through β-enolizable methyl groups and (or) the β-, or more remote, methylene sites. Ketone **2***b* was prepared by repeated methylation of the commerically available parent ketone with MeI/$NaNH_2$/Et_2O and then subjected to the usual homoenolization conditions. A glc analysis of the neutral product, isolated by pentane extraction, (>90% yields), revealed the presence of slowly increasing amounts (Table 1) of one new ketone (1710 cm^{-1}, δ_C 215.3), which was found to be isomeric with **2***b* by precise mass measurement. Samples for characterization were readily obtained by preparative glc. The ^{13}Cmr spectrum of the new ketone contained signals (δ_C, $CDCl_3$) for five methyl carbons, two of which are equivalent, at 14.0, 14.1, 20.0, and 24.3 (2), seven methylene, one methine, and a quaternary carbon, in addition to the carbonyl carbon signal. Clearly one methyl carbon has become a methylene carbon and the ^{13}C data accord well with those expected for **3***b*. An authentic sample of **3***b* was synthesized independently. Treatment of *N-tert*-butyl isobutyraldehyde imine, prepared according to House *et al.* (11), with *n*-butyllithium followed by the addition of *n*-butyl bromide gave *N-tert*-butyl 2,2-dimethylhexanal imine **7**. Hydrolysis of **7** afforded 2,2-dimethylhexanal (**8**), which was reacted immediately with propane-1,3-dithiol, as described by Seebach (12), to provide dithiane **9** (Scheme 2) in 75% yield. After lithiation of **9** with butyllithium, reaction with 1-bromo-2-methylhexane (**10**) gave dithiane **11** in 76% yield. Bromide **10** was prepared from the corresponding alcohol,

Can. J. Chem. Downloaded from www.nrcresearchpress.com by 88.85.125.76 on 09/07/12
For personal use only.

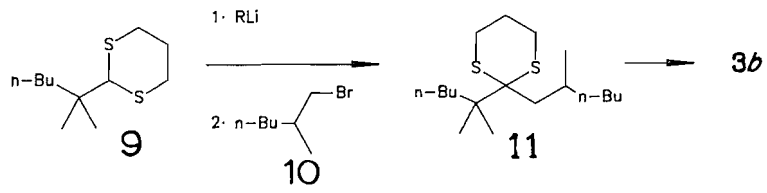

SCHEME 2

obtained from allyl alcohol in 77% yield by the method of Crandall and Clark (13), through reaction of its tosylate with sodium bromide in DMSO. Hydrolysis of **11** gave ketone **3*b***, in 67% yield, which was identical by ir, ms, and ^{1}H and ^{13}Cmr spectra with the rearrangement product from **2*b***. Treatment of **3*b*** with *t*-BuO$^-$/*t*-BuOH at 195°C for as long as 300 h led simply to the recovery of starting material in good yield (>80%) with no evidence of the presence of any isomeric ketone. Thus, **3*b*** is formed irreversibly from β-enolate **5*b***, or its equivalent. We found no evidence of a second β-enolate rearrangement leading to **4*b***.

As in the di-*tert*-butyl ketone system, experiments in deuterated media were carried out with **2*b*** and **3*b*** separately. Samples of **2*b*-d_x** isolated after 75 and 200 h in *t*-BuO$^-$/*t*-BuOD at 195°C contained 0.25 and 0.48 atoms ^{2}H/molecule, respectively, by mass spectrometry and each gave rise to an ^{2}Hmr spectrum containing a single peak corresponding to that expected for the α-methyl deuterons. Upon the addition of increasing amounts of Eu(fod)$_3$, this signal exhibited the same shifts as those found for the α-methyl protons in the ^{1}Hmr spectrum. Thus, ^{2}H exchange occurred only at the α-methyl carbons with no evidence of proton abstraction from the methylene carbons. For the analogous test with **3*b***, samples were first treated with MeO$^-$/MeOD by refluxing overnight to provide [7,7-$^2H_2$]-**3*b***, 1.96 atoms ^{2}H/molecule, which was heated at 195°C for 150 and 300 h in *t*-BuO$^-$/*t*-BuOD. After isolation of these **3*b*-d_x** samples, the α-deuterons were back-exchanged with MeO$^-$/MeOH before mass spectrometric analysis, which indicated incorporations of 0.67 and 0.88 atoms ^{2}H/molecule. The ^{13}C and ^{2}Hmr spectra of these samples showed that exchange occurred only at the α-methyl sites and from these data for **2*b*** and **3*b*** approximate rate constants for exchange at the α-methyl sites are 10 and 20 × 10^{-7} s^{-1}, respectively. Thus, the results for these two acyclic systems **2*a*** and **2*b*** are similar, although the β-exchange processes are somewhat slower for the latter case. It is interesting that proton abstraction from the β-methylene sites was not observed for either **2*b*** or **3*b***. From the exchange rates, β-enolate formation at the methyl carbons is faster for the less hindered ketones **3*a, b***, presumably reflecting differences in strain energy in the β-enolates **5*a, b*** vs. **6*a, b***, as noted earlier.

One other ketone, 2,4-dimethyl-2,4-dicyclohexylpentan-3-one (**2*c***), was also examined but even after heating with *t*-BuO$^-$/*t*-BuOH for >200 h at temperatures up to 210°C there was no evidence of rearrangement and **2*c*** was recovered in 85–90% yields. Perhaps steric crowding precludes the formation of the requisite β-enolate **5*c*** (R = cyclo-C_6H_{11}) that could lead to rearrangement.

(b) α-Phenyl ketones

From the results for **2*a*** and **2*b*** it was apparent that proton abstraction from the α-methyl carbons proceeds at rates comparable to those found for this process at β-methylene sites in several polycyclic ketones (2), but the competition between the modes of cleavage as denoted by *a* and *b* for **5** is strongly biased toward path *a*. The presence of a suitable substituent R in **5**, however, could serve to stabilize the incipient carbanion formed via path *b* to favour generation of the chain-extended isomer **3**. To examine this possibility, we selected 2,4-dimethyl-2,4-diphenyl-3-pentanone (**2*d***) as a model system, although it was realized that cleavage of the Haller–Bauer type through an intermediate species **12** could become a major competitive reaction. For example, ketones **13** and **14** (R = ethyl, dimethylallyl, benzyl) undergo this cleavage exclusively upon treatment with *t*-BuO$^-$/*t*-BuOH (14, 15). However, the more hindered carbonyl group in **2*d*** could render the rearrangement process more likely, since "ideally, the site of Haller–Bauer cleavage should not be subjected to any element of serious steric compression" (15). Also, cleavage *b* in **5*d*** leads to a benzylic carbanion. Thus, one could anticipate a closer competition between the two cleavages of **5*d*** than in the **5*a, b*** systems and this proved to be the case. Earlier investigations had shown that the *tert*-butyl esters formed in the Haller–Bauer cleavage (see **12**) do not survive under the conditions employed and the corresponding carboxylic acids are isolated.

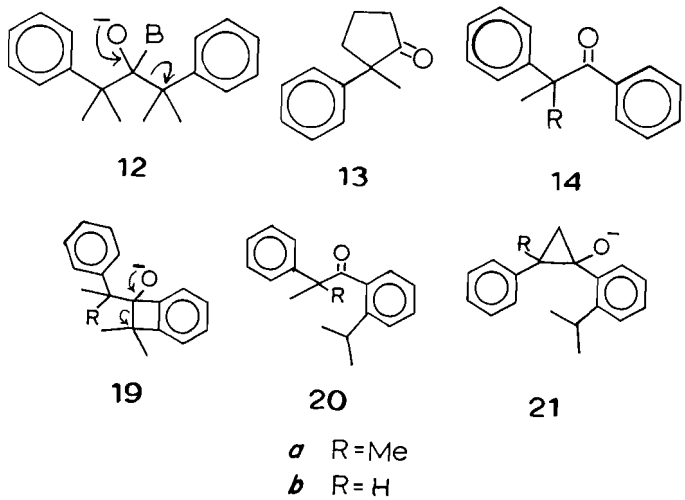

Treatment of **2*d*** with *t*-BuO$^-$/*t*-BuOH at 185°C following our usual methods with a slightly modified isolation procedure gave a neutral fraction containing, by glc analysis, four principal components with small amounts (<2%) of minor materials. These neutral products were isolated by pentane extraction after dilution of the reaction mixture with water and the addition of concentrated NH_4Cl solution to avoid the formation of emulsions. The aqueous layer was then acidified to pH ~1 before extraction with ether to isolate the acidic product. The glc analyses of the acidic fractions after methylation with CH_2N_2 revealed the presence of three esters in relative amounts that varied with reaction time. Several preliminary experiments were carried out using an oven that was subsequently found to have poor thermal stability over the long reaction times employed. Thus, although their reproducibility was poor, these experiments gave a qualitative picture of the sequence of

Can. J. Chem. Downloaded from www.nrcresearchpress.com by 88.85.125.76 on 09/07/12
For personal use only.

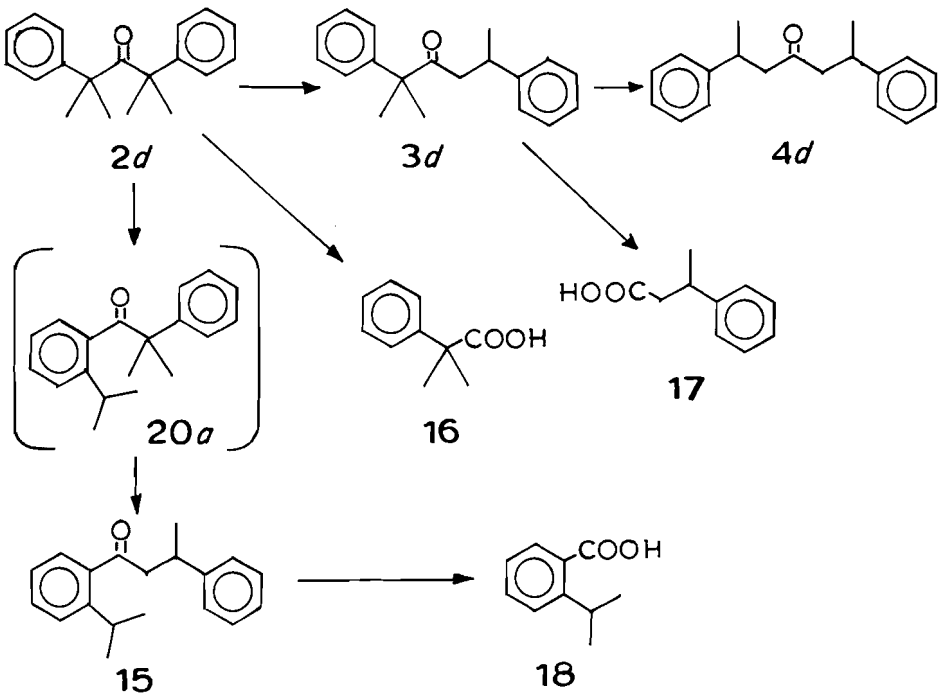

SCHEME 3

Can. J. Chem. Downloaded from www.nrcresearchpress.com by 88.85.125.76 on 09/07/12
For personal use only.

appearance of the various products and provided samples of each component for identification. Reproducible results were obtained from a series of runs in which the tubes were immersed in an oil-bath at 185 ± 1°C. The combined neutral and acidic fractions isolated typically represented >90% yields in each run. Samples of each component could be obtained by preparative glc or by chromatography on silica. Their structures were readily deduced from their ir and nmr spectra and the identity of each was confirmed by independent synthesis.

In the neutral fractions recovered from reactions for up to 136 h, the major component was easily shown to be the initial ketone **2***d* accompanied by three new components, which were found to be ketonic (ir, ^{13}Cmr) and isomeric with **2***d* by precise mass measurement. The first new ketone to appear in the neutral product exhibited carbonyl absorption at 1710 cm^{-1} with δ_C 211.0. The ^{13}Cmr spectrum contained signals for three methyl (21.4, 24.8, 25.1), one methylene (46.1), one methine (34.9), and a quaternary carbon (52.1) in the high field region. These data are clearly compatible with structure **3***d* and this was confirmed by its synthesis. The reaction of 2-methyl-2-phenylpropanal with 2-phenylpropyl magnesium bromide gave 2-methyl-2,5-diphenyl-3-hexanol, which was oxidized to **3***d*. The relative amount of **3***d* in the neutral fraction was found to increase slowly over ca. 100 h and then decrease in the product isolated after longer reaction times.

The second new ketone (1720 cm^{-1}), initially appearing more slowly than **3***d*, became the major component in the neutral fractions isolated after reaction times >200 h. Its ^{13}C spectrum contained three, equally intense, absorptions for methyl, methylene, and methine carbons in the sp^3 region. While a single methyl signal was found (δ_C 21.9), the methylene and methine absorptions each consisted of a pair of closely spaced signals at δ_C 51.7, 51.9 and 35.2, 35.3, respectively. In addition to two carbonyl peaks, δ_C 208.8, 208.7, signals for phenyl carbons were found at 126.2, 126.8 (2), 128.5 (2), and 146.2. In contrast to the equivalence of the methyl carbons, the methyl protons gave rise to a pair of equally intense doublets at δ 1.17 and 1.21 with J = 7 Hz for each. The ^{1}H spectrum also contained a broad singlet, δ 7.20 (10 H), a broadened "sextet" centred at δ 3.30, and a multiplet at 2.6; these two multiplets exhibited a 1:2 intensity ratio with the total equal to that of the methyl absorptions. These data are consistent with those expected for **4***d* as a 1:1 mixture of diastereomers.

Small amounts of the same mixture were obtained from a four-step preparative sequence analogous to that employed for the synthesis of **3***b*. Reaction of lithio 2-(2-phenylpropyl)-1,3-dithiane with β-bromocumene followed by hydrolysis gave **4***d* in low yield. In both cases, **4***d* was isolated as an oil but attempts to crystallize the mixture from MeOH at −70°C afforded colourless crystals, mp 40–45°C. The nmr spectra of the crystalline material indicated that the proportion of diastereomers changed to ca. 2:1, since the lower field methyl doublet (δ 1.21) and the higher field methine (δ_C 35.2) and methylene (δ_C 51.7) signals were twice as intense as their counterparts at δ 1.17 and δ_C 35.3, 51.9, respectively.

The third new ketone (1690 cm^{-1}, δC 205.3), which was the minor component in the neutral product from reactions of up to 136 h, gave rise to absorptions for three methyl (δ_C 22.1, 24.2_0, 24.2_4), one methylene (51.4), and two methine carbons (29.3, 35.8) in the high field region of its ^{13}Cmr spectrum. In the ^{1}H spectrum, a pair of overlapping methyl doublets, δ 1.13, 1.16, each with J = 6.5 Hz, and a septet, δ 3.10, J = 6.5 Hz, readily revealed the presence of an isopropyl group. The remaining methyl protons gave rise to a doublet, δ 1.33, J = 6.9 Hz, due to coupling with a methine proton at δ 3.47 appearing as a broadened sextet, which upon irradiation of the 1.33 ppm doublet collapsed to a four-line pattern representing the X part of an ABX pattern. The methylene protons gave rise to the AB portion of this pattern: δ_A 3.08, δ_B 3.19, J_{AB} = 16.4 Hz, J_{AX} = 7.8 Hz, J_{BX} = 6.5 Hz. Although the aryl proton absorption, 7.1–7.4 (m, 9H) was not particularly informative, seven protonated aryl carbon signals were resolved, two of which were twice as intense as the other five: δC 125.3, 126.3, 126.5, 126,8, 126.9 (2), 128.5 (2), 130.7; these signals were accom-

TABLE 2. Product distributions[a] from the reaction of **2***d* with *t*-BuO$^-$/*t*-BuOH at 185°C

	Neutral fraction					Acid fraction[b]			
Time (h)	Yield[c]	**2***d*	**3***d*	**4***d*	**15**	Yield[c]	**16**	**17**	**18**
30	67	90	8	2	—	24	60	32	8
68	63	70	23	6	<1	30	58	33	8
100	50	62	27	10	~1	40	43	45	11
136	42	60	22	16	<2	50	39	49	12
270	25	25	5	60	10	65	40	50	10

[a]Determined by glc analysis on SE-30 columns, estimated precision ±2%, and by ^{13}Cmr.
[b]Assayed by ^{13}Cmr and,after silylation, by glc on SE-30 columns.
[c]Given as the relative proportion, on a molar basis, of the isolated products, recovered in ≥90% yields.

Can. J. Chem. Downloaded from www.nrcresearchpress.com by 88.85.125.76 on 09/07/12
For personal use only.

panied by three peaks for fully substituted sp^2 carbon: δ_C 139.5, 146.2, 147.4. These data led to its tentative identification as 1-*o*-cumyl-3-phenyl-1-butanone **15** and this was confirmed by subsequent experiments described later.

The two major components of the acidic fractions were expected to be the methyl esters of 2-methyl-2-phenylpropionic acid (**16**) and 3-phenylbutyric acid (**17**) through Haller–Bauer cleavage of **2***d* and **3***d* as a result of addition at the carbonyl carbon by the alkoxide base, the collapse of which generates the benzylic cumyl anion as the leaving group (see **12**). The structures of these esters were confirmed, after isolation by preparative glc, by comparison with authentic samples obtained by methylation of the commercially available carboxylic acids. The third ester in the acidic fraction was shown to be isomeric with them by precise mass measurement. Its nmr spectra clearly showed the presence of an isopropyl group δ 1.24 (d, J = 7 Hz, 6H), δ_C 24.0; δ 3.73, (septet, J = 7 Hz, 1 H), δ_C 29.6, a methoxyl group (δ 3.86, δ_C 51.8) together with four equally intense protonated carbon signals (δ_C 125.5, 126.2, 129.9, 131.8), signals for two fully substituted carbons (130.0, 149.7), and a carboxyl carbon (168.7). The aryl protons gave rise to three multiplets centred at δ 7.20 (m, 1H), 7.40 (m, 2H), 7.75 (bd, J ~ 8 Hz, 1H). These data served to identify this ester as methyl 2-isopropylbenzoate and its properties were found to be identical to those of an authentic sample prepared from **18** using 2-isopropylacetophenone via the haloform reaction and methylation with CH_2N_2/Et_2O.

For the initial experiments, the compositions of the acidic fractions were assessed by glc analysis of the mixtures after methylation. In subsequent runs, these data were obtained from the ^{13}C spectra of the acid mixtures and by glc analysis after silylation (16) of the mixtures. The compositions of the neutral fractions were determined by ^{13}Cmr and glc analysis.

From the distribution of the various components in the neutral and acidic fractions (Table 2), it was apparent that skeletal rearrangement through β-enolization at the methyl groups does indeed compete with Haller–Bauer cleavage, in contrast to the situation found earlier for the less hindered ketones **13** and **14** (14, 15). In addition, a third process was discovered leading to the formation of **15**. The sequence **2***d* → **3***d* → **4***d* is readily explicable in terms of the β-enolate intermediates, **5***d* and **6** *d*, respectively, as in the saturated acyclic examples. However, the formation of **6***d* is a much more favoured process for the α-phenyl system, even though it competes with α-enolization.

Experiments with **2***d* in *t*-BuO$^-$/*t*-BuOD showed that ^{2}H exchange involved only the aryl protons since only aryl ^{2}H absorption was evident in the ^{2}Hmr spectra of the recovered **2***d*–d_x samples; none was detected at the methyl sites. Deuterium assays by mass spectrometry showed incorporations of 3.5 and 5.3 atoms ^{2}H/molecule after 16 and 88 h, respectively. Thus, the cleavage of β-enolate **5***d* proceeds exclusively through path *b*, in contrast to the results for the saturated acyclic systems. The regiospecificity of the cleavage of **5***d* is presumably governed by the fact that the incipient tertiary anion formed by this cleavage is benzylic. Similarly, one could anticipate that the formation of **6***d* would lead to the generation of **4***d* preferentially, which is entirely consistent with the observation that **4***d* is the major neutral component in the product isolated after long reaction times.

The relative ease of aryl exchange is not unexpected since aryl protons are more acidic than alkyl protons (10*b*). Proton abstraction would be expected to occur at each position on the aryl rings (17) and the formation of an *ortho*-phenyl anion could lead to the cyclobutoxide, or γ-enolate, **19***a*. Analogous species have been generated in a few saturated polycyclic systems under comparable conditions (18). Ketonization of **19***a* to the benzylic anion will lead to **20***a* and this should be a favoured route. Upon its formation, **20***a* can undergo rearrangement through one of the β-enolizable methyl groups to form **15**, i.e., via **21***a*, or suffer Haller–Bauer cleavage to produce 2-isopropylbenzoic acid. This sequence clearly accounts for the presence of these unusual products from the homoenolization of **2***d*. However, no material having structure **20***a* had been isolated. Consequently ketone **20***a* was synthesized and its behaviour upon treatment with *t*-BuO$^-$/*t*-BuOH examined.

Benzyl magnesium bromide was reacted with 2-isopropylbenzonitrile to give 2-isopropylphenyl benzyl ketone in 70% yield. Methylation with LDA/MeI/THF afforded the α-methyl derivative **20***b*, which in a second methylation cycle gave the desired α,α-dimethyl derivative **20***a*. The glc retention time of **20***a* was found to be very slightly shorter than that for **2***d* under the conditions employed for the analysis of the neutral products and the presence of a small amount of **20***a* could have escaped detection. In any event, it was found that **20***a* reacts relatively rapidly under the homoenolization conditions employed to produce a mixture of **15** and **18**, the latter isolated after methylation with CH_2N_2/Et_2O. The half-life for the disappearance of **20***a* was ca. 8 h at 185°C; the results for a series of experiments are summarized in Table 3. These results show that Haller–Bauer cleavage of **20***a* is somewhat faster than the β-enolate rearrangement to **15**. Careful examination of the nmr spectra of the **20***a* samples recovered from these runs failed to reveal the presence of any **2***d*, indicating that **19***a* → **20***a* is not reversible

From these results, the fate of **2***d* upon treatment with *t*-BuO$^-$/*t*-BuOH can be summarized as in Scheme 3.

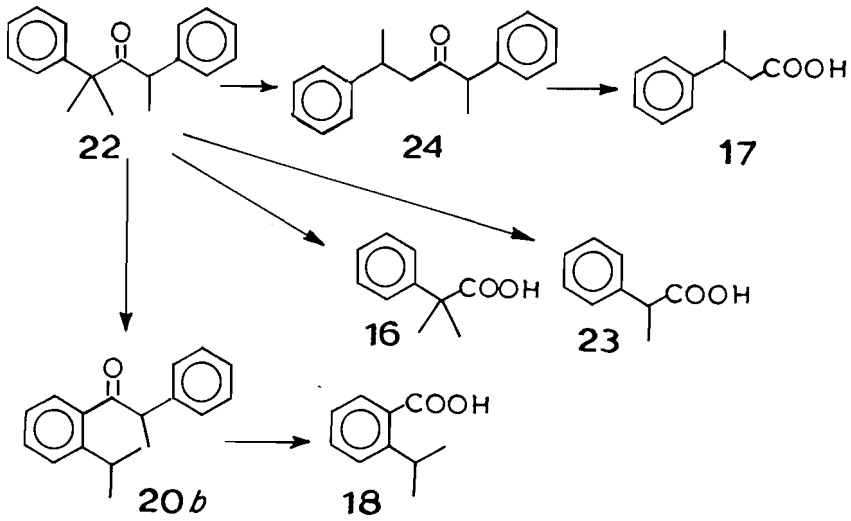

SCHEME 4

TABLE 3. Product distribution[a] from the treatment of **20***a* with *t*-BuO$^-$/*t*-BuOH at 185°C

Time (h)	**20***a*	**15**	**18**
6	66	14	20
12	35	28	37
26	11	37	52
52	2	34	64

[a]>90% recovery.
[b]Proportions of **15** and **20***a* determined by glc with an SE-30 column.

From the observation that β-enolization at the α-methyl groups in **3***d* competes favourably with α-enolization to generate **4***d* , it was of interest to compare the behaviour of 2-methyl-2,4-diphenyl-3-pentanone (**22**) with that of its fully methylated analog **2***d*. From a series of experiments in which **22** was heated at 185°C in *t*-BuO$^-$/*t*-BuOH for varying periods, the methylated acidic product was found to contain four esters, three of which were found to arise from **16, 17**, and **18**. The fourth ester, the major component in the acidic product from relatively short runs, was expected to be methyl 2-phenylpropionate arising from Haller–Bauer cleavage of **22**. This was confirmed by comparison with an authentic sample prepared from the commercially available carboxylic acid. The neutral fractions contained two new components in addition to decreasing amounts of **22**. The expected *o*-isopropyl derivative **20***b* was readily identified since an authentic sample was available from the preparative sequence employed to obtain **20***a*. The major neutral component in the products from the longer runs appeared to be a 1:1 mixture of diastereomers as anticipated for 2,5-diphenyl-3-hexanone (**24**), the ketone which would arise through β-enolization at one of the *gem*-dimethyl carbons in **22**. An authentic sample of **24** was obtained by a method analogous to that employed for the preparation of **3***b*. Lithiation of the dithiane formed from 2-phenylpropanal and 1,3-propanedithiol followed by reaction with β-bromocumene and hydrolysis gave in low yield the same 1:1 mixture of diastereomers **24** together with other unidentified material. An attempted alternative sequence utilizing the reaction of 2-phenylpropanal with the Grignard reagent from β-bromocumene, followed by oxidation, gave a different mixture of diastereomers **24** in low yield. The ^{13}Cmr spectrum indicated this mixture to be enriched in one of the two forms. The distribution of components in the neutral and acidic fractions after various reaction times was assessed by glc analysis; these results are collected in Table 4. The fate of **22** upon treatment with *t*-BuO$^-$/*t*-BuOH is summarized in Scheme 4.

(*c*) *Summary*

The data for the acyclic saturated ketones **2***a, b* show that proton abstraction from the α-methyl sites proceeds at rates comparable to those found for the corresponding sites in a variety of cyclic ketones (2). In contrast to the cyclic systems, however, the acyclic ketones rearrange slowly to **3***a, b*, showing that cleavage of the intermediate **5***a, b*, or equivalent species, leads to both primary (path *a*) and tertiary (path *b*) incipient carbanions. In the cyclic systems, only the former pathway has been observed. We suggest that the relative stabilities of **2***a, b* vs. **3***a, b* may be responsible. The carbonyl stretching frequencies differ by ca. 30 cm^{-1}, indicating a significant difference in the C—C(O)—C bond angle, which may destabilize **2***a, b* by a few kcal/mol. A similar difference has been shown to give 100% regioselectivity in the homoketonization of 2-acetoxydeltacyclane (19) for which the two possible modes of cleavage involve secondary carbanionic sites. We suggest that the difference in the stabilities of **2***a, b* and **3***a, b* alters the regioselectivity of the cleavage of **5***a, b* rendering the "unexpected" mode *b* competitive with regeneration of the initial ketone. Introduction of the α-phenyl groups in **2***d* renders cleavage of **5***d* regiospecific since no ^{1}H/^{2}H exchange was observed at the methyl carbons in **2***d*. Cleavage of **5***d* to generate a benzylic carbanionic site (path *b*) leading to **3***d* is clearly dominant, although Haller–Bauer type cleavage to acidic product becomes significant. Presumably, steric hindrance to carbonyl addition by *t*-BuO$^-$ in **2***d* renders β-enolate rearrangement more favourable energetically in contrast to the exclusive cleavage found for the less hindered **13** and **14**. If Haller–Bauer cleavage could be suppressed, there is some promise that β-enolization could be useful for chain extension and, perhaps, ring expansion in α-aryl substituted cyclic systems. Studies directed along these lines are currently in progress.

Can. J. Chem. Downloaded from www.nrcresearchpress.com by 88.85.125.76 on 09/07/12
For personal use only.

TABLE 4. Product distribution[a] from the reaction of **22** with *t*-BuO$^-$/*t*-BuOH at 185°C

	Neutral fraction				Acid fraction[b]				
Time (h)	Yield[c]	**22**	**24**	**20***b*	Yield[c]	**23**	**16**	**17**	**18**
15	65	90	10	—	35	70	30	—	—
100	35[d]	28	60	7	65	50	15	33	2
200	25[d]	20	60	15	75	25	15	55	5

[a]Determined by glc analysis, SE-30 column, estimated precision ±2%.
[b]The glc assay after methylation of the total fraction with CH_2N_2/Et_2O.
[c]Given as the relative proportion, on a molar basis, of the isolated material, recovered in >90% yields.
[d]Neutral fractions contained ca. 5% unidentified material.

Experimental

Boiling points and melting points are uncorrected Gas–liquid chromatography was carried out on Varian 920, 3300, and 3700 instruments using columns of SE-30, DEGS, Carbowax 4000 or 20M on Chromosorb W, as indicated. Thin-layer chromatography was done on Kieselgel 60 F_{254} plates unless otherwise indicated. Tetrahydrofuran and ether were dried over sodium and freshly distilled before use. Undecan-6-one, 1,3-diphenyl-2-propanone, 2-phenylpropanol, β-bromocumene, ketones **2***a*, **3***a*, **4***a*, and the carboxylic acids **16**, **17**, and **23** were available commercially. The preparations of the remaining compounds are described below.

Infrared spectra were recorded with a Beckman 4250 instrument and mass spectra were obtained on a Varian MAT-311A system, at 70 eV (direct inlet). The ^{1}H and ^{13}Cmr spectra of each of the compounds were obtained to confirm their identities and those spectra were recorded with Varian XL-100, -200, or -300 spectrometers. Carbon, hydrogen, and sulfur analyses were performed by Chemalytics Inc., Tempe, Arizona.

*5,5,7-Trimethyl- and 5,5,7,7-tetramethylundecan-6-one (23*b)

To a stirred suspension of freshly powdered anhydrous sodium amide (13.7 g) in 1 L of anhydrous ether under a nitrogen atmosphere was added a solution of 6-undecanone (10 g) in 80 mL of dry ether. The mixture was stirred vigorously for 3 h under gentle reflux and then freshly distilled methyl iodide (84 g) in 80 mL of dry ether was added slowly. The mixture was stirred for 24 h at room temperature. After hydrolysis of excess $NaNH_2$ by the addition of water, the crude product was isolated by ether extraction and found to contain three components by glc analysis (10% Carbowax 4000), none of which corresponded to the starting ketone. The total product was recycled through the methylation procedure and after the third cycle a single product, isolated by preparative glc, exhibited properties consistent with those expected for 5,5,7-trimethylundecan-6-one; ir (liquid film): 1700 cm^{-1}; ^{1}Hmr ($CDCL_3$)δ: 0.88 (t, $J \sim 7$ Hz, 6H), 1.01 (d, $J \sim 6.5$ Hz, 3H), 1.11 (s, 3H), 1.12 (s, 3H), 2.95 (m, 1H); ^{13}Cmr ($CDCl_3$)δ: CH_3, 14.0 (2), 18.1, 24.06, 24.12; CH_2, 22.9, 23.4, 27.0, 29.7, 34.0, 39.2; CH, 39.6; quat C, 48.0; C=O, 219.3.

A fourth cycle, during which the reaction mixture was refluxed for 22 h after the addition of the methyl iodide solution, gave a new ketone (13.4 g), essentially pure by glc analysis. Distillation under reduced pressure furnished pure **2***b*, bp 128–130°C/15 Torr (1 Torr = 133.3 Pa); ir (liq. film): 1675 cm^{-1}; ^{1}Hmr ($CDCl_3$)δ: 0.98 (t, $J \sim 6.5$ Hz, 6H), 1.23 (s, 12H); ^{13}Cmr ($CDCl_3$)δ: CH_3, 14.0, 26.3(2); CH_2, 23.4, 27.2, 41.6; quat C, 49.4; C=O, 218.2. Anal. calcd. for $C_{15}H_{30}O$: C 79.57, H 13.36; found: C 79.43, H 13.64.

*5,5,8-Trimethyl-6-dodecanone (3*b)

(*i*) N-tert-*Butyl-2,2-dimethylhexanal imine (7)*

A solution of *N-tert*-butyl isobutyraldehyde imine (16.2 g, 0.127 mol), prepared according to House *et al.* (11), in dry tetrahydrofuran (70 mL) was cooled to −20°C and a solution of butyllithium (65 g, 2 M in hexane) was added. The mixture, which turned yellow almost immediately, was allowed to warm to 0°C and this temperature was maintained as *n*-butyl bromide (26 g, 0.18 mol) was added slowly. After 30 min, saturated sodium chloride solution (300 mL) was added. The aqueous layer was extracted with ether and the extracts added to the organic layer, which was then dried over anhydrous $MgSO_4$. After removal of the solvent under reduced pressure, the residue was distilled to furnish a fraction (17.2 g) boiling in the range 85–95°C/70–100 Torr, containing two components in a 4:1 ratio. The major product, isolated by preparative glc (20% SE-30), slowly crystallized on standing and was the desired imine **7** (57% yield); mp 104–105°C; ir (mull); 2990, 2960, 2890, 1675, 1470, 1370, 1230 cm^{-1}; ^{1}Hmr ($CDCl_3$)δ: 0.95 (s, 6H), 1.08 (s, 9H), 7.23 (s, 1H, -CH=N); ^{13}Cmr ($CDCl_3$)δ: CH_3, 14.1, 25.0(2), 29.8(3); CH_2, 23.6, 26.7, 40,6; CH, 164.3; C, 38.5, 56.0; ms: 183 (M^+). The minor product was not identified.

(*ii*) *Dithiane* **9**

Imine **7** (14.2 g, 0.08 mol) was dissolved in hexane (50 mL) and 20% aqueous acetic acid (130 mL) was added. After 15 min, sufficient NaCl was added to saturate the aqueous layer and the product isolated by repeated extraction with pentane. After evaporation of the solvent, the extracts furnished essentially pure 2,2-dimethylhexanal (**8**) (4.7 g, 47% yield); ^{1}Hmr ($CDCl_4$)δ: 1.03 (s, 6H), 9.33 (s, 1H, CHO); ^{13}Cmr ($CDCl_3$)δ: CH_3, 14.0, 21.4(2); CH_2, 23.6, 26.7, 37.3; CHO, 205.1; quat C, 45.7.

Aldehyde **8** (1.6 g) was dissolved in chloroform (40 mL) and propane-1,3-dithiol (1.3 mL) was added at room temperature (12). After stirring for 1 h, the solution was cooled to 0°C and BF_3/Et_2O (0.5 mL) was added. After standing overnight at 6°C, a small amount of water had separated. The $CHCl_3$ layer was extracted three times with cold 7% aqueous potassium hydroxide solution and once with water before drying over K_2CO_3. The residual oil obtained after evaporation of the solvent under reduced pressure was distilled to furnish **9** (2 g, 75% yield), bp 93°C/0.55 Torr; ^{1}Hmr ($CDCl_3$)δ: 0.9 (t, $J \sim 7$ Hz, 3H), 1.06 (s, 6H), 3.93 (s, 1H); ^{13}Cmr ($CDCl_3$)δ: CH_3, 14.1, 25.4(2); CH_2, 23.4, 25.9, 26.2, 31.4(2), 40.2; CH, 60.9; quat C, 38.0. Anal. calcd. for $C_{11}H_{22}S_2$: C 60.48, H 10.15, S 29.36; found: C 60.70, H 10.30, S 29.70. Exact mass calcd. for $C_{11}H_{22}S_2$: 218.1163; found: 218.1165.

(*iii*) *Dithiane* ***11***

A solution of 2-methylhexan-1-ol (5.0 g), prepared from allyl alcohol in 77% yield as described by Crandall and Clark (13), in dry pyridine (40 mL) was cooled to 0°C and tosyl chloride (24 g) was added with stirring. After stirring for 30 min, the reaction mixture was stored at 0°C overnight before the addition of ice-cold water (70 mL). The product was extracted with Et_2O (3 × 50 mL) and the combined extracts washed with cold 10% aqueous HCl, 10% $NaHCO_3$ solution, and water before drying over $MgSO_4$. Removal of the solvent gave a slightly yellow oil (10.2 g, 88%) containing a single component by tlc. This oil was dissolved in DMSO (40 mL), and NaBr (10 g, was added with swirling. After 5 days, the crude product was isolated by ether extraction and purified by distillation to give 1-bromo-2-methylhexane (**10**) (6 g, 88% yield) boiling at 105–106°C/100 Torr; ^{13}Cmr ($CDCl_3$)δ: CH_3, 14.0, 18.8; CH_2, 22.8, 29.1, 34.6, 41.6; CH, 35.3.

Dithiane **9** (3.3 g) was dissolved in dry tetrahydrofuran (20 mL) under an argon atmosphere. After cooling to −30°C, *n*-butyllithium (7 mL, 2 M in hexane) was added. The colorless solution became

Can. J. Chem. Downloaded from www.nrcresearchpress.com by 88.85.125.76 on 09/07/12
For personal use only.

deep red and then developed a yellow tinge. The temperature was maintained at −15°C for 18 h and then raised to 0°C. After **10** (2.7 g) was added, the yellow colour slowly faded. The mixture was kept at 6°C for 2 days before the reaction was quenched by pouring the mixture into water. The crude product (4.4 g) was isolated by pentane extraction. Distillation under reduced pressure yielded dithiane **9** (1.1 g) and dithiane **11** (2.4 g, 76% yield based on reacted **9**), bp 138°C/0.05 Torr; ir (liquid film): 2925, 2873, 1470, 1459, 1418, 1383 cm^{-1}; ^{1}Hmr ($CDCl_3$)δ: 0.90 (t, $J \sim 6$ Hz, 3H), 0.92 (t, $J \sim 6$ Hz, 3H), 1.05 (d, $J \sim 7$ Hz, 3H), 1.12 (s, 6H), 2.83 (bt, $J \sim 6$ Hz, 4H). Anal. calcd. for $C_{18}H_{36}S_2$: C 68.28, H 11.46, S 20.25; found: C 67.99, H 11.21, S 20.70. Exact mass calcd. for $C_{18}H_{36}S_2$: 316.2258; found: 316.2252.

(*iv*) *Ketone* **3***b*

A solution of dithiane **11** (2.4 g) in 90% aqueous methanol (50 mL) containing mercuric oxide (2.4 g and mercuric chloride (5.1 g) was heated under reflux with stirring for 3 h. After cooling, the reaction mixture was filtered and diluted with water (250 mL) before ether extraction. The combined extracts were washed with concentrated ammonium chloride solution. After drying, the solvent was evaporated to furnish essentially pure **3***b* as an oil (1.15 g, 67% yield). Bulb-to-bulb distillation at 100°C/0.05 Torr furnished an analytical sample; ir ($CHCl_3$): 1710 cm^{-1}; ^{1}Hmr ($CDCl_3$)δ: 0.88 (t, $J \sim 6$ Hz, 6H), 0.86 (d, $J \sim 6$ Hz, 3H), 1.08 (s, 6H), 2.35 (dd, 2H); ^{13}Cmr ($CDCl_3$)δ: CH_3, 14.0, 14.1, 20.0, 24.3(2); CH_2, 22.9, 23.4, 26.9, 29.3, 36.7, 39.7, 44.3; CH, 28.4; quat C 47.5; C=O, 215.4. Anal. calcd. for $C_{15}H_{30}O$: C 79.58, H 13.36; found: 79.32, H 13.29, Exact mass calcd. for $C_{15}H_3O$: 226.2289; found: 226.2290.

*2-Methyl-2,4-diphenyl- and 2,4-dimethyl-2,4-diphenyl-3-pentanone (**22**, **2**d)*

With the methylation procedure described above for 6-undecanone, 1,3-diphenyl-2-propanone gave, after three cycles, the tetramethyl derivative **2***d* in 60% yield after crystallization from EtOH, mp 111–112°C (lit.(20) mp 110–115°C (dec.)); ir ($CHCl_3$): 1690 cm^{-1}; ^{1}Hmr ($CDCl_3$)δ: 1.26 (s, 12H), 7.1 (bs, 10H); ^{13}Cmr ($CDCl_3$)δ: CH_3, 27.8; aryl CH, 125.8(2), 126.4, 128.3(2); quat C, 52.9, 144.3; C=O, 213.0. Anal. calcd. for $C_{19}H_{22}O$: C 85.66, H 8.32; found: C 85.52, H 8.41. Exact mass calcd. for $C_{19}H_{22}O$: 266.1671; found: 266.1673.

A single methylation cycle furnished a mixture of di- and trimethyl derivatives from which, through repeated recrystallizations from ethanol, the trimethyl ketone **22** could be isolated in ca. 50% yield, mp 56–57°C; ir ($CHCl_3$): 1708 cm^{-1}; ^{1}Hmr ($CDCl_3$)δ: 1.28 (d, $J \sim 6.5$ Hz, 3H), 1.39 (s, 3H), 1.51 (s, 3H), 3.82 (q, $J \sim 6.5$ Hz, 1H), 7.5 (m, 10H); ^{13}Cmr ($CDCl_3$)δ: CH_3, 21.8, 24.4, 25.6; CH, 47.4; quat C, 53.2; C=O, 213.2; aryl CH, 126.5(3), 126.9, 127.5(2), 128.3(2), 128.6(2); aryl C, 141.7, 143.0. Exact mass calcd. for $C_{18}H_{20}O$: 252.1514; found: 252.1518.

*2,4-Dimethyl-2,4-dicyclohexylpentan-3-one (**2**c)*

Hydrogenation of **2***d* (1.5 g) in glacial acetic acid (30 mL) and perchloric acid (20 mL) over PtO_2 at 380 kPa for 100 h furnished ketone **2***c* as a low melting solid (1.4 g, 88% yield). After recrystallization from methanol, **2***c* had mp 49–50°C; ir ($CHCl_3$): 1675 cm^{-1}; ^{1}Hmr ($CDCl_3$)δ: 1.12 (s, 6H); ^{13}Cmr ($CDCl_3$)δ: CH_3, 22.8; CH_2, 26.8, 27.2(2), 28.1(2); CH, 45.1; quat C, 52.8; C=O, 218.1. Anal. calcd. for $C_{19}H_{34}O$: C 81.94, H 12.32, found: C 81.68, H 12.62. Exact mass calcd. for $C_{19}H_{34}O$: 278.2610; found: 278.2612.

*2-Methyl-2,5-diphenyl-3-hexanone (**3**d)*

A solution of β-bromocumene (1.9 g) in anhydrous Et_2O (20 mL) containing Mg turnings (0.23 g) was treated with 2 drops of 1,2-dibromoethane before refluxing under argon for 1.5 h. After cooling to −70°C, the reaction mixture was treated with 2-methyl-2-phenylpropanal (1.4 g), which had been prepared as described by Schaffner and co-workers (21) with the Doering oxidation step (22). After warming to room temperature, ether extraction of the reaction mixture gave a crude product that, by glc analysis, contained a major component (~75%) accompanied by two minor components. This product was treated with Jones' reagent (23) until the colour persisted. The aqueous layer was separated, extracted with Et_2O, and the combined extracts dried before evaporation of the solvent. The crude product (0.5 g) was found to contain **3***d*, 2-methyl-2-phenylpropionic acid, and some unidentified material by tlc. A sample of **3***d* separated by tlc was identified by glc (SE-30) and its physical properties were identical to those found for **3***d* from the homoenolization experiments with **2***d*: ir (CCl_4): 3100, 3075, 3040, 2970, 2940, 1710, 1590 cm^{-1}; ^{1}Hmr ($CDCl_3$)δ: 1.08 (d, $J \sim 7$ Hz, 3H), 1.33 (s, 3H), 1.46 (s, 3H); ^{13}Cmr ($CDCl_3$)δ: CH_3, 21.4, 24.8, 25.1; CH_2, 46.1; CH, 34.9; quat C, 52.1; C=O, 211.0; aryl CH, 126.6(3), 126.7, 126.8(2), 128.2(2), 128.6(2); quat C, 143.5, 146.4. Exact mass calcd. for $C_{19}H_{22}O$: 266.1671; found: 266.1668.

*2,6-Diphenyl-4-heptanone (**4**d)*

Following a sequence analogous to that employed to generate **3***b*, this preparation required 2-(2-phenylpropyl)-1,3-dithiane, which was obtained (12) from metallated 1,3-dithiane (1.2 g) upon reaction with β-bromocumene (2 g) near 0°C for 15 h. The dithiane was isolated by pentane extraction (1.2 g, 50%) and distilled under reduced pressure, bp 130°C/0.01 Torr; ^{1}Hmr ($CDCl_3$)δ: 1.23 (d, $J \sim 7$ Hz, 3H), 2.95 (m, 1H), 3.56 (t, $J \sim 7$ Hz, 1H); ^{13}Cmr ($CDCl_3$)δ: CH_3, 22.3; CH_2, 26.0, 29.8, 30.1, 36.2; CH, 43.6, 45.1; aryl CH, 126.2, 127.0(2), 128.4(2); quat C, 145.7. Exact mass calcd. for $C_{13}H_{18}S_2$: 238.0852; found: 238.0858.

Metallation of this dithiane followed by reaction with β-bromocumene and hydrolysis as described above for **3***b* gave a mixture of products containing small amounts of **4***d* as revealed by glc analysis and comparison with samples obtained in the homoenolization experiments with **2***d*. Material isolated from homoenolization of **2***d* as a 1:1 mixture of diastereomers had the following properties: ir (CCl_4): 3150, 2820, 2650, 1720, 1495, 1450 cm^{-1}; ^{1}Hmr ($CDCl_3$)δ: 1.17 (d, $J \sim 7$ Hz, 3H), 1.21 (d, $J \sim 7$ Hz, 3H), 2.35–2.80 (m, 4H), 3.1–3.5 (m, 2H); ^{13}Cmr ($CDCl_3$)δ: CH_3, 21.9; CH_2, 51.7, 51.8; CH, 35.2, 35.3; aryl CH, 126.2, 126.8(2), 128.5(2); quat C, 146.2; C=O, 208.5, 208.6. Exact mass calcd. for $C_{19}H_{22}O$: 266.1671; found: 266.1668.

Attempted recrystallization from methanol at −70°C gave a mixture, mp 40–45°C, which was significantly enriched in one of the diastereomeric forms and for which the 1.21 ppm doublet was enhanced in the ^{1}H spectrum while the higher field methylene and methine signals were the more intense in the ^{13}C spectrum.

Methyl 2-isopropylbenzoate

With vigorous stirring, 2-isopropylacetophenone (0.80 g) was added to a mixture of NaOH (4 g) and Br_2 (1.2 g) in ice-water (10 mL) while the temperature was maintained near 0°C with a cold brine bath. After 1 h, the reaction mixture was allowed to warm to room temperature and stirring was continued overnight. After thorough ether extraction, the aqueous phase was treated with $Na_2S_2O_5$ (0.5 g in 10 mL of H_2O) and then acidified with concentrated HCl solution. Ether extraction of the acidic aqueous phase afforded 2-isopropylbenzoic acid (0.70 g, 85% yield), mp 60–62°C; ^{13}Cmr ($CDCl_3$)δ: CH_3, 24.0(2): CH, 29.4; aryl CH, 125.6, 126.5, 131.0, 132.8; aryl C, 128.4, 151.0; C=O, 174.5.

Treatment of an ethereal solution of the acid (0.65 g) with excess CH_2N_2/Et_2O gave methytl 2-isopropylbenzoate (0.67 g, 95% yield); ir (CCl_4): 1728 cm^{-1}; ^{1}Hmr ($CDCl_3$)δ: 1.26 (d, $J = 7$ Hz, 6H), 3.74 (septet, $J = 7$ Hz, 1H), 3.87 (s, 3H), 7.1–7.8 (m, 4H); ^{13}Cmr ($CDCl_3$)δ: CH_3, 24.0(2); CH, 29.6; CH_3O, 51.8; aryl CH, 125.5, 126.2, 129.9, 131.8; aryl C, 130.0, 149.7; C=O, 168.7. Exact mass calcd. for $C_{11}H_{14}O_2$: 178.0994; found: 178.0995.

*Methyl esters of **16**, **17**, and **23***

Treatment of the corresponding carboxylic acids, which were commercially available, with excess CH_2N_2/Et_2O afforded authentic samples of the esters. (a) Methyl 2-methyl-2-phenylpropionate (**16**): ir (CCl_4): 1730 cm^{-1}; ^{1}Hmr ($CDCl_3$)δ: 1.52 (s, 6H), 3.43 (s, 3H), 7.1 (bs, 5H); ^{13}Cmr ($CDCl_3$)δ: CH_3, 26.5; C, 46.5; CH_3O, 51.8; aryl CH, 125.6(2), 126.7, 128.4(2); aryl C, 144.8; C=O, 176.8. (b) Methyl 3-phenylbutyrate (**17**): ir (CCl_4): 1728 cm^{-1}; ^{1}Hmr ($CDCl_3$)δ: 1.27 (d, $J = 7.5$ Hz, 3H), 2.45 (m, 1H), 2.60 (m, 1H), 3.30 (m, 1H), 3.57 (s, 3H) 7.15 (bs, 5H); ^{13}Cmr ($CDCl_3$)δ: CH_3, 21.8; CH, 36.5; CH_2, 42.7; CH_3O, 51.3; aryl CH, 126.4, 126.7(2), 128.5(2); aryl C, 145.8; C=O, 172.6. (c) Methyl 2-phenylpropionate (**23**): ir (CCl_4): 1735 cm^{-1};

Can. J. Chem. Downloaded from www.nrcresearchpress.com by 88.85.125.76 on 09/07/12
For personal use only.

Can. J. Chem. Downloaded from www.nrcresearchpress.com by 88.85.125.76 on 09/07/12
For personal use only.

^{1}Hmr ($CDCl_3$)δ: 1.50 (d, J = 7 Hz, 3H), 3.67 (s, 3H), 3.71 (q, J = 7 Hz, 1H), 7.33 (bs, 5H).

Benzyl phenyl ketones ***20***a, b

Following the standard Sandmeyer procedure, 2-isopropylbenzonitrile was prepared from 2-isopropylaniline in 38% yield, bp 100–101°C/5 Torr; ir (CCl_4); 2230 cm^{-1}; ^{1}Hmr ($CDCl_3$)δ: 1.05 (d, $J \sim 7$ Hz, 6H), 3.33 (septet, $J \sim 7$ Hz, 1H); ^{13}Cmr ($CDCl_3$)δ: CH_3, 23.1; CH, 32.5; aryl CH, 126.1, 126.6, 132.9, 133.2; quat C, 111.8, 152.2; CN, 118.0. Exact mass calcd. for $C_{10}H_{11}N$: 145.0891; found: 145.0895.

To a cooled solution (0°C) of benzylmagnesium bromide in anhydrous ether (300 mL), prepared from benzyl bromide (10.5 g) and magnesium turnings (2.2 g), was slowly added 2-isopropylbenzonitrile (10.5 g) in dry ether (15 mL). The reaction mixture was heated under gentle reflux for 20 h and then the reaction was quenched by adding concentrated HCl (50 mL) in water (150 mL). This mixture was heated on a steam bath for 1 h and, after cooling, the product was extracted with ether. After drying the extracts over anhydrous sodium sulfate and removal of the solvent, the residue was distilled under reduced pressure to yield 2-isopropylphenyl benzyl ketone in 70% yield (11.8 g); bp 130°C/1 Torr; ir ($CHCl_3$): 1695 cm^{-1}; ^{1}Hmr ($CDCl_3$)δ: 1.10 (d, $J \sim$ 7 Hz, 6H), 3.20 (septet, $J \sim 7$ Hz, 1H), 4.03 (s, 2H); ^{13}Cmr ($CDCl_3$)δ: CH_3, 24.1; CH_2, 49.7; CH, 29.4; C=O, 202.6; aryl CH, 125.2, 126.3, 126.8, 126.9, 128.5(2), 129.6(2), 130.7; quat C, 134.2, 138.8, 147.6. Exact mass calcd. for $C_{17}H_{18}O$: 238.1358: found: 238.1356.

A solution of lithium diisopropylamide (LDA) was prepared in a flame-dried flask under nitrogen by the dropwise addition of *n*-butyllithium (17.5 mL, 1.6 M in hexane) to a cooled solution of diisopropylamine (2.8 g, 0.028 mol) in freshly distilled tetrahydrofuran. After stirring the resulting solution of LDA at 0°C for 15 min, a solution of 2-isopropylphenyl benzyl ketone (6 g, 0.025 mol) in 10 mL of THF was added dropwise and the reaction mixture stirred for 15 min. To this solution methyl iodide (7.1 g, 0.05 mol) was added slowly and the temperature allowed to rise to ambient. After stirring for 5 h, 100 mL of water was added and the product isolated by ether extraction (2 × 75 mL). After drying and evaporating the solvent, the residue was crystallized from methanol to furnish the monomethyl derivative **20***b* (4.2 g, 67% yield); mp 65–67°C; ir ($CHCl_3$): 1692 cm^{-1}; ^{1}Hmr ($CDCl_3$)δ: 0.88 (d, $J \sim$ 7 Hz, 3H), 1.20 (d, $J \sim 7$ Hz, 3H), 1.55 (d, $J \sim 7$ Hz, 3H), 2.93 (septet, $J \sim 7$ Hz, 1H), 4.35 (q, $J \sim 7$ Hz, 1H), 7.05–7.35 (m, 9H); ^{13}Cmr ($CDCl_3$)δ: CH_3, 17.8, 23.8, 24.5; CH, 29.8, 52.1; C=O, 205.8; aryl CH, 125.1, 126.4(2), 127.0, 128.2(2), 128.7(2), 130.3; quat C, 139.6, 139.8, 147.4. Exact mass calcd. for $C_{18}H_{20}O$: 252.1514; found: 252.1517.

The above procedure using **20***b* as starting material with a twofold excess of LDA and a fivefold excess of methyl iodide furnished **20***a* in 60% yield, mp 33–34°C; ir ($CHCl_3$); 1685 cm^{-1}; ^{1}Hmr ($CDCl_3$)δ: 1.18 (d, $J \sim 7$ Hz, 6H), 1.38 (s, 6H), 2.76 (septet, $J \sim 7$ Hz, 1H), ^{13}Cmr ($CDCl_3$)δ: CH_3, 24.4, 26.2; CH, 31.0; quat C, 52.1; C=O, 209.9; aryl CH, 124.5, 125.3, 125.9, 126.4(2), 127.0, 128.6(2), 129.2; quat C, 139.2, 143.2, 146.3. Exact mass calcd. for $C_{19}H_{22}O$: 266.1671; found: 266.1670.

*2,5-Diphenyl-3-hexanone (****24****)*

Following the procedures described for the preparation of dithiane **9** above, 2-(1-phenylethyl)-1,3-dithiane was prepared in 80% yield from 2-phenylpropanal; bp 115°C/0.05 Torr; ^{1}Hmr ($CDCl_3$)δ: 1.42 (d, J = 7 Hz, 3H), 1.7–2.1 (m, 2H), 2.5–2.8 (m, 4H), 3.03 (m, 1H), 4.16 (d, $J \sim 7$ Hz, 1H), 7.15 (bs, 5H); ^{13}Cmr ($CDCl_3$)δ: CH_3, 18.5; CH_2, 25.6, 30.3, 30.7, CH, 44.6, 54.6: aryl CH: 126.7, 127.5(2), 128.0(2); aryl C, 142.8. Exact mass calcd. for $C_{12}H_{16}S_2$: 224.0693; found: 224.0690.

Lithiation of this dithiane in the usual way followed by the addition of β-bromocumene gave a mixture of products, which was hydrolyzed to furnish a 1:1 mixture of the diastereomers of **24** in low yield after tlc separation. This sample was identical to that isolated from the homoenolization of **22**; ir (CCl_4): 1720 cm^{-1}; ^{1}Hmr ($CDCl_3$)δ: 1.08 (d, J = 7 Hz, 3H), 1.18 (d, J = 7 Hz, 3H), 1.29 (d, J = 7 Hz, 3H), 1.31 ((d, J = 7 Hz, 3H), 2.4–2.9 (m, 4H), 3.1–3.45 (m, 2H), 3.52 (q, J = 7 Hz, 1H), 3.67 (q, J = 7 Hz, 1H), 7.0–7.4 (m, 20H); ^{13}Cmr ($CDCl_3$)δ: CH_3, 17.2(2), 21.5, 21.8; CH_2, 49.1, 49.5; CH, 35.1, 35.4, 53.5(2); aryl CH, 128.9(2), 128.8(2), 128.4(2), 128.3(2), 128.0(2), 127.8(2), 127.1, 127.0, 126.7(4), 126.2, 126.1; aryl C, 140.2, 140.3, 146.0, 146.1; C=CO, 207.5, 207.4. Exact mass calcd. for $C_{18}H_{20}O$: 252.1514; found: 252.1515.

An alternative synthesis of **24** was briefly examined but gave even poorer results than those just described. Following the procedure used to prepare **3***d*, β-bromocumene (2.0 g) was dissolved in dry Et_2O (20 mL) containing magnesium turnings (0.25 g), and 2 drops of 1,2-dibromoethane were added before refluxing for 1.5 h. After cooling to −70°C, 2-phenylpropanal (1.34 g) was added and the low temperature maintained for 1 h before allowing the mixture to warm to room temperature. The crude product was isolated by ether extraction and treated with Jones' reagent until the colour persisted. Preparative tlc of the product mixture isolated by ether extraction afforded a sample whose ^{13}Cmr spectrum indicated it to be a 3:1 mixture of the diastereomers of **24**.

Homoenolization experiments

The general procedure for these experiments has been described in detail previously (8) and was employed for the examinations of **2***a, b, c* and **3***a, b*. The nature of the products obtained from the reactions of **2***d*, **3***d*, **20***a*, and **22**, however, necessitated modification of the isolation procedures. The contents of the individual reaction tubes were poured into 20 volumes of water and some concentrated ammonium chloride solution added before extraction of the neutral fraction with pentane. The aqueous layer was then acidified to pH ~1 with either dilute H_2SO_4 or HCl solution and the acidic products extracted with ether. In the initial experiments after drying over $MgSO_4$, the ether extract was concentrated and treated with diazomethane in ether to convert the acids to their methyl esters. In later runs, the acid fraction was silylated (16) for analysis. The product compositions were determined by glc analysis using DEGS or Carbowax 4000 columns for **2***a, b* and **3***a, b* while SE-30 columns were most suitable for the products from the reactions of **2***d*, **3***d*, **20***a*, and **22**. In the latter experiments it was found that chromatography over silica gel before glc analysis removed small amounts of polymeric material from the neutral fractions, thereby improving the assessment of their composition. Preparative glc furnished samples of the various components in these mixtures for identification and characterization.

In the experiments involving **2***d*, recrystallization of the neutral fraction permitted separation of ~70% of the starting material from the product. Subsequent column chromatography on silica impregnated with 10% silver nitrate using pentane:ether (3:1) as eluent gave **2***d* as the first fraction, a mixture of **3***d* and **15** as the second fraction, and **4***d* essentially pure as the third fraction. Pure **3***d* could be isolated by repeated chromatography of the second fraction on $AgNO_3$-impregnated silica tlc plates.

To examine the $^1H/^2H$ exchange processes involving the α-methyl sites in **2***a, b, d* and **3***a, b*, these ketones were heated with *tert*-butyl alcohol-*o*-*d*, (99% deuterated, D_2O content <250 μg/mL) as solvent; the results of these experiments are described in the text.

Acknowledgements

We are grateful for the financial support provided by the Natural Sciences and Engineering Council of Canada.

1. A. NICKON and J. L. LAMBERT. J. Am. Chem. Soc. **84**, 4604 (1962); **88**, 1905 (1966.
2. N. H. WERSTIUK. Tetrahedron. **39**, 205 (1983).
3. A. K. CHENG, A. K. GHOSH, and J. B. STOTHERS. Can. J. Chem. **62**, 1385 (1984).
4. V. PATEL and J. B. STOTHERS. Can. J. Chem. **58**, 2728 (1980).
5. N. H. WERSTIUK and S. YEROUSHALMI. Can. J. Chem. **58**, 1601 (1980).
6. M. B. RAMPERSAD and J. B. STOTHERS. J. Chem. Soc. Chem. Commun. 709 (1976).
7. R. A. DYLLICK-BRENZINGER and J. B. STOTHERS. J. Chem. Soc. Chem. Commun. 108 (1979).

8. A. L. JOHNSON, J. B. STOTHERS, and C. T. TAN. Can. J. Chem. **53**, 212 (1975).
9. N. H. WERSTIUK and G. TIMMINS. Can. J. Chem. **63**, 526 (1985).
10. (*a*) D. J. CRAM. *In* Fundamentals of carbanion chemistry. Academic Press, New York. 1965. p. 65; (*b*) pp. 20–31.
11. H. O. HOUSE, W. C. LIANG, and P. D. WEEKS. J. Org. Chem. **39**, 3102 (1974).
12. D. SEEBACH. Synthesis, 17 (1969).
13. J. C. CRANDALL and A. C. CLARK. J. Org. Chem. **37**, 4236 (1972).
14. T. D HOFFMAN and D. J. CRAM. J. Am. Chem. Soc. **91**, 1000 (1969).
15. L. A. PAQUETTE, J. P. GILDAY, and C. S. RA. J. Am. Chem. Soc. **109**, 6858 (1987).
16. C. C. SWEENLEY, R. BENTLEY, M. MAKITA, and W. W. WELLS. J. Am. Chem. Soc. **85**, 2497 (1963).
17. D. H. HUNTER and J. B. STOTHERS. Can. J. Chem. **51**, 2884 (1973).
18. A. K. CHENG, A. K. GHOSH, and J. B. STOTHERS. Can. J. Chem. **62**, 1385 (1984), and references therein.
19. A. NICKON, D. F. COVEY, G. D. PANDIT,and J. J. FRANK. Tetrahedron Lett. 3681 (1975).
20. J. R. GOULD, M. B. ZIMMT, N. J. TURRO, B. H. BARETZ, and G. F. LEHR. J. Am. Chem. Soc. **107**, 4607 (1985).
21. H. KUNTZEL, H. WOLF, and K. SCHAFFNER. Helv. Chim. Acta, **54**, 868 (1971).
22. J. R. PARIKH and W. V. E. DOERING. J. Am. Chem. Soc. **89**, 5505 (1967).
23. K. BOWDEN, L. M. HEILBRON, E. R. H. JONES, and B. C. L. WEEDON. J. Chem. Soc. 39 (1946).
24. A. STOESSL, G. L. ROCK, and J. B. STOTHERS. Can. J. Chem. **67**, 1302 (1989).

Can. J. Chem. Downloaded from www.nrcresearchpress.com by 88.85.125.76 on 09/07/12
For personal use only.

Molecular recognition of a human blood group determinant by a plant lectin

LOUIS T. J. DELBAERE, MARGARET VANDONSELAAR, AND LATA PRASAD
Department of Biochemistry, University of Saskatchewan, Saskatoon, Sask., Canada S7N 0W0

J. WILSON QUAIL
Department of Chemistry, University of Saskatchewan, Saskatoon, Sask., Canada S7N 0W0

JOYCE R. PEARLSTONE, MICHAEL R. CARPENTER, AND LAWRENCE B. SMILLIE
MRC Group in Protein Structure and Function, Department of Biochemistry, University of Alberta, Edmonton, Alta., Canada T6G 2H7

AND

PANDURANG V. NIKRAD, ULRIKE SPOHR, AND RAYMOND U. LEMIEUX
Department of Chemistry, University of Alberta, Edmonton, Alta., Canada T6G 2G2

Received January 11, 1990

This paper is dedicated to Professor Arthur S. Perlin on the occasion of his 67th birthday

LOUIS T. J. DELBAERE, MARGARET VANDONSELAAR, LATA PRASAD, J. WILSON QUAIL, JOYCE R. PEARLSTONE, MICHAEL R. CARPENTER, LAWRENCE B. SMILLIE, PANDURANG V. NIKRAD, ULRIKE SPOHR, and RAYMOND U. LEMIEUX. Can. J. Chem. **68**, 1116 (1990).

The lectin IV of *Griffonia simplicifolia* (GS4) specifically binds the terminal tetrasaccharide unit of the Lewis b human blood group determinant (Le^b). The single crystal X-ray analysis of the complex with Le^b-OMe has demonstrated that the binding site on the lectin is a shallow depression with a negatively charged aspartate side chain at the bottom of the cavity. In addition to this aspartate, a serine and an asparagine side chain provide the polar groups that hydrogen bond to the three hydroxyl groups of Le^b, which has been termed the key polar grouping for complex formation. A notable characteristic of the binding site is that five aromatic amino acid side chains (one Phe, two Tyr, and two Trp residues) surround these polar interactions and make van der Waals contacts with the tetrasaccharide. Thus, as predicted from previous solution binding studies, extensive nonpolar interactions are involved, which contribute importantly both to the specificity of the reaction and the stability of the noncovalent complex that is formed. These results represent the first structural example of the molecular recognition of a human blood group determinant by the receptor site of a protein. Extensive sequence homology exists between GS4 and the concanavalin A (Con A), pea, and favin lectins. The main hydrophilic groups of the carbohydrate-binding site of GS4 and Con A are aspartate, asparagine, and serine residues; the homology suggests that the serine is replaced by asparagine in the case of the pea and favin lectins. It appears probable that these two latter lectins possess very similar, if not identical, specificities.

Key words: lectin, carbohydrate, molecular recognition, binding.

LOUIS T. J. DELBAERE, MARGARET VANDONSELAAR, LATA PRASAD, J. WILSON QUAIL, JOYCE R. PEARLSTONE, MICHAEL R. CARPENTER, LAWRENCE B. SMILLIE, PANDURANG V. NIKRAD, ULRIKE SPOHR et RAYMOND U. LEMIEUX. Can. J. Chem. **68**, 1116 (1990).

La lectine IV du *Griffonia simplicifolia* (GS4) se lie spécifiquement à l'unité tétrasaccharide terminale du déterminant du groupe sanguin humain Lewis b (Le^b). Une analyse par diffraction des rayons-X effectuée sur un cristal unique de son complexe avec le Le^b-OMe a permis de démontrer que le site de liaison de la lectine est une légère dépression au fond de laquelle on retrouve une chaîne latérale d'aspartate chargée négativement. En plus de cet aspartate, des chaînes latérales de sérine et d'asparagine fournissent des groupements polaires qui forment des points hydrogènes avec les trois groupements hydroxyles du Le^b; il s'agit du groupement polaire clé pour la formation de complexes. Le fait que cinq chaînes latérales formées d'acides aminés aromatiques entourent ces interactions dipolaires et qu'elles établissent des contacts de van der Waals avec le tétrasaccharide est une caractéristique notable de ce site de liaison. Tel que prédit à partir d'études antérieures de liaisons en solution, il existe donc de nombreuses interactions non-polaires qui apportent une contribution importante tant à la spécificité de la réaction qu'à la stabilité du complexe non-covalent qui se forme. Ces résultats correspondent au premier exemple de reconnaissance moléculaire d'un déterminant de groupe sanguin humain par le site récepteur d'une protéine. Il existe une homologie séquentielle importante entre le GS4, la concanavaline A (Con A) et les lectines de pois et de favine. Les groupements hydrophiles principaux du site de liaison de l'hydrate de carbone du GS4 et du Con A sont des résidus aspartate, asparagine et sérine; dans le cas des lectines de pois et de favine, l'homologie suggère de remplacer la sérine par l'asparagine. Il semble probable que ces deux dernières lectines possèdent des spécificités très semblables, sinon identiques.

Mots clés : lectine, hydrate de carbone, reconnaissance moléculaire, liaison.

[Traduit par la revue]

The process of molecular recognition is fundamental to an understanding of all living processes. A wide variety of proteins, such as enzymes and antibodies, function as receptors for the specific recognition and binding of distinct molecules. Lectins are proteins which are of widespread occurrence in tissues and which possess at least two sites (one per subunit) that are designed specifically to recognize and bind complex carbohydrate structures (1, 2). Lectins do not possess enzymic properties and are not products of an immune response. Their role in tissues appears diverse and is probably related to the organization and transport of biological macromolecules (1–3). This communication provides the first detailed X-ray analysis of a complex that involves the molecular recognition of a human blood group determinant. These results combined with the

Can. J. Chem. Downloaded from www.nrcresearchpress.com by 88.85.125.76 on 09/07/12
For personal use only.

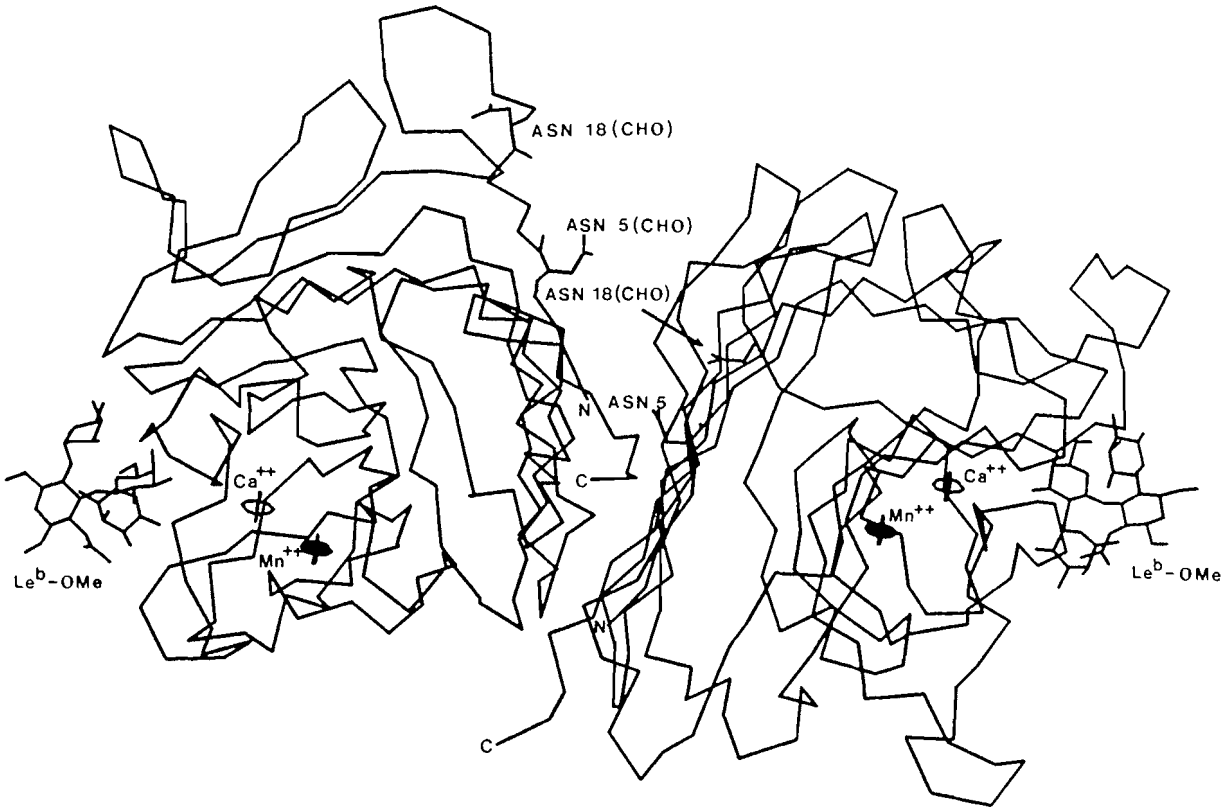

FIG. 1. The polypeptide chain folding of each subunit of the molecular dimer of GS4; only the α carbon atoms are illustrated. The binding sites of the Le^b-OMe are on opposite sides of the dimer. The N- and C-termini of each subunit are indicated. CHO refers to covalently attached oligosaccharide.

recently reported crystal structure for the concanavalin A (Con A) complex, Con A/α-D-Man-OMe (4), appear to provide insight toward an appreciation of the full specificities of the Con A, favin, and pea lectins.

Con A was the first lectin to have its crystal structure determined (5, 6). Furthermore, the preliminary description of the carbohydrate-binding site of a lectin corresponded to that of Con A (7, 8). Carver *et al.* (9) identified the four loops at the surface of this protein that form the combining site for α-D-Man-OMe; they also showed that a more stable complex is formed with α-D-Man(1 → 6)[α-D-Man(1 → 3)]D-Man than with the monosaccharide. The carbohydrate-binding site of favin was described in the structure of the favin/glucose complex (10). The crystal structure of native pea lectin (11) and the pea lectin/trimannose complex (12) have also been reported. The amino acid sequences of the leguminous lectins, Con A, favin, and pea lectin, have been published (13–15). Their specificities are reported to be related to mannose/glucose derived saccharides (1, 2). On the other hand the lectin IV of *Griffonia simplicifolia* (GS4) is known to bind specifically the surfaces held in common by the Lewis b (Le^b) and Y human blood group determinants (16, 17), which are the tetrasaccharide units α-L-Fuc(1→2)β-D-Gal(1→3)[α-L-Fuc(1→4)]β-DGlcNAc– and α-L-Fuc(1 → 2)β-D-Gal(1 → 4)[α-L-Fuc(1 → 3)β-D-GlcNAc–, respectively.

As displayed in Fig. 1, GS4 is a heterodimeric metalloglycoprotein and each subunit contains one Ca^{2+}, one Mn^{2+}, and one binding site for Le^b-OMe, the methyl glycoside of Le^b. There are two Lewis b tetrasaccharides bound per GS4 molecular heterodimer in the GS4/Le^b-OMe complex. The native GS4 and complexes of GS4 both with Le^b-OMe and a large variety of derivatives obtained by chemical alterations were reported to crystallize isomorphously in space group $P4_22_12$ (18). The crystal structure of the native GS4 was solved by the molecular replacement method (19) with the use of favin coordinates (10), pea lectin coordinates (11), and the aid of the amino acid sequence (20). The structure of the GS4/Le^b-OMe complex was also solved and least-squares refined (21, 22). Subsequent analysis showed that the true space group is $P4_2$ (23). Further refinement in space group $P4_2$ at 2.8 Å resolution gave an R index of 0.21 for 6844 reflections with $F > 4\sigma(F)$.[1] The crystal system is tetragonal with unit cell dimensions $a = 78.9$ Å, $c = 89.1$ Å with one molecular heterodimer in the asymmetric unit. Details of the crystallographic analysis are given elsewhere (23). The overall folding of the polypeptide chain of each subunit is presented in Fig. 1. Each subunit has two major antiparallel β-sheets, one six-stranded and the other seven-stranded, which are similar to those that occur in the subunits of Con A (4–6), pea (11), and favin (10) lectins. Both subunits of GS4 contain 243 amino acid residues, which are identical except for five residues where heterogeneity was observed (20). It has been demonstrated by chemical analysis that one subunit has a covalently linked oligosaccharide at Asn 5 and Asn 18 whereas the second subunit of the molecular heterodimer has N-linked carbohydrate only at Asn 18 (20) (see Fig. 1). The association of the monomers of GS4 is different from that occurring in the Con A (4–6), pea (11), and favin (10) lectins,

[1]The coordinates of the α carbon atoms for the two subunits of GS4 are available and may be purchased from the Directory of Unpublished Data, CISTI, National Research Council of Canada, Ottawa, Ont., Canada K1A 0S2.

Can. J. Chem. Downloaded from www.nrcresearchpress.com by 88.85.125.76 on 09/07/12
For personal use only.

Can. J. Chem. Downloaded from www.nrcresearchpress.com by 88.85.125.76 on 09/07/12
For personal use only.

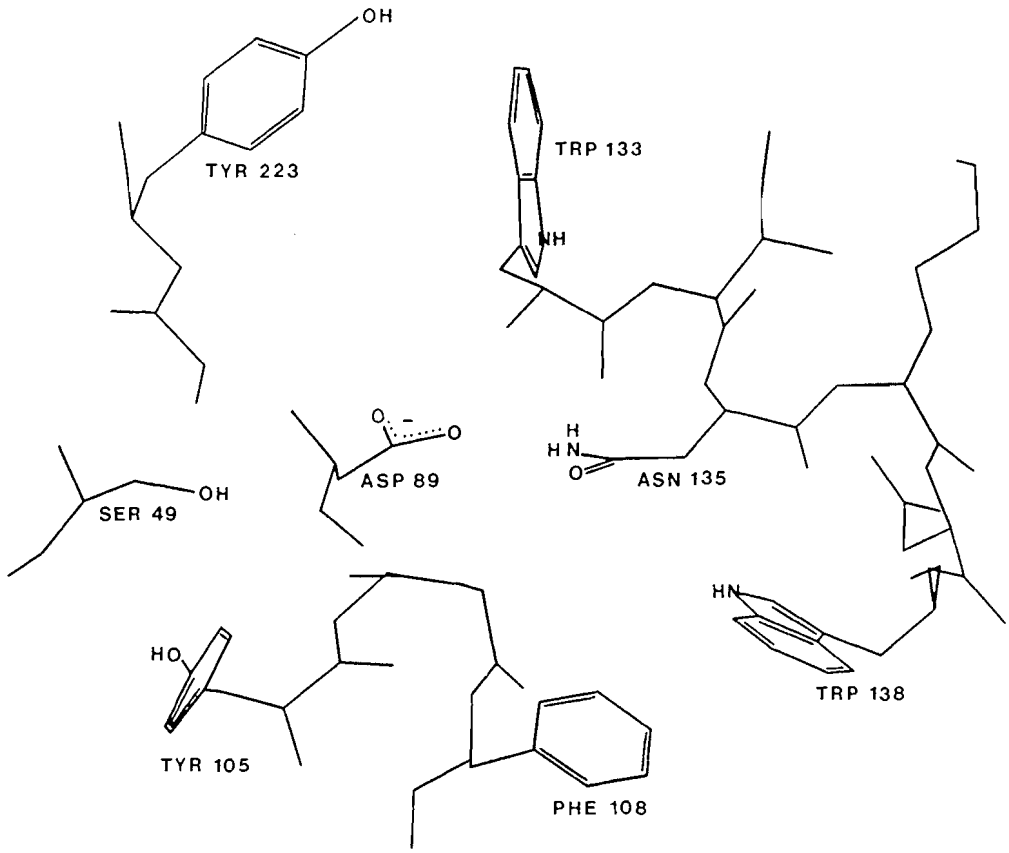

FIG. 2. Amino acid residues of GS4 that are present in the combining site for Le^b-OMe. This view is from the direction of the tetrasaccharide towards the protein. Selected non-carbon atoms are illustrated. It is expected that, at higher resolution, immobilized water molecules will be found to be present.

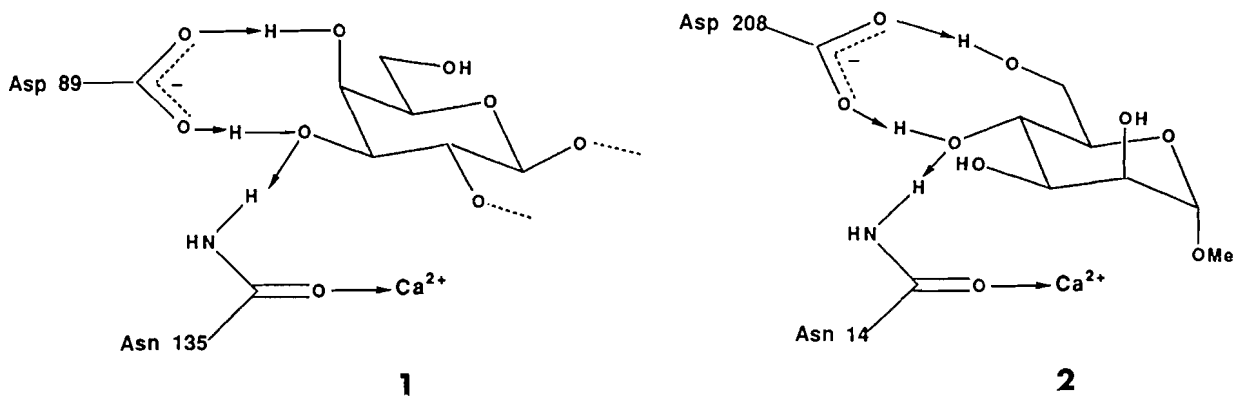

FIG. 3. Comparison of a key polar interaction for the binding of the β-D-Gal unit of the Le^b-OMe tetrasaccharide by GS4 (**1**) with that (**2**) for the binding of α-D-Man-OMe by Con A (4). In both cases the positive calcium ion cooperates with the negative carboxylate group in enhancing the charge delocalization for the strengthening of the intervening hydrogen bonds.

possibly due to the involvement of a portion of the covalently linked oligosaccharides in the interactions between the subunits of GS4. The ligands for the Ca^{2+} and Mn^{2+} cations are analogous to those reported for Con A (6, 24), pea (11), and favin (10) lectins. The Le^b-OMe noncovalent binding sites are located on opposite sides of the GS4 dimer (see Fig. 1) and the electron density is in accord with the expectation (17) that the Le^b-OMe molecule is bound in the same conformation in which it exists in aqueous solution (25).

The disposition of the amino acid residues of GS4 that bind Le^b-OMe is presented in Fig. 2. Three hydrophilic amino acid residues are directly involved in the binding. Two of these residues were found to have unusual features in that Asp 89 is involved in the *cis*-peptide linkage between Ala 88 and Asp 89 and the carbonyl group of the Asn 135 side chain is coordinated to the Ca^{2+} ion. However, since our preliminary communication of this work (26), an essentially analogous situation (see Fig. 3) has been found (4) to exist for the binding of methyl α-D-mannopyranoside by Con A. A particularly striking characteristic of the other amino acid residues that form the combining

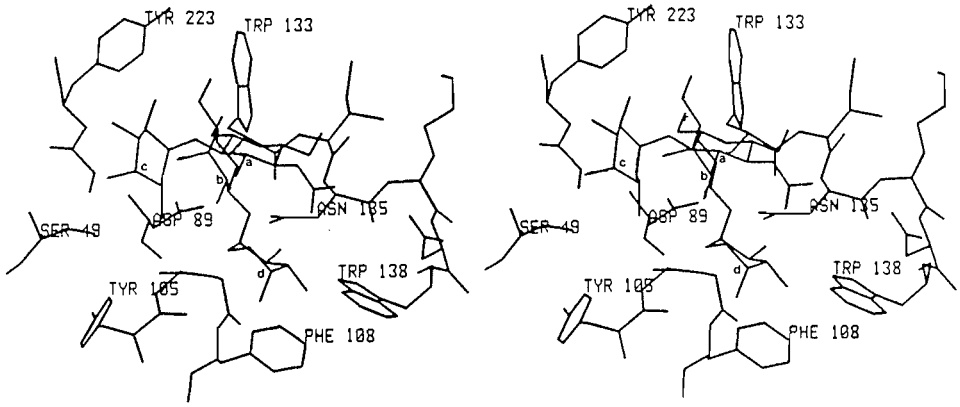

FIG. 4. Stereo illustration of the Le^b-OMe bound in the receptor site of GS4. The Asp 89 side chain is at the bottom of this cavity. This view is approximately the same as that in Fig. 2. The monosaccharide units of Le^b-OMe are denoted as follows: a, β-D-GlcNAc; b, β-D-Gal; c, α-L-Fuc(1 → 4); d, α-L-Fuc(1 → 2).

TABLE 1. Known and probable contributions ot the formation of the combining sites of the GS4, Con A (4), favin (10), and pea (11) lectins

GS4		Con A		Favin or pea
Amino acid residues*	Interactions†	Amino acid residues*	Interactions‡	Amino acid residues§
Key polar interactions				
AD(89)G	OD1 → HO-4b OD2 → HO-3b	AD(208)G	OD1 → HO-6 OD2 → HO-4	YVAD(82)GFT
IN(135)K	NH_2 ← OH-3b NH_2 ← OH-2d	PN(14)T	NH_2 ← OH-4	TFYN(126)AAW
RS(49)S	HO(S) → HO-4c	GS(168)S	—	AVKN(40)TVG
Other interactions				
TW(133)I	H-5b	TY(12)P		FDTF(124)NAA
GY(223)	H-6b's	GL(99)Y	NH ← O-5, NH ← O-6	TGAE(213)YAT‖
		GLY(100)K	NH ← O-6	
DY(105)G	H-6c's	ST(226)G	—	PQTG(98)GGY
DW(138)N	OH-2d,O3-d	DI(17)G	—	NAAW(129)DPS
GF(108)L	H-2d, O-3d, O-4d	GR(228)LL	NH ← O-3	GGGY(101)LGV

*The central numbered amino acid unit is that which is either known or which may interact with the oligosaccharide; A, Ala; D, Asp; E, Glu; F, Phe; G, Gly; I, Ile; K, Lys; L, Leu; N, Asn; P, Pro; Q, Gln; R, Arg; S, Ser; T, Thr; V, Val; W, Trp; Y, Tyr.

†With the Le^b-OMe for which the b, c, and d units are β-D-Gal, α-L-Fuc(1 → 4), and α-L-Fuc(1 → 2), respectively.

‡With α-D-Man-OMe (4).

§Both are reported to possess affinities for mannose/glucose. For the pea lectin the sequence number is one less, except for entry‖ where the sequence number is greater by five.

‖In the case of the pea lectin, alanine 221 replaces threonine 216.

site of GS4, except for the diglycine bridge between Tyr 105 and Phe 108, is that all of these have aromatic side chains that reside near the periphery of the complex. The amino acid side chains, which provide the key polar interaction, are toward the bottom of the shallow combining site.

Figure 4 shows a stereo drawing of the Le^b tetrasaccharide as it is bound in the complex with GS4. The GlcNAc-OMe group is not involved in any direct interactions with amino acid residues of GS4; this finding is in agreement with extensive inhibition (17) and thermodynamic studies of the binding of Le^b-OMe and several Le^b-OMe analogs (27). As was to be expected both from the cross-reaction with the Y tetrasaccharide and from the results obtained on probing the combining site with modified Le^b-OMe structures (17), the polar amino acid side chains hydrogen bond to the HO-3 and HO-4 groups of the β-D-Gal unit and to the HO-4 group of the α-L-Fuc(1 → 4) unit. An additional polar interaction involves the HO-2 group of the α-L-Fuc(1 → 2) unit. These polar interactions are surrounded by the five aromatic amino acids that make several van der Waals contacts with three of the four monosaccharide residues of Le^b-OMe.

The interactions between the Le^b-OMe tetrasaccharide and amino acid residues of GS4 are presented in Table 1. A further polar interaction, which has the hydroxyl group of Ser 49 hydrogen bonded to Tyr 105, was identified. The hydroxyl group of Ser 49 serves as proton acceptor from HO-4 of the α-L-Fuc(1 → 4) unit. As indicated, several interactions appear to be lipophilic in character (17). The 2.8 Å resolution structure appears to have Tyr 223 in lipophilic interaction with the β-D-Gal unit and with its hydroxyl group in contact with the aqueous phase.

As mentioned above, GS4 was found to possess extensive sequence homology with the Con A, favin, and pea lectins. A detailed comparison and alignment of the amino acid sequences

Can. J. Chem. Downloaded from www.nrcresearchpress.com by 88.85.125.76 on 09/07/12
For personal use only.

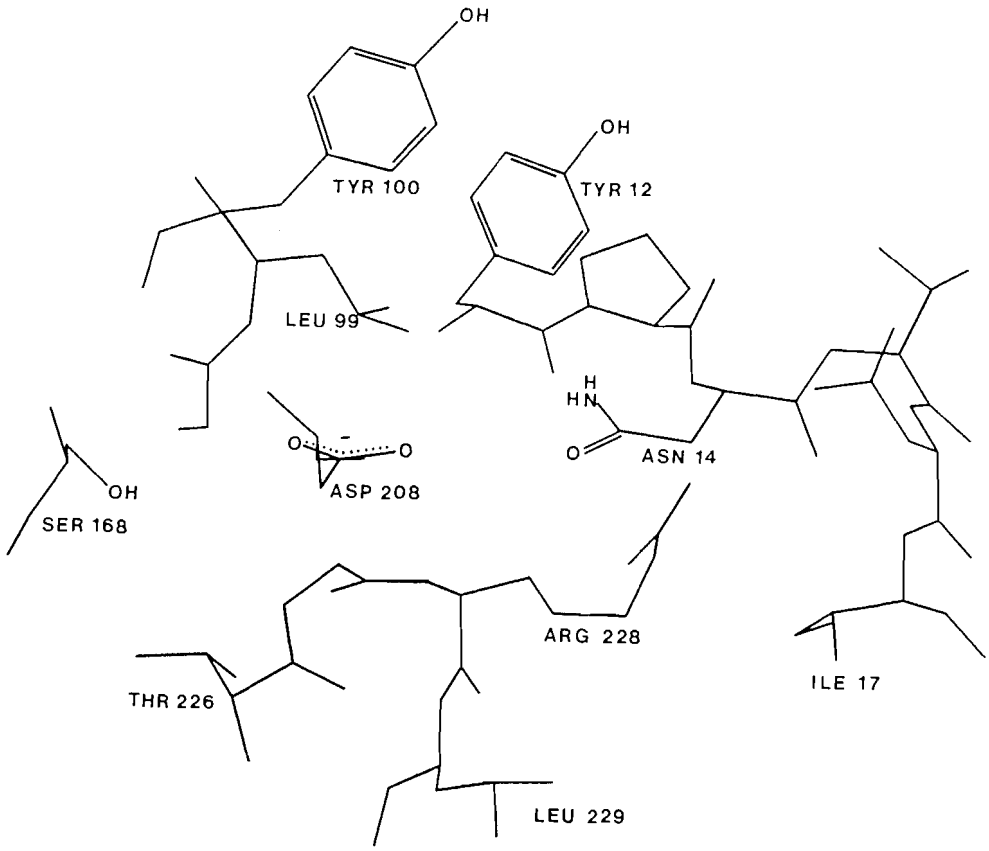

FIG. 5. The combining site in Con A as recently proposed (4) and extended to the regions that are homologous with the combining site of GS4. Selected non-carbon atoms are illustrated. This combining site should be compared with that of GS4 as shown in Figs. 2 and 4.

of GS4 with related lectins is underway. Also, the key polar interaction between GS4 and Le^b-OMe was found to be very similar to that between Con A and α-D-Man-OMe (Fig. 3). Indeed, in addition to Asp 89 and Asn 135 of GS4 being in sequence positions corresponding to Asp 208 and Asn 14 of Con A, Ser 49 of GS4 is equivalent to Ser 168 in Con A. Thus, it can be expected that the expression of the full specificity for Con A will prove to involve Ser 168 in a hydrogen bonding interaction with an appropriate oligosaccharide. Indeed, it is truly remarkable that the same tripeptide unit, namely, Ala-Asp-Gly, is found not only in all four lectins presented in Table 1, but also in seven other lectins listed in the recent review by Franz (2). Furthermore, Rini *et al.* (28) have found that Asp 81 of the pea lectin is involved in the binding of α-D-Man(1 → 3)[α-D-Man(1 → 6)]α-D-Man-OMe and Becker and Reeke (29) have reported the participation of Asp 82 in the binding of glucose by the favin lectin. Also, not only do the asparagine units that participate in the key polar interactions for the GS4 and Con A lectins correspond in sequence, but asparagine residues are found at the same sequence positions both in the favin and pea lectins (see Table 1) and in the lectins mentioned above and reviewed by Franz (2). For the favin and pea lectins, the adjacent amino acid residues are identical but this is not so for the corresponding asparagines of the GS4 and Con A lectins. These changes in structural features produce different topographies and are therefore expected to affect specificity of binding. In view of its widespread occurrence, the cooperation of anionic carboxylate and cationic Ca^{2+} for the strengthening of hydrogen-bonded networks may be a general binding property of lectins that contain Ca^{2+}. Furthermore, the region involving the combining site of these homologous lectins appears to contain an identical structural motif, which is responsible for binding oligosaccharides; this moiety consists of (i) the Ca^{2+} and Mn^{2+} cations with appropriate ligands, (ii) an Asn side chain that has the carbonyl group coordinated to the Ca^{2+} ion and the $-NH_2$ unit available for hydrogen bonding, (iii) a conserved tripeptide unit, Ala-Asp-Gly, which has a *cis*-peptide linkage between the Ala and Asp residues with the Asp side chain at the bottom of the depression and available for interaction with oligosaccharide.

Examination of Fig. 5 shows that the combining site that is proposed for the Con A lectin (the coordinates of Con A were obtained from the Protein Data Bank (30)) has several amino acid units with spatial dispositions very similar to those in the combining site of the GS4 lectin. However, these are mainly different types in that Trp 133, Trp 138, Phe 108, and Tyr 105 of the GS4 lectin are replaced by Tyr 12, Ile 17, Leu 229, and Thr 226 in the Con A lectin. Clearly, therefore, lipophilic interactions play a major role in determining the specificity of lectin affinities for oligosaccharides. In this regard, it is noteworthy that Tyr 223 in GS4 and Tyr 100 in Con A appear similarly disposed in space. These occur in sequences Gly-Tyr 223 and Gly-Leu-Tyr 100. In Fig. 5 the leucine 99 unit projects its side chain into the corresponding region of the GS4 combining site that accepts the α-L-Fuc(1 → 4) unit, see Fig. 4, and therefore the presence of Leu 99 must be an important reason that the Con A lectin does not bind Le^b-OMe. The peptide units of the favin and pea lectins, which fall into the sequence homology for the GS4 lectin, are so similar in primary structure (see Table 1) as to suggest that these two lectins have identical specificities.

Of major importance is the discovery arising from this study that the structural features of the GS4/Le^b-OMe complex are in good general accord with the kind of expectations that were

Can. J. Chem. Downloaded from www.nrcresearchpress.com by 88.85.125.76 on 09/07/12
For personal use only.

based on the results of a systematic probing of the combining site using structurally slightly altered modifications of the Le^b-OMe tetrasaccharide (17, 27). Most noteworthy in this regard is the confirmation of the presence of an extensive contribution to the formation of the complex by lipophilic interactions. In fact, probing experiments have indicated that similarly extensive nonpolar interactions are present in the complexes between oligosaccharides and all the lectins and monoclonal antibodies that have been studied to date (31–36). Lemieux (37) has suggested that the stabilities of these complexes are importantly related to the exchange of interactions with water of amphiphilic regions of both the oligosaccharides and the combining site, with the interactions with water after the complex is formed. It was considered that the exchanges of polar interactions are mainly concerned with the provision of high fidelity to the specificity of the complexation. These notions were not previously expected for the association of such highly hydrophilic substances, like oligosaccharides, with proteins and may have a bearing on molecular recognition in general. It is anticipated that the X-ray structures of the wide array of isomorphous crystals (18) that have been obtained for complexes of GS4 with analogs of Le^b-OMe, and for which the thermodynamic parameters for their formation are known (38), will shed more light on this important matter, which is directly related to the role played by water.

Acknowledgements

The authors thank Drs. F. L. Suddath and H. Einspahr, and Drs. G. N. Reeke, Jr. and J. W. Becker for providing atomic coordinates of pea lectin and favin, respectively. This research was supported by grants from the Medical Research Council of Canada to L.T.J.D. and to L.B.S., and from the Natural Sciences and Engineering Research Council of Canada to R.U.L.

1. I. E. Leiner, N. Sharon, and I. J. Goldstein. The lectins. Properties, functions and applications in biology and medicine. Academic Press, New York. 1986. pp. xi–xvi.
2. H. Franz. Advances in lectin research. Vol. 1. VEB Verlag Volk and Gesundheit, Berlin, 1988. pp. 73–134.
3. K. Drickamer. Carbohydrate recognition in cellular function. 1989 Ciba Foundation Symposium 145, John Wiley and Sons, New York. pp. 45–61.
4. Z. Derewenda, J. Yariv, J. R. Helliwell, A. J. Kalb (Gilboa), E. J. Dodson, M. Z. Papiz, T. Wan, and J. Campbell. EMBO J. **8**, 2189 (1989).
5. K. D. Hardman and C. F. Ainsworth. Biochemistry, **11**, 4910 (1972).
6. J. W. Becker, G. N. Reeke, Jr., J. L. Wang, B. A. Cunningham, and G. M. Edelman. J. Biol. Chem. **250**, 1513 (1975).
7. K. D. Hardman and C. F. Ainsworth. Biochemistry, **15**, 1120 (1976).
8. J. W. Becker, G. N. Reeke, Jr., B. A. Cunningham, and G. M. Edelman. Nature, **259**, 406 (1976).
9. J. P. Carver, A. E. Mackenzie, and K. D. Hardman. Biopolymers, **24**, 49 (1985).
10. G. N. Reeke, Jr. and J. W. Becker. Science, **234**, 1108 (1986).
11. H. Einspahr, E. H. Parks, K. Suguna, E. Subramanian, and F. L. Suddath. J. Biol. Chem. **261**, 16518 (1986).
12. J. M. Rini. Ph.D. Thesis, University of Toronto, Toronto, Canada. 1987.
13. B. A. Cunningham, J. L. Wang, M. J. Waxdal, and G. M. Edelman. J. Biol. Chem. **250**, 1503 (1975).
14. B. A. Cunningham, J. J. Hemperly, T. P. Hopp, and G. M. Edelman. Proc. Natl. Acad. Sci. U.S.A. **76**, 3218 (1976).
15. T. J. V. Higgins, P. M. Chandler, G. Zurawski, S. C. Button, and D. Spencer. J. Biol. Chem. **258**, 9544 (1983).
16. S. Shibata, I. J. Goldstein, and D. A. Baker. J. Biol. Chem. **257**, 9324 (1982).
17. U. Spohr, O. Hindsgaul, and R. U. Lemieux. Can. J. Chem. **63**, 2644 (1985).
18. M. Vandonselaar, L. T. J. Delbaere, U. Spohr, and R. U. Lemieux. J. Biol,. Chem. **262**, 10848 (1987).
19. M. G. Rossmann. *In* Molecular replacement method. *Edited by* M. G. Rossmann. Gordon and Breach, New York. 1972. pp. 1–276.
20. P. V. Nikrad, J. R. Pearlstone, L. B. Smillie, and R. U. Lemieux. Abstracts, The Third Symposium of the Protein Society, Seattle, WA. July 29–August 2, 1989. S162.
21. J. H. Konnert and W. A. Hendrickson. Acta Crystallogr. Sect. A: Cryst. Phys. Differ. Theor. Gen. Crystallogr. **A36**, 344 (1980).
22. M. G. Vincent and J. P. Priestle. J. Appl. Crystallogr. **18**, 185 (1985).
23. L. T. J. Delbaere, M. Vandonselaar, L. Prasad, J. W. Quail, P. V. Nikrad, J. R. Pearlstone, M. R. Carpenter, L. B. Smillie, U. Spohr, and R. U. Lemieux. Trans. Am. Crystallogr. Assoc. In press.
24. K. D. Hardman, R. C. Agarwal, and M. J. Freiser. J. Mol. Biol. **157**, 69 (1982).
25. H. Thøgersen, R. U. Lemieux, K. Bock, and B. Meyer. Can. J. Chem. **60**, 44 (1982).
26. L. T. J. Delbaere, M. Vandonselaar, L. Prasad, J. W. Quail, U. Spohr, and R. U. Lemieux. American Crystallographic Association Meeting, July 28, 1989, Seattle, WA. Abstracts of Papers, **17**, V5.
27. U. Spohr and R. U. Lemieux. Carbohydrate Res. **174**, 211 (1988).
28. J. M. Rini, K. D. Hardman, H. Einspahr, F. L. Suddath, and J. P. Carver. American Crystallographic Association Meeting, July 28, 1989, Seattle, WA. Abstracts of Papers, **17**, V4.
29. J. W. Becker and G. N. Reeke, Jr. Trans. Am. Crystallogr. Assoc. In press.
30. F. C. Bernstein, T. F. Koetzle, G. J. B. Williams, E. F. Meyer, Jr., M. D. Brice, J. R. Rodgers, O. Kennard, T. Shimanoucki, and M. Tasumi. J. Mol. Biol. **112**, 535 (1977).
31. R. U. Lemieux, T. C. Wong, J. Liao, and E. A. Kabat. Mol. Immunol. **21**, 751 (1984).
32. O. Hindsgaul, D. P. Khare, M. Bach, and R. U. Lemieux. Can. J. Chem. **63**, 2653 (1985).
33. R. U. Lemieux, A. P. Venot, U. Spohr, P. Bird, G. Mandal, N. Morishima, O. Hindsgaul, and D. R. Bundle. Can. J. Chem. **63**, 2664 (1985).
34. U. Spohr, N. Morishima, O. Hindsgaul, and R. U. Lemieux. Can. J. Chem. **63**, 2659 (1985).
35. R. U. Lemieux, O. Hindsgaul, P. Bird, S. Narasimhan, and W. W. Young, Jr. Carbohydr. Res. **178**, 293 (1988).
36. R. U. Lemieux, R. Cromer, and U. Spohr. Can. J. Chem. **66**, 3083 (1988).
37. R. U. Lemieux. Chem. Soc. Rev. **18**, 347 (1989).
38. U. Spohr, R. Cromer, and R. U. Lemieux. Abstracts, XIVth International Carbohydrate Symposium, Stockholm, Sweden, August 14–19, 1988. C 14.

Can. J. Chem. Downloaded from www.nrcresearchpress.com by 88.85.125.76 on 09/07/12
For personal use only.

Novel synthesis of monosulphated methyl α-D-galactopyranosides

ABDUL RASHID[1] AND WILLIAM MACKIE[1]
Astbury Department of Biophysics, University of Leeds, Leeds LS2 9JT, U.K.
IAN J. COLQUHOUN
AFRC Institute of Food Research, Norwich Laboratory, Colney Lane, Norwich NR4 7UA, U.K.
AND
DORIANO LAMBA
Istituto di Strutturistica Chimica "Giordano Giacomello", C.N.R. – Area della Ricerca di Roma, C.P. No 10-I-00016 Monterotondo Stazione, Roma, Italy

Received November 15, 1989

This paper is dedicated to Professor Arthur S. Perlin on the occasion of his 67th birthday

ABDUL RASHID, WILLIAM MACKIE, IAN J. COLQUHOUN, and DORIANO LAMBA. Can. J. Chem. **68**, 1122 (1990).

The syntheses of the methyl α-D-galactopyranoside 2-, 3-, 4-, and 6-sulphates (**11**, **12**, **16**, and **21** respectively) have been achieved using trimethylamine – sulphur trioxide as the sulphating agent. The procedure used is high yielding and requires shorter reaction times than reported previously. Each compound was obtained in a crystalline form as the potassium salt. Improved syntheses are described of the 3,4-isopropylidene acetal **2** of the methyl α-D-galactopyranoside and methyl 2-*O*-acetyl 4,6-*O*-benzylidene α-D-galactopyranoside **8**, which are starting materials in the preparation of the 2- and 3-sulphates (**11** and **12** respectively). An efficient route has been devised for the synthesis of methyl 2,3,6-tri-*O*-acetyl-α-D-galactopyranoside **14** using a base-catalysed transesterification (C4-OH → C6-OH).

Key words: synthesis, methyl α-D-galactopyranoside, monosulphates.

ABDUL RASHID, WILLIAM MACKIE, IAN J. COLQUHOUN et DORIANO LAMBA. Can. J. Chem. **68**, 1122 (1990).

Utilisant le complexe triméthylamine – trioxyde de soufre comme agent sulfatant, on a réalisé la synthèse des α-D-galactopyranoside de méthyle 2-, 3-, 4- et 6-sulfates (**11**, **12**, **16**, et **21** respectivement). La méthode utilisée fournit d'excellents rendements et requiert des temps de réaction qui sont beaucoup plus courts que ceux utilisés antérieurement. On a obtenu les sels de potassium de chacun des composés sous une forme cristalline. On décrit des synthèses améliorées de l'acétal 3,4-isopropylidénique **2** de l'α-D-galactopyranoside de méthyle ainsi que du 2-*O*-actéyl-4,6-*O*-benzylidène-α-D-galactopyranoside de méthyle (**8**) qui sont des produits de départ pour la préparation des 2- et 3-sulfates (respectivement **11** et **12**). On a aussi mis au point une voie efficace pour la synthèse du 2,3,6-tri-*O*-acétyl-α-D-galactopyranoside de méthyle (**14**) qui fait appel à une transestérification catalysée par les bases (C4-OH → C6-OH).

Mots clés : synthèse, α-D-galactopyranoside de méthyle, monosulfates.

[Traduit par la revue]

Introduction

Sulphated carbohydrates are widely distributed in plants and animals. In animals, they occur in the glycosaminoglycans (chondroitins, keratan and dermatan sulphates) of the extracellular matrix of tissues such as cartilage, ligament, skin, cornea, and synovial fluid, in heparin which has anti-coagulant and anti-lipaemic properties, in brain and nerve tissue as sulphated cerebrosides (1, 2). In plants, they occur in the intercellular and cell wall region polysaccharides of brown and red algae (fucoidan, carrageenan) (3).

Of particular interest to us are the carrageenans. Structurally, these polysaccharides are based on an alternating sequence of α-(1 → 3)- and β-(1 → 4)-linked D-galactosyl residues, although the individual carrageenan samples differ according to the location of sulphate and the degree of sulphation as well as the occurrence of 3,6-anhydro-D-galactose residues (4).

Carrageenans are widely employed in the food industry as gelling agents due to their ability to form thermoreversible gels (5). It has been suggested that double-helical polysaccharide chains are involved in gel formation (6, 7) and there is evidence that cations associated with sulphate groups play an important role in the mechanism of gelation (8, 9). However, the exact function of the counterion is not well understood and it has been suggested that nonspecific competition by cations for water may also be important in promoting the interactions amongst polysaccharide chains that lead to the formation of a gel network, as well as specific conformational transitions of the polysaccharide chains (10–12).

Results from detailed structural studies on the polysaccharides are complex (13, 14). In consequence, we have endeavoured to explore the use of low molecular weight model compounds for obtaining reliable stereochemical data (15, 16). For example, X-ray crystallographic studies can provide information on hydrogen bonding and cation coordination that may be useful for modelling the polymer chains. High resolution ^{1}H and ^{13}C nmr, in both the solution and the solid state, may provide complementary information relevant to the biopolymer structure.

Suitable model compounds that could provide interesting stereochemical data on the polysaccharide chains of carrageenans are the methyl glycosides of galactose monosulphates. At the outset of our investigation, the only example of a definitive synthesis of such compounds was that of 4-(barium sulphate) of methyl α-D-galactopyranoside reported by Harris and Turvey (17). The compound was obtained in a modest yield from reaction of pyridine – sulphur trioxide with 2,3,6-tri-*O*-benzoyl-α-D-galactopyranoside. During the course of the present investigation, Vliegenthart and co-workers (18) reported the syntheses of sodium methyl α-D-galactopyranoside 2- and 3-sulphates, essentially using a similar sulphation procedure to the one employed by Harris and Turvey.

We now present the results of our own novel approach to the synthesis of potassium methyl α-D-galactopyranoside 2-, 3-, 4-

[1]Authors to whom correspondence may be addressed.

Printed in Canada / Imprimé au Canada

Can. J. Chem. Downloaded from www.nrcresearchpress.com by 88.85.125.76 on 09/07/12
For personal use only.

Can. J. Chem. Downloaded from www.nrcresearchpress.com by 88.85.125.76 on 09/07/12
For personal use only.

and 6-sulphates (**11**, **12**, **16**, and **21** respectively), using trimethylamine – sulphur trioxide as the sulphating agent. This sulphating agent has advantages over others in that the reaction times are shorter, the work-up is simple, and the product yields are high.

Results and discussion

For the synthesis of methyl α-D-galactopyranoside 2-sulphate **11**, the required intermediate, 3,4-*O*-isopropylidene-α-D-galactopyranoside **2**, was prepared by isopropylidenation of methyl α-D-galactopyranoside using a modification of the Liptak method (19). This procedure gave no significant amounts of the unwanted isomer **3**. Compound **2** was converted to the 6-*O*-trityl derivative **4** in the standard manner. Sulphation of **4** with trimethylamine – sulphur trioxide in dimethylformamide at 50–60°C for 30 min yielded **5**, which after removal of the protecting groups furnished **11** in 88% yield.

In the synthesis of methyl α-D-galactopyranoside 3-sulphate **12**, the intermediate methyl 2-*O*-acetyl-4,6-*O*-benzylidene-α-D-galactopyranoside **8** was obtained using the regioselective acetylation of methyl 4,6-*O*-benzylidene-α-D-galactopyranoside **6** via the stannylene intermediate **7** (20). Sulphation of **8** with trimethylamine – sulphur trioxide gave the protected sulphate **10**, which after deprotection gave **12** in 82% yield.

The intermediate methyl 2,3,4-tri-*O*-acetyl-6-*O*-trityl-α-D-galactopyranoside **13** was synthesized according to published procedure (23). Detritylation of **13** with a solution of chloroform saturated with hydrogen chloride gas at 0°C, followed by quenching the reaction with saturated aqueous sodium bicarbonate, led exclusively to the formation of methyl 2,3,6-tri-*O*-acetyl-α-D-galactopyranoside **14**. This C4 → C6 base-catalysed transesterification is well documented in the glucose series (21, 22). However, in the galactose series, attempts to prepare 1,2,3,6-tetra-*O*-acetyl-D-galactose from the corresponding 1,2,3,4-tetra-*O*-acetyl compound by acetyl migration in dilute alkali have led to complex mixtures of products (21). It is probable that the reaction time in alkali is critical and should be as short as possible.

Methyl α-D-galactopyranoside 4-sulphate **16** was obtained in an 86% yield from sulphation of **14** followed by subsequent removal of the acetyl groups with methanolic sodium methoxide.

In the synthesis of methyl α-D-galactopyranoside 6-sulphate **21**, it was appropriate to use the already available intermediate **13** to prepare the compound methyl 2,3,4-tri-*O*-acetyl-α-D-galactopyranoside **17** as described in the literature (23). Thus, to our surprise, detritylation of **13** with hydrogen chloride – chloroform at 0°C as before, followed by quenching the reaction with water, led to a mixture of 2,3,6-tri-*O*-acetyl **14** as the major product with **17** as a minor component. This result was in contrast to the published report (23) in which compound **17** was claimed to be the exclusive product, although no spectral data on the product are reported.

To overcome the problem of acetyl migration, it was decided to employ benzoyl as protecting groups since these are less prone to migration. Thus methyl 2,3,4-tri-*O*-benzoyl-α-D-galactopyranoside **19** was prepared from the corresponding 2,3,4-tri-*O*-benzoyl-6-*O*-trityl-α-D-galactopyranoside **18** by treatment with aqueous acetic acid. Sulphation of **19** with trimethylamine – sulphur trioxide followed by benzoyl deprotection using methanolic sodium methoxide furnished the 6-sulphate **21** in 88% yield.[2]

[2]Some preparations contained compound **16** as a minor impurity presumably arising as a result of benzoyl migration.

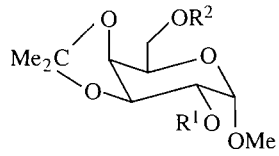

2 $R^1 = R^2 = H$
4 $R^1 = H, R^2 = Tr$
5 $R^1 = SO_3K, R^2 = Tr$

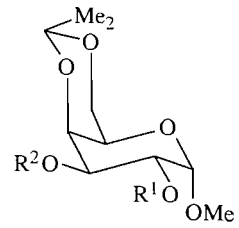

3 $R^1 = R^2 = H$

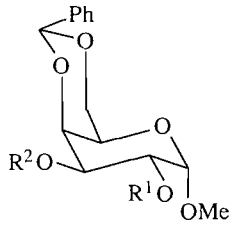

6 $R^1 = R^2 = H$
8 $R^1 = Ac, R^2 = H$
9 $R^1 = H, R^2 = Ac$
10 $R^1 = Ac, R^2 = SO_3Na$

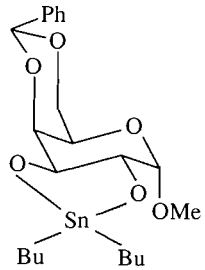

7

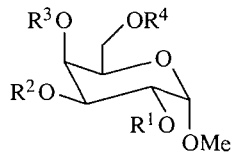

1 $R^1 = R^2 = R^3 = R^4 = H$
11 $R^2 = R^3 = R^4 = H, R^1 = SO_3K$
12 $R^1 = R^3 = R^4 = H, R^2 = SO_3K$
13 $R^1 = R^2 = R^3 = Ac, R^4 = Tr$
14 $R^1 = R^2 = R^4 = Ac, R^3 = H$
15 $R^1 = R^2 = R^4 = Ac, R^3 = SO_3Na$
16 $R^1 = R^2 = R^4 = H, R^3 = SO_3K$
17 $R^2 = R^2 = R^3 = Ac, R^4 = H$
18 $R^1 = R^2 = R^3 = Bz, R^4 = Tr$
19 $R^1 = R^2 = R^3 = Bz, R^4 = Tr$
20 $R^1 = R^2 = R^3 = Ac, R^4 = SO_3Na$
21 $R^1 = R^2 = R^3 = H, R^4 = SO_3K$

(Tr = Ph_3C-)

The sulphates **11**, **12**, **16**, and **21** were readily isolated as either the sodium or the potassium salts, each of which was usually crystalline.

The structures of the four sulphated monosaccharide potassium salts **11**, **12**, **16**, and **21** were confirmed by ^{13}C and ^1H nmr spectroscopy (Tables 1–3). The spectroscopic data are in general agreement with those published earlier (18) for the sodium salts of these compounds. In particular, protons α to the sulphate group are found to be deshielded by 0.4–0.7 ppm in comparison with corresponding protons in methyl α-D-galactopyranoside. The presence of a sulphate group causes an increase in the ^{13}C chemical shift of 6–8 ppm for the α carbons and a decrease of 1–2 ppm for the β carbons. Knowledge of these typical changes will be of value in interpreting the nmr spectra of sulphated oligo- and polysaccharides.

TABLE 1. ^{13}C nuclear magnetic resonance data for potassium methyl α-D-galactopyranoside monosulphates **11**, **12**, **16**, and **21**

Compound	Chemical shift[a]						
	C-1	C-2	C-3	C-4	C-5	C-6	OCH_3
11	98.38	76.38	69.11	70.80	71.55	62.12	55.88
12	100.16	67.65	78.36	68.34	71.22	62.19	56.01
16	100.00	69.01	69.25	78.34	70.84	61.94	55.94
21	100.14	68.79	69.72	69.98	69.26	68.39	55.85

[a]In ppm relative to internal 1,4-dioxane in D_2O (δ 67.4) at 25°C.

TABLE 2. ^1H nuclear magnetic resonance data for potassium methyl α-D-galactopyranoside monosulphates **11**, **12**, **16**, and **21**

Compound	Chemical shift[a]							
	H-1	H-2	H-3	H-4	H-5	H-6	H-6′	OCH_3
11	5.13	4.44	3.93	4.03	3.92	3.75	3.76	3.43
12	4.90	3.98	4.48	4.32	3.95	3.75	3.75	3.43
16	4.83	3.84	3.94	4.68	4.03	3.78	3.76	3.37
21	4.83	3.82	3.80	4.00	4.13	4.16	4.15	3.41

[a]In ppm relative to internal acetone in D_2O (δ 2.225) at 25°C.

TABLE 3. ^1H nuclear magnetic resonance coupling constant data (Hz) for the monosulphates **11**, **12**, **16**, and **21**

Compound	$J_{1,2}$	$J_{2,3}$	$J_{3,4}$	$J_{4,5}$	$J_{5,6}$	$J_{5,6'}$	$J_{6,6'}$
11	3.8	10.2	3.5	1.0	4.1	8.1	−11.8
12	3.9	10.2	3.2	1.1	4.2	8.3	−11.8
16	4.0	10.4	3.4	0.6	4.3	8.2	−11.9
21	3.9	10.3	3.4	1.0	4.2	8.2	−11.0

Experimental

Methyl α-D-galactopyranoside was purchased from Sigma Chemical Company and the trimethylamine – sulphur trioxide complex was obtained from Aldrich Chemical Company. Melting points were determined in capillary tubes with a Stuart melting point apparatus and are uncorrected. Optical rotations were measured at 22°C with a Thorn type 243 automatic polarimeter using a 0.1 dm cell. Elemental analyses were performed by the analytical service of the Department of Chemistry, University of Leeds.

The purity of the products was determined by tlc on silica gel 60 (Merck) with detection by charring with 5% sulphuric acid in ethanol. Column chromatography was performed on silica gel 60 (Merck, 70–230 mesh) and fractions were monitored by tlc. Unless otherwise indicated, the solvent systems used for chromatography were (v/v): A, 5:1 ethyl acetate – methanol; B, 1:1 ethyl acetate – petroleum ether (bp 60–80°C); C, 6:1 ethyl acetate – acetone; D, 4:1 ethyl acetate – methanol; E, 3:2 ethyl acetate – methanol; F, 2:1 ethyl acetate – methanol; G, ethyl acetate; H, 1:1 ethyl acetate – methanol; J, 2:3 ethyl acetate – petroleum ether (bp 60–80°C). Organic solvents were generally dried with anhydrous magnesium sulphate.

The nmr spectra were recorded at 25°C either on a Bruker AM-200 spectrometer at NMR Service, Area della Ricerca di Roma, C.N.R., Roma, or on a Jeol GX-400 spectrometer at the AFRC Laboratory, Norwich. ^1H chemical shifts were expressed in ppm relative to TMS using either TMS itself ($CDCl_3$ solutions) or acetone (δ 2.225 ppm, D_2O and CD_3OD solutions) as internal references. ^{13}C chemical shifts were also expressed relative to TMS using dioxan (δ 67.4 ppm, D_2O solutions) or solvent peaks ($CDCl_3$ 77.0 ppm, CD_3OD 49.0 ppm) as internal references.

Methyl 3,4-O-isopropylidene-α-D-galactopyranoside **2**

To a suspension of dry methyl-α-D-galactopyranoside **1** (5.72 g, 0.03 mol) in dry 2,2-dimethoxypropane (150 mL) was added *p*-toluenesulphonic acid monohydrate (0.3 g, 1.6 mmol). The reaction was stirred at room temperature for 48 h (the solid gradually dissolved) after which water (10 mL) was added. After 1 h (tlc showed a single product R_f 0.5, solvent A), the solvents were evaporated *in vacuo* and the residue chromatographed on silica (solvent C) to yield the product as a white solid. This solid was dissolved in acetone and precipitated with hexane to afford a crystalline product (6.2 g, 91%), mp 98–100°C (lit. (24) mp 97–98°C); $[\alpha]_D$ +147° (*c* 1, chloroform); ^1H nmr data (D_2O) δ: 4.75 (d, 1H, $J_{1,2}$ 3.7 Hz, H-1), 4.35 (dd, 1H, $J_{3,4}$ 5.4 Hz, $J_{4,5}$ 2.2 Hz, H-4), 4.19 (dd, 1H, $J_{2,3}$ 8.0 Hz, $J_{3,4}$ 5.4 Hz, H-3), 4.11 (ddd, 1H, $J_{4,5}$ 2.2 Hz, $J_{5,6}$ 4.3 Hz, $J_{5,6'}$ 7.9 Hz, H-5), 3.82 (dd, 1H, $J_{5,6}$ 4.3 Hz, $J_{6,6'}$ −11.8 Hz, H-6), 3.76 (dd, 1H, $J_{5,6'}$ 7.9 Hz, $J_{6,6'}$ −11.8 Hz, H-6′), 3.71 (dd, 1H, $J_{1,2}$ 3.7 Hz, $J_{2,3}$ 8.0 Hz, H-2), 3.38 (s, 3H, OMe), 1.47 (s, 3H, Me), 1.333 (s, 3H, Me).

Methyl 3,4-O-isopropylidene-6-O-trityl-α-D-galactopyranoside **4**

A solution of **2** (3.5 g, 15 mmol) and chlorotriphenylmethane (4.2 g, 15.1 mmol) in dry pyridine (50 mL) was kept at room temperature for 48 h, and then poured into ice-water (500 mL). The solvent was decanted from the sticky solid, and the solid was washed several times with water and finally taken up in acetone. Evaporation of the acetone under reduced pressure and chromatography of the residue (silica, solvent B) gave the product as a colourless foam, R_f 0.5 (5 g, 70%), mp 61–64°C (lit. (18) mp 60–61°C); $[\alpha]_D$ +49° (*c* 1, chloroform); ^1H nmr data ($CDCl_3$) δ: 7.50–7.22 (m, 15H, Tr), 4.74 (d, 1H, $J_{1,2}$ 4.0 Hz, H-1), 4.21 (dd, 1H, $J_{3,4}$ 5.8 Hz, $J_{4,5}$ 1.9 Hz, H-4), 4.17 (dd, 1H, $J_{2,3}$ 10.3 Hz, $J_{3,4}$ 5.8 Hz, H-3), 4.01 (dt, 1H, $J_{4,5}$ 1.9 Hz, $J_{5,6}$ 6.3 Hz, $J_{5,6'}$ 6.3 Hz, H-5), 3.78 (ddd, 1H $J_{1,2}$ 4.0 Hz, $J_{2,OH}$ 6.5 Hz, $J_{2,3}$ 10.3 Hz, H-2), 3.46 (s, 3H, OMe), 3.45 (dd, 1H, $J_{5,6}$ 6.3 Hz, $J_{6,6'}$ −9.5 Hz, H-6), 3.36 (dd, 1H, $J_{5,6'}$ 6.3 Hz, $J_{6,6'}$ −9.5 Hz, H-6′), 2.24 (d, 1H, $J_{2,OH}$ 6.5 Hz, OH), 1.44 (s, 3H, Me), 1.33 (s, 3H, Me).

Methyl 3,4-O-isopropylidene-6-O-trityl-α-D-galactopyranoside 2-(potassium sulphate) **5**

To a solution of methyl 3,4-*O*-isopropylidene-6-*O*-trityl-α-D-galactopyranoside **4** (3.36 g, 7 mmol) in dry dimethylformamide (50 mL) was added trimethylamine – sulphur trioxide (2.1 g, 15 mmol), and the

Can. J. Chem. Downloaded from www.nrcresearchpress.com by 88.85.125.76 on 09/07/12
For personal use only.

Can. J. Chem. Downloaded from www.nrcresearchpress.com by 88.85.125.76 on 09/07/12
For personal use only.

reaction mixture heated with stirring at 50–60°C for 30 min (tlc then shows reaction to be complete, R_f 0.4, solvent D). After cooling, water (50 mL) was added to the reaction and the solution kept at room temperature for a further 30 min, the pH adjusted to neutrality by the addition of aqueous potassium bicarbonate, and the solvents removed under reduced pressure. The residue was taken up in methanol (50 mL), the solution filtered, and the filtrate evaporated to dryness. The residue was purified by chromatography on silica (solvent D) to afford the product as an amorphous solid (3.8 g, 90%). Recrystallized from isopropanol, mp 155–158°C (dec.); $[\alpha]_D$ +54° (*c* 1, methanol); ^{1}H nmr data (D_2O/acetone-d_6) δ: 7.25–7.65 (m, 15H, Tr), 5.14 (d, 1H, $J_{1,2}$ 3.2 Hz, H-1), 4.35 (dd, 1H, $J_{1,2}$ 3.2 Hz, $J_{2,3}$ 8.3 Hz, H-2), 4.34 (dd, 1H, $J_{3,4}$ 5.0 Hz, $J_{4,5}$ 3.2 Hz, H-4), 4.19 (dd, 1H, $J_{2,3}$ 8.3 Hz, $J_{3,4}$ 5.0 Hz, H-3), 4.15 (ddd, 1H, $J_{4,5}$ 3.2 Hz, $J_{5,6}$ 4.2 Hz, $J_{5,6'}$ 8.1 Hz, H-5), 3.30 (dd, 1H, $J_{5,6}$ 4.2 Hz, $J_{6,6'}$ −11.8 Hz, H-6), 3.38 (dd, 1H, $J_{5,6'}$ 8.1 Hz, $J_{6,6'}$ −11.8 Hz, H-6'), 3.41 (s, 3H, OMe), 1.46 (s, 3H, Me), 1.31 (s, 3H, Me); ^{13}C nmr δ: 145.50, 129.92, 128.90, 128.24 (Ph_3C), 109.90 (Me_2C), 99.84 (C-1), 75.61, 75.52, 75.33 (C-2/3/4, Ph_3C), 68.01 (C-5), 64.54 (C-6), 56.03 (OMe), 30.50 and 29.81 (Me_2C). Anal. calcd. for $C_{29}H_{31}KO_9S \cdot 2H_2O$: C 55.23, H 5.55, S 5.07; found: C 54.94, H 5.20, S 4.68.

Methyl α-D-galactopyranoside 2-(potassium sulphate) ***11***

Compound **5** (3.5 g, 5.8 mmol) was dissolved in a mixture of absolute ethanol (15 mL) – 50% acetic acid (15 mL), and the solution heated under reflux for 4 h (tlc then shows formation of a new product, R_f 0.5, solvent E). After cooling the reaction, the solvent was removed under reduced pressure, the residue coevaporated from ethanol, redissolved in ethanol (20 mL), and the solution neutralized with saturated aqueous potassium bicarbonate. The solvent was evaporated, the residue taken up in methanol, the solution filtered, and the filtrate evaporated to dryness. Chromatography of the residue (silica, solvent F) gave the product as a colourless solid which was crystallized from absolute ethanol (1.5 g, 88%), mp 185–190°C (dec.); $[\alpha]_D$ +100° (*c* 1, water). For the ^{13}C and ^{1}H nmr data, see Tables 1–3. Anal. calcd. for $C_7H_{13}KO_9S \cdot 3H_2O$: C 23.59, H 5.30, S 8.98; found: C 22.62, H 4.70, S 8.75.

*Methyl 4,6-benzylidene-2-*O*-acetyl-α-D-galactopyranoside* ***8***

A mixture of methyl 4,6-benzylidene-α-D-galactopyranoside **6** (2.82 g, 10 mmol) and dibutyltin oxide (2.48 g, 10 mmol) in dry methanol (100 mL) was heated under reflux for 2 h (the solution becomes clear) and then cooled. Evaporation of the solvent under reduced pressure gave a white solid **7**. This was dissolved in dry dioxan (50 mL), and to the solution was added triethylamine (2 mL, 15 mmol), followed by acetyl chloride (1 mL, 15 mmol) at 5°C. The reaction was allowed to warm to room temperature, stirred overnight, quenched with water (10 mL), and the solvents evaporated under reduced pressure. The residue was taken up in ethyl acetate (200 mL), washed with water (twice), dried, and the solvent evaporated to leave the crude product, R_f 0.6, solvent G. This was purified by chromatography on silica, first eluting with a mixture of ethyl acetate – petroleum ether 1:1 (200 mL), which is discarded, and then with ethyl acetate, to give the product as a white crystalline solid, which was crystallized from ethanol (2.5 g, 78%), mp 170–175°C (lit. (25) mp 168–174°C); $[\alpha]_D$ +140° (*c* 1, chloroform); H nmr data ($CDCl_3$) δ: 5.20 (dd, 1H, $J_{1,2}$ 3.6 Hz, $J_{2,3}$ 9.5 Hz, H-2), 4.88 (d, 1H, $J_{1,2}$ 3.6 Hz, H-1), 3.39 (s, 3H, OMe), 2.15 (s, 3H, OAc).

*Methyl 4,6-*O*-benzylidene-2-*O*-acetyl-α-D-galactopyranoside 3-(sodium sulphate)* ***10***

A mixture of 4,6-benzylidene-2-*O*-acetyl-α-D-galactopyranoside **8** (1.2 g, 4 mmol) and trimethylamine – sulphur trioxide complex (1.3 g, 10 mmol) in dry dimethylformamide (25 mL) was heated at 50–60°C for 30 min with stirring. Water (50 mL) was then added to the reaction mixture, and after 1 h the reaction was neutralized with aqueous sodium bicarbonate solution and the solvents evaporated under reduced pressure. The residue was dissolved in more water, the pH again adjusted to neutrality by adding aqueous sodium bicarbonate, and the solvents evaporated. The residue was dissolved in methanol (50 mL), the solution filtered, and the filtrate evaporated to dryness. Chromatography of the residue on silica (solvent D) afforded the product as an amorphous solid (1.5 g, 90%), R_f 0.5, recrystallized from ethanol, mp 160–165°C (dec); $[\alpha]_D$ +118° (*c* 1, methanol); H nmr data (D_2O) δ: 7.38–7.56 (m, 5H, aromatic), 5.70 (s, 1H, H-benz.), 4.93 (d,1H, $J_{1,2}$ 3.7 Hz, H-1), 4.69 (dd, 1H, $J_{3,4}$ 3.4 Hz, $J_{4,5}$ 4.6 Hz, H-4), 4.59 (dd, 1H, $J_{2,3}$ 10.2 Hz, $J_{3,4}$ 3.4 Hz, H-3), 4.18 (m, 2H, H6H6'), 4.04 (dd, 1H, $J_{1,2}$ 3.7 Hz, $J_{2,3}$ 10.2 Hz, H-2), 3.91 (m, 1H, H-5), 3.41 (s, 3H, OMe), 1.85 (s, 3H. OAc); ^{13}C nmr δ: 182.12 (MeCO), 152.74, 130.68, 129.51, 127.22 (PhC), 102.09 (C-1), 100.77 (PhC), 76.60, 75.40, 69.68, 66.70 (C-2/3/4/5), 63.45 (C-6), 58.18 (OMe), 24.63 (MeCO). Anal. calcd. for $C_{16}H_{19}NaO_{10}S \cdot 2H_2O$: C 41.55, H 4.97, S 6.92; found: C 41.88, H 4.90, S 6.35.

Methyl α-D-galactopyranoside 3-(potassium sulphate) ***12***

A solution of **10** (1.4 g) in 60% aqueous acetic acid (20 mL) was heated under reflux for 30 min. The cooled solution was evaporated to dryness, the residue taken up in dry methanol (20 mL) and treated with 1 M sodium methoxide in methanol solution (5 mL). After 30 min, the reaction mixture was acidified with Dowex-50 (H^+), the resin filtered, and the filtrate neutralized with aqueous potassium bicarbonate and evaporated to dryness. The residue was chromatographed on silica, first washing through with ethyl acetate – methanol 2:1, and then with ethyl acetate – methanol 1:1 to elute the required product as a white solid, R_f 0.5, solvent E; crystallized from dichloromethane and methanol (0.8 g, 82%), mp 180–185°C (dec.); $[\alpha]_D$ +126° (*c* 0.7, water). For the ^{13}C and ^{1}H nmr data, see Tables 1–3. Anal. calcd. for $C_7H_{13}KO_9S \cdot 2H_2O$: C 24.06, H 4.88, S 9.19; found: C 23.45, H 4.30, S 8.70.

*Methyl 2,3,4-tri-*O*-acetyl-6-*O*-trityl-α-D-galactopyranoside* ***13***

A solution of methyl α-D-galactopyranoside **1** (dried by heating at 110°C *in vacuo*) (5.72 g, 0.03 mol) and chlorotriphenylmethane (8.6 g, 0.031 mol) in dry pyridine (100 mL) was stirred at room temperature for 4 days (tlc then shows formation of product, R_f 0.4, solvent D). Acetic anhydride (10 ml, 0.2 mol) was added and the reaction allowed to proceed for a further 12 h. The contents were then poured into ice-water (500 mL), the product filtered, washed with absolute ethanol, and dried. Crystallization from ethanol gave the product as a white solid (12.5 g, 76%), mp 170–173°C (lit. (23) mp 167–169°C); $[\alpha]_D$ +60° (*c* 1, chloroform); ^{1}H nmr data ($CDCl_3$) δ: 7.20–7.41 (m, 15H, Tr), 5.53 (dd, 1H, $J_{3,5}$ 3.3 Hz, $J_{4,5}$ 1.2 Hz, H-4), 5.35 (dd, 1H, $J_{2,3}$ 10.7 Hz, $J_{3,4}$ 3.3 Hz, H-3), 5.08 (dd, 1H, $J_{1,2}$ 3.7 Hz, $J_{2,3}$ 10.7 Hz, H-2), 4.93 (d, 1H, $J_{1,2}$ 3.7 Hz, H-1), 4.04 (ddd, 1H, $J_{4,5}$ 1.2 Hz, $J_{5,6}$ 6.1 Hz, $J_{5,6'}$ 7.3 Hz, H-5), 3.39 (s, 1H, OMe), 3.31 (dd, 1H, $J_{5,6}$ 6.1 Hz, $J_{6,6'}$ −9.4 Hz, H-6), 3.05 (dd, 1H, $J_{5,6'}$ 7.3 Hz, $J_{6,6'}$ −9.4 Hz, H-6'), 2.07 (s, 3H, OAc), 1.97 (s, 3H, OAc), 1.90 (s, 3H, OAc).

*Methyl 2,3,6-tri-*O*-acetyl-α-D-galactopyranoside* ***14***

Compound **13** (5 g) was treated with a solution of chloroform saturated with hydrogen chloride gas at 0°C. After 10 min (tlc indicated reaction to be complete) the contents of the reaction were poured into a saturated aqueous sodium bicarbonate solution (50 mL). The organic layer was rapidly separated, dried, and evaporated to dryness. Chromatography of the residue on silica (solvent B) yielded the product as a syrup (2.5 g, 88%); $[\alpha]_D$ +150° (*c* 1, chloroform); ^{1}H nmr data ($CDCl_3$) δ: 5.25 (d, 1H, $J_{1,2}$ 3.6 Hz, H-1), 5.23 (dd, 1H, $J_{2,3}$ 10.6 Hz, $J_{3,4}$ 3.2 Hz, H-3), 4.97 (dd, 1H, $J_{3,4}$ 3.2 Hz, $J_{4,5}$ 1.0 Hz, H-4), 4.35 (dd, $J_{5,6}$ 6.0 Hz, $J_{6,6'}$ −11.0 Hz, H-6), 4.21 (dd, 1H, $J_{5,6'}$ 7.4 Hz, $J_{6,6'}$ −11.0 Hz, H-6'), 4.12 (dd, 1H, $J_{1,2}$ 3.6 Hz, $J_{2,3}$ 10.6 Hz, H-2), 4.04 (ddd, 1H, $J_{4,5}$ 1.0 Hz, $J_{5,6}$ 6.0 Hz, $J_{5,6'}$ 7.4 Hz, H-5), 3.39 (s, 4H, OMe, OH), 2.09 (s, 3H, OAc), 2.07 (s, 6H, 2OAc); ^{13}C nmr δ: 170.83, 170.37, 170.03 ($3CH_3CO$), 97.03 (C-1), 69.96 (C-4), 68.0 (C-3), 67.58, 67.41 (C-2/5), 62.86 (C-6), 55.14 (OMe), 20.79, 20.72, 20.67 ($3CH_3CO$). Anal. calcd. for $C_{13}H_{20}O_9$: C 48.75, H 6.25; found: C 48.42, H 6.50.

*Methyl 2,3,6-tri-*O*-acetyl-α-D-galactopyranoside 4-(sodium sulphate)* ***15***

To a solution of methyl 2,3,6-tri-*O*-acetyl-α-D-galactopyranoside **14** (3.2 g, 10 mmol) in dry dimethylformamide (50 mL) was added trimethylamine – sulphur trioxide (3.5 g, 25 mmol.) and the reaction

Can. J. Chem. Downloaded from www.nrcresearchpress.com by 88.85.125.76 on 09/07/12
For personal use only.

mixture heated with stirring at 50–60°C for 30 min, after which tlc (solvent D) revealed a main product having R_f 0.7. Water (50 mL) was then added; after a further 30 min the pH of the reaction was adjusted to neutrality by the addition of aqueous sodium bicarbonate solution, and the solvents were evaporated under reduced pressure. The residue was taken up in methanol (50 mL), the solution filtered, and the filtrate concentrated to dryness. Chromatography of the residue on silica (solvent D) afforded the product as a white solid (4.0 g, 91%), crystallized from ethanol, mp 170–175°C; $[\alpha]_D$ +50° (*c* 1, methanol); ^{1}H nmr data (D_2O) δ: 4.94 (d, 1H, $J_{1,2}$ 3.6 Hz, H-1), 4.13 (dd, 1H, $J_{3,4}$ 3.0 Hz, $J_{4,5}$ 0.5 Hz, H-4), 3.98 (ddd, 1H, $J_{4,5}$ 0.5 Hz, $J_{5,6}$ 4.4 Hz, $J_{5,6'}$ 8.0 Hz, H-5), 3.89 (dd, 1H, $J_{2,3}$ 10.4 Hz, $J_{3,4}$ 3.0 Hz, H-3), 3.79 (dd, 1H, $J_{1,2}$ 3.6 Hz, $J_{2,3}$ 10.4 Hz, H-2), 3.74 (dd, 1H, $J_{5,6}$ 4.4 Hz, $J_{6,6'}$ −11.9 Hz, H-6), 3.72 (d, 1H, $J_{5,6'}$ 8.0 Hz, $J_{6,6'}$ −11.9 Hz, H-6′), 3.37 (s, 3H, OMe), 1.89 (s, 3H, OAc), 1.87 (s, 3H, OAc), 1.85 (s, 3H, OAc); ^{13}C nmr δ: 170.62 ($3CH_3CO$), 180.54 ($3CH_3CO$), 101.23 (C-1), 77.57, 71.44 (C-3/4), 70.42 (C-2/5), 61.78 (C-6), 55.71 (OMe), 24.26 ($3CH_3CO$). Anal. calcd. for $C_{13}H_{19}NaO_{12}S\cdot H_2O$: C 35.45, H 4.77, S 7.27; found: C 34.86, H 4.40, S 6.68.

Methyl α-D-*galactopyranoside 4-(potassium sulphate)* **16**

Compound **15** (2.5 g) was dissolved in dry methanol (50 mL) and to the solution added methanolic 0.1 M sodium methoxide (10 mL) at room temperature. After 1 h, the reaction was complete as shown by tlc (solvent E), R_f 0.4. The solution was acidified with Amberlite IRC-50 (H^+), the resin filtered, and the filtrate neutralized with saturated aqueous potassium bicarbonate and concentrated to dryness. The residue was chromatographed on silica, eluting with ethyl acetate – methanol 2:1 to afford the product as a white solid (2.0 g, 86%), crystallized from aqueous isopropanol, mp 200–205°C (dec.); $[\alpha]_D$ +103° (*c* 1, water). For the ^{13}C and ^{1}H nmr data, see Tables 1–3. Anal. calcd. for $C_7H_{13}KO_9S\cdot 2H_2O$: C 24.06, H 4.88, S 9.19; found: C 23.20, H 4.40, S 8.50.

*Methyl 2,3,4-tri-*O*-benzoyl-*α*-D-galactopyranoside* **19**

Dry methyl α-D-galactopyranoside (5.72 g, 0.03 mol) and trityl chloride (8.6 g, 0.031 mol) in anhydrous pyridine (100 mL) were stirred together at room temperature for 24 h. Benzoyl chloride (17 mL, 0.15 mol) was then added dropwise with cooling and the reaction allowed to continue for a further 20 h after which the contents were poured into ice-water (1000 mL). The syrupy precipitate was dissolved in ethyl acetate (200 mL) and then washed with 0.1 M HCl, saturated aqueous sodium bicarbonate, water, dried, and concentrated to a syrup. Methyl 2,3,4-tri-*O*-benzoyl-6-*O*-trityl-α-D-galactopyranoside **18** was obtained as a white solid (19 g, 86%), R_f 0.8 (solvent J); ^{1}H nmr data ($CDCl_3$) δ: 8.06–7.12 (m, 1H, 3PhCO, Tr), 6.01 (dd, 1H, $J_{3,4}$ 3.3 Hz, $J_{4,5}$ 0.9 Hz, H-4), 5.96 (dd, 1H, $J_{2,3}$ 10.3 Hz, $J_{3,4}$ 3.3 Hz, H-3), 5.54 (dd, 1H, $J_{1,2}$ 3.6 Hz, $J_{2,3}$ 10.3 Hz, H-2), 5.23 (d, 1H, $J_{1,2}$ 3.6 Hz, H-1), 4.27 (dt, 1H, $J_{4,5}$ 0.9 Hz, $J_{5,6}$ 7.0 Hz, $J_{5,6'}$ 7.0 Hz, H-5), 3.68 (dd, 1H, $J_{5,6}$ 7.0 Hz, $J_{6,6'}$ −14.0 Hz, H-6), 3.43 (s, 3H, OMe), 3.27 (dd, 1H, $J_{5,6'}$ 7.0 Hz, $J_{6,6'}$ −14.0 Hz, H-6′); ^{13}C nmr δ: 166.05, 165.53, 165.30 ($3C_6H_5CO$), 129.88–126.96 ($3C_6H_5CO$, Tr), 97.42 (C-1), 86.95 (Ph_3C), 69.60 (C-4), 69.27 (C-3), 68.43 (C-5), 67.83 (C-2), 61.54 (C-6), 55.52 (OMe).

Compound **18** (10 g) was dissolved in 80% aqueous acetic acid (100 mL) and the solution heated under reflux for 2 h, cooled, and concentrated to a syrup. The product **19** was purified by column chromatography on silica (solvent J) and obtained as an amorphorus solid (6 g, 91%), R_f 0.4; ^{1}H nmr data ($CDCl_3$) δ: 7.96–7.13 (m, 15H, 3PhCO), 6.00 (dd, 1H, $J_{3,4}$ 3.2 Hz, $J_{4,5}$ 0.5 Hz, H-4), 5.95 (dd, 1H, $J_{2,3}$ 10.5 Hz, $J_{3,4}$ 3.2 Hz, H-3), 5.54 (dd, 1H, $J_{1,2}$ 3.5 Hz, $J_{2,3}$ 10.5 Hz, H-2), 5.23 (d, 1H, $J_{1,2}$ 3.5 Hz, H-1), 4.65 (dt, 1H, $J_{4,5}$ 0.5 Hz, $J_{5,6}$ 7.0 Hz, $J_{5,6'}$ 7.0 Hz, H-5), 3.69 (dd, 1H, $J_{5,6}$ 7.0 Hz, $J_{6,6'}$ −11.0 Hz, H-6), 3.43 (s, 3H, OMe), 3.28 (dd, 1H, $J_{5,6'}$ 7.0 Hz, $J_{6,6'}$ −11.0 Hz, H-6′); ^{13}C nmr δ: 166.06, 165.53, 165.30 ($3C_6H_5CO$), 129.79–128.33 ($3C_6H_5CO$), 97.42 (C-1), 69.28 (C-3/4), 68.43, 67.83 (C-2/5), 61.55 (C-6), 55.53 (OMe).

*Methyl 2,3,4-tri-*O*-benzoyl-*α*-D-galactopyranoside 6-(sodium sulphate)* **20**

To a solution of methyl 2,3,4-tri-*O*-benzoyl-α-D-galactopyranoside **19** (2.5 g, 5 mmol) in dry dimethylformamide (50 mL) was added trimethylamine – sulphur trioxide (1.4 g, 10 mmol) and the reaction mixture heated with stirring at 50–60°C for 30 min, after which tlc (solvent D) revealed a main product having R_f 0.7. Water (50 mL) was then added to the cooled reaction mixture and, after a further 30 min, the pH of the reaction was adjusted to neutrality by the addition of aqueous sodium bicarbonate solution, and the solvents were evaporated under reduced pressure. The residue was taken up in methanol (50 mL), the solution filtered, and the filtrate evaporated to dryness. The residual solid was washed with ether, dried, and crystallized from ethanol to afford the product as a white solid (2.7 g, 90%), mp 165–170°C (dec.); $[\alpha]_D$ +44° (*c* 1, methanol); ^{1}H nmr data (CD_3OD) δ: 8.07–7.21 (m, 15H, $3C_6H_5CO$), 5.97 (dd, 1H, $J_{3,4}$ 3.3 Hz, $J_{4,5}$ 1.2 Hz, H-4), 5.90 (dd, 1H, $J_{2,3}$ 10.6 Hz, $J_{3,4}$ 3.3 Hz, H-3), 5.67 (dd, 1H, $J_{1,2}$ 3.3 Hz, $J_{2,3}$ 10.6 Hz, H-2), 5.27 (d, 1H, $J_{1,2}$ 3.3 Hz, H-1), 5.65 (dt, 1H $J_{4,5}$ 1.2 Hz, $J_{5,6}$ 6.7 Hz, $J_{5,6'}$ 6.7 Hz, H-5), 4.16 (dd, 1H, $J_{5,6}$ 6.7 Hz, $J_{6,6'}$ −11.0 Hz, H-6), 4.15 (dd, 1H, $J_{5,6'}$ 6.7 Hz, $J_{6,6'}$ −11.0 Hz, H-6′), 3.53 (s, 3H, OMe); ^{13}C nmr δ: 134.73, 134.61, 134.42 ($3C_6H_5CO$), 131.02–129.22 ($3C_6H_5CO$), 98.94 (C-1), 70.84 (C-4), 70.56 (C-3), 68.60 (C-2), 66.96 (C-6), 56.14 (OMe). Anal. calcd. for $C_{28}H_{25}NaO_{12}S$; C 55.26, H 4.11, S 5.26; found: C 54.95, H 4.15, S 5.05

Methyl α-D-*galactopyranoside 6-(potassium sulphate)* **21**

A solution of **18** (2.5 g) in dry methanol (30 mL) was treated with methanolic 0.5 M sodium methoxide (3 mL) at room temperature. After 1 h the reaction was complete as shown by tlc (solvent E), R_f 0.5. The solution was acidified with Amberlite IRC-50 (H^+), the resin filtered, and the filtrate neutralized with saturated aqueous potassium bicarbonate and concentrated to dryness. The residue was chromatographed on silica, eluting with ethyl acetate – methanol 1:1 to afford the product as a white solid, crystallized from isopropanol and methanol (1.05 g, 88%), mp 210–215°C (dec); $[\alpha]_D$ +77° (*c* 1, water). For the ^{13}C and ^{1}H nmr data, see Tables 1–3. Anal. calcd. for $C_7H_{13}KO_9S\cdot 3H_2O$: C 23.59, H 5.33, S 8.98; found: C 22.90, H 4.65, S 9.20.

Acknowledgements

We thank Dr. C. W. J. Fishwick, Department of Chemistry, University of Leeds, and Dr. A. L. Segre, NMR Service, Area della Ricerca di Roma, C.N.R., Roma Italy, for their interest and advice. The provision of financial support by the AFRC (to A.R.) and by C.N.R. (Progetto Finalizzato Chimica Fine II) (to D.L.) is gratefully acknowledged.

1. R. W. JEANLOZ. *In* The carbohydrates. *Edited by* W. Pigman and D. Horton. Academic Press, New York. 1970. pp. 589–625.
2. J. M. MCKIBBIN. *In* The carbohydrates. *Edited by* W. Pigman and D. Horton. Academic Press, New York. 1970. pp. 711–738.
3. W. MACKIE and R. D. PRESTON. *In* Algal physiology and biochemistry. *Edited by* W. D. P. Stewart. Blackwell, Oxford. 1974. pp. 40–85.
4. E. E. PERCIVAL and R. H. MCDOWELL. *In* Chemistry and enzymology of marine algal polysaccharides. Academic Press, New York. 1967.
5. V. J. MORRIS and G. R. CHILVERS. Carbohydr. Poly. **3**, 129 (1983).
6. S. ARNOTT, W. E. SCOTT, D. A. REES, and C. G. A. MCNAB. J. Mol. Biol. **90**, 253 (1974).
7. E. R. MORRIS, D. A. REES, and G. ROBINSON. J. Mol. Biol. **138**, 349 (1980).
8. M. TAKO and S. NAKAMURA. Carbohydr. Res. **155**, 200 (1986).
9. M. TAKO, S. NAKAMURA, and Y. KOHDA. Carbohydr. Res. **16**, 247 (1987).
10. P. S. BELTON, G. R. CHILVERS, V. J. MORRIS, and S. F. TANNER. Int. J. Biol. Macromol. **6**, 303 (1984).
11. P. S. BELTON, V. J. MORRIS, and S. F. TANNER. Int. J. Biol. Macromol. **7**, 53 (1985).
12. P. S. BELTON, R. H. WILSON, and D. H. CHENERY. Int. J. Biol. Macromol. **8**, 247 (1986).
13. J. J. CAEL, D. L. W. KWOK, S. S. BHATTACHARJEE, and S. L. PATT. Macromolecules, **18**, 819 (1985).

14. H. CHANZY, B. HENRISSAT, M. VINCENDON, S. F. TANNER, and P. S. BELTON. Carbohydr. Res. **160**, 1 (1987).
15. D. LAMBA, C. BURDEN, W. MACKIE, and B. SHELDRICK. Carbohydr. Res. **155**, 11 (1986).
16. D. LAMBA, W. MACKIE, B. SHELDRICK, P. BELTON, and S. TANNER. Carbohydr. Res **180**, 183 (1988).
17. M. J. HARRIS and J. R. TURVEY. Carbohydr. Res. **9**, 397 (1969).
18. R. R. CONTRERAS, J. P. KAMERLING, J. BREG, and J. F. G. VLIEGENTHART. Carbohydr. Res. **179**, 411 (1988).
19. A. LIPTAK, P. FUGEDI, J. KEREKGYARTO, and P. NANASI. Carbohydr. Res. **113**, 225 (1983).
20. R. M. MUNAVU and H. SZMANT. J. Org. Chem. **41**, 1832 (1976).
21. B. HELFERICH and H. BREDERECK. Ber. **64**, 2411 (1931).
22. P. J. ARCHBALD, M. D. FENN, and A. B. ROY. Carbohydr. Res. **93**, 177 (1981).
23. D. M. MACKIE and A. S. PERLIN. Carbohydr. Res. **24**, 67 (1972).
24. A. STOFFYN and P. STOFFYN. J. Org. Chem. **32**, 4001 (1967).
25. H. B. BOREN, P-J. GAREGG, L. KENNE, L. MARON, and S. SVENSSON. Acta Chem. Scand. **26**, 644 (1972).

Can. J. Chem. Downloaded from www.nrcresearchpress.com by 88.85.125.76 on 09/07/12
For personal use only.

The two solid-state conformations of nefopam methiodide, a quaternary ammonium salt of the analgesic drug

ROBERT GLASER[1]
Department of Chemistry, Ben Gurion University of the Negev, Beersheva 84105, Israel
AND
ANDRÉ MICHEL[1] AND MARC DROUIN
Département de chimie structurale, Université de Sherbrooke, Sherbrooke (Québec), Canada J1K 2R1

Received, December 8, 1989

This paper is dedicated to Professor Arthur S. Perlin on the occasion of his 67th birthday[2]

R. GLASER, A. MICHEL, and M. DROUIN. Can. J. Chem. **68**, 1128 (1990).

The solid-state structure of nefopam methiodide, a quaternary ammonium salt of nefopam hydrochloride (a non-narcotic analgesic drug), has been determined by single crystal X-ray diffraction analysis. Nefopam methiodide gives crystals belonging to the monoclinic $P2_1/c$ space group and, at 298 K, a = 10.001(1), b = 9.928(1), c = 17.598(1) Å, β = 94.41(1)°, V = 1742.2(2) Å^3, Z = 4, $R(F)$ = 0.086, and $R_w(F)$ = 0.108. Due to disorder, the boat (flattened chair) and twist-chair (flattened chair) conformations of the 2,5-benzoxazocine eight-membered ring were both observed in the crystal with 55:45 occupancy, respectively. Positional disorder was also observed for the iodide counterion, which showed occupancies of 81:9.5:9.5.

Key words: nefopam, analgesic, X-ray crystallography, conformation.

R. GLASER, A. MICHEL et M. DROUIN. Can. J. Chem. **68**, 1128 (1990).

Faisant appel à la diffraction des rayons-X sur un cristal unique, on a déterminé la structure du méthiodure de néfopam, un sel d'ammonium quaternaire obtenu à partir du chlorhydrate de néfopam (un analgésique non-narcotique). Le méthiodure de néfopam donne des cristaux monocliniques qui appartiennent au groupe d'espace $P2_1/c$, avec a = 10.001(1), b = 9.928(1) et c = 17.598(1) Å, β = 94.41(1), V = 1742.2 Å^3, Z = 4, $R(F)$ = 0.086 et $R_w(F)$ = 0.108. À cause du désordre, les conformations bateau (chaise aplatie) et chaise croisée (chaise aplatie) du cycle à huit chaînons de la 2,5-benzoxazocine existent toutes les deux dans le cristal; les quantités relatives sont 45:55. On a aussi observé du désordre de positions pour le contre-ion iodure; les quantités relatives sont 81 : 9,5 : 9,5.

Mot clés : néfopam, analgésique, diffraction des rayons-X, conformation.

[Traduit par la revue]

Introduction

Nefopam hydrochloride (5-methyl-1-phenyl-3,4,5,6-tetrahydro-1*H*-2,5-benzoxazocine hydrochloride, **1**) is a non-narcotic

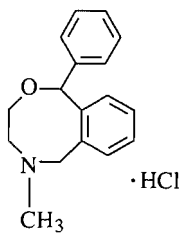

1

analgesic drug (1, 2). It has an equatorial *N*-methyl group orientation (**e**) in the crystalline state for both the racemic modification and for the chiral crystal (3, 4). The molecules in both types of crystal have similar geometries ((1*R*,5*R*)/(1*S*,5*S*) and (1*S*,5*S*) configuration, respectively (3)) in which the octagonal ring is twisted into the boat (flattened chair) conformation (4), **1e**. This is similar to the important boat-chair conformation having C_s symmetry observed for cyclooctane (5, 6).[3] In structure **1e**, the phenyl ring resides in a relatively sterically unhindered *exo*-type ring position *trans* to the methyl (3, 4).

Recently, ^{1}H and ^{13}C NMR evidence has been presented showing that acidic aqueous solutions (pH 1 or pD 1) of crystalline equatorial *N*-methyl racemic nefopam hydrochloride

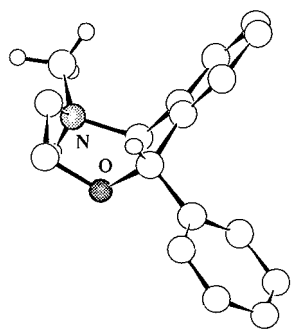

(+)-**1e**

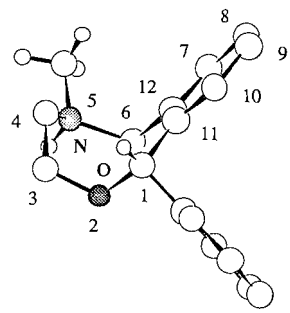

(±)-**1e**

(±)-**1e** show two slow exchange limit (SEL) $^+$NHCH$_3$ (or $^+$NDCH$_3$) diastereomeric species **1a,e** (ca. 1:1) differing in the stereochemistry of the *N*-methyl group (3, 8). The same two *N*-protonated diastereomeric species (**1a,e** ratio ca. 3:2) also exist in dichloromethane or chloroform solutions of crystalline (±)-**1e** or (+)-**1e**·H$_2$O (3, 8). A prototropic shift/nitrogen

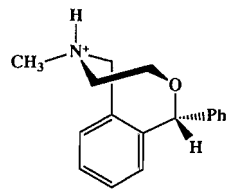

1e

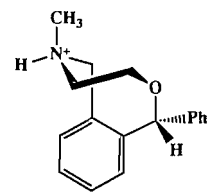

1a

inversion mechanism interconverts the two diastereomeric species in either aqueous medium or in the chlorinated organic solvent (3, 8).

While the boat (flattened chair) has been shown to be the

[1]Authors to whom correspondence may be addressed.

[2] "... חכמתו מתקיימת ..." "... *his wisdom shall endure* ..." Pirke Aboth, chapter III, verse 12.

[3]Also C. Vergelatti, S. Raymond, and F. Brisse. Unpublished results.

Printed in Canada / Imprimé au Canada

Can. J. Chem. Downloaded from www.nrcresearchpress.com by 88.85.125.76 on 09/07/12
For personal use only.

Can. J. Chem. Downloaded from www.nrcresearchpress.com by 88.85.125.76 on 09/07/12
For personal use only.

conformation for both solution species (3, 8), other benzoxazocine conformations are known, e.g., the twist-chair (flattened chair) has been found for the X-ray crystallographically determined structure of free base (±)-8,9-dimethoxy-3-methyl-1-phenyl-3,4,5,6-tetrahydro-1*H*-2,3-benzoxazocine (9), **2**. In the case of nefopam hydrochloride **1**, molecular mechanics has also shown this conformation to be comparable in energy to that of the boat (flattened chair) (4).

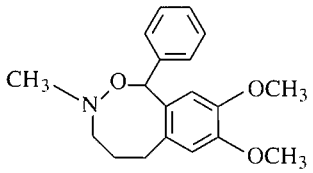

2

Some of the ^{1}H NMR resonances for the equatorial *N*-methyl epimer **1e** were observed to be broadened (the diastereotopic C(6) methylenic-*H*, in particular) (3, 8). This necessitated lowering the probe temperature to 233 K in order to sharpen them up (3, 8). However, no new resonances were readily apparent in the low temperature spectrum, and thus the boat (flattened chair) conformation **1e** was proposed as the major species in equilibrium with a *hidden partner* (8). This was in contradistinction to the line-shapes for the axial *N*-methyl **1a** species, since all the resonances for this epimer were found to be sharp in the ambient temperature ^{1}H NMR spectrum (8).

The ^{1}H and ^{13}C NMR spectral parameters of the nefopam methiodide quaternary ammonium salt **3** have recently been

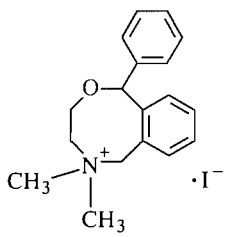

3

reported (10). Using trideuteriomethyl iodide, two isotopomeric **3**-d_3 diastereomers were produced as kinetic products of the quaternization (ca. 20% excess of equatorial *N*-CD_3 product was noted) (10). At ambient probe temperature, all the resonances were found to be ca. 3 times broader at half-height relative to that measured for an internal standard (10). The observation of this phenomenon suggested that conformational heterogeneity was also apparent for the quaternary salt (10). The time-averaged vicinal coupling constants and difference NOE experiments were readily interpreted as showing a preponderance of the boat (flattened chair) conformation species **4** within the equilibrium mixture solution (10). Based upon the earlier molecular mechanics studies (4), the second species was assigned as the putative twist-chair (flattened chair) conformation **5** (10). This paper reports the single-crystal X-ray diffraction analysis of the quaternary ammonium salt **3**, and the observation of both benzoxazocine conformations **4** and **5** in the disordered crystal.

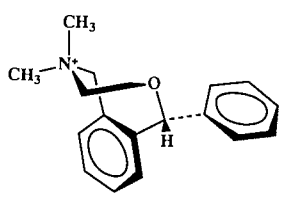

4

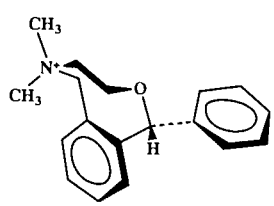

5

Results and discussion

Crystals of (±)-nefopam methiodide **3** belonging to the monoclinic space group $P2_1/c$ were obtained by vapour diffusion of acetone into an absolute ethanol solution of the salt. The crystal data are provided in Table 1. Due to disorder in the crystal, the boat (flattened chair) and twist-chair (flattened chair) conformations of the 2,5-benzoxazocine eight-membered ring were both observed in the solid state with 55:45 occupancy, respectively. Positional disorder was also observed for the iodide counterion, which showed occupancies of 9.5:81:9.5.

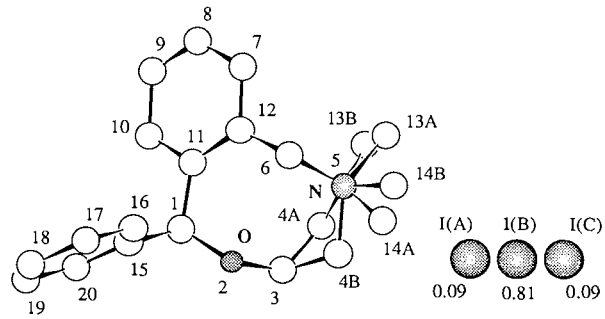

6

The atomic parameters *x*, *y*, and *z* for the boat (flattened chair) conformer (molecule **3A**), and the twist-chair (flattened chair) (molecule **3B**) conformer are listed in Table 2. The numbering scheme for the skeleton is provided in structure **6**, while that for the aliphatic protons is depicted in structure **7** (molecule **3A**) and in structure **8** (molecule **3B**). Intramolecular distances and

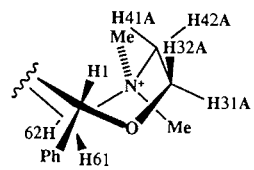

7

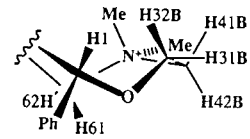

8

angles are given in Table 3, and selected torsion angles are presented in Table 4. Tables of thermal parameters, hydrogen atom coordinates, and structure factors have been deposited.[4]

Perusal of the octagonal-ring torsion angles in Table 4 shows that the **3A** boat (flattened chair) conformation is very similar to that found for both (±)-**1e** and (+)-**1e**·H_2O (4) (see **3A** versus (+)-**1e** and (±)-**1e** for a pictorial comparison).

[4]Hydrogen atom fractional coordinates, isotropic thermal parameters (B_{iso}), and corresponding occupancy factors for (±)-nefopam methiodide (**3**); anisotropic thermal parameters (×100) for non-hydrogen atoms with esd's in parentheses; and tables of observed and calculated structure factors have been deposited and may be purchased from the Depository of Unpublished Data, CISTI, National Research Council of Canada, Ottawa, Ont., Canada K1A 0S2.

Tables of isotropic thermal parameters and hydrogen atom coordinates have also been deposited with the Cambridge Crystallographic Data Centre, and can be obtained on request from the Director, Cambridge Crystallographic Data Centre, University Chemical Laboratory, Lensfield Road, Cambridge CB2 1EW, U.K.

TABLE 1. Crystallographic details for (±)-nefopam methiodide **3**

	$C_{18}H_{21}NOI$
FW, amu	394.82
Space group	$P2_1/c$
a, Å	10.001(1)
b, Å	9.928(1)
c, Å	17.598(1)
β, deg	94.41(1)
V, Å^3	1742.2(2)
Z	4
ρ_{calcd}, g cm^{-3}	1.505
Linear absorption coefficient, cm^{-1}	145.70
Temperature, K	298
Crystal size, mm	0.08 × 0.25 × 0.30
Radiation	Graphite-monochromated Cu $K_{\bar{\alpha}}$ (λ = 1.5418 Å)
Collection range	$\pm h, +k, +l$ $(-11 \leq h \leq 11, 0 \leq k \leq 11, 0 \leq l \leq 21)$
2θ limits	$4.0° \leq 2\theta \leq 143.9°$
Scan type	ω–2θ
Scan width, deg	1.0 + 0.35 tanθ
Scan speed, deg min^{-1}	2.0
Background time/scan time	0.33
Unique data	3378
Unique data with $I_{net} \geq 2.5\sigma(I_{net})$	2690
No. of variables	205
$R(F)$	0.086
$R_w(F)$	0.108
Weighting factor, w	Unit weights
Goodness of fit[a]	4.324

[a]Goodness of fit = SQRT[$(\Sigma_i\{w_i(|F_{obs}|_i - |F_{calc}|_i|)\}^2)$/(no. of reflections − no. of parameters)].

TABLE 2. Fractional coordinates, B_{eq}, and corresponding occupancy factors for (±)-nefopam methiodide (**3**), esd's in parentheses

Atom	x	y	z	B_{eq}	Occupancy
I(A)	0.505(2))	1.147(2)	0.617(1)	10.0(4)	0.09
I(B)	0.3975(1)	1.1442(1)	0.6166(1)	4.89(1)	0.81
I(C)	0.292(2)	1.145(2)	0.617(1)	9.0(3)	0.09
C(1)	1.077(2)	0.839(1)	0.610(1)	5.5(6)	1.00
O(2)	0.950(1)	0.834(1)	0.568(1)	4.6(4)	1.00
C(3)	0.866(2)	0.949(2)	0.572(1)	8.9(11)	1.00
C(4A)	0.803(2)	0.981(2)	0.637(1)	3.8(4)	0.55
C(4B)	0.738(5)	0.926(5)	0.592(3)	8.9(11)	0.45
N(5)	0.729(1)	0.863(1)	0.673(1)	8.3(7)	1.00
C(6)	0.829(1)	0.746(1)	0.697(1)	5.5(7)	1.00
C(7)	0.976(2)	0.778(2)	0.816(1)	5.5(7)	1.00
C(8)	1.095(2)	0.812(2)	0.854(1)	5.9(7)	1.00
C(9)	1.201(2)	0.852(2)	0.820(1)	6.0(7)	1.00
C(10)	1.190(2)	0.860(2)	0.737(1)	5.9(7)	1.00
C(11)	1.072(1)	0.829(1)	0.698(1)	5.2(6)	1.00
C(12)	0.962(1)	0.785(1)	0.734(1)	4.7(6)	1.00
C(13A)	0.670(3)	0.924(3)	0.748(2)	5.8(6)	0.55
C(13B)	0.725(3)	0.956(3)	0.740(2)	5.0(6)	0.55
C(14A)	0.617(3)	0.821(3)	0.621(2)	5.4(5)	0.45
C(14B)	0.594(3)	0.797(3)	0.664(2)	5.4(6)	0.45
C(15)	1.157(1)	0.729(1)	0.577(1)	5.0(6)	1.00
C(16)	1.112(2)	0.595(2)	0.577(1)	6.3(8)	1.00
C(17)	1.185(2)	0.495(2)	0.547(1)	6.2(7)	1.00
C(18)	1.308(2)	0.523(2)	0.518(1)	6.4(8)	1.00
C(19)	1.355(2)	0.656(2)	0.516(1)	6.4(8)	1.00
C(20)	1.277(1)	0.755(2)	0.548(1)	5.5(7)	1.00

[a]Anisotropically refined atoms are given in the form of the isotropic equivalent displacement parameter defined as: $B_{eq} = [(8/3)\pi^2]\Sigma_i\Sigma_j U_{ij}a^*_i a^*_j a_i a_j$.

Can. J. Chem. Downloaded from www.nrcresearchpress.com by 88.85.125.76 on 09/07/12
For personal use only.

TABLE 3. Bond lengths and bond angles for (±)-nefopam methiodide (**3**); esd's in parentheses

(*a*) Bond lengths (Å)

Common part			
C(1)—O(2)	1.42(2)	C(9)—C(10)	1.45(2)
C(1)—C(11)	1.55(2)	C(10)—C(11)	1.36(2)
C(1)—C(15)	1.50(2)	C(11)—C(12)	1.38(2)
O(2)—C(3)	1.42(2)	C(15)—C(16)	1.41(2)
N(5)—C(6)	1.57(2)	C(15)—C(20)	1.37(2)
C(6)—C(12)	1.49(2)	C(16)—C(17)	1.37(2)
C(7)—C(8)	1.36(2)	C(17)—C(18)	1.39(2)
C(7)—C(12)	1.45(2)	C(18)—C(19)	1.40(3)
C(8)—C(9)	1.32(2)	C(19)—C(20)	1.39(2)
Molecule A		Molecule B	
C(3)—C(4A)	1.38(3)	C(3)—C(4B)	1.37(6)
C(4A)—N(5)	1.55(3)	C(4B)—N(5)	1.55(5)
N(5)—C(13A)	1.61(3)	N(5)—C(13B)	1.51(4)
N(5)—C(14A)	1.45(3)	N(5)—C(14B)	1.50(4)

(*b*) Bond angles (deg)

Common part			
O(2)—C(1)—C(11)	115(1)	C(6)—C(12)—C(7)	117(1)
O(2)—C(1)—C(15)	105(1)	C(6)—C(12)—C(11)	126(1)
C(11)—C(1)—C(15)	113(1)	C(7)—C(12)—C(11)	118(1)
C(1)—O(2)—C(3)	117(1)	C(1)—C(15)—C(16)	121(1)
N(5)—C(6)—C(12)	117(1)	C(1)—C(15)—C(20)	121(1)
C(8)—C(7)—C(12)	120(1)	C(16)—C(15)—C(20)	118(1)
C(7)—C(8)—C(9)	123(2)	C(15)—C(16)—C(17)	120(1)
C(8)—C(9)—C(10)	119(1)	C(16)—C(17)—C(18)	121(2)
C(9)—C(10)—C(11)	120(1)	C(17)—C(18)—C(19)	120(2)
C(1)—C(11)—C(10)	114(1)	C(18)—C(19)—C(20)	120(2)
C(1)—C(11)—C(12)	125(1)	C(15)—C(20)—C(19)	123(2)
C(10)—C(11)—C(12)	121(1)		
Molecule A		Molecule B	
O(2)—C(3)—C(4A)	123(2)	O(2)—C(3)—C(4B)	116(3)
C(3)—C(4A)—N(5)	115(2)	C(3)—C(4B)—N(5)	114(3)
C(4A)—N(5)—C(6)	111(2)	C(4B)—N(5)—C(6)	117(2)
C(4A)—N(5)—C(13A)	106(2)	C(4B)—N(5)—C(13B)	119(3)
C(4A)—N(5)—C(14A)	110(2)	C(4B)—N(5)—C(14B)	102(2)
C(6)—N(5)—C(13A)	109(4)	C(6)—N(5)—C(13B)	107(2)
C(6)—N(5)—C(14A)	113(2)	C(6)—N(5)—C(14B)	104(2)
C(13A)—N(5)—C(14A)	109(2)	C(13B)—N(5)—C(14B)	106(2)

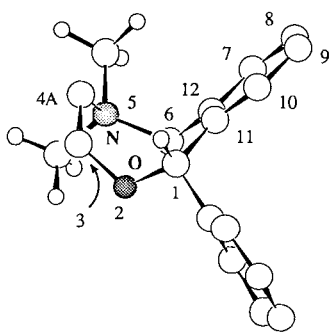

3A

The *gauche* (synclinal) conformation oxydimethyleneamino fragment occupies the "boat" region of the boat (flattened chair) ring in **3A**. The staggered boat region of this conformation is similar to that found for the cyclooctane boat-chair (refs. 5, 6, and footnote 3) conformation, but differs in that the "chair" region of the cycle is distorted such that O(2) moves close to the nearly planar region denoted by C(1), C(6), C(11), and C(12) (and other benzo-ring atoms). This flattening of the chair region markedly reduces transannular nonbonded interactions in the benzoxazocine ring (e.g., that between H(1) and H(41A) in structure **7**). For instance, the internuclear distance between H(1) and the *endo*-oriented H(41A) is 2.26 Å in the MMX88 (11) molecular mechanics model of boat-chair cyclooctane **9**, versus 2.96 Å in a model of **3A** based on hydrogens geometrically placed on the X-ray crystallographically determined heavy-atom skeleton (C—H bond distance set at 1.08 Å). The latter value is similar to the 2.76 and 3.10 Å H(1)···H(41A) distances in crystalline (±)-**1e** and (+)-**1e**·H_2O, respectively (4). Flattening of the chair region by "pushing" C(11) "up" into the C(1,6,12) plane in **9** should result in a compensating torque around the C(1)—C(11) bond, thereby moving H(1ax) "down" and farther away from *endo*-H(41A).

Placement of a nonprotonated atom (oxygen) at the junction between the boat and chair regions in **1–3** also lessens the very severe transannular nonbonded interaction found in the parent hydrocarbon. This involves cyclooctane *endo*-oriented methylene protons ligated to carbons corresponding to O(2) and C(6). In addition, benzoxazocine-O(2) occupancy at the above-mentioned "junction" removed unfavorable torsional interactions found in

Can. J. Chem. Downloaded from www.nrcresearchpress.com by 88.85.125.76 on 09/07/12
For personal use only.

TABLE 4. Comparison of selected torsion angles (deg) for (±)-nefopam methiodide boat (flattened chair) conformation (**3A**) and (±)-nefopam methiodide twist-chair (flattened chair) conformation (**3B**), versus those for boat (flattened chair) conformation in (+)-**1e**/(±)-**1e** and for twist-chair (flattened chair) conformation in (±)-**2**; esd's in parentheses refer to the last digit printed

Angle	**3A**[a]	(+)-**1e**[b]	(±)-**1e**[b]	**3B**[a]	(±)-**2**[c]
C(11)—C(1)—O(2)—C(3)	−72(1)	−78.1(2)	−82.7(2)	−71(1)	−61.2(2)
C(1)—O(2)—C(3)[d]—C(4)[e]	72(2)	74.9(3)	63.8(2)	128(3)	134.0(2)
O(2)—C(3)[d]—C(4)[e]—N(5)[d]	48(1)	48.0(3)	57.7(2)	−62(2)	−77.2(3)
C(3)[d]—C(4)[e]—N(5)[d]—C(6)	−60(1)	−64.3(3)	−59.3(2)	43(2)	53.9(4)
C(4)[e]—N(5)[d]—C(6)—C(12)	−42(1)	−41.0(3)	−49.1(2)	−88(1)	−88.0(4)
N(5)[d]—C(6)—C(12)—C(11)	81(1)	79.3(3)	79.1(2)	83(1)	80.8(4)
C(6)—C(12)—C(11)—C(1)	2(1)	4.7(4)	3.2(3)	2(1)	8.7(4)
C(12)—C(11)—C(1)—O(2)	−15(1)	−17.0(4)	−6.5(2)	−15(1)	−29.5(3)
C(3)[d]—C(4)[e]—N(5)[d]—C(13)[e]	−178(2)	169.4(3)	174.2(2)	−88(3)	[f]
C(3)[d]—C(4)[e]—N(5)[d]—C(14)[e]	66(2)	[f]	[f]	156(4)	[f]
C(13)[e]—N(5)[d]—C(6)—C(12)	73(3)	84.5(3)	76.5(2)	48(2)	[f]
C(14)[e]—N(5)[d]—C(6)—C(12)	−166(2)	[f]	[f]	160(2)	[f]
O(2)—C(1)—C(15)—C(16)	58(1)	91.3(3)	58.7(2)	58(1)	95.3(3)
C(11)—C(1)—C(15)—C(20)	111(2)	149.4(3)	115.0(2)	111(2)	148.9(3)

[a](1*S*) Configuration.
[b](1*S*, 5*S*) Configuration.
[c](1*S*, 3*R*) Configuration.
[d]Atoms no. 3 and 5 for (±)-**2**, are respectively N(3) and C(5), while they are respectively C(3) and N(5) in all other structures.
[e]For (+)-**1e** and (±)-**1e**, atoms no. 4, 13, and 14 are C(4, 13, 14); in **3A** they are C(4A, 13A, 14A); and in **3B** they are C(4B, 13B, 14B).
[f]Not applicable.

boat-chair cyclooctane **9** (20.8° H(1eq)—C(1)—C(2)—H(2eq) torsion angle from the MMX88 (11) model). The sp^2 hybridization for benzoxazocine-C(12) removed this interaction on the other side. The MMX88 calculated model for boat-chair **9** has octagonal-ring torsion angles that are very similar to those found by low temperature single-crystal X-ray diffraction analysis of a cyclooctane-thiourea adduct.[3]

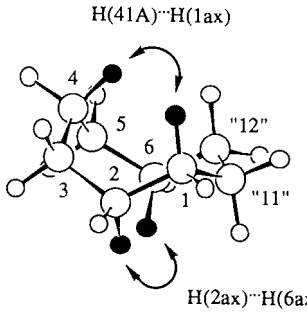

9

Inspection of the octagonal-ring torsion angles in Table 4 also shows that the twist-chair (flattened chair) conformation of **3B** is very similar to that found for **2** (9) (see **3B** versus **2** for a pictorial comparison). In addition, the pitch (or twist) of the phenyl ring around the C(1)—C_{ipso} bond in **3A** (and in **3B**) was found to be very similar to that in (±)-**1e**, while that for twist-chair (flattened chair) **2** was similar to that in (+)-**1e**.

Some of the Table 3 bond lengths involving atoms N(5), C(3, 4A/B, 13A/B, 14A/B) appear longer or shorter than expected (e.g., N—C(13A) is particularly long: 1.61(3) Å, while C(4A)—C(3) and C(4B)—C(3) are particularly short: 1.38(3) and 1.37(6) Å, respectively). The skeletal disorder concerning these very same atoms probably lies at the root of the problem.

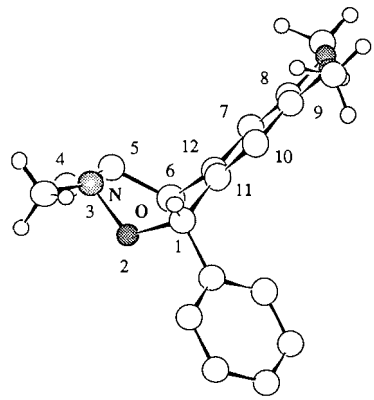

2

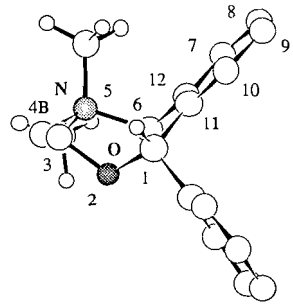

3B

While the disorder then does present a problem, one must remember that the X-ray diffraction analysis was undertaken to study the molecular conformational geometry of the quaternary ammonium salt. When viewed in this light, it was indeed fortuitous that the skeletal disorder occurred, since it provided two different views of the molecule. The presence of two conformational types, and the assignment of their molecular geometries, is clear and undisputable, in spite of the fact that disorder in the crystal resulted in non-optimal final $R(F)$ and $R_w(F)$ values. The relatively large values of $R(F)$ and $R_w(F)$ are explained by the model for the iodine atom refinement, combined with the occurrence of a disordered structure. The existence of three iodine subsites accounts for anisotropic vibrations into a non-harmonic potential well. The validity of the model used is corroborated by interatomic distances of C(4A)···I(A) = 3.40(3) Å, C(4B)···I(A) = 3.26(5) Å, and C(7)···I(C) = 3.28(2) Å (where I(C) is symmetry related). Such values for close contacts are in accordance with the van der

Can. J. Chem. Downloaded from www.nrcresearchpress.com by 88.85.125.76 on 09/07/12
For personal use only.

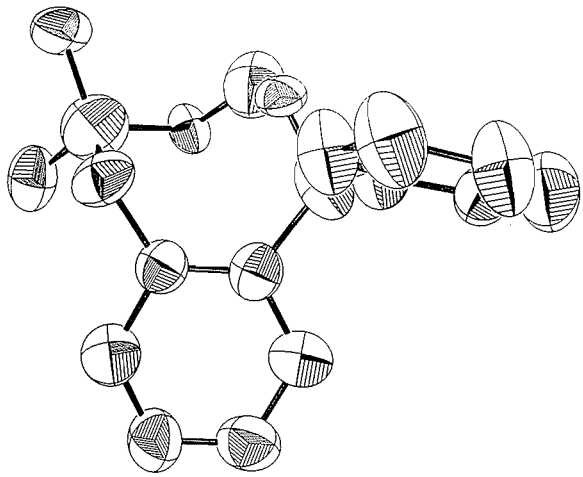

FIG. 1. ORTEP drawing of boat-(flattened chair) conformation of (±)-nefopam methiodide **3A**.

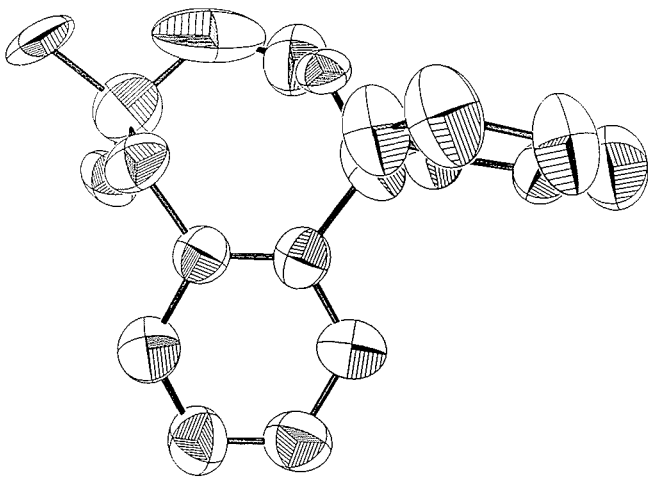

FIG. 2. ORTEP drawing of twist-chair-(flattened chair) conformation of (±)-nefopam methiodide **3B**.

Waals radii deduced by Nyburg and Faerman (12), who determined the effective nonbonding shapes of halogen atoms from crystal data. Furthermore, the attractive van der Waals forces associated with such short distances can account for the anharmonicity. ORTEP drawings showing ellipsoids of thermal motion for atoms in **3A** and **3B** are depicted in Figs. 1 and 2, respectively.

Comparison of solution-state vs. solid-state conformational preferences for nefopam HCl/MeI

Molecule **3B** provides the first direct observation of a non-boat (flattened chair) conformation for the benzoxazocine skeleton of nefopam. As noted above, line-broadening of ^{1}H resonances for **1e** (and particularly for **3**) showed the existence of a rapid conformational equilibrium in CD_2Cl_2 solution (3, 8). Determination of the appropriate vicinal coupling constants for the -NCH_2CH_2O- fragment together with the use of Lambert's *R*-factor method (13) enabled the estimation of the time-averaged O(2)—C(3)—C(4)—N(5) dihedral angle (3, 8). Lambert's *R*-factor stands for a *ratio* of vicinal coupling constants ($R = (J_{aa} + J_{ee})/(J_{ae} = J_{ea})$) (12). In this method, the electronegative and orientation effects of X,Y-substituents in the -XCH_2CH_2Y- fragment are canceled by using a ratio of coupling constants (12). Thus, the O(2)—C(3)—C(4)—N(5) dihedral angles for the axial and equatorial *N*-methyl **1a,e** diastereomers in CD_2Cl_2 solution were estimated to be 53 ± 2° and 58 ± 2°, respectively (3, 8). These compared quite favorably with the X-ray crystallographically determined value of 57.7(2)° for (±)-**1e**, and the molecular mechanics determined 59.5° and 53.6° values for boat (flattened chair) **1e** and **1a**, respectively (4). Since the O(2)—C(3)—C(4)—N(5) dihedral angle is ca. 80 ± 3° for the twist-chair (flattened chair) conformation of **1** (molecular mechanics (4)), the experimentally determined values clearly point to a solution-state preference for the boat (flattened chair) geometry.

Nuclear Overhauser effect (difference-NOE) experiments were also consistent with boat (flattened chair) conformational preferences for **1e,a** in solution (8). Yet, line-broadening does show that another conformation is present for **1e**, albeit in minor amounts (3, 8). The equatorial *N*-methyl diastereomer of phendimetrazine mesylate **10** was used as a model for non-time-

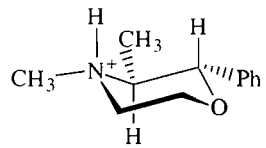

10

averaged vicinal coupling constants in the *gauche* arrangement for the **1e** -NCH_2CH_2O- fragment (14). The study confirmed the time-averaged nature of the vicinal coupling constant values for the **1e** fragment (14).

As noted above, line-broadening for solutions of **3** appeared to be even more pronounced than that found for **1e** (10). Again, Lambert's method allows us to estimate a ca. 54° value for the O(2)—C(3)—C(4)—N(5) dihedral angle (10). The 48(1)° and −62(2)° values found for the (1*S*) enantiomer of solid-state (±)-**3A** and (±)-**3B**, respectively, show that the solution-state time-averaged value is consistent with a boat (flattened chair) preference for **3** in solution. The 55:45 **3A:3B** occupancy shows that only a slight conformational preference was found for **3** in the crystal. However, it remains to be proven whether the conformational disorder is dynamic or static.

The solid-state CP-MAS ^{13}C NMR spectrum of crystalline **3** was recorded in order to search for externally diastereotopic resonances from the two diastereomeric conformations. Only four of the six aliphatic ^{13}C resonances were found in the solid-state spectrum. A fairly sharp δ 85.33 C(1) signal was observed from the crystalline sample, but the C(3, 6) resonances are evidently overlapped at δ 66.97 (width at half-height ca. 3.1 times that for C(1)). Two *N*-methyl carbon resonances were observed at δ 54.46 and 50.17. Their assignment was confirmed by a dipolar dephasing experiment based on less efficient solid-state relaxation for methyl carbons (vis-à-vis methylene and methine carbons). After a suitable delay period was introduced prior to FID acquisition, *N*-CH_3 and $C_{quaternary}$ magnetization was still noted in the spectrum. While two species were not directly observed in the solid-state spectrum, the absence of a clearly defined signal from C(4) is consistent with the disorder for that atom. In comparison, time-averaged fast exchange limit resonances from all six aliphatic carbons were clearly assigned in the solution-state ^{13}C NMR (CD_2Cl_2) spectrum of **3** (δ 86.51 C(1), 65.61 C(3), 58.20 C(4), 68.09 C(6), 53.20 C(13), and 51.12 C(14)) (10). The δ 53.20 and 51.12 signals were assigned to internally diastereotopic equatorial and axial *N*-methyl carbons, respectively, via ^{1}H homonuc-

Can. J. Chem. Downloaded from www.nrcresearchpress.com by 88.85.125.76 on 09/07/12
For personal use only.

lear NOE experiments and an XHCORR $^{13}C/^{1}H$ correlation spectrum (10).

Studies are currently underway to force the nefopam benzoxazocine ring into structures having new stable conformations. Preliminary results have shown that appropriate derivatization of nefopam can afford compounds having predominantly the new twist-chair (flattened chair) conformation.[5]

Experimental

Nefopam methiodide was prepared by reaction of methyl iodide with nefopam free base in methanol. Nefopam hydrochloride was a gift of Mr. David Donnell of 3M Riker (United Kingdom). Dissolution in absolute ethanol followed by vapor diffusion of acetone yielded clear, colorless, crystalline prisms, belonging to the monoclinic system $P2_1/c$; melting point 253–256°C (dec.) (uncorrected).

Intensity data were collected at 298 K on an Enraf–Nonius CAD-4 automatic diffractometer. Table 1 provides crystallographic and data collection details. The NRCVAX programs (16) were used for centering, indexing, and data collection. The unit cell dimensions were obtained by a least-squares fit of 24 centered reflections in the range of $40° \leq 2\theta \leq 50°$. Reflections were measured with a constant scan speed of 2°/min. During data collection, the intensities of two standard reflections were monitored after every 60 min. No decay was observed.

The structure was solved by the application of direct methods and refined by least squares using the NRCVAX program (16). Unitary weights were used. Since the minimum and maximum transmission factors were respectively 0.13(1) and 0.23(1), an empirical absorption correction was applied. An isotropic extinction coefficient was included in the refinement (17) to account for secondary extinction effects (18); its value was 1.40(9). Atomic scattering factors stored in the NRCVAX program were those of Cromer and Waber (19). Hydrogen atomic positions were geometrically placed at 1.08 Å; they were assigned isotropic thermal parameters of their respective attached atoms but were not refined. Iodine subsites I(A) and I(C) and carbon (C(4A), C(4B), C(13A), C(13B), C(14A), and C(14B)) positions were refined isotropically and all other non-H atoms anisotropically. At convergence the final discrepancy indices on F were $R(F) = 0.086$ and $R_w(F) = 0.108$ for the 2690 reflections with $I_{net} \geq 2.5\sigma(I_{net})$ and 205 variables.[6] The residual positive and negative electron densities in the final map were 1.14 e/Å ($x,y,z = 0.4343, 0.7670, 0.3873$) near iodine subsite I(A) and −1.50 e/Å ($x,y,z = 0.6485, 0.7469, 0.3900$) near iodine subsites I(B) and I(C). The maximum shift/σ was 0.114. The occupancy factors for iodine subsites I(A), I(B), and I(C) and carbon atoms C(4A/B), C(13A/B), and C(14A/B) were refined. Upon convergence, the relative occupation for molecules A:B was found to be 55:45, while the relative occupation for I(A):I(B):I(C) was found to be 9.5:81:9.5.

The minimized energy geometry of the molecular mechanics calculated model compounds was determined by the MMX88 program (11), performed on a Micro VAX-II computer under Micro VMS V4.5. MMX88 is an enhanced version of Allinger's MM2 program (20) with MMP1 π-subroutines (21) incorporated for localized π-electron systems. Ball and stick structures were drawn with the BALL AND STICK 2.2 program (7). The ORTEP drawings were produced showing a 50% probability level for the ellipsoids of thermal motion.

Solid-state ^{13}C NMR (25.13 MHz) spectra were recorded on a Chemagnetics M100 solid-state Fourier transform spectrometer operating in the CP-MAS mode. Hexamethylbenzene (17.35 ppm CH_3) was used as an external secondary reference. An evolution delay period of 25 μs was used in the dipolar dephasing experiment (15).

[5]R. Glaser, J. Blumenfeld, K. Maartmann-Moe, and S. Geresh. Unpublished results.

[6]The final discrepancy index $R(F)$ is defined as $R(F) = (\Sigma_i||F_{obs}|_i - |F_{calc}|_i|)/(\Sigma_i|F_{obs}|_i)$; the weighted value R_w is defined as $R_w(F) = \mathrm{SQRT}[(\Sigma_i\{w_i(|F_{obs}|_i - |F_{calc}|_i|)\}^2)/(\Sigma_i\{w_i(|F_{obs}|_i)\}^2)]$, and the particular weighting factor w_i used is given in Table 1.

Acknowledgments

Gratitude is expressed to the Israel Center for Psychobiology, Charles E. Smith Family Foundation, for a research grant extended to R.G. Thanks are given to Dr. Fred Morin (McGill University) for recording the solid-state CP-MAS NMR spectra.

1. M. W. Klohs, M. D. Draper, F. J. Petracek, K. H. Ginzel, and O. N. Ré. Arzneim.-Forsch. (Drug Res.) **22**, 132 (1972).
2. R. C. Heel, R. N. Brogden, G. E. Pakes, T. M. Speight, and G. S. Avery. Drugs, **19**, 249 (1980).
3. R. Glaser, S. Cohen, D. Donnell, and I. Agranat. J. Pharm. Sci. **75**, 772 (1986).
4. R. Glaser, G. Frenking, G. H. Loew, D. Donnell, S. Cohen, and I. Agranat. J. Chem. Soc. Perkin Trans. 2, 113 (1989).
5. J. E. Anderson, E. D. Glazer, D. L. Griffith, R. Knorr, and J. D. Roberts. J. Am. Chem. Soc. **91**, 1386 (1969).
6. A. L. Anet. Top. Curr. Chem. **45**, 169 (1974).
7. N. Müller and A. Falk. BALL AND STICK molecular graphics program for Apple Macintosh computers. Johannes Kepler University, Linz, Austria. Version 2.2. 1989.
8. R. Glaser, G. Frenking, G. H. Loew, D. Donnell, and I. Agranat. New J. Chem. **12**, 953 (1988).
9. J. B. Bremner, E. J. Browne, P. E. Davis, C. L. Raston, and A. H. White. Aust. J. Chem. **33**, 1323 (1980).
10. R. Glaser, A. Peleg, and S. Geresh. Magn. Reson. Chem. In Press.
11. MMX88, Serena Software Inc., P.O.B. 3076, Bloomington, Indiana 47402-3076.
12. S. C. Nyburg and C. H. Faerman. Acta Crystallogr. Sect. B: Struct. Sci. **B41**, 274 (1985).
13. (*a*) J. B. Lambert. J. Am. Chem. Soc. **89**, 1836 (1967); (*b*) Acc. Chem. Res. **4**, 87 (1971).
14. R. Glaser. Magn. Reson. Chem. **27**, 1142 (1989).
15. (*a*) S. J. Opella and G. Frey. J. Am. Chem. Soc. **101**, 5854 (1979); (*b*) S. J. Opella, G. Frey, and B. P. Cross. J. Am. Chem. Soc. **101**, 5856 (1979).
16. E. J. Gabe, F. L. Lee, and Y. LePage. The NRCVAX crystal structure system in crystallographic computing. *In* Data collection, structure determination, proteins, and data bases. Vol. 3. *Edited by* G. M. Sheldrick, C. Kruger, and R. Goddard. Clarendon Press, Oxford. 1985. pp. 167–174.
17. A. C. Larson. Acta Crystallogr. **23**, 664 (1967).
18. W. H. Zachariasen. Acta Crystallogr. **16**, 1139 (1963).
19. D. T. Cromer and J. T. Waber. *In* International tables for X-ray crystallography. Vol. IV. *Edited by* J. A. Ibers and W. C. Hamilton. Kynoch Press, Birmingham. 1974. pp. 99–101. Table 2.2B. (Present distributor Kluwer Academic Publishers, Dordrecht.)
20. N. L. Allinger. J. Am. Chem. Soc. **99**, 8127 (1977).
21. N. L. Allinger and J. T. Sprague. J. Am. Chem. Soc. **95**, 3893 (1973).

Can. J. Chem. Downloaded from www.nrcresearchpress.com by 88.85.125.76 on 09/07/12
For personal use only.

Left- and right-handed chiral nematic mesophase of (trityl)(alkyl)cellulose derivatives

BRIAN R. HARKNESS AND DEREK G. GRAY[1]

Paprican and Department of Chemistry, Pulp and Paper Research Centre, McGill University, Montreal, P.Q., Canada H3A 2A7

Received December 12, 1989

This paper is dedicated to Professor Arthur S. Perlin on the occasion of his 67th birthday

BRIAN R. HARKNESS and DEREK G. GRAY. Can. J. Chem. **68**, 1135 (1990).

A series of novel specifically substituted 6-*O*-trityl-2,3-*O*-alkyl cellulose derivatives have been prepared by the reaction of triphenylmethyl (trityl) cellulose in DMSO with powdered sodium hydroxide and an alkyl iodide (iodohexane, iodopentane, and iodobutane). These derivatives form lyotropic chiral nematic mesophases that exhibit both left- and right-handed twists. The dilute solution circular dichroism due to the phenyl chromophores along the chain does not correlate with the twist sense of the tertiary structures. However, a striking difference in the optical activity of the phenyl chromophores was observed in mesophases with the opposite twist sense. This may reflect some molecular factor responsible for the change in the macroscopic twist sense, or it may be due to the chirality of the helicoidal tertiary structure of the mesophase.

Key words: cellulose, trityl, mesophase, cholesteric, chiroptical.

BRIAN R. HARKNESS et DEREK G. GRAY. Can. J. Chem. **68**, 1135 (1990).

En faisant réagir de la triphénylméthyl (trityl) cellulose avec de l'hydroxyde de sodium et des iodures d'alkyles (iodohexane, iodopentane et iodobutane) en solution dans le DMSO, on a préparé une série de nouvelles 6-*O*-trityl-2,3-*O*-alkyl celluloses spécifiquement substituées. Ces dérivés forment des mésophases nématiques chirales lyotropes qui présentent des déviations vers la gauche ainsi que vers la droite. Des solutions diluées présentent un dichroïsme circulaire qui est dû aux chromophores phényles de la chaîne; il n'y a pas de corrélation entre ces spectres et le sens de rotation des structures tertiaires. Toutefois, les mésophases de sens de rotation opposés présentent des différences remarquables dans l'activité optique des chromophores phényles. Cette différence pourrait être le reflet de facteurs moléculaires responsables pour le changement dans le sens macroscopique de rotation ou bien elle pourrait être due à la chiralité de la structure hélicoïdale tertiaire de la mésophase.

Mots clés : cellulose, trityl, mésophase, cholestérique, chiroptique.

[Traduit par la revue]

Introduction

Many cellulose derivatives form lyotropic chiral nematic (cholesteric) liquid crystalline phases that exhibit reflection bands at specific wavelengths in the visible region due to the selective reflection of one component of circularly polarized light by the supramolecular helicoidal structure. The handedness of the reflected component depends on the twist sense of the helicoidal structure. Cellulose derivatives have been found to form both right-handed (1) and left-handed (2) chiral nematic structures. In some cases a chiral nematic inversion or change in twist sense may occur as the result of a chemical modification of the polymer (3, 4), a change in the solvent (2, 5), or a change in the temperature of the mesophase (6).

6-*O*-Triphenylmethyl-2,3-*O*-benzyl cellulose (TBzC) (7) and 6-*O*-triphenylmethyl-2,3-*O*-pentyl cellulose (TPeC) (8) form lyotropic liquid crystalline phases that exhibit chiral nematic reflection colours. In both of these cases the chiral nematic structure has a right-handed twist sense. Circular dichroism (CD) spectra of these polymers in dilute solution show peaks that correspond to the phenyl chromophores along the chain. These signals are the result of the perturbation of the phenyl electronic transitions by the chiral cellulose backbone. The signs and magnitudes of the phenyl CD bands were found to change markedly as the polymer concentration was increased above the critical concentration for liquid crystal formation. Although the formation of a liquid crystalline phase influences the apparent CD signals for the phenyl chromophores, it is not known whether a change in the twist sense of the chiral nematic structure influences this chiroptical activity.

In a continuation of our study of the chiroptical properties of triphenylmethyl (trityl) cellulose derivatives, we have prepared several new cellulose-based polymers with trityl groups at position six of the anhydroglucose units and alkyl groups at positions two and three. We find that this family of polymers forms both left-handed and right-handed lyotropic chiral nematic liquid crystalline phases. This observation has presented a unique opportunity to probe the relationship between the chiral nematic twist sense and the chiroptical activity of the phenyl chromophores in dilute solution and in the liquid crystalline state.

Experimental

Materials

Trityl cellulose was prepared by the reaction of regenerated cellulose (regenerated from cellulose acetate: Kodak; viscosity (ASTM-A) 27 ± 10) with triphenylmethyl chloride in pyridine according to the method of Hearon *et al.* (9). Trityl cellulose was alkylated according to a procedure similar to that described by Isogai *et al.* (10). Approximately 7–10 g of trityl cellulose was added to 300 mL of dry DMSO and allowed to dissolve. The clear solution was degassed with nitrogen for about 30 min. To the stirring solution was added 12 molar equivalents of sodium hydroxide per mole of polymeric hydroxyl groups (9 molar equivalents of base for the preparation of THeC1). The sodium hydroxide was pulverized with a mortar and pestle, or with a domestic coffee grinder prior to use. One hour following the addition of the sodium hydroxide, 12 molar equivalents of an alkyl iodide (iodobutane, iodopentane, or iodohexane) were added dropwise over 3 h (9 molar equivalents of iodohexane for the preparation of THeC1). The solution was stirred at 50°C for 18 h, then poured into 700 mL of methanol. The precipitate was filtered and dried under vacuum. The product was further purified by reprecipitation from tetrahydrofuran into methanol. A water wash of the filtered precipitate completed the purification process. The final yields of the polymers were greater than 85%.

General analysis

^{1}H NMR spectra were recorded with a Varian XL300 spectrometer at a frequency of 300 MHz. The spectra were recorded in chloroform-d_1 with tetramethylsilane as the internal reference. A small quantity of D_2O was added to the NMR solutions. The degrees of substitution of the 6-*O*-trityl-2,3-*O*-alkyl cellulose derivatives were determined by

[1]Author to whom correspondence may be addressed.

Can. J. Chem. Downloaded from www.nrcresearchpress.com by 88.85.125.76 on 09/07/12
For personal use only.

integrating the ^{1}H NMR signals (which are proportional to the number of protons) and comparing the intensity of the side-group proton signals to the intensity of the signals from the cellulose backbone protons.

Infrared spectra of thin polymer films cast from chloroform were recorded with an Analect AQS-18 FTIR spectrometer. The mass average molar masses, $\overline{M}_w$, were measured in tetrahydrofuran with a Chromatix KMX6 long-angle laser light scattering photometer. Measurements of the Rayleigh factors for each solution were made at a scattering angle of 6–7°. The values for the specific refractive index increment dn/dc were measured with a Brice–Phoenix differential refractometer.

Solution properties

Concentrated solutions were prepared by placing approximately 0.15 g of the polymer into small vials and adding spectrograde chloroform or tetrahydrofuran to the polymer until an isotropic solution formed. The solvent was allowed to evaporate slowly over several days until the desired concentration had been reached. The vials were then weighed to determine the polymer concentration. The polymer solutions were quickly removed from the vials and placed as a thin layer between glass plates. The plates were sealed with epoxy to minimize solvent evaporation. The samples for UV–CD measurements were prepared as thin films (~0.1 mm) between quartz plates. During sample preparation some solvent evaporation occurred and therefore the actual polymer concentrations may be somewhat higher than the recorded value.

The dilute solution measurements were made on solutions of TPeC1 and THeC2 dissolved in spectrograde THF or chloroform, placed into 1.0 and 0.1 cm quartz solution cells at ambient temperature.

Circular reflectivity and circular dichroism spectra were recorded with a Jasco J-500 spectropolarimeter. Absorbance spectra were recorded with a Pye Unicam SP-150 UV–visible spectrometer equipped with a Mettler hot stage that heated the sample at a rate of 1 deg/min.

Results and discussion

Synthesis and characterization

The polymers 6-*O*-trityl-2,3-*O*-butyl cellulose (TBuC), 6-*O*-trityl-2,3-*O*-pentyl cellulose (TPeC), and 6-*O*-trityl-2,3-*O*-hexyl cellulose (THeC) were synthesized from trityl cellulose using a procedure similar to that described by Isogai *et al.* (10). These workers found that cellulosic hydroxyl groups can be alkylated by reacting cellulose, dissolved in a SO_2–DEA–DMSO solvent system, with sodium hydroxide and an appropriate alkyl iodide. A modification of these conditions has been successful in preparing 6-*O*-trityl-2,3-*O*-benzyl cellulose from trityl cellulose dissolved in DMSO (7). Unfortunately, this procedure was not as effective in promoting high degrees of substitution for the longer chain alkyl derivatives. As shown in Table 1, approximately one alkyl group substituted per anhydroglucose unit for both TBuC1 and TPeC1. The alkylating procedure was improved by grinding the sodium hydroxide into a very fine powder with the aid of a domestic coffee grinder. This modification resulted in much higher degrees of substitution, as shown for the polymers TBuC2, TPeC2, and THeC2. This improvement is likely due to the higher reactive surface area of the powdered sodium hydroxide as compared to the more granular form obtained upon hand grinding.[2] The lower DS for THeC1 resulted from the use of 9 rather than 12 molar equivalents of sodium hydroxide and iodohexane.

Figure 1 shows the 300 MHz ^{1}H NMR spectrum for TPeC2. The group of signals between 0.5 and 1.7 ppm can be assigned to most of the pentyl group protons. The signals between 2 and 5 ppm can be assigned to the cellulose backbone protons as well as to the pentyl protons adjacent to the ether linkage. The signals between 6.7 and 8 ppm are assigned to the trityl protons, and the sharp peak at 4.7 ppm is due to HOD present in the solution.

[2]T. Kondo. Personal communication.

TABLE 1. Degrees of substitution and molecular weights for a series of trityl-alkyl cellulose derivatives

Polymer	DS trityl	DS alkyl	Total DS	$\overline{M}_w$ (g/mol)
TBuC1	1.06	1.08	2.14	70 000
TPeC1	1.06	0.87	1.93	189 000
THeC1	1.06	1.21	2.27	166 000
TBuC2	1.03	1.74	2.77	166 000
TPeC2	1.03	1.82	2.85	144 000
THeC2	1.03	1.92	2.95	158 000

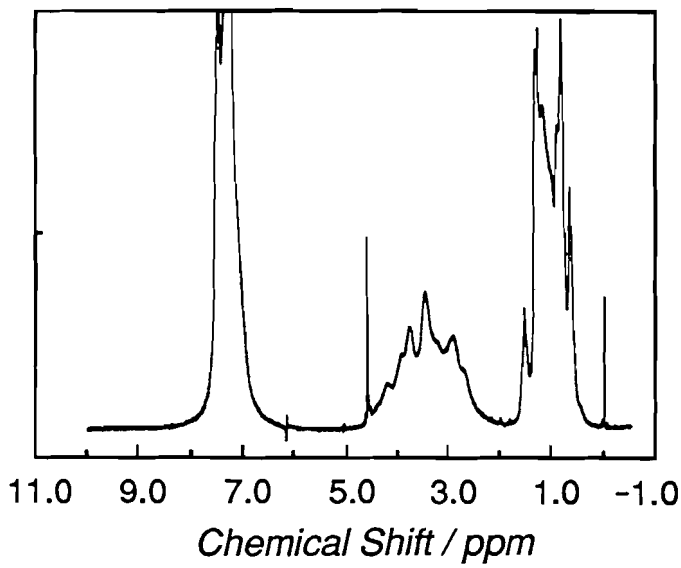

FIG. 1. 300 MHz ^{1}H NMR spectrum of TPeC2.

The NMR results were supported by the FTIR spectra, which showed only very small hydroxyl stretching bands for the polymers with high degrees of substitution. These results indicate that the described procedure is an effective method for alkylating trityl cellulose.

The mass average molar masses, $\overline{M}_w$, for these polymers are listed in Table 1.

Chiroptical properties

Concentrated solutions of the polymers in tetrahydrofuran and chloroform form liquid crystalline phases displaying anisotropy and microscopic textures when observed as thin layers under a polarizing microscope. Several of these mesophases exhibit chiral nematic reflection colours when dissolved in a particular solvent at a specific polymer concentration. The chiroptical properties of one of these polymers, 6-*O*-trityl-2,3-*O*-pentyl cellulose (TPeC1), has already been discussed in a previous paper (8). This polymer was found to form a right-handed chiral nematic structure when dissolved in tetrahydrofuran or chloroform. The reflection band wavelength was found to increase with an increase in temperature and decrease with an increase in the polymer concentration.

The 6-*O*-trityl-2,3-*O*-alkyl cellulose derivatives listed in Table 1 were found to form liquid crystalline phases above polymer concentrations of approximately 36 ± 4 mass percent polymer in tetrahydrofuran and 26 ± 4 mass percent polymer in chloroform.

The optical properties of the liquid crystalline solutions were strongly influenced by the chemical differences between the polymers. Several of these mesophases exhibited chiral nematic

Can. J. Chem. Downloaded from www.nrcresearchpress.com by 88.85.125.76 on 09/07/12
For personal use only.

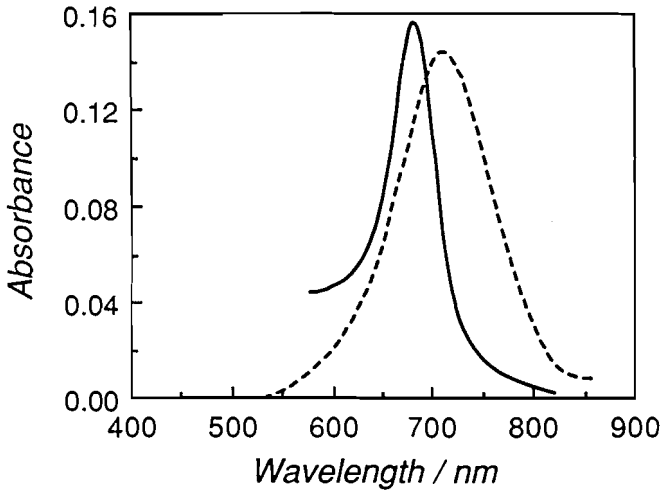

FIG. 2. Apparent absorption spectra of TPeC1/THF (solid line) and THeC2/THF (dashed line) mesophases at polymer concentrations of 51 and 66 mass percent respectively.

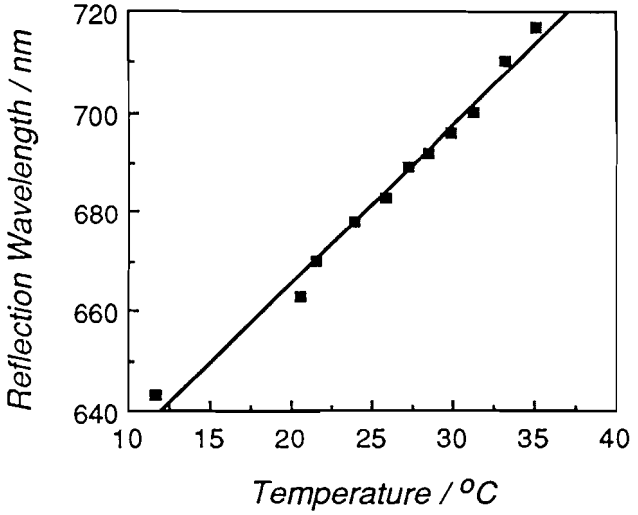

FIG. 3. Reflection wavelength as a function of temperature for a THeC2/THF mesophase at a concentration of 66 mass percent polymer.

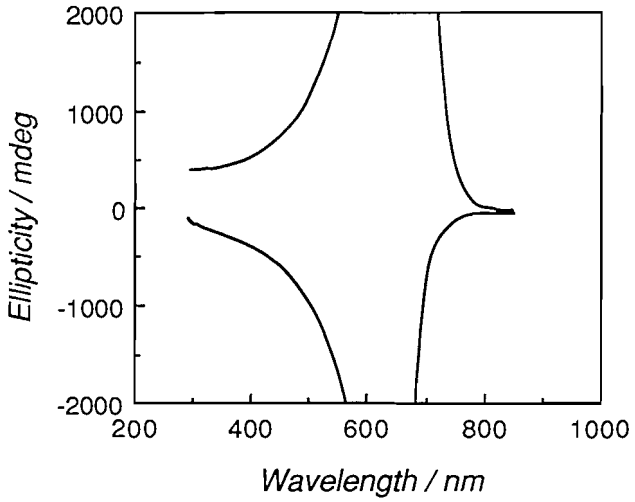

FIG. 4. Apparent circular dichroism spectra for the mesophases THeC2/THF (positive band) and TPeC1/THF (negative band) at concentrations of 66 and 46 mass percent polymer respectively.

reflection colours in tetrahydrofuran or chloroform, whereas others did not. Figure 2 shows the apparent absorbance spectra for mesophases of TPeC1 (solid line) and THeC2 (dashed line) in tetrahydrofuran at concentrations of 51 mass percent polymer and 66 mass percent polymer respectively. The reflection band for the THeC2 mesophase is much broader than the band for the TPeC1 mesophase. This indicates a higher degree of order and more perfect alignment of the chiral nematic axis in the less viscous TPeC1/THF mesophase.

The pitch, P, of the chiral nematic structure is determined from the wavelength of maximum reflectivity, λ_0, according to the relationship $\lambda_0 = \bar{n}P$, where $\bar{n}$ is the average refractive index of the mesophase (12). Due to the volatility of tetrahydrofuran and chloroform, $\bar{n}$ could not be measured accurately and, as a result, only the values of the reflection wavelengths are quoted in this report. The reflection wavelength for the THeC2/THF mesophase increases with an increase in temperature. As shown in Fig. 3, the increase in the reflection wavelength is almost linear with respect to temperature, with a value of 3.2 nm/deg C for $d(\bar{n}P)/dT$. The TPeC1/$CHCl_3$ mesophase exhibits a reflection band that is more sensitive to temperature (8), with a value of 7.2 nm/deg C for $d(\bar{n}P)/dT$.

The reflection wavelength as a function of temperature has also been measured for the mesophases TBzC/$CHBr_3$, TPeC1/$CHCl_3$, THeC2/THF, and TBuC1/$CHCl_3$ and in all of these cases the pitch increased with an increase in the temperature. This is the usual behavior for most cellulose derivatives although some show a decrease in the wavelength with increasing temperature (13), and a reversal of temperature dependence can occur in the two-phase region (14).

The reflection wavelengths for the mesophases TBzC/$CHBr_3$, TPeC1/$CHCl_3$, THeC2/THF, and TBuC1/$CHCl_3$ decrease with an increase in the polymer concentration. Again, this is the usual type of behavior although there have been reports of cellulose derivatives that show an increase in pitch as the polymer concentration is increased (13, 15). A change in the twist sense with a change in polymer concentration has been reported for the mesophase cellulose dicarbanilate/pyridine (13).

The circular reflectivity spectra for the mesophases THeC2/THF and TPeC1/THF, at concentrations of 66 and 46 mass percent polymer respectively, are shown in Fig. 4. The reflection for the TPeC1/THF mesophase shows negative ellipticity indicating that the right-handed component of the circularly polarized light is selectively reflected. The mesophase TPeC1/THF therefore has a right-handed chiral nematic structure. The reflection band for the THeC2/THF mesophase shows positive ellipticity, indicating that the left-handed circularly polarized component is selectively reflected. The mesophase THeC2/THF therefore has a left-handed chiral nematic structure. Table 2 lists the twist sense of the chiral nematic structures for the polymers in Table 1 that exhibit reflection colours in the visible region. The twist sense of the mesophases formed from TBzC (7) are also included in this list.

The difference in the handedness of the mesophases THeC2/THF and TPeC1/THF is another example of a change in the chiral nematic twist sense brought about by a change in the nature of the side groups attached to the cellulose backbone. It has been reported that a change in the handedness of cellulose acetate mesophases occurs when the unsubstituted hydroxyl groups on the polymer are trifluoroacetylated (3). Ethyl cellulose also shows a change in the twist sense when the remaining hydroxyl groups are acetylated (4) or ethylated (16). The twist sense of hydroxypropyl cellulose changes from right-handed to

Can. J. Chem. Downloaded from www.nrcresearchpress.com by 88.85.125.76 on 09/07/12
For personal use only.

TABLE 2. The chiral nematic twist sense for cast films and lyotropic mesophases of some trityl-alkyl cellulose derivatives

Polymer	Twist sense	
	THF	$CHCl_3$
TBuC1	?	R-H[a]
TBuC2	?	R-H[b]
TPeC1	R-H[a,b]	R-H[a,b]
TPeC2	?	R-H[b]
TH3C1	?	R-H[b]
THeC2	L-H[a,b]	R-H[b]
TBzC	R-H[a]	R-H[a]

[a]Lyotropic solution exhibited a chiral nematic reflection band in the visible.

[b]Cast film exhibited a chiral nematic reflection band in the visible region.

R-H: Forms a right-handed mesophase.

L-H: Forms a left-handed mesophase.

?: Handedness not determined due to absence of visible reflection band.

left-handed upon attachment of acetoacetoxy groups to the polymer (17).

The results discussed above clearly indicate that derivatives of trityl cellulose are capable of forming both left- and right-handed chiral nematic mesophases depending on the nature of the side groups at positions two and three of the anhydroglucose units. It is not clear how the substitution of achiral groups onto the cellulose backbone affects the chirality of the chiral nematic mesophases formed by these derivatives. There have been several theoretical explanations for the observations of chiral nematic inversions in poly(γ-benzyl-L-glutamate)(PBLG) liquid crystals that occur with changes in solvent and temperature (18–21). A change in the optical activity of the polymer molecules can result in a change in the chiral nematic twist sense, although this is not a necessary condition for inversion. It has been shown (7, 8) that the phenyl chromophores of trityl cellulose derivatives show optically active electronic transitions in the ultraviolent region of the CD spectrum. This allows an examination of the chiroptical activity of these chromophores in the mesophase and in dilute solution.

The formation of a liquid crystalline phase from dilute solution can change the sign and magnitude of the optical activity observed from the trityl chromophores attached to the cellulose backbone of TPeC1 (8) and TBzC (7). However, it was not known what effect a change in the chiral nematic twist sense would have on this chiroptical activity since these derivatives formed only right-handed chiral nematic structures. It has been observed for lyotropic mesophases of poly(γ-benzyl-L-glutamate)(PBLG) (22), and thermotropic mesophases of poly(γ-benzyl L-glutamate-*co*-γ-dodecyl L-glutamates) (23), that the CD for the phenyl side groups changes sign when a change in the chiral nematic twist sense occurs. The CD spectrum for the phenyl transitions in mesophases of THeC2 (solid line) and TPeC1 (dashed line) in tetrahydrofuran at concentrations of 42 and 49 mass percent polymer, respectively, are shown in Fig. 5. It is apparent that the CD signals from the phenyl chromophores in the left-handed mesophase, THeC2, give a signal that is opposite in sign to the signal from the phenyl chromophores in a right-handed mesophase, TPeC1. It has been observed that all of the trityl cellulose derivatives that form right-handed chiral

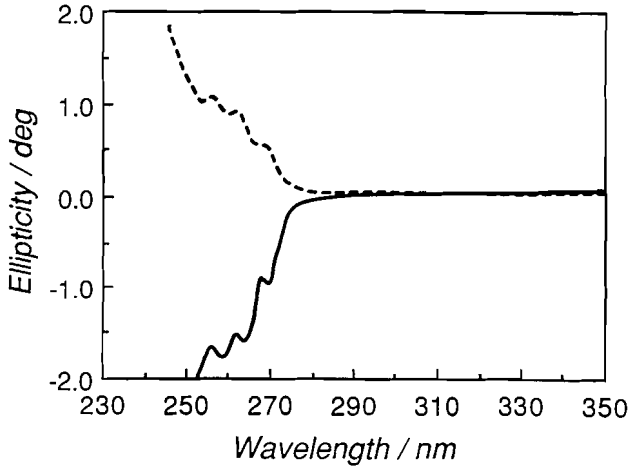

FIG. 5. CD spectra for THeC2/THF (solid line) and TPeC1/THF (dashed line) mesophases at concentrations of 42 and 49 mass percent polymer respectively.

nematic structures also show positive CD signals from the phenyl chromophores when in the mesomorphic state. The mesophase THeC2/THF has a left-handed chiral nematic structure and negative CD signals from the phenyl chromophores. These results suggest that the twist sense of mesophases formed by trityl cellulose derivatives correlates with the sign of the CD bands that arise from the phenyl chromophores in the mesophase.

Interestingly, it was observed that the phenyl CD bands for the THeC2/$CHCl_3$ mesophase were positive, like those observed in the right-handed mesophases. This suggests that there may be a solvent dependent change in the chiral nematic twist sense from left-handed in tetrahydrofuran to right-handed in chloroform. Unfortunately, the THeC2/$CHCl_3$ mesophase did not exhibit chiral nematic reflection colours in the lyotropic state, but reflection colours observed from thin films of THeC2, cast from chloroform, indicate that the frozen-in chiral nematic structure has a right-handed twist sense. This does not prove conclusively that the mesophase of THeC2/$CHCl_3$ is right-handed as it has been reported that the sign of CD peaks from chiral nematic reflection bands in cast films can be sensitive to residual linear orientation (24). If linear effects are present, then a rotation of the sample in the incident beam would be expected to alter the sign and magnitude of the reflection band. Rotation of the film sample by 90° in a direction orthogonal to the incident beam did not result in a change in the sign of the circular reflectivity band, and only a small change in the magnitude of the signal was observed. These results strongly indicate that there is in fact a solvent-dependent twist sense for mesophases of THeC2, which may be related to a difference in the conformation of this polymer in the two solvents.

In dilute solution, trityl cellulose derivatives show circular dichroism as a result of the chiral interaction between the phenyl chromophores and the cellulose backbone. If a change in polymer conformation is responsible for the change in twist sense, then this may be reflected in the dilute solution optical activity from the phenyl chromophores of THeC2 and TPeC1 in THF.

Figure 6 shows the dilute solution CD spectra for TPeC1 (solid line) and THeC2 (dashed line) in tetrahydrofuran. There are two phenyl electronic transitions that give rise to the CD bands in the region 210–280 nm. The ^1L_b transition exhibits negative ellipticity and characteristic fine structure with a maximum around 261 nm. The ^1L_a transition with its maximum

Can. J. Chem. Downloaded from www.nrcresearchpress.com by 88.85.125.76 on 09/07/12
For personal use only.

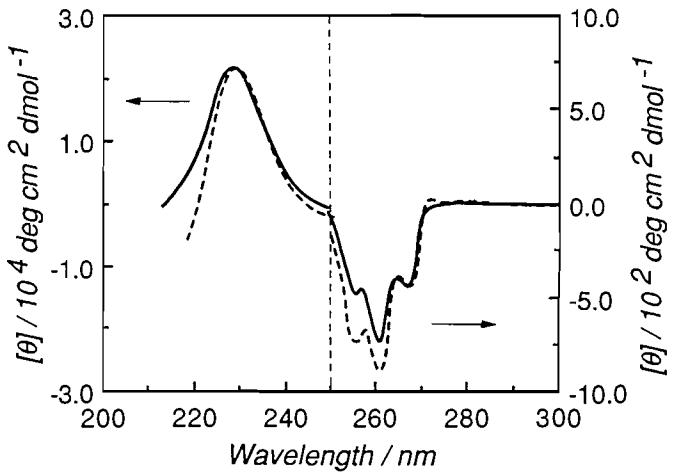

FIG. 6. Dilute solution CD spectra for TPeC1 (solid line) and THeC2 (dashed line) in tetrahydrofuran.

around 228 nm shows positive ellipticity. A comparison of the two spectra reveals that there are no changes in the signs of the CD bands, with the bands showing almost identical molar ellipticities. The similarity between the two spectra does not indicate a difference in the conformation of the trityl chromophores relative to the cellulose backbone for the two polymers. This result does not preclude the possibility that there are conformational differences in other regions of the polymer, such as the glycosidic linkage, that are responsible for the difference in the chirality of the liquid crystalline helicoidal structures. Since there does not appear to be a helical contribution to the dilute solution optical activity, as evidenced by the absence of exciton splitting of the bands, it is difficult to determine whether there is a difference in the conformation of the glycosidic linkages.

It is apparent from Fig. 6 that the dilute solution optical activity does not provide a basis for predicting the twist sense of the chiral nematic phases formed from THeC2 and TPeC1 in THF. The dilute solution CD spectra of THeC2 in chloroform and THF were identical, giving no indication of why the chiral nematic twist sense of this polymer is solvent dependent. It can be concluded that the difference in chiral nematic twist sense does not appear to be the result of a conformational change in the trityl group, although it is possible that the difference may be the result of other conformational changes in the polymer that are not reflected in the optical activity of the phenyl chromophores.

It was noted earlier that the formation of a chiral nematic mesophase from trityl-alkyl cellulose derivatives can alter dramatically the sign and magnitude of the CD signals from the phenyl chromophores. This is evident when comparing the dilute solution spectra in Fig. 6 with the spectra obtained in the mesophase (Fig. 5). The changes in the spectra due to mesophase formation may result from a tertiary helicoidal arrangement of chromophores enforced by the chiral nematic structure (11). Alternatively, the change in the sign and magnitude of the CD signal may be an artifact that results when CD measurements are made on a sample that is also linearly dichroic and linearly and circularly birefringent (25).

Conclusion

Several new specifically substituted trityl-alkyl cellulose derivatives with high degrees of alkyl substitution have been prepared by reacting trityl cellulose, dissolved in DMSO, with powdered sodium hydroxide and an alkyl iodide. These cellulose derivatives form chiral nematic mesophases with a right- or left-handed twist sense depending on the nature of the side-group substitution and the solvent. Dilute solution optical activity from the trityl group phenyl chromophores did not change when different alkyl groups were attached to the trityl cellulose backbone. Differences in the optical activity of the phenyl groups were observed in mesophases with opposite twist sense. Whether this indicates a molecular factor responsible for the twist sense of the mesophase or simply reflects the chirality of the chiral nematic phase is not yet clear.

Acknowledgements

We thank the Natural Sciences and Engineering Research Council of Canada for support; B.R.H. thanks Domtar Inc. for a G.S. Thomlinson II graduate fellowship.

1. R. S. WERBOWYJ and D. G. GRAY. Mol. Cryst. Liq. Cryst. **34**, 97 (1976).
2. P. ZUGENMAIER and P. HAURAND. Carbohydr. Res. **160**, 369 (1987).
3. A. M. RITCEY, K. R. HOLME, and D. G. GRAY. Macromolecules, **21**, 2914 (1988).
4. J. X. GUO and D. G. GRAY. Macromolecules, **22**, 2086 (1989).
5. M. SIEKMEYER and P. ZUGENMAIER. Makromol. Chem. Rapid Commun. **8**, 511 (1987).
6. T. YAMAGISHI, T. FUKUDA, T. MIYAMOTO, and J. WATANABE. *In* Cellulose structural and functional aspects. *Edited by* J. F. Kennedy, G. O. Phillips, and P. A. Williams. Ellis Horwood, Chichester. 1990. p. 391.
7. B. R. HARKNESS and D. G. GRAY. Macromolecules, **23**, 1452 (1990).
8. B. R. HARKNESS and D. G. GRAY. Liq. Cryst. In press.
9. W. N. HEARON, G. D. HIATT, and C. R. FORDYCE. J. Am. Chem. Soc. **65**, 2449 (1943).
10. A. ISOGAI, A. ISHIZU, and J. NAKANO. J. Appl. Polym. Sci. **31**, 341 (1986).
11. F. D. SAEVA. *In* Liquid crystals. *Edited by* F. D. Saeva. Marcel Dekker, New York. 1979. p. 249.
12. H. L. DEVRIES. Acta. Crystallogr. **4**, 219 (1951).
13. U. VOGT and P. ZUGENMAIER. Ber. Bunsen-ges. Phys. Chem. **89**, 1217 (1985).
14. S. FORTIN and G. CHARLET. Macromolecules, **22**, 2286 (1989).
15. H. STEINMAIER and P. ZUGENMAIER. Carbohydr. Res. **173**, 75 (1988).
16. D. R. BUDGELL. Ph.D. thesis, McGill University, 1989.
17. W. P. PAWLOWSKI, R. D. GILBERT, R. E. FORNES, and S. T. PURRINGTON. J. Polym. Sci. Polym. Phys. **25**, 2293 (1987).
18. T. V. SAMULSKI and E. T. SAMULSKI. J. Chem. Phys. **67**, 824 (1977).
19. K. CZARNIECKA and E. T. SAMULSKI. Mol. Cryst. Liq. Cryst. **63**, 205 (1981).
20. H. KIRMURA, M. HOSINO, and H. NAKANO. J. Phys. Soc. Jpn. 1584 (1982).
21. M. A. OSIPOV. Chem. Phys. **96**, 259 (1985).
22. I. UEMATSU and Y. UEMATSU. Adv. Polym. Sci. **59**, 37 (1984).
23. J. WATANABE and T. NAGASE. Macromolecules, **21**, 171 (1988).
24. A. M. RITCEY, G. CHARLET, and D. G. GRAY. Can. J. Chem. **66**, 2229 (1988).
25. Y. SHINDO and Y. OHMI. J. Am. Chem. Soc. **107**, 91 (1985).

Can. J. Chem. Downloaded from www.nrcresearchpress.com by 88.85.125.76 on 09/07/12
For personal use only.

Complexes of carbohydrates with metal cations. XVI.[1] Di-D-fructose and di-L-sorbose dianhydrides

STEPHEN JOHN ANGYAL AND DONALD CHADWICK CRAIG
School of Chemistry, University of New South Wales, Kensington, N.S.W. 2033, Australia
AND
JACQUES DEFAYE AND ANDRÉE GADELLE[2]
Laboratoires de chimie, Département de recherche fondamentale, Centre d'études nucléaires de Grenoble, 85 X, 38041 Grenoble, France
Received November 30, 1989
This paper is dedicated to Professor Arthur S. Perlin on the occasion of his 67th birthday

STEPHEN JOHN ANGYAL, DONALD CHADWICK CRAIG, JACQUES DEFAYE, and ANDRÉE GADELLE. Can. J. Chem. **68**, 1140 (1990).

Di-D-fructose 2′,1:2,1′-dianhydrides form complexes with metal cations if the two anomeric carbon atoms have the same configuration. Such anomers have the central 1,4-dioxane ring in a flexible form; complex formation involves O-1, O-1′, O-3, and O-3′, as confirmed by the X-ray crystal structure of the strontium complex of the β,β-dipyranose anomer. The α,β-anomers, and dianhydrides containing only furanose rings, do not form such complexes.
Key words: difructose dianhydrides, complex formation with cations, crystal structure of complex, chromatographic separation on ion-exchange resins.

STEPHEN JOHN ANGYAL, DONALD CHADWICK CRAIG, JACQUES DEFAYE et ANDRÉE GADELLE. Can. J. Chem. **68**, 1140 (1990).

Les 2′,1:2,1′-dianhydrides du di-D-fructose forment des complexes avec les cations métalliques si les deux atomes de carbone anomériques possèdent la même configuration. Dans de tels anomères, le cycle 1,4-dioxane central existe dans une conformation flexible; comme il a été établie par diffraction des rayons-X sur le complexe de strontium de l'anomère β,β-dipyranose, la formation de complexe implique les atomes O-1, O-1′, O-3 et O-3′. Les anomères α,β ainsi que les dianhydrides ne contenant que des cycles furanoses ne forment pas de tels complexes.
Mots clés : dianhydrides du difructose, formation de complexes avec les cations, structure cristalline du complexe, séparation par chromatographie sur des résines échangeuses d'ions.

[Traduit par la revue]

Introduction

The reaction of D-fructose or inulin with strong aqueous acids or with anhydrous hydrogen fluoride yields a mixture of difructose dianhydrides of which nine diastereomers have been isolated and characterized (2–5). To separate them, chromatographic methods are employed; five of the anhydrides have been separated from each other by reverse-phase high-performance liquid chromatography (HPLC) (6). It seemed desirable to ascertain whether chromatography on cation-exchange resins in the calcium form (7) would be suitable for their separation. In principle, this method does not seem to offer much promise because fructosides do not form strong complexes with cations (8): fructofuranosides do not complex, α-fructopyranosides form only very weak complexes at O-4–O-5, and β-fructopyranosides weak ones at O-4–O-5 and O-2–O-3. However, complexing involving hydroxyl groups of both fructose moieties may be favourable (9); in fact, it was found that one isomer, di-β-D-fructopyranose 2′,1:2,1′-dianhydride (**1**), complexes quite strongly. In this paper we describe the structure of this complex.

Results and discussion

Six of the dianhydrides have the 2′,1:2,1′ structure, that is, the anomeric carbon atom of each fructose moiety is linked to O-1 of the other one. (We shall use abbreviated names for them, for example, αF,βP for α-D-fructofuranose β-D-fructopyranose dianhydride.) The complexing ability of these six di-D-fructose 2′,1:2,1′-dianhydrides was compared by running them on TLC plates of cation-exchange resins in the calcium form (8). The R_f values are shown in Table 1. The same order was found for the retention times of these anhydrides on a "Sugar PAK 1" (Waters) HPLC column (an ion-exchange column in the Ca^{2+} form) (Table 1), confirming again that the HPLC separation on such a column is due to complex formation with the cation (9). It appears that all but the first two anhydrides could be separated from each other on a preparative ion-exchange column (7).

TABLE 1. TLC mobilities (R_f) and HPLC retention times (min) of di-fructose and di-sorbose 2′,1:2,1′-dianhydrides

Dianhydrides	R_f	Retention times (min)
αF,βF D-fructose	0.87	3.8
βF,βF D-fructose	0.86	3.8
αF,βP D-fructose	0.83	4.5
αP,βP D-fructose	0.78	4.8
βF,βP D-fructose	0.76	
βP,βP D-fructose	0.55	7.9
αP,βP L-sorbose	0.85	
αP,αP L-sorbose	0.70	7.7
αP,αP DL-sorbose		4.1

Table 1 shows that anhydrides with only furanose rings do not form complexes; those with one or two pyranose rings complex weakly; but one anhydride, the βP,βP isomer (**1**), complexes well, being strongly retained on the TLC plate and on the HPLC column. This strong complexing must be due to the involvement of oxygen atoms from both fructose moieties; its occurrence with just one isomer must be due to conformational factors.

In all of these anhydrides, the two fructose moieties are connected by a 1,4-dioxane ring. When C-2 and C-2′ have differing configurations, the dioxane ring, in its chair form, has

[1]For part XV, see ref. 1.
[2]Équipe CNRS SDI 5509.

Printed in Canada / Imprimé au Canada

Can. J. Chem. Downloaded from www.nrcresearchpress.com by 88.85.125.76 on 09/07/12
For personal use only.

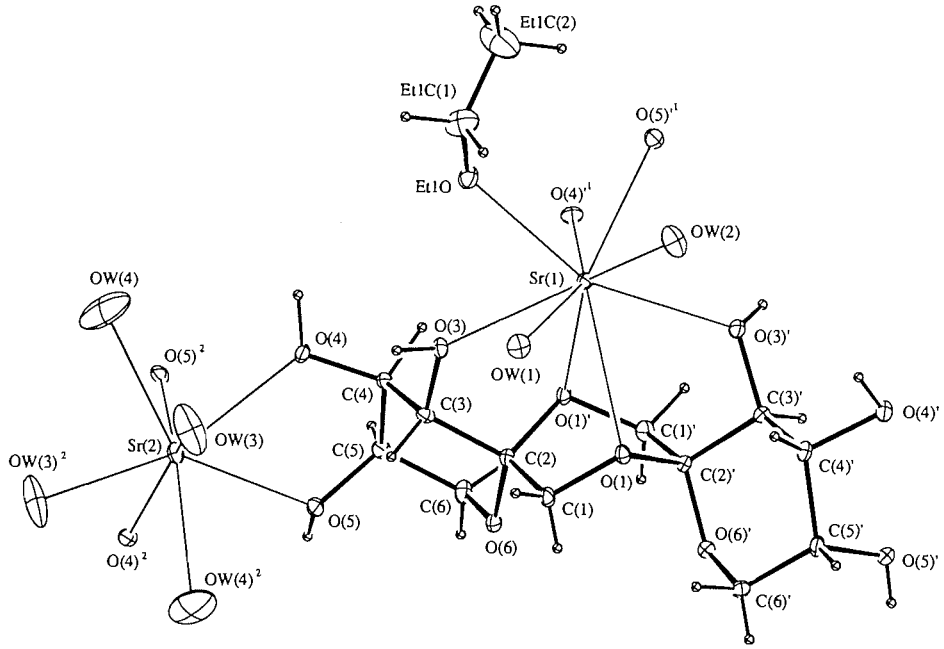

FIG. 1. ORTEP plot of the strontium complex of di-β-D-fructopyranose 2′,1:2,1′-dianhydride, showing the atomic numbering scheme. The coordination of O(4)′ and O(5)′ to another strontium ion is not shown.

O-6 and O-6′ in axial disposition and C-3 and C-3′ in equatorial positions; a stable arrangement. An example is the αP,βP isomer (**2**), the conformation of which has been determined by X-ray crystallography (2). However, if the configurations of C-2 and C-2′ are the same, the dioxane ring in its chair form would have an axial carbon and an equatorial oxygen atom attached to it: an unfavourable arrangement. This is the case with the βP,βP isomer (**3**). Pedersen and co-workers (10) have shown that, in the crystal as well as in solution, this compound is found with the dioxane ring in a boat form, not only owing to the anomeric effect related to the 1,4-dioxane ring but also to the exo-anomeric effect related to the fructose moieties.

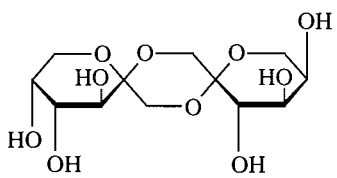

1

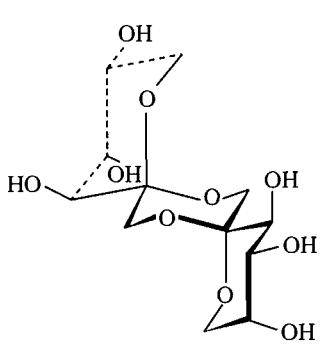

2

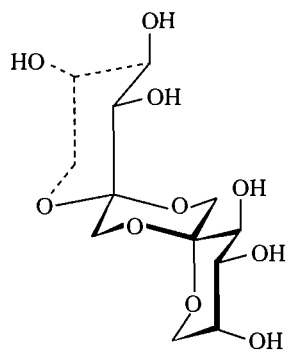

3

When the dioxane ring is in a chair form it is not possible for both of its oxygen atoms to be coordinated to the same cation. This is, however, possible in the skew or boat forms; moreover, both O-3 and O-3′ can be close to both ring oxygen atoms. It was therefore postulated that the complex formation of **1** is tetradentate and involves O-1, O-1′, O-3, and O-3′. In the βF,βP isomer, O-3 of the furanose ring cannot come close to O-1, although the dioxane ring must be in a flexible form here too; hence only tridentate complexing is possible, which is weaker (R_f 0.76). In the difuranose (βF,βF), both O-3 and O-3′ are unfavourably located for complex formation; hence complex formation is negligible.

Similar considerations apply to the di-L-sorbose dianhydrides (11). In the αP,αP isomer, the two anomeric centres have the same configuration; the compound differs from the βP,βP isomer of di-D-fructose dianhydride (**1**) only in the configuration of C-5 and C-5′. It complexes well with calcium ions, the R_f value being 0.70, only slightly higher than that of **1**. The difference is accounted for by the lack of *cis* hydroxyl groups on C-4 and C-5. By contrast, the αP,βP isomer of L-sorbose has R_f 0.85, indicating the absence of complex formation. Similarly, the mixed anhydride α-D-sorbopyranose α-L-sorbopyranose dianhydride (10) has two anomeric centres of differing configuration (α-D and α-L) and does not form a complex. It is so insoluble in water that it is not detected on the TLC plate but it emerges from the HPLC column after 4.1 min, compared with 7.7 min for the α-D, α-D isomer. The mixed anhydride β-D-fructopyranose α-L-sorbopyranose 2′,1:2,1′-dianhydride[3] has two anomeric centres of the same configuration (β-D and α-L); it also complexes well (R_f 0.65).

To prove the suggested location of the complexing site, we investigated the shifts caused by lanthanide ions in the ^{1}H NMR spectra (12). Addition of europium salts caused a small upfield shift of all of the signals in the spectrum of the βP,βP isomer; however, praseodymium salts shifted only the signal of H 3,3′

[3]Provided by Dr. C. Pedersen; preparation not yet published.

Can. J. Chem. Downloaded from www.nrcresearchpress.com by 88.85.125.76 on 09/07/12
For personal use only.

Can. J. Chem. Downloaded from www.nrcresearchpress.com by 88.85.125.76 on 09/07/12
For personal use only.

TABLE 2. Non-hydrogen positional coordinates; esd in parentheses

Atom	x	y	z	Atom	x	y	z
Sr(1)	0.3052(1)	0.2374(1)	0.2140(1)	C(5)	0.1407(5)	0.0407(3)	0.0557(10)
Sr(2)	0.0000	0.0000	0.3955(1)	C(6)	0.2405(6)	0.0413(3)	−0.0262(11)
Cl(1)	0.4490(1)	0.3051(1)	−0.2940(3)	C(1)′	0.3971(6)	0.1445(3)	−0.0626(10)
Cl(2)	0.8822(2)	0.0797(1)	0.8771(3)	C(2)′	0.4907(5)	0.1581(3)	0.0385(9)
Cl(3)	0.1700(2)	0.1580(1)	0.6698(3)	C(3)′	0.5357(5)	0.2108(3)	−0.0014(9)
O(1)	0.4598(3)	0.1600(2)	0.2000(6)	C(4)′	0.6329(5)	0.2223(3)	0.0893(9)
O(3)	0.2109(4)	0.1548(2)	0.3101(6)	C(5)′	0.7075(5)	0.1766(3)	0.0809(10)
O(4)	0.0395(3)	0.0851(2)	0.2494(6)	C(6)′	0.6558(6)	0.1256(3)	0.1051(11)
O(5)	0.1328(4)	−0.0018(2)	0.1659(6)	OW(1)	0.3518(5)	0.2159(2)	0.5030(7)
O(6)	0.3237(4)	0.0528(2)	0.0774(7)	OW(2)	0.4123(6)	0.3121(2)	0.3315(8)
O(1)′	0.3077(4)	0.1426(2)	0.0345(6)	OW(3)	0.0645(9)	0.0515(4)	0.6295(11)
O(3)′	0.4591(4)	0.2495(2)	0.0275(6)	OW(4)	−0.1479(10)	0.0588(6)	0.4958(14)
O(4)′	0.6809(4)	0.2679(2)	0.0276(6)	OW(5)	0.6631(14)	0.0224(4)	0.3698(22)
O(5)′	0.7514(4)	0.1789(2)	−0.0713(7)	Et1O	0.1447(4)	0.2638(2)	0.3622(7)
O(6)′	0.5656(4)	0.1188(2)	0.0134(7)	Et1C(1)	0.1296(10)	0.3042(5)	0.4664(15)
C(1)	0.4131(5)	0.1119(3)	0.2431(10)	Et1C(2)	0.1040(16)	0.3551(5)	0.4100(17)
C(2)	0.3151(5)	0.1023(2)	0.1476(9)	Et2O	0.5000	0.0000	0.5456(42)
C(3)	0.2195(5)	0.1039(2)	0.2429(9)	Et2C(1)	0.5790(65)	−0.0067(33)	0.6538(99)
C(4)	0.1245(5)	0.0911(3)	0.1471(9)	Et2C(2)	0.5000	0.0000	0.7644(56)

TABLE 3. Bond distances; esd in parentheses*

Bond	Length (Å)	Bond	Length (Å)
Sr(1)—O(1)	2.847(5)	C(2)′—O(1)	1.447(9)
Sr(1)—O(3)	2.596(4)	O(1)—C(1)	1.431(8)
Sr(1)—O(1)′	2.889(5)	C(2)—C(3)	1.500(10)
Sr(1)—O(3)′	2.598(5)	C(3)—C(4)	1.531(10)
Sr(1)—OW(1)	2.618(6)	C(4)—C(5)	1.531(10)
Sr(1)—OW(2)	2.589(6)	C(5)—C(6)	1.488(11)
Sr(1)—Et1O	2.554(5)	C(6)—O(6)	1.441(10)
Sr(1)—O(4)′[a]	2.645(5)	O(6)—C(2)	1.413(8)
Sr(1)—O(5)′[a]	2.578(5)	C(3)—O(3)	1.437(8)
Sr(2)—O(4)	2.580(5)	C(4)—O(4)	1.429(9)
Sr(2)—O(5)	2.635(5)	C(5)—O(5)	1.453(9)
Sr(2)—OW(3)	2.553(8)	C(2)′—C(3)′	1.518(9)
Sr(2)—OW(4)	2.610(10)	C(3)′—C(4)′	1.525(10)
Sr(2)—O(4)[b]	2.580(5)	C(4)′—C(5)′	1.532(10)
Sr(2)—O(5)[b]	2.635(5)	C(5)′—C(6)′	1.494(11)
Sr(2)—OW(3)[b]	2.553(8)	C(6)′—O(6)′	1.434(9)
Sr(2)—OW(4)[b]	2.610(10)	O(6)′—C(2)′	1.428(8)
C(1)—C(2)	1.547(10)	C(3)′—O(3)′	1.439(8)
C(2)—O(1)′	1.426(8)	C(4)′—O(4)′	1.435(8)
O(1)′—C(1)′	1.440(9)	C(5)′—O(5)′	1.431(9)
C(1)′—C(2)′	1.546(11)		

*Superscripts refer to the symmetry transformations:
[a] $x - 1/2, 1/2 - y, -z$.
[b] $-x, -y, z$.

TABLE 4. Selected bond angles; esd in parentheses

Bonds	Angle (°)	Bonds	Angle (°)
C(1)—O(1)—C(2)′	109.8(6)	C(4)—C(5)—C(6)	110.9(6)
C(2)—O(6)—C(6)	112.9(5)	O(6)—C(6)—C(5)	112.2(6)
C(2)—O(1)′—C(1)′	111.4(5)	O(1)′—C(1)′—C(2)′	109.3(6)
C(2)′—O(6)′—C(6)′	113.5(6)	O(1)—C(2)′—O(6)′	111.3(6)
O(1)—C(1)—C(2)	111.0(6)	O(1)—C(2)′—C(1)′	108.9(6)
O(6)—C(2)—O(1)′	111.7(6)	O(1)—C(2)′—C(3)′	107.2(6)
O(6)—C(2)—C(1)	107.8(6)	O(6)′—C(2)′—C(1)′	107.6(6)
O(6)—C(2)—C(3)	109.0(5)	O(6)′—C(2)′—C(3)′	109.3(5)
O(1)′—C(2)—C(1)	107.5(5)	C(1)′—C(2)′—C(3)′	112.6(6)
O(1)′—C(2)—C(3)	107.1(5)	O(3)′—C(3)′—C(2)′	108.0(5)
C(1)—C(2)—C(3)	113.7(6)	O(3)′—C(3)′—C(4)′	111.2(6)
O(3)—C(3)—C(2)	108.2(5)	C(2)′—C(3)′—C(4)′	112.6(6)
O(3)—C(3)—C(4)	110.5(5)	O(4)′—C(4)′—C(3)′	109.8(6)
C(2)—C(3)—C(4)	112.4(6)	O(4)′—C(4)′—C(5)′	109.3(5)
O(4)—C(4)—C(3)	109.2(6)	C(3)′—C(4)′—C(5)′	111.2(6)
O(4)—C(4)—C(5)	109.5(5)	O(5)′—C(5)′—C(4)′	105.6(6)
C(3)—C(4)—C(5)	110.3(6)	O(5)′—C(5)′—C(6)′	110.3(7)
O(5)—C(5)—C(4)	107.1(6)	C(4)′—C(5)′—C(6)′	112.2(6)
O(5)—C(5)—C(6)	112.3(6)	O(6)′—C(6)′—C(5)′	114.0(6)

upfield, the other signals moving only slightly. The correlation between lanthanide-induced shifts and structure has only been studied (12) for tridentate complexes. The interpretation in case of tetradentate complexing is uncertain; all that can be safely concluded is that O-3 and O-3′ are involved in complex formation.

To establish the nature of complex formation, an X-ray crystal analysis of a complex was carried out. Suitable crystals were obtained of a complex of the βP,βP isomer with strontium chloride containing three strontium cations for two anhydride molecules. The structure is discussed in the next section. Two strontium ions were found to be coordinated, indeed, to O-1, O-1′, O-3, and O-3′ of the dianhydride, making it very probable that the same coordination would occur in solution too. The third strontium ion is coordinated only to O-4 and O-5 of two molecules; such bidentate complexing is, by past experience (9), not likely to persist in solution to any extent.

There are three known D-fructose dianhydrides that have, not the 2′,1:2,1′-, but the 2′,1:2,3′- structure. In these, there are no hydroxyl groups suitably placed for tetradentate complexing even when the 1,4-dioxane ring is in a flexible form, and they do not form complexes with cations: β-D-fructofuranose β-D-fructopyranose 2′,1:2,3′-dianhydride (2) and α-D-fructofuranose β-D-fructofuranose 2′,1:2,3′-dianhydride (4) both have R_f values of 0.85.

Crystal structure

The crystals investigated contain 1.5 strontium and 3 chloride ions for each anhydride molecule, and include water and ethanol of crystallization. Figure 1 shows a view of the complex with the

TABLE 5. Selected torsional angles; esd in parentheses

Bonds	Angle (°)	Bonds	Angle (°)
C(2)′—O(1)—C(1)—C(2)	−62.8(7)	C(2)—C(3)—C(4)—O(4)	170.7(5)
O(6)′—C(2)′—O(1)—C(1)	−62.6(7)	C(2)—C(3)—C(4)—C(5)	50.3(8)
C(1)′—C(2)′—O(1)—C(1)	55.8(7)	O(4)—C(4)—C(5)—O(5)	−45.1(7)
C(3)′—C(2)′—O(1)—C(1)	177.9(5)	O(4)—C(4)—C(5)—C(6)	−167.9(6)
C(6)—O(6)—C(2)—O(1)′	−56.9(7)	C(3)—C(4)—C(5)—O(5)	75.1(7)
C(6)—O(6)—C(2)—C(1)	−174.8(6)	C(3)—C(4)—C(5)—C(6)	−47.8(9)
C(6)—O(6)—C(2)—C(3)	61.3(7)	O(5)—C(5)—C(6)—O(6)	−66.8(8)
C(5)—C(6)—O(6)—C(2)	−61.3(8)	C(4)—C(5)—C(6)—O(6)	53.0(9)
O(6)—C(2)—O(1)′—C(1)′	−61.2(7)	O(1)′—C(1)′—C(2)′—O(1)	4.9(8)
C(1)—C(2)—O(1)′—C(1)′	56.9(7)	O(1)′—C(1)′—C(2)′—O(6)′	125.6(6)
C(3)—C(2)—O(1)′—C(1)′	179.4(5)	O(1)′—C(1)′—C(2)′—C(3)′	−113.8(7)
C(2)—O(1)′—C(1)′—C(2)′	−63.5(7)	O(1)—C(2)′—C(3)′—O(3)′	−58.3(7)
C(6)′—O(6)′—C(2)′—O(1)	−58.7(8)	O(1)—C(2)′—C(3)′—C(4)′	64.8(7)
C(6)′—O(6)′—C(2)′—C(1)′	−177.8(6)	O(6)′—C(2)′—C(3)′—O(3)′	−179.1(6)
C(6)′—O(6)′—C(2)′—C(3)′	59.6(8)	O(6)′—C(2)′—C(3)′—C(4)′	−55.9(8)
C(5)′—C(6)′—O(6)′—C(2)′	−57.3(9)	C(1)′—C(2)′—C(3)′—O(3)′	61.4(8)
O(1)—C(1)—C(2)—O(6)	126.2(6)	C(1)′—C(2)′—C(3)′—C(4)′	−175.5(6)
O(1)—C(1)—C(2)—O(1)′	5.6(8)	O(3)′—C(3)′—C(4)′—O(4)′	−68.6(7)
O(1)—C(1)—C(2)—C(3)	−112.8(7)	O(3)′—C(3)′—C(4)′—C(5)′	170.3(6)
O(6)—C(2)—C(3)—O(3)	−178.6(5)	C(2)′—C(3)′—C(4)′—O(4)′	170.1(6)
O(6)—C(2)—C(3)—C(4)	−56.3(7)	C(2)′—C(3)′—C(4)′—C(5)′	49.0(8)
O(1)′—C(2)—C(3)—O(3)	−57.5(7)	O(4)′—C(4)′—C(5)′—O(5)′	−45.5(8)
O(1)′—C(2)—C(3)—C(4)	64.8(7)	O(4)′—C(4)′—C(5)′—C(6)′	−165.7(7)
C(1)—C(2)—C(3)—O(3)	61.1(7)	C(3)′—C(4)′—C(5)′—O(5)′	75.8(7)
C(1)—C(2)—C(3)—C(4)	−176.6(6)	C(3)′—C(4)′—C(5)′—C(6)′	−44.3(9)
O(3)—C(3)—C(4)—O(4)	−68.3(7)	O(5)′—C(5)′—C(6)′—O(6)′	−69.1(8)
O(3)—C(3)—C(4)—C(5)	171.3(6)	C(4)′—C(5)′—C(6)′—O(6)′	48.3(9)

Can. J. Chem. Downloaded from www.nrcresearchpress.com by 88.85.125.76 on 09/07/12
For personal use only.

atomic numbering scheme.[4] The positional coordinates of the atoms (other than hydrogen) are shown in Table 2, bond distances in Table 3, selected bond angles in Table 4, and selected torsional angles in Table 5. The crystal structure is complex and shows several interesting features. Every oxygen atom of the anhydride is coordinated to a cation, except O-6 and O-6′. There are two different locations for the three strontium ions. Two are in ninefold coordination to O-1, O-1′, O-3, and O-3′ of one anhydride, O-4′ and O-5′ of another anhydride molecule, two water molecules, and one ethanol molecule. The third strontium cation, which lies on a crystallographic twofold axis, is in eightfold coordination: it bridges two anhydrides, being attached only to O-4 and O-5 of the two anhydrides, in addition to four water molecules. The coordination polyhedra are of irregular shapes. The Sr—O-1 and Sr—O-1′ distances are longer than the average Sr—O distances; these two oxygen atoms are bonded to two carbon atoms each and hence appear to form weaker coordination bonds than the others.

The conformation of the dianhydride in the strontium complex is remarkably similar to that of the uncomplexed βP,βP isomer of which the structure has been determined (10) but not yet published;[5] however, Dr. Pedersen kindly sent us his results. The 1,4-dioxane ring is also in the $^{O,O}B$ boat form; O-3 and O-3′ are in positions where they can coordiante to Sr^{2+} ions with the usual Sr—O distance. That is, the site for fourfold coordination is present in the molecule in its preponderant conformation and no change of conformation occurs when the complex is formed.

Experimental

α-D-Fructofuranose β-D-fructofuranose 2′,1:2,3′-dianhydride was a gift from Dr. Takao Uchiyama; the other dianhydrides were prepared as described (2, 3, 11). TLC was carried out on ion-exchange plates (Polygram Ionex-25 SA, from Macherey–Nagel GmbH, 5160 Düren, Germany) at ambient temperature (8), HPLC on a Sugar PAK 1 column (Waters) at 93°C. NMR spectra were recorded with a Bruker AM-500 spectrometer.

Lanthanide-induced shifts

^{1}H NMR data for β-D-fructopyranose β-D-fructopyranose 2′,1:2,1′-dianhydride: δ (D_2O): 3.80 (m, $J_{4,5}$ 3.5, $J_{5,6eq}$ 1.2, $J_{5,6ax}$ 2.0 Hz, H-5), 3.78 (d), $J_{1,1'}$ −12.5 Hz, H-1), 3.76 (dd, $J_{6eq,6ax}$ −12.5 Hz, H-6_{eq}), 3.72 (dd, $J_{3,4}$ 10.0 Hz, H-4), 3.52 (dd, H-6_{ax}), 3.51 (d, H-3), 3.47 (d, H-1′). The data shown for this isomer in ref. 2 are, erroneously, those for the αP,βP isomer. Addition of 0.01 equiv. of $PrCl_3$ caused the following induced shifts: H-1, −0.03; H-1′, −0.05; H-3, −0.21; H-4, −0.02; H-5, −0.01; H-6, 0.02; H-6′, −0.02.

Preparation of the crystalline strontium complex

The βP,βP isomer readily forms crystalline 1:1 complexes with

[4]Tables of atomic parameters with standard deviations, interatomic distances, interatomic angles, and rotational angles may be purchased from the Depository of Unpublished Data, CISTI, National Research Council of Canada, Ottawa, Ont., Canada K1A 0S2.

Tables of atomic parameters, interatomic distances and angles have also been deposited with the Cambridge Crystallographic Data Centre, and can be obtained on request from The Director, Cambridge Crystallographic Data Centre, University Chemical Laboratory, Lensfield Road, Cambridge CB2 1EW, U.K.

[5]NOTE ADDED IN PROOF: Described by J. A. Kanters, A. Schouten, J. Kroon, M. Mathloutli, J. H. van der Maas, and B. Lutz. Acta Crystallogr. Sect. C: Cryst. Struct. Commun. **C45**, 1934 (1989).

$CaCl_2$, $SrCl_2$, $BaCl_2$, or $LaCl_3$ when ethanol is added in small aliquots to a concentrated aqueous solution of an equimolecular mixture of the salt and the dianhydride; for example, Anal. calcd. for $C_{12}H_{20}O_{10}\cdot CaCl_2\cdot 2H_2O$: C 30.38, H 5.06, Ca 9.07, Cl 14.98; found: C 30.46, 30.35; H 5.35, 5.59, Ca 8.05, 8.13; Cl 15.36, 15.08. These 1:1 complexes form very thin long needles, unsuitable for X-ray crystal analysis.

When a large excess of $SrCl_2$ was used, the thin needles appeared readily but, on standing in solution, gradually changed into stout prisms. When this change was complete, the crystals were collected: they proved to be 2:3 complexes, suitable for X-ray analysis.

Crystal data

$C_{12}H_{20}O_{10}\cdot(SrCl_2)_{1.5}\cdot(H_2O)_5\cdot(C_2H_5OH)_{1.5}$ $M = 721.3$

Orthorhombic, space group $P2_12_12$, $a = 13.132(2)$, $b = 25.757(5)$, $c = 8.596(1)$ Å, $V = 2907.6(8)$ Å^3, $D_c = 1.65$ g cm^{-3}, $Z = 4$, $\mu_{Mo} = 30.20$ cm^{-1}. Crystal size 0.17 × 0.16 × 0.21 mm, $2\theta_{max} = 50°$, maximum and minimum transmission factors 0.55 and 0.66. The number of reflections was 2303 considered observed out of 2912 unique data. Final residuals R, R_w were 0.036, 0.048. Changing enantiomers resulted in R, R_w of 0.070, 0.094, so the original assignment seems correct.

Structure determination

Reflection data were measured with an Enraf–Nonius CAD-4 diffractometer in $\theta/2\theta$ scan mode using graphite monochromatized molybdenum radiation (λ 0.7107 Å). Data were corrected for absorption. Reflections with $I > 3\sigma(I)$ were considered observed. The structure was determined by direct phasing and Fourier methods. Hydrogen atoms for the carbohydrate moiety were located in a difference Fourier, positions for those of the coordinated ethanol were calculated, and all were assigned thermal parameters equal to those of the atom to which bonded. Hydrogen atoms were not located for the water molecules and the second ethanol, which was disordered about a 2-fold axis. Positional and anisotropic thermal parameters for the non-hydrogen atoms were refined using full-matrix least squares. Reflection weights used were $1/\sigma^2(F_o)$, with $\sigma(F_o)$ being derived from $\sigma(I_o) = [\sigma^2(I_o) + (0.04I_o)^2]^{1/2}$. The weighted residual is defined as $R_w = (\Sigma w\Delta^2/\Sigma wF_o^2)^{1/2}$. Atomic scattering factors and anomalous dispersion parameters were from International tables for X-ray crystallography (13). Structure solution was by MULTAN 80 (14) and refinement used BLOCKLS, a local version of ORFLS (15). ORTEP-II (16) running on a Macintosh IIcx was used for the structural diagram, and an IBM 3090 computer was used for the calculations.

1. S. J. Angyal. Carbohydr. Res. In press.
2. J. Defaye, A. Gadelle, and C. Pedersen. Carbohydr. Res. **136**, 53 (1985).
3. J. Defaye, A. Gadelle, and C. Pedersen. Carbohydr. Res. **174**, 323 (1988).
4. T. Taniguchi and T. Uchiyama. Carbohydr. Res. **107**, 255 (1982).
5. T. Taniguchi, M. Sawada, T. Tanaka, and T. Uchiyama. Carbohydr. Res. **177**, 13 (1988).
6. E. Rajakylä. J. Chromatogr. **353**, 1 (1986).
7. S. J. Angyal, G. S. Bethell, and R. J. Beveridge. Carbohydr. Res. **73**, 9 (1979).
8. S. J. Angyal and J. A. Mills. Aust. J. Chem. **32**, 1993 (1979).
9. S. J. Angyal. Adv. Carbohydr. Chem. Biochem. **47**, 1 (1989).
10. K. Bock, C. Pedersen, J. Defaye, and A. Gadelle. Abstr. Pap. Europ. Carbohydr. Symp., 3rd, Grenoble (1985). p. 75.
11. J. Defaye, A. Gadelle, and C. Pedersen. Carbohydr. Res. **152**, 89 (1986).
12. S. J. Angyal, D. Greeves, L. Littlemore, and V. A. Pickles. Aust. J. Chem. **29**, 1231 (1976).
13. J. A. Ibers and W. C. Hamilton. International tables for X-ray crystallography. Vol. 4. Kynoch Press, Birmingham. 1974.
14. P. Main. MULTAN 80. University of York, England. 1980.
15. W. R. Busing, K. O. Martin, and H. A. Levy. ORFLS, Oak Ridge National Laboratory, Tennessee, U.S.A. 1962.
16. C. K. Johnson. ORTEP-II, Oak Ridge National Laboratory, Tennessee, U.S.A. 1976.

Can. J. Chem. Downloaded from www.nrcresearchpress.com by 88.85.125.76 on 09/07/12
For personal use only.

Two-dimensional POMMIE carbon–proton chemical shift correlated ^{13}C NMR spectrum editing

BRUCE COXON

Center for Analytical Chemistry, National Institute of Standards and Technology, Gaithersburg, MD 20899, U.S.A.

Received December 11, 1989

This paper is dedicated to Professor Arthur S. Perlin on the occasion of his 67th birthday

BRUCE COXON. Can. J. Chem. **68**, 1145 (1990).

Two pulse sequences are described for acquisition of two-dimensional, carbon–proton chemical shift correlated ^{13}C NMR spectra by the "phase oscillations to maximize editing technique". One of these sequences provides two-dimensional, carbon–proton chemical shift correlated spectra in which the ^1H–^1H coupling constants are present in the ^1H chemical shift dimension, whereas the other sequence includes a bilinear rotation decoupling unit that removes the vicinal ^1H–^1H couplings in this dimension. Extensions of these techniques to generation of two-dimensional, carbon–proton chemical shift correlated CH, CH_2, and CH_3 ^{13}C NMR subspectra from linear combinations of three two-dimensional data sets are described. Decreased residual signals in the edited 2D subspectra have been achieved by Pascal programs that include six floating point coefficients, and a method for their calibration is discussed. Results are reported for troleandomycin (**1**).

Key words: ^{13}C nuclear magnetic resonance, carbon–proton chemical shift correlation, DEPT, Pascal programs, POMMIE, two-dimensional NMR spectrum editing, troleandomycin.

BRUCE COXON. Can. J. Chem. **68**, 1145 (1990).

On décrit deux séquences de pulsation qui permettent de faire l'acquisition de spectres RMN bidimensionnels du ^{13}C, avec corrélation des déplacements chimiques carbone–proton, par la «technique des oscillations de phase dans le but de maximiser l'édition». Une de ces séquences fournit des spectres bidimensionnels avec corrélation des déplacements chimiques carbone–proton dans laquelle les constantes de couplage ^1H–^1H sont présentes dans la dimension du déplacement chimique du ^1H; l'autre séquence comporte une unité de découplage bilinéaire de la rotation qui élimine les couplages vicinaux ^1H–^1H de cette dimension. On décrit des extensions de ces techniques qui permettent, à partir de combinaisons linéaires de trois données en deux dimensions, de générer des sous-spectres RMN bidimensionnels du ^{13}C des CH, des CH_2 et des CH_3, avec corrélation des déplacements chimiques carbone–hydrogène. On a diminué les signaux résiduels dans les sous-spectres 2D édités en faisant appel à des programmes en Pascal comportant six coefficients à point flottant; on discute d'une méthode pour leur calibration. On rapporte les résultats obtenus avec la troléandomycine (**1**).

Mots clés : résonance magnétique nucléaire du ^{13}C, corrélation des déplacements chimiques carbone–proton, DEPT, programme en Pascal, POMMIE, édition de spectres RMN bidimensionnels, troléandomycine.

[Traduit par la revue]

Introduction

Polarization transfer techniques have made a significant contribution to the analytical power of nuclear magnetic resonance (NMR) methods. Many one-dimensional (1D) and two-dimensional (2D) NMR methods are based on these techniques, as are several procedures for NMR spectrum editing, which may be defined as the selective display of the resonances of individual molecular features. The **D**istortionless **E**nhancement by **P**olarization **T**ransfer (DEPT) technique (1, 2) has played a major role in the development of heteronuclear NMR spectrum editing or structure selective methods, and both 1D (1, 2) and 2D (3–6) implementations of these methods have been described.

A number of practical advantages have been claimed for an alternative polarization transfer technique, namely, the **P**hase **O**scillations to **MaxiMI**ze **E**diting (POMMIE) method (7, 8), which in its 1D form is similar to DEPT, except that the polarization transfer pulse (θ) in the latter method is supplanted by a pair of successive 90° pulses that are arranged to have a variable phase difference ϕ. The intensities of ^{13}C NMR signals acquired by the POMMIE technique (7, 8) have the same theoretical dependences on the phase shift ϕ as do the corresponding DEPT intensities on the pulse flip angle θ (1, 2). These dependences are $CH = k \sin x$, $CH_2 = k \sin 2x$, and $CH_3 = 3k (\sin x + \sin 3x)/4$, where $k = \gamma_H/\gamma_C$, and $x = \phi$ or θ.

2D heteronuclear, chemical shift correlation NMR (9, 10) has proved to be one of the more useful techniques for the structural analysis of organic and inorganic materials (11). This paper describes the use of two pulse sequences for 2D POMMIE, chemical shift correlated spectrum editing as alternative processes for simplifying interpretation of the shift correlated spectrum. Refinement of the 2D editing computations has been realized by introducing six floating point coefficients into the linear combinations of data that are used to compute the subspectra. The methods have been tested on the macrocyclic antibiotic, troleandomycin (**1**, the tri-*O*-acetyl derivative of oleandomycin (12)).

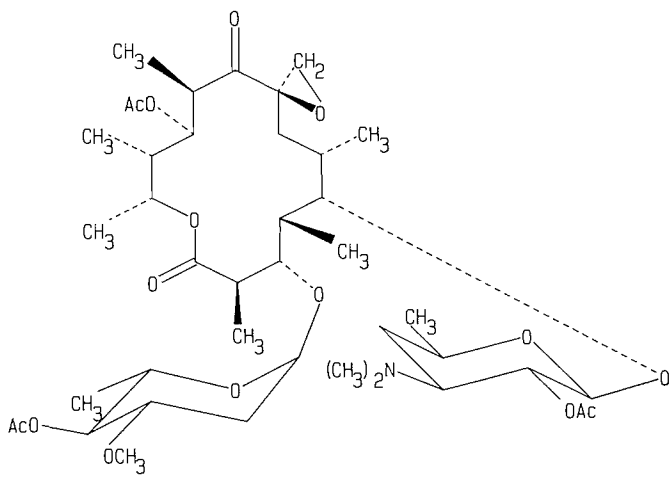

1

Can. J. Chem. Downloaded from www.nrcresearchpress.com by 88.85.125.76 on 09/07/12
For personal use only.

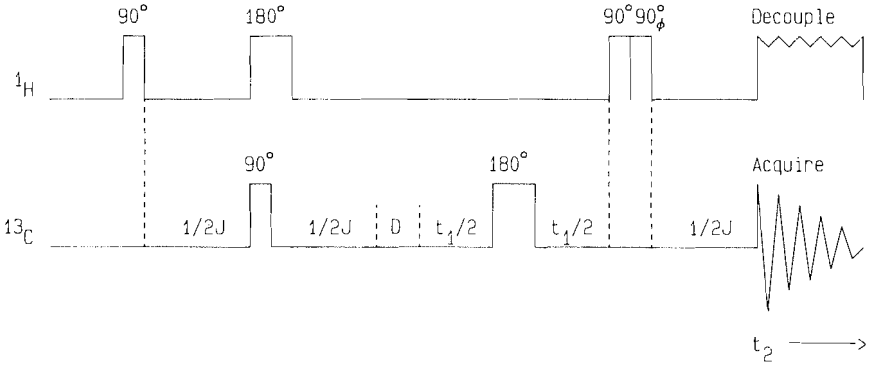

FIG. 1. Pulse sequence for 2D POMMIE, carbon–proton chemical shift correlated, ^{13}C NMR spectroscopy. J is an average value of the coupling constant between directly bonded proton and carbon nuclei, D is a delay equal to the width of the ^1H 180° pulse, and ϕ is the RF phase difference of the adjoining ^1H 90° pulses. Phase programs are listed in Table 1.

Experimental

Materials

A 0.2 mol L^{-1} solution of troleandomycin (**1**) in 1:1 v/v chloroform-*d*:dimethylsulfoxide-d_6 was used.

Measurement of ^{13}C NMR spectra

^{13}C NMR spectra were recorded at 100.6 MHz and at 300 K, by use of the Bruker[1] DISR88 program (version 880101.0) with a Bruker Instruments model WM-400 spectrometer that was equipped with a 5 mm dual frequency carbon–proton probe, digital frequency generation, a process controller, and an Aspect 3000 data system with array processor. The pulse power of the proton decoupler at 400 MHz was increased by means of a Henry Radio selective power amplifier, which afforded a gain of 10.5 db once the output was filtered through four parallel pairs of crossed diodes and a 400 MHz bandpass filter. In this manner, the ^1H 90° pulse width was decreased to 8.1 μs. The ^{13}C 90° pulse width was 9.3 μs. The transmitter and decoupler offsets were set to the centers of the respective frequency ranges for **1**. The ^{13}C chemical shifts are referenced to internal tetramethylsilane.

2D POMMIE, carbon–proton chemical shift correlated, ^{13}C NMR spectra with ^1H–^1H coupling in the F_1 dimension were acquired by use of the pulse sequence 90°(H)–1/2J–180°(H)90°(C)–1/2J–D–t_1/2–180°(C)–t_1/2–90°(H)90°(H,ϕ)–1/2J–acquire ^{13}C, decouple ^1H (sequence A, see Fig. 1) with the phase programs shown in Table 1.

The corresponding 2D POMMIE, carbon–proton chemical shift correlated spectra with vicinal ^1H–^1H decoupling in the F_1 dimension (13) were obtained by means of the sequence 90°(H)–t_1/2–90°(H)–1/2J–180°(H)90°(C,x)240°(C,y)90°(C,x)–1/2J–90°(H)–t_1/2–1/2J–180°(H)90°(C)–1/2J–90°(H)90°(H,ϕ)180°(C)–1/2J–acquire ^{13}C, de couple ^1H (sequence B, see Fig. 2), in conjunction with the phase programs in Table 1.

Phase comparability for data sets acquired by using ϕ = 45°, 90°, and 135° (angle set a) was ensured by the somewhat empirical procedure of adjusting the relative lengths of the contiguous 90°(H) and 90°(H,ϕ) pulses; i.e., the first of these pulses was lengthened by 1.2 μs, whereas the second pulse 90°(H,ϕ) was shortened by 1.2 μs. These adjustments are slightly larger than those (+1.0 and −1.0 μs) required for matching with the phase propagation delay of 2.0 μs that is defined by hardware delay lines in the Bruker process controller. The data acquisition conditions included the use of 4096 (t_2) × 128 (t_1) point data sets, zero-filled to 256 points in the t_1 dimension, two dummy scans with 64 scans per spectrum for all values of ϕ, spectral widths of 1.8 and 10.4 kHz in the F_1 and F_2 dimensions, respectively, and WALTZ-16 composite pulse ^1H decoupling (14) in the F_2 dimension. An average delay 1/2J(CH) = 3.52 ms was used, together with a pulse recycle time of 2.2 s.

[1]Certain commercial equipment, instruments, or materials are identified in this paper to specify adequately the experimental procedure. Such identification does not imply recommendation by the National Institute of Standards and Technology, nor does it imply that the materials or equipment are necessarily the best available for the purpose.

TABLE 1. Phase cycles for 2D POMMIE carbon–proton chemical shift correlated ^{13}C NMR spectrum editing

Pulse	Phase program[a]
90°(H)	*x*
180°(H)	*x, x, x, x, −x, −x, −x, −x*
90°(C)	*x, x, x, x, x, x, x, x, y, y, y, y, y, y, y, y, −x, −x, −x, −x, −x, −x, −x, −x, −y, −y, −y, −y, −y, −y, −y, −y*
180°(C)	*x, x, x, x, −x, −x, −x, −x, y, y, y, y, −y, −y, −y, −y, −x, −x, −x, −x, x, x, x, x, −y, −y, −y, −y, y, y, y, y*
90°(H)	*x, −x, y, −y*
90°(H,ϕ)	45°, 225°, 135°, 315°, or *y, −y, −x, x,* or 135°, 315°, 225°, 45°
Receiver	*x, −x, y, −y, x, −x, y, −y, y, −y, −x, x, y, −y, −x, x, −x, x, −y, y, −x, x, −y, y, −y, y, x, −x, −y, y, x, −x*

[a]The phase cycles for 2D POMMIE carbon–proton correlation with BIRD ^1H–^1H decoupling were the same, except that the phases for the BIRD pulse subsequence were
90°(H): *x, x, x, x, y, y, y, y, −x, −x, −x, −x, −y, −y, −y, −y*
180°(H): y, y, y, y, −x, −x, −x, −x, −y, −y, −y, −y, x, x, x, x, −y, −y, −y, −y, x, x, x, x, y, y, y, y, −x, −x, −x, −x
90°(C, *x*): *x, x, x, x, −x, −x, −x, −x*; 240°(C, *y*): *y, y, y, y, −y, −y, −y, −y*; 90°(C, *x*): *x, x, x, x, −x, −x, −x, −x*
90°(H): *x, x, x, x, y, y, y, y, −x, −x, −x, −x, −y, −y, −y, −y*, and for the ^{13}C refocussing pulse,
180°(C): *x, x, x, x, −x, −x, −x, −x, y, y, y, y, −y, −y, −y, −y*

Data processing

2D POMMIE, carbon–proton chemical shift correlated, ^{13}C NMR subspectra were computed from the following algorithm:

$$\text{(Scheme A)}\quad CH_2 = \text{Data(45)} - a\cdot\text{Data(135)} - b\cdot\text{Data(90)}$$
$$CH_3 = \text{Data (45)} + c\cdot\text{Data(135)} - d\cdot\text{Data(90)}$$
$$CH = \text{Data(90)} - e\cdot CH_2 - f\cdot CH_3$$

where Data(45), Data(90), and Data(135) are the 2D data sets that were acquired by use of the sampling angles ϕ = 45°, 90°, and 135°, respectively, and a–f are six floating point coefficients. Both dimensions of the time–domain data were subjected to sine-bell squared apodization, with a window shift of $\pi/2$.

Can. J. Chem. Downloaded from www.nrcresearchpress.com by 88.85.125.76 on 09/07/12
For personal use only.

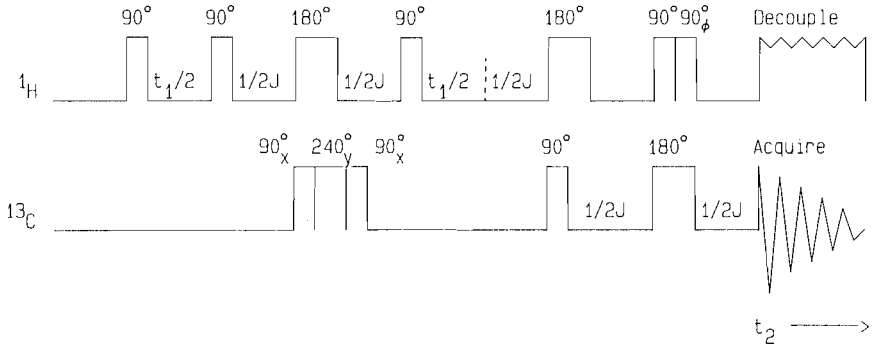

FIG. 2. Pulse sequence for 2D POMMIE, carbon–proton chemical shift correlated, ^{13}C NMR spectroscopy with BIRD ^{1}H–^{1}H decoupling. Definitions of parameters are the same as for Fig. 1. Phase programs are shown in Table 1.

Calibration of the six floating point coefficients

After the three complete 2D POMMIE, chemical shift correlated data sets had been acquired (usually overnight), a separate 1D calibration run was performed in which only the first row of each data matrix was collected (Bruker NE = 1). However, an increased number of scans (e.g., 1024 instead of 64) was done to increase the signal:noise ratio in the calibration spectra. The calculations in scheme A were then implemented consecutively in 1D dual display mode, and the values of the constants a–f were optimized by successive interactive knob adjustments to give good editing and residue reduction of the appropriate signals. For pulse sequence A, typical values of the coefficients were $a = 0.73$, $b = 0.33$, $c = 1.19$, $d = 1.55$, $e = -0.21$, and $f = 0.01$, and for sequence B, $a = 0.74$, $b = 0.37$, $c = 1.23$, $d = 1.59$, $e = -0.19$, and $f = 0.03$. These values may be compared with the ideal values $a = 1$, $b = 0$, $c = 1$, $d = 1.414$, $e = 0$, and $f = 0$.

Pascal program for 2D NMR spectrum editing

Earlier Pascal programs (6, 15) that had been written in fixed point format for 2D DEPT and 2D POMMIE J(CH)-resolved ^{13}C NMR spectrum editing were modified to include (a) keyboard entry of six floating point coefficients at program start, (b) floating point arithmetic on the six coefficients, (c) the 2D data matrix dimensions (size of free induction decay × number of spectra acquired) are read automatically from the data file and printed for inspection, and (d) the results of the floating point computations are converted to fixed point format before storage to the hard disk. A listing of this Pascal program (FPT6SIRE) is available on request. The compile-time option :H (an instruction to use the firmware floating point package) in the Bruker PASCOM program (version 880808.0) was used to speed the editing computations in floating point mode.

Results and discussion

The original version of the 1D DEPT method (1) required the acquisition of three heteronuclear NMR spectra, by use of a different value of the polarization transfer pulse flip angle (θ) for each. Angle set a ($\theta = 45°$, 90°, and 135°) has often been used for 1D DEPT spectrum editing, although use of the modified set $\theta = 30°$, 90°, and 150° (angle set b) is computationally advantageous for 2D DEPT NMR spectrum editing (4–6).

In previous work (15), a pulse sequence for 2D POMMIE J(CH)-resolved ^{13}C NMR was used to explore three methods for the automated acquisition of data for 2D spectrum editing and, when compared with the 2D DEPT J(CH)-resolved spectrum editing technique (6), the 2D POMMIE version was found to have the particular advantage that the programming of additional delays (3) into the sequence was not necessary in order to ensure equalization of the phases of the data sets (15). For these techniques (6, 15), angle set b was used for either θ or ϕ, because it allows the 2D J(CH)-resolved ^{13}C NMR subspectra to be computed from the simple 1:1 data combinations:

(Scheme B) CH = Data(90)

CH_2 = Data(30) − Data(150)

CH_3 = Data(30) + Data(150) − Data(90)

which were programmed in Pascal, in rapid fixed point arithmetic (for example, a computation time of 1.33 min for processing of three 4096 × 64 point data sets, with optimized array addressing). By contrast, use of the more traditional angle set a requires that at least one floating point coefficient be used in the linear combinations (1).

Attempts to perform 2D POMMIE, carbon–proton chemical shift correlated, ^{13}C NMR spectrum editing by using pulse sequences A and B, in conjunction with angle set b and computation scheme B, have revealed many cases where the residues in the 2D edited subspectra are unexpectedly large, despite the use of a probehead with good RF homogeneity (16). For molecules of biological interest, it is often difficult to obtain aesthetically pleasing 2D DEPT or 2D POMMIE, carbon–proton chemical shift correlated CH_2 subspectra. This difficulty appears to be largely due to the unique properties of methylene groups. In biomolecules, these groups often contain nonequivalent protons that split the CH_2 correlation cross peak into two to five or more components (sometimes an AB quartet with an extra central line), which tend to exaggerate the *relative* intensities of CH and CH_3 residues in the CH_2 subspectra by a factor of two to five, or more. Longer spin–spin relaxation times (T_2) for typical CH_3 carbon nuclei may also contribute to this effect, and if there are F_1 ridges in the spectra, then these artifacts are relatively emphasized, too.

In practice, the accuracy of 1D and 2D POMMIE spectrum editing experiments may be influenced (16) by several effects, including (a) lateral displacements of the ^{13}C intensity – phase shift (ϕ) dependence curves caused by the use of insufficient decoupler pulse power, (b) amplitude mismatch in the two sampling angle quadrants, $0° < \phi < 90°$, $90° < \phi < 180°$, and (c) signal phase mismatch in the two quadrants. Because of these limitations, the present experiments have been conducted at high decoupler pulse power (110 W). Although phase matching of all types of signals obtained in the two sampling angle (ϕ) quadrants has been achieved by adjustment of the relative lengths of the adjacent 90°(H) and 90°(H, ϕ) pulses (see Figs. 1 and 2 and the Experimental), this technique did not provide an amplitude match in the two ϕ quadrants. Therefore, this match has been improved by optimization of the six coefficients in computation scheme A. The use of spectrum editing computations with up to six or more floating point coefficients is now more feasible than before, because of improvements in Pascal programs and compilers.

Can. J. Chem. Downloaded from www.nrcresearchpress.com by 88.85.125.76 on 09/07/12
For personal use only.

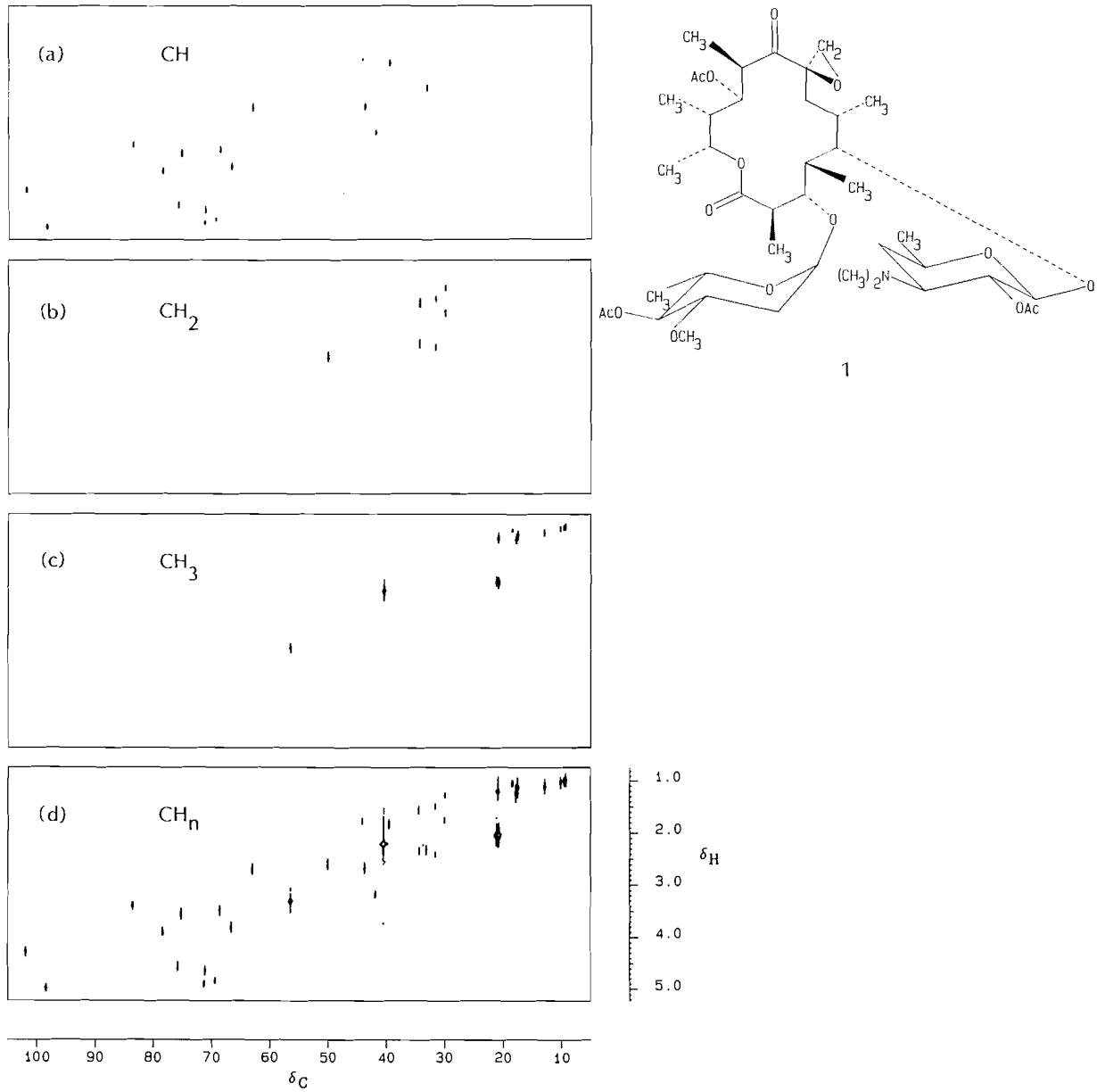

FIG. 3. Contour plots of the 2D POMMIE, carbon–proton chemical shift correlated, ^{13}C NMR spectra of troleandomycin (**1**, 0.2 mol L^{-1} in 1:1 v/v chloroform-*d*:dimethylsulfoxide-d_6). The CH, CH_2, and CH_3 subspectra in (a)–(c) were obtained from editing computations with six floating point coefficients (see scheme A), on raw data acquired by means of the sampling phase shifts $\phi = 45°$, 90°, and 135°. The unedited CH_n spectrum in (d) is the data from $\phi = 135°$.

In other work (16) on carbohydrate derivatives at low decoupler pulse power (10 W), alternative strategies for 2D POMMIE NMR spectrum editing have been tested, particularly adjustment of the sampling angle ϕ to values other than those of angle sets a or b, in order to achieve equalization of the amplitudes of certain specific resonances measured in the two quadrants of ϕ. For example, in studies of the 2D POMMIE, *J*(CH)-resolved ^{13}C NMR spectrum editing of a mixture of seven methyl glycopyranosides, the sampling angle set $\phi = 40°/96°/152°$ was used, and the three raw data matrices were processed in linear combinations with *two* floating point coefficients (16). However, the methods discussed in the present paper represent an optimized and refined technique in which high decoupler pulse power is used to force the ^{13}C intensity – sampling angle ϕ dependence curves to approach theoretical behavior, which allows use of the symmetrically related angles $\phi = 45°$ and 135° (or 30° and 150°).

In the present work, sampling angle set a was favored over angle set b, because the theoretical methylene carbon intensity function $CH_2 = k \sin 2\phi$ has amplitude maxima (without regard to algebraic sign) at $\phi = 45°$ and 135°. Extraction of the maximum methylene carbon amplitudes from the experiment tends to counteract any weakness in the methylene cross peaks caused by spin coupling between nonequivalent methylene protons. At $\phi = 30°$ and 150°, the theoretical CH_2 intensities are only 87% of those at $\phi = 45°$ and 135°. Linear combinations of the three data matrices with six floating point coefficients are then used to correct any remaining amplitude discrepancies in resonances measured in the two ϕ quadrants.

Computation scheme A includes "on the fly" reduction of

Can. J. Chem. Downloaded from www.nrcresearchpress.com by 88.85.125.76 on 09/07/12
For personal use only.

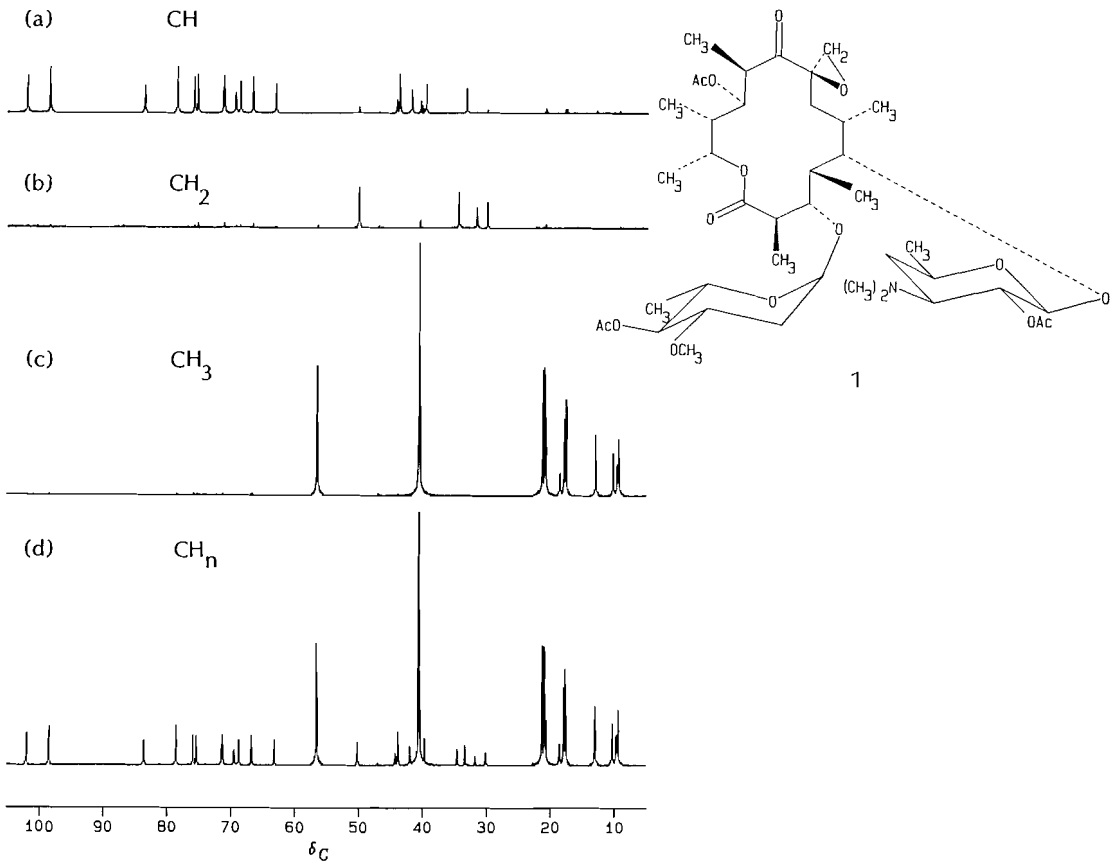

FIG. 4. F_2 projections of the 2D POMMIE, carbon–proton chemical shift correlated, ^{13}C NMR spectra of troleandomycin (**1**) shown in Fig. 3.

CH_2 and CH_3 residues in the CH 2D subspectrum by subtraction from Data(90) of small fractions *e* and *f*, respectively, of the CH_2 and CH_3 subspectra that have just been computed. These subtractions are performed while the corresponding 4096 point segments of Data(90) and the CH_2 and CH_3 subspectra are still in memory, thus minimizing disk access time. With a compile-time instruction to use the resident firmware floating point package, the current Pascal program with six floating point coefficients requires approximately 1 h (on the Bruker Aspect 3000 computer) to process three 4096 × 128 point data matrices, a time that is reasonably short for practical use. Without the firmware floating point package, the program computation times are a factor of 3.8 longer.

The complete 2D POMMIE, carbon–proton chemical shift correlated, ^{13}C NMR spectrum of a solution of troleandomycin is shown in Fig. 3d, a spectrum that was acquired by using pulse sequence A with $\phi = 135°$. Figures 3a–3c display the CH, CH_2, and CH_3 subspectra that were computed from the three raw data matrices (Data(45), Data(90), and Data(135)) by use of six floating point coefficients in scheme A. In Fig. 3b, three out of four of the methylene carbon signals appear as unresolved AB quartets. The separate CH_2 subspectrum supports the interpretation that each pair of cross peaks that have the same ^{13}C chemical shift but different proton chemical shifts is associated with the same methylene carbon nucleus, and not with carbon nuclei of other types that are accidentally equivalent in the carbon dimension.

An indication of the efficiency of the 2D spectrum editing is given by the F_2 projections of the 2D POMMIE, carbon–proton chemical shift correlated spectra shown in Fig. 4. The complete projection spectrum that was measured by use of $\phi = 135°$ is shown in Fig. 4d, in which the strong intensities of the methyl carbon signals are noteworthy. Nevertheless, the methyl residues in the CH and CH_2 subspectra (Fig. 4a and 4b, respectively) are effectively suppressed by the editing computation with six floating point coefficients.

The application of pulse sequence B and computation scheme A to troleandomycin gave a similar set of edited correlation subspectra and corresponding F_2 projections, except that the CH cross peaks were distinctly narrowed by the **BI**linear **R**otation **D**ecoupling (BIRD) unit in sequence B. The BIRD subsequence removes the vicinal $^1H-^1H$ couplings in the F_1 dimension (13), but not the geminal $^1H-^1H$ couplings in the methylene groups. Another difference in the results from the sequences performed with and without BIRD decoupling was that the latter technique produced an extra line in the center of the methylene AB quartet at lowest field (δ_C 34.38), thus further diluting the effective intensity of the methylene carbon correlation cross peaks. The origin and variability of these methylene correlation artifacts (5) has recently been discussed (17). They are thought to arise because the BIRD pulse sequence transfers some spin coherence between nonequivalent methylene protons, and a theoretical analysis has suggested that the artifacts may or may not be observed for particular methylene carbon atoms, because of a cyclic dependence on the chemical shift separation of the methylene protons (17).

Pascal programs based on scheme A may also be used for suppression of the residual signals in the edited subspectra

Can. J. Chem. Downloaded from www.nrcresearchpress.com by 88.85.125.76 on 09/07/12
For personal use only.

obtained by selective 2D DEPT carbon–proton chemical shift correlation (4, 5), and the 2D DEPT *J*(CH)-resolved (6) and 2D POMMIE *J*(CH)-resolved (15) methods.

Acknowledgment

Thanks are due to T. Alexander of the Food and Drug Administration, Washington, DC, for a sample of troleandomycin (**1**).

1. D. M. Doddrell, D. T. Pegg, and M. R. Bendall. J. Magn. Reson. **48**, 323 (1982).
2. D. T. Pegg, D. M. Doddrell, and M. R. Bendall. J. Chem. Phys. **77**, 2745 (1982).
3. M. H. Levitt, O. W. Sorensen, and R. R. Ernst. Chem. Phys. Lett. **94**, 540 (1983).
4. T. T. Nakashima, B. K. John, and R. E. D. McClung. J. Magn. Reson. **57**, 149 (1984).
5. T. T. Nakashima, B. K. John, and R. E. D. McClung. J. Magn. Reson. **59**, 124 (1984).
6. B. Coxon. J. Magn. Reson. **66**, 230 (1986).
7. J. M. Bulsing, W. M. Brooks, J. Field, and D. M. Doddrell. J. Magn. Reson. **56**, 167 (1984).
8. J. M. Bulsing and D. M. Doddrell. J. Magn. Reson. **61**, 197 (1985).
9. G. Bodenhausen and R. Freeman. J. Magn. Reson. **28**, 471 (1977).
10. R. Freeman and G. A. Morris. J. Chem. Soc. Chem. Commun. 684 (1978).
11. A. E. Derome. *In* Modern NMR techniques for chemistry research. Pergamon Press, Oxford. 1987. pp. 245–258.
12. W. D. Celmer and D. C. Hobbs. Carbohydr. Res. **1**, 137 (1965).
13. A. Bax. J. Magn. Reson. **53**, 517 (1983).
14. A. J. Shaka, J. Keeler, and R. Freeman. J. Magn. Reson. **53**, 313 (1983).
15. B. Coxon. Magn. Reson. Chem. **26**, 449 (1988).
16. B. Coxon. *In* NMR applications in biochemistry and food. *Edited* by A. S. Serianni and J. Finley. Plenum Press, New York, NY. In press.
17. A. D. Bain, D. W. Hughes, and H. N. Hunter. Magn. Reson. Chem. **26**, 1058 (1988).

Can. J. Chem. Downloaded from www.nrcresearchpress.com by 88.85.125.76 on 09/07/12
For personal use only.

Synthesis of optically active cyclohexanone analogs of the plant hormone abscisic acid[1]

NANCY LAMB AND SUZANNE R. ABRAMS[2]

Plant Biotechnology Institute, National Research Council of Canada, 110 Gymnasium Place, Saskatoon, Sask., Canada S7N 0W9

Received November 24, 1989

This paper is dedicated to Professor Arthur S. Perlin on the occasion of his 67th birthday

NANCY LAMB and SUZANNE R. ABRAMS. Can. J. Chem. **68**, 1151 (1990).

The abscisic acid analogs (−)-(4*R*,5*R*)-, (+)-(4*S*,5*S*)-, and (−)-(4*S*,5*R*)-4(1*E*,3*Z*)-4-(4-carboxy-3-methyl-1,3-butadienyl)-4-hydroxy-3,3,5-trimethylcyclohexanones (dihydroabscisic acids), and (−)-(4*S*,5*R*)-, (+)-(4*R*,5*S*)-, and (−)-(4*R*,5*R*)-4(*Z*)-4-hydroxy-4-(5-hydroxy-3-methylpent-3-en-1-ynyl)-3,3,5-trimethylcyclohexanones were synthesized from a common precursor, (−)-(6*R*)-2,2,6-trimethylcyclohexan-1,4-dione, which was readily prepared by the fermentation of oxoisophorone with bakers' yeast.

Key words: abscisic acid, dihydroabscisic acid, acetylenic analogs, optically active analogs, plant growth regulators.

NANCY LAMB et SUZANNE R. ABRAMS. Can. J. Chem. **68**, 1151 (1990).

Utilisant comme produit de départ commun la (−)-(6*R*)-2,2,6-triméthylcyclohexane-1,4-dione que l'on peut préparer facilement par fermentation de l'oxoisophorone à l'aide du levain de boulanger, on a synthétisé les analogues suivants de l'acide abscissique : les (−)-(4*R*,5*R*)-, (+)-(4*S*,5*S*)- et (−)-(4*S*,5*R*)-4(1*E*,3*Z*)-4-(4-carboxy-3-méthylbuta-1,3-dièn yl)-4-hydroxy-3,3,5-triméthylcyclohexanones (acides dihydroabscissiques) ainsi que les (−)-(4*S*,5*R*)-, (+)-(4*R*,5*S*)- et (−)-(4*R*,5*R*)-4(*Z*)-4-hydroxy-4-(5-hydroxy-3-méthylpent-3-èn-1-ynyl)-3,3,5-triméthylcyclohexanones.

Mots clés : acide abscissique, acide dihydroabscissique, analogues acétyléniques, analogues optiquement actifs, régulateurs de croissance des plantes.

[Traduit par la revue]

Can. J. Chem. Downloaded from www.nrcresearchpress.com by 88.85.125.76 on 09/07/12
For personal use only.

Introduction

The plant hormone abscisic acid (ABA, **1**) is widely distributed in higher plants and is involved in the regulation of many developmental phases and stress responses including germination, dormancy, transpiration, and abscission (1). Many structural analogs of ABA have been synthesized for establishing structure–activity relationships and for developing practical plant growth regulators (2).

The natural hormone has the (S)-(+) configuration (Fig. 1) and is active in bioassays involving growth inhibition, germination inhibition, and reduction of transpiration by stomatal closure, when applied exogenously to plants (3, 4). The unnatural (*R*)-(−) enantiomer is as active as natural ABA in germination and growth inhibition, but is inactive in stomatal closure (3, 4). The metabolism of the two antipodes proceeds at different rates in plant cells, and is thought to lead to different products (5).

One of the goals of our research program is to develop ABA-like compounds that will enhance the hardiness of crop plants toward extreme climatic conditions such as cold and drought (6). Of a number of compounds tested in collaboration with other research groups, we find that racemic ABA and the known (7) analog racemic dihydroabscisic acid, (±)-**2**, are active in inducing cold tolerance in a brome grass tissue culture assay (8). Furthermore, both (±)-ABA and (±)-**2** have antitranspirant activity in Douglas fir seedlings that have been subjected to water stress.[3]

Another ABA analog (±)-4(*Z*)-(4α,5β)-4-hydroxy-4-(5-hydroxy-3-methylpent-3-en-1-ynyl)-3,3,5-trimethylcyclohexanone, (±)-**3**, which has an acetylenic group in the side chain (9), has recently been demonstrated to promote the germination of barley and stimulate the appearance of the enzyme α-

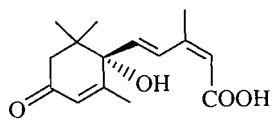

1

(+)-*S*-abscisic acid

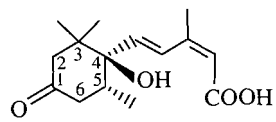

2

(−)-(4*R*, 5*R*)-dihydroabscisic acid

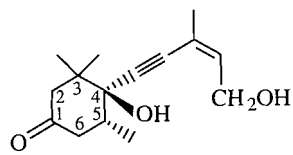

3

(−)-(4*S*, 5*R*)

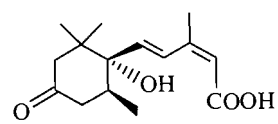

4

(+)-(4*S*, 5*S*)-dihydroabscisic acid

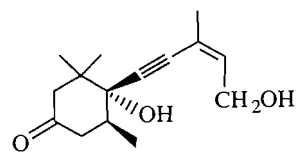

6

(+)-(4*R*, 5*S*)

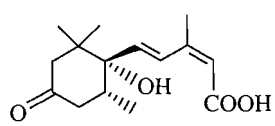

5

(−)-(4*S*, 5*R*)-dihydroabscisic acid

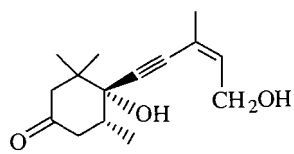

7

(−)-(4*R*, 5*R*)

FIG. 1.

[1]NRCC No. 31223.

[2]Author to whom correspondence may be addressed.

[3]T. Blake, Department of Forestry, University of Toronto, personal communication.

amylase.[4] To better understand the mechanisms by which these compounds function as growth regulators and their metabolism in plants, we have undertaken the synthesis and biological testing of both the (+) and (−) enantiomers of optically pure ABA analogs.

The literature has several reports on the synthesis of optically active ABA-like compounds and carotenoids (10–14). Some of these preparations involve the use of expensive resolving agents and tedious resolution procedures. This paper reports an efficient and inexpensive synthesis of the (−)-(4*R*,5*R*) isomer of dihydroabscisic acid (**2**),[5] the (+)-(4*S*,5*S*) enantiomer (**4**), and the (−)-(4*S*,5*R*) epimer (**5**). The acetylenic analog (−)-4(*Z*)-(4*S*,5*R*)-4-hydroxy-4-(5-hydroxy-3-methylpent-3-en-1-ynyl)-3,3,5-trimethylcyclohexanone (**3**), as well as the corresponding (+)-(4*R*,5*S*) enantiomer (**6**) and the (−)-(4*R*,5*R*) epimer (**7**) have also been obtained (Fig. 1).

Results and discussion

Similar to the procedure of Mayer and co-workers (12, 13), our synthesis started with (−)-(6*R*)-2,2,6-trimethylcyclohexan-1,4-dione (**9**), which was readily prepared by the fermentation of oxoisophorone (**8**) with bakers' yeast according to the method of Leuenberger *et al.* (15) (Scheme 1). Regioselective reduction of diketone **9** was achieved with lithium tri-*sec*-butylborohydride (L-Selectride^R) (16). The thermodynamically less stable *trans* ketol (−)-(4*R*,6*R*)-4-hydroxy-2,2,6-trimethylcyclohexanone (**10**) was obtained as the major product. Some *cis* ketol of low optical purity, i.e., a mixture of compounds **11** and **12**, was also isolated, indicating that some epimerization of the methyl group at C6 had occurred.

For the synthesis of ABA analogs **2**, **3**, **5**, and **7**, which have the (5*R*) configuration (see Fig. 1), the *trans* ketol **10** was first protected as the *tert*-butyldimethylsilyl ether **13** (Scheme 1). The ^{1}H nuclear magnetic resonance (nmr) spectrum of **13** showed an apparent quintet at 4.08 ppm (J = 3.2 Hz) for the CHOSi proton. The observed coupling is consistent with the pattern expected for an equatorial proton, which usually has axial–equatorial and equatorial–equatorial coupling constants of 2–6 Hz. A doublet of doublets of quartets at 3.16 ppm with J = 13.2, 5.3, and 6.4 Hz was observed for the C*H*CH$_3$ proton, and the coupling constant of 13.2 Hz was indicative of a proton in the axial position. These nmr data demonstrated that conformation **13***a* with the silyl ether group in the axial position and an equatorial methyl group at C6 was preferred over **13***b*, which has strong 1,3-diaxial interaction between the methyl groups at C2 and C6 (see Scheme 1). The desired side chain containing an acetylenic group required for compounds **3** and **7** was then introduced by treating **13** with the dianion generated between (*Z*)-3-methylpent-2-en-4-yn-1-ol and two equivalents of *n*-butyllithium. A mixture of two addition products in an 8:1 ratio as determined by gas chromatographic (gc) analysis (DB1701 column) was obtained. The major product (retention time 20.05 min) was assigned the structure **14** with the (1*S*,6*R*) configuration, which was most likely formed by the well-documented preferential axial attack of cyclohexanone **13***a* by the acetylide anion (7, 9, 10, 12–14, 17). The minor product (retention time 19.77 min) was tentatively assigned as the (1*R*,6*R*) isomer **15**. The stereochemistry of compounds **14** and **15** was differentiated by studying the nuclear Overhauser enhancement (nOe) in the ^{1}H nmr spectra of their derivatives (see below). The (1*R*,6*S*) isomer **31** (see Scheme 4), which could be distinguished from **14** and **15** by gc analysis (retention time 19.11 min), was absent from the product mixture, therefore indicating that epimerization at the C6 position of the starting material **13** did not occur prior to the addition reaction.

The mixture of **14** and **15** was acetylated and then desilated to give compounds **16** and **17**, which could be separated by flash column chromatography followed by preparative thin-layer chromatography (tlc). Compounds **16** and **17** were separately oxidized and hydrolyzed to give the desired ABA analog (−)-4(*Z*)-(4*S*,5*R*)-4-hydroxy-4-(5-hydroxy-3-methylpent-3-en-1-ynyl)-3,3,5-trimethylcyclohexanone (**3**) (10) and the (−)-(4*R*,5*R*) epimer (**7**), respectively.

At this point in the synthesis, the optical purity of the acetylenic analog **3** obtained was examined by treating it with (−)-(2*R*,3*R*)-2,3-butanediol to form the ketal **18** (Scheme 2) (10, 18). Analysis of **18** by gc on a DB1701 column showed only one component with retention time of 18.57 min, whereas the diastereomeric ketal **19** prepared in the same fashion from the (+)-(4*R*,5*S*) enantiomer **6** (see below) had a longer retention time of 18.76 min. Furthermore, both the ^{1}H and ^{13}C nmr spectra of ketal **18** demonstrated that it was a single compound, with signals distinctly different from those of the diastereomeric ketal **19** (see Experimental). Ketalization of the racemic acetylenic analog (±)-**3** (9) under the same conditions afforded a product with gc and nmr data that are consistent with a 1:1 mixture of compounds **18** and **19**.

To continue with the synthesis of (−)-(4*R*,5*R*)-dihydroabscisic acid (**2**), the carbonyl group in compound **3** was protected as the ketal to form **20** (Scheme 3). Reduction of **20** with sodium bis(2-methoxyethoxy)aluminium hydride (Redal^R) (19) gave compound **21** with the desired pentadienol side chain. After deketalization by acid-catalyzed hydrolysis to give **22**, the allylic alcohol was oxidized with manganese(IV) oxide to the aldehyde **23**. Further oxidation of **23** using a mixture of manganese(IV) oxide, sodium cyanide, acetic acid, and methanol (20) gave (−)-(4*R*,5*R*)-methyl dihydroabscisate (**24**), which was readily hydrolyzed to the desired ABA analog (−)-(4*R*,5*R*)-dihydroabscisic acid (**2**).

The conversion of compound **7** to (−)-(4*S*,5*R*)-dihydroabscisic acid (**5**) followed the same sequence of reactions (see Scheme 3). To confirm the stereochemistry at C4 of this series of compounds, an nOe experiment was performed with ketals **21** and **26**. When the C1′ olefinic proton doublet at 5.94 ppm in the ^{1}H nmr spectrum of ketal **21** was irradiated, an nOe of approximately 5% was observed for the multiplet at 1.34–1.42 ppm assigned to the two axial protons at C7 and C11. Likewise, an nOe of about 7% was observed for the doublet at 5.94 ppm when the multiplet at 1.34–1.42 was irradiated. On the other hand, no significant nOe was observed for the corresponding olefinic and axial proton signals when the ^{1}H nmr spectrum of ketal **26** was recorded under the same experimental conditions. These results support the assignment of epimeric structures **21** and **26** to the two ketals. The dienol group in compound **21** is in the axial position, with the olefinic proton at C1′ of the side chain in close proximity to the axial protons at C7 and C11 of the cyclohexane ring. The isomer **26** has an

[4]R. Hill, Department of Plant Science, University of Manitoba, personal communication.

[5]For the convenience of discussion, the same numbering system will be adopted for dihydroabscisic acid (**2**) and compound **3** in this paper (see Fig. 1). In the literature, the racemic form of structure **2** is also known as 2′,3′-dihydroabscisic acid (ref. 7) and [1α,1(2*Z*,4*E*),6β]-5-(1-hydroxy-2,2,6-trimethyl-4-oxocyclohexyl)-3-methyl-2,4-pentadienoic acid (Chem. Abstr. **96**, 1321F (1982); CAS registry no. 81749-10-2).

Can. J. Chem. Downloaded from www.nrcresearchpress.com by 88.85.125.76 on 09/07/12
For personal use only.

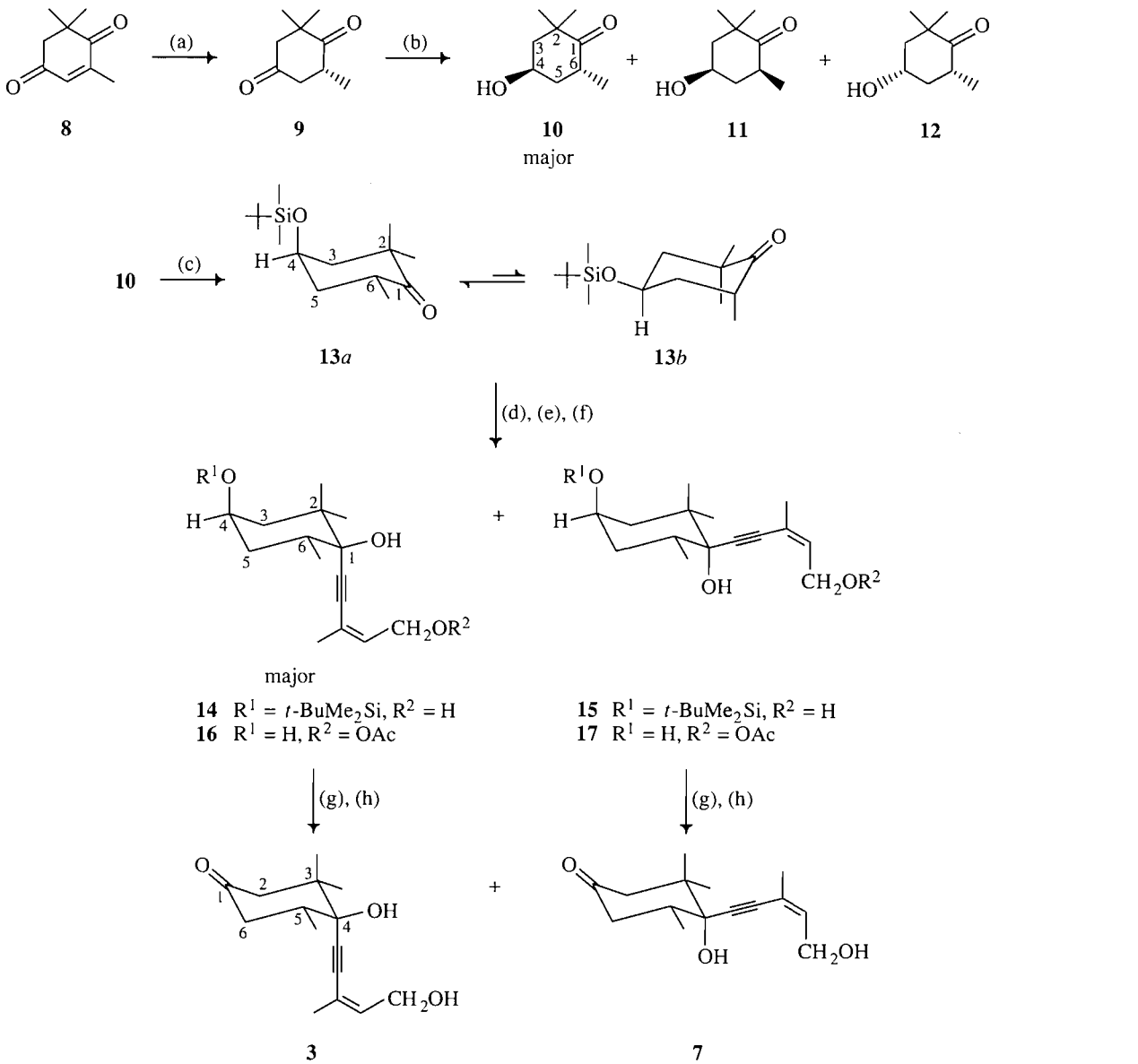

SCHEME 1. (a) Bakers' yeast; (b) L-Selectride^{R}; (c) *t*-BuMe$_2$SiCl, imidazole; (d) (*Z*)-3-methylpent-2-en-4-yn-1-ol, 2 *n*-BuLi; (e) Ac_2O, pyridine; (f) HOAc, H_2O; (g) pyridinium dichromate; (h) NaOH, MeOH.

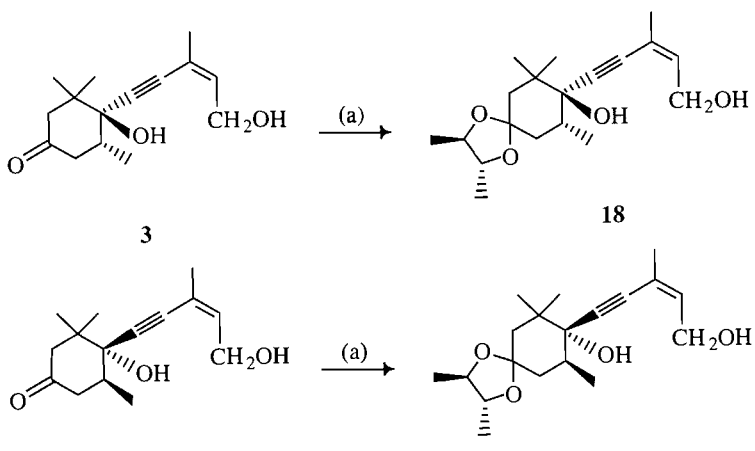

SCHEME 2. (a) (−)-(2*R*,3*R*)-2,3-butanediol, pyridinium *p*-tosylate.

Can. J. Chem. Downloaded from www.nrcresearchpress.com by 88.85.125.76 on 09/07/12
For personal use only.

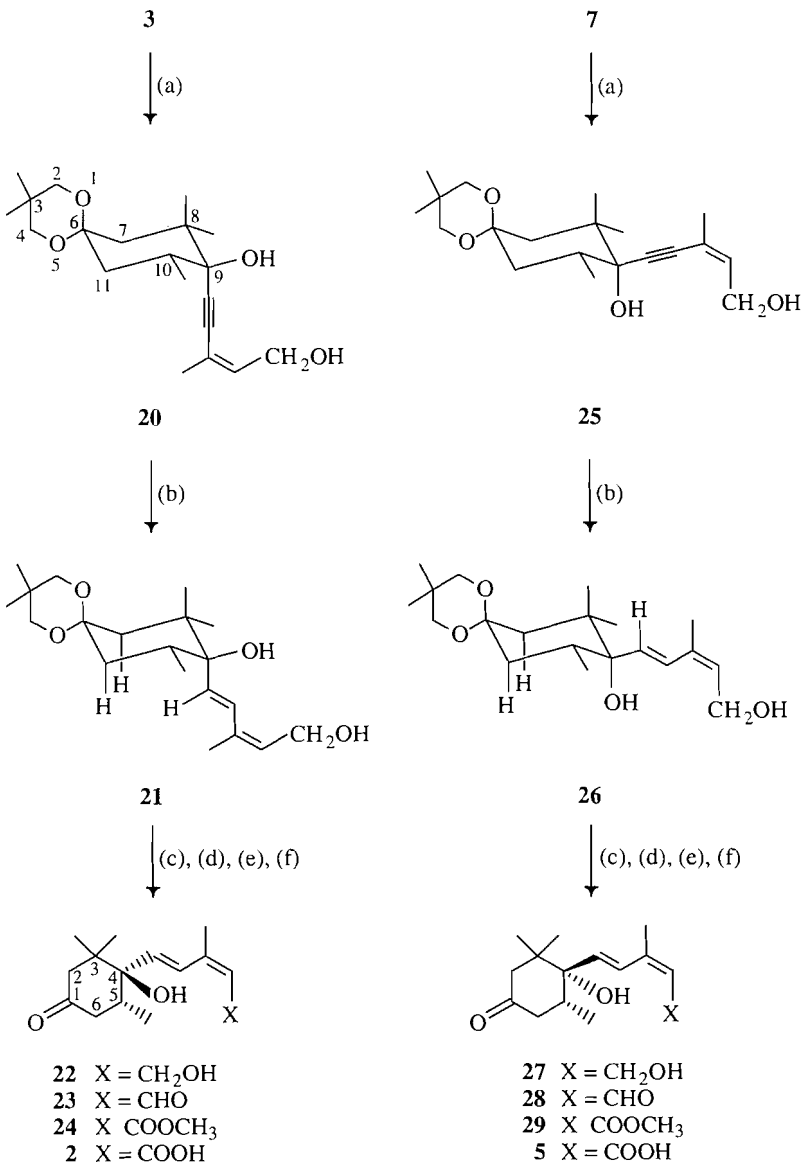

SCHEME 3. (a) 2,2-Dimethyl-1,3-propanediol, pyridinium *p*-tosylate; (b) Redal^{R}; (c) HCl, H_2O; (d) MnO_2; (e) MnO_2, NaCN, HOAc, MeOH; (f) KOH.

equatorial dienol side chain and the olefinic protons are too far away from the protons at C7 and C11 for nOe to be observed.

Our attention was next turned to the synthesis of ABA analogs **4** and **6**, both of which possess the (5*S*) configuration. The starting material required was (+)-(4*R*,6*S*)-4-hydroxy-2,2,6-trimethylcyclohexanone (**11**), which was readily obtained from the epimerization of ketol **10** under basic conditions (15). The conversion of **11** to the (+)-(4*R*,5*S*) acetylenic ABA analog **6** and to (+)-(4*S*,5*S*)-dihydroabscisic acid (**4**) followed a sequence of reactions similar to that employed in the synthesis of the (−) isomers (see Scheme 4). It is worth noting that, unlike the conversion of silyl ether **13** to a mixture of compounds **14** and **15** (see above), only one addition product **31** was obtained in the reaction between silyl ether **30** and the dianion of (*Z*)-3-methylpent-2-en-4-yn-1-ol.

As in the synthesis of (−) enantiomer **3**, the optical purity of the (+) acetylenic analog **6** obtained was established by converting it to a single ketal **19**, which could be differentiated from the diastereomeric ketal **18**, obtained from **3**, by gc and nmr analyses (see above and Scheme 2).

The ester (−)-(4*R*,5*R*)-methyl dihydroabscisate (**24**) and its (+)-(4*S*,5*S*) enantiomer (**37**) were found to be resolvable on the Chiracel OD chiral high performance liquid chromatography (hplc) column using 10% isopropanol and 90% hexane as the eluent at a flow rate of 1.0 mL min^{-1} (21, 22). Compound **24** had a retention time of 10.7 min, whereas its enantiomer **37** had a shorter retention time of 8.7 min under these conditions. Both the ester **24** and its enantiomer **37** obtained in our synthesis were found to be 100% optically pure by this method of analysis.

Furthermore, the optical purity of our synthetic (−)-(4*R*,5*R*)-dihydroabscisic acid (**2**) and its enantiomer (+)-(4*S*,5*S*)-dihydroabscisic acid (**4**) was confirmed by recording the ^{1}H nmr spectra of their sodium salts in D_2O with γ-cyclodextrin as the chiral complexing agent (23, 24). Under these conditions, the

Can. J. Chem. Downloaded from www.nrcresearchpress.com by 88.85.125.76 on 09/07/12
For personal use only.

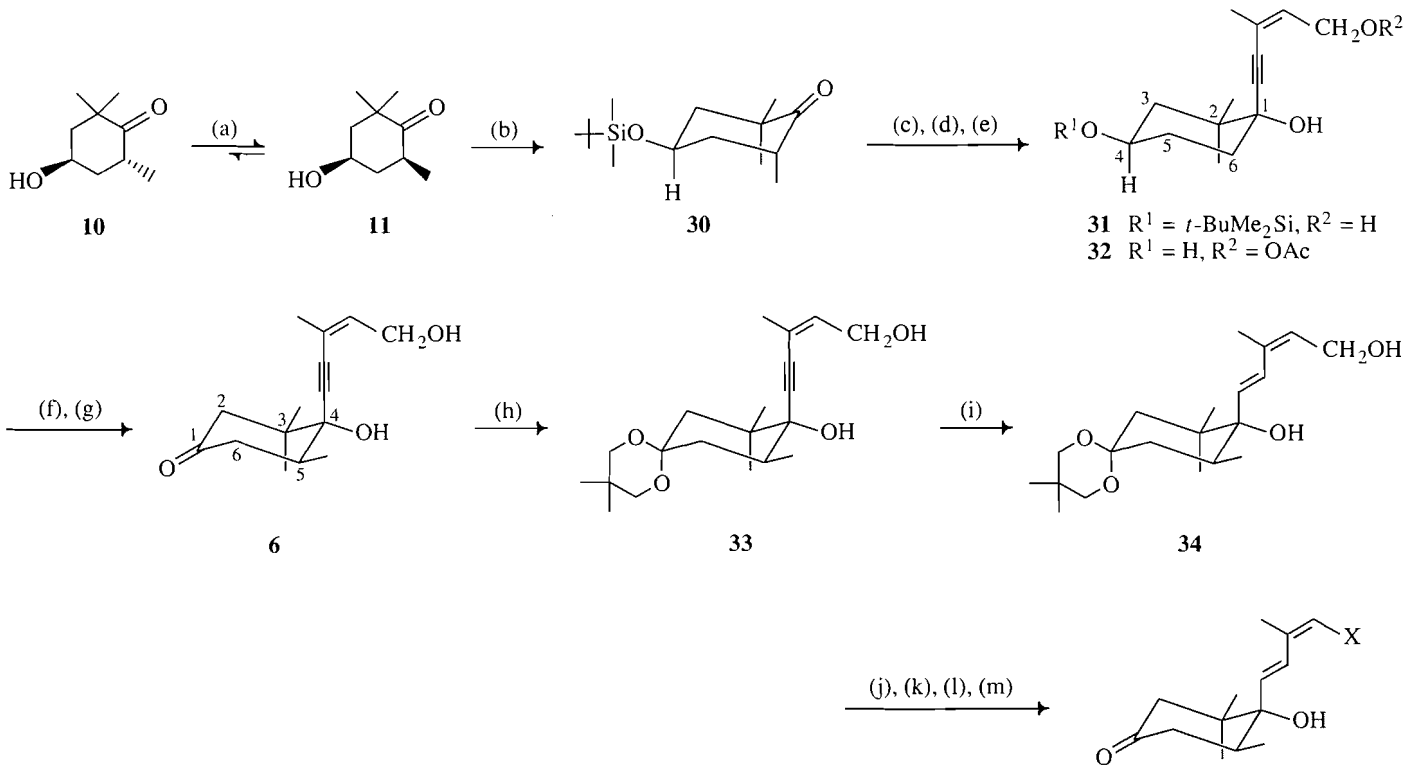

SCHEME 4. (a) NaOH; (b) *t*-BuMe$_2$SiCl, imidazole; (c) (*Z*)-3-methylpent-2-en-4-yn-1-ol, 2 *n*-BuLi; (d) Ac_2O, pyridine; (e) HOAc, H_2O; (f) pyridinium dichromate; (g) NaOH, MeOH; (h) 2,2-dimethyl-1,3-propanediol, pyridinium *p*-tosylate; (i) Redal^R; (j) HCl, H_2O; (k) MnO_2; (l) MnO_2, NaCN, HOAc, MeOH; (m) KOH.

spectra of mixtures of **2** and **4** showed doubling of the two vinyl proton doublets at 6.2 ppm and 7.3 ppm, as well as the doublet at 2.6 ppm due to the axial proton at C2, as two diastereomeric complexes were formed between cyclodextrin and the salts of compounds **2** and **4**. Doubling of signals was not observed when spectra of the synthetic samples of **2** and **4** were separately recorded under the same conditions.

An attempt was made to synthesize the (−) analogs **2** and **3** from (−)-(6*R*)-2,2,6-trimethylcyclohexan-1,4-dione (**9**) by a more direct route depicted in Scheme 5. Initial attempts to protect the less hindered ketone group in **9** by ketalization with ethylene glycol and *p*-toluenesulfonic acid as catalyst (25) resulted in loss of optical activity and a mixture of mono- and diketals. More success was met when treatment of **9** with 1.1 equivalent of 2,2-dimethyl-1,3-propanediol and a catalytic amount of pyridinium *p*-tosylate proceeded in 100% regioselectivity to give the monoketal **38**, which was optically active. The ^{1}H nmr spectrum of **38** did not show any doubling of the signals when γ-cyclodextrin was added as the chiral complexing agent (see above). Under the same conditions, two sets of doublet of doublets at about 2.3–2.6 ppm were observed for the equatorial proton at C7 of the racemate (±)-**38**, which was prepared from (±)-**9** (25). Since doubling of the C7 proton signals could be detected in the spectrum of a 4:1 mixture of **38** and its racemate, the monoketal **38** was estimated to be at least 90% optically pure. The acetylenic analog **3** and the (−)-dihydroabscisic acid **2** were prepared from **38** by the route shown in Scheme 5 and were found to be approximately 85% optically pure using the different methods described above.

The optically active ABA analogs obtained are being subjected to various biological tests involving germination and induction of cold hardiness. The (−)-(4*S*,5*R*) acetylenic analog **3** has been found to be more potent than its racemic counterpart in stimulating the release of α-amylase in the germination of barley.[6] The metabolism of the optically active analogs in plants is currently under investigation. Details of these studies will be reported elsewhere.

Experimental

General

Melting points (mp) are uncorrected and were recorded on an Ernst Leitz Wetzlar hot-stage melting point apparatus. Gas chromatographic (gc) separations were carried out with a Varian 3700 instrument equipped with a DB-1701 or a DB-5 capillary column (J and W Scientific, 30 m) and a flame ionization detector. Helium at a flow rate of about 2.5 cm min^{-1} was used as the carrier gas. High performance liquid chromatographic (hplc) analyses were carried out with an instrument consisting of a Spectra-Physics SP8700 solvent delivery

[6]R. Hill, Department of Plant Science, University of Manitoba, personal communication.

Can. J. Chem. Downloaded from www.nrcresearchpress.com by 88.85.125.76 on 09/07/12
For personal use only.

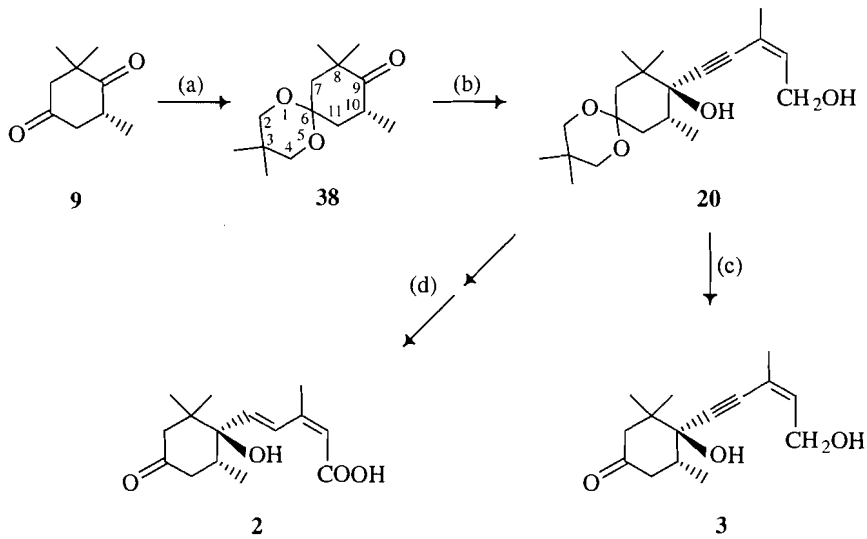

SCHEME 5. (a) 2,2-Dimethyl-1,3-propanediol, pyridinium tosylate; (b) (*Z*)-3-methylpent-2-en-4-yn-1-ol, 2 *n*-BuLi; (c) HCl, H_2O; (d) see Scheme 3.

system and a Spectroflow 773 variable wavelength absorbance detector (Kratos Analytical Instrument). Infrared (ir) spectra were recorded on a Perkin–Elmer 257 grating infrared spectrophotometer using $CHCl_3$ as solvent and matching NaCl cavity cells (0.2 mm). Proton nuclear magnetic resonance (^{1}H nmr, 360 MHz) spectra and carbon-13 (^{13}C nmr, 90.55 MHz) spectra were recorded on a Bruker AM-360-WB spectrometer with $CDCl_3$ as solvent. The 90 MHz ^{1}H nmr spectra were recorded on a Perkin–Elmer EM390 nmr spectrometer. ^{1}H chemical shifts (δ) and coupling constants (J) are reported as if they are first order. The abbreviations ax and eq are used to indicate axial and equatorial protons, respectively. Low resolution mass spectra were obtained by using a DB-5 column (60 m) in a Finnigan–Mat 4000 E instrument with an Incos 2300 data system in the electron impact (eims) or chemical ionization (cims) mode. Mass spectral data are reported in mass to charge units (m/z) with the relative intensities as percentages of the base peak given in parentheses. High resolution mass spectra (hrms) were recorded in the electron impact mode using a VG70-250SEQ instrument with a Digital PDP 11/73 data system. Unless otherwise stated, all spectroscopic analyses were performed on intermediates and products that were at least 95% pure by gc analysis. Elemental analyses (Anal.) were performed by the Microanalytical Laboratory of the Department of Chemistry at the University of Alberta.

Flash column chromatography was performed using E. Merck silica gel 60 (230–400 mesh). E. Merck precoated glass plates of silica gel 60 F254 (0.25 or 1.0 mm) were used in preparative thin-layer chromatography (tlc). E. Merck silica gel 60 F254 plates (0.2 mm) with aluminium sheet backing were used in analytical tlc. Ultraviolet active materials were detected under an ultraviolet (uv) lamp. The plates were then dipped into a solution of phosphomolybdic acid and slowly heated on a hot plate to visualize the spots. Preparative tlc was also performed on the Chromatotron (Harrison Research) with circular glass plates precoated with silica gel F254 (1, 2, or 4 mm), where the radial flow of eluent and sample were centrifugally accelerated.

The solvent tetrahydrofuran (THF) was dried by distillation from sodium and benzophenone. *N,N*-Dimethyl formamide (DMF) was dried by distillation from calcium hydride and was stored over molecular sieves.

*(−)-(6R)-2,2,6-Trimethylcyclohexan-1,4-dione (**9**)*

Compound **9** was prepared according to the procedure reported by Leuenberger *et al.* (15). Active dry yeast (Fleischmann's Quick Rise, 12 g) suspended in warm distilled water (450 mL, 45°C) was added to a solution of sucrose (BDH, 25 g) in distilled water (500 mL). The resulting mixture was stirred at room temperature for 30 min. Oxoisophorone (**8**) (Fluka, 10.0 g, 0.065 mol) was then added, followed by distilled water (50 mL) and anti-foaming agent (Antifoam C Emulsion, Sigma, 4 drops). A gentle stream of air was bubbled through the mixture while it was stirred at room temperature for 9 days and, starting on the 5th day, extra portions of yeast (5 g) and sucrose (10 g) were added daily. The fermentation was terminated after 9 days by filtering the mixture through a bed of Celite^R by suction. The filtrate was extracted with CH_2Cl_2 (3 × 150 mL). The organic extract was dried over anhydrous Na_2SO_4 and concentrated to give yellowish oily crystals (8.5 g), which were recrystallized from ether-hexane (1:1) to give diketone **9** as colorless needles (4.4 g, 44%); mp 93–94°C (lit. (15) mp 91–92°C); $[\alpha]_D$ −269.2° (*c* 0.98, CH_3OH) (lit. (15) $[\alpha]_D$ −270° (*c* 0.4, CH_3OH)); ir: 1720 cm^{-1}; ^{1}H nmr (90 MHz) δ: 1.05 (d, J = 6 Hz, 3H, $CHCH_3$), 1.02 and 1.10 (2s, 6H, $2CH_3$), 2.3–4.4 (m, 5H, CH_2 and CH).

*(−)-(4R,6R)-4-Hydroxy-2,2,6-trimethylcyclohexanone (**10**)*

A solution of (−)-(6*R*)-2,2,6-trimethyl-1,4-cyclohexandione (**9**) (2.0 g, 13 mmol) in dry THF (50 mL) was stirred under argon and cooled to −65°C with a Dry Ice – acetone bath. Lithium tri-*sec*-butylborohydride (L-Selectride^R, Aldrich, 1 M in THF, 15 mL, 15 mmol) was added slowly such that the temperature of the reaction mixture did not rise above −60°C. Thirty minutes after the addition of L-Selectride^R was completed, the reaction mixture was poured, with stirring, into an ice-cold mixture of saturated NaCl (100 mL) and 1 M HCl (20 mL). The organic and aqueous layers were separated and the aqueous layer was extracted with CH_2Cl_2. The combined THF and CH_2Cl_2 layers were washed with H_2O, saturated $NaHCO_3$, and H_2O. Then most of the solvent was removed by evaporation. The residue was dissolved in hexane (30 mL) and cooled in an ice-water bath. A mixture of 30% H_2O_2 and water was added. After 2 h of stirring the aqueous and hexane layers were separated. The aqueous layer was extracted with CH_2Cl_2. The hexane and CH_2Cl_2 layers were combined, washed successively with H_2O, saturated $NaHSO_3$, H_2O, saturated $NaHCO_3$, H_2O, and dried over anhydrous Na_2SO_4. Evaporation of solvent gave a pale yellow liquid (2.3 g), which on purification by flash chromatography (75% ether + 25% hexane) gave *trans* ketol **10** as a colorless oil (1.2 g, 60%), tlc R_f 0.4 (75% ether + 25% hexane). The product, **10**, crystallized on storage at −10°C and was recrystallized from ether–hexane to give colorless needles, mp 45.0–47.5°C (lit. (15) mp 49.5–50.5°C); $[\alpha]_D$ −108.9° (*c* 1.06, CH_3OH) (lit. (15) $[\alpha]_D$ −113.9° (*c* 0.8, CH_3OH)); ir: 3460, 1700 cm^{-1}; ^{1}H nmr δ: 1.01 (d, J = 6.9 Hz, 3H, $CHCH_3$), 1.02 (s, 3H, CH_3), 1.33 (s, 3H, CH_3), 1.66 (ddd, J = 13.9, 13.9, 3.4 Hz, 1H, H-5_{ax}), 1.77 (dd, J = 14.5, 3.8 Hz, 1H, H-3_{ax}), 1.96 (ddd, J = 14.5, 3.8, 3.2 Hz, 1H, H-3_{eq}), 2.10 (dddd, J =

Can. J. Chem. Downloaded from www.nrcresearchpress.com by 88.85.125.76 on 09/07/12
For personal use only.

13.9, 5.6, 4.4, 3.2 Hz, 1H, H-5_{eq}), 3.14 (m, 1H, H-6_{ax}), 4.2 (quintet or dddd, J = 3.5 Hz, 1H, H-4_{eq}); eims m/z: 156 (M^+, 10), 138 (8), 88 (41), 83 (89), 56 (100).

A more polar product was also isolated as a colorless oil from the flash column. It was identified as the partially racemized *cis* ketol (i.e., a mixture of **11** and **12**) (0.52 g, 26%), tlc R_f 0.3; $[\alpha]_D$ −65.7° (*c* 1.02, CH_3OH) (lit. (15) (−)-*cis*-ketol **12**, $[\alpha]_D$ −104.2° (*c* 0.8, CH_3OH); mp 51.5–52.5°C). The spectral data of the product were identical to those described below for *cis* ketol **11**.

(−)-(4R,6R)-4-tert-Butyldimethylsiloxy-2,2,6-trimethylcyclohexanone (13)

A mixture of *trans* ketol **10** (115 mg, 0.73 mmol), *tert*-butyldimethylsilyl chloride (Aldrich, 202 mg, 1.27 mmol), imidazole (100 mg, 1.47 mmol), and dry DMF (3 mL) was stirred at room temperature under an argon atmosphere for 1.5 h. Then water was added and the mixture was extracted with ether (3×). The ether extract was washed with saturated NaCl and dried over anhydrous Na_2SO_4. Evaporation of solvent gave a colorless oil (325 mg), which was distilled using the Kugelrohr apparatus. After some forerun that was discarded, the desired silyl ether **13** was collected as a colorless oil at 150–180°C, 9–10 Torr (1 Torr = 133.3 Pa) (156 mg, 80%). The product solidified on storage at −10°C to form colorless crystals, mp 29.5–31.5°C; $[\alpha]_D$ −65.1° (*c* 1.06, CH_3OH); ir: 1710 cm^{-1}; ^1H nmr δ: 0.06 and 0.07 (2s, 6H, CH_3SiCH_3), 0.89 (s, 9H, $3CH_3$), 0.98 (s, 3H, CH_3), 0.98 (d, J = 6.4 Hz, 3H, $CHCH_3$), 1.32 (s, 3H, CH_3), 1.57 (ddd, J = 13.4, 13.2, 2.7 Hz, H-5_{ax}), 1.65 (dd, J = 14.2, 3.4 Hz, 1H, H-3_{ax}), 1.88 (ddd, J = 14.2, 3.3, 3.2 Hz, 1H, H-3_{eq}), 1.99 (dddd, J = 13.4, 5.3, 3.3, 3.2 Hz, 1H, H-5_{eq}), 3.16 (ddq, J = 13.2, 5.3, 6.4 Hz, 1H, H-6_{eq}), 4.08 (quintet or dddd, J = 3.2 Hz, 1H, H-4_{eq}); eims m/z: 255 (M^+ − 15, 1), 213 (60), 171 (78), 121 (43), 75 (100). Exact Mass (hrms) calcd. for $C_{15}H_{30}O_2Si$: 270.2015; found: 270.2015.

(−)-1(Z)-(1S,4R,6R)- and (−)-1(Z)-(1R,4R,6R)-1-(5-Acetoxy-3-methylpent-3-en-1-ynyl)-2,2,6-trimethylcyclohexan-1,4-diol (16 and 17)

A solution of *Z*-3-methylpent-2-en-4-yn-1-ol (Fluka, 1.60 g, 16.7 mmol) in dry THF (20 mL) under an argon atmosphere was cooled to about −60°C in a Dry Ice – acetone bath. *n*-Butyllithium (Aldrich, 1.6 M in hexane, 19 mL, 30.4 mmol) was added dropwise with stirring. After all the *n*-butyllithium had been added the reaction mixture, which was orange in color, was allowed to warm up to −5°C over 30 min. Then it was again cooled to −60°C and a solution of silyl ether **13** (2.7 g, 10 mmol) in dry THF (20 mL) was added dropwise. After the addition had been completed the reaction mixture was allowed to warm to 0°C over 90 min before it was poured into water and extracted with ether (3×). The combined organic extracts were washed with saturated NaCl (2×) and dried over anhydrous Na_2SO_4. Evaporation of solvent gave a yellow oil (4.5 g) as the crude product. Purification of the product by flash column chromatography (75% ether + 25% hexane as eluent) followed by distillation (Kugelrohr, 180–200°C, 0.03 Torr) gave a mixture of compounds **14** and **15** as a yellow oil (2.82 g, 76% yield), gc retention times (DB1701 column, 70–240°C at 10°C min^{-1}) 20.05 min and 19.77 min, ratio of peak areas about 8:1, respectively.

The mixture of compounds **14** and **15** (2.82 g, 7.6 mmol) was dissolved in pyridine (15 mL). A mixture of acetic anhydride (2.35 g, 23.0 mmol) and pyridine (5 mL) was added, followed by 4-dimethylaminopyridine (Aldrich, 32 mg, 0.26 mmol). The reaction mixture was stirred at room temperature for 1 h, poured into water, and extracted with hexane (3×). The combined organic extract was washed with saturated NaCl and dried over anhydrous Na_2SO_4. Removal of solvent gave a mixture of acetates as a pale yellow oil (3.72 g), which was desilated without purification to give compounds **16** and **17** by the procedure below. Gas chromatographic analysis of the crude acetate mixture (DB1701 column, 70–240°C at 10°C min^{-1}) showed two components in the ratio of 8:1 (retention times 20.26 min and 20.12 min, respectively).

The crude acetates obtained in the above procedure were stirred with glacial acetic acid (30 mL) and H_2O (10 mL), and the mixture was heated to 70°C under argon for 20 h. After cooling to room temperature, the reaction mixture was diluted with water and extracted with $CHCl_3$ (3×). The organic extract was washed with H_2O, then with saturated $NaHCO_3$, and dried over anhydrous Na_2SO_4. Evaporation of solvent gave a yellow oil (2.98 g) as the crude product. Separation by flash column chromatography (75% ether + 25% hexane) followed by preparative tlc (same eluent) gave compounds **16** (1.26 g, 56% overall yield) and **17** (0.15 g, 7% overall yield).

Compound **16**, colorless oil; gc (DB5 column, 70–240°C at 10°C min^{-1}) retention time 18.37 min; tlc (90% ether + 10% hexane) R_f about 0.30; $[\alpha]_D$ −18.4° (*c* 1.02, CH_3OH); ir: 3610, 3400, 1735 cm^{-1}; ^1H nmr δ: 1.05 (d, J = 6.6 Hz, $CHCH_3$), 1.08 and 1.22 (2s, 6H, $2CH_3$), 1.55–1.75 (m, 4H, $2CH_2$), 1.89 (m, 3H, vinyl CH_3), 2.03 (s, 3H, CH_3COO), 2.34 (m, 1H, $CHCH_3$), 4.02 (m, 1H, CHOH), 4.71 (dd, J = 7.0, 1.0 Hz, 2H, CH_2O), 5.77 (ddq, J = 7.0, 7.0, 1.5 Hz, 1H, =CH); ^{13}C nmr δ: 16.05, 20.88, 23.08, 23.28, and 27.39 ($5CH_3$), 38.77 (C2), 31.92, 40.12 and 44.47 (CH_2 and CH), 62.80 and 67.55 (CH_2O and CHOH), 79.01 (COH), 84.89 and 95.33 (2 acetylenic C), 123.52 (=C), 130.03 (=CH), 170.83 (C=O); eims m/z: 234 (M^+ − 60, 6), 178 (28), 148 (100).

Compound **17**, colorless oil; gc (DB5 column, 70–240°C at 10°C min^{-1}) retention time 18.50 min; tlc (90% ether + 10% hexane) R_f about 0.35; $[\alpha]_D$ −28.3° (*c* 0.92, CH_3OH); ir: 3630, 3500, 1735 cm^{-1}; ^1H nmr δ: 1.05 (s, 3H, CH_3), 1.06 (d, J = 5.2 Hz, 3H, $CHCH_3$), 1.27 (s, 3H, CH_3), 1.43 (ddd, J = 14.6, 2.5, 2.5 Hz, 1H, H-3_{eq}), 1.52 (dddd, J = 14.3, 3.9, 2.5, 2.5 Hz, 1H, H-5_{eq}), 1.68 (ddd, J = 14.3, 12.6, 3.3 Hz, 1H, H-5_{ax}), 1.76 (dd, J = 14.6, 3.5 Hz, 1H, H-3_{ax}), 1.89 (m, 3H, vinyl CH_3), 2.03 (s, 3H, CH_3COO), 2.33 (m, 1H, $CHCH_3$), 4.07 (m, 1H, CHOH), 4.72 (dd, J = 7.0, 1.0 Hz, 2H, CH_2O), 5.76 (ddq, J = 7.0, 7.0, 1.5 Hz, 1H, =CH); ^{13}C nmr δ: 16.81, 20.91, 23.21, 26.78, and 27.13 ($5CH_3$), 38.17 (C2), 30.77, 35.75, and 40.29 ($2CH_2$ and CH), 62.79 and 67.04 (CH_2O and CHOH), 76.53 (COH), 83.52 and 97.37 (2 acetylenic C), 123.62 (=C), 129.99 (=CH), 170.86 (C=O); eims m/z: 234 (M^+ − 60, 3), 178 (10), 148 (100).

(−)-4(Z)-(4S,5R)-4-Hydroxy-4-(5-hydroxy-3-methylpent-3-en-1-ynyl)-3,3,5-trimethylcyclohexanone (3)

To a solution of compound **16** (1.21 g, 4.1 mmol) in CH_2Cl_2 (50 mL) was added pyridinium dichromate (Aldrich, 5.0 g, 13.3 mmol). The mixture was stirred at room temperature for 5 h before it was filtered through a short column of Florisil^R. The residue and Florisil^R were rinsed with ether and CH_2Cl_2 and the rinsing was combined with the filtrate. Evaporation of solvent gave a pale yellow oil (1.35 g), which was purified by flash chromatography (75% ether + 25% hexane) to give a keto-acetate as colorless crystals (1.02 g, 84%). A small sample of the product was recrystallized twice from ether–hexane to give colorless needles, mp 120.0–122.0°C ((±)-keto-acetate mp 104–106°C); $[\alpha]_D$ −22.9° (*c* 0.99, CH_3OH); ir: 1720 cm^{-1}; ^1H nmr δ: 0.98 (s, 3H, CH_3), 1.14 (m, 3H, $CHCH_3$), 1.20 (s, 3H, CH_3), 1.92 (d, J = 1.4 Hz, 3H, vinyl CH_3), 2.03 (s, 3H, CH_3COO), 2.10 (dd, J = 14.3, 1.5 Hz, 1H, H-2_{eq}), 2.31 (m, 4H, $CHCH_3$, CH_2 at C6 and OH), 2.65 (d, J = 14.3 Hz, 1H, H-2_{ax}), 4.74 (dd, J = 7.1, 0.9 Hz, 2H, CH_2O), 5.84 (ddq, J = 7.1, 7.1, 1.5 Hz, 1H, =CH); eims m/z: 292 (M^+, about 2), 232 (18), 176 (45), 148 (54), 120 (31), 106 (100). Exact Mass (hrms) calcd. for $C_{17}H_{24}O_4$: 292.1675; found: 292.1650. Anal. calcd. for $C_{17}H_{24}O_4$: C 69.82, H 8.28%; found: C 69.50, H 8.32%.

The keto-acetate (1.0 g, 3.4 mmol) was hydrolyzed by stirring with 5 M NaOH (1 mL) and methanol (30 mL) at room temperature for 1 h. The solution was then concentrated, and the residue was diluted with H_2O and extracted with ether. The organic extract was washed with H_2O and dried over anhydrous Na_2SO_4. Evaporation of solvent gave a yellow oil (0.86 g), which after purification by flash column chromatography (75% ether + 25% hexane) gave the desired compound **3** as colorless crystals (0.74 g, 87%). A small sample of the product was recrystallized from ether–hexane to give colorless plates, mp 97–98°C ((±)-**3** mp 92–98°C, lit. (9) (±)-**3** was an oil); $[\alpha]_D$ −25.8° (*c* 0.93, CH_3OH); ir: 3400, 1710 cm^{-1}; ^1H nmr δ: 0.98 (s, 3H, CH_3), 1.14 (m, 3H, $CHCH_3$), 1.20 (s, 3H, CH_3), 1.91 (m, 3H, vinyl

Can. J. Chem. Downloaded from www.nrcresearchpress.com by 88.85.125.76 on 09/07/12
For personal use only.

CH_3), 2.08 (d, J = 14.3 Hz, 1H, H-2_{ax}), 2.30 (m, 3H, CH_2 at C6 and C*H*CH_3), 2.66 (dd, J = 14.3, 0.7 Hz, 1H, H-2_{eq}), 4.32 (d, J = 5.4 Hz, 1H, CH_2OH), 5.91 (ddq, J = 6.7, 6.6, 1.5 Hz, 1H, =CH); ^{13}C nmr δ ($CDCl_3/C_6D_6$, 1:1): 16.43, 20.60, 23.04, and 25.74 (4q, $4CH_3$), 37.33 (d, CH), 41.98 (s, C3), 46.92, 52.82, and 61.15 (3t, $3CH_2$), 77.22 (s, COH), 86.19 and 93.05 (2s, 2 acetylenic C), 119.65 (s, =C), 136.55 (d, =CH), 208.48 (s, C=O); cims m/z: 250 (M^+, 11), 232 (2), 179 (33), 165 (31), 163 (21), 152 (40), 148 (56), 139 (42), 123 (38), 55 (100). Exact Mass (hrms) calcd. for $C_{15}H_{22}O_3$: 250.1569; found: 250.1575. Anal. calcd. for $C_{15}H_{22}O_3$: C 71.95, H 8.86%; found: C 71.84, H 8.79%.

(−)-4(Z)-(4R,5R)-4-Hydroxy-4-(5-hydroxy-3-methylpent-3-en-1-ynyl)-3,3,5-trimethylcyclohexanone (7)

Compound **17** (140 mg, 0.47 mmol) was oxidized with pyridinium dichromate (850 mg, 2.26 mmol) in CH_2Cl_2 (15 mL) by the procedure described above (see the conversion of compound **16** to compound **3**) to give a keto-acetate as a colorless oil (90 mg, 70%), $[\alpha]_D$ −26.0° (*c* 0.78, CH_3OH); ir: 3630, 1730 cm^{-1}; ^{1}H nmr δ: 1.03 (s, 3H, CH_3), 1.17 (d, J = 6.3 Hz, 3H, CHCH_3), 1.19 (s, 3H, CH_3), 1.89 (m, 3H, vinyl CH_3), 1.95 (dd, J = 13.8, 2.3 Hz, 1H, H-2_{eq}), 2.04 (s, 3H, CH_3COO), 2.16 (ddd, J = 13.2, 3.8, 2.3 Hz, 1H, H-6_{eq}), 2.31 (ddq, J = 12.4, 3.8, 6.3 Hz, 1H, C*H*CH_3), 2.39 (dd, J = 13.2, 12.4 Hz, 1H, H-6_{ax}), 2.73 (br d, J = 13.8 Hz, 1H, H-2_{ax}), 4.73 (dd, J = 7.0, 0.9 Hz, 2H, CH_2O), 5.81 (ddq, J = 7.0, 7.0, 1.5 Hz, 1H, =CH); ms m/z: 232 (M^+ − 60, 24), 176 (47), 148 (41), 120 (23), 106 (100). Exact Mass (hrms) (M^+ − 60 peak) calcd. for $C_{15}H_{20}O_2$: 232.1463; found: 232.1485.

The keto-acetate (90 mg, 0.3 mmol) was hydrolyzed by treating with 5 M KOH (5 drops) and methanol (10 mL) as described above to give compound **7** as a colorless oil (69 mg, 92%) that would not crystallize ((±)-**7** crystallized on storage at −10°C to give colorless crystals, mp 72.5–79.5°C); $[\alpha]_D$ −16.4° (*c* 0.62, CH_3OH); ir: 3630, 1710 cm^{-1}; ^{1}H nmr δ: 1.03 (s, 3H, CH_3), 1.17 (d, J = 6.4 Hz, 3H, CHCH_3), 1.19 (s, 3H, CH_3), 1.88 (m, 3H, vinyl CH_3), 1.96 (dd, J = 13.8, 2.3 Hz, 1H, H-2_{eq}), 2.16 (ddd, J = 13.3, 3.4, 2.3 Hz, 1H, H-6_{eq}), 2.32 (m, 1H, C*H*CH_3), 2.39 (ddd, J = 13.3, 12.8, 0.8 Hz, 1H, H-6_{ax}), 2.72 (ddd, J = 13.8, 0.8, 0.8 Hz, 1H, H-2_{ax}), 4.29 (dd, J = 6.8, 1.0 Hz, 2H, CH_2OH), 5.88 (ddq, J = 6.8, 6.8, 1.5 Hz, 1H, =CH); ^{13}C nmr δ: 16.76, 23.13, 24.98, and 25.41 (4q, $4CH_3$), 37.64 (d, CH), 43.06 (s, C3), 44.25, 49.48, and 61.27 (3t, $3CH_2$), 75.25 (s, COH), 84.47 and 94.85 (2s, 2 acetylenic C), 120.26 (s, =C), 136.08 (d, =CH), 210.86 (s, C=O); ms m/z: 250 (M^+, very weak), 232 (5), 179 (23), 165 (66), 106 (100). Exact Mass (hrms) calcd. for $C_{15}H_{22}O_3$: 250.1569; found: 250.1570.

(−)-8(Z)-(2R,3R,8S,9R)-8-(5-Hydroxy-3-methylpent-3-en-1-ynyl)-2,3,7,7,9-pentamethyl-1,4-dioxaspiro[4,5]decan-8-ol (18)

A mixture of (−)-4(*Z*)-(4*S*,5*R*)-4-hydroxy-4-(5-hydroxy-3-methylpent-3-en-1-ynyl)-3,3,5-trimethylcyclohexanone (**3**) (7.8 mg, 0.03 mmol), (−)-(2*R*,3*R*)-butanediol (Aldrich, 23.6 mg, 0.26 mmol), pyridinium *p*-tosylate (Aldrich, 3.7 mg, 0.01 mmol), and benzene (4 mL) was heated to reflux under a Dean–Stark separator for 15 h (10, 18). The reaction mixture was then allowed to cool to room temperature, washed with saturated Na_2CO_3 and water, and dried over anhydrous Na_2SO_4. Evaporation of solvent gave a colorless oil (10 mg), which was purified on the Chromatotron (1 mm silica gel plate, 75% ether + 25% hexane) to give ketal **18** as a colorless oil (6.8 mg, 70%), gc retention time (DB1701 column, 70–240°C at 10°C min^{-1}) 18.57 min; $[\alpha]_D$ −30.0° (*c* 0.6, CH_3OH); ir: 3620 cm^{-1}; ^{1}H nmr δ: 1.04 (d, J = 6.5 Hz, 3H, CHCH_3 at C9), 1.08 and 1.11 (2s, 3H each, $2CH_3$), 1.18 and 1.22 (2d, J = 6.0 Hz, 3H each, CHCH_3 at C2 and C3), 1.70 (m, 2H, H-10), 1.52 (dd, J = 14.1, 2.6 Hz, 1H, H-6_{eq}), 1.76 (d, J = 14.1 Hz, 1H, H-6_{ax}), 1.86 (q, J = 1.1 Hz, 3H, vinyl CH_3), 2.22 (m, 1H, C*H*CH_3 at C9), 3.50 and 3.60 (2dq, J = 8.3, 6.0 Hz, 1H each, C*H*CH_3 at C2 and C3), 4.28 (dd, J = 6.7, 0.9 Hz, 2H, CH_2OH), 5.84 (ddq, J = 6.7, 6.7, 1.5 Hz, 1H, =CH); ^{13}C nmr δ: 16.17, 16.88, 17.10, 21.27, 23.27, and 27.38 (6q, $6CH_3$), 34.63 (d, C9), 39.84 (s, C7), 43.80 and 46.57 (2t, C6 and C10), 61.31 (t, CH_2OH), 77.37 and 78.27 (2d, C2 and C3), 78.47 (s, C8), 85.48 and 94.09 (2s, 2 acetylenic C), 107.15 (s, C5), 120.47 (s, =C), 135.73 (d, =CH); cims (isobutane) m/z: 321 (M^+ + 1, very weak), 305. Exact Mass (hrms) calcd. for $C_{19}H_{30}O_4$: 322.2144; found: 322.2135.

(−)-(9Z)-(9S,10R)-9-(5-Hydroxy-3-methylpent-3-en-1-ynyl)-3,3,8,8,10-pentamethyl-1,5-dioxaspiro[5,5]undecan-9-ol (20)

A mixture of (−)-4(*Z*)-(4*S*,5*R*)-4-hydroxy-4-(5-hydroxy-3-methylpent-3-en-1-ynyl)-3,3,5-trimethylcyclohexanone (**3**) (620 mg, 2.49 mmol), 2,2-dimethyl-1,3-propanediol (Aldrich, 460 mg, 4.4 mmol), pyridinium *p*-tosylate (Aldrich, 19 mg, 0.07 mmol), and benzene (18 mL) was heated to reflux under a Dean–Stark separator for 4 h. The reaction mixture was then allowed to cool to room temperature, and washed with saturated Na_2CO_3, saturated NaCl, and water. After drying over anhydrous Na_2SO_4 and evaporation of solvent, a yellow oil was obtained as the crude product (1 g). Purification by flash column chromatography (75% ether + 25% hexane) gave the desired ketal **20** as a pale yellow oil (750 mg, 90%); $[\alpha]_D$ −29.4° (*c* 1.02, CH_3OH); ir: 3610, 3440, 1110, and 1090 cm^{-1}; ^{1}H nmr δ: 0.83, 1.04, 1.05, 1.06, 1.09, and 1.11 (15H, $5CH_3$), 1.53–1.61 (m, 2H, 2 axial H at C7 and C11), 1.84 (m, 3H, vinyl CH_3), 1.98 (ddd, J = 13.8, 3.4, 3.4 Hz, 1H, H-11_{eq}), 2.18 (m, 1H, CH), 2.51 (dd, J = 14.3, 3.2 Hz, 1H, H-7_{eq}), 3.36 and 3.38 (2dd, J = 11.3, 1.9 Hz, 2H, 2 equatorial H at C2 and C4), 3.55 (d, J = 11.3 Hz, 2H, 2 axial H at C2 and C4), 4.29 (br s, 2H, CH_2OH), 5.50 (ddq, J = 6.7, 6.7, 1.5 Hz, 1H, =CH); eims (trimethylsilyl ether) m/z: 408 (M^+ of trimethylsilyl ether), 155 (100). Exact Mass (hrms) (trimethylsilyl ether) calcd. for $C_{23}H_{40}O_4Si$: 408.2696; found: 408.2718.

(−)-9(1E,3Z)-(9R,10R)-9-(5-Hydroxy-3-methyl-1,3-pentadienyl)-3,3,8,8,10-pentamethyl-1,5-dioxaspiro[5,5]undecan-9-ol (21)

A solution of (−)-(9*Z*)-(9*S*,10*R*)-9-(5-hydroxy-3-methylpent-3-en-1-ynyl)-3,3,8,8,10-pentamethyl-1,5-dioxaspiro[5,5]undecan-9-ol (**20**) (730 mg, 2.2 mmol) in dry THF (50 mL) was stirred under an argon atmosphere and cooled with an ice-water bath. Sodium bis(2-methoxyethoxy)aluminium hydride (Redal^R, Aldrich, 3.4 M in toluene, 1.3 mL, 4.4 mmol) was added dropwise. Some frothing occurred as the Redal^R was added. The reaction mixture was stirred at 0°C until the frothing subsided. Then another portion of Redal^R (0.7 mL, 2.2 mmol) was added. After 1.5 h of stirring at 0°C followed by 1 h at room temperature, the reaction was worked up by pouring into H_2O and extracting with ether (3×). The combined organic extracts were washed with saturated NaCl and dried over anhydrous Na_2SO_4. Evaporation of solvent gave a colorless oil (about 1 g) as the crude product, which was usually hydrolyzed by the procedure described below to give compound **22** without purification. A small amount of the crude product was purified on the Chromatotron (75% ether + 25% hexane) to give the desired ketal **21** as a colorless oil; $[\alpha]_D$ −64.4° (*c* 1.02, CH_3OH); ir: 3600, 1600, 1100, 975, 910 cm^{-1}; ^{1}H nmr δ: 0.76, 0.78, 0.85, 1.05, and 1.12 (4s, 1d, 15H, $5CH_3$), 1.34–1.42 (m, 2H, 2 axial H at C7 and C11), 1.85 (d, J = 0.9 Hz, 3H, vinyl CH_3), 1.97 (ddd, J = 14.0, 3.5, 3.5 Hz, 1H, H-11_{eq}), 2.16 (m, 1H, CH), 2.29 (dd, J = 14.6, 3.2 Hz, 1H, H-7_{eq}), 3.40 (m, 2H, 2 equatorial H at C2 and C4), 3.57 and 3.58 (2d, J = 11.2, 11.4 Hz, respectively, 2H, 2 axial H at C2 and C4), 4.31 (d, J = 6.9 Hz, 2H, CH_2OH), 5.54 (t, J = 7 Hz, 1H, =CH), 5.94 (d, J = 15.6 Hz, 1H, =CH), 6.68 (d, J = 15.6 Hz, 1H, =CH).

(−)-4(1E,3Z)-(4R,5R)-4-Hydroxy-4-(5-hydroxy-3-methyl-1,3-pentadienyl)-3,3,5-trimethylcyclohexanone (22)

The crude ketal **21** obtained in the above procedure was hydrolyzed by stirring with 1 M HCl (5 drops) and acetone (50 mL) at room temperature for 2 h. After concentration of the acetone solution, saturated $NaHCO_3$ was added and the mixture was extracted with ether. The organic layer was dried with anhydrous Na_2SO_4 and concentrated to give a yellow oil as the crude product. Flash column chromatography using 90% ether + 10% hexane as eluent gave the desired compound **22** as a colorless oil (338 mg, 60%) that would not crystallize ((±)-**22** crystallized on standing at room temperature and was recrystallized from ether–hexane to give colorless crystals, mp 128°C (sharp));

Can. J. Chem. Downloaded from www.nrcresearchpress.com by 88.85.125.76 on 09/07/12
For personal use only.

Can. J. Chem. Downloaded from www.nrcresearchpress.com by 88.85.125.76 on 09/07/12
For personal use only.

$[\alpha]_D$ −41.6° (*c* 0.98, CH_3OH); ir: 3610, 3450, 1710, 1610, 975 cm^{-1}; ^1H nmr δ: 0.84 (d, *J* = 6.3 Hz, $CHCH_3$), 0.89 and 1.01 (2s, 6H, CH_3), 1.88 (d, *J* = 0.8 Hz, 3H, vinyl CH_3), 2.1–2.3 (m, 4H, H-2_{eq}, CH_2 at C6 and $CHCH_3$), 2.46 (d, *J* = 15.8 Hz, 1H, H-2_{ax}), 4.31 (d, *J* = 7.0 Hz, 2H, CH_2OH), 5.59 (t, *J* = 7.0 Hz, 1H, =CH), 6.07 (d, *J* = 15.6 Hz, 1H, =CH), 6.81 (dd, *J* = 15.6, 0.4 Hz, 1H, =CH); ^{13}C nmr δ: 15.91, 20.78, 22.78, and 25.18 (4q, $4CH_3$), 37.39 (d, CH), 41.64 (s, C3), 47.08, 52.88, and 58.34 (3t, $3CH_2$), 78.12 (s, COH), 128.36, 128.64, and 128.96 (3d, 3 =CH), 134.40 (s, =C), 209.55 (s, C=O); eims (trimethylsilyl ether) *m/z*: 324 (M^+ of trimethylsilyl ether, 3), 73 (100). Exact Mass (hrms) (trimethylsilyl ether) calcd. for $C_{18}H_{32}O_3Si$: 324.2121; found: 324.2109.

*(−)-4(1*E*,3*Z*)-(4*R*,5*R*)-4-Hydroxy-4-(3-methyl-5-oxo-1,3-pentadienyl)-3,3,5-trimethylcyclohexanone (**23**)*[7]

To a solution of compound **22** (300 mg, 1.2 mmol) in acetone (30 mL) was added manganese oxide (2.08 g, 24 mmol). The mixture was stirred at room temperature under a drying tube for 1 h before the manganese oxide was removed by filtration. The solid residue was rinsed with acetone and the rinsing was combined with the filtrate. Evaporation of acetone gave the crude aldehyde **23**, which was usually oxidized to ester **24** (see below) without purification.

A small amount of aldehyde **23** was purified by preparative tlc (90% ether + 10% hexane) followed by recrystallization from ether–hexane to give colorless crystals, mp 106.0–108.5°C; $[\alpha]_D$ −64.5° (*c* 0.38, CH_3OH); ir: 3550, 1715, and 1665 cm^{-1}; ^1H nmr δ: 0.89 (d, *J* = 6.4 Hz, 3H, $CHCH_3$), 0.93 and 1.04 (2s, 6H, $2CH_3$), 2.11 (d, *J* = 1.1 Hz, 3H, vinyl CH_3), 2.15–2.42 (m, CH_2 at C6 and $CHCH_3$), 2.17 (dd, *J* = 14.9, 2.5 Hz, H-2_{eq}), 2.48 (d, *J* = 14.9 Hz, 1H, H-2_{ax}), 5.90 (d, *J* = 7.7 Hz, 1H, =CH), 6.49 and 7.50 (2d, *J* = 15.4 Hz, 2H, 2 =CH), 10.21 (d, *J* = 8.0 Hz, 1H, HC=O). Exact Mass (hrms) calcd. for $C_{15}H_{22}O_3$: 250.1569; found: 250.1575.

*(−)-(4*R*,5*R*)-Methyl dihydroabscisate (**24**)*[8]

Crude aldehyde **23** (about 1.2 mmol) obtained from the above procedure was dissolved in methanol (30 mL). Manganese oxide (1.79 g, 20 mmol), sodium cyanide (87 mg, 1.7 mmol), and glacial acetic acid (0.10 g, 1.6 mmol) were added. The mixture was stirred at room temperature for 5 h before it was filtered through Celite^R. The manganese oxide residue and Celite was rinsed with methanol and the rinsing was combined with the filtrate. The combined rinsing and filtrate was then concentrated, and the residue was partitioned between ether and H_2O. The ether layer was separated, dried over anhydrous Na_2SO_4, and concentrated to give a yellow oil (283 mg) as crude product. Purification on the Chromatotron (4 mm silica gel plate, 90% ether + 10% hexane) gave (−)-(4*R*,5*R*)-methyl dihydroabscisate (**24**) as colorless crystals (199 mg, 70% overall yield). Part of the product was recrystallized from ether–hexane to give colorless needles, mp 117.0–119.5°C; $[\alpha]_D$ −62.7°C (*c* 0.90, CH_3OH); hplc (Chiracel OD column (20, 21), 0.46 cm × 25 cm, 10% isopropanol + 90% hexane at 1.0 mL min^{-1}) retention time 10.7 min; ir: 3600, 1710 cm^{-1}; ^1H nmr δ: 0.88 (d, *J* = 6.3 Hz, 3H, $CHCH_3$), 0.92 and 1.04 (2s, 6H, $2CH_3$), 2.03 (d, *J* = 1.2 Hz, 3H, vinyl CH_3), 2.15 (dd, *J* = 16.0, 15.0 Hz, H-6_{ax}), 2.15 (dd, *J* = 15.0, 2.5 Hz, H-2_{eq}), 2.30–2.40 (m, 2H, $CHCH_3$ and H-6_{eq}), 2.46 (d, *J* = 14.9 Hz, 1H, H-2_{ax}), 3.69 (s, 3H, OCH_3), 5.74 (s, 1H, =CH), 6.46 (d, *J* = 16.0 Hz, 1H, =CH), 7.91 (dd, *J* = 16.0, 0.6 Hz, 1H, =CH); ^{13}C nmr δ: 16.00, 21.28, 22.87, and 25.25 (4q, $4CH_3$), 37.40 (d, CH), 41.71 (s, C3), 47.10 (t, CH_2), 51.10 (q, CH_3O), 52.92 (t, CH_2), 78.14 (s, COH), 117.62, 129.41, and 135.15 (3d, 3=CH), 149.41 (s, =C), 166.51 (s, OC=O), 209.12 (s, C=O); eims *m/z*: 280 (M^+, 2), 192 (35), 164 (23), 123 (100). Exact Mass (hrms) calcd. for $C_{16}H_{24}O_4$: 280.1675; found: 280.1664. Anal. calcd. for $C_{16}H_{24}O_4$: C 68.53, H 8.63%; found: C 68.67, H 8.74%.

*(−)-(4*R*,5*R*)-Dihydroabscisic acid (**2**)*[9]

A mixture of (−)-(4*R*,5*R*)-methyl dihydroabscisate (**24**) (166 mg, 0.6 mmol), 2 M KOH (6 mL), and methanol (3 mL) was stirred at room temperature for 4 h. Most of the methanol was then evaporated. The residue was diluted with H_2O, extracted with ether, and the ether extract was discarded. The aqueous layer was acidified with 1 M HCl and then extracted with $CHCl_3$. The $CHCl_3$ layer gave, after drying over anhydrous Na_2SO_4 and evaporation of solvent, (−)-(4*R*,5*R*)-dihydroabscisic acid (**2**) as white crystals (118 mg, 78%). Part of the product was recrystallized from $CHCl_3$–hexane to give white crystals, mp 177–184°C (lit. (7) (±)-**2** mp 193.5°C); $[\alpha]_D$ −65.2° (*c* 0.66, CH_3OH); ir: 2800–3200, 1715, 1690 cm^{-1}; ^1H nmr δ: 0.89 (d, *J* = 6.4 Hz, $CHCH_3$), 0.93 and 1.06 (2s, 6H, $2CH_3$), 2.08 (s, 3H, vinyl CH_3), 2.14–2.43 (m, 4H, $CHCH_3$, CH_2 at C6 and H-2_{eq}), 2.47 (d, *J* = 14.9 Hz, 1H, H-2_{ax}), 5.77 (br s, 1H, =CH), 6.50 and 7.88 (2d, *J* = 16.0 Hz, 2H, 2 =CH); eims (trimethylsilyl ether) *m/z*: 338 (M^+, 2), 192 (30), 73 (100). Exact Mass (hrms) (trimethylsilyl ether) calcd. for $C_{18}H_{30}O_4Si$: 338.1913; found: 338.1921. Anal. calcd. for $C_{15}H_{22}O_4$: C 67.63, H 8.33%; found: C 67.21, H 8.30%.

*(−)-(9*Z*)-(9*R*,10*R*)-9-(5-Hydroxy-3-methylpent-3-en-1-ynyl)-3,3,8,8,10-pentamethyl-1,5-dioxaspiro[5,5]undecan-9-ol (**25**)*

(−)-4(*Z*)-(4*R*,5*R*)-4-Hydroxy-4-(5-hydroxy-3-methylpent-3-en-1-ynyl)-3,3,5-trimethylcyclohexanone (**7**) (130 mg, 0.52 mmol) was treated with a mixture of 2,2-dimethyl-1,3-propanediol (160 mg, 1.53 mmol), pyridinium *p*-tosylate (9 mg, 0.04 mmol), and benzene (4 mL) according to the procedure described above for the conversion of compound **3** to ketal **20**. The desired ketal **25** was obtained as a pale yellow oil (149 mg, 89%); $[\alpha]_D$ −27.8° (*c* 1.2, CH_3OH); ir: 3610, 3440, 1110, and 1090 cm^{-1}; ^1H nmr δ: 0.84 (s), 1.04 (s), 1.08 (s), 1.09 (d, *J* = 6.8 Hz), and 1.16 (s) (15H, $5CH_3$), 1.52 (d, *J* = 14.1 Hz, 1H, H-7_{ax}), 1.58 (dd, *J* = 13.4, 13.2 Hz, 1H, H-11_{ax}), 1.83 (ddd, *J* = 13.4, 3.7, 2.9 Hz, 1H, H-11_{eq}), 1.87 (m, *J* = 1 Hz, 3H, vinyl CH_3), 2.11 (dd, *J* = 14.1, 2.8 Hz, 1H, H-7_{eq}), 2.13–2.22 (m, 1H, $CHCH_3$), 3.35–3.41 (m, 2H, 2 equatorial H at C2 and C4), 3.58 and 3.54 (2d, *J* = 11.9 and 12.6 Hz, respectively, 2H, 2 axial H at C2 and C4), 4.29 (d, *J* = 6.7 Hz, 2H, CH_2OH), 5.84 (ddq, *J* = 6.7, 6.7, 1.5 Hz, 1H, =CH). Exact Mass (hrms) (M^+ − 18 peak) calcd. for $C_{20}H_{30}O_3$: 318.2195; found: 318.2188.

*(−)-9(1*E*,3*Z*)-(9*S*,10*R*)-9-(5-Hydroxy-3-methyl-1,3-pentadienyl)-3,3,8,8,10-pentamethyl-1,5-dioxaspiro[5,5]undecan-9-ol (**26**)*

(−)-(9*Z*)-(9*R*,10*R*)-9-(5-Hydroxy-3-methylpent-3-en-1-ynyl)-3,3,8,8,10-pentamethyl-1,5-dioxaspiro[5,5]undecan-9-ol (**25**) (149 mg, 0.44 mmol) was reduced with sodium bis(2-methoxyethoxy)aluminium hydride (Redal^R, Aldrich, 3.4 M in toluene, 0.8 mL, 2.48 mmol) by the procedure described above for the preparation of compound **21**. The crude product **26** obtained was usually hydrolyzed by the procedure described below to give compound **27** without purification. A small amount of the crude product was purified on the Chromatotron (75% ether + 25% hexane) to give the desired ketal **26** as a colorless oil; ir: 3600, 1600, 1100, 975, 910 cm^{-1}; ^1H nmr δ: 0.76 (d, *J* = 6.9 Hz), 0.83 (s), 0.84 (s), 1.02 (s), and 1.06 (s) (15H, $5CH_3$), 1.57 (d, *J* = 14.1 Hz, 1H, H-7_{ax}), 1.59 (dd, *J* = 13.0, 12.7, 1H, H-11_{ax}), 1.84 (ddd, *J* = 12.7, 3.6, 2.7 Hz, 1H, H-11_{eq}), 1.85 (d, *J* = 0.9 Hz, 3H, vinyl CH_3), 2.08 (dd, *J* = 14.1, 2.7 Hz, 1H, H-7_{eq}), 2.16 (ddq, *J* = 13.0, 3.6, 6.8 Hz, 1H, $CHCH_3$), 3.30–3.50 (m, 2H, 2 equatorial H at C2 and C4), 3.56 and 3.60 (2d, *J* = 11.7, 11.5 Hz, respectively, 2H, 2 axial H at C2 and C4), 4.30 (d, *J* = 7.0 Hz, 2H, CH_2OH), 5.54 (dd, *J* = 7.0, 6.8 Hz, 1H, =CH), 5.70 (d, *J* = 15.8 Hz, 1H, =CH), 6.60 (d, *J* = 15.8 Hz, 1H, =CH).

[7]Alternatively, this compound can also be named as (−)-1(2*Z*,4*E*)-(1*R*,6*R*)-5-(1-hydroxy-2,2,6-trimethyl-4-oxocyclohexyl)-3-methyl-2,4-pentadienal.

[8]This compound can also be named as (−)-1(2*Z*,4*E*)-(1*R*,6*R*)-5-(1-hydroxy-2,2,6-trimethyl-4-oxocyclohexyl)-3-methyl-2,4-pentadienoic acid, methyl ester, or (−)-4(1*E*,3*Z*)-(4*R*,5*R*)-4-(4-carbomethoxy-3-methyl-1,3-butadienyl)-4-hydroxy-3,3,5-trimethylcyclohexanone.

[9]This compound can also be named as (−)-1(2*Z*,4*E*)-(1*R*,6*R*)-5-(1-hydroxy-2,2,6-trimethyl-4-oxocyclohexyl)-3-methyl-2,4-pentadienoic acid, or (−)-4(1*E*,3*Z*)-(4*R*,5*R*)-4-(4-carboxy-3-methyl-1,3-butadienyl)-4-hydroxy-3,3,5-trimethylcyclohexanone. See footnote 5.

Can. J. Chem. Downloaded from www.nrcresearchpress.com by 88.85.125.76 on 09/07/12
For personal use only.

(−)-4-(1E,3Z)-(4S,5R)-4-Hydroxy-4-(5-hydroxy-3-methyl-1,3-pentadienyl)-3,3,5-trimethylcyclohexanone (27)

The crude ketal **26** obtained in the above procedure was hydrolyzed by stirring with 1 M HCl (4 drops) and acetone (5 mL) at room temperature for 1 h. Working up in the manner previously described followed by purification on the Chromatotron (4 mm silica gel plate, 90% ether + 10% hexane) gave the desired compound **27** as a colorless oil (33 mg, 30% overall yield); $[\alpha]_D$ −18.3° (*c* 1.1, CH_3OH); ir: 3620, 1700 cm^{-1}; ^1H nmr δ: 0.86 (d, *J* = 6.5 Hz, $CHCH_3$), 0.88 and 0.93 (2s, 6H, CH_3), 1.86 (d, *J* = 1.1 Hz, 3H, vinyl CH_3), 1.90 (dd, *J* = 13.6, 2.2 Hz, 1H, H-2_{eq}), 2.18 (ddd, *J* = 13.5, 4.3, 2.2 Hz, 1H, H-6_{eq}), 2.23–2.33 (m, 1H, $CHCH_3$), 2.41 (t, *J* = 13.5 Hz, 1H, H-6_{ax}), 2.82 (d, *J* = 13.6 Hz, H-2_{ax}), 4.31 (m, 2H, CH_2OH), 5.59 (dd, *J* = 7.0, 6.3 Hz, 1H, =CH), 5.73 (d, *J* = 15.7 Hz, 1H, =CH), 6.69 (d, *J* = 15.7 Hz, 1H, =CH); ^{13}C nmr δ: 16.03, 20.72, 24.51, and 24.59 (4q, $4CH_3$), 36.83 (d, CH), 42.85 (s, C3), 45.11, 51.46, and 58.34 (3t, $3CH_2$), 77.78 (s, COH), 126.70, 128.28, and 134.02 (3d, 3 =CH), 134.51 (s, =C), 211.45 (s, C=O). Exact Mass (hrms) calcd. for $C_{15}H_{24}O_3$: 252.1725; found: 252.1708.

(−)-4(1E,3Z)-(4S,5R)-4-Hydroxy-4-(5-oxo-3-methyl-1,3-pentadienyl)-3,3,5-trimethylcyclohexanone (28)

Compound **27** (30 mg, 0.11 mmol) was oxidized with manganese oxide (420 mg, 4.8 mmol) to give aldehyde **28** by the procedure previously described (see the preparation of compound **23**). The crude aldehyde **28** was usually oxidized to ester **29** (see below) without purification.

A small amount of aldehyde **28** was purified by preparative tlc (90% ether + 10% hexane) to give a colorless oil; $[\alpha]_D$ −39.5° (*c* 0.77, CH_3OH); ir: 3610, 3450, 1700, and 1665 cm^{-1}; ^1H nmr δ: 0.89 (d, *J* = 6.4 Hz, 3H, $CHCH_3$), 0.96 (s, 6H, $2CH_3$), 1.93 (dd, *J* = 13.6, 2.2 Hz, H-2_{eq}), 2.08 (d, *J* = 1.1 Hz, 3H, vinyl CH_3), 2.20–2.46 (m, CH_2 at C6 and $CHCH_3$), 2.84 (d, *J* = 13.6 Hz, 1H, H-2_{ax}), 5.90 (d, *J* = 7.8 Hz, 1H, =CH), 6.16 (dd, *J* = 15.47, 0.4 Hz, 1H, =CH), 7.40 (d, *J* = 15.7 Hz, 1H, =CH), 10.20 (d, *J* = 7.8 Hz, 1H, HC=O).

(−)-(4S,5R)-Methyl dihydroabscisate (29)

Crude aldehyde **28** (about 0.11 mmol) obtained from the above procedure was reacted with a mixture of methanol (5 mL), manganese oxide (310 mg, 3.56 mmol), sodium cyanide (35 mg, 0.71 mmol), and glacial acetic acid (35 mg, 0.58 mmol) (see preparation of ester **24**). The desired product (−)-(4*S*,5*R*)-methyl dihydroabscisate (**29**) was obtained as colorless crystals (21 mg, 70% overall yield). Part of the product was recrystallized from ether–hexane at 0°C to give colorless plates, mp 105–108°C; $[\alpha]_D$ −40.6° (*c* 1.03, CH_3OH); ir: 1700 cm^{-1}; ^1H nmr δ: 0.87 (d, *J* = 6.5 Hz, 3H, $CHCH_3$), 0.94 and 0.96 (2s, 6H, $2CH_3$), 1.91 (dd, *J* = 13.6, 2.2 Hz, 1H, H-2_{eq}), 2.01 (d, *J* = 1.2 Hz, 3H, vinyl CH_3), 2.20 (ddd, *J* = 13.6, 4.2, 2.2 Hz, H-6_{eq}), 2.33 (m, 1H, $CHCH_3$), 2.44 (dd, *J* = 13.6, 13.0 Hz, 1H, H-6_{ax}), 2.86 (d, *J* = 13.6 Hz, 1H, H-2_{ax}), 3.70 (s, 3H, OCH_3), 5.72 (s, 1H, =CH), 6.09 (d, *J* = 15.9 Hz, 1H, =CH), 7.81 (d, *J* = 15.9 Hz, 1H, =CH); eims *m/z*: 280 (M^+, 4), 192 (43), 164 (24), 123 (100). Exact Mass (hrms) calcd. for $C_{16}H_{24}O_4$: 280.1675; found: 280.1649.

(−)-(4S,5R)-Dihydroabscisic acid (5)

(−)-(4*S*,5*R*)-Methyl dihydroabscisate (**29**) (15 mg, 0.05 mmol) was hydrolyzed with 2 M KOH (3 mL) and methanol (3 mL) as previously described to give (−)-(4*S*,5*R*)-dihydroabscisic acid (**5**) as a colorless oil (13 mg, 90%); $[\alpha]_D$ −34.5° (*c* 0.89, CH_3OH); ir: 2800–3500, 1680 cm^{-1}; ^1H nmr δ: 0.88 (d, *J* = 6.4 Hz, $CHCH_3$), 0.95 and 0.96 (2s, 6H, $2CH_3$), 1.91 (dd, *J* = 13.6, 2.1 Hz, 1H, H-2_{eq}), 2.04 (d, *J* = 1.2 Hz, 3H, vinyl CH_3), 2.21 (ddd, *J* = 13.4, 4.1, 2.1 Hz, H-6_{eq}), 2.35 (m, 1H, $CHCH_3$), 2.44 (dd, *J* = 13.4, 12.7 Hz, 1H, H-6_{ax}), 2.86 (d, *J* = 13.6 Hz, 1H, H-2_{ax}), 5.75 (s, 1H, =CH), 6.14 and 7.79 (2d, *J* = 16.1 Hz, 2H, 2=CH); ^{13}C nmr δ: 16.05, 21.48, 24.58, and 24.63 ($4CH_3$), 43.00 (C3), 36.67, 45.03, and 51.42 (CH and $2CH_2$), 78.00 (COH), 151.77, 140.60, 127.72, and 116.99 (4 =C), 170.63 (COOH), 211.26 (C=O); eims *m/z*: 266 (M^+, about 2), 248 (5), 192 (29), 164 (67), 123 (100). Exact Mass (hrms) calcd. for $C_{15}H_{22}O_4$: 266.1518; found: 266.1519.

(+)-(4R,6S)-4-Hydroxy-2,2,6-trimethylcyclohexanone (11)

A mixture of (−)-(4*R*,6*R*)-4-hydroxy-2,2,6-trimethylcyclohexanone (**10**) (300 mg, 0.19 mmol), 5 M NaOH (1 mL), and ethanol (10 mL) was heated to 85°C for 24 h under an argon atmosphere. Then most of the ethanol was removed by evaporation. The residue was dissolved in ether, and the solution was washed with water. After drying over anhydrous Na_2SO_4 and evaporation of the solvent, a pale yellow oil (255 mg) was obtained. Purification by flash chromatography (75% ether + 25% hexane) gave unreacted *trans* ketol **10** (46 mg); $[\alpha]_D$ −102.3° (*c* 0.92, CH_3OH), followed by the desired *cis* ketol **11** as a colorless oil (195 mg, 73% based on starting material consumed). The product **11** solidified on storage at −10°C and was recrystallized from ether–hexane to give colorless needles, mp 48.0–50.0°C (lit. (15) mp 52–53°C); $[\alpha]_D$ +95.0° (*c* 0.88, CH_3OH) (lit. (15) $[\alpha]_D$ +107.4° (*c* 0.8, CH_3OH)); ^1H nmr δ: 0.96 (d, *J* = 6.5 Hz, 3H, $CHCH_3$), 1.00 and 1.14 (2s, 3H each, $2CH_3$), 1.35 (ddd, *J* = 12.4, 12.4, 11.3 Hz, 1H, H-5_{ax}), 1.53 (dd, *J* = 12.2, 11.5 Hz, 1H, H-3_{ax}), 2.00 (ddd, *J* = 12.2, 4.2, 3.5 Hz, H-3_{eq}), 2.22 (m, 1H, H-5_{eq}), 2.67 (m, 1H, H-6_{ax}), 4.25 (tt, *J* = 11.3, 4.3 Hz, 1H, H-4_{ax}); eims *m/z*: 156 (M^+, 10), 138 (8), 83 (66), 74 (50), 69 (60), 57 (100).

(+)-(4R,6S)-4-tert-Butyldimethylsiloxy-2,2,6-trimethylcyclohexanone (30)

The *cis* ketol **11** (66 mg, 0.42 mmol) was treated with a mixture of *tert*-butyldimethylsilyl chloride (130 mg, 0.86 mmol), imidazole (73 mg, 1.07 mmol), and dry DMF (2 mL) by the procedure described above for the conversion of *trans* ketol **10** to silyl ether **13**. After working up and purification by distillation (Kugelrohr, 150–180°C, 8–10 Torr), the desired silyl ether **30** was obtained as a colorless oil (111 mg, 99%); $[\alpha]_D$ +58.0° (*c* 0.98, CH_3OH); ir: 1710 cm^{-1}; ^1H nmr δ: 0.07 (s, 6H, CH_3SiCH_3), 0.87 (s, 9H, $3CH_3$), 0.98 (d, *J* = 6.5 Hz, 3H, $CHCH_3$), 1.03 and 1.17 (2s, 3H each, $2CH_3$), 1.43 (ddd, *J* = 13.6, 12.8, 11.0 Hz, 1H, H-5_{ax}), 1.58 (dd, *J* = 13.1, 11.1 Hz, 1H, H-3_{ax}), 1.89 (ddd, *J* = 13.1, 4.3, 3.5 Hz, 1H, H-3_{eq}), 2.11 (m, 1H, H-5_{eq}), 2.68 (ddq, *J* = 12.8, 6.5, 6.5 Hz, 1H, H-6_{ax}), 4.24 (tt, *J* = 11.0, 4.4 Hz, 1H, H-4_{ax}); cims (isobutane) *m/z*: 271 (M^+ + 1). Exact Mass (hrms) calcd. for $C_{15}H_{30}O_2Si$: 270.2015; found: 270.2004.

(+)-1(Z)-(1R,4R,6S)-4-tert-Butyldimethylsiloxy-1-(5-hydroxy-3-methylpent-3-en-1-ynyl)-2,2,6-trimethylcyclohexanol (31)

Silyl ether **30** (5.7 g, 21 mmol) was treated with *Z*-3-methylpent-2-en-4-yn-1-ol (3.0 g, 32 mmol) and *n*-butyllithium (1.6 M in hexane, 40 mL, 63 mmol) by the procedure described for the conversion of silyl ether **13** to compounds **14** and **15**. The desired product **31** was obtained as a colorless oil (4.9 g, 64%), which solidified on storage at 0°C to give colorless crystals, gc (DB1701 column, 70–240°C at 10°C min^{-1}) retention time 19.11 min; mp 89–94°C; $[\alpha]_D$ +19.1° (*c* 0.82, CH_3OH); ir: 3620 cm^{-1}; ^1H nmr δ: 0.03 (s, 6H, CH_3SiCH_3), 0.86 (s, 9H, $3CH_3$), 1.01 (s, 3H, CH_3), 1.05 (d, *J* = 6.5 Hz, 3H, $CHCH_3$), 1.11 (s, 3H, CH_3), 1.40, 1.55, and 1.73 (3m, $2CH_2$), 1.89 (d, *J* = 1.0 Hz, 3H, vinyl CH_3), 1.92–2.00 (m, 1H, $CHCH_3$), 3.83 (tt, *J* = 10.8, 5.2 Hz, 1H, CHOSi), 4.32 (m, 2H, CH_2OH), 5.86 (ddd, *J* = 6.7, 6.7, 1.5 Hz, 1H, =CH); cims (isobutane) *m/z*: 367 (M^+ + 1), 349.

(+)-1(Z)-(1R,4R,6S)-1-(5-Acetoxy-3-methylpent-3-en-1-ynyl)-2,2,6-trimethylcyclohexan-1,4-diol (32)

Compound **31** (2.5 g, 6.9 mmol) was reacted with acetic anhydride (2.5 g, 18.6 mmol), pyridine (25 mL), and 4-dimethylaminopyridine (32 mg, 0.2 mmol) by the procedure previously described for the acetylation of compounds **14** and **15**. A small amount of the crude acetate obtained was purified on the Chromatotron (1 mm silica gel plate, 50% ether + 50% hexane) to give a colorless oil, gc (DB1701 column, 70–240°C at 10°C min^{-1}) retention time 19.37 min; $[\alpha]_D$ +17.6° (*c* 1.07, CH_3OH); ir: 3610, 3500, 1735 cm^{-1}; ^1H nmr δ: 0.03 (s, 6H, CH_3SiCH_3), 0.86 (s, 9H, $3CH_3$), 1.01 (s, 3H, CH_3), 1.05 (d, *J* = 6.5 Hz, 3H, $CHCH_3$), 1.11 (s, 3H, CH_3), 1.37, 1.56, and 1.73 (3m, $2CH_2$), 1.90 (d, *J* = 1.3 Hz, 3H, vinyl CH_3), 1.96 (m, 1H, $CHCH_3$), 2.03 (s, 3H, CH_3C=O), 3.84 (tt, *J* = 11.0, 5.0 Hz, 1H, CHOSi), 4.74 (dd, *J* = 7.1, 0.9 Hz, CH_2O), 5.79 (dd, *J* = 7.1, 7.1, 1.5 Hz, 1H, =CH); eims *m/z*: 348 (M^+ − 60); cims (isobutane) *m/z*: 409 (M^+ + 1), 349.

Can. J. Chem. Downloaded from www.nrcresearchpress.com by 88.85.125.76 on 09/07/12
For personal use only.

The crude acetate was desilated by heating (80°C) with glacial acetic acid (30 mL) and water (10 mL) to give, after work-up and purification, the desired product **32** as a colorless oil (1.46 g, 73% overall yield); $[\alpha]_D$ +23.8° (*c* 0.4, CH_3OH); ir: 3610, 1735 cm^{-1}; ^1H nmr δ: 1.03 (s, 3H, CH_3), 1.06 (d, *J* = 6.5 Hz, 3H, $CHCH_3$), 1.12 (s, 3H, CH_3), 1.37 and 1.57 (2m, H-3_{ax} and CH_2 at C5), 1.70 (ddd, *J* = 12.7, 4.6, 2.3 Hz, 1H, H-3_{eq}), 1.91 (d, *J* = 1.3 Hz, vinyl CH_3), 2.00 (m, 1H, $CHCH_3$), 2.04 (s, 3H, $CH_3C{=}O$), 3.84 (m, 1H, $CHOH$), 4.77 (d, *J* = 7.3 Hz, CH_2O), 5.70 (ddd, *J* = 7.1, 7.1, 1.5 Hz, 1H, =CH); ^{13}C nmr δ: 16.43, 20.73, 20.95, 23.17, and 26.96 ($5CH_3$), 39.92 (C2), 35.86, 41.76, and 46.38 (CH and $2CH_2$), 62.89 and 66.10 (CHOH and CH_2O), 78.31 (COH), 85.43 and 95.17 (2 acetylenic C), 123.68 (=C), 129.96 (=CH), 171.04 (C=O); eims *m/z*: 294 (M^+, very weak), 234 (10), 148 (100).

(+)-4(Z)-(4R,5S)-4-Hydroxy-4-(5-hydroxy-3-methylpent-3-en-1-ynyl)-3,3,5-trimethylcyclohexanone (6)

Compound **32** (1.44 g, 4.9 mmol) was oxidized with pyridinium dichromate (6.07 g, 16.1 mmol) in CH_2Cl_2 (30 mL) as previously described (see preparation of compound **3**). A keto-acetate was obtained as colorless needles (0.94 g, 70%), mp 118.0–120.0°C; $[\alpha]_D$ +20.5° (*c* 0.58, CH_3OH); ir, ^1H and ^{13}C nmr identical with those of the (−) enantiomer.

The keto-acetate (0.94 g, 3.2 mmol) was hydrolyzed by stirring with 5 M NaOH (1 mL) and methanol (25 mL) at room temperature for 1 h. After work-up and purification, the desired product (+)-4(*Z*)-(4*R*,5*S*)-4-hydroxy-4-(5-hydroxy-3-methylpent-3-en-1-ynyl)-3,3,5-trimethylcyclohexanone (**6**) was obtained as colorless crystals (0.80 g, 100%), mp 96.5–98.0°C; $[\alpha]_D$ +22.3° (*c* 0.53, CH_3OH); ir, ^1H and ^{13}C nmr identical with those of the (−)-(4*S*,5*R*) enantiomer **3**.

8(Z)-(2R,3R,8R,9S)-8-(5-Hydroxy-3-methylpent-3-en-1-ynyl)-2,3,7,7,9-pentamethyl-1,4-dioxaspiro[4,5]decan-8-ol (19)

(+)-4(*Z*)-(4*R*,5*S*)-4-Hydroxy-4-(5-hydroxy-3-methylpent-3-en-1-ynyl)-3,3,5-trimethylcyclohexanone (**6**) (5.3 mg, 0.02 mmol) was treated with a mixture of (−)-(2*R*,3*R*)-butanediol (12 mg, 0.13 mmol), pyridinium *p*-tosylate (2 mg, 0.008 mmol), and benzene (4 mL) according to the procedure described above for the conversion of compound **3** to ketal **18**. After work-up and purification, ketal **19** was obtained as a colorless oil (2 mg, 30%), gc retention time (DB1701 column, 70–240°C at 10°C min^{-1}) 18.76 min; ^1H nmr δ: 1.05 (d, *J* = 6.6 Hz, 3H, $CHCH_3$ at C9), 1.10 and 1.12 (2s, 3H each, $2CH_3$), 1.19 and 1.21 (2d, *J* = 5.7 Hz, 6H, $CHCH_3$ at C2 and C3), 1.54–1.71 and 1.83 (2m, H-6 and H-10), 1.86 (d, *J* = 1.2 Hz, 3H, vinyl CH_3), 2.22 (m, 1H, $CHCH_3$ at C9), 3.58 (m, 2H, $CHCH_3$ at C2 and C3), 4.30 (br s, 2H, CH_2OH), 5.84 (ddq, *J* = 6.7, 6.7, 1.5 Hz, 1H, =CH); ^{13}C nmr δ: 16.17, 16.88, 17.10, 21.27, 23.27, and 27.38 (6q, $6CH_3$), 34.98 (d, C9), 39.58 (s, C7), 43.97 and 47.90 (2t, C6 and C10), 61.31 (t, CH_2OH), 77.37 and 78.27 (2d, C2 and C3), 78.47 (s, C8), 85.48 and 94.09 (2s, 2 acetylenic C), 107.27 (s, C5), 120.47 (s, =C), 135.73 (d, =CH).

(+)-(9Z)-(9R,10S)-9-(5-Hydroxy-3-methylpent-3-en-1-ynyl)-3,3,8,8,10-pentamethyl-1,5-dioxaspiro[5,5]undecan-9-ol (33)

Compound **6** was ketalized to give **33**; $[\alpha]_D$ +27.1° (*c* 0.90, CH_3OH), by the procedure described above for the preparation of the (−) enantiomer **20**.

(+)-9(1E,3Z)-(9S,10S)-9-(5-Hydroxy-3-methyl-1,3-pentadienyl)-3,3,8,8,10-pentamethyl-1,5-dioxaspiro[5,5]undecan-9-ol (34)

Compound **34** was obtained by reducing compound **33** with Redal^R (see preparation of compound **21**) and was hydrolyzed to give compound **35** (see below) without purification.

(+)-4(1E,3Z)-(4S,5S)-4-Hydroxy-4-(5-hydroxy-3-methyl-1,3-pentadienyl)-3,3,5-trimethylcyclohexanone (35)

Compound **34** was hydrolyzed with 1 M HCl and acetone as previously described to give the desired product **35**; $[\alpha]_D$ +42.6° (*c* 1.03, CH_3OH).

(+)-4(1E,3Z)-(4S,5S)-4-Hydroxy-4-(5-oxo-3-methyl-1,3-pentadienyl)-3,3,5-trimethylcyclohexanone (36)

Aldehyde **36** was prepared by the oxidation of compound **35** with manganese oxide (see conversion of compound **22** to **23**), and was further oxidized to (+)-(4*S*,5*S*)-methyl dihydroabscisate (**37**) without purification.

(+)-(4S,5S)-Methyl dihydroabscisate (37)

Aldehyde **36** was reacted with MnO_2, NaCN, methanol, and glacial acetic acid according to the procedure previously described to give (+)-(4*S*,5*S*)-methyl dihydroabscisate (**37**) as colorless needles, mp 117.5–118.5°C; $[\alpha]_D$ +65.7° (*c* 0.9, CH_3OH); hplc (Chiracel OD column, 10% isopropanol + 90% hexane at 1.0 mL min^{-1}) retention time 8.7 min.

(+)-(4S,5S)-Dihydroabscisic acid

(+)-(4*S*,5*S*)-Methyl dihydroabscisate (**37**) was hydrolyzed with 2 M KOH and methanol to give (+)-(4*S*,5*S*)-dihydroabscisic acid (**4**) as colorless crystals, mp 173–180°C; $[\alpha]_D$ +63.5° (*c* 1.17, CH_3OH).

(−)-(10R)-3,3,8,8,10-Pentamethyl-1,5-dioxaspiro[5,5]undecan-9-one (38)

A mixture of (−)-(6*R*)-2,2,6-trimethyl-1,4-cyclohexandione (**9**) (924 mg, 6.0 mmol), 2,2-dimethyl-1,3-propanediol (791 mg, 7.6 mmol), pyridinium *p*-tosylate (34 mg, 0.13 mmol), and benzene (15 mL) was heated to reflux under a Dean–Stark water separator for 4 h. The reaction mixture was allowed to cool to room temperature before it was washed with H_2O, and dried over anhydrous Na_2SO_4. Evaporation of solvent gave a pale yellow oil (1.43 g) as the crude product, which was distilled using the Kugelrohr apparatus (80–100°C, 0.03 Torr) to give pure ketal **38** as a colorless oil (1.31 g, 91%); $[\alpha]_D$ +87.7° (*c* 1.10, CH_3OH); ir: 1710 cm^{-1}; ^1H nmr δ: 0.85 (s, 3H, CH_3), 0.91 (d, *J* = 6.6 Hz, 3H, $CHCH_3$), 0.97 (s, 6H, $2CH_3$), 1.16 (s, 3H, CH_3), 1.56 (dd, *J* = 13.5, 13.5 Hz, H-11_{ax}), 1.58 (d, *J* = 14.2 Hz, H-7_{ax}), 2.38 (ddd, *J* = 13.5, 5.3, 3.8 Hz, 1H, H-11_{eq}), 2.47 (dd, *J* = 14.2, 3.8 Hz, 1H, H-7_{eq}), 2.85 (m, 1H, $CHCH_3$), 3.41 and 3.48 (2dd, *J* = 11.4, 1.6 Hz, 2H, 2 equatorial H at C2 and C4), 3.53 and 3.61 (2d, *J* = 11.4 Hz, 2H, 2 axial H at C2 and C4); ms *m/z*: 240 (M^+, 0.58), 141 (27), 155 (98), 83 (27), 69 (100).

(−)-(9Z)-(9S,10R)-9-(5-Hydroxy-3-methylpent-3-en-1-ynyl)-3,3,8,8,10-pentamethyl-1,5-dioxaspiro[5,5]undecan-9-ol (20)

Ketal **38** (1.31 g, 5.5 mmol) was reacted with *Z*-3-methylpent-2-en-4-yn-1-ol (0.65 g, 6.7 mmol) and *n*-butyllithium (1.6 M in hexane, 8 mL, 12.8 mmol) in dry THF by the procedure described for the preparation of compounds **14** and **15** (see above). The crude product obtained (yellow oil, 2.6 g) was purified by flash column chromatography (75% ether + 25% hexane) followed by distillation using the Kugelrohr apparatus (about 250°C, 0.06 Torr) to give compound **20** as a colorless oil (1.40 g, 77%); $[\alpha]_D$ −30.0° (*c* 1.05, CH_3OH); ir and ^1H nmr identical to those reported above for compound **20**.

Hydrolysis of compound 20

To a solution of ketal **20** (200 mg, 0.6 mmol) in acetone (5 mL) was added 1 M HCl (2 drops). The mixture was stirred at room temperature for 1.5 h before saturated $NaHCO_3$ was added to neutralize the acid. Most of the solvent was then evaporated. The residue was dissolved in ether and washed with saturated NaCl. The ether layer was separated and dried over anhydrous Na_2SO_4. Evaporation of ether gave a colorless oil (145 mg), which was purified on the Chromatotron (2 mm silica gel plate, 75% ether + 25% hexane) to give compound **3** as colorless crystals (123 mg, 80%), mp 85–93°C. A small sample of the product was recrystallized from ether–hexane to give colorless plates, mp 92–98°C; $[\alpha]_D$ −25.0° (*c* 0.68, CH_3OH); ir, ^1H and ^{13}C nmr identical to those reported above for compound **3**.

Acknowledgements

We are grateful to Balco Canfor Reforestation Centre Ltd. and Dr. G. A. Hunt for providing part of the financial support under the Industrial Research Assistance Program (IRAP). We also thank Angela C. Shaw for technical assistance, Ted Mazurek for performing the NMR studies, Lawrence Hogge and Doug Olson for mass spectral analyses, and Drs. M. S. C. Pedras, G. Abrams, and L. A. K. Nelson for helpful discussion.

1. F. T. ADDICOTT and H. R. CARNS. *In* Abscisic acid. *Edited by* F. T. Addicott. Praeger, New York. 1983. Chap. 1 and references therein.
2. D. C. WALTON. *In* Abscisic acid. *Edited by* F. T. Addicott. Praeger, New York. 1983. Chap. 4 and references therein.
3. E. SONDHEIMER, E. C. GALSON, Y. P. CHANG, and D. C. WALTON. Science, **174**, 829 (1971).
4. W. R. CUMMINS and E. SONDHEIMER. Planta, **111**, 365 (1973).
5. B. V. MILBORROW. *In* Abscisic acid. *Edited by* F. T. Addicott. Praeger, New York. 1983. Chap. 3 and references therein.
6. S. R. ABRAMS. Canadian Chemical News, July/August 1989. pp. 15–17.
7. T. ORITANI and K. YAMASHITA. Agric. Biol. Chem. **46**, 817 (1982).
8. (*a*) M. J. T. REANEY and L. V. GUSTA. Plant Physiol. **83**, 423 (1987); (*b*) T. H. H. CHEN and L. V. GUSTA. Plant Physiol. **73**, 71 (1983).
9. T. ORITANI and K. YAMASHITA. Agric. Biol. Chem. **37**, 1215 (1973).
10. G. SAUCY. U.S. Patent 4153615 (1979).
11. K. MORI. Tetrahedron Lett. 723 (1973).
12. F. KIENZLE, H. MAYER, R. E. MINDER, and H. THOMMEN. Helv. Chim. Acta, **61**, 2609 (1978).
13. F. KIENZLE and H. MAYER. Helv. Chem. Acta, **61**, 2616 (1978).
14. T. ORITANI and K. YAMASHITA. Agric. Biol. Chem. **37**, 1115 (1973).
15. H. G. LEUENBERGER, W. BOGUTH, E. WIDMER, and R. ZELL. Helv. Chim. Acta, **59**, 1832 (1976).
16. H. C. BROWN and S. KRISHNAMURTHY. J. Am. Chem. Soc. **94**, 7159 (1972).
17. (*a*) E. C. ASHBY and J. T. LAEMMLE. Chem. Rev. **75**, 521 (1975); (*b*) D. CAINE and T. L. SMITH, JR. J. Am. Chem. Soc. **102**, 7568 (1980); (*c*) I. KUWAJIMA, E. NAKAMURA, and K. HASHIMOTO. Tetrahedron, **39**, 975 (1983); (*d*) J. A. FINDLAY, D. N. DESAI, G. C. LONERGAN, and P. S. WHITE. Can. J. Chem. **58**, 2827 (1980); (*e*) G. L. OLSON, H. C. CHEUNG, K. D. MORGAN, R. BORER, and G. SAUCY. Helv. Chim. Acta, **59**, 567 (1976); (*f*) G. F. HENNION and F. X. O'SHEA. J. Am. Chem. Soc. **80**, 614 (1958).
18. H. HIEMSTRA and H. WYNBERG. Tetrahedron Lett. 2183 (1977).
19. T. K. JONES and S. E. DENMARK. Org. Synth. **64**, 182 (1986).
20. E. J. COREY, M. W. GILMAN, and B. E. GANEM. J. Am. Chem. Soc. **90**, 5616 (1968).
21. I. D. RAILTON. J. Chromatogr. **402**, 371 (1987).
22. Y. OKAMOTO, M. KAWASHIMA, and K. HATADA. J. Chromatogr. **363**, 173 (1986).
23. D. GREATBANKS and R. PICKFORD. Magn. Reson. Chem. **25**, 208 (1987).
24. S. R. ABRAMS, M. J. T. REANEY, G. D. ABRAMS, T. MAZUREK, A. C. SHAW, and L. V. GUSTA. Phytochemistry, **28**, 2885 (1989).
25. O. ISLER, H. LINDLAR, M. MOTAVON, R. RUEGG, G. SAUCY, and P. ZELLAR. Helv. Chim. Acta, **39**, 2041 (1956).

Can. J. Chem. Downloaded from www.nrcresearchpress.com by 88.85.125.76 on 09/07/12
For personal use only.

The crystal and molecular structures of adamantanecarboxylic acid at 173 and 280 K

FRANCINE BÉLANGER-GARIÉPY AND FRANÇOIS BRISSE[1]

Département de Chimie, Université de Montréal, C.P. 6128, Succ. A, Montréal (Qué.), Canada H3C 3J7

AND

PIERRE D. HARVEY, DENIS F. R. GILSON,[1] AND IAN S. BUTLER[1]

Department of Chemistry, McGill University, 801 Sherbrooke Street West, Montreal, P.Q., Canada H3A 2K6

Received September 19, 1989

This paper is dedicated to Professor Arthur S. Perlin on the occasion of his 67th birthday

BÉLANGER-GARIÉPY, FRANÇOIS BRISSE, PIERRE D. HARVEY, DENIS F. R. GILSON, and IAN S. BUTLER. Can. J. Chem. **68**, 1163 (1990).

The crystal structure of adamantanecarboxylic acid, tricyclo[3.3.1.1^{3,7}] decan-1-carboxylic acid $C_{10}H_{15}COOH$, has been determined by X-ray diffraction at two temperatures, 173 and 280 K. At both temperatures, the unit cells are triclinic, space group $P\bar{1}$, and each contains two molecules. At 173 K, a = 6.452(3), b = 6.681(2), c = 11.510(3) Å, α = 80.84(2)°, β = 87.22(3)°, γ = 74.11(3)°; V = 471.10 Å^3, D_x = 1.271 g cm^{-3}, μ(CuKα) = 6.46 cm^{-1}. The structure was solved by direct-methods. The least-squares refinement, based on 1347 observed reflections converged to R = 0.0485 and R_w = 0.0415. At 280 K, a = 6.503(2), b = 6.849(2), c = 11.620(4) Å, α = 77.11(2)°, β = 85.77(2)°, γ = 76.34(2)°; V = 490.11 Å^3, D_x = 1.221 g cm^{-3}, μ(CuKα) = 6.21 cm^{-1}, R = 0.0874, and R_w = 0.0512 for 828 observed reflections. The low-temperature form is ordered while at room temperature the molecule is disordered. In the structure of the high-temperature phase, the adamantyl group takes two distinct orientations, in a 60:40 proportion, at about 14° from one another. The carboxylic group also has two orientations differing by about 170°. The geometry of the adamantane skeleton is not affected by the presence of the carboxylic group. The molecules form centrosymmetric dimers through hydrogen bonds of the O—H---O type. The O---O distances range between 2.616(11) and 2.752(15) Å. The order-disorder transition is interpreted using the Guthrie–McCullough approach.

Key words: adamantanecarboxylic acid, order–disorder transition, crystal structure.

BÉLANGER-GARIÉPY, FRANÇOIS BRISSE, PIERRE D. HARVEY, DENIS F. R. GILSON, et IAN S. BUTLER. Can. J. Chem. **68**, 1163 (1990).

On a déterminé la structure cristalline de l'acide adamantanecarboxylique, l'acide tricyclo[3.3.1.1^{3,7}] décane-1-carboxylique, $C_{10}H_{15}COOH$, par diffraction des rayons-X à deux températures, soit 173 et 280 K. Aux deux températures, les mailles élémentaires appartiennent au groupe d'espace $P\bar{1}$ et chacune contient deux molécules. A 173 K, a = 6,452(3), b = 6,681(2), et c = 11,510(3) Å, α = 80,84(2), β = 87,22(3),et γ = 74,11(3)°; V = 471,10 Å^3, D_x = 1,271 g cm^{-3}, μ(CuKα) = 6,46 cm^{-1}. On a détermine la structure par méthodes directes et on l'a affinée par la méthode des moindres carrés jusqu'à des valeurs respectives de R = 0,0485 et R_w = 0,0415 pour 1347 réflexions observées. A 280 K, a = 6,503(2), b = 6,849(2) et c = 11,620(4) Å, α = 77,11(2), β = 85,77(2) et γ = 76,34(2)°, V = 490,11 Å^3, D_x = 1,221 g cm^{-3}, μ(CuKα) = 6,21 cm^{-1}, R = 0,0874 et R_w = 0,0512 pour 828 réflexions observées. La forme qui existe à basse température est ordonnée alors que, à la température ambiante, la molécule est désordonnée. Dans la structure de la molécule telle qu'elle existe à haute température, le groupe adamantyle adopte deux orientations distinctes, qui existent dans des proportions de 60:40 et qui diffèrent par 14°. Le groupe carboxylique a aussi deux orientations différentes, à 170° l'une de l'autre. La géométrie du squelette adamantane n'est pas affectée par la présence du groupement carboxylique. Les molécules forment des dimères centrosymétriques par le biais de ponts hydrogènes du type O—H---O. Les distances O---O varient de 2,616(11) à 2,752(15) Å. On interprète la transition ordre–désordre en fonction de l'approche de Guthrie–McCullough.

Mots clés : acide adamantanecarboxylique, transition ordre–désordre, structure cristalline.

[Traduit par la revue]

Introduction

The cage hydrocarbon adamantane is a well-known example of a solid that undergoes an order–disorder transition (1), occurring in this case at 208 K (2). Substitution does not necessarily prevent the occurrence of such transitions, even when a strongly interacting group, such as a hydrogen bonding substituent, is present (3–7). In 1-hydroxyadamantane, the transition temperature is 353 K (6). In the 2-hydroxy-compound, there are two phase transitions, at 318 and 382 K, respectively (7). Thus, both compounds have their transitions moved to much higher temperatures. In *dl*-camphor the melting temperature is 451 K, and there are transitions at 204 and 350 K, with the major disordering occurring at the lower temperature (8). If the keto-group is reduced to the alcohol, to give *dl*-borneol, the major transition shifts to 346 K and the melting point to 487 K (9). Based on these, and other cases, it is apparent that the principal effect of the hydroxyl substituent is to raise the transition and melting temperatures, but not to prevent the occurrence of a disordered high-temperature phase.

In contrast, the transition in 1-adamantanamyne hydrochloride (10) occurs at 124 K, with an entropy change of 2.51 J K^{-1} mol^{-1}, and in the 1-carboxylic acid derivative (11) at 251 K with an entropy change of 8.96 J K^{-1} mol^{-1}. In both of these compounds, the entropy changes are too small for complete order–disorder transitions. In the case of the amine hydrochloride salt, the crystal structure determination of the high temperature phase confirmed the presence of an ordered phase (12).

The carboxylic acid compound seemed to be an excellent candidate for the determination of the crystal structures both above and below the phase transition temperature. The IR and Raman spectra showed only small changes at the phase transition (11) and the absence of large factor group splittings indicated that the site symmetry must be similar in the two phases, which is consistent with the relatively low transition

[1]Authors to whom correspondence may be addressed.

Can. J. Chem. Downloaded from www.nrcresearchpress.com by 88.85.125.76 on 09/07/12
For personal use only.

Can. J. Chem. Downloaded from www.nrcresearchpress.com by 88.85.125.76 on 09/07/12
For personal use only.

entropy. The lack of coincidence between vibrational frequencies in the IR and Raman spectra suggested that a centrosymmetric structure occurs. This was supported by the local frequencies of the carboxylic acid group, which showed that dimers exist. In this paper, the X-ray structures of 1-adamantyl carboxylic acid at 173 and 280 K are presented.

Experimental

The low temperature form

The crystal selected for X-ray structure analysis was a platelet bounded by {001}, {101}, {010} whose dimensions were 0.02 × 0.15 × 0.36 mm. The unit cell dimensions were obtained from 25 well-centered reflections in the range $40° \leq 2\theta \leq 60°$. The X-ray data were measured on a Nonius CAD-4 diffractometer using graphite-monochromatized CuKα radiation, λ(CuKα) = 1.54178 Å, and equipped with a modified Nonius low-temperature attachment. The intensities were collected by the ω–2θ scan technique with a scan width defined by $\Delta\omega = (1.00 + 0.14 \tan\theta)°$, within the sphere of reflection limited by $2\theta_{max} = 140.0°$ and $-7 \leq h \leq 7$, $-7 \leq k \leq 8$, $-14 \leq l \leq 14$. The orientation of the crystal was monitored every 100 measurements while the intensities were checked every hour using seven standard reflections. The largest intensity fluctuation during the measurement of 3515 reflections was 1.9%. After averaging of the equivalent reflections (R of averaging 0.045), 1347 reflections, $I \geq 1.96\sigma(I)$, were retained for structure determination and refinement. No absorption correction was applied as the absorption coefficient for the copper radiation is small.

The structure was solved by direct-methods (MULTAN 80).[2] A full-matrix weighted least-squares refinement was conducted, based on F's using isotropic then anisotropic temperature factors for all non-hydrogen atoms. All the H-atoms were found on a difference Fourier synthesis. They were included in the refinement with isotropic temperature factors. The function minimized was $\Sigma w(|F_o| - |F_c|)^2$. Convergence of the refinement was attained when $R = 0.0485$, $R_w = 0.0415$, and $S = 2.092$ for 183 refined parameters.[3] The weights were derived from the counting statistics, $w = 1/\sigma^2(F)$. The maximum and the average values of (Δ/σ) were 0.004 and 0.000, respectively. The residual electron density fluctuations on final difference Fourier synthesis were +0.25 and −0.23 e Å^{-3}.

The room temperature form

Another crystal was used for the room temperature data collection. The dimensions of the crystal were 0.03 × 0.08 × 0.18 mm. The unit cell dimensions were obtained from 25 well-centred reflections in the range $40° \leq 2\theta \leq 60°$. The intensity data were collected in the same conditions as for the low-temperature form up to $2\theta_{max} = 140.0°$. In this case, the intensities of the reference reflections decreased by about 20% over the duration of the data collection. This was attributed to the slow sublimation of the compound at this temperature. After averaging of the equivalent reflections of the 3616 measured reflections, only 831 with $I \geq 1.96\sigma(I)$ were considered observed (66%).

The stucture was solved by direct-methods using SHELX. At first, atoms O(1), O(2), C(0), C(1) of the carboxylic group were clearly visible while another six peaks, attached to C(1), suggested that the adamantyl ring system could be disordered over two or more sites. A succession of structure factor calculations and difference Fourier syntheses revealed most of the other non-hydrogen atoms. Then, in another difference Fourier synthesis, it was recognized that the carboxylic group was also disordered. Thus, it was concluded that the adamantanecarboxylic acid at 280 K was disordered in two orientations with only C(I) being common to both individuals. Assuming equally populated orientations, set **A** and set **B**, the space group could then be $P1$ rather than $P\bar{1}$. Solution of the structure in the $P1$ space group (without averaging the reflections) did not bring about any improvement. Thus, the $P1$ space group was retained. All atoms were refined isotropically with C—C distances constrained to 1.54 Å and occupancy factors of 0.50. At convergence, the thermal parameters associated with molecule **A** were found to by systematically lower than those for molecule **B**. Therefore, a few more refinement cycles were performed with fixed B values, this time adjusting the occupancy factors. This refinement indicated that the occupancy factor for molecule **A** was 0.60 and 0.40 for molecule **B**. Accordingly, fixed

TABLE 1. Final atomic coordinates and their esd's (×10^4) and U_{eq} (Å^2, × 10^3) for adamantanecarboxylic acid at 173 K[a]

Atom	X	Y	Z	U_{eq}
		Molecule **1**		
O(1)	5903(3)	−3326(3)	3806(2)	30
O(2)	2705(2)	−3209(2)	4666(1)	29
C(0)	3816(3)	−2465(3)	3922(2)	21
C(1)	2940(3)	−479(3)	3064(2)	19
C(2)	499(4)	387(4)	3216(2)	24
C(3)	−324(4)	2415(4)	2346(2)	23
C(4)	792(4)	4066(4)	2579(2)	28
C(5)	3224(4)	3214(4)	2427(2)	27
C(6)	4057(4)	1194(4)	3297(2)	24
C(7)	3453(4)	−917(4)	1790(2)	22
C(8)	2602(4)	1110(4)	926(2)	25
C(9)	165(4)	1956(4)	1086(2)	26
C(10)	3731(4)	2752(4)	1170(2)	27

[a] $U_{eq} = (1/3)\,\Sigma_i\Sigma_j U_{ij} a^*_i a^*_j \mathbf{a}_i \cdot \mathbf{a}_j$.

TABLE 2. Final atomic coordinates and their esd's (×10^4) and U_{eq} (Å^2, × 10^3) for adamantanecarboxylic acid at 280 K[a,b]

Atom	X	Y	Z	U_{eq}
		Molecule **2A**		
O(1)	2700(10)	−3265(9)	4649(7)	51
O(2)	5730(11)	−3531(11)	3713(8)	67
C(0)	3962(16)	−2580(15)	3849(11)	55
C(1)	3059(7)	−470(7)	3053(4)	38
C(2)	4746(11)	−114(11)	2028(7)	56
C(3)	3835(13)	1954(12)	1131(9)	62
C(4)	1802(12)	1719(13)	696(9)	68
C(5)	171(12)	1416(12)	1630(8)	50
C(6)	1070(12)	−664(11)	2503(7)	57
C(7)	2589(13)	1306(11)	3676(7)	65
C(8)	1743(13)	3341(12)	2798(8)	60
C(9)	3375(13)	3647(12)	1798(8)	62
C(10)	−289(13)	3183(11)	2332(9)	63
		Molecule **2B**		
O(1)	5971(15)	−3158(15)	3897(11)	58
O(2)	2900(16)	−2842(15)	4858(11)	72
C(0)	3915(18)	−2317(17)	3966(13)	26
C(2)	591(13)	299(14)	3286(10)	48
C(3)	−210(16)	2283(14)	2401(11)	36
C(4)	902(16)	3963(16)	2592(13)	76
C(5)	3233(16)	3270(16)	2361(11)	63
C(6)	4155(16)	1096(14)	3214(10)	53
C(7)	3354(16)	−786(14)	1807(9)	51
C(8)	2530(17)	1301(17)	906(12)	63
C(9)	132(17)	1993(17)	1166(11)	74
C(10)	3609(17)	2795(16)	1146(13)	67

[a] $U_{eq} = (1/3)\,\Sigma_i\Sigma_j U_{ij} a^*_i a^*_j \mathbf{a}_i \cdot \mathbf{a}_j$.
[b] Atom C(1) is common to both molecules **2A** and **2B**.

[2] The programs used here are modified versions of NRC-2, data reduction, NRC-10, bond distances and angles and NRC-22, mean planes; MULTRAN80, multisolution program; SHELX, program for structure determination and ORTEP, stereodrawings (13–16).

[3] $R = \Sigma \| F_o| - |F_c| \| / \Sigma |F_o|$, $R_w = [\Sigma w(|F_o| - |F_c|)^2 / \Sigma w |F_o|^2]^{1/2}$. $S = [\Sigma w(|F_o| - |F_c|)^2/(m - n)]^{1/2}$.

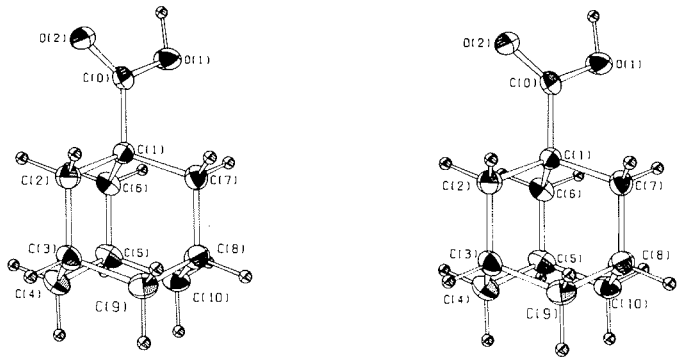

FIG. 1. Stereopair showing the structure of adamantanecarboxylic acid, the low temperature form, with atomic numbering. The ellipsoids correspond to 50% probability, except for hydrogens, which are shown as spheres of arbitrary size.

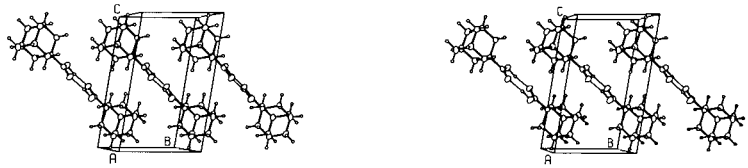

FIG. 2. Packing of the low temperature form of adamantanecarboxylic acid. Atoms are represented by spheres of arbitrary size. Hydrogens, except H(OH), are omitted for clarity.

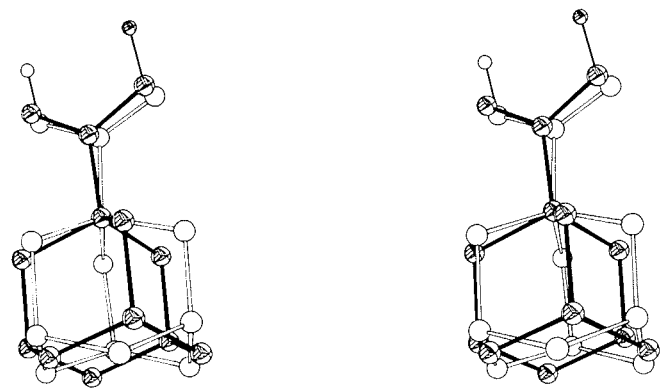

FIG. 3. Stereopair showing the two disordered molecules of adamantanecarboxylic acid in the high temperature phase. In order to differentiate the two molecules, the bonds of molecule **2B** (occupancy factor = 0.40) were blackened while their ellipsoids are not hatched. All the atoms are shown as spheres of arbitrary size.

normalized values of 0.60 and 0.40 were set for molecules **A** and **B** respectively. At this time, the constraints were removed and a full-matrix weighted least-squares refinement, based on F's was performed. All the H-atoms were fixed at idealized positions (C—H = 1.08 Å, isotropic U = 0.06 Å^2). At this stage, a difference Fourier synthesis showed peaks of 0.3 e Å^{-3} at reasonable positions for the hydrogen atoms of the carboxylic groups. The positions of these H-atoms and their isotropic temperature factors were refined. The function minimized was $\Sigma w(|F_c| - |F_o|)$.[2] In the last refinement cycles, three reflections (−1 0 1, 1 1 2, and 0 2 3) were given zero weight as they were clearly suffering from extinction. At convergence, the final agreement indices were R = 0.0874 and R_w = 0.0512 with weights derived from the counting statistics $w = 1/\sigma^2(F)$, while S = 2.068 for 235 refined parameters. The maximum and the average values of (Δ/σ) are 0.27 and 0.02, respectively. A final difference Fourier synthesis was essentially featureless, with general background between −0.24 to 0.26 e Å^{-3}.

The scattering curves for the nonhydrogen atoms were taken from Cromer and Mann (17) and those the H-atoms from Stewart, Davidson, and Simpson (18).

Results and discussion

The final atomic coordinates and the equivalent U_{eq} of the adamantanecarboxylic acid are presented in Table 1[4] for the low-temperature phase (molecule **1**), and in Table 2 for the high-temperature phase (molecules **2A** and **2B**). The atomic numbering adopted is given on the stereoview of the molecule **1** shown in Fig. 1. The packing of molecule **1** of the low-temperature phase is shown in Fig. 2. The molecular structure of the high-temperature phase (molecule **2**) is represented as stereopairs in Figs. 3 and 4. The bond distances, angles, and torsion angles of interest are compared in Table 3.

[4]Tables of atomic positions for hydrogen atoms, least-squares planes, anisotropic temperature factors and structure factor tables of the X-ray determinations of the low and the high tempertaure forms of the adamantanecarboxylic acid have been deposited and may be purchased from the Depository of Unpublished Data, CISTI, National Research Council of Canada, Ottawa, Ont., Canada K1A 0S2.

Can. J. Chem. Downloaded from www.nrcresearchpress.com by 88.85.125.76 on 09/07/12
For personal use only.

Can. J. Chem. Downloaded from www.nrcresearchpress.com by 88.85.125.76 on 09/07/12
For personal use only.

TABLE 3. Bond distances (Å), bond angles (deg), and torsion angles (deg) with their esd's for adamantanecarboxylic acid at 173 K (**1**) and at 280 K (molecule **2A** and **2B**)

	Distance		
Bond	**1**	**2A**	**2B**
O(1)—C(0)	1.321(3)	1.278(14)	1.329(16)
O(2)—C(0)	1.222(3)	1.199(13)	1.218(18)
C(0)—C(1)	1.511(3)	1.540(12)	1.480(14)
C(1)—C(2)	1.534(3)	1.577(9)	1.590(11)
C(2)—C(3)	1.532(3)	1.575(12)	1.515(15)
C(3)—C(4)	1.535(3)	1.505(12)	1.558(15)
C(4)—C(5)	1.527(4)	1.476(12)	1.501(16)
C(5)—C(6)	1.529(3)	1.565(11)	1.602(16)
C(6)—C(1)	1.548(3)	1.530(9)	1.471(11)
C(1)—C(7)	1.543(3)	1.511(9)	1.503(11)
C(7)—C(8)	1.530(3)	1.540(12)	1.575(16)
C(8)—C(9)	1.531(4)	1.528(12)	1.547(16)
C(9)—C(3)	1.530(3)	1.496(12)	1.486(18)
C(8)—C(10)	1.539(4)	1.500(13)	1.453(16)
C(10)—C(5)	1.529(4)	1.566(12)	1.508(19)
	Angle		
Bonds	**1**	**2A**	**2B**
O(1)—C(0)—O(2)	122.7(2)	122.2(10)	119.7(12)
O(1)—C(0)—C(1)	114.0(2)	115.9(9)	117.2(10)
O(2)—C(0)—C(1)	123.3(2)	121.9(9)	121.8(11)
C(0)—C(1)—C(2)	111.3(2)	106.6(6)	109.6(7)
C(0)—C(1)—C(6)	108.4(2)	106.6(6)	105.2(7)
C(0)—C(1)—C(7)	110.0(2)	114.6(6)	114.7(7)
C(1)—C(2)—C(3)	109.8(2)	108.9(6)	108.5(8)
C(2)—C(3)—C(4)	109.7(2)	106.3(7)	109.5(9)
C(3)—C(4)—C(5)	109.3(2)	114.2(8)	108.4(10)
C(4)—C(5)—C(6)	109.8(2)	107.1(7)	110.3(9)
C(5)—C(6)—C(1)	109.6(2)	108.3(6)	111.1(8)
C(6)—C(1)—C(2)	108.9(2)	107.8(5)	109.2(6)
C(6)—C(1)—C(7)	108.5(2)	111.3(5)	110.7(6)
C(1)—C(7)—C(8)	109.8(2)	110.3(6)	110.5(8)
C(7)—C(8)—C(10)	108.7(2)	107.3(7)	107.5(10)
C(8)—C(10)—C(5)	109.4(2)	109.4(7)	116.0(11)
C(10)—C(5)—C(6)	109.6(2)	108.5(7)	103.1(9)
C(7)—C(8)—C(9)	109.9(2)	109.2(7)	106.8(9)
C(8)—C(9)—C(3)	109.5(2)	112.6(7)	109.6(10)
C(9)—C(3)—C(2)	109.7(2)	107.6(7)	111.8(9)
C(2)—C(1)—C(7)	109.7(2)	109.7(5)	107.4(6)
C(9)—C(3)—C(4)	109.4(2)	109.6(8)	110.5(9)
C(4)—C(5)—C(10)	109.7(2)	111.1(7)	109.8(10)
C(9)—C(8)—C(10)	109.6(2)	110.8(7)	109.3(10)
	Torsion angle		
Bonds	**1**	**2A**	**2B**
O(1)—C(0)—C(1)—C(2)	177.8(2)	−171.4(8)	180.0(10)
O(1)—C(0)—C(1)—C(6)	−62.5(2)	−56.4(10)	−62.8(12)
O(1)—C(0)—C(1)—C(7)	56.0(3)	67.2(10)	59.1(13)
O(2)—C(0)—C(1)—C(2)	−2.7(3)	7.6(12)	−12.9(15)
O(2)—C(0)—C(1)—C(6)	117.0(2)	122.5(10)	104.4(13)
O(2)—C(0)—C(1)—C(7)	−124.5(2)	−113.9(10)	−133.8(12)
C(0)—C(1)—C(2)—C(3)	179.1(2)	175.9(7)	175.5(8)
C(0)—C(1)—C(6)—C(5)	179.2(2)	−176.9(7)	−174.7(8)
C(0)—C(1)—C(7)—C(8)	−178.9(2)	178.8(7)	−176.2(8)
C(1)—C(2)—C(3)—C(4)	−60.2(2)	−58.4(8)	−62.6(10)
C(2)—C(3)—C(4)—C(5)	59.9(3)	61.7(9)	62.7(12)

TABLE 3. (*concluded*)

Bonds	Torsion angle		
	1	**2A**	**2B**
C(3)—C(4)—C(5)—C(6)	−60.1(3)	−63.6(9)	−57.9(12)
C(4)—C(5)—C(6)—C(1)	60.2(3)	62.2(8)	58.0(11)
C(5)—C(6)—C(1)—C(2)	−59.7(2)	−62.8(7)	−57.1(9)
C(6)—C(1)—C(2)—C(3)	59.7(2)	61.8(7)	60.8(9)
C(1)—C(2)—C(3)—C(9)	59.9(2)	59.0(8)	60.3(11)
C(2)—C(3)—C(9)—C(8)	−60.2(3)	−60.6(9)	−61.8(12)
C(3)—C(9)—C(8)—C(7)	59.8(3)	60.2(9)	60.0(12)
C(9)—C(8)—C(7)—C(1)	−59.0(3)	−58.0(8)	−62.3(10)
C(8)—C(7)—C(1)—C(2)	58.4(2)	59.0(7)	61.7(9)
C(7)—C(1)—C(2)—C(3)	−58.9(2)	−59.5(7)	−59.3(9)
C(1)—C(6)—C(5)—C(10)	−60.3(3)	−57.7(8)	−59.1(11)
C(6)—C(5)—C(10)—C(8)	60.8(3)	62.8(9)	61.8(13)
C(5)—C(10)—C(8)—C(7)	−60.8(3)	−63.5(9)	−61.2(13)
C(10)—C(8)—C(7)—C(1)	61.0(2)	62.2(8)	54.9(11)
C(8)—C(7)—C(1)—C(6)	−60.4(2)	−60.2(8)	−57.4(1)
C(7)—C(1)—C(6)—C(5)	59.7(2)	57.6(7)	61.0(9)
C(3)—C(4)—C(5)—C(10)	60.4(3)	54.7(10)	55.1(12)
C(4)—C(5)—C(10)—C(8)	−59.8(3)	−54.7(9)	−55.7(14)
C(5)—C(10)—C(8)—C(9)	59.4(3)	55.6(9)	54.3(14)
C(10)—C(8)—C(9)—C(3)	−59.6(3)	−57.8(10)	−56.0(13)
C(8)—C(9)—C(3)—C(4)	60.1(3)	54.6(10)	60.4(12)
C(9)—C(3)—C(4)—C(5)	−60.4(3)	−54.3(10)	−60.8(12)

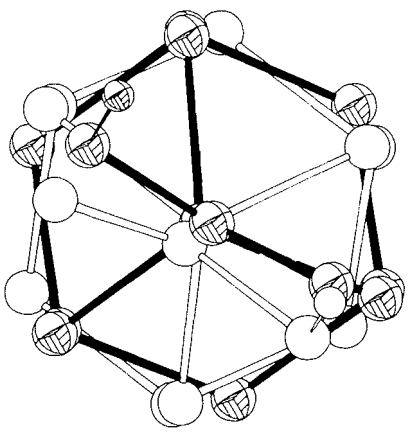

FIG. 4. View down the C(0)—C(1) bond of the room temperature form. The bonds of molecule **2B** are blackened.

The adamantane ring system

The C—C bonds of the low temperature phase of the adamantane ring system range from 1.527(4) to 1.548(3) Å, with a mean value of 1.534 Å, which is close to the expected value of 1.544 Å for C(sp^3)—C(sp^3) bond in diamond or 1.542 Å in adamantane-1,3,5,7-tetracarboxylic acid (21) whose structure is closely related to that of diamond. In the room-temperature phase, more distortions are observed. The C—C bonds in the adamantyl group **2A** or **2B** range from 1.453(16) to 1.602(16) Å, but the average value is 1.528 Å. The low-temperature distances are, on the average, nearly identical to those reported by Donohue and Goodman for adamantane itself (19), or in the theoretical calculations of Gleicher and Schleyer (20). In our structure at 173 K, the C—C—C bond angles range from 108.4(2) to 111.3(2)°, with a mean value of 109.5°, which is the expected tetrahedral angle. At 280 K, the C—C—C bond angles are not as well defined, since they take values in a larger range, from 103.1(9) to 116.0(11)°, but have a mean value of 109.5°. There are no significant differences in either the bond distances or angles when this molecule is compared to adamantane or its derivatives (19, 21).

The adamantane skeleton consists of four fused cyclohexane rings, the torsion angles for each of these rings are compared in Table 3. These angles suggest that each ring has a nearly perfect chair conformation. The overall mean torsion angles of 59.9° for molecule **1**, 59.2 and 59.8° respectively for molecule **2A** and **2B** is very close to the expected value of 60° for a perfectly staggered chair conformation with tetrahedral bond angles. All these values agree well with the corresponding quantities in some related compounds such as 1-adamantanol (24), or adamantanamine hydrochloride (12). The adamantane cage is quite rigid and its geometry is not affected by substitution and crystal packing forces.

The C(1)—C(0) bond with value of 1.511(3) Å for molecule **1** (at 173 K) agrees well with the value 1.523(1) Å reported for adamantane-1,3,5,7-tetracarboxylic acid (21) or the value of 1.522(17) Å in 2-aminoadamantane-2-carboxylic acid hydrobromide (22) and the values of 1.523(4) and 1.513(4) Å in bicyclo[2.2.2]octane-1,4-dicarboxylic acid (23). At 280 K, the two C(1)—C(0) distances with values of 1.540(12) and 1.480(14) Å show the effect of the disorder.

The bond distances and angles in the carboxylic group are normal when compared to the corresponding quantities in adamantane-1,3,5,7-tetracarboxylic acid (21) or in bicyclo[2.2.2]octane-1,4-dicarboxylic acid (23). The carboxylic group of atoms, [C(0),C(1),O(1),O(2)], is planar at low temperature and at room temperature.

The *syn*-planar arrangement Cβ—Cα—C = O is adopted for the carboxylic group. The torsion angle O(2)—C(0)—C(1)—C(2) has a value of −2.7(3)° for molecule **1**. This torsion angle is

Can. J. Chem. Downloaded from www.nrcresearchpress.com by 88.85.125.76 on 09/07/12
For personal use only.

TABLE 4. Distances (Å) and angles (deg) involving hydrogen bonds in adamantanecarboxylic acid at 173 and 280 K

	Distance			Angle
O—H---O	O—H	H---O	O---O	O—H—O
At 173 K, molecule **1**				
O(i)—H(O1)---O(2)[a]	1.00(3)	1.65(3)	2.642(2)	171(3)
At 280 K, molecule **2A**				
O(1)—H(O1)---O(2)[a]	1.05(2)	1.79(2)	2.616(11)	132(2)
Molecule **2B**				
O(1)—H(O1)---O(2)[a]	0.99(2)	1.79(2)	2.752(15)	165(2)

[a] $1-x, -1-y, 1-z$.

7.6(12)° and −12.9(15)°, respectively for molecule **2A** and molecule **2B**. This syn-planar conformation of the Cβ—Cα—C = O group is generally observed in saturated carboxylic acids (25). The deviation observed here from the *syn*-planar arrangement is small compared to that reported for adamantane-1,3,5,7-tetracarboxylic acid (21) where it takes the value of 17.0(2)° and the value of about 30° in the case of bicyclo[2.2.2] octane-1,4-dicarboxylic acid (23).

Molecular disorder

As mentioned in the Experimental section, at 280 K, the molecule of adamantancarboxylic acid is present in the crystal with two distinct orientations in a 60:40 ratio. The disorder observed can be described in terms of rotation of the adamantyl group and another rotation of the carboxylic group. No major change in site of factor group symmetry occurs when going from the high-temperature phase to the low-temperature phase. In the room temperature form, molecule **2B** is almost unchanged in position from the low temperature structure, and molecules **2A** and **2B** deviate from one another by a rotation around the pseudo-threefold axis by about 14°. Similarly, the carboxylic group of **2A** is at 168.4° of the corresponding group in **2B**. This situation may be more clearly appreciated in Fig. 4.

The adamantyl group has an almost threefold symmetry. It also has three non-crystallographic mirror planes, plane *1* [C(1),C(7),C(8),C(4)], plane *2* [C(1),C(6),C(5),C(9)], plane *3* [C(1),C(2),C(3),C(10)]. The dihedral angles between these planes is close to 120° for **1** and for **2A** and **2B**. Plane *3* is nearly coplanar with the carboxylic group in molecules **1**, **2A** and **2B**. The dihedral angle between the carboxylic group of atoms and plane *3* is only 3.2, 8.3, and 11.1° respectively for **1**, **2A**, and **2B**.

The structure is stabilized by strong hydrogen bonds. Apart from these hydrogen bonds, there are no other short contacts. The hydrogen bond distances and angles are compared in Table 4. The projection of the molecules **2A** and **2B** down C(1)—C(0) bond shows the C—O bond directions to be skewed with respect to the bonds covalently linked to C(1). The molecules are interconnected to form the cyclic hydrogen-bonded dimer which is the most commonly observed motif in the solid state (25). The middle of each hydrogen-bonded dimer lines on a crystallographic center of symmetry and this arrangement persists through the phase transition.

Interpretation of the entropy of transition in compounds of this type has often been based upon the Guthrie–McCullough equation, $S = R \ln (N_1/N_2)$, where N_1 and N_2 are the numbers of distinguishable positions in the two different phases (26). However, the entire entropy change should not be attributed to this configurational contribution, since the contribution due to any volume change is neglected. In the case of adamantyl carboxylic acid, the entropy change is, according to the Guthrie–McCullough approach, equivalent to $R \ln 3$. In adamantanamine hydrochloride, the entropy of transition is 2.51 J K^{-1} mol^{-1} (10). If we attribute the entropy of transition to the volume term and assume that the coefficients of thermal expansion and of compression are similar in adamantane carboxylic acid and in the amine salt, and that the molar volume changes at the transition are the same, then the configurational contribution to the entropy change in adamantyl carboxylic acid is reduced to 6.46 J K^{-1} mol^{-1}, or $R \ln 2.2$. This is in reasonable agreement with the observation reported here that there are two distinguishable molecules in the unit cell.

Acknowledgements

We wish to thank the Natural Science and Engineering Research Council of Canada for its financial support. We are also grateful to Dr. M. Simard for the X-ray data collection and to Dr. J. Britten for helpful discussion.

1. N. G. PARSONAGE and L. A. K. STAVELEY. Disorder in crystals. Clarendon Press, Oxford. 1978.
2. S. S. CHANG and E. F. WESTRUM. J. Phys. Chem. **64**, 1547 (1980).
3. T. CLARK, T. MC.O. KNOX, H. HACKLE, and M. A. MCKERVEY. J. Chem. Soc. Faraday Trans. 1,**73**, 1224 (1977).
4. I. S. BUTLER, H. B. R. COLE, D. F. R. GILSON, P. D. HARVEY, and J. MCFARLANE. J. Chem. Soc. Faraday Trans. 2, **82**, 525 (1986).
5. P. D. HARVEY, D. F. R. GILSON, and I. S. BUTLER. Can. J. Chem. **65**, 1757 (1987).
6. R. M. PAROLI, N. T. KAWAI, G. LORD, I. S. BUTLER, and D. F. R. GILSON. Can. J. Chem. **66**, 1973 (1988).
7. C. SCHALLER, I. S. BUTLER, and D. F. R. GILSON. Unpublished results.
8. K. L. SCHAFER and U. WAGNER. Z. Elektrochem. **62**, 328 (1958).
9. J. G. ASTON. *In* Physics and chemistry of the organic solid state. *Edited by* D. Fox, M. M. Lasco, and A. Weissberger. Interscience, London. 1963. p. 543.
10. P. D. HARVEY, D. F. R. GILSON, and I. S. BUTLER. J. PHYS. CHEM. **91**, 1267 (1987).
11. P. D. HARVEY, D. F. R. GILSON and I. S. BUTLER. J. Phys. Chem. **90**, 136 (1986).
12. F. BÉLANGER-GARIÉPY, F. BRISSE, P. D. HARVEY, I. S. BUTLER, and D. F. R. GILSON. Acta Crystallogr. Sect. C, **43**, 756 (1987).
13. F. R. AHMED, S. R. HALL, M. E. PIPPY, and C. P. HUBER. J. Appl. Crystallogr. **6**, 309 (1973); Accession Nos 133–147.
14. P. MAIN, S. J. FISKE, S. E. HULL, L. LESSINGER, G. GERMAIN, J. DECLERCQ, and M. M. WOOLFOSON. MULTAN80. A system of

Can. J. Chem. Downloaded from www.nrcresearchpress.com by 88.85.125.76 on 09/07/12
For personal use only.

computer programs for the automatic solution of crystal structures from X-ray diffraction data. Universities of York, England, and Louvain, Belgium. 1980.
15. G. M. SHELDRICK. Program for crystal structure determination. SHELX. Univ. of Cambridge, England. 1976.
16. C. K. JOHNSON. ORTEP, REPORT ORNL-3794. Oak Ridge National Laboratory. TN. 1965.
17. D. T. CROMER and J. B. MANN. Acta Crystallogr. Sect. A, **24**, 321 (1968).
18. R. F. STEWART, E. R. DAVIDSON, and W. T. SIMPSON. J. Chem. Phys. **42**, 3175 (1965).
19. J. DONOHUE and S. H. GOODMAN. Acta Crystallogr. **22**, 353 (1967).
20. G. J. GLEICHER and P. VON R. SCHLEYER. J. Am. Chem. Soc. **89**, 582 (1967).
21. O. ERMER. J. Am. Chem. Soc. **110**, 3747 (1988).
22. K. K. CHACKO and R. ZAND. Acta Crystallogr. Sect. B. **29**, 2681 (1973).
23. O. ERMER and J. D. DUNITZ. Helv. Chim. Acta **52**, 1861 (1969).
24. J. P. AMOUREUX, M. BEE, C. GORS, V. WARIN, and F. BAERT. Cryst. Struct. Commun. **8**, 449 (1979).
25. L. LEISEROWITZ. Acta Crystallogr. Sect. B, **32**, 775 (1976).
26. J. B. GUTHRIE and J. P. MCCULLOUGH. J. Phys. Chem. Solids, **18**, 28 (1961).

Can. J. Chem. Downloaded from www.nrcresearchpress.com by 88.85.125.76 on 09/07/12
For personal use only.

Spruce budworm (*Choristoneura fumiferana*) antifeedants 2. Structure–activity relationship among some functionalized decalin compounds[1]

T. H. CHAN,[2] K. R. GUERTIN, AND C. V. C. PRASAD
Department of Chemistry, McGill University, Montreal, P.Q., Canada H3A 2K6

AND

A. W. THOMAS, G. M. STRUNZ, AND A. SALONIUS
Forestry Canada – Maritimes Region, Fredericton, N.B., Canada E3B 5P7

Received November 2, 1989

This paper is dedicated to Professor Arthur S. Perlin on the occasion of his 67th birthday

T. H. CHAN, K. R. GUERTIN, C. V. C. PRASAD, A. W. THOMAS, G. M. STRUNZ, and A. SALONIUS. Can. J. Chem. **68**, 1170 (1990).

Several compounds, each possessing a polyoxygenated decalin structure, were synthesized and tested for antifeedant activities against the spruce budworm, *Choristoneura fumiferana*. Definite biological activity was observed for some of these compounds. A structure–activity relationship was discussed on the basis of these results.

Key words: decalin, synthesis, antifeedant, spruce budworm.

T. H. CHAN, K. R. GUERTIN, C. V. C. PRASAD, A. W. THOMAS, G. M. STRUNZ et A. SALONIUS. Can. J. Chem. **68**, 1170 (1990).

On a synthétisé plusieurs composés, possédant chacun une structure décalinique polyoxygénée, et on a vérifié leur activité contre la tordeuse des bourgeons de l'épinette, *Choristoneura fumiferana*. Quelques-uns de ces composés présentent une activité biologique non ambiguë. Sur la base de ces résultats, on discute d'une relation structure–activité.

Mots clés : décaline, synthèse, tordeuse des bourgeons de l'épinette.

[Traduit par la revue]

Introduction

The spruce budworm, *Choristoneura fumiferana*, is an insect pest that inflicts huge damage to the forest resource in eastern North America. In eastern Canada, the larvae of the budworm begin to feed on the buds or the newly opened shoots of the host tree in mid-May, and consume the greatest amount of foliage during their sixth instar in late June. A strategy that has been considered for pest control is to employ antifeedants to interfere with the feeding behaviour of insects. The approach may offer advantages over conventional methods of pest control since antifeedant could protect current year foliage while leading indirectly to budworm mortality without being generally toxic (2).

In screening programs, a number of natural products have been found to have antifeedant activity, e.g., azadirachtin (**1**) (3), clerodin (**2**) (4), and Nic-1 (**3**) (5). For the spruce budworm (6), an active compound, specionin (**4**), has been isolated from the leaves of *Catalpa speciosa* Warder (Bignoniaceae) (7). The chemical synthesis of specionin has recently been reported (8).

Because of the complexity of the structures of the known antifeedants (**1–4**), chemical synthesis of any of these compounds is considered a major challenge and not likely to be used in any large-scale application. A more practical approach is to prepare simpler analogs of these compounds. However, there has been relatively little study of structure–activity relationship with respect to antifeedant activity (9). There is therefore no guiding principle for the design of these simpler analogs.

Although their carbon skeletons or presumed biogenetic origin may differ widely, most insect antifeedants discovered so far share a common feature, namely, they are polyoxygenated molecules. Synthetic compounds **5**, **6**, and **7**, which have partial structures in common with azadirachtin (10) and clerodin (11), were found to exhibit antifeedant activities. In the case of the spruce budworm, we previously found that the iridoid derivative **8** has moderate but definite antifeeding activity (1).

In this paper, we report on the synthesis of a number of oxygenated decalins and examine them as potential antifeedants against spruce budworm. These compounds, though only remotely resembling clerodin (**2**), azadirachtin (**1**), and Nic-1 (**3**) in structure, provide a rigid framework to explore the structure–activity relationship.

Chemical synthesis

Recently, we described a new annelation reaction based on tandem Michael–Claisen condensation of the siloxydiene **9** with α,β-unsaturated ketones (12). The reaction has been used to construct the 9-methyldecalin and the hydrindan (13) systems, and in the syntheses of some sesquiterpenes (14). Since both clerodin (**2**) and azadirachtin (**1**) as well as many terpenoid natural products are disubstituted at the C-4 (steroid numbering) position, we decided to examine the use of the annelation reaction for the synthesis of polyoxygenated decalin compounds with similar dimethyl substituents.

Reaction of the siloxydiene **9** with the enone **10** promoted by titanium tetrachloride provided the Michael adduct as a mixture of *E* and *Z* isomers, **11***a* and **11***b* (*E*/*Z* = 4.0:1) respectively. Claisen cyclization of the major adduct **11***a* could be achieved under basic conditions by treatment with potassium *tert*-butoxide to give the decalone **12** in good yield. Alternatively, the *E*/*Z* mixture of **11** could be cyclized to the decalone **12** by treatment with lithium thiophenoxide as previously reported (12) (Scheme 1).

Methylation of **12** with K_2CO_3/CH_3I in acetonitrile gave a mixture of *C*- and *O*-methylated products, **13**, **14**, and **15**, in 35, 28, and 28% yields respectively. The *O*-methyl compound **15** could readily be distinguished from the two isomeric *C*-methyl compounds, **13** and **14**, on the basis of their spectroscopic data.

[1]For previous paper on this subject, see ref. 1.
[2]Author to whom correspondence may be addressed.

Can. J. Chem. Downloaded from www.nrcresearchpress.com by 88.85.125.76 on 09/07/12
For personal use only.

Can. J. Chem. Downloaded from www.nrcresearchpress.com by 88.85.125.76 on 09/07/12
For personal use only.

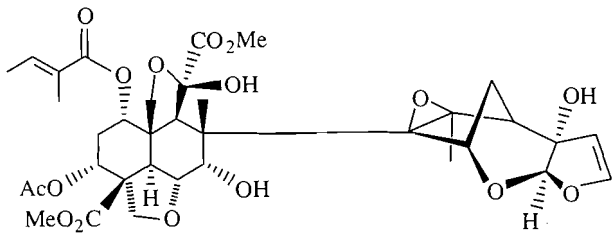

1

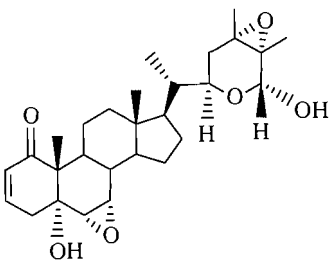

3

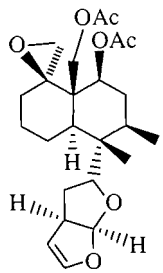

2

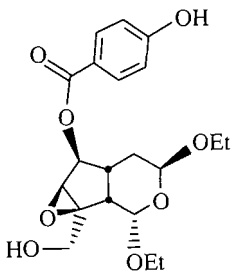

4

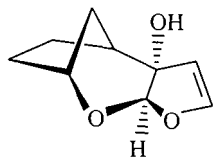

5

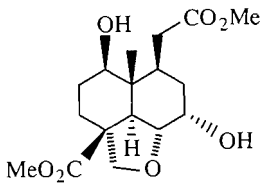

6

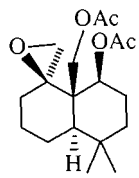

7

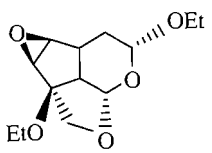

8

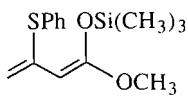

9

The assignment of the *trans* stereochemistry to compound **14** is based on chemical correlation according to Scheme 2. Compound **14** was thioketalized to **16** with ethanedithiol. Replacement of the thiophenyl group in **16** by a methoxy group was accomplished by reflux in sodium methoxide/methanol to give **17**. Raney nickel reduction of **17** gave the known compound **18** with *trans* ring junction stereochemistry (15). Reduction of **18** with lithium aluminum hydride followed by acid hydrolysis gave the known compound **19** as reported (15).

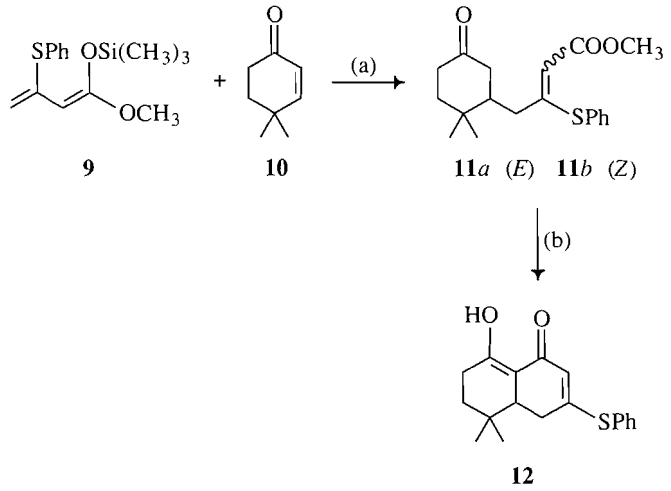

(a) $TiCl_4$, CH_2Cl_2, -78°C, 2.5 h, 57%; (b) KOt-Bu, THF, room temp., 1 h, 70%

SCHEME 1

With the stereochemistry of **14** thus firmly established, compound **13** must then have the *cis* ring junction stereochemistry.

The preferred formation of the *cis* compound **13** over the *trans* isomer **14** in the methylation of **12** under basic conditions is somewhat unexpected. We previously found that in the methylation of the parent decalone **20** with methyl iodide, using either KO-*t*-Bu or Bu_4NOH as the base, the *trans* isomer **21** was formed preferentially over the *cis* isomer **22** in a ratio of 9:4 (12). We therefore examined the methylation of the decalone **12** in greater detail under a variety of conditions. The selectivity as well as the yields of each reaction are given in Table 1. In all cases, the *cis* isomer **13** was formed preferentially, with stereoselectivity ranging from a low of 1.1:1 to a high of 7:1. The selectivity may be attributed to the steric hindrance of the C-4 axial methyl group in anion **23** to the approaching electrophile in forming **14**. When the counterion M^+ is larger (Cs^+, K^+, or Bu_4N^+) and less coordinating to the anion, or the solvent more polar (CH_3CN), relatively more of the *trans* compound **14** is formed because, in the transition state, the

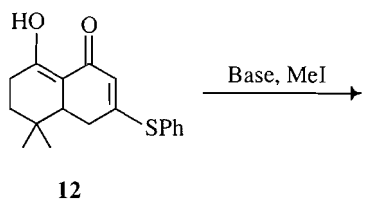

12

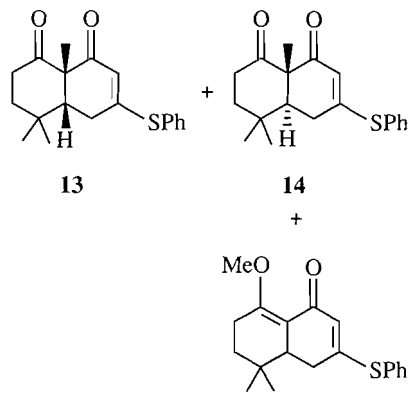

13 14 + 15

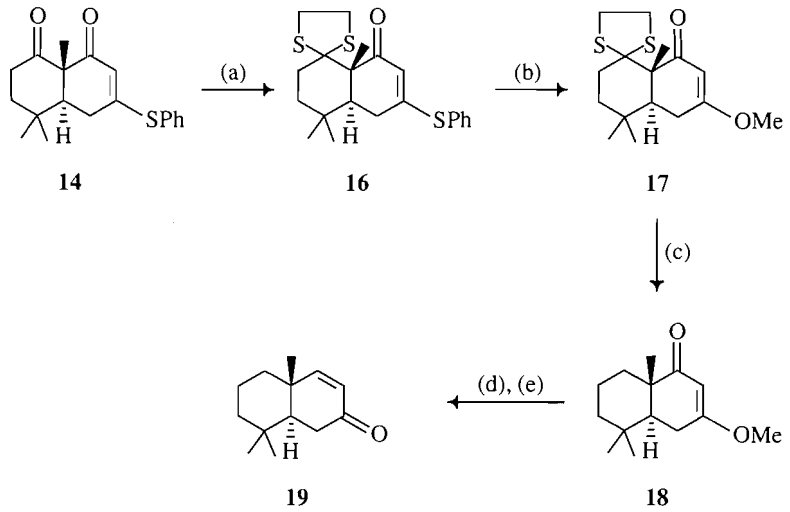

(a) $HSCH_2CH_2SH$, *p*-TSA, benzene, refilux, 100%; (b) MeONa, MeOH, reflux 24 h, 60%; (c) Raney nickel, EtOH, reflux, 6 h, 85%; (d) $LiAlH_4$, ether, reflux 1 h; (e) 20% HCl/MeOH, room temp., 6 h, 74% from **18**

SCHEME 2

electrophile is farther away and is less subject to steric effect. Also, the degree of *O*-methylation seems to be significant when the M^+ is larger and less coordinating than Li^+.

The *O*-methyl isomer **15** can of course be recycled back to the starting decalone **12** by hydrolysis of the enol ether. Alternatively, it was deprotonated by lithium hexamethyldisilazide (LHMDS) to the anion **24**. Methylation of **24** with methyl iodide gave the *O*,*C*-dimethyl compound **25**, which was not isolated but hydrolysed to give a mixture of **13** and **14** in a ratio of 4:1. This two-step route therefore also offers an efficient way to prepare **13** selectively. This sequence of annelation–alkylation may well be useful for the synthesis of drimanic sesquiterpenes, especially for compounds such as sicannin (**26**) (16) where the stereochemistry of the ring junction is *cis*.

Reduction of **13** with $NaBH_4/CH_3OH$ or $LiAlH(O\text{-}t\text{-}Bu)_3$/THF gave the alcohol **27** stereoselectively in quantitative yield (Scheme 4). The stereochemistry of the hydroxy group in **27** was assigned on the basis of ^1H nmr. The methine hydrogen at 3.15 ppm showed both large (11 Hz) and small (5 Hz) coupling constants expected of an axial hydrogen. Protection of the hydroxy group of **27** was achieved with *tert*-butyldimethylsilyl triflate/2,6-lutidine to give the TBDMS ether **28**. Refluxing in sodium methoxide/methanol converted **28** to the methoxy compound **29**. Similar conditions converted **27** to the corresponding alcohol **30**, albeit in poor yield.

On the other hand, reduction of the *trans* isomer **14** with

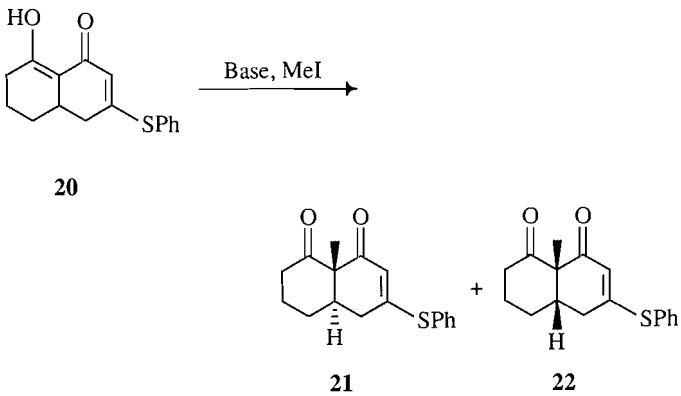

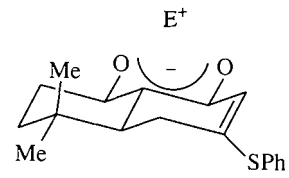

23

$NaBH_4$ (Scheme 5) led to the diol **31***a* and the epimeric alcohol **31***b* (as a mixture of stereoisomers). The relative proportion of the two compounds obviously depended on the amount of reducing agent used. The assignment of stereochemistry of the two hydroxy groups in **31***a* is based on ^1H nmr as well as on the presumed axial attack of the hydride from the less hindered side. Acetylation of **31***a* with acetic anhydride/pyridine gave the diacetate **32** as the major product.

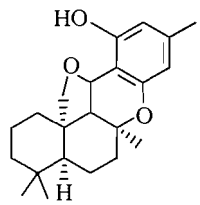

Sicannin **26**

Biological assay

Two sets of biological assays were conducted on ten of the synthetic compounds as well as on three simple commercially available ketoesters (**33**, **34**, **35**) for comparison purposes. Each bioassay involved feeding laboratory-colony spruce budworm larvae on artificial diet (17) containing 0.2% (wet weight) of the test compounds. In the assay, newly emerged 2nd-instar larvae were reared individually at 26°C, 17 h photoperiod, 50 replicates per test compound. At the point at which approximately 50% of the controls had reached the final (6th) instar, the larvae were sacrificed and their development stage determined. The mean development stage (instar) of larvae on each treatment diet was determined (mean instar in Tables 2 and 3) as well as the proportion of 6th instars. Because the data

Can. J. Chem. Downloaded from www.nrcresearchpress.com by 88.85.125.76 on 09/07/12
For personal use only.

TABLE 1. Methylation reaction of the dione **12**

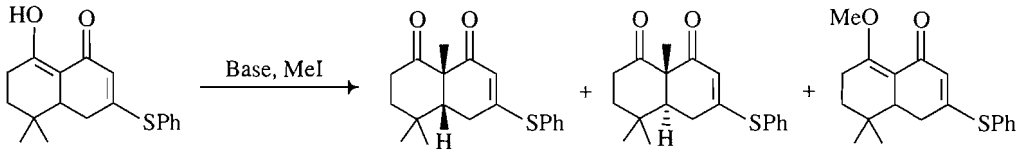

12 **13** **14** **15**

Conditions	Temperature (°C)	Time (h)	% Yield[a] **13** and **14**	Ratio[b] **13**:**14**	% Yield[a] **15**	% Recovered[a] **12**
BuLi, −78°C/CH_3I, THF	50	262	50	4.2:1	2	13
$K_2CO_3/CH_3CN/CH_3I$	82	26	63	1.2:1	28	0
$Cs_2CO_3/CH_3CN/CH_3I$	82	4	56	1.2:1	24	4
Cs_2CO_3/THF/CH_3I	66	72	49	2.0:1	11	0
$Ag_2O/CH_3CN/CH_3I$	82	75	19	4.0:1	20	39
$Bu_4NOH/C_6H_6/CH_3I$	80	141	22	1.1:1	1	46
(i) TlOEt/C_6H_6, (ii) CH_3I	42	216	15	7:1	5	32

[a]Refers to isolated yield (after chromatography).
[b]Ratios were determined from the ^1H nmr spectrum of the crude reaction mixture.

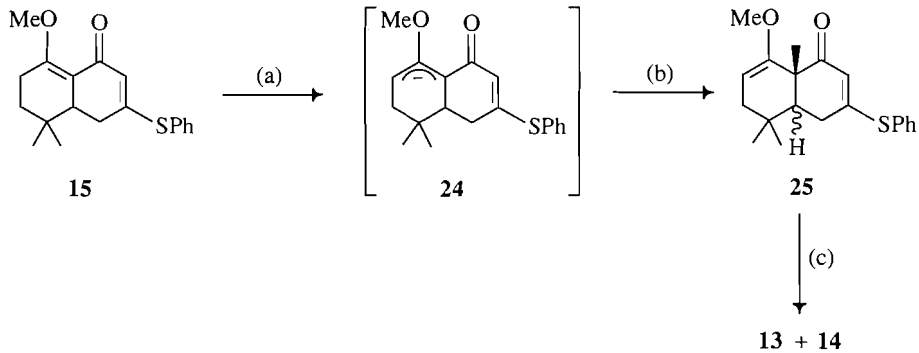

15 **24** **25**

13 + **14**

(a) LHMDS, THF, −23°C, 1 h; (b) MeI, −23°C, 6 h, (c) H^+/H_2O, 79% from **15**

SCHEME 3

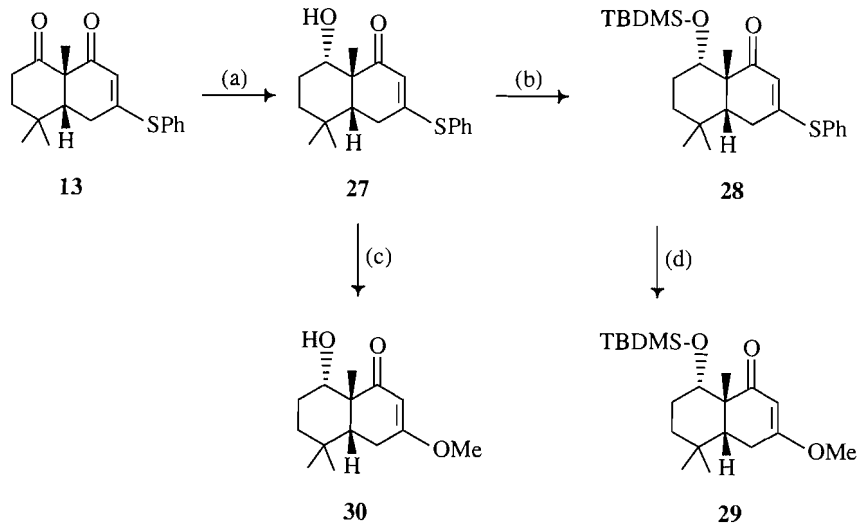

13 **27** **28**

30 **29**

(a) $NaBH_4$, MeOH, 0°C, 6 h, 100%; (b) TBDMS triflate, 2,6-lutidine, CH_2Cl_2, room temp., 6 h, 77%; (c) MeONa, MeOH, reflux, 4 days, 33%; (d) MeONa, MeOH, reflux, 5 days 83%.

SCHEME 4

Can. J. Chem. Downloaded from www.nrcresearchpress.com by 88.85.125.76 on 09/07/12
For personal use only.

Can. J. Chem. Downloaded from www.nrcresearchpress.com by 88.85.125.76 on 09/07/12
For personal use only.

TABLE 2. Biological assays

Compound		Mean instar	% of 6th instars
Control	a	5.20	46
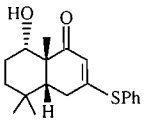 **27**	a	5.20	24
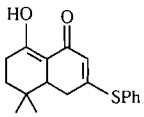 **12**	ab	4.98	26
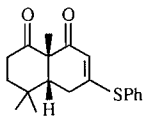 **13**	bc	4.60	8
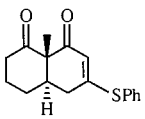 **21**	c	4.42	8
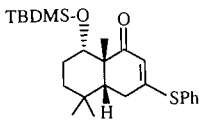 **28**	c	4.30	10
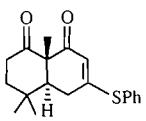 **14**	c	4.34	4

TABLE 3. Biological assays

Compound	Mean instar	% of 6th instars
Control	5.12	42
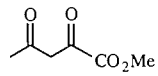 **35**	4.98	43
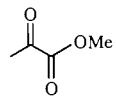 **34**	5.10	35
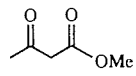 **33**	5.04	38
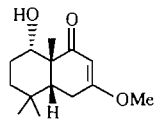 **30**	5.04	30
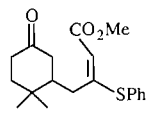 **11*a***	5.08	30
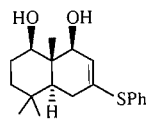 **31*a***	5.02	18
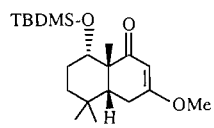 **29**	4.74	14

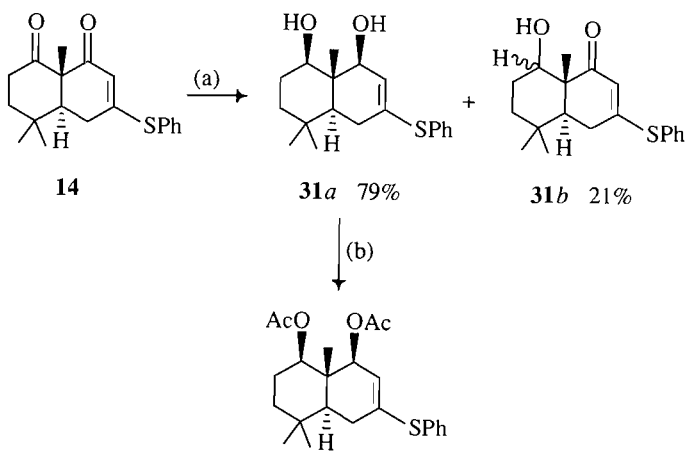

(a) $NaBH_4$, MeOH, 0°C, 18 h; (b) Ac_2O, pyridine, DMAP (cat.), CH_2Cl_2, room temp., 49 h, 85%.

SCHEME 5

are clearly nonparametric, the rank transformation approach (18) was used for the purposes of statistical analysis. In each set of biological assays, all the observations (i.e., the instar of each of the 350 larvae in set 1, 400 in set 2) were ranked from the largest to the smallest, with average ranks assigned in cases of ties. The compounds were then listed in descending order according to their mean rank values (Tables 2 and 3). A one-way analysis of variance applied to the rank values allowed us to test nonparametrically for intercompound differences (19, 20). Significant differences were detected between the compounds in the first set of biological assays (Table 2) and a Tukey-type multiple comparison test, using rank sums instead of means, was performed to locate the differences (19, 20). Compounds followed by the same letter were not significantly different ($P > 0.05$) in their effect on the development rate of budworm larvae. No significant difference was found between the compounds in the second set of biological assays (Table 3).

The biological assay showed that the development of larvae

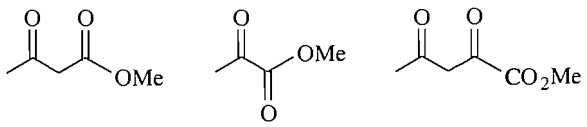

33 34 35

reared from second instar on test diets was significantly retarded by compounds **14**, **21**, **28**, and **13**, but not by the other compounds. The levels of activity of these compounds are comparable to that of compound **8** reported previously (1).

Several conclusions can be drawn from the structure–activity relationship observed so far. The absence of activity in the acyclic compounds (**33**, **34**, **35**) and the monocyclic compound **11** suggests that the two oxygen functions have to be fixed in their relative positions. The nature of the oxygen function is of critical importance, with the hydroxy group generally giving the inactive compounds. Comparing compounds **28** and **29**, electronic effect on the carbonyl group may be a factor in influencing activity. On the other hand, comparing compounds **14** and **21**, the *gem*-dimethyl group appears to have little influence at all.

Conclusion

The observation of definite biological activity in this series of easily accessible synthetic compounds gives hope that much more active compounds can be designed. On the basis of the structure of azadirachtin and clerodin, our next step in this structure–activity study will be to replace the angular methyl group in **21** by an oxygenated methyl group.[3]

Experimental

Melting points were determined on a Gallenkamp block and are uncorrected. The ^{1}H nmr spectra were taken on Varian XL-300 and XL-200 instruments and the data are reported in ppm relative to the $CHCl_3$ reference line with the multiplicity, coupling constants, and number of protons given in parentheses. The ir spectra were recorded on an Analect AQS-18 FT-IR instrument. Electron impact (EI) mass spectra were recorded at 70 eV on either a Dupont 21-492B or Kratos MS25RFA instrument and are reported as *m/z* (relative intensity %). Ammonia chemical ionization (CI) mass spectra were recorded on a Hewlett–Packard 5980A instrument. Column chromatography was performed on Merck silica gel 60 (230–400 mesh). All glassware was predried in an oven at approximately 200°C before using.

*Methyl 3-phenylthio-4-(3'-oxo-6',6'-dimethylcyclohexyl)-but-2-enoate (**11**a, **11**b)*

To a stirred solution of 4,4-dimethyl-2-cyclohexen-1-one (0.50 g; 0.53 mL; 4.02 mmol) and the siloxydiene **9** (1.80 g; 6.43 mmol; 1.6 equiv.) in dry methylene chloride (20 mL) under argon at −78°C was added titanium tetrachloride (0.49 mL; 4.42 mmol; 1.1 equiv.) dropwise. After 2 h 15 min the mixture was allowed to warm to room temperature, then poured into aqueous sodium bicarbonate and extracted twice with 20-mL portions of methylene chloride. The combined extracts were dried (Na_2SO_4) and concentrated to give 1.84 g of yellow semisolid residue. Flash chromatography on silica gel (eluent: 25% ethyl acetate/hexane) provided the *E* (mp 146–148°C) and *Z* (mp 134–136°C) isomers of **11** in a ratio of 4:1 in 57% yield.

The *E* isomer **11***a* had ir ($CHCl_3$, cm^{-1}): 3013, 2965, 1709, 1697, 1599, 1341, 1176; ^{1}H nmr ($CDCl_3$, ppm): 7.42–7.58 (m, 5H), 5.28 (s, 1H), 3.58 (s, 3H), 3.42–1.48 (m, 9H), 1.12 (s, 3H), 1.08 (s, 3H); ms: 332 ($M^{+\cdot}$, 39), 301 (16), 219 (26), 176 (29), 134 (29), 55 (100). Exact mass calcd. for $C_{19}H_{24}O_3S$: 332.145; found: 332.148.

The *Z* isomer **11***b* had ir ($CHCl_3$, cm^{-1}): 3013, 2965, 1707, 1581, 1436, 1177; ^{1}H nmr ($CDCl_3$, ppm): 7.67–7.10 (m, 5H), 5.82 (s, 1H), 3.77 (s, 3H), 2.87–1.23 (m, 9H), 0.73 (s, 3H), 0.40 (s, 3H); ms: 332 ($M^{+\cdot}$, 56), 300 (16), 258 (39), 223 (41), 205 (60), 149 (49), 110 (60), 28 (100). Exact mass calcd. for $C_{19}H_{24}O_3S$: 332.145; found: 332.141.

*3-Phenylthio-5,6,4a,8a-tetrahydro-5,5-dimethyl-(4*H,7H*)napthalen-1,8-dione (**12**)*

To a stirred solution of the *E* adduct **11***a* (3.99 g; 12.0 mmol) in dry THF (60 mL) under argon at 0°C was added potassium *tert*-butoxide (2.05 g; 18.3 mmol; 1.5 equiv.). The mixture was then allowed to warm to room temperature. After 1 h, the solvent was removed *in vacuo* and the residue taken into methylene chloride (50 mL) and washed with 10 mL of saturated NH_4Cl solution. The extract was dried (Na_2SO_4) and concentrated to give a crude yellow crystalline material. Flash chromatography on silica gel (eluent: 20% ethyl acetate/hexane) provided the dione **12** in 70% yield as a bright canary-yellow-colored solid, mp 124–126°C. **12** had ir ($CHCl_3$, cm^{-1}): 2934, 1617, 1594, 1558, 1270, 1249; ^{1}H nmr ($CDCl_3$, ppm): 7.50–7.40 (m, 5H), 5.41 (s, 1H), 2.73–2.13 (m, 5H), 1.65–1.47 (m, 2H), 1.04 (s, 3H), 0.88 (s, 3H), 15.15 (s, 1H); ms: 300 ($M^{+\cdot}$, 78), 298 (100), 283 (37), 255 (35), 244 (60), 191 (50), 135 (96), 110 (52). Exact mass calcd. for $C_{18}H_{20}O_2S$: 300.118; found: 300.121.

*Representative methylation of the decalone (**12**)*

To a stirred solution of the dione **12** (100 mg; 0.33 mmol) and dried potassium carbonate (69 mg; 0.50 mmol; 1.5 equiv.) in dry acetonitrile (5.0 mL) under argon at room temperature was added methyl iodide (0.21 mL; 3.33 mmol; 10.0 equiv.). The reaction flask was then fitted with a condenser and warmed to reflux. After 26 h at this temperature, the mixture was allowed to cool down to room temperature. The solvent was removed *in vacuo* and the residue taken into 20 mL of methylene chloride and washed with 10 mL of water. The aqueous phase was further extracted with 10 mL of methylene chloride. The combined organic phases were dried (Na_2SO_4) and concentrated to give a crude yellow residue. Flash chromatography on silica gel (eluent: 30% ethyl acetate/hexane) provided the *cis* compound **13** (mp 116–117°C) and the *trans* compound **14** (mp 132–134°C) in a ratio of 1.2:1 in 63% yield. Further elution of the column with 80% ethyl acetate/hexane afforded the *O*-methyl product **15** in 28% yield.

cis-**13** had ir ($CHCl_3$, cm^{-1}): 2966, 1717, 1646, 1591, 1230, 1097; ^{1}H nmr ($CDCl_3$, ppm): 7.44–7.56 (m, 5H), 5.44 (d, J = 2.2 Hz, 1H), 2.89 (ddd, J = 2.2, 6.3, 19 Hz, 1H), 2.57 (d, J = 19 Hz, 1H), 2.29 (dt, J = 3.5, 14 Hz, 1H), 2.06 (d, J = 6.3 Hz, 1H), 2.50–2.70 (m, 1H), 1.52–1.83 (m, 2H), 1.36 (s, 3H), 1.02 (s, 6H); ms: 314 ($M^{+\cdot}$, 9), 217 (17), 176 (63), 148 (39), 110 (32), 85 (24), 77 (56), 67 (100). Exact mass calcd. for $C_{19}H_{22}O_2S$: 314.134; found: 314.135.

trans-**14** had ir (B)r, cm^{-1}): 2950, 1718, 1648, 1590, 1250; ^{1}H nmr ($CDCl_3$, ppm): 7.40–7.55 (m, 5H), 5.35 (d, J = 1.8 Hz, 1H), 2.70 (ddd, J = 1.8, 12.2, 17.7 Hz, 1H), 2.40–2.63 (m, 4H), 1.58–1.90 (m, 2H), 1.41 (s, 3H), 1.11 (s, 3H), 1.09 (s, 3H); ms: 314 ($M^{+\cdot}$, 8), 258 (3), 217 (7), 200 (9), 176 (78), 148 (70), 110 (41), 85 (47), 77 (70), 67 (100), 39 (68).

15 had ^{1}H nmr ($CDCl_3$, ppm): 7.34–7.58 (m, 5H), 5.44 (d, J = 1.6 Hz, 1H), 3.73 (s, 3H), 2.12–2.65 (m, 5H), 1.58 (s, 3H), 1.22–1.56 (m, 2H), 0.88 (s, 3H).

trans-*6'-Phenylthio-3',4',4a',8a'-tetrahydro-4',4',8a'-trimethyl-spiro[1,3-dithiolane-2,1'(2'*H*)-naphthalen]-8'(5'*H*)-one (**16**)*

To a stirred solution of the dione **14** (1.26 g; 4.0 mmol) in 70 mL of benzene was added a catalytic amount of *p*-toluenesulfonic acid and 1,2-ethanedithiol (1.0 mL; 12.0 mmol). The mixture was then refluxed (Dean–Stark) and the reaction followed by tlc (eluent: 20% ethyl acetate/hexane). At the end of the reaction the mixture was diluted with 50 mL of ether and washed with 10% sodium bicarbonate solution. The solvent was evaporated *in vacuo* and the compound purified by column chromatography (eluent: 20% ethyl acetate/hexane) to give **16** in almost quantitative yield. **16** had ^{1}H nmr ($CDCl_3$, ppm): 7.43 (s, 5H), 5.32 (s, 1H), 3.00–3.80 (m, 4H), 1.43–2.73 (m, 7H), 1.38 (s, 3H), 0.93 (s, 6H); ms: 390 (6), 331 (28), 298 (40), 283 (20), 255 (18), 244 (24), 229 (29), 191 (25), 176 (29), 155 (19), 135 (46),

[3]T. H. Chan, A. Schwerdtfeger, A. W. Thomas, G. M. Strunz, and A. Salonius. Manuscript in preparation.

Can. J. Chem. Downloaded from www.nrcresearchpress.com by 88.85.125.76 on 09/07/12
For personal use only.

131 (46), 118 (33), 110 (57), 107 (33), 77 (28), 55 (39), 41 (45), 28 (100). Exact mass calcd. for $C_{21}H_{26}OS_3$: 390.115; found: 390.111.

trans-*6'-Methoxy-3',4',4a',8a'-tetrahydro-4',4',8a'-trimethyl-spiro-[1,3-dithiolane-2,1'(2'H)-naphthalen]-8'(5'H)-one (17)*

To a well-stirred solution of **16** (0.78 g; 2.0 mmol) in dry methanol (40 mL) under nitrogen was added sodium methoxide (0.55 g; 10.0 mmol) and the mixture refluxed for 24 h. The solvent was removed *in vacuo* and the residue extracted with 100 mL of ether. The ether layer was washed with 10 mL of water and then dried (Na_2SO_4). The solvent was removed *in vacuo* and the crude product purified by column chromatography (eluent: 30% ethyl acetate/hexane) to give **17** in 60% yield. The starting compound **16** was also recovered in 30% yield. **17** had ^{1}H nmr ($CDCl_3$, ppm): 5.13 (s, 1H), 3.30 (s, 3H), 3.10–3.80 (m, 4H), 1.50–2.53 (m, 7H), 1.20 (s, 3H), 0.98 (s, 3H), 0.95 (s, 3H); ms: 312 (44), 253 (53), 155 (68), 139 (42), 131 (100), 122 (20), 118 (47), 98 (38), 69 (48), 55 (45). Exact mass calcd. for $C_{16}H_{24}O_2S_2$: 312.122; found: 312.125.

trans-*3-Methoxy-5,6,4a,8a,7,8-hexahydro-5,5,8a-trimethyl-(4H)-naphthalen-1-one (18)*

To a stirred solution of **17** (0.62 g; 2.0 mmol) in 50 mL of ethanol was added 3.0 g of Raney nickel and the mixture was stirred for 6 h. At this point the reaction mixture was refluxed for another 6 h, the catalyst removed by filtration, and the solvent removed *in vacuo*. The crude product was purified by column chromatography (eluent: 20% ethyl acetate/hexane). The product was then crystallized from hexane to give **18**, mp 55–57°C, in 85% yield. The spectral properties of **18** are identical in all respects to the reported values (15). **18** had ^{1}H nmr ($CDCl_3$, ppm): 5.18 (s, 1H), 3.78 (s, 3H), 1.18–2.55 (m, 9H), 1.08 (s, 3H), 0.98 (s, 3H), 0.93 (s, 3H); ms: 222 (37), 207 (23), 151 (17), 139 (32), 109 (24), 98 (100), 68 (35), 41 (26), 28 (47). Exact mass calcd. for $C_{14}H_{22}O_2$: 222.162; found: 222.160.

trans-*5,6,4a,8a,7,8-Hexahydro-5,5,8a-trimethyl-(4H)naphthalen-3-one (19)*

To a stirred solution of **18** (111 mg; 0.5 mmol) in 40 mL of dry ether under nitrogen was added lithium aluminum hydride (19 mg; 2.0 mmol). After 30 min, once again LAH (19 mg; 2.0 mmol) was added and the solution refluxed for 1 h. Then, the excess LAH was destroyed by adding 2.0 mL of ethyl acetate. The mixture was diluted with 50 mL of ether, washed with 10% aqueous HCl, and then dried (Na_2SO_4). The solvent was removed *in vacuo* and the crude product treated with 20% HCl/methanol and stirred for 6 h. The solvent was removed again and the crude product extracted with ether. The ether extracts were washed with 10 mL of saturated sodium chloride solution and then dried (Na_2SO_4). The crude product was chromatographed (eluent: 15% ethyl acetate/hexane) to give **19** in 74% yield. The spectral properties were identical in all respects to the reported values (15). **19** had ^{1}H nmr ($CDCl_3$, ppm): 6.65 (d, J = 10 Hz, 1H), 5.67 (d, J = 10 Hz, 1H), 1.10–2.60 (m, 9H), 1.10 (s, 3H), 0.92 (s, 3H), 0.88 (s, 3H); ms: 192 (49), 177 (22), 151 (29), 150 (87), 135 (55), 121 (44), 109 (52), 79 (30), 69 (97), 55 (47), 41 (52), 28 (100). Exact mass calcd. for $C_{13}H_{20}O$: 192.151; found: 192.150.

cis-*3-Phenylthio-5,6,4a,8a,7,8-hexahydro-5,5,8a-trimethyl-(4H,7H)-naphthalen-1-one (27)*

To a stirring solution of the dione **13** (0.51 g; 1.62 mmol) in dry methanol (25 mL) under argon at 0°C was added sodium borohydride (0.080 g; 2.10 mmol; 1.3 mol equiv.). The mixture was then stirred for 6 h at which time water (2.0 mL) was added and the mixture allowed to warm to room temperature. The solvent was then removed *in vacuo* and the residue taken into 30 mL of methylene chloride and washed with 10 mL of water. The extract was dried ($MgSO_4$) and concentrated *in vacuo* to give **27** as a white solid in 100% yield. This material appeared to be quite pure by tlc (one spot) and ^{1}H nmr. The product could be further purified by recrystallization from absolute ethanol as white needles, mp 180–182°C. **27** had ir ($CHCl_3$, cm^{-1}): 3460, 3005, 2961, 1629, 1593, 1139, 1026; ^{1}H nmr ($CDCl_3$, ppm): 7.42–7.53 (m, 5H), 5.35 (d, J = 2.8 Hz, 1H), 4.81 (d, J = 10.6 Hz, exch. D_2O, 1H), 3.16 (ddd, J = 11.6, 10.6, 4.6 Hz, 1H), 2.92 (ddd, J = 19.1, 4.6, 2.8 Hz, 1H), 2.50 (dd, J = 19.1, 1 Hz, 1H), 1.21–1.89 (m, 5H), 1.47 (s, 3H), 0.96 (s, 3H), 0.77 (s, 3H); ms: 316 ($M^{+\cdot}$, 10), 217 (100), 176 (54), 148 (54), 139 (71), 108 (80), 67 (67), 43 (91), 39 (85). Exact mass calcd. for $C_{19}H_{24}O_2S$: 316.150; found: 316.144.

cis-*3-Phenylthio-5,6,4a,8a,7,8-hexahydro-5,5,8a-trimethyl-(4H)-naphthalen-8α(tert-butyldimethylsiloxy)-1-one (28)*

To a stirred solution of the hydroxydecalone **27** (0.32 g; 1.01 mmol) and 2,6-lutidine (0.30 mL; 0.27 g; 2.53 mmol; 2.5 equiv.) in dry methylene chloride (1.0 mL) under argon at room temperature was added *tert*-butyldimethylsilyl trifluoromethanesulfonate (0.35 mL; 0.40 g; 1.52 mmol; 1.5 equiv.) dropwise. After 5 h, the mixture was diluted with 20 mL of methylene chloride and washed with 10 mL of 10% sodium carbonate solution. The aqueous layer was further extracted with 10 mL of methylene chloride. The combined extracts were dried ($MgSO_4$) and concentrated *in vacuo* to give a crude oily liquid. Flash chromatography on silica gel (eluent: 5% ethyl acetate/hexane) afforded **28** in 77% yield as fine white crystals, mp 64–67°C. **28** had ir (Nujol, cm^{-1}): 1646, 1606, 1289, 1250, 1073, 1042; ^{1}H nmr ($CDCl_3$, ppm): 7.38–7.54 (m, 5H), 5.38 (d, J = 1.4 Hz, 1H), 2.81–3.00 (bm, 1H), 2.42 (dd, J = 17.0, 5.2 Hz, 1H), 1.72–1.90 (m, 3H), 1.49–1.67 (m, 1H), 1.28 (s, 3H), 1.19 (s, 3H), 0.98 (s, 3H), 0.84 (s, 9H), 0.01 (s, 3H), −0.12 (s, 3H); ms: 415 ($M^{+\cdot}$ − 15, 3), 373 (100), 249 (38), 217 (35), 75 (58), 57 (21), 41 (37). Exact mass calcd. for $C_{25}H_{39}O_2SSi$ (CI, NH_3, $M^{+\cdot}$ + 1): 431.244; found: 431.244.

cis-*3-Methoxy-5,6,4a,8a,7,8-hexahydro-5,5,8a-trimethyl-(4H)naphthalen-8α(tert-butyldimethylsiloxy)-1-one (29)*

To a stirred solution of sodium methoxide (1.74 mmol; prepared by dropwise addition of 10.0 mL of methanol to 41.8 mg of sodium hydride) in dry methanol under argon at room temperature was added **28** (150 mg; 0.38 mmol). The reaction flask was then fitted with a condenser and warmed to reflux. After 5 days, the mixture was allowed to cool and the solvent was removed *in vacuo*. The residue was taken into 20 mL of methylene chloride and washed with 10 mL of water. The organic layer was dried ($MgSO_4$) and concentrated *in vacuo*. The crude product was subjected to flash chromatography on silica gel (eluent: 8% ethyl acetate/hexane) to give 101.4 mg (83%) of **29** as fine waxy crystals, mp 68–70°C. **29** had ir ($CHCl_3$, cm^{-1}): 2929, 2856, 1627, 1381, 1079, 841; ^{1}H nmr ($CDCl_3$, ppm): 5.36 (d, J = 0.8 Hz, 1H), 3.82 (bm, 1H), 3.64 (s, 3H), 2.78 (m, 1H), 2.28 (dd, J = 17.8, 5.7 Hz, 1H), 1.50–1.90 (m, 5H), 1.31 (s, 3H), 1.13 (s, 3H), 0.95 (s, 3H), 0.79 (s, 9H), 0.02 (s, 3H), −0.08 (s, 3H); ms: 337 ($M^{+\cdot}$ − 15, 6), 297 (23), 296 (43), 295 (100), 171 (40), 139 (35), 101 (24), 89 (46), 75 (43), 73 (45), 41 (40). Exact mass calcd. for $C_{20}H_{37}O_3Si$ (CI, NH_3, $M^{+\cdot}$ + 1): 353.251; found: 353.251.

cis-*3-Methoxy-5,6,4a,8a,7,8-hexahydro-5,5,8a-trimethyl-(4H)naphthalen-8α-hydroxy-1-one (30)*

For compound **27**: This reaction (and work-up) was carried out as indicated above for **29** on a 100 mg (0.32 mmol) scale using 10.0 equivalents of sodium methoxide in 5.0 mL of methanol. The reaction required 4 days to reach completion. The crude residue after work-up was chromatographed (eluent: 25% ethyl acetate/hexane), providing **30** in 33% yield. **30** had ir ($CHCl_3$, cm^{-1}): 3420, 1620, 1237, 1179, 1155, 1076; ^{1}H nmr ($CDCl_3$, ppm): 5.22 (d, J = 1.8 Hz, 1H), 5.12 (d, J = 10.8 Hz, exch. D_2O, 1H), 3.69 (s, 3H), 3.17 (ddd, J = 11.0, 10.8, 5.3 Hz, 1H), 2.77 (ddd, J = 19.1, 6.8, 1.8 Hz, 1H), 2.36 (d, J = 19.1 Hz, 1H), 1.59–1.90 (m, 3H), 1.23–1.50 (m, 2H), 1.46 (s, 3H), 0.91 (s, 3H), 0.70 (s, 3H); ms: 238 ($M^{+\cdot}$, 2), 220 (8), 205 (5), 139 (100), 122 (46), 107 (70), 98 (88), 69 (57), 55 (36), 41 (34), 39 (29). Exact mass calcd. for $C_{14}H_{23}O_3$ (CI, NH_3, $M^{+\cdot}$ + 1): 239.165; found: 239.165.

trans-*3-Phenylthio-5,6,4a,8a,7,8-hexahydro-5,5,8a-trimethyl-naphthalen-8β-hydroxy-1β(1H,4H)-ol (31a)*

To a stirred solution of the *trans*-decalone **14** (250 mg; 0.796 mmol) in dry methanol (10.0 mL) under argon at 0°C was added sodium borohydride (39.1 mg; 1.03 mmol; 1.3 mol equiv.) in one portion. After 18 h of stirring at this temperature, water (1.0 mL) was added

Can. J. Chem. Downloaded from www.nrcresearchpress.com by 88.85.125.76 on 09/07/12
For personal use only.

dropwise and the mixture allowed to come to room temperature. The solvent was then removed *in vacuo* and the residue taken into 30 mL of methylene chloride and washed with 10 mL of water. The organic phase was dried ($MgSO_4$), filtered, and evaporated *in vacuo*. The crude residue was subjected to flash chromatography on silica gel (eluent: 23% ethyl acetate/hexane) to give **31***a* in 79% yield (mp 102–104°C), as well as a mixture of the two monoreduced species **31***b* in 21% yield.

31*a* had ir ($CHCl_3$, cm^{-1}): 3200–3500 (b), 2931, 2870, 1476, 1086, 1019; ^1H nmr ($CDCl_3$, ppm): 7.26–7.42 (m, 5H), 5.43 (d, J = 1.5 Hz, 1H), 4.20 (bm, 1H), 3.53–3.63 (ddd, J = 10.5, 5.2, 3.2 Hz, 1H), 2.95 (d, J = 3.9 Hz, exch. D_2O, 1H), 2.63 (d, J = 3.2 Hz, exch. D_2O, 1H), 2.11–2.18 (m, 2H), 1.25–1.70 (m, 5H), 0.94 (s, 3H), 0.88 (s, 3H), 0.81 (s, 3H); ms: 318 ($M^{+\cdot}$, 3), 300 (5), 209 (71), 191 (58), 109 (96), 69 (89), 43 (100). Exact mass calcd. for $C_{19}H_{26}O_2S$: 318.165; found: 318.169.

31*b* had ir ($CHCl_3$, cm^{-1}): 3463, 3008, 2963, 1636, 1629, 1287; ^1H nmr ($CDCl_3$, ppm): 7.25–7.50 (m, 5H, isomers A,B), 5.32 (s, 1H, isomer A), 5.27 (d, J = 1.8 Hz, 1H, isomer B), 4.38 (s, exch. D_2O, 1H, isomer A), 4.11 (m, 1H, isomer A), 3.75 (m, 1H, isomer B), 2.64 (s, exch. D_2O, 1H, isomer B), 2.24–2.63 (m, 2H, isomers A,B), 1.15–1.82 (m, 5H, isomers A,B), 1.14 (s, 3H, isomer B), 1.07 (s, 3H, isomer A), 0.99 (s, 3H, isomer A), 0.98 (s, 3H, isomers A,B), 0.93 (s, 3H, isomer B); ms: 316 ($M^{+\cdot}$, 7), 301 (4), 217 (100), 139 (45), 109 (48), 67 (47), 43 (96), 41 (61), 39 (51).

trans-*3-Phenylthio-5,6,4a,8a,7,8-hexahydro-5,5,8a-trimethyl-1β,8β-diacetoxy-(1H,4H)naphthalene (32)*

To a stirred solution of **17** (0.62 g; 2.0 mmol) in 50 mL of ethanol (0.33 mL; 4.1 mmol; 6.0 equiv.), and acetic anhydride (0.39 mL; 4.1 mmol; 6.0 equiv.) in dry methylene chloride (8.0 mL) under argon at room temperature was added a catalytic amount of 4-dimethylaminopyridine (DMAP). After 49 h the mixture was diluted with 20 mL of methylene chloride and washed with 10 mL of water. The organic phase was then dried ($MgSO_4$) and evaporated *in vacuo*. The crude residue was chromatographed (eluent: 20% ethyl acetate/hexane) to give the diacetate **32** (mp 104–107°C) in 85% yield. **32** had ir ($CHCl_3$, cm^{-1}): 2933, 1736, 1373, 1260, 1026; ^1H nmr ($CDCl_3$, ppm): 7.27–7.38 (m, 5H), 5.32–5.39 (m, 2H), 4.73 (dd, J = 10.7, 5.2 Hz, 1H), 2.13–2.20 (m, 2H), 2.00 (s, 3H), 1.99 (s, 3H), 1.54–1.71 (m, 2H), 1.35–1.53 (m, 3H), 1.08 (s, 3H), 0.89 (s, 3H), 0.81 (s, 3H); ms: 402 ($M^{+\cdot}$, 3), 359 (4), 342 (25), 191 (17), 173 (25), 105 (21), 91 (31), 43 (100). Exact mass calcd. for $C_{23}H_{31}O_4S$ (CI, NH_3, $M^{+\cdot}$ + 1): 403.194; found: 403.194.

Acknowledgement

Financial support from NSERC and FCAR is gratefully acknowledged.

1. T. H. CHAN, Y. J. ZHANG, F. SAURIAL, A. W. THOMAS, and G. M. STRUNZ. Can. J. Chem. **65**, 1853 (1987).
2. K. MUNAKATA. *In* Control of insect behaviour by natural products. *Edited by* D. L. Wood, R. M. Silverstein, and M. Nakajima. Academic Press, New York. 1970.
3. I. KUBO, A. MATSUMOTO, T. MATSUMOTO, and J. A. KLOCOE. Tetrahedron, 489 (1986); W. KRAUS, M. BOKEL, A. KLENK, and H. POHNL. Tetrahedron Lett. **26**, 6435 (1985); H. B. BROUGHTON, S. V. LEY, A. M. A. ALAWIN, D. J. WILLIAMS, and E. D. MORGAN. J. Chem. Soc. Chem. Commun. 46 (1986).
4. D. H. R. BARTON, H. T. CHEUNG, A. D. CROSS, L. M. JACKMAN, and M. MARTIN-SMITH. J. Chem. Soc. 5061 (1961).
5. M. J. BEGLEY, L. CROMBIE, P. J. HAM, and D. A. WHITING. J. Chem. Soc. Perkin Trans. 1, **296**, 304 (1976).
6. G. M. STRUNZ, P. GIGUERE, and A. W. THOMAS. J. Chem. Ecol. **12**, 251 (1986).
7. C. C. CHANG and K. NAKANISHI. J. Chem. Soc. Chem. Commun. 605 (1983).
8. E. VAN DER EYCKEN, A. DE BRUYN, J. VAN DER EYCKEN, P. CALLANT, and M. VANDEWALLE. Tetrahedron, **42**, 5385 (1986); E. VAN DER EYCKEN, A. JANSSENS, and M. VANDEWALLE. Tetrahedron Lett. **28**, 3519 (1987); D. P. CURRAN, P. B. JACOBS, R. L. ELLIOTT, and B. H. KIM. J. Am. Chem. Soc. **109**, 5280 (1987).
9. Y. KOJIMA and N. KATO. Tetrahedron, **37**, 2527 (1981).
10. S. V. LEY, D. SANTAFIANOS, W. M. BLANCY, and M. S. J. SIMMONDS. Tetrahedron Lett. **28**, 221 (1987); M. G. BRASCA, H. B. BROUGHTON, D. CRAIG, S. V. LEY, A. A. SOMOVILLA, and P. L. TOOGOOD. Tetrahedron Lett. **29**, 1853 (1988); A. P. BRUNETIERE, M. LECLAIRE, S. BHATNAGAR, J. Y. LALLEMAND, and J. COSSY. Tetrahedron Lett. **30**, 341 (1989); S. V. LEY, A. A. SOMOVILLA, H. B. BROUGHTON, D. CRAIG, A. M. Z. SLAWIN, P. L. TOOGOOD, and D. J. WILLIAMS. Tetrahedron, **45**, 2143 (1989).
11. S. V. LEY, D. NEUHAUS, N. S. SIMKINS, and A. J. WHITTLE. J. Chem. Soc. Perkin Trans. 1, 2157 (1982).
12. T. H. CHAN and C. V. C. PRASAD. J. Org. Chem. **52**, 110 (1987).
13. C. V. C. PRASAD and T. H. CHAN. J. Org. Chem. **54**, 3242 (1989).
14. C. V. C. PRASAD and T. H. CHAN. J. Org. Chem. **52**, 120 (1987).
15. E. WENKERT and B. P. STRIKE. J. Am. Chem. Soc. **86**, 2044 (1964).
16. K. HIRAI, K. T. SUZUKI, and S. NOZOE. Tetrahedron, **27**, 6057 (1971).
17. A. MCMORRAN. Can. Entomol. **97**, 58 (1965).
18. W. J. CONOVER and R. L. IMAN. Am. Stat. **35**, 124 (1981).
19. SAS User's Guide: Statistics, Version 5. 1985 Edition. SAS Institute Inc., Cary, N.C., U.S.A.
20. J. H. ZAR. Biostatistical analysis. 2nd ed. Prentice–Hall, New York. 1984.

Can. J. Chem. Downloaded from www.nrcresearchpress.com by 88.85.125.76 on 09/07/12
For personal use only.

The crystal structure of 1,2-dibenzoyl-1-*tert*-butylhydrazine, a nonsteroidal ecdysone agonist, and its effects on spruce budworm (*Choristoneura fumiferana*)

T. H. CHAN,[1] A. ALI, AND J. F. BRITTEN
Department of Chemistry, McGill University, Montreal, Que., Canada H3A 2K6
AND
A. W. THOMAS, G. M. STRUNZ, AND A. SALONIUS
Forestry Canada – Maritimes Region, Fredericton, N.B., Canada E3B 5P7

Received December 8, 1989

This paper is dedicated to Professor Arthur S. Perlin on the occasion of his 67th birthday

T. H. CHAN, A. ALI, J. F. BRITTEN, A. W. THOMAS, G. M. STRUNZ, and A. SALONIUS. Can. J. Chem. **68**, 1178 (1990).

The crystal structure of 1,2-dibenzoyl-1-*tert*-butylhydrazine (**1**), a nonsteroidal ecdysone agonist, has been established by direct methods and refined to a final *R* value of 0.038 for 2502 observed reflections. The crystals belong to the monoclinic system, $a = 10.5114(7)$, $b = 31.557(3)$, $c = 11.1578(8)$ Å, $\beta = 113.210(6)°$, and the space group is $P2_1/n$. The N—N bond in **1** was found to adopt a *gauche* conformation with a dihedral angle of −71.8° or −58.1°. The two amide functions adopt different planar conformations. The compound is found to have a potent effect on the development of spruce budworm (*Choristoneura fumiferana*) larvae, causing early apolysis and subsequent mortality at 0.2–10 ppm concentration in artificial diet.

Key words: ecdysone, agonist, spruce budworm, 1,2-dibenzoyl-1-*tert*-butylhydrazine.

T. H. CHAN, A. ALI, J. F. BRITTEN, A. W. THOMAS, G. M. STRUNZ et A. SALONIUS. Can. J. Chem. **68**, 1178 (1990).

On a déterminé la structure cristalline de la 1,2-dibenzoyl-1-*tert*-butylhydrazine (**1**), un agoniste non-stéroïdal de l'ecdysone, à l'aide de méthodes directes et on l'a affinée jusqu'à une valeur finale de *R* de 0,038 pour 2502 réflexions observées. Les cristaux sont monocliniques, groupe d'espace $P2_1/n$, avec $a = 10{,}5114(7)$, $b = 31{,}557(3)$ et $c = 11{,}1578(8)$ Å et $\beta = 113{,}210(6)°$. On a trouvé que la liaison N—N du composé **1** adopte une conformation *gauche* avec un angle dièdre allant de −71,8 à −58,1°. Les deux fonctions amides adoptent des conformations planaires différentes. On a trouvé que le composé possède une activité importante vis-à-vis du développement de la larve de la tordeuse des bourgeons de l'épinette (*Choristoneura fumiferana*); à des concentrations allant de 0,2 à 10 ppm dans des diètes artificielles, il cause une apolyse précoce et une mortalité subséquente.

Mots clés : ecdysone, agoniste, tordeuse des bourgeons de l'épinette, 1,2-dibenzoyl-1-*tert*-butylhydrazine.

[Traduit par la revue]

Introduction

The spruce budworm, *Choristoneura fumiferana*, is an insect pest that causes considerable damage to the forest resource in eastern North America, threatening the wood supply from large areas of forest in eastern Canada. The damage is caused by the 2nd instar to the 6th instar larvae, which feed on the buds, newly opened shoots, and needles of the host tree from mid-May to late June. Efforts to control the spruce budworm up to now have relied on the spraying of insecticides.

Recently, we have examined some alternative approaches to the control of spruce budworm. One strategy that has been studied is to employ antifeedants to interfere with the feeding behaviour of insects (1, 2). Another line of attack is to intervene in the insect's development. The terpenoid juvenile hormone and the steroid ecdysone are known to regulate insect metamorphosis and development (3). While much research has been carried out with juvenile hormone mimics (4), compounds that only interfere with pupation do not appear to be the most useful control agents for insects that, like the spruce budworm, inflict their damage during the larval stages. On the other hand, relatively little attention has been focused on the interference of ecdysone functions as a mean of insect control. In 1988, 1,2-dibenzoyl-1-*tert*-butylhydrazine (**1**) was reported to mimic the action of 20-hydroxyecdysone (**2**) in competing for the same receptor sites (5). Furthermore, the compound was found to be extremely potent at promoting the onset of molting in larvae of the tobacco hornworm (*Manduca sexta*) (6). We have therefore investigated the effects of **1** on the spruce budworm.

[1]Author to whom correspondence may be addressed.

Biological assays

Compound **1** and its parent compound, 1,2-dibenzoylhydrazine (**3**), were synthesized by standard procedures. The compound was incorporated into artificial diet to give concentrations of 0.2, 1, 10, 100 ppm wet weight, and was offered to spruce budworm larvae from a laboratory colony. Diet subjected to the same solvent treatment but with no compound was used as a control. Full-strength artificial diet (7) was used for one set of assays beginning with 2nd instar larvae, whereas 40% diet (1 part diet:1.5 parts Alphacel) was used for another set beginning with 6th instar larvae.

Compound **1** caused early apolysis, seen as head-capsule

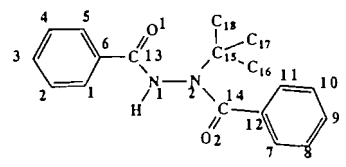

1

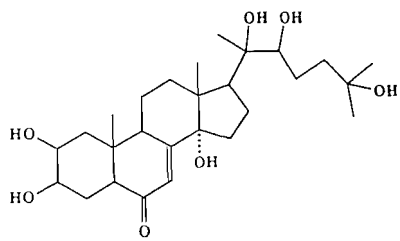

2

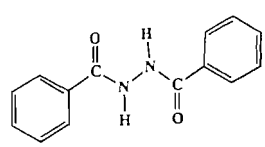

3

Can. J. Chem. Downloaded from www.nrcresearchpress.com by 88.85.125.76 on 09/07/12
For personal use only.

slippage, in 100% of the 2nd instar larvae at 10 ppm and 100 ppm, and all the larvae died before reaching the 3rd instar. At a concentration of 1 ppm, compound **1** had no effect on the development of 2nd instar larvae to 6th instars. No 6th instar survived to a pupa when fed 10 and 100 ppm of **1**. The no effect level for 6th instar larvae was 0.2 ppm.

In contrast, neither larval development from 2nd instar to 6th instar nor development of 6th instar larvae to pupae were affected by any concentration of **3** up to 100 ppm.

Crystal structure

The significant activity observed for **1** is encouraging in the context of the possible use of ecdysone agonists for control of the spruce budworm. From the chemistry point of view, a fundamental question is why **1** should behave as an ecdysone agonist (5, 6) when the two compounds, **1** and **2**, are structurally so different. Furthermore, any explanation will have to take into consideration the fact that **3**, the parent compound of **1**, fails to show significant activities in this and other bioassays (6). Molecular modelling, which has been used extensively in the field of drug design, may offer an understanding of the structure–activity relationship. A prerequisite of any meaningful molecular modelling calculation is the precise structure of an active compound obtained by X-ray structure determination. Towards this end, we have determined the crystal structure of **1**.

The title compound (**1**) was prepared by reacting *tert*-butylhydrazine with benzoyl chloride in aqueous sodium hydroxide solution. It was recrystallized from ethanol–water to give crystals with mp 174°C. A crystal approximately 0.20 × 0.20 × 0.20 mm was mounted on a glass fibre. The room temperature intensity data were collected using Cu $K_{\bar{\alpha}}$ radiation (λ = 1.54178 Å) on an Enraf–Nonius CAD4 diffractometer under NRCCAD (8) control with on-line profile fitting. Twenty seven reflections (70° < 2θ < 90°) were used for the cell determination. A θ/2θ collection of $\pm h$, $+k$, $+l$ set of reflections with $2\theta_{max}$ = 99.7° yielded 4529 measurements. The 400, 004, and −181 reflections were each measured after every 80 reflections and varied less than 0.7%. There were 3421 unique reflections, and 2502 with $I > 2.5\ \sigma_I$ were used for refinement. σ_I is given by (peak + m^2 background)$^{1/2}$, where m is the peak-to- background measurement time ratio.

Crystal data:

$C_{18}H_{20}N_2O_2$ MW 296.37 g mol^{-1}

Monoclinic, $P2_1/n$ (non-standard $P2_1/c$, no. 14), a = 10.5114(7) Å, b = 31.557(3) Å, c = 11.1578(8) Å, β = 113.210(6)°, V = 3401.6(4) Å^3 at 21°; Z = 8, ρ_c = 1.157 Mg m^{-3}, μ = 0.58 mm^{-1} (no absorption correction).

Data reduction, structure solution, and structure refinement were carried out using the NRCVAX (9) program system on a Silicon Graphics IRIS 3130. Direct methods (SOLVER (9)) revealed all non-hydrogen atoms for two independent molecules. Full-matrix least-squares refinement and a Fourier difference map revealed all hydrogen atoms. The final refinement, on 558 parameters (non-hydrogen atoms anisotropic) for 84 atoms, based on observed wF's, was weighted with $w = (\sigma_F^2 + 0.00001\ F^2)^{-1}$ and gave residuals R = 0.038, R_w = 0.027, and S = 2.06 where $R = \Sigma||F_o| - |F_c||/\Sigma F_o$, $R_w = [\Sigma(w(|F_o| - |F_c|)^2)/\Sigma(wF_o^2)]^{1/2}$, and $S = [\Sigma(w(|F_o| - |F_c|)^2)/(\text{number of reflections minus number of parameters})]^{1/2}$. The largest shift/error was 0.112 and the major features of the final difference map were a hole of −0.14 e/Å^3 and a peak of 0.12 e/Å^3. The secondary extinction coefficient refined to 1.57 (8).

TABLE 1. Final atomic coordinates of **1**

Atom	x	y	z	B_{iso}[a]
O(1)A	0.5393(2)	0.06019(7)	0.7579(2)	5.8
O(2)A	0.5840(2)	0.13797(7)	1.0279(2)	4.7
N(1)A	0.7586(3)	0.07944(8)	0.8779(3)	3.6
N(2)A	0.7254(2)	0.09344(8)	0.9806(2)	3.4
C(1)A	0.8383(4)	0.0287(1)	0.7023(4)	5.3
C(2)A	0.8732(5)	0.0112(1)	0.6058(5)	6.5
C(3)A	0.7801(6)	0.0098(1)	0.4809(5)	6.3
C(4)A	0.6518(6)	0.0255(2)	0.4502(4)	8.8
C(5)A	0.6153(5)	0.0431(2)	0.5452(4)	7.6
C(6)A	0.7090(4)	0.0448(1)	0.6726(3)	3.6
C(7)A	0.7636(5)	0.1780(1)	0.8580(4)	5.7
C(8)A	0.7574(7)	0.2071(1)	0.7641(6)	8.1
C(9)A	0.6351(7)	0.2157(2)	0.6640(6)	8.2
C(10)A	0.5170(6)	0.1962(2)	0.6567(5)	8.0
C(11)A	0.5213(5)	0.1675(1)	0.7525(4)	5.8
C(12)A	0.6458(4)	0.1581(1)	0.8532(3)	4.0
C(13)A	0.6599(4)	0.0617(1)	0.7708(3)	4.0
C(14)A	0.6468(3)	0.1291(1)	0.9592(3)	3.7
C(15)A	0.7424(4)	0.0625(1)	1.0885(3)	3.9
C(16)A	0.8147(6)	0.0855(2)	1.2166(4)	5.8
C(17)A	0.6013(5)	0.0461(2)	1.0769(5)	6.2
C(18)A	0.8305(7)	0.0252(2)	1.0776(5)	7.1
O(1)B	0.8874(2)	0.80103(7)	0.0551(2)	5.2
O(2)B	0.9481(2)	0.90919(7)	0.0175(2)	5.4
N(1)B	0.6895(3)	0.8387(1)	−0.0061(3)	3.8
N(2)B	0.7449(3)	0.87296(8)	−0.0479(2)	3.7
C(1)B	0.5584(5)	0.7632(1)	0.0362(4)	6.2
C(2)B	0.4991(6)	0.7311(1)	0.0812(6)	8.2
C(3)B	0.5827(7)	0.7057(1)	0.1795(6)	8.0
C(4)B	0.7210(6)	0.7109(2)	0.2296(5)	9.7
C(5)B	0.7780(5)	0.7427(1)	0.1832(5)	7.6
C(6)B	0.6984(4)	0.7696(1)	0.0881(3)	4.0
C(7)B	0.7690(4)	0.9039(1)	0.2183(4)	4.7
C(8)B	0.7859(5)	0.9052(1)	0.3470(5)	6.1
C(9)B	0.9072(6)	0.8909(1)	0.4412(5)	6.9
C(10)B	1.0111(5)	0.8760(1)	0.4086(4)	6.8
C(11)B	0.9942(4)	0.8750(1)	0.2798(4)	5.4
C(12)B	0.8718(4)	0.8888(1)	0.1829(3)	3.8
C(13)B	0.7685(4)	0.8037(1)	0.0445(3)	3.8
C(14)B	0.8604(4)	0.8905(1)	0.0450(3)	4.1
C(15)B	0.7133(4)	0.8755(1)	−0.1917(3)	4.6
C(16)B	0.7132(7)	0.9220(2)	−0.2285(5)	6.8
C(17)B	0.8189(6)	0.8502(2)	−0.2243(5)	7.0
C(18)B	0.5685(6)	0.8574(2)	−0.2650(5)	7.0

[a] B_{iso} is the mean of the principal axes of the thermal ellipsoid.

The final atomic coordinates[2] are given in Table 1. Bond distances and bond angles are given in Tables 2 and 3 respectively.

There are two molecules (labelled as A and B) in the asymmetric unit. Molecule A is shown in the stereo ORTEP (10) in Fig. 1. While the two molecules A and B are very similar in their conformations, they are not identical. A least-squares pairwise

[2]Tables of observed and calculated structure factors, anisotropic thermal parameters, hydrogen atom parameters, hydrogen geometry, and torsion angles may be purchased from the Depository of Unpublished Data, CISTI, National Research Council of Canada, Ottawa, Ont., Canada K1A 0S2.

Can. J. Chem. Downloaded from www.nrcresearchpress.com by 88.85.125.76 on 09/07/12
For personal use only.

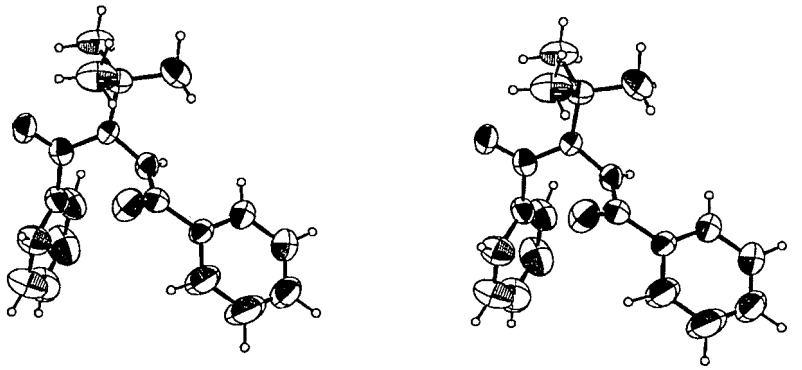

FIG. 1. Stereo ORTEP of molecule A (50% probability for non-hydrogen atoms. Hydrogen atoms are shown with arbitrary size for clarity).

TABLE 2. Bond distances

Bond	Distance (Å) A	B
O(1)—C(13)	1.219(5)	1.211(5)
O(2)—C(14)	1.226(5)	1.230(5)
N(1)—N(2)	1.394(4)	1.394(4)
N(1)—C(13)	1.356(5)	1.362(5)
N(2)—C(14)	1.360(4)	1.365(4)
N(2)—C(15)	1.506(4)	1.507(4)
C(1)—C(2)	1.382(6)	1.384(7)
C(1)—C(6)	1.364)6)	1.367(6)
C(2)—C(3)	1.351(7)	1.364(8)
C(3)—C(4)	1.348(8)	1.346(9)
C(4)—C(5)	1.378(7)	1.370(7)
C(5)—C(6)	1.375(5)	1.359(6)
C(6)—C(13)	1.481(5)	1.491(5)
C(7)—C(8)	1.375(7)	1.376(6)
C(7)—C(12)	1.371(6)	1.373(6)
C(8)—C(9)	1.36(1)	1.370(7)
C(9)—C(10)	1.36(1)	1.364(8)
C(10)—C(11)	1.389(7)	1.378(7)
C(11)—C(12)	1.380(6)	1.385(5)
C(12)—C(14)	1.492(5)	1.496(5)
C(15)—C(16)	1.514(5)	1.525(6)
C(15)—C(17)	1.527(6)	1.522(6)
C(15)—C(18)	1.532(6)	1.527(6)
Hydrogen bonds:		
O(2A)—N(1B)[a]	2.885(4)	
O(2B)—N(1A)[b]	2.857(4)	

[a]Related to N(1B) by (1-x, 1-x, 1-z).
[b]Related to N(1A) by (2-x, 1-y, 1-z).

TABLE 3. Bond angles

Bonds	Angle (deg) A	B
N(2)—N(1)—C(13)	120.2(3)	120.0(3)
N(1)—N(2)—C(14)	116.7(3)	115.2(3)
N(1)—N(2)—C(15)	117.6(2)	116.8(2)
C(14)—N(2)—C(15)	123.3(3)	123.0(3)
C(2)—C(1)—C(6)	120.3(4)	121.2(4)
C(1)—C(2)—C(3)	120.6(5)	118.9(5)
C(2)—C(3)—C(4)	119.7(4)	120.7(5)
C(3)—C(4)—C(5)	120.4(4)	119.6(5)
C(4)—C(5)—C(6)	120.6(4)	121.7(5)
C(1)—C(6)—C(5)	118.3(4)	117.9(4)
C(1)—C(6)—C(13)	123.9(3)	123.8(3)
C(5)—C(6)—C(13)	117.6(4)	118.3(4)
C(8)—C(7)—C(12)	120.3(5)	121.2(4)
C(7)—C(8)—C(9)	120.4(5)	119.3(5)
C(8)—C(9)—C(10)	120.3(5)	120.6(4)
C(9)—C(10)—C(11)	119.9(5)	119.9(4)
C(10)—C(11)—C(12)	120.0(5)	120.4(4)
C(7)—C(12)—C(11)	119.1(4)	118.6(4)
C(7)—C(12)—C(14)	121.7(3)	122.1(3)
C(11)—C(12)—C(14)	119.0(4)	119.1(4)
O(1)—C(13)—N(1)	121.2(3)	122.3(3)
O(1)—C(13)—C(6)	123.2(3)	122.7(3)
N(1)—C(13)—C(6)	115.6(3)	114.9(3)
O(2)—C(14)—N(2)	121.3(3)	122.3(3)
O(2)—C(14)—C(12)	121.2(3)	120.6(3)
N(2)—C(14)—C(12)	117.5(3)	116.9(3)
N(2)—C(15)—C(16)	107.5(3)	108.3(3)
N(2)—C(15)—C(17)	110.3(3)	110.5(3)
N(2)—C(15)—C(18)	108.6(3)	107.8(3)
C(16)—C(15)—C(17)	110.6(4)	111.3(4)
C(16)—C(15)—C(18)	110.5(4)	108.8(4)
C(17)—C(15)—C(18)	109.4(4)	110.0(4)

fitting of the non-hydrogen atoms of A and B, performed with QUANTA[3] on the IRIS 3130 gave an rms displacement of 0.355 Å. Tables 2 and 3 illustrate the geometric similarities. In the discussion below, relevant comparisons are made.

The phenyl groups

The atoms of each of the two phenyl groups are coplanar. However, the two carbonyl groups to which they are bonded are not coplanar with the phenyl rings. The torsion angles defined by C(1)—C(6)—C(13)—O(1) and by C(7)—C(12)—C(14)—O(2) are −149.6(4)° (or −153.8(4)° for B) and 114.3(4)° (or 122.0(4)° for B) respectively, considerably different from the 180° (or 0°) expected. Furthermore, the relative orientation of the two phenyl rings is given by the dihedral angle of 66.3(2)° (or 60.8(2)° for B).

The tert*-butyl group*

The bond distances and angles in the *tert*-butyl group compare well with other *tert*-butyl groups in the literature (11). The bond distance in A of the N(2)—C(15) linkage, 1.506(4) Å

[3]The QUANTA progam is available from Polygen Corporation, 200 Fifth Ave., Waltham, MA 02254, U.S.A.

Can. J. Chem. Downloaded from www.nrcresearchpress.com by 88.85.125.76 on 09/07/12
For personal use only.

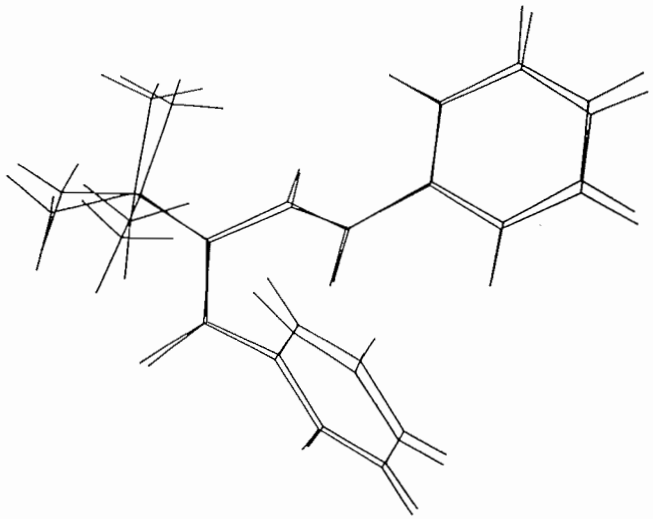

FIG. 2. Least-squares pairwise (non-hydrogen atoms) fitting of molecules A and B.

(1.507(4) Å for B), is within the expected range of 1.47 Å for the normal C—N single bond.

The hydrazine linkage

While the two amide functions adopt the expected planar structure, the amide bearing the N-H has the *s-cis* conformation (O(1)—C(13)—N(1)—N(2)) whereas the amide bearing the N-*tert*-butyl group has the *s-trans* conformation (O(2)—C(14)—N(2)—N(1)). Clearly, the steric size of the *tert*-butyl group causes the phenyl group to be directed away. For N(1), which bears the hydrogen, the nitrogen has an sp^2 hybridized structure with the bond angle for A of N(2)—N(1)—C(13) at 120.2(3)° (120.0(3)° for B). On the other hand, the other nitrogen, N(2), which bears the *tert*-butyl group, is distorted from the perfect trigonal structure, with N(1)—N(2)—C(14) = 116.7(3)°, N(1)—N(2)—C(15) = 117.6(2)°, and C(14)—N(2)—C(15) = 123.3(3)°(115.2(3)°, 116.8(2)°, and 123.0(3)° respectively for B). The N—N bond adopts a *gauche* conformation with a dihedral angle (ϕ) of −71.8° in A (−58.1° in B) for C(13)—N(1)—N(2)—C(14). Such a *gauche* effect has been observed for other hydrazine derivatives (12).

Packing

The crystal, which readily cleaves to give thin needles, shows hydrogen bonding only along the *a* direction, involving N(1) and O(2) atoms of alternating A and B molecules (see Table 2). van der Waals interactions are responsible for the three-dimensional stability.

Conclusions

The crystal structure of **1** reveals some interesting features. Possibly because of the steric effect of the *tert*-butyl group, the two amide functions in **1** adopt different conformations. Furthermore, in the *gauche* conformation of the hydrazine linkage, the carbonyl group of C(13) is away from the *tert*-butyl group. The two carbonyl oxygen atoms are therefore placed in positions relative to each other that would be expected to be different in diacylhydrazines not possessing the bulky *tert*-butyl group. Obviously, it remains to be seen whether this is the factor responsible for the structure–activity difference of **1** and **3**. In view of the potent biological effect of **1** on spruce budworm, further investigation in this area is clearly warranted.

Experimental

1,2-Dibenzoylhydrazine (**3**) was obtained commercially from Aldrich. 1,2-Dibenzoyl-1-*tert*-butylhydrazine (**1**) was synthesized according to the following procedure. Benzoyl chloride (1.12 g, 8 mmol) was added dropwise to a cooled (0°C) solution of *tert*-butylhydrazine hydrochloride (0.50 g, 4 mmol) in aqueous sodium hydroxide (0.30 g, 8 mmol) solution. White precipitate started to appear after 30 min. After 2 h, the white precipitate was filtered and recrystallized from ethanol and water (1:1) to give **1**, mp 174°C, in 78% yield. Compound **1** had IR ($CHCl_3$, cm^{-1}): 3073, 1698, 1610; ^1H NMR ($CDCl_3$, ppm): 1.60 (s, 9H), 7.49 (m, 10H).

Acknowledgements

We thank NSERC for financial support of this research. We are also grateful to Drs. E. J. Gabe and Y. Lepage of the X-ray Diffraction Laboratory, Chemistry Division, National Research Council of Canada, Ottawa, for the collection of X-ray data.

1. T. H. CHAN, Y. J. ZHANG, F. SAURIO, A. W. THOMAS, and G. M. STRUNZ. Can. J. Chem. **65**, 1853 (1987).
2. T. H. CHAN, K. GUERTIN, C. V. C. PRASAD, A. W. THOMAS, G. M. STRUNZ, and A. SALONIUS. Can. J. Chem. **68**, 1169 (1990).
3. G. A. KERKUT and L. I. GILBERT (*Editors*). Comprehensive insect physiology, biochemistry, and pharmacology: Endocrinology I. Vol. 7. Pergamon, Oxford. 1985.
4. G. T. BROOKS. J. Pestic. Sci. **12**, 113 (1987).
5. K. D. WING. Science, **241**, 467 (1988).
6. K. D. WING, R. A. SLAWECKI, and G. R. CARLSON. Science, **241**, 470 (1988).
7. G. T. HARVEY. Can. Entomol. **106**, 353 (1974); A. MCMORRAN. Can. Entomol. **97**, 58 (1965).
8. E. J. GABE and Y. LEPAGE. ACA Meeting, June 1986, McMaster University, Hamilton, Ont. Paper PA23.
9. E. J. GABE, F. L. LEE, and Y. LEPAGE. J. Appl. Crystallogr. **22**, 384 (1989).
10. C. K. JOHNSON. ORTEP-II. Report ORNL-5138. Oak Ridge National Laboratory, Oak Ridge, TN. 1976.
11. F. BRISSE, D. THORAVAL, and T. H. CHAN. Can. J. Chem. **64**, 739 (1986).
12. S. WOLFE. Acc. Chem. Res. **5**, 102 (1972).

Can. J. Chem. Downloaded from www.nrcresearchpress.com by 88.85.125.76 on 09/07/12
For personal use only.

Relative reactivity of three oxygen lone pairs of an α-nucleophile in S_N2 reactions

J. L. WOLK, M. R. HAJNAL, AND S. HOZ[1]
Department of Chemistry, Bar-Ilan University, Ramat-Gan, Israel, 52100

AND

R. M. TARKKA AND E. BUNCEL[1]
Department of Chemistry, Queen's University, Kingston, Ont., Canada K7L 3N6

Received December 11, 1989

This paper is dedicated to Professor Arthur S. Perlin on the occasion of his 67th birthday

J. L. WOLK, M. R. HAJNAL, S. HOZ, R. M. TARKKA, and E. BUNCEL. Can. J. Chem. **68**, 1182 (1990).

The S_N2 reaction of $H_2C{=}NO^-$ with CH_3Cl was investigated at the AM1, STO-3G, and 6-31 + G* levels. Three modes of approach of CH_3Cl to the oxygen of the nucleophile were examined: *syn* and *anti* to the lone pair on the nitrogen in the molecular plane, and an approach along the π system of the oximate anion. The AM1 method differed markedly from the two *ab initio* methods, both in the reactivity order of the three geometries as well as in the relative stabilities of the products. The reactivity order calculated at the STO-3G and the 6-31 + G* levels was *syn* > π > *anti* (AM1 order: *anti* > *syn* > π). Product stability order calculated by the two *ab initio* methods was *syn* > *anti* > π (AM1 order: *anti* > *syn* > π). Excellent agreement was obtained between percent bond elongations at the transition state predicted by the equation suggested by Shaik, Schlegel, and Wolfe, and the activation barriers calculated at the 6-31 + G* level. The relevance of the calculations with respect to the α-effect is also discussed.

Key words: oxygen lone pairs, aximate, S_N2, *ab initio*.

J. L. WOLK, M. R. HAJNAL, S. HOZ, R. M. TARKKA et E. BUNCEL. Can. J. Chem. **68**, 1182 (1990).

On a étudié la réaction S_N2 du $H_2C{=}NO^-$ avec le CH_3Cl aux niveaux AM1, STO-3G et 6-31 + G*. On a examiné trois modes d'approche du CH_3Cl et de l'oxygène du nucléophile : dans le plan moléculaire, *syn* et *anti* par rapport à la paire d'électrons non partagée de l'azote ainsi qu'une approche le long du système π de l'anion oximate. Il existe des différences importantes entre la méthode AM1 et les deux méthodes *ab initio*; elles se manifestent dans l'ordre de réactivité des trois géométries ainsi que dans les stabilités relatives des produits. L'ordre de réactivité, calculé aux niveaux STO-3G et 6-31 + G*, est *syn* > π > *anti* (avec AM1: *anti* > *syn* > π). La stabilité des produits, telle que calculée par les méthodes *ab initio*, est *syn* > *anti* > π (avec AM1: *anti* > *syn* > π). On a obtenu un excellent accord entre les pourcentages d'élongation des liaisons telles que prédites par l'équation suggérée par Shaik, Schlegel et Wolfe et les barrières à l'activitation calculées aux niveaux 6-31 + G*. On discute aussi de la relation entre ces calculs et l'effet α.

Mots clés : paire d'électrons non partagée de l'oxygène, oximate, S_N2, *ab initio*.

[Traduit par la revue]

Introduction

In simple alkoxides such as CH_3O^-, the three lone pairs on the oxygen atom, after rehybridization, have cylindrical symmetry (C_{3v}). Therefore, in S_N2 reactions, all the approach directions of the electrophile having the same angle with the C_3 symmetry axis are energetically equivalent. However, in oximate anions such as **1**, the three lone pairs are not equivalent because of the

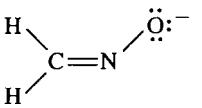

1

asymmetric electronic environment. One lone pair is associated with the π system, one is located *syn* to the lone pair on the nitrogen, and one is located *anti* to it, as illustrated in Fig. 1.

Although the term ambident nucleophile (1) usually applies to a nucleophile having two separate reactive sites, this definition could be extended to the single site, i.e., the oxygen atom of the present system. In this case, it would apply to the distinct lone pairs or directions of approach to oxygen rather than to different atoms on the nucleophile.

The purpose of this work was therefore to compare the reactivity of **1** in the three modes of approach in an S_N2 reaction with CH_3Cl as a model electrophile. In addition, since the oximate anion is frequently used to explore the α-nucleophilicity phenomenon (2), we have also examined the compatibility of the relatively fast semi-empirical AM1 method for future structure–reactivity studies.

Methods

The AM1 calculations (3) were carried out on an IBM 3081 computer using the AMPAC program version 2.10. The STO-3G (4*a*) and 6-31 + G* (4*b*) calculations were performed on an IBM 3090 computer using Gaussian 86 (4*c*). The optimized geometries of the reactants, transition states, and products of eq. [1],

[1] $H_2C{=}NO^-\cdots CH_3Cl \rightarrow [H_2C{=}NO\cdots CH_3\cdots Cl]^{-\ddagger}$
$\rightarrow H_2C{=}NOCH_3\cdots Cl^-$

for all three modes of approach (*syn*, *anti*, and π), were calculated at all three levels. In all cases, the S_N2 collinear geometry of O···C···Cl was enforced. The π geometry was enforced by fixing the CNOC dihedral angle at 90°. Transition states were characterized by a single negative force constant associated with the asymmetric stretching frequency of O···C···Cl. Each 6-31 + G* transition state was further characterized by a frequency analysis. In all three cases (π, *syn*, and *anti*), one large (ca. 500 cm^{-1}) negative frequency associated with the reaction coordinate was obtained. In the case of the *syn* and *anti* geometries, this was accompanied by another much smaller (ca. 50 cm^{-1}) negative frequency, associated with out-of-plane bending of the nucleophile. It is thus clear that the reported transition states are located in the immediate vicinity of the stationary points, having practically the same energy.

[1]Authors to whom correspondence may be addressed.

Printed in Canada / Imprimé au Canada

Can. J. Chem. Downloaded from www.nrcresearchpress.com by 88.85.125.76 on 09/07/12
For personal use only.

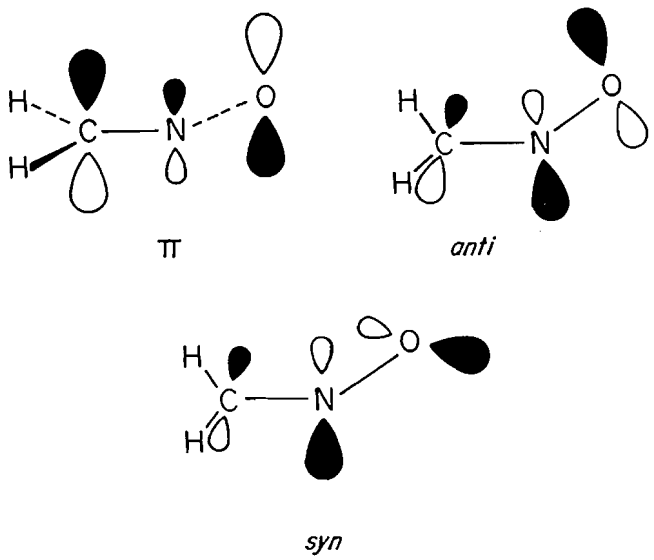

FIG. 1. Illustrations of the three molecular orbitals for oximate anion associated with the π, *anti*, and *syn* lone pairs, respectively. The HOMO is associated with the π oxygen lone pair, while the highest two subjacent occupied molecular orbitals are associated with the *syn* and *anti* oxygen lone pairs, respectively.

Results and discussion

Energies and geometries of ground states, transition states, and products

The energies of the various species at the three levels of calculation, together with the equilibrium and activation enthalpies, are given in Table 1. The geometries are given in Table 2. At the 6-31 + G* level, the reactant complex did not optimize in the *anti* geometry. While the CH_3Cl residue remained in the molecular plane during the optimization, the CON angle steadily increased. Scanning of the potential surface over a large range of CON angles revealed a shallow region between 130° and 160° in which the energy changes only by 0.7 kcal. The angle of 142° was hence arbitrarily assigned as the CON angle of the reactants. For the transition state and the products, the optimization procedure gave the local minima at the angles indicated in Table 2.

Examination of Table 1 reveals that the three levels of calculation give markedly different results for the kinetics and thermodynamics of the reactions. Assuming that the 6-31 + G* calculations are more reliable than the other two methods, the δH^0 values for the latter methods deviate equally from the 6-31 + G* values, though in opposite directions. The two *ab initio* methods predict the processes to be exothermic, whereas AM1 predicts the processes to be iso- or endothermic. More interesting is the relative order of stability of the products. While the two *ab initio* methods predict the stability order *syn* > *anti* > π, the AM1 order is *anti* > *syn* > π. The destabilization of the π-type product relative to the others in all three methods likely stems from disruption of allylic conjugation attendant to fixing the π lone pair as a covalent bond.

To ascertain whether the *syn–anti* stability order is affected by the chloride anion present in the products, the optimized geometries of the two methylformaldoximate conformers (**2**, R = CH_3) were calculated at the 6-31 + G* level.

The calculations showed that, in this system as well, the *syn* is more stable than *anti*, although by a larger margin (8.2 kcal/mol). A similar stability order was found for the parent

TABLE 1. Energies of reactants, products, and transition states calculated at the AM1, STO-3G, and 6-31 + G* levels, and reaction and activation enthalpies[a]

		AM1	STO-3G	6-31 + G*
Reactants	*syn*	−39.24	−659.6130	−667.3583
	anti	−39.37	−659.6121	−667.3566
	π	−38.93	−659.2127	−667.3573
Products	*syn*	−35.86	−659.7221	−667.4204
	anti	−39.56	−659.7157	−667.4152
	π	−32.54	−659.7128	−667.4114
Transition state	*syn*	−21.61	−659.6111	−667.3483
	anti	−22.59	−659.6076	−667.3426
	π	−18.13	−659.6086	−667.3447
$\delta H^{\ddagger}$	*syn*	17.63	1.19	6.28
	anti	16.78	2.82	8.79
	π	20.8	2.57	7.91
δH°	*syn*	3.38	−68.46	−38.97
	anti	−0.19	−65.01	−36.77
	π	6.39	−62.81	−33.95

[a]The *ab initio* calculated energies of the species are given in au. The rest of the data are in kcal/mol.

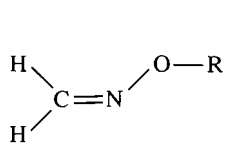

2 *syn*

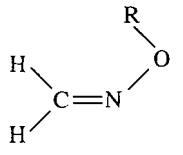

2 *anti*

R = H	−168.84811 au	R = H	−168.83763 au
R = Me	−207.87571 au	R = Me	−207.86268 au

oxime (**2**, R = H) (for previous calculations see ref. 5). It is interesting to compare this stability order with that of the model system **3** in which the opposite stability order was found for X = CH_2 or O as compared to X = C(H)OH (6).

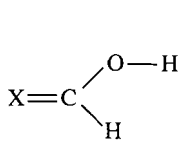

3 *syn*

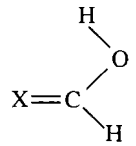

3 *anti*

Several factors were considered to be the cause of this stability order for **3**, including electrostatic interactions, lone pair – lone pair interactions, hydrogen bonding, and nonbonded aromaticity (6). It seems, however, that in the oxime series, **2**, the most crucial factor is the lone pair – lone pair repulsion between the pairs on the oxygen and on the nitrogen. This destabilizing interaction becomes diminished when the lone pair on the oxygen is utilized for formation of the covalent bond.

Theoretical work by several groups (7) has shown that the protons in the *syn* and *anti* conformers of formic acid (**3**, X=O) are of different acidity. In other words, the two in-plane oxygen lone pairs differ in their basicity. This idea was used to draw important conclusions concerning the mechanism of enzymatic reactions catalyzed by proton transfer to a carboxylate residue (8), and more recently by Rebek and co-workers to design and prepare a new class of chelating agents in which the lone pair *syn* to the C=O function was utilized to ligate the metal cation (9).

Can. J. Chem. Downloaded from www.nrcresearchpress.com by 88.85.125.76 on 09/07/12
For personal use only.

TABLE 2. Main structural parameters for reactants, products, and transition state of the reaction $CH_2NO^- + CH_3Cl$[a]

		AM1	STO-3G	6-31 + G*
	syn			
Reactants	C—Cl	1.776	1.839	1.840
	O—C	2.572	2.607	2.809
	N—O	1.222	1.323	1.292
	C—N	1.323	1.320	1.278
	CON	131.7	103.5	98.7
	ONC	121.8	118.5	118.8
	anti			
	C—Cl	1.775	1.839	1.833
	O—C	2.575	2.660	2.839
	N—O	1.221	1.321	1.291
	C—N	1.325	1.322	1.279
	CON	116.6	132.5	142.0[b]
	ONC	121.7	118.7	118.8
	π			
	C—Cl	1.773	1.833	1.836
	O—C	2.575	2.673	2.821
	N—O	1.222	1.322	1.291
	C—N	1.324	1.322	1.279
	CON	135.9	99.6	109.8
	ONC	121.7	118.3	118.5
	syn			
Products	C—Cl	2.953	3.333	3.552
	O—C	1.465	1.453	1.426
	N—O	1.311	1.408	1.349
	C—N	1.295	1.282	1.252
	CON	121.3	108.0	111.5
	ONC	118.5	110.6	113.0
	anti			
	C—Cl	2.947	3.242	3.445
	O—C	1.459	1.450	1.420
	N—O	1.291	1.398	1.345
	C—N	1.294	1.281	1.256
	CON	115.6	115.8	119.2[b]
	ONC	133.6	120.3	120.3
	π			
	C—Cl	2.947	3.298	3.528
	O—C	1.460	1.453	1.426
	N—O	1.322	1.433	1.380
	C—N	1.293	1.281	1.251
	CON	116.8	107.6	111.6
	ONC	118.2	111.5	112.7
	syn			
Transition state	C—Cl	2.216	1.925	2.179
	O—C	1.848	2.191	2.155
	N—O	1.311	1.336	1.305
	C—N	1.307	1.310	1.269
	CON	122.8	108.7	108.8
	ONC	119.7	117.9	117.7
	anti			
	C—Cl	2.187	1.949	2.214
	O—C	1.857	2.132	2.149
	N—O	1.244	1.336	1.303
	C—N	1.308	1.308	1.271
	CON	114.3	125.8	129.0
	ONC	123.2	120.5	119.6
	π			
	C—Cl	2.227	1.951	2.215
	O—C	1.826	2.128	2.129
	N—O	1.263	1.348	1.314
	C—N	1.306	1.308	1.268
	CON	117.9	109.2	112.0
	ONC	120.2	117.1	117.1

TABLE 2 (*concluded*)

[a]Bond lengths in Å, angles in degrees.
[b]See text.

The results of the present study suggest, therefore, that in using the oximate function for chelation, the molecular system should be designed in such a way as to position the cation in the complex *syn* to the lone pair on nitrogen. Since the difference in the stability of the two isomers in formic acid is 4.5 kcal (7), whereas in the oxime system it is significantly larger (6.6 kcal), the geometrical requirements in the oxime seem to be more important than in the carboxylate system.

With respect to $\delta H^{\neq}$ values (Table 1), the three levels of calculation also give differing results. However, the STO-3G method gives values closer to 6-31 + G* than does AM1.

According to classical physical organic chemistry considerations, the reactivity order should be governed by product stability and (or) the energy of the HOMO. According to all three methods of calculation, the HOMO is associated with the π system. The MOs associated with the *syn* and *anti* lone pairs on oxygen are subjacent to the HOMO and in the plane of the molecule (Fig. 1). However, since the energies of the highest three occupied molecular orbitals are all contained within a range of 4 kcal (at the 6-31 + G* level), it is not surprising that $\delta H^{\neq}$ in the π approach is not the smallest (Table 1). A relatively higher barrier for this approach is expected on the basis of relative product stability. The importance of the latter factor is expected to be more dominant in late transition states. The relative *syn–anti* activity, in all methods, corresponds to product stability and is apparently governed as well by the lone pair – lone pair pair repulsion effect.

Relevance of the calculation to the α-effect phenomenon

The results of the calculations are also pertinent with respect to the α-effect, as was stated in the introduction. Oximate anion, as a representative α-nucleophile, possesses a lone pair of electrons on the atom adjacent to the nucleophilic center, and such nucleophiles have often been observed to show enhanced reactivity compared to normal nucleophiles of the same basicity (pK_a). Several factors have been advanced, the most common being ground-state destabilization, transition state stabilization, stabilization of α-nucleophilic products, solvation effects, and a variety of other causes including intramolecular hydrogen bonding, etc. (2).

These factors have been discussed in a number of articles and reviews (2), and it is not our purpose to analyze them at present. As we pointed out previously (2*b*), since the α-phenomenon is one of enhanced reactivity, the important point is that reaction of an α-nucleophile involves a decrease in the free energy of activation, and therefore, in principle, ground state destabilization and transition state stabilization could act in concerted fashion, resulting in the overall rate enhancement. However, we have already shown that ground state destabilization affects both nucleophilicity and basicity, and therefore cannot be the origin of the α-effect (2*i*). Therefore, the lone pair – lone pair interaction may enhance the relative reactivity of the *syn* lone pair

Can. J. Chem. Downloaded from www.nrcresearchpress.com by 88.85.125.76 on 09/07/12
For personal use only.

compared to the other lone pairs, but the ground state destabilization it causes is not the foundation of the α-effect.

From the results we have obtained, it must be concluded that this study does not provide the key to the enigma of the α-effect, nor does it prove or disprove any of the existing theories. A more elaborate theoretical study would be needed for this purpose.

Transition state bond elongation model

We now address some of the geometrical features of the transition state as calculated at the 6-31 + G* level. Recently, Shaik, Schlegel, and Wolfe (10) reported an interesting relationship between the percent of elongation of the bonds of the central carbon atom to the nucleophile and the leaving group at the transition state of the S_N2 reactions ($Y^- + CH_3X \rightleftharpoons YCH_3 + X^-$). Percent bond elongation of the C—X bond is defined in eq. [2], and in a corresponding expression will apply to the C—Y bond.

$$[2] \quad \%\,CX = 100(d^{\ddagger}_{CX} - d^{\circ}_{CX}) \qquad (d = \text{bond length})$$

Using the data of some 30 S_N2 reactions calculated at the 4-31G level, they found a remarkable correlation between the percent bond elongation (%CX) and the activation barrier (eq. [3]).

$$[3] \quad \%CX = 0.76\,\delta H^{\ddagger} + 14$$

The data in Tables 1 and 2 allow an analysis of the present S_N2 reaction, $H_2C{=}NO^- + CH_3Cl \rightleftharpoons H_2C{=}NOCH_3 + Cl^-$, in both the forward and the reverse directions. It was found that for all three modes of approach, the percent C···O bond elongation at the transition state is 50 ± 1%, while for the C···Cl bond the elongation is 19 ± 1%. Using eq. [3] with the activation barriers in the forward and reverse directions to calculate the corresponding bond elongation at the transition state, we found that this equation predicts bond elongations with a very high degree of precision (±2% of our calculated 6-31 + G* values). This remarkable correlation with our data lends credence to the aforementioned equation, which is based on 4-31G data, showing it to be an effective tool in predicting transition state geometries from activation parameters in the gaseous phase.

1. V. Gold (*Editor*). Glossary of terms used in physical organic chemistry. Pure Appl. Chem. **55**, 1281 (1983).
2. (*a*) N. J. Fina and J. O. Edwards. Int. J. Chem. Kinet. **5**, 1 (1973); (*b*) S. Hoz and E. Buncel. Isr. J. Chem. **26**, 313 (1985); (*c*) W. P. Jencks and J. Carriuolo. J. Am. Chem. Soc. **82**, 1778 (1960); (*d*) J. O. Edwards and R. G. Pearson. J. Am. Chem. Soc. **84**, 16 (1962); (*e*) J. D. Aubort and R. F. Hudson. J. Chem. Soc. Chem. Commun. 1342 (1969); (*f*) J. D. Aubort, R. F. Hudson, and R. C. Woodcock. Tetrahedron Lett. **14**, 2229 (1973); (*g*) M. Laloi-Diard, J. F. Verchere, P. Gosselin, and F. Terrier. Tetrahedron Lett. **25**, 1267 (1984); (*h*) E. Buncel and I. H. Um. J. Chem. Soc. Chem. Commun. 595 (1986); (*i*) S. Hoz and E. Buncel. Tetrahedron Lett. **24**, 4777 (1983).
3. (*a*) M. J. S. Dewar, E. G. Zoebisch, E. F. Healy, and J. J. P. Stewart. J. Am. Chem. Soc. **107**, 3902 (1985); (*b*) M. J. S. Dewar and H. S. Rzepa. J. Am. Chem. Soc. **100**, 58 (1978).
4. (*a*) W. J. Hehre, R. F. Stewart, and J. A. Pople. J. Chem. Phys. **51**, 2657 (1969); (*b*) J. Chandrasekhar, J. G. Andrade, and P. v. R. Schleyer. J. Am. Chem. Soc. **103**, 5609 (1981); (*c*) G. W. Spitznagel, T. Clark, J. Chandrasekhar, and P. v. R. Schleyer. J. Comput. Chem. **3**, 363 (1982); (*d*) M. Frisch, J. S. Binkley, H. B. Schlegel, K. Raghavachari, R. Martin, J. J. P. Stewart, F. Bobrowitz, D. DeFrees, R. Seeger, R. Whiteside, D. Fox, E. Fluder, and J. A. Pople. GAUSSIAN-86, Release C, Carnegie Mellon University, Pittsburgh, PA.
5. (*a*) D. Liotard, A. Dargelos, and M. Chaillet. Theor. Chim. Acta, **31**, 325 (1973); (*b*) A. Dargelos, D. Liotard, and M. Chaillet. Theor. Chim. Acta, **38**, 79 (1975); (*c*) M. A. Robb and I. G. Csizmadia. J. Chem. Phys. **50**, 1819 (1969); (*d*) L. Radom, W. J. Hehre, and J. A. Pople. J. Chem. Soc. A, 2299 (1971); (*e*) L. Radom, W. J. Hehre, and J. A. Pople. J. Am. Chem. Soc. **93**, 289 (1971); (*f*) P. D. Adeney, W. J. Bouma, L. Radom, and W. R. Rodwell. J. Am. Chem. Soc. **102**, 4069 (1980).
6. (*a*) K. B. Wiberg and K. E. Laidig. J. Am. Chem. Soc. **110**, 1872 (1988); (*b*) J. R. Larson, N. D. Epiotis, and F. Bernardi. J. Am. Chem. Soc. **100**, 5713 (1978).
7. M. R. Peterson and I. G. Csizmadia. J. Am. Chem. Soc. **101**, 1076 (1979), and references cited therein.
8. R. D. Gandour. Bioorg. Chem. **10**, 169 (1981).
9. L. Marshall, K. Parris, J. Rebek, Jr., S. V. Luis, and M. I. Burguete. J. Am. Chem. Soc. **110**, 5192 (1988).
10. S. S. Shaik, H. B. Schlegel, and S. Wolfe. J. Chem. Soc. Chem. Commun. 1322 (1988).

Can. J. Chem. Downloaded from www.nrcresearchpress.com by 88.85.125.76 on 09/07/12
For personal use only.

Structural requirements for molecular recognition by the Neurokinin receptors

FRANÇOIS LEMAY, CHAKIB AMEZIANE HASSANI, AND ANDRÉ G. MICHEL[1]

Laboratoire de chimie structurale, Département de chimie, Université de Sherbrooke, Sherbrooke (Québec), Canada J1K 2R1

Received December 13, 1989

This paper is dedicated to Professor Arthur S. Perlin on the occasion of his 67th birthday

FRANÇOIS LEMAY, CHAKIB AMEZIANE HASSANI, and ANDRÉ G. MICHEL. Can. J. Chem. **68**, 1186 (1990).

Populations of lower energy conformers have been generated by conformational energy calculations, using empirical energy functions, for the C-terminal pentapeptide of Substance P (CH_3-CO-Phe-Phe-Gly-Leu-Met-NH_2), Neurokinins A and B (CH_3-CO-Phe-Val-Gly-Leu-Met-NH_2), and Eledoisin (CH_3-CO-Phe-Ile-Gly-Leu-Met-NH_2). The C-terminal sequences are greatly conserved in the Neurokinin and Tachychinin families of peptides and are mainly responsible for the molecular recognition. These sequences differ in the nature of the second residue. This substitution interferes with the recognition processes and modulates the specificities. A procedure based on a random generation of conformers, followed by energy minimizations, has been applied to produce the populations of conformers for the three pentapeptides. The conformational properties of the lower energy conformers have been analysed and compared with respect to the substitution of the second residue. Earlier nuclear magnetic resonance data as well as structure–activity relationship results have been interpreted in light of the proposed stable conformers. It is shown that the selectivity towards the NK3 receptor requires a structure with a restrained flexibility introduced at the second N-terminal residue. The selectivity towards the NK1 receptor is shown to be related to the presence of a constrained structure at the Gly residue. These structures suggest further chemical modifications be introduced in order to produce more selective and stable analogues.

Key words: peptide conformation, empirical energy, Neurokinin, molecular recognition.

FRANÇOIS LEMAY, CHAKIB AMEZIANE HASSANI et ANDRÉ G. MICHEL. Can. J. Chem. **68**, 1186 (1990).

Les populations des conformères les plus stables ont été générées par calculs conformationnels à l'aide de fonctions empiriques, pour les pentapeptides C-terminaux de la Substance P (CH_3-CO-Phe-Phe-Gly-Leu-Met-NH_2), des Neurokinines A et B (CH_3-CO-Phe-Val-Gly-Leu-Met-NH_2) ainsi que de l'Eledoisine (CH_3-CO-Phe-Ile-Gly-Leu-Met-NH_2). Ces séquences sont communes à ces familles de peptides et considérées comme responsable de la reconnaissance moléculaire par les récepteurs correspondants. Une procédure consistant à générer des structures aléatoires et ensuite à minimiser leurs énergies a été utilisée pour constituer les populations regroupant les conformères les plus stables pour les trois séquences considérées. Ces structures sont présentées et des résultats antérieurs obtenus par résonance magnétique nucléaire sont interprétés. Les hypothèses formulées à propos des relations structures–activités sont également reconsidérées à partir des résultats obtenus. Finalement, il est proposé que la sélectivité caractérisant le récepteur NK3 est reliée à la présence d'une rigidification conformationnelle au niveau du second résidu. En ce qui concerne le récepteur NK1, il est montré que des contraintes au niveau de résidu Gly sont de nature à augmenter la spécificité. Ces structures permettent de suggérer des modifications chimiques à effectuer sur ces peptides afin d'en augmenter la spécificité.

Mots clés : conformation de peptides, énergies empiriques, Neurokinine, reconnaissance moléculaire.

Introduction

In recent years, the important role played by endogenous peptides was demonstrated in various physiological mechanisms. Particularly, it was shown that Substance P may be the mediator of sensory stimuli, as well as the originator of the antidromic vasodilatation, increasing vascular permeability. Nevertheless, some years after the discovery of Substance P and its homologues in the families of Neurokinin and Tachykinin (Table 1) their structure–activity relationships remain undefined. Many biological studies have been done on these peptides to establish structural congruencies to account for their selectivities (1–9).

Physico-chemical studies like NMR (Nuclear Magnetic Resonance) (10–16) and CD (Circular Dichroïsm) experiments (17) as well as conformational analysis by molecular mechanics (18–22) have tried to establish their conformational properties. Divergent conclusions have been reached in many cases.

The NMR studies on Substance P and its fragments or analogues have postulated the formation of hydrogen bonds. It was suggested that a C-terminal carbonyl group might form an H-bond with the primary amide protons of Gln^5 and Gln^6 residues (11, 15). Another hypothesis was to involve the Phe^7 amide proton (12, 13). All these studies suggested a folded U-shape configuration for the C-terminal end (25). Nevertheless, other structure–activity relationship studies (7) and NMR investigations (16) postulated an extended structure for this part of the peptide.

Examining the results of theoretical calculations by empirical energy methods, it was obvious that the size of the problem, as well as the number of degrees of freedom, prevented a systematic search (20, 22). Consequently, the results presented did not give a complete picture of the conformational space accessible to these molecules. Generally these studies concentrated on frequently observed structures, rather than giving a description of the overall conformational behaviour of these peptides (31, 32).

From structure–activity relationship studies it was shown that the conformational study could be limited to the C-terminal hexapeptide, which retains a large portion of the activity (2). Moreover, the substitution of residue 6 in the hexapeptide SP(6–11) (23, 24) was shown to modulate the activity, but the C-terminal pentapeptide Phe-X-Gly-Leu-Met-NH_2 was common to all active peptides, with X = Phe (Tyr), Val, or Ile for Substance P, Neurokinin A/B, and Eledoisin, respectively.

These observations suggested that we concentrate the conformational analysis on the pentapeptides SP(7–11), NK(6–10), and EL(7–11) presented in Table 1, assuming that the spatial requirements for the recognition are included in those sequences. The size of the sequences allowed us to explore a significant part of the conformational space by empirical energy

[1]Author to whom correspondence may be addressed.

Can. J. Chem. Downloaded from www.nrcresearchpress.com by 88.85.125.76 on 09/07/12
For personal use only.

TABLE 1. Amino acid sequences of Substance P, Neurokinin A and B, Eledoisin, and the pentapeptides SP(7–11), NK(6–10), EL(7–11)

Peptides	Code	Sequences
Neurokinins		
Substance P	SP	Arg^1-Pro^2-Lys^3-Pro^4-Gln^5-Gln^6-Phe^7-Phe^8-Gly^9-Leu^{10}-Met^{11}-NH_2
Neurokinin A	NKA	His^1-Lys^2-Thr^3-Asp^4-Ser^5-Phe^6-Val^7-Gly^8-Leu^9-Met^{10}-NH_2
Neurokinin B	NKB	Asp^1-Met^2-His^3-Asp^4-Phe^5-Phe^6-Val^7-Gly^8-Leu^9-Met^{10}-NH_2
Tachykinin		
Eledoisin	EL	$pGlu^1$-Pro^2-Ser^3-Lys^4-Asp^5-Ala^6-Phe^7-Ile^8-Gly^9-Leu^{10}-Met^{11}-NH_2
Pentapeptides		
Substance P(7–11)	SP(7–11)	Ac-Phe^7-Phe^8-Gly^9-Leu^{10}-Met^{11}-NH_2
Neurokinin A/B(6–10)	NK(6–10)	Ac-Phe^6-Val^7-Gly^8-Leu^9-Met^{10}-NH_2
Eledoisin(7–11)	EL(7–11)	Ac-Phe^7-Ile^8-Gly^9-Leu^{10}-Met^{11}-NH_2

calculations. Particularly, the influences of the nature of the residue in position 8 (7 for NK) could be related to the corresponding specificities towards receptors NK1, NK2, and NK3.[2] In light of the generated conformations, the NMR data as well as structure–activity relationships should be reconsidered.

Method

The investigation of the conformational space for the three pentapeptides SP(7–11), NK(6–10), and EL(7–11) shown in Table 1 was undertaken by empirical energy calculations using the system of programs PEPSEA (26). This system proceeds in three successive steps.

First, values are randomly generated for each variable dihedral angle selected in the sequence by the user. Then the conformational energy of the corresponding starting conformers is calculated using the ECEPP/2 force field (27). For the purpose of this application an *effective* dielectric constant of 2 was used (33). Using this value, the ECEPP force field was shown to reproduce CNDO/2 calculations on hydrogen bonding in peptidic molecules (33). Subsequently, the energies are minimized by the conjugated gradient techniques, varying the values of the predefined variable angles. The resulting sets of conformers are sorted and analyzed.

This procedure was applied to each of the three forementioned pentapeptides. The peptidic sequences were built from the standard fragments included in ECEPP/2 (27). The calculations included terminal groups CH_3CO- (Ac) and NH_2 at the N-terminal and C-terminal ends respectively. The 15 dihedral angles considered as variable for the generation and energy minimization processes were all ϕ, ψ, $\chi^{1,1}$ angles and $\chi^{2,1}$ for Leu. All other $\chi^{m,n}$ side-chain dihedral angles were set in the *trans* conformation, except for $\chi^{2,1} = 90°$ for the Phe residues. Sets of values were randomly generated for the 15 variable dihedral angles. The corresponding conformers were built for the three pentapeptides and their conformational energies minimized. This generation–minimization procedure was repeated as soon as duplicates frequently appeared, requiring 1000 runs. The three resultant populations of conformers were sorted by increasing values of the conformational energies.

For the 20 most stable conformers, the remaining interactions between side chains were eliminated by energy minimizations, varying all the dihedral angles simultaneously.

Conformational energies were computed relative to the energy of the α-helix structures considered as the global minima. The α-helix conformational energies were obtained by the procedure described above, keeping an α-helix backbone constant and varying the side-chain orientations. The conformational energies of 200 randomly generated orientations of the side chains were energy-minimized.

The calculations were done on CRAY X-MP (The Ontario Center for Large Scale Computation, Toronto, Ont.) and on an IBM 4381, VM/CMS operating system (Computing Center, Université de Sherbrooke, Québec). The SYBYL molecular modeling system was used for the display, plotting, and fitting of the molecular structures (28). Dihedral angles are given according to the IUPAC–IUB Commission on Biochemical Nomenclature (29).

Results

Table 2 presents the values of the conformational energies[3] obtained for the 20 most stable conformers. The corresponding conformations have been coded in accordance with the conventional letter-coded partition of the [ϕ, ψ] maps (30).

The differences observed between the three peptides reflect the influence of the substitution of residue 6(7) on the global conformations: for each peptide, the same 1000 random conformers were used as starting points, and the minimization processes converged in different ways for each peptide, depending on the nature of residue 6(7), to reach the conformers given in Table 2.

It is worth noting that relatively high energy values of 5.32, 6.16, and 6.86 kcal/mol correspond to the 20 most stable conformers. This observation reflects highly restricted conformations. Many substructures are common to the three sequences, like DCC* for SP(5–11) no. 5, no. 10, EL(7–11) no. 12, NK(6–10) no. 13, no. 17; AAA observed for SP(7–11) no. 1, no. 2, EL(7–11) no. 1, no. 8, NK(6–10) no. 1, no. 5, no. 7; EAA for SP(7–11) no. 3, EL(7–11) no. 19, NK(6–10) no. 14; AEC*A for SP(7–11) no. 13, EL(7–11) no. 6 and NK(6–10) no. 8. The last three residues of SP(7–11) no. 20, EL(7–11) no. 4 (Fig. 1a), and NK(6–10) no. 18 adopt the C*CC structure. Relatively few structures share the same conformation for the five residues: SP(7–11) no. 6, no. 13, and NK(6–10) no. 2, no. 8, SP(7–11) no. 5 and EL(7–11) no. 2, no. 15, NK(6–10) no. 5, no. 14, no. 18, and EL(7–11) no. 8, no. 19, no. 4.

Many characteristic structures are found within those stable conformers. C_7 hydrogen bonds are present in many structures, as shown in Table 2. Most of the residues coded C adopt the C_7^{eq} and C* the C_7^{ax} inducing a γ-turn in the sequence. SP(7–11) no. 20, EL(7–11) no. 4 (Fig. 1a), and NK(6–10) no. 18 adopt the C_7 helix for the terminal tripeptide. Figure 1b shows the C_7 conformation for Gly in SP(7–11) no. 19 while Fig. 1c shows the same conformation observed for Leu in EL(7–11) no. 13. Moreover, C_{10} hydrogen bonds are common as shown in Table 2. Among those, many β turns have been found in the most

[2]The nomenclature for the receptors is in accordance with the recommendations of the committee for the Substance P and Neurokinin Symposium (July, 1986, Montréal, Canada.)

[3]Conformational energies are relative to the value calculated for the α-helix structure, following a procedure described in Methods.

Can. J. Chem. Downloaded from www.nrcresearchpress.com by 88.85.125.76 on 09/07/12
For personal use only.

TABLE 2. Distribution of the 20 most stable structures for the three pentapeptides

No.	SP(7–11) Codes[a]	SP(7–11) Energies[b]	EL(7–11) Codes[a]	EL(7–11) Energies[b]	NK(6–10) Codes[a]	NK(6–10) Energies[b]
	P P G L M h h l e e e e y u t		P I G L M h l l e e e e y u t		P V G L M h a l e e e l y u t	
	A A A A A	0.00	A A A A A	0.00	A A A A A	0.00
1	A A A D F	6.12	A A A D C	6.66	A A A C A	5.86
2	A A A A A*	6.33	D C C*A C	7.95	E G G A E	6.54
3	E A A C C	6.75	F C D*E A*	9.25	E A* A* A* F	8.24
4	A C B*A C	7.58	D A C*C C	9.76	A C D*A A	8.48
5	D C C*A C	8.27	F F C*A A	10.04	A A A A A	8.76
6	E G G A E	8.28	A E C*A A	10.42	E A D A E	9.54
7	E E C*G F	9.03	D D C*A C	10.53	A A A C F	9.85
8	E G C*G A	9.15	A A A A A	10.57	A E C*A G	10.06
9	F C D*A A	9.16	C A C*C E	10.83	C F C*A A	10.25
10	D C C*A E	9.35	E E E C A	11.61	E A C*G A	10.48
11	C C D*D A*	9.48	D E F* A C	11.64	A* C C*G F	10.77
12	E A B E A*	10.20	C E C*D F	11.87	C E A* A* G	10.83
13	A E C*A G	10.39	E E A C E	11.94	D C C* C A*	11.53
14	E F A*C A	10.52	C A C*D E	12.30	E A A E A*	11.61
15	F C D C C	10.59	D C C*A C	12.30	E D E* E A	11.93
16	E E A* A* C	10.82	E E A C A*	12.33	D D E C E	12.14
17	D D D*C C	10.88	E C C*A C	12.63	D C C*D A	12.25
18	A C A*G F	11.15	A F A*G F	12.73	D A C*C C	12.61
19	C B C*C E	11.29	E A A E A*	12.79	E A* C*D A*	12.71
20	E F C*C C	11.44	C A A*G A	12.82	E F C* E A*	12.72

[a]Codes have been determined as defined in ref. 24.

[b]Energies are conformational energies relative to the α helix and expressed in kcal/mol. C C* indicates residues involved in a C_{10} structure. C indicates residues involved in a C_7 structure.

stable structures: SP(7–11) no. 1, no. 2, no. 4, EL(7–11) no. 1, no. 15, no. 17, NK(6–10) no. 1, no. 4, no. 7, no. 12. This conformation is illustrated by NK(6–10) no. 4 on Fig. 1d.

Other types of hydrogen bonds have been observed, inducing non-classical U-turns, like SP(7–11) no. 3, no. 6, no. 7, no. 9, no. 10, no. 13, EL(7–11) no. 11, no. 16, no. 19, and in NK(6–10) no. 2, no. 3, no. 14 (Fig. 1e) the structure of EL(7–11) no. 19 illustrates such folded structures. Hydrogen bonds have been located with SYBYL (28) using the geometrical constraints of 1.8 Å ≤ d(CO--NH) ≤ 2.5 Å and the angle N—H—O ≥ 120°.

Discussion

Examining Table 2 and comparing the series of conformers obtained for the three pentapeptides, it appears that the substitution differentiating the three sequences generates very different populations of conformers. The trend to create intramolecular hydrogen bonds is reflected in the three peptides, generating rigidified structures. A large predominance of conformations where the Gly residue adopts a structure with positive ϕ's (* code) is observed for all the structures. Nevertheless, structure–activity studies (9) have shown that the substitution of Gly by D-Ala seriously affected the activities. The observation would suggest that we reject star-coded conformations. Our results diverge from this conclusion, suggesting that the substitution of Gly by D-Ala affects the activity for other reasons than conformational modifications.

Folded structures have been postulated by most of the NMR studies (11, 12, 14, 16). Particularly, the NH group of Phe^7 in SP analogues has been shown to form hydrogen bonds with a carbonyl group close to the C-terminal end (12). Some of our structures support this observation: mainly SP(7–11) no. 11, no. 12, EL(7–11) no.3, no. 19 (Fig. 1e), NK(6–10) no. 3, no. 14, no. 20 form hydrogen bonds between NH of $Phe^{7(6)}$ and the carbonyl of Met. Another possibility, compatible with NMR results, is SP(7–11) no. 3, involving the carbonyl group of Leu. Table 2 reveals that many conformers are in agreement with the possibility of forming a C_7 hydrogen bond between the carbonyl group of Gly and the NH of Met, as postulated by other NMR (500 MHz) results (11, 16). This situation is illustrated in Fig. 1c.

Very few structures corroborate the hypothesis of an extended structure, even for the last three residues, as proposed by structure–activity relationship studies (7) and NMR results (16). This might be attributed to the low value of the dielectric constant used in the calculations, favoring the formation of intramolecular interactions.

A very NK3-selective analogue [Pro^7]NKB (7) was also studied by NMR at 500 MHz (16) and possible values for torsional angles were suggested. Examining our results, we found that the structure of NK(6–10) no. 4 (Fig. 1d) was compatible with these results. Furthermore, Val^7 of NK(6–10) no. 4 was substituted by Pro(down), and the conformational energy minimized. The resultant structure shown in Fig. 2 in superposition with NK(6–10) no. 4 adopts a conformation in agreement with the NMR results (16), preferring a C_7 hydrogen bond between the carbonyl group of Pro and the NH of Leu, instead of the β turn originally present in NK(6–10) no. 4 (Fig. 1d). Other structure–activity relationship studies emphasized the importance of a rigidification at residue 7, increasing the

Can. J. Chem. Downloaded from www.nrcresearchpress.com by 88.85.125.76 on 09/07/12
For personal use only.

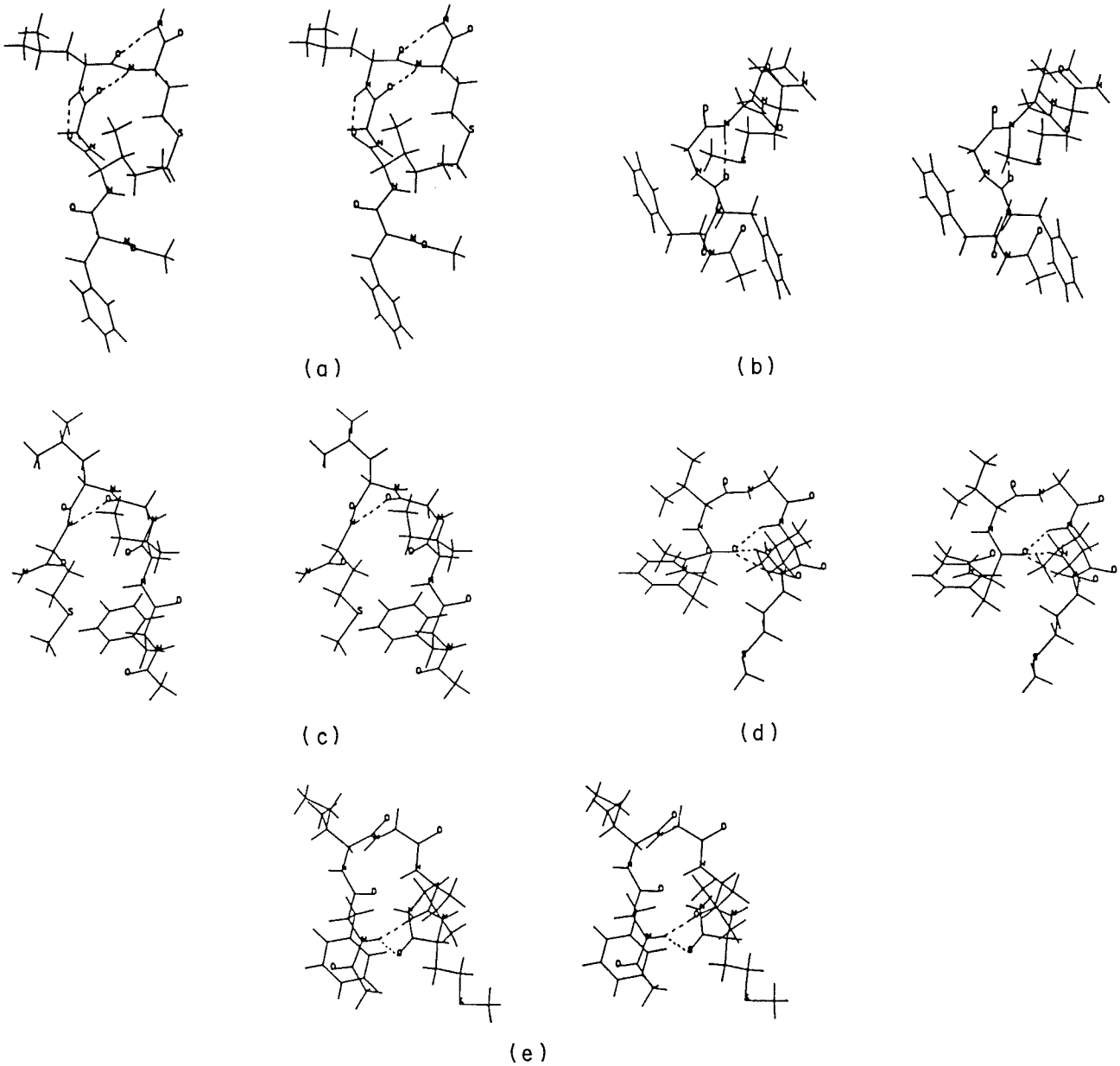

FIG. 1. Stereographic representations of characteristic structures. (a) EL(7–11) no. 4: C_7 helix conformation for the C-terminal tripeptide. (b) SP(7–11) no. 19: C_7 conformation for the Gly residue. (c) EL(7–11) no. 13: C_7 conformation for the Leu residue. (d) NK(6–10) no. 4: β turn involving Val and Gly. (e) EL(7–11) no. 19: implication of the Phe^7 NH in a hydrogen bond, inducing a folded structure. Dotted lines represent possible hydrogen bonds.

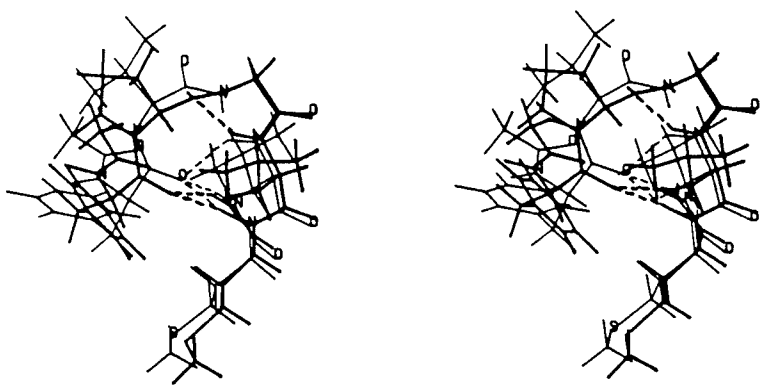

FIG. 2. Stereographic superpositions of NK(6–10) no. 4 (thin lines) with [Pro^7]NK(6–10) no. 4 (dark). Dotted lines represent possible hydrogen bonds.

Can. J. Chem. Downloaded from www.nrcresearchpress.com by 88.85.125.76 on 09/07/12
For personal use only.

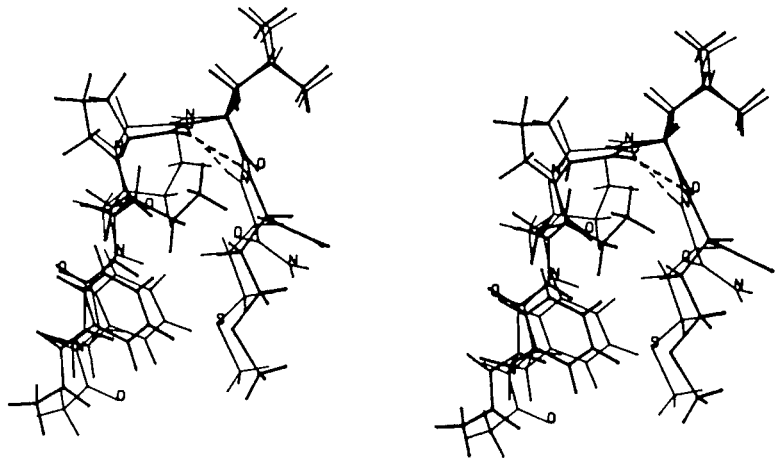

FIG. 3. Stereographic superposition of EL(7–11) no. 13 (thin lines) with [Pro^9]EL(7–11) no. 13 (dark). Dotted lines represent possible hydrogen bonds.

selectivity by N-methylation, introducing an unusual Sarcosin (Sar) residue (1).

Consequently, the structure of NK(6–10) no. 4 appears to be a good model for further designs of very selective substrates of the NK3 receptor.

Pharmacological studies have shown that highly selective compounds to the NK1 receptor have a geometrically constrained residue in position 9 (1, 7). Particularly, the presence of a Pro^9 in [pGlu^6]SP(6–11) and Sar^9 in other SP active fragments induced very high degrees of specificity to the NK1 receptor (1, 8). Examining our results, it appeared that the geometrical requirements for compatibility with a Pro substitution are achieved by the structure EL(7–11) no. 13. We substituted Gly^9 by a Pro^9(flat structure: $\phi = -57.6°$) in this structure. The resulting structure after energy minimization is presented in Fig. 3, in superposition with EL(7–11) no. 13. Again, the rigidity is assumed by a C_7 hydrogen bond between the carbonyl group of Gly^9 and the NH of Met^{11}. The structure presented in Fig. 2 accommodates the substitution by a Sar^9 residue. Consequently, EL(7–11) no. 13 appears to possess the structural requirements for NK1 receptor selectivity.

In conclusion, the strategy based on random generation of peptidic structures, followed by energy minimization, has been shown to generate populations of pertinent conformers, compatible with NMR results. The method appears to be an excellent alternative when a systematic conformational search of conformations is prohibitive. It has been demonstrated that the conformational properties of the C-terminal pentapeptides in Neurokinins, Substance P, and Eledoisin contain the structural requirements for molecular recognition by the NK1 and NK3 receptors. Model compounds have also been described, suggesting further synthesis of more selective compounds.

Acknowledgements

We thank the Natural Sciences and Engineering Research Council of Canada for computer time on the CRAY X-MP allowed to A.M. The F.C.A.R. is acknowledged for financial support to F.L. We are grateful to Professor D. Regoli for fruitful discussions.

1. D. REGOLI, G. DRAPEAU, S. DION, and R. COUTURE. Trends Pharmacol. Sci. **9**, 290 (1988).
2. D. REGOLI, G. DRAPEAU, S. DION, and P. D'ORLEANS-JUSTE. Life Sci. **40**, 109 (1987).
3. D. REGOLI, E. ESCHER, and J. MIZRAHI. Pharmacology, **28**, 301 (1984).
4. K. FOLKERS, D. CHANG, I. YAMAGUSHI, Y. WAN, G. RACKUR, and G. FISHER. *In* Substance P. *Edited by* U.S. Von Euler and B. Pernow. Raven Press, New York. 1977. p. 19.
5. R. COUTURE, A. FOURNIER, J. MAGNAN, S. ST-PIERRE, and D. REGOLI. Can. J. Physiol. Pharmacol. **57**, 1427 (1979).
6. E. ESCHER, R. COUTURE, C. POULOS, N. PINAS, J. MIZRAHI, D. REGOLI, and D. THEODOROPOULOS. J. Med. Chem. **25**, 1317 (1982).
7. S. LAVIELLE, G. CHASSAING, O. PLOUX, D. LOEUILLET, J. BESSEYRE, S. JULIEN, A. MARQUET, O. CONVERT, J.-C. BEAUJOUAN, Y. TORRENS, L. BERGSTRÖM, M. SAFFROY, and J. GLOWINSKI. Biochem. Pharmacol. **37**, 41 (1988).
8. R. LAUFER, C. GILON, M. CHOREV, and Z. SELINGER. J. Med. Chem. **29**, 1284 (1986).
9. S. BLUMBERG and V. I. TEICHBERG. Biochem. Biophys. Res. Commun. **99**, 752 (1981).
10. H. KAWAKI, A. OTTER, H. BEIERBECK, and G. KOTOVYCH. J. Biomol. Struct. Dyn. **3**, 795 (1986).
11. G. CHASSAING, O. CONVERT, and S. LAVIELLE. Eur. J. Biochem. **154**, 77 (1986).
12. G. ESPOSITO, L. SETTENBRI, and G. C. VISCOMI. J. Chem. Soc. Perkin Trans. 2, 1313 (1988).
13. A. RIBEIRO, O. JARDETZKY, C. GILON, D. TEITELBAUM, and M. CHOREV. Biopolymers, **22**, 247 (1983).
14. F. INAGAKI, T. MIYAZAWA, N. YANAIHARA, and M. OTSUKA. *In* Proceedings of the 15th Symposium on Peptide Chemistry. *Edited by* T. Shiba. Protein Research Foundation, Osaka. 1987. p. 103.
15. G. CHASSAING, O. CONVERT, and S. LAVIELLE. Bioch. Bioph. Acta, **873**, 397 (1986).
16. D. LOEUILLET, O. CONVERT, S. LAVIELLE, and G. CHASSAING. Int. J. Pept. Protein Res. **33**, 171 (1989).
17. B. MEHLIS, M. RUEGER, M. BECKER, M. BIENERT, H. NIEDRICH, and P. OEHME. Int. J. Pept. Protein Res. **15**, 20 (1980).
18. P. MANAVALAN and F. A. MOMANY. Int. J. Pept. Protein Res. **20**, 351 (1982).
19. G. V. NIKIFOROVICH, Y. BALODIS, and G. I. CHIPPENS. *In* Peptides. Proceedings of the 16th European Peptide Symposium. *Edited by* K. Bruwfekdt. Scriptor, Copenhagen. 1981. p. 631.
20. M. COTRAIT and M. HOSPITAL. Biochem. Biophys. Res. Commun. **109**, 1123 (1982).
21. M. COTRAIT. Int. J. Pept. Protein Res. **22**, 110 (1983).
22. M. COTRAIT and M. HOSPITAL. Int. J. Pept. Protein Res. **28**, 450 (1986).
23. R. MICHELOT, M. MAYER, S. MAGNENEY, J. THIERRY, and P. POTIER. *In* Substance P and Neurokinin. *Edited by* J. L. Henry, R.

Can. J. Chem. Downloaded from www.nrcresearchpress.com by 88.85.125.76 on 09/07/12
For personal use only.

Couture, A. C. Cuello, G. Pelletier, and R. Quirion. Springer-Verlag, New York. 1987. p. 158.
24. M. CHOREV, C. GILON, U. WORMSER, Z. Y. FRIEDMAN, and Z. SELINGER. *In* Peptide. Proceedings of the 16th European Peptide Symposium. *Edited by* K. Brumfeldt. Scriptor, Copenhagen. 1981. p. 451.
25. B. E. B. SANDBERG and L. L. IVERSON. J. Med. Chem. **25**, 1009 (1982).
26. A. G. MICHEL and C. AMEZIANE HASSANI. PEPSEA: A program to search for peptidic structures. Univ. of Sherbrooke, 1989.
27. M. J. BROWNAN, L. M. CARRUTHERS, K. L. KASHUBA, F. A. MOMANY, M. S. POTTLE, S. P. ROSEN, and S. M. RUMSEY. QCPE, **11**, 286 (1975).
28. SYBYL program Version 5.2. A system of computer programs for interactive molecular modeling and computer assisted drug design. Tripos Associates, St-Louis, MO. 1989.
29. IUPAC–IUB Commission on Biochemical Nomenclature. J. Mol. Biol. **52**, 1 (1970).
30. S. S. ZIMMERMAN, M. S. POTTLE, G. NÉMETHY and H. A. SCHERAGA. Macromolecules, **10**, 1 (1977).
31. P. N. LEWIS, F. A. MOMANY, and H. A. SCHERAGA. Isr. J. Chem. **11**, 212 (1973).
32. P. Y. CHOU and G. D. FASMAN. J. Mol. Biol. **115**, 135 (1977).
33. F. A. MOMANY, L. M. CARRUTHERS, R. F. MCGUIRE, and H. A. SCHERAGA. J. Phys. Chem. **78,** 1595 (1974).

Can. J. Chem. Downloaded from www.nrcresearchpress.com by 88.85.125.76 on 09/07/12
For personal use only.

^{13}C CP/MAS NMR spectra of poly-β-D(1→4) mannose: mannan

R. H. MARCHESSAULT[1] AND M. G. TAYLOR[2]

Xerox Research Centre of Canada, 2660 Speakman Drive, Mississauga, Ont., Canada L5K 2L1

AND

W. T. WINTER

SUNY–ESF, Chemistry Department, Syracuse, NY 13210, U.S.A.

Received December 7, 1989

This paper is dedicated to Professor Arthur S. Perlin on the occasion of his 67th birthday

R. H. MARCHESSAULT, M. G. TAYLOR, and W. T. WINTER. Can. J. Chem. **68**, 1192 (1990).

^{13}C solid-state NMR spectra (CP/MAS) were recorded for mannan polymorphs: mannan I ("ivory nut") and mannan II (*Codium fragile*). These pure mannans, poly-β-(1→4) mannopyranose, show a single resonance for each carbon of the chemical repeat unit. This is the expected result based on the crystalline $P2_12_12_1$ and $I222$ symmetries. The T_1 values were also recorded and the results are compared to those for cellulose obtained from the literature. The much lower mobility of C-6, even in noncrystalline mannan, compared to native cellulose is attributed to the epimeric difference at C-2 between cellulose and mannan allowing intramolecular hydrogen bonding in the former but not the latter.

Key words: mannan, solid state NMR, T_1 relaxation, polysaccharide, ivory nut.

R. H. MARCHESSAULT, M. G. TAYLOR et W. T. WINTER. Can. J. Chem. **68**, 1192 (1990).

On a déterminé les spectres RMN du ^{13}C à l'état solide (CP/MAS) de mannanes polymorphes : le mannane I («noix d'ivoire») et le mannane II (*Codium fragile*). Ces mannanes purs, des poly-β-(1→4)mannopyranoses, ne présentent qu'une raie pour chaque atome de carbone de l'unité chimique de base. Ce résultat est en accord avec des symétries cristallines $P2_12_12_1$ et $I222$. On a aussi mesuré les valeurs T_1 et on les a comparées avec celles rapportées dans la littérature pour la cellulose. La mobilité du C-6, même dans du mannane qui n'est pas cristallin, est beaucoup plus faible que celle observée dans la cellulose; cette différence est attribuée au fait que l'épimère en C-2 de la cellulose permet une laison hydrogène intramolécuaire ce qui n'est pas le cas avec l'épimère présent dans le mannane.

Mots clés : mannane, RMN à l'état solide, relaxation T_1, polysaccharide, noix d'ivoire.

[Traduit par la revue]

Cellulose and mannan are often compared because they are both β(1→4) linked carbohydrate polymers based on D-glucose and D-mannose respectively, i.e., they differ only in configuration at C-2. They are frequently found together in plant cell walls and both show polymorphism (1). In the native state both may act as skeletal material, cellulose mostly in land plants and mannan in certain green algae.

In gymnosperm cells, mannans, in the form of the copolysaccharides glucomannans and galactoglucomannans, occur concurrently with cellulose microfibrils. It has been shown that these so-called hemicelluloses are oriented parallel to the microfibrils (2) but there is no evidence of mannan crystallization in this natural occurrence. Nevertheless, cellulose microfibrils can be made to serve as a crystallization template for mannan, producing an epitaxial crystallization of the mannan chains with their fibre axes parallel to that of cellulose (3).

In addition to its structural role, mannan also functions as a reserve substance in seeds. In this form it is found either as pure mannan, e.g., in the endosperms of palm, date, and coffee beans, or as galactomannan, e.g., in the endosperms of legumes such as locust bean or guar. In the latter, galactose residues occur as single substituents linked α(1→6) to the mannan backbone in an irregular fashion. Depending on the plant species, galactomannans have ratios of galactose to mannose ranging from zero to unity. The endosperm of date palm, commonly called "ivory nut", has no galactose while the endosperm of "fenugreek" seeds has almost one galactose per mannose residue in the backbone (4).

In this study we have used the cross-polarization and magic-angle spinning (CP/MAS) technique to acquire ^{13}C NMR spectra of the insoluble, crystalline mannans from ivory nut (mannan I) and *Codium fragile* (mannan II) in order to enrich the solid-state structure models derived from diffraction methods.

Fibre diagrams for mannan I were first recorded by Frei and Preston (5). Their unit cell parameters and three-dimensional structure models were further refined by Nieduszynsky and Marchessault (6). The proposed space group for the orthorhombic unit cell was $P2_12_12_1$. As in cellulose, the fiber repeat of 10.3 Å corresponds to an extended disaccharide residue with a twofold screw axis relating contiguous mannosyl residues. Thanks to the high quality electron diffraction data from lamellar single crystals of mannan I, the required systematic absences of the baseplane reciprocal lattice net are unequivocal (3, 7), resulting in a two-chain unit cell with anti-parallel chains, as required by the $P2_12_12_1$ space group. Accordingly, a single anhydromannose residue is the asymmetric unit. The occurrence of anti-parallel chains in the native crystalline form of mannan is in direct contrast with proposed models of cellulose (8, 9).

While the X-ray analysis for mannan II is not nearly as advanced, the proposed space group, $I222$ (personal communication, S. Arnott, St. Andrews University), also implies a single anhydromannose residue as the asymmetric unit. As in the mannan I structure, this naturally occurring polymorph involves an anti-parallel packing of regular twofold helices although the arrangement is less dense than in mannan I and is thought to involve a hydrated form of the polymer.

[1]Chemistry Department, McGill University, 3420 University, Montreal, P.Q., H3A 2A7.

[2]Esso Petroleum Canada Research, P.O. Box 3022, Sarnia, Ont., N7T 7M1.

Printed in Canada / Imprimé au Canada

Can. J. Chem. Downloaded from www.nrcresearchpress.com by 88.85.125.76 on 09/07/12
For personal use only.

Can. J. Chem. Downloaded from www.nrcresearchpress.com by 88.85.125.76 on 09/07/12
For personal use only.

Experimental

Two samples of mannan were studied: ivory nut mannan powder from ground nuts of *Phytelephas macrocarpa* and algal mannan from *Codium fragile*. The first sample is a pure mannan I as shown by X-ray powder diffraction and has been used in previous work (3, 7). Additionally, a whole ivory nut was mounted on a lathe and turned down into a cylinder for direct insertion in the rotor. The second sample, which is predominantly mannan II, was prepared by Dr. H. Chanzy of the CERMAV/CNRS, Grenoble, and was purified in the manner described by Preston (1). X-ray diffraction analysis has shown that while this sample is predominantly mannan II, it has a minor mannan I component.

^{13}C NMR spectra were acquired at ambient temperature on a Bruker CXP200 spectrometer operating at an observation frequency of 50.3 MHz. Spectra were acquired using polarization transfer from ^{1}H to ^{13}C with Hartmann–Hahn matching radiofrequency fields of 60 MHz and a recycling time of 5 s. Samples were rotated at the magic angle at rates of 2.5–3.5 kHz. Chemical shift values were assigned by reference to the resonance at 32.9 ppm (10) relative to TMS arising from a small piece of crystalline polyethylene (NBS/1475) included with the samples. Spin lattice (T_1) relaxation times were measured using the pulse sequence of Torchia (11) with delay times between 10 and 400 s, acquiring 224 scans at each value of the delay time. Intensities in the transformed spectra were measured both as peak heights and by peak integration.

Discussion

The CP/MAS spectra of mannan I and II are shown in Fig. 1. The most notable feature of both spectra is that they both show exactly six resonances corresponding to the six carbons in the anhydromannan asymmetric unit. The breadth of the resonances is greater for mannan II in keeping with the lower level of crystalline perfection of this sample, as evidenced by X-ray line broadening.[3] It is noteworthy that C-1 and C-4 resonances are distinctly different from those of cotton cellulose, provided the assignments are the same (cf. Table 1). Assuming the correlation between chemical shift and the glycosidic dihedral angles is the same as for cellulose, this implies a distinctly different set of conformational angles (ϕ, ψ) as defined in ref. 7. The angles ϕ, ψ, which define the conformational relation of successive anhydromannopyranose residues, are reported as $-93°$ and $-147°$ for cellulose (8) and $-81°$ and $-161°$ for mannan I (7). These values are based on the atom sequence (O-5, C-1, O-1, C-4′, C-5′). Additionally, the differing C-2 epimers of cellulose and mannan may contribute to these chemical shift differences. Assuming that the C-2 epimer difference does not have an influence on the correlation data of Horii *et al.* (13), the observed chemical shift for C-6 in Fig. 1 corresponds to the O-6 oxygen in the *gt* arrangement (i.e., O-6 is *gauche* with respect to O-5 and *trans* with respect to C-4), supporting the diffraction-based modeling for mannan I. A similar refinement for mannan II (S. Arnott, private communication) also proposes a *gt* O-6 conformer.

Comparison of the CP/MAS spectra of native celluloses whose lateral order is known to differ (*Valonia* vs. cotton) has been helpful in furthering the interpretation of their spectra. *Valonia* cellulose with near 100% crystallinity has well-defined C-1 and C-4 multiplets and lacks so-called amorphous phase resonances. By contrast, cotton shows less-resolved multiplets and displays well-defined noncrystalline resonances, in keeping with its lower perfection in lateral order. While there has been considerable controversy (14) in the interpretation of the multiplets for cellulose, the two-chain unit cell with a $P2_1$ space group and the screw axis parallel to the chain direction leads one to expect that the asymmetric unit in cotton involves two glucose residues.

[3]The subsidiary maxima for mannan II at ~80 and 60 ppm probably reflect a well-defined, hydrogen-bonded, noncrystalline component as in CP-MAS spectra of cellulose I and II (18).

TABLE 1. ^{13}C chemical shifts (ppm relative to TMS) from the 50.3 MHz CP/MAS spectra of mannan and cotton

	C-1	C-4	C-2, C-3, C-5	C-6
Mannan I	102.0	81.4	76.3 72.5 70.3	62.4
Mannan II	102.4	83.0	75.0 72.5 70.9	62.9
Cotton	106–104	89	75.3–71.6	65.5

A simplification develops when a $P2_12_12_1$ space group is operative, as is the case for the ivory nut mannan; here the well-resolved single resonances at C-1 and C-4 are in sharp contrast to the multiplets observed for C-1 and C-4 resonances in the cotton and *Valonia* cellulose spectra (14). The narrowness of the resonances leaves little doubt concerning the good lateral order in ivory nut, especially in contrast with the broader resonances in *Codium fragile* (mannan II). The latter, in keeping with its $I222$ space group, does not display multiplets. The greater breadth of the resonances for the *Codium* polymer is indicative of lower lateral order, compared to mannan I, reminiscent of a similar difference between cellulose I and II.

Spin lattice relaxation times

Figure 2 shows partially relaxed spectra for ivory nut mannan acquired with relaxation delays of 10 s (A) and 150 s (B) as well as their difference spectrum (C). The difference between the spectra indicates there are at least two components in the sample with different spin lattice relaxation times. The difference spectrum, which is the spectrum of the component with the shorter relaxation time, presumably represents the noncrystalline fraction of the mannan. For short relaxation delays or under the normal CP pulse sequence, the observed spectra are superpositions of the spectra representative of both the crystalline and noncrystalline fractions of the mannan. The spectrum of the crystalline material can be extracted by allowing a longer relaxation delay during which the signals due to the more rapidly relaxing component decay. As seen in Fig. 2B, the resulting spectrum shows excellent resolution of all six peaks with linewidths much smaller than those observed in the spectrum of the noncrystalline fraction (Fig. 2C).

It was necessary to consider the composite nature of the spectra in calculating T_1 values from the relaxation data. Intensity data were measured from peak integrals rather than peak heights because of the large difference in line widths for the two components. The use of integrals does introduce errors where broad peaks are strongly overlapping, i.e., in the region from 70 to 80 ppm. T_1 values and relative contributions for each of the two components were calculated by fitting the integrated intensity vs. relaxation delay data to two-component exponential decays using nonlinear regression. The T_1 values for both components along with their relative fractions for each line in the mannan I spectrum are tabulated in Table 2.

These data can be compared with relaxation measurements for cotton cellulose (12, 16). Two-phase behavior was also noted for the ^{13}C T_1 relaxation in cellulose with the two components assigned to the crystalline and amorphous region. The values of the relaxation times determined for mannan are uniformly longer than those measured for cotton cellulose (12, 16). The most striking difference is noted for the short T_1 values

Can. J. Chem. Downloaded from www.nrcresearchpress.com by 88.85.125.76 on 09/07/12
For personal use only.

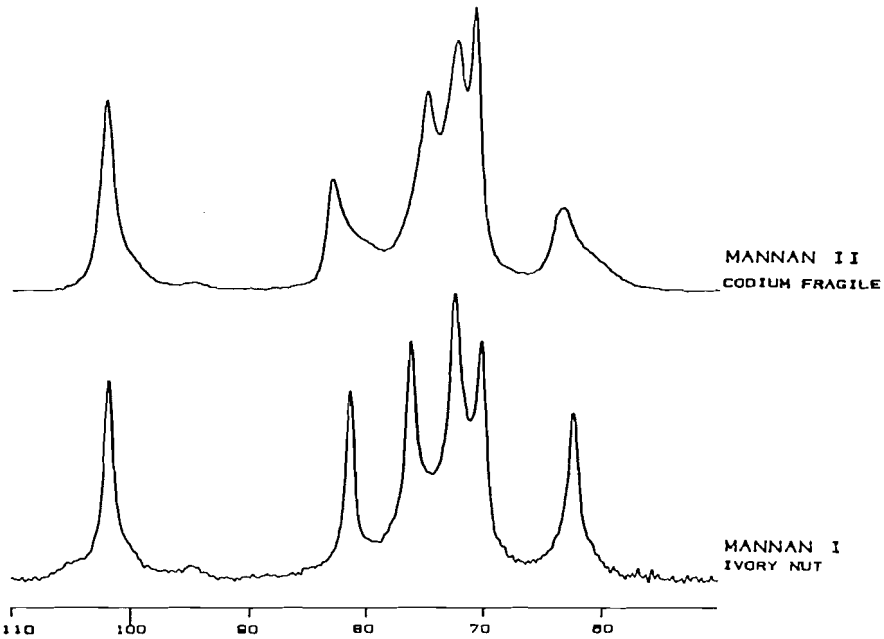

FIG. 1. ^{13}C CP/MAS NMR spectra of ivory nut and *Codium fragile* mannans. The samples are polymorphic and the unit cells are referred to as mannan I and mannan II, respectively.

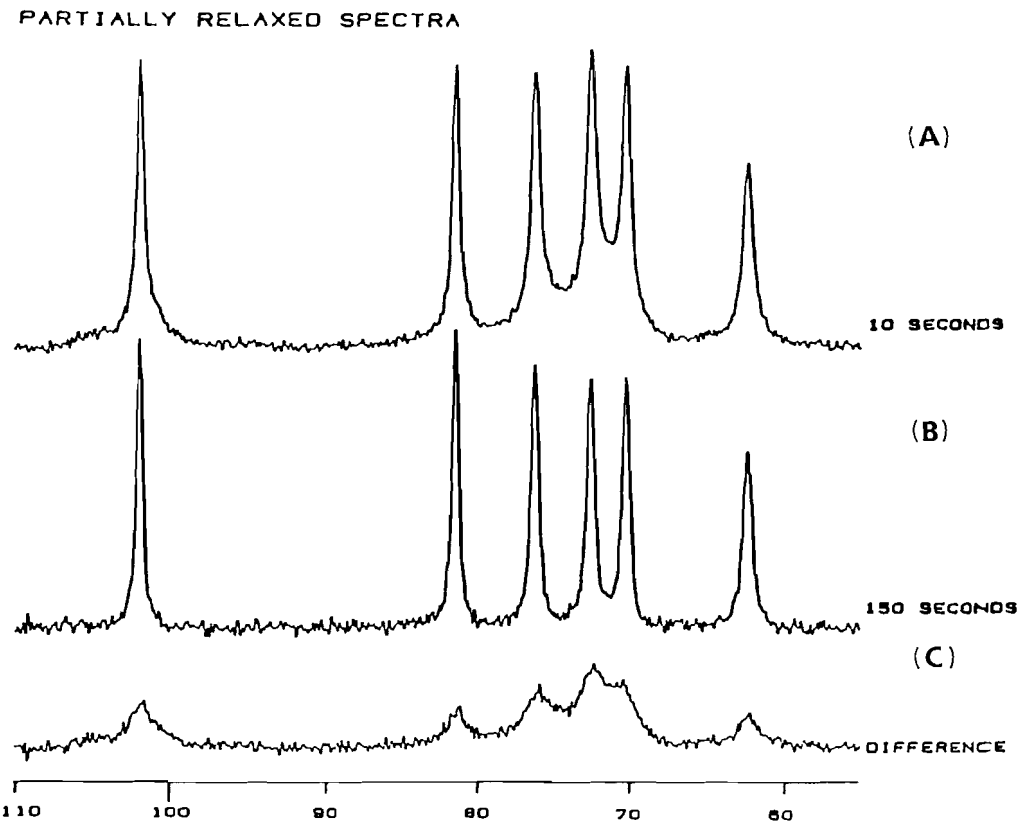

FIG. 2. ^{13}C CP/MAS NMR spectra of ivory nut mannan acquired with relaxation delays of 10 s (A), 150 s (B), and their difference (C).

assigned to the amorphous component in each polysaccharide. The T_1 values for the amorphous component of mannan are similar for all of the carbon resonances, while a large variation is observed in the case of amorphous cellulose. In particular, the observed T_1 for C-6 in amorphous cellulose is much shorter than the T_1's found for the other carbons, in contrast to the present data for mannan where the C-6 carbon T_1 is the second largest observed. This difference probably reflects greater restriction of the motional freedom of the hydroxymethyl group in amorphous mannan relative to cellulose. Such a conclusion would be expected on the basis of an intramolecular H-bond for O-6 in native cellulose vs. an intermolecular H-bond for O-6 in mannan (6, 7), an inevitable consequence of the configurational differences at C-2. In addition, cellulose hydrogen bonds into a

TABLE 2. ^{13}C T_1 relaxation times and parameters for mannan I from ivory nut

	C-1	C-4	C-2, C-3, C-5			C-6
Integral range (ppm)	107–97	85–79	79–74.5	74.5–71.5	71.5–68.5	65.5–59.5
Crystalline T_1 (s)	406	423	375	336	373	386
Noncrystalline T_1 (s)	26	39	23	21	24	33
Crystalline fraction (percent)	57	68	53	50	39	22

sheet-like structure whereas mannan hydrogen bonds into a three-dimensional network (6, 7).

Decomposition of the relaxation decay into two components should yield an estimate of the relative amounts of the crystalline and amorphous fractions in the sample. As seen inTable 2, a wide variation is noted in the relative crystalline fraction for the individual carbon resonances. Each of the resonances should in principle provide the same estimate of the degree of crystallinity of the sample. The discrepancy may result from the use of cross polarization for the generation of ^{13}C magnetization in the T_1 measurement. If the cross-polarization efficiencies for the two components of a particular line are not equal, the two components are not proportionally represented in the total initial ^{13}C magnetization. The subsequent relaxation decay faithfully represents the biased initial magnetization, leading to an incorrect estimate of the relative fractions of the two components. This difficulty could be circumvented by generating the ^{13}C magnetization by the normal single pulse method; however, it would be necessary to allow relaxation delays on the order of five times the longest T_1 value between pulses, leading to a prohibitively lengthy acquisition.

Conclusions

This study supports the concept that space group symmetry is an essential component of the interpretation of ^{13}C CP/MAS spectra of crystalline polymers. One signal for each carbon in the asymmetric unit provides a rational basis for understanding the differences between the multiplet-dominated cotton spectrum compared to the singlet resonances in the mannan spectrum. The observed differences in C-1 and C-4 chemical shifts between cellulose and mannan certainly derive from the ϕ, ψ dihedral differences for these two polysaccharides, but unfortunately it is not possible to partition the differences in chemical shifts between intra- (conformational) and inter-molecular influences. X-ray and electron diffraction data on crystalline fibers (6) and lamellar single crystals (7) are consistent with this conclusion.

In the case of the α-D-(1→4) glucans a linear correlation between crystallographic ϕ, ψ values and the C-1 and C-4 chemical shifts for the crystalline cyclomaltose hydrates has been shown (15, 17). Horii *et al.* (13) have proposed a similar correlation for the β-D-(1→4) glucans and the data for cellulose and mannan fit reasonably well on their plot. This kind of correlation is valuable to support diffraction-based modelling for crystalline polysaccharides. The agreement for the O-6 rotamer position (based on chemical shift correlation) between the X-ray fiber diffraction analysis and this study is very satisfying. Of equal significance is the striking difference in relaxation behaviour of C-6 in cotton vs. mannan. This observation, for samples of equal crystallinity, has structural implications. With the test of time, it appears more and more that the unique feature of native cellulose is the O-2...O-6 intramolecular H-bond. Because of the axial vs. equatorial orientation of O-2 in mannan compared to cellulose, such an intramolecular H-bond is not possible in mannan. Intramolecular H-bonds can be considered to allow greater translational and rotational freedom of individual chains; hence C-6 in cellulose would be expected to have a shorter T_1 than for mannan, especially in the noncrystalline regions.

Acknowledgements

W. T. Winter wishes to acknowledge partial support of his contribution to this work by the Donors of the Petroleum Research Fund administered by the American Chemical Society, and by the Xerox Research Centre of Canada.

1. R. D. PRESTON. Physical biology of plant cell walls. Chapman and Hall, London. 1974. pp. 239–255.
2. C. Y. LIANG, K. H. BASSETT, E. A. MCGINNES, and R. H. MARCHESSAULT. TAPPI, **43**, 1017 (1960).
3. H. CHANZY, M. DUBÉ, R. H. MARCHESSAULT, and J. F. REVOL. Biopolymers, **18**, 887 (1979).
4. P. ANDREWS, L. HOUGH, and J. K. N. JONES. J. Chem. Soc. (1952) 2744.
5. E. FREI AND R. D. PRESTON. Proc. R. Soc. B: **169**, 27 (1968).
6. I. A. NIEDUSZYNSKI and R. H. MARCHESSAULT. Can. J. Chem. **50**, 230 (1972).
7. H. CHANZY, S. PÉREZ, D. P. MILLER, G. PARADOSSI, and W. T. WINTER. Macromolecules, **20**, 2407 (1987).
8. A. SARKO and R. MUGGLI. Macromolecules, **7**, 486 (1979).
9. K. H. GARDNER and J. BLACKWELL. Biopolymers, **13**, 1975 (1974).
10. D. L. VANDERHART. J. Chem. Phys. **84**, 1196 (1986).
11. D. A. TORCHIA and A. SZABO. J. Magn. Reson. **49**, 107 (1982); D. A. TORCHIA. J. Magn. Reson. **30**, 613 (1978).
12. R. TEEAAR and E. LIPPMAA. Polym. Bull. (Berlin), **12**, 315 (1984).
13. F. HORII, A. KIRAI, and R. KITAMARU. Polym. Bull. (Berlin), **10**, 357 (1983).
14. R. H. ATTALLA and D. L. VANDERHART. Science, **223**, 283 (1984).
15. R. P. VEREGIN, C. A. FYFE, R. H. MARCHESSAULT, and M. G. TAYLOR. Carbohydr. Res. **160**, 41 (1987).
16. F. HORII, A. HIRAI, and R. KITAMARU. J. Carbohydr. Chem. **3**, 641 (1984).
17. H. SAITO, G. IZUMI, T. MAMIZUKA, S. SUZUKI, and R. TABETA. Chem. Commun. 1386 (1982).
18. C. A. FYFE, R. L. DUDLEY, P. J. STEPHENSON, Y. DESLANDES, G. K. HAMER, and R. H. MARCHESSAULT. J. Macromol. Sci. Rev. Macromol. Chem. Phys. C**23**, 187 (1983).

Can. J. Chem. Downloaded from www.nrcresearchpress.com by 88.85.125.76 on 09/07/12
For personal use only.

Application of FT-Raman spectroscopy to the study of selected organometallic complexes and proteins[1]

STEVEN M. BARNETT, FRANÇOIS DICAIRE, and ASHRAF A. ISMAIL[2]

Department of Chemistry, McGill University, 801 Sherbrooke Street West, Montreal, P.Q., Canada H3A 2K6

Received January 2, 1990

This paper is dedicated to Professor Arthur S. Perlin on the occasion of his 67th birthday

STEVEN M. BARNETT, FRANÇOIS DICAIRE, and ASHRAF A. ISMAIL. Can. J. Chem. **68**, 1196 (1990).

The study of colored organometallic complexes by dispersive Raman spectroscopy has been limited due to fluorescence or photodecomposition caused by the visible laser used as the excitation source. As a solution to this problem, FT-Raman spectroscopy with a near-infrared laser source has been useful in lowering fluorescence or photolysis in these samples. To investigate the utility of this technique, we have obtained and assigned the FT-Raman spectra of a series of arene chromium tricarbonyl complexes and of cyclopentadienyl manganese tricarbonyl. Some bands previously unobserved by dispersive Raman spectroscopy were seen, including a band assigned to a ^{13}CO satellite in the spectrum of methylbenzoate chromium tricarbonyl. In addition, FT-Raman data for bovine serum albumin (BSA) and Protein-A are presented.

Key words: FT-Raman spectroscopy, metal carbonyl, proteins, organometallics, near infrared.

STEVEN M. BARNETT, FRANÇOIS DICAIRE et ASHRAF A. ISMAIL. Can. J. Chem. **68**, 1196 (1990).

L'étude des complexes organométalliques colorés par la spectroscopie Raman de dispersion a été limitée par la fluorescence ou la photodécomposition causées par les lasers visibles utilisés comme sources d'excitation. Pour solutionner ce problème, la spectroscopie Raman par transformée de Fourier à l'aide d'une source laser proche infrarouge s'est avérée utile pour diminuer la fluorescence ou la photolyse dans ces échantillons. Dans le but de définir l'utilité de cette technique, on a déterminé les spectres FT-Raman d'une série de complexes d'arènes chrome tricarbonyle et de cyclopentadiényl manganèse tricarbonyle. On a pu observé un certain nombre de bandes qui n'avaient pas été observées antérieurement par spectroscopie Raman de dispersion, y compris une bande attribuée à un satellite ^{13}CO du spectre du benzoate de méthyle chrome tricarbonyle. De plus, on présente des données de FT-Raman relatives au sérum d'albumine de bovins (SAB) et à la protéine-A.

Mots clés : spectroscopie FT-Raman, métal carbonyle, protéines, organométalliques, proche infrarouge.

[Traduit par la revue]

Introduction

Since the first synthesis of arene chromium tricarbonyl complexes in 1957, the chemical reactivities of this class of complexes have been extensively investigated (1, 2). Recently, we have employed certain arene chromium tricarbonyl derivatives as probes of enzyme binding sites (3) and as markers in infrared immunoassay (IRIA), a new assay technique employing FT-IR spectroscopy as the method of detection (4). The infrared characterization of these compounds has been undertaken by several groups (5, 6) but Raman studies have been limited to date due to the rapid thermal or photolytic decomposition of a large number of arene chromium tricarbonyl complexes under visible laser irradiation.

One approach to circumventing fluorescence and photodecomposition in Raman experiments is through the use of a near-infrared (NIR) laser in place of a visible laser as the excitation source. For samples containing molecules with low-lying electronic states, visible laser excitation puts the molecules in a virtual energy state that couples readily to adjacent electronic states, resulting in fluorescent de-excitation or photodecomposition. Irradiation of such samples with a NIR laser puts the molecules in a virtual energy state that lies between the electronic ground state and the first excited electronic state, thus avoiding both fluorescence and photodecomposition. However, the use of NIR lasers results in reduced sensitivity of the Raman measurements for two reasons. First, scattering efficiency decreases as the fourth power of the wavelength of excitation. Therefore, the intensity of the scattered signal using a NIR laser is 10 to 20 times lower than that using a visible laser. Second, the detectors suitable for near-IR measurements are not as sensitive as the ultrasensitive photomultiplier detectors used in the visible region. A successful approach to overcoming these problems has involved the use of interferometry and Fourier transform (FT) techniques for signal processing.

The use of the FT spectrometer has had a considerable impact on infrared spectroscopy in recent years. This is due to the three principal advantages of FT spectrometry: high throughput, wavelength accuracy, and multiplexing, that is, the simultaneous detection of all wavelengths. The first FT-Raman experiment was performed by Chandry *et al.* in 1964 (7) but went largely unnoticed until Hirschfeld and Chase (8, 9) and Murphy and co-workers (10) reintroduced FT-Raman spectroscopy in 1986. Several manufacturers of FT-IR instrumentation have recently adapted their spectrometers to perform FT-Raman measurements. As a result, IR and Raman spectra can be recorded using the same optical bench with two different sources and detectors. In addition, Raman data can be processed using the FT-IR software.

FT-Raman spectroscopy has proved very successful in a variety of applications, especially in the study of dyes (9, 11) and polymers (12, 13). In this paper, we will present some examples of the application of FT-Raman spectroscopy to the study of organometallic complexes, as well as the FT-Raman spectra of two proteins employed in our laboratory in the synthesis of protein-organometallic conjugates.

Experimental

The arene chromium tricarbonyl complexes were prepared from chromium hexacarbonyl by a previously described method (14).

[1]Presented in part at the 72nd Canadian Chemical Conference and Exhibition, Victoria, B.C., June 4–8, 1989.

[2]Author to whom correspondence should be addressed.

Can. J. Chem. Downloaded from www.nrcresearchpress.com by 88.85.125.76 on 09/07/12
For personal use only.

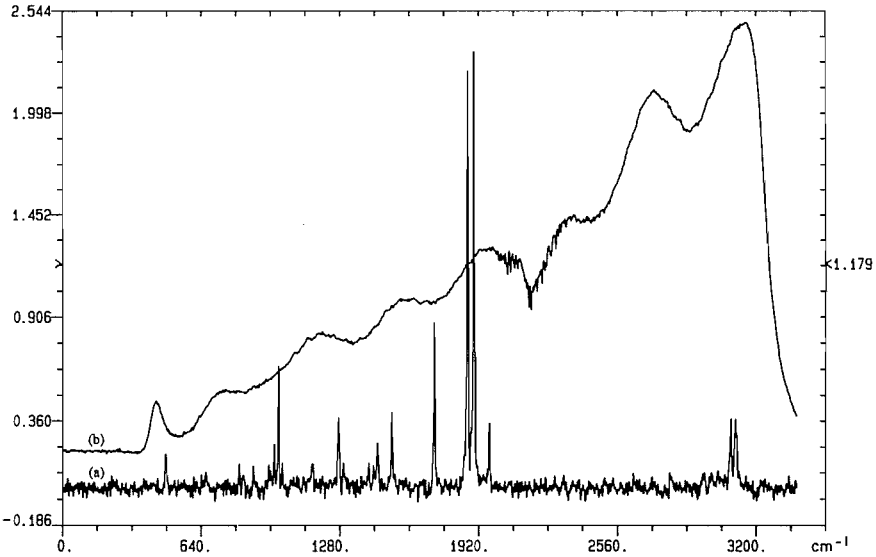

FIG. 1 (*a*) Unratioed FT-Raman spectrum of methylbenzoate chromium tricarbonyl and (*b*) instrument response curve of spectrometer.

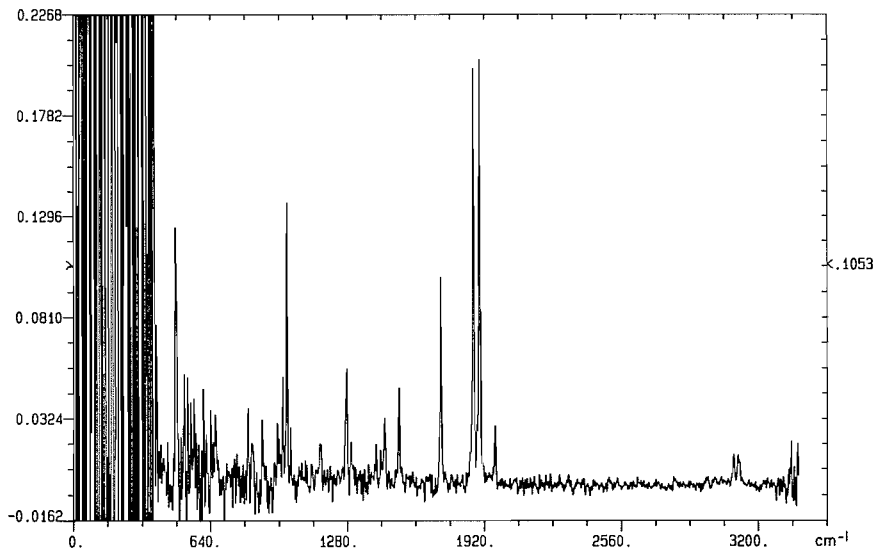

FIG. 2. FT-Raman spectrum of methylbenzoate chromium tricarbonyl ratioed against instrument response curve.

Bovine serum albumin (BSA) and Protein-A were used without purification (Sigma).

FT-Raman spectra were obtained using a Bomem DA-3 or Michelson spectrometer equipped with an indium–gallium–arsenide detector and configured to collect back-scattered radiation at a 180° angle. The excitation source was a Nd:YAG laser operating at 1064 nm. The laser power was typically 0.5 W for solids and 1 W for solution samples.

Solid samples were analyzed in 1-mm id glass capillary tubes. Saturated solutions of methylbenzoate chromium tricarbonyl and cyclopentadienyl manganese tricarbonyl in carbon tetrachloride were prepared in 10-mm glass vials. Protein samples were dissolved in phosphate buffered saline (0.01 M phosphate, 0.15 M NaCl), pH 7.2, in the concentration range of 1–5 mg/mL. The temperature of solution samples was monitored with a Fluke 2170A digital thermometer.

Results

The FT-Raman spectrum of methylbenzoate chromium tricarbonyl in the solid phase is shown in Fig. 1. As a result of the multiplexing advantage of FT-Raman spectroscopy, the complete spectral region can be covered at 4 cm^{-1} resolution in a matter of seconds. The ν(CO) peaks are clearly discernible in this spectrum at 1870, 1898, and 1970 cm^{-1}. However, the low-energy vibrations are missing due to the use of filters necessary to reduce the intensity of the Rayleigh line. The loss of information content in the low-frequency region can be best appreciated by ratioing the spectrum of methylbenzoate chromium tricarbonyl against the instrument response, as shown in Fig. 2. FT-Raman spectroscopy also allows for the recording of solution spectra of transition metal carbonyl complexes whereas photodecomposition of these complexes under visible-laser irradiation is often a particularly severe problem. Figure 3 shows the FT-Raman spectrum of cyclopentadienyl manganese tricarbonyl in carbon tetrachloride. After irradiation of 1 mL of solution with 1 W of power for 15 min, the sample temperature increased from 23 to 28°C.

The band positions from the FT-Raman spectra of a number of arene chromium tricarbonyl complexes, together with band assignments based on previous assignments in the literature (5, 6), are listed in Table 1. The corresponding data for cyclo-

Can. J. Chem. Downloaded from www.nrcresearchpress.com by 88.85.125.76 on 09/07/12
For personal use only.

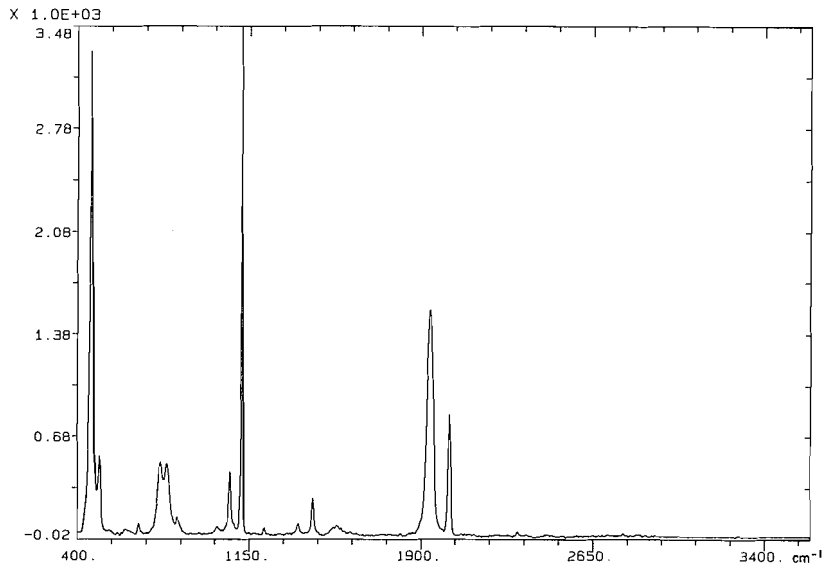

FIG. 3. FT-Raman spectrum of a saturated solution of cyclopentadienyl manganese tricarbonyl solution in carbon tetrachloride.

TABLE 1. FT-Raman band assignments for a series of arene chromium tricarbonyl complexes, $ArCr(CO)_3$

Frequency (cm^{-1})						
Ar = $C_6H_5COOCH_3$						
Solid	Solution	Ar = $C_6H_5COONHS$	Ar = $C_6H_5OCH_3$	Ar = $C_6H_5CH_3$	Ar = $C_6H_3(CH_3)_3$	Assignment
	2952 w					CH stretch
	2844 w					
1970 wm	1989 m	1976 wm	1937 m	1937 m	1946 m	CO stretch a_1
1898 vs	1924 s	1901 vs	1882 vs	1891 vs	1866 vs	CO stretch e
1870 vs		1890 vs	1845 vs	1853 vs	1852 vs	
1856 w						^{13}CO stretch a_1
1717 m	1731 m	1772 vw				CO ketone stretch
1552 wm	1518 m	1520 wm	1531 wm	1462 w	1538 w	Aromatic
	1452 m	1453 w	1435 wm	1444 w		CC stretch
	1436 w					
	1412 wm					
	1391 vw					
	1294 wm					C—OMe stretch
		1301 w				C—ONHS stretch
		1276 w				
	1147 w	1154 w	1147 wm	1208 w		CH i.p. bend
	1108 wm					
	1053 wm					
	1009 w					
997 m	994 m	992 wm	991 m	998 s	998 w	CC stretch ring breath
	787 w		782 wm	782 wm		CH o.p. bend
	651 vw	653 vw	666 wm	665 wm	675 w	CrC—O bend
447 w	471 m	474 w	488 m	485 wm	483 w	Cr—CO stretch

pentadienyl manganese tricarbonyl (15) are presented in Table 2. It should be pointed out that the total measurement time for the acquisition of all these spectra was approximately one hour, which is less than the time required to record a comparable spectral region for a single sample using a conventional Raman spectrometer with the same signal-to-noise ratio at $4\,cm^{-1}$ resolution.

The advantage of using FT-IR software to treat FT-Raman data is illustrated by the example shown in Fig. 4, where the broad CH stretching peak in the FT-Raman spectrum of cyclopentadienyl manganese tricarbonyl is deconvoluted to show weak CH stretching bands at 3146, 3118, 3106, and $3098\,cm^{-1}$ in addition to the strong CH stretching band at $3130\,cm^{-1}$. Fourier deconvolution was also used in the case of methylbenzoate chromium tricarbonyl to isolate a weak shoulder on the $1870\,cm^{-1}$ peak, which is assigned to a ^{13}C satellite of the $1898\,cm^{-1}$ peak.

The FT-Raman spectrum of BSA in the solid state is shown in Fig. 5. The Raman spectrum of BSA has been previously obtained by dispersive methods (16, 17), and the results of the

Can. J. Chem. Downloaded from www.nrcresearchpress.com by 88.85.125.76 on 09/07/12
For personal use only.

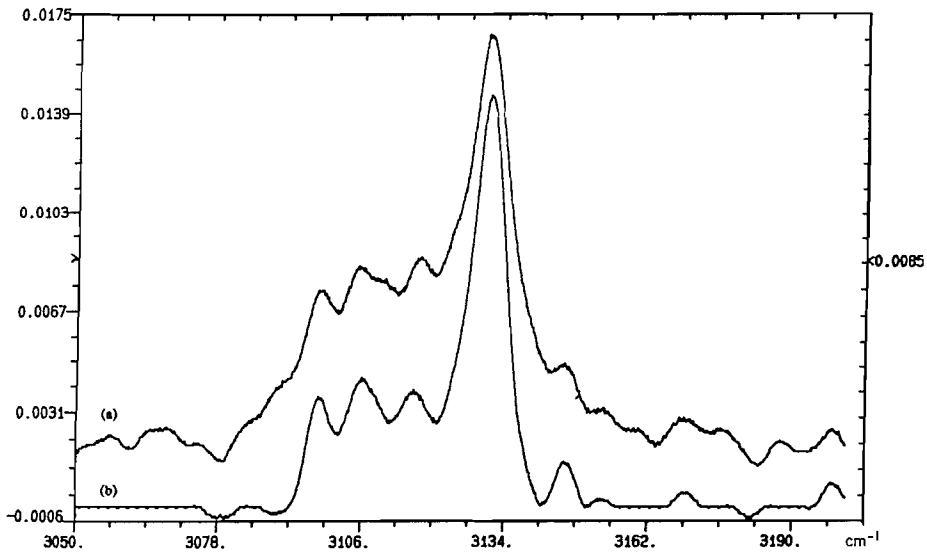

FIG. 4. FT-Raman spectrum in the CH stretching region of cyclopentadienyl manganese tricarbonyl: (*a*) before and (*b*) after deconvolution.

TABLE 2. FT-Raman band assignments for cyclopentadienyl manganese tricarbonyl

Frequency (cm^{-1})		
Solid	Solution	Assignment
3146 vvw		
3130 m		CH stretch
3118 vw		
3106 vw		
3098 vw		
2095 wm		
2016 s	2035 s	CO stretch a_1
2005 w		
1944 s	1938 s	CO stretch e
1922 s		
1916 m		
1424 wm	1423 m	CC stretch e_1
1360 w	1365 w	CC stretch e_2
	1215 vw	CH i.p. bend e_2
1114 s	1115 s	Ring breath a_1
1107 w		
1078 w	1064 m	CH o.p. bend e_2
1066 wm		
1061 wm		
1005 vw	1011 vw	CH i.p. bend e_1
	667 w	MnC—O bend
604 vvw		
549 vvw		
538 vvw		
500 w	496 m	Mn—CO stretch
486 w		
389 vw		

TABLE 3. Band assignments for BSA and Protein-A (ProA)

Frequency (cm^{-1})		
BSA	ProA	Assignment
2915 s	2889 s	CH stretch
2870 s		
1659 s	1665 m	Amide I
1610 w		Tyr
1590 vw		
	1490 wm	
1452 s	1445 m	CH bend
	1425 w	
	1372 w	
1337 m		CH bend
1317 m		
	1229 wm	
1203 w		Tyr + Phe
1177 w		Tyr
1157 w		CN bend
1127 w		
	1101 w	
1032 w		Phe
	1032 w	
1010 s		Phe, Trp
	1003 w	
956 m		C—N—N bend (α)
938 m	936 m	
898 w	901 w	
851 w	855 w	Tyr
825 w		Tyr
	757 m	
747 w		
506 w		S—S stretch

earlier work have been used in assigning the peaks in the FT-Raman spectrum. The FT-Raman spectrum of Protein-A has also been obtained, and some assignments have been made by comparison of the spectrum with that of BSA. The data for these two proteins are shown in Table 3. Attempts to obtain the FT-Raman spectrum of BSA in solution were unsuccessful at 1 and 2 W of laser power. When the power was increased to 4 W, sample heating became significant; after 15 min of laser irradiation, the sample temperature was 47°C, at which temperature BSA is subject to denaturation.

Discussion

FT-Raman spectroscopy offers many advantages with respect to traditional Raman spectroscopy. It is particularly useful for samples where fluorescence or photolysis by visible laser

Can. J. Chem. Downloaded from www.nrcresearchpress.com by 88.85.125.76 on 09/07/12
For personal use only.

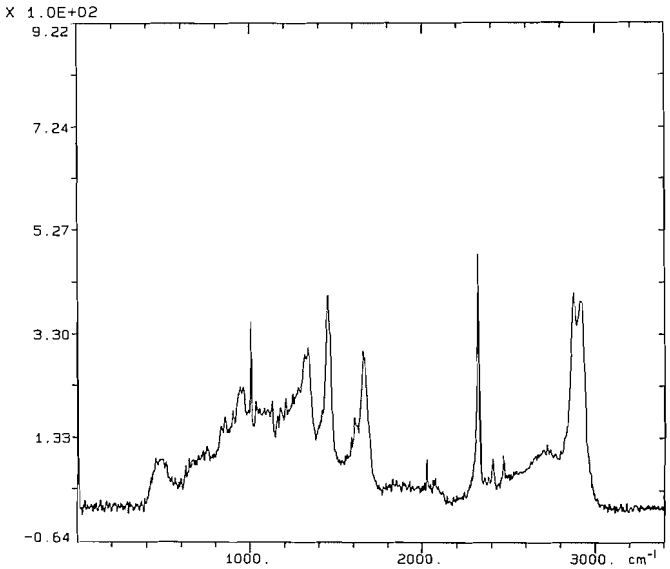

FIG. 5. FT-Raman spectrum of bovine serum albumin in the solid state.

irradiation is a problem. In addition, the entire Raman spectrum can be scanned in a much shorter time than with traditional Raman spectroscopy. Finally, the adaptation of FT-IR spectrometers for FT-Raman measurements allows the extensive FT-IR data handling capabilities to be applied to FT-Raman spectroscopy. As a result of these features, the development of FT-Raman spectroscopy should vastly extend the applicability of Raman spectroscopy.

In the present study FT-Raman spectroscopy has proved useful in obtaining the Raman spectra of colored organometallic complexes in both the solid and the solution phase without photolytic dissociation of the complexes. It has also provided a means for acquisition of protein spectra free of fluorescent background. Denaturation of protein samples has not been found under the conditions employed in our work. Lin and Koenig (17) determined that the Raman band at 934 cm^{-1} in the spectrum of BSA, due to skeletal stretching, was indicative of BSA in an α-helical conformation and that upon heat denaturation, this peak became very weak or disappeared. This peak was strong in the FT-Raman spectra of BSA and Protein-A, indicating that no significant denaturation occurred under NIR-laser irradiation with the laser powers employed (0.5–1 W). However, from the studies described above, it appears that the application of FT-Raman spectroscopy in the study of proteins in solutions is, at present, limited due to several factors: the weak scattering efficiency as a result of the use of a NIR laser for irradiation; the low concentrations of the proteins in solution that must be maintained in order to mimic physiological conditions and avoid formation of aggregated species; and the susceptibility of proteins to denaturation upon heating, limiting the laser power that can be employed. Sample heating could be alleviated through the use of the same cooling accessories as employed in traditional Raman experiments, such as spinning sample cells.

Acknowledgement

We would like to thank Dr. Henry Buijs for use of the FT-Raman facilities at Bomem Inc. One of us (F.D.) is grateful for a Pestcon Graduate Scholarship. This work was sponsored in part by an FCAR grant and a grant from Bomem Inc.

1. R. DAVIS and L. A. P. KANE-MAGUIRE. *In* Comprehensive organometallic chemistry. Vol. 3. *Edited by* G. Wilkinson, F. G. A. Stone, and E. W. Abel, Pergamon Press, Oxford, 1982.
2. M. CAIS, D. FRAENKEL, and K. WEIDENBAUM. Coord. Chem. Rev. **16**, 27 (1975).
3. J. TAGUCHI and A. A. ISMAIL. Paper presented at the 57th Conference of l'Association canadienne-française pour l'avancement des sciences, May, 1989; J. Taguchi and A. A. Ismail. To be published.
4. (*a*) A. A. ISMAIL, P. BROSSIER, P. CHERET, and G. JAOUEN. Clin. Biochem. **22**, 297 (1989); (*b*) P. BROSSIER, F. MARIET, M. SALMAIN, G. JAOUEN, and A. A. ISMAIL. Immunoanal. Biol. Spéc. **13**, 9 (1989).
5. D. M. ADAMS and A. SQUIRE. J. Chem. Soc. Dalton Trans. 558 (1974).
6. D. M. ADAMS, R. E. CHRISTOPHER, and D. C. STEVENS. Inorg. Chem. **14**, 1562 (1975).
7. G. W. CHANDRY, H. A. GEBBIE, and C. HELSUM. Nature, **203**, 1052 (1964).
8. T. HIRSCHFELD and B. CHASE. Appl. Spectrosc. **40**, 133 (1986).
9. D. B. CHASE. J. Am. Chem. Soc. **108**, 7485 (1986).
10. D. J. MOFFATT, H. BUIJS, and W. F. MURPHY. Appl. Spectrosc. **40**, 1079 (1986).
11. C. G. ZIMBA, V. M. HALLMARK, J. D. SWALEN, and J. F. RABOLT. Appl. Spectrosc. **41**, 721 (1987).
12. R. J. ANGELO, H. MIURA, K. H. GARDNER, D. B. CHASE, and A. D. ENGLISH. Macromolecules, **22**, 117 (1989).
13. R. G. MESSERSCHMIDT and D. B. CHASE. Appl. Spectrosc. **43**, 11 (1989).
14. C. A. L. MAHAFFY and P. L. PAUSON. Inorg. Synth. **19**, 154 (1979).
15. I. J. HYAMS, R. T. BAILEY, and E. R. LIPPINCOTT. Spectrochim. Acta, **23A**, 273 (1967).
16. M. C. CHEN and R. C. LORD. J. Am. Chem. Soc. **98**, 990 (1976).
17. V. J. C. LIN and J. L. KOENIG. Biopolymers, **15**, 203 (1976).

Can. J. Chem. Downloaded from www.nrcresearchpress.com by 88.85.125.76 on 09/07/12
For personal use only.

Synthesis, NMR spectroscopy, and crystal structure of the 1:2 host: guest complex of 18-crown-6 with lithium phenoxide[1]

KIMBERLY A. WATSON AND SUZANNE FORTIER[2]
Department of Chemistry, Queen's University, Kingston, Ont., Canada K7I 3N6

MICHAEL P. MURCHIE, JOHN W. BOVENKAMP,[2] AND ANDRE RODRIGUE
Defence Research Establishment Ottawa, Ottawa, Ont., Canada K1A 0Z4

GERALD W. BUCHANAN[2]
Ottawa–Carleton Chemistry Institute, Carleton University, Ottawa, Ont., Canada K1S 5B6

AND

CHRISTOPHER I. RATCLIFFE
Chemistry Division, National Research Council of Canada, Ottawa, Ont., Canada K1A 0R6

Received October 30, 1989

This paper is dedicated to Professor Arthur S. Perrin on the occasion of his 67th birthday

KIMBERLY A. WATSON, SUZANNE FORTIER, MICHAEL P. MURCHIE, JOHN W. BOVENKAMP, ANDRE RODRIGUE, GERALD W. BUCHANAN, and CHRISTOPHER I. RATCLIFFE. Can. J. Chem. **68**, 1201 (1990).

The title complex crystallizes in the space group *Pcab* with a = 16.019(7), b = 19.62(1), c = 15.847(5) Å, and Z = 8. The structure was solved by direct methods and refined by full matrix least-quares calculations to a residual, R, of 0.083. The monomeric structure lacks a true centre of symmetry although the two lithiums have similar chemical environments. Each lithium cation is coordinated to three different oxygens of the hexaether and to both phenoxide oxygens. The hexaether is slightly elongated allowing both Li(1) and Li(2) to lie in the cavity formed by the crown with values of −0.077 and 0.074 Å, respectively, out of the plane approximated by the six oxygens. Both cations are strongly associated with the phenol moieties. The distances between the lithium and the phenoxide oxygens range from 1.859–1.893 Å, while distances of 1.940–2.420 Å are found with the ether oxygens. The Li(1)—Li(2) distance is found to be relatively short at 2.35 (2) Å.

Evidence for motion in the 18-crown-6 portion of the solid complex has been obtained from ^{13}C CPMAS NMR spectroscopy. At 298 K, a dipolar washout phenomenon occurs since the motional correlation times are of the order of the inverse of the ^{1}H decoupling field amplitude. At lower temperatures, the motion becomes slow enough to permit resolution of the chemical shift differences of unique carbon sites of the crown ether. Consistent with the X-ray analysis, only five resonances are evident for the phenoxide carbons, indicating that the two aromatic rings are nearly equivalent in their crystallographic environment. The solution ^{13}C spectrum shows only five resonances in total down to 188 K indicative of rapid conformational averaging of all the 18-crown-6 carbon resonances and rapid rotation about the O-phenyl bond.

Key words: crown ethers, NMR, stereochemistry, dynamics, X-ray.

KIMBERLY A. WATSON, SUZANNE FORTIER, MICHAEL P. MURCHIE, JOHN W. BOVENKAMP, ANDRE RODRIGUE, GERALD W. BUCHANAN et CHRISTOPHER I. RATCLIFFE. Can. J. Chem. **68**, 1201 (1990).

Le composé mentionné dans le titre cristallise dans le groupe d'espace *Pcab* avec a = 16.019(7), b = 19,62(1) et c = 15,847(5) Å et Z = 8. On a résolu la structure par des méthodes directes et on l'a affinée par la méthode des moindres carrés jusqu'à une valeur de R = 0,083. La structure monomère ne possède pas de vrai centre de symétrie même si les deux atomes de lithium se trouvent dans des environnement chimiques semblables. Chaque cation lithium est coordonné à trois oxygènes différents de l'hexaéther et aux deux groupements phénolates. L'hexaéther est partiellement allongé et les deux Li(1) et Li(2) se trouvent respectivement à −0,077 et à +0,074 Å du plan approximatif formé par les six oxygènes dans la cavité formée par la couronne. Les deux cations sont fortement associés aux oxygènes des phénols. Les distances entre le lithium et les oxygènes des phénols varient de 1,859 à 1,893 Å alors que les distances entre les lithium et les oxygènes des éthers varient de 1,940 à 2,420 Å. On a trouvé que la distance Li(1)—Li(2) est relativement courte à 2,35(2) Å.

En se basant sur des données de spectroscopie rmn CPMAS due ^{13}C, on a pu mettre en évidence un mouvement de l'éther 18-couronne-6. A 298 K, il se produit un phénomène d'annulation dipolaire qui résulte du fait que les temps de corrélation des mouvements sont du même ordre de grandeur que l'inverse de l'amplitude du champ de découplage du ^{1}H. A des températures plus basses, le mouvement devient suffisamment lent pour permettre la résolution des différences dans les déplacements chimiques des sites uniques des carbones de l'éther couronne. En accord avec l'analyse des rayons-X, on n'observe que cinq bandes de résonance pour les carbones du phénolate; ces résultats indiquent que les deux cycles aromatiques sont pratiquement équivalents dans leur environnement cristallographique. Au total, le spectre du ^{13}C ne présente que cinq raies jusqu'à 188 K; ces résultats indiquent qu'il s'opère un équilibre conformationnel rapide de toutes les résonances des carbones de la 18-couronne-6 et une rotation rapide autour de la liaison O-phényle.

Mots clés: éthers couronniques, RMN, stéréochimie, dynamiques, rayons-X.

[Traduit par la revue]

---

[1]NRCC No. 31404.
[2]Authors to whom correspondence may be addressed.

Can. J. Chem. Downloaded from www.nrcresearchpress.com by 88.85.125.76 on 09/07/12
For personal use only.

Can. J. Chem. Downloaded from www.nrcresearchpress.com by 88.85.125.76 on 09/07/12
For personal use only.

Introduction

Since Pedersen (1) reported the first synthesis of crown ether complexes, over four hundred crystal structure analyses of crown ether complexes have been carried out and it is now well understood that several factors, such as host–guest size compatibility, ligand substituents, anion and solvent effects, have an influence on the resulting structure and stoichiometry of these complexes.

Over the last few years, we have studied crown ether complexes with unusual host:guest ratios, that is ratios that would not be expected on the basis of the host:guest size compatibility criterion. For example, several 1:2 and 1:3 host:guest complexes of 18-crown-6 macrocyclic ethers with potassium and sodium salts (2) and 1:2 host-guest complexes of 15-crown-5 macrocyclic ethers with sodium and lithium salts (3) were synthesized. Crystal structure analyses were carried out on several of these complexes (3, 4) and in each case it was clear that the structural characteristics and stoichiometry were a result of concerted host, guest, anion, and solvent effects.

In the present work, we report the synthesis, solution and solid state NMR study, and X-ray crystal structure determination of the 1:2 host:guest complex of 18-crown-6 with lithium phenoxide. Few lithium complexes of 18-crown-6 have been reported to date and this study was undertaken to characterize the complexation of the lithium ions by this host. We were also interested in comparing these results with those of several complexes of alkali metal phenoxide salts with macrocyclic ethers, obtained from similar solvents, and exhibiting unusual host: guest ratios.

Experimental

Commercial anhydrous diethyl ether was dried over sodium wire. Hexane was dried over molecular sieves. Reagent grade tetrahydrofuran was distilled from lithium aluminum hydride using a Stedman column and a variable take-off still head. Commercial 18-crown-6 was precipitated as the acetonitrile complex (5) and the acetonitrile was removed under vacuum; mp 40.5–41.0°C (lit. (6) mp 39–40°C). Lithium phenoxide was prepared as described in ref. 7.

The complexation reactions, the preparation of samples for elemental analysis and the preparation of melting point and NMR spectroscopic samples were carried out in a Dri-Lab (Vacuum Atmospheres Corp.) under an argon atmosphere.

Synthesis of 18-crown-6·2LiOPh

In a typical reaction, LiOPh (6.49 mmol) was dissolved in a mixture of diethyl ether (40 mL) hexane (20 mL). The 18-crown-6 (2.17 mmol), dissolved in hexane (15 mL), was added to the LiOPh solution. A white precipitate was formed after less than 5 min. The reaction mixture was stirred overnight at room temperature. The precipitate was isolated by suction filtration and then dried under vacuum (<0.001 Torr) in a drying pistol at 56°C for 15 h. The white solid had a melting point of 143.5–146.0°C and was identified by proton NMR spectroscopy and elemental analysis of 18-crown-6·2LiOPh. *Anal.* calcd.: C 62.06, O 7.38, Li 2.99; found: C 61.73, O 7.16, Li 3.27. The yield of 18-crown-6·2LiOPh was 1.88 mmol which corresponds to an 87% yield based on 18-crown-6.

Preparation of a crystalline sample of 18-crown-6·2LiOPh

Suitable crystals of 18-crown-6·2LiOPh were obtained from a solution of the complex (0.19 g) in anhydrous tetrahydrofuran (10 mL). The solution was slowly evaporated to dryness in an argon atmosphere.

X-ray crystal structure analysis of 18-crown-6·2LiOPh

Pertinent data about the crystal used and the measurement of diffraction intensities are summarized in Table 1. The crystal used in the diffraction experiment was mounted inside a glass capillary in a moisture-free environment. The intensity data were collected on an Enraf-Nonius CAD-4 diffractometer using CuKα (λ = 1.5418 Å) radiation. The intensities were collected by the ω/2θ scanning procedure and two reflections were measured after every 7200 s of exposure time to check on the stability of the crystal. No evidence of crystal decay was detected. The data were corrected for Lorentz and polarization effects; absorption corrections were not considered necessary. The structure was solved routinely by direct methods using the program MULTAN 80 (8). The positions of sixteen of the total of thirty four hydrogen atoms were found in the difference Fourier map, the remaining eighteen were calculated. The structure was refined by full-matrix least squares using all reflections with $I > 3\sigma(I)$. Anisotropic temperature factors were used for the non-hydrogen atoms. The hydrogen atoms were assigned isotropic temperature factors equal in magnitude to the equivalent isotropic temperature factors of their parent atoms. They were included in the calculations but they were not refined. The function minimized was $\Sigma w||F_o| - |F_c||^2$, where $w = 1/\sigma^2(|F_o|)$. A correction for isotropic secondary extinction effect was included in the refinement. The scattering factors were taken from Cromer and Waber (9). All calculations were done on a PDP 11/23 computer using the Enfra-Nonius SDP program package (10).

TABLE 1. Crystal data[a]

Parameter	Crystal data
Molecular formula	$Li_2O_8C_{24}H_{34}$
Molecular weight	464.42
Space group; Z	*Pcab*; 8
a, Å	16.019(7)
b, Å	19.62(1)
c, Å	15.847(5)
V, Å^3	4980.8
Number of reflections used for the determination of unit cell parameters; 2θ range, deg	25; 9–27
Density (calcd.), g cm^{-3}	1.238
Number of measured reflections	2651
Number of observed reflections, $I > 3\sigma(I)$	1778
2 θ range scanned, deg	1–50
μ(CuKα), cm^{-1}	7.062
Crystal dimensions, mm	0.38 × 0.32 × 0.25
Isotropic secondary extinction correction, g	2.09×10^{-7}
Final R; R_w	0.083; 0.096
Largest shift/error in final least-squares cycle, Δ/σ	0.00
Maximum and minimum residual electron density in final difference Fourier map, e Å^{-3}	0.355; −0.299
Standard deviation of an observation of unit weight, σ	2.635

[a]Estimated standard deviations are shown in parentheses.

Nuclear magnetic resonance spectra

The ^{13}C CPMAS spectra were recorded at 45.3 MHz using a Bruker CXP-180 NMR spectrometer and a Doty Scientific variable temperature probe. Cross polarization time was 0.5 ms with the rf field amplitude being ca. 60 kHz. The number of transients was 1000 at room temperature and 72 at 210 K. The sweep width was 20 kHz and the recycle times were 60 s at room temperature and 80 s at 210 K. Normally 2K data points were collected with zero filling to 8 K before Fourier transformation. At room temperature the magic angle spinning rate was 41.1 kHz and at 210 K the rate was 3.8 kHz. The chemical shifts were measured relative to external solid hexamethylbenzene (HMB) and converted to the TMS scale via the factor of 16.9 ppm which is the chemical shift of the CH_3 group of HMB.

The solution phase ^{13}C NMR spectra were obtained using a Varian

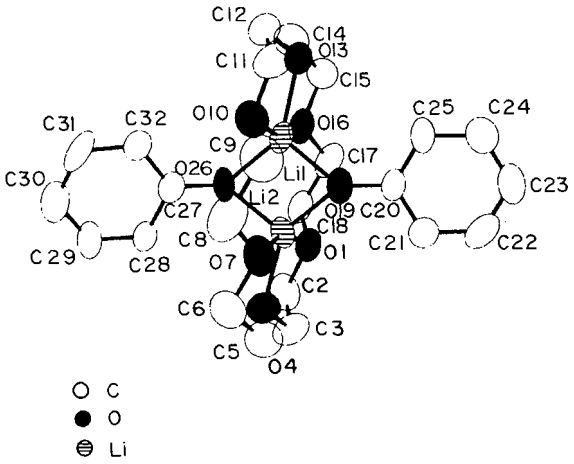

FIG. 1. ORTEP diagram of 18-crown-6·2LiOPh

XL-200 spectrometer operating at 50.3 MHz. Normal sweep width was 10 kHz with 32K data points and complete ^1H noise decoupling. Samples were ca. 0.2 M in 5 mm tubes using dimethoxyethane-d_{10} as solvent. Normally a 45° observing pulse was applied with delays of 1 s. Temperatures were calibrated using a copper–constantan thermocouple and are deemed accurate to within 2°C.

Results and discussion

Crystal structure of 18-crown-6·LiOPh

An ORTEP (11) drawing of the complex showing the atom numbering scheme is given in Fig. 1. The fractional coordinates and equivalent isotropic temperature factors of the non-hydrogen atoms are presented in Table 2. Lithium–oxygen bond distances and angles appear in Table 3; average and range of bond distances and angles of the macrocycle and of the phenoxides are given in Table 4; and macrocyclic ring torsion angles are presented in Table 5.

Host geometry and conformation

The cavity outlined by the oxygens of the hexaether is slightly elongated, with values of 5.454(6), 6.202(6), and 5.366(7) Å for O(1)---O(10), O(4)---O(13), and O(7)---O(16), respectively. The elliptical arrangement of the oxygens of the hexaether allows both Li^+ cations to be accommodated in the crown cavity while keeping a sufficient Li^+—Li^+ separation of 2.35(2) Å. The ether oxygens form an approximate plane with all oxygens pointing toward the centre of the cavity. They are found alternately, ca. 0.026 Å above and below their mean plane.

In a regular hexaether conformation all torsion angles about C—C bonds are synclinal and those about C—O bonds are antiperiplanar (12). From Table 5 is is evident that these values are present in some portions of the structure, but substantial deviations are present in other regions. For example, two of the six O—C—C—O networks have torsional angles which are >25° larger than the "regular" value of 60°. These deviations, combined with some lesser contractions of C—C—O—C angles result in an elliptical cavity shape for the 18-membered ring.

The C—C bond lengths in the macrocycle exhibit the characteristic (13, 14) shortening with an average value of 1.498 Å. The C—O bond lengths have an average value of 1.427 Å and the O—C—C and C—O—C angles have average values of 109.3° AND 113.5°, respectively, which are consistent with previous studies on related systems (13, 14).

Host–guest interactions

Although the two lithium cations are not related by crystallo-

TABLE 2. Final fractional coordinates and equivalent eotropic temperature factors with estimated standard deviations in parentheses

Atom	x	y	z	B_{eq}(Å^2)[a]
O1	0.6677(4)	0.0836(3)	−0.0501(4)	4.8(2)
O4	0.7884(4)	0.0865(3)	0.0665(4)	5.3(2)
O7	0.7436(5)	0.1721(3)	0.1981(4)	5.5(2)
O10	0.5552(4)	0.1944(3)	0.2443(4)	5.0(2)
O13	0.4280(4)	0.1897(3)	0.1307(4)	5.2(2)
O16	0.4820(4)	0.1088(3)	0.0017(4)	5.1(2)
O19	0.6176(4)	0.2051(3)	0.0587(4)	4.4(2)
P26	0.6013(4)	0.0714(3)	0.1385(4)	4.5(2)
C2	0.7379(4)	0.0390(5)	−0.0556(6)	6.3(3)
C3	0.8102(6)	0.0728(6)	−0.0187(6)	6.0(3)
C5	0.8479(7)	0.1199(6)	0.1144(8))	7.1(3)
C6	0.8150(7)	0.1277(6)	0.2040(6)	6.2(3)
C8	0.7039(7)	0.1798(6)	0.2766(6)	6.6(3)
C9	0.6285(7)	0.2269(6)	0.2702(7)	7.0(3)
C11	0.4834(7)	0.2361(5)	0.2566(7)	6.1(3)
C12	0.4121(6)	0.1972(5)	0.2207(6)	5.3(3)
C14	0.3701(6)	0.1485(6)	0.0849(7)	6.2(3)
C15	0.3991(6)	0.1415(6)	−0.0049(6)	5.9(3)
C17	0.5204(6)	0.1033(5)	−0.0799(6)	5.3(3)
C18	0.5904(7)	0.0539(5)	−0.0759(6)	5.2(3)
C20	0.6191(6)	0.2603(4)	0.0112(5)	3.5(2)
C21	0.6892(6)	0.2783(5)	−0.0330(6)	4.5(3)
C22	0.6898(6)	0.3373(6)	−0.0826(6)	5.6(3)
C23	0.6261(7)	0.3818(5)	−0.0822(7)	5.8)
C24	0.5548(7)	0.3638(5)	−0.0410(6)	5.7(3)
C25	0.5513(6)	0.3038(5)	0.0082(6)	4.8(3)
C27	0.6080(6)	0.0253(5)	0.1973(5)	3.8(2)
C28	0.6753(6)	−0.0242(5)	0.1949(5)	3.7(2)
C29	0.6820(7)	−0.0727(5)	0.2570(6)	4.8(2)
C30	0.6319(7)	−0.0781(5)	0.3226(7)	6.1(3)
C31	0.5645(7)	−0.0312(6)	0.3279(6)	5.9(3)
C32	0.5542(6)	0.0200(5)	0.2658(6)	4.7(3)
Li1	0.541(1)	0.1528(9)	0.118(1)	4.9(4)
Li2	0.6771(1)	0.124(1)	0.075(1)	5.7(5)

[a] $B = (4/3)\sum_i\sum_j \beta_{ij}(\mathbf{a}_i \cdot \mathbf{a}_j)$.

TABLE 3. Oxygen – alkali metal bond lengths and angles with estimated standard deviations in parentheses

Bonds	Length (Å)	Bonds	Angle (deg)
Li(1)—O(10)	2.170(13)	O(10)—Li(1)—O(13)	82.1(5)
Li(1)—O(13)	1.967(13)	O(10)—Li(1)—O(16)	160.5(7)
Li(1)—O(16)	2.249(13)	O(10)—Li(1)—O(19)	101.2(6)
Li(1)—O(19)	1.853(12)	O(10)—Li(1)—O(26)	96.3(5)
Li(1)—O(26)	1.890(12)	O(13)—Li(1)—O(16)	80.4(5)
Li(2)—O(1)	2.141(14)	O(13)—Li(1)—O(19)	117.1(6)
Li(2)—O(4)	1.934(13)	O(13)—Li(1)—O(26)	139.7(7)
Li(2)—O(7)	2.416(15)	O(16)—Li(1)—O(19)	94.2(5)
Li(2)—O(19)	1.873(13)	O(16)—Li(1)—O(26)	91.7(5)
Li(2)—O(26)	1.885(13)	O(19)—Li(1)—O(26)	102.8(6)
		O(1)—Li(2)—O(4)	81.9(5)
		O(1)—Li(2)—O(7)	157.5(6)
		O(1)—Li(2)—O(19)	98.7(5)
		O(1)—Li(2)—O(26)	104.3(7)
		O(4)—Li(2)—O(7)	78.4(5)
		O(4)—Li(2)—O(19)	141.5(8)
		O(4)—Li(2)—O(26)	115.0(6)
		O(7)—19)	90.2(6)
		O(7)—Li(2)—O(26)	93.8(5)
		O(19)—Li(2)—O(26)	102.2(6)

Can. J. Chem. Downloaded from www.nrcresearchpress.com by 88.85.125.76 on 09/07/12
For personal use only.

TABLE 4. Average and range in the bond lengths (Å) and angles (deg) for the macrocyclic rings and phenoxides with estimated standard deviations in parentheses

Parameter	Value	Parameter	Value
Macrocyclic ring			
Average C—C	1.497(10)	Average C—O	1.427(8)
Range of C—C	1.457–1.526(11)	Range of C—O	1.384–1.478(9)
Average C—O—C	113.6(6)	Average C—C—O	108.7(6)
Range of C—O—C	110.7–116.2(6)	Range of C—C—O	104.5–114.0(7)
Phenoxides			
O(19)—C(20)	1.318(7)	O(26)—C(27)	1.304(7)
O(19)—C(20)—C(21)	121.3(7)	O(26)—C(27)—C(28)	120.5(6)
O(19)—C(20)—C(25)	120.8(7)	O(26)—C(27)—C(32)	124.0(7)
Average C—C	1.386(9)	Average C—C—C	120.2(7)
Range of C—C	1.317–1.452(9)	Range of C—C—C	115.5–125.1(7)

TABLE 5. Macrocyclic ring torsional angles (estimated standard deviations in parentheses)

Bonds	Angle (deg)
O(1)—C(2)—C(3)—O(4)	60.(1)
C(2)—C(3)—O(4)—C(5)	−179.1(8)
C(3)—O(4)—C(5)—C(6)	−177.9(8)
O(4)—C(5)—C(6)—O(7)	−65.)1)
C(5)—C(6)—O(7)—C(8)	176.0(8)
C(6)—O(7)—C(8)—C(9)	179.9(8)
O(7)—C(8)—C(9)—O(10)	85.1(1)
C(8)—C(9)—O(10)—C(11)	167.4(8)
C(9)—O(10)—C(11)—C(12)	176.0(8)
O(10)—C(11)—C(12)—O(13)	−63.4(9)
C(11)—C(12)—O(13)—C(14)	174.8(8)
C(12)—O(13)—C(14)—C(15)	−175.5(8)
O(13)—C(14)—C(15)—O(16)	60.1(1)
C(14)—C(15)—O(16)—C(17)	−175.8(8)
C(15)—O(16)—C(17)—C(18)	−163.9(8)
O(16)—C(17)—C(18)—O(1)	−86.6(9)
C(17)—C(18)—O(1)—C(2)	−172.8(8)
C(18)—O(1)—C(2)—C(3)	−173.6(8)

graphic symmetry, they have nearly identical chemical environments. Both Li^+ cations lie in the approximate plane defined by the donor ether oxygens, with distances of −0.077 and 0.074 Å for Li(1) and Li(2), respectively, out of the mean plane. The lithium cations are located along the direction of elongation of the elliptically shaped cavity and are colinear with O(4) and O(13). Each lithium is coordinated to three diffferent oxygens of the crown ether and to both oxygens of the phenoxide moieties.

In their study of the environments of alkali cations complexed to ethers, Chakrabarti and Dunitz (15) found that the cations always lie close to the bisecting plane through the oxygen atom. They predicated that, for optimal complexation with lithium, a polyether ligand should have a cavity (M---O distances) of approximately 2 Å and should also have the C—O—C bisectors of the ether groups converging to one point. With a polyether ligand accommodating two lithium guests, we expect to see some deviations from these predictions and indeed we find some lengthening of the Li---O distances. The lithium cations are found, nevertheless, as predicted, near the C—O—C bisector planes of the ether groups. Li(1) is at distances of 0.35, 0.05, and 0.43 Å from the C(9)—O(10)—C(11), C(12)—O(13)—C(14), and C(15)—O(16)—C(17) bisector planes, respectively. Li(2) is at distances of 0.31, 0.05, and 0.57 Å from the C(18)—O(1)—C(2), C(3)—O(4)—C(5), and C(6)—O(7)—C(8) bisector planes, respectively. In each case the three bisector planes intersect approximately in a line such that each lithium is near this line of intersection and also in the plane defined by the ether–oxygens.

The lithium ether–oxygen distances range from 1.934–2.416 Å with an average value of 2.146 Å. The lithium phenoxide–oxygen distances range from 1.853–1.890 Å, with an average value of 1.875 Å. Thus, stronger interactions exist between the Li^+ ions and the phenoxide oxygens than between the Li^+ ions and the ether oxygens. The range in lithium ether–oxygen distances reported to date is 1.950–2.531 Å (16). Although the two lithium cations interact strongly with the phenoxide–oxygens to form an aggregate, as expected for these ions in ethereal solvents (3), the relatively large cavity of the 18-crown-6 host allows both lithium cations to coordinate to the regular hexaether host with all the oxygens participating in the coordination of the lithium guests. This is in contrast to the lithium ether–oxygen interaction observed in 18-crown-6·2LiSCN·$2H_2O$ (17), where it was believed that the hydrogen bonding of the water molecules to the ether–oxygen atoms was necessary for coordination of the lithium cations to the crown host. Clearly, in our structure, the two lithium cations are accommodated by the crown ether without the aid of hydrogen bonding.

The 18-crown-6-·2LiOPh complex contains an Li_2O_2 four membered ring defined by Li(1), O(19), Li(2), and O(26). The Li(1)---Li(2) distance is short, with a value of 2.35(2) Å. A search of all the entries in the Cambridge Structural Data Base (16) for Li^+---Li^+ separations revealed a range of distances between 2.299 and 2.759 Å with a mean value of 2.565 Å, based on 46 observations.

In our study of macrocyclic complexes with alkali metal–phenoxide salts, we have observed that the competition between the hard anion and the macrocyclic ligand can give rise to unusual host:guest stoichiometry and unexpected structural characteristics. For example, in both the 15-crown-5·2LiOPh (3) and the dicyclohexano-18-crown-6 (isomer A)·2NaOPh (4) complexes, the formation of the phenoxide aggregate predominates and the cations are pulled out of the host cavity. In the 15-crown-5·2LiOPh complex the aggregate consists of a dimer containing an Li_2O_2 four-membered ring, also observed in our structure. In dicyclohexano-18-crown-6 (isomer A)·2NaOPh it is a tetramer of sodium phenoxides that is formed. Similarly, in the dicyclohexano-18-crown-6 (isomer B)·2KOPh complex (4), the potassium ions are pulled out of the host cavity and a

Can. J. Chem. Downloaded from www.nrcresearchpress.com by 88.85.125.76 on 09/07/12
For personal use only.

potassium phenoxide dimer is observed. However, the tendency to form aggregates in ethereal solutions does not preclude the possibility of obtaining an optimal host:guest coordination geometry. The present, 18-crown-6·2LiOPh, complex exhibits a strong phenoxide aggregate formation, in addition to a host:guest geometry where both lithium cations lie in the cavity outlined by the 18-crown-6.

The ability of a crown host to accommodate more than one guest in a nested position has been observed in complexes where the host cavity is large compared to the size of the guest ions. For example, in dibenzo-24-crown-8·2KNCS (18) the crown ring surrounds both potassium cations in a nearly planar geometry and all the ether–oxygens interact with the potassium cations, analogous to what is observed for the present complex.

Solid state and solution NMR spectra of 18-crown-6·2LiOPh

^{13}C CPMAS spectrum

The solid phase ^{13}C NMR spectra of this material as a function of temperature are presented in Fig. 2. At 298 K, a broad crown ether resonance containing no discernable fine structure is observed centered at *ca.* 70 ppm. At 310 K this resonance is considerably more broadened so that essentially no crown ether carbon signal was observed. Further temperature increases caused sample melting. Lowering the sample temperature sharpens this resonance and some discernable fine structure is apparent at 210 K. Before discussing the origin of the fine structure at low temperature however, the high temperature broadening phenomenon merits clarification.

Similar broadening has been observed recently in other 18-crown-6 complexes (19, 20) and can be attributed to a "dipolar washout" phenomenon. Under conditions where molecular motion has a correlation time of the order of the inverse of the decoupling field amplitude, the incoherent field generated by the motion destructively interferes with the coherent ^1H decoupling field. As a result, the ^1H decoupling field is rendered ineffective and hence a broad dipolar ^1H coupled ^{13}C resonance is observed (21, 22). In the presence of a decoupling field of amplitude 60 Hz, this broadening is maximal for $\tau_C = (1/2)\pi\gamma H_1 = (1/2)\mu \times 60\ \text{Hz} = 2.7 \times 10^{-6}$ S. At temperatures below 298 K, the crown ether resonance sharpens since the correlation time for molecular motion becomes too slow for the above conditions to be met.

With regard to the type of motion involved here, a model is required which allows a large amplitude motion consistent with the NMR data while at the same time preserving the X-ray crystallographic conformation of the 18-crown-6 moiety. The motion must be sufficient to cause an averaging of ^1H—^{13}C dipolar coupling. From other evidence on related 18-crown-6 complexes (20), the motion must also be sufficient to average the ^1H—^1H dipolar couplings and reduce the width and change the sign of the ^{13}C chemical shift anisotropy. The model proposed for the present complex and related systems (20) is one where the entire macrocycle reorients such that the O—CH_2—CH_2—O units exchange positions around the ring. Each unit must simultaneously readjust to fit the local conformation of each site visited, thereby keeping the crystallographic structure unchanged. This type of motion is analogous to a small cyclic molecule undergoing simultaneous reorientation and ring puckering.

A more subtle broadening of the crown ether line near 70 ppm occurs when the correlation time for motion becomes of the same order as the inverse of the chemical shift difference (in Hz). In the slow motional limit, separate resonances will be discernable for each unique carbon type should the chemical shift differences be sufficiently large.

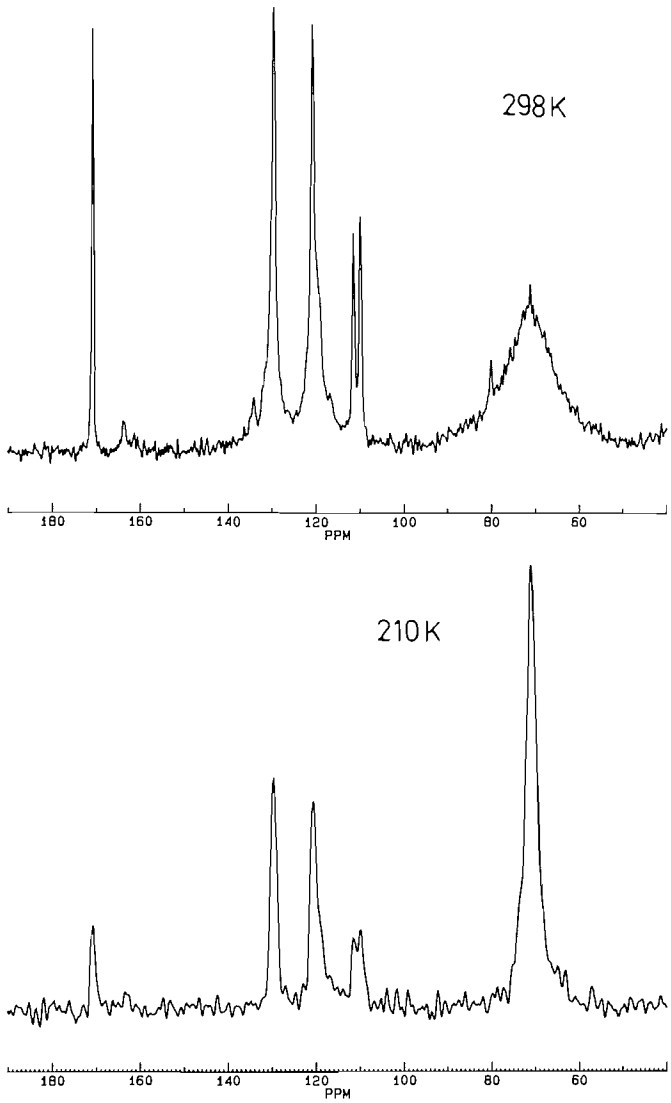

FIG. 2. 45.3 MHz ^{13}C solid phase NMR spectra at 298 and 210 K.

The X-ray results indicate that there are no elements of symmetry in the structure, so that in principle, one anticipates twelve unique ^{13}C resonances in the solid phase spectrum. In fact considerably less than this number are observed due to nearly equivalent chemical shifts and the inherently low resolution (*ca.* 20 Hz linewidth) of solid state ^{13}C spectra. The expanded spectrum showing the crown ether region at 210 K is depicted in Fig. 3. From spectral deconvolution techniques, four overlapping resonances appear to be present, at $\partial_C = 70.2$, 71.4, 72.5, and 73.3 ppm with relative intensities of *ca.* 8:2:1:1.

It is of interest to examine the above results in terms of the torsional environments of each of the twelve unique carbon atoms of the macrocycle. If hydrogens are ignored, then each carbon is present in four torsional networks, either as a central or a terminal atom as indicated in Table 6.

Although the dihedral angle dependence of ^{13}C chemical shifts in these particular types of networks has not been delineated, the effects are well documented experimentally for both central and terminal atoms of related C—C—C—C and C—C—C—O arrangements (23–25). In every instance carbons experiencing *gauche* interactions are shielded by *ca.* 5 ppm rela-

Can. J. Chem. Downloaded from www.nrcresearchpress.com by 88.85.125.76 on 09/07/12
For personal use only.

TABLE 6. Individual carbon torsional environments

Carbon	Torsion angle			
	O—C*—C—O	C—O—C*—C	C*—C—O—C	C—C—O—C*
2	60.0	173.6	179.1	172.8
3	60.0	179.1	173.6	177.9
5	65.0	177.9	176.0	179.1
6	65.0	176.0	177.9	179.9
8	85.0	179.9	167.4	176.0
9	85.0	167.4	179.9	176.0
11	63.4	176.0	174.8	167.4
12	63.4	174.8	176.0	175.5
14	60.0	175.5	175.8	174.8
15	60.0	175.8	175.5	163.9
17	86.6	163.9	172.8	175.8
18	86.6	172.8	163.9	173.6

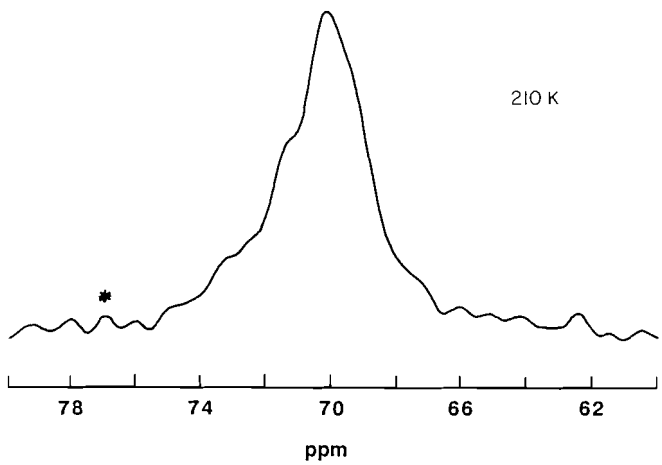

FIG. 3. Expanded crown ether carbon region of ^{13}C spectrum at 210 K.

tive to their counterparts in *trans* orientations. In view of the similarities in the bond angles for sp^3 hybridized carbon and oxygen atoms, it is reasonable to assume a qualitatively similar angular dependence of ^{13}C chemical shifts in O—C—C—O and C—C—O—C networks.

Examination of data in Table 6 shows that eight of the twelve carbons are in rather similar environments, namely they have O—C—C—O angles near 60° and three transoid interactions in the C—C—O—C fragment. Hence the broad resonance centered near 70.2 ppm is deemed to contain unresolved resonances due to C-2,3,5,6,11,12,14, and 15.

For C-8,9,17, and 18 expansion of the O—C—C—O angles to values near 85° is expected to lead to deshielding of the ^{13}C resonances (26). Based on a consideration of the torsional angles, identical chemical shifts are predicted for C-8 and 9, so that the intensity two line at 71.4 ppm is attributed to these carbons. Finally, C-17 and C-18 will likely be the most deshielded and the resonances at 72.5 and 73.2 ppm can be attributed to these sites.

It must be pointed out that in the interpretation of these data, one cannot rule out other contributions to the ^{13}C shifts of the macrocycle such as anisotropic and steric effects of the aromatic rings of the guest LiOPh species, however such influences probably play a lesser role than do the dihedral angle factors.

The solid phase ^{13}C shifts of the phenoxide carbons are also of interest. Since there are no true symmetry elements in the crystal structure, one anticipates twelve resonances in the range of chemical shifts from 100–175 p.p.m. (27). In fact only five are clearly evident. The low intensity signals at ∂_C = 110.0 and 111.9 arise from C-23 and C-30 *i.e.* those sites which are *para* to the carbon-bearing oxygen. At 120.5 is found the resonance for the *ortho* carbons C-21, 25, 28, and C-32, while the *meta* sites resonate near 130.0 ppm. Finally the phenoxide carbons appear at 170.9 ppm. This pattern of chemical shifts suggests that the two aromatic rings are very nearly equivalent in their crystallographic environment. There is, however, non-equivalence between each aromatic moiety as evidenced by the two observed *para* carbon resonances.

For comparison, the ^{13}C CPMAS spectrum of lithium phenoxide itself shows four resonances at ∂_C = 114, 119, 132, and 164. The relative intensities of these lines are 1:2:2:1 as expected on the basis of the above assignments.

From the temperature dependence of these solid state spectra and the dipolar washout temperature, it is also possible to estimate the activation energy for the macrocyclic motion using methods described in our previous work (19, 20). In the present case E_a is ca. 48 kJ/mol.

Solution ^{13}C NMR studies

In dimethoxyethane-d_{10} at 298 K the ^{13}C spectrum of this complex exhibits only five resonances at ∂_C = 167.9, 129.6, 120.1, 114.2, and 71.4 ppm. This is indicative of rapid conformational averaging of all the 18-crown-6 resonances on the NMR timescale as well as rapid rotation about the O—phenyl bond. Upon lowering the temperature to 188 K, the ^{13}C spectra undergo no appreciable changes other than minor temperature-dependent chemical shifts. Thus the aforementioned stereochemical phenomena remain rapid on the NMR timescale at this temperature in solution.

A further point concerns the state of aggregation of these species in solution. The solid phase ^{13}C shifts for the para carbon of the phenoxide moiety are consistent with a phenoxide dimer (7, 28). In solution, however, it has been shown (28) for lithium phenoxide itself that the species present in dimethoxyethane is the tetramer. This possibility cannot be ruled out unambiguously in the present work.

To conclude, a limitation exists in the analysis as presented for the solid phase ^{13}C spectra and their correlation with torsional angles. The X-ray data were obtained at 300 K and these data are employed in an attempt to interpret ^{13}C CPMAS spectra at

Can. J. Chem. Downloaded from www.nrcresearchpress.com by 88.85.125.76 on 09/07/12
For personal use only.

temperatures that are nearly 100° lower. Ideally, only X-ray data obtained at comparable temperatures should be utilized, however in the present instance the quality of the crystals prevents this from being carried out.

1. C. J. PEDERSEN. J. Am. Chem. Soc. **89**, 7017 (1967).
2. A. RODRIGUE, J. W. BOVENKAMP, B. V. LACROIX, R. A. B. BANNARD, and G. W. BUCHANAN. Can. J. Chem. **64**, 808 (1986).
3. M. P. MURCHIE, J. W. BOVENKAMP, A. RODRIGUE, K. A. WATSON, and S. FORTIER. Can. J. Chem. **66**, 2515 (1988).
4. M. E. FRASER, S. FORTIER, A. RODRIGUE, and J. W. BOVENKAMP. Can. J. Chem. **64**, 816 (1986).
5. C. L. LIOTTA. U. S. Patent No. 3,997,562 (1976).
6. C. J. PEDERSEN. J. Am. Chem. Soc. **89**, 7017 (1967).
7. L. M. JACKMAN and C. W. DEBROSSE. J. Am. Chem. Soc. **105**, 4177 (1983).
8. P. MAIN, S. J. FISKE, S. E. HULL, L. LESSINGER, G. GERMAIN, J.-P. DECLERCQ, and M. M. WOOLFSON. MULTAN80. A system of computer programs for the automatic solution of crystal structures from X-ray diffraction data. Univs. of York, England and Louvain, Belgium. 1980.
9. D. T. CROMER and J. T. WABER. International tables for X-ray crystallography. Vol. IV. Kynoch Press, Birmingham. 1974.
10. Enraf-Nonius. Structure determination package. Revised by B. A. Frenz. Enraf-Nonius, Delft. 1979.
11. C. K. JOHNSON. ORTEP. Report ORNL-3794, Oak Ridge National Laboratory, TN. 1965.
12. J. D. DUNITZ, M. DOBLER, P. SEILER, and R. P. PHIZACKERLEY. Acta Crystallogr. Sect. B, **30**, 2733 (1974).
13. M. E. FRASER, S. FORTIER, A. RODRIGUE, and J. W. BOVENKAMP. Can. J. Chem. **64**, 816 (1986).
14. D. E. FENTON, M. MERCER, N. S. POONIA, and M. R. TRUTER. J. Chem. Soc. Chem. Commun. **66**, (1972).
15. P. CHAKRABARTI and J. DUNITZ. Helv. Chem. Acta, **65**, 1482 (1982).
16. F. H. ALLEN, S. BELLARD, M. D. BRICE, B. A. CARTWRIGHT, A. DOUBLEDAY, H. HIGGS, T. HUMMELINK, B. G. HUMMELINK-PETERS, O. KENNARD, W. D. S. MOTHERWELL, J. R. RODGERS, and D. G. WATSON. Acta. Crystallogr. B, **35**, 2331 (1979).
17. P. GROTH. Acta Chem. Scand. A, **36**, 109 (1982).
18. M. MERCER and M. R. TRUTER. J. Chem. Soc. Dalton, 2469 (1973).
19. G. W. BUCHANAN, C. MORAT, J. P. CHARLAND, C. I. RATCLIFFE, and J. A. RIPMEESTER. Can. J. Chem. **67** 1212 (1989).
20. G. W. BUCHANAN, C. MORAT, C. I. RATCLIFFE, and J. A. RIPMEESTER. J. Chem. Soc. Chem. Commun. 1306 (1989).
21. W. P. ROTHWELL and J. S. WAUGH. J. Chem. Phys. **74**, 2721 (1981).
22. D. SAWELACK, W. P. ROTHWELL, and J. S. WAUGH. J. Chem. Phys. **73**, 2559 (1980).
23. G. W. BUCHANAN, R. A. KIRBY, C. I. RATCLIFFE, and J. A. RIPMEESTER. Tetrahedron Lett. **28**, 4783 (1987).
24. G. W. BUCHANAN, M. Z. KHAN, J. A. RIPMEESTER, J. W. BOVENKAMP, and A. RODRIGUE. Can. J. Chem. **65**, 2564 (1987).
25. N. K. WILSON and J. B. STOTHERS. Top. Stereochem. **8**, 1 (1973).
26. G. W. BUCHANAN, R. A. KIRBY, and J. S. TSE. Unpublished results.
27. G. E. MACIEL and J. J. NATTERSTAD. J. Chem. Phys. **42**, 2427 (1965).
28. L. M. JACKMAN and B. D. SMITH. J. Am. Chem. Soc. **110**, 3829 (1988).

Can. J. Chem. Downloaded from www.nrcresearchpress.com by 88.85.125.76 on 09/07/12
For personal use only.

Liquid chromatographic retention behaviour and separation of chlorophenols on a β-cyclodextrin bonded-phase column. Part III. Diaromatic chlorophenols

MICHAEL PALEOLOGOU

Pulp and Paper Research Institute of Canada, 570 St, John's Blvd, Pointe Claire, P.Q., Canada H9R 3J9

AND

SONG LI AND WILLIAM C. PURDY[1]

Department of Chemistry, McGill University, 801 Sherbrooke St. West, Montreal, P.Q., Canada H3A 2K6

Received December 13, 1989

This paper is dedicated to Professsor Arthur S. Perlin on the occasion of his 67th birthday

MICHAEL PALEOLOGOU, SONG LI, and WILLIAM C. PURDY. Can. J. Chem. **68**, 1208 (1990).

The liquid chromatographic retention behaviour of 16 diaromatic phenols and chlorophenols (PCB metabolic analogues) on a β-cyclodextrin bonded-phase column was investigated with respect to mobile-phase composition, pH, temperature, and ionic strength. The mechanistic aspects of retention of these compounds on the β-cyclodextrin column were studied and compared to other reversed-phase columns. Comparison is also made to the liquid chromatographic retention behaviour and separation of monoaromatic chlorophenols on the same column. The size, shape, and spatial geometry of each substrate appears to affect retention and selectivity. Most of the evidence suggests that inclusion complex formation, which involves hydrophobic interactions with the interior of the cavity and/or van der Waals interactions of the chlorine substituents with the backbone of the cavity, provides the physical basis for the resolution of these positional isomers. Under certain chromatographic conditions, however, it appears that, for certain congeners, all or part of the molecule is excluded from the cyclodextrin cavity; in such cases a normal-phase or mixed chromatographic mechanism is postulated based on the interaction of the substrates with the secondary hydroxyls on the periphery of the cyclodextrin moieties. The gradient–elution separation of 14 out of 16 of this type of compound on a single chromatogram is also reported and discussed.

Key words: biphenylols, chlorobiphenylols, biphenyldiols, liquid chromatographic retention behaviour, gradient-elution separation, β-cyclodextrin bonded-phase column.

MICHAEL PALEOLOGOU, SONG LI et WILLIAM C. PURDY. Can. J. Chem. **68**, 1208 (1990).

Faisant varier la composition de la phase mobile, le pH, la température et la force ionique, on a étudié le comportement de seize phénols et chlorophénols diaromatiques (analogues de métabolites de BPC) lors de leur chromatographie liquide de rétention dans une colonne remplie d'une phase liée à de la β-cyclodextrine. On a étudié les aspects mécanistiques de la rétention de ces composés sur la colonne de β-cyclodextrine et on les a comparés à ceux d'autres colonnes de phase inversée. On a aussi effectué une comparaison avec le comportement et la séparation par chromatographie liquide de chlorophénols monoaromatiques sur la même colonne. Il semble que la rétention et la sélectivité soient affectées par la grosseur, la forme et la géométrie spatiale de chaque substrat. La plupart des données obtenues suggère que la formation d'un complexe d'inclusion, qui implique les interactions hydrophobes avec l'intérieur de la cavité et/ou des interactions de van der Waals des substituants chlore avec le squelette de la cavité, fournisse la base physique pour la résolution de ces isomères de position. Toutefois, dans certaines conditions chromatographiques, il semble que, pour certains congénères, l'ensemble ou une partie de la molécule est exclu de la cavité de la cyclodextrine; dans de telles conditions, on envisage un mécanisme chromatographique de phase normale ou mixte qui serait basé sur l'interaction du substrat avec les groupements hydroxyles secondaires à la périphérie de la portion cyclodextriné. On rapporte aussi la séparation, sur un seul chromatogramme et en faisant appel à un gradient d'élution, de quatorze des seize composés de ce type et on discute ce résultat.

Mots clés : biphénols, chlorobiphénols, biphényldiols, comportement lors de la chromatographie liquide de rétention, séparation par gradient d'élution, colonne remplie d'une phase liée à la β-cyclodextrine.

[Traduit par la revue]

Introduction

In two previous publications (1, 2) we discussed the liquid chromatographic (LC) retention behaviour and separation of monoaromatic chlorophenols on a β-cyclodextrin (CD) bonded-phase column. It is the purpose of this paper to extend these investigations to diaromatic chlorophenols of a biphenyl-type structure (see Fig. 1). Stable CD bonded phases were first described in the literature in 1984 (3). These packings consist of chiral CD molecules linked to silica gel via a 6- to 10-atom non-nitrogen-containing spacer arm. Both the linkage and the CD are hydrolytically stable under standard LC conditions. The attachment is such that the CD molecules remain physically intact.

Cyclodextrins are torus-shaped cyclic oligosaccharides formed by the action of *Bacillus macerans* amylase on starch. These molecules contain six to twelve glucose units bonded through

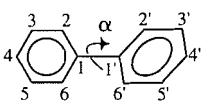

FIG. 1. Biphenyl structure. The numbers indicate the positions of substistituents. α indicates the relative angle between the phenyl rings.

α-(1, 4)-glycosidic linkages. The physical shape of the molecule is that of a truncated cone, with an internal cavity whose dimensions are determined by the number of glucose units. Due to the orientation of the glucose units, there are no hydroxyls on the interior of the cavity thus rendering it hydrophobic.

When using aqueous-organic mobile phases in LC employing CD bonded-phase stationary phases, retention is thought to be predominantly due to inclusion complex formation. The stability of the CD adducts varies markedly with the size of the CD cavity and/or with the structure of the substrate. Hydrogen bonding (4), van der Waals interactions (5, 6), hydrophobic interactions (6, 7), release of high-energy water (5), and com-

[1]Author to whom correspondence should be addressed.

Can. J. Chem. Downloaded from www.nrcresearchpress.com by 88.85.125.76 on 09/07/12
For personal use only.

Can. J. Chem. Downloaded from www.nrcresearchpress.com by 88.85.125.76 on 09/07/12
For personal use only.

binations of these have been proposed to explain inclusion phenomena.

CD-bonded phases were demonstrated to be particularly adept in resolving structural isomers (8) such as the *ortho-*, *meta-*, and *para-* forms of many monoaromatic compounds. We have previously reviewed the LC retention behaviour and separation of monoaromatic chlorophenols (1, 2). A few researchers have investigated the interactions of diaromatic compounds with CD-bonded stationary phases; Fujimura *et al.* (9) and Kawaguchi *et al.* (10) have extensively reported on the retention behaviour and separation of napthalene and substituted napthalenes on diamino-β-CD and ethylenediamine-β-CD bonded-phase columns, respectively. Armstrong *et al.* (11) have described the separation of 80 compounds, including a number of diaromatic analogues, from their isomers using hydrolytically stable β-CD bonded-phase columns obtained from Advanced Separation Technologies, Inc., Whippany, NJ (12). Issaq *et al.* (13), using the same type of column, have examined the effect of mobile-phase composition, temperature, and pH on the retention of a selected group of compounds including napthalene and biphenyl. Finally, Weaver and van Lier (14) have reported the separation of 2-, 3- and 4-hydroxybiphenyls on a β-CD bonded-phase column.

All studies discussed to this point dealt with the LC retention behaviour and/or separation, on a CD bonded-phase column, of structural isomers of relatively small diaromatic molecules with one or two substituents. Here we extend these investigations to structural isomers with more than one or two substituents on the benzene rings. A class of compounds that we found particularly suited for the study of diaromatic phenols and chlorophenols is the chlorinated and non-chlorinated biphenylols and biphenyldiols (PCB metabolic analogues). Sixteen commercially available members of this family of compounds were chosen for our studies (see Table 1). These compounds were chosen because they present a number of distinct features: (*1*) Biphenyl is non-planar in solution (15, 16) and the angle between the two benzene rings is affected by the nature and the position of the substituents (17) (see Fig. 1). Wide stereochemical diversity can exist in biphenyl as a result of its three-dimensional structure, especially when seen in combination with the diversity arising from the degree of substitution and spatial geometry of the substituents on either or both of the benzene rings. (*2*) The largest possible diameter of a chloro-substituted biphenylol is about 7.1 Å which is very close to the diameter of the β-CD cavity (7.8 Å). One would, therefore, expect a close fit for many of these compounds into the cavity. The length of unsubstituted biphenyl is 9.1 Å as compared to 7.8 Å for the length of the cavity. This would allow for maximum interaction with the cavity and possibly hydrogen bonding with the hydroxyls in the periphery of the cavity. (*3*) The pK_a's of the various biphenylol isomers vary depending on the position of the substituents and the number of substituents (see Table 1). Thus by varying the pH of the mobile phase one can examine both the chromatographic behaviour of both the neutral and anionic forms of these compounds. (*4*) There exists a large variation in the solubility of the various biphenylols in common reversed phase mobile phases. This difference is quite substantial between biphenylols and biphenyldiols.

This paper investigates the LC retention behaviour of chlorinated and non-chlorinated biphenylols and biphenyldiols on a β-CD column with respect to mobile-phase composition, pH, temperature and ionic strength. This behaviour is compared with the results previously obtained with the structurally simpler monoaromatic chlorophenols (1). Based on the findings of this study conditions were chosen for the isocratic and gradient-elution separation of these compounds.

Experimental

The LC system consisted of a Waters Model 590 pump, a Rheodyne Model 7125 injector with a 10-μL loop, and a Model Spectroflow 773 variable wavelength uv–vis detector equipped with a 8-μL cell. For the gradient-elution separations an additional Waters Model M-6000 pump was used along with a Waters Model 660 solvent programmer. The chromatograms were obtained by using a Microohm Model SE 120 strip-chart recorder. The column temperature was controlled through a Heto Model 623 water bath.

A Cyclobond I, 250 × 4.6 mm column was obtained from Advanced Separation Technologies (Whippany, NJ). The Cyclobond I column has β-CD chemically bonded to a spherical silica gel support through a five-atom, non-nitrogen-containing spacer arm. The preparation and characterization of this column was fully described elsewhere (12). When not in use, the column was stored in 100% methanol. The column performance appeared to be unchanged for a period of about 3 months.

The effect of pH on the retention time of biphenylols was investigated by changing the pH of the aqueous part of the mobile phase from 4 to 6 using triethylamine–acetate buffers (0.01M). The effect of ionic strength on retention time was examined by varying the concentration of triethylamine buffer (pH = 4.0) in the aqueous part of the mobile phase from 0.01 to 0.1 M. The ionic strength study was performed at pH = 4.0 since at this pH all biphenylols are likely to be in their neutral form. The pK_a of all compounds, was determined from plots of retention time vs. pH on a PRP-1 prepacked analytical column obtained from Hamilton (18), in 60:40 (v/v) methanol:water.

The mobile phase was degassed by bubbling helium into it before use. The flow rate was 1.0 mL/min and the column back-pressures at this flow rate ranged from 1600 to 2200 psi. All compounds were dissolved in methanol to give concentrations of 0.02–0.1 mM. Typically 2 μL of these standard reference compounds were injected. The retention times and elution order were established from consecutive injections of the individual standards. The precision associated with the measured retention times for the various standards ranged from 5–10%. The wavelength utilized for detection was 290 nm. Since almost all ions and molecules, including the typical volume indicators, such as Cl^-, Br^-, I^- etc., partially bind to β-CD, they cannot be directly employed to determine column void volumes or times. For this reason, a special procedure by Hinze *et al.* (19) was used to estimate the void volume of the column which was found to be 3.1 mL at a flow rate of 1 mL/min.

HPLC grade methanol was obtained from Fisher Scientific Co., triethylamine from Aldrich and acetic acid from J. J. Baker Chemical Co. Water was deionized by passing distilled water through a Barnstead Water purification system. Biphenylol, biphenyldiol, chlorobiphenylol, and chlorobiphenyldiol standards were purchased from Chem Service.

Discussion

Effect of mobile-phase composition

The effect of mobile-phase composition on the capacity factor of biphenylols, chlorobiphenylols, and biphenyldiols was investigated by changing the methanol–water ratio in the mobile phase from 40/60 to 100/0 (v/v). In this set of experiments the mobile phase contained no buffer.

It was previously shown that a linear relationship exists between the log of the capacity factor, k, and the volume fraction of methanol in methanol/water mixtures used as mobile phases in reversed-phase chromatography (20–22). The shapes of plots such as these are assumed to be due to structural variations in the solvent system as the concentration of the organic modifier is changed. The fact that in the case of metha-

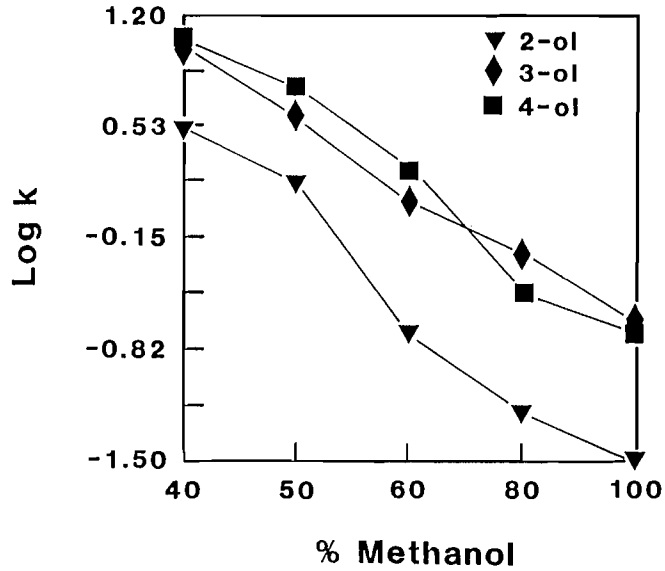

FIG. 2. Effect of mobile-phase composition on the logarithm of the capacity factor for biphenylols. Conditions: column, Cyclobond I (β-cyclodextrin bonded-phase); no buffer was used in the mobile phase; flow rate 1 mL/min; t_o = 3.1 min; ambient temperature.

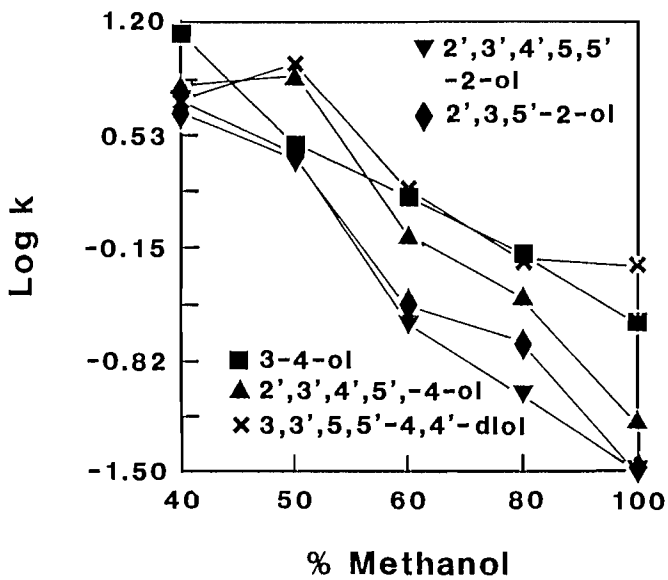

FIG. 3. Effect of mobile-phase composition on the logarithm of the capacity factor for chlorinated biphenylols. Conditions as in Fig. 2.

nol–water mixtures a linear relationship exists over almost the whole composition range was explained in terms of the ability of methanol to act as both a proton donor and acceptor (21).

By plotting log k vs. methanol content in the mobile phase for the various biphenylols, chlorobiphenylols, and biphenyldiols we found that the curves obtained are mostly linear (see Figs. 2–4) as would be expected if a reversed mechanism of retention was in operation. This is not the case, however, for 3,3′,5,5′-tetrachloro-4,4′-biphenyldiol, and 2′,3′,4′,5′ tetrachloro-4-biphenylol (see Fig. 3) which present local maxima at around 50% methanol. These maxima may be taken as suggestive evidence that in CD-bonded-phase chromatography one or more mechanisms of retention, in addition to the reversed-phase mechanism encountered with hydrocarbonaceous bonded-phases (hydrophobic interactions), may be in operation (e.g. van der

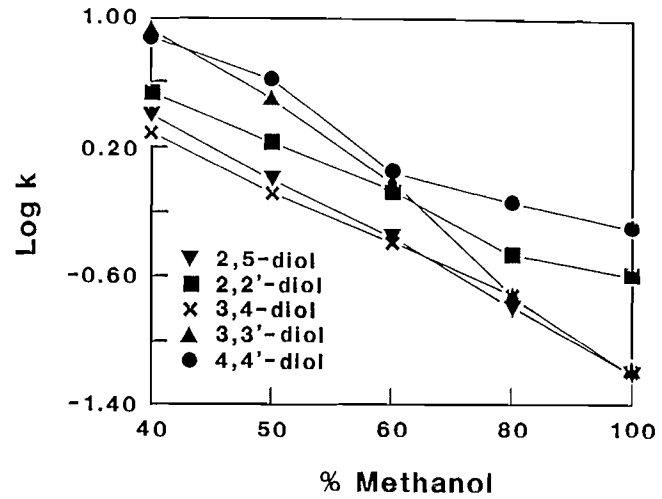

FIG. 4. Effect of mobile-phase composition on the logarithm of the capacity factor for biphenyldiols. Conditions as in Fig. 2.

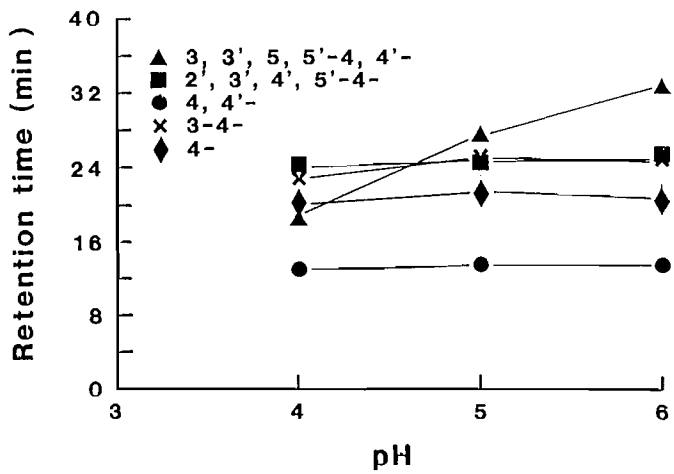

FIG. 5. Effect of pH on the retention time of diaromatic chlorophenols. Conditions: column, Cyclobond I (β-cyclodextrin bonded-phase); mobile phase, 50:50 methanol:water (0.01 M in triethylamine acetate buffer); flow rate: 1 mL/min; t_o = 3.1 mL; ambient temperature.

Waals interactions of the chlorine subtituents with the backbone of the cavity). Similar behaviour was observed by Chang and Wu (23) with nitrophenols, on a γ-CD column, with 2-propanol as the organic modifier and Paleologou *et al.* (1) with highly chlorinated monoaromatic chlorophenols, on a β-cyclodextrin column, with methanol as the organic modifier.

It should also be noted that for all biphenylols and particularly the more highly chlorinated ones, the shape of the peaks was affected by the mobile-phase composition; peaks became sharper (smaller width) as well as more symmetrical as the methanol content increased.

Effect of pH

The effect of pH on the retention time of biphenylols, chlorobiphenylols, and biphenyldiols was investigated by changing the pH of the aqueous part of the mobile phase (50/50: methanol/water) from 4 to 6 using triethylamine buffers (0.01 M). From plots of retention time vs. pH (e.g. see Fig. 5) it appears that for all compounds, except one, there is no change in retention time with pH in the range examined. This situation can be rationalized in terms of the pK_a's of these compounds (see Table 1). It should be pointed here that one can expect marked

Can. J. Chem. Downloaded from www.nrcresearchpress.com by 88.85.125.76 on 09/07/12
For personal use only.

TABLE 1. Diaromatic phenols and chlorophenols: retention parameters

No.	Compound	pK_a^a	t_R^b (min)	t_R^c (min)	ΔH^d (kcal/mol)
1	3,4-Biophenyldiol	9.3	5.6	4.0	—
2	2,5-Biphenyldiol	11.0	5.8	4.4	−7.2
3	2,2′-Biphenyldiol	9.4	6.1	4.7	—
4	3,3′-Biphenyldiol	10.0	9.6	6.1	−9.8
5	2-Biphenyldiol	10.9	9.4	7.8	—
6	2′,5′-Dichloro-2-biphenylol	11.0	9.3	8.8	−8.4
7	2′,3,5′-Trichloro-2-biphenylol	9.0	10.7	11.3	−10.5
8	4,4′-Dichloro-3,3′-biphenyldiol	8.3	10.8	11.3	−9.9
9	2′,3′,4′,5,5′-Pentachloro-2-biphenylol	9.6	12.1	12.7	—
10	4,4′-Biphenyldiol	10.0	13.0	12.7	−14.0
11	3-Biphenylol	10.6	16.3	14.1	−9.5
12	4-Biphenylol	10.2	20.1	16.7	−8.9
13	2′,3′,4′,5′-Tetrachloro-3-biphenylol	—	—	18.4	—
14	3-Chloro-4-biphenylol	8.6	22.7	19.2	−9.7
15	2′,3′,4′,5′-Tetrachloro-4-biphenylol	10.1	24.1	25.9	−8.5
16	3,3′,5,5′-Tetrachloro-4,4′-biphenyldiol	6.0	18.9	34.7	−13.6

[a]In 60:40 methanol:water.
[b]Retention time at pH = 4.0; t_0 = 3.1 mL.
[c]Retention time at gradient elution conditions; t_0 = 3.1 mL.
[d]In 50:50 methanol:water.

effects on the retention as long as the pH of the mobile phase is within one unit of the pK_a of a given compound.

All compounds examined, except one, have pK_a values which exceed the maximum of the pH range examined by more than one pH unit and therefore are expected to remain in their neutral form throughout this range. In the case of 3,3′,5,5′-tetrachloro-4,4′-biphenyldiol, however (see Fig. 5), an increase in retention time is observed with increasing pH. This change can also be rationalized on the basis of the pK_a of this compound (see Table 1) which is quite a bit lower than the rest of the chlorophenols (pK_a = 6.0). It should be remembered at this point that binding to the CD lowers the pK_a's of chlorophenols (24) and therefore brings them closer to the pH range examined. Furthermore, since the mobile phase contains methanol, the apparent pH of the mobile phase is actually higher than that of the aqueous phase (25); these two effects are likely to position the pK_a of 3,3′,5,5′-tetrachloro-4,4′-biphenyldiol well within the limits of the pH range examined; this is probably the reason that the effect of pH on retention begins quite early on (see Fig. 5). The increase in retention time with increasing pH for 3,3′,5,5′-tetrachloro-4,4′-biphenyldiol confirms an earlier observation (1) that the chlorophenolate anions bind to the CD more tightly than the corresponding neutral forms. No reasonable explanation has yet been provided in the literature concerning this unusual phenomenon.

At pH = 4.0 all diaromatic phenols and chlorophenols are expected to be in their neutral form and therefore, valid comparisons can be made between these and the monoaromatic chlorophenols (1), under the same conditions, regarding the extent of their participation in the inclusion process. Table 1 presents the retention times of all diaromatic phenols under these conditions.

The biphenylols elute in the order 4- >3- >2- analogous to the monochlorophenols which also elute in this same order (1). This is likely to be due to the linear geometry of the 4-substituted analogs which allows full penetration into the CD cavity both ways along the axis of symmetry of the molecule (assuming that the aromatic C—OH bond lies on this axis). In such a case the β-CD cavity sees a diameter (projected width) of 4.3 Å and therefore this molecule can very easily enter this cavity from end to end. The 3-substituted analogs, on the other hand, can penetrate the cavity to a limited extent because of the phenyl substituent at the 3-position; in this case the CD cavity sees a diameter of 7.9 Å which is slightly larger than the diameter of the opening of the CD cavity itself. The 2-substituted analogs limit penetration even further because of the closeness of the phenyl substituent to the —OH group since the cavity still sees a diameter of 7.9 Å We previously showed that monoaromatic chlorophenols which have a substituent in the 2- or 6-position, and especially both these positions, present low retention times as compared to 4-substituted monoaromatic chlorophenols (1). Similar behaviour was also observed by Chang *et al.* (26) for the positional isomers of cresol and chlorophenol regardless of mobile phase composition and for nitrophenols when the methanol content in the mobile phase is less than 30%. The validity of these assumptions was confirmed by Armstrong (27) who used X-ray crystal structures (28–30) for the production of computer projected images of inclusion complexes of *o*-, *m*-, and *p*-nitrophenol and other isomers with α-CD as well as β-CD.

The retention time for 4-biphenylol is significantly higher than that of 4-chlorophenol (20.1 vs. 6.5 min). This can be rationalized in terms of the whole molecule (both benzene rings) entering the CD cavity and interacting with it. Since, in fact, one ring is at a slight angle with respect to the other (15, 16), it is likely that the two rings interact differently with the cavity and probably in a complementary fashion. The retention time for 3-biphenylol is also significantly higher than that of 3-chlorophenol (16.3 vs. 6.2 min). If this molecule were to be entering the cavity with the —OH group first, at all times, then one would expect a retention time similar to 3-chlorophenol since only one of the two benzene rings would have entered the CD cavity and this only partially. It, therefore, appears that the cavity can also be entered by way of the unsubstituted benzene ring. The high retention time of 2-biphenylol as compared to 2-chlorophenol (9.4 vs. to 5.8 min) can be rationalized using a similar argument.

Can. J. Chem. Downloaded from www.nrcresearchpress.com by 88.85.125.76 on 09/07/12
For personal use only.

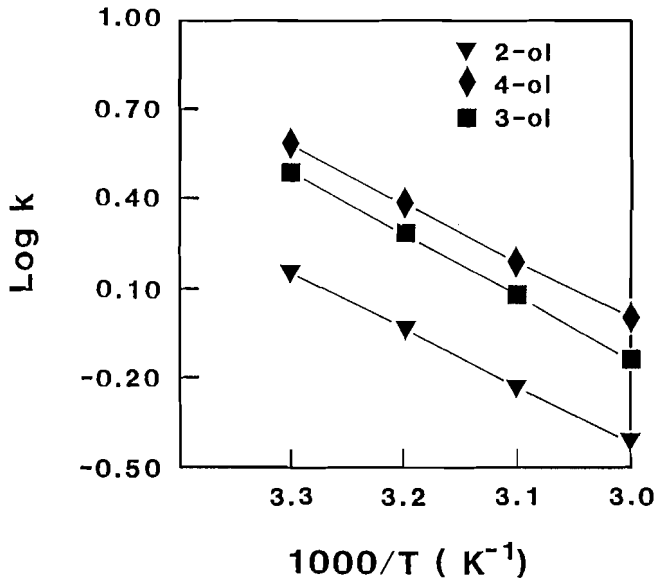

FIG. 6. van't Hoff plot for the retention of biphenylols in the 30–60°C temperature range. Conditions: column, Cyclobond I (β-cyclodextrin bonded-phase); mobile phase, 50:50 methanol:water (no buffer was used in the mobile phase); flow rate, 1 mL/min; t_o = 3.1 mL.

In the case of chloro-substituted biphenylols the following observations can be made regarding their retention behaviour. For 3-chloro-4-biphenylol, for example, the retention time is very similar to 4-biphenylol (22.7 vs. 20.1 min); this may be ascribed to the linear geometry of both these molecules which can allow full penetration into the cavity as illustrated above. The retention time is slightly higher in the former case because of the closer fit of one of the two benzene rings into the CD cavity as a result of the chlorine substituent; the cavity in the latter case sees a diameter of 5.64 Å as compared to 4.26 Å in the former case. Chlorine, as well as other substituents, are also known to affect the angle between the two benzene rings in biphenyl-type compounds (17), thereby leading to a three-dimensional interaction with the cavity. For 2′,3′,4′,5′-tetrachloro-4-biphenylol the retention time is even higher (24.1 min) probably due to the increased interactions between the second benzene ring and the cavity because of its numerous chlorine substituents; the cavity sees a diameter of 7.03 Å in this case, suggesting an almost perfect fit in the cyclodextrin cavity. A similar argument can be made to justify the greater retentions times of 2′,3′,4′,5′-tetrachloro-3-biphenylol (d = 7.03 Å for that part of the molecule that can enter the CD cavity, t_R = 20.5 min) as compared to 3 biphenylol (d = 4.26 Å, t_R = 16.3 min) and 2′,3,5′-trichloro-2-biphenylol (d = 7.03 Å, t_R = 10.7 min) and 2′,3′,4,5,5′-pentachloro-2-biphenylol (d = 7.03 Å, t_R = 12.1 min) as compared to 2-biphenylol (d = 4.26 Å, t_R = 9.4 min). In the case of biphenyls hydroxylated in the 2-position, only one benzene ring is likely to enter the cavity at a time and therefore, these retention times are likely to reflect, to some extent, weighted averages of the retention times of the corresponding monoaromatic chlorophenols and chlorobenzenes.

Effect of temperature

The effect of temperature on the retention time of biphenylols, chlorobiphenylols, and biphenyldiols was investigated in the temperature range 20–60°C with a mobile phase that was 50/50 (v/v) methanol:water. In this set of experiments the mobile phase contained no buffer. In all cases a decline in retention time with increasing temperature is observed (e.g. see Fig. 6 for biphenylols). This is likely to follow the decrease in the binding constant to the β-CD with increasing temperature. The temperature effect appears to increase in the order biphenyldiols<biphenylols<chlorobiphenylols. Moreover, the decline in retention with temperature is quite regular suggesting the same mechanism of retention at different temperatures for any given compound. An exception to this trend is 3,3′,5,5′-tetrachloro-4,4′-biphenyldiol that presents very high retention times for temperatures below 40°C.

The effect of temperature on retention is largely determined by the enthalpy of eluite interaction with the stationary phase. The enthalpy can be evaluated from the slope of van't Hoff plots, that is plots of log k versus the reciprocal of the absolute temperature (31, 32). When the equilibrium for eluite binding by the stationary phase can be written in terms of a single eluite species and a single bound species, then the enthalpy of this particular binding process is easily obtained. Figure 6 presents van't Hoff plots for the three biphenylols. Since all three of these compounds as well as all other diaromatic chlorophenols, except one, present pK_a's significantly above the pH of the mobile phase, a single eluite species and a single bound species is likely to exist. In addition, since these plots are quite linear, it is possible to determine the enthalpy of binding from the slope of the van't Hoff plots. These values are given in Table 1. From the intercept of van't Hoff plots it is theoretically possible to calculate the change in the corresponding entropy as well. This is difficult, however, because with bonded phases the phase ratio cannot be clearly defined (31). Given the relative bulkiness of biphenylols (4.26 Å projected diameter, assuming that one ring enters the cavity) and especially substituted biphenylols (5.64 to 7.03 Å depending on number and position of substituents) in comparison to the diameter of the β-CD cavity (7.8 Å at the front and 6 Å at the back) it is likely that the complexation is mostly governed by enthalpy and not entropy (33). This is because of the increased contribution or van der Waals interactions ($\Delta H<0$, $\Delta S<0$) in the binding process. Among the binding forces proposed for inclusion phenomena only hydrophobic interactions are governed by entropy. These would be of significance only in the case of relatively small substrates. Evidence supporting this hypothesis is also provided by gas chromatography using β-CD as the stationary phase (34) and di- and tri-substituted benzenes as the substrates; the retention and selectivity are quite appreciable despite the complete absence of hydrophobic interactions.

Deviations from linearity do exist for some of these compounds (e.g. 2,5-biphenyldiol, 2′,5′-dichloro-2-biphenylol, 4,4′-biphenyldiol, 4,4′-dichloro-3,3′-biphenyldiol and 3,3′,5,5′-4,4′-biphenyldiol). Non-linear van't Hoff plots in RPC can be expected whenever one of the following three conditions hold (31): (*1*) the eluite exists in two or more forms having different capacity factors; (*2*) the eluite is retained by two or more mechanisms due to the heterogeneity of the stationary phase surface containing more than one type of binding site; (*3*) eluite exists in more than one form and the surface is heterogeneous.

In the case of 2,5-biphenyldiol, for example, the non-linear van't Hoff plot is likely to be due to condition (*2*) being in effect. At T = 40°C ($10^3/T$ = 3.20) a break is observed in its van't Hoff plot. This break is likely to correspond to the dissociation of the CD-2,5-biphenyldiol complex at this temperature. 2,5-Biphenyldiol is not likely to fully enter the cavity because it has a phenyl substituent *ortho*- to one of the hydroxyl groups. Other biphenyldiols (e.g. 4,4′-) present breaks at a higher temperature (50°C) while the remaining ones present quite linear behaviour throughout the temperature range exam-

Can. J. Chem. Downloaded from www.nrcresearchpress.com by 88.85.125.76 on 09/07/12
For personal use only.

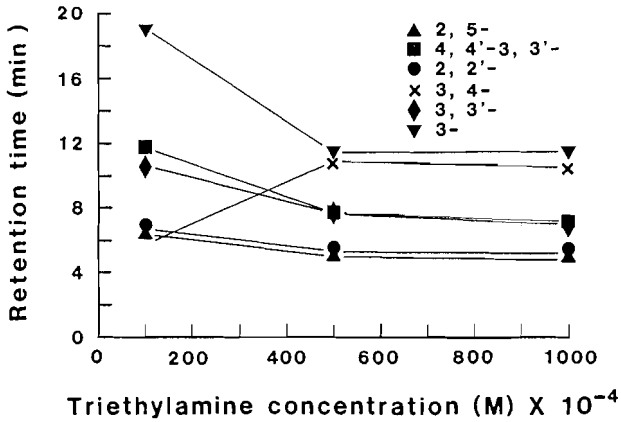

FIG. 7. Effect of ionic strength on the retention time of diaromatic chlorophenols. Conditions: column, Cyclobond I (β-cyclodextrin bonded-phase); mobile phase, 50:50 methanol:water (buffered to pH = 4.0 with triethylamine acetate); flow rate, 1 mL/min; t_o = 3.1 mL; ambient temperature.

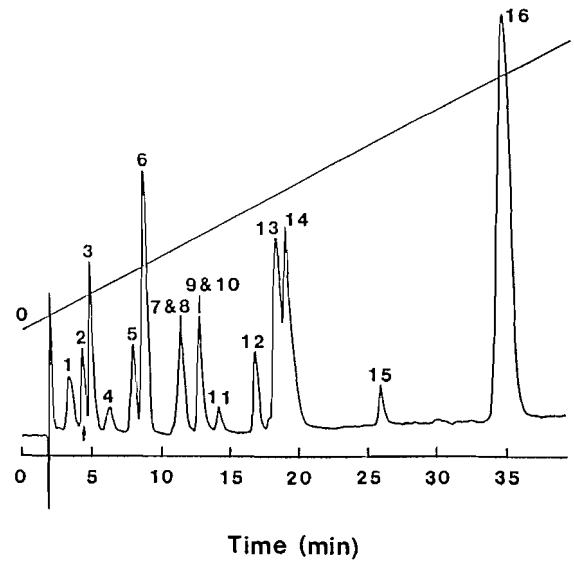

FIG. 8. Gradient elution separation of diaromatic chlorophenols. Bands are identified in Table 1. Conditions: column, Cyclobond I (β-cyclodextrin bonded-phase); mobile phase gradient, 27–73% methanol/aqueous buffer (0.01 M triethylamine acetate, pH = 4.0); flow rate, 1.0 mL/min; T: 50°C; detector, UV at 280 nm.

ined. From the above observations it appears that the inclusion mechanism of retention in CD-bonded phase RPC, affects the shape of van't Hoff plots. Non-linear van't Hoff plots on a β-CD column were also obtained by Issaq *et al.* (13) with various amino acids and Paleologou *et al.* (1) with some monoaromatic chlorophenols.

In the case of 3,3',5,5'-tetrachloro-4,4'-biphenyldiol the van't Hoff plot is also non-linear. The curvature in this plot is likely to be due to condition (3) being in effect since the pK_a of this compound is close to the pH of the mobile phase; this means that the eluite species is likely to exist in two forms (non-ionized and ionized). Since in the case of this compound there was more than one kind of eluite species, the van't Hoff plot yielded the overall retention enthalpy which is a weighted average of the enthalpies for the binding of the species. Similar behaviour was previously observed in the case of most monoaromatic tri-, tetra-, and pentachlorophenols with pK_a's close to the pH of the mobile phase (1). No enthalpies of binding were calculated for those compounds whose van't Hoff plots did not present any appreciable degree of linearity. Selectivity is affected very slightly, if at all, by changing the temperature. In this regard β-CD columns appear to behave like other reversed-phase columns (35).

Effect of ionic strength

The effect of ionic strength on the retention time of biphenylols and chlorobiphenylols was investigated in the concentration range of 0.01 to 0.1 M triethylamine–acetate (for aqueous part of mobile phase pH = 4.0) in a 50/50 methanol:water mobile phase. In the case of biphenyldiols (see Fig. 7) an initial decline in retention is observed in the electrolyte concentration range between 0–0.05 M followed by a plateau in the 0.05–0.1 M range. The effect of ionic strength on biphenylols and chlorobiphenylols is similar to that observed; in the case biphenyldiols, it is, however, more pronounced. An exception to the above behaviour is presented by 3,4-biphenyldiol whose retention increases in the 0.01–0.05 M ionic strength range while stabilizing in the 0.05–0.10M range. This phenomenon is likely to be due to the disruption of intramolecular hydrogen bonding in this compound by increasing ionic strength and the resulting increased interaction of its hydroxyls with the secondary hydroxyls at the periphery of the cavity; as a result of their electrical charge, both the triethylammonium cation and the acetate anion can be expected to be involved in the formation of more powerful hydrogen bonds with a given aromatic hydroxyl as compared to such a bond with an adjacent neutral hydroxyl (36).

Resolution is also affected by ionic strength. The peak shapes of chlorophenols and especially the most chlorinated ones, become sharper (shorter width) and more symmetrical with increasing buffer concentration. The selectivity of the separation of chlorophenols is affected very slightly, if at all, by the ionic strength as evidenced by the absence of any changes in the elution order of chlorophenols with increasing ionic strength. Since the presence of an electrolyte in the mobile phase does not affect the selectivity. it is possible to couple the β-CD bonded-phase column with an electrochemical detector (2).

Horvath *et al.* (37) showed that in RPC employing hydrocarbonaceous bonded phases, increasing ionic strength augments the capacity factors of neutral solutes. This effect has been ascribed to the increasing surface tension of the eluent and the concomitant increase in the energy required for cavity formation (38). As seen in Fig. 7, however, exactly the opposite behaviour is observed in the case of a CD-bonded silica stationary phase. This type of behaviour was previously encountered with monoaromatic chlorophenols as well and was rationalized in terms of the triethylamine cations including into the cavity thus competing with the substrate molecules (1).

Separation

After studying the liquid chromatographic retention behaviour of diaromatic chlorophenols with respect to mobile-phase composition, pH, temperature and ionic strength conditions were chosen for the isocratic separation of these compounds. Even though each category of chlorobiphenylols (2-, 3-, 4-) could be separated into its member components with reasonable resolution and selectivity, significant overlaps existed between the retention time ranges of the various categories which prevented the isocratic separation of all chlorophenols on the same chromatogram. A gradient-elution separation was, therefore, attempted.

Table 1 and Fig. 8 present the retention times and the gradient-elution separation, respectively, of 14 out of the 16 diaromatic chlorophenols within 35 minutes of injection of the mixture.

Can. J. Chem. Downloaded from www.nrcresearchpress.com by 88.85.125.76 on 09/07/12
For personal use only.

This separation was achieved with a linear mobile phase gradient of 1%/min increase in methanol (solvent B) beginning with a 27:73 methanol/water (solvent A) mobile phase. The temperature was 50°C, the buffer concentration 0.01 M triethylamine acetate (TEAA) and the pH = 4.0. The design of this gradient was based on our previous experience with the gradient elution separation of monoaromatic chlorophenols on a β-CD column (2). We have thus established in this paper that the well-known selectivity of CD columns can be extended to polysubstituted and non-substituted diaromatic phenols such as the chlorinated and non-chlorinated biphenylols and biphenyldiols.

Acknowledgement

The authors are indebted to the Natural Sciences and Engineering Research Council of Canada for financial support of this work.

1. M. Paleologou, S. Li, and W. C. Purdy. J. Chromratogr. Sci. In press.
2. M. Paleologou, S. Li, and W.C. Purdy. J. Chromratogr. Sci. In press.
3. D. W. Armstrong. J. Liq. Chromatogr. **7**(S-2): 353 (1984).
4. F. Cramer and W. Kampe. J. Am. Chem. Soc. **87**, 1115 (1965).
5. R. L. VanEtten, J. F. Sebastian, G. A. Clowes, and M. L. Bender. J. Am. Chem. Soc. **89**, 3242 (1967).
6. I. Tabushi, Y. Kiyosuke, T. Sugimoto, and K. Yamamura. J. Amer. Chem. Soc. **100**, 916 (1978).
7. M. Komiyama and M. L. Bender. J. Am. Chem. Soc. **100**, 2259 (1978).
8. W. Hinze. Sep. Purif. Methods. **10**(2). 159 (1981).
9. K. Fujimura, T. Ueda, and T. Ando. Anal. Chem. **55**, 446 (1983).
10. Y. Kawaguchi, M. Tanaka, M. Nakae, K. Funazo, and T. Shono. Anal. Chem. **55**, 1852 (1983).
11. D. W. Armstrong, W. DeMond, A. Alak, W. L. Hinze, T. E. Riehl, and K. H. Bui. Anal. Chem. **57**, 234 (1985).
12. D. W. Armstrong and W. J. DeMond. J. Chromatogr. Sci. **22**, 411 (1984).
13. H. J. Issaq, M. L. Glennon, D. E. Weiss, and S. D. Fox. *In* Ordered media in chemical separations. *Edited by* W. Hinze and D. W. Armstrong. Am. Chem. Soc. Washington, DC. 1987. pp. 260–271.
14. D. E. Weaver and R. B. L. van Lier. Anal. Biochem. **154**, 590 (1986).
15. R. M. Barret and D. Steele. J. Mol. Struct. **11**, 105 (1972).
16. E. D. Schmid and B. Broza. J. Chem. Phys. **56**, 6267 (1972).
17. K. L. E. Kaiser. Environ. Pollut. **7**, 93 (1974).
18. S. Li, M. Paleologou, and W.C. Purdy. Can. J. Chem. To be published.
19. W. L. Hinze, T. E. Riehl, D. W. Armstrong, W. DeMond, A. Alak, and T. Ward. Anal. Chem. **57**, 247 (1985).
20. K. Karch, I. Sebastian, I. Halasz, and H. J. Englehardt. J. Chromatogr. **122**, 171 (1976).
21. B. L. Karger, J. R. Gant, A. Hartkopf, and P. H. Weiner. J. Chromatogr. **128**, 65 (1976).
22. L. R. Snyder, J. W. Dolan, and J. R. Gant. J. Chromatogr. **165**, 3 (1979).
23. C. A. Chang and Q. Wu. Anal. Chim. Acta. **189**, 293 (1986).
24. K.A. Connors and J. M. Lipari. J. Pharm. Sci. **65**, 379 (1976).
25. R. G. Bates. CRC Critical Rev. Anal. Chem. 247 (1981).
26. C. A. Chang, Q. Wu, and D.W. Armstrong. J. Chromatogr. **354**, 454 (1986).
27. R. D. Armstrong. *In* Ordered media in chemical separations. *Edited by* W. Hinze and D. W. Armstrong. Am. Chem. Soc. Washington, DC. 1987. pp. 272–279.
28. K. Harata, U. Hisahi, and J. Tanaka. Bull. Chem. Soc. Jpn. **51**, 1627 (1978).
29. K. Harata. Bull. Chem. Soc. Jpn. **51**, 1416 (1977).
30. F. Iwqsaki and Y. Kawano. Acta Crystallogr. **34**, 1286 (1977).
31. W.R. Melander and C. Horvath. *In* High performance liquid chromatography — advances and perspectives. Vol. 2. *Edited by* C. Horvath. Academic Press, New York, NY. 1980. pp. 113–319.
32. L. R. Snyder. J. Chromatogr. **179**, 167 (1979).
33. Y. Matsui and K. Mochida. Bull. Chem. Soc. Jpn. **52**(10). 2808 (1979).
34. E. Smolkova-Keulemansova and L. Sojak. *In* Ordered media in chemical separations. *Edited by* W. Hinze and D. W. Armstrong. Am. Chem. Soc. Washington, DC. 1987. pp. 247–259.
35. H. Colin, J. C. Diez-Masa, G. Guiochon, T. Czajkowska, and I. Miedziak. J. Chromatogr. **167**, 41 (1978).
36. J. T. Edsall. *In* Biophysical chemistry. Vol. 1. Academic Press Inc., New York, NY. 1958. pp. 62–63.
37. C. Horvath, W. Melander, and I. Molnar. Anal. Chem. **49**, 142 (1977).
38. C. Horvath, W. Melander, and I. Molnar. J. Chromatogr. **125**, 129 (1976).

Can. J. Chem. Downloaded from www.nrcresearchpress.com by 88.85.125.76 on 09/07/12
For personal use only.

Minor saponins from the starfish *Asterias forbesi*

JOHN A. FINDLAY AND ZHENG-QUAN HE
Department of Chemistry, University of New Brunswick, Fredericton, N.B. Canada E3B 6E2

AND

BARBARA BLACKWELL
Plant Research Centre, Research Branch, Ottawa, Ont., Canada K1A 0C6

Received January 18, 1990

This paper is dedicated to Professor Arthur S. Perlin on the occasion of his 67th birthday

JOHN A. FINDLAY, ZHENG-QUEN HE, and BARBARA BLACKWELL. Can. J. Chem. **68**, 1215 (1990).

The structures of three new saponins from the starfish *Asterias forbesi* have been elucidated by spectroscopic means. Forbeside F is the hydrate of the monosodium salt of 6α-*O*-{β-D-fucopyranosyl(1→4)-*O*-[β-D-quinovopyranosyl(1→2)]-*O*-β-D-quinovopyranosyl(1→3)-*O*-6-deoxy-β-D-xylo-hexos-4-ulopyranosyl}-20*S*-hydroxy-3β-sulfo-oxy-5α-cholest-9(11)-en-23-one. Forbeside G is the hydrate of the monosodium salt of 6α-*O*-{[β-D-quinovopyranosyl(1→2)]-*O*-β-D-quinovopyranosyl(1→3)-*O*-6-deoxy-β-D-xylo-hexos-4-ulopyranosyl}-20*S*-hydroxy-3β-sulfo-oxy-5α-cholest-9(11)-en-23-one. Forbeside H is the monosodium salt of 6α-*O*-{[β-D-quinovopyranosyl(1→2)]-β-D-xylopyranosyl(1→3)-β-D-quinovopyranosyl}-20*S*-hydroxy-3β-sulfo-oxy-5α-cholest-9(11)-en-23-one.

Key words: *Asterias forbesi*; forbesides F, G, and H; starfish saponins; sterol glycosides.

JOHN A. FINDLAY, ZHENG-QUEN HE et BARBARA BLACKWELL. Can. J. Chem. **68**, 1215 (1990).

En se basant sur des méthodes spectroscopiques, on a élucidé les structures des trois nouvelles saponines isolées de l'étoile de mer *Asterias forbesi*. Le forbeside F est l'hydrate du sel de monosodium de la 6α-*O*- (β-D-fucopyranosyl(1→4)-*O*-[β-D-quinovopyranosyl(1 → 2)]-*O*-β-D-quinovopyranosyl(1 → 3)-*O*-6-désoxy-β-D-xylo-hexos-4-ulopyranosyl)-20*S*-hydroxy-3β-sulfo-oxy-5α-cholest-9(11)-èn-23-one. Le forbeside G est l'hydrate du sel de monosodium de la 6α-*O*([β-D-quinovopyranosyl(1→2)]-*O*-β-quinovo pyranosyl(1 → 3)-*O*-6-désoxy-β-D-hexos-4-ulopyranosyl}-20*S*-hydroxy-3β-sulfo-oxy-5α- cholest-9(11)-èn-23-one. Le forbeside H est le sel de monosodium de la 6α-*O*([β-D-quinovopyranosyl(1→2)]-β-D-xylopyranosyl(1→3)-β-D-quinovopyranosyl)-20*S*-hydroxy-3β-sulfo-oxy-5α-cholest-9(11)-èn-23-one.

Mots clés : *Asterias forbesi*; forbesides F, G et H; saponines de l'étoile de mer; stérol glycosides.

[Traduit par la revue]

Recently we reported (1, 2) the structures of three major saponins, designated forbesides A, B, and C, from the starfish *Asterias forbesi* (Desor). These were deduced totally by spectroscopic means. We now report the isolation from the same source of three new saponins, two of which, F and G, are structurally related to forbeside C, **1**, and the third, H, to forbeside A, **4**.

The FAB^+ mass spectrum of forbeside F, **2**, displays a prominent pseudomolecular ion at m/z 1159 corresponding to M^+ ($C_{51}H_{83}O_{24}SNa$) + 2H + Na and major fragments at m/z 1039 ($M^+ - NaSO_4 + Na + H$) and 623 (M^+ − aglycone − H + Na). Substantial fragments at m/z 477 (623−146), 331 (477−146), and 185 (331−146) attest to the attachment of three deoxyhexose units. The ^{13}C nmr spectrum indicates a total of 51 carbons, 27 of which were readily assigned to the thornasterol-3-*O*-sulfate aglycone by comparison of chemical shift and multiplicity with those of forbeside C (see Table 1). In addition to featuring four anomeric carbon signals, the downfield region displays signals at δ 90.4 and 92.7 ppm, the unusual chemical shifts associated with carbons 3 and 4, respectively, of the unique hydrated form of the 6-deoxy-xylo-4-hexulose unit as found in forbeside C. A comparison of the remaining chemical shifts shows a remarkably close correspondence of all the carbohydrate carbon signals with those of forbeside C, **1**, except for the signals assigned to the terminal fucose and the signal at δ 81.6 ppm assigned to the glycosidic linked C2 of the non-terminal fucose unit of the latter. Instead, forbeside F displays a signal at δ 73.7 ppm appropriate for C2 of a β-linked fucose unit. Hence we tentatively formulated forbeside F as **2**. Corroboration of this conclusion was obtained from 500 MHz 2D ^1H–^1H COSY and 2D hydrogen carbon correlation (HETCOR)

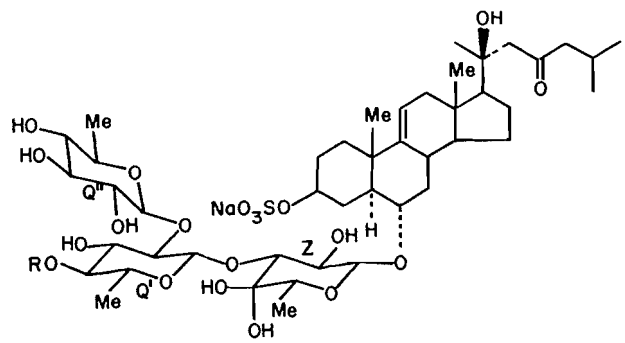

1, FORBESIDE C R =

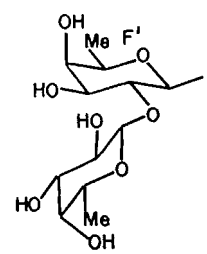

2, FORBESIDE F R =

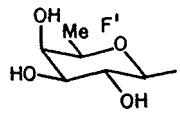

3, FORBESIDE G R = H

Can. J. Chem. Downloaded from www.nrcresearchpress.com by 88.85.125.76 on 09/07/12
For personal use only.

Can. J. Chem. Downloaded from www.nrcresearchpress.com by 88.85.125.76 on 09/07/12
For personal use only.

TABLE 1. Comparative ^{13}C chemical shifts (δ, ppm) for forbeside C, **1**; F, **2**; G, **3**; A, **4**; H, **5** in pyridine-d_5/D_2O (5:1)

	1[a]	**2**[b]	**3**[b]		**4**[c]	**5**[d]
1	35.9	35.9	35.3		35.8	35.4
2	29.2	29.2	28.6		28.8	28.7
3	78.0	78.2	77.8		77.9	77.7
4	30.6	30.6	30.0		30.3	30.1
5	49.1	49.0	48.4		48.3	48.5
6	79.9	79.9	79.4		80.3	79.5
7	41.2	41.2	40.9		40.9	40.7
8	35.3	35.3	34.7		35.2	34.8
9	145.4	145.4	144.8		145.3	144.9
10	38.3	38.2	37.8		38.2	37.8
11	116.7	116.7	116.2		116.9	116.2
12	42.3	42.3	41.8		42.4	41.9
13	41.5	41.5	40.6		41.5	41.0
14	54.0	53.9	53.4		54.0	53.5
15	23.2	23.2	22.7		23.2	22.8
16	25.1	25.1	24.5		25.0	24.6
17	59.2	59.1	58.5		58.7	58.7
18	13.6	13.6	13.0		13.6	13.1
19	19.3	19.5	18.7		19.3	18.8
20	73.9	73.9	73.6		73.7	73.5
21	26.7	26.8	26.2		26.6	26.3
22	55.2	55.3	54.8		55.3	54.8
23	212.3	212.3	212.5		212.0	212.5
24	53.9	53.9	53.4		53.9	54.8
25	24.6	24.5	24.0		24.7	24.0
26	22.6	22.6	22.1		22.7	22.2
27	22.5	22.5	22.0		22.6	22.0
Z1	104.5	104.8	103.8	Q1	103.7	103.5
2	73.1	73.1	73.0	2	73.7	73.5
3	90.4	90.4	90.0	3	88.5	88.9
4	92.7	92.7	92.2	4	74.1	73.8
5	73.1	72.1	72.6	5	71.9	71.5
6	13.4	13.4	12.9	6	17.9	17.7
Q'1	103.5	104.4	103.2	X1	105.1	103.6
2	83.4	83.4	83.9	2	81.6	83.6
3	74.7	74.9	74.8	3	75.0	75.1
4	84.8	84.5	73.4	4	79.4	69.5
5	73.1	73.5	72.2	5	64.0	66.1
6	18.0	18.1	17.5	Q''1	105.1	105.2
Q''1	105.8	105.7	105.2	2	75.4	75.4
2	76.0	75.9	75.3	3	76.1	76.4
3	76.5	76.5	75.9	4	75.4	76.3
4	75.5	75.5	74.9	5	73.5	73.4
5	73.9	74.0	73.4	6	18.4	18.1
6	18.0	17.6	17.2			
F'1	102.3	103.4				
2	81.6	73.7				
3	74.5	74.4				
4	71.6	71.8				
5	71.6	71.5				
6	16.6	16.7				

[a]From ref. 2.
[b]Assignments by comparison with **1** assisted by 500 MHz HETCOR data.
[c]By comparison with assignments for versicoside A in pyridine-d_5 (5).
[d]Assignments by comparison with **4** assisted by 500 MHz HETCOR data.

TABLE 2. Comparative ^1H nmr chemical shifts (δ, ppm) for sugars in forbeside C, **1**; F, **2**; G, **3**; A, **4**; H, **5** in pyridine-d_5/D_2O (5:1)

	1[a]	**2**[b]	**3**[b]		**4**[c]	**5**[b]
Z 1	4.99	5.01	5.03	Q'1	4.83	4.92
2	4.33	4.33	4.35	2	3.98	4.00
3	4.07	4.12		3	3.89	3.97
4				4	3.56	3.61
5	3.99	3.98	4.00	5	3.71	3.81
6	1.77	1.77	1.80	6	1.59	1.65
Q'1	5.11	5.08	5.06	X1	5.07	5.09
2	3.96	3.95	4.03	2	4.00	4.00
3	4.16	4.15	4.11	3	4.22	4.24
4	3.57	3.61	3.86	4	4.22	4.19
5	3.99	3.90	3.71	5α	3.79	3.77
6	1.72	1.71	1.83	5β	4.41	4.08
Q''1	5.06	5.08	5.05	Q''1	5.16	5.14
2	3.99	4.01	3.92	2	4.06	4.04
3	4.08	4.08	4.22	3	4.09	4.14
4	3.86	3.85	3.62	4	3.95	3.90
5	3.68	3.70	3.85	5	3.69	3.76
6	1.83	1.84	1.52	6	1.83	1.84
F'1	4.84	4.82				
2	4.41	4.33				
3	4.18	4.19				
4	4.08	4.10				
5	3.93	4.01				
6	1.48	1.51				

[a]From ref. 2.
[b]Assignments from 500 MHz ^1H–^1H COSY data.
[c]From ref. 1.

experiments, which permitted rigorous assignment of ^1H chemical shifts for the tetrasaccharide side chain that are in excellent agreement with those assigned to the first four sugars of forbeside C, **1** (Table 2). The assignments and connectivity of the latter were determined by nOe difference experiments in conjunction with ^1H–^1H COSY and 2D relayed coherence transfer (2D-RCT) experiments. Thus forbeside F is the hydrate of the monosodium salt of 6α-*O*-(β-D-fucopyranosyl(1→4)-*O*-[β-D-quinovopyranosyl(1→2)]-*O*-β-D-quinovopyranosyl-(1→3)-*O*-6-deoxy-β-D-xylo-hexos-4-ulopyranosyl)-20*S*-hydroxy-3β-sulfo-oxy-5α-cholest-9(11)-en-23-one, **2**.

Forbeside G displays a weak ion (3%) *m/z* 987 corresponding to M^- ($C_{45}H_{73}O_{20}SNa$) − H and a prominent *m/z* 965 (82%) ion corresponding to M^- − Na in the FAB^- mass spectrum. Other prominent ions at *m/z* 947 (965 − H_2O), 865 (965 − $C_6H_{12}O$ side chain by reverse aldol), 847 (865 − H_2O), 511 (aglycone + H − Na), 493 (511 − H_2O), 411 (511 − $C_6H_{12}O$), and 393 (411 − H_2O) are consistent with formulation **3**. The ^{13}C nmr spectrum revealed the presence of 45 carbons, 27 of which were assignable to the thornasterol-3-*O*-sulfate aglycone and the remaining 18 to the oligosaccharide moiety. As in the case of forbesides C and F, two distinctive signals could be assigned to C3 (δ 90.0 ppm) and C4 (δ 92.7 ppm) of the hydrated form of a 6-deoxy-xylo-4-hexulose unit Z. Examination of the ^1H–^1H COSY spectrum of forbeside G permitted assignment of ^1H signals for each of the quinovose units Q', Q'' and unit Z. HETCOR data allowed assignment of the ^{13}C signals for the trisaccharide side chain. The close correlation of ^{13}C and ^1H signals with their counterparts in forbesides C and F except for Q'4 leaves no doubt that forbeside G possesses structure **3**, the hydrate of the monosodium salt of 6α-*O*-{[β-D-quinovopyranosyl(1→2)]-*O*-β-D-quinovopyranosyl(1→3)-*O*-6-deoxy-β-D-xylo-hexos-4-ulopyranosyl}-20*S*-hydroxy-3β-sulfo-oxy-5α-cholest-9(11)-en-23-one.

The base peak of the FAB^- mass spectrum of forbeside H is at *m/z* 935, corresponding to M^- ($C_{44}H_{71}O_{19}SNa$) − Na. Significant ions also appear at *m/z* 957 (M^- − H), 835 (935 − $C_6H_{12}O$), 917 (935 − H_2O), 511 (aglycone + H − Na), 411 (511 − $C_6H_{12}O$), and 393 (411 − H_2O) showing parallel fragmentation to that of forbeside G. Inspection of the ^{13}C nmr

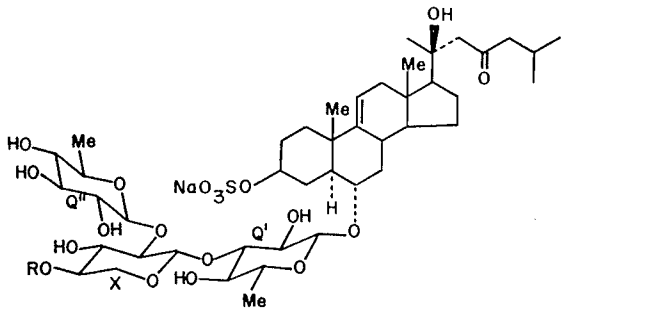

4, FORBESIDE A R =

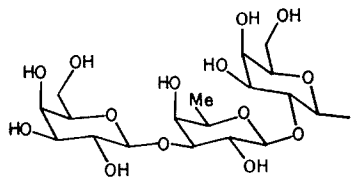

5, FORBESIDE H R = H

spectrum showed the high field region to be identical to that of forbeside G (see Table 1); thus they must share the same aglycone. Confirmation of a trisaccharide side chain in forbeside H was confirmed by the presence of signals for three anomeric protons plus signals appropriate for two 6-deoxy hexose units and a pentapyranose in addition to those assigned to the aglycone. The 500 MHz ^1H–^1H COSY data allowed assignment of ^1H chemical shifts for each sugar unit and allowed their identification as two quinovose units and a xylose moiety from signal multiplicity and J values. A HETCOR experiment permitted assignment of ^{13}C signals in the trisaccharide chain and revealed the location of interglycosidic linkages via glycosylation shifts. Comparison of ^{13}C chemical shifts with those assigned to forbeside A showed a close correlation for all signals due to the aglycone and the first three sugars except for the X4 signal, which appears at δ 79.4 ppm in the latter since it is a site of interglycosidic linkage and at δ 69.5 ppm in forbeside H. Thus we conclude that forbeside H has structure **5**, the monosodium salt of 6α-*O*-{[β-D-quinovopyranosyl(1 → 2)]-β-D-xylopyranosyl(1→3)-β-D-quinovopyranosyl}-20*S*-hydroxy-3β-sulfo-oxy-5α-cholest-9(11)-en-23-one.

We are not aware of any previous reports of asterosaponins possessing a tetrasaccharide side chain and the only previously reported steroidal trisaccharides of starfish origin appear to be the sepositoides A, B, C, and D from *Echinaster sepositus*, which feature a three-sugar chain cyclized between C3 and C6 and lack sulfate moieties (3).

Experimental

The nmr spectra were recorded on Varian 200 and Bruker AM-500 NMR spectrometers using tetramethylsilane as internal reference. $^1H/^1H$ correlation (COSY) spectra were acquired as 512 FLO's of 2K data points and 3.3 kHz spectral window, using a 90° pulse of 22 μs and a recycle time of 3.3 s. Spectra were processed using sine-bell squared functions shifted π/4 in F1 and were zero-filled in F1 for a final digital resolution of 3.2 Hz/pt. $^1H/^{13}C$ correlation (HETCOR) spectra were acquired as 256 F10's of 4K data points with a 3 s recycle time and 14 kHz and 2.8 kHz spectral windows in F2 (^{13}C) and F1 (^1H), respectively. The data matrix was zero-filled in F1, processed using sine-bell squared functions shifted π/2 in F2 and π/4 in F1, and plotted as power spectra. FAB mass spectra were recorded on a Kratos MS50 instrument using Xenon as ionizing gas. Optical rotations were measured on a Perkin Elmer 241 polarimeter. Preparative tlc was performed with precoated silica gel F254 (1 mm) and KC18F reverse phase (0.25 mm) plates.

Isolation of forbesides F, G, and H

The starfish, *Asterias forbesi*, were collected at Indian Point, Bay of Fundy, Canada, on September 26, 1988, and frozen. The frozen animals (20 kg, wet wt) were defrosted and cut into small pieces and extracted with cold methanol (40 L). The total aqueous methanolic extract was filtered and the filtrate was concentrated on a rotary evaporator at 30°C. The aqueous extract thus obtained (4 L) was passed through a column of Amberlite XAD-2 (1 kg, 30–50 mesh). The column was washed with distilled water (2 L) and then eluted with methanol (4 L). The methanol eluate was concentrated to small volume (250 mL) and then treated with cold acetone (2.5 L) to give the crude glycoside mixture (12 g, yellow powder).

The crude glycoside mixture (10 g) was dissolved in $CHCl_3/CH_3OH/H_2O$ (66:44:5), filtered, and the filtrate was chromatographed on a silica gel (500 g, 230–400 mesh) column and eluted with the same solvent system, yielding 15 fractions. Fraction 3 afforded the previously reported (4) forbesides E1, E2, and E3. Fraction 4 (248 mg) was rechromatographed on ptlc plates (1 mm, 50 mg/plate) using the solvent system *n*-BuOH/EtOAc/H_2O (5:1:1) to yield forbeside F (36 mg) and a mixture of forbesides G and H (62 mg). By similar treatment, fraction 5 (300 mg) yielded forbeside E (30 mg) (6), forbeside F (50 mg), and a mixture of forbesides G and H (50 mg). The pure forbesides G (50 mg) and H (40 mg) were finally obtained by successive column chromotography over a Merck Lichroprep RP-18 reverse phase column (20 g) using CH_3OH/H_2O (7:3) as solvent, followed by purification on reverse phase ptlc using the same solvent system. Forbeside A (600 mg) was obtained from fraction 13 by repeated silica gel column chromatography.

Forbeside F, **2**: colorless powder, mp 208°C; $[\alpha]^{20}$ +11.6° (*c* 0.010, H_2O). FAB$^+$ ms (magic bullet) *m/z* (%): 1159 (9.7, $M^+ + Na + 2H$), 1157 (8.0, $M^+ + Na$), 1139 (5.0, $M^+ + Na - H_2O$), 1056 (2.5), 1039 (7.0), 1019 (3.0), 993 (2.7), 639 (2.3), 477 (4.1), 461 (4.8), 331 (4.7), 285 (7.0).

Forbeside G, **3**: colorless powder, mp 194°C; $[\alpha]^{20}$ −4.7° (*c* 0.010, H_2O). FAB$^-$ ms (glycerol) *m/z* (%): 987 (3, $M^- - H$), 965 (82, $M^- - Na$), 947 (28.2 $M^- - Na - H_2O$), 865 (47.4), 847 (48.8), 701 (9.6), 659 (10.9), 555 (16.2), 539 (22.6), 533 (24.0), 511 (47.6), 493 (28.0), 439 (39.9), 411 (100), 393 (67.1), 377 (16.4), 353 (19.4), 309 (15.5).

Forbeside H, **5**: colorless powder, mp 188°C; $[\alpha]^{20}$ −4.7° (*c* 0.010, H_2O). FAB$^-$ ms (glycerol) *m/z* (%): 957 (13, $M^- - H$), 935 (100, $M^- - Na$), 917 (11.7, $M^- - Na - H_2O$), 835 (89.2), 819 (9.9), 777 (17.9), 689 (14.5), 639 (10.8), 585 (10.9), 557 (20.1), 539 (26.0), 411 (48.5), 393 (67.3).

Acknowledgements

This study was supported by a grant from the Natural Sciences and Engineering Research Council of Canada. The assistance of the Huntsman Marine Laboratory in collecting organisms is gratefully acknowledged.

1. J. A. FINDLAY, M. JASEJA, D. J. BURNELL, and J.-R. BRISSON. Can. J. Chem. **65**, 1384 (1987).
2. J. A. FINDLAY, M. JASEJA, and J.-R. BRISSON. Can. J. Chem. **65**, 2605 (1987).
3. R. RICCIO, E. DE SIMONE, A. DINI, E. FINAMORE, L. MINALE, C. PIZZA, F. SENATORE, and F. ZOLLO. Tetrahedron Lett. **22**, 1557 (1981).
4. J. A. FINDLAY and Z.-Q. HE. J. Nat. Prod. In press.
5. Y. ITAKURA, T. KOMORI, and T. KAWASAKI. Liebig's Ann. Chem. 2079 (1983).
6. J. A. FINDLAY, Z.-Q. HE, and M. JASEJA. Can. J. Chem. **67**, 2078 (1989).

Can. J. Chem. Downloaded from www.nrcresearchpress.com by 88.85.125.76 on 09/07/12
For personal use only.

The electrocatalytic hydrogenation of fused polycyclic aromatic compounds at Raney nickel electrodes: the influence of catalyst activation and electrolysis conditions[1]

DENIS ROBIN, MICHEL COMTOIS, ANNA MARTEL, RENÉ LEMIEUX, AMOY KAM CHEONG, GÉRARD BELOT, AND JEAN LESSARD[2]

Laboratoire d'électrochimie, Université de Sherbrooke, Sherbrooke (Qué.), Canada J1K 2R1

Received December 1, 1989

This paper is dedicated to Professor Arthur S. Perlin on the occasion of his 67th birthday

DENIS ROBIN, MICHEL COMTOIS, ANNA MARTEL, RENÉ LEMIEUX, AMOY KAM CHEONG, GÉRARD BELOT, and JEAN LESSARD. Can. J. Chem. **68**, 1218 (1990).

The electrocatalytic hydrogenation (ECH) of phenanthrene, anthracene, and naphthalene has been investigated under constant current at Raney nickel electrodes in a mixed aqueous organic medium. The influence of various parameters on the efficiency of the process determined by the current efficiency (a measure of the competition between hydrogenation and hydrogen evolution, the only two electrochemical processes occurring), the extent of hydrogenation (yield of octahydro-derivatives), and the conversion rate was studied with phenanthrene. The best conditions were ethylene glycol or propylene glycol as cosolvent containing between 1.5 to 5% of water, a neutral or slightly acidic medium containing boric acid (0.1 M) as buffer (initial pH of 2.6, final pH of 6.0–6.2), sodium chloride or tetrabutylammonium chloride as supporting electrolyte, a temperature of 80°C, and a current density of 42 to 84 mA/cm^2. The most active electrodes (consisting of Raney Ni particles dispersed in a nickel matrix and surrounded by a layer of porous nickel) were obtained by leaching the dispersed alloy particles at 75°C for 7 h in 30% aqueous sodium hydroxide. The electrohydrogenation stopped at derivatives with a single aromatic ring, namely the octahydrophenanthrenes, octahydroanthracenes, and tetralin. In a non-buffered medium, tetrahydrophenanthrene could be obtained with selectivities of 80% or better.

Key words: electrocatalytic hydrogenation, Raney nickel electrodes, phenanthrene, anthracene, naphthalene.

DENIS ROBIN, MICHEL COMTOIS, ANNA MARTEL, RENÉ LEMIEUX, AMOY KAM CHEONG, GÉRARD BELOT et JEAN LESSARD. Can. J. Chem. **68**, 1218 (1990).

On a étudié l'hydrogénation électrocatalytique (HEC) du phénanthrène, de l'anthracène et du naphtalène à courant constant sur des électrodes de nickel de Raney en milieu eau-solvant organique. L'étude de l'influence de divers paramètres sur l'efficacité de l'électrohydrogénation du phénanthrène déterminée par l'efficacité de courant (une mesure de la compétition entre hydrogénation et dégagement d'hydrogène, les deux seuls processus électrochimiques observés), le degré d'hydrogénation (rendement en octahydrophénanthrènes) et le taux de conversion, a conduit à définir les meilleurs conditions, soit : l'éthylène glycol ou le propylène glycol contenant entre 1,5 et 5% d'eau comme solvant, un milieu neutre ou légèrement acide contenant de l'acide borique (0,1 M) comme tampon (pH initial de 2,6–2,7 et pH final de 6,0–6,2), le chlorure de sodium ou de tétrabutylammonium comme électrolyte-support, une température de 80°C et une densité de courant de 42 à 84 mA/dm^2. Les électrodes sont faites de particules de nickel de Raney dispersées dans une matrice de nickel et entourées d'une couche de nickel poreux. Les plus actives provenaient d'une lixiviation des particules d'alliage précurseur à 75°C pendant 7 h dans de l'hydroxyde de sodium à 30%. L'électrohydrogénation s'est arrêtée aux dérivés possédant un seul noyau aromatique, soit les octahydrophénanthrènes, les octahydroanthracènes et la tétraline. En solution non tamponnée, on a obtenu le tétrahydrophénanthrène avec des sélectivités égales ou supérieures à 80%.

Mots clés : hydrogénation électrocatalytique, électrodes de nickel Raney, phénanthrène, anthracène, naphtalène.

Introduction

The electrocatalytic hydrogenation (ECH) of an unsaturated organic molecule in aqueous or mixed aqueous-organic media involves first the formation of chemisorbed hydrogen at a cathode with a low hydrogen overvoltage (transition metal) by reduction of water or hydronium ion (reaction [1] where M is the metallic surface and (H)M chemisorbed hydrogen). Hydrogenation then proceeds as in catalytic hydrogenation, that is by reaction of the adsorbed substrate (Y=Z)M, with chemisorbed hydrogen (reactions [3] and [4]).

[1] $2H_2O(H_3O^+) + 2e^- + M \rightarrow 2(H)M + 2OH^-(H_2O)$

[2] $Y{=}Z + M \rightarrow (Y{=}Z)M$

[3] $(Y{=}Z)M + (H)M \rightarrow (\dot{Y}{-}ZH)M$

[4] $(\dot{Y}{-}ZH)M + (H)M \rightarrow (YH{-}ZH)M$

[5] $(YH{-}ZH)M \rightarrow YH{-}ZH + M$

Electrocatalytic hydrogenations have been carried out since the beginning of the century (4–7). It has been suggested quite early that electrochemical reductions in aqueous media, on cathodes of spongy transition metals, might involve reaction of the unsaturated substance with adsorbed hydrogen (8). This has been confirmed in a number of mechanistic studies of ECH at Raney nickel (9–11), at nickel black (12, 13), at platinized platinum (Pt/Pt) (10, 12–21), at PTFE-bound platinum black (22, 23), at smooth platinum (24, 25), at Raney platinum iridium (26), at PTFE-bound palladium black (27), and at Raney ruthenium–iridium (28).

ECH has the following advantages over catalytic hydrogenation. Firstly, the kinetic barrier due to the splitting of the hydrogen molecule is completely bypassed, as is the mass transport of the poorly soluble hydrogen molecule. Thus the use of hydrogen gas, elevated temperatures and pressures can be avoided. Secondly, the fact that a cathodic potential is applied to the catalyst in ECH can in some cases diminish or even prevent the adsorption of poisons (3, 10, 11). A limitation of the ECH method with substrates that are difficult to hydrogenate comes from the competition between hydrogenation (steps [3]

[1]Part IV in the series "Electrocatalytic hydrogenation of organic compounds". For parts I, II, and III, see refs. 1, 2, and 3.

[2]Author to whom correspondence should be addressed.

Can. J. Chem. Downloaded from www.nrcresearchpress.com by 88.85.125.76 on 09/07/12
For personal use only.

and [4]) and the formation of molecular hydrogen from chemisorbed hydrogen (reactions [6] and/or [7], respectively the Heyrovský and Tafel steps of the hydrogen evolution reaction (29)) (9, 10, 30).

[6] $H(M) + H_2O + e^- \rightarrow H_2 + M + OH^-$

[7] $H(M) + (H)M \rightarrow H_2 + M$

When compared to electrohydrogenation by the electronation–protonation (EP) process (reactions [8] to [11]), ECH has the

[8] $Y{=}Z + e^- \rightarrow [Y{=}Z]^{\cdot -}$

[9] $[Y{=}Z]^{\cdot -} + H_2O \rightarrow \dot{Y}{-}ZH + OH^-$

[10] $\dot{Y}{-}ZH + e^- \rightarrow \ddot{\overline{Y}}{-}ZH$

[11] $\ddot{\overline{Y}}{-}ZH + H_2O \rightarrow YH{-}ZH + OH^-$

advantage of requiring less energy. Indeed the formation of chemisorbed hydrogen by reduction of water on a low hydrogen overvoltage cathode (reaction [1]) requires a less negative potential than the electronation (reaction [8]) of most functional groups of organic chemistry (at the exception of the nitro group family).

The advantages of ECH over catalytic hydrogenation and direct electrochemical reduction (EP process)[3] make it a method of general interest for the hydrogenation of functional groups in organic molecules. For example, electrohydrogenations of interest in synthesis have been reported at various high area catalytic electrodes: nickel (1–3, 7, 9–11, 33–44), platinum (4, 6, 10, 21, 30, 44–51), palladium (4, 5, 30, 34, 35, 44, 50), and rhodium (30, 44). The functional groups electrohydrogenated include triple bonds (33, 37, 38), double bonds (4, 7, 34, 37, 41, 42), aromatic rings (1, 5, 6, 21, 30, 45–48), carbonyl groups (1, 9, 10, 16, 37, 40, 44, 49–51), imines (1, 37, 44), oximes (37), nitriles (35, 37, 44), heterocycles (36, 40), nitro groups (hydroxylamines) (1–3, 37), hydrazines (2), and bromides (42).

The efficiency of electrocatalytic hydrogenations is determined by the competition between hydrogenation (reactions [3] and [4]) and hydrogen evolution (reactions [6] and/or [7]). The relative rates of these two processes are affected by the strength of the bond to be hydrogenated and by a number of factors which influence the adsorption of the organic substrate, the coverage of the electrode by chemisorbed hydrogen, and/or the activity of chemisorbed hydrogen such as the electrode material (17, 30, 44), the electrode surface and, for a given electrode, the current density (polarization of the electrode) (44), the concentration of the substrate (9–11, 30), the pH of the solution (9, 31), the organic cosolvent (30) and the presence of any molecule that can be adsorbed on the electrode (11), the supporting electrolyte, and the temperature (36).

In this paper, we report the results of a study of the influence of the electrode activation and electrolysis conditions (pH, buffer, supporting electrolyte, solvent, temperature, current density) on the ECH of phenanthrene at a Raney Ni cathode. Anthracene and naphthalene were also electrohydrogenated under the best conditions found with phenanthrene.

Results and discussion

The electrohydrogenations were carried out on a 1 mmol scale, at constant current, on electrodes consisting of Raney Ni particles embedded in a Ni matrix (see below), and were stopped after the passage of the charge required for complete hydrogenation of the substrate. The catholyte was analysed by vapour phase chromatography (vpc). The 100% mass balance obtained in the vast majority of experiments show that the sole process competing with hydrogenation (reactions [3] and [4]) was hydrogen evolution (reactions [6] and/or [7]). The current efficiency is then a measure of the relative importance of the two processes. The current efficiency diminished gradually as the electrolysis proceeded due to the diminution of the rate of hydrogenation with the concentration of the substrate (9–11, 30). Because the freshly activated Raney Ni electrodes were filled with adsorbed-hydrogen, generally between 0.7 to 1.1 mmol of active hydrogen depending on the amount of catalyst as shown by open-circuit (catalytic) hydrogenations (see below), the current efficiency was usually higher than 100% up to a charge of 3 F/mol under the best conditions. The potential of the working electrode was measured at a current density of 84 mA/dm^2 (geometric area) in ethylene glycol – water 98.5:1.5 (v/v). It corresponds to the potential for reduction of the medium to hydrogen and varied with the pH and temperature as expected. Thus, it was less negative (reduction of water easier) at pH 2.6 (0.1 M H_3BO_3), −0.7 V against the saturated calomel electrode (SCE), than in alkaline medium (0.3 M (n-Bu)$_4$NOH), −1.0 V vs. SCE (T = 80°C). And it was less negative at higher temperatures, −0.7 V at 80°C and −0.85 V vs. SCE at 50°C (pH 2.6).

The working electrodes were prepared in the following way. First, particles of Raney alloy were suspended in a nickel bath and electroplating was carried out on a stainless steel grid to give a coating consisting of particles of alloy embedded in deposited nickel (1, 52). The Raney nickel electrode was then obtained by leaching out the aluminum in aqueous sodium hydroxide according to procedures described for the different preparations of Raney Ni (53). Scanning electron microscopic studies before and after leaching have shown that the particles of Raney alloy, and of Raney nickel after leaching, are held in a nickel matrix, each particle being surrounded by a layer of nickel (54). This nickel layer must be porous since leaching of the alloy did occur through it as shown by analysis of Ni and Al by X-ray powder diffraction (XRPD) before and after leaching (54).

ECH of phenanthrene

We studied the influence of the cathode activation, the pH of the solution, the buffer, the supporting electrolyte, the solvent, the temperature, and the current density on the efficiency of the ECH of phenanthrene (**1**). The products observed were 9,10-dihydrophenanthrene (**2**), tetrahydrophenanthrene (**3**), and the octahydrophenanthrenes **4** (asymmetric) and **5** (symmetric). The efficiency of electrohydrogenation was evaluated from the

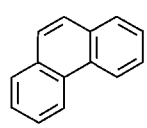

1

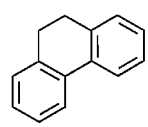

2 (di)

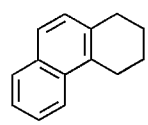

3 (tetra)

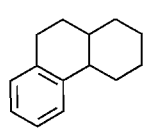

4 (octa-as)

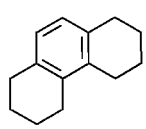

5 (octa-s)

[3]For a discussion on common features and differences of ECH, catalytic hydrogenation, and direct electrochemical reduction, see refs. 9, 31, and 32.

Can. J. Chem. Downloaded from www.nrcresearchpress.com by 88.85.125.76 on 09/07/12
For personal use only.

TABLE 1. ECH of phenanthrene at Raney Ni electrodes in ethylene glycol – water 98.5:1.5 (v/v): effect of conditions (temperature and time) of leaching in 30% aqueous NaOH (w/v)[a]

	Leaching		Electrode[b]			Yield of products (%)[c]			
Entry	T (°C)	Time (h)	NiAl composition[a] (w/w)	Specific area (BET) (m^2/g)	Conversion (%)	Di (**2**)	Tetra (**3**)	Octa (**4** + **5**) (**4**/**5**)	Current efficiency (%)
1	—	—	69:31	6×10^{-4}	0	—	—	—	0
2	50	1	97.5:2.5		9	13	87	0	4
3	25–75[e]	7	98:2	21.5	56	21	70	9 (0.6)	32
4	25–75[e]	17	99.3:0.7		82	16	72	12 (0.6)	52
5	75	7	99.6:0.4	20.6	80	15	65	19 (0.6)	53
6	92	7			72	20	70	10 (0.75)	39
7	105–110	7	97.3:2.7	14.0	63	20	69	10 (0.75)	26
8[f]	75	7			70	20	64	16 (0.8)	44

[a]Electrolysis conditions: 1.1 mmol of phen (9 mM); 0.29 M $NaBF_4$; pH = 6 (initial) to 8 (final); T = 80°C; J = 42 mA/dm^2 (geometric area); charge passed (Q) = 7–8 F/mol.

[b]Amount of Raney alloy 0.7–0.8 g (58–62% of alloy in the matrix).

[c]The conversion rate and yield of products were determined by glc analysis. The yields are based on converted phenanthrene. Material balance ≥99%.

[d]By X-ray fluorescence.

[e]The Raney alloy electrode was immersed in the NaOH bath at 25°C then the bath was heated to 75°C on a hot plate.

[f]The electrode (0.6 g of alloy, 54%) was rinsed under an atmosphere of H_2 after leaching.

current efficiency, the extent of hydrogenation (the yield of octahydrophenanthrenes), and the conversion rate. The best conditions should give the highest current efficiency together with the best yield of octahydrophenanthrenes at high conversion (~100%).

The cathode

The effect of the particle size of the precursory alloy, of the quantity of Raney Ni (proportional to the quantity of deposited alloy), and of the conditions of leaching on the efficiency of electrohydrogenation of phenanthrene was investigated. Changing the range of the size of particles from 38–125 μm, to 53–106 μm, then to 45–75 μm had no detectable effect.

Increasing the quantity of Raney alloy from 0.71 g (55% of alloy in the matrix) to 1.2 g (69%)[4] caused an increase of the current efficiency from 40 to 47% and of the yield of octahydrophenanthrenes from 43% to 65%. The charge passed was 14 F/mol and the conversion of phenanthrene was 97–100% under the conditions used (ethylene glycol – water 98.5:1.5 (v/v); 0.1 M NaCl; 0.1 M H_3BO_3; pH = 2.7 (initial) to 6.0 (final), T = 80°C; J = 84 mA/dm^2 (geometrical area)). By increasing the surface of the support, for instance by using a reticulated vitreous carbon support, it was possible to increase the amount of alloy to 3 to 4 g (60 to 68% of alloy in the matrix). This resulted in a further increase of the current efficiency to 50–56% after complete conversion of phenanthrene (Q = 14 F/mol) and of the yield of octahydrophenanthrenes to 100% (**4**/**5** = 0.8 to 0.9). However, the material balance dropped to 70% due to loss of material by adsorption on the catalyst. The latter type of electrodes was not used for the studies reported below. With the first type of electrodes (stainless steel grid support), the electrohydrogenations were quite reproducible. For instance, four electrolyses on electrodes containing similar amounts of Raney Ni (from 0.75 to 0.85 g of deposited alloy (58–60%)) gave current efficiencies in the range of 42–44% and yields of octahydrophenanthrenes varying from 55 to 58%.

[4]On a given support, the percentage of alloy in the nickel matrix was usually higher, the larger the amount of deposited alloy, but not always.

Table 1 reports the results of a study of the influence of leaching on the efficiency of the electrohydrogenation of phenanthrene. Because the particles of alloy are covered with a layer of porous nickel, leaching required more forceful conditions (longer reaction time and/or higher temperature) than those reported for the preparations of Raney Ni from powdered Raney alloy (53). At an unactivated (unleached) electrode, hydrogen evolution was the sole process observed (Table 1, entry 1). Leaching at 50°C for 1 h in 30% aqueous NaOH (w/v) led to very little hydrogenation (entry 2). Immersing the electrode in the NaOH solution at 25°C then digesting at 75°C for 17 h (entry 4) produced an electrode with the same efficiency as one prepared by immersion at 75°C then digested at that temperature for 7 h (entry 5). A shorter leaching time (entry 3) or a higher temperature of leaching (entries 6 and 7) gave less efficient electrodes. The most efficient electrodes had the smallest content of aluminum together with a specific area of 20–21 m^2/g (entry 5). The decrease of efficiency at higher temperatures of leaching (entries 6 and 7) appears related mainly to a decrease in the specific area. Indeed, Freel *et al.* (55) have shown that the specific area of powdered Raney Ni decreases upon increasing the temperature of leaching above 100°C due to an increase of the size of the pores. The least active Raney nickel catalysts (W1 and W8) are obtained by leaching at temperatures above 100°C (53).

The most active form of powdered Raney Ni (W6) is prepared by leaching at 50°C followed by washing under H_2 atmosphere (53). However, an electrode rinsed under H_2 after leaching and immediately immersed into the cell showed no improvement of efficiency (entry 8). The smaller conversion rate, current efficiency, and percentage of octahydrophenanthrenes in entry 8 as compared to entry 5 probably reflects the smaller quantity of Raney Ni on the electrode.

We studied the effect of passing a charge of 400 coulombs (hydrogen evolution) before adding the substrate and found that there was practically no effect on the efficiency. Open-circuit hydrogenation (catalytic hydrogenation) of phenanthrene showed that an electrode (0.76 g of alloy, 57%) on which hydrogen was evolved contained about 0.48 mmol of active hydrogen

Can. J. Chem. Downloaded from www.nrcresearchpress.com by 88.85.125.76 on 09/07/12
For personal use only.

TABLE 2. Influence of pH and buffer on ECH of phenanthrene at Raney Ni electrodes in ethylene glycol – water 98.5:1.5 (v/v)[a]

Entry	Weak acid	pH_i[b]	pH_f[b]	Conversion (%)	Yield of products (%)[c] Di (2)	Tetra (3)	Octa (as/s) (4 + 5) (4/5)	Current efficiency (%)
1[d]	None	>13	>13	12	0	100	0	16
2	None	10.0[e]	11.9	65	9	88	3 (0.5)	18
3	None	7.1	11.9	86	8	87	6 (1.5)	25
4	None	3.0[f]	11.9	94	7	86	6 (1)	27
5	None	7.0	11.8	94	6	80	13 (1.4)	29
6	Glycine 0.10 M	6.1	10.0	65	8	90	3 (>8)[g]	19
7	Citric 0.05 M	3.5[e]	6.4	38	13	76	11 (1)	11
8	Succinic 0.10 M	2.6	5.1	25	12	56	36 (0.8)	9
9	Acetic 0.10 M	2.6	6.2	82	13	76	12 (1)	25
10	Boric 0.05 M	2.7	10.4	100	4	39	58 (1)	44
11	Boric 0.10 M	2.6–2.7	6.0–6.2	97–100[h]	4–7[h]	30–38[h]	55–65 (0.8–0.9)[h]	42–47[h]
12	Boric 0.15 M	2.5	5.7	100	6	46	49 (0.6)	41
13	Boric 0.20 M	2.5	5.0	95	12	61	27 (0.4)	33

[a]Electrolysis conditions: 1.1 mmol of phenanthrene (9 mM); 0.1 M NaCl; T = 80°C; Q = 14 F/mol. For entries 1 to 3: J = 42 mA/dm^2; electrodes, 0.75–0.81 g of alloy (59%). For entries 4 to 13: J = 84 mA/dm^2; electrodes, 0.90–1.0 g of alloy (62–64%).
[b]pH_i = pH at the beginning of the electrolysis, pH_f = pH at the end. The pH meter was calibrated using buffers in aqueous solution. Buffers with pH values of 9.96 and 3.68 in water gave values of 10.69 and 4.65, respectively, in 98.5:1.5 (v/v) ethylene glycol – water.
[c]See footnote *c* of Table 1.
[d]Supporting electrolyte: 0.3 M (n-Bu_4NOH); Q = 4 F/mol.
[e]pH value obtained by adding NaOH.
[f]pH value obtained by adding HCl.
[g]The symmetric isomer **5** was not detected.
[h]Range obtained from 10 different electrolyses. Electrodes, 0.75–1.2 g of alloy (58–69%).

and an electrode (0.68 g of alloy, 59%) used without evolving hydrogen contained a little more, 0.66 mmol.

A Raney Ni electrode stored in dilute aqueous sodium hydroxide (0.1 to 1 M) for a month was almost as efficient as an electrode used immediately after leaching. The loss of efficiency was important, however, when the electrode was kept in absolute ethanol. The Raney Ni catalysts are usually stored in 0.1 M aqueous sodium hydroxide or in absolute ethanol. Loss of catalytic activity was observed when powdered Raney Ni was kept in absolute alcohol (56).

Although repeated use of the same electrode does lead to some loss of efficiency, the lifetime of electrodes made of Raney Ni particles embedded in a nickel matrix is much longer than that of an electrode made of powdered Raney Ni (37, 39–44).[5] A rapid loss of activity was reported for the latter type of Raney Ni electrodes and it was attributed to the agglomeration of the finely divided (dark) powder into larger size particles (lighter in colour) (58). In catalytic hydrogenation, agglomeration of powdered metal catalysts is a well known deactivation process (59). The agglomeration of catalyst particles dispersed in a metallic matrix, if not prevented completely, is considerably slowed down (2).

pH and buffer

As shown in reaction [1], the ECH process produces hydroxide ions at the surface of the cathode so the pH near the surface is most probably higher than in the bulk solution and the pH of an unbuffered electrolysis medium increases as the electrolysis proceeds. The effect of pH of the bulk solution on the efficiency of ECH of phenanthrene was investigated and the results are reported in Table 2. In an alkaline medium (0.3 M (n-$Bu)_4NOH$ as supporting electrolyte, entry 1), the efficiency was very poor even after the passage of only 4 F/mol.[6] At pH 10–12, the results were better (entry 2). The efficiency was improved further by commencing the electrolysis at lower pH values (entries 3 to 5). Thus, contrary to catalytic hydrogenations over Raney Ni (60) and to ECH of acetone at Raney Ni (9), ECH of phenanthrene becomes less efficient as the basicity increases. The addition of a weak acid at concentrations of 0.05 to 0.1 M allowed to keep the pH below 10 up to a charge of 14 F/mol (entries 5 to 12). The use of a carboxylic acid had a detrimental effect on the efficiency of ECH as shown by the lower conversion rates and current efficiencies in entries 6 to 9 as compared to entry 5, acetic acid (entry 9) being the least detrimental. However, the uses of boric acid to buffer the solution (entries 10 to 13) led to an appreciable improvement of the efficiency of the hydrogenation process as seen from the high conversion of phenanthrene, the higher current efficiencies, and better yields of octahydrophenanthrenes. The optimum concentration of boric acid was in the range of 0.05–0.1 M (entries 10 and 11). At higher concentrations, the hydrogenation efficiency did diminish (entries 12 and 13). The concentration of boric acid had also an effect on the ratio of asymmetric-to-symmetric octahydrophenanthrenes (see entries 10 to 13).

The negative influence of organic carboxylic acids can be explained by their adsorption on Raney Ni, adsorption strong enough to displace phenanthrene. A decrease in the concentration of adsorped phenanthrene would thus lead to a decrease in the rate of hydrogenation (reactions [3] and [4]) and to a lower

[5]Under continuous operation conditions (flow cell), there was no significant loss of activity after 200 h of electrolysis for the ECH of various organic substrates (2, 57).

[6]Better results were reported for the ECH of phenanthrene in ethanol–water 67:33 (v/v) containing (n-$Bu)_4NOH$ at room temperature for a charge of 6 F/mol (1): 94% conversion; 36% of **2**, 44% of **3**, and 6% of **4** + **5**; current efficiency of 46%.

Can. J. Chem. Downloaded from www.nrcresearchpress.com by 88.85.125.76 on 09/07/12
For personal use only.

TABLE 3. Influence of the supporting electrolyte on ECH of phenanthrene at Raney Ni electrodes in ethylene glycol – water 98.5:1.5 (v/v)[a]

Entry	Supporting electrolyte MX	Conversion (%)	Yield of products (%)[b] Di (**2**)	Tetra (**3**)	Octa (as/s) (**4** + **5**) (**4**/**5**)	Current efficiency (%)
1[c]	NaCl	97–100	4–7	30–38	55–65 (0.8–0.9)	42–47
2	NaBr	97	8	49	42 (0.6)	37
3	NaH_2PO_4[d]	58	10	71	17 (1)	18
4	NaI	17	18	71	12 (1)	5
5	KCl	98	6	41	55 (0.9)	42
6	n-Bu_4NCl	99	7	27	66 (0.9)	46
7	Me_4NCl	99	7	55	37 (0.8)	38
8	Na_2SO_4[e]	100	8	63	30 (0.8)	36

[a]Electrolysis conditions: 1.1 mmol of phenanthrene (9 mM); 0.1 M MX; 0.1 M H_3BO_3; pH = 2.6–2.7 (initial) to 6.0–6.2 (final); T = 80°C; J = 84 mA/dm^2; Q = 14 F/mol. Electrodes: amount of alloy, 0.88–0.96 g (62–63%).

[b]See footnote *c* of Table 1.

[c]Taken from Table 2, entry 11.

[d]pH = 4.3–6.5. Phosphoric acid was added to bring down the initial pH to 4.3.

[e]No H_3BO_3 present since Na_2SO_4 was not soluble enough in 98.5:1.5 (v/v) ethylene glycol – water containing H_3BO_3: pH = 3.0–11.8; J = 43 mA/dm^2.

efficiency of the ECH process. The positive influence of boric acid could be related to an activation of the hydrogenation process (reactions [3] and [4]) and/or to an inhibition of hydrogen evolution (reactions [6] and/or [7]) due to a pH effect or to other effects which have to be investigated. At concentrations higher than 0.1 M, adsorption of boric acid could become important enough to slow down the hydrogenation process.

Supporting electrolyte

As shown in Table 3 for the NaX series (entries 1 to 4), the efficiency of ECH of phenanthrene depends on the anion of the supporting electrolyte and decreases in the order NaCl > NaBr >> NaH_2PO_4 >> NaI. This order most probably reflects the increasing strength of adsorption of the anions on Raney Ni, that is the increasing tendency to poison the catalyst. Chloride ions have been reported to poison Raney Ni in the catalytic hydrogenation of styrene (61). Furthermore, the rate of catalytic hydrogenation of organic halides on Raney Ni has been shown to decrease in the order chlorides > bromides >> iodides (61) and this could be due to poisoning of the catalysts by the halide ions produced in the hydrogenolysis (62), the poisoning effect of the soft iodide ions being much greater than that of the bromide or chloride ions. Open circuit experiments under the same conditions as those used for the electrolyses of phenanthrene confirmed the inhibiting effect of chloride ions in catalytic hydrogenation and showed the strong inhibiting effect of iodide ions. In the absence of halide ions, of the 1.1 mmol of phenanthrene initially present, 33% was hydrogenated and 1.15 mmol of active hydrogen was consumed to give 5% of **2** and 28% of **3**. In the presence of 0.1 M sodium chloride, 15% of phenanthrene was hydrogenated and only 0.5 mmol of hydrogen was used to give 3% of **2** and 14% of **3**. In the presence of 0.1 M sodium iodide, no hydrogenation occurred at all. Sulfate anions are probably not adsorbed on Raney nickel and the fact that sodium chloride (entry 1) was as efficient as sodium sulfate (entry 8) as supporting electrolyte shows that the application of a cathodic potential to the catalyst must diminish considerably or even prevent the adsorption of chloride ions, and in general the adsorption of poisons that are not too strongly adsorbed (3, 10, 11). This constitutes an advantage of ECH over catalytic hydrogenation as pointed out in the Introduction. The lower efficiency of ECH in entry 8 as compared to entry 1 probably reflects the absence of boric acid. Sodium sulfate was not soluble enough in the electrolysis medium containing 0.1 M boric acid.

The cation of the supporting electrolyte appears to have little effect on the efficiency of ECH as seen from entry 1 and entries 5 to 7 of Table 3. The efficiency decreases slightly in the order (n-Bu)$_4$NCl ≥ NaCl ≥ KCl > Me_4NCl.

For the electrolyses of Table 1, sodium tetrafluoroborate (0.29 M) was used as supporting electrolyte. Under the electrolysis conditions, it was rapidly hydrolysed to boric acid and hydrofluoric acid (reaction [2]) as shown by potentiometric titration. This explains why the pH varied little (between 6 and 8) during the electrolyses (Q = 7–8 F/mol). The supporting electrolyte was then sodium fluoride. The ECH was quite efficient (see entry 5 of Table 1) since boric acid was present and fluoride ions should not be adsorbed strongly on Raney Ni (even in the absence of a negative potential).

[12] $NaBF_4 + 3H_2O \rightarrow B(OH)_3 + 3HF + NaF$

Solvent

The best organic cosolvents are those that are less organic as found also for the ECH of phenol at a Pt/C or Rh/C cathode (30). For instance, very little hydrogenation of phenanthrene was observed with THF as cosolvent (current efficiency ~5% after Q = 4 F/mol) and little hydrogenation was observed with tertiobutanol (current efficiency ≤15%). This is most probably due to the adsorption of the organic solvent competing with the adsorption of the organic substrate as found with organic acids (see above). The effect is to diminish the effective concentration of adsorbed substrate and thus to inhibit the hydrogenation process (reactions [3] and [4]). The results of Table 4 show that ethylene glycol is superior to methanol as cosolvent (entries 1 and 2). Propylene glycol is as good as ethylene glycol (entries 4 and 5) whereas diethylene glycol is less good (entry 3) probably because it is more strongly adsorbed on Raney Ni and/or more viscous. The results of entries 5 to 8 also show the influence of

Can. J. Chem. Downloaded from www.nrcresearchpress.com by 88.85.125.76 on 09/07/12
For personal use only.

TABLE 4. Influence of solvent on the ECH of phenanthrene at Raney Ni electrodes[a]

Entry	Organic solvent	% water (v/v)	T (°C)	Conversion (%)	Yield of products (%)[b] Di (**2**)	Tetra (**3**)	Octa (as/s) (**4** + **5**) (**4**/**5**)	Material balance (%)	Current efficiency (%)
1	Methanol	1.5	60	77	8	79	12 (0.5)	99	23
2	Ethylene glycol	1.5	60	90	9	45	45 (0.6)	99	38
3	Diethylene glycol	1.5	80	71	6	65	28 (1.5)	99	26
4	Propylene glycol	1.5	80	98	6	29	65 (0.6)	100	46
5[c]	Ethylene glycol	1.5	80	97–100	4–7	30–38	55–65 (0.8–0.9)	99–100	42–47
6	Ethylene glycol	5	80	95	3	20	77 (1.2)	100	47
7	Ethylene glycol	10	80	95	4	28	54 (0.7)	86	37
8	Ethylene glycol	20	80	97	2	13	60 (0.9)	75	37

[a]Electrolysis conditions: 1.1 mmol of phenanthrene (9 mM); 0.1 M NaCl; 0.1 M H_3BO_3; pH = 2.6–2.7 (initial) to 6.0–6.2 (final); J = 84 mA/dm^2; Q = 14 F/mol. Electrodes: amount of alloy, 0.71–0.78 g (58–60%).
[b]See footnote *c* of Table 1.
[c]Taken from Table 2, entry 11.

TABLE 5. Effect of temperature and current density on the ECH of phenanthrene at Raney Ni electrodes in 98.5:1.5 (v/v) ethylene glycol – water[a]

Entry	T (°C)	J[b] (mA/dm^2)	Conversion (%)	Yield of products (%)[c] Di (**2**)	Tetra (**3**)	Octa (as/s) (**4**) (**4**/**5**)	Current efficiency (%)
1	50	84	73	8	32	60 (0.8)	32
2	60	84	90	9	45	45 (0.6)	38
3	70	84	86	5	28	70 (1.1)	41
4[d]	80	84	97–100	4–7	30–38	55–65 (0.8–0.9)	42–47
5	90	84	93	5	38	58 (0.9)	41
6[e]	80	42	65	9	74	15 (0.7)	78
7[e]	100	42	30	10	73	13 (1)	40
8	80	21	98	13	65	21 (0.9)	31
9	80	42	100	5	32	63 (0.85)	46
10	80	104	95	10	59	31 (0.5)	34

[a]Electrolysis conditions: 1.1 mmol of phenanthrene (9 mM); 0.1 M NaCl; 0.1 M H_3BO_3; pH = 2.6–6.0; Q = 14 F/mol. Electrodes: 0.85–0.95 g of alloy (62–64%).
[b]Based on the geometric area.
[c]See footnote *c* of Table 1.
[d]Taken from Table 2, entry 11.
[e]Electrolysis conditions: 0.29 M $NaBF_4$; pH = 6–8; Q = 3.8 F/mol.

the amount of water. Larger quantities of water appear to favor the formation of octahydrophenanthrenes (entry 6). However, increasing the percentage of water beyond 5% caused material losses as shown by the lower material balance of entries 7 and 8. We were not able to account fully for these losses. Small amounts of diphenic acid resulting from the oxidation of phenanthrene were found in the anodic compartment for the electrolyses of entries 7 and 8. There was no loss due to sublimation or evaporation of phenanthrene or its derivatives. Only very small amounts of organic products were recovered by washing thoroughly the electrodes recovered from the electrolyses with organic solvents or by heating them under vacuum.

Temperature

The effect of temperature on the ECH of phenanthrene was studied, from 25°C to 56°C, in methanol–water 98.5:1.5 (v/v) containing 0.3 M lithium perchlorate as supporting electrolyte (pH = 7–8). The current efficiency after 4 F/mol increased from 30 to 61%. In ethylene glycol – water 98.5:1.5 (v/v) under the usual conditions (see Table 5 entries 1 to 4), an increase of temperature from 50 to 80°C caused an increase of the current efficiency at Q = 14 F/mol from 32 to about 44%. The current efficiency dropped slightly at 90°C (entry 5). A significant drop of current efficiency and conversion rate occurred at 100°C (compare entries 6 and 7 where the charge passed was 3.8 F/mol only). Thus, upon increasing the temperature up to 80–90°C, the rate of hydrogenation increases more rapidly than that of hydrogen evolution. At temperatures above 90°C, the situation appears to be reversed. The rate of ECH of pyridine at Raney Ni was reported to be influenced by the temperature between 20 and 50°C (36). In that paper, there is no indication of the direction of the effect but it can probably be assumed that an increase in rate was observed.

Current density

The effect of increasing the current density from 21 to 104 mA/dm^2 (geometric area) on the current efficiency after 14 F/mol is shown in Table 5. From 21 (entry 8) to 42 mA/dm^2 (entry 9), the small increase in cathodic polarization associated

Can. J. Chem. Downloaded from www.nrcresearchpress.com by 88.85.125.76 on 09/07/12
For personal use only.

TABLE 6. ECH of phenanthrene 9,10-dihydrophenanthrene, tetrahydrophenanthrene, anthracene, and naphthalene at Raney Ni electrodes in 98.5:1.5 (v/v) ethylene glycol – water[a]

Entry	Substrate	Charge (F/mol)	Conversion (%)	Yield of products (%)[b] Di (2)	Tetra (3)	Octa (as/s) (4 + 5) (4/5)	Current efficiency (%)
1[c]	Phenanthrene	14	97–100	4–7	30–38	55–65 (0.8–0.9)	42–47
2	Dihydro phen (**2**)	14	92	8	38	54 (1.1)	28
3		30	99	1	6	93 (1.5)	19
4	Tetrahydro phen (**3**)	14	80	2	20	77 (0.9)	17
5	Anthracene (**6**)	14	100	12	52	36 (0.3)	36
6	Naphthalene (**11**)	2.1	51	—	51	—	100
7		7.7	99	—	99	—	52
8		9.7	100	—	100	—	42

[a]Electrolysis conditions: 1.1 mmol of substrate (1.6 mmol for naphthalene); 0.1 M NaCl; 0.1 M H_3BO_3; pH = 2.6–2.7 to 6.6.4; T = 80°C.
[b]See footnote *c* of Table 1.
[c]Taken from Table 2, entry 11.

with the increase of current density favors hydrogenation over hydrogen evolution which leads to an increase of both current efficiency and extent of hydrogenation (yield of octahydrophenanthrenes). There is little change between 42 (entry 9) and 84 mA/dm^2 (entry 5). Further increase favors hydrogen evolution over hydrogenation as shown by the diminution of the current efficiency and of the extent of hydrogenation in entry 10. For the ECH of acetone, De Hemptinne and Jungers (9) reported that beyond a certain current density, the rate of hydrogen evolution increased with the current density while the rate of hydrogenation remained constant. This would be translated by a drop in current efficiency as observed in this work and others (30).

A current density of 84 mA/dm^2 (42 mA/dm^2 in a few cases) was used throughout this work to evaluate the influence of the various parameters on the efficiency of ECH of phenanthrene. Such low current density reflects the low concentration of substrate (9–11) together with the difficulty of hydrogenation of aromatic rings.

ECH of hydrogenated derivatives of phenanthrene

In catalytic hydrogenation, the initial rate of hydrogenation, that is the ease of hydrogenation of fused polycyclic aromatics increases with the number of rings (benzene < naphthalene < phenanthrene) and only one ring is saturated at a time (63). In ECH, under the best conditions defined above (ethylene glycol – water 98.5:1.5 (v/v); 0.1 M NaCl; 0.1 M H_3BO_3; T = 80°C; J = 84 mA/dm^2), the octahydrophenanthrenes are not electrohydrogenated at all. The strength of the π bond of a single aromatic ring is such that hydrogen evolution becomes much faster than hydrogenation and is the sole electrochemical process occurring. The ECH of tetrahydrophenanthrene was more difficult than that of phenanthrene as expected. This is shown by the lower conversion rate and much lower current efficiency of entry 3, Table 6, as compared to entry 1. Thus it was possible, under basic conditions, to electrohydrogenate phenanthrene to tetrahydrophenanthrene with interesting selectivities and good conversions (see Table 2, entries 3 to 5). Long ago, Breteau (5) reported the ECH of phenanthrene to tetrahydrophenanthrene in acid medium at Pd/Pt—Ir. No yield was given but the tetrahydro derivative was the sole product identified. Catalytic hydrogenation of phenanthrene over Raney Ni in dry ethanol under more vigorous conditions (100°C, 127 atm) using a limited quantity of hydrogen is less selective, giving some 55% of tetrahydro derivative together with 28% of 9,10-dihydro derivative (and 8% of octahydrophenanthrenes) at 53% conversion (64).

Catalytic hydrogenation of phenanthrene results in the initial saturation of the 9,10 positions and can be stopped at the dihydro stage if the catalyst is not too active (65). In ECH at Raney Ni, the difference in the rate of hydrogenation of phenanthrene and dihydrophenanthrene is not sufficient to allow the selective formation of the dihydro derivative even below 50% conversion.

The highest proportion of dihydrophenanthrene was obtained in basic aqueous ethanol at room temperature (1). The conversion of 9,10-dihydrophenanthrene to tetrahydrophenanthrene cannot occur directly. Disproportionation to phenanthrene and tetrahydrophenanthrene over Raney Ni was shown to occur to an extent of 40% after 6 h at 150°C under pressure (100–140 atm of N_2) (64). We cannot exclude the possibility that some disproportionation does take place under the conditions of ECH, that is at temperatures of 25 to 80°C and at atmospheric pressure. However, the conversion of 9,10-dihydrophenanthrene to tetrahydrophenanthrene (Table 6, entries 2 and 3) probably involves either dehydrogenation to phenanthrene followed by hydrogenation to readily hydrogenated dihydro derivatives or isomerization of 9,10-dihydrophenanthrene to those same dihydroderivatives through partial dehydrogenation and double bond migration. Dihydrophenanthrenes with a double bond in a terminal ring should be readily hydrogenated. That dehydrogenation could occur under the electrolysis conditions was suggested by the fact that small amounts of 9,10-dihydrophenanthrene (2 to 4%) were detected in the attempts to electrohydrogenate the octahydrophenanthrenes (uncontaminated by the dihydroderivative). Surprisingly, no tetrahydrophenanthrene was detected. Dihydrophenanthrene was also detected in the ECH of uncontaminated tetrahydrophenanthrene (Table 6, entry 4).

ECH of anthracene (6) and naphthalene (11)

They were electrohydrogenated under the best conditions found with phenanthrene and the results are recorded in Table 6, entries 5 to 8. The electrohydrogenation of anthracene (entry 5) was somewhat less efficient than that of phenanthrene (entry 1) as shown by the lower current efficiency and lower yield of

Can. J. Chem. Downloaded from www.nrcresearchpress.com by 88.85.125.76 on 09/07/12
For personal use only.

octahydro derivatives. The proportion of symmetric and asymmetric isomers differ in the two series. The electrohydrogenation of naphthalene was quite selective, giving tetralin (**12**) in a high chemical yield and with a good current efficiency (entry 7). As with phenanthrene, the derivatives with a single aromatic ring could not be hydrogenated further, hydrogen evolution being much faster and the sole electrochemical process observed. Entries 2 and 3, and entries 6 to 8 illustrate clearly the decrease of current efficiency (the decrease in the rate of hydrogenation with respect to that of hydrogen evolution) as the number of coulombs is increased (as the concentration of the organic substrate decreases).

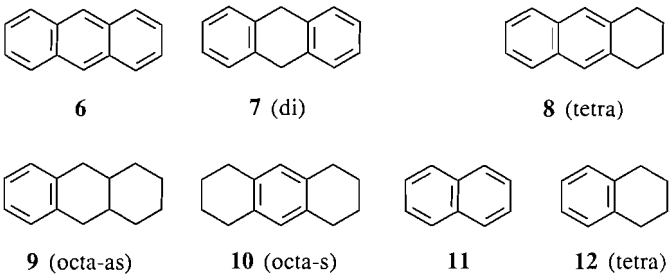

6 **7** (di) **8** (tetra)

9 (octa-as) **10** (octa-s) **11** **12** (tetra)

Conclusion

In ECH of organic compounds, the efficiency of electrohydrogenation is determined by the relative rates of two competing processes, namely the addition of chemisorbed hydrogen to the organic substrate (hydrogenation: reactions [3] and [4]) and the formation of molecular hydrogen from chemisorbed hydrogen (hydrogen evolution: reactions [6] and/or [7]). In this paper, using phenanthrene as substrate and a Raney nickel cathode consisting of particles of Raney nickel embedded on a nickel matrix, we have shown that the relative rate of the two processes is influenced by a number of factors: the activation of the cathode, the pH of the solution, the buffer, the supporting electrolyte, the cosolvent, the amount of water, the temperature, and the current density. The best conditions with the most active electrode (leaching at 75°C for 7 h) were a pH of 2.6–6.2 with boric acid as buffer, sodium chloride or tetrabutylammonium chloride as supporting electrolyte, ethylene glycol or propylene glycol containing between 1.5 to 5% (v/v) of water as solvent, a temperature of 80°C, and a current density of 42 to 84 mA/dm^2. A weak organic acid as buffer had a detrimental effect probably because its adsorption displaced some of the adsorbed phenanthrene and thus caused a decrease in the rate of hydrogenation. For the same reason, the more organic the cosolvent, the less efficient was the electrohydrogenation as found also by Miller and Christensen (30) for the ECH of phenol on a Pt/Pt cathode. An alkaline medium did favor hydrogen evolution over electrohydrogenation and the ECH was quite inefficient at pH > 13 contrarily to what was reported for the ECH of acetone at Raney Ni (10). The hydrogenation to hydrogen evolution ratio increased upon increasing the temperature from 25 to 80°C and when increasing the current density from 21 to 42 mA/dm^2 and started to decrease at temperatures above 90°C and current densities higher than 84 mA/dm^2. Poisoning of Raney Ni by chloride ions, which was observed in catalytic hydrogenation (61), is prevented or at least significantly diminished by cathodic polarization of the catalyst in ECH.

Under the best conditions, a charge equivalent to the full saturation of the aromatic compound led to complete conversion. With phenanthrene and anthracene, a mixture of octahydro derivatives (60% with phenanthrene, 36% with anthracene) and tetrahydro derivatives (34% with phenanthrene, 52% with anthracene) was obtained with current efficiencies of 45% and 36%, respectively. With naphthalene, the yield of tetralin was 99% and the current efficiency 50%. Complete conversion of phenanthrene or anthracene to octahydro derivatives could be achieved either by increasing the charge to about 30 F/mol with concomitant diminution of current efficiency (15–20%) or by increasing the amount of catalyst with concomitant loss of material due to adsorption. Tetrahydrophenanthrene was obtained with very good selectivities (≥80%) in the absence of boric acid. Full saturation of the aromatics could not be achieved. A single aromatic ring has a stronger π bond than that of fused polycyclic aromatics and the rate of hydrogenation of octahydro derivatives of phenanthrene and anthracene, and of tetralin is then much slower than hydrogen evolution. ECH of compounds with a single aromatic ring has been achieved at room temperature and atmospheric pressure at platinum cathodes in acidic solutions (6, 21, 30, 45, 46).

Compared to catalytic hydrogenation, the advantages of the ECH process are real due to the prevention or the minimization of poisoning and due to milder conditions of temperature and pressure as illustrated in the ECH of anthracene, phenanthrene, and naphthalene to tetrahydro or octahydro derivatives (see refs. 63–65 for catalytic hydrogenation of these substrates). It is also possible that polarization of the catalyst increases the rate of catalytic hydrogenation (11).

Finally, it is noteworthy that the electrohydrogenation of the polycyclic aromatics studied in this work by the ECH method can be accomplished at potentials of −0.7 to −1.0 V vs. SCE depending on the pH, and thus requires much less energy than electrohydrogenation by the electronation–protonation process. The electronation of these molecules necessitates potentials of −1.9 V (anthracene) to −2.5 V (phenanthrene, naphthalene) vs. SCE (66), which requires 23 to 40 kcal more energy than the ECH process.

Experimental

Vapor phase chromatographic (vpc) analyses were performed on a Hewlett Packard (HP) 5710A chromatograph equipped with a flame ionization detector and an HP 3390A integrator, using a DB-5 (dimethyldiphenylpolysiloxane) fused capillary column 30 m long at 160°C.

The following aromatic compounds were commercially available: phenanthrene from BDH (95%); 9,10-dihydrophenanthrene (≥97%), anthracene and tetralin (99%) from Aldrich Chemical, and naphthalene (>99%) from Fisher Scientific. Tetrahydrophenanthrene (>99%) was prepared from naphthalene according to the method described by Haworth (67). Asymmetric octahydrophenanthrene (100%) was synthesized from cyclohexanone and 1-bromo-1-ethylcyclohexane according to the method described by Perlman *et al.* (68). Symmetric octahydrophenanthrene (95.5%) was obtained by catalytic hydrogenation over Raney Ni as described by Durland and Atkins (64) followed by flash chromatographic separation on Merck silica gel 60 (230–400 mesh) and contained 4.5% of 9,10-dihydrophenanthrene. The authentic samples were characterized by their ir, ^{1}H nmr, and mass spectra.

Methanol, 2-propanol, and THF were distilled before use. Ethylene glycol (ACS, Anachemia), propylene glycol (USP, Baker), and diethylene glycol (Reagent, Fisher Scientific) were used without purification. Tetraethylammonium hydroxide (40% aqueous solution) was purchased from Aldrich Chemical, sodium tetrafluoroborate (pract.) from Fluka, boric acid (ACS) from Analar, and the Raney alloy particles (Ni–Al 50:50 (w/w)) from Aldrich Chemical (38–125 μm), BDH (45–125 μm), or Fluka (38–75 μm).

Can. J. Chem. Downloaded from www.nrcresearchpress.com by 88.85.125.76 on 09/07/12
For personal use only.

Can. J. Chem. Downloaded from www.nrcresearchpress.com by 88.85.125.76 on 09/07/12
For personal use only.

Raney Ni electrodes (1, 53)

A 60 mesh stainless steel grid (3 cm × 4 cm) to which was fixed a copper or stainless steel wire was heated at 80°C for 30 min in a bath containing NaOH (30 g/L), K_3PO_4 (30 g/L), and K_2SiO_3 (10 g/L). After washing thoroughly with distilled water and drying at 150°C, it was immersed in a 1 L beaker containing 550 mL of a plating solution made of 28% aqueous NH_4OH (200 mL/L), $NiCl_2.6H_2O$ (213 g/L), and NH_4Cl (30 g/L), pH = 8–9, with the stainless steel grid as the cathode and a cotton bag containing nickel beads (nickel shots (99%), Anachemia or BDH) (300 g) surrounding a graphite rod as the anode. Nickel was plated at 500 mA with a McKee-Pederson mp-1026 or a Sorrensen SRL 20-25 power supply. The current efficiency for Ni deposition varied between 94 and 96%. For the codeposition of Ni and alloy particles, Raney alloy particles (7 to 10 g) were added to the above plating bath and maintained in suspension by magnetic stirring. Plating was carried out at 500 mA for 60 min. In order to obtain about the same amount of particles on both faces of the cathode, the latter was turned around twice, after 8 min then after 33 min. The grid was placed at an angle of about 20° with respect to the vertical lead (held in a glass tube) to ensure a better contact with the flowing particles. The electrode was washed thoroughly with distilled water, dried in air, and weighed after removing the loosed particles by gentle brushing. The quantity of deposited Ni evaluated from the charge passed (95% current efficiency) was 0.53 g. The amount of deposited alloy particles varied between 0.7 and 1.2 g and the percentage of deposited alloy from 55 to 69%. The same bath could be used for many platings provided 0.9 g of alloy was added after each plating and concentrated NH_4OH was added to maintain the pH between 8 and 9. The electrode was activated by immersing it in a 125 mL Nalgene beaker containing a 30% (w/v) NaOH solution (80 mL) heated to the desired temperature. The most active electrodes were obtained by digesting at 75 ± 5°C for 7 h. The electrode was then washed thoroughly with distilled water and used immediately or kept in a 4% (w/v) NaOH solution until used.

Electrolyses

The electrolyses were carried out with a Princeton Applied Research (PAR) 173 or an Electrosynthesis Company (ESC) 410 or a G. Bank Electronic Wenking potentiostat having an ESC 640 or a PAR 379 coulometer and an ammeter connected to the auxiliary circuit. A two compartment jacketed glass H-cell (volume of each compartment: 150 mL) having a Nafion-324 (E.I. du Pont de Nemours & Co) membrane (~5 cm^2) as separator was connected to a Haake F423 constant temperature circulating bath filled with water (25–50°C) or ethylene glycol (60–100°C). The counter electrode was a graphite rod (7 mm) or a platinum grid (~10 cm^2) or plate (~5 cm^2). The cell voltages varied between 20 and 40 V for i = 20 mA. A Cole Parmer saturated calomel electrode, placed in a compartment separated from the working electrode by a fritted glass disc positioned near the surface of the electrode facing the counter electrode, was used to monitor the cathode potential.

The supporting electrolyte (generally 25 mmol) and a weak acid (generally 25 mmol) were dissolved in 250 mL of an organic solvent containing water in the required volumic proportions (generally 246 mL of ethylene glycol and 3.8 mL of water). The pH of the solution was measured at ca. 25°C with a Sargent Welch 6000 pH meter and a Cole Parmer glass electrode which was calibrated using aqueous solutions of commercial buffers. The solution was then poured in the cell (125 mL in each compartment), heated to the required temperature while deaerated (N_2 or Ar). The activated cathode and the counter electrode were immersed in the cell, the organic substrate (1.12 mmol, 9 mM solution) was added, and a constant current was immediately circulated. The cathodic solution was stirred magnetically. Aliquots (0.5 mL) were extracted with ether after the addition of a saturated NaCl solution (1 mL) and analysed by vpc. In the case of phenanthrene and naphthalene, the products were identified by comparison of retention times with those of authentic samples. The yields and mass balance were determined by comparison of peak areas with those of standard solutions of authentic samples using bibenzyl (phenanthrene) or biphenyl (naphthalene) as internal standard. In the case of anthracene, the products were identified by gc–ms (system NSB HP5970 with a quadrupolar filter)[7] and the proportions of starting material and products were evaluated by comparison of peak areas assuming a similar response to the detector. The mass balance was determined by extracting the cathodic solution with ether followed by the usual work-up and weighing the residue. For phenanthrene and naphthalene, the mass balance determined by isolation of the crude product was similar to that determined by vpc. For most electrolyses, the anodic compartment was also extracted with ether and the residue was weighed (2 to 8 mg) and analysed by vpc.

Acknowledgements

Financial support from the Natural Sciences and Engineering Research Council of Canada and the "Ministère de l'Enseignement Supérieur et de la Science du Québec" is gratefully acknowledged. We thank Mr. M. Drouin and Mr. Y. Couture for very helpful assistance, and Mrs. S. Thériault for typing the manuscript.

1. G. Belot, S. Desjardins, and J. Lessard. Tetrahedron Lett. **25**, 5347 (1984).
2. A. Cyr, P. Huot, G. Belot, and J. Lessard. Electrochim. Acta. **35**, 147 (1990).
3. A. Vélin-Prikidánovics and J. Lessard. J. Appl. Electrochem. In press.
4. S. Fokin. Z. Elektrochem. **12**, 749 (1906).
5. M. P. Breteau. Bull. Soc. Chim. Fr. Sér. 4, **9**, 764 (1911).
6. F. Fichter and R. Stocker. Chem. Ber. **47**, 2015 (1914).
7. U. Pomilio. Z. Elektrochem. **21**, 444 (1915).
8. W. M. Leslie and J. A. V. Butler. Trans. Faraday Soc. **32**, 989 (1936).
9. X. De Hemptinne and J. C. Jungers. Z. Physik. Chem. N.F. **15**, 137 (1958).
10. X. De Hemptinne. Acad. R. Belg. Cl. Sci. Mém. **32**, 5 (1961).
11. I. V. Kirilyus and M. A. Zhuk. Sov. Electrochem. **8**, 967 (1972).
12. I. V. Kudryasmov and V. L. Kochetkov. Kinet. I Katal. **11**, 692 (1970).
13. N. P. Ratiani, A. É. Kakhadze, A. A. Michri, and A. G. Pshenichnikov. Sov. Electrochem. **11**, 1305 (1975).
14. F. Nagy, I. Teces, and G. Horányi. Acta Chim. Budapest, **37**, 295 (1963); G. Y. Horányi, S. Szabo, J. Solt, and F. Nagy. Acta Chim. Budapest, **71**, 239 (1972).
15. L. D. Burke, C. Kimball, and F. A. Lewis. Trans. Faraday Soc. **60**, 913 (1964).
16. X. De Hemptinne and K. Schunk. Ann. Soc. Sci. Bruxelles, Sér. 1, **80**, 289 (1966); X. De Hemptinne and K. Schunk. Trans. Faraday Soc. **65**, 591 (1969); P. Florequin, K. Feyaerts, B. Juliam, and X. De Hemptinne. Bull. Soc. Chem. Belg. **85**, 195 (1976); K. Fayaerts and X. De Hemptinne. Bull. Soc. Chem. Belg. **87**, 265 (1978).
17. M. Byrne and A. T. Kuhn. J. Chem. Soc. Faraday Trans. I, **68**, 355 (1972).
18. D. N. Barra and H. M. Hulburt. J. Electrochem. Soc. **120**, 1333 (1973).
19. M. Byrne and A. T. Kuhn. J. Electroanal. Chem. **60**, 75 (1975).
20. K. Fujikawa and H. Kita. J. Chem. Soc. Trans. I, **75**, 2638 (1979).
21. K. Sasaki, A. Kunai, J. Harada, and S. Nakabori. Electrochem. Acta, **28**, 671 (1983).
22. H. J. Davitt and L. F. Albright. J. Electrochem. Soc. **118**, 236 (1971).
23. S. H. Langer and G. P. Sakellaropoulos. J. Electrochem. Soc. **122**, 1619 (1975).
24. Z. Takehara. Electrochim. Acta, **15**, 999 (1970).
25. H. Kita, T. Nakamura, H. Itoh, and H. Kano. Electrochim.

[7]We thank Dr. Christiane Ayotte from INRS Santé, Montréal, for the gc–ms analyses and interpretations of the mass spectra.

Acta, **23**, 405 (1978); K. SHIMADZU and H. KITA. Electrochim. Acta, **24**, 1085 (1979).
26. A. D. SEMENOVA, N. V. KROPOTOVA, and G. D. VOVCHENKO. Elektrokhimiya, **10**, 1233 (1974).
27. G. P. SAKELLAROPOULOS and S. H. LANGER. J. Catal. **67**, 77 (1981).
28. A. D. SEMENOVA, K. I. YANKOVSKII, N. V. KROPOTOVA, and G. D. VOVSCHENKO. Zh. Fiz. Khim. **54**, 2397 (1980).
29. K. J. VETTER. Electrochemical kinetics. Theoretical and experimental aspects. Academic Press, New York. 1967. pp. 516, 517.
30. L. L. MILLER and L. CHRISTENSEN. J. Org. Chem. **43**, 2059 (1978).
31. F. BECK. Int. Chem. Eng. **19**, 1 (1979).
32. M. D. BIRKETT, A. T. KUHN, and G. C. BOND. Catalysis, **6**, 61 (1985).
33. K. N. CAMBELL and E. E. YOUNG. J. Am. Chem. Soc. **65**, 965 (1943).
34. K. JUNGHANS. Chem. Ber. **107**, 3191 (1974).
35. K. KRISHNAN and H. V. K. UDUPA. Proc. Intl. Symp. Ind. Electrochem. SAEST India, 25 (1976); K. KRISHNAN and H. V. K. UDUPA. Trans. SAEST, **13**, 761 (1978).
36. I. V. KIRILYUS, G. K. MURZATOVA, and D. V. SOKOL'SKII. Sov. Electrochem. **15**, 1330 (1979).
37. T. CHIBA, M. OKIMOTO, H. NAGAI, and Y. TAKATA. Bull. Chem. Soc. Jpn. **56**, 719 (1983).
38. D. V. SOKOL'SKII, I. V. KIRILYUS, U. B. BEKENOVA, and G. K. MURZATOVA. Sov. Electrochem. **20**, 525 (1984).
39. K. PARK, P. N. PINTAURO, M. M. BAIZER, and K. NOBE. J. Electrochem. Soc. **132**, 1850 (1985).
40. T. MATSUE, T. YAMADA, H. TAKAHASHI, and T. OSA. Bull. Chem. Soc. Jpn. **59**, 3690 (1986).
41. T. YAMADA, T. OSA, and T. MATSUE. Chem. Lett. 995 (1987).
42. T. YAMADA, T. OSA, and T. MATSUE. Chem. Lett. 1992 (1987).
43. T. YAMADA, N. FUJIMOTO, T. MATSUE, and T. OSA. Denki Kagaku, **56**, 175 (1988).
44. M. A. CASEDEI and D. PLETCHER. Electrochim. Acta, **33**, 117 (1988).
45. W. D. BANCROFT and A. B. GEORGE. Trans. Electrochem. Soc. **57**, 399 (1930).
46. M. V. SITARAMAN and U. V. RAMAN. Curr. Sci. **16**, 23 (1947).
47. S. ONO and T. YAMAUCHI. Bull. Chem. Soc. Jpn. **25**, 404 (1952); S. ONO and T. HAYASHI. Bull. Chem. Soc. Jpn. **26**, 11 (1953); S. ONO and T. HAYASHI. Bull. Chem. Soc. Jpn. **26**, 232 (1953).
48. R. A. MISRA and B. L. SHARMA. Electrochim. Acta, **24**, 727 (1979).
49. D. PLETCHER and M. RAZAQ. Electrochim. Acta, **26**, 819 (1981).
50. T. NONAKA, M. TAKAHASHI, and T. FUCHIGAMI. J. Electrochem. Soc. Jpn. **51**, 129 (1983); Bull. Chem. Soc. Jpn. **56**, 2584 (1983).
51. G. HORÁNYI. Electrochim. Acta, **31**, 1095 (1986).
52. Y. ODA, H. OTOUMA, and E. ENDOH. U.S. Pat. 4 302 322 (1981); E. ENDOH, H. OTOUMA, and T. MORIMOTO. Int. J. Hydrogen Energy, **13**, 207 (1988).
53. R. L. AUGUSTINE. Catalytic hydrogenation. Marcel Dekker Inc., New York. 1965. pp. 26–30.
54. Y. CHOQUETTE, H. MENARD, and L. BROSSARD. Int. J. Hydrogen Energy, **14**, 21 (1990).
55. J. FREEL, W. J. M. PETERS, and R. B. ANDERSON. J. Catalysis, **14**, 247 (1969).
56. H. A. SMITH, W. C. BEDOIT JR., and J. F. FUSEK. J. Am. Chem. Soc. **71**, 3769 (1949).
57. S. DESJARDINS, G. BELOT, and J. LESSARD. Unpublished results.
58. K. PARK, P. N. PINTAURO, M. M. BAIZER, and K. NOBE. J. Appl. Electrochem. **16**, 941 (1986).
59. C. N. SATTERFIELD. Heterogeneous catalysis in practice. McGraw-Hill, New York. 1980. p. 143.
60. R. L. AUGUSTINE. Catalytic hydrogenation. Marcel Dekker Inc., New York. 1965. p. 46.
61. J. N. PATTISON and E. F. DEGERING. J. Am. Chem. Soc. **73**, 611 (1951).
62. E. SCHWENK, D. PAPA, and H. F. GINSBERG. Eng. Chem. Anal. Ed. **15**, 576 (1943).
63. R. L. AUGUSTINE. Catalytic hydrogenation. Marcel Dekker Inc., New York. 1965. pp. 74–77.
64. J. R. DURLAND and H. ADKINS. J. Am. Chem. Soc. **60**, 1501 (1938).
65. A. BURGER and E. MOSETTIG. J. Am. Chem. Soc. **57**, 2731 (1935); **58**, 1857 (1936).
66. L. MEITES and P. ZUMAN. CRC handbook series in organic electrochemistry. CRC Press Inc., Cleveland, OH. pp. 422–425; 602–605.
67. R. D. HAWORTH. J. Chem. Soc. 1125 (1932).
68. D. PERLMAN, D. DAVIDSON, and M. T. BOGERT. J. Org. Chem. **1**, 288 (1936).

Can. J. Chem. Downloaded from www.nrcresearchpress.com by 88.85.125.76 on 09/07/12
For personal use only.

Vinylpyridinium ionomers. III. Influence of the matrix glass transition temperature on the dynamic mechanical properties of random acrylate-based systems[1]

DENIS DUCHESNE[2] AND ADI EISENBERG[3]

Department of Chemistry, McGill University, 801 Sherbrooke St. W., Montreal, Que., Canada H3A 2K6

Received November 27, 1989

This paper is dedicated to Professor Arthur S. Perlin on the occasion of his 67th birthday

DENIS DUCHESNE and ADI EISENBERG. Can. J. Chem. **68**, 1228 (1990).

The thermal and dynamic mechanical properties of random butyl acrylate- and plasticized ethyl acrylate-based vinylpyridinium ionomers have been investigated. The properties of the ionomers were found to be dependent on the glass transition temperature of the matrix material. Ionomers having a glass transition temperature lower than ca. 25°C exhibited all the features associated with the presence of phase-separated microdomains or clusters while the materials with higher glass transition temperatures were not. It was also observed that the dispersion associated with the vinylpyridinium clusters for a butyl acrylate-based ionomer with 12 mol% of ionic units occurs at ca. 25°C. This value is very close to that observed previously by Otocka and Eirich in their study of a butadiene-based vinylpyridinium ionomer with the same ion content.

Key words: ionomers, plasticization, clustering, glass transition, dynamic mechanical properties.

DENIS DUCHESNE et ADI EISENBERG. Can. J. Chem. **68**, 1228 (1990).

On a examiné les propriétés dynamiques et mécaniques d'ionomères du vinylpyridinium basés sur de l'acrylate de butyle et de l'acrylate d'éthyle plastifié. On a trouvé que les propriétés des ionomères dépendent de la température de transition vitreuse du matériel de la matrice. Les ionomères possédant une température de transition vitreuse inférieure à environ 25°C présentent toutes les caractéristiques associées à la présence des microdomaines ou des agrégats séparés par des phases; ce n'est pas le cas avec les matériaux dont les températures de transition vitreuse sont plus élevées. On a aussi observé que la dispersion associée aux agrégats de vinylpyridinium d'un ionomère basé sur l'acrylate de butyle et contenant 12 mol% d'unités ioniques se produit à environ 25°C. Cette valeur est très semblable de celle observée antérieurement par Otocka et Eirich dans leur étude d'un ionomère de vinylpyridinium basé sur le butadiène et contenant la même quantité d'ion.

Mots clés : ionomères, plastification, agrégation, transition vitreuse, propriétés dynamiques et mécaniques.

[Traduit par la revue]

Introduction

In other publications of this series (1, 2), rheological evidence was presented to support the hypothesis that the formation of phase-separated microdomains or clusters does not occur in ethyl acrylate- and styrene-based vinylpyridinium ionomers. Indeed, the investigation of their dynamic mechanical properties has shown that the properties of the materials, aside from an increase in the glass transition temperature with increasing ion content, were unaltered by the incorporation of up to 24.2 mol% of vinylpyridinium units. This is in contrast with the results obtained by Otocka and Eirich (3, 4), for butadiene-based vinylpyridinium ionomers. Not only did they observe a large increase in the glass transition temperature of the materials with increasing ion concentrations, they also observed the appearance of a second inflexion point in the Young's modulus versus temperature curves and a decrease in the slope of the same curves in the transition regions. They concluded that all these modifications in the rheological properties of the butadiene–vinylpyridinium ionomers were most probably due to the formation of ionic aggregates and that these, according to their stress relaxation data, had a decomposition temperature of ca. 25°C.

A comparison of all these data suggests that while the butadiene–vinylpyridinium ionomers appear to be clustered, cluster formation in the ethyl acrylate- and styrene-based vinylpyridinium ionomers does not occur, possibly because their glass transition temperatures are higher than the vinylpyridinium cluster decomposition temperature previously reported by Otocka and Eirich, or because no clusters exist in these styrene or ethyl acrylate ionomers.

Another factor that could be invoked to explain the absence of clusters in the ethyl acrylate-based ionomers is the dielectric constant of the matrix, which is higher than that for the butadiene-based system. Eisenberg and co-workers (5) have compared the stress–relaxation behaviour of ethyl acrylate–sodium acrylate copolymers with that of styrene–sodium methacrylate copolymers and concluded that clusters become rheologically significant at higher ion contents in the former system. The threshold concentration values above which the clusters start to dominate the rheological behaviour were found to be 6 mol% and 12 mol% for the styrenic system and the acrylic system, respectively. Neppel *et al.* (6, 7), using Raman spectroscopy techniques, showed that the degree of solubility of multiplets is higher in the acrylates than in styrene. Hence, both the glass transition temperature and the dielectric constant of the matrix material seem to be parameters of utmost importance for cluster formation.

Many studies, reviewed elsewhere (8–10), have dealt with the influence of the ion structure as well as the dielectric constant of the matrix material on the formation of clusters. None, as yet, has specifically tried to establish the effect of the matrix glass transition temperature alone on cluster formation. In order to do this, the viscoelastic properties of the low glass transition temperature butyl acrylate-based vinylpyridinium ionomers as well as those of plasticized ethyl acrylate-based ionomers were investigated. The plasticizer, dimethyl malonate, was chosen to match the dielectric constant of the ethyl acrylate matrix so as to allow for the examination of the effect of one parameter alone, i.e., the glass transition. The results of

[1]This paper is based, in part, on Duchesne's Ph.D. dissertation "Structure–property relations of vinylpyridinium ionomers". McGill University, 1985.

[2]Present address: 3M Canada Inc., P.O. Box 5757, London, Ont., Canada N5A 4T1.

[3]To whom all correspondence should be addressed.

Can. J. Chem. Downloaded from www.nrcresearchpress.com by 88.85.125.76 on 09/07/12
For personal use only.

this investigation will be compared with the results that already exist on butadiene- (3, 4), styrene- (1), and ethyl acrylate-based (2) vinylpyridinium ionomers to obtain a better understanding of the effect of the matrix glass transition on cluster formation in vinylpyridinium ionomers.

Experimental

Materials

Ethyl acrylate (Aldrich, 98%, inhibited with 200 ppm of monoethylether hydroquinone) and butyl acrylate (Aldrich, 98%, inhibited with 10–50 ppm of monoethylether hydroquinone) were fractionally distilled under reduced pressure, discarding the first and last 10% of the distillate. The monomers were then stored under a nitrogen atmosphere at −20°C prior to use. 4-Vinylpyridine (Aldrich, 98%) was treated the same way.

Benzoyl peroxide (Baker, 99%) benzene (Fisher, reagent grade), hexanes (A&C, technical grade), and methanol (A&C, technical grade) were used without further purification.

Polymerization

The copolymers were prepared by the free radical copolymerization in solution. The amount of initiator necessary to get the required polymerization rate and molecular weight was assumed to be the same as that for the monomer constituting the major part of the copolymer.

For each mixture, the monomers were transferred through a double-tipped needle under flowing nitrogen into an ampoule and kept under nitrogen. Next, the solvent was weighed and the calculated amount of benzoyl peroxide (to get the desired molecular weight) was added and dissolved in the solvent. Once the catalyst was dissolved completely, the solvent–catalyst mixture was transferred through a double-tipped needle under flowing nitrogen into the ampoule already containing the monomers, and again kept under a nitrogen atmosphere.

Each ampoule was immediately degassed by several freeze–thaw cycles under vacuum (10^{-2} mm Hg), sealed off under vacuum, and immersed in a thermostatted bath preset to 56°C or 60°C. The polymerization time varied with the nature of the comonomers and the composition of the mixtures. The conversions were kept low to give less than 30% compositional heterogeneity in the copolymers. Subsequently, the ampoules were opened and the copolymers isolated by precipitation in a 10 volume excess of hexanes.

The gel-forming copolymers were soaked overnight in fresh non-solvent. Following this step, they were removed from the non-solvent. To insure total dryness, all the copolymers were placed in a drying oven at 60°C under reduced pressure (1 mm Hg) until constant weight was reached. The details of the copolymerization runs are given in Tables 1, 2, and 3.

Analysis

The vinylpyridine content was determined by potentiometric titration using a solution of perchloric acid in glacial acetic acid according to the procedures described by Burleigh *et al.* (11). These results were further verified for the series of ethyl acrylate-4-vinylpyridine copolymers by elemental analysis. Variations between the different techniques were less than 0.2 mol%.

Molecular weight determination

An approximate molecular weight for at least one copolymer of each series was obtained by measuring their intrinsic viscosities, [η], in acetone solutions. The determinations were made at 25°C (BuA) and 30°C (EA) using a Ubbelhode viscometer. The values of K and a were taken as $K = 6.8 \times 10^{-5}$ dl/g and $a = 0.75$ for the BuA (12) copolymers and 20×10^{-5} dl/g and $a = 0.66$ for the EA copolymers (13). The intrinsic viscosities ranged from 0.7 to 1.5 dl/g corresponding to molecular weights of $2–6 \times 10^5$ g-mol^{-1}.

Copolymer modification

Materials

Methyl iodide (A&C, reagent grade) was fractionally distilled under nitrogen and in the absence of light a few hours before use.

Tetrahydrofuran (THF) was dried by refluxing over potassium metal and benzophenone until the deep purple colour characteristic of the potassium–benzophenone complex persisted. It was then distilled directly into the flask containing the polymer. Absolute ethanol (100%, Consolidated Alcohols Ltd.) and hexanes (A&C, technical grade) were used without further purification.

TABLE 1. Copolymerization conditions

Copolymer	Bz_2O_2 × 10^2 M	Solvent	T (°C)
Ea-4-VP	0.78	benzene*	56
BuA-4-VP	2.8	benzene†	60

*60 wt%.
†50 wt%.

TABLE 2. Monomer feed, copolymer composition, polymerization time, yield, and intrinsic viscosity for ethyl acrylate-4-vinyl-pyridine (EA-4-VP) copolymers

Vinylpyridine content in				
Monomer feed (mol%)	Copolymer (mol%)	Polymerization time, (min)	Yield (%)	[η]
0	0	10	10.1	0.7
0.47	1.6	30	12.4	—
1.5	5.1	95	12.1	—
2.3	7.6	125	12.7	1.5
3.4	10.5	205	14.5	—
5.6	16.0	300	14.4	1.0

TABLE 3. Monomer feed, copolymer composition, polymerization time, yield, and intrinsic viscosity for butyl acrylate-4-vinly-pyridine (BuA-4-VP) copolymers

Vinylpyridine content in				
Monomer feed (mol%)	Copolymer (mol%)	Polymerization time (min)	Yield (%)	[η]
2.2	4.6	60	26.7	0.75
6.2	12.3	150	30.4	—
8.6	18.6	170	22.0	—

Quaternization

The vinylpyridinium copolymers were obtained by the reaction of the vinylpyridine copolymers with methyl iodide. The procedure given below is a combination of those described by Otocka and Eirich (3, 4), Selb and Gallot (14), and Gauthier and Eisenberg (15).

The 4-vinylpyridine copolymers were quaternized by adding a five-fold excess of methyl iodide to a boiling 3% copolymer solution. The mixture was then refluxed under nitrogen for 2 h. The final products had a yellow colouration most probably due to the presence of triiodide ions. The solvents in which the reactions were conducted, ethanol for the EA copolymers and THF for the BuA copolymers were chosen to avoid the precipitation of quaternized material during the reaction.

The ionomers were recovered by precipitation into 10 volumes of stirred hexanes. The gel-forming materials were soaked overnight in the non-solvent and then dried in a vacuum over at 60°C for at least 24 h.

Analysis

The extent of quaternization of the ethyl acrylate- and butyl acrylate-based vinylpyridinium ionomers was determined by NMR

Can. J. Chem. Downloaded from www.nrcresearchpress.com by 88.85.125.76 on 09/07/12
For personal use only.

spectroscopy (Varian XL-200, Varian T-60). The ionomers were found to be at least 80% quaternized. This value was obtained by taking the ratio of the peak intensity for the PY+CH_3I^- protons (*N*-methyl-4-vinylpyridinium iodide (4-VPQ): 4.65 ppm) to the peak intensity for some of the protons on the pendant ethyl or butyl acrylate groups.

Plasticization

The plasticized ethyl acrylate-4-vinylpyridium iodide (EA-4-VPQ) 10.5 mol% samples were prepared by mixing pieces of the previously dried rubbery material with dimethyl malonate (Aldrich, 99%) in a compression mold. The mixtures were then molded at pressures no higher than 2000 psi at 70°C for 1 h and were used without further treatment. The plasticizer content was determined by measuring the difference in weight for the samples before performing the dynamic mechanical testing and after that, once the samples had been heated at 80°C under reduced pressures until a constant weight was reached. It is assumed that no loss of plasticizer occurred during the testing since dimethyl malonate has a boiling point of 182°C (19).

Calorimetry

The glass transition temperatures of the non-quaternized copolymers and the ionomers were determined using a Perkin and Elmer Differential Scanning Calorimeter (D.S.C.-II). The determinations were done on samples weighing about 10 mg. Indium and n-octane were used to calibrate the instrument. The calibration and experimental runs were carried out at a heating rate of 20°C min^{-1}. Prior to the determination of their glass transition temperatures, all the samples were dried for at least 48 h in a vacuum oven at 60°C.

The non-ionic copolymers were annealed at Tg+20°C for 5 min and quenched before each scan. Three scans were usually made to ensure reproducibility, the last one being retained.

The alkyl acrylate ionomers were annealed at Tg+10°C for 5 min, quenched, and then scanned. Three runs were also made, the last one being retained.

In all cases the values obtained for the glass transition temperature were reproducible within 2°C.

Dynamic mechanical measurements

The dynamic mechanical properties were investigated with a torsional pendulum which is described elsewhere (17). The frequency varied from ca. 3 Hz in the glassy region to ca. 0.03 Hz in the low modulus region. Rectangular samples obtained by compression molding of 0.7 to 0.9 g of polymer at a temperature of Tg+20°C and at pressures no higher than 2000 psi were used in this study. All samples were subjected to the same drying procedures as those adopted for the calorimetry study.

The experiments were performed under a nitrogen atmosphere. Heating rates of 1–2°C min^{-1} were employed and the temperature was controlled to ±1°C. The values of the shear storage modulus (G′), the shear loss modulus (G″), and the loss tangent (tan delta) acquired and calculated by a computerized system, were obtained directly.

Results

*Butyl acrylate-*N*-methyl-4-vinylpyridinium iodide ionomers*

The variation of the shear storage modulus (G′) with the temperature for a series of butyl acrylate ionomers with 4.6 to 18.3 mol% of 4-VPQ ions (BuA-4-VPQ) is plotted in Fig. 1. It can be seen that as the ion content increases, the curves shift upward in temperature, and the shapes of the curves are modified extensively in the glass to rubber transition region with noticeable broadening.

The loss tangent curves, shown in Fig. 2, display two distinct relaxations. The high temperature relaxation is seen to gain in intensity as more ions are incorporated and, at high levels, to become the dominant one. The position of both relaxations depends to a different degree on the ion content, as can be seen in Fig. 3. The low temperature relaxation moves progessively upward in temperature at a rate of about 1°/mol% while the high temperature relaxation is shifted at a rate of about 4.3°/mol%.

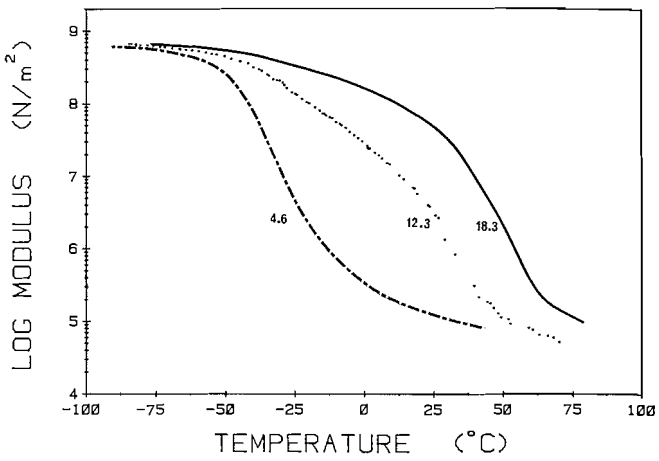

FIG. 1. Shear storage modulus as a function of temperature for butyl acrylate-*N*-methyl-4-vinylpyridinium iodide ionomers.

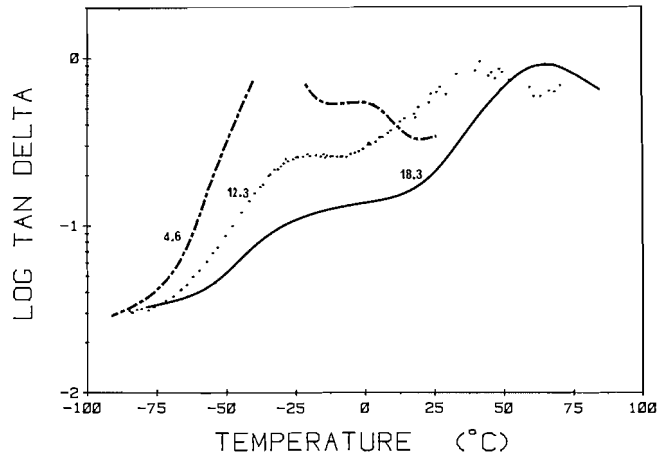

FIG. 2. Loss tangent as a function of temperature for butyl acrylate-*N*-methyl-4-vinylpyridinium iodide ionomers

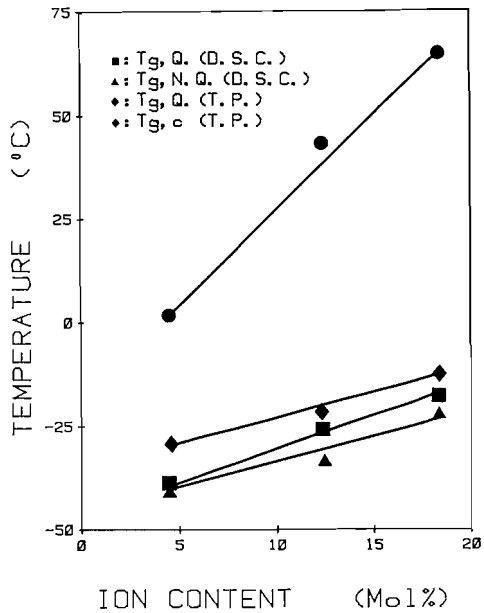

FIG. 3. Glass transition temperature (Tg) as a function of ion content as determined by D.S.C. and dynamic mechanical measurements (T.P.) for the non-quaternized (N.Q.) and quaternized (Q.) poly(butyl acrylate-co-4-vinylpyridine) copolymers, and high temperature peak position (Tg, c) as a function of ion content for the quaternized copolymers.

Can. J. Chem. Downloaded from www.nrcresearchpress.com by 88.85.125.76 on 09/07/12
For personal use only.

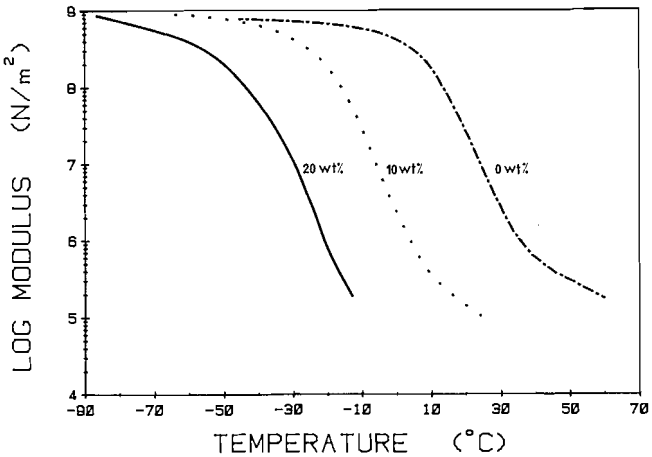

FIG. 4. Shear storage modulus as a function of temperature for ethyl acrylate-*N*-methyl-4-vinylpyridinium iodide ionomers plasticized with dimethyl malonate (DMM).

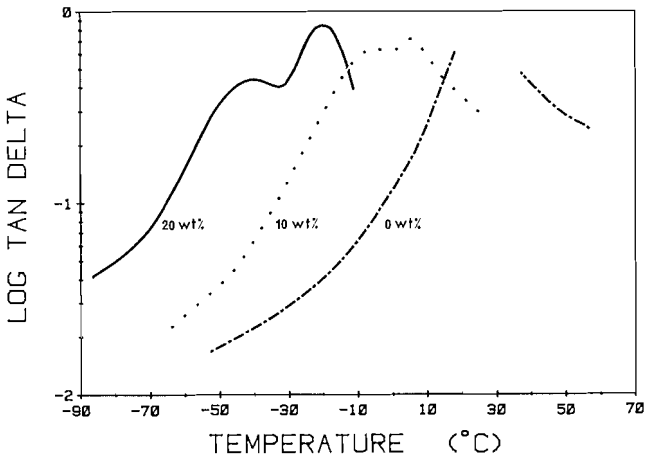

FIG. 5. Loss tangent as a function of temperature for ethyl acrylate-*N*-methyl-4-vinylpyridinium iodide ionomers plasticized with dimethyl malonate (DMM).

Only one transition is detected by calorimetry. Its position, also plotted in Fig. 3, is influenced by the ion concentration in the same way as the low temperature relaxation detected by dynamic mechanical measurements. For the sake of comparison, results obtained for the non-quaternized copolymers (N.Q.) are also presented.

*Plasticized ethyl acrylate-*N*-methyl-4-vinylpyridinium iodide ionomers*

The dynamic mechanical properties of an ethyl acrylate-based vinylpyridinium ionomer (EA-4-VPQ) 10.5 mol% plasticized with dimethyl malonate (DMM) were investigated. Figure 4 shows the variation of the shear storage modulus with temperature for samples of poly(ethyl acrylate) with 0, 10, 20 wt% of dimethyl malonate which was used as a plasticizer. A marked shift downward in temperature is observed as the amount of plasticizer increases. Along with this shift, the 20 wt% sample also exhibits some broadening in the glass to rubber transition region.

Similarly, the loss tangent curves, Fig. 5, move progressively downward in temperature indicating, as expected, a severe depression of the glass transition temperature with increasing plasticizer content. More importantly, the 10 and 20 wt% sample display two relaxations. The significance of this second relaxation will be discussed in detail in the next section.

Discussion

The damping behaviour of BuA-4-VPQ ionomers indicates that these materials are phase-separated. Indeed, the appearance of a high temperature relaxation can easily be related to the formation of clusters. As can be seen in Fig. 2, the high temperature relaxation gains substantially in intensity relative to the low temperature relaxation as the ion concentration increases.

In the light of these results, it is believed that the low temperature relaxation is due to microbrownian segmental motions associated with the glass transition of the ion-poor region, while the high temperature relaxation is associated with the same phenomenon in the ion-rich phase. Thus, the BuA-4-VPQ ionomers fall in the same category of ionomeric material as, among others, styrene – sodium methacrylate (18), styrene – sodium-*p*-styrene sulfonate (19), ethyl acrylate – sodium acrylate copolymers, sulfonated ethylene – propylene rubbers (EPDM) (20), and carboxylated polypentenamers (9).

The plot for the unplasticized EA ionomer in Fig. 5, along with results for a more extensive ion concentration range reported in ref. 2, tend to indicate that the EA ionomers are not clustered. By contrast, it is clear that ionomers based on BuA are clustered. The question of whether clustering takes place because the butyl acrylate matrix has a lower glass transition temperature or a lower dielectric constant than the ethyl acrylate matrix will now be addressed. The plasticization experiments provide the answer.

The results in Figs. 4 and 5 suggest that phase separation is induced and progressively enhanced as the glass transition is depressed by the addition of the plasticizer. As the plasticizer content increases, clusters are formed which have observable mechanical properties of their own. It should be noted that the plasticizer mimics the backbone: therefore, the clustering cannot be ascribed to changes in the dielectric constant, but only to changes in Tg. Thus, vinylpyridinium ionomers with a low glass transition temperature should be clustered while those with high glass transition temperature should not. Similar observations have been made in a parallel study for the poly(styrene-co-4-vinyl pyridine) system (21). Furthermore, while the dielectric constant of the matrix increases the solubility limit of the multiplets, it will not prevent cluster formation by itself unless it has a very high value, as in the case of the polyphosphates (22).

In the light of these results, it now seems surprising that the low concentration (<10 mol%) EA-4-VPQ ionomers did not show any sign of phase separation. It appears that these materials are a borderline case, and would probably be clustered if their glass transition temperatures were a few degrees lower.

Conclusions

The BuA-4-VPQ ionomers were shown to behave like clustered materials. In addition, the investigation of the viscoelastic properties of EA-4-VPQ 10.5 mol% samples plasticized with DMM suggest that while the EA ionomers are not clustered, in the absence of plasticizer, the plasticized samples are clustered, and that the essential condition for vinyl pyridinium ions to form clusters in this material is a lowering of the matrix glass transition temperature.

1. S. GAUTHIER, D. DUCHESNE, and A. EISENBERG. Macromolecules, **20**, 760 (1987).
2. D. DUCHESNE, and A. EISENBERG. J. Polym. Sci. To be published.
3. E. P. OTOCKA, and F. R. EIRICH. J. Polym. Sci. Part A-2, **6**, 921 (1968).

Can. J. Chem. Downloaded from www.nrcresearchpress.com by 88.85.125.76 on 09/07/12
For personal use only.

4. E. P. OTOCKA, and F. R. EIRICH. J. Polym. Sci. Part A-2, **6**, 933 (1968).
5. A. EISENBERG, H. MATSUURA, and T. TSUTSUI. J. Polym. Sci. Polym. Phys. **18**, 479 (1980).
6. A. NEPPEL, I. S. BULTER and A. EISENBERG. Macromolecules, **12**, 948 (1979).
7. A. NEPPEL, I. S. BUTLER, and A. EISENBERG. J. Polym. Sci. Polym. Phys. **17**, 2145 (1979).
8. A. EISENBERG and M. KING. Ion-containing polymers. Academic Press, New York. 1977.
9. W. J. MACKNIGHT and T. R. EARNEST. J. Polym. Sci., Macromol. Rev. **16**, 41 (1981).
10. R. LONGWORTH. *In* Developments in ionic polymers–I. *Edited by* A. Wilson and H. Prosser. Applied Science Publishers, Essex. 1983, Chap. 3.
11. J. E. BURLEIGH, O. F. MCKINNEY, and M. G. BARKER. Anal. Chem. **31**, 10 (1959), **31**, 1684 (1959).
12. E. SAINI and L. TROSSARELLI. Atti. Accad. Sci. Torino, Classe Sci. Fis. Mat. Nat., **90**, 410 (1955–56).
13. H. SUMITOMO and Y. HACHIHAMA. Kobunshi Kagaku. **10**, 544 (1953).
14. J. SELB and Y. GALLOT. J. Polym. Sci. Polym. Lett. **13**, 615 (1975).
15. S. GAUTHIER and A. EISENBERG. Polym. Prepr. Am. Chem. Soc. Div. Polym. Chem. **22**, 2 (1981); **22**, 293 (1981).
16. R. C. WEAST. (*Editor*). Handbook of chemistry and physics. 56th ed. CRC Press, Cleveland. 1975.
17. B. CAYROL. Ph.D. Thesis, McGill University, Montreal. 1982.
18. A. EISENBERG and M. NAVRATIL. Macromolecules. **6**, 604 (1973).
19. M. RIGDHAL and A. EISENBERG. J. Polym. Sci. Polym. Phys. **19**, 1641
20. P. AGARWAL, H. S. MAKOWSKI, and R. D. LUNDBERG. Macromolecules. **13**, 1679 (1980).
21. D. WOLLMANN and A. EISENBERG. To be published.
22. A. EISENBERG, H. FARB, and L. G. COOL. J. Polym. Sci. Part A-2. **4**, 855 (1966).

Can. J. Chem. Downloaded from www.nrcresearchpress.com by 88.85.125.76 on 09/07/12
For personal use only.

Xα local spin density calculations of the 1:1 hydrogen-bonded complexes formed by water, ammonia, and hydrogen fluoride

E. C. VAUTHIER
Département de Recherches Physiques, Université P. et M. Curie, 4 Place Jussieu, Paris, France

V. BARONE
Dipartimento di Chimica, Università di Napoli, via Mezzocannone 4, Napoli, Italia

C. MINICHINO
Dipartimento di Chimica, Università della Basilicata, Potenza, Italia

AND

S. FLISZÁR
Département de Chimie, Université de Montréal, C.P. 6128, Succ. A, Montréal (Qué), Canada H3C 3J7

Received December 7, 1989

This paper is dedicated to Professor Arthur S. Perlin on the occasion of his 67th birthday

E. C. VAUTHIER, V. BARONE, C. MINICHINO, and S. FLISZÁR. Can. J. Chem. **68**, 1233 (1990).

The dissociation energies of the 1:1 hydrogen-bonded complexes formed by NH_3, H_2O, and HF were computed in the LCGTO-Xα local spin density approximation using extended basis sets. Attention was given to the appropriate selection of α. The order of stability of the various complexes reflects well their acid–base properties, in general agreement with experimental data and refined post Hartree–Fock computations.

Key words: hydrogen bonds, Xα method, local spin density method.

E. C. VAUTHIER, V. BARONE, C. MINICHINO et S. FLISZÁR. Can. J. Chem. **68**, 1233 (1990).

Les énergies de dissociation des complexes à liaison hydrogène formés par NH_3, H_2O et HF ont été calculées dans l'approximation LCGTO-Xα à densité de spin locale, à l'aide de bases étendues. La sélection de la valeur appropriée de α a été analysée. L'ordre de stabilité de ces complexes traduit bien leurs propriétés acide–base, en bon accord avec résultats expérimentaux et les meilleurs calculs post Hartre–Fock.

Mots clés : liaisons d'hydrogène, méthode Xα, methode à densité spin locale.

Can. J. Chem. Downloaded from www.nrcresearchpress.com by 88.85.125.76 on 09/07/12
For personal use only.

Introduction

The importance of hydrogen bonding has long been recognized. This study considers the various possible 1:1 complexes formed by water, ammonia, and hydrogen fluoride on two counts, namely for the physics underlying hydrogen bond formation and as an illustration of applications of density functional theory (DFT) in energy calculations involving the Xα approximation (1) for solving the equations of the local spin density (LSD) approach (2).

The merits of DFT, by far the most useful non-empirical alternative to configuration interaction calculations, are well demonstrated by applications to inorganic chemistry (3), i.e, in an area where the familiar wave function methods meet with formidable computational demands. LSD is presently the method of choice for the more complex systems involving several "heavier" atoms, namely transition metals. In the LCGTO approach, where the molecular orbitals are expanded as linear combinations of Gaussian type orbitals, full advantage is taken from the standard techniques of traditional *ab initio* calculations, namely as regards optimizations of basis sets (4). In short, thanks to these developments, the LCGTO-Xα(LSD) form of DFT now represents a manageable tool for the study of inorganic systems.

As regards organic molecules, the LCGTO-Xα(LSD) method was recently tested (5) in calculations of their total (kinetic + potential) energies, using the computational technology developed by Dunlap, Connolly, and Sabin (6). The attempt was a successful one: calculated energies were generally well within experimental uncertainties. The tentative hypothesis was that the LCGTO-Xα(LSD) method effectively mimics correlated calculations, although there is presently no formal justification for this contention. Briefly, it was assumed in this brute force approach that the energy should be right if α is properly selected. Here we proceed with the same philosophy, building on the quality of the results obtained in this fashion, and offer simple didactic examples. This work should be regarded as a first exploration in the field of intermolecular interactions, with special reference to the energetics of hydrogen bond formation. Our motivation rests with the suspicion that, in spite of its acknowledged merits in the description of electronic properties (e.g., multipole moments, ionization potentials, and transition energies), the Xα approach still suffers from difficulties in coping with subtle energy differences. The emphasis is on the general aspects regarding the proper use of Xα(LSD) theory in the field of "non-bonded" interactions. Possible further numerical improvements are left to future considerations.

The selection of α

Ever since the appearance of the Xα method, the way of selecting α has been a fundamental problem (1, 7). This is where we stand with our projected calculations of dimerization energies. Our results indicate that the "correct" α values — i.e., the α's corresponding to experimental energies — of monomeric H_2O and NH_3 differ from one another by as much as ~0.005; approximately the same difference is found between HF and H_2O and, finally, the difference between NH_3 and HF is as high as ~0.01. Under these circumstances, how can we pick the appropriate α values for the various possible hydrogen-bonded complexes involving H_2O, NH_3, and HF? In the Xα approach, the total energy is linear in α, i.e., if $E^0 = E^0(\alpha^0)$ is the energy

Printed in Canada / Imprimé au Canada

Can. J. Chem. Downloaded from www.nrcresearchpress.com by 88.85.125.76 on 09/07/12
For personal use only.

obtained for α^0, that deduced for $\alpha = \alpha^\circ + \Delta\alpha$ is

$$[1] \quad E = E^0 + (\alpha - \alpha^0)(\partial E/\partial\alpha)$$

Clearly, a relatively small uncertainty in the estimate of α rapidly translates into a large error for E. For example, $\Delta\alpha = 0.001$ and $\partial E/\partial\alpha$ values ranging from -20.86 to -28.59 au for the complexes considered here correspond to errors of $\sim$13–18 kcal mol^{-1} in dimerization energy and would put a stop to our hopes of doing thermochemistry using Xα(LSD) calculations.

Now we focus attention on the selection of $\alpha = \alpha_{AB}$ for the complex AB formed from monomers A and B with α values α_B, respectively. We tentatively select a common α value, α^0, and calculate the energies E^0_A, E^0_B, and E^0_{AB} for the monomers (A and B) and the complex AB, respectively. The corresponding *correct* energies are, from eq. [1],

$$E_A = E^0_A + (\alpha_A - \alpha^0)(\partial E_A/\partial\alpha)$$

$$E_B = E^0_B + (\alpha_B - \alpha^0)(\partial E_B/\partial\alpha)$$

$$E_{AB} = E^0_{AB} + (\alpha_{AB} - \alpha^0)(\partial E_{AB}/\partial\alpha)$$

The dimerization energy $\Delta E = E_{AB} - E_A - E_B$ is thus

$$\Delta E = [E^0_{AB} - E^0_A - E^0_B] + (\alpha_{AB} - \alpha^0)(\partial E_{AB}/\partial\alpha) - (\alpha_A - \alpha^0)(\partial E_A/\partial\alpha) - (\alpha_B - \alpha^0)(\partial E_B/\partial\alpha)$$

The term in square brackets would represent the correct answer if, instead of α^0, we had used the correct α's throughout our calculations, namely, the appropriate α_A and α_B for the monomers and the correct α_{AB} for the complex. As things are, the term in square brackets differs in principle from the true ΔE, and the error is

$$(\alpha_{AB} - \alpha^0)(\partial E_{AB}/\partial\alpha) - (\alpha_A - \alpha^0)(\partial E_A/\partial\alpha) - (\alpha_B - \alpha^0)(\partial E_B/\partial\alpha)$$

Here we inquire under what conditions this error vanishes. The answer is the dimerization energy, $E^0_{AB} - E^0_A - E^0_B$, calculated for a common α^0 minimizes the error if we use $\alpha^0 = \alpha_{AB}$, with α_{AB} given by eq. [2]:

$$[2] \quad \alpha_{AB} = \frac{\alpha_A(\partial E_A/\partial\alpha) + \alpha_B(\partial E_B/\partial\alpha)}{(\partial E_A/\partial\alpha) + (\partial E_B/\partial\alpha)}$$

Of course, the same reasoning also holds for the formation of higher polymers, i.e.

$$[3] \quad \alpha = \frac{\Sigma_i n_i\alpha_i(\partial E_i/\partial\alpha)}{\Sigma_i n_i(\partial E_i/\partial\alpha)}$$

for a complex containing n_A, n_B, ... n_i molecules with α values α_A, α_B, ... α_i and derivatives $\partial E_A/\partial\alpha$, $\partial E_B/\partial\alpha$, ..., $\partial E_i/\partial\alpha$, respectively. Equation [3] is the same as that used earlier for molecules containing n_A, n_B, ..., n_i atoms A, B, etc., in which case α_i and $\partial E_i/\partial\alpha$ represent atomic parameters (5). Note that eqs. [2] and [3] follow from the linearity of E in α, eq. [1], which is an integral part of the Xα theory, in an approximation which neglects higher order terms due to wave function variations. In actual practice, the α's obtained from a match of Xα computations with experimental energies also reflect the approximations involved in the present form of Xα(LSD) theory, including the treatment of correlation, not to mention the orbital and auxiliary basis set limitations. Nevertheless, this analysis also indicates — and this is an important point — that any reasonable common α° ($\neq \alpha_{AB}$) will do for the computation of ΔE. Indeed, the residual error

$$(\alpha_{AB} - \alpha^0)[(\partial E_{AB}/\partial\alpha) - (\partial E_A/\partial\alpha) - (\partial E_B/\partial\alpha)]$$

is small because $(\partial E_{AB}/\partial\alpha) \simeq (\partial E_A/\partial\alpha) + (\partial E_B/\partial\alpha)$. This point has been verified by detailed calculations which indicate that the computed ΔE's are almost independent of α^0. The results reported in this work were obtained using eq. [2] and the α's corresponding to the experimental atomization energies of the monomers, a strategy which minimizes the errors and gives the atomization energies of the complexes with reference to the experimental energies of the atoms.

Thermochemical data

All Xα(LSD) calculations are made for molecules at 0 K when all the atoms are stationary in their equilibrium positions. The total ground-estate energy of a molecule is then

$$[4] \quad E = \Sigma_i E_i^{atom} - \Delta E_a^*$$

where E_i^{atom} is the ground-state energy of the isolated atom i and ΔE_a^* the atomization energy of that molecule. Let us first examine the data required for comparisons with experiment, namely, with dimerization enthalpies.

The energy of an isolated atom, E^{atom}, is taken (with the appropriate change in sign) as the sum of its ionization potentials. With the conversion factor 1 hartree = 27.2106 eV, we obtain from the tabulation given by Moore (8) $E_N^{atom} = -54.6121$, $E_O^{atom} = -75.1102$, $E_F^{atom} = -99.8065$, and $E_H^{atom} = -0.5$ hartree. These energies are used in calculations of E, eq. [4], together with the appropriate experimental ΔE_a^* results. The latter are deduced from eq. [5].

$$[5] \quad \Delta E_a^* = \Sigma_i n_i[\Delta H_f^0(A_i) - \frac{5}{2}RT] + \text{ZPE} + (H_T - H_0) - \Delta H_f^0$$

where ΔH_f^0 is the standard enthalpy of formation of the molecule in the gas phase and $\Delta H_f^0(A_i)$ that of the isolated atom A_i, with n_i = number of atoms A_i found in the molecule. We have used (9) $\Delta H_f^0(H) = 52.09$, $\Delta H_f^0(N) = 113.0$, $\Delta H_f^0(O) = 59.54$, and $\Delta H_f^0(F) = 18.86$ kcal mol^{-1} for the atoms and (10) $\Delta H_f^0(H_2O) = -57.80$, $\Delta H_f^0(NH_3) = -10.97$, and $\Delta H_f^0(HF) = -65.14$ (9) kcal mol^{-1} for the molecules. ZPE is the zero point energy (evaluated in the harmonic oscillator approximation) and $(H_T - H_0)$ the heat content. ZPE + $H_T - H_0$ values of 15.25 (H_2O), 22.94 (NH_3), and 7.99 kcal mol^{-1} (HF) were deduced from the vibrational frequencies given in ref. 11*a* (for H_2O and NH_3) and ref 11*b*, (for HF). Finally, we obtain from eqs. [4] and [5] the experimental energies $E = -76.4804$ (H_2O), -56.5858 (NH_3), and -100.5314 hartree (HF), with 1 hartree = 627.51 kcal mol^{-1}.

The dimerization energy ΔE_{dim} for the reaction A + B → AB is defined as follows

$$[6] \quad \Delta E_{dim} = E_{AB} - E_A - E_B$$

and the corresponding enthalpy change is, in the gas phase,

$$[7] \quad \Delta H_{298} = \Delta E_{dim} + \Delta(\text{ZPE} + H_T - H_0)$$

where $\Delta(\text{ZPE} + H_T - H_0)$ represents the value of the complex AB minus the values of the monomers A and B. We have used $\Delta(\text{ZPE} + H_T - H_0) = 1.663$ (water), 1.035 (ammonia), and 0.443 kcal mol^{-1} (hydrogen fluoride) (12). For the H_2O,HF complex we have deduced $\Delta(\text{ZPE} + H_T - H_0) = 1.72$ kcal mol^{-1} from the frequencies reported in ref. 13. Finally, for the H_2O,NH_3 and HF,NH_3 complexes, we have used frequencies calculated at the Hartree–Fock level in the basis described below for the geometries. Comparisons between calculated and observed frequencies of H_2O, NH_3, and HF indicated that (as usual) calculated frequencies should be reduced by $\sim$10%. A

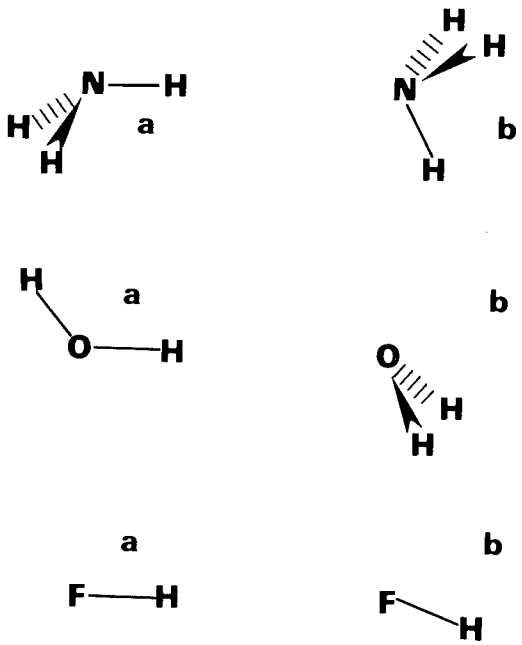

SCHEME 1. Positioning of the monomers as they occur in the complexes. The $H_2NH\cdots NH_3$, $H_2NH\cdots OH_2$, $HOH\cdots NH_3$, $HOH\cdots OH_2$, $HOH\cdots FH$, $FH\cdots NH_3$, $FH\cdots OH_2$, and $FH\cdots FH$ complexes are combinations of (*a*) and (*b*), where (*a*) always refers to the first molecule indicated in these formulas.

balanced evaluation led to $\Delta(ZPE + H_T - H_0) \simeq 1.84$ and 1.87 kcal mol^{-1} for the H_2O,NH_3 and HF,NH_3 complexes, respectively.

The stage is set. All we need now are the energies E_{AB} of the complexes. They are the target of our Xα(LSD) calculations.

Outline of LCGTO-Xα(LSD) calculations

The calculations were performed using the program developed by Dunlap, Connolly, and Sabin (6), which includes the fitting methods for the charge density and the Xα exchange potentials to sets of auxiliary Hermite gaussian functions and the use of two *s*-type bond-centered auxiliary functions. No bond-centered functions were used for the hydrogen bonds because tests indicated that they have no effect on the results. The sampling points for the exchange potentials were determined by taking each tenth point of the Herman–Skillman radial mesh (14) and an angular mesh consisting of the twelve vertices of a regular icosahedron (15) — a procedure which may require future attention for the reasons indicated below.

It is now well-known that the quantitative description of hydrogen bonds by HF + CI methods requires at least double ζ bases augmented by two sets of polarization functions and one set of diffuse functions. Since basis sets optimized at the HF level are generally also adequate for LSD computations (4) provided, of course, that reasonably extended, flexible bases are used, we have selected the following two orbital basis sets. For nitrogen and oxygen we started with Dunning's $(9s5p) \rightarrow [4s2p]$ set (16). For N we added one uncontracted *s* (ζ = 0.0639), one uncontracted *p* (ζ = 0.0639) (17), and two uncontracted *d* primitives (ζ = 0.90 and 0.13) (18). For oxygen, on the other hand, we added one *s* (ζ = 0.0845), one *p* (ζ = 0.0845), and two *d* functions (ζ = 1.04 and 0.14) (18). Fluorine was described using Dunning's $(10s6p) \rightarrow [10s4p]$ set (19) to which we added one uncontracted *s* (ζ = 0.1076), one uncontracted *p* (ζ = 0.1076) (17), and two *d* functions (ζ = 1.06 and 0.18) (18). For hydrogen we have used Dunning's $(5s) \rightarrow [3s]$ set (19), to which two *p* functions were added with ζ = 1.0 and 0.08 (18). This concludes the description of basis 1. Our basis 2 is the same as above, with the addition of one set of diffuse *p* functions on N (ζ = 0.048), on O (ζ = 0.059), and on F (ζ = 0.074) (20). The selected auxiliary functions were $(9s5p3d)$ for N and O, $(11s4p4d)$ for F, and $(5s5p)$ for H (5).

TABLE 1. α and $\partial E/\partial\alpha$ values for monomers[a]

Molecule		Basis 1 α	Basis 1 $\partial E/\partial\alpha$, au	Basis 2 α	Basis 2 $\partial E/\partial\alpha$, au
NH_3	(a)	0.774578	−10.426	0.774563	−10.426
	(b)	0.774182	−10.432	0.774154	−10.432
H_2O	(a)	0.769162	−12.234	0.769164	−12.233
	(b)	0.769469	−12.229	0.769464	−12.229
HF	(a)	0.764424	−14.291	0.764388	−14.290
	(b)	0.764420	−14.291	0.764423	−14.290

[a]Basis 1: $(9,5,2/5,2) \rightarrow [4,2,2/3,2]$ plus diffuse (*sp*) functions for H_2O and NH_3; $(10,6,2/5,2) \rightarrow [6,4,2/3,2]$ plus diffuse (*sp*) function for HF. Basis 2: the same, plus additional diffuse *p* functions for N, O, and F.

Although we have not performed a comprehensive study of basis set effects, test computations indicated that they are quite similar in HF + CI and in Xα(LSD) computations. For example, with the addition of two sets of polarization functions and one set of diffuse functions to a double ζ basis set, the computed Xα and MP2 dimerization energies of water decrease from 13 to 6.5 and from 12.7 to 5.4 kcal mol^{-1}, respectively.

Results

The equilibrium geometries of the monomers and the various complexes were fully optimized by means of conventional Hartree–Fock calculations using Dunning's double ζ basis (16) augmented with single polarization functions (20).[1] The corresponding dimerization energies fall in the usual range of HF results obtained from medium size basis sets, e.g. −5.0 (water), −2.4 (ammonia), and −5.1 kcal mol^{-1} (hydrogen fluoride). The structure of the water dimer resembles that deduced by Dannenberg (21) at the MP2/6-31G* level, with a slightly bent hydrogen bond. Now we can proceed with Xα(LSD) calculations.

The first step consists in an evaluation of the appropriate α and $\partial E/\partial\alpha$ parameters corresponding to the experimental energies of the monomers, for use in eq. [2]. This was easily done using an initial guess, α^0, for α, which yields an approximate value of $E^0 = E^0(\alpha^0)$. Next, we estimated an improved value, $\alpha = \alpha^0 + \Delta\alpha$, using the experimental energy and eq. [1], and repeated the procedure until convergence was attained. In prac-

[1]Hartree–Fock geometries were used here for practical convenience because they are presently easier to obtain via a simultaneous optimization of all geometrical parameters than in the Xα approach. It should be added that Xα equilibrium geometries of diatomic molecules are in general good agreement with their experimental counterparts, e.g., 1.74 (calcd.) vs. 1.73 bohr (exptl.) for HF. Hartree–Fock bond distances, on the other hand, are systematically too short, by ~0.02 bohr, both in the dimers and in the monomers. As a result, we benefit here from error cancellations in the computation of Xα dimerization energies, a point which was carefully tested for the HF dimer, using both Hartree–Fock and Xα bond distances, as well as available experimental data. The uncertainties associated with the present selection of geometries should not exceed ~0.15 kcal mol^{-1} in dimerization energy.

Can. J. Chem. Downloaded from www.nrcresearchpress.com by 88.85.125.76 on 09/07/12
For personal use only.

TABLE 2. Calculated energies of complexes for α values predicted by eq. [2] and corresponding $\partial E/\partial\alpha$ values

Complex	Basis 1			Basis 2		
	α	E	$\partial E/\partial\alpha$, au	α	E	$\partial E/\partial\alpha$, au
$H_2NH\cdots NH_3$	0.774380	−113.1790	−20.862	0.774358	−113.1795	−20.863
$H_2NH\cdots OH_2$	0.771820	−133.0739	−22.661	0.771811	−133.0737	−22.661
$HOH\cdots HN_3$	0.771472	−133.0804	−22.676	0.771461	−133.0803	−22.675
$HOH\cdots OH_2$	0.769315	−152.9713	−24.471	0.769314	−152.9714	−24.471
$HOH\cdots FH$	0.766607	−177.0183	−26.529	0.766610	−177.0185	−26.529
$FH\cdots NH_3$	0.768541	−157.1478	−24.749	0.768509	−157.1474	−24.748
$FH\cdots OH_2$	0.766750	−177.0336	−26.541	0.766729	−177.0336	−26.541
$FH\cdots FH$	0.764422	−201.0731	−28.591	0.764406	−201.0740	−28.591

TABLE 3. Reaction energies and enthalpies for hydrogen bond formation, kcal/mol

Complex	ΔE_{dim}			Δ(ZPE + H_T − H_0)	ΔH^0 (298.15 K)		
	Xα(1)	Xα(2)	MU[a]		Xα(1)	Xα(2)	Exp.[b]
$H_2NH\cdots NH_3$	−4.64	−4.96	−4.1	1.035	−3.60	−3.92	−4.1±0.4
$H_2NH\cdots OH_2$	−4.83	−4.71	−4.1				
$HOH\cdots NH_3$	−8.91	−8.85	−9.0	1.84	−7.07	−7.01	
$HOH\cdots OH_2$	−6.59	−6.65	−7.8	1.663	−4.93	−4.99	−5.2±1.5
$HOH\cdots FH$	−4.08	−4.20					
$FH\cdots NH_3$	−19.20	−18.95	−16.3	1.87	−17.33	−17.08	
$FH\cdots OH_2$	−13.68	−13.68	−13.4	1.72	−11.96	−11.96	−6.2±1.0
$FH\cdots FH$	−6.46	−7.03	−7.6	0.443	−6.02	−6.59	−7.0±1.5

[a]Results of Umeyama and Morokuma (23).
[b]The experimental results are extracted from ref. 24 ($H_2NH\cdots HN_3$); ref. 25 ($HOH\cdots OH_2$); ref. 26 ($FH\cdots OH_2$), and ref. 27 ($FH\cdots FH$).

tice, with a little experience as regards the initial guess, two calculations suffice. However, at this stage we met with a minor but disturbing computational imperfection — which is not there to stay — linked to the numerical fittings of the Xα exchange potentials: it turned out that the results slightly depend (≤0.3 kcal mol^{-1}) on how the reference axes are defined. To get around this difficulty, we positioned each monomer (with its own optimized geometry) as closely as possible as it is found in the complex. This simply means that each monomer had to be computed twice in order to determine the appropriate α and $\partial E/\partial\alpha$ parameters. The relative positions of the monomers are indicated in Scheme 1 and the results are given in Table 1. It is clear that, at this level, the enrichment of the basis set has little influence on the results. (The use of Huzinaga's (9*s*5*p*) orbital basis (22), which has proven adequate for the study of organic molecules, yield slightly higher α values (5)).

It is now straightforward to deduce the appropriate α's for the complexes from eq. [2] by means of the results given in Table 1. These are the α values which were used in our Xα(LSD) energy calculations for the complexes. The results are indicated in Table 2. Finally, with the help of the appropriate experimental energies of the monomers, the energies thus calculated for the complexes lead to the energies, eq. [6], and enthalpies, eq. [7], of dimerization indicated in Table 3.

In closing, our curiosity was attracted by the following point. The exchange-correlation energies $\alpha(\partial E/\partial\alpha)$, which are easily back-calculated from the data reported in Table 1 for the monomers and Table 2 for the complexes, change in going from the monomers to the corresponding complexes. Here we inquired about these changes by subtracting the $\alpha(\partial E/\partial\alpha)$ values of the monomers from those of the complexes: they appear to follow the pattern exhibited by the complexation energies (Table 4). These results are offered for what they are — namely, an observation which may, or may not, lend itself to future interpretations.

TABLE 4. Variation of exchange-correlation energies upon complex formation

Complex	ΔE_{xc}, kcal mol^{-1}	
	Basis 1	Basis 2
$H_2NH\cdots NH_3$	−1.9	−2.4
$H_2NH\cdots OH_2$	−2.9	−2.9
$HOH\cdots NH_3$	−4.8	−4.8
$HOH\cdots OH_2$	−3.9	−4.4
$HOH\cdots FH$	−1.9	−2.9
$FH\cdots NH_3$	−12.5	−12.5
$FH\cdots OH_2$	−10.1	−10.6
$FH\cdots FH$	−4.3	−5.3

Discussion

The calculated dimerization enthalpies of ammonia, water, and hydrogen fluoride nicely agree with their experimental counterparts (Table 3). There is some controversy, however, regarding the reported experimental values. For example, the result quoted for water (25) was obtained from infrared spectroscopy and is in line with experiments exploited in terms of the second virial coefficient, leading to $\Delta H_{298} = -5.5$ kcal mol^{-1} (28). The latter results were challenged (29) on the grounds of new measurements, suggesting $\Delta H_{298} = -3.6 \pm 0.5$ kcal mol^{-1}. We feel it is not our role to discuss the experimental aspects involved in the admittedly difficult measurements of

Can. J. Chem. Downloaded from www.nrcresearchpress.com by 88.85.125.76 on 09/07/12
For personal use only.

dimerization enthalpies. In the main, the experimental results can be classified as either "high" or "low", e.g. −5.2 vs. −3.7 for water and −7.0 vs. −4.6 kcal mol^{-1} for hydrogen fluoride (30). Our present Xα results consistently support the more negative values (Table 3). The theoretical results of Umeyama and Morokuma (23) also point in that direction. In contrast, the most recent Hartree–Fock + CI calculations favor the less negative results (31, 32). The difference between the present Xα and the HF + CI calculations using comparable basis sets is nearly constant for the dimers of NH_3, H_2O, and HF. As regards the $FH\cdots OH_2$ complex, in spite of the present differences between the two theoretical approaches and without engaging into any final assessment on the accuracy of our results, it seems clear that the experimental value quoted for the formation of this complex probably requires revision.

The questions concerning dimerization energies are not yet quite settled, neither on the experimental nor on the theoretical side. As regards the Xα approach, additional investigations are certainly in order. On the whole, however, even in this first brute force attempt, Xα(LSD) theory has revealed its promising potential, perhaps beyond expectation. In any case, our results consistently reflect the trends in the complexation energy which would be anticipated from a consideration of the basicities and/or acidities of the species involved.

Conclusions

The use of the Xα approximation for solving the LSD equations raises the notorious problem concerning the appropriate selection of α. It now appears that the α to be used in energy calculations of a molecular complex is the weighted average of the α's of the individual molecules entering the composition of that complex. This result is a direct consequence of the linear dependence of the energy on α, which is an integral part of Xα(LSD) theory, and does not involve the introduction of any new hypothesis. The results thus obtained mirror the genuine qualities of the Xα(LSD) method. The formation of hydrogen bonded complexes — an example where small errors in the evaluation of α rapidly translate into important errors in computed dimerization energies — illustrates the merits of the present LCGTO-Xα(LSD) approach. Calculated complexation energies are of the quality of conventional post Hartree–Fock computations, thus suggesting that, in its present form, correlation has been effectively (though not explicitly) incorporated in our applications of Xα(LSD) theory. Beyond the absolute numerical values, the point is that this theory is adequate both in systems consisting of light atoms (in which case correlation is only a perturbation to the HF treatment) and in situations involving heavy atoms, i.e., systems still lying outside the reach of conventional HF + CI computations because of the huge amount of many-body effects.

Can. J. Chem. Downloaded from www.nrcresearchpress.com by 88.85.125.76 on 09/07/12
For personal use only.

Acknowledgements

The financial support given by the Natural Sciences and Engineering Research Council of Canada is gratefully acknowledged. We thank the "Conseil Scientifique du Centre de Calcul Vectoriel pour la Recherche (CCVR)", École Polytechnique de Palaiseau, France, for computational facilities made available.

1. W. Kohn and L. J. Sham. Phys. Rev. **140**, A1133 (1965); R. Gáspár. Acta Phys. Acad. Sci. Hung. **3**, 263 (1954); J. C. Slater. Phys. Rev. **81**, 385 (1951); J. C. Slater. Adv. Quantum Chem. **6**, 1 (1972); J. C. Slater. The self-consistent field for molecules and solids. Vol. 4. McGraw-Hill, New York. 1974.
2. U. von Barth and L. Hedin. J. Phys. C: Solid State Phys. **5**, 1629 (1972).
3. D. R. Salahub. Adv. Chem. Phys. **69**, 447 (1987); J. P. Dahl and J. Avery (*Editors*). Local density approximation in quantum chemistry and solid state physics. Plenum, New York. 1984; S. Lundqvist and N. H. March (*Editors*). Theory of the inhomogeneous electron gas. Plenum, New York. 1983.
4. J. Andzelm, E. Radzio, and D. R. Salahub. J. Comput. Chem. **6**, 520 (1985); E. Radzio, J. Andzelm, and D. R. Salahub. J. Comput. Chem. **6**, 533 (1985).
5. S. Fliszár, S. Rioux, J. Andzelm, C. Minichino, and E. C. Vauthier. Can. J. Chem. **66**, 3166 (1988); S. Fliszár. *In* NATO ASI Series, 1989. In press.
6. B. I. Dunlap, J. W. D. Connolly, and J. R. Sabin. J. Chem. Phys. **71**, 4993 (1970); H. Sambe and R. H. Felton. J. Chem. Phys. **62**, 1122 (1975).
7. R. Gáspár and Á. Nagy. Theoret. Chim. Acta, **72**, 393 (1987); Á. Nagy. Int. J. Quantum Chem. **31**, 269 (1987); R. Gáspár. Acta Phys. **35**, 213 (1974); K. Schwarz. Phys. Rev. B, **5**, 2466 (1972).
8. C. E. Moore. Natl. Stand. Ref. Data Ser. (US Natl. Bur. Stand.) NSRD-NBS, **34**, 1 (1970).
9. D. R. Stull and G. C. Sinke. Adv. Chem. Ser. **18**, 1 (1956).
10. J. D. Cox and G. Pilcher. Thermochemistry of organic and organometallic compounds. Academic Press, London, New York. 1970; M. W. Chase, J. L. Curnutt, J. R. Downey, R. A. McDonald, A. N. Syverud, and E. A. Valenzuela. JANAF thermochemical tables, 1982 (Supplement); J. Phys. Chem. Ref. Data, **11**, (3), 695 (1982).
11. (*a*) G. Herzberg. Molecular spectra and molecular structure. II. Infrared and Raman spectra of polyatomic molecules. D. van Nostrand Reinhold Co., New York. 1968; (*b*) G. Herzberg. Molecular spectra and molecular structure. Spectra of diatomic molecules. D. van Nostrand Co., Inc., Princeton, NJ. 1967.
12. P. A. Kollman. *In* Modern theoretical chemistry. Vol. IV. Methods of electronic structure theory. *Edited by* H. Schaefer. Plenum, New York. 1988. Chap. 3.
13. D. G. Lister and P. Palmieri. J. Mol. Struct. **39**, 295 (1977).
14. F. Herman and S. Skillman. Atomic structure calculations. Prentice-Hall, Englewood Cliffs, NH. 1963.
15. A. H. Stroud. Approximate calculation of multiple integrals. Prentice-Hall, Englewood Cliffs, NJ. 1971.
16. T. H. Dunning, Jr. J. Chem. Phys. **53**, 2823 (1970).
17. T. Clark, J. Chandrasekhar, J. W. Spitznagel, and P. von R. Schleyer. J. Comp. Chem. **4**, 294 (1983).
18. J. G. C. M. van Duijneveldt-van de Rijdt and F. B. van Duijneveldt. J. Mol. Struct. **89**, 185 (1982).
19. T. H. Dunning, Jr. J. Chem. Phys. **55**, 716 (1971).
20. P. J. Hay and T. H. Dunning, Jr. *In* Modern theoretical chemistry, methods of electronic structure theory. Vol. III. *Edited by* H. Schaefer. Plenum, New York. 1977. p. 10.
21. J. J. Dannenberg. J. Phys. Chem. **92**, 6869 (1988).
22. S. Huzinaga. J. Chem. Phys. **42**, 1293 (1965).
23. H. Umeyama and K. Morokuma. J. Am. Chem. Soc. **99**, 1316 (1977).
24. J. E. Lowder. J. Quant. Spectrosc. Radiation Transfer, **10**, 1085 (1970).
25. H. A. Gebbie, W. J. Burrough, J. E. Harris, and R. J. Jones. Nature, **221**, 143 (1969).
26. R. K. Thomas. Proc. R. Soc. London, A, **344**, 579 (1975).
27. E. U. Franck and F. Meyer. J. Electrochem. **63**, 577 (1959).
28. R. A. Bohlander and H. A. Gebbie. Nature (London), **253**, 523 (1975).
29. L. A. Curtiss, D. J. Frurip, and M. Blander. J. Chem. Phys. **71**, 2703 (1970).
30. L. A. Curtiss and M. Blander. Chem. Rev. **88.** 827 (1988).
31. K. Szalewicz, S. J. Cole, W. Kolos, and R. J. Bartlett. J. Chem. Phys. **89**, 3662 (1988).
32. M. Kofranek, H. Lischka, and A. Karpfen. Chem. Phys. **121**, 137 (1988).

NMR and conformational study of branched oligosaccharides containing 2,3-disubstituted residues of α-L-rhamnose

GRIGORY M. LIPKIND, NIKOLAY E. NIFANT'EV, ALEXANDER S. SHASHKOV, AND NIKOLAY K. KOCHETKOV
N. D. Zelinsky Institute of Organic Chemistry, Academy of Sciences of the U.S.S.R., Moscow, U.S.S.R.

Received December 18, 1989

This paper is dedicated to Professor Arthur S. Perlin on the occasion of his 67th birthday

GRIGORY M. LIPKIND, NIKOLAY E. NIFANT'EV, ALEXANDER S. SHASHKOV, and NIKOLAY K. KOCHETKOV. Can. J. Chem. **68**, 1238 (1990).

^1H and ^{13}C NMR spectra have been recorded and the nuclear Overhauser enhancements (in D_2O), after pre-irradiation of the anomeric protons, have been measured for tri- and tetrasaccharides containing 2,3-disubstituted residues of α-L-rhamnose and the corresponding disaccharides. The proximity of the conformational states of the disaccharide units in these branched oligosaccharides and in the corresponding disaccharides has been shown, on the basis of both the nOe experimental data and theoretical conformational analysis. This conclusion is also confirmed by data for glycosylation effects in the ^{13}C NMR spectra of the oligosaccharides.

Key words: branched oligosaccharides, ^1H and ^{13}C NMR spectra, conformations.

GRIGORY M. LIPKIND, NIKOLAY E. NIFANT'EV, ALEXANDER S. SHASHKOV et NIKOLAY K. KOCHETKOV. Can. J. Chem. **68**, 1238 (1990).

On a déterminé les spectres RMN du ^1H et du ^{13}C et on a évalué les eOn (dans le D_2O, après irradiation des protons anomériques) de tri- et de tétrasaccharides contenant des résidues 2,3-disubstitués du α-L-rhamnose ainsi que des disaccharides correspondants. En se basant sur les données expérimentales relatives aux eOn ainsi que sur les résultats d'une analyse conformationnelle théorique, on a montré que les états conformationnels des unités disaccharides de ces oligosaccharides ramifiés ressemblent à ceux des disaccharides correspondants. Cette conclusion est confirmée par les données relatives aux effets de glycosylation sur les spectres RMN de ^{13}C des oligosaccharides.

Mots clés : oligosaccharides ramifiés, spectres RMN du ^1H et du ^{13}C, conformations.

[Traduit par la revue]

Can. J. Chem. Downloaded from www.nrcresearchpress.com by 88.85.125.76 on 09/07/12
For personal use only.

Introduction

The spatial shape of branched polysaccharides depends mainly on the conformational features of the branch points. The branch points with vicinal substitution are the most conformationally rigid, because in this case the chemically nonbonded monosaccharide residues are in close proximity and interact with one another. The conformational properties of such branched oligosaccharides may cause considerable anomalies in chemical shift values in the NMR spectra, as is clear from the spectral data for both the branch points and the corresponding disaccharide fragments (1). The analysis of such differences in chemical shifts is important both for study of the spatial structure of branched oligosaccharide chains and for the extension of computer analysis of natural polysaccharide structures (on the basis of ^{13}C NMR data (2)) to the case of branched polysaccharides.

We earlier studied ^1H and ^{13}C NMR spectra and carried out the conformational analysis for several branched trisaccharides containing the galactose residue bis-glycosylated both at O3,O4 (3) and O2,O3 (4). These ^{13}C NMR data allowed us to carry out the primary structure analysis of branched polysaccharides containing a galactose residue at the branch point (5).

The present work deals with conformational analysis, on the basis of both NMR and theoretical calculations, for α-methylglycosides of branched trisaccharides with vicinal substitution at positions 2 and 3 of the α-L-rhamnopyranose residue. Such an investigation allows us to examine the stereochemical case when one of the vicinal substituents is equatorial and the other one axial, with neighbouring positions (1 and 4 in our case) lacking bulky substituents, i.e., a hydroxymethyl group.

The trisaccharides **1–4** of common formula:

X(1–2([Y(1–3)] αLRha-*O*Me

1 X = Y = αLRha

2 X = Y = βDGlc

3 X = Y = αDMan

4 X = Y = βLFuc

have been examined. The trisaccharides **1–4** differ from each other either by the absolute configuration of the substituents (D, L) or by the configuration of their anomeric centres (α, β). At the same time each separate trisaccharide has the same glycosyl residue.

It is important to mention that the anomeric centre of the rhamnose residue in the branch point has the α configuration in all examples. This choice is due to the α configuration of (1–2)-linked mannose and rhamnose residues in the overwhelming majority of natural polysaccharides (6).

Besides the trisaccharides **1–4**, we examined the tetrasaccharide **5** containing the same branched trirhamnose fragment as **1**:

αLRha(1–2)[αLRha(1–3)]αLRha(1–2)αLRha-OMe

5

as well as the trisaccharide **6** of the main chain of this tetrasaccharide:

αLRha(1–2)αLRha(1–2)αLRha-OMe

6

The comparison of the spectral and conformational properties of oligosaccharides **1**, **5**, and **6** was made to prove the competence of "trisaccharide approximation" for the branch points in oligo- and polysaccharides.

We need data concerning model disaccharides of the following type:

Printed in Canada / Imprimé au Canada

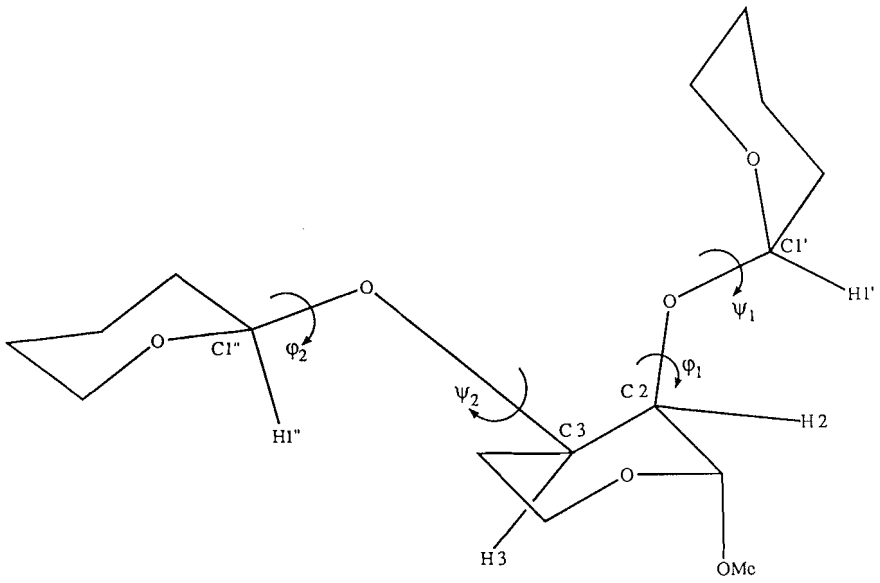

SCHEME 1

X(1–2)αLRha-OMe and Y(1–3)αLRha-OMe

7 X = αLRha	**8** Y = αLRha
9 X = βDGlc	**10** Y = βDGlc
11 X = αDMan	**12** Y = αDMan
13 X = βLFuc	**14** Y = βLFuc

Since the disaccharides **7–10** were investigated previously (7, 8), we present the new data only for the disaccharides **11–14**.

It is well known that the experimental data essential for conformational analysis, and which could be obtained from ^{1}H NMR spectra, are the values of the nOe's, which reflect the spatial proximity of different protons in the molecule. Thus the nOe values caused by pre-irradiation of the anomeric protons in oligosaccharides **1–6** and **11–14** have been measured. As far as concerns ^{1}H NMR spectra recorded for solutions in D_2O, the nOe parameters reflect the conformational states of the oligosaccharides in aqueous solution. Here we also pay attention to the glycosylation effects in ^{13}C NMR spectra of oligosaccharides **1–14**, which are sensitive to conformations of the glycosidic linkages.

Theoretical conformational analysis of the oligosaccharides was carried out on the basis of molecular mechanics using atom – atomic potential functions.

The angles of rotation around the interunit glycosidic linkage are the conformational parameters of oligosaccharide chains. For the trisaccharides **1–4** these angles are given in Scheme 1. The angles of rotation around the C1′—O and O—C2 bonds of the X(1–2)αLRha units are designated respectively as φ_1 and ψ_1. For units Y(1–3)αLRha the angles of rotation around the C1″—O and O—C3 bonds are respectively φ_2 and ψ_2. The primed numbers refer to the X residue and the double primed numbers to the residue Y. All four angles are zero for the *cis* orientation of the corresponding C—H and C—O bonds.

Results and discussion

The nOe data obtained by pre-irradiation of H-1′ and H-1″ residues X and Y in **1–4** are given in Table 1. The nOe data for the tetrasaccharide **5** and the linear trisaccharide **6** are given in Table 2. The data in Tables 1 and 2 show that the nOe's were observed not only for the resonances of protons related to the pre-irradiated monosaccharide or glycosylated moiety but also for those of protons of the other monosaccharide moiety (e.g., Y, after pre-irradiation of H-1′ of X in the trisaccharide **1**).

For purposes of comparison of the nOe values for disaccharide units in branched trisaccharides with those for the corresponding disaccharides, the nOe data for **7–14** are listed in Table 3.

Calculation of the optimal conformations of **1–6** was based on minimization of the potential energies of the molecules by variation of φ_1, ψ_1, φ_2 and ψ_2, using, as initial approximations, the data on the optimal conformations for the disaccharide units of **1–6** (7, 8).

After determination of the lowest-energy conformer of the trisaccharide, the cross section of its potential surface was drawn (conformational maps), φ_1–ψ_1 (with φ_2 and ψ_2 fixed at their optimal values) and φ_2–ψ_2 (with φ_1 and ψ_1 at the optimal values). Such conformational maps demonstrate the range of admissible values of the rotation angles in the trisaccharide being studied.

The parametrization of the force field for calculations of branched trisaccharide conformations is given in ref. 3. It was shown that the energy of nonbonded interactions for the disaccharide units of trisaccharides was best calculated using the Scott and Scheraga function (9), and interactions of the nonbonded carbohydrate residues, using the Momany *et al.* (10) or Zhurkin *et al.* (11) potentials, suggested for the calculation of molecular packing in crystals. As was shown (12), the potentials in the calculations of the conformations of oligosaccharides in aqueous solution are those of "medium force". The parametrization of other minor components of the energy is also dealt with in ref. 8. The data on the structures of the anomers of Glc, Man, Rha residues for conformational calculations were taken from neutron diffraction studies (13–15). The coordinates of the βLFuc residue were obtained by mirror reflection of the βDGal residue coordinates (16). The valency angle of the glycoside-bond oxygen (17) was an average value (116.7°).

The conformational analysis of **1–4** allowed both calculation of the nOe's and comparison with the experimental values. The variation of signal intensity f_s^d for a proton d on pre-irradiation of a proton s can be calculated using the formula reported by

Can. J. Chem. Downloaded from www.nrcresearchpress.com by 88.85.125.76 on 09/07/12
For personal use only.

TABLE 1. The nOe (%) observed upon pre-irradiation of anomeric protons of the trisaccharides **1–4**

Trisaccharide	Observed nOe			
	Pre-irradiation of H-1′		Pre-irradiation of H-1″	
αLRha(1–2)αLRha-OMe αLRha(1–3)αLRha-OMe **1**	H-2,2′	14.6(1)	H-2″	8.0(0.8)
	H-1	0.5	H-3	10.6(1)[a]
	H-3″,5″	5.1(0.3)	H-2	2.2(0.2)
βDGlc(1–2)αLRha-OMe βDGlc(1–3)αLRha-OMe **2**	H-3′,5′	17.0(1.7)	H-3″,5″	19.0(2.0)
	H-2	9.6(1)	H-3	9.3(1.0)
αDMan(1–2)αLRha-OMe αDMan(1–3)αLRha-OMe **3**	H-2′	7.8(1.3)	H-2″,3	19.2(2.0)
	H-2	5.8(1.0)	H-2	9.8(1.0)
	H-1	7.2(1.2)	H-5′	3.8(0.4)
βLFuc(1–2)αLRha-OMe βLFuc(1–3)αLRha-OMe **4**	H-2′[b]		H-2″[b]	
	H-3′	6.4(1.0)	H-3″	7.7(0.8)
	H-5′	9.5(1.4)	H-5″	8.5(0.9)
	H-1	6.2(1.0)	H-2	3.2(0.3)
	H-2	6.4(1.0)	H-3	9.3(1.0)

[a]The relative nOe values are given in parentheses. The nOe value for the α-proton of the aglycon was accepted as unity.

[b]The nOe was not determined due to a "pseudo-indor" effect, as a consequence of the close location of the H-1′ and H-1″ signals.

TABLE 2. The nOe (%) observed upon pre-irradiation of anomeric protons of the oligosaccharides **5** and **6**

Oligosaccharide	Observed nOe					
	Pre-irradiation of H-1′[a,b]		Pre-irradiation of H-1″		Pre-irradiation of H-1	
5	H-2′	7.5	H-2″	7.5	H-2	6.1
	H-2	10.8	H-3	11.5	H-5′	5.0
	H-3″,5″	6.5	H-2	1.1	H-2‴	13.4
6	[c]		[c]		H-2	5.8
					H-5′	6.2
					H-2‴	12.3
					H-1‴	0.3

[a]Numeration of the protons H-1, H-1′ and H-1″ is the same as in the trisaccharides **1–4**; H-1‴ is the anomeric proton of the "reducing" rhamnopyranose residue.

[b]Protons with one, two, and three primes and without primes correspond to terminal non-reducing, reducing, and middle rhamnopyranose residues respectively.

[c]The nOe values upon pre-irradiation of H-1′ and H-1″ are not determined because of the overlap of H-1′ and H-1″ signals.

Shirmer *et al.* (18), taking into account the influence of adjacent protons on the nOe for proton d. For the comparison with the experimental data, the average values of the nOe $\langle f_s^d \rangle$ (s = H-1, H-1′, H-1″) were calculated and Boltzmann probabilities were considered for all possible conformations of each trisaccharide:

$$\langle f_s^d \rangle = \frac{\sum_{\varphi_1}\sum_{\psi_1}\sum_{\varphi_2}\sum_{\psi_2} (f_s^d)_{\varphi_1,\psi_1,\varphi_2,\psi_2} \exp(-\Delta U_{\varphi_1,\psi_1,\varphi_2,\psi_2}/kT)}{\sum_{\varphi_1}\sum_{\psi_1}\sum_{\varphi_2}\sum_{\psi_2} \exp(-\Delta U_{\varphi_1,\psi_1,\varphi_2,\psi_2}/kT)}$$

To minimize the time on the computer, only those values of φ and ψ that correspond to conformations with relative energy ≤3 kcal/mol on cross sections of the potential surface were considered. Each step in the accepted range was 10°.

The optimal values of φ_1, ψ_1, φ_2, and ψ_2 in the lowest-energy conformations of **1–4** are listed in Table 4, as well as calculated values of the nOe f_s^d for the optimal conformers. Table 5 contains the calculated values of the nOe $\langle f_s^d \rangle$ and their relative values used for comparison with the corresponding observed values. The deviations from additivity in the ^{13}C NMR spectra of **1–4** are given in Table 6. Tables 7 and 8 contain ^1H and ^{13}C NMR spectral data for **1–14** (see Experimental).

αLRha(1–2)[αLRha(1–3)]αLRha-OMe (*1*)

As well as for the disaccharides **7** and **8** (Table 3), pre-irradiation of H-1′ and H-1″ in **1** caused considerable nOe, first of all on the protons of the carbon atoms forming the glycosidic linkages, H-2 and H-3 (Table 1). At the same time the considerable nOe between protons of the nonbonded rhamnose residues in **1** has been observed. The pre-irradiation of H-1′ of the X residue caused an nOe for the resonances of H-3″ and H-5″ of Y to have a total value of 5.1% (Table 1). This effect is clearly seen in the nOe spectrum of the trisaccharide **1** (Fig. 1) obtained upon pre-irradiation of H-1′. This result demonstrates the close proximity of the X and Y rhamnose residues, first of all in the region of H-1′ and H-3″, H-5″.

After minimization of the potential energy, two low-energy conformers of the trisaccharide **1** have been found, in which units with (1–2) and (1–3) bonds with equal conformational states are presented, AA in one case and BB in the other (Table 4). The symbols A and B correspond to optimal conformations with the rotation angles φ and ψ (50, 20° and 40, −30° respectively) for the disaccharides **7** and **8** (see Table 3 in refs. 7 and 8). The molecular model of the optimal conformation BB of the trisaccharide **1** is presented in Fig. 2.

Conformations AB and BA for the trisaccharide **1** have high energy, shown in the cross section of the potential surface of the trisaccharide **1** (Fig. 3). If the (1–3)-bonded unit has conformation B with $\psi_2 < 0°$ (Fig. 3b), then the (1–2)-bonded unit may also have only negative values of ψ_1 (conformation B). In this case the region of positive values of ψ_1, which corresponds to

Can. J. Chem. Downloaded from www.nrcresearchpress.com by 88.85.125.76 on 09/07/12
For personal use only.

TABLE 3. The nOe (%) observed upon pre-irradiation of anomeric protons H-1′ of the disaccharides **7**–**14**

Disaccharide	Observed nOe						
	H-1	H-2	H-2,2′	H-2′	H-2′,5′	H-3′	H-5′
αLRha(1–2)αLRha-OMe **7**		8.6		5,6			
βDGlc(1–2)αLRha-OMe **9**	1.0	10.5			11.5	8.9	
αDMan(1–2)αLRha-OMe **11**	7.1		15.9				
βLFuc(1–2)αLRha-OMe **13**	4.1	8.1				4.9	6.7
	H-2	H-3	H-2′	H-3′	H-5′	H-3′,5′	
αLRha(1–3)αLRha-OMe **8**		11.0	9.1				
βDGlc(1–3)αLRha-OMe **10**		4.6	1.8			7.5	
αDMan(1–3)αLRha-OMe **12**	10.0	5.7	7.5				
βLFuc(1–3)αLRha-OMe **14**	4.9	9.1		6.0	7.8		

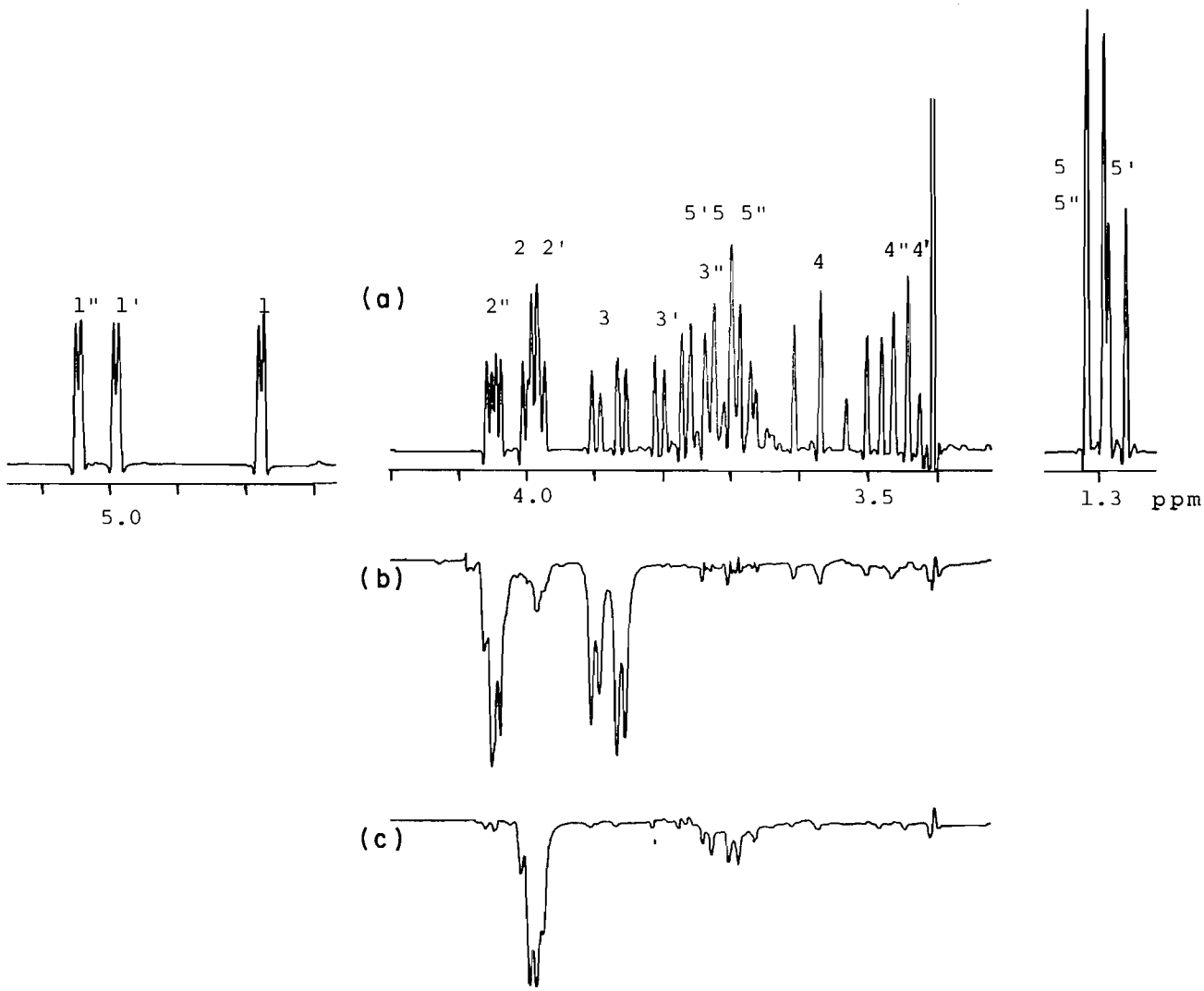

FIG. 1. (a) The ^{1}H NMR spectrum of the trisaccharide **1** αLRha(1–2)[αLRha(1–3)]αLRha-OMe. The nOe spectra obtained by pre-irradiation of (b) H-1″ and (c) H-1′.

state A, becomes energetically forbidden (Fig. 3a) for inadmissible proximity of X and Y residues. However, if the (1–3)-bonded unit has conformation A, then the (1–2)-bonded unit strives for state A as well (Fig. 3c), because in this case the optimal packing of the two nonbonded rhamnose residues X and Y is possible. At the same time, in each unit of the trisaccharide **1**, both preferred conformers A and B for the disaccharides **7** and **8** are possible.

As for conformers C (φ, ψ −40, −20°) of the disaccharides **7** and **8** (7, 8) with a *trans* orientation of the aglycon along the

Can. J. Chem. Downloaded from www.nrcresearchpress.com by 88.85.125.76 on 09/07/12
For personal use only.

Can. J. Chem. Downloaded from www.nrcresearchpress.com by 88.85.125.76 on 09/07/12
For personal use only.

TABLE 4. Angles of rotation (deg), energies E (kcal/mol), and the calculated nOe values f_s^d (%) for optimal conformations of the trisaccharides **1–4**

Trisaccharide	Conformer	φ_1	ψ_1	φ_2	ψ_2	E	nOe on pre-irradiation of H-1′ H-1	H-2	H-2″	H-3″	H-5″	H-1″ H-2	H-3	H-5′
1	AA	55.0	13.5	60.3	15.1	−7.4		10		15			11	
	BB	39.0	−37.1	49.2	−25.1	−8.2	1	17			6		20	
2	AB	57.7	19.0	53.9	−28.8	−7.1		14	6				19.5	
	BB	40.6	−24.1	39.0	−48.0	−6.7		22					18.0	
3	AA	−59.0	−37.6	−61.5	−35.1	−8.7	29	4				14	4	6.5
4	AA	−56.9	−25.1	−54.1	−39.0	−6.8	24	5				22	4	
	BB	−20.0	36.8	−21.3	35.0	−5.6		25					20	

TABLE 5. The calculated average nOe values $\langle f_s^d \rangle$ (%) as well as their relative values (in parentheses)

Trisaccharide	Observed nOe: Pre-irradiation of H-1′		Pre-irradiation of H-1″	
1	H-2′	13.5(0.8)	H-2″	14(0.8)
	H-1	2(0.1)	H-2	1.5(0.1)
	H-2	17(1.0)	H-3	17(1)
	H-3″ H-5″	4 5(0.5)		
2	H-2′	7(0.4)	H-2″	6(0.3)
	H-3′ H-5′	18 18(1.9)	H-3″ H-5″	16 17(1.8)
	H-1	2(0.1)	H-3	18(1.0)
	H-2	19(1.0)		
	H-2″	2(0.1)		
3	H-2′	11.1(1)	H-2″	10.3(1)
	H-1	16(1.4)	H-2	10.1(1)
	H-2	11.1(1)	H-3	10.5(1)
			H-5′	3.1(0.3)
4	H-3′	6.4(1.0)	H-3″	7.7(0.8)
	H-5′	9.5(1.4)	H-5″	8.5(0.9)
	H-1	6.2(1)	H-2	3.2(0.3)
	H-2	6.4(1)	H-3	9.3(1)

TABLE 6. Deviations from additivity Δ^a (ppm) in ^{13}C NMR spectra of the trisaccharides **1–4** for C-1–C-6, C-1′, and C-1″ atoms

Trisaccharide	C1	C2	C3	C4	C5	C6	C1′	C1″
1	0.6	−0.2	0.2	0.5	0.3	0.6	−0.4	0.3
2	0.6	−0.5	−0.2	−0.4	0.1	0.0	−0.2	0.1
3	0.2	0.5	0.2	0.1	0.0	0.1	0.0	0.4
4	0.1	−0.8	0.4	−0.6	−0.2	0.0	−0.3	0.6

[a] $\Delta = \delta_{exp.} - \delta_{calc.}$; $\delta_{calc.} = \delta_1 + \delta_2 - \delta_{MR}$, where $\delta_{exp.}$ and $\delta_{calc.}$ are observed and calculated chemical shifts of carbon atoms in the trisaccharides; δ_1 and δ_2 in the (1–2)- and (1–3)-linked disaccharides; δ_{MR} in methyl-α-L-rhamnopyranoside.

C1′—O5′ bond (thought to be unfavorable due to the *exo*-anomeric effect (19)), these are not stabilized in the case of the trisaccharide **1** by additional dispersion interactions of the X and Y residues; that is why the corresponding conformers (AC, CC etc.) have high energy.

The results of conformational analysis for the trisaccharide **1** are in accordance with the observed nOe values. If in the conformation AA protons H-1′ and H-3″ are in close proximity (r(H-1′–H-3″) = 2.4 Å), then in the conformation BB (Fig. 2) the protons H-1′ and H-5″ become close (r(H-1′–H-5″) = 2.4 Å). The equilibrium of the two forms causes the nOe's for the resonances on both H-3″ and H-5″ protons upon pre-irradiation of H-1′. In fact the calculated value of $f_{H\text{-}1'}^{H\text{-}3''}$ in the AA conformation is 15% ($f_{H\text{-}1'}^{H\text{-}5''}$ = 0%), while the value $f_{H\text{-}1'}^{H\text{-}5''}$ in the BB conformation is 6% ($f_{H\text{-}1'}^{H\text{-}3''}$ = 0%, Table 4). The calculated average values of $\langle f_{H\text{-}1'}^{H\text{-}3''} \rangle$ and $\langle f_{H\text{-}1'}^{H\text{-}5''} \rangle$ turn out to be almost equal (4 and 5% respectively, Table 5). We also note that, in accordance with experimental data (Table 1), the ratio of sums of the average values $(\langle f_{H\text{-}1'}^{H\text{-}3''} \rangle + \langle f_{H\text{-}1'}^{H\text{-}5''} \rangle)/(\langle f_{H\text{-}1'}^{H\text{-}2'} \rangle + \langle f_{H\text{-}1'}^{H\text{-}2'} \rangle)$ is approximately 1:3 (Table 5).

TABLE 7. ^{1}H NMR data for oligosaccharides **1**–**6** and **11**–**14** (D_2O)

Compound	Residue	Chemical shifts (ppm)								Coupling constants (Hz)						
		H-1	H-2	H-3	H-4	H-5	H-6	H-6′	OMe	$J_{1,2}$	$J_{2,3}$	$J_{3,4}$	$J_{4,5}$	$J_{5,6}$	$J_{5,6'}$	$J_{6,6'}$
1	αLRha-(1→2)	5.01	4.01	3.80	3.45	3.75	1.29			1.6	3.4	9.6	9.6	6.2		
	αLRha-(1→3)	5.06	4.06	3.73	3.48	3.71	1.32			1.7	3.4	9.6	9.6	6.2		
	αLRha-OMe	4.80	4.01	3.90	3.59	3.73	1.32		3.42	1.6	3.4	9.6	9.6	6.2		
2	βDGlc-(1→2)	4.67	3.36	3.52	3.41–3.48		3.92	3.75		7.9	9.1	9.1		1.7	4.4	12.9
	βDGlc-(1→3)	4.71	3.33	3.46	3.41–3.48		3.89	3.72		8.0	9.1	9.1		1.7	4.5	12.8
	αLRha-OMe	4.94	4.30	3.96	3.66	3.74	1.32		3.41	1.7	3.1	9.4	9.4	6.0		
3	αDMan-(1→2)	4.97	3.94	3.84	3.70	3.69[a]	3.82[a]	3.82[a]		1.8	3.4	9.9	9.9			
	αDMan-(1→3)	5.01	3.92	3.86	3.68	3.84[a]	3.82[a]	3.82[a]		1.6	3.5	9.9	9.9			
	αLRha-OMe	4.86	4.19	3.89	3.54	3.71	1.30		3.39	1.7	3.5	9.6	9.6	6.3		
4	βLFuc-(1→2)	4.45	3.51	3.62	3.74	3.76	1.26			7.9	9.8	3.4	1.0	6.6		
	βLFuc-(1→3)	4.50	3.54	3.65	3.73	3.78	1.25			7.9	9.8	3.4	1.0	6.4		
	αLRha-OMe	4.85	4.23	3.92	3.55	3.71	1.32		3.41	1.8	3.6	9.7	9.7	6.2		
5	αLRha-(1→2)	5.00	3.99	3.78	3.42	3.73	1.30			1.7	3.3	9.5	9.5	6.4		
	αLRha-(1→3)	5.07	4.05	3.71	3.46	3.75	1.31			1.8	3.3	9.6	9.6	6.3		
	→2,3)-αLRha-(1→2)	5.12	4.16	3.95	3.59	3.78	1.28			1.8	3.1	9.5	9.5	6.4		
	αLRha-OMe	4.75	3.93	3.82	3.46	3.66	1.26		3.39	1.7	3.2	9.5	9.5	6.3		
6	αLRha-(1→2)	4.97	4.07	3.79	3.45	3.75	1.29			1.7	3.4	9.5	9.5	6.3		
	→2)-αLRha-(1→2)	5.12	4.08	3.90	3.48	3.73	1.27			1.8	3.5	9.5	9.5	6.2		
	αLRha-OMe	4.76	3.93	3.83	3.47	3.69	1.32		3.40	1.7	3.4	9.5	9.5	6.2		
11	αDMan-(1→2)	4.94	3.95	3.88	3.66	3.89	3.79	3.74		1.6	3.2	9.6	9.6	2.6	4.9	12.0
	αLRha-OMe	4.79	3.97	3.79	3.43	3.66	1.29		3.39	1.7	3.3	9.7	9.7	6.1		
12	αDMan-(1→3)	4.98	3.97	3.88	3.68	3.87	3.83	3.74		1.6	3.3	9.6	9.6	3.2	5.2	12.0
	αLRha-OMe	4.72	4.13	3.79	3.48	3.69	1.30		3.38	1.7	3.3	9.6	9.6	6.2		
13	βLFuc-(1→2)	4.41	3.53	3.65	3.76	3.78	1.28			7.5	9.9	3.3	1.0	6.6		
	αLRha-OMe	4.83	4.07	3.73	3.44	3.70	1.31		3.42	1.6	3.5	9.7	9.7	6.1		
14	βLFuc-(1→3)	4.48	3.56	3.68	3.77	3.81	1.27			7.5	9.8	3.3	1.1	6.6		
	αLRha-OMe	4.75	4.12	3.89	3.56	3.73	1.33		3.42	1.6	3.4	9.6	9.6	6.2		

[a]The position of this signal was determined using the 2D COSY RCT experiment.

Can. J. Chem. Downloaded from www.nrcresearchpress.com by 88.85.125.76 on 09/07/12
For personal use only.

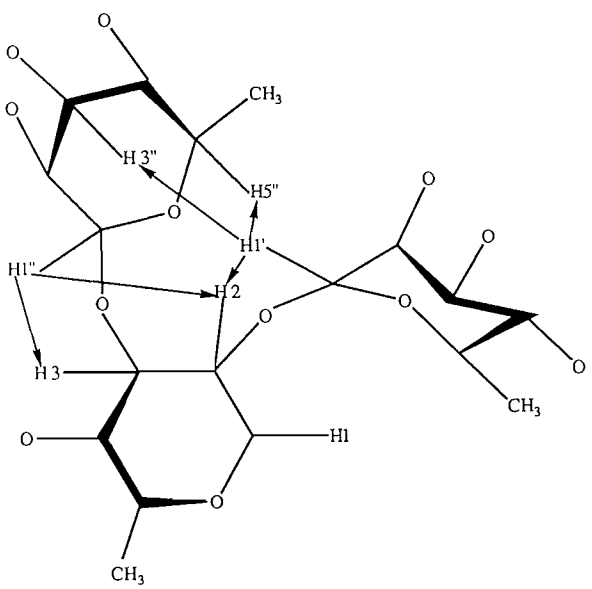

FIG. 2. Molecular model of low-energy conformer BB of the trisaccharide **1** αLRha(1–2) [αLRha(1–3)]αLRha-OMe. The optimal rotation angles are given in Table 4. Arrows show the protons with the fixed nOe's.

The conformers A ($\varphi \sim 60°$, $\psi \sim 15°$) in the αLRha(1–2)αLRha and αLRha(1–3)αLRha units are optimal, while the conformers B with $\varphi > 0°$ and $\psi < 0°$ ($\psi \sim -40°$) turn out to be of high energy according to the HSEA method (19). At the same time the reality of the ψ_2 value in the region between -30 and $-60°$ (see Fig. 2b) is proved by the presence of the nOe (2.2%, Table 1) for the H-2 proton upon pre-irradiation of H-1″ (as well as with the strong nOe for H-3). Within the range of ψ_2 values mentioned, the protons H-1″ and H-2 may be in close proximity and cause the nOe. Observation of the small nOe for the resonance of H-1 upon pre-irradiation of H-1′ (Table 1) also indicates the possibility of ψ_1 values near $-40°$. Thus, the conformer BB is actually present in aqueous solution of **1**. This conclusion also follows from the observed nOe for the resonance H-5″. The theoretical ratio of average values $\langle f^{H\text{-}2}_{H\text{-}1''}\rangle/\langle f^{H\text{-}3}_{H\text{-}1''}\rangle$ in the (1–3)-linked unit, as well as the $\langle f^{H\text{-}2}_{H\text{-}1'}\rangle/\langle f^{H\text{-}2}_{H\text{-}1'}\rangle$ ratio in the (1–2)-linked unit, is 1:10 (Table 5).

To summarize the conformational analysis for the trisaccharide **1**, one could mention that, in spite of some decrease of conformational freedom in its disaccharide units, the conformational freedom does not differ much from that in the corresponding free disaccharides **7** and **8**. Thus, in conformer BB the deviations of φ_2 and ψ_2 are considerable and approximately the same as in the disaccharide **8** (compare contours of relative

TABLE 8. ^{13}C NMR chemical shifts for oligosaccharides **1–14** and methyl α-L-rhamnopyranoside **15** (D_2O)

Compound	Residue	C-1	C-2	C-3	C-4	C-5	C-6	OMe
1	αLRha-(1→2)	103.05	71.6	71.45	73.4	70.75	18.1	
	αLRha-(1→3)	103.6	71.45	71.6	73.3	70.55	18.0	
	αLRha-OMe	100.9	78.8	78.8	73.3	70.2	18.1	56.3
7	αLRha-(1→2)	103.5	71.5	71.6	73.5	70.5	17.9	
	αLRha-OMe	101.0	79.8	71.5	73.6	70.0	17.9	56.1
8	αLRha-(1→3)	103.3	71.1	71.1	73.0	70.0	17.6	
	αLRha-OMe	101.8	70.8	79.0	72.4	69.6	17.6	56.1
5	αLRha-(1→2)	103.05	71.6	71.55	73.7	70.6	18.2	
	αLRha-(1→3)	103.6	71.5	71.7	73.45	70.85	18.1	
	→2,3)-αLRha-(1→2)	102.0	78.6	78.55	73.3	71.0	18.2	
	αLRha-OMe	101.0	79.5	71.55	73.35	70.1	18.1	56.3
6	αLRha-(1→2)	103.6	71.4	71.4	73.35	70.65	18.0	
	→2)-αLRha(1→2)	102.2	79.65	71.15	73.45	70.5	18.0	
	αLRha-OMe	101.0	79.55	71.4	73.45	70.0	18.0	56.2
15	αLRha-OMe	102.5	71.6	71.9	73.3	69.7	18.0	56.0
2	βDGlc-(1→2)	105.3	74.75	77.0	70.8	77.2	62.0	
	βDGlc-(1→3)	105.1	74.8	77.0	70.9	77.2	62.0	
	αLRha-OMe	101.3	80.0	81.0	72.5	69.8	18.1	56.25
9	βDGlc-(1→2)	105.5	74.8	77.0	70.7	77.2	62.1	
	αLRha-OMe	101.2	81.0	71.6	73.7	69.7	17.9	56.1
10	βDGlc-(1→3)	105.0	74.9	77.3	71.1	77.2	62.2	
	αLRha-OMe	102.0	71.2	81.5	72.5	69.7	18.2	56.1
3	αDMan-(1→2)	99.5	71.65	71.65	67.85	74.5	62.2	
	αDMan-(1→3)	97.95	71.75	71.9	67.85	74.0	62.2	
	αLRha-OMe	98.9	72.15	74.7	71.75	70.1	18.15	56.35
11	αDMan-(1→2)	99.5	71.7	71.7	68.1	74.2	62.3	
	αLRha-OMe	99.1	76.0	70.9	73.4	70.05	18.0	56.25
12	αDMan-(1→3)	97.5	71.6	71.75	67.85	73.9	62.1	
	αLRha-OMe	102.05	67.2	75.45	71.6	69.75	18.05	56.1
4	βLFuc-(1→2)	103.45	71.85	74.2	72.7	72.6	16.9	
	βLFuc-(1→3)	103.0	71.65	74.2	72.7	72.5	16.8	
	αLRha-OMe	100.0	76.0	79.05	71.95	69.95	18.05	56.1
13	βLFuc-(1→2)	103.7	71.7	74.05	72.65	72.3	16.8	
	αLRha-OMe	100.45	79.2	70.9	73.95	69.9	17.9	56.2
14	βLFuc-(1→3)	102.35	71.9	74.2	72.7	72.4	16.8	
	αLRha-OMe	101.95	69.2	79.7	71.9	69.65	18.15	56.15

energy Δ 3 kcal/mol in Fig. 2b in this paper, and Fig. 2 in ref. 8). On the contrary, in conformer AA there is considerable conformational freedom in the (1–2)-linked unit, which is close to that in the disaccharide **7** (compare Fig. 2c in this paper and Fig. 3 in ref. 7). The closeness of the conformational states of the disaccharide units in the trisaccharide **1** as well as in the free disaccharides **7** and **8** is apparent in the nOe data: the ratio values of the nOe for H-2′ and H-2 upon pre-irradiation of H-1′, and that for H-2″ and H-3 upon pre-irradiation of H-1′ in the units of the trisaccharide **1** coincide well with the ratio values observed in the case of the corresponding disaccharides **7** and **8** (Tables 1, 3, and 5).

Our study of the tetrasaccharide **5** shows that the presence of aglycon for the bis-glycosylated α-L-rhamnopyranose residue does not cause any significant conformational deviations of the branch point. This becomes clear from the fact that, upon pre-irradiation of H-1′ for the αLRha(1–2)αLRha unit of **5** (here we use the same plots for protons as in **1**), strong nOe's are observed for the resonances H-3″ and H-5″ of the residue Y. In this case as well as in the trisaccharide **1**, the sum of the nOe's on H-2′ and H-2 is 3-fold higher than that for the resonances of H-3″ and H-5″ (Tables 1 and 2). As well, in **5** and in **1**, upon pre-irradiation of H-1″ the ratio of the nOe's for H-2″ and H-3 is 0.7/0.8 (Tables 1 and 2).

In fact, in the tetrasaccharide **5**, the aglycon in the form of the α-methylrhamnoside residue and the substituents X and Z are placed on opposite sides of the best four-atom plane of the branched rhamnose residue and do not interact with each other. The molecular model of the optimal conformation of **5** with rotation angles φ_1, 40; ψ_1, −31; φ_2, 49; ψ_2, −25; φ_3, 51; and ψ_3, 15° (the latter two angles correspond to αLRha(1–2)αLRha-OMe) is shown in Fig. 4.

The nOe data for the (1–2)-linked rhamnotriose core chain of the tetrasaccharide **1** and for the trisaccharide **6** are equal. For

Can. J. Chem. Downloaded from www.nrcresearchpress.com by 88.85.125.76 on 09/07/12
For personal use only.

Can. J. Chem. Downloaded from www.nrcresearchpress.com by 88.85.125.76 on 09/07/12
For personal use only.

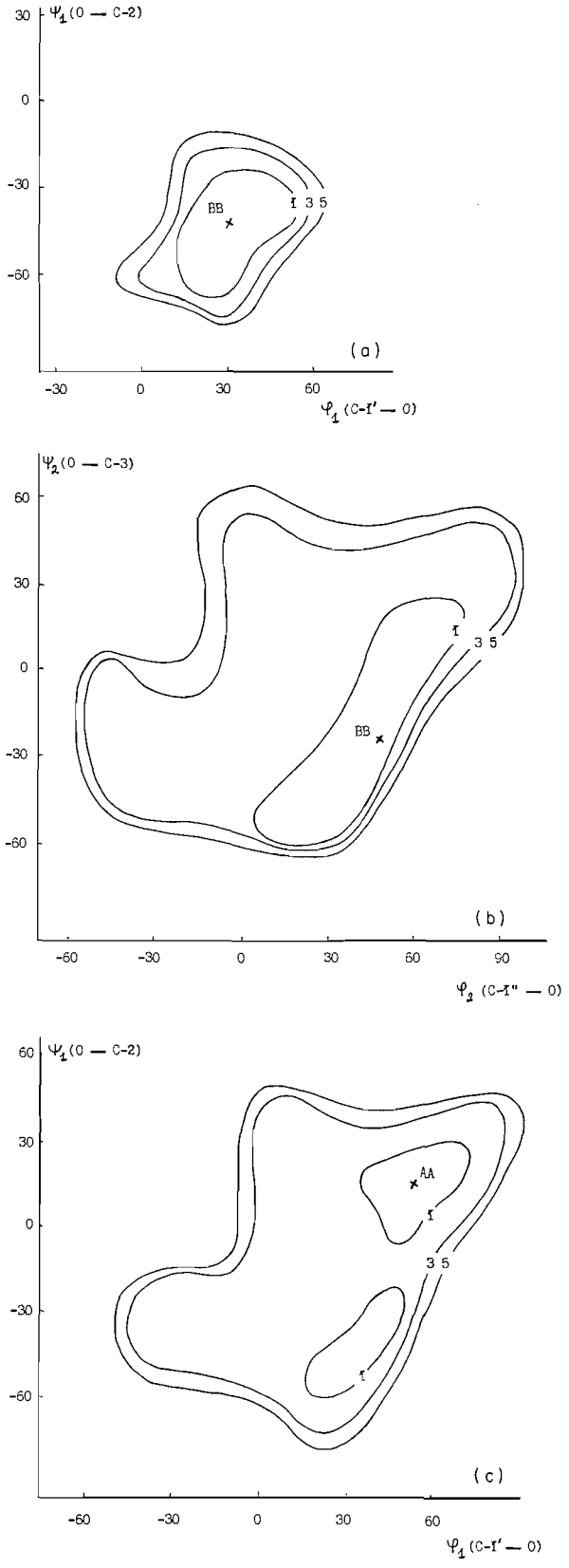

FIG. 3. Cross sections of potential surface for the trisaccharide **1** αLRha(1–2) [αLRha(1–3)]αLRha-OMe. (a) $\varphi_1 - \psi_1$ ($\varphi_2 = 49.2$, $\psi_2 = -25.1°$, Table 4); (b) $\varphi_2 - \psi_2$ ($\varphi_1 = 39.0$, $\psi_1 = -37.1°$); (c) $\varphi_1 - \psi_1$ ($\varphi_2 = 60.3$, $\psi_2 = 15.1°$);

The equipotentials of relative energy of Δ 1, Δ 3, and Δ 5 kcal/mol are given, × denotes the positions of local minima.

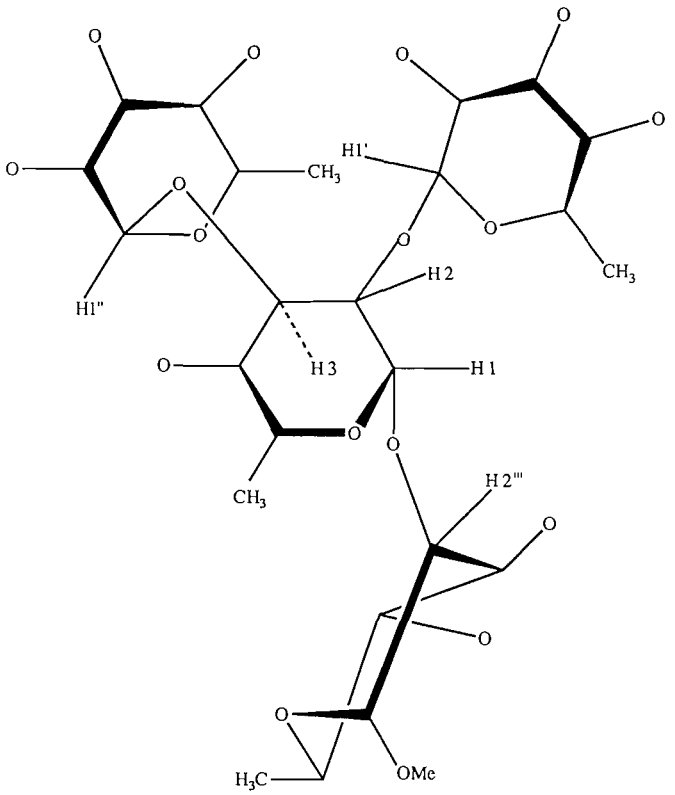

FIG. 4. Molecular model of the predominant conformer for the tetrasaccharide **5** αLRha(1–2)[αLRha(1–3)]αLRha(1–2)αLRha-OMe (see text).

example, in both cases, upon pre-irradiation of H-1 of the central L-rhamnose residue, the observed nOe's for the protons H-2, H-5′, and H-2‴ are almost equal (H-2‴ corresponds to the "reducing residue" of rhamnose Z), Table 2.

Thus, the conformational properties of branched trisaccharides with a 2,3-disubstituted α-rhamnose (or α-mannose) residue are preserved in the polysaccharide chain.

βDGlc(1–2)[βDGlc(1–3)]αLRha-OMe (2)

After pre-irradiation of H-1′ in the (1–2)-linked unit of **2** the nOe is observed only for H-2 of the rhamnose residue, and it is 40% less than the sum of nOe's for H-3′ and H-5′ of the irradiated residue βDGlc. Analogously, in the (1–3)-linked unit the nOe for H-3 after pre-irradiation of H-1″ is 50% less than the sum of nOe's for H-3″ and H-5″ (Table 1).

Both βDGlc substituents of the rhamnose residue in the trisaccharide **2** are separated and do not interact with each other in the majority of the admissible conformations; that is why the conformational possibilities for the disaccharide units are almost the same as for the free disaccharides **9** and **10** (7). This is clear from comparison of cross section $\varphi_2 - \psi_2$ (Fig. 5) and the conformational map of the disaccharide **10** (Fig. 5 (7)). Therefore, all four possible conformers AA, AB, BA, and BB in the trisaccharide **2** do exist (A and B are the optimal conformational states of the disaccharide units, see Table 3 (7)). Among the listed conformers the AB one is of lowest energy (Table 4). This conformer is additionally stabilized by means of dispersional interactions of two glucose residues (their energy is −2 kcal/mol). The molecular model of the AB conformer is presented in Fig. 6.

According to calculations for all conformers of the trisaccharide **2**, after pre-irradiation of the anomeric protons, the nOe's are possible only on the protons at the carbon atoms of the

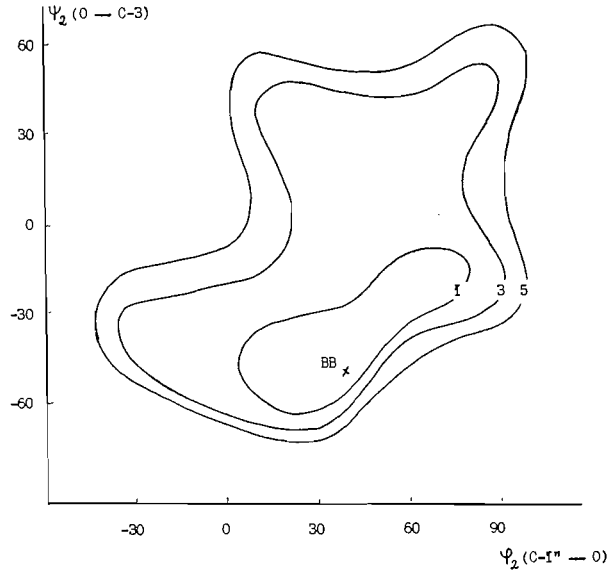

FIG. 5. Cross sections of potential surface for the trisaccharide **2** βDGlc(1–2)[βDGlc(1–3)]αLRha-OMe. $\varphi_2 - \psi_2$ ($\varphi_1 = 40.6$, $\psi_1 = -24.1°$); see legend to Fig. 3.

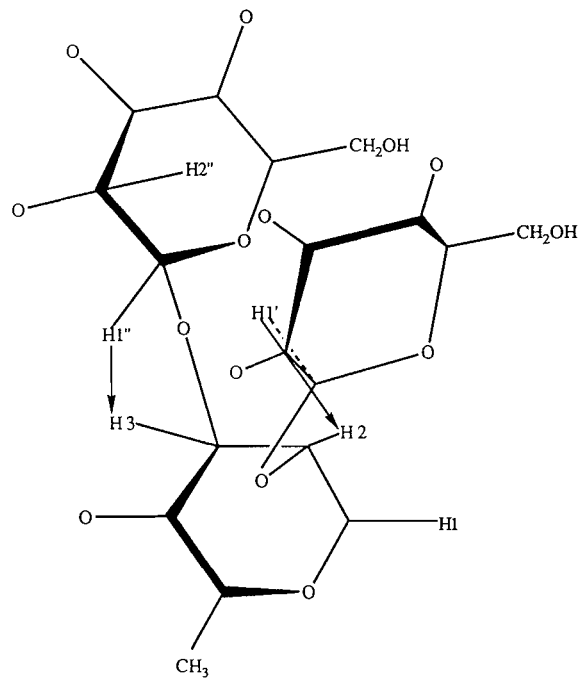

FIG. 6. Molecular model of the low-energy conformer AB of the trisaccharide **2** βDGlc(1–2)[βDGlc(1–3)]αLRha-OMe; see legend to Fig. 2.

rhamnose residue forming the glycosidic linkages: for H-2 on pre-irradiation of H-1′ and for H-3 on pre-irradiation of H-1″ (Table 5). However, H-1′ and H-2″ in the AB conformation are in spatial proximity as well (Fig. 6); we failed to determine the corresponding effects on pre-irradiation of H-1′ because the positions of the H-1′ and H-1″ signals are too close to each other. The data for the statistical calculation of the nOe's are listed in Table 5. As well as in the (1–2)- and (1–3)-linked units, the ratio of average values $(\langle f^{H\text{-}3'}_{H\text{-}1'}\rangle + \langle f^{H\text{-}5'}_{H\text{-}1'}\rangle)/\langle f^{H\text{-}2}_{H\text{-}1'}\rangle$ and $(\langle f^{H\text{-}3''}_{H\text{-}1''}\rangle + \langle f^{H\text{-}5''}_{H\text{-}1''}\rangle)/f^{H\text{-}3}_{H\text{-}1''}\rangle$ is equal to 1.8/1.9. The same ratio of the nOe's under discussion is experimentally observed (Table 1). It should

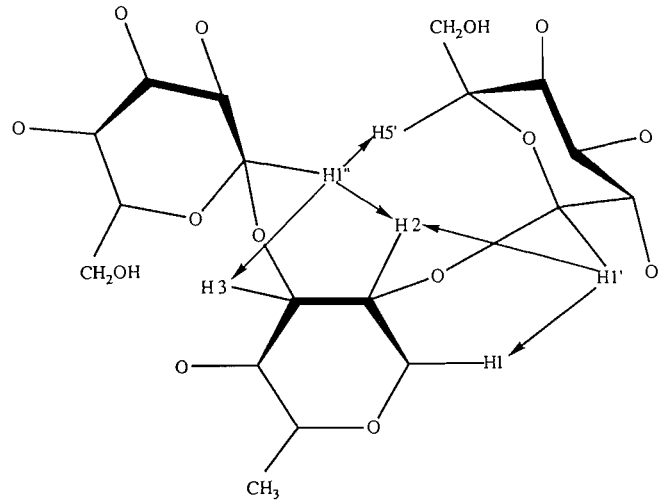

FIG. 7. Molecular model of preferred conformer AA of the trisaccharide **3** αDMan(1–2)[αDMan(1–3)]αLRha-OMe; see legend to Fig. 2.

be noted that similar values of the nOe's are observed for the disaccharides **9** and **10** (Table 3). This means that the conformational states of both disaccharide units in the trisaccharide **2** and in the disaccharides **9** and **10** are similar.

αDMan(1–2)[αDMan(1–3)]αLRha-OMe (3)

Trisaccharide **3** differs from trisaccharide **1** by the absolute configuration of the X and Y substituents at the rhamnopyranose residue. Due to this fact (see ref. 20), upon pre-irradiation of the anomeric proton in each disaccharide unit significant nOe is observed not only for the proton linked to the α-carbon atom of the aglycon (i.e., for H-2 and H-1 in the (1–2)-linked unit and for H-3 and H-2 in the (1–3)-linked unit, Table 1). The same situation exists for the disaccharides **11** and **12** (Table 3). The change of absolute configuration of the X and Y substituents in the trisaccharide **3** relative to the trisaccharide **1** causes a turn in the average planes of the X and Y residues of ≃180° and proton H-1″ in **3** is located in the region between the X and Y residues (Fig. 2). Indeed, the pre-irradiation of H-1″ causes the nOe for the resonance of H-5′ (3.8%, Table 1).

One preferred conformer is localized on the potential surface of **3** with rotation angles listed in Table 4. The molecular model of this conformer is drawn in Fig. 7. Two disaccharide units of this structure have the conformation A ($\varphi \simeq -60°$, $\psi \simeq -40°$) of the corresponding disaccharides **11** and **12** (see Table 2, ref. 7), i.e., it has the AA designation. In the optimal conformation found, the protons H-1″ and H-5′ are in close proximity (r(H-1″–H-5′) = 2.4 Å). The existence of the nOe for H-5′ after pre-irradiation of H-1″ (Table 1) indicates the significant statistical weight of the proposed AA conformation of **3**. We should point out that, in the AA conformation of **3**, not only the protons H-1″ and H-5′ are within the distance of van der Waals contacts, but also H-1″ and H-2 on one side and H-2″ and H-6′ on the other (Fig. 7). Thus this conformation is stabilized by effective dispersion interactions of the X and Y residues, with an energy of ca. −2 kcal/mol. This circumstance determines, in **3**, the location of the lowest energy contour Δ 1 kcal/mol for the cross sections on the potential energy surface φ_1–ψ_1 and φ_2–ψ_2 (Fig. 8) at values for the rotation angles of $\varphi < -30°$ and $\psi < -30°$. At other allowable values of φ and ψ of **3**, the residues X and Y are separated and do not interact with each other. Therefore the

Can. J. Chem. Downloaded from www.nrcresearchpress.com by 88.85.125.76 on 09/07/12
For personal use only.

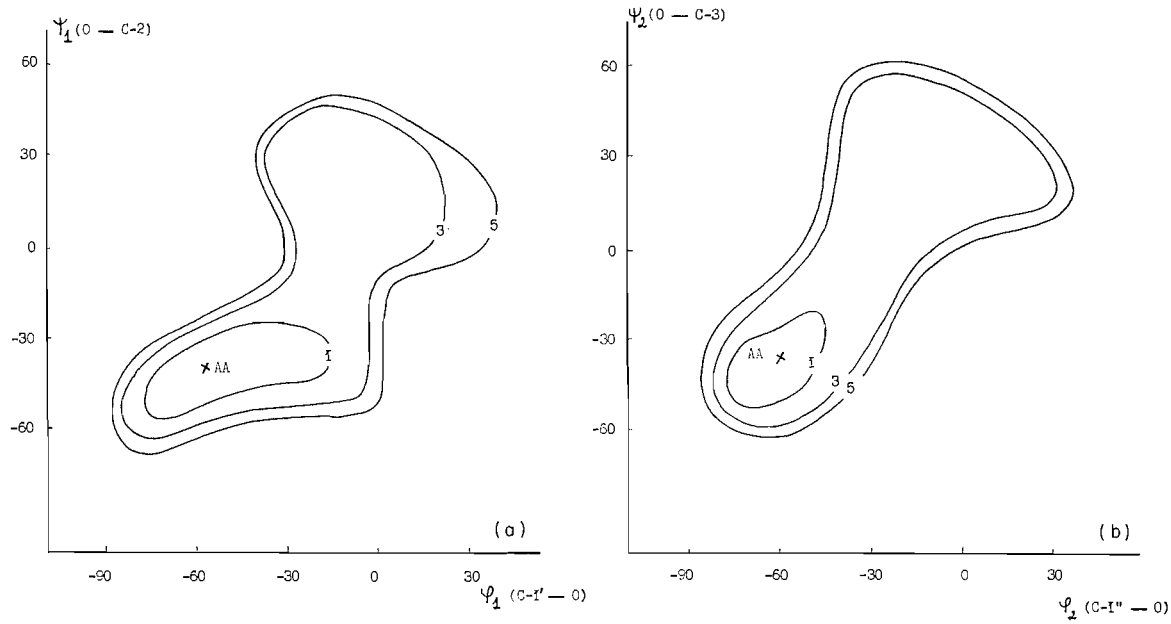

FIG. 8. Cross sections of potential surface for the trisaccharide **3** αDMan(1–2)[αDMan(1–3)]αLRha-OMe. (a) $\varphi_1 - \psi_1$ ($\varphi_2 = -61.5, \psi_2 = -35.1°$); (b) $\varphi_2 - \psi_2$ ($\varphi_1 = -59.0, \psi_1 = -37.6°$); see legend to Fig. 3.

contour forms of relative energy Δ 3 kcal/mol on cross sections (Fig. 8) and conformational maps of the free disaccharides **11** and **12** are equal.

Thus conformational state A of the disaccharide units (which in the free disaccharides **11** and **12** are assigned the statistical weight of 75% (7)) are additionally stabilized in the trisaccharide **3** by nonbonded interactions between two α-D-mannose residues, so that conformer AA is preferable for **3**.

The nOe value between H-1″ and H-5′ of the nonbonded mannose residues depends mainly on conformational possibilities of the disaccharide units in **3**. In this calculation they are determined by the φ_1–ψ_1 and φ_2–ψ_2 cross sections (in Fig. 8). The fact that the ratio of the nOe's for H-5′ and H-2 after pre-irradiation of H-1″ is 0.4 according to the experimental data (Table 1), while the calculated value is 0.3 (Table 5), indicates an acceptable description of the conformational flexibility of **3**.

In optimal conformation AA of **3**, for the (1–2)-linked unit the calculated value $f_{H\text{-}1'}^{H\text{-}1}$ is several times higher than $f_{H\text{-}1'}^{H\text{-}2}$ (Table 4). Similarly, for the (1–3)-linked unit the value of $f_{H\text{-}1''}^{H\text{-}2}$ is much higher than $f_{H\text{-}1''}^{H\text{-}3}$ (Table 4), but in statistical calculations the average value $\langle f_{H\text{-}1'}^{H\text{-}1} \rangle$ is higher than $\langle f_{H\text{-}1'}^{H\text{-}2} \rangle$ by only 1.4-fold (Table 5). The experimental ratio is 1.3 (Table 1). The values $\langle f_{H\text{-}1''}^{H\text{-}2} \rangle$ and $\langle f_{H\text{-}1''}^{H\text{-}3} \rangle$, taking into account the possible deviations of φ and ψ, are equal (Table 5). Due to overlapping of the H-2″ and H-3 signals, we failed to determine exactly the experimental nOe values for H-3 after pre-irradiation of H-1″ (Table 1). At the same time both the ratio of the sum of the observed nOe for the H-2″, H-3 protons and the nOe for H-2, as well as the ratio of the above-mentioned average values $(\langle f_{H\text{-}1''}^{H\text{-}3} \rangle + \langle f_{H\text{-}1''}^{H\text{-}2} \rangle)/\langle f_{H\text{-}1''}^{H\text{-}2} \rangle$, is 2:1 (Tables 1 and 5).

It should be noted that the calculated nOe values for H-2 and H-3 protons on pre-irradiation of H-1″ are equal (Table 5), whereas the observed nOe for H-2 of **12** is 2-fold higher than that for H-3 (Table 3). This fact may indicate the possibility of considerable differences in the conformational states of the αDMan(1–3)αLRha unit in the trisaccharide **3** and in the disaccharide **12**. But this is not the case. The decrease of the relative nOe value on H-2 in **3** is caused by additional spatial proximity (up to 2.6 Å) of this proton with H-1′ of the mannose residue of the (1–2)-linked unit, which is absent in the disaccharide **12**. In accordance with the conformational analysis, the conformer A (φ,ψ −60,−40°) of **12** remains predominant for the corresponding unit of **3**.

βLFuc(1–2)[βLFuc(1–3)]αLRha-OMe (4)

The X and Y residues in **4** differ from those in **3** by two-configuration parameters: absolute and anomeric configurations. That is why the observed regularities in spectra of these trisaccharides should be almost the same (20). Actually the commensurable nOe's are observed on pre-irradiation of H-1′ for H-1 and H-2 in the trisaccharide **3** as well as in **4** and on pre-irradiation of H-1″ for H-2 and H-3 of the rhamnose residue (Table 1). However, upon pre-irradiation of H-1′ as well as H-1″ of **4**, the nOe's on the protons of the nonbonded residues (Y for H-1′ and X for H-1″) were not observed.

The β configuration of the fucopyranosyl residues leads to increased conformational freedom of the disaccharides **13** and **14** in comparison with the disaccharides **11** and **12** (see refs. 7 and 8), which is preserved in the disaccharide units of the trisaccharide **4**; as before, the limit of admissible values for angles ψ_1 and ψ_2 ranges from −60 to +60°. This means that for the above-mentioned rotation angles the inadmissible van der Waals contacts between two nonbonded fucose residues do not appear. The molecular model of the lowest-energy conformation AA of **4**, in which the predominant conformers A (φ,ψ −50,−30°) of the disaccharide units are presented, is shown in Fig. 9. The spatial structure of **4** (Fig. 9) explains the relative decrease of the nOe value on H-2 on pre-irradiation of either H-1′ or H-1″ in this trisaccharide, in comparison with the disaccharides **13** and **14** (see the data in Tables 1 and 3). As for the trisaccharide **3**, this result for **4** is caused by the spatial proximity of H-2 to a greater number of protons than in the selected disaccharides **13** and **14**. It should be noted that the calculations present only a qualitative picture of the observed nOe's because of the absence of the definite X-ray structure of the β-L-fucopyranose residue (compare Tables 1 and 5).

Can. J. Chem. Downloaded from www.nrcresearchpress.com by 88.85.125.76 on 09/07/12
For personal use only.

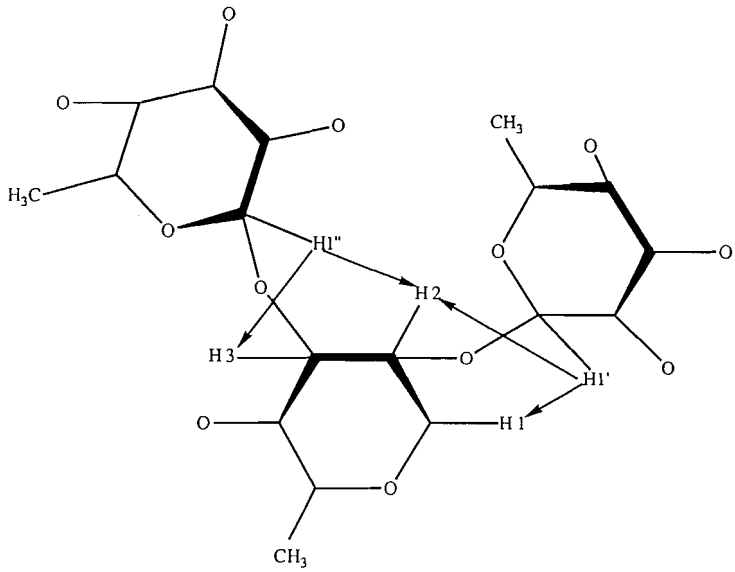

FIG. 9. Molecular model of low-energy conformer AA of the trisaccharide **4** βLFuc(1–2)[βLFuc(1–3)]αLRha-OMe; see legend to Fig. 2.

Glycosylation effects

The changes in chemical shifts of the carbon atom signals in the ^{13}C NMR spectra while transferring from mono- to disaccharides (the glycosylation effects) are directly connected with the spatial structure of the disaccharides formed. It was shown earlier that there is a distinct dependence between glycosylation effect values and nonbonded interactions of glycon and aglycon protons placed near a glycosidic linkage (20–22). Thus for "γ-*gauche*" interactions between anomeric proton H-1′ and the equatorial proton at the β position of the aglycon (which could be realized in (1–3)-linked glycosylgalactosides and glycosylmannosides (glycosylrhamnosides)), the glycosylation effects for C-β (C-4 in the first case and C-2 in the second one) could be −3 to −5 ppm (23), i.e., chemical shifts for the above-mentioned atoms are observed at a higher field. At the same time the glycosylation-effect values for linear oligo- and polysaccharides are preserved (24), so their ^{13}C NMR spectra could be calculated according to an additive scheme.

Upon investigation of branched oligosaccharides, a question arises — whether there is a similar correlation between glycosylation effects and spatial proximity of protons (as well as other atoms) for the different monosaccharide residues.

The analysis of a series of methyl-β-D-galactopyranoside derivatives glycosylated at neighbouring OH-3 and OH-4 or at OH-2 and OH-3 (1) showed that chemical shifts of the carbon atoms in branched trisaccharides, calculated with the use of an additive scheme on the basis of the spectra of the corresponding disaccharides and methyl-β-D-galactopyranoside, definitely differ from experimental data. It was found that deviations (about −3 ppm) of chemical shift values calculated by the additive scheme from the experimental values do correlate with the conformational changes that take place in disaccharide units of branched trisaccharides, in comparison with the corresponding free disaccharides.

The aim of this paper is the investigation of the dependence of the glycosylation effect on spatial structure for branched trisaccharides having vicinal substitution at axial OH-2 and equatorial OH-3 of the α-L-rhamnopyranose residue.

^{13}C NMR spectral data both for the disaccharides **7**–**14**, corresponding to disaccharide units of trisaccharides, and the trisaccharides **1**–**4** (see Tables 7 and 8 in Experimental), allow us to calculate the deviation from additivity Δ (ppm), which represents the difference between the observed ^{13}C chemical shifts of the trisaccharide and the shift calculated according to the additive scheme, $\Delta = \delta_{exp} - \delta_{calc.}$ (see Table 6).

The deviations from additivity Δ in the ^{13}C NMR spectra of **1**–**4** for all the carbon atoms of the α-L-rhamnopyranose residue at branch points and C-1′, C-1″ of the X and Y residues (for the other atoms of the X and Y groups, Δ-values are equal to 0) are presented in Table 6. It is obvious that in all cases the Δ-values are in the −0.6 to +0.6 ppm range, i.e., they practically correlate with the ordinary deviations of chemical shifts in the ^{13}C NMR spectra of oligosaccharides (experimental error is near ±0.5 ppm).

Thus the chemical shift values for the ^{13}C NMR spectra of the branched oligosaccharides **1**–**4** represent additive values related to the chemical shifts of the corresponding disaccharides. This means that the conformational states of disaccharide units in the trisaccharides **1**–**4** are close to the conformational states of free disaccharides. This conclusion was reached previously on the basis of the nOe data and conformational calculations for **1**–**4**.

It should be noted that chemical shifts of carbon atoms at the branch point (2,3-disubstituted α-L-rhamnopyranose residue) in the tetrasaccharide **5** are close to the chemical shift values of the carbon atoms (without prime) of the corresponding trisaccharides **1** and **6**. Thus the positions of C-3 and C-4 signals in **1** and **5** practically coincide; the same is true for the C-1 signals in **5** and **6** (Table 8).

The data obtained for **1**–**4** mean that chemical shifts of branch points having vicinal substituents at OH-2 and OH-3 of the α-rhamnopyranose (or α-mannopyranose) residue could be calculated according to an additive scheme.

Experimental

1D and 2D NMR experiments were performed on samples dissolved in D_2O at 40–55°C using Bruker WM-250 (for ^1H) and AM-300 (for ^{13}C) spectrometers. The reference for the ^1H and ^{13}C NMR spectra was acetone (2.225 and 31.45 ppm, respectively). Assignments of the ^1H NMR spectra (Table 7) were accomplished using COSY and RCT 2D experiments (COSY RCT of the standard Bruker software for

Can. J. Chem. Downloaded from www.nrcresearchpress.com by 88.85.125.76 on 09/07/12
For personal use only.

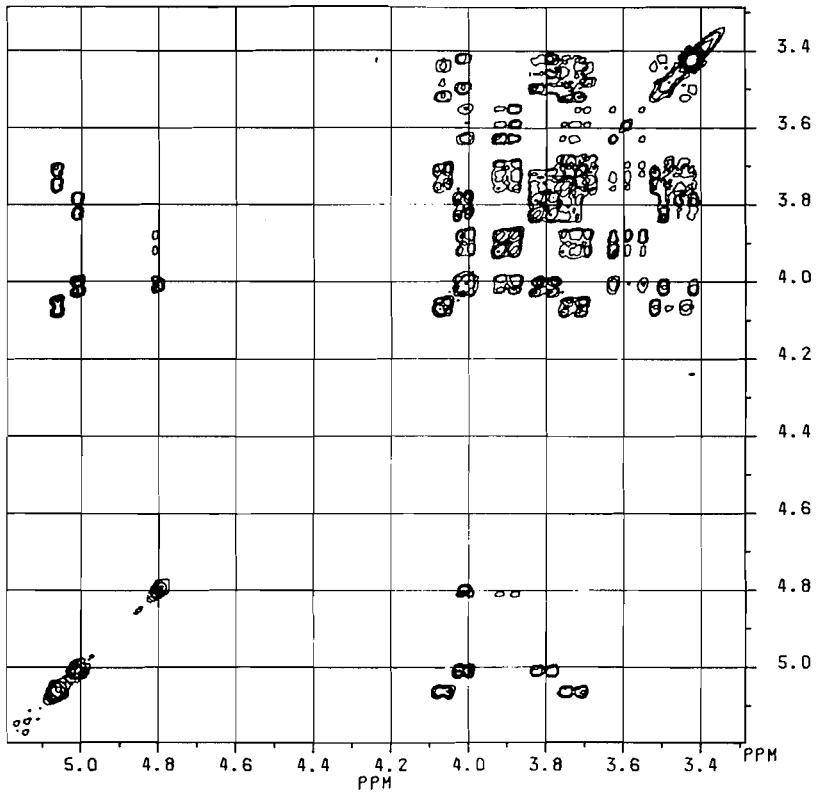

FIG. 10. COSY RCT contour plots of the trisaccharide **1** αLRha(1–2)[αLRha(1–3)]αLRha-OMe in D_2O (area of the ring proton resonances).

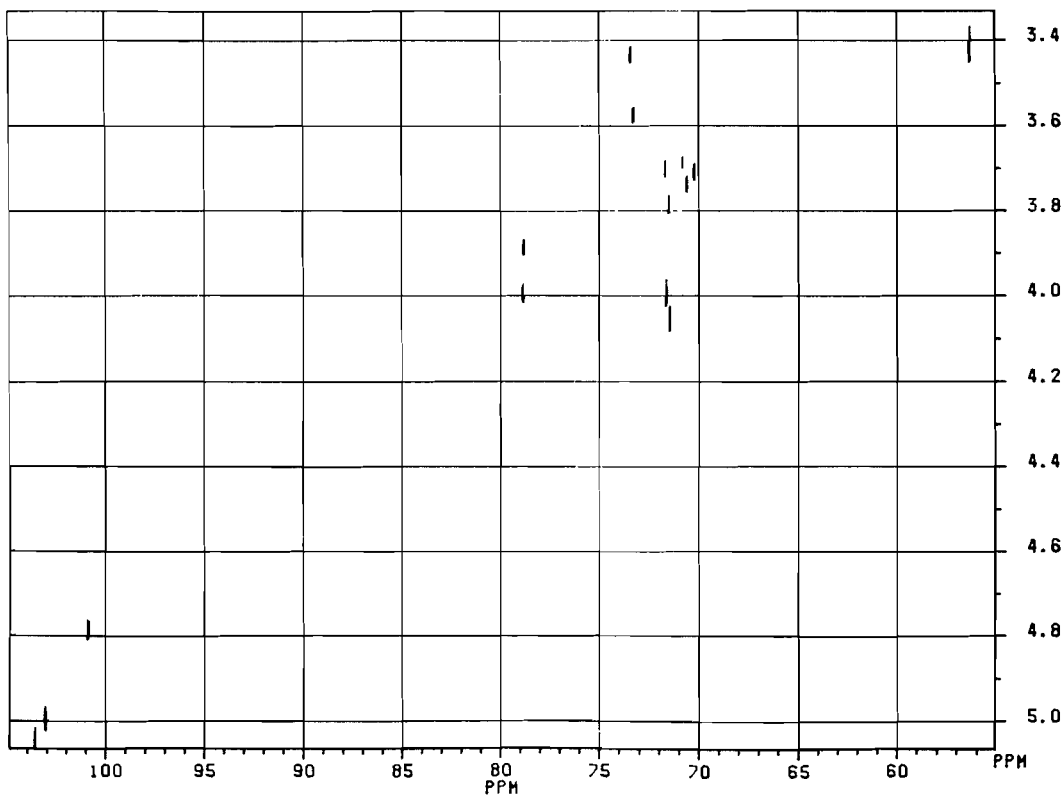

FIG. 11. Contour plot of the $^1H-^{13}C$ correlated spectrum of the trisaccharide **1** αLRha(1–2)[αLRha(1–3)]αLRha-OMe (the area of both ring proton and carbon atom resonances).

Can. J. Chem. Downloaded from www.nrcresearchpress.com by 88.85.125.76 on 09/07/12
For personal use only.

ASPECT-2000). The HDO signal suppressing upon the relaxation delay (1 s) D_2 was 33 ms ($1/4J$; J = 7.5 Hz). Spectral windows were ca. 500 Hz (the region of the pyranose ring protons only). Data sets consisting of 256 t_1 experiments each with 512 data points were zero-filled to 512 data points. Prior to Fourier transformation the FIDs were multiplied with a sine-bell window function (not shifted). Typical COSY RCT contour plots are represented in Fig. 10.

The nOe experiments were performed in the difference mode within the tOe technique (25) with D_1 (pre-irradiation time) 0.5 s and D_2 (the relaxation delay) 0.8 s using the NOEMULT program of the standard Bruker software. The pre-irradiated signal area in the difference spectra was taken as 100%. The nOe's are expressed as the ratio of integrated intensities of the observed and saturated proton resonances.

In cases where, upon pre-irradiation of the anomeric proton of one residue, significant pre-irradiation of the anomeric proton of the other residue occurs, both irradiations might cause the nOe on the same proton d; for example, due to the close position of H-1′ and H-1″ signals in the H NMR spectrum of **2** (Table 7), during pre-irradiation of H-1″, proton H-1′ was also affected. Thus the registered value of nOe on the H-2 ("proton d") is a result of the pre-irradiation not only of H-1″, but H-1′ as well. The nOe values x and y on the d proton caused by the first and second irradiation were calculated from the solution of the equilibrium system:

$$I'_d = x\,I'_{H\text{-}1'} + y\,I'_{H\text{-}1''}$$

$$I''_d = x\,I''_{H\text{-}1'} + y\,I''_{H\text{-}1''}$$

where I'_d, $I'_{H\text{-}11'}$, and $I'_{H\text{-}1''}$ are the integral intensities of the differential nOe spectra signals of protons d, H-1′, and H-1″ on pre-irradiation of H-1′; I''_d, $I''_{H\text{-}1'}$, and $I''_{H\text{-}1''}$ are the same on pre-irradiation of H-1″.

The assignments of the ^{13}C NMR spectra (Table 8) were made in a straightforward manner by using 2D ^1H–^{13}C correlated spectroscopy (XHCORRD program of the Bruker software for ASPECT-3000). The typical spectral window was 500 Hz for ^1H and 5000 for ^{13}C (the region, respectively, of pyranose ring protons or carbon atoms only). Data sets consisting of 256 t_1 experiments each with 2K data points were zero-filled to 512 data points. For detection of ^1J correlations D_3 was set to 3.2 ms and D_4 to 1.6 ms ($1/2J$ and $1/4J$, respectively; J = 155 Hz). FIDs were multiplied with a square sine-bell window function (not shifted) in both directions, prior to Fourier transformation. A typical spectrum is represented in Fig. 11. The syntheses of **1**–**6** and **11**–**14** will be published elsewhere.

1. G. M. Lipkind, A. S. Shashkow, O. A. Nechaev, V. I. Torgov, V. N. Shibaev, and N. K. Kochetkov. Bioorg. Khim. **15**, 1366 (1989).
2. G. M. Lipkind, A. S. Shashkov, Y. A. Knirel, E. V. Vinogradov, and N. K. Kochetkov. Carbohydr. Res. **175**, 59 (1988).
3. G. M. Lipkind, A. S. Shashkov, O. A. Nechaev, V. I. Torgov, V. N. Shibaev, and N. K. Kochetkov. Carbohydr. Res. **195**, 11 (1989).
4. G. M. Lipkind, A. S. Shashkov, O. A. Nechaev, V. I. Torgov, V. N. Shibaev, and N. K. Kochetkov. Carbohydr. Res. 195, 27 (1989).
5. G. M. Lipkind, A. S. Shashkov, and N. K. Kochetkov. Carbohydr. Res. In press.
6. G. M. Lipkind and N. K. Kochetkov. Bioorg. Khim. **10**, 1670 (1984).
7. S. S. Mamyan, G. M. Lipkind, A. S. Shashkov, N. E. Byramova, A. V. Nikolaev, and N. K. Kochetkov. Bioorg. Khim. **14**, 205 (1988).
8. G. M. Lipkind, A. S. Shashkov, Y. A. Knirel, and N. K. Kochetkov. Bioorg. Khim. **12**, 771 (1986).
9. R. A. Scott and H. A. Scheraga. J. Chem. Phys. **44**, 3052 (1966).
10. F. A. Momany, L. M. Curruthers, R. F. McGuire, and H. A. Scheraga. J. Chem. Phys. **78**, 1595 (1974).
11. V. V. Zhurkin, V. I. Poltev, and V. A. Florentjev. Molek. Biol. **14**, 1116 (1980).
12. G. M. Lipkind, V. B. Verovsky, and N. K. Kochetkov. Carbohydr. Res. **133**, 1 (1984).
13. G. A. Jeffrey, K. K. McMullan, and Sh. Takagi. Acta Crystallogr. Sect. B: Struct. Crystallogr. Cryst. Chem. **B35**, 728 (1977).
14. G. A. Jeffrey, and Sh. Takagi. Acta Crystallogr. Sect. B: Struct. Crystallogr. Cryst. Chem. **B33**, 738 (1977).
15. Sh. Takagi and G. A. Jeffrey. Acta Crystallogr. Sect. B: Struct. Crystallogr. Cryst. Chem. **B34**, 2551 (1978).
16. Sh. Takagi and G. A. Jeffrey. Acta Crystallogr. Sect. B: Struct. Crystallogr. Cryst. Chem. **B35**, 902 (1979).
17. S. Arnott and W. E. Scott. J. Chem. Soc. Perkin Trans. 2, 324 (1972).
18. R. E. Shirmer, J. H. Noggle, J. P. Davis, and P. A. Hart. J. Am. Chem. Soc. **92**, 3266 (1970).
19. H. Thøgersen, R. U. Lemieux, K. Bock, and B. Meyer. Can. J. Chem. **60**, 44 (1982).
20. G. M. Lipkind, A. S. Shashkov, S. S. Mamyan, and N. K. Kochetkov. Carbohydr. Res. **181**, 1 (1988).
21. N. K. Kochetkov, O. S. Chizhov, and A. S. Shashkov. Carbohydr. Res. **133**, 173 (1984).
22. K. Bock, A. Brignole, and B. W. Siglerskjold. J. Chem. Soc. Perkin Trans. 2, 1711 (1986).
23. A. S. Shashkov, A. I. Usov, Y. A. Knirel, B. A. Dmitriev, and N. K. Kochetkov. Bioorgan. Khim. **7**, 1364 (1981).
24. A. S. Shashkov, G. M. Lipkind, Y. A. Knirel, and N. K. Kochetkov. Magn. Reson. Chem. **26**, 735 (1988).
25. G. Wagner and K. Wüthrich. J. Magn. Reson. **33**, 675 (1979).

Can. J. Chem. Downloaded from www.nrcresearchpress.com by 88.85.125.76 on 09/07/12
For personal use only.

Photocyclisations de cétoacétals aromatiques en vue d'une approche synthétique de la crombénine

FRANÇOISE COTTET, LOUIS COTTIER ET GÉRARD DESCOTES

Laboratoire de chimie organique II, Université Lyon I, Unité associée n° 463 du Centre national de la recherche scientifique, 69622 Villeurbanne, France

Reçu le 8 août 1989

Cet article est dédié au Professeur Arthur S. Perlin à l'occasion de son 67e anniversaire

FRANÇOISE COTTET, LOUIS COTTIER et GÉRARD DESCOTES. Can. J. Chem. **68**, 1251 (1990).

La crombénine **1** est un spiropeltogynoïde présentant une structure spiroacétalique. Une approche de sa synthèse a été entreprise à partir d'orthocarbonylphénoxyisochromanne avec pour étape clef une réaction de photocyclisation de type Norrish II. En série isochromannique, le cycle aromatique induit une réaction secondaire de cyclisation sur le radical benzylique compétitive avec la réaction de spirocyclisation. Cependant, la présence de substituant électroattracteur ou encombrant en C-4′ diminue la formation du dérivé bicyclique de type [4.3.1] et oriente la photolyse vers le produit de structure spirannique.

Mots clés : acétals, isochromène, photocyclisation, spiroacétals.

FRANÇOISE COTTET, LOUIS COTTIER and GÉRARD DESCOTES. Can. J. Chem. **68**, 1251 (1990).

Crombenin **1** is a spiropeltogynoid compound with a spiroacetal moiety. A similar structure was synthesized starting from an orthocarbonylphenoxyisochroman by a Norrish type II photocyclisation. With an isochroman compound, the aromatic ring induces benzyl radical formation to give chiefly a bicyclic [4.3.1] derivative. However, with the introduction of electron-withdrawing or bulky substituents at C-4′, this side reaction is limited and the spiranic product becomes preponderant.

Key words: acetals, isochroman, photocyclisation, spiroacetals.

La crombénine **1** (R = OH) (1, 2) est une substance isolée en très faible quantité de l'«Acacia crombei». Sa structure, identifiée à partir de l'un de ses dérivés tétra-*O*-méthylé **1** (R = OMe) (3), possède un motif spiroacétalique (figure 1) présent dans de nombreuses substances biologiquement actives (4–8). Ayant étudié différentes réactions de spirocyclisation par voie photochimique de systèmes cétoacétaliques, une approche de la synthèse de la crombénine a été entreprise ayant pour étape clef une réaction de photocyclisation de type Norrish II.

En effet, les résultats obtenus en série glycosidique (9, 10) et en série tétrahydropyrannique (11–13) permettent d'envisager la synthèse de la crombénine ou de ses analogues selon un schéma rétrosynthétique en quatre étapes (Schéma 1). La condensation d'un phénol orthocarbonylé **A** avec un isochromène **B** ou un dérivé, devrait donner un acétal **C** qui, par photolyse, serait transformé en produit spirannique **D**. Selon la nature de la fonction hydroxyle sur le cycle furannique, une simple oxydation ou une déshydratation suivie d'une oxydation conduirait au composé **E** possédant la fonction cétone souhaitée. Ainsi, compte tenu des résultats obtenus avec les phénylglucosides orthocarbonylés (9), cette séquence réactionnelle a d'abord été étudiée en série tétrahydropyrannique puis elle a été étendue à des substrats isochromanniques.

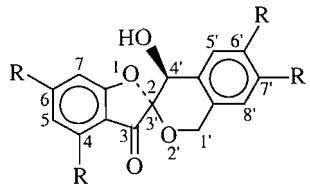

2(3′)*R* : 4′*R* ou 2(3′)*S* : 4′*S*

1 R = OH crombénine
1 R = OMe tetra-OMe-crombénine

FIG. 1. Crombénine.

Résultats

Synthèse des acétals

La fonction aldéhydique a été choisie comme groupe chromophore, car elle aurait permis d'accéder à un alcool secondaire en C-3 directement oxydable. La condensation directe entre l'aldéhyde salicylique et le dihydropyranne n'ayant pu être réalisée, le tétrahydropyrannyloxy-2 benzaldéhyde **6** a été synthétisé à partir de l'alcool *o*-hydroxy-benzylique **2**. L'estérification sélective de la fonction alcool primaire selon Nagao *et al.* (14), suivie de l'acétalisation avec le dihydropyranne, d'une saponification et d'une oxydation ménagée, permet d'obtenir l'aldéhyde **6** recherché (Schéma 2).

La synthèse des différents cétoacétals aromatiques **7** (tableau 1) a été récemment publiée en série hétérocyclique (15). En série isochromannique, l'acétal **10** a été obtenu par condensation en milieu alcalin de la chlorhydrine **9** issue de l'isochromène **8** (16) avec l'*ortho*-hydroxy-acétophénone selon la méthode décrite par Bakassian *et al.* (17) (Schéma 3).

En effet, l'isochromène, comme le dihydropyranne, réagit avec une solution d'eau de javel (18) pour donner un mélange *cis* + *trans* de chlorhydrines **9** isomères instables à température ambiante. L'attribution de la configuration a été réalisée à partir des dérivés acétylés **11** par comparaison en rmn ^{1}H des constantes de couplage entre les protons H-3 et H-4 avec celles des hydroxy-5 méthoxy-6 dihydro-5,6 [2*H*] pyrannes décrites par Chmielewski et Zamojski (19); l'isomère *trans* présente une constante de couplage inférieure à celle de l'isomère *cis* (pour **16** : *cis*, J_{3-4} = 3,1 Hz; *trans*, J_{3-4} = 2,6 Hz). Les dérivés **9** instables sont soumis à l'état brut à l'action de l'*ortho*-hydroxy-acétophénone qui sert de solvant et de réactif. Le produit de condensation obtenu **10**, de configuration *trans*, est alors estérifié par le *N*-acétylimidazole en **12** (20) ou silylé en **13** (Schéma 3).

*Photolyse des acétals **6**, **7**, **10**, **12** et **13***

Contrairement aux résultats antérieurs (9, 13), la photolyse de l'aldéhyde **6** donne un mélange complexe subissant une dégradation importante lors de la séparation sur une colonne de silice. En conséquence, le groupe chromophore aldéhydique a été remplacé par un groupe acétyle.

Printed in Canada / Imprimé au Canada

Can. J. Chem. Downloaded from www.nrcresearchpress.com by 88.85.125.76 on 09/07/12
For personal use only.

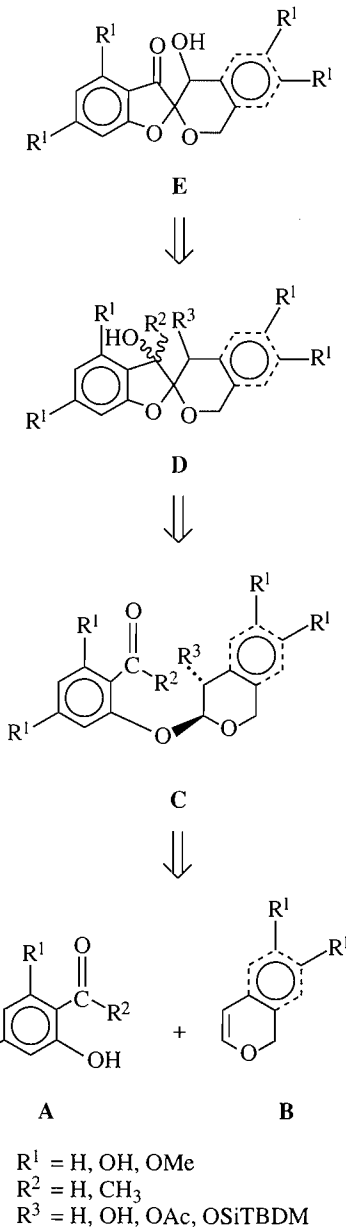

SCHÉMA 1. Schéma rétrosynthétique de la synthèse de la crombénine.

Avec les acétals cétoniques **7**, la réaction de cyclisation en composés spiranniques **14** dépend de la nature des substituants sur le cycle aromatique (tableau 1). La photolyse de **7***a* non substitué donne un mélange de quatre diastéréoisomères **14***a* détectés en rmn ^1H par la présence de quatre singulets pour les groupes méthyles quaternaires. Ces alcools isomères **14***a* sont déshydratés ($POCl_3$ + pyridine) afin d'établir la structure et le pourcentage des seuls isomères *cis–trans* au niveau du cycle tétrahydropyrannique. La structure des produits insaturés **15***a* (conformation avec la liaison C2—O1 axiale, isomère *cis–trans*) a été déterminée selon les méthodes spectrales précédemment signalées en série hétérocyclique (11, 12, 21) et en série glucosidique (9, 10, 22). La position axiale de la liaison C2—O1 résulte de la comparaison des déplacements chimiques des carbones C-2, C-3′, C-5′ entre les composés **15***a* et les dérivés spiranniques (11, 12) non aromatiques, compte tenu des effets d'un groupement acétate en C-3′ (23). Ainsi, en rmn ^{13}C, les déplacements chimiques observés et calculés pour les

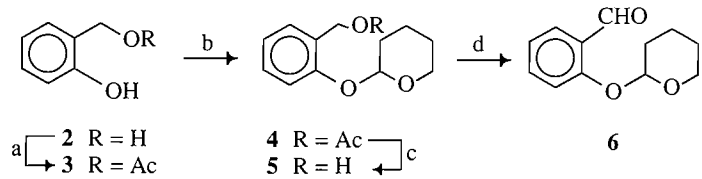

a : Ac_2O, BF_3OEt_2 (84%)
b : DHP, PPTS (32%)
c : NaOH, EtOH (94%)
d : PCC (69%)

SCHÉMA 2. Synthèse du tétrahydropyrannyloxy-2 benzaldéhyde **6**.

carbones C-2, C-3′, C-5′ sont voisins à 2 ppm près (**15***a*, δ C-*i* (obs.–calc.) : *cis*, C-2 (107,5–106,9), C-3′ (71–72,7), C-5′ (24,7–22,7); *trans*, C-2 (105,9–105,3), C-3′ (69,7–68,5), C-5′ (19,0–18,9)). En rmn ^1H, la multiplicité des signaux du proton H-3′ permet d'attribuer respectivement aux isomères **15***a* la configuration *cis* et *trans* (**15***a* *cis*, δ : 5,5 (dd, J = 6 et 10 Hz); *trans*, δ : 5,05 (t, J = 3 Hz)). Enfin, le rapport de l'intégrale de ces signaux (5,5 et 5,05 ppm) montre pour ce mélange d'isomères *cis–trans*, une proportion égale à 78 : 22. Comme la déshydratation de **4***a* a été faite en milieu basique, la cyclisation radicalaire du produit **7***a* conduit au même mélange d'isomères *cis–trans*.

L'introduction de deux substituants méthoxy **7***c* sur le cycle aromatique modifie fortement la formation des produits spiranniques (tableau 1). Cette diminution de réactivité photochimique pour **7***c*, a déjà été observée pour d'autres cétones aromatiques (24, 25). Différents auteurs (24, 25) ont montré qu'avec un groupement méthoxy, l'état triplet de plus basse énergie prend un caractère $\pi\pi^*$ défavorisant une réaction de type Norrish II. De plus, Scaiano et coll. (26) ont relié la constante de vitesse d'abstraction d'un atome d'hydrogène à la valeur du paramètre σ d'Hammett. Des valeurs négatives (pour CH_3O-, $\sigma = -0{,}12$) (27) favorisent un état triplet $\pi\pi^*$ et entrainent une baisse de réactivité qui n'a pu être compensée par la présence d'un nouveau groupe chromophore éthoxalyle (COCOOEt) ayant un coefficient d'absorption plus élevé (28, 29). Une valeur positive de σ correspond à une augmentation de la population de l'état triplet $n\pi^*$ et permet ainsi d'expliquer le faible pourcentage de composé spirannique **14***b* obtenu avec des substituants acétoxy (pour CH_3COO-, $\sigma = +0{,}31$) (27) sur le cycle aromatique carbonylé.

L'irradiation des acétals isochromanniques **10**, **12** et **13** conduit à des composés spiranniques **16** ou bicycliques **17** (Schéma 4) dont les proportions varient avec la nature du substituant en position 4′. L'alcool **10** donne préférentiellement le dérivé bicyclique [4.3.1] **17***a* avec un rendement de 41%. La structure a été établie par rmn et confirmée par l'analyse cristallographique (figure 2). Le spectre rmn ^1H montre un seul singulet pour le méthyle quaternaire en C-2 et deux singulets pour les protons H-1 et H-6. L'absence de constante de couplage entre H-6 et H-7 résulte de la valeur de l'angle dièdre H-6—C-6—C-7—H-7 voisin de 90°. Par contre, le signal correspondant à H-7 est un doublet (J = 9 Hz) résultant du couplage avec l'hydrogène de l'hydroxyle secondaire. L'irradiation de l'ester **12** permet l'isolement, après purification, d'isomères spiranniques **16***b* (10%) et du régioisomère **17***b* (24%).

La présence de quatre stéréoisomères **16***b* est décelée par le nombre de singulets (huit) en rmn ^1H correspondant au méthyle quaternaire et à celui du groupe acétate. Le rapport des

Can. J. Chem. Downloaded from www.nrcresearchpress.com by 88.85.125.76 on 09/07/12
For personal use only.

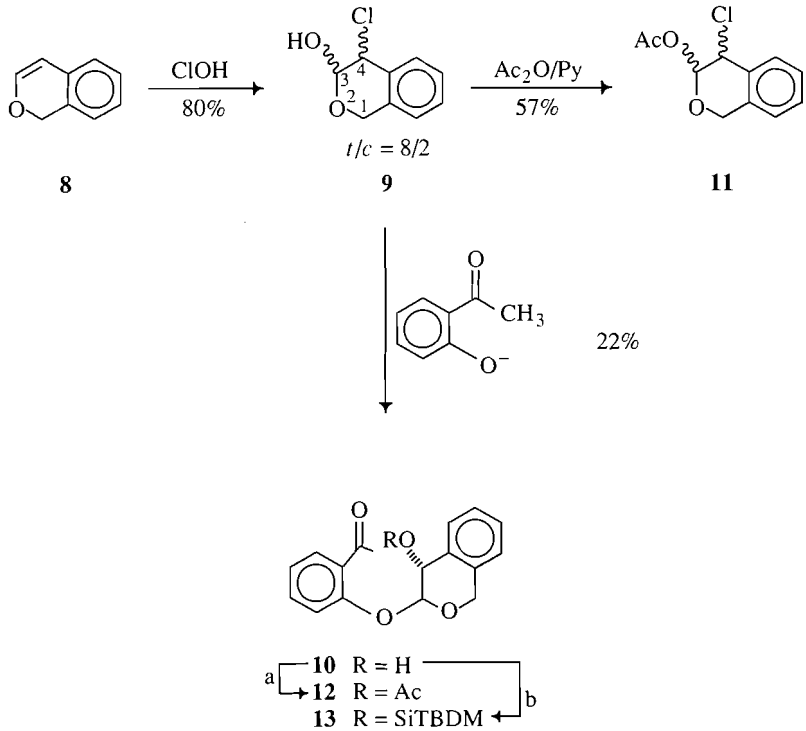

a : NaH, THF, N-Ac imidazole, 80%
b : TBDMSiCl, imidazole, DMF,71%

SCHÉMA 3. Synthèse des acétals isochromanniques.

TABLEAU 1. Photolyse des cétoacétals **7**

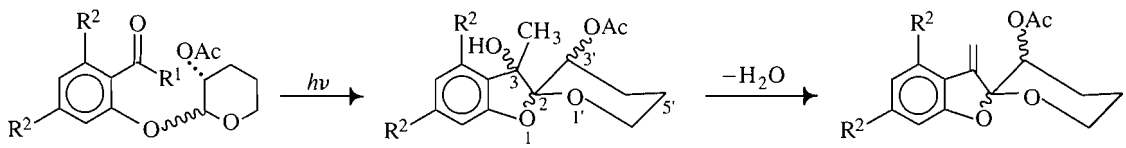

	R^1	R^2	%*	%	(c/t)
a	Me	H	87	72	(78 : 22)
b	Me	OAc	20	—	
c	Me	OMe	Traces	Traces	
d	COOEt	OMe	0	0	

*Pourcentage calculé par rmn ^{1}H.

intégrales de ces singulets indique que les quatre diastéréoisomères **16***b* sont dans des proportions pratiquement équivalentes (3 : 3 : 2 : 2).

Enfin, la photolyse du dérivé silylé **13** semble produire majoritairement le composé spirannique **16***c* (70%). En effet, si la purification du photolysat obtenu par chromatographie sur silice conduit à la dégradation des produits, le spectre rmn ^{1}H (350 MHz) du produit brut révèle la présence du mélange des isomères spiranniques **16***c* et du composé **17***c*.

Discussion des résultats

La photolyse des acétals aromatiques de type **C** comportant un groupe chromophore acétyle conduit à des composés de structure spirannique **D** en série hétérocyclique. En série isochromannique, la présence d'un second noyau aromatique induit une réaction secondaire de cyclisation sur le radical benzylique, compétitive avec la réaction de spirocyclisation.

Cette photocyclisation conduisant à des dérivés bicycliques de type [4.3.1] peut résulter d'une proximité plus grande du groupe carbonyle avec un des atomes d'hydrogène benzylique par rapport à l'atome d'hydrogène acétalique car un tel facteur peut intervenir dans la régiosélectivité d'une telle réaction radicalaire (30). De plus, la formation du dérivé bicyclique **17***a* peut s'expliquer en supposant une vitesse d'homolyse plus grande pour l'hydrogène benzylique étant donné la faible valeur de l'angle dièdre ($\theta_1 = 30°$) formé par la liaison C-1′—H-1′ et

Can. J. Chem. Downloaded from www.nrcresearchpress.com by 88.85.125.76 on 09/07/12
For personal use only.

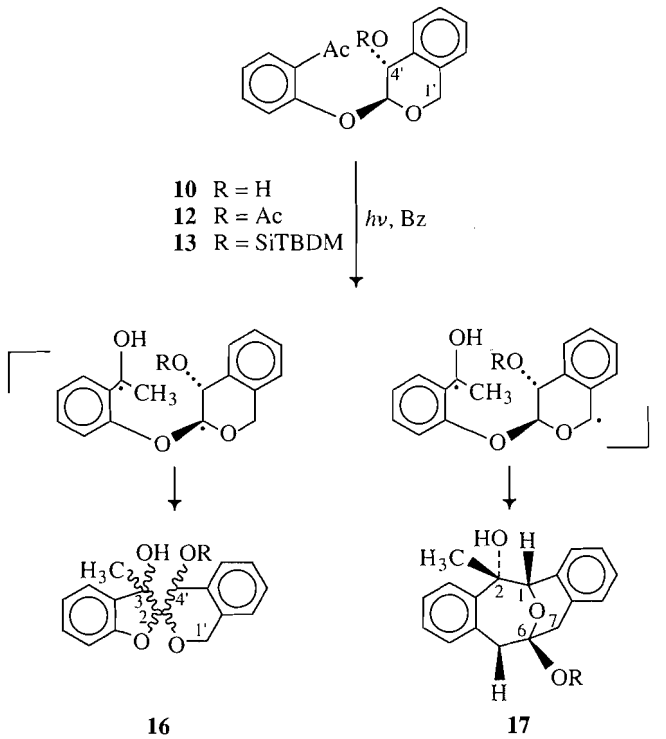

a R = H
b R = Ac
c R = SiTBDM

SCHÉMA 4. Photolyse des acétals isochromanniques.

TABLEAU 2. Photolyse* des cétoacétals **10**, **12** et **13**

Acétals	% **16**	% **17**
10 R = H		41†
12 R = Ac	10†	24
13 R = SiTBDM	70‡	14

*Taux de transformation : 75–80%.
†Rendement déterminé par rapport à la quantité d'acétal qui a effectivement réagi après purification par chromatographie.
‡Rendement estimé d'après le spectre rmn.

l'orbitale *p* non liante de l'atome d'oxygène (Schéma 5) (31–33). En outre, selon Leroy (34), l'énergie de stabilisation SE d'un radical benzylique (45,19 kJ mol^{-1}) est supérieure à celle d'un radical acétalique (−8,11 kJ mol^{-1}) alors que l'enthalpie de clivage de liaison (BDE) est inférieure de 52,7 kJ mol^{-1} (367,5 au lieu de 420,2). Ainsi, l'ensemble de ces facteurs stériques et énergétiques justifierait la formation du composé bicyclique **17**.

Ayant précédemment constaté l'influence favorable d'un groupement acétate en C-2 sur le processus de photocyclisation des glycosides (10, 22), il nous a semblé utile d'acétyler la fonction alcool. La présence d'un tel groupement modifie sensiblement la conformation de la partie tétrahydropyrannique (**10** *trans*, R = H, J_{3-4} = 2,6 Hz; **12**, R = Ac, J_{3-4} = 0) et probablement la valeur des angles θ_1 et θ_2. En outre, il est vraisemblable d'envisager selon Giese et coll. (35) une interaction stabilisante entre l'orbitale *p* occupée par un électron isolé (SOMO) et l'orbitale σ* (LUMO) de la liaison C-4—OAc.

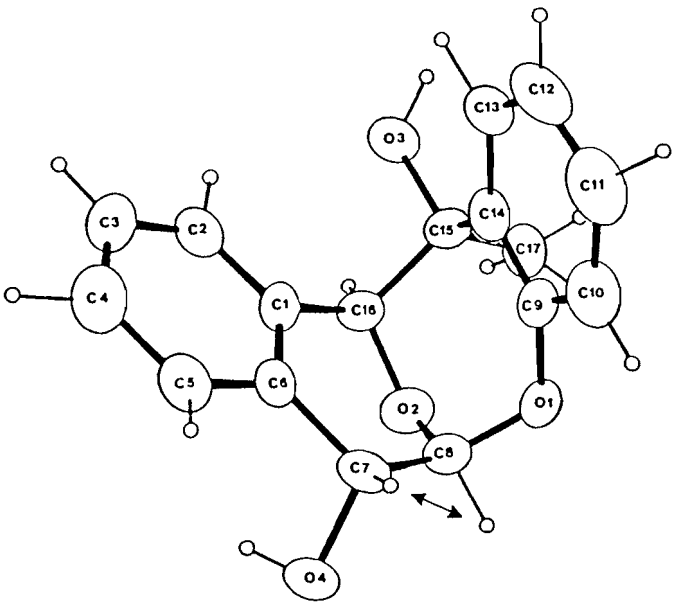

FIG 2. Analyse cristallographique de **17***a*. (La numérotation des atomes de **17***a* dans ce schéma est différente de celle du schéma 5.)

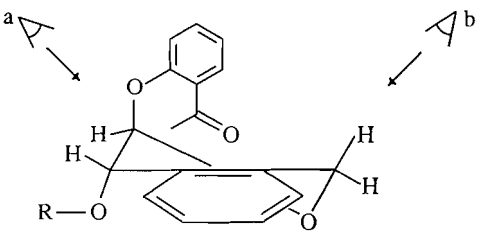

10 R = H
12 R = Ac
13 R = SiTBDM

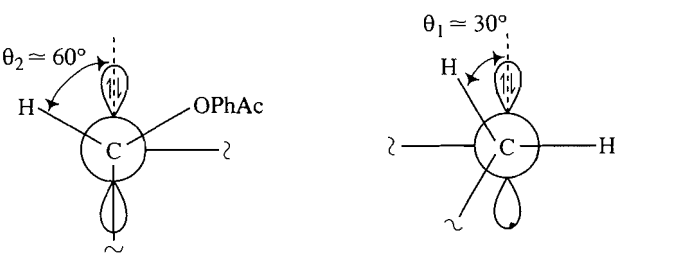

a : liaison C—H acétalique b : liaison C—H benzylique

SCHÉMA 5. Représentation des acétals isochromanniques.

Enfin, les résultats avec le composé **13** montrent que l'introduction du groupe *tert*-butyldiméthylsilyle oriente la photolyse vers la spirocyclisation. La présence d'un tel groupement encombrant doit vraisemblablement modifier la conformation de la partie hétérocyclique (**13**, R = SiTBDM, J_{3-4} = 2 Hz) éloignant le groupe carbonyle des hydrogènes benzyliques.

En conséquence, l'application de ces résultats initiaux en série tétrahydropyrannique et en série isochromannique au diméthoxy-6,7 isochromène devrait être envisagée pour la synthèse ultérieure de la tétra-*O*-méthyl crombénine **1** (R = OMe) et de la crombénine **1** (R = OH).

Can. J. Chem. Downloaded from www.nrcresearchpress.com by 88.85.125.76 on 09/07/12
For personal use only.

Can. J. Chem. Downloaded from www.nrcresearchpress.com by 88.85.125.76 on 09/07/12
For personal use only.

Partie expérimentale

Les points de fusion non corrigés ont été déterminés sur un appareil Buchi. Les spectres rmn ^1H (60, 80 et 350 MHz) et masse, ont été tracés à température ambiante respectivement avec les spectromètres suivants : Varian EM 360, Cameca, Bruker WP.80 CW, Varian série 634 et Varian Match 5 à 70 eV. Les chromatographies «flash» ont été réalisées avec de la silice Merck (230–400 mesh).

Synthèse des acétals tétrahydropyranniques et isochromanniques

Synthèse de l'acétate de salicyle ***3***

À 50 g (0,4 mol) d'alcool *o*-hydroxybenzylique **2** dissous dans 300 mL d'éther et refroidis à 0°C, sont ajoutés goutte à goutte 48 mL (0,5 mol) d'anhydride acétique puis 1 mL d'éthérate de trifluorure de bore. Le mélange, agité pendant 4 h à 15°C, est neutralisé avec 44 g d'hydrogénocarbonate de sodium dissous dans 100 mL d'eau glacée. Après extraction avec 200 mL d'éther, lavage à l'eau et séchage sur sulfate de sodium, l'évaporation du solvant donne 65 g de produit **3** brut. Le composé **3** (4,8 g) est purifié par chromatographie (hexane/acétate d'éthyle, 3 : 2) donnant 4,16 g (0,025 mol) de **3** (rendement 84%); liquide; rmn ^1H 60 MHz ($CDCl_3$) δ : 7,6 (large s, 1H, OH), 7,1 (m, 4H, arom.), 5,05 (s, 2H, CH_2O), 2,0 (s, 3H, CH_3COO) ppm. Anal. calc. pour $C_9H_{10}O_3$: C 65,05, H 6,07; tr. : C 64,95, H 6,05.

Synthèse de l'acétate de tétrahydropyrannyloxy-2-benzyle ***4***

Le composé **4** a été préparé selon la méthode décrite par Miyashita *et al.* (36) à partir de 1,9 g (0,011 mol) de **3**, 1,5 mL (0,017 mol) de dihydropyranne et 0,3 g de paratoluène sulfonate de pyridinium. Le produit brut (1,4 g) est purifié par deux chromatographies successives (hexane/acétate d'éthyle, 4 : 1, puis dichlorométhane) donnant 0,915 g (3,6 mmol) de **4** (rendement 32%) et 1 g (6 mmol) d'alcool **3**; solide; *F* 48–49°C; rmn ^1H 60 MHz ($CDCl_3$) δ : 7,2 (m, 4H, arom.), 5,5 (m, 1H, OCHO), 5,2 (s, 2H, CH_2OCO), 3,8 (m, 2H, CH_2O), 2,05 (s, 3H, CH_3COO), 1,9 (m, 6H, $(CH_2)_3$) ppm. Anal. calc. pour $C_{14}H_{18}O_4$: C 67,18, H 7,25; tr. : C 67,10, H 7,23.

Synthèse de l'alcool tétrahydropyrannyloxy-2 benzylique ***5***

L'acétate **4** (2,5 g, 0,01 mol) dilué dans 20 mL d'éthanol est saponifié à 18°C pendant 1 h par une solution éthanolique de soude (10 mL de soude 2 N et 10 mL d'éthanol). Après évaporation de l'éthanol, le résidu est repris avec 50 mL d'éther. Après lavage à l'eau, séchage, filtration et évaporation, le produit brut (2 g) est chromatographié (hexane/acétate d'éthyle, 4 : 1) donnant 1,95 g (9,4 mmol) d'alcool **5** (rendement 94%); liquide; rmn ^1H 60 MHz ($CDCl_3$) δ : 7,2 (m, 4H, arom.), 5,35 (s, 1H, OCHO), 4,6 (s, 2H, CH_2OH), 3,9 (m, 2H, CH_2O), 2,55 (large s, 1H, OH), 1,8 (m, 6H, $(CH_2)_3$). Anal. calc. pour $C_{12}H_{16}O_3$: C 69,21, H 7,74; tr. : C 69,17, H 7,73.

Synthèse du tétrahydropyrannyloxy-2 benzaldéhyde ***6***

À la solution de 1,75 g (8 mmol) de chlorochromate de pyridinium dans 16 mL de dichlorométhane, sont ajoutés 0,1 g d'acétate de sodium anhydre puis 1,13 g (54 mmol) d'alcool **5** dilué dans 8 mL de dichlorométhane. Après 3 h d'agitation à température ambiante, le mélange est filtré sur Célite, dilué avec 20 mL d'éther, lavé à l'eau puis séché sur sulfate de sodium. Après filtration et évaporation, la chromatographie (hexane/acétate d'éthyle, 9 : 1) du produit brut (1 g) donne 0,78 g (38 mmol) d'aldéhyde **6** (rendement 69%); liquide; rmn ^1H 60 MHz ($CDCl_3$) δ : 10,4 (s, 1H, CH=O), 7,5 (m, 4H, arom.), 5,4 (s, 1H, OCHO), 3,8 (m, 2H, CH_2O), 1,8 (m, 6H, $(CH_2)_3$) ppm. Anal. calc. pour $C_{12}H_{14}O_3$: C 69,88, H 6,84; tr. : C 69,66, H 6,63.

Synthèse du chloro-4-isochromannol-3 ***9***

Une solution de 1,87 g (14,2 mmol) d'isochromène (16) dans 3 mL de tétrahydrofuranne est ajoutée à l'abri de la lumière et sous azote à 2,5 g de phosphate de potassium monopotassique solubilisé dans 3,4 mL d'eau distillée. Puis 7,9 mL d'une solution aqueuse d'hypochlorite de sodium (48° chlorométriques) sont ajoutés à 0°C goutte à goutte pendant 40 min. La solution, revenue à température ambiante, est évaporée puis extraite à l'éther. Après lavage à l'eau, séchage et évaporation, le produit **9** instable (2,1 g, rendement 80%) est utilisé à l'état brut; produit huileux; rmn ^1H 60 MHz ($CDCl_3$) δ : 7,35 (m, 4H, arom.), 5,5 (m, 1H, CHCl), 5,1 (m, 1H, CHOH), 4,9 (s, 2H, CH_2), 2,5 (large s, 1H, OH) ppm.

Synthèse de l'acétoxy-3-chloro-4- isochromanne ***11***

Sous azote et à l'abri de la lumière, on mélange 0,5 g (2,7 mmol) de chlorhydrine **9** avec 6,5 mL de pyridine anhydre, 16 mg de diméthylamino-4-pyridine et 5,1 mL (54 mmol) d'anhydride acétique. Après 3 h d'agitation à température ambiante, le mélange est concentré, repris avec 30 mL d'éther, neutralisé avec une solution aqueuse d'hydrogénocarbonate de sodium, puis lavé à l'eau. Après séchage, filtration et évaporation, le résidu (588 mg) est purifié par chromatographie (hexane/acétate d'éthyle, 7 : 3) donnant 350 mg (1,5 mmol) d'ester instable **11** (rendement 57%); solide; *F* 46–51°C; rmn ^1H 250 MHz ($CDCl_3$) δ : 7,35 (m, 4H, arom.), 4,96 (s, 1H, H-1), 6,38 (d, J = 2,6 Hz, H-3 *trans*), 6,37 (d, J = 3,1 Hz, H-3 *cis*), 5,13 (d, J = 3,1 Hz, H-4 *cis*), 4,94 (d, J = 2,6 Hz, H-4 *trans*), 2,15 (s, CH_3COO, *cis*), 2,08 (s, CH_3COO, *trans*) ppm. Anal. calc. pour $C_{11}H_{11}ClO_3$: C 58,29, H 4,89, Cl 15,64; tr. : C 58,60, H 4,70, Cl 15,60.

Synthèse de l'(acétyl-2'-phénoxy)3-isochromannol-4 ***10***

À une suspension de 0,874 g d'hydrure de sodium dans 20 mL d'éther anhydre sont additionnés sous azote et goutte à goutte 5 mL (41,5 mmol) d'*o*-hydroxy-acétophénone. Après l'arrêt du dégagement d'hydrogène, le mélange est dilué avec 60 mL d'*o*-hydroxy-acétophénone. Puis on ajoute 2,8 g (15 mmol) de chlorhydrine **9** solubilisée dans 10 mL d'*o*-hydroxy-acétophénone. Après 2 h d'agitation à température ambiante, le milieu est dilué avec 200 mL d'éther puis refroidi à 0°C avant l'addition de 52 mL d'une solution de soude à 5%. Après décantation, la phase organique est lavée avec cette solution basique pour éliminer l'*o*-hydroxy-acétophénone résiduelle. Après lavage à l'eau, séchage sur sulfate de magnésium et évaporation, le produit brut (2 g) est chromatographié (dichlorométhane/acétate d'éthyle, 85 : 15, plus 1% de pyridine) donnant 0,952 g (3,35 mmol) d'acétal **10** (rendement 22%); solide; *F* 73–74°C; rmn ^1H 80 MHz ($CDCl_3$) δ : 7,3 (m, 8H, arom.), 5,7 (d, J = 2,6 Hz, 1H, OCHO), 4,81 (s, 2H, CH_2O), 4,7 (d, J = 2,6 Hz, 1H, CHOH), 2,75 (large s, 1H, OH), 2,2 (s, 3H, $COCH_3$). Anal. calc. pour $C_{17}H_{16}O_4$: C 71,81, H 5,67; tr. : C 71,78, H 5,65.

Synthèse de l'(acétyl-2'-phénoxy)-3 acétoxy-4-isochromanne ***12***

Une solution d'alcool **10** (0,916 g, 3,2 mmol) dans 5 mL de tétrahydrofuranne est ajoutée, sous azote et goutte à goutte, à une suspension de 0,169 g d'hydrure de sodium (3,9 mmol) dans 3 mL de tétrahydrofuranne. Après 30 min d'agitation à température ambiante, 1,278 g de *N*-acétylimidazole (11,6 mmol) dilué dans 3 mL de tétrahydrofuranne sont ajoutés. Après 12 h d'agitation, le mélange est évaporé, repris avec 30 mL d'éther, lavé à l'eau puis séché sur sulfate de sodium. Après filtration et évaporation, le produit brut est chromatographié (dichlorométhane) donnant 0,875 g (2,6 mmol) d'acétate **12** (rendement 80%); solide; *F* 106–107°C; rmn ^1H 80 MHz ($CDCl_3$) δ : 7,4 (m, 8H, arom.), 5,9 (s, 2H, OCHO et CH—$OCOCH_3$), 4,9 (s, 2H, OCH_2), 2,15 (s, 3H, CH_3COO), 2,1 (s, 3H, $COCH_3$) ppm. Anal. calc. pour $C_{19}H_{18}O_5$: C 69,93, H 5,56; tr. : C 69,92, H 5,36.

Synthèse de l'(acétyl-2'-phénoxy)-3-tertiobutyldiméthylsilyloxy-4-isochromanne ***13***

De l'imidazole (0,874 g, 12,8 mmol) puis 0,968 g de chlorure de tertiobutyldiméthylsilyle (6,4 mmol) sont ajoutés à température ambiante à une solution de 0,912 g d'alcool **10** (3,2 mmol) dans 3,2 mL de diméthylformamide. Après 3 h d'agitation, le milieu réactionnel est dilué à 25 mL d'éther de pétrole. La phase inférieure est extraite trois fois avec 20 mL d'éther de pétrole. Les phases organiques sont lavées 2 fois avec 5 mL d'eau et séchées sur sulfate de sodium. Après filtration et évaporation, le produit brut (1,456 g) est chromatographié (hexane/acétate d'éthyle, 9 : 1) donnant 0,910 g (2,3 mmol) de produit silylé **13** (rendement 71%); solide; *F* 99–100°C; rmn ^1H 80 MHz ($CDCl_3$) δ : 7,35 (m, 8H, arom.), 5,8 (d, J = 2 Hz, 1H, OCHO), 4,9 (s déformé, 3H, OCH_2 et CHOSi), 2,2 (s, 3H, $COCH_3$), 0,9 (s, 9H, $SiC(CH_3)_3$), 0,13 et 0,1 (2s, 6H, $Si(CH_3)_2$). Anal. calc. pour $C_{23}H_{30}O_4Si$: C 69,31, H 7,59; tr. : C 68,84, H 7,59.

Can. J. Chem. Downloaded from www.nrcresearchpress.com by 88.85.125.76 on 09/07/12
For personal use only.

Photolyse des cétoacétals

Les irradiations ont été réalisées dans les conditions opératoires déjà décrites (22). La lampe est munie d'un filtre Vycor. Le solvant utilisé est l'acétonitrile ou le benzène.

7*a* : 7,2 g (26 mmol) de **7***a* dissous dans 600 mL d'acétonitrile ont été irradiés pendant 5 h. Après évaporation du solvant, le produit brut (7,4 g) est chromatographié (hexane/acétate d'éthyle, 3 : 2) donnant 6,28 g du mélange des stéréoisomères **14***a* (rendement 87%); liquide visqueux qui cristallise en partie lentement; rmn ^{1}H, 60 MHz (C_6D_6) δ : 7,15 (m, 4H, arom.), 5,5 et 5,05 (m, 1H, CH—OCOCH$_3$), 4,05 et 3,5 (m, 2H, CH_2O), 3,3 (s, 1H, OH), 1,9 et 1,7 (2s, 3H, CH_3COO), 1,5 (m, 4H, $(CH_2)_2$), 1,3 et 1,1 (2s, 3H, C—CH_3) ppm; rmn ^{13}C ($CDCl_3$) δ : 1,81, 1,80, 1,73 et 1,71 (4s, 3H, C—CH_3) ppm. Anal. calc. pour $C_{15}H_{18}O_5$: C 64,73, H 6,52; tr. : C 64,68, H 6,46.

Déshydratation des alcools isomères ***14***a

Selon la méthode décrite par Bernasconi *et al.* (9) 2 g (7,2 mmol) d'alcools **14***a* dans 15 mL de pyridine sont traités avec une solution d'oxychlorure de phosphore (2,1 mL, 23 mmol) dans 3,5 mL de pyridine. Le produit brut obtenu (1,76 g) est chromatographié (dichlorométhane/hexane/éther, 30 : 20 : 2) donnant 1,35 g (5,2 mmol) des isomères **15***a* (rendement 72%); liquide; rmn ^{1}H 60 MHz (C_6D_6) δ : 7,5–6,8 (m, 4H, arom.), 5,5 (dd, J = 6 et 10,4 Hz, 1H, CHOCOCH$_3$ *trans*), 5,05 (t, J = 3 Hz, 1H, CHOCOCH$_3$ *cis*), 4,8 (2 dd, J = 2,2 Hz, C=CH_2), 4,35–3 (m, 2H, -CH_2O), 2,2–0,8 (m, 4H, $(CH_2)_2$), 1,7–1,3 (2s, 3H, CH_3COO) ppm; rmn ^{13}C ($CDCl_3$) **15***a cis*, δ : 169,1 (C=O), 158,5 (C-3), 138,9, 134,1 (carbones quaternaires aromatiques), 129,6 (C-4), 129,03 (C-6), 122,1 (C-7), 119,8 (C-5), 107,5 (C-2), 80,8 (=CH_2), 71 (C-3′), 62,85 (C-6′), 25,2 (C-4′), 24,7 (C-5′), 20,2 (CH_3) ppm; **15***a trans*, δ : 169,3 (C=O), 157,9 (C-3), 139,6, 133,6 (carbones quaternaires aromatiques), 129,6 (C-4), 128,4 (C-6), 123,8 (C-7), 120,3 (C-5), 105,9 (C-2), 80,9 (=CH_2), 69,7 (C-3′), 63,4 (C-6′), 24,1 (C-4′), 21 (CH_3), 19 (C-5′) ppm. Anal. calc. pour $C_{15}H_{16}O_4$: C 67,73, H 6,50; tr. : C 67,71, H 6,46.

7*b* : 0,947 g (2,4 mmol) de **7***b* dissous dans 50 mL de benzène est irradié pendant 8 h. Le produit brut (0,940 g) obtenu après évaporation est chromatographié (hexane/acétate d'éthyle, 3 : 2) donnant 0,264 g (0,6 mmol) de produit initial **7***b* et 0,153 g (0,4 mmol) de composé spirannique **14***b* (rendement 20%); liquide; rmn ^{1}H 60 MHz ($CDCl_3$) δ : 7 (s, 2H, arom.), 5,8–5,4 (m, 1H, CHOCOCH$_3$), 4,4–3,5 (m, 2H, OCH_2), 2,3 et 2,28 (2s, 9H, CH_3COO), 1,85 (large s, 3H, CH_3), 2,9–1,6 (m, 5H, $(CH_2)_2$ et OH) ppm.

7*c* : 2,3 g (2,6 mmol) de **7***c* dissous dans 52 mL d'acétonitrile sont irradiés pendant 10 h. Après évaporation, 0,810 g de photoproduits sont déshydratés comme **14***a*. Le produit brut (0,619 g) obtenu, est chromatographié (hexane/acétate d'éthyle, 3 : 2) donnant des traces (19 mg) de produit insaturé **15***c*; liquide; rmn ^{1}H 60 MHz ($CDCl_3$) δ : 6,3 (m, 2H, arom.), 5,75 et 5,2 (2s, 2 × 2H, C=CH_2), 5,1 (m, 1H, CH—OCOCH$_3$), 4,1 (m, 2H, OCH_2), 3,9 et 3,85 (2s, 2 × 3H, OCH_3), 2,0 (m, 4H, $(CH_2)_2$), 2,15 et 1,9 (2s, 2 × 3H, CH_3COO) ppm.

10 (R = H) : 0,66 g (2,3 mmol) de produit **10** solubilisé dans 46 mL d'acétonitrile est irradié pendant 4 h. Après évaporation, le produit brut est purifié par deux chromatographies successives (dichlorométhane/acétate d'éthyle, 4 : 1, puis hexane/acétate d'éthyle, 1 : 1) donnant 0,167 g (0,6 mmol) de **10** et 0,204 g (0,7 mmol) de dérivé bicyclique **17***a* (rendement 41%); solide; F 149–150°C; rmn ^{1}H 80 MHz ($CDCl_3$) δ : 7,05 (m, 8H, arom.), 5,6 (s, 1H, OCHO), 4,75 (s, 1H, C-1—H), 4,35 (d, J = 9 Hz, 1H, C-7—H), 2,1 (d, J = 9 Hz, C-7—OH), 2,08 (s, 1H, C-2—OH), 1,8 (s, 3H, CH_3) ppm. Anal. calc. pour $C_{17}H_{16}O_4$: C 71,82, H 5,67; tr. : C 71,50, H 5,68.

12 (R = Ac) : 0,602 g (1,8 mmol) d'acétal acétylé **12** dans 37 mL de benzène est irradié pendant 12 h. Après évaporation, le produit brut est chromatographié (dichlorométhane/acétate d'éthyle, 9,5 : 0,5) donnant 0,060 g (0,18 mmol) d'acétate spirannique **16***b* (R = OAc) et 0,145 g (0,43 mmol) d'isomères bicycliques **17***b* (R = OAc); composé **16***b* (rendement 10%); solide; F 146–151°C; rmn ^{1}H 350 MHz ($CDCl_3$) δ : 7,3 (m, 4 × 8H, arom.), 6,6–6,5–5,9–5,8 (4s, 4 × 1H, CHOCOCH$_3$), 5,29–5,26–4,98–4,89 (4d, J = 15 Hz, 4 × 2H, C-1′—H_2), 3,2 (large s, 1H, OH), 2,13–2,10–1,95–1,92 (4s, 4 × 3H, CH_3COO), 1,83–1,79–1,77–1,74 (4s, 4 × 3H, C-3—CH_3) ppm; pour les CH_2 benzyliques deux isomères sur quatre sont observés; composé **17***b* (rendement 24%); solide; F 158–159°C; rmn ^{1}H 80 MHz ($CDCl_3$) δ : 7,1 (m, 8H, arom.), 5,8 (s, 1H, OCHO), 5,7 (s, 1H, CH—OCOCH$_3$), 4,95 (s, 1H, C-1—H), 2,3 (s, 1H, OH), 2,1 (s, 3H, CH_3COO), 1,9 (s, 3H, CH_3—C-2) ppm. Anal. calc. pour $C_{19}H_{18}O_5$: C 69,93, H 5,56; tr. : C 69,72, H 5,65.

13 (R = SiTBDM) : 0,5 g (1,3 mmol) d'acétal silylé **13** est irradié pendant 6 h. Après évaporation, le produit brut est analysé par rmn sans purification; rendement en produit spirannique **16***c* d'après le rapport des intégrales en rmn : 70%; rmn ^{1}H 350 MHz ($CDCl_3$) δ : 7,2 (m, 8H, arom.), 5,30–5,22–4,98–4,88 (4d, J = 15 Hz, 4 × 1H, C-1′—H), 5,30–5,29–5,25–5,21 (4s, 4 × 1H, C-4′—H), 1,84–1,79–1,77–1,75 (4s, 4 × 3H, C-3—CH_3), 0,8 (m, 9H, $C(CH_3)_3$), 0,1 (m, 6H, $Si(CH_3)_2$) ppm; **17***c* (rendement estimé d'après la rmn : 14%); rmn ^{1}H 350 MHz ($CDCl_3$) δ : 7,2 (m, 8H, arom.), 5,95 (s, 1H, C-6—H), 5,84 (s, 1H, C-7—H), 4,95 (s, 1H, C-1—H), 1,92 (s, 3H, C-2—CH_3) ppm.

Analyse cristallographique du composé ***17***a

Les données cristallographiques[1] sont :

$C_{17}H_{16}O_4$ PM = 284,30

Monoclinique, groupe d'espace Pc, a = 8,987(1), b = 8,784(1), c = 17,279(2) Å, β = 92,31(1)°, V = 1362,9(5) Å^3, F_{000} = 600, μ = 7,7 cm^{-1}, z = 4, ρ_c = 1,38 Mg m^{-3}.

Le cristal (prisme 0,10 × 0,10 × 0,20 mm) est étudié sur un diffractomètre automatique Enraf–Nonius (λ(Mo-Kα) = 0,71073 Å, scan ω/2θ = 1, t_{max} = 60 s); l'enregistrement donne 3010 reflections dont 2727 uniques (R_{int} = 0,045) et 2436 avec $I > \sigma(I)$. La structure est résolue à l'aide des méthodes directes. Après affinements en isotrope puis en anisotrope (R = 0,061) des atomes non-hydrogènes, les atomes d'hydrogène sont localisés dans la même différence de Fourier (entre 0,52 et 0,24 e Å^{-3}). Le meilleur affinement par matrice complète de la structure donne : $R = \Sigma||F_o| - |F_c||/\Sigma|F_o| = 0,055$, $R_w = (\Sigma w(|F_o| - |F_c|)^2/\Sigma w|F_o|^2)^{1/2} = 0,053$, $w = 1/\sigma^2|F_o|^2 = [\sigma^2(I) + (0,04F_o^2)^2]^{-1/2}$, S_w = 1,10, NV = 474. Les tableaux des différentes valeurs sont confiés au «Dépôt de données non publiées».[2]

1. E. V. Brandt, D. Ferreira et D. G. Roux. J. Chem. Soc. Perkin Trans. 1, 1879 (1981).
2. M. Tindale et D. G. Roux. Phytochemistry, **13**, 829 (1974).
3. E. V. Brandt, D. Ferreira et D. G. Roux. J. Chem. Soc. Chem. Commun. 392 (1972).
4. D. A. Evans, C. E. Sacks, R. A. Whitney et N. G. Mandel. Tetrahedron Lett. **8**, 727 (1978).
5. P. R. McGuirk et D. B. Collum. J. Org. Chem. **49**, 843 (1984).
6. H. Redlich et W. Francke. Angew. Chem. Int. Ed. Engl. **8**, 630 (1980).
7. K. Hintzer, R. Weber et V. Schurig. Tetrahedron Lett. **22**, 55 (1981).
8. C. Iwata, K. Hattori, S. Uchida et T. Imanischi. Tetrahedron Lett. **28**, 2995 (1984).
9. C. Bernasconi, L. Cottier, G. Descotes, J. P. Praly et G. Remy. Carbohydr. Res. **115**, 105 (1983).
10. G. Remy, L. Cottier et G. Descotes. J. Carbohydr. Chem. **1**, 37 (1982).
11. C. Bernasconi, L. Cottier et G. Descotes. Bull. Soc. Chim. Fr. 107 (1977).
12. L. Cottier, G. Descotes, M. F. Grenier et F. Metras. Tetrahedron, **37**, 2515 (1981).

1. L'analyse cristallographique a été réalisée par L. Toupet au Laboratoire de physique cristalline (Université de Rennes, U.A. CNRS 804, 35042 Rennes, France), que nous remercions vivement.

2. Les différents tableaux sont disponibles. On peut les acheter en s'adressant au Dépôt de données non publiées, ICIST, Conseil national de recherches ou Canada, Ottawa (Ont.), Canada K1A 0S2.

On peut également se les procurer en s'adressant au directeur, Cambridge Crystallographic Data Centre, University Chemical Laboratory, Lensfield Road, Cambridge CB2 1EW, Royaume-Uni.

13. T. KOZLUK, L. COTTIER et G. DESCOTES. Tetrahedron, **37**, 1875 (1981).
14. Y. NAGAO, E. FUJITA, T. KONNO et M. YAGI. Synthesis, 81 (1983).
15. F. COTTET, L. COTTIER, G. DESCOTES et R. M. SRIVASTAVA. J. Heterocycl. Chem. **25**, 1481 (1983).
16. F. COTTET, L. COTTIER et G. DESCOTES. Synthesis, 497 (1987).
17. G. BAKASSIAN, F. CHIZAT, D. SINOU et G. DESCOTES. Bull. Soc. Chim. Fr. **1**, 621 (1969).
18. J. C. SOULA et G. DESCOTES. Bull. Soc. Chim. Fr. **31**, 2636 (1964).
19. M. CHMIELEWSKI et A. ZAMOJSKI. Rocz. Chem. **46**, 1767 (1972).
20. H. A. STAAB. Angew. Chem. **12**, 407 (1962).
21. L. COTTIER et G. DESCOTES. J. Heterocycl. Chem. 1271 (1977).
22. G. REMY, L. COTTIER et G. DESCOTES. Can. J. Chem. **58**, 2660 (1980).
23. H. J. SCHNEIDER et V. HOPPEN. J. Org. Chem. **43**, 3866 (1978).
24. N. C. YANG, D. S. MCCLURE, S. L. MUROV, J. J. HOUSER et R. DUSENBERY. J. Am. Chem. Soc. **89**, 5466 (1967).
25. P. J. WAGNER, A. E. KEMPPAINEN et H. N. SCHOTT. J. Am. Chem. Soc. **85**, 5604 (1973).
26. P. J. WAGNER, R. J. TRUMAN et J. C. SCAIANO. J. Am. Chem. Soc. **107**, 7093 (1985).
27. O. EXNER. *Dans* Correction analysis in chemistry. *Éditeurs* : N. B. Chapman et I. Shorter. Plenum Press, New York. 1978. Chap. 10.
28. J. C. GRAMAIN, R. REMUSON et D. VALLEE. J. Org. Chem. **50**, 710 (1985).
29. S. P. PAPPAS, B. C. PAPPAS et J. E. BLACKWELL. J. Org. Chem. **32**, 3066 (1967).
30. N. J. TURRO et D. S. WEISS. J. Am. Chem. Soc. **90**, 2185 (1968).
31. D. J. PASTO, R. KRASNANSKY et C. ZERCHER. J. Org. Chem. **52**, 3062 (1987).
32. V. MALATESTA et J. C. SCAIANO. J. Org. Chem. **47**, 1455 (1982).
33. V. MALATESTA et K. U. INGOLD. J. Am. Chem. Soc. **103**, 609 (1981).
34. G. LEROY. Int. J. Quantum Chem. **23**, 271 (1983).
35. K. G. KORTH, R. SUSTMANN, J. DUPUIS et B. GIESE. J. Chem. Soc. Perkin Trans. 2, 1453 (1986).
36. M. MIYASHITA, A. YOSHIKOSHI et P. A. GRIECO. J. Org. Chem. **42**, 3772 (1977).

Can. J. Chem. Downloaded from www.nrcresearchpress.com by 88.85.125.76 on 09/07/12
For personal use only.

Dodecylammonium-glutamate Schiff bases of retinal

ANIL K. SINGH, CAMILLE SANDORFY, AND JANOS H. FENDLER

Département de chimie, Université de Montréal, C.P. 6128, Succursale A, Montréal (Québec), Canada H3C 3J7

Received December 22, 1989

This paper is dedicated to Professor Arthur S. Perlin on the occasion of his 67th birthday

ANIL K. SINGH, CAMILLE SANDORFY, and JANOS H. FENDLER. Can. J. Chem. **68**, 1258 (1990).

Dodecylammonium glutamate (**4**) has been prepared from dodecylamine (**2**) and *l*-glutamic acid (**3**) in ethanol and in aqueous ethanol. The obtained crystalline glutamic acid salt of dodecylamine (**4**) has been characterized by absorption, FTIR, ^{1}H NMR, ^{13}C NMR, and mass spectroscopy. Reaction of all-*trans* retinal (**5**) with the α-amino group of **4** gave a Schiff base (**6**), which was protonated by the α-COOH group of the glutamyl residue. However, the protonated Schiff base underwent acid-catalyzed hydrolysis to **2** + **3** + **5**. Some of **5** reacted with **2** to give the corresponding Schiff base. The proposed structures have been substantiated by *in situ* absorption, FTIR, and ^{1}H NMR spectroscopy.

Key words: retinal Schiff base, retinal, rhodopsin model, dodecylammonium glutamate, Schiff-base protonation.

ANIL K. SINGH, CAMILLE SANDORFY et JANOS H. FENDLER. Can. J. Chem. **68**, 1258 (1990).

On a préparé le glutamate de dodécylammonium (**4**) en faisant réagir la dodécylamine (**2**) avec l'acide *l*-glutamique, dans l'éthanol et dans l'éthanol aqueux. On a caractérisé le sel cristallin **4** à l'aide des spectroscopies infrarouge par transformation de Fourier, RMN du ^{1}H et du ^{13}C, d'absorption et de masse. La réaction du rétinal complètement *trans* (**5**) avec le groupement α-amino du produit **4** conduit à la base de Schiff **6**. Le produit **6** se protone sous l'action du groupement α-COOH du résidu glutamyle. Toutefois, la base de Schiff protonée subit une hydrolyse catalysée par les acides qui fournit les produits **2**, **3**, et **5**. Une partie du produit **5** a réagi avec le produit **2** pour donner la base de Schiff correspondante. Les structures proposées sont proposées sur la base des spectres RMN du ^{1}H, d'absorption et infrarouge par transformation de Fourier qui ont été déterminés *in situ*.

Mots clés : base de Schiff rétinal, rétinal, modèle de rhodopsine, glutamate de dodécylammonium, protonation de la base de Schiff.

[Traduit par la revue]

Introduction

A major class of biological pigments contain the polyene aldehyde retinal attached to the apo-protein via a Schiff base linkage (Fig. 1) (1–3). The imine linkage is formed by the reaction of the aldehyde group of retinal and the ε-amino group of a lysine residue in the protein. It is believed that the imine nitrogen in rhodopsins is protonated, though the exact mechanism of their protonation is not known (4). To provide chemical clarification to several striking structural and functional features of rhodopsins, bio-organic models involving retinylidene Schiff bases (**1**) have been used extensively. In most of the model

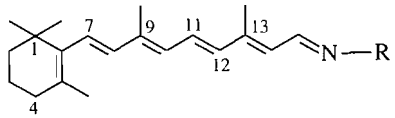

1*a*: R = *n*-butyl
1*b*: R = *n*-propyl
1*c*: R = *tert*-butyl
1*d*: R = peptide

compounds of rhodopsin, an alkyl amine (mostly *n*-butyl, *n*-propyl, and *tert*-butyl amine) has been used to prepare the retinylidene Schiff base (4, 5), although a few models involving polymeric amino compounds (6, 7) and amino esters and acids (8) have also been reported. These model compounds have not shown, however, a red shift of the absorption spectra comparable to that observed in vivo for the Schiff base chromophore in rhodopsin. Protonation of the imine group, hydrogen bonding, and electrostatic perturbations of the chromophore by charged protein residues have been proposed to be responsible for shifting the absorption maximum of rhodopsins (4, 9, 10). This postulate has prompted the use of model Schiff bases that have negative charges in their vicinity (11).

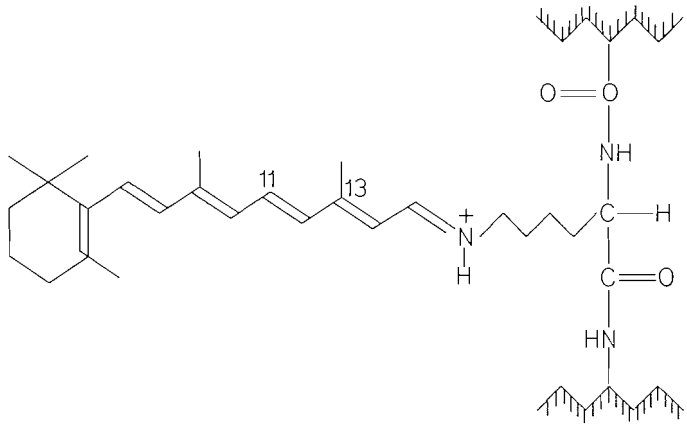

FIG. 1. Retinal attached to lysine via a protonated Schiff base linkage (11-*cis*, visual pigments, all-*trans* and 13-*cis*, bacteriorhodopsin).

A retinylidene Schiff base incorporating an amino acid residue provides a better model since it possesses a potentially intrinsic negative charge. The relative insolubility of amino acids in organic solvents and the instability of the retinylidene Schiff bases in the presence of hydrophobic carboxylates (e.g., CF_3COO^-) and water have hampered the development of a practical methodology for the preparation of retinylidene – amino acid Schiff bases. We have overcome these difficulties by taking advantage of reversed micelles. Recently, we reported that amino acids incorporated into sodium bis(2-ethylhexyl)sulfosuccinate- (AOT) solubilized water pools in heptane reacted with retinal to give Schiff bases (12). The small amounts of amino acids that could be incorporated into reversed micelles have, however, limited the preparative utility of this approach. Advantage has been taken of alkylammonium surfactants that contained amino acid counterions to form Schiff bases in orga-

Can. J. Chem. Downloaded from www.nrcresearchpress.com by 88.85.125.76 on 09/07/12
For personal use only.

nic solvents. The present report describes the formation of retinylidene Schiff bases of dodecylammonium glutamate and their protonation in methanol.

Experimental

All experiments using retinal and its derivatives were performed in the dark with dim red illumination. Dodecylamine (**2**), *l*-glutamic acid (**3**), and all-*trans* retinal (**5**) were obtained from the Aldrich Chemical Company. The solvents (Aldrich, spectral grade) were stored over a 4 Å Linde type molecular sieve and were freshly distilled under N_2 before use. UV–VIS absorption spectra were measured on a Varian Carey 16 spectrophotometer. NMR spectra were recorded on either a 300 or a 400 MHz Bruker NMR spectrometer. FTIR spectra were measured on a Nicolet 5 DXB FTIR spectrophotometer with a 2 cm^{-1} resolution. Mass spectra were recorded on a MS 50 TATC (Cratos) spectrometer. Thin-layer chromatographic analyses were done on silanized Si-60 reverse phase plates (Merck RP-2) using anhydrous and freshly distilled methanol as a solvent.

Dodecylammonium glutamate (4)

Two methods were used to prepare **4**:

1. An ethanolic (97%) solution (5 mL) of dodecylamine (**2**, 0.63 g, 3.4 mmol) was added to *l*-glutamic acid (**3**, 0.50 g, 3.4 mmol) in a round-bottom flask. The white suspension was stirred (Teflon) at ambient temperature. A very thick white creamy mass appeared after 20 min of vigorous stirring. The white mass was washed with 100 mL ethanol–water (1:1) and benzene. The white powder (**4**, 1 g) was dried under vacuum.

2. *l*-Glutamic acid (**3**, 0.50 g) was suspended in 6 mL water and the mixture was stirred (Teflon) to dissolve the maximum amount of the acid. An ethanolic solution (5 mL) of dodecylamine (**2**, 0.70 g) was then slowly added to the glutamic acid suspension in water, which resulted in complete dissolution of the contents of the flask, giving a clear solution. The solution was further stirred for 2 h at ambient temperature. Benzene (10 mL) was added to the reaction mixture and the solvent was removed on a rotary evaporator. The white crystalline material (**4**), obtained in quantitative yield, was dried over P_2O_5 under vacuum; mp 168–169°C; IR (Nujol) ν: 3040, 3022, 2982, 2972, 2878, 2848, 2540, 2498, 2437, 2086, 1664, 1604, 1529, 1518, 1508, 1403, 1364, 1328, 1298, 1220, 1150, 974, 931, 681 cm^{-1}; ^1H NMR (D_2O, 400 MHz) δ: 0.844 (3H, t, CH_3), 1.260 (18H, br s, CH_2), 1.638 (2H, m, -CH_2), 2.0–2.16 (2H, m, glu-C_α-CH_2-), 2.29–2.40 (2H, m, glu-C_α-C-CH_2-), 2.927 (2H, t, -CH_2-N^+H_3), 3.727 (1H, t, glu-C_α-H); ^{13}C NMR (D_2O, 100.62 MHz) δ: 14.56 (CH_3), 23.32–29.71 (-CH_2), 33.72 (-CH_2COO^-), 40.24 (-$CH_2N^+H_3$), 55.35 (C_α), 175.17 (C_α-COO^-), 181.13 (glu-C_γ-COO^-); mass, *m/e* (% rel. int.): 186 (50), 130 (100).

*Reactions of all-*trans *retinal (5) with dodecylammonium glutamate (4)*

1. A solution of all-*trans* retinal (**5**, 4×10^{-5} M) in dodecylammonium glutamate (**4**, 1×10^{-2} M in anhydrous MeOH) was kept in the dark at ambient temperature. The progress of the reaction was monitored by UV–VIS absorption measurements. The reaction mixture had faint yellow coloration in the beginning and exhibited a UV–VIS absorption band at 371 nm due to retinal. After 30 min of reaction, an intense UV–VIS band appeared at 361 nm and a small band appeared at 457 nm. On further standing, the reaction mixture showed a decrease in the absorbance of the 361-nm band and an increase in the 457-nm band. The reaction mixture acquired a deep yellow color after 1 h.

2. Dodecylammonium glutamate (**4**, 0.0166 g, 0.05 mmol) and all-*trans* retinal (**5**, 0.0142 g, 0.05 mmol) were dissolved in CD_3OD. The dark brown solution was allowed to stand in the dark at 4°C overnight before NMR analyses: **6**: ^1H NMR (300 MHz, CD_3OD) δ: 0.89 (3H, t, -CH_3-CH_2-), 1.04 (6H, s, C_1-Me_2), 1.28 (18H, s, -$(CH_2)_9$), 1.49 (2H, m, -CH_2-), 1.64 (2H, m, -CH_2-CH_2-CH_2), 1.71 (3H, s, C_5-Me), 2.02 (3H, s, C_9-Me), 2.05 (2H, m, DO_2C-CH_2-CH_2-), 2.18 (3H, s, C_{13}-Me), 2.46 (2H, m, DO_2C-CH_2-CH_2-), 2.90 (2H, t, D_3N^+-CH_2-CH_2-), 3.54 (1H, m, C_α-H), 6.08 (1H, d, $J_{14,15}$ = 10 Hz, H_{14}), 6.16 (1H, d, $J_{7,8}$ = 16 Hz, H_8), 6.21 (1H, d, $J_{10,11}$ = 11.9 Hz), 6.30 (1H, d, J = 16 Hz, H_7), 6.45 (1H, d, $J_{11,12}$ = 15 Hz, H_{12}), 7.01 (1H, d,d, $J_{11,12}$ = 15 Hz, $J_{10,11}$ = 11.6 Hz, H_{11}), 8.48 (1H, d, $J_{14,15}$ = 10 Hz, H_{15}).

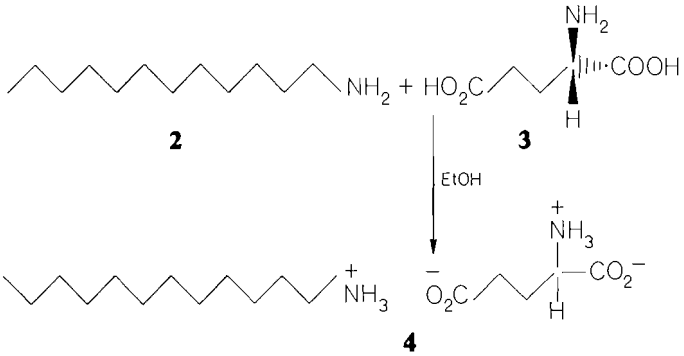

SCHEME 1

Results and discussion

Reaction of dodecylamine (2) with l*-glutamic (3) acid*

Dodecylamine (**2**) can react with the two carboxyl groups of *l*-glutamic acid (**3**) (Scheme 1). The chemical reaction leading to amide formation between dodecylamine and the -COOH group of glutamic acid is not considered, as the reaction is unlikely to be feasible at ambient temperature in the absence of a catalyst. It has been found (13) that amide bonds betwen amine and acid are formed at elevated temperatures.

Glutamic acid (**3**) is insoluble in ethanol and sparingly soluble in water. However, when an alcoholic solution of dodecylamine (**2**) was added to a water suspension of glutamic acid, the reaction mixture became completely transparent, indicating the modification of the molecular forces present in glutamic acid and dodecylamine. The properties of glutamic acid were changed by dodecylamine, even in the presence of relatively small amounts of water when the solid glutamic acid reacted with dodecylamine in 97% ethanol. Removal of solvent afforded a crystalline material that showed melting (168°C) behavior different from glutamic acid, as well as dodecylamine. The white crystalline solid was soluble only in alcohols and water, in which it foamed. It showed UV absorption bands at 204 and 275 nm. IR spectra of the solid showed a complex band with sharp peaks between 2950 and 2850 cm^{-1}, with major strong peaks located at 2851, 2918, 2953, and 2994 cm^{-1}. A continuous absorption with several small and broad peaks at 2731, 2598, 2543, 2496, and 2430 cm^{-1} was indicative of the presence of the ammonium group. Very intense IR absorption at 1640, 1604, and 1526 cm^{-1} indicated the presence of the COO^- group. A medium intensity (relative to the COO^- band at 1604 cm^{-1}) IR band at 1664 was also present. The IR data indicated the compound to be a salt of dodecylamine and glutamic acid.

A comparison of the ^1H NMR spectra of the reaction product with those of glutamic acid and dodecylamine confirmed the mono-salt structure **4**. The methylene group adjacent to the -NH_2 group in **2** resonates at δ 2.62 as a broad triplet, but this signal was absent in the product, and a new broad triplet appeared at δ 2.93. In glutamic acid (**3**), the two methylene groups of the side chain resonate as a complex multiplet between δ 1.50 and 2.50. However, in the product, the two side-chain methylene groups showed two complex multiplets centered at δ 2.33 and 2.07. The two multiplets are separated by a width of 1 δ. The C_α-*H* showed a triplet at δ 3.73 as against a multiplet at

Can. J. Chem. Downloaded from www.nrcresearchpress.com by 88.85.125.76 on 09/07/12
For personal use only.

Can. J. Chem. Downloaded from www.nrcresearchpress.com by 88.85.125.76 on 09/07/12
For personal use only.

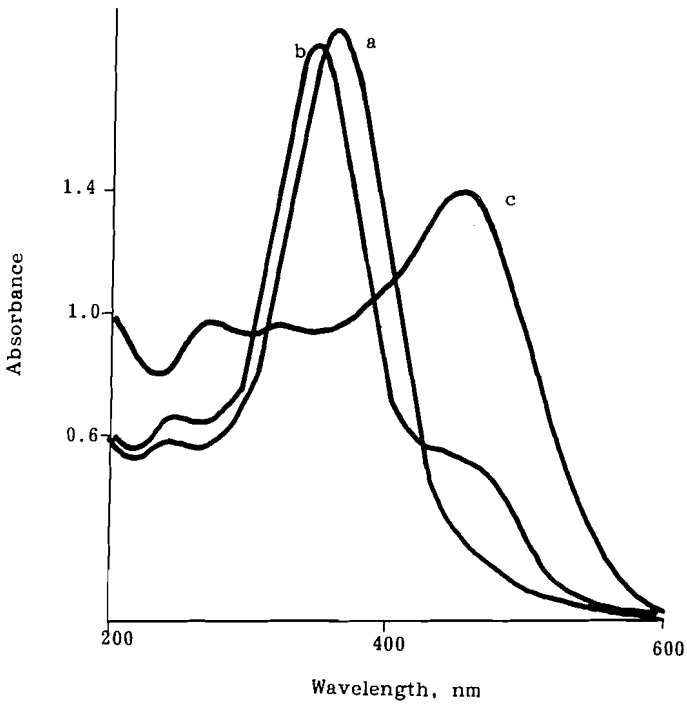

FIG. 2. Absorption spectra of a reaction mixture containing 4.5×10^{-5} M all-*trans* retinal (**5**) and dodecylammonium glutamate (**4**) in MeOH: (a) 0 h, (b) after 1 h, and (c) after 40 h.

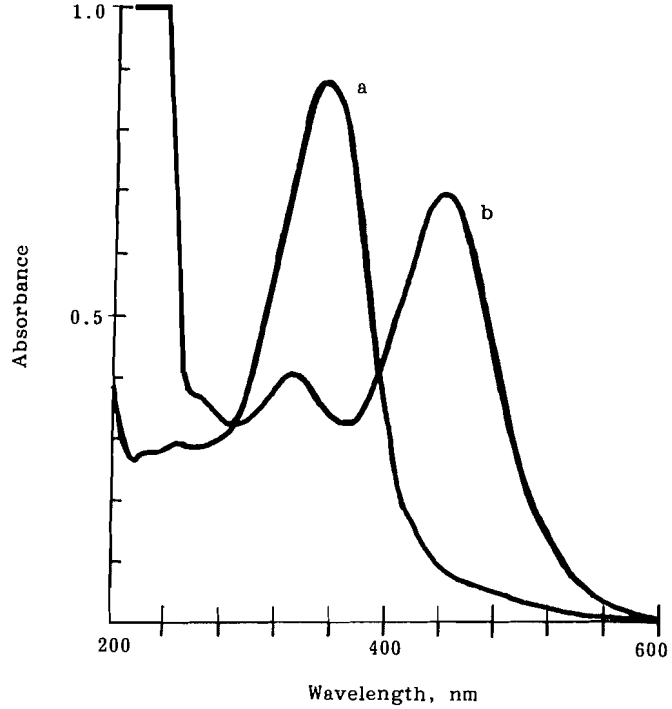

FIG. 3. Absorption spectra showing protonation of methanolic 5.9×10^{-5} M Schiff base **6** by excess CF_3COOH: (a) Schiff base formed between retinal (**5**) and dodecylammonium glutamate (**4**) in MeOH and (b) red shift after addition of CF_3COOH.

δ 3.25 in glutamic acid. The fact that the resonance frequency of the side-chain methylene group is perturbed shows that it is the side-chain carboxyl which reacted with the dodecylamine (**2**).

Further confirmation of structure **4** was obtained by ^{13}C NMR spectral analysis. Thus, the signal for the C_α-COO^- group of glutamic acid was seen unperturbed in the product resonating at δ 175.17. Similarly, the C_α carbon was seen at δ 55.35. Any change in chemical polarity around the C_α carbon is expected to influence its resonance frequency. Resonance frequency at δ 55.35 in the product was similar to the resonance frequency of C_α in glutamic acid (**3**).

Mass spectral analysis of **4** showed prominent peaks at *m/e* 186 (50%) due to $[C_{12}H_{28}N]^+$ and at *m/e* 130 (100%, base peak) due to $[C_5H_6O_4]^+$, which could readily be formed by breaking away NH_3 from the glutamic part of the molecule.

*Reaction of dodecylamine-glutamate (4) with all-*trans *retinal (5)*

Reaction of all-*trans* retinal (**5**) and dodecylammonium glutamate (**4**) was first studied by following absorption changes in a mixture of **5** (4×10^{-5} M) and **4** (10^{-2} M) in methanol. All of the retinal reacted with **5** within 30 min. Two UV–VIS bands were present in the absorption spectrum of the mixture (Fig. 2). The major band at 361 nm and a minor band at 457 nm accounted for ca. 90% and 10% of the retinylidene chromophore, respectively. Keeping the reaction mixture at ambient temperature in the dark resulted in the formation of a major band at 462 nm and a minor band at 327 nm (Fig. 2c).

The band at 361 nm is most likely to be due to a Schiff base formed from retinal. The Schiff base may undergo protonation by the glutamic acid part of **4** in methanolic solution, giving a protonated Schiff base with an absorption band at 457 nm. In due course, most of the Schiff base underwent protonation and gave a major band at 462 nm. However, the protonated Schiff base accounted for only ca. 59% of the retinylidene (assuming

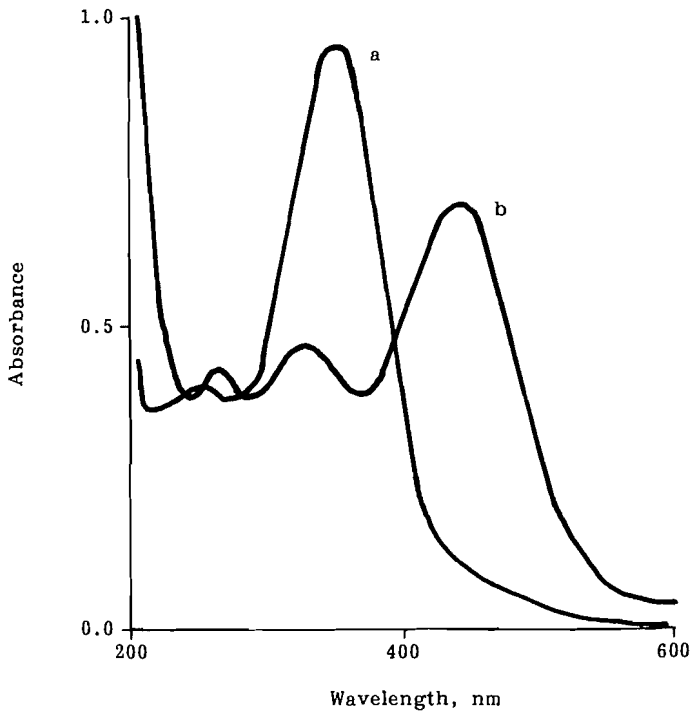

FIG. 4. Absorption spectra showing protonation of 5.9×10^{-5} M methanolic Schiff base **6** by excess 3-chloropropionic acid (CPA): (a) Schiff base **6** before addition of CPA and (b) after addition of CPA.

its absorbance to be 51 800 M^{-1} cm^{-1}) (14) chromophore. Thus, ca. 41% of the chromophore was lost in the synthetic mixture. That a Schiff base of retinal was formed in methanolic **4** could be confirmed by the fact that addition of CF_3COOH or 3-chloropropionic acid caused the 361-nm band to red shift to 440 nm (Figs. 3 and 4).

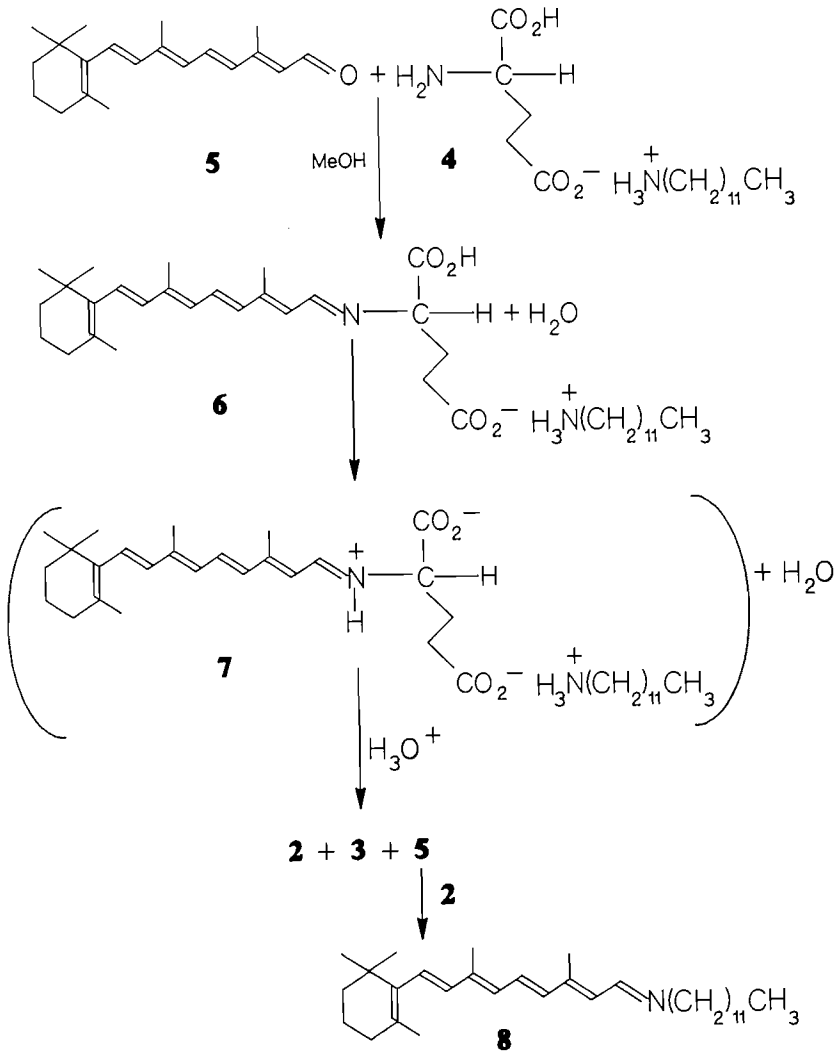

SCHEME 2

To further characterize the Schiff base formed, the reaction of **4** and retinal was studied by ^{1}H NMR spectroscopy. **4** and **5** were dissolved in CD_3OD in equimolar amounts and allowed to react at 4°C overnight. The proton ^{1}H NMR of the reaction mixture showed no signal corresponding to the aldehyde proton (δ 10.12; *J*, 8 Hz) (15) of retinal, indicating that most of the retinal had reacted. The NMR spectrum was characterized by the signals that were indicative of the presence of retinylidene, glutamic, and dodecyl moieties. Thus, a triplet at δ 0.89 was due to the CH_3 group of the dodecyl radical. The 18 methylene protons of the dodecyl group showed up as a broad singlet at δ 1.28. A sharp triplet at δ 2.89 was due to the -CH_2 group adjacent to the N^+H_3 group of the dodecylammonium residue. A multiplet at δ 1.64 corresponded to β-CH_2 of the dodecylammonium part. The α- and β-methylenes (H_3N^+-C_α-H_2-$C_\beta H_2$-) in the dodecylammonium part of **4** appeared as a sharp triplet at δ 2.92 and multiplet at δ 1.64 respectively. Hence, the dodecylammonium part of **4** remained unchanged after reaction with retinal. Therefore, it is the glutamic part which reacted with retinal. The most likely functional group of glutamic acid that can react with retinal is its amino function. The nucleophilic amino group can react with the electrophilic aldehyde group of retinal to give the corresponding Schiff base. That such reaction does occur is clear from the ^{1}H NMR spectrum of the reaction product. A doublet at δ 8.48 with coupling constant of 10 Hz is due to the C_{15} retinylidene proton. The C_{15} aldehyde proton of retinal is expected to show up as a doublet at δ 10.12. Other signals due to the retinylidene moiety were seen as expected. The protons of the glutamic side chain were seen as very complex multiplets centered at δ 2.05 and δ 2.47. The C_α-H of the glutamyl residue was seen at δ 3.54 as a multiplet. Appearance of minor doublets in δ 8.60–8.70 indicated the presence of an isomeric retinylidene group; however, the doublet at δ 8.48 was the major component (>80%). Proton decoupling experiments established that the dd at δ 7.01 and doublets at δ 6.42 and δ 6.21 are due to C_{11}, C_{12}, and C_{10} of the retinylidene unit, respectively, as irradiation at δ 7.01 caused the doublets at δ 6.42 and δ 6.21 to become singlets. Irradiation of the multiplet at δ 1.63 caused the triplet at δ 2.90 to become singlet. Hence, the t at 2.90 was due to the C_α-H_2 group of the dodecylammonium part. Irradiation at δ 2.40 caused simplification of the multiplet between δ 1.96 and 2.18 (except the intense, merged singlet at δ 2.02 due to the C_9-Me group of retinylidene). There was no change, however, in the multiplet at δ 3.55. Therefore, the complex multiplets belong to the methylene groups in the glutamyl side chain. Thus, the α-amino group of the glutamic acid part of **4** reacted with retinal to give Schiff base **4**. Reversed phase preparative TLC (silica gel 60-silanized, Merck RP-2, MeOH) of a 24-h reaction mixture gave two yellow bands with R_f values of 0.73 and 0.13. Further analysis (RP TLC) of the

Can. J. Chem. Downloaded from www.nrcresearchpress.com by 88.85.125.76 on 09/07/12
For personal use only.

band with R_f 0.73 showed it to be a mixture of two components with close R_f values (0.72 and 0.75). ^{1}H NMR of the front fraction showed it to be a mixture of retinal (13%) and all-*trans*-*N*-retinylidene-*n*-dodecylamine (87%, estimated from the integral intensity of doublets at δ 10.05, -CHO, and δ 8.36, -CH=N-). The lower fraction was found to contain the Schiff base of retinal and glutamic acid as the major components and minor amounts of dodecylamine. The 400 MHz, ^{1}H NMR spectrum of this fraction showed the doublet due to Schiff base proton (C_{15}-H=N-) at δ 8.30, as against δ 8.47 for the Schiff base proton of **6**. The olefinic region was too complex to be due to one isomer.

It appears that the α-amino group of **4** reacts with retinal to give the corresponding Schiff base **6**. The alkylammonium ion pair remains intact. The polarity of the $-N^+H_3$ group of dodecylamine is not reversed, hence there is no reaction with the electrophilic -CHO group of retinal (**5**). The Schiff base **6** undergoes protonation by the α-COOH group of the glutamyl residue. However, the Schiff base is not stable and the ion pairs get separated. The Schiff base may then undergo acid-catalyzed hydrolysis, giving retinal and **4** or dodecylamine and glutamic acid. Some of the dodecylamine reacts with retinal, giving the corresponding Schiff base **8** (Scheme 2).

In the Schiff base formation between retinal and alkylamine, a dehydrating agent (often anhydrous Na_2SO_4 or molecular sieves) is added to the reaction mixture in order to shift the equilibrium of the reaction towards the imine. However, in the reaction of retinal with **4**, in spite of the formation of H_2O, the equilibrium is completely shifted towards the formation of **6**. Though Schiff base **6** is formed in solution, it is not feasible to isolate and keep it at room temperature. In solution, the stability of **6** is limited, but it remains intact at −10°C for a day. The color of the solution indicates the nature of the products formed: the imine solution is generally yellow, whereas the imminium ion solution is characteristically deep orange to deep brown. Black residues appeared in the synthetic solutions kept for a few days even in the freezer.

It is important to comment on the absorption spectral characteristics of the synthetic solution in which **4** is present in 250 mole excess over retinal. There is a band at 457 nm corresponding to the protonated form **7**. It is believed that the protonation of an imine linkage in **6** is caused intramolecularly by the proton of the adjacent C_α-COOH group. The contribution of intermolecular protonation is not significant, as the amount of the protonated form of **6** is no more than 10% in the beginning.

The preparation of compound **4** was undertaken in the hope that it would form reversed micelles (16) in hydrocarbon solvents. A retinylidene Schiff base incorporated in a reversed micellar system containing glutamic acid would be a very attractive model because glutamic or aspartic acids are believed to be responsible for the protonation of rhodopsin's chromophore (17–20). Unfortunately, alkylammonium carboxylate **4** did not dissolve in hydrocarbon solvents, obviating the possibility of forming its reversed micelles. Nevertheless, the results obtained here present a new methodology for the preparation of biologically important Schiff bases between hydrophobic aldehydes and relatively insoluble amino acids. Further, they demonstrate that intramolecular association of the imine nitrogen with nearby H atoms can cause a bathochromic shift in the absorption spectra of rhodopsins. The imine bond may be protonated by the labile protons of the apo-protein and further stabilized by H-bonded counterions involving a few water molecules. It has recently been shown that there are, indeed, a few water molecules present in the vicinity of the chromophore of rhodopsins (21). Compound **6** serves as a good model for rhodopsins as far as through-space influence (11) of ion pairs and negatively charged (e.g., -COOH side chain) groups of the apo-protein are concerned.

Acknowledgments

Support of this work by the Natural Sciences and Engineering Research Council of Canada is gratefully acknowledged. Anil K. Singh thanks the Director of ITT (Bombay, India) for granting him a special leave of absence.

1. G. WALD. Science, **162**, 230 (1967).
2. T. SCHRECKENBACH, B. WALCKHOFF, and D. OESTERHELT. Eur. J. Biochem. **76**, 499 (1977).
3. A. R. OSEROFF and R. H. CALLENDER. Biochemistry, **13**, 4243 (1974).
4. C. SANDORFY and D. VOCELLE. Can. J. Chem. **64**, 2251 (1986).
5. R. S. BECKER. Photochem. Photobiol. **48**, 309 (1988), and references cited therein.
6. E. K. S. VIJAIKUMAR and P. BALRAM. Photochem. Photobiol. **39**, 667 (1984).
7. P. K. DAG, R. S. BECKER, B. HEMMASI, and E. BAYER. J. Am. Chem. Soc. **101**, 239 (1979).
8. C. RABILLER and D. DANHO. Helv. Chim. Acta, **67**, 1254 (1984).
9. K. NAKANISHI, V. BALOGH-NAIR, M. ARNABOLDI, K. TSUJIMOTO, and B. HONIG. J. Am. Chem. Soc. **102**, 7945 (1980).
10. M. ARNABOLDI, M. G. MOTTO, K. TSUJIMOTO, V. BALOGH-NAIR, and K. NAKANISHI. J. Am. Chem. Soc. **101**, 7082 (1979).
11. M. SHEVES, K. NAKANISHI, and B. HONIG. J. Am. Chem. Soc. **101**, 7086 (1979).
12. A. K. SINGH, C. SANDORFY, and J. H. FENDLER. Can. J. Chem. In press.
13. A. KITAHARA. Bull. Chem. Soc. Jpn. **28**, 234 (1955).
14. K. A. FREEDMAN and R. S. BECKER. J. Am. Chem. Soc. **108**, 1245 (1986).
15. D. J. PATEL. Nature, **221**, 825 (1969).
16. J. H. FENDLER. Membrane mimetic chemistry. Wiley–Interscience, New York. 1982.
17. L. S. LUSSIER, C. SANDORFY, H. LETHANH, and D. VOCELLE. J. Phys. Chem. **91** 2282 (1987).
18. H. G. KHORANA, G. E. GERBER, W. C. HERLIHY, C. P. GRAY, R. J. ANDEREGG, K. NIHEI, and K. BIEMANN. Proc. Natl. Acad. Sci. U.S.A. **76**, 5046 (1979).
19. Y. A. OVCHINNIKOV, N. G. ABDULAEV, M. Y. FEIGINA, A. V. KISELEV, and N. A. LOBANOV. FEBS Lett. **100**, 219 (1979).
20. P. A. HARGRAVE, J. M. MCDOWELL, D. R. CURTIS, J. K. WANG, E. JUSZCZAK, S. FONG, J. K. M. RAO, and P. ARGOS. Biophys. Struct. Mech. **9**, 235 (1983).
21. N. A. DENCHER, M. B. DRESSELHAUSE, G. PAPADOPOULOS, G. ZACCAI, and G. BUILDT. *In* Proceedings of the Yamada Conference XXI on Molecular Physiology of Retinal Proteins. *Edited by* T. Hara. Yamada Science Foundation, Osaka. 1988. p. 109.

Can. J. Chem. Downloaded from www.nrcresearchpress.com by 88.85.125.76 on 09/07/12
For personal use only.

Conformational analysis and complete assignment of the proton and carbon NMR spectra of ouabain and ouabagenin

DEANE D. MCINTYRE, MARKUS W. GERMANN, AND HANS J. VOGEL[1]

Division of Biochemistry, Department of Biological Sciences, University of Calgary, Calgary, Alta., Canada T2N 1N4

Received June 12, 1989[2]

DEANE D. MCINTYRE, MARKUS W. GERMANN, and HANS J. VOGEL. Can. J. Chem. **68**, 1263 (1990).

The ^1H and ^{13}C NMR spectra of the cardenolide ouabain and its aglycon ouabagenin have been completely assigned by two-dimensional NMR techniques, including phase-sensitive COSY and carbon–proton correlation (HETCOR, HMQC, and COLOC) spectra. The major conformer of these two compounds in solution is all-chair as determined from proton–proton coupling constants and is similar to that in the crystal lattice as previously determined by X-ray diffraction. The conformations of the A and D rings of ouabain in water are somewhat different than in DMSO/$CDCl_3$ (2:1). At lower temperatures (−20°C) signals from two conformers in slow exchange were readily observed in the ^{13}C spectra, with an approximate ratio of 1:7. Molecular mechanics and dynamics calculations indicate that the conformational process responsible for this involves a chair/twist-boat interconversion of the A ring, with the all-chair conformer highly preferred.

Key words: ouabain, conformational analysis, 2-D NMR, molecular mechanics, molecular dynamics.

DEANE D. MCINTYRE, MARKUS W. GERMANN et HANS J. VOGEL. Can. J. Chem. **68**, 1263 (1990).

En se basant sur des techniques de RMN bidimensionnelles, y compris des spectres COSY sensibles aux phases ainsi que des corrélations (HETCOR, HMQC et COLOC) de spectres carbone–proton, on a pu attribuer toutes les bandes des spectres RMN du ^1H et du ^{13}C du cardénolide ouabaine et de son aglycone ouabagénine. En se basant sur les constantes de couplage proton–proton, on a démontré que ces deux composés en solution n'existent que sous des conformations chaises semblables à celles qu'on a observées antérieurement, á l'aide de la diffraction des rayons-X, dans la structure cristalline. En solution dans l'eau, les conformations des cycles A et D sont légèrement différentes de celles que l'on peut observer dans le DMSO/$CDCl_3$ (2:1). Dans les spectres du ^{13}C, mesurés à des températures plus basses (−20°C), on a observé les signaux des deux conformères en équilibre lent et présents dans un rapport approximatif de 1 : 7. Des calculs dynamiques et de mécanique moléculaire indiquent que le processus conformationnel responsable pour ces observations implique une interconversion chaise/bateau-croisé du cycle A; toutefois, le conformère préféré n'implique que des chaises.

Mots clés : ouabaïne, analyse conformationnnelle, RMN 2-D, mécanique moléculaire, dynamique moléculaire.

[Traduit par la revue]

Introduction

The cardenolide ouabain **1** (3-[(6-deoxy-α-L-mannopyranosyl) oxy]1,5,11α,14,19-pentahydroxycard-20(22)enolide) is obtained from the seeds of *Strophanthus gratus*. Upon acid hydrolysis, it yields its aglycon ouabagenin **2** (1,3,5,11,14,19- hexahydroxycard-20(22)enolide) and rhamnose (1). The cardenolides are of importance in the treatment of heart disease (2) and, in the case of ouabain, also for the treatment of cancer (3). In studies involving the interactions of ouabain and ouabagenin with Na^+, K^+-adenosine triphosphatase, it has been observed that ouabagenin is a reversible inhibitor while the interaction with ouabain is pseudo-irreversible (4, 5).

NMR spectroscopy has been the method of choice for the determination of the chemical structure of natural products (6, 7). However, obtaining the complete proton spectral assignments of cardenolides and steroids in general has been difficult due to severe signal overlap in the 1.0–2.5 ppm chemical shift range, even at high (>10 T) magnetic fields (6). The carbon-13 NMR spectra of steroids generally do not suffer from this problem as the signals are dispersed over a much larger chemical shift range, and they have consequently been used to assign NMR spectra of steroids by making comparisons with appropriate model compounds (7). However, the recent introduction of a variety of two-dimensional NMR techniques has made it possible to assign the ^1H NMR spectra of steroids without a need for model compounds. Once the task of assignment has been completed the solution conformation of the molecule can be determined from the dihedral angles between vicinal protons as deduced from the coupling constants obtained via the Karplus relationship. If necessary this can be supplemented by internuclear distances determined from nOe data (6).

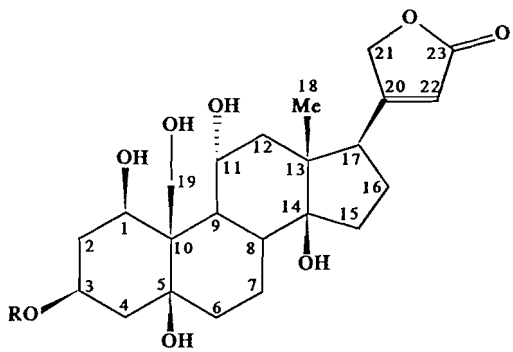

1, R = H

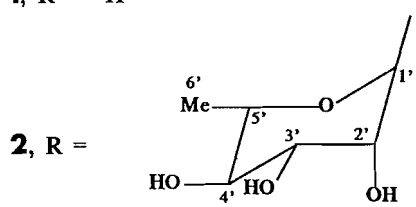

2, R =

In this work, we report the complete assignment of both the proton and ^{13}C NMR spectra of ouabain and ouabagenin. For ouabain, the conformation was determined in two solvent systems, a 2:1 mixture of dimethylsulphoxide–chloroform, and in water. Molecular dynamics and molecular mechanics calculations were also used to further explore the nature of conformational processes. Some carbon-13 NMR assignments have been reported previously (8), and the solution conformation of the E

[1]Author to whom correspondence may be addressed.

[2]Revision received February 12, 1990.

Can. J. Chem. Downloaded from www.nrcresearchpress.com by 88.85.125.76 on 09/07/12
For personal use only.

Can. J. Chem. Downloaded from www.nrcresearchpress.com by 88.85.125.76 on 09/07/12
For personal use only.

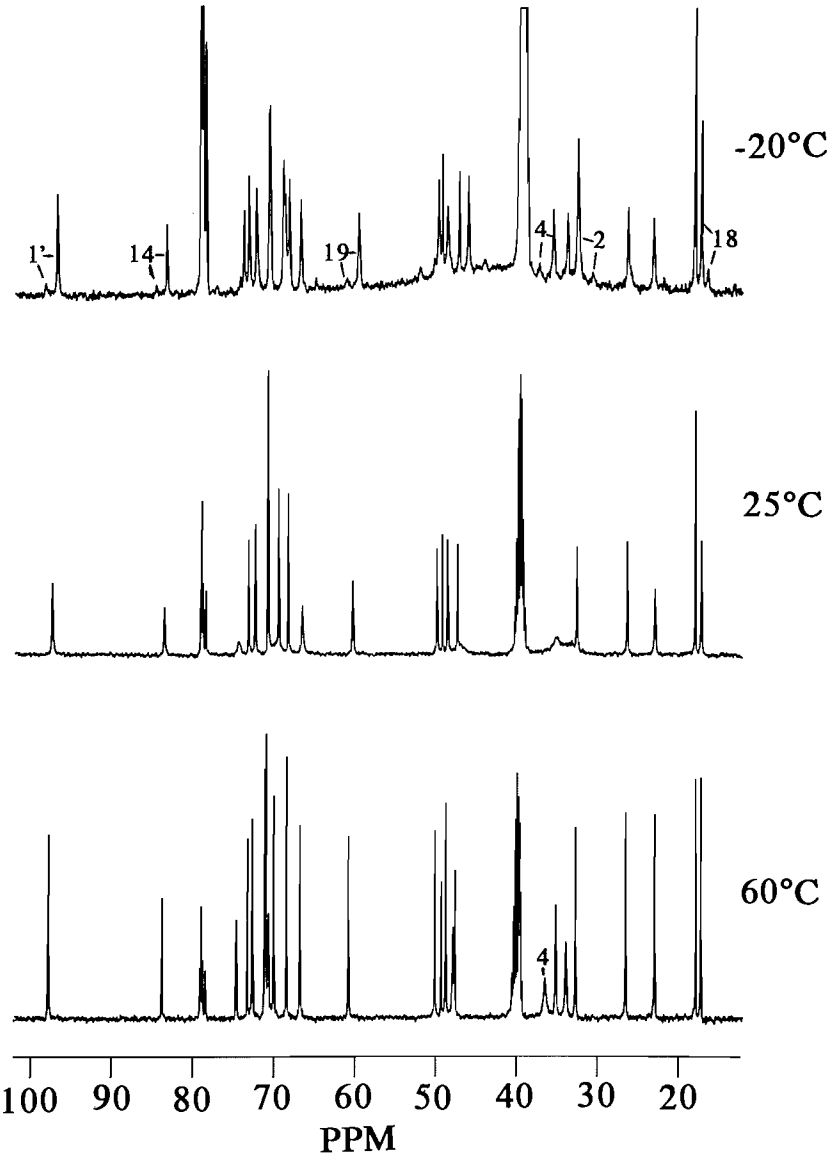

FIG. 1. Carbon-13 NMR spectra (proton decoupled) of ouabain in DMSO/$CDCl_3$ (2:1) solution at −20°C, 25°C, and 60°C. Representative signals in slow exchange at −20°C are indicated. At 25°C, a number of signals are broad, indicating that they are in intermediate exchange. The spectrum obtained at 60°C indicates that all signals, with the exception of C-4 (labelled), are in fast exchange.

ring relative to the D ring of various cardenolides has been determined by ^{1}H NMR (9).

Experimental

Ouabain (as the octahydrate) and ouabagenin were both obtained from Sigma Chemical Co., St Louis, Missouri, U.S.A., and were used as received. The samples for NMR were prepared by dissolving 40 mg of ouabain or 25 mg of ouabagenin in 0.5 mL of a 2:1 dimethylsulphoxide-d_6/chloroform-d mixture with tetramethylsilane added as an internal reference for both ^{1}H and ^{13}C. This solvent mixture is the same as that used previously in the assignment of the ^{13}C spectrum of ouabain (8). For the HMQC (heteronuclear multiple quantum coherence) experiment, ouabain was twice exchanged with D_2O in order to eliminate the signal from the water of hydration. A saturated solution of ouabain in D_2O was also prepared with 2,2-dimethyl-2-silapentane-5-sulphonate added as an internal standard.

All NMR spectra were obtained on a Bruker AM-400 spectrometer operating in the FT mode at a frequency of 400.1 MHz for ^{1}H and 100.6 MHz for ^{13}C. All two-dimensional NMR spectra were obtained using standard Bruker software. Phase-sensitive COSY spectra were obtained using a spectral width of 2500 Hz, 16 scans per t_1 increment, a 1.4 s recycle time, and a data matrix of 1024 ($F1$) × 2048 ($F2$) that was zero-filled once in each dimension prior to apodization with a standard sine bell function and transformation. HETCOR spectra, optimized for ^1J C–H = 130 Hz (10), and COLOC (correlation by long-range coupling) spectra, optimized for ^{2}J C–H = 5 Hz (11), were obtained using a spectral width of 11 000 Hz in $F2$ (carbon) and 2500 Hz in $F1$ (proton) with decoupling in both dimensions, using a 128 ($F1$) × 2048 ($F2$) matrix that was zero-filled to 512 × 4096 prior to apodization with a Lorentz–Gauss function and transformation. The resulting spectra were background subtracted, and are presented in the magnitude mode. HMQC spectra were obtained in the phase-sensitive mode without decoupling using a bilinear (BIRD) pulse (12) and a 128 ($F1$) (carbon) × 256 ($F2$) (proton) matrix that was zero-filled to 512 × 1024 prior to apodization with a Lorentz–Gauss function and transformation. A delay of 0.4 s was inserted between the BIRD and HMQC pulses.

Relaxation times were determined by using the standard inversion–recovery technique, with composite pulse decoupling and cycling of the delay times. The resulting data were fitted to an exponential function using standard Bruker software. The attached proton test (APT) spectra (13) were obtained with a delay time of 7.4 ms (ca. $1/J$).

TABLE 1. Chemical shifts (referred to TMS), carbon–proton coupling constants, and relaxation times for ouabain and ouabagenin dissolved in DMSO-d_6/$CDCl_3$ (2:1)

	Ouabain						Ouabegenin
	Chemical shift, ppm			^1J (C–H), Hz	T_1, s		Chemical shift, ppm
Carbon	60°C	25°C	−20°C	60°C	60°C	25°C	60°C
1	70.60	[a]	68.59, 64.80	154	0.31	[a]	71.28
2	33.81	33.09	32.30, 30.52	126	0.18	[a]	[a]
3	69.95	69.41	68.77	148	0.36	0.21	65.68
4	36.38	[a]	35.35, 37.07	126	0.18	[a]	[a]
5	74.54	74.36	73.64		2.4	1.3	75.16
6	35.04	34.89	33.59	126	0.19	[a]	35.31
7	22.85	22.78	22.93	126	0.18	0.12	22.85
8	39.56	[a]	[a]	127	0.56	[a]	39.46
9	47.78	46.70	45.68, 43.81	123	[a]	[a]	47.92
10	47.53	47.27	47.02		2.9	1.9	47.41
11	66.72	66.48	66.64, 64.79	142	0.38	0.24	66.49
12	48.69	48.52	48.48	129	0.19	0.13	48.53
13	49.24	49.15	49.11		3.3	1.8	49.12
14	83.69	83.51	83.18, 84.44		3.4	1.7	83.53
15	32.63	32.44	32.30	128	0.19	0.11	32.53
16	26.44	26.22	26.11	131	0.22	0.13	26.35
17	50.04	49.81	49.57	135	0.36	0.25	49.97
18	17.15	17.05	17.04, 16.23	125	0.62	0.34	17.14
19	60.74	60.28	59.47, 60.94	141	0.22	0.14	61.01
20	174.90	175.15	175.28		1.8	0.77	174.80
21	73.16	73.09	73.02	138	0.26	0.15	73.08
22	116.42	116.36	116.35		0.44	0.25	116.41
23	173.59	173.69	173.85	10(^{2}J)	9.6	2.4	173.49
1′	97.76	97.37	96.66, 98.14	167	0.43	0.23	
2′	70.95	70.75	70.41	148	0.49	[a]	
3′	71.06	70.75	70.52	148	0.43	[a]	
4′	72.58	72.31	72.11	157	0.43	0.24	
5′	68.39	68.25	68.06	180	0.41	0.24	
6′	17.77	17.80	17.83	126	0.84	0.34	

[a]Signal not observed due to chemical exchange or overlap.

Can. J. Chem. Downloaded from www.nrcresearchpress.com by 88.85.125.76 on 09/07/12
For personal use only.

Molecular mechanics and dynamics calculations were carried out on a Silicon Graphics Iris 4D/25G workstation using the Quanta software package (Polygen, Waltham, MA), which employs the CharmM force field (14). A dielectric constant of 1 was used for most simulations, but separate mechanics calculations with higher dielectric constants did not influence the results. Typically, molecular structures were energy-minimized using 200 steps of conjugate gradient minimization. In the calculation of root-mean-square (RMS) values only heteroatoms were considered. For the molecular dynamics simulations (Verlet dynamics), energy-minimized molecules were heated to 300 K over 5 ps, followed by a 10 ps equilibration at 300 K. Simulations were then run for 1000 ps using 10^{-3} ps time steps. Shake constraints were applied to all bonds containing a hydrogen atom (15).

Results

Carbon-13 NMR spectroscopy of ouabain

The carbon-13 NMR spectrum of ouabain obtained in DMSO/$CDCl_3$ at 25°C (Fig. 1) showed several broad signals, suggesting that an intermediate exchange process was occurring at this temperature. All signals were in fast exchange at 60°C, and therefore most experiments were performed at this temperature. The number of protons attached to each carbon was determined by means of an attached proton test (APT). In addition a spectrum was recorded without decoupling during acquisition, from which the carbon–proton coupling constants were obtained. The T_1 relaxation times were determined at both 25 and 60°C. From these data, initial tentative assignments were made. Upon cooling the sample to −20°C a large number of signals split into two components (approximate ratio 7:1) and the system is clearly in slow chemical exchange at this temperature (*vide supra*).

A proton–carbon correlation spectrum (HETCOR spectrum) (Fig. 2) was obtained at 60°C and all expected cross peaks were observed. A number of cross peaks, corresponding to those carbons in intermediate exchange, were missing in a HETCOR spectrum obtained at 25°C. To assign the quaternary carbon atoms, a COLOC spectrum, optimized for a 5-Hz long-range coupling constant, was obtained. From these carbon–proton correlation spectra, it was possible to obtain ^{13}C assignments (Table 1) for all carbon atoms with the exception of C-2, C-4, and C-6. These ^{13}C resonances were later assigned from the HETCOR and HMQC spectra using ^1H assignments, as will be discussed later.

As indicated in Table 1, the chemical shifts of some carbons, notably those in the A and B rings, were quite temperature dependent, and a pronounced upfield shift was observed with increasing temperature. The ^{13}C relaxation times (Table 1) are unexceptional for a molecule of this nature, and are considerably shorter at 25°C than at 60°C due to the combined effects of chemical exchange and longer correlation times in the reasonably viscous solvent system employed.

Can. J. Chem. Downloaded from www.nrcresearchpress.com by 88.85.125.76 on 09/07/12
For personal use only.

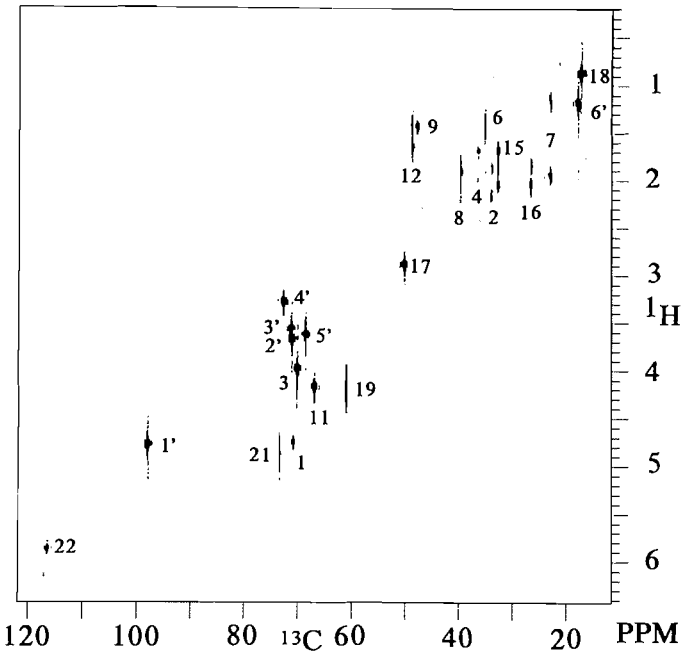

FIG. 2. Proton-decoupled HETCOR spectrum of ouabain, obtained at 60°C.

Proton NMR spectroscopy of ouabain

Approximate chemical shifts for all ouabain protons in DMSO/$CDCl_3$ were obtained in the first instance by inspection of the HETCOR spectrum; however, at this juncture, due to the uncertain assignments of C-2, C-4, and C-6 as indicated above, the assignments of the corresponding protons could only be considered tentative. In addition, due to the fact that the decoupled HETCOR spectrum does not decouple vicinal diastereomeric protons of methylene groups from each other, it is not possible to obtain accurate chemical shifts of such protons from a HETCOR spectrum alone. This unfavourable situation is made even more complex by the frequent occurrence of an artifact located between the two methylene doublets (16). Inspection of the HMQC spectrum (Fig. 3), in which this artifact does not occur, and which generally gives narrower cross peaks in the proton dimension than the HETCOR spectra, gave more accurate chemical shifts in this case.

To obtain proton chemical shifts of ouabain accurate to 0.01 ppm and to furthermore obtain the proton–proton coupling constants, a phase-sensitive COSY spectrum was obtained at fairly high digital resolution (1.2 Hz in $F2$). From this spectrum (Fig. 4), the proton assignments were straightforward. Beginning with the rhamnose moiety, the anomeric proton at 4.75 ppm was readily identified on the basis of its chemical shift. The remaining rhamnose protons were assigned from the COSY connectivity, ending with the 6′ methyl group at 1.16 ppm. All proton assignments, along with proton–proton coupling constants, are tabulated in Table 2. The coupling constants that could not be obtained directly from the one-dimensional spectra were obtained by measurement of the active coupling in expanded plots of the phase-sensitive COSY spectrum. Under the experimental conditions, the rhamnose hydroxyl protons were in slow exchange, and thus they were readily assignable from the COSY spectrum.

The steroid protons were assigned in an analogous fashion. Starting from H-1 (4.72 ppm), the connectivity between all A-ring protons was traced out. The B- and C-ring protons form

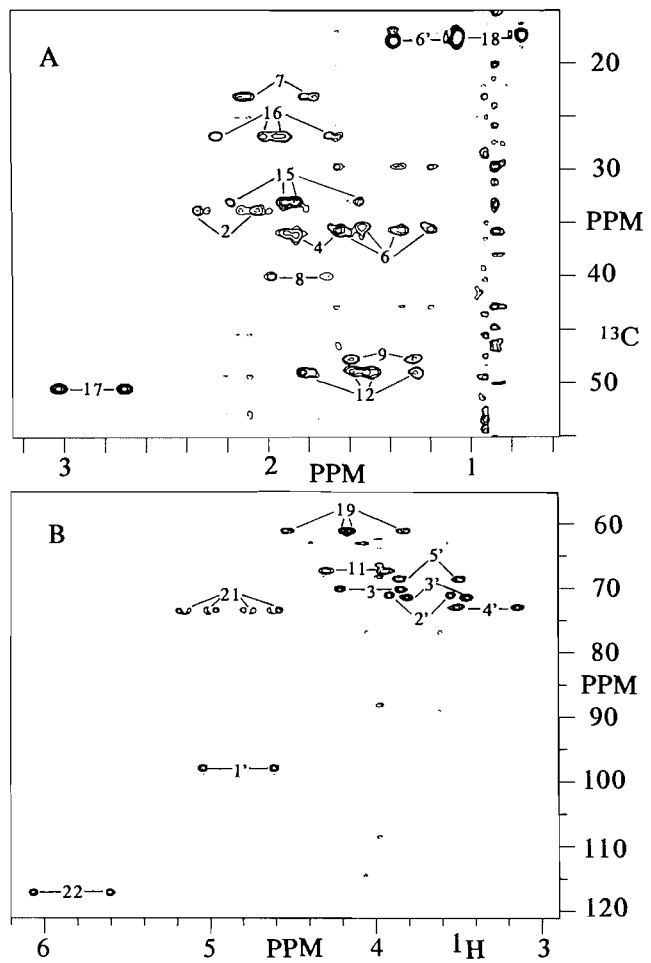

FIG. 3. Carbon-coupled HMQC spectra of ouabain, obtained in the phase-sensitive mode at 60°C. Panel (A) shows the upfield region of the spectrum, and panel (B) the downfield region. Each proton appears as a characteristic doublet parallel to the $F2$ axis; note the cross-peak shape, which is better defined compared to the HETCOR spectrum.

one extended spin system, which was assigned starting from H-11 at 4.15 ppm. The D-ring protons were assigned starting from H-17 at 2.86 ppm. Assignment of the remaining protons, including the methyl protons on C-18 as well as H-21 and H-22, was obvious from inspection of the one-dimensional spectrum. A NOESY spectrum, obtained at −20°C using a 250-ms mixing time, showed a fairly intense cross peak between the anomeric proton and H-3 of the steroid. This observation confirms the point of attachment of the sugar to the steroid moiety. In the solvent system used, the hydroxyl groups attached to the steroid are in fast or intermediate exchange with the remaining water peak at 3.20 ppm, and thus could not be assigned.

With the unambiguous proton assignments now in hand, it then became possible to complete and cross-check the assignment of the ^{13}C spectrum, as indicated in Table 1. It is noteworthy from the data in Table 1 that the previously reported ^{13}C assignments (8), which were based mainly on comparisons with model compounds, are partly in error.

To define the conformation of the ouabain molecule in solution, the proton–proton coupling constants, accurate to 1 Hz, were obtained from the appropriate cross sections of the phase sensitive COSY spectrum, measured parallel to the $F2$ axis. These are also included in Table 2. The conformation of ouabain in water was also studied by recording a phase-sensitive

Can. J. Chem. Downloaded from www.nrcresearchpress.com by 88.85.125.76 on 09/07/12
For personal use only.

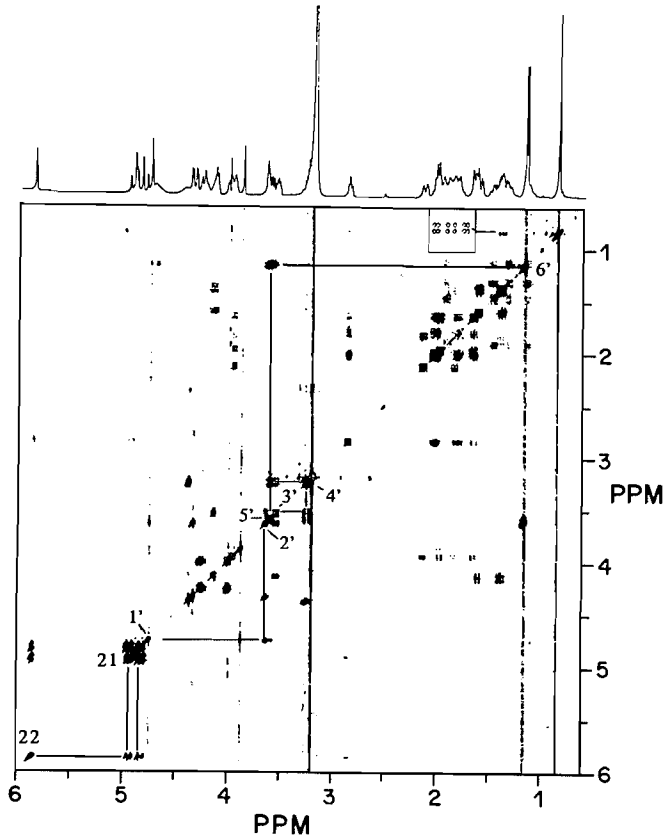

FIG. 4. Phase-sensitive COSY spectrum of ouabain obtained at 60°C. Representative connectivities are indicated by lines joining the diagonal and cross peaks arising from the carbohydrate and steroid H-21–H-22 protons. The insert shows an expansion of the 12β–18 cross peak, illustrating its fine structure; these were used to obtain the proton–proton coupling constants. The one-dimensional ^1H spectrum is shown above the *F2* axis.

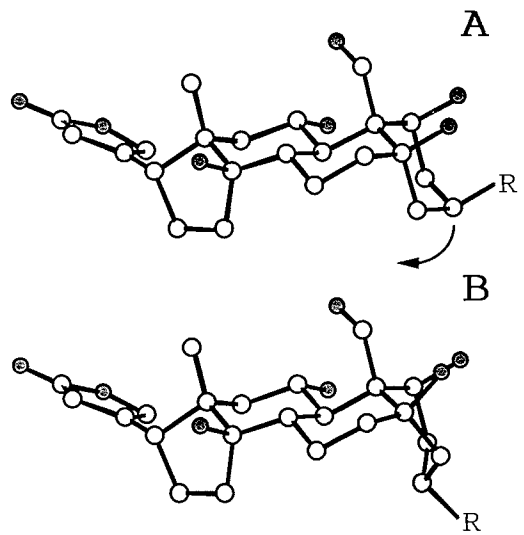

FIG. 5. Structures of ouabagenin (R = H) and ouabain (R = Rha) of the two conformers, observed in the MM calculations. (A) A ring in chair conformation; (B) A ring in twist conformation.

COSY spectrum at 60°C. This was assigned and analyzed as described above, and the resulting chemical shifts and coupling constants are included in Table 2. One-dimensional proton spectra were obtained in DMSO/$CDCl_3$ at temperatures between 60°C and −20°C. However, due to broadening resulting from high solvent viscosity, it was not possible to resolve signals arising from the minor conformer. Attempts to clarify this matter by using two-dimensional nOe/exchange spectroscopy at −20°C (slow exchange domain) and at 25°C (intermediate exchange domain) with a variety of mixing times were not successful. This has prevented us from determining the conformation of the minor form. Attempts at obtaining spectra in other solvents were hampered by low solubility.

Carbon-13 and proton NMR spectroscopy of ouabagenin

Carbon-13 NMR spectra of ouabagenin were obtained at temperatures ranging from 60°C to −20°C. As expected, most of the chemical shifts, with the exception of those near the point of attachment of the rhamnose in ouabain, namely C-2, C-3, and C-4, were within 0.5 ppm of the values observed in ouabain. They are tabulated in Table 1 for three different temperatures, 60°C, 25°C, and −20°C. Upon cooling of the sample, a number of signals broadened, and finally split into two signals in a manner analogous to that observed in ouabain. The approximate ratio of the components was again 7:1.

Following the same procedure as used for ouabain, the proton spectrum of ouabagenin was assigned from a phase-sensitive COSY spectrum obtained in DMSO/$CDCl_3$ at 60°C, a temperature at which the molecule is in fast chemical exchange. The resulting chemical shifts and coupling constants are tabulated in Table 2. As expected, most of the chemical shifts were close (within 0.03 ppm) to the values observed in ouabain, with the exception of the methylene protons attached to C-2 and C-4. No change was observed in the shift of H-3 despite the fact that this proton is vicinal to the rhamnose ring in ouabain.

Discussion

The chemical shifts and proton–proton coupling constants obtained in DMSO/$CDCl_3$ were almost identical in both compounds studied, which indicates that their conformations are similar. Hence the conformation of the steroid is not affected to a great extent by the presence of the rhamnose ring in ouabain. From the coupling constants the approximate dihedral angles were determined via the Karplus relationship. Molecular models were then constructed which would satisfy the calculated dihedral angles without imposing unrealistic steric crowding or strained bonds. One unique conformation was obtained, which therefore reasonably represents the conformation of the molecule in solution. All six-membered rings of the steroid portions of both ouabain and ouabagenin were found to be in the chair conformation, in complete agreement with the data from X-ray studies of both molecules (17–19). Thus, the extensive intermolecular hydrogen bonding that was observed in the crystal lattice did not influence the conformation of these compounds.

Ouabain in water has a conformation that is very similar to that in DMSO/$CDCl_3$; however, one significant difference is that the A-ring chair is less flat, as could be deduced from the observation that the H-1, H-2 coupling constants are approximately equal in DMSO/$CDCl_3$ (7 and 6 Hz), but are quite different in D_2O (8 and 3 Hz). Minor differences also occur in the conformation of the D ring, with this five-membered ring being flatter in DMSO/$CDCl_3$ than in D_2O. Moreover, in the latter solvent the D-ring conformation is closer to the 16β envelope than the 14β envelope found in DMSO/$CDCl_3$ and in the crystal lattice (17). The rhamnose ring of ouabain was found to be in the chair conformation, which is in agreement with the

TABLE 2. Proton chemical shifts (δ, ppm from TMS) and proton–proton coupling constants (Hz) for ouabain and ouabagenin at 60°C in DMSO-d_6/$CDCl_3$ (2:1) solution, and ouabain at 60°C in D_2O solution (DSS reference)

Proton	Ouabain (DMSO/$CDCl_3$)		Ouabain (D_2O)	
1	4.72	J 1,2α = 7; J 1,2β = 6	5.11	J 1,2α = 8; J 1,2β = 3
2α	1.83	J 2α,2β = 15; J 2α,3 = 9	2.08	J 2α,2β = 16; J 2α,3 = 8
2β	2.14	J 2β,3 = 5	2.24	J 2β,3 = 7
3	3.95	J 3,4α = 5; J 3,4β = 5	4.19	J 3,4α = 5; J 3,4β = 4
4α	1.66	J 4α,4β = 19	1.78	J 4α,4β = 16
4β	1.98		2.21	
6α	1.49	J 6α,6β = 13; J 6α,7α = 6 J 6α,7β = 5	1.58	J 6α,6β = 13; J 6α,7α = 5 J 6α,7β = 4
6β	1.33	J 6β,7α = 6; J 6β,7β = 3	1.45	J 6β,7α = 5; J 6β,7β = 3
7α	1.14	J 7α,7β = 13; J 7α,8 = 9	1.31	J 7α,7β = 13; J 7α,8 = 9
7β	1.92	J 7β,8 = 3	1.93	J 7β,8 = 4
8	1.88	J 8,9 = 12	1.86	J 8,9 = 12
9	1.40	J 9,11 = 9	1.62	J 9,11 = 9
11	4.15	J 11,12α = 5; J 11,12β = 9	4.15	J 11,12α = 4; J 11,12β = 11
12α	1.61	J 12α,12β = 14	1.75	J 12α,12β = 16
12β	1.39	J 12β,18 = 3	1.53	
15α	1.99	J 15α,15β = 15; J 15α,16α = 5 J 15α,16β = 4	2.21	J 15α,15β = 16; J 15α,16α = 4 J 15α,16β = 6
15β	1.65	J 15β,16α = 8; J 15β,16β = 4 J 15β,17 = 4	1.78	J 15β,16α = 10; J 15β,16β = 6 J 15β,17 = 3
16α	1.81	J 16α,16β = 14; J 16α,17 = 9	1.86	J 16α,16β = 16; J 16α,17 = 7
16β	2.02	J 16β,17 = 11	2.25	J 16β,17 = 8
17	2.86		2.95	
18	0.85		0.95	
19a	4.00	J 19a,19b = 14	4.16	J 19a,19b = 12
19b	4.26		4.35	
21a	4.84	J 21a,21a = 19; J 21a,22 = 2	5.01	J 21a,21a = 19; J 21a,22 = 4
21b	4.92	J 21b,22 = 2	5.02	J 21b,22 = 4
22	5.84		6.00	
1′	4.75	J1′,2′ = 2	4.92	J 1′,2′ = 2
2′	3.64	J 2′,3′ = 3	3.90	J 2′,3′ = 3
2′ OH	4.33	J 2′,2′OH = 6		
3′	3.54	J 3′,4′ = 9	3.80	J 3′,4′ = 10
3′ OH	4.14	J 3′,3′OH = 5		

crystal structure. The fact that the aglycon of ouabain exists in solution in the same conformation as that of ouabagenin supports the notion that the irreversible inhibition of the Na^+, K^+-adenosine triphosphatase by ouabain is probably associated with the rhamnose ring (4, 5).

The nature of the conformational processes that affect these two molecules does not depend on the rhamnose moiety: similar behaviour was observed for both ouabain and ouabagenin. In fact, in ouabain, the exchange process was also observed for the anomeric carbon of the rhammose ring. As all the carbons that are bound to, or are directly attached to, the A ring (with the exception of C-3) exhibited chemical exchange, it appears reasonable to presume that the major conformational process that causes the observed temperature-dependent effects involves this ring. However, C-14 and C-18 also exhibited similar behaviour. It is possible, but not likely in view of the similar ratios of signal intensity, that this represents a distinct chemical exchange process. In principle, all carbons, regardless of their distance from the A ring, should exhibit separate signals. In practice, due to accidental chemical shift equivalence, this is not always the case. From the populations and the chemical shift differences between the two conformers, it can be calculated (20) that the free energy difference $\Delta G°$ and the free energy of activation (major → minor) $\Delta G°^{\ddagger}$ are approximately 4.6 and 58 kJ/mol, respectively. These values are reasonable for ring reversion of cyclohexane rings with annelated substituents (21). Thus, we hypothesize that the conformational process that is responsible for the observed chemical exchange involves interconversion of the chair form of the A ring with a higher energy conformer (see below). The major conformation at −20°C corresponds to that determined in the fast exchange regime at 60°C. However, in the absence of information about the proton–proton coupling constants for the minor conformer it is not possible to deduce its conformation unambiguously.

Molecular dynamics (MD) and molecular mechanics (MM) simulations can be used to obtain additional insight into conformational processes that have been detected by NMR studies (22). To help define the nature of the minor conformer, calculations were performed for ouabagenin with the E ring removed. One initial structure, corresponding to the major conformer, was constructed in which all six-membered rings of the steroid portion are in the chair conformation and subsequently energy minimized (see Fig. 5A). The observation of the minor NMR resonances at low temperatures for both ouabagenin and ouabain, combined with model building studies, prompted us to construct two additional conformers in which the

Can. J. Chem. Downloaded from www.nrcresearchpress.com by 88.85.125.76 on 09/07/12
For personal use only.

TABLE 2. (*concluded*)

Proton	Ouabain (DMSO/$CDCl_3$)		Ouabain (D_2O)	
4′	3.24	J 4′,5′ = 10	3.45	J 4′,5′ = 10
4′ OH	4.38	J 4′,4′OH = 5		
5′	3.60	J 5′,6′ = 6	3.83	J 5′,6′ = 6
6′	1.16		1.29	
Proton	Ouabagenin			
1	4.72	J 1,2α = 8; J 1,2β = 7		
2α	1.80	J 2α,2β = 14; J 2α,3 = 10		
2β	2.05	J 2β,3 = 5		
3	3.96	J 3,4α = 5; J 3,4β = 5		
4α	1.58	J 4α,4β = 14		
4β	2.03			
6α	1.51	J 6α,6β = 13; J 6α,7α = 4 J 6α,7β = 4		
6β	1.34	J 6β,7α = 6; J 6β,7β = 4		
7α	1.14	J 7α,7β = 14; J 7α,8 = 9		
7β	1.93	J 7β,8 = 4		
8	1.87	J 8,9 = 13		
9	1.38	J 9,11 = 9		
11	4.12	J 11,12α = 5; J 11,12β = 9		
12α	1.60	J 12α,12β = 14		
12β	1.39			
15α	1.99	J 15α,15β = 12; J 15α,16α = 4 J 5α,16β = 4		
15β	1.66	J 15β,16α = 8; J 15β,16β = 4 J 15β,17 = 4		
16α	1.80	J 16α,16β = 14; J 16α, 17 = 9		
16β	2.03	J 16β,17 = 12		
17	2.86			
18	0.85			
19a	4.00	J 19a,19b = 14		
19b	4.25			
21a	4.82	J 21a,21b = 19; J 21a,22 = 3		
21b	4.92	J 21b,22 = 2		
22	5.84			

A ring assumes two different boat conformations. Upon energy minimization both boat conformers converged to the same twist structure, which is intermediate between the two boat conformers (see Fig. 5B) with an RMS deviation of 0.014 Å and an energy difference of 0.04 kJ/mol. A comparison of the twist and chair conformation (RMS deviation 0.27 Å) demonstrates that the all-chair conformation is energetically favoured by 32.6 kJ/mol. We have also investigated the conformational changes in the A ring (using a boat conformation as the starting structure) in molecular dynamics simulations by monitoring the C10-C1-C2-C3 torsion angle. This calculation demonstrated a rapid interconversion of the two boat forms on the picosecond time scale (0.5–1 ps). This considerable conformational freedom of the A ring indicates the presence of only relatively small energy barriers between the two boat conformations. In this MD simulation we also observed the conversion of the boat forms to the all-chair conformer, which occurs only infrequently (200–300 ps). No changes in the conformations of the other steroid rings were observed. Using the chair conformer as the starting structure, the boat conformers were not obtained over a 1000-ps simulation. Thus, both MM and MD calculations indicate that the all-chair conformation is the preferred structure for the A ring, corresponding to the major conformer observed in the NMR studies. In addition, the MD simulations suggest that the NMR-observed minor conformation may correspond to two rapidly interconverting boat forms of ring A that are in fast exchange on the NMR time scale.

Acknowledgements

This work was supported by grants from the Medical Research Council and Natural Sciences and Engineering Research Council of Canada (MRC, NSERC). H.J.V. and M.W.G. are the recipients of a scholarship and a postdoctoral fellowship from the Alberta Heritage Foundation for Medical Research (AHFMR), which also provided the funds for the purchase of the NMR spectrometer. Funding for the Silicon Graphics workstation and associated software was provided by the Erna and Victor Hasselblad Foundation, Göteborg, Sweden.

1. The Merck Index. 8th ed. Merck, Rahway, NJ. 1976. p. 896.
2. W. H. LEWIS and M. P. F. ELVIN-LEWIS. *In* Medical botany: plants affecting man's health. John Wiley and Sons, New York, NY. 1977.
3. R. M. BAKER. Banbury Rep. **2**, 237 (1979); Chem. Abstr. **92**, 122474c (1979).
4. E. T. WALLICH, F. DOWD, J. C. ALLEN, and A. SCHWARTZ. J. Pharmacol. Exp. Ther. **189**, 434 (1974).

Can. J. Chem. Downloaded from www.nrcresearchpress.com by 88.85.125.76 on 09/07/12
For personal use only.

5. A. YODA. Mol. Pharmacol. **9**, 51 (1973).
6. W. R. CROASMUN and R. M. K. CARSON. *In* Two dimensional NMR spectroscopy: applications for chemists and biochemists. VCH, Weinheim. 1987. Chap. 7.
7. J. W. BLUNT and J. B. STOTHERS. Org. Magn. Reson. **9**, 439 (1977).
8. L. BROWN, H. T. ANDREW, R. THOMAS, T.R. WATSON, and J. L. E. NEMORIN. J. Chem. Soc. Perkin Trans. 1, 1779 (1981).
9. R. HINTSCHE, R. MEGGES, D. PFEIFFER, H.J. PORTIUS, W. SCHOENFIELD, and K. R. H. REPKE. Eur. J. Med. **20**, 9 (1985).
10. G. A. MORRIS and L.D. HALL. J. Am. Chem. Soc. **103**, 4703 (1981).
11. H. KESSLER, C. GRIESINGER, J. ZARBOCK, and H.R. LOOSLI. J. Magn. Reson. **57**, 331 (1984).
12. A. BAX and S. SUBRAMANIAN. J. Magn. Reson. **67**, 565 (1986).
13. G. A. MORRIS and R. FREEMAN. J. Am. Chem. Soc. **101**, 760 (1979).
14. B. R. BROOKS, R. E. BRUCCOLERI, B. D. OLAFSON, D. J. STATES, S. SWAMINATHAN, and M. KARPLUS. J. Comput. Chem. **4**, 187 (1983).
15. W. F. VAN GUNSTEREN and H. J. C. BERENDSEN. Mol. Phys. **34**, 1311 (1977).
16. M. PERPICK-DUMONT, W. F. REYNOLDS, and R. G. ENRIQUEZ. Magn. Reson. Chem. **26**, 358 (1988).
17. A. MESSERSCHMIDT. Cryst. Struct. Commun. **9**, 1185 (1980).
18. K. GO and G. KARTHA. Cryst. Struct. Commun. **10**, 1329 (1981).
19. K. GO and G. KARTHA. Acta. Crystallogr. Sect.C: Cryst. Struct. Commun. **C39**, 376 (1983).
20. J. SANDSTRÖM. *In* Dynamic NMR spectroscopy. Academic Press, London. 1982. Chaps. 6 and 7.
21. J. D. ROBERTS and M. C. CASERIO. *In* Basic principles of organic chemistry. 2nd ed. Benjamin, Menlo Park, CA. 1977. Chap. 12.
22. B. A. DAWSON, H. W. AVDOVICH, W.-W. SY, G. A. NEVILLE, and L. A. COLEBROOK. Can. J. Spectrosc. **34**, 107 (1989).

Can. J. Chem. Downloaded from www.nrcresearchpress.com by 88.85.125.76 on 09/07/12
For personal use only.

Synthèse d'isoxazoles substitués en α de l'azote par une chaine alkyle ou alcényle

JEAN-CLAUDE CHERTON, MARC LANSON,[1] DAÏF LADJAMA, YVETTE GUICHON ET JEAN-JACQUES BASSELIER

Laboratoire de chimie organique structurale, Unité Associée n° 455, Université Pierre et Marie Curie, 8 Rue Cuvier, Bat. F, 7ème étage, Paris CEDEX 05, 75005, France

Reçu le 14 février 1989[2]

JEAN-CLAUDE CHERTON, MARC LANSON, DAÏF LADJAMA, YVETTE GUICHON et JEAN-JACQUES BASSELIER. Can. J. Chem. **68**, 1271 (1990).

Diverses synthèses d'isoxazoles particuliers et d'accès difficile : les isoxazoles dits « α-*N* substitués » portant en α de l'azote une longue chaîne alkyle ou alcényle, sont présentées. La classique cycloaddition dipolaire-1,3 est la méthode de choix dans le cas de substituants alkyles. Comme méthode compatible avec des chaînes alcényles, l'action de l'hydroxylamine sur les époxy-énones constitue une nouvelle voie univoque. Si l'on dispose d'« isoxazoles α-*O* substitués » d'accès plus facile, leur isomérisation est une voie rapide et générale. Enfin, l'action des magnésiens sur le bromométhyl-3 méthyl-5 isoxazole est une méthode originale et efficace.

Mots clés : isoxazoles, substitution en α de l'azote.

JEAN-CLAUDE CHERTON, MARC LANSON, DAÏF LADJAMA, YVETTE GUICHON, and JEAN-JACQUES BASSELIER. Can. J. Chem. **68**, 1271 (1990).

Several syntheses of special isoxazoles bearing a long alkyl or alkenyl side chain in the α position of the nitrogen are presented. A very convenient route in the case of an alkyl side chain is the classical 1,3-dipolar cycloaddition of a nitrile-oxide to a vinyl acetate. Although it is a rather long approach, the reaction of hydroxylamine with enone-epoxides represents a new and unequivocal method compatible with alkenyl side chains. The isomerisation of the easily synthesized isoxazoles bearing such substitutents α to the oxygen, by the reaction of their isoxazolium salts with hydroxylamine, is a fast and general method. Another very convenient access to "α-*N* substituted" isoxazoles is the coupling of magnesium compounds with 3-bromomethyl 5-methyl isoxazole.

Key words: isoxazoles, substitution in the α position of nitrogen.

Nous nous intéressons dans la perspective de leurs activités biocides à des isoxazoles substitués en α des hétéroatomes par une ou deux longues chaînes alkyle ou alcényle (1).[3] L'accès à des isoxazoles 3,5 disubstitués par ces groupements, de même qu'à des isoxazoles simplement « α-*O* substitués » est aisément réalisable (1[3] et 2–7). En revanche, les isoxazoles du type « α-*N* substitués » (cf. schéma 1), sont connus pour être beaucoup moins accessibles, même pour des substituants simples, et très peu sont décrits (8–10). Le substituant alcényle, dans le cas présent, peut entraîner une difficulté de synthèse supplémentaire. Nous présentons ici différents accès à de tels isoxazoles particuliers.

Résultats et discussion

Pour l'élaboration des isoxazoles α-*N* substitués, nous avons soit adapté des méthodes connues, soit développé de nouvelles voies de synthèse.

Voie A : cycloadditions dipolaires-1,3 d'oxydes de nitriles sur des alcynes (réf. 4) ou des alcènes (réf. 5)

1. *Isoxazoles* **4** α-N *monosubstitués*

Un accès univoque peut s'envisager par addition dipolaire-1,3 d'oxydes de nitriles **1** sur l'acétylène (4) et nous avons utilisé l'acétate de vinyle **2***a* comme équivalent synthétique de ce dipolarophile dans une méthode indirecte (11). Sa condensation avec des oxydes de nitrile à groupe alkyle ou alcényle, conduit régiosélectivement aux isoxazolines **3** (isolées ou non selon les cas), qui sont aromatisées en isoxazoles α-*N* par chauffage en milieu acide (cf. schéma 2 et tableau 1). Cette méthode[4] a l'avantage d'impliquer des matières premières et des précurseurs commerciaux ou d'accès facile : acétate de vinyl, bromure d'alkyle ou d'alcényle, aldéhydes.

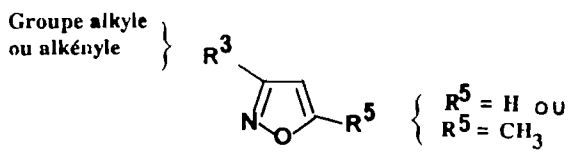

SCHÉMA 1. Isoxazoles α-*N* substitués.

2. *Isoxazoles* α-N **6** *méthylés en position 5*

Nous avons employé l'acétate d'isopropényle **2***b* comme équivalent synthétique du dipolarophile propyne dans la méthode indirecte via les isoxazolines **5** (cf. schéma 2). Le (décène-9 yl)-3 méthyl-5 isoxazole (**6***c*) est ainsi obtenu, mais en faible rendement (~20%) car il se forme une quantité importante (~40%) de furoxanne **1**′ (13) lors de la préparation de l'isoxazoline **5***c*.

Voie B : action de l'hydroxylamine sur des composés carbonylés

Nous avons d'abord retenu les énones[5] comme précurseurs carbonylés des isoxazoles α-*N*. En effet, une transformation *énone* → *isoxazole* a été obtenue par Büchi et Vederas (14) dans le cas des β-ionones, par action de l'hydroxylamine suivie d'une oxydation. Nous avons donc synthétisé des énones telles

[1]Partie de thèse soutenue a l'Université Pierre et Marie Curie, Paris, 1987.

[2]Révision reçue le 9 mars 1990.

[3]Synthèse d'« isoxazoles α-*O* substitués » soumis au Can. J. Chem., J. C. Cherton, M. Lanson, D. Ladjama, N. Lefèvre et J. J. Basselier.

[4]La déprotonation par les bases, du méthyle du méthyl-3 isoxazole, suivie d'une alkylation (voie de type C) n'est pas une voie d'accès aux isoazoles **4** puisque ce synthon, fragile en milieu basique, est de plus d'obtention difficile. L'action de l'hydroxylamine sur les β-cétoaldéhydes est hautement régiosélective mais conduirait dans notre cas aux isomères α-*O* substitués (12).

[5]L'action de l'hydroxylamine sur les β-dicétones (10, 18) et les ynones (19) conduit à des mélanges d'isoxazoles de types α-*N* et α-*O* substitués (9, 20).

Can. J. Chem. Downloaded from www.nrcresearchpress.com by 91.121.58.235 on 09/07/12
For personal use only.

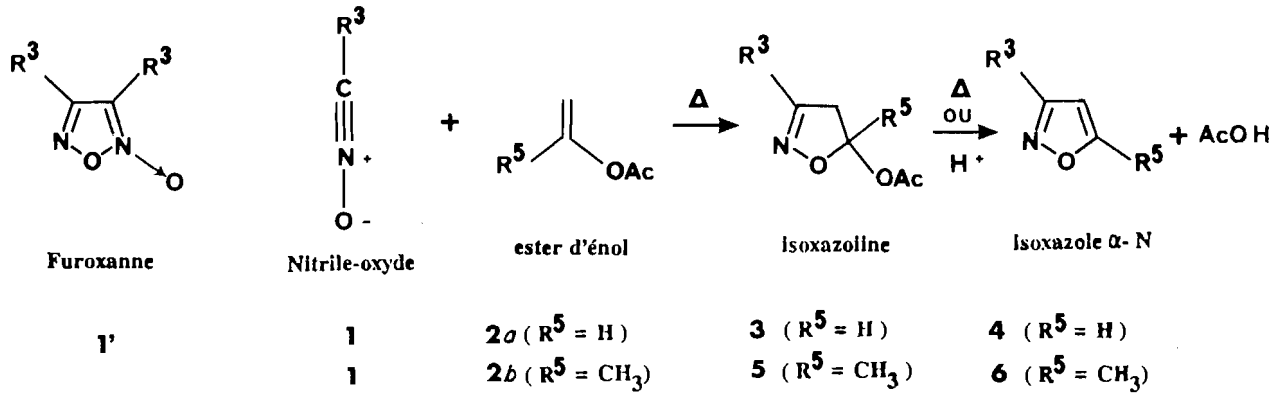

SCHÉMA 2. Synthèse d'isoxazoles α-*N* substitués par cycloaddition dipolaire-1,3 (voie A).

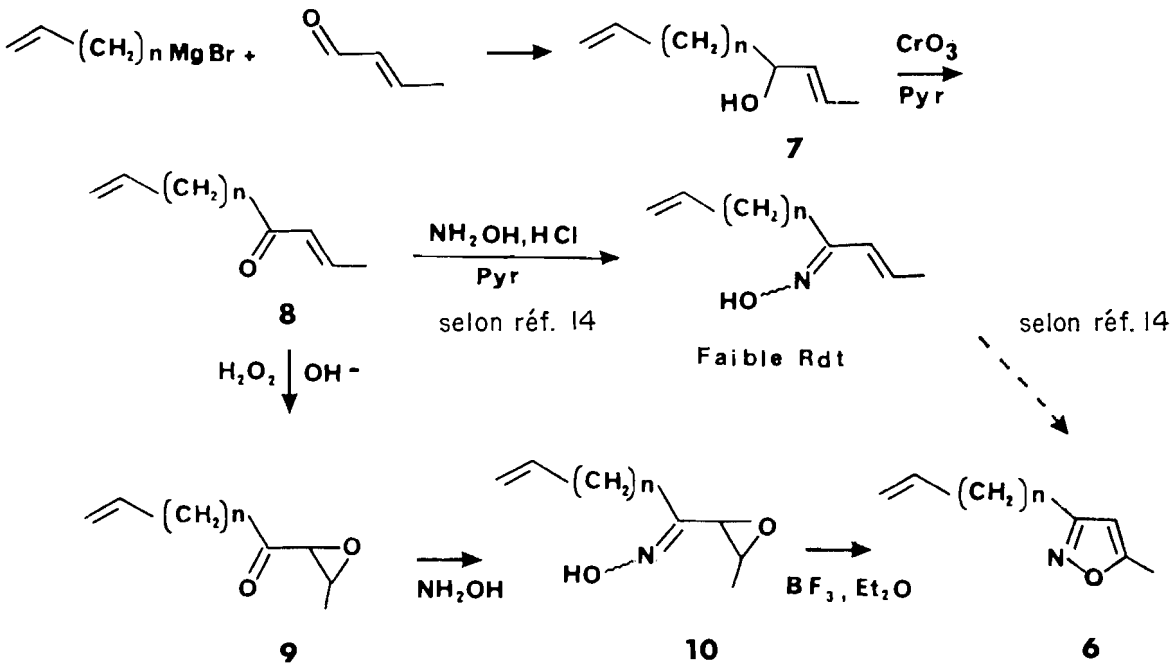

SCHÉMA 3. Voie des époxy-énones **9** (voie B).

que **8** par action du magnésien approprié sur le crotonal suivie d'une oxydation de l'alcool allylique **7** résultant selon la méthode de Ratcliffe (15). Toutefois, la transposition de la méthode de Büchi aux énones **8** s'est avérée décevante dès la première étape (1), (cf. schéma 3). Ceci provient de la difficulté d'obtention des oximes d'énones (16). Aussi avons nous procédé par action de l'hydroxylamine non pas sur les énones **8** mais sur les époxy-énones **9**. Ces dernières sont obtenues par époxydation sélective de la double liaison de l'énone avec l'eau oxygénée en milieu alcalin. Leur conversion en isoxazoles **6** a nécessité une mise au point de chacune des étapes. L'action de l'hydroxylamine en l'absence de solvant supprime la coupure en α du carbonyle masqué qui se produit en présence de pyridine (17). La cyclisation des oximes d'époxy-énones **10** a été effectuée en milieu acide doux (BF_3/Et_2O), pour éviter l'hydrolyse des oximes et éventuellement l'isomérisation des doubles liaisons terminales (cf. schéma 3 et tableau 2).

Cette synthèse partant d'époxy-énones a un rendement global faible. C'est néanmoins une méthode sûre, univoque et compatible avec des chaînes alcényles.

Voies C : partant d'isoxazoles

1. *Isomérisation des isoxazoles* α-O *substitués* (Voie C_1)

Nous avons appliqué *à l'échelle préparative* la méthode d'isomérisation des isoxazoles de Kashima et al. (21)[6] en quaternarisant les isoxazoles α-*O* **11** (1), (cf. schéma 4). Les méthyl-2 isoxazoliums **12** cristallisent parfois difficilement à cause de la présence d'une longue chaîne lipophile, et nous avons dû, pour chaque cas, rechercher l'anion le plus favorable (cf. schéma 4 et tableau 3). Nous nous sommes volontairement limités aux cas les plus simples où les isoxazoliums cristallisent. Néanmoins, même dans le cas contraire, cette méthode semble être une voie d'accès très intéressante aux isoxazoles α-*N* substitués.

[6]La difficulté de synthèse des isoxazoles de type α-*N*-substitués est bien connue (8–10) et les tentatives négatives concernant le simple *tert*-butyl-3 méthyl-5 isoxazole ont incité Kashima à rechercher une méthode générale d'accès à ces isoxazoles α-*N*. Cette synthèse fait appel aux sels de methyl-2 isoxazoliums (21, 22). L'action de l'hydroxylamine (sous forme $NHOH^-$) se traduit finalement par une inversion des hétéroatomes du cycle.

Can. J. Chem. Downloaded from www.nrcresearchpress.com by 91.121.58.235 on 09/07/12
For personal use only.

Can. J. Chem. Downloaded from www.nrcresearchpress.com by 91.121.58.235 on 09/07/12
For personal use only.

TABLEAU 1. Isoxazoles α-*N* monosubstitués **4** et **6***c*
Voie A (cf. schéma 2)

Nitrile-oxyde **1**				
R^3	Méthode de préparation*	Dipolarophile **2**	Isoxazoline **3** (Rdt %)	Isoxazole (Rdt %)
			3*a*	
$-(CH_2)_7$	b	**2***a*	Non isolée	**4***a* (60)
$-(CH_2)_8$	b	**2***a*	**3***b* (65)	**4***b* (48)
nDec	b	**2***a*	**3***c* (60)	**4***c* (54)
Et	a	**2***a*	**3***d* (72)	**4***d* (55)
			5*c*	
$-(CH_2)_8$	b	**2***b*	Non isolée	**6***c* (20)

*Méthode a : à partir du dérivé nitré (Kornblum et Ungnade (25*a*)). Méthode b : à partir des chloroaldoximes (Larsen et Torssell (26)).

TABLEAU 2. Obtention des isoxazoles α-*N* **6** à partir des époxy-énone **9**
Voie B (cf. schéma 3)

n	Obtention d l'alcool allylique (Rdt %)	Oxydation (Rdt %)	Epoxydation (Rdt %)	Oximation (Rdt %)*	Cyclisation (Rdt %)
2	**7***a* (56)	**8***a* (54)	—	—	—
3	**7***b* (45)	**8***b* (57)	**9***b* (35)	**10***b* (78)	**6***b* (16)
8	**7***c* (60)	**8***c* (86)	**9***c* (76)	**10***c* (76)	**6***c* (40)
9	**7***d* (50)	**8***d* (84)	**9***d* (70)	**10***d* (78)	**6***d* (35)

*Rendement en produit brut.

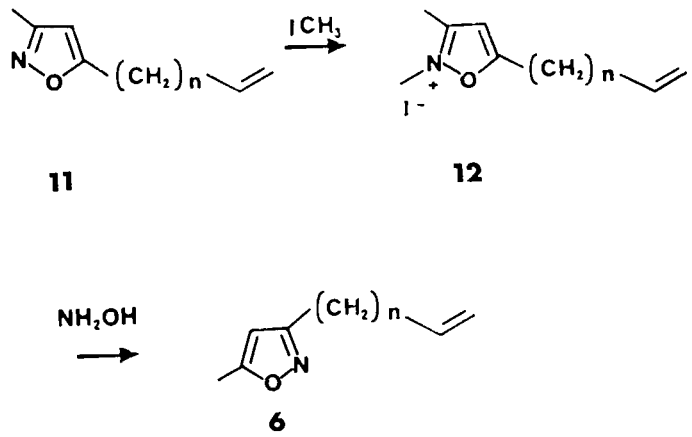

SCHÉMA 4. Voie des isoxazoliums **12** (voie C_1).

2. *Synthèse originale par action des magnésiens sur le bromométhyl isoxazole* **6**g (Voie C_2)

Nous avons utilisé le motif méthyl-3 isoxazole non pas comme nucléophile,[7] mais comme électrophile. Le point de départ est l'isoxazole ester **6***e* obtenu (23) à partir de l'acétyl-pyruvate d'éthyle. Sa réduction par le borohydrure de sodium conduit à l'isoxazole alcool **6***f* dont l'extraction a nécessité une

[7]La métallation/alkylation du diméthyl-3,5 isoxazole ne convient pas à l'obtention des isoxazoles α-*N*, puisque la déprotonation par des bases variées se fait sur le méthyle en position 5 (1) et conduit aux isoxazoles α-*O* substitués.

TABLEAU 3. Obtention des isoxazoles α-*N* **6** à partir des isoxazoliums **12**
Voie C_1 (cf. schéma 4)

n	RX	X^- final	Isoxazolium (Rdt %)	Isomère α-N (Rdt %)
2	CH_3I	I^-	**12***a* (45)	**6***a* (25)
3	$(CH_3)_2SO_4$	ClO_4^-	Ne cristallise pas	—
3	CH_3I	I^-	**12***b* (72)*	**6***b* (54)
8	CH_3I	I^-	Ne cristallise pas	—
8	$(CH_3)_2SO_4$	ClO_4^-	Ne cristallise pas	—
9	CH_3I	I^-	Ne cristallise pas	—
9	$(CH_3)_2SO_4$	ClO_4^-	**12***d* (45)	**6***d* (27)

*Cristallise au bout d'une semaine.

mise au point. La bromation fournit l'isoxazole bromé **6***g* dont le couplage avec le magnésien approprié s'est effectué sans difficulté (cf. schéma 5). Cette nouvelle méthode générale semble la plus efficace de celles que nous avons jusqu'ici testées pour produire des isoxazoles α-*N* substitués.

Ces isoxazoles α-*N* substitués dont les propriétés biologiques seront présentées indépendamment ont servi de synthons dans l'élaboration d'isoxazoles substitués de part et d'autre des hétéroatomes (1).[3]

Partie expérimentale

Les spectres d'absorption infrarouge ont été enregistrés sur un appareil Pye Unicam modèle SP3-200 (film liquide entre pastilles de NaCl, ou en pastilles de KBr, bandes d'absorption exprimées en cm^{-1} avec les abréviations suivantes : L, large; F, forte; m, moyenne; f, faible). Les spectres de rmn ^1H et de rmn ^{13}C ont été enregistrés sur des appareils Bruker WP 80, WM 250 et WM 500. Sauf indication contraire tous les spectres ont été effectués dans le $CDCl_3$. Les déplacements chimiques sont exprimés en ppm par rapport au TMS pour les spectres de rmn ^1H et par rapport au pic central du $CDCl_3$ choisi comme référence (77,1 ppm) pour les spectres de rmn ^{13}C (avec les abréviations suivantes : s, singulet; d, doublet; t, triplet; q, quadruplet; m, multiplet; M, massif). Les spectres de masse et de masse exacte ont été enregistrés sur des spectrographes MS 30 et MS 50 sous impact électronique à 70 eV par M^lle^ J. Mercier que nous remercions. Les pics sont exprimés en *m/z* avec, entre parenthèses, leur intensité relative. Les analyses élémentaires ont été executées au service de microanalyse de l'Université Pierre et Marie Curie ou au service de microanalyse du CNRS à Vernaison. Les points de fusion non corrigés ont été déterminés de façon instantanée au banc de Kofler.

Pour les composés intermédiaires tels que les isoxazoles **3** ou encore les énones **8**, les époxy-énones **9**, les oximes d'époxy-énones **10** et les sels d'isoxazolium **12**, les caractéristiques structurales sont souvent plus succintes en raison d'éventuelles instabilités. Ces composés sont alors utilisés directement sans purification.

Voie A (tableau 1)

1. *Synthèse des isoxazoles* **4** *monosubstitués en position 3*

Isoxazolines-2, **3**. L'isoxazoline **3***d* a été obtenue selon la méthode de Mukaiyama et Hoshino (24) à partir du dérivé nitré correspondant, lui-même obtenu selon la méthode de Kornblum et Ungnade (25*a*), méthode a). *Acétoxy-5- éthyl-3 isoxazoline-2* (**3***d*) : (72%), *F* 44°C; ir : 3020(m), 2960(m), 1740(F), 1230(F), 960(m); rmn ^1H : 6, 7 (dd, 1H), 3,1 (m, 2H), 2,4 (q, 2H), 2 (s, 3H), 1,1 (t, 3H).

Les isoxazolines-2 **3***b* et **3***c* sont synthétisées selon la méthode de Larsen et Torssell (26) (méthode b), à partir des aldéhydes correspondants, ainsi que l'isoxazoline **3***a* qui a été oxydée directement à l'état brut sans être isolée. *Acétoxy-5 (décène-8 yl)-3 isoxazoline-2* (**3***b*) : (65%), *F* 44°C; ir (chloroforme) : 3020(F), 2940(F), 2880(m), 1760(F), 1230(F), 1060(m); rmn ^1H : 6,7 (dd, 1H), 5,6 (m, 1H), 4,9 (m, 2H), 3 (m, 2H), 2,3 (m, 2H), 2 (s, 3H), 1,3 (m, 14H); masse : M^+ 267,

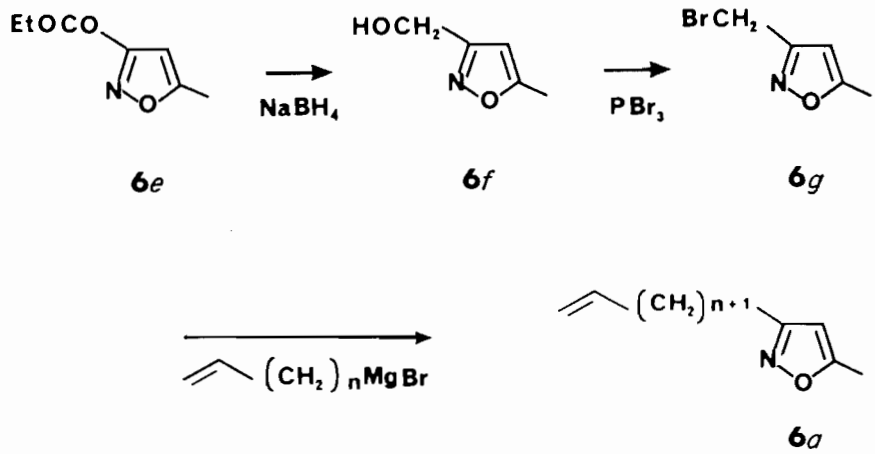

SCHÉMA 5. Action des magnésiens sur le bromométhyl-3 méthyl-5 isoxazole (voie C_2).

96(30), 83(60), 55(70), 43(100), 41(100). Anal. calc. pour $C_{15}H_{25}NO_3$: C 67,38, H 9,42, N 5,24; tr. : C 67,57, H 9,48, N 5,47. *Acétoxy-5 décyl-3 isoxazoline-2* (**3***c*) : (60%), *F* 65°C, ir (chloroforme) : 3020(m), 2940(m), 2860(m), 1760(F), 1470(f), 1420(f), 1380(f), 1220(F), 1050(m), 960(m); rmn ^{1}H : 6,7 (dd, 1H), 3,1 (m, 2H), 2,45 (m, 2H), 2 (s, 3H), 1,2 (m, 16H), 0,85 (m, 3H). Anal. calc. pour $C_{15}H_{27}NO_3$: C 66,88, H 10,10, N 5,20: tr. : C 66,97, H 10,03, N 5,23.

Isoxazoles **4**. On porte à reflux pendant 3 h un mélange de 50 mL d'éthanol, contenant 25 mmol de l'isoxazoline-2 acétoxylée et 1 mL d'acide chlorhydrique 12 N. Après retour à température ambiante, le solvant est chassé sous vide. Le résidu est repris à l'éther et neutralisé par une solution aqueuse de bicarbonate. Après séchage sur $MgSO_4$ la phase organique est concentrée puis distillée. *(Nonène-8 yl)-3 isoxazole* (**4***a*) : (60%), Eb_1 75–78°C; ir : 3080(f), 2920(F), 2840 (m), 1640(m), 1570(m), 1420(m); rmn ^{1}H : 2(m, 2H), 2,7 (t, 7 Hz, 2H), 5.0 (2H), 5,8 (1H), 6,2 (d, 2 Hz, 1H), 8,3 (d, 2 Hz, 1H); rmn ^{13}C : 25,7, 28,2, 28,8, 28,9, 29,0, 33,7, 103,8, 114,1, 138,0, 158.0, 162,8; masse : M^+ 192, 110(10), 97(10), 96(45), 83(73), 55(64), 54(30), 41(100). Anal. calc. pour $C_{12}H_{19}NO$: C 75,97, H 10,47, N 6,33; tr. : C 75,78, H 10,55, N 6,45. *(Decène-9 yl)-3 isoxazole* (**4***b*) : (48%), Eb_1 80°C; ir : 3080(f), 2920(F), 2840(m), 1640(m), 1570(m), 1420(m); rmn ^{1}H : 2(m, 2H), 2,7 (t, 7 Hz, 2H), 5,0 (2H), 5,8 (1H), 6,1 (d, 2 Hz, 1H), 8,7 (d, 2 Hz, 1H); rmn ^{13}C : 25,8, 28,3, 28,9, 29,1, 29,2, 29,3, 33,8, 103,9, 114,1, 139,1, 158,0, 163,0; masse : M^+ 207; 96(30), 83(50), 55(60), 41(100). Anal. calc. pour $C_{13}H_{21}NO$: C 75,31, H 10,20, N 6,75; tr. : C 75,13, H 10,27, N 6,44. *Décyl-3 isoxazole* (**4***c*) : (54%), $Eb_{0,5}$ 88°C; ir : 2920(F), 2860(m), 1570(m), 1420(m), 1120(m); rmn ^{1}H : 2,6 (t, 7 Hz, 2H), 6,2 (d, 3 Hz), 8,3 (d, 2 Hz, 1H); rmn ^{13}C : 14,1, 22,7, 25,9, 28,4, 29,2, 29,3, 29,6, 31,9, 103,9, 158,0, 163,0; masse : M^+ 209, 110(15), 97(10), 96(50), 83(100), 43(30), 41(50). Anal. calc. pour $C_{13}H_{23}NO$: C 74,59, H 11,07, N 6,69; tr. : C 74,78, H 10.96, N 6,88. *Ethyl-3 isoxazole* (**4***d*) : (55%), Eb_{760} 138–139°C; ir : 2960(m), 1570(F), 1470(m), 1420(F), 1130(F), 1070(m), 870(F), 780(m); rmn ^{1}H : 1,2 (t, 7 Hz, 3H) 2,7 (q, 7 Hz, 2H), 6,2 (1H), 8,3 (1H); rmn ^{13}C : 12,5, 19,3, 103,6, 158,0, 164,0; masse : M^+ 97, 69(60), 68(100), 41(40). Anal. calc. pour C_4H_7NO : C 61,83, H 7,26, N 14,42; tr. : C 61,47, H 7,41, N 14,70.

2. *Synthèse de l'isoxazole* **6***c via l'isoxazoline* **5***c*

La méthode de Larsen est appliquée à un mélange équimoléculaire de 11 mmol de l'oxime de l'undécénal (2 g) et d'acétate d'isopropényle (1,1 g). Après évaporation du solvant (chloroforme), l'addition de 100 mL d'heptane au milieu réactionnel provoque la précipitation du furoxanne correspondant **1′** (1,46 g, 37%), *F* 96–97°C; ir (KBr) : 2880(F), 1610(m), 1410(m), 1360(m), 1000(f), 820(m); rmn ^{1}H : 5,75 (M, 2H), 5,0 (M, 4H), 1,25 (M, 32H).

La distillation sous vide du filtrat renfermant l'isoxazoline brute **5***c* conduit à l'isoxazole **6***c* (512 mg, 20% par rapport à l'oxime), $Eb_{0,05}$ 110–112°C. Ce composé présente les mêmes caractéristiques spectroscopiques que l'isoxazole **6***c* obtenu par la voie B.

Voie B (tableau 2)

1. *Synthèse des précurseurs*

Enones **8**a–d. Elles sont obtenues selon la réf. 14 à partir des alcools allyliques **7** eux mêmes synthétisés selon la réf. 27. *Octadiène-2,7 one-4* (**8***a*) : (54%), Eb_{12} 70°C (litt. (28) Eb_{15} 72°C). *Nonadiène-2,8 one-4* (**8***b*) : (57%), Eb_{14} 94°C (litt. (28) Eb_{17} 98°C). *Tétradecadiène-2,13 one-4* (**8***c*) : (86%), $Eb_{0,5}$ 106°C; ir : 2920(F), 2860(m), 1690(f), 1670(m), 1640(m), 1440(m), 990(f), 970(m), 910(F), 740(F); rmn ^{1}H : 6,85 (1H, qd, 16 Hz, 7 Hz), 6,12 (1H, qd, 16 Hz, 1 Hz), 5,8 (1H, m) 4,9 (2H, m), 2,5(2H, t, 7,5 Hz), 2,05 (2H, m), 1,90 (3H, dd, 6,9 Hz, 1,25 Hz), 1,60 (2H, m), 1,30 (10H, M); rmn ^{13}C : 200,6, 142,2, 139,2, 132, 114, 40,1, 33,8, 29,7, 29,4, 29,1, 24,3, 18,2; masse : M^+ 208, 193(20), 123(40), 84(50), 69(100), 55(20), 41(50). Anal. calc. pour $C_{14}H_{24}O$: C 80,71, H 11,61, O 7,68; tr. : C 80,88, H 11,65, O 7,47. *Pentadécadiène-2,14 one-4* (**8***d*) : (84%), $Eb_{0,3}$ 123°C; ir : 3080(f), 2920(F), 2860(F), 1695(m), 1670(F), 1630(F), 1460(m), 995(f), 970(m), 910(m); rmn ^{1}H : 6,65 (1H, qd, 16 Hz, 6 Hz), 5,7 (2H, m), 4,6 (2H, m), 2,4 (2H, t, 7 Hz), 2,2–1 (19H, M); rmn ^{13}C : 200,5, 141,9, 139,2, 132,2, 114,2, 40,2, 33,8, 29,4, 29,1, 29,0, 24,3, 18,0. Anal. calc. pour $C_{15}H_{26}O$: C 81,02, H 11,79, O 7,20; tr. : C 80,98, H 11,88, O 7,14.

Epoxy-énones **9** : elles sont obtenues selon la méthode de House et Reif (29). *(Méthyl-3 oxiranyl-2)-1 hexène-5 one* (**9***b*) : (35%), Eb_{14} 108°C; ir : 1710(F), 1650(m), 1420(m), 1000(f), 970(m), 920(m); rmn ^{1}H : 5,70 (m, 1H), 4,9 (M, 2H), 3,1 (d, 1,6 Hz, 1H), 3,07 (dq, 5,2 Hz, 1,6 Hz, 1H), 2,37 (t, 2H), 2 (m, 2H), 1,60 (m, 2H), 1,33 (d, 5,2 Hz, 3H); rmn ^{13}C : 207, 137,0, 115,2, 60,4, 54,1, 36,1,32,8, 22,0, 17,3. *(Méthyl-3 oxiranyl-2)-1 undecène-10 one-1* (**9***c*) : (76%), Eb_1 118–120°C; ir : 3100(f), 2950(F), 2880(m), 1720(F), 1650(f), 1420(f), 1380(f), 1000(f), 980(f), 920(f); masse : 83(30), 69(60), 67(30), 55(100), 43(60), 41(80); rmn ^{1}H : 5,80 (m, 1H), 4,9 (M, 2H), 3,17 (d, 1,9 Hz, 1H), 3,13 (dq, 4,9 Hz, 1,9 Hz, 1H), 2,37 (m, 2H), 2 (m, 2H), 1,60 (m, 2H), 1,40 (d, 9 Hz, 3H), 1,29–1,25 (M, 10H); rmn ^{13}C : 207,9, 139,2, 114,2, 60,6, 54,3, 37,2, 33,8, 23,2, 17,5. Anal. calc. pour $C_{14}H_{22}O_2$: C 74,95, H 10,78, O 14,26; tr. : C 75,03, H 10,93, O 14,04. *(Méthyl-3 oxiranyl-2)-1 dodécène-11 one-1* (**9***d*) : (60%), $Eb_{0,3}$ 128°C; ir : 3080(f), 2920(F), 2860(F), 1710(F), 1640(m), 1460(m), 1380(m), 1000(m), 980(m), 910(F), 850(m); rmn ^{1}H : 5,70 (m, 1H), 4,8 (M, 2H), 3,0 (M, 2H), 2,25 (d, 2,2 Hz, 2H), 1,9 (m, 2H), 1,30 (d, 5,0 Hz, 3H); rmn ^{13}C : 207,4, 139,0, 114,2, 60,5, 54,0, 37,0, 33,7, 23,1, 17,5; masse : 99(50), 84(30), 69(90), 55(100), 43(55), 41(100). Anal. calc. pour $C_{15}H_{24}O_2$: C 75,58, H 10,99, O 13,42; tr. : C 75,03, H 10,93, O 13,38.

Oximes d'époxy-énones **10** (16)

(Méthyl-3 oxiranyl-2)-1 undécène-10 one-1 oxime (**10***c*). On traite par 0,72 g (10 mmol) de chlorhydrate d'hydroxylamine dans 1,2 mL d'eau 1,86 g (8 mmol) d'époxy-énone **9***c* sous agitation à température ambiante pendant 2 h. La phase organique est décantée, lavée à l'eau (3

Can. J. Chem. Downloaded from www.nrcresearchpress.com by 91.121.58.235 on 09/07/12
For personal use only.

Can. J. Chem. Downloaded from www.nrcresearchpress.com by 91.121.58.235 on 09/07/12
For personal use only.

× 5 mL), puis étendue d'éther. Après séchage sur Na_2SO_4, on concentre sous vide. Le résidu n'est pas distillé en raison de sa fragilité, il est utilisé directement pour la cyclisation en isoxazole (76%).

L'oxime d'époxy-énone **10***b* est préparée de la même manière ainsi que l'oxime **10***d* qui est utilisée immédiatement. (*Méthyl-3 oxiranyl-2)-1 hexène-5 one-1 oxime* (**10***b*) : (78%), ir : 3300(large), 3080(f), 2980(m), 2640(m), 1650(m), 1440(F), 1000(m), 940(F), 860(m); rmn ^{1}H : 12,2 (1H, mobile), 5,6 (1H, m), 4,8 (2H, m), 3,1 (1H, d, 2 Hz), 2,9 (1H, qd, 5 Hz, 2 Hz), 2 (4H, m), 1,5 (2H, m), 1,3 (3H, d, 5 Hz). (*Méthyl-3 oxiranyl-2)-1 dodecène-11 one-1 oxime* (**10***d*) : (78%).

2. *Isoxazoles* α-N *substitués* **6**

(*Décène-9 yl)-3 méthyl-5 isoxazole* (**6***c*). On porte à reflux pendant 4 h un mélange de 1,45 g (6,1 mmol) d'oxime d'époxy-énone **10***c* dans 60 mL de benzène anhydre et 0.7 mL (6 mmol) de BF_3/Et_2O. Après retour à température ambiante, la solution est étendue avec 60 mL d'éther, puis lavée à l'eau (4 × 60 mL) jusqu'à pH neutre. La phase organique est séchée sur $MgSO_4$. Le solvant est chassé sous vide. Le résidu obtenu est distillé (40%), Eb_1 (Kugelrohr) 140°C; rmn ^{1}H : 5,8 (d, 0,7 Hz, 1H), 5,8 (m, 1H), 5,0 (M, 2H), 2,58 (t, 2H), 2,35 (d, 0,7 Hz, 3H), 2 (m, 2H), 1,6 (m, 2H), 1,3 (M, 10H); rmn ^{13}C : 168,2, 164,2, 139,1, 114,1, 101,2, 33,8, 29,5, 29,2, 29,1, 29,0, 28,3, 26,1, 12,2. Masse exacte calc. pour $C_{14}H_{23}NO$: 221,1780; tr. : 221,1775.

Les isoxazoles **6***b* et **6***d* ont été préparés de la même manière. *Méthyl-5 (pentène-4 yl)-3 isoxazole* (**6***b*) : (16%), $Eb_{0,2}$ 37°C; rmn ^{1}H : 5,8 (d, 0,6 Hz, 1H), 5,8 (m, 1H), 5,0 (m, 2H), 2,61 (t, 2H), 2,38 (d, 0,6 Hz, 3H), 2,1 (m, 4H), 1,7 (m, 2H); rmn ^{13}C : 168,9, 163,9, 137,8, 115,1, 101,2, 33,0, 27,4, 25,4, 12,1; masse : M^+ 151 (45), 55(50), 44(45), 43(80), 41(100). Masse exacte calc. pour $C_9H_{13}NO$: 151,0997; tr. : 151,0996. *Méthyl-5 (undécène-10 yl)-3 isoxazole* (**6***d*) : (35%), $Eb_{0,7}$ 120°C; rmn ^{1}H : 5,8 (d, 0.7 Hz, 1H), 5,8 (m, 1H), 5,0 (M, 2H), 2,53 (t, 2H), 2,3 (d, 0,7 Hz, 3H), 2 (m, 2H), 1,6 (m, 2H), 1,5–1 (M, 12H); rmn ^{13}C : 168,8, 164,1, 139,0, 114,0, 101,1, 33,7, 29,3, 29,1, 28,9, 28,2, 25,9, 12,1; masse : M^+ 235, 149(30), 110(70), 97(100), 55(50), 43(45), 41(65). Anal. calc. pour $C_{15}H_{25}NO$: C 76,54, H 10,70, N 5,95; tr. : C 76,65, H 10,80, N 6,12.

Voie C_1 : *Isomérisations des isoxazoles* α-O *substitués* ***11*** (tableau 3)

Isoxazoliums ***12***

Les iodures d'isoxazoliums **12***a* et **12***b* sont préparés selon la méthode de Lampe et Smolinska (22) à partir des isoxazoles α-*O* substitués **11** correspondants (1).[3] *Iodure de (butène-3 yl)-5 diméthyl-2,3 isoxazolium* (**12***a*) : (45%), *F* <50°C (éther diéthylique); ir : 1640(f), 1600(m), 1540(m), 1480(m), 1420(m), 1000(m), 900(f); rmn ^{1}H : 7,1 (s, 1H), 5,8 (m, 1H), 5,0 (m, 2H), 4,5 (s, 3H), 3 (t, 7,4 Hz, 2H), 2,6 (s, 3H), 2,4 (m, 2H); rmn ^{13}C : 172,8, 158,2, 133,7, 114,8, 105,8, 36,6, 27,7, 23,1, 10,0. *Iodure de diméthyl-2,3 (pentène-4 yl)-5 isoxazolium* (**12***b*) : (72%), *F* <50°C (acétate d'éthyle); ir : 1640(f), 1610(f), 1550(f), 1050(f), 1000(f), 980(f), 930(m), 860(f), 650(m); rmn ^{1}H : 7,1 (s, 1H), 5,8 (m, 1H), 5,1 (m, 2H), 4,5 (s, 3H), 3 (t, 7,4 Hz, 2H), 2,9 (s, 3H), 2,2 (m, 2H), 1,8 (m, 2H); rmn ^{13}C : 176,1, 160,2, 136,2, 116,4, 108,6, 40,9, 32,4, 26,0, 25,5, 14,2. *Perchlorate de diméthyl-2,3 (undécène-10 yl)-5 isoxazolium* (**12***d*) : il est obtenu selon la méthode de Woodward et Olofson (30) (47%), *F* <50°C (acétone); rmn ^{1}H : 6,6 (s, 1H), 5,8 (m, 1H), 4,9 (m, 2H), 4,2 (s, 3H), 2,8 (t, 7,4 Hz, 2H), 2,6 (s, 3H), 2,0 (m, 2H), 1,7 (m, 2H), 1,4–1 (M, 12H); rmn ^{13}C : 176,8, 160,8, 139,2, 114,2, 107,8, 38,6, 33,8, 26,8, 26,6, 12,4.

Action de l'hydroxylamine sur les isoxazoliums ***12***

Les isoxazoles α-*N* **6***a*, **6***b* et **6***d* ont été préparés à partir des isoxazoliums correspondants selon la méthode de Kashima *et al.* (21). (*Butène-4 yl)-3 méthyl-5 isoxazole* (**6***a*) : (25%), Eb_{15} 82°C; rmn ^{1}H : 5,80 (M, 2H), 5,0 (m, 2H), 2,7 (t, 2H), 2,4 (m, 2H), 2,36 (s, 3H); rmn ^{13}C : 169,1, 163,6, 137,1, 115,7, 101,3, 32,2, 25,6, 12,2; masse : M^+ 137, 55(55), 43(100), 41(40). Anal. calc. pour $C_8H_{11}NO$: C 70,04, H 8,08, N 10,21; tr. : C 70,00, H 8,26, N 10,30. *Méthyl-5 (pentényl-4 yl)-3 isoxazole* (**6***b*) : (54%). *Méthyl-5 (undécène-10 yl)-3 isoxazole* (**6***d*) : (27%). Les composés **6***b* et **6***d* présentent les mêmes caractéristiques physiques que ceux obtenus par la voie B.

Voie C_2 : *À partir du bromomèthyl-3 méthyl-5 isoxazole* (**6***g*)

Méthyl-5 isoxazole carboxylate-3 d'éthyle (**6***e*) : On utilise la méthode de Baraldi *et al.* (23) (69%), Eb_{20} 124°C (litt. (23) Eb_{18} 112°C). *Hydroxyméthyl-3 méthyl-5 isoxazole* (**6***f*) : Afin d'éviter les problèmes d'extraction, nous avons modifié la méthode de Baraldi *et al.* (23). À une solution de 6,2 g (0.04 mol) de méthyl-5 isoxazole carboxylate-3 d'éthyle **6***e* dissous dans 84 mL d'éthanol absolu refroidi par un bain de glace, on ajoute 3,3 g (0,087 mol) de borohydrure de sodium par petites quantités. On laisse sous agitation à température ambiante pendant 3 h puis on neutralise le milieu réactionnel avec une solution concentrée de HCl. Le solvant est chassé sous vide, puis le résidu est saturé par du sulfate d'ammonium et extrait à l'éther. La phase éthérée est séchée sur sulfate de magnésium, évaporée au rotovapor, puis distillée sous vide (75%), Eb_{15} 120°C (litt. (23) Eb_{15} 120°C). *Bromométhyl-3 méthyl-5 isoxazole* (**6***g*) : À une solution de 25 mL be benzène anhydre refroidie à −10°C et contenant 2,9 g (0,01 mol) de PBr_3 et 0,6 mL de pyridine, on ajoute un mélange de 0,4 mL pyridine et de 5,6 g (0,05 mol) d'hydroxyméthyl-3 méthyl-5 isoxazole (**6***f*) en maintenant la température à −5°C durant l'addition. On agite ensuite pendant 1 h à −10°C, puis à température ambiante pendant 24 h. Le mélange est distillé, le distillat est étendu d'éther et lavé à l'eau, séché sur sulfate de magnésium. L'éther est chassé sous vide (59%), Eb_{15} 105°C; ir : 3150(m), 1610(F), 1480(F), 1450(F), 1270(F), 1230(F), 1150(F), 1020(F), 920(F), 810(F), 760(F), 710(F), 620(m); rmn ^{1}H : 5,9 (s, 1H), 4,2 (s, 2H), 2,3 (s, 3H); rmn ^{13}C : 170,3, 160,8, 101,5, 20,7, 12,1; masse : M^+ 177–175, 96(60), 43(100).

Attaque du bromométhyl-3 méthyl-5 isoxazole par les magnésiens

Butène-4 yl)-3 méthyl-5 isoxazole (**6***a*): À 17 mL (0,01 mol) du magnésien du bromure d'allyle refroidi par un bain de glace, on ajoute goutte à goutte 1,87 g (0,01 mol) du bromométhyl-3 méthyl-5 isoxazole (**6***g*) dilué dans 2 mL d'éther anhydre. Après 12 h d'agitation, le mélange réactionnel est traité par une solution de HCl concentré jusqu'à neutralité, puis extrait à l'éther. L'éther est chassé sous vide et l'huile obtenue est distillée (64%), et présente les mêmes caractéristiques physiques et spectroscopiques que l'isoxazole obtenu par la voie des isoxazoliums.

1. M. Lanson. Thèse de doctorat, Paris (1987).
2. D. J. Brunelle. Tetrahedron Lett. **22**, 3699 (1981).
3. G. Bianchi et M. De Amici. J. Chem. Soc. Chem. Commun. 962 (1978).
4. B. J. Wakefield et D. J. Wright. J. Chem. Soc. 1165 (1970).
5. A. Barco, S. Benetti et G. P. Pollini. Synthesis, 837 (1977).
6. R. G. Micetich. Can. J. Chem. **48**, 2006 (1970).
7. C. Kashima, S. Tobe, N. Sugiyama et M. Yamamoto. Bull. Chem. Soc. Jpn. **46**, 310 (1973).
8. D. H. Hoskin et R. A. Olofson. J. Org. Chem. **47**, 5222 (1982).
9. C. Kashima. Chem. Lett. 1455 (1982).
10. F. Imura. Nippon Kagaku Zasshi, **77**, 1855 (1956); Chem. Abstr. **53**, 5127f (1959).
11. R. Paul et S. Tchelitcheff. Bull. Soc. Chim. Fr. 2215 (1962).
12. M. Ceresole. Ber. **17**, 812 (1884).
13. R. G. Micetich. Can. J. Chem. **48**, 467 (1970).
14. G. Büchl et J. C. Vederas. J. Am. Chem. Soc. **94**, 9128 (1972).
15. R. W. Ratcliffe. Org. Synth. **55**, 84 (1955).
16. T. M. Chau, C. Beauté, S. Cornuel et N. Thoai. Tetrahedron Lett. **45**, 4316 (1971).
17. L. I. Klimova et N. N. Suvorov. Khim. Prir. Soedin. **2**, 325 (1966); Chem. Abstr. **67**, 54332 m (1966).
18. M. F. Couturier. C. R. Acad. Sci. **150**, 928 (1910).
19. H. Feuer. J. Org. Chem. **29**, 935 (1964).
20. C. Kashima, Y. Yamamoto, Y. Omote et Y. Tsuda. Bull. Chem. Soc. Jpn. **50**, 543 (1977).
21. C. Kashima, K. Arai, S. Imada et Y. Tsuda. Bull. Chem. Soc. Jpn. **51**, 1844 (1978).
22. W. Lampe et J. Smolinska. Rocz. Chem. **28**, 163 (1954).

23. P. G. BARALDI, D. SIMONI, F. MORODER, S. MANFREDINI, L. MUCCHI et F. DALLA VECCHIA. J. Heterocycl. Chem. **19**, 557 (1982).
24. T. MUKAIYAMA et T. HOSHINO. J. Am. Chem. Soc. **82**, 5339 (1960).
25. (*a*) N. KORNBLUM et H. E. UNGNADE. Org. Synth. **38**, 75 (1958); (*b*) A. J. FATIADI. Synthesis, 65 (1976).
26. K. E. LARSEN et K. B. G. TORSSELL. Tetrahedron, **40**, 2985 (1984).
27. E. R. COBURN. Org. Synth. **55**, 84 (1955).
28. M. BORTOLOSSI, R. BLOCH et J. M. CONIA. Bull. Soc. Chim. Fr. 2726 (1975).
29. H. O. HOUSE et D. J. REIF. J. Am. Chem. Soc. **79**, 6491 (1957).
30. R. B. WOODWARD et R. A. OLOFSON. Tetrahedron Suppl. n° **7**, 415 (1966).

Can. J. Chem. Downloaded from www.nrcresearchpress.com by 91.121.58.235 on 09/07/12
For personal use only.

Studies in aryltin chemistry. Part 6.[1] Crystal and molecular structures of tetra(*p*-methylsulphonylphenyl)tin(IV) and tetra(*p*-methylsulphinylphenyl)tin(IV) monohydrate[2]

IVOR WHARF
Department of Chemistry and Chemical Technology, Dawson College, 3040 Sherbrooke St. W., Montreal, Que., Canada H3Z 1A4

MICHEL G. SIMARD
Département de chimie, Université de Montréal, C.P. 6128, Succ. A., Montreal, Que., Canada H3C 3J7

AND

HENRY LAMPARSKI
Department of Chemistry, McGill University, 801 Sherbrooke St. W., Montreal, Que., Canada H3A 2K6

Received September 8, 1989

IVOR WHARF, MICHEL G. SIMARD, and HENRY LAMPARSKI. Can. J. Chem. **68**, 1277 (1990).

Tetrakis(*p*-methylsulphonylphenyl)tin(IV) and tetrakis(*p*-methylsulphinylphenyl)tin(IV) *n*-hydrate have been prepared and their spectra (ir 1350–400 cm^{-1}; nmr, ^1H, ^{13}C, ^{119}Sn) and X-ray crystal structures are reported. The first compound is monoclinic, space group $C2/c$, $Z = 4$, with $a = 21.589(6)$, $b = 6.207(3)$, $c = 22.861(11)$ Å, $\beta = 93.80(3)°$ (22°C); the structure was solved by the direct method and refined by full-matrix least squares calculations to $R = 0.043$ for 2755 observed reflections. It has 2 molecular symmetry with the methyl group and one oxygen atom completely disordered in both $CH_3S(O_2)$ groups in the asymmetric unit. The second compound is tetragonal, space group $P4_2/n$, $Z = 2$, with $a = b = 15.408(6)$, $c = 6.379(2)$ Å (−100°C); the structure was solved by the Patterson method and refined by full-matrix least squares calculations to $R = 0.060$ for 1209 observed reflections. It has $\bar{4}$ molecular symmetry with the whole asymmetric unit disordered. Water molecules occupy positions on parallel 4_2 axes but molecular packing requirements prevent all sites having 100% occupancy giving $n \sim 1$ for the hydrate.

Key words: Tetra-aryltins, crystal structures, sulphone, sulphoxide, hydrogen-bonding.

IVOR WHARF, MICHEL G. SIMARD et HENRY LAMPARSKI. Can. J. Chem. **68**, 1277 (1990).

On a préparé le tétrakis(*p*-méthylsulfonylphényl)étain(IV) et le *n*-hydrate du tétrakis(*p*-méthylsulfinylphényl)étain(IV) et on a déterminé leurs spectres ir (de 1350 à 400 cm^{-1}) et rmn du ^1H, du ^{13}C et du ^{119}Sn ainsi que leurs structures cristallines par diffraction des rayons-X. Le premier composé est monoclinique, groupe d'espace $C2/c$, $Z = 4$, avec $a = 21,589(6)$, $b = 6,207(3)$ et $c = 22,861(11)$ Å et $\beta = 93,80(3)°$ (22°C); on a affiné la structure par la méthode directe et on l'a affinée par la méthode des moindres carrés jusqu'à une valeur de $R = 0,043$ pour 2755 réflexions observées. Il possède symétrie moléculaire 2 alors que le groupement méthyle ainsi que l'atome d'oxygène sont complètement désordonnés dans les deux groupements $CH_3S(O_2)$ de l'unité asymétrique. Le second composé est tétragonal, groupe d'espace $P4_2/n$, $Z = 2$, avec $a = b = 15,408(6)$ et $c = 6,379(2)$ Å (−100°C); on a résolu la structure par la méthode de Patterson et on l'a affinée par la méthode des moindres carrés jusqu'à une valeur de $R = 0,060$ pour 1209 réflexions observées. Il possède une symétrie moléculaire $\bar{4}$ et l'unité asymétrique dans son ensemble est désordonnée. Les molécules d'eau occupent des positions parallèles aux axes 4_2; toutefois, l'empilement moléculaire ne permet pas à tous les sites d'être occupés à 100% et l'hydrate est à $n \sim 1$.

Mots clés : tétra-arylétains; structures cristallines; sulfone; sulfoxyde; liaison hydrogène.

[Traduit par la revue]

Introduction

Although the eight tetra-aryltin structures reported to date (2, 3) have $\bar{4}$ molecular symmetry, the specific tetragonal space group adopted depends on the phenyl ring substituents present. Usually substituted tetra-aryltins are prepared from the appropriate aryl bromide but if the substituent is itself a functional group, this can react further, yielding other tetra-aryltins. Here we report two new Ar_4Sn obtained by oxidation of the methylthio groups of $(p\text{-}CH_3SC_6H_4)_4Sn$ (**1**) to $CH_3S(O)$ or $CH_3S(O_2)$.

Oxidation of a sulphide to a sulphone is readily accomplished at room temperature with several oxidants (4*a*), including that used here, *m*-chloroperbenzoic acid (*m*-CPBA). Since crystal structures of compounds with an —$S(O_2)$— unit joined to aryl and alkyl groups concurrently (5–10) including two with the $CH_3S(O_2)$— moiety (11, 12), show no example where the C—S—C_{ar} unit and phenyl ring are coplanar, we undertook an X-ray diffraction study of $(p\text{-}CH_3S(O_2)C_6H_4)_4Sn$ (**2**), to determine the effect of this large unsymmetric *para*-substituent on the choice of space group for the compound.

Partial oxidation of (**1**) to give $(p\text{-}CH_3S(O)C_6H_4)_4Sn$ (**3**) using *m*-CPBA is unpredictable (4*b*) requiring careful temperature control (13) to prevent formation of sulphone groups whose presence can be detected from the infrared spectra of the products. Since **1** has the CH_3—S bond coplanar with the phenyl ring, equal numbers of *R* or *S* configuration $CH_3S(O)$— groups will be formed, enabling **3** with this disorder to have effective fourfold symmetry. However, infrared spectra show authentic samples of **3** also contain hydrogen-bonded lattice water, another potential cause of disorder. An X-ray diffraction study of **3** was therefore carried out to determine the nature of the disorder at each sulphur atom, as well as hydrogen bonding and the amount of lattice water in the crystal.

Experimental

Tetra(*p*-methylthiophenyl)tin (**1**) was a previous preparation (2) while *m*-CPBA (Aldrich) was used as received. All solvents were

[1]For Part 5, see ref. 1.

[2]Presented in part by I.W. at the 3rd North American Chemical Congress, Toronto, Canada, June, 1988, Inorganic Division, Paper 334.

Can. J. Chem. Downloaded from www.nrcresearchpress.com by 88.85.125.76 on 09/07/12
For personal use only.

TABLE 1. Crystallographic data[a]

Parameter	Value	
	2	**3**
Composition	$(p\text{-}CH_3S(O)_2C_6H_4)_4Sn$ $C_{28}H_{28}O_8S_4Sn$	$(p\text{-}CH_3S(O)C_6H_4)_4Sn.nH_2O$ (n = 1, 2) $C_{28}H_{28}O_4S_4Sn.n(H_2O)$ (n = 1, 2)
MW	739.47	693.49–711.51
Crystal system	Monoclinic	Tetragonal
Space group	$C2/c$	$P4_2/n$
a (Å)	21.589(6)	15.408(6)
b (Å)	6.207(3)	15.408(6)
c (Å)	22.861(11)	6.379(2)
β (deg)	93.80(3)	—
V (Å^3)	3056.7	1514.4
d_c (g cm^{-3})	1.607	1.521
Z	4	2
μ (cm^{-1})	97.3	97.0
Crystal size (mm)	0.023 × 0.33 × 0.39	0.10 × 0.13 × 0.32
T_m (°C)	22	−100
Scan speed (deg min^{-1})	4	2
Independent reflections	2907	1699
Acceptance level $I/\sigma(I) \geq$	3.0	3.0
Observed reflections	2755	1219
Transmission factors	0.14–0.80	0.27–0.43
$R = \Sigma(F_o - F_c)/\Sigma F_o$	0.043	0.060
$R_w = [\Sigma w(F_o - F_c)^2/\Sigma w F_o^2]$	0.050	0.069
$S = [\Sigma w(F_o - F_c)^2/(m - n)]$	2.27	2.59
Final ΔF map (e Å^{-3})	1.50–0.48 (5 peaks)	0.95 (1 peak)
distance from Sn and/or S (Å)	0.82–1.14	0.33
Background (± e Å^{-3})	0.45	0.40
Shift-to-σ ratio, maximum	0.14	0.22
average	0.02	0.04

[a] $2\theta_{max}$ = 140° and scan width = (1.00 + 0.14 tan θ)°.

stored over molecular sieves except anhydrous ether (Fisher). Other experimental details, e.g. micro-analyses and infrared (Nujol mull) 1350–500 cm^{-1} and nmr (^{13}C, ^{119}Sn) spectra were as described elsewhere (1, 14); proton nmr spectra ($CDCl_3$ solution) were obtained using a Varian T-60 instrument.

Preparations

*Tetra(*p*-methylsulphonylphenyl)tin (2)*

Solid *m*-CPBA (85%; 11.08 g) was added over 1½ h to a well-stirred dichloromethane (20 mL) solution of **1** (3.34 g) kept at −8°C. Further CH_2Cl_2 (75 mL) was added to the mixture which was then stirred for 2½ h at room temperature. Dissolving the white suspension with (1/1) CH_2Cl_2/ether (200 mL) followed by adding ether (300 mL) to the clear filtrate gave the *product* as a white powder. This was redissolved in CH_2Cl_2 (300 mL), then reprecipitated with ether (300 mL), and dried in vacuum overnight; yield 67%; dec. > 355°C; ir data, (1308, 1305)*vs($\nu_{as}(SO_2)$), 1296s, 1290sh, 1281sh, 1266wm, 1195wmsp, 1189wmsp, (1153, 1151)*vs($\nu_s(SO_2)$), 1117w, 1094sh, 1091m, 1061wmsp, 1013msp, 975sh, 967sm, 960s, 949sh, 824msp, 821sh, 814msp, 775*s($\nu(CH_3—S)$), 733wbr, 715wm, 708w, 554sh, 551*vs, 543*s, (534, 530)*vs; ^{1}H nmr δ: 3.07 (s, 3H), 7.67–8.05 (q, 4H). *Anal.* calcd. for $C_{28}H_{28}O_8S_4Sn$: C 45.5, H 3.8; found: C 45.0, H 3.8.

*Tetra(*p*-methylsulphinylphenyl)tin* n*-hydrate (3)*

A solution of *m*-CPBA (85%; 4.20 g) in CH_2Cl_2 (100 mL) was added dropwise over 1½ h to a well-stirred CH_2Cl_2 (20 mL) solution of (**1**) (3.05 g) kept at −12°C. The stirred mixture was allowed to slowly warm to room temperature (4 h) and the clear solution obtained washed with saturated aqueous solutions of $NaHCO_3$ (4 × 80 mL) and NaCl (100 mL). The organic layer was dried over anhydrous $MgSO_4$ (2 days) and then evaporated under vacuum to a clear glassy solid. This was recrystallised from much acetone (~1 L) to yield a fine white powder which was dried in a vacuum for 2 days; yield 55%; mp 265–267°C; ir data, 3440s, vbr (ν(OH)); 1298m, 1262w, 1189w, 1107w, 1088vs,sp, 1060m,sp, (1052vs, (1036, 1033, 1029)vs)*(ν(SO)), 1011vs,sp, 952s, 938m, 859w, 813s, 720w, 681wm ($\nu(CH_3—S)$), 629w,sp, 509s, 487sm; ^{1}H nmr δ: 2.23 (s, 1H), 2.79 (s, 3H), 7.73 (s, 4H); ^{13}C nmr δ: 43.76 (CH_3), 123.82 (*m*-C, J = 53.6 Hz, ^{119}Sn—C), 137.68 (*o*-C, J = 40.4 Hz, ^{119}Sn—C), 139.91 (*i*-C, J = 534.5 Hz, ^{119}Sn—C), 147.79 (*p*-C, J = 11.9 Hz, ^{119}Sn—C); ^{119}Sn nmr: −129.10 ppm (ext. $Sn(CH_3)_4$). Anal. calcd. for $C_{28}H_{28}O_4S_4Sn.nH_2O$: ($n$ = 1) C 48.5, H 4.4; (n = 2) C 47.3, H 4.5; found: C 47.5, H 4.5.

X-ray structure analysis

Data collection for both compounds followed previous procedures (2, 15); the specific parameters are given in Table 1. The structures were solved using MULTAN (**2**) or the Patterson method (**3**), followed by difference Fourier calculations. Final cycles introduced H-atoms at fixed positions (d(C—H) = 1.08 Å) followed by anisotropic refinement of all non-hydrogen atoms.

For **2**, the disordered solutions for the *para*-substituents obtained in both space groups (Cc and $C2/c$) showed the symmetry from the disorder was not imposed by the centrosymmetric $C2/c$ space group. This space group was retained for the final refinements with methyl group and oxygen atom positions related by disorder, treated together. Individual weights based on counting statistics applied in the last cycles ($w = 1/\sigma^2(F) + 0.0002F^2$), and isotropic temperature factors of the hydrogen atoms fixed at U(phenyl H) = 0.07 Å^2 and U(methyl H) = 0.10 Å^2, gave the refinement indicators presented in Table 1.

In the case of **3**, a high residual peak beside the initial sulphur atom in the second ΔF map which showed disorder existed was assigned to a second sulfur atom position. The model including Sn and the two sulphur atoms (occupancy = 0.65/0.35) revealed nearly all the disorder associated with the *para*-thiophenyl group, there being two

Can. J. Chem. Downloaded from www.nrcresearchpress.com by 88.85.125.76 on 09/07/12
For personal use only.

Can. J. Chem. Downloaded from www.nrcresearchpress.com by 88.85.125.76 on 09/07/12
For personal use only.

orientations using C(1) and Sn as a common pivot. The disorder involving the $CH_3S(O)$— groups was considered next. Only one methyl group could be localised for each sulphur atom, indicating that the disorder involved the oxygen atoms. For the major occupancy model (**A**, 0.70(2)) two oxygen positions on each side of the C(4)—S—CH_3 plane were introduced at first, from the computed ΔF map, but on refinement that giving local *S*-chirality at the sulphur was further divided to account for large anisotropic temperature factors. In contrast, for the minor occupancy model (**B**, 0.30(2)) only one oxygen position (local *R*-chirality) could be found. Oxygen atoms corresponding to water molecules were found distributed over three special positions ($4f$) along the 4_2 screw axis with an occupancy ratio of 1:3:1, and the total occupancy giving $H_2O/Sn = 1.24 \pm 0.40$. In the final cycles, ten reflections suffering extinction were rejected and individual weights ($w = 1/\sigma^2(F)$) based on counting statistics were applied. Fixed hydrogen isotropic temperature factors at U(phenyl H) = 0.05 Å^2 and U(methyl H) = 0.07 Å^2 gave refinement indicators presented in Table 1.

Refined coordinates for all non-hydrogen atoms for both compounds are listed in Table 2 while selected bond lengths and angles are listed in Tables 3. The remaining data are on deposit.[3]

Results

The compounds reported here are best identified by their infrared spectra which may be compared with the spectrum of the starting material (**1**).[4] Even though complete assignments for $CH_3S(O_n)C_6H_5$ (n = 0, 1, 2) have been made (16) and the infrared spectrum of *p*-bromothioanisole was assigned earlier (17), enabling $CH_3SO(O_n)$— group absorptions to be readily identified, the oxidation states of sulphur atoms in the various products of *m*-CPBA oxidation were monitored empirically using the strong peaks labelled (⊕), (*), and (≠) in the spectra of **1**, **2**, and **3**, respectively. Only two of the many attempted preparations of **3** had infrared spectra with no peaks characteristic of CH_3S— or $CH_3S(O_2)$— groups. The NMR spectra (^1H, ^{13}C, ^{119}Sn; $CDCl_3$ solution) of both samples also showed that only *p*-methylsulphinyl groups were present in each case.

[p-$CH_3S(O_2)C_6H_4]_4Sn$ (2)

This is the first fully characterised tetra-aryltin with less than fourfold symmetry. However, the deviation is small with $I4_1/a$ being the related minimal non-isomorphic supergroup for the $C2/c$ space group (18). The two *p*-$CH_3S(O_2)C_6H_4$— parts of the asymmetric unit (Fig. 1) differ principally in the orientation of the ordered S=O bond of each *para*-substituent with respect to the adjacent phenyl ring (Table S5). The rings themselves show fewer changes from ideal benzene ring values (Table S6) than other phenylmetal systems (19). While intramolecular interactions involving ring *meta*-H atoms and adjacent methylsulphonyl group are significant, it is more likely that intermolecular interactions cause the differing geometries of the two $CH_3S(O_2)$— moieties. Molecules pack in the crystal by interleaving *p*-$CH_3S(O_2)C_6H_4$ groups attached to tins on parallel 2 axes (Fig. S2). With each *para*-substituent disordered (interchange of CH_3 with an O atom) each group may be characterised as *exo-* or *endo-* depending on the orientation of its methyl radical with respect the inversion centre relating neighbouring groups of different Ar_4Sn (Fig. S3). Many of the interatomic distances between the possible *exo–exo*, *endo–endo*, and *exo–endo* pairs of asymmetric units from adjacent molecules are less than van der Waals indicating considerable strain in the crystal lattice but most are still allowed (Table S7). The few which are clearly unrealistically short suggest complete disorder does not occur at these points in the crystal. However, any ordering is localised at each position and does not give rise to any long range order in the lattice which remains for all practical purposes completely disordered.

[p-$CH_3S(O)C_6H_4]_4Sn.n$-H_2O (3)

Compound **3** has the usual $\bar{4}$ molecular symmetry for tetraorganotins although a new space group, $P4_2/n$, is used. The asymmetric unit (Fig. 2) is almost completely disordered with only the Sn—C_{ipso} bond ordered. The phenyl ring of model (**A**) shows the elongation expected when attached to a metal atom (19) (Table S12) but the phenyl ring of the minor occupancy model (**B**) is not well defined. Thus the large distortions observed may simply be artefacts from the solution of the structure. In contrast the four well-defined $CH_3S(O)$— groups of the asymmetric unit agree with the infrared data (ν(S=O)) for **3** with the peak at 1052 cm^{-1} assigned to the shorter non-hydrogen bonded $\rangle$S=O moiety of model **B** (20, 21) while the three lower frequencies may be assigned to the three longer possibly hydrogen-bonded S=O bonds in model **A** (22–24). It must be noted, however, that lattice effects could account for the splitting of ν(S=O) seen here.

The hydrogen bonding noted above — the distinctive feature of this Ar_4Sn structure — involves water molecules lying on 4_2 axes parallel to the Ar_4Sn columns in the unit cell (Fig. S5). The water molecules occupy sites grouped in threes, although only one site in each group at a time can be occupied, giving $n \simeq 2$ with full occupancy. Since the sites are surrounded by pairs of methylsulphoxide groups (Fig. S6), inspection of shorter intermolecular distances (Table S14) shows that the methyl radical from a model **B** $CH_3S(O)$— group clearly prevents the occupation of these sites by water molecules. With each $CH_3S(O)$— group in the structure described by the orientation of the sulphoxide oxygen with respect to the adjacent water column as *exo-* (O(1A) or O(1B) or *endo-* (O(2A) or O(3A)), the possible H-bonding environments of the lattice water molecules (Table S15) include a water molecule held in place by (*a*) four, (*b*) two, or (*c*) one oxygen(s) from *endo*-sulphoxide groups. However, since neighbouring water molecules can also hydrogen-bond in the column, we may assume that if *both* surrounding $CH_3S(O)$— groups are described by model **A**, each group of three sites will be occupied by a water molecule giving an occupancy of 0.46–0.52 and $n = 0.98 \pm 0.06$. Whether an asymmetric unit is assigned to model **A** or **B** depends on the packing of pairs of units related by inversion centres in the unit cell. If both such $CH_3S(O_2)$— units are *exo-* conformation then only the d(O---O) value (2.73 Å) when *both* oxygens belong to the minor model **B** is physically reasonable, although this value still implies considerable intermolecular strain, which may account for the distortion of the phenyl ring of model **B**. If the two groups are *exo-* *endo-* then both may belong to model **A**, giving predicted occupancy factrns, model **A**, 0.75, and model **B**, 0.25, with $n = 1.125$, a value close to that given by water molecule occupancy factors. However, the occupancy factors

[3]Tables of H-atom positions, anisotropic temperature factors, observed and calculated structure factors, and least-squares planes data (S1-4; S8-11) and others referred to in the text, as well as Figs. S1—S6, may be purchased from the Depository of Unpublished Data, CISTI, National Research Council of Canada, Ottawa, Ont., Canada K1A 0S2.

[4]IR data (1350–450 cm^{-1}) for (*p*-$CH_3SC_6H_4)_4Sn$: 1320m, 1298w, 1252m, 1193m, 1113wm, 1102s, 1061vs, 1050wm, 1047sh, 1009s, sp, 967sm, 955m, 838w, 805vs, 783m, 731m ($\nu(CH_3—S)$), 709sm, 631w, (492, 490)vs, 467wm.

Can. J. Chem. Downloaded from www.nrcresearchpress.com by 88.85.125.76 on 09/07/12
For personal use only.

TABLE 2. Atomic coordinates and equivalent isotropic temperature factors for all non-hydrogen atoms of the two structures

(*a*) Compound **2**, $(p\text{-}CH_3SO_2C_6H_4)_4Sn$ (X,Y,Z, $\times 10^4$; Sn and Sn, $\times 10^5$; and U_{eq}, $\times 10^3$)

Atom	X	Y	Z	U_{eq}
Sn	50000	16735(5)	75000(8)	35
S(1)	72663(5)	77676(18)	87634(5)	53
S(2)	39417(6)	−38830(18)	97342(4)	57
O(11)	7670(2)	8463(7)	8337(2)	105
O(12)	7512(6)	6598(16)	9260(4)	94
O(13)	6985(5)	9397(16)	9088(5)	86
O(21)	4331(2)	−3312(6)	10242(1)	91
O(22)	3297(3)	−3316(23)	9746(8)	73
O(23)	3965(9)	−6105(8)	9587(7)	57
C(11)	5739(2)	3641(5)	7884(2)	37
C(12)	5628(2)	4896(6)	8363(2)	47
C(13)	6092(2)	6179(7)	8629(2)	49
C(14)	6672(2)	6183(6)	8405(2)	43
C(15)	6797(2)	4936(7)	7927(2)	51
C(16)	6327(2)	3643(6)	7663(2)	46
C(17)	7642(10)	5929(24)	9269(7)	94
C(18)	6872(9)	10078(22)	9013(8)	86
C(21)	4655(2)	−182(6)	8194(1)	39
C(22)	4141(2)	−1518(6)	8111(2)	48
C(23)	3916(2)	−2691(7)	8574(2)	51
C(24)	4220(2)	−2493(7)	9126(2)	43
C(25)	4736(2)	−1207(6)	9220(2)	48
C(26)	4952(2)	−46(6)	8753(2)	44
C(27)	3151(4)	−3073(36)	9776(13)	73
C(28)	3964(14)	−6706(11)	9594(12)	57

(*b*) Compound **3**, $(p\text{-}CH_3SOC_6H_4)_4Sn\cdot nH_2O$ (n = 1, 2) (X,Y,Z, $\times 10^4$; O $\times$ 10^3; and $U_{eq} \times 10^3$)

Atom	X	Y	Z	U_{eq}	Occupancy
SN	2500	2500	2500	31	0.25
S(A)	−814(3)	767(4)	−2831(8)	53	0.70
S(B)	−1047(12)	998(10)	−2650(33)	93	0.30
O(1A)	−52(2)	−18(2)	−345(4)	60	0.20
O(2A)	−169(2)	115(2)	−198(4)	75	0.25
O(3A)	−160(2)	96(2)	−136(4)	75	0.25
O(1B)	−73(2)	35(3)	−413(5)	118	0.30
O(10)	−250	250	132(5)	132	0.19
O(11)	−250	250	34(7)	132	0.06
O(12)	−250	250	247(7)	118	0.06
C(1)	1457(5)	1989(5)	664(12)	34	1.00
C(2A)	1580(11)	1266(8)	−755(12)	44	0.70
C(3A)	924(9)	893(8)	−1776(24)	47	0.70
C(4A)	92(14)	1238(12)	−1620(22)	40	0.70
C(5A)	−38(10)	1951(13)	−272(26)	55	0.70
C(6A)	640(14)	2318(12)	810(23)	45	0.70
C(7A)	−716(11)	1358(11)	−5199(27)	87	0.70
C(2B)	1597(31)	1387(24)	−855(59)	66	0.30
C(3B)	767(20)	1161(17)	−2000(44)	33	0.30
C(4B)	29(35)	1369(31)	−1178(51)	40	0.30
C(5B)	−198(24)	1975(31)	274(46)	48	0.30
C(6B)	594(24)	2191(32)	1359(50)	45	0.30
C(7B)	−1375(33)	2019(25)	−3837(54)	65	0.30

*$U_{eq} = (1/3)\sum_i\sum_j U_{ij}a_i^*a_j^*\mathbf{a}_i\cdot\mathbf{a}_j$.

Can. J. Chem. Downloaded from www.nrcresearchpress.com by 88.85.125.76 on 09/07/12
For personal use only.

TABLE 3. Selected bond distances and bond angles

(*a*) (p-$CH_3S(O_2)C_6H_4)_4Sn$

(*i*) Bond distances (Å)

Bond	Distance: Phenyl I (X = 1)	Distance: Phenyl II (X = 2)
Sn—C(X1)	2.150(3)	2.134(3)
S(X)—O(X1)	1.417(5)	1.432(4)
S(X)—O(X2)	1.421(10)	1.438(7)
S(X)—O(X3)	1.415(10)	1.421(6)
S(X)—C(X4)	1.773(4)	1.774(4)
S(X)—C(X7)	1.782(17)	1.789(11)
S(X)—C(X8)	1.781(16)	1.782(8)

(*ii*) Bond angles (deg)

Bonds	Angle	Bonds	Angle
C(11)—Sn—C(11)[a]	110.77(13)	C(21)—Sn—C(21)[a]	114.68(13)
C(11)—Sn—C(21)	106.80(13)	C(11)—Sn—C(21)[a]	108.90(13)

Bonds	Angle: Phenyl I (X = 1)	Angle: Phenyl II (X = 2)
Sn—C(X1)—C(X2)	118.8(3)	122.4(3)
Sn—C(X1)—C(X6)	121.4(3)	119.1(2)
S(X)—C(X4)—C(X3)	118.3(3)	120.3(3)
S(X)—C(X4)—C(X5)	120.2(3)	118.2(3)
C(X4)—S(X)—O(X1)	108.1(2)	107.7(2)
C(X4)—S(X)—O(X2)	107.8(5)	105.9(6)
C(X4)—S(X)—O(X3)	108.5(4)	105.5(6)
C(X4)—S(X)—C(X7)	103.2(6)	106.2(7)
C(X4)—S(X)—C(X8)	104.4(6)	108.8(8)
O(X1)—S(X)—O(X2)	119.4(5)	116.1(6)
O(X1)—S(X)—O(X3)	116.6(5)	113.8(6)
O(X1)—S(X)—C(X7)	111.5(6)	113.4(7)
O(X1)—S(X)—C(X8)	107.7(6)	111.6(8)
O(X2)—S(X)—C(X8)	108.4(7)	106.3(9)
O(X3)—S(X)—C(X7)	108.0(7)	109.5(9)

(*b*) (p-$CH_3S(O)C_6H_4)_4Sn.nH_2O$

(*i*) Bond distances (Å)

Bond	Distance: Model **A** (X = A)	Distance: Model **B** (X = B)
Sn—C(1X)	2.136(8)	
C(4X)—S(X)	1.75(2)	1.99(5)
S(X)—C(7X)	1.77(2)	1.82(4)
S(X)—O(1X)	1.57(3)	1.46(4)
S(X)—O(2X)	1.58(3)	
S(X)—O(3X)	1.56(3)	

TABLE 3. (*concluded*)

(*ii*) Bond angles (deg)

Bonds	Angle	Bonds	Angle
C(1)—Sn—C(1)[b]	113.3(3)	C(1)—Sn—C(1)[c]	107.6(3)

Bonds	Angle: Model **A** (X = A)	Angle: Model **B** (X = B)
Sn—C(1X)—C(2X)	122.7(7)	121(2)
Sn—C(1X)—C(6X)	121.2(9)	116(2)
C(3X)—C(4X)—S(X)	122.5(13)	118(3)
C(5X)—C(4X)—S(X)	118.7(14)	107(3)
C(4X)—S(X)—C(7X)	95.6(8)	100(2)
C(4X)—S(X)—O(1X)	112.0(12)	103(2)
C(4X)—S(X)—O(2X)	105.5(13)	
C(4X)—S(X)—O(3X)	105.8(12)	
C(7X)—S(X)—O(1X)	99.9(11)	115(2)
C(7X)—S(X)—O(2X)	103.9(13)	
C(7X)—S(X)—O(3X)	118.5(12)	

[a] $1 - x, y, 3/2 - z$.
[b] $1/2 - x, 1/2 - y, z$.
[c] $1/2 + x, y, 1/2 + z$.

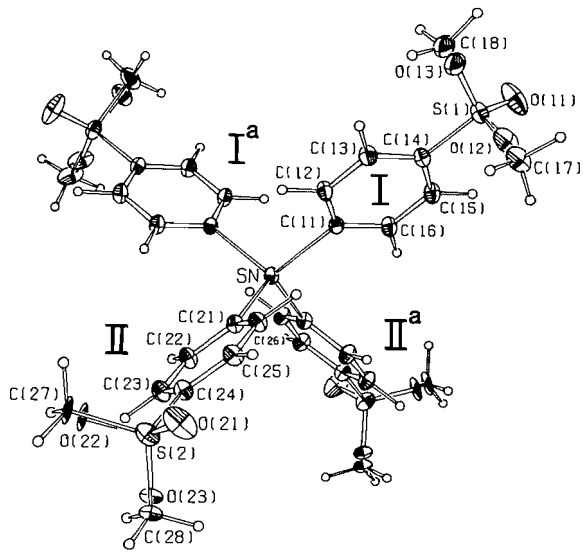

FIG. 1. View of the disordered (p-$CH_3S(O_2)C_6H_4)_4Sn$ molecule shown perpendicular to the 2 axis (*a*: $1 - x, y, 3/2 - z$) with the numbering scheme used for the structure.

for the two models of the asymmetric unit are better defined and on this basis we consider compound **3** is best described as a mono-hydrate.

Discussion

Empirical force field calculations (25) indicate that ground state isolated Ar_4Sn molecules will have $\bar{4}$ symmetry while Kitaigorodsky earlier proposed (26*a*) that the most efficient close packing of such quasi-spherical $\bar{4}$ molecules requires the use of tetragonal space groups with $I\bar{4}$, $P42_1c$, and $P4_2/n$ preferred. In addition, he predicted that as larger and more complex *para*-substituents make the Ar_4Sn less spherical, less

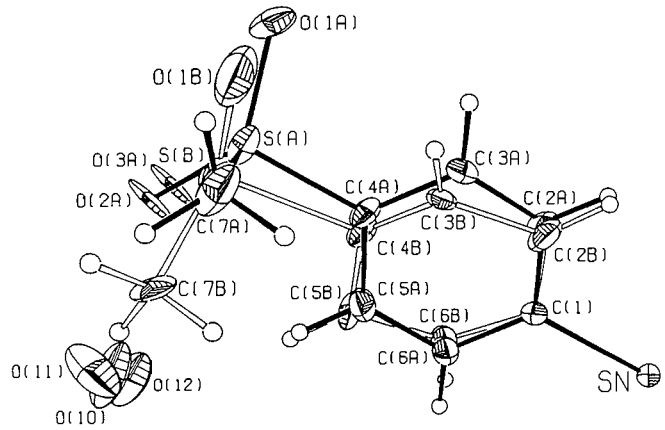

FIG. 2. The asymmetric unit, with numbering scheme, for (p-$CH_3S(O)C_6H_4)_4Sn.nH_2O$; darkened bonds stand for the major occupancy model **A**.

symmetric space groups would be favoured with a concomitant lowering of molecular symmetry. The structure of **2** is consistent with those predictions. Furthermore, since the molecule with the disorder seen here could easily have $\bar{4}$ symmetry, it is presumably the need for efficient crystal packing which determines the choice of space group.

In contrast, compound **3** with *para*-groups of similar size and complexity crystallises in the previously unused close-packed tetragonal space group, $P4_2/n$, and retains $\bar{4}$ molecular symmetry. Presumably the hydrogen bonding network promotes dense packing in the lattice even though when neighbouring *exo*-$CH_3S(O)$— groups interact, the considerable steric strain has to be relieved by distorting the full asymmetric unit. The exact amount of H-bonding (and degree of hydration) is therefore a balance between the increased lattice energy it creates and the unfavourable energy changes due to the larger intermolecular repulsions and phenyl ring distortions required. The importance of bulky *para*-substituents is shown also by the crystal data for (p-$EtOC_6H_4)_4Sn$ (26*b*, 27). However, the space group ($P2_1/a$) is not related to any tetragonal space group, and since tin atoms lie on general positions, a more detailed analysis of this structure is clearly necessary.

Acknowledgements

The financial support of the "fonds FCAR, Programme ACSAIR" of the Government du Québec is gratefully acknowledged. The authors (I.W., H.L.) also thank Professor M. Onyszchuk, McGill University, for the use of his laboratory, where part of this work was carried out.

1. I. WHARF. Inorg. Chim. Acta, **159**, 41 (1989).
2. I. WHARF and M. G. SIMARD. J. Organomet. Chem. **332**, 85 (1987) and references therein.
3. V. K. BELSKY, A. A. SIMONENKO, V. O. REIKHSFELD, and I. E. SARATOV. J. Organomet. Chem. **224**, 125 (1983).
4. T. DURST. *In* Comprehensive organic chemistry. Vol. 3. Part 11. *Edited by* D. N. Jones. Pergamon, Oxford. 1979. (*a*) p. 174; (*b*) pp. 124–126.
5. I. C. PAUL, S. M. JOHNSON, L. A. PAQUETTE, J. H. BARRETT, and R. J. HALUSKA. J. Am. Chem. Soc. **90**, 5023 (1968).
6. J. BERTHOU, G. JÉMINET, and A. LAURENT. Acta Crystallogr. B**28**, 2480 (1972).
7. C. O. HAAGENSEN. Acta Crystallogr. B**34**, 3143 (1978).
8. I. TICKLE, J. HESS, A. VOS, and J. B. F. N. ENGBERTS. J. Chem. Soc. Perkin Trans. II, 460 (1978).
9. L. A. PAQUETTE, P. CHARUMILIND, M. C. BOHM, R. GLEITER, L. S. BLASS, and J. CLARDY. J. Am. Chem. Soc. **105**, 3136 (1983).
10. J. M. M. SMITS, P. T. BEURSKENS, J. R. M. SMITS, V. PARTHASARATHI, A. A. M. HOUWEN-CLAASSEN, and A. J. H. KLUNDER. J. Crystallogr. Spectrosc. Res. **18**, 1 (1988).
11. N. M. BLATON, O. M. PEETERS, and C. J. DERANTER. Cryst. Struct. Commun. 1357 (1982).
12. C. HOUTTEMANE, J. C. BOIVIN, G. NOWOGROCKI, D. J. THOMAS, J. P. BONTE, and M. DEBAERT. Acta Crystallogr. C**39**, 585 (1983).
13. R. A. AMOS. J. Org. Chem. **50**, 1311 (1985).
14. I. WHARF. Can. J. Spectrosc. **31**, 27 (1986).
15. I. WHARF, L. PIEHLER, B. M. SAILOFSKY, M. ONYSZCHUK, and M. G. SIMARD. Can. J. Chem. **65**, 639 (1987).
16. M. BOUQUET, G. CHASSAING, J. CORSET, J. FAVROT, and J. LIMOWZI. Spectrochim. Acta, **37**A, 727 (1981).
17. J. H. S. GREEN, D. J. HARRISON, W. KYNASTON, and D. W. SCOTT. Spectrochim. Acta, **26**A, 1515 (1970).
18. T. HAHN (*Editor*). International tables for crystallography. Vol. A. D. Reidel Publishing Co., Boston, MA. 1983. p. 183.
19. M. R. CHURCHILL, K. L. KAIRA, and M. Y. VERDIS. Inorg. Chem. **12**, 1656 (1973).
20. V. DE LA CAMP and H. HOPE. Acta Crystallogr. B**26**, 846 (1970).
21. A. DUCSMAN, I. KAPOVITS, I. KÖVESDI, A. KALMAN, and L. PARKANYI. J. Mol. Struct. **127**, 135 (1985).
22. B. DAHLEN. Acta Crystallogr. B**29**, 595 (1973); B**30**, 642 (1974).
23. F. TODA, K. TANAKA, and T. C. W. MAK. Chem. Lett. 2085 (1984).
24. P. CHARPIN, E. DUÑACH, H. B. KAGAN, and F. R. THEOBALD. Tetrahedron Lett. **27**, 2989 (1986).
25. M. G. HUTCHINGS, J. D. ANDOZE, and K. MISLOW. J. Am. Chem. Soc. **97**, 4553 (1975).
26. A. I. KITAIGORODSKY. Organic chemical crystallography. Consultants Bureau, New York, NY. 1961. (*a*) p. 120; (*b*) p. 406.
27. I. G. ISMAILZADE and G. S. ZHDANOW. Dokl. Akad. Nauk. SSSR. **68**, 95 (1949).

Can. J. Chem. Downloaded from www.nrcresearchpress.com by 88.85.125.76 on 09/07/12
For personal use only.

Electrochemical preparation and properties of the mixed-crystalline hexavanadates $M_xM'_{4-x}V_6O_{16}$, M, M' = NH_4, K, Rb, Cs

E. ANDRUKAITIS, P. W. M. JACOBS, AND J. W. LORIMER[1]

Department of Chemistry, The University of Western Ontario, London, Ont., Canada N6A 5B7

Received December 21, 1989

E. ANDRUKAITIS, P. W. M. JACOBS, and J. W. LORIMER. Can. J. Chem. **68**, 1283 (1990).

Coherent deposits of oriented, crystalline $M_xM'_{4-x}V_6O_{16+\delta}$, with M, M' = K, Rb, Cs, or NH_4, $0.0 \leq x \leq 4.0$ and $0.00 \leq \delta \leq 0.13$, have been prepared electrochemically on various conducting substrates from metavanadate solutions containing ammonium or alkali metal cations, singly or in combination. Chemical analysis and X-ray diffraction show that the deposits consist of a continuous series of mixed crystals based on the isomorphic end members $M_4V_6O_{16}$ and $M'_4V_6O_{16}$.

The deposits can be oxidized electrochemically, with removal of M and M' atoms, and the products can be used as cathodes for insertion of lithium, with the largest capacity achieved about 1.0 mol% of total vanadium. Cycling of the electrodes improves capacity, with insertion of lithium reaching 25 mol% of total vanadium. This gain in capacity results from further removal of alkali metal or ammonium ions from the electrode during the oxidation step of the cycling process.

The results extend the range of composition of homogeneous phases in the system $(NH_4)_2O$–K_2O–V_2O_4–V_2O_5.

Key words: alkali metal hexavanadates, electrochemical preparation.

E. ANDRUKAITIS, P. W. M. JACOBS et J. W. LORIMER. Can. J. Chem. **68**, 1283 (1990).

On a préparé des dépôts cohérents qui contiennent des cristaux orientés de $M_xM'_{4-x}V_6O_{16+\delta}$, avec M, M' = K, Rb, Cs ou NH_4, $0{,}0 \leq x \leq 4{,}0$ et $0{,}00 \leq \delta \leq 0{,}13$, par la méthode de voltammétrie cyclique sur des substrats divers et dans des solutions de metavanadates qui contiennent des cations des métaux alcalins ou d'ammonium seuls ou des combinations de tels ions. L'analyse chimique et la diffraction des rayons X ont démontré que les dépôts comprennent une série continue de cristaux mixtes basée sur les membres terminaux $M_4V_6O_{16}$ et $M'_4V_6O_{16}$.

L'oxydation électrochimique mène à une perte d'atomes M, et la réduction suivante rend possible l'insertion de lithium, avec une capacité maximum de 1 mol% du vanadium total. La voltammétrie cyclique a réussi à agrandir la capacité jusqu'à 25 mol% du vanadium total. Cet agrandissement résulte de la perte supplémentaire de M^+ et de NH_4^+ de l'électrode pendant l'étape d'oxydation.

Les résultats prolongent le domaine de composition des phases homogènes dans le système $(NH_4)_2O$–K_2O–V_2O_4–V_2O_5.

Mots clés : hexavanadates de métaux alcalins, préparation électrochimique.

Can. J. Chem. Downloaded from www.nrcresearchpress.com by 91.121.58.235 on 09/07/12
For personal use only.

Introduction

Vanadium oxides are useful materials for use as cathodes in lithium batteries (1); lithium ions can be inserted into the oxides during discharge, and removed during charge. Previous work from this laboratory (2–4) has been concerned with preparation of pure vanadium oxides via electrochemical deposition to form coherent deposits which can be used directly as electrodes. This method of preparation has potential advantages over other methods for both fundamental and practical studies: the electrodes are free of the customary, but extraneous, polymeric binders and materials to enhance conductivity. The route of preparation involves electrodeposition of diammonium (2) or tetraammonium hexavanadates (3) or vanadium pentoxide gels (4).

Mixed-valence alkali metal hexavanadates have been made by melting metal oxide and a vanadium oxide at high temperature (5, 6), and the corresponding ammonium compounds have been prepared by controlled precipitation and oxidation in solution (7). Regions of existence have also been established in part for the system $M_2O \cdot VO_2 \cdot V_2O_5$, where M = K or NH_4 (5–7). As an alternate route to synthesis of similar compounds, Goncharenko and Suvorova (8) deposited a mixed-valence vanadium oxide hydrate with approximate formula $3K_2O \cdot 2VO_2 \cdot 5V_2O_5 \cdot 15H_2O$ on a platinum cathode at room temperature. The electrochemical properrties of this material, especially as an insertion cathode for lithium, have not been investigated. The anodic deposition of diammonium hexavanadate near room temperature and its use in insertion electrodes (2) led to a reinvestigation of the work of Goncharenko, and it was found that the cathodic deposits actually consisted of $M_4V_6O_{16}$, where M = NH_4 or K (3). Either the diammonium or tetraammonium hexavanadates, prepared at or near room temperature, can be decomposed by controlled heating to V_2O_5 and to other oxides in which vanadium has mixed oxidation states, but maintain their coherence on the substrate.

In the course of investigation of the cathodic deposits (3), it was found possible to prepare, by electrochemical methods, new mixed-crystal hexavanadates of general formula $M_xM'_{4-x}V_6O_{16}$, with M, M' = K, Rb, Cs, or NH_4. This paper gives detailed chemical and X-ray analyses of several members of the mixed crystalline series, including the new Rb and Cs end members, and also gives some results on their electrochemical properties, especially those relating to ion insertion.

Experimental

The materials and methods of analysis were as described previously (2, 3). Solutions of K, Rb, or Cs metavanadates were prepared by adding stock 1 mol/L RbOH or CsOH to a saturated aqueous solution of NH_4VO_3, followed by boiling to remove ammonia. Solutions of RbOH or CsOH were prepared by passing a solution of RbCl or CsCl through an ion exchange column (in hydroxide form) or from commercial aqueous RbOH or CsOH solutions (50 mass%). Solutions containing both K^+ and NH_4^+ were made by saturating a solution with NH_4VO_3 at 40°C and adding K_2SO_4 to various concentrations of 0.0, 0.05, 0.10, and 0.5 mol/L. Mixtures of various combinations of Cs^+ with NH_4^+, Rb^+ or K^+, and Rb^+ with K^+ were made by combining these vanadate solutions in the desired proportions.

Electrochemical depositions used a cell operated at 40°C with platinum electrodes and one of the above solutions as electrolyte. Both constant current, density 0.1 mA/cm^2, or cyclic voltammetry, at scan rate 50 mV/s between potentials 0.0 and −0.7 V (SCE) for about 2000 cycles, were used to prepare deposits. Potentials and currents

[1]To whom correspondence should be addressed.

Can. J. Chem. Downloaded from www.nrcresearchpress.com by 91.121.58.235 on 09/07/12
For personal use only.

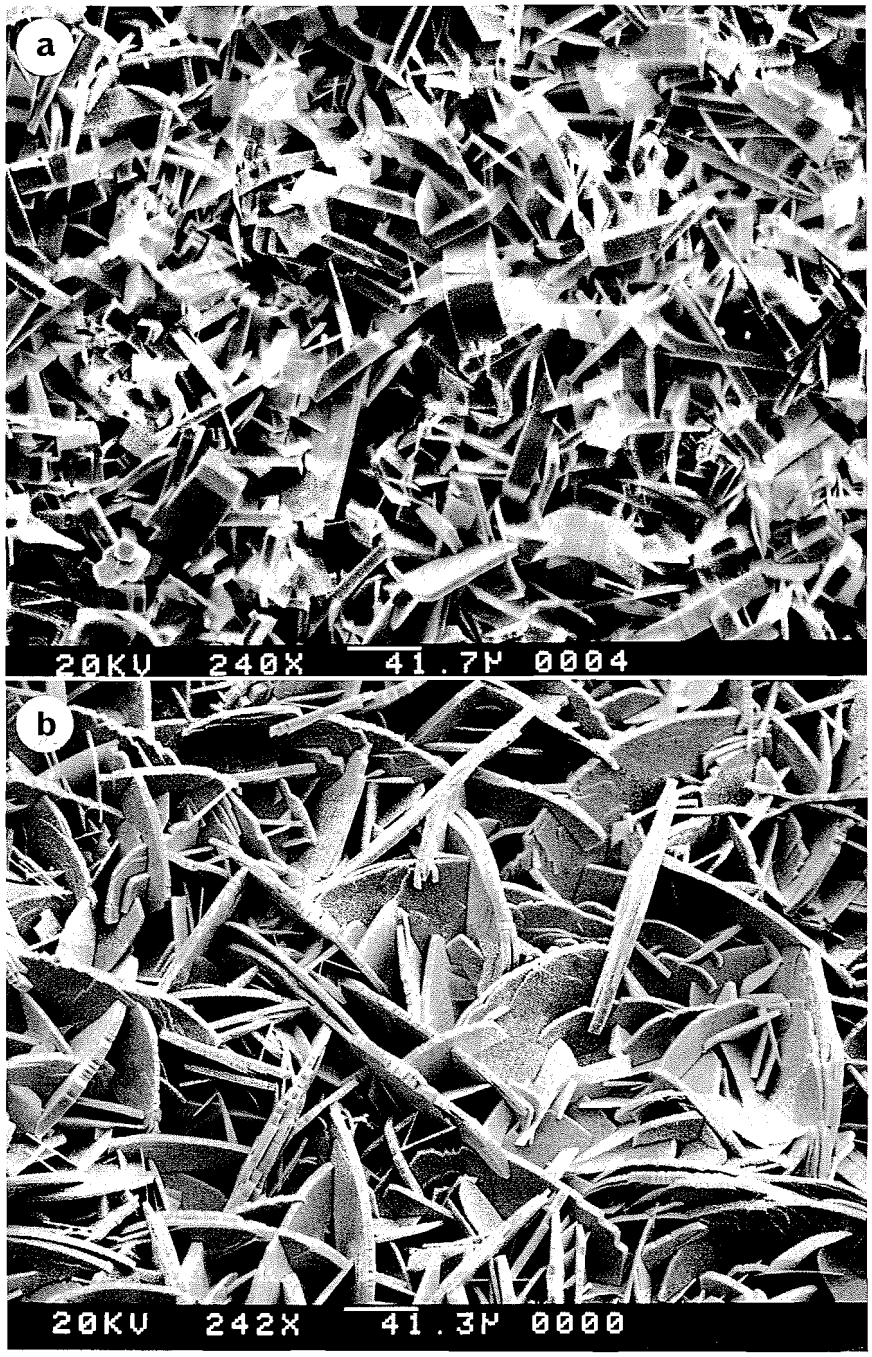

FIG. 1. SEM photographs of cathodic electrodeposits. (*a*) $Rb_4V_6O_{16}$ from $RbVO_3$ solution. Magnification ×240, bar length 41.7 μm. (*b*) $Cs_4V_6O_{16}$ from $CsVO_3$ solution, ×380, bar 26.3 μm.

were applied using a PAR Model 273 potentiostat interfaced to a microcomputer and graphics plotter.

The deposits were analyzed by scanning electron microscopy (SEM), with simultaneous energy-dispersive X-ray analysis (EDX). Direct X-ray diffraction of the deposits on their substrates was performed on a Rigaku rotation anode diffractometer (Bragg-Brentano focussing, curved graphite single crystal monochromator) using Cu $K\alpha_1$ radiation, $\lambda = 0.15405$ nm. Diffraction patterns were analyzed by iterative least squares to obtain refined values of the lattice parameters. Chemical analyses (2, 3) were done for NH_4 by the Kjeldahl method, for NH_4, K, Rb, and Cs by the gravimetric tetraphenylborate method, and for total vanadium, V(IV) and V(V) by redox titration (2). Densities were measured using a Berman density balance, with toluene as the buoyancy liquid, to which a drop of Triton X-100 was added to improve wetting.

All ion insertions were performed at constant current. Open circuit measurements of the potential were made for the insertion of lithium into the deposits and for cycles of oxidation–reduction to study insertion of lithium after an oxidation step; here a solution of 0.1 mol/L $LiClO_4$ in dry propylene carbonate was used, with a Ag–AgCl reference electrode (potential 3.550 V vs. Li^+/Li). The following sequence was controlled by computer. Constant current, density between 0.1 to 1 mA/cm^2, was passed for a measured time. The current was then turned off, the cell was allowed to equilibrate under

TABLE 1. Chemical and gravimetric analysis of deposits made by constant current (0.1 mA/cm^2) at a Pt cathode from saturated aqueous vanadate solutions at 40°C

Solution (mass/mg sample)	EDX analysis	Mass% of ion	Mole ratio V(IV)/V(V)	Mass% total V	Formula of deposit from analysis
NH_4VO_3	No alkali metal ion	11.385 11.35[a]	0.4771	48.30	$(NH_4)_{3.994}V_6O_{15.95}$ $(NH_4)_{3.982}V_6O_{15.46}$
KVO_3	K only	21.78	0.4728	42.52	$K_{4.004}V_6O_{16.04}$
$RbVO_3$	Rb only	37.84	0.4535	33.75	$Rb_{4.009}V_6O_{16.08}$
$CsVO_3$	Cs only	48.70	0.4948	30.1	$Cs_{4.013}V_6O_{15.84}$[b]

[a]Analyzed by volumetric Kjeldahl method.
[b]Composition calculated assuming charge balance; see text.

TABLE 2. Chemical analysis of deposits made galvanostatically, current density 0.1 mA/cm^2, from a solution of NH_4VO_3 (0.2 mol/L + specified concentrations of K_2SO_4), 40°C

Solution of 0.2 M NH_4VO_3 + K_2SO_4 (mol/L)	Mass% NH_4^+	Mass% V(IV)	Mass% total V	$(NH_4)_xK_{4-x}V_6O_{16+\delta}$ values in formula		EDX value $4-x$
				x	δ	
No K_2SO_4	11.33	15.6	48.3	3.990	0.028	0.02
0.048	7.71	15.2	46.2	2.820	0.010	1.32
0.096	5.94	14.9	45.4	2.214	0.012	1.78
0.57	1.90	13.9	43.3	0.744	0.036	3.20
KVO_3 only	0.00	13.3	42.3	0.000	0.056	4.00[a]

[a]Assuming $x = 0$ for deposit from KVO_3 solution for comparison with chemical analysis (see text).

stirring for 1 min, then the open circuit potential was measured after stirring was stopped. Current was again passed, and the procedure was repeated until the maximum insertion of lithium had occurred.

Results and discussion

Formation and nature of deposits

(a) Phases containing a single alkali metal or ammonium cation

Details of the formation and morphology of cathodic deposits of the single phases tetraammonium and tetrapotassium hexavanadate, $(NH_4)_4V_6O_{16+\delta}$ and $K_4V_6O_{16+\delta}$, have been described elsewhere (3). The black deposits formed on platinum were usually grown to thicknesses up to 100 μm, with a surface density up to about 10 mg/cm^2. SEM photographs of the deposit made in solutions of KVO_3 and NH_4VO_3 have been given in ref. 3; the deposits made from solutions of $RbVO_3$ and $CsVO_3$ are shown in Figs. 1(*a*) and (*b*). SEM shows the crystals to have a preferred orientation with length about 50 μm and thickness about 5–10 μm. From NH_4VO_3 solution (3), the crystals are uniform in size (about 50 × 5 μm) and shape, with form and orientation the same as for anodic electrodeposits (2) with respect to their faces, but with a higher packing density. From KVO_3 solutions (3), densely-packed deposits are also formed; rosette-shaped crystalline masses, which appear to arise from secondary nucleation and growth at long electrolysis times, overlie a finer-grained deposit. $RbVO_3$ solutions tend to give much thicker crystals, Fig. 1(*a*), which vary in size from about 5 × 50 μm to 50 × 50 μm square, with a range of 5–50 μm in thickness. For $CsVO_3$ solutions, the deposit is shown in Fig. 1(*b*); the crystals are uniform in size (about 100 × 5 μm).

Chemical analyses after air drying are given in Table 1. The tetrarubidium and tetracesium hexavanadates have not been reported previously. While gravimetric analysis cannot distinguish between the alkali metal ions K, Rb, or Cs, EDX confirmed that only one type of alkali metal ion was present in each case. The general formula can therefore be written $M_aV(IV)_bV(V)_cO_d$, where M = K, NH_4, Rb, or Cs. The analytical data for the NH_4, K, and Rb compounds permit calculation of the ratios a/c, b/c, and d/c, and these values (normalized to $b + c = 6$) are given in Table 1. The ratio of total vanadium to metal or ammonium is stoichiometric for $M_4V_6O_{16}$ (*i.e.*, 1.5) within the experimental error of about 0.3%. Charge balance ($2d/c = a/c + 4b/c + 5$) is also satisfied to 0.5% or better. However, the mole ratio V(IV)/V(V) is variable, and is therefore the only source of non-stoichiometry. In the case of the Cs compound, samples of only about 15 mg were available, so the analysis for vanadium is inaccurate. The values in Table 1 for Cs have therefore been found by assuming charge balance. The formula can thus be written $M_4V(IV)_bV(V)_{6-b}(V)O_d$, with $(b + c)/a = 6$ and again normalized to $b + c = 6$, as above, which gives $d = 17 - b/2 = 16 + \delta$. The data in Table 1 and from other experiments give $-0.05 \leq \delta \leq 0.13$, so that departures from ideal stoichiometry are small.

(b) Mixed crystal phases containing two alkali metal or ammonium cations

Only minor differences in packing and crystal morphology are found in deposits made from solutions containing either single alkali metal or ammonium vanadates or their mixtures. Chemical analyses of several deposits formed at varying ratios of K^+ to NH_4^+ are given in Table 2 and of Cs^+ to NH_4^+ in Table 3. Varying the concentration of K^+ in solution produces a continuous series of mixed crystals of formula

Can. J. Chem. Downloaded from www.nrcresearchpress.com by 91.121.58.235 on 09/07/12
For personal use only.

Can. J. Chem. Downloaded from www.nrcresearchpress.com by 91.121.58.235 on 09/07/12
For personal use only.

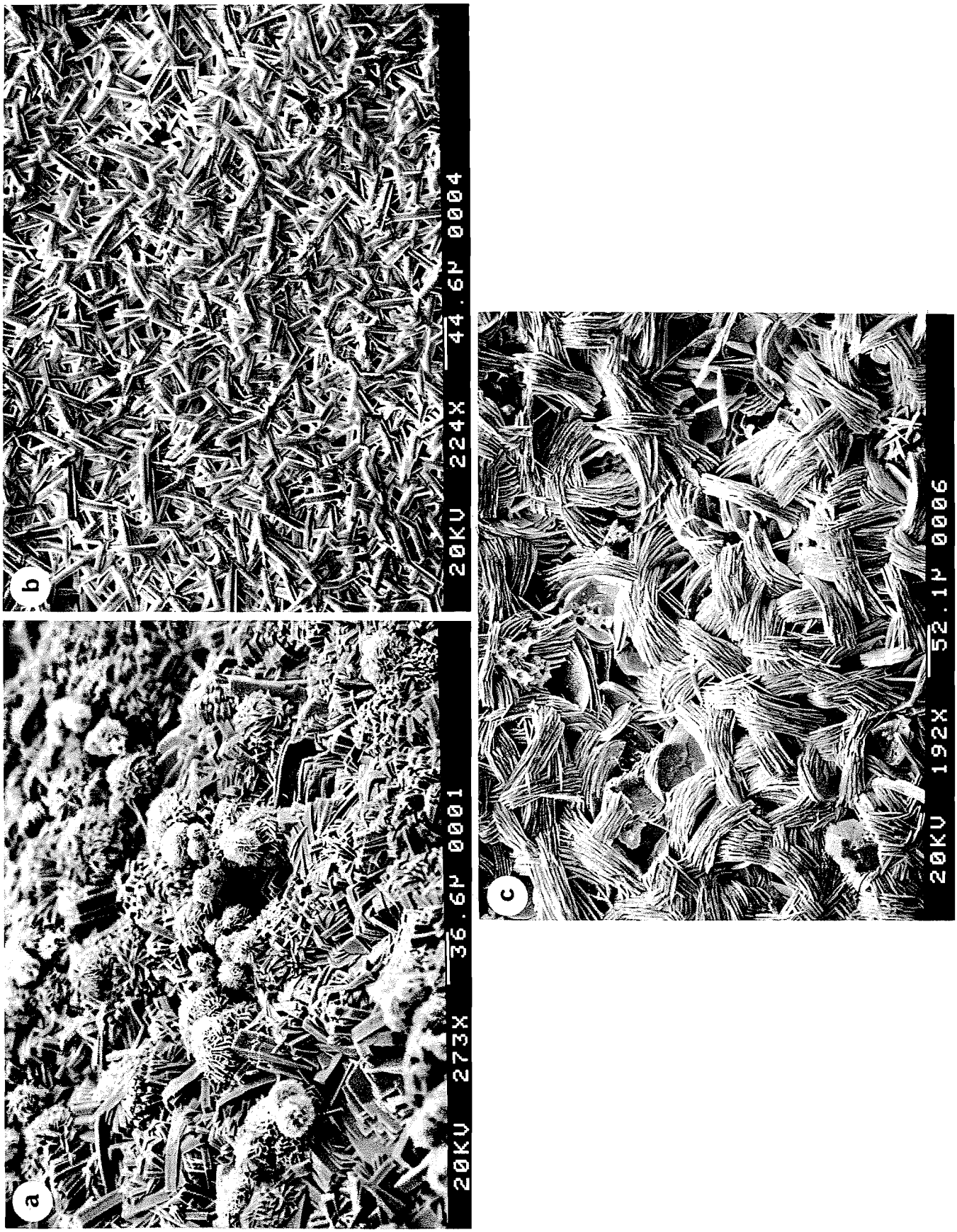

FIG. 2. SEM photographs of cathodic electrodeposits. (*a*) $K_{1.33}Rb_{2.67}V_6O_{16}$. Magnification ×273, bar length 37 μm. (*b*) $K_2Cs_2V_6O_{16}$, ×224, bar 45 μm. (*c*) $K_{1.33}Cs_{2.67}V_6O_{16}$, ×192, bar 52 μm.

TABLE 3. Chemical analysis of deposits made galvanostatically, current density 0.1 mA/cm^2, from a solution of NH_4VO_3 and $CsVO_3$, 0.2 mol/L, 40°C

Solution of 0.1 M NH_4VO_3 + $CsVO_3$ (mol/L)	Mass% NH_4^+	Mass% V(IV)	Mass% total V	$(NH_4)_xCs_{4-x}V_6O_{16+\delta}$ values in formula for x	δ	EDX value $4-x$
No $CsVO_3$	11.33	15.6	48.3	3.990	0.028	0.00
0.1	3.99	10.1	34.8	1.92	0.130	2.18
0.2	2.45	10.95	33.5	1.28	0.02	2.84
$CsVO_3$ only	0.00	9.98	30.3	0.00	0.014	4.00[a]
$RbVO_3$ only	0.27	10.36	33.9	0.12	0.082	Only Rb present

[a]Assuming $x = 0$ for deposit from $CsVO_3$ solution for comparison with chemical analysis (see text).

$(NH_4)_xM_{4-x}V_6O_{16+\delta}$, where M = K or Cs, $0.00 \leq \delta \leq 0.13$ and $0.0 \leq x \leq 4.0$. Similar phases $M_xM'_{4-x}V_6O_{16+\delta}$, with $M \neq M' = K$, Rb, Cs, NH_4 can also be made from appropriate combinations of starting solutions. If only NH_4VO_3 is present, tetraammonium hexavanadate is formed, but as the amount of $M' = K^+$, Rb^+, or Cs^+ increases in solution, the value of x decreases continuously until in an $M'VO_3$ solution $x = 0$ is reached, corresponding to $M'_4V_6O_{16}$. Again δ varies over the small range 0.00 to 0.13, with a mean value for all analyses of 0.08. The amounts of K, Rb, and Cs were not determined because of interference of NH_4^+, which is always present to some extent as an unavoidable contaminant; their values $4 - x$ were found by difference from the amount of ammonium (x). However, semi-quantitative estimation of the mole ratio of alkali metal ion to total vanadium can be obtained from EDX. In $(NH_4)_xK_{4-x}V_6O_{16+\delta}$, the absolute error is large (>10%), but the presence of K^+ is confirmed. If the value $x = 0$ is assigned to the deposit from KVO_3 solution (*i.e.*, $K_4V_6O_{16}$), the EDX values show the same trend as the chemical analyses with better than 2% agreement for the three intermediate mixed cation phases analyzed, Table 2. For the two phases $(NH_4)_xCs_{4-x}V_6O_{16+\delta}$ in Table 3, EDX confirms the presence of Cs^+, but the agreement for the mole ratios is poorer; the large atomic weight of Cs makes analysis of NH_4^+ and V less accurate for a given sample size.

In SEM photographs of deposits containing both K and NH_4 (6), a large amount of secondary nucleation and growth was apparent as overlying rosette-shaped crystalline masses. The underlying layer was similar to that for the corresponding phases containing only a single type of ion. For deposits containing both K and Rb, a change in the mole ratio K/Rb from 1/2 to 2, Fig. 2(*a*), causes no perceptible change in overall crystal morphology. However, for deposits containing both K and Cs, Fig. 2(*b*,*c*), a mole ratio K/Cs of 1 produces rod-shaped crystals, while a ratio of 1/2 produces compact stacks of thin sheets.

(c) X-ray analyses of phases containing alkali metal or ammonium cations

X-ray diffraction data are given in Table 4 for the new compounds $Rb_4V_6O_{16}$ and $Cs_4V_6O_{16}$. The assumption that the unit cell is tetragonal, as in the corresponding K and NH_4 compounds, leads to successful indexing by iterative least squares. Of 35 observed lines, there are 19 matches between the Rb and Cs compounds; note the interchange in *d*-spacing between the (312) and (411) reflections. Table 5 summarizes the unit cell dimensions and densities, the latter showing that there are always two formula units in the unit cell. The measured densities tend to be somewhat less than those calculated from the unit cell dimensions because of the difficulty in wetting the very small crystals in the buoyancy liquid.

The ionic radii of Cs^+, Rb^+, NH_4^+, and K^+ are 0.166, 0.149, 0.146, and 0.134 nm, respectively, obtained (for consistency) by subtracting the Pauling radius for Cl^- (0.181 nm) from the interionic distances in alkali metal or ammonium chloride crystals with the NaCl structure (9). Plots of the a lattice dimension and the volume a^2c of the unit cell are linear in the ionic radius, as shown in Fig. 4, but the dimension c (the V—O layers lie in the [001] plane) increases more rapidly at smaller ionic radii. For comparison, the lattice dimensions a, b, c and volume for the monoclinic dimetal and diammonium hexavanadates, $M_2V_6O_{16}$, are given; for these, the V—O layers lie in the [100] plane and the monoclinic angle $\beta = 96.75°$ is constant (10). Thus, as expected, the expansion on adding larger cations is mainly in a direction perpendicular to the interplanar spacing between sheets of V and O atoms for both di- and tetrametalhexavanadates. Also as expected, for a particular insertion cation, the volumes of the unit cells for $M_4V_6O_{16}$ are larger than those for $M_2V_6O_{16}$, the difference increasing slightly as the cation becomes larger.

The vanadate phases containing a mixture of pairs of K, Rb, Cs, and NH_4 have not been described before. Because x varies continuously, only a few X-ray patterns with accompanying chemical analyses will be given. Table 5 gives lattice parameters for phases that have been analyzed by EDX and by chemical methods; the experimental diffraction patterns for $(NH_4)_xK_{4-x}V_6O_{16}$, with $x = 0.000$, 0.744, 2.114, 2.820, and 3.990, are given in Fig. 3. The progression from one pure phase to the other as NH_4^+ is replaced by K^+ is apparent: all major peaks in the one phase can be seen in the other, with minor shifts in their diffraction angles.

Plots of the lattice parameters and volume are almost linear in x in $M_{4-x}K_xV_6O_{16}$, Fig. 5, which is to be expected for completely random mixing of the two different ions on their lattice sites. The width of the diffraction peaks is greatest near $x = 2$, *i.e.*, equal proportions of M and M′ atoms, indicating a diminution of long-range order when two cations are present.

Sodium or lithium metavanadate solutions do not yield electrodeposits containing these two ions. Some reasons for this behaviour have been discussed elsewhere (2).

Can. J. Chem. Downloaded from www.nrcresearchpress.com by 91.121.58.235 on 09/07/12
For personal use only.

Can. J. Chem. Downloaded from www.nrcresearchpress.com by 91.121.58.235 on 09/07/12
For personal use only.

TABLE 4. X-ray diffraction of polycrystalline tetrarubidium hexavanadate, $Rb_4V_6O_{16.02}$, and tetracesium hexavanadate, $Cs_4V_6O_{16.02}$

			$Rb_4V_6O_{16.02}$					$Cs_4V_6O_{16.02}$			
				d-spacing/nm				*d*-spacing/nm			
h	*k*	*l*	θ/degree	Obs.	Calc.	Relative intensity	θ/degree	Obs.	Calc.	Relative intensity
2	0	0	9.99	0.444	0.4452	4				
1	1	1					10.235	0.4335	0.4337	11
2	1	0					11.145	0.3985	0.3998	12
2	0	1	12.84	0.347	0.3480	19	12.475	0.3566	0.3576	60
2	1	1	13.795	0.3230	0.3242	38	13.44	0.3314	0.3321	100
2	2	0	14.175	0.3145	0.3148	10	14.16	0.3149	0.3161	12
3	0	0					14.93	0.2990	0.2980	42
3	1	0	15.91	0.2810	0.2816	100	15.85	0.2820	0.2827	45
2	2	1	16.19	0.2763	0.2742	7	16.04	0.2788	0.2793	4
1	1	2					16.52	0.2709	0.2697	7
3	0	1					16.755	0.2672	0.2666	4
3	1	1	17.885	0.2508	0.2514	4	17.555	0.2554	0.2554	5
3	2	0	18.18	0.2469	0.2470	4	18.065	0.2484	0.2480	19
2	1	2	18.73	0.2310	0.2285	1	18.75	0.2396	0.2390	31
3	2	1	19.86	0.2267	0.2258	3				
4	0	0	20.255	0.2225	0.2226	25	20.165	0.2234	0.2235	6
4	1	0	20.905	0.2159	0.2160	40	20.82	0.2167	0.2168	23
3	3	0	21.54	0.2098	0.2099	22	21.455	0.2106	0.2107	18
3	0	2	22.21	0.2038	0.2033	7				
4	1	1	22.49	0.2014	0.2014	23	312	22.01	0.2055	0.2052	27
4	2	0	22.765	0.1991	0.1991	44				
3	1	2	22.96	0.1975	0.1982	5	411	22.205	0.2038	0.2038	24
3	3	1	23.09	0.1964	0.1964	9				
4	2	0					22.67	0.1998	0.1999	19
0	0	3					22.82	0.1986	0.1988	19
2	0	3					25.015	0.1822	0.1815	6
4	0	2					25.55	0.1786	0.1788	46
4	2	1	24.245	0.1876	0.1875	2				
5	1	0	26.14	0.1748	0.1746	4	26.01	0.1756	0.1753	19
4	1	2	26.88	0.1704	0.1708	5				
3	3	2	27.395	0.1674	0.1677	5	26.58	0.1721	0.1721	17
5	1	1	27.51	0.1668	0.1667	12	27.29	0.1680	0.1682	9
4	2	2	28.415	0.1619	0.1621	2	27.65	0.1660	0.1660	5
5	2	1	29.50	0.1584	0.1585	30	28.82	0.1598	0.1599	19
4	4	0	29.265	0.1576	0.1574	6	29.12	0.1583	0.1580	4

TABLE 5. Unit cell dimensions[a] and density for polycrystalline deposits of tetragonal $M_4V_6O_{16}$ $M_xM'_{4-x}V_6O_{16}$

			Density/g cm^{-3}	
Compound	*a*/nm	*c*/nm	Obs.	Calculated from unit cell
$K_4V_6O_{16}$[b]	0.8878 ± 0.0005	0.5227 ± 0.0006	2.77 ± 0.04	2.89 ± 0.01
$(NH_4)_4V_6O_{16}$[b]	0.8917 ± 0.0007	0.5587 ± 0.0007	2.32 ± 0.02	2.37 ± 0.01
$Rb_4V_6O_{16}$	0.8904 ± 0.0006	0.5581 ± 0.0012	3.36 ± 0.02	3.39 ± 0.01
$Cs_4V_6O_{16}$	0.8940 ± 0.0003	0.5964 ± 0.0006	3.78 ± 0.03	3.81 ± 0.01
$(NH_4)_xK_{4-x}V_6O_{16}$				
$x = 2.82$	0.8908 ± 0.0005	0.5492 ± 0.0007		2.56 ± 0.01
$x = 2.22$	0.8904 ± 0.0006	0.5453 ± 0.0008		2.58 ± 0.01
$x = 0.74$	0.8872 ± 0.0016	0.5369 ± 0.0018		2.76 ± 0.02
$(NH_4)_xCs_{4-x}V_6O_{16}$				
$x = 1.92$	0.8905 ± 0.0007	0.5849 ± 0.0060		3.12 ± 0.06

[a]Error limits are ± 1 std. dev.
[b]Reference 7.

Can. J. Chem. Downloaded from www.nrcresearchpress.com by 91.121.58.235 on 09/07/12
For personal use only.

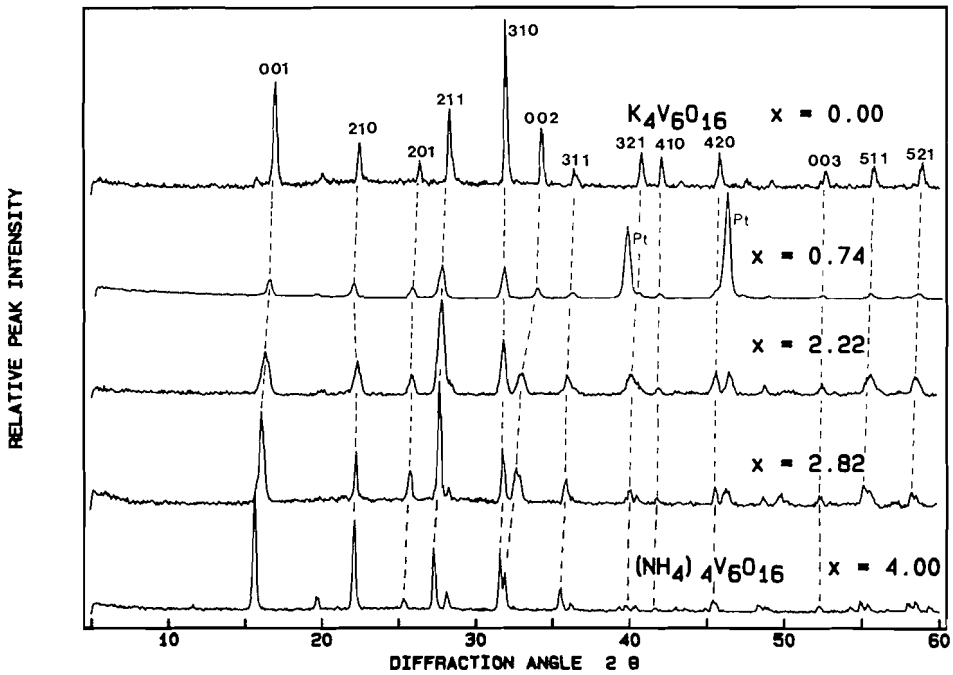

FIG. 3. X-ray diffraction for $(NH_4)_xK_{4-x}V_6O_{16}$, with principal reflections identified. The large shifts with x of the 00 l reflections are apparent. For $x = 0.74$, sample is sufficiently thin to show lines from the Pt substrate. All intensities are relative to the most intense line in each pattern.

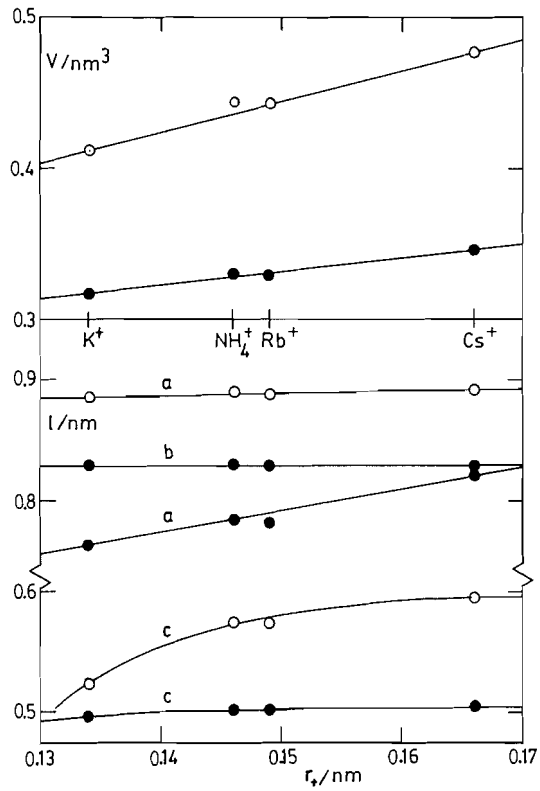

FIG. 4. Dependence of lattice parameter l and volume V of unit cells on ionic radius r_+ in $M_2V_6O_{16}$ (8) (closed circles; parameters a, b, c) and in $M_4V_6O_{16}$ (open circles; a, c).

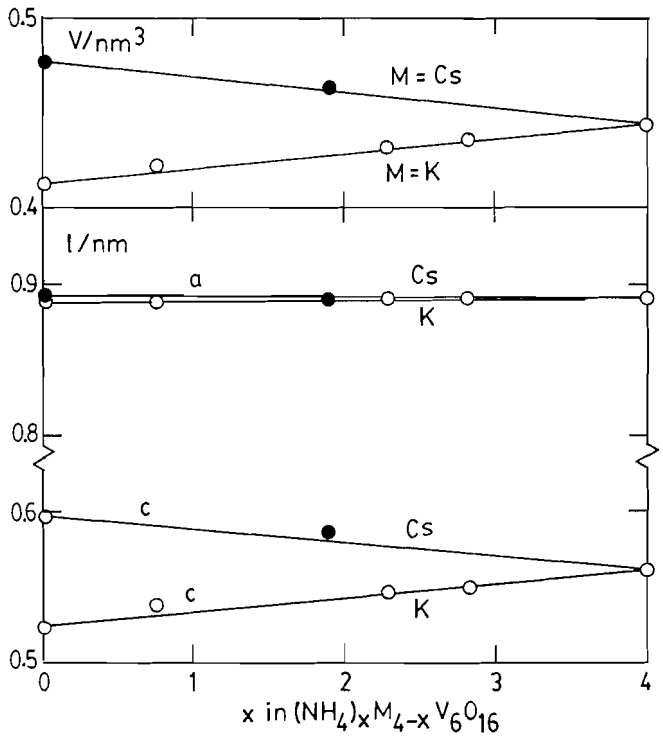

FIG. 5. Dependence of lattice parameter l and volume V of unit cells in $(NH_4)_xM_{4-x}V_6O_{16}$ on x for M = K (open circles), M = Cs (closed circles).

Insertion of alkali cations and protons

Only limited insertion of lithium occurs in unheated deposits of $(NH_4)_4V_6O_{16}$, corresponding to the α phase for lithium vanadium bronzes; the value of x in $Li_x(NH_4)_4V_6O_{16}$ is 0.05 (Fig. 6). Similarly, very little lithium can be inserted into the deposits containing K^+, with $x = 0.085$ for $K_{3.852}V_6O_{16}$ and $x = 0.025$ for $K_4V_6O_{16}$ (Fig. 7). Repetitive electrochemical oxidation and reduction of the deposit leads, as shown by chemical analysis and EDX, to cumulative loss of small amounts of K and NH_4 and a corresponding loss of V(IV). The K or NH_4 can be replaced by Li. After only a few such cycles, plateaus can be seen which indicate phase changes as lithium is inserted (Figs. 6, 7). The analyses show, again, that non-stoichiometry arises from a change in the V(IV)/V(V) ratio to

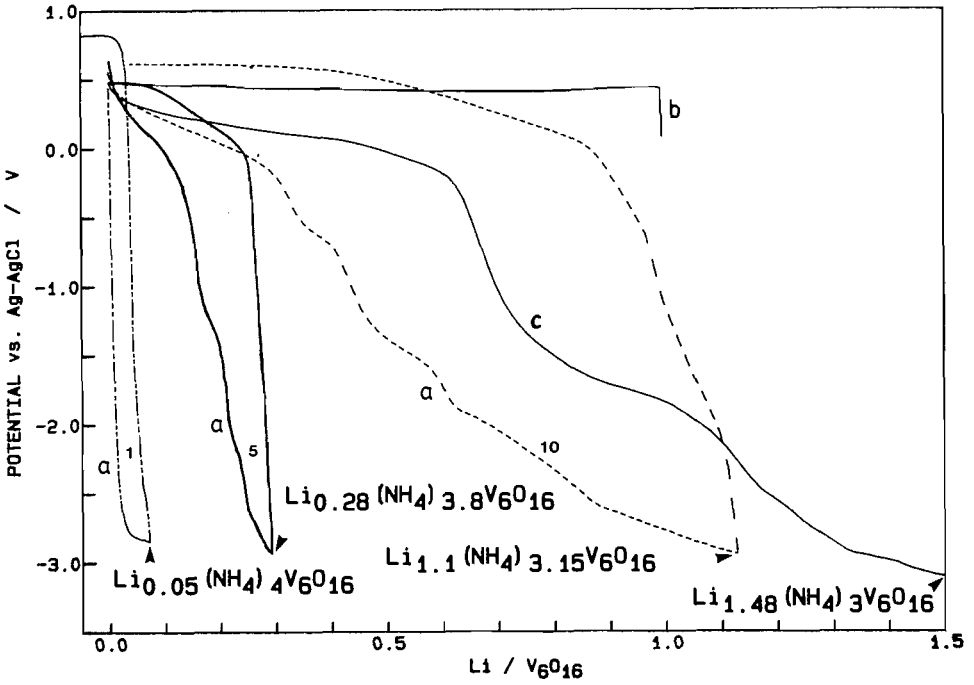

FIG. 6. Open circuit potentials for insertion of lithium into $(NH_4)_4V_6O_{16}$; (*a*) not oxidized; (*b*) after electro-oxidation by 6.7 C of charge; (*c*) subsequent insertion of Li. Numbers are cycles of insertion and removal. Compositions given for end of insertion process (arrows).

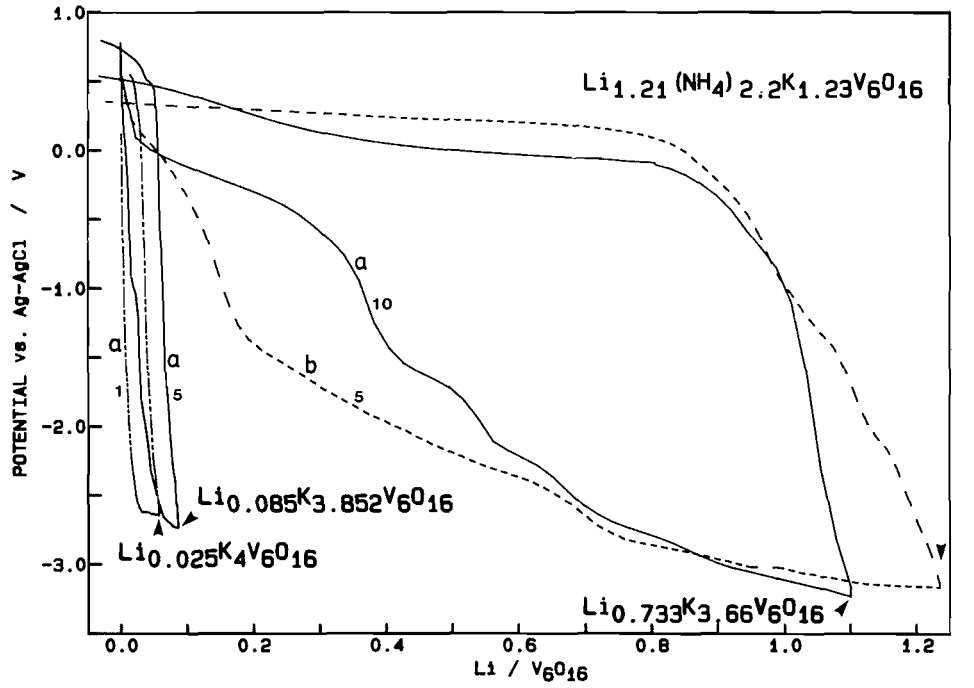

FIG. 7. Open circuit potentials for insertion of lithium into (*a*) $K_4V_6O_{16}$; (*b*) $(NH_4)_{2.67}K_{1.33}V_6O_{16}$. Numbers are cycles of insertion and removal. Compositions given for end of insertion process (arrows).

compensate for removal of M^+, but that the ratio O/V(total) remains unchanged. The formula consistent with the data is thus $(2 - x)M_2O \cdot (2 + x)V_2O_5 \cdot (1 - x)V_2O_4 = M_{4-2x}V_6O_{16}$, and loss of 1 M^+ is accompanied by loss of 1 V^{4+} and gain of a V^{5+}. Subsequent electrochemical insertion of lithium then takes place in two steps, the first involving replacement of the $M^+ = Cs^+$, Rb^+, NH_4^+, or K^+ lost during the previous oxidation, and decrease of the V(V)/V(IV) ratio to its initial value of 2. The second step is accompanied by a large drop in potential and involves insertion of sufficient lithium to reduce the V(V)/V(IV) ratio to less than 2. These processes can be summarized, using salt formulas, as:

$$M_{4-2x}V_6O_{16} \xrightarrow{+\,2xLi^+ + 2xe^-} M_{4-2x}Li_{2x}V(IV)_2V(V)_4O_{16}$$

$$\xrightarrow{+\,2yLi^+ + 2ye^-} M_{4-2x}Li_{2(x+y)}V(IV)_{2(2+y)}V(V)_{2(2-y)}O_{16}$$

Can. J. Chem. Downloaded from www.nrcresearchpress.com by 91.121.58.235 on 09/07/12
For personal use only.

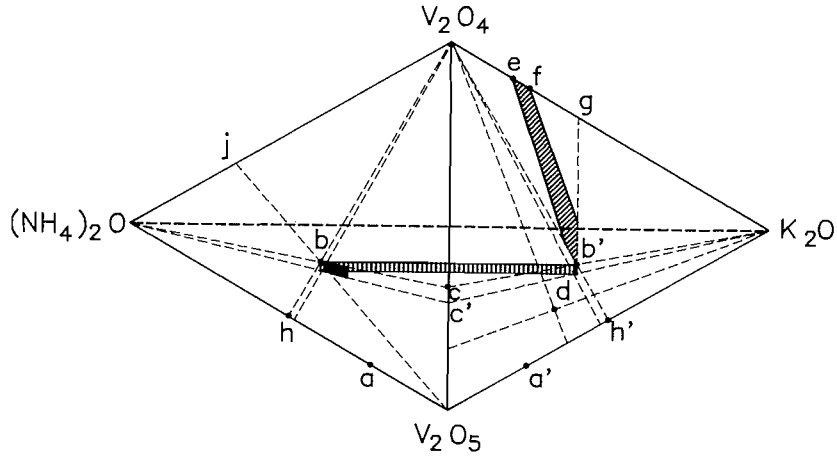

FIG. 8. Compositions of homogeneous phases in the quaternary system $(NH_4)_2O$–V_2O_4–K_2O–V_2O_5. a, a': $(NH_4)_2V_6O_{16}$, $K_2V_6O_{16}$ (6); b, b': $(NH_4)_4V_6O_{16}$, $K_4V_6O_{16}$ (7); c: V_3O_7; d: $3K_2O \cdot 5V_2O_5 \cdot V_2O_4$ (4); e: $K_2V_8O_{17}$; f: $K_2V_6O_{13}$; g: $K_4V_3O_7$; h, h': NH_4VO_3, KVO_3; j: $(NH_4)_2V_3O_7$. Diagonal hatching: results of ref. 5; solid shading: results of ref. 7; vertical hatching: this paper.

The compositions at various stages of cycling are given for a few electrode deposits in Figs. 6 and 7. The $K_2V_3O_8$ electrodes are the most resistant to oxidation–reduction processes, probably because removal of the smaller K^+ from between the V—O layers is more difficult than removal of the larger cations.

In an attempt to remove K^+ or NH_4^+ and insert lithium from other hexavanadate electrodes, similar reduction–oxidation experiments were performed in propylene carbonate solutions containing 0.5 mol/L $LiClO_4$. The results of these experiments are also given in Fig. 7. The initial low amount of insertion of Li^+ is to be expected because of the presence of K^+ or NH_4^+ between the V—O layers. Previously, anodic deposits of $(NH_4)_2V_6O_{16}$ were found to insert Li up to $x = 1.44$ in $Li_x(NH_4)_2V_6O_{16}$. The anodic deposits contain only half as much NH_4^+ as the cathodic deposits, although both yield V_2O_5 on thermal decomposition (2, 3).

Relation to other vanadate phases

Pouchard *et al.* (5) plotted a composition diagram showing the ranges of existence of homogeneous solid phases, named by them Φ-phases, of the form $K_{4-x}V_{6+2x}O_{16+2x\pm k}$, in the ternary system V_2O_5–V_2O_4–K_2O, and prepared by them by synthesis at high temperatures. They interpreted precision density measurements on a series of compounds in terms of the above formula, and claimed that it implied a double non-stoichiometry involving replacement of K^+ with $(VO)_2$ units, starting with the phase $K_4V_6O_{16}$ ($x = 0$), which has the minimum density for the system. Their formula is equivalent to $(2 - x/2)K_2O \cdot (2 - 3x/2 \pm k)V_2O_5 \cdot (1 + 5x/2 \mp k)V_2O_4$, which shows clearly that removal of 1 K^+ is accompanied by a net gain of 5/2 O^{2-} + 5 V^{4+} and a loss of 3 V^{5+}, *i.e.*, a net reduction of vanadium. Bernard *et al.* (7) extended this diagram to include the isomorphous compounds $(NH_4)_xV_6O_{16}$ made by precipitation near room temperature, and which also contained variable proportions of V(IV) and V(V). In their compounds, removal of NH_4^+ is accompanied by an increase in V^{5+}, as in our experiments. Figure 8 contains a further extension of this diagram to include the mixed crystals described in this paper, which are prepared electrochemically and contain both NH_4^+ and K^+. The quaternary system is plotted on a tetrahedral diagram with vertices $(NH_4)_2O$, V_2O_4, K_2O, V_2O_5. The mixed crystals are stoichiometric in the M/V(total) ratio, but not in the V(IV)/V(V) ratio, and thus exhibit a different type of non-stoichiometry than the compounds of Pouchard *et al.* (5), but are similar to those of Bernard *et al.* (7). Their compositions lie on a narrow surface bounded by the line bb' (on the plane $(NH_4)_2O$–c–K_2O) and a corresponding line on the plane $(NH_4)_2O$–c'–K_2O, where $b = (NH_4)_4V_6O_{16}$, $b' = K_4V_6O_{16}$, $c = V_6O_{14} = 2V_2O_5 \cdot V_2O_4$ and $c' = V_6O_{14+d} = (2 + d)V_2O_4$, with $d = 0.13$ the maximum observed value corresponding to non-stoichiometry. All other observed data lie on the two front faces of the tetrahedron. The V(V) hexavanadates a, a' (5), the Φ-phases of Pouchard *et al.* (5), the phases of Bernard *et al.* (7), and the single phase d reported by Goncharenko and Suvorova (8) are also shown, along with a number of characteristic compositions for the system. The phase reported in ref. 8 probably contains ammonium, so that its position is questionable. Several other phases which exist over small composition ranges in the V_2O_5-rich part of the K_2O–V_2O_5–V_2O_4 system (see ref. 6) have not been included in Fig. 6.

Extensive data on the products of electrochemical oxidation described above are not available, and therefore have not been included on the diagram. For hexavanadates containing only one type of M atom, these products are located in the same area as the products of Bernard *et al.* (7) for NH_4^+, and a corresponding area on the K_2O–V_2O_4–V_2O_5 part of the diagram. Products containing two types of M atom are located inside the volume defined by the plane $bb'c$ and the similar plane through point c'.

Conclusions

The compounds $Rb_4V_6O_{16+d}$ and $Cs_4V_6O_{16+d}$ and the mixed crystal phases $M_xM'_{4-x}V_6O_{16+\delta}$, with M, M' = K, Rb, Cs, NH_4, described in this paper, extend the range of known homogeneous solid phases in the general system M_2O–M'_2O–V_2O_5–V_2O_4. The non-stoichiometry of these compounds relative to the ideal stoichiometry of mixed crystals arises from varying ratios of V_2O_4 to V_2O_5, but with constant ratio of oxygen to total vanadium. Non-stoichiometry can be produced during preparation by excess reduction at a cathode, or by subsequent electro-oxidation. The series of tetrametal or tetraammonium hexavanadates, with average oxidation state for vanadium 14/3, is analogous to the series of dimetal hexavanadates with oxidation state 5. The unit cells of the tetragonal tetrametal (or ammonium) hexavanadates are larger than those of the corresponding monoclinic dimetal hexavanadates, but the differences in volume are more than those required to accom-

Can. J. Chem. Downloaded from www.nrcresearchpress.com by 91.121.58.235 on 09/07/12
For personal use only.

modate two more ions, indicating that the presence of V(IV) results in an expanded and less distorted lattice with higher symmetry. The tetrametal hexavanadate lattice is sufficiently open to permit limited replacement of one of the ions K^+, Rb^+, Cs^+, or NH_4^+ with Li^+, but at a very slow rate, unless the lattice is subjected to severe cyclic oxidation and reduction.

Acknowledgements

This research was sponsored by the Natural Sciences and Engineering Research Council of Canada (NSERC) under a Strategic Grant (G1651). E.A. thanks NSERC and the Ontario Ministry of University Affairs for the award of studentships. Thanks are also due to Professor G. Starkey for making X-ray equipment available. SEM and EDX analyses were performed at Surface Science Western.

1. J. DESILVESTRO and O. HAAS. J. Electrochem. Soc. **137**, 5C (1990).
2. E. ANDRUKAITIS, P. W. M. JACOBS, and J. W. LORIMER. Solid State Ionics, **27**, 19 (1988).
3. E. ANDRUKAITIS, P. W. M. JACOBS, and J. W. LORIMER. Solid State Ionics. **37**, 157 (1990).
4. E. ANDRUKAITIS, P. W. M. JACOBS, and J. W. LORIMER. J. Power Sources, **26**, 475 (1988).
5. M. POUCHARD, J. GALY, L. RABARDEL, and P. HAGENMULLER. C.R. Hebd. Acad. Sci. **264**, 1943 (1967).
6. P. HAGENMULLER. *In* Comprehensive inorganic chemistry. Vol. 4. *Edited by* J. C. Bailar, H. J. Emeléus, R. Nyholm, and A. F. Trotman-Dickinson. Pergamon Press. 1973. pp. 583–588.
7. J. BERNARD, F. THEOBALD, and A. VIDONNE. Bull. Soc. Chim. Fr. **6**, 2108 (1970).
8. A. S. GONCHARENKO and O. A. SUVOROVA. Zh. Prikl. Khim. **33**, 846 (1960); J. Appl. Chem. USSR, **33**, 847 (1960).
9. Joint Committee on Powder Diffraction Standards, US Dept. of Commerce. NBS crystal data. Vol. II. 3rd ed. 1973.
10. A. D. KELMERS. J. Inorg. Nucl. Chem. **21**, 45 (1961).

Can. J. Chem. Downloaded from www.nrcresearchpress.com by 91.121.58.235 on 09/07/12
For personal use only.

Self-association of caffeine in aqueous solution: an FT-IR study[1]

MICHAEL FALK, MANUEL GIL,[2] AND NEREA IZA[2]

Atlantic Research Laboratory, National Research Council of Canada, Halifax, N.S., Canada B3H 3Z1

Received November 10, 1989

MICHAEL FALK, MANUEL GIL, and NEREA IZA. Can. J. Chem. **68**, 1293 (1990).

Spectra of caffeine in D_2O solution (0.003 to 0.129 M) were studied by Fourier-transform infrared spectroscopy. Spectral changes in the carbonyl stretching region were interpreted in terms of the self-association equilibria resulting from the stacking of caffeine molecules. Absence of isosbestic points indicated the occurrence of more than two spectroscopically distinct caffeine species. A simple monomer–dimer–polymer model was employed, in which the successive equilibria are governed by two association constants, K_d for the formation of dimers and K_p for the formation of trimers and larger polymers. The value K_d = 158.1 L mol^{-1} was taken from a recent ultraviolet study by Iza *et al.* and the value K_p = 27 L mol^{-1} was derived from the analysis of infrared band profiles sharpened by Fourier self-deconvolution. From these values of K_d and K_p, the weight fractions of monomers, dimers, and polymers were calculated for every caffeine concentration and their individual molar absorptivity spectra were derived. In agreement with the earlier work of Maevsky and Sukhorukov, it was found that stacking association causes shifts of both C=O stretching fundamentals to higher wavenumbers. The monomer-dimer shifts are smaller than the dimer-polymer shifts. Analogous shifts were observed for the stacking self-association of 1,3-dimethyluracil in D_2O. The shifts to higher wavenumbers are probably caused by the diminished hydrogen bonding of water to C=O groups of the stacked bases.

Key words: caffeine, self association, infrared spectroscopy, base stacking.

MICHAEL FALK, MANUEL GIL et NEREA IZA. Can. J. Chem. **68**, 1293 (1990).

Nous avons étudié les spectres de la caféine dans des solutions de D_2O (0.003 à 0.129 M) par la spectroscopie infrarouge à transformée de Fourier. La variation des spectres dans la region de vibration de valence des groupes C=O a été interpreté en termes des équilibres impliquant l'auto-association par empilage de molécules de caféine. L'absence de points isosbestiques a indiqué l'existence d'au moins trois espèces distinctes de caféine. Nous avons employé un modèle monomère–dimère–polymère, dans lequel les équilibres successifs sont controlés par deux constantes d'association, K_d pour la dimérization et K_p pour la formation de trimères et de polymères plus grands. La valeur K_d = 158.1 L mol^{-1} a été prise de l'étude récente faite par Iza et al., tandis que la valeur K_p = 27 L mol^{-1} a été derivée de l'analyse des profiles de bandes infrarouges obtenues par auto-déconvolution. A partir des valeurs de K_d et K_p, nous avons calculé la fraction en poids des monomères, dimères et polymères pour chaque concentration de caféine, ce qui nous a permis de calculer leurs spectres individuels. En accord avec les travaux antérieurs de Maevsky et Sukhorukov, nous avons trouvé que l'association par empilage cause des déplacements de vibrations de valence des groupes C=O vers les hautes fréquences. Les déplacements monomère–dimère sont moins grands que les déplacements dimère–polymère. Nous avons aussi observé des déplacements analogues pour l'auto-association du 1,3-dimethyluracil dans du D_2O. Des tels déplacements vers les hautes fréquences semblent avoir comme origine la diminution des formations de liaisons hydrogène entre l'eau et les groupes C=O des bases empilées.

Mots clés : caféine, auto-association, spectroscopie infrarouge, empilage de bases.

Can. J. Chem. Downloaded from www.nrcresearchpress.com by 88.85.125.76 on 09/07/12
For personal use only.

Introduction

Like other purine bases, caffeine molecules in aqueous solution aggregate by plane-to-plane stacking (1–3). This type of molecular self-association is recognized as a key biophysical process, responsible for the stacking of purine–pyrimidine base pairs and hence for the double-helix structure of nucleic acids (4). Stacking interactions are also important in connection with the pharmacological action of caffeine (5) and the interaction between caffeine and nucleic acids (6).

Stacking of purine and pyrimidine bases is accompanied by major changes in the electronic spectrum. Particularly striking is the characteristic diminution of the intensity of absorption near 260 nm (the so-called hypochromic effect), well documented experimentally and understood theoretically (7–10).

In contrast to the electronic spectrum, the effect of base stacking on the vibrational spectrum has not been studied theoretically and was not clearly demonstrated until the recent work of Maevsky and Sukhorukov (11). These workers recorded spectra in the carbonyl stretching region for caffeine and for several other purine and pyrimidine bases in D_2O solution. In spite of the relatively low accuracy of their experimental data, obtained by dispersive spectroscopy, they detected shifts of peak position with solute concentration and succeeded in separating the observed spectra mathematically into contributions from monomeric molecules and stacked molecules.

We believe that vibrational spectra can offer information regarding the molecular details of base-stacking interactions, which is potentially as valuable as that obtained from the electronic spectras. Therefore, we have repeated the work of Maevsky and Sukhorukov using Fourier-transform infrared spectroscopy. The higher quality of FT-IR spectral data permitted us to use Fourier self-deconvolution, which demonstrated directly the occurrence of component bands in the experimental spectra. The data were of sufficient quality to permit an analysis in terms of a three-component model, which yielded the individual spectra of caffeine monomers, dimers, and higher polymers.

Experimental

Caffeine solutions. Solutions of caffeine (from Sigma Chemical company) in D_2O (from MSD Isotopes, Division of Merck Frosst Canada, Inc) were prepared gravimetrically. The lower concentration limit was 0.003 M, imposed by the photometric accuracy of the interferometer system. The upper concentration limit was 0.129 M, imposed by the solubility of caffeine in D_2O. The spectral accuracy increased with caffeine concentration.

Spectroscopy. Absorption spectra were recorded on a Bomem model

[1]NRCC No. 31522.

[2]On leave of absence, February–July 1989, from Departamento de Quimica Fisica, Facultad de Ciencias Quimicas, Universidad Complutense, 28040 Madrid, Spain.

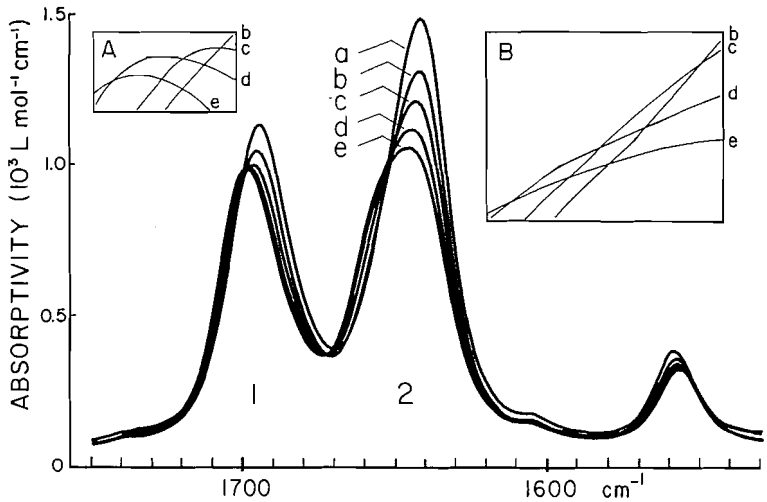

FIG. 1. Apparent molar absorptivity of caffeine in D_2O at the following concentrations: 0.010 M (*a*), 0.025 M (*b*), 0.050 M (*c*), 0.090 M (*d*), and 0.129 M (*e*). Inserts A and B: enlarged regions of intersections near 1699 and 1651 cm^{-1}, respectively.

DA3.02 FT-IR spectrometer, used with a potassium bromide beamsplitter and a mercury cadmium telluride detector, at a resultion of 2 cm^{-1} with 2500 interferograms co-added for each spectrum. The spectral range was 2000–1000 cm^{-1} and a detailed study was made of the carbonyl stretching region, 1750–1530 cm^{-1}. The temperature was 25°C.

Cells and experimental procedure. The spectra were recorded using a sealed liquid cell with CaF_2 windows and an optical path $b = 0.00289$ cm, calculated from the interference fringes recorded with the empty cell. The raw spectra were recorded in the sequence S_1 (cell with pure D_2O), S_2 (cell with one of the caffeine solutions), S_3 (empty beam). The transmittance of the solvent, T_1, and that of the solution, T_2, were obtained by ratioing the raw spectra:

[1a] $$T_1 = S_1/S_3$$

[1b] $$T_2 = S_2/S_3$$

The corresponding absorbances were obtained from $A_1 = \log(1/T_1)$ and $A_2 = \log(1/T_2)$. The absorbance of caffeine, A, at each concentration C (mol/L) was obtained from

[2] $$A = A_2 - A_1$$

and the apparent molar absorptivity of caffeine, ϵ, was determined from

[3] $$\epsilon = A/(b.C)$$

(The term "apparent" is used to indicate that ϵ is a function of C, as Beer's law is not obeyed).

Procedure and Results

Experimental spectra

Figure 1 shows the apparent molar absorptivity spectra for concentrations from 0.010 to 0.129 M, each of them the average of two to four individual measurements. The spectrum of caffeine in the region of the carbonyl stretching fundamentals consists of two major absorption bands: band 1 at 1692 to 1700 cm^{-1}, due to the stretching of the isolated carbonyl, C=O(2), and band 2 at 1641 to 1647 cm^{-1}, due to the stretching of the conjugated carbonyl, C=O(6) (see Fig. 2). A less intense third band, at about 1560 cm^{-1}, is due to C=N and C=C stretching vibrations of the purine ring and will not be discussed further. These vibrational band assignments for caffeine are well established (12). Changes of peak position, peak absorptivity, and halfwidth with concentration are recorded in Table 1. At increasing concentrations of caffeine, bands 1 and 2 shift to higher frequencies and increase their halfwidth. At the same time, their peak intensities are diminished, but in quite a different manner for the two bands. The intensity of band 1 undergoes an initial diminution with increasing caffeine concentration and then becomes concentration-independent. The intensity of band 2, on the other hand, undergoes a larger diminution which continues all the way to the highest concentrations.

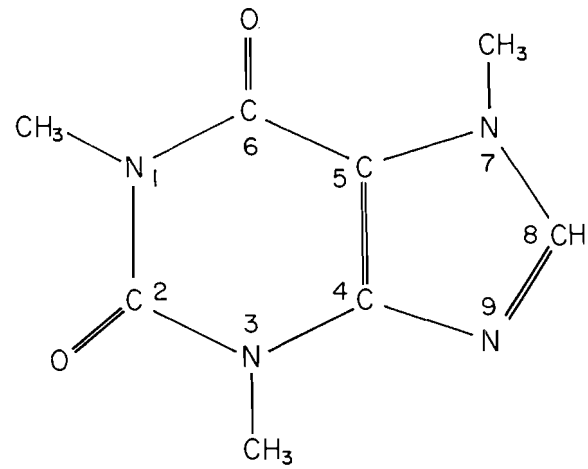

FIG. 2. Molecular structure of caffeine.

In our analysis of the spectra in terms of the self-association equilibria, we have assumed that each absorption band is a composite of contributions from several absorbing molecular species. Band 1 has an approximately Lorentzian shape at all concentrations and reveals its composite nature only indirectly, by the shift of its peak position and by slight broadening with increasing concentration. Band 2 also shifts and broadens, but, in addition, it also reveals the presence of underlying components more directly, by the appearance of a high-wavenumber shoulder at higher concentrations.

Absence of isosbestic points

In choosing the appropriate model to represent the spectral changes due to caffeine association, an important observation is that the apparent absorptivity curves in Fig. 1 intersect over a range of points and not over a single point. This has been

Can. J. Chem. Downloaded from www.nrcresearchpress.com by 88.85.125.76 on 09/07/12
For personal use only.

TABLE 1. Peak position (cm^{-1}), peak absorptivity (L mol^{-1} cm^{-1}) and halfwidth (cm^{-1}) of the carbonyl stretching fundamentals of caffeine in D_2O

	Band 1			Band 2		
Concentration	Position	Absorptivity	Halfwidth	Position	Absorptivity	Halfwidth
			Observed spectra			
0.003	1694.4±2.0*	1290±341	22.8±3.9	1641.5±0.4	1375±50	22.5±0.7
0.005	1694.1±0.6	1056±126	24.3±0.7	1641.5±0.1	1435±49	24.0±0.4
0.010	1694.8±0.2	1094±25	25.0±0.0	1641.9±0.0	1430±4	26.0±0.7
0.025	1695.7±0.3	986±24	25.7±1.5	1642.6±0.1	1250±32	27.7±0.6
0.050	1697.1±0.0	942±1	26.5±0.0	1643.7±0.0	1151±1	30.0±0.0
0.090	1698.9±0.0	935±1	26.3±0.4	1645.1±0.1	1059±1	32.5±0.0
0.100	1699.0±0.0	937±2	26.0±0.0	1645.4±0.1	1047±2	33.0±0.0
0.129	1699.5±0.1	930±11	26.0±0.0	1646.6±0.1	999±3	33.3±0.0
			Calculated spectra			
Monomer	1693.5±0.3	1476±20	25.0	1640.5±0.1	1920±40	23.0
Dimer	1695.2±1.0	840±15	24.0	1643.9±0.3	1267±65	25.0
Polymer	1703.7±0.7	1267±185	19.0	1658.6±0.6	1200±160	25.0

*Numbers following the ± symbol are standard deviations for the observed spectra and estimated standard errors for the calculated spectra.

verified by the examination of the points of intersection of the four most accurate absorptivity curves (corresponding to the four highest concentrations). The points of intersection form a regular pattern (inserts, Fig. 1), unlikely to arise from spectroscopic inaccuracy. The absence of a single isosbestic point indicates that aqueous caffeine solutions contain more than two distinct molecular species in equilibrium. Therefore, the analysis of the spectral data should be based on a model recognizing the existence of at least three molecular species. We have consequently adopted a simple three-species model, described below.

The monomer–dimer–polymer model

Our model, which follows that used by several earlier workers (13, 14) assumes that monomeric caffeine molecules (M) associate in aqueous solution to form dimers (M_2), trimers (M_3), etc., in a series of successive association equilibria:

[4*a*] $M + M = M_2$

[4*b*] $M + M_2 = M_3$

[4*c*] $M + M_3 = M_4, \ldots$ etc.

In general, each polymeric species of caffeine should possess a distinct spectrum, but as the size of the polymer increases, these spectra should converge. In the present model, we have assumed that monomers, dimers, and trimers possess distinct spectra, but that the spectrum of trimers is already the same as that of all the higher polymers. If the concentrations of the molecular species are defined as C_1, C_2, C_3, etc., then mass balance requires

[5] $$C = C_1 + 2C_2 + 3C_3 + 4C_4 + \ldots$$

If we also assume that ratios of activity coefficients are nearly unity, concentrations may be used instead of activities. In general, the association process must be governed by an infinite set of equilibrium association constants,

[6a] $$K_2 = C_2/(C_1.C_1)$$

[6b] $$K_3 = C_3/(C_2.C_1)$$

[6c] $$K_4 = C_4/(C_3.C_1) \ldots \text{ etc.}$$

The numerical values of the constants in the Series K_2, K_3, K_4, ... are likely to converge. We have assumed that the convergence already occurs at the second term, so that the association constants take only two distinct values, which we will call K_d (for the dimerization step) and K_p (for all the following polymerization steps), i.e.:

[7a] $$K_d = K_2$$

[7b] $$K_p = K_3 = K_4 = K_5 = \ldots$$

We will also introduce for the concentrations of caffeine species the symbols $C_m = C_1$, $C_d = C_2$, and $C_p = C_3 + C_4 + C_5 + \ldots$, appropriate to our model. Equations [5]–[7] lead to the following relation between the equilibrium constants, K_d and K_p, and the monomer concentration, C_m:

[8] $$C = C_m + \frac{K_d.C_m^2}{1 - K_p.C_m} + \frac{K_d.C_m^2}{(1 - K_p.C_m)^2}$$

For any values of K_d, K_p, and C, eq. [8] can be solved for C_m by iteration. Once C_m is known, the dimer concentration can be calculated from $C_d = K_d.C_m^2$ (eq. [6*a*]) and the weight fractions of the three components can be obtained as follows:

[9a] $$\text{Monomer fraction: } F_m = C_m/C$$

[9b] $$\text{Dimer fraction: } F_d = 2.C_d/C = 2.K_d.C_m^2/C$$

[9c] $$\text{Polymer fraction: } F_p = N_p.C_p/C = 1 - F_m - F_d$$

(where N_p is the average size of polymers larger than the dimer at caffeine concentration C.)

At low concentrations of caffeine, 0.25×10^{-3} to 1×10^{-3} M, the association equilibrium is mainly between monomers and dimers and the dimerization constant, K_d = 160 L mol^{-1}, has been determined with good accuracy from ultraviolet spectra (15, 16). At higher caffeine concentrations, trimers and higher polymers are also present and the isodesmic model (1, 17, 18) has been used to calculate an apparent single association constant, K, from various physico-chemical measurements (19–24). The values of K calculated under the isodesmic model tend to be in the range 8–12 L mol^{-1} and appear to be concentration-dependent (1). A two-constant monomer–dimer–polymer mod-

Can. J. Chem. Downloaded from www.nrcresearchpress.com by 88.85.125.76 on 09/07/12
For personal use only.

TABLE 2. Positions (cm^{-1}) and estimated fractional intensities of the deconvolved components H and L

Spectrum in Fig. 3	Concentration (M)	Component H		Component L	
		Position	Fractional intensity†	Position	Fractional intensity†
a	0.01	*	0±10%	1639.9	100±10%
b	0.025	*	14±8%	1640.0	86±8%
c	0.050	1657.2	24±6%	1640.9	76±6%
d	0.090	1657.2	35±5%	1640.7	65±5%
e	0.129	1657.0	45±4%	1640.0	55±4%

*There is a large uncertainty due to a superimposed side-band of the much larger L component.
†Numbers following the ± symbol represent estimated standard error.

el, identical with the one described here, was used by Iza *et al.* (15, 16) to obtain the values $K_d = 158.1$ L mol^{-1} and $K_p = 18.1$ L mol^{-1} from the ultraviolet spectra of caffeine in the concentration range 1×10^{-3} to 5×10^{-3} M. We have adopted their value of K_d derived from ultraviolet data as the best available, but for K_p we have used a value estimated from the results of Fourier deconvolution of the infrared spectra, as explained below.

Fourier self-deconvolution

The object of Fourier self-deconvolution of a spectrum is to reduce the effect of natural broadening of absorption bands and to reveal band structure that could not be originally observed (25). The main problem is that as one increases the resolution by decreasing the halfwidth parameter HW and by increasing the narrowing factor NF, the side-lobes also increase, until they become difficult to distinguish from real features. We have followed the usual criteria for choosing HW and NF to minimize the possibility of error (26), but in addition we have used the following criterion to distinguish real band components from artifacts of deconvolution: The former should exhibit gradual and regular changes as a function of caffeine concentration, and their position and intensity should be relatively insensitive to small changes of deconvolution parameters.

The software for Fourier self-deconvolution was provided by Bomem, Inc. and is based on the method of ref. 25. Using the criteria of ref. 26 and the additional criterion stated above, we were led to the following optimal choice of deconvolution parameters: Lorentzian lineshape function, HW = 35 and NH = 2.8. This choice of parameters resulted in the series of deconvolved spectra shown in Fig. 3. Under these conditions band 1 did not resolve, but band 2 resolved into two components, the high-frequency component H at about 1657 cm^{-1} and a low-frequency component L at about 1640 cm^{-1}. The positions of H and L were constant to within 1 cm^{-1} and their relative intensities varied in a regular manner, that of H increasing and that of L decreasing with increasing caffeine concentration. Peak positions and fractional intensities of H and L are recorded in Table 2. Fractional intensities were calculated respectively as $H/(H + L)$ and $L/(H + L)$, where H and L are the peak heights of the two components, measured above a baseline traced through the peaks of the surrounding small bands, which are artifacts of deconvolution. Peaks H and L have the same bandshape and halfwidth (imposed by the deconvolution procedure), so that peak heights are a fair measure of relative band areas.

It is clear from the concentration behaviour of the deconvolved components H and L, that they represent respectively polymers and monomers, but as no distinct intermediate feature

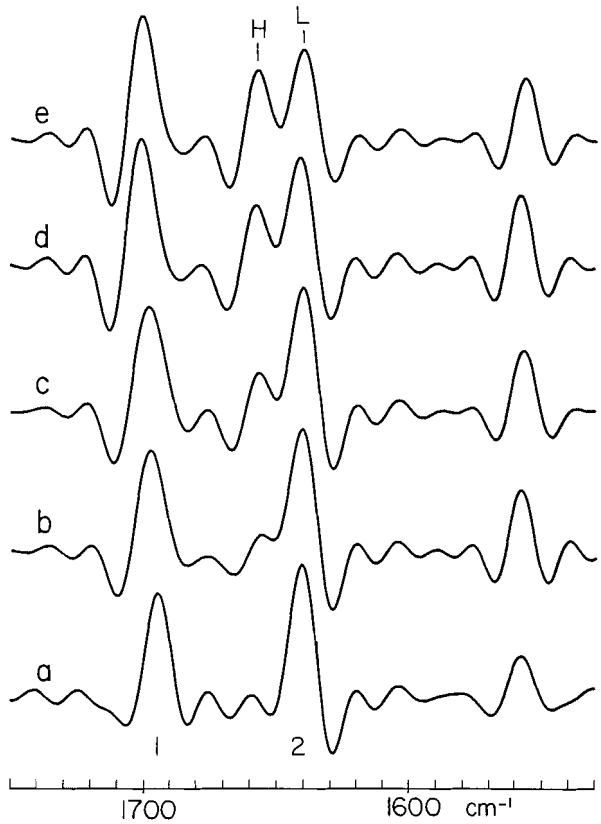

FIG. 3. Spectra obtained by self-deconvolution of the spectra in Fig. 1.

is observed, either H or L must include the dimer contribution. The ambiguity is resolved by the plots, shown in Fig. 4, of the polymer fraction, F_p, versus the caffeine concentration. F_p was calculated from eqs. [8] and [9], assuming $K_d = 158.1$ L mol^{-1} and a wide range of values of K_p. Similarly calculated values of the dimer fraction plus polymer fraction, $F_d + F_p$, are also plotted.

The rectangles in Fig. 4 represent the fractional intensity of H from Table 2. It is immediately apparent that the approximately linear increase of the fractional intensity of H with caffeine concentration is inconsistent with this band representing dimers *and* polymers, but plausible for a band representing only polymers. This finding is in agreement with other indications that the monomer–dimer wavenumber shift is much smaller than the monomer–polymer shift (see below), which makes it likely that

Can. J. Chem. Downloaded from www.nrcresearchpress.com by 88.85.125.76 on 09/07/12
For personal use only.

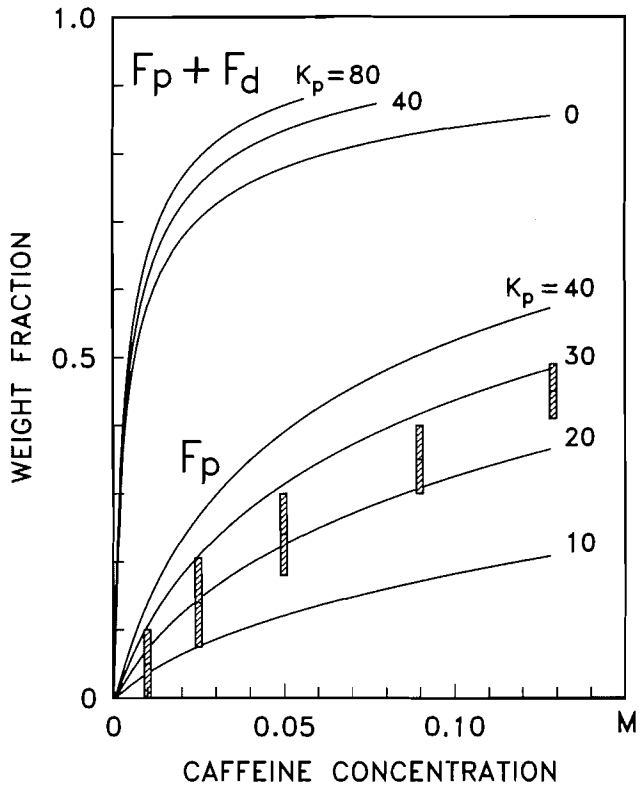

FIG. 4. Lower curves: Polymer weight fraction, F_p, calculated for K_d = 158.1 L mol^{-1} and different values of K_p. Upper curves: Similar plots for the sum of polymer and dimer weight fractions, $F_p + F_d$. Rectangles: Experimental values of the intensity fraction $H/(H + L)$ for the deconvolved components H and L of band 2.

the monomer and dimer absorptions remain unresolved by the deconvolution.

Analysis of the data in Fig. 4 allowed us to bracket the value of K_p as 27 ± 10 L mol^{-1}. This value agrees reasonably well with the value of 18.1 L mol^{-1} derived from ultraviolet spectra (19, 20). In addition, an analysis of the dependence of peak position of bands 1 and 2 with caffeine concentration (Table 1) yielded independent estimates of the polymer fraction, F_p, consistent with K_p = 158 L mol^{-1} and K_p = 27 L mol^{-1}. This gave us confidence in the above values, which we have adopted in subsequent calculations.

Weight fractions

Given the values of K_d and K_p, the weight fractions of the monomers, dimers, and polymers can be calculated by eqs. [8] and [9] for the caffeine concentrations employed in the present study (Table 3). Subject to the correctness of our model, it can be seen that between C = 0.003 M and C = 0.129 M, the dimer contribution changes relatively little, while the contribution of polymers increases and that of monomers decreases. The value of the parameter N_p, the average size of polymers larger than the dimer, varies only from 3.0 to 3.5. Therefore, in our concentration range, the contribution of polymers greater than the trimer is not very great, and the spectrum of "polymers" that we shall compute will be largely based on that of trimers.

Spectra of monomers, dimers, and polymers

The key assumption of the monomer–dimer–polymer model is that at each spectral point the total absorbance of caffeine in water, A, can be expressed as a sum of absorbance contributions from monomers, A_m, dimers, A_d, and "polymers", A_p:

TABLE 3. Molecular composition of caffeine solutions in the concentration range investigated in the present work. Calculated from eq. [9] for K_d = 158.1 L mol^{-1} and K_p = 27 L mol^{-1}

Caffeine concentration fraction C	Average polymer size N_p	Monomer weight fraction F_m	Dimer weight fraction F_d	Polymer weight F_p
0.003	3.052	0.614	0.357	0.029
0.005	3.075	0.521	0.429	0.050
0.010	3.121	0.400	0.505	0.095
0.025	3.216	0.263	0.547	0.190
0.050	3.327	0.183	0.529	0.288
0.090	3.463	0.130	0.483	0.387
0.100	3.492	0.122	0.472	0.406
0.129	3.571	0.104	0.444	0.452

[10] $$A = A_m + A_d + A_p.$$

Dividing eq. [10] by the optical path, b, and the total concentration of caffeine, C, we get:

[11] $$\epsilon = A/(b.C) = A_m/(b.C) + A_d/(b.C) + A_p/(b.C)$$

where ϵ is the apparent absorptivity of caffeine at concentration C, an experimentally derived quantity. Using the following definitions of the molar absorptivities of monomers, dimers, and polymers (per caffeine unit),

[12a] $$\epsilon_m = A_m/(b.C_m)$$

[12b] $$\epsilon_d = A_d/(b.2.C_d)$$

[12c] $$\epsilon_p = A_p/(b.N_p.C_p)$$

and introducing the definitions of weight-fractions, F_m, F_d, and F_p, from eq. [9] we obtain:

[13] $$\epsilon = F_m.\epsilon_m + F_d.\epsilon_d + F_p.\epsilon_p,$$

which holds at every spectral point.

Equation [13] contains one known quantity, ϵ, three parameters, F_m, F_d, F_p, calculable from K_d and K_p, and three unknown quantities, ϵ_m, ϵ_d, ϵ_p, to be calculated. To solve for the three unknowns, we require three equations and these are provided by using eq [13] three times, with experimental ϵ data for three caffeine concentrations. For this purpose we chose the absorptivity data for C = 0.01, 0.05, and 0.09 M, henceforth designated $\epsilon(1)$, $\epsilon(2)$, $\epsilon(3)$, respectively. This leads to a system of three simultaneous equations,

[14a] $$\epsilon(1) = F_m(1).\epsilon_m + F_d(1).\epsilon_d + F_p(1).\epsilon_p$$

[14b] $$\epsilon(2) = F_m(2).\epsilon_m + F_d(2).\epsilon_d + F_p(2).\epsilon_p$$

[14c] $$\epsilon(3) = F_m(3).\epsilon_m + F_d(3).\epsilon_d + F_p(3).\epsilon_p$$

which contains three experimental quantities, $\epsilon(1)$, $\epsilon(2)$, $\epsilon(3)$, three unknown quantities, ϵ_m, ϵ_d, ϵ_p, and nine weight fractions, forming 3 × 3 matrix [**F**]. Designating the observed quantities as the vector $[\epsilon_{obs}]$ and the quantities to be calculated as the vector $[\epsilon_{calc}]$, the above three equations can be expressed in matrix form as

[15] $$[\epsilon_{obs}] = [\mathbf{F}].[\epsilon_{calc}]$$

so that

[16] $$[\epsilon_{calc}] = [\mathbf{F}^{-1}].[\epsilon_{obs}]$$

Can. J. Chem. Downloaded from www.nrcresearchpress.com by 88.85.125.76 on 09/07/12
For personal use only.

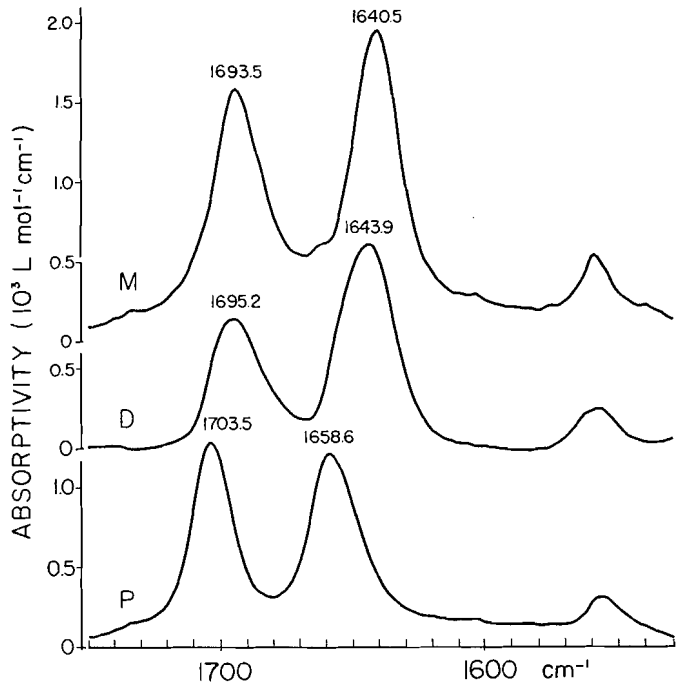

FIG. 5. Molar absorptivity of caffeine monomers (M), dimers (D), and polymers (P), calculated from eq. [16].

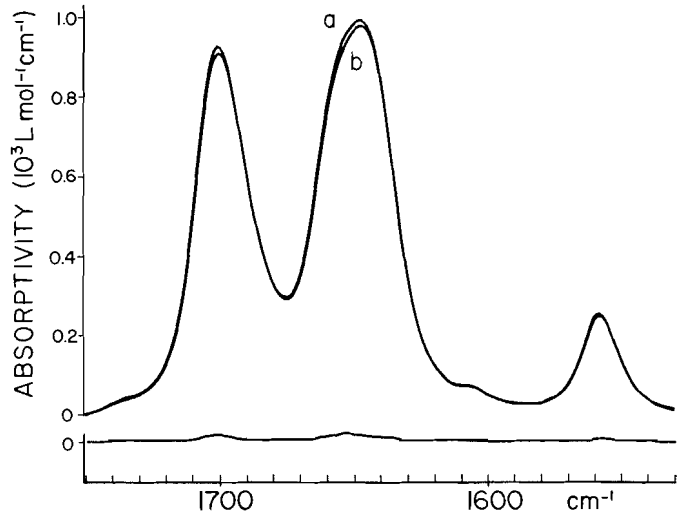

FIG. 6. Comparison of calculated (*a*) and observed (*b*) spectra for caffeine concentration 0.129 mol L^{-1}. Bottom: Difference (*a*) − (*b*).

where the matrix $[\mathbf{F}^{-1}]$ is the inverse of $[\mathbf{F}]$. In our procedure, we have calculated the nine components of the matrix $[\mathbf{F}]$ and inverted it to obtain $[\mathbf{F}^{-1}]$. The nine components of $\mathbf{F}^{-1}$ yielded the nine coefficients used to derive the calculated spectra, at each spectral point, from the observed spectra via eq. [16]. The calculations were performed on a personal computer.

The calculated absorptivity spectra of monomers, dimers and polymers are shown in Fig. 5; their peak positions, peak absorptivities, and halfwidths are recorded in the lower part of Table 1. The standard errors on these spectral parameters were estimated from their variation when K_p is changed from 27 to 18 L mol^{-1}. The derived absorptivity spectra of monomers, dimers, and polymers are physically reasonable, with good band shapes and smaller halfwidths than in the original spectra. Figure 6 shows the agreement between the observed ϵ spectrum for 0.129 M caffeine solution and the corresponding spectrum calculated by eq. [14], (using our values of ϵ_m, ϵ_d, and ϵ_p derived from spectra of 0.01, 0.05, and 0.09 M caffeine solutions). The maximum disagreement is about 2.0%, which is reasonable, as the standard deviation of individual measurements of the experimental spectra is of the order of 1%.

When the numerical parameters of the monomer–dimer–polymer model, K_d and K_p, are varied away from the values 158.1 and 27 L mcl^{-1}, respectively, the quality of the fit remains nearly equally good mathematically, but the derived spectra of monomers, dimers, and polymers display increasing negative regions, larger halfwidths and complex band shapes. We conclude that within the monomer–dimer–polymer model the above values of the association parameters are optimal.

The monomer–dimer wavenumber shifts turned out to be quite small: $+1.7 \pm 1.0$ cm^{-1} and $+3.4 \pm 3$ cm^{-1}, respectively, for bands 1 and 2. As the halfwidths of these bands are 20 to 25 cm^{-1}, it is not surprising that the monomer and dimer contributions remain unresolved, either in the original spectra or upon self-deconvolution.

The monomer–polymer shifts are considerably larger: $+10.2 \pm 0.8$ cm^{-1} and $+18.1 \pm 0.6$ cm^{-1}, respectively, for bands 1 and 2. These spectral differences are large enough to allow two spectral components to be easily resolved by deconvolution (and nearly resolved in the original spectra) for band 2 but not for band 1.

The intensity of the dimer bands is lower by 40–50% than that of the monomer bands. For band 2 the intensity of the polymers is about the same as that of the dimers, but for band 1 it is about half-way between that of the monomers and that of the dimers. The origin of these complex intensity changes due to stacking is not understood at the present.

General discussion

The model. The decomposition of the vibrational spectrum into contributions of three distinct species seems well warranted by the superior photometric and wavenumber accuracy of the FT-IR data. The use of a three-species model leads to more detailed information on the effect of base stacking on the spectrum than could be obtained from a two-component model, such as that used in ref. 11.

Values of the association constants. The association constant for the formation of the dimer, K_d, appears to be considerably larger than that for the formation of the larger aggregates, K_p. This implies a larger negative free energy for the dimerization step. It seems likely that the enthalpy change is the same for each association step, but that the entropy change is greater for the formation of the larger aggregates, because of their greater stiffness. The importance of the entropy contribution in the formation of stacking complexes has been emphasized by Gill *et al.* (2). The diminution of K with the degree of association of purine has been noted by Ts'o (1).

Spectroscopic effects of stacking. We have confirmed the observation of Maevsky and Sukhorukov (11) that base stacking causes shifts of carbonyl stretching fundamentals to higher wavenumbers. The direction and magnitude of the monomer–polymer shifts we have found are in almost exact agreement with those reported in ref. 11. The new and somewhat unexpected finding is that only about 20% of the overall shift due to stacking occurs in the first association step (dimer formation)

Can. J. Chem. Downloaded from www.nrcresearchpress.com by 88.85.125.76 on 09/07/12
For personal use only.

and about 80% occurs in the subsequent step (trimer formation). This is an important clue to the origin of the shift, which appears to be due to diminished hydration of the carbonyl groups upon stacking.

The C=O groups of monomeric caffeine molecules in D_2O solution can be assumed to be fully hydrated. In the stacked dimer, steric hindrance may prevent full hydration of C=O groups, but due to the relative flexibility of the dimer structure, the resulting "dehydration" effect is likely to be relatively small. Already with the trimer, however, the structure may be much more rigid so that the extent of carbonyl dehydration may approach that encountered in an infinitely long stack.

Full hydration of carbonyl groups typically brings about a wavenumber lowering of C=O stretching fundamentals by about 20 cm^{-1}. For example, the wavenumber of the C=O stretching fundamental of acetone dissolved in a large excess of D_2O is lowered by 22 cm^{-1} with respect to pure liquid acetone (27) and by 18 cm^{-1} with respect to acetone dissolved in dioxane (28). Thus the magnitude of the monomer–polymer shifts for the carbonyl stretching fundamentals of caffeine is consistent with partial dehydration of C=O groups upon stacking.

Related systems. We have also recorded spectra of 1,3-dimethyluracil in D_2O. Our results show that C=O stretching fundamentals shift to higher wavenumbers with increasing concentration, similarly to what had been reported by Maevsky and Sukhorukov (11). We have not made a detailed analysis of these shifts, but qualitatively the spectral behaviour of dimethyluracil upon stacking resembles that of caffeine. The shifts of carbonyl fundamentals of purine and pyrimidine bases upon stacking in solution appear to be universal and are analogous to those observed in the spectra of nucleic acids and polynucleotides upon helix-coil transition (11).

1. P. O. P. Ts'o, J. S. Melvin, and A. S. Olson. J. Am. Chem. Soc. **85**, 1289 (1963).
2. S. J. Gill, M. Downing, and G. F. Sheats. Biochemistry, **6**, 272 (1967).
3. A. Cesàro, E. Russo, and V. Crescenzi. J. Phys. Chem. **80**, 335 (1976).
4. R. Rymdén and P. Stilbs. Biophys. Chem. **21**, 145 (1989).
5. I. B. Syed. J. Am. Pharm. Assoc. **16**, 568 (1975).
6. H. Lang. Stud. Biophys. **55**, 137 (1976).
7. G. J. Thomas, Jr., and K. Kyogoku. J. Am. Chem. Soc. **89**, 4170 (1967).
8. W. B. Gratzer and C. W. F. McClare. J. Am. Chem. Soc. **89**, 4224 (1967).
9. C. R. Cantor and P. R. Schimmel. Biophysical chemistry. Part I. W. H. Freeman, San Francisco. 1980. p. 399.
10. J. F. Constant, P. Laûgaa, B. P. Roques, and J. Lhomme. Biochemistry, **27**, 3997 (1988).
11. A. A. Maevsky and B. I. Sukhorukov. Nucl. Acids Res. **8**, 3029 (1980).
12. J. De Taeye and T. Zeegers-Huyskens. J. Pharm. Sci. **74**, 660 (1985); Spectrosc. Lett. **19**, 299 (1986).
13. L. A. Laplanche, H. B. Thompson, and M. T. Rogers. J. Phys. Chem. **69**, 1482 (1965).
14. M. D. Joesten and L. J. Schaad. Hydrogen bonding. Marcel Dekker, New York. 1974. p. 281.
15. N. Iza, M. Gil, J. L. Montero, and J. Morcillo. J. Mol. Struct. **175**, 25 (1988).
16. N. Iza. Phil Doct., Univ. Complutense. Madrid, 1988.
17. D. Pörschke and F. Eggers. Eur. J. Biochem. **26**, 490 (1972).
18. J.-L. Dimicoli and C. Hélène. J. Am. Chem. Soc. **95**, 1036 (1973).
19. P. O. P. Ts'o. *In* Basic principles of nucleic acid chemistry. *Edited by* P. O. P. Ts'o. Academic Press. New York. 1974. Chap. 1, pp. 453–584.
20. H. Fritsche, I. Petri, H. Schutz, K. Weller, P. Sedmera, and H. Lang. Biophys. Chem. **11**, 109 (1980).
21. H. Høiland, A. Skauge, and I. Stokkeland. J. Phys. Chem. **88**, 6350 (1984).
22. A. L. Thakkar, L. G. Tensmeyer, R. B. Hermann and W. L. Wilham. J. Chem. Soc. Chem. Commun. **9**, 524 (1970).
23. L. Ramaswamy and D. Anbananthan. Acustica, **51**, 190 (1982).
24. P. Hemmes, A. A. Maevski, V. A. Buckin, and A. P. Sarvazyan. J. Phys. Chem. **84**, 699 (1980).
25. J. K. Kauppinen, D. J. Moffat, H. H. Mantsch, and D. Cameron. Appl. Spectrosc. **35**, 271 (1981).
26. W.-J. Wang and P. R. Griffiths. Computer enhanced Spectrosc. **1**, 157 (1983).
27. M. Falk and P. F. Seto. Unpublished results.
28. B. Z. Gorbunov and Yu. I. Naberukhin. Zhur. Strukt. Khim. **15**, 8 (1974).

Can. J. Chem. Downloaded from www.nrcresearchpress.com by 88.85.125.76 on 09/07/12
For personal use only.

Identification of some L-numbered *Lycopodium* alkaloids

WILLIAM A. AYER,[1] LOIS M. BROWNE, A. WARREN ELGERSMA, AND PETER P. SINGER
Department of Chemistry, University of Alberta, Edmonton, Alta., Canada T6G 2G2

Received February 22, 1990

WILLIAM A. AYER, LOIS M. BROWNE, A. WARREN ELGERSMA, and PETER P. SINGER. Can. J. Chem. **68**, 1300 (1990).

The pioneering research on Lycopodium alkaloids carried out by R. H. F. Manske and L. Marion led to the characterization of a large number of alkaloids. Many of these alkaloids were designated by numbers preceded by an L (e.g., L1, which has since been shown to be dihydrolycopodine). While the identity of many of these alkaloids has now been established, several remain unreported. We have examined samples of alkaloids L15, L16, L17, L18, L22, L24, L25, L26, L28, L29, L31, and L35, obtained from Marion's collection, by GC–MS and GC–IR, and report herein the identity of these alkaloids and alkaloid mixtures. Most of the samples proved to be mixtures of known alkaloids. Acetylannofoline (**5**), a component of alkaloid L17, and 5,15-oxidolycopodane (**9**), a component of alkaloids L28 and L31, are identified for the first time as natural products. A complete listing of the L-numbered alkaloids is provided.

Key words: Lycopodium alkaloids, alkaloids, acetylannofoline, oxidolycopodane.

WILLIAM A. AYER, LOIS M. BROWNE, A. WARREN ELGERSMA et PETER P. SINGER. Can. J. Chem. **68**, 1300 (1990).

Les travaux de pionniers réalisés par R. H. F. Manske et par L. Marion sur les alcaloïdes du Lycopodium ont conduit à la caractérisation d'un grand nombre d'alcaloïdes. Plusieurs de ces alcaloïdes ont été désignés par des chiffres précédés de la lettre L (par example, L1; il a depuis été établi qu'il s'agit de la dihydrolycopodine). Même si l'identité de plusieurs de ces alcaloïdes a maintenant été établie, plusieurs n'ont pas été réétudiés. Faisant appel à la SM/CPG et à l'IR/CPG, on a donc réexaminé des échantillons des alcaloïdes L15, L16, L17, L18, L22, L24, L25, L26, L28, L29, L31 et L35 qui ont été obtenus de la collection de Marion et on rapporte ici l'identité de ces alcaloïdes et de ces mélanges d'alcaloïdes. L'acétylannofoline (**5**), un composant de l'alcaloïde L17, et le 5,15-oxidolycopodane (**9**), un composant des alcaloïdes L28 et L31, n'avaient jamais été identifiés antérieurement comme produits naturels. On fournit une liste complète des alcaloïdes désignés par L et un numéro.

Mots clés : alcaloïdes du Lycopodium, alcaloïdes, acétylannofoline, oxidolycopodane.

[Traduit par la revue]

Introduction

The presence of alkaloids in the genus *Lycopodium* (family Lycopodiaceae) was first noted in 1881. An extensive investigation of these compounds did not commence until the 1940's, and it was not until the late 1950's and early 1960's that the structures of these alkaloids began to be clarified. In Canada the study of the chemistry of the *Lycopodium* alkaloids was pioneered by R. H. F. Manske and L. Marion, who isolated and characterized a large number of alkaloids from various species of the club moss. Since that time the structures of about 100 alkaloids classified into 16 structure types have been established and their chemistry has been the subject of several reviews (1–4). However, the structures of a number of alkaloids originally characterized by Manske and Marion remain unreported (4). In the past few years we have been fortunate to come into possession of many of the original *Lycopodium* samples of Manske and Marion. Several of the alkaloids that were isolated over 40 years ago and whose structure or identity remain to be resolved were found in their sample collection. We have reexamined the samples of alkaloids L15 (*L. tristachyum*), L16 and L17 (*L. obscurum*), L18 (*L. clavatum*), L22, L24, and L25 (*L. lucidulum*), L26 (*L. sabinaefolium*), L28, L29, and L31 (*L. annotinum*), and L35 (*L. densum*) and report herein their identity.

Results and discussion

The alkaloid identification was based on GC/MS (5) examination coupled with GC/IR (6) examination of the sample to rapidly establish the structure. A reference library of MS and IR spectra of known alkaloids was prepared from over 35 authentic samples available to us. In each GC/MS and GC/IR analysis a library search algorithm program was used to search the sample spectrum against the data base to find the best match to a sample spectrum. When the sample was found to be a mixture of alkaloids and sufficient sample was available, the components were separated and the identity of the alkaloids was verified by spectral analysis including high resolution MS and NMR and by comparison with authentic samples.

In the early 1940's Marion and Manske began their chemical investigation of the genus *Lycopodium* with the hypothesis that similarities of alkaloid constituents were indicative of botanical similarities and that this information could form the basis of a chemotaxonomical classification of the genus. Accordingly, several *Lycopodium* species were investigated, their alkaloids isolated, characterized, and designated with an L number. In early 1944 examination of the alkaloids of *L. tristachyum* Pursh led to the isolation of nicotine, lycopodine, L13 (later found to be identical with lycopodine), L14 (subsequently identified as anhydrodihydrolycopodine (7)), and L15. Alkaloid L15 (reported as $C_{20}H_{31}NO_4$) (8) was analyzed by GC/MS and found to comprise one major and one minor component with molecular ions of m/z 247 and 263, respectively. Analysis of the sample by GC/IR confirmed the presence of two components and identified lycopodine (**1**) as the major alkaloid in the mixture. Since the components of the mixture eluted almost simultaneously from the GC column, it was not possible to identify unambiguously the minor alkaloid of L15. Thus alkaloid L15 was separated by chromatography into its components. The least polar compound from the mixture was found to be identical with an authentic sample of lycopodine. The more polar compound was identified as flabelliformine (**2**) (9) by spectral analysis and by comparison with an authentic sample.

The chemical investigation in 1944 of the alkaloids of *L. obscurum* var. *dendroideum* (10) yielded lycopodine, L13, obscurine, and two new alkaloids: L16 and L17. Alkaloid L16 ($C_{16}H_{25}NO$) was reported by these authors to be isomeric with

[1]Author to whom correspondence may be addressed.

Can. J. Chem. Downloaded from www.nrcresearchpress.com by 88.85.125.76 on 09/07/12
For personal use only.

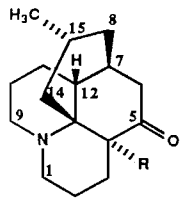

1 R = H
2 R = OH

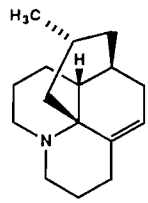

3

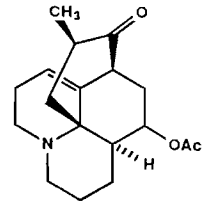

4

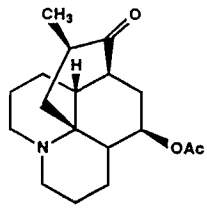

5

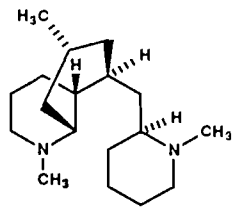

6

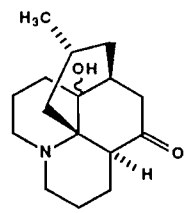

7 α-OH
8 β-OH

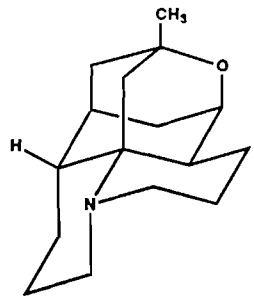

9

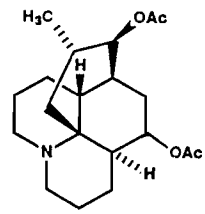

10

lycopodine and L13. Analysis of alkaloid L16 by GC/MS revealed that it is a 1:1 mixture of two compounds with molecular ions of m/z 247 and 231. Subsequent examination of L16 by GC/IR confirmed the presence of two alkaloids and identified these as lycopodine (**1**) and anhydrodihydrolycopodine (**3**). Alkaloid L17 was examined by GC/MS and GC/IR and found to be a 2:1 mixture of alkaloids. The minor component was identical with acetylacrifoline (**4**) (11). The major alkaloid was shown to be acetylannofoline (**5**) (12).

Later in 1944 *L. clavatum* L. of North American origin was examined and found to contain nicotine, lycopodine, L19 (subsequently found to be identical with L34 and shown to be clavolonine) (13, 14), and L18 (reported as $C_{11}H_{19}NO$ and isolated as its picrate) (15). Alkaloid L18 was examined by GC/MS and found to contain two alkaloids (ratio 3:1) each with a molecular ion at m/z 278 ($C_{18}H_{34}N_2$, HRMS) and with very similar fragmentation patterns. GC/IR confirmed that alkaloid L18 was a mixture and that each of the component alkaloids contained *N*-methyl functionality (2780 cm^{-1}). Attempted separation of the sample by chromatography was unsuccessful. Analysis of the ^1H NMR spectrum of the mixture revealed the structural similarity of each component. Each component contains two *N*-methyl groups (δ 2.16, 2.28 (major); 2.25, 2.26 (minor)) and a secondary methyl (δ 0.84 (major); 0.92 (minor)). The spectral properties of the minor component are identical with those of *N,N*-dimethylphlegmarine[2] (**6**) (16). We believe that the major component is an isomer of this compound.

[2]We thank Dr. J. C. Braekman for copies of the spectra of this compound.

A total of nine alkaloids were isolated from *L. lucidulum* Michx. by Manske and Marion in 1946 (17). Besides nicotine, lycopodine, and L13, the remaining alkaloids include L20 (18), L21 (later shown to be luciduline) (19), L22 (reported as $C_{16}H_{27}NO$), L23 (subsequently found to be isolycodoline (**7**)) (20), L24 (reported as $C_{16}H_{25}NO$), and L25 (reported as $C_{16}H_{25}NO_2$). We examined alkaloid L22 by GC/MS and GC/IR. Each analysis revealed that it was a mixture of two alkaloids (ratio 3:2), one of which was lycopodine (**1**). The other component of the mixture shows a molecular ion at m/z 263 ($C_{16}H_{25}NO_2$) and was found to closely match isolycopodine (**7**) in the GC/IR library. Separation of the sample by chromatography led to the isolation of lycopodine and isolycopodine, identical in all respects with authentic samples. Analysis of alkaloids L24 and L25 by GC/MS and GC/IR revealed that each was a single compound. Alkaloid L24 was identified as lycopodine (**1**) while alkaloid L25 was found to be identical with isolycopodine (**7**) (L23).

In a continuation of their studies, Manske and Marion reported that *L. sabinaefolium* Willd. contained four alkaloids: nicotine, lycopodine, alkaloid L13, and alkaloid L26 (reported as $C_{15}H_{25}NO$) (21). Alkaloid L26 was analyzed by GC/MS and GC/IR. It was found to be a pure compound with a molecular formula of $C_{16}H_{27}NO$ (HRMS) and its IR spectrum matched perfectly with that of dihydrolycopodine (22) from the library of known alkaloids. Further analysis of the sample was not undertaken due to the small sample size.

In 1947 it was reported that *L. annotinum* var. *acrifolium* contained a different alkaloid spectrum than other varieties of *L. annotinum*. In addition to annotinine and acrifoline (L27), four

Can. J. Chem. Downloaded from www.nrcresearchpress.com by 88.85.125.76 on 09/07/12
For personal use only.

TABLE 1. Lycopodium alkaloids: the "L" numbers

L no.	Molecular weight	Molecular formula	Name (reference)
L1	249	$C_{16}H_{27}NO$	Dihydrolycopodine (complanatine, L26) (22)
L2	291	$C_{18}H_{31}NO_2$	*O*-Acetyldihydrolycopodine (1)
L3	291	$C_{18}H_{31}NO_2$	*O*-Acetyldihydrolycopodine (1)
L4	231	$C_{16}H_{25}N$	Anhydrodihydrolycopodine (7)[a]
L5	288	$C_{18}H_{28}N_2O$	Flabellidine (30)
L6			Mixture: α- and β-obscurine (31)
L7	275	$C_{16}H_{21}NO_3$	Annotinine (32)
L8	263	$C_{16}H_{25}NO_2$	Lycodoline (L30) (24)
L9			Mixture: lycopodine and acetyllofoline
L10			Structure not reported and sample unavailable
L11	288	$C_{16}H_{21}NO_3$	Annotine (33)
L12	305	$C_{18}H_{25}NO_3$	*O*-Acetylacrifoline (11)
L13	247	$C_{16}H_{25}NO$	Lycopodine[b]
L14	231	$C_{16}H_{25}N$	Anhydrodihydrolycopodine (7)[a]
L15*			Mixture: lycopodine and flabelliformine (9)
L16*			Mixture: lycopodine and anhydrodihydrolycopodine (7)
L17*			Mixture: acetylannofoline (12) and acetylacrifoline (33)
L18*			Mixture: *N,N*-dimethylphlegmarine and isomer
L19	263	$C_{16}H_{25}NO_2$	(L34), clavolonine (13, 14)
L20	263	$C_{16}H_{25}NO_2$	6α-Hydroxylycopodine (18)
L21	207	$C_{13}H_{21}NO$	Luciduline (19)
L22*			Mixture: lycopodine and isolycodoline (L23) (20)
L23	263	$C_{16}H_{25}NO_2$	Isolycodoline (epilycodoline, pseudoselagine) (20)
L24*	247	$C_{16}H_{25}NO$	Lycopodine
L25*	263	$C_{16}H_{25}NO_2$	Isolycodoline (epilycodoline, pseudoselagine) (20)
L26*	249	$C_{16}H_{27}NO$	Dihydrolycopodine (L1) (22)
L27	261	$C_{16}H_{23}NO_2$	Acrifoline (26, 27)
L28*			Mixture: lycopodine and oxidolycopodane (**1**)
L29*	261	$C_{16}H_{23}NO_2$	Acrifoline (26, 27)[c]
L30	263	$C_{16}H_{25}NO_2$	Lycodoline (L8) (24)
L31*			Mixture: *O*-acetyllofoline and oxidolycopodane (**1**)
L32	262	$C_{16}H_{26}N_2O$	Cernuine (34)
L33	278	$C_{16}H_{26}N_2O_2$	Lycocernuine (34)
L34	263	$C_{16}H_{25}NO_2$	Clavolonine (L19) (13, 14)
L35*			Mixture: lycopodine, flabelliformine (9), and lycodoline (24)

*Alkaloids identified recently in this or other studies in our laboratories.

[a]Identical with L14, identified as anhydrodihydrolycopodine by Marion and Manske (Dr. Marion's laboratory notebook 698, p. 15). This identity was confirmed by GC/MS and GC/IR.

[b]Identified as lycopodine by Marion and Manske (Dr. Marion's laboratory notebook 698, p. 57). Eleven samples of L13 isolated from several *Lycopodium* species were found to be composed mainly of lycopodine by GC/MS and GC/IR.

[c]We thank T. Chua, Alberta Heritage Undergraduate Summer Research Assistant, 1986, for this identification.

previously unreported alkaloids were isolated and designated numbers L28–L31 (23). Subsequent investigations revealed that L30 was identical with L8, which has been shown to possess structure **8** and has been named lycodoline (24). The structures of L28, L29, and L31 have not been reported to date. L28 (reported as $C_{17}H_{27}NO_2$) was analyzed by GC/MS. It was shown to be a mixture of two compounds, each of which has a molecular weight of 247 with similar but not identical mass spectral fragmentation patterns. Analysis by GC/IR confirmed the presence of two components and revealed that one of the components was lycopodine (**1**). The mixture was separated by chromatography over alumina. The less polar component, L28-1, was identified as lycopodine by comparison of its spectral properties with those of an authentic sample. The more polar component, L28-2, was isolated as an optically active, air-sensitive oil. The HRMS confirmed its molecular weight as m/z 247 and established the molecular formula as $C_{16}H_{25}NO$. The base peak at m/z 174 ($M^+ - C_4H_9O$) is consistent with oxygen functionality on the "bridge atoms" (C-8, C-14, C-15). Examination of the IR spectrum of L28-2 revealed the absence of hydroxyl or carbonyl functional groups and thus the oxygen of L28-2 must be present as an ether. This was corroborated by its ^{13}C NMR spectrum, which showed oxygenated carbons at δ 74.3 (CH) and 72.3 (C). The ^1H NMR spectrum of L28-2 revealed a methyl singlet (δ 1.15) and this suggested that L28-2 may have structure **9**. 5,15-Oxidolycopodane (**9**) has not been isolated previously from natural sources although it has been prepared synthetically in a series of reactions from lycopodine (25). To confirm the identity of **9**, we oxidized dihydrolycopodine with lead tetraacetate. The oxidation product obtained was identical in all respects (MS, IR, ^1H and ^{13}C NMR) with L28-2. In earlier studies in these laboratories alkaloid L29 was identified as acrifoline (26, 27) by comparison (TLC, IR, MS) with an authentic sample.

Another unidentified alkaloid isolated from *L. annotinum*, L31 (reported as $C_{20}H_{29}NO_4$), was also found to be a mixture of two components by GC/MS: $C_{16}H_{25}NO$ (m/z 247) and $C_{20}H_{31}NO_4$ (m/z 359). The presence of two components in

Can. J. Chem. Downloaded from www.nrcresearchpress.com by 88.85.125.76 on 09/07/12
For personal use only.

TABLE 2. Compounds in the GC/MS and GC/IR library*

Molecular weight	Molecular formula	Name	Molecular weight	Molecular formula	Name
207	$C_{13}H_{21}NO$	Luciduline	274	$C_{17}H_{26}N_2$	Dihydroobscurinine
231	$C_{16}H_{25}N$	Anhydrodihydrolycopodine*	274	$C_{17}H_{26}N_2O$	Sauroxine
242	$C_{16}H_{22}N_2$	Lycodine	275	$C_{16}H_{21}NO_3$	Annotine
242	$C_{15}H_{18}N_2O$	Huperzine A (selagine)	275	$C_{16}H_{21}NO_3$	Annotinine
245	$C_{16}H_{23}NO$	Fawcettidine	278	$C_{16}H_{26}N_2O_2$	Lycocernuine
247	$C_{16}H_{25}NO$	Lycopodine	279	$C_{16}H_{25}NO_3$	Alopecuridine
248	$C_{16}H_{28}N_2$	Dihydrodeoxycernuine	291	$C_{18}H_{29}NO_3$	Clavine
249	$C_{16}H_{27}NO$	Dihydrolycopodine	291	$C_{17}H_{25}NO_3$	Lyconnotine
258	$C_{16}H_{22}N_2O$	Des-*N*-methyl-β-obscurine	303	$C_{18}H_{25}NO_3$	Acetylacrifoline
260	$C_{16}H_{24}N_2O$	Des-*N*-methyl-α-obscurine	305	$C_{18}H_{27}NO_3$	Acetylannofoline*
261	$C_{16}H_{23}NO_2$	Acrifoline	305	$C_{18}H_{27}NO_3$	Dehydro-α-lofoline
261	$C_{16}H_{23}NO_2$	Serratidine	305	$C_{18}H_{27}NO_3$	Dehydrofawcettiine
262	$C_{16}H_{26}N_2O$	Cernuine	305	$C_{18}H_{27}NO_3$	Dihydro-*O*-acetylacrifoline
263	$C_{16}H_{25}NO_2$	Clavolonine	307	$C_{18}H_{29}NO_3$	α-Lofoline
263	$C_{16}H_{25}NO_2$	Flabelliformine	307	$C_{18}H_{29}NO_3$	Fawcettiine (β-lofoline)
263	$C_{16}H_{25}NO_2$	Isolycodoline	307	$C_{18}H_{29}NO_3$	Lycoclavine
263	$C_{16}H_{25}NO_2$	Lucidioline	320	$C_{18}H_{28}N_2O_3$	Acetyllycocernuine*
263	$C_{16}H_{25}NO_2$	Lycodoline	321	$C_{18}H_{28}NO_4$	*N*-Acetylalopecuridine
263	$C_{16}H_{25}NO_2$	Lycofoline	323	$C_{18}H_{29}NO_4$	Lycofawcine
264	$C_{16}H_{28}N_2O$	Dihydrodeoxylycocernuine	333	$C_{19}H_{27}NO_5$	Acetylannopodine
265	$C_{16}H_{27}NO_3$	Dihydroclavolonine	349	$C_{20}H_{31}NO_4$	Acetyllofoline
272	$C_{17}H_{24}N_2$	Isoobscurinine*	349	$C_{20}H_{31}NO_4$	Acetylfawcettiine
272	$C_{17}H_{24}N_2$	Obscurinine	349	$C_{20}H_{31}NO_4$	Acetyllycoclavine
274	$C_{16}H_{26}N_2O$	α-Obscurine	367	$C_{23}H_{29}NO_3$	Alopecurine

*Alkaloids not present in the GC/MS library.

Can. J. Chem. Downloaded from www.nrcresearchpress.com by 88.85.125.76 on 09/07/12
For personal use only.

L31 was confirmed by GC/IR analysis, which indicated the presence of compound **9** and acetyllofoline. The components were separated by chromatography over alumina to give L31-1, identified as oxidolycopodane (**9**) by comparison with an authentic sample, and L31-2, identified as acetyllofoline (**10**) by comparison with an authentic sample (28).

The last species of *Lycopodium* investigated by these workers was a species indigenous to New Zealand, *L. densum* Labill. This plant, which has a lower than usual total alkaloid content, contains lycopodine, L34 (identified as clavolonine) (12, 13), and alkaloid L35 (reported as $C_{14}H_{21}NO_2$) (29). GC/MS analysis revealed that alkaloid L35 is a mixture of three components (ratio 5:1:2) with molecular ions of m/z 247 ($C_{16}H_{25}NO$), 263 ($C_{16}H_{25}NO_2$), and 263 ($C_{16}H_{25}NO_2$). Examination of the mixture by GC/IR indicated that these alkaloids were lycopodine (**1**), flabelliformine (**2**) (9), and lycodoline (L8) (**8**) (24), respectively. Alkaloid L35 was separated by chromatography. Comparison of the spectral data of each compound isolated with those of authentic samples confirmed their identity.

The Lycopodium alkaloids have proven to be a rich source of chemically interesting compounds. In total there were 35 alkaloids designated with an L number by Manske and Marion. The structures or identity of the majority of these alkaloids were determined previously. Table 1 presents a complete list of all of the L-numbered alkaloids. They are presented in order of increasing L number, and the table includes their molecular weight, molecular formula, name, and reference to their structure determination.

Experimental

Materials and methods

The alkaloids used in compiling the library of spectra are listed in order of increasing molecular weight in Table 2.

GC/MS and GC/IR

Alkaloid samples were prescreened by GC using the conditions described below. Initially retention indices were calculated with respect to lycopodine. Over the time period for this study, however, the retention index of some standards changed enough to warrant this data unacceptable for identification purposes. Analysis of the alkaloid sample by GC/MS was performed on a HP5985 MS system using an HP5840A gas chromatograph with a 18835 splitless capillary inlet. The samples (1–2 μL, c = 1 mg/mL) were injected onto a fused silica capillary column (12 m × 0.32 mm i.d.) coated with an SE-54 equivalent. (Conditions: flow rate 4 mL/min; carrier gas He; temperatures: injector 280°C, detector 300°C, oven 80°C (1 min), 80–300°C at 20°/min, 300°C (5 min).) The gas chromatograph was connected to the mass spectrometer by an open split interface (MS: positive ion mode; ionizing beam 70 eV; temperatures: source 200°C, transfer line 300°C; mass range 35–500; 50 scans/min). The MS of authentic samples of alkaloids were entered into a GC/MS library and test samples identified by computer match when possible (5). Analysis of the alkaloids by GC/IR was performed on a HP5965A IRD system. The samples (1–2 μL, c = 1 mg/mL) were injected onto an Ultra 2 capillary column (conditions: carrier gas He; temperature: injector 200°C, oven 80°C (1 min), 80–290°C at 20°/min, 290°C (5 min)). The gas phase IR spectra of known alkaloids were entered into the GC/IR library. The gas phase IR spectra of the unknown alkaloids were compared to library spectra by computer using a library search algorithm. The spectrum search parameters were developed and the accuracy of the match between the sample spectrum and known spectrum was assessed and a match quality number assigned. Match quality numbers greater than 950 (maximum 1000) were considered to be identical with an authentic sample. The best match was visually inspected for confirmation of identity.

5,15-Oxidolycopodane (9)

Alkaloid L28 (*L. annotinum*) was chromatographed over alumina (eluant: CH_2Cl_2–CH_3OH (2%) gradient) to give two compounds. The less polar constituent was identified as lycopodine by comparison with an authentic sample. The more polar component was identified as

oxidolycopodane (**9**) (25): $[\alpha]_D$ 51° (*c* 0.019, CH_3OH); FTIR: 2964, 2925, 2860, 1442, 1132, 1110 cm^{-1}; ^1H NMR (360 MHz, $CDCl_3$) δ: 3.63 (1H, m, H-5), 3.36 (1H, td, *J* = 3.5, 14.5 Hz, H-1e), 3.19 (1H, td, *J* = 3.5, 12.0 Hz, H-9e), 2.64 (1H, dd, *J* = 2.0, 12.0 Hz, H-14a), 2.53 (1H, dm, *J* = 2.0, 12.5 Hz, H-1a), 2.05 (1H, m, H-4), 1.97 (1H, m, H-2a), 1.89 (2H, m, H-3a, H-6a), 1.78 (1H, m, H-10e), 1.73 (1H, ddd, *J* = 2.5, 2.5, 12.0 Hz, H-11), 1.70 (2H, m), 1.67 (1H, m, H-10), 1.63 (1H, m), 1.60 (1H, m), 1.55 (1H, ddd, *J* = 2.0, 4.0, 12.0 Hz, H-8a), 1.47 (1H, m, H-3e), 1.40 (1H, m), 1.27 (1H, dm, *J* = 13 Hz, H-2a), 1.15 (3H, s, H-16), 1.06 (1H, d, *J* = 12.0 Hz, H-14e); ^{13}C NMR (75.5 MHz, $CDCl_3$) δ: 74.3 (d, C-5), 72.3 (s, C-15), 54.3 (s, C-13), 46.8 (d, C-12), 47.4 (t, C-9), 47.0 (t, C-1), 43.9 (t, C-14), 42.1 (t, C-8), 33.9 (d, C-7), 31.4 (d, C-4), 31.0 (t, C-6), 29.2 (q, C-16), 26.5 (t, C-10), 25.6 (t, C-11), 24.6 (t, C-3), 18.6 (t, C-2); HREIMS (probe) 70 eV, *m/z* (rel. int.) calcd. for $C_{16}H_{25}NO$: 247.1936; found: 247.1944; (47), 191 (10), 190 (60), 176 (10), 175 (15), 174 ($C_{12}H_{16}N$, 100), 163 (17), 146 (10).

Transformation of dihydrolycopodine to compound ***9***

$Pb(OA)_4$ (100 mg) and I_2 (catalytic amount) were added to a solution of dihydrolycopodine (26 mg) in CH_2Cl_2 (5 mL). The reaction mixture was irradiated for 16 h using a 75-W light bulb. H_2O (10 mL) was added and the layers separated. The aqueous fraction was extracted several times with CH_2Cl_2, then basified (aq. NH_3) and extracted exhaustively with CH_2Cl_2. The CH_2Cl_2 layer was subjected to acid–base work-up in the usual way. The resultant CH_2Cl_2 fraction was concentrated to give an oil (14.5 mg) that was shown to be a mixture of 3 components (TLC). Chromatography over Al_2O_3 gave dihydrolycopodine (5.4 mg) and 5,15-oxidolycopodane (8.0 mg). The third component decomposed before it was fully characterized.

Acknowledgements

We thank T. Chua (Alberta Heritage Undergraduate Summer Research Assistant) for the earlier identification of alkaloid L29, Dr. J. C. Braekman for spectra of *N*,*N*-dimethylphlegmarine, J. Hoyle for the GC/IR analyses, and the Natural Sciences and Engineering Research Council of Canada for financial support. Special thanks are due to Dr. O. E. Edwards, formerly of the National Research Council, Ottawa, for providing us with Dr. Marion's collection of Lycopodium alkaloids and the lab books describing their isolation, and Prof. D. B. MacLean for providing many reference samples over the years.

1. D. B. MacLean. *In* The alkaloids. Vol. 10. *Edited by* R. H. F. Manske. Academic Press, New York. 1968.
2. W. A. Ayer. *In* MTP international review of science. Series 1, Vol. 9. *Edited by* D. H. Hey and K. F. Wiesner. University Park Press, Baltimore. 1973. p. 1.
3. D. B. MacLean. *In* The alkaloids. Vol. 14. *Edited by* R. H. F. Manske. Academic Press, New York. 1973.
4. D. B. MacLean. *In* The alkaloids. Vol. 16. *Edited by* A. Brossi. Academic Press, New York. 1985.
5. R. V. Gerard and D. B. MacLean. Phytochemistry, **25**, 1143 (1986).
6. W. Herres. *In* HRGC-FTIR: capillary gas chromatography – Fourier transform infrared spectroscopy. Huthig, New York. 1987. p. 1.
7. F. A. L. Anet. Tetrahedron Lett. No. 20, 13 (1960).
8. L. Marion and R. H. F. Manske. Can. J. Res. **22B**, 1 (1944).
9. M. Curcumelli-Rodostamo and D. B. MacLean. Can. J. Chem. **40**, 1068 (1962).
10. R. H. F. Manske and L. Marion. Can. J. Res. **22B**, 53 (1944).
11. G. S. Perry and D. B. MacLean. Can. J. Chem. **34**, 1189 (1956).
12. G. C. Kasitu. Ph.D. Thesis, University of Alberta, Edmonton, Alberta. 1988. pp. 90–97.
13. R. H. Burnell and D. R. Taylor. Tetrahedron, **15**, 173 (1961).
14. R. H. Burnell and D. R. Taylor. Chem. Ind. (London), 1239 (1960).
15. L. Marion and R. H. F. Manske. Can. J. Res. **22B**, 137 (1944).
16. L. Nyembo, A. Goffin, C. Hootele, and J. C. Braekman. Can. J. Chem. **56**, 851 (1978).
17. R. H. F. Manske and L. Marion. Can. J. Res. **24B**, 57 (1946).
18. W. A. Ayer, J. A. Berezowsky, and D. A. Law. Can. J. Chem. **41**, 649 (1963).
19. W. A. Ayer, N. Masaki, and D. S. Nkunika. Can. J. Chem. **46**, 3631 (1968).
20. W. A. Ayer, B. Altenkirk, R. H. Burnell, and M. Moinas. Can. J. Chem. **47**, 449 (1969).
21. L. Marion and R. H. F. Manske. Can. J. Res. **24B**, 63 (1946).
22. W. A. Harrison, M. Curcumelli-Rodostamo, D. F. Carson, L. R. C. Barclay, and D. B. MacLean. Can. J. Chem. **39**, 2086 (1961).
23. R. H. F. Manske and L. Marion. J. Am. Chem. Soc. **60**, 2126 (1947).
24. W. A. Ayer and G. Iverach. Can. J. Chem. **42**, 2514 (1964).
25. W. A. Ayer and K. Piers. Chem. Commun. 541 (1965).
26. W. N. French and D. B. MacLean. Chem. Ind. (London), 658 (1960).
27. W. N. French and D. B. MacLean. Can. J. Chem. **39**, 2100 (1961).
28. W. A. Ayer, A. N. Hogg, and A. C. Soper. Can. J. Chem. **42**, 949 (1964).
29. R. H. F. Manske. Can. J. Chem. **31**, 894 (1953).
30. S. N. Alam, K. A. H. Adams, and D. B. MacLean. Can. J. Chem. **42**, 2456 (1964).
31. W. A. Ayer and G. G. Iverach. Can. J. Chem. **38**, 1823 (1960).
32. K. Wiesner, W. A. Ayer, L. R. Fowler, and Z. Valenta. Chem. Ind. (London), 564 (1957).
33. W. A. Szarek, K. A. H. Adams, M. Curcumelli-Rodostamo, and D. B. MacLean. Can. J. Chem. **42**, 2584 (1964).
34. W. A. Ayer, J. K. Jenkins, S. Valverde-Lopez, and R. H. Burnell. Tetrahedron Lett. 2201 (1964).

Can. J. Chem. Downloaded from www.nrcresearchpress.com by 88.85.125.76 on 09/07/12
For personal use only.

α-(Dialkylamino)-α-pyrrolylacetonitriles. A potpourri of useful synthetic transformations[1]

BRIAN L. BRAY[2] AND JOSEPH M. MUCHOWSKI[3]

Syntex Research, Institute of Organic Chemistry, 3401 Hillview Avenue, Palo Alto, CA 94304, U.S.A.

Received February 27, 1990

BRIAN L. BRAY and JOSEPH M. MUCHOWSKI. Can. J. Chem. **68**, 1305 (1990).

α-(Dialkylamino)-α-(pyrrol-2-yl)acetonitriles (**3**) are versatile intermediates that are readily converted into regiochemically pure 2-bromo-6-dialkylamino-1-azafulvenes and 5-bromo-2-acylpyrroles (acyl = CHO, COR). In addition, **3** (R^1 = H), **4** (R^1 = H), and the β-substituted compound **9** are transformed easily and under mild conditions, via the corresponding α-methylthio compounds (e.g., **7***a*), into the methyl pyrrole carboxylates **8***a*, **8***b*, and **10**, respectively.

Key words: α-(dialkylamino)-α-(pyrrol-2-yl)acetonitriles, 5-bromo-2-acylpyrroles, methyl pyrrole carboxylates.

BRIAN L. BRAY et JOSEPH M. MUCHOWSKI. Can. J. Chem. **68**, 1305 (1990).

Les α-(dialkylamino)-α-(pyrrol-2-yl)acétonitriles (**3**) sont des intermédiaires versatiles qui peuvent facilement être transformés en 2-bromo-6-dialkylamino-1-azafulvènes et en 5-bromo-2-acylpyrroles (acyle = CHO, COR) qui sont régiochimiquement purs. De plus, utilisant des conditions douces impliquant un passage par les composés α-méthylthio correspondants (comme le produit **7***a*), on a pu facilement transformer les composés **3** (R^1 = H), **4** (R^1 = H) ainsi que le composé β-substitué (**9**) dans les pyrrolecarboxylates de méthyle respectifs, **8***a*, **8***b* et **10**.

Mots clés : α-(dialkylamino)-α-(pyrrol-2-yl)acétonitriles, 5-bromo-2-acylpyrroles, pyrrolecarboxylates de méthyle.

[Traduit par la revue]

Can. J. Chem. Downloaded from www.nrcresearchpress.com by 88.85.125.76 on 09/07/12
For personal use only.

It was recently reported (1) that α-(dimethylamino)-α-pyrrolylacetonitriles were useful precursors of alkyl pyrrolyl ketones and were particularly valuable for the synthesis of 3-alkanoylpyrroles. This publication shows that these "Strecker type" nitriles undergo a number of other synthetically important transformations, some of which are uniquely characteristic of α-(dialkylamino)-α-pyrrolylacetonitriles.

The previously unreported α-dialkylamino nitriles **3***b* and **3***c* (Scheme 1) were synthesized by the reaction of excess sodium cyanide with the iminium salts **2***b* and **2***c*, which in turn were obtained from pyrrole and the appropriate dialkylamide under Vilsmeier–Haack (2) conditions. This process is analogous to that which has been used (1) to synthesize **3***a*.

The bromination of the α-dialkylamino nitriles **3***a–d* with *N*-bromosuccinimide in tetrahydrofuran (THF) occurred rapidly at −78°C to give predominantly, if not exclusively, the corresponding 5-bromo compounds **4***a–d* (Scheme 2). These substances, though isolable, were unstable, and were used without purification in subsequent reactions. For example, hydrolysis of **4***b–d* (see Experimental) gave 5-bromopyrrole-2-carboxaldehyde (**6***b*), 2-benzoyl-5-bromopyrrole (**6***c*), and 2-*n*-nonanoyl-5-bromopyrrole (**6***d*), respectively. These hydrolyses proceeded via intermediate 1-azafulvenes, which, in the case of **5***b* and **5***c* were easily isolable, stable entities. Compound **5***b* has recently been shown to be a valuable precursor of a wide variety of 5-substituted pyrrole-2-carboxaldehydes (3).

The bromination of **3** at C-5 is an important observation because it demonstrates that the α-dialkylaminoacetonitrile group is an activating substituent, even though formally at the aldehyde or ketone level of oxidation. This is of obvious synthetic significance since the direct bromination of 2-acylpyrroles occurs to give a mixture of the 4-bromo (kinetic product) and the 5-bromo compounds in which the latter is usually the minor product (4).

The dianions corresponding to **3***a* and **4***a*, which were generated with lithium diisopropylamide at low temperature,

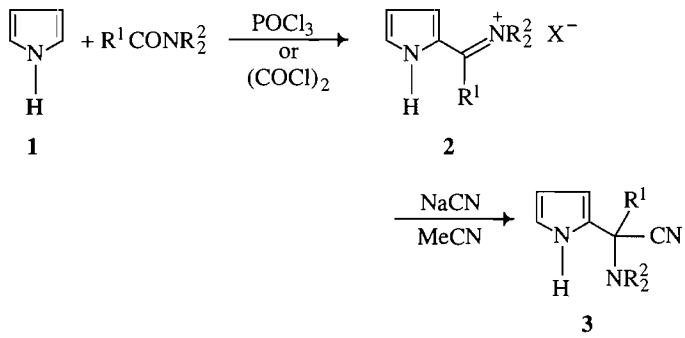

1 **2** **3**

a, R^1 = H, R^2 = Me
b, R^1 = H, R^2 = *i*-Pr
c, R^1 = Ph, R^2 = Me

SCHEME 1

upon reaction with dimethyl disulfide gave the isolable but unstable methylthio compounds **7***a* and **7***b* (Scheme 3). On brief treatment with aqueous methanolic sodium hydroxide, these compounds gave the methyl esters **8***a* or **8***b* in ca. 60% yield. Methyl pyrrole-3-carboxylate (**10**) was obtained in an analogous manner from the known (1) α-dimethylaminoacetonitrile derivative **9**.

The formation of the above esters presumably takes place by addition of hydroxide ion to the *anti* thioimidate salts (**11**, Scheme 4) and subsequent stereoelectronically controlled fragmentation (5) of the tetrahedral intermediate **12** to the thiol ester **13**. Base-catalysed methanolysis of the thiol ester would provide the observed methyl esters.

The above process constitutes an exceedingly mild means of oxidation of pyrrole carboxaldehydes to the corresponding carboxylic acid esters. It has precedent in the work of Jonczyk *et al.* (6) who have reported that α-methylthio-α-dialkylaminoacetonitriles can be hydrolytically converted into *N*,*N*-dialkylamides or alkyl acetic acids. In addition, Boche and co-workers (7) have shown that *N*,*N*-dialkylamides are generated on acidic hydrolysis of α-trimethylsilyloxy-α-dimethylaminoacetonitriles.

In summary, α-(dialkylamino)-α-pyrrolylacetonitriles are not only useful precursors of alkanoylpyrroles (1) but, in

[1]Contribution no. 804 from the Institute of Organic Chemistry.
[2]Syntex Research Postdoctorate Fellow, 1987–1989.
[3]Author to whom correspondence may be addressed.

Printed in Canada / Imprimé au Canada

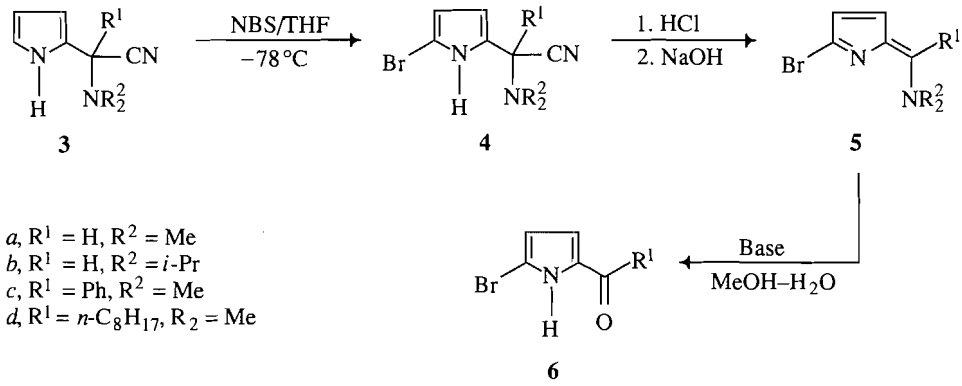

3 4 5 6

SCHEME 2

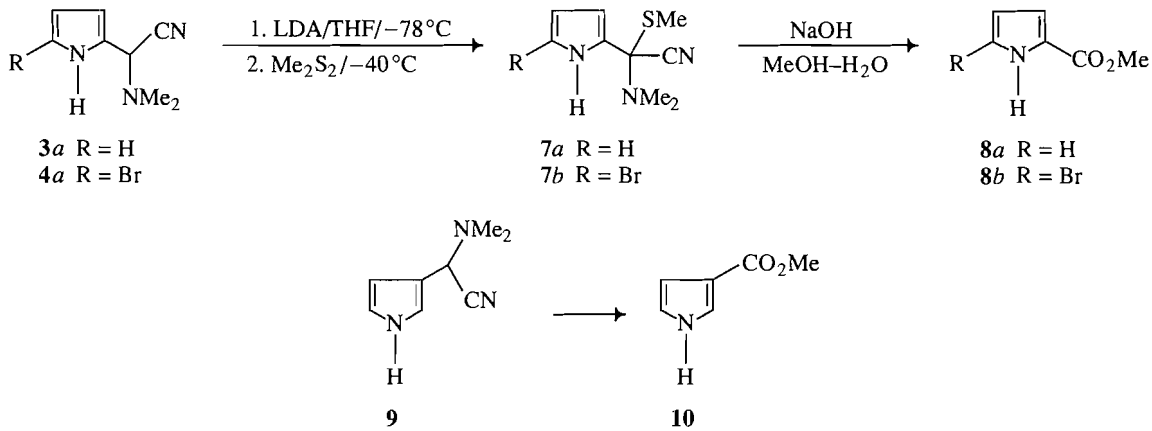

3a R = H
4a R = Br
7a R = H
7b R = Br
8a R = H
8b R = Br

9 10

SCHEME 3

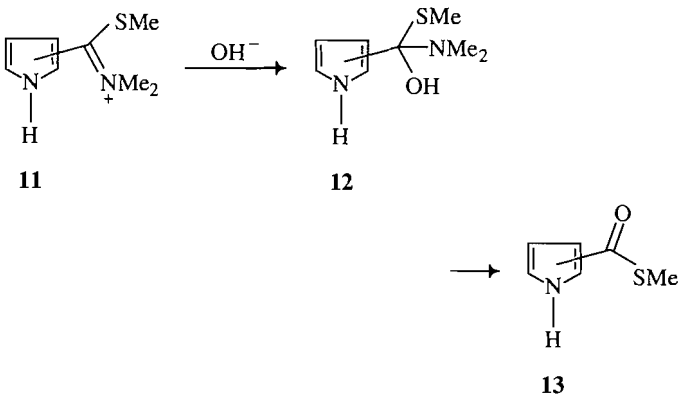

11 12 13

SCHEME 4

addition, can be converted with ease into 5-bromo-6-dialkylamino-1-azafulvenes, methyl pyrrolyl carboxylates, and 5-bromo-2-acylpyrroles. Because the α-(dialkylamino)-α-pyrrolylacetonitrile substituent is activating, at least when at C-2 of the pyrrole nucleus, such compounds are likely to find considerable utility in the synthesis of regiochemically pure 5-substituted-2-acylpyrroles.

Experimental

The melting points were determined in a Mel-Temp melting point apparatus and are not corrected. The infrared spectra were measured as dispersions in potassium bromide with a Nicolet 5 PC FT infrared spectrophotometer. The ^{1}H nmr spectra were measured with a Varian EM-360 or a Bruker WM 300 nmr spectrometer in deuteriochloroform and are expressed as parts per million (δ) from internal tetramethylsilane. When exchangeable protons were present, the data are given for deuterium oxide exchanged spectra.

The terms "worked up in the usual manner" or the "usual work-up" signify that the extract was dried over anhydrous magnesium sulfate and evaporated *in vacuo*.

The α-(dimethylamino)-α-pyrrolylacetonitriles **3***a*, **3***d*, and **9** were prepared by the method of Bray and Muchowski (1).

Tetrahydrofuran was distilled from benzophenone ketyl before use.

N,N-*Diisopropylpyrrole-2-formiminium chloride* **2**b

A solution of *N*,*N*-diisopropylformamide (28.9 g, 224 mmol) in anhydrous dichloromethane (50 mL) was added dropwise at 0°C to a stirred solution of oxalyl chloride (28.4 g, 224 mmol) in the same solvent (500 mL) over a 0.25 h period. After 0.33 h at 0°C, a solution of pyrrole (15.0 g, 224 mmol) in dichloromethane (50 mL) was added dropwise with stirring over a 0.25 h period. The reaction mixture was then stirred at room temperature for 0.33 h. The solvent was removed *in vacuo* and the resulting solid was washed with dry acetone and then dried *in vacuo* to provide the hygroscopic salt **2***b* (48 g, 100% yield), which was pure as judged by nmr spectroscopy. Three recrystallizations of the salt from dry ethyl acetate gave an analytical specimen, mp 212–213°C; ir: 3441, 1644 cm^{-1}; nmr (300) δ: 1.52 (d, 6H, J = 6.9 Hz, CH*Me*$_2$), 1.62 (d, 6H, J = 6.6 Hz, CH*Me*$_2$), 4.13 (sept, 1H, J = 6.9 Hz, *CH*Me$_2$), 4.79 (sept, 1H, J = 6.6 Hz, *CH*Me$_2$), 6.61 (m, 1H, $J_{3,4}$ = 4.4 Hz, $J_{4,5}$ ≈ 2.2 Hz, H-4),[4] 7.24 (bd, 1H, H-3), 7.54 (dd, 1H, $J_{4,5}$ ≈ 2.2 Hz, $J_{3,5}$ ≈ 1.0 Hz, H-5), 9.83 (bs, 1H, CH=N). Anal. calcd. for $C_{11}H_{19}ClN_2$: C 61.53, H 8.92, N 13.04; found: C 61.60, H 8.73, N 12.82.

*α-(Diisopropylamino)-α-(pyrrol-2-yl)-acetonitrile (3*b)

A slurry of the nmr pure iminium salt **26** (23 g, 108 mmol) and sodium cyanide (26.5 g, 540 mmol) in acetonitrile (750 mL) was stirred

[4]H-4 is coupled to the iminium proton by ~0.5 Hz.

Can. J. Chem. Downloaded from www.nrcresearchpress.com by 88.85.125.76 on 09/07/12
For personal use only.

Can. J. Chem. Downloaded from www.nrcresearchpress.com by 88.85.125.76 on 09/07/12
For personal use only.

at 23°C for 12 h. About 75% of the solvent was removed *in vacuo* and then ether (300 mL) was added. The organic solution was washed successively with water and saturated sodium chloride solution and then it was dried over anhydrous potassium carbonate. The solvent was removed *in vacuo* and the solid so obtained was recrystallized from hexane–ether to provide pure **3***b*, mp 113–115°C; ir: 3331, 2234 cm^{-1}; nmr (300) δ: 1.07 (d, 6H, J = 6.67 Hz, CH*Me*$_2$), 1.26 (d, 6H, J = 6.67 Hz, CH*Me*$_2$), 3.23 (sept, 2H, J = 6.67 Hz, *CH*Me$_2$), 4.96 (bs, 1H, CHN),[5] 6.19 (m, 1H, $J_{3,4}$ = 3.57 Hz, $J_{4,5}$ = 2.68 Hz, H-4), 6.37 (m, 1H, $J_{3,4}$ = 3.57 Hz, $J_{3,5}$ = 1.52 H, H-3),[6] 6.77 (m, 1H, $J_{4,5}$ = 2.68 Hz, $J_{3,5}$ = 1.52 Hz, H-5).[6] Anal. calcd. for $C_{12}H_{19}N_3$: C 70.20, H 9.33, N 20.46; found: C 70.31, H 9.41, N 20.70.

*α-(Dimethylamino)-α-phenyl-α-(pyrrol-2-yl)acetonitrile (**3**c)*

A solution of *N*,*N*-dimethylbenzamide (10.0 g, 67 mmol) in phosphorus oxychloride (10.0 g, 67 mmol) was left at room temperature, with protection from moisture, for 2 h. A solution of pyrrole (4.5 g, 67 mmol) in dry dichloromethane (200 mL) was added to the crystalline iminimum salt and the mixture was stirred for 20 h at 23°C. The resulting solution was concentrated *in vacuo* and the iminium salt **2***c* was dissolved in acetonitrile (400 mL). Powdered anhydrous potassium cyanide (65 g, 1.0 mol) was added with stirring. The light yellow colored reaction mixture rapidly became black. Stirring at 23°C was continued for 3.5 h and then the solvent was removed *in vacuo*. The black colored solid was partitioned between ether and water. The ether phase was separated, combined with an ether extract of the aqueous phase, and then it was washed successively with water and saturated salt solution. The ether solution was dried over anhydrous potassium carbonate and the deeply colored solution was stirred with activated charcoal (35 g). Filtration of the mixture and evaporation of the filtrate to dryness *in vacuo* gave **3***c* as a solid (11.7 g, 78%) that was pure as judged by nmr spectroscopy. Recrystallization of this material from hexane–ether gave the analytically pure material (9.1 g, 61% yield), mp 84–85°C; ir: 2234 cm^{-1}; nmr (300) δ: 2.26 (s, 6H, NMe$_2$), 6.07 (dd, 1H, $J_{3,4}$ = 3.52 Hz, $J_{4,5}$ = 2.81 Hz, H-4), 6.39 (dd, 1H, $J_{3,4}$ = 3.52 Hz, $J_{3,5}$ = 1.54 Hz, H-3), 6.70 (dd, 1H, $J_{3,5}$ = 1.54 Hz, $J_{4,5}$ = 2.81 Hz, H-5), 7.31–7.40 (m, 3H, H-3′,4′,5′), 7.69 (2H, H-2′,6′). Anal. calcd. for $C_{14}H_{15}N_3$: C 74.63, H 6.71, N 18.65; found: C 74.70, H 6.87, N 18.40.

*2-Bromo-6-diisopropylamino-1-azafulvene (**5**a)*

N-Bromosuccinimide (2.23 g, 12.5 mmol) was added to a stirred solution of **3***b* (2.57 g, 12.5 mmol) in dry THF (100 mL) at −78°C. The reaction mixture was stirred at this temperature for 4 h, removed from the cooling bath and, when the reaction temperature had reached ambient, the solvent was removed *in vacuo*. The residue (**4***b*) was dissolved in methanol (50 mL), 0.5 M HCl (50 mL) was added, and after 0.33 h at room temperature the deeply colored solution was poured into water. After extraction with ether (discarded) the aqueous phase was adjusted to pH 12 with 10 wt.% sodium hydroxide solution. The azafulvene precipitated out of solution. The mixture was extracted with ether, the extract was washed with saturated salt solution, and then it was dried over sodium sulfate. The solvent was removed *in vacuo* and the residual solid was crystallized from hexane–ether to give pure **5***a* (2.57 g, 80% yield), mp 110–112°C; ir: 1616 cm^{-1}; nmr (300) δ: 1.31 (d, 6H, J = 6.73 Hz, CH*Me*$_2$), 1.35 (d, 6H, J = 6.73 Hz, CH*Me*$_2$), 3.81 (sept, 1H, J = 6.73 Hz, *CH*Me$_2$), 6.31 (d, 1H, $J_{3,4}$ = 3.78 Hz, H-3), 6.40 (sept, 1H, J = 6.73 Hz, *CH*Me$_2$), 6.89 (d, 1H, $J_{3,4}$ = 3.78 Hz, H-4), 7.01 (s, 1H, H-6).[7] Anal. calcd. for $C_{11}H_{17}BrN_2$: C 51.37, H 6.66, N 10.89; found: C 51.45, H 6.71, N 10.85.

*2-Bromo-6-phenyl-6-dimethylamino-1-azafulvene (**5**c)*

N-Bromosuccinimide (1.46 g, 8.22 mmol) was added to a stirred solution of **3***c* (1.85 g, 8.22 mmol) in dry THF (50 mL) at −78°C. The solution was stirred at −78°C for 3 h and then warmed to 23°C over a 0.5 h period. The solvent was removed *in vacuo* and the solid residue (**4***c*) was dissolved in methanol (75 mL). Sodium hydroxide solution (10 wt.%, 20 mL) was added and the reaction mixture was stirred at room temperature for 5 min. The slurry was poured into an HCl (1 M, 150 mL) – ice (100 g) mixture and the resulting solution was extracted with ether. The aqueous phase was adjusted to pH 12 by the addition of 10 wt.% sodium hydroxide solution (the azafulvene precipitates). The mixture was shaken with ether and the azafulvene solution was processed as described for **5***a*. The solid produced in this way (1.96 g, 86%) was pure as judged by its nmr spectrum. Recrystallization from hexane–ether gave the analytically pure material (1.79 g, 78% yield), mp 160–162°C; ir: 1592 cm^{-1}; nmr (300) δ: 2.97 (s, 3H, NMe), 3.99 (s, 3H, NMe), 6.20 (q, 2H, $J_{3,4}$ = 3.95 Hz, H-3,4), 7.32 (m, 2H), 7.47 (m, 3H). Anal. calcd. for $C_{13}H_{13}BrN_2$: C 56.33, H 4.72, N 10.10; found: C 56.04, H 4.78, N 9.87.

*5-Bromopyrrole-2-carboxaldehyde (**6**a)*

A solution of the azafulvene **5***a* (0.100 g, 0.389 mmol) in methanol (20 mL) containing 10 wt.% sodium hydroxide solution (10 mL) was stirred at room temperature for 5 h. The reaction mixture was poured into 1 N HCl (50 mL) and the product was extracted into dichloromethane solution. After the usual work-up the aldehyde **6***a* was obtained as a pure crystalline solid (0.060 g, 88% yield), mp 94–96°C (lit. (8) mp 93–94°C).

*5-Bromo-2-benzoylpyrrole (**6**c)*

A solution of the azafulvene **5***c* (0.40 g, 1.4 mmol) in methanol (25 mL) containing sodium acetate (0.60 g, 7.2 mmol) and water (10 mL) was heated at reflux temperature for 22 h. The cooled solution was poured into saturated sodium chloride solution and the product was extracted into ether. After the usual work-up, the solid that was obtained was recrystallized from hexane – ethyl acetate to give pure **6***c* (0.33 g, 92% yield), mp 137–138°C; ir: 3430, 1632 cm^{-1}; nmr (300) δ: 6.30 (d, 1H, $J_{3,4}$ = 3.99 Hz, H-4), 6.79 (d, 1H, $J_{3,4}$ = 3.99 Hz, H-3), 7.54 (m, 3H), 7.87 (m, 2H). This substance tenaciously retained water of crystallization (exchangeable nmr absorption at δ 1.62). Anal. calcd. for $C_{11}H_8BrNO \cdot 0.1H_2O$: C 52.44, H 3.28, N 5.56; found: C 52.31, H 3.33, N 5.61.

*5-Bromo-2-n-nonanoylpyrrole (**6**d)*

N-Bromosuccinimide (0.33 g, 1.8 mmol) was added, at −78°C, to a stirred solution of the α-aminonitrile **3***d* (0.48 g, 1.8 mmol, purified just prior to use by passing through a column of Act II neutral alumina (25 g/g nitrile) with 4:1 hexane – ethyl acetate) in dry THF (35 mL) and after 2 h at this temperature it was left to reach ambient conditions over a 0.5 h period. The solvent was removed *in vacuo*, the residue (**4***d*) was dissolved in methanol (10 mL), and 10 wt.% sodium hydroxide solution (10 mL) was added. After agitation for 0.5 h, 0.05 M HCl (50 mL) was added and the product was extracted into ether. The crude product was purified by flash chromatography on silica gel using hexane – ethyl acetate (4:1) as the eluting solvent. The solid (0.30 g, 58% yield), which was pure as judged by nmr spectroscopy, was recrystallized from pentane to give analytically pure **6***d*, mp 66–67°C; ir: 3441, 3231, 1645 cm^{-1}; nmr (300) δ: 0.87 (t, 3H, J = 7.0 Hz, Me), 1.26–1.40 (m, 10H, $(CH_2)_5$), 1.70 (m, 2H, CH_2), 2.71 (t, 2H, J = 7.5 Hz, $COCH_2$), 6.23 (d, 1H, $J_{3,4}$ = 3.92 Hz, H-4), 6.80 (d, 1H, $J_{3,4}$ = 3.92 Hz, H-3). Anal. calcd. for $C_{13}H_{20}BrNO$: C 54.55, H 7.04, N 4.89; found: C 54.21, H 7.04, N 4.55.

*Methyl pyrrole-2-carboxylate (**8**a)*

A solution of *n*-butyllithium in hexane (1.6 M, 17.6 mL, 28.1 mmol) was added to a stirred solution of diisopropylamine (2.97 g, 29.3 mmol) in anhydrous THF (100 mL) maintained at −78°C in a nitrogen atmosphere. After 10 min, a solution of the α-dimethylamino nitrile **3***a* (1.82 g, 12.2 mmol) in dry THF (10 mL) was added. Stirring was continued at −78°C for 0.5 h and then at −40°C for a further 0.5 h. A solution of dimethyl disulfide (1.27 g, 13.4 mmol) in dry THF (10 mL) was added at −40°C and stirring was continued at this temperature for 0.25 h and then at 0°C for 0.5 h. The reaction mixture

[5]This proton is coupled to H-3 and H-5 by ca. 0.5–1 Hz.

[6]These coupling constants obtained after decoupling from the absorption at δ 4.96.

[7]The diisopropylamino group is *syn* to the azafulvene nitrogen atom. The one-proton absorptions at 3.81 and 6.40 were assigned to the *i*-Pr CH groups, which were proximal and distal to the azafulvene nitrogen atom. The basis for this assignment will be discussed in a future publication.

was poured into saturated aqueous ammonium chloride solution and the product was extracted with ether. After the usual work-up, a light colored crystalline solid (**7***a*, 2.5 g), which rapidly darkened, was obtained; nmr (60) δ: 1.98 (s, 3H, SMe), 2.35 (s, 6H, NMe_2), 6.03 (t, 1H, H-4), 6.42 (dd, 1H, $J_{3,4}$ = 3.6 Hz, $J_{3,5}$ = 1.4 Hz, H-3), 6.78 (dd, 1H, $J_{3,5}$ = 1.4 Hz, $J_{4,5}$ = 1.9 Hz, H-5). Crude **7***a* from above, in methanol (30 mL) and 5 wt.% sodium hydroxide (15 mL), was stirred at room temperature for 0.33 h and the reaction mixture was poured into water. The pH of the solution was adjusted to 6 with sodium dihydrogen phosphate and the product was extracted into dichloromethane. After the usual work-up, the crude product was taken up in ether (75 mL) and treated with activated charcoal. Removal of the solvent and purification of the solid by flash chromatography on silica gel using hexane – ethyl acetate as the eluting solvent gave pure **8***a* (0.96 g, 63% yield) as a white solid, mp 73–75°C (lit. (9) mp 69–70°C).

*Methyl 5-bromopyrrole-2-carboxylate (**8**b)*

Compound **3***a* was monobrominated in the same manner as described for **4***b* (see preparation of **5***a*). The monobromo compound **4***a* was converted into **8***b* in the same manner as described above for **8***a* except that the reaction with dimethyl disulfide was conducted for 1 h at −78°C and that the elution solvent for the chromatographic purification was hexane – ethyl acetate (7:1). Compound **8***b* (pure by nmr spectroscopy) was obtained as a solid (56% yield), which on recrystallization from hexane had mp 105–106°C (lit. (8) 102–103°C).

*Methyl pyrrole-3-carboxylate (**10**)*

The compound was prepared from **9** in exactly the same manner as described for **8***a* except that chromatographic purification was not required. The ester **10** (pure by nmr spectroscopy) was produced as a solid (74% yield), which on recrystallization from hexane–ether gave a pure sample (60% yield), mp 88–90°C (lit. (10) mp 86–87°C).

1. B. L. Bray and J. M. Muchowski. J. Org. Chem. **53**, 6115 (1988).
2. G. Hazebroucq. Ann. Pharm. Fr. **24**, 793 (1966); Chem. Abstr. **67**, 10854d (1967); C. Jutz. Adv. Org. Chem. **9** (Part 1), 225 (1976).
3. B. L. Bray, P. Hess, J. M. Muchowski, and M. E. Scheller. Helv. Chim. Acta, **71**, 2053 (1988).
4. R. A. Jones and G. P. Bean. *In* The chemistry of pyrroles. Academic Press, London. 1977. pp. 133–135.
5. P. Deslongchamps. *In* Stereoelectronic effects in organic chemistry. Pergamon Press, Oxford. 1983. pp. 118–147.
6. A. Jonczyk, Z. Owczarczyk, M. Makosza, and J. Winiarski. Bull. Soc. Chim. Belg. **96**, 303 (1987).
7. G. Boche, F. Bosold, and M. Niessner. Tetrahedron Lett. **23**, 3255 (1982).
8. H. J. Anderson and S.-H. Lee. Can. J. Chem. **43**, 409 (1965).
9. J. W. Harbuck and H. Rapoport. J. Org. Chem. **37**, 3618 (1972).
10. H. Rapoport and C. D. Wilson. J. Org. Chem. **26**, 1102 (1961).

Can. J. Chem. Downloaded from www.nrcresearchpress.com by 88.85.125.76 on 09/07/12
For personal use only.

A theoretical study of silyl anions and radicals. Change of mechanism from vertex inversion to edge inversion with increasing substitution by halogens

A. C. HOPKINSON AND C. F. RODRIQUEZ
Department of Chemistry, York University, North York, Ont., Canada M3L 1P3
AND
M. H. LIEN
Department of Chemistry, National Chung-Hsing University, Taichung, Taiwan 400

Received July 28, 1989[1]

A. C. HOPKINSON, C. F. RODRIQUEZ, and M. H. LIEN. Can. J. Chem. **68**, 1309 (1990).

Structures for trivalent silyl anions $SiH_nF_{(3-n)}^-$ and $SiH_nCl_{(3-n)}^-$, where n takes values from 0 to 3, have been optimized at the HF/6-31++G* level and single point calculations made at the MP2/6-31++G* level (core included). SiH_3^- and ions containing one halogen invert by the vertex mechanism in which the lone-pair has π-symmetry, and the monosubstituted ions have high barriers (SiH_2F^- 45.2 kcal/mol and SiH_2Cl^- 44.0 kcal/mol). Further substitution by halogens results in a change to the edge inversion mechanism involving a T-shaped transition structure with the lone-pair coplanar with the ligands. Barriers (kcal/mol) at the MP2/6-31++G* level including ZPE are lower than for the monosubstituted ions and are $SiHF_2^-$ 35.0, SiF_3^- 35.9, $SiHCl_2^-$ 28.4, and $SiCl_3^-$ 32.5. In $SiLi_3^-$ edge inversion is preferred, but the surface is much flatter and the barrier is low (9.8 kcal/mol). Trivalent silyl radicals $SiH_nF_{(3-n)}$, $SiH_nCl_{(3-n)}$ and $SiF_nCl_{(3-n)}$ (with n having values 0 to 3) have also been examined with the 6-31++G* basis set, with optimization at the UHF level and single point calculations at the UMP2 level. Radicals SiH_3, SiH_2F, SiH_2Cl, and $SiHCl_2$ all invert by the vertex mechanism. Increased halogenation results in a change of mechanism and SiF_3, $SiCl_3$, SiF_2Cl, and $SiFCl_2$ invert by the edge mechanism. For radical $SiHF_2$ the calculated barriers for the two mechanisms are almost identical with the higher level of theory slightly favouring edge inversion.

Key words: inversion mechanism, halogenated silyl radicals and anions.

A. C. HOPKINSON, C. F. RODRIQUEZ et M. H. LIEN. Can. J. Chem. **68**, 1309 (1990).

Opérant au niveau HF/6-31++G*, on a optimisé les structures des anions silyles trivalents $SiH_nF_{(3-n)}^-$ et $SiH_nCl_{(3-n)}^-$ dans lesquels n varie de 0 à 3 et on a effectué des calculs ponctuels au niveau MP2/6-31++G* (y compris le noyau). L'inversion des ions SiH_3^- et ceux contenant un halogène se produit par un mécanisme de sommet dans lequel la paire libre possède une symétrie π et les ions monosubstitués possèdent des barrières élevées (SiH_2F^-, 45,2 kcal/mol; SiH_2Cl^-, 44,0 kcal/mol). La substitution par d'autres halogènes provoque un changement vers un mécanisme d'inversion des arêtes impliquant une structure de transition en forme de T et une paire libre coplanaire avec les ligands. Au niveau MP2/6-31++G*, incluant l'EPZ, les barrières (kcal/mole) des ions monosubstitués sont plus faibles, soit 35,0 pour le $SiHF_2^-$, 35,9 pour le SiF_3^-, 28,4 pour le $SiHCl_2^-$ et 32,5 pour le $SiCl_3^-$. Pour le $SiLi_3^-$, le mécanisme d'inversion des arêtes est le préfére; toutefois, la surface est beaucoup plus plane et la barrière est faible (9,8 kcal/mol). On a aussi étudié les radicaux silyles trivalents $SiH_nF_{(3-n)}$, $SiH_nCl_{(3-n)}$ et $SiF_nCl_{(3-n)}$ (dans lesquels n peut prendre des valeurs allant de 0 à 3) à l'aide de l'ensemble de base 6-31++G*, d'une optimisation au niveau UHF et de calculs ponctuels au niveau UMP2. Les radicaux SiH_3, SiH_2F, SiH_2Cl et $SiHCl_2$ s'inversent tous par un mécanisme de sommet. Une augmentation de l'halogénation provoque un changement de mécanisme et les radicaux SiF_3, $SiCl_3$, SiF_2Cl et $SiFCl_2$ s'inversent par un mécanisme d'arête. Pour le radical $SiHF_2$, les barrières calculées pour les deux mécanismes sont pratiquement identiques; le niveau de théorie le plus élevé favorise légèrement l'inversion d'arête.

Mots clés : mécanisme d'inversion, les radicaux et les anions silyles trivalents.

[Traduit par la revue]

Inversion of a pyramidal molecule AX_3 (**1**, X = Y = Z. C_{3v} point group) usually proceeds through a planar trigonal structure **2** which has D_{3h} symmetry. When X = Y = Z = H, the magnitude of the barrier to inversion increases as A becomes more electropositive due to the greater stabilization of the pyramidal structure through HOMO-LUMO interactions (1).

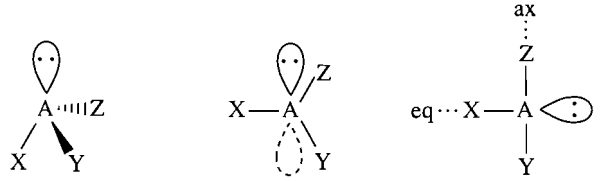

1 **2** **3**

The barriers to inversion of hydrides from the second row, then, are larger than those for analogous molecules from the first row and the silyl anion SiH_3^- has a much larger barrier than the methyl anion CH_3^- (26 kcal/mol (2) compared with 0.5 kcal/mol (3)). Replacing the hydrogens with atoms which are π-donors or σ-acceptors raises the barrier to inversion (2–7) and halogens, which have both these properties, are particularly effective (calculated barriers of CH_2F^- and SiH_2F^- are 24 and 58 kcal/mol, respectively). Increasing the number of halogen substituents should further increase the barrier to inversion by this vertex mechanism, but recent studies (8) have shown that inversion at phosphorus surrounded by electronegative substituents occurs by a different mechanism involving edge-inversion through the T-shaped transition structure, **3**. In **2** the lone-pair on the central atom is destabilised by π-interaction with lone-pairs on the halogens, while in **3** the lone-pair on the central atom is coplanar with the ligands and is available for σ-donation to the halogens.

Previously we reported barriers to inversion for monosubstituted silyl anions (9) and the discovery that increasing halogen substitution in the isolelectronic phosphines results in a change in the inversion mechanism stimulated us to extend our work to polyhalogenated silyl anions.

The parent silyl radical, SiH_3, is pyramidal (10) and the barrier to inversion in radicals R_3Si are sufficiently large that optically active silanes react via the radical with retention of

[1]Revision received March 7, 1990.

Can. J. Chem. Downloaded from www.nrcresearchpress.com by 88.85.125.76 on 09/07/12
For personal use only.

configuration (11), i.e., bimolecular reactions of the radicals are faster than unimolecular inversion. Radical $SiCl_3$ is bent further out of plane than $Si(CH_3)_3$ (12) and it appears that, as in the methyl radical (13), halogens will increase the barrier to inversion of silyl radicals. For a radical, where the out-of-plane orbital at the radical centre formally contains only one electron, there is less π-repulsion with lone-pairs on the substituents in transition structure **4** than in the corresponding structure **2** for the anion. Nevertheless, it seemed possible that even in silyl radicals structure **5**, with the unpaired electron in an orbital coplanar with the ligands, might be preferred over structure **4**. We therefore optimized structures **4** and **5** for radicals $SiH_nF_{(3-n)}$, $SiH_nCl_{(3-n)}$, and $SiF_nCl_{(3-n)}$ where n has values from 0 to 3.

4 **5**

Previous *ab initio* molecular orbital studies on polyhalogenated silyl radicals have focussed on calculating heats of formation (14, 15) or inversion (16) via transition structure **5**, but while this work was in progress Garrison and Goddard (17) predicted, on the basis of a theoretical study, that SiF_3 undergoes inversion through the T-shaped transition structure, **5**.

Computational method

Structures **1–5** and the pyramidal radicals were initially optimized at the HF/6-31+G* level of theory (3, 18) and then subsequently at the HF/6-31++G* level, using gradient methods in the Monstergauss (19) and Gaussian 82 (20) programs. The 6-31+G* basis set has diffuse *s*- and *p*-functions on only the silicon and halogen atoms whereas the 6-31++G* basis set also has diffuse *s*-functions on hydrogen. The results from the two basis sets are very similar with the larger basis set giving better energies by as much as 0.8 kcal/mol for SiH_3^-. Structures from the two basis sets are almost identical and only for the axial bonds in anions **3** are there significant differences (by up to 0.03 Å). Only the results from the larger basis set are included in this work.

Single point calculations on the optimised structures at the MP2/6-31++G* level (21) (including inner shells) were used to assess the effect of correlation energy. Total energies at both levels of calculation are given in Table 1. Harmonic frequency calculations on the optimised geometries provided zero-point energies and the number of imaginary frequencies was used to characterize the critical points as being either minima or transition structures.

Results and discussion

(A) Silyl anions

(I) Structural details and barriers to inversion

Pyramidal SiH_3^- has a bond angle of 96.7° (Table 2) and the HOMO, which formally holds the lone-pair on silicon, has a_1 symmetry with the largest contribution coming from the valence shell *s*-functions on silicon. The Si—H bonds then have little *s*-character and a large amount of *p*-character. Distortion of the pyramidal anion to form trigonal transition structure **2** imposes sp^2 character on the silicon atom with the lone-pair in the out-of-plane non-bonding π-orbital. This increase in *s*-character on vertex inversion results in a shortening of the Si—H bond by 0.062 Å and localization of more negative charge on the silicon atom (−0.668 compared with −0.202). By contrast, in transition structure **3** the axial Si—H bonds are longer than in the pyramidal ion by 0.352 Å while the equatorial bond is shorter by 0.032 Å. Also in **3** most of the negative charge resides on the axial hydrogens (−0.736) and the silicon has a large positive charge (+0.663). Transition structures **2** and **3** then have opposite characteristics; **2** concentrates the negative charge on silicon and **3** has a decrease in negative charge on silicon.

TABLE 1. Total energies[a] of silyl anions and radicals

Anion	HF/6-31++G*	MP2/6-31++G*	ZPE[b,c]
SiH_3^-	−290.61580	−290.71575	12.9
SiH_2F^-	−389.54692	−389.82961	10.5
$SiHF_2^-$	−488.49243	−488.95917	7.8
SiF_3^-	−587.45258	−588.10404	4.7
SiH_2Cl^-	−749.59765	−749.83125	10.1
$SiHCl_2^-$	−1208.57783	−1208.94944	6.7
$SiCl_3^-$	−1667.55501	−1668.06920	2.5
$SiLi_3^-$[d]	−311.19575	−311.37122	2.4
Radical	**UHF/6-31++G***	**UMP2/6-31++G***	**ZPE[b,c]**
SiH_3	−290.60726	−290.68703	14.4
SiH_2F	−389.53193	−389.79179	11.9
$SiHF_2$	−488.46536	−488.90587	8.9
SiF_3	−587.39996	−588.02006	5.6
SiH_2Cl	−749.56461	−749.78101	11.3
$SiHCl_2$	−1208.52169	−1208.87786	7.6
$SiCl_3$	−1667.47632	−1667.97478	3.4
SiF_2Cl	−947.42468	−948.00477	4.9
$SiFCl_2$	−1307.45010	−1307.98986	4.2

[a]Total energy in hatrees.
[b]Zero-point energy (unscaled) in kcal/mol.
[c]Harmonic frequency calculations showed all structures to be minima.
[d]Calculations on $SiLi_3^-$ use the 6-31+G* basis set.

In pyramidal SiX_3^- where X is Cl and F, the bond angles (100.5° and 96.5°, respectively) are also considerably less than tetrahedral. On inversion similar structural changes to those found for SiH_3^- occur. Halogens are powerful σ-withdrawing substituents but they also function as π-donors. In pyramidal $SiCl_3^-$ σ-withdrawal dominates and the population analysis shows the silicon to be positively charged (+0.347). Inversion by the vertex mechanism leads to a dramatic charge reversal with the silicon in **2** (X = Y = Z = Cl) having a charge of −0.406. Much of this charge results from π-donation from Cl to Si, and examination of the gross orbital populations of valence shell functions of π-symmetry (3*p*, 4*p*, *d* and diffuse *p*-function) showed silicon to have a valence shell π-population of 2.3 e and the chlorines to have a population of 1.9 e, i.e., the silicon functions as a π-acceptor although it formally has a lone pair of π-symmetry. On vertex inversion of $SiCl_3^-$ then electron density is taken away from the electronegative chlorine atoms and placed on the electropositive silicon. The change in electron density is more pronounced than in the parent SiH_3^- with the results that halogen substitution increases the barrier to inversion by the vertex mechanism.

The π-crowding in transition structures **2** results in a rapid increase in the barriers to vertex inversion as the number of halide substituents increases. In ions $SiH_nF_{(3-n)}^-$ structures **2** are not always bound despite the inclusion of diffuse functions and we illustrate the effect of increasing numbers of halide substituents by using ions containing chlorine. The barriers to

Can. J. Chem. Downloaded from www.nrcresearchpress.com by 88.85.125.76 on 09/07/12
For personal use only.

TABLE 2. Structural parameters[a] for silyl anions

Ion	Structure 1			Structure 2			Structure 3		
	r	θ		r	θ		r_{ax}	r_{eq}	θ
SiH_3^-	1.534	96.7		1.472	120.0		1.886	1.502	82.9
SiF_3^-	1.668	96.5		high π 1.619[b]	120.0		1.747	1.656	85.7
				low π 1.750	120.0				
$SiCl_3^-$	2.210	100.5		high π 2.116[b]	120.0		2.506	2.116	91.4
				low π 2.438	120.0				
SiH_2F^-	SiH 1.540	∠HSiH 94.3		SiH 1.457	∠HSiF 114.7		C_sSiH 1.796	1.521	∠HSiH 81.4
	SiF 1.699	∠HSiF 98.1		SiF 1.654			SiF 1.789		∠FSiH 84.4
							C_{2v} 1.715	1.662	80.6
$SiHF_2^-$	SiH 1.547	∠HSiF 96.3		SiH 1.438	∠HSiF 126.3		C_{2v} 1.778	1.527	83.7
	SiF 1.682	∠FSiF 97.2		SiF 1.632			C_sSiH 1.794	1.654	∠HSiF 82.0
							SiF 1.746		∠FSiF 85.1
SiH_2Cl^-	SiH 1.524	∠HSiCl 95.2		SiH 1.459	∠HSiCl 114.8		dissociates into $SiH_2 + Cl^-$		
	SiCl 2.284	∠HSiH 94.5		SiCl 2.147					
$SiHCl_2^-$	SiH 1.512	∠HSiCl 93.5		SiH 1.448	∠HSiCl 124.1		2.497	1.490	83.5
	SiCl 2.242	∠ClSiCl 99.7		SiCl 2.118					
$SiLi_3^-$[c]	2.505	81.8		2.399	120.0		2.560	2.628	78.6

[a]Bond lengths in Å and bond angles in degrees.
[b]"high π" has lone-pair out of plane, formally in $p\pi$ on Si; "low π" has lone-pair in σ-system.
[c]Calculated using the Monstergauss program.

Can. J. Chem. Downloaded from www.nrcresearchpress.com by 88.85.125.76 on 09/07/12
For personal use only.

inversion (in kcal/mol) via structure **2** are SiH_3^-, 26.5; SiH_2Cl^-, 44.0; $SiHCl_2^-$, 67.7; and $SiCl_3^-$, 99.8 (Table 3).

The T-shaped structure **3** has axial bonds which are markedly longer than those of **1**, while the equatorial bonds are slightly shorter. For all ions, except $SiCl_3^-$, the bond angles are smaller than 90°, leaving all the ligands on the opposite side of the central atom from the lone-pair. In ions with both hydrogen and halogen atoms, the halogens always occupy the axial position. For SiH_2F^- both T-shaped ions are transition structures to inversion (one imaginary frequency) but the structure with F in the axial position (C_s symmetry) is 14.6 kcal/mol below the other structure (C_{2v}). For $SiHF_2^-$ the T-shaped isomer with both fluorines axial (C_{2v}) is 14.3 kcal/mol lower in energy than the unsymmetrical isomer (C_s). For $SiHCl_2^-$ the isomer with both chlorines axial is stable while the unsymmetrical isomer loses the axial chlorine to form Cl^- solvated by SiHCl (this combination is 14 kcal/mol higher in energy than the structure with C_{2v} symmetry).

Structure **3** for $SiCl_3^-$ has a larger positive charge on Si than in the pyramidal ion (+0.559 compared with +0.347) and the π-population of the formally vacant $3p$-orbital on silicon is only 0.19, ie., there is less π-donation to silicon than in structure **2**. In structure **3**, then, the negative charge is on the more electronegative element, chlorine. The overall effect of substitution by halogens in **3** then is to transfer negative charge onto the halogens and to stabilize **3** relative to **1**. The effect is largest in the fluorinated ions where the barriers to edge inversion (in kcal/mol) via structure **3** are SiH_3^-, 83.6; SiH_2F^-, 52.9; $SiHF_2^-$, 35.0; and SiF_3^-, 35.9. In both the chloro- and fluoro-substituted ions substitution by the third halogen (in the equatorial position) results in little change.

The unusual bond lengths in the T-shaped transition structures, **3**, can be rationalised qualitatively by analysing the occupied valence shell molecular orbitals of SiH_3^-. The molecular orbitals have major contributions from s, p_y, and p_z-functions on silicon and the s-functions on the hydrogen atoms, with minimal contributions from the d-orbitals on silicon (from a 6-31++G*($5d$) basis set calculation the largest gross orbital population from the d-orbital is 0.07 from the d_{z^2} orbital). The occupied valence shell molecular orbitals, 6, 7, 8, and 9, have symmetries a_1 (eigenvalue −0.47 hartree), b_2 (−0.22 hartree), a_1 (−0.21 hartree), and a_1 (−0.04 hartree). The major atomic orbital contributions to these molecular orbitals are sketched in Fig. 1.

The most tightly bound molecular orbital, **6**, has largest coefficients on the two s-functions describing the $3s$ atomic orbital of silicon, with smaller coefficients on the s-functions of the equatorial hydrogen and almost zero contributions from the axial hydrogens. This molecular orbital then is largely localised on silicon, considerably more tightly bound than the other valence shell orbitals, and essentially represents the $3s$ electrons on silicon which are not significantly involved in the bonding. The major contributors to molecular orbital **7** (b_2 symmetry) are the p_y functions on silicon and the s-functions on the axial hydrogens, providing bonding between silicon and the axial hydrogens. Similarly molecular orbital **8** consists of the p_z-functions on silicon in phase with the s-functions on the equatorial hydrogen and this orbital describes the Si—H equatorial bond. Molecular orbital **9** is the most delocalised with major coefficients on the diffuse functions of the axial hydrogen (−ve) and the diffuse s-function on the silicon (+ve). Smaller contributions from the p_z-functions on silicon and the diffuse s-function on the equatorial hydrogen are also antibonding.

The unusual bond lengths of structure **3** for SiH_3^- are easily understood in terms of these valence shell molecular orbitals. The equatorial Si—H bond is a normal bond resulting mainly from the bonding interaction in molecular orbital **8**, with small offsetting bonding and antibonding contributions from molecular orbitals **6** and **9**. The bonds from silicon to the axial hydrogens result from interactions in molecular orbitals **7** (strongly bonding) and **9** (weakly antibonding) and these two bonds are weak and long. Orbitals **7** and **9** are essentially the

TABLE 3. Barriers to inversion (kcal/mol) for anions $SiH_nX^-_{(3-n)}$

Planar anion		Symmetry	Number of imaginary frequencies	Barrier to inversion[c] HF/6-31++G*	Barrier to inversion[c] MP2/6-31++G*	Dissociation energy[d] to give X^- ([1])	Ionisation potential of anion[e]	Dissociation energy[d] to give H ([3])
SiH_3^-	**2**	(D_{3h})	1	29.2	26.5	—	19.3[f]	
	3	(C_{2v})	2	81.8	83.6			63.0
SiH_2F^-	**2**	(C_{2v})[a]	1	49.0	45.2	73.8	24.5	
	3	(C_s)	1	58.1	52.9			62.4
$SiHF_2^-$	**2**	(C_{2v})[a]	1	85.3	79.3	77.9	34.5	
	3	(C_{2v})	1	44.6	35.0			61.2
SiF_3^-	**2**	(D_{3h})[a]	1	153.7	139.0	79.2	53.7	
	3	(D_{3h})[b]	3	82.9	54.8			—
	3	(C_{2v})	1	45.8	35.9			
SiH_2Cl^-	**2**	(C_{2v})	1	49.8	44.0	40.7	32.7	
	3	dissociates into $SiH_2 + Cl^-$			—			62.2
$SiHCl_2^-$	**2**	(C_{2v})	1	76.2	67.7	46.3	46.0	
	3	(C_{2v})	1	25.9	28.4			60.9
$SiCl_3^-$	**2**	(D_{3h})	1	110.4	99.8			
	3	(D_{3h})[b]	3	47.3	43.1	48.8	60.1	—
	3	(C_{2v})	1	32.5	32.5			
$SiLi_3^-$	**2**	(D_{3h})	—	15.9[g]				
	3	(C_{2v})	—	9.8[g]				—

[a]HOMO has a positive energy.
[b]Lowest electronic configuration with D_{3h} symmetry has lone-pair in a_1 orbital. These collapse, without barrier, into the structure with C_{2v} symmetry.
[c]Includes correction for zero-point energy (unscaled).
[d]Energies at MP2/6-31++G*, including zero-point energy (unscaled).
[e]Ionisation potentials (kcal/mol) calculated by differences in energy of $SiH_nX^-_{(3-n)}$ and $SiH_nX_{(3-n)}$ (at MP2/6-31++G*, and UMP2/6-31++G* repectively), and including zero-point energy (unscaled). These energies are estimated electron affinities.
[f]Experimental electron affinity of SiH_3 is 33.2 kcal/mol (23).
[g]At the HF/6-31++G* level, without zero-point energies.

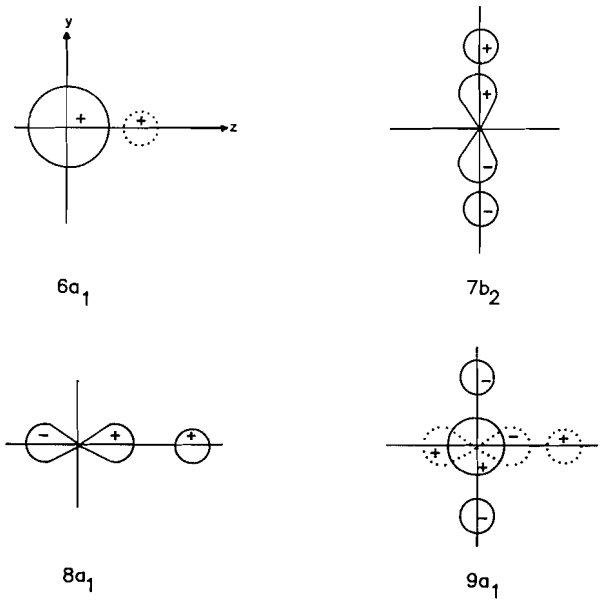

FIG. 1. Major atomic orbital contributions to the occupied valence shell molecular orbitals of T-shaped SiH_3^-. Dotted lines are for more minor, but significant contributors.

bonding and non-bonding molecular orbitals of a three-centre 4-electron system (22), a system which is known to result in weak bonds. In a three-centre 4-electron system the terminal atoms carry the majority of the electron density and such structures are favoured when the terminal atoms are more electronegative than the central atom. In SiH_3^- the axial hydrogens carry a large negative charge (−0.7357), much larger than that on the equatorial hydrogen (−0.1918). When a halogen replaces a hydrogen atom in structure **3** it occupies the axial position since this is the position in which it can obtain the largest amount of negative charge.

(II) Reactions in competition with inversion

The high inversion barriers in silyl anions could make alternative reactions competitive. Halogens stabilize singlet silylenes (by π-donation) and also support negative charges, and the dissociation reaction in eq. [1] is likely to occur, particularly in solution where X^- can be solvated.

[1] $SiH_nX^-_{(3-n)} \rightarrow SiH_nX_{(2-n)} + X^-$

In the gas phase negative ions lose electrons at relatively low energies ([2]).

[2] $SiH_nX^-_{(3-n)} \rightarrow SiH_nX_{(3-n)} + e$

The Si—H bond is considerably weaker than the Si—halogen bonds and homolysis of this bond yields radical anion $SiH_{(n-1)}X^-_{(3-n)}$ plus hydrogen atom

[3] $SiH_nX^-_{(3-n)} \dashrightarrow SiH_{(n-1)}X^-_{(3-n)} + H$

Energies for reactions [1] to [3] at the MP2/6-31++G* level are included in Table 3.

In eq. [1] all species are closed shell and molecular orbital calculations should give reliable estimates. Here it should be noted that attempts to optimize structure **3** for SiH_2Cl^- and also for $SiHCl_2^-$ (with one chlorine in the equatorial position) led to silylenes and the chloride anion. In reactions [2] and [3] the reactant anions have one more electron pair than the products and inclusion of correlation energy is important to describe

Can. J. Chem. Downloaded from www.nrcresearchpress.com by 88.85.125.76 on 09/07/12
For personal use only.

TABLE 4. Structural parameters[a] for silyl radicals

	Pyramidal radical			Structure **4**			Structure **5**			
Radical		r	θ		r	θ		r_{ax}	r_{eq}	θ
SiH_3		1.475	110.9[b]		1.462	120.0		1.600	1.492	92.2
SiH_2F	SiH	1.473	∠HSiH 111.4	SiH	1.452	∠HSiH 129.1	C_s SiH	1.570	1.480	∠HSiH 94.9
	SiF	1.609	∠HSiF 108.4	SiF	1.604		SiF	1.639		∠HSiF 94.1
							C_{2v}	1.553	1.615	89.8
$SiHF_2$	SiH	1.470	∠HSiF 108.5	SiH	1.441	∠FSiF 111.3	C_{2v}	1.627	1.469	95.0
	SiF	1.593	∠FSiF 106.7	SiF	1.589		C_s SiH	1.585	1.598	∠HSiF 90.9
							SiF	1.620		∠FSiF 94.1
SiF_3		1.580	107.8	π-radical	1.583	120.0		1.609	1.583	95.9
				(σ-radical	1.593)[c]					
SiH_2Cl	SiH	1.471	∠HSiH 111.3	SiH	1.454	∠HSiH 126.2	C_s SiH	1.553	1.475	∠HSiH 96.7
	SiCl	2.070	∠HSiCl 108.6	SiCl	2.053		SiCl	2.204		∠HSiCl 93.5
							C_{2v}	1.558	2.093	89.8
$SiHCl_2$	SiH	1.467	∠HSiCl 108.4	SiH	1.448	∠ClSiCl 116.7	C_{2v}	2.140	1.466	96.5
	SiCl	2.056	∠ClSiCl 110.4	SiCl	2.038					
							C_s SiH	1.557	2.055	∠HSiCl 93.4
							SiCl	2.188		∠ClSiCl 97.5
$SiCl_3$		2.047	109.7[d]	π-radical	2.030	120.0		2.149	2.039	100.6
				(σ-radical	2.128)[c]					
SiF_2Cl	SiF	1.583	∠FSiF 106.8	SiF	1.587	∠FSiCl 122.7	C_s SiCl	2.149	1.581	∠FSiCl 96.4
	SiCl	2.037	∠FSiCl 108.8	SiCl	2.018		SiF	1.607		∠FSiF 96.9
							C_{2v}	1.615	2.044	96.8
$SiFCl_2$	SiF	1.587	∠FSiCl 107.6	SiF	1.592	∠FSiCl 117.6	C_{2v}	2.129	1.582	97.1
	SiCl	2.041	∠ClSiCl 111.2	SiCl	2.023					
							C_s SiF	1.613	2.040	∠FSiCl 98.1
							SiCl	2.171		∠ClSiCl 99.7

[a]Bond lengths in Å, angles in degrees.
[b]Experimental bond angle 110.6°, ref. 10.
[c]Unpaired electron in σ-system, radical constrained to have D_{3h} symmetry.
[d]Experimental estimate of ∠ClSiCl is 109.9°, ref. 12..

these processes. The calculated electron affinities of radicals $SiH_nX_{(3-n)}$ and the Si—H dissociation energies of the anions then are expected to be underestimated. Some estimate of the errors incurred here are provided by comparison of the calculated electron affinity of SiH_2 (19.3 kcal/mol) with the experimental value of 33.2 kcal/mol (23). Indeed the electron affinity of SiH_2 cannot be calculated satisfactorily even at much higher levels of theory (24).

From the data in Table 3 only one ion, SiH_2Cl^-, has a dissociation energy lower than the inversion barrier and the energy difference is small. For all other anions inversion occurs at considerably lower energy than dissociation. The calculated energies for electron loss from anions SiH_3^-, $SiHF_2^-$, and SiH_2Cl^- are all lower than the calculated barriers to inversion, but it must be remembered that the electron affinities are all underestimated due to errors inherent in the method. It therefore seems likely that both SiH_3^- and $SiHF_2^-$ will invert at lower energies than that required for electron loss. On a more definitive note, anions SiF_3^-, $SiHCl_2^-$, and $SiCl_3^-$ all undergo inversion at energies lower than those calculated for reactions [1] and [2]. For each of these anions the transition structure for inversion has the T-shaped structure **3**. The barrier to inversion in SiF_3^- of 35.9 kcal/mol compares with barriers of 53.8 and 64.6 kcal/mol for PF_3 and SF_3^+, i.e., as the central atom becomes more electropositive the barrier to edge inversion decreases. A similar trend was found for inversion by the vertex mechanism (1).

(III) $SiLi_3^-$

Electropositive substituents are stabilising in carbanions (3, 25) and failure to include polarisation functions in the basis set leads to an overemphasis on π-stabilization and an overestimation of the stabilization energy (3). At the 4-31+G level both H_2CBeH^- and $H_2CBH_2^-$ are planar, but singlet CH_2Li^- is pyramidal with a low barrier to inversion (3.2 kcal/mol) (3). By contrast preliminary calculations on $SiLi_3^-$ show the pyramidal structure (C_{3v}) to be at a minimum and this anion has the smallest XSiX bond angle (81.8°) of all the silyl anions. These small angles are consistent with a recent study on $SiLi_4$ where the global minimum on a rather flat surface was found to have bond angles of ~84° and to have C_{2v} symmetry rather than the expected tetrahedral structure (26). Our study of lithiated silyl anions is incomplete but the initial calculations at the 6-31+G* level show the inversion barrier of $SiLi_3^-$ to be low, 9.8 kcal/mol through the T-shaped structure, **3**, and 15.9 kcal/mol through **2**.

(B) Silyl radicals

(I) Structural details

The pyramidal silyl radicals all have bond angles close to the ideal tetrahedral angle. The parent SiH_3 is slightly flatter than the ideal angle but halogen substitution leads to an increase in the pyramidality and in SiF_3 the bond angle is 107.8° (Table 4). For $SiH_nF_{(3-n)}$ the bond lengths are similar to those reported previously (14) and show the same trend, a shortening of both

Can. J. Chem. Downloaded from www.nrcresearchpress.com by 88.85.125.76 on 09/07/12
For personal use only.

TABLE 5. Calculated inversion barriers in silyl radicals

Planar radical	Point group	Symmetry of half-filled molecular orbital	Number of imaginary frequencies	Barrier to inversion[a]	
				UHF/6-31++G*	UMP2/6-31++G*
SiH_3	D_{3h}	π	1	6.7	4.9
	C_{2v}	σ	0	66.2	66.3
SiH_2F	C_{2v}	π	1	17.1	14.8
	C_s	σ	1	50.3	46.1
$SiHF_2$	C_{2v}	π	1	38.4	35.4
	C_{2v}	σ	1	42.3	34.9
SiF_3	D_{3h}	π	0	81.0	74.5
	D_{3h}	σ	3	51.3	36.0
	C_{2v}	σ	1	41.1	33.7
SiH_2Cl	C_{2v}	π	1	13.8	11.2
	C_s	σ	0	57.3	55.5
$SiHCl_2$	C_{2v}	π	1	24.4	21.4
	C_{2v}	σ	1	38.7	35.4
$SiCl_3$	D_{3h}	π	0	41.7	38.5
	D_{3h}	σ	2	46.0	35.7
	C_{2v}	σ	1	39.5	34.0
SiF_2Cl	C_{2v}	π	0	64.4	59.9
	C_s	σ	1	38.3	32.5
$SiFCl_2$	C_{2v}	π	0	51.6	48.0
	C_{2v}	σ	1	36.4	31.9

[a]Barriers in kcal/mol, include correction for zero-point energy.

Si—H and Si—X bonds as the number of halogens attached to silicon increases. When all three ligands are identical, structure **4** was assumed to have bond angles of 120°, but in the unsymmetrically substituted planar π-radicals the bond angles involving the more electronegative substituents are smaller than 120°, e.g. in SiH_2X, $\angle HSiX < \angle HSiH$; in $SiHX_2$, $\angle XSiX < \angle XSiH$; in $SiFCl_2$, $\angle ClSiF < \angle ClSiCl$; and in SiF_2Cl, $\angle FSiF < \angle ClSiF$. The bond lengths in **4** are slightly shorter than in the pyramidal radicals, consistent with a change to higher *s*-character in the bonding in planar radicals.

In structure **5** the ax—Si—eq angle is slightly larger than 90° and increases with the size of the atoms to a maximum value of 100.6° in $SiCl_3$. The axial bonds are markedly longer than in the pyramidal radicals (by ~0.03 Å for Si—F, ~0.1 Å for Si—H and ~0.085 Å for Si—Cl) while the equatorial bonds are almost unchanged. These are similar but less pronounced structural changes than those found in the T-shaped transition structures for the silyl anions and also for PF_3 (8*b*). In the T-shaped radicals SiX_3 the HOMO has a_1 symmetry and, as in the anions, is antibonding between silicon and each of the ligands. The largest contributors to this orbital are the diffuse and valence *s*-functions on Si and functions on the axial atoms (*s* for X = H, the *p*-functions directed toward silicon for X = F and Cl). This orbital, then, is largely responsible for the longer Si-axial bond lengths. Addition of another electron to this molecular orbital forms the anions SiH_3^-, SiF_3^-, and $SiCl_3^-$ and results in further elongation of the axial bond lengths (to 1.886, 1.747, and 2.506 Å, respectively, compared to 1.600, 1.609, and 2.149 Å in the radicals). By comparison the equatorial bonds are only slightly longer in the anions than in the radicals (for X = H, 1.502 Å compared with 1.492 Å; for X = Cl, 2.116 Å compared with 2.039 Å; and for X = F, 1.656 Å compared with 1.583 Å).

In T-shaped silyl radicals containing both halogens and hydrogen atoms the halogens always occupy the axial position. For SiH_2F structure **5** with C_s symmetry is better than the C_{2v} structure by 7.6 kcal/mol; for $SiHF_2$ the isomer with both fluorines in the axial position (C_{2v} symmetry) is better than the equatorially substituted isomer (C_s) by 3.0 kcal/mol; for SiH_2Cl the C_s structure is better than the C_{2v} one by 1.3 kcal/mol; and for $SiHCl_2$ the C_{2v} structure is the better one by 7.2 kcal/mol. For radicals containing both halogens, structures with fluorine in the equatorial position are the best. For SiF_2Cl and $SiFCl_2$ the differences are 2.5 and 2.6 kcal/mol, respectively.

(II) Barriers to inversion in radicals

For SiH_3, **4** is a transition structure, only 4.9 kcal/mol above the pyramidal structure. The T-shaped structure **5** is at a high minimum, 66.3 kcal/mol above **5**, and is clearly of no importance to the inversion process.

The barriers to inversion for silyl radicals in Table 5 show that, as for both silyl anions (9) and phosphines $PH_nF_{(3-n)}$ (7, 8*a*), inclusion of halogens greatly increases the barrier to inversion. Fluorine is more effective than chlorine and, assuming inversion occurs through transition structure **4**, each additional fluorine atom increases the barrier by approximately twice the increase resulting from addition of the previous fluorine, i.e. SiH_2F has a barrier 9.9 kcal/mol higher than SiH_3, $SiHF_2$ 20.6 kcal/mol higher than SiH_2F, and SiF_3 39.1 kcal/mol higher than $SiHF_2$. As with SiH_3, the π-radicals SiF_3 and $SiCl_3$ are both at high minima, 74.5 and 38.5 kcal/mol, respectively, above the pyramidal structures. However, for both $SiCl_3$ and SiF_3 the D_{3h} structures, in which the unpaired electron is in the σ-system (in an orbital of a_1 symmetry), are

Can. J. Chem. Downloaded from www.nrcresearchpress.com by 88.85.125.76 on 09/07/12
For personal use only.

TABLE 6. Estimates of dissociation energies[a] for silyl radicals from eq. [4]

	ΔH^0 (0 K)	Literature	Expt[d]
(*a*) Si—H breaking reactions			
$SiHF_2$	30.9	41.7[b]	
$SiHCl_2$	38.1		
SiH_2F	48.9	59.2[b]	
SiH_2Cl	50.7		
SiH_3	61.3	70.1[b], 72.4[c]	64
(*b*) Si—Cl breaking reactions			
SiF_2Cl	55.5		
$SiFCl_2$	59.1		
$SiCl_3$	62.1	67.9[c]	66
$SiHCl_2$	73.8		
SiH_2Cl	81.6		
(*c*) Si—F breaking reactions			
SiF_3	104.1	106.6[b]	123
SiF_2Cl	107.6		
$SiFCl_2$	110.6		
$SiHF_2$	122.2	123.6[b]	
SiH_2F	128.2	129.5[b]	

[a]Energies in kcal/mol from MP2/6-31++G* level, including corrections for ZPE.
[b]Using calculated heats of formation from ref. 14.
[c]ΔH (298 K) from ref. 15.
[d]Reference 30.

lower in energy than the π-radicals. These latter structures have more than one imaginary frequency, i.e. they are not transition structures to inversion, and relaxing the requirement that all bond angles are 120° leads to collapse into the lower energy T-shaped structures **5**.

For all T-shaped structures **5**, with the exception of the parent SiH_3, there is one imaginary vibrational frequency involving out-of-plane motion, i.e., **5** is a transition structure for inversion. *In polyhalogenated radicals $SiF_nCl_{(3-n)}$ and for $SiHF_2$ **5** is lower than **4** and inversion will occur through edge inversion.* Halogen substitution at silicon then increases the barrier to inversion, but the effect is less drastic than suggested by using **4** as the model for the transition structure since for heavily substituted radicals the alternative edge inversion mechanism becomes operative.

The effect of halogen substituents on the relative energy of **5** can be understood by comparison with square-planar silanes and methanes. Square-planar SiH_4 is much closer in energy to the tetrahedral structure than for CH_4 (95 kcal/mol at the HF/3-21G* level compared with 170 kcal/mol at HF/3-21G*) (27, 28), and the stabilization is largely attributed to interaction between the hydrogen atoms and a silicon *d*-orbital of b_{1g} symmetry. The situation in the T-shaped SiH_3 is somewhat similar, with the three hydrogens occupying three vertices of the square and the unpaired electron the fourth. Here the energy difference of 66.3 kcal/mol between the pyramidal and T-shaped structures is somewhat smaller than in SiH_4, although comparison is difficult since the levels of theory used here are considerably higher. In square-planar SiH_4 all the valence electrons are in σ-orbitals leaving an empty *p*-orbital of π-symmetry on silicon and π-donating ligands are strongly stabilising. At the 3-21G* level the tetrahedral/square-planar difference is reduced to 75 kcal/mol. Similarly in T-shaped silyl radicals both fluorine and chlorine are π-donors and their inclusion reduces the pyramidal/T-shaped difference from 67 kcal/mol in SiH_3 to as low as 31.9 kcal/mol in $SiFCl_2$.

(III) Dissociation reactions in silyl radicals

The barriers to inversion in silyl radicals are substantial and it is possible that dissociation may occur at lower energies. In general, dissociation of a bond leads to breaking an electron pair and the products have less correlation energy than the reactant, making it impossible to obtain accurate dissociation energies from Hartree–Fock calculations. However, singlet silylenes are lower in energy than the triplets (27) and the isogyric

[4] SiXYZ (doublet) → SiXY (singlet) + Z (doublet)

reaction given in eq. [4] then gives a lower limit to the dissociation energy of the radical.

Dissociation energies at 0 K, calculated by taking the difference in electronic and zero-point energies and using eq. [3] are given in Table 6. We did not attempt to correct these energies to room temperature since Ho *et al.* (15) have shown that empirical corrections, considerably larger than the small thermal energies, have to be *added* in order to duplicate the experimental heats of atomisation of SiH_n, $SiCl_n$, and SiH_nCl_n. The values given in Table 6 then are expected to be *underestimates* of the dissociation energies. Only for one radical, $SiHF_2$, is the dissociation energy lower than the calculated inversion barrier but even here the difference is small (3.9 kcal/mol) and at an even higher level of theory the calculated dissociation energy of 42.7 kcal/mol (14) is higher than the inversion barrier of 34.8 kcal/mol. We conclude then that all halogenated silyl radicals undergo inversion at lower energies than that required for dissociation.

From Table 6 the relative bond strengths are Si—H < Si—Cl < Si—F. For any given type of dissociation, e.g., Si—H, the total dissociation energy is determined mainly by the kind of bond being broken but also depends on the stability of the silylene being produced. Fluorine (29) and, to a lesser extent, chlorine both stabilise singlet silylenes by π-donation and consequently dissociation reactions in which SiF_2 and $SiCl_2$ are products require less energy than reactions producing SiHF and SiHCl, while those producing SiH_2 are the least favourable.

Conclusions

The barrier to inversion in SiH_3 (4.9 kcal/mol) is much smaller than that in the silyl anion, SiH_3^- (26.5 kcal/mol) and both species invert through the trigonal structure with the non-bonding electron(s) in the out-of-plane *p*-orbital, i.e., they undergo vertex inversion. Replacement of one hydrogen by a fluorine results in an increase in the barrier by 9.9 kcal/mol for the radical and 18.7 kcal/mol in the anion, but the vertex inversion mechanism is preferred. A second fluorine substitution further destabilizes the transition structure for vertex inversion and both $SiHF_2$ and $SiHF_2^-$ invert by the edge inversion mechanism and have similar barrier (~35.0 kcal/mol) at the MP2/6-31++G* level. A third fluorine substituent destabilises the transition structure for vertex inversion even further but has little effect on inversion by the edge inversion mechanism. Similar, less pronounced, trends are found with chlorine substitution and all triply halogenated silyl anions and radicals invert by the edge inversion mechanism.

Acknowledgements

We thank Natural Sciences and Engineering Council of Canada for financial support. We wish to thank a referee for useful suggestions about the bonding in the T-shaped structures.

Can. J. Chem. Downloaded from www.nrcresearchpress.com by 88.85.125.76 on 09/07/12
For personal use only.

1. C. C. LEVIN. J. Am. Chem. Soc. **97**, 5649 (1975).
2. A. E. REED and P. v. R. SCHLEYER. Chem. Phys. Lett. **133**, 553 (1987).
3. G. W. SPITZNAGEL, T. CLARK, J. CHANDRASEKHAR, and P. v. R. SCHLEYER. J. Comp. Chem. **3**, 363 (1982).
4. A. C. HOPKINSON and M. H. LIEN. Int. J. Quant. Chem. **18**, 1371 (1980).
5. J. M. LEHN. Fort. Chem. Forsch. **15**, 311 (1970).
6. A. SCHMIEDEKAMP, S. SKAARUP, P. PULAY, and J. E. BOGGS. J. Chem. Phys. **66**, 5769 (1977).
7. S. YABUSHITA and M. S. GORDON. Chem. Phys. Lett. **117**, 321 (1985).
8. (*a*) D. A. DIXON, A. J. ARDUENGO, III, and T. FUKUNAGA. J. Am. Chem. Soc. **108**, 2461 (1986); (*b*) A. J. ARDUENGO, III, D. A. DIXON, and D. C. ROE. J. Am. Chem. Soc. **108**, 6821 (1986); (*c*) D. A. DIXON and A. J. ARDUENGO, III. J. Chem. Soc. Chem. Commun. 498 (1987); (*d*) A. J. ARDUENGO, III, D. A. DIXON, D. C. ROE and M. KLINE,. J. Am. Chem. Soc. **110**, 4437 (1988).
9. A. C. HOPKINSON and M. H. LIEN. Tetrahedron, **37**, 1105, (1981).
10. R. L. MOREHOUSE, J. J. CHRISTIANSEN, and W. GORDY. J. Chem. Phys. **45**, 1751 (1966).
11. (*a*) H. SAKURAI, M. MURAKAMI, and M. KUMADA. J. Am. Chem. Soc. **91**, 519 (1969); (*b*) A. G. BROOK and J. M. DUFF. J. Am. Chem. Soc. **91**, 2119 (1969).
12. R. V. LLOYD and M. T. ROGERS. J. Am. Chem,. Soc. **95**, 2459 (1977).
13. F. BERNARDI and N. EPIOTIS. Prog. Theoret. Org. Chem. **2**, 47 (1977).
14. E. W. IGNACIO and H. B. SCHLEGEL. J. Chem. Phys. In press.
15. P. HO, M. E. COLTRIN, J. S. BINKLEY, and C. F. MELIUS. J. Phys. Chem. **89**, 4647 (1985).
16. J. MOC, Z. LATAJKA, and H. RATAJCZAK. Chem. Phys. Lett. **136**, 122 (1987).
17. B. J. GARRISON and W. A. GODDARD, III. J. Chem. Phys. **87**, 1307 (1987).
18. J. A. POPLE and P. C. HARIHARAN. Theor. Chim. Acta, **28**, 213 (1978).
19. M. R. PETERSON and R. A. POIRIER. Monstergauss program. Department of Chemistry, University of Toronto, Ont., Canada.
20. J. S. BINKLEY, M. FRISCH, K. RAGHAVACHARI, D. DEFREES, H. B. SCHLEGEL, R. WHITESIDE, E. FLUDER, R. SEEGER, and J. A. POPLE. Gaussian 82, Release A. Carnegie-Mellon University, Pittsburgh, U.S.A.
21. C. MØLLER and M. S. PLESSET. Phys. Rev. **46**, 618 (1934); J. A. POPLE, J. S. BINKLEY, and R. SEEGER. Int. J. Quantum Chem. Symp. **10**, 1 (1976); R. KRISHNAN and J. A. POPLE. Int. J. Quantum Chem. **14**, 91 (1978); R. KRISHNAN, M. J. FRISCH, and J. A. POPLE. J. Chem. Phys. **72**, 4244 (1980).
22. F. A. COTTON and G. WILKINSON. Advanced inorganic chemistry. 2nd ed. Wiley 1966. p. 407.
23. K. J. REED and J. I. BRAUMAN. J. Chem. Phys. **61**, 4830 (1974).
24. J. A. POPLE, P. v. R. SCHLEYER, J. KANETI, and G. W. SPITZNAGEL. Chem. Phys. Lett. **145**, 359 (1988); M. T. NGUYEN. J. Mol. Struct. Theochem. **164**, 391 (1988).
25. A. PROSS, D. J. DEFREES, B. A. LEVI, S. K. POLLACK, L. RADOM, and W. J. HEHRE. J. Org. Chem. **48**, 1693, (1981).
26. P. v. R. SCHLEYER and A. E. REED. J. Am. Chem. Soc. **110**, 4453 (1988).
27. M. B. KROGH-JESPERSEN, J. CHANDRASEKHAR, E. U. WURTHWEIN, J. B. COLLINS, and P. v. R. SCHLEYER. J. Am. Chem. Soc. **102**, 2263 (1980).
28. W. J. HEHRE, L. RADOM, P. v. R. SCHLEYER, and J. A. POPLE. Ab initio molecular orbital theory. Wiley, New York. 1986. p. 432f.
29. B. T. LUKE, J. A. POPLE, M. B. KROGH-JESPERSEN, Y. APELOIG, M. KARNI, J. CHANDRASEKHAR, and P. v. R. SCHLEYER. J. Am. Chem. Soc. **108**, 270 (1986).
30. R. WALSH. Acc. Chem. Res. **14**, 246 (1981).

Can. J. Chem. Downloaded from www.nrcresearchpress.com by 88.85.125.76 on 09/07/12
For personal use only.

Thermal diffusion of weak electrolytes: aqueous phosphoric and iodic acids

LÜ HUI AND DEREK G. LEAIST[1]

Department of Chemistry, University of Western Ontario, London, Ont., Canada N6A 5B7

Received October 27, 1989

LÜ HUI and DEREK G. LEAIST. Can. J. Chem. **68**, 1317 (1990).

Soret coefficients of aqueous phosphoric acid and aqueous iodic acid are determined conductimetrically at 25°C. As the molality of phosphoric acid drops from 0.05 toward 0.00 mol kg^{-1}, the enthalpy of transport jumps from 2 to 15 kJ mol^{-1}. For iodic acid, a stronger electrolyte, the corresponding increase is smaller, from 12 to 17 kJ mol^{-1}. Equations are developed for the enthalpy of transport of 1:1 weak electrolytes. The equations are used to evaluate the reactive enthalpy of transport and the intrinsic enthalpies of transport of the ionized and molecular forms of phosphoric and iodic acids. Equating the enthalpies of transport of the acid molecules and the acid anions provides estimates of single-ion enthalpies of transport. Thermal diffusion measurements are reported for potassium dihydrogen phosphate and potassium iodate to help interpret the results.

Key words: thermal diffusion, enthalpy of transport, Soret coefficients, weak electrolytes, phosphoric acid, iodic acid.

LÜ HUI et DEREK G. LEAIST. Can. J. Chem. **68**, 1317 (1990).

Opérant à 25°C et faisant appel à une méthode conductimétrique, on a déterminé les coefficients de Soret des acides phosphorique et iodique aqueux. Lorsque la molalité de l'acide phosphorique diminue de 0,05 vers 0,00 mol kg^{-1}, l'enthalpie de transport passe rapidement de 2 à 15 kJ mol^{-1}. Pour l'acide iodique, qui est un électrolyte plus fort, l'augmentation correspondante est plus faible et elle passe de 12 à 17 kJ mol^{-1}. On a développé des équations pour l'enthalpie de transport d'électrolytes faibles 1:1. On a utilisé les équations pour évaluer l'enthalpie de transport réactive ainsi que les enthalpies intrinsèques de transport des formes ionisées et moléculaires des acides phosphorique et iodique. Lorsqu'on établit une équation entre les enthalpies de transport des molécules d'acide et les anions d'acide, on obtient une bonne évaluation des enthalpies de transport des ions uniques. Afin d'aider dans l'interprétation des résultats, on rapporte aussi des mesures de diffusion thermique pour le phosphate diacide de potassium ainsi que l'iodate de potassium.

Mots clés : diffusion thermique, enthalpie de transport, coefficients de Soret, électrolytes faibles, acide phosphorique, acide iodique.

[Traduit par la revue]

Can. J. Chem. Downloaded from www.nrcresearchpress.com by 88.85.125.76 on 09/07/12
For personal use only.

1. Introduction

A temperature gradient applied to an electrolyte solution causes the dissolved ions to diffuse relative to the solvent (1, 2). The thermally-driven diffusion of strong electrolytes has been the subject of a number of studies (1–11). In the work reported here, thermal diffusion measurements are reported for aqueous phosphoric acid ($pK_a = 2.15$), a "weak" electrolyte (12), and aqueous iodic acid ($pK_a = 0.80$), an "almost strong" electrolyte (13–15).

In contrast to a strong electrolyte, a weak electrolyte can diffuse in different chemical forms, e.g. $HA \rightleftharpoons H^+ + A^-$. The enthalpy of transport of a solute that exists as a mixture of rapidly-equilibrating species consists of a contribution from the intrinsic enthalpies of transport of the species and another, usually smaller, contribution from the enthalpy change of the chemical reaction (16–18). The treatment developed in the present study is used to estimate the intrinsic enthalpies of transport of the molecular and ionized forms of iodic and phosphoric acids and the reactive component of the total enthalpy of transport. To help interpret the results, thermal diffusion measurements are also reported for the potassium salts of the acids. No thermal diffusion data appear to have been reported previously for iodates or phosphates (11).

2. Experimental

The solutions were prepared from BDH reagent grade materials and distilled deionized water. The phosphoric acid solutions were analyzed by potentiometric titration against standard alkali.

Conductance methods for the determination of the Soret coefficients of electrolytes are well developed (1–8). The cells used in the present study were of the pattern described by Agar and Turner (3). The cells held short columns of solutions (height 0.9–1.2 cm) between copper thermostat blocks maintained at 20 or 30°C. Thermal diffusion of the ions was followed by measuring changes in electrical resistance across pairs of small platinum electrodes at fixed levels near the top and bottom of the solution column. Details of the equipment and procedure have been reported (19).

Published densities (20, 21), conductances (13, 15, 20–23), and isothermal diffusion data (24–27) were used to evaluate the Soret coefficients from the measured resistance changes. Since no diffusion coefficients appear to have reported for aqueous HIO_3 or KIO_3, a few isothermal diffusion measurements were made on these electrolytes. A simplified version of Harned's conductimetric procedure was employed (24).

3. Results

Thermal diffusion in a convection-free solution leads to a steady state in which the diffusion of solute driven by the temperature gradient is balanced by ordinary diffusion back down the thermally-induced concentration gradient. The Soret coefficient defined by (1, 2)

$$[1] \quad \sigma = -(1/m)(\mathrm{d}m/\mathrm{d}T)_{\text{steady-state}}$$

gives the relative change in solute molality per degree at steady state. Positive σ values indicate thermal diffusion to the colder parts of the solution.

The enthalpy of transport of an electrolyte is related to its Soret coefficient by the following identity (1, 2)

$$[2] \quad H^* = (\nu_+ + \nu_-)RT^2\sigma(1 + m\,\mathrm{d}\ln\gamma_\pm/\mathrm{d}m)_T$$

ν_+ and ν_- give the number of moles of cations and anions per mole of fully dissociated electrolyte, m is the total electrolyte molality, and $\gamma_\pm$ is the stoichiometric mean ionic activity coefficient. The enthalpy of transport may be interpreted as the heat absorbed to keep the solution at constant temperature when solute diffuses out of a volume element of solution (1, 2).

[1]To whom correspondence should be addressed.

Can. J. Chem. Downloaded from www.nrcresearchpress.com by 88.85.125.76 on 09/07/12
For personal use only.

Soret coefficients were determined conductimetrically at molalities from 0.001 to 0.2 mol kg^{-1} at the mean cell temperature 25°C. The results are given in Tables 1–5. The reported σ values represent average values from two or three runs at each composition. The values of σ were reproducible within 2–4%, except at the lowest molalities where the reproducibility was poorer, about 5%. Published activity coefficient data (12, 13, 28–33) were used to calculate enthalpies of transport (H^*) from the measured Soret coefficients, as listed in Tables 1–5 and plotted against the square root of the ionic strength I in Fig. 1.

KH_2PO_4

A short extrapolation to zero ionic strength gives 4.3 kJ mol^{-1} for the limiting enthalpy of transport of aqueous KH_2PO_4. If Cl^- is arbitrarily assigned conventional enthalpy of transport 0 kJ mol^{-1} at ionic strength 0.01 mol kg^{-1}, the conventional (1, 4–6, 11) ionic enthalpies of transport of K^+ and $H_2PO_4^-$ are, respectively, 2.0 and 1.4 kJ mol^{-1}.

In addition to K^+ and $H_2PO_4^-$ ions, aqueous KH_2PO_4 solutions contain traces of H^+, HPO_4^{2-}, and molecular H_3PO_4 species due to the equilibria $H_2PO_4^- \rightleftharpoons H^+ + HPO_4^{2-}$ ($K_2 = 6.2 \times 10^{-8}$) (34, 35) and $H_3PO_4 \rightleftharpoons H^+ + H_2PO_4^-$ ($K_1 = 7.14 \times 10^{-3}$) (12). These minor species may be neglected here because their concentrations are very small. This simplification is supported by the observation that the limiting slope $dH^*/dI^{1/2}$ agrees qualitatively with the value -10.8 kJ $kg^{1/2}$ $mol^{-3/2}$ expected for a simple 1:1 electrolyte (11). Moreover, previously measured (27) isothermal diffusion coefficients of aqueous KH_2PO_4 extrapolate correctly to the limiting Nernst value for a strong 1:1 electrolyte.

K_2HPO_4

Thermal diffusion measurements were made on aqueous K_2HPO_4 solutions to provide additional information about aqueous phosphates. As the molality drops to 0.001 mol kg^{-1}, the slope of H^* against $I^{1/2}$ is increasing, and it exceeds the limiting value -32.4 kJ $kg^{1/2}$ $mol^{-3/2}$ suggested by theory for a 1:2 strong electrolyte (11). This behaviour may be due to the dissociation of $KHPO_4^-$ ion pairs, or to the hydrolysis reaction $HPO_4^{2-} + H_2O \rightleftharpoons H_2PO_4^- + OH^-$ ($K_h = 1.6 \times 10^{-7}$). It was not possible to estimate the limiting value of H^* reliably.

No attempts were made to measure thermal diffusion of K_3PO_4. Since this salt hydrolyzes extensively, its diffusion is a complicated ternary process involving coupled transport of $K^+ + OH^-$ (26).

KIO_3

Table 3 gives the Soret coefficients for the potassium salt of iodic acid. Extrapolation leads to the value 6.2 kJ mol^{-1} for the salt's limiting enthalpy of transport. The conventional enthalpy of transport of the IO_3^- ion has the value 4.2 kJ mol^{-1}. For comparison, the conventional enthalpies of transport of the ions IO_4^- and ClO_4^- are 1.5 and -0.8 kJ mol^{-1}, respectively (11). Table 3 includes the values of the isothermal diffusion coefficient D that were obtained for aqueous KIO_3 solutions. The limiting value of D, 1.393×10^{-9} m^2 s^{-1}, was calculated by using the Nernst relation $D^0 = 2D_+D_-/(D_+ + D_-)$ and the limiting ionic diffusion coefficients $D_+(K^+) = 1.958 \times 10^{-9}$ and $D_-(IO_3^-) = 1.081 \times 10^{-9}$ m^2 s^{-1}. The ionic diffusion coefficients were calculated from the limiting ionic conductances (15) $\Lambda_+^0 = 0.007354$ and $\Lambda_-^0 = 0.004060$ S m^{-2} mol^{-1} by using the identity $D_i = RT\Lambda_i^0/F^2z_i^2$.

H_3PO_4

The results of the experiments and calculations on aqueous phosphoric acid are given in Table 4. Both the Soret coefficient and the enthalpy of transport of the acid increase sharply as the concentration drops toward zero. This behavior is not surprising in view of the large intrinsic enthalpy of transport of the H^+ ions (11) that are produced by dissociation of the dilute acid.

The sharp curvature of the plot of H^* against $I^{1/2}$ (Fig. 1) makes the direct extrapolation of H^* highly unreliable. (Similar difficulties are encountered in the extrapolation of the acid's molar conductivity to the limiting value.) A better approach is to estimate the limiting enthalpy of transport of the dissociated acid by appealing to the additivity rule (1–6), and extrapolating the enthalpy of transport of the hypothetical fully dissociated electrolyte $H^+ + H_2PO_4^-$ estimated from strong electrolyte data as follows: $H^*(H^+ + H_2PO_4^-) = H^*(KH_2PO_4) + H^*(HCl) - H^*(KCl)$. The extrapolation of $H^*(H^+ + H_2PO_4^-)$ estimated from the measured enthalpies of transport of KH_2PO_4, HCl (10), and KCl (6) is shown in Fig. 1 (lower dashed curve). This procedure gives 15.4 kJ mol^{-1} for the limiting enthalpy of transport of phosphoric acid. This value is based on neglect of the second and third stages of dissociation of the acid.

HIO_3

The Soret coefficient and enthalpy of transport of HIO_3 (Table 5) are less sensitive to changes in concentration than for H_3PO_4 because the former is almost fully ionized at the concentrations used in the present study. As the molality of the acid drops from 0.05 toward 0.00 mol kg^{-1}, for example, the degree of dissociation, α, of HIO_3 increases from about 0.83 to 1.00 (13), whereas α for H_3PO_4 changes from 0.35 to 1.00 (12). Extrapolation of $H^*(HCl) + H^*(KIO_3) - H^*(KCl)$ (upper dashed curve in Fig. 1) leads to the value 17.3 kJ mol^{-1} for the limiting enthalpy of transport of HIO_3.

The values of the isothermal diffusion coefficients for aqueous HIO_3 are listed in Table 5. The limiting value of D was calculated according to Nernst's equation using $D(H^+) =$

TABLE 1. Soret coefficients and enthalpies of transport of aqueous KH_2PO_4 at 25°C

m/mol kg^{-1}	$10^3\sigma/K^{-1}$	H^*/kJ mol^{-1}	$1 + d \ln \gamma_\pm / d \ln m$
0.000	2.9[a]	4.3[a]	1.000
0.002	2.60	3.75	0.975
0.005	2.52	3.58	0.962
0.010	2.44	3.42	0.948
0.030	2.32	3.14	0.916
0.050	2.43	3.22	0.896
0.100	2.37	3.02	0.861

[a]Extrapolated value.

TABLE 2. Soret coefficients and enthalpies of transport of aqueous K_2HPO_4 at 25°C

m/mol kg^{-1}	$10^3\sigma/K^{-1}$	H^*/kJ mol^{-1}	$1 + d \ln \gamma_\pm / d \ln m$
0.000	—	—	1.000
0.001	4.75	9.93	0.943
0.002	4.17	8.53	0.923
0.005	3.88	7.65	0.889
0.010	3.89	7.42	0.860
0.030	3.68	6.64	0.814
0.050	3.80	6.75	0.801

TABLE 3. Soret coefficients, enthalpies of transport, and isothermal diffusion coefficients of aqueous KIO_3 at 25°C

m/mol kg^{-1}	$10^9 D$/m^2 s^{-1}	$10^3\sigma$/K^{-1}	H^*/kJ mol^{-1}	$1 + d \ln \gamma_\pm / d \ln m$
0.000	1.393[a]	4.2[b]	6.2[b]	1.000
0.002	1.35	3.86	5.57	0.976
0.005	1.34	3.72	5.30	0.963
0.010	1.32	3.62	5.08	0.950
0.020	1.29	3.57	4.92	0.933
0.030	1.26	3.58	4.88	0.922
0.050	1.21	3.61	4.83	0.905
0.100	1.13	3.72	4.83	0.879
0.200	1.04	4.11	5.14	0.846

[a]Nernst value.
[b]Extrapolated value.

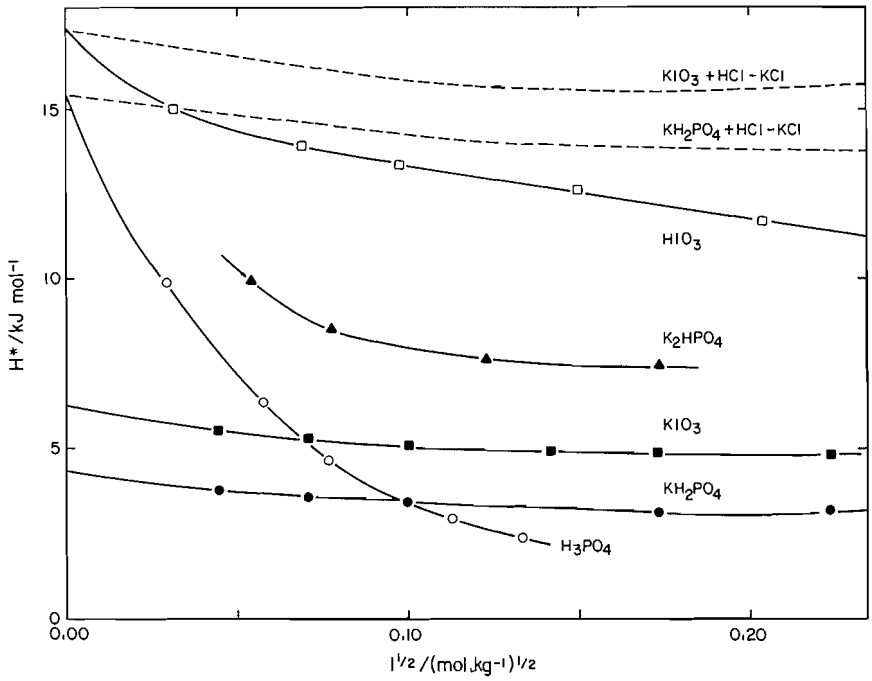

FIG. 1. Plot of measured enthalpies of transport against the square root of the ionic strength for aqueous HIO_3, H_3PO_4, K_2PO_4, KIO_3, and KH_2PO_4 at 25°C. The dashed curves give the enthalpies of transport estimated for the hypothetical fully dissociated acids $H^+ + IO_3^-$ and $H^+ + H_2PO_4^-$.

TABLE 4. Soret coefficients and enthalpies of transport of aqueous H_3PO_4 at 25°C

m/mol kg^{-1}	$10^3\sigma$/K^{-1}	H^*/kJ mol^{-1}	$1 + d \ln \gamma_\pm / d \ln m$
0.000	10.4[a]	15.4[a]	1.000
0.001	7.50	9.89	0.892
0.005	5.68	6.35	0.756
0.010	4.72	4.67	0.670
0.030	3.24	2.99	0.624
0.050	2.66	2.35	0.597

[a]Extrapolated value.

9.317×10^{-9} and $D(IO_3^-) = 1.081 \times 10^{-9}$ m^2 s^{-1} (15). Previous studies (25, 36–39) have shown that diffusion data for dilute weak acids can be analyzed to estimate the diffusion coefficient of the molecular form of the acid, D_0. But in this case, only a small portion of dilute aqueous iodic acid diffuses in molecular form. As a result, it was not possible to obtain a reliable value of D_0. It is likely, however, that the value of D_0 for the molecular HIO_3 species is close to 1.081×10^{-9} m^2 s^{-1}, the diffusion coefficient of IO_3^-. (The diffusion coefficients of $H_2PO_4^-$ and the structurally similar molecular H_3PO_4 species, for example, are 0.86×10^{-9} and 0.87×10^{-9} m^2 s^{-1} (25, 40).)

4. Discussion

Polymeric species, such as $H(H_2PO_4)^-$ or $H(IO_3)_2^-$, complicate the properties of concentrated solutions of phosphoric and iodic acids in water (12, 13). But a negligible proportion of the total acid exists as these secondary species provided the acid molality is kept below about 0.05 mol kg^{-1}. For the purposes of the present study, dilute aqueous solutions of phosphoric acid or iodic acid will be treated as simple weak electrolytes subject to the single equilibrium reaction $HA \rightleftharpoons H^+ + A^-$.

Recently, Agar and Lin (18) developed the thermodynamic theory for thermal diffusion of a solute that exists in two

Can. J. Chem. Downloaded from www.nrcresearchpress.com by 88.85.125.76 on 09/07/12
For personal use only.

TABLE 5. Soret coefficients, enthalpies of transport, and isothermal diffusion coefficients of aqueous HIO_3 at 25°C

m/mol kg^{-1}	$D/10^{-9}$ m^2 s^{-1}	$\sigma/10^{-3}$ K^{-1}	H^*/kJ mol^{-1}	$1 + d \ln \gamma_\pm / d \ln m$
0.000	1.937[a]	11.7[b]	17.3[b]	1.000
0.001	1.88	10.4	15.0	0.977
0.005	1.79	9.90	13.9	0.950
0.010	1.73	9.88	13.4	0.916
0.025	1.61	10.0	12.6	0.854
0.050	1.46	10.0	11.7	0.792
0.100	1.33	9.90	10.0	0.682
0.200	1.28	9.51	8.4	0.595

[a]Nernst value.
[b]Extrapolated value.

rapidly-equilibrating forms: $nA \rightleftharpoons A_n$. Adapting their results to the problem under discussion leads to the exact expression

[3] $$H^* = t_0 H_0^* + t_\pm H_\pm^* + H_r^*$$

for the enthalpy of transport of a 1:1 weak electrolyte. H_0^* and $H_\pm^*$ stand for the intrinsic enthalpies of transport per mole of the molecular (HA) and ionized ($H^+ + A^-$) forms of the electrolyte. t_0 and $t_\pm$ are transport numbers which give the fractions of the total electrolyte transported as HA or $H^+ + A^-$ (by definition, $t_0 + t_\pm = 1$). H_r^*, the reactive contribution to the enthalpy of transport, is given by

[4] $$H_r^* = [t_\pm - (dm_\pm/dm)]\Delta_r H$$

where $\Delta_r H$ is the enthalpy change of the dissociation reaction $HA = H^+ + A^-$, $m_\pm = \alpha m$ is the molality of the ionized portion of the electrolyte, and $dm_\pm/dm$ measures the change in the ionized electrolyte molality with the total electrolyte molality, under equilibrium conditions. If $t_\pm$ is greater than $dm_\pm/dm$, diffusion tends to remove ions faster than they are produced by dissociation; the subsequent dissociation required to maintain local equilibrium then makes a contribution to the enthalpy of transport of the same sign as the enthalpy of dissociation. Conversely, H^* and H_r^* will have opposite signs if $t_\pm < dm_\pm/dm$.

The generally accepted value of the enthalpy of dissociation of dilute aqueous phosphoric acid is -7.9 kJ mol^{-1} at 25°C (41). The value of $\Delta_r H$ for iodic acid is somewhat uncertain; calorimetric (14), conductance (15), and solubility measurements (42) lead to the discordant values -2.8, -4.6, and -10.0 kJ mol^{-1}, respectively. Without obvious reasons to dismiss any of these careful determinations, the simple arithmetic mean value -5.8 kJ mol^{-1} will be naively adopted.

Values of $t_\pm$ and $dm_\pm/dm$ are also required to estimate the reactive enthalpy of transport. $dm_\pm/dm$ was calculated from the extents of dissociation recommended by Pitzer and Silvester (12) (for phosphoric acid) and by Pethybridge and Prue (13) (for iodic acid). The transport numbers were evaluated by using the dilute-solution transport equations (43–45)

[5] $$j_i = -(c_i D_i/RT)\nabla \tilde{\mu}_i$$

for the flux densities of H^+, A^-, and molecular HA species (designated by subscripts +, −, and 0 respectively). c_i and $\nabla\tilde{\mu}_i$ are the concentrations (in moles per unit volume) and the gradients in the electrochemical potential of the species. The conditions of electroneutrality ($j_+ = j_-$) and local chemical equilibrium ($\tilde{\mu}_0 = \tilde{\mu}_+ + \tilde{\mu}_-$) may be used to show that the fraction of electrolyte transported in ionic form is given by

[6] $$t_\pm = \frac{j_-}{j_- + j_0} = \frac{\alpha D_+ D_-/(D_+ + D_-)}{(1-\alpha)D_0 + \alpha[D_+ D_-/(D_+ + D_-]}$$

(An approach similar to the one used here has been used to analyze the reactive enthalpy of transport of aqueous sulfuric acid (19) subject to the bisulfate/sulfate equilibrium.)

TABLE 6. Reactive enthalpy of transport of aqueous H_3PO_4 at 25°C

m/mol kg^{-1}	α	$t_\pm$	$dm_\pm/dm$	H_r^*/kJ mol^{-1}
0.000	1.000	1.000	1.000	0.00
0.001	0.895	0.885	0.824	−0.48
0.005	0.679	0.657	0.553	−0.82
0.010	0.590	0.566	0.423	−1.13
0.030	0.423	0.399	0.285	−0.90
0.050	0.354	0.332	0.234	−0.77

TABLE 7. Reactive enthalpy of transport of aqueous HIO_3 at 25°C

m/mol kg^{-1}	α	$t_\pm$	$dm_\pm/dm$	H_r^*/kJ mol^{-1}
0.000	1.000	1.000	1.000	0.00
0.001	0.994	0.993	0.989	−0.02
0.005	0.974	0.971	0.951	−0.12
0.010	0.951	0.946	0.910	−0.21
0.025	0.896	0.885	0.814	−0.41
0.050	0.828	0.812	0.698	−0.66
0.100	0.744	0.722	0.598	−0.72

Tables 6 and 7 list the estimates of the reactive enthalpy of transport together with the supplementary values of $t_\pm$, $dm_\pm/dm$, and α. The calculations indicate negative reactive enthalpies for both phosphoric and iodic acids. Iodic acid has larger reactive enthalpies of transport because its enthalpy of dissociation is larger. The magnitude of H_r^* for each acid passes through a maximum at a molality near K^{-1}, where similar amounts of the associated and dissociated forms of the acid are present (18).

Study of Tables 6 and 7 indicates that the fraction of acid transported in the ionized form is less than the fraction of total acid that is dissociated, i.e. $t_\pm < \alpha$. This behavior stems from the relatively low mobility of the dissociated electrolyte: the motion of H^+ and A^- through the solvent meets greater frictional resistance than the motion of the single associated species HA (25, 36–39).

Can. J. Chem. Downloaded from www.nrcresearchpress.com by 88.85.125.76 on 09/07/12
For personal use only.

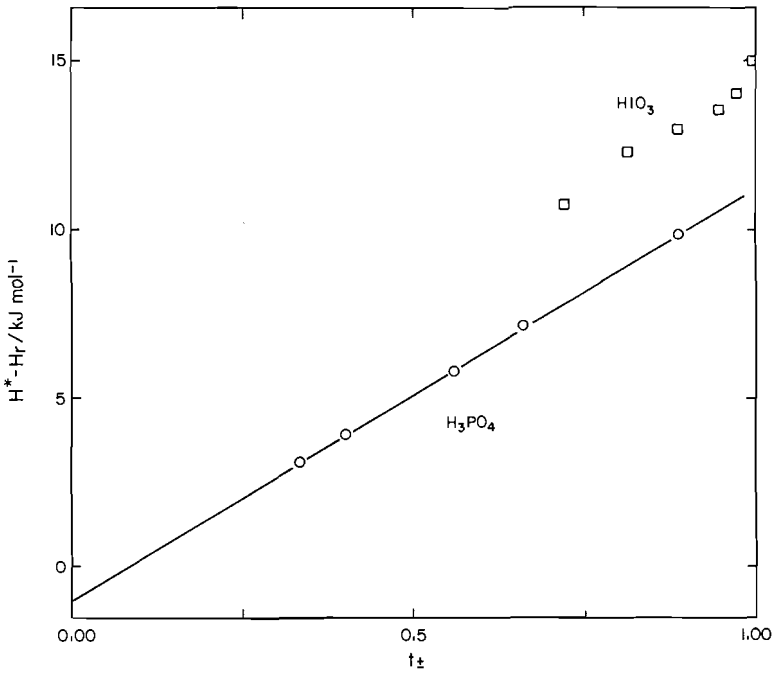

FIG. 2. Intrinsic enthalpy of transport of aqueous phosphoric acid and iodic acid plotted against the transport number of the ionized form of the acid.

The intrinsic enthalpy of transport can be evaluated by subtracting the reactive enthalpy of transport from the measured total enthalpy of transport: $t_0H_0^* + t_\pm H_\pm^* = H^* - H_r^*$. In Fig. 2, the intrinsic enthalpies of transport obtained in this manner are plotted against $t_\pm$, the transport number of the dissociated form of the acids. A linear extrapolation to $t_\pm = 0$ for phosphoric acid gives the value -1.0 kJ mol^{-1} for H_0^*, the enthalpy of transport of the molecular H_3PO_4 species. The corresponding extrapolation for iodic acid is long and unreliable due to the larger values of $t_\pm$ for this "almost strong" acid. It appears, however, that the extrapolation for iodic acid runs parallel to the extrapolation for phosphoric acid, but is shifted upwards by 2–4 kJ mol^{-1}. This observation leads to the tentative value 2 ± 1 kJ mol^{-1} for the enthalpy of transport of the molecular HIO_3 species.

It is intriguing that the difference between the enthalpies of transport of the H_3PO_4 and HIO_3 molecules appears to mirror the difference in the enthalpies of transport of the $H_2PO_4^-$ and IO_3^- ions [$H^*(H_2PO_4^-) - H^*(IO_3^-) = H^*(KH_2PO_4) - H^*(KIO_3)$ at low ionic strength (see Fig. 1)].

The comparison provides circumstantial evidence, but not proof, that the enthalpies of transport of the anion/molecule pairs $H_2PO_4^-/H_3PO_4$ and IO_3^-/HIO_3 are nearly identical. This suggestion is not unreasonable on physical grounds since the acid anions and the acid molecules are structurally very similar. Moreover, the relatively low charge densities of the $H_2PO_4^-$ and IO_3^- anions would tend to reduce the distortion of the structure of the nearby solvent.

If the enthalpies of transport of the acid molecules and anions are indeed nearly identical, it is then possible to evaluate single-ion enthalpies of transport. Adopting -1.0 kJ mol^{-1} for the enthalpy of transport of $H_2PO_4^-$ and molecular H_3PO_4 species, for example, leads to the corresponding values 16.4, 5.3, and 0.9 kJ mol^{-1} for the limiting enthalpies of transport of the ions H^+, K^+, and IO_3^-.

The quoted single-ion enthalpies of transport are speculative and remain to be checked by thermal diffusion measurements on other ion/molecule pairs. Nevertheless, progress along these lines may provide a practical scale of single-ion enthalpies of transport that is acceptably close to the true value of these elusive but theoretically-important quantities.

Acknowledgment

The authors thank the Natural Sciences and Engineering Research Council for financial support of this work.

1. J. N. AGAR. Advances in electrochemistry and electrochemical engineering. *Edited by* P. Delahay and C. W. Tobias. Interscience, New York. 1963. Chap. 2.
2. H. J. V. TYRRELL. Diffusion and heat flow in liquids. Butterworths, London. 1961.
3. J. N. AGAR and J. C. R. TURNER. J. Phys. Chem. **64**, 1000 (1960).
4. J. N. AGAR and J. C. R. TURNER. Proc. R. Soc. (London) A**255**, 307 (1960).
5. P. N. SNOWDON and J. C. R. TURNER. Trans. Faraday Soc. **56**, 1409 (1960).
6. P. N. SNOWDON and J. C. R. TURNER. Trans. Faraday Soc. **56**, 1812 (1960).
7. N. H. SAGERT and W. G. BRECK. Trans. Faraday Soc. **57**, 436 (1961).
8. A. D. PAYTON and J. C. R. TURNER. Trans. Faraday Soc. **58**, 55 (1962).
9. L. G. LONGSWORTH. J. Phys. Chem. **61**, 1557 (1957).
10. J. LIN, J. A. BIERLEIN, and J. G. BECSEY. J. Solution Chem. **3**, 827 (1974).
11. N. TAKEYAMA and K. NAKASHIMA. J. Solution Chem. **17**, 305 (1988).
12. K. S. PITZER and L. F. SILVESTER. J. Solution Chem. **5**, 269 (1976).
13. A. D. PETHYBRIDGE and J. E. PRUE. Trans. Faraday Soc. **63**, 2019 (1967).

Can. J. Chem. Downloaded from www.nrcresearchpress.com by 88.85.125.76 on 09/07/12
For personal use only.

14. E. M. WOOLLEY, J. O. HILL, W. K. HANNAN, and L. G. HEPLER. J. Solution Chem. **7**, 385 (1978).
15. L. E. STRONG and A. D. PETHYBRIDGE. J. Solution Chem. **16**, 841 (1987).
16. B. BARANOWSKI, A. E. DE VRIES, A. HARING, and R. PAUL. Adv. Chem. Phys. **16**, 101 (1969).
17. J. C. JOHNSON and A. L. BEYERLEIN. J. Phys. Chem. **82**, 1430 (1978).
18. J. N. AGAR and J. LIN. J. Solution Chem. **16**, 973 (1987).
19. D. G. LEAIST. J. Solution Chem. **18**, 651 (1989).
20. E. W. WASHBURN (*Editor*). International critical tables. McGraw Hill, New York. 1929.
21. C. M. MASON and J. B. CULVERN. J. Am. Chem. Soc. **71**, 2387 (1949).
22. M.-C. JUSTICE, R. BURY, and J.-C. JUSTICE. Electrochim. Acta, **16**, 687 (1971).
23. R. M. FUOSS and C. A. KRAUS. J. Am. Chem. Soc. **55**, 476 (1933).
24. O. W. EDWARDS and E. O. HUFFMAN. J. Phys. Chem. **63**, 1830 (1959).
25. D. G. LEAIST. J. Chem. Soc. Faraday Trans. 1, **80**, 3041 (1984).
26. D. G. LEAIST. J. Solution Chem. **14**, 709 (1985).
27. R. A. NOULTY and D. G. LEAIST. J. Phys. Chem. **91**, 1655 (1987).
28. S. GOLDMAN, R. G. BATES, and R. A. ROBINSON. J. Solution Chem. **3**, 593 (1974).
29. J. M. STOKES. Trans. Faraday Soc. **41**, 685 (1945).
30. C. W. CHILDS, C. J. DOWNES, and R. F. PLATFORD. Aust. J. Chem. **26**, 863 (1973).
31. E. A. GUGGENHEIM and J. C. TURGEON. Trans. Faraday Soc. **51**, 747 (1955).
32. K. S. PITZER. J. Phys. Chem. **77**, 268 (1973).
33. K. S. PITZER and G. MAYORGA. J. Phys. Chem. **77**, 2300 (1973).
34. A. K. GRZYBOWSKI. J. Phys. Chem. **62**, 555 (1938).
35. R. G. BATES and S. F. ACREE. J. Res. Natl. Bur. Std. (U.S.) **34**, 373 (1945).
36. G. T. A. MÜLLER and R. H. STOKES. Trans. Faraday Soc. **53**, 642 (1957).
37. L. A. DUNN and R. H. STOKES. Aust. J. Chem. **18**, 285 (1965).
38. E. L. HOLT and P. A. LYONS. J. Phys. Chem. **69**, 2341 (1965).
39. V. VITAGLIANO and D. A. LYONS. J. Am. Chem. Soc. **78**, 4538 (1956).
40. M. SELVARATNAM and M. SPIRO. Trans. Faraday Soc. **61**, 360 (1965).
41. D. P. WAGMAN, W. H. EVANS, V. B. PARKER, I. HALOW, S. M. BAILEY, and R. H. SCHUMM. Natl. Bur. Stand. (U.S.) Tech. Note 270-3. Government Printing Office, Washington. 1968.
42. R. W. RAMETTE and D. A. PALMER. J. Solution Chem. **13**, 637 (1984).
43. A. R. GORDON. J. Chem. Phys. **5**, 522 (1937).
44. W. H. STOCKMAYER. J. Chem. Phys. **33**, 1291 (1960).
45. D. G. LEAIST. J. Chem. Soc. Faraday Trans. 1, **78**, 3069 (1982).

Can. J. Chem. Downloaded from www.nrcresearchpress.com by 88.85.125.76 on 09/07/12
For personal use only.

Synthesis and multinuclear magnetic resonance study of some tin(IV) complexes of pyridine-2-thiolate and related ligands, and the X-ray structural analysis of $Sn(C_5H_4NS)_4 \cdot C_5H_5NS$[1]

LESLIE C. DAMUDE, PHILIP A. W. DEAN,[2] VEERAGATHY MANIVANNAN, RADHEY S. SRIVASTAVA,[3] AND JAGADESE J. VITTAL[2]

Department of Chemistry, University of Western Ontario, London, Ont., Canada N6A 5B7

Received January 16, 1990

LESLIE C. DAMUDE, PHILIP A. W. DEAN, VEERAGATHY MANIVANNAN, RADHEY S. SRIVASTAVA, and JAGADESE J. VITTAL. Can. J. Chem. **68**, 1323 (1990).

Tin metal reacts with 2,2′-dithiobis (pyridine) in refluxing toluene to give the pyridine-2-thiolate complex $Sn(C_5H_4NS)_4$, **1***a*. Multinuclear (^{77}Se, ^{119}Sn) magnetic resonance shows that ligand redistribution occurs in **1***a*:$Sn(EPh)_4$ (E = S or Se) mixtures to give $Sn(EPh)_{4-x}(C_5H_4NS)_x$. From the pattern of the ^{119}Sn chemical shifts of these series, compared with that of $Sn(EPh)_{4-x}(SR)_x$ (R = simple alkyl or aryl group), the complexes are shown to be five-coordinate $Sn(EPh)_3(C_5H_4NS\text{-}N,S)$ when x = 1 and six-coordinate $Sn(EPh)_{4-x}(C_4H_4NS\text{-}S)_{x-2}(C_5H_4NS\text{-}N,S)_2$ when x = 2–4. Reaction of $Sn(SPh)_2$ and $(C_5H_4NS)_2$ yields pure $Sn(SPh)_2(C_5H_4NS)_2$. The ^{13}C NMR spectrum of $Sn(C_5H_4NS\text{-}S)_2$ $(C_5H_4NS\text{-}N,S)_2$ is an exchange average down to 178 K, probably as a result of fluxionality. The series $Sn(EPh)_{4-x}(L')_x$ (E = Se, L′ = 5-nitropyridine- or quinoline-2-thiolate, x = 0–4; E = S or Se, L′ = pyridine-2-thiolate-*N*-oxide, x = 0–2) can be prepared *in situ* by redox between $Sn(EPh)_4$ and the disulfide $(L')_2$. Treatment of **1***a* with X_2 (X = Br or E- gives $SnX_{4-x}(C_5H_4NS\text{-}N,S)_x$ (x = 2 or 3), which have been characterized by NMR, and provides a new synthesis of the known dihalo complexes.

In a recrystallization of **1***a* from CH_2Cl_2:hexane $Sn(C_5H_4NS)_4 \cdot C_5H_5NS$, **2**, was obtained, probably as a result of hydrolysis. The structure of **2** has been solved by single crystal X-ray diffraction techniques. The compound crystallizes in the orthorhombic space group *Pbca* (No. 61) with a unit cell of dimensions a = 17.132(2) Å, b = 15.337(2) Å, c = 21.268(3) Å, and Z = 8. Full-matrix least-squares on F led to agreement factors R = 0.0439 and R_w = 0.0426 for 3145 independent reflections with $F_o > 2.5\sigma$ (F_o) and 206 variables. The molecule $Sn(C_5H_4NS\text{-}S)_2(C_5H_4NS\text{-}N,S)_2$ has highly distorted octahedral coordination about the tin atom, with the monodentate ligands in *cis* positions and the bidentate ligands attached with mutually *cis* nitrogen atoms. The Sn—S distances are 2.463(2)–2.542(2) Å and the Sn—N distances are 2.332(2) and 2.324(2) Å. The N—Sn—S angles in the chelate rings are 64.2(2) and 65.1(1)°. The molecule of pyridine-2-thione in the lattice is hydrogen-bonded to the N atom of one of the monodentate ligands in the tin complex, with a N—H···N hydrogen bond distance of 1.92(7) Å.

Key words: pyridine-2-thiolate, selenium-77 NMR, tin-119 NMR, tin(IV) complexes, X-ray analysis.

LESLIE C. DAMUDE, PHILIP A. W. DEAN, VEERAGATHY MANIVANNAN, RADHEY S. SRIVASTAVA, et JAGADESE J. VITTAL. Can. J. Chem. **68**, 1323 (1990).

L'étain métallique réagit avec la 2,2′-dithiobis (pyridine), dans le toluène au reflux, pour donner le complexe pyridine-2-thiolate, $Sn(C_5H_4NS)_4$, **1***a*. La résonance magnétique multi-noyaux (^{77}Se, ^{119}Sn) démontre que, dans des mélanges de **1***a*: $Sn(EPh)_4$ où E = S ou Se, il se produit une redistribution des ligands et la formation de composés du type $Sn(EPh)_{4-x}(C_5H_4NS)_x$. En se basant sur une comparaison des déplacements chimiques du ^{119}Sn dans les composés de cette série avec ceux observés dans les produits $Sn(EPh)_{4-x}(SR)_x$ où R = groupements aryles ou alkyles simples, on a démontré que, si x = 1, les complexes sont les entités penta-coordonnées $Sn(EPh)_3(C_5H_4NS\text{-}N,S)$ alors que, si x = 2–4, les complexes sont les entités hexa-coordonnées $Sn(EPh)_{4-x}(C_5H_4NS\text{-}S)_2$. La réaction du $Sn(SPh)_2$ avec le $(C_5H_4NS)_2$ fournit du $Sn(SPh)_2(C_5H_4NS)_2$ à l'état pur. Même lorsqu'on abaisse la température jusqu'à 178 K, le spectre rmn du ^{13}C du $Sn(C_5H_4NS\text{-}S)_2(C_5H_4NS\text{-}N,S)_2$ est un spectre moyen résultant probablement d'un mécanisme de fluxion. Faisant appel à une réaction redox *in situ* entre le $Sn(EPh)_4$, et le disulfure $(L')_2$, on peut préparer les produits de la série $Sn(EPh)_{4-x}(L')_x$ (E = Se, L′ = 5-nitropyridine- ou quinoléine-2-thiolate, x = 0–4; E = S ou Se, ′ L′ = pyridine-2-thiolate N-oxyde, x = 0–2). Le traitement du produit **1***a* par du X_2 (X = Br ou I) fournit les complexes $SnX_{4-x}(C_5H_4NS\text{-}N,S)_x$ (x = 2 ou 3) que l'on a caractérisés par rmn; ces réactions fournissent une nouvelle synthèse de ces complexes dihalogénés connus.

Lors de la recristallisation du produit **1***a* dans un mélange de CH_2Cl_2 : hexane, on obtient le $Sn(C_5H_4NS)_4 \cdot C_5H_4NS$, **2**, qui provient probablement d'une hydrolyse. On a déterminé la structure du composé **2** par des techniques de diffraction des rayons-X effectuées sur des cristaux uniques. Le composé donne des cristaux orthorhombiques qui appartiennent au groupe d'espace *Pbca* (No. 61) avec une maille unitaire dont les dimensions sont a = 17,132(2), b = 15,337(2) et c = 21,268(3) Å et Z = 8. On a affiné la structure par la méthode des moindres carrés jusqu'à des valeurs respectives de R = 0,0439 et R_w = 0,0426 pour 3145 réflexions indépendantes avec $F_o > 2{,}5\sigma(F_o)$ et 206 variables. La molécule de $Sn(C_5H_4NS\text{-}N,S)_2(C_5H_4NS\text{-}N,S)_2$ est caractérisée par une coordination octaédrique très déformée autour de l'atome d'étain; les ligands monodentates sont attachés aux positions *cis* et lis ligands bidentates sont attachés aux atomes d'azote qui sont mutuellement *cis*. Les distance Sn—S varient de 2,463(2) à 2,542(2) Å alors que les distances Sn—N sont égales à 2,332(2) et 2,324(2) Å. Les angles N—Sn—S des cycles chélates sont égaux à 64,2(2) et 65,1(1)°. La molécule de pyridine-2-thione présente dans le réseau est reliées par une liaison hydrogène avec l'atome d'azote de l'un des ligands du complexe d'étain; la longueur de la liaison hydrogène N—H···N est égale à 1,92(7) Å.

Mots clés : pyridine-2-thiolate, ^{77}Se RMN, ^{119}Sn RMN, complexes d'étain, analyses des rayons-X.

[Traduit par la revue]

---

[1]No reprints available.

[2]Authors to whom correspondence may be addressed.

[3]On leave from Department of Chemistry, M. G. Degree College, Gorakhpur 273001, India.

Can. J. Chem. Downloaded from www.nrcresearchpress.com by 88.85.125.76 on 09/07/12
For personal use only.

Can. J. Chem. Downloaded from www.nrcresearchpress.com by 88.85.125.76 on 09/07/12
For personal use only.

Introduction

In previous work from this laboratory (1), multinuclear magnetic resonance was used to characterize several new species of the type $Sn(EPh)_{4-x}(E'Ph)_x$ (E, E' = S, Se, Te). The probe nuclei were ^{119}Sn, ^{77}Se, and ^{125}Te,[4] and equilibrium mixtures of the species with mixed phenylchalcogenates were produced either by oxidation of $Sn(EPh)_2$ with $Ph_2E'_2$ (for E = S or Se; E' = S, Se or Te) or by ligand redistribution between $Sn(SPh)_4$ and $Sn(SePh)_4$.

In an extension of the earlier work, we present here a multinuclear magnetic resonance study of species of the type $Sn(EPh)_{4-x}(pyt)_x$ (E = S or Se;[5] pyt = pyridine-2-thiolate or related ligand). Pyridine-2-thiolates are known to be versatile ligands. Modes of attachment that have been established include monodentate terminal bonding through S with (e.g. refs. 3–5) or without (e.g. ref. 6) weak intramolecular M···N interaction, monodentate bridging through S, with weak M···N interaction (7), N,S-chelation, with various degrees of distortion caused by the small bite of the ligand (e.g. refs. 6, 8–11), and bidentate N,S-bridging (e.g. refs. 7, 12–15). Of particular relevance to the present work, chelation has been established in *cis*-$SnCl_2(C_5H_4NS\text{-}N,S)_2$ by X-ray analysis (9). The compound was found to be monomeric in methylisobutylketone (16), but no evidence seems to be available regarding the exact nature of the Sn(IV)–pyt^- interaction for this or related (16) dihalo tin complexes in solution. Tin-119 NMR is very senstitive to changes in the coordination number of tin(IV) (17) and so should be of use for determining the denticity of pyt^- in Sn(IV)-pyt^- complexes. Using ^{119}Sn NMR, we show here that in the series $Sn(EPh)_{4-x}(pyt)_x$ the pyt^- behaves as a chelate when $x = 1$ or 2, while both bidentate and monodentate pyt^- ligands occur when $x = 3$ or 4. The result for $x = 4$ is supported by an X-ray analysis of $Sn(C_5H_4NS)_4 \cdot C_5H_5NS$.

Experimental

Materials

The disulfides R_2S_2 (R = Et, Pr^n, $PhCH_2$, 4-C_6H_4Me, 4-$C_6H_4NO_2$, 2-pyridyl, 2-(5-nitropyridyl), or 2-pyridyl-*N*-oxide), and 2-mercaptopyridine (all from Aldrich), as well as diphenyldiselenide (from Aldrich or Strem) showed no significant impurities by NMR (^1H, ^{13}C, ^{77}Se, as appropriate), and were used as received.

Literature syntheses were used for $Sn(SPh)_2$ (18), and $Sn(EPh)_4$ (E = S or Se) (19). Standard methods (20) were used for the synthesis of Ar_2S_2 (Ar = Ph, 2-MeC_6H_4, 4-ClC_6H_4, or 2-quinolinyl) from the corresponding thiols. The purity of these disulfides was checked using ^{13}C NMR.

Tin(IV) thiolates or selenolates, and 2,2′-dithiobis(pyridine-*N*-oxide) were handled under an atmosphere of Ar or N_2. Solvents for use in synthesis or in the preparation of NMR samples were dried over 3 Å molecular sieves and sparged with Ar before use.

Synthesis

$Sn(SPh)_2(C_5H_4NS)_2$. This was synthesized by the oxidative addition of 2,2′-dithiobis(pyridine) to $Sn(SPh)_2$. The tin(II) compound (0.205 g, 0.608 mol) and $(C_5H_4NS)_2$ (0.134 g, 0.608 mmol) were stirred together in ca. 20 mL of CH_2Cl_2 under nitrogen for 48 h. After this time, the mixture was filtered and the filtrate was concentrated in vacuo then left at 5°C for crystallization to occur. The yellow product was separated by filtration, washed with an ice-cold mixture of CH_2Cl_2 and hexane (1:10 v:v), and dried *in vacuo*. Yield 0.210 g (62%). Mp 142–143°C. *Anal.* calcd. for $C_{22}H_{18}N_2S_4Sn$ (mol. wt. 557.34): C 47.41, H 3.25, N 5.02; found: C 47.37, H 3.20, N 5.04.

*$Sn(C_5H_4NS)_4$, 1*a. Following ref. 19, this compound was prepared from tin powder and 2,2′-dithiobis(pyridine) in refluxing toluene. In a typical reaction, tin powder 1.50 g (12.6 mmol) was refluxed with 4.18 g (19.0 mmol) of 2,2′-dithiobis(pyridine) in ca. 75 mL of toluene for ca. 18 h under N_2. The yellow supernatant liquid was separated by decantation. The excess tin was washed with toluene then CH_2Cl_2 and these washings were combined with the initial decantate. Removal of the solvent on a rotary evaporator gave the crude material. This was dissolved in CH_2Cl_2 and the yellow product was precipitated with hexane and separated by filtration. A second crop resulted from keeping the filtrate at 5°C overnight. Yield 4.88 g (92%). Mp 137–138°C. *Anal.* calcd. for $C_{20}H_{16}N_4S_4Sn$ (mol. wt. 559.30): C 42.95, H 2.88; found: C 43.33, H 3.20. Carbon-13 NMR ($CDCl_3$, 294 K): 162.5, 145.5, 137.6, 125.8, 118.9.

Conversion of $Sn(C_5H_4NS)_4$ to $Sn(C_5H_4NS)_4 \cdot C_5H_5NS$, 2. In attempting to obtain single crystals of $Sn(C_5H_4NS)_4$ for X-ray analysis, solvents that had not been dried were used. Yellow crystals, which proved to be $Sn(C_5H_4NS)_4 \cdot C_5H_5NS$, were grown by layering hexane onto a filtered solution of $Sn(C_5H_4NS)_4$ in CH_2Cl_2 then refrigerating the mixture overnight. *Anal.* calcd. for $C_{25}H_{21}N_5S_5Sn$ (mol. wt. 670.49): C 44.79, H 3.16, N 10.45; found: C 45.03, H 2.95, N 10.21. Carbon-13 NMR ($CDCl_3$, 213 K): 175.5, 138.5, 133.5, 114.1 (C_5H_5NS); 161.1, 146.0, 138.5, 126.4 ($J(^{119}Sn—^{13}C) \approx 35$ Hz), 120.0 ($Sn(C_5H_4NS)_4$). At 294 K, the ^{13}C NMR spectrum is similar but noticeably broader.

Reaction of $Sn(C_5H_4NS)_4$ with I_2 and Br_2. Reaction of $Sn(C_5H_4NS)_4$ with ≥ 1 mol. equiv. of I_2 or Br_2 in CH_2Cl_2 caused formation of poorly soluble $Sn(C_5H_4NS)_2X_2$, which are known compounds (16). For example, when a solution of 1.03 g (1.83 mmol) of $Sn(C_5H_4NS)_4$ in 10 mL of CH_2Cl_2 was mixed with a solution of 0.473 g (1.86 mmol) of I_2 in 20 mL of CH_2Cl_2, yellow $Sn(C_5H_4NS)_2I_2$ was precipitated. The yellow iodo complex was separated by filtration, washed with a little cold CH_2Cl_2, and dried under vacuum. Yield 0.83 g (76%). Mp 281–283°C (lit. (16) mp 271–273°C). *Anal.* calcd. for $C_{10}H_8I_2N_2S_2Sn$ (mol. wt. 592.79): C 20.26, H 1.36; found: C 20.02, H 1.28. Synthesis of $Sn(C_5H_4NS)_2X_2$ from $Sn(C_5H_4NS)_4$ avoids the use of air-sensitive SnX_2.

Nuclear magnetic resonance spectra

NMR samples were prepared and NMR spectra measured and referenced as reported in earlier papers from these laboratories (1, 21). Typically, the number of mol of solute per litre of solvent was 0.1–0.2 for $Sn(SPh)_4$ or $Sn(C_5H_4NS)_4$ and ca. 0.05–0.1 for $Sn(SePh)_4$. Spectra were obtained from samples at ambient probe temperature unless noted otherwise. Linewidths in the ^{77}Se NMR spectra were below 10 Hz, and those in the ^{119}Sn NMR spectra in the range 10–70 Hz, except as noted.

Collection and reduction of X-ray data

A well-developed, light yellow crystal of **2** of suitable quality was mounted on a glass fibre in air. A preliminary photographic examination indicated the unique orthorhombic space group *Pbca* (No. 61) (22). The crystal density was determined to be 1.61(5) g cm^{-3} by flotation in mixtures of carbon tetrachloride and bromoform.

The data collection was carried out on an Enraf-Nonius CAD4F diffractometer using an incident-beam monochromator and Mo Kα (0.71073 Å) radiation (23). Cell constants and an orientation matrix were determined and refined by using the angular settings for 20 high angle reflections with $28.2 < 2\theta < 35.82$. Intensity data were recorded at variable scan speeds chosen to optimize counting statistics within a maximum time per datum of 60 s. Background estimates were made by extending the scan by 25% on each side. Standard reflections 043, 600, 040, 006 were monitored every 120 min of X-ray exposure time and showed −2.5% decay over the total period of 109.2 h. In all, 5329 observations and 172 standards were recorded. Corrections were applied for Lorentz, monochromator and crystal polarization, background radiation effects and crystal decay, using the Structure Determination Package (24) running on a PDP11/23+ computer. The absorption coefficient was 13.0 cm^{-1} and a Gaussian absorption correction was applied (25). The transmission factors ranged from

[4]The natural abundances of ^{119}Sn, ^{77}Se, ^{125}Te, and ^{13}C are 8.58, 7.58, 6.99, and 1.108, respectively; their relative receptivities, D^C, are 25.6, 3.01, 12.7, and 1, respectively (2).

[5]To date, neither $Sn(TePh)_2$ nor $Sn(TePh)_4$ has been isolated pure.

TABLE 1. Summary of X-ray structure determination

Compound	$SnS_4N_4C_{20}H_{20}\cdot C_5H_5NS$
Formula weight	670.490
Crystal system	Orthorhombic
Space group	*Pbca* (No. 61)
Cell dimensions (Å)	a = 17.132(2)
	b = 15.337(2)
	c = 21.268(3)
Temperature, °C	23
Cell volume (Å^3)	5588(2)
Z	8
Density, g cm^{-3}, obsd; calcd.	1.61(5), 1.594
Approximate crystal dimensions (mm)	0.176 × 0.152 × 0.308
Face indices	{100}, {010}, {001},
	{111}, except 1$\bar{1}$1,
	210, $\bar{2}$10, 110, $\bar{1}$10
Crystal-detection (mm), t.o.a. (deg)	205, 2.5
Aperture (mm), vertical; horizontal	4.0, 0.8 + 0.35 tan θ
ω-scan widths, before, after	0.11, 0.111
Scan mode, width (deg)	ω – 2θ, 6.0 + 0.35 tan θ
Index, θ ranges	$-1 \le h \le 20; -1 \le k \le 18; -1 \le \ell \le 25$
	$3.0 \le 2\theta \le 50$
Scan speed (deg min^{-1})	1.177–4.12
Decay, absorption corrections	Yes, Gaussian
Absorption coefficient (cm^{-1}); grid size	13.0, 10 × 12 × 16
R (F) for average, before, after	0.032, 0.030
Number of data averaged	612
No. of unique data, significance	4915 > 0
Top residual peak (e. Å^{-3}), coordinates	0.851, 0.1754, −0.0661, 0.2833

0.8217 to 0.7373. Equivalent reflections were averaged before and after the absorption correction.

Crystal data and the experimental conditions are shown in Table 1.

Solution and refinement of the structure

The tin atom was located by Patterson heavy atom methods using SDP programs running on a PDP11/23+ computer (26). All the remaining non-hydrogen atoms, including those of a molecule of C_5H_5NS, were located in subsequent difference Fourier syntheses and refined by full-matrix least-squares techniques on F using the SHELX-76 software (27). Scattering factors for neutral, non-hydrogen atoms were taken from ref. 28. All the non-carbon atoms were assigned anisotropic thermal parameters. Refinement converged at R = 0.0580 and R_w = 0.0700. At this stage, all the 20 hydrogen atoms attached to the carbon atoms were successfully located in a difference Fourier syntheses, with electron density ranging from 0.259 to 0.777 e Å^{-3}. An electron density of 0.533 e Å^{-3} was found near the N atom of the free C_5H_5NS showing that this molecule is present in the thione rather than the thiol form. The 20 hydrogen positions were calculated (C—H = 0.95 Å) while a common isotropic thermal parameter was refined in the least squares cycles. The positional and the isotropic thermal parameters of the N—H proton were refined in the least square cycles at later stages.

An inspection of F_o and F_c suggested that an extinction parameter should be refined. With the use of 3145 observations with $F_o > 2.5\sigma(F_o)$, and a weighting scheme utilizing weights of the form $w = 1/\text{sig}^2(F_o) + g(F_o)^2$, where g = 0.000135, refinement of 206 variables converged at agreement factors R = 0.0439 R_w = 0.0426 where $R = \Sigma||F_o| - |F_c||/\Sigma|F_o|$ and $R_w = [\Sigma w(|F_o| - |F_c|)^2/wF_o^2]^{1/2}$. The final least-square cycles had a maximum shift/esd of 0.0820 on U of C(22). In the analysis of a total difference Fourier synthesis, there were seven peaks with electron density greater than 0.510 e Å^{-3}; of these, the largest one was associated with C(33) at a distance of 0.68 Å and the remainder were of no chemical significance. An analysis of the data as a function of F_o, 2θ, and Miller indices showed no unusual trends. The extinction parameter refined to 0.000233 (14).

Positional and U(equiv) thermal parameters for the refined atoms are given in Table 2. Tables of hydrogen atom parameters, anisotropic thermal parameters, root-mean-square amplitudes of vibration, weighted least-squares planes, torsion angles, and structure factors have been deposited as supplementary material.[6]

Elemental microanalysis

Microanalyses for C, H, and N were carried out by Guelph Chemical Laboratories, Ltd.

Results and discussion

Synthesis

Tin metal reacts with 2,2′-dithiobis(pyridine), **3***a*, in refluxing toluene to produce yellow $Sn(C_5H_4NS)_4$, **1***a*:

[1] $Sn + 2(C_5H_4NS)_2 \rightarrow Sn(C_5H_4NS)_4$

This preparation parallels the straightforward synthesis of $Sn(SPh)_4$ that was reported recently (19). Under the conditions used to produce **1***a*, tin metal does not react with either 2,2′-dithiobis(5-nitropyridine), **3***b*, or 2,2′-dithiobis(quinoline), **3***c*. We note, however, that Sn(IV) species containing 5-nitropyridine-2-thiolate and quinoline-2-thiolate are well established, e.g. the dichlorotin(IV) complexes (16). We were able to obtain ^{119}Sn NMR spectroscopic evidence for $Sn(5\text{-}NO_2\text{—}C_5H_3NS)_4$, **1***b*, and $Sn(C_9H_6NS)_4$, **1***c* in reaction mixtures containing $Sn(SePh)_4$ and the appropriate dithio compound, **3***b* or **3***c* (see below).

When **1***a* was crystallized from CH_2Cl_2–hexane that had not been dried, hydrolysis apparently occurred and the product was yellow $Sn(C_5H_4NS)_4\cdot C_5H_5NS$, **2**. This compound has been fully characterized by X-ray analysis (see below).

Reaction of **1***a* with one or more mole equivalents of Br_2 or I_2

[6]Copies may be purchased from the Depository of Unpublished Data, CISTI, National Research Council of Canada, Ottawa, Ont., Canada K1A 0S2.

Can. J. Chem. Downloaded from www.nrcresearchpress.com by 88.85.125.76 on 09/07/12
For personal use only.

Can. J. Chem. Downloaded from www.nrcresearchpress.com by 88.85.125.76 on 09/07/12
For personal use only.

TABLE 2. Positional ($\times 10^4$) and thermal ($\times 10^2$) parameters and their estimated standard deviations

Atom	x	y	z	U_{eq}* (Å)
Sn	1001.7(2)	2272.8(3)	2186.7(2)	3.28(1)
S(1)	−443.6(9)	1963(1)	2339.7(8)	4.30(5)
S(2)	918(1)	3876(1)	2301.4(8)	4.56(5)
S(3)	2366(1)	2024(1)	2536.0(9)	4.59(5)
S(4)	1006(1)	1999(1)	1045.5(8)	4.44(5)
S(5)	7730(1)	3082(2)	372(1)	7.77(8)
N(1)	555(3)	2316(3)	3222(2)	3.7(1)
N(2)	1682(4)	5060(5)	1561(3)	8.1(3)
N(3)	1279(3)	853(3)	2496(3)	3.7(1)
N(4)	−485(3)	1606(4)	815(3)	4.9(2)
N(5)	9175(3)	3476(4)	714(3)	4.7(2)
C(11)	−214(4)	2184(4)	3122(3)	4.1(2)
C(12)	−746(4)	2227(5)	3614(3)	5.0(2)
C(13)	−462(4)	2393(5)	4204(3)	5.6(2)
C(14)	321(4)	2511(5)	4313(4)	5.5(2)
C(15)	823(4)	2483(4)	3801(3)	4.8(2)
C(21)	1591(4)	4156(4)	1713(3)	3.9(2)
C(22)	1980(3)	3583(4)	1438(3)	2.9(1)
C(23)	2498(5)	3748(5)	999(4)	6.2(2)
C(24)	2651(5)	4594(5)	823(4)	6.6(2)
C(25)	2264(5)	5243(6)	1099(4)	6.7(2)
C(31)	2028(4)	969(4)	2668(3)	4.0(2)
C(32)	2465(5)	272(5)	2909(3)	5.1(2)
C(33)	2110(5)	−529(5)	2946(4)	6.0(2)
C(34)	1357(5)	−636(5)	2768(4)	6.2(2)
C(35)	937(4)	64(4)	2550(4)	5.1(2)
C(41)	207(4)	1266(4)	963(3)	4.2(2)
C(42)	328(5)	372(5)	1041(4)	6.5(2)
C(43)	−318(5)	−161(6)	963(4)	7.9(3)
C(44)	−1015(5)	148(6)	805(4)	7.3(2)
C(45)	−1086(5)	1039(5)	744(4)	6.6(2)
C(51)	8453(4)	3780(5)	543(4)	5.4(2)
C(52)	8392(5)	4695(5)	500(4)	6.7(2)
C(53)	8999(5)	5212(6)	622(4)	7.5(2)
C(54)	9729(5)	4873(6)	785(4)	7.3(3)
C(55)	9799(5)	4010(5)	832(4)	5.9(2)

*$U_{eq} = (1/3)\,\Sigma_i\,\Sigma_j\,U_{ij}a_i^*\cdot a_j^*\cdot a_i\cdot a_j$.

in CH_2Cl_2 gives clean conversion to $Sn(C_5H_4NS)_2X_2$ (X = Br or I) (reaction [2], $x = 2$). The dihalo complexes are already known (16).

[2] $Sn(C_5H_4NS)_4 + (x/2)\,X_2 \rightarrow Sn(C_5H_4NS)_{4-x}X_x + (x/2)\,(C_5H_4NS)_2$

The replacement of only two of the four $C_5H_4NS^-$ ligands of **1***a* in this experiment suggests that there are inequivalent bonding modes for $C_5H_4NS^-$ in $Sn(C_5H_4NS)_4$. For comparison, $Sn(EPh)_4$ (E = S or Se) can be converted to SnX_4 (via $Sn(EPh)_{4-x}X_x$) by addition of X_2 (X = Br or I).[7]

Nuclear magnetic resonance studies

The ^{13}C NMR spectrum of **1***a* in $CDCl_3$ or CH_2Cl_2 consists of only five resonances from room temperature to 178 K. Therefore in solution, the $C_5H_4NS^-$ ligands either are equivalent or are made equivalent by an averaging process. Clearly the ^{13}C NMR spectrum does not allow a distinction between four-coordinate $Sn(C_5H_4NS\text{-}S)_4$ and a higher coordinate species. The ^{119}Sn NMR spectrum of **1***a* in CH_2Cl_2 at ambient probe temperature consists of a singlet with $\delta_{Sn} = -516$, shielded by over 560 ppm relative to the resonance of $Sn(SPh)_4$ (Table 3). This change is very much larger than the difference between $\delta_{Sn}(Sn(SPh)_4)$ and δ_{Sn} for other simple $Sn(SR)_4$, as shown by data for several representative series $Sn(SPh)_{4-x}(SR)_x$ (Table 4). Equilibrium mixtures containing all members of these series are most easily produced by the reaction of R_2S_2 with $Sn(SPh)_2$:

[3] $Sn(SPh)_2 + R_2S_2 \rightarrow Sn(SPh)_{4-x}(SR)_x$ (equilibrium mixture)

Thus δ_{Sn} for **1***a* is apparently inconsistent with a structure containing only monodentate S-bonded $C_5H_4NS^-$. Monodentate bonding of $C_5H_4NS^-$ through nitrogen would be expected to result in shielding of the tin nucleus, but there do not appear to be any cases in which the ligand binds in this manner, so we discard this possibility.[8] Increase of the coordination number of tin from four to five or six is known to result in a significant increase in nuclear shielding at tin (17). Accordingly δ_{Sn} for **1***a* points to a coordination number of greater than four at tin. This possibility is supported strongly by the NMR data for $Sn(EPh)_4$ (E = S or Se): **1***a* mixtures and related systems, and is confirmed by an X-ray analysis of **2**.

The ^{13}C NMR spectrum of **2** in $CDCl_3$ exhibits signals from both $Sn(C_5H_4NS)_4$ and free C_5H_5NS, which is known to exist mainly as the thione tautomer in solution (31). Separate signals for the two components can be observed at ambient probe temperature, but the overall spectrum is sharper at reduced temperatures. Evidently there is slow intermolecular exchange of $C_5H_4NS^-$ between the tin complex and the free thione at ambient probe temperature which can be stopped at lower temperatures.

(i) $Sn(SePh)_{4-x}(C_5H_4NS)_x$

As the ratio of the two components is changed in $Sn(SePh)_4$: **1***a* mixtures, a total of five ^{119}Sn NMR signals and four ^{77}Se NMR signals is observed. Evidently the redistribution shown in reaction [4] (E = Se) occurs. Typically, several ^{119}Sn and

[4] $[(4-x)/4]\,Sn(EPh)_4 + (x/4)\,Sn(C_5H_4NS)_4 \rightleftharpoons Sn(EPh)_{4-x}(C_5H_4NS)_x$ (equilibrium mixture)

^{77}Se signals are observed for each sample, showing that multiple species coexist at equilibrium, as is frequently found in ligand scrambling processes. From their order of appearance, the signals are readily assignable to individual members of the series $Sn(SePh)_{4-x}(C_5H_4NS)_x$ (Table 3). Of particular significance is the pattern of the sequential differential ^{119}Sn chemical shifts, $\delta_{Sn}[Sn(EPh)_{4-x}(L')_x] - \delta_{Sn}[Sn(EPh)_{4-x+1}(L')_{x-1}]$ (or, more generally, $\delta_{Sn}[SnL_{4-x}L'_x] - \delta_{Sn}[SnL_{4-x+1}L'_{x-1}]$), hereinafter abbreviated $\Delta\delta_{Sn,x}$, which is quite unlike that found in the simple series $Sn(SePh)_{4-x}(SPh)_x$ (1). For $x = 1$, 2, 3, and 4, $\Delta\delta_{Sn,x} = -216$, -302, 51, and 84, respectively. The large negative values for $x = 1$ and 2 we attribute to substitution of $SePh^-$ by bidentate $C_5H_4NS^-$, with changes from four coordination to five coordination, and from five coordination to six coordination, respectively. Thus the complexes with $x = 1$ and 2 are $Sn(SePh)_3(C_5H_4NS\text{-}N,S)$, with kernel $SnSe_3NS$, and $Sn(SePh)_2(C_5H_4NS\text{-}N,S)_2$, with kernel $SnSe_2N_2S_2$, respectively. The values of $\Delta\delta_{Sn,x}$ for $x = 3$ and 4 are positive and of smaller magnitude. We associate these with the replacement of $SePh^-$ by a monodentate S-bonded $C_5H_4NS^-$. In the series $Sn(SePh)_{4-x}(SPh)_x$, replacement of $SePh^-$ by SPh^- leads to a diminution of ^{119}Sn shielding by ca. 45 ppm per substitution (1). Thus it is evident that the $C_5H_4NS^-$ complex with

[7]P. A. W. Dean and V. Manivannan. Unpublished results.

[8]In contrast, *3a* is known to act as an N-donor exclusively, e.g. ref. 30.

TABLE 3. NMR data for $SnL_{4-x}(L')_x$ (L' = pyridine-2-thiolate or related ligand) in CH_2Cl_2 at 293 ± 2 K

L'	L	x	δ_{Sn}[a]	δ_{Se}[b]	$^1J(^{119}Sn—^{77}Se)$[c] (Hz)
Pyridine-2-thiolate	$PhSe^-$[d]	0	−132.7[e]	183.4[e]	1584[e]
		1[f]	−349	237.6	1529
		2[g]	−651	327.9	1427
		3[h]	−600	353.6	1535
		4	−516		
	PhS^-[i]	0	49.5[e]		
		1[f]	−151		
		2[g]	−425[j]		
		3[h]	−476		
	PhS^-, $PhSe^-$[k]	2	−535	309.0	1463
	I^-	0[l]	−1755		
		1[l,m]	−1583		
		2[n,o]	−1380		
		3[n,p]	−835		
	Br^-[n]	2[o]	−783		
		3	−617		
	Br^-, I^-	2[k]	−1082		
5-Nitropyridine-2-thiolate	$PhSe^-$[q]	1[f]	−312	235.0	1595[r]
		2[g]	−631	333.1	1542[r]
		3[h]	−610	393.3	1717
		4	−528		
Quinoline-2-thiolate	$PhSe^-$[s]	1[f]	−338	247.8	1534
		2[g]	−615[t]	335.5	1402
		3[h]	−562	376.4	1507[r]
		4	−457		
Pyridine-2-thiolate-*N*-oxide	PhS^-[u]	1[f]	−161		
		2[g]	−352[v]		
	$PhSe^-$[u]	1[f]	−374	260.2	1563
		2[g]	−557[w]	317.0[x]	≈1400
	PhS^-, $PhSe^-$[k]	2	−451[v]	301.0[x]	[y]
Pyridine-2-thiolate, Pyridine-2-thiolate-*N*-oxide[z]	PhS^-		−389		

[a]Relative to external pure $SnMe_4$ at 295 K; reproducibility between different equilibrium mixtures ±2 ppm.

[b]Relative to external pure Me_2Se at 295 K; reproducibility between different equilibrium mixtures ±0.2 ppm.

[c]Estimated error ±5 Hz except as noted.

[d]In $Sn(C_5H_4NS)_4$:$Sn(SePh)_4$ or $Sn(SePh)_4$:$(C_5H_4NS)_2$ mixtures.

[e]From ref. 1.

[f]$Sn(\eta^2\text{-}L')L_3$ (see text).

[g]$Sn(\eta^2\text{-}L')_2L_2$ (see text).

[h]$Sn(\eta^1\text{-}L')(\eta^2\text{-}L')_2L$ (see text).

[i]In $Sn(C_5H_4NS)_4$:$Sn(SPh)_4$, $Sn(C_5H_4NS)_4$:Ph_2S_2 or $Sn(SPh)_4$:$(C_5H_4NS)_2$ mixtures.

[j]This signal was broad in some mixtures.

[k]$Sn(\eta^2\text{-}L')_2(L)(L'')$, formed at equilibrium when solutions containing $Sn(\eta^2\text{-}L')_2(L)_2$ and $Sn(\eta^2\text{-}L')_2(L'')_2$ are mixed.

[l]In $Sn(C_5H_4NS)_4$:SnI_4 mixtures.

[m]Broad signal ($\Delta\nu_{1/2} \approx 140$ Hz).

[n]In $Sn(C_5H_4NS)_4$:X_2 mixtures.

[o]$Sn(\eta^2\text{-}C_5H_4NS)_2X_2$ is poorly soluble.

[p]Broad line ($\Delta\nu_{1/2} \approx 730$ Hz).

[q]In $Sn(SePh)_4$:2,2′-dithiobis(5-nitropyridine) mixtures.

[r]Estimated error ±10 Hz.

[s]In $Sn(SePh)_4$:2,2′-dithiobis(quinoline) mixtures.

[t]$\Delta\nu_{1/2} \approx 350$ Hz.

[u]In $Sn(EPh)_4$:2,2′-dithiobis(pyridine-*N*-oxide) mixtures.

[v]$\Delta\nu_{1/2} \approx 240$ Hz.

[w]$\Delta\nu_{1/2} \approx 125$ Hz.

[x]$\Delta\nu_{1/2} \approx 60$ Hz.

[y]Could not be observed.

[z]In a 1:0.5:0.5 mixture of $Sn(SPh)_4$:$(C_5H_4NS)_2$:$(C_5H_4SNO)_2$.

Can. J. Chem. Downloaded from www.nrcresearchpress.com by 88.85.125.76 on 09/07/12
For personal use only.

TABLE 4. Tin-119 NMR chemical shifts for some series $Sn(SPh)_{4-x}(SR)_x$ in CH_2Cl_2 at 293 ± 2 K.[a]

R	δ_{Sn}[b]			
	$x = 1$	$x = 2$	$x = 3$	$x = 4$
Ph	49.5[c]	49.5[c]	49.5[c]	49.5[c]
Me	77.3	105.4	133.7	162.0[d]
Et	72.3	94.4	116.1	137.5[e]
Pr^n	72.1	94.9	117.8	140.7
Bu^n	72.4	95.1	118.0	140.8
$PhCH_2$	68.2	87.9	108.9	130.8
2-C_6H_4Me	47.0	45.0	43.4	42.2
4-C_6H_4Me	48.6	47.6	46.6	45.7
4-C_6H_4Cl	48.6	47.6	46.7	46.2
4-$C_6H_4NO_2$	47.6	46.3	46.1?	[f]

[a]In 1:1 mixtures of $Sn(SPh)_2$ and R_2S_2.
[b]Estimated error in differential chemical shifts ±0.2 ppm; reproducibility of individual chemical shifts is probably poorer.
[c]From ref. 1.
[d]δ_{Sn} = 165 for neat $Sn(SMe)_4$ (29).
[e]δ_{Sn} = 138 for neat $Sn(SEt)_4$ (29).
[f]Could not be observed with certainty: probably isochronous with the signal of $Sn(SPh)(S\{4\text{-}C_6H_4NO_2\})_3$.

$x = 3$ is $Sn(SePh)(C_5H_4NS\text{-}S)(C_5H_4NS\text{-}N,S)_2$, with the kernel $SnSeS_3N_2$, while that with $x = 4$ is $Sn(C_5H_4NS\text{-}S)_2$ $C_5H_4NS\text{-}N,S)_2$, with the kernel SnS_4N_2. The last conclusion is in accord with the chemical evidence from halogen oxidation of **1***a* (see above), and also means that the five-line ^{13}C NMR spectrum observed for $Sn(C_5H_4NS)_4$ down to 178 K (see above) must be an exchange average.[9] The observation of separate ^{77}Se NMR spectra, with ^{119}Sn satellites, for the individual species $Sn(SePh)_{4-x}(C_5H_4NS)_x$ at 293 K shows that intermolecular exchange of $SePh^-$ is slow on the timescales of $^1J(^{119}Sn—^{77}Se)$ and $\Delta\delta_{Se}$, and therefore, presumably, of $\Delta\delta_{Sn}$ also, under these conditions. As a result, it is not possible to conclude from the observation of separate ^{119}Sn signals for this series that intermolecular exchange of $C_5H_4NS^-$ must also be slow here. However, exchange of the chelate ligands is evidently slow on the timescale of $\Delta\delta_{Sn}$ for the series $Sn(SPh)_2(C_5H_4NS\text{-}N,S)_2$-$(C_5H_4SNO\text{-}O,S)_n$ at 293 K (see (*iv*) below). Therefore we believe that it is rapid intramolecular (rather than intermolecular) exchange that simplifies the ^{13}C NMR spectrum of **1***a* at 293 K. The observation of ^{119}Sn satellites ($J(^{119}Sn—^{13}C)$ ≈ 35 Hz) about the 126.4 ppm resonance in the ^{13}C NMR spectra of **1***a* and **2** at 213 K shows that the exchange is certainly intramolecular at this temperature.

The ^{119}Sn and ^{77}Se NMR data are insufficient to allow the deduction of finer detail about the coordination kernel of tin in the complexes with mixed ligands, such as the coordination geometry and geometrical isomeric form. Undoubtedly the six-coordinate species are distorted octahedral, as reported for $SnCl_2(C_5H_4NS\text{-}N,S)_2$ (9). Either trigonal bipyramidal or square pyramidal geometry is possible for $Sn(SePh)_3(C_5H_4NS\text{-}N,S)$, but in any case this molecule must be fluxional to account for the occurrence of only one ^{77}Se NMR signal. With regard to the ^{77}Se NMR data, it is also interesting to note that $^1J(^{119}Sn—^{77}Se)$ shows only a 10% reduction in magnitude on changing from four-coordinate $Sn(SePh)_4$ to six-coordinate $Sn(SePh)_2$-$(C_5H_4NS\text{-}N,S)_2$. On the basis of a change from sp^3 to sp^3d^2 hybridization, a larger reduction might have been anticipated. Most likely the effects of substitution and change in hybridization almost cancel. Consistent with the existence of competing effects, both ^1J and δ_{Se} vary irregularly across the whole series (Table 3).

The series $Sn(SePh)_{4-x}(C_5H_4NS)_x$ can be generated in $Sn(SePh)_4$: **3***a* mixtures also (reaction [5], E = Se). However, the redox

[5] $Sn(EPh)_4 + (x/2)\,(C_5H_4NS)_2 \rightleftharpoons Sn(EPh)_{4-x}(C_5H_4NS)_x + (x/2)\,Ph_2E_2$ (equilibrium mixture)

reaction is very slow to reach equilibrium at room temperature. For example a 1:2 mixture was still changing slowly after one week. At that time a mixture of the species with x = 2–4 existed.

(ii) $Sn(SPh)_{4-x}(C_5H_4NS)_x$

This series is generated most easily from $Sn(SPh)_4$: **1***a* mixtures in CH_2Cl_2 (reaction [4], E = S). The same species can be generated over a matter of hours-days in $Sn(SPh)_4$: **3***a* or **1***a*: Ph_2S_2 mixtures (c.f. reaction [5]). As expected, a total of five species exists in the series. The ^{119}Sn NMR chemical shifts are given in Table 3. By comparison with data for simple complexes of the type $Sn(SPh)_{4-x}(SR)_x$ (Table 4), which can be accounted for on the basis of first or second order additivity models (37), the chemical shifts of $Sn(SPh)_{4-x}(C_5H_4NS)_x$ show irregular behaviour. For this latter series, $\Delta\delta_{Sn,x} = -201$ and -274 for $x = 1$ and 2, respectively, significantly larger than the values of -51 and -40 for $x = 3$ and 4, respectively. On this basis the pyridine-2-thiolate complexes are five-coordinate $Sn(SPh)_3$-$(C_5H_4NS\text{-}N,S)$ and six-coordinate $Sn(SPh)_{4-x}(C_5H_4NS\text{-}S)_{x-2}$-$(C_5H_4NS\text{-}N,S)_2$ (x = 2–4).

According to ^{119}Sn NMR measurements, $Sn(SPh)_2(C_5H_4NS)_2$ is the only species present at equilibrium when $Sn(SPh)_4$ and **1***a* or **3***a* are mixed in a 1:1 ratio in CH_2Cl_2. (The reaction of **1***a* with Ph_2S_2 is too slow to be useful.) Consistent with this observation, $Sn(SPh)_2(C_5H_4NS)_2$ can be isolated pure from a 1:1 mixture of $Sn(SPh)_2$ and **3***a* (see Experimental section).

When a solution of $Sn(SPh)_2(C_5H_4NS\text{-}N,S)_2$ is mixed with a solution containing $Sn(SePh)_2(C_5H_4NS\text{-}N,S)_2$ as the main component,[10] a major new ^{119}Sn NMR signal appears together with a corresponding new ^{77}Se NMR signal. The chemical shift of the new ^{119}Sn resonance is close to the midpoint of those of the $Sn(EPh)_2(C_5H_4NS\text{-}N,S)_2$ parents, and it is evident that scrambling of EPh^- anions has occurred to give $Sn(SPh)$-$(SePh)(C_5H_4NS\text{-}N,S)_2$.

(iii) $Sn(SePh)_{4-x}(SR')_x$ (R' = 5-nitro-2-pyridyl or 2-quinolinyl)

Although the parent compounds **1***b* and **1***c* were not isolated, these two series of complexes could be prepared in CH_2Cl_2 by the reaction of $Sn(SePh)_4$ with the appropriate $(R'S)_2$ (**3***b* or **3***c*). These redox reactions parallel [5]. The reactions are slow at ambient probe temperature, e.g. 1:1 mixtures had not reached equilibrium after a week. Nevertheless, it was possible to characterize all members of both series by ^{77}Se and/or ^{119}Sn NMR, and these data are given in Table 3. The similarity with

[9]Similarly, tin(IV) dialkyldithiocarbamates, with the solid-state structure $Sn(dtc\text{-}S)_2$ $(dtc\text{-}S,S')_2$ (32, 33), show equivalencing of dtc groups by ^{13}C NMR at ambient probe temperature (34). Tin(IV) xanthates, of analogous structure in the solid state (35), show equivalencing of ligands by ^{13}C NMR down to 183 K (36).

[10]Unlike $Sn(SPh)_2(C_5H_4NS)_2$, $Sn(SePh)_2(C_5H_4NS)_2$ always occurs as one component of an equilibrium mixture.

Can. J. Chem. Downloaded from www.nrcresearchpress.com by 88.85.125.76 on 09/07/12
For personal use only.

Can. J. Chem. Downloaded from www.nrcresearchpress.com by 88.85.125.76 on 09/07/12
For personal use only.

data for the series $Sn(SePh)_{4-x}(C_5H_4NS)_x$ is obvious, and the data can be accounted for in a like manner.

(iv) $SnX_{4-x}(C_5H_4NS)_x$ (X = Br or I or a mixture of these)

For $x = 2$ or 3, these complexes can be prepared *in situ* in CH_2Cl_2 according to reaction [2]. Their ^{119}Sn NMR spectra are readily assigned on the basis of the order of appearance of the signals, and the assignments are given in Table 3. As expected from the chemical shifts reported for $SnBr_6^{2-}$,[11] δ_{Sn} for $SnBr_{4-x}(C_5H_4NS\text{-}N,S)_x$ decreases with decreasing x. The iodo analogues are even more shielded as anticipated on the basis of the normal halogen dependence, which is observed for tin(IV).[12] A mixture of $SnBr_2(C_5H_4NS\text{-}N,S)_2$ and $SnI_2(C_5H_4NS\text{-}N,S)_2$ provides evidence for $SnBrI(C_5H_4NS\text{-}N,S)_2$. Overall, the pattern of ^{119}Sn chemical shifts for the halo complexes is very similar to those of various analogous halo-substituted xanthates of Sn(IV) (36).

Extension of $SnX_{4-x}(C_5H_4NS)_x$ to include the species with $x = 1$ can be made using **1***a* or $SnX_2(C_5H_4NS)_2$:SnX_4 mixtures. For instance, the complex with $x = 1$, X = I, gives a resonance at −1583 ppm, between those of $SnI_2(C_5H_4NS\text{-}N,S)_2$ and SnI_4. The signal of the trioiodo complex is significantly more shielded than that of $SnI_3(SPh)$ (−935 ppm).[7] This indicates a five-coordinate structure for $SnI_3(C_5H_4NS\text{-}N,S)$.

(iv) $Sn(EPh)_{4-x}(C_5H_4SNO)_x$

2,2′-Dithiobis (pyridine-*N*-oxide), $(C_5H_4SNO)_2$, is poorly soluble in CH_2Cl_2, but at the concentration used here dissolves over a period of ca. 1 h in the presence of 2 mol. equiv. of $Sn(SPh)_4$. When this reaction is followed by ^{119}Sn NMR, the first new signal to appear is at −161 ppm. This can be assigned to $Sn(SPh)_3(C_5H_4SNO)$. At equilibrium a second, significantly broader, new signal is observed at −352 ppm and can be attributed to $Sn(SPh)_2(C_5H_4SNO)_2$. The equilibrium mixture is far from statistical: $Sn(SPh)_3(C_5H_4SNO)$ is present in minor amount relative to $Sn(SPh)_4$ and $Sn(SPh)_2(C_5H_4SNO)_2$. A 1:1 $Sn(SPh)_4$:$(C_5H_4SNO)_2$ mixture at equilibrium contains only $Sn(SPh)_2(C_5H_4SNO)_2$. The large values of $\Delta\delta_{Sn,x}$, −211 and −191 ppm for $x = 1$ and 2, respectively, point to chelation by the $C_5H_4SNO^-$ ligand, which is a well-established feature of its coordination behaviour (e.g. refs. 40–42). Accordingly, the species with $x = 1$ and 2 must have the chelated structures $Sn(SPh)_3(C_5H_4SNO\text{-}O,S)$ and $Sn(SPh)_2(C_5H_4SNO\text{-}O,S)_2$, respectively.

Mixtures of $Sn(SePh)_4$ and $(C_5H_4SNO)_2$ behave very much like those containing $Sn(SPh)_4$. The species $Sn(SePh)_{4-x}(C_5H_4SNO\text{—}O,S)_x$ ($x = 1$ or 2) have been characterized by ^{77}Se and ^{119}Sn NMR (Table 3).

When a solution of $Sn(SPh)_2(C_5H_4SNO\text{-}O,S)_2$ is mixed with a solution of $Sn(SPh)_2(C_5H_4NS\text{-}N,S)_2$ a new species occurs in equilibrium with the two component complexes. This new species has a ^{119}Sn resonance at −389 ppm, between the signals of the two parent complexes, and is clearly the redistribution product $Sn(SPh)_2(C_5H_4NS\text{-}N,S)(C_5H_4SNO\text{-}O,S)$. Similarly, $Sn(SPh)(SePh)(C_5H_4SNO\text{-}O,S)_2$ may be detected by ^{77}Se and ^{119}Sn NMR in mixtures of $Sn(SPh)_2(C_5H_4SNO\text{-}O,S)_2$ and $Sn(SePh)_2(C_5H_4SNO\text{-}O,S)_2$.

Crystal structure of $Sn(C_5H_4NS)_4 \cdot C_5H_5NS$, 2

The crystal structure of **2** consists of $Sn(C_5H_4NS)_4$ molecules and pyridine-2-thione molecules. The N—H proton of the thione is hydrogen bonded to an uncoordinated N atom of one of the ligands attached to Sn(IV), with an N(5)—H···N(4) hydrogen bond distance of 1.92(7) Å. There are close nonbonded contacts of 2.71(6) Å between H(5) and H(45), 2.75(7) Å between H(5) and C(45) and 2.935(9) Å between N(4) and N(5). Figure 1 gives a perspective view of the $Sn(C_5H_4NS)_4$ molecule. A view of the lattice thione has been deposited.[6] The bond distances and angles for $Sn(C_5H_4NS)_4$ are given in Table 2. Those for the thione have been deposited.[6]

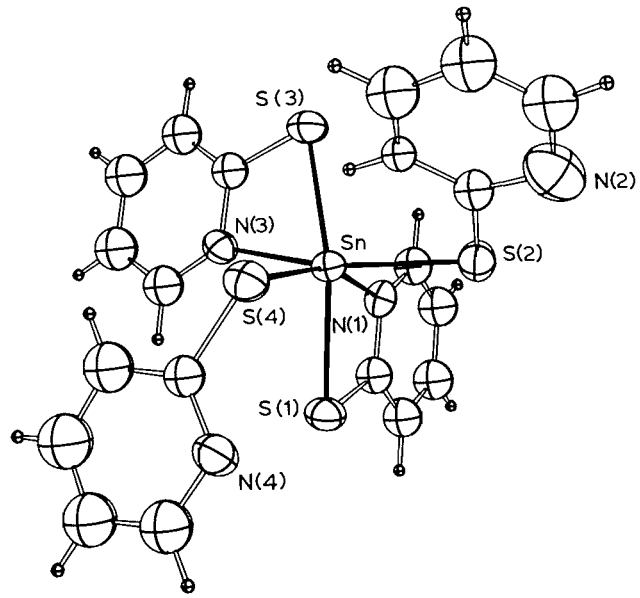

FIG. 1. Perspective view of the molecule $Sn(C_5H_4NS\text{-}S)_2(C_5H_4NS\text{-}N,S)_2$ in **2**.

As can be seen in Fig. 1, the monomeric $Sn(C_5H_4NS)_4$ has highly distorted octahedral coordination about Sn(IV). Of the four $C_5H_4NS^-$ ligands, two are monodentate and S-bonded with the two sulphur atoms in mutually *cis* positions, while the other two are bidentate, coordinating through their N and S atoms such that the two S atoms are *trans* and the two N atoms are *cis*. The configuration of $Sn(C_5H_4NS\text{-}S)_2(C_5H_4NS\text{-}N,S)_2$ is very similar to that reported for $Sn(C_5H_4NS\text{-}N,S)_2Cl_2$, **4** (9).

The Sn—S bond distances are 2.542(2) and 2.483(2) Å for the chelated ligands and 2.475(2) and 2.463(2) Å for the monodentate ligands. The distances from Sn to the S of the monodentate ligands are slightly lower than those of $Sn(SPh)_4$bpy, which are in the range of 2.502(1)–2.497(1) Å (43). In the chelate rings, the Sn—S bond distances are slightly lower than those found in $Sn(S_2CNEt_2)_4$ (32), $Sn(S_2CNMe_2)_4$ (33), or $Sn(S_2COEt)_4$ (35). The Sn—N bond distances (2.332(5) and 2.324(5) Å) and the Sn—S bond distances in the chelate rings are all higher than the corresponding distances observed in **4** and, consistent with these increased bond lengths, the chelate bite angles are 64.2(2) and 65.1(1)° in $Sn(C_5H_4NS)_4$ compared to 66.2(3) and 66.0(3)° in **4**. These differences may be due to either electronegativity differences between the Cl and S donor atoms, or crowding effects of phenyl rings, or both. The C—S bond distances of the coordinated ligands ranges from 1.740(7) to 1.779(7) Å with an average of 1.754(2) Å. For the chelating ligands, the C—S bond distances are shorter than for the monodentate ligands (Table 5). The C—N and C—C bond distances of the ligands are normal and warrant no further discussion.

The angle S(1)—Sn—S(3) between the mutually *trans* sulfur

[11] δ_{Sn} for $(Bu_4N)_2[SnBr_6]$ in CH_2Cl_2 is −2064 at 243 K (38), −2074 ppm at 307 K (39).

[12] The ^{119}Sn resonance of SnI_6^{2-} has not yet been observed (38, 39).

TABLE 5. Bond distances and angles for $Sn(C_5H_4NS\text{-}S)_2(C_5H_4NS\text{-}N,S)_2$ in **2**

(*a*) Bond distances

Atom 1	Atom 2	Distance (Å)	Atom 1	Atom 2	Distance (Å)	Atom 1	Atom 2	Distance (Å)
Sn	S(1)	2.542(2)	Sn	N(1)	2.332(5)	Sn	S(2)	2.475(2)
Sn	S(3)	2.483(2)	Sn	N(3)	2.324(5)	Sn	S(4)	2.463(2)
S(1)	C(11)	1.743(7)	N(1)	C(11)	1.348(8)	N(1)	C(15)	1.340(8)
C(11)	C(12)	1.390(9)	C(12)	C(13)	1.371(9)	C(13)	C(14)	1.372(9)
C(14)	C(15)	1.388(9)	S(2)	C(21)	1.755(7)	N(2)	C(21)	1.432(9)
N(2)	C(25)	1.428(10)	C(21)	C(22)	1.298(8)	C(22)	C(23)	1.329(9)
C(23)	C(24)	1.375(10)	C(24)	C(25)	1.331(10)	S(3)	C(31)	1.740(7)
N(3)	C(31)	1.347(8)	N(3)	C(35)	1.349(8)	C(31)	C(32)	1.402(9)
C(32)	C(33)	1.373(10)	C(33)	C(34)	1.355(10)	C(34)	C(35)	1.372(10)
S(4)	C(41)	1.779(7)	N(4)	C(41)	1.333(8)	N(4)	C(45)	1.357(9)
C(41)	C(42)	1.397(10)	C(42)	C(43)	1.386(11)	C(43)	C(44)	1.329(11)
C(44)	C(45)	1.378(11)						

(*b*) Bond angles

Atom 1	Atom 2	Atom 3	Angle (deg)	Atom 1	Atom 2	Atom 3	Angle (deg)	Atom 1	Atom 2	Atom 3	Angle (deg)
N(1)	Sn	S(1)	64.2(2)	S(2)	Sn	S(1)	96.69(6)	S(2)	Sn	N(1)	82.0(1)
S(3)	Sn	S(1)	148.22(6)	S(3)	Sn	N(1)	91.8(1)	S(3)	Sn	S(2)	100.26(6)
N(3)	Sn	S(1)	89.3(1)	N(3)	Sn	N(1)	80.0(2)	N(3)	Sn	S(2)	156.2(1)
N(3)	Sn	S(3)	65.1(1)	S(4)	Sn	S(1)	95.57(6)	S(4)	Sn	N(1)	159.4(1)
S(4)	Sn	S(2)	105.48(6)	S(4)	Sn	S(3)	105.43(6)	S(4)	Sn	N(3)	96.8(1)
C(11)	S(1)	Sn	82.3(2)	C(11)	N(1)	Sn	99.6(4)	C(15)	N(1)	Sn	139.5(4)
C(15)	N(1)	C(11)	120.6(5)	N(1)	C(11)	S(1)	113.6(5)	C(12)	C(11)	S(1)	125.4(5)
C(12)	C(11)	N(1)	121.0(6)	C(13)	C(12)	C(11)	117.7(7)	C(14)	C(13)	C(12)	121.7(7)
C(15)	C(14)	C(13)	118.1(7)	C(14)	C(15)	N(1)	120.9(6)	C(21)	S(2)	Sn	97.7(2)
C(25)	N(2)	C(21)	115.0(7)	N(2)	C(21)	S(2)	118.1(5)	C(22)	C(21)	S(2)	118.7(5)
C(22)	C(21)	N(2)	123.3(6)	C(23)	C(22)	C(21)	118.9(6)	C(24)	C(23)	C(22)	123.1(8)
C(25)	C(24)	C(23)	119.5(8)	C(24)	C(25)	N(2)	120.2(8)	C(31)	S(3)	Sn	83.0(2)
C(31)	N(3)	Sn	98.5(4)	C(35)	N(3)	Sn	140.9(5)	C(35)	N(3)	C(31)	120.6(6)
N(3)	C(31)	S(3)	113.4(5)	C(32)	C(31)	S(3)	126.2(5)	C(32)	C(31)	N(3)	120.4(6)
C(33)	C(32)	C(31)	117.9(7)	C(34)	C(33)	C(32)	120.9(8)	C(35)	C(34)	C(33)	119.9(8)
C(34)	C(35)	N(3)	120.2(7)	C(41)	S(4)	Sn	101.7(2)	C(45)	N(4)	C(41)	116.9(6)
N(4)	C(41)	S(4)	117.5(5)	C(42)	C(41)	S(4)	119.6(6)	C(42)	C(41)	N(4)	122.9(6)
C(43)	C(42)	C(41)	116.5(8)	C(44)	C(43)	C(42)	122.6(9)	C(45)	C(44)	C(43)	117.2(9)
C(44)	C(45)	N(4)	123.9(8)								

atoms is 148.22(6)°, while the angle N(1)—Sn—N(3) between the mutually *cis* nitrogen atoms is 80.0(2)°. The angles N(1)—Sn—S(3) and N(3)—Sn—S(1) are 91.8(1) and 89.3(1)°, respectively. To our knowledge, *trans* S atoms and *cis* N atoms are a feature of all the other structurally characterized octahedral complexes having two chelated $C_5H_4NS^-$ ligands (6, 8, 44).

Each of the ligands is planar within experimental error. The tin atom is practically in the same plane as three of the ligands, but is out of the plane of one of the monodentate ligands probably due to hydrogen bonding. The Sn—S(4)—C(41)—N(4) and the Sn—S(4)—C(41)—C(42) torsional angles are 94.7(5) and −86.7(6)°, respectively. Between the two bidentate ligands, the interplanar angle is 96.2(2)°. The relative position of these two ligands is very similar to that observed for **4**.

The successful location and refinement of a hydrogen atom 1.04 Å from N(5) of the lattice C_5H_5NS confirms that this species is pyridine-2-thione. The thionic C—S bond distance of 1.667(8) is shorter than the average C—S bond distance (1.754(2) Å) observed here for the ligands attached to Sn(IV) and this can be attributed to multiple bonding occurring in the thione. Overall, the dimensions of C_5H_5NS in **2** are very similar to those found in the pure thione (45), as well as to those of the lattice thione in $[Cu(C_5H_5NS)_4](ClO_4)\cdot 2C_5H_5NS$ (46), and therefore they are not discussed further.

Acknowledgments

This work was made possible by funding from the Natural Sciences and Engineering Research Council of Canada. We are grateful to V. M. Richardson and S. England of this Department for expert technical assistance in obtaining some of the NMR spectra. One of us (J.J.V.) would like to thank Professor N. C. Payne of this Department, for providing the X-ray diffraction and computer facilities and computer programs, as well as for his keen interest and support.

1. P. A. W. DEAN and R. S. SRIVASTAVA. Inorg. Chim. Acta, **105**, 1 (1985).
2. R. K. HARRIS. Nuclear magnetic resonance spectroscopy. Pitman, London. 1983. p. 230.
3. A. P. BOZOPOULOS, S. C. KOKKOU, P. J. RENTZEPERIS, and P. KARAGIANNIDIS. Acta Crystallogr. C**40**, 944 (1984).
4. A. CASTINEIRAS, W. HILLER, J. STRAHLE, J. BRAVO, J. S. CASAS,

Can. J. Chem. Downloaded from www.nrcresearchpress.com by 88.85.125.76 on 09/07/12
For personal use only.

M. GAYOSO, and J. SORDO. J. Chem. Soc. Dalton Trans. 1945 (1986).
5. H. PREUT, F. HUBER, and K.-H. HENGSTMANN. Acta Crystallogr. C**44**, 468 (1988).
6. P. MURA, B. G. OLBY, and S. D. ROBINSON. J. Chem. Soc. Dalton Trans. 2101 (1985).
7. S. WANG and J. P. FACKLER. Inorg. Chem. **28**, 2615 (1989).
8. S. R. FLETCHER and A. C. SKAPSKI. J. Chem. Soc. Dalton Trans. 635 (1972).
9. M. MASAKI, S. MATSUNAMI, and H. UEDA. Bull. Chem. Soc. Jpn. **51**, 3298 (1978).
10. P. MURA and S. D. ROBINSON. Acta Crystallogr. C**41**, 1798 (1984).
11. S. G. ROSENFIELD, H. P. BERENDS, L. GELMINI, D. W. STEPHAN, and P. K. MASCHARAK. Inorg. Chem. **26**, 2792 (1987).
12. K. UMAKOSHI, I. KINOSHITA, and S. OOI. Inorg. Chim. Acta, **127**, L41 (1987).
13. M. A. CIRIANO, F. VIGURI, L. A. ORO, A. TIRIPICCHIO, and M. TIRIPICCHIO-CAMELLINI. Angew. Chem. **99**, 452 (1987); Angew. Chem. Int. Ed. Engl. **26**, 444 (1987).
14. K. UMAKOSHI, I. KINISHITA, A. ICHIMURA, and S. OOI. Inorg. Chem. **26**, 3551 (1987).
15. R. KUMAR, V. S. J. DE MEL, and J. P. OLIVER. Organometallics, **8**, 2488 (1989).
16. M. MASAKI and S. MATSUNAMI. Bull. Chem. Soc. Jpn. **49**, 3274 (1976).
17. J. D. KENNEDY and W. MCFARLANE. *In* Multinuclear NMR. *Edited by* J. Mason. Plenum, New York. 1987. Chap. 11 and references therein.
18. J. J. I. ARSENAULT and P. A. W. DEAN. Can. J. Chem. **61**, 1516 (1983).
19. R. KUMAR, H. E. MABROUK, and D. G. TUCK. J. Chem. Soc. Dalton Trans. 1045 (1988).
20. L. FIELD. *In* Organic chemistry of sulfur. *Edited by* S. Oae. Plenum, New York. 1977. Chap. 7.
21. P. A. W. DEAN and J. J. VITTAL. Can. J. Chem. **66**, 2443 (1988), and references therein.
22. International tables for X-ray crystallography. Vol. A. D. Reidel Publishing Company, Dordrecht, The Netherlands, 1983.
23. Enraf-Nonius CAD4F Users Manual. Enraf-Nonius, Delft, The Netherlands. 1982.
24. Enraf-Nonius Structure Determination Package. SDP-PLUS, Version 3.0. 1985.
25. A. C. T. NORTH, D. C. PHILLIPS, and F. S. MATHEWS. Acta Crystallogr. A**24**, 351 (1968).
26. G. M. SHELDRICK. SHELXS-86, structure solving program. University of Gottingen, F.R.G. 1986.
27. G. M. SHELDRICK. SHELX-76, Program for crystal structure determination. University of Cambridge, England. 1976.
28. D. T. CROMER and D. LIBERMAN. J. Chem. Phys. **53**, 1891 (1970).
29. J. D. KENNEDY and W. MCFARLANE. J. Chem. Soc. Perkin II, 146 (1974).
30. M. M. KADOOKA, E. HILTI, L. G. WARNER, and K. SEFF. Inorg. Chem. **15**, 1186 (1976), and references therein.
31. M. WITANOWSKI and L. STEFANIAK. Bull. Pol. Acad. Sci. Chem. **35**, 305 (1987).
32. C. S. HARRELD and E. O. SCHLEMPER. Acta Crystallogr. B**27**, 1964 (1971).
33. J. POTENZA, R. J. JOHNSON, and D. MASTROPAOLO. Acta Crystallogr. B**32**, 941 (1976).
34. H. L. M. VAN GAAL, J. W. DIESVELD, F. W. PIJPERS, and J. G. M. VAN DER LINDEN. Inorg. Chem. **18**, 3251 (1979).
35. C. L. RASTON, P. R. TENNANT, A. H. WHITE, and G. WINTER. Aust. J. Chem. **31**, 1493 (1978).
36. D. DAKTERNIEKS, R. W. GABLE, and G. WINTER. Inorg. Chim. Acta, **75**, 185 (1983).
37. C. J. JAMESON and J. MASON. *In* Multinuclear NMR. *Edited by* J. Mason. Plenum, New York. 1987. Chap. 3 and references therein.
38. R. COLTON, D. DAKTERNIEKS, and C.-A. HARVEY. Inorg. Chim. Acta, **61**, 1 (1982).
39. K. B. DILLON and A. MARSHALL. J. Chem. Soc. Dalton Trans. 1245 (1984).
40. B. L. BARNETT, H. C. KRETSCHMAR, and F. A. HARTMAN. Inorg. Chem. **16**, 1834 (1977).
41. SEIK WENG NG, CHEN WEI, V. G. KUMAR DAS, and T. C. W. MAK. J. Organomet. Chem. **334**, 283 (1987); J. Organomet. Chem. **334**, 295 (1987).
42. M. V. CASTANO, A. SANCHEZ, J. S. CASAS, J. SORDO, J. L. BRIANSO, J. F. PINIELLA, X. SOLANS, G. GERMAIN, T. DEBAERDEMAEKER, and J. GLASER. Organometallics, **7**, 1897 (1988).
43. J. L. HENCHER, M. KHAN, F. F. SAID, R. SIELER, and D. G. TUCK. Inorg. Chem. **21**, 2787 (1982).
44. F. A. COTTON, P. E. FANWICK, and J. W. FITCH III. Inorg. Chem. **17**, 3254 (1978).
45. U. OHMS, H. GUTH, A. KUTOGLU, and C. SCHERINGER. Acta Crystallogr. B**38**, 831 (1982).
46. S. C. KOKKOU and V. SCHRAMM. Acta Crystallogr. C**41**, 1040 (1985).

Can. J. Chem. Downloaded from www.nrcresearchpress.com by 88.85.125.76 on 09/07/12
For personal use only.

Analysis of the kinetics of the thermal decomposition of pentafluoroethane

VIKTORYA AVIYENTE AND YÜKSEL INEL[1]
Chemistry Department, Bogaziçi University, Bebek 80815, Istanbul, Turkey
Received, July 19, 1989[2]

VIKTORYA AVIYENTE and YÜKSEL INEL. Can. J. Chem. **68**, 1332 (1990).

The thermal decomposition of pentafluoroethane has been studied experimentally over the temperature range 1180–1470 K under 3500 torr pressure by Tschuikow-Roux and co-workers (1). Although the principal process which occurred at around 1200 K was the elimination of hydrogen fluoride, the formation of radicals by carbon–carbon bond scission is suggested at around 1400 K. In this article the C_2HF_5 molecule has been submitted to a treatment in terms of the RRKM theory to test plausible activated complex models and to explain the formation of different products at different temperatures. The hydrogen fluoride elimination reaction is modeled after a four-membered ring for the activated complex whereas two different approaches (Gorin model and the criterion of minimum state density) have been used to explain the C—C bond rupture. In this work it is confirmed satisfactorily by calculation of the rate energy dependences for the different mechanisms that, at around 1200 K, the alkene (C_2F_4) is the dominant product; as the temperature approaches 1400 K carbon–carbon bond rupture becomes feasible.

Key words: RRKM, bond rupture, HF elimination, pyrolysis, rate coefficient.

VIKTORYA AVIYENTE et YÜKSEL INEL. Can. J. Chem. **68**, 1332 (1990).

La décomposition thérmale du pentafluorure d'éthane a été étudiée sous une pression de 3500 torr au laboratoire à des temperatures allant de 1180 à 1470 K par Tschuikow-Roux et ses collaborateurs (1). Le produit principal obtenu dans les conditions mentionnées, C_2F_4. résulte de l'élimination du fluorure d'hydrogène. Des produits secondaires ont aussi été obtenus par la scission de la liaison C—C au fur et à mesure que la temperature augmente. Dans cet article la molecule C_2HF_5 a été soumise à un traitement théorique, RRKM, dans l'intention de tester des modèles pour le complexe activé, formé pendant l'état de transition. La reaction d'élimination du fluorure d'hydrogène est expliquée en se servant d'un cycle à quatre chatnons comme modèle pour l'état de transition; deux modèles différents sont utilisés afin de rationaliser la rupture de la liaison carbonique.

Mot clés : RRKM, rupture de liaison, élimination du fluorure d'hydrogène, pyrolyse, constante de vitesse.

Introduction

The thermal decomposition of simple alkyl fluorides has received considerable attention in the seventies. The experimental investigations have shown that at temperatures where first product formation occurs, the principal mode of decomposition is via molecular elimination of hydrogen fluoride. Data on the experimental thermal decomposition of pentafluoroethane, C_2HF_5, in a single pulse shock tube, over the temperature range 1180–1470 K under 3500 torr pressure has been reported by Tschuikow-Roux *et al.* (1). As is claimed in that article the principal primary process in the pyrolysis of pentafluoroethane is the molecular elimination of hydrogen fluoride

[1] $C_2HF_5 \rightarrow C_2F_4 + HF$

The first order rate constant k_1 is given by

[2] $k_1/s^{-1} = 10^{13.6\pm0.4} \exp(-71.600 \pm 2.400 \text{ kcal mol}^{-1})/2.303RT$

From the knowledge of k_1 it was possible to evaluate the rate constant k_2 for the reaction

[3] $C_2HF_5 \rightarrow CHF_2^{\cdot} + CF_3^{\cdot}$

as

[4] $k_2/s^{-1} = 10^{16.6\pm0.6} \exp(-93.500 \pm 5.200 \text{ kcal mol}^{-1})/2.303RT$

The purpose of our work is to subject the thermal decomposition of C_2HF_5 to a theoretical treatment in terms of RRKM theory with the intent to test plausible activated complex models which would explain the experimental results.

[5a] $C_2HF_5 + M \rightarrow C_2HF_5^* + M \xrightarrow{k_{a1}(E^*)} [C_2HF_5^+] \rightarrow C_2F_4 + HF$

[5b] $C_2HF_5 + M \rightarrow C_2HF_5^* + M \xrightarrow{k_{a2}(E^*)} [C_2HF_5^+] \rightarrow CHF_2^{\cdot} + CF_3^{\cdot}$

First, the hydrogen fluoride elimination reaction is considered using a four-membered ring for the activated complex; next, the C—C bond scission reaction is analyzed. Two different models are employed for the second step. In the first model the activated complex is treated as a decomposing diatomic molecule in which the atoms have the masses of the actual fragments; in the second model the critical configuration has a value of the reaction coordinate such that the density of accessible internal states of the molecule is minimized. The significance of the centrifugal contributions to the loose activated complexes is also discussed.

Computational section

As is already known, to carry out the calculations mentioned above one needs to know the geometries as well as the vibrational frequencies of the energized molecule and the activated complex. In this study it has been assumed that the energized molecule has the same parameters as the molecule itself (2); these are given in Table 1. Besides, the molecule has

[1]Author to whom correspondence should be addressed.
[2]Revision received January 16, 1990.

Printed in Canada / Imprimé au Canada

Can. J. Chem. Downloaded from www.nrcresearchpress.com by 88.85.125.76 on 09/07/12
For personal use only.

TABLE 1. The parameters of pentafluoroethane

Parameter	Value
Vibrational frequencies[a] (cm^{-1})	1218, 1198, 1111, 867, 725, 654, 523, 361, 3008, 217, 1393, 1309, 1145, 577, 413, 1359, 247, 74[b]
Moments of inertia[c] (amu Å^2)	147.86, 211.04, 243.76
Moment of inertia for internal rotation[c] (amu Å^2)	37.05
Symmetry number for internal rotation[d]	3
Collision diameter[e] (Å)	4.39

[a]Reference 2*a*.
[b]This vibrational frequency is included if the molecule is considered a vibrator.
[c]The moments of inertia have been calculated using the molecular structure given in ref. 2*b*.
[d]The symmetry number for internal rotation is taken into account if the molecule is considered a rotor.
[e]Reference 3.

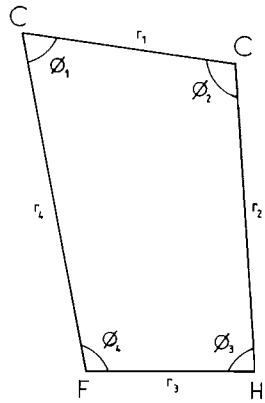

FIG. 1. The transition state for HF elimination.

TABLE 2. The parameters of the activated complex for H—F elimination reaction

Bond orders[a]: 1.5, 0.0259, 0.5, 0.0259
Bond lengths[a] (Å): 1.42, 2.04, 0.9, 2.28
Moments of inertia (amu Å^2): 171.39, 192.90, 341.11
Vibrational frequencies:
(*a*) The out-of-ring vibrational frequencies (cm^{-1}): 1218, 1198, 1111, 725, 654, 361, 1393, 1145, 577, 413, 1359, 523
(*b*) The in-plane ring frequencies (cm^{-1}): 2927, 1062, 484, 211
(*c*) The out-of-plane ring vibrational frequency (cm^{-1}): 50
$\delta = 0.4741$
$\phi_1 = 71°$
$\phi_2 = 101.58°$
$\phi_3 = 86.47°$
$\phi_4 = 100.95°$
Critical energy (kcal mol^{-1}): $E_0 = 70.72$
Entropy of activation (eu) $\Delta S^{\ddagger}_{1400\,K} = -1.94$[c]
$\Delta S^{\ddagger}_{1400\,K} = -1.94$[c]

[a]Bond orders and bond lengths are given in the following order: C—C, C—H, H—F, C—F.
[b]The molecule is treated as a rotor.
[c]The molecule is treated as a vibrator.

been treated as a vibrator as well as a rotor with an internal rotation around the C—C bond to see how this would affect the results. The parameters of the activated complex have been described using semi-empirical relationships.

I. HF elimination

HF elimination from pentafluoroethane is considered the reverse of HF addition to C_2F_4. The transition state for the reaction under consideration is characterized by six parameters. The first four parameters are bond orders of the four bonds involved in the reaction, the fifth parameter is the partial formal charge separation along the breaking bonds, and the sixth parameter is any one of the interior angles of the quadrilateral formed by the interacting bonds. In the model used by Maltman *et al.* (4), it is assumed that if the approach of the reactants is relatively unhindered their intermolecular interaction can be roughly described by the Kihara potential for interaction of linear core systems. The shortest distance between the two breaking bonds is maximized. By applying these principles the partial formal charge separation δ has been calculated to be 0.4741 and the angle ϕ_1 71°. Using the analytical expressions given by these workers the angles ϕ_2, ϕ_3 and ϕ_4 have been evaluated as $\phi_2 = 101.58°$, $\phi_3 = 86.47°$, $\phi_4 = 100.95°$. As seen from Fig. 1, the activated complex does not have any internal rotation, so σ^+, the symmetry number for internal rotation is taken as 1. The vibrational frequencies of the complex have been classified as described below and shown in Table 2.

(1) The out-of-ring vibrational frequencies: These are the C—F stretches and the CF_2 group bendings, a total of 12 frequencies.

(2) The in-plane ring vibrational frequencies: The values of the bond orders for the forming bonds were calculated assuming generalized bond order conservation, i.e., the sum of the transition state bond orders plus the partial formal charge separation equals the sum of the initial bond orders. The description of the transition state geometry was completed using Pauling's rule (5), which correlates bond lengths to bond orders. Finally, the vibrational frequencies were calculated from the partial bonds by means of Badger's rule (6).

(3) The out-of-plane ring vibrational frequency: The out-of-plane ring vibration is separable (by symmetry (7)) from the other ring modes. Its value was treated as an adjustable parameter; it was adjusted to best fit the experimental $\Delta S^{\ddagger}$ value.

II. The C—C bond rupture reaction

The experimentally observed high pre-exponential factor suggests a loose transition state. Two models which satisfy this condition have been used:

1. Model I (Gorin Model)

In this approach the critical configuration is located at the maximum of the potential energy surface separating reactants from products. The reaction coordinate is treated by considering the complex as a decomposing diatomic molecule in which the atoms have the masses of the actual fragments. The distance $\langle R_c \rangle$, the average value of the critical bond length, is large enough to validate the assumption mentioned above, the basic assumption in the Gorin theory (8). $\langle R_c \rangle$ was given by Tschuikow-Roux (9) as

$$[6] \quad \langle R_c \rangle = 1.3092(2a/kT)^{1/6}$$

where a is the constant in the attractive potential energy expression $V = -a/R^6$ and has been calculated by taking into account the electrostatic, inductive, and dispersion contribution from the two radicals. The fragments formed by the dissociation

Can. J. Chem. Downloaded from www.nrcresearchpress.com by 88.85.125.76 on 09/07/12
For personal use only.

Can. J. Chem. Downloaded from www.nrcresearchpress.com by 88.85.125.76 on 09/07/12
For personal use only.

of the molecule are assumed to have the same geometry and vibrational frequencies as the free radicals. There are five active internal rotational degrees of freedom which include the figure axis rotation plus two doubly degenerate tumblings of the $CHF_2^{\cdot}$ and $CF_3^{\cdot}$ groups about their own axis. The 12 vibrational frequencies of the complex are the frequencies of the $CHF_2^{\cdot}$ and $CF_3^{\cdot}$ radicals as shown in Table 3 (10).

2. Model II (Bunker and Pattengill Model)

The proposal was to locate the critical configuration where the density of states along the reaction coordinate is minimized and to predict that this bottleneck should represent the critical configuration or dividing surface of the RRKM theory (11). In studies where the potential energy of the reaction coordinate is represented by a Morse function, the criterion of minimum state density gives a value of r^+ at the critical configuration less than the value of r^+ at the rotational barrier. In this study where the reaction coordinate is assumed to be the C—C bond extension, $V(r^+)$, the potential energy is given by

$$[7] \quad V(r^+) = D\{1 - \exp[-\beta(r^+ - r_e)]\}^2 + E_z^+ - E_z^m$$

where

$$[8] \quad D = \Delta H^0_0 + E_z^m - E_z^p$$

$$[9] \quad \beta = (f/2D)^{1/2}$$

In [7], [8], [9] ΔH^0_0 is the bond dissociation energy at 0 K, E_z^m is the zero point energy of the reactant molecule, E_z^p is the zero point energy of the radicals produced, and f is the C—C stretching force constant. The rocking motions of the $CF_3^{\cdot}$ and $CHF_2^{\cdot}$ groups lower the frequencies of the molecule according to

$$[10] \quad \nu = \nu_i \exp[-\alpha(r^+ - r_e)] \qquad (i = 1, \ldots 4)$$

where ν_i represents the rocking vibrational frequencies and α is an adjustable parameter. The parameters for this model are given in Table 4.

Results and discussion

Collisions between molecules at a given temperature produce energized molecules with an equilibrium distribution of energy (the Maxwell–Boltzmann distribution which enables the fraction of molecules energized in the range E to $E + \delta E$ to be calculated as

$$[11] \quad K(E)\delta E = \frac{N(E)\exp(-E/kT)\delta E}{Q_2}$$

where $N(E)$ is the density of states of the molecule at energy E and Q_2 is the partition function for active degrees of freedom. On the other hand, the fraction of molecules reacting in the range E to $E + \delta E$ is expressed as

$$[12] \quad \frac{k_a(E)}{k_a(E) + w} K(E)\delta E$$

which under high pressure transforms into

$$[13] \quad \frac{k_a(E)}{w} K(E)\delta E$$

In eqs. [12] and [13] w is the rate constant for the backward reaction of the energized molecule,

$$[14] \quad C_2HF_5^* + M \xrightarrow{w} C_2HF_5 + M$$

Substitution of [11] in [13] will yield the final form for the fraction of molecules reacting in the energy range E to $E + \delta E$:

$$[13] \quad \frac{k_a(E)}{w} \times \frac{N(E)\exp(-E/kT)\delta E}{Q_2}$$

The fact that the ratio of the products formed via paths [5*a*] to [5*b*] is given by the ratio of the microcanonical rate coefficients $k_{a1}(E^*)$ to $k_{a2}(E^*)$ is confirmed when this ratio is evaluated using expression [15]. Figures 2 to 5 tend to rationalize the experimental results by comparing the rate coefficients for HF elimination with the ones for C—C bond breaking reactions. The RRKM calculation was carried out by using the equation

$$[16] \quad k_a(E^*) = L^+ W^+(E^* - E_0)/hN(E^*)$$

in which L^+ is a statistical factor given by $\alpha\sigma/\sigma^+$ (α is the number of optical isomers of the complex and is taken to be 1 for reactions [5*a*] and [5*b*]; σ and σ^+ are the symmetry numbers for the molecule and the complex respectively), W^+ is the sum of the transition state energy levels from 0 to $E^* - E_0$, E_0 is the activation energy.

An explanation of the calculated results has been given in what follows. The average energy a molecule needs to react is given by the classical value as $E_0 + skT$, where s is the number

TABLE 3. The parameters of the activated complex for C—C bond scission reaction (MODEL I)

Vibrational frequencies[a] (cm^{-1}): 3000, 1166, 700, 650, 1317, 1175, 1087, 703, 1251(2), 512(2)
Moments of inertia[b] (amu Å^2): 885.99, 922.42, 156.46
Moment of inertia for internal rotation[b] (amu Å^2): 39.18
Critical energy (kcal mol^{-1}): $E_0 = 96.77$
Number of internal rotations: $r^+ = 5$
Entropy of activation (eu): $\Delta S^{\ddagger}_{1400\,K} = 16.28$[c]
$\Delta S^{\ddagger}_{1400\,K} = 16.73$[d]
Symmetry number for internal rotations: 2, 1
Symmetry number for overall rotations: 3

[a]References 10 and 12.
[b]The moments of inertia have been calculated using the geometries given in refs. 10, 12, and 13.
[c]The molecule is treated as a rotor.
[d]The molecule is treated as a vibrator.

TABLE 4. The parameters of the activated complex for the C—C bond scission reaction (MODEL II)

Vibrational frequencies (cm^{-1}): 1218, 1198, 1111, 725, 654, 523, 3008, 1393, 1309, 1145, 577, 1359. 361 exp $[-\alpha(r^+ - 1.525)]$, 217 exp $[-\alpha(r^+ - 1.525)]$, 413 exp $[-\alpha(r^+ - 1.525)]$, 247 exp $[-\alpha(r^+ - 1.525)]$,
Moments of inertia (amu Å^2): 473.34, 503.03, 155.55
Moment of inertia for internal rotation (amu Å^2): 38.05
f(dynes cm^{-1})[a] : 540.000
α[a] : 0.80
ΔH_0^0 (Kcal.mol^{-1})[b] : 91.1
Critical energy (kcal mol^{-1}): $E_0 = 84.86$
Entropy of activation (eu): $\Delta S^{\ddagger}_{1400\,K} = 9.11$[c]
$\Delta S^{\ddagger}_{1400\,K} = 9.56$[d]
Critical bond length (Å): 3.075

[a]Reference 3.
[b]Reference 15.
[c]The molecule is treated as a rotor.
[d]The molecule is treated as a vibrator.

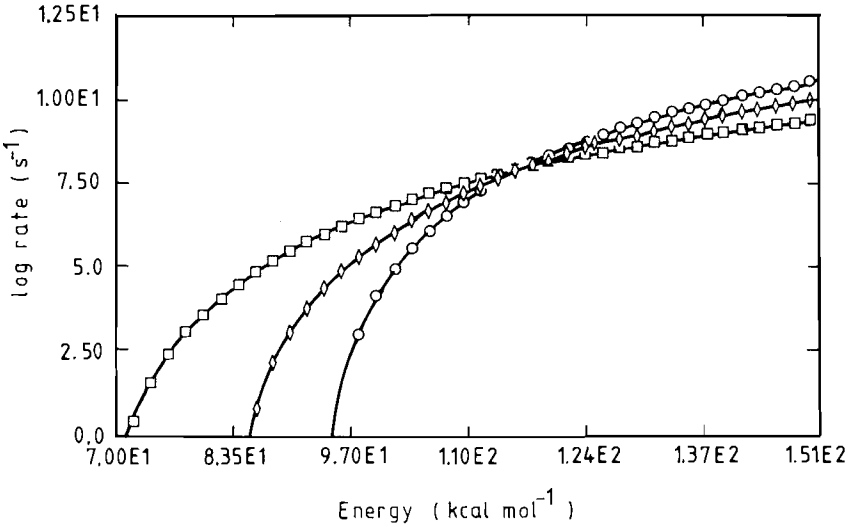

FIG. 2. Calculated rate coefficients (logarithmic scale) versus total energy. HF elimination (squares), C—C bond cleavage model I (circles), model II (diamond). The molecule is considered a vibrator at $T = 1400$ K.

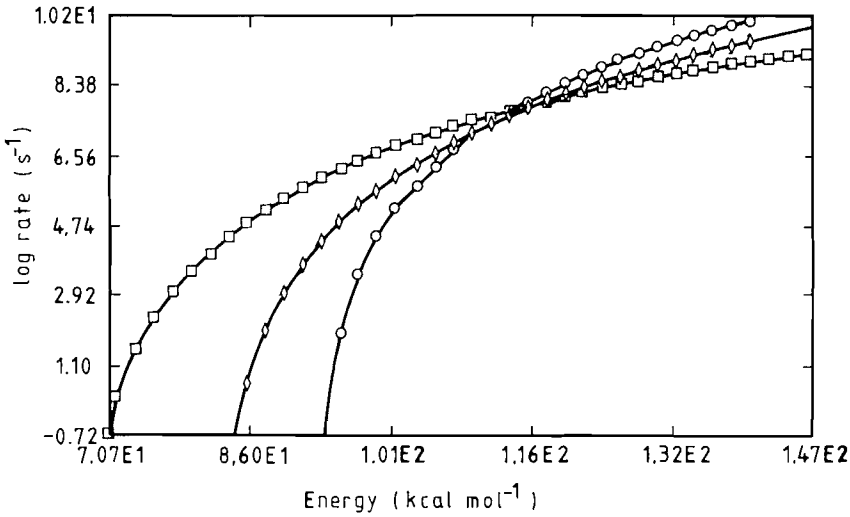

FIG. 3. Calculated rate coefficients versus total energy. HF elimination (squares), C—C bond cleavage model I (circles), model II (diamond). The molecule is considered a vibrator at $T = 1200$ K.

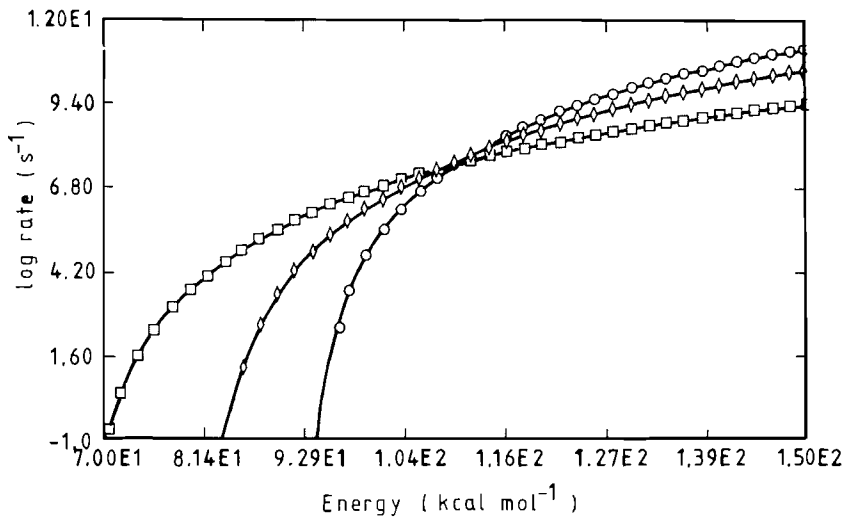

FIG. 4. The contribution of centrifugal effects to rate coefficients versus total energy. HF elimination (squares), C—C bond cleavage model I (circles), model II (diamond). The molecule is considered a vibrator at $T = 1400$ K.

Can. J. Chem. Downloaded from www.nrcresearchpress.com by 88.85.125.76 on 09/07/12
For personal use only.

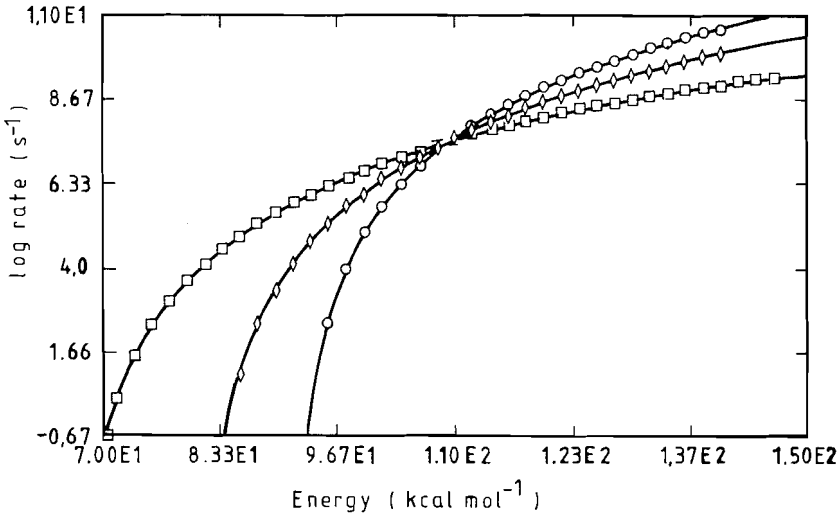

FIG. 5. The contribution of centrifugal effects to rate coefficients versus total energy. HF elimination (squares), C—C bond cleavage model I (circles), model II (diamond). The molecule is considered a vibrator at $T = 1200$ K.

TABLE 5. Experimental and calculated values for $k^{\infty}(s^{-1})$

	k^{∞}	
Reaction	Experimental	Calculated
[5a]	264.13	186.03[a] 152.20[b]
[5b]	100.64	303.27[a] (Model I) 723.1[b] (Model I) 142.9[a] (Model II) 214.38[b] (Model II)

[a]The molecule is treated as a vibrator.
[b]The molecule is treated as a rotor.

of degrees of freedom. At 1400 K, for HF elimination, this value is around 118 kcal mol^{-1}, whereas for C—C rupture, it is 144 kcal mol^{-1} (Model I) and 132.15 kcal mol^{-1} (Model II), respectively. In Fig. 2 the curves for the rate coefficients versus total energy cross at 116 kcal mol^{-1}. At this point, the rate for reaction [5*b*] starts to overcome the rate for reaction [5*a*]; although molecules would prefer to give products with low activation energy, the microcanonical rate constants favor radical formation so that products from both channels are observed. At 1200 K (Fig. 3) the crossing point at 113 kcal mol^{-1}. Under these conditions, the average energy possessed by molecules undergoing HF elimination is also 113 kcal mol^{-1}. When the rate coefficient for reaction [5*b*] starts to dominate, the excited molecules will already have reacted producing the alkene and HF. The contribution of the centrifugal effects to the rate coefficients supports the experimental results quite well. At 1400 K, the crossing point shifts to 110 kcal mol^{-1} (Fig. 4), at 1200 K it shifts to 109 kcal mol^{-1} (Fig. 5) so that C—C cleavage is observed only at high temperatures. The Waage–Rabinovitch approximation which has been used for this purpose has the form

$$[17] \quad k'_a(E^*) = k_a(E^*)/F$$

and

$$[18] \quad F = \{1 + [s + (r/2) - 1](I^+/I - 1)RT/(E_0 + a'E_z)\}^{-1}$$

where $k'_a(E^*)$ is the corrected rate coefficient, s and r are the number of active vibrational and rotational degrees of freedom, I^+ and I are the moments of inertia of the complex and the molecule, respectively, E_z is the zero point energy of the molecule, and a' is a parameter which can be calculated from the properties of the molecule. Table 5 compares the average experimental and calculated values for the unimolecular rate constants at high pressures. Consideration of these values favors Model II over Model I for the C—C bond rupture reaction. This is in agreement with Hase's proposal (11) which suggests that the unimolecular rate is overestimated by Gorin since the energized reactant molecules and critical configurations are not in kinematic equilibrium.

Another minor contribution of this work was the decision on whether the molecule should be treated as a rotor or as a vibrator. The entropy of activation was found experimentally to be $\Delta S^{\ddagger}_{1400\,K} = -1.37 \pm 1.8$ eu for HF elimination and $\Delta S^{\ddagger}_{1400\,K} = 12.35 \pm 2.8$ eu for C—C bond rupture reaction. These values support the treatment of the molecule as a vibrator when compared with the calculated results in Tables 2, 3, and 4.

Our future objective is to use Model II together with variational RRKM theory (14) to rationalize the experimental results for other fluoroethanes.

Acknowledgements

The research described herein was supported by the Bogaziçi University Research Fund.

1. E. TSCHUIKOW-ROUX, G. E. MILLWARD, and W. J. QUIRING. J. Phys. Chem. **75**, 3493 (1971).
2. (*a*) W. F. EDGELL and C. E. MAY. J. Chem. Phys. **22**, 1808 (1954); (*b*) B. BEAGLEY, M. O. JONES, and P. YAVARI. J. Mol. Struct. **71**, 203 (1981),
3. V. AVIYENTE. Ph.D. Thesis, Bogaziçi University, Istanbul, Turkey. 1983.
4. K. R. MALTMAN, E. TSCHUIKOW-ROUX, and K. H. JUNG. J. Phys. Chem. **78**, 1035 (1974).
5. L. PAULING. J. Am. Chem. Soc. **69**, 542 (1947).
6. (*a*) R. M. BADGER. J. Chem. Phys. **2**, 128 (1934); J. Chem. Phys. **3**, 710 (1935); Phys. Rev. **48**, 284 (1935); (*b*) D. R. HERSCHBACH and V. W. LAURIE. J. Chem. Phys. **35**, 458 (1961).

Can. J. Chem. Downloaded from www.nrcresearchpress.com by 88.85.125.76 on 09/07/12
For personal use only.

7. K. S. PITZER. Quantum chemistry. Prentice-Hall, Inc., Englewood Cliffs, NJ. 1953. p. 449.
8. E. GORIN. Acta Physicochim. URSS, **6**, 691 (1938).
9. E. TSCHUIKOW-ROUX. J. Phys. Chem. **72**, 1009 (1968).
10. T. G. CARVER and L. ANDREWS. J. Chem. Phys. **50**, 5100 (1969).
11. (*a*) D. L. BUNKER and M. PATTENGILL. J. Chem. Phys. **48**, 772 (1968); (*b*) W. L. HASE. J. Chem. Phys. **57**, 730 (1972); (*c*) W. L. HASE. J. Chem. Phys. **64**, 2442 (1976).
12. D. E. MILLIGAN and M. E. JACOX. J. Chem. Phys. **48**, 2265 (1968).
13. M. T. ROGERS and L. D. KISPERT. J. Chem. Phys. **46**, 3193 (1967).
14. W. L. HASE, S. L. MONDRO, R. J. DUCHOVIC, and D. M. HIRST. J. Am. Chem. Soc. **109**, 2916 (1987).
15. S. W. BENSON. J. Chem. Educ. **42**, 502 (1965).

Can. J. Chem. Downloaded from www.nrcresearchpress.com by 88.85.125.76 on 09/07/12
For personal use only.

Polycarboxylate diaza crown ethers derived from *R,R*-(+)-tartaric acid: synthesis and complexation of metal ions

ASHOK ANANTANARAYAN AND THOMAS M. FYLES

Department of Chemistry, University of Victoria, Victoria, B.C., Canada V8W 2Y2

Received November 21, 1989

ASHOK ANANTANARAYAN and THOMAS M. FYLES. Can. J. Chem. **68**, 1338 (1990).

The synthesis and complexation properties of polycarboxylate diaza crown ethers based on *R,R*-(+)-tartaric acid are described. Cesium carbonate mediated macrocyclization of a bis-tosylamide precursor with a bis-tosylate precursor provided the protected crown ethers. Photochemical deprotection of the tosylamides and hydrolysis of the carboxamides yielded dicarboxylic and tetracarboxylic acid derivatives of 1,10-diaza-18-crown-6. *N*-Methylenecarboxylate (*N*-acetate) derivatives were prepared by *N*-alkylation with bromoacetic acid. The synthetic and purification procedures developed provide samples of the ligands in a metal-free form. Acidity and stability constants for complexation of alkali metal, alkaline earth, late- and post-transition metal cations were determined by potentiometric titration. The ligands form complexes which show enhancement of stability by charge–charge and chelate interaction with the carboxylates. In comparison with crown ether polycarboxylates these aza crown ethers showed a selectivity for softer metal ions relative to alkali and alkaline earth metal ions. *N*-Methylenecarboxylate chelate ligands were found to bind almost all types of metal ions, due to a highly co-operative array of charge–charge, chelate and crown ether interactions.

Key words: aza crown ether synthesis, tartaric acid, potentiometric titration, cation complexation, aminocarboxylate complexone.

ASHOK ANANTANARAYAN et THOMAS M. FYLES. Can. J. Chem. **68**, 1338 (1990).

On décrit la synthèse et les propriétés de complexation d'éthers couronnes diaza polycarboxyliques préparées à partir de l'acide *R,R*-(+)-tartrique. Le carbonate de césium permet de réaliser une macrocyclisation d'un précurseur bis-tosylamide avec un autre précurseur bis-tosylate et d'obtenir des éthers couronnes protégés. La déprotection photochimique des tosylamides et l'hydrolyse des carboxamides fournit les dérivés dicarboxylique et tétracarboxylique de la 1,10-diaza-18-couronne-6. On a préparé des dérivés *N*-méthylènecarboxylates (*N*-acétates) par le biais d'une *N*-alkylation avec de l'acide bromoacétique. Les méthodes de synthèse et de purification développées fournissent des échantillons des ligands qui sont exempts de métal. Faisant appel à une titration potentiométrique, on a déterminé l'acidité et les constantes de stabilité pour la complexation des cations des métaux alcalins, alcalino-terreux ainsi que des métaux de la fin de (ou qui suivent) la période de transition. Les ligands forment des complexes qui présentent une augmentation de la stabilité par des interactions charge–charge et de chélate avec les groupements carboxylates. Par comparaison avec les éthers couronnes portant des groupements carboxylates, les éthers couronnes diaza présentent une sélectivité pour les ions des métaux mous par rapport aux ions des métaux alcalins ou alcalino-terreux. On a trouvé que les ligands chélates *N*-méthylènecarboxylates se lient à pratiquement tous les types d'ions métalliques; cette caractéristique est due à un arrangement très coopératif d'interactions charge–charge, de chélate et d'éthers couronnes.

Mots clés : synthèse d'éthers couronnes aza, acide tartrique, titration potentiométrique, complexation des cations, complexion par un aminopolycarboxylate.

[Traduit par la revue]

Metal ion recognition by synthetic and naturally occurring ligands is a complex process involving a cooperative match of the complementary properties of the host and the guest. A key factor in the design of new ligands with unique complexation behaviors is the choice of ligand donor sites (1). Within a class of ligands, such as the crown ethers or cryptands, clear changes in selectivity of cation binding are provoked by substitution of the oxygen donors of a parent ring system for nitrogen or sulfur donor sites (2). Such substitutions alter the primary character of the donor (Lewis basicity) as well as the geometrical and conformational properties of the ligand (3). Thus in a system involving highly cooperative binding interactions, donor atom substitution can profoundly influence binding selectivity.

Our interest in ligand design has centered on crown ethers derived from *R,R*-(+)-tartaric acid: the di-, tetra-, and hexa-acids illustrated at the top of Fig. 1 (4–6). The tartarate derived units impart rigidity to the ligands, leading to well defined conformations, and the carboxylates, when ionized, provide a strong electrostatic field which greatly enhances complex stability for alkali metal and alkaline earth cations. Despite the favorable Coulombic interactions, binding of heavy metal cations occurs only to a limited extent due to a mismatch of the hard oxygen donor set and the softer guest cations (6). An obvious ligand modification which might lead to stabilized crown ether type complexes of heavier cations would be the substitution of some of the donor atoms for N or S. We have previously reported dithia crown ethers bearing four carboxylates (7); the purpose of this report is to describe the chemistry of the diaza polycarboxylate crown ethers illustrated in the lower part of Fig. 1. The ligands are derivatives of 1,10-diaza-18-crown-6 (**2.2**); the trivial names assigned (6) reflect the parent crown ether and the number of carboxylic acid groups from tartaric acid ($\mathbf{A_n}$) and *N*-methylene acetic acid units ($\mathbf{D_n}$).

The synthesis of aza crown ethers has been recently reviewed (8, 9) and the core methods have been successfully exploited by many groups. Of the two "classic" approaches, macrocyclization of a diamine with a diacid chloride to give a diamide which is reduced to the amine (10) was not suitable due to the presence of other reducible groups. The other "classic" route due to Richman and Atkins involves cyclization of a bis-tosylamide precursor with a suitable bis-alkylating agent (11). We have previously used a related approach to prepare dithia polycarboxylate crown ethers (7) following the procedure of Kellogg and co-workers in the use of cesium carbonate to generate a nucleophile (12). These workers also report the use of the same base system for the synthesis of protected diaza

Can. J. Chem. Downloaded from www.nrcresearchpress.com by 88.85.125.76 on 09/07/12
For personal use only.

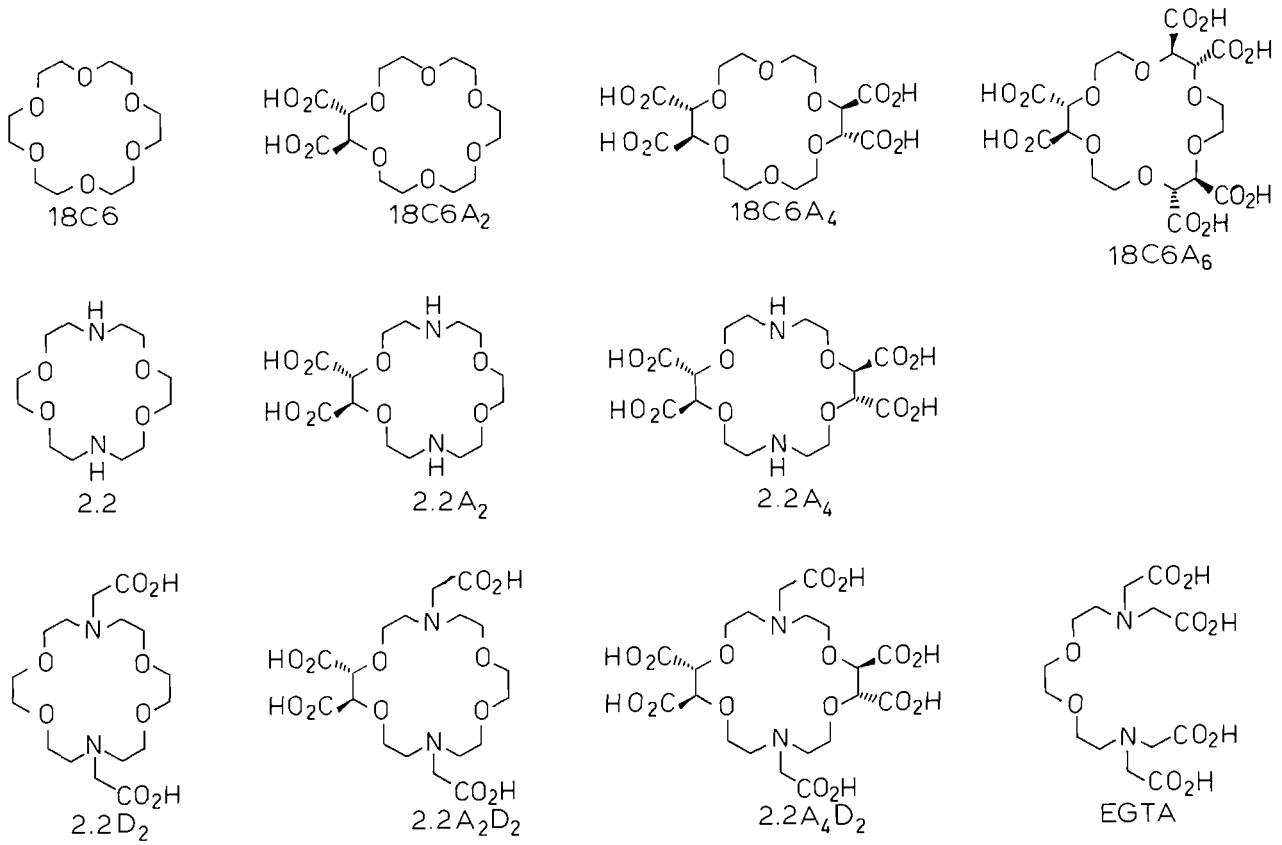

FIG. 1. Structures of oxa and aza crown ethers derived from tartaric acid showing incremental structural variations. Names are derived from 18-crown-6 (**18C6**) or 1,10-diaza-18-crown-6 (**2.2**) by addition of carboxylic acid units from tartaric acid ($\mathbf{A_n}$) (4–6), or *N*-methylene acetic acid ($\mathbf{D_n}$).

macrocycles (13, 14). A recent report provides further evidence of the general utility of the Kellogg modified Richman–Atkins cyclization using a metal carbonate as the base (15).

Despite all this excellent precedent, the synthesis of these ligands presented an additional challenge in that the neutral forms illustrated in Fig. 1 cannot exist at any pH. Zwitterionic and multiply charged forms of these amino acids ensure that they will be water soluble at all pH values, will resist extraction into organic solvents, and will bind to conventional chromatographic supports. Moreover, we expected that the ligands would show some affinity for most types of cations. The situation is exacerbated for the *N*-methylene carboxylates **2.2A$_2$D$_2$** and **2.2A$_4$D$_2$** as most procedures for the direct production of related complexones such as EDTA give the product in a vast excess of salt (16). For EDTA, the excess of NaCl may be ignored as the stability constant for complexation of Na^+ is only $50\,M^{-1}$ (16). This is negligibly small for many applications of the ligand and does not impede crystallization of the metal free ligand or a complexed form (17).

The diaza polycarboxylate crown ethers bear superficial similarity to aminopolycarboxylate complexones, particularly EGTA (Fig. 1). The ligands share a similar set of donors and bear similar negative charges in basic solution. At least one of the parent ligands, **2.2D$_2$**, is capable of achieving a chelate geometry similar to that found in simple aminopolycarboxylate complexones. The crystal structures of two copper complexes of **2.2D$_2$** (18–20) show encapsulated Cu^{2+} held in a geometry similar to a glycinate or EDTA complex. The ligand is relatively undistorted and the majority of the torsion angles are close to normal values for crown ether complexes. Moreover, the units which would be occupied by carboxylates from the tartaric acid residues are in open positions about the complex. The steric demands might therefore be modest. Unfortunately, all attempts to crystallize the aza crowns of Fig. 1 or their metal ion complexes have so far been fruitless. This report therefore examines the complexation chemistry of the ligands in solution only from the perspective of stability constants.

Results and discussion

Ligand synthesis

Our synthetic approach based on macrocyclization of a bis-sulfonamide is outlined in Fig. 3; the synthesis of the required precursors is sketched in Fig. 2. The diol **3** and the bis-toluenesulfonate **4** were prepared for related syntheses (7) via thallous ethoxide mediated alkylation of **1** followed by hydrolysis of the bis-tetrahydropyranyl ether **2**. A somewhat simplified procedure suitable for large scale is given in the Experimental section. The bis-toluenesulfonate **4** was converted into the bis-phthalimide derivative **5** in 92% purified yield, and was then subjected to hydrazinolysis to obtain the crude diamine **6** in 70% yield as a yellow oil. Attempted purification by distillation or salt formation was not successful and hence **6** was used as such for the next step. The bis-sulfonamide **7** was obtained as a white solid in 75% yield from **6** using a modified Schotten–Baumann technique.

Although the average yield per step was high, the overall

Can. J. Chem. Downloaded from www.nrcresearchpress.com by 88.85.125.76 on 09/07/12
For personal use only.

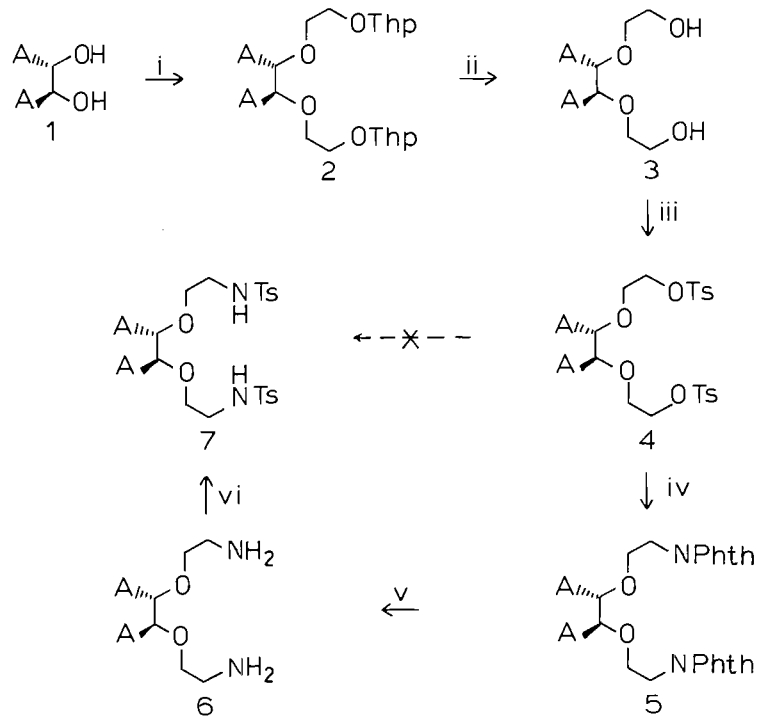

FIG. 2. Preparation of precursors. Conditions: (*i*) (*1*) TlOEt/DMF (*2*) $BrCH_2CH_2OThp$; (*ii*) H_3O^+/MeOH; (*iii*) TsCl/Et_3N/CH_2Cl_2; (*iv*) KNPhth/DMF; (*v*) H_2NNH_2/EtOH; (*vi*) TsCl. Abbreviations: OThp, tetrahydropyranyloxy-; Ts, *p*-toluenesulfonyl-; NPhth, phthalimido-; A, $(CH_3)_2NC{=}O$.

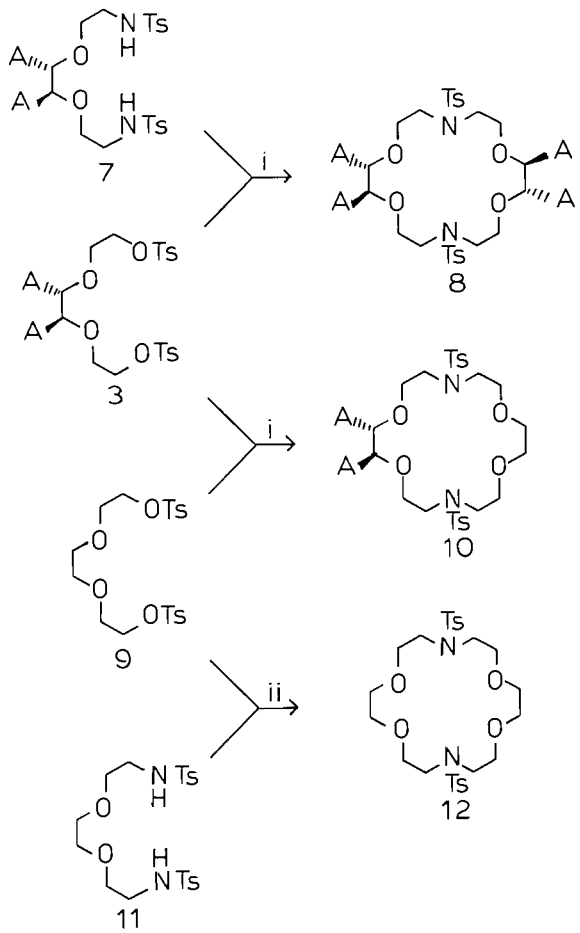

FIG. 3. Preparations of protected macrocycles. Conditions: (*i*) Cs_2CO_3/DMF/rt; (*ii*) K_2CO_3/DMF/50°C. Abbreviations as in Fig. 2.

yield was not. It was thus desirable to explore other shorter routes leading to **7**. Direct conversion of **4** to **7** using *p*-toluenesulfonamide salts was unfortunately not feasible. A model study using octyl bromide as the alkylating agent showed that dialkylation was a major reaction pathway. Subsequently, other workers have reported a macrocyclization method based on bis-alkylation of *p*-toluenesulfonamide (21); we did not observe any **8** in our attempts to convert **4** directly to **7**. A more direct route leading to **7** directly from **1** using tosylaziridine (22) was similarly unsuccessful. Tosylaziridine polymerized under strongly basic conditions (the dianion of **1**) and was unreactive under neutral conditions (**1** alone).

Figure 3 sketches the macrocyclization reactions leading to protected crown ethers **8**, **10**, and **12**. The macrocyclization was performed using cesium carbonate according to the method of Vriesema *et al.* (13), at a concentration of 0.05 M in the sulfonamide **7** with excess solid cesium carbonate. The bis-toluenesulfonate (**3** or **9** (23)) was added over 2–3 h and the reaction was essentially complete in 12–15 h at room temperature. The crown ether products had a high affinity for alumina, hence chromatographic losses were sometimes high. Deactivated alumina (Brockmann III) gave consistent results; overall yields of purified product from the cyclization were 75% on average. As Fig. 3 also shows, K_2CO_3 could be substituted for Cs_2CO_3 in the synthesis of **12** from **9** and **11** (11), with no significant loss in yield. K_2CO_3, however, requires a higher temperature (40–50°C) in keeping with its lower solubility in DMF (14, 15).

In principle, hydrolysis of **8** and **10** should lead to the parent aza crown ethers $\mathbf{2.2A_4}$ and $\mathbf{2.2A_2}$ respectively. The sulfonamides are, however, known to require vigorous conditions for their removal (11). As expected, hydrochloric acid was found to be insufficient. The tetraacid **17** was, however, obtained in good yield (Fig. 4). Prolonged reflux in HCl was of no avail; the

Can. J. Chem. Downloaded from www.nrcresearchpress.com by 88.85.125.76 on 09/07/12
For personal use only.

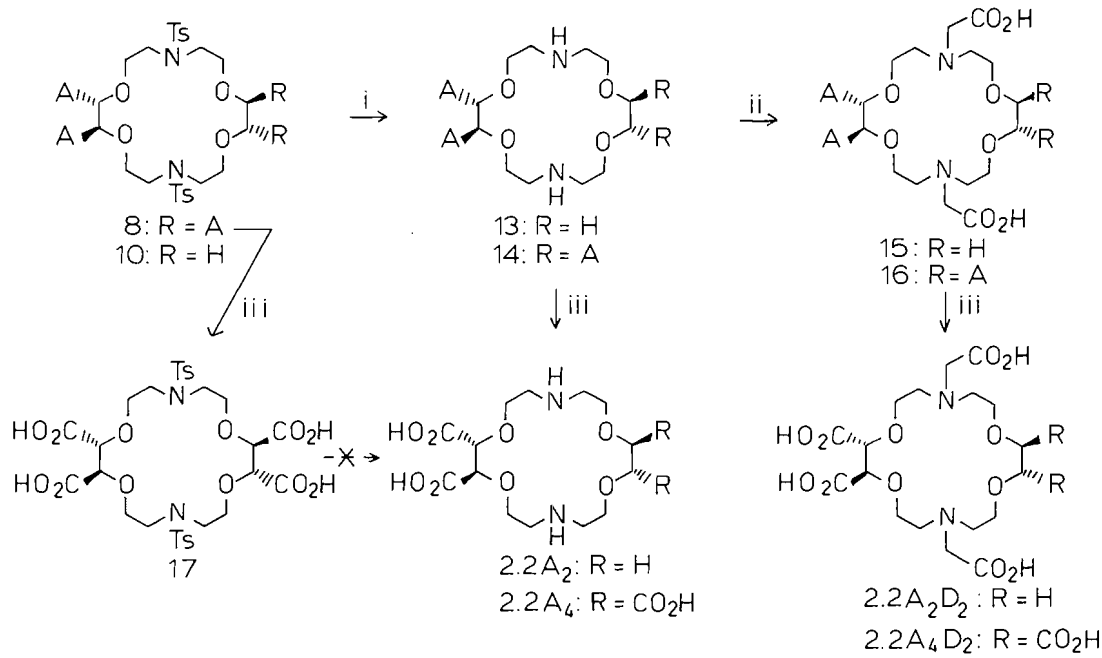

FIG. 4. Deprotections and *N*-alkylation of aza crown ether carboxylic acids. Conditions: (*i*) hν/dimethoxybenzene/hydrazine; (*ii*) HO_2CCH_2Br/Li_2CO_3; (*iii*) H_3O^+ (see text). Abbreviations as in Fig. 2.

tetraacid was recovered unchanged. Concentrated H_2SO_4 (11) at 100°C completely charred the reaction mixture, and no organic product could be isolated. HBr/AcOH/phenol (24) is the other common reagent for sulfonamide cleavage; some diethanolamine (from crown ether cleavage) and phenol (from the reagent) were the only products isolated from an attempt to deprotect **8**.

Lithium aluminum hydride is reported to be an effective reagent for sulfonamide removal (25), but it is inappropriate for **8** or **10** as the carboxamides would undergo reduction as well. Dissolving metal reductions using sodium amalgam (15, 21, 26), or Li or Ca (21) in liquid ammonia, are other reductive cleavage reagents. Since carboxylates are known to be relatively resistant to dissolving metal reductions, the tetraacid **17** was chosen as the starting material. Reductive methods typically require a large excess of metal to be used. For the tetraacid **17**, the first four equivalents form the tetra-salt, hence stoichiometry required at least 8 equiv. of metal. On workup, the ^1H NMR of an aqueous extract showed that the crown ether **2.2A$_4$** was indeed present. However, separation of the charged, water soluble crown ether from an eight-fold excess of salt (Li^+ or Ca^{2+}), to obtain "metal free" ligands, proved to be impossible. Attempted precipitation of Ca^{2+} with oxalate or carbonate was not successful, probably due to binding of Ca^{2+} by the ligand. Similarly, direct crystallization of the product was not possible. Ion exchange chromatography also did not succeed as the ligand could not be recovered from the resin.

Direct photochemical deprotection of arylsulfonamides is known (27), but the low reported yields give the reaction little practical unity. Attempted photolysis of **8** at 254 nm as a dilute solution in isopropanol produced the deprotected crown tetraamide **14** in poor yields (<25%) as a mixture that was difficult to separate. An improved photochemical procedure, exploiting the photosensitized electron transfer reactions of arylsulfonamides (28), finally achieved the required cleavage and left a product which could be purified. In our hands the most successful conditions utilized a ten-fold molar excess of *p*-dimethoxybenzene as sensitizer and hydrazine as the reducing agent. The crude diamines were purified to ^1H NMR "purity" by a tedious sequence of extractions and ion exchange chromatography.

The carboxamides of **13** and **14** are readily hydrolyzed in aqueous acids to give the desired crown ethers in an excess of dimethylammonium salt. In order to separate the crown ether from this inevitable byproduct, it was most convenient to manipulate a mixture of salts which was soluble in organic solvent. To this end, hydrolysis of the carboxamides (**13** or **14**) was achieved using a stoichiometric amount of *p*-toluenesulfonic acid in water. The reaction mixture was evaporated to dryness, dissolved in chloroform/methanol (1:1), and chromatographed using Sephadex LH-20. Fractions were collected and analyzed by ^{13}C NMR; the crown ethers **2.2A$_2$** or **2.2A$_4$** eluted near the void volume as their bis-toluenesulfonate salts. These were further purified by re-chromatography using a small amount of additional *p*-toluenesulfonic acid to ensure complete protonation of the ligands.

The ^{13}C NMR spectra of **2.2A$_4$** showed a pH dependence whereby "extra" resonances appeared at intermediate pH (3–6). At the extremes of pH (2 or 12), the expected four line spectra were observed for the ligand (plus signals for the counterion). The purified samples had the expected spectral properties (^1H and ^{13}C NMR, IR) but resisted reproducible elemental analysis. No constant level of hydration could be achieved, and the anhydrous samples were extremely moisture sensitive. The homogeneity of the anhydrous ligands was established by potentiometric titration using the pronounced end-point between pH 5 and 8 to indicate the formation of the bis-zwitterion (addition of base; 2 equiv. for **2.2A$_2$** and 4 equiv. for **2.2A$_4$**). In both cases the calculated equivalent weights were within 2% of the expectation values.

Reagents for the introduction of N—CH_2CO_2H side chains on amines are haloacetic acids (17) or their esters (29). Ethyl bromoacetate could not be used as the alkylating agent, probably due to competing amination of the esters. Alkylation

Can. J. Chem. Downloaded from www.nrcresearchpress.com by 88.85.125.76 on 09/07/12
For personal use only.

Can. J. Chem. Downloaded from www.nrcresearchpress.com by 88.85.125.76 on 09/07/12
For personal use only.

of crown ether **2.2A$_2$** or **2.2A$_4$** with bromoacetic acid in a buffered medium gave the expected alkylated product as judged by ^{13}C NMR. As before, the large excess of buffer required (either as alkali metal carbonate or tertiary ammonium chloride) made separation of the crown ether from the reaction mixture an extremely difficult task. Ultimately, bromoacetic acid in stoichiometric aqueous Li_2CO_3 proved to be the reagent of choice. The intermediate amides **15** and **16** were not purified, but were directly hydrolysed with stoichiometric amounts of *p*-toluenesulfonic acid to give samples of the N—CH_2CO_2H derivatives in excess lithium toluenesulfonate. Repeated gel permeation chromatography on LH20 as before gave **2.2A$_2$D$_2$** and **2.2A$_4$D$_2$** (as water soluble deliquescent solids) in 55–60% yields as their *p*-toluenesulfonate salts. An elemental analysis of **2.2A$_2$D$_2$** dihydrate was obtained and the same sample showed the expected equivalent weight. Alternatively, an anhydrous sample gave the expected equivalent weight. However, despite extensive gel permeation, **2.2A$_4$D$_2$** failed to give a satisfactory titrimetric equivalent weight. The presence of a substoichiometric amount of Li^+ was determined by atomic absorbance measurement. Presumably a lithium complex is formed which resists the separation as a lithium toluenesulfonate salt during chromatography. Consequently, the structure proof for **2.2A$_4$D$_2$** rests entirely on the spectra obtained. Unfortunately, our inability to purify this ligand has prevented the successful determination of acidity and stability constants for complexation.

Complexation of cations

Complex formation in solution can be described in terms of a cumulative formation constant β_{lmh} defined by the equilibrium between l ligands of charge $z-$, m cations of charge $y+$, and h protons (reaction [1])

$$[1]\quad lL^{z-} + mM^{y+} + hH^+ \rightleftharpoons lL^{z-}mM^{y+}hH^+$$

$$[2]\quad \beta_{lmh} = \frac{[lL^{z-}mM^{y+}hH^+]}{[L^{z-}]^l[M^{y+}]^m[H^+]^h}$$

Since ligand and complex activity coefficients are unknown, the β_{lmh} values are typically defined in terms of concentrations. The errors introduced are minimized by the use of a constant ionic strength, low ligand concentration, and corrections to the calibration of the pH electrode (below). Stepwise formation constants as would apply to the association of a partly protonated ligand with a metal ion can be derived from the β_{lmh} for the system (4, 6).

To render the cumulative formation constants entirely in terms of concentrations, it is necessary to convert from the pH meter reading (pH_m) to the concentration of H^+ (pC_{H^+}). A linear relationship is assumed (30–34):

$$[3]\quad pH_m = (s)^*(pC_{H^+}) + b$$

where "s" is a slope, typically very close to 1 and "b" an intercept. Both parameters, and the effective value of pK_w for the supporting electrolyte can be determined from a strong acid – strong base titration. We follow the procedure of Jameson and Wilson in the definitions (34),

$$[4]\quad \log K_w = (pH_{m1} + pC_{HO^-}) + pC_{H^+} - pH_{m2}$$

where pH_{m1} refers to the pH meter reading in the alkaline region and pH_{m2} to the pH meter reading in the acidic region of a strong acid/strong base titration. At every point in the titration, it is possible to calculate stoichiometric H^+ and HO^- concentrations corrected for dilution. In the strong acid buffer region (up to pH 2.5) the average value of $pC_{H^+} - pH_{m2}$ is $-b$. In the strong base buffer (>pH 11.5) an average value for $pH_{m1} + pC_{HO^-}$ when added to $-b$ gives $-pK_w$. The measured pH_m can thus be used to calculate the hydrogen ion concentration and using these values, the β values obtained will be true concentration constants containing no activity terms. The thermodynamic values may be obtained by calculating an activity correction using a modified Debye–Huckel expression (35, 36).

General trends

Table 1 presents the acidity and stability constant data for the ligands. The numbers tabulated are all cumulative constants; stepwise formation constants for the association of the metal ion with partially protonated forms of the ligand are given in parentheses. The values of l, m, and h serve to define the complex stoichiometry. The value of $h = -1$ indicates an hydroxo complex (see below). The value of r in square brackets is a "goodness-of-fit" parameter derived from the standard deviation in titer given by the program (37) divided by the experimental titer increment (usually 3 μL to give 18 points per equivalent of ligand titrated). Table 2 gives an abbreviated summary of the primary (β_{110}) complexes of the ligands, together with data on other ligands for comparison purposes.

The acidity constants follow expected trends consistent with the basic protonations occurring on nitrogen, and the acidic protonations occurring on carboxylate oxygen. As the ligands become progressively more negatively charged, the amines become more basic. For example, in the case of **2.2A$_2$**, the amines are deprotonated from a species that has a formal charge of −2. Compared to **2.2**, this causes a +0.3 increment in the first pK_a. The increment can be seen for the second amino group as well. The amino groups of **2.2A$_2$D$_2$** are less basic than **2.2A$_4$**, although both are tetraanionic ligands. This trend is in line with expectations, since the nitrogen on **2.2A$_2$D$_2$** is tertiary.

Most of the carboxylic acid groups in these ligands are strongly acidic (6). Only one weakly acidic carboxyl ($pK_a > 3$) was detected in every case. The other carboxyls were all more strongly acidic (<2.5) and outside the range of the pH-metric technique. These values are again in the expected range, compared for example with EGTA or **18C6A$_4$**.

An inspection of the data for the aza ligands with Group I or II cations reveals that they are quite unselective. For example, the Na^+, K^+, and Cs^+ complexes of **2.2A$_4$** have stability constants around $\log \beta = 3$. Thus metal ion size makes little difference in stability. As noted previously the "cation size – ligand cavity match" concept holds less well for charged oxa crown ethers (6), and this is confirmed in the aza series. Although larger and more polarizable ions like Cs^+ should be favored by the nitrogen donors, this effect is probably overwhelmed by the electrostatic effects.

The role of the nitrogen donors is more clearly seen in the complexes of the transition metal ions, Cd^{2+} and Pb^{2+}. Even with the neutral parent **2.2**, these ions form stronger complexes than do the harder alkali metals, and this tendency is retained and enhanced as the ligand charge increases. The ligand selectivities do not change in order (apparently the Irving–Williams order for the limited set available), nor in magnitude as the ligand charge increases. Along the sequence **2.2**, **2.2A$_2$**, **2.2A$_4$** the complex stability does increase in a regular manner.

Electrostatic ion binding and chelate interactions

One of the rationales for this study was the expectation that an anionic ligand environment would act to stabilize the

TABLE 1. Logarithm of the cumulative formation constant of the ligands studied[a]

Metal	*lmh*	log K_a when ligand = **2.2A$_2$**	**2.2A$_4$**	**2.2A$_2$D$_2$**
H^+ [a]	101	9.37	10.63	9.88
	102	17.86 (8.49)	19.81 (9.18)	18.53 (8.65)
	103	21.04 (3.18)	23.90 (4.09)	22.18 (3.65)
	104	—	26.35 (2.45)	—
		[r = 0.65]	[r = 0.3]	[r = 0.6]
Na^+	110	—	2.8	3.2
	111	—	—	12.5 (2.6)
			[r = 0.2]	[r = 0.15]
K^+	110	2.0	3.1	3.3
	111	—	—	12.7 (2.8)
		[r = 0.5]	[r = 0.3]	[r = 0.25]
Cs^+	110	3.2	3.2	2.8
	111	12.4 (3.0)	13.1 (2.5)	12.4 (2.5)
		[r = 0.65]	[r = 0.2]	[r = 0.13]
Tl^+	110	2.7	3.7	5.4
	111	—	13.3 (2.7)	14.2 (4.3)
		[r = 0.35]	[r = 0.2]	[r = 0.2]
Ca^{2+}	110	3.9	6.6	9.0
	111	12.4 (3.0)	15.2 (4.6)	16.7 (6.8)
	11−1	7.9 (6.6)[c]	—	—
		[r = 0.3]	[r = 1.1]	[r = 1.2]
Sr^{2+}	110	4.2	6.7	10.4
	111	12.5 (3.1)	15.2 (4.6)	17.3 (7.4)
	11−1	7.8 (7.1)[c]	—	—
		[r = 0.1]	[r = 0.32]	[r = 0.3]
Ba^{2+}	110	4.3	6.6	10.2
	111	12.6 (3.2)	15.7 (5.1)	17.3 (7.4)
	11−1	7.8 (7.2)[c]	—	—
		[r = 0.1]	[r = 0.4]	[r = 1.0]
La^{3+}	110	5.5	9.3	13.5
	111	13.2 (3.9)	17.0 (6.4)	19.4 (9.5)
	11−1	10.1 (4.6)[c]	—	—
		[r = 0.2]	[r = 0.7]	[r = 0.8]
Ni^{2+}	110	4.9	6.4	10.1
	111	13.3 (3.9)	15.0 (4.4)	17.4 (7.5)
	11−1	9.8 (5.5)[c]	10.5 (6.3)[c]	—
		[r = 0.45]	[r = 0.2]	[r = 0.8]
Cu^{2+}	110	9.1	11.3	14.2
	111	14.6 (5.2)	18.3 (7.7)	20.2 (10.3)
	11−1	14.7 (8.0)[c]	—	—
		[r = 0.3]	[r = 1.1]	[r = 0.5]
Zn^{2+}	110	5.1	7.7	10.2
	111	13.5 (4.1)	15.9 (5.3)	17.2 (7.3)
	11−1	11.2 (6.5)[c]	12.5 (7.8)	—
		[r = 0.3]	[r = 0.26]	[r = 0.6]
Cd^{2+}	110	7.3	10.0	12.9
	111	14.5 (5.1)	17.1 (6.5)	18.5 (8.6)
	11−1	12.7 (8.9)[c]	—	—
		[r = 0.3]	[r = 0.3]	[r = 0.8]
Pd^{2+}	110	8.5	12.1	14.1
	111	15.6 (6.2)[c]	18.4 (7.8)	20.0 (10.1)
		[r = 1.2]	[r = 0.7]	[r = 1.05]

[a]log β_{lmh} values: determined in 0.1 M TMAN at 25°C, uncertainty in log β_{lmh} = ±0.2, ±0.1 in pK_a.
[b]Negative logarithm of dissociation constants; follows convention of pK_a.
[c]Stepwise formation constant for MOH + L; see text. —, complex of that stoichiometry not detected under the experimental conditions.

complexes. A number of points bear out this expectation. Firstly, divalent and trivalent ions are bound more strongly than monovalent ions. Secondly, the complexes of the fully deprotonated ligands with divalent ions show a regular increase in stability with increasing charge. For example, the Ca^{2+}, Cd^{2+}, and Cu^{2+} triad all experience 10^2–10^3 fold enhancement in stability for every two carboxylates added. Trivalent metal ions, like La^{3+}, experience an even larger increase (10^4) for every two additional carboxylates. Thirdly, most complexes undergo significant destabilization on ligand protonation. This effect was also observed in the oxa series, as were complexes of multiply protonated ligands (6). No diprotonated complexes were detected in the aza series.

There are two structural possibilities for the monoprotonated aza crown complexes; (*1*) *N* protonation, with loss of a donor site and creation of a positive charge in the macrocyclic binding site, or (*2*) carboxylate protonation with loss of remote electrostatic stabilization only. The latter possibility is supported by similar magnitudes of destabilization for the oxa and aza series: **2.2A$_2$** and **2.2A$_4$** with alkaline earth cations destabilized by log β_{110} − log β_{111} = 1.31 on average compared with 1.35 for the same cations and **18C6A$_2$**, **18C6A$_4$**, and **18C6A$_6$** (Table 2). In addition, the parent crown ethers **2.2** and **2.2D$_2$**, which lack these extra carboxylates, do not show protonated complexes.

To an extent therefore, the expectation of electrostatic stabilization appears to be fulfilled. However, there are a number of other features of the data that argue for an insignificant role for the ligand charge *per se*. Chief among these is the substantial difference in stability between **2.2A$_4$** and **2.2A$_2$D$_2$**; the divalent ion complexes of the latter are on average a thousand-fold more stable than the former yet the overall charges are identical (4−). The differences are even more pronounced for the 2− charged ligands **2.2A$_2$** and **2.2D$_2$** (4.7 in log β). Furthermore, there is a relatively modest difference between the divalent ion complexes of **2.2D$_2$** and **2.2A$_2$D$_2$** (1.3 in log β for an increase in charge from 2− to 4− compared with 2.1 in log β for the same ions and charge increment in the oxa series). There can be little doubt that a chelate interaction involving the *N*-acetate unit (N—CH_2—CO_2^-) is much more stabilizing than a remote charge, or an equivalent interaction involving a O—CH—CO_2^- unit. From the difference in log β for **2.2A$_2$** and **2.2D$_2$** (averaged over divalent ions) this stabilization can be estimated to be of the order of 20 kJ per chelate interaction at constant charge. Viewed from another perspective, introduction of two charges to **2.2** to generate **2.2A$_2$** gives a stabilization of the order of 8 kJ per charge, while the introduction of two *N*-acetates to **2.2** to generate **2.2D$_2$** gives a stabilization of 25 kJ per chelate and charge introduced. Either way the *N*-acetates bring substantial stability to the complexes of divalent ions. The same is apparently true for Tl^+, but not for the alkali metals.

We have previously analyzed the data for the oxa series to show that carboxylate participation in a chelate interaction is a recurring feature of the complexation process. A similar treatment of the data for the aza crown ether series yields substantially the same conclusions. The method involves a division of the complexation free energy into a "crown ether" part plus an electrostatic part which is scaled by the extent of protonation of the ligand (6, 39). In terms of log β values,

$$[5]\quad (\log \beta_{obs})^2 = (\log \beta_C)^2 + 2\Phi \log \beta_C \log \beta_E + (\Phi \log \beta_E)^2$$

Can. J. Chem. Downloaded from www.nrcresearchpress.com by 88.85.125.76 on 09/07/12
For personal use only.

TABLE 2. Logarithm of stepwise stability constants for complexation[a]

		log β_{lmh} when ligand =								
Metal	*lmh*	**2.2A$_2$**	**2.2A$_4$**	**2.2A$_2$D$_2$**	**2.2**	**2.2D$_2$**[f]	EGTA[g]	**18C6A$_2$**[h]	**18C6A$_4$**[h]	**18C6A$_6$**[h]
Na^+	110	—[k]	2.8	3.2	0.8[l]	?[p]	[o]	3.3	4.5	5.4
K^+	110	2.0	3.1	3.3	2.0[m]	3.9	[o]	4.2	4.8	5.3[i]
Tl^+	110	2.7	3.7	5.4	2.2[d]	?[p]	4.4	5.7	4.8[i]	5.8[i]
Ca^{2+}	110	3.9	6.6	9.0	1.8[c]	8.4	10.9	5.6	8.6	9.8
Sr^{2+}	110	4.2	6.7	10.4	2.6[c]	8.3	8.5	5.9	8.0	10.4
Ba^{2+}	110	4.3	6.6	10.2	3.0[c]	7.6	8.4	6.5	7.2	9.5
La^{3+}	110	5.5	9.4	13.5	6.2[n]	12.2	15.8	?[p]	?[p]	12.7[j]
Ni^{2+}	110	4.9	6.5	10.1	2.5[e]	7.4	11.8	?[p]	?[p]	?[p]
Cu^{2+}	110	9.1	11.3	14.3	6.2[e]	14.5	17.7	3.9	5.3	7.1
Zn^{2+}	110	5.1	7.7	10.2	3.2[e]	8.4	12.9	3.7	4.0	6.3
Cd^{2+}	110	7.3	10.0	12.9	5.25[e]	11.1	16.1	3.0	7.9	9.3
Pb^{2+}	110	8.5	12.2	14.1	6.9[e]	13.5	11.8	?[p]	9.8[j]	?[p]

[a]Determined at 25°C, I = 0.1 M with Me_4NNO_3 in water; uncertainty in log β_{lmh} = ±0.1. The literature constants chosen were determined in H_2O, using similar methods unless otherwise indicated.
[b]Logarithm of dissociation constants; follows the convention of pK_a.
[c]Reference 49.
[d]Reference 50.
[e]Reference 51.
[f]Reference 52.
[g]Reference 53.
[h]Reference 6.
[i]Monoprotonated complex; 110 complex is less stable. see ref. 6.
[j]P. J. Dutton, T. M. Fyles, and P. D. Wotton. Unpublished values ±0.5.
[k]Not detected under the experimental conditions.
[l]Determined using ISE; ref. 54.
[m]MeOH solvent; ref. 55.
[n]MeOH solvent; ref. 56.
[o]Estimated to be very weak.
[p]?, stability constant not known.

where log β_{obs} is the formation constant for the complex, log β_C is the formation constant for a neutral reference compound (**2.2** in this case), and Φ is the scaling factor which takes values from zero for a neutral ligand form to 1 for a maximally deprotonated form. The unknown in [5] is log β_E, the electrostatic component of the binding. The three terms on the right hand side of [5] are proportional to the interaction of the macrocycle alone, the cooperative or chelating interaction of the carboxylates acting on a cation in the macrocycle and the purely electrostatic interaction, respectively. Expressed as percentages, the three terms describe the apparent cooperativity of the binding. The results are given in Table 3. In all cases, and as found in the oxa series as well, about 40–50% of the interaction energy can be ascribed to cooperative or chelating interactions. The donors are both tartro and *N*-acetate derived, yet this distinction cannot be found in the data. This implies that the ion binding process ignores whether the donor comes from the tartro units or the *N*-acetates.

Cooperative chelate interactions are also a dominant feature in the solid state chemistry of the oxa crown ethers (38), and can be seen in the published structures of **2.2D$_2$** copper complexes (18–20). We are therefore tempted to ascribe the energy differences noted above to the difference between five-membered chelate rings containing O vs. N as donors in the unit X—C—CO_2^-.

In summary, a generalized electrostatic effect is of minor importance in these crown ethers. The more important interactions are chelation of the ion, presumably located within the macrocyclic cavity, by donor carboxylates appended to the periphery. The tartro units provide one mode of coordination, while the *N*-acetates provide a more effective mode.

Hydroxo complexes

Many of the metals studied have important hydroxo complexes in alkaline media and the hydroxide ion is thus a competing ligand. On the other hand, cationic hydroxo complexes (e.g. $NiOH^+$) can still bind with the ligands of this study (Table 1). The complexes thus formed can be described as a sum of formation equilibria [6] and [7] (where the subscript −1 refers to addition of one OH^-):

[6] $MOH^+ \rightleftharpoons M^{2+} + HO^-$ $\quad 1/\beta_{01\text{-}1}$

[7] $L + M^{2+} + OH^- \rightleftharpoons LMOH^+$ $\quad \beta_{11\text{-}1}$

The reaction of interest is the stepwise association of the metal hydroxide with the ligand,

[8] $MOH^+ + L \rightleftharpoons LMOH^+$

whence the stepwise log K for the LMOH complex would be given by log $\beta_{11\text{-}1}$ − log $\beta_{01\text{-}1}$.

A few such complexes were detected, especially with ligands of lower charge and lower donor number (**2.2A$_2$**) (Table 1). A striking feature regarding these complexes is that they are almost as stable as, or in some cases more stable than, the primary 110 complexes. In the case of Group II complexes with **2.2A$_2$**, the $\beta_{11\text{-}1}$ complexes are more stable than the β_{110} complexes by a factor of 10^3. Alkaline earth cations are expected to bind weakly to the nitrogen and strongly to a hard ligating site. Addition of hydroxide would provide an additional

Can. J. Chem. Downloaded from www.nrcresearchpress.com by 88.85.125.76 on 09/07/12
For personal use only.

TABLE 3. Contributions to ion binding[a] calculated by eq. [5] (39)

Metal	Complex *lmh*	Ligand[b] **2.2A$_2$** %CE	%CO	%EL	**2.2A$_4$** %CE	%CO	%EL	**2.2A$_2$D$_2$** %CE	%CO	%EL
Tl^+	110	66	30	4	35	48	17	17	48	35
	111	—	—	—	79	20	1	41	46	13
Ca^{2+}	110	21	50	29	7	40	53	4	32	64
	111	73	24	3	28	50	22	15	48	37
Sr^{2+}	110	38	47	15	16	47	37	6	38	56
	111	89	10	1	50	41	8	24	50	26
Ba^{2+}	110	49	42	9	21	49	30	9	42	49
	111	97	3	0	51	41	8	30	50	20
Ni^{2+}	110	26	50	24	15	47	38	6	37	57
	111	76	22	2	49	42	9	22	50	28
Cu^{2+}	110	46	43	11	30	50	20	19	49	32
	111	—	—	—	77	21	2	53	40	7
Zn^{2+}	110	39	47	14	17	49	34	10	43	47
	111	86	13	1	53	39	8	33	49	18
Cd^{2+}	110	52	40	8	28	49	23	17	48	35
	111	—	—	—	78	21	1	53	39	7
Pb^{2+}	110	65	31	4	32	49	19	24	50	26
	111	—	—	—	87	13	0	63	33	4

[a]%CE = crown ether alone; %CO = co-operative interaction, %EL = electrostatics alone; calculated using **2.2** as a reference point.

[b]—, inappropriate, since the protonated complex is less stable compared to the parent crown **2.2**.

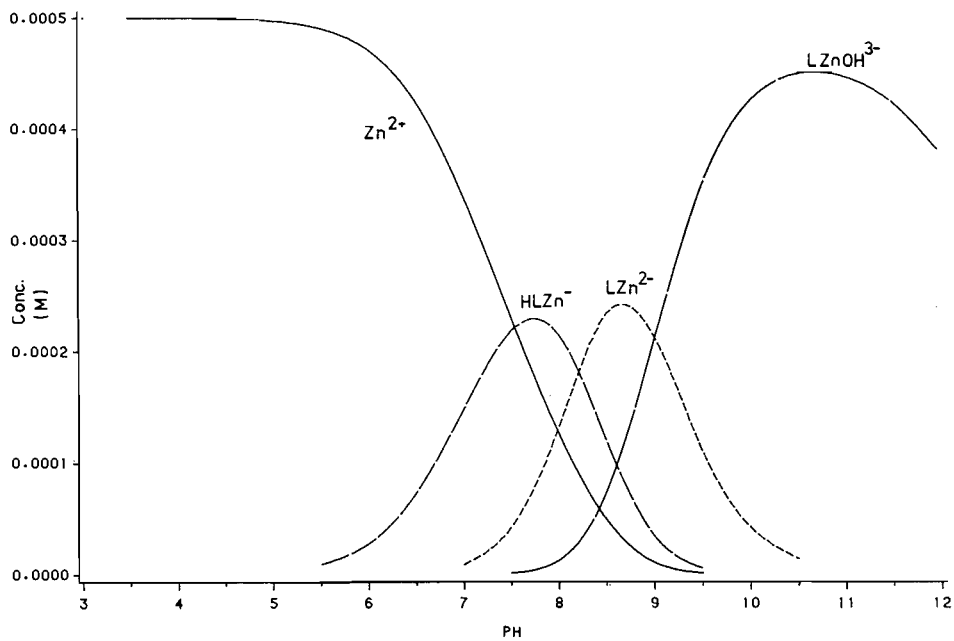

FIG. 5. Species concentration as a function of pH calculated for an equimolar mixture of Zn^{2+} and **2.2A$_4$** at 5×10^{-4} M.

hard donor, while maintaining a potentially high coordination number. In the higher charged ligands (**2.2A$_4$**) the statistical factor (four carboxylate donors) and the high charge acts to displace the hydroxide. Very few hydroxo complexes were detected in this case. Similarly in the case of **2.2A$_2$D$_2$**, the strong chelate donors completely prevent hydroxide ligation.

Speciation plots for **2.2A$_4$** in the presence of an equivalent of zinc are shown in Fig. 5. The binding occurs in the alkaline regions (pH > 7) as can be seen by a sharp drop in free Zn^{2+} concentration. Both the "primary" complex of the deprotonated ligand and the monoprotonated complex play a relatively minor role in the solution compared to the dominant role played by the hydroxo complex. Similar hydroxo complexes of aminopolycarboxylate complexones are known (16), but they

Can. J. Chem. Downloaded from www.nrcresearchpress.com by 88.85.125.76 on 09/07/12
For personal use only.

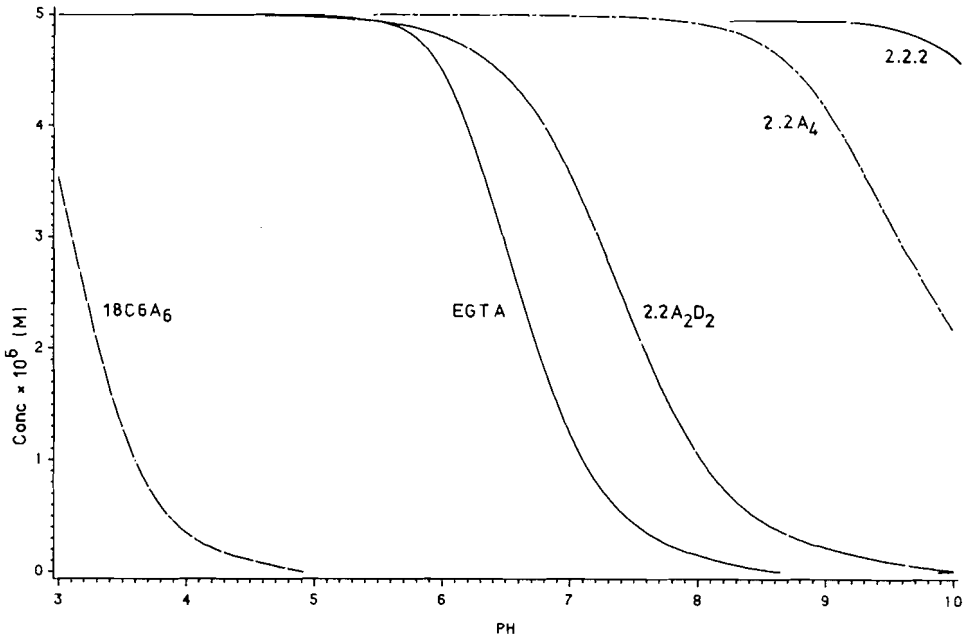

FIG. 6. Free calcium concentration as a function of pH calculated for an equimolar mixture of various ligands and Ca^{2+} at 5×10^{-6} M.

play only a minor role in solutions dominated by the "primary" 1:1 complexes.

Interligand comparisons

The polycarboxylate crown ethers, both oxa and aza, are effective cation complexing agents and compare favorably with neutral ligands, such as the cryptands, and with charged aminopolycarboxylates, such as EDTA. Table 2 provides an overview for comparisons between the ligands.

As noted previously, the oxa crown carboxylates form a number of protonated complexes (6). Protonation on carboxylate reduces complex stability but the metal ion remains effectively bound even in acidic solutions. In contrast, *N*-protonation results in significant destabilization in the aza crowns and EGTA and catastrophic destabilization in cryptand **2.2.2**. Comparisons are readily made in Fig. 6, where free Ca^{2+} concentrations have been calculated for an equimolar mixture of metal ion and ligand at 5×10^{-6} M. The relative concentrations at high pH reflect the relative stability constants for Ca^{2+} complexation. The persistence of the Ca^{2+} complex to pH 7 and below reflects the ability of the ligand to bind metal ions despite protonation. Clearly, the oxa crowns achieve this most effectively.

The close similarities, and significant differences due to donor atom substitution between the oxa and aza crowns have been examined above. Equally close similarities exist between the aza crowns and aminopolycarboxylate complexones such as EDTA and EGTA. With some exceptions, the formation constants of **2.2A$_2$D$_2$** are closely similar to EGTA as might be expected from the charge, donor set and the appropriate dimensions of EGTA (a rearranged "isomer" of **2.2A$_2$D$_2$** lacking a triethylene glycol bridge). The differences between EDTA and EGTA have been ascribed to a pre-organization effect in which the entropy term for the latter would be larger (40). Since the entropy associated with EGTA and **2.2A$_2$D$_2$** complexation must be significantly different in its detail, our results suggest that there is also a "cavity size" component as well. Relative to EDTA, EGTA or **2.2A$_2$D$_2$** apparently have difficulty bringing in all the available donor interactions. That the **2.2** cavity is too large for transition metal cations has been noted previously (41, 42); potentially this could result in a decrease in the number of coordinated donors.

We attempted to approach this question from the view point of the linear free energy relationships which had been described by Hancock and co-workers for the estimation of the stability constants for complexation by aminopolycarboxylates (41, 42). The approach seeks to relate unidentate binding constants for complexation of a cation by acetate and ammonia to the overall formation constant for the aminopolycarboxylate (43–45). Statistical or steric correction factors based on the number of each donor type are included. We envisaged using the available correlations, which work reasonably well for simple cases, and by simple variation of the donor number terms, derive a "best-fit" to the aza crown data. The results were considerably more scattered than for simple complexones, but "best-fits" were typically achieved using only one nitrogen donor site. Whether this is an artifact or reflects some underlying chemistry is not known.

An alternative linear free energy approach to the characterization of ligands is the use of the stability index, Q, and related derived parameters (46). As above, the results were considerably more scattered than for simple ligands but consistently indicated that the aza crowns of this study were more typical of class b behaviors. This is in general agreement with the size of the macrocycle which would favor larger cations.

Taken together, all the trends point to a close relationship of the aza crown series to crown ethers, and a somewhat more distant relationship to aminopolycarboxylates. The complex stabilities approach similar values but the ligand characteristic of a cavity maintained by its periphery and providing a flexible, but defined donor array are evident. As in all productive binding events, the strong complexes arise from a strong cooperativity of the various cavity, electrostatic, and chelate interactions. At the same time however, the relatively weak complexes of the alkali metals still represent significant enhancement over the neutral parent. One result is that the aza crowns described here,

Can. J. Chem. Downloaded from www.nrcresearchpress.com by 88.85.125.76 on 09/07/12
For personal use only.

Can. J. Chem. Downloaded from www.nrcresearchpress.com by 88.85.125.76 on 09/07/12
For personal use only.

and in particular **2.2A$_2$D$_2$**, have significant affinity for all types of cations and could serve as a general purpose cation binding agent. It remains to be seen if this molecular promiscuity can be turned to any chemical advantage.

Experimental

Melting points were taken on a Riechardt hot stage microscope (uncorrected). Proton NMR spectra were recorded with a Perkin-Elmer R32 (90 MHz, CW) or Bruker WM 250 (250 MHz, FT) spectrometer in $CDCl_3$ solvent with Me_4Si as internal standard or in D_2O with external Me_4Si in $CDCl_3$ as reference. Carbon NMR spectra were recorded at 62.8 MHz (WM 250) in $CDCl_3$ with the central solvent line as standard (77.0 ppm relative to Me_4SI) or in D_2O with a frequency reference for this solvent previously calibrated against external Me_4Si in $CDCl_3$. The mass spectra were recorded with a Finnegan 3300 GC-MS instrument with methane chemical ionization. IR spectra were recorded on a Perkin Elmer 283. Optical rotations were recorded on a Perkin Elmer 141 instrument; concentrations were in g/mL. Elemental analyses were performed by Canadian Microanalytical Services, New Westminster, B.C., and are quoted in percentages.

(2R,3R)-N,N,N′,N′-*Tetramethyl-2,3-bis(2-(tetrahydropyranyloxy)-ethoxy]succinamide (2)*

Thallous ethoxide (126 g, 0.5 mol) was added dropwise via syringe to a solution of (2*R*,3*R*)-*N*,*N*,*N*′,*N*′-tetramethyltartaramide **1** (48.6 g, 0.24 mol) in 3.5 L of dry dimethylformamide (DMF). The resultant slurry was mechanically stirred under an inert atmosphere and warmed to 50°C, whereupon 2-(2-bromoethoxy)tetrahydropyran (7) (130 g, 0.62 mol) was added in one portion. The mixture was heated at 65°C for a further 14 h and cooled. The thallous bromide was removed by filtration, and the solvent was removed by evaporation at reduced pressure. The oily product was dissolved in CH_2Cl_2 and filtered through a pad of Celite, the eluent evaporated, and the final traces of DMF removed by evaporation at high vacuum. The crude sample (100.5 g, 92%, predominantly **2** by ^{1}H NMR) could be used without further purification. Spectral data are given in Table 4.

Alternatively, crude **2** was purified by chromatography on neutral alumina (1 kg/100 g of **2**, column diameter 80 mm) using 1% MeOH/CH_2Cl_2. Fractions (400 mL) were collected and **2** eluted first. The appropriate fractions were combined and evaporated to yield **2** as a light yellow oil, in ca. 60% yield.

(2R,3R)-N,N,N′,N′-*Tetramethyl-2,3-bis(2-hydroxyethyl)succinamide (3)*

The crude bis(tetrahydropyranyl) ether **2** (92 g, 0.2 mol) was dissolved in 250 mL of methanol, 2 drops of concentrated HCl was added, and the mixture was stirred at reflux for 1 h, cooled, and evaporated. The oil was dissolved in water and extracted with 2 × 100 mL portions of ether, and the water layer was evaporated at high vacuum until a solid was obtained. Trituration using a minimum volume of ether/THF (1:9) gave **3** (42.5 g, 73%) as a white solid, mp 100–102°C. Spectral data are given in Table 4.

When pure **2** was subjected to hydrolysis as described, the diol **3** was obtained as a white solid in nearly quantitative yield. Infrared (KBr) 3500 br 1650 cm^{-1}. Anal. calcd. for $C_{12}H_{24}N_2O_6$: C 49.28, H 8.28, N 9.58; found: C 48.94, H 8.04, N 9.45.

(2R,3R)-N,N,N′,N′-*Tetramethyl-2,3-bis(2-(tosyloxy)ethoxy)succinamide (4)*

The diol **3** (23 g, 78 mmol) was dissolved in CH_2Cl_2 (200 mL) and triethylamine (20 mL) at 10°C, and solid *p*-toluenesulfonyl chloride (30.5 g, 160 mmol) was added. The mixture was stirred at ambient temperature for 24 h, diluted with a further 200 mL of CH_2Cl_2, extracted with 3 × 100 mL portions of cold 1 M HCl, followed by 5 × 100 mL portions of ice-cold water, dried over Na_2SO_4, and evaporated to a solid gum. The gum was triturated to a solid with a minimum of ether. This purity was sufficient for the subsequent steps (yield = 35.8 g, 78%). An analytical sample was obtained by recrystallization from ether/THF, mp 105–107°C. Spectral data are given in Table 4. Anal. calcd. for $C_{26}H_{36}N_2O_{10}S_2$: C 51.96, H 6.04, N 4.66, S 10.68; found: C 51.74, H 6.06, N 4.65, S 10.72.

(2R,3R)-N,N,N′,N′-*Tetramethyl-2,3-bis(2-(phthalimidoethoxy))-succinamide (5)*

The ditosylate **4** (20 g, 33 mmol) and potassium phthalimide (13 g, 70 mmol) were mixed in 400 mL of dry DMF. Distilled diethylamine (2 mL) was added as a solid–liquid phase transfer catalyst. The mixture was stirred at 50–60°C for 8 h under an inert atmosphere. The clear solution obtained was evaporated under reduced pressure and then evaporated at high vacuum overnight. The gummy product obtained was suspended in CH_2Cl_2 (500 mL) and the slurry stirred for 30 min. The precipitated solids were removed by filtration and the CH_2Cl_2 evaporated to give the crude diphthalimide **5** in quantitative yield (18.3 g). Recrystallization from 95% ethanol gave pure **5** as a white solid (16.7 g, 92%), mp 204–205°C. $[\alpha]_D = +46°$ ($c = 1.05$, CH_2Cl_2) $M^{+\cdot} = 550$. ^{1}H and ^{13}C spectral data are listed in Table 4. Anal. calcd. for $C_{28}H_{30}N_4O_8$: C 61.06, H 5.49, N 10.17; found: C 60.98, H 5.46, N 10.19.

(2R,3R)-N,N,N′,N′-*Tetramethyl-2,3-bis(2-aminoethyl)succinamide (6)*

The diphthalimide **5** (16.6 g, 30 mmol) was suspended in 300 mL of ethanol. Hydrazine hydrate (3.5 g, 70 mmol) was added and the mixture heated to 50°C with mechanical stirring. A thick precipitate formed over 3 h. This was stirred for a further 2 h and cooled. Most of the precipitated phthalhydrazide was removed by filtration. The filtrate was then concentrated and brought to pH 3–4 by cautious addition of cold 1 M HCl. Any remaining phthalhydrazide was thus precipitated and removed by filtration. The filtrate was cautiously concentrated and passed through a strongly basic (IRA 400) anion exchange resin. The alkaline fractions were combined and evaporated to yield the diamine **6** as a yellow oil (6.2 g, 70%, predominantly **6** by ^{1}H NMR) which was used without further purification (^{1}H NMR in Table 4).

(2R,3R)-N,N,N′,N′-*Tetramethyl-2,3-bis(2-tosylamidoethoxy)succinamide (7)*

The diamine **6** (6.2 g, 21 mmol) was dissolved in 100 mL of water. Potassium carbonate (5.5 g, 40 mmol) and *p*-toluenesulfonyl chloride (8.0 g, 42 mmol) were added in portions at room temperature over an hour. The reaction mixture was then stirred at 50°C for a further 4 h. It was then cooled and neutralized with 1 M HCl to pH 6–7. Crushed ice was added to complete precipitation. The solid was filtered and recrystallized from aqueous methanol to yield **7** as a white solid (9.4 g, 75%) mp 82–84°C. $[\alpha]_D = +41°$ ($c = 0.98$, CH_2Cl_2); $M^{+\cdot} = 598$. Spectral data are given in Table 4. Anal. calcd. for $C_{26}H_{38}O_8S_2N_4 \cdot 2H_2O$: C 49.17, H 6.67, N 8.82, S 10.11; found: C 49.09, H 6.62, N 8.83, S 10.15.

(2R,3R,11R,12R)-N,N,N′,N′,N″,N″,N‴,N‴-*Octamethyl-1,4,10,13-tetraoxa-7,16-ditosylazacyclooctadecane-2,3,11,12-tetracarboxamide (8)*

The bis-sulfonamide **7** (5.98 g, 10 mmol) and cesium carbonate (9.8 g, 30 mmol) were mixed in 200 mL of dry DMF and stirred for 1.5 h at ambient temperature under an inert atmosphere. The ditosylate **4** (6.0 g, 10 mmol) in 100 mL of DMF was added dropwise over a period of 2 to 3 h. The mixture was stirred for a further 20 h at ambient temperature. The solvent was removed under reduced pressure to obtain a solid paste. This was suspended in 200 mL of CH_2Cl_2 and stirred for 30 min. The precipitated solids were filtered and the solvent and the residual DMF were removed by evaporation at high vacuum. The resulting solid (predominantly **8** by ^{1}H NMR) was chromatographed on neutral alumina (Brockmann III, 180 g) using CH_2Cl_2 as eluent. The crown eluted after 6 or 7 column volumes of solvent had passed through. The appropriate fractions were combined and evaporated to yield **8** as a white solid (6.7 g, 79%). This could be further purified by recrystallization from 95% methanol: mp = 194–196°C; $[\alpha]_D = +74°$ ($c = 1$, CH_2Cl_2); $M^{+\cdot} = 854$; IR (KBr) 1655 cm^{-1}. Spectral data are given in Table 4. Anal. calcd. for

Can. J. Chem. Downloaded from www.nrcresearchpress.com by 88.85.125.76 on 09/07/12
For personal use only.

TABLE 4. ^1H and ^{13}C NMR data for new compounds prepared[a,b]

Cmpd.		Me_2N	C=O	HCO	OCH_2CH_2X[c]		R	
5	^1H	2.75, 3.0	—	4.7	3.8 s		7.6–7.9 m	—
	^{13}C	35.4, 37.0	167.9, 168.7	76.1	65.6	37.7	123.1, 123.3, 132.0, 133.8	—
6	^1H	2.9, 3.2	—	4.8	2.85 A_2B_2	3.6 J = 7 Hz	NH 2.8 br	—
7	^1H	2.9, 3.1	—	4.7	3.1 A_2B_2	3.6 J = 7 Hz	Ar 7.2, 7.8 AB J = 8 Hz NH 5.8 t	CH_3 2.4
	^{13}C	35.8, 37.0	168.6	76.5	68.0	42.9	126.9, 129.5, 137.0, 143.0	21.2
8	^1H	2.9, 3.1	—	4.7	3.4 A_2B_2	3.8 J = 7 Hz	7.2, 7.8 AB J = 8 Hz	2.4
	^{13}C	35.6, 37.5	168.9	76.5	49.8	69.5	127.1, 129.7, 136.2, 143.3	21.4
10	^1H	2.9, 3.1	—	4.7	3.5 br m		7.2, 7.7 AB J = 8 Hz	2.4
	^{13}C	35.7, 37.4	169.2	76.9	69.3 70.8 49.2	70.5 49.1	127.1, 129.8, 136.7, 143.4	21.5
13	^1H	2.9, 3.15	—	4.8	3.6	2.8 m	—	—
	^{13}C	35.3, 36.8	168.9	75.7	67.8 69.8 49.1	69.5 49.0	—	—
14	^1H	2.9, 3.1	—	4.8	3.7	2.9 br	—	—
	^{13}C	35.6, 37.4	168.6	73.8	63.5	49.7	—	—
17	^1H	—	—	4.3	3.5	3.8 m	7.2, 7.8 AB J = 8 Hz	2.4
	^{13}C	—	170.8	80.6	49.5	71.9	127.1, 130.5, 138.1, 144	21.3
2.2A$_2$	^1H	—	—	4.7	3–4 br m		—	—
	^{13}C	—	172.3	78.6	65.3 69.5 46.8	65.5 46.7	—	—
2.2A$_4$	^1H	—	—	4.7	3.4 A_2B_2	3.8 J = 7 Hz	—	—
	^{13}C	—	172.6	78.9	46.7	65.8	—	—
2.2A$_2$D$_2$	^1H	—	—	4.7	3–4 br m		—	—
	^{13}C	—	168.2, 172.2	78.9	63.6 69.8 54.0	64.4 53.2	—	—
2.2A$_4$D$_2$	^1H	—	—	4.8	3.4 br 4.0 br		—	—
	^{13}C	—	170.7	78.5	65.5 46.4	53.2	—	—

[a]In $CDCl_3$ versus TMS or D_2O versus ext. TMS.
[b]—, inappropriate.
[c]X = OR, NR.

$C_{38}H_{58}O_{12}N_6S_2$: C 53.26, H 6.93, N 9.62, S 7.35; found: C 53.04, H 6.91, N 9.55, S 7.32.

*(2R,3R)-N,N,N',N'-Tetramethyl-1,4,10,13-tetraoxa-7,16-ditosyl-azacyclooctadecane-2,3-dicarboxamide (**10**)*

The preparation of **10** was identical to **8** except that the bis-sulfonamide **9** (23) was used in place of **7**. Amounts: **9**, 4.5 g (10 mmol); Cs_2CO_3, 9.75 g (30 mmol); **4**, 6.0 g (10 mmol). Yield: 5.8 g (81%); mp = 62–64°C; $[\alpha]_D$ = +46° (c = 1, CH_2Cl_2); $M^{+\cdot}$ = 712; IR (KBr) cm^{-1} 1650. Spectral data are given in Table 4. Anal. calcd. for $C_{32}H_{48}N_4S_2O_{10}$: C 53.89, H 6.79, N 7.86, S 8.99; found: C 53.71, H 6.81, N 7.54, S 9.11.

*Preparation of 1,10-ditosylaza-4,7,13,16-tetraoxacyclooctadecane (**12**)*

The bis-sulfonamide **9** (2.2 g, 4.9 mmol) was mixed with finely powdered, oven-dried K_2CO_3 (2.0 g, 14.8 mmol) in 125 mL of dry DMF under nitrogen. The mixture was heated at 50°C for 2 h. Triethylene glycol ditosylate **11** (11) (2.25 g, 4.9 mmol) in 75 mL of DMF was added dropwise over 3 h. The mixture was stirred under

Can. J. Chem. Downloaded from www.nrcresearchpress.com by 88.85.125.76 on 09/07/12
For personal use only.

nitrogen at 50°C for a further 24 h. The reaction mixture was then concentrated and the last traces of DMF removed by evaporation at high vacuum. The solid mass obtained was suspended in CH_2Cl_2 and the solids were removed by filtration. The solvent was then evaporated to afford crude **12**. This could be purified by direct crystallization, albeit with difficulty, from aqueous methanol. Yield = 1.95 g, 70%. The spectral properties were in accord with expectations, mp = 161°C; Lit. (11) mp = 163–164°C.

(2R,3R,11R,12R)-1,4,10,13-tetraoxa-7,16-ditosylazacyclooctadecane-2,3,11,12-tetracarboxylic acid (17)

The tetraamide crown **8** (4.0 g, 4.7 mmol) was dissolved in 75 mL of 50% methanol. Concentrated HCl (15 mL) was added and the solution stirred at reflux for 4 h. The reaction mixture was cooled and passed through a column of strongly acidic cation exchange resin. The acidic fractions were combined and evaporated to give a pasty solid. Recrystallization from water/methanol (4:1) afforded **17** (2.4 g, 71%). This was used without further purification. Spectral data are listed in Table 4.

(2R,3R,11R,12R)-N,N,N′,N′,N″,N″,N‴,N‴-*Octamethyl-1,4,10,13-tetraoxa-7,16-diazacyclooctadecane-2,3,11,12-tetracarboxamide (14)*

The tetraamide bis-sulfonamide crown **8** (2 g, 2.3 mmol), hydrazine hydrate (2.3 g, 46 mmol), and *p*-dimethoxybenzene (3.1 g, 23 mmol) were dissolved in 500 mL of 80% EtOH. The solution was degassed by bubbling Ar through for half an hour. The mixture was photolysed in a preparative photoreactor using a high pressure Hannovia lamp for 1.5 h. The solvent was then evaporated to dryness to obtain a yellow pasty mass. This was taken up in deionized water (100 mL) and washed with 4 × 100 mL portions of ether. The aqueous layer was then passed through a strongly basic ion exchange resin (previously activated with Me_4NOH and washed well with deionized water). The alkaline fractions were combined and evaporated. The last traces of remnant hydrazine were removed by evaporation at high vacuum. The resulting yellow oil was partly decolorized by stirring an aqueous solution with 10% Pd–charcoal followed by saturation with SO_2 gas. *p*-Toluenesulfonic acid (0.95 g, 5 mmol) was then added, followed by filtration to remove the charcoal. The aqueous filtrate was washed with ether (4 × 50 mL) and rechromatographed on a basic resin as before, to yield **14** as a light yellow brittle foam. The product had to be stored under inert atmosphere in the absence of light. Yield = 0.77 g, 60%; $M^{+\cdot}$ = 546. Spectral data are given in Table 4.

(2R,3R)-N,N,N′,N′-*Tetramethyl-1,4,10,13-tetraoxa-7,16-diazacyclooctadecane-2,3-dicarboxamide (13)*

The experimental procedure for photodeprotection of **10** to **13** was identical to the one described for the preparation of **14**. Amounts: **10**, 2.0 g (2.8 mmol); *p*-dimethoxybenzene, 3.1 g (23 mmol); hydrazine hydrate, 2.3 g (46 mmol); 80% EtOH, 500 mL; photolysis time, 1.5 h. Yield: 0.66 g, 58%. Spectral data are listed in Table 4.

(2R,3R,11R,12R)-1,4,10,13-Tetraoxa-7,16-diazacyclooctadecane-2,3,11,12-tetracarboxylic acid bis(hydrogen toluenesulfonate) (2.2A$_4$)

The tetraamide diaza crown **14** (0.55 g, 1 mmol) and *p*-toluenesulfonic acid (1.2 g, 6.3 mmol) were dissolved in 10 mL of distilled deionized water and stirred at reflux for 24 h. The water was evaporated and the residue was examined by ^{13}C NMR. The two *N*-methyl resonances of the carboxamides had collapsed into a single peak at 37 ppm, thus indicating completion of hydrolysis. The reaction mixture was then evaporated under high vacuum to a brown powder. This was dissolved in a minimum of $CHCl_3$/MeOH (1:1) and loaded onto a 5 cm by 45 cm column of LH-20 Sephadex (ca. 250 mg of compound per 100 g of Sephadex). The column was eluted with the same solvent as above and fractions (10 mL) were collected. These were examined by ^{13}C NMR. The early fractions contained the crown ether **2.2A$_4$** and these were concentrated and rechromatographed as before to yield **2.2A$_4$** (0.57 g, 74%) as its bis-toluenesulfonate salt as a light brown deliquescent solid, mp >200 (dec.); $[\alpha]_D$ = +62° (*c* = 1.0, H_2O); IR (KBr) 3500–2500 (br), 1720 cm^{-1}. Spectral data are listed in Table 4. Equivalent weight: calcd. for 4 equiv. to pH 7 end-point: 195.5 g/equiv.; found: 193.5 g/equiv.

(2R,3R)-1,4,10,13-Tetraoxa-7,16-diazacyclooctadecane-2,3-dicarboxylic acid bis(hydrogen toluenesulfonate) (2.2A$_2$)

The preparation of **2.2A$_2$** from **13** was identical to the preparation of **2.2A$_4$**. Amounts: **13**, 0.5 g (1.2 mmol); *p*-toluenesulfonic acid, 0.95 g (5 mmol). Yield: 0.64 g (77%), mp 180°C (dec.); $[\alpha]_D$ = +39° (*c* = 0.9, H_2O), IR (KBr) 3500–2600 (br), 1730 cm^{-1}. Spectral data are listed in Table 4. Equivalent weight: calcd. for 2 equivalents to a pH 7 end-point: 347 g/equiv.; found: 340.4 g/equiv.

(2R,3R)-1,4,10,13-Tetraoxa-7,16-diazacyclooctadecane-2,3-dicarboxylic acid N,N′-*diacetic acid bis(hydrogen toluenesulfonate) (2.2A$_2$D$_2$)*

Crown ether **13** (0.25 g, 0.618 mmol) was mixed in 20 mL of aqueous methanol (1:2) containing suspended Li_2CO_3 (0.275 g, 3.72 mmol). Purified bromoacetic acid (0.173 g, 1.24 mmol) was added in portions with stirring. After the CO_2 evolution had ceased, the mixture was stirred at reflux for 4 h. Examination by ^{13}C NMR showed new peaks at ca. 178 and 51 ppm. (CO and NCH_2CO_2). The CH_2—Br resonance at 20 ppm had also disappeared. The mixture was now taken up in 5 mL deionized of water and purified *p*-toluenesulfonic acid (0.71 g, 3.7 mmol) was added. A minimum amount of water was added to homogenize the mixture. This was then heated at reflux for 24 h. A ^{13}C NMR of the crude mixture revealed that the carboxamides had hydrolyzed (collapse of *N*-methyls). The desired crown ether **2.2A$_2$D$_2$** was isolated from the reaction mixture by repeated gel permeation chromatography on LH-20 Sephadex as described for the preparation of **2.2A$_2$** and **2.2A$_4$** to obtain **2.2A$_2$D$_2$** as a light yellow deliquescent solid. Yield: 0.29 g (60%); mp 195°C (dec.) $[\alpha]_D$ = +32° (*c* = 0.5, H_2O). Spectral data are listed in Table 4. Anal. calcd. for $C_{32}H_{44}O_{18}N_2S_2.2H_2O$: C 45.47, H 5.73, N 3.32; found: C 45.32, H 5.86, N 3.96. Equivalent weight: calcd. for 2 equivalents to a pH 7 end-point: 422 g/equiv.; found: 415.6 g/equiv.

(2R,3R,11R,12R)-1,4,10,13-Tetraoxa-7,16-diazacyclooctadecane-2,3,11,12-tetracarboxylic acid N,N′-*diacetic acid bis(hydrogen toluenesulfonate) (2.2A$_4$D$_2$)*

The preparation of **2.2A$_4$D$_2$** from **14** was identical to that described for **2.2A$_2$D$_2$**. Amounts: **14**, 0.2 g (0.36 mmol); bromoacetic acid, 0.10 g (1.46 mmol); Li_2CO_3, 0.17 g (2.9 mmol); *p*-toluenesulfonic acid.H_2O, 0.56 g (2.9 mmol). Yield: 0.17 g (51%); mp 188°C (dec.). Spectral data given in Table 4. Neither a satisfactory elemental analysis, nor a titrimetric equivalent weight could be obtained. All samples were contaminated with 0.5–0.8 equiv. of Li^+.

Stability constant determination

Solutions of acid (0.05 M HNO_3) and base (0.05 M tetramethylammonium hydroxide (TMAOH)) were prepared and standardized against the primary standards TRIS (tris-hydroxymethylaminomethane) for HNO_3 or potassium acid phthalate for TMAOH. A constant ionic strength was maintained (0.1 M) by the addition of tetramethylammonium nitrate (TMAN) to both the standard acid and base, as well as by using a 0.1 M TMAN medium for titrations. Standard metal ion solutions (0.05 M) were made from the corresponding nitrates. All reagents were analytical grade or better and were dried before use. Standard ligand solutions (approximately 2×10^{-2} M) were made from thoroughly evacuated samples of the ligand bis-toluenesulfonate salts. The equivalent weight was determined from the average of several titrations and was used to establish ligand homogeneity and purity before the stability constant determinations.

The general procedures and apparatus have been described previously (4, 6). The following is an abbreviated outline which incorporates some recent modifications and controls. The electrode system was calibrated using commercially available buffers at pH 2.00 and pH 9.18 and linearity was confirmed at pH 6.86 and 4.01. For pK_a determinations, a 4 mL solution of the ligand (approximately 4×10^{-4} M) in 0.1 M TMAN was titrated with standardized Me_4NOH

containing 0.1 M TMAN to beyond the strong acid – strong base end point (60 μL per ligand equivalent with 0.05 M base) in 2–4 μL aliquots (minimum 18 points per ligand equivalent). The data file was processed using SCOGS (37) to yield β_{l0h} for the ligand.

Other checks and controls were as follows:

(*a*) The carbonate content in the base was determined by a strong acid – strong base titration against standardized HNO_3 (I = 0.1 with Me_4NNO_3). The effective pK_a's of CO_3^{2-} were determined to be log β_{110} = 9.73 and log β_{111} = 16.73. These, together with the concentration of carbonate, were included in the calculations.

(*b*) Slope and intercept corrections (34) for the pH meter as discussed in the text were also used in the calculations. The slope correction was found to be very small and was ignored (i.e., s = 1) but an intercept correction of −0.23 was determined and used.

(*c*) The pK_{medium} (13.78) was determined (34) using the same strong acid – strong base curve.

(*d*) The validity of the above procedure was checked by determining pK_a and log β (Ca^{2+}) values of EDTA and EGTA. Satisfactory agreement with the literature was obtained in all cases (better than ±0.2 in log β).

For stability constant determinations, two procedures were used. One followed the procedure for pK_a determination directly, with the addition of an equivalent of metal nitrate solution to the free acid before titration with the base. The other used the solution resulting from the pK_a titration by addition of an equivalent of metal nitrate to the basic solution. This mixture was then back titrated with standardized 0.05 M HNO_3 (containing 0.1 M TMAN) to the starting acidic pH. The second method, however, is inappropriate for metals which form insoluble hydroxo complexes. Both methods gave comparable β_{lmh} values. The hydroxo complexes for the relevant metal ions were chosen from the literature (47). These values had been determined under similar conditions to the present study (nitrate salts at 25°C and I = 0.1 M). The values for the various metal ions were as follows: log β (species): 0.7 [$CaOH^+$, $SrOH^+$, $BaOH^+$]; 4.7 [$LaOH^{2+}$]; 4.3 [$NiOH^+$]; 5.7 [$CuOH^+$]; 13.1 [$Cu(OH)_2$]; 16.9 [$Cu_2(OH)_2^{2+}$]; 33.7 [$Cu_3(OH)_4^{2+}$]; 4.7 [$ZnOH^+$]; 9.86 [$Zn(OH)_2$]; 5.7 [$Zn(OH)_3^-$]; 3.8 [$CdOH^+$]; 6.9 [$PbOH^+$]; 10.8 [$Pb(OH)_2$]; 13.3 [$Pb(OH)_3^-$].

All computations utilized the program SCOGS (37) adapted for the corrections to the pH. The standard deviation in titer reported by the program was divided by the titer increment from the experiment to yield a composite goodness-of-fit parameter, r, reported in Table 1. Since all the titrations were done under closely similar conditions, r reflects the quality of the modeling done by SCOGS. The reliability of the values, assessed from reproducibility between duplicate solution preparations from salts is ±0.1 in pK_a and ±0.2 in log β. Computations of species distribution as a function of pH was done using the algorithm COMPLEX (48) adapted for use on a microcomputer.

Acknowledgements

The continuing support of the University of Victoria and the Natural Sciences and Engineering Research Council of Canada is gratefully acknowledged.

1. J. M. LEHN. Struct. Bonding, **16**, 1 (1973).
2. B. DIETRICH. *In* Inclusion compounds. Vol. 2. *Edited by* J. L. Atwood, J. E. D. Davies, and D. D. MacNichol. Academic Press, London. 1984. Chap. 10. p. 337.
3. N. F. CURTIS. *In* Coordination chemistry of macrocyclic compounds. *Edited by* G. A. Melson. Plenum Press, New York. 1979. p. 219.
4. L. A. FREDERICH, T. M. FYLES, N. P. GURPRASAD, and D. M. WHITFIELD. Can. J. Chem. **59**, 1724 (1981).
5. J. P. BEHR, J. M. GIRODEAU, R. C. HAYWARD, J. M. LEHN, and J. P. SAUVAGE. Helv. Chim. Acta, **63**, 2096 (1980).
6. P. J. DUTTON, T. M. FYLES, and S. A. MCDERMID. Can. J. Chem. **66**, 1097 (1988).
7. A. ANANTANARAYAN, P. J. DUTTON, T. M. FYLES, and M. J. PITRE. J. Org. Chem. **51**, 752 (1986).
8. G. W. GOKEL, D. M. DISHONG, R. A. SCHULTZ, and V. J. GATTO. Synthesis, 997 (1982).
9. K. E. KRAKOWIAK, J. S. BRADSHAW, and D. J. ZAMECKA-KRAKOWIAK. Chem. Rev. **89**, 929 (1989).
10. B. DIETRICH, J. M. LEHN, and J. P. SAUVAGE. Tetrahedron, **29**, 1647 (1973).
11. J. E. RICHMAN and T. J. ATKINS. J. Am. Chem. Soc. **96**, 2268 (1974).
12. J. BUTER and R. M. KELLOGG. J. Org. Chem. **46**, 4481 (1981).
13. B. K. VRIESEMA, J. BUTER, and R. M. KELLOGG. J. Org. Chem. **49**, 110 (1984).
14. G. DIJKSTRA, W. H. KRUIZINGA, and R. M. KELLOGG. J. Org. Chem. **52**, 4230 (1987).
15. F. CHAVEZ and A. D. SHERRY. J. Org. Chem. **54**, 2990 (1989).
16. A. E. MARTELL and R. M. SMITH. Critical stability constants. Vol. 1. Plenum Press, New York. 1974. p. 204.
17. G. SCHWARZENBACH, A. WILLI, and R. O. BACH. Helv. Chim. Acta, **30**, 1303 (1947); R. SMITH, J. L. BULLOCK, F. C. BERSWORTH, and A. E. MARTELL. J. Org. Chem. **14**, 355 (1949); F. P. DWYER and F. C. GARVIN. J. Am. Chem. Soc. **81**, 2955 (1959).
18. T. UECHI, I. UEDA, M. TAZAKI, M. TAKAGI, and K. UENO. Acta Crystallogr. Sect. B, **B38**, 433 (1982).
19. P. GLUZINSKI, J. W. KRAJEWSKI, and Z. URBANCZYK-LIPOWSKA. Cryst. Struct. Commun. **11**, 1589 (1982).
20. P. GLUZINSKI, J. W. KRAJEWSKI, Z. URBANCZYK-LIPOWSKA, G. D. ANDREETTI, and G. BOCELLI. Acta Crystallogr. **C40**, 778 (1984).
21. F. BOTTINO, M. DI GRAZIA, P. FINOCCHIARO, F. R. FRONCZEK, A. MAMO, and S. PAPPALARDO. J. Org. Chem. **53**, 3521 (1988).
22. W. GAUSS, P. MOSER, and G. SCHWARZENBACH. Helv. Chim. Acta, **35**, 2359 (1952); A. E. MARTIN, T. M. FORD, and J. E. BULKOWSKI. J. Org. Chem. **47**, 412 (1982).
23. W. P. REEVES and M. L. BAHR. Synthesis, 823 (1970).
24. E. HASKELL and S. P. BOWLUS. J. Org. Chem. **41**, 159 (1976).
25. E. BUHLEIER, W. RASSHOFER, W. WEHNER, F. LUPPERTZ, and F. VÖGTLE. Justus Liebegs Ann. Chem. 1344 (1977).
26. B. M. TROST, H. C. ARNDT, P. E. STREGE, and T. R. VERHOEVEN. Tetrahedron Lett. 3477 (1976).
27. D. MELLIER, J. P. PETE, and C. PORTELLA. Tetrahedron Lett. 4559 (1971).
28. T. HAMADA, A. NISHIDA, and O. YONEMITSU. J. Am. Chem. Soc. **108**, 140 (1986).
29. S. KULSTAD and L. A. MALMSTEN. Acta Chem. Scand. Sect. B, **33**, 469 (1979).
30. W. A. E. MCBRYDE. Analyst, **94**, 337 (1969).
31. W. A. E. MCBRYDE. Analyst, **96**, 739 (1971).
32. G. R. HEDWIG and H. K. J. POWELL. Anal. Chem. **43**, 1206 (1971).
33. A. AVDEEF and J. J. BUCHER. Anal. Chem. **50**, 2137 (1978).
34. R. F. JAMESON and M. F. WILSON. J. Chem. Soc. 2607 (1972).
35. W. J. HAMER and Y.-C. WU. J. Phys. Chem. Ref. Data, **1**, 1047 (1972).
36. P. C. MEIER. Anal. Chim. Acta, **236**, 363 (1982).
37. I. G. SAYCE. Talanta, **15**, 197 (1968); **18**, 653 (1971).
38. P. J. DUTTON, F. R. FRONCZEK, T. M. FYLES, R. D. GANDOUR, and V. V. SURESH. To be published.
39. R. J. ADAMIC, E. M. EYRING, S. PETRUCCI, and R. A. BARTSCH. J. Phys. Chem. **89**, 3752 (1985).
40. A. EVERS, R. D. HANCOCK, A. E. MARTELL, and R. J. MOTEKAITIS. Inorg. Chem. **28**, 2189 (1989).
41. V. J. THOM, M. S. SHAIKJEE, and R. D. HANCOCK. Inorg. Chem. **25**, 2992 (1986).
42. R. D. HANCOCK. Pure Appl. Chem. **58**, 1445 (1986).
43. R. D. HANCOCK and F. MARSICANO. J. Chem. Soc. Dalton, 1096 (1976).
44. R. D. HANCOCK and G. J. MCDOUGALL. J. Coord. Chem. **6**, 163 (1977).

Can. J. Chem. Downloaded from www.nrcresearchpress.com by 88.85.125.76 on 09/07/12
For personal use only.

45. F. MULLA, F. MARSICANO, B. S. NAKANI, and R. D. HANCOCK. Inorg. Chem. **24**, 3076 (1985).
46. E. NIEBOER and W. A. E. MCBRYDE. Can. J. Chem. **51**, 2512 (1973).
47. L. G. SILLEN and A. E. MARTELL. Stability constants of metal ion complexes. Chem. Soc. Special Publication, No. 17 (1964); No. 24 (1971).
48. G. GINZBURG. Talanta, **23**, 149 (1976).
49. G. ANDEREGG. Helv. Chim. Acta, **58**, 1218 (1975).
50. M. KODAMA and E. KIMURA. Bull. Chem. Soc. Jpn. **49**, 2465 (1976).
51. F. ARNAUD-NEU, B. SPIESS, and M. J. SCHWING-WEILL. Helv. Chim. Acta, **60**, 2633 (1977).
52. C. A. CHANG and M. E. ROWLAND. Inorg. Chem. **22**, 3866 (1983).
53. G. ANDEREGG. Helv. Chim. Acta, **47**, 1801 (1964).
54. B. DIETRICH. Thèse de Doctorat, Université Louis Pasteur. 1973.
55. H. K. FRENSDORF. J. Am. Chem. Soc. **93**, 600 (1971).
56. G. ANDEREGG. Helv. Chim. Acta, **64**, 1790 (1981).

Can. J. Chem. Downloaded from www.nrcresearchpress.com by 88.85.125.76 on 09/07/12
For personal use only.

The crystal structure and thermal expansion of the CCl_4 adduct of Dianin's compound

WALTER ABRIEL[1] AND ANDRÉ DU BOIS
Institut für Anorganische Chemie and SFB 173 der Universität, Callinstr. 9, D-3000 Hannover, Federal Republic of Germany
AND
MAREK ZAKRZEWSKI AND MARY ANNE WHITE[2]
Department of Chemistry, Dalhousie University, Halifax, N.S., Canada B3H 4J3

Received August 16, 1989[3]

WALTER ABRIEL, ANDRÉ DU BOIS, MAREK ZAKRZEWSKI, and MARY ANNE WHITE. Can. J. Chem. **68**, 1352 (1990).

The crystal structure of the title compound has been determined by single crystal X-ray diffraction data collected at 293 K, and refined to a final R_w of 0.057. The crystals are rhombohedral, space group $R\bar{3}$, with a = 27.134(8) Å, c = 10.933(2) Å, and Z = 18. The mole ratio of Dianin's compound (4-*p*-hydroxyphenyl-2,2,4-trimethylchroman) to CCl_4 is 6:1. The guest molecules are disordered. X-ray powder diffraction was carried out in the temperature range from 10 to 300 K. From this, the thermal expansion coefficients for the ***a***- and ***c***-axes and the volume have been determined.

Key words: thermal expansion, crystal structure, clathrate.

WALTER ABRIEL, ANDRÉ DU BOIS, MAREK ZAKRZEWSKI et MARY ANNE WHITE. Can. J. Chem. **68**, 1352 (1990).

La structure cristalline du composé mentionné dans le titre a été déterminée par diffraction des rayons-X sur un cristal unique, à l'aide données recueillies à 293 K et affinées jusqu'à une valeur finale de R_w de 0,057. Les cristaux sont rhomboédriques, groupe d'espace $R\bar{3}$ avec a = 27,134(8) et c = 10,933(2) Å et Z = 18. Le rapport molaire entre le composé de Dianin (4-*p*-hydroxyphényl-2,2,4-triméthylchromane) et le CCl_4 est de 6 : 1. Les molécules hôtes sont désordonnées. La diffraction des rayons-X sur les poudres a été réalisée à des températures allant de 10 à 300 K. A partir de ces données, on a pu déterminer les coefficients d'expansion thermique pour les axes ***a*** et ***c*** ainsi que pour le volume.

Mots clés : coefficients d'expansion thermique, structure cristalline, clathrate.

[Traduit par la revue]

Introduction

4-*p*-Hydroxyphenyl-2,2,4-trimethylchroman, **1**, also known as Dianin's compound (1), forms clathrates by crystallization with many solvents (2, 3). In all reported adducts, it crystallizes in the space group $R\bar{3}$ (4, 5). The general structure of the host lattice consists of the hexamers of **1**, held together by a ring of hydrogen bonds involving the phenolic hydroxy groups. The monomeric units of the hexamers alternately point up and down from this ring, and groups of hexamers form chains of hourglass shaped cages. The upper half of each cage consists of three molecules of **1** from one hexamer, and the lower half is three molecules of **1** from another hexamer. The cage is held together at the roof and floor by the hydrogen-bond network, and at the waist by van der Waals forces between the molecules. The cages are quite large, free volume about 180 Å^3, and can accommodate even bulky molecules (2).

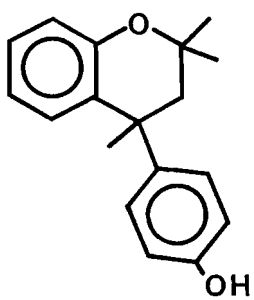

1

Clathrates can be used to investigate many interesting properties of matter, and one of the purposes of our ongoing clathrate studies is to examine the effect of guest molecules on the properties of the host lattice. The Dianin clathrate system is particularly interesting because it has the rare feature of a stable empty host lattice (5). The structure of the CCl_4 clathrate has not been reported previously, and knowledge of the structure, and particularly the guest occupancy, was required for the analysis of our recent calorimetric results (6). We are also interested in the effect of the number and type of guests in the host lattice on the cavity itself. We report here the structure of the CCl_4 adduct of **1**, as determined by single crystal X-ray diffraction at T = 293 K.

The effect of anharmonic interactions within clathrates has been proposed as the origin of the unusual thermal conductivities of clathrate hydrates (7) and in order to test the generality of this effect in other clathrates, we have recently measured the thermal conductivities (White and Zakrzewski, unpublished results) and thermal expansion of the empty and ethanol adducts of Dianin's compound. For comparison, we report here the thermal expansion coefficients for all significant lattice parameters for the CCl_4 adduct of Dianin's compound, based on X-ray powder diffraction determinations of the lattice parameters in the temperature range from 10 to 300 K.

Experimental

Dianin's compound (**1**) was prepared from phenol and mesityl oxide according to the method of Baker *et al.* (2), and isolated as the ethanol adduct. This was converted to the unsolvated form of **1** by bubbling CO_2 gas through a basic solution of the ethanol adduct in H_2O (2). The resultant white powder was dissolved in carbon tetrachloride to produce the CCl_4 adduct of **1** (2). Single crystals were obtained by slow evaporation; samples for the X-ray powder diffraction were obtained by rapid recrystallization. The observed melting point was 159–160°C, in agreement with the literature value (2). Chemical analysis gave the following composition in mass % (theoretical composition for host to

[1]Present address: Institut für Anorganische Chemie, P.O. Box 397, Universität Regensburg, Federal Republic of Germany.
[2]Author to whom correspondence should be addressed. Telephone: 902/424-3894, BITNET: MAWHITE@AC.DAL.CA.
[3]Revision received March 14, 1990.

Printed in Canada / Imprimé au Canada

Can. J. Chem. Downloaded from www.nrcresearchpress.com by 88.85.125.76 on 09/07/12
For personal use only.

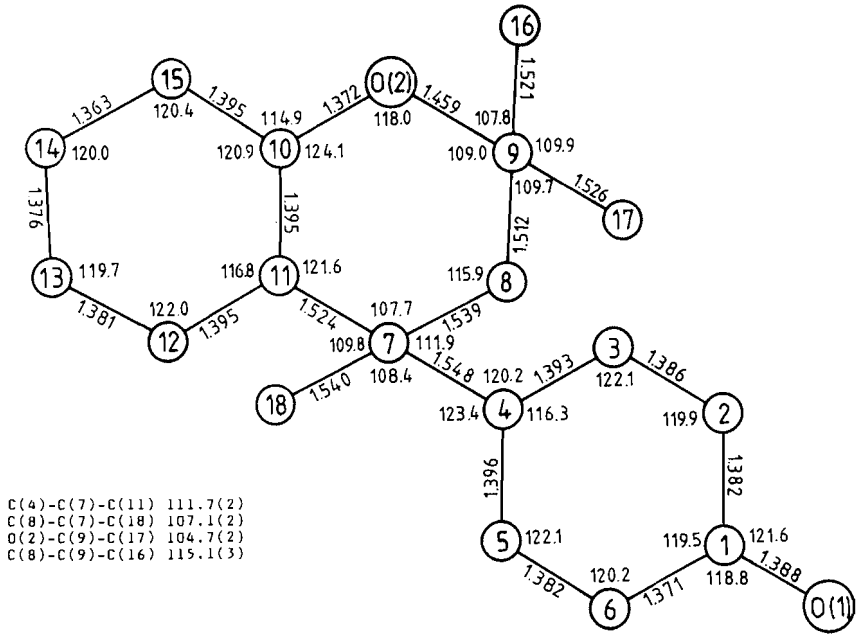

FIG. 1. Bond distances (Å) and angles (deg) for 4-*p*-hydroxyphenyl-2,2,4-trimethylchroman. The hydrogens are not shown.

guest ratio of 6:1 given in parentheses): C, 73.45 ± 0.2 (74.2); H, 7.1 ± 0.1 (6.86); Cl, 9.5 ± 0.1 (8.04). The errors quoted are precisions not accuracies.

Weissenberg photographs (CuKα) of a needle-shaped crystal showed Laue symmetry $\bar{3}$ with systematically absent reflections indicating a rhombohedral lattice. The crystal faces were: (2$\bar{1}$0), ($\bar{2}$10), (1$\bar{2}$0), ($\bar{1}$20), (110), ($\bar{1}\bar{1}$0), {001}. The crystal volume was 4.8×10^{-2} mm^3 with diameter of 0.68 mm in [001]. The X-ray data collection at 293 K was performed with a SIEMENS AED2 diffractometer using graphite monochromatized MoKα radiation. Accurate cell parameters from 33 reflections in the θ range 7.3 to 21.5° gave a = 27.134(8) Å, c = 10.933(2) Å. Intensity data collection: maximum $\sin\theta/\lambda = 0.704$ Å^{-1}; range of hkl 35, $\bar{1}$8, 0 to 35, 38, 15 in the ω-scan mode (minimum scan angle 1.2°, scan time maximum 36 s). Reflections $\bar{5}$55, 555, and $\bar{6}$82 were used for standard intensity measurements; intensity variation was less than 1%. 8374 measured reflections yielded 4259 unique reflections (R_{int} = 0.064); 2498 reflections with $F > 3\sigma(F)$ were regarded as observed. Numerical absorption correction (μ = 1.5 cm^{-1}) was applied with a min./max. transmission of 0.96/0.97.

X-ray powder diffraction experiments in the temperature range from 10 to 300 K were performed with a recently developed Guinier-diffractometer using Ge-monochromatized CuKα_1 radiation. A detailed description of the set up is given elsewhere (8). The powder sample was sieved to use the particles less than 50 μm in size. This procedure was chosen because grinding larger crystals produced structural defects and decomposition, as shown by the high background scattering and line broadening in the diffraction diagram. The diffractograms were recorded with a step width of 0.01° and a counter time of 4 s per step in the range $4° < \theta < 24°$.

Results[4]

Single crystal diffraction

The structural calculations were carried out in the space group $R\bar{3}$ (#148), *i.e.* that found by Flippen *et al.* (4) for other clathrates of Dianin's compounds, starting with refinement of the atomic parameters of the host structure. A subsequent ΔF synthesis yielded the positions of the CCl_4 guest molecules.

The refinement of the site occupancy factors for the atoms of the guest CCl_4 molecules yielded the values 0.514(9) for C(19), 0.983(5) for Cl(1), and 0.489(2) for Cl(2), indicating a 6:1 ratio of host-to-guest species. This contradicts the results of ref. 2 in which it is stated that two CCl_4 molecules occupy each cage. However, the theoretical atomic composition is also given incorrectly in ref. 2, and a 6:1 ratio is much closer to what one would expect on the basis of the chemical analysis of our sample (*e.g.* the theoretical mass % of Cl would be 8.04 for 6:1). Furthermore, we have measured the densities of single crystals of our sample using a calibrated pycnometer and found ρ = 1.262 ± 0.005 g cm^{-3} at T = 296 K. Using the lattice constants and thermal expansion determined here (*vide infra*), this gives a ratio of host-to-guest molecules of (5.94 ± 0.05):1.

For the final refinement of all structural parameters (on F) the site occupancy parameters for CCl_4 were fixed with the values 1.0 and 0.5 for Cl(1) and Cl(2), respectively. The hydrogen atoms were refined with geometrical constraints together with the adjacent C or O atom. The final refinement's results are R = 0.084, $R_w = \Sigma\Delta F\sqrt{W}/\Sigma F_o\sqrt{W}$ = 0.057 (with $W = 1/\sigma^2(F)$), S(GOF) = 3.92, maximum shift/esd 0.001 in the last cycle of refinement (195 parameters), $0.14 \geq \Delta \geq -0.2$ e/Å^3 from final ΔF synthesis. Neutral atom scattering factors were taken from International tables (9). The program used was STRUCSY from the diffractometer software package. A complete listing of the refined structural parameters is given in Table 1.

For the structure of the host compound, the previously reported atomic positions (4) were confirmed with only small deviations of the bond geometry (see Fig. 1).

The CCl_4 guest molecule is two-fold disordered in the cage (Fig. 2). The atom Cl(1) occupies the centre of the waist in the cage, consequently this position belongs to both guest molecules with a site occupancy factor of 100%. The CCl_4 molecule is almost a regular tetrahedron with the following bond distances (not corrected for libration) and bond angles: C(19)—Cl(1), 1.67(1) Å; C(19)—Cl(2), 1.702(4) Å; Cl(1)—C(19)—Cl(2), 108.5(1)°; and Cl(2)—C(19)—Cl(2), 110.5(2)°. We assumed

[4]A complete list of observed structure factors, anisotropic displacement parameters, the experimental lattice parameters (a, c, V) for the range from 10 to 300 K, coefficients of polynomials describing the temperature variation of the lattice parameters may be purchased from the Depository of Unpublished Data, CISTI, National Research Council of Canada, Ottawa, Ont., Canada K1A 0S2.

Can. J. Chem. Downloaded from www.nrcresearchpress.com by 88.85.125.76 on 09/07/12
For personal use only.

TABLE 1. Fractional atomic coordinates ($\times 10^4$) and equivalent isotropic displacement factors ($Å^2 \times 10^4$) estimated as 1/3 trace of the orthogonalized matrix U (definition in ref. 12).

Atom	Site	x	y	z	U_{eq}
O(1)	18f	651(1)	1202(1)	9815(2)	447
H(O)	18f	829(1)	918(1)	9927(2)	492
O(2)	18f	871(1)	2621(1)	3740(2)	374
C(1)	18f	888(1)	1617(1)	8915(2)	332
C(2)	18f	1401(1)	1757(1)	8368(2)	366
H(2)	18f	1602(1)	1570(1)	8634(2)	403
C(3)	18f	1615(1)	2163(1)	7447(2)	322
H(3)	18f	1973(1)	2260(1)	7076(1)	354
C(4)	18f	1328(1)	2437(1)	7042(2)	266
C(5)	18f	817(1)	2292(1)	7636(2)	304
H(5)	18f	615(1)	2483(1)	7401(2)	334
C(6)	18f	602(1)	1890(1)	8557(2)	323
H(6)	18f	248(1)	1795(1)	8948(2)	356
C(7)	18f	1574(1)	2874(1)	5984(2)	278
C(8)	18f	1645(1)	2607(1)	4804(2)	296
H(81)	18f	1924(1)	2904(1)	4295(2)	325
H(82)	18f	1779(1)	2353(1)	5035(2)	325
C(9)	18f	1111(1)	2262(1)	4057(2)	296
C(10)	18f	874(1)	2984(1)	4616(2)	318
C(11)	18f	1196(1)	3125(1)	5688(2)	287
C(12)	18f	1171(1)	3523(1)	6456(2)	349
H(12)	18f	1392(1)	3628(1)	7195(2)	384
C(13)	18f	837(1)	3760(1)	6189(3)	410
H(13)	18f	832(1)	4032(1)	6740(3)	451
C(14)	18f	521(1)	3608(1)	5129(3)	429
H(14)	18f	287(1)	3773(1)	4948(3)	472
C(15)	18f	539(1)	3227(1)	4347(3)	378
H(15)	18f	318(1)	3119(1)	3609(3)	415
C(16)	18f	648(1)	1731(1)	4685(3)	400
H(161)	18f	796(1)	1487(1)	4902(3)	441
H(162)	18f	521(1)	1835(1)	5408(3)	441
H(163)	18f	335(1)	1535(1)	4130(3)	441
C(17)	18f	1263(1)	2103(1)	2833(2)	419
H(171)	18f	1421(1)	1860(1)	2967(2)	461
H(172)	18f	927(1)	1907(1)	2341(2)	461
H(173)	18f	1537(1)	2442(1)	2418(2)	461
C(18)	18f	2170(1)	3352(1)	6360(3)	391
H(181)	18f	2335(1)	3629(1)	5718(3)	430
H(182)	18f	2137(1)	3532(1)	7087(3)	430
H(183)	18f	2409(1)	3192(1)	6522(3)	430
C(19)*	6c	0	0	3469(9)	400
Cl(1)	3b	0	0	5000	856
Cl(2)*	18f	658(1)	499(1)	2976(2)	934

*Site occupancy factor = 1/2.

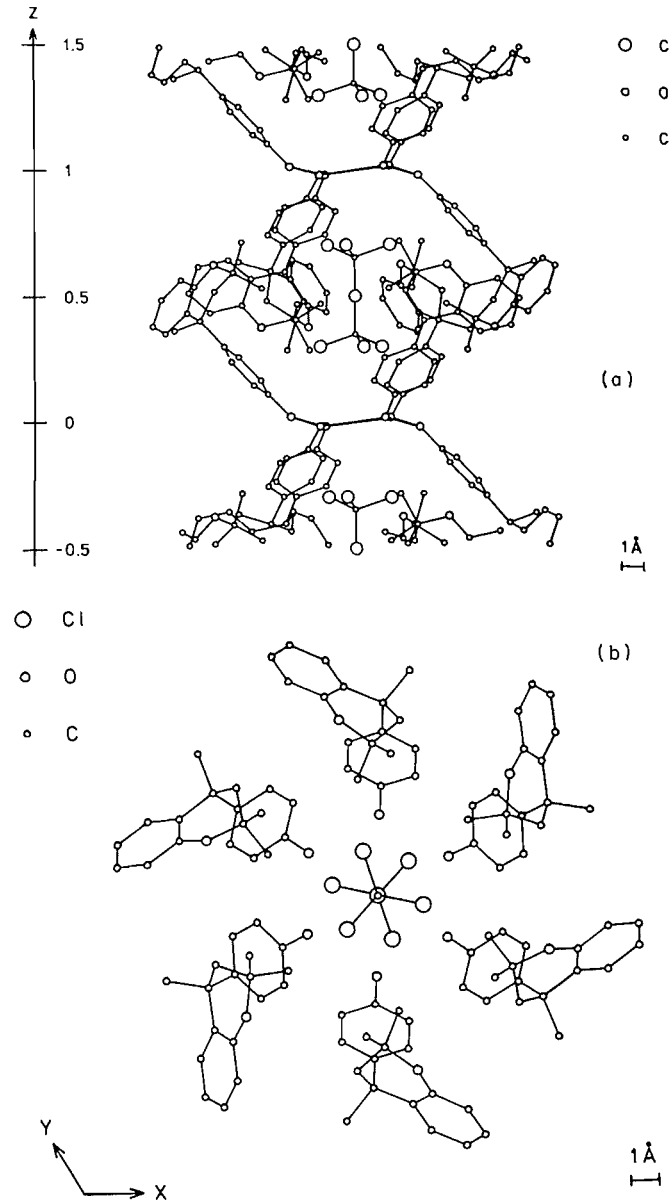

FIG. 2. The crystal structure of the CCl_4 adduct of Dianin's compound (plot program SCHAKAL (10)): (*a*) the stacking of the host lattice along the *c* axis; two cages per translation unit contain one CCl_4 molecule, (*b*) the crystal structure viewed along [001].

that the rigid CCl_4 molecule is librating about its centre of mass, and checked this model by calculating a generalized R-index for the agreement of observed and calculated U_{ij} (11). With the anisotropic displacement parameters from our structure determination we calculated for CCl_4 an R-factor of 0.058, indicating consistency of the model. The angular displacement of the libration is shown by the librational tensor L, where the values given are in degrees^2 for orthogonal axes:

$$\Lambda = \begin{vmatrix} 51.8 & 0 & 0 \\ 0 & 51.8 & 0 \\ 0 & 0 & 113.6 \end{vmatrix}$$

and the centre of gravity for the librational movement is at 0.0004, 0.0005, 0.3401 according to the T tensor (in Å^2):

$$T = \begin{vmatrix} 0.0379 & 0.0 & 0.0 \\ 0.0 & 0.0379 & -0.0002 \\ 0.0 & -0.0002 & 0.0690 \end{vmatrix}$$

The closest host–guest distances found were Cl(1)—H(163) (H(163) bonded to C(16)), 3.91 Å; Cl(2)—H(161) (H(161) bonded to C(16)), 3.09 Å; Cl(2)—C(1), 3.13 Å.

Powder diffraction

The lattice parameters were determined by least-squares fit to the 11 most intense reflections unambiguously assignable. As no change of symmetry occurred down to 10 K the space group $R\bar{3}$ was assumed for all diagrams.

The unit cell dimensions along the ***a*** and ***c*** axes, and the unit cell volume are shown in Fig. 3 as functions of temperature.

Can. J. Chem. Downloaded from www.nrcresearchpress.com by 88.85.125.76 on 09/07/12
For personal use only.

Can. J. Chem. Downloaded from www.nrcresearchpress.com by 88.85.125.76 on 09/07/12
For personal use only.

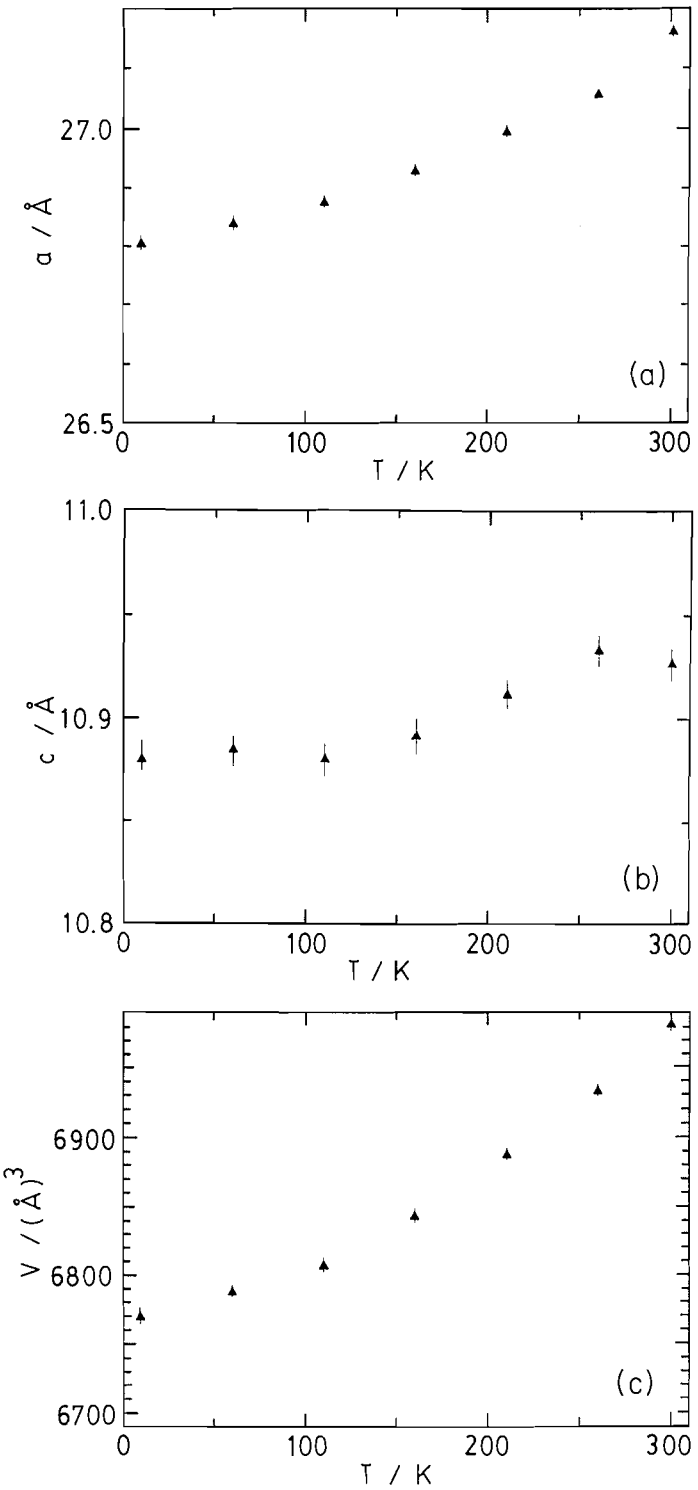

FIG. 3. Lattice parameters and unit cell volume of the CCl_4 adduct of Dianin's compound as a function of temperature: (*a*) along the ***a*** axis, (*b*) along the ***c*** axis, (*c*) unit cell volume.

Interpolation of the powder data to $T = 293$ K gives lattice parameters $a = 27.143(9)$ Å, $c = 10.928(8)$ Å in excellent agreement with those from the single crystal work, $a = 27.134(8)$ Å, $c = 10.933(2)$ Å.

Discussion

From the crystallographic results we find that the CCl_4 guest molecules are librating in the cage. The librational tensor (*vide supra*) reveals that the guest molecule is experiencing root-mean-squared amplitudes of vibration of 10.7° with respect to the ***c***-axis, and 7.2° with respect to two orthogonal axes in the ***ab*** plane. Using the method of Cruickshank (13), and moments of inertia corresponding to our determination of the bond lengths and angles ($I_x = I_y = 4.457 \times 10^{-38}$ g cm^2, $I_z = 4.601 \times 10^{-38}$ g cm^2), we determine the average librational frequencies of the CCl_4 molecules to be 40 cm^{-1} about the ***x*** and ***y*** axes, and 27 cm^{-1} about the *z* axis. From ^{35}Cl NQR studies of CCl_4 in ***1***, these librational frequencies have been determined to be 47 and 37 cm^{-1}, respectively (14).

Throughout the temperature range from 10 to 300 K the CCl_4 guest causes an increase in *a* of about 0.6%, and insignificant change in *c*, in comparison with the lattice parameters (15) for the empty host lattice. This can be contrasted with the ethanol adduct (15) in which the presence of the guest decreases *a* at low temperatures, but increases it above about 200 K. In the ethanol adduct, *c* is increased by about 0.5% at all temperatures. One of the differences between the CCl_4 adduct and the ethanol adduct is that the latter has a dimer guest in the cage. As we have shown with the single crystal work here, CCl_4 has only one guest per cage. The lack of expansion along the ***c*** axis in the CCl_4 adduct, relative to the expansion caused by the ethanol guest dimer, may be due to "free" space in the unoccupied half of the cage of the host lattice in the CCl_4 adduct.

The Dianin host lattice is, as stated above, held together predominantly by hydrogen bonds. In the region of the ring of hydrogen-bonded phenolic groups, we find the O····O distance in the CCl_4 adduct of **1** to be 2.857(3) Å, which is very similar to that found in the ethanol adduct of **1**, 2.85(1) Å (4). This is a longer distance than is found in the CCl_4 adduct of 4-*p*-hydroxyphenyl-2,4-dimethylchroman, 2.77 Å (16), which shows the appreciable role of the second methyl group at carbon-2 in **1**. In general, O····O bond distances in hydrogen-bonded systems such as ices, hydrates, and hydroxy compounds range from 2.7 to 2.9 Å (16); we are at the upper end of this range. Although we are unable to determine the true position of the hydrogen in this hydrogen bond, we expect that it will be unsymmetric with respect to the neighbouring oxygens, and possibly dynamically disordered at room temperature. This effect has been observed recently by solid state ^{2}H nmr (17).

We now turn our attention to the coefficients of thermal expansion, α_i ($= i^{-1}\, \mathrm{d}i/\mathrm{d}T$, $i = a, c, V$) for the CCl_4 adduct of **1**. These were calculated from polynomials fit to the appropriate lattice constant data. The thermal expansions, α_a and α_V, are shown in Fig. 4; the points shown were calculated directly from lattice parameter changes at neighbouring temperatures. The thermal expansion along the ***c*** axis, α_c, is given in Table 2.

The overall thermal expansion, α_V, is positive throughout the investigated temperature range, as is α_a. The thermal expansion along the ***c*** axis is very small especially at low temperatures; this was noticed also for the unsolvated Dianin's compound and the ethanol adduct.

In comparison with the empty host lattice, α_a is larger for the CCl_4 adduct only for $T < 100$ K and $T > 200$ K; in the intermediate temperature region α_a is essentially the same with and without the CCl_4 guest. The thermal expansion along ***c*** is virtually unchanged by the presence of the CCl_4 guest. Since α_V is dominated by α_a ($\alpha_V = 2\alpha_a + \alpha_c$), it shows the same trends as α_a with respect to the presence of the CCl_4 guest. α_a and α_V for the CCl_4 adduct of **1** are smaller than for the ethanol adduct

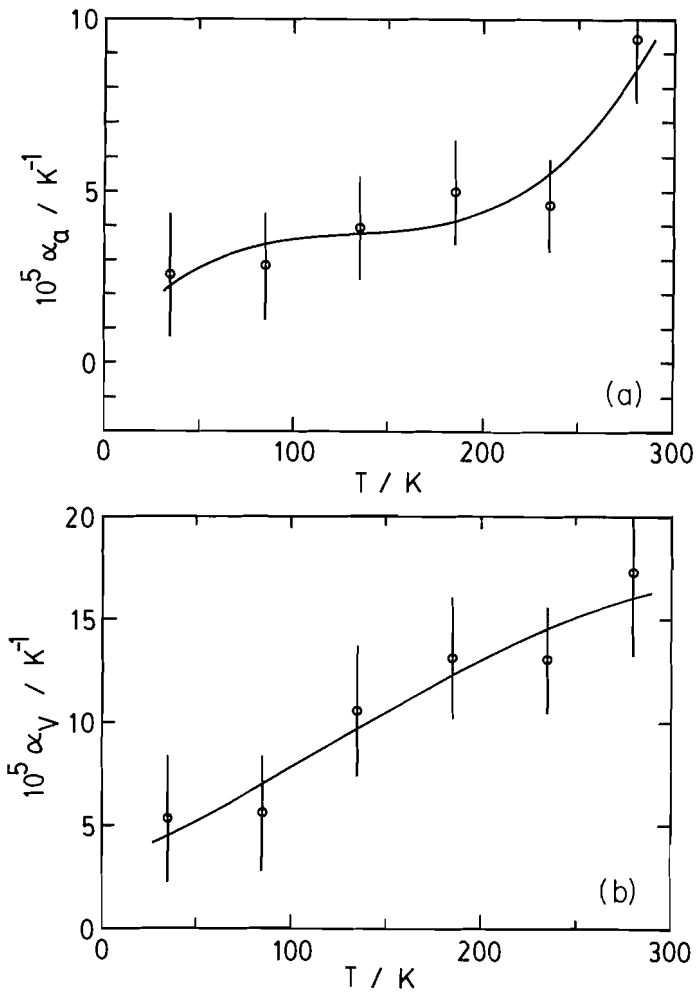

FIG. 4. Thermal expansion coefficient of CCl_4 adduct of Dianin's compound as a function of temperature: (*a*) along the ***a*** axis, (*b*) for the unit cell volume.

throughout the temperature region examined, *i.e.* the CCl_4 adduct is intermediate in thermal expansion between the empty host lattice and the ethanol adduct.

The origin of the unusual thermal conductivities of some clathrates has been attributed to the interactions of the low-frequency optic modes of the guest molecules with the acoustic modes of the host lattice (7). These interactions are due to anharmonicity in the interaction potential, and they should be manifest in other physical properties such as increased thermal expansion. We have recently shown (White and Zakrzewski, unpublished results) that the thermal expansion correlates with the thermal conductivity of the empty and ethanol adducts of Dianin's compound as one would expect for this model. A further test of the importance of guest–host interactions will be the measurement of the thermal conductivity of the CCl_4 adduct of **1**; if this hypothesis is correct, the intermediate thermal expansion of the CCl_4 adduct shoud lead to a thermal resistivity higher than that of the empty clathrate and lower than that of the ethanol adduct.

TABLE 2. Thermal expansion along the ***c*** axis, α_c, for the CCl_4 adduct of Dianin's compound

T/K	$10^5\ \alpha_c/K^{-1}$
50	0.7±0.5
100	1.2±0.5
150	1.8±0.8
200	2.3±0.8
250	2.8±0.8
300	3.3±0.8

Acknowledgements

Financial support by the Deutsche Forschungsgemeinschaft (to W.A.), the Fonds der Chemischen Industrie (to W.A.), NATO (to M.A.W. and W.A.), and the Natural Sciences and Engineering Research Council of Canada (to M.A.W.) is gratefully acknowledged. We also thank Professor R. J .C. Brown for a useful discussion and one of the referees for helpful comments concerning librational analysis.

1. A. P. DIANIN. J. Rus. Phys.-Chem. Soc. **46**, 1310 (1914).
2. W. BAKER, A. J. FLOYD, J. W. F. MCOMIE, G. POPE, A. S. WEAVING, and J. H. WILD. J. Chem. Soc. 2010 (1956).
3. A. GOLDUP and G. W. SMITH. Sep. Sci. **6**, 791 (1971).
4. J. L. FLIPPEN, J. KARLE, and I. L. KARLE. J. Am. Chem. Soc. **92**, 3749 (1970).
5. D. D. MACNICOL. *In* Inclusion compounds. Vol. 2. *Edited by* J. L. Atwood, J. E. D. Davies, and D. D. MacNicol. Academic Press, London. 1984. Chap. 1.
6. M. A. WHITE and M. ZAKRZEWSKI, J. Incl. Phen. Mol. Recog. Chem. **8**, 215 (1990).
7. J. S. TSE and M. A. WHITE. J. Phys. Chem. **92**, 5006 (1988).
8. W. ABRIEL and U. BISMAYER. Phase Transitions **15**, 49 (1989).
9. International tables for X-ray crystallography. Vol. IV. Kynoch Press, Birmingham. 1974.
10. E. KELLER. Chem. Unserer Zeit, **14**, 56 (1980).
11. B. T. M. WILLIS and A. W. PRYOR. Thermal vibrations in crystallography. Cambridge University Press, London. 1975.
12. R. X. FISCHER and E. TILLMANNS. Acta Crystallogr. C**44**, 775 (1988).
13. D. W. J. CRUICKSHANK. Rev. Mod. Phys. **30**, 163 (1958).
14. L. PANG and E. A. C. LUCKEN. J. Incl. Phenom. **5**, 245 (1987).
15. M. ZAKRZEWSKI, M. A. WHITE, and W. ABRIEL. J. Phys. Chem. **94**, 2203 (1990).
16. A. F. WELLS. Structural inorganic chemistry. 5th ed. Oxford University Press, Oxford. 1984.
17. T. BERNHARD, H. ZIMMERMANN, and H. HAEBERLEN. J. Chem. Phys. **92**, 2178 (1990).

Can. J. Chem. Downloaded from www.nrcresearchpress.com by 88.85.125.76 on 09/07/12
For personal use only.

X-ray structural and nuclear magnetic resonance study of open chain and macrocyclic thioether complexes[1]

C. Robert Lucas,[2] Shuang Liu, and Michael J. Newlands
Department of Chemistry, Memorial University of Newfoundland, St. John's, Nfld., Canada A1B 3X7

and

Eric J. Gabe
Division of Chemistry, National Research Council of Canada, Ottawa, Ont., Canada K1A 0R9

Received December 14, 1989

C. Robert Lucas, Shuang Liu, Michael J. Newlands, and Eric J. Gabe. Can. J. Chem. **68**, 1357 (1990).

Preparations of the thiophenophane and open chain thioether complexes $MX_2 \cdot$BBTE (M = Pd; X = Cl, I) (M = Pt; X = Cl) (BBTE = 1,2-bis(benzylthio)ethane) and $MX_2 \cdot$L (M = Pd; X = Cl, Br, I, SCN) (M = Pt; X = Cl) (L = 2,5,8-trithia[9](2,5)thiophenophane) are described. The molecular structure of $PdBr_2 \cdot$L which contains a weak thiophene-sulfur-to-palladium interaction has been determined: space group $P2_1/n$, a = 8.3569(3), b = 16.3254(15), c = 11.1462(3) Å, β = 92.833(4)°, Z = 4, R_f = 0.060, R_w = 0.058. The electronic, low frequency ir, and ^{13}C nmr spectra are described. Variable temperature ^1H nmr spectra are discussed and it is concluded that the open chain complexes undergo rapid conformational exchange at room temperature but are configurationally rigid unless the temperature is increased. In contrast, the macrocyclic complexes undergo very limited conformational and no configurational exchange up to their decomposition temperatures. They are also nonfluxional in the same temperature range. Chemical exchange of acidic ligand hydrogens and a metal–ligand dissociative equilibrium were also detected when X = SCN.

Key words: thiophene, thioether, macrocyclic metal complexes.

C. Robert Lucas, Shuang Liu, Michael J. Newlands et Eric J. Gabe. Can. J. Chem. **68**, 1357 (1990).

On décrit les préparations de complexes du thiophénophane et de thioéthers en chaîne ouverte de formule $MX_2 \cdot$BBTE (M = Pd; X = Cl ou I) (M = Pt; X = Cl) (BBTE = 1,2-bis(benzylthio)éthane) et $MX_2 \cdot$L (M = Pd; X = Cl, Br, I ou SCN) (M = Pt; X = Cl) (L = 2,5,8-trithia[9](2,5)thiophénophane). On a déterminé la structure du $PdBr_2 \cdot$L qui contient une interaction faible entre le soufre du thiophène et le palladium : groupe d'espace $P2_1/n$, a = 8,3569(3), b = 16,3254(15) et c = 11,1462(3) Å, β = 92,833(4)°, Z = 4, R_f = 0,060 et R_w = 0,058. On décrit les spectres électroniques, ir à basse fréquence et rmn du ^{13}C. On discute des spectres rmn du ^1H à température variable et on en conclut que, à la température ambiante, les complexes avec des chaînes ouvertes subissent des échanges conformationnels rapides; toutefois, ils sont rigides d'un point de vue configurationnel, à moins que l'on augmente la température. Par ailleurs, lorsqu'on soumet les complexes avec des macrocycles à des températures allant jusqu'à leurs températures de décomposition, ils ne subissent que des échanges conformationnels et configurationnels très limités. Dans le cas où X = SCN, on a aussi détecté un échange chimique impliquant les hydrogènes acides agissant comme ligands ainsi qu'un équilibre métal ligand impliquant une dissociation.

Mots clés : thiophène, thioéther, complexes métalliques de macrocycles.

[Traduit par la revue]

Introduction

As part of our continuing interest in the effects of structural constraint in sulfur-donor ligands (1) we have prepared several Pd and Pt derivatives of the ligand L and of BBTE (1,2-bis(benzylthio)ethane).

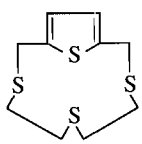

L

Structures and properties of complexes formed by sulfur-donor ligands in general and by sulfur-donor macrocycles in particular are of interest because they are often unusual (2). Their unusual nature derives from a combination of the electronic properties of thioether sulfur (3), the flexibility of polythioether chains (4), the conformational preferences of polythioether macrocycles (5), and the ability of polythioether ligands to be involved in fluxional processes (6). In order to assess the extent to which the unusual properties are controlled by stereochemical aspects in the ligand, we have carried out a variety of studies, some of which are described in this report.

Since rigidity associated with the aromatic thiophene ring is the structural constraint we have imposed on ligand L, we are able, in this study to explore at the same time the possibility of thiophene coordination. Conventionally, thiophene is considered to coordinate poorly to transition metals although there are several recent examples in which M—S(thiophene) distances have been found that are roughly equal to the sum of the covalent radii of divalent sulfur and the metal involved (7–15). In addition, there are compounds in which weaker interactions occur that can be detected spectroscopically and for which the M—S distance is much longer (16). Thus, it seems that the metal—S(thiophene) interaction is not inherently weak but rather that the conditions under which strong M—S(thiophene) interactions can be formed are not yet fully understood. Since hydrodesulfurization of thiophenes is a major industrial process that may involve M—S(thiophene) coordination, it is important to understand the controlling factors.

In our complexes, chelation by L using adjacent thioether sulfurs places the thiophene ring near the metal. Once there, its sulfur atom may choose whether or not to coordinate by rotating the plane of the thiophene ring about the bonds to substituents in its 2- and 5-positions so that the metal–sulfur distance varies. Part of our objective in this study was to see whether the M—S(thiophene) distance will be long or short under these conditions. This report also describes the unexpected rigidity

[1]NRCC No. 31606.

[2]Author to whom all correspondence should be addressed.

Can. J. Chem. Downloaded from www.nrcresearchpress.com by 88.85.125.76 on 09/07/12
For personal use only.

Can. J. Chem. Downloaded from www.nrcresearchpress.com by 88.85.125.76 on 09/07/12
For personal use only.

of these macrocyclic complexes, the nmr spectra of which clearly show several consequences of structural constraint. Interpretation of these spectra owes much to earlier work by Abel and co-workers (2, 17), Cross *et al.* (18, 19), and Hunter and Massey (19, 20) and as a point of departure from their studies we began by examining spectra of complexes formed by 1,2-bis(benzylthio)ethane, BBTE, an open chain dithioether which lacks some of the constraints we later found in the macrocyclic ligand, L.

Experimental

Commercially available reagents were obtained from the Aldrich Chemical Co. Inc., or from Morton Thiokol Alfa Products Inc., and were used without further purification. We have previously described the preparation of L (21). Spectroscopic data were obtained using the following instruments: ir, Perkin Elmer Model 283; uv/vis, Cary Model 17; nmr General Electric 300-NB; mass spectra, V.G. micromass 7070 HS. X-ray data were collected using an Enraf Nonius CAD-4 diffractometer. Analyses were performed by Canadian Microanalytical Services Ltd.

Preparative

(a) $C_{16}H_{18}S_2$ (BBTE)

Sodium metal (2.3 g, 0.10 mol) was dissolved in commercial absolute ethanol (300 mL) under an atmosphere of dry nitrogen and 1,2-ethanedithiol (4.7 g, 0.050 mol) added. The solution was refluxed for 5 min and then benzyl bromide (17.1 g, 0.100 mol) in dry benzene (150 mL) was added dropwise. The mixture was refluxed for 1 h, volatiles removed on a rotary evaporator, and the residue extracted with $CHCl_3$. The extract was washed, dried over anhydrous $MgSO_4$, and evaporated to give an oil that was crystallized from ethanol at 0°C as white crystals. mp 32–34°C. Yield 11.5 g (84%). Mass spectrum: parent ion 274 $[C_{16}H_{18}S_2]^+$. Nuclear magnetic resonance ($CDCl_3$, ppm from TMS int. std.), ^{1}H: 2.53 (s, 4H) —CH_2CH_2—, 3.52 (s, 4H) $PhCH_2$, 7.23 (m, 10H) C_6H_5.

(b) $PdCl_2$·BBTE

Solutions of *cis*-$PdCl_2(PhCN)_2$ (153 mg, 0.400 mmol) in acetone (20 mL) and BBTE (110 mg, 0.400 mmol) in CH_2Cl_2 (10 mL) were mixed and the solvents allowed to evaporate at room temperature until orange crystals had formed. The solid was separated, washed with acetone and then ether, and dried in vacuum. mp 184–185°C (dec). Yield 229 mg (79%). *Anal.* calcd. for $C_{16}H_{18}Cl_2PdS_2$: C 42.54, H 4.02, Cl 15.70, Pd 23.55; found: C 42.77, H 4.01, Cl 15.60, Pd 22.60.

(c) PdI_2·BBTE

A solution of *cis*-$PdCl_2(PhCN)_2$ (153 mg, 0.400 mmol) in acetone (20 mL) was treated with a solution of $AgCF_3SO_3$ (205 mg, 0.800 mmol) in acetone (30 mL). The resulting precipitate was removed and discarded and to the filtrate solutions of KI (133 mg, 0.800 mmol) in H_2O (5 mL) and BBTE (110 mg, 0.400 mmol) in CH_2Cl_2 (10 mL) were added in that order. The purple solution was filtered quickly and the solvent allowed to evaporate slowly at room temperature until a purple solid appeared. The solid was separated, washed, and dried in vacuum. mp 179–180°C (dec). Yield 190 mg (75%). *Anal.* calcd. for $C_{16}H_{18}I_2PdS_2$: C 30.26, H 2.86, Pd 16.76; found: C 30.39, H 2.87, Pd 15.90.

(d) $PtCl_2$·BBTE

Potassium trichloro(ethylene)platinate(II) (74 mg, 0.20 mmol) was dissolved in acetone (15 mL) and the solution filtered. BBTE (60 mg, 0.22 mmol) in CH_2Cl_2 (10 mL) was added and the mixture filtered. The filtrate was allowed to evaporate at room temperature until yellow crystals formed. The solid was separated, washed with acetone and then ether, and dried in vacuum. mp 180–186°C (dec). Yield 86 mg (80%). *Anal.* calcd. for $C_{16}H_{18}Cl_2PtS_2$: C 35.54, H 3.36, Cl 13.12; found: C 35.99, H 3.56, Cl 12.93.

(e) PdX_2·L (X = Cl, Br, I, SCN)

Preparations of these complexes were analogous to those containing BBTE. Thus, the chloro complex was prepared directly from *cis*-$PdCl_2(PhCN)_2$ but for X = Br, I, or SCN, chloride was first removed using $AgCF_3SO_3$ and the appropriate halide or pseudohalide added as its potassium salt KX before the ligand solution was added.

$PdCl_2$·L: orange, mp 223–226°C (dec). Yield 85%. *Anal.* calcd. for $C_{10}H_{14}Cl_2PdS_4$: C 27.31, H 3.21, Cl 16.13, Pd 24.19; found: C 27.21, H 3.20, Cl 16.29, Pd 22.90.

$PdBr_2$·L: red, mp 210–213°C (dec). Yield 85%. *Anal.* calcd. for $C_{10}H_{14}Br_2PdS_4$: C 22.72, H 2.67, Br 30.23, Pd 20.12; found: C 21.96, H 2.58, Br 29.71, Pd 17.60.

PdI_2·L: purple, mp 237–240°C (dec). Yield 83%. *Anal.* calcd. for $C_{10}H_{14}I_2PdS_4$: C 19.28, H 2.27, I 40.76, Pd 17.09; found: C 19.43, H 2.28, I 37.74, Pd 15.50.

$Pd(SCN)_2$·L: red, mp 169–170°C (dec). Yield 77%. *Anal.* calcd. for $C_{12}H_{14}N_2PdS_6$: C 29.72, H 2.91, Pd 21.94; found: C 29.71, H 2.91, Pd 22.50.

(f) $PtCl_2$·L

This yellow complex was prepared in the same way as its BBTE analogue. mp 235–240°C (dec). Yield 79%. *Anal.* calcd. for $C_{10}H_{14}Cl_2PtS_4$: C 22.73, H 2.67, Pt 36.91; found: C 23.00, H 2.75, Pt 36.40.

X-ray

A summary of the crystal data for $PdBr_2$·L is in Table 1. The diffraction intensities were collected at 295 K using the $\theta/2\theta$ scan technique with profile analysis (22) at a scan speed of 4°/min. Three standards were measured after every 100 reflections and no significant crystal decay was detected. Space groups were determined by systematic absences. Unit cell parameters in Table 2 were obtained by a least-squares refinement of the setting angles for 46 reflections ($35° \leq 2\theta \leq 45°$). Lorentz and polarization factors were applied and corrections were made for absorption.

The structure was solved with MULTAN (23) plus a difference Fourier map and refined by full matrix least-squares with counting statistics weights. H-atom positions were calculated but their parameters were not refined. All heavier atoms were refined anisotropically. All calculations were performed with the NRCVAX Crystal Structure programs (24). Scattering factors were taken from the usual source (25). The final atomic positional parameters, the equivalent isotropic temperature factors and important bond lengths and angles are listed in Tables 2 and 4. Anisotropic thermal parameters, a full listing of bond lengths and angles and final structure factors are available as supplementary data.[3] Figure 1 shows a view of the molecule and its atomic numbering scheme.

Results and discussion

The infrared and electronic spectra (Table 3) are consistent with *cis*-planar arrangements of donor atoms (26, 27) and the X-ray results (Fig. 1) confirm that structure for $PdBr_2$·L. In addition, however, there is a weak thiophene-sulfur-to-palladium interaction, revealed by the X-ray study which probably occurs in the other PdX_2·L complexes (X = Cl, Br, I, SCN) as well.

Complexes such as these are known (28) to exhibit *d–d* transitions, ligand-to-metal charge transfer (LMCT), and metal-to-ligand charge transfer (MLCT) bands all of which overlap in the same region of the spectrum. Therefore, no specific assignments have been made although it should be noted that the lowest energy band in each case moves to higher energy in the sequence I < Br < Cl and Pd < Pt as would be expected for LMCT. Furthermore, the highest energy band ($\sim$40 000 cm^{-1} in solution or $\sim$28 000 cm^{-1} in mull spectra) moves very little as X changes in MX_2·L or MX_2·BBTE but rises in energy when M changes from Pd to Pt, again as expected for LMCT. It is

[3]A complete set of data may be purchased from the Depository of Unpublished Data, CISTI, National Research Council of Canada, Ottawa, Ont., Canada K1A 0S2.

Can. J. Chem. Downloaded from www.nrcresearchpress.com by 88.85.125.76 on 09/07/12
For personal use only.

TABLE 1. Crystal data for $PdBr_2 \cdot L$

Parameter	Value
Empirical formula	$C_{10}H_{14}Br_2PdS_4$
Formula weight	528.68
Crystal dimensions, mm	0.10 × 0.10 × 0.20
Space group	Monoclinic $P2_1/n$
a, Å	8.3569(3)[a]
b, Å	16.3254(15)
c, Å	11.1462(3)
β, deg	92.833(4)
Z (molecules/cell)	4
$F(000)$, electrons	1031.91
Vol, Å^3	1518.81
d_{calc}, g/cm^3	2.312
Linear absorption coefficient (μ) mm^{-1}	6.93
Radiation, Å	λ = 0.70930 (MoKα$_1$)
2θ (max), deg	49.9
No. reflections measured	4158
No. unique reflections	2652
No. unique reflection $I_{net} > n\sigma(I_{net})$	1446 (n = 2.5)
Last least sq. cycle calc. with	17 atoms 105 parameters 1446 reflections
R_f (sig. refl.)	0.060[b]
R_w (sig. refl.)	0.058[c]
Goodness of fit (last cycle)	1.780[d]
R_f (all refl.)	0.120[b]
R_w (all refl.)	0.066[c]
Max. shift/σ	1.026
Last D-map:	
Deepest hole, e/Å^3	−1.330
highest peak, e/Å^3	1.350
Sec. ext. coeff.	0.69(7)

[a]Throughout this work esd's are in parentheses and refer to the last digit printed.
[b]$R_f = \Sigma||F_o| - |F_c||/\Sigma|F_o|$.
[c]$R_w = [\Sigma w(|F_o| - |F_c|)^2/\Sigma(w|F_o|)^2]^{1/2}$ where $w = 1/\sigma^2 I$.
[d]Goodness of fit = $[\Sigma w(|F_o| - |F_c|)^2/(\text{No. of refl.} - \text{No. of parameters})]^{1/2}$.

TABLE 2. Positional and thermal parameters and equivalent isotropic temperature factors for $PdBr_2 \cdot L$

Atom	x	y	z	B_{iso}[a]
Pd	0.11671(13)	0.40399(6)	0.48133(9)	2.52(5)
Br1	−0.13314(20)	0.36972(12)	0.37460(16)	5.19(10)
Br2	0.23534(21)	0.45936(11)	0.30220(15)	4.81(9)
S1	0.3209 (4)	0.24573(22)	0.4228 (3)	2.45(15)
S2	0.3495 (4)	0.43730(22)	0.5846 (3)	2.91(17)
S3	0.0173 (4)	0.35233(20)	0.6527 (3)	2.35(16)
S4	0.0472 (5)	0.08858(23)	0.5635 (4)	4.16(20)
C1	0.3356 (16)	0.1487 (8)	0.4859 (12)	2.6 (6)
C2	0.4539 (18)	0.1469 (9)	0.5728 (13)	3.2 (7)
C3	0.5259 (15)	0.2241 (9)	0.5924 (12)	2.6 (7)
C4	0.4690 (14)	0.2837 (8)	0.5215 (12)	2.2 (6)
C5	0.5065 (16)	0.3729 (9)	0.5251 (13)	3.1 (7)
C6	0.3252 (16)	0.3931 (9)	0.7332 (12)	3.3 (7)
C7	0.1557 (17)	0.3973 (8)	0.7662 (11)	2.9 (6)
C8	0.0803 (16)	0.2462 (8)	0.6596 (12)	2.8 (6)
C9	−0.0140 (15)	0.1948 (8)	0.5668 (13)	3.1 (7)
C10	0.2042 (17)	0.0890 (9)	0.4567 (13)	3.6 (7)

[a]B_{iso} is the mean of the principal axes of the thermal ellipsoid.

TABLE 3. Spectral data

Compound	ν(M—X)[a] cm^{-1}	Colour	λ$_{max}$ in nm (ε) Solutions[c]	Mulls[d]
$PdCl_2 \cdot BBTE$	300,324	Orange	390 (2 000) 360 (sh) 310 (sh) 255 (24 000)	405 330
$PdI_2 \cdot BBTE$	[b]	Purple	480 (4 000) 410 (sh) 280 (30 000) 255 (sh)	500 415 340
$PtCl_2 \cdot BBTE$	318,329	Yellow	360 (300) 315 (2 000) 250 (30 000)	
$PdCl_2 \cdot L$	324,341	Orange	395 (1 000) 310 (sh) 250 (14 000)	400 325
$PdBr_2 \cdot L$	225,238	Red	415 (800) 355 (sh) 260 (13 000)	425 325
$PdI_2 \cdot L$	[b]	Purple	480 (2 500) 260 (18 000)	490 350
$Pd(SCN)_2 \cdot L$	[b]	Red	425 (800) 350 (sh) 300 (16 000) 260 (sh)	480 (sh) 435 360
$PtCl_2 \cdot L$	318,330	Yellow	360 (200)[e]	380 225

[a]Nujol; medium or strong bands.
[b]Not found.
[c]CH_2Cl_2.
[d]Nujol.
[e]N,N-Dimethylformamide.

therefore tempting to suggest the former to be X → M LMCT and the latter to be S → M LMCT.

The conformation of the ligand in solid $PdBr_2 \cdot L$ (Fig. 1) is the same as that in $[CuL_2]^+$ (21) and $(CuCl_2 \cdot L)_2$ (16) and as in the case of the copper(II) complex of L, there is a weak apical thiophene-sulfur-to-metal interaction in $PdBr_2 \cdot L$. Apical bonds in five or six coordinate palladium complexes tend to be longer than their equatorial counterparts. For example, the axial and average equatorial lengths in the five coordinate $PdBr_2$ complex of 1,4,7-trithiacyclononane are 3.125 and 2.266 Å, respectively (29), while the corresponding lengths in the six coordinate Pd(II) complex of 1,4,7,10,13,16-hexathiacyclooctadecane are 3.273 and 2.309 Å (30). In comparison, the apical (thiophene) and average basal Pd—S distances in $PdBr_2 \cdot L$ are 3.1817(3) and 2.279 Å, respectively. The apical distance to the thiophene-sulfur of $PdBr_2 \cdot L$ is significantly less than the sum (3.40 Å) (31) of the van der Waals' radii of Pd and S. The palladium atom lies in the plane defined by the two coordinated thioether sulfurs and the two bromines and the bond angles at Pd deviate no more than 3.38° and on average only 1.78° from ideal values. Bond lengths, angles and other details of the $PdBr_2 \cdot L$ structure are in Tables 1, 2, and 4.

Although not common, bonds between thiophene-sulfur and Re, Fe, Ru, Rh, Cu(I), Ag, and B have been identified using X-ray techniques (7–15). These bonds have lengths that are more or less equal to the sum of the covalent radii of M and S although establishment of an appropriate covalent radius for calculation of apical bond lengths for metals such as Pd, Cu(I), Cu(II), or Ag(I) that form apical bonds reluctantly or whose complexes are subject to Jahn–Teller distortion is problematical. Other weaker interactions that involve bond lengths greater

Can. J. Chem. Downloaded from www.nrcresearchpress.com by 88.85.125.76 on 09/07/12
For personal use only.

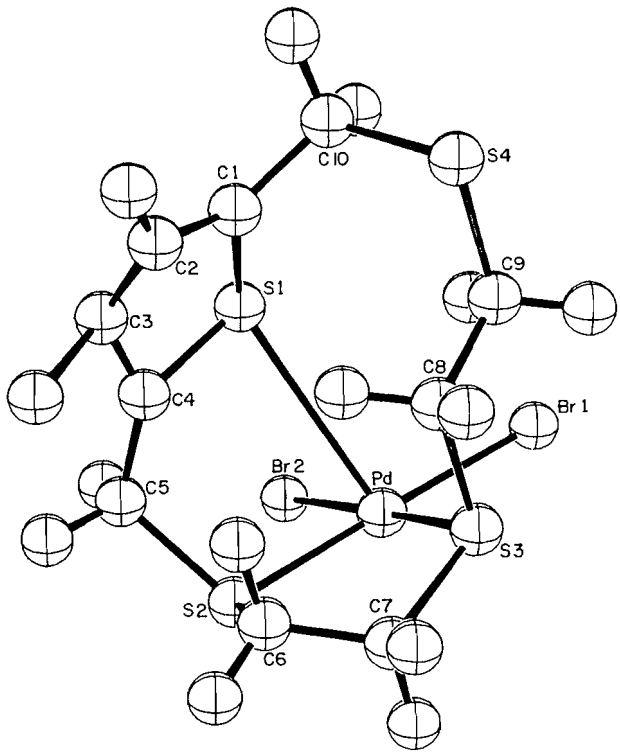

FIG. 1. ORTEP drawing of $PdBr_2 \cdot L$.

TABLE 4. Selected bond lengths and angles in $PdBr_2 \cdot L$

Bond	Distance (Å)	Bonds	Angle (deg)
Pd—Br(1)	2.417(2)	Br(1)—Pd—Br(2)	93.38(7)
Pd—Br(2)	2.446(2)	Br(1)—Pd—S(2)	178.95(12)
Pd—S(1)	3.182(4)	Br(1)—Pd—S(3)	89.14(10)
Pd—S(2)	2.277(3)	Br(2)—Pd—S(2)	87.34(11)
Pd—S(3)	2.282(4)	Br(2)—Pd—S(3)	177.41(11)
S(1)—C(1)	1.735(14)	S(2)—Pd—S(3)	90.15(13)
S(1)—C(4)	1.730(13)	Pd—S(2)—C(5)	106.8(4)
S(2)—C(5)	1.831(15)	Pd—S(2)—C(6)	103.5(4)
S(2)—C(6)	1.828(15)	Pd—S(3)—C(7)	100.8(5)
S(3)—C(7)	1.825(13)	Pd—S(3)—C(8)	105.8(5)
S(3)—C(8)	1.811(13)	S(1)—C(1)—C(2)	110.2(10)
S(4)—C(9)	1.808(14)	S(1)—C(1)—C(10)	118.1(10)
S(4)—C(10)	1.814(16)	C(1)—C(2)—C(3)	112.5(12)
C(1)—C(2)	1.350(20)	C(2)—C(3)—C(4)	115.2(12)
C(1)—C(10)	1.491(19)	S(1)—C(4)—C(3)	109.9(10)
C(2)—C(3)	1.409(21)	S(1)—C(4)—C(5)	120.7(10)
C(3)—C(4)	1.327(19)	Br(1)—Pd—S(1)	99.8(3)
C(4)—C(5)	1.489(19)	Br(2)—Pd—S(1)	83.7(4)
C(6)—C(7)	1.483(20)	S(1)—Pd—S(2)	81.0(3)
C(8)—C(9)	1.521(19)	S(1)—Pd—S(3)	95.3(4)
		Pd—S(1)—C(1)	133.3(3)
		Pd—S(1)—C(4)	87.3(3)

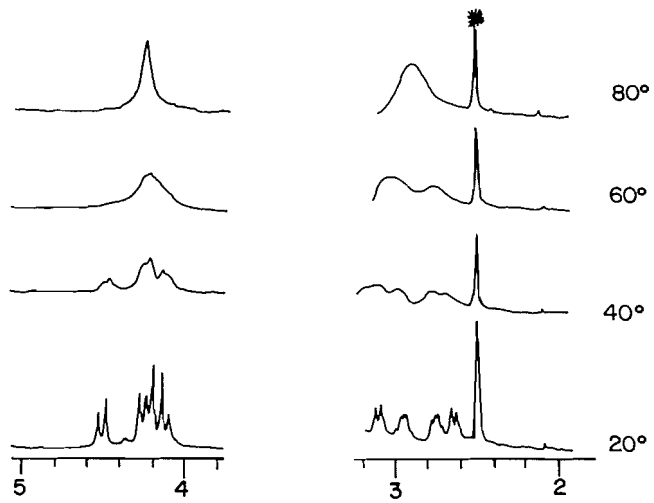

FIG. 2. ^1H nmr spectra of $PdCl_2 \cdot BBTE$ (* is d_6-DMSO).

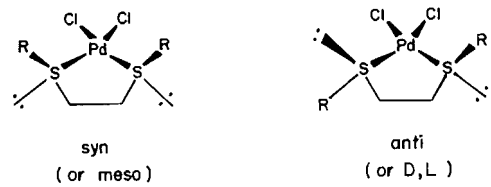

FIG. 3. Isomers of $PdCl_2 \cdot BBTE$ (R = $PhCH_2$).

than the sum of the usual covalent radii but less than the sum of the van der Waals' radii are also known such as that involving ligand L and Cu(II) (16). These interactions are analogous to the long apical M—S distances of 3.12 and 3.27 Å in macrocyclic polythioether complexes (29, 30) (*vide supra*) in the sense that they influence spectroscopic and other properties of the complexes but are weaker than other shorter M—S bonds in those molecules. The palladium bromide and related complexes of ligand L, described herein may be considered part of this latter group since the presence of the M—S(thiophene) interaction influences the rigidity of the molecules as observed by nmr (*vide infra*) even through the M—S(thiophene) distance is greater than the sum of the usual covalent radii of M and S.

The 300 MHz nmr spectra of all the BBTE complexes are similar and for the sake of brevity only that of $PdCl_2 \cdot BBTE$ (Fig. 2) will be discussed. At room temperature in d_6-dimethylsulfoxide it consists of a typical phenyl multiplet at 7.4 ppm from internal tetramethylsilane, a pair of partially overlapped AB quartets near 4.3 ppm due to benzylic methylenes and four distinct multiplets of equal intensity near 2.8 ppm due to $—CH_2CH_2—$ of the chelate ring. The integrated intensities of these three regions are in the ratio 10:4:4 as required. The occurrence of two sets of quartets near 4.3 ppm suggests two isomers (Fig. 3) are present in solution in the ratio 42%:58%. That which is present in the smaller amount has more de-shielded benzylic methylenes and is probably the *syn* isomer (19). The fact that only two AB quartets are seen may be attributed to conformational averaging of the axial and equatorial environments of the benzylic methylene hydrogens in each isomer so that only one averaged benzyl group is detected per isomer.

For analysis of the $—CH_2CH_2—$ portion of the spectrum near 2.8 ppm, the arguments applied by Hunter and Massey (20) to spectra of $PdCl_2 \cdot BISE$ (BISE = 1,2-bis(isopropylseleno)ethane) are appropriate. Thus, the observation at room temperature of two AA'BB' multiplets, one with widely separated components (~0.45 ppm) and another with narrowly separated ones (~0.2 ppm), all of which are of similar intensity, is consistent with the presence of nearly equal amounts of two isomers, both of which are undergoing reversal of their ring conformations that is rapid on the nmr time scale. This is the same conclusion already reached by examination of the benzylic methylene portion of the spectrum.

As the temperature of the solution is increased, the signals

TABLE 5. ^{1}H nmr chemical shifts[a] in ppm vs. TMS

^{1}H nmr chemical shift					
$PdCl_2 \cdot L$	$PdBr_2 \cdot L$	$PdI_2 \cdot L$	$Pd(SCN)_2 \cdot L$	$PtCl_2 \cdot L$[d]	Assignment
7.12 (d)[b]	7.20 (d)[b]	7.18 (d)[b]	7.24 (d)[b]	7.13 (d)	H3
6.90 (d)[b]	6.97 (d)[b]	6.94 (d)[b]	7.01 (d)[b]	6.88 (d)	H2
4.50 (d)[c]	4.75 (d)[c]	4.96 (d)[c]	4.57 (s)	4.57 (d)[c]	H5A
4.18 (d)[c]	4.42 (d)[c]	4.65 (d)[c]		4.40 (d)[c]	H5B
4.08 (d)[c]	4.15 (d)[c]	4.14 (d)[c]	4.16 (d)[c]	4.13 (d)[c]	H10A
3.96 (d)[c]	4.02 (d)[c]	3.98 (d)[c]	4.06 (d)[c]	4.04 (d)[c]	H10B
3.15 (m)	3.20 (m)	3.17 (m)	3.39 (m)	3.04	H7B
3.08 (m)	3.17 (m)	3.15 (m)	2.84 (m)	3.00	H8B
3.07 (m)	3.13 (m)	3.02 (m)	3.35 (m)	2.89	H7A
2.94 (m)	3.00 (m)	2.96 (m)	3.58 (m)	2.85	H6A
2.78 (m)	2.86 (m)	2.90 (m)	3.07 (m)	2.80	H9B
2.45 (m)	2.55 (m)	2.53 (m)	2.70 (m)	2.48	H6B
2.29 (m)	2.35 (m)	2.29 (m)	2.60 (m)	2.32	H9A
0.61 (m)	0.67 (m)	0.64 (m)	0.70 (m)	0.54	H8A

[a] In d_6-dmso.
[b] J = 3.5 Hz.
[c] J = 13.9 Hz.
[d] ^{195}Pt satellites not detected.

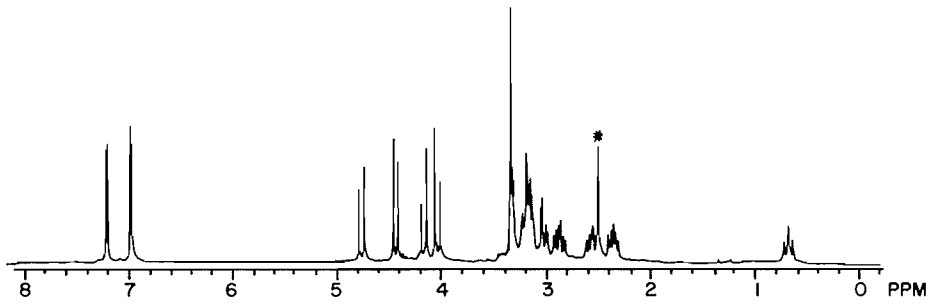

FIG. 4. ^{1}H nmr spectrum of $PdBr_2 \cdot L$ at room temperature.

near 4.3 ppm begin to coalesce as do those near 2.8 ppm until both become broad singlets at 353 K. These observations are consistent with the onset of rapid interconversion of the two isomers by either simultaneous or consecutive inversions at the two coordinated S-atoms (17, 20). Coalescence at 353 K for $PdCl_2 \cdot$BBTE may be compared to coalescences at 400 K (20) for $PdCl_2 \cdot$BISE or 240 K for $Mo(CO)_4 \cdot$BBTE (19). These are in accordance with the known trends in kinetic barriers to inversion as one changes either the identity of the inverting atom or the electropositive character of the metal to which the inverting atom is bound.

Thus, we may conclude that at room temperature the Pd and Pt complexes of BBTE are undergoing rapid exchange of the chelate ring conformations and of the axial and equatorial orientations of the lone pairs on the sulfurs. The complexes remain configurationally rigid, however, until the temperature is raised several tens of degrees when inversions at coordinated sulfurs interconvert the *syn* and *anti* isomers.

The 300 MHz ^{1}H nmr spectra of the complexes $MX_2 \cdot L$ (M = Pd, Pt; X = Cl, Br, I, SCN; L = 2,5,8-trithia[9](2,5)thiophenophane) are all similar (Table 5) and we shall therefore discuss in detail only that of $PdBr_2 \cdot L$ (Fig. 4) for which we also have X-ray structural data (Fig. 1). Subsequently, we will discuss the two differences between spectra of $PdBr_2 \cdot L$ and $Pd(SCN)_2 \cdot L$, the latter being the only member of the series for which significant differences occur. Spectral assignments are in Table 5.

At room temperature, H2 and H3, the two aromatic hydrogens give signals that are doublets near 7.2 and 7.0 ppm, respectively. These hydrogens are chemically non-equivalent as a result of the asymmetric way in which palladium is bound to the macrocycle. The non-equivalence of these hydrogens indicates the absence of a 1,4-heteroatom fluxionality involving S2, S3, and S4 similar to that reported for the nitrogen donor complex $Pd(non)_2^{2+}$ (non = 1,4,7-triazacyclononane) (6). This conclusion is supported by the ^{13}C spectrum (Table 6) which shows nine signals assigned by ^{13}C—^{1}H COSY and Attached Proton Test to all but one of the ten carbons in the molecule. The missing signal is due to C7 and is expected to be obscured by the solvent signal. Were the molecule fluxional only five signals would be expected.

This molecule is rigid in another respect as well. The hydrogens of every —CH_2— in the molecule are non-equivalent up to at least 120°C which indicates that inversions at S2 and S3 are not occurring. In the case of $PdCl_2 \cdot$BBTE, coalescence of the room temperature methylene signals to broad singlets has already occurred at 80°C and for $PdBr_2 \cdot L$ an even lower coalescence temperature, might be expected (17). Clearly, however, the rigidity of $PdBr_2 \cdot L$ is such that non-dissociative inversions at S2 and S3 are prevented even at 120°C.

Can. J. Chem. Downloaded from www.nrcresearchpress.com by 88.85.125.76 on 09/07/12
For personal use only.

TABLE 6. ^{13}C nmr chemical shifts[a] in ppm vs. TMS

^{13}C nmr chemical shift				
$PdCl_2 \cdot L$	$PdBr_2 \cdot L$	$Pd(SCN)_2 \cdot L$	$PtCl_2 \cdot L$	Assignment
146.3	146.2	146.7	147.0	C4
134.7	134.8	135.1	136.3	C3
134.7	134.8	134.6	136.3	C1
124.8	124.8	125.5	125.4	C2
[b]	[b]	38.4	39.1	C7
37.9	38.3	37.6	38.2	C5
35.7	35.8	35.5	36.1	C8
34.8	35.4	35.4	35.4	C6
30.1	30.2	30.0	30.4	C10
27.6	28.3	27.5	27.9	C9
		117.8		SCN
		117.3		SCN
		122.0		SCN[c]

[a] ^1H decoupled; in d_6-dmso.
[b] Obscured by solvent.
[c] Due to Pd species produced by ligand dissociation; cf $Pd(SCN)_4^{2-}$ at 119.0 ppm (34).

Unlike $PdCl_2 \cdot$BBTE, the two quartets near 4.5 ppm in the spectrum of $PdCl_2 \cdot L$ are due not to the presence of two isomers but rather to two different CH_2 groups in the same molecule. In fact, because S2 and S3 are part of a macrocyclic ring in which a third sulfur (S1) is also interacting with the metal, the only configuration possible for the five-membered chelate ring formed by L corresponds to the *syn* isomer of $PdCl_2 \cdot$BBTE. The remainder of the spectrum of $PdCl_2 \cdot L$ involves separate signals for each of the eight hydrogens comprising the two $-CH_2CH_2-$ units. One of these hydrogens is in a unique environment that is evidently much more shielded than the others since its signal is at comparatively high field (0.67 ppm). This is designated as H8A and is the hydrogen on C8 that lies over the center of the thiophene ring (Fig. 1) and is therefore subjected to the shielding effect of the induced ring current in the aromatic π-system. Because of the rigidity of the molecule, the conformations available to the chelate ring, $PdS2CH_2CH_2S3$, are strictly limited. For example, the envelope conformation which requires both sulphur lone-pairs to be simultaneously axial or simultaneously equatorial is not possible. It is this envelope conformation that is usually the transition state between two half-chair conformations and in its absence a pseudo-librational route between the two half-chair conformations is likely to be of sufficiently low kinetic barrier as to be undetectable by nmr (32). In either half-chair conformation, the $-CH_2CH_2-$ unit will be an ABCD spin system and the two such systems are unrelated by any symmetry element. Therefore, two ABCD spectra would be expected if conformational exchange is slow or one averaged ABCD spectrum if it is rapid. In view of the predicted low barrier to conformational exchange and our earlier observation of rapid conformational exchange in $PdX_2 \cdot$BBTE we would anticipate just one ABCD pattern at room temperature as is observed (Fig. 4). This interpretation is supported by the absence of change in these signals up to at least 120°C by which temperature any barrier to this conformational exchange must surely have been overcome.

The other $-CH_2CH_2-$ unit is also an ABCD system. As a result of steric crowding, due at least in part to the Pd–S1 interaction, conformational possibilities in this region of the molecule are also strictly limited and the spectrum observed at room temperature is consistent with the rigid structure in Fig. 1.

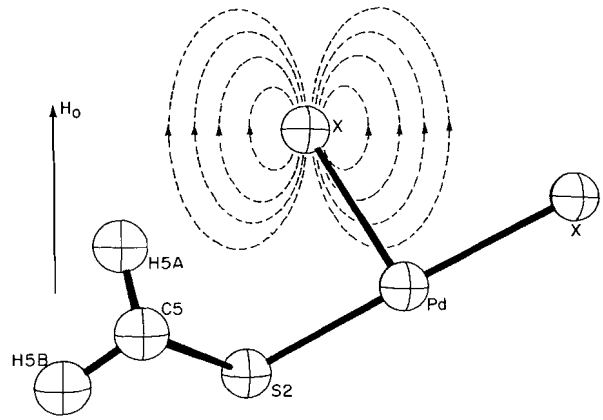

FIG. 5. Neighbour effects at H5A and H5B from X in $PdX_2 \cdot L$.

As the solution is warmed to 120°C, the two pairs of peaks that comprise the H5A–H5B quartet at ~4.5 ppm *move away* from each other with, however, no change in the coupling. The total movement is 0.02 ppm for the more shielded pair and 0.06 ppm for the lower field pair. There is no other change in the entire system. This curious behaviour is observed to a greater or lesser extent for all members of the $MX_2 \cdot L$ series and is a neighbour anisotropic effect made possible by the rigid orientations of H5A and H5B with respect to the atom X (Fig. 5).

As the temperature is raised, thermal enhancement of the bending vibration of H5A—C5—H5B occurs. In this vibrational mode, movement of one of the hydrogens is at a nearly constant radius from X whereas the other's motion is along a radius from X. Therefore, the extent of deshielding by this neighbour anisotropic contribution of X will vary with temperature for the nearer, more deshielded hydrogen but will remain more or less constant for the more distant and less deshielded hydrogen.

There is a second manifestation of this neighbour effect made possible by stereochemical rigidity. The quartet due to H5A and H5B moves to lower field as X changes from Cl to Br to I but the shift is in the wrong direction for an electronegativity effect. However, it can be attributed to a deshielding neighbour effect in which larger, more polarizable I will experience induced circulation of its electrons more readily than Cl. The induced field which is deshielding at H5A and H5B will therefore be larger for I than for Cl. This explanation is supported by the fact that the chemical shift difference between H5A and H5B is essentially the same for all X (i.e. both hydrogens are affected proportionally the same as X is varied) and J_{gem} is the same in all cases.

The spectrum of $Pd(SCN)_2 \cdot L$ shows two major differences from those of all other complexes in this series. The first difference is that free ligand peaks are present and grow in intensity as the temperature is raised. This indicates that formation of $Pd(SCN)_2 \cdot L$ is an equilibrium process and that the formation is exothermic. The second striking difference is that the H5A—H5B signal is a singlet. The only way this can occur while maintaining all other hydrogens distinctive is by dissociative interchange of H5A and H5B. It is known (33) that M—SCN systems are usually bent (~110°) and that the N atom is appreciably basic (34). The pK_a's (35) of DMSO (35.1), $PhCH_3$ (44.0), and $PhCH_2SPh$ (30.8) suggest that H5A and

Can. J. Chem. Downloaded from www.nrcresearchpress.com by 88.85.125.76 on 09/07/12
For personal use only.

H5B should be significantly acidic and may therefore interchange by a process involving intermediate residence on the basic nitrogen of thiocyanate either in the same or a different molecule. Why the thiocyanate complex should dissociate its ligand so readily when none of the other complexes in this study show any sign of dissociation until they reach their decomposition temperatures may be due to the fact that S-bonded SCN is a better π-acid than halide and its presence weakens the *trans* M—S bond.

In conclusion the complexes $MX_2 \cdot L$ have been shown to involve pseudo-square pyramidal coordination with a weak interaction between the metal and a thiophene-sulfur in the apical position. This interaction contributes to an unexpected rigidity in these complexes which do not undergo either fluxional processes or sulfur inversions up to at least 120°. These results are in contrast with the behaviour of complexes formed by tridentate N-donor macrocycles and simple chelating dithioethers, respectively. Furthermore, unexpected effects on the nmr spectra of $MX_2 \cdot L$ species as X or temperature are varied have been identified as consequences of this rigidity and an uncommon acid–base reaction between a C—H bond and the nitrogen of a coordinated thiocyanate has been observed. The complexes $MX_2 \cdot L$ have been shown to be surprisingly robust and rigid except when X = SCN. These findings are of interest for a variety of reasons not the least of which involves an improved understanding of the behaviour in solution of these or related substances that may be used as chemotherapeutic agents or catalysts.

Acknowledgements

Financial assistance by Memorial University of Newfoundland in the form of a Hatcher Scholarship (S.L.) and an operating grant (C.R.L.) and by the Natural Sciences and Engineering Research Council of Canada is gratefully acknowledged. Collection of mass spectral data was carried out by Dr. B. Gregory and Miss M. Baggs.

1. C. R. Lucas, S. Liu, M. J. Newlands, J. P. Charland, and E. J. Gabe. Can. J. Chem. **68**, 644 (1990).
2. E. W. Abel, P. D. Beer, I. Moss, K. G. Orrell, V. Šik, P. A. Bates, and M. B. Hursthouse. J. Chem. Soc. Chem. Commun. 978 (1987).
3. C. R. Lucas. Can. J. Chem. **64**, 1758 (1986).
4. J. A. Clarkson, R. Yagbasan, P. J. Blower, and S. R. Cooper. J. Chem. Soc. Chem. Commun. 1244 (1989).
5. S. R. Cooper. Acc. Chem. Res. **21**, 141 (1988).
6. G. Hunter, A. McAuley, and T. W. Whitcombe. Inorg. Chem. **27**, 2634 (1988).
7. A. L. Spek, A. J. M. Duisenberg, G. C. van Stein, and G. van Koten. Acta Crystallogr. C**41**, 374 (1985).
8. G. C. van Stein, G. van Koten, K. Vrieze, A. L. Spek, E. A. Klop, and C. Brevard. Inorg. Chem. **24**, 1367 (1985).
9. M. Draganjac, C. J. Ruffing, and T. B. Rauchfuss. Organometallics, **4**, 1909 (1985).
10. R. A. Sanchez-Delgado, R. L. Marquez-Silva, J. Puga, A. Tiripicchio, and M. Tiripicchio Camellini. J. Organomet. Chem. **316**, C35 (1986).
11. J. D. Goodrich, P. N. Nickias, and J. P. Selegue. Inorg. Chem. **26**, 3426 (1987).
12. J. R. Lockemeyer, T. B. Rauchfuss, A. L. Rheingold, and S. R. Wilson. J. Am. Chem. Soc. **111**, 8828 (1989).
13. M. G. Choi and R. J. Angelici. J. Am. Chem. Soc. **111**, 8753 (1989).
14. E. C. Constable, R. P. G. Henney, and D. A. Tocher. J. Chem. Soc. Chem. Commun. 913 (1989).
15. J. Chen, L. M. Daniels, and R. J. Angelici. J. Am. Chem. Soc. **112**, 199 (1990).
16. C. R. Lucas, S. Liu, M. J. Newlands, J. P. Charland, and E. J. Gabe. Can. J. Chem. **67**, 639 (1989).
17. E. W. Abel, S. K. Bhargava, and K. G. Orrel. Prog. Inorg. Chem. **32**, 1 (1984).
18. R. J. Cross, D. S. Rycroft, D. W. A. Sharp, and H. Torrens. J. Chem. Soc. Dalton Trans. 2434 (1980).
19. R. J. Cross, G. Hunter, and R. C. Massey. J. Chem. Soc. Dalton Trans. 2015 (1976).
20. G. Hunter and R. C. Massey. J. Chem. Soc. Dalton Trans. 2007 (1976).
21. C. R. Lucas, S. Liu, M. J. Newlands, J. P. Charland, and E. J. Gabe. Can. J. Chem. **66**, 1506 (1988).
22. D. F. Grant and E. J. Gabe. J. Appl. Crystallogr. **11**, 114 (1978).
23. G. Germain, P. Main, and M. M. Woolfson. Acta Crystallogr. A**27**, 368 (1971).
24. E. J. Gabe, F. L. Lee, and Y. LePage. *In* Crystallographic computing 3. *Edited by* G. Sheldrick, C. Kruger, and R. Goddard. Clarendon Press, Oxford. 1985. p. 167.
25. International tables for X-ray crystallography. Vol. IV. Kynoch Press, Birmingham, England. 1974. p. 99. Table 2.2B.
26. S. G. Murray and F. R. Hartley. Chem. Rev. **81**, 365 (1981).
27. K. Nakamoto. Infrared and Raman spectra of inorganic and coordination compounds. 4th ed. Wiley, Toronto. 1986. p. 283.
28. A. B. P. Lever. Inorganic electronic spectroscopy. 2nd ed. Elsevier, New York. 1984. pp. 341 *et seq*, 544 *et seq*.
29. K. Wieghardt, H. J. Küppers, E. Raabe, and C. Krüger. Angew. Chem. Int. Ed. **25**, 1101 (1986).
30. A. J. Blake, R. O. Gould, A. J. Lavery, and M. Schröder. Angew. Chem. Int. Ed. **25**, 274 (1986).
31. A. Bondi. J. Phys. Chem. **68**, 441 (1964).
32. E. W. Abel, S. K. Bhargava, K. G. Orrell, and V. Šik. J. Chem. Soc. Dalton Trans. 2073 (1982).
33. W. R. Scheidt, Y. J. Lee, D. K. Geiger, K. Taylor, and K. Hatano. J. Am. Chem. Soc. **104**, 3367 (1982).
34. J. A. Kargol, R. W. Crecely, and J. L. Burmeister. Inorg. Chem. **18**, 2532 (1979).
35. E. Block. Reactions of organosulfur compounds. Academic Press, New York. 1978. p. 46.

Can. J. Chem. Downloaded from www.nrcresearchpress.com by 88.85.125.76 on 09/07/12
For personal use only.

Palladium-catalysed arylation of peracetylated glycals, III.[1] Crystal structure of a by-product: mechanistic implications

VÉRONIQUE BELLOSTA

Laboratoire de recherches organiques, Unité associée n° 476 du Centre national de la recherche scientifique, École supérieure de physique et chimie industrielles de la ville de Paris, 10 rue Vauquelin, 75005 Paris, France

STANISLAS CZERNECKI[2]

Laboratoire de chimie des glucides, Université Pierre et Marie Curie, T 74-E6. 4 Pl. Jussieu, 75005 Paris, France

AND

DANIÈLE AVENEL, SAÏD EL BAHIJ, AND HÉLÈNE GILLIER-PANDRAUD

Laboratoire de chimie structurale biomoléculaire, Université Paris-Nord, 74 rue Marcel Cachin, 93000 Bobigny, France

Received March 22, 1989[3]

VÉRONIQUE BELLOSTA, STANISLAS CZERNECKI, DANIÈLE AVENEL, SAÏD EL BAHIJ, and HÉLÈNE GILLIER-PANDRAUD. Can. J. Chem. **68**, 1364 (1990).

Reinvestigation of the structure of (4,6-di-*O*-acetyl-2,3-dideoxy-α-D-*erythro*-hex-2-enopyranosyl)benzene, obtained by the title reaction, is described. The α anomeric configuration was clearly established by X-ray diffraction methods on the deacetylated compound. The sugar moiety exhibits a distorted half-chair $^0H_5$ conformation. Circular dichroism data are included. These new data demonstrate the stereospecificity of intermediate arylpalladium *syn* addition on the α face of the glycal. The resulting adduct collapses in two different ways: *syn* elimination of acetatohydridopalladium leading to **3**, *trans* elimination of palladium acetate affording **5**.

Key words: *C*-glycosides, palladium, X-ray diffraction.

VÉRONIQUE BELLOSTA, STANISLAS CZERNECKI, DANIÈLE AVENEL, SAÏD EL BAHIJ et HÉLÈNE GILLIER-PANDRAUD. Can. J. Chem. **68**, 1364 (1990).

La structure du (di-*O*-acétyl-4,6-didésoxy-2,3-α-D-*érythro*-hexéno-2-pyrannosyl) benzène, obtenu par la réaction du titre, est réétudiée. La configuration anomérique est clairement établie comme étant α par diffraction des rayons X sur le composé déacétylé. La conformation du cycle glucidique est demi-chaise $^0H_5$ déformée. Des données de dichroïsme circulaire sont fournies. Ces nouvelles données démontrent la stéréospécificité de la *syn*-addition de l'arylpalladium intermédiaire sur la face α du glycal. L'adduit formé conduit ensuite à **3** par *syn*-élimination d'acétatohydruropalladium ou à **5** par *trans*-élimination d'acétate de palladium.

Mots clés : *C*-glycosides, palladium, diffraction des rayons-X.

Introduction

We previously demonstrated that the title reaction constitutes a new synthesis of *C*-glycosides (1). When 3,4,6-tri-*O*-acetyl-1,5-anhydro-2-deoxy-D-*arabino*-hex-1-enitol (tri-*O*-acetyl-D-glucal **1**) and its D-*lyxo* isomer (tri-*O*-acetyl-D-galactal **2**) were reacted with an aromatic compound in the presence of acetic acid and palladium acetate, 2,3-unsaturated α-D-*C*-glycopyranosides **3** and **4** were obtained in acceptable yields (43–67%).

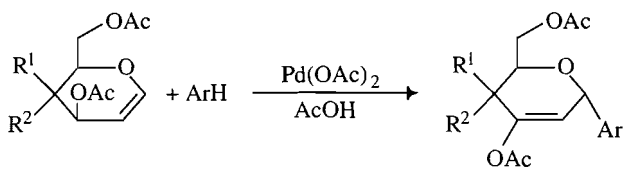

1 R^1 = H, R^2 = OAc
2 R^1 = OAc, R^2 = H

3 R^1 = H, R^2 = OAc
4 R^1 = OAc, R^2 = H

Unambiguous determination of the anomeric structures of **3** and **4** was rather difficult because only one anomer was obtained, thus methods using comparisons such as the γ-effect rule in ^{13}C nmr (2), which assigns the less shielded C-1 or C-5 signals to the *cis* anomer (β-D) (3, 4), were precluded. Furthermore, due to the presence of a double bond between C-2 and C-3, the values of the coupling constants $^3J_{1-2}$ (2.5–3.9 Hz) (1) were compatible with both configurations.

The structures of these compounds were finally determined unambiguously by X-ray diffraction for **4** (5) and by 250 MHz ^1H nmr for **3** and **4** after transformation of the enol-ester function into the parent oxime (6).

From tri-*O*-acetyl-D-glucal **1** and benzene a by-product **5** was isolated (≅10%), to which the β configuration was initially assigned.

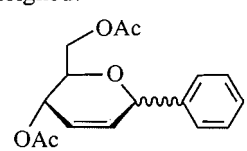

5

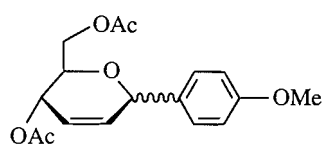

6

Comparison of the specific rotation of **5** ($[\alpha]_D^{20}$ +3.3° (*c* 1.34, $CHCl_3$)) with the sole example of 2,3-dideoxy-2,3-unsaturated aryl-*C*-glycoside described in the literature at that time, **6** (7) ($[\alpha]_D^{20}$ +250° (*c* ≅ 1, CH_2Cl_2)), clearly indicated that the anomeric configurations were different. Since **6** was claimed (7) to be the α anomer,[4] the β configuration was

[1]For preceding papers see refs. 1 and 5.

[2]Author to whom correspondence may be addressed.

[3]Revision received March 23, 1990.

[4]When this paper was in preparation the $SnCl_4$ promoted arylation of tri-*O*-acetyl-D-glucal **1** by means of anisole was reinvestigated by Casiraghi *et al.* (8) and the β-D-configuration was assigned to **6** by X-ray diffraction.

Printed in Canada / Imprimé au Canada

Can. J. Chem. Downloaded from www.nrcresearchpress.com by 88.85.125.76 on 09/07/12
For personal use only.

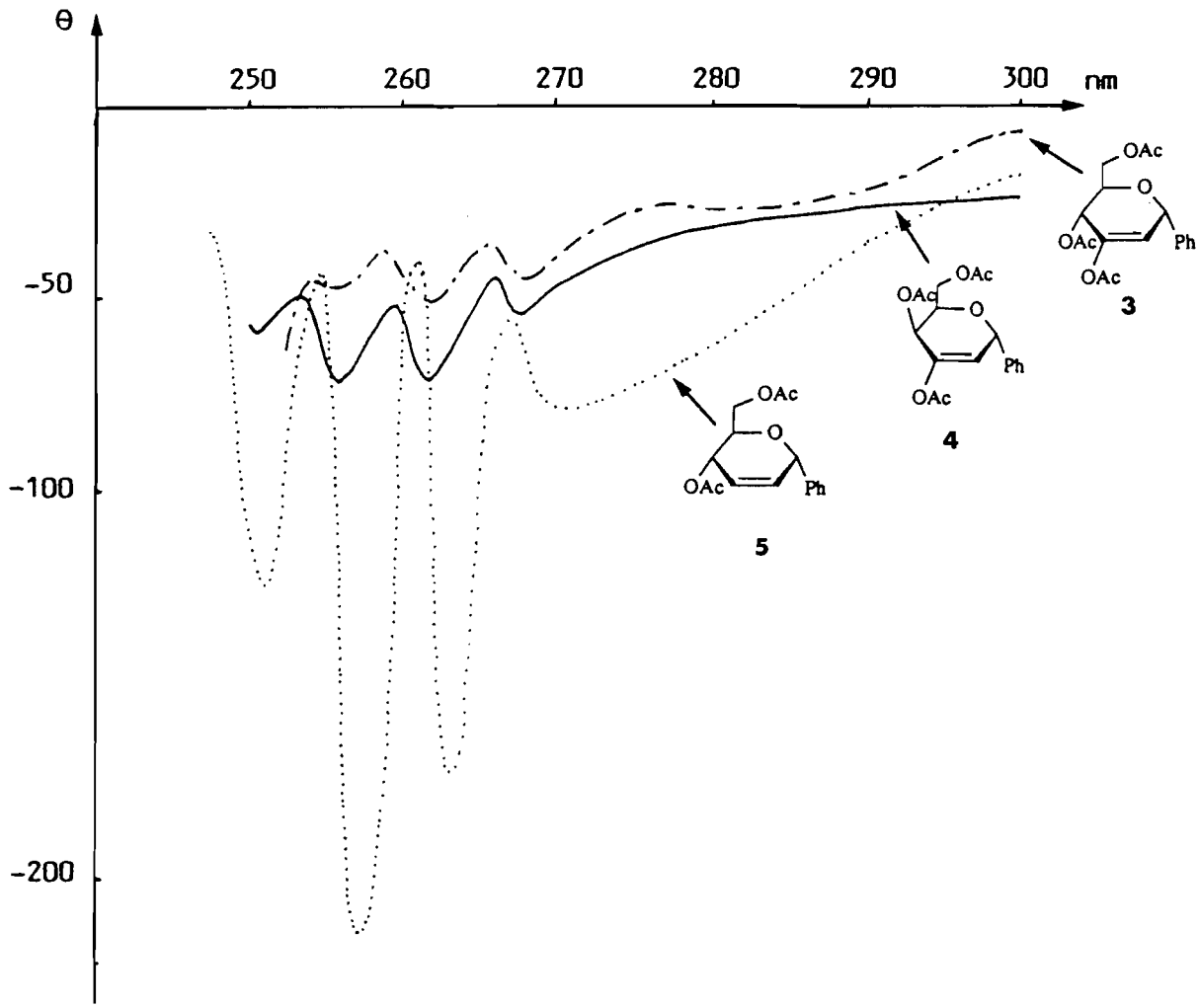

FIG. 1. Circular dichroism spectra of *C*-glycosides **3**, **4**, **5** recorded in 95% ethanol.

assigned to **5**. Rigorously, the aromatic ring was not the same in **5** and **6**, but we observed, in the series of aryl 2,3-unsaturated α-D-*C*-glycopyranosides derived from tri-*O*-acetyl-D-galactal, that the specific rotation was weakly influenced by the nature of this group (1).

We were not very confident in this assignment because several exceptions to Hudson's rules of isorotation were observed by different authors (9) for alkyl-2,3-dideoxy-hex-2-enopyranosides. Moreover the $^3J_{4-5}$ value observed for **5** (6.8 Hz in $CDCl_3$, 7 Hz in C_6D_6) appeared to us a little too small for a quasi-axial–axial relationship between H-4 and H-5. Meanwhile, several anomeric pairs of 2,3-unsaturated D-*C*-glycosides (3, 10–12) and *C*-nucleosides (13) appeared in the literature. Generally the coupling constant $^3J_{4-5}$ for the conformationally stable β-D anomer with all groups in the quasi-equatorial or equatorial position is high (8.7–9.4 Hz). For the conformationally more flexible α-D anomer this value is usually smaller (3.3–7 Hz). When the specific rotations were given (3, 10, 11), it was found that these compounds do not obey Hudson's rules of isorotation.

All these data prompted us to reinvestigate the structure assignment of compound **5**.

Results and discussion

Circular dichroism

Since compound **5** was not crystalline, we decided to examine its circular dichroism (cd) curves and to compare them with those of compounds **3** and **4** of known anomeric configuration. We have observed for a variety of aryl-*C*-glycosides that the sign of the Cotton effect is determined by the anomeric configuration and is not influenced by changes in conformation or by different substitutions at C-2, C-3, or C-4 (14).

Figure 1 shows that all three compounds give very similar curves, indicating the same spatial arrangement of the two chromophores present in the molecule (15). Consequently the α configuration should be assigned to compound **5**.

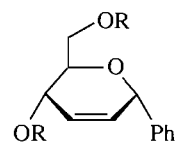

5 R = Ac
5' R = H

Furthermore, it has to be noticed that for these α-D anomers a negative Cotton effect is observed, whereas a positive one is observed for α-D-*C*-glycosides with no 2,3-unsaturation (11).

X-ray diffraction

Finally we were able to obtain crystals suitable for X-ray diffraction from the deacetylated derivative **5'**. The crystal-

Can. J. Chem. Downloaded from www.nrcresearchpress.com by 88.85.125.76 on 09/07/12
For personal use only.

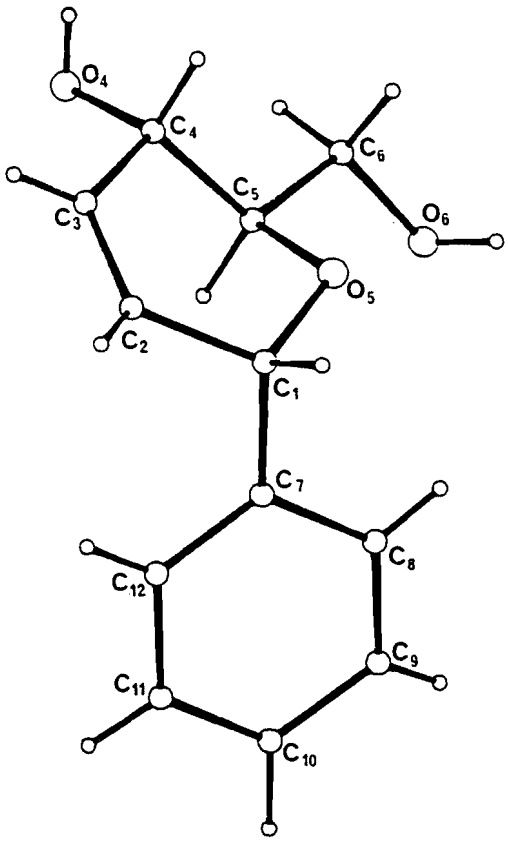

FIG. 2. ORTEP (16) representation of the molecule and atomic numbering.

lographically observed structure (ORTEP (16)) and atomic numbering are shown in Fig. 2. Coordinates and isotropic thermal parameters for carbon and oxygen atoms are listed in Table 1. Interatomic distances and bond angles are given in Tables 2 and 3.

Although the X-ray data determined only the relative position of the atoms, the certainty with respect to the chirality of C(4) and C(5) unambiguously established the α configuration of C(1). The enopyranoid ring of **5′** exhibits a distorted half-chair $^{0}H_{5}$ conformation in which C(1), C(2), C(3), C(4) are coplanar (π), C(5) and O(5) deviating disymmetrically by 0.53 and 0.25 Å respectively on both sides of this π plane. The ring deformation is related to the torsion angles listed in Table 4.

The dihedral angle between the π and benzene planes is 57.3°. This deviation from perpendicularity is related to the distortion of the $^{0}H_{5}$ enopyranoid ring. The values of the exocyclic torsion angles O(5)C(1)C(7)C(8) (−142.1(6)°) and O(5)C(1)C(7)C(12) (41.1(4)°) indicate that the conformation around the C(1)—C(7) bond approaches the energetic minimum of the "axial perpendicular" conformation of phenylcyclohexane (17).

Twelve molecules related to **5′** have already been characterized by X-ray diffraction (5, 18). Among these 13 enopyranoid rings, the ideal $^{0}H_{5}$ conformation was adopted by three of them (18*a–c*); in five others, this conformation was slightly distorted (8, 18*d–g*); in the remaining five (compound **5′** and refs. 18*e*, *h*, and *i*) a significant deformation towards the E_5 conformation was observed and C(5) deviates from the π plane at least 0.2 Å more than O(5). This deformation could be related neither to the size of the enopyranoid ring substituents nor to the conformation

TABLE 1. Coordinates and isotropic thermal parameters of carbon and oxygen atoms

Atom	*x*	*y*	*z*	*U*
C(1)	0.3323(2)	0.3413(6)	0.6614(8)	0.041(4)
C(2)	0.3276(2)	0.2863(6)	0.8952(10)	0.053(5)
C(3)	0.3718(3)	0.2009(6)	0.9867(8)	0.053(5)
C(4)	0.4315(2)	0.1581(5)	0.8768(8)	0.038(4)
C(5)	0.4408(2)	0.2725(5)	0.6879(7)	0.032(3)
C(6)	0.4952(2)	0.2257(5)	0.5460(7)	0.043(4)
C(7)	0.3335(2)	0.5263(5)	0.6308(9)	0.039(4)
C(8)	0.3155(2)	0.6345(7)	0.7880(9)	0.051(5)
C(9)	0.3151(3)	0.8032(7)	0.7491(10)	0.062(6)
C(10)	0.3330(3)	0.8627(6)	0.5547(11)	0.061(6)
C(11)	0.3508(2)	0.7551(6)	0.3945(10)	0.059(6)
C(12)	0.3508(2)	0.5897(7)	0.4310(10)	0.053(5)
O(4)	0.4844(2)	0.1722(4)	1.0196(5)	0.051(3)
O(5)	0.3853(1)	0.2668(3)	0.5589(4)	0.037(2)
O(6)	0.5070(1)	0.3463(4)	0.3848(5)	0.045(3)

TABLE 2. Bond lengths (Å)

Atoms	Length (Å)
C(1)—C(2)	1.520(8)
C(2)—C(3)	1.303(7)
C(3)—C(4)	1.486(7)
C(4)—C(5)	1.511(6)
C(5)—O(5)	1.429(5)
O(5)—C(1)	1.432(5)
C(5)—C(6)	1.507(6)
C(4)—O(4)	1.438(5)
C(6)—O(6)	1.424(5)
C(1)—C(7)	1.522(6)
C(7)—C(8)	1.370(7)
C(8)—C(9)	1.397(8)
C(9)—C(10)	1.355(9)
C(10)—C(11)	1.379(8)
C(11)—C(12)	1.368(6)
C(12)—C(7)	1.392(5)

TABLE 3. Bond angles (deg)

Atoms	Angle (deg)
O(5)C(1)C(2)	110.5(4)
C(1)C(2)C(3)	121.7(5)
C(2)C(3)C(4)	123.1(5)
C(3)C(4)C(5)	108.8(4)
C(4)C(5)O(5)	107.8(3)
C(5)O(5)C(1)	113.0(3)
C(2)C(1)C(7)	114.4(4)
O(5)C(1)C(7)	110.6(3)
C(3)C(4)O(4)	111.7(4)
C(5)C(4)O(4)	109.0(3)
C(4)C(5)C(6)	113.4(4)
O(5)C(5)C(6)	107.7(3)
C(5)C(6)O(6)	111.7(3)
C(12)C(7)C(8)	117.9(4)
C(7)C(8)C(9)	120.8(6)
C(8)C(9)C(10)	120.3(5)
C(9)C(10)C(11)	119.4(5)

Can. J. Chem. Downloaded from www.nrcresearchpress.com by 88.85.125.76 on 09/07/12
For personal use only.

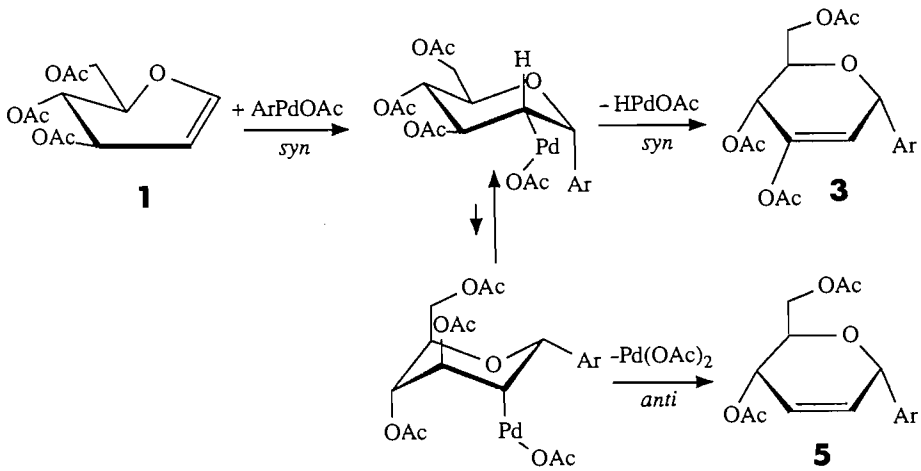

SCHEME 1. General picture of the arylation of **1**.

TABLE 4. Enopyranoid ring torsion angles (deg)

Atoms	Angle (deg)
O(5)C(1)C(2)C(3)	8.3(4)
C(1)C(2)C(3)C(4)	3.5(5)
C(2)C(3)C(4)C(5)	19.0(4)
C(3)C(4)C(5)O(5)	−52.9(4)
C(4)C(5)O(5)C(1)	69.6(4)
C(5)O(5)C(1)C(2)	−45.3(4)

change at C(4). It could rather be ascribed to the crystal field constraints.

Mechanistic implications

The better knowledge of the stereochemical outcome of the reaction affords a new insight into its mechanism, as exemplified for **1** in Scheme 1.

As proposed in our previous paper (1), the main product (**3**) is formed by a *syn* addition of an arylpalladium (ArPdOAc) from the α face of the glycal followed by a *syn* elimination of hydridoacetatopalladium.

Since the anomeric configuration of **5** was initially incorrectly assigned, a *syn* addition of ArPdOAc from the β face of the glucal followed by a *syn* elimination of $Pd(OAc)_2$ was initially evoked (1) to explain its formation. At that time, the stereochemistry of HPdOAc elimination was well documented (19), whereas that of $Pd(OAc)_2$ loss was not known.

Finally the *stereospecificity* of the initial attack of ArPdOAc to the glucal is demonstrated by the fact that **3** and **5** have the same anomeric configuration. Consequently, only one σ-alkyl palladium intermediate is generated from which **3** is formed by the usual *syn* elimination of HPdOAc and **5** by *anti* elimination of $Pd(OAc)_2$ after conformational change. It has been recently demonstrated (13) with rigid structures that the steric requirements for an *anti* elimination of palladium acetate is a *trans*-diaxial arrangement of palladium and β-acetate.

It is unclear why attack of the organopalladium reagent on the pyranoid glycal double bond for π-complex and σ-adduct formation should be stereospecific. Daves and co-workers also observed (13) that the Pd-mediated reactions of various pyranoid glycals with (1,3-dimethyl-2,4-dioxo 1,2,3,4-tetrahydropyrimidin-5-yl)mercuric acetate occurred regio- and stereospecifically to form, in each case, a single σ-alkylpalladium intermediate. The same stereospecificity was observed in our laboratory in the Pd-mediated arylation of three enones derived from glycals (20).

Experimental

General procedures are the same as indicated before (1).

*(4,6-Di-O-acetyl-2,3-dideoxy-α-D-*erythro*-hex-2-enopyranosyl)-benzene* **5** was prepared as previously reported (1) and characterized as follows: oil; R_f 0.59 (pet. ether:ether, 1:2); $[\alpha]_D^{20}$ +3.3° (*c* 1.34, $CHCl_3$); ν_{max} (film): 1735 (ester), 1690 (C=C), 730 (*cis*-alkene) cm^{-1}; uv (95% ethanol) ε_{257} = 553; ^1H nmr δ ($CDCl_3$; 250 MHz): 2.07 (s, 3H, $OCOCH_3$), 2.09 (s, 3H, $OCOCH_3$), 3.85 (ddd, 1H, H-5, J_{4-5} = 6.8 Hz), 4.10 (dd, 1H, H-6, J_{5-6} = 5.9 Hz and $|J_{6-6'}|$ = 12 Hz, 4.27 (dd, 1H, H-6′, $J_{5-6'}$ = 3.1 Hz), 5.32 (m, 1H, H-4), 5.33 (m, 1H, H-1), 5.99 (ddd, 1H, H-2 or H-3), 6.19 (ddd, 1H, H-2 or H-3), 7.27–7.45 (m, 5H, Ph); δ (C_6D_6; 250 MHz): 1.67 (s, 3H, $OCOCH_3$), 1.69 (s, 3H, $OCOCH_3$), 3.93 (ddd, 1H, H-5, J_{4-5} = 7 Hz), 4.12 (dd, 1H, H-6′, $J_{5-6'}$ = 3.2 Hz), 4.28 (dd, 1H, H-6, J_{5-6} = 6 Hz and $|J_{6-6'}|$ = 12 Hz), 5.13 (dd, 1H, H-1, J_{1-4} = 2.4 Hz), 5.44 (ddd, 1H, H-4), 5.76 (ddd, 1H, H-2, J_{2-3} = 10.3 Hz, J_{2-1} = 2.9 Hz, and J_{2-4} = 1.5 Hz), 5.88 (ddd, 1H, H-3, J_{3-1} = 2 Hz and J_{3-4} = 2.5 Hz), 6.87–7.20 (m, 5H, Ph); ^{13}C nmr δ ($CDCl_3$, 77.05 60 MHz): 20.62 and 20.90 (2 × $OCOCH_3$), 62.9 (C-6), 65.11 (C-4), 69.51 (C-5), 73.6 (C-1), 124.9 (C-3), 131.5 (C-2), 127.8, 128.11, 128.4, 138.97 (C phenyl); mass spectrum (70 eV) *m/e*: 290 (M^+) 105 (100%) (Ph-C≡O^+). Anal. calcd. for $C_{16}H_{18}O_5$ (290.3): C 66.19, H 6.25; found: C 66.16, H 6.17.

*(2,3-Dideoxy-α-D-*erythro*-hex-2-enopyranosyl)benzene* **5′**

A solution of **5** (100 mg, 0.34 mmol) in MeOH (4 mL) was stirred in the presence of 15 mg of Amberlite IRN-78 (OH^-) for 16 h at room temperature. After completion of the reaction was indicated by tlc (pet. ether:ether, 1:2) the reaction mixture was filtered. Removal of solvent gave a crude product, which was purified by flash column chromatography (silica gel; $CHCl_3$:MeOH, 98:2) to give **5′** (54 mg, 77%); mp 101–102°C (cyclohexane, diethyl ether, absolute ethanol); R_f 0.55 ($CHCl_3$:MeOH, 9:1); $[\alpha]_D^{20}$ −52° (*c* 0.97, MeOH). Anal. calcd. for $C_{12}H_{14}O_3$ (206): C 69.90, H 6.80; found: C 68.79, H 6.90.

Circular dichroism spectra were recorded on a Jobin et Yvon dicrograph III at room temperature with 1- or 2-cm cells. The compounds were dissolved in 95% EtOH to a concentration of ca. 0.6 mg/mL.

X-ray diffraction

A thin elongated plate (0.08 × 0.2 × 0.6 mm), obtained by

Can. J. Chem. Downloaded from www.nrcresearchpress.com by 88.85.125.76 on 09/07/12
For personal use only.

crystallization from a (cyclohexane, diethyl ether, absolute ethanol) solution, was mounted on an automatic Philips PW 1100 diffractometer. The orthorhombic cell parameters were obtained by least-squares refinement with the 2θ values of 25 reflections ($20 < \theta < 50°$) for monochromatized CuK_α radiation: $a = 21.338(5)$, $b = 8.161(2)$, $c = 6.209(1)$ Å, $V = 1081.2(6)$ Å^3, space group $P2_12_12_1$, $Z = 4$, $\rho_c = 1.27$ g cm^{-3}. Intensities were collected in the following conditions: room temperature, $2\theta_{max} = 138°$; $-24 < h < 24$, $-9 < k < 9$, $0 \leq l < 7$; θ–2θ scan mode; $\mu = 6.57$ cm^{-1}. Of the 4386 collected intensities, 1193 were independent and, on the criterion $I > 2.5\sigma(I)$, 1112 were considered observed above background.

The carbon and oxygen atom positions, obtained by multisolution direct methods (DEVIN program (21)), were refined by a full-matrix least-squares procedure (SHELX (22)). The H atoms were located on difference electron-density maps calculated at intermediate stages of the refinement. In the final cycles, positional parameters for all atoms were refined. Anisotropic thermal parameters were varied only for the carbon and oxygen atoms. The final values of the residuals $R(F)$ $(\Sigma(|F_o| - |F_c|)/\Sigma|F_o|)$ and $R(WF)$ $(\Sigma(|F_o| - |F_c|) \times W^{1/2}/\Sigma|F_o| \times W^{1/2})$ with $W = 1/\sigma^2(F)$ were respectively 0.08 and 0.066. The highest residual electron density on the difference map was 0.4 e Å^{-3}. Tables of anisotropic thermal parameters, hydrogen atom coordinates, and a listing of structure factor amplitudes have been deposited.[5]

Acknowledgements

We are grateful to Doctor Jacques Bolard (Dept. Rech. Phys., Univ. P. et M. Curie, Paris, France) for the use of his circular dichroism apparatus.

1. S. Czernecki and V. Dechavanne. Can. J. Chem. **61**, 533 (1983).
2. J. B. Stothers. Carbon-13 NMR spectroscopy. Academic Press, New York. 1972. Chap. 3.
3. R. D. Dawe and B. Fraser-Reid. J. Chem. Soc. Chem. Commun. 1180 (1981); J. Org. Chem. **49**, 522 (1984).
4. L. V. Dunkerton and A. J. Serino. J. Org. Chem. **47**, 2812 (1982); L. V. Dunkerton, J. M. Euske, and A. J. Serino. Carbohydr. Res. **171**, 89 (1987).
5. H. Gillier-Pandraud, R. Brahmi, V. Bellosta-Dechavanne, and S. Czernecki. Can. J. Chem. **63**, 491 (1985).
6. V. Bellosta and S. Czernecki. Carbohydr. Res. **171**, 279 (1987).
7. G. Grynkiewicz and A. Zamojski. Z. Naturforsch. **35B**, 1024 (1980).
8. G. Casiraghi, M. Cornia, L. Colombo, G. Rassu, G. Gasparri Fava, M. Ferrari Belicchi, and L. Zetta. Tetrahedron Lett. **29**, 5549 (1988).
9. (*a*) H. H. Baer and Z. S. Hanna. Can. J. Chem. **59**, 889 (1981); (*b*) R. U. Lemieux, K. A. Watanabe, and A. A. Pavia. Can. J. Chem. **47**, 4413 (1969); (*c*) B. Fraser-Reid, B. J. Carthy, N. L. Holder, and M. Yunker. Can. J. Chem. **49**, 3038 (1971).
10. M. Brakta, F. Le Borgne, and D. Sinou. J. Carbohydr. Chem. **6**, 307 (1987).
11. F. G. De las Heras, H. San Felix, and P. Fernandez-Resa. Tetrahedron, **39**, 1617 (1983).
12. S. J. Danishefsky, S. De Ninno, and P. Lartey. J. Am. Chem. Soc. **109**, 2082 (1987).
13. J. C.-Y. Cheng, U. Hacksell, and G. D. Daves, Jr. J. Org. Chem. **52**, 3083 (1987).
14. V. Bellosta. Doctoral Thesis, Université P. et M. Curie, Paris, France. 1987.
15. K. Nakanishi, H. W. Park, R. Takeda, J. T. Vasquez, and W. Wiesler. Stereochemistry of organic and bioorganic transformations. *Edited by* W. Bartmann. Verlag Chemie, Weinheim. 1987. pp. 303–319.
16. C. K. Johnson. ORTEP, Report ORNL-3794. Oak Ridge National Laboratory, Oak Ridge, TN. 1965.
17. N. L. Allinger and M. T. Tribble. Tetrahedron Lett. 3259 (1971).
18. (*a*) Z. Ruzic-Toros, V. Rojic, and B. Kojic-Prodic. Acta Crystallogr. Sect. B: Struct. Crystallogr. Cryst. Chem. **B36**, 607 (1980); (*b*) J. W. Krajewski, Z. Urbanczyk-Lipowska, P. Gluzinski, J. Bleidelis, and A. Kemme. Acta Crystallogr. Sect. B: Struct. Crystallogr. Cryst. Chem. **B35**, 2625 (1979); (*c*) B. Kojic-Prodic. Acta Crystallogr. Sect. B: Struct. Crystallogr. Cryst. Chem. **B35**, 1162 (1979); (*d*) M. Cesario, J. Guilhem, and J. C. Martin. Carbohydr. Res. **71**, 1 (1979); (*e*) J. W. Krajewski, P. Gluzinski, Z. Urbanczyk-Lipowska, A. Banaszek, K. Vangehr, and P. Luger. Carbohydr. Res. **125**, 203 (1984); (*f*) J. Lopez de Lerma, S. Martinez-Carrera, and S. Garcia-Blanco. Acta Crystallogr. Sect. B: Struct. Crystallogr. Cryst. Chem. **B29**, 537 (1973); (*g*) B. Kojic-Prodic, V. Rogic, and Z. Ruzic-Toros. Acta Crystallogr. Sect. B: Struct. Crystallogr. Cryst. Chem. **B32**, 1833 (1976); (*h*) Z. Ruzic-Toros, B. Kojic-Prodic, and E. Coffou. Acta Crystallogr. Sect. B: Struct. Crystallogr. Cryst. Chem. **B37**, 877 (1981); (*i*) L. M. Wingert, J. R. Ruble, and G. A. Jeffrey. Carbohydr. Res. **128**, 1 (1984).
19. P. M. Henry and G. A. Ward. J. Am. Chem. Soc. **94**, 673 (1972).
20. R. Benhaddou. Doctoral Thesis, Université P. et M. Curie, Paris, France. 1988.
21. C. Riche. Acta Crystallogr. Sect. A: Cryst. Phys. Diffr. Theor. Gen. Crystallogr. **A29**, 133 (1973).
22. G. Sheldrick. SHELX, program for crystal structure determination. Univ. of Cambridge, England. 1976.

[5]These tables may be purchased from the Depository of Unpublished Data, CISTI, National Research Council of Canada, Ottawa, Ont., Canada K1A 0S2.

Can. J. Chem. Downloaded from www.nrcresearchpress.com by 88.85.125.76 on 09/07/12
For personal use only.

Ozonolyses of 1,4-disubstituted 1,3-cyclohexadienes and of related compounds in methanol

KARL GRIESBAUM,[1] HENRI MERTENS, AND IN CHAN JUNG
Engler-Bunte-Institut, Bereich Petrochemie, Universität Karlsruhe (TH), D-7500 Karlsruhe, Germany

Received November 10, 1989

KARL GRIESBAUM, HENRI MERTENS, and IN CHAN JUNG. Can. J. Chem. **68**, 1369 (1990).

Ozonolyses of 1,4-dimethyl- (**5***a*) and of 1-methyl-4-isopropyl-1,3-cyclohexadiene (**5***b*) in methanol occur stepwise by sequential cleavage of the two double bonds. Monoozonolysis products are the corresponding compounds **6** and **7**, and diozonolysis products are the corresponding cyclic peroxides **19, 20**, and **21**. By contrast, ozonolysis of the non-conjugated diene 2,5-dimethyl-1,5-hexadiene (**13**) in methanol occurs by simultaneous mono- and diozonolysis to give **14, 16***a*, **18***a*, and **20***a*.

Key words: ozonolysis, 1,3-cyclohexadienes, 3-hydroperoxy-1,2-dioxanes, 2,5-bis-hydroperoxy-2,5-dimethoxyhexane, 3-hydroxy-1,2-dioxanes, 3,6-dimethoxy-1,2-dioxanes.

KARL GRIESBAUM, HENRI MERTENS et IN CHAN JUNG. Can. J. Chem. **68**, 1369 (1990).

L'ozonolyse, dans le méthanol, des 1,4-diméthyl- (**5***a*) et 1-méthyl-4-isopropyl-cyclohexa-1,3-diène (**5***b*) se produit par des clivages par étape des deux doubles liaisons. Les produits de monoozonolyse sont les composés **6** et **7** alors que les produits de diozonolyse sont les peroxydes cycliques correspondants **19, 20** et **21**. Par opposition, l'ozonolyse dans le méthanol d'un diène non-conjugué, comme le 2,5-diméthyl-hexa-1,5-diène (**13**), provoque des mono- et des di-ozonolyses simultanées qui fournissent les produits **14, 16***a*, **18***a* et **20***a*.

Mots clés : ozonolyse, cyclohexa-1,3-dièns, 3-hydroperoxy-1,2-dioxanes, 2,5-bis-hydroperoxy-2,5-diméthoxyhexane, 3-hydroxy-1,2-dioxanes, 3,6-diméthoxy-1,2-dioxanes.

[Traduit par la revue]

Can. J. Chem. Downloaded from www.nrcresearchpress.com by 88.85.125.76 on 09/07/12
For personal use only.

Introduction

Ozonolysis reactions of conjugated cyclic diolefins in participating solvents have not been studied extensively, and essential details concerning the course of events are unknown. Ozonolysis of 1,3-cyclohexadiene gave a mixture of oxalic acid and succinic acid (1); ozonolysis of 1-methyl-4-isopropyl-1,3-cyclohexadiene in methanol, followed by reduction with sodium iodide in acetic acid, gave 2-methyl-3,6-dioxoheptane (2). Ozonolysis of naphthalene (**1***a*) and of the substituted naphthalenes **1***b*–*d* in methanol afforded in each case the hemiperacetal **2***a*, and **1***d* gave, additionally, the peracetal **2***d* (3). Compounds **3** and **4** have been postulated, yet not proven, as intermediates for **2***a* and **2***d*, respectively. Similar results were reported for the ozonolysis of 1-methylnaphthalene (4) and of substituted 2-methoxynaphthalenes (5) in methanol.

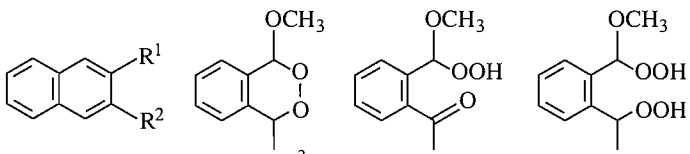

1 **2** **3** **4**

	R^1	R^2	R^3
a	H	H	H
b	CH_3	CH_3	H
c	OH	H	H
d	OCH_3	H	CH_3

The results of these ozonolysis reactions did not reveal (a) whether ozone attack at the two double bonds of the diene systems occurred simultaneously or consecutively, (b) the direction of cleavage, and (c) the nature of the primary cleavage products. In line with our continued interest in the ozonolysis of conjugated dienes (6), we have now studied the ozonolysis of the cyclodienes **5***a* and **5***b*, and of the acyclic substrates **13** and **15** in methanol at ca. −75°C.

Results and discussion

Monoozonolyses of the dienes 5a, 5b, *and 13*

Treatment of **5***a* with 0.7 molar equivalents of ozone gave the two monoozonolysis products **6***a* and **7***a* in a ratio of 3:2, as shown by ^{1}H nmr analysis of the fresh ozonolysis product. Compound **7***a* could be isolated and structurally assigned by spectroscopic methods. At room temperature it decomposed slowly to give a mixture of **8***a* and **9***a*. Compound **6***a* was less stable and decomposed when we tried to isolate it. Hence its structural assignment is based only on its ^{1}H nmr data, which were obtained from the mixture of **6***a* and **7***a* in the crude reaction product, and on the fact that reduction of this mixture with dimethyl sulfide gave *Z*-**8***a* and *E*-**8***a* (ratio 1:2) as the sole products.

Treatment of **5***b* with ca. 0.8 molar equivalents of ozone afforded a peroxidic product mixture from which ca. 3% of **7***b*, 5% of **7***c*, 6% OF **8***b* (unknown stereochemistry), 2% of *E*-**8***c*, 2% of *Z*-**8***c*, 1% of **10***b*, and 0.1% of **10***c* have been isolated. While **6***b* and **6***c* could not be positively identified in the product mixture, there is indirect evidence for their transient existence from the results of the diozonolysis of **5***b* as reported below. We assume, by analogy with **6***a*, that **6***b* and **6***c* are labile and undergo rapid decomposition, possibly in part by oxygen transfer to the double bonds of **8***b* and **8***c* to give epoxides **10***b* and **10***c*, respectively.

The isolated hydroperoxides **7***b* and **7***c* decomposed spontaneously in $CDCl_3$, and within ca. 18 h as neat samples at room temperature, to give **8***b* and **8***c*, respectively. In $CDCl_3$/pyridine they were stable for several hours. Reductions of **7***b* and **7***c* with dimethyl sulfide also afforded **8***b* and **8***c*, respectively. Compound **8***b* of unknown geometry as well as *Z*-**8***c* and *E*-**8***c* have been identified by comparison of their ^{1}H nmr and mass spectral data with those published in the literature (7). Epoxides **10***b* and **10***c* have been tentatively identified based on their ^{1}H nmr data.

[1]Author to whom correspondence may be addressed.

Printed in Canada / Imprimé au Canada

Can. J. Chem. Downloaded from www.nrcresearchpress.com by 88.85.125.76 on 09/07/12
For personal use only.

The relative proportions of the ozonolysis products in the crude reaction mixture could not be determined by glc analysis due to the thermal instability of **7***b* and of **7***c*, nor by ^{1}H nmr analysis due to overlap of diagnostic signals. Immediate reduction of a fresh ozonolysis product mixture with dimethyl sulfide afforded **8***b* and **8***c* in relative amounts of 70 and 30%.

The above results show that ozone attack at the conjugated diene systems of **5***a* and **5***b* occurs stepwise and that, probably for steric reasons, attack at the methyl substituted double bond of **5***b* is approximately 2.3 times faster than attack at the isopropyl substituted double bond. The direction of cleavage in the monoozonolysis of **5***a*, which gave **11***a* and **12***a* in approximately equal amounts as primary cleavage products, is not in line with the experience that trialkyl substituted double bonds are almost exclusively cleaved to give the higher substituted carbonyl oxide. We believe that the stepwise attack of ozone at **5***a* and **5***b* is due to the fact that the oxygenated functional groups that are formed in allylic positions to the remaining double bonds of the monoozonolysis products **6** and **7** deactivate these double bonds against further ozone attack. Similarly, the relatively high proportion of **7***a* formed in the ozonolysis of **5***a* can be ascribed to resonance stabilization of the positive centre of the carbonyl oxide moiety in **12***a* by the neighbouring double bond.

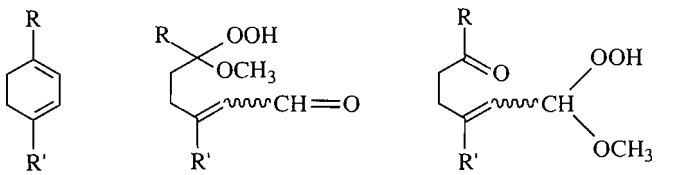

5 **6** **7**

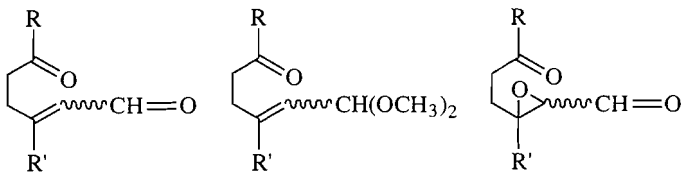

8 **9** **10**

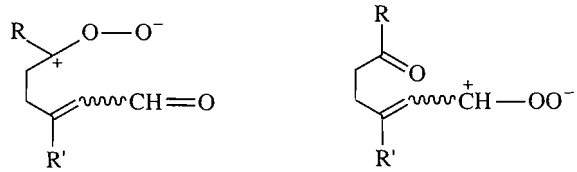

11 **12**

a: R = R' = CH_3
b: R = CH_3, R' = $(CH_3)_2CH$
c: R = $(CH_3)_2CH$, R' = CH_3

To test the above hypotheses concerning the reasons for the stepwise ozone attack and for the direction of cleavage, we investigated the monoozonolysis of the non-conjugated diene **13**. Treatment of **13** with 0.7 molar equivalents of ozone gave a mixture of **14** (52%),[2] **16***a* (23%), **19***a* (7%), *cis*-**20***a* (10%), and *trans*-**20***a* (8%), as shown by ^{1}H nmr analysis. Hydroperoxides **14** and **16***a* have been isolated and characterized by their ^{1}H nmr spectra as well as by reduction with triphenyl phosphine to give **15** and **17***a*, respectively. Monoozonolysis of **13** followed by immediate reduction with triphenyl phosphine afforded **15** and **17***a* in a ratio of 54:46.

From these results it can be concluded that, in contrast to the conjugated diene **5***a*, the two double bonds in **13** are almost simultaneously attacked by ozone to give approximately equal amounts of mono- and diozonolysis products. This is ascribed to the fact that the functional groups introduced by monoozonolysis are so remote from the remaining double bond that they do not decrease its reactivity towards ozone attack. It can be further concluded that ozone cleavage of the double bonds in **13** occurs predominantly in one direction only, with formation of the higher substituted carbonyl oxides, since there was no indication for the presence of either **15** or **17***a* in the product mixture.

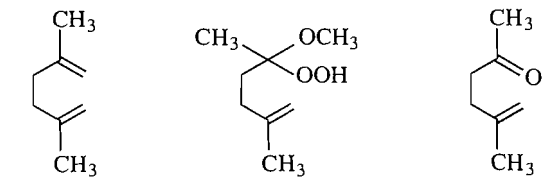

13 **14** **15**

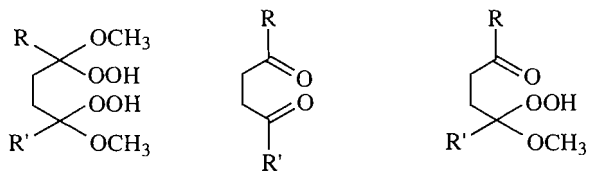

16 **17** **18**

a: R = R' = CH_3
b: R = CH_3, R' = $(CH_3)_2CH$

Diozonolyses of 5a, 5b, *and* **13** *and ozonolysis of some model compounds*

Diozonolysis of **5***a* gave 70–80% of **16***a* along with small amounts, each, of **19***a*, *cis*- and *trans*-**20***a*, and *cis*- and *trans*-**21***a*. After warm-up to room temperature and evaporation of the solvent, the contents of **19***a* (33%),[3] *cis*-**20***a* (12%), *trans*-**20***a* (19%), *cis*-**21***a* (11%), and *trans*-**21***a* (24%) had considerably increased at the expense of that of **16***a*, which had virtually disappeared.

Diozonolysis of **13** and oznonolysis of **14** gave similar results: Immediately after completion of the reaction, **16***a* was the major product in selectivities of 65% and 85%, respectively, but after warm-up to room temperature **16***a* had again disappeared. Thus, the aged product mixture derived from the ozonolysis of **13** contained **19***a* (12%), *cis*-**20***a* (12%), *trans*-**20***a* (11%), *cis*-**21***a* (20%), and *trans*-**21***a* (45%), yet none of **16***a*. From such mixtures, *cis*-**20***a* (in admixture with 30% of the *trans* isomer), *trans*-**20***a* (in admixture with 10% of the *cis* isomer), *cis*-**21***a*, and *trans*-**21***a* have been isolated.

Ozonolysis of **15** gave a mixture of **17***a* (27%)[2] and **19***a* (73%), from which **19***a* has been isolated. There was no indication for the presence of **18***a*.

Diozonolysis of **5***b* and subsequent warm-up to room temperature gave a product mixture from which **19***b*, **19***c*, and **21***b*, each of unknown stereochemistry, as well as *cis*-**20***b*, *trans*-**20***b*, *cis*-**20***c*, *trans*-**20***c*, and a mixture of **17***b* and **22**

[2]Relative product distribution. The products derived from the $=CH_2$ moiety are not included in the material balance.

[3]Relative product distribution. The products derived from the =CH—CH= moiety are not included in the material balance.

have been isolated. Due to overlap of diagnostic signals, the relative amounts of these compounds in the product mixture could not be determined by ^1H nmr spectroscopy. Ozonolyses of **8***b* and of **8***c* gave mixtures of **17***b* (58%), **19***b* (31%), **22** (11%), and of **17***b* (41%), **19***c* (32%), **22** (27%), respectively.

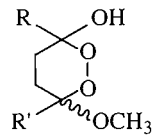

19

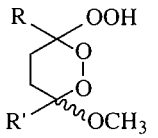

20

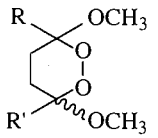

21

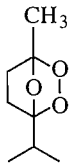

22

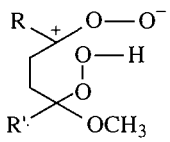

23

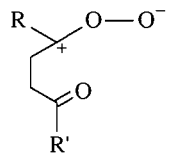

24

a: R = R' = CH_3
b: R = CH_3, R' = $(CH_3)_2CH$
c: R = $(CH_3)_2CH$, R' = CH_3

The hemiperacetals **19***a*, **19***b*, and **19***c* of unknown stereochemisty have been characterized by their ^1H and ^{13}C nmr spectra, by elemental analysis, and by reduction with dimethyl sulfide to give the corresponding diketones of structure **17**. Their formation is explained by ozone cleavage of monoozonolysis products **14** and **6, 7, 8**, respectively, to give γ-keto hydroperoxides of structure **18**, which subsequently undergo intramolecular acetalization. In the latter reaction, the equilibrium is apparently completely shifted towards the side of the hemiperacetal, since **19***a*, **19***b*, and **19***c* showed no positive hydroperoxide test with lead tetraacetate (8).

The hydroperoxyperoxides **20***a*, **20***b*, and **20***c* have been characterized by their ^1H and ^{13}C nmr spectra, by positive hydroperoxide tests with lead tetraacetate (8), and by reduction with dimethyl sulfide to give the corresponding diketones of structure **17** and dimethyl sulfoxide in molar ratios of 1:2. The stereochemical assignments are based on the assumptions (a) that in **20***a* the methyl group at the hydroperoxy substituted carbon atom and in **20***b* and **20***c* the isopropyl groups assume equatorial positions in the preferred conformations owing to the relatively high *A* values (9*a*), and (b) that, by analogy with results obtained for other substituted 6-membered rings (9*b*), the signals of the CH_3O groups in the equatorial position of *cis*-**20***a* (δ = 3.39), and of *cis*-**20***c* (δ = 3.40) as well as the signal of the axial CH_3 group of *cis*-**20***b* (δ = 1.50) appear downfield from the corresponding signals of *trans*-**20***a* (δ = 3.36) *trans*-**20***c* (δ = 3.36) and *trans*-**20***b* (δ = 1.37).

The formation of compounds **20***b* and **20***b,c* can be rationalized by further ozone cleavage of the monoozonolysis products **14** and **6**, respectively, to give intermediates of structure **23**. In the latter, the carbonyl oxide moiety can react either intramolecularly with the hydroperoxide group of **23** to give **20** or intermolecularly with methanol to give **16**, which subsequently forms **20** by intramolecular displacement of methanol. We could not find experimental evidence for the first reaction path, i.e., the intramolecular reaction of **23** to give **20**, and to our knowledge trapping of a carbonyl oxide by a hydroperoxide is hitherto unknown. The second reaction path via a bis-hydroperoxide of structure **16** is obviously responsible for the formation of **20***a* following the diozonolysis of **5***a* and of **13** since, as reported above, **20***a* was in each case formed at the expense of the precursor **16***a* upon warm-up of the fresh ozonolysis mixture. In support of this reasoning, it was found that authentic **16***a* in $CDCl_3$ was converted into a mixture containing 30% of *cis*-**20***a*, 30% of *trans*-**20***a*, 22% of cis-**21***a*, and 18% of *trans*-**21***a* when it was kept at room temperature overnight.

A priori, one had also to consider a third mode of formation for compounds **20**, viz. hydrolysis of methoxy hydroperoxides of types **6, 14, 16**, or **18** by trace amounts of water to give hydrogen peroxide, which in turn reacts with hemiperacetals of structure **19** to give **20**. If this were truely an alternative, one should also expect the formation of **20***a* in the ozonolysis of **15**. It should provide **18***a* as the primary product. This could undergo partial hydrolysis to give H_2O_2, which in turn could react with **19***a* to give **20***a*, whereas none of the intermediates **16***a* or **23***a*, required for the formation of **20***a* by the alternate routes, can be derived from **15**. As reported above, ozonolysis of **15** gave **17***a* and **19***a*, yet not detectable amounts of **20***a*, thus ruling out the third potential mode of formation for compounds **20**.

The cyclic peroxides **21***a* and **21***b* were characterized by their ^1H and ^{13}C nmr spectra, by elemental analysis, and by reduction with triphenyl phosphine to give the corresponding diketones of structure **17**. Both **21***a* and **21***b* are remarkably stable, as evidenced by the fact that reduction with sodium iodide or with triphenyl phosphine did not occur at room temperature but had to be performed at ca. 60°C. The stereochemical assignments of *cis*- and *trans*-**21***a* are again based on the assumptions (a) that due to the larger *A* value (9*a*), the methyl groups in *trans*-**21***a* assume equatorial positions in the preferred conformation, and (b) that the signals of the resulting axial CH_3O groups appear upfield (9*b*) (δ = 3.34) from those of the axial and equatorial CH_3O groups (δ = 3.38) in *cis*-**21***a*. The stereochemistry of isolated **21***b* could not be assigned on the basis of the above arguments, since only one isomer was obtained.

The formation of the cyclic peroxides **21** can be rationalized by reaction of compounds **19** or **20** with methanol. This view is supported by the fact that the yield of isolated **21***b* from the diozonolysis of **5***b* could be increased to 31% when the crude product mixture was treated with *p*-toluenesulfonic acid for 20 h, i.e., when the acetalization of **19***b* and **20***b* was catalyzed by acid.

The structure of ozonide **22** was proven through the independent preparation of **22** by the ozonolysis of a mixture of **8***b* and **8***c* in pentane and by reduction of **22** with triphenyl phosphine to give **17***b*. The formation of **22** from **5***b* is rationalized by intramolecular cycloaddition of the carbonyl oxide moieties with the carbonyl groups of intermediates **24***b* and **24***c*. The fact that **22** is obtained even in methanol as a solvent indicates that this cycloaddition competes favourably with the trapping of the carbonyl oxide by methanol.

In summary, the work described in this paper has shown that the course of the ozonolysis of conjugated dienes deviates considerably from that of similarly structured non-conjugated dienes both in the sequence of ozone attack and in the direction of cleavage of the two double bonds. Furthermore, the previously postulated (4, 5) intermediacy of 1,4-bis-methoxyhydroperoxides like **4** has now been proven by the isolation of **16***a*, and it was shown that they serve not only as precursors for compounds like **2***d* or **21**, but that they react also to give the hitherto unknown class of compounds **20**.

Can. J. Chem. Downloaded from www.nrcresearchpress.com by 88.85.125.76 on 09/07/12
For personal use only.

Can. J. Chem. Downloaded from www.nrcresearchpress.com by 88.85.125.76 on 09/07/12
For personal use only.

Experimental

General methods

The ^{1}H nmr and ^{13}C nmr spectra were recorded on a Bruker WM 250 and, only where it is specifically mentioned, on a Bruker WP 60 or on a Bruker WH 300; ir spectra on a Beckman Acculab 1; and gc/ms spectra on a Hewlett–Packard 5985 B instrument. The glc analyses were carried out on a Shimadzu model 6A using a glass column 0.3 × 300 cm, 5% Nitrilesiliconoil XE 60 on Chromosorb G.

Monoozonolysis of **5**a

A solution of 0.3 g (2.8 mmol) of **5***a* (10) in 10 mL of methanol was treated with 0.7 molar equivalents of ozone at −75°C. The mixture was flushed with nitrogen and evaporated at room temperature with a water aspirator to leave 0.51 g of a colourless liquid residue; ^{1}H nmr analysis ($CDCl_3$, Me_4Si) showed the presence of **6***a* (δ: 1.36 (s, 3H), 2.00 (s, 3H), 3.34 (s, 3H), 5.91 (d, J = 7.7 Hz, 1H), 7.88 (br s, 1H), 9.94 (d, J = 7.7 Hz, 1H)) and of **7***a* (data, see below) in a ratio of 3:2. From 0.5 g of the residue 72 mg (13% yield) of **7***a* were isolated by flash chromatography (11) (column 2.5 × 50 cm; 60 g Florisil; 1 L of pentane and diethyl ether, 7:3; fractions of 50 mL) in fractions 7–9.

1-Hydroperoxy-1-methoxy-3-methyl-6-oxo-2-heptene (**7***a*):[4] Colourless liquid; ir (film), ν: 3400 (OOH), 1715 (C=O), 1680 (C=C) cm^{-1}; ^{1}H nmr ($CDCl_3$, Me_4Si), δ: 1.75 (d, J = 0.8 Hz, 3H), 2.19 (s, 3H), 2.26–2.65 (m, 4H), 3.52 (s, 3H), 5.27 (dd, J = 6.3 Hz and 0.8 Hz, 1H), 5.44 (d, J = 6.3 Hz, 1H), 9.28 (s, 1H); ^{13}C nmr ($CDCl_3$, Me_4Si), δ: 22.88 q, 26.78 t, 29.98 q, 41.52 t, 55.12 q, 104.67 d, 120.88 d, 142.51 s, 208.33 s.

Decomposition of **7**a

A sample of 0.3 g of neat **7***a* was kept at room temperature for 16 days; ^{1}H nmr analysis ($CDCl_3$, Me_4Si) showed the presence of 8% of *Z*-**8***a* (δ: 1.97 (d, J = 1.3 Hz, 3H), 2.19 (s, 3H), 5.88 (dd, J = 7.9 and 1.3 Hz, 1H), 9.97 (d, J = 7.9 Hz, 1H)); of 4% of *E*-**8***a* (δ: 2.19 (s, 6H), 5.83 (d, J = 7.8 Hz, 1H), 9.99 (d, J = 7.8 Hz, 1H)); 43% of *Z*-**9***a* (δ: 1.75 (s, 3H), 2.16 (s, 3H), 3.31 (s, 6H), 5.02 (d, J = 6.2 Hz, 1H), 5.30 (d, J = 6.2 Hz, 1H)); and 43% of *E*-**9***a* (δ: 1.73 (s, 3H), 2.16 (s, 3H), 3.30 (s, 6H), 5.02 (d, J = 6.4 Hz, 1H), 5.22 (d, J = 6.4 Hz, 1H)).

Monoozonolysis of **5**a *followed by reduction with dimethyl sulfide*

A solution of 0.3 g (2.8 mmol) **5***a* in 10 mL of methanol was ozonized with 0.7 molar equivalents of ozone at −75°C. The reaction product was flushed with nitrogen, admixed with 0.16 g (2.6 mmol) of dimethyl sulfide, kept at room temperature for 18 h, and then evaporated at room temperature with a water aspirator to leave 0.7 g of a colourless liquid residue. Gas–liquid chromatographic analysis (60–180°C at 10°C/min) with the help of authentic samples showed the presence of *Z*-**8***a* (t_R = 20.46 min) and of *E*-**8***a* (t_R = 22.77 min) in a ratio of 1:2.

Monoozonolysis of **5**b

A solution of 1.07 g (7.9 mmol) of **5***b* in 25 mL of methanol was ozonized with 0.8 molar equivalents of ozone at −78°C. The reaction product was flushed with nitrogen and evaporated, at room temperature and 18 Torr (1 Torr = 133.3 Pa), to leave 1.81 g of a liquid residue. By flash chromatography (11) (column 2 × 100 cm; 100 g of Florisil; 2 L of pentane/diethyl ether, 7:3; fractions of 50 mL), 79 mg (3.3%) of **7***b* (fractions 20–27) and 119 mg (5.0%) of **7***c* (fractions 11–16) were isolated. Flash chromatography of a second sample (column 2 × 100 cm; 123 g of silica gel; 2 L of pentane/diethyl ether, 7:3, followed by 1 L of diethyl ether: fractions of 50 mL) provided 637 mg of a mixture of **8***b* (51%), **8***c* (37%), **10***b* (11%), and **10***c* (1%). Separation of this mixture by the hplc method (column 1.6 × 25 cm; Lichrosorb Si 100; 10 bar (1 bar = 100 kPa); pentane/diethyl ether, 3:7) gave 110 mg (6%) of **8***b*, 34 mg (1.8%) of *E*-**8***c*, 45 mg (2.4%) of *Z*-**8***c*, 24 mg (1.1%) of **10***b*, and 1.8 mg (0.1%) of **10***c*.

1-Hydroperoxy-1-methoxy-3-isopropyl-6-oxo-2-heptene (**7***b*):[4] Colourless, viscous liquid; ir (film), ν: 3350 (OOH), 1710 (C=O), 1663 (C=C) cm^{-1}; ^{1}H nmr ($CDCl_3$/pyridine-d_5, Me_4Si), δ: 1.03 (dd, J = 6.8 and 0.7 Hz, 6H), 2.16 (s, 3H), 2.21–2.63 (m, 5H), 3.51 (s, 3H), 5.27 (dd, J = 6.3 and 0.7 Hz, 1H), 5.42 (d, J = 6.3 Hz, 1H).

1-Hydroperoxy-1-methoxy-3,7-dimethyl-6-oxo-2-octene (**7***c*):[4] Colourless, viscous liquid; ir (film), ν: 3370 (OOH), 1710 (C=O), 1665 (C=C) cm^{-1}; ^{1}H nmr ($CDCl_3$/pyridine-d_5, Me_4Si), δ: 1.10 (d, J = 6.9 Hz, 6H), 1.74 (d, J = 1.1 Hz, 3H), 2.15–2.72 (m, 5H), 3.51 (s, 3H), 5.28 (dd, J = 6.0 and 1.2 Hz, 1H), 5.44 (d, J = 6.0 Hz, 1H).

3-Isopropyl-6-oxo-2-heptenal (**8***b*; unknown stereochemistry): Colourless, viscous liquid; glc (60–160°C at 4°C/min), t_R = 50.16 min; ^{1}H nmr (60 MHz, $CDCl_3$, Me_4Si), δ: 1.11 (d, J = 6.8 Hz, 6H), 2.19 (s, 3H), 2.29–2.76 (m, 5H), 5.89 (d, J = 7.7 Hz, 1H), 10.00 (d, J = 7.7 Hz, 1H). The data are identical with those reported for **8***b* in the literature (7).

E-*3,7-Dimethyl-6-oxo-2-octenal* (*E*-**8***c*): Colourless, viscous liquid; glc (60–160°C at 4°C/min), t_R = 55.23 min; ^{1}H nmr (60 MHz, $CDCl_3$, Me_4Si), δ: 1.11 (d, J = 6.8 Hz, 6H), 2.19 (d, J = 1.3 Hz, 3H), 2.41–2.80 (m, 5H), 5.83 (dq, J = 8.0 and 1.3 Hz, 1H), 10.00 (d, J = 8.0 Hz, 1H). The data are identical with those reported for *E*-**8***c* in the literature (7).

E-*3,7-Dimethyl-6-oxo-2-octenal* (*Z*-**8***c*): Colourless, viscous liquid; glc (60–160°C at 4°C/min), t_R = 47.33 min; ^{1}H nmr (60 MHz, $CDCl_3$, Me_4Si), δ: 1.11 (d, J = 6.9 Hz, 6H), 1.97 (d, J = 1.5 Hz, 3H), 2.50–2.84 (m, 5H), 5.88 (dq, J = 8.0 and 1.5 Hz, 1H), 9.99 (d, J = 7.9 Hz, 1H). The data are identical with those reported for *Z*-**8***c* in the literature (7).

2-Isopropyl-2-(3-oxo)-butyl-3-formyl-oxirane (**10***b*): Slightly yellow liquid; ^{1}H nmr (60 MHz, $CDCl_3$, Me_4Si), δ: 0.90 (d, J = 6.6 Hz, 3H), 1.01 (d, J = 6.6 Hz, 3H), 2.17 (s, 3H), 1.56–2.83 (m, 5H), 3.35 (d, J = 4.6 Hz, 1H), 9.54 (d, J = 4.6 Hz, 1H); ei-ms (rel. intensity, %), *m/e*: 184 (0.5) $(M)^+$, 155 (51) $(M - CHO)^+$, 141 (77) $(M - CH_3CO)^+$, 71 (23) $((CH_3)_2CHCO)^+$, 43 (100) $(CH_3CO)^+$; ci-ms (rel. intensity, %), *m/e*: 185 (27) $(M + 1)^+$. Since the compound was not pure (yellow), no elemental analysis was performed.

2-Methyl-2-(3-oxo-4-methyl)-pentyl-3-formyl-oxirane (**10***c*): ^{1}H nmr (60 MHz, $CDCl_3$, Me_4Si), δ: 0.96 (d, J = 6.8 Hz, 6H), 1.73 (s, 3H), 3.93 (d, J = 4.4 Hz, 1H), 9.44 (d, J = 4.4 Hz, 1H). Insufficient amount for elemental analysis.

Reduction of **7**b

To a solution of 23 mg (0.1 mmol) of **7***b* in C_6D_6, 13 mg (0.21 mmol) of dimethyl sulfide was added and the mixture was kept at room temperature for 17 h; ^{1}H nmr analysis (60 MHz, $CDCl_3$, Me_4Si) showed the signals of *E*- and *Z*-**8***b*, methanol (δ = 3.26), dimethyl sulfide (δ = 1.75), and dimethyl sulfoxide (δ = 1.79).

Reduction of **7**c

In the same way, 17 mg (0.08 mmol) of **7***c* was reduced with 5.6 mg (0.09 mmol) of dimethyl sulfide to give *E*- and *Z*-**8***c*, methanol, and dimethyl sulfoxide.

Monoozonolysis of **5**b *followed by reduction with dimethyl sulfide*

A solution of 1.04 g (7.6 mmol) of **5***b* in 20 mL of methanol was ozonized with 0.7 molar equivalents of ozone at −78°C. The mixture was flushed with nitrogen and admixed with 0.71 g (11.5 mmol) of precooled (−20°C) dimethyl sulfide. The mixture was briefly agitated, allowed to warm up to room temperature overnight, kept at room temperature for 5 h, and then evaporated at 20°C and 18 Torr to leave 2.44 g of a colourless liquid; glc analysis (60–160°C at 4°C/min) showed the peaks of **8***b* (t_R = 50.13 min), *E*-**8***c* (t_R = 55.04 min), and *Z*-**8***c* (t_R = 47.30 min). The relative peak areas of **8***b* and of *E*-**8***c* + *Z*-**8***c* were 70% and 30%, respectively. By flash chromatography (column 2 × 10 cm; 8 g silica gel; 250 mL of pentane/diethyl ether, 99:1, 250 mL pentane/diethyl ether, 3:2), 581 mg (3.46 mmol) of a mixture containing **8***b* and of **8***c* was isolated.

Monoozonolysis of ***13***

A solution of 0.95 g (8.7 mmol) of **13** in 20 mL of methanol was ozonized with 0.7 molar equivalents of ozone at −78°C.

A sample of the crude reaction product was immediately analyzed by ^{1}H nmr ($CDCl_3$, Me_4Si), to show the presence of **14** (52%),[2] **16***a* (23%), **19***a* (7%), *cis*-**20***a* (10%), and *trans*-**20***a* (8%). Then triphenyl

[4]Due to decomposition of the neat substance no elemental analysis has been performed.

Can. J. Chem. Downloaded from www.nrcresearchpress.com by 88.85.125.76 on 09/07/12
For personal use only.

phosphine was added to the sample and the mixture was kept at room temperature for 10 min; ^{1}H nmr analysis showed the presence of **15** (δ: 1.72 (s, 3H), 2.14 (s, 3H), 1.84–2.59 (m, 4H), 4.65 (s, 1H), 4.73 (s, 1H)) and of **17***a* (δ: 2.19 (s, 6H), 2.72 (s, 4H)) in a molar ratio of 54:46.

The remainder of the crude ozonolysis product was warmed up to room temperature and evaporated at 18 Torr to leave 1.3 g of a peroxidic liquid residue. By flash chromatography (column 2.5 × 50 cm; 80 g silica gel; 2 L of pentane/diethyl ether, 75:25; fractions of 50 mL), 560 mg (35%) of **14** (fractions 4 and 5) and 30 mg (1.6%) of **16***a* (fractions 28–33) were isolated.

2-Methyl-5-hydroperoxy-5-methoxy-1-hexene (**14**):[4] Colourless liquid; ir (film), ν: 3320 (OOH), 1645 (C=C) cm^{-1}; ^{1}H nmr ($CDCl_3$, Me_4Si), δ: 1.36 (s, 3H), 1.75 (s, 3H), 1.80–188 (m, 2H), 2.04–2.13 (m, 2H), 3.32 (s, 3H), 4.70 (s, 2H), 7.74 (s, 1H); ^{13}C nmr ($CDCl_3$, Me_4Si), δ: 18.97, 22.51, 32.04, 33.24, 48.92, 107.04, 109.84, 145.27.

2,5-Bis-hydroperoxy-2,5-dimethoxyhexane (**16***a*;[4] probably a mixture of *meso*- and *rac*-**16***a* in nearly equal amounts): Colourless liquid; ^{1}H nmr ($CDCl_3$, Me_4Si), δ: 1.29 and 1.32 (s, each, CH_3) 1.50–2.05 (m, CH_2CH_2), 3.34 (s, CH_3O), 8.54 and 8.82 (s, each, OOH); ^{13}C nmr ($CDCl_3$, Me_4Si), δ: 18.37, and 18.67, 29.72 and 29.84, 48.93 and 48.97, 106.70 and 106.75.

Reduction of ***14***

Triphenyl phosphine was added to a solution of one drop of **14** in 0.6 mL of $CDCl_3$ and the mixture was kept at room temperature for 10 min; ^{1}H nmr analysis (Me_4Si) showed the presence of **15**.

Reduction of ***16***a

16*a* was completely converted into **17***a* by the above method, as shown by ^{1}H nmr analysis.

Diozonolysis of ***5***a

A solution of 0.3 g (2.8 mmol) of **5***a* in 10 mL of methanol was ozonized at −78°C until it turned blue, and excess ozone was removed by flushing with nitrogen. A sample of the crude reaction product was immediately analyzed by ^{1}H nmr ($CDCl_3$, Me_4Si) which showed the presence of ca. 75% of **16***a* (δ = 1.29, 1.32) and small amounts, each, of **19***a* (δ = 1.40), *cis*-**20***a* (δ = 1.51), *trans*-**20***a* (δ = 1.46), *cis*-**21***a* (δ = 1.41), and *trans*-**21***a* (δ = 1.30).

The remainder of the crude reaction product was warmed up to room temperature and evaporated at ca. 20 Torr to leave 0.49 g of a liquid residue; ^{1}H nmr analysis ($CDCl_3$, Me_4Si) showed the presence of **19***a* (33%), *cis*-**20***a* (12%), *trans*-**20***a* (19%), *cis*-**21***a* (11%), and *trans*-**21***a* (24%), whereas the signals of **16***a* had disappeared.

Diozonolysis of ***13***

(*a*) *Determination of the product distribution*

A solution of 0.1 g (0.90 mmol) of **13** in 10 mL of methanol was ozonized at −78°C until it turned blue. The excess of ozone was removed by flushing with nitrogen and the solution was evaporated at room temperature and 18 Torr to leave 1.39 g of a liquid residue. Immediate ^{1}H nmr analysis ($CDCl_3$, Me_4Si) showed the presence of **16***a* (65%, δ = 1.29, 1.32), **19***a* (12%, δ = 1.40), *cis*-**20***a*(10%, δ = 1.51), *trans*-**20***a* (8%, δ = 1.46), and *cis*-**21***a* (5%, δ = 1.41); ^{1}H nmr analysis of a sample that was kept at room temperature overnight showed the presence of **19***a* (12%), *cis*-**20***a* (12%), *trans*-**20***a* (11%), *cis*-**21***a* (20%), and *trans*-**21***a* (45%, δ = 1.30), whereas the signals of **16***a* had disappeared.

(*b*) *Isolation of stereoisomers of* ***20***a *and* ***21***a

A solution of 1.90 g (17.3 mmol) of **13** in 30 mL of methanol was ozonized at −78°C until the solution turned blue, and excess ozone was removed by flushing with nitrogen. The crude reaction product was warmed up to room temperature and evaporated at 20°C and 18 Torr to leave 2.43 g of a yellow liquid residue. Flash chromatography of the residue (column 2 × 100 cm; 122 g of silica gel; 2 L of pentane/diethyl ether, 4:1, and 0.5 L of diethyl ether; fractions of 50 mL) gave 830 mg of a mixture of *cis*- and *trans*-**21***a* in fractions 10 and 11 and 630 mg of a mixture of *cis*- and *trans*-**20***a* and *cis*-**21***a* in fractions 12–20. From fractions 10 and 11, 143 mg (5%) of *cis*-**21***a* and 531 mg (17.5%) of *trans*-**21***a* were isolated by hplc separation (column 3 × 10 cm; Lichrosorb Si 60; 10 bar; pentane/diethyl ether, 9:1). Fractions 12–20 were again submitted to flash chromatography under the same conditions to give 473 mg of a 1:1 mixture of *cis*- and *trans*-**20***a*. From the latter mixture, *cis*- and *trans*-**20***a* could be enriched, yet not completely separated from each other, by hplc separation (conditions as above).

cis-*3-Hydroperoxy-6-methoxy-3,6-dimethyl-1,2-dioxane* (*cis*-**20***a*; in admixture with 30% of *trans*-**20***a*): Colourless liquid; ir (film), ν: 3400 (OOH) cm^{-1}; ^{1}H nmr (60 MHz, $CDCl_3$, Me_4Si), δ: 1.44 (s, 3H), 1.51 (s, 3H), 1.60–2.16 (m, 4H), 3.39 (s, 3H), 8.59 (s, 1H); ^{13}C nmr ($CDCl_3$, Me_4Si), δ: 19.33, 19.60, 26.62, 29.75, 49.19, 102.64, 107.13. Anal. calcd. for $C_7H_{14}O_5$: C 47.18, H 7.92; found: C 47.10, H 7.81. Addition of a drop of *cis*-**20***a* to lead tetraacetate in benzene resulted in the spontaneous development of gas bubbles.

trans-*3-Hydroperoxy-6-methoxy-3,6-dimethyl-1,2-dioxane* (*trans*-**20***a*; in admixture with 10% of *cis*-**20***a*): Colourless solid; ir (film), ν: 3400 (OOH) cm^{-1}; ^{1}H nmr (60 MHz, $CDCl_3$, Me_4Si), δ: 1.31 (s, 3H), 1.46 (s, 3H), 1.53–2.16 (m, 4H), 3.36 (s, 3H), 8.36 (s, 1H); ^{13}C nmr ($CDCl_3$, Me_4Si), δ: 19.71, 19.81, 28.23, 31.00, 49.98, 103.37, 107.58. Addition of *trans*-**20***a* to lead tetraacetate in benzene resulted in the spontaneous development of gas bubbles.

cis-*3,6-Dimethyl-3,6-dimethoxy-1,2-dioxane* (*cis*-**21***a*): Colourless liquid; ^{1}H nmr ($CDCl_3$, Me_4Si), δ: 1.41 (s, 6H), 1.60–210 (m, 4H), 3.38 (s, 6H); ^{13}C nmr ($CDCl_3$, Me_4Si), δ: 19.70 (q, J = 29.9 Hz), 30.90 (t, J = 32.0 Hz), 49.71 (q, J = 44.0 Hz), 102.31 (s).

trans-*3,6-Dimethyl-3,6-dimethoxy-1,2-dioxane* (*trans*-**21***a*): Colourless liquid; ^{1}H nmr ($CDCl_3$, Me_4Si), δ: 1.30 (s, 6H), 1.50–2.10 (m, 4H), 3.34 (s, 6H); ^{13}C nmr ($CDCl_3$, Me_4Si), δ: 19.92, 29.69, 49.01, 101.72. Anal. calcd. for $C_6H_{16}O_4$: C 54.53, H 9.15; found: C 54.52, H 8.97.

Ozonolysis of ***14***

A solution of 0.1 g (0.63 mmol) of **14** in 10 mL of methanol was ozonized at −78°C until it turned blue. Excess ozone was removed by flushing with nitrogen and the solvent was evaporated at room temperature and ca. 20 Torr to leave 0.13 g of a liquid residue. Immediate ^{1}H nmr analysis ($CDCl_3$, Me_4Si) showed the presence of **16***a* (85%; δ = 1.29, 1.32), **19***a* (5%; δ = 1.40), *cis*-**20***a* (7%; δ = 1.51), and *trans*-**20***a* (3%, δ = 1.46).

Ozonolysis of ***15*** *and isolation of* ***19***a

A solution of 1.51 g (13.4 mmol) of **15** in 25 mL of methanol was ozonized at −74°C until it turned blue, and excess ozone was removed by flushing with nitrogen. A small sample was immediately analyzed by ^{1}H nmr ($CDCl_3$, Me_4Si) to show the presence of **17***a* (27%,[2] δ = 2.19 and 2.72) and of **19***a* (73%, δ = 1.32, 1,39, 3,34). The remainder of the product mixture was evaporated at 20°C and 20 Torr to leave 1.8 g of a liquid residue. By flash chromatography (column 2 × 100 cm; 120 g of silica gel; 1 L of pentane/diethyl ether, 4:1, fractions of 50 mL), 433 mg (20%) of **19***a* was isolated in fractions 14–23.

3-Hydroxy-6-methoxy-3,5-dimethyl-1,2-dioxane (**19***a*, unknown stereochemistry): Colourless solid, mp 68°C; ir (CCl_4), ν: 3620, 3480 cm^{-1}; ^{1}H nmr ($CDCl_3$, Me_4Si), δ: 1.32 (s, 3H), 1.40 (s, 3H), 1.60–2.10 (m, 4H), 3.03 (s, 1H), 3.35 (s, 3H); ^{13}C nmr ($CDCl_3$, Me_4Si), δ: 19.89, 25.13, 29.63, 29.95, 49.16, 99.43, 101.76. Anal. calcd. for $C_7H_{14}O_4$: C 51.84, H 8.70; found: C 51.88, H 8.37.

Diozonolysis of ***5****b*

(*a*) *Isolation of* ***19***b, ***19***c, cis-***20***b, trans-***20***b, cis-***20***c, and trans-***20***c

A solution of 3.07 g (22.6 mmol) of **5***b* in 50 mL of methanol was ozonized at −75°C until it turned blue. Excess ozone was removed by flushing with nitrogen and the reaction mixture was immediately evaporated at 20°C and 18 Torr to leave 5.42 g of a liquid residue. Immediate separation of the residue by flash chromatography (column 2 × 100 cm; 125 g of silica gel; 0.5 L of pentane/diethyl ether, 9:1, 2 L of pentane/diethyl ether, 4:1, 1 L of pentane/diethyl ether, 2:1, 0.5 L of diethyl ether; fractions of 50 mL) gave 45 mg of a 1:1 mixture of **21***b* and **22** in fractions 7–9, 1.15 g of a 1:2 mixture of **20***b* (*cis* + *trans*), and of **20***c* (*cis* + *trans*) in fractions 16–40, and 1.84 g of a mixture of **17***b*, **19***b*, **19***c*, and formic acid in fractions 50–63. Fractions 16–40 were further separated by the hplc method (column 1.6 × 25 cm;

Can. J. Chem. Downloaded from www.nrcresearchpress.com by 88.85.125.76 on 09/07/12
For personal use only.

Lichrosorb Si 100; 11 bar; pentane/diethyl ether, 4:1) to give 192 mg of mixture A, containing *cis*- and *trans*-**20***b* and *trans*-**20***c*, 516 mg of mixture B containing *cis*-**20***b* and *trans*-**20***c* and 402 mg of mixture C, containing *cis*-**20***b* and *cis*- and *trans*-**20***c*. Further hplc separation under the same conditions gave 42 mg (0.9%) of *trans*-**20***b* from mixture A, 125 mg (2.7%) of *cis*-**20***c* from mixture C, as well as 74 mg (1.6%) of *cis*-**20***b* and 573 mg (12.3%) of *trans*-**20***c* from a combination of mixture B and the by-products obtained from the separation of mixtures A and C. The hplc separation of fractions 50–63 from the flash chromatography gave 42 mg (1%) of **19***b* and 137 mg (3.2%) of **19***c*.

3-Hydroxy-3-methyl-6-methoxy-6-isopropyl-1,2-dioxane (**19***b*): Colourless solid, mp 31°C; ^{1}H nmr ($CDCl_3$, Me_4Si), δ: 0.92 (d, J = 7.0 Hz, 3H), 0.97 (d, J = 7.0 Hz, 3H), 1,39 (s, 3H), 1.45–2.30 (m, 5H), 3.30 (s, 3H); ^{13}C nmr ($CDCl_3$, Me_4Si), δ: 16.50, 17.40, 21.15, 25.65, 28.82, 29.89, 48.19, 99.00, 104.38.

3-Hydroxy-3-isopropyl-6-methyl-6-methoxy-1,2-dioxane (**19***c*): Colourless viscous liquid; ^{1}H nmr ($CDCl_3$, Me_4Si), δ: 0.97 (d, J = 6.9 Hz, 3H), 0.98 (d, J = 6.9 Hz, 3H), 1.31 (s, 3H), 1.20–2.10 (m, 5H), 2.95 (s, 1H), 3.34 (s, 3H); ^{13}C nmr ($CDCl_3$, Me_4Si), δ: 15.94, 16.81, 20.22, 24.81, 29.52, 35.80, 49.05, 101.30, 101.51. Anal. (of a 1:1 mixture of **19***b* and **19***c*) calcd. for $C_9H_{18}O_4$: C 56.82, H 9.54; found: C 56.46, H 9.31.

cis-*3-Hydroperoxy-3-methyl-6-methoxy-6-isopropyl-1,2-dioxane* (*cis*-**20***b*): Colourless solid, mp 77°C; ir (CCl_4), ν: 3460 (OOH) cm^{-1}; ^{1}H nmr (300 MHz, $CDCl_3$, Me_4Si), δ: 0.94 (d, J = 6.8 Hz, 3H), 0.95 (d, J = 6.8 Hz, 3H), 1.50 (s, 3H), 1.67–2.16 (m, 4H), 2.19 (sept, J = 6.9 Hz, 1H), 3.35 (s, 3H), 8.42 (s, 1H); ^{13}C nmr ($CDCl_3$, Me_4Si), δ: 16.19, 16.48, 19.48, 24.53, 27.69, 31.90, 49.61, 106.27, 108.13. Addition of *cis*-**20***b* to lead tetraacetate in benzene resulted in the spontaneous development of gas bubbles.

trans-*3-Hydroperoxy-3-methyl-6-methoxy-6-isopropyl-1,2-dioxane* (*trans*-**20***b*): Colourless solid, mp 68°C; ir (CCl_4), ν: 3500 (OOH) cm^{-1}; ^{1}H nmr ($CDCl_3$, Me_4Si), δ: 0.91 (d, J = 6.8 Hz, 3H), 0.96 (d, J = 6.8 Hz, 3H), 1.37 (s, 3H), 1.53–2.02 (m, 4H), 2.03 (sept, J = 6.8 Hz, 1H), 3.31 (s, 3H), 8.15 (s, 1H); ^{13}C nmr ($CDCl_3$, Me_4Si), δ: 16.44, 17.40, 20.19, 21.83, 26.34, 30.04, 48.30, 104.98, 106.46. Addition of *trans*-**20***b* to lead tetraacetate in benzene resulted in the spontaneous development of gas bubbles.

cis-*3-Hydroperoxy-3-isopropyl-6-methyl-6-methoxy-1,2-dioxane* (*cis*-**20***c*): Colourless, viscous liquid; ir (CCl_4), ν: 3380 (OOH) cm^{-1}; ^{1}H nmr ($CDCl_3$, Me_4Si), δ: 0.98 (d, J = 7.0 Hz, 3H), 0.99 (d, J = 6.9 Hz, 3H), 1.44 (s, 3H), 1.65–2.20 (m, 4H), 2.36 (sept, J = 7.0 Hz, 1H), 3.40 (s, 3H), 8.43 (s, 1H); ^{13}C nmr ($CDCl_3$, Me_4Si), δ: 16.58, 16.81, 19.78, 23.23, 30.51, 31.53, 50.13, 103.83, 110.48. Addition of *cis*-**20***c* to lead tetraacetate in benzene resulted in the spontaneous development of gas bubbles.

trans-*3-Hydroperoxy-3-isopropyl-6-methyl-6-methoxy-1,2-dioxane* (*trans*-**20***c*): Colourless, viscous liquid; ir (film), ν: 3510 (OOH) cm^{-1}; ^{1}H nmr ($CDCl_3$, Me_4Si), δ: 0.97 (d, J = 6.8 Hz, 3H), 0.99 (d, J = 6.8 Hz, 3H), 1.29 (s, 3H), 1.34–2.10 (m, 4H), 2.39 (sept, J = 6.9 Hz, 1H), 3.36 (s, 3H), 7.92 (s, 1H); ^{13}C nmr ($CDCl_3$, Me_4Si), δ: 16.62, 17.41, 19.15, 19.93, 29.41, 30.32, 49.03, 101.93, 109.75. Anal. calcd. for $C_9H_{18}O_5$: C 52.41, H 8.80; found: 52.70, H 8.68. Addition of *trans*-**20***c* to lead tetraacetate in benzene resulted in the spontaneous development of gas bubbles.

(*b*) *Isolation of* ***21***b

Ozonolysis of **5***b* was repeated as described above for (a), but the crude reaction product was kept at room temperature for 27 h before it was evaporated. By flash chromatography (column 2 × 100 cm; 119 g of silica gel; pentane/diethyl ether, 9:1, fractions of 50 mL), 340 mg (7.3%) of **21***b* was obtained in fractions 6–9.

3-Methyl-6-isopropyl-3,6-dimethoxy-1,2-dioxane (**21***b*): Colourless liquid; ^{1}H nmr (300 MHz, $CDCl_3$, Me_4Si), δ: 0.90(d, J = 6.8 Hz, 3H), 0.95 (d, J = 6.8 Hz, 3H), 1.28 (s, 3H), 1.35–2.17 (m, 5H), 3.29 (s, 3H), 3.33 (s, 3H); ^{13}C nmr ($CDCl_3$, Me_4Si), δ: 16.49, 17.42, 20.43, 20.91, 29.03, 29.93, 47.94, 48.78, 100.96, 104.08. Anal. calcd. for $C_{10}H_{20}O_4$: C 58.80, H 9.87; found: C 58.95, H 9.66.

Reductions of hemiperacetals of structure ***19***

(*a*) *Reduction of* ***19***a: A solution of 23 mg (0.14 mmol) of **19***a* and 19 mg (0.30 mmol) of dimethyl sulfide in $CDCl_3$ was kept at room temperature for 5 days; ^{1}H nmr analysis (Me_4Si) showed the presence of **17***a* and of dimethyl sulfoxide (δ = 2.64) in a ratio of 1:1.

(*b*) *Reduction of* ***19***b *and* ***19***c: A solution containing 31 mg (0.16 mmol) of a 1:1 mixture of **19***b* and **19***c* and 32 mg (0.5 mmol) of dimethyl sulfide in $CDCl_3$ was kept at room temperature for 6 days; ^{1}H nmr analysis (Me_4Si) showed the presence of **17***b* (δ = 1.11, 2.19, 2.72) and of dimethyl sulfoxide (δ = 2.63) in a ratio of 1:1.

Reductions of hydroperoxyperoxides of structure ***20***

(*a*) *Reduction of* ***20***a: A solution containing 15 mg (0.08 mmol) of a 1:1 mixture of *cis*- and *trans*-**20***a*, and 25 mg (0.4 mmol) of dimethyl sulfide in 0.5 mL of $CDCl_3$ was kept at room temperature for 2 weeks; ^{1}H nmr analysis (Me_4Si) showed the presence of **17***a* (δ = 2.19, 2.71) and of dimethyl sulfoxide (δ = 2.63) in a ratio of 1:2.

(*b*) *Reduction of* ***20***b *and* ***20***c: Solutions containing dimethyl sulfide and *cis*-**20***b*, *trans*-**20***b*, *cis*-**20***c*, and *trans*-**20***c*, respectively, in $CDCl_3$ were kept at room temperature for ca. 1 week, each; ^{1}H nmr analysis (Me_4Si) showed in each case the presence of **17***b* and of dimethyl sulfoxide (δ = 2.62) in a ratio of 1:2.

Reductions of the cyclic peracetals of structure ***21***

(*a*) *Reduction of* cis- *and* trans-***21***a: A solution of **21***a* (*cis*:*trans* = 1:1) and triphenyl phosphine in $CDCl_3$ was heated to 60°C for 6 days; ^{1}H nmr analysis (Me_4Si) showed the presence of **17***a* (δ = 2.19 and 2.71).

(*b*) *Reduction of* ***21***b: A solution of 18.5 mg (0.09 mmol) of **21***b* and 47.5 mg (0.18 mmol) of triphenyl phosphine in 0.6 mL of $CDCl_3$ was kept at room temperature for 3 days; ^{1}H nmr analysis (Me_4Si) showed no change in the composition. The solution was heated to 60°C for 4 days; ^{1}H nmr analysis showed the presence of **17***b* and of the remaining **21***b* in a ratio of 2:1.

Ozonolysis of ***5***b *followed by acid catalysis*

A solution of 1.95 g (13.6 mmol) of **5***b* in 50 mL of methanol was ozonized at −74°C until it turned blue. Excess ozone was removed by flushing with nitrogen, the mixture was warmed up to room temperature, admixed with 50 mg of *p*-toluenesulfonic acid monohydrate, and stirred at room temperature for 20 h. Then 10 mg of potassium carbonate was added, stirring was continued for 1 h, and the solvent was evaporated at 20°C and 18 Torr. From the residue, 861 mg (31%) of **21***b* was isolated by flash chromatography in fractions 8–12 (column 2 × 100 cm; 120 g of silica gel; 1 L of pentane/diethyl ether, 9:1, fractions of 50 mL).

Preparation of ***22*** *by ozonolysis of* ***8***b *and* ***8***c *in pentane*

A solution of 581 mg (3.46 mmol) of a mixture of **8***b* and **8***c* in 50 mL of pentane was ozonized at −60°C until it turned blue. Excess ozone was flushed off with nitrogen, the mixture was warmed up to room temperature, pentane was largely evaporated, and the residue was submitted to flash chromatography (column 2 × 100 cm; 60 g of silica gel; 2 L of pentane/diethyl ether, 49:1; fractions of 50 mL) to give 93 mg (17%) of **22** in fractions 8–16.

1-Methyl-4-isopropyl-2,3,7-trioxabicyclo[2.2.1]heptane (**22**): Colourless liquid; ^{1}H nmr ($CDCl_3$, Me_4Si), δ: 1.06 (d, J = 6.9 Hz, 3H), 1.09 (d, J = 7.0 Hz, 3H), 1.67 (s, 3H), 1.76–2.41 (m, 5H); ^{13}C nmr ($CDCl_3$, Me_4Si), δ: 14.96, 17.35, 17.76, 28.99, 30.83, 34.92, 110.66, 115.37. Anal. calcd. for $C_8H_{14}O_3$: C 60.74, H 8.92; found: C 60.46, H 8.74.

Reduction of ***22***

A solution of 31 mg (0.20 mmol) of **22** and 154 mg (0.59 mmol) of triphenyl phosphine in 0.3 mL of $CDCl_3$ was kept at room temperature for 3 days; ^{1}H nmr analysis (Me_4Si) showed the presence of **17***b*.

1. A. T. Menyailo, I. E. Prokrovskaya, and A. K. Ykoleva. Neftekhimiya, **7**, 70 (1967).
2. W. I. Fanta and W. F. Erman. J. Org. Chem. **33**, 1656 (1968).

3. P. S. BAILEY, S. S. BATH, F. DOBINSON, F. J. GARCIA-SHARP, and C. D. JOHNSON. J. Org. Chem. **29**, 697 (1964).
4. R. H. CALLIGHAN and M. H. WILT. J. Org. Chem. **26**, 5212 (1961).
5. J. J. PAPPAS, W. P. KEAVENEY, M. BERGER, and R. V. RUSH. J. Org. Chem. **33**, 787 (1968).
6. K. GRIESBAUM and G. ZWICK. Chem. Ber. **119**, 229 (1986), and references cited therein.
7. G. RÜCKER and U. MOLLS. Liebigs Ann. Chem. **5**, 608 (1979).
8. R. CRIEGEE, H. PILZ, and H. FLYGARE. Ber. Dtsch. Chem. Ges. **72**, 1799 (1939).
9. H. GÜNTHER. NMR-Spektroskopie. Georg Thieme Verlag, Stuttgart. 1973. (*a*) p. 264; (*b*) p. 77.
10. W. T. BRADY, S. J. NORTON, and J. KO. Synthesis, **7**, 704 (1985).
11. W. C. STILL, M. KAHN, and A. MITRA. J. Org. Chem. **43**, 2923 (1978).

Can. J. Chem. Downloaded from www.nrcresearchpress.com by 88.85.125.76 on 09/07/12
For personal use only.

Reactions of thiyl radicals with phenothiazines and other antioxidants in aqueous solutions. A pulse radiolysis study

MANOHAR LAL AND H. S. MAHAL

Chemistry Division, Bhabha Atomic Research Centre, Trombay, Bombay-400 085, India

Received December 8, 1989

MANOHAR LAL and H. S. MAHAL. Can. J. Chem. **68**, 1376 (1990).

Reaction rate constants of thiyl radicals with phenothiazines, promethazine (PMZ), chlorpromazine (CPZ), prochlorperazine (PPZ), trimeperazine tarterate (TPZ), and other antioxidants, e.g., ascorbic acid and 2,2-azinobis(3-ethyl benzthiazoline-6 sulphonate) (ABTS) have been estimated using pulse radiolysis technique. In general they are quite high (10^8–10^9 M^{-1} s^{-1}). The *k* values for cysteine, cysteamine, mercaptoethanol, and mercaptopropionic acid with similar structures and molecular weights are more or less similar for PMZ, CPZ, and PPZ.

Rate constants are lower in value for PenṠ, DṪT, DṪE and GuṠ radicals of phenothiazines showing that they are dependent upon the structure and the molecular weight of the compound.

Rate constants are the same whether the thiyl radicals are generated from thiols or their corresponding disulphides. The *k* values for chlorine-containing phenothiazines, chlorpromazine, and prochlorperazine are higher than those of promothazine

Key words: pulse radiolysis, thiyl radicals, phenothiazines, ABTS, ascorbic acid.

MANOHAR LAL et H. S. MAHAL. Can. J. Chem. **68**, 1376 (1990).

Faisant appel à la technique de la radiolyse pulsée, on a évalué les constantes de vitesse de réaction du radical thiyle avec les phénothiazines, prométhazine (PMZ), chlorpromazine (CPZ), prochlorpérazine, (PPZ) et tartrate de trimépérazine (TPZ) ainsi que d'autres antioxydants comme l'acide ascorbique et le 2,2-azinobis(3-éthylbenzothiazoline-6-sulfonate) (ABTS). Généralement, les constantes de vitesse sont très élevées (10^8–10^9 M^{-1} s^{-1}). Les valeurs de *k* pour la cystéine, la cystéinemaine, le mercaptoéthanol et l'acide mercaptopropanoïque qui possèdent des structures et des poids moléculaires semblables ressemblent aux valeurs obtenues pour la PMZ, la CPZ et la PPZ.

Les valeurs des constantes de vitesse de réaction des radicaux PenṠ, DṪT, DṪE et GuṠ avec les phénothiazines sont plus faibles; ces résultats démontrent que les valeurs de *k* dépendent de la structure et du poids moléculaire du composé.

Les constantes de vitesse des réactions des radicaux thiyles sont constantes quelles que soient les sources, thiols ou disulfures, de ces radicaux. Les valeurs de *k* pour les phénothiazines contenant du chlore, comme la chlorpromazine et la prochlorpérazine, sont plus élevées que celle pour la prométhazine.

Mots clés : radiolyse pulsée, radicaux thiyles, phénothiazines, ABTS, acide ascorbique.

[Traduit par la revue]

Introduction

Radiation protection of DNA, enzymes bacteriophage and mammals by thiols has been the subject of considerable interest in the past (1–3). The protective effect is known to be due to (*i*) the scavenging of potentially damaging primary species and (*ii*) the repair of the biological molecules by hydrogen transfer:

[1] $RH + \dot{H}, \dot{O}H \rightarrow \dot{R} + H_2, H_2O$

[2] $\dot{R} + RSH \rightarrow RH + R\dot{S}$

Thiyl radicals thus formed are very reactive (4). Their fate and reations with other molecules are of considerable importance in biological and biochemical processes.

Reactions of thiyl radicals with two phenothiazines and other antioxidants have been reported earlier (4*a*, 8, 12).

We have extended these studies to thiyl radicals generated from a variety of thiols and their corresponding disulphides to see if there is any difference in reactivity. In the earlier studies (4*a*) reactions of dithiothreitol radical with the phenothiazines could not be investigated because of their low signals. This prompted us to investigate the reactions of DṪT, DṪE radicals and radical anions with phenothiazines and other antioxidants. Phenothiazines are being used in psychiatric and anti-inflammatory treatment. Recent studies have shown that chlorpromazine HCl (CPZ), promethazine HCl (PMZ), prochlorperazine (PPZ), and trimeprazine tartrate (TPZ) are effective in the radiosensitization of hypoxic bacterial and mammalian cells *in vitro* and in mouse solid tumour *in vivo* (5–7). In addition to the first two phenothiazines we have also investigated the reactions of thiyl radicals with the last two phenothiazines. Effect of pH on the reaction of DṪT, DṪE, and GuṠ radicals with phenothiazines has been studied.

The metabolism, pharmacology, and toxicology of these compounds have been studied earlier and it has been suggested that free radicals are generated and expected to play an important role in the mechanism of toxic action of these compounds. In view of this, the fact that thiols are radiation protective agents and that variety of enzymes and proteins in biological systems contain the thiol group and disulphide bridges from which thiyl radicals may be generated, it is important and of interest to explore the reactions of thiyl radicals with phenothiazines and antioxidants and the reactions of phemothiazine radicals with other molecules.

Experimental

2,2-Azinobis(3-ethylbenzthiazoline-6 sulphonate) (ABTS), ascorbic acid, and other reagents were of A grade from Sigma Chemical Co. Prochlorperazine (PPZ) and trimeprazine tartrate (TPZ) were of pharmaceutical grade from May and Baker and were supplied to us by courtesy Dr. B. B. Singh of Biology Group, BARC, Bombay. Promethazine HCl (PMZ) and chlorpromazine (CPZ) were a gift from May and Baker Ltd., England. These two compounds were later procured from Sigma. Similar results were obtained with compounds from the two sources.

The pulse radiolysis set up (9) used in these investigations employs 25 ns pulses of 7 MeV electrons from a linear accelerator. Typical dose per pulse is ~13 Gy as evaluated by thiocyanate dosimetry. All solutions were prepared in Nano pure water of conductivity ~0.06 μS. Phosphate buffers of pH ~3.6 and 6.4 (total phosphate concentration

Can. J. Chem. Downloaded from www.nrcresearchpress.com by 88.85.125.76 on 09/07/12
For personal use only.

10 mM) were used in experiments with ABTS or ascorbic acid/thiol or disulphide solution. In the case of phenothiazines, however, some turbidity was observed when phenothiazine and thiol or disulphide were dissolved in the buffer. The signal obtained in these mixtures was too weak to be analyzed properly. Weak signals had also been reported earlier (4*a*) when similar experiments were carried out with dithiol DTT. The pH of the reaction mixtures viz. 3.5–3.7 and 6.4–6.7 used in these studies was adjusted using $HClO_4$ and NaOH. These pH values were chosen because we wanted to study the reactions of neutral DTT or DTE radicals and DTT or DTE radical anions which are formed in equilibrium [3] with a pk ~5.3 (10, 11) (see later).

It can be seen that at pH ~3.5 the majority of the radicals would be in the neutral form **I** and at pH ~6.7 they would be in the radical anion form **II**. For each experiment fresh solutions were prepared. In the case of mercaptoethanol (βME) and mercaptopropionic acid (βMPA) the aqueous solutions of phenothiazines or antioxidants were saturated with N_2O in a glass irradiation cell with rubber septum. After saturating, small amount of the liquid (βME or βMPA) was added to the cell via the septum. It is assumed that contribution from the oxygen content in the few μlitres of βME or βMPA is negligible.

[3] 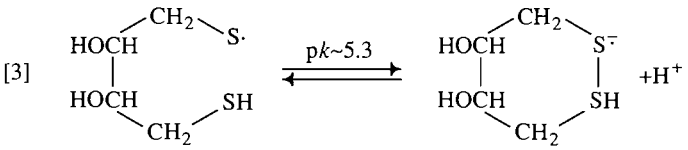

I **II**

The structures of thiols, disulphides, ABTS, ascorbic acid, and phenothiazines used are given in Scheme 1, along with their shortforms

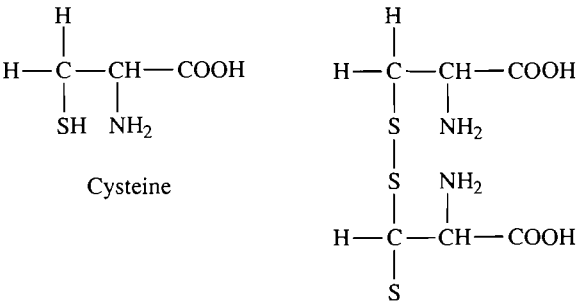

Cysteine

Cystine

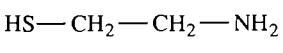

Cysteamine

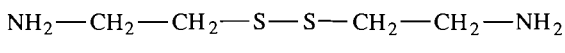

Cystamine

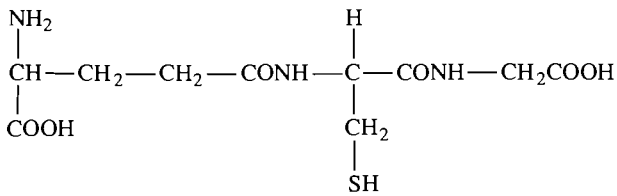

Reduced glutathione (GuSH)

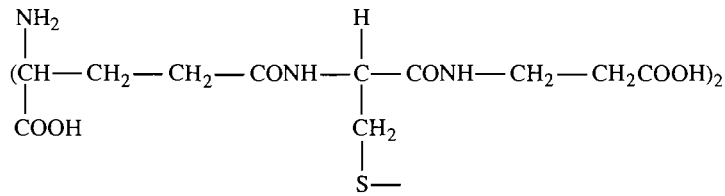

Oxidized glutathione (GuSSGu)

Results and discussion

(I) N_2O-saturated thiol or disulphide – ABTS solutions

On pulse radiolysis of N_2O-saturated solutions containing ABTS a characteristic absorption immediately after the pulse was observed at 415 nm. This is known to be due to the $ABTS^{+}$ radical cation (12) formed according to reaction [4]

[4] $ABTS + \dot{O}H \rightarrow ABTS^{+} + OH^{-}$

Similar absoprtion was observed at 415 nm when N_2O-saturated aqueous solutions containing thiol or disulphide (2.5 mM) and ABTS (5–20 × 10^{-5} M) were pulse radiolysed. At these concentrations and with known $k_{\dot{O}H + \text{thiols/djsulphide}}$ and $k_{\dot{O}H + ABTS}$ it can be shown that the majority of $\dot{O}H$ radicals react with thiol/disulphide to give thiyl radicals according to reactions [5] and [6]. Reaction [6] is known to give ~50% of $R\dot{S}$ radicals when compared with other modes of reactions of $\dot{O}H$ with disulphides (11*b*).

[5] $RSH + \dot{O}H \rightarrow R\dot{S} + H_2O$

[6] $RSSR + \dot{O}H \rightarrow R\dot{S} + RSOH$

Can. J. Chem. Downloaded from www.nrcresearchpress.com by 88.85.125.76 on 09/07/12
For personal use only.

Can. J. Chem. Downloaded from www.nrcresearchpress.com by 88.85.125.76 on 09/07/12
For personal use only.

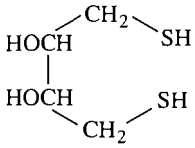

Dithiothreitol (DTT)

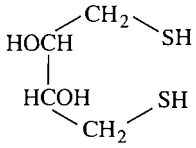

Dithioerythreitol (DTE)

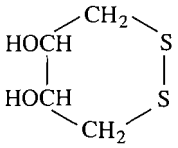

Oxidized dithiothreitol

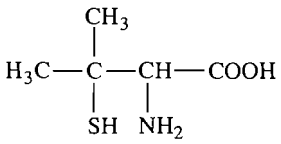

Penicillamine (PenSH)

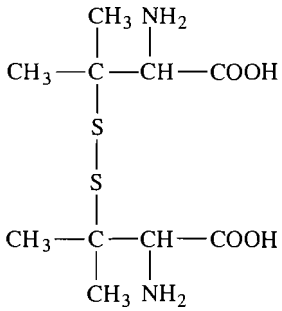

Penicillamine disulphide (PenssPen)

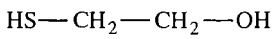

Mercaptoethanol (βME)

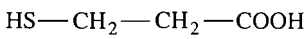

Mercaptopropianic acid (βMPA)

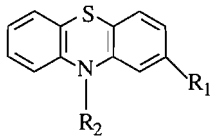

Phenothiazine

	R_1	R_2
Promethazine (PMZ^+)	H	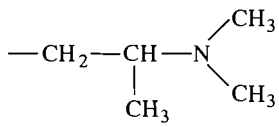
Chlorpromethazine (CPZ^+)	Cl	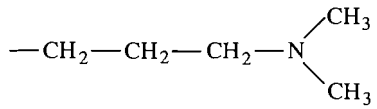
Prochlorperazine (PPZ^+)	Cl	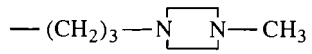
Trimeprazine tartrate (TPZ^+)	H	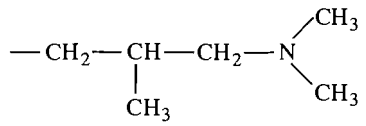

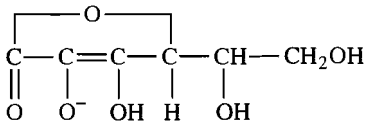

Ascorbic acid (AH^-)

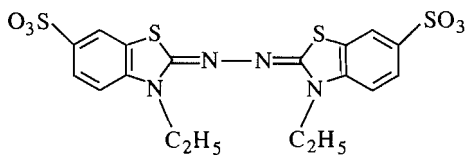

2,2'-Azinobis(3-ethylbenzthiazoline-6-sulphonic acid) (ABTS)

SCHEME 1

TABLE 1. Rate constant of reaction between thiyl radical and ABTS and AH^-

Compound	$k_{RS + ABTS} \times 10^{-8}$ M s			$k_{RS + AH^-} \times 10^{-8}$ M s		
	pH	Present[c]	Ref. 12	pH	Present[c]	Ref. 4*a*
Cysteine	3.75	10.0	5.0[a]	6.9	13.0	12[b]
Cystine	3.75	11.0		6.9	11.0	
Cysteamine	3.75	30.0	24.0[a]	6.9	20.0	13[b]
Cystamine	3.75	28.0		6.9	17.0	
Penicillamine	3.75	2.7		6.9	4.5	4.9[b]
Panicillamine disulphide	3.75	2.5		6.9	4.8	
Glutathione reduced	3.75	6.0	3.3[a]	6.9	3.6	6.0[b]
Glutathione oxidized	3.75	6.1		6.9	4.2	
Dithiothreitol	3.75	3.0		6.9	5.0	
Dithioerythreitol	3.75	4.0		6.9	4.0	
Mercaptoethanol	3.75	14.0		6.9	10.0	

[a]pH ~7.0, ref. 12.
[b]pH ~6.5, ref. 4*a*.
[c]Error within ± 20%.

$R\dot{S}$ radical can then react with ABTS according to reaction [7] and can dimerise according to reaction [7*a*].

[7] $R\dot{S} + ABTS \rightarrow RS^- + ABTS^{+}$

[7*a*] $R\dot{S} + R\dot{S} \rightarrow RSSR$

The formation of $ABTS^{+}$ at 415 nm was exponential with time for all thiols and disulphides. The first order rate constants when plotted against [ABTS] gave straight lines. The small intercept observed on the Y-axis in few cases appears to be due to reaction [7*a*]. Bimolecular rate constants have been evaluated from the slopes of these plots and are presented in Table 1. Bimolecular rate constants obtained earlier (12) in the case of a few thiols are also given in Table 1 for comparison.

(II) N_2O-saturated thiols/disulphides – ascorbic acid solutions

On pulse radiolysis of N_2O-saturated ascorbic acid solutions at pH ~6.4 a characteristic absorption at 360 nm due to $A^{\cdot}$ formed via reaction [8] was observed (13)

[8] $AH^- + \dot{O}H \rightarrow A^{\cdot} + H^+ + OH^-$

Very similar absorption at 360 nm was observed in N_2O-saturated solutions containing thiol/disulphide (2.5 mM) and ascorbic acid 5–20 × 10^{-5} M at pH 6.4. The absorption spectrum is similar to the one observed in the absence of thiol/disulphide. This is attributed to $A^{\cdot}$ formed according to reactions [5], [6], and [9].

[9] $AH^- + R\dot{S} \rightarrow A^{\cdot} + H^+ + RS^-$

The absorption grows exponentially and is first order in AH^- concentration. Bimolecular rate constants for reaction [9] as evaluated from the slopes of the respective plots of first order rate constant versus $[AH^-]$ are presented in Table 1. The small intercept on *Y*- axis appears to be due to reaction [7*a*]. Table 1 also show the rate constants for a few thiols evaluated earlier (4*a*).

(III) N_2O-Saturated thiol/disulphide and phenothiazine solutions

On pulse radiolysis of N_2O-saturated aqueous solutions containing thiol/disulphide and phenothiazines at pH 3.6 and 6.5, a characteristic absorption between 510–525 nm due to phenothiazine radical cations was observed. The concentrations of sulphur compounds and phenothiazines were chosen in such a way that most of the $\dot{O}H$ radicals in N_2O-saturated solutions react with thiol/disulphide to give thiyl radical according to

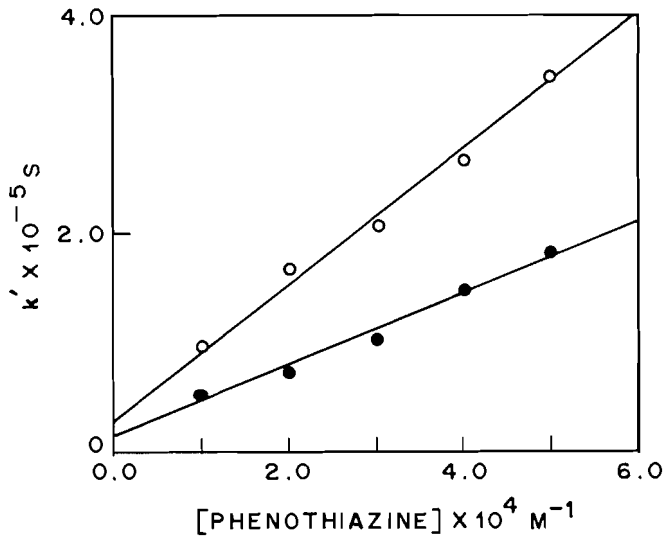

FIG. 1. Plot of first order rate constant (k') for the formation of absorption in N_2O-saturated solutions of PPZ^+ and cysteine ○; PMZ^+ and cysteine ●. Cysteine concentrations ~5 × 10^{-3} M.

reactions [5] and [6]. Thiyl radicals thus formed react with phenothiazines under investigation to give radical cations of the latter absorbing between 510 and 525 nm. Besides promethazine (PMZ^+) and chlorpromazine (CPZ^+) on which some work has been reported earlier (4*a*, 14), we have now studied two other phenothiazines viz. prochlorperazine (PPZ^+) and trimeprazine tartrate (TPZ^+). As the pk_a values for the side chain nitrogen atom of promethazine and chlorpromazine is 9.3 (15), it is expected that the phenothiazines would exist in the cationic form at the experimental pH values. The reactions of a variety of thiyl radicals have been investigated with the four drugs (reactions [10]–[13]).

[10] $R\dot{S} + PMZ^+ \rightarrow PMZ^{2+} + RS^-$

[11] $R\dot{S} + CPZ^+ \rightarrow CPZ^{2+} + RS^-$

[12] $R\dot{S} + PPZ^+ \rightarrow PPZ^{2+} + RS^-$

[13] $R\dot{S} + TPZ^+ \rightarrow TPZ^{2+} + RS^-$

Transient spectra of the radical cations formed in reactions [10]–[13] revealed maxima at 510, 525, 515, and 510 nm,

Can. J. Chem. Downloaded from www.nrcresearchpress.com by 88.85.125.76 on 09/07/12
For personal use only.

Can. J. Chem. Downloaded from www.nrcresearchpress.com by 88.85.125.76 on 09/07/12
For personal use only.

respectively, for PMZ^{2+}, CPZ^{2+}, PPZ^{2+}, and TPZ^{2+}. Our λ_{max} for PMZ^{2+} and CPZ^{2+} differed only slightly from those reported earlier (4*a*, 14). The *k* values for reactions [10]–[13] have been evaluated from the data obtained at the above wavelengths. Formation of radical cations in all four phenothiazines at the two pH's were found to be exponential with time and first order in phenothiazine concentration for all thiols and disulphides. The first order rate constants when plotted against phenothiazine concentrations gave straight lines. A typical plot of *k'* in the case of cysteine against $[PPZ^+]$ and cysteine against $[PMZ^+]$ is shown in Fig. 1. Bimolecular rate constants are derived from the slopes of these plots. It can be seen that there is an intercept on the *y* axis which appears to be due to reaction [7*a*].

In view of the complex nature of our system it is rather difficult to eliminate the intercept. To keep the ratio $k_{\dot{O}H + RSH}[RSH]/k_{\dot{O}H + phenothiazine}$ [phenothiazine] high, the thiol concentration is to be kept high. On the other hand, in order that the majority of the e^-_{aq} are converted to $\dot{O}H$ radicals the ratio $k_{e^-_{aq} + N_2O}[N_2O]/k_{e^-_{aq} + RSH}[RSH]$ should be high and therefore the thiol concentration has to be kept low. We have used 5×10^{-3} M thiol in these experiments. Taking the saturation concentration of N_2O as 2.5×10^{-2} M, $k_{e^-_{aq} + N_2O} \sim 9 \times 10^9\ M^{-1}\ s^{-1}$ and $k_{e^-_{aq} + RSH} \sim 1 \times 10^{10}\ M^{-1}\ s^{-1}$ for most thiols and disulphides except GuSH, it can be seen that about 82% of electrons are converted to $\dot{O}H$ radicals which would give $G(R\dot{S}) \sim 5.0$. Even though reduction in $\dot{O}H$ radicals would reduce the concentration of $R\dot{S}$ radicals in the system it wold not have any effect on the reactions of $R\dot{S}$ radicals with the phenothiazines and on the kinetics. In some cases the signal was low at low phenothiazine concentrations because of the competing reaction [7*a*]. High concentrations of both phenothiazines (4×10^{-4} M) and thiols (5×10^{-3} M) were taken and the rate constant evaluated by the average of four such experiments. Even at these concentrations reaction [7*a*] would occur to some extent (~5%). Rate constants thus obtained agreed to within 10% of the *k* values evaluated from straight line plots.

The results of Tables 1 and 2 demonstrate certain important common features.

(*i*) In general the rate constants are quite high (10^8–$10^9\ M^{-1}\ s^{-1}$), and seem to depend upon the individual thiyl radical, the antioxidant, and the phenothiazine. Minor differences with earlier reported results for ABTS and AH^- are within the limits of experimental error.

(*ii*) Rate constants increase with decreasing size of the thiyl radical. Rate constants for cysteine, cysteamine, mercaptoethanol, and mercaptoproprionic acid which have quite similar structure and molecular weight, however are more or less similar for PPZ^+, CPZ^+, and PMZ^+.

(*iii*) Rate constants are lower for the radicals PenṠ and GuṠ. The low value for PenṠ could be due to steric hindrance caused by the two methyl groups attached to the carbon atom that is close to the sulphur atom. The somewhat lower *k* value for GuS could be ascribed to its bulkiness.

(*iv*) Rate constants are the same whether the thiyl radicals are generated from thiol or the corresponding disulphide. This confirms the earlier finding that thiyl radicals are formed in both reactions [5] and [6].

(*v*) Rate constants are higher for chlorpromazine and prochlorperazine as compared to promethazine, which can be explained on the basis of the higher oxidation potential of the PMZ^{2+}/PMZ^+ couple as compared to that of CPZ^{2+}/CPZ^+ (14, 16). The oxidation reaction of phenothiazines by $\dot{O}H$ radicals takes place by a number of processes (14). The high rate constants for various processes in the two systems suggest the same explanation for all competing reactions.

TABLE 2. Rate constant of reaction between thiyl radicals and phenothiazines[a]

		$k_{R\dot{S} + Phenothiazines} \times 10^{-8}$ M s [b]			
	pH	PPZ^+	CPZ^+	PMZ^+	TPZ^+
Cysteine	6.5	6.2	18(3.0)	3.1(0.87)	13.4
Cystine	6.5	7.1	20	2.8	12.4
GuSH	6.5	4.6	11	2.0	8.0
GuSSGu	6.5	4.9	13	1.0	8.1
Cysteamine	6.5	9.1	19.0(1.7)	3.5(0.67)	8.8
Cystamine	6.5	8.6	11.0	2.2	9.0
PenSH	6.5	2.9	9.0(1.2)	1.6(0.27)	4.8
PenSSPen	6.5	3.4	7.5	1.9	4.0
ME	6.5	8.0	19.0	2.9	7.7
MPA	6.5	6.0	17.0	2.2	4.2

[a]Values in parentheses are from ref. 4*a*; values in Table 2 are an average of at least four independent determinations.
[b]Error within ±20%.

Even though we have not evaluated the rate constants for individual processes in our system, similar reactions may be involved in the reactions of thiyl radicals with the phenothiazines and higher oxidation potential for PMZ^+ as compared to CPZ^+ may be the cause for the low rate constant in the case of promethazine.

(*vi*) In general our rate constants are higher than those reported earlier (4*a*). The experimental conditions used in this study are very much similar to those in ref. 4*a*. (The dosage ~10 Gy and concentrations of reactants were more or less same. The pH used was 3.0.) The difference in pH as compared to ours should not affect the results, as the thiyl radicals will be neutral radicals in the pH range 3.0–6.5. In view of this it is rather difficult to explain the differences in *k* values in the two cases.

(IV) (a) N_2O-saturated DTT/DTE–phenothiazine solutions

As mentioned earlier, the authors of ref. 4*a* were not able to get good signals for the phenothiazine radical cation in dithiothreitol/phenothiazine mixtures. On the other hand, we have been able to get good formation signals with all four phenothiazines. A typical signal is shown in Fig. 2. The inset in Fig. 2 gives a straight line from which the first order rate constant (*k'*) is calculated. The pseudo first order rate constant (*k'*) versus phenothiazine concentrations are straight lines. The bimolecular rate constants are derived from the slope of these straight lines and are presented in Table 3. The low rate constants for DṪT and DṪE radicals appear to be due to the cyclic structure of DṪT and DṪE radicals (see **I** and **II** in reaction [3]) which may sterically hinder the approach towards the phenothiazines. The reason of very low signals in 4*a* in DTT/phenothiazines in N_2O-saturated aqueous solutions is not clearly known.

(b) Effect of pH on $k_{DṪT/DṪE + phenothiazines}$

Experiments have been carried out in N_2O-saturated aqueous solutions for DTT, DTE, and GuSH/phenothiazine mixtures. Thiyl radicals are generated in reaction of $\dot{O}H$ radicals with thiols. DṪT and DṪE radicals are known to exist in equilibrium (reaction [3]) with a p*k* value of 5.3 (10, 11). The pH's chosen were 3.6 and 6.4 with a view to investigate the reactions of

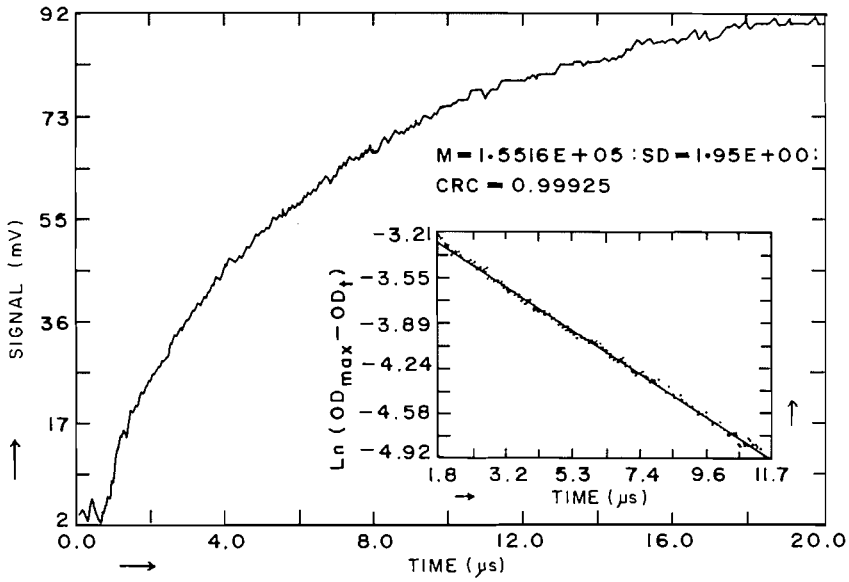

FIG. 2. Formation trace of the radical cation TPZ^{2+} observed at 515 nm after a 25 ns pulse (13 GY) on a N_2O-saturated trimeprazine tartrate (4×10^{-4} M) and dithiothreitol (5×10^{-3} M); aqueous solutions at pH ~6.5. Inset shows the straight line plot of ln ($OD_{max} - OD_t$) vs. time. Points derived from the formation trace and the straight line is the least square fit.

TABLE 3. Effect of pH on the rate constants

	$k_{\dot{R}S + \text{phenothiazines}} \times 10^{-8}$ M s [a]							
	CPZ^+		TPZ^+		PMZ^+		PPZ^+	
Thiols	pH = 3.6	pH = 6.4	pH = 3.6	pH = 6.4	pH = 3.6	pH = 6.4	pH = 3.6	pH = 6.4
GuSH	14.0	11.0	8.1	8.0	1.6	2.0	—	—
GuSSGu	13.2	13.0	8.0	7.8	1.7	1.0	—	—
DTE	2.2	5.6	4.2	10.0	0.5	1.0	1.8	4.2
DTT	3.0	6.6	2.0	15.5	0.4	0.9	1.6	4.0

[a]Error within ±20%.

neutral DṪT or DṪE radical and DTT or DTE radical anion with phenothiazines. It can be seen that at pH 3.6, DṪT and DṪE radicals would exist almost entirely in the neutral form **I** and at pH 6.4 they would exist in the radical anion form **II**. The results of this study are shown in Table 3. The results of GuSH and GuSSGu at pH 3.6 and 6.4 are also shown in Table 3 for comparison.

As can be seen, there is no difference in rate constants for GuṠ radical at the two pH's. The rate constants for neutral DṪT and DṪE species **I** is about ½ that of the DTT and DTE radical anion species **II** for all phenothiazines. This might be explained as follows:

At pH ~3.6 and 6.4 all drugs chlorpromazine, promethazine, prochlorperazine, and trimeprazine tartrate are present in cationic forms $CPZH^+$, $PPZH^+$, $PMZH^+$, and $TPZH^+$, respectively (pk_a ~9.3). Thus the reactions of DTT and DTE radical anions at pH 6.4 with phenothiazine cations would be expected to be faster than the reactions of neutral DṪT and DṪE radicals at pH 3.6 with phenothiazine cations. The fact that there is no variation in the rate constants of GuṠ radicals with phenothiazine radical cation at the two pH's suggest that GuṠ radicals at either pH remain a neutral species.

The results of this study demonstrate that thiyl radicals are strong oxidizing species. Each thiyl radical generated from all thiols and disulphides can take up one electron from the four phenothiazines, ABTS, and ascorbic acid with considerable ease. The rate constants range between ~10^8–10^9 M^{-1} s^{-1} depending on the nature of the thiyl radicals and the reactants. In view of the complex nature of the systems under investigations no attempt has been made to correlate the rate constants with redox properties of thiyl radicals.

The radicals formed thus are quite reactive and may be responsible for cell damage and other biological problems. Our studies should therefore be relevant.

Acknowledgements

The authors wish to thank Dr. R. M. Iyer, Director, Chemical Group and Dr. J. P. Mittal, Head, Chemistry Division, for their keen interest during the course of this work.

1. (*a*) Panel on radiation damage to the biological molecular information system with special regard to the role of —SH groups, IAEA Vienna. 1969; (*b*) A. PHIL and T. SANNER. *In* Radiation protection and sensitisation. *Edited by* H. L. Moroson and M. Quintiliani. Taylor and Fransis Ltd., London, 1970. p. 43; (*c*) Z. M. Bacq. Chemical protection against ionising radiation. Charles C. Thomas Springfield, IL. 1965.
2. (*a*) P. ALEXANDER and A. CHARLESBY. *In* Radiobiology sympo-

Can. J. Chem. Downloaded from www.nrcresearchpress.com by 88.85.125.76 on 09/07/12
For personal use only.

sium. Butterworth, London, 1954, p.49; (*b*) G. E. ADAMS. *In* Advances in radiation chemistry. Vol. 3. *Edited by* M. Burton and J. L. Magee, 1972, p. 125.
3. LAL, W. S. LIN, G. M. GAUCHER, and D. A. ARMSTRONG. Int. J. Radiat. Biol. **28**, 549 (1975).
4. (*a*) L. G. FORNI, J. MONIG, V. O. MORA-ARELLANO, and R. L. WILLSON. J. Chem. Soc. Perkin Trans. II, 961 (1983); (*b*) M. Tamba, G. Simone, and M. QUINTILIANI. Int. J. Radiat. Biol. **50**, 495 (1986).
5. M. A. SHENOY, B. B. SINGH, and A. R. GOPAL-AYENGAR. NATURE, **248**, 415 (1974).
6. K. C. GEORGE, V. T. SRINIVASAN, and B. B. SINGH. Int. J. Radiat. Biol. **38**, 661 (1980).
7. (*a*) M. A. SHENOY and B. B. SINGH. Indian J. Exp. Biol. **18**, 791 (1980); (*b*) K. C. GEORGE and B. B. SINGH. Indian J. Expl. Biol. **22**, 305 (1984).
8. E. PELIZZETTI, D. MEISEL, W. A. MULAC, and P. NETA. J. Am. Chem. Soc. **101**, 6954 (1979).
9. (*a*) S. N. GUHA. Ph.D. Thesis, Bombay University, 1987; (*b*) S. N. GUHA, P. N. MOORTHY, K, KISHORE, D. B. NAIK, and K. N. RAO. Proc. Indian Acad. Sci. **99**, 261 (1987).
10. J. L. REDPATH. Radiat. Res. **54**, 364 (1973).
11. (*a*) P. C. CHAN and B. H. J. BIELSKI. J. Am. Chem. Soc. **95**, 5504 (1973); (*b*) K.-D. ASMUS. Radioprotectors and anticarcinogens. *Edited by* O. F. Nygaard and M. G. Simic. Academic Press, Inc. 1983. p. 24.
12. B. S. WOLFENDEN and R. L. WILLSON. J. Chem. Soc. Perkin Trans. II, 805 (1982).
13. B. H. J. BIELSKI and A. O. ALLEN. J. Am. Chem. Soc. **92**, 3793 (1970).
14. D. BAHNEMANN, K. D. ASMUS, and R. L. WILLSON. J. Chem. Soc. Perkin Trans. II, 1661 (1983).
15. A. HULSHOFF and J. H. PERRIN. Pharm. Acta. Helv. **51**, 65 (1976).
16. D. BAHNEMANN, K. D. ASMUS, and R. L. WILLSON. J. Chem. Soc. Perkin Trans. II, 1669 (1983).

Can. J. Chem. Downloaded from www.nrcresearchpress.com by 88.85.125.76 on 09/07/12
For personal use only.

^{1}H and ^{19}F NMR conformational studies of the monofluorostyrenes in solution. Comparison with theory and vapor phase behavior

TED SCHAEFER AND RUDY SEBASTIAN
Department of Chemistry, University of Manitoba, Winnipeg, Man., Canada R3T 2N2

Received January 16, 1990

TED SCHAEFER and RUDY SEBASTIAN. Can. J. Chem. **68**, 1383 (1990).

The parameters for the high resolution ^{1}H and ^{19}F NMR spectra of 2-, 3-, and 4-fluorostyrene are reported for solutions in CS_2 and acetone-d_6 at 300 K. The populations of the planar *cis* and *trans* conformers of 2- and 3-fluorostyrene are deduced from the long-range coupling constants involving the *meta* and α protons. These populations are insensitive to solvent and appear to be in reasonable agreement with previous 6-31G MO computations for the free molecule; they are also compared with populations deduced from recent rotational and vibronic spectra. The long-range coupling constants for the protons of 4-fluorostyrene imply an internal barrier to rotation about the exocyclic carbon–carbon bond very similar to that in styrene, in agreement with the 6-31G results. The signs of the coupling constants involving ^{19}F and the protons in the side chain are reported and discussed in terms of coupling mechanisms for the three molecules. An earlier surmise, of a positive σ electron contribution to the coupling constant over six bonds in an all-*trans* arrangement, is confirmed for the *meta* and *trans*-β protons in 3-fluorostyrene.

Key words: monofluorostyrenes, ^{1}H and ^{19}F NMR, conformations, long-range coupling mechanisms, MO calculations of internal barriers.

TED SCHAEFER et RUDY SEBASTIAN. Can. J. Chem. **68**, 1383 (1990).

On a déterminé les paramètres pour les spectres RMN à haute résolution du ^{1}H et du ^{19}F des 2-, 3- et 4-fluorostyrènes, en solutions dans le CS_2 et dans l'acétone-d_6, à 300 K. On a déduit les populations des conformères plans *cis* et *trans* présents dans les 2- et 3-fluorostyrènes en se basant sur les constantes de couplage à longue distance impliquant les protons *méta* et α. Ces populations sont insensibles à la nature des solvants et elles semblent en bon accord avec des prévisions faites antérieurement en se basant sur des calculs d'OM effectués au niveau 6-31G, sur la molécule libre; on a aussi comparé ces résultats avec les populations qui ont récemment été déduites de spectres de rotation et de vibration. Les constantes de couplage à longue distance qui sont observées dans le 4-fluorostyrène impliquent que la barrière interne à la rotation autour de la liaison carbone–carbone exocyclique est très semblable à celle qui est observée dans le styrène; cette conclusion est en accord avec les prédictions faites à l'aide de calculs au niveau 6-31G. On rapporte aussi les signes des constantes de couplage entre le ^{19}F et les protons de la chaine latérale et on en discute en fonction de mécanismes de couplage opérant dans ces trois molécules. Pour les protons *méta* et *trans*-β du 3-fluorostyrène, on confirme la prédiction antérieure à l'effet que, dans un arrangement complètement *trans*, il existe une contribution σ électronique positive à la constante de couplage à travers six liaisons.

Mots clés : monofluorostyrènes, RMN du ^{1}H et du ^{19}F, conformations, mécanismes de couplage à longue distance, calculs d'OM des barrières internes.

[Traduit par la revue]

Introduction

Recent microwave and electronic spectroscopic studies of 2-fluorostyrene (2FS) and 3-fluororstyrene (3FS) in the vapor phase disagree in some respects as to the internal rotational potentials and, again, with parts of the predictions from 6-31G MO computations (1–6). The present NMR studies of these molecules in polar and nonpolar solvents provide conformational information relevant to these discrepancies. In addition, the work reported here includes a conformational study of 4-fluorostyrene (4FS), meant to assess the change in the internal rotational potential of styrene caused by the substituent. It turns out that the solvent dependence of the conformational populations is weak for 2FS and 3FS. These populations for 3FS agree reasonably well with microwave and theoretical data but not with the jet spectroscopic results. For 2FS, the solution and theoretical data are moderately compatible, but disagree with the gas phase spectoscopic results.

In the vapor phase at 260 K, the microwave spectrum (5) provides no evidence for the presence of **2**, the *cis* conformer of 2FS. The absence of this conformer is also noted in the single vibronic level fluorescence spectra of a supersonic jet (1). By way of contrast, 6-31G MO computations for the two conformations suggest a ratio of near 2:1 for the *trans*/*cis* populations at 300 K (6).

The spectra of 3FS in a supersonic jet (2) imply a *cis*/*trans* ratio of 3:1, apparently (3) that found at room temperature with

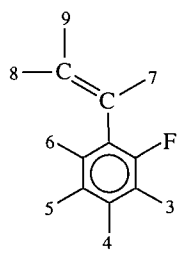

θ = 180°

1

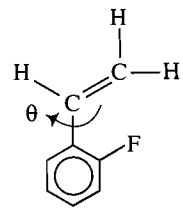

θ = 0°

2

the high resolution electronic absorption spectrum. Yet the microwave spectrum of 3FS, while detecting both conformers, **3** and **4**, has this ratio as $1.15^{+0.34}_{-0.21}$ at 260 K (4), in rather better agreement with *ab initio* molecular orbital calculations with a

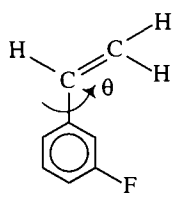

θ = 0°

3

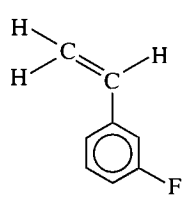

θ = 180°

4

Can. J. Chem. Downloaded from www.nrcresearchpress.com by 88.85.125.76 on 09/07/12
For personal use only.

TABLE 1. ^1H and ^{19}F NMR spectral parameters for the monofluorostyrenes in CS_2/C_6D_{12} and acetone-d_6 solutions at 300 K, excluding coupling constants between the vinyl protons and ring nuclei in the benzene moiety

	4-Fluorostyrene		3-Fluorostyrene		2-Fluorostyrene	
Parameter	CS_2/C_6D_{12}[a]	Acetone-d_6[b]	CS_2/C_6D_{12}[a]	Acetone-d_6[b]	CS_2/C_6D_{12}[a]	Acetone-d_6[b]
ν_2	2174.807(1)[c,e]	2248.060(1)	2091.847(1)	2170.359(1)	12475.396(1)	12404.570(1)
ν_3	2064.006(1)	2126.945(1)	14000.663(1)	13940.211(1)	2068.563(1)	2131.750(1)
ν_4	13805.691(1)[d]	13718.449(1)	2045.552(1)	2106.288(1)	2132.447(1)	2190.679(1)
ν_5	2064.006(1)	2126.945(1)	2149.723(1)	2208.156(1)	2096.536(1)	2149.506(1)
ν_6	2174.807(1)	2248.060(1)	2112.191(1)	2181.303(1)	2208.739(1)	2279.156(1)
$\nu_7(\alpha)$	1976.500(1)	2021.062(1)	1978.837(1)	2026.130(1)	2036.123(1)	2064.373(1)
$\nu_8(cis)$	1670.666(1)	1723.547(1)	1700.297(1)	1760.046(1)	1719.590(1)	1766.251(1)
$\nu_9(trans)$	1540.115(1)	1563.701(1)	1565.626(1)	1593.247(1)	1583.865(1)	1616.115(1)
^2J_g	0.870(1)[e]	0.901(1)	0.804(1)	0.817(1)	1.239(1)	1.218(1)
^3J_c	10.859(1)	10.959(1)	10.827(1)	10.931(1)	11.191(1)	11.271(2)
^3J_t	17.495(1)	17.639(1)	17.482(1)	17.618(1)	17.690(1)	17.775(1)
$^3J_{23}$	8.554(2)	8.600(1)	9.878(1)[f]	10.428(1)[f]	10.569(1)[f]	11.068(2)[f]
$^3J_{34}$	8.360(1)	8.858(1)	8.278(1)[f]	8.789(1)[f]	8.245(1)	8.290(1)
$^3J_{45}$	8.360(1)[f]	8.858(1)[f]	8.238(1)	8.284(1)	7.360(1)	7.382(1)
$^3J_{56}$	8.554(2)	8.600(1)	7.698(1)	7.727(1)	7.774(1)	7.783(1)
$^4J_{24}$	5.328(1)[f]	5.453(1)[f]	2.581(1)	2.627(1)	5.156(1)[f]	5.288(1)[f]
$^4J_{35}$	2.757(1)	2.826(1)	5.902(1)[f]	6.086(1)[f]	1.179(1)	1.177(2)
$^4J_{26}$	2.352(1)	2.379(1)	1.591(1)	1.583(1)	7.524(1)	7.769(1)
$^4J_{46}$	5.328(1)	5.453(1)	0.976(1)	0.945(1)	1.752(1)	1.754(1)
$^5J_{25}$	0.395(1)	0.395(1)	0.395(1)	0.411(1)	(−)0.145(1)[g]	(−)0.095(2)[g]
$^5J_{36}$	0.395(1)	0.395(1)	(+)0.1071(1)[g]	(+)0.203(1)[g]	0.376(1)	0.379(1)
Calculated trans.	896	896	1024	1090	1024	1024
Assigned trans.	705	703	828	795	703	697
Observed peaks	320	370	550	595	550	545
Largest diff.	0.022	0.017	0.018	0.020	0.018	0.022
Root-mean-square deviation	0.009	0.006	0.007	0.007	0.007	0.009

[a]5.0 mol% in a solution of CS_2, containing also 10.0 mol% C_6D_{12}, 0.5 mol% TMS, and 0.25 mol% of C_6F_6.
[b]5.0 mol%, containing also 0.5 mol% TMS and 0.25 mol% of C_6F_6.
[c]In Hz at 300.135$_2$ MHZ to high frequency of internal TMS.
[d]In Hz at 282.369 MHz to high frequency of internal C_6F_6; note that on the δ scale, C_6F_6 has a δ of −163 ppm (relative to $CFCl_3$ and therefore more shielded).
[e]Numbers in parentheses are standard deviations in the last significant figure.
[f]The marked solvent dependence of ^nJ (H,F) within the benzene ring is well known (46).
[g]Signs assumed on the basis that ^5J (H,F) in fluorobenzene derivatives becomes algebraically larger in more polar solvents, as experienced in this laboratory. Note also that ^5J (H,F) is positive in 3-fluorobenzaldehyde (47) and in 3-fluorotoluene (41), but is negative in 2-fluorobenzaldehyde (47) and in 2-fluorotoluene (43).

minimal basis set (7) and also with 6-31G MO computations (6). In solution (see below) the *cis* conformer is only slightly the more abundant at 300 K. In early work (8–10) the internal rotational barriers in 4FS and 3FS are discussed in terms of twofold symmetry; in view of recent experimental work on styrene (11, 12) and of theoretical work on styrene (13, 14) and 4FS (6), these terms are inappropriate.

Experimental

The three fluorostyrenes were prepared as 5.0 mol% solutions in CS_2/C_6D_{12} and acetone-d_6 (see Table 1 for details). These solutions were filtered into 5 mm o.d. NMR sample tubes, were degassed by five cycles of the freeze–pump–thaw procedure, and were then flame-sealed under vacuum to produce symmetrical tops. The ^1H and ^{19} NMR spectra were accumulated on a Bruker AM 300 spectrometer in a manner described before (15). Certain relative signs of $^1H,^{19}F$ coupling constants were also found (see below).

INDO and CNDO MO FPT computations (16, 17) were performed on a Amdahl 5870 system; *ab initio* molecular orbital computations, with geometry optimization (see the caption to Fig. 2), utilized the same computer and the program GAUSSIAN 86 (18).

Results and discussion

Spectral analyses

The ^1H and ^{19}F NMR spectra were analyzed with the program NUMARIT (19), extensively modified in this laboratory. The spectral parameters are to be found in Tables 1 and 2. Figure 1 shows parts of the ^1H NMR spectra of the α proton in the three compounds, together with their theoretical simulations. We discuss interring $^1H,^1H$ couplings first, most being known about their θ dependence.

The conformational equilibria based on $^5J_{37}$ and $^5J_{57}$

(i) 2-Fluorostyrene

The coupling constant between the α and *meta* protons in styrene has been examined theoretically (20–23), one study (23) strongly implying a predominant σ electron mechanism. In other words, $^5J_{37}$, analogous to that in **1**, is expected to be small whereas $^5J_{57}$ should be large for the all-*trans* arrangement of the five intervening bonds. Furthermore, it has been argued (24) that $^5J_{57}$ is proportional to $\sin^2(\theta/2)$, therefore vanishing in **2** when $\theta = 0°$ and attaining its maximum value in **1**, when $\theta = 180°$. The argument is based on the insensitivity of $^5J_{37}$ or $^5J_{57}$ to nonplanarity of the molecule, in 2,6-dichlorostyrene (20), for example, among others (24), and also that $^5J_{37}$ in 2,5-dichlorostyrene (20) is very small, corresponding to predominance of conformer **1** above. The argument implies that $^5J_{37}$ in styrene behaves like the analogous coupling constant in benzaldehyde (25) but not like that in toluene (26, 27).

Can. J. Chem. Downloaded from www.nrcresearchpress.com by 88.85.125.76 on 09/07/12
For personal use only.

TABLE 2. Coupling constants between the olefinic protons and the protons and fluorine nuclei in the ring for the monofluorostyrenes at 300 K[a]

	4-Fluorostyrene		3-Fluorostyrene		2-Fluorostyrene	
Parameter	CS_2/C_6D_{12}[a]	Acetone-d_6[b]	CS_2/C_6D_{12}[a]	Acetone-d_6[b]	CS_2/C_6D_{12}[a]	Acetone-d_6[b]
$^4J_{27}$	−0.525(1)[c]	−0.523(1)	−0.507(1)	−0.494(1)	0.485(1)	0.494(2)
$^4J_{67}$	−0.525(1)	−0.523(1)	−0.522(1)	−0.520(1)	0.572(1)	0.575(1)
$^5J_{37}$	0.378(1)	0.375(1)	0.867(1)	0.907(1)	0.220(1)	0.214(2)
$^5J_{57}$	0.378(1)	0.375(1)	0.310(1)	0.314(1)	0.537(1)	0.544(2)
$^6J_{47}$	0.235(1)	0.217(1)	−0.203(1)	−0.199(1)	−0.233(1)	−0.238(1)
$^5J_{28}$	±0.047(1)	±0.048(1)	±0.02$_0$[e]	±0.020(10)[e]	0.298(1)	0.345(2)
$^5J_{68}$	±0.047(1)	±0.048(1)	±0.069(1)	±0.069(1)	±0.086(1)	±0.076(1)
$^6J_{38}$	±0.015[e]	±0.015(10)[e]	0.296(1)	0.310(1)	±0.082(1)	±0.086(2)
$^6J_{58}$	±0.015[e]	±0.015(10)[e]	±0.02$_0$[e]	±0.020(10)[e]	±0.01$_0$[e]	0.010(10)[e]
$^7J_{48}$	−0.592(2)	−0.589(1)	0.247(1)	0.253(1)	0.222(1)	0.226(1)
$^5J_{29}$	0.168(1)	0.172(1)	0.164(1)	0.169(1)	0.285(1)	0.300(2)
$^5J_{69}$	0.168(1)	0.172(1)	0.175(1)	0.176(1)	0.085(1)	0.083(1)
$^6J_{39}$	±0.015[e]	±0.015(10)[e]	0.574(1)	0.590(1)	±0.035	(+)0.030(10)
$^6J_{59}$	±0.015[e]	±0.015(10)[e]	0.062(1)	0.060(1)[d]	±0.01$_0$[e]	±0.010(10)[e]
$^7J_{49}$	−0.764(1)	−0.762(1)	0.310(1)	0.315(1)	0.284(1)	0.295(1)

[a]For the solutions described in Table 1.
[b]Note that H-7 is the α proton of the vinyl group and that H-9 is the *trans*-β proton.
[c]Numbers in parentheses are the standard deviations in the last significant figure.
[d]The sign is an accidental by-product of the double resonance experiments.
[e]These numbers are obtained from assessments of peak shapes and are not optimized.

In 4-methylstyrene in acetone-d_6 solution, $^5J_{37} = {}^5J_{57} =$ 0.377 (1) Hz (24), the same as that in 4-fluorostyrene (Table 2). For evenfold barriers to internal rotation about the C_{sp^2}—C_{sp^2} bond, the expectation value of $<\sin^2(\theta/2)>$ is 0.5 (see caption to Fig. 2). Hence $^5J_{180}$ is 2 (0.376_5) or 0.753 (3) Hz for 4FS, taking the average values of $^5J_{37}$ in the two solutions of Table 1. This result is now applied to the conformational equilibria for 2FS and 3FS.

The sum of $^5J_{37}$ and $^5J_{57}$ in 2FS is 0.757 (2) and 0.758 (4) Hz in CS_2/C_6D_{12} and acetone-d_6 solutions, respectively, equal to that in 4FS, within experimental error. On the assumption that the fluorine substituent in 2FS does not alter significantly the intrinisic magnitude of $^5J_{37}$, the population of the *trans* conformer, **1**, follows as 0.71 (1) in the nonpolar and as 0.72 (1) in the polar solvent at 300 K. This result implies that the conformational equilibrium is independent of solvent and, indeed, the STO-3G and 6-31G MO computations (6) suggest that the dipole moment of **1** is larger that that of **2** by only 0.01 D. The former computations have the *trans* form as 1.91 kJ/mol more stable, corresponding to a fractional *trans* population of 0.68, if differences in zero point energy between **1** and **2** are ignored; the latter basis gives the same population. These energy differences imply a population of about 0.30 for the *cis* conformer at 260 K, the temperature of the microwave experiments. Yet no spectral lines due to this conformer could be found (5). The same statement applies to the $S_1 \leftarrow S_0$ fluorescence excitation spectra in a supersonic jet (1). The gas phase experiments yield a barrier to planarity for the *trans* form of 0.19 (2) and 0.18 (5) kJ/mol (1, 5) while the 6.31G basis has the energy of the nonplanar as 0.04 kJ/mol lower than the planar *trans* form. The potential function given by this basis yields an average value of 16° for the dihedral angle between the vinyl and benzene planes at 300 K; the microwave data fit an angle of about 14° at 260 K. One might speculate that the density of vibrational and rotational states for the *trans* form is much larger for the *cis* form, which, according to the MO computations (6), is planar and has a barrier of 0.7 kJ/mol to rotation by 15° about the C_{sp^2}—C_{sp^2} bond. If this speculation were correct, then it would follow that entropy effects cause the very low abundance of the *cis* conformer in the vapor but also that the solvent molecules damp out these states in the NMR experiment.

The populations of **1** and **2** for 2FS in solution were based on a two-site analysis. The internal rotational potential given by the 6-31G basis yields $<\sin^2(\theta/2)>$ as 0.735 at 300 K, contributions from nonplanar conformations now being included. Hence $^5J_{37}$ follows as 0.735 (0.758) or 0.557 Hz, whereas $^5J_{57}$ becomes 0.201 Hz. The corresponding STO-3G potential has $<\sin^2(\theta/2)>$ as 0.675 at 300 K, suggesting $^5J_{37}$ as 0.512 Hz and $^5J_{57}$ as 0.246 hz. The differences in the coupling constants reflect the differences in the barrier heights predicted by the two bases; the minimal basis set has this height as 16.0 kJ/mol at $\theta = 90°$, some 2.4 kJ/mol larger than found with the split-valence basis. The means of the coupling constants obtained from the two theoretical potentials are rather near those found in solution.

For styrene itself, the 6-31G potential agrees quite closely with experiment (14) but the STO-3G potential (13) overestimates the barrier height by about 3.5 kJ/mol. It is conceivable that the solvent raises the barrier height in styrene. Quadrupolar splittings in the high resolution NMR spectra of deuterated styrene, in solvents of low polarity, are used (28) to deduce a twofold internal barrier of 16.7 ± 1.6 kJ/mol, close to the twofold component of 16.3 ± 0.1 kJ/mol given by the minimal basis (13); the free molecule, however, has a substantial fourfold component in the barrier (11). The temperature dependence of $^6J_{47}$ in 3,5-dichlorostyrene in acetone-d_6 and CD_2Cl_2 solutions (22) is interpreted to mean that the fourfold component is quite different than for styrene, that the barrier height in the former solvent is the same as in gaseous styrene, and that the height increases by 2.3 ± 1.5 kJ/mol in the chlorinated solvent. The nonpolar molecule, ethylbenzene, displays no solvent dependence of the barrier to rotation about the exocyclic C_{sp^2}—C_{sp^3} bond (29).

Can. J. Chem. Downloaded from www.nrcresearchpress.com by 88.85.125.76 on 09/07/12
For personal use only.

Can. J. Chem. Downloaded from www.nrcresearchpress.com by 88.85.125.76 on 09/07/12
For personal use only.

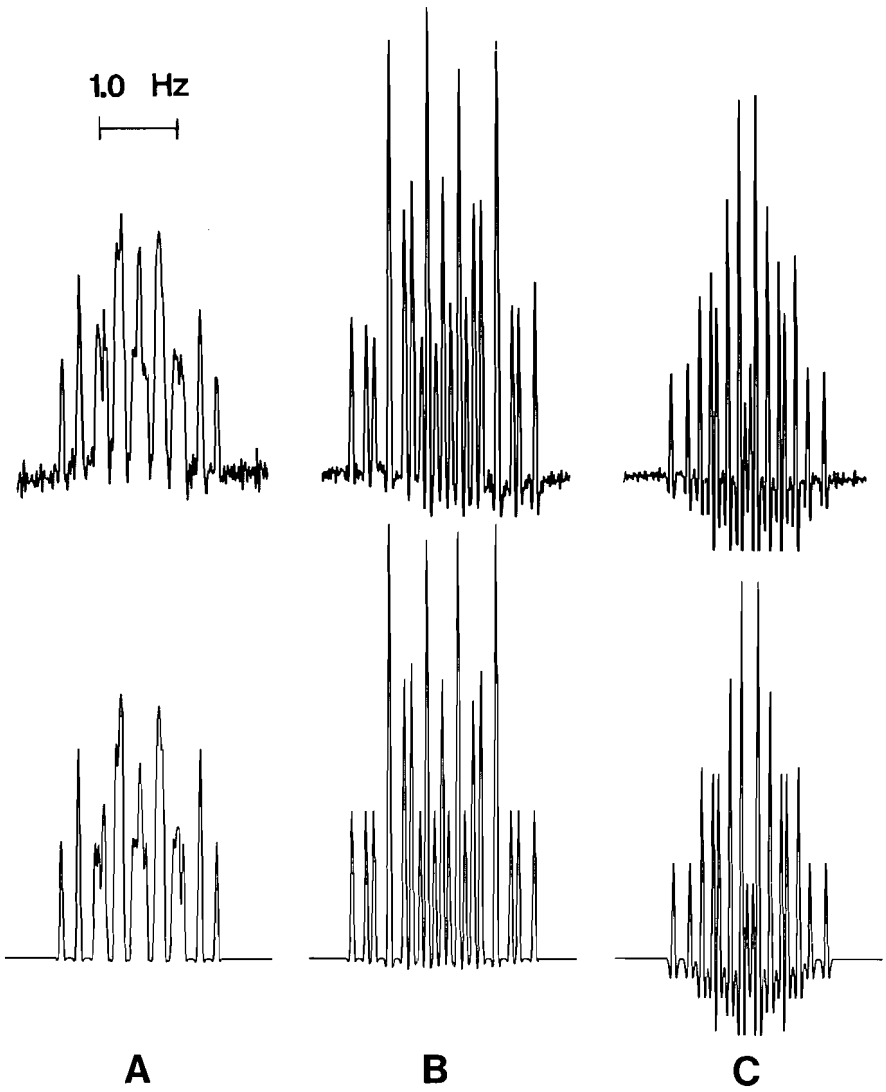

FIG. 1. The bands at lowest frequency of the ^{1}H NMR spectra at 300.135 MHz of the α protons in 2-, 3-, and 4-fluorostyrene are shown in A, B, and C, respectively, for 5.0 mol% solutions in acetone-d_6 and a probe temperature of 300 K. The splittings arise from long-range coupling interactions with all the ^{1}H and ^{19}F nuclei in the benzene ring. The theoretical spectra are produced with the spectral parameters in Tables 1 and 2 and each transition has a linewidth at half height of 0.04 Hz. The digital resolution is 0.005 Hz per point; the smallest spacings in B, for example, are about 0.07 Hz.

In summary, in both polar and nonpolar solutions at 300 K, the *cis* conformer of 2FS has an abundance of near 30%. In the gas phase, this conformer appears to be absent.

(ii) 3-Fluorostyrene

$^5J_{57}$ is 0.310 (1) and 0.314 (1) Hz in the CS_2 and acetone-d_6 solutions, respectively, implying that the conformational equilibrium is essentially independent of solvent polarity. The computed dipole moments of the *cis* and *trans* conformers, **3** and **4**, differ by less than 0.01 D (6). If $^5J_{180}$ is 0.753 (3) Hz, as in 4FS,[1] then a two-site analysis indicates that the fractional abundance of the *trans* form is 0.312 (3) /0.753 (3) or 0.41 (1) in both solvents.

The 6-31G energy of this form is 0.53 kJ/mol higher than that of the *cis* form, corresponding to a fractional population of 0.45 at 300 K if the computed energies are identified with free energies. The STO-3G computations have the *cis* form favored by only 0.20 kJ/mol. The gas phase electronic absorption spectrum at room temperature has an intensity ratio favoring the *cis* conformer by 3:1, or by 2.7 kJ/mol in free energy (3). However, the microwave spectra imply a free energy difference of only 0.3 ± 0.5 kJ/mol at 260 K, the *cis* form predominating (4). All methods agree that the *cis* conformer is most stable. The solution data imply a solvent independence of the conformational equilibrium. Table 3 summarizes the conformational populations suggested by the various methods.

$^6J_{47}$ as an indicator of the internal rotational barriers

$^6J_{47}$ in Hz for styrene has been written (24) as $-0.448 \sin^2\theta - 0.149$ on the assumption that the internal rotational barrier in the gas phase (11, 12) is the same as in acetone-d_6 solution. For 3,5-dichlorostyrene, $^6J_{47}$ is taken as $-0.670 \sin^2\theta - 0.130$, based on its temperature dependence in acetone-d_6 and CD_2Cl_2 solutions (22). The values of $^6J_{47}$ of 2FS and 3FS do not display a marked solvent dependence (Table 2). At 300 K,

[1]In unpublished work in this laboratory, it was shown that ^5J(H,CHO) in 4-fluorobenzaldehyde is essentially unchanged from its value in benzaldehyde, this coupling being a purely σ electron mediated interaction.

TABLE 3. Populations of *cis* conformers of 2-fluorostyrene and 3-fluorostyrene in various states by different methods

Method	State	Temperature/K	P(*cis*) 2FS	P(*cis*) 3FS	Reference
Microwave	Vapor	260	0	0.53(5)	4, 5
Fluoresence[a]	Vapor	—	0	0.75	1, 2
Electronic absorption	Vapor	~298	—	0.75	3
NMR[b]	Solution	300	0.29(1)	0.59(1)	This work
6-31G[c]	Free molecule	300	0.32	0.55	6

[a]Vibronic fluoresence spectra of a jet, suggested (1, 2) to have a room temperature conformer distribution.
[b]Based on long-range coupling constants between ring and vinylic protons in CS_2/C_6D_{12} and acetone-d_6 solutions.
[c]Based on the computed energy differences between the *cis* and *trans* conformers, uncorrected for zero point energy differences.

the STO 3G and 6-31G MO potentials (6) have $<\sin^2\theta>$ as 0.108 and 0.157, respectively, for 2FS and are 0.118 and 0.170 for 3FS. The smaller values of $<\sin^2\theta>$ from the minimal basis set reflect the higher computed internal barriers. The ensuing $^6J_{47}$ numbers obtained from these $<\sin^2\theta>$ values and the relationships above can be summarized as follows. For 2FS, the 6-31G potential yields $^6J_{47}$ as −0.219 and −0.235 Hz, the observed value being −0.238 (1) Hz in acetone-d_6 solution, whereas the STO-3G potential yields −0.197 and −0.202 Hz from the two relationships above. By way of contrast, for 3FS the 6-31G potential has $^6J_{47}$ as −0.225 and −0.244 Hz, rather larger in magnitude than the measured value of −0.199 (1) Hz, while the STO-3G potential has $^6J_{47}$ as −0.201 and −0.209 Hz.

Now, the 6-31G potential agrees best with the experimental potential for styrene in the gas phase. If this agreement holds true for 3FS in the gas phase, as is consistent with the microwave data (4), then $^6J_{47}$ implies a barrier in solution larger by about 3 kJ/mol than in the gas phase; this follows from the STO-3G potential (6), which has the barrier height as 3.4 kJ/mol larger than that from the 6-31G basis. Both parameterizations of ^6J imply such an increase.

However, a variety of potentials probably would be consistent with the $^6J_{47}$ numbers in Table 2. Hence it is best to conclude that the internal rotational potential may be somewhat larger for 3-fluorostyrene in acetone-d_6 solution, where $^6J_{47}$ is −0.199 (1) Hz, than it is for styrene in the same solution, where $^6J_{47}$ is −0.227 (3) Hz. This conclusion follows simply from the $\sin^2\theta$ dependence of $^6J_{47}$. The internal barrier in 3,5-dichlorostyrene is also higher than in styrene, based on the same comparison.

A caveat concerns the intrinsic substituent dependence of the predominantly σ−π coupling constant, $^6J_{47}$. The somewhat analogous coupling constant in 3-fluorotoluene, at −0.593 (2) Hz (30), is indeed slightly smaller in magnitude than the −0.602 (2) Hz for toluene (27) in the same solvent. Furthermore, in 3-fluorobenzaldehyde, $^6J_{47}$ is +0.045 (1) Hz (25), whereas it cannot be detected in benzaldehyde. In view of the detailed discussion of the coupling mechanisms in toluene (26, 27) and styrene (21) it seems possible that the fluorine substituent in 3FS causes a small intrinsic positive change in $^6J_{47}$. If so, then the increased barrier relative to styrene in solution is not established.

The long-range $^1H,^1H$ coupling constants for the β-olefinic protons

(i) Five-bond coupling constants

$^5J_{28}$ and $^5J_{68}$ were not detected for styrene (31) but occur as ±0.045 (1) Hz in 4-methylstyrene (24) and as ±0.048 (1) Hz in 4FS in both solvents of Table 2. Both the valence bond and molecular orbital models probably overestimate their positive magnitudes (20) for θ = 180°, that is, for J_{28} in **4**, for example. For $^5J_{68}$ in **4**, the latter model predicts a very small, negative value, probably arising from a direct or proximate coupling mechanism. Indeed, $^5J_{68}$ is −0.15 (4) Hz in 2,5-dichlorostyrene (20); if the latter exists entirely as one planar conformer, then ^5J is about −0.15 Hz for H-8 and H-*ortho* in a *cis* orientation. $^5J_{28}$ and $^5J_{68}$ are less than 0.1 Hz in magnitude for 2FS and 3FS and, since their signs are unknown, will not be further discussed.

The negative, proximate contribution to $^5J_{28}$ is not present in $^5J_{29}$ and $^5J_{69}$. Hence the latter have larger magnitudes, at about 0.17 Hz in styrene (31) as well as in 4FS and 3FS. $^5J_{69}$ is slightly larger than $^5J_{29}$ in 3FS, suggesting a small σ electron contribution, largest for an all-*trans* orientation of the intervening bonds. Such a contribution is also consistent with the small $^5J_{69}$ of 0.085 Hz in 2FS, for which the all-*trans* orientation is less prevalent (conformational bias) than in 4FS and 3FS.

(ii) Six-bond coupling constants

$^6J_{38}$ and $^6J_{58}$, computed as negative by both valence bond and molecular orbital methods (20), have not been detected in styrene (31) and are clearly very small in 4FS, as is $^6J_{58}$ in 3FS and 2FS (Table 2).

For the all-*trans* coupling path, $^6J_{39}$ and $^6J_{59}$ are predicted as positive (20), presumably due to a positive σ electron component. Again, these coupling constants have not been observed for styrene and are small in 4FS. However, the ^7J (H-3,CH_3) in β-methylstyrene (24) implies a π electron contribution of −0.08 Hz to these coupling constants for nearly planar conformations. Hence the very small values of $^6J_{39}$ and $^6J_{59}$ in 4FS may well arise from cancellation of the two components. Our INDO MO FPT computations give −0.12 and 0.09 Hz for $^6J_{39}$ in the two planar conformers, suggesting -0.01_5 Hz in 4FS; this result is consistent with observation (Table 2). For 3FS, our INDO MO FPT calculations give $^6J_{59}$ as 0.15 Hz in the *cis* conformer, **3**, and as −0.08 Hz in the *trans* conformer, **4**; the latter has an abundance of 41%, according to the discussion in a previous section. Accordingly, $^6J_{59}$ follows as 0.06 Hz, consistent with the measured value of +0.06 Hz.

(iii) Seven-bond coupling constants

$^7J_{48}$ and $^7J_{49}$ are attributed to π electron coupling mechanisms (20). In 4-methylstyrene, ^8J (H-8,CH_3) and ^8J (H-9,CH_3) are 0.26 Hz in magnitude (24), giving a measure of the π electron contributions to $^7J_{48}$ and $^7J_{49}$. In styrene itself, $^7J_{48}$ is 0.24 Hz, whereas $^7J_{49}$ is 0.28 Hz (31). The difference in mag-

Can. J. Chem. Downloaded from www.nrcresearchpress.com by 88.85.125.76 on 09/07/12
For personal use only.

TABLE 4. Some INDO MO and CNDO/2 MO FPT values of $^1H,^{19}F$ spin–spin coupling constants in Hz, involving the side-chain protons for the monofluorostyrenes with 6-31 G geometries

	$^nJ_7$[a]			$^nJ_8$[a]			$^nJ_9$[a]		
θ/deg	2FS	3FS	4FS	2FS	3FS	4FS	2FS	3FS	4FS
0[b,c]	−0.35	3.26	0.09	−6.13	0.26	−0.31	−0.85	0.36	−0.29
90	1.24	−0.33	1.20	0.50	−0.09	−0.03	1.48	0.20	0.20
180	—[e]	0.33	0.09	−0.16	0.15	−0.31	0.12	0.97	−0.29
0[b,d]	−0.12	2.43	−0.02	−4.66	0.08	−0.01	−0.16	0.13	0.00
90	0.35	0.17	0.02	0.46	0.10	0.03	1.16	0.29	0.09
180	−1.10	0.58	−0.02	−0.03	0.02	−0.01	0.30	0.49	0.0

[a]The number of formal intervening bonds, n, varies from 4 to 7, of course. See the text for the numbering of the protons in the olefinic group.
[b]The planar molecule has the angle, θ, as zero and, for 2FS and 3FS, the double bond of the side chain is then oriented *cis* to the fluorine substitutents.
[c]This block refers to the INDO MO FPT results.
[d]This block refers to the CNDO/2 MO FPT results.
[e]The computation did not converge for this number.

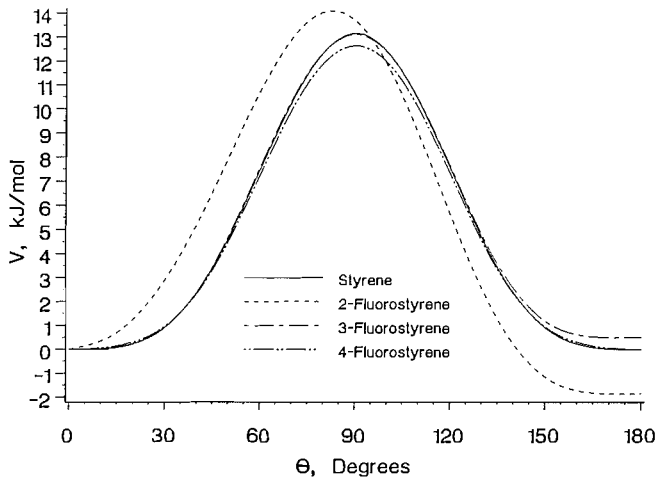

FIG. 2. The 6-31G MO potentials for rotation about the exocyclic carbon–carbon bond are displayed for styrene and the three monofluorostyrenes. A conformational angle, θ, of 180° corresponds to a *trans* orientation of the C—F and C=C bonds in 2-fluoro and 3-fluorostyrene. The curves result from a fit of the computed energies at intervals of 15° in θ. For styrene, the curve represents the internal potential (all energies in kJ/mol), $V = 13.19\ (15)\ \sin^2\theta - 3.18\ (15)\ \sin^2 2\theta$, the number in parentheses being the standard error in the fit of the computed energies (14) to twofold, in $\sin^2\theta$, and fourfold, in $\sin^2 2\theta$, components. This potential agrees to within combined experimental error with the components deduced from vibronic fluoresence data (11). For 4-fluorostyrene, the computed energies (6) are fit by twofold and fourfold components of 12.67 (3) and −3.02 (3), respectively, if an eightfold term of 0.08 (3) is included. The theoretical curves essentially coincide for the θ values accessible to the molecule at ambient temperatures. For 3-fluorostyrene, the theoretical potential is $V = 0.33\ \sin^2(\theta/2) + 12.97\ \sin^2\theta + 0.19\ \sin^2(3\theta/2) - 3.19\ \sin^2 2\theta - 0.09\ \sin^2 3\theta + 0.03\ \sin^2 4\theta$, the standard error in the fit of the energies (6) being 0.03. The presence of the onefold (0.33) and threefold (0.19) terms accounts for greater stability of the *cis* conformer. The computed potential for 2-fluorostyrene is $V = -4.66\ \sin^2(\theta/2) + 14.63\ \sin^2\theta + 2.82\ \sin^2(3\theta/2) - 2.84\ \sin^2 2\theta$, the standard error in each component being 0.04. The onefold and threefold components oppose each other in establishing the stability of the *trans* conformer.

nitude between $^7J_{48}$ and $^7J_{49}$ rises to 0.06 Hz in 2FS and 3FS. The difference is not reproduced by our INDO MO FPT computations. However, the magnitudes themselves are not drastically different from those in styrene, as is reasonable in terms of the internal rotational potentials sketched in Fig. 2.

The long-range $^1H,^{19}F$ coupling constants

The signs of the H,F coupling constants for the vinylic protons, all of which are 0.2 Hz or larger in magnitude, were determined by $^1H\{^1H\}$ experiments (32, 33) in the normal way and were based on the positive values of ^4J (H,F) and ^3J (H,F) within the aromatic ring. The signs are given in Table 2. Table 4 contains theoretical values for these coupling constants for planar and perpendicular conformations of the three molecules in question. Figure 3 shows an example of a sign determination.

(i) 4-Fluorostyrene

To a reasonable approximation (23), the CNDO/2 numbers for ^nJ (H,F) in Table 4 represent transmission of nuclear spin state information via the σ electron framework, while the INDO numbers also include contributions from π electrons and from σ–π interactions. Comparison of the theoretical results for 4FS indicates than $^6J_{47}$, $^7J_{48}$, and $^7J_{49}$ are dominated by π electron mechanisms, the CNDO/2 values being very small or zero. This indication is expected on the basis of previous theoretical data for the corresponding H,H interactions (20). Because the composite hyperfine interaction parameter, Q^F_{CF}, is positive, however, unlike Q^H_{CH}, the computed values of $^6J_{47}$, $^7J_{48}$, and $^7J_{49}$ are of opposite sign to the corresponding coupling constants in the parent molecule, styrene.

$^6J_{47}$ ia a σ–π coupling constant, predominantly, and accordingly has its largest value, 1.20 Hz, at θ = 90°. A pure σ–π coupling constant is proportional to $\sin^2\theta$. For 4FS, the 6-31 G potential has $<\sin^2\theta>$ as 0.171 at 300 K. If this potential were to apply to 4FS in CS_2 solution, $^6J_{47}$ would follow as 0.171 (1.20) or 0.205 Hz. The experimental value of 0.235 (1) Hz is somewhat larger than this, perhaps because a small term in $\cos^2\theta$, apparently present for $^6J_{47}$ in styrene (20, 22), is neglected. In our opinion, however, the rather good agreement between experiment and theory above is coincidental.

One might argue as follows. The long-range coupling

Can. J. Chem. Downloaded from www.nrcresearchpress.com by 88.85.125.76 on 09/07/12
For personal use only.

Can. J. Chem. Downloaded from www.nrcresearchpress.com by 88.85.125.76 on 09/07/12
For personal use only.

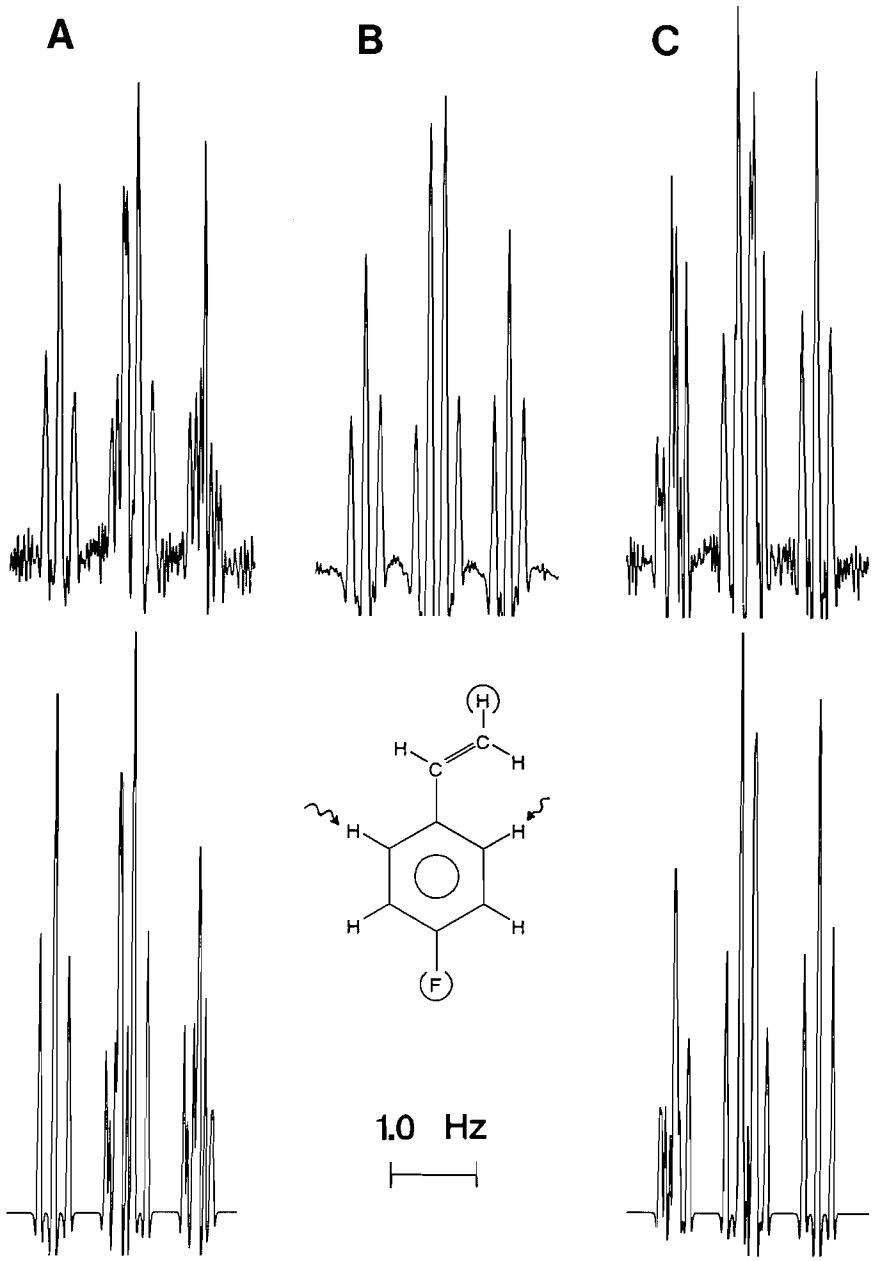

FIG. 3. The band at lowest frequency of H-9 in the ^{1}H NMR spectrum of 4-fluorostyrene in acetone-d_6 solution is shown in B. A geminal coupling of 0.90 Hz (Table 1), a ^7J (H, F) of ± 0.76 Hz, and a ^5J (H, F) of 0.17 Hz to H-2 and H-6 account for the structure of the band. In A this band has the given appearance when a second radiofrequency field of an amplitude roughly equal to 1 Hz is centered at 2255.48 Hz to high frequency of internal TMS, corresponding to irradiation of peaks due to H-2 and H-6. For these peaks the spin states of H-3 and F-4 are the same if $^3J_{23}$ and $^4J_{24}$ have the same sign, as they do (48–52). Qualitatively, it is clear in A that ^7J (H-9, F)/^4J (H,F) < 0 simply because the peaks in the multiplet at low frequency are perturbed in intensity or split when the peaks in the H-2 region are irradiated to high frequency of the shift position of H-2. The theoretical spectrum below the experimental one in A was computed with the program DOR (53), as modified in this laboratory to accommodate eight spins. The agreement between theory and experiment is not exact, depending as it does on the theoretical intensity of the irradiating field, but is sufficiently close to show that ^7J (H-9,F) is negative, ^4J (H,F) being positive (51, 52). A check is provided by the experimental and theoretical bands in C, corresponding to irradiation at 2241.04 Hz. Note that a positive sign of ^7J would have resulted in marked perturbations of that "triplet" in A and C, which was not, in fact, strongly altered in the double resonance experiment.

constants involving fluorine in 4FS should be proportional to Q^F_{CF} for the C—F bond. In toluene and 4-fluorotoluene, ^6J (H,CH_3) and ^6J (F,CH_3) are a measure of Q^H_{CH} and the composite (34, 36) Q^F_{CF} at the position *para* to the methyl group (26, 35). The former coupling constant is -0.602 (2) Hz (27), the latter 1.15 (2) Hz (35). Hence Q^H_{CH}/Q^F_{CF} is -0.52_3. In styrene $^7J_{48}$ is 0.237 (3) Hz (31), so that $^7J_{48}$ in 4FS should be 0.237 (3)/-0.52_3 or -0.45 Hz. However, $^7J_{48}$ in 4FS is measured as -0.59 Hz, implying a larger magnitude of Q^F_{CF} in 4FS than in 4-fluorotoluene. The methyl group is a π electron donor, whereas the vinyl group is electronically neutral (37). Hence the former will act to repress somewhat the π electron donation of the fluorine substituent, with the consequence that the double-bond character of the C—F bond in 4FS is larger

Can. J. Chem. Downloaded from www.nrcresearchpress.com by 88.85.125.76 on 09/07/12
For personal use only.

than in 4-fluorotoluene. The larger double-bond character increases Q^{F}_{CF} because it facilitates the transmission of electron spin density into the $2p_z$ orbital on fluorine (38). Given this interpretation, it still follows that $^6J_{47}$ in styrene, at −0.227 (3) Hz, should be much smaller in magnitude than $^6J_{47}$ in 4FS, measured, however, as 0.235 Hz in CS_2 solution. This is so, whatever the effect (21, 22) of the $=CH_2$ moiety on the spin polarizability of the π system of the olefinic group.

The theoretical calculations (Table 4) give $^6J_{48}$ as only about half as large as measured, but of correct sign. $^7J_{49}$ is even larger in magnitude, at −0.76 Hz (Table 2), whereas theory has $^7J_{49}$ almost equal to $^7J_{48}$ for a planar molecule, just as for the analogous coupling parameters in styrene itself. The larger magnitude measured for $^7J_{49}$ is reminiscent of the hyperfine splitting constants in the allyl radical (39, 40), these being somewhat different for the two protons bonded to the carbon atom of the methylene group; the larger Q^{H}_{CH} occurs for the C—H bond placed *cis* to the central C—H bond, just as in 4FS. A similar remark applies to the corresponding coupling constants in styrene.

It is also noted that the ratio of the $^7J_{48}$ values of styrene and 4FS is 0.40 whereas for $^7J_{49}$ it is 0.37, all values applying to the acetone-d_6 solutions.

The present discussion illustrates the difficulties involved in the use of ^nJ (H,F) in the conformational analysis of 4FS. The signs are understood but not their magnitudes, unlike their counterparts in styrene. Note, further, that $^6J_{47}$ is sensitive to solvent, intrinsically so, as strongly implied by the solvent independence of the (conformationally dependent) long-range H,H coupling parameters of 4FS (Table 2). The intrinsic solvent dependence of the H,F couplings of the olefinic protons is also present for 2FS and 3FS.

(ii) 3-Fluorostyrene

As expected, $^5J_{37}$ is calculated as strongly stereospecific by both CNDO/2 and INDO MO methods (Table 2). Comparison with similar computations for 3-fluorotoluene (41) suggests that the magnitudes will be overestimated, as is borne out by the measured value, near 0.9 Hz (Table 1). Furthermore, the INDO numbers imply a negative $^5J_{37}$ for θ values near 90°. That a coupling like $^5J_{37}$ is positive for planar conformations, defined by θ = 0° and 180°, and negative for certain intermediate conformations, has been shown for 3,5-difluoro derivatives of toluene, ethylbenzene, and isopropyl benzene (42). In the toluene derivative it is small and negative, all θ values being sampled equally at 300 K, whereas in the isopropyl compound $^5J_{37}$ is larger and positive as a consequence of the predominance of conformations described by θ values near 0° and 180°. The latter description also applies to 3FS, so that the large and positive $^5J_{37}$ is qualitatively reasonable.

Unlike the corresponding H,H coupling constants, it is not clear whether $^5J_{37}$ in 3FS vanishes for θ = 0°. A coupling constant as large as 0.1 Hz may well exist for such a conformation in the alkyl compounds above (42). Were this coupling constant to vanish, then the populations of 0.59 for the *cis* form of 3FS, deduced in a previous section, together with the measured value of 0.87 Hz in CS_2 solution, would imply a value near 1.5 Hz for $^5J_{37}$ at θ = 180° in 3FS, not far from the value of about 1.7 Hz suggested (42) for the alkyl compounds. In other words, the measured values of $^5J_{37}$ for 3FS can be said to be reasonably consistent with its conformational behaviour but are no more than that.

$^6J_{38}$ and $^6J_{39}$ are striking because they are so large compared to the apparently vanishing analogous coupling constants in styrene (31) or 4FS, for example. Theory (Table 1) reproduces their positive sign and also has $^6J_{39} > {}^6J_{38}$, as measured. In fact, for a two-site analysis, the INDO values and the experimental populations of the planar conformers together yield $^6J_{39}$ as 0.61 Hz, in good agreement with the measured values of 0.57 and 0.59 Hz in the two solutions. A similar treatment of the INDO numbers for $^6J_{38}$ gives a value of 0.21 Hz, substantially lower than the 0.30 Hz found by experiment.

The large theoretical values of $^6J_{39}$ for the all-*trans* conformation (θ = 180°) imply a substantial positive σ electron contribution over six bonds for this conformation, therefore accounting at least partly for the larger magnitude of $^6J_{39}$ relative to $^6J_{38}$. The σ-electron contribution to $^6J_{39}$ in styrene for such a conformation is also computed (20) as positive (the π electron contributions are of course of opposite sign for the long-range H,H and H,F coupling constants under consideration); note that $^6J_{59}$ in 3FS is positive (Table 2) and has been discussed in a previous section.

(iii) 2-Fluorostyrene

Because the *trans* conformer of 2FS is about 70% abundant in both solvents, the available theoretical data in Table 4 imply a negative $^4J_{27}$; its value is actually near 0.5 Hz (Table 2). The disagreement is reminiscent of 2-fluorotoluene (43), where negative values of ^4J are also found by INDO MO FPT computations for θ = 0° and 180° and are attributed to a faulty estimate of the proximate component of the coupling constant for a *cis* orientation of the bonds carrying the coupled nuclei. The use of model compounds (43) showed that ^4J must be positive for a *cis* arrangement of the C—F and C—H bonds, that is, for a conformation analogous to the *trans* form of 2FS. The large positive value of 1.24 Hz computed at θ = 90° for 2FS arises from the σ–π mechanism, of course. It is probable that, as for 2-fluorotoluene (43), the computations give values algebraically too small for $^4J_{27}$ for all θ values. That $^6J_{47}$ in 2FS differs by only 0.01 Hz or less from its magnitude in styrene is a strong indication that conformers with large θ values are not heavily populated at 300 K. The 6-31G potential for 2FS has $<\sin^2\theta>$ as less than 0.2 at this temperature, so that only a part of the observed value of 0.5 Hz for $^4J_{27}$ comes from this source.

Turning to $^5J_{28}$, the large and negative value computed for the *cis* form is again a consequence of the proximity of the C—H and C—F bonds and, in this semiempirical formulation that estimates only the contact interactions, of the overlap of the 1*s* orbital on hydrogen with the 2*s* orbital on fluorine, as previously discussed (43). The measured value is 0.298 (1) Hz in CS_2 solution and, although only about 30% of the molecules are in the *cis* form, this number indicates too large a magnitude for the computed proximate and negative component of $^5J_{28}$. That such a component is present, however, is suggested by the increase of 0.05 Hz, or 16%, in $^5J_{28}$ when 2FS is transferred to the acetone-d_6 medium. According to $^5J_{57}$, the *trans* form is more stable in this solvent and hence the negative, proximate component of $^5J_{28}$ should decrease in importance. While the intrinsic solvent dependence may account for part of the increase in $^5J_{28}$, the relative magnitude of the change is much larger for $^5J_{28}$ than for the other long-range H,F coupling constants in Table 2. A measurement of $^5J_{28}$ and its signs in 2,5-difluorostyrene and, say, 2-fluoro-6-chlorostyrene, might allow an assessment of the proximate coupling mechanism.

Note that proximate interactions also give rise to negative $^5J_{28}$ in styrene itself, that is, for the corresponding H,H coupling constant (20).

According to theory, $^5J_{29}$ is again negative in the less abundant *cis* conformer of 2FS, unlike the theoretical result for the analogous coupling constant in styrene (20), implying a relayed, proximity pathway. However that may be, the measured $^5J_{29}$ is near 0.3 Hz, implying that $^5J_{29}$ is positive and sizeable for the *trans* conformer.

(iv) A comparison of long-range $^1H,^1H$ and $^1H,^{19}F$ coupling constants

Because Q^F_{CF} and Q^H_{CH} are of opposite sign, it is expected that the $\sigma-\pi$, dependent on $\sin^2\theta$, and the π, dependent on $\cos^2\theta$, electron contributions to ^nJ (H,F) and ^nJ(H,H) are also of opposite sign. This is true for styrene and 4FS. When coupling between ^{19}F on the ring and protons on the side chain occurs predominantly via the σ electron system, experience has it that ^nJ (H,F) and ^nJ (H,H) usually have the same sign. This is borne out by $^5J_{37}$ in styrene and $^5J_{37}$ in 3FS, presumably also by the corresponding $^5J_{29}$ values in 2FS and styrene. Again, $^6J_{39}$ in 3FS is positive, as is $^6J_{59}$; the conformational bias ensures a positive σ electron contribution to the latter H,H coupling constant, but the former coupling constant has significant σ and π electron contributions of the same sign, positive.

A number of the long-range H,H coupling constants in styrene and its derivatives have π and σ electron contributions of opposite sign, $^6J_{38}$ and $^6J_{39}$ being examples (20, 31), and hence are often very small; these contributions often reinforce each other for the H,F coupling constants, leading to larger magnitudes. However, the stereospecificty of the latter may not be as strong as for the former; for example, $^5J_{37}$ in 3FS may not be zero in **4** while this is very likely true for the analogous H,H coupling constant.

The intra group spectral parameters

The chemical shifts of the olefinic protons in Table 1 in principle could be discussed in terms of the models developed by Reynolds and co-workers (37) for a series of 4-substituted styrenes, including 4FS. Fluorine is apparently an anomaly in these models (37), so that the shifts will not be discussed further, except to note that the differences between the chemical shifts of the β-protons, for example, in CS_2 solutions are 0.435, 0.449, and 0.452 ppm for 4FS, 3FS, and 2FS, respectively. In acetone-d_6 solution, these differences are 0.533, 0.556, and 0.500, as compared to 0.570 ppm in styrene (31). It has been shown (44) that solvent shifts for 4-substituted styrene derivatives are inconsistent with the reaction field model. It is apparent, from the numbers above and from Table 1, that a similar remark applies to 2FS and 3FS.

The geminal coupling constants in 4-substituted styrenes are sensitive to field and resonance effects from the substituent (37). In styrene, ^2J is 1.05 Hz in acetone-d_6 solution (31). In 2FS, ^2J rises to 1.22 Hz (Table 1), not much more than the 1.11 Hz found for 4-methylstyrene (24), but considerablly smaller than the 1.66 Hz in 2-vinylpyridine (45). A perusal of the θ dependent long-range coupling constants for these molecules shows that ^2J is not obviously related to θ in 2FS. The well-known solvent dependence of ^nJ (H,F) within a fluorophenyl group is documented in the references to Table 1. The generally somewhat larger values of ^nJ (H,H) within a phenyl group for more polar solvents is a common observation in this laboratory and is not an artifact of the spectral analyses. The vicinal coupling constants within the vinyl group behave in a similar manner (Table 1).

Acknowledgments

We are grateful to the Natural Sciences and Engineering Research Council of Canada for a grant-in-aid of research, and to the referees for cogent criticism.

1. J. M. Hollas and M. Z. Bin Hussein. Chem. Phys. Lett. **154**, 14 (1989).
2. J. M. Hollas and M. Z. Bin Hussein. Chem. Phys. Lett. **154**, 228 (1989).
3. J. M. Hollas and M. Z. Bin Hussein. J. Mol. Spectrosc. **135**, 59 (1989).
4. R. M. Villamañān and J. L. Alonso. Chem. Phys. Lett. **159**, 97 (1989).
5. R. M. Villamañān, J. C. Lopez, and L. Alonso. J. Am. Chem. Soc. **111**, 6487 (1989).
6. T. Schaefer and R. Sebastian. Chem. Phys. Lett. **163**, 212 (1989).
7. W. M. Ralowski, P. J. Mjoberg, and J. E. Almlof. J. Chem. Soc. Faraday Trans. 2, **71**, 1109 (1975).
8. L. A. Carreira and T. G. Towns. J. Mol. Struct. **37**, 85 (1977).
9. W. M. Ralowski, P. J. Mjoberg, and S. O. Ljunggren. J. Mol. Struct. **30**, 1 (1976).
10. J. M. Hollas, E. Khalilipour, and S. N. Thakar. J.Mol. Spectrosc. **73**, 240 (1978).
11. J. M. Hollas, H. Musa, T. Ridley, P. H. Turner, and K. H. Weisenberger. J. Mol. Spectrosc. **94**, 437 (1982).
12. W. Caminati, B. Vogelsanger, and A. Bauder. J. Mol. Spectrosc. **128**, 384 (1988).
13. T. Schaefer and G. H. Penner. Chem. Phys. Lett. **114**, 526 (1985).
14. C. W. Bock, M. Trachtman, and P. George. Chem. Phys. **93**, 431 (1985).
15. T. Schaefer, J. Peeling, and R. Sebastian. Can. J. Chem. **63**, 3219 (1985).
16. J. A. Pople, J. W. McIver, Jr., and N. S. Ostlund. J. Chem. Phys. **49**, 2960 (1968); **49**, 2965 (1968).
17. P. Dobosh and N. S. Ostlund. OCPE, **11**, 281 (1975).
18. M. J. Frisch, J. S. Binkley, H. B. Schlegel, K. Raghavachari, C. F. Melius, R. L. Martin, J. J. P. Steward, F. W. Bobrowicz, C. F. Rohlfig, L. R. Kahn, D. J. Defrees, R. Seeger, R. A. Whiteside, D. J. Fox, E. M. Fluder, and J. A. Pople. Carnegie–Mellon Quantum Publishing Unit, Pittsburgh, PA. 1984.
19. J. S. Martin, A. R. Quirt, and K. E. Worvill, The NMR program library. Daresbury Laboratory, Daresbury, U.K.
20. M. Barfield, C. J. Macdonald, I. R. Peat, and W. F. Reynolds. J. Am. Chem. Soc. **93**, 4195 (1971).
21. R. Laatikainen and E. Kolehmainen. J. Magn. Reson. **65**, 89 (1985).
22. R. Laatikainen, E. Kolehmainen, T. Kuokkanen, and K. Tupperainen. J. Magn. Reson. **78**, 9 (1988).
23. I. R. Peat and W. F. Reynolds. Can. J. Chem. **52**, 2403 (1974).
24. T. Schaefer, R. Sebastian, and G. H. Penner. Can J. Chem. **66**, 584 (1988).
25. T. Schaefer and C. S. Takeuchi. Can. J. Chem. **67**, 827 (1989).
26. R. Wasylishen and T. Schaefer. Can. J. Chem. **50**, 1852 (1972).
27. T. Schaefer, R. Sebastian, and G. H. Penner. Can. J. Chem. **63**, 2597 (1985).
28. K. L. Facchine, S. W. Staley, P. C. M. van Zijl, P. K. Mishra, and A. A. Bothner-By. J. Am. Chem. Soc. **110**, 4900 (1988).
29. T. Schaefer, G. H. Penner, and R. Sebastian. Can. J. Chem. **65**, 873 (1987).

Can. J. Chem. Downloaded from www.nrcresearchpress.com by 88.85.125.76 on 09/07/12
For personal use only.

30. T. SCHAEFER, W. DANCHURA, and W. NIEMCZURA. Can. J. Chem. **56**, 2233 (1978).
31. H. NIES, H. BAUER, K. ROTH, and D. REWICKI. J. Magn. Reson. **39**, 521 (1980).
32. W. A. FREEMAN and R. ANDERSON. J. Chem. Phys. **37**, 2053 (1962).
33. J. P. MAHER and D. F. EVANS. Proc. Chem. Soc. (London), 208 (1961).
34. D. R. EATON, A. D. JASEY, W. D. PHILLIPS, and R. E. BENSON. Mol. Phys. **5**, 407 (1962).
35. R. WASYLISHEN and T. SCHAEFER. Can. J. Chem. **49**, 94 (1971).
36. R. J. COOK, J. R. ROWLANDS, and D. H. WHIFFEN. Mol. Phys. **7**, 31 (1963).
37. G. K. HAMER, I. R. PEAT, and W. F. REYNOLDS. Can. J. Chem. **51**, 897 (1973).
38. J. R. BOLTON. *In* Radical ions. *Edited by* E. T. Kaiser and L. Kevan. J. Wiley and Sons, New York. 1968. p. 26.
39. R. W. FESSENDEN and R. H. SCHULER. J. Chem. Phys. **39**, 2147 (1963).
40. R. W. FESSENDEN. J. Phys. Chem. **71**, 74 (1967).
41. T. SCHAEFER, W. DANCHURA, and W. NIEMCZURA. Can. J. Chem. **56**, 2233 (1978).
42. T. SCHAEFER, C. S. TAKEUCHI, and S. E. SVEINSON. Can. J. Chem. **66**, 1490 (1988).
43. T. SCHAEFER, C. S. SEBASTIAN, R. P. VEREGIN, and R. LAATIKAINEN. Can J. Chem. **61**, 29 (1983).
44. G. K. HAMER and W. F. REYNOLDS. Can. J. Chem. **46**, 3813 (1968).
45. J. B. ROWBOTHAM and T. SCHAEFER. Can.J. Chem. **52**, 136 (1974).
46. H. M. HUTTON, B. RICHARDSON, and T. SCHAEFER. Can J. Chem. **45**, 1795 (1967).
47. R. WASYLISHEN and T. SCHAEFER. Can. J. Chem. **49**, 3216 (1971).
48. A. D. BUCKINGHAM and K. A. MCLAUCHLAN. Proc. Chem. Soc. (London), 144 (1963).
49. A. SAUPE. Z. NATURFORSCH. A: Astrophys. Phys. Phys. Chem. **19A**, 161 (1964); **20A**, 572 (1965).
50. R. FREEMAN. J. Chem. Phys. **43**, 3087 (1965).
51. W. R. MONIZ and E. LUSTIG. J. Chem. Phys. **50**, 1905 (1969).
52. H. S. GUTOWSKY, C. H. HOLM, A. SAIKA, and G. A. WILLAIMS. J. Am. Chem. Soc. **79**, 4596 (1957).
53. G. GOVIL and D. H. WHIFFEN. Mol. Phys. **12**, 449 (1967).

Can. J. Chem. Downloaded from www.nrcresearchpress.com by 88.85.125.76 on 09/07/12
For personal use only.

^{1}H and ^{13}C NMR studies of the conformational mobility of 1,2-dimethoxybenzene in solution

TED SCHAEFER, RUDY SEBASTIAN, ALBERTA LEMIRE,[1] AND GLENN H. PENNER[2]
Department of Chemistry, University of Manitoba, Winnipeg, Man., Canada R3T 2N2

Received January 24, 1990

TED SCHAEFER, RUDY SEBASTIAN, ALBERTA LEMIRE, and GLENN H. PENNER. Can. J. Chem. **68**, 1393 (1990).

^{1}H NMR and ^{13}C NMR spectral data are presented for 1,2-dimethoxybenzene-α,α'-^{13}C, as well as for a number of other anisole derivatives. For the title molecule, the coupling constants between the ^{13}C nucleus in the side chain and the *para* ring proton or ^{13}C nucleus in the benzene ring show that the expectation value of $\sin^2\theta$ is very near 0.2 at 300 K, where θ is the angle by which the methoxy groups twist out of the aromatic plane. This value of $\langle\sin^2\theta\rangle$ is much larger than that of 0.05 for anisole in solution, emphasizing the greater conformational mobility of the methoxy groups in 1,2-dimethoxybenzene (DMB). Long-range coupling constants between the methyl and ring protons in DMB are also discussed and compared with those in anisole and some of its derivatives. The preponderance of conformations with large values of θ, thought to occur in the vapor, disappears in solution at ambient temperatures. Under these conditions, the molecule is perhaps best described as preferring a planar conformation in which, however, the methoxy groups undergo excursions in θ whose average value is near 25°.

Key words: 1,2-dimethoxybenzene, conformational behaviour, internal mobility, long-range coupling constants, ^{1}H and ^{13}C NMR.

TED SCHAEFER, RUDY SEBASTIAN, ALBERTA LEMIRE et GLENN H. PENNER. Can. J. Chem. **68**, 1393 (1990).

On présente des données relatives aux spectres RMN du ^{1}H et du ^{13}C pour des 1,2-diméthoxybenzène-α,α'-^{13}C ainsi que pour un certain nombre d'autres dérivés de l'anisole. Pour la molécule mentionnée dans le titre, les constantes de couplage entre le noyau ^{13}C de la chaîne latérale et le proton attaché en position *para* du cycle ou avec le noyau ^{13}C du noyau benzénique montrent que, à 300 K, la valeur attendue pour le $\sin^2\theta$ (où θ est l'angle de torsion du groupement méthoxyle par rapport au plan du noyau aromatique) se situe très près de 0,2. Cette valeur de $\langle\sin^2\theta\rangle$ est beaucoup plus importante que la valeur de 0,05 observée pour l'anisole en solution et elle démontre que les groupements méthoxyles du 1,2-diméthoxybenzène possèdent une mobilité conformationnelle beaucoup plus grande. On discute aussi des constantes de couplage à longue distance entre les protons des groupements méthyles du DMB et ceux du cycle et on les compare à celles observées dans l'anisole et dans quelques-uns de ses dérivés. Les conformations caractérisées par des valeurs élevées de θ, qui existeraient d'une façon prépondérante en phase gazeuse, disparaîtraient en solution, à la température ambiante. Dans ces conditions, la molécule semble exister dans une conformation plane dans laquelle les valeurs moyennes des angles θ des groupements méthoxyles sont de l'ordre de 25°.

Mots clés : 1,2-diméthoxybenzène, comportement conformationnel, mobilité interne, constantes de couplage à longue distance, RMN du ^{1}H et du ^{13}C.

[Traduit par la revue]

Introduction

The conformational behaviour of 1,2-dimethoxybenzene (DMB), veratrole, has been studied extensively with somewhat mixed results. Early STO-3G MO computations, with geometries based on calculations for anisole, have the 0°,90° (see **1**)

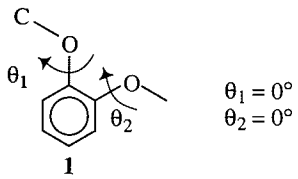

1

as 0.1 kJ/mol more stable than the planar or 0°,0° conformation, for example (1). The nonplanar conformations have a fourfold statistical weight, of course, so that they are expected to be predominant in the gas phase. The photoelectron spectrum of DMB in this phase is indeed in much better agreement with that expected for the 0°,90° than for the planar conformer (1). In the crystalline solid state, however, the planar conformation is prevalent for DMB derivatives (1–4), very likely caused by crystal packing forces. In solution, therefore, an intermediate situation may well prevail.

Nonplanarity of DMB in solution is indicated by partition coefficients (1), the temperature dependence of the dipole moment (5), dielectric relaxation times (6), ^{1}H and ^{13}C NMR chemical shifts (7–9), and by the energetics of charge-transfer complexes formed by its derivatives (10).

More recently, the vibrational spectra of crystalline DMB (11, 12) have been interpreted (11) in terms of the coexistence of planar and nonplanar conformers. The methoxy torsional frequencies do not distinguish between the two planar conformers, those characterized by 0°,0° and 0°,180° (11). The barrier to rotation about the C_{sp^2}—O bond was assessed at about 60 kJ/mol in the solid (11). In this connection, STO-3G MO computations, extensively geometry-optimized, find the 0°,0° conformer as most stable, whereas the 0°,90° conformation is higher in energy by about 2 kJ/mol and the 0°,180° is even higher at 12 kJ/mol (11, 13). It is stated that solvation or packing forces in condensed media can overcome these energy differences (11), perhaps accounting for the long-range proton–proton coupling constants (14), ^{13}C NMR chemical shifts, and ^{13}C spin-lattice relaxation times (15) for DMB in solution, all of which are interpreted as consistent with a predominantly planar conformer. However, ^{17}O NMR chemical shifts, measured at 348 K in acetonitrile solution (16), indicate that the methoxy groups of DMB rotate out of the benzene plane by an amount larger than does the methoxy group in 2-methylanisole.

The dipole moment of DMB in benzene solution at 303 K is 1.32 D (5) and is consistent (17) with a conformational mixture of planar conformers, namely, 0°,0° (70%) and 0°,180° (30%).

[1]Present address: Atomic Energy of Canada Limited, Pinawa, Manitoba.

[2]Present address: Department of Chemistry and Biochemistry, University of Guelph, Guelph, Ontario.

Can. J. Chem. Downloaded from www.nrcresearchpress.com by 88.85.125.76 on 09/07/12
For personal use only.

Can. J. Chem. Downloaded from www.nrcresearchpress.com by 88.85.125.76 on 09/07/12
For personal use only.

A more detailed investigation (18) of the dipole moments of DMB and some of its derivatives in benzene solution at 298 K shows that the measured values are compatible with a variety of conformational mixtures; the most likely appear (18) to be 0°,0° (40%) and 0°,90° (60%). Molecular mechanics computations (19) imply the coexistence of the conformers specified by 0°,0°; 0°,180°; 0°,90°; 90°,90°; they also imply an increase in the dipole moment as the temperature rises. It is noted that the dipole moment of DMB depends on the solvent in which it is measured, that it increases monotonically with temperature in benzene solution and for the liquid, and that it levels off at 363 K in decalin or paraffin oil (5).

Finally, phosphorescence spectroscopy of DMB in various organic solvents at 1.4 K indicates the existence of three conformers, depending on the solvent, and probably assignable to 0°,0°; 0°,180°; and 0°,90° (20). Furthermore, a photoinduced conversion between two conformers, very likely the planar ones, is observed.

Consideration of all these data suggests that DMB is conformationally mobile at ambient temperatures, that the mobility depends on the solvent, and that too small a number of conformations has been taken into account in the interpretation of at least some of the measurements. Ideally, a reliable calculation of the internal rotational potential surface for the free molecule should be combined with a reliable intermolecular force field, appropriate to each solution or state, in order to reproduce the experimental data in a satisfactory manner. This procedure is beyond our ability at present.

In this report we present new ^{1}H NMR and ^{13}C NMR data for DMB and some of its derivatives in solution and these are used to provide some conformational information.

While this work was in progress, Konschin (13) presented STO-3G MO computations on DMB, gave an extensive justification of the utility of such computations, and used geometry optimization procedures. We had done similar computations. Although our optimizations were somewhat more complete, we noted that there was good agreement with his energy for the most stable conformer of DMB. In the original version of this paper, the computations were used to discuss conformational populations and dipole moments in the various states of DMB. One referee objected to this discussion and it is now absent. The interested reader may ask for a copy.

Experimental

The 2-bromo and 2-fluoroanisole-α-^{13}C were prepared from the corresponding phenol derivatives as described previously for other anisoles (21). The 1,2-dimethoxybenzene-α,α′-^{13}C was made as follows. Catechol, 0.26 g, was dissolved in 2 mL of DMSO, to which was added 0.55 g of powdered KOH. After addition of 0.68 g of $^{13}CH_3I$ (95 at.%, MSD Isotopes), the mixture was stirred overnight. It was then diluted with 20 mL of water and stirred for 0.5 h. Extraction with CH_2Cl_2 (4 × 25 mL) and washing with water (3 × 25 mL) was followed by drying with anhydrous $MgSO_4$. Filtration and rotary evaporation gave 0.30 g of the desired product.

The 4,5-dibromo-1,2-dimethoxybenzene was synthesized as follows. In 50 mL of ethanol there was dissolved 15 g of DMB. Also, 12.5 g of Br_2 was added to 50 mL of ethanol, considerable heating occurring during the addition. The bromine solution was then added to the solution of DMB and the mixture was stirred for 2 h. On addition of 200 mL of water, an oil precipitated and 7.7 g of this oil was removed with a dropper. The oil was dissolved in 1 mL of methanol and stored in a refrigerator overnight. A few long needles of crystal formed. Addition of two drops of water caused a separation into two layers. Cooling in a refrigerator for several hours yielded crystals, which were isolated by filtration and washed with 1 mL of cold hexane. The yield was 0.25 g, mp 90°C (lit. (33) mp 91°C). The mass spectrum was consistent with the desired product. The ^{1}H NMR spectrum in benzene solution was also characteristic but showed a small amount of what was very likely the monobromo compound. All other compounds came from Aldrich.

Samples for NMR analysis were prepared in various solvents and at concentrations given in the tables below. These solutions were transferred to 5 mm o.d. NMR sample tubes by filtration through cotton wool. The tubes were degassed by several cycles of the freeze–pump–thaw procedure and were then flame-sealed.

^{1}H NMR and ^{13}C NMR spectra were obtained on an AM300 Bruker spectrometer at a probe temperature of 300 K by procedures previously described (see tables). The ^{1}H NMR spectrum of 1,2-dimethoxybenzene-α,α′-^{13}C was measured on a WH90 Bruker spectrometer, modified to allow clean decoupling (two frequencies of irradiation) of the two bands of the methyl protons arising from $^1J(^1H,^{13}C)$.

Results and discussion

The NMR spectral data

^{1}H NMR spectra were analyzed with the computer program NUMARIT (22). The ^{1}H NMR spectra were of a quality very similar to those previously illustrated for anisole and some of its derivatives (23–25). $^nJ(^{13}C,^{13}C)$ values were found from $^{13}C\{^1H\}$ NMR spectra by inspection. Figure 1 displays the proton-decoupled ^{13}C NMR spectrum of the aromatic carbon nuclei for 1,2-dimethoxybenzene-α,α′-^{13}C, demonstrating the resolution of the smallest coupling constant of 0.17_5 Hz. Tables 1–5 present the spectral parameters for the various molecules.

Conformational deductions from $^6J(^1H,^{13}CH_3)$ and $^5J(^{13}C,^{13}C)$

The important number in Table 1 is the coupling over six bonds between the ^{13}C nucleus and the ring proton in 1,2-DMB-α,α′-^{13}C. Its value is -0.13 ± 0.01 Hz. $^6J(H,^{13}C)$ is a σ–π coupling (21, 24, 26) and is therefore proportional to the expectation value, $\langle \sin^2 \theta \rangle$, θ being the angle by which the methoxy group twists out of the benzene plane. At θ = 90° this coupling is -0.63 ± 0.01 Hz (21, 24, 26). Consequently, $\langle \sin^2 \theta \rangle$ for DMB in benzene-d_6 solution is 0.21 ± 0.02 at 300 K. For anisole in CS_2, $^6J(H,^{13}C)$ is $\pm 0.030 \pm 0.005$ Hz (24), emphasizing the larger conformational mobility in DMB.

A similar mobility in acetone-d_6 is indicated by $^5J(^{13}C,^{13}C)$ for DMB in Table 2, given as $0.17_5 \pm 0.01$ Hz. This coupling also depends on $\langle \sin^2 \theta \rangle$ and, from a detailed discussion (21), can be assessed as 0.95 ± 0.03 Hz at θ = 90°. Hence $\langle \sin^2 \theta \rangle$ is 0.18 ± 0.02 at 300 K. The *weak* indication that DMB is somewhat less conformationally mobile in the polar acetone-d_6 solution than in benzene-d_6 solution is supported by the lower dipole moment of DMB in polar than in nonpolar solvents.

$^5J(^{13}C,^{13}C)$ for 2-bromoanisole-α-^{13}C was not apparent in the spectrum, suggesting a conformation in which the methoxy group is much more strongly confined to the benzene plane than is DMB. In 2-fluoroanisole-α-^{13}C this coupling (Table 1) has a value, 0.08 ± 0.02 Hz, intermediate between those in DMB and 2-bromoanisole, implying also an intermediate conformational mobility of the methoxy group in 2-fluoroanisole. When the methyl group of the methoxy moiety lies *trans* to the *ortho* substituent, the steric interaction occurs via the oxygen atom and should then be similar for DMB and 2-fluoroanisole. Accordingly, the larger conformational mobility in DMB is quite likely a consequence of the greater π electron donation by oxygen, thereby decreasing the mobile bond order of the other C_{sp^2}—O bond.

The trends in $^{2,3,4}J(^{13}C,^{13}C)$ for the three compounds in Table 2 are consistent with the relative conformational mobilities deduced from $^5J(^{13}C,^{13}C)$. This statement follows from

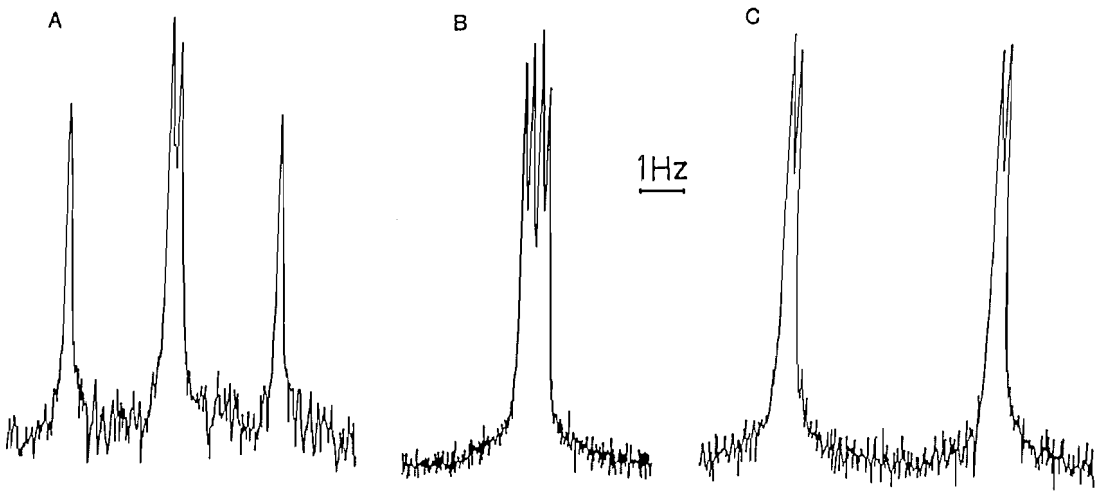

FIG. 1. The proton-decoupled ^{13}C NMR spectra at 75.486 MHz and 300 K of the aromatic nuclei of a 4 mol% solution of 1,2-dimethoxybenzene-α,α′-^{13}C in acetone-d_6 are displayed. The experimental conditions for spectral accumulation are given in great detail in ref. 21. In A, the doublet of doublets arises from C-1 and C-2, in B the four peaks come from C-4 and C-5, and in C they are due to C-3 and C-6. The important coupling constant (see text), $^5J(C\text{-}4,OCH_3) \equiv {}^5J(C\text{-}5,OCH_3)$, is cleanly resolved and has a magnitude of $0.17_5 \pm 0.01$ Hz, as shown by repeated experimental runs.

TABLE 1. ^1H NMR spectral parameters[a] for a 5 mol% solution in benzene-d_6 of 1,2-dimethoxybenzene-α,α′-^{13}C at 90.02 MHz and 298 K

Parameter	Value	Parameter	Value
$\nu(CH_3)$	148.3[b]	^5J(H-3,^{13}C)	0.277(6)
$\nu_3 = \nu_6$	439.307(4)	^6J(H-4,^{13}C)	−0.133(10)
$\nu_4 = \nu_5$	454.258(4)[c]	$^5J(^{13}C,^{13}C)$	0.000(7)
$^3J_{34}$	7.989(4)	Calcd. transitions	128.
$^3J_{45}$	7.589(6)	Assigned transitions	80.
$^4J_{35}$	1.571(5)	Peaks observed	36.
$^5J_{36}$	0.253(6)	Largest difference	0.039
^4J(H-3,^{13}C)	−0.050(8)	RMS deviation	0.021
^5J(H-4,^{13}C)	0.128(6)		

[a]The methyl protons are being decoupled.
[b]In Hz at 90.020 MHz to high frequency of an arbitrary frequency; ^1J(H,^{13}C) is 143.56 Hz.
[c]Numbers in parentheses are standard deviations in the last significant figure.

the observations on $^{2,3,4}J(^{13}C,^{13}C)$ for a variety of anisole derivatives (21).

Long-range $^1H,^1H$ coupling constants

$^5J(H,CH_3) \equiv {}^5J$ is −0.152(0) and −0.155(0) Hz for anisole in CS_2/C_6D_{12} and acetone-d_6 solutions, respectively (23). This proximate coupling constant is highly stereospecific (14, 25, 27, 28), all the available evidence being that it vanishes for the proton in the *ortho* C—H bond lying *trans* to the methyl group; hence ^5J is a precise indicator of methoxy group orientations in *meta*-substituted anisole derivatives, for example (25). As a proximate coupling constant, ^5J is very sensitive to the distance between the methyl protons and the proton in the ring C—H bond placed *cis* to the methyl group (14, 27). INDO MO FPT computations imply an approximate $\cos^4\theta$ dependence of ^5J, where θ is zero for the *cis* orientation, but also that ^5J increases in magnitude by, for example, about 0.04 Hz when θ is zero and the COC angle decreases by 1° (14, 27). The theoretical indications, therefore, are that substituents placed *ortho* to the methoxy group may enhance the magnitude of ^5J simply by compression of the angles at the methoxy moiety so as to decrease the average distance between the bonds carrying the coupled protons.

Table 3 presents precise analyses of the ^1H NMR spectra of 2-bromoanisole in CS_2/C_6D_{12} and acetone-d_6 solutions. The magnitudes of ^5J, at 0.322(1) and 0.329(0) Hz in the two solutions, are indeed rather larger than those, expected as 0.304(0) and 0.310(0) Hz, from the corresponding values for anisole in the two solvents. Based on $^5J(^{13}C,^{13}C)$ for 2-bromoanisole-α-^{13}C (Table 2) and anisole-α-^{13}C (21), in both of which this coupling constant is very small, if indeed present, the increased magnitude of $^5J(H,CH_3)$ in the former compound is reasonably attributed to bond-angle compression.

Table 4 contains the ^1H NMR spectral parameters of DMB in CS_2/C_6D_{12} and in C_6D_6 solutions. ^5J is smaller by 0.03 Hz in magnitude than for 2-bromoanisole in CS_2 solution but only 0.01 Hz smaller in magnitude than expected for a *cis* conformer of anisole in the same solution. $^6J(H,^{13}C)$ and $^5J(^{13}C,^{13}C)$ for anisole and DMB, as discussed in the previous section, both indicate much larger deviations from planarity for DMB than for anisole. Hence, the rather similar values of ^5J for the two molecules in CS_2/C_6D_{12} most likely arise from a partial compensation by two phenomena present in DMB: the decrease in magnitude of ^5J caused by larger out-of-plane excursions of the methoxy groups is counteracted by an increase due to bond-angle compression. Evidence for the latter comes from our own STO-3G MO computations as well as from published calculations of this kind (see Figs. 2 and 3 of ref. 11); the COC angle in planar DMB is computed as 0.7° smaller than in planar anisole and the CCH angle at the *ortho* C—H bond is also decreased by 0.6°, bringing the *ortho* proton nearer the methyl group. The subtle interplay of the two phenomena, together with the extreme distance dependence of ^5J, renders moot a further disentanglement.

A final point concerns the accuracy of ^5J. The ^1H NMR spectrum of DMB arises from an $AA'BB'X_3X_3'$ spin system, the ring protons being rather tightly coupled. The symmetry of the spin system, together with the presence of other small long-range coupling constants, entailed a correlation of ^5J of as large as 0.12 with another spectral parameter. Consequently, the ^1H NMR spectrum of 4-bromo-1,2-dimethoxybenzene in

Can. J. Chem. Downloaded from www.nrcresearchpress.com by 88.85.125.76 on 09/07/12
For personal use only.

TABLE 2. ^{13}C NMR chemical shifts and $^{n}J(^{13}C,^{13}C)$ for some 2-substituted anisoles in acetone-d_6 at 300 K

Parameter	2-Br[a]	2-F[b]	2-OCH_3[c]	Parameter	2-Br	2-F	2-OCH_3
δ_α	56.38	56.34	—	$(-)^2J$(C,C-1)[d]	2.05	2.19	2.33
δ_1	156.83	148.70	150.44	$(+)^3J$(C,C-2)	3.26	2.76	2.52
δ_2	111.95	153.24	150.44	$(+)^3J$(C,C-6)	4.94	4.74	4.77
δ_3	133.88	116.57	112.94	$(+)^4J$(C,C-3)	0.28	0.23	0.17
δ_4	122.51	121.60	121.52	$(+)^4J$(C,C-5)	0.55	0.42	0.38
δ_5	129.58	125.40	121.52	$(+)^5J$(C,C-4)	<0.05	0.08(2)	0.17$_5$
δ_6	113.17	114.58	112.94				

[a]6.4 mol%.
[b]3 mol%; ^1J(C,F) = −243.98, ^2J(C-1,F) = 10.49, ^2J(C-3,F) = 18.04, ^3J(C-4,F) = 6.83, ^3J(C-6,F) = 1.87, ^4J(C-5,F) = 3.97, ^4J(C-α,F) < 0.03 Hz.
[c]<5 mol%; enriched at both methyl sites.
[d]The coupling constants are reproducible to within 0.01 Hz.

TABLE 3. ^1H NMR spectral parameters for 2-bromoanisole in CS_2 and acetone-d_6 solutions at 300 K

$\nu(CH_3)$	1134.622(1)[a]	1164.770(0)[b]	$^5J_{36}$	0.251(1)[a]	0.253(1)[b]
ν_3	2217.068(1)[c]	2264.746(1)[d]	^5J(H-6,CH_3)	−0.322(1)	−0.329(0)
ν_4	2015.764(1)	2062.890(1)	^6J(H-3,CH_3)	0.000(1)	0.000(0)
ν_5	2145.282(1)	220.972(1)	^6J(H-5,CH_3)	0.092(1)	0.088(0)
ν_6	2026.817(1)	2122.128(1)	^7J(H-4,CH_3)	−0.042(1)	−0.043(1)
$^3J_{34}$	7.841(1)	7.874(1)	Calcd. transitions	256	256
$^3J_{45}$	7.423(1)	7.435(1)	Assigned transitions	250	232
$^3J_{56}$	8.218(1)	8.274(1)	Peaks observed	84	96
$^4J_{35}$	1.633(1)	1.624(1)	Largest difference	0.017	0.013
$^4J_{46}$	1.407(1)	1.406(1)	RMS deviation	0.004	0.003

[a]For a 2.5 mol% solution in CS_2 containing also 10 mol% of C_6D_{12} and 0.5 mol% TMS.
[b]For a 2.5 mol% solution in acetone-d_6 containing also 0.5 mol% TMS.
[c]In Hz at 300.135$_2$ MHz to high frequency of internal TMS.
[d]Numbers in parentheses are standard deviations in the last significant figure.

CS_2/C_6D_{12} was also analyzed (Table 5). Here the symmetry is broken and the two ^5J values in fact are not very different from those in DMB. It may be significant that ^5J for the methoxy group placed *para* to the bromine substituent is nearly 0.01 Hz smaller in magnitude than the other ^5J because the dipole moment of this molecule has been interpreted (18) to mean that this methoxy group is conformationally more mobile than the one situated *meta* to bromine. The remote bromine substituent is nevertheless a minor perturber of the methoxy conformations and the data in Table 5 are taken as a confirmation of the accuracy of ^5J in Table 4. Furthermore, a 10 mol% solution of 4,5-dibromo-1,2-dimethoxybenzene in C_6D_6 solution gave a simple spectrum from which ^5J was deduced as 0.30(1) Hz, again very similar to the data in Tables 4 and 5.

Turning to ^6J(H,CH_3) and ^7J(H,CH_3), these coupling constants are interpretable as follows. The latter is −0.043(0) Hz for anisole in a CS_2/C_6D_{12} solvent (23) and arises via (23) an attractive nonbonded interaction in which a group orbital of π symmetry for the methyl group is used to form an aromatic cycle in the planar conformer. The transmission of nuclear spin state information via this cycle is interrupted in a perpendicular orientation of the methoxy group (23) and it might be expected that a twist of 45° would markedly reduce the efficacy of the external aromatic cycle. In DMB, ^7J is −0.043(0) Hz in CS_2/C_6D_{12} and implies that, on average, θ is rather less than 45°. Because $\langle\sin^2\theta\rangle$ is near 0.2, arc sin $\langle\sin^2\theta\rangle^{1/2}$ is near 25°, substantially larger than that of 13°, following for anisole from its $\langle\sin^2\theta\rangle$ of 0.05 at 300 K (25). A vanishing ^7J in DMB, or one greatly reduced in magnitude, would have indicated very large excursions in θ, on average. The ^7J in 2-bromoanisole cannot be used in this discussion because it correlates significantly with other spectral parameters (footnote to Table 5) and in consequence is not known accurately.

^6J(H,CH_3) also vanishes for perpendicular conformations of the methoxy group (23) and has a significant magnitude only for the *meta* C—H bond oriented *cis* to the methyl group. In anisole it is 0.049(0) Hz in CS_2/C_6D_{12} (23), being an average of two values, one essentially zero and the other near 0.1 Hz in magnitude. For DMB, ^6J in CS_2/C_6D_{12} is 0.087(1) Hz for the favored orientation, consistent with somewhat greater average θ values than in anisole (see discussion of ^6J in ref. 23). ^6J for the nonfavored bond orientations is indeed small but not zero; according to the proposed coupling mechanism (23), this coupling constant arises from a five-bond pathway involving the aromatic cycle, the other ^6J from a three-bond pathway. In 4-bromo-1,2-dimethoxybenzene (Table 5), ^6J is 0.090(1) Hz, roughly as expected.

In summary, the long-range coupling constants involving the ^{13}C nucleus and the protons of the methyl group in DMB are consistent with a description in which the methoxy groups move out of the ring plane with rather greater facility than does the methoxy group in anisole; the average deviation from planarity in solution is roughly twice as large in DMB. The spectral data are consistent with the planar being the conformation of lowest energy for DMB in solution, as previously suggested from other NMR data (14, 15). The most simple description then is that the methoxy groups undergo large excursions from planarity, of varying amplitudes but with an average value near 25° for the

Can. J. Chem. Downloaded from www.nrcresearchpress.com by 88.85.125.76 on 09/07/12
For personal use only.

TABLE 4. The ^{1}H NMR spectral parameters for 1,2-dimethoxybenzene in CS_2/C_6D_{12} and C_6D_6 solutions at 300 K

Parameter	Value	Parameter	Value		
$\nu(CH_3)$	1104.623(0)[a]	1027.977(1)[b]	^6J(H-3,CH_3)	±0.011(0)[a,c]	±0.010(0)
$\nu_3 = \nu_6$[e]	2006.085(1)[d]	1997.418(1)	^7J(H,CH_3)	−0.043(0)	−0.049(0)
$\nu_4 = \nu_5$	2020.107(1)[d]	2049.506(1)	^7J(CH_3,CH_3)	0.000(0)	0.000(0)
$^3J_{34}$	7.985(1)[f]	7.986(2)	Calcd. transitions	1445	1538
$^3J_{45}$	7.551(1)	7.568(2)	Assigned transitions	951	786
$^4J_{35}$	1.517(0)	1.522(0)	Peaks observed	859	759
$^5J_{36}$	0.224(1)	0.228(1)	Largest difference	0.022	0.023
^5J(H,CH_3)	−0.294(1)	−0.309(1)	RMS deviation	0.008	0.011
^6J(H-4,CH_3)	0.087(1)	0.077(1)			

[a]For a 6.0 mol% solution in CS_2 containing also 10 mol% of C_6D_{12} and 0.5 mol% TMS.
[b]For a 6.0 mol% solution in C_6D_6containing also 0.5 mol% TMS.
[c]^6J(H-3,CH_3) is definitely nonzero.
[d]For a 2.5 mol% solution in CS_2/C_6D_{12}, these numbers are 2007.07 for ν_3 and 2021.18 for ν_4.
[e]In Hz at 300.135$_2$ MHz to high frequency of internal TMS.
[f]Numbers in parentheses are standard deviations in the last significant figure.

TABLE 5. ^{1}H NMR spectral parameters for a 2.5 mol% solution of 4-bromo-1,2-dimethoxybenzene in CS_2 solution[a] at 300 K

Parameter	Value	Parameter	Value
$\nu(CH_3$-1)	1115.667(0)[b,c]	J(H-5,CH_3)	0.090(1)
$\nu(CH_3$-2)	1111.394(0)	J(H-6,CH_3)	0.0[d]
ν_3	2046.069(0)	J(H-3,CH_3)	0.0[d]
ν_5	2058.560(1)	J(H-5,CH_3)	−0.019(1)[e]
ν_6	1975.580(0)	J(CH_3,CH_3)	0.0[d]
$^3J_{56}$	8.514(1)	Calcd. transitions	816
$^4J_{35}$	2.301(1)	Assigned transitions	645
$^5J_{36}$	0.150(1)	Peaks observed	51
^5J(H-3,CH_3)	−0.305(0)	Largest difference	0.016
^5J(H-6,CH_3)	−0.297(0)	RMS deviation	0.005

[a]Containing also 10 mol% C_6D_{12} and 0.5 mol% TMS.
[b]In Hz at 300.135$_2$ MHz to high frequency of internal TMS.
[c]Numbers in parentheses are the standard deviations in the last significant figure.
[d]Decoupling experiments indicate no evidence for the presence of these coupling constants.
[e]There are large correlations with other parameters, in particular one of 0.32 with $\nu(CH_3$-2).

twist angle, θ, at 300 K. This description, for liquid solutions of DMB, is possibly preferable to those in which equilibria between conformers with rather definite values of θ_1 and θ_2 (see **1**) have been postulated. The chemical shifts, discussed below, are consistent with this description.

Some chemical shift comparisons

A recent interpretation of ^{17}O and aromatic ^{13}C NMR chemical shifts (29) in some series of anisole derivatives can be taken to imply that these shifts in DMB in solution provide no evidence for conformations in which the methoxy groups take on large θ values of the kind implied by the photoelectron spectra in the vapor (1) or by the STO-3G MO calculations below. The ^{13}C NMR chemical shifts of the methoxy groups and the spin-lattice relaxation times of the ^{13}C nuclei of DMB (15) are consistent with this implication.

Again, the ^{1}H NMR chemical shifts of benzene (30), anisole (24), and DMB (Table 4) for 2.5 mol% solutions in CS_2/C_6D_{12} show that $\delta_{3,6}$ and $\delta_{4,5}$ are 0.055 and 0.048 larger at 300 K than expected on the basis of additivity of substituent effects. In other words, the ring protons are less shielded than expected from additivity. It has been argued (31) that H-6 in 2-X-anisoles is deshielded by steric crowding arising from the coplanar methoxy group buttressed by X as small as chlorine. This proximity shift is estimated as twice the deviation from the additivity shift. For DMB, therefore, its value is 0.11 ppm, about one third of the value of 0.32 ppm estimated (31) for 2-chloroanisole. Now, steric crowding is very sensitive to interatomic distances and hence the steric crowding in planar DMB, with an effective X of oxygen in the planar 0°,0° conformer, is anticipated as much smaller than for an X of chlorine. Furthermore, H-4 and H-5 are deshielded, relative to additivity expectations, by nearly as much as H-3 and H-6 in DMB. The simple explanation is that one methoxy group hinders the π electron donation of the other somewhat, leading to less shielding of the ring protons than calculated from additivity; then the methyl protons in DMB should be more shielded in DMB than in anisole, as should the ^{17}O nuclei, as observed (16, 24, 29). Consequently, the ^{1}H NMR chemical shifts of DMB are consistent with other NMR data. Large populations of, for example, the 0°,90° conformer would presumably cause much larger deviations for H-4 and H-5, the *para* proton in anisole being shielded by 0.436 ppm relative to benzene in CS_2/C_6D_{12} (25, 30).

From the viewpoint of the conformational behaviour of DMB in solution, perhaps the most interesting chemical shifts are those of C-6 in a series of *ortho*-substituted anisoles (32). These are shown (32) to contain a screening term due to steric compression by the planar *cis* conformation of the methoxy group. The striking result is that, while 2-fluoroanisole and DMB display somewhat smaller steric compression than, say, 2-bromoanisole, the conclusion must be (Tables 1 and 3 of ref. 32) that DMB in solution does not evince large populations of conformers with θ magnitudes such as are implied by experiment and theory for the vapor.

Acknowledgements

We are grateful to the Natural Sciences and Engineering Research Council of Canada for financial assistance.

1. G. M. ANDERSON, P. A. KOLLMAN, L. N. DOMELSMITH, and K. N. HOUK. J. Am. Chem. Soc. **101**, 2344 (1979).
2. J. CAILLET. Acta Crystallogr. Sect. B: Struct. Crystallogr. Cryst. Chem. **B38**, 1786 (1982).
3. S. C. NYBURG and C. H. FAERMAN. J. Mol. Struct. **140**, 347 (1986).

Can. J. Chem. Downloaded from www.nrcresearchpress.com by 88.85.125.76 on 09/07/12
For personal use only.

4. W. HUMMEL, K. HUML, and H.-B. BURGE. Helv. Chim. Acta, **71**, 1291 (1988).
5. L. M. DIBELLO, H. M. MCDEVITT, and D. M. ROBERTI. J. Phys. Chem. **72**, 1405 (1968).
6. D. M. ROBERTI and C. P. SMYTH. J. Am. Chem. Soc. **82**, 2106 (1960).
7. J. S. MARTIN and B. P. DAILEY. J. Chem. Phys. **39**, 1722 (1963).
8. K. S. DHAMI and J. B. STOTHERS. Can. J. Chem. **44**, 2855 (1966).
9. W. KITCHING, I. DEJONGE, W. ADCOCK, and A. N. ABEYWICKREMA. Org. Magn. Reson. **14**, 502 (1980).
10. A. ZWEIG, J. E. LEHNSEN, and M. A. MURRAY. J. Am. Chem. Soc. **85**, 3933 (1963).
11. H. KONSCHIN, H. TYLLI, and B. WESTERMARK. J. Mol. Struct. **102**, 279 (1983).
12. V. P. NOVIKOV, A. V. YARKOV, A. F. SOLOTNOV, and O. A. RAEVSKII. Izv. Akad. Nauk SSSR, Ser. Khim. 1047 (1985).
13. H. KONSCHIN. J. Mol. Struct. (Theochem), **168**, 293 (1988).
14. T. SCHAEFER and R. LAATIKAINEN. Can. J. Chem. **61**, 224 (1983).
15. A. MAKRIYANNIS and S. FESIK. J. Am. Chem. Soc. **104**, 6462 (1982).
16. M. A. WYSOCKI, P. W. JARDON, G. J. MAINS, E. J. EISENBRAUN, and D. W. BOYKIN. Magn. Reson. Chem. **25**, 331 (1987).
17. H. LUMBROSO, C. LIÉGEOIS, L. TESTAFERRI, and M. TIECCO. J. Mol. Struct. **144**, 121 (1986).
18. O. EXNER and V. JEHLIČKA. Collect. Czech. Chem. Commun. **48**, 1030 (1983).
19. H. DODZIUK. Pol. J. Chem. **57**, 535 (1983).
20. T. BACHÉ, C. BRÄUCHLE, and J. VOITLÄNDER. Chem. Phys. Lett. **144**, 226 (1988).
21. T. SCHAEFER and G. H. PENNER. Can. J. Chem. **66**, 1635 (1988).
22. J. S. MARTIN, A. R. QUIRT, and K. E. WORVILL. The NMR program library, Daresbury Laboratory, Daresbury, UK.
23. T. SCHAEFER and R. SEBASTIAN. J. Magn. Reson. **73**, 541 (1987).
24. T. SCHAEFER and R. SEBASTIAN. Can. J. Chem. **67**, 1148 (1989).
25. T. SCHAEFER and R. SEBASTIAN. Can. J. Chem. **67**, 1027 (1989).
26. T. SCHAEFER, R. LAATIKAINEN, T. A. WILDMAN, J. PEELING, G. H. PENNER, J. BALEJA, and K. MARAT. Can. J. Chem. **62**, 1592 (1984).
27. T. SCHAEFER, S. R. SALMAN, T. A. WILDMAN, and G. H. PENNER. Can. J. Chem. **63**, 782 (1985).
28. R. W. CRECELY, K. W. MCCRACKEN, and J. H. GOLDSTEIN. Tetrahedron, **25**, 877 (1969).
29. I. I. SCHUSTER, M. PARVEZ, and A. J. FREYER. J. Org. Chem. **53**, 5819 (1988).
30. T. SCHAEFER, R. SEBASTIAN, and G. H. PENNER. Can. J. Chem. **63**, 2597 (1985).
31. R. H. CONTRERAS, M. B. FERRARO, D. G. DEKOWALEWSKI, and L. DIAZ. Magn. Reson. Chem. **23**, 296 (1985).
32. R. R. BIEKOFSKY, A. B. POMILIO, R. H. CONTRERAS, D. G. DEKOWALEWSKI, and J. C. FACELLI. Magn. Reson. Chem. **27**, 158 (1989).
33. H. W. UNDERWOOD, O. L. BARIL, and G. C. TOONE. J. Am. Chem. Soc. **52**, 4087 (1930).

Can. J. Chem. Downloaded from www.nrcresearchpress.com by 88.85.125.76 on 09/07/12
For personal use only.

New plastoquinones from the brown alga *Desmarestia menziesii*

PATRICIO RIVERA AND FEDERICO PODESTÁ
Departamento de Quimica, Facultad de Ciencias, Universidad de Chile, Casilla 653, Santiago de Chile, Chile
AND
MANUEL NORTE,[1] FERNANDO CATALDO, AND ANTONIO G. GONZÁLEZ
Centro de Productos Naturales Orgánicos "Antonio González", Instituto Universitario de Bio-Orgánica, Universidad de La Laguna, Carretera de La Esperenza, 2, 38206, La Laguna, Tenerife, España

Received November 15, 1989

PATRICIO RIVERA, FEDERICO PODESTÁ, MANUEL NORTE, FERNANDO CATALDO, and ANTONIO G. GONZÁLEZ. Can. J. Chem. **68**, 1399 (1990).

Two new plastoquinones have been isolated from the brown alga *Desmarestia menziesii*. The structures of these metabolites have been elucidated by spectral analysis.

Key words: *Desmarestia menziesii*, brown algae, *Desmarestiaceae*, plastoquinones, spectral analysis.

PATRICIO RIVERA, FEDERICO PODESTÁ, MANUEL NORTE, FERNANDO CATALDO et ANTONIO G. GONZÁLEZ. Can. J. Chem. **68**, 1399 (1990).

On a isolé deux nouvelles plastoquinones des algues brunes *Desmarestia menziesii*. On a élucidé les structures de ces métabolites à l'aide d'analyses spectrales.

Mots clés : *Desmarestia menziesii*, algues brunes, *Desmarestiaceae, plastoquinones, analyse spectrale.*

[Traduit par la revue]

Introduction

Brown algae belonging to the families *Sargassaceae* and *Cystoseiraceae* are known to produce diterpenes of mixed biogenesis, which are believed to be employed in chemical defence against predators (1). In fact, these families of seaweeds are characterized as offering more resistance than other algae to their potent predators, sea urchins, and some of these metabolites are inhibitors of the mitotic cell division in the fertilized sea urchin egg assay (2). On the other hand, few data on secondary metabolites of the brown algae belonging to the family *Desmarestiaceae* have been published, previous studies being limited to the hormonal secretions of its eggs (3). The only study we know was that done on *Desmarestia aculeata*, which reports the presence of plastoquinone-9 and a new C-27 sterol (4).

In this paper we report the isolation and structural elucidation of two new diterpenes of mixed biogenesis from the brown alga *Desmarestia menziesii* (J. Agardt), collected near the Antarctic peninsula (Chilean Base Arturo Prat), in January 1985. The air-dried alga was extracted with acetone and the resulting extract was partitioned between diethyl ether and water. After evaporation to dryness of the ether layer, the compounds were obtained by standard silica gel and Sephadex LH-20 chromatographies.

Desmarestial **1** had a molecular formula of $C_{27}H_{38}O_4$ (HRMS m/z: 426.2820; calcd.: 426.2825). The IR absorptions at 3600 cm^{-1} (hydroxyl group) and the UV band at λ = 266 nm (ϵ = 2170) were indicative of the presence of a quinol moiety. The NMR spectra exhibited signals for a dialkylated quinol ring: ^{13}C NMR δ: 153.8 (s), 127.0 (s), 115.4 (d), 148.8 (s), 125.4 (d), and 137.6 (s); ^1H NMR, two *meta* coupled (J = 2.9 Hz) proton resonances at δ 6.96 and 6.82. The presence of a formyl group at C-6 instead of the usual methyl group at this position, characteristic of this type of compound, was established as follows. The IR of **1** showed an absorption at 1650 cm^{-1} together with a band in the UV spectrum at λ 232 nm characteristic of an α,β-unsaturated carbonyl group. It was confirmed by the deshielded chemical shifts of the aromatic protons described above and also

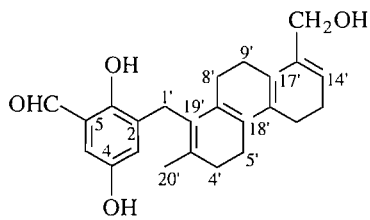

1

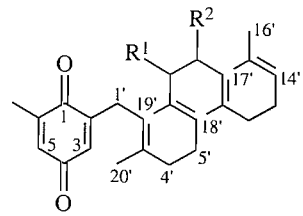

2 : R^1 = H, R^2 = OH
3 : R^1 = R^2 = OH

by the MS fragmentation, which showed a peak at m/z 151 due to the fragment $C_8H_7O_3^+$.

The acyclic nature of the diterpene component was evident since the NMR spectrum showed the presence of four olefinic protons and four vinylic methyl groups, implying four unsaturations with *E* geometry in accordance with their chemical shifts (Table 1). The absence of one methyl group in the last isoprene unit in the diterpenic side chain was evident from its carbon NMR spectrum. It was replaced by an isolated allylic alcohol (^1H: δ 4.03 (s); ^{13}C: δ 69.2 (t)), which was long-range correlated in the homonuclear COSY experiment with the olefinic protons at δ 5.40 (H-14′) and also with the vinylic methyl group at δ 1.69 (Me-17′). The proton and carbon NMR chemical shifts of **1** were fully assigned by using homo- and heteronuclear COSY experiments (Table 1).

Compound **2**, oil, $[\alpha]_D$ +2.01 (*c* 0.9, $CHCl_3$), had a molecular formula of $C_{27}H_{38}O_3$ (HRMS m/z: 410.2816; calcd.: 410.2821). This compound possesses a 6-methyl-2-propenyl-1,4-benzoquinone system in accordance with its spectroscopic data: IR: 1650 cm^{-1}; UV, λ: 251 nm (ϵ = 21 000); ^1H NMR δ: 6.47 and 6.54 (each 1H, br m); ^{13}C NMR δ: 188.1 (s), 146.0 (s), 132.5 (d), 188.2 (s), 133.3 (d), 146.0 (s), 16.2 (q); MS m/z: 175.0.

The diterpenic part of this molecule was characterized as a (2′*E*, 6′*E*, 10′*E*, 14′*E*) hydroxygeranyl geranyl derivative. The methine from the hydroxy group, which appeared in the ^1H NMR spectrum at δ 4.44, was correlated on a COSY (^1H–^1H) map with the olefinic proton centered at δ 5.16 and also with

[1]Author to whom correspondence may be addressed.

Printed in Canada / Imprimé au Canada

Can. J. Chem. Downloaded from www.nrcresearchpress.com by 91.121.58.235 on 09/07/12
For personal use only.

TABLE 1. NMR spectral data for compounds **1** and **2**

	1[a]		**2**	
Position	^{13}C	^{1}H	^{13}C[b]	^{1}H[c]
1	158.8	—	188.1	—
2	127.0	—	146.0	—
3	115.4	6.82 d, 2.9	132.5	6.47 m
4	148.8	—	188.2	—
5	125.4	6.96 d, 2.9	133.3	6.54 m
6	137.6	—	146.0	—
7	196.4	9.79 s	16.2	2.08 d, 2.0
1′	29.9	3.35 d, 7.3	27.5	3.12 d, 7.4
2′	121.1	5.30 t, 7.3	118.6	5.20 m
3′	* 134.2	—	138.2	—
4′	# 39.9	1.98 m	39.7	2.07 m
5′	× 27.0	2.14 m	26.6	2.07 m
6′	124.8	5.09 m	127.5	5.16 m
7′	* 137.6	—	143.1	—
8′	# 39.2	1.98 m	48.3	2.12 m
9′	× 26.0	2.14 m	66.0	4.44 dd, 8.0 6.5
10′	124.2	5.09 m	127.8	5.16 m
11′	* 134.4	—	139.5	—
12′	# 39.7	1.98 m	39.7	2.07 m
13′	× 26.5	2.14 m	26.6	2.07 m
14′	126.9	5.40 t, 6.7	124.2	5.16 m
15′	135.1	—	132.0	—
16′	69.2	4.03 s	25.9	1.67 s
17′	13.9	1.69 s	16.8	1.66 s
18′	16.1	1.59 s	17.9	1.66 s
19′	16.2	1.59 s	16.4	1.62 s
20′	16.1	1.67 s	16.4	1.59 s

[a]Assignments made by homo and heteronuclear COSY.
[b]Assignments made by comparison with **1** and related compounds.
[c]Assignments made by homonuclear COSY.
#, ×, *: interchangeable.

the methylene centered at δ 2.12. This type of correlation established that the possible positions for the OH group in the diterpenic side chain were the carbons C-5′, C-9′, or C-13′. Its actual location was impossible to deduce from the correlation observed in the homonuclear COSY map or by decoupling experiments because the signals from the olefin and from the methylene protons overlapped in both cases.

However, a choice was made on the basis of the mass spectrum fragmentations. Thus, the C(8′)—C(9′) bond cleavage divided the molecule into two fragments at m/z 257 $(C_{17}H_{21}O_2)^+$ and at m/z 153 $(C_{10}H_{17}O)^+$, the hydroxyl being placed in the latter. Furthermore, the fragment at m/z 69 $(C_5H_9)^+$ precludes its location at C-13′ and, consequently, the hydroxyl group must be at C-9′.

Together with these compounds we also isolated another diterpene that has physical and spectroscopic data identical with those reported for compound **3** (5). In the experimental part we give the ^{13}C NMR chemical shifts, which have not been previously reported.

Experimental

IR and UV spectra were recorded on a Perkin–Elmer model 257 and model 402 spectrophotometer, respectively. Optical rotations were determined for solution in $CHCl_3$ with a Perkin–Elmer model 241 polarimeter. NMR spectra were recorded on a Bruker WP-200 SY spectrometer (200 MHz), chemical shifts are reported relative to Me_4Si (δ = 0), and coupling constants are given in hertz. The 2D-NMR spectra were obtained using Bruker microprograms. Low and high resolution mass spectra were obtained from a VG Micromass ZAB-2F spectrometer. Silica gel column chromatography, TLC, and preparative layer chromatography (PLC) were performed on silica gel 60 G, from Merck. The TLC plates were developed by spraying with 6 N sulphuric acid and heating. Sephadex LH-20 obtained from Pharmacia was used for gel filtration chromatography. All solvents were purified by standard techniques. Anhydrous sodium sulfate was used for drying solutions.

The air-dried and ground alga (1.2 kg), collected in January 1985 near the Chilean base Arturo Prat in the Antarctic peninsula, was extracted three times with acetone. Evaporation of the solvent afforded a dark-green oil (60 g), which was chromatographed on Si gel (5 × 100 cm; increasing concentrations of ethyl acetate in *n*-hexane as the eluent).

Fractions of 200 mL were collected and those exhibiting similar TLC profiles were combined. Compounds **1** and **2** eluted in the 20% fraction and **3** in the 30% fraction. All the products were purified and the chlorophyll removed by successive chromatographies on a Sephadex LH-20 column with $CHCl_3$: MeOH: *n*-hexane (1:1:2), to afford pure **1** (40 mg), **2** (30 mg), **3** (30 mg), and demosterol (≈3 g). Their structures were established on the basis of the following spectroscopic data.

*Compound **1**: (2′E, 6′E, 10′E, 14′E)-2-(15′hydroxymethylgeranylgeranyl)-6-formylquinol*

Amorphous solid, mp 98–100°C; IR ν_{max} $CHCl_3$: 3600, 3500–3100, 3030, 1700, 1600, and 1450 cm^{-1}; UV λ_{max}: 232, 266 nm (ε = 2170, 4300); HRMS, m/z calcd. for $C_{27}H_{38}O_4$: 426.2825; found: 426.2820; MS m/z (rel. int. %): 426.30 (1), 175.00 (69), 151.00 (99), 135.02 (100), 93.05 (95), 68.98 (91), 68.00 (57), 67.05 (77). For NMR spectral data see Table 1.

*Compound **2**: (2′E, 6′E, 10′E)-2-(9′-hydroxygeranylgeranyl)-6-methyl-1,4-benzoquinone*

Yellow oil; $[\alpha]_D$ +2.0 (*c* 0.94, $CHCl_3$); UV λ_{max}: 250 nm (ε = 21 000); IR ν_{max} $CHCl_3$: 3650, 3550–3100, 3020, 3000, 2940, 2920, 1650, 1640, and 1600 cm^{-1}; HRMS, m/z calcd. for $C_{27}H_{38}O_3$: 410.2821; found: 410.2816; MS m/z (rel. int. %): 410.25 (3), 392.25 (4), 175.05 (100), 151.10 (4), 68.95 (77). For NMR spectral data see Table 1.

*Compound **3**: (2′E, 6′E, 10′E)-2-(8′,9′-dihydroxygeranylgeranyl)-6-methyl-1,4-benzoquinone*

Yellow oil; $[\alpha]_D$ −15.0 (*c* 0.40, $CHCl_3$). Physical and spectroscopic data were identical with those published for one of the benzoquinone constituents of *Sargassum tortile*. We add the ^{13}C NMR spectral data (50 MHz, $CDCl_3$), δ: 12.27 (q), 16.1 (q), 16.2 (q), 17.0 (q). 17.8 (q), 25.8 (q), 26.6 (t), 27.6 (t), 39.2 (t), 39.8 (t), 70.3 (d), 80.9 (d), 118.5 (d), 123.7 (d), 124.1 (d), 128.0 (d), 131.8 (d), 132.4 (d), 133.3 (s), 134.7 (s), 139.7 (s), 141.1 (s), 146.4 (s), 148.8 (s), 188.0 (s), and 188.5 (s).

Acknowledgments

This research was supported by grants from the Plan Nacional (FAR 88-0500). P.R. thanks the Ministry of Education of Spain for a post-doctoral fellowship. F.C. thanks A.I.E.T.I. for a fellowship. We thank Prof. María Eliana Ramírez (Museo de Historia Natural, Santiago de Chile) for identifying the alga.

1. B. BANAIGS, C. FRANCISCO, E. GONZÁLEZ, L. CODAMIER, and W. FENICAL. Tetrahedron Lett. **23**, 3271 (1982); B. AMICO, G. ORIENTE, M. PIATELLI, G. RUBERTO, and F. R. FRANCZECK. Tetrahedron, **40**, 1721 (1984).
2. B. BANAIGS, J. TESTE, and C. FRANCISCO. J. Org. Chem. **51**, 1115 (1986).
3. D. G. MÜELLER, A. PETERS, G. GASSMAN, W. BOLAND, F. J. MARNER, and L. JAENICKE. Naturwissenschaften, **69**, 290 (1982).
4. J. A. FINDLAY and A. D. PATIL. Phytochemistry, **24**, 366 (1985).
5. M. ISHITSUKA, T. KUSUMI, Y. NOMURA, T. KONNO, and H. KAKISAWA. Chem. Lett. 1269 (1979).

Can. J. Chem. Downloaded from www.nrcresearchpress.com by 91.121.58.235 on 09/07/12
For personal use only.

The homogeneous thermal conversion of methane to higher hydrocarbons in the presence of ethylene

ALAIN R. BOSSARD AND MARGARET H. BACK
Department of Chemistry, University of Ottawa, Ottawa, Ont., Canada K1N 6N5

Received February 9, 1990

ALAIN R. BOSSARD and MARGARET H. BACK. Can. J. Chem. **68**, 1401 (1990).

The pyrolysis of mixtures of methane and ethylene has been studied over the temperature range 774–853 K at total pressures below atmospheric to explore the effectiveness of ethylene as a catalyst for conversion of methane to higher hydrocarbons. Pyrolysis of ethylene alone at these temperatures yields ethane, propylene, butene-1, and butadiene as the major volatile products. In the lower temperature region the addition of methane increased the rate of production of ethane through the chain propagation reaction,

$$C_2H_5 + CH_4 \rightarrow C_2H_6 + CH_3$$

thus effecting the conversion of methane to ethane. The rates of formation of butene-1 and butadiene were not appreciably altered and that of propylene was increased only at low pressures of ethylene. At higher temperatures methane caused a substantial increase in the rate of production of propylene, the result of the increasing importance of the methyl radical in the propagation reactions. Thus ethylene can efficiently convert methane to ethane or to propylene depending on the temperature of the reaction. Addition of small quantities of butene-1, which acted as a secondary initiator, to the mixtures increased considerably the overall rate of the conversion of methane. A mechanism is discussed which accounts for the main features of the reactions.

Key words: methane, ethylene, kinetics, pyrolysis, catalysis.

ALAIN R. BOSSARD et MARGARET H. BACK. Can. J. Chem. **68**, 1401 (1990).

Dans le but de déterminer l'efficacité de l'éthylène comme catalyseur pour la conversion du méthane en hydrocarbures de masses plus élevées, on a étudié la pyrolyse de mélanges de méthane et d'éthylène, à des températures allant de 774 à 853 K, à des pressions totales inférieures à la pression atmosphérique. À ces températures, la pyrolyse de l'éthylène seul fournit de l'éthane, du propylène, du but-1-ène et du butadiène comme produits volatils majeurs. Dans la région de températures plus basses, l'addition de méthane provoque une augmentation de la vitesse de production de l'éthane par le biais d'une réaction de propagation en chaîne,

$$C_2H_5 + CH_4 \rightarrow C_2H_6 + CH_3$$

qui affecte ainsi la conversion du méthane en éthane. Les vitesses de formation du but-1-ène et du butadiène ne sont pas beaucoup modifiées et celle du propylène n'est augmentée qu'à des basses pressions d'éthylène. Aux températures plus élevées, l'addition de méthane provoque une augmentation importante de la vitesse de production du propylène; ce résultat est dû à l'augmentation de l'importance du radical méthyle dans les réactions de propagation. L'éthylène peut donc transformer le méthane en éthane ou en propylène, dépendant de la température de la réaction. Lorsqu'on ajoute aux mélanges de faibles quantités de but-1-ène qui agit comme initiateur secondaire, les mélanges augmentent considérablement les vitesses globales de conversion du méthane. On discute d'un mécanisme qui tient compte des principales caractéristiques des réactions.

Mots clés : méthane, éthylène, cinétique, pyrolyse, catalyse.

[Traduit par la revue]

Introduction

In the search for simple and efficient mechanisms for conversion of methane into fuels of higher carbon number, the major research effort has been directed to the development and improvement of catalytic processes (1–3). Homogeneous reactions have received less attention, mainly because the high temperatures necessary to induce decomposition of methane also lead to rapid conversion to carbon (4, 5). To interrupt the process at the stage where a reasonable yield of higher hydrocarbon is produced has proved difficult.

One approach to this problem is the use of a sensitizer that induces the decomposition of methane at lower temperatures where carbon is not so rapidly formed. A system has been described using small quantities of oxygen, which gives good yields of methanol (6). For production of hydrocarbon fuels, however, the sensitizer must be a hydrocarbon and must not only provide radicals for the attack on methane but also induce a chain reaction mechanism for the formation of products. A sensitizer that fulfills these requirements is ethylene and the present paper describes the results of the use of this reactant in the conversion of methane to higher hydrocarbons over the temperature range 774–853 K at pressures below atmospheric.

Description of the system

At temperatures in the neighborhood of 800 K ethylene reacts by a chain reaction mechanism, initiated by the bimolecular reaction of ethylene,

[1] $$2C_2H_4 \rightarrow C_2H_3 + C_2H_5$$

and followed by addition, abstraction, decomposition, and isomerization reactions of the ethyl, vinyl, and other radicals (7). The four major products, methane, ethane, propylene, and 1-butene, constitute about 80% of the products volatile at room temperature. Methane and ethane, the only saturated products, are formed by hydrogen abstraction by the corresponding radical,

[2] $$CH_3 + C_2H_4 \rightarrow CH_4 + C_2H_3$$

[3] $$C_2H_5 + C_2H_4 \rightarrow C_2H_6 + C_2H_3$$

Products formed from radical combination reactions, for example, propane and butane, are formed in minute amounts (7–9), indicating that the chain length is long. Thus ethane formed by combination of methyl radicals would be negligible compared to that formed by reaction [3]. Similarly, the only important source of methane is reaction [2]. Methyl and ethyl radicals are

Can. J. Chem. Downloaded from www.nrcresearchpress.com by 88.85.125.76 on 09/07/12
For personal use only.

Can. J. Chem. Downloaded from www.nrcresearchpress.com by 88.85.125.76 on 09/07/12
For personal use only.

the most stable radicals in this system and are the only radicals for which abstraction competes with addition or decomposition. Propylene and butene-1 are formed by addition of radicals to ethylene followed by isomerization and decomposition reactions.

When methane is added to the system the additional reaction forming ethane may occur

[4] $C_2H_5 + CH_4 \rightarrow C_2H_6 + CH_3$

Direct dissociation of methane will be negligible at these temperatures. Thus methane enters the propagation reactions in the chain mechanism and is converted to ethane. If the amount of methane is small so that the actual and the relative concentrations of the radicals in the system are not altered, the relative initial rates of formation of ethane in the presence and absence of methane may be expressed as follows (10):

$$[5] \quad \frac{(R^0_{C_2H_6})_a}{R^0_{C_2H_6}} = 1 + \frac{k_4[CH_4]}{k_3[C_2H_4]}$$

The efficiency of the conversion of methane to ethane in this system depends on the ratio of rate constants k_4/k_3, and the relative concentration of methane and ethylene. The rate constants k_4 and k_3 have similar values (11) so that increasing the ratio of methane to ethylene should enhance the conversion of methane to ethane. As the concentration of methane is increased, however, and reaction [4] becomes the dominant source of ethane, ethyl radicals are converted to methyl radicals and the characteristics of the chain mechanism of the ethylene reaction are altered. The products formed from reactions of methyl radicals will become more important while the relative rate of formation of ethane will be reduced. The ratio CH_4/C_2H_4 is therefore an important factor in the efficiency of the conversion of methane to ethane.

Equally important is the absolute concentration of ethylene. As the initiator, ethylene controls the overall rate of the reaction, and a reduction in its concentration to allow a high ratio of CH_4/C_2H_4 inevitably reduces the rate of conversion of methane. Thus the high ratio CH_4/C_2H_4 favouring reaction [4] must be balanced by sufficient sensitizer to provide a reasonable rate. The purpose of the present study was to search for conditions where pyrolysis of mixtures of methane and ethylene would give a maximum efficiency for conversion of methane to ethane.

Experimental

The experiments were performed in a static pyrolysis system using a cylindrical quartz reaction cell of 0.21 L. The cell was placed in the center of a three-zone furnace, Lindberg model no. 54457, which controlled the temperature to within ±2 K. Mixtures were admitted to the reactor by expansion from calibrated volumes and samples were removed for analysis at the end of an experiment.

Mixtures of the reactants were prepared using spherical mixing flasks designed with a minimum of connecting tubing. The reactant present in lower concentration was introduced first. Rapid admission of a higher pressure of the second reactant caused convection currents that provided rapid mixing. Tests of the mixtures showed that homogeneous mixtures were achieved in less than one hour.

Products were analyzed using a Hewlett Packard gas chromatograph model 5710A with flame detector. Two columns were required for separation of the products from the large quantities of reactants. A silica gel column (40/60 mesh, 1.5 m × 6.5 mm) at 30°C separated the small quantities of the product ethane from the large amounts of methane and ethylene. A Durapak column (phenylisocyanate/Porasil C, 80/100 mesh, 6 m × 6.5 mm) maintained at 25°C was used for the products propylene and butene-1. Both columns were calibrated with a certified mixture, ethane 450 ppm, propylene 109 ppm, and butene-1 53 ppm, in ethylene, obtained from Matheson Gas Products, Whitby, Ont.

TABLE 1. Initial pressure of ethylene and ratios of methane to ethylene in the experiments

Temperature (K)	Pressure of C_2H_4 (Torr)	$\frac{CH_4}{C_2H_4}$
774	200	0.1, 0.5, 1.0
	100	1.0, 2.0, 3.0
	50	1.0, 3.0, 5.0, 8.0
	25	1.0, 3.0, 5.0, 8.0
	14	13.2, 20
824	50	4.0, 7.0
	25	4.0, 7.0
	12.5	4.0, 7.0
853	50	4.0, 7.0
	25	4.0, 7.0
	12.5	4.0, 7.0

Research grade ethylene (99.99%), research grade butene-1 (99.9%), and research grade methane (99.99%) were obtained from Matheson Gas Products, Whitby, Ont. and, except for rigorous degassing, were used without further purification. Impurities in the reactants were too small to affect the kinetics of the reaction, but correction to the yield of ethane, due to this impurity in the ethylene and the methane, was made where necessary.

Results

Ethylene and mixtures of methane and ethylene were pyrolyzed at 774, 824, and 853 K. A summary of the conditions for the experiments at each temperature is given in Table 1. In addition, experiments with small quantities (~4%) of butene-1 added to the mixtures of ethylene and methane were performed at 774 and 853 K.

A. Pyrolysis of ethylene

As reported in previous studies (12), propylene was the major product followed by butene-1 and ethane in comparable amounts. 1,3-Butadiene was of lesser importance. Methane was also a product but was not of course measurable in the presence of added methane. At these temperatures auto-acceleration of the rate was observed at all pressures, as illustrated in Figs. 1 and 2, which also show yields in the presence of methane, and initial rates were obtained by extrapolation of the ratio

$$\frac{(\text{yield product})_t}{t}$$

to zero time. This function was usually linear and the uncertainty in the initial rate was about ±30%. Auto-acceleration is caused by secondary initiation by products, principally butene-1, and is observed at conversions as low as 0.01% (12).

For each pressure of ethylene the rate of product formation was determined as a function of the initial pressure of ethylene. The order of the initial rate of formation of the three major products over the pressure range 25–200 Torr (1 Torr = 133.3 Pa) was for ethane, 2.0, for propylene, 2.7, and for butene-1, 2.3, in good agreement with previous measurements.

The thermal reactions of ethylene at these temperatures involve a complex set of parallel and interacting chain propagation reactions of the ethyl and vinyl radicals, following initiation by reaction [1]. The mechanism proposed by Back and Martin

Can. J. Chem. Downloaded from www.nrcresearchpress.com by 88.85.125.76 on 09/07/12
For personal use only.

(7) is based on the original suggestion by Kossiakoff and Rice (13) and substantiated by Quinn (14) that isomerization and decomposition of the normal radicals formed by addition of radicals to ethylene is not important until the chain has reached C_6 or possibly C_5. For these radicals isomerization can compete with further addition and the isomerized radical readily decomposes to give the products propylene and butene-1, regenerating the ethyl or methyl radicals. Thus methane and ethane are the result of radical abstraction from ethylene while propylene and butene-1 are the result of radical addition to ethylene. The vinyl radical undergoes similar reactions (although the abstraction is a simple exchange and hence unobservable) leading to butadiene and other products more unsaturated than propylene and butene-1. Since the measurement of such products was not the purpose of this study, reactions of the vinyl radical will not be considered further.

The following series of reactions represents a simplified scheme for the formation of methane, ethane, propylene, and butene-1 for which only the reactions of the methyl, ethyl, and higher saturated radicals need be considered.

[1] $2C_2H_4 \rightarrow C_2H_3 + C_2H_5$

[2] $CH_3 + C_2H_4 \rightarrow CH_4 + C_2H_3$

[3] $C_2H_5 + C_2H_4 \rightarrow C_2H_6 + C_2H_3$

[6] $C_2H_5 + C_2H_4 \leftrightarrows C_4H_9$

[7] $C_4H_9 + C_2H_4 \rightarrow 1\text{-}C_6H_{13}$

[8] $1\text{-}C_6H_{13} \rightarrow 2\text{-}C_6H_{13}$

[9] $2\text{-}C_6H_{13} \rightarrow C_3H_6 + 1\text{-}C_3H_7$

[10] $1\text{-}C_3H_7 + C_2H_4 \rightarrow 1\text{-}C_5H_{11}$

[11] $1\text{-}C_5H_{11} \rightarrow 2\text{-}C_5H_{11}$

[12] $2\text{-}C_5H_{11} \rightarrow C_3H_6 + C_2H_5$

[13] $1\text{-}C_6H_{13} \rightarrow 3\text{-}C_6H_{13}$

[14] $3\text{-}C_6H_{13} \rightarrow C_4H_8 + C_2H_5$

[15] $3\text{-}C_6H_{13} \rightarrow C_5H_{10} + CH_3$

[16] $CH_3 + C_2H_4 \rightleftarrows C_3H_7$

[t] $2C_2H_5 \rightarrow C_4H_{10}$

where [t] indicates the termination reaction.

Although several radicals are important in the mechanism, initiation and termination reactions of the ethyl radical probably control the total radical concentration. Assuming a steady-state concentration of radicals, the concentration of ethyl radicals may be expressed as follows:

$$[17] \quad [C_2H_5] = \left(\frac{k_1}{k_t}\right)^{1/2}[C_2H_4]$$

As discussed earlier, ethane is formed entirely by reaction [2] and the rate of formation of ethane is, therefore,

$$[18] \quad R_{C_2H_6} = k_3[C_2H_5][C_2H_4] = k_3\left(\frac{k_1}{k_t}\right)^{1/2}[C_2H_4]^2$$

The rate of formation of ethane was observed to be second order, in accord with this expression.

Butene-1 is formed by decomposition of the 3-hexyl radical, reaction [14], and its rate of formation may be expressed as follows:

$$[19] \quad R_{C_4H_8} = (1 - a)b\frac{k_6[C_2H_4]}{k_{-6} + k_7[C_2H_4]} \cdot k_7[C_2H_5][C_2H_4]$$

where a and b are the fractions $k_8/(k_8 + k_{13})$ and $k_{14}/(k_{14} + k_{15})$ respectively. Since the order of the rate of formation of butene-1 was observed to be slightly greater than two, the term in the denominator, $k_7[C_2H_4]$, makes a significant contribution. In other words, reaction [6] is not completely equilibrated under the conditions of these experiments.

Propylene is formed through reactions [9] and [12] and its rate of formation therefore involves two terms, as follows:

$$[20] \quad R_{C_3H_6} = a \cdot \frac{k_6[C_2H_4]}{k_{-6} + k_7[C_2H_4]} \cdot k_7[C_2H_5][C_2H_4] + k_{10}K_{16}[CH_3][C_2H_4]^2$$

or, expressing the concentration of methyl radicals in terms of the concentration of ethyl radicals:

$$[CH_3] = (1 - b)(1 - a) \cdot \frac{k_6[C_2H_4]}{k_{-6} + k_7[C_2H_4]} \cdot \frac{k_7}{k_2}[C_2H_5]$$

eq. [20] becomes

$$[21] \quad R_{C_3H_6} = a \cdot \frac{k_6[C_2H_4]}{k_{-6} + k_7[C_2H_4]} \cdot k_7[C_2H_5][C_2H_4] + (1 - b)(1 - a) \cdot \frac{k_6[C_2H_4]}{k_{-6} + k_7[C_2H_4]} \cdot \frac{k_{10}K_{16}k_7}{k_2}[C_2H_5][C_2H_4]^2$$

assuming equilibration of the propyl radicals by reaction [16]. The first term will give an order of the rate similar to that of butene-1 while the second term will lead to a higher order, due to the formation of the propyl radical by reaction [16]. Since the observed order for the rate of formation of propylene was 2.7, and in previous studies has always been observed to be greater than that for butene-1, formation through the reaction of propyl radicals must make a significant contribution.

The different orders for the rates of formation of these products are illustrated by the change in the ratios of the rates, $R_{C_3H_6}/R_{C_2H_6}$ and $R_{C_3H_6}/R_{C_4H_8}$, with increasing pressure of ethylene, shown in Fig. 3.

$$[22] \quad \frac{R_{C_3H_6}}{R_{C_2H_6}} = a \cdot \frac{k_6[C_2H_4]}{k_{-6} + k_7[C_2H_4]} \cdot \frac{k_7}{k_3} + (1 - b)(1 - a)\frac{k_6[C_2H_4]}{k_{-6} + k_7[C_2H_4]} \cdot \frac{k_{10}K_{16}k_7}{k_3k_2}[C_2H_4]$$

$$[23] \quad \frac{R_{C_3H_6}}{R_{C_4H_8}} = \frac{a}{b(1 - a)} + \frac{(1 - b)}{b} \cdot \frac{k_{10}K_{16}}{k_2}[C_2H_4]$$

Equation [22] predicts a dependence on ethylene pressure slightly greater than linear, because of the ratio $k_6[C_2H_4]/(k_{-6} + k_7[C_2H_4])$, while eq. [23] predicts a linear dependence. Both predictions are supported by the experimental data. Although this mechanism is greatly oversimplified it gives a general picture of the reactions leading to the three main products, ethane, propylene, and butene-1, which are used as the main indicators of changes in the mechanism that occur on addition of methane to the system.

Butadiene was also measured in the presence and absence of methane. It is most probably formed through a similar series of reactions involving the vinyl radical. Reactions of these unsaturated radicals are, however, not as well understood as those of the saturated radicals and the development of an expression for the rate of formation of butadiene would involve too many approximations and assumptions to allow reasonable credibility. The effect of methane on the rate of formation of

Can. J. Chem. Downloaded from www.nrcresearchpress.com by 88.85.125.76 on 09/07/12
For personal use only.

butadiene and other more unsaturated products will therefore not be discussed further.

B. Pyrolysis of mixtures of ethylene and methane

Addition of methane to ethylene increased the rate of formation of ethane at all temperatures and pressures of ethylene. At 774 K the rate of formation of propylene was unaffected at 100 and 200 Torr of ethylene but was significantly increased at 25 and 50 Torr. These effects are shown in Figs. 1 and 2. At 774 K the rate of formation of butene-1 was slightly decreased at the two lowest pressures while the rate of formation of butadiene was not appreciably altered at any pressure of ethylene. At the highest temperature the reduction in the rate of formation of butene-1 was more pronounced but the rate of formation of butadiene was not much affected.

The fact that at 100 and 200 Torr of ethylene ethane was the only product whose rate of formation was increased by the addition of methane is strong indication that the only new propagation reaction introduced under these conditions is the abstraction of hydrogen from methane by ethyl radicals, reaction [4], and that the contribution by this reaction is not sufficient to alter appreciably the relative concentrations of radicals in the system. Under these conditions, as discussed earlier, the relative initial rates of formation of ethane may be described by eq. [5]. With the limited data available the function was linear up to a ratio of methane/ethylene of about two and from the slope of the linear portion a value of k_4/k_3 of 1.0 was obtained. This value is consistent with other values of this ratio measured with different additives at the same temperature by the same method, as shown in Table 2.

At the lower pressures of ethylene at 774 K and at all pressures at the higher temperatures, addition of methane enhanced considerably the rate of formation of propylene, and also altered the rate of formation of butene-1. Under these conditions, where the distribution of radicals in the chain mechanism is changed, the relative rates of formation of ethane cannot be expressed by the simple eq. [5]. When the relative concentration of radicals in the system changes, the main chain-carrying radical may change, with consequent changes in the termination steps and even in the total radical concentration. Nevertheless changes in the distribution of products may be examined as qualitative indication of changes in the mechanism induced by the presence of methane.

At the fractional conversions used in the present experiments the ratios of the products were unchanged during the course of the reaction. Therefore, secondary reactions of the products are not perturbing the chain propagation reactions and changes in the ratios of the products are due to the presence of methane.

In the presence of methane the two new reactions of most importance will be the following abstraction reactions:

[4] $C_2H_5 + CH_4 \rightarrow C_2H_6 + CH_3$

[24] $C_2H_3 + CH_4 \rightarrow C_2H_4 + CH_3$

As mentioned earlier, only for the methyl, ethyl, and vinyl radicals is abstraction from ethylene or methane sufficiently fast to compete with decomposition or addition to ethylene. For example, the products propane and butane are always very minor and no evidence was observed for increasing importance in the presence of methane. There is also no direct evidence for the occurrence of reaction [24] and the expressions for the rates of formation of the products presented later will not include this reaction. These expressions will therefore be qualitative and have not been used to estimate values for ratios of rate constants involved in the mechanism.

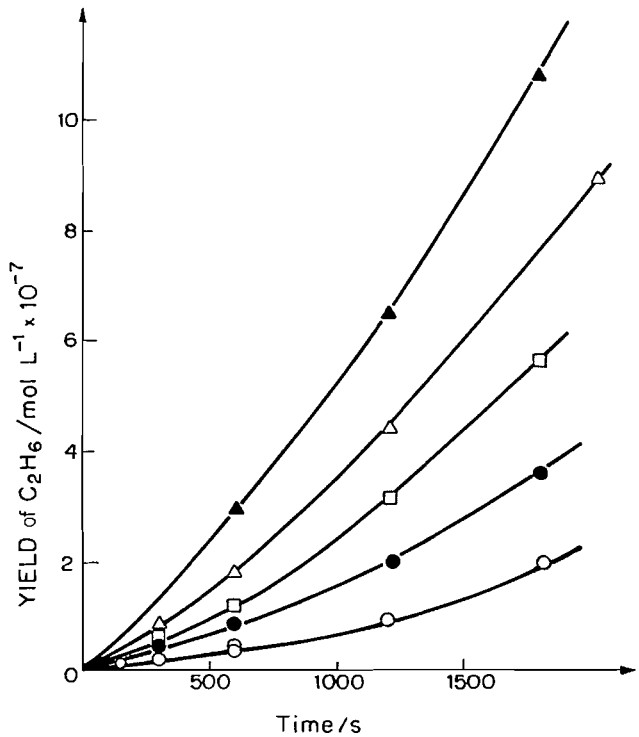

FIG. 1. Yield of ethane as a function of time at 774 K with an initial pressure of ethylene of 50 Torr. Pressure of CH_4 (Torr), ○: 0; ●: 50; □: 150; △: 250; ▲: 400.

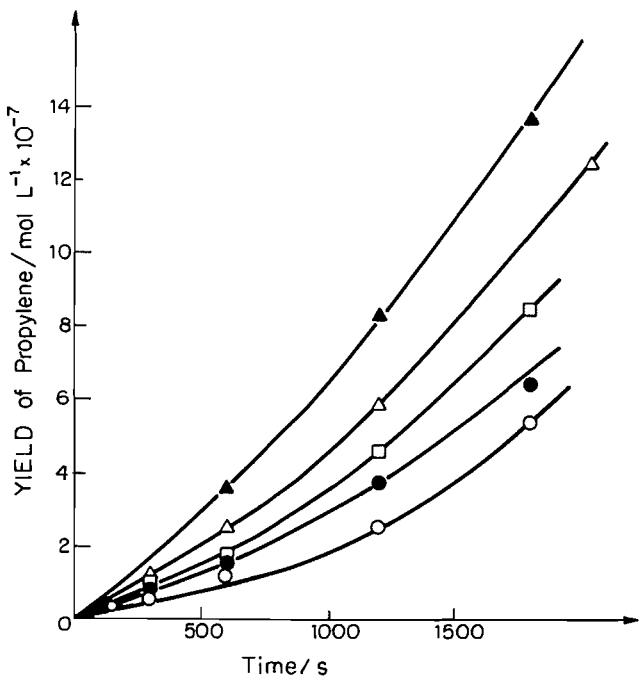

FIG. 2. Yield of propylene as a function of time at 774 K with an initial pressure of ethylene of 50 Torr. Pressure of CH_4 (Torr), ○: 0; ●: 50; □: 150; △: 250; ▲: 400.

As a first approximation we assume that the concentration of ethyl radicals is unchanged in the presence of methane and given, as before, by eq. [17]. Under these conditions the rate of formation of butene-1 will be unchanged, as expressed by eq. [19]. The rates of formation of ethane and propylene will be given as follows, still assuming equilibration of the propyl radical.

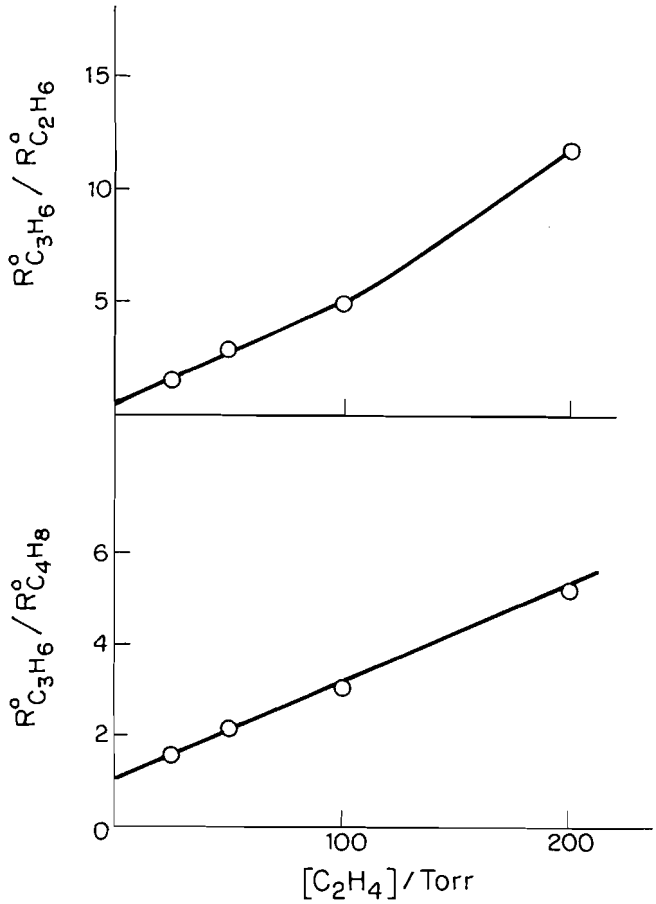

FIG. 3. The ratios $R^0_{C_3H_6}/R^0_{C_2H_6}$ and $R^0_{C_3H_6}/R^0_{C_4H_8}$ as a function of the initial pressure of ethylene obtained in the pyrolysis of ethylene at 774 K.

TABLE 2. Relative rate constants for abstraction of hydrogen by ethyl radicals for the following reactions

E $C_2H_5 + C_2H_4 \rightarrow C_2H_6 + C_2H_3$

R $C_2H_5 + RH \rightarrow C_2H_6 + R$

RH	k_R/k_E at 774 K	Reference
CH_4	1.0	Present work
H_2	50	15
C_2H_6	8	10
C_3H_8	23	16
i-C_4H_{10}	38	16
C_6H_6	4	17
C_7H_8	17	17

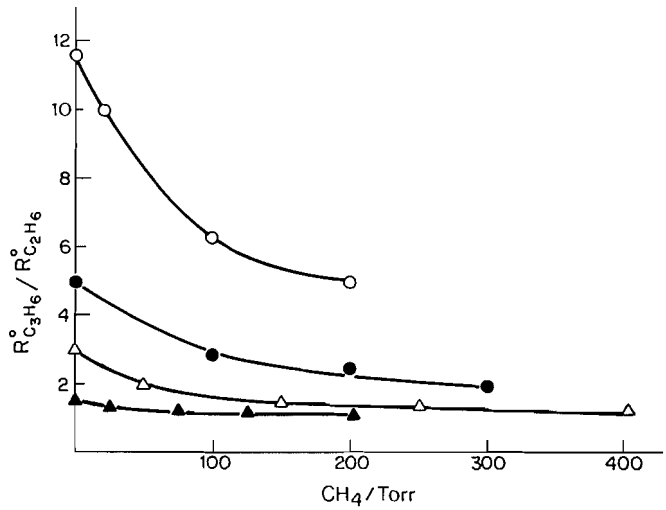

FIG. 4. The ratio $R^0_{C_3H_6}/R^0_{C_2H_6}$ as a function of the pressure of methane from the pyrolysis of the mixtures at 774 K. Initial pressure of ethylene (Torr), ○: 200; ●: 100; △: 50; ▲: 25.

$$[25]\quad R_{C_2H_6} = [C_2H_5](k_3[C_2H_4] + k_4[CH_4])$$

$$[26]\quad R_{C_3H_6} = [C_2H_5]\left\{a\cdot\frac{k_6[C_2H_4]}{k_{-6} + k_7[C_2H_4]}\cdot k_7[C_2H_4] + (1-b)(1-a)\cdot\frac{k_6[C_2H_4]}{k_{-6} + k_7[C_2H_4]}\cdot\frac{k_{10}K_{16}k_7}{k_2}[C_2H_4]^2 + \frac{k_{10}K_{16}}{k_2}[C_2H_4][CH_4]\right\}$$

In the presence of methane the rate of formation of ethane is increased directly through reaction [4] while the rate of formation of propylene is increased through the increasing importance of the methyl radical, the consequent formation of the propyl radical, and the sequence of reactions [10]–[12].

Letting the fraction $k_6[C_2H_4]/(k_{-6} + k_7[C_2H_4]) = X$, the expression for the ratios of rates $R_{C_3H_6}/R_{C_2H_6}$ and $R_{C_3H_6}/R_{C_4H_8}$ are given as follows:

$$[27]\quad \frac{R_{C_3H_6}}{R_{C_2H_6}} = \frac{a.X.k_7[C_2H_4] + (1-b)(1-a)X\dfrac{k_{10}K_{16}k_7[C_2H_4]^2}{k_2} + \dfrac{k_{10}K_{16}}{k_2}[C_2H_4][CH_4]}{k_3[C_2H_4] + k_4[CH_4]}$$

$$[28]\quad \frac{R_{C_3H_6}}{R_{C_4H_8}} = \frac{a}{b(1-a)} + \frac{(1-b)}{b}\cdot\frac{k_{10}K_{16}}{k_2}[C_2H_4] + \frac{1}{b(1-a)}\frac{k_{10}K_{16}[CH_4]}{k_2k_7X}$$

These ratios are shown as a function of the pressure of methane in Figs. 4 and 5. The changes in these ratios can be understood on the basis of the changes in the relative concentrations of the ethyl and methyl radicals. The ratio $R_{C_3H_6}/R_{C_2H_6}$ at first decreases with added methane due to the importance of reaction [4], before the concentration of the ethyl radical is significantly altered. As the balance of the two radicals gradually shifts toward the methyl radical, the final term in the numerator will eventually dominate the route to propylene and as a result the influence of methane on the two rates will tend to cancel. As illustrated in Fig. 4 the ratio approached a constant value at high pressures of methane.

The importance of the final term in the rate of formation of propylene is also illustrated by the ratio $R_{C_3H_6}/R_{C_4H_8}$. When this term is not important this ratio will be independent of the concentration of methane. This was the case for the experiments

Can. J. Chem. Downloaded from www.nrcresearchpress.com by 88.85.125.76 on 09/07/12
For personal use only.

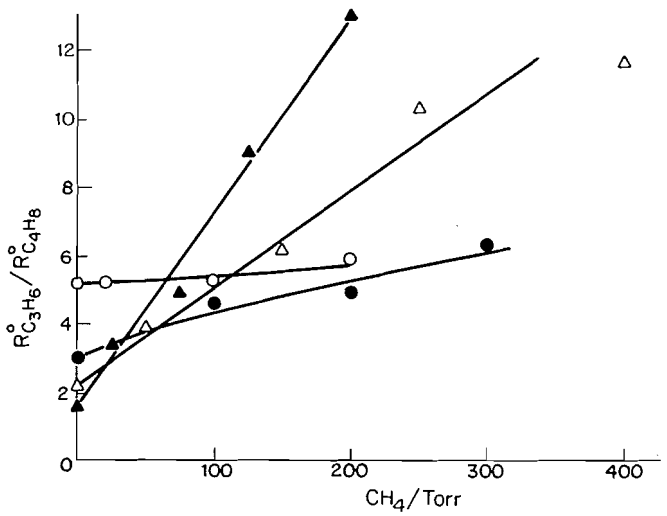

FIG. 5. The ratio $R^0_{C_3H_6}/R^0_{C_4H_8}$ as a function of the pressure of methane from the pyrolysis of the mixtures at 774 K. Initial pressure of ethylene (Torr), ○: 200; ●: 100; △: 50; ▲: 25.

with the highest pressure of ethylene, 200 Torr, and is consistent with the observed decrease in the ratio $R_{C_3H_6}/R_{C_2H_6}$ under the same conditions. At lower pressures of ethylene the final term becomes more important and the ratio $R_{C_3H_6}/R_{C_4H_8}$ increases linearly with increasing concentration of methane. Both ratios show that this term assumes increasing importance as the pressure of ethylene is lowered and is the dominant source of propylene at the lowest pressure of ethylene. Moreover, as predicted by eq. [28], the value of the ratio $R_{C_3H_6}/R_{C_4H_8}$ in the absence of methane is greatest for the highest pressure of ethylene. The results show therefore that the simple mechanism outlined earlier accounts satisfactorily for the effects observed on the rate of product formation by the addition of methane.

As discussed at the beginning of this section, the interpretation of the relative rates of formation of ethane in the presence and absence of methane in terms of eq. [5] was possible only for the experiments at the two highest pressures of ethylene. It is nevertheless useful to examine the magnitude of the increase in the rates of both products ethane and propylene in the presence of methane under the other conditions of the experiments, mainly as a means of assessing the efficiency of the conversion of methane. The relative rates of formation of ethane and propylene in the presence and absence of methane R^0_a/R^0, are shown as a function of the ratio CH_4/C_2H_4 for the three temperatures of the reaction in Fig. 6. At 774 K ethane is the product most affected by the addition of methane but by 824 K the increase in the rate of formation of propylene is significantly greater than the increase in the rate of formation of ethane, particularly at the lowest pressure. At the highest temperature, however, the effect of methane on the rates of formation of both products had diminished and no longer appears to increase linearly with the ratio CH_4/C_2H_4.

Probably of more significance than the relative rates is the actual rate of conversion of methane into higher molecular weight products. Since the conversion of both ethylene and methane was kept low in these experiments, in order to obtain measurements of the initial rates, the rate of conversion of methane must be estimated from the rate of formation of products. The two reactions that consume methane are [4] and [24]. The increase in rate of formation of ethane, which is the difference between the rate in the presence of methane, R^0, and

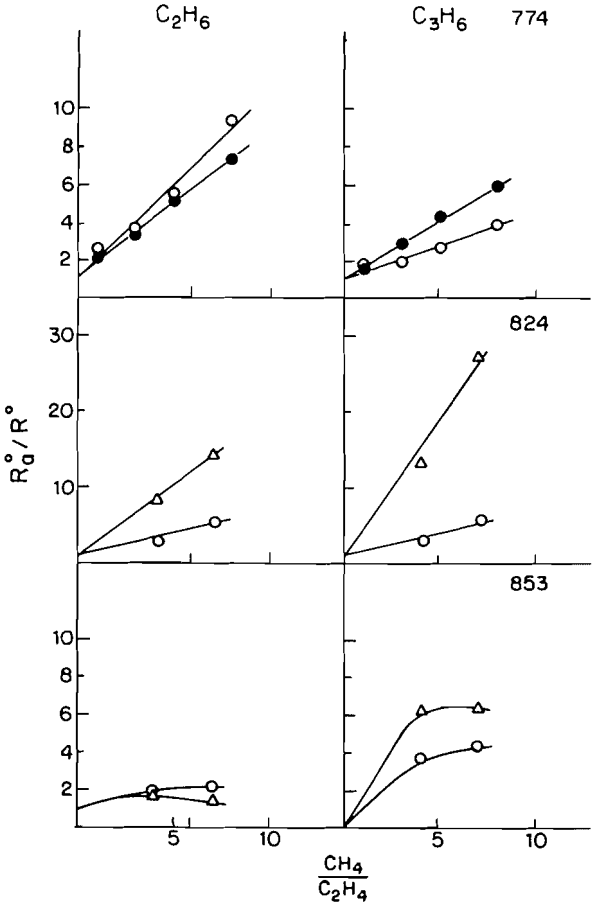

FIG. 6. Relative rates of formation in the presence and absence of methane, R^0_a/R^0, of the products ethane and propylene at the three temperatures of the reaction as a function of CH_4/C_2H_4. Initial pressure of ethylene (Torr), ○: 50; ●: 25; △: 12.5.

in the absence of methane, R^0_a, may be equated to a rate of loss of methane,

$$R^0_a - R^0 = \text{rate loss methane}$$

The conversion of methane was calculated from the measurements of the initial rates for all the experiments at each temperature. The highest rate of conversion was 2×10^{-5} percent·s^{-1}, measured at the highest temperature, 853 K, with 50 Torr ethylene and 200 Torr methane. This rate was actually not very different over the whole range of temperature because of the compensating effects of temperature, pressure, and relative rates.

C. Pyrolysis of mixtures of ethylene, methane, and butene-1

A rate of conversion of this magnitude is not likely to find application in industrial processing operations. Even though this estimate is a lower limit, the actual rate is probably no more than two or three times greater. An improved rate of conversion could be achieved only through an increase in the rate of the overall reaction of ethylene. At higher tempratures the rate of the reaction was greatly increased but experiments under these conditions showed that the mechanism was significantly different, leading to changes in the interpretation. These results will be reported separately. In the region of temperature of the present experiments the rate of the reaction could be increased only by the addition of a new source of initiation of radicals.

The rate of the thermal reaction of ethylene at these

Can. J. Chem. Downloaded from www.nrcresearchpress.com by 88.85.125.76 on 09/07/12
For personal use only.

TABLE 3. Pyrolysis of mixtures of ethylene, methane, and butene-1

Temperature (K)	Initial pressure of reactants (Torr)			Initial rate of formation of products (mol L^{-1} s^{-1} × 10^9)	
	C_2H_4	1-C_4H_8	CH_4	C_2H_6	C_3H_6
774	50	0	0	0.04	0.13
	50	2	0	2.2	6.8
	50	1.7	400	4.4	7.0
853	50	0	0	1.0	0.7
	50	1.9	0	39	180
	50	1.6	400	76	150

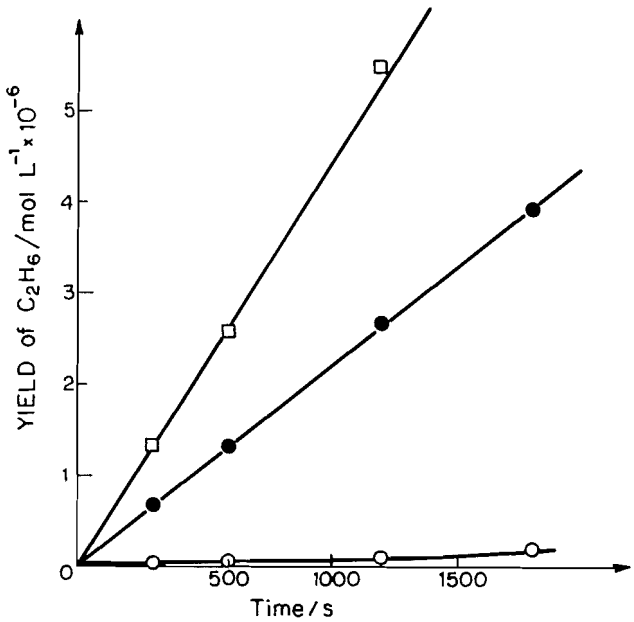

FIG. 7. Yield of ethane as a function of time from the pyrolysis of mixtures of ethylene, methane and butene-1 at 774 K. Initial pressures (Torr), ○: 50 (C_2H_4), 0 (CH_4), 0 (1-C_4H_8); ●: 50 (C_2H_4), 0 (CH_4), 2 (1-C_4H_8); □: 50 (C_2H_4), 400 (CH_4), 2 (1-C_4H_8).

temperatures is strongly auto-accelerated, as illustrated in Figs. 1 and 2, due to secondary initiation by the product butene-1. Furthermore, previous studies had shown that addition of butene-1 to thermally reacting ethylene caused an increase in the rate of the reaction, and, if the quantities of butene-1 were not too large, the products of the reaction were unchanged (12). Small quantities of butene-1 were therefore added to the mixtures of ethylene and methane in order to increase the overall rate of the reaction and the conversion of methane. Experiments were done at 774 and 853 K with mixtures of ethylene containing about 4% butene-1 in the presence and absence of methane. In the absence of methane the rate of formation of all products from the reaction of ethylene was substantially increased, as observed in previous studies. In the presence of methane the rate of formation of ethane was increased while the rates of formation of propylene and butene-1 were unaffected. The results are summarized in Table 3 and illustrated in Fig. 7.

The result clearly showed that butene-1 acted as a new initiator for the chain reaction of ethylene, through rapid thermal dissociation, increasing the rate of the overall reaction.

$$C_4H_8 \rightarrow CH_3 + C_3H_5$$

The extent of the conversion of methane in these experiments may be estimated from the difference between the rate of formation of ethane in the presence of methane and in the absence of methane, as in the experiments without butene-1. At 853 K with 400 Torr of methane the percentage conversion of methane per second was 5×10^{-4}. The addition of butene-1 therefore gave considerable improvement in the rate of conversion of methane.

Conclusions

The pyrolysis of mixtures of methane and ethylene leads to the direct conversion of methane to ethane and propylene, through participation of methane in the chain propagation reactions of the ethylene pyrolysis. The overall rate of the conversion may be enhanced by the addition of compounds that provide an increased rate of initiation. An advantage of the system is that methane is converted exclusively to hydrocarbon product.

Acknowledgments

The authors thank the Department of Energy, Mines and Resources, Canada, for the award of a contract in support of this project. They also thank Dr. J. Z. Galuszka, ERL, CANMET, for his continued interest in the project.

1. J. S. LEE and S. T. OYAMA. Catal. Rev. Sci. Eng. **30**, 249 (1988).
2. C.-H. LIN, J.-X. WANG, and J. H. LUNSFORD. J. Catal. **111**, 302 (1988).
3. I. T. ALI EMESH and Y. AMENOMIYA. J. Phys. Chem. **90**, 4785 (1986).
4. C.-J. CHEN, M. H. BACK, and R. A. BACK. Can. J. Chem. **54**, 3175 (1976).
5. M. H. BACK and R. A. BACK. Pyrolysis: theory and industrial practice. *Edited by* L. F. Albright, B. L. Crynes, and W. H. Corcoran. Academic Press, New York. 1983.
6. H. D. GESSER, N. R. HUNTER, and C. B. PRAKASH. Chem. Rev. **85**, 235 (1985).
7. M. H. BACK and R. MARTIN. Int. J. Chem. Kinet. **11**, 757 (1979).
8. D. DELLISTE, C. RICHARD, and R. MARTIN. J. Chim. Phys. **78**, 655 (1981).
9. A. L. MACKENZIE, P. D. PACEY, and J. H. WIMALASENA. Can. J. Chem. **61**, 2033 (1983).
10. S. I. AHONKHAI and M. H. BACK. Can. J. Chem. **66**, 578 (1988).
11. J. A. KERR and S. J. MOSS. CRC handbook of bimolecular and termolecular gas reactions. Vol. I. CRC Press, Boca Raton, FL. 1981.
12. G. AYRANCI and M. H. BACK. Int. J. Chem. Kinet. **13**, 897 (1981).
13. A. KOSSIAKOFF and F. O. RICE. J. Am. Chem. Soc. **65**, 590 (1943).
14. C. P. QUINN. Trans. Faraday Soc. **59**, 2543 (1963).
15. H.-X. ZHANG and M. H. BACK. Int. J. Chem. Kinet. **22**, 21 (1990).
16. S. I. AHONKHAI, X.-H. LIN, and M. H. BACK. Int. J. Chem. Kinet. **21**, 1 (1989).
17. H.-X. ZHANG, S. I. AHONKHAI, and M. H. BACK. Can. J. Chem. **67**, 1541 (1989).

Can. J. Chem. Downloaded from www.nrcresearchpress.com by 88.85.125.76 on 09/07/12
For personal use only.

Approaches to the tetracyclic eudistomins: the synthesis of N(10)-acetyleudistomin L[1]

IAN W. J. STILL[2] AND JURIS R. STRAUTMANIS

J. Tuzo Wilson Research Laboratories, Erindale Campus, University of Toronto, Mississauga, Ont., Canada L5L 1C6

Received August 24, 1989

IAN W. J. STILL and JURIS R. STRAUTMANIS. Can. J. Chem. **68**, 1408 (1990).

The successful synthesis of the tetracyclic ring system present in eudistomins C, E, K, and L involves a convergent approach to N(10)-acetyleudistomin L from 5-bromo-*N'*-hydroxytryptamine and a suitably protected cysteinal derivative. Ring C in the eudistomin was constructed by a modified Pictet–Spengler reaction and the unique 1,3,7-oxathiazepine ring (ring D) by an unprecedented intramolecular sila-Pummerer reaction. An interesting diastereoselectivity is observed in the former process. The formation of an alternative seven-membered ring cyclization product under certain conditions in the sila-Pummerer reaction is also described.

Key words: eudistomins, 1,3,7-oxathiazepine, Pictet–Spengler, sila-Pummerer.

IAN W. J. STILL et JURIS R. STRAUTMANIS. Can. J. Chem. **68**, 1408 (1990).

Une bonne synthèse du système tétracyclique présent dans les eudistomines C, E, K et L implique une approche convergente vers la N(10)-acétyleudistomine L, à partir de la 5-bromo-*N'*-hydroxytryptamine et d'un dérivé cystéinal protégé d'une façon appropriée. On a construit le cycle C de l'eudistomine en faisant appel à une réaction modifiée de Pictet–Spengler et on est parvenu à former le cycle unique de la 1,3,7-oxathiazépine (cycle D) en effectuant une réaction intramoléculaire de sila-Pummerer qui n'avait jamais été réalisée antérieurement. On décrit que, dans certaines conditions de la réaction de sila-Pummerer, il y a une formation alternative d'un cycle à sept chaînons.

Mots clés : eudistomines, 1,3,7-oxathiazépine, Pictet–Spengler, sila-Pummerer.

[Traduit par la revue]

Can. J. Chem. Downloaded from www.nrcresearchpress.com by 91.121.58.235 on 09/07/12
For personal use only.

Introduction

In 1984, Rinehart and co-workers (1) reported the structure determination of 15 indole alkaloids, collectively termed eudistomins, which had been isolated from the tunicate (ascidian) organism *Eudistoma olivaceum*. Several reports of additional eudistomins, and the related compound eudistomidin A, have since appeared (2–5). Eudistomins C, E, K, and L (**1***a–d*,

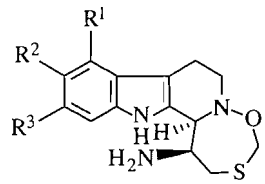

1*a*, R^1 = H, R^2 = OH, R^3 = Br
b, R^1 = Br, R^2 = OH, R^3 = H
c, R^1 = R^2 = H, R^3 = Br
d, R^1 = R^3 = H, R^2 = Br

respectively) have been shown to contain the unique 1,3,7-oxathiazepine ring as ring D of the tetracyclic system. These compounds have been shown to possess strong antiviral activity against the *Herpes simplex* virus (HSV-1) as well as certain types of in vivo antitumour activity (5*d*). Several early attempts towards the synthesis of this class of compound have appeared (6–8). Since our earlier preliminary communication (9), Nakagawa *et al.* have reported a second successful approach (10).[3] We present here a detailed account of our synthesis of N(10)-acetyleudistomin L **2**, a simple analogue of eudistomins of the 1,3,7-oxathiazepine type.

Our general approach to the synthesis of **2** is outlined in Scheme 1. At the time this work was initiated, not only was there no literature precedent for the synthesis of the 1,3,7-oxathiazepine ring present in **2**, but there also existed no literature precedents for the N(2)-hydroxylated tetrahydro-β-carbolines such as **3**. We envisaged the construction of ring D in **2** as being carried out by a Pummerer-type reaction strategy (11), or perhaps the sila-Pummerer modification (12), while the construction of ring C in **3** might best be accomplished by a modification of the classical Pictet–Spengler reaction, via an intermediate nitrone (6). The details of the synthesis of the key intermediates **4** and **5** and the convergent synthesis of **2** are described in the following section.

Results and discussion

According to the plan we had established by our retrosynthetic analysis (Scheme 1), we first set out to prepare 5-bromo-*N'*-hydroxytryptamine **4**. 5-Bromoindole **6** is commercially available and may also be prepared from indole, using a procedure originally reported by Thesing *et al.* (13). The known 5-bromotryptamine **10** (14) is prepared via the intermediacy of the 3-carboxaldehyde **8** (15) and nitro-olefin **9** (14) (Scheme 2). We have been able to devise a modification to the reduction of **9** that allows us to prepare **4** by a two-stage reduction procedure, in 65–70% overall yield (Scheme 3).

The first reduction step (**9** → **11**) is based upon a procedure reported by Varma and Kabalka (16), our earlier attempt to achieve the reduction of **9** to the hydroxylamine **4** directly, based upon another procedure of Kabalka and co-workers (17) and using a BH_3·THF complex catalyzed by $NaBH_4$, having been completely unsuccessful. We feel that an important factor in the success of this nitro-olefin reduction is the necessity for the hydroxylic solvent. Under our conditions, the active reducing agent is likely a trimethoxyborohydride formed by reaction of borohydride anion with excess methanol. The nitronate anion initially formed from **9** has thus only trimethoxyborane with which to complex, and further reduction does not occur, in the absence of an electrophilic reducing agent (e.g., borane) or a more powerful hydride reducing agent (e.g., $LiAlH_4$). Interestingly, no protection of the indole N-H proton is necessary during this reduction, as observed independently by others (18).

[1]Abstracted in part from the Ph.D. thesis of J. R. Strautmanis, University of Toronto, 1989.

[2]Author to whom correspondence may be addressed.

[3]Since this manuscript was submitted, two very interesting alternative synthetic strategies have been reported: see ref. 43.

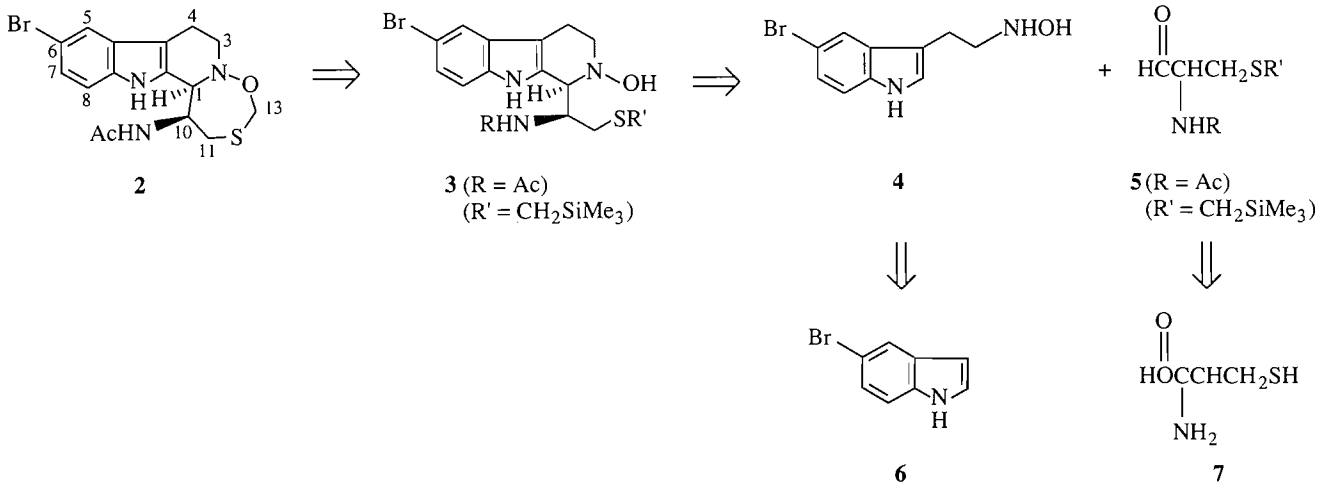

2 3 (R = Ac) (R' = CH_2SiMe_3) 4 5 (R = Ac) (R' = CH_2SiMe_3)

6 7

SCHEME 1

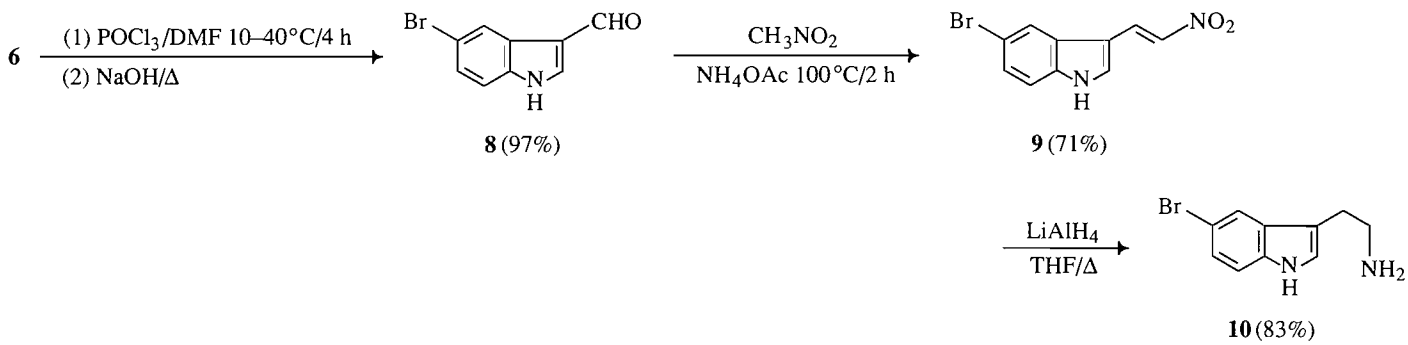

8 (97%) 9 (71%) 10 (83%)

SCHEME 2

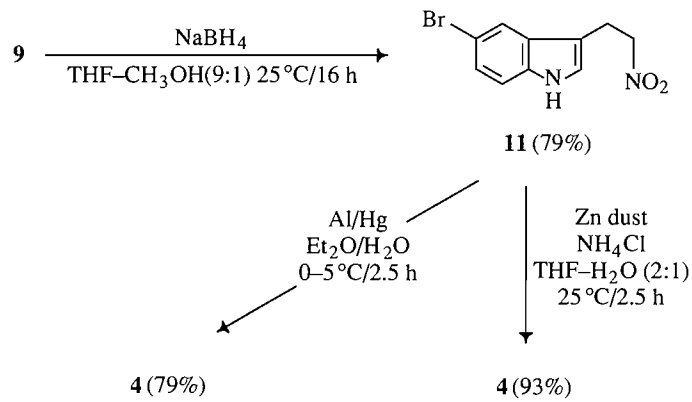

11 (79%) 4 (79%) 4 (93%)

SCHEME 3

Finally, the preparation of 5-bromo-*N'*-hydroxytryptamine **4** was readily achieved by aluminum amalgam reduction of the saturated nitro compound **11**. Aluminum amalgam reduction of nitro compounds to hydroxylamines is well established and, indeed, this was the route taken by Cava and co-workers (6) in their preparation of an analogous (non-brominated) *N'*-hydroxytryptamine. The zinc reduction of saturated nitro compounds to hydroxylamines, in the presence of a mild proton source and in a variety of solvents, is also well established in the literature (19). Due mainly to the more convenient preparation of the reducing agent, we preferred to use the zinc reduction for the preparation of 5-bromo-*N'*-hydroxytryptamine. Besides the work of Cava (6) and the present work, the only other preparation of *N'*-hydroxytryptamines was reported by Cohen and Heath-Brown (20), using zinc/ammonium chloride reduction of the corresponding nitro compounds in 95% ethanol.

We obtained **4** as a pale beige, sticky and sometimes foamy, substance, identified primarily on the basis of its ^{1}H NMR spectrum, in which the *NHOH* protons were characteristically observed as a broad singlet (2H) at δ 5.5 ppm, exchangeable by treatment with D_2O. In sharp contrast, the NH_2 protons in the corresponding tryptamine **10** appeared as a broad singlet (2H) at δ 1.7. The indole N-H proton in **10** appeared at δ 9.8, again in sharp contrast with **4**, where the corresponding proton appears at δ 8.2, an exceptionally shielded position for indole N-H protons in our series of compounds. We were never able to crystallize 5-bromo-*N'*-hydroxytryptamine nor achieve its purification in any other way. Hydroxylamines have often been characterized as their hydrogen oxalate salts (21). Treatment of the crude hydroxylamine, however, in dry ether with dried oxalic acid gave a beige precipitate, with a broad melting point, which we were unable to recrystallize. Neither a satisfactory ^{1}H NMR spectrum nor a satisfactory mass spectrum could be obtained for this material. Attempts to prepare the hydrochloride salt of **4** likewise led to intractable products. We decided to proceed with the hydroxylamine and to use the freshly prepared, crude free base in the subsequent reactions. Subsequently, the presence of the hydroxylamine was amply verified by irrefutable evidence for the identity of the reaction products derived from it.

The next phase of our strategy involved the construction of a suitable cysteine-derived moiety. The desired aldehyde **5** was chosen as the key intermediate because the aldehyde functionality is required for the modified Pictet–Spengler reaction (6)

Can. J. Chem. Downloaded from www.nrcresearchpress.com by 91.121.58.235 on 09/07/12
For personal use only.

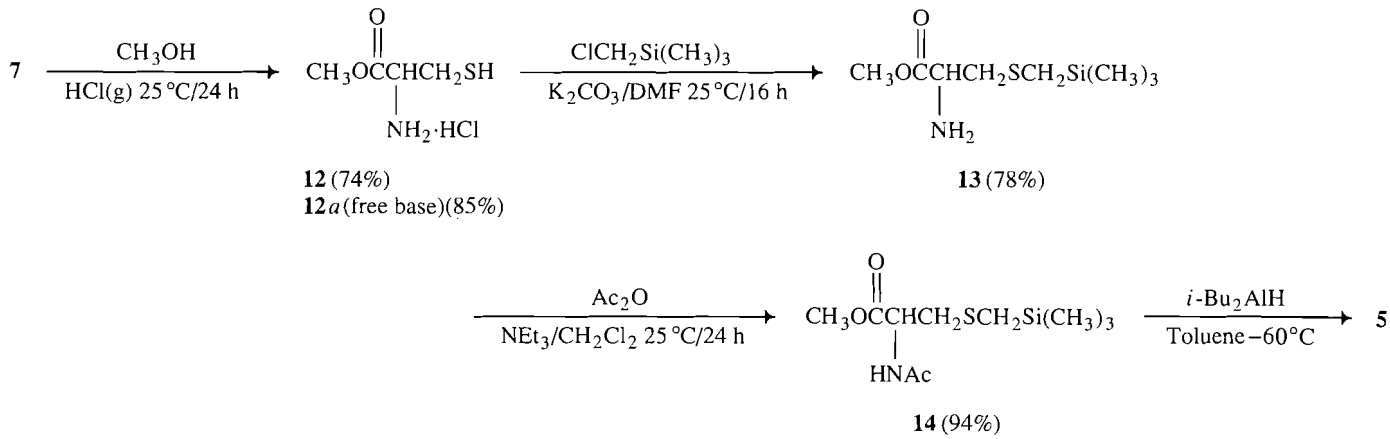

12 (74%)
12*a* (free base)(85%)

13 (78%)

14 (94%)

SCHEME 4

with the *N'*-hydroxytryptamine **4** above to construct ring C (Scheme 1). For the purposes of our sila-Pummerer ring closure strategy for ring D (Scheme 1) we first converted the -SH group in **7** into the trimethylsilylmethyl analogue **13**, using a procedure modified from that reported by Shimizu and Ogata (22).

Protection of the amino group is also essential to avoid the well-known dimerization of α-amino acid esters or aldehydes. We initially discarded the idea of using the more common Boc and Cbz groups frequently used for this purpose, on the grounds that compounds of type **1** would likely be sensitive to both acid hydrolysis and to hydrogenolysis because of the (expected) labile nature of ring D. The first of these assumptions has now been found to be erroneous and we will return to this point later. In the event, *N*-acetylation, to give **14**, was employed in this step, immediately following the *S*-alkylation step.

The methyl ester **12** (23) was thought to be the most convenient derivative of L-cysteine to serve as a precursor of the required aldehyde **5**. Diisobutylaluminum hydride (DIBAL) reduction of esters to the corresponding aldehyde is well established in the literature (24), including recent applications in which protected α-amino aldehydes are prepared from the corresponding protected α-amino esters (25). The synthesis of **5** is outlined in Scheme 4.

With the exception of the final aldehyde **5**, all the products in Scheme 4 were obtained in optically active form. Attempts to purify **5** by chromatography on silica gel led to optically inactive material, as has been noted previously for α-amino aldehydes (26). Subsequent work on the ring C closure (q.v.) was to reveal, however, that use of the unpurified aldehyde **5** was justified, in terms of a satisfactory diastereomeric outcome. The yield in the reduction step (40–50%) was also disappointing, although significantly better than for the corresponding ethyl ester analogue. In spite of these problems, we were able to obtain **5** conveniently by the route outlined and the chemical purity of the crude aldehyde was adequately demonstrated by its IR and ^{1}H NMR spectra, notably the peaks at 2727 and 1736 cm^{-1} in the former and the singlet at δ 9.6 in the latter showing the expected integration.

With the key intermediates **4** and **5** in hand, we next turned our attention to the closure of ring C of the eudistomin skeleton, by the modified Pictet–Spengler strategy. Before proceeding to this, however, we wish to briefly present the results of some preliminary experiments, by an alternative approach.

We reasoned initially that an intermediate such as **15** would be useful as a means not only for introducing an α-thio substituent at the methyl site, by standard methodology, but also for later introduction of the C-10 amino group by reductive amination, probably in a stereoselective fashion. Attempts to carry out a classical Pictet–Spengler reaction with pyruvic aldehyde **16** (or its dimethyl acetal) and 5-bromotryptamine **10**, however, were completely without success. We have also synthesized 6-bromo-1,2,3,4-tetrahydro-β-carboline **17**, by adapting the procedure used by Ho and Walker (27) for the parent tetrahydro-β-carboline, and were able to oxidize it by sodium tungstate-catalyzed oxidation with H_2O_2 (28) to the cyclic nitrone **18**, which we had also considered as a potential intermediate in our synthesis, through addition of a suitable 2-carbon nucleophile at C-1. The yield of **18** that we obtained, however, was less than 20% and this approach was not pursued.

Returning to our modified Pictet–Spengler strategy using **4**, a chance discovery, using acetone in the presence of silica gel and subsequently duplicated with acetaldehyde, enabled us to demonstrate not only the intermediacy of the nitrone intermediates **19***a*,*b* but also the fact that these were stable, isolable compounds. It was subsequently found that nitrone formation was more effectively catalyzed by anhydrous magnesium sulfate. Subsequent cyclization with trifluoroacetic acid, also at 25°C, readily produced the model 2-hydroxy-1,2,3,4-tetrahydro-β-carbolines **20***a*,*b*. With our original preparation of **15** in mind, we have also successfully employed 2-methyl-1,3-dithiane-2-carbaldehyde **21** (29) in this two-step sequence, to produce **23**, via **22**, in 42% overall yield. This has established **21** as a viable alternative to pyruvic aldehyde and its derivatives for such Pictet–Spengler reactions. Because of our successful application of the cysteinal derivative **5** in this sequence, however, no attempt to hydrolyze the dithioacetal unit in **23** or to proceed further with this approach was made.

The intermediate aldonitrones, **19***b* and **22**, were very easily distinguished by the characteristic one-proton signal at δ ~6.4 ppm in the ^{1}H NMR spectrum. The comparable protons (at C-1) in the cyclized products **20***b* and **23**, on the other hand, appeared much further upfield at δ ~4.1 ppm. Compounds **20***b* and **23** were also easily distinguished by showing the presence of three, rather than four, aromatic protons and, additionally, by the presence of two exchangeable hydrogens (indole N-H and N-OH). The assignment of the *Z* configuration to the single isomer obtained in each case for **19***b* and **22** is based on numerous literature precedents. The mass spectral breakdown of **19***b* versus that of **20***b* is also very diagnostic, a Cope-type *syn*-elimination of a β-hydrogen being characteristic of the

Can. J. Chem. Downloaded from www.nrcresearchpress.com by 91.121.58.235 on 09/07/12
For personal use only.

Can. J. Chem. Downloaded from www.nrcresearchpress.com by 91.121.58.235 on 09/07/12
For personal use only.

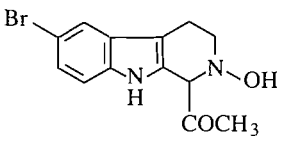

15

CH_3COCHO

16

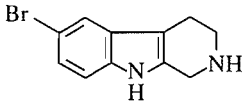

17

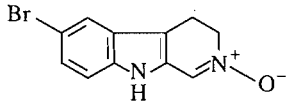

18

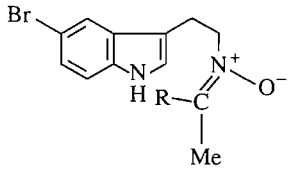

19*a*, R = CH_3
b, R = H

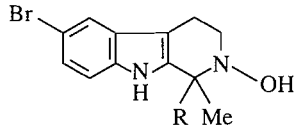

20*a*, R = CH_3
b, R = H

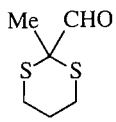

21

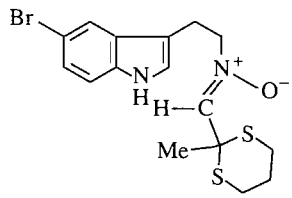

22

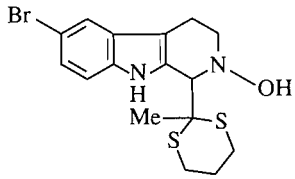

23

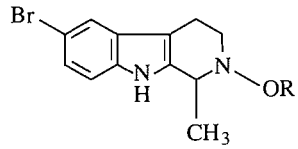

24*a*, R = $SiMe_3$
b, R = Ac

former, whereas a *retro*-Diels–Alder fragmentation, already well documented for simpler 1,2,3,4-tetrahydro-β-carbolines (30), is the major pathway in **20***b*. Both processes originate with initial electron ejection from the indole nitrogen atom. The model compound **20***b* was further characterized by the formation of its *O*-trimethylsilyl and *O*-acetyl derivatives **24***a*,*b*.

Having firmly established the generality of the modified Pictet–Spengler reaction with the *N'*-hydroxytryptamine **4**, we next carried out the reaction of **4** with the desired cysteinal **5**. This time the intermediate nitrone was cyclized immediately, without purification, under the conditions described above for the model compounds, to afford the desired 2-hydroxy-1,2,3,4-tetrahydro-β-carboline **25***a* in 24% yield, after recrystallization. Compound **25***a* has been fully characterized by IR, (400 MHz) ^1H and ^{13}C NMR, mass spectral, and elemental analyses.

An attempt was made to purify the intermediate nitrone but this was not entirely successful as some contaminants were still present after column chromatography on alumina. The impure nitrone, however, did show certain characteristic spectroscopic features, which we have discussed above for the previously described nitrones (**19***b* and **22**), including the characteristic aldonitrone proton in the ^1H NMR at δ 6.6 ppm and the Cope-type mass spectral fragmentation.

Our preparation of the N(2)-hydroxy-1,2,3,4-tetrahydro-β-carboline **25***a* by the modified Pictet–Spengler reaction led to its isolation as a single diastereoisomer that was optically inactive. Since, as discussed above, the diisobutylaluminum hydride reduction of the optically active α-acetamido ester **14** led to crude, unpurified intermediate **5**, concurrent racemization at the α-carbon of this cysteine derivative, even without subjection to the potentially racemizing conditions of silica gel chromatography, cannot be ruled out. Alternatively, it is possible that the observed racemization occurred subsequently to give the compound presently under scrutiny, the ring C cyclized compound **25***a*. It was reported, however, by Nakagawa *et al.* (10) that *both* nitrone formation *and* the Pictet–Spengler cyclization, carried out under similar but not identical conditions to our own, proceeded with retention of enantiomeric purity.

In our case, nitrone formation in dichloromethane, in the presence of magnesium sulfate, would appear less likely to cause racemization than the more acidic conditions of the modified Pictet–Spengler reaction, in the presence of trifluoroacetic acid. Under the latter conditions, O-protonation of the nitrone, followed by deprotonation at the chiral carbon, might be expected to give the *N*-hydroxyenamine **26**. Chirality is thus lost and, upon reprotonation of **26**, the racemic ring C cyclized compound is obtained.

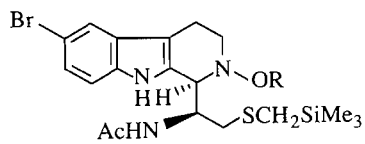

25*a* R = H
b R = $SiMe_3$

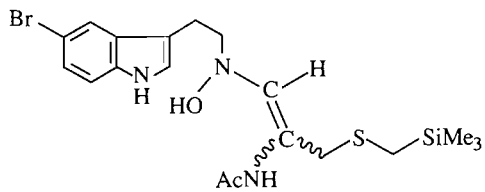

26

The correct explanation for this disappointing stereochemical outcome must remain conjectural for the present. More encouragingly, the observation of but a single set of signals in either the ^{13}C NMR spectrum or the (400 MHz) ^1H NMR spectrum of **25***a* verified that the ring C cyclized compound is a single diastereomer. The chiral centre at C(10) originates in L-cysteine and is racemized as described above, while the other centre, at C(1), is formed by what apparently is a diastereoselective process during the modified Pictet–Spengler cyclization. In our investigation of this reaction, we have found no evidence for a second diastereomeric compound being formed, a result essentially similar to that reported very recently by Nakagawa *et al.* (10), who reported preferred formation of one diastereomer (8:1 to 41:1 preference) at −78°C in trifluoroacetic acid.

In related literature examples, Ottenheijm and co-workers (7) obtained mixtures of diastereomers (with respect to the stereochemistry at C(1) and C(10)) in the modified Pictet–Spengler cyclization, using cysteine aldehydes in their work towards the

Can. J. Chem. Downloaded from www.nrcresearchpress.com by 91.121.58.235 on 09/07/12
For personal use only.

eudistomins. This result is complicated, however, by their use, in the cyclization, of a hydroxylamine derived from the ethyl ester of tryptophan, although the reaction conditions for the cyclization were otherwise similar to ours. It is also noteworthy that carbamate groups were used for the cysteine amino group protection in both the other approaches cited (7, 10), whereas we used an amide protecting group.

We were able to determine the relative stereochemistry at C(1) and C(10) only after formation of the oxathiazepine ring (q.v.). As it turned out, we had fortuitously obtained the correct diastereomer of the N(2)-hydroxy-1,2,3,4-tetrahydro-β-carboline **25***a*, bearing the substituents at C(1) and C(10) in the same relative orientation as in the naturally occurring eudistomin L (**1***d*). We interpret this observation by proposing a model **27** for the modified Pictet–Spengler cyclization[4] similar

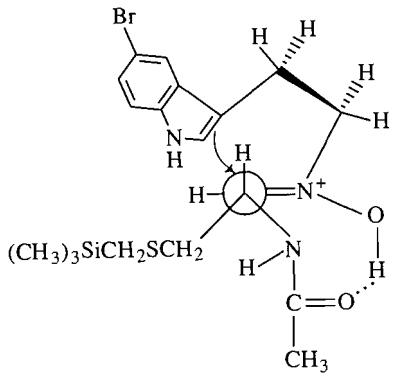

27

to that suggested by Czarnocki, MacLean, and Szarek (31) to explain the diastereoselectivity observed by these authors in the classical Pictet–Spengler reaction of β-phenylethylamines and aldehydes derived from carbohydrates, in the synthesis of isoquinoline alkaloids. This can be regarded as a variant of the model proposed by Cram and Elhafez (32) for nucleophilic attack at a double bond adjacent to a chiral centre. A related case of asymmetric induction in the 1,3-addition of Grignard reagents to nitrones has been very recently reported by Jenkins and co-workers (33).

In keeping with the above model structure, the amide carbonyl stretching vibration of **25***a* is observed in the IR at 1632 cm^{-1}, indicative of a very pronounced hydrogen bonded character. Interestingly, in the mass spectrum of **25***a* no evidence for a *retro*-Diels–Alder fragmentation was observed. As the model compound **23** has revealed, however, 2-hydroxy-1,2,3,4-tetrahydro-β-carbolines with relatively complex substituents at C(1) may prefer to undergo fragmentation by cleavage of the C(1)—C(10) bond, as in the present case. Compounds **20***a*, **20***b*, **23**, and **25***a* are amongst the first members of a new subclass of C(1)-substituted, N(2)-hydroxylated 1,2,3,4-tetrahydro-β-carbolines, which promise to be of considerable synthetic potential.

We were now in a position to complete our construction of the tetracyclic eudistomin skeleton in **1** by proceeding to the closure of ring D, using the sila-Pummerer intramolecular cyclization alluded to earlier. For this it was necessary to form the corresponding sulfoxide from **25***a*. Before proceeding to this, however, we reacted **25***a* by standard methodology to obtain the *O*-trimethylsilyl analogue **25***b* (for reasons which we will return to later) in 90% yield. Treatment of the sulfide **25***a* with *m*-chloroperbenzoic acid in THF, under the conditions shown (Scheme 5), gave the sulfoxide **28***a* as a pale yellow solid, in 67% yield. Compound **28***a* displayed a strong sulfoxide band at 1007 cm^{-1} (KBr) in its IR spectrum. This vibration is at a much lower value than that usually observed for sulfoxide bands, and two possible explanations are suggested. The sulfoxide oxygen may hydrogen-bond to either the indole N—*H* or the hydroxylamine N—O—*H* group in a manner similar to that suggested to account for the low value of the amide C=O band (1632 cm^{-1}) in sulfide **25***a*. (Significantly, the C=O band in **28***a* is found at 1661 cm^{-1} (KBr)). Alternatively, the low value of the sulfoxide band in **28***a* may be a manifestation of the β-effect of the trimethylsilyl group (34), which increases the contribution of the dipolar sulfoxide resonance structure. Based upon its (400 MHz) ^1H NMR spectrum, sulfoxide **28***a* appeared to be, as expected, a mixture of diastereomers. No further purification of the diastereomeric mixture was attempted as it was not anticipated that this would pose any problems in the next step. After a number of unsuccessful cyclization attempts in hot THF, benzene, or toluene, heating a 0.02 M solution of sulfoxide **28***a* in either acetonitrile or dimethylformamide (Scheme 5) was found to give the desired N(10)-acetyleudistomin L **2** in 20% yield, after chromatography on alumina. Compound **2** could be recrystallized from benzene and has been fully characterized by IR, ^{13}C NMR and ^1H NMR (Tables 1 and 2), and mass spectral analysis. The proposed structure has further been verified by a single crystal X-ray structure determination.[5,6]

This novel ring closure is assumed to proceed via an initial (concerted or stepwise) elimination of trimethylsilanolate ion, followed by attack on the dicoordinate sulfonium ion unit in **29** by the hydroxylamino oxygen atom, as shown. Besides the hydroxylamino oxygen, there are a number of potential nucleophiles present to intercept **29**, including both the indole nitrogen and C(3) sites, the acetamide nitrogen and oxygen atoms, and the hydroxylamine nitrogen atom, as well as the DMF or acetonitrile present, any water formed by condensation of two molecules of trimethylsilanol, and trimethylsilanolate ion itself. Such alternative pathways likely occur to some extent because, as noted above, the desired cyclization product **2** is obtained in relatively low yield. The use of a solvent of high dielectric constant, to minimize ion-pair formation in **29**, appears to be essential. None of the possible side products could be identified from the complex mixture remaining after separation of **2**.

While it is not known from the above cyclization whether the free hydroxyl group in **29**, or its anion, carries out the final nucleophilic 7-*endo*-trig (35) ring closure, we reasoned that the reaction might be facilitated by the use of the sulfoxide derived from the *O*-trimethylsilylated analogue **25***b* referred to above. Desilylation *in situ* by the trimethylsilanolate ion (to form hexamethyldisiloxane) might be expected to generate the

[4]This model shows only formation of the 1*S*,10*S* enantiomer. An equal amount of the 1*R*,10*R* enantiomer is also formed because of the racemization discussed above.

[5]Crystals of (±)-N(10)-acetyleudistomin L **2** were obtained by recrystallization from benzene as slightly discolored blocks. All work was performed on an Enraf–Nonius CAD4 diffractometer (graphite monochromatized MoK$\bar{\alpha}$ radiation, λ = 0.71069 Å; hexagonal plate of overall dimensions 0.212 × 0.237 × 0.375 mm) and gave the following crystal data: $C_{16}H_{18}BrN_3O_2S \cdot \frac{1}{2}C_6H_6$, M_r = 435.4, monoclinic, space group $C2/c$ with a = 15.492(2) Å, b = 21.425(6) Å, c = 12.184(2) Å, β = 100.87(1)°, V = 3971 Å^3, D_x = 1.456 g cm^{-1} for Z = 8, μ(MoK$\bar{\alpha}$) = 21.7 cm^{-1}, F(000) = 1784, T = 298 K.

[6]Full details of the crystallographic structure will be published elsewhere.

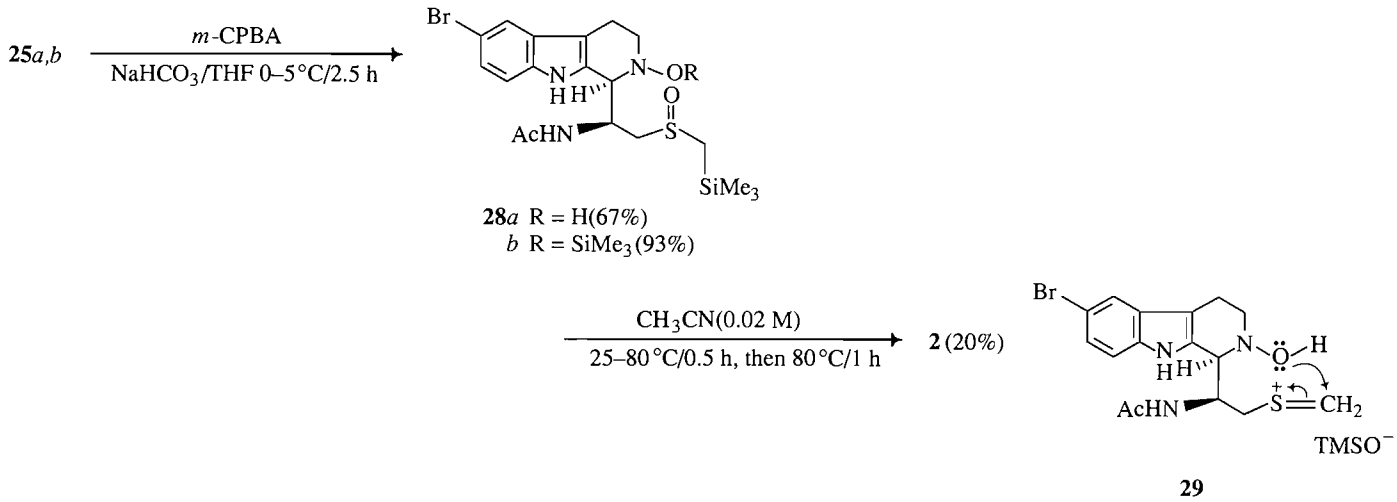

SCHEME 5

TABLE 1. ^{1}H NMR data (ppm, multiplicity, ^3J(Hz)) for compounds **25***a*, **2**, and **30**[a]

Proton	**25***a*[b]	**2**[c]	**30**[c]
H(1)	4.08 s	4.13 br s	3.92 d (10.3)
H(3)	2.97 m	3.11 td (11.0, 4.3)	2.96 td (14.0, 4.5)
H(3)	3.35 m	3.58 m	3.33 dd (13.3, 4.9)
H(4)	2.68 br s	2.88 m	2.50 dd (15.0, 4.5)
H(4)		2.76 m	3.09 td (13.0, 4.5)
H(5)	7.53 s	7.53 s	7.61 d (1.8)
H(7)	7.13 dd (8.5, 1.8)	7.17 dd (8.6, 1.8)	7.26 dd (8.7, 1.8)
H(8)	7.28 d (8.5)	7.12 d (8.6)	7.09 d (8.7)
H(10)	4.60 m	5.00 m	3.70 m
H(11)	2.44 m	2.76 m	2.67 dd (14.3, 9.5)
H(11)	2.85 dd (13.3, 5.3)	3.30 d (14.6)	3.59 br d (15.0)
H(13)	1.84 s	4.80 d (9.0)	4.95 d (15.0)
H(13)		4.94 d (9.0)	5.21 d (15.0)
$COCH_3$	1.81 s	1.73 s	2.04 s
$CSi(CH_3)_3$	0.03 s	—	—
$OSi(CH_3)_3$	—	—	0.20 s
O-H	8.29 s (exch)	—	—
N(10)-H	7.52 d	6.59 d (9.9)	6.68 br s
ind N-H	10.66 s (exch)	8.93 br (exch)	—

[a]The spectroscopic assignments in Tables 1 and 2 for these spectra recorded on a Varian XL-400 spectrometer were made on the basis of analysis of data obtained in the individual ^{13}C and ^{1}H NMR spectra, ^{1}H/^{13}C HETCOR (two-dimensional correlation spectroscopy), and homonuclear proton spin decoupling experiments. A comparison with data contained in a recent review of ^{13}C NMR data for indole alkaloids (44) also proved useful in assigning the quaternary carbon signals in **25***a*.
[b]In DMSO-d_6.
[c]In $CDCl_3$.

oxy-anion analogue of **29** and thus enable the ring closure to proceed more efficiently. Accordingly, we converted **25***b* into **28***b*, under conditions identical to those used for the formation of **28***a*, in 93% yield. This type of *in situ* generation of oxy-anions has been used recently by Eguchi and co-workers (36) and by Harpp and Gingras (37), and appeared, in our case, to have the additional advantage of avoiding the generation of water from the self-condensation of trimethylsilanol formed during the reaction of **28***a*.

After a number of unsuccessful attempts in refluxing solvents of low polarity, in which we obtained no identifiable products, heating sulfoxide **28***b* in acetonitrile at 80°C for 1 h gave the unexpected tetracyclic compound **30**, containing the 1,3-thiazepine ring shown, as the only identifiable product,[7] in 17% yield. Compound **30** was characterized by IR, ^{13}C and ^{1}H NMR (Tables 1 and 2), and mass spectral analysis. The formation of **30** may be viewed as involving initial deprotonation at the indole N—*H* by the (eliminated) trimethylsilanolate ion, followed by ring closure at the nucleophilic site so generated. A faint spot on TLC analysis indicated the presence of only a trace of the desired eudistomin **2**. It is possible that future work with an indole N-protected derivative would be instructive in

[7]The I.U.P.A.C. name for **30** is 10-acetamido-6-bromo-2-trimethylsilyloxy-1,2,3,4,10,11-hexahydro-13*H*-1,3-thiazepino[3,4,5-*l*,*m*]-β-carboline.

Can. J. Chem. Downloaded from www.nrcresearchpress.com by 91.121.58.235 on 09/07/12
For personal use only.

Can. J. Chem. Downloaded from www.nrcresearchpress.com by 91.121.58.235 on 09/07/12
For personal use only.

TABLE 2. ^{13}C NMR data (ppm) for compounds **25***a*, **2**, and **30**[a]

Carbon	**25***a*[b]	**2**[c]	**30**[c]
C(1)	65.34	68.89	64.82
C(3)	54.64	54.75	47.54
C(4)	18.98	20.54	15.96
C(4a)	108.26	108.76	109.84
C(4b)	127.89	127.88	128.51
C(5)	119.89	120.59	121.48
C(6)	111.00	112.59	112.94
C(7)	123.06	124.56	124.82
C(8)	113.01	112.95	110.22
C(8a)	135.07	135.70	134.74
C(9a)	133.80	131.84	133.14
C(10)	49.23	46.86	55.15
C(11)	37.00	32.10	37.21
C(13)	17.36	71.00	46.80
C=O	168.94	170.30	170.14
$COCH_3$	22.91	23.24	23.62
$CSi(CH_3)_3$	−1.72	—	—
$OSi(CH_3)_3$	—	—	−0.39

[a]The spectroscopic assignments in Tables 1 and 2 for these spectra recorded on a Varian XL-400 spectrometer were made on the basis of analysis of data obtained in the individual ^{13}C and ^{1}H NMR spectra, $^{1}H/^{13}C$ HETCOR (two-dimensional correlation spectroscopy), and homonuclear proton spin decoupling experiments. A comparison with data contained in a recent review of ^{13}C NMR data for indole alkaloids (44) also proved useful in assigning the quaternary carbon signals in **25***a*.

[b]In DMSO-d_6.

[c]In $CDCl_3$.

attempting to steer the ring closure in the desired direction of initial disiloxane, and subsequent oxathiazepine (eudistomin L) ring, formation.

The structure determination of the thiazepino-β-carboline **30** was essentially an exercise in determining the site of closure for the fourth ring formed in this competing sila-Pummerer reaction. The various possible sites for ring closure by nucleophilic attack on the sulfonium ion intermediate **29** have already been enumerated. The presence of IR bands at 3260 (NH) and 1646 (C=O) cm^{-1} in **30** eliminated the amide group of **28***b* as the intramolecular nucleophile. The base peak at m/z = 75 (C_2H_7OSi) in the mass spectrum indicated retention of the N—$OSiMe_3$ unit and hence ruled out six-membered ring closure involving the hydroxylamino nitrogen atom. It remained to distinguish between **30**, formed by ring closure at the indole nitrogen atom, and the spiroindolenine **31**, formed by alterna-

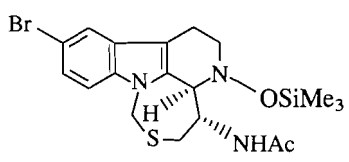

30

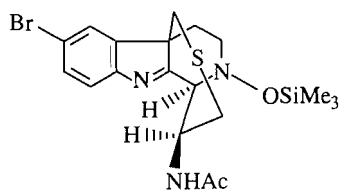

31

tive ring closure at C-3 of the indole unit. Firstly, the signal pattern for the protons on the benzene ring in the ^{1}H NMR spectrum of **30** was very similar to that found in all of our previous indoles and did not suggest an indolenine. The absence in the ^{13}C NMR spectrum of a signal for an imine carbon also tended to discount the indolenine. A third factor in allowing us to eliminate structure **31** was the observation of a fragmentation pattern in the mass spectrum of **30** which included a major (93%) *retro*-Diels–Alder reaction, clearly unlikely in the spiroindolenine **31** because of the quaternary carbon atom at the indole 3-position.

The stereochemistry at C(1) and C(10) in the earlier modified Pictet–Spengler cyclization of ring C is retained in the molecule during the alternative sila-Pummerer reaction producing **30**. However, instead of the H(1) axial – H(10) equatorial relationship found in N(10)-acetyleudistomin L **2**, compound **30** displays an H(1) axial – H(10) axial stereochemical relationship. This is because the fused 1,3-thiazepine ring has necessarily closed in the opposite direction to that for the oxathiazepine ring in the formation of **2**. These two processes require internal rotation of the substituent at C(1) in opposite directions and thus give the different relative stereochemistry observed at C(1) and C(10) as a result of this conformational change. The assignment of the H(1),H(10) *trans*-diaxial relationship in **30** is supported by the signal assigned to H(1) in the ^{1}H NMR spectrum, which appears as a doublet at δ 3.92 ppm, with a coupling constant $^{3}J_{H(1),H(10)}$ = 10.3 Hz. This should be contrasted with the signal assigned to H(1) in **2**, which appears as a broad singlet at δ 4.13 ppm, with a width at half height ($W_{1/2}$) of 5.2 Hz, indicating a small H(1),H(10) coupling constant and, therefore, according to the Karplus relationship, a *cis* relationship of H(1) and H(10). The stereochemistry of the racemic **30**, therefore, we believe to be as shown.

A number of unsuccessful attempts have been made to effect the removal of the N(10)-acetyl protecting group in **2** and to generate the free amine. Attempted ammonolysis of **2**, or hydrazinolysis in refluxing ethanol, returned largely the starting acetamide. Treatment with lithium hydroxide, potassium hydroxide, or sodium methoxide was without effect at 25°C but caused extensive decomposition of the molecule at higher temperatures (60–100°C). Interestingly, similar efforts under acidic conditions were also unsuccessful, treatment with 0.5 M hydrochloric acid in tetrahydrofuran–water (3:1) returning compound **2** even after 16 h at 50°C. This may indicate effective protection of the O,S mixed acetal functionality in the molecule by preferred protonation at the adjacent nitrogen atom. Clearly, the use of an amine protecting group that is acid-labile, in contrast to our initial concerns, is likely to prove more viable.

The preparation of N(10)-acetyleudistomin L **2** and the novel, 1,3,7-oxathiazepine ring system it contains had never been reported until recently (9, 10). Additionally, the present work represents the first successful example of a ring closure by an application of the sila-Pummerer reaction. In spite of the difficulty described in removing the *N*-acetyl protecting group, we believe the general synthetic strategy employed provides a versatile approach to the synthesis of eudistomins of this structural type and to the novel 1,3,7-oxathiazepine ring system in general. Further synthetic studies in this area and an investigation of the potentially interesting thiazepine-fused product **30** are continuing.

Experimental

Most of the intermediates and reagents used in this study were obtained from commercial suppliers and were used without further purification. 1,3-Dithiane, however, was freshly sublimed prior to use. Solutions of hydrogen peroxide (30% solution in water) and *n*-butyllithium (1.8 M and 2.5 M in hexanes) were titrated before use. Dry DMF, nitromethane, and dichloromethane were obtained by distillation from P_2O_5 and stored over 3 Å molecular sieves. Methanol was

Can. J. Chem. Downloaded from www.nrcresearchpress.com by 91.121.58.235 on 09/07/12
For personal use only.

distilled from magnesium methoxide and acetonitrile and triethylamine were distilled from calcium hydride and stored over 3 Å molecular sieves. Absolute ethanol, pyridine (Analar^R grade), and benzene (ACS grade) were used without further purification. THF, diethyl ether, and toluene were freshly distilled from sodium/benzophenone immediately before use.

The silica gel (Merck) used in flash chromatography or chromatography was grade 60, 230–400 mesh, 60 Å. The R_f values used in several chromatographic separations are taken from the corresponding analytical TLC separations on plastic sheets coated with silica gel 60 F_{254} (Merck) or aluminum sheets coated with aluminum oxide 60 F_{254} (Merck), run under the solvent conditions specified. The neutral alumina (BDH) used was deactivated by long storage (>5 years). Preparative thin-layer chromatographic plates were from Merck; silica gel code: 13792; alumina code: Typ T.

Short-path (molecular) distillations were carried out on a Kugelrohr apparatus. Melting points were determined in open-ended glass capillary tubes on an Electrothermal melting point apparatus and are uncorrected.

Infrared spectra were run as KBr pellets or neat films on NaCl discs, as indicated, on a Nicolet 5DXB Fourier transform infrared spectrometer. ^{1}H NMR spectra were routinely run at 60 MHz on a Varian EM360-L spectrometer in $CDCl_3$, DMSO-d_6, and acetone-d_6, using tetramethylsilane as internal standard, or in D_2O, using sodium 2,2-dimethyl-2-silapentane-5-sulfonate (DSS) as internal standard. Additionally, ^{13}C and 400 MHz ^{1}H NMR spectra were run on a Varian XL 400 instrument. Mass spectra were routinely run under electron impact conditions on a VG11-250S instrument at 70 eV, unless otherwise stated. Optical rotations were measured on an Optical Activity Ltd polarimeter, model AA-10, path length 2 dm. Elemental analyses were performed by the Scandinavian Microanalytical Laboratory, Box 25, DK-2730 Herlev, Denmark.

*5-Bromoindole-3-carbaldehyde, **8***

Following the procedure of Smith (15), phosphorus oxychloride (13.5 mL, 0.147 mol) was added to dry DMF (110 mL) stirring at 10°C under nitrogen, dropwise during 15 min. To the solution at 15–20°C was added 5-bromoindole **6** (21.1 g, 0.108 mol), dissolved in dry DMF (125 mL), dropwise during 15 min. The reaction mixture was warmed to 35–40°C during 1.5 h; it turned to a yellow paste and, after 2 h at 35–40°C, was cooled to 25°C during 1.5 h, poured onto crushed ice (1850 g), and allowed to warm to 25°C during 3 h, giving a clear pink solution. Sodium hydroxide (26.0 g), dissolved in water (95 mL), was added dropwise to give a yellow solution containing a white precipitate. This was quickly brought to boiling for 2 min, and allowed to stand at 25°C overnight. The beige solid was collected by filtration, washed with water (4 L), and dried to give **8** (23.45 g, 97%), mp 202–203.5°C. Compound **8** obtained in this manner was suitable for use in subsequent reactions. Recrystallization from 35% ethanol (90% recovery) gave **8**, mp 204.5–205°C (lit. (38) mp 205°C); IR (KBr) ν: 3211, 2837, 1642 cm^{-1}; ^{1}H NMR (DMSO-d_6) δ: 11.2 (br s, 1H, exch, *ind-NH*), 9.9 (s, 1H, *CHO*), 8.3 (s, 1H, *H-2*), 8.2 (m, 1H, *H-4*), 7.4 (m, 2H, *H-6*, *H-7*) ppm; MS *m/z* (%): 225 (95), 224 (80), 223 (100), 222 (85), 196 (14), 194 (15), 169 (10), 167 (9), 143 (18).

*2-(5′-Bromo-3′-indolyl)-1-nitroethene, **9***

Following the procedure of Young (39), nitromethane (110 mL) was added to the aldehyde **8** (9.20 g, 41.1 mmol) and ammonium acetate (1.05 g, 13.3 mmol) under nitrogen. The reaction mixture was refluxed (oil bath, 110–120°C) for 2 h. The dark solution was allowed to stand at 25°C overnight, forming red crystals that were collected by suction filtration. The crystals were washed with toluene (2 × 50 mL) and dried to give **9** (7.80 g, 71%), mp 196.5–198.5°C. Recrystallization from methanol (70% recovery) did not raise the melting point (lit. (14) mp 192–193.5°C); IR (KBr) ν: 3454, 1602, 1522, 1477, 1310, 1295, 1272, 1203, 1117 cm^{-1}; ^{1}H NMR (DMSO-d_6) δ: 12.0 (br s, 1H, exch, *ind-NH*), 8.4 (d, J = 14 Hz, 1H, *vinylic H*), 8.3 (s, 1H, *H-2*), 8.2 (m, 1H, *H-4*), 8.1 (d, J = 14 Hz, 1H, *vinylic H*), 7.3 (m, 2H, *H-6*, *H-7*) ppm; MS *m/z* (%): 268 (90), 266 (95), 221 (60), 219 (55), 141 (100).

*5-Bromotryptamine, **10***

Following a general procedure by Ho *et al.* (14), dry THF (25 mL) was added to lithium aluminum hydride (1.00 g, 26.6 mmol) under nitrogen at 0–5°C dropwise, to give a grey slurry, followed by the nitroolefin **9** (1.25 g, 4.68 mmol), dissolved in dry THF (20 mL), during 20 min. The reaction mixture was refluxed for 4 h and stirred at 25°C for a further 18 h, before adding cold water (30 mL) dropwise at 0–5°C, followed by diethyl ether (50 mL). Filtration through Celite was followed by extraction of the aqueous layer with ether. The combined extracts were washed with 2 M HCl (3 × 40 mL). The combined aqueous extracts were rewashed with ether (2 × 25 mL), basified with concentrated NaOH, and extracted thoroughly with ether (3 × 40 mL). The ether layer was dried (Na_2SO_4) and concentrated to give **10** (0.93 g, 83%) as an amber oil. IR (CH_2Cl_2) ν: 3469, 3375, 3140, 3055, 2936, 2863, 1610, 1590, 1568, 1460, 1420, 1095 cm^{-1}; ^{1}H NMR ($CDCl_3$) δ: 9.8 (br s, 1H, exch, *ind-NH*), 7.7 (d, J = 1.5 Hz, 1H, *H-4*), 7.2 (m, 2H, *H-7*, *H-8*), 6.9 (s, 1H, *H-2*), 3.0 (m, 4H, -CH_2CH_2-), 1.7 (br s, 2H, exch, NH_2) ppm; ^{13}C NMR (DMSO-d_6)[8] δ: 22.8 (*ind-CH_2*), 39.3 (*CH_2-N*), 109.5 (*C-3*), 111.2 (*C-5*), 113.6 (*C-7*), 120.5 (*C-4*), 123.6 (*C-6*), 125.2 (*C-2*), 128.8 (*C-3a*), 135.0 (*C-7a*) ppm; MS *m/z* (%): 240 (15), 238 (15), 211 (60), 210 (60), 209 (60), 208 (60), 130 (25), 129 (35).

*2-(5′-Bromo-3′-indolyl)-1-nitroethane, **11***

To the nitroolefin **9** (4.6 g, 17.2 mmol) dissolved in dry THF (80 mL) and methanol (10.3 mL) was added, portionwise during 10 min, sodium borohydride (0.92 g, 24.3 mmol). On being stirred at 25°C for 1 h, the reaction mixture foamed and became lighter in colour. Cold water (170 mL) and cold 1 M HCl (50 mL) were added and the THF and methanol were evaporated at a bath temperature of 30–35°C. The dark-brown, oily residue was taken into dichloromethane (100 mL), the aqueous layer was extracted with dichloromethane (2 × 25 mL), the combined organic layers were washed (5% $NaHCO_3$ aq., saturated NaCl), dried (Na_2SO_4), and concentrated to give **11** (4.62 g, 100%), as a dark-brown, thick oil. Column chromatography on silica gel, eluting with dichloromethane, gave **11** (3.65 g, 79%) (R_f 0.40) as a beige solid. Recrystallization from hexanes–chloroform (3:1) (78% recovery) gave pure **11** (2.83 g) as golden yellow needles, mp 91–92.5°C. (Concentration of the mother liquor gave **11** (0.80 g), which, combined with similar concentrates from other preparations and rechromatographed, gave **11** suitable for use in subsequent reactions.) IR (KBr) ν: 3411, 3133, 2968, 1551, 1543, 1385, 1095, 801 cm^{-1}; ^{1}H NMR ($CDCl_3$) δ: 8.1 (br s, 1H, *ind-NH*), 7.6 (s, 1H, *H-4*), 7.2 (s, 2H, *H-6*, *H-7*), 6.9 (d, J = 3 Hz, 1H, *H-2*), 4.6 (t, J = 7 Hz, 2H, *CH_2NO_2*), 3.3 (t, J = 7 Hz, 2H, *ind-CH_2*) ppm; MS *m/z* (%): 270 (50), 268 (50), 224 (35), 223 (80), 222 (35), 221 (80), 210 (20), 208 (20), 143 (100). Anal. calcd. for $C_{10}H_9BrN_3O_2$: C 44.63, H 3.37, Br 29.70, N 10.41; found: C 44.59, H 3.40, Br 29.87, N 10.30.

*5-Bromo-N′-hydroxytryptamine, **4***

Method A: Following a procedure similar to that reported by Fieser and Fieser (40) for the preparation of aluminum amalgam, and by Shin *et al.* (41) for the aluminum amalgam reduction of saturated nitro compounds to hydroxylamines, aluminum powder (0.52 g, 19.3 mmol), washed with 1 M NaOH (50 mL), then with water (25 mL), swirled in 0.5% $HgCl_2$ (90 mL) for 1.25 min, and washed successively with water (30 mL), 95% ethanol (30 mL), and diethyl ether (2 × 25 mL), was covered with ether (15 mL), under nitrogen. The saturated nitro compound **11** (0.60 g, 2.23 mmol) in ether (30 mL) was added dropwise during 0.5 h. Water (2 × 5 drops) was added, effervesence was observed at the metal surface, and the reaction mixture was stirred at 25°C for 2.5 h with water (25 drops total) added periodically. Ether (50 mL) was added, the solids removed by suction filtration through Celite and washed with ether (2 × 25 mL), and the combined organic extracts washed with saturated NaCl (75 mL), dried (Na_2SO_4), and concentrated to give **4** (0.45 g, 79%) as a light yellow oil. The IR and NMR spectra of **4** prepared in this manner were essentially identical to those obtained using Method B (see below).

[8]This spectrum was recorded for the hydrochloride salt.

Can. J. Chem. Downloaded from www.nrcresearchpress.com by 91.121.58.235 on 09/07/12
For personal use only.

Method B: Following a procedure by Corey and Estreicher (42), zinc dust (0.36 g, 5.51 mmol) was washed with 17.5% ammonium chloride solution (10 mL) for 1–2 min and with water (2 × 10 mL), and was added to the saturated nitro compound **11** (0.25 g, 0.93 mmol), dissolved in THF (10 mL) and water (5 mL) containing ammonium chloride (0.10 g, 1.87 mmol), under nitrogen. Unwashed zinc dust (0.10 g, 1.53 mmol) was added and the reaction mixture stirred at 25°C for 2.5 h. Diethyl ether (50 mL) was added, the solids were removed by filtration through Celite and washed with ether (2 × 25 mL), and the clear, colourless filtrate concentrated. The residue was dissolved in dichloromethane (50 mL), washed with saturated NaCl (25 mL), dried (Na_2SO_4), and concentrated to give **4** (0.22 g, 93%), as a pale beige, resinous material. Compound **4** obtained in this manner was used in subsequent reactions without further purification. IR (film) ν: 3428, 3264, 2921, 2858, 1617, 1566, 1460, 1422, 1266, 1097, 1051, 883, 793 cm^{-1}; ^1H NMR ($CDCl_3$) δ: 8.2 (br s, 1H exch, *ind-NH*), 7.7 (s, 1H, *H-4*), 7.2 (m, 2H, *H-6*, *H-7*), 6.9 (m, 1H, *H-2*), 5.5 (br s, 2H, exch, *NHOH*), 3.1 (m, 4H, CH_2CH_2) ppm; ^{13}C NMR (DMSO-d_6)[9] δ: 23.0 (*ind-*CH_2), 51.9 (CH_2-*N*), 109.5 (*C-3*), 111.1 (*C-5*), 113.5 (*C-7*), 120.5 (*C-4*), 123.5 (*C-6*), 125.0 (*C-2*), 128.9 (*C-3a*), 135.0 (*C-7a*) ppm; MS *m/z* (%): 256 (6), 254 (11), 252 (6), 240 (14), 238 (25), 236 (19), 234 (9), 211 (87), 210 (100), 209 (90), 208 (93), 129 (50); MS (CI) *m/z* (%): 266 (22), 264 (28), 257 (22), 255 (30), 241 (83), 240 (26), 239 (100), 238 (100), 237 (17), 224 (66), 222 (67), 211 (31), 210 (32), 209 (32), 208 (25).

L-Cysteine methyl ester hydrochloride, 12

L-Cysteine (18.3 g, 0.151 mol) was slurried in dry methanol (350 mL) and hydrogen chloride was bubbled into the reaction mixture for 5 min at 25°C, accompanied by periodic cooling (ice bath). The reaction mixture was stirred at 25°C for 21 h, before concentrating to a volume of 100 mL. Diethyl ether (250–300 mL) and isopropyl alcohol (25–50 mL) were added and a white precipitate began to form. After standing overnight at 25°C, the white solid was collected by filtration, washed with isopropyl alcohol (2 × 25 mL) and ether (2 × 50 mL), and dried to give **12** (18.80 g, 73%), mp 134–138°C (lit. (23) mp 143°C); $[\alpha]_D^{25}$ −2.5° (*c* 10.0, MeOH) (lit. (23) $[\alpha]_D^{32}$ −3.0° (*c* 10, MeOH)). Storage of the filtrate at −15°C for 24 h gave a second crop of **12** (2.88 g, 11%), mp 136–139°C; IR (KBr) ν: 2990, 2843, 2642, 1747 cm^{-1}; ^1H NMR (D_2O) δ: 4.2 (t, *J* = 5 Hz, 1H, *CH*), 3.6 (s, 3H, CH_3), 2.9 (d, *J* = 5 Hz, 2H, CH_2) ppm.

L-Cysteine methyl ester, 12a

The hydrochloride **12** (11.2 g, 0.0653 mol) was dissolved in water (85 mL) containing sodium bicarbonate (9.70 g, 0.115 mol). The solution was saturated with sodium chloride and extracted thoroughly with dichloromethane. The combined organic extracts were washed (saturated NaCl), dried (Na_2SO_4), and concentrated to give the free base, **12***a* (7.50 g, 85%), as a slightly purple-tinged oil. IR (film) ν: 3380, 3311, 3000, 2954, 2846, 2568, 1738 cm^{-1}; ^1H NMR ($CDCl_3$) δ: 3.8 (s, 3H, CH_3), 3.7 (t, *J* = 5 Hz, 1H, *CH*), 2.8 (d, *J* = 5 Hz, 2H, CH_2), 1.8 (br s, 3H, exch, NH_2, *SH*) ppm.

S-*(Trimethylsilylmethyl)-L-cysteine methyl ester, 13*

To the free base **12***a* (7.45 g, 0.0551 mol), dissolved in dry DMF (250 mL) under nitrogen, was added potassium carbonate (15.9 g, 0.115 mol) and chloromethyltrimethylsilane (10.0 mL, 0.0688 mol) and the reaction mixture was stirred at 25°C for 16 h. The pale yellow, cloudy reaction mixture was concentrated *in vacuo* (bath temperature 40°C) and the orange paste so obtained was partitioned between water (200 mL) and diethyl ether (250 mL). The aqueous layer was extracted with ether (2 × 50 mL) and the combined ether extracts washed (saturated NaCl) and concentrated. The residual oil was taken into dichloromethane (125 mL), washed (saturated NaCl), dried (Na_2SO_4), and concentrated to give a yellow oil. Kugelrohr distillation gave **13** (9.52 g, 78%), bath temperature 120–125°C/0.20 Torr (1 Torr = 133.3 Pa), $[\alpha]_D^{25}$ +16.5° (*c* 7.0, CH_2Cl_2), as a colorless, mobile liquid. IR (film) ν: 3380, 3311, 2956, 2895, 1738, 1679, 1248, 844 cm^{-1}; ^1H NMR ($CDCl_3$) δ: 3.7 (s, 3H, CH_3), 3.6 (m, 1H, *CH*), 2.8 (m, 2H, CH_2S), 1.8 (s, 2H, SCH_2Si), 1.7 (br s, 2H, exch, NH_2), 0.1 (s, 9H, $Si(CH_3)_3$) ppm. Compound **13** was used in subsequent reactions immediately after distillation, as storage at room temperature for several hours caused considerable darkening.

N-*Acetyl-S-(trimethylsilylmethyl)-L-cysteine methyl ester, 14*

To the free base **13** (9.52 g, 0.0430 mol) in dry dichloromethane (350 mL) were added triethylamine (28.0 mL, 0.201 mol) and acetic anhydride (7.5 mL, 0.0795 mol) and the reaction mixture was stirred under nitrogen at 25°C for 22 h. The beige mixture was diluted with dichloromethane (50 mL), washed with water (100 mL), 1 M HCl (2 × 100 mL), 10% $NaHCO_3$ solution (2 × 50 mL), water (100 mL), and saturated NaCl (100 mL), dried (Na_2SO_4), and concentrated to give a thick oil. Kugelrohr distillation gave **14** (10.69 g, 94%), bath temperature 180–190°C/0.20 Torr, $[\alpha]_D^{25}$ +35.0° (*c* 5.0, toluene), as a beige-tinged oil. IR (film) ν: 3286, 3065, 2954, 2898, 2847, 1749, 1658, 1250, 848 cm^{-1}; ^1H NMR ($CDCl_3$) δ: 6.4 (br d, 1H, *NH*), 4.8 (m, 1H, *CH*), 3.7 (s, 3H, OCH_3), 3.0 (d, *J* = 6 Hz, 2H, CH_2S), 2.1 (s, 3H, $COCH_3$), 1.8 (s, 2H, SCH_2Si), 0.1 (s, 9H, $Si(CH_3)_3$) ppm; MS *m/z* (%): 263 (12), 217 (19), 216 (14), 204 (48), 173 (21), 158 (33), 133 (28), 100 (62), 73 (100); HRMS observed: 263.1006; calcd. for $C_{10}H_{21}NO_3SSi$: 263.1011. Anal. calcd. for $C_{10}H_{21}NO_3SSi$: C 45.59, H 8.04, N 5.32, S 12.17; found: C 45.34, H 8.03, N 5.47, S 12.22.

N-*Acetyl-S-(trimethylsilylmethyl)-L-cysteine aldehyde, 5*

To compound **14** (2.15 g, 8.13 mmol), dissolved in dry toluene (81 mL) under nitrogen, was added a 1.0 M solution of diisobutylaluminum hydride in toluene (21.0 mL, 0.021 mol) at −60°C during 20 min. Some effervesence was observed and the colorless reaction mixture was stirred at −60°C for 2.5 h. Methanol (2.2 mL), followed by sodium potassium tartrate (22 g) dissolved in water (100 mL), was added dropwise at −60°C and the reaction mixture was allowed to warm to room temperature. Diethyl ether (100 mL) was added, the organic layer was separated, the aqueous layer extracted with ether (100 mL), and the combined organic extracts washed (saturated NaCl), dried (Na_2SO_4), and concentrated to give a yellow, very viscous oil. Flash chromatography on silica gel, eluting with dichloromethane – ethyl acetate (1:1), gave **5** (1.04 g, 55%) (R_f 0.25), as a clear oil; IR (film) ν: 3286, 3065, 2957, 2897, 2825, 2727, 1736, 1654, 1249, 847 cm^{-1}; ^1H NMR ($CDCl_3$) δ: 9.6 (s, 1H, *CHO*), 6.4 (br s, 1H, *NH*), 4.7 (m, 1H, *CH*), 3.0 (d, *J* = 6 Hz, 2H, CH_2S), 2.1 (s, 3H, $COCH_3$), 1.8 (s, 2H, SCH_2Si), 0.1 (s, 9H, $Si(CH_3)_3$) ppm; MS *m/z* (%): 233 (5), 204 (16), 174 (40), 173 (28), 159 (37), 158 (55), 133 (52), 105 (41), 73 (100). Compound **5** was normally used in the subsequent reactions in the crude form, without purification, immediately after preparation.

6-Bromo-1,2,3,4-tetrahydro-β-carboline, 17

5-Bromotryptamine (**10**) hydrochloride (1.43 g, 5.19 mmol) in water (19.0 mL) was heated at 90°C (water bath). Glyoxylic acid monohydrate (0.52 g, 5.62 mmol) in water (1.0 mL) was added dropwise during 1 min, and the reaction mixture was adjusted to pH 3.5 by the addition of KOH (0.31 g, 5.52 mmol) in water (1.5 mL) and several drops of concentrated HCl. A beige precipitate formed, the reaction mixture was stirred at 25°C for 2 h, and a green-beige solid was collected by filtration and washed with water (2 × 5 mL). The solid was resuspended in water (10 mL) containing concentrated HCl (1.5 mL) and brought to the boil. Concentrated HCl (1.5 mL) was added; the reaction mixture was boiled for 0.5 h and then allowed to cool to room temperature. A grey solid was collected by filtration and washed with water (2 × 5 mL). The solid was resuspended in water (10 mL) and the mixture was adjusted to pH 12 with a concentrated solution of KOH. After 1 h at 40°C, a beige solid was collected by filtration, washed with water (3 × 5 mL) and dried to give crude **17** (0.92 g, 71%), mp 225–227°C. Recrystallization from methanol (65% recovery, 2 crops) gave **17**, mp 234–237°C; IR (KBr) ν: 3444, 3302, 3131, 3027, 2909, 2840, 2727, 1436, 798 cm^{-1}; ^1H NMR (DMSO-d_6) δ: 11.0 (s, 1H, exch, *ind-NH*), 7.6 (m, 1H, *H-5*), 7.2 (m, 2H, *H-7*, *H-8*), 3.9 (s, 2H, *H-1*), 3.2 (m, 3H, N(2)-H, exch, *H-3*),

[9]This spectrum was recorded for the hydrogen oxalate salt.

Can. J. Chem. Downloaded from www.nrcresearchpress.com by 91.121.58.235 on 09/07/12
For personal use only.

2.6 (m, 2H, *H-4*) ppm; MS *m/z* (%): 252 (25), 251 (10), 250 (30), 249 (10), 223 (95), 222 (10), 221 (100), 220 (15). Anal. calcd. for $C_{11}H_{11}BrN_2$: C 52.61, H 4.42, Br 31.82, N 11.16; found: C 52.79, H 4.63, Br 31.65, N 11.06.

6-Bromo-3,4-dihydro-β-carboline 2-oxide, ***18***

Following the procedure of Murahashi and co-workers (28), to compound **17** (0.46 g, 1.83 mmol), dissolved in 95% ethanol (46 mL) at 0–5°C, was rapidly added sodium tungstate dihydrate (0.05 g, 0.152 mmol). A 30% aqueous solution of hydrogen peroxide (0.65 mL, 5.73 mmol) in 95% ethanol was added dropwise during 15 min and the reaction mixture was stirred at 0–5°C for 1.5 h. Water (20 mL) was added, the reaction mixture stirred at 25°C for 2 h, dichloromethane (100 mL) was added, and the organic layer washed (dilute $NaHSO_3$ (2 × 25 mL), saturated NaCl (50 mL)), and concentrated. Column chromatography on neutral alumina, eluting with dichloromethane–methanol (85:15), gave **18** (0.08 g, 17%), as a beige amorphous solid that was not recrystallized. ^{1}H NMR (DMSO-d_6) δ: 11.4 (br s, 1H, exch, *ind-NH*), 7.8 (s, 1H, *H-1*), 7.7 (m, 1H, *H-5*), 7.3 (m, 2H, *H-7, H-8*), 4.2 (t, *J* = 8 Hz, 2H, *H-3*), 3.2 (t, *J* = 8 Hz, 2H, *H-4*) ppm.

N-*[2′-(5″-Bromo-3″-indolyl)ethyl]-2-propanimine* N-*oxide,* ***19****a*

Acetone (7 mL) was added to a solution of **4** (0.275 g, 1.1 mmol) in dry dichloromethane (16 mL). The reaction mixture was stirred in the presence of silica gel for 3 h, during which time the colour went from light yellow to deep brown. After removal of the solvent the residue was dissolved in dichloromethane and the resulting solution washed (5% $NaHCO_3$, saturated NaCl), dried (Na_2SO_4), and concentrated to give 0.29 g of material. Chromatography on a preparative TLC plate using CH_2Cl_2:MeOH = 9:1 gave **19***a* (0.26 g, 80%), mp 65–70°C, used in the subsequent reaction without further purification. ^{1}H NMR ($CDCl_3$) δ: 9.3 (s, 1H, exch, *NH*), 7.7 (s, 1H, *H-4″*), 7.3 (s, 2H, *H-6″, H-7″*), 7.0 (d, 1H, *H-2″*), 4.1 (t, 2H, *H-1′*), 3.3 (t, 2H, *H-2′*), 2.2 (s, 3H, CH_3), 1.7 (s, 3H, CH_3) ppm; MS *m/z* (%): 296 (4), 278 (16), 223 (65), 209 (40), 70 (100).

N-*[2′-(5″-Bromo-3″-indolyl)ethyl] acetaldimine* N-*oxide,* ***19****b*

To **4** (1.28 g, 5.02 mmol) in dry dichloromethane (115 mL), under nitrogen and cooled to 0–5°C, was added acetaldehyde (1.0 mL, 17.7 mmol) and anhydrous magnesium sulfate (5.15 g, 42.8 mmol). The reaction mixture was stirred for 8 h and allowed to warm to 25°C during 1 h. The pink-tinged reaction mixture was filtered and concentrated to give a beige solid. Column chromatography on neutral alumina, eluting with dichloromethane–methanol (96:4), gave **19***b* (0.65 g, 46%) (R_f 0.50), as a beige foam, mp 60–70°C; IR (KBr) *ν*: 3553, 3483, 3417, 3239, 2925, 1618, 1457, 1385, 1166, 1103 cm^{-1}; ^{1}H NMR ($CDCl_3$) δ: 9.4 (br s, 1H, *ind-NH*), 7.8 (s, 1H, *H-4″*), 7.3 (m, 2H, *H-6″, H-7″*), 7.1 (d, *J* = 2 Hz, 1H, *H-2″*), 6.6 (q, *J* = 6 Hz, 1H, *HC*=*N*), 4.1 (t, *J* = 7 Hz, 2H, *H-1′*), 3.4 (t, *J* = 7 Hz, 2H, *H-2′*), 1.9 (d, *J* = 6 Hz, 3H, CH_3) ppm; MS *m/z* (%): 223 (90), 221 (100), 210 (18), 208 (17). Compound **19***b* could be used in subsequent reactions without prior chromatographic purification.

6-Bromo-1,1-dimethyl-2-hydroxy-1,2,3,4-tetrahydro-β-carboline, ***20****a*

The nitrone **19***a* (0.07 g, 2.3 mmol) was stirred briefly in a solution of CH_2Cl_2 (10 mL) with trifluoroacetic acid (0.5 mL) and the solution was refluxed for 6 h. Solvent was evaporated and the residue (0.06 g) taken up in CH_2Cl_2. The CH_2Cl_2 solution was washed (5% $NaHCO_3$), dried (Na_2SO_4), and concentrated to give 0.04 g of residue. Recrystallization ($CHCl_3$/*n*-hexane) gave 10 mg (15%) of **20***a*, mp 158–160°C; ^{1}H NMR ($CDCl_3$) δ: 7.8 (s, 1H, exch, *N-H*), 7.5 (s, 1H, *H-5*), 7.2 (s, 2H, *H-7, H-8*), 3.2 (t, 2H, *H-3*), 2.7 (t, 2H, *H-4*), 1.5 (s, 6H, CH_3) ppm.

6-Bromo-2-hydroxy-1-methyl-1,2,3,4-tetrahydro-β-carboline, ***20****b*

To the chromatographed nitrone **19***b* (0.10 g, 0.36 mmol) in dry dichloromethane (10 mL), under nitrogen at 25°C, was added trifluoroacetic acid (0.3 mL, 0.40 mmol). The reaction mixture darkened and was stirred at 25°C for 20 h. Dichloromethane (25 mL) was added and the reaction mixture washed (5% $NaHCO_3$ solution (2 × 25 mL), saturated NaCl (25 mL)), dried (Na_2SO_4), and concentrated to give crude **20***b* (0.09 g, 90%), as a beige solid, mp 175–180°C. Compound **20***b* could not be further purified. (Later preparations gave **20***b*, mp 190–193°C.) IR (KBr) *ν*: 3551, 3413, 3346, 3237, 2974, 2921, 2901, 2848, 2826, 1639, 1616, 1440, 1305 cm^{-1}; ^{1}H NMR (acetone-d_6)[10] δ: 10.4 (br s, 1H, exch, *ind-NH*), 7.6 (s, 1H, *H-5*), 7.5 (br s, 1H, exch, *N-OH*), 7.4 (m, 2H, *H-7, H-8*), 4.2 (q, *J* = 7 Hz, 1H, *H-1*), 3.0 (m, 4H, *H-3, H-4*), 1.6 (d, *J* = 7 Hz, 3H, CH_3) ppm; MS *m/z* (%): 282 (27), 280 (29), 265 (16), 264 (19), 263 (19), 262 (24), 261 (15), 260 (14), 237 (95), 235 (100); HRMS observed: 280.0204, 282.0206; calcd. for $C_{12}H_{13}BrN_2O$: 280.0197, 282.0221.

6-Bromo-1-methyl-2-trimethylsilyloxy-1,2,3,4-tetrahydro-β-carboline, ***24****a*

To crude **20***b* (0.27 g, 0.96 mmol) in dry dichloromethane (48 mL) under nitrogen at 0–5°C was added *N*-(trimethylsilyl)imidazole (0.20 mL, 1.36 mmol) at once, and the reaction mixture was stirred at 0–5°C for 1.5 h. The ice-bath was removed, dichloromethane (50 mL) was added, and the amber-coloured reaction mixture was washed (water (3 × 75 mL), saturated NaCl (50 mL)), dried (Na_2SO_4), and concentrated to give a brown solid. Flash chromatography on silica gel, eluting with dichloromethane–acetone (96:4), gave **24***a* (0.08 g, 24%) (R_f 0.40) as a colourless glassy solid, mp 47–67°C; IR (KBr) *ν*: 3420, 3322, 2962, 2933, 2905, 2846, 1439, 1250, 842 cm^{-1}; ^{1}H NMR ($CDCl_3$) δ: 7.7 (br s, 1H, *ind-NH*), 7.5 (s, 1H, *H-5*), 7.1 (m, 2H, *H-7, H-8*), 3.9 (br q, 1H, *H-1*), 3.2 (m, 2H, *H-3*), 2.8 (m, 2H, *H-4*), 1.4 (d, *J* = 7 Hz, 3H, CH_3), 0.2 (s, 9H, $Si(CH_3)_3$) ppm; MS *m/z* (%): 354 (37), 352 (34), 339 (33), 337 (32), 238 (16), 237 (100), 236 (35), 235 (98), 234 (20), 75 (20), 73 (28).

2-Acetoxy-6-bromo-1-methyl-1,2,3,4-tetrahydro-β-carboline, ***24****b*

To compound **20***b* (0.10 g, 0.36 mmol), slurried in dry dichloromethane (7 mL) under nitrogen at 25°C, was added triethylamine (0.25 mL, 1.88 mmol). Acetic anhydride (0.05 mL, 0.53 mmol) was added and the reaction mixture stirred at 25°C for 5 h. Dichloromethane (50 mL) was added and the organic phase was washed (water (4 × 50 mL), saturated NaCl (50 mL)), dried (Na_2SO_4), and concentrated to give a brown oil. Column chromatography on silica gel, eluting with dichloromethane–acetone (90:10), gave **24***b* (0.06 g, 55%) (R_f 0.25) as a beige solid, mp 151–153°C. Recrystallization from ethyl acetate – hexane (1:1) gave **24***b* as beige crystals, mp 155–156.5°C; IR (KBr) *ν*: 3370, 3068, 2968, 2920, 2844, 1732, 1242, 1009 cm^{-1}; ^{1}H NMR ($CDCl_3$–acetone-d_6) δ: 9.1 (br s, 1H, *ind-NH*), 7.6 (d, *J* = 2 Hz, 1H, *H-5*), 7.2 (s, 2H, *H-7, H-8*), 4.4 (q, *J* = 7 Hz, 1H, *H-1*), 3.5 (m, 2H, *H-3*), 2.8 (t, *J* = 7 Hz, 2H, *H-4*), 2.1 (s, 3H, $COCH_3$), 1.5 (d, *J* = 7 Hz, 3H, CH_3) ppm; HRMS observed: 322.0310, 324.0294; calcd. for $C_{14}H_{15}BrN_2O_2$: 322.0304, 324.0292.

2-Methyl-1,3-dithiane-2-carbaldehyde, ***21***

This was prepared by the procedure of Seebach (29) from 2-methyl-1,3-dithiane, in turn prepared by methylation of 1,3-dithiane (29). Kugelrohr distillation gave **21** (2.30 g, 60%), bath temperature 140–150°C/7.0 Torr (lit. (29) bp 60°C/0.06 Torr), as a pale yellow liquid; IR (film) *ν*: 2962, 2924, 2865, 2814, 2702, 1717 cm^{-1}; ^{1}H NMR ($CDCl_3$) δ: 9.0 (s, 1H, *CHO*), 3.2–1.8 (complex m, 6H, *H-4, H-5, H-6*), 1.5 (s, 3H, CH_3) ppm.

N-*[2′-(5″-bromo-3″-indolyl)ethyl]-2-methyl-1,3-dithiane-2-carbaldimine* N-*oxide,* ***22***

To 5-bromo-*N′*-hydroxytryptamine **4** (0.50 g, 1.96 mmol) in dry dichloromethane (40 mL) under nitrogen and at 0–5°C, was added **21** (0.40 g, 2.46 mmol), in dry dichloromethane (20 mL), followed by anhydrous magnesium sulfate (1.90 g, 15.8 mmol). The reaction mixture was stirred at 0–5°C for 8 h and allowed to warm to 25°C during 1 h before filtering and concentrating to give a white solid. Column chromatography on neutral alumina, eluting with dichloromethane–methanol (97.5:2.5), gave **22** (0.65 g, 83%) (R_f 0.50). Recrystallization from dichloromethane gave white, granular crystals, mp 182–184°C; IR (KBr) *ν*: 3230, 3081, 2935, 2901, 2825, 1584,

[10]Compound **20***b* was not very soluble in this solvent, hindering complete interpretation of the spectrum.

Can. J. Chem. Downloaded from www.nrcresearchpress.com by 91.121.58.235 on 09/07/12
For personal use only.

1459, 1420, 1173, 1146, 879, 799 cm^{-1}; ^1H NMR ($CDCl_3$) δ: 9.1 (br s, 1H, *ind-NH*), 7.7 (s, 1H, *H-4″*), 7.3 (s, 2H, *H-6″*, *H-7″*), 7.0 (br d, 1H, *H-2″*), 6.7 (s, 1H, *HC=N*), 4.1 (t, *J* = 7 Hz, 2H, *H-1′*), 3.3 (t, *J* = 7 Hz, 2H, *H-2′*), 3.0–2.4 (m, 6H, *H-4*, *H-5*, *H-6*), 1.8 (s, 3H, CH_3) ppm; MS *m/z* (%): 400 (4), 398 (4), 384 (4), 382 (8), 380 (4), 223 (100), 221 (99), 210 (78), 208 (80), 133 (96), 59 (36). Anal. calcd. for $C_{16}H_{19}BrN_2OS_2$: C 48.12, H 4.80, Br 20.01, N 7.01, S 16.01; found: C 48.11, H 4.90, Br 20.21, N 7.00, S 16.01.

6-Bromo-2-hydroxy-1-(2′-methyl-1′,3′-dithian-2′-yl)-1,2,3,4-tetrahydro-β-carboline, ***23***

To the nitrone **22** (0.32 g, 0.80 mmol), in dry dichloromethane (50 mL) under nitrogen at 25°C, was added trifluoroacetic acid (0.14 mL, 1.88 mmol) and the reaction mixture was stirred for 18 h. Dichloromethane (50 mL) was added and the yellow reaction mixture washed (5% $NaHCO_3$ solution (2 × 75 mL), saturated NaCl), dried (Na_2SO_4), and concentrated to give a beige solid. Column chromatography on neutral alumina, eluting with dichloromethane–methanol (99:1), gave **23** (0.16 g, 50%) (R_f 0.70) as a white solid, mp 75–90°C; IR (KBr) *ν*: 3403, 2957, 2913, 2845, 1637, 1618, 1460 cm^{-1}; ^1H NMR ($CDCl_3$) δ: 9.4 (br s, 1H, *ind-NH*), 7.6 (s, 1H, *H-5*), 7.2 (s, 2H, *H-7*, *H-8*), 6.9 (br s, 1H, *N-OH*), 4.7 (s, 1H, *H-1*), 3.7–2.6 (br m, 8H, *H-3*, *H-4*, *H-4′*, *H-6′*), 2.2 (m, 2H, *H-5′*), 1.3 (s, 3H, CH_3) ppm; ^{13}C NMR ($CDCl_3$) δ: 19.2 (*C-4*), 24.0 (CH_3), 26.8 (*C-4′*, *C-6′*), 27.7 (*C-5′*), 52.3 (*C-3*), 55.0 (*C-2′*), 67.7 (*C-1*), 111.2 (*C-4a*), 112.5 (*C-8*), 112.6 (*C-6*), 120.8 (*C-5*), 124.6 (*C-7*), 128.3 (*C-4b*), 131.6 (*C-9a*), 134.4 (*C-8a*) ppm; MS *m/z* (%): 400 (2), 398 (2), 384 (4), 383 (9), 382 (8), 381 (8), 380 (5), 349 (18), 347 (18), 309 (13), 307 (17), 267 (77), 265 (76), 251 (60), 250 (59), 249 (96), 248 (62), 247 (64), 245 (24), 133 (100).

1-[1′-Acetamido-2′-(trimethylsilylmethylthio)ethyl]-6-bromo-2-hydroxy-1,2,3,4-tetrahydro-β-carboline, ***25***a

To 5-bromo-*N′*-hydroxytryptamine **4** (1.90 g, 7.45 mmol) in dry dichloromethane (175 mL) under nitrogen at 0–5°C was added *N*-acetyl-*S*-(trimethylsilylmethyl)-L-cysteine aldehyde **5** (2.80 g, 12.0 mmol), in dry dichloromethane (175 mL), followed by anhydrous magnesium sulfate (12.5 g, 104 mmol). The light yellow mixture was stirred at 0–5°C for 8 h and allowed to warm to 25°C during 1 h, before filtering and concentrating to give the intermediate nitrone (3.87 g) as a fluffy yellow solid. IR (KBr) *ν*: 3275, 3080, 2956, 2923, 2896, 1655, 1248, 847 cm^{-1}; ^1H NMR ($CDCl_3$) δ: 9.3 (br s, 1H, *ind-NH*), 7.7 (s, 1H, *H-4″*), 7.3 (m, 3H, *H-6″*, *H-7″*, *NH-Ac*), 7.0 (br d, 1H, *H-2″*), 6.6 (d, *J* = 6 Hz, 1H, *H—C=N*), 4.7 (m, 1H, *H-2*), 3.9 (br t, *J* = 7 Hz, 2H, CH_2-N^+), 3.3–2.5 (m, 4H, *ind-*CH_2, CH_2S), 2.1–1.7 (m, 5H, SCH_2Si, CH_3), 0.1 (s, 9H, $Si(CH_3)_3$) ppm; MS *m/z* (%): 471 (2), 469 (2), 454 (9), 452 (9), 335 (44), 334 (100), 333 (52), 332 (89), 224 (71), 223 (56), 222 (72), 221 (50), 211 (31), 210 (96), 209 (37), 208 (96), 143 (59), 73 (87).

To the crude nitrone, (3.87 g, 8.23 mmol) in dry dichloromethane (350 mL) under nitrogen was added trifluoroacetic acid (2.40 mL, 32.3 mmol), and the reaction mixture was stirred at 25°C for 20 h. The dark brown reaction mixture was washed (5% $NaHCO_3$ (2 × 125 mL), saturated NaCl (100 mL)), dried (Na_2SO_4), and concentrated to give a beige solid. Recrystallization from ethyl acetate gave **25***a* (0.86 g, 25%, based on **4**), as a beige amorphous solid, mp 214–216°C; IR (KBr) *ν*: 3546, 3469, 3414, 3328, 3092, 2954, 2922, 2847, 1632, 1542, 1250, 854 cm^{-1}; ^1H NMR (DMSO-d_6):[11] see Table 1; ^{13}C NMR (DMSO-d_6):[11] see Table 2; MS *m/z* (%): 471 (2), 469 (2), 454 (16), 452 (15), 368 (12), 366 (14), 335 (10), 334 (28), 333 (12), 332 (29), 268 (22), 267 (99), 266 (25), 265 (100), 73 (40). Anal. calcd. for $C_{19}H_{28}BrN_3O_2SSi$: C 48.50, H 6.00, Br 16.98, N 8.93, S 6.82; found: C 48.35, H 6.03, Br 16.81, N 8.90, S 6.80.

1-[1′-Acetamido-2′-(trimethylsilylmethylthio)ethyl]-6-bromo-2-trimethylsilyloxy-1,2,3,4-tetrahydro-β-carboline, ***25***b

To **25***a* (0.56 g, 1.19 mmol), slurried in dry dichloromethane (50 mL) under nitrogen and at 0–5°C, was added *N*-(trimethylsilyl)imidazole (0.25 mL, 1.70 mmol). The reaction mixture was stirred at 0–5°C until all the solids dissolved. Dichloromethane (50 mL) was added and the reaction mixture washed (water (3 × 100 mL), saturated NaCl (100 mL)), dried (Na_2SO_4), and concentrated, to give **25***b* as a pale yellow solid (0.60 g, 90%), mp 85–100°C; IR (KBr) *ν*: 3312, 3076, 2957, 2909, 2844, 1656, 1248, 844 cm^{-1}; ^1H NMR ($CDCl_3$)[11] δ: 8.9 (br s, 1H, *ind-NH*), 7.6 (s, 1H, *H-5*), 7.2 (m, 2H, *H-7*, *H-8*), 6.4 (br s, 1H, *NH-Ac*), 4.5 (m, 2H, *H-1*, *H-10*), 3.5–2.6 (m, 6H, *H-3*, *H-4*, *H-11*), 2.0 (s, 3H, CH_3), 1.8 (s, 2H, *H-13*), 0.2 (s, 9H, $OSi(CH_3)_3$), 0.1 (s, 9H, $Si(CH_3)_3$) ppm; MS *m/z* (%): 544 (0.2), 543 (0.2), 542 (0.2), 541 (0.19), 528 (2), 526 (2), 340 (21), 339 (100), 338 (20), 337 (95), 249 (19), 247 (17), 75 (12), 73 (35).

1-[1′-Acetamido-2′-(trimethylsilylmethylsulfinyl)ethyl]-6-bromo-2-hydroxy-1,2,3,4-tetrahydro-β-carboline, ***28***a

To compound **25***a* (0.94 g, 2.0 mmol) in dry THF (60 mL) under nitrogen was added sodium bicarbonate (0.60 g, 7.13 mmol). At 0–5°C *m*-chloroperoxybenzoic acid (80%, 0.60 g, 2.78 mmol) in dry THF (40 mL) was added dropwise during 20 min. The reaction mixture was stirred at 0–5°C for 2 h, dichloromethane (125 mL) was added, and the solution was washed (2.5% $Na_2S_2O_3$ (2 × 100 mL), saturated NaCl (100 mL)), dried (Na_2SO_4), and concentrated to give a yellow solid. This residue was taken into dichloromethane (25 mL) at reflux, cooled to room temperature, and allowed to stand at 25°C overnight. A pale yellow solid was collected by filtration and washed with dichloromethane (2 × 5 mL) to give **28***a* (0.65 g, 67%), mp 170–175°C; IR (KBr) *ν*: 3352, 3271, 2952, 2920, 2842, 1661, 1507, 1251, 1006, 848 cm^{-1}; ^1H NMR (DMSO-d_6)[11] δ: 10.7 (br s, 1H, exch, *ind-NH*), 8.3 (s, 1H, exch, *N-OH*), 7.8 (br d, 1H, *NH-Ac*), 7.6 (s, 1H, *H-5*), 7.3 (m, 2H, *H-7*, *H-8*), 4.8 (br m, 1H, *H-10*), 4.1 (br s, 1H, *H-1*), 3.2–2.5 (br m, 6H, *H-3*, *H-4*, *H-11*), 2.3 (s, 2H, *H-13*), 1.9 (s, 3H, CH_3), 0.15 (s, 9H, $Si(CH_3)_3$) ppm; MS *m/z* (%): 487 (3), 485 (3), 470 (16), 468 (16); HRMS observed: 466.0601, 468.0602; calcd. for $C_{19}H_{25}BrN_3O_2SSi$ ($M^+ - H, H_2O$): 466.0582, 468.0604.

N(10)-Acetyleudistomin L, ***2***

To sulfoxide **28***a* (0.34 g, 0.70 mmol) was added dry acetonitrile (34 mL) under nitrogen. The reaction mixture was brought to reflux (oil bath temperature 100°C) during 0.5 h. During this time the solid dissolved and the light yellow reaction mixture was heated at reflux for a further 1 h. The solvent was removed and the residue chromatographed on neutral alumina, eluting with dichloromethane–methanol (98.5:1.5), to give N(10)-acetyleudistomin L **2** (0.045 g, 20%) (R_f 0.70) as a white solid, mp 193.5–195.5°C, after trituration with diethyl ether. Recrystallization from benzene gave crystals suitable for X-ray crystal structure determination (q.v.). IR (KBr) *ν*: 3410, 3229, 3100, 2920, 2847, 1653, 1510, 1446, 1309, 1041, 793 cm^{-1}; ^1H NMR ($CDCl_3$): see Table 1; ^{13}C NMR ($CDCl_3$): see Table 2; MS *m/z* (%): 397 (17), 395 (17), 312 (24), 310 (24), 282 (15), 280 (17), 267 (23), 266 (99), 265 (2), 264 (100), 250 (13), 249 (26), 248 (15), 247 (25), 186 (11), 185 (17), 168 (24); HRMS, observed: 395.0303; calcd. for $C_{16}H_{18}BrN_3O_2S$: 395.0301.

1-[1′-Acetamido-2′-(trimethylsilylmethylsulfinyl)ethyl]-6-bromo-2-trimethylsilyloxy-1,2,3,4-tetrahydro-β-carboline, ***28***b

To compound **25***b* (0.27 g, 0.50 mmol) in dry dichloromethane (25 mL) under nitrogen at 0–5°C was added sodium bicarbonate (0.20 g, 2.38 mmol), followed by *m*-chloroperoxybenzoic acid (80%, 0.12 g, 0.56 mmol) in dry dichloromethane (10 mL) dropwise during 10 min. The reaction mixture was stirred at 0–5°C for 1 h, dichloromethane (50 mL) was added, and the organic phase washed (2% $Na_2S_2O_3$ (2 × 40 mL), 5% $NaHCO_3$ (2 × 40 mL), saturated NaCl (25 mL)), dried (Na_2SO_4), and concentrated to give crude **28***b* (0.26 g, 93%) as a pale yellow–beige solid, mp 95–105°C. Compound **28***b* was used without further purification in the subsequent reaction. IR (KBr) *ν*: 3412, 3083, 2958, 2905, 2847, 1654, 1252, 1015, 844 cm^{-1}; ^1H NMR ($CDCl_3$)[11] δ: 10.2 (s, 1H, *ind-NH*), 7.6 (s, 1H, *H-5*), 7.1 (s, 2H, *H-7*, *H-8*), 6.7 (br s, 1H, *NH-Ac*), 4.3 (br s, 2H, *H-1*, *H-10*), 3.3–2.5 (m, 6H, *H-3*, *H-4*, *H-11*), 2.3–2.1 (2s, 2H, *H-13*), 2.0 (s, 3H, CH_3), 0.2 (s, 18H, $Si(CH_3)_3$, $OSi(CH_3)_3$) ppm.

[11]For ease of reference, we have retained the eudistomin numbering in these NMR spectral assignments.

*10-Acetamido-6-bromo-2-trimethylsilyloxy-1,2,3,4,10,11-hexahydro 13*H*-1,3-thiazepino[3,4,5-1,*m*]-β-carboline, **30***

The sulfoxide **28***b* (0.24 g, 0.43 mmol) was slurried in dry acetonitrile (27 mL) under nitrogen, and the solution brought to reflux during 0.5 h (oil bath temperature 100°C). All the solids dissolved and the reaction mixture was refluxed for 1 h. The solvent was removed and the yellow residue chromatographed on a preparative thin-layer (neutral) alumina plate, eluting with dichloromethane–methanol (98:2), to give **30** (0.035 g, 17%) (R_f 0.85) as a white solid. Recrystallization from 95% ethanol (35% recovery) gave pure **30** as white leaflets, mp 230–234.5°C; IR (KBr) ν: 3551, 3475, 3417, 3260, 3081, 2959, 2935, 2895, 2841, 1646, 1618, 1570, 1249, 935, 889, 844 cm^{-1}; ^1H NMR ($CDCl_3$):[11] see Table 1; ^{13}C NMR ($CDCl_3$):[11] see Table 2; MS *m/z* (%): 469 (0.5), 467 (0.5), 454 (7), 452 (7), 384 (24), 382 (24), 380 (9), 378 (8), 338 (8), 336 (9), 268 (18), 267 (94), 266 (30), 265 (93), 264 (13), 77 (22), 75 (100), 73 (25).

X-ray crystallography[6]

Unit cell dimensions were based upon 25 reflections ($11.2 < \theta < 16.9°$). Intensity data collection (ω–2θ scans over scan ranges ($0.65 + 0.35 \tan\theta$)°, max. scan time = 60 s, octants h, k, $\pm l$ with $2\theta \leq 55°$, and an additional 1762 symmetry related data with negative h and k indices and $2\theta \leq 30°$) gave a total of 6752 data. Scan rates were conditional on information collected in prescans. Three standards collected every 7500 s suffered small (~6%) losses in intensity.

Lorentz, polarization, and crystal decay corrections applied to all reflections. Exclusion of 906 systematically absent or zero F_{obs} data and averaging 1764 symmetry equivalent reflections ($R_{merge}(F) = 0.031$) gave a final data set of 3872 reflections. Structure solution: Patterson function (Br), followed by standard least-squares and Fourier calculations. Hydrogen atoms located in ΔF maps have been allowed to refine. Full matrix least-squares refinements minimizing $\Sigma_i w\Delta F^2$ converged (max. $\Delta/\sigma = 0.26$) to final residuals $R(wR) = 0.044(0.047)$ for 1967 observed data with $I \geq 3\sigma(I)$. Weights: $w = 4F^2[\sigma^2(I) + ((0.033)F^2)^2]^{-1}$, and a final ΔF Fourier contains residual peaks up to 0.74 e $Å^{-3}$ close to Br and the solvent molecule in the lattice.

Acknowledgements

Financial support of this work by the J. P. Bickell Foundation and, in part, by an operating grant from the Natural Sciences and Engineering Research Council of Canada is gratefully acknowledged, as is the award of an NSERC Postgraduate Scholarship, 1984–1988 (to J.R.S.). We also acknowledge the important experimental contribution to the investigation made by Mr. Eric Endrizzi, undergraduate research participant, in effecting the synthesis of compounds **19***a* and **20***a*. We are indebted to Dr. Jeffery F. Sawyer for the crystallographic structure determination of **2**.

1. (*a*) K. L. Rinehart, Jr., J. Kobayashi, G. C. Harbour, R. G. Hughes, Jr., S. A. Mizsak, and T. A. Scahill. J. Am. Chem. Soc. **106**, 1524 (1984); (*b*) J. Kobayashi, G. C. Harbour, J. Gilmore, and K. L. Rinehart, Jr. J. Am. Chem. Soc. **106**, 1526 (1984).
2. J. Kobayashi, H. Nakamura, Y. Ohizumi, and Y. Hirata. Tetrahedron Lett. **27**, 1191 (1986).
3. K. L. Rinehart, Jr., J. Kobayashi, G. C. Harbour, J. Gilmore, M. Mascal, T. G. Holt, L. S. Shield, and F. Lafargue. J. Am. Chem. Soc. **109**, 3378 (1987).
4. K. F. Kinzer and J. H. Cardellina II. Tetrahedron Lett. **28**, 925 (1987).
5. (*a*) J. W. Blunt, R. J. Lake, M. H. G. Munro, and T. Toyokuni. Tetrahedron Lett. **28**, 1825 (1987); (*b*) R. J. Lake, M. M. Brennan, J. W. Blunt, M. H. G. Munro, and L. K. Pannell. Tetrahedron Lett. **29**, 2255 (1988); (*c*) R. J. Lake, J. D. McCombs, J. W. Blunt, M. H. G. Munro, and W. T. Robinson. Tetrahedron Lett. **29**, 4971 (1988); (*d*) R. J. Lake, J. W. Blunt, and M. H. G. Munro. Aust. J. Chem. **42**, 1201 (1989).
6. S.-Y. Han, M. V. Lakshmikantham, and M. P. Cava. Heterocycles, **23**, 1671 (1985).
7. R. Plate, R. H. M. van Hout, H. Behm, and H. C. J. Ottenheijm. J. Org. Chem. **52**, 555 (1987).
8. M. Nakagawa, J.-J. Liu, K. Ogata, and T. Hino. J. Chem. Soc. Chem. Commun. 463 (1988).
9. I. W. J. Still and J. R. Strautmanis. Tetrahedron Lett. **30**, 1041 (1989).
10. M. Nakagawa, J.-J. Liu, and T. Hino. J. Am. Chem. Soc. **111**, 2721 (1989).
11. S. Yasuda, T. Hirasawa, and M. Hanaoka. Tetrahedron Lett. **28**, 2399 (1987).
12. A. G. Brook. Acc. Chem. Res. **7**, 77 (1974).
13. J. Thesing, G. Semler, and G. Mohr. Chem. Ber. **95**, 2205 (1962).
14. B. T. Ho, W. M. McIsaac, and L. W. Tansey. J. Pharm. Sci. **58**, 563 (1969).
15. G. F. Smith. J. Chem. Soc. 3842 (1954).
16. R. S. Varma and G. W. Kabalka. Synth. Commun. **15**, 151 (1985).
17. M. S. Mourad, R. S. Varma, and G. W. Kabalka. J. Org. Chem. **50**, 133 (1985).
18. F. Yamada, T. Hasegawa, M. Wakita, M. Sugiyama, and M. Somei. Heterocycles, **24**, 1223 (1986).
19. R. Huie and W. R. Cherry. J. Org. Chem. **50**, 1531 (1985).
20. A. Cohen and B. Heath-Brown. J. Chem. Soc. 7179 (1965).
21. (*a*) P. M. Wovkulich and M. R. Uskokovic. Tetrahedron, **41**, 3455 (1985); (*b*) W. Oppolzer, S. Siles, R. L. Snowden, B. H. Bakker, and M. Petrzilka. Tetrahedron, **41**, 3497 (1985).
22. S. Shimizu and M. Ogata. J. Org. Chem. **53**, 5160 (1988).
23. L. Zervas and I. Photaki. J. Am. Chem. Soc. **84**, 3887 (1962).
24. E. Winterfeldt. Synthesis, 617 (1975).
25. A. P. Kozikowski, T. R. Nieduzak, T. Konoike, and J. P. Springer. J. Am. Chem. Soc. **109**, 5167 (1987).
26. A. Ito, R. Takahashi, and Y. Baba. Chem. Pharm. Bull. **23**, 3081 (1975).
27. B. T. Ho and K. E. Walker. Org. Synth. **51**, 136 (1971).
28. M. Mitsui, S.-I. Zenki, T. Shiota, and S.-I. Murahashi. J. Chem. Soc. Chem. Commun. 874 (1984).
29. D. Seebach. Synthesis, 17 (1969).
30. J. Gynther. Acta Chem. Scand. **B42**, 433 (1988).
31. Z. Czarnocki, D. B. Maclean, and W. A. Szarek. Can. J. Chem. **64**, 2205 (1986).
32. D. J. Cram and F. A. Abd Elhafez. J. Am. Chem. Soc. **74**, 5828 (1952).
33. M. P. Cowling, P. R. Jenkins, and K. Cooper. J. Chem. Soc. Chem. Commun. 1503 (1988).
34. E. W. Colvin. Silicon in organic synthesis. Butterworths, London. 1981. pp. 15–20.
35. J. E. Baldwin. J. Chem. Soc. Chem. Commun. 734 (1976).
36. M. Ohno, M. Ido, and S. Eguchi. J. Chem. Soc. Chem. Commun. 1530 (1988).
37. D. N. Harpp and M. Gingras. J. Am. Chem. Soc. **110**, 7737 (1988).
38. G. Cavallini and V. Ravenna. Farmaco (Pavia) Ed. Sci. **13**, 105 (1958); Chem. Abstr. **52**, 20126 (1958).
39. E. H. P. Young. J. Chem. Soc. 3493 (1958).
40. L. F. Fieser and M. Fieser. Reagents for organic synthesis. Vol. 1. J. Wiley and Sons, New York. 1967. pp. 20–22.
41. C. Shin, M. Masaki, and M. Ohta. Bull. Chem. Soc. Jpn. **43**, 3219 (1970).
42. E. J. Corey and H. Estreicher. J. Am. Chem. Soc. **100**, 6294 (1978).
43. (*a*) P. H. H. Hermkens, J. H. van Marseveen, C. G. Kruse, and H. W. Scheeren. Tetrahedron Lett. **30**, 5009 (1989); (*b*) M. P. Kirkup, B. B. Shankar, S. McCombie, A. K. Ganguly, and A. T. McPhail. Tetrahedron Lett. **30**, 6809 (1989).
44. M. R. Yagudaev. Chem. Nat. Comp. (Engl. Transl.), **22**, 1 (1986).

Can. J. Chem. Downloaded from www.nrcresearchpress.com by 91.121.58.235 on 09/07/12
For personal use only.

A ^{19}F magic angle spinning nuclear magnetic resonance and infrared analysis of the adsorption of alkali metal fluorides onto montmorillonite clay

FATHI M. ASSEID, CATHERINE V. A. DUKE, AND JACK M. MILLER[1]

Department of Chemistry, Brock University, St. Catharines, Ont., Canada L2S 3A1

Received June 26, 1989[2]

FATHI M. ASSEID, CATHERINE V. A. DUKE, and JACK M. MILLER. Can. J. Chem. **68**, 1420 (1990).

Alkali metal fluorides have been adsorbed onto montmorillonite clay K10, and the resulting reagents analysed by ^{19}F magic angle spinning nuclear magnetic resonance and infrared spectroscopy. The complexes M_3SiF_6, $MAlF_4$, and M_3AlF_6 are readily formed, the particular complex depending on M, the loading, and the drying temperature employed. Chemisorption of fluoride to give surface -Si-F groups also occurs under certain conditions.

Key words: MAS NMR, alkali metal fluorides, adsorption, montmorillonite clay, infrared.

FATHI M. ASSEID, CATHERINE V. A. DUKE et JACK M. MILLER. Can. J. Chem. **68**, 1420 (1990).

On a fait adsorber des fluorures des métaux alcalins sur de la glaise montmorillonite K10 et on a analysé les réactifs qui en résultent par le biais de l'angle magique en résonance magnétique nucléaire du ^{19}F et par la spectroscopie infra-rouge. Il se forme facilement des complexes de M_3SiF_6, $MAlF_4$ et M_3AlF_6; la nature des complexes formés dépend de M, de la charge ainsi que de la température utilisée pour le séchage. Dans certaines conditions, il se produit aussi de la chemisorption des fluorures pour donner des groupements -Si-F superficiels.

Mots clés : MAS RMN, fluorures des métaux alcalins, adsorption, glaise montmorillonite, infra-rouge.

[Traduit par la revue]

Can. J. Chem. Downloaded from www.nrcresearchpress.com by 88.85.125.76 on 09/07/12
For personal use only.

Introduction

The fluorination of oxide catalysts causes changes in catalytic activity. Fluorinated alumina has been studied extensively, and fluorination generally leads to significant increases in reactivity (1), but much less has been done on fluorinated aluminosilicates, since these materials already have high catalytic activity, and fluorination often reduces their reactivity (2). Fluorinated oxides are typically studied by IR spectroscopy of adsorbed model compounds (3). Other techniques such as X-ray photoelectron spectroscopy and X-ray diffraction have been used as well, and there are also a few examples of the use of ^{19}F NMR spectroscopy, the most recent of these being the papers by Schlup and Vaughan (4, 5).

We are currently studying fluorinated oxides using ^{19}F magic angle spinning (MAS) NMR spectroscopy. MAS is a line narrowing technique that significantly improves the resolution of peaks in the spectrum of a solid, and allows direct determination of the isotropic chemical shift, whereas without MAS the isotropic shift can only be found indirectly. ^{29}Si MAS NMR has been extensively used to analyse zeolites and silicates because silicon has a low chemical shift anisotropy (CSA), and therefore the line broadening can be removed at easily achievable spinning rates. ^{19}F MAS NMR has received much less attention, however; two recently described applications are in the analysis of fluorinated polymers (6), and of fluorohydroxyapatite (7). We have found ^{19}F MAS to be a very effective tool in the analysis of inorganic fluorides (8), and have applied the technique to MF-alumina (9) and MF-silica (16) reagents. In these reagents, the complexes M_3AlF_6 and M_3SiF_6 are readily formed on the alumina or silica surface at temperatures of 100–200°C. We are now extending our study to look at MF-montmorillonite K10 clay.

Experimental

NH_4F (Aldrich), NaF and KF (BDH), and RbF and CsF (Alfa) were used without further purification. Montmorillonite K10 clay (surface area 220–270 $m^2 g^{-1}$) was obtained from Fluka. K10 is a commercial support material prepared by acid washing. Our samples had an extractable iron content of between 0.3 and 1.3%. On removing iron by five successive extractions with 50 mL of 3 M HNO_3, we extracted a total of 1.3% iron, after which no significant additional iron could be removed. (The material contained about 3% iron, according to Fluka spec sheets, so the difference is presumably tightly bonded iron.) We could not detect a change in either our IR or ^{19}F results if we extracted iron and other soluble ions, so further work was carried on with the material as purchased. XRD powder patterns do not show detectable levels of quartz. Sodium, potassium, and calcium are all below 0.1% extractable, with additional found in lattice sites. The silica gel was Merck Kieselgel 100, 70–230 mesh.

The MF-K10 reagents were prepared at loadings of 0.5, 2.0, 3.5, 5.0, and 10.0 mmol MF per g K10 by dissolving the appropriate quantity of MF in water and adding the solution to K10 clay to form a slurry. The water was removed on a rotary evaporator until the reagent had caked to the wall of the flask, and the reagents were then dried in air at various temperatures. RbF-silica and CsF-silica were also prepared, at a loading of 5.0 mmol g^{-1}. In a typical preparation, KF-K10 (3.5 mmol g^{-1}) was prepared by dissolving 2.03 g of KF in 25 cm^3 of water, and adding 10.0 g of K10 to form a slurry. The water was then removed until the clay had caked onto the side of the flask, and the resulting reagent was dried in air.

IR spectra were obtained on an Analect FX6260 Fourier transform spectrometer, attached to a MAP-66 data system. Samples were prepared as KBr discs, using a KBr/reagent ratio of about 20:1 by weight.

NMR spectra were obtained on a Bruker AC200 instrument at 188.3 MHz, using our home-built ^{19}F MAS probe. Samples were spun in Delrin rotors at about 3300 Hz. Since this spinning rate is considerably less than the CSA of fluorine (the CSA of KF is 323 ppm, which is equivalent to 65 kHz in a 200-MHz field, for example (10)), spinning side bands are seen in most of the spectra. Some of the spectra, especially those of the NaF-K10 reagents, showed broad unresolved peaks, probably because of the low spinning rate. Peaks were referenced to external $CFCl_3$, using the usual convention that upfield peaks are more negative.

Results and discussion

Each of the MF-K10 reagents was prepared at several loadings and dried over a range of temperatures. The loadings

[1]Author to whom correspondence may be addressed.

[2]Revision received January 15, 1990.

Can. J. Chem. Downloaded from www.nrcresearchpress.com by 88.85.125.76 on 09/07/12
For personal use only.

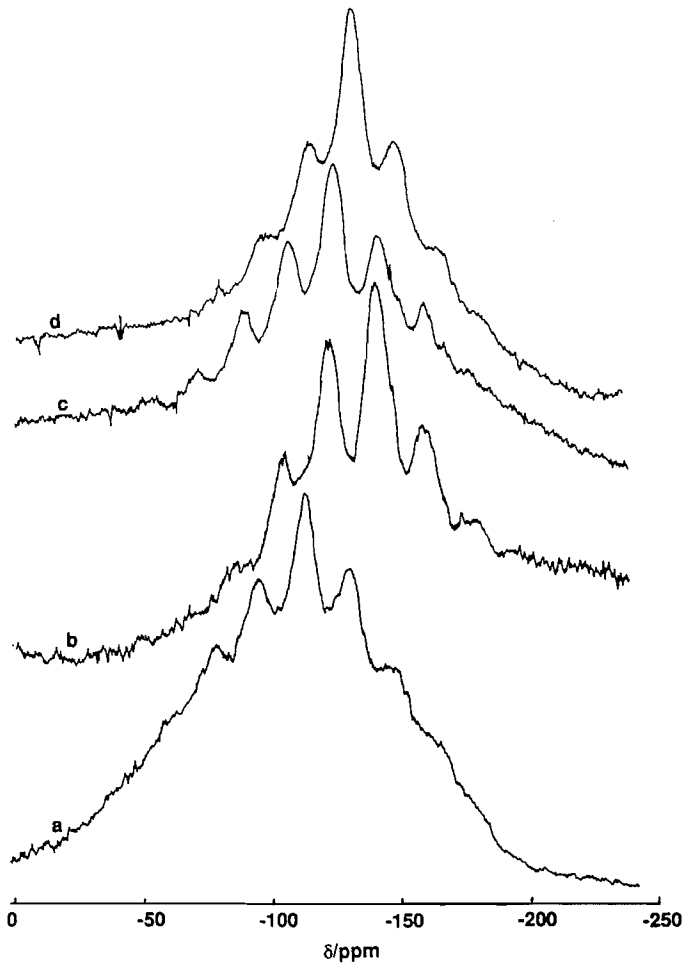

FIG. 1. ^{19}F MAS NMR spectra of (a) CsF-K10, (b) RbF-K10, (c) KF-K10, and (d) NH_4F-K10. Reagent loading is 5.0 mmol g^{-1}; reagents dried at 100°C.

range from 0.5 mmol g^{-1}, which is less than monolayer coverage, to 10.0 mmol g^{-1}, which should be well above the level of monolayer coverage. As the reagents were analysed, certain trends became apparent. The ^{19}F MAS NMR spectra of the reagents at a loading of 5.0 mmol g^{-1} and dried at 100°C are shown in Figs. 1 and 2 together with the spectrum of a mixed sample of $KAlF_4$ and K_3AlF_6. The corresponding IR spectra are shown in Figs. 3 and 4. The IR spectra of all the reagents except NaF-K10 show a band at about 740 cm^{-1}, which coincides with the position of the AlF_4^- band (lit. value for ν_3 for AlF_4^- is 760 cm^{-1} in the molten phase (11)). This suggests that either AlF_4^- or SiF_6^{2-} (or both) is being formed (lit. value for ν_3 for SiF_6^{2-} is 740 cm^{-1} (12)). The ^{19}F NMR spectrum of KF-K10 shows that SiF_6^{2-} is present, rather than AlF_4^-, with a peak at −129 ppm; the literature value for the ν_3 band of K_2SiF_6 is −129 ppm in the solid state (13), whereas the $KAlF_4$ sample has a peak at −155 ppm. SiF_6^{2-} is also formed on NH_4F-K10 in preference to AlF_4^-, the sample having an NMR peak at −136 ppm (lit. value (14) for NH_4AlF_4 is −147 ppm). On RbF-K10 both species are formed: the NMR spectrum shows two strong bands, at −123 and at −141 ppm, and although there is superposition of spinning side bands, two species are clearly present. RbF-silica shows a peak at −122 ppm, with an IR band at 740 cm^{-1}, and the chemical shift in RbF-alumina is −139 ppm, IR evidence indicating that the species present on

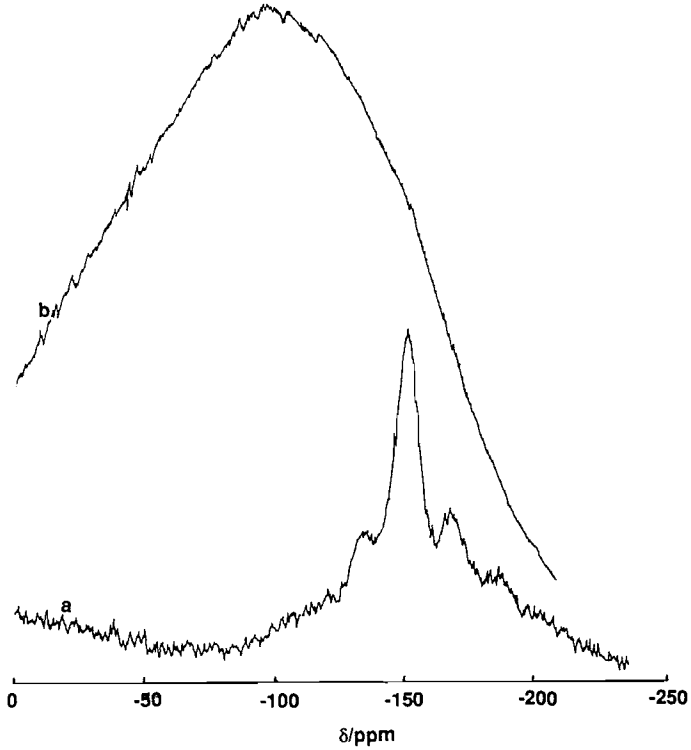

FIG. 2. ^{19}F MAS NMR spectra of (a) $KAlF_4/K_3AlF_6$ and (b) NaF-K10 (5.0 mmol g^{-1}, dried at 100°C).

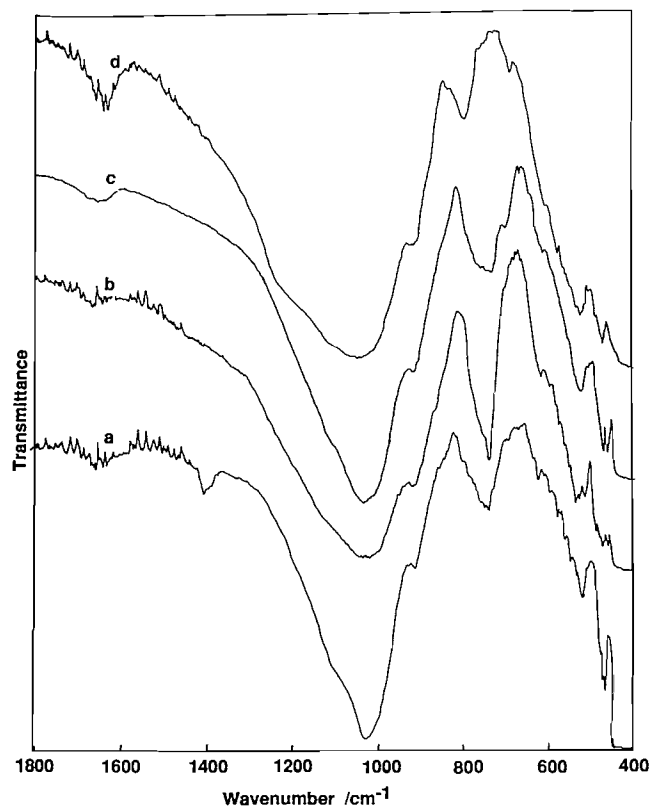

FIG. 3. IR spectra of (a) CsF-K10, (b) RbF-K10, (c) KF-K10, and (d) NaF-K10. Reagent loading is 5.0 mmol g^{-1}; reagents dried at 100°C.

Can. J. Chem. Downloaded from www.nrcresearchpress.com by 88.85.125.76 on 09/07/12
For personal use only.

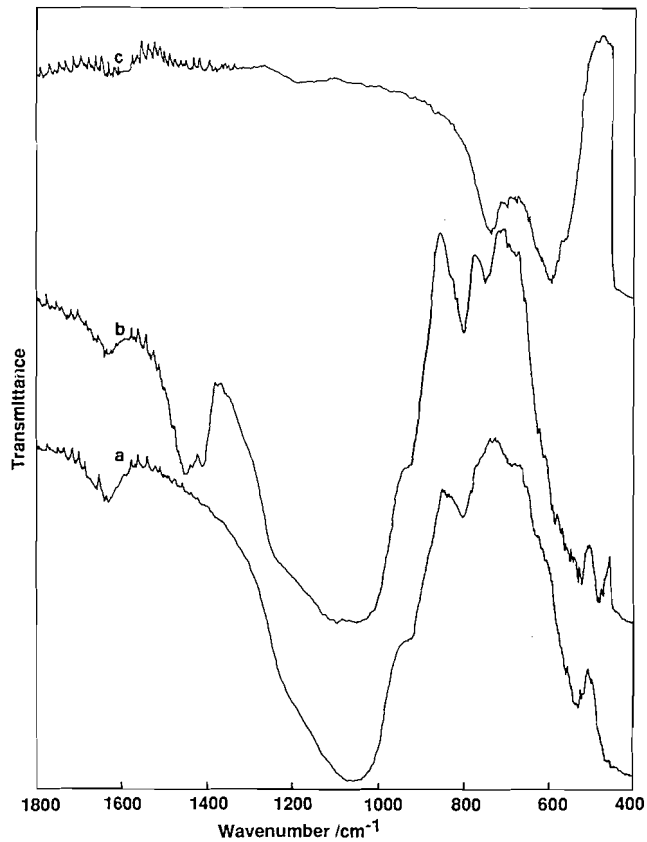

FIG. 4. IR spectra of (a) K10, (b) NH_4F-K10 (5.0 mmol g^{-1}, dried at 100°C), and (c) $KAlF_4/K_3AlF_6$.

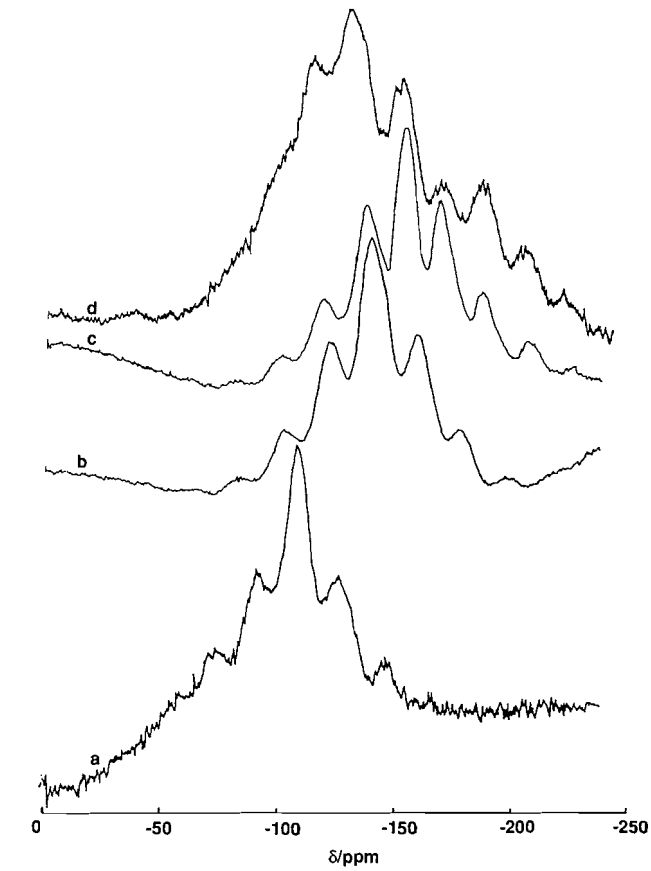

FIG. 5. ^{19}F MAS NMR spectra of (a) CsF-K10, (b) RbF-K10, (c) KF-K10, and (d) NH_4F-K10. Reagent loading is 5.0 mmol g^{-1}; reagents dried at 600°C.

this reagent is Rb_3AlF_6. The chemical shifts for $RbAlF_4$ and Rb_3AlF_6 should be close, since the chemical shifts for K_3AlF_6 and $KAlF_4$ are the same (the $KAlF_4$ and K_3AlF_6 peaks are not resolvable in these spectra because of their broadness). The IR spectrum of CsF-K10 also shows a band at 740 cm^{-1}, but this is probably due only to AlF_4^- with no SiF_6^{2-}. The ^{19}F MAS spectrum of CsF-K10 shows a peak at −113 ppm; CsF-alumina shows a peak at −115 ppm, which is due to Cs_3AlF_6 (IR band at 570 cm^{-1}; lit. value for AlF_6^{3-} (15), 568 cm^{-1}), whereas CsF-silica has an NMR peak at −92 ppm with an IR band at 740 cm^{-1}. The downfield shift of 37 ppm from −129 ppm for K_2SiF_6 to −92 ppm for Cs_2SiF_6 compares to a downfield shift of 42 ppm from −155 ppm for $KAlF_4$ to the −113 ppm peak found for CsF-K10. The NMR spectrum of NaF-K10 shows only a broad, unresolved peak, probably due to large dipolar interactions and (or) high CSA. In this case, a much higher spinning speed than is possible in our setup would be required to obtain a decent spectrum. The IR spectrum of the NaF-K10 reagent shows that there has been no formation of complex fluoride. It is possible instead that chemisorption has occurred to give -Si-F groups, or that F^- is dispersed over the surface.

The ^{19}F MAS spectra of the reagents dried at 600°C are shown in Fig. 5, and it can be seen that various changes have occurred on heating the reagents in air. As we found with NH_4F-silica, $(NH_4F)_2SiF_6$ on K10 readily decomposes at temperatures of 200°C and above, giving off, presumably, NH_3 and SiF_4. The HF that is formed then chemisorbs to the surface; the ^{19}F NMR spectrum of NH_4F-K10 shows a set of asymmetrical peaks, which indicates that the fluorine is no longer in a symmetrical environment, and is probably in the form of -Si-F surface groups as in NH_4F-silica (16). K_2SiF_6 is stable up to 400°C, depending on the loading of KF, with decomposition occurring at around 500°C (lower at lower loadings), but whereas F^- remains after the decomposition of K_2SiF_6 on KF-silica, AlF_4^- and (at high loadings) AlF_6^{3-} are formed when K_2SiF_6 decomposes on KF-K10. RbF-K10 behaves similarly: at 600°C Rb_2SiF_6 decomposes, forming some AlF_6^{3-} and leaving AlF_4^- intact. Cs_2SiF_6 does not form on CsF-K10, and CsF-K10 appears to be unchanged on heating. The ^{19}F MAS spectra of KF-K10 (3.5 mmol g^{-1}) dried at temperatures of 200°C, 400°C, and 600°C are given in Fig. 6, and clearly show the transition from SiF_6^{2-} to AlF_4^-; the IR band at 740 cm^{-1} becomes very much weaker in intensity as SiF_4 is given off, and is now only present as a shoulder. The IR spectra of RbF-K10 (5.0 mmol g^{-1}) dried at several temperatures are given in Fig. 7, and these show the loss in intensity of the 740 cm^{-1} band as SiF_4 is given off, and the appearance of a new band at 570 cm^{-1} due to Rb_3AlF_6. The IR spectrum of NaF-K10 at 600°C shows bands forming at 740 and 580 cm^{-1}, which suggests that the complexes Na_3AlF_6 and $NaAlF_4$ are forming, although the ^{19}F NMR still consists of an unresolvable broad peak. The 740 cm^{-1} peak is probably not due to Na_2SiF_6, as we would expect this to decompose, as on KF-K10. Therefore, on NaF-K10 dried at 100°C, F^- is probably dispersed over the surface rather than chemisorbed.

The ^{19}F MAS spectra of all the reagents (except NaF-K10) at the low loading of 0.5 mmol g^{-1}, which is rather less than monolayer coverage, are very similar and show a peak with nonsymmetrical spinning side bands, which is superimposed on a very broad underlying peak (Fig. 8). None of the reagents

Can. J. Chem. Downloaded from www.nrcresearchpress.com by 88.85.125.76 on 09/07/12
For personal use only.

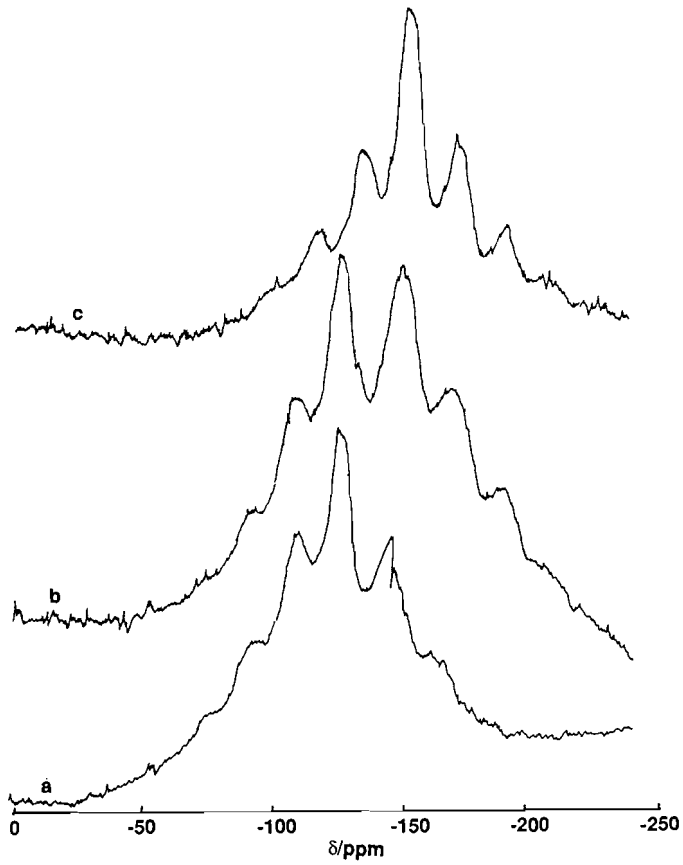

FIG. 6. ^{19}F MAS NMR spectra of KF-K10 (5.0 mmol g^{-1}) dried at (a) 200°C, (b) 400°C, and (c) 600°C.

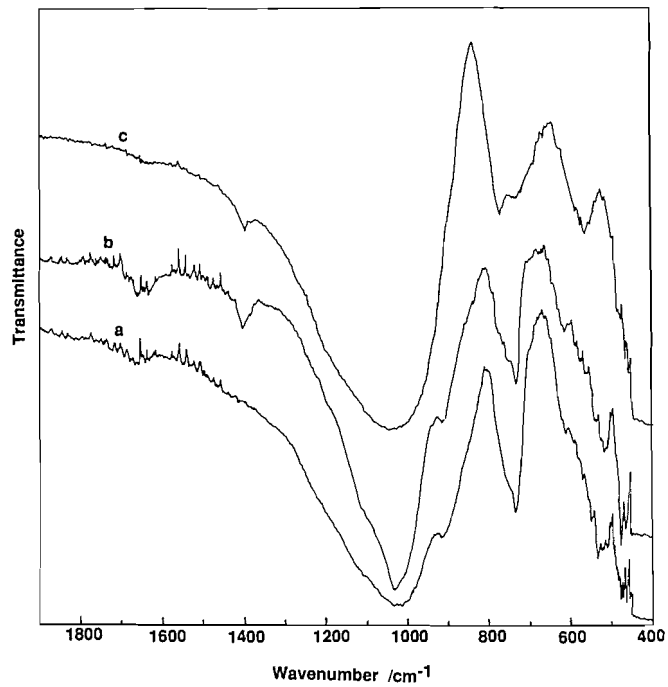

FIG. 7. IR spectra of RbF-K10 (5.0 mmol g^{-1}) dried at (a) 100°C, (b) 200°C, and (c) 600°C.

shows a 740 cm^{-1} band in its IR spectra and hence no SiF_6^{2-} or AlF_4^- is forming. Presumably then, chemisorption is occurring, with -Si-F groups forming on the surface. Chemisorbed fluorine is present on NH_4F-alumina at fluorine concentrations

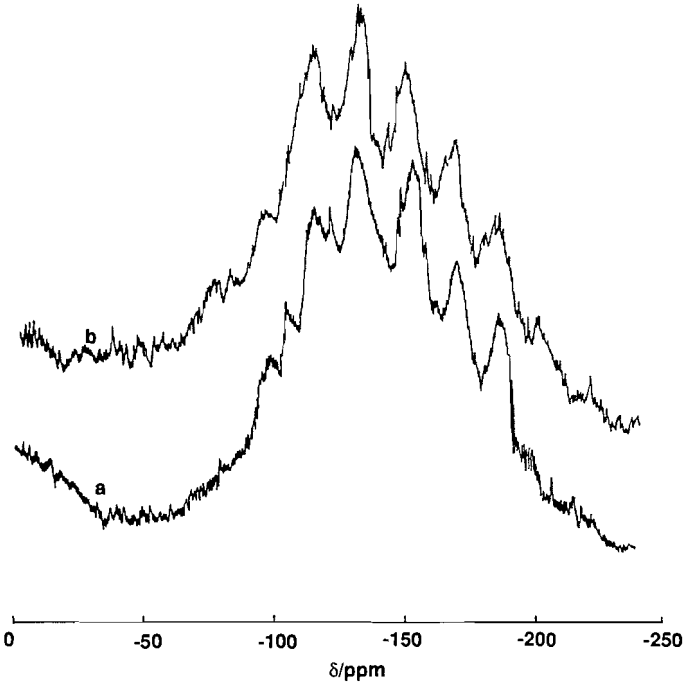

FIG. 8. ^{19}F MAS NMR spectra of (a) CsF-K10 and (b) RbF-K10. Reagent loading is 0.5 mmol g^{-1}; reagents dried at 100°C.

TABLE 1. Ionic radii of the M^+ ions

Ion	Radius/pm[a]
Na^+	97
K^+	133
NH_4^+	143
Rb^+	147
Cs^+	167

[a]CRC Handbook of Chemistry and Physics.

of less than about 5% by weight, which is equivalent to a loading of 2.6 mmol g^{-1} of MF, but at higher concentrations $(NH_4)_3AlF_6$ is formed. Most of the reagents, at the higher loading of 2.0 mmol g^{-1}, form a complex fluoride species. An exception is CsF-K10, which forms $CsAlF_4$ at the still higher loading of 5.0 mmol g^{-1}.

The varying behaviour of the MF-K10 reagents can probably be attributed to the different cation size of M^+ (see Table 1). NH_4F-K10, KF-K10, and RbF-K10 all behave similarly in initially forming M_2SiF_6, and these cations are similar in size, whereas NaF (Na^+ much smaller) appears to be dispersed over the K10 surface, and CsF (Cs^+ much larger) forms $CsAlF_4$ and Cs_3AlF_6. It is possible that Na^+ diffuses right through the open aluminosilicate structure, and that it only migrates to the external surface on heating; the local concentration of NaF will then become high enough to form Na_3AlF_6 and $NaAlF_4$. Cs^+ is large and less strongly polarizing (i.e., softer) than the other M^+ cations, and will therefore be attracted to the more polarizable (softer) AlO_4^{5-} tetrahedra rather than to the SiO_4^{4-} tetrahedra.

To conclude, complex fluorides form when MF is adsorbed onto montmorillonite K10, the particular species formed depending on the loading of MF, the drying temperatures, and the cation employed.

Acknowledgements

We would like to thank NSERC for an operating grant (to J.M.M.), and Mr. T. R. B. Jones for technical assistance with the NMR instrument.

1. V. R. CHOUDHARY. Ind. Eng. Chem. Prod. Res. Dev. **16**, 12 (1977).
2. A. K. GHOSH and R. A. KYDD. J. Catal. **103**, 399 (1987).
3. P. O. SCOKART, S. A. SELIM, J. P. DAMON, and P. G. ROUXHET. J. Colloid Interface Sci. **70**, 209 (1979).
4. J. R. SCHLUP and R. W. VAUGHAN. J. Catal. **85**, 311 (1984).
5. J. R. SCHLUP and R. W. VAUGHAN. J. Catal. **99**, 304 (1986).
6. S. F. DEC, R. A. WIND, and G. E. MACLEL. Macromolecules, **20**, 2754 (1987).
7. J. P. YESINOWSKI and M. J. MOBLEY. J. Am. Chem. Soc. **105**, 6191 (1983).
8. J. H. CLARK, E. M. GOODMAN, D. K. SMITH, S. J. BROWN, and J. M. MILLER. J. Chem. Soc. Chem. Commun. 657 (1986).
9. T. ANDO, S. J. BROWN, J. H. CLARK, D. G. CORK, T. HANAFUSA, J. ICHIHARA, J. M. MILLER, and M. S. ROBERTSON. J. Chem. Soc. Perkin Trans. 2, 1133 (1986).
10. B. R. APPLEMAN and B. P. DAILEY. *In* Advances in magnetic resonance. Vol. 7. *Edited by* J. S. Waugh. Academic Press, New York. 1974.
11. B. GILBERT, G. MAMANTOV, and G. M. BEGUN. Inorg. Nucl. Chem. Lett. **10**, 1123 (1974).
12. R. B. BADACHHAPE, G. HUNTER, L. D. MCCORY, and J. L. MARGRAVE. Inorg. Chem. **5**, 929 (1966).
13. Y. YOSHIOKA, N. NAKAMURA, and H. CHIHARA. Bull. Chem. Soc. Jpn. **61**, 3037 (1988).
14. YU. A. BUSLAEV, V. V. PESHKOV, and R. L. DAVIDOVICH. Spectrosc. Lett. **7**, 147 (1974).
15. M. J. REISFELD. Spectrochim. Acta, **29A**, 1923 (1973).
16. C. V. A. DUKE, J. M. MILLER, and J. H. CLARK. Spectrochim. Acta. In press.

Can. J. Chem. Downloaded from www.nrcresearchpress.com by 88.85.125.76 on 09/07/12
For personal use only.

Photochemistry of 2-azido-2-alkyl-3-oxobutanoic esters and amides[1]

OLIVER E. EDWARDS[2]
Division of Chemistry, National Research Council of Canada, Ottawa, Ont., Canada K1A 0R6

AND

WERNER RANK[3]
Department of Chemistry, Laurentian University, Sudbury, Ont., Canada P3E 2C6

Received November 30, 1989

OLIVER E. EDWARDS and WERNER RANK. Can. J. Chem. **68**, 1425 (1990).

Photolysis of 2-alkyl-2-azido-3-oxobutanoic esters and amides gave products resulting from alkyl or acyl migration onto nitrogen. The resulting ketimimes could be isolated in moderate purity, but the *N*-acyl imines were rapidly converted into solvation products or enamides (*N*-acetyl dehydroamino acid esters) resulting from double bond migration. Mechanisms for formation of these products are discussed. The *N*-(2-azido-2-methyl-3-oxobutanoyl) derivative of the diketopiperazine from L-valyl-L-proline gave a stereoisomer of the cyclol tripeptide unit of ergovaline.

Key words: *N*-acyl imines, mechanism of 2-azido-3-keto ester photolysis, cyclol tripeptide synthesis, ergovaline.

OLIVER E. EDWARDS et WERNER RANK. Can. J. Chem. **68**, 1425 (1990).

La photolyse des esters et des amides des acides 2-alkyl-2-azido-3-oxobutanoïques fournit des produits qui proviennent de migrations d'alkyles ou d'acyles vers l'azote. L'état de pureté des cétimines qui en résultent est correct; toutefois, les imines *N*-acylées se transforment rapidement en produits de solvatation ou en ènamides (esters des *N*-acétyl déhydroamino acides) qui résultent d'une migration de double liaison. On discute des mécanismes de formation de ces produits. La dérivé *N*-(2-azido-2-méthyl-3-oxobutanoyle) de la dicétopipérazine provenant de la L-valyl-L-proline fournit un stéréoisomère de l'unité tripeptide cyclol de l'ergovaline.

Mots clés : imines *N*-acylées, mécanisme de photolyse des esters 2-azido-2-céto, synthèse de l'unité tripeptide cyclol, ergovaline.

[Traduit par la revue]

Can. J. Chem. Downloaded from www.nrcresearchpress.com by 88.85.125.76 on 09/07/12
For personal use only.

A number of biologically active molecules contain units derivable from *N*-acyl imines (**1**), such as carbinolamides (**2**, R^3 = H), carbinolamide ethers (**2**, R^3 = alkyl), and peptides containing dehydroamino acid units as in **3**. These include the 6-

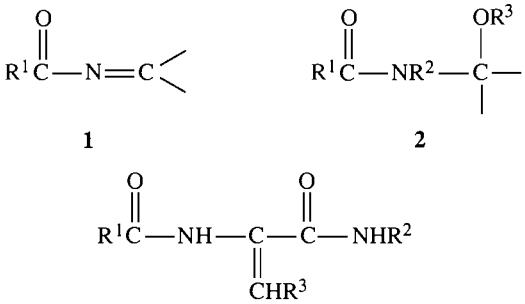

1 **2**

3

methoxy β-lactam antibiotics (1), pederin (2), maytansine (3), bicyclomycin (4), and many ergot alkaloids (5). A review of natural dehydroamino acid derivatives was presented by Bycroft (6*a*) and more recent examples were cited by Steglich and co-workers (6*b*).

Interest in the mechanism of the photochemical formation of *N*-acyl imines and enamides from α-azido carbonyl compounds (7), possible extension of the reaction to α-azido-β-keto esters and amides, and the potential of the reaction for the synthesis of natural products and agents for chemotherapy prompted us to examine the photolysis of 2-alkyl-2-azido-3-oxobutanoic esters and amides.

[1]Issued as NRCC No. 31519. Presented in part at the 63rd Canadian Chemical Conference, Ottawa, June 3–6, 1980.

[2]Author to whom correspondence may be addressed at Department of Chemistry, Carleton University, Ottawa, Ont., Canada, K1S 5B6.

[3]NRCC research associate 1974–1976.

Results

The preparation of 2-alkyl-2-azido derivatives of 3-oxobutanoic esters was carried out using apparent S_N2 displacement on the corresponding bromides (eq. [1]). The mechanism of this

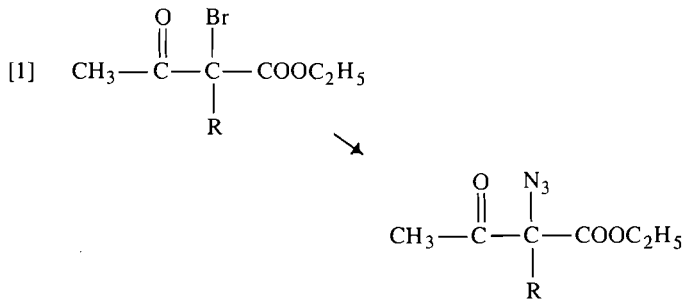

displacement has been studied in these laboratories (8). Good yields of azides **4***a* and **4***b* were obtained.

As a model for subsequent peptide work, the α-azidoketo amide **7** was prepared as shown in eq. [2]. A by-product of the bromination of **5** with pyridinium perbromide was the crystalline tribromide **8**.

The only primary products characterized from the photolysis of azides **4***a* and **4***b* in dichloromethane were the imines **10** (27%) (Scheme 1) and **16** (30%) (Scheme 3). The former was relatively stable, surviving heating in pyridine or distillation at 100°C *in vacuo*. However, **16** isomerized readily to the benzaldimine **18**. This was not isolated, but its hydrolysis product, benzaldehyde, appeared on handling of **16**.

The *N*-acyl imine primary products **9** and **15** formed in the photolysis of azides **4a** and **4b**, respectively, were not isolated as such, since they readily converted into the enamides **11** (27%)

[2] 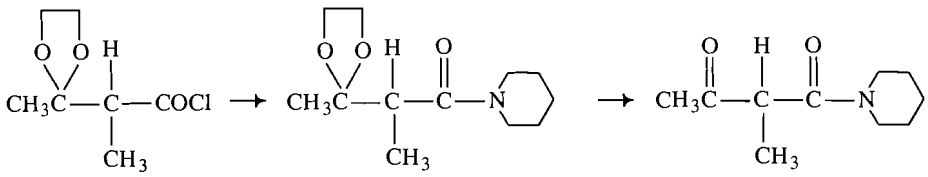

5

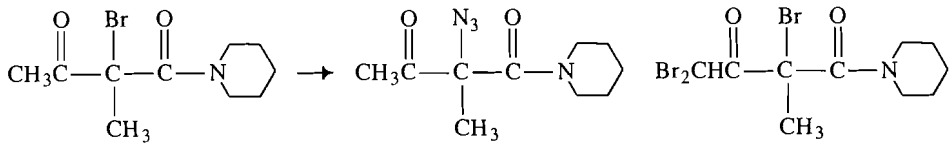

6 7 8

and **17** (21%), even on rapid chromatography on neutral silica gel, heating in dry pyridine, or distillation *in vacuo*. The presence and yields of **9** and **15** were also deduced from the isolation of derivatives (Schemes 1 and 3). *N*-Acyl imines **9** and **15** were trapped efficiently upon irradiation of the azides using 254-nm lamps in methanol (Schemes 2 and 4) or ethanol, or by the use of 300-nm lamps and an acid catalyst such as *p*-toluenesulfonic acid or trifluoroacetic acid. The resulting carbinolamide ethers **12**, **14** (44%), and **19** (26%) were well characterized. Finally, **14** was converted into the 2,4-dinitrophenylhydrazone of ethyl 2-oxobutanoate, confirming the skeleton.

Photolysis of the α-azidoketo amide **7** was only studied in methanol. The products characterized were *N*-(2-acetamido-2-methoxypropanoyl) piperidine **20** (26%) and *N*-(2-methoxy-2-methylamino-3-oxobutanoyl) piperidine **21** (11%).

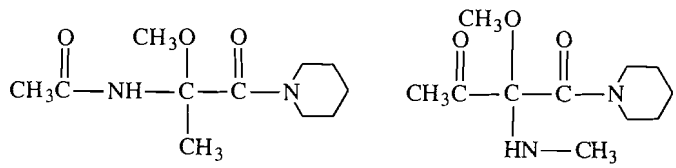

20 21

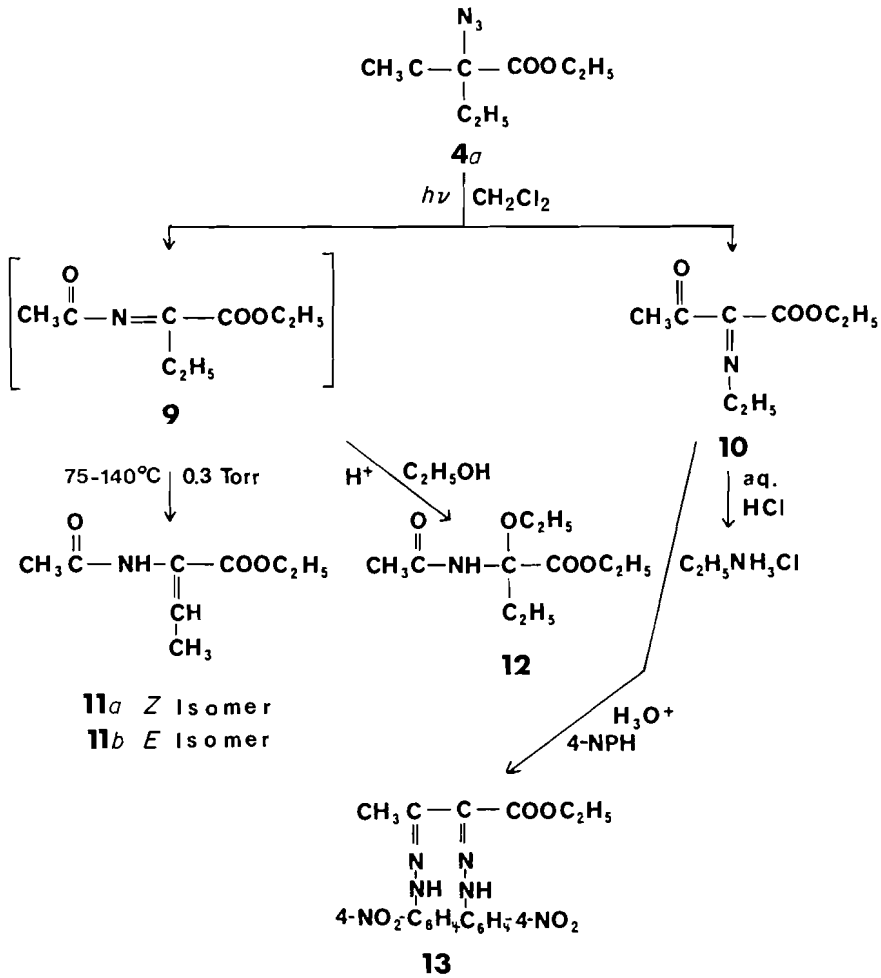

SCHEME 1

Can. J. Chem. Downloaded from www.nrcresearchpress.com by 88.85.125.76 on 09/07/12
For personal use only.

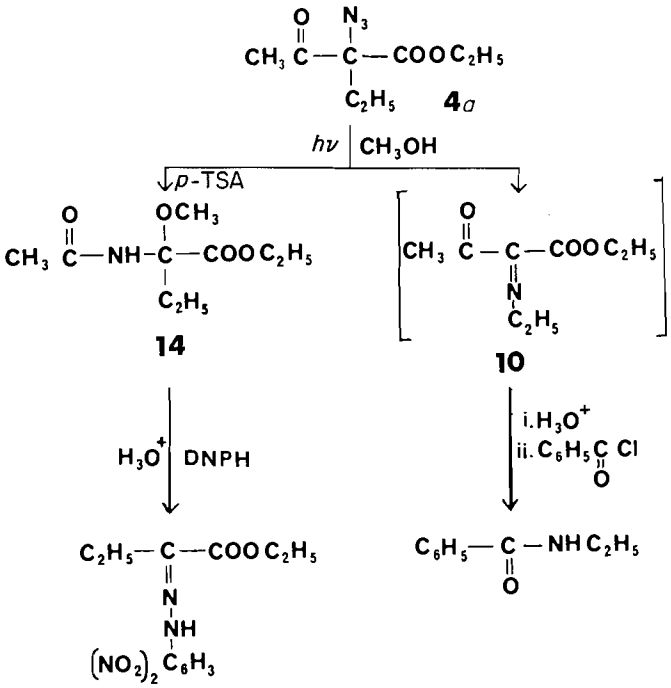

SCHEME 2

One objective of our research was to explore an *N*-acyl imine route for the synthesis of a cycloltripeptide unit found in therapeutically valuable ergot alkaloids. The only syntheses of these appear to be those of Hofmann and co-workers (9, 15). The cycloltripeptide portion in ergovaline (**22**, R = lysergyl) can be envisioned to arise from the hydrated diketopiperazine appropriately substituted with an *N*-acyl imine function (**23***a*). Thus the photochemical generation of such a unit seemed attractive.

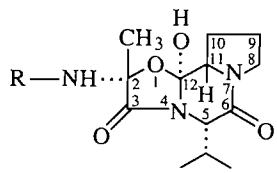

22

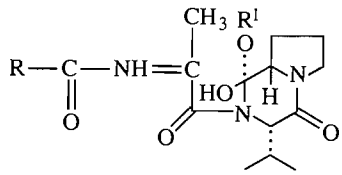

23*a* $R^1 = H$
23*b* $R^1 = CH_3$

The preparation of the α-azidoketo lactam **28** from the diketopiperazine L-prolyl-L-valyl lactam **24** (9) was achieved as outlined in Scheme 5. Mixtures were obtained at each stage. The main *N*-(2-methyl-3-oxobutanoyl) diketopiperazine **26** was converted to a mixture of crystalline and amorphous bromo compounds **27**. No well-characterized products were obtained when the amorphous bromo compound(s) were subjected to azide exchange and subsequent photolysis. However, the crys-

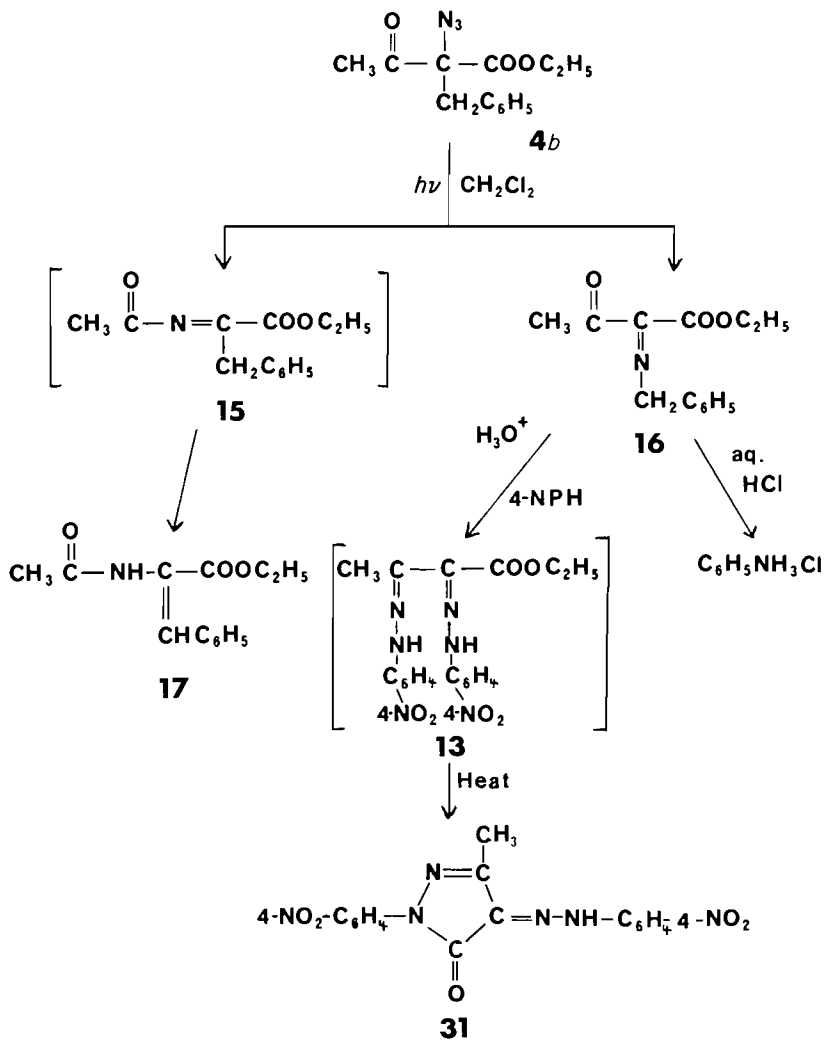

SCHEME 3

Can. J. Chem. Downloaded from www.nrcresearchpress.com by 88.85.125.76 on 09/07/12
For personal use only.

Can. J. Chem. Downloaded from www.nrcresearchpress.com by 88.85.125.76 on 09/07/12
For personal use only.

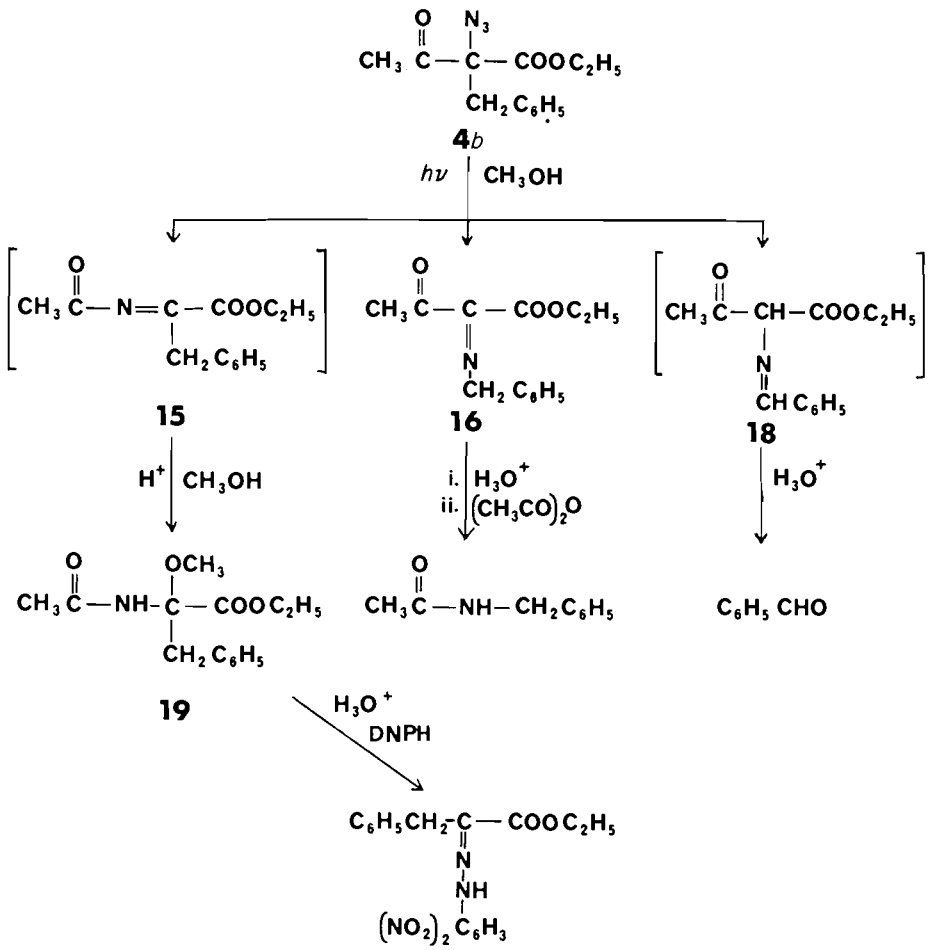

SCHEME 4

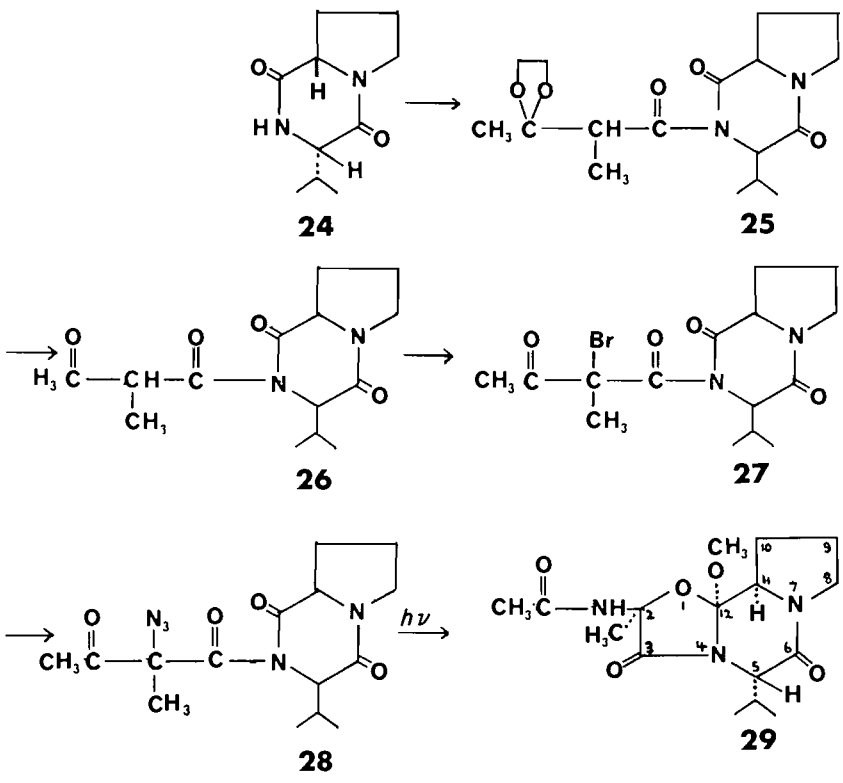

SCHEME 5

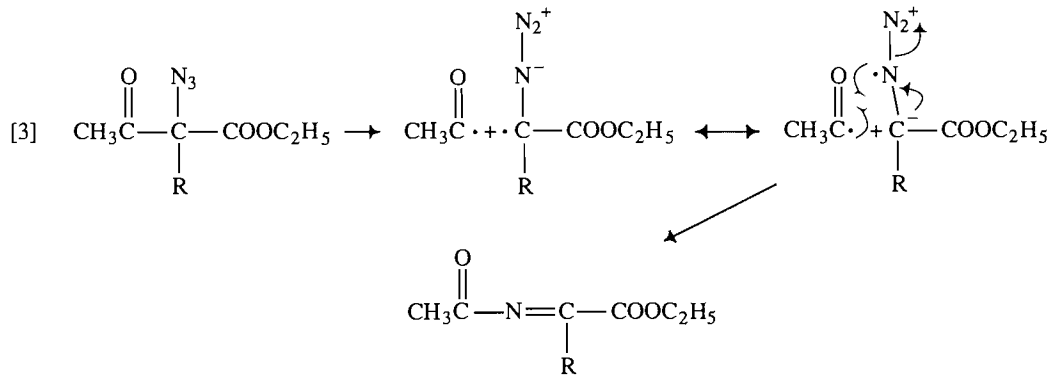

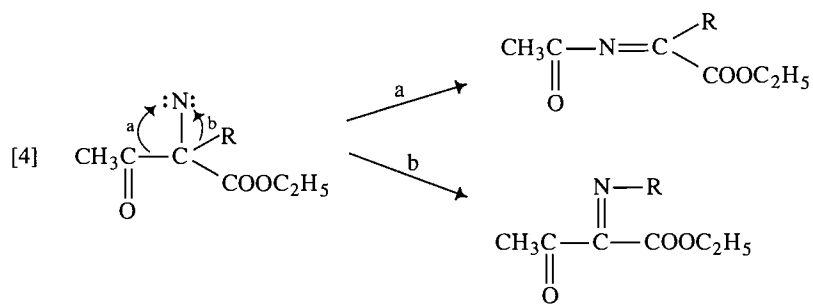

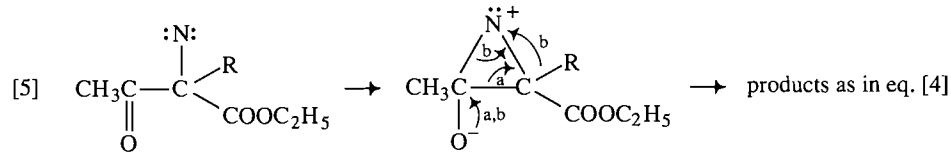

31

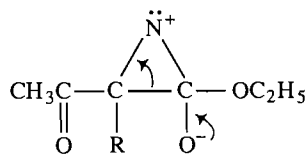

32

talline isomer **27** was converted to the α-azidoketo lactam **28**, which according to its ^{1}Hmr spectrum was a mixture of two isomers. Photolysis of the mixture in methanol followed by treatment with acidic methanol and subsequent chromatography of the products on alumina gave 17% of a crystalline methyl ether **29** related to the *N*-acetyl derivative of the cycloltripeptide unit of ergovaline (9). An X-ray crystallographic analysis by Przybylska and Ahmed (10) confirmed the structural assignment and established the stereochemistry of the product as being 2*S*,5*S*,11*R*,12*S*-acetamido-3,6-dioxo-5-isopropyl-10b-methoxy-2-methyl-perhydro-8-*H*-oxazolo[3,2-*a*]pyrrolo[2,1-*c*]-pyrazine. It was thus a D-proline derivative with the configuration at C-2 opposite to that of the natural ergot alkaloid tripeptides.

Discussion

The longest wavelengths of light used for the above photolyses (centered at 300 nm) could excite either the azido group or the ketone carbonyl and thus three mechanisms seem plausible: The first (eq. [3]) involves a Norrish type 1 fission after $n \rightarrow \pi^*$ excitation of the ketone. The other two mechanisms in eqs. [4] and [5] involve the well-known photochemical cleavage of an azide to nitrogen and a singlet nitrene.

The mechanism described in eq. [3] seems unlikely. To produce the *N*-acyl imine the two radicals would have to combine before diffusing apart and before decarbonylation of the acetyl radical. In addition, the formation of the imines **10** and **16** cannot be explained readily.[4]

The singlet nitrene mechanism in eq. [4] can account for both acyl (route "a") and alkyl (route "b") migration. However, singlet nitrenes react with alcohols to give *N*-alkoxy compounds (11*b*), none of which were observed. A possible alternative mechanism is that the zwitterion **31** shown in eq. [5] forms very rapidly and, in its turn, rearranges rapidly to the main primary products. The zwitterion is internally neutralized, hence not very nucleophilic.[5] Some support for the zwitterion **31** comes from the failure to observe ethoxy carbonyl migration. According to Saunders *et al.* (12), lowering of the electron density on groups retarded their migration onto singlet nitrenes. Thus if the

[4]A referee suggested that $n \rightarrow \pi^*$ photoexcitation of the carbonyl would lead to rapid internal energy transfer to the azide group. We consider that this would likely result in formation of a triplet nitrene (11*a*), which would abstract hydrogen instead of rearranging.

[5]A referee pointed out that the nitrene may simply rearrange much faster than it can undergo bimolecular reaction.

Can. J. Chem. Downloaded from www.nrcresearchpress.com by 88.85.125.76 on 09/07/12
For personal use only.

Can. J. Chem. Downloaded from www.nrcresearchpress.com by 88.85.125.76 on 09/07/12
For personal use only.

singlet nitrene mechanism (eq [4]) were operative, one would expect a significant migration of the ethoxycarbonyl group, which has a higher electron density on its carbonyl carbon than that on the ketone carbonyl.[6] In contrast, the same electron density differential should favor formation of zwitterion **31** over the alternative **32**, thus leading to the products actually observed. We thus favor the mechanism in eq. [5], with the assumption that the initial nitrene has such a short lifetime that its reaction with solvent is negligible.

The facile isomerization of *N*-acyl imines, when the appropriate hydrogen is available, to the thermodynamically more stable enamides was also observed in our work on photolysis of a 9α-azido-11-keto steroid (unpublished work with T. Sano). Two other photochemical studies have reported production of *N*-acyl imines as very reactive intermediates (13, 14).

The moderately good yields of *N*-acyl imine derived products from the α-azido-β-keto esters and amides encouraged us to attempt a cycloltripeptide synthesis. However, the lack of stereochemical control in the reaction sequence in Scheme 5 was disappointing. The pure lactam **24** gave a mixture of two ketal lactams (**25**). These may have been diastereoisomers at C-2′. However, inversion of the asymmetric center of proline cannot be excluded since facile inversion of this center has previously been observed as a base-catalysed or thermal reaction of diketopiperazines derived from this amino acid (5, 9, 15). This facile isomerization at the proline center obviously occurred at one of the steps in Scheme 5. In addition, acid-catalysed isomerization of the cycloltripeptide units of the ergot alkaloids had been shown (16) to involve inversion at C-2, so the formation of the unwanted isomer **29** is not too surprising. Of course the cyclization of a solvated diketopiperazine such as **23*b*** could lead to a mixture of isomers at the new asymmetric centers C-2 and C-12.

Because of the isolation in this case of a modest yield of only one isomer, the method may be of limited utility for the preparation of other ergot peptides. Nevertheless, this study provided in principle another example of the potential of *N*-acyl imines as intermediates in synthetic sequences. Furthermore, the establishment of the structure of the cycloltripeptide **29** by X-ray analysis is noteworthy, since only two other related structures have been determined by X-ray methods (16, 17). Considering that in less complex α-azidoketo systems such as **4*a*** the yield of *N*-acyl imine derived products is around 45%, this method might prove useful for the generation of carbinolamide ether or dehydro-amino acid (enamide) units of natural products less prone to isomerizations than the diketopiperazine derivatives reported in this paper.

Experimental

Infrared (ir) spectra were obtained with a Perkin–Elmer grating spectrometer, model 257, using dichloromethane as solvent. Proton magnetic resonance (^{1}Hmr) and ^{13}C magnetic resonance (^{13}Cmr) spectra were recorded with a Bruker WP-80 FT spectrometer. The ^{1}H chemical shift data are quoted in δ units and refer to solutions in deuterochloroform using tetramethylsilane as internal reference. Optical rotations were measured with a Perkin–Elmer polarimeter. Mass spectral data were recorded on a VG 707E instrument. The photolytic experiments were carried out using a Rayonet photochemical reactor with lamps giving peak emission at 254 or 300 nm. Preparative layer chromatography (plc) was carried out on 20 × 20 cm glass plates precoated with silica. Neutralized "flash" silica gel refers to silica gel (230–400 mesh) that has been neutralized by treatment with pyridine in ethyl acetate. Unless otherwise stated, anhydrous sodium sulfate was used for drying organic solutions. Solvents were usually removed on a rotary evaporator using a water aspirator and bath temperatures of 30–40°C. Melting points and boiling points are uncorrected.

*Ethyl 2-azido-2-ethyl-3-oxobutanoate (**4**a)*

Alkylation of ethyl acetoacetate with bromoethane in the presence of sodium ethoxide gave ethyl 2-ethyl-3-oxobutanoate (18), bp 92–98°C at 24 Torr (1 Torr = 133.3 Pa), in a yield of 78%. Dropwise addition of bromine to an aqueous suspension of this material furnished ethyl 2-bromo-2-ethyl-3-oxobutanoate (18), bp 110–115°C at 20 Torr, in a yield of 91%. To a solution of 19.32 g of ethyl 2-bromo-2-ethyl-3-oxobutanoate in 40 mL of dimethylformamide was added portionwise 5.83 g of sodium azide over 20 min, during which time the temperature was kept below 30°C by cooling. After continued stirring for 6 h at room temperature the crude azide was isolated by extractive work-up with ether. Fractional distillation gave 73% of pure azide **4*a*** boiling at 60–63°C at 0.8 Torr. Spectral and analytical data supported the structural assignment; ir ν_{max}: 2110, 1740, 1725 cm^{-1}; ^{1}Hmr: 4.37 (2H, q, J = 7 Hz), 2.3 (3H, s), 2.07 (2H, q, J = 7 Hz), 1.35 (3H, t, J = 7 Hz), 0.93 (3H, t, J = 7 Hz). Anal. calcd. for $C_8H_{13}N_3O_3$: C 48.23, H 6.58, N 21.10; found: C 48.46, H 6.73, N 21.31.

*Ethyl 2-azido-2-benzyl-3-oxobutanoate (**4**b)*

Alkylation of ethyl acetoacetate with benzyl bromide in the presence of sodium ethoxide gave ethyl 2-benzyl-3-oxobutanoate (18), bp 103–105°C at 0.3 Torr, in a yield of 83%. Dropwise addition of bromine to an aqueous suspension of this material furnished ethyl 2-benzyl-2-bromo-3-oxobutanoate (18), bp 98–101°C at 0.1 Torr, in a yield of 76%. To a solution of 10.76 g of ethyl 2-benzyl-2-bromo-3-oxobutanoate in 20 mL of dimethylformamide was added portionwise 2.57 g of sodium azide while the temperature was maintained below 30°C by cooling. After continued stirring for 6 h at room temperature the crude azide was isolated by extractive work-up with ether. Fractional distillation gave 68% of pure azide **4*b*** boiling at 106–108°C at 0.3 Torr. Spectral and analytical data supported the structural assignment; ir ν_{max}: 2120, 1740, 1725 cm^{-1}; ^{1}Hmr: 7.38 (5H, s), 4.33 (2H, q, J = 7 Hz), 3.33 (2H, s), 2.22 (3H, s), 1.30 (3H, t, J = 7 Hz). Anal. calcd. for $C_{13}H_{15}N_3O_3$: C 59.76, H 5.79, N 16.08; found: C 59.90, H 5.88, N 16.21.

*Photolysis of ethyl 2-azido-2-ethyl-3-oxobutanoate (**4**a)*

1. In dichloromethane

(*a*) A solution of 690 mg of azide **4*a*** in 75 mL of dry dichloromethane was flushed with argon, then irradiated in a Vycor flask for 6.5 h at 10°C using 254-nm lamps. After distilling off the dichloromethane the residue had ir absorptions at ν_{max}: 3400, 2120 (residual azide), 1737, 1702, and 1679 cm^{-1}. Its ^{1}Hmr spectrum showed no enamide to be present. The residue was taken up in hexane/benzene (1:1, v/v) and adsorbed on a column of 4 g of neutralized flash silica gel. The same solvent eluted 268 mg of a material that was rich in imine **10** but contained some azide **4*a***. Elution with benzene, and then dichloromethane, gave 39 mg of unidentified products. Further elution with dichloromethane containing methanol (5%, v/v) yielded 247 mg of a material rich in enamide **11**. The azide-containing material was irradiated for another 2 h in 50 mL of dry dichloromethane and purified again by chromatography on 1.9 g of neutralized flash silica gel. Elution with hexane/benzene (1:1, v/v) gave 202 mg of a material that consisted of approximately 80% (by ^{1}Hmr ratios) of imine **10**, corresponding to a yield of 27%.

(*b*) A comparable photolysis of 450 mg of **4*a*** gave 457 mg of crude material. This was heated in 0.5 mL of dry pyridine for 1 h in a bath at 124°C. After removal of the pyridine *in vacuo* the remaining brown liquid was distilled in a Kugelrohr at a pressure of 0.3 Torr. Three fractions were collected: 94 mg boiling up to 75°C; 142 mg boiling at 75–130°C, and 49 mg boiling at 130–140°C. The middle fraction of 142 mg contained most of the enamide **11**. Purification by plc on silica

[6]The ^{13}Cmr shift of the ketone carbonyl (>200 ppm) relative to an ester carbonyl (ca. 170 ppm) is in accord with this electron density.

Can. J. Chem. Downloaded from www.nrcresearchpress.com by 88.85.125.76 on 09/07/12
For personal use only.

gel (two plates of 1000 μm) using chloroform containing (5% v/v) methanol as solvent gave 49 mg (14%) of enamide **11***a* (R_f 0.39) followed closely by 45 mg (13%) of enamide **11***b*. (The yields are adjusted for unreacted azide.)

(*c*) In some of the photolyses in dichloromethane, crystalline ethylamine hydrochloride separated. This must have arisen from the hydrolysis of **10**, presumably a result of moisture accidentally present in the photolysate. The maximum yield obtained was 7%.

2. In methanol

(*a*) A solution of 323 mg of azide **4***a* in 40 mL of methanol was irradiated at 10°C for 3 h using 300-nm lamps. After irradiation, 200 mg of *p*-toluenesulfonic acid hydrate was added and the solution was left for 3 h at room temperature. It was then evaporated at 25°C *in vacuo* and the residue distributed between dichloromethane and aqueous sodium carbonate. The dichloromethane extracts yielded 255 mg of an oil, which was distilled in a Kugelrohr apparatus at 0.1 Torr. After a forerun of 28 mg (below 90°C) a main fraction of 124 mg was collected between 90 and 125°C. The main fraction was nearly pure methoxy compound **14**, some of which was also present in the forerun. The estimated yield of **14** was 44%, representing a minimum yield of *N*-acyl imine **9** as a primary product.

(*b*) The material from a comparable photolysis of 606 mg of azide **4***a* was hydrolyzed (60 mL methanol, 0.3 mL conc. hydrochloric acid, 0.5 mL water) for 1 h at room temperature. The methanol was removed *in vacuo* and the residue was distributed between water and dichloromethane. The water layers were concentrated to a volume of 2 mL and then treated for 1 h under Schotten–Baumann conditions with 300 mg of benzoyl chloride and 20% of aqueous sodium hydroxide. Extraction with dichloromethane gave 194 mg of a crude material. Purification by plc on silica gel (1 plate of 1000 μm) using chloroform containing ethanol (5%, v/v) furnished 132 mg (27%) of pure *N*-ethyl benzamide with a melting point of 69°C. This material was identical to an authentic sample. This represents a minimum yield of the imine **10** in this photolysis.

3. In ethanol

A solution of 430 mg of azide **4***a* in 80 mL of absolute ethanol was irradiated in a Vycor vessel for 2.5 h at 8°C using 254-nm lamps. The photolysate was then treated with 446 mg of *p*-toluenesulfonic acid hydrate for 1 h at 30°C. Concentration at 40°C *in vacuo* gave a material that was distributed between dichloromethane and aqueous sodium bicarbonate. The organic layers gave 323 mg of a crude oil that was purified by plc using silica gel (3 plates of 1000 μm) and chloroform containing ethanol (10% v/v). Zone extraction (R_f 0.5) gave 124 mg (26%) of ethoxy compound **12**.

Characterization and derivatization of the photolysis products from azide **4**a

Ethyl 2-acetamido-2-butenoate (11)

The enamide isomers **11** were further purified by plc, short path distillation at 100°C and 0.3 Torr, and recrystallization.

trans *Isomer (Z isomer) 11*a: The isomer with the higher R_f value crystallized from ethyl acetate/hexane upon cooling. The long flat needles had a melting point of 44–45°C. The spectral data supported the structural assignment; ir ν_{max}: 3400 (m), 1725 (m), 1680 (s) cm^{-1}; ^{1}Hmr: 7.7 (1H, br) 6.99 (1H, q, J = 8 Hz), 4.30 (2H, q, J = 7 Hz), 2.08 (3H, s), 2.07 (3H, d, J = 8 Hz), 1.35 (3H, t, J = 7 Hz); ^{13}Cmr: 169.1 (s), 164.7 (s), 127.7 (d), 126.3 (s), 61.5 (d), 24.2 (t), 14.3 (t). Reference 19 described this compound as an oil and assigned it the *Z* geometry illustrated below.

cis *Isomer (E isomer) 11*b: The isomer with the lower R_f value crystallized from ethyl acetate/hexane as sheaves of needles with a melting point of 64–65°C. Its spectral data supported the structural assignment; ν_{max}: ir 3405, 1692 cm^{-1}; ^{1}Hmr: 7.29 (1H, br), 6.80 (1H, q, J = 7 Hz), 4.23 (2H, q, J = 7 Hz), 2.13 (3H, s), 1.77 (2H, d, J = 7 Hz), 1.30 (3H, s). Reference 22 reported a melting point of 66.5°C while ref. 20 reported a melting point of 61°C for a mixture rich in this isomer. In ref. 22 the *E* geometry was assigned to this isomer as illustrated below:

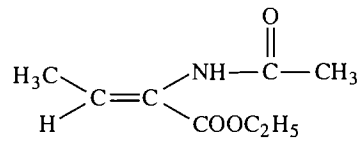

11*a* *Z* isomer

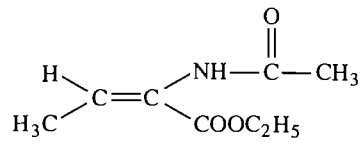

11*b* *E* isomer

Ethyl 2-ethylimino-3-oxobutanoate (10)

The imine **10** was further purified by repeated plc on neutralized flash silica gel using hexane/benzene (1:1, v/v) as developing system. The nearly pure material so obtained was an oil with the following spectral data: ir ν_{max}: 1737, 1702 cm^{-1}; ^{1}Hmr: 4.55 (2H, q, J = 7 Hz), 3.61 (2H, q, J = 7 Hz), 2.45 (3H, s), 1.35 (6H, t, J = 7 Hz; at 60 MHz the two methyl triplets were separated by approx. 2 Hz); ^{13}Cmr: 197.0, 163.8, 159.4, 61.6, 50.0, 24.3, 15.3, 14.2. EI-MS: 171 (0.6), 156 (2.2), 144 (3.3), 128 (20), 101 (3), 98 (8.6), 56 (100). Mol. wt. calcd. for $C_8H_{13}NO_3$: 171 (the fragments with e/z 128 and 98 correspond to a loss of $CH_3CO\cdot$ and $\cdot COOC_2H_5$ respectively, while the base peak at 56 probably corresponds to the ion $CH_3CH_2N^+{=}CH\cdot$).

Imine **10** was further characterized by its conversion to the bis-4-nitrophenylhydrazone derivative. For this purpose a solution of 100 mg of **10** in 1 mL of ethanol and 0.05 mL of concentrated hydrochloric acid was left at room temperature for 1 h. After addition of 50 mg of sodium acetate, 200 mg of 4-nitrophenylhydrazine, and 1 mL of ethanol the mixture was heated under reflux for 20 min. A crystalline material separated, and was removed by filtration. Then 0.1 mL of acetic acid was added to the filtrate. This mixture was heated under reflux for 1 h to give a second bath of crystals. The combined solids were washed with water to remove salts, leaving 123 mg (51%) of a sparingly soluble product with a melting point of 290°C (dec.). Recrystallization from chloroform/ethanol gave pure ethyl 2,3-dioxobutanoate bis-hydrazone **13** melting at 292–294°C (dec.). It gave ^{1}Hmr signals in pyridine-d_5 at 8.5–7.0 (pyridine + Ar H), 4.90 (4H, s, 2NH + H_2O), 4.13 (2H, q, J = 7 Hz), 2.25 (3H, s), 1.24 (3H, t, J = 7 Hz). Anal. calcd. for $C_{18}H_{18}N_6O_6$: C 52.17, H 4.38, N 20.28; found (sample dried for 5 h at 140°C and 0.1 Torr): C 51.01, H 4.26, N 20.38.

Ethyl 2-acetamido-2-methoxybutanoate (14)

The methoxy compound **14** was further purified by plc on silica gel using chloroform containing methanol (5%, v/v). The material so obtained (R_f 0.5) was distilled over a short path at 90°C and 0.05 Torr. It crystallized from ethyl acetate and melted at 71.5–72.5°C. The reported melting point (19) is 80–81°C, but their ^{1}Hmr data were identical to ours. Spectral and analytical data supported the structure assigned to **14**; ir ($CHCl_3$) ν_{max}: 3410, 1730, 1688 cm^{-1}; ^{1}Hmr: 6.73 (1H, b), 4.30 (2H, q, J = 7 Hz), 3.25 (3H, s), 2.45–1.9 (2H, m), 2.06 (3H, s), 1.30 (3H, t, J = 7 Hz), 0.80 (3H, t, J = 7 Hz); ^{13}Cmr: 170.2, 169.5, 88.4, 62.1, 51.3, 28.3, 23.6, 14.1, 7.7. Anal. calcd. for $C_9H_{17}NO_4$: C 53.19, H 8.43, N 6.89; found: C 52.96, H 8.47, N 6.87.

Methoxy compound **14** was further characterized by its conversion to the 2,4-dinitrophenyldrazone derivative. For this purpose a solution of 64 mg of **14** in 3 mL of ethanol containing 108 mg of 2,4-dinitrophenylhydrazine in suspension was heated gently while concentrated hydrochloric acid was added dropwise. After a clear reddish solution was obtained, 0.5 mL of water was added and the solution was cooled. Crystalline ethyl 2-oxobutanoate 2,4-dinitrophenylhydrazone separated, melting at 135°C. Recrystallization from ethanol gave a 2,4-dinitrophenylhydrazone melting at 139–141°C (lit. (23) mp

142°C). It gave ^{1}Hmr signals at 9.20 (1H, d, J = 2 Hz), 8.6–7.8 (2H, m), 4.49 (2H, q, J = 7 Hz), 2.78 (2H, q, J = 7 Hz), 1.45 (3H, t, J = 7 Hz), 1.27 (3H, t, J = 7 Hz).

Ethyl 2-acetamido-2-ethoxybutanoate (12)

The ethoxy compound **12** was characterized by crystallization from ether/hexane, giving a product with a melting point of 78–79°C. The melting point reported in the literature (19) was 102–104°C. The structural assignment of the product was supported by its spectral and analytical data; ir ν_{max}: 3415, 1730, 1685 cm^{-1}; ^{1}Hmr: 6.85 (1H, s), 4.33 (2H, q), 3.1–3.7 (2H, m), 1.8–2.7 (2H, m), 2.08 (3H, s), 1.31 (3H, t, J = 7 Hz), 1.20 (3H, t, J = 7 Hz), 0.80 (3H, t, J = 7 Hz). Anal. calcd. for $C_{10}H_{19}NO_4$: C 5.28, H 8.82, N 6.45; found: C 55.49, H 8.82, N 6.40.

Photolysis of ethyl 2-azido-2-benzyl-3-oxobutanoate (4b)

1. In dichloromethane

(*a*) A solution of 618 mg of the azide **4***b* in 80 mL of dry dichloromethane was placed in a Vycor vessel and flushed with dry argon. It was then irradiated at 15°C for 4 h using 300-nm lamps. The yellow photolysate was then concentrated *in vacuo* to give 605 mg of an oil with ir signals at ν_{max} 3400, 1737, 1702, and 1681 cm^{-1} and ^{1}Hmr signals at 2.15 (weak singlet) and at 4.75, 3.85, 2.40, 2.20, and 1.95 (strong to medium singlets). The oil was taken up in a benzene/hexane mixture (1:1, v/v) and adsorbed onto a column (1.4 × 11 cm) of neutralized flash silica gel. Elution with a mixture of benzene/hexane (3:7, v/v) gave 228 mg of an oil very rich in the imine **16**. Further elution with the same solvent, then benzene, gave 94 mg of a mixture of unidentified products. Elution with dichloromethane gave another 44 mg of a mixture of unidentified products. Finally, elution with dichloromethane containing methanol (5%, v/v) gave 241 mg of an orange oil rich in enamide **17**. This oil was further purified by plc on silica gel (2 plates of 1000 μm) using chloroform containing ethanol (3%, v/v) as developing system. Zone extraction (R_f 0.2) furnished 146 mg (26%) or nearly pure enamide **17**.

(*b*) In a comparable experiment at 5°C crystalline benzylamine hydrochloride (25%) separated during the photolysis. Formation of this product presumably arose by hydrolysis of imine **16**, a result of moisture being present in the photolysate.

2. In methanol

(*a*) A solution of 300 mg of azide **4***b* in 60 mL of dry methanol was purged with nitrogen and then irradiated using a 100-W Hanovia lamp in an immersion well of Vycor glass cooled with circulating methanol at ca. −55°C. The outer vessel was immersed in a Dry Ice – acetone bath. Monitoring by ir spectroscopy showed that the azide signal at 2120 cm^{-1} diminished in intensity while new peaks at 1705 and 1680 cm^{-1} apeared. After 2 h of irradiation only a little amount of azide remained. Evaporation of the photolysate at 30°C *in vacuo* gave 242 mg of an oil that showed four main spots on tlc (CCl_4/EtOAc = 4:3). The oil showed ir absorptions at 3410 (w), 2120 (w), 1735 (s), 1705 (s), 1685 (s), 1645 (w), 1605 (w), and 1585 (w) cm^{-1}. The ^{1}Hmr spectrum showed two pairs of signals at 4.8 and 2.5 and at 4.0 and 2.2 consistent with the presence of the imine **16** and the *N*-acyl imine **15**. These two major components were present in nearly equal amounts (ca. 25% each). The ^{1}Hmr spectrum showed only weak methoxy signals at 3.30 and 3.35.

(*b*) A solution of 1.13 g of azide **4***b* in 170 mL of methanol was irradiated in two portions in a Vycor vessel at 10°C using 254-nm lamps. After 3 h only a small amount of azide remained (ir). Removal of the methanol *in vacuo* gave a material that was adsorbed from benzene onto 200 g of neutral alumina, activity III. Elution with benzene gave an early eluate of 203 mg of a mixture. Further elution with benzene and with benzene/dichloromethane (1:1, v/v) gave a second eluate of 405 mg, which was rich in the methoxy compound **19**. Chloroform and methanolic chloroform eluted another 181 mg of a mixture. The early eluate was further purified by plc on silica gel (2 plates of 1000 μm) using chloroform containing methanol (5%, v/v) as developing system. Extraction of the fastest zone (R_f 0.8) gave 65 mg of a material that contained roughly 40% of benzaldehyde accompanied by a number of other components. The second eluate yielded a total of 299 mg (26%) of crystalline methoxy compound **19**.

(*c*) A solution of 77 mg of azide **4***b* in 80 mL of methanol was irradiated in a Vycor vessel for 5 h at 10°C using 300-nm lamps. After concentration of the photolysate to a volume of 3 mL the remainder was treated with 1 mL of 6 N sulfuric acid for 1 h at room temperature and 0.5 h at 55°C. The remaining methanol was then removed *in vacuo*. After addition of 5 mL of water, extraction with dichloromethane removed the neutral and acidic products. The dichloromethane extracts were washed with aqueous sodium carbonate. Evaporative work-up gave 481 mg of neutral oil that was rich in the methoxy compound **19**. The acidic aqueous fraction was made strongly basic with sodium hydroxide. Extraction with dichloromethane, and evaporative work-up of the extracts, gave 108 mg of basic products. This material was acetylated to furnish 116 mg (26%) of nearly pure *N*-benzylacetamide, thus indicating that the photolysis produced a minimum yield of 26% of imine **16**.

Characterization and derivatization of the photolysis products from azide 4b

Ethyl 2-acetamido-3-phenylpropenoate (ethyl 2-acetamidocinnamate) (17)

Enamide **17** was further purified by plc on silica gel (plate of 1000 μm) using chloroform containing methanol (5%, v/v) as developing system. The material obtained by zone extraction (R_f 0.5) was distilled in a Kugelrohr apparatus at 145°C and 0.05 Torr to give pure **17** as characterized by the following spectral and analytical data: ir ($CHCl_3$) ν_{max}: 3350, 1680 cm^{-1}; ^{1}Hmr: 7.96 (1H, br s), 7.70 (1H, s), 7.25 (5H, s), 4.13 (2H, q, J = 7 Hz), 2.13 (3H, s), 1.02 (3H, t, J = 7 Hz); ^{13}Cmr: 169.0 (s), 164.9 (s), 135.3 (s), 128.5–126.8, 125.0 (d), 61.6 (t), 23.9 (q), 13.4 (q). Anal. calcd. for $C_{13}H_{15}NO_3$: C 66.93, H 6.48, N 6.01; found: C 66.81, H 6.44, N 5.95. According to its spectral data, **17** was mainly one geometric isomer, different from the one described by Hersheid *et al.* (21), which had a melting point of 98°C.

Ethyl 2-acetamido-2-methoxy-3-phenylpropanoate (19)

The methoxy compound **19** was recrystallized from acetone/hexane to give pure **19** melting at 100–101°C (lit. (19) mp 98°C). The spectral and analytical data supported the assigned structure; ir ($CHCl_3$)ν_{max}: 3415, 1730, 1690 cm^{-1}; ^{1}Hmr: 7.03 (5H, s), 6.47 (1H, br s), 4.31 (2H, q, J = 7 Hz), 3.95 (1H, d, J = 13 Hz), 3.25 (1H, d, J = 13 Hz), 3.30 (3H, s), 2.06 (3H, s), 1.32 (3H, t, J = 7 Hz); ^{13}Cmr: 169.8 (s), 134.7 (d), 130.2, 128.3 and 127.3 (d), 88.6 (s), 62.4 (t), 51.7 (q), 41.0 (t), 24.0 %q), 14.2 (q). Anal. calcd. for $C_{14}H_{19}NO_4$: C 63.38, H 7.22, N 5.28; found: C 63.53, H 7.30, N 5.16.

Methoxy compound **19** was further characterized by its conversion to the 2,4-dinitrophenylhydrazone derivative. For this purpose 40 mg of **19** was dissolved in 1 mL of ethanol. Then a hot solution of 77 mg of 2,4-dinitrophenylhydrazine in 3 mL of ethanol and 0.5 mL of concentrated hydrochloric acid was added. After 1.5 h, 0.5 mL of water was added and the mixture was allowed to stand for 2 h at room temperature. Concentration *in vacuo* gave a residue that was distributed between dichloromethane and 4 N sulfuric acid. The dichloromethane extracts were washed first with 3 N sulfuric acid and then with water. After drying, the solution was concentrated *in vacuo* to yield 57 mg of an orange coloured gum. Purification by plc on silica gel (2 plates of 500 μm) using chloroform containing ethanol (2%, v/v) gave 3 mg of a fast moving (R_f 0.6) crystalline material, followed closely by 13 mg of an amorphous material. Crystals combined from several runs were recrystallized from dichloromethane/ether to give the pure ethyl 3-phenyl-2-oxopropanoate 2,4-dinitrophenylhydrazone with a melting point of 132°C. Its spectral and analytical data supported the assigned structure; ^{1}Hmr: 9.12–8.10 (3H, m), 7.28 (5H, s), 4.36 (2H, q, J = 7 Hz), 3.95 (2H, s), 1.32 (3H, t, J = 7 Hz). Anal calcd. for $C_{17}H_{16}N_4O_6$: C 54.84, H 4.33, N 15.05; found: C 54.62, H 4.24, N 15.04. The amorphous material had an ^{1}Hmr spectrum nearly identical to that of the crystalline hydrazone, except for the benzyl methylene signal at 4.10 (2H, s). Thus the two materials must be the *syn* and *anti* isomers of the 2,4-dinitrophenylhydrazone.

Can. J. Chem. Downloaded from www.nrcresearchpress.com by 88.85.125.76 on 09/07/12
For personal use only.

Can. J. Chem. Downloaded from www.nrcresearchpress.com by 88.85.125.76 on 09/07/12
For personal use only.

Ethyl 2-benzylimino-3-oxobutanoate (16)

The crude imine **16** was estimated to be 75% pure but contained some benzaldehyde and a variety of minor impurities (^{1}Hmr). Although the sample could not be obtained pure, its structural identity was confirmed by the following spectral data: ir ν_{max}: 1737, 1702 cm^{-1}; ^{1}Hmr: 7.38 (5H, s), 4.75 (2H, s), 4.39 (2H, q, J = 7 Hz), 2.44 (3H, s), 1.36 (3H, t, J = 7 Hz); ^{13}Cmr: 196.7(s), 163.3(s), 159.3(s), 128.3, 127.7 and 127.2(d), 61.6(d), 58.5(d), 24.2(q), 13.8(q). The presence of benzaldehyde in most samples was confirmed by the ^{1}Hmr signal at δ 10.0 and ^{13}Cmr signals at 192.2 and 134.4 ppm. The benzaldehyde impurity was also confirmed by its conversion to a 4-nitrophenylhydrazone that had a melting point of 190°C and a mixture melting point with an authentic sample of 191°C.

Imine **16** was further characterized by its hydrolysis and subsequent derivatization with 4-nitrophenylhydrazine. For this purpose a solution of 75 mg of the best sample of imine **16** in 1 mL of ethanol (95%) and 0.1 mL of concentrated hydrochloric acid was left for 2 h at room temperature. Concentration *in vacuo* gave a residue that was taken up in dichloromethane. After washing with sodium bicarbonate solution, the dichloromethane was evaporated and 2 mL of ethanol and 207 mg of 4-nitrophenylhydrazine were added. The mixture was heated to boiling for 5 min and left overnight under argon. Evaporation of the ethanol *in vacuo* gave a residue that was partially soluble in chloroform. The insoluble material was filtered off and consisted of 26 mg of high melting crystals. The chloroform filtrate was washed with 3 N sulfuric acid and water. Evaporation of the chloroform gave a material that was purified by plc on silica gel (one plate of 1000 μm) using chloroform containing methanol (10%, v/v) as developing system. Zone extraction gave 2 mg of high melting crystals and 12 mg of benzaldehyde 4-nitrophenylhydrazone. The high melting crystals were sparingly soluble in hot chloroform or diglyme but could be recrystallized from dry pyridine to give a material melting at 292–294°C. This material showed no melting point depression with ethyl 2,3-dioxobutanoate bis-4-nitrophenylhydrazone **13** prepared from the imine **10**. However, its ^{1}Hmr spectrum showed no signals corresponding to an ethyl ester group. Therefore, the high melting crystals are most probably the pyrazolone **33**, formed also upon heating of the hydrazone **13**.

Preparation and photolysis of azide 7

Ethyl 3,3-ethylenedioxy-2-methylbutanoate

To a solution of 35 g of ethyl 2-methyl-3-oxobutanoate (Aldrich) in 40 mL of chloroform (ethanol-free) was added 35 g of ethylene glycol and 1 g of *p*-toluenesulfonic acid. The mixture was heated to gentle boiling to remove the chloroform and water (approximately 3.5 mL) during a period of 6 h. Fractional distillation of the residue gave 37 g (80%) of the ketal ester boiling at 58°C at a pressure of 0.1 Torr. The material showed ^{1}Hmr signals at 4.20 (2H, q, J = 7 Hz), 4.02 (4H, s), 2.81 (1H, q, J = 7 Hz), 1.43 (3H, s), and 1.29 (6H, t, J = 7 Hz).

3,3-Ethylenedioxy-2-methylbutanoic acid

To a solution of 4.35 g of ethyl 3,3-ethylenedioxy-2-methylbutanoate in 50 mL of dioxane–water (1:1 v/v) was added 5 g of potassium hydroxide. The initial two-phase mixture was stirred at 35°C and became homogeneous after 6 h. Stirring was continued for another hour, then the bulk of the solvents was removed under reduced pressure. The residue was dissolved in 30 mL of water and washed with dichloromethane. The aqueous solution was then acidified and extracted with chloroform. Evaporation of the solvent gave 3.0 g (81%) of the ketal acid, with the following ^{1}Hmr data: 9.8 (1H, br s), 4.03 (4H, s), 2.83 (1H, q, J = 7 Hz), 1.45 (3H, s), 1.33 (3H, d, J = 7 Hz).

3,3-Ethylenedioxy-2-methylbutanoyl chloride

A solution of 1.18 g of 3,3-ethylenedioxy-2-methylbutanoic acid in 10 mL of dry dichloromethane was cooled to 0°C under dry argon. Then a solution of 2.15 g of oxalyl chloride in 4 mL of dry dichloromethane was added. After 5 min at 0°C the mixture was allowed to warm and then was kept at room temperature. Gas evolution ceased after 30 min, and after another 30 min the solvent and excess oxalyl chloride were removed under reduced pressure. The residual oil was distilled over a short path to give 1.1 g of the ketal acid chloride boiling at 65°C at a pressure of 0.3 Torr.

N-*(3,3-Ethylenedioxy-2-methylbutanoyl)-piperidine*

To a solution of 376 mg of 3,3-ethylenedioxy-2-methylbutanoyl chloride in 5 mL of pentane was added slowly with stirring a solution of 400 mg of piperidine in 5 mL of dichloromethane. After complete addition the reaction mixture was washed with dilute sulfuric acid, followed by a washing with dilute sodium carbonate solution. Evaporation under reduced pressure gave 433 mg (66%) of crude ketal amide **8**. Distillation over a short path of 0.5 Torr and 100°C gave pure amide **8**. Spectral and analytical data were in agreement with the structural assignment; ir ν_{max}: 3410 (br), 1625 cm^{-1}; ^{1}Hmr: 3.93 (4H, s), 3.53 (4H, br s), 3.07 (1H, q, J = 7 Hz), 1.60 (6H, br s), 1.37 (3H, s), 1.20 (3H, d, J = 7 Hz). Anal. calcd. for $C_{12}H_{21}NO_3$: C 63.41, H 9.31, N 6.16; found: C 63.19, H 9.41, N 6.28.

N-*(2-Methyl-3-oxobutanoyl)-piperidine (5)*

To a solution of 111 mg of *p*-toluenesulfonic acid hydrate in 5 mL of water was added 79 mg of *N*-(3,3-ethylenedioxy-2-methylbutanoyl)-piperidine. After stirring for 10 h at room temperature the reaction mixture was made alkaline by adding sodium carbonate. Extraction with dichloromethane gave 647 mg (100%) of the keto amide **5** with the correct spectral data; ir ν_{max}: 3450 (br), 1725, 1645, 1635 cm^{-1}; ^{1}Hmr: 3.70 (1H, q, J = 7 Hz), 3.87–3.35 (4H, br s), 2.23 (3H, s), 1.67 (6H, br s), 1.37 (3H, d, J = 7 Hz).

N-*(2-Bromo-2-methyl-3-oxobutanoyl)-piperidine (6)*

(a) Bromination with bromine: To a stirred solution of 1.49 g of keto amide **5** and 100 mg of *p*-toluenesulfonic acid hydrate in 4 mL of dichloromethane was added slowly a solution of 800 mg of bromine in 4 mL of dichloromethane. After initial rapid uptake of bromine an excess persisted for 10 min. The reaction mixture was washed with a dilute solution of sodium carbonate and then concentrated under reduced pressure to give a crude residue of 1.85 g. According to its ^{1}Hmr spectrum, this residue still contained starting keto amide **9**. Therefore this residue was subjected to a repeat bromination and work-up to give a crude product weighing 1.98 g. This material was absorbed from benzene onto 40 g of neutral alumina (activity II). Elution with benzene gave 1.08 (50%) of nearly pure bromoketo amide **6**.

(b) Bromination with pyridinium bromide perbromide: To a solution of 560 mg of the keto amide **5** in 2 mL of dry pyridine was added 1.5 g of pyridinium bromide perbromide. The reaction mixture was stirred for 6 h at room temperature, during which time some hydrobromide crystallized. Removal of the pyridine *in vacuo* at 35°C left a residue that was taken up in dichloromethane (10 mL) and washed with dilute sulfuric acid (3 mL). The dichloromethane solution was then washed with a dilute solution of sodium thiosulfate and dried. Evaporation under reduced pressure gave a residue that contained much starting material (^{1}Hmr). The bromination was repeated with 3 mL of pyridine and 2 g of pyridinium bromide perbromide. A reaction time of 17 h at room temperature in the dark, followed by the above work-up, gave a residue that was extracted with dry ether. The ether-soluble component was 715 mg of a pale yellow gum. A crude purification by adsorption onto 20 g of neutral alumina (activity II) and elution with ether gave 585 mg of products followed by 84 mg of starting material. The product mixture was separated by plc on silica gel (4 plates of 100 μm) using a mixture of ethyl acetate/hexane (6:4, v/v) as eluent. Extraction of the front zone (R_f 0.8) gave 202 mg of an almost pure, fast moving solid material. A second zone yielded 245 mg of a pure, slower moving oily material.

The slower moving material proved to be the desired *N*-(2-bromo-2-methyl-3-oxobutanoyl)-piperidine **6** (30%) with correct spectra data: ir ν_{max}: 1720, 1710, 1640 cm^{-1}; ^{1}Hmr: 3.52 (4H, br s), 2.48 (3H, s), 2.04 (3H, s), 1.65 (6H, br s).

The fast moving material was further purified by filtering of a dichloromethane solution through a short column of neutral alumina (activity IV). Evaporation of the solvent gave a material that crystallized as prisms from ethyl acetate/hexane. This material proved to be

Can. J. Chem. Downloaded from www.nrcresearchpress.com by 88.85.125.76 on 09/07/12
For personal use only.

N-(2,4,4-tribromo-2-methyl-3-oxobutanoyl)-piperidine (**8**) melting at 82–83°C. Spectral and analytical data corroborated the structural assignment; ir ν_{max}: 1741, 1651, 1619 cm^{-1}; uv (95% ethanol) λ_{max}: 269 nm (ϵ 1000); ^{1}Hmr: 6.52 (1H, s), 3.67 (4H, br), 2.18 (3H, s), 1.63 (6H, br); ^{13}Cmr: 190.4, 164.5, 59.7, 48.1 (br), 45.0 (br), 36.2, 27.2, 25.4, 24.1 (at −30°C the broad signals at 48.1 and 45.0 sharpened to singlets at 48.6 and 44.6, with small shift changes in other signals). Anal. calcd. for $C_{10}H_{14}Br_3NO_2$: C 28.60, H 3.36, N 3.34, Br 57.09; found: C 28.69, H 3.58, N 3.70, Br 56.10.

N-*(2-Azido-2-methyl-3-oxobutanoyl)-piperidine (7)*

Lithium azide (570 mg) was dissolved in 5 mL of dry dimethylformamide by heating. After cooling to 10°C a solution of 875 mg of bromoketo amide **6** in 5 mL of dry dimethylformamide was added. After 20 min at room temperature the main portion of the solvent was removed under reduced pressure and a bath temperature of 60°C. The residue was dissolved in dichloromethane, then the solution was washed with water, dried, and concentrated. The residue of 838 mg, containing a little dimethylformamide, was distilled over a short path. At a pressure of 0.1 Torr and a temperature of 130°C a colourless oil (657 mg, 88%) was obtained, which proved to be the desired azidoketo amide **7**. It had ir ν_{max}: 2105, 1721, 1651 cm^{-1}; ^{1}Hmr: 3.47 (4H, br s), 2.30 (3H, s), 1.73 (3H, s), 1.63 (6H, br s). Anal calcd. for $C_{10}H_{16}N_4O_2$: C 53.55, H 7.19, N 24.99; found: C 53.43, H 7.26, N 24.87.

Photolysis of N-*(2-azido-2-methyl-3-oxobutanoyl)-piperidine 7*

A solution of 310 mg of azidoketo amide **7** in 80 mL of dry methanol under argon was irradiated for 4 h at 10°C in a Vycor vessel using lamps with a peak emission at 254 nm. After addition of 130 mg of *p*-toluenesulfonic acid hydrate, the photolysate was warmed to 40°C and then left at room temperature for another hour. The photolysate was neutralized with a saturated aqueous solution of sodium bicarbonate and then concentrated under reduced pressure to a volume of 5 mL. After addition of 5 mL of water, extraction with dichloromethane (3 × 15 mL) and chloroform (10 mL) led to the isolation of 286 mg of an oily material. Separation of the products by plc using silica gel (2 plates of 1000 μm) and methanol/chloroform (1:9, v/v) gave 165 mg of a fast moving material (R_f 0.6) and 36 mg of a slower moving material (R_f 0.4). According to its ^{1}Hmr spectrum, the fast moving material was mainly methoxy compound **20**. Further purification by plc using methanol-washed alumina and ethanol-free chloroform gave a material isolated from the main zone (R_f 0.36), which was once more purified by plc using silica gel and methanol/chloroform (1:9, v/v). Zone extraction gave a faintly coloured oil (83 mg, 26%), which proved to be almost pure[7] *N*-(2-acetamido-2-methoxypropionyl)-piperidine (**20**) according to its spectral data; ir ν_{max}: 3375, 1677, 1617 cm^{-1}; ^{1}Hmr: 7.7 (1H, br), 4.0–3.4 (5H, m), 3.21 (3H, s), 2.07 (3H, s), 1.93 (3H, s), 1.69 (6H, br m); ^{13}Cmr: 168.9, 168.0, 87.0, 51.6, 47.0, 45.0, 26.4, 26.0, 25.7, 24.4, 23.0. CI-MS: 229 (94.5), 197 (100), 170 (17), 155 (50). Mol. wt. calcd. for $C_{11}H_{20}N_2O_3$: 228.

The slower moving pure material, which crystallized on standing, proved to be *N*-(2-methoxy-2-methylamino-3-oxobutanoyl)-piperidine (**21**) (36 mg, 11%) with a melting point of 121–123°C (needles from ethyl acetate/hexane). Spectral data, ir ν_{max}: 3450, 3420, 1722, 1653 cm^{-1}; ^{1}Hmr: 5.7 (1H, br), 3.5–3.2 (4H, br m), 3.18 (3H, s), 2.30 (3H, s), 1.61 (6H, br s); ^{13}Cmr: 207.8, 155.1, 87.8, 50.2, 45.0, 25.7, 24.3, 23.9, 21.8. CI-MS: 229 (94.5), 197 (100), 185 (7), 149 (75), 112 (35). Mol. wt. calcd. for $C_{11}H_{20}N_2O_3$: 228.

A second photolysis under comparable conditions was carried out with 274 mg of azidoketo amide **7** in 40 mL of methanol containing 159 mg of trifluoroacetic acid. After irradiation for 2.5 h the photolysate was concentrated under reduced pressure and the residue was dissolved in dichloromethane. This solution was washed with a saturated solution of sodium bicarbonate, and concentrated under reduced pressure to yield 250 mg of an oily product exhibiting only weak azide absorption. Purification of this material by plc using alumina (2 plates of 1000 μm) and chloroform gave 15 mg of a fast moving material that proved to be the starting azidoketo amide **7**. Zone extraction of a slower moving material (R_f 0.7) gave 79 mg (30% based on unrecovered **7**) of the 2-acetamido-2-methoxy compound **20**.

Preparation and photolysis of azido lactam 28

L-Prolyl-L-valyl lactam (24)

The diketopiperazine **24** was prepared from L-prolyl-L-valine methyl ester (an oil with $[\alpha]_D$ −55° (*c* 0.95, ethanol)), which in turn was prepared from benzyloxycarbonyl-L-prolyl-L-valine methyl ester (an oil with $[\alpha]_D$ −60° (*c* 1.01, ethanol) by hydrogenolysis over 30% Pd on charcoal in ethanol. The L-prolyl-L-valine methyl ester (3.49 g) was placed in a small flask equipped with a short air condenser. The ester was then cyclized by heating for 3 h in a bath at 110°C and at a pressure of 12 Torr. The residue was triturated with ethyl acetate/hexane, leaving a crystalline solid that was filtered off. The soluble material was heated again as above leading to the isolation of a second batch of crystals. After a third heating a total of 1.23 g (41%) of crystalline diketopiperazine **24** was collected. After recrystallization from ethyl acetate/hexane this material had a melting point of 190°C and $[\alpha]_D$ −156° (*c* 1.0, ethanol) (lit. (9) mp 192°C; $[\alpha]_D$ −159°).

N-*(3,3-Ethylenedioxy-2-methylbutanoyl)-prolyl-valyl lactam (25)*

A solution of 2.75 g of 3,3-ethylenedioxy-2-methylbutanoyl chloride in 3 mL of dry chloroform was added to a cooled solution of 2.67 g of diketopiperazine **24** and 1.66 g of 4-dimethylaminopyridine in 5 mL of dry chloroform. The resulting mixture was heated to reflux for 6.5 h and then left at room temperature for 9 h. After dilution with chloroform the solution was washed with dilute sulfuric acid and a saturated solution of sodium bicarbonate. Evaporation of the solvent followed by oil pump evacuation (40°C, 0.5 Torr) gave 4.5 g of an oily residue. This residue was dissolved in ethyl acetate/hexane (1:1, v/v) whereby a precipitate of 403 mg of unreacted diketopiperazine **24** was formed. Concentration of the filtrate led to the isolation of 3.6 g of a material that was rich in isomeric *N*-acylated diketopiperazines (ketal lactams) **25**. This material was dissolved in benzene and adsorbed onto 30 g of neutral alumina (activity III). Elution with benzene and dichloromethane gave 3.0 g of a principal eluate, which proved to be a mixure of isomers of the desired ketal lactam **25** and esters of ethylene glycol (^{1}Hmr). Further elution with dichloromethane and chloroform containing ethanol (0.75%, v/v) gave 207 mg of material rich in L-prolyl-L-valyl lactam **24**, followed by an isomer of **24**.

Spectral analysis of the principal eluate indicated that it consisted of similar amount of two isomeric ketal lactams **25** with the following ^{1}Hmr data: two doublets at 4.93 (J = 4 Hz) and 4.70 (J = 5 Hz), two singlets at 3.90 and 3.77, three major methyl signals at 1.25, 1.13, and 1.02, and a set of weaker methyl signals. In addition the ^{1}Hmr spectrum indicated the presence of minor impurities with signals at 4.33 and 2.0 and 1.92, suggesting the presence of a glycol ester and acetates or methyl ketones. These minor impurities could be removed at 90°C and 0.1 Torr.

N-*(2-Methyl-3-oxobutanoyl)-prolyl-valyl lactam (26)*

A mixture of 5.7 g of the isomeric ketal lactams **25** and 1 mL of tetrahydrofuran gave a syrup, which was stirred for 4 min at room temperature with 80% (v/v) aqueous trifluoroacetic acid. The reaction mixture was then concentrated by evaporation at 25°C and a pressure of 0.1 Torr (25 min). The residue was dissolved in 15 mL dichloromethane and the solution was washed with water followed by 5 mL of a saturated solution of sodium bicarbonate. The aqueous phases were extracted again with dichloromethane. Removal of the solvent from the combined dichloromethane extracts gave 4.39 g of an oily residue. When this residue was dissolved in ether a first crop of 878 mg of crystals separated. Addition of hexane to the mother liquor gave a second crop of 1.1 g of crystals. The combined crystalline material was recrystallized from acetone/hexane to give 1.54 g of a mixture of isomeric keto lactams **26** with a melting point of 150°C. Upon evaporation the mother liquors gave 2.4 g of an amorphous material, which was adsorbed from benzene onto 20 g of neutral alumina (activity III). The first eluates upon evaporation gave 1.1 g of a material that upon dissolution in ether gave another 303 mg of the keto lactam **26** melting at 150°C. The mother liquor contained more keto lactams and a glycol

[7]All the spectra showed evidence of contaminants.

Can. J. Chem. Downloaded from www.nrcresearchpress.com by 88.85.125.76 on 09/07/12
For personal use only.

ester, which could be distilled at 90°C and 2×10^{-3} Torr. Later eluates contained crystals of prolyl-valyl lactam **24** and an isomeric keto lactam. The crystalline keto lactam mixture **26** (1.54 g) was separated by fractional crystallization from acetone/hexane. The main component **26*a*** crystallized as blades with a melting point of 155°C, while the minor component **26*b*** formed complex prisms with a melting point of 109°C.

The major keto lactam **26*a*** was further purified by plc on silica gel using chloroform containing methanol (5%, v/v). The prisms so obtained had a melting point of 158–160°C (dec.) and $[\alpha]_D$ +41° (*c* 0.8, ethanol). The spectral and analytical data supported the structural assignment as *N*-(2-methyl-3-oxobutanoyl)-prolyl-valyl lactam; ir ν_{max}: 1722, 1668, cm^{-1}; ^{1}Hmr: 4.96 (1H, d, J = 9 Hz), 4.3 (2H, m), 3.55 (2H, m), 2.29 (3H, s) 1.40 (3H, d, J = 7 Hz), 1.08 (6H, d, J = 6 Hz); ^{13}Cmr: 205.0, 170.9, 170.7, 165.3, 63.7, 59.9, 56.5, 45.5, 31.4, 29.6, 28.2, 22.8, 19.6, 13.1. Anal. calcd. for $C_{15}H_{22}N_2O_4$: C 61.20, H 7.53, N 9.52; found: C 61.02, H 7.50, N 9.35.

The minor keto lactam **26*b*** was recrystallized from acetone/hexane to give pure **26*b*** with a melting point of 108–109°C and $[\alpha]_D$ +174° (*c* 0.9, ethanol). The spectral and analytical data suported the structural assignment; ^{1}Hmr: 4.98 (1H, d, J = 9 Hz), 4.55 (1H, q, J = 15, J_2 = 7 Hz), 4.3 (1H, t, J = 7 Hz), 3.6 (2H, m), 2.25 (3H, 5), 1.39 (3H, d, J = 7 Hz), 1.09 (3H, d, J = 7 Hz), 0.98 (3H, d, J = 7 Hz). Anal. calcd. for $C_{15}H_{22}N_2O_4$: C 61.20, H 7.53, N 9.52; found: C 61.06, H 7.60, N 9.48.

N-(2-Bromo-2-methyl-3-oxobutanoyl)-prolyl-valyl lactam (27)

Bromination of keto lactams **26** using *N*-bromosuccinimide in THF or using bromine in the presence of trifluoroacetic acid in CH_2Cl_2 gave bad mixtures of products. Using bromine in dry pyridine gave reasonable yields of isomeric monobromoketo lactams. However, the best and most convenient procedure employed the pyridinium bromide perbromide complex.

A solution of 211 mg of quite pure keto lactam **26*a*** (mp 153°C) in 1 mL of dry pyridine was cooled in ice. After addition of 269 mg of pyridinium bromide perbromide the mixture was stirred in the dark at room temperature for 5 h. Concentration under reduced pressure at 30°C gave a residue that was dissolved in 15 mL of dichloromethane and then washed with 5 n sulfuric acid followed by a dilute solution of sodium thiosulfate. Concentration of the dichloromethane solution gave 251 mg of a frothy material from which, upon treatment with ether, a flocculent solid separated. Concentration of the filtrate and treatment of the residue with hexane gave a first crop of 114 mg of nearly pure bromoketo lactam **27** and a second crop of 52 mg of a mixture contining bromoketo lactam **27** and ca. 40% of the parent keto lactam **26*a***. The mixture of **27** and **26*a*** could be separated by chromatography using neutral alumina (activity III) and benzene. The total yield of crystalline bromoketo lactam **27** based on unrecovered **26*a*** was 60%. Recrystallization from dichloromethane gave colourless short needles of bromoketo lactam **27** with a melting point of 107°C and $[\alpha]_D$ 42° (*c* 0.5, ethanol). The spectral and analytical data supported the structural assignment; ir ν_{max}: 1733, 1669 cm^{-1}; ^{1}Hmr: 4.92 (1H, d, J = 9.5 Hz), 4.29 (1H, t, J = 8 Hz), 3.55 (2H m), 2.52 (3H, s), 2.00 (3H, s), 1.10 (3H, d, J = 6.5 Hz), 1.05 (3H, d, J = 6.5 Hz). Anal. calcd. for $C_{15}H_{21}BrN_2O_4$: C 48.26, H 5.63, N 7.50; found: C 48.49, H 5.80, N 7.44.

The mother liquor from the bromination contained mainly material giving ^{1}Hmr signals at 2.0 and 2.5 characteristic of the bromoketo lactam. However, the characteristic doublet at 4.9 arising from the lactam moiety was replaced by a complex multiplet, suggesting the presence of a mixture of isomers. Attempts to use this material in subsequent reactions led to bad mixtures.

N-(2-Azido-2-methyl-3-oxobutanoyl)-prolyl-valyl lactams (28)

To replace the bromo group of **27** by the azide function, "neutralized" lithium azide was prepared from commercial lithium azide. For this purpose lithium azide was dissolved in methanol and the pH of the solution adjusted to a value of 7.5 by addition of a dilute solution of perchloric acid in methanol. The neutralized solution was evaporated to dryness and the solid residue was dried at 100°C *in vacuo*. A solution of 75 mg of bromoketo lactam **27** in 0.5 mL of hot dimethylformamide was cooled to room temperature. A solution of 100 mg of neutralized lithium azide in 0.5 mL of dimethylformamide was added and the mixture was stirred at room temperature for 15 min. Concentration at 25°C and 0.3 Torr gave a residue that was taken up in 10 mL of dichloromethane. After washing twice with 5 mL of water and extraction of the aqueous washings with dichloromethane, the combined extracts of dichloromethane were concentrated to give 59 mg of an oil. This oil was purified through a short column of neutral alumina (0.3 g, activity III) using dichloromethane as solvent. The first eluates yielded 48 mg (71%) of the azidoketo lactams **28** free of bromoketo lactam **27**. The spectral data of this material suggested that there were at least two isomers present: It had ir signals at ν_{max} 2110, 1720, and 1670 cm^{-1}, and ^{1}Hmr signals at 1.03 and 1.13 (superimposed on other partially resolved signals), 1.60 (weak), 1.69 (less than half the intensity expected for a methyl group), and at 2.30 (a singlet integrating to approximately 3H). In comparable experiments it was observed that the ^{1}Hmr signal at 1.60 was nearly as intense as the one at 1.69. The factor influencing the signal ratio was not determined. Attempts to separate the isomers on alumina led to major loss of material without success. Therefore, the isometric mixture of azidoketo lactams **28** was used as such for the photolytic studies.

Photolysis of N-(2-azido-2-methyl-3-oxobutanoyl)-prolyl-valyl lactams 28

A solution of 72 mg of isomeric azidoketo lactams **28** in 12 mL of pure methanol was irradiated for 5 h at 10°C in a Vycor vessel using lamps with a peak emission at 300 nm. Most of the azido group had disappeared (ir) after 4 h. The photolysate was concentrated to give a material that exhibited only a very weak methoxy signal in the ^{1}Hmr spectrum. Therefore the material was dissolved in 3 mL of methanol containing 55 mg of trifluoroacetic acid and stirred at room temperature for 1.5 h. Then the mixture was neutralized using a few drops of a saturated solution of sodium bicarbonate and evaporated to dryness. The residue was taken up in dichloromethane and washed with a saturated solution of sodium bicarbonate. Evaporation of the solvent gave 49 mg of a gum, which was dissolved in ether. After addition of hexane, 16 mg of a gum separated. An ether solution of this gum led to the isolation of 5 mg of slowly crystallizing methoxy cycloltripeptide **29**. The soluble material was recycled through the methanol/trifluoroacetic acid treatment to give another 4 mg for a total of 9 mg (12%) of the methoxy cycloltripeptide **29**.

In comparable experiments the total product from the photolysis was adsorbed from dichloromethane onto a 40-fold weight ratio of neutral alumina (activity III). Elution with dichloromethane and chloroform removed undesired products, while elution with chloroform containing methanol (10%, v/v) eluted the methoxy cycloltripeptide **29** in a maximum yield of 17% The methoxy cycloltripeptide **29** crystallized from acetone/dichloromethane to give square plates or rods with a melting point of 176–178°C and $[\alpha]_D$ +60° (*c* 1.0, methanol). The spectral and analytical data supported the structural assignment; ^{1}Hmr: 6.30 (1H, s), 3.34 (3H, s), 1.90 (3H, s), 1.68 (3H, s), 1.08 (3H, d, J = 7 Hz), 1.03 (3H, d, J = 6 Hz); ^{13}Cmr: 186.0, 185.0, 179.0, 86.2, 63.4, 62.1, 49.9, 28.4, 23.6, 22.9, 20.2, 19.4. Anal. calcd for $C_{16}H_{25}N_2O_5$: C 56.62, H 7.43, N 12.38; found: C 56.73, H 7.52, N 12.48.

An X-ray crystallographic analysis (10) confirmed the gross structural assignment and established the stereochemistry of the product as being 2*S*,5*S*,11*R*,12*S* - acetamido - 3,6-dioxo-5 - isopropyl-10b-methoxy-2-methyl-perhydro-8*H*-oxazolo[3,2-*a*]pyrrolo[2, 1-*c*]-pyrazine.

Acknowledgements

We thank Professor J. W. ApSimon for the opportunity to finish this work at Carleton University, H. Seguin for microanalyses, Dr. I. C. P. Smith, L. Turner, and K. Bourque for ^{13}Cmr spectra, and the Mass Spectrometry Center, University of Ottawa, for the mass spectra.

1. R. M. WILLIAMS. Tetrahedron Lett. **22**, 2341 (1981), and references therein.

2. T. MATSUMOTO, M. YANAGIYA, S. MAENO, and S. YASUDA. Tetrahedron Lett. 6297 (1968).
3. S. M. KUPCHAN, Y. KOMODA, W. A. COURT, G. Y. THOMAS, R. M. SMITH, A. KARIM, C. J. GILMORE, R. C. HALTIWANGER, and R. F. BRYAN. J. Am. Chem. Soc. **94**, 1354 (1972).
4. A. SOMEYA, M. ISEKI, and N. TANAKA. J. Antibiot. **31**, 712 (1978); N. TANAKA, M. ISEKI, T. MIYOSHI, A. AOKI, and H. IMANAKA. J. Antibiot. **29**, 155 (1976).
5. A. STOLL, A. HOFMANN, and TH. PETRZILKA. Helv. Chim. Acta, **34**, 1544 (1951).
6. (*a*) B. W. BYCROFT. Nature, **224**, 595 (1969); B. W. BYCROFT. *In* Comprehensive organic chemistry. Vol. 5. *Edited by* D. H. R. Barton and W. D. Ollis. Pergamon Press, New York. 1979. pp. 241–287. (*b*) U. REDEKER, N. ENGEL, and W. STEGLICH. Tetrahedron Lett. **22**. 4263 (1981).
7. W. A. COURT, O. E. EDWARDS, C. GRIECO, W. RANK, and T. SANO. Can. J. Chem. **53**, 463 (1975).
8. O. E. EDWARDS and C. GRIECO. Can. J. Chem. **52**, 3561 (1974).
9. P. A. STADLER, A. J. FREY, H. OTT, and A. HOFMANN. Helv. Chim. Acta, **47**, 1911 (1964).
10. M. PRZYBYLSKA and F. R. AHMED. Acta Crystallogr. Sect. B: Struct. Crystallogr. Cryst. Chem. **B37**, 168 (1981).
11. (*a*) I. BROWN and O. E. EDWARDS. Can. J. Chem. **45**, 2599 (1967); (*b*) Can. J. Chem. **47**, 2751 (1969); W. LWOWSKI, R. DEMAURIAC, T. W. MATTINGLY, JR., and E. SCHEIFFELE. Tetrahedron Lett. 3285 (1964); R. KREHER and G. H. BOCKHORN. Angew. Chem. **76**, 681 (1964).
12. W. H. SAUNDERS and J. C. WARE. J. Am. Chem. Soc. **80**, 3328. (1958); W. H. SAUNDERS and E. A. CARESS. J. Am. Chem. Soc. **86**, 861 (1964).
13. Y. L. CHOW and A. C. H. LEE. Can. J. Chem. **45**, 311 (1967).
14. E. CAVALIERI and D. GRAVEL. Can. J. Chem. **48**, 2727 (1970).
15. H. OTT, A. J. FREY, and A. HOFMANN. Tetrahedron, **19**, 1675 (1963).
16. A. T. MCPHAIL, G. A. SIM, A. J. FREY, and H. OTT. J. Chem. Soc. (B), 377 (1966).
17. H. HEBERT. Acta Crystallogr. Sect. B: Struct. Crystallogr. Cryst. Chem. **B35**, 2978 (1979).
18. P. L. STOTTER and K. A. HILL. Tetrahedron Lett. 4067 (1972).
19. T. IWASAKI, H. HORIKAWA, H. MATSUMOTO, and M. MIYOSHI. Bull. Chem. Soc. Jpn. **52**, 826 (1979).
20. H. POISEL and U. SCHMIDT. Chem. Ber. **108**, 2547 (1975); U. SCHMIDT and E. OHLER. Angew. Chem. Int. Ed. Engl. **15**, 42 (1976); H. POISEL and U. SCHMIDT. Angew. Chem. Int. Ed. Engl. **15**, 294 (1976).
21. J. D. M. HERSCHEID, H. P. H. SCHOLTEN, M. W. TIJHUIS, and H. C. J. OTTENHEIJM. Recl. Trav. Chim. Pay-Bas, **100**, 73 (1981).
22. (*a*) C. G. SHIN, K. NANJO, E. ANDO, and J. YOSHIMURA. Bull. Chem. Soc. Jpn. **47**, 3109 (1974); (*b*) C. G. SHIN, M. HAYAKAWA, T. SUZUKI, A. OHTSUKA, and J. YOSHIMURA. Bull. Chem. Soc. Jpn. **51**, 550 (1978).
23. E. VOGEL and H. SCHINZ. Helv. Chim. Acta, **33**, 116 (1950).

Can. J. Chem. Downloaded from www.nrcresearchpress.com by 88.85.125.76 on 09/07/12
For personal use only.

The mechanism of the infrared laser induced multiphoton decomposition of ethyl alcohol[1]

J. W. GOODALE, D. K. EVANS,[2] M. IVANCO, AND ROBERT D. MCALPINE
Atomic Energy of Canada Limited, Research Company, Chalk River Nuclear Laboratories, Chalk River, Ont., Canada K0J 1J0

Received February 19, 1990

J. W. GOODALE, D. K. EVANS, M. IVANCO, and ROBERT D. MCALPINE. Can. J. Chem. **68**, 1437 (1990).

The infrared laser induced multiphoton decomposition of ethyl alcohol has been studied in experiments with iodine as a radical scavenger and the deuterium substituted form CH_3CD_2OH of the alcohol. These experiments show that the principal product, C_2H_4, arises from a concerted molecular elimination, as do most of the CH_4 and CH_3CHO. The C_2H_6 product results from recombination of the nascent methyl radicals formed in the minor bond breaking channel.

Key words: ethyl alcohol, multiphoton decomposition.

J. W. GOODALE, D. K. EVANS, M. IVANCO et ROBERT D. MCALPINE. Can. J. Chem. **68**, 1437 (1990).

Par le biais d'expériences réalisées à l'aide de la forme deutérée CH_3CD_2OH de l'alcool et utilisant l'iode comme piège à radical, on a étudié la décomposition multiphotonique induite par un laser infrarouge de l'alcool éthylique. Ces expériences démontrent que le produit principal, le C_2H_4, se forme par une élimination moléculaire concertée, comme c'est aussi le cas pour la majeure partie du CH_4 et du CH_3CHO. Le C_2H_6 qui se forme provient d'une recombinaison des radicaux méthyles naissants qui se forment par une voie mineure de bris de liaison.

Mots clés : alcool éthylique, décomposition multiphotonique.

[Traduit par la revue]

Can. J. Chem. Downloaded from www.nrcresearchpress.com by 88.85.125.76 on 09/07/12
For personal use only.

Introduction

There have been a number of studies of the infrared laser induced multiphoton decomposition (MPD) of ethyl alcohol over the past few years (1–13), and several reaction channels have been proposed to explain the product mix observed. In those papers, the channel ratios as a function of conditions such as fluence or pressure have been well documented. In this study, we are interested in the route to the products and have not been concerned with the channel ratios. The following three molecular reactions [1*a*,*b*,*c*] and the simple radical cleavage reaction [1*d*] have been deduced as the major decomposition channels for the MPD of ethyl alcohol:

$$[1a] \quad C_2H_5OH \rightarrow C_2H_4 + H_2O$$

$$[1b] \quad \rightarrow CH_3CHO + H_2$$

$$[1c] \quad \rightarrow CH_4 + H_2CO$$

$$[1d] \quad \rightarrow CH_3\cdot + H_2COH\cdot$$

The identification of the major channels suggested above is primarily based on final stable product analysis. For MPD, the molecular channel [1*a*] is believed to predominate but, in pyrolysis studies, other free radical channels, which lead to the products CH_3CHO and H_2, are reported to be most important (14). One recent report discusses the relative importance of molecular and radical channels for several alcohols (13).

In the present work, we have performed two types of experiments in an effort to clarify the mechanism of the decomposition: (i) experiments using iodine as a free radical scavenger and (ii) decomposition of the selected deuterium substituted form, CH_3CD_2OH, of ethyl alcohol. In the latter, the location of the deuterium atoms in the product molecules allows determination of the mechanism leading to several of the decomposition products.

We find that, at moderate fluences, the product C_2H_6 arises only via a radical channel involving combination of two methyl radicals, while the products C_2H_4 and CH_3CHO are produced through molecular channels. CH_4 is found to come mainly from a molecular elimination with little arising from abstraction by a methyl radical, generated through reaction [1*d*].

Experimental

A temporally smooth CO_2 laser operating at 2 Hz with a pulse duration of about 60 ns was used in all of the experiments reported here. The undeuterated alcohol was irradiated with the 9P(16) line (9.250 μm) while the deuterated species were irradiated with the 10P(14) line (10.532 μm). The beam was focused with a 54 cm focal length lens to an area of 0.005 cm^2 into a 12.6 cm path length Pyrex cell onto which NaCl windows were sealed with an epoxy. The focusing geometry was used to avoid damage to the windows at the fluences used for decomposition. The pressures of the ethyl alcohol vapour ranged from 0.067 to 1.33 kPa.

The protiated alcohol was dried as reported in ref. 12, while the deuterated alcohols (M.S.D. Isotopes) were used with only vacuum degassing. FTIR and mass spectrometric analyses were done to confirm the locations of the deuterium atoms.

Measurements of ethyl alcohol depletion and product formation, following MPD, were performed using a Hewlett–Packard 5995 GC/MS system in the Single-Ion-Monitor (SIM) mode. The cracking patterns of the isotopically labelled decomposition products were characteristic of the labelled site and thus accurate determinations of the location of the deuterium atoms in the parent ethyl alcohols and in the products of decomposition were possible. By judiciously choosing the sites of deuteration of the ethyl alcohol, we were able to use this procedure to help in determining the mechanism of multiphoton decomposition. While experiments were performed with several deuterated forms of ethyl alcohol, the majority of this deuterium atom location work was done using the CH_3CD_2OH form, for which the ion masses selected for identification of the products are at 15–20, 26–34, and 41–48 amu. The CH_3CD_2OH form provided definitive comments on the decomposition mechanism and only results from experiments with that isotopic form are discussed. The masses chosen identified both protiated and deuterated species of the major decomposition products (ethene, ethane, ethyne, ethenal, methane, and carbon dioxide). These products, and ethyl alcohol, were also measured quantitatively by comparing their peak areas against standards.

The gas chromatographic column (Porapac P, 2.44 m long × 3.2 mm outside diameter stainless steel) separates ethyl alcohol and product molecules effectively under the following column conditions. With a helium carrier gas flow rate of approximately 25 cm^3/min, the column temperature was initially set to 60°C and held at that temperature for 4 min, then raised at a rate of 16°/min to 140°C where

[1]Issued as AECL No. 10214.

[2]Author to whom correspondence may be addressed.

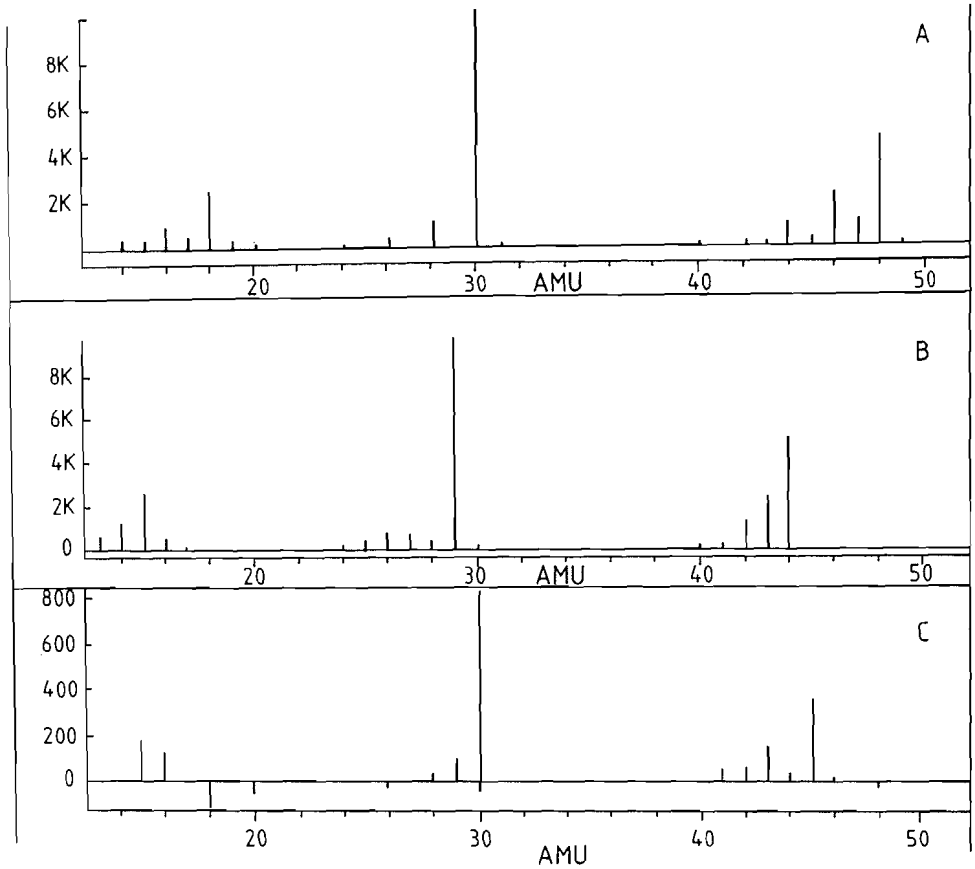

FIG. 1. The mass spectra of reference compounds (A and B) and of gas chromatographically separated products of MPD of CH_3CD_2OH (C). The location of the deuterium atoms is unique, and allows a clear interpretation of the decomposition mechanism as discussed in the text.

it was held for 25 min. The same GC/MS system was used in the quantitative analysis of the $C_2H_5OH + I_2$ irradiations, although the column temperature program was changed slightly (60°C for 10 min, then 10°C/min to 150°C where it was held for 30 min).

In some of the experiments, significant amounts of diethoxymethane were found. This only occurred after the cell had been used with iodine and is a result of reaction among the iodine, adsorbed ethyl alcohol, and the epoxy used to glue on the sodium chloride windows. This reaction was shown to be the source of the diethoxymethane both through atom balance calculations and by irradiating ethyl alcohol in a newly prepared cell. No diethoxymethane was found immediately after irradiation in the cell that had never been exposed to iodine. Iodine was added to the mixture of ethyl alcohol and decomposition products and the cell allowed to sit for 3 days. At the end of this time, another analysis was performed and diethoxymethane was found. This showed that the diethoxymethane was not a MPD product but its appearance was an artifact of a reaction not related to the photochemistry.

Results and discussion

Ethyl alcohol plus iodine

As reported earlier (12), the addition of O_2 as a radical scavenger had no effect on the molecular elimination reactions [1*a*], [1*b*], or [1*c*]; however, it completely suppressed the production of ethane. This indicated that ethane is produced following the radical reaction [1*d*], which produces $CH_3\cdot$ radicals. Our experiments with I_2 as a radical scavenger support the proposition that ethane results from radical combination, as methyl iodide is a new product and essentially no C_2H_6 is found when I_2 is present. Similarly, iodine additions had no effect on the other reaction products, indicating reactions [1*a*], [1*b*], and [1*c*] are molecular and only [1*d*] produces significant quantities of free radicals ($CH_3\cdot$). The lack of an effect on the quantity of methane produced indicates that the principle after-pulse reaction of the $CH_3\cdot$ radicals is for two to combine, and very little, if any, abstraction to form methane occurs. Also, unlike the mechanism suggested for pyrolysis (14), the CH_3CHO is produced by a molecular channel in the laser induced process.

Labelled ethyl alcohol

An example of determining the location of the deuterium atom(s) in acetaldehyde is shown in Fig. 1. Figure 1(A) and 1(B) show the mass spectra of fully deuterated (with up to about 10% protiated as purchased) and fully protiated acetaldehyde. The spectra are presented with the background subtracted from the signal of the GC peak. By examining Fig. 1(C) we can determine the number of deuterium atoms present and their location in the acetaldehyde product molecule. The major mass at *m/e* 45, CH_3CDO, shows there is exactly one deuterium atom in the molecule (*m/e* 44, CH_3CHO, has a small signal and *m/e* 48, CD_3CDO, has no signal). The mass at *m/e* 30 shows the presence of the CDO^+ ion, while the mass at *m/e* 15 shows that of the CH_3^+ ion. The molecule is thus CH_3CDO. Similar methods are used for the other product molecules.

In this report, information on the reaction mechanism has been determined by the IRMPD of deuterated species of ethyl alcohol and by analyzing the mass spectra of the reaction products. The following scheme is proposed.

$$[2] \quad CH_3CD_2OH \rightarrow H_2C{=}CD_2 + H_2O$$

$$[3] \quad \rightarrow CH_3CDO + HD$$

$$[4a] \quad \rightarrow CH_4 + D_2CO$$

$$[4b] \quad CH_3D + DCOH$$

$$[5] \quad \rightarrow CH_3\cdot + \cdot D_2COH$$

Can. J. Chem. Downloaded from www.nrcresearchpress.com by 88.85.125.76 on 09/07/12
For personal use only.

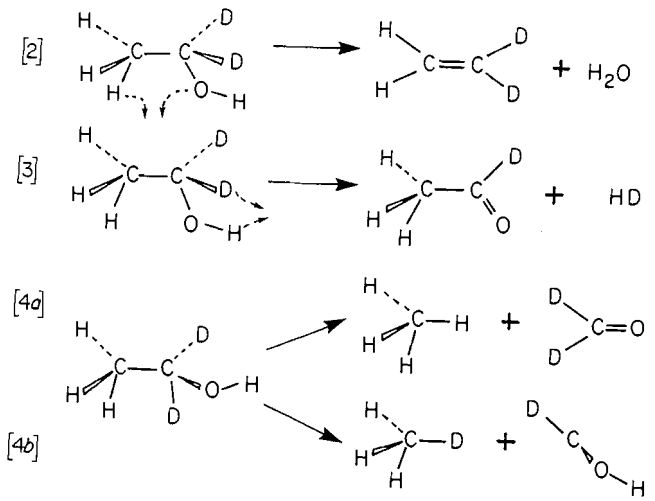

FIG. 2. The probable pathway for the decomposition mechanism producing the major products is indicated by the arrows. The molecular fragments leave by a concerted molecular process where the bonds of the products are formed while the reactant bonds are broken. Equation numbers are the same as in the text.

In ethyl alcohol MPD experiments, the major decomposition product was C_2H_4 with about 10–15% as much C_2H_6, slightly more than 5% as much CH_3CHO, and about 5% as much CH_4. The channel ratios were in agreement with previous reports. In this work, the interest was in how the products arise, not in their relative proportions.

Reactions [2]–[4] are shown pictorially in Fig. 2, where the mechanistic details can be more clearly seen. Molecular models were useful in visualizing the channels suggested as credible combinations of the normal modes of vibration of ethyl alcohol.

In reaction [2] the only isotopic form of ethene produced throughout the pressure range of 0.067–0.8 kPa, at a fluence of 25 J/cm^2, is CH_2=CD_2, indicating the reaction involves the removal of a C2 hydrogen and the -OH group to form water. No measurement of the water formed was made. Similarly, in reaction [3], the only isotopic form of acetaldehyde observed was CH_3CDO, consistent with a concerted elimination of HD across the CO bond. The gas chromatograph system used is not able to measure $m/e < 10$, so that no determination of the HD was possible here. There appears to be no involvement of the methyl hydrogens in this reaction. From product analysis, there are approximately equal quantities of CH_4 and CH_3D found after irradiation and their ratio is independent of starting pressure. A ratio near unity and the fact that there are two deuterium atoms on the α carbon of the starting ethyl alcohol, compared to the single hydrogen atom in the hydroxyl group, suggests a preference for reaction [4*a*], that is, a concerted molecular elimination of the methyl group with the hydrogen of the hydroxyl group. A physical model of the ethyl alcohol molecule shows that this is a possible mechanism. Reaction [5], at low pressure, produces only CH_3—CH_3; however, as the ethyl alcohol pressure increases, there appears to be a change in the mechanism and, by 1.33 kPa, equal quantities of CH_3—CH_3 and CH_3—CH_2D are produced. The experiments done for this study did not provide any further information on the changes resulting from increased pressure.

Conclusions

The infrared laser induced decomposition of ethyl alcohol leading to the products ethene, acetaldehyde, and methane has been shown to proceed mainly through molecular channels. Ethane is formed by efficient bimolecular recombination of methyl radicals (formed by a minor free radical channel) to the exclusion of abstractions to form methane. The preponderance of molecular eliminations is contrary to what was deduced for pyrolysis studies where products are formed largely by free radical channels (14).

1. L. SELWYN, R. A. BACK, and C. WILLIS. Chem. Phys. **32**, 323 (1979).
2. W. C. DANEN. J. Am. Chem. Soc. **101**, 1187 (1979).
3. R. B. BHATNAGAR. Ph.D. Thesis, University of Hull, England (1979).
4. A. GANDINI and R. A. BACK. J. Photochem. **18**, 241 (1982).
5. Z.-B. ZHANG, W.-S. ZHU, P.-R. ZHU, Y.-Y. ZHAO, J.-R. XU, C. ZHU, and Z.-Q. WU. Wuli, **11**, 151 (1982).
6. W.-S. ZHU, Z.-B. ZHANG, P.-R. ZHU, Y.-Y. ZHAO, L.-M. ZHANG, T.-Y. REN, A.-Z. ZHANG, and W.-Z. JIN. Jinguang, **9**, 199 (1983).
7. T. MAJIMA, S. ARAI, T. YAMAUCHI, and T. ISHII. Reza Kagaku Kenkyu, **6**, 67 (1984).
8. S. R. DE A. LEITE, P. C. ISOLANI, and J. M. RIVEROS. Can. J. Chem. **62**, 1380 (1984).
9. C. J. SHAW. Ph.D. Thesis, University of Hull, England (1984).
10. V. N. BAGRATASHVILI, M. V. KUZMIN, R. R. OSMANOV, F. N. PUTILIN, and L. N. VERESHCHAGINA. Chem. Phys. Lett. **120**, 211 (1985).
11. G. P. ZHITNEVA and S. YA. PSHEZHETSKII. Khim. Vys. Energ. **18**, 176 (1985).
12. R. A. BACK, D. K. EVANS, R. D. MCALPINE, E. M. VERPOORTE, M. IVANCO, J. W. GOODALE, and H. M. ADAMS. Can. J. Chem. **66**, 857 (1988).
13. G. P. ZHITNEVA, I. A. MARKINA, and S. A. PSHEZHETSKII. Laser Chem. **8**, 259 (1988).
14. J. A. BARNARD and H. W. D. HUGHES. Trans. Faraday Soc. **56**, 55 (1960).

Can. J. Chem. Downloaded from www.nrcresearchpress.com by 88.85.125.76 on 09/07/12
For personal use only.

Average local ionization energies on the molecular surfaces of aromatic systems as guides to chemical reactivity

PER SJOBERG
Nobel Chemicals, Nobel Industries Sweden, S-691 85 Karlskoga, Sweden
AND
JANE S. MURRAY, TORE BRINCK, AND PETER POLITZER[1]
Department of Chemistry, University of New Orleans, New Orleans, LA 70148, U.S.A.

Received January 3, 1990

PER SJOBERG, JANE S. MURRAY, TORE BRINCK, and PETER POLITZER. Can. J. Chem. **68**, 1440 (1990).

The average ionization energy, $\bar{I}(r)$, is introduced and is demonstrated to be useful as a guide to chemical reactivity in aromatic systems. $\bar{I}(r)$ is rigorously defined within the framework of self-consistent-field molecular orbital (SCF-MO) theory and can be interpreted as the average energy needed to ionize an electron at any point in the space of a molecule. An *ab initio* SCF-MO approach has been used to calculate $\bar{I}(r)$ at the 6-31G* level, using STO-3G optimized geometries. $\bar{I}(r)$ has been computed on molecular surfaces defined by the contour of constant electronic density equal to 0.002 electrons/bohr^3, for a series of aromatic systems. This surface $\bar{I}(r)$ provides site specific predictions for preferred positions of electrophilic aromatic substitution. Relative reactivity toward electrophiles increases as the magnitudes of the smallest $\bar{I}(r)$ values ($\bar{I}_{min}$) for these systems decrease. An excellent relationship, with a correlation coefficient of 0.99, has been found between the Hammett constants and $\bar{I}_{min}$; this allowed us to predict the values of these constants for the substituents NHF and NF_2, for which they were previously not known.

Key words: average local ionizations energy, chemical reactivity, electrophilic aromatic substitution, molecular surfaces, Hammett constants.

PER SJOBERG, JANE S. MURRAY, TORE BRINCK et PETER POLITZER. Can. J. Chem. **68**, 1440 (1990).

On introduit le concept d'énergie moyenne d'ionisation locale, $\bar{I}(r)$, et on démontre qu'il est un guide utile pour prédire la réactivité chimique dans les systèmes aromatiques. On définit $\bar{I}(r)$ d'une façon rigoureuse dans le cadre de la théorie des orbitales moléculaires en champ auto-cohérent (OM-CAC) et on peut l'interpréter comme l'énergie moyenne nécessaire pour ioniser un électron dans un point quelconque de l'espace d'une molécule. On a utilisé une approche *ab initio* d'OM-CAC pour calculer $\bar{I}(r)$ au niveau 6-31G*, en utilisant des géométries optimisées au niveau STO-3G. Pour une série de systèmes aromatiques, on a aussi calculé $\bar{I}(r)$ sur les surfaces moléculaires définies par le contour d'une densité électronique constante de 0,002 électrons/bohr^3. Cette $\bar{I}(r)$ de surface fournit des prédictions spécifiques au site pour les positions préférées par les substitutions aromatiques électrophiles. La réactivité relative vis-à-vis des électrophiles augmente avec une diminution des amplitudes des valeurs $\bar{I}(r)$ les plus faibles $\bar{I}_{min}$ de ces systèmes. On a obtenu une excellente corrélation, avec un coefficient de corrélation de 0,99, entre les constantes de Hammett et les valeurs de $\bar{I}_{min}$; cette corrélation nous permet de prédire les valeurs de ces constantes pour les substituants NHF et NF_2 pour lesquels ils n'étaient pas encore connus.

Mots clés : énergie moyenne d'ionisation locale, réactivité chimique, substitution aromatique électrophile, surfaces moléculaires, constantes de Hammett.

[Traduit par la revue]

Introduction

The interpretation and prediction of molecular reactive behavior is a continuing focus of our computational studies (1–5). In this work we introduce the average local ionization energy, $\bar{I}(r)$, and show its applicability in predicting sites and relative reactivities for electrophilic attack in aromatic systems.

$\bar{I}(r)$ is rigorously defined within the framework of self- consistent-field molecular orbital (SCF-MO) theory, as given by eq. [1]:

$$[1] \quad \bar{I}(r) = \sum_i \frac{\rho_i(r)|\epsilon_i|}{\rho(r)}$$

$\rho_i(r)$ is the electronic density of the ith molecular orbital at the point r, ϵ_i is the orbital energy, and $\rho(r)$ is the total electronic density. Since Koopmans' theorem justifies regarding the orbital energies as good approximations to the ionization potentials of the respective electrons (6), $\bar{I}(r)$ can be interpreted as the average energy needed to ionize an electron at any particular point in the space of the molecule. Thus, the positions where $\bar{I}(r)$ has its lowest values are the points at which are found, on the average, the highest energy electrons.

In this study, we have computed $\bar{I}(r)$ for a series of benzene derivatives, **I–IX**, on three-dimensional surfaces encompassing the molecules. These results will be discussed in relation to the experimentally observed reactive behavior of the repective molecules. Understanding and predicting the effects of substituents on electrophilic aromatic substitution reactions has long been an objective of both fundamental and practical interests (7, 8).

Methods and procedure

An *ab initio* SCF-MO approach (GAUSSIAN 82 (9)) has been used to compute 6-31G* wave functions for systems **I–IX**

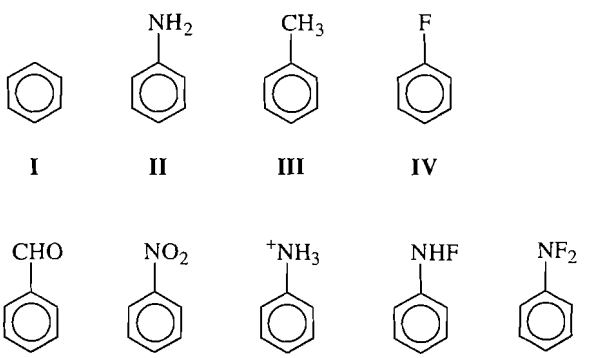

I **II** **III** **IV**

V **VI** **VII** **VIII** **IX**

[1]To whom correspondence should be addressed.

Printed in Canada / Imprimé au Canada

Can. J. Chem. Downloaded from www.nrcresearchpress.com by 88.85.125.76 on 09/07/12
For personal use only.

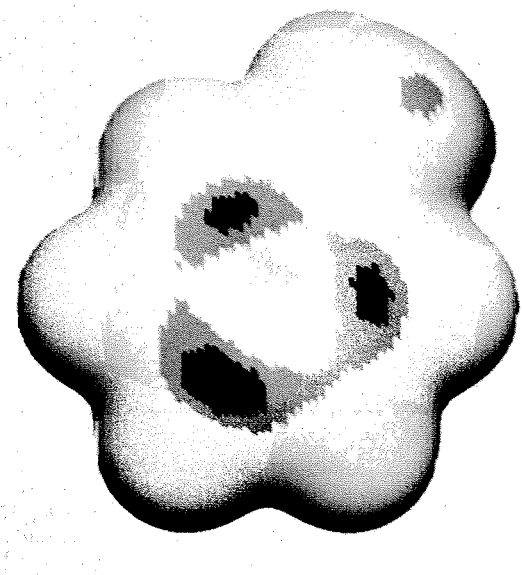

FIG. 1. Calculated $\bar{I}(r)$ on the molecular surface of aniline (**II**). Black is for $\bar{I}(r) < 11.84$ eV; gray is for $11.84 \text{ eV} < \bar{I}(r) < 12.11$ eV.

using STO-3G optimized geometries. These wave functions have then been used to calculate $\bar{I}(r)$ (eq. [1]) on the three-dimensional surfaces corresponding to the contour of constant electronic density equal to 0.002 electron/bohr^3. It has been shown, for a group of diatomic molecules and for methane, that this contour gives physically reasonable molecular dimensions, and encompasses at least 95% of the electronic charge (10–12). This surface is defined in terms of a molecular property, the electronic density function $\rho(r)$, and therefore reflects features such as bond formation, lone pairs, etc. that are unique to a molecule. This means of designating a molecular surface is in contrast to earlier methods in which it has been defined as the outer surface of a set of intersecting spheres centered on the nuclei of the molecule (12–22); such surfaces cannot take into account the very properties that are characteristic of a molecule. (This point has also been discussed by Bader *et al.* (23).) We have recently shown that the molecular electrostatic potential computed on the surface defined by the 0.002 contour is useful in studies of recognition interactions (24), and also permits predictions of sites for nucleophilic attack (25); the latter poses problems when two-dimensional plots are used.

Results

Figure 1 shows $\bar{I}(r)$ plotted on the molecular surface of aniline, **II**. The lowest average ionization energies are found above the *ortho* and *para* positions; slightly higher ones are associated with the amine lone pair.

In Table 1 are presented the locations and magnitudes of the smallest $\bar{I}(r)$ values, $\bar{I}_{min}$, for molecules **I**–**IX**. These are the points at which the least amount of energy is required to remove an electron from the surface; thus these sites are expected to be the most reactive toward electrophiles. (We have verified that there is no significant change in the magnitude of the surface $\bar{I}_{min}$ (less than 1% decrease) when the surface is defined by the 0.001 electrons/bohr^3 contour instead of the 0.002.) Also included in Table 1 is the energy of the highest occupied molecular orbital (HOMO) in each molecule. According to Koopmans' theorem (6), this should represent a good estimate of its ionization potential.

TABLE 1. Calculated 6-31G* $\bar{I}_{min}$ values, HOMO energies and Hammett constants[a] for **I**–**VIII**

Molecule	$\bar{I}_{min}$ (eV)	HOMO energy (eV)	Hammett constants[a] for substituent	
			σ_p	σ_m
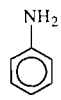 II	11.51 (*para*) 11.69 (*ortho*) 11.71 (*ortho*) 12.08 (amine N)	−7.87	−0.57	−0.09
III	11.93 (*ortho*) 11.96 (*ortho*) 11.96 (*para*) 12.08 (*meta*) 12.10 (*meta*)	−8.68	−0.14	−0.06
I	12.12 (C)	−9.00	0.00	0.00
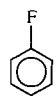 IV	12.31 (*para*) 12.44 (*ortho*) 12.45 (*ortho*)	−9.11	0.06	0.34
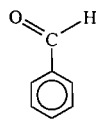 V	12.55 (*meta*) 12.59 (*meta*)	−9.44	0.47	0.41
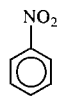 VI	13.03 (*meta*) 13.04 (*meta*)	−9.97	0.81	0.71
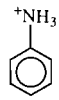 VII	16.58 (*para*) 16.59 (*meta*)	−13.59	[b]	[b]
VIII	12.22 (*para*) 12.24 (*ortho*) 12.38 (*ortho*)	−8.77	(0.06)[c]	[b]
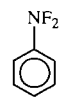 IX	12.73 (*para*) 12.78 (*meta*) 12.81 (*ortho*)	−9.53	(0.49)[c]	(0.54)[c]

[a]Hammett constants are taken from Exner (28).
[b]Hammett constant for $^+NH_3$ not available.
[c]Estimated Hammett constants, using correlation shown in Fig. 2.

Can. J. Chem. Downloaded from www.nrcresearchpress.com by 88.85.125.76 on 09/07/12
For personal use only.

Can. J. Chem. Downloaded from www.nrcresearchpress.com by 88.85.125.76 on 09/07/12
For personal use only.

The minimum values of $\bar{I}(r)$ on the surface of unsubstituted benzene are located above the carbons and have magnitudes of 12.12 eV. The magnitude of the HOMO energy is considerably less, 9.00 eV, and is in good agreement with the experimentally-determined ionization potential of benzene, 9.24 eV (26). This difference between the magnitude of $\bar{I}_{min}$ and the HOMO energy brings out the interesting point that there is quite a significant likelihood of finding inner, more tightly-bound electrons on the molecular surface. Comparison of the magnitude of $\bar{I}_{min}$ and the HOMO energies in Table 1 shows that this is true as well for the other molecules that have been studied.

$\bar{I}_{min}$ values of **II–IV** are found over the *ortho* and *para* positions (Table 1), consistent with the observed *ortho-* and *para*-directing tendencies of NH_2, CH_3, and F (7, 8). In the case of toluene (**III**), there are also minima in $\bar{I}(r)$ above the *meta* positions. These are larger than the *ortho* and *para* values, suggesting a lesser tendency for *meta* substitution. The magnitudes of $\bar{I}_{min}$ relative to that of benzene indicate whether the respective substituents activate or deactivate the benzene ring toward electrophilic attack. Aniline and toluene have $\bar{I}_{min}$ values lower than that of benzene, while those of fluorobenzene are higher. These results are in agreement with the well-known activating effects of NH_2 and CH_3 and the deactivating tendency of F (7, 8).

The surface $\bar{I}_{min}$ of **V** and **VI** are greater than those of benzene, and are above the *meta* positions. These findings reflect the established deactivating and *meta*-directing tendencies of the CHO and NO_2 groups (7, 8).

The substituent NH_3^+ is known to have the interesting property of being a *meta–para* director and to strongly deactivate the benzene ring toward electrophilic substitution (7, 8). Our calculated $\bar{I}_{min}$ for **VII** are fully consistent with these observations, being the largest in Table 1 and located over the *meta* and *para* positions.

Experimental reactivity data are not available for the NHF and NF_2 derivatives of benzene; accordingly our findings for **VIII** and **IX** constitute predictions for the effects of these substituents. The $\bar{I}_{min}$ values of **VIII** are found over the *ortho* and *para* positions, while **IX** shows the feature of having an $\bar{I}_{min}$ over all three types of positions: *ortho*, *meta*, and *para*, as was found for toluene. Our results suggest that the NF_2 group is less specific than the substituents in **II** and **IV–VIII** in directing electrophilic aromatic substitution. The $\bar{I}_{min}$ values of **VIII** are only slightly larger than those of benzene, while those of **IX** are intermediate between those of benzaldehyde (**V**) and nitrobenzene (**VI**) (see Table 1.) These data indicate that NF_2 is a significantly stronger deactivator of the aromatic ring than NHF.

Discussion

Our $\bar{I}(r)$ computations provide position specific predictions for preferred sites of aromatic electrophilic substitution. In addition, the magnitudes of the $\bar{I}_{min}$ values for each molecule (Table 1) are indicative of the relative activating and deactivating tendencies of the various substituents (relative to benzene itself).

The ability of $\bar{I}(r)$ to order the reactivities of **I–VII** led us to investigate the possibility of $\bar{I}(r)$ correlating with the Hammett constants, σ_p and σ_m (27, 28). The latter are established measures of the electron-withdrawing and -donating tendencies of substituents on aromatic rings, with reference to the *para* and *meta* positions. σ_p and σ_m are listed in Table 1 for the substituents in **I–VI**.

We have found an excellent correlation between the Hammett constant σ_p or σ_m and the corresponding $\bar{I}_{min}$. The relationship is shown in Fig. 2; the linear correlation coefficient is 0.99. This correlation strongly suggests tht our calculated $\bar{I}_{min}$ values are good indices of the relative electron-withdrawing and -donating effects of substituents on benzene rings.

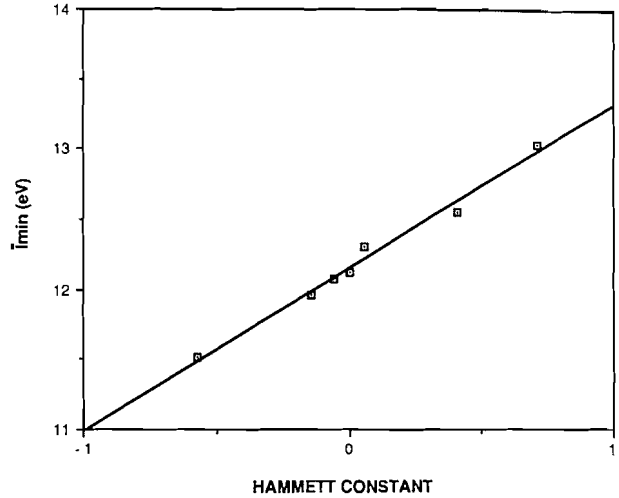

FIG. 2. Correlation between $\bar{I}_{min}$ and Hammett constants for six aromatic systems. Data are from Table 1. The least squares equation of the line is $y = 12.1547 + 1.1643x$, with a correlation coefficient of 0.99.

The correlation shown in Fig. 2 allows us to predict Hammett constants that have not yet been determined. For example, we predict σ_p for NHF to be 0.06 and σ_p and σ_m for NF_2 to be 0.49 and 0.54, respectively. Thus, NF_2 is expected to be a relatively strongly electron-withdrawing substituent, intermediate between CHO and the more powerful electron-attracting CN and NO_2 groups, whereas NHF is apparently, overall, a very weak attracter of electronic charge. (In view of the fact that Hammett's treatment did not include charge substituents, we have not estimated values for NH_3^+.)

We have recently presented a procedure that allows the inductive constant σ_I of a substituent X to be estimated from the calculated molecular electrostatic potential of X—NH_2 (29). For X = NF_2, we find σ_I to be 0.53. Since $\sigma_p \approx \sigma_I + \sigma_R$ (28), where σ_R describes resonance effects, then we can also predict that $\sigma_R \approx -0.04$ for NF_2. Our estimated σ_I for NHF is 0.43; a corresponding σ_R value of -0.37 is predicted [σ_R(NHF) $\approx$ 0.06–0.43]. These σ_R predictions for NHF and NF_2 are indicative of NHF being a significantly stronger resonance donor of charge than NF_2; presumably the nitrogen lone pair can more readily be delocalized to the ring when this is opposed by only one fluorine rather than two.

We also investigated $\bar{I}(r)$ at the 3-21G level (using STO-3G geometries) and obtained results generally similar to the 6-31G*. However, the latter basis set provides smoother surface $\bar{I}(r)$ representations and yields a better correlation with the Hammett constants. (The correlation coefficient between $\bar{I}_{min}$ computed at the 3-21G level and the Hammett constants is 0.94, compared to 0.99 for the 6-31G*.) This improvement in our $\bar{I}(r)$ data at the 6-31G* level reflects the nature of the property; $\bar{I}(r)$ depends on the goodness of the densities $\rho_i(r)$ and $\rho(r)$ at any specific point r and therefore improves with a larger, more flexible basis set.

Summary

In this study, we have introduced a new molecular property, $\bar{I}(r)$, the average local ionization energy, and have demonstrated

its usefulness as a guide to chemical reactivity in aromatic systems. $\bar{I}(r)$ is rigorously defined within the framework of self-consistent-field molecular orbital theory and can be interpreted as the average energy needed to remove an electron at any point in space r. Thus those regions where $\bar{I}(r)$ has its smallest values can be viewed as having, on the average, the highest energy electrons, most reactive toward electrophiles.

For a series of aromatic systems, we have computed $\bar{I}(r)$ on molecular surfaces defined by the contour of constant electronic density equal to 0.002 electrons/bohr^3. This surface $\bar{I}(r)$ provides site specific predictions of preferred positions for electrophilic aromatic substitution. The relative reactivities of these systems toward electrophiles increase as the magnitudes of the smallest $\bar{I}(r)$ values ($\bar{I}_{min}$) decrease. An excellent relationship, with a correlation coefficient of 0.99, is found between the Hammett constant σ_p or σ_m and the corresponding $\bar{I}_{min}$. This has allowed us to predict the σ_p and/or σ_m values for the substituents NHF and NF_2.

Acknowledgement

We greatly appreciate the support of this work by the Office of Naval Research through contract #N00014-85-K-0217.

1. P. POLITZER and K. C. DAIKER. *In* The force concept in chemistry. *Edited by* B. M. Deb. Van Nostrand Reinhold, New York. 1981. p. 294.
2. P. POLITZER and D. G. TRUHLAR (*Editors*). Chemical applications of atomic and molecular electrostatic potentials. Plenum Press, New York. 1981.
3. P. POLITZER, P. R. LAURENCE, and K. JAYASURIYA. Environ. Health Perspect. **61**, 191 (1985) (Special Issue on Structure–activity correlation in mechanism studies and procedure toxicology).
4. P. POLITZER and J. S. MURRAY. *In* Structure and reactivity (molecular structure and energetics). *Edited by* J. F. Liebman and A. Greenberg. VCH Publishers, New York. 1988. Chap. 1.
5. P. POLITZER and J. S. MURRAY. *In* Theoretical biochemistry and molecular biophysics: A comprehensive survey. *Edited by* D. L. Beveridge and R. Lavery. Adenine Press. In press.
6. T. A. KOOPMANS. Physica, **1**, 104 (1933).
7. R. T. MORRISON and R. N. BOYD. Organic chemistry. 3rd ed. Allyn & Bacon, Boston. 1973. Chap. 11.
8. F. A. CAREY and R. J. SUNDBERG. Advanced organic chemistry, Part A: Structure and mechanisms. Plenum Press, New York. 1977. Chap. 9.
9. GAUSSIAN 82: J. S. BINKLEY, M. J. FRISCH, D. J. DEFREES, R. KRISHNAN, R. A. WHITESIDE, H. B. SCHLEGEL, E. M. FLUDER, and J. A. POPLE; GAUSSIAN 82, Carnegie-Mellon Quantum Chemistry Publishing Unit, Pittsburgh, PA.
10. R. F. W. BADER, W. H. HENNEKER, and P. E. CADE. J. Chem. Phys. **46**, 3341 (1967).
11. R. F. W. BADER and H. J. T. PRESTON. Theor. Chim. Acta, **17**, 384 (1970).
12. S. D. KAHN, C. F. PARR, and W. J. HEHRE. Int. J. Quantum Chem. Quantum Chem. Symp. **22**, 575 (1988).
13. B. PULLMAN, D. PERAHIA, and D. CAUCHY. Nucl. Acids Res. **6**, 3821 (1979).
14. P. K. WEINER, R. LANGRIDGE, J. M. BLANEY, R. SCHAEFER, and P. A. KOLLMAN. Proc. Natl. Acad. Sci. (U.S.) **79**, 709 (1982).
15. M. L. CONNOLLY. Science, **221**, 709 (1983).
16. P. A. BASH, N. PATTABIRAMAN, C. HUANG, T. E. FERRIN, and R. LANGRIDGE. Science, **222**, 1325 (1983).
17. M. M. FRANCL, R. F. HOUT, JR., and W. J. HEHRE. J. Am. Chem. Soc. **106**, 563 (1984).
18. P. QUARENDON, C. B. NAYLOR, and W. G. J. RICHARDS. J. Mol. Graph. **2**, 4 (1984).
19. M. L. CONNOLLY. J. Am. Chem. Soc. **107**, 1118 (1985).
20. J. P. RITCHIE. J. Am. Chem. Soc. **107**, 1829 (1985).
21. J. M. BURRIDGE, P. QUARENDON, C. A. REYNOLDS, and P. J. GOODFORD. J. Mol. Graph. **5**, 165 (1987).
22. G. A. ARTECA, V. B. JAMMAL, P. G. MEZEY, J. S. YADAV, M. A. HERMSMEIER and T. M. GUND. J. Mol. Graph. **6**, 45 (1988).
23. R. F. W. BADER, M. T. CARROLL, J. R. CHEESEMAN, and C. J. CHANG. J. Am. Chem. Soc. **109**, 7968 (1987).
24. P. SJOBERG, J. S. MURRAY, T. BRINCK, P. EVANS, and P. POLITZER. J. Mol. Graph. In press.
25. P. SJOBERG and P. POLITZER. J. Phys. Chem. In press.
26. H. WATANABE. J. Chem. Phys. **22**, 1565 (1954); **26**, 542 (1957).
27. L. P. HAMMETT. Physical organic chemistry. McGraw-Hill, New York, 1940.
28. O. EXNER. Correlation analysis of chemical data. Plenum Press, Czechoslovakia. 1988.
29. J. S. MURRAY and P. POLITZER. Chem. Phys. Lett. **152**, 364 (1988).

Can. J. Chem. Downloaded from www.nrcresearchpress.com by 88.85.125.76 on 09/07/12
For personal use only.

Synthesis and X-ray crystal structure of the 3,5-dimethylpyrazolato copper(I) trimer, [Cu (pz″)]$_3$

MARTIN K. EHLERT, STEVEN J. RETTIG, ALAN STORR, ROBERT C. THOMPSON, and JAMES TROTTER
Department of Chemistry, University of British Columbia, 2036 Main Mall, Vancouver, B.C., Canada V6T 1Y6

Received December 19, 1989

MARTIN K. EHLERT, STEVEN J. RETTIG, ALAN STORR, ROBERT C. THOMPSON, and JAMES TROTTER. Can. J. Chem. **68**, 1444 (1990).

A moderately high-yield, high temperature synthesis of the title compound is reported. Crystals of tris[(3,5-dimethylpyrazolato-N^1,N^2)copper(I)] are triclinic, a = 12.360(4), b = 14.637(4), c = 12.358(4) Å, α = 105.29(2), β = 119.83(2), γ = 93.99(3)°, Z = 4 (trimers, two per asymmetric unit), space group $P\bar{1}$. The structure was solved by heavy atom methods and was refined by full-matrix least-squares procedures to R = 0.034 and R_w = 0.038 for 3877 reflections with $I \geq 3\sigma(I)$. The structure consists of trimeric molecules with an unusually short average Cu—N distance of 1.852 Å. The central Cu_3N_6 nine-membered rings are planar to within 0.07 Å. The trimer units are linked in pairs about centres of symmetry by weak Cu···Cu interactions averaging 2.946 Å.

Key words: pyrazolato copper (I) timer, copper (I) pyrazolate.

MARTIN K. EHLERT, STEVEN J. RETTIG, ALAN STORR, ROBERT C. THOMPSON et JAMES TROTTER. Can. J. Chem. **68**, 1444 (1990).

Faisant appel à une méthode de synthèse impliquant une température élevée, on a préparé le produit mentionné dans le titre avec un assez bon rendement. Les cristaux du tris[(3,5-diméthylpyrazolato-N^1,N^2)cuivre(I)] sont tricliniques et ils appartiennent au groupe d'espace $P\bar{1}$, avec a = 12,360(4), b = 14,637(4) et c = 12,358(4) Å, α = 105,29(2), β = 119,83(2) et γ = 93,99(3)° et Z = 4 (deux trimères par unité asymétrique). On a affiné la structure par la méthode des atomes lourds et on l'a affinée par la méthode des moindres carrés jusqu'à des valeurs respectives de R = 0,034 et R_w = 0,038 pour 3877 reflexions avec $I \geq 3\sigma(I)$. La structure est formée de molécules trimères dans lesquelles la distance moyenne Cu—N, 1,852 Å, est anormalement courte. Les cycles centraux à neuf chaînons de Cu_3N_6 sont plans à moins de 0,07 Å. Des interactions Cu···Cu faibles, de distance moyenne 2,946 Å, retiennent les unités de trimère par paires autour de centres de symétrie.

Mots clés : trimère pyrazolato-cuivre (I), pyrazolat de cuivre (I).

[Traduit par la revue]

Introduction

A novel and efficient synthesis of the title compound has resulted unexpectedly from an attempt to prepare the polymetric copper(II) 3,5-dimethylpyrazolato species [Cu(pz″)$_2$]$_x$. Our interest in the latter material stems from the magnetic exchange properities exhibited by such infinite-chain polymers, with the pyrazolate ligands acting as propagating pathways between the interacting Cu centres (1). The trimeric copper(I) compound, [Cu(pz″)]$_3$, reported here was obtained as colorless crystals which provided excellent samples for data collection in an X-ray structure determination. The central nine-membered ring structure, Cu_3N_6, is qualitatively planar and the rings are arranged in pairs in the crystal lattice. The structure is discussed in relation to similar M(I) pyrazolate species (M = Cu, Ag, or Au) (2–4).

Experimental

Synthesis of [Cu(pz″)]$_3$, **1**

A mixture of $Cu(OH)_2$ (~0.3 g) and 3,5-dimethylpyrazole (Hpz″) (~4.0 g) was heated under a nitrogen atmosphere at 130°C for 10 days. The reaction mixture turned dark brown within a few minutes and within a day large colorless cyrstals could be seen forming on the sides of the reaction flask. At the end of the reaction period the mixture was allowed to cool to room temperature and was then extracted with acetone to remove excess Hpz″. This procedure also allowed the separation of the insoluble colorless crystals of [Cu(pz″)]$_3$ from a fine reddish-brown powder, chracterized as the [Cu(pz″)$_2$]$_x$ polymer, which was also produced in the reaction. Thus most of the reddish-brown powder was separated by suspending in acetone and decanting from the colorless crystals. Final separation of pure samples of the colorless crystals was achieved by manual separation under a microscope. The yields of the copper containing products were estimated at ~70% for [Cu(pz″)]$_3$ and ~30% for [Cu(pz″)$_2$]$_x$. *Anal.* calcd. for $C_{15}H_{21}Cu_3N_6$: C 37.85, H 4.45, N 17.66; found: C 38.00, H 4.43, N 17.45.

Physical characterization

[Cu(pz″)]$_3$ was found to be insoluble in both polar and non-polar organic solvents. It is indefinitely stable towards air and moisture. Differential scanning calorimetry (Mettler DSC 20 cell and TC 10 TA processor) shows the compound to be thermally stable to ~300°C at which temperature it decomposes without melting. The infrared spectrum (4000–250 cm^{-1}) was obtained as a Nujol mull on a Perkin-Elmer Model 598 spectrophotometer. Frequencies (cm^{-1}): 3120 w, 2734 w, 2720 w, 2283 w, 2122 w, 1535 wsh, 1524 s, 1509 wsh, 1438 s, 1421 s, 1358 wsh, 1345 s, 1150 s, 1125 wsh, 1059 s, 1043 w, 1029 wsh, 979 w, 769 s, 662 w, 659 m, 601 w, 464 m, 428 m (Nujol bands omitted, s = strong, m = medium, w = weak, sh = shoulder).

X-ray crystallographic analysis

A crystal *ca* 0.10 × 0.20 × 0.20 mm in size was mounted in a general orientation. Unit-cell parameters were refined by least-squares on setting angles for 25 reflections (2θ = 26.6–33.8°) measured on a diffractometer with Mo-$K\alpha$ radiation (λ = 0.71069 Å). Crystal data at 21°C are as follows:

$C_{15}H_{21}Cu_3N_6$ fw = 476.01

Triclinic, a = 12.360(4), b = 14.637(4), c = 12.358(4) Å, α = 105.29(2), β = 119.83(2), γ = 93.99(3)°, V = 1816(3) Å^3, Z = 4, ρ_c = 1.741 Mg m^{-3}, F(000) = 960, μ(Mo-$K\alpha$) = 35.0 cm^{-1}. Absent reflections: none, space group $P\bar{1}$ (reduced cell, Donnay convention) from structure analysis. Since the a and c axes are nearly equal in length and the β angle is close to 120° there was a possibility that the crystal lattice was actually hexagonal. No lattice transformations to a true hexagonal unit cell were found.

Intensities were measured with graphite-monochromated Mo-$K\alpha$ radiation on a Rigaku AFC6S diffractometer. An ω–2θ scan at 32° min^{-1} over a range of (1.31 + 0.35 tan θ) degrees in ω (with up to eight

Can. J. Chem. Downloaded from www.nrcresearchpress.com by 91.121.58.235 on 09/07/12
For personal use only.

Can. J. Chem. Downloaded from www.nrcresearchpress.com by 91.121.58.235 on 09/07/12
For personal use only.

TABLE 1. Final atomic coordinates (fractional) and B(eq)

Atom	x	y	z	B(eq)
Cu(1)	0.44003(6)	0.10767(5)	−0.09545(7)	3.22(3)
Cu(2)	0.30478(7)	0.11095(5)	0.06924(6)	3.29(3)
Cu(3)	0.60085(6)	0.10500(5)	0.20688(7)	3.19(3)
Cu(4)	0.87956(6)	0.39355(6)	1.01873(7)	3.16(3)
Cu(5)	0.72124(7)	0.38634(5)	0.71761(7)	3.30(3)
Cu(6)	1.02170(7)	0.39304(5)	0.85631(6)	3.23(3)
N(1)	0.2704(4)	0.1159(3)	−0.1717(4)	3.1(2)
N(2)	0.2125(4)	0.1179(3)	−0.1002(4)	3.1(2)
N(3)	0.3964(4)	0.1144(3)	0.2436(4)	3.1(2)
N(4)	0.5241(4)	0.1112(3)	0.3039(4)	3.2(2)
N(5)	0.6831(4)	0.1140(3)	0.1178(4)	2.9(2)
N(6)	0.6141(4)	0.1148(3)	−0.0109(4)	2.9(2)
N(7)	0.7051(4)	0.3862(3)	0.9368(4)	3.1(2)
N(8)	0.6369(4)	0.3822(3)	0.8051(4)	2.9(2)
N(9)	0.7983(4)	0.3797(3)	0.6204(4)	3.1(2)
N(10)	0.9269(4)	0.3827(3)	0.6789(4)	3.2(2)
N(11)	1.1108(4)	0.3883(3)	1.0266(4)	2.9(2)
N(12)	1.0499(4)	0.3883(3)	1.0952(4)	2.9(2)
C(1)	0.1852(6)	0.1275(4)	−0.2859(6)	3.6(2)
C(2)	0.0742(4)	0.1363(5)	−0.2885(6)	3.9(2)
C(3)	0.0932(5)	0.1299(4)	−0.1711(6)	3.3(2)
C(4)	0.3637(6)	0.1246(4)	0.3334(6)	3.3(2)
C(5)	0.4682(6)	0.1274(4)	0.4513(6)	3.7(2)
C(6)	0.5668(6)	0.1192(4)	0.4298(6)	3.3(2)
C(7)	0.8073(5)	0.1272(4)	0.1581(5)	3.0(2)
C(8)	0.8200(6)	0.1370(4)	0.0550(6)	3.5(2)
C(9)	0.6974(5)	0.1285(4)	−0.0484(5)	2.8(2)
C(10)	0.2187(6)	0.1268(5)	−0.3868(6)	4.9(3)
C(11)	0.0084(6)	0.1348(5)	−0.1182(6)	4.4(2)
C(12)	0.2312(6)	0.1297(5)	0.2982(6)	4.3(2)
C(13)	0.7035(6)	0.1205(5)	0.5221(6)	4.5(3)
C(14)	0.9058(5)	0.1285(5)	0.2926(6)	4.1(2)
C(15)	0.6519(6)	0.1324(4)	−0.1828(6)	3.8(2)
C(16)	0.6205(5)	0.3757(4)	0.9723(6)	3.4(2)
C(17)	0.4985(5)	0.3676(4)	0.8674(6)	3.7(2)
C(18)	0.5134(5)	0.3715(4)	0.7649(6)	3.5(2)
C(19)	0.7493(6)	0.3694(4)	0.4931(6)	3.6(2)
C(20)	0.8459(6)	0.3641(4)	0.4674(5)	3.8(2)
C(21)	0.9556(6)	0.3732(4)	0.5861(6)	3.4(2)
C(22)	1.2293(5)	0.3766(4)	1.0996(5)	2.9(2)
C(23)	1.2463(5)	0.3680(4)	1.2159(5)	3.4(2)
C(24)	1.1320(5)	0.3764(4)	1.2099(5)	2.9(2)
C(25)	0.6631(6)	0.3738(5)	1.1072(6)	4.9(3)
C(26)	0.4162(6)	0.3681(5)	0.6289(6)	4.2(2)
C(27)	0.6105(6)	0.3639(5)	0.4030(6)	4.8(3)
C(28)	1.0888(6)	0.3750(5)	0.6194(6)	4.7(3)
C(29)	1.3170(5)	0.3718(4)	1.0504(6)	3.8(2)
C(30)	1.0958(6)	0.3725(4)	1.3072(5)	3.9(2)

TABLE 2. Bond lengths (Å) with estimated standard deviations in parentheses[a]

Atom	Atom	Distance	Atom	Atom	Distance
Cu(1)	Cu(3)′	2.944(2)	N(10)	C(21)	1.337(6)
Cu(1)	N(1)	1.852(5)	N(11)	N(12)	1.387(5)
Cu(1)	N(6)	1.845(4)	N(11)	C(22)	1.338(6)
Cu(2)	N(2)	1.858(4)	N(12)	C(24)	1.339(6)
Cu(2)	N(3)	1.853(4)	C(1)	C(2)	1.371(8)
Cu(3)	N(4)	1.852(4)	C(1)	C(10)	1.495(8)
Cu(3)	N(5)	1.853(4)	C(2)	C(3)	1.380(8)
Cu(4)	Cu(6)″	2.947(2)	C(3)	C(11)	1.484(8)
Cu(4)	N(7)	1.851(4)	C(4)	C(5)	1.372(8)
Cu(4)	N(12)	1.846(4)	C(4)	C(12)	1.484(8)
Cu(5)	N(8)	1.846(4)	C(5)	C(6)	1.378(7)
Cu(5)	N(9)	1.857(4)	C(6)	C(13)	1.491(8)
Cu(6)	N(10)	1.857(4)	C(7)	C(8)	1.401(7)
Cu(6)	N(11)′	1.851(4)	C(7)	C(14)	1.487(7)
N(1)	N(2)	1.382(6)	C(8)	C(9)	1.381(7)
N(1)	C(1)	1.343(6)	C(9)	C(15)	1.485(7)
N(2)	C(3)	1.343(6)	C(16)	C(17)	1.385(8)
N(3)	N(4)	1.381(6)	C(16)	C(25)	1.487(8)
N(3)	C(4)	1.336(6)	C(17)	C(18)	1.382(7)
N(4)	C(6)	1.339(6)	C(18)	C(26)	1.487(8)
N(5)	N(6)	1.385(5)	C(19)	C(20)	1.383(8)
N(5)	C(7)	1.337(6)	C(19)	C(27)	1.491(8)
N(6)	C(9)	1.346(6)	C(20)	C(21)	1.379(8)
N(7)	N(8)	1.393(6)	C(21)	C(28)	1.481(8)
N(7)	C(16)	1.334(6)	C(22)	C(23)	1.388(7)
N(8)	C(18)	1.332(7)	C(22)	C(29)	1.480(7)
N(9)	N(10)	1.372(6)	C(23)	C(24)	1.393(7)
N(9)	C(19)	1.333(7)	C(24)	C(30)	1.489(7)

[a]Primed and double-primed atoms have coordinates related to those in Table 1 by the symmetry operations: $1 - x, -y, -z$; and $2 - x, 1 - y, 2 - z$; respectively.

rescans, background/scan time ratio = 0.5) was employed. Data were measured to $2\theta = 55°$. The intensities of three check reflections, measured every 150 reflections throughout the data collection, showed only small random fluctuations. After data reduction,[1] an empirical absorption correction, based on azimuthal scans for four reflections, was applied which resulted in relative transmission factors ranging from 0.84 to 1.00. Of the 8714 reflections measured, 8329 were unique ($R_{int} = 0.026$) and 3877 (46.5%) of these had intensities greater than or equal to $3\sigma(F^2)$ above background where $\sigma^2(F^2) = (S^2(C + 4B) + (0.03(F_o^2))^2)/Lp^2$ with S = scan rate, C = scan count, B = total background count, and Lp = Lorentz-polarization factors.

The structure was solved by conventional heavy atom methods, the six crystallographically independent copper atoms being positioned from the Patterson map and the remaining non-hydrogen atoms from subsequent difference Fourier syntheses. All non-hydrogen atoms were refined with anisotropic thermal parameters and hydrogen atoms were fixed in idealized positions (methyl group orientations based on difference map peaks, C—H = 0.98 Å, $U_H = 1.2U_{bonded\ atom}$). Scattering factors for all atoms and anomalous dispersion corrections for the non-hydrogen atoms were taken from ref. 5. The weighting scheme $w = 1/\sigma^2(F)$, where $\sigma^2(F)$ is derived from the previously defined $\sigma^2(F)$, gave uniform average values of $w(|F_o| - |F_c|)^2$ over ranges of both $|F_o|$ and $\sin\theta/\lambda$ and was employed in the final stages of full-matrix refinement of 433 variables. Reflections with $I < 3\sigma(I)$ were not included in the refinement. Convergence was reached at $R = 0.034$ and $R_w = 0.038$ for 3877 reflections with $I \geq 3\sigma(I)$. The function minimized was $\Sigma w(|F_o| - |F_c|)^2$, $R = \Sigma\,||F_o| - |F_c||/\Sigma|F_o|$ and $R_w = (\Sigma w(|F_o| - |F_c|)^2/\Sigma w|F_o|^2)^{1/2}$.

On the final cycle of refinement the maximum parameter shift corresponded to 0.002σ. The mean error in an observation of unit weight was 1.45. The final difference map showed maximum fluctuations of −0.42 to 0.43 e Å^{-3}. The final positional and equivalent isotropic thermal parameters for the non-hydrogen atoms appear in Table 1. Bond lengths and angles are listed in Tables 2 and 3. Hydrogen

[1]All computations performed using the TEXSAN–TEXRAY Structure Analysis Package which includes versions of the following: AGNOST, absorption corrections, by J. A. Ibers; ORFLS, full-matrix least-squares, and ORFFE, function and errors, by W. R. Busing, K. O. Martin and H. A. Levy; DIRDIF, phase extension and refinement of difference structures, by P. T. Beurskens; ORTEP II, illustrations, by C. K. Johnson.

TABLE 3. Bond angles (deg) with estimated standard deviations in parentheses

Atom	Atom	Atom	Angle	Atom	Atom	Atom	Angle
Cu(3)′	Cu(1)	N(1)	99.2(1)	C(2)	C(3)	C(11)	131.5(6)
Cu(3)′	Cu(1)	N(6)	87.4(1)	N(3)	C(4)	C(5)	109.1(5)
N(1)	Cu(1)	N(6)	173.4(2)	N(3)	C(4)	C(12)	121.0(5)
N(2)	Cu(2)	N(3)	175.3(2)	C(5)	C(4)	C(12)	129.9(5)
Cu(1)′	Cu(3)	N(4)	100.4(1)	C(4)	C(5)	C(6)	106.1(5)
Cu(1)′	Cu(3)	N(5)	86.0(1)	N(4)	C(6)	C(5)	109.2(5)
N(4)	Cu(3)	N(5)	173.5(2)	N(4)	C(6)	C(13)	120.2(5)
Cu(6)″	Cu(4)	N(7)	99.5(1)	C(5)	C(6)	C(13)	130.5(6)
Cu(6)″	Cu(4)	N(12)	85.8(1)	N(5)	C(7)	C(8)	108.6(5)
N(7)	Cu(4)	N(12)	174.7(2)	N(5)	C(7)	C(14)	121.1(5)
N(8)	Cu(5)	N(9)	175.2(2)	C(8)	C(7)	C(14)	130.4(5)
Cu(4)″	Cu(6)	N(10)	99.7(1)	C(7)	C(8)	C(9)	106.0(5)
Cu(4)″	Cu(6)	N(11)	86.7(1)	N(6)	C(9)	C(8)	109.0(5)
N(10)	Cu(6)	N(11)	173.6(2)	N(6)	C(9)	C(15)	120.7(5)
Cu(1)	N(1)	N(2)	119.2(3)	C(8)	C(9)	C(15)	130.2(5)
Cu(1)	N(1)	C(1)	133.6(4)	N(7)	C(16)	C(17)	109.6(5)
N(2)	N(1)	C(1)	107.1(4)	N(7)	C(16)	C(25)	120.6(5)
Cu(2)	N(2)	N(1)	119.8(3)	C(17)	C(16)	C(25)	129.8(5)
Cu(2)	N(2)	C(3)	131.3(4)	C(16)	C(17)	C(18)	105.6(5)
N(1)	N(2)	C(3)	108.8(4)	N(8)	C(18)	C(17)	109.5(5)
Cu(2)	N(3)	N(4)	120.4(3)	N(8)	C(18)	C(26)	120.7(5)
Cu(2)	N(3)	C(4)	131.4(4)	C(17)	C(18)	C(26)	129.9(5)
N(4)	N(3)	C(4)	108.1(4)	Cu(6)	N(10)	C(21)	133.3(4)
Cu(3)	N(4)	N(3)	118.3(3)	N(9)	N(10)	C(21)	107.9(4)
Cu(3)	N(4)	C(6)	134.1(4)	Cu(6)	N(11)	N(12)	120.2(3)
N(3)	N(4)	C(6)	107.5(4)	Cu(6)	N(11)	C(22)	131.1(4)
Cu(3)	N(5)	N(6)	120.1(3)	N(12)	N(11)	C(22)	108.5(4)
Cu(3)	N(5)	C(7)	131.3(4)	Cu(4)	N(12)	N(11)	120.6(3)
N(6)	N(5)	C(7)	108.4(4)	Cu(4)	N(12)	C(24)	131.3(4)
Cu(1)	N(6)	N(5)	120.7(3)	N(11)	N(12)	C(24)	107.8(4)
Cu(1)	N(6)	C(9)	131.1(4)	N(1)	C(1)	C(2)	109.3(5)
N(5)	N(6)	C(9)	108.0(4)	N(1)	C(1)	C(10)	120.1(5)
Cu(4)	N(7)	N(8)	118.3(3)	N(9)	C(19)	C(20)	108.7(5)
Cu(4)	N(7)	C(16)	134.0(4)	N(9)	C(19)	C(27)	121.1(5)
N(8)	N(7)	C(16)	107.5(4)	C(20)	C(19)	C(27)	130.2(6)
Cu(5)	N(8)	N(7)	120.0(3)	C(19)	C(20)	C(21)	106.0(5)
Cu(5)	N(8)	C(18)	132.0(4)	N(10)	C(21)	C(20)	109.0(5)
N(7)	N(8)	C(18)	107.9(4)	N(10)	C(21)	C(28)	120.8(5)
Cu(5)	N(9)	N(10)	120.4(3)	C(20)	C(21)	C(28)	130.2(5)
Cu(5)	N(9)	C(19)	131.1(4)	N(11)	C(22)	C(23)	108.7(5)
N(10)	N(9)	C(19)	108.5(4)	N(11)	C(22)	C(29)	120.9(5)
Cu(6)	N(10)	N(9)	118.7(3)	C(23)	C(22)	C(29)	130.4(5)
C(2)	C(1)	C(10)	130.6(6)	C(22)	C(23)	C(24)	106.1(5)
C(1)	C(2)	C(3)	106.9(5)	N(12)	C(24)	C(23)	108.9(5)
N(2)	C(3)	C(2)	107.9(5)	N(12)	C(24)	C(30)	121.5(5)
N(2)	C(3)	C(11)	120.6(5)	C(23)	C(24)	C(30)	129.6(5)

Can. J. Chem. Downloaded from www.nrcresearchpress.com by 91.121.58.235 on 09/07/12
For personal use only.

parameters, anisotropic thermal parameters, torsion angles, intermolecular contacts, least-squares planes, and structure factors have been deposited.[2]

Results and discussion

The first report of a coinage metal pyrazolate compound (silver(I) pyrazolate) appeared 100 years ago (6). It was not until more recently that Singh *et al.* reported the isolation of a gray diamagnetic Cu(I) pyrazolate material from the reaction of $Cu(acac)_2$ with hydrazine (7). To this they assigned the formulation [Cu(pz″)] although the calculated and found analytical data provided do not agree with this composition. At the same time Okkerson *et al.* reported the [Cu(pz)] and [Cu(5-Mepz)] species to be at least trimeric on the basis of mass spectrometric data (8). Since these reports a low yield synthesis and crystal structure of the trimer $[Cu(3,5\text{-}Ph_2pz)]_3$ (where 3,5-Ph_2pz = 3,5-diphenylpyrazolate) has been reported (4) and [Cu(pz)] and [Cu(pz″)] have been isolated as insoluble white polymeric materials (9). We report here a moderately high-yield, high temperature synthesis of crystalline $[Cu(pz'')]_3$ via the reaction of $Cu(OH)_2$ with molten Hpz″:

$$\text{excess Hpz}'' + Cu(OH)_2 \xrightarrow[130°C]{N_2} \underset{\text{colorless}}{[Cu(pz'')]_3} + \underset{\text{reddish-brown}}{[Cu(pz'')_2]_x} + ?$$

[2]Supplementary material mentioned in the text may be purchased from the Depository of Unpublished Data, CISTI, National Research Council of Canada, Ottawa, Ont., Canada K1A 0S2.

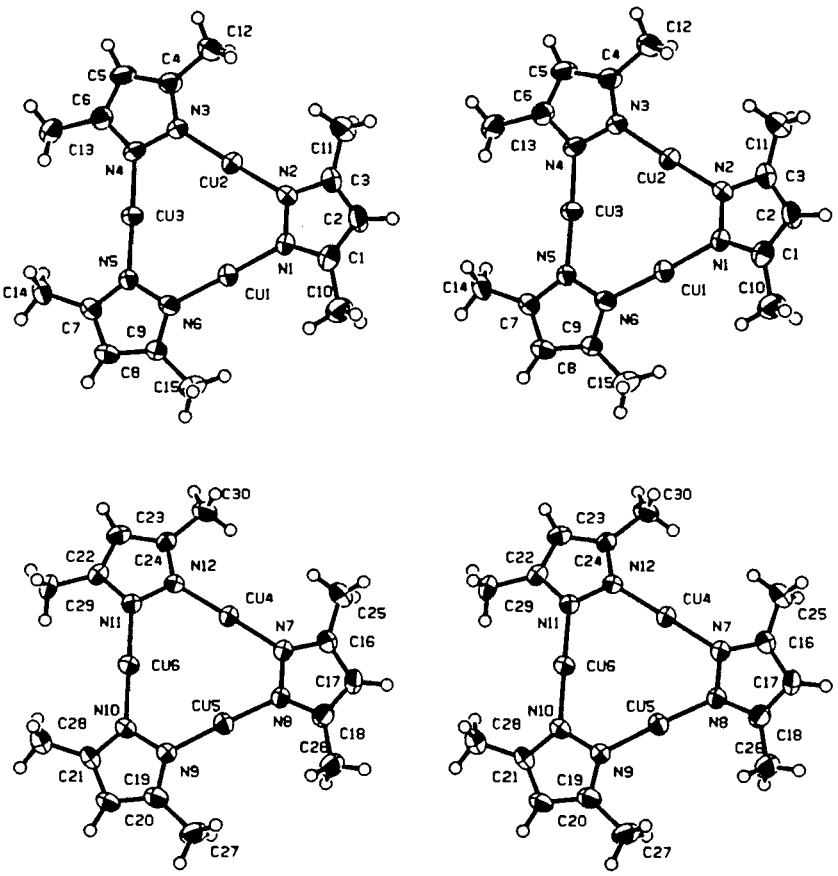

FIG. 1. Stereoscopic views of the two crystallographically independent molecules of tris[(3,5-dimethyl-pyrazolato-N',N^2)copper(I)]; 50% probability thermal ellipsoids are shown for the non-hydrogen atoms.

Obviously the Cu(II) reactant is being partially reduced in this reaction and consequently the pyrazole reactant must be oxidized. Oxidation of pyrazoles, albeit with more common oxidants, has been documented (10). The structure of the title compound consists of trimeric molecules (Fig. 1) linked in pairs (Fig. 2) by weak Cu...Cu interactions.

Related Ag(I) and Au(I) pyrazolate compounds have been recorded in the literature (2, 3) and an unusual Cu(II) complex, $[Cu_3(\mu_3\text{-}OH)(\mu\text{-}pz)_3(Hpz)_2(NO_3)_2]\cdot H_2O$, containing as a central feature a nine-membered metallocycle, common to all the $[M(3,5\text{-}R_2pz)]_3$ (M = Cu, Ag, or Au) structures, has also been reported (11). Selected structural parameters for $[M(3,5\text{-}R_2pz)]_3$ complexes are collected in Table 4 and relate to the general trimetallocycle formulation:

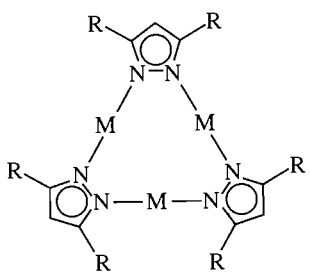

Of the five compounds listed in Table 4, compounds **1** and **4** exhibit essentially planar nine-membered M_3N_6 rings (those in **1** are planar to within 0.07 Å) whereas compounds **2**, **3**, and **5** show a marked puckering in the molecular arrangements. Interestingly the Cu(II) complex mentioned above (11) contains an almost planar Cu_3N_6 ring with Cu—N bond lengths ranging 1.917–1.972 (average 1.945 Å) and Cu···Cu intramolecular distances of 3.324–3.365 (average 3.351 Å). The same molecular arrangement as depicted above was also found in the structure of 3,5-dimethylpyrazole (Hpz″) itself (12). The structure of Hpz″ consists of planar trimeric units with strongly H-bonded hydrogen atoms between the three pyrazole molecules replacing the M atoms of the $[M(3,5\text{-}R_2pz)]_3$ metallocycles.

The present structure (Figs. 1 and 2) displays two strikingly unique features when compared with the structures of compounds **2**–**5**. The first is the shortening by ~0.2 Å of the Cu—N bonds relative to a standard Cu(I)—N single bond length. (The average Cu—N distance in the Cu(I) complex $[HBpz_3]Cu(CO)$ is 2.046 Å (13)). This observation would indicate that a considerable Cu($d\pi$)–pz″(π^*) interaction is augmenting the σ-bonding between the Cu and N atoms. Evidence for this interaction can be seen in the lengthening of the distances within the pyrazole rings, particularly the N—N bond (1.381–1.385, average 1.383 Å), when compared to the corresponding distances (average 1.334 Å) observed in the structure of $[Hpz'']_3$ (12). In the latter compound the hydrogen bonds linking the molecules into trimer units cannot interact with the π^* orbitals of the pz″ rings. The infrared spectra of the two compounds provide additional evidence in that the band attributed primarily to a $\nu_{C=N}$ mode is shifted from ~1599 cm^{-1} in $[Hpz'']_3$ to ~1524 cm^{-1} in

Can. J. Chem. Downloaded from www.nrcresearchpress.com by 91.121.58.235 on 09/07/12
For personal use only.

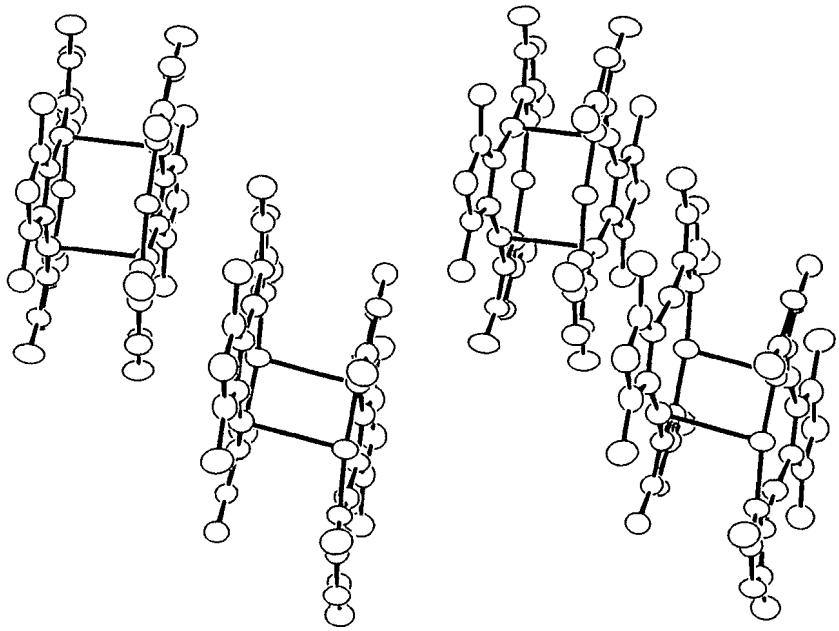

FIG. 2. Stereoscopic view tris[(3,5-dimethylpyrazolato-N^1,N^2)copper(I)] showing the trimer–trimer Cu...Cu interactions.

TABLE 4. Selected structural parameters for $[M(3,5\text{-}R_2pz)]_3$ species (distances in Å)

Compound	1	2	3	4	5
M	Cu	Cu	Ag	Au	Au
R	Me	Ph	Ph	Ph	CF_3
M—N (obs)	1.845–1.858	2.041–2.105	2.08–2.09	1.978	1.89–1.96
Average	1.852	2.081	2.085		1.93
M—N (est)[a]	2.04	2.04	2.19	2.06	2.06
M···M intra	3.195–3.257	3.280–3.406	3.305–3.486	3.368	3.344–3.355
Average	3.218	3.339	3.388		3.348
M···M inter	2.946			7.567	3.998
Reference	This work	4	3	3	2

[a]Reference 14.

$[Cu(pz'')]_3$, consistent with a weakening of the bonds in the pz″ rings of the Cu trimer. The second unique feature is the arrangement of the trimer units within the crystal lattice. Only in the present structure is there an intermolecular (between trimers) M···M separation shorter than the intramolecular M···M distance. In compounds **2**–**4** the individual trimer units are clearly non-interacting whereas in the present example the trimers are arranged in pairs about crystallographic inversion centres with two Cu atoms from one M_3N_6 metallocycle being positioned close to two Cu atoms from the second unit (see Fig. 2). The mean intertrimer Cu—Cu distance of 2.946 Å is close to the sum of van der Waals radii (2.86 Å) (14) and thus the interaction holding the trimers together must necessarily be weak. Interestingly only two of the Cu atoms in each trimer are involved in these weak Cu···Cu interactions, the third Cu atom being positioned above the centre of a pz″ ring at the opposite end of the inversion-related trimer unit (average Cu···pz″ ring mean plane = 3.272 Å). The only related trimeric structure to show similar intermolecular interactions is the $[AuC(OEt)=N(p\text{-tolyl})]_3$ complex (15). In this structure the intramolecular Au···Au distances are reported at 3.224, 3.288, and 3.299 Å with one intermolecular Au···Au distance of 3.244 Å responsible for joining the trimers in pairs. In this example the nature of the interaction is not specified but again is likely to be weak since the distance observed is of the same order as the sum of van der Waals radii (~3.22 Å) (14).

Acknowledgments

We thank the Natural Sciences and Engineering Research Council of Canada for financial support and the University of British Columbia Computing Centre for assistance.

1. M. K. EHLERT, S. J. RETTIG, A. STORR, R. C. THOMPSON, and J. TROTTER. Can. J. Chem. **67**, 1970 (1989).
2. B. BOVIO, F. BONATI, and G. BANDITELLI. Inorg. Chim. Acta, **87**, 25 (1984).
3. H. H. MURRAY, R. G. RAPTIS, and J. P. FACKLER, JR. Inorg. Chem. **27**, 26 (1988).
4. R. G. RAPTIS and J. P. FACKLER, JR. Inorg. Chem. **27**, 4179 (1988).
5. International tables for X-ray crystallography. Vol. IV. Kynoch press, Birmingham. 1974. pp. 99–102 and 149.
6. E. BUCHNER. Chem. Ber. **22**, 2163 (1889).
7. C. B. SINGH, S. SATPATHY, and B. SAHOO. J. Inorg. Nucl. Chem. **35**, 3947 (1973).
8. H. OKKERSON, W. L. GROENEVELD, and J. REEDIJK. Recl. Trav. Chim. Pays-Bas, **92**, 945 (1973).

Can. J. Chem. Downloaded from www.nrcresearchpress.com by 91.121.58.235 on 09/07/12
For personal use only.

9. G. A. ARDIZZOIA, G. L. MONICA, M. A. ANGARONI, and F. CARIATI. Inorg. Chim. Acta, **158**, 159 (1989).
10. K. SCHOFIELD, M. R. GRIMMETT, and B. R. T. KEENE. Heteroaromatic nitrogen compounds: the azoles. Cambridge University Press, Cambridge. 1976. p. 154.
11. F. B. HULSBERGEN, R. W. M. TEN HOEDT, C. G. VERSCHOOR, J. REEDIJK, and A. L. SPEK. J. Chem. Soc. Dalton Trans. **539** (1983).
12. J. A. S. SMITH, B. WEHRLE, F. AGUILAR-PARRILLA, H. H. LIMBACH, M. C. FOCES-FOCES, F. H. CANO, J. ELGUERO, A. BALDY, M. PIERROT, M. M. T. KHURSHIB, and J. B. LARCOMBE-MCDOUALL. J. Am. Chem. Soc. **111**, 7304 (1989).
13. M. R. CHURCHILL, B. G. DEBOER, F. J. ROTELLA, and O. M. A. SALAH. Inorg. Chem. **14**, 2051 (1975).
14. W. W. PORTERFIELD. Inorganic chemistry. A unified approach. Addison-Wesley. Reading, MA. 1984. p. 166.
15. A. TIRIPICCHIO, M. T. CAMELLINI, and G. MINGHETTI. J. Organomet. Chem. **171**, 399 (1979).

Can. J. Chem. Downloaded from www.nrcresearchpress.com by 91.121.58.235 on 09/07/12
For personal use only.

Sulfonyl esters. 2. CS cleavage in some substitution reactions of nitrobenzenesulfonates

JAMES CLAYTON BAUM, JIMAT BOLHASSAN, RICHARD FRANCIS LANGLER,[1] PAUL JOSEPH PUJOL, AND RAJ KUMAR RAHEJA

Department of Chemistry, Florida Institute of Technology, Melbourne, FL 32901-6988, U.S.A.

Received May 23, 1989[2]

JAMES CLAYTON BAUM, JIMAT BOLHASSAN, RICHARD FRANCIS LANGLER, PAUL JOSEPH PUJOL, and RAJ KUMAR RAHEJA. Can. J. Chem. **68**, 1450 (1990).

An attempt to explore aromatic sulfonate esters as agents for the condensation of alcohols with mercaptans revealed an unusual process for sulfonate esters: CS bond rupture. Two mechanistic possibilities for CS bond rupture are explored: (i) radical anion intermediacy via single electron transfer and (ii) nucleophilic aromatic substitution. Both experiments and molecular orbital computations are presented to support the conclusion that nucleophilic aromatic substitutions are occurring.

Key words: sulfonyl esters, nitrobenzenesulfonates, CS bond rupture.

JAMES CLAYTON BAUM, JIMAT BOLHASSAN, RICHARD FRANCIS LANGLER, PAUL JOSEPH PUJOL et RAJ KUMAR RAHEJA. Can. J. Chem. **68**, 1450 (1990).

Lorsqu'on a essayé d'utiliser les esters d'acides sulfoniques aromatiques comme agents de condensation des alcools avec les mercaptans, on a observé une réaction inusitée pour ce type de composé, à savoir une rupture de la liaison CS. On a exploré deux possibilités mécanistiques pour expliquer ces scissions : (i) un intermédiaire radical-anion se formant par le transfert d'un seul électron et (ii) une réaction de substitution aromatique nucléophile aromatique. On présente des expériences ainsi que des calculs d'orbitales moléculaires qui suggèrent que les réactions se produisent par le biais de substitutions aromatiques nucléophiles.

Mots clés : esters d'acides sulfoniques, nitrobenzènesulfonates, rupture de la liaison CS.

[Traduit par la revue]

Introduction

We recently reported (1) that phenyl methanesulfonate induces the condensation of *p*-tolyl mercaptan with primary alcohols, as shown in eq. [1]. Further study of this chemistry led to the observation that *p*-nitrophenyl methanesulfonate condensed with the mercaptan leaving the alcohol largely unused (eq. [2]).

[1] $PhOSO_2CH_3 + CH_3C_6H_4SH + CH_3CH_2OH \xrightarrow[HMPA]{2\ NaH} CH_3C_6H_4SCH_2CH_3$

[2] $O_2NC_6H_4OSO_2CH_3 + CH_3C_6H_4SH + CH_3CH_2OH \xrightarrow[HMPA]{2\ NaH} CH_3C_6H_4SC_6H_4NO_2$

1

In an attempt to examine nitro-substituted sulfonates that might induce alcohol–mercaptan condensation, a study of the chemistry of a linkage isomeric nitrophenyl sulfonate **2** was undertaken.

Results and discussion

Reaction of **2** with ethanol and *p*-tolyl mercaptan furnished the surprising results shown in eq. [3]. There appears to be only one example of a sulfonate ester substitution reaction leading to CS bond rupture (2) (see eq. [4]). There are, however, several known examples of CS bond rupture in reactions of related

[3] $O_2NC_6H_4SO_2OPh + CH_3C_6H_4SH + CH_3CH_2OH \xrightarrow[HMPA]{2\ NaH} O_2NC_6H_4SC_6H_4CH_3$

1 (63%)

[4] $Ph_2CHSO_2OAr \longrightarrow Ph_2CHOAr + SO_2$

[5] $O_2NC_6H_4SO_2OPh + CH_3C_6H_4SH \xrightarrow[HMPA]{NaH} \mathbf{1}\ (67\%) + CH_3C_6H_4SC_6H_4SO_2OPh\ \mathbf{3}\ (16\%)$

sulfonyl-containing structures (3, 4). Repetition of the eq. [3] reaction in the absence of ethanol permitted the isolation of **1** in the same yield, along with a modest yield of **3**. Thus a role for ethanol in the formation of **1** can be dismissed from consideration.

The unexpected CS rupture in the reactions of **2** with mercaptide anions prompted us to examine nitroaryl sulfonates to establish the relative propensities for CS and CO rupture. The behaviour of the ideal dinitrosulfonate ester **4** was modelled with the aid of the linkage isomeric dinitrosulfonates **5***a* and **5***b*.

The reactions of these dinitrosulfonate esters with *p*-tolyl mercaptide anions in HMPA are depicted below.

Assuming that methyl substitution diverts *x*% of product formation to the other ring, a simple calculation on the results in eqs. [6] and [7] leads to the conclusion that the ratio of the yields of **1** formed by CS rupture to the yields of **1** formed by CO rupture would be ca. 19:1 in the hypothetical reaction of **4** with *p*-tolyl mercaptide anions!

Two reasonable mechanisms may be advanced to account

[1]Author to whom correspondence may be addressed at the Department of Chemistry, Mount Allison University, Sackville, N.B., Canada E0A 3C0.

[2]Revision received April 18, 1990.

Printed in Canada / Imprimé au Canada

Can. J. Chem. Downloaded from www.nrcresearchpress.com by 88.85.125.76 on 09/07/12
For personal use only.

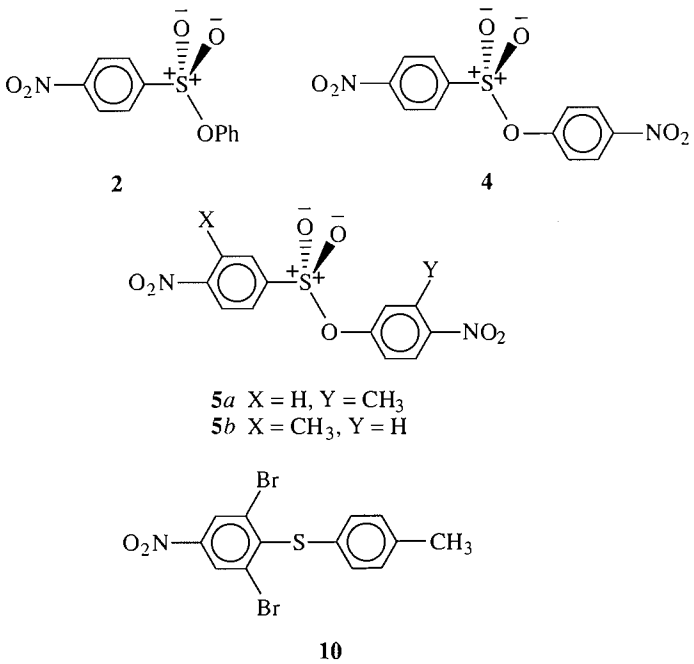

2 4

5*a* X = H, Y = CH_3
5*b* X = CH_3, Y = H

10

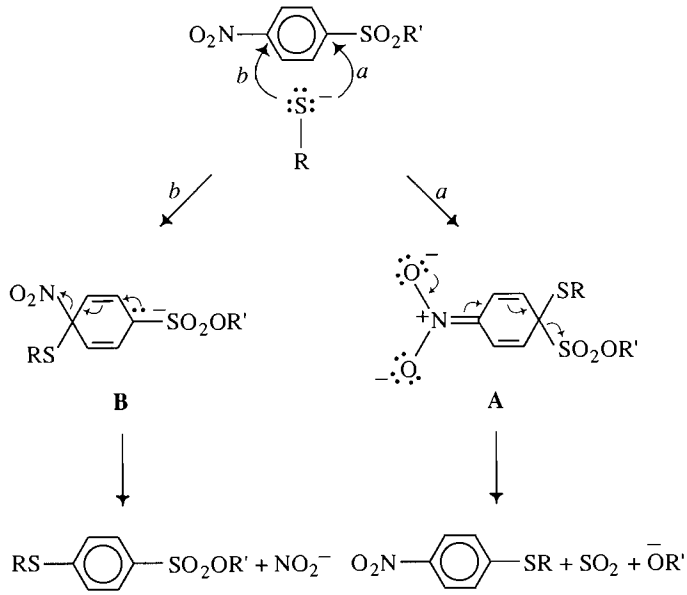

SCHEME 1

for the surprisingly facile CS bond rupture observed for the reactions of the bis(nitroaryl) sulfonates **5***a*, **5***b*. Reaction might proceed through a Meisenheimer complex (**A**) as shown in Scheme 1. Alternatively, the mercaptide anion could transfer an electron to the sulfonate ester, converting it into the corresponding radical anion as depicted in Scheme 2.

To explore Scheme 1, semi-empirical molecular orbital computations were carried out on the linkage isomers **5***a* and **5***b*. The ZINDO calculated LUMOs, presented in Fig. 1, indicate that nucleophilic attack should occur preferentially on the sulfonyl-substituted phenyl ring in accord with experiment.

Given that hard–soft acid–base arguments (5) militate against nucleophilic attack by mercaptide anions (soft) at nitrogen or sulfur (hard), the computations suggest a straightforward choice between soft acid sites: nitro-bearing carbon and sulfonyl-bearing carbon. Sulfonyl-bearing carbon has the larger LUMO coefficient, indicating that attack there will lead to a more strongly stabilized transition state (5). This analysis should also satisfactorily rationalize the results portrayed in eq. [5].

In contrast to the reaction of **5***a*, **5***b* undergoes a modest amount of nucleophilic attack on the nitrophenoxy ring. This may be rationalized by an examination of the NLUMO of **5***b* (6). The preferred soft acid site on that ring is the oxygen-bearing carbon (NLUMO coefficient: −0.319) rather than the nitro-bearing carbon (NLUMO coefficient: −0.176). The computed difference in energies between the NLUMO and the LUMO for **5***a* is 0.443 eV. The corresponding value for **5***b* is 0.279 eV, suggesting a relative enhancement for the role of the NLUMO in the chemistry of **5***b*.

ZINDO calculations were performed on **4** and its radical anion **4**$^{\cdot-}$. These computations were intended to reveal the nature and propensities of the radical anion in order to assess the viability of the Scheme 2 mechanism. Figure 2 presents selected bond length changes computed for the conversion **4** → **4**$^{\cdot-}$. The greatest *contractions* in bond length are computed for those bonds which are actually ruptured during one or more of the reactions reported herein. On this basis the Scheme 2 mechanism seems improbable.

It is our view that the substitution reactions reported in eqs. [3], [6], and [7] proceed through Meisenheimer complexes as portrayed in the Scheme 1 mechanism. However, aryl sulfonates can be drawn into electron transfer reactions (7, 8).

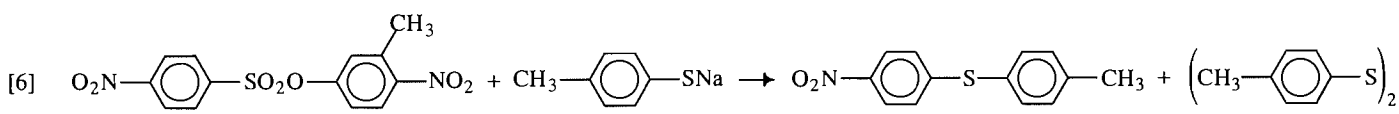

5*a* **1** (16%)

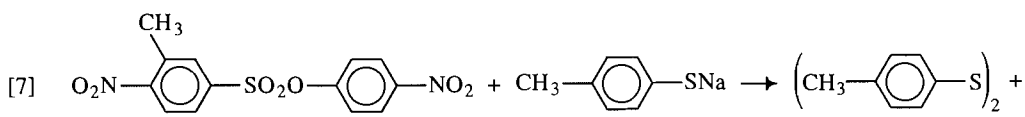

5*b*

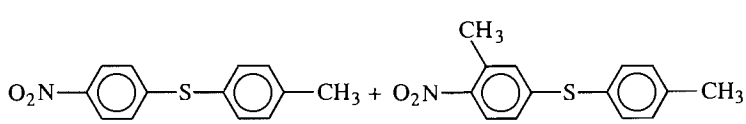

1 Relative yield: (11%) **6** Relative yield: (89%)

Can. J. Chem. Downloaded from www.nrcresearchpress.com by 88.85.125.76 on 09/07/12
For personal use only.

Can. J. Chem. Downloaded from www.nrcresearchpress.com by 88.85.125.76 on 09/07/12
For personal use only.

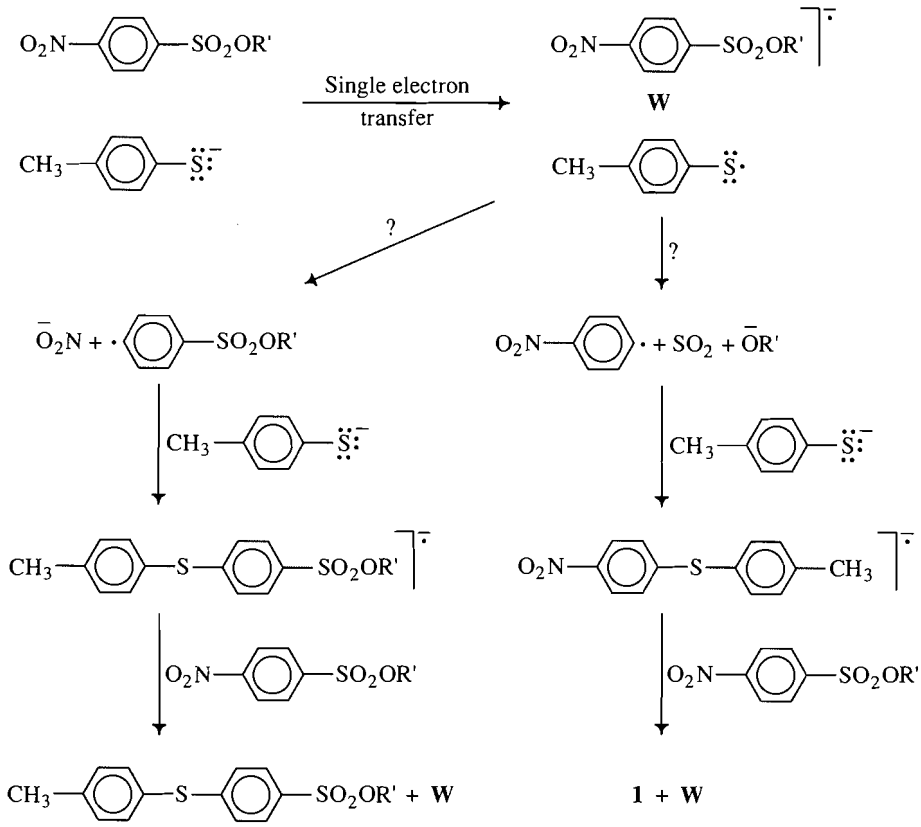

SCHEME 2

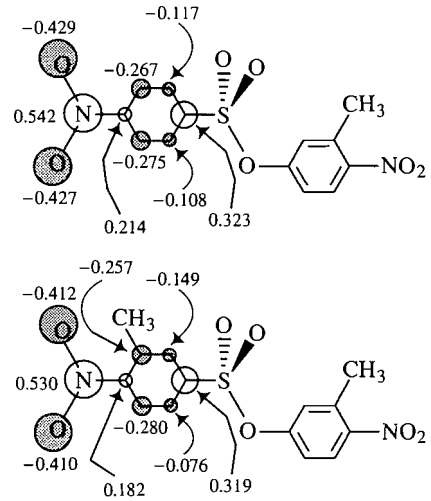

FIG. 1. ZINDO calculated lowest unoccupied molecular orbitals for **5***a* and **5***b*.

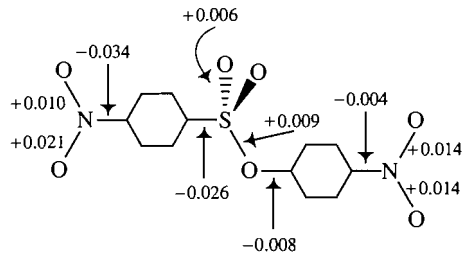

FIG. 2. Some calculated bond length changes (Å) induced by conversion of **4** into **4**$^{\cdot-}$.

Equation [8] presents a final nitroaryl sulfonate ester – mercaptide anion reaction.[3]

In the eq. [8] reaction, it seems extremely likely that the mesylate group is replaced first so that both products arise via the intermediacy of **10**. The formation of **9** is an appropriate reaction for a SET mechanism similar to the one outlined in Scheme 2.

In conclusion, it appears that nitroaromatic compounds may be involved in reactions proceeding through radical anions or in reactions proceeding through Meisenheimer complexes. Introduction of a sulfonate linkage onto a nitro-bearing phenyl ring appears to shift pathway preference toward nucleophilic aromatic substitution.

Computational methods

All computations were performed using the ZINDO molecular orbital method (9). The ZINDO program is available as part of the QUIPU molecular modelling package from the Quantum Theory Project, University of Florida.

The ground state geometries were obtained at the INDO/1 level, including *d*-orbitals on sulfur and using a BFGS updated Hessian search with Newton–Raphson optimization. The restricted Hartree–Fock method was used for the closed shell neutral molecule. For the radical anion (open shell) system, an unrestricted Hartree–Fock calculation with annihilation was employed. The INDO/S option was employed to determine the HOMO and LUMO eigenvalues and eigenvectors using Matago–Nishimoto repulsion integrals and fixed ground state geometries.

[3]Since this reaction was conducted early in our research program, an equivalent of ethanol was present to check for *p*-tolyl ethyl sulfide formation.

[8] 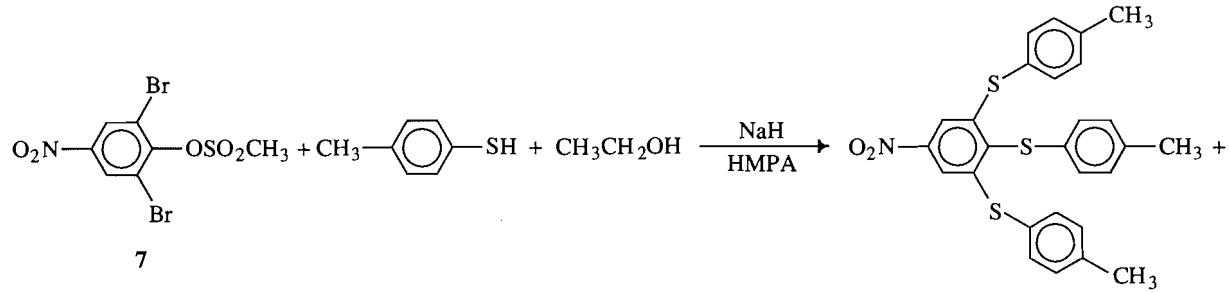

7

8

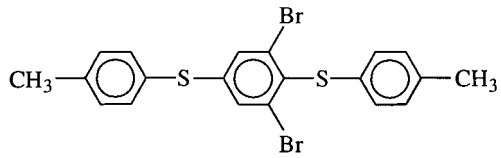

9

Can. J. Chem. Downloaded from www.nrcresearchpress.com by 88.85.125.76 on 09/07/12
For personal use only.

ZINDO calculated structural parameters for dimethyl sulfone are closer to experimental values than those obtained by 3-21G computations (10). ZINDO spectroscopic predictions agree well with experimentally determined ultraviolet spectra on a series of five substituted phenyl methanesulfonates. ZINDO spectroscopic predictions were systematically superior to those obtained by CNDO/UV computations.

Experimental

General

The ir spectra were recorded on a Perkin–Elmer 237B grating spectrophotometer. Ultraviolet spectra were run on a Beckman DU-2 spectrophotometer. The nmr spectra were obtained on a Varian EM360A instrument using TMS as the internal standard. Melting points were determined on a Gallenkamp MFB-595 capillary melting point apparatus and are uncorrected.

Preparation of phenyl p*-nitrobenzenesulfonate* **2**

A solution of phenol (0.43 g, 4.5 mmol) and triethylamine (0.45 g, 4.5 mmol) in pyridine (50 mL) was cooled with an ice/water bath. *p*-Nitrobenzenesulfonyl chloride (1.0 g, 4.5 mmol) was added in small portions. The ice/water bath was removed and the reaction mixture stirred overnight.

Chloroform extraction followed by acid washing gave crude sulfonate ester (0.98 g). The crude was recrystallized from methanol affording colorless crystals (0.67 g, 2.4 mmol, 54%, mp 118.1–118.6°C). The product had R_f 0.66 on analytical tlc plates when developed with chloroform; ir ($CHCl_3$): 1540, 1390, 1355, and 1150 cm^{-1}; nmr ($CDCl_3$) δ: 8.36 (2H, d, J = 8 Hz), 8.06 (2H, d, J = 8 Hz), 7.30 (3H, m), and 6.96 (2H, m). Anal. calcd. for $C_{12}H_9NO_5S$: C 51.60, H 3.24; found: C 51.58, H 3.22.

Reaction of **2** *with ethoxide and* p*-tolyl mercaptide anions*

Sodium hydride (0.65 g, 27 mmol) was suspended in HMPA[4] (30 mL). A solution of absolute ethanol (0.63 g, 13 mmol) in HMPA (10 mL) was added dropwise over 5 min. The reaction mixture was stirred at ambient temperature for 5 min. A solution of *p*-tolyl mercaptan (1.71 g, 13 mmol) in HMPA (10 mL) was added dropwise over 10 min. The reaction mixture was stirred at ambient temperature for 5 min. The nitrosulfonate **2** (3.82 g, 13 mmol) was added and the reaction mixture stirred at ambient temperature for 2 h. After about 10 min the homogeneous reaction mixture was rust colored.

The reaction mixture was poured into water (400 mL) containing 10% HCl (5 mL). The resultant mixture was extracted with diethyl ether (three 100-mL aliquots). The wet organic layer was concentrated. The residue was added to water (100 mL) and the resultant mixture washed with diethyl ether (three 100-mL aliquots). The combined ether layers were extracted with 2.5% NaOH (two 100-mL portions). The organic layer was dried ($MgSO_4$) and concentrated, yielding crude *p*-nitrophenyl *p*-tolyl sulfide **1** (3.79 g).

The crude was recrystallized from methanol, affording impure nitrosulfide **1** (2.71 g). The recrystallized nitrosulfide was chromatographed on silica gel (250 g) employing carbon tetrachloride elution (100-mL fractions). Fractions 11–18 were combined and concentrated, furnishing clean nitrosulfide **1** (2.130 g, 8.6 mmol, 63%). After recrystallization from methanol, the chromatographed nitrosulfide was shown to be identical to previously obtained material (2) by ir, nmr, tlc, mp, and mixture mp.

Reaction of **2** *with* p*-tolyl mercaptide anions*

Sodium hydride (0.36 g, 15 mmol), *p*-tolyl mercaptan (1.73 g, 13 mmol), and the nitrosulfonate **2** (3.82 g, 13 mmol) were reacted in HMPA (40 mL) as above.

The crude was subjected to column chromatography on silica gel (400 g) employing hexanes, carbon tetrachloride, and chloroform as sequential eluants. Nitrosulfide **1** (2.23 g, 9.1 mmol, 66.7%) was obtained along with a sulfonate ester mixture (1.67 g). The mixture was chromatographed on silica gel (200 g) employing 1:1 carbon tetrachloride/chloroform elution. Sulfide–sulfonate ester **3** (0.78 g, 2.1 mmol, 16%) was obtained. After recrystallization from methanol, the product had mp 52.3–53.5°C, R_f, 0.75 upon development with 1:1 chloroform/carbon tetrachloride; ir ($CHCl_3$); 1380 and 1180 cm^{-1}; nmr ($CDCl_3$) δ: 7.6 (2H, d, J = 9 Hz), 7.25 (6H, m), and 2.40 (3H, s); ms m/e: 356 (M, 33.9%), 263 (26%), 199 (100%), and 184 (64%). Anal. calcd. for $C_{19}H_{16}O_3S_2$: C 64.02, H 4.52; found: C 64.15, H 4.36. Fractions 13–19 were combined and concentrated, giving unchanged nitrosulfonate **2** (0.47 g).

Preparation of the dinitrosulfonate ester **5**a

p-Nitro-*m*-methylphenol (0.69 g, 4.5 mmol), triethylamine (0.45 g, 4.5 mmol), and *p*-nitrobenzenesulfonyl chloride (0.99 g, 4.5 mmol) in pyridine (50 mL), reacted as above, gave recrystallized **5***a* (0.85 g, 2.5 mmol, 56%, mp 131.4–132.2°C). The product had R_f 0.25 on analytical tlc plates when developed with 1:1 carbon tetrachloride/chloroform; ir ($CHCl_3$): 1540, 1395, 1350, and 1190 cm^{-1}; nmr ($CDCl_3$) δ: 8.40 (2H, d, J = 8 Hz), 8.06 (2H, d, J = 8 Hz), 7.90 (1H, d, J = 8 Hz), 6.96 (2H), and 2.35 (3H, s); ms m/e: 338 (M^+, 3.2%), 321 (31.8%), and 122 (100%). Anal. calcd. for $C_{13}H_{10}N_2O_7S$: C 46.15, H 2.97; found: C 46.10, H 2.81.

Preparation of p*-nitro-*m*-methylphenyl benzenesulfonate*

p-Nitro-*m*-methylphenol (5.00 g, 32 mmol), triethylamine (3.30 g, 32 mmol), and benzenesulfonyl chloride (5.75 g, 32 mmol) were reacted in pyridine (50 mL) following the procedure outlined for the preparation of phenyl *p*-nitrobenzenesulfonate **2**.

[4]HMPA is hexamethylphosphoramide $[(CH_3)_2N]_3PO$. HMPA is toxic and carcinogenic (11).

Can. J. Chem. Downloaded from www.nrcresearchpress.com by 88.85.125.76 on 09/07/12
For personal use only.

The crude nitrosulfonate was recrystallized from methanol, affording nitrosulfonate (6.85 g, 23 mmol, 71%, mp 75–76°C). The product had R_f 0.67 on analytical tlc plates developed with 1:1 chloroform/carbon tetrachloride; ir ($CHCl_3$): 1525, 1382, 1348, and 1190 cm^{-1}; nmr ($CDCl_3$) δ: 7.40 (8H, m), 2.53 (3H, s); ms *m/e*: 293 ($M^{\ddagger}$, 0.35%) and 77 (100%). Anal. calcd. for $C_{13}H_{11}NO_5S$: C 53.23, H 3.78; found: C 53.21, H 3.72.

Preparation of p-*nitro*-m-*methylphenyl benzyl sulfide*

Sodium hydride (0.41 g, 17 mmol) was added to HMPA (30 mL). A solution of benzyl thiol (2.1 mL, 16 mmol) in HMPA (10 mL) was added dropwise over 5 min. *p*-Nitro-*m*-methyl-phenyl benzenesulfonate (5.00 g, 17 mmol) was added and the reaction mixture stirred at ambient temperature for 2 h.

The reaction mixture was subjected to the extraction procedure outlined under "Reaction of **2** with ethoxide and *p*-tolyl mercaptide anions".

Crude product was chromatographed on silica gel (400 g) employing carbon tetrachloride elution followed by chloroform elution. Dibenzyl disulfide (0.63 g) was isolated. The *p*-nitro-*m*-methylphenyl benzyl sulfide so obtained was recrystallized from methanol, furnishing clean yellow needles (0.85 g, 3.3 mmol, 20%, mp 58.3–59.2°C). The nitrosulfide had R_f 0.51 on analytical tlc plates developed with carbon tetrachloride; ir ($CHCl_3$): 1525 and 1340 cm^{-1}; nmr ($CDCl_3$) δ: 7.86 (1H, d), 7.20 (7H, m), 4.16 (2H, s), and 2.53 (3H, s); ms *m/e*: 259 ($M^{\ddagger}$, 10%) and 91 (100%). Anal. calcd. for $C_{14}H_{13}NO_2S$: C 64.84, H 5.05; found: C 64.77, H 4.96.

Preparation of p-*nitro*-m-*methyl benzenesulfonyl chloride*

p-Nitro-*m*-methylphenyl benzyl sulfide (3.99 g, 15 mmol) was suspended in a solution of glacial acetic acid (25 mL) and water (3 mL). Chlorine (ca. 200 mL/min) was bubbled through the mixture for 9.75 g. Ice/water cooling was used as required to maintain the reaction temperature below 30°C.

Chloroform extraction followed by base washing gave a crude residue. The residue was rectified at reduced pressure, yielding *p*-nitro-*m*-methyl benzenesulfonyl chloride (2.73 g, 11 mmol, 75%, bp 142–148°C/1.6 Torr) (1 Torr = 133.3 Pa). *p*-Nitro-*m*-methyl benzenesulfonyl chloride had ir ($CHCl_3$): 1540, 1385, 1355, and 1175 cm^{-1}; nmr ($CDCl_3$) δ: 8.10 (3H, s) and 2.70 (3H, s).

Preparation of **5** b

p-Nitrophenol (0.61 g, 4.3 mmol), triethylamine (0.47 g, 4.6 mmol), and *p*-nitro-*m*-methylbenzene sulfonyl chloride (1.03 g, 4.3 mmol) were reacted in pyridine (50 mL). Procedure and work-up were the same as those outlined for the preparation of the dinitrosulfonate ester **5***a*.

Recrystallized **5***b* (0.69 g, 2.0 mmol, 46%, mp 120–121°C) had R_f 0.34 on analytical tlc plates developed with 3:2 carbon tetrachloride/methylene chloride; ir ($CHCl_3$): 1530, 1400, 1350, and 1175 cm^{-1}; nmr ($CDCl_3$) δ: 8.30 (2H, d), 7.96 (3H, m), 7.23 (2H, d), and 2.66 (3H, s); ms *m/e*: 338 ($M^{\ddagger}$, 27%), 200 (100%), and 136 (78%). Anal. calcd. for $C_{13}H_{10}N_2O_7S$: C 46.15, H 2.97; found: C 46.21, H 2.68.

Reaction of dinitrosulfonate **5** a *with* p-*tolyl mercaptide anions*

Sodium hydride (0.05 g, 2.2 mmol) was added to HMPA (10 mL). A solution of *p*-tolyl mercaptan (0.29 g, 2.3 mmol) in HMPA (5 mL) was added dropwise. The dinitrosulfonate **5***a* (0.75 g, 2.2 mmol) was added and the reaction mixture stirred for 2 h. The reaction mixture was subjected to the extraction procedure outlined under "Reaction of **2** with ethoxide and *p*-tolyl mercaptide anions".

Crude product was chromatographed on silica gel (30 g), affording a mixture of *p*-tolyl disulfide and the nitrosulfide **1** (0.21 g). The mixture was rechromatographed on silica gel (25 g), furnishing clean nitrosulfide **1** (0.11 g).

Preparation of p-*nitro*-m-*methylphenyl* p-*tolyl sulfide* **6**

Sodium hydride (0.32 g, 13 mmol) was suspended in HMPA (30 mL). *p*-Tolyl mercaptan (1.69 g, 13.7 mmol) in HMPA (10 mL) was added dropwise over 5 min. *p*-Nitro-*m*-methylphenyl benzenesulfonate (4.00 g, 13.6 mmol) was added and the reaction mixture stirred at ambient temperature for 2 h.

The reaction mixture was subjected to the same extraction procedure as the **5***a* mixture.

Crude product was chromatographed on silica gel (400 g), affording *p*-tolyl disulfide (0.80 g, 3.2 mmol) and the nitrosulfide **6** (1.51 g, 5.8 mmol, 43%, mp 45.6–45.9°C). The nitrosulfide **6** had R_f 0.63 on analytical tlc plates developed with carbon tetrachloride; ir ($CHCl_3$): 1510 and 1340 cm^{-1}; nmr ($CDCl_3$) δ: 7.86 (1H, d), 7.16 (6H, m), 2.50 (3H, s), and 2.33 (3H, s); ms *m/e*: 259 ($M^{\ddagger}$, 100%), 198 (29%), and 123 (14%). Anal. calcd. for $C_{14}H_{13}NO_2S$: C 64.84, H 5.05; found: C 64.71, H 4.98.

Reaction of dinitrosulfonate **5** b *with* p-*tolyl mercaptide anions*

Sodium hydride (0.05 g, 2.3 mmol) was suspended in HMPA (10 mL). A solution of *p*-tolyl mercaptan (0.26 g, 2.1 mmol) in HMPA (5 mL) was added dropwise over 1 min. The dinitrosulfonate ester **5***b* (0.70 g, 2.0 mmol) was added and the reaction mixture stirred at ambient temperature for 2 h.

The reaction mixture was subjected to the same extraction procedure as the **5***a* and **6** mixtures.

The crude product was chromatographed on silica gel (70 g), affording *p*-tolyl disulfide (0.13 g, 0.5 mmol) and a mixture containing *p*-nitro-*m*-methylphenyl *p*-tolyl sulfide **6** (0.07 g) and *p*-nitrophenyl *p*-tolyl sulfide **1** (0.009 g). The sulfide mixture was homogeneous on tlc. The sample was split in half. The presence of each sulfide was confirmed by the addition of 15-mg aliquots of each sulfide, which induced the expected changes for appropriate signals in the nmr spectra of the mixtures.

Preparation of o-*dibromo*-p-*nitrophenyl methanesulfonate* **7**

o-Dibromo-*p*-nitrophenol (4.98 g, 16 mmol), triethylamine (1.70 g, 16 mmol), and methanesulfonyl chloride (1.93 g, 16 mmol) were reacted in dry pyridine (25 mL). Procedure and work-up were the same as those outlined under "Preparation of the dinitrosulfonate ester **5***a*". Recrystallized *o*-dibromo-*p*-nitrophenyl methanesulfonate (3.83 g, 10 mmol, 61%, mp 135–136°C) had R_f 0.77 on analytical tlc plates developed with chloroform; ir ($CHCl_3$): 1540, 1390, 1355, and 1190 cm^{-1}; uv (CH_3OH) λ_{max}: 385 (s, ε 172), 270 (ε 7352), and 224 (ε 16 176) nm; nmr ($CDCl_3$) δ: 8.46 (2H, s) and 3.56 (3H, s). Anal. calcd. for $C_7H_5Br_2NO_5S$: C 22.42, H 1.34; found: C 22.44, H 1.30.

Reaction of **7** *with ethoxide and* p-*tolyl mercaptide anions*

Sodium hydride (0.66 g, 27 mmol) was added to HMPA (30 mL). A solution of ethanol (0.62 g, 13 mmol) in HMPA (10 mL) was added dropwise over 5 min. Upon completion of the addition, a solution of *p*-tolyl mercaptan (1.71 g, 13 mmol) in HMPA (10 mL) was added dropwise over 5 min. The nitrodibromomesylate (5.24 g, 14 mmol) was added and the reaction mixture stirred at ambient temperature for 2 h. The reaction color changed from khaki to red, then to yellow, and finally orange within the first 15 min. The orange color persisted until the end of the reaction.

The reaction mixture was subjected to the extraction procedure outlined under "Reaction of **2** with ethoxide and *p*-tolyl mercaptide anions".

The crude residue was twice chromatographed on silica gel, affording pale yellow crystals of 3,4,5-tris(thio-*p*-tolyl) nitrobenzene **8** (0.73 g, 1.4 mmol, 32%). Upon recrystallization from methanol the product had mp 144–144.5°C, R_f 0.40 on analytical tlc plates developed with carbon tetrachloride; ir ($CHCl_3$): 1520 and 1340 cm^{-1}; uv (CH_3OH) λ_{max}: 395 (s, ε 2060), 375 (ε 2681), 253 (ε 56 666), and 207 (ε 157 575); nmr ($CDCl_3$) δ: 7.2 (14H, m), 2.43 (6H, s), and 2.36 (3H, s). Anal. calcd. for $C_{27}H_{23}NO_2S_3$: C 66.22, H 4.73; found: C 66.30, H 4.60.

In addition, colorless crystals of 2,6-dibromo-1,4-bis(thio-*p*-tolyl) benzene **9** (0.76 g, 1.5 mmol, 23%) were obtained. Upon recrystallization from methanol the product had mp 93.5–94°C, R_f 0.35 on analytical tlc plates developed with hexanes; ir ($CHCl_3$): 1560 and 1500 cm^{-1}; uv (CH_3OH) λ_{max}: 300 (ε 9070), 275 (ε 18 500), and

220 (ε 31 111); nmr ($CDCl_3$) δ: 7.20 (10H, m), 2.33 (3H, s), and 2.23 (3H, s). Anal. calcd. for $C_{20}H_{16}Br_2S_2$: C 50.01, H 3.35; found: C 49.95, H 3.33.

Acknowledgements

The authors acknowledge the guidance of one of the referees in producing the final form of the experimental part of this manuscript. Professor M. Zerner has kindly provided access to the ZINDO program utilized in the computational part of this study.

1. R. F. Langler and N. A. Morrison. Can. J. Chem. **65**, 2385 (1987).
2. J. F. King and M. Aslam. Can. J. Chem. **57**, 3278 (1979).
3. (*a*) B. A. Kent and S. Smiles. J. Chem. Soc. 422 (1934); (*b*) W. J. Evans and S. Smiles. J. Chem. Soc. 181 (1935).
4. (*a*) H. O. Fong, W. R. Hardstaff, D. G. Kay, R. F. Langler, R. H. Morse, and D. N. Sandoval. Can. J. Chem. **57**, 1206 (1979); (*b*) J. F. King and K. C. Khemani. Can. J. Chem. **63**, 619 (1985).
5. I. Fleming. Frontier orbitals and organic chemical reactions. Wiley, New York. 1976.
6. (*a*) G. Klopman. J. Am. Chem. Soc. **90**, 223 (1968); (*b*) L. Salem. J. Am. Chem. Soc. **90**, 543 (1968); **90**, 553 (1968).
7. K. A. Durkin, R. F. Langler, and N. A. Morrison. Can. J. Chem. **66**, 3070 (1988).
8. J. C. Carnahan, Jr., W. D. Closson, J. R. Ganson, D. A. Juckett, and K. S. Quaal. J. Am. Chem. Soc. **98**, 2526 (1976).
9. J. Ridley and M. Zerner. Theor. Chim. Acta, **32**, 111 (1973).
10. W. J. Pietro, M. M. Francl, W. T. Hehre, D. J. Defrees, J. A. Pople, and J. S. Binkley. J. Am. Chem. Soc. **104**, 5039 (1982).
11. N. I. Sax. Dangerous properties of industrial materials. Van Nostrand Rheinhold, New York. 1979. p. 721.

Can. J. Chem. Downloaded from www.nrcresearchpress.com by 88.85.125.76 on 09/07/12
For personal use only.

The structure of the antigenic lipopolysaccharide O-chain produced by *Escherichia hermannii* ATCC 33650 and 33652[1]

LINDA M. BEYNON, DAVID R. BUNDLE, AND MALCOLM B. PERRY
Institute for Biological Sciences, National Research Council, Ottawa, Ont., Canada K1A 0R6

Received February 20, 1990

LINDA M. BEYNON, DAVID R. BUNDLE, and MALCOLM B. PERRY. Can. J. Chem. **68**, 1456 (1990).

High resolution two-dimensional ^{1}H and ^{13}C nuclear magnetic resonance at 500 MHz was used in combination with molecular modelling to solve the structures of the antigenic O-polysaccharides produced by *Escherichia hermannii* strains ATCC 33650 and 33652. Classical structural methods such as methylation analysis, selective and partial hydrolysis, and periodate oxidations confirmed that the O-polysaccharides had a branched tetrasaccharide repeating unit with the structure:

$$\begin{array}{l}\rightarrow 4)\text{-}\beta\text{-D-Glc}p\text{-}(1\rightarrow 2)\text{-}\alpha\text{-D-Rha}p\text{-}(1\rightarrow 3)\text{-}\beta\text{-D-Rha}p\text{-}(1\rightarrow \\ \qquad\qquad\qquad\qquad\qquad\qquad\qquad\qquad\qquad\qquad\qquad\quad 3 \\ \qquad\qquad\qquad\qquad\qquad\qquad\qquad\qquad\qquad\qquad\qquad\quad \uparrow \\ \qquad\qquad\qquad\qquad\qquad\qquad\qquad\qquad\qquad\qquad\qquad\quad 1 \\ \qquad\qquad\qquad\qquad\qquad\qquad\qquad\qquad\qquad\qquad\qquad\quad \alpha\text{-D-Gal}p\end{array}$$

Key words: *Escherichia hermannii*, lipopolysaccharide, magnetic resonance, polysaccharide.

LINDA M. BEYNON, DAVID R. BUNDLE et MALCOLM B. PERRY. Can. J. Chem. **68**, 1456 (1990).

Faisant appel à une combinaison de résonance magnétique nucléaire du ^{1}H et ^{13}C bidimensionnelle à haute résolution (500 MHz) et de modelage moléculaire, on a résolu les structures des O-polysaccharides antigéniques produits par les souches ATCC 33650 et 33652 d'*Escherichia hermannii*. Les méthodes classiques de détermination de structure, comme l'analyse des méthylations, les hydrolyses sélectives et partielles ainsi que les oxydations par le periodate, ont permis de confirmer que l'unité de base qui se répète dans les O-polysaccharides est un tétrasaccharide ramifié possédant la structure :

$$\begin{array}{l}\rightarrow 4)\text{-}\beta\text{-D-Glc}p\text{-}(1\rightarrow 2)\text{-}\alpha\text{-D-Rha}p\text{-}(1\rightarrow 3)\text{-}\beta\text{-D-Rha}p\text{-}(1\rightarrow \\ \qquad\qquad\qquad\qquad\qquad\qquad\qquad\qquad\qquad\qquad\qquad\quad 3 \\ \qquad\qquad\qquad\qquad\qquad\qquad\qquad\qquad\qquad\qquad\qquad\quad \uparrow \\ \qquad\qquad\qquad\qquad\qquad\qquad\qquad\qquad\qquad\qquad\qquad\quad 1 \\ \qquad\qquad\qquad\qquad\qquad\qquad\qquad\qquad\qquad\qquad\qquad\quad \alpha\text{-D-Gal}p\end{array}$$

Mots clés : *Escherichia hermannii*, lipopolysaccharide, résonance magnétique, polysaccharide.

[Traduit par la revue]

Introduction

Escherichia hermannii is described as an atypical biogroup of *Escherichia coli*. Wounds, sputum, lungs, and stools account for the source of human isolates; however, the incidence and clinical significance of the organism has not been investigated (1). Our interest in *E. hermannii* arose from the fact that some strains of the organism were falsely identified by cross-serological reactions as the important human pathogen *E. coli* O157:H7 (2). Subsequent investigations in our laboratory revealed that the structural chemical basis for this cross-serological activity resided in the presence of common epitopes involving 1,2-linked 4-acetamido-4,6-dideoxy-α-D-mannopyranosyl residues contained in their respective lipopolysaccharide O-chains (3, 4). The LPS O-chains of the cross-reacting strains of *E. hermannii* were found to be composed of repeating pentasaccharide units in linear unbranched homopolymers containing 1,2- and 1,3-linked 4-acetamido-4,6-dideoxy-α-D-mannopyranosyl residues (5), having a very close structural similarity to the M antigen found in the LPS O-chains of *Brucella melitensis* (6).

Since no chemical analyses have been reported on *E. hermannii* species it was of interest to determine if all strains of *E. hermannii* were of one serotype, showing serological cross-reaction with *Brucella* or *E. coli* O157 polysaccharide antigens. The findings in this paper record that two of the three strains of *E. hermannii* (ATCC 33650 and 33652) carried in the American Type Culture Collection have identical LPS O-chains composed of tetrasaccharide repeating units containing D-galactose, D-glucose, and D-rhamnose (1:1:2), totally unrelated to the *Brucella* and *E. coli* O157 LPS O-chains, which contain *N*-acylated common 4-amino-4,6-dideoxy-D-mannose residues. The third *E. hermannii* ATCC strain (ATCC 33651) has been found to have a unique LPS antigenic O-chain of an unbranched polymer containing only 1,3-linked β-D-rhamnopyranosyl residues (7).

Results and discussion

Extraction of *E. hermannii* (ATCC 33650) cells by a modified lysozyme phenol–water extraction procedure (8), followed by ultracentrifugation (105 000 × *g*) of the concentrated dialyzed aqueous phase, afforded LPS (ca. 5% yield based on dry cell weight). The LPS was treated with hot dilute acetic acid to yield an insoluble lipid A (15%) and Sephadex G-50 gel filtration of the concentrated water soluble products afforded polysaccharide O-chain (K_{av} 0.03, 43%), core oligosaccharide (K_{av} 0.77, 11%), and a fraction containing phosphate and 3-deoxy-D-*manno*-octulosonic acid (K_{av} 0.99, 9%).

The lyophilized O-polysaccharide had $[\alpha]_D$ +55.4° (*c* 0.54, water). Anal. found: C 40.61, H 6.01, N nil, ash, nil%. Preparative paper chromatography of the polysaccharide hydrolyzate afforded (a) D-galactose (R_{Gal} 1.00), which had [α] +78° (*c* 0.3, water) and which on reduction and acetylation gave galactitol hexaacetate having mp and mixture mp 166°C, and on GLC (program A) it gave a single peak with T_{GA} 1.01; (b) D-glucose (R_{Gal} 1.20) having $[\alpha]_D$ +52° (*c* 0.04, water), which on reduction and acetylation gave D-glucitol hexaacetate, mp and mixture mp 99°C and $[\alpha]_D$ +10° (*c* 0.2, $CHCl_3$), and which

[1]NRCC No. 31631.

Can. J. Chem. Downloaded from www.nrcresearchpress.com by 88.85.125.76 on 09/07/12
For personal use only.

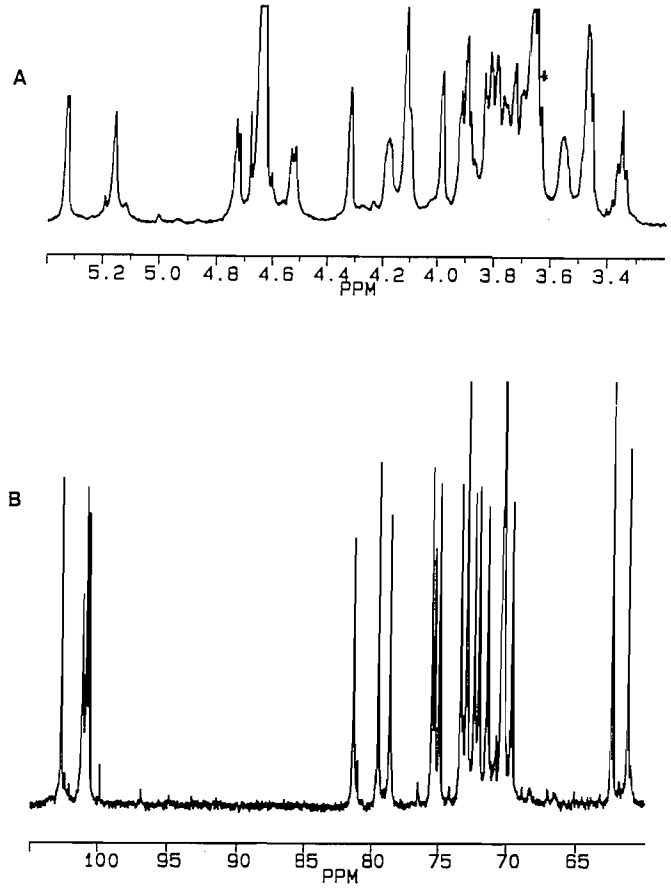

FIG. 1. (A) The 500 MHz ^{1}H NMR spectrum of the chromatographically purified *E. hermannii* O-polysaccharide. The spectral window covers the region δ 5.4–3.2 ppm, which includes the ring proton resonances. (B) The 125 MHz ^{13}C NMR spectrum of the O-polysaccharide. The ^{13}C resonances occurring in the displayed spectral region δ 105.0–60 ppm correspond to carbon atoms directly bonded to the protons displayed in A.

on GLC (program A) gave a single peak with T_{GA} 1.00; and (c) D-rhamnose (R_{Gal} 1.97) having $[\alpha]_D$ −8° (*c* 0.4, water), which on methanolysis afforded crystalline methyl α-D-rhamnopyranoside having mp and mixture mp 106°C, and $[\alpha]_D$ +62° (*c* 0.4, water), and the derived rhamnitol pentaacetate gave a single peak on GLC (program A) with T_{GA} 0.61. The assigned configurations were confirmed from the GLC analysis of the acetate and trimethylsilyl derivatives of derived 2-(+)-butyl glycosides (9, 10). Quantitative analysis of the polysaccharide constituent sugars by GLC (program A) of the derived alditol acetates of the hydrolysis products (11) showed D-galactose, D-glucose, and D-rhamnose to be present in the exact molar ratios of 1:1:2.

Four anomeric resonances were observed in both the ^{1}H and ^{13}C NMR spectra of the O-polysaccharide (Figs. 1A and 1B), suggesting a repeating unit based on a tetrasaccharide structure. The ^{1}H NMR spectrum of the O-antigen showed four equal intensity anomeric proton signals at δ 5.32 (d, 1H, $J_{1,2}$ 3.5 Hz), 5.16 (bs, 1H), 4.72 (bs, 1H), and 4.54 (d, 1H, $J_{1,2}$ 8 Hz) (Fig. 1). Consistent with the ^{1}H NMR spectrum, the ^{13}C NMR spectrum showed four distinct anomeric carbon resonances, δ 102.7, 101.1, 100.8, and 100.7, having $^1J_{C,H}$ values of 162, 170, 171, and 160 Hz respectively (Fig. 1B). Proton resonances at δ 1.32 with corresponding ^{13}C signals at δ 17.5 confirmed the presence of 6-deoxyhexose residues, while the heteronuclear

TABLE 1. ^{1}H NMR chemical shifts[a] of O-polysaccharide

Monosaccharide residue	H-1	H-2	H-3	H-4	H-5	H-6
a	5.323	3.824	3.901	3.981	4.178	3.79 3.72
b	5.150	4.317	4.101	3.640	3.890	1.321
c	4.732	4.117	3.663	3.470	3.465	1.342
d	4.521	3.343	3.645	3.662	3.562	3.78 3.75

[a]First-order chemical shifts were measured for solutions in D_2O at 37°C, and are referenced to internal 1% (v/v) acetone (δ 2.225 ppm).

TABLE 2. ^{13}C NMR chemical shifts[a] in O-polysaccharide

Monosaccharide residue	C-1[b]	C-2	C-3	C-4	C-5
a	101.13 (172)	69.65	70.32	70.40	72.36
b	100.87 (173)	78.63	75.26	72.91	70.27
c	100.68 (162)	71.41	81.33	72.04	72.91
d	102.69 (163)	73.35	74.92	79.50	75.49

[a]Chemical shifts were measured for solutions in D_2O at 37°C as expressed relative to 1% (v/v) internal acetone (δ 31.07 ppm).
[b]Value in parentheses: one-bond heteronuclear coupling constant in hertz.

coupling constants indicated the presence of two α- and two β-linked hexopyranose residues in the O-polysaccharide repeating unit.

Both ^{1}H and ^{13}C NMR spectra suggested that the structure of the polysaccharide repeating unit was based on a tetrasaccharide element, and detailed two-dimensional NMR experiments were used to unambiguously assign the structure of the polysaccharide using the absolute configuration of the component monosaccharides as the only non-spectroscopic technique. Homonuclear correlated (COSY) (12) and relayed coherence transfer (relayed COSY) (13) two-dimensional experiments allowed an almost complete assignment of the 26 proton resonances (Table 1), since the ^{1}H NMR spectrum showed very good dispersion (Fig. 2). In combination with ^{13}C/^{1}H correlation (14), the residual ^{1}H resonances were assigned, together with a complete assignment of the ^{13}C NMR spectrum (Table 2). Based upon the ^{1}H and ^{13}C chemical shifts (15–17) and the heteronuclear ^1J values (18), the polysaccharide contained α-D-galactopyranosyl, α-D-rhamnopyranosyl, β-D-rhamnopyranosyl, and β-D-glucopyranosyl residues. These four hexopyranose residues were labelled **a**–**d** based upon the chemical shift ordering of the ^{1}H anomeric resonances. This designation was used to track the dipolar coupling and residue sequence subsequently revealed by nOe experiments.

Phase sensitive NOESY (19) experiments (Fig. 3) served to establish the sequence of the monosaccharide residues in the polysaccharide and, in the case of the β-linked hexopyranose units (β-D-Glc*p* and β-D-Rha*p*), intra-residue nOe's that result from 1,3 diaxial relaxation between H-1, H-3, and H-5 atoms also confirmed the anomeric configuration. Monosaccharide **a** (α-D-Gal*p*) exhibits strong nOe's between H1**a**, H2**a**, and H3**b**, suggesting that residue **a** was α1,3 linked to **b**. The absence

Can. J. Chem. Downloaded from www.nrcresearchpress.com by 88.85.125.76 on 09/07/12
For personal use only.

Can. J. Chem. Downloaded from www.nrcresearchpress.com by 88.85.125.76 on 09/07/12
For personal use only.

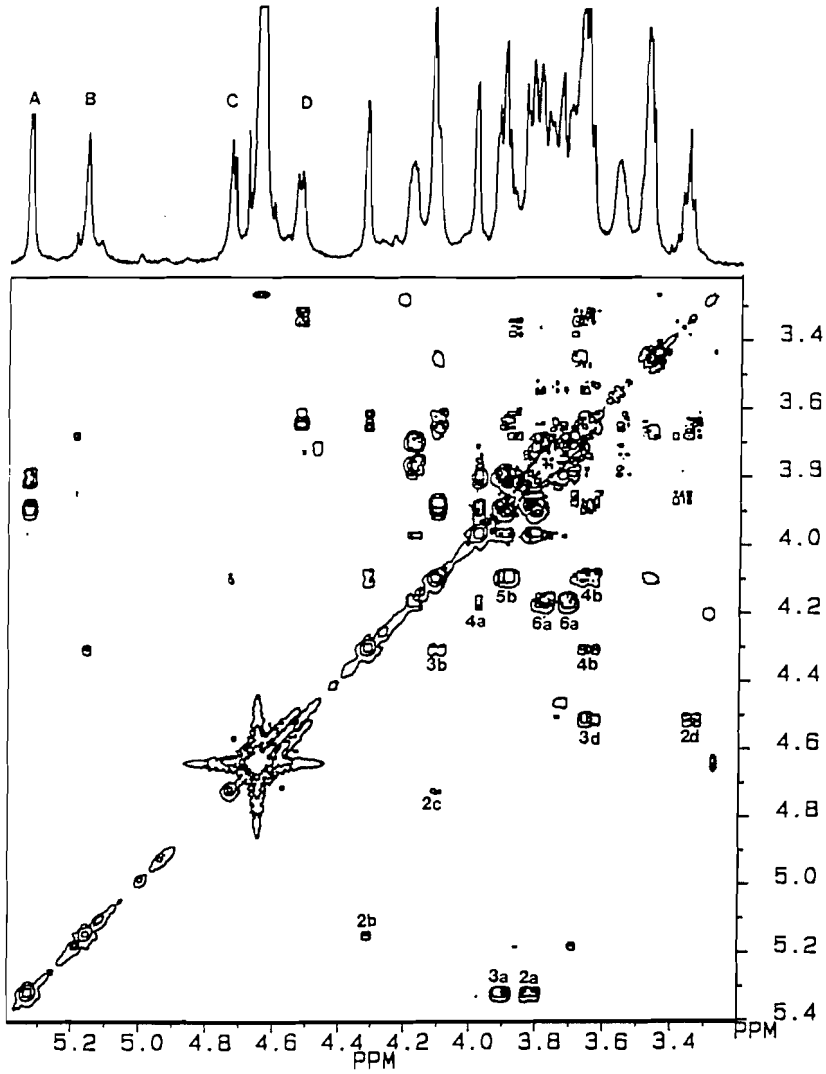

FIG. 2. Relayed coherence transfer experiment. The anomeric resonances 1a → 1d provide a point of entry for assignment of other ring protons. Magnetization transfer occurred during a fixed delay of 30 ms, which emphasizes spin networks with $^3J \approx 10$ Hz.

of any other nOe connectivities between **a** and either **d** or **c** suggests that **a** is a terminal unsubstituted residue. In comparison, residue **b** was correlated to residues **d** or **c** by an extensive network of inter-residue nOe cross peaks. These involved H1**b**, H2**b**, H1**c**, H1**d**, H2**c**, and either or both of H3**c**/H4**d**, resonances that are virtually coincident. Weaker cross peaks to H5**d** and H5**c**/H4**c** were also observed (Table 3). Thus it was not immediately clear whether unit **b** was glycosidically linked to residue **d** or **c**. The latter β-D-Rha*p* possessed nOe's between H1**c**, H3**c**, and H5**c**, and the magnitude of the cross peak between H1**c**/H3**c** suggested an additional nOe involving the coincident resonance H4**d**. Finally, residue **d** (β-D-Glc*p*) was concluded to be β1,2 linked to the α-D-Rha*p* unit **b**, since H1**d** showed strong cross peaks to H2**b**, H3**d**, and H5*d*. Based upon this data (Table 3, Fig. 4) the simplest linkage sequence was **d** → **b** → **c** with residue **a** as a branch point on **b**. The $^{13}C/^{1}H$ correlation map was consistent with this since it indicated that positions C4**d** and C3**c** were glycosylated as each carbon resonance experienced characteristic glycosylation shifts (Table 2) (17). Combining the ^{13}C NMR chemical shift with ^{1}H nOe data, the basic repeating unit structure was concluded to be

(**d**) (**b**) (**c**)

→4)-β-D-Glc*p*-(1→2)-α-D-Rha*p*-(1→3)-β-D-Rha*p*-(1→

3
↑
1

α-D-Gal*p*

(**a**)

Inter- and intra-residue nOe's extracted from the NOESY experiment (Fig. 3) agree with predicated nOe's (Table 3). These were calculated from a molecular model of the proposed polysaccharide repeating unit using the GESA algorithm (20) adapted to take account of motional averaging about the glycosidic linkages. Ensemble averaged nOe's were also calculated by the full matrix treatment (21). The overlap of crucial proton resonances H3**c**/H4**d** and H3**d**/H4**b** introduces a degree of uncertainty into the assignment of sequence linkage position for residues **c** and **d**. To place the NMR structural assignment upon a rigorous basis, classical chemical methods that included specific degradation and methylation analysis were used (Scheme 1).

Can. J. Chem. Downloaded from www.nrcresearchpress.com by 88.85.125.76 on 09/07/12
For personal use only.

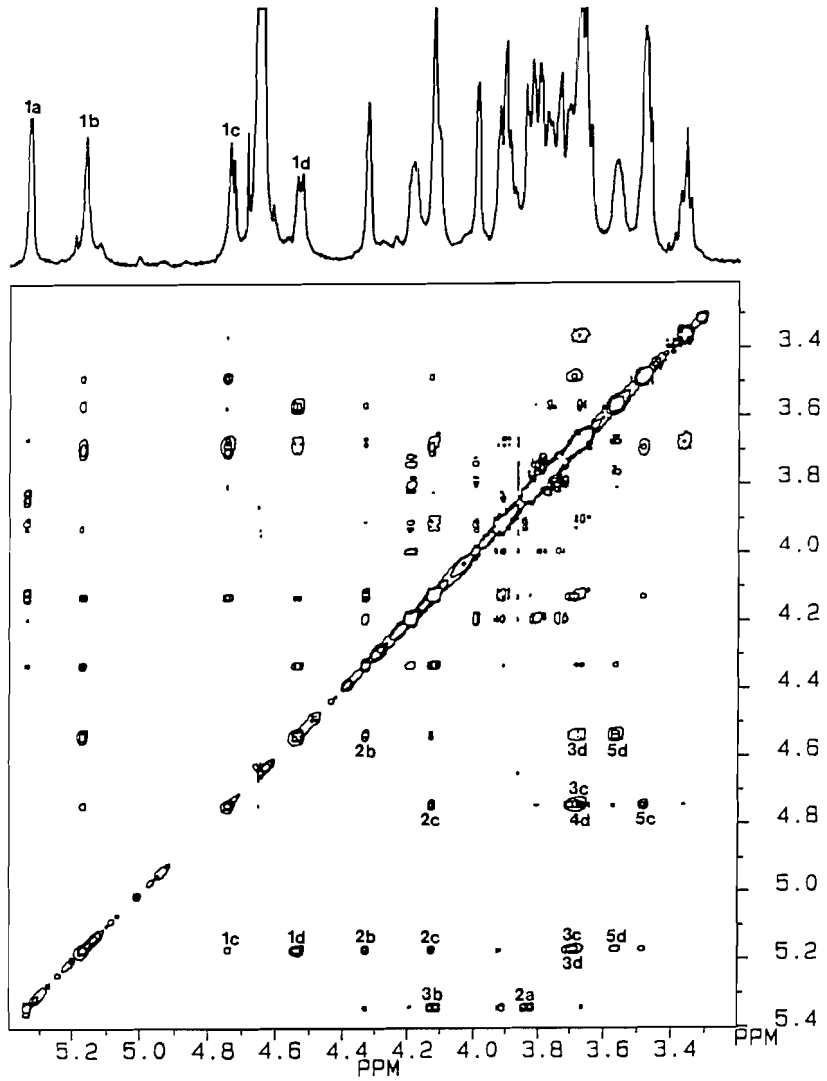

FIG. 3. Phase-sensitive NOESY experiments used to sequence the O-polysaccharide repeating unit. Dipolar coupling is evident for protons within the same ring and across the glycosidic oxygen atom as illustrated schematically in Fig. 4.

TABLE 3. Glycosidic torsional angles and the observed[a] and predicted nOe's[b]

	αDGal(1→3)αDRha	(1→2)α-D-Rha(1→3)	(1→3)β-D-Rha(1→4)	(1→4)β-D-Glc(1→2)
Glycosidic torsional angles, ϕ, ψ[a]	−53°/−15°	−47°/−7°	55°/5°	57°/16°
Observed nOe's (cross-peak intensity)	H2**a**(H1**a**) s H3**b**(H1**a**) s	H2**b**(H1**b**) s H1**c**(H1**b**) m H2**c**(H1**b**) s H3**c**(H1**b**) s H1**d**(H1**b**) s H5**d**(H1**b**) w H5**c**(H1**b**) w	H2**c**(H1**c**) s H3**c**(H1**c**) s H5**c**(H1**c**) s H4**d**(H1**c**) s	H3**d**(H1**d**) s H5**d**(H1**d**) s H2**b**(H1**d**) s
Predicted nOe's	H2**a**(H1**a**) s H3**b**(H1**a**) s	H2**b**(H1**b**) s H1**c**(H1**b**) w H2**c**(H1**b**) w H3**c**(H1**b**) s H1**d**(H1**b**) s H5**d**(H1**b**) w H4**c**(H1**b**) w	H2**c**(H1**c**) s H3**c**(H1**c**) m H5**c**(H1**c**) s H4**d**(H1**c**) s H1**b**(H1**c**) w	H3**d**(H1**d**) s H5**d**(H1**d**) s H2**d**(H1**d**) m H2**b**(H1**d**) s H1**b**(H1**d**) s

[a]The magnitude of observed nOe's was estimated from the height of cross-peak cross sections or one-dimensional nOe difference spectra.
[b]Predicted nOe's were ranked on the basis of nOe's calculated from a distance matrix of the repeating unit.
[c]Torsion angles are defined as ϕ H1—C1—O1—C_x and ψ C1—O1—C_x—H_x.

Can. J. Chem. Downloaded from www.nrcresearchpress.com by 88.85.125.76 on 09/07/12
For personal use only.

GLC–MS analysis of the reduced ($NaBD_4$) and acetylated products of the hydrolyzed methylated O-polysaccharide (Table 4) indicated the repeating unit to be a branched tetrasaccharide consisting of non-reducing D-galactopyranose end groups, 3-*O*-substituted D-rhamnopyranosyl units, 4-*O*-substituted D-glucopyranosyl units, and branch points of D-rhamnopyranose substituted at the *O*-2 and *O*-3 positions. The glycose sequence and anomeric configurations of the linkages in the O-chain were determined by degradation methods.

Selected acid hydrolysis (0.5 M trifluoroacetic acid, 1 h, 100°C) followed by Sephadex G-50 gel filtration chromatography of the concentrated hydrolyzate gave a major high molecular weight product (**1**) (K_{av} 0.06) composed of D-glucose and D-rhamnose (1:2). Methylation analysis (Table 4) of **1** gave 3,4-di-*O*-methyl-D-rhamnose, 2,4-di-*O*-methyl-D-rhamnose, and 2,3,6-tri-*O*-methyl-D-glucose (1:1:1.1). The new appearance of 3,4-di-*O*-methyl-D-rhamnose shows that the non-reducing D-galactopyranose end group was the single side substituent attached to the 2-*O*-glycosidically substituted D-rhamnopyranosyl residue contained in the unbranched linear backbone of the O-chain. The ^1H and ^{13}C spectra (Table 5) of the degraded O-chain are consistent with the proposed trisaccharide repeating unit present in the backbone structure and to assignment in the native O-chain of the α and β configurations to the D-galactopyranosyl and D-glucopyranosyl residues respectively.

The sequence of the three glycose residues in the O-chain backbone was established through periodate oxidation studies. The periodate oxidized and reduced ($NaBH_4$) O-chain, on Smith type hydrolysis (22) and subsequent Bio-Gel P2 gel chromatographic separation of the hydrolyzate, gave a major product (**2**) (K_{av} 0.65), which on TLC exhibited two spots having R_f 0.48 and 0.42 (ca. 1:2.5). GLC–MS (program C) analysis of the methylated mixed product **2** gave two peaks for derivatives **2***a* and **2***b* having T_{MS} 1.58 and 2.45 (ca. 2.3:1). The GLC–CI-MS of **2***a* (Table 6) gave a fragmentation pattern consistent with the structure:

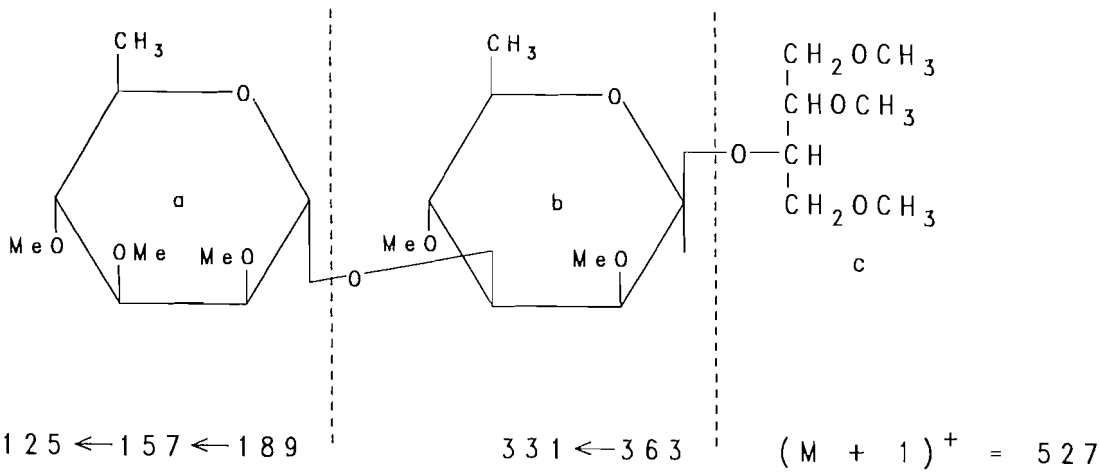

The GLC–CI-MS fragmentation pattern of **2***b* (Table 6) suggested that it was an artifact produced during the Smith-type hydrolysis and has the possible structure:

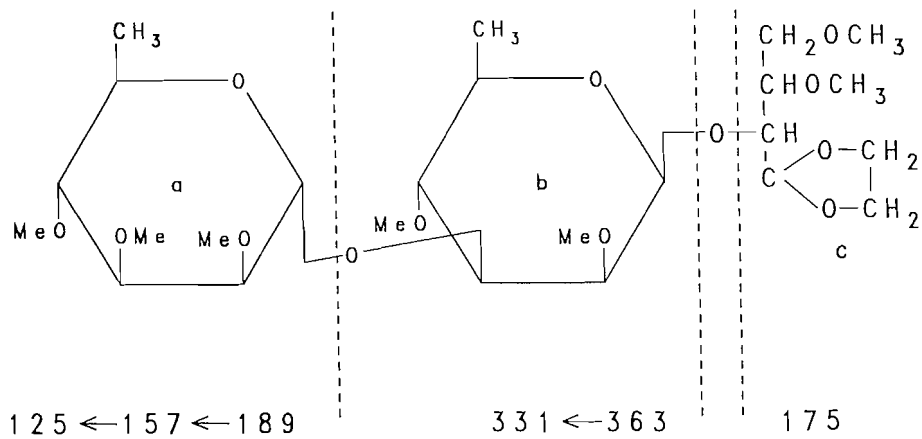

GLC–MS analysis of the reduced ($NaBD_4$) and acetylated hydrolysis products of methylated **2** (Table 4) showed it to give 2,3,4-tri-*O*-methyl-D-rhamnose and 2,4-di-*O*-methyl-D-rhamnose (1.2:1) consistent with the proposed structure **2***a* and of the linkage sequence →2)-D-Rha*p*-(1→3)-D-Rha*p*-(1→4)-D-Glc*p*-(1→ in the backbone of the O-chain. Periodate oxidation of **2** followed by Smith-type hydrolysis and preparative paper chromatography afforded a major product **3** (R_{Gal} 1.75), having $[\alpha]_D$ −110° (*c* 0.2, water), composed of D-rhamnose and glycerol (1:1) and identified as β-D-rhamnopyranosyl-(1→2)-glycerol by methylation analysis and from its ^{13}C NMR spectrum, which showed an anomeric carbon signal (δ 100.19)

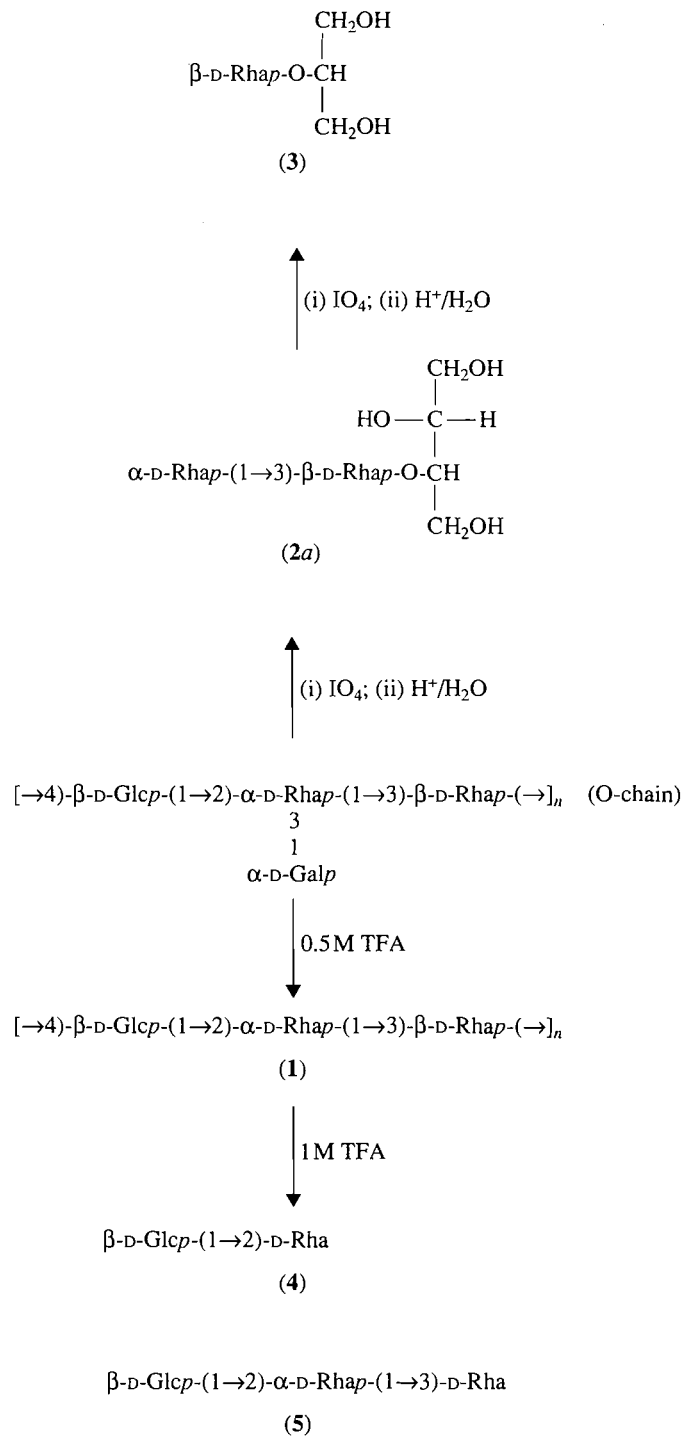

SCHEME 1. Degradation of *E. hermannii* LPS O-chain by hydrolytic and periodate oxidation methods.

having a $J_{C,H}$ coupling of 159 Hz. The identification of **3**, considered in connection with the identified presence of an α and a β configuration present in its precursor **2***a* (Table 5), indicates that the backbone structure of the O-chain contains the sequence →4)-β-D-Glc*p*-(1→2)-α-D-Rha*p*-(1→3)-β-D-Rha*p*-(1→.

Further confirmation of the structure of the O-chain was obtained by partial hydrolysis of the native O-chain (1 M trifluoroacetic acid, 95°C, 45 min) followed by Bio-Gel P2 gel filtration chromatography of the products, affording a disaccharide **4** (23%) (K_{av} 0.82) and a trisaccharide **5** (12%) (K_{av} 0.61). Both products were chromatographically pure by TLC and had R_f 0.34 and 0.27 respectively.

Oligosaccharide **4** was composed of D-glucose and D-rhamnose (1:1) and GLC–MS (program C) of methylated **4** showed two peaks (T_{MS} 0.89 and 0.91) giving identical mass spectral fragmentation patterns (Table 6) consistent with the structure:

Can. J. Chem. Downloaded from www.nrcresearchpress.com by 88.85.125.76 on 09/07/12
For personal use only.

TABLE 4. GLC–MS analysis of the products of methylation analysis of the O-chain of *E. hermannii* ATCC 33650 and its degradation products

Methylated glycitol derivative	Molar ratios						
			Degradation products[b]				
	T_{GM}[a]	LPS O-chain	**1**	**2**	**3**	**4**	**5**
1,5-Di-*O*-acetyl-2,3,4-tri-*O*-methyl-D-rhamnitol	0.68	—	—	1.2	1.0	—	—
1,2,5-Tri-*O*-acetyl-3,4-di-*O*-methyl-D-rhamnitol	0.87	—	1.0	—	—	1.0	1.0
1,3,5-Tri-*O*-acetyl-2,4-di-*O*-methyl-D-rhamnitol	0.93	1.0	1.0	1.0	—	—	0.6
1,5-Di-*O*-acetyl-2,3,4,6-tetra-*O*-methyl-D-glucitol	1.00	—	—		—	1.2	0.8
1,5-Di-*O*-acetyl-2,3,4,6-tetra-*O*-methyl-D-galactitol	1.06	0.7	—	—	—	—	—
1,2,3,5-Tetra-*O*-acetyl-4-*O*-methyl-D-rhamnitol	1.12	1.0	—	—	—	—	—
1,4,5-Tri-*O*-acetyl-2,3,6-tri-*O*-methyl-D-glucitol	1.31	1.0	1.1	—	—	—	—

[a]GLC (program B) retention time relative to 1,5-di-*O*-acetyl-2,3,4,6-tetra-*O*-methyl-D-glucitol = 1.00.

[b]Degradation products: **1**, degraded O-chain from selective hydrolysis; **2**, periodate oxidation product D-Rha*p*-(1→3)-D-Rha*p*-(1→2)-erythritol; **3**, periodate oxidation product D-Rha*p*-(1→2)-glycerol; **4**, partial hydrolysis product D-Glu*p*-(1→2)-D-Rha; **5**, partial hydrolysis product D-Glu*p*-(1→2)-D-Rha*p*-(1→3)-D-Rha.

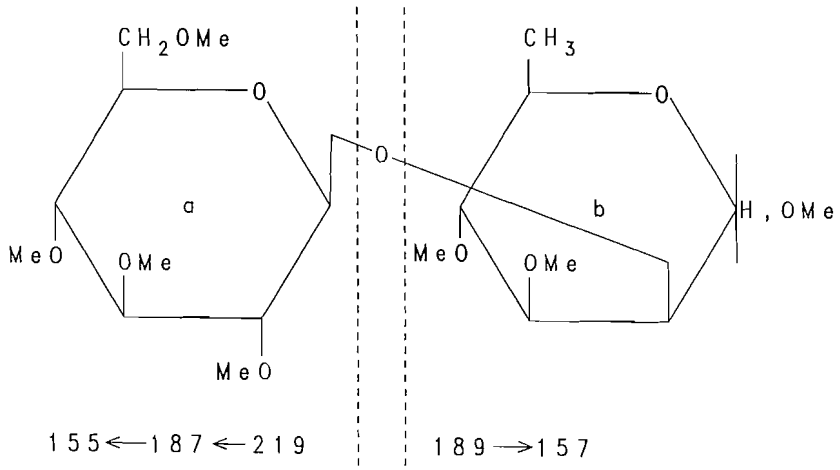

Hydrolysis of methylated **4** gave 2,3,4,6-tetra-*O*-methyl-D-glucose and 3,4-di-*O*-methyl-D-rhamnose (1.2:1). The ^{1}H NMR spectrum (Table 5) of **4** showed the anomeric proton signal of the D-glucopyranosyl residue at δ 4.50 (d, 1H, $J_{1,2}$ = 8 Hz), allowing **4** to be assigned the structure β-D-glucopyranosyl-(1→2)-D-rhamnose.

Oligosaccharide **5** was composed of D-glucose and D-rhamnose (1:2). GLC–MS (program C) analysis of methylated **5** gave a single peak (T_{MS} 2.31), giving a MS spectrum (Table 6) consistent with the structure:

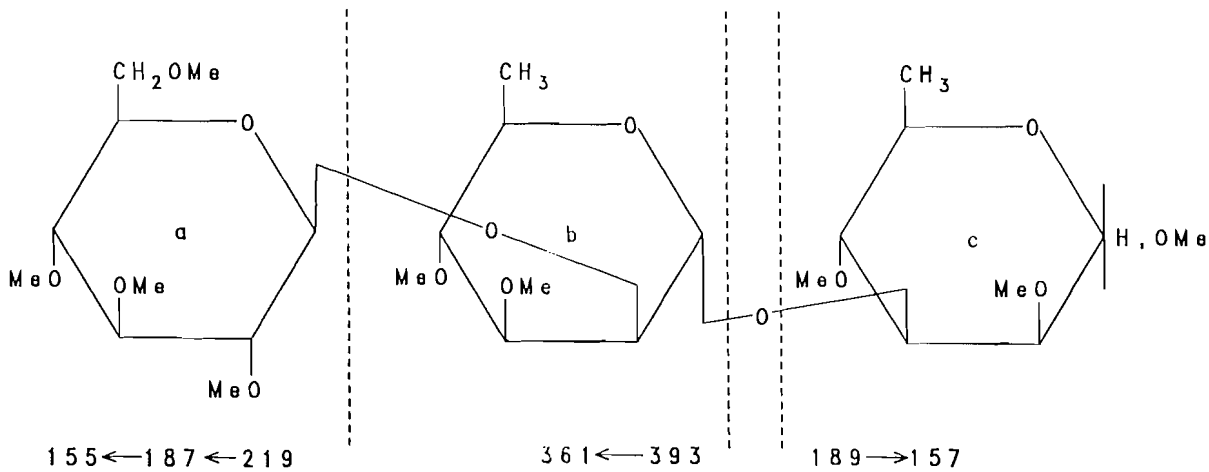

Can. J. Chem. Downloaded from www.nrcresearchpress.com by 88.85.125.76 on 09/07/12
For personal use only.

TABLE 5. NMR data for *E. hermannii* ATCC 33650 O-chain and derived oligosaccharides

Compound	^{1}H NMR data				^{13}C NMR data	
	δ[a] (ppm)	$J_{1,2}$ (Hz)	Integral (no. of H's)	Assignment[b]	δ[c] (ppm)	Assignment[d]
Selectively hydrolyzed polysaccharide	5.15	s	1	2-α-D-Rha	102.37	4-β-D-Glc
→4)-β-D-Glc-(1→2)-α-D-Rha-(1→3)-β-D-Rha-(1→	4.71	s	1	3-β-D-Rha	101.09	2-α-D-Rha
1	4.53	8	1	4-β-D-Glc	100.67	3-β-D-Rha
	1.30	5	6	CH_3 of Rha	61.03	C6 of 4-β-D-Glc
	1.35				17.54	CH_3 of 2-α-D-Rha
					17.39	CH_3 of 3-β-D-Rha
Smith product	5.03	s	1	α-D-Rha	103.10	α-D-Rha
α-D-Rha-(1→3)-β-D-Rha-(1→2)-Ery	4.75	s	1	β-D-Rha	100.58	3-β-D-Rha
2*a*	1.30	m	6	CH_3 of Rha	63.13	C4 of Ery
					62.18	C1 of Ery
					17.60	CH_3 of α-D-Rha
					17.45	CH_3 of 3-β-D-Rha
β-D-Rha-(1→2)-Gly	4.80	s	1	β-D-Rha	100.19	β-D-Rha
3	1.30	m	3	CH_3 of Rha	62.31	C1, C3 of Gly
					61.70	
					17.60	CH_3 of Rha
Partial hydrolysis products	5.23	s	0.6	2-α-D-Rha	104.80	β-D-Glc-(1→2)-β-D-Rha
β-D-Glc-(1→2)-D-Rha	4.95	s	0.3	2-β-D-Rha	102.76	β-D-Glc-(1→2)-α-D-Rha
4	4.50	9	1.0	β-D-Glc	94.39	2-β-D-Rha
	1.25	m	3.0	CH_3 of Rha	92.99	2-α-D-Rha
					61.51	C6 of α-D-Glc
					17.53	CH_3 of 2-α-D-Rha
β-D-Glc-(1→2)-α-D-Rha-(1→3)-D-Rha-ol	5.08	s	1.0	2-α-D-Rha	100.63	β-D-Glc
5	4.47	9	1.0	β-D-Glc	98.87	2-α-D-Rha
	1.30	m	6.0	CH_3 of Rha	61.60	C6 β-D-Glc
					59.63	C1 3-β-D-Rha-ol
					17.95	CH_3 of 2-α-D-Rha
					15.36	CH_3 of 3-β-D-Rha-ol

[a]Chemical shift relative to internal acetone assigned at δ 2.23 downfield from external sodium 4,4-dimethyl-4-silapentane-1-sulphonate (DSS).
[b]2-α-D-Rha denotes the anomeric proton of a 2-linked α-D-rhamnopyranosyl residue. The absence of a numerical prefix indicates a terminal non-reducing group.
[c]Chemical shift relative to internal acetone assigned at 31.07 ppm downfield from external DSS.
[d]As for *b*, but for anomeric ^{13}C nuclei.

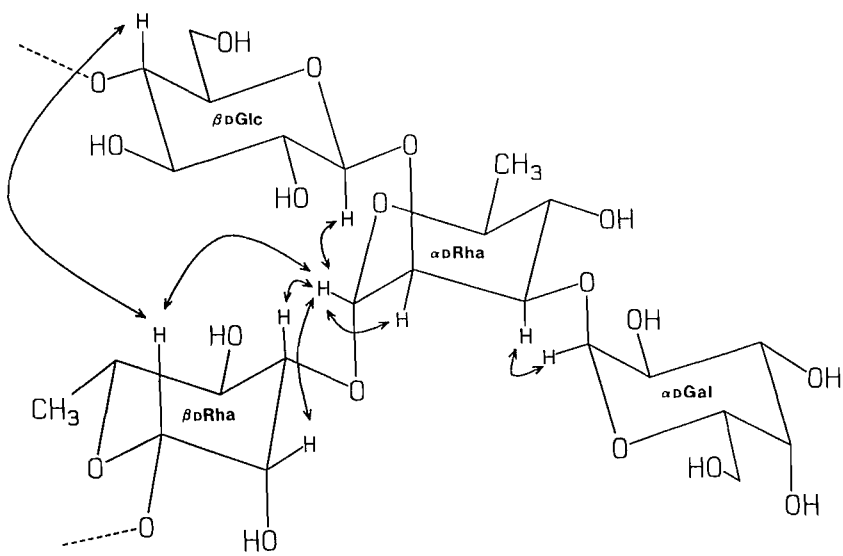

FIG. 4. The chemical structure of the *E. hermannii* ATCC 33650 and 33652 O-polysaccharides illustrating the network of observed nOe used to sequence the arrangement of four monosaccharide residues.

Can. J. Chem. Downloaded from www.nrcresearchpress.com by 88.85.125.76 on 09/07/12
For personal use only.

Can. J. Chem. Downloaded from www.nrcresearchpress.com by 88.85.125.76 on 09/07/12
For personal use only.

TABLE 6. GLC–MS analysis of methylated oligosaccharide degradation products of LPS O-chain

Methylated oligosaccharide	T_{MS}[a]	Mass spectral fragment ions											
		$[M+H]^+$	$[aA_1]$	$[aA_2]$	$[aA_3]$	$[bA_1]$	$[abA_1]$	$[abA_2]$	$[cA_1]$	$[abJ_1]$	$[cbA_1]$	$[cbA_2]$	$[cbA_3]$	$[bcJ_1]$	$[abcJ_1]$
α-D-Rha*p*-(1→3)-β-D-Rha*p*-(1→2)-erythritol **2***a*	1.58	527 (1.5)	189 (15.3)	157 (4.5)	125 (8.4)	—	363 (100)	331 (3.0)	147 (0.5)	—	—	—	—	—	—
α-D-Rha*p*-(1→3)-β-D-Rha*p*-(1→2)-X[b] **2***b*	2.45	555 (0.4)	189 (18.3)	157 (4.9)	125 (8.7)	—	363 (100)	331 (3.4)	175 (6.6)	—	—	—	—	—	—
β-D-Glc*p*-(1→2)-D-Rha **4**	0.89 0.91	—	219 (4.4)	187 (29.6)	155 (6.7)	189 (69.5)	—	—	—	249 (81.8)	—	—	—	—	—
β-D-Glc*p*-(1→2)-α-D-Rha*p*-(1→3)-D-Rha **5**	2.31	—	219 (13.5)	187 (100)	155 (17.4)	—	393 (4.9)	361 (24.2)	189 (4.5)	—	363 (5.9)	331 (23.2)	299 (12.8)	249 (32.4)	423 (26.1)

[a]GLC retention times relative to methylated sucrose (program C).
[b]X = artifact produced by Smith type hydrolysis (see text).

Methylation analysis of **5** (Table 4) gave 2,3,4,6-tetra-*O*-methyl-D-glucose, 3,4-di-*O*-methyl-D-rhamnose, and 2,4-di-*O*-methyl-D-rhamnose (0.8:1:0.6). The ^1H and ^{13}C NMR data on **5** and reduced ($NaBH_4$) **5** (Table 5) are consistent with **5** being assigned the structure β-D-glucopyranosyl-(1→2)-α-D-rhamnopyranosyl-(1→3)-D-rhamnose, the α-D configuration being assigned to the non-reducing D-rhamnopyranosyl residue from the $J_{C,H}$ (169.5 Hz) value of the anomeric carbon signal at δ 100.6, assigned to that residue. The O-chain polysaccharide is thus chemically confirmed to have the structure:

$$\begin{array}{c}\rightarrow 4)\text{-}\beta\text{-D-Glc}p\text{-}(1\rightarrow 2)\text{-}\alpha\text{-D-Rha}p\text{-}(1\rightarrow 3)\text{-}\beta\text{-D-Rha}p\text{-}(1\rightarrow \\ 3 \\ \uparrow \\ 1 \\ \alpha\text{-D-Gal}p\end{array}$$

Figure 5 illustrates a molecular model representation of the polysaccharide repeating unit, showing the orientation of each glycosidic linkage and the proximity of the protons that lead to the network of nOe's used to sequence the polymer.

The LPS core oligosaccharide had $[\alpha]_D$ +98.9° (*c* 0.9, water) and was composed of D-glucose, D-galactose, 2-amino-2-deoxy-D-glucose, and D-*glycero*-D-*manno*-heptose in the molar ratio 3.8:1.0:0.9:1.0.

A parallel study of the LPS of *E. hermannii* ATCC 33652 showed that it had a polysaccharide O-chain having an identical structure with that of the *E. hermannii* ATCC 33650 strain.

Experimental

Cell growth and production of lipopolysaccharide

Escherichia hermannii (ATCC 33650 and 33652) were first grown in BHI (50 mL) in 250-mL baffled Erlenmeyer flasks incubated overnight at 37°C and 250 rpm, followed by transfer to BHI (1 L) in 4-L baffled Erlenmeyer flasks and further incubation at 37°C for 7 h at 200 rpm. The 1-L growths were used to inoculate a fermentor (28 L Microferm, New Brunswick Scientific) containing 28 L BHI and antifoam (5 mL). The bacteria were grown at 37°C at 200 rpm with aeration 25 L/min for 18 h. Growths were killed by phenol at a final concentration of 0.75% and, after keeping at 4°C for 4 h, the cells (ca. 350 g wet weight) were collected using a Sharples centrifuge. Collected cells were extracted with stirred 48% (w/v) aqueous phenol (12 min, 65°C) and, following low speed centrifugation at 4°C, the separated aqueous and phenol phases were collected, dialyzed against tap water until phenol-free, and the retentates were lyophilized. The lyophilized products dissolved in water (100 mL) were treated with ribonuclease and deoxyribonuclease (6 h, 37°C) followed by protease K (4 h, 37°C) and, following removal of insolubles, the LPS were obtained as precipitated gels by ultracentrifugation (105 000 × g, 16 h, 4°C). Yields: 3.1 g aqueous phase LPS; 0.3 g phenol phase LPS.

LPS (0.5 g) dissolved in 1.5% (v/v) acetic acid (100 mL) were heated for 2 h on a boiling water bath and, following removal of precipitated lipid A from the cooled solution by low speed centrifugation, the centrifugates were lyophilized. The lyophilizates dissolved in 0.05 M aqueous pyridinium acetate (5 mL, pH 4.7) were fractionated on a column (2.5 × 85 cm) of Sephadex G-50 (Pharmacia Fine Chemicals) using the same buffer as the eluant. The column eluate was monitored using a Waters 402 refractometer and fractions (10 mL) of the eluates were collected.

Analytical methods

Quantitative colorimetric methods used were (a) the phenol – sulfuric acid method for neutral glycoses (23), (b) the modified Elson–Morgan method for aminodeoxyhexoses (24), (c) the method of Chen *et al.* for phosphate (25), and (d) the periodate oxidation – thiobarbituric acid method for 3-deoxy-D-*manno*-octulosonate (26).

GLC was done with a Hewlett–Packard 5830A gas chromatograph fitted with a flame ionization detector and a model 18850A electronic

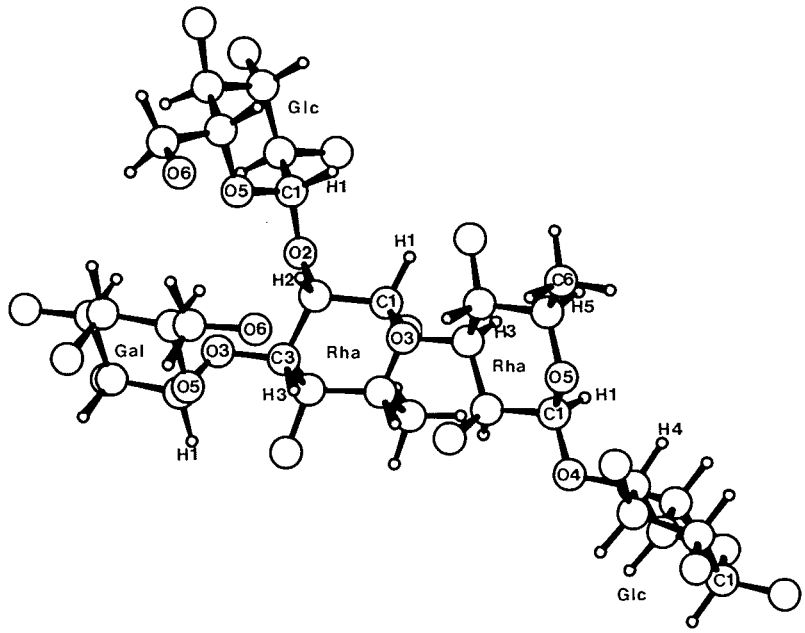

FIG. 5. The pentasaccharide sequence →4)-β-D-Glc*p*-(1→2)-[α-D-Gal*p*-(1→3)]-α-D-Rha*p*-(1→3)-β-D-Rha*p*-(1→4)-β-D-Glc*p*-(1→ is displayed in its minimum energy conformation. The network of nOe's arise from the proximity of anomeric protons (H-1) and the protons attached to the respective linkage carbon atoms are readily appreciated: H1**d**/H2**b**, H1**a**/H3**b**, H1**b**/H3**c**, and H1**c**/H4**d**.

integrator. For glycose derivative analysis, an OV 17 fused silica capillary column (0.32 mm diam. × 25 m) 007 series bonded phase (Quadrex Corp.) using temperature programs (A) 180°C (delay 2 min) – 240°C at 4°C/min, (B) 180°C (delay 2 min) – 240°C at 2°C/min, and (C) 220°C–280°C at 7°C/min. Retention times are quoted relative to D-glucitol hexaacetate (T_{GA}), 1,5-di-*O*-acetyl-2,3,4,6-tetra-*O*-methyl-D-glucitol (T_{GM}), or fully methylated sucrose (T_{MS}). GLC–MS analyses were made using a Hewlett–Packard 5985B system and GLC programs A–C with an ionization potential of 70 eV. Glycose configurations were determined by GLC of the acetylated or trimethylsilylated derived 2-(+)-butyl glycosides (9, 10).

TLC was carried out using preformed glass plates coated with silica gel 60 (Merck) using 1-propanol/concentrated ammonium hydroxide/water (6:3:1 v/v) as the mobile phase.

Gel filtrations were performed on columns of Sephadex G-50 (2 × 100 cm) or Bio-Gel P-2 (200–400 mesh) (1.6 × 100 cm).

Total hydrolysis of oligo- and polysaccharide samples (1 mg) was made in sealed tubes with 2 M trifluoroacetic acid at 100°C for 15 h followed by concentration to dryness.

Optical rotations were determined in 10-cm microtubes using a Perkin–Elmer 402 polarimeter, and concentrations were made by rotary evaporation below 45°C.

Hydrolysis methods

Selective hydrolysis (removal of D-galactopyranosyl non-reducing end groups) of O-polysaccharide (50 mg) was done with 0.5 M trifluoroacetic acid (100 mL) at 100°C for 1 h, followed by lyophilization.

Partial hydrolysis of O-polysaccharide (140 mg) to yield oligosaccharides was effected with 1 M trifluoroacetic acid (100 mL) at 95°C for 45 min, followed by evaporation to dryness.

Methylation analyses

Samples (1–2 mg) were methylated according to the Hakomori method (27) and the products were isolated by partition between dichloromethane and water. Methylated products were hydrolyzed with 2 M trifluoroacetic acid at 100°C for 16 h or 4 M trifluoroacetic acid at 125°C for 1 h, followed by evaporation to dryness. Released methylated glycoses were reduced ($NaBD_4$) and acetylated by heating with acetic anhydride and pyridine (1:1 v/v) at 95°C for 30 min, followed by direct GLC–MS (program B) analysis.

Periodate oxidation (ref. 22)

Polysaccharide (85 mg) in water (10 mL) containing sodium metaperiodate (0.2 g) was kept for 3 days in the dark at 20°C and, following the destruction of excess periodate with ethylene glycol (0.2 mL), the product was reduced by the addition of sodium borohydride (0.5 g). After 16 h at 20°C, excess borohydride was destroyed by acidification with 50% acetic acid and the product was recovered by lyophilization of the dialysed reaction mixture. Treatment of the polyol with 0.5 M trifluoroacetic acid (10 mL) for 24 h at 20°C, followed by lyophilization and Bio Gel P-2 gel filtration chromatography, afforded oligosaccharides.

Nuclear magnetic resonance spectroscopy

Polysaccharide and oligosaccharide samples were lyophilized from deuterium oxide and were dissolved at concentrations of 20 and 50 mg/500 μL. Spectra were recorded for samples in 5-mm tubes at 500 MHz for ^1H and 125 mHz for ^{13}C on a Bruker AM-500 spectrometer. Proton spectra were recorded at 303 and 310 K and ^{13}C spectra were recorded at 310 K employing ~1-W WALTZ decoupling as previously described (28).

Homonuclear two-dimensional spectroscopy was performed with Bruker DISNMRP software. COSY (12, 29) and NOESY (19) experiments were performed with suppression of the HOD resonance as previously described (6, 28). Mixing times of 100 and 150 ms were employed for NOESY experiments. Relayed COSY (13) experiments were carried out with fixed delays of 30 and 80 ms in two separate experiments to optimize coherence transfer for large and small scalar couplings (30). All homonuclear experiments were performed with quadrature detection in the F_1 dimension, and a total of $256t_1$ increments of 96 scans each (64 scans for COSY experiments) were recorded with a minimum delay between pulses of 1.2 s and a sweep width of 2500 Hz. The time domain data matrix was zero filled to either 1024 × 1024 or 2048 × 2048 points and, following resolution enhancement in both dimensions by a modified sine-bell function, the doubly transformed data were processed to give magnitude spectra. NOESY experiments were performed in the phase-sensitive mode (19). The symmetrical matrix was symmetrized about the diagonal for presentation and to reduce t_1 noise.

Heteronuclear shift correlation spectroscopy (14) was performed with quadrature detection in F_1 (31, 32), and a total of $64t_1$ increments

Can. J. Chem. Downloaded from www.nrcresearchpress.com by 88.85.125.76 on 09/07/12
For personal use only.

of 320 scans each were recorded for a spectral width in F_2 of 7800 Hz and 1500 Hz in F_1. Data were processed to give after zero filling a matrix ($t_1 \times t_2$) of 256 × 8192 points, and, following resolution enhancement, double transformation gave power spectra. Fixed delays of τ_1 = 3.4 ms and τ_2 = 1.7 ms were employed to select all multiplicities, and a recycle delay of ca. 1 s (one proton T_1) was used.

Potential energy calculations

Potential energy calculations using the GESA (20, 21) algorithm were performed for a hypothetical pentasaccharide unit β-D-Glc*p*-(1→2)-[α-D-Gal*p*-(1→3)]-α-D-Rha*p*-(1→3)-β-D-Rha*p*-(1→4)-β-D-Glc*p*, using coordinates generated from X-ray or neutron diffraction data as previously described (28). Atomic coordinates for α-D-galactopyranose residues were obtained from neutron diffraction data (33) while those for D-rhamnopyranose units were derived by bond modification of neutron diffraction data for α-D-mannopyranoside (34). The atomic coordinates for the heavy atoms of β-D-glucopyranose were taken from X-ray data (35).

Acknowledgements

We thank Mr. Fred Cooper for GLC–MS analyses, Mr. D. W. Griffith for the production of cells, and Ms. Leann MacLean for technical assistance.

1. D. J. Brenner, B. R. Davis, A. G. Steigerwalt, C. F. Riddle, A. C. McWhorter, S. D. Allen, J. J. Farmer, Y. Saitho, and G. R. Fanning. J. Clin. Microbiol. **15**, 703 (1986).
2. A. A. Borczyk, H. Lior, and B. Ciebin. Int. J. Food Microbiol. **4**, 247 (1987).
3. M. B. Perry, L. MacLean, and D. W. Griffith. Can. J. Biochem. Cell Biol. **64**, 21 (1985).
4. M. B. Perry, D. R. Bundle, M. A. J. Gidney, and H. Lior. J. Clin. Microbiol. **26**, 2391 (1988).
5. M. B. Perry and D. R. Bundle. Infect. Immun. **58**, 1391 (1990).
6. D. R. Bundle, J. R. Cherwonogrodzky, and M. B. Perry. Biochemistry, **26**, 8717 (1987).
7. M. B. Perry and J. R. Richards. Carbohydr. Res. In press.
8. K. G. Johnson and M. B. Perry. Can. J. Microbiol. **22**, 29 (1976).
9. K. Leontein, B. Lindberg, and J. Lonngren. Carbohydr. Res. **62**, 359 (1978).
10. G. R. Gerwig, J. P. Kamerling, and J. F. G. Vliegenthart. Carbohydr. Res. **62**, 349 (1978).
11. S. W. Gunner, J. K. N. Jones, and M. B. Perry. Can. J. Chem. **39**, 1892 (1961).
12. W. P. Aue, E. Bartholdi, and R. R. Ernst. J. Chem. Phys. **64**, 2229 (1976).
13. G. Wagner. J. Magn. Reson. **55**, 151 (1983).
14. A. Bax and G. Morris. J. Magn. Reson. **42**, 501 (1981).
15. K. Bock and H. Thogersen. Annu. Rep. NMR Spectrosc. **13**, 1 (1982).
16. K. Bock and C. Pedersen. Adv. Carbohydr. Chem. Biochem. **41**, 27 (1983).
17. K. Bock, C. Pedersen, and H. Pedersen. Adv. Carbohydr. Chem. Biochem. **42**, 193 (1984).
18. K. Bock and C. Pedersen. Chem. Soc. Perkin Trans. 2, 293 (1984).
19. G. Bodenhausen, H. Kogler, and R. R. Ernst. J. Magn. Reson. **58**, 370 (1984).
20. H. Paulsen, T. Peters, V. Sinnwell, R. Lebuhn, and B. Meyer. Liebigs Ann. Chem. 951 (1984).
21. T. Peters, J.-R. Brisson, and D. R. Bundle. Can. J. Chem. **68**, 979 (1990).
22. I. J. Goldstein, G. W. Hay, B. A. Lewis, and F. Smith. Methods Carbohydr. Chem. **5**, 361 (1970).
23. M. Dubois, K. A. Gilles, K. A. Hamilton, P. A. Rebers, and F. Smith. Anal. Chem. **28**, 350 (1956).
24. R. Gatt and R. Berman. Anal. Biochem. **15**, 167 (1965).
25. P. S. Chen, T. Y. Toribara, and H. Warner. Anal. Chem. **28**, 1756 (1956).
26. D. Aminoff. Biochem. J. **81**, 384 (1961).
27. S. Hakomori. J. Biochem. (Tokyo), **55**, 205 (1964).
28. D. R. Bundle, M. Gerken, and M. B. Perry. Can. J. Chem. **64**, 255 (1986).
29. K. A. Nagayama, A. Kumar, K. Wuthrich, and R. R. Ernst. J. Magn. Reson. **40**, 321.
30. A. Bax and G. Drobny. J. Magn. Reson. **61**, 306 (1985).
31. A. Bax. J. Magn. Reson. **53**, 517 (1983).
32. V. Rutar. J. Magn. Reson. **58**, 306 (1984).
33. S. Takagi and G. A. Jeffrey. Acta Crystallogr. Sect. B: Struct. Crystallogr. Cryst. Chem. **B35**, 902 (1979).
34. G. A. Jeffrey, R. K. McMullan, and S. Takagi. Acta Crystallogr. Sect. B: Struct. Crystallogr. Cryst. Chem. **B33**, 728 (1977).
35. F. Arene, A. Neuman, and F. Longchambon. C.R. Acad. Sci. Ser. C, **288**, 331 (1979).

Can. J. Chem. Downloaded from www.nrcresearchpress.com by 88.85.125.76 on 09/07/12
For personal use only.

COMMUNICATION

A study of thermodynamic acidities of enols with the semiempirical computational method AM1

NICK HENRY WERSTIUK AND DAVID ANDREW[1]
Department of Chemistry, McMaster University, Hamilton, Ont., Canada L8S 4M1

Received January 2, 1990

NICK HENRY WERSTIUK and DAVID ANDREW. Can. J. Chem. **68**, 1467 (1990).

Using the semiempirical computational method AM1 we have computed the enthalpies of ionization of enols **1**–**21** and correlated these values with solution and estimated pK_a's. From this initial study it appears that, in general, it is possible to predict the pK's of acyclic enols within ±1 pK_a unit. On the basis of this correlation we predict the pK_a's of 1-hydroxy-1,3-butadiene (3-butenal enol) (9.7) and 1,1-difluoroacetone enol (9.6) and suggest that the previously estimated pK_a of 1,1-dichloroacetone enol (6.2) is low by approximately 3 pK units. We find computationally (this has been established experimentally) that the *Z*-enol of phenylacetaldehyde is less acidic than the *E*-enol.

Key words: enols, acidities, computational studies, AM1.

NICK HENRY WERSTIUK et DAVID ANDREW. Can. J. Chem. **68**, 1467 (1990).

Utilisant la méthode de calculs semi-empiriques AM1, on a calculé les enthalpies d'ionisation des énols **1**–**21** et on a établi une corrélation entre les résultats de ces calculs et les valeurs observées en solution ainsi qu'avec les valeurs estimées des pK_a. Sur la base de cette étude initiale, il semble que, en général, il est possible de prédire les valeurs des pK d'énols acycliques à ±1 unité de pK_a. Sur la base de cette corrélation, on peut prédire les valeurs des pK_a du 1-hydroxy-buta-1,3-diène (énol du but-3-ènal) (9,7) et de l'énol de la 1,1-difluoroacétone (9,6) et suggérer que la valeur de 6,2, estimée antérieurement pour le pK_a de l'énol de la 1,1-dichloroacétone, est environ 3 unités de pK_a trop basse. Sur la base des calculs — qui ont été confirmés d'une façon expérimentale — le énol-*Z* du phénylacétaldéhyde est moins acide que l'énol-*E*.

Mots clés :

[Traduit par la revue]

Enols are important intermediates in organic chemistry. The pK_a's of a number of these transient species have been obtained experimentally, mainly through the elegant work of Kresge and co-workers (1–7).[2] Guthrie, in elaborating a thermochemical approach for predicting the enol content of a simple ketone, estimated the pK_a's of 24 enols by a LFER method (8, 9).

To expand studies on the enthalpies of ionization[3,4] with the semiempirical computational method AM1 (10), we undertook a study of enols to establish whether the pK_a's of these transient species can be estimated computationally. We calculated heats of formation of 1-formylfluorene enol (**1**), mandelic acid enol (**2**), diphenylacetaldehyde enol (**3**), phenylacetaldehyde enol (**4**), methoxyacetophenone enol (**5**), acetophenone enol (**6**), isobutyraldehyde enol (**7**), acetone enol (**8**), and acetaldehyde enol (**9**) and the corresponding enolates. To extend this study to the ionization of an anionic species, heats of formation of the enol of pyruvate (CH_2=CH(OH)CCO-$^+$, neutralized by a unit positive charge, and its enolate (CH_2=CH(O-)COO-$^+$ were

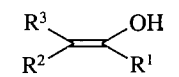

1, R^1 = H; R^2 = R^3 = fluorenyl
2, R^1 = R^2 = OH; R^3 = Ph
3, R^1 = H; R^2 = R^3 = Ph
4, R^1 = H; R^2 = Ph; R^3 = H
5, R^1 = Ph; R^2 = H; R^3 = OMe
6, R^1 = Ph; R^2 = R^3 = H
7, R^1 = H; R^2 = R^3 = Me
8, R^1 = Me; R^2 = R^3 = H
9, R^1 = R^2 = R^3 = H
10, R^1 = COONa; R^2 = R^3 = H
11, R^1 = Me; R^2 = OMe; R^3 = H
12, R^1 = $PhCH_2$; R^2 = R^3 = H
13, R^1 = (*E*)-PhCH=CH; R^2 = R^3 = H
14, R^1 = *p*-MeO-Ph; R^2 = R^3 = H
15, R^1 = Me; R^2 = H; R^3 = Cl
16, R^1 = Me; R^2 = H; R^3 = Br
17, R^1 = COOEt; R^2 = R^3 = H
18, R^1 = CH_2Cl; R^2 = H; R^3 = Cl
19, R^1 = *p*-NO_2Ph; R^3 = R^3 = H
20, R^1 = Me; R^2 = H; R^3 = Ph
21, R^1 = Me; R^2 = R^3 = Cl

calculated as well.[5] The optimized structures of these species including the location of the positive charge are shown as **1ON** and **1ONE**, respectively. Enol **1ON** is a planar species with the carboxylate oxygens symmetrically disposed with respect to the positive charge. Enolate **1ONE** is twisted; one carboxylate

[1]Recipient of a Natural Sciences and Engineering Research Council of Canada Summer-Student Research Scholarship, 1988.

[2]Also A. J. Kresge, personal communication. We thank Professor Kresge for providing us with the pK_a (11.57) of the enol of sodium pyruvate prior to publication.

[3]Computations (RHF) were carried out using AM1 or AMPAC, Version 2.1, which was ported to Sun 3/60 and IBM RT computers.

[4]The enthalpy of ionization of an enol EH is given by the equation

$$\Delta H_i = [\Delta H_f(E^-) - \Delta H_f(EH)] + \Delta H_f(H^+)$$

The geometries of EH and E^- were fully optimized in each case using the AM1 default parameters. $\Delta H_f(H^+)$ = 364.2 kcal/mol.

[5]It is possible within AM1 to use a point charge to represent an alkali metal cation. While ΔH_i for CH_2=CH(OH)COO^- is 450 kcal/mol, for CH_2=CH(OH)COO^+ it is 377.8 kcal/mol. It is clear from these values and Fig. 1(a) that this "ion pairing" is necessary in the case of anions in order to compute ΔH_i's that correlate with solution acidities. It is interesting to note also that the computed ΔH_i for the enol hydroxyl of CH_2=CH(OH)COOH is 345.0 kcal/mol. From eq. [1], the pK_a is estimated to be 9.4 in solution. Based on this value—it cannot be obtained experimentally—ionization of the carboxyl group of the enol of pyruvic acid followed by ion pairing in solution lowers the acidity of the enol by approximately 2.1 pK units.

Can. J. Chem. Downloaded from www.nrcresearchpress.com by 88.85.125.76 on 09/07/12
For personal use only.

Can. J. Chem. Downloaded from www.nrcresearchpress.com by 88.85.125.76 on 09/07/12
For personal use only.

TABLE 1. Thermodynamic parameters and acidity constants of enols

Enol	ΔH_f(enol) (kcal/mol)	ΔH_f(enolate) (kcal/mol)	ΔH_i	pK_a Experimental[a]	pK_a Estimated[c]
1	29.9	−11.4	322.9	7.4[b]	
2	−102.4	−141.2	325.4	6.5	
3	16.4	−15.4	332.4	9.4	
4	−11.4	−36.9	338.7	9.5	
5	−46.2	−60.5	349.9	10.86	
6	−4.6	−15.5	353.3	10.34	
7	−50.1	−59.6	354.7	11.63	
8	−39.5	−43.5	360.2	10.94	
9	−33.5	−37.2	360.5	10.50	
10	−232.4	−218.8	377.8	11.57	
11	−77.8	−84.6	357.3		10.9
12	−11.0	−20.1	355.1		11.5
13	7.9	−3.2	353.1		11.1
14	−42.7	−53.8	353.1		11.2
15	−49.6	−63.1	350.7		10.4
16	−38.0	−55.2	347.0		10.3
17	−118.6	−137.0	345.8		9.2
18	−55.0	−76.1	343.1		9.0
19	−0.9	−24.9	340.2		10.0
20	−17.0	−41.1	340.0		11.8 (9.2)[d]
21	−54.1	−76.5	341.4		6.2 (9.4)[e]

[a]Taken from refs. 1–7 (see also footnote 2) unless stated otherwise.
[b]Taken from ref. 11.
[c]Taken from refs. 8 and 9 unless stated otherwise.
[d]Obtained from ΔH_i and eq. [1].
[e]Obtained from ΔH_i and eq. [1].

oxygen and the enolate oxygen interact with the positive charge. The ΔH_f data, ΔH_i's, and solution pK_a's of enols **1–10** are given in Table 1. The pK_a of **1** was obtained by Harcourt and More O'Farrell (11), and Kresge and co-workers have determined the pK_a's of **2–10** (1–7).[2] We also computed the ΔH_f's of methoxyacetone enol (**11**), the non-conjugated isomer of phenylacetone enol (**12**), 4-phenylbuten-2-one enol (**13**), *p*-methoxyacetophenone enol (**14**), chloroacetone enol (**15**), bromoacetone enol (**16**), ethyl pyruvate enol (**17**), 1,3-dichloroacetone enol (**18**), *p*-nitroacetophenone enol (**19**), and phenylacetone enol (**20**), 1,1-dichloroacetone enol (**21**), and their enolates (Table 1). The pK_a's of enols **11–21** have been estimated by Guthrie (8, 9). A correlation of the pK_a's and ΔH_i's of enols **1–21** is presented and discussed in this communication.

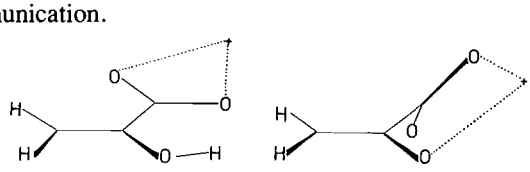

10N 10NE

Figure 1(a) shows a plot of the experimental pK_a's of enols **1–10** versus the computed ΔH_i's. Figure 1(b) shows a similar plot for enols **11–21**; this group of 11 enols was selected from the series of 24 studied by Guthrie to provide the widest range of structural types and acidities. Figure 1(c) shows a plot of both sets of data with the values for enols **20** and **21** excluded. Linear least-squares analysis yields slopes of 0.086, 0.121, and 0.090, for plots (a), (b), and (c), respectively. The equation of the regression line defined in Fig. 1(a) is shown as eq. [1] and the correlation coefficient is 0.88. Considering the wide range of structures studied, the narrow range of pK_a's, and the fact that ΔS_i (solution) is assumed to be invariant through the series, the correlation of the combined data is remarkable. Even though the uncertainties in the slope and intercept are high it appears that this method will be useful for estimating pK_a's of acyclic enols within ±1 pK unit.[6]

$$[1] \quad pK_a = 0.086(\pm 0.033)\Delta H_i - 20.0(\pm 11.6)$$

For the enols studied, we find, in general, that AM1 predicts *s-cis* isomers to be 1.6–3.8 kcal lower in energy than the *s-trans* isomers. There is some experimental support for this result. On the basis of the magnitude of the =CH-OH vicinal coupling constant (8.88 Hz), Capon and Guo (12) have suggested that (*E*)-1-hydroxy-1,3-butadiene exists in an *s-cis* conformation in 90:10 DMSO–CH_3OH. A smaller coupling constant (5.53 Hz) was taken as evidence that the *s-trans* conformer is the stablest species in the case of the *Z*-enol. However, AM1 predicts that *s-cis* conformers are the stablest structures in both cases. It is possible that the *Z*-enol exists as a twisted *s-cis* conformer in this medium to reduce steric inhibition to hydrogen bonding. Based on a computed ΔH_i of 345.1 kcal/mol, we predict the pK_a of (*E*)-1-hydroxy-1,2-butadiene to be 9.7.

The results obtained for the *E*- and *Z*-enols and enolates of phenylacetaldehyde and the enol and enolates of mandelic acid illustrate the potential utility of these computational studies. AM1 computes ΔH_i of the *E*-enol of phenylacetaldehyde to be 1.2 kcal/mol lower than ΔH_i of the *Z*-enol; this translates into a

[6]The equation of the line given in Fig. 1(c) is

$$pK_a = 0.90(\pm 0.027)\Delta H_i - 21.3(\pm 9.30)$$

The correlation coefficient is 0.86.

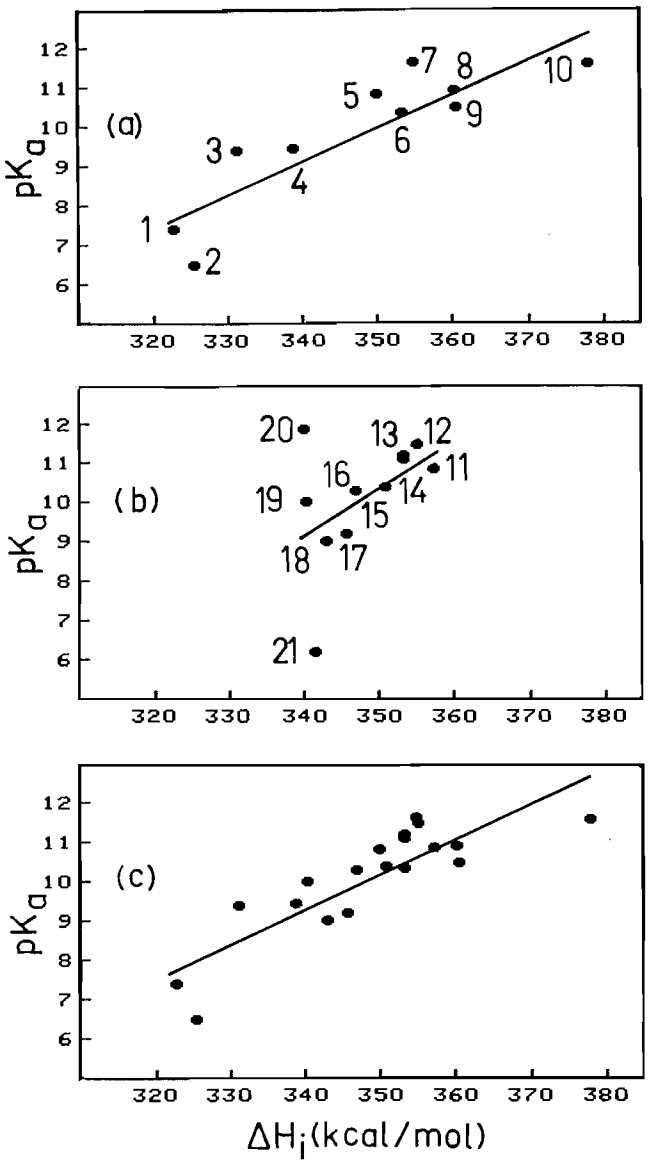

FIG. 1. (a) Plot of pK_a versus ΔH_i for enols **1–10**; (b) plot of pK_a versus ΔH_i for enols **11–21**; (c) plot of pK_a versus ΔH_i for enols **1–19**.

slightly higher pK_a ($\Delta pK = 0.10$) for the *Z* isomer than the *E* isomer. Kresge and co-workers have shown that the solution pK_a's of the *E*- and *Z*-enols are 9.46 and 9.76 ($\Delta pK = 0.30$), respectively (7). By studying a number of conformers of mandelic acid enol we find that, unlike the case of phenylacetaldehyde enol, ionization of the hydroxyl group *cis* to phenyl is preferred over ionization of the *trans* hydroxyl by 1.9 kcal/mol.

The difference between the pK_a (11.8) of phenylacetone enol (**20**) estimated by Guthrie (9) and the value (9.2) obtained using the computed ΔH_i deserves comment. According to AM1, the planar *Z*-enolate is 2.2 kcal/mol lower in energy than the *E*-enolate. One possible source of the difference between these predicted pK_a's is that solvation of the oxygen of *o*-phenyl phenolate used to estimate the pK_a of **20** is maximized only if the phenyl ring is twisted out of conjugation with the phenolate π-system. To probe the effect of deconjugating the phenyl group of the *Z*-enolate of **20**, the heat of formation was computed as a function of the phenyl twist angle. Based on the ΔH_f's of the planar *Z*-enolate and the 90° conformer, resonance stabilization by the phenyl group is 12.8 kcal/mol in the gas phase; a 30° twist results in only a small destabilization relative to the planar species. Based on eq. [1], the pK_a of the 90° conformer is predicted to be 10.5, which is closer to the value estimated by Guthrie. However, it seems unlikely that a highly twisted *Z*-enolate of phenylacetone could be the stablest species because the planar *E* isomer, in which solvation of the oxygen is not sterically inhibited, is only 2.2 kcal/mol higher in energy relative to the planar *Z* isomer. In this respect it is interesting to note that Kresge and co-workers used the experimentally determined pK_a of **4** to estimate the pK_a (9.75) of **20** (13).

Based on the plots shown in Fig. 1, it appears that the pK_a (6.2) estimated for 1,1-dichloroacetone enol (**21**) by Guthrie (9) is approximately 3 pK units too low. The reason for this is not clear, but it appears that the inductive effect of two chlorines has been overestimated. Here we predict that 1,1-difluoroacetone enol will be less acidic (ΔH_i = 343.7, pK_a = 9.6) than 1,2-dichloroacetone enol (predicted pK_a = 9.4). This is undoubtedly due to the +R effect of fluorine (14).

Acknowledgements

We thank the Natural Sciences and Engineering Research Council of Canada for financial support and IBM Canada Ltd. for donating an IBM RT computer through the auspices of a McMaster – IBM Canada Ltd. Cooperative project.

1. Y. CHIANG, A. J. KRESGE, Y. S. TANG, and S. WIRZ. J. Am. Chem. Soc. **106**, 460 (1984).
2. Y. CHIANG, A. J. KRESGE, and J. WIRZ. J. Am. Chem. Soc. **106**, 6392 (1984).
3. Y. CHIANG, A. J. KRESGE, and P. A. WALSH. J. Am. Chem. Soc. **108**, 6314 (1986).
4. Y. CHIANG, M. HOJATTI, J. R. KEEFE, A. J. KRESGE, N. P. SCHEPP, and J. WIRZ. J. Am. Chem. Soc. **109**, 4000 (1987).
5. Y. CHIANG, A. J. KRESGE, and E. T. KROGH. J. Am. Chem. Soc. **110**, 2600 (1988).
6. Y. CHIANG, A. J. KRESGE, and N. P. SCHEPP. Abstracts of the 72nd Canadian Chemical Conference. Victoria, British Columbia. June 4–8, 1989. Abstract No. 544.
7. Y. CHIANG, A. J. KRESGE, P. A. WALSH, and Y. YIN. J. Chem. Soc. Chem. Commun. 869 (1989).
8. J. P. GUTHRIE and P. A. CULLIMORE. **57**, 240 (1979).
9. J. P. GUTHRIE. Can. J. Chem. **57**, 1177 (1979).
10. N. H. WERSTIUK. Can. J. Chem. **66**, 2958 (1988).
11. M. P. HARCOURT and R. A. MORE O'FARRELL. J. Chem. Soc. Chem. Commun. 822 (1987).
12. B. CAPON and B. GUO. J. Am. Chem. Soc. **110**, 514 (1988).
13. J. R. KEEFE, A. J. KRESGE, and Y. YIN. J. Am. Chem. Soc. **110**, 8201 (1988).
14. O. A. REUTOV, I. P. BELETSKAYA, and K. B. BUTIN. *In* CH-acids. Pergamon Press, Oxford. 1978. Chap. II, p. 52.

Can. J. Chem. Downloaded from www.nrcresearchpress.com by 88.85.125.76 on 09/07/12
For personal use only.

A characterization and catalytic study of Y zeolite supported Ni/Cu bimetallics

BRENDAN COUGHLAN AND MARK A. KEANE[1]
Physical Chemistry Laboratories, University College, Galway, Eire

Received October 4, 1989

BRENDAN COUGHLAN and MARK A. KEANE. Can. J. Chem. **68**, 1471 (1990).

A wide range of CuNiNaY and CuNiKY zeolites were prepared by ion exchange. The location of both Ni^{2+} and Cu^{2+} cations within the zeolite framework was monitored after various stages of thermal treatment and the reduction process of the transition metal ions in a flowing hydrogen atmosphere was investigated and correlated with reduction time and temperature. The metallic phase generated on reduction was characterized by X-ray diffraction line broadening. The catalytic activity of the reduced zeolites in the hydrogenation of benzene is discussed in the light of these physical characterizations.

Key words: zeolites, supported Ni/Cu bimetals, cation location, crystallite size, catalysis.

BRENDAN COUGHLAN et MARK A. KEANE. Can. J. Chem. **68**, 1471 (1990).

On a préparé une grande variété de zéolites des types CuNiNaY et CuNiKY par échange d'ions. On a déterminé la position des cations Ni^{2+} et Cu^{2+} dans le squelette des zéolites après divers stages du traitement thermique; de plus, on a examiné le processus de réduction des ions des métaux de transition dans un atmosphère formé d'un flux d'hydrogène et on a établi une corrélation avec le temps et la température de réduction. En se basant sur l'élargissement des rais de diffraction des rayons-X, on a caractérisé la phase métallique qui est générée lors de la réduction. À la lumière de ces caractérisations physiques, on discute de l'activité catalytique des zéolites réduits lors de l'hydrogénation du benzène.

Mots clés : zéolites, position des cations, grosseur cristalline, catalyse.

[Traduit par la revue]

1. Introduction

In the 1950's there was a strong interest in heterogeneous catalysis by alloys, due to the alleged validity of the Rigid Band Model (RBM). According to this model, upon alloying, the holes in the *d*-band of the transition metals could be filled (1). For the Ni/Cu system, Hall and Emmett (2) quote the critical composition of 40% Ni/60% Cu for a complete filling of the *d* holes. A number of reports that contradict the RBM (5–7) have since been presented. The majority of studies on the physical and catalytic properties of Ni/Cu bimetallics (2–10) deal with unsupported systems, i.e., films or powders. In some cases, reduction in hydrogen has been shown to generate a copper-rich phase that envelops a nickel-rich phase, i.e., the "cherry model" (6). In the case of highly dispersed alloy particles, some authors (9, 10) have considered the possibility of the formation of single phase microcrystals with unsegregated surfaces and a variety of metallic combinations that do not correspond to bulk alloys. For this reason, Sinfelt (11) has chosen the term "bimetallic clusters" rather than alloys in referring to highly dispersed supported bimetallic systems.

It has been shown by many workers that hydrogen reduction of Zeolite Y exchanged with Ni^{2+} and Cu^{2+} ions results in the formation of an alloy (12–15). The published results suggest that during reduction at temperatures above 690 K some of the Ni^{2+} and Cu^{2+} ions form large metal particles on the outer surface of the zeolite crystals. Total alloy reduction was found to occur on silica at 773 K (16). In addition, calcining prior to reduction resulted in the formation of much larger alloy particles (16) as opposed to the case of zeolites where precalcination yields smaller crystallites (13). The techniques normally employed to characterize monometallic catalysts are also applicable to the study of bimetallic systems. X-ray diffraction (11), H_2 chemisorption (3), and magnetic methods (12–14, 16) have all been used with varying success.

Data for 40 reactions over Ni/Cu alloys have been summarized by Ponec (17). In agreement with the Rigid Band Model, Hall and Emmet (2) observed a marked drop in hydrogenation activity over Ni/Cu films at 40% Ni/60% Cu. By comparison, the retarding effect of copper has also been observed at 70% Ni/30% Cu (18, 19). The catalytic activity of nickel with respect to benzene hydrogenation was found to decrease slowly with increasing copper concentration at temperatures below 373 K (20, 21) and to increase at higher temperatures (20). van Barneveld and Ponec (21) have attributed a positive alloy effect to an inhibition of side reactions. Indeed, copper addition has been found to suppress the rate of benzene hydrogenolysis to methane (22).

Bimetallic zeolites constitute an important chapter in the development of heterogeneous catalysts. There remains, however, much scope for further research. Additional data on the degree of reduction and crystallite sizes of the nickel and copper components supported on NaY and KY will be reported in this paper. The catalytic activity of these bimetallics, which also serves to characterize the system, will be discussed.

2. Experimental

The nickel/copper Y Zeolites were prepared by first exchanging with nickel cations as described previously (23). The dried zeolite was then refluxed with solutions of Cu $(NO_3)_2$, the concentrations of which were determined by assuming an exchange efficiency level of 80%. For copper exchange levels greater than ca. 7 Cu^{2+} per unit cell (U.C.), the exchange procedure was repeated. To prevent hydrolytic Na^+ or K^+ loss or exchange of hydroxylic nickel species, i.e., to ensure stoichiometric exchange, the pH of the nitrate solutions was kept at ca. 6. All the samples were air dried at 373 K for 24 h and stored over saturated NH_4Cl prior to analysis. Thermal analyses were conducted using a Perkin Elmer thermobalance operating in the TG mode to measure water loss and in the DTG mode to measure the rate of change of water loss as a function of temperature; the temperature was scanned at 40 K min^{-1} in the range 294–773 K under a nitrogen purge of 20 cm^3 min^{-1}. Atomic absorption (Ni^{2+} and Cu^{2+} concentrations) and flame emission (Na^+ and K^+ concentrations) techniques, using a Perkin Elmer 360 atomic absorption spectrophotometer, were employed to determine the cation contents.

The percent reduction of Ni^{2+} and (or) Cu^{2+} ions, supported on both

[1]Author to whom correspondence may be addressed. Present address: Chemistry Department, The University of Glasgow, Glasgow G12 8QQ, Scotland.

Can. J. Chem. Downloaded from www.nrcresearchpress.com by 91.121.58.235 on 09/07/12
For personal use only.

Can. J. Chem. Downloaded from www.nrcresearchpress.com by 91.121.58.235 on 09/07/12
For personal use only.

NaY and KY carriers, in flowing hydrogen was measured using a Na^+ back exchange technique. In each case, 3 g of hydrated sample, in pellet form (1.18–1.70 mm diameter), was reduced in a fixed bed catalytic reactor (23), in a 120 cm^3 min^{-1} stream of hydrogen at 723 K for 18 h. After reduction, the samples were stored over saturated NH_4Cl and the water content was determined. The hydrated reduced zeolite (100 mg), in powder form, was immersed in 50 cm^3 of 1 M $NaNO_3$ and the resultant suspension refluxed for 24 h. In this process, the Na^+ ions will be exchanged with the unreduced Ni^{2+} and (or) Cu^{2+} cations. On filtering the solution, the filtrate was made up to 100 cm^3 and analyzed for Ni^{2+} and Cu^{2+} ion concentration by atomic absorption in the 0–5 ppm range. The procedure was also repeated using the unreduced zeolite as a blank. The degree of reduction (α) is then given by:

$$\frac{\text{ppm } TM^{2+} \text{ in unred. sample} - \text{ppm } TM^{2+} \text{ in red. sample}}{\text{ppm } TM^{2+} \text{ in unred. sample}}$$

where TM^{2+} represents the Ni^{2+} or Cu^{2+} transition metal ions. Metal (Ni^{2+} and Cu^{2+}) reduction was also measured by an iodometric titration described elsewhere (23). The latter technique only gives the total level of metal cation reduction and does not differentiate between the individual levels of Ni^{2+} and Cu^{2+} reduction. Nevetheless, the total metal cation reduction levels measured by both Na^+ back exchange and iodometric titrations were in very close agreement (within ±4%). The possibility of a reoxidation of the small metal particles during the Na^+ back exchange process can be ruled out.

Examination of the samples for the presence of nickel and copper crystallites was performed by studying X-ray line broadening (Jeol JDX-85 diffractometer) around the nickel line at a 2θ angle of 52.2° and the copper line at a 2θ of 50.8° under the following conditions: time constant = 4; voltage = 30 kV; current = 20 mA; scan time = 0.5 min^{-1}; counts/s = 8 × 10^2; radiation = CoKα. A correction for instrument broadening under identical conditions was made using Ni and (or) Cu powder in a NaY/KY matrix.

All catalytic reactions were carried out under atmospheric pressure in a fixed bed tubular glass reactor (24, 25) operating in the differential mode at 473 K. The catalysts were pelletized without binder using a pressure of 4000 kg cm^{-1} and sieved in the mesh range 1.18–1.70 mm. Catalyst activation was the same as for the degree of reduction measurements (23, 26). Benzene was fed into the reactor from a precision motor driven syringe at a flow rate of 2.0 cm^3 h^{-1}. Product analysis was carried out using a Pye Unicam GCV chromatograph with a flame ionization detector. Mol% conversion to cyclohexane after 6 h on stream was used as a point of comparison between different catalysts. Full details of the experimental procedure are given elsewhere (24, 25).

Diffraction patterns of all the catalysts, before and after use in catalysis, were obtained to ensure maintenance of sample crystallinity. Infrared spectroscopy in the range 1200–350 cm^{-1} was also used as a check on crystallinity. The band at ca. 395 cm^{-1} has been assigned to a breathing of the pore opening in zeolites (27) and is thus the most sensitive to changes in crystallinity.

3. Results and discussion

The chemical compositions of the CuNiNaY and CuNiKY samples prepared by ion exchange are given in Tables 1 and 2. It may be noted that on back exchange of the Cu^{2+} ions into NiNaY and NiKY some of the Ni^{2+} ions are displaced. Sample crystallinity, monitored by X-ray diffraction and IR techniques, was maintained after the preparation of all the tabulated samples.

The reduction process in a wide range of monometallic (nickel and copper) Y Zeolites has been investigated in these laboratories (23, 26, 28). The degree of reduction of Ni^{2+} cations supported on Y Zeolites has been shown to be strongly dependent on the pretreatment conditions and nickel loading (23). The level of reduction is also dependent on the location of the metal cations within the zeolite lattice (26). The accessible nickel cations were found to be preferentially reduced while the migration of Ni^{2+} ions into the supercage was retarded with progressive reduction. The overall degree of reduction was also shown to be promoted by using lower heating and hydrogen flow rates and inhibited with sample precalcination (23). Most of the

TABLE 1. Chemical composition of CuNiNaY samples prepared by ion exchange of NiNaY by Cu^{2+} ions

Zeolite sample	Na^+/U.C.	Ni^{2+}/U.C.	Cu^{2+}/U.C.	Water content (wt.%)
NaY	58.00	—	—	24.79
NiNaY-7.58	53.22	2.20	—	25.40
CuNiNaY-14.34[a]	49.54	2.20	1.96	25.61
CuNiNaY-21.69	45.16	2.15	4.14	25.88
CuNiNaY-31.55	38.69	2.14	7.01	26.14
CuNiNaY-49.03	29.26	2.08	12.14	26.93
NiNaY-21.35	45.82	6.19	—	26.51
CuNiNaY-29.03	40.16	5.98	2.44	27.41
CuNiNaY-36.48	35.14	5.63	4.95	27.53
CuNiNaY-46.55	29.29	5.31	8.19	27.80
CuNiNaY-69.41	16.54	3.63	16.50	28.12
NiNaY-34.24	37.37	9.93	—	26.94
CuNiNaY-43.38	31.71	9.79	2.79	26.97
CuNiNaY-48.21	28.16	9.48	4.50	27.51
CuNiNaY-57.45	23.58	9.25	7.41	27.84
CuNiNaY-69.31	16.77	6.14	13.96	28.40
NiNaY-63.17	22.40	18.32	—	29.06
CuNiNaY-67.48	19.16	16.94	2.63	29.04
CuNiNaY-69.38	17.76	15.41	4.71	28.86
CuNiNaY-71.52	16.32	13.11	7.63	28.70
CuNiNaY-75.62	13.99	8.06	13.87	28.43

[a]Total transition metal ion content.

TABLE 2. Chemical composition of CuNiKY samples prepared by ion exchange of NiKY by Cu^{2+} ions

Zeolite sample	K^+/U.C.	Ni^{2+}/U.C.	Cu^{2+}/U.C.	Water content (wt.%)
KY	58.00	—	—	22.13
NiKY-11.14	51.42	3.23	—	22.70
CuNiKY-17.83[a]	46.55	3.21	1.96	23.11
CuNiKY-25.00	42.45	3.21	4.04	23.56
CuNiKY-34.00	37.34	3.18	6.79	24.71
CuNiKY-52.45	26.39	3.10	12.11	26.41
NiKY-23.31	44.35	6.76	—	23.41
CuNiKY-30.79	39.34	6.59	2.34	23.66
CuNiKY-39.38	34.20	6.36	5.06	25.11
CuNiKY-46.03	30.19	6.04	7.31	26.04
CuNiKY-65.72	18.16	5.46	13.69	27.14
NiKY-36.14	36.34	10.48	—	24.69
CuNiKY-44.62	31.40	10.40	2.54	24.89
CuNiKY-48.38	28.94	10.16	3.87	25.16
CuNiKY-57.69	23.90	9.97	6.76	26.65
CuNiKY-68.10	18.19	7.64	12.11	27.13
NiKY-69.45	17.62	20.14	—	27.84
CuNiKY-73.03	15.44	19.31	1.87	27.76
CuNiKY-76.59	13.18	17.21	5.00	27.58
CuNiKY-78.28	12.20	15.56	7.14	27.89
CuNiKY-77.93	12.00	10.24	12.36	28.14

[a]Total transition metal cation content.

Can. J. Chem. Downloaded from www.nrcresearchpress.com by 91.121.58.235 on 09/07/12
For personal use only.

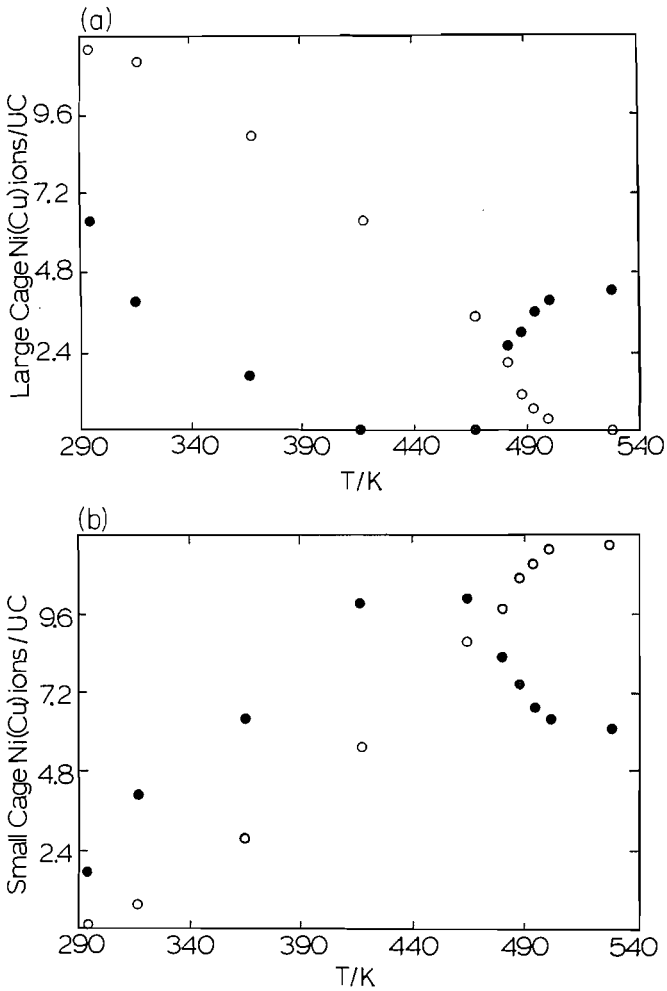

FIG. 1. Variation in the number of (a) large cage and (b) small cage Ni^{2+} (○) and Cu^{2+} (●) cations with increasing temperature on calcining $Cu_{8.0}Ni_{11.8}KY$ in a stream of nitrogen (120 cm^3 min^{-1}).

phenomena encountered with Ni^{2+} reduction are also associated with the Cu^{2+} system (28). However, the greater freedom of the copper ions to migrate into the supercages results in the equilibrium level of reduction being reached sooner than is the case for Ni^{2+} reduction, but the greater acidity associated with the monometallic copper samples ultimately results in an overall lower level of metal reduction.

There have been no published data on the nature of the competitive migration of metal ions in a bimetal exchanged zeolite. By employing a back exchange technique, the location of Ni^{2+} and Cu^{2+} ions in the zeolite lattice during different calcination steps and hence the effect of sample pretreatment on ion location and reduction was probed. In this case, the rehydrated calcined samples were treated with 2 M CsCl to remove any cation species present in the supercage. Because of its size, the Cs^+ ion is restricted from entering the sodalite units or hexagonal prisms. The number of Ni^{2+} and Cu^{2+} cations remaining in the small cages was then determined by atomic absorption. Figure 1 illustrates the migration of Ni^{2+} and Cu^{2+} in a $Cu_{8.0}$ $Ni_{11.8}$ KY sample at elevated temperatures. The Cs^+ back exchange measurements have yielded some very intriguing results. Although the Cu^{2+} ions are preferably admitted into the small cages at lower temperatures (<423 K), at higher temperatures the migrating Ni^{2+} ions exchange out the short-lived $S_I/S_{I'}$ Cu^{2+} (as well as the indigenous K^+ ions) and locate the entire

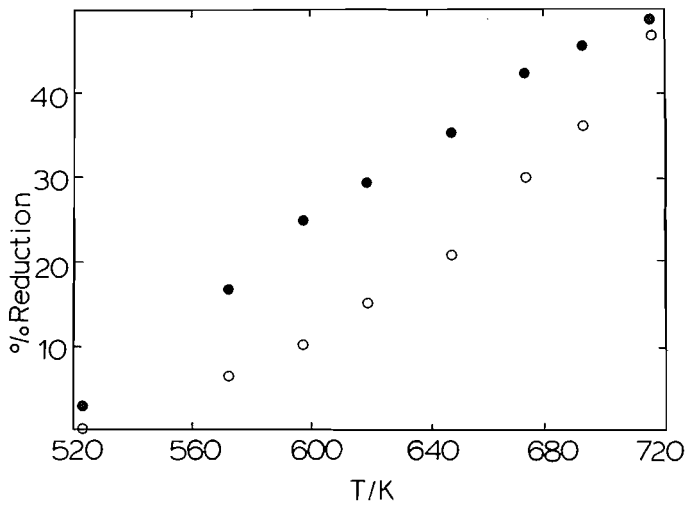

FIG. 2. Variation in the level of reduction (after 18 h) of Ni^{2+} (○) and Cu^{2+} (●) cations supported on $Cu_{7.3}Ni_{6.0}KY$ with increasing reduction temperature.

Ni^{2+} compliment within the small cavities. This reversal in migratory behavior may be explained by a greater relative ease of shedding the cationic water coating exhibited by the Cu^{2+} ions. From the DTG measurements, the Cu^{2+} ions are stripped of their water molecules at a lower temperature (446 K) than the Ni^{2+} ions (456 K) and locate preferentially in the small cages. A reversal in selectivity for the $S_I/S_{I'}$ sites occurs at 423 K. The location of the two metal ions within the zeolite lattice is such as to minimize the free energy of the system. The Ni^{2+} ions, in locating preferentially at the well-shielded S_I sites, lower the overall potential energy of the zeolite system. As a direct consequence, the number of Cu^{2+} ions located in the supercages is greater than that observed for the monometallic samples (28).

Figure 2 follows the variation in degree of metal cation reduction of a CuNiKY sample with reduction temperature. The supported copper ions are preferably reduced at lower temperatures, with Ni^{2+} reduction more evident at temperatures greater than 623 K. Although this is empirically identical to the situation encountered for the monometallic samples (23, 28), the level of reduction of both metal ions is lower. The reduction vs. time curves for the same sample are given in Fig. 3. Both curves are characterized by a gradual attainment of the equilibrium percent reduction value. The reduction behaviour is the same as that observed for the monometallic samples but the time necessary for the equilibrium reduction value to be attained is lower for the single metal component systems (23, 28), i.e., ca. 16 h for the Ni^{2+} exchanged zeolites and ca. 14 h for the Cu^{2+} exchanged zeolites compared with ca. 18 h for the Ni^{2+}/Cu^{2+} exchanged zeolites. The lengthy hydrogen treatment again indicates the involvement of a slow diffusion of hydrogen molecules to the inaccessible metal ions. The presence of Cu^{2+} ions in the open supercages must serve to restrict the passage of hydrogen molecules to the hidden Ni^{2+} ions.

Table 3 serves to show the effects of diluting NiNaY and NiKY samples with Cu^{2+} ions on the level of metal ion reduction. It is clear that the addition of Cu^{2+} suppresses Ni^{2+} reduction, the inhibitory effect increasing as the Ni^{2+}/Cu^{2+} ratio gets smaller. At the same time, the degree of Cu^{2+} reduction increases with copper content. However, the individual degree of reduction of the metal ions is lower than for the monometal samples (26, 28), as is the overall degree of reduction. The potassium based samples, with their lower associated

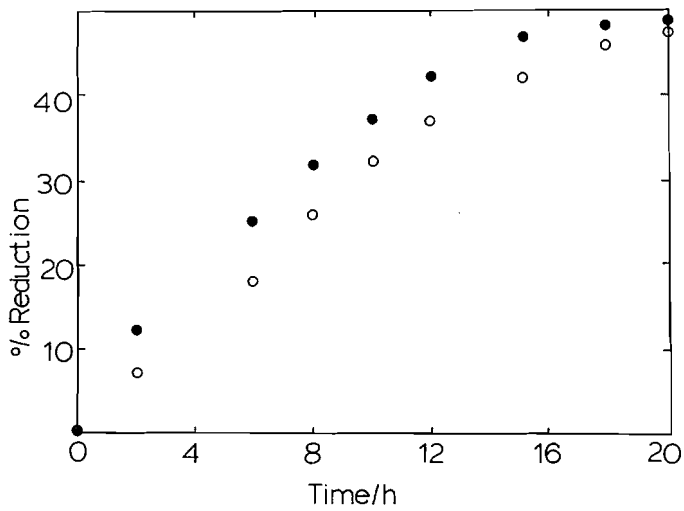

FIG. 3. Variation in the level of reduction (at 723 K) of Ni^{2+} (○) and Cu^{2+} (●) cations supported on $Cu_{7.3}Ni_{6.0}KY$ with increasing time.

TABLE 3. Effect of Cu^{2+} exchange on % Ni^{2+} reduction at 723 K

Zeolite sample	Ni^{2+}/Cu^{2+}	% Ni^{2+} reduction			
		NH_3 treated		Untreated	
		Ni^{2+}	Cu^{2+}	Ni^{2+}	Cu^{2+}
NiNaY-21.35	—	96.28	—	80.77	—
CuNiNaY-29.03	2.45	88.77	97.96	66.90	7.38
CuNiNaY-36.48	1.13	83.35	95.54	58.24	28.11
CuNiNaY-46.55	0.65	79.10	93.37	54.00	39.20
CuNiNaY-69.41	0.22	49.48	84.16	31.05	46.12
NiNaY-63.17	—	87.86	—	53.54	—
CuNiNaY-67.48	6.44	84.13	94.25	38.36	5.36
CuNiNaY-69.38	3.21	72.20	88.76	29.41	18.33
CuNiNaY-71.52	1.72	59.36	84.13	21.26	29.67
CuNiNaY-75.62	0.58	43.14	79.86	13.50	39.40
NiKY-23.31	—	77.16	—	67.65	—
CuNiKY-30.79	2.82	74.63	96.18	54.37	14.13
CuNiKY-39.38	1.26	67.20	90.34	50.06	33.86
CuNiKY-46.03	0.83	65.42	89.34	47.32	48.10
CuNiKY-52.45	0.40	63.14	88.42	44.12	59.13
NiKY-69.45	—	88.74	—	53.13	—
CuNiKY-73.03	10.32	86.13	98.22	48.86	8.80
CuNiKY-76.59	3.42	78.20	92.16	37.34	21.24
CuNiKY-79.28	2.17	66.13	88.73	30.41	32.14
CuNiKY-77.93	0.83	58.16	86.20	19.00	44.84

acidity (29), in accordance with the monometal samples (26, 28), exhibit a higher level of Ni^{2+} and Cu^{2+} reducibility. From the cation location data, the Cu^{2+} cations are displaced into the supercages where they are preferentially reduced (28), generating an acid function that ultimately inhibits reduction, particularly of the Ni^{2+} cations. Increasing the copper ion concentration promotes this effect with an overall lowering of Ni^{2+} reducibility.

To address further the role of acidity in inhibiting the reduction process, it was decided to investigate the effect of neutralizing the acidic centres by the adsorption of a base, NH_3, which, because of its small size may diffuse into the pore structure and "poison" the small cage Bronsted acid sites. The ammonia was adsorbed at 323 K by passing a stream of the gas at a flow rate of 120 cm^3 min^{-1} over the prereduced sample for a period of 15 min, which was sufficient to allow the temperature of the zeolite bed to fall back to 423 K after the initial temperature rise due to the heat of adsorption. Hydrogen was then reintroduced and the sample was flushed for 6 h at 423 K and treated for a further 24 h in a 120 cm^3 min^{-1} flow. Treating the samples with NH_3 has resulted in a marked increase in the overall degree of reduction; both metal cations exhibit higher levels of reduction over the untreated samples, Cu^{2+} ions in particular (Table 3). Nevertheless, the reduction of divalent nickel in the bimetallic sample is again less than that determined for the NiNaY and NiKY samples (26, 28). By analogy with electrochemistry, where the reducibility of metal ions is effectively measured by electrode potentials ($Ni^{2+}/Ni = -0.25$ V; $Cu^{2+}/Cu = +0.34$ V), it is to be expected that when the added complication of acidity is removed the Cu^{2+} ions are preferably reduced.

TABLE 4. Effect of Cu^{2+} exchange on Ni^0 and Cu^0 crystallite size after reduction at 723 K

Zeolite sample	Ni^{2+}/Cu^{2+}	% Ni^{2+} reduction			
		NH_3 treated		Untreated	
		Ni^0	Cu^0	Ni^0	Cu^0
NiNaY-21.35	—	25.00	—	26.31	—
CuNiNaY-29.03	2.45	23.24	18.14	20.35	[a]
CuNiNaY-36.48	1.13	21.62	22.30	16.68	15.13
CuNiNaY-46.55	0.65	20.40	28.54	15.33	25.24
CuNiNaY-69.41	0.22	13.76	37.38	[a]	32.16
NiNaY-63.17	—	68.56	—	59.20	—
CuNiNaY-67.48	6.44	66.13	19.27	54.33	[a]
CuNiNaY-69.38	3.21	60.45	21.54	50.14	12.13
CuNiNaY-71.52	1.72	57.12	26.63	46.20	22.25
CuNiNaY-75.62	0.58	46.66	36.34	38.86	29.76
NiKY-23.31	—	24.23	—	27.00	—
CuNiKY-30.79	2.82	23.34	15.33	20.31	[a]
CuNiKY-39.38	1.26	20.88	18.50	18.42	14.40
CuNiKY-46.03	0.83	20.14	20.52	17.00	12.30
CuNiKY-52.45	0.40	18.66	29.65	13.54	34.36
NiKY-69.45	—	65.34	—	54.14	—
CuNiKY-73.03	10.32	63.10	15.70	50.00	[a]
CuNiKY-76.59	3.42	59.00	17.45	48.26	[a]
CuNiKY-79.28	2.17	57.54	18.23	47.08	20.75
CuNiKY-77.93	0.83	48.13	24.50	38.35	30.44

[a]Crystallites were undetected by X-ray diffraction.

The state of the two metals in bimetallic zeolites has been poorly characterized. The majority of studies have been concerned with obtaining evidence of interaction between the atoms of the two metallic components. The metal phases generated were characterized by X-ray line broadening using the Scherrer formula:

$$d = K\lambda/\beta \cos\theta$$

which relates the mean particle diameter (d) to the X-ray broadening (β) of the diffraction lines. In accordance with the work of Jenkins and deVries (30), a value of 0.9 was chosen for K. The lower limit of detection for this method is ca. 5 nm, with the result that it gives no information on the state of metal in the internal pore structure. X-ray line broadening is therefore diagnostic of the presence of nickel and (or) copper metal located on the external surface. It was observed that the peaks due to nickel ($2\theta = 52.2°$) and copper ($2\theta = 51.5°$) metal in the monometallic samples were shifted closer together (Ni^0: $2\theta = 52.0°$; Cu^0: $2\theta = 51.5°$) in the bimetallic samples. This observa-

Can. J. Chem. Downloaded from www.nrcresearchpress.com by 91.121.58.235 on 09/07/12
For personal use only.

TABLE 5. Effect of Cu^{2+} exchange on the hydrogenation activity of NiNaY and NiKY; $W/F = 134.1$ g mol^{-1} h, $T = 473$ K

Zeolite sample	Ni^{2+}/Cu^{2+}	Mol% C_6H_{12} (6 h on stream)	
		NH_3 treated	Untreated
NiNaY-21.35	—	46.13	54.14
CuNiNaY-29.03	2.45	41.40	43.20
CuNiNaY-36.48	1.13	35.30	34.12
CuNiNaY-46.55	0.65	28.14	16.13
CuNiNaY-69.41	0.22	21.00	4.45
NiNaY-63.17	—	74.00	0.65
CuNiNaY-67.48	6.44	68.14	0.60
CuNiNaY-69.38	3.21	63.24	0.53
CuNiNaY-71.52	1.72	49.00	1.10
CuNiNaY-75.62	0.58	40.10	5.33
NiKY-23.31	—	73.11	76.20
CuNiKY-30.79	2.82	68.86	63.60
CuNiKY-39.38	1.26	62.23	50.00
CuNiKY-46.03	0.83	48.74	22.14
CuNiKY-52.45	0.40	41.13	12.36
NiKY-69.45	—	96.55	79.14
CuNiKY-73.03	10.32	89.13	72.86
CuNiKY-76.59	3.42	86.00	59.30
CuNiKY-79.28	2.17	70.12	31.46
CuNiKY-77.93	0.83	58.86	23.33

tion suggests that there is an interaction between Ni^0 and Cu^0 generating two phases of an alloy: a nickel-rich phase corresponding to $2\theta = 52.0°$ and copper-rich phase at $2\theta = 51.5°$. From the data presented in Table 4, it can be deduced that reduction at 723 K results in nickel and copper phases on the external zeolite surface. It may be noted that as the level of copper exchange is increased, copper particle growth is promoted whereas the nickel phase is in the form of much smaller crystallites. This is in agreement with the conclusion of a number of workers (13, 14) that, in the bimetal zeolite, the higher reduction temperatures facilitate the diffusion of the more volatile copper component. In this study, the formation of larger copper crystallites is also the result of the increased level of Cu^{2+} reduction with copper exchange. As expected, the crystallite size of both metal components was increased with NH_3 treatment. In addition, the introduction of a precalcination step was observed to inhibit particle growth.

The catalytic hydrogenation of benzene over nickel Y Zeolites has been well characterized in a number of reports from these laboratories (24, 25, 31). The reaction conditions used in this study have already been successfully employed for comparing the catalytic activities of different nickel catalysts (25, 31). Under these conditions, cyclohexane is the primary product with trace amounts of methylcyclopentane isolated in the product mixture. The metal function promotes the hydrogenation reaction whereas skeletal isomerization occurs at the acid sites (31). Surface acidity has been shown to promote methylcyclopentane and ultimately coke formation (31). A knowledge of the nature of the metal surface is an essential prerequisite for a proper understanding of catalytic activity. In particular, the degree of cation reduction and the resultant dispersion of the active metal will have a direct influence on catalytic behaviour. Monometallic CuY Zeolites were catalytically inactive towards benzene hydrogenation at reaction temperatures up to 473 K. Nevertheless, the levels of benzene conversion over the supported nickel metal decreased markedly with increasing copper concentration, Table 5. This would seem to vindicate the theoretical approach that interprets catalytic action in terms of the chemical properties of nickel metal and regards the copper phase merely as a diluent. Such an approach predicts a simple type of additive behaviour. The inhibiting effect may be rationalized in terms of the lower degree of Ni^{2+} reduction in the Ni/Cu exchanged zeolites, which was increased with NH_3 treatment and is reflected by higher benzene conversions, Table 5. It should be noted that the less acidic potassium-based catalysts generated higher levels of cyclohexane.

TABLE 6. Effect of the Cu^{2+} exchange of NiNaY and NiKY on the level of coke formation; $W/F = 134.1$ g mol^{-1} h, $T = 473$ K

Zeolite sample	Ni^{2+}/Cu^{2+}	% Residual carbon
NiNaY-63.17	—	5.04
CuNiNaY-67.44	6.44	4.80
CuNiNaY-69.38	3.21	3.46
CuNiNaY-71.52	1.72	2.44
CuNiNaY-75.62	0.58	2.20
NiKY-69.45	—	4.46
CuNiKY-73.03	10.32	4.00
CuNiKY-76.59	3.42	2.94
CuNiKY-79.28	2.17	2.00
CuNiKY-77.93	0.83	1.76

Hydrogenation activity has been shown to decrease with time on stream as a result of the generation of occluded polynuclear aromatic molecules, which restrict access to the intracrystalline metal sites (24, 31). To test if coke deposition was operative in this study, the residual carbon contents of a number of spent catalysts were measured and the results are presented in Table 6. The extent of coking was lowered upon copper addition to the nickel zeolites as evidenced by the lower residual carbon contents of the spent catalysts. The presence of copper metal must therefore serve to suppress the side reactions that initiate coke formation (24, 31). Moreover, only trace amounts of methylcyclopentane were generated during catalysis over the bimetallic zeolites. The incorporation of copper into nickel zeolites may also modify the adsorption and activity of any reaction intermediates. In fact the inhibition of coke formation with copper exchange has actually resulted in an increase in cyclohexane formation over the more acidic nickel-rich NaY samples, *i.e.*, CuNiNaY-71.52 and CuNiNaY-75.62, as shown in Table 5.

4. Conclusions

The interaction between Ni^{2+} and Cu^{2+} ions during calcination and reduction was investigated. Although Cu^{2+} ions are preferably admitted into the small cages at lower temperatures (<473 K), the migrating Ni^{2+} ions exchange out these small cage Cu^{2+} ions at higher temperatures. In the absence of zeolite acidity the Cu^{2+} ions are preferably reduced and the resultant copper metal phase is in the form of larger metal crystallites. In the scope of this study, Ni^0/Cu^0 alloy formation was not observed. Nevertheless, some bimetallic interplay does occur as a result of an intimate emplacement of the metals, which lowers the hydrogenation activity of the nickel component.

1. N. F. MOTT and H. JONES. The theory of the properties of metals and alloys. Clarenden Press, Oxford, England. 1936. p. 196; N. F. MOTT. Proc. Phys. Soc. (London), **47**, 571 (1935).

Can. J. Chem. Downloaded from www.nrcresearchpress.com by 91.121.58.235 on 09/07/12
For personal use only.

2. W. K. HALL and P. H. EMMET. J. Phys. Chem. **62**, 816 (1958).
3. N. D. LANG and H. EHRENREICH. Phys. Rev. B, **168**, 605 (1968).
4. G. M. STOCKS, R. W. WILLIAMS, and J. S. FAULKNER. Phys. Rev. **4**, 4390 (1971).
5. T. A. SPOONER and J. K. A. CLARKE. Ber. Bunsen-ges. **76**, 1187 (1972).
6. W. M. H. SACHTLER and G. J. H. DORGELO. J. Catal. **4**, 654 (1965).
7. V. PONEC and W. M. H. SATCHLER. J. Catal. **24**, 250 (1972).
8. K. WATANABE, M. HASHIBA, and T. YAMASHINA. Surf. Sci. **61**, 483 (1976).
9. D. F. OLLIS. J. Catal. **23**, 131 (1971).
10. D. W. HOFFMANN. J. Catal. **27**, 234 (1972).
11. J. D. SINFELT. J. Catal. **29**, 308 (1973).
12. W. G. REMAN, A. H. ALI, and G. C. A. SCHUIT. J. Catal. **20**, 374 (1971).
13. Z. MASKOS and J. H. C. VAN HOOFF. J. Catal. **66**, 73 (1980).
14. W. ROMANOWSKI. React. Kinet. Catal. Lett. **4**, 129 (1976).
15. J. GREZECHOWIAK and Z. MASKOS. Appl. Chem. **1**, 63 (1975).
16. S. D. ROBERTSON, S. C. KLOET, and W. M. H. SACHTLER. J. Catal. **39**, 234 (1975).
17. V. PONEC. J. Quantum Chem. **12**, (1977).
18. E. I. EVKZERIKHIM and G. D. LYUBARSKI. Kinet. Katal. **7**, 1085 (1966).
19. P. W. REYNOLDS. J. Chem. Soc. 265 (1950).
20. P. VAN DER PLANK and W. M. H. SATCLER. J. Catal. **12**, 35 (1968).
21. W. A. A. VAN BARNEVELD and V. PONCE. Recl. Trav. Chim. Pays-Bas, **93**, 243 (1974).
22. G. A. MARTIN and J. A. DALMON. J. Catal. **75**, 233 (1982).
23. B. COUGHLAN and M. A. KEANE. J. Catal. In press.
24. M. A. KEANE. *In* A catalytic and characterization study of the effects of alkali metal cations on nickel and other transition metals in Y zeolite catalysts. Ph.D. Thesis (Vol. I and II), National University of Ireland (1988), and references therein.
25. B. COUGHLAN and M. A. KEANE. Zeolites. In press.
26. B. COUGHLAN and M. A. KEANE. J. Catal. Submitted.
27. E. M. FLANIGEN, H. KHATAMI, and H. A. SZYMAUSKI. Molecular sieve zeolites. Adv. Chem. Ser. **101**, 201 (1971).
28. B. COUGHLAN and M. A. KEANE. J. Chem. Soc. Faraday Trans. **86**, 1007 (1990).
29. B. COUGHLAN and M. A. KEANE. J. Colloid Interface Sci. In press.
30. R. JENKINS and J. L. DE VRIES. *In* Worked examples of X-ray analysis. 2nd ed. Phillips Technical Library, Macmillan. 1978.
31. B. COUGHLAN and M. A. KEANE. Zeolites. Submitted.

Can. J. Chem. Downloaded from www.nrcresearchpress.com by 91.121.58.235 on 09/07/12
For personal use only.

Electronic effects of heterocyclic substituents. Spectroscopical and theoretical (AM1) study in a series of heterocyclic carboxaldehydes

C. CATIVIELA[1] AND J. I. GARCIA

Instituto de Ciencia de Materiales de Aragón, Departamento de Química Orgánica y Química Física, Universidad de Zaragoza-C.S.I.C., 50009 Zaragoza, Spain

Received January 10, 1990

C. CATIVIELA and J. I. GARCIA. Can. J. Chem. **68**, 1477 (1990).

The electronic effects of a series of 18 heterocyclic carboxaldehydes (furans, thiophenes, pyrroles, and pyridines) have been studied by means of the correlation existing between ^{13}C chemical shifts of the carbonylic carbon and calculated total and π charges (AM1). The implications of this theoretical model to explain polar and resonance contributions to the total electronic effect are discussed.

Key words: heterocyclic substituents, electronic effects, ^{13}C NMR, DSP models.

C. CATIVIELA et J. I. GARCIA. Can. J. Chem. **68**, 1477 (1990).

Les effets électroniques d'une série de 18 aldéhydes hétérocycliques ont été etudiés à partir de la corrélation établie entre les déplacements chimiques du carbone carbonylique en RMN du ^{13}C et les charges, totales et π, calculées avec la méthode AM1. On discute de l'utilisation possible d'un modèle de ce type pour expliquer les contributions polaires et résonantes à l'effet électronique total.

Mots clés : substituants hétérocycliques, effets électroniques, RMN du ^{13}C, modèles biparamétriques.

[Traduit par la revue]

Introduction

The use of different parameters to describe the effects of substituents on a molecule has been of increasing interest in recent years, especially in Structure–Properties Relationship (SPR) methodology (1). Nevertheless, there are no systematic studies with regard to the use of such parameters when the substituent is a heterocyclic group. We previously reported (2, 3) the hypothesis that structural characteristics in an additive model could be used to describe heterocyclic substituents. Using a different approach, we now want to report our first results in determining the electronic effect of heterocyclic substituents by means of ^{13}C NMR spectroscopy.

The quantitative determination of the magnitude of the electronic effects of substituents has up to now been based on measuring their influence on reaction rates or the position of chemical equilibria. Over the last years, however, the effects of substituents on ^{13}C NMR chemical shifts have been increasingly used for this purpose. It has become evident that in suitable systems the influence of substituents on these shifts is predominantly a consequence of their polar and resonance effects. The most widely used systems for this study have been the shifts of the *para* ring carbons in benzenes (4) and of the side-chain carbons of ring-substituted styrenes (5, 6). Considerably less attention has been paid to the aromatic carbonyl compounds, although the understanding of the ways in which substituents modify the electronic environment of this site is of great interest because of the importance of this group in organic chemistry. Only very recently, an extensive work of Budesinsky and Exner (7) that deals with a series of substituted methyl benzoates has been published. Consequently, we have chosen to deal with a series of 18 heterocyclic carboxaldehydes as suitable models for determining the electronic influence of the corresponding heterocyclic fragments on the formyl moiety (Fig. 1).

Results and discussion

Formyl ^{13}C NMR chemical shifts of heterocyclic carboxaldehydes **1–18** relative to benzaldehyde (**19**) are collected in

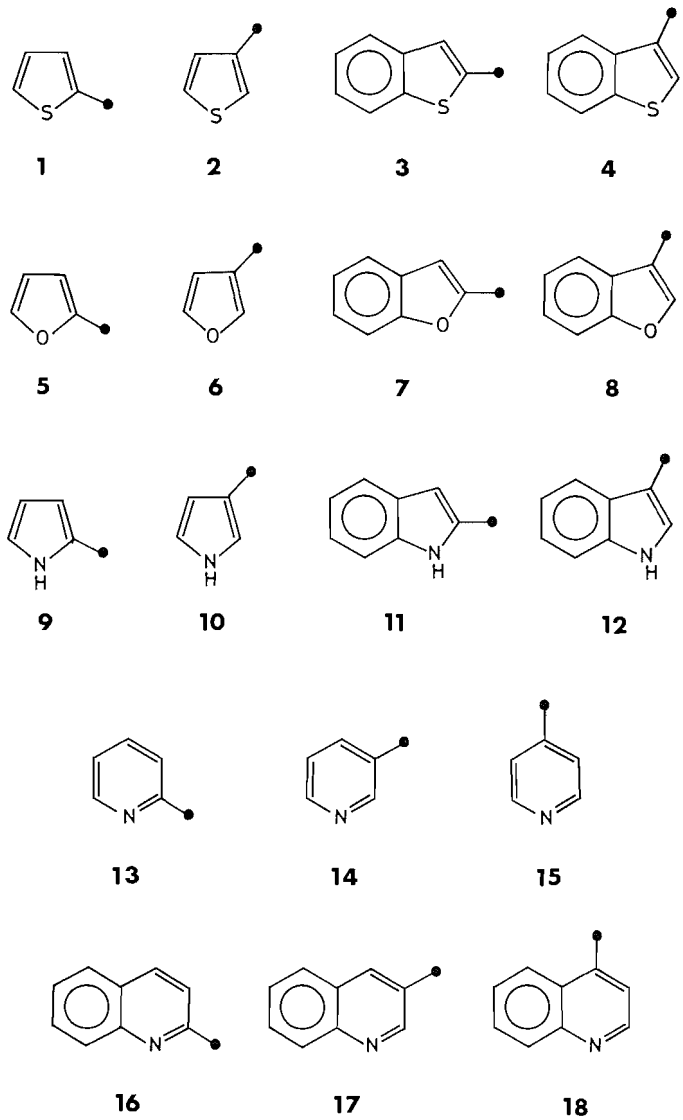

FIG. 1. Heterocyclic substituents included in the present study.

[1]Author to whom correspondence may be addressed.

Printed in Canada / Imprimé au Canada

Can. J. Chem. Downloaded from www.nrcresearchpress.com by 91.121.58.235 on 09/07/12
For personal use only.

TABLE 1. Experimental SCS values, relative to benzaldehyde (192 ppm), and atomic total and π-charges of the carbonyl carbon of compounds **1–19**

Compound	Δδ	q_C^{Tot}	q_C^{π}	Δq_C^{Tot}	Δq_C^{π}
1	−8.4	0.2450	−0.0197	0.0220	−0.0126
2	−6.4	0.2403	−0.0141	0.0173	−0.0070
3	−6.8	0.2430	−0.0189	0.0200	−0.0118
4	−6.1	0.2398	−0.0142	0.0168	−0.0071
5	−13.9	0.2535	−0.0220	0.0305	−0.0149
6	−8.0	0.2506	−0.0162	0.0276	−0.0091
7	−12.6	0.2486	−0.0203	0.0256	−0.0132
8	−7.7	0.2519	−0.0180	0.0289	−0.0109
9	−11.7	0.2483	−0.0191	0.0253	−0.0120
10	−5.9	0.2538	−0.0170	0.0308	−0.0099
11	−10.1	0.2412	−0.0170	0.0182	−0.0103
12	−7.7	0.2540	−0.0191	0.0310	−0.0120
13	1.5	0.2352	0.0117	0.0122	0.0188
14	−0.6	0.2290	−0.0104	0.0060	−0.0033
15	0.2	0.2200	−0.0083	−0.0030	−0.0012
16	2.0	0.2331	0.0127	0.0101	0.0198
17	−1.9	0.2290	−0.0106	0.0060	−0.0035
18	0.1	0.2187	−0.0064	−0.0043	0.0002
19	0.0	0.2230	−0.0071	0.0000	0.0000

Table 1. As can be seen, chemical shifts cover a range of ca. 16 ppm, which seems to be broad enough to monitor substituent-induced changes. In substituted benzaldehydes and methyl benzoates, for instance, Substituent-induced Changes in chemical Shifts (SCS) cover a range of only ca. 3 ppm.

At first sight (Table 1), the great importance of the heteroatom in the heterocyclic ring appears evident. Thus, the whole range of 16 ppm is covered by compounds that are substituted at position 2, whereas 3- and 4-substituted compounds only cover about half of this range, ca. 8 ppm. Furans and pyrroles (**5–12**) show the most marked differences in shielding when comparing positions 2 and 3. Thiophenes and pyridines (**1–4, 13–18**) show comparatively fewer important differences in this respect.

As far as the heterocyclic families are concerned, five-membered heterocycles (**1–12**) show upfield shifts with respect to benzaldehyde (negative values of Δδ) that are in good accordance with the π-excessiveness of this type of heterocycle, and hence with the electron-donating character that is generally attributed to them.

On the other hand, six-membered heterocycles show downfield shifts (positive values of Δδ) in the case of 2- and 4-substitution (**13, 15, 16, 18**), whereas 3-substituted pyridine and quinoline carboxaldehydes (**14, 17**) show negative values of Δδ. These results are also in accordance with the π-deficient character of pyridines, which leads to an electron-withdrawing character at positions 2 and 4. Position 3 does not show the same effect because of the lack of resonance between the probe site and the heteroatom.

In any case, Δδ values of pyridines are, in absolute terms, much less important than those of the corresponding π-excessive heterocycles. This is undoubtedly due to the electron-withdrawing character of the probe site itself. This character of the formyl group leads to strong positive interactions with electron-donating substituents (such as π-excessive heterocycles) and to competitive interactions with electron-withdrawing substituents, such as pyridines, which diminish the overall SCS. These interactions, probe site – substituent, have already been described for analogous systems with similar effects on chemical reactivity (8).

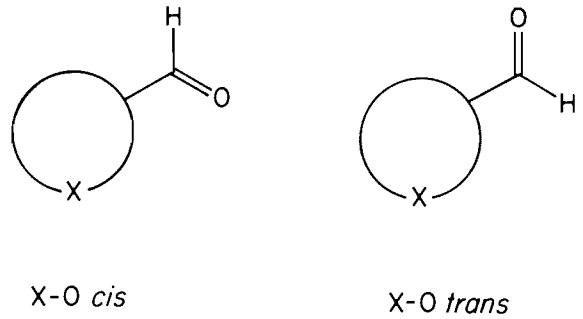

FIG. 2. X–O *cis* and X–O *trans* arrangements of the formyl group with respect to the heteroatom of the heterocyclic substituent.

As a consequence, the ^{13}C NMR chemical shift in these systems is a useful probe for electron-donating substituents, whereas it is less useful for electron-accepting substituents.

The ordering of electron-donating ability for the heterocyclic families studied is the following: furans > pyrroles > thiophenes > pyridines. However, the true dependence between the electronic character and the chemical shifts observed seems to be a complex relationship involving the type of heteroatom and the substitution position of the heterocyclic ring. To study this relationship in depth, theoretical calculations have been performed with the whole set of these structures.

Experimental chemical shifts have been frequently related to calculated changes in electron densities. The theoretical justification for investigating such a relationship arises from a consideration of terms related to the nuclear screening constant. It is generally accepted that for carbon chemical shifts, the paramagnetic constant governs the total shielding (5, 9). Using a number of assumptions, it is possible to represent this term by means of the well-known Karplus–Pople equation (10):

$$[1]\quad \sigma^{A}_{para} = \frac{-e^2\hbar^2}{2m^2c^2\,\Delta E}\langle r^{-3}\rangle_{2p}\left(\sum_{A} Q_A + \sum_{B\neq A} Q_B\right)$$

Although the Karplus–Pople equation provides a relatively solid theoretical framework for investigating the origin of chemical shifts, the correlations between these magnitudes and calculated charges are generally approached from an empirical perspective, because of the difficulty of dealing with the average excitation energy (AEE) term, ΔE. In our case, we have chosen the empirical approach, assuming the chemical similarity of the whole set of heterocyclic carboxaldehydes.

For this purpose, AM1 (11) formalism has been employed throughout the work. Bond lengths and valency angles have been fully optimized in all cases. Structures were kept planar to save computer time, and the two possible arrangements of the formyl group, X–O *cis* and X–O *trans* (Fig. 2), have been considered. Some calculations with full geometrical optimization were performed, however, to test the reliability of AM1 results. The formyl group remained planar in all cases, in agreement with experimental gas phase and *ab initio* studies (12, 13). This result proves the actual improvement of AM1 over the MNDO (14) method in representing rotation around single bonds in conjugated systems.

Conformational preferences calculated by AM1 also agree well with the available experimental gas phase and *ab initio* studies in all but one case, namely, that of thiphene-2-carboxaldehyde (**1**). AM1 gives the S–O *trans* conformation as 4.8 kJ mol^{-1} more stable than the corresponding S–O *cis* conformation, whereas *ab initio* 3-21G//3-21G calculations (13) give the converse preference with a difference in stability of 2.8 kJ

Can. J. Chem. Downloaded from www.nrcresearchpress.com by 91.121.58.235 on 09/07/12
For personal use only.

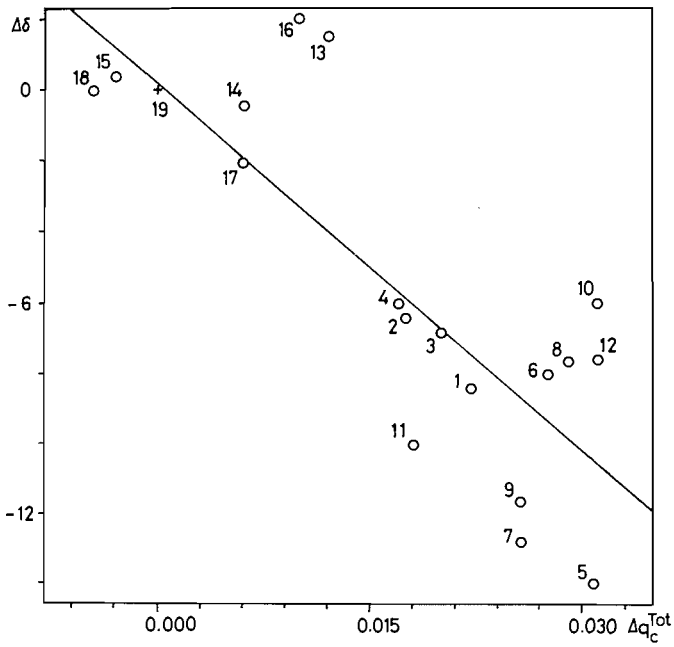

FIG. 3. Plot of Δq_C^{Tot} vs. $\Delta\delta$ (values relative to benzaldehyde, +).

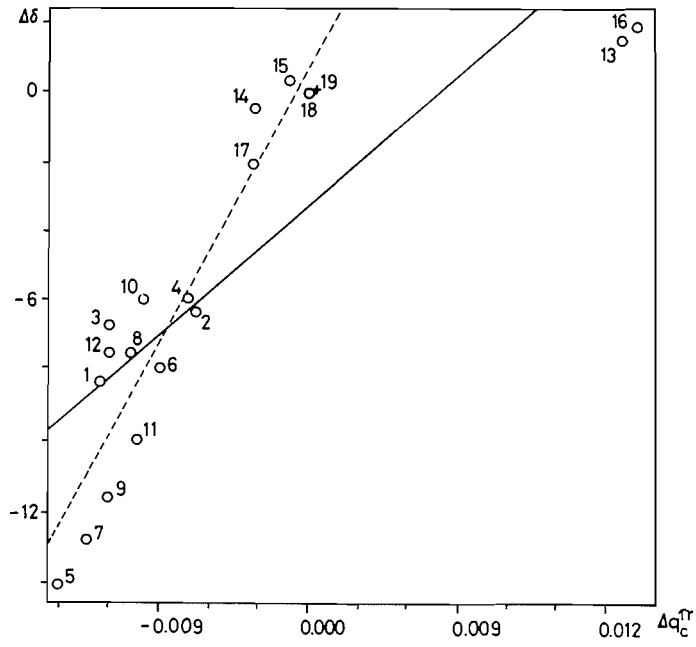

FIG. 4. Plot of Δq_C^{π} vs. $\Delta\delta$ (values relative to benzaldehyde, +). The dashed line corresponds to the regression line excluding compounds **13** and **16**.

mol^{-1}. This result, which can be logically extended to the corresponding benzo[*b*] derivative **3**, can be accounted for by the overestimation of lone pair – lone pair repulsions that have already been noticed with the AM1 method (15).

Because of this overestimation, charge distribution is comparatively less reliable for these compounds. C—O bond polarity in **1**, for instance, is calculated to be higher in the S–O *trans* conformation, whereas the converse tendency is found in *ab initio* STO-3G//STO-3G calculations (13). We have consequently decided to use the values corresponding to AM1 minima (even for compounds **1** and **3**) in order to be consistent with the method throughout the work.

Table 1 collects some of the results of AM1 calculations: total (q_C^{Tot}) and π (q_C^{π}) atomic charge density on the carbonylic carbon as established by Mulliken Population Analysis, and differences of atomic charge density relative to benzaldehyde (Δq_C^{Tot}, Δq_C^{π}).

Figure 3 plots the Δq_C^{Tot} values versus the corresponding $\Delta\delta$ ones. The slope is −343.8 ppm/electron, corresponding to the following regression line:

[2] $\Delta\delta = 0.3 - 343.8\ (\pm 128.1)\ \Delta q_C^{Tot}$

$r = 0.809,\ s = 3.0,\ n = 19,\ F_{1,17} = 32.09\ (p < 0.001)$

Although the model is highly significant from a statistical point of view, indicating that substituent-induced chemical shifts are systematic and electronic in origin, the standard error, *s*, is very large, which gives rise to a considerable scatter around the regression line. Moreover, total atomic charges do not predict the correct direction of chemical shifts. Electron-donating substituents, such as furans or pyrroles, are associated with an increased positive total atomic charge at the carbonyl carbon, i.e., a decreased electronic population at this site, whereas they induce upfield chemical shifts. This type of trend, which is contrary to chemical intuition, has already been noticed for other carbonyl compounds (5, 16), and it is generally explained by the strong relationship existing between changes in σ, π, and total atomic charges (5, 17).

This apparent contradiction vanishes, however, when considering only π charges. Figure 4 plots the corresponding Δq_C^{π} values versus $\Delta\delta$, giving a slope of 420.8 ppm/electron, in the right direction. This plot corresponds to the regression line:

[3] $\Delta\delta = -3.3 + 420.8\ (\pm 144.3)\ \Delta q_C^{\pi}$

$r = 0.831,\ s = 2.9,\ n = 19,\ F_{1,17} = 37.83\ (p < 0.001)$

If we examine the plot, it appears evident that 2-pyridine and 2-quinoline carboxaldehydes (**13, 16**) are placed at a considerable distance from the rest of the compounds. By discarding these two compounds, the remaining 17 carboxaldehydes fit the following regression line, the dashed line in Fig. 4:

[4] $\Delta\delta = 0.8 + 867.9\ (\pm 177.4)\ \Delta q_C^{\pi}$

$r = 0.937,\ s = 1.6,\ n = 17,\ F_{1,15} = 108.75\ (p < 0.001)$

As can be seen, not only does the statistical quality of the model improve, but the intercept approaches zero, as expected, and its value is within the standard error of the model (1.6 ppm). This fact confirms that compounds **13** and **16** are outliers in the regression sense. Two main explanations for this result are possible.

Firstly, the previously mentioned overestimation of lone-pair repulsions, which are known to be important in 2-substituted pyridines, could account for the observed deviation. So, whereas the $\Delta\delta$ values are shifted downfield by about 2 ppm with respect to 4-pyridine and 4-quinoline carboxaldehydes (**15, 18**), the difference in electron density is as large as 0.0200 electrons, which corresponds to a difference of 17.4 ppm, following the model. This difference in electron density is by far the most important noticed in all the families of compounds.

On the other hand, the breakdown in the regression line could be explained by the competitive interaction between two electron-withdrawing groups, such as 2-pyridine (or quinoline) and the formyl group. This phenomenon has been described, for instance, in the case of gas phase acidities of substituted benzaldehydes (8). Electron-donating substituents have a precise linear relationship when using the corresponding σ_R

Can. J. Chem. Downloaded from www.nrcresearchpress.com by 91.121.58.235 on 09/07/12
For personal use only.

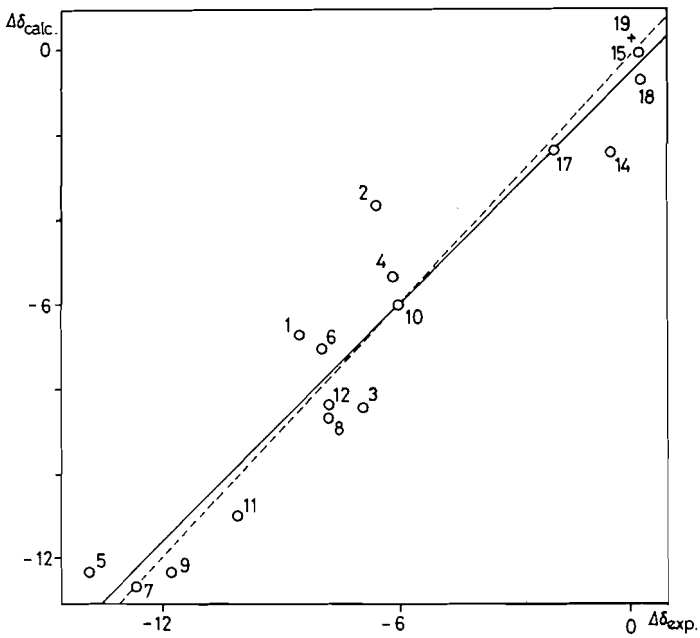

FIG. 5. Plot of experimental vs. calculated values of Δδ (values relative to benzaldehyde, +) corresponding to the DSP model, eq. [5]. The dashed line represents the bisectrix line.

values, whereas electron-withdrawing substituents lead to a breakdown of the regression line, with a slope of zero with respect to σ_R values.

As these two explanations are not mutually exclusive, it is very difficult to attribute the extent to which each contributes to the observed deviation. Further experimental and (or) theoretical work seems necessary in order to solve this question.

Returning to eq. [4], it is possible to verify that this model explains about 88% of the observed variation in chemical shifts. This means that the electron-donating or -accepting ability of heterocyclic substituents, quantified by means of their ^{13}C NMR chemical shifts, is fundamentally due to changes in π-electron density induced by the heterocycle on the probe site. The probe site used in the present work, the formyl group, appears to be quite sensitive to these electronic changes, as the high value of the slope, 867.9 ppm/electron, indicates.

The π-electron density changes can be ideally separated into polar and resonance contributions. Some authors have claimed (12) that resonance effects are more important at position 2 than they are at position 3 in the case of furans, pyrroles, and pyridines. This difference may explain why the observed SCS are more important at position 2 in these families of compounds. Equation [4] also shows the same trend except for compounds **11** and **12**. Indole-3-carboxaldehyde (**12**) is predicted to have an upfield chemical shift with respect to indole-2-carboxaldehyde (**11**). AM1 calculations did in fact show that the resonance is more important in compound **12** than in compound **11**. The π-bond order between the carbonylic carbon and the heterocyclic carbon linked to it is, for instance, 0.2493 for compound **12** and only 0.2289 for compound **11**. This result is in accordance with the known chemical reactivity of compound **12** (18).

We feel that two main conclusions can be extracted from this point of the discussion. On the one hand, the Δq_C^{π} values calculated by AM1 are fundamentally dominated by resonance contributions. On the other hand, polar contributions, which must always be more important on position 2, would explain the great difference between positions 2 and 3 as well as the anomalous result obtained for compounds **11** and **12** when eq. [4] is applied.

The separation of polar and resonance effects, either experimentally or theoretically, is a formidable task, which has only been partially achieved for the more simple substituents. It is clear, however, that any serious attempt to understand the electronic effects of heterocyclic substituents should deal with this matter.

In a preliminary attempt to evaluate these contributions from a theoretical point of view, we have calculated the 19 structures of the carboxaldehydes with the formyl group perpendicular to the aromatic ring. In this manner, changes in atomic charges can be fundamentally attributed to polar effects. Several Dual Substituent Parameter (DSP) models, based on quantum mechanics indices, have been tested, the best fit being obtained with the following equation:

$$[5]\quad \Delta\delta = 0.5 - 193.9\ (\pm 33.8)\ \Delta P_{CO}^{Tot} - 395.1\ (\pm 78.1)\ \Delta q_O^{90}$$

$$r = 0.965,\ s = 1.3,\ n = 17,\ F_{2,14} = 94.14\ (p < 0.001)$$

Where ΔP_{CO}^{Tot} represents the polarity of the C—O bond in planar structures (defined as the difference between the atomic charges of the carbon and the oxygen atoms), relative to benzaldehyde, mainly attributed to resonance contributions, and Δq_O^{90} is the atomic charge of the carbonylic oxygen, relative to benzaldehyde, when the formyl group is perpendicular to the aromatic ring, and therefore mainly attributed to polar contributions. Figure 5 plots experimental versus calculated Δδ values corresponding to eq. [5]. As can be seen, experimental trends for compounds **11** and **12** are now reproduced by the model.

Although we feel that this and similar results should be taken with extreme caution, the interest in modelling electronic effects in heterocyclic systems undoubtedly requires a more extensive experimental and theoretical effort in this direction, which will be the subject of future work.

Conclusions

Theoretical and experimental work leading to a better knowledge of the electronic effects of heterocyclic substituents and their transmission mechanisms is of prime importance for incorporating this class of molecular fragments into Structure–Properties Relationship studies. We have shown that ^{13}C NMR chemical shifts of the side chain of aromatic heterocyclic systems can be an excellent tool for monitoring the electronic effects of this type of substituent with respect to the classical benzene systems, taking the phenyl group as reference. Theoretical calculations have shown that the SCS are electronic in origin, and mainly due to changes in the π-electron distribution on the probe site. This change in π-electron density could be tentatively attributed to resonance effects, but some preliminary studies, as well as some discrepancies in experimental results, indicate that polar effects may play a part. We suggest that further experimental and theoretical work is necessary to determine precisely the part played by polar and resonance effects in this family of compounds.

Experimental

Heterocyclic carboxaldehydes **1, 2, 5, 9, 12–15, 17**, and **18** are commercial and were used as purchased. The remaining aldehydes **3, 4, 6–8, 10, 11**, and **16** were prepared following previously described procedures, and purified to obtain analytically pure samples.

^{13}C NMR spectra were recorded at room temperature on a Bruker

Can. J. Chem. Downloaded from www.nrcresearchpress.com by 91.121.58.235 on 09/07/12
For personal use only.

WP 80 SY spectrophotometer using $CDCl_3$ as solvent in all but the case of compound **12**, which presents a weak solubility in this solvent. To obtain comparable chemical shifts, several spectra were recorded in mixtures of DMSO-d_6 and $CDCl_3$, and the corresponding δ value was extrapolated to pure $CDCl_3$.

Theoretical calculations were performed using the AMPAC (19) package of quantum mechanical programs, running on a DEC-VAX 8300 computer under the VMS operating system.

1. C. HANSCH and A. LEO. *In* Substituent constants for correlation analysis in chemistry and biology. Wiley, New York, NY. 1979.
2. C. CATIVIELA, J. I. GARCIA, J. ELGUERO, D. MATHIEU, and R. PHAN TAN LUU. Quant. Struct.–Act. Relat. **6**, 173 (1987).
3. C. CATIVIELA, J.-L. DEJARDIN, J. ELGUERO, J. I. GARCIA, E. GONZALEZ, and J. A. MAYORAL. Collect. Czech. Chem. Commun. **55**, 72 (1990).
4. (*a*) J. BROMILOW, R. T. C. BROWNLEE, V. O. LOPEZ, and R. W. TAFT. J. Org. Chem. **44**, 4766 (1979); (*b*) J. BROMILOW, R. T. C. BROWNLEE, D. J. CRAIK, M. SADEK, and R. W. TAFT. J. Org. Chem. **45**, 2429 (1980).
5. D. J. CRAIK and R. T. C. BROWNLEE. Prog. Phys. Org. Chem. **14**, 1 (1983).
6. (*a*) W. F. REYNOLDS, A. GOMES, A. MASON, D. W. MACINTYRE, R. G. MAUNDER, T. ATES, H. E. WONG, G. K. KRAMER, and R. PEAT. Can. J. Chem. **61**, 2367 (1983); (*b*) D. A. R. HAPPER. J. Chem. Soc. Perkin Trans. 2, 1673 (1984).
7. M. BUDESINSKY and O. EXNER. Magn. Reson. Chem. **27**, 585 (1989).
8. R. W. TAFT and R. D. TOPSOM. Prog. Phys. Org. Chem. **16**, 1 (1987).
9. P. SOHAR. *In* Nuclear magnetic resonance spectroscopy. Vol. II. CRC Press, Boca Raton, FL. 1983.
10. M. KARPLUS and J. A. POPLE. J. Chem. Phys. **38**, 2803 (1963).
11. M. J. S. DEWAR, E. G. ZOEBISCH, E. F. HEALY, and J. J. P. STEWART. J. Am. Chem. Soc. **107**, 3902 (1985).
12. I. G. JOHN, G. L. D. RITCHIE, and L. RADOM. J. Chem. Soc. Perkin Trans. 2, 1601 (1987).
13. R. BENASSI, U. FOLLI, L. SCHENETTI, and F. TADDEI. J. Chem. Soc. Perkin Trans. 2, 961 (1987).
14. M. J. S. DEWAR and W. THIEL. J. Am. Chem. Soc. **99**, 4899 (1977).
15. W. M. FABIAN. J. Comput. Chem. **9**, 369 (1988).
16. M.-T. BERALDIN, E. VAUTHIER, and S. FLISZÁR. Can. J. Chem. **60**, 160 (1982).
17. S. FLISZÁR, G. CARDINAL, and M.-T. BERALDIN. J. Am. Chem. Soc. **104**, 5287 (1982).
18. R. LIVINGSTONE. *In* Rodd's chemistry of carbon compounds. Vol. IVA. Elsevier, Amsterdam. 1973.
19. Program AMPAC. Dewar Group (1986).

Can. J. Chem. Downloaded from www.nrcresearchpress.com by 91.121.58.235 on 09/07/12
For personal use only.

Thione–thiol tautomerism and stability of 2- and 4-mercaptopyridines and 2-mercaptopyrimidines

STEFAN STOYANOV,[1] IVAN PETKOV, LIUDMIL ANTONOV, and TATYANA STOYANOVA
Department of Chemistry, University of Sofia, Sofia 1126, Bulgaria

AND

PETROS KARAGIANNIDIS[1] and PARASKEVAS ASLANIDIS
Department of General and Inorganic Chemistry, Aristotelian University of Thessaloniki, Thessaloniki 54006, Greece

Received December 22, 1989

STEFAN STOYANOV, IVAN PETKOV, LIUDMIL ANTONOV, TATYANA STOYANOVA, PETROS KARAGIANNIDIS, and PARASKEVAS ASLANIDIS. Can. J. Chem. **68**, 1482 (1990).

The possible thione–thiol tautomerism of 2- and 4-mercaptopyridines, 2-mercaptopyrimidine, and 4,6-dimethyl-2-mercaptopyrimidine in solution is studied by means of absorption (UV–VIS) spectroscopy. In accordance with earlier observations, polar solvents and self-association shift the apparent tautomeric equilibrium significantly towards the thione form. In dilute solutions of nonpolar solvents the thiol form predominates. On standing, significant changes are observed in the absorption spectra of these tautomeric compounds in ethanol, dioxane, and water. The time course of the tautomerization, followed spectrophotometrically, reveals quantitative transformation of the thiol form to the corresponding symmetrical disulfides. The influence of concentration, temperature, and irradiation with indirect sunlight are discussed. This thione–disulfide process is reversible in water, starting either from the tautomeric thione or from its symmetrical disulfide, implying a possible importance in biological systems.

Key words: thione–thiol tautomerism, absorption spectra, thiol–disulfide oxidation, mercaptopyridines and pyrimidines.

STEFAN STOYANOV, IVAN PETKOV, LIUDMIL ANTONOV, TATYANA STOYANOVA, PETROS KARAGIANNIDIS et PARASKEVAS ASLANIDIS. Can. J. Chem. **68**, 1482 (1990).

Faisant appel à la spectroscopie d'absorption UV–VIS, on a étudié les possibilités de tautomérie dans les 2- et 4-mercaptopyridines, la 2-mercaptopyrimidine et la 4,6-diméthyl-2-mercaptopyrimidine en solution. Comme on l'avait observé antérieurement, l'utilisation de solvants polaires et l'auto-association déplacent fortement l'équilibre tautomère apparent vers la forme thione. Si on laisse reposer des solutions de ces composés dans l'éthanol, le dioxane et l'eau, on observe des changements importants dans les spectres d'absorption. Lorsqu'on détermine d'une façon spectrophotométrique la tautomérisation en fonction du temps, on note qu'il se produit une transformation quantitative de la forme thiol en disulfures symétriques correspondants. On discute de l'influence de la concentration, de la température et de l'irradiation par de la lumière solaire indirecte. Dans l'eau, ce processus thione–disulfure est réversible en partant soit de la thione tautomère ou de son disulfure symétrique; ce résultat indique qu'il pourrait avoir une certaine importance dans les systèmes biologiques.

Mots clés : tautomérie thione–thiol, spectre d'absorption, oxydation thiol–disulfure, mercaptopyridines et pyrimidines.

[Traduit par la revue]

Can. J. Chem. Downloaded from www.nrcresearchpress.com by 91.121.58.235 on 09/07/12
For personal use only.

Introduction

It is well known that organic molecules bearing a mobile H atom undergo rapid and facile tautomeric transformations. Pyridines and pyrimidines substituted with an SH or an OH group at the 2 or 4 positions are fundamentally tautomeric heterocyclic systems and many theoretical and experimental studies have been reported (1–9). It is generally accepted that in solution both pyridine and pyrimidine substituted at the 2 or 4 position by potentially tautomeric groups XH (X = O or S) exist in lactam or thione forms rather than in lactim or thiol forms (Scheme 1).

X-ray crystallography (10, 11) revealed that 2-mercaptopyridine–pyridine-2-thione (**1**⇄**3**) exist as H-bonded dimers of **3** in the solid state. However, Beak *et al.* (8), on the basis of the UV spectra of 2- and 4-thiosubstituted pyridines in the gas phase, suggested that mercapto forms **1** and **5** are dominant in vapour. This was also confirmed from photoelectron spectroscopy (12). To approach the vapour phase environment, Beak *et al.* (8, 13–15) used dilute solutions in nonpolar solvents and concluded that the effect of self-association in **1**⇄**3** can significantly shift the apparent tautomeric equilibrium in solution. On the other hand, thiols are considered to be the most active groups found in cells and they are easily oxidized to the rather more stable disulfides, which can be reduced easily and completely back to thiols (16). It may be expected that resistance to oxidation of possible thiol forms to the corresponding disulfides **17**–**20** will influence this tautomeric thione–thiol equilibrium.

Thus the aim of this study is to investigate in detail some factors, including the nature of the solvent, stability, temperature, and concentration, that may influence this equilibrium.

Results and discussion

The absorption spectra of **1**⇄**3** in cyclohexane (Fig. 1) at different concentrations confirm the earlier observations (13, 15) that self-association can significantly shift the apparent tautomeric equilibrium in solution. Using the changing ratio in optical densities at λ_{max} of bands assigned to the thione and thiol chromophores as a function of concentration (13–15, 17), it is possible to evaluate the equilibrium constant of association (K_{assoc}), which is $(8.6 \pm 0.7) \times 10^4$ L mol^{-1}, i.e., an order of magnitude less than the value reported by Beak *et al.* (13).

Additional evidence for the existence of self-association is presented in Fig. 2, where the absorption spectra **1**⇄**3** in cyclohexane at different temperatures are presented. Evidently the monomer–dimer equilibrium is shifted towards the monomer thiol form **1** when the stable dimers of **3** are broken up by heating or dilution. The change in K_{assoc} for **1**⇄**3** in cyclohexane as a function of temperature allows calculation of the thermodynamic parameters ΔG^0_{assoc} (293 K) = −27.6 kJ mol^{-1}, $\Delta H^0_{assoc} = -49.6 \pm 2.5$ kJ mol^{-1}, and $\Delta S^0_{assoc} = -18.2 \pm 2.0$

[1]Authors to whom correspondence may be addressed.

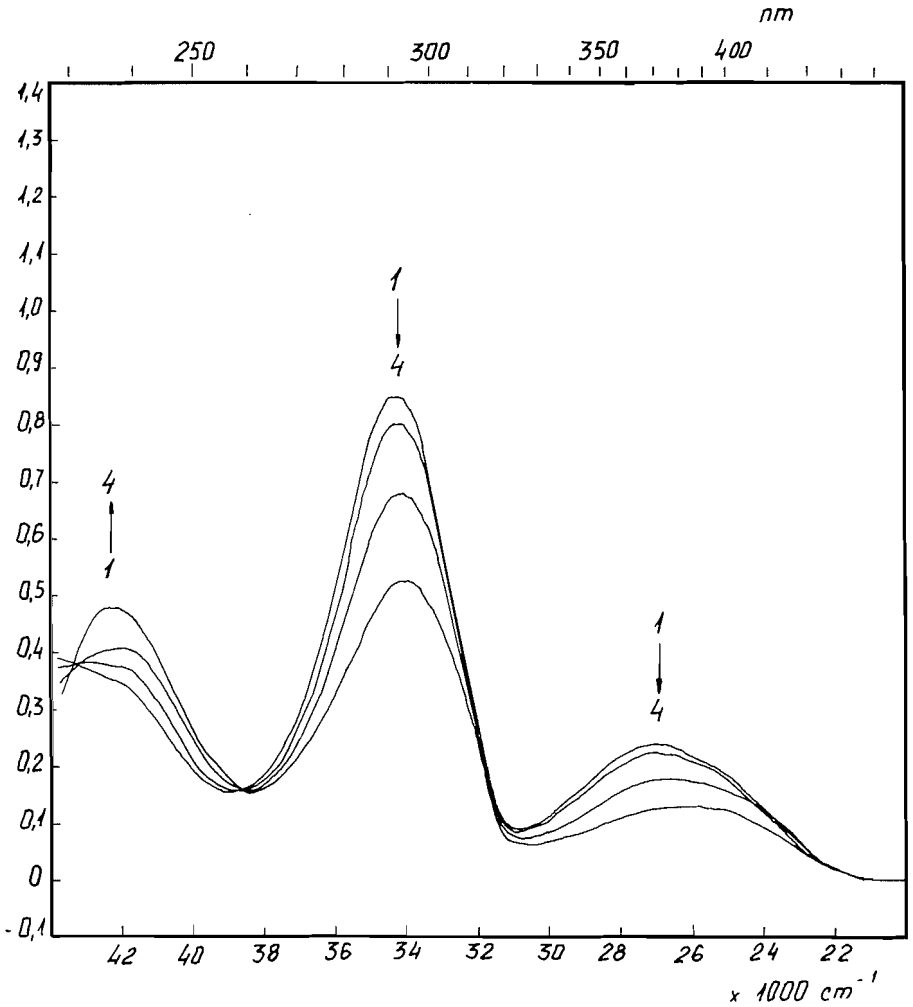

FIG. 1. Absorption spectra of **1**⇄**3** in cyclohexane at different concentrations: 1, 5.77×10^{-5} M; 2, 2.89×10^{-5} M; 3, 1.15×10^{-5} M; 4, 5.77×10^{-6} M; $c \cdot l$ = const.

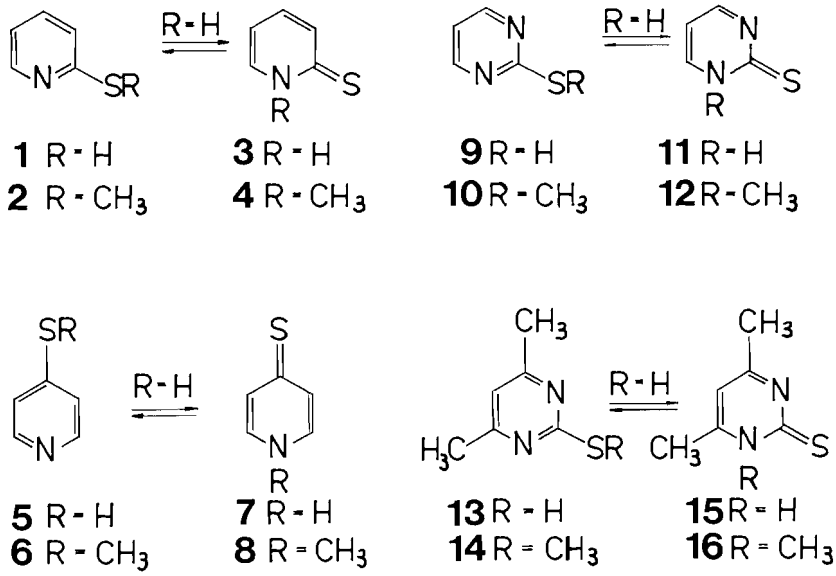

SCHEME 1

Can. J. Chem. Downloaded from www.nrcresearchpress.com by 91.121.58.235 on 09/07/12
For personal use only.

Can. J. Chem. Downloaded from www.nrcresearchpress.com by 91.121.58.235 on 09/07/12
For personal use only.

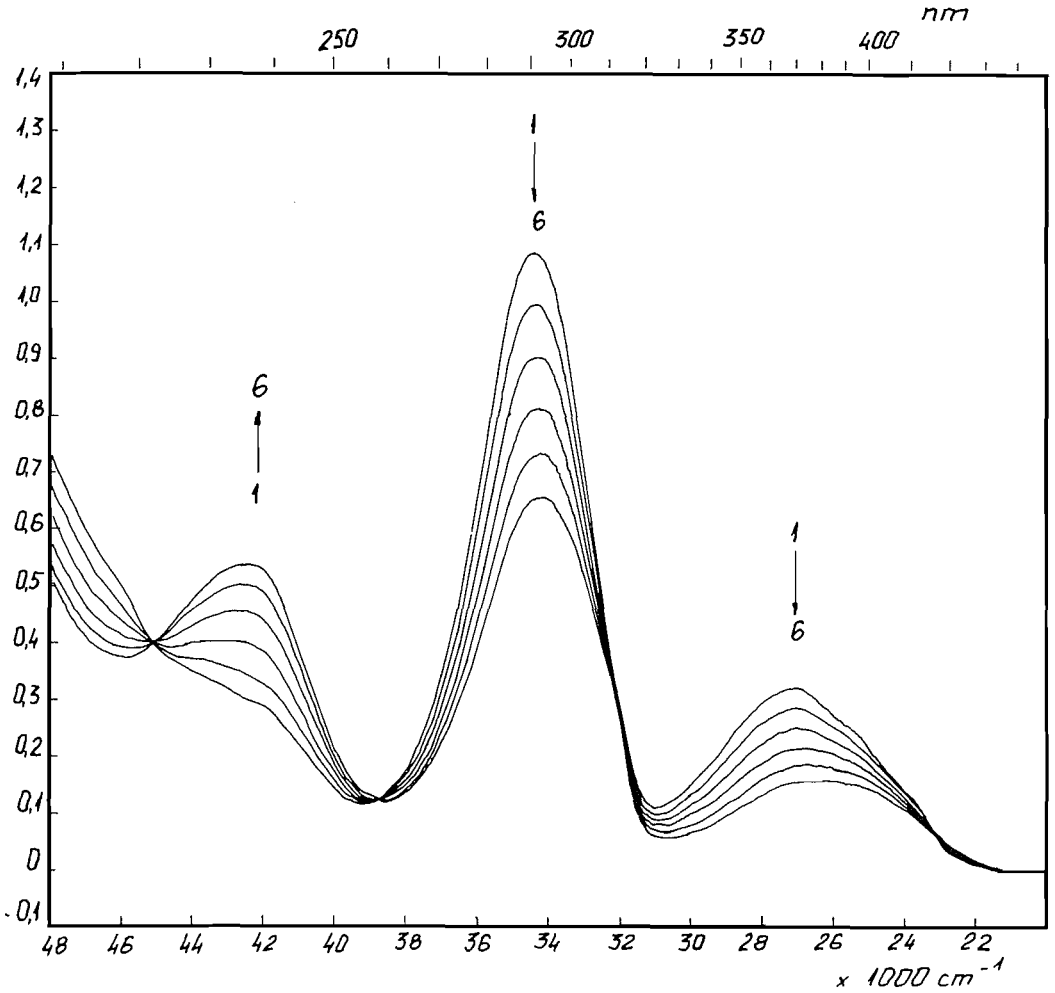

FIG. 2. Absorption spectra of **1**⇄**3** in cyclohexane, $c = 1.33 \times 10^{-4}$ M, $l = 0.5$ cm, at different temperatures: 1–6, from 293 K to 343 K.

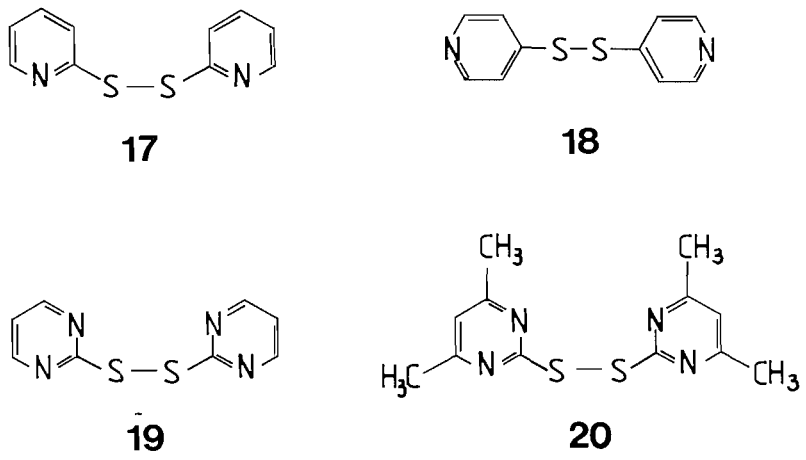

SCHEME 2

eu, confirming earlier suggestions that **3** is somewhat less associated than its oxygen analog (15, 18, 19). The absorption spectra of **13**⇄**15** in water and ethanol exhibit spectral features of the thione form **15**, whereas in cyclohexane tautomeric equilibrium is shifted almost completely towards the thiol form **13**. Further evidence for the existence of thiol form **13** could be obtained by measuring the absorption spectra, in different volume ratios of dichloromethane and cyclohexane, of **13**⇄**15**. Because the thione form **15** is dominant in CH_2Cl_2, addition of cyclohexane shifts the tautomeric equilibrium towards the thiol form **13**. The opposite is observed when CH_2Cl_2 is added to the solution of **13**⇄**15** in cyclohexane. Obviously the nature of the solvent significantly shifts the apparent tautomeric equilibrium between isomers. Thus the solvent that is able to participate in

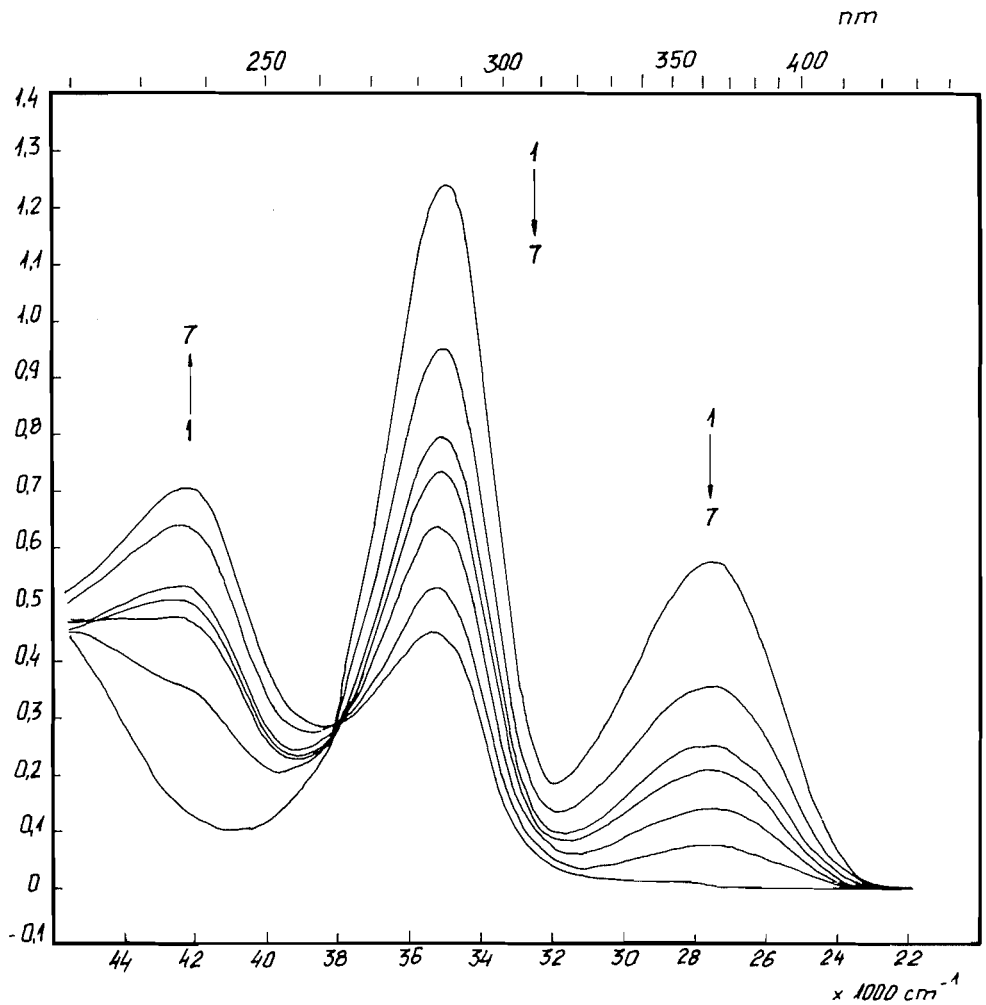

FIG. 3. Absorption spectra of **1**⇄**3** in ethanol, l = 2 cm, $c = 9.73 \times 10^{-5}$ M, in dark, recorded with time: 1, initial solution: 2, after–71 h; 3, 136 h; 4, 164 h; 5, 210 h; 6, 329 h; 7, 486 h.

hydrogen bonding, that can compete with the self-association and also participate in differential solvation of different dipoles of the associated and unassociated species, is responsible for such a shift (15, 17). Therefore, on dilution in dichloroethane, **1**⇄**3** and **9**⇄**11** reveal an apparent shift of tautomeric equilibrium towards the thiol forms **1** and **9**, while addition of ethanol, keeping the total concentration constant, leads back to formation of the thione forms **3** and **11**.

Qualitatively these observations are in accordance with the effect of self-association favoring the thione tautomer, the well-known rule that a more polar thione tautomer is preferentially stabilized in the more polar solvents, and with the proton donating ability of ethanol, which favors the thione form (1, 8, 14, 17, 20). Indeed in ethanol and water the tautomeric equilibrium is shifted almost exclusively towards the thione forms **3**, **7**, **11**, and **15**. Such large differences for tautomeric equilibria in nonpolar solvents and alcoholic or aqueous solution should not be regarded as surprising, since at dilution of $\leq 10^{-5}$ M in nonpolar solvents the position of the equilibrium might be expected to be close to that in the gas phase.

During the course of spectral studies in ethanol and water it was noticed that the absorption spectra of these tautomeric compounds reveal significant changes on standing at ambient laboratory conditions in the dark or in indirect sunlight. The absorption spectra of **1**⇄**3** in ethanol, recorded during 20 days in the dark, are presented in Fig. 3. The observed spectral features, i.e., appearance of a new maximum at 240 nm, disappearance of the maximum at 360 nm, and the ratio of absorbances $A_{\lambda_{240}}/A_{\lambda_{285}}$ at the end of the process, could be due to slow formation of the thermodynamically more stable thiol form **1** or to the corresponding oxidation product, 2,2′-pyridinedisulfide, **17**. Such a relatively slow process also takes place in ethanol with **5**⇄**7**, **9**⇄**11**, and **13**⇄**15**, leading irreversibly to almost quantitative transformation of the thione structures. The absorption characteristics of the corresponding thiols and disulfides may be expected to be very similar since the parent chromophore is the same and only the molar intensity should be doubled due to the noncoplanar structure of disulfides (21, 22). Therefore the IR, NMR, and TLC data for the final product of 2-pyridinethione transformation were compared with those for the corresponding disulfide **17**, showing full coincidence. The spectral characteristics of the individual thione forms and other disulfides together with the model N-CH_3 and S-CH_3 derivatives are presented in Table 1.

Additional evidence for the structure of the transformation products from the thione forms **3**, **7**, **11**, and **15** in ethanol comes from the quantitative comparison of their spectral data with those of disulfides **17**⇄**20**, taking into account the fact that two

Can. J. Chem. Downloaded from www.nrcresearchpress.com by 91.121.58.235 on 09/07/12
For personal use only.

TABLE 1. Spectral data of the individual thione forms, N-CH_3 and S-CH_3 model compounds, and corresponding symmetrical disulfides

Our data[a]									
Compounds studied	λ (nm)	ϵ^b	$\frac{\epsilon_{\lambda_1}}{\epsilon_{\lambda_2}}$	Model compound	Solvent	λ (nm)	ϵ^b	$\frac{\epsilon_{\lambda_1}}{\epsilon_{\lambda_2}}$	Reference
17	237	15930	1.61	**2**	C_2H_5OH	249	7400	2.39	6
	283	9940				292.5	3100		
					C_2H_5OH	248	10400	2.55	8
						291	4080		
3	286	12750	2.15	**4**	C_2H_5OH	287	12900	2.03	8
	362.6	5940				357	6370		
					C_2H_5OH	210	8700	1.83[c]	6
						284	11000		
						355	6000		
18	246	17630		**6**	C_2H_5OH	263	11800		8
7	231	7330	0.33	**8**	C_2H_5OH	231	6520	0.26	8
	341.5	22320				348	25000		
19	239	17640	4.14	**10**	C_2H_5OH	251	15850	7.93	3
	278s	4260				286s	2000		
11	214	2060	4.08	**12**	H_2O	279	18200	6.45	7
	291	23000			pH 9	344	2820		
	373	5640							
20	243	22070	2.55	**14**	H_2O[d]	210	3980	0.29	2
	273s	8650			pH 7	250	13800		
15	240	11230	5.91[c]	**16**	H_2O	220	10715	6.76[c]	2
	289	22500			pH 7	277	17380		
	360	3810				332	2570		

[a]In ethanol.
[b]L mol^{-1} cm^{-1}.
[c]$\epsilon_{\lambda_2}/\epsilon_{\lambda_3}$.
[d]4-Methyl derivative.

moles of thione are oxidized through the corresponding thiol to one mole of symmetrical disulfide according to the following reaction (22):

[1] $2\,RSH + 1/2\,O_2 \rightarrow RSSR + H_2O$

where R is the corresponding pyridine or pyrimidine.

The estimated percentages of conversion to disulfides **17–20** in ethanol according to eq. [1] are 90, 89, 86, and 100%, respectively. Also, excellent agreement with the shape and positions of the absorption maxima is observed. When the concentrations used were less than 1×10^{-4} M, the process of thione–disulfide oxidation proceeded almost quantitatively. The changes in absorbances A_i at λ_{max} of the thione form with time were analyzed as being first-order kinetics, using the least-squares method. As Beak *et al.* (13–15) have shown, the evaluation of the effect of self-association is essential for reliable interpretation of solution data. Therefore, different concentrations were used to determine the rate constants (K_{obs}) of thione–disulfide oxidation and the data obtained are tabulated in Table 2.

These results clearly show that this oxidation is relatively slow and a marked dependence on the concentration is observed. Using Scheme 3, it is possible to explain the influence of concentration on K_{obs}. Upon dilution, the monomer–dimer equilibrium is shifted from the dimeric species where only the thione chromophore is observed (13) to the monomeric species where both tautomeric forms are possible. The thiol–disulfide oxidation takes place subsequently and the tautomeric equilibrium is restored again. Finally all the thione molecules are oxidized to the corresponding disulfide. At higher concentrations ($>1 \times 10^{-4}$ M), the calculated values of K_{obs} decrease (Table 2) and the relationship between $\ln(A_0/A_i)$ and τ(s) deviates from linearity due to the relative resistance of the self-associated thione form towards oxidation and the domination of dimer species in solution. When a deoxygenated solution of **9⇄11** in ethanol is used, the thione–sulfide transformation proceeds very slowly (Table 2), confirming our suggestion about the nature of the process involved.

A number of solvents, of different types, were used in order to evaluate their influence on the thione–thiol equilibrium and the thione–disulfide transformation. In CH_3CN, CH_2Cl_2, and $CHCl_3$ the thione form predominates and the rate of oxidation to the corresponding disulfides is rather slow.

In dioxane, the thione form also predominates but the thione–disulfide transformation proceeds relatively rapidly. However, the observed spectrum **1⇄3** differs slightly from that of the corresponding disulfide in the same solvent (Fig. 4) and only after 24 h does the final spectrum correspond to about 90% of the theoretically expected amount of **17**. This transformation is also enhanced by a decrease in the concentration of the initial thione (Table 2) and by an increase in the temperature (Table 3).

However, the addition of water partly restores the thione spectrum. Thus it is possible to observe the absorption characteristics of the thiol form along with those of the forming disulfide. The temperature and concentration dependence are readily accommodated by the well-known tendency of **3** to form

Can. J. Chem. Downloaded from www.nrcresearchpress.com by 91.121.58.235 on 09/07/12
For personal use only.

TABLE 2. Rate constants of thione–disulfide oxidation (K_{obs}) for the compounds investigated

Compounds studied	Solvent	$C \times 10^5$ (mol L^{-1})	K_{obs} (s^{-1})	$\tau_{1/2}$ (h)
3 → 17	Ethanol	97.30	$(4.05 \pm 0.76) \times 10^{-7}$	475.41
	Ethanol	9.73	$(1.92 \pm 0.04) \times 10^{-6}$	100.46
	Ethanol	3.01	$(3.39 \pm 0.15) \times 10^{-6}$	56.74
	Ethanol	0.20	$(5.02 \pm 0.12) \times 10^{-6}$	38.39
	Dioxane	17.64	$(5.29 \pm 0.36) \times 10^{-4}$	0.36
	Dioxane	8.61	$(6.24 \pm 0.18) \times 10^{-4}$	0.31
	Ethanol	3.18	$(7.03 \pm 0.10) \times 10^{-4}$	0.27
	Dioxane	1.89	$(8.72 \pm 0.21) \times 10^{-4}$	0.22
	Water	2.23	$(3.67 \pm 0.52) \times 10^{-7}$	525.11
	Water[a]	7.65	$(6.53 \pm 0.55) \times 10^{-7}$	294.71
7 → 18	Ethanol	3.02	$(1.13 \pm 0.04) \times 10^{-6}$	170.89
	Ethanol[a]		$(2.29 \pm 0.11) \times 10^{-6}$	84.14
	Dioxane	12.08	$(4.19 \pm 0.10) \times 10^{-5}$	4.59
	Dioxane	8.31	$(9.23 \pm 0.06) \times 10^{-5}$	2.09
	Dioxane	2.61	$(1.84 \pm 0.04) \times 10^{-4}$	1.05
	Water	1.14	$(3.90 \pm 0.87) \times 10^{-7}$	493.69
	Water[a]	5.95	$(6.95 \pm 0.52) \times 10^{-7}$	277.03
11 → 19	Ethanol	49.03	$(8.83 \pm 1.00) \times 10^{-8}$	2179.70
	Ethanol	9.01	$(2.72 \pm 0.07) \times 10^{-6}$	70.92
	Ethanol	4.90	$(4.12 \pm 0.12) \times 10^{-6}$	46.71
	Ethanol[b]	1.0	$(1.74 \pm 0.15) \times 10^{-7}$	1005.75
	Ethanol	0.98	$(4.09 \pm 0.39) \times 10^{-6}$	47.11
	Dioxane	40.26	$(1.24 \pm 0.10) \times 10^{-4}$	1.55
	Dioxane	13.21	$(2.19 \pm 0.11) \times 10^{-4}$	0.88
	Dioxane	9.86	$(2.21 \pm 0.07) \times 10^{-4}$	0.87
	Dioxane	4.29	$(3.80 \pm 0.08) \times 10^{-4}$	0.51
	Dioxane	1.59	$(7.25 \pm 0.98) \times 10^{-4}$	0.27
	Water	1.11	$(5.82 \pm 0.83) \times 10^{-7}$	331.02
	Water[a]	6.25	$(9.75 \pm 0.75) \times 10^{-7}$	197.48
14 → 20	Dioxane	32.71	$(3.86 \pm 0.54) \times 10^{-5}$	4.98
	Dioxane	13.41	$(1.39 \pm 0.11) \times 10^{-4}$	1.40
	Dioxane	8.01	$(1.67 \pm 0.05) \times 10^{-4}$	1.17
	Dioxane	3.78	$(3.90 \pm 0.05) \times 10^{-4}$	0.49
	Dioxane	1.67	$(5.40 \pm 0.10) \times 10^{-4}$	0.36

[a]In indirect sunlight.
[b]Deoxygenated with argon.

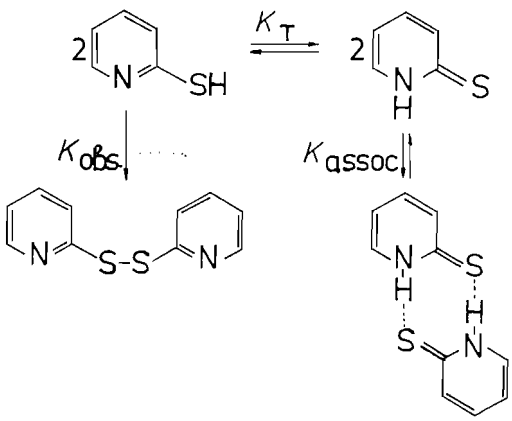

SCHEME 3

stable dimers that are broken up by heating or dilution. In water, the most polar solvent, the thione form dominates initially, but the thione–disulfide transformation is restored on standing at ambient conditions. The values of K_{obs} (Table 2) are relatively smaller than in ethanol. Surprisingly, when almost all the thione molecules of **9** are converted to the corresponding disulfide **19**, additional standing in the dark leads to the formation of ca. 85% of the initial thione form **9**. When dilute solutions (10^{-4}–10^{-5} M) of the model disulfides **17**–**20** in water are allowed to stand in the dark an almost complete transformation of the original spectrum, corresponding to that of the thiones, is observed. Moreover, additional standing in indirect sunlight induces reversion to the initial disulfide as shown by eq. [2]:

$$[2]\quad \text{Thione} \underset{\text{dark}}{\overset{\text{light}}{\rightleftharpoons}} \text{disulfide}$$

This practical thiol–disulfide redox system could have some importance in biological systems and resembles the reaction known as "disulfide interchange" (23), in which a thiol reacts with a disulfide to give a different thiol and disulfide pair as products. Thus the disulfides **17** and **18** investigated have been extensively used for the modification and estimation of protein thiol groups (24).

Apparently, in these potentially tautomeric heterocyclic systems, understanding the effects of molecular environment along with the relative stability of the thiol form may be pertinent to important aspects of their biological action.

Can. J. Chem. Downloaded from www.nrcresearchpress.com by 91.121.58.235 on 09/07/12
For personal use only.

Can. J. Chem. Downloaded from www.nrcresearchpress.com by 91.121.58.235 on 09/07/12
For personal use only.

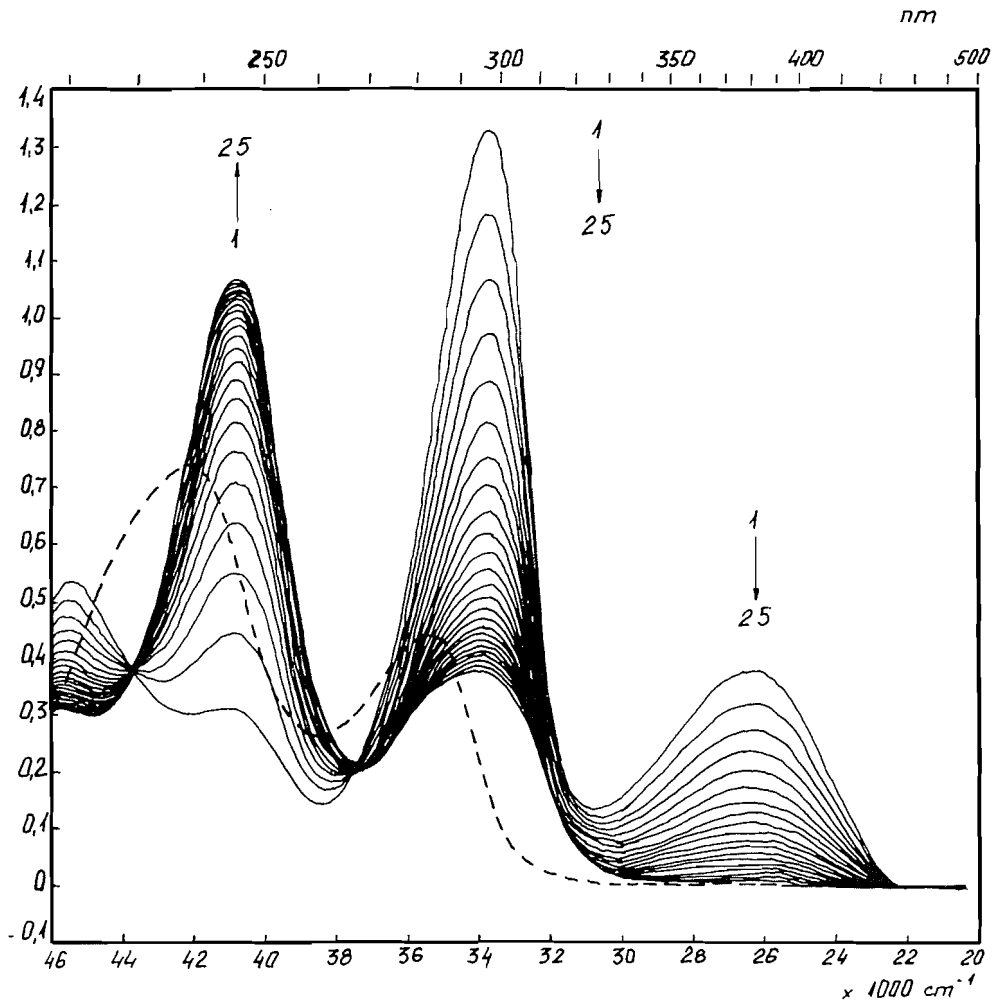

FIG. 4. Absorption spectra of **1**⇄**3** in dioxane, $c = 4.71 \times 10^{-5}$ M; recorded in dark with 3 min 21 s time interval; (---), **17** in dioxane.

TABLE 3. Values of K_{obs} at different temperatures for thione–disulfide oxidation in dioxane

Compounds studied	T (K)	$C \times 10^5$ (mol L^{-1})	$K_{obs} \times 10^4$ (s^{-1})	$\tau_{1/2}$ (h)
3 → **17**	293	5.74	4.35±0.40	0.44
	313	5.43	9.95±2.14	0.19
	333	5.99	33.18±9.91	0.06
11 → **18**	293	4.29	3.80±0.08	0.51
	303	4.97	6.20±0.37	0.31
	313	4.61	7.25±0.69	0.27
	323	4.56	7.55±0.81	0.26
14 → **19**	293	3.78	3.90±0.05	0.49
	303	3.51	7.66±0.51	0.25
	313	3.88	8.18±0.98	0.24

Irradiation of solutions, even with indirect sunlight, leads to an increase of K_{obs}, or it enhances the thione–disulfide transformation (Table 2). Further studies are underway to clarify the influence of irradiation on the position of the tautomeric thione–thiol equilibrium in solution.

Experimental

Pyridine-2-thione, pyrimidine-2-thione, 4,6-dimethylpyrimidine-2-thione (Fluka), and pyridine-4-thione (Aldrich) were purified following the procedures described (25, 26) to obtain analytically pure materials. The IR, NMR, and absorption properties were consistent with those expected for the assigned structures. The disulfides **17**–**20** were prepared from the corresponding thiones through oxidation with equimolar amounts of H_2O_2 in water at room temperature and recrystallized from aqueous ethanol. The elemental analysis, mp (26, 27), and ^{1}H NMR for **17**–**19** are in accordance with those expected for the structures. For **20**: mp 166–168°C; ^{1}H NMR ($CDCl_3$) δ: 6.68 (s, H5.5′), δ 2.32 (s, CH_3). Anal. calcd. for $C_{12}H_{14}N_4S_2$: C 51.80, H 5.04, N 20.14, found: C 51.50, H 5.02, N 20.03.

The UV–VIS absorption spectra were obtained at appropriate temperatures on a Specord UV–VIS spectrophotometer with cells ranging from 0.01 to 10 cm. The temperature was kept constant within ±0.2°C by circulating thermostatted water in the cell holder. Spectrograde solvents were used as received in all measurements.

1. A. R. KATRITZKY and J. M. LOGOWSKI. Adv. Heterocycl. Chem. **1**, 312 (1963).
2. J. R. MARSHALL and J. WALKER. J. Chem. Soc. 1004 (1951).
3. M. P. V. BEARLAND and J. F. W. MCOMIE. J. Chem. Soc. 3716 (1952).
4. A. ALBERT and G. B. BARLIN. J. Chem. Soc. 2384 (1959).
5. R. A. JONES and A. R. KATRITZKY. J. Chem. Soc. 3610 (1958).
6. V. S. KOROBKOV, A. V. VOROPAEVA, and I. H. FELDMAN. Zh. Obshch. Khim. **31**, 3136 (1961).
7. A. ALBERT and G. B. BARLIN. J. Chem. Soc. 3129 (1959).
8. P. BEAK, I. S. FRY, JR., J. LEE, and F. STEELA. J. Am. Chem. Soc. **98**, 171 (1976).
9. J. ELGUERO, C. MARZIN, A. R. KATRITZKY, and P. LINDA. The tautomerism of heterocycles. *Edited by* A. R. Katritsky and A. J.

Boulton. Adv. Heterocycl. Chem. (Suppl. 1), Academic Press, New York.
10. B. R. RENFOLD. Acta Crystallogr. **6**, 707 (1953).
11. U. H. OHMS, H. GUTH, A. KUTOGLU, and C. SCHERINGER. Acta Crystallogr. Sect. B: Struct. Crystallogr. Cryst. Chem. **B38**, 831 (1982).
12. M. J. COOK, S. EL-ABBADY, A. R. KATRITZKY, C. GUIMAN, and S. PFISTER-GUILLOUZO. J. Chem. Soc. Perkin Trans. **2**, 1652 (1977).
13. P. BEAK, J. B. COVINGTON, and S. G. SMITH. J. Am. Chem. Soc. **98**, 8284 (1976).
14. P. BEAK. Acc. Chem. Res. **10**, 186 (1977).
15. P. BEAK, J. B. COVINGTON, S. G. SMITH, J. M. WHITE, and J. M. ZEIGER. J. Org. Chem. **45**, 1354 (1980).
16. E. E. REID. Organic chemistry of biovalent sulfur. Vol. III. Chemical Publ. Co., New York. 1960. pp. 362–462.
17. P. BEAK, J. B. COVINGTON, and J. M. WHITE. J. Org. Chem. **45**, 1354 (1980).
18. M. H. KROCKOV, C. M. LEE, and H. G. MAUTNER, J. Am. Chem. Soc. **87**, 892 (1965).
19. N. KULEVSKY and W. REINEKE. J. Phys. Chem. **72**, 339 (1968).
20. O. BENSAUDE, M. CHEVRIER, and J. E. DUBOIS. J. Am. Chem. Soc. **101**, 2433 (1979).
21. E. CAMPAIGNE, J. TSURUGI, and W. W. MEYER. J. Org. Chem. **26**, 2486 (1961).
22. O. OHNO and SH. OAE. Organic Chemistry of Sulfur. *Edited by* S. Oae. Plenum Press, New York and London. 1977. pp, 155–160.
23. T. M. KITSON. J. Chem. Educ. **65**, 829 (1988).
24. K. BROCKLENURST. Methods Enzymol. **87C**, 427 (1982).
25. J. RENAULT. Ann. Chem. **10**, 135 (1955).
26. H. KING and L. L. WARE, J. Chem. Soc. 873 (1939).
27. W. MACKWALD, W. KLEMM, and H. TRABERT. Chem. Ber. **33**, 1559 (1900).

Can. J. Chem. Downloaded from www.nrcresearchpress.com by 91.121.58.235 on 09/07/12
For personal use only.

Liquides de toupies symétriques : leur tenseur de polarisabilité optique intrinsèque via deux expériences sous champ statique : CH_3CN

CLAUDE BROT

Laboratoire de physique de la matière condensée, Unité de recherche n° 190, associée au Centre national de la recherche scientifique, Université de Nice – Sophia Antipolis – Parc Valrose, 06034 Nice CEDEX, France

Reçu le 19 décembre 1989

CLAUDE BROT. Can. J. Chem. **68**, 1490 (1990).

On montre qu'en combinant pour un liquide un résultat expérimental de résonance magnétique nucléaire sous champ électrique avec sa constante de Kerr on peut obtenir des informations sur l'anisotropie optique de la molécule, car toutes les propriétés électriques statiques moléculaires s'éliminent. On emploie la formalisme des tenseurs d'incrément de polarisabilité en phase liquide développé par l'auteur pour les fluides de molécules quasi-ellipsoïdales. S'aidant de l'équation constitutive de la réfractivité dans le modèle utilisé, on peut obtenir les deux composantes distinctes du tenseur d'incrément de polarisabilité optique des molécules toupies symétriques constituant le liquide. On passe alors aux éléments de polarisabilité intrinsèque (*in vacuo*) par un calcul faisant intervenir le volume et la forme moléculaire (élongation de l'ellipsoïde) ainsi que l'indice de réfraction du liquide. Pour le cas de l'acétonitrile pur l'accord avec des mesures en phase vapeur publiées est excellent : On trouve, en unités 10^{-40} C^2 m^2 J^{-1}, la valeur 5,06 pour la polarisabilité moyenne et la valeur 2,52 pour son anisotropie, alors qu'une étude expérimentale publiée utilisant la diffusion dépolarisée de la lumière en phase gazeuse fournit respectivement les valeurs 4,96 et 2,49 à $\lambda = 633$ nm. Finalement et accessoirement, on suggère que les intercorrélations dipolaires dans l'acétonitrile sont peu importantes. En effet un formalisme analogue pour le calcul du moment permanent à partir de la permittivité statique fournit une valeur en accord à 1% près avec la valeur mesurée dans le gaz.

Mots clés : tenseurs de polarisabilité, liquides, constante de Kerr, RMN.

CLAUDE BROT. Can. J. Chem. **68**, 1490 (1990).

NMR line splitting under a strong static electric field (EF-NMR) allows one to measure the average alignment (second spherical harmonic) of the molecule studied under the influence of the field. This average alignment (per unit squared field) can be formulated theoretically by an expression involving the permanent dipole moment, the anisotropy of the static polarizability, etc. and possibly orientational intercorrelations within the liquid. On the other hand the Kerr constant per molecule can be represented by the *same* expression, multiplied by a factor that is independent of any *static* electrical property of the molecule (for a gas this factor would be simply proportional to the anisotropy of the *optical* polarizability). Consequently the ratio of the above experimental results contains information bearing only on the optical properties. The formalism of the "tensor of polarizability increment" developed by the author for liquids made up of ellipsoidal molecules is employed. It is shown that by combining the above ratio with the constitutive equation for the refractivity of the liquid, the two distinct principal elements of the tensor of polarizability increment of the symmetric top molecules constituting the liquid are immediately obtained. Using then the molecular volume, a van der Waals estimate for the elongation of the molecule, and the index of refraction of the liquid, one can calculate the elements of the optical polarizability tensor *in vacuo*. The method is illustrated by neat acetonitrile for which the necessary experimental data exist in the literature. One finds, in units 10^{-40} C^2 m^2 J^{-1}, 5.06 for the mean polarizability and 2.52 for its anisotropy. A published experimental study using depolarized light scattering in the gas phase indicates that the corresponding figures are 4.96 and 2.49 respectively at $\lambda = 633$ nm. Finally and accessorily, it is suggested that dipolar intercorrelations are weak in acetonitrile. Indeed, using an analogous formalism for the static permittivity of the liquid, a value for the permanent moment of the molecule is deduced. This value is within 1% of the experimental gas value.

Key words: polarizability tensors, liquids, Kerr constant, NMR.

I. Introduction

Nous utiliserons le tenseur des «polarisabilités incrémentielles» en phase liquide, dont la théorie a été développée dans des articles antérieurs (1–3). La molécule est supposée ellipsoïdale et immergée dans un continuum de permittivité relative ε. Un élément de ce tenseur, diagonalisé dans les axes moléculaires, s'écrit :

$$[1] \quad \alpha_{jj}^{*} = C_{jj} f_{jj} \alpha_{jj} - C_{jj} \frac{abc}{3} 4\pi\varepsilon_0(\varepsilon - 1)$$

Attention: Malgré une notation identique à celles d'auteurs antérieurs pour une polarisabilité effective en phase condensée, nos α^* en sont différents : ce sont des quantités *incrémentielles*, positives ou négatives. Ils sont exactement nuls si la molécule est remplacée par un ellipsoïde homogène ayant même permittivité que le milieu environnant, ce qui rend notre approche autoconsistante.

α_{jj} est l'élément correspondant de la polarisabilité *in vacuo*; a, b et c sont les demi axes principaux de la cavité ellipsoïdale, supposée homothétique de l'enveloppe van der Waals de la molécule; ε_0 égale $(4\pi)^{-1}$ dans le système esu, ou égale $8{,}854 \times 10^{-12}$ F m^{-1} dans le système SI. Pour les α ou les α^* la correspondance numérique entre ces systèmes est 10^{-24} esu = $1{,}11264\ 10^{-40}$ C^2 m^2 J^{-1}.

C_{jj} est l'élément du tenseur facteur de champ de cavité :

$$[2] \quad C_{jj} = \varepsilon/(\varepsilon - S_j(\varepsilon - 1))$$

$$[3] \quad S_z = \frac{abc}{2}\int_0^{\infty} \frac{\mathrm{d}s}{(s + c^2)^{3/2}(s + a^2)^{1/2}(s + b^2)^{1/2}} \text{ etc.}$$

$$\sum_{j=x,y,z} S_j = 1$$

$\boldsymbol{f}$ est le facteur tensoriel de champ interne pour la molécule dans sa cavité ellipsoïdale (éviter la confusion avec le facteur de champ de réaction) :

$$[5] \quad f_{jj} = \left\{1 - \frac{\varepsilon - 1}{\varepsilon} S_j \left[1 + (1 - S_j)\frac{3\alpha_{jj}}{abc\,4\pi\varepsilon_0}\right]\right\}^{-1}$$

Printed in Canada / Imprimé au Canada

Can. J. Chem. Downloaded from www.nrcresearchpress.com by 91.121.58.235 on 09/07/12
For personal use only.

Can. J. Chem. Downloaded from www.nrcresearchpress.com by 91.121.58.235 on 09/07/12
For personal use only.

Dans l'équation [1] le premier terme représente un effet d'induction sur la molécule, corrigé par le facteur de champ interne et par la présence de la cavité virtuelle. Le deuxième terme, négatif, représente un effet analogue pour la portion de continuum qui a été supposée soustraite. Nous ferons usage des formules obtenues précédemment pour la constante de Kerr K et pour la moyenne du second harmonique sphérique sous champ électrique statique, qu'on obtient à partir du dédoublement de certaines raies RMN provoqué par ce champ (EF-NMR). Les deux types d'expérience font intervenir le moment dipolaire permanent, si il existe, ainsi que les polarisabilités *statiques*. Les polarisabilités statiques *incrémentielles* sont celles définies plus haut, équations [1]–[5]. Nous les affectons d'un indice supérieur s. L'effet Kerr fait intervenir de plus les polarisabilités à fréquence optique. Nous les affectons d'un indice supérieur l (pour «lumière»). Elles sont analogues à celles définies par [1]–[5], sauf que partout la permittivité ε doit être remplacée par le caré de l'indice n^2.

II. Principe de la méthode

Commençons par l'effet Kerr. On a montré (2) qu'en négligeant les termes dus aux hyperpolarisabilités (cf. section finale) :

$$[6] \quad \frac{K}{N} = \frac{1}{30n^2kT\varepsilon_0}\left[\Gamma^{ls*} + \frac{\Lambda^{ls*}}{kT}\right]$$

N est le nombre de molécules par unité de volume.

Les quantités dans le crochet sont explicitées dans la référence 2 pour une toupie générale. Pour une toupie symétrique, en adoptant O_Z comme axe principal, notant $\alpha_\parallel = \alpha_{zz}$ et $\alpha_\perp = \alpha_{xx} = \alpha_{yy}$, avec la même convention pour les éléments incrémentiels correspondants, et puisque nécessairement le moment permanent μ est le long de O_Z, les formules données dans la référence 2 se réduisent à

$$[7] \quad \Gamma^{ls*} = (\alpha_\parallel^{l*} - \alpha_\perp^{l*})(\alpha_\parallel^{s*} - \alpha_\perp^{s*})$$

$$[8] \quad \Lambda^{ls*} = (\alpha_\parallel^{l*} - \alpha_\perp^{l*})(f_z^s\mu)^2$$

d'où

$$[9] \quad \frac{K}{N} = \frac{1}{30n^2kT\varepsilon_0}(\alpha_\parallel^{l*} - \alpha_\perp^{l*})\left[(\alpha_\parallel^{s*} - \alpha_\perp^{s*}) + \frac{(f_z^s\mu)^2}{kT}\right]$$

Passons au dédoublement des raies RMN (spin $> \frac{1}{2}$) sous l'effet d'un fort champ électrique statique E. Si on connait la constante de couplage quadrupolaire du noyau étudié, situé sur l'axe moléculaire, ce type d'expérience permet d'obtenir «l'alignement» moyen de l'axe moléculaire sous l'effet du champ, c.-à-d. la moyenne du second harmonique sphérique de l'angle θ entre l'axe moléculaire et le champ. Nous avons montré (3) que

$$[10] \quad \frac{\langle \frac{3}{2}\cos^2\theta - \frac{1}{2}\rangle}{E^2} = \frac{1}{15kT}\left[(\alpha_\parallel^{s*} - \alpha_\perp^{s*}) + \frac{(f_z^s\mu)^2}{kT}\right]$$

où E est le champ de Maxwell appliqué; les contributions en E^4 sont ici négligées, comme il est usuel.

Les formules [9] et [10] sont rigoureuses, dans le cadre du modèle, c'est-à-dire seulement si l'environnement de chaque molécule anisotrope est un quasi-continuum, en pratique un solvant de petites molécules isotropes. Dans un liquide pur de molécules anisotropes il faut mettre en facteur des équations [9] et [10] un facteur d'intercorrélation G dont la différence avec l'unité représente les possibles corrélations orientationnelles (4–6).

Il est remarquable, et tout à fait utile pour notre but, que ce facteur serait le même pour les équations [9] et [10], car le champ statique appliqué fait réagir les orientations possiblement corrélées de manière identique dans les deux case.

En divisant l'équation [9] par l'équation [10] on obtient donc, même pour un liquide pur, aussi bien polaire que non polaire :

$$[11] \quad \frac{K/N}{\langle \frac{3}{2}\cos^2 - \frac{1}{2}\rangle/E^2} = \frac{1}{2n^2\varepsilon_0}\left(\alpha_\parallel^{l*} - \alpha_\perp^{l*}\right)$$

où figure maintenant seulement des quantités optiques.

Les composantes de polarisabilité de cette équation sont du type «incrémentiel». Nous devons maintenant atteindre par elles leurs analogues intrinsèques, c'est-à-dire *in vacuo*. Mais d'abord il nous manque une équation. Celle-ci nous est donnée par l'équation constitutive de la réfractivité pour notre modèle des polarisabilités incrémentielles. Cette équation s'écrit pour un liquide pur (7) :

$$[12] \quad \mathrm{Tr}\alpha^{l*} = 0$$

Cette équation est évidente car elle signifie que si on ménage dans le liquide pur une cavité ayant le volume moléculaire moyen, qu'on y inserre une molécule identique à celles du liquide et qu'on laisse le système fluctuer, on n'a en moyenne rien changé. Elle donne pour n^2, si l'on connait les éléments *in vacuo* α_{jj}, des résultats voisins mais en meilleur accord avec l'expérience que la formule de Lorenz–Lorentz (7). Elle est aussi plus cohérente avec le modèle employé ici.

Pour une toupie symétrique, en dénotant l'anisotropie optique incrémentielle

$$[13] \quad \alpha_\parallel^{l*} - \alpha_\perp^{l*} = \Delta^{l*}$$

on tire de l'équation [12] :

$$[14] \quad \alpha_\parallel^{l*} = (2/3)\Delta^{l*}, \qquad \alpha_\perp^{l*} = -(1/3)\Delta^{l*}$$

Il suffira ensuite de résoudre les deux systèmes correspondants d'équations [1]–[5] pour obtenir les deux composantes distinctes du tenseur de polarisabilité optique *in vacuo*.

III. Illustrations par l'acétonitrile liquide

Nous considérons le liquide CH_3CN, très polaire, pour lequel il existe dans la littérature à la fois une mesure de constante de Kerr (4) et une mesure EF-NMR du noyau N (8). Nous adoptons la température 293 K pour notre illustration, et le système SI.

Premièrement la constante de Kerr. Il existe deux définitions usuelles pour cette constante, B et K, reliées par la formule

$$[15] \quad K = B\lambda/n$$

$$[16] \quad B = (n_\parallel - n_\perp)/E^2\lambda$$

avec les notations usuelles.

À la longueur d'onde $\lambda = 633 \times 10^{-9}$ m où l'indice $n = 1{,}34$, Beevers et Khanarian (4), à 293 K, ont mesuré $B = 49{,}9 \times 10^{-14}$ m V^{-2}. On en tire :

$$K = 23{,}57 \times 10^{-20}\ \mathrm{m^2\ V^{-2}}$$

$1/N$, qui figure dans le membre de gauche de notre équation [11], est égal au volume par molécule dans le liquide : $1/N = 10^{-6}M/dN_a$ où la masse molaire $M = 41{,}05$ et la densité à 293 K est $d = 0{,}7857$ (9). N_a et le nombre d'Avogadro. Ceci donne successivement :

Can. J. Chem. Downloaded from www.nrcresearchpress.com by 91.121.58.235 on 09/07/12
For personal use only.

[17] $1/N = 86{,}76 \times 10^{-30}\ \mathrm{m}^3$

[18] $K/N = 20{,}45 \times 10^{-48}\ \mathrm{m}^5\ \mathrm{V}^{-2}$

Nous passons à la mesure EF-NMR.

Sous un champ de $4 \times 10^6\ \mathrm{V\ m^{-1}}$ Hilbers et MacLean (8) ont déduit $\langle 3\cos^2\theta - 1\rangle = 0{,}82 \times 10^{-4}$ à 300 K. Ceci donne :

$$\langle \tfrac{3}{2}\cos^2\theta - \tfrac{1}{2}\rangle / E^2 = 2{,}56 \times 10^{-18}\ \mathrm{m^2\ V^{-2}}$$

Il nous faut ramener cette quantité à la valeur qu'elle aurait à 293 K, température adoptée ici. Pour ceci nous remarquons que pour une molécule très polaire comme CH_3CN le deuxième terme du crochet de notre équation [10] est largement dominant. Donc le membre de gauche de cette équation est très sensiblement inversement proportionnel au carré de la température. Ceci nous fournit à 293 K :

[19] $\langle \tfrac{3}{2}\cos^2\theta - \tfrac{1}{2}\rangle / E^2 = 2{,}684 \times 10^{-18}\ \mathrm{m^2\ V^{-2}}$

Utilisant les résultats expérimentaux [18] et [19] dans notre équation [11] nous obtenons :

$$\Delta^{l*} = \alpha_{\parallel}^{l*} - \alpha_{\perp}^{l*} = 2{,}42 \times 10^{-40}\ \mathrm{J^{-1}\ C^2\ m^2}$$

d'où, avec [14] : $\alpha_{\parallel}^{l*} = 1{,}615$ et $\alpha_{\perp}^{l*} = -0{,}8075$ en unités $10^{40}\ \mathrm{J^{-1}\ C^2\ m^2}$.

Pour obtenir les polarisabilités correspondantes *in vacuo*, nous devons résoudre le système d'équations [1]–[5] (avec $\varepsilon = n^2$), ce qui est faisable algébriquement. Dans ce système figure la quantité $4\pi a^2 c/3$ qui est le volume par molécule, $1/N$, donné par [17]. Il est nécessaire aussi d'estimer S_z (d'où $S_x = S_y = (1 - S_z)/2$). Pour ce faire nous utilisons les longueurs de liaison et les rayons de van der Waals tabulés (9) :

longueur C—C : 1,541 Å, longueur C—N : 1,158 Å
rayon de van der Waals de N : 1,5 Å
rayon de van der Waals moyen du méthyle : 2 Å

Un dessin à l'échelle montre que l'enveloppe de van der Waals de la molécule est légèrement piriforme (10), car le rayon du méthyle est supérieur à celui de l'azote. On peut cependant circonscrire cette enveloppe par un ellipsoïde de révolution de demi grand axe 3,125 Å et de demi petit axe 2,23 Å. Ceci donne un «volume de la molécule» égal à $65{,}1 \times 10^{-30}\ \mathrm{m^3}$. La différence entre le volume disponible par molécule (équation [17]) et cette valeur est évidemment attribuable à l'espace intermoléculaire nécessaire au mouvement thermique. Nous allons supposer que la cavité est homothétique à l'ellipsoïde de van der Waals de la molécule. Ceci est une simplification indispensable ici bien que des arguments partant sur les amplitudes de libration permettent de croire qu'elle est légèrement plus sphérique (7).

L'élongation c/a est donc alors $3{,}125/2{,}23 = 1{,}4$. Cette valeur est voisine de celle adoptée pour l'acétonitrile dans la référence 11. Les tables de la référence 12 indiquent qu'alors $S_z = 0{,}25$.

La résolution du système [1]–[5] donne alors successivement, en unités $10^{-40}\ \mathrm{C^2\ m^2\ J^{-1}}$:

[20] $\alpha_{\parallel}^{l} = 6{,}746, \qquad \alpha_{\perp}^{l} = 4{,}22$

d'où, pour la polarisabilité moyenne et son anisotropie :

[21] $\bar{\alpha}^{l} = (1/3)\mathrm{Tr}\,\alpha^{l} = 5{,}06$ et $\alpha_{\parallel}^{l} - \alpha_{\perp}^{l} = 2{,}52$

Nous pouvons comparer les valeurs [21] avec celles mesurées *directement* en phase vapeur par mesure de l'intensité de la diffusion dépolarisée de la lumière : À $\lambda = 633$ nm la référence 13 donne, dans les mêmes unités que ci-dessus :

[22] $\bar{\alpha}^{l} = 4{,}96$ et $\alpha_{\parallel}^{l} - \alpha_{\perp}^{l} = 2{,}49$

L'accord est excellent. La précision atteinte (1–2%) est même probablement fortuite, car il est vraisemblable que les ingrédients expérimentaux que nous avons utilisés (constante de Kerr et surtout EF-NMR) étaient affectées d'une erreur probable au moins égale.

L'adoption d'une cavité sphérique ($S_z = \frac{1}{3}$ dans nos équations) change peu la polarisabilité moyenne, mais fournit une anisotropie très sousestimée : $1{,}98 \times 10^{-40}\ \mathrm{C^2\ m^2\ J^{-1}}$.

IV. Discussion et conclusion

Nous avons dit Section II que dans notre expression de la constante de Kerr nous négligeons les termes d'hyperpolarisabilité. La validité de cette hypothèse mérite brève discussion. En principe ces termes peuvent s'obtenir directement par des mesures de production des harmoniques successifs d'une fréquence lumineuse sous champ électrique statique. La littérature ne fournit que peu de ces mesures, et encore avec de larges limites d'erreur. Il existe pourtant une étude (14) qui porte sur une série de méthanes substitués polaires à l'état vapeur en utilisant à la fois la mesure de l'effet Kerr, la dépolarisation de la lumière et les hyperpolarisabilités de la littérature; on conclut de cette étude que le terme d'orientation dipolaire (correspondant à notre équation [8]) est largement dominant. Le terme d'alignement d'anisotropie (notre eq. [7]) en représentent seulement quelques pour-cent et les termes d'hyperpolarisabilité encore moins. On retiendra de ceci que pour les corps polaires le fait de négliger les hyperpolarisabilités n'est pas grave, mais qu'il faudrait être beaucoup plus prudent pour des corps non polaires.

Nous passons à l'examen des possibles intercorrélations d'orientation représentées par $(G - 1)$ où G est un facteur de Kirkwood généralisé que nous avons omis dans nos équations [9] et [10] puisqu'il s'élimine de notre équation [11]. Il est rappelé que $(G - 1)$ théoriquement une combinaison du facteur de Kirkwood dipolaire $g_k = g_1$, de son analogue g_2 construit sur le deuxième harmonique sphérique moyen de l'angle θ_{ij} entre molécules, et enfin d'un facteur g_3 qui fait intervenir des intercorrélations à trois corps. La forme exacte de cette combinaison est controversée, deux formulations différentes ayant été proposées (5, 6).

Nous nous bornerons ici à examiner les possibles intercorrélations *polaires* dans l'acétonitrile liquide. La littérature (4, 11) donne g_k voisin de 0,75, mais ce chiffre est obtenu à partir de la formule de Kirkwood–Frohlich originelle qui suppose une cavité moléculaire sphérique. Voyons quel serait son analogue dans le cas d'une cavité ellipsoïdale. Pour ce faire nous utilisons l'équation constitutive de la permittivité statique dans ce modèle [1]. Elle s'écrit pour une toupie générale, en l'absence d'intercorrélations :

[23] $\Sigma[\alpha_{jj}^{s*} + f_j^{s2}\mu_j^2/kT] = 0 \qquad (j = x,y,z)$

Pour une toupie symétrique ($\mu \parallel O_Z$) l'équation [23] peut s'écrire :

[24] $$\mu^2 = -\frac{kT}{(f_z^s)^2}(2\alpha_{xx}^{s*} + \alpha_{zz}^{s*})$$

(Le signe négatif n'est pas surprenant car dans notre définition [1] le deuxième terme négatif domine à cause de la valeur élevée de ε).

Il est alors facile via nos équations [1], [5] et [24] de calculer μ selon le modèle. La valeur expérimentale de ε à 293 K est ε = 37,5 (15). Pour les polarisabilités statiques *in vacuo* α_{jj} nous utilisons nos valeurs des équations [20] augmentées empiriquement de 5% pour tenir compte des contributions atomiques. Nous obtenons $\mu_{\text{modèle}} = 13{,}0 \times 10^{-30}$ C m = 3,90 D. La littérature (16) donne la valeur 3,92 D obtenue par effet Stark sur le spectre microonde, et 3,96 D obtenue par mesure du viriel diélectrique. Si on adopte une valeur moyenne probable μ_{gaz} = 3,94 D, nous obtenons :

$$[25] \quad g_B = \mu^2_{\text{modèle}}/\mu^2_{\text{gaz}} = 0{,}98$$

où nous avons défini un nouveau paramètre de corrélation polaire g_B qui diffère de celui de Kirkwood en ce sens que dans un modèle à cavité ellipsoïdale prolate les plus proches voisines sont plus éloignées dans les directions axiales que dans les directions transverses (et l'inverse pour une cavité oblate).

Le fait que g_B soit indistinguable de l'unité vues les erreurs expérimentales probables indique que les corrélations polaires sont inexistantes ou peu importantes dans l'acétonitrile liquide.

Il est par contre difficile d'avoir des données sur les corrélations d'alignement représentées par $(g_2 - 1)$. Une étude expérimentale dynamique (17) (largeurs de Raie Raman et Rayleigh comparées) amène à conclure que $(g_2 - 1)$ est probablement positif, mais cette déduction dépend du modèle adopté, où intervient aussi un facteur de corrélation dynamique à priori inconnu. Une étude radiocristallographique semble permettre une conclusion analogue (18). Par contre, une étude (19) par simulation numérique de CH_3CN (potentiel représenté par 3 centres LJ + 3 charges sur atomes) montre pour le modèle utilisé de faibles corrélations d'alignement au-delà des premières molécules voisines en direction transverse. Quant au paramètre de corrélation à trois corps $(g_3 - 1)$, il semble impossible à évaluer avec certitude présentement, ni par voie théorique, ni par voie expérimentale.

Pour conclure nous revenons sur les articles originaux dont nous avons utilisé les données expérimentales : aussi bien les auteurs ayant travaillé à l'aide de la EF-NMR (8) que ceux ayant utilisé l'effet Kerr (4) interprétent leur résultat à l'aide d'un champ interne résultant d'une cavité supposée sphérique. À 293 K les premiers trouvent pour $\langle P_2(\cos\theta)\rangle/E^2$ la valeur $2{,}68 \times 10^{-18}$ m^2 V^{-2} (notre équation [19]) et les deuxièmes trouvent 2,13 dans les mêmes unités. À notre avis cette divergence est causée par l'utilisation d'une cavité sphérique. Notre traitement, par contre, nous semble réconcilier les deux types de mesure d'une part entre elles, d'autre part avec la valeur connue de l'anisotropie optique de la molécule CH_3CN.

1. C. Brot. Mol. Phys. **45**, 543 (1982).
2. C. Brot. Mol. Phys. **53**, 891 (1984).
3. C. Brot. J. Mol. Liq. **40**, 79 (1989).
4. M. S. Beevers et G. Khanarian. Aust. J. Chem. **33**, 2585 (1980).
5. A. D. Buckingham et R. E. Raab. J. Chem. Soc. **6B**, 2341 (1957).
6. J. D. Ramshaw, D. W. Schaeffer, J. S. Waugh et J. M. Deutch. J. Chem. Phys. **54**, 1239 (1971).
7. C. Brot. Mol. Phys. **43**, 1021 (1981).
8. C. W. Hilbers et C. MacLean. Mol. Phys. **17**, 517 (1969).
9. R. C. Weast (*Éditeur*). CRC handbook of chemistry and physics. CRC Press, Boca Raton, FL. 1980.
10. E. Satie. Trois morceaux en forme de poire. Éditions Salabert, Paris. 1910.
11. C. J. F. Bootcher et P. Bordewijk. Theory of electric polarization. Elsevier, Amsterdam. 1978.
12. A. B. Myers et R. R. Birge. J. Chem. Phys. **74**, 3514 (1981).
13. M. P. Bogaard, A. D. Buckingham, R. K. Pierens et A. H. White. J. Chem. Soc. Faraday Trans. 1, **74**, 3008 (1978).
14. A. K. Burnham, L. W. Buxton et W. H. Flygare. J. Chem. Phys. **67**, 4990 (1977).
15. Table of dielectric constants of pure liquids. NBS Circular. 1951.
16. A. L. McClellan. Tables of experimental dipole moments. W. H. Freeman, San Francisco and London. 1963.
17. G. D. Patterson et J. E. Griffiths. J. Chem. Phys. **63**, 2406 (1975).
18. Von A. Kratochwill, J. U. Weidner et H. Zimmermann. Ber. Bunsen-Ges. Phys. Chem. **77**, 408 (1973).
19. D. M. F. Edwards, P. A. Madden et I. R. McDonald. Mol. Phys. **51**, 1141 (1984).

Can. J. Chem. Downloaded from www.nrcresearchpress.com by 91.121.58.235 on 09/07/12
For personal use only.

Zinc 3,5-dimethylpyrazolate complexes: synthesis and structural studies. The crystal and molecular structure of $[Zn_2(dmpz)_4(Hdmpz)_2]$

MARTIN K. EHLERT, STEVEN J. RETTIG, ALAN STORR, ROBERT C. THOMPSON, and JAMES TROTTER
Department of Chemistry, University of British Columbia, 2036 Main Mall, Vancouver, B.C., Canada V6T 1Y6

Received January 16, 1990

MARTIN K. EHLERT, STEVEN J. RETTIG, ALAN STORR, ROBERT C. THOMPSON, and JAMES TROTTER. Can. J. Chem. **68**, 1494 (1990).

Zinc metal reacts with excess 3,5-dimethylpyrazole (Hdmpz) in the presence of O_2 to produce materials of composition $Zn(dmpz)_2(Hdmpz)_y$. Thermolysis of these materials results in the loss of Hdmpz and the formation of the $[Zn(dmpz)_2]_x$ polymer. Under appropriate conditions the pure dimer $[Zn_2(dmpz)_4(Hdmpz)_2]$ can be obtained in high yield. Crystals of bis[μ-(3,5-dimethylpyrazolyl-N^1,N^2)]bis[(3,5-dimethylpyrazolyl)(3,5-dimethylpyrazole)zinc(II)] are orthorhombic, a = 17.009(2), b = 29.239(2), c = 13.590(2) Å, Z = 8, space group *Fddd*. The structure was solved by heavy atom methods and was refined by full-matrix least-squares procedures to R = 0.037 and R_w = 0.042 for 913 reflections with $I \geq 3\ \sigma(I)$. The structure of $[Zn_2(dmpz)_4(Hdmpz)_2]$ contains nearly planar doubly dmpz bridged Zn_2 units capped at each end by strongly hydrogen-bonded dmpz···Hdmpz units. The zinc atoms display pseudotetrahedral coordination geometry with Zn—N = 1.991(3) (bridging) and 2.025(3) Å (terminal), and N—Zn—N = 99.6(2)–113.8(2)°.

Key words: zinc 3,5-dimethylpyrazolate complexes, crystal structure.

MARTIN K. EHLERT, STEVEN J. RETTIG, ALAN STORR, ROBERT C. THOMPSON et JAMES TROTTER. Can. J. Chem. **68**, 1494 (1990).

Le zinc métallique réagit avec un excés de 3,5-diméthylpyrazole (Hdmpz), en présence de O_2, pour donner des produits de composition $Zn(dmpz)_2(Hdmpz)_y$. La thermolyse de ces produits conduit à une perte de Hdmpz et à la formation de polymère $[Zn(dmpz)_2]_x$. Dans des conditions appropriées, on a obtenu le dimère $[Zn_2(dmpz)_4(Hdmpz)_2]$ avec un excellent rendement. Les cristaux du bis[μ-(3,5-diméthylpyrazolyl-N^1,N^2)]bis[(3,5-diméthylpyrazolyl)(3,5-diméthylpyrazole)zinc(II)] sont orthorhombiques, a = 17,009(2), b = 29,239(2) et c = 13,590(2) Å, Z = 8 et groupe d'espace *Fddd*. On a résolu la structure par la méthode aux atomes lourds et on l'a affinée par la méthode des moindres carrés (matrice complète) jusqu'à des valeurs de R = 0,037 et R_w = 0,042 pour 913 réflexions avec $I \geq 3\sigma(I)$. La structure du $[Zn_2(dmpz)_4(Hdmpz)_2]$ contient des unités pratiquement planes de Zn_2 doublement pontés à des dmpz et capées à chaque extrémité par des unités dmps···Hdmpz fortement liées par des ponts hydrogènes. Les atomes de zinc présentent une géométrie de coordination pseudotétraédrique avec des longueurs de liaison Zn—N de pont de 1,991(3) et terminale de 2,025(3) Å et des angles N—Zn—N allant de 99,6(2) à 113,8(2)°.

Mots clés : composés du zinc 3,5-diméthylpyrazolate, structure cristalline.

[Traduit par la revue]

Introduction

Our interest in binary metal pyrazolates is part of a continuing investigation of complexes incorporating, as an exobidentate uninegative ligand, the pyrazolate moiety or its C-substituted derivatives (1, 2). The present account details our studies on zinc complexes incorporating the 3,5-dimethylpyrazolyl bridging ligand, ranging from a bimetallic, dimeric species of composition $[Zn_2(dmpz)_4(Hdmpz)_2]$, through a larger oligomer, to the polymeric $[Zn(dmpz)_2]_x$ material (Hdmpz = 3,5-dimethylpyrazole, dmpz = 3,5-dimethylpyrazolate). The dimeric species has been structurally characterized through a single crystal X-ray diffraction study. This represents the first binary zinc pyrazolate structure determination. Related poly(1-pyrazolate)borate zinc complexes were first reported by Trofimenko *et al.* some time ago (3). More recently, zinc and boron centres were featured in a number of polynuclear pyrazolyl bridged spiro species (4) and a variety of pyrazolyl gallate ligands have been used to complex divalent zinc ions (5–7). Bonati *et al.* have employed bis(1-pyrazolyl)methanes to complex zinc metal ions (8, 9) and Seel and Rodrian refer briefly to the complex $Na_2[Znpz_4]$ (pz = pyrazolate) (10). In addition, the vibrational assignments of a number of binary zinc pyrazolates have been discussed (11).

None of the above mentioned reports contains X-ray structure determinations, but recently a number of structural reports relevant to the present study have appeared. A report by Driessen *et al.* describes a compound in which the zinc centre is "tetrahedrally" coordinated by two 3,5-dimethylpyrazolyl moieties, one neutral 3,5-dimethylpyrazole, and a nitrate anion (12); Verweij *et al.* report a zinc complex in which the zinc is coordinated by the N2 atoms of two 3-methyl-5-phenylpyrazole molecules and two bromide anions in a distorted tetrahedral fashion (13); and Haanstra *et al.* describe a novel structure consisting of chains of zinc atoms linked by a bridging 1,8-bis(3,5-dimethylpyrazolyl)-3,6-dithiaoctane ligand (14). Of more than passing interest to the present study is a report on the binding of pyrazole in crystalline binary and tertiary complexes of liver alcohol dehydrogenase (15). In these complexes the pyrazole is directly bound to the active site zinc atom (with a Zn—N bond distance of 2.1 Å), and has a marked inhibitory effect on the enzyme function.

Experimental

Synthesis of $[Zn_2(dmpz)_4(Hdmpz)_2]$

Cleaned zinc metal shot (3.505 g, 53.61 mmol) and 3,5-dimethyl pyrazole (3.340 g, 34.75 mmol) were heated together with stirring, under dioxygen at 90°C. Sufficient acetone was added dropwise to the reaction mixture for the Hdmpz to dissolve completely, but without allowing the resultant solution to reflux (~3 mL acetone). After ~2 h a fine white precipitate was visible and this accumulated during the reaction. The reaction was allowed to proceed for 45 h. Acetone was added periodically throughout the reaction to maintain the Hdmpz in solution. The reaction mixture was then cooled to room temperature and extracted with 40 mL of acetone in small portions, suction filtered, the insolubles washed with a further 200 mL of acetone and then dried

Can. J. Chem. Downloaded from www.nrcresearchpress.com by 91.121.58.235 on 09/07/12
For personal use only.

Can. J. Chem. Downloaded from www.nrcresearchpress.com by 91.121.58.235 on 09/07/12
For personal use only.

in vacuo at room temperature for ~30 min. A fine white powder was collected in 99% yield based on the zinc metal reacted. *Anal.* calcd. for $[Zn_2(dmpz)_4(Hdmpz)_2]$: C 51.22, H 6.30, N 23.89; found: C 50.92, H 6.37, N 23.90.

Attempts to perform the above reaction in neat, molten Hdmpz, without the presence of acetone, necessitated the use of a higher temperature (Hdmpz mp = 108°C) and resulted in the production of a material of non-stoichiometric composition. Cleaned zinc metal shot (3.53 g, 54.0 mmol) and Hdmpz (5.88 g, 61.2 mmol) were reacted with stirring under a dioxygen atmosphere at 130°C for 48 h. a low yield (0.030 g) of a fine white powder was obtained as the zinc-containing product. Elemental analysis of the sample yielded the following results. Found: C 48.67, H 5.76, N 22.70. These results suggest the nominal composition, $Zn(dmpz)_2 \cdot 0.323Hdmpz$: *Anal.* calcd.: C 48.66, H 5.83, N 22.70. Evidence to be presented later suggests the material is a mixture of $[Zn_2(dmpz)_4(Hdmpz)_2]$ and higher oligomers of the formulation $Zn_x(dmpz)_{2x}$ which may or may not contain Hdmpz.

The dimer $[Zn_2(dmpz)_4(Hdmpz)_2]$ was obtained in crystalline form, suitable for single crystal X-ray diffraction studies, by reacting zinc metal with neat molten Hdmpz, without stirring, in the presence of limited dioxygen. A 2 g piece of zinc metal shot was covered with excess Hdmpz in a test tube. The tube was flushed with N_2 gas and then sealed with parafilm into which a pinhole was punched. The lower end of the tube was then maintained at 115°C for 5 days. After ~20 h, small colorless crystals could be seen forming on the zinc shot as well as near the Hdmpz/atmosphere interface. At the end of the reaction period the mixture was cooled and then extracted with acetone to remove excess Hdmpz and yield the insoluble, well formed, colorless crystals of $[Zn_2(dmpz)_4(Hdmpz)_2]$.

Synthesis of the $[Zn(dmpz)_2]_x$ polymer

Samples of material of composition $Zn(dmpz)_2$ were prepared on a 5–10 mg scale by thermolysis directly in differential scanning calorimetry (DSC) aluminum sample pans in the calorimeter. Two routes were employed: the first from $[Zn_2(dmpz)_4(Hdmpz)_2]$) heated at 240°C for 30 min and the second from the dimer/oligomer mixture heated at 170°C for 45 min. *Anal.* calcd. for $Zn(dmpz)_2$: C 46.99, H 5.53, N 21.92; found: (from $[Zn(dmpz)_4(Hdmpz)_2]$ C 46.75, H 5.35, N 21.76 and (from dimer/oligomer mixture) C 46.68, H 5.40, N 21.79. The material produced in these experiments is assumed to be polymeric, with an infinite chain structure, by analogy with the known structures of other binary metal(II) pyrazolates (1, 16). At higher temperatures the DSC thermogram shows that the onset of decomposition of the $[Zn(dmpz)_2]_x$ polymer, without melting, occurs at ~305°C.

Attempts to grow single crystals of the polymer were unsuccessful. Zinc shot was combined with excess Hdmpz without stirring in a nitrogen-filled tube at 175°C for 24 h. Air was allowed to diffuse slowly into the mixture. At the cessation of the reaction colorless crystals with the same morphology as those of $[Zn_2(dmpz)_4(Hdmpz)_2]$ and a fine white solid had grown as a coating on the zinc shot. Due to the presence of intractable decomposition products, the latter was not characterized further.

Physical characterization

Infrared spectra (4000–400 cm^{-1}) were recorded on a Perkin-Elmer Model 598 spectrometer. Samples were mulled in Nujol and sandwiched between KBr plates. Infrared frequencies are listed in Table 1.

Differential scanning calorimetry measurements were obtained with a Mettler DSC 20 Standard Cell and TC10 TA Processor.

X-ray powder diffraction patterns were recorded in the range 5–60° in 2θ using a Rigaku Rotaflex rotating anode X-ray powder diffractometer (Ni filtered Cu $K\alpha$ radiation). A simulated powder X-ray diffraction pattern for $[Zn_2(dmpz)_4(Hdmpz)_2]$ was generated using the computer program LAZY PULVERIX (17).

Single crystal X-ray analysis of $[Zn_2(dmpz)_4(Hdmpz)_2]$

A crystal *ca.* 0.20 × 0.25 × 0.34 mm in size was mounted in a general orientation. Unit-cell parameters were refined by least-squares on setting angles for 25 reflections (2θ = 20–39°) measured on a

TABLE 1. Infrared frequencies (cm^{-1})[a]

$Zn_2(dmpz)_4(Hdmpz)_2$	$[Zn(dmpz)_2]_x$
3113 w	3113 w
2735 w	2740 w
	2665 w
2380 w,b	
	2263 w
	2117 w
1860 w,b	
1570 w,b,sh	1566 w
1537 w,sh	
1525 s	1529 s
1511 m,sh	1509 w,sh
1430 s	1421 s
1344 s	1337 s
1328 m	1325 s
1140 m	1142 s
1088 w	1088 m
1047 s,sh	
1041 s	1041 s
988 w	979 w
870 w,b	
796 m	796 w,sh
	786 m,sh
	779 s
769 s	772 s
	751 s
758 m	
751 w	
666 w	662 w
599 w	602 w
461 w	458 w
439 w	

[a]Nujol bands omitted, s = strong, m = medium, w = weak, b = broad, sh = shoulder.

diffractometer with Mo-$K\alpha$ radiation (λ = 0.71069 Å). Crystal data at 21°C are as follows

$C_{30}H_{44}N_{12}Zn_2$ f.w. = 703.52

Orthorhombic, a = 17.009(2), b = 29.239(2), c = 13.590(2) Å, V = 6759(1) $Å^3$, Z = 8, ρ_c = 1.383 Mg m^{-3}, $F(000)$ = 2944, μ(Mo-$K\alpha$) = 14.9 cm^{-1}. Absent reflections: hkl; $h + k$, $k + l$, odd; $0kl$, $k + l \neq 4n$; and $hk0$, $h + k \neq 4n$, uniquely indicate the space group $Fddd$.

Intensities were measured with graphite-monochromated Mo-$K\alpha$ radiation on a Rigaku AFC6S diffractometer. An ω–2θ scan at 32° min^{-1} over a range of (1.10 + 0.35 tan θ) degrees in ω (with up to 8 rescans, background/scan time ratio = 0.5) was employed. Data were measured to 2θ = 55°. The intensities of three check reflections, measured every 150 reflections throughout the data collection, showed only small random fluctuations. After data reduction,[1] an empirical absorption correction based on azimuthal scans for three reflections was applied, resulting in relative transmission factors ranging from 0.88 to 1.00. Of the 2128 independent reflections measured, 913 (42.9%) had intensities greater than or equal to $3\sigma(F^2)$ above background where $\sigma^2(F^2) = (S^2(C + 4B) + (0.035(F_o^2))^2)/Lp^2$ with S =

[1]All computations performed using the TEXSAN – TEXRAY Structure Analysis Package which includes versions of the following: AGNOST, absorption corrections, by J. A. Ibers; ORFLS, full-matrix least-squares, and ORFFE, function and errors, by W. R. Busing, K. O. Martin and H. A. Levy; DIRDIF, phase extension and refinement of difference structures, by P. T. Beurskens; ORTEP II, illustrations, by C. K. Johnson.

Can. J. Chem. Downloaded from www.nrcresearchpress.com by 91.121.58.235 on 09/07/12
For personal use only.

TABLE 2. Final atomic coordinates (fractional) and B(eq)

Atom	x	y	z	B(eq)
Zn	0.51484(3)	1/8	1/8	3.14(3)
N(1)	0.4380(2)	0.1779(1)	0.1253(5)	3.5(2)
N(2)	0.3584(2)	0.1697(1)	0.1245(4)	3.8(2)
N(3)	0.5841(1)	0.1229(2)	0.2430(2)	2.9(1)
C(1)	0.3195(2)	0.2091(2)	0.119(1)	3.7(2)
C(2)	0.3740(3)	0.2438(1)	0.1180(4)	4.3(2)
C(3)	0.4470(2)	0.2234(1)	0.122(1)	3.5(2)
C(4)	0.2314(3)	0.2095(2)	0.1174(6)	5.2(3)
C(5)	0.5271(2)	0.2440(2)	0.1247(7)	5.2(3)
C(6)	0.5607(2)	0.1216(2)	0.3378(3)	3.1(2)
C(7)	5/8	1/8	0.3980(4)	3.5(3)
C(8)	0.4751(2)	0.1171(2)	0.3631(4)	4.8(3)

TABLE 3. Bond lengths (Å) with estimated standard deviations

Atom	Atom	Distance	Atom	Atom	Distance
Zn	N(1)	2.025(3)	C(1)	C(2)	1.374(7)
Zn	N(3)	1.991(3)	C(1)	C(4)	1.498(6)
N(1)	N(2)	1.375(4)	C(2)	C(3)	1.379(6)
N(1)	C(3)	1.340(5)	C(3)	C(5)	1.491(6)
N(2)	C(1)	1.332(6)	C(6)	C(7)	1.369(5)
N(3)	N(3)′	1.396(5)	C(6)	C(8)	1.502(5)
N(3)	C(6)	1.348(5)			

scan speed, C = scan count, B = total background count, and Lp = Lorentz-polarization factor.

The structure was solved by conventional heavy atom methods, the coordinates of the zinc atom being determined from the Patterson function and those of the remaining non-hydrogen atoms from a subsequent difference Fourier synthesis. The non-hydrogen atoms were refined with anisotropic thermal parameters and the hydrogen atoms were fixed in calculated positions (N—H, C—H = 0.98 Å, B_H = 1.2 $B_{\text{bonded atom}}$). A difference map shows the N—H proton to be disordered about the twofold axis (rather than lying on the C_2 axis). Scattering factors for all atoms and anomalous dispersion corrections for the non-hydrogen atoms were taken from ref. 18. The weighting scheme $w = 1/\sigma^2(F)$, where $\sigma^2(F)$ is derived from the previously defined $\sigma^2(I)$, gave uniform average values of $w(|F_o| - |F_c|)^2$ over ranges of both $|F_o|$ and sin θ/λ and was employed in the final stages of full-matrix refinement of 101 variables. Reflections with $I < 3\sigma(I)$ were not included in the refinement. Convergence was reached at $R = 0.037$ and $R_w = 0.042$ for 913 reflections with $I \geq 3\sigma(I)$. The function minimized was $\Sigma w(|F_o| - |F_c|)^2$, $R = \Sigma||F_o| - |F_c||/\Sigma|F_o|$ and $R_w = (\Sigma w(|F_o| - |F_c|)^2/\Sigma w|F_o|^2)^{1/2}$.

On the final cycle of refinement the maximum parameter shift corresponded to 0.02σ. The mean error in an observation of unit weight was 1.43. The final difference map showed maximum fluctuations of -0.25 to 0.35 e Å^{-3}. The final positional and equivalent isotropic thermal parameters for the non-hydrogen atoms appear in Table 2. Bond lengths and angles are listed in Tables 3 and 4. Hydrogen parameters, anisotropic thermal parameters, torsion angles, intermolecular contacts, least-squares planes, and structure factors have been deposited.[2].

Results and discussion

The dimeric species $[Zn_2(dmpz)_4(Hdmpz)_2]$ can be formed in virtually quantitative yield by the reaction of zinc metal with excess Hdmpz in the presence of dioxygen at 90°C. The reaction involves the oxidation of zinc by molecular oxygen with the formation of the zinc complex and water. X-ray diffraction quality crystals of the dimer can be grown by a slight modification of the procedure used to prepare the material in bulk. The molecular structure (Fig. 1) consists of two zinc atoms bridged by two pyrazolate ions with each zinc atom being end-capped by a pyrazolate ion and a netural Hdmpz molecule. Strong hyrogen bonding occurs between the capping ligands [N(2)—H(1)···N(2) (x, 1/4 − y, 1/4 − z), H···N = 1.77, N···N = 2.612(7) Å, N—H···N = 141°] with the unique hydrogen atom being disordered between two possible sites. The molecule has exact (crystallographic) D_2 and approximate D_{2h} symmetry (with crystallographic twofold axes passing through the zinc and C(7) atoms). The zinc atoms are coordinated in a pseudotetrahedral fashion (N—Zn—N = 99.6(2) − 113.8(2)°) and are separated by a non-bonded distance of 3.748(1) Å in the qualitatively planar (to within 0.064(3) Å) six-membered Zn_2N_4 ring. The dihedral angles between normals to the central and terminal ZnN_2 planes is 87.9°. The bridging Zn—N distance of 1.991(3) Å is significantly shorter than the terminal Zn—N distance of 2.025(3) Å. This is consistent with the lengthening of the pyrazolyl N—N bond in the bridging ring to 1.395(5) Å and is also indicative of significant $p\pi$–$d\pi$ interaction between the pyrazolyl group and the metal (19). The effect is not as dramatic as that reported for the planar three-coordinate nickel complex $(\mu\text{-pz})_2[Ni(NO)]_2$ (20) in which the corresponding N—N distance is 1.457(4) Å. The Zn—N distances are similar to values of 1.981(5)–2.053(5) Å reported for other Zn(II) pyrazolate and pyrazole structures (12–14).

The infrared data for $[Zn_2(dmpz)_4(Hdmpz)_2]$ (Table 1) reflect the presence of strong hydrogen bonding in the molecule with the appearance of two broad ν_{NH} vibration bands centered at ~2380 and ~1860 cm^{-1}, significantly shifted from the broad band centered at ~3000 cm^{-1} in solid Hdmpz and the band at 3484 cm^{-1} in CCl_4 solutions of the ligand (21). Similar band shifts, involving ν_{OH} vibrations, have long been recognized as occurring in metal dimethylglyoxime complexes containing strong intramolecular hydrogen bonding (22). Bellamy *et al.* (23, 24) have examined in some detail correlations between infrared frequency shifts and hydrogen bond distances in crystals. The empirical correlation of Bellamy and Owen (24) predicts a frequency shift of about 2000 cm^{-1} for an intermolecular hydrogen bond with a N—H···N distance of 2.612 Å. The shifts we observe are less than this, which is no doubt at least partly due to the non-linear intramolecular N—H···N hydrogen bond. In addition, it should be noted that there is considerable uncertainty in the predicted shift due to its strong dependence on distance at short N···N distances. In $[Zn(dmpz)_2]_x$ these ν_{NH} bands are, as expected, missing as is the broad medium intensity band occuring at 870 cm^{-1} in the dimer. This latter band is likely associated with a N—H deformation vibration although it has been assigned previously to a C—H bending out-of-plane motion (21). Consistent with our assignment, this band is also missing in the spectrum of Nadmpz. The ring stretching (in plane) vibration which occurs at 1596 cm^{-1} in solid Hdmpz and CCl_4 solutions of the ligand (21) has been reported to shift to lower frequencies on coordination of Hdmpz to metals, for example: to 1556 cm^{-1} in $Co(Hdmpz)_2Cl_2$ (25), 1573 cm^{-1} in $Au(Hdmpz)(PPh_3)(BF_4)$, and 1575 cm^{-1} in Au(Hdmpz)Cl and $Au(Hdmpz)_2Cl$ (26). This band occurs at even lower frequencies in the coordinated deprotonated ligand: 1530 cm^{-1} in $[Cu(dmpz)]_x$ (25), 1512 cm^{-1} in $[Co(dmpz)_2]_x$ (25), and 1529

[2]Supplementary material mentioned in the text may be purchased from the Depository of Unpublished Data, CISTI, National Research Council of Canada, Ottawa, Ont., Canada K1A 0S2.

TABLE 4. Bond angles (deg) with estimated standard deviations[a]

Atom	Atom	Atom	Angle	Atom	Atom	Atom	Angle
N(1)	Zn	N(1)″	99.6(2)	N(2)	C(1)	C(2)	107.7(4)
N(1)	Zn	N(3)	113.8(2)	N(2)	C(1)	C(4)	120.3(4)
N(1)	Zn	N(3)″	111.1(2)	C(2)	C(1)	C(4)	131.9(5)
N(3)	Zn	N(3)″	107.4(2)	C(1)	C(2)	C(3)	106.7(4)
Zn	N(1)	N(2)	120.1(2)	N(1)	C(3)	C(2)	109.2(4)
Zn	N(1)	C(3)	133.2(3)	N(1)	C(3)	C(5)	120.3(4)
N(2)	N(1)	C(3)	106.6(3)	C(2)	C(3)	C(5)	130.6(4)
N(1)	N(2)	C(1)	109.8(3)	N(3)	C(6)	C(7)	109.4(3)
Zn	N(3)	N(3)′	125.9(1)	N(3)	C(6)	C(8)	120.5(4)
Zn	N(3)	C(6)	126.5(2)	C(7)	C(6)	C(8)	130.0(4)
N(3)′	N(3)	C(6)	107.2(2)	C(6)	C(7)	C(6)′	106.6(5)

[a]Here and elsewhere in this report, ′ and ″ refer to symmetry operations: x, $1/4 - y$, $1/4 - z$; and $5/4 - x$, $1/4 - y$, z; respectively.

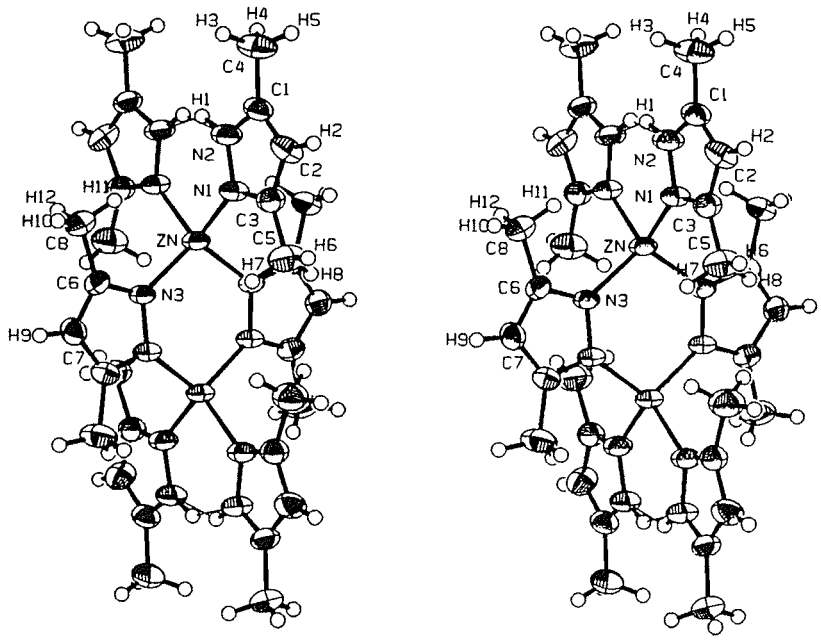

FIGURE 1. Stereoscopic view of the $[Zn_2(dmpz)_4(Hdmpz)_2]$ molecule; 50% probability thermal ellipsoids are shown for the non-hydrogen atoms.

cm^{-1} in $[Zn(dmpz)_2]_x$ (present work). In spite of the fact that there are two crystallographically unique 3,5-dimethylpyrazole rings in $[Zn_2(dmpz)_4(Hdmpz)_2]$ and, moreover, that formally there are both neutral and deprotonated ligands present in this compound, only one band assignable to this ring stretching vibration is observed at 1525 cm^{-1}. On the basis of the low frequency observed for this vibration, one may conclude that all of the ligands are effectively anionic. This is somewhat surprising in the case of the capping ligands and is likely a consequence of the very strong hydrogen bonding associated with these ligands. The remainder of the infrared spectrum of the dimer is almost indistinguishable from that of the polymer $[Zn(dmpz)_2]_x$ with the exception of a weak unassigned band at 458 cm^{-1} in the polymer which appears as two bands at 439 and 461 cm^{-1} in the dimer, the former frequency presumably associated with the capping ligands and the latter with the bridging ligands. The band occurs at 412 cm^{-1} in solid Hdmpz.

When the experimental conditions used to obtain the dimer $[Zn_2(dmpz)_4(Hdmpz)_2]$ (reaction [1]) are altered somewhat a new product of nominal composition $Zn(dmpz)_2 \cdot 0.323Hdmpz$ is obtained (reaction [2]).

$$[1]\quad 2Zn + xs\ Hdmpz \xrightarrow[90°C,\ stirring,\ 45\ h]{O_2,\ acetone} [Zn_2(dmpz)_4(Hdmpz)_2] + 2H_2O$$

$$[2]\quad Zn + xs\ Hdmpz \xrightarrow[130°C,\ stirring,\ 48\ h]{O_2} Zn(dmpz)_2 \cdot 0.323Hdmpz + H_2O$$

Interestingly, DSC studies show that while the products of [1] and [2] can both be converted to the polymeric material $[Zn(dmpz)_2]_x$, the conditions for doing so differ. The DSC thermogram of the dimer (from [1]) shows an endothermic event at 230°C (ΔH = 150 kJ mol^{-1}). Weight difference measurements show a weight loss over the event of 28% representing the loss of two neutral Hdmpz ligands; moreover, elemental analysis of the product confirmed the composition $Zn(dmpz)_2$. On the other hand the DSC thermogram of the product of reaction [2]

Can. J. Chem. Downloaded from www.nrcresearchpress.com by 91.121.58.235 on 09/07/12
For personal use only.

shows an endothermic event at 178°C (with no event at 230°C) and elemental analysis of the product of this thermolysis also confirmed the loss of neutral Hdmpz.

These observations seem to rule out the possibility that the product mixture formed in [2] is merely a mixture of the dimer and the polymer since, if this were the case, the thermogram would be expected to show an endothermic event at 230°C. Further evidence that at least one different compound is present in the product mixture from [2] comes from powder X-ray diffraction experiments. Thus, powder X-ray diffraction patterns were obtained for the dimer, $[Zn_2(dmpz)_4(Hdmpz)_2]$, the polymer $[Zn(dmpz)_2]_x$, and the product mixture from [2]. The pattern for the latter clearly shows the presence of the dimer, but lines corresponding to those of the polymeric species are all shifted from their positions in the pure polymer. We interpret this as indicating the presence of oligomeric species as described below. A computer simulation of the powder X-ray diffraction pattern of $[Zn_2(dmpz)_4(Hdmpz)_2]$ using parameters from the single crystal X-ray structure determination shows that the lattice *d*-spacings from the experimental powder diffraction pattern are consistent with those of the single crystal structure; however, peak intensities from the simulated and experimental patterns differ, suggesting preferred orientation in the powder sample.

It thus appears that the reaction between Hdmpz and Zn under the conditions specified in [2] produces a mixture of dimer and larger oligomers likely of the type $Zn_x(dmpz)_{2x}\cdot 2Hdmpz$ in which each oligomer is end-capped with the dmpz···Hdmpz units as for the dimer. This material, like the dimer, gives polymeric $Zn(dmpz)_2$ on heating. Some insight into the growth mechanism for the polymer comes from the observations in the DSC studies on the dimer/oligomer mixture. Namely that (*i*) separate events corresponding to the loss of neutral Hdmpz from different oligomers do not occur and (*ii*) the single endothermic event which does occur takes place at a lower temperature than that observed for the pure dimer. It appears that the larger $Zn_x(dmpz)_{2x}\cdot 2Hdmpz$ oligomers dissociate neutral Hdmpz molecules at a lower temperature than does the dimer and, moreover, that these oligomers and/or reactive intermediates formed on Hdmpz dissociation from them facilitate dissociation of Hdmpz from the dimer at this lower temperature.

In summary, Zn reacts with excess Hdmpz in the presence of O_2 to produce materials of composition $Zn(dmpz)_2(Hdmpz)_y$. Under appropriate conditions the pure dimer $[Zn_2(dmpz)_4(Hdmpz)_2]$ can be obtained in high yield and in crystalline form suitable for single crystal X-ray diffraction studies. The latter studies revealed a doubly dmpz bridged Zn_2 unit capped at each end by strongly, intramolecularly, H-bonded dmpz···Hdmpz units. A sample of composition $Zn(dmpz)_2\cdot 0.323Hdmpz$ is considered to be a mixture of the dimer and other oligomers of the type $Zn_x(dmpz)_{2x}\cdot 2Hdmpz$. Thermolysis of these materials results in the loss of Hdmpz and the formation of polymeric $[Zn(dmpz)_2]_x$. The temperature at which this occurs appears to depend on oligomer size with the polymerization proceeding at around 230°C in the case of pure dimer and at lower temperatures in the presence of larger oligomers.

Acknowledgments

We thank the Natural Sciences and Engineering Research Council of Canada for financial support. Elemental analyses were performed by Mr. P. Borda of this department.

1. M. K. Ehlert, S. J. Rettig, A. Storr, R. C. Thompson, and J. Trotter. Can. J. Chem. **67**, 1970 (1989).
2. S. J. Rettig, A. Storr, and J. Trotter. Can. J. Chem. **66**, 2194 (1988) and references therein.
3. J. P. Jesson, S. Trofimenko, and D. R. Eaton. J. Am. Chem. Soc. **89**, 3148 (1967).
4. J. Bielawski, T. G. Hodgkins, W. J. Layton, K. Niedenzu, P. M. Niedenzu, and S. Trofimenko. Inorg. Chem. **25**, 87 (1986).
5. K. S. Chong, S. J. Rettig, A. Storr, and J. Trotter. Can. J. Chem. **55**, 4166 (1977).
6. K. S. Chong, S. J. Rettig, A. Storr, and J. Trotter. Can. J. Chem. **56**, 1212 (1978).
7. K. S. Chong, S. J. Rettig, A. Storr, and J. Trotter. Can. J. Chem. **58**, 1091 (1980).
8. A. Lorenzotti, A. Cingolani, G. G. Lobbia, D. Loenesi, and F. Bonati. Gazz. Chim. Ital. **117**, 191 (1987).
9. D. Leonesi, A. Cingolani, G. G. Lobbia, A. Lorenzotti, and F. Bonati. Gazz. Chim. Ital. **117**, 491 (1987).
10. F. Seel and J. Rodrian. Liebigs Ann. Chem. 1794 (1974).
11. J. G. Vos and W. L. Groeneveld. Inorg. Chim. Acta, **27**, 173 (1978).
12. W. L. Driessen, H. L. Blonk, R. A. G. de Graaff, and J. Reedijk. Acta Crystallogr. Sect. C, **43**, 1516 (1987).
13. P. D. Verweij, F. J. Rietmeijer, R. A. G. de Graaff, A. Erdonmez, and J. Reedijk. Inorg. Chim. Acta, **163**, 223 (1989).
14. W. G. Haanstra, W. L. Driessen, J. Reedijk, U. Turpeinen, and R. Hamalainen. J. Chem. Soc. Dalton Trans. 2309 (1989).
15. H. Eklund, J. P. Samama, and L. Wallen. Biochem. **21**, 4858 (1982).
16. M. K. Ehlert *et al.* To be published.
17. K. Yvon, W. Jeitschko, and E. Parthe. J. Appl. Cryst. **10**, 73 (1977).
18. International tables for X-ray crystallography. Vol. IV. Kynoch Press, Birmingham. 1974. pp. 99–102 and 149.
19. K. D. Gallicano, N. L. Paddock, S. J. Rettig, and J. Trotter. J. Am. Chem. Soc. To be published.
20. K. S. Chong, S. J. Rettig, A. Storr, and J. Trotter. Can. J. Chem. **57**, 3090 (1979).
21. A. Zecchina, L. Cerruti, S. Coluccia, and E. Borello. J. Chem. Soc. Sect. B, 1363 (1967).
22. K. Nakamoto. Infrared spectra of inorganic and coordination compounds. 2nd ed. Wiley–Interscience New York. 1969.
23. L. J. Bellamy and R. J. Pace. Spectrochim. Acta, **25**A, 319 (1969).
24. L. J. Bellamy and A. J. Owen. Spectrochim. Acta, **25**A, 329 (1969).
25. C. B. Singh, S. Satpathy, and B. Sahoo. J. Inorg. Nucl. Chem. **35**, 3949 (1973).
26. G. Banditelli, A. L. Bandini, G. Minghetti, and F. Bonati. Can. J. Chem. **59**, 1241 (1981).

Can. J. Chem. Downloaded from www.nrcresearchpress.com by 91.121.58.235 on 09/07/12
For personal use only.

Kinetics and mechanism of oxidation of iodide ion by the molybdenum (VI) – hydrogen peroxide system

CONCHITA ARIAS, FERNANDO MATA, AND JOAQUIN F. PEREZ-BENITO

Departmento de Quimica Fisica, Facultad de Quimica, Universidad de Barcelona, Marti i Franques, 1, 08028 Barcelona, Spain

Received January 5, 1990

CONCHITA ARIAS, FERNANDO MATA, and JOAQUIN F. PEREZ-BENITO. Can. J. Chem. **68**, 1499 (1990).

The kinetics of oxidation of potassium iodide by hydrogen peroxide in aqueous perchloric acid has been studied both in the absence and in the presence of sodium molybdate by means of the initial-rates method. The law found for the total initial reaction rate is

$$r_t = k_1 [I^-][H_2O_2] + k_2 [I^-][H_2O_2][[H^+] + k_3 [I^-][MoO_4^{2-}][H^+] / (a + [H^+])$$

The activation energies associated with rate constants k_1, k_2, and k_3 are 52 ± 1, 49 ± 1, and 42 ± 3 kJ mol^{-1}, respectively. A mechanism in agreement with the experimental kinetic data is proposed, according to which rate constants k_1, k_2, and k_3 correspond to the oxidations of iodide ion by H_2O_2, $H_3O_2^+$ and H_2MoO_5, respectively.

Key words: catalysis, hydrogen peroxide, iodide ion, kinetics, molybdate ion.

CONCHITA ARIAS, FERNANDO MATA et JOAQUIN F. PEREZ-BENITO. Can. J. Chem. **68**, 1499 (1990).

Faisant appel à la méthode des vitesses initiales et opérant tant en présence qu'en absence de molybdate de sodium, on a étudié la cinétique de l'oxydation de l'iodure de potassium par le peroxyde d'hydrogène dans l'acide perchlorique aqueux. La loi régissant la vitesse de réaction initiale globale est :

$$r_t = k_1 [I^-][H_2O_2] + k_2 [I^-][H_2O_2][[H^+] + k_3 [I^-][MoO_4^{2-}][H^+] / (a + [H^+])$$

Les énergies d'activation associées avec les constantes de vitesse k_1, k_2 et k_3 sont respectivement 52 ± 1, 49 ± 1 et 42 ± 3 kJ mol^{-1}. On propose un mécanisme en accord avec les données cinétiques expérimentales et selon lequel les constantes de vitesse k_1, k_2 et k_3 correspondent respectivement aux oxydations des ions iodures par le H_2O_2, le $H_3O_2^+$ et H_2MoO_5.

Mots clés : catalyse, peroxyde d'hydrogène, ion iodure, cinétique, ion molybdate.

[Traduit par la revue]

Introduction

The reaction between iodide ion and hydrogen peroxide in aqueous solution (overall stoichiometry: $3I^- + H_2O_2 + 2H^+ \rightarrow I_3^- + 2H_2O$) has been the subject of kinetic study for over a century (1–10). In particular, it has been established that several oxyanions, such as molybdate ion, have a catalytic effect on that reaction, what has been shown to be useful for the analytical determination of microquantities of those oxyanions (11–14). However, the kinetics of the iodide – hydrogen peroxide reaction in the presence of molybdenum(VI) as catalyst is not so well-known as that of the uncatalyzed reaction, and, as a result, there is considerable argument not only about the mechanism, but also as far as the rate law is concerned (15–17).

To clarify this matter, we have studied the reaction between iodide ion and hydrogen peroxide in aqueous solution both in the absence and in the presence of molybdenum(VI). The results are presented and discussed in detail in this paper.

Experimental section

All chemical reagents used in this work were supplied by Merck (analytical grade). The solvent was water previously purified by double distillation. The oxidant was hydrogen peroxide and the reductant potassium iodide. The kinetic runs were always done in perchloric acid aqueous media. After preparation, the stock solutions were deoxygenated by bubbling nitrogen (previously purified) through them.

The concentration of the hydrogen peroxide stock solution was determined by titration with potassium permanganate (previously standardized with sodium oxalate). The concentration of the perchloric acid stock solution was determined by titration with sodium hydroxide (previously standardized with potassium hydrogenphthalate). In the experiments with catalyst, the concentration of the sodium molybdate stock solution was determined by means of a Beckman DB-GT UV-vis spectrophotometer, by reduction of Mo(VI) to Mo(V) with tin(II) chloride and further complexation with potassium thiocyanate, measuring the absorbance of the molybdenum(V)–thiocyanate complex at 460 nm (18).

The kinetic runs were done in a volumetric flask provided with a double-wall system to allow peripheral circulation of water, so that the constancy of temperature during the runs was ensured. A constant flow of nitrogen was passed through the solutions during the runs to prevent possible interferences from oxygen. The concentration of iodine liberated in the iodide – hydrogen peroxide reaction was measured at regular intervals of time by titration with sodium thiosulfate (Tritisol reagent 0.1 N) using starch as indicator.

Results

The iodine liberated in the reaction was selected as the rate-monitoring species. Since iodide ion was also present in the experiments as a reactant, the following equilibrium has to be considered (19, 20):

[1] $I_2 + I^- \rightleftarrows I_3^-$

Consequently, the iodine liberated was present partially as I_2 and partially as I_3^-. While the use of a spectrophotometric method for monitoring the reaction would allow the determination of only one of those species, the use of a titration method (with thiosulfate ion as reductant and starch as indicator) allows the determination of the total $I_2 + I_3^-$ concentration. This is due to the fact that although the spectra of I_2 and I_3^- are very different, their respective redox properties are similar. Therefore titration was preferred over the spectrophotometric method.

The concentration of iodine liberated ($I_2 + I_3^-$) was determined at regular time intervals by titration with sodium thiosulfate. The results from four typical runs can be seen in Fig. 1. The kinetic data were deduced by using the initial-rates method to experiments done both in the absence and in the presence of molybdate ions. In the presence of molybdate ions, the total initial reaction rate (r_t) can be written as:

Printed in Canada / Imprimé au Canada

Can. J. Chem. Downloaded from www.nrcresearchpress.com by 91.121.58.235 on 09/07/12
For personal use only.

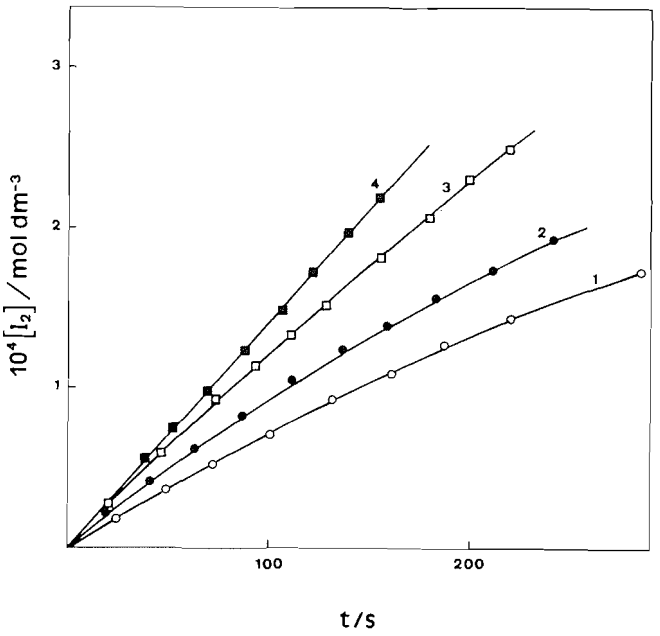

FIG. 1. Typical concentration of iodine vs. time plots. *1*: $[I^-] = 3 \times 10^{-2}$ mol dm^{-3}, $[H_2O_2] = 5 \times 10^{-4}$ mol dm^{-3}; *2*: $[I^-] = 5 \times 10^{-2}$ mol dm^{-3}, $[H_2O_2] = 5 \times 10^{-4}$ mol dm^{-3}; *3*: $[I^-] = 3 \times 10^{-2}$ mol dm^{-3}, $[H_2O_2] = 1 \times 10^{-3}$ mol dm^{-3}; *4*: $[I^-] = 1.5 \times 10^{-2}$ mol dm^{-3}, $[H_2O_2] = 5 \times 10^{-3}$ mol dm^{-3}. In all four cases: [Mo(VI)] = 5×10^{-7} mol dm^{-3}, $[H^+] = 5 \times 10^{-3}$ mol dm^{-3}, ionic strength = 0.20 mol dm^{-3} ($NaClO_4$), temperature 125.0°C.

[2] $r_t = r_u + r_c$

where r_u and r_c stand, respectively, for the contributions of the uncatalyzed and catalyzed reactions to the total initial rate. By doing the same experiment both in the presence and in the absence of molybdate ion, it was possible to determine r_t and r_u, respectively; the difference between them gave the value of r_c.

As can be seen in Fig. 2, r_t, r_u, and r_c are all directly proportional to the reductant concentration; i.e., both the uncatalyzed and the catalyzed reactions are first order in iodide ion. However, albeit both r_t and r_u increase linearly with the oxidant concentration, r_c is independent of that concentration (Fig. 3). Thus the kinetic orders of hydrogen peroxide are unity in the uncatalyzed reaction and zero in the catalyzed one.

As far as the hydrogen ion concentration is concerned, although the r_u vs. $[H^+]$ plot is linear (intercept different from zero), both the r_t vs. $[H^+]$ and r_c vs. $[H^+]$ plots are curves (Fig. 4). As can be seen in Fig. 5 for two typical sets of experimental conditions, $1/r_c$ increases linearly as increasing $1/[H^+]$. It can then be concluded that there are two distinct pathways involved in the uncatalyzed reaction, one zero order in hydrogen ion and the other first order, whilst the catalyzed reaction has non-definite kinetic order in hydrogen ion.

On the other hand, the values of r_t and r_c corresponding to various molybdate ion concentrations are given in Table 1. We can see that r_c is directly proportional to $[MoO_4^{2-}]$; i.e., the catalyzed reaction is first order as far as the catalyst is concerned.

Hence, the rate law found for the total reaction is:

[3] $$r_t = k_1[I^-][H_2O_2] + k_2[I^-][H_2O_2][H^+] + k_3[I^-][MoO_4^{2-}][H^+]/(a + [H^+])$$

where k_1 and k_2 are the rate constants corresponding to the two pathways involved in the uncatalyzed reaction (zero order and first order in H^+, respectively), and k_3 is the rate constant of the catalyzed reaction. Parameter a can be obtained from the $1/r_c$ vs. $1/[H^+]$ plots given in Fig. 5, its value at 25.0°C being $(1.00 \pm 0.03) \times 10^{-2}$ mol dm^{-3}. The activation parameters (energies, enthalpies, and entropies) associated with the rate constants have been determined from their variation with temperature (Fig. 6) by means of the Arrhenius and Eyring equations, and the results are given in Table 2. It is important to notice that since the total kinetic orders associated with rate constants k_1, k_2, and k_3 (second order, third order, and a non-definite order, respectively) are different, no kinetic nor mechanistic information can be inferred from a comparison of their corresponding activation entropies (21–23).

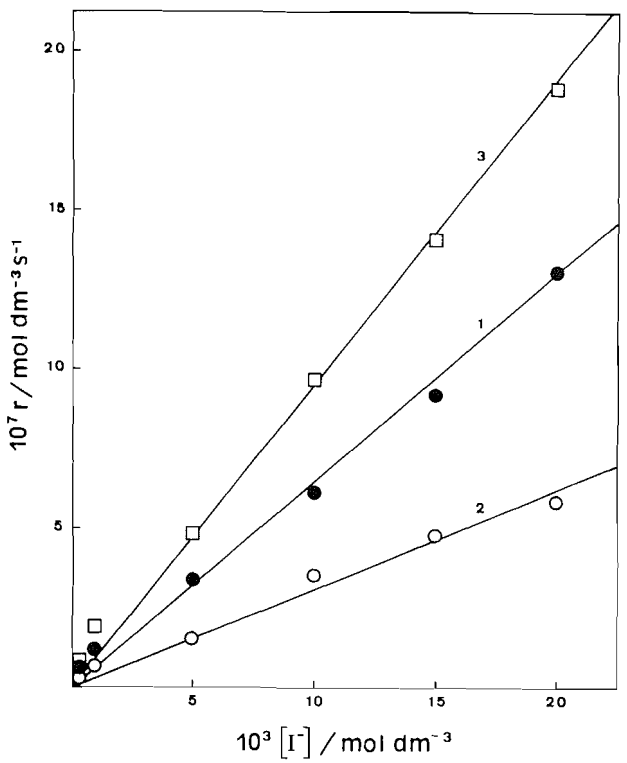

FIG. 2. Dependence of the reaction rates (*1*: r_u; *2*: r_c; *3*: r_t) on the iodide ion concentration. $[H_2O_2] = 5 \times 10^{-3}$ mol dm^{-3}, [Mo(VI)] = 5×10^{-7} mol dm^{-3}, $[H^+] = 5 \times 10^{-3}$ mol dm^{-3}, ionic strength = 0.20 mol dm^{-3} ($NaClO_4$), temperature = 25.0°C.

Discussion

According to the kinetic data obtained in this work, the overall mechanism that can be proposed for the oxidation of iodide ion by the molybdenum(VI) – hydrogen peroxide system is as follows:

[4] $$H_2O_2 + H^+ \overset{K_4}{\rightleftharpoons} H_3O_2^+$$

[5] $$H_2MoO_4 + H_2O_2 \overset{K_5}{\rightleftharpoons} H_2MoO_5 + H_2O$$

[6] $$H_2MoO_5 \overset{K_6}{\rightleftharpoons} HMoO_5^- + H^+$$

[7] $$I^- + H_2O_2 \xrightarrow{k_7} HIO + OH^-$$

[8] $$I^- + H_3O_2 \xrightarrow{k_8} HIO + H_2O$$

[9] $$I^- + H_2MoO_5 + H_2O \xrightarrow{k_9} HIO + H_2MoO_4 + OH^-$$

[10] $$I^- + HIO \xrightarrow{k_{10}} I_2 + OH^-$$

Can. J. Chem. Downloaded from www.nrcresearchpress.com by 91.121.58.235 on 09/07/12
For personal use only.

Can. J. Chem. Downloaded from www.nrcresearchpress.com by 91.121.58.235 on 09/07/12
For personal use only.

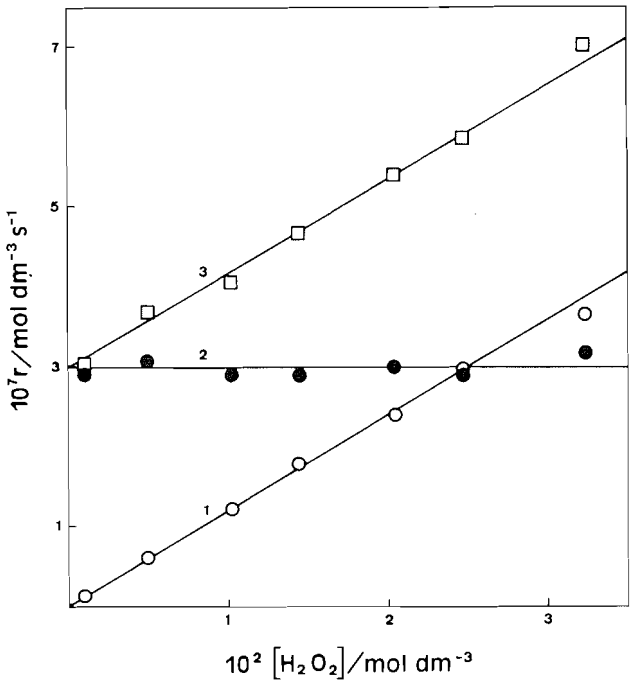

FIG. 3. Dependence of the reaction rates (*1*: r_u; *2*: r_c; *3*: r_t) on the hydrogen peroxide concentration. $[I^-] = 1 \times 10^{-3}$ mol dm^{-3}, $[Mo(VI)] = 5 \times 10^{-7}$ mol dm^{-3}, $[H^+] = 5 \times 10^{-3}$ mol dm^{-3}, ionic strength = 0.20 mol dm^{-3} ($NaClO_4$), temperature = 25.0°C.

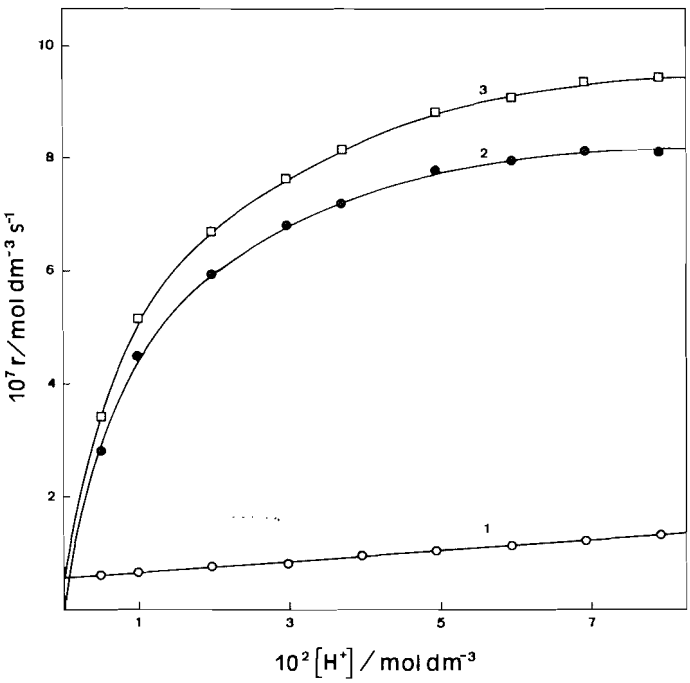

FIG. 4. Dependence of the reaction rates (*1*: r_u; *2*: r_c; *3*: r_t) on the hydrogen ion concentration. $[I^-] = 1 \times 10^{-3}$ mol dm^{-3}, $[H_2O_2] = 5 \times 10^{-3}$ mol dm^{-3}, $[Mo(VI)] = 5 \times 10^{-6}$ mol dm^{-3}, ionic strength = 0.20 mol dm^{-3} ($NaClO_4$), temperature = 25.0°C.

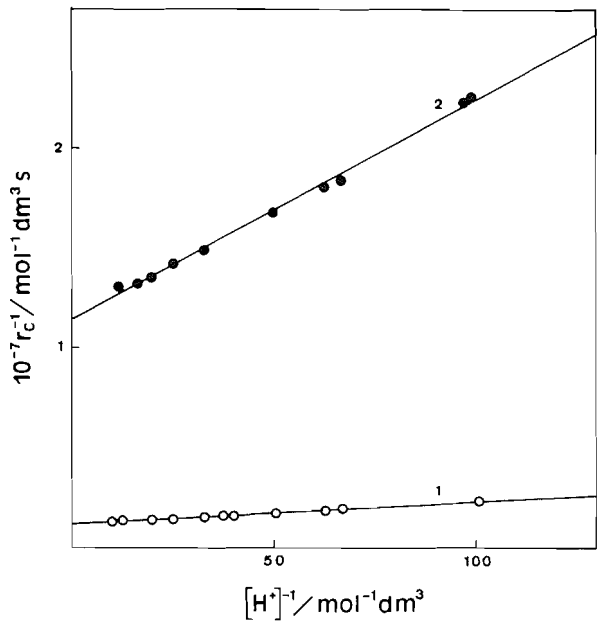

FIG. 5. $1/r_c$ vs. $1/[H^+]$ plots. *1*: $[Mo(VI)] = 5 \times 10^{-6}$ mol dm^{-3}; *2*: $[Mo(VI)] = 5 \times 10^{-7}$ mol dm^{-3}. In both cases: $[I^-] = 1 \times 10^{-3}$ mol dm^{-3}, $[H_2O_2] = 1 \times 10^{-3}$ mol dm^{-3}, ionic strength = 0.20 mol dm^{-3} ($NaClO_4$), temperature = 25.0°C.

TABLE 1. Rates at various molybdenum(VI) concentrations for the oxidation of iodide ion (1×10^{-3} mol dm^{-3}) by hydrogen peroxide (5×10^{-3} mol dm^{-3}) at $[H^+] = 5 \times 10^{-2}$ mol dm^{-3}, ionic strength = 0.20 mol dm^{-3} ($NaClO_4$) and 25.0°C

10^6 [Mo(VI)] (mol dm^{-3})	$10^7 r_t$ (mol dm^{-3} s^{-1})	$10^7 r_c$ (mol dm^{-3} s^{-1})	r_c/[Mo(VI)] (s^{-1})
0.00	1.02	0.00	—
0.10	1.18	0.16	0.160
0.50	1.83	0.81	0.162
1.00	2.54	1.52	0.152
1.50	3.31	2.29	0.153
2.00	4.05	3.03	0.152
3.00	5.63	4.61	0.154
4.00	7.26	6.24	0.156
5.00	8.66	7.64	0.153
6.00	9.99	8.97	0.150
7.00	11.49	10.47	0.150
8.00	13.12	12.10	0.151

TABLE 2. Activation parameters associated with each rate constant[a]

Rate constant	E_a (kJ mol^{-1})	$\Delta H^{\ddagger}$ (kJ mol^{-1})	$-\Delta S^{\ddagger}$ (J K^{-1} mol^{-1})
k_1	52±1	50±1	116±3
k_2	49±1	46±1	104±4
k_3	42±3	40±3	68±11

[a]The activation entropies are referred to the 1 mol dm^{-3} standard state.

First, we have considered in reaction [4] the equilibrium of protonation of hydrogen peroxide to enhance its oxidizing power, due to the fact that the electron density of $H_3O_2^+$ is lower than that of H_2O_2; i.e., $H_3O_2^+$ is a better oxidant than H_2O_2. Given the dissociation constants of molybdic acid (24), the predominant form of molybdenum(VI) in the perchloric acid media used in this work was H_2MoO_4. This species reacts reversibly with H_2O_2 in reaction [5] to form H_2Mo0_5; actually, the existence of peroxymolybdic acid, as well as that of other peroxyderivatives of molybdenum(VI), is already known (25, 26). The equilibrium between peroxymolybdic acid and hydrogenperoxymolybdate ion has been depicted in reaction [6].

On the other hand, since there are three rate constants involved in the experimental rate law (eq. [3]), it seems

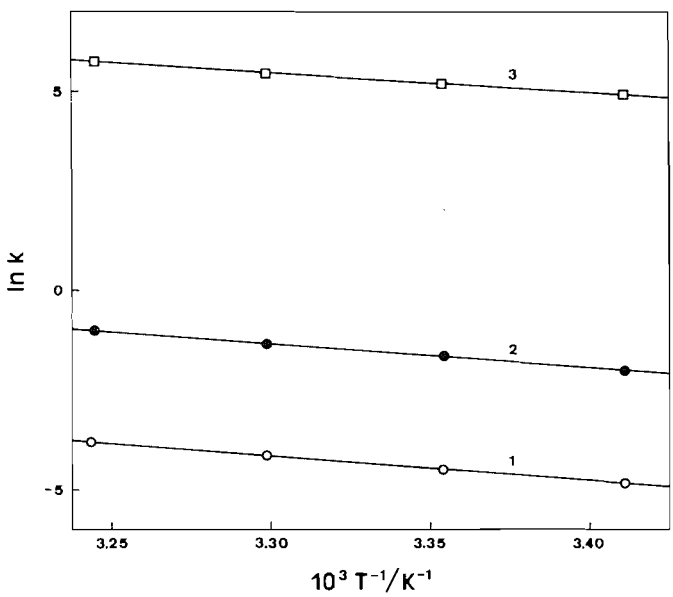

FIG. 6. Dependence of the experimental rate constants (*1*: k_1; *2*: k_2; *3*: k_3) on temperature. $[I^-] = 1 \times 10^{-3}$ mol dm^{-3}, $[H_2O_2] = 5 \times 10^{-3}$ mol dm^{-3}, [Mo(VI)] = 5×10^{-7} mol dm^{-3} (only for plot *3*), $[H^+] = 5 \times 10^{-3}$ mol dm^{-3}, ionic strength = 0.20 mol dm^{-3} ($NaClO_4$).

reasonable to conclude that there are also three active oxidants capable of reacting with iodide ion in rate-determining steps. In the mechanism proposed, these oxidants are H_2O_2, $H_3O_2^+$ and H_2MoO_5. These three species oxidize iodide ion to hypoiodous acid (reactions [7]–[9]). Finally, iodine is formed in reaction [10] by the well-known reaction between iodide ion and hypoiodous acid (8, 27).

It is important to notice that the oxidation of iodide ion by hydrogenperoxymolybdate ion has not been postulated. This is because the electron density of $HMoO_5^-$ is much higher than that of H_2MoO_5. Therefore, $HMoO_5^-$ is a much worse oxidant than H_2MoO_5. Moreover, the nucleophilic attack of I^- on $HMoO_5^-$ is considerably impeded by the fact that they are like-charged ions. It should also be noticed that reaction [9] can perfectly well be an elementary step, for, although it requires the trimolecular encounter of an ion and two molecules, one of the two molecules is the solvent. In this step, reaction [9], the catalyst H_2MoO_4 is recuperated.

The mechanism proposed for the uncatalyzed reaction (reactions [4], [7], [8], and [10]) is consistent with the ones proposed by other authors for the same reaction (5, 7, 27, 28). As far as the catalyzed reaction is concerned, albeit the mechanism given in reactions [5], [6], and [9] differs notably from previous proposals (16, 17), it is in better agreement with the experimental rate law (eq. [3]) found in this work.

Since iodine was selected as the rate-monitoring species, we can write for the total reaction rate:

$$[11] \quad r_t = d[I_2]/dt = k_{10}[I^-][HIO]$$

and, considering that reactions [7]–[9] are rate-determining, for the step given by reaction [10] is very fast (8, 27), the rate of formation of iodine must be given by the total rate of formation of hypoiodous acid through reactions [7]–[9]:

$$[12] \quad r_t = k_7[I^-][H_2O_2] + k_8[I^-][H_3O_2^+] + k_9[I^-][H_2MoO_5]$$

On the other hand, the concentrations of the intermediates $H_3O_2^+$ and H_2MoO_5 can be deduced from the equilibrium laws associated with reactions [4]–[6]:

$$[13] \quad [H_3O_2^+] = K_4[H_2O_2]_T[H^+] / (1 + K_4[H^+])$$

$$[14] \quad [H_2MoO_5] = K_5[H_2O_2][MoO_4^{2-}]_T[H^+] / z$$

z being defined as follows:

$$[15] \quad z = [H^+] + (K_6 + [H^+])K_5[H_2O_2]$$

It should be noticed that $[H_2O_2]_T$ in eq. [13] stands for the total concentration of hydrogen peroxide ($H_2O_2 + H_3O_2^+$) present in the experiments, whereas $[MoO_4^{2-}]_T$ in eq. [14] stands for the total concentration of catalyst ($H_2MoO_4 + H_2MoO_5 + HMoO_5^-$), that is, the initial concentration of sodium molybdate used to prepare the solutions.

Since the concentration of hydrogen ion in the experiments was relatively low, provided that the value of K_4 is low enough and that the value of K_5 is high enough, the following approximations can be applied:

$$[16] \quad K_4[H^+] \ll 1$$

$$[17] \quad [H^+] \ll (K_6 + [H^+])K_5[H_2O_2]$$

These approximations are indeed reasonable, for $H_3O_2^+$ is a very acidic species, since a very low value (2×10^{-5} at 25.0°C) has been reported for K_4 (28). This means that the free form of hydrogen peroxide (H_2O_2) was predominant in the experiments and, therefore, the total concentration of hydrogen peroxide $[H_2O_2]_T$ can also be approximately written in eq. [13] as $[H_2O_2]$. Moreover, it is well-known (25) that molybdenum(VI) is easily peroxidized (i.e., K_5 is very high). From eqs. [13]–[17], and by substituting $[H_2O_2]$ for $[H_2O_2]_T$, we obtain:

$$[18] \quad [H_3O_2^+] = K_4[H_2O_2][H^+]$$

$$[19] \quad [H_2MoO_5] = [MoO_4^{2-}]_T[H^+] / (K_6 + [H^+])$$

Finally, substitution of eqs. [18] and [19] in eq. [12] leads to:

$$[20] \quad r_t = k_7[I^-][H_2O_2] + K_4k_8[I^-][H_2O_2][H^+] + k_9[I^-][MoO_4^{2-}]_T[H^+] / (K_6 + [H^+])$$

We can see that the theoretical rate law (eq. [20]) based on the mechanism proposed is perfectly coherent with the experimental rate law found in this work (eq. [3]). A comparison of both rate laws (theoretical and experimental) leads to the following identities for the experimental rate constants k_1, k_2, and k_3, and the parameter a appearing in eq. [3]: $k_1 = k_7$, $k_2 = K_4k_8$, $k_3 = k_9$, and $a = K_6$. Hence the activation parameters given in Table 2 for the experimental rate constants k_1 and k_3 are actually the ones corresponding to the oxidations of iodide ion by hydrogen peroxide (eq. [7]) and peroxymolybdic acid (eq. [9]), respectively, whereas the activation parameters given in Table 2 for the experimental rate constant k_2 have only an apparent character, since they are actually combinations of the activation parameters corresponding to the oxidation of iodide ion by $H_3O_2^+$ (reaction [8]) and the thermodynamic parameters corresponding to the protonation of hydrogen peroxide (reaction [4]). We can also see in Table 2 that the true activation energy found for the I^-–H_2MoO_5 reaction (42 ± 3 kJ mol^{-1}) is considerably lower than both the true activation energy for the I^-–H_2O_2 reaction (52 ± 1 kJ mol^{-1}) and the apparent activation energy for the I^-–$H_3O_2^+$ reaction (49 ± 1 kJ mol^{-1}). It can then be concluded that the actual role of molybdenum(VI) as a catalyst of the reaction is to decrease the energetic barrier associated with the oxidation of iodide ion.

Can. J. Chem. Downloaded from www.nrcresearchpress.com by 91.121.58.235 on 09/07/12
For personal use only.

1. A. G. V. HARCOURT and W. ESSON. J. Chem. Soc. **20**, 460 (1867).
2. A. A. NOYES and W. O. SCOTT. Z. Phys. Chem. **18**, 118 (1895); **14**, 692 (1896).
3. J. BRODE. Z. Phys. Chem. **49**, 208 (1904).
4. E. ABEL. Z. Phys. Chem. **136**, 161 (1928).
5. H. A. LIEBHAFSKY and A. MOHAMMAD. J. Am. Chem. Soc. **55**, 3977 (1933); J. Phys. Chem. **38**, 857 (1934).
6. J. WEISS. Ann. Rep. **44**, 60 (1947).
7. F. BELL, R. GILL, D. HOLDEN, and W. F. K. WYNNE-JONES. J. Phys. Colloid Chem. **55**, 874 (1951).
8. J. O. EDWARDS. Chem. Rev. **50**, 455 (1952); J. Am. Chem. Soc. **76**, 1540 (1954).
9. B. SURFLEET and P. A. H. WYATT. J. Chem. Soc. (A), 1564 (1967).
10. C. ARIAS, F. MATA, and J. F. PEREZ-BENITO. An. Quim. In press.
11. A. K. BABKO, G. S. LISETSKAYA, and G. F. TSARENKO. Zh. Anal. Khim. **23**, 1342 (1968).
12. G. SVEHLA. Analyst (London), **94**, 513 (1969).
13. F. F. GAAL, V. I. SOROS, and V. J. VAJGAND. Anal. Chim. Acta, **84**, 127 (1976).
14. M. KATAOKA, K. NISHIMURA, and T. KAMBARA. Talanta, **30**, 941 (1983).
15. G. SVEHLA and L. ERDEY. Microchem. J. **7**, 206 (1963).
16. F. GARCIA and J. GOMEZ. Rev. Soc. Quim. Mex. **13**, 222 (1969).
17. R. H. SMITH and J. KILFORD. Int. J. Chem. Kinet. **8**, 1 (1976).
18. E. B. SANDELL. Colorimetric determination of traces of metals. 3rd ed. Interscience, New York. 1959. p. 644.
19. H. M. DAWSON and E. SPIVEY. J. Chem. Soc. 1838 (1932).
20. J. F. PEREZ-BENITO, E. BRILLAS, and C. ARIAS. Can. J. Chem. **68**, 79 (1990).
21. D. M. GOLDEN. J. Chem. Educ. **48**, 235 (1971).
22. R. K. BOYD. J. Chem. Educ. **55**, 84 (1978).
23. P. J. ROBINSON. J. Chem. Educ. **55**, 509 (1978).
24. Y. SASAKI and L. G. SILLEN. Acta Chem. Scand. **18**, 1014 (1964).
25. J. A. CONNOR and E. A. V. EBSWORTH. Adv. Inorg. Chem. Radiochem. **6**, 279 (1964).
26. O. BORTOLINI, L. BRAGANTE, F. DI FURIA, and G. MODENA. Can. J. Chem. **64**, 1189 (1986).
27. J. BARRETT and A. E. BEEZER. Educ. Chem. **14**, 42 (1977).
28. J. O. EDWARDS. Peroxide reaction mechanism. Wiley, New York. 1962. p. 85.

Can. J. Chem. Downloaded from www.nrcresearchpress.com by 91.121.58.235 on 09/07/12
For personal use only.

The formation of *N*-alkylporphyrins during epoxidation of ethylene catalyzed by iron(III) *meso*-tetrakis(2,6-dichlorophenyl)porphyrin

TAKU NAKANO

Department of Pharmaceutical Sciences, Toyama Medical and Pharmaceutical University, 2630 Sugitani, Toyama, 930-01, Japan

TEDDY G. TRAYLOR

Department of Chemistry, University of California, San Diego, La Jolla, CA 92093, U.S.A.

AND

DAVID DOLPHIN

Department of Chemistry, University of British Columbia, 2036 Main Mall, Vancouver, B.C., Canada V6T 1Y6

Received December 19, 1989

TAKU NAKANO, TEDDY G. TRAYLOR, and DAVID DOLPHIN. Can. J. Chem. **68**, 1504 (1990).

During the epoxidation of ethylene using iron *meso*-tetrakis(2,6-dichlorophenyl)porphyrin chloride and iodosopentafluorobenzene several *N*-alkylporphyrins were formed. The major product was 21-carboxymethyl-5,10,15,20-tetrakis(2,6-dichlorophenyl)porphyrin. This was derived, by oxidation, from the corresponding 21-formylmethyl complex which in turn was obtained from the initially formed *N*-hydroxyethylporphyrin, a compound not isolated due to its ready oxidation.

Key words: *N*-alkylporphyrins, suicide labelling, cytochrome P-450, hemin catalysis, epoxidation, oxidation.

TAKU NAKANO, TEDDY G. TRAYLOR et DAVID DOLPHIN. Can. J. Chem. **68**, 1504 (1990).

Lors de l'époxydation de l'éthylène à l'aide de la *méso*-tétrakis(2,6-dichlorophényl)porphyrine et de l'iodosopentafluorobenzène, il se forme plusieurs *N*-alkylporphyrines. Le produit principal est la 21-carboxyméthyl-5,10,15,20-tétrakis(2,6-dichlorophényl)porphyrine. Ce produit est formé par oxydation du complexe 21-formylméthyle correspondant qui est lui-même obtenu à partir de la *N*-hydroxyéthylporphyrine qui se forme initialement, mais qui n'a pas été isolée à cause de son oxydation très facile.

Mots clés : *N*-alkylporphyrines, marquage suicide, cytochrome P-450, catalyse héminique, époxydation, oxydation.

[Traduit par la revue]

Can. J. Chem. Downloaded from www.nrcresearchpress.com by 91.121.58.235 on 09/07/12
For personal use only.

Introduction

Suicide inactivation during the metabolism of alkenes and alkynes results in *N*-alkylation of the heme prosthetic group of cytochromes P-450 (1). These reactions have been mimicked using simple iron tetraphenylporphyrins (2, 3) and the roles of σ-iron alkylporphyrins, their interconvertability to *N*-alkylporphyrins (4), their roles in nature (5), and as models for cytochrome P-450 (6) have been reviewed.

Normally, alkylation of a terminal alkene results in *N*-alkylation at the less substituted terminal C-atom (**1**). However, Mansuy and co-workers (7) have shown that the *N*-alkylation of iron *meso*-tetrakis(*p*-chlorophenyl)porphyrin by several terminal alkenes resulted in substitution, **2**, at the more substituted carbon atom (C-2). These reactions were complicated by apparent subsequent oxidation of the alcohol to the corresponding carboxylic acid (**2** → **3**). If oxidation occurs before or during alkylation then the observation of substitution at C-2 could be more complicated than had been suggested.

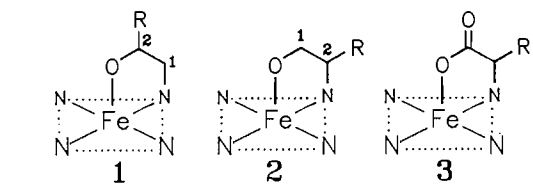

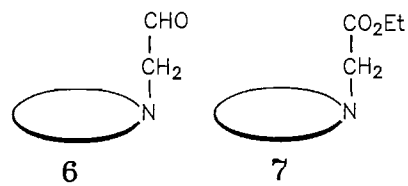

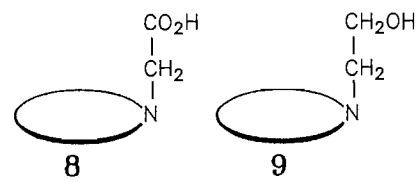

N = *meso*-Tetrakis(2,6-dichlorophenyl)porphyrin

5

Results and discussion

To understand and further explore the *N*-alkylation process we have studied the catalysis of epoxidation of the simplest alkene, ethylene. In a typical experiment iron *meso*-tetrakis(2,6-dichlorophenyl)porphyrin chloride (**4**) (8) in CH_2Cl_2 was cooled in a CCl_4 – dry ice bath and the solution saturated with ethylene. Excess iodosopentafluorobenzene was added and the reaction mixture allowed to warm to room temperature. After addition of further iodosopentafluorobenzene and standing for 1.5 h the original brown solution had turned greenish brown with a broad Soret band at 433 nm and additional broad peaks at 355, 565, and 643 nm. Demetallation ($FeCl_2$/HCl/CH_3CO_2H) followed by chromatography (silica gel) gave several fractions with identical optical spectra (Fig. 1). Elution with CH_2Cl_2 gave *meso*-tetrakis(2,6-dichlorophenyl)porphyrin (**5**) (8) followed by 21-formylmethyl-5,10,15,20-tetrakis(2,6-dichlorophenyl)-porphyrin (**6**) and then 21-ethoxycarbonylmethyl-5,10,15,20-tetrakis(2,6-dichlorophenyl)porphyrin (**7**).[1] Continued elution with CH_2Cl_2/acetone (9:1) gave 21-carboxymethyl-5,10,15,20-tetrakis(2,6-dichlorophenyl)porphyrin (**8**).

The optical spectra (Fig. 1) of all the *N*-alkylporphyrins are

[1] Ethanol for this esterification came from the $FeCl_2$ reduction of the ethylene oxide which was the principal product in the reaction.

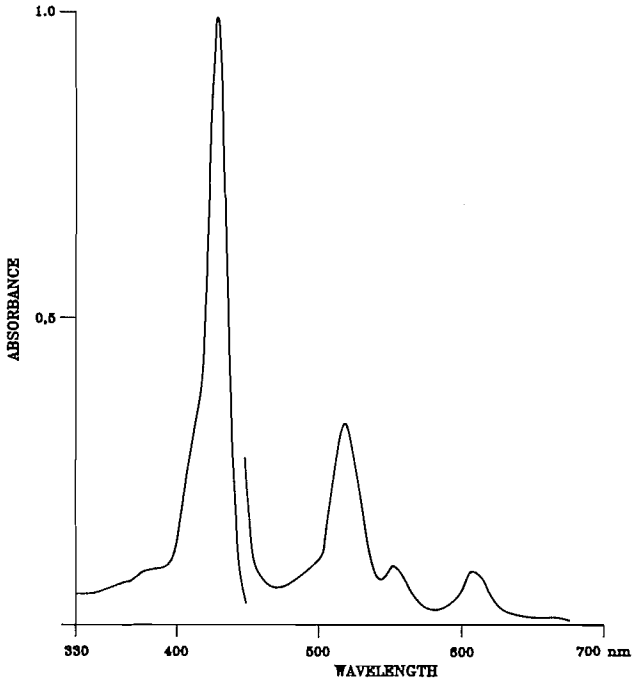

FIG. 1. Optical spectrum (CH_2Cl_2) of the *N*-alkylporphyrins **6–8**.

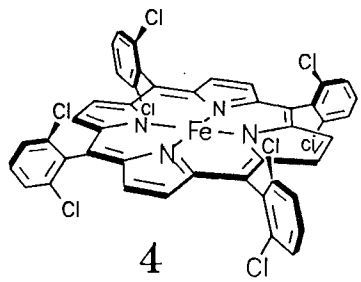

similar to those previously reported for the *N*-alkylation with 4,4-dimethyl-1-pentene (2). Traces of other *N*-alkylated species with similar optical spectra were not further characterized.

Remetallation of **6** followed by treatment with C_6F_5IO in CH_2Cl_2 gave **8** (after demetallation), showing that oxidation of the *N*-formylmethyl to the *N*-carboxymethyl group readily occurs under the reaction conditions for *N*-alkylation.

We presume that the absence of the *N*-hydroxyethylhemin (**9**) results from its rapid oxidation to carboxaldehyde and then to the carboxylic acid. Preliminary experiments on the epoxidation of 1-hexene using **4** and even more electron deficient porphyrins chlorinated on the β-positions of the porphyrin itself (9) show that these less basic porphyrins exhibit less of a tendency towards alkylation. We have proposed that the first step in alkene epoxidation (and *N*-alkylation) is a one-electron transfer from the olefin to the hemin (8). Since ethylene has a higher oxidation potential than other homologous alkenes the rate of formation of the *N*-hydroxyethyl complex with the less basic porphyrin could well be slower than its oxidation to the carboxaldehyde.

The observation that oxidation can occur after *N*-alkylation suggests that Mansuy's observation (3) of *N*-alkylation at C-2 of the alkene occurred independently of its oxidation to the *N*-carboxyalkyl complex (**3**). In fact, our initial proposal of a common intermediate for both epoxidation, *N*-alkylation, and substrate rearrangement can account for *N*-alkylation at both C-1 and C-2 of a terminal alkene.

The scheme shows formation of an olefin π-cation radical (**11**) via a one-electron oxidation of the olefin by the oxoferryl [Fe(IV)] porphyrin π-cation radical (**10**). Radical dimerization via route *a* could give a "primary carbonium ion" (**12**).[2] This common intermediate could then give epoxide (route *c*), product rearrangement (route *d*) and *N*-alkylation at C-1 (route *e*) while radical dimerization via route *b* would give the more stable "secondary carbonium ion" (**13**) which upon *N*-alkylation would give the alkylation at C-2 (route *f*) observed by Mansuy (3).

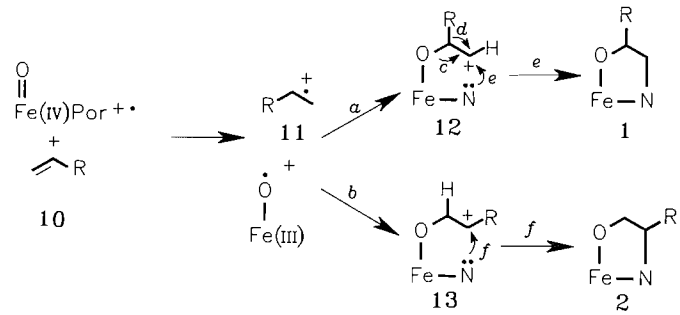

Experimental

Iron *meso*-tetrakis(2,6-dichlorophenyl)porphyrin chloride (**4**) (46 mg) in CH_2Cl_2 (40 mL) was placed in a 100 mL three-necked flask fitted with an ethylene-gas-bubbler and spinning bar. The solution was cooled in a CCl_4 – dry ice bath and ethylene was passed into the solution until saturation. Iodosylpentafluorobenzene (148 mg) was added and the solution stirred as a steady stream of ethylene was passed through the solution. The reaction mixture was then allowed to warm to room temperature and stirring continued until the optical spectrum showed no further formation of *N*-alkyl hemin (~1.5 h). At this time the original brown solution had changed to a green brown color with a broad Soret band at 433 nm and broad peaks at 355, 565, and 643 nm.

The mixture was taken to dryness on a rotatory evaporator and the *N*-alkylhemin was demetallated by treatment under N_2 with $FeCl_2$ (1 g) in concentrated HCl (2 mL) and acetic acid (38 mL). The solution immediately turned green. After 2 h, CH_2Cl_2 (50 mL) was added and air was passed through the mixture for a few minutes. Water (40 mL) was added and the separated organic layer was washed with aliquots of water (15 mL) until neutral. The organic layer was dried over anhydrous Na_2SO_4, filtered, and the filtrate chromatographed over silica gel to afford several fractions with identical optical spectra. Elution with CH_2Cl_2 gave *meso*-tetrakis(2,6-dichlorophenyl)porphyrin (**5**) (25 mg, 53%) and 21-formylmethyl-5,10,15,20-tetrakis(2,6-dichlorophenyl)porphyrin (**6**) (3.4 mg, 7.4%) and 21-ethoxycarbonylmethyl-5,10,15,20-tetrakis(2,6-dichlorophenyl)porphyrin (**7**) (0.9 mg, 2%). Continued elution with CH_2Cl_2:acetone (9:1, v:v) gave 21-carboxymethyl-5,10,15,20-tetrakis(2,6-dichlorophenyl)porphyrin (**8**) (6.8 mg, 14.8%).

The same products were obtained as above when (*i*) the ethylene was scrubbed by passing it through alkaline mercuric cyanide to remove any contaminating acetylene and (*ii*) the reaction was carried out under pressure in a stainless steel pressure tube.

21-Formylmethyl-5,10,15,20-tetrakis(2,6-dichlorophenyl)porphyrin (6)

An analytical sample was recrystallized from CH_2Cl_2. *Anal.* calcd. for $C_{46}Cl_8H_{24}N_4O$: C 59.26, H 2.59, N 6.01; found: C 59.18, H 2.54, N 5.99. ^1H NMR ($CDCl_3$, 270 MHz) δ −3.26 (s, 2H, N-CH_2CHO), −2.15 (s, 1H, N—*H*), 6.84 (s, 1H, N—CH_2CHO), 8.00 (s, 2H, pyrr. *a*, *b*), 8.38 (q, AB-system, J = 4.88 Hz, 4H, pyrr. *c*, *d*, *g*, *h*), 8.69 (d pyrr. *e*, *f*), 7.65–7.86 (c, 12H, ph). IR ($CHCl_3$) 1729 cm^{-1} (*N*—CH_2*CHO*). λ_{max}^{nm} (log ε) (CH_2Cl_2) 317 (4.11), 354 (4.23), 379

[2]Molecular addition of the radical cation to the O—Fe—N unit is also consistent with our findings.

Can. J. Chem. Downloaded from www.nrcresearchpress.com by 91.121.58.235 on 09/07/12
For personal use only.

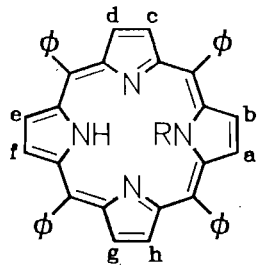

(4.39), 427 (5.46), 487 (3.56), 519 (4.28), 552 (3.73), 606 (3.71), 665 (2.91). *m/e* 930 ($M^+ + 4 - 3H$).

21-Ethoxycarbonylmethyl-5,10,15,20-tetrakis(2,6-dichlorophenyl)-porphyrin (7)

Crystallized from CH_2Cl_2/hexane. ^1H NMR ($CDCl_3$, 270 MHz) δ −3.22 (s, N—CH_2COOCH$_2$CH$_3$), −2.16 (s, 1H, N—*H*), 0.56 (t, 3H, *J* = 7.02 Hz, *N*—CH_2COOCH$_2$C*H*$_3$), 3.00 (q, 2H, *J* = 7.02 Hz, N—CH_2COO*CH*$_2$CH$_3$), 8.05 (d, 2H, pyrr. *a*, *b*), 8.43–8.34 (c, 4H, pyrr. *c*, *d*, *g*, *h*), 8.67 (d, 2H, pyrr. *e*, *f*), 7.86–7.63 (c, 12H, ph.). *m/e* 976 ($M^+ + 4$), 930 ($M^+ + 4 - HOCH_2CH_3$).

21-Carboxymethyl-5,10,15,20-tetrakis(2,6-dichlorophenyl)porphyrin (8)

Crystallized from CH_2Cl_2/hexane. ^1H NMR ($CDCl_3$, 270 MHz) δ −3.93 (c, 2H, N—CH_2COOH), −2.14 (s (broad), 1H, N—*H*), 7.79 (s, 2H, pyrr. *a*, *b*), 8.40 (q, (accompanied by smaller but wider q), AB-system *J* = 4.55 Hz, 4H, pyrr. *c*, *d*, *g*, *h*), 8.67 (s (broad), 2H, pyrr. *e*, *f*), 7.64–7.89 (c, 12H, ph.). IR ($CHCl_3$) 1725 cm^{-1} (N—CH_2*COOH*). *m/e* 904 ($M^+ + 4 - CO_2$).

Acknowledgements

This work was supported by the U.S. National Institutes of Health (DK17989 (DD)), the U.S. National Science Foundation (CHE87-2164 (TGT)), and the Natural Sciences and Engineering Research Council of Canada. Thanks are due to Mr. M. Morikoshi for measuring the NMR spectra.

1. P. R. Ortiz de Montellano. *In* Cytochrome P-450. *Edited by* P. R. Ortiz de Montellano. Plenum, New York. 1986.
2. T. Mashiko, D. Dolphin, T. Nakano, and T. G. Traylor. J. Am. Chem. Soc. **107**, 3735 (1985).
3. D. Mansuy, L. Devocelle, I. Artaud, and J.-P. Battoni. Nouv. J. Chim. **9**, 711 (1985).
4. D. Dolphin, A. Matsumoto, and C. Shortman. J. Am. Chem. Soc. **111**, 411 (1989).
5. J.-I. Setsune and D. Dolphin. Can. J. Chem. **65**, 459 (1987).
6. D. Mansuy. Pure Appl. Chem. **59**, 759 (1987).
7. I. Artaud, L. Devocelle, J.-P. Battioni, J.-P. Girault, and D. Mansuy. J. Am. Chem. Soc. **109**, 3782 (1987).
8. T. G. Traylor, T. Nakano, B. E. Dunlap, P. S. Traylor, and D. Dolphin. J. Am. Chem. Soc. **108**, 2482 (1986).
9. T. Wijesekera, A. Matsumoto, D. Dolphin, and D. Lexa. To be published.

Can. J. Chem. Downloaded from www.nrcresearchpress.com by 91.121.58.235 on 09/07/12
For personal use only.

Excited state dipole moments and polarizabilities of some aromatic alkenes and alkynes

HEMANT K. SINHA, PAUL C. P. THOMSON, AND KEITH YATES
Department of Chemistry, Lash Miller Chemical Laboratories, University of Toronto, Ont., Canada M5S 1A1
Received February 14, 1990

HEMANT K. SINHA, PAUL C. P. THOMSON, and KEITH YATES. Can. J. Chem. **68**, 1507 (1990).

Electric field induced changes in the optical absorption spectra (electrochromism) have been used to obtain the excited state dipole moments and polarizabilities of styrene, 2-vinylnaphthalene, 2-naphthylacetylene, and 9-vinylanthracene. Excited state dipole moments of the order of 4–6 debye have been obtained for all these molecules except for 9-vinylanthracene, for which the excited state dipole moment is zero within experimental error. These results support earlier proposals of the involvement of charge transfer excited states in the fast and efficient acid-catalysed photohydration reactions of this type of substrate. 9-Vinylanthracene, on the other hand, under similar conditions reacts differently to give a dimer as the major photoproduct, and its reaction is not subject to acid catalysis. These results shed light on the importance of charge transfer excited states on the efficiency of photohydration reactions.

Key words: electrochromism, excited state, dipole moments, polarizabilities.

HEMANT K. SINHA, PAUL C. P. THOMSON et KEITH YATES. Can. J. Chem. **68**, 1507 (1990).

On a utilisé les changements induits par les champs électriques sur les spectres d'absorption optique (électrochromisme) pour obtenir les moments dipolaires ainsi que les polarisabilités des états excités du styrène, du 2-vinylnaphtalène, du 2-naphtylacétylène et du 9-vinylanthracène. Pour toutes les molécules étudiées, excepté le 9-vinylanthracène, on a obtenu des moments dipolaires des états excités qui étaient de l'ordre de 4 à 6 debye; dans le cas exceptionnel, le moment dipolaire de l'état excité est égal à zéro, dans les limites des erreurs expérimentales. Ces résultats supportent les propositions qui avaient été formulées antérieurement concernant l'implication des états excités du transfert de charge dans les réactions rapides et efficaces de photohydratation, catalysées par les acides, de ce type de substrat. Le 9-vinylanthracène, soumis aux mêmes conditions expérimentales, réagit toutefois différemment et conduit à la formation prépondérante d'un dimère comme photoproduit et cette réaction n'est pas catalysée par les acides. Ces résultats mettent en relief l'importance des états excités des transferts de charge sur l'efficacité des réactions de photohydratation.

Mots clés : électrochromisme, état excité, moments dipolaires, polarisabilités.

[Traduit par la revue]

Introduction

Electrochromism (electric field induced change in the extinction coefficient) is probably the best known method for direct detection of the charge distribution in molecules in both their ground and excited states. Initially developed by Labhart, Czekalla, and Liptay, this method has been successfully used to obtain the ground and excited state electrical properties, such as dipole moments and polarizabilities, of both polar and nonpolar molecules (1–8).

For polar molecules, the ground state dipole moment of the molecule and the change in dipole moment on electronic excitation are the principal components that contribute to the electric field perturbation of the absorption spectrum. On the other hand, for nonpolar molecules it is the change in the induced dipole moment that contributes most to the electric field perturbation, and this is reflected in a change in the polarizability upon electronic excitation. Recent investigations by Liptay and co-workers (7) and Ponder and Mathies (8) have indicated that conjugated polyenes undergo large changes in polarizability upon electronic excitation, and the solution phase and gas phase polarizabilities of polyenes are very different. Excited state dipole moments of the order of 1–4 debye obtained for some symmetric polyenes have been explained as a result of symmetry breaking perturbations, either due to single bond rotation or inhomogeneous local solvent interactions. Several other experiments on aromatic systems have been carried out to evaluate the accuracy of various theoretical approximations involved in quantum mechanical calculations (9).

In this paper, we deal with the results of electrochromic measurements from a different viewpoint, namely to find support for the proposed mechanistic features of photohydration reactions. Recently, it has been observed that aromatic alkenes, alkynes, and allenes, on electronic excitation, can be directly protonated in neutral water or in dilute aqueous sulphuric acid solution, to produce appropriate carbocation intermediates (10–13), which lead efficiently to photohydration products. These reactions are catalysed by H_3O^+ as well as by general acids and are very fast in comparison to the corresponding ground state reactions (14). To explain the mechanistic features of these reactions, it has been proposed that a strongly polar excited state S_1 may be responsible for these fast excited state protonation reactions, as illustrated in structure **I**.

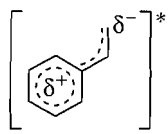

I

We believe that a high degree of charge transfer in the singlet excited states of these normally nonpolar molecules is the driving force for fast protonation reactions. Since electrochromism is the best method for direct detection of the difference in the charge distributions between the ground and excited states, it should be a valuable tool to probe the excited state charge transfer characteristics of those molecules which undergo efficient photohydration reactions. In turn this should shed light on the mechanism of photohydration reactions.

Theory

Liptay and Czekalla (1, 2) and Labhart (3) were the first to provide the necessary theoretical expression describing the changes in the optical absorption due to the application of a strong external electric field. According to them, the field induced change in the molar extinction coefficient ($\Delta\epsilon$) is given

Can. J. Chem. Downloaded from www.nrcresearchpress.com by 91.121.58.235 on 09/07/12
For personal use only.

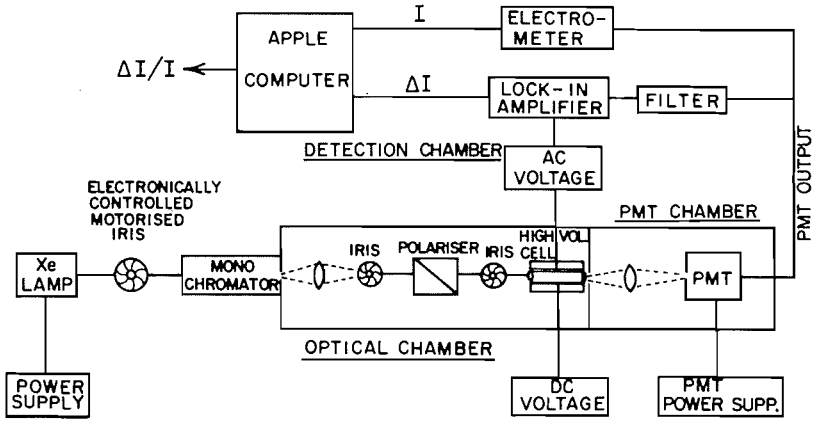

FIG. 1. Block diagram of electric field spectrometer.

by

$$[1]\quad \Delta\epsilon = F_{\text{int}}^2\epsilon\left[A_\chi + B_\chi/15h\frac{d/d\nu(\epsilon/\nu)}{(\epsilon/\nu)} + C_\chi/30h^2\frac{d^2/d\nu^2(\epsilon/\nu)}{(\epsilon/\nu)}\right]$$

where

$$[2]\quad A_\chi = 1/30(3\cos^2\chi - 1)\beta^2[3(\hat{m}\cdot\mu_g)^2 - \mu_g^2] + 3\beta(\alpha_{gm} - \bar{\alpha}_g)$$

$$[3]\quad B_\chi = 5\beta(\mu_g\cdot\Delta\mu) + 15/2\Delta\bar{\alpha} + (3\cos^2\chi - 1)\beta[3(\hat{m}\cdot\mu_g)(\hat{m}\cdot\Delta\mu) - (\mu_g\cdot\Delta\mu)] + 3/2(\Delta\alpha_m - \Delta\bar{\alpha})$$

$$[4]\quad C_\chi = 5\Delta\mu^2 + (3\cos^2\chi - 1)[3(\hat{m}\cdot\Delta\mu)^2 - \Delta\mu^2]$$

In the above equations F_{int} is the corrected electric field at the location of the molecule in solution, μ_g and α_g are the ground state dipole moment and polarizability, $\Delta\mu$ and $\Delta\alpha$ are the change in the dipole moment and polarizability upon electronic excitation, $\hat{m}$ is a unit vector in the direction of the transition moment, and χ is the angle between the electric field and polarization direction of the exciting light.

The formulation of eq. [1] is basically attributable to two effects, the orientation effect and the band shift effect. The orientation effect results from the anisotropic distribution of molecular orientation induced by the applied field. Therefore a polar molecule will tend to align its dipole moment with the field, and a nonpolar molecule whose ground state polarizability is anisotropic will tend to align the axis of greatest polarizability with the field. These effects are reflected in A_χ. The band shift effect will occur due to the interaction of the electric field with the electronic energy levels of a molecule. This interaction results in the change in the energy of the electronic transition if the ground state dipole moment and the polarizability are different from those in the excited state. Therefore the magnitude of the band shift effect is proportional to the change in the dipole moment and polarizability upon electronic excitation to the excited states. These effects are manifested in B_χ and C_χ.

Experimental

The complete setup of the electric field spectrometer designed in our laboratory can be divided into three chambers: optical chamber, pmt chamber, and detection chamber (see Fig. 1). Light from a 1000-W Xe lamp was collimated using a Kratos lamp housing and then passed through a water (or solvent) filter to prevent overheating of the monochromator (Kratos GM252) entrance lens/slit, and then through a motorized iris diaphragm (see Discussion later) before being dispersed by the grating. The monochromatic light is then further collimated onto a Glan–Thompson polarizing prism fitted with an iris diaphragm. The polarizer was mounted on a 360° rotable mount (Optikon) for accurately determining the angle of polarization. Polarized light is then allowed to fall on the quartz window of the high voltage cell (see Discussion later) of 10 cm path length before impinging on the photomultiplier tube (pmt) (Thorn Emi 9906B). The pmt was provided with a mu-metal shield to protect the tube from the background magnetic and electric fields from the field generating apparatus. As shown in Fig. 1, the optical chamber section just after the monochromator was enclosed in a light-tight housing made from aluminium sheet. The exit window of the cell was pressed against the opening of the aluminium sheet that separates the optical and pmt chambers, with the help of a Teflon ring. Since the quartz window and the opening of the aluminium sheet have the same dimensions, only light that travels through the sample cell will be collected by the pmt in the pmt chamber. This arrangement avoids stray light detection by the pmt.

The detection chamber mainly comprises electronic components. Figure 2 shows the block diagram of the electronics used in the construction. The ac field generating apparatus consists of an audio oscillator that supplies a 500-Hz sine wave to an audio amplifier. This amplifies the signal and then drives a step-up transformer to obtain the final ac potential applied to the cell (24 kV ptp). This potential was dropped across a voltage divider to provide a reference signal (1 V rms) for the lock-in amplifier and to give a 1-μV test signal. The dc power supply was also custom-built and can provide a variable dc potential ranging from 10 to 30 kV.

The output of the pmt was fed into a lock-in amplifier (PAR 128) tuned to ω (500 Hz) and an electrometer (Keithly 172). A custom-built additional filter tuned to ω was very helpful in reducing the noise level, and allowing work in the very sensitive region of the lock-in amplifier. The pmt output voltage was controlled by a negative feedback unit to maintain a particular voltage (light intensity) during the data collection at each wavelength. Since the light intensity varies considerably (20:1) across the full wavelength region (230–700 nm), some method of attenuation was required to maintain constant light intensity. The negative feedback unit controls the light level passing through the cell in two ways. A small degree of attenuation could be effected by varying the power to the lamp, but for higher attenuation a motorized iris was utilized. The output from the lock-in amplifier (ΔI) and the electrometer (I) are then digitized by an A/D converter, ratioed, and stored in an Apple IIe computer for further calculation.

Details of the cell used in this experiment are shown in Fig. 3. The cell body consisted of a Teflon tube fitted with two polished, hemicylindrical hollow stainless-steel electrodes, leaving a gap of 5.2 ± 0.1 mm between the parallel faces. Oil was circulated through the hollow cell to maintain constant temperature. Threaded plastic rings were used to hold the quartz window in place. Since high voltages of the order of 10–40 kV were to be used, 15-cm Teflon rings were

Can. J. Chem. Downloaded from www.nrcresearchpress.com by 91.121.58.235 on 09/07/12
For personal use only.

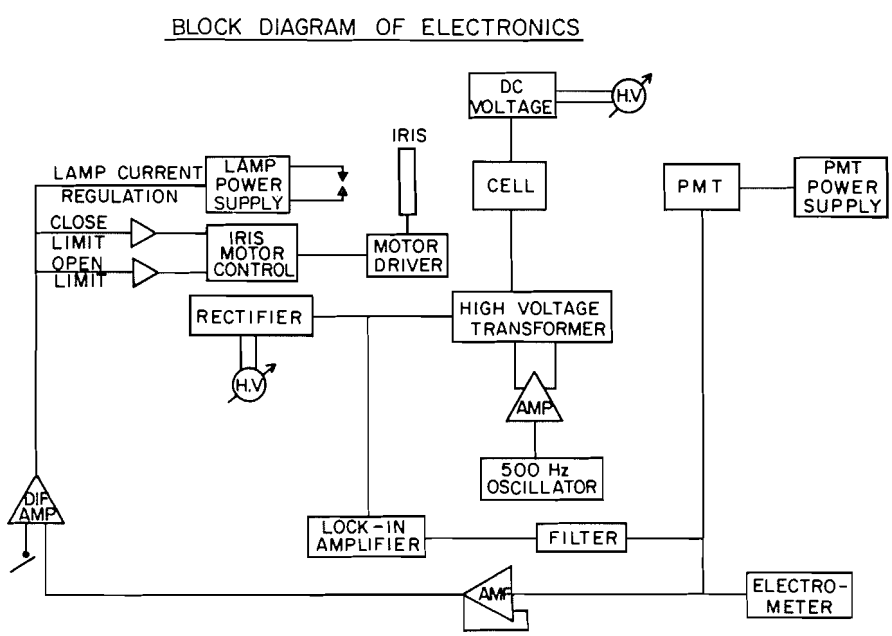

FIG. 2. Block diagram of electronics used in electric field spectrometer.

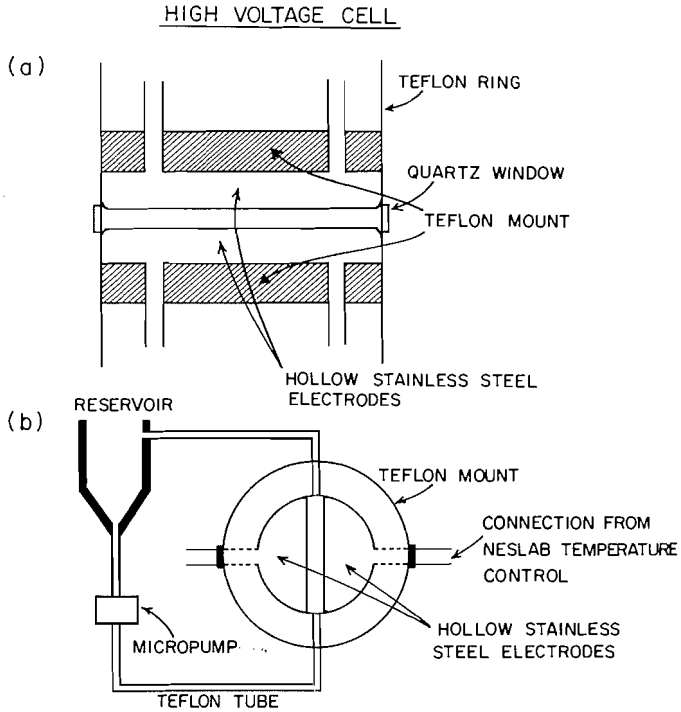

FIG. 3. Diagram of high voltage cell: (a) lateral view; (b) front view.

attached at each end as a safety precaution, and also to prevent the possibility of arc-over. The solution was circulated continuously from a reservoir to the cell by a micropump, to avoid any significant photochemical decomposition of the compound due to prolonged exposure to light.

Since the ac voltage was applied with a dc bias, the total field strength is given by $F_{ext} = \sqrt{2F_{ac}F_{dc}}$. The external electric field F_{ext} was converted to internal electric field F_{int} by taking into account the spherical cavity approximation, which is given by

$$F_{int} = F_{ext}\frac{3\xi}{2\xi + 1}$$

where ξ is the dielectric constant of the solvent used. The change in the molar extinction coefficient $\Delta\epsilon$ was obtained from the equation

$$\Delta\epsilon = -1/2.303cl\frac{I_F - I_{F=0}}{I_{F=0}}$$

where I_F and $I_{F=0}$ are the transmitted light intensities with and without the applied electric field, c is the concentration of the solute, and l is the pathlength of the cell. The data points were collected at two or three different angles χ. For each data point, depending on the signal strength, 5000–10 000 counts were taken over a period of 5–15 min and averaged. The derivative terms in eq. [1] were computed from a digitized absorption spectrum. The values of $\Delta\epsilon$ obtained from the electric field experiment were then least-squares fitted to zero, first, and second derivative terms to obtain A_χ, B_χ, and C_χ, and then the molecular parameters were calculated by using eqs. [2]–[4]. *p*-Nitroaniline (PNA) and *N,N*-dimethyl-*p*-nitroaniline (DMPNA) were subjected to electric field study as test samples to determine the accuracy of our instrument, since these molecules have already been studied by Liptay (4). The close agreement between the present and reported results (Table 1) indicates that the signals obtained from our instrument are not due to any experimental artifacts.

TABLE 1. Ground and excited state dipole moments of *p*-nitroaniline and *N,N*-dimethyl-*p*-nitroaniline[a]

Compound	μ_g[b]	μ_e[b]	μ_g[c]	μ_e[c]
p-Nitroaniline	5.5±0.2	13.7±0.5	5.6	13.7
N,N-Dimethyl-*p*-nitroaniline	5.7±0.2	13.8±0.4	5.1	13.0

[a]Dipole moments are in debye units.
[b]Results obtained from this work.
[c]Results reported by Liptay (4).

Styrene (STY), 2-vinylnapththalene (VN), and 9-vinylanthracene (VA) were obtained from Aldrich chemicals and recrystallized from appropriate solvents. 2-Naphthylacetylene (NA) was synthesized by the earlier reported method (15) and purified by vacuum sublimation. Spectrograde dioxane from Aldrich chemicals was used as solvent, without further purification.

Results

The electric field spectra of STY, VN, NA, and VA are shown in Fig. 4. The discrete points are the values of $\Delta\epsilon$ obtained

Can. J. Chem. Downloaded from www.nrcresearchpress.com by 91.121.58.235 on 09/07/12
For personal use only.

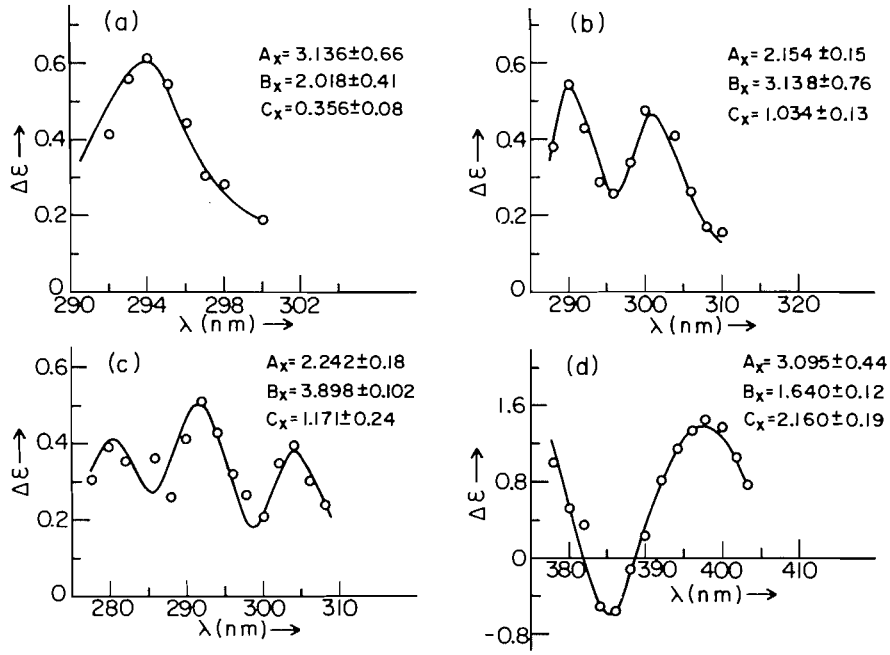

FIG. 4. Electric field spectra of (a) STY; (b) VN; (c) NA; and (d) VA in dioxane at $\chi = 0$. The parameters obtained after multiple linear regression fit to the experimental points are shown on the side of each curve.

TABLE 2. Dipole moments and polarizabilities of aromatic alkenes and alkynes[a]

Compound	$\Delta\tilde{\alpha}$	$\Delta\alpha_m$	$\Delta\mu$	$\hat{m}\Delta\mu$	$\alpha_{gm} - \tilde{\alpha}_g$
Styrene	16.3±4	33.9±4	6.0±2	6.5±2	9.2±3
2-Vinylnaphthalene	30.8±4	56.2±4	3.9±1	3.5±1	12.0±3
2-Naphthylacetylene	37.5±4	70.8±4	5.0±1	5.4±1	15.0±3
2-Vinylanthracene	16.8±2	33.8±2	≃0	—	0.2±1

[a]All measurements were made in dioxane solution at 25°C. Dipole moments are in debye and polarizabilities are in Å^3.

from the electric field experiment. The solid lines are the theoretical curves obtained by a stepwise multiple linear regression fit of the experimental points to eq. [1]. The excellent fit between the experimental data points and theoretical curve indicates that the experimental results are accurately described by eq. [1].

If the molecule has the symmetry of the C_{2v} point group, as in the case of PNA and DMPNA, the calculation of the individual molecular parameters contained in eqs. [2]–[4] becomes simpler because of the definite directions of the dipole moment and transition moment vectors. Since the hydrocarbon molecules investigated here do not belong to the C_{2v} point group, some simplification of eqs. [2]–[4] is required to obtain the molecular parameters from A_χ, B_χ, and C_χ. In our derivation the ground state dipole moments of all these molecules have been assumed to be zero. This assumption is supported by the fact that the reported dipole moment μ_g of STY is close to zero (0–0.13 *D*) (16) and μ_g has been found to be zero or close to zero for various polyenes studied by Liptay *et al.* (17) and Ponder and Mathies (8). Molecular orbital calculations also show that the ground state dipole moments of these molecules are indeed very small.[1] Moreover, this assumption will not introduce any serious errors in the calculation of the change in the dipole moment upon electronic excitation ($\Delta\mu$), which is obtained from C_χ term.

Our experiments yield nonzero values of C_χ for all these molecules except for VA. These large values of C_χ, which give a measure of $\Delta\mu$ of the order of 4–6 debye, indicate that these molecules are quite polar in their Franck–Condon (FC) excited states. However, $\Delta\mu$ was found to be close to zero for VA, within experimental error. The values of $\hat{m}\cdot\Delta\mu$ were calculated by assuming that $\hat{m}$ and $\Delta\mu$ are parallel, which is reasonable for these molecules. The close agreement between the values of $\hat{m}\cdot\Delta\mu$ and $\Delta\mu$ indicate that the change in the dipole moment and transition moment directions are indeed nearly parallel. Setting $\mu_g = 0$, values of $\Delta\tilde{\alpha}$ and $\Delta\alpha_m$ can be calculated from B_χ and the values of $\alpha_{gm} - \tilde{\alpha}_g$ can be obtained from A_χ. All the molecular parameters are compiled in Table 2. The argument that the difference between the change in dipole moments for benzene or naphthalene and anthracene derivatives could be due to a change in the nature of their lowest electronic state can be ruled out on the basis of following points. For example, in benzene and naphthalene derivatives the lowest electronic states are of ^1L_b character, which is polarized along the long molecular axis, and in anthracene derivatives they are of ^1L_a character, polarized along the short molecular axis. In the case of STY, VN, and NA, since the substituents (vinyl group) are present along the

[1]P. Martin, I. G. Csizmadia, and K. Yates. Unpublished results.

Can. J. Chem. Downloaded from www.nrcresearchpress.com by 91.121.58.235 on 09/07/12
For personal use only.

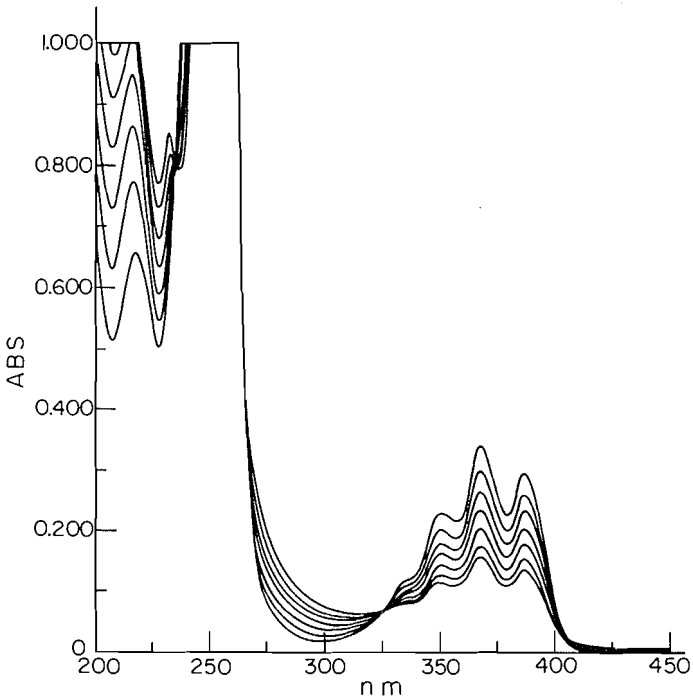

FIG. 5. Absorption changes of VA in acetonitrile on irradiation with 254-nm light. The irradiation was carried out on a Rayonet RPR-100 reactor. The time of irradiation was increased by 5 min from top trace to bottom trace.

long molecular axis, any change in the charge distribution on electronic excitation involving the substituents will be reflected in their ^1L_b type transition. On the other hand, since in VA the substituent is present along the short axis, any change will be more pronounced in its ^1L_a type transition. The fact that there is no change in the dipole moment of VA on electronic excitation could be due to the lack of coplanarity of the vinyl group and the anthracene ring in the ground state because of steric reasons. In fact, the angle between the vinyl group and anthracene ring in the ground state was calculated to be 60° ± 10° from molecular polarizability work (19). This is also manifested by the fact that the absorption spectrum of VA maintains a strong resemblance to that of the parent anthracene. Based on the results of this electric field study one would predict that VA may not undergo any appreciable photohydration reaction.

Figure 5 shows the change in the uv/vis absorption spectra of VA in pure acetonitrile (degassed with argon) upon irradiation with 254-nm uv light. Similar changes were observed when acetonitrile/water in 50% v/v was used as solvent. The major photoproduct obtained in both solvent systems is the same and was identified as a dimer resulting from intermolecular addition across the 9,10 positions of the anthracene moiety. This reaction of VA is completely different from that other aromatic alkenes/alkynes studied here. For example, STY, NA, and VN do not react in pure acetonitrile solvent to any appreciable extent, and in aqueous solution give exclusive and efficient photoaddition of water (10–15).

Discussion

In the case of polar aromatic molecules containing a donor and an acceptor group, a large change in the dipole moment upon electronic excitation is often detectable, which reflects the redistribution of electronic charges in the electronically excited state. However, this is the first time that large changes in the dipole moment have been detected in simple aromatic hydrocarbons containing an alkyne or alkene moiety as a side chain (Table 2). Though the concept of sudden polarization is well documented in the literature from both an experimental and theoretical point of view (20), this process is generally associated with a twisting of a central bond, thereby localizing the charge separation. Furthermore, changes in the dipole moment of the order of 1–3 debye for centrosymmetric polyenes, as observed by Ponder and Mathies (8), have again been attributed to the symmetry-breaking phenomena due to single bond rotations. In our experiments, since we are dealing with the FC excited states, it is very evident that in these molecules electronic excitation and charge separation are concurrent processes. These molecules behave more like electron donor–acceptor systems, where the aromatic ring acts as an electron donor and the alkene or alkyne moiety acts as an electron acceptor.

In the excited state, these molecules (VN, NA, and STY) are approximately 10^{11}–10^{13} times more reactive towards protonation than the corresponding ground states (10–15). This rate effect has been found to increase further on substituting electron donor groups on the aromatic ring, which is expected to further facilitate the charge transfer process. In the proposed mechanism of photohydration reactions, Wan and Yates (10) pointed out that the S_1 states (thermally relaxed first excited singlet states) probably possess a high degree of charge transfer, as shown by structure **I** for the styrene. This has also been postulated by a number of previous workers in their studies of the photoprotonation of aromatic alkenes and cycloalkenes (21, 22). Since alkenes and alkynes are generally known to undergo stabilizing twisting or bending motions upon electronic excitation (23–26), these molecules probably have a twisted or bent relaxed structure in the S_1 state. We believe that charge separation in the FC excited state is the driving force for the twisting or bending in these alkenes and alkynes, hence providing strong solvent stabilization due to the effective interaction between the solvent dipoles and the localized positive and negative charges on the solute. Twisting and the localization of charges would be further helpful in the efficient photoprotonation reaction, since the carbon being protonated is effectively rehybridized before proton transfer takes place. A change in the dipole moment of the order of 4–5 debye in VN and NA amounts to approximately 20% displacement of charges, if the centers of gravity of positive and negative charges are localized at the center of the naphthalene ring and β carbon atom respectively.

The changes in the polarizability upon electronic excitation in case of VN (31 Å^3) and NA (37 Å^3) are far larger than that observed for the parent naphthalene (1.4 Å^3) (9). These large excited state polarizabilities could create a large reaction field in the solution phase, which could explain the observed large excited state dipole moment of these simple hydrocarbon molecules. The value of $\Delta\alpha_m$ for VN and NA, which is nearly twice the value of $\Delta\bar{\alpha}$, suggests that the excited state polarizability is highly anisotropic and that the major change in the polarizability takes place along the direction of transition moment. Since the long wavelength transitions in 2-substituted naphthalenes, such as VN and NA, are known to be polarized along the long axis (29), from the values obtained for $\hat{m}\cdot\Delta\mu$ and $\Delta\alpha_m$ it can be concluded that the electronic transition directly affects the charge distribution around the alkene or alkyne moiety.

Can. J. Chem. Downloaded from www.nrcresearchpress.com by 91.121.58.235 on 09/07/12
For personal use only.

Can. J. Chem. Downloaded from www.nrcresearchpress.com by 91.121.58.235 on 09/07/12
For personal use only.

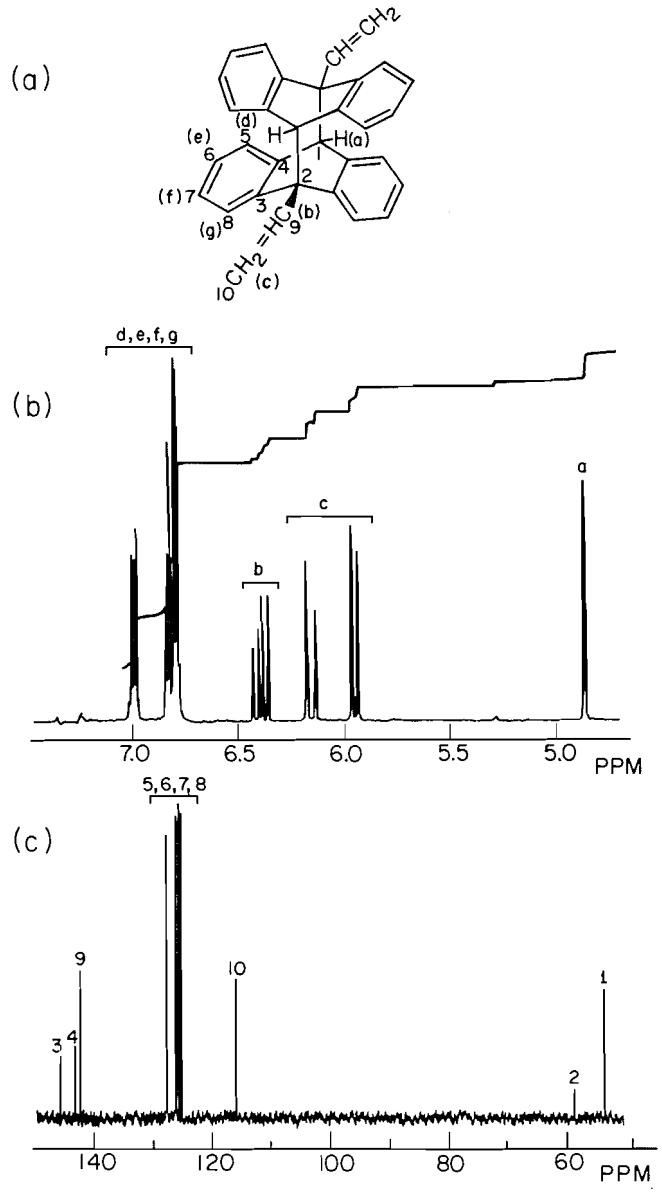

FIG. 6. Molecular structure of the dimer of (a) VA; (b) ^{1}H nmr chemical shifts; (c) ^{13}C nmr chemical shifts.

The study of the photophysics and photochemistry of VA suggests that, for aromatic alkenes and alkynes, other reaction pathways dominate, if significant charge separation in the excited state cannot take place. Since for VA the change in the dipole moment on electronic excitation is zero, which is indicative of no charge separation, the dominant photochemical reaction involves only the anthracene moiety and gives a photodimerization product leaving the alkene moiety intact. As mentioned earlier, the unreactive nature of the vinyl group in VA could be due to the lack of coplanarity between the anthracene ring and vinyl group in the ground state, and hence in the FC excited state, which leads to little or no conjugation or charge transfer. From this study it is quite clear that planarity of the initially excited system is required to bring about efficient charge separation in the excited states of these types of molecules. The type of photodimerization found for VA has been reported for a number of meso-substituted anthracenes in the litarature (27, 28). From this study it appears that photohydration is not necessarily a general reaction for all alkenes and alkynes. The change in the polarizability of VA on electronic excitation closely resembles that of anthracene itself (17 Å^3). This further supports the ineffective nature of the alkene moiety towards charge reorganization in VA.

The complete characterization of the dimer from VA was carried out by spectroscopic techniques. Irradiation of a solution (either 50:50 acetonitrile/water or pure acetonitrile) of VA with 254-nm uv light resulted in a white precipitate. A similar precipitate was also observed by Ebeid *et al.* in methanol, but the product was not characterized (30). The anthracene-like absorption (387, 368, 351 nm) completely disappeared in the absorption spectrum of the product, which is as expected because of the loss of conjugation across the whole anthracene system. The ^{13}C and ^{1}H nmr spectra are consistent with the proposed structure of the dimer (see Fig. 6). COSY, ATP, and HECTOR techniques were used to identify the ^{1}H and ^{13}C chemical shifts, which are shown in Fig. 6(b, c). The dimer (mp 178 ± 2°C) does not appear to be stable at high temperature, since it breaks down during the mass spectral analysis to give the monomeric mass (*m/e* 204) as the major peak. However, careful analysis revealed a small peak at *m/e* 408, corresponding to the dimeric mass. Such decompositions of anthracene dimers to give monomer at temperatures greater than 200°C have been reported in the literature (18). The complete details of the structural analysis, along with the X-ray studies, will be published later.

Acknowledgements

Grateful acknowledgement is made to the Natural Sciences and Engineering Research Council of Canada for continued financial support. We thank Wolfgang Panning for his cooperation in designing the electronics involved in the construction of the instrument.

1. W. LIPTAY and J. CZEKALLA. Z. Naturforsch. A, **15**, 1072 (1960).
2. W. LIPTAY and J. CZEKALLA. Ber. Bunsen-ges. Phys. Chem. **65**, 721 (1961).
3. H. LABHART. Chimia, **15**, 20 (1961).
4. W. LIPTAY. *In* Excited states. Vol. 1. *Edited by* E. C. Lim. Academic Press, New York. 1974. p. 129.
5. R. MATHIES and L. STRYER. Proc. Natl. Acad. Sci. U.S.A. **73**, 2169 (1975).
6. W. LIPTAY, R. WORTMAN, R. BÖHM, and N. DETZER. Chem. Phys. **120**, 429 (1988).
7. R. WORTMAN, K. ELICH, and W. LIPTAY. Chem. Phys. **124**, 395 (1988).
8. M. PONDER and R. MATHIES. J. Phys. Chem. **87**, 5090 (1983).
9. R. MATHIES and A. C. ALBRECHT. J. Chem. Phys. **60**, 2500 (1974).
10. P. WAN and K. YATES. Rev. Chem. Intermed. **5**, 157 (1984).
11. P. WAN, S. C. CULSHAW, and K. YATES. J. Am. Chem. Soc. **104**, 2509 (1982).
12. P. WAN and K. YATES. J. Org. Chem. **48**, 869 (1983).
13. P. KALANDEROPOULOS and K. YATES. J. Am. Chem. Soc. **108**, 6290 (1986).
14. J. MCEWEN and K. YATES. J. Am. Chem. Soc. **109**, 5800 (1987).
15. P. WAN. Ph.D. Thesis, University of Toronto. 1983.
16. A. L. MCCLELLAN. *In* Tables of experimental dipole moments. W. H. Freeman, San Francisco. 1963.
17. W. LIPTAY, W. WALZ, W. BAUMANN, H. J. SCHLOSSER, H. DECKERS, and N. DETZER. Z. Naturforsch. A, **26**, 2020 (1971).
18. E. A. CHANDROSS. J. Chem. Phys. **43**, 4175 (1965).
19. T. C. WERNER. *In* Modern fluorescence spectroscopy. Vol. 2. *Edited by* E. L. Wehry. Plenum Press, New York. 1976. p. 298.

20. L. SALEM. Acc. Chem. Res. **12**, 87 (1979), and references therein.
21. P. KROPP. J. Org. Photochem. **4**, 1 (1979), and references therein.
22. P. KROPP. J. Am. Chem. Soc. **95**, 4611 (1973).
23. L. SALEM and C. ROWLAND. Angew. Chem. Int. Ed. Engl. **11**, 92 (1972).
24. L. SALEM and W. D. STOHRER. J. Chem. Soc. Chem. Commun. 140 (1975).
25. W. G. DAUBEN, L. SALEM, and N. J. TURRO. Acc. Chem. Res. **8**, 41 (1975).
26. C. K. INGOLD. J. Chem. Soc. 2991 (1954).
27. D. O. CAWAN and R. L. DRISKO. *In* Elements of organic photochemistry. Plenum Press, New York. 1976. Chap. 2.
28. M. A. CASTELLAN and M. R. CALAS. C.R. Seances Acad. Sci. Paris, **281**, 221 (1975).
29. H. H. JAFFE and M. ORCHIN. *In* Theory and application of ultraviolet spectroscopy. Wiley and Sons, New York. 1962. p. 303.
30. E. M. EBEID, M. A. EL-GAMEL, and S. E. MORSI. Photochem. Photobiol. **44**, 547 (1986).

Can. J. Chem. Downloaded from www.nrcresearchpress.com by 91.121.58.235 on 09/07/12
For personal use only.

Retinylidene Schiff bases in surfactant-solubilized water pools in heptane

ANIL K. SINGH, CAMILLE SANDORFY, AND JANOS H. FENDLER[1]

Département de chimie, Université de Montréal, C.P. 6128, Succursale A, Montréal (Québec), Canada H3C 3J7

Received January 26, 1990

ANIL K. SINGH, CAMILLE SANDORFY, and JANOS H. FENDLER. Can. J. Chem. **68**, 1514 (1990).

All-*trans*-retinal (**1**) was reacted with *n*-butylamine in sodium bis(2-ethylhexyl)sulfosuccinate (AOT) reverse micelles in heptane to form all-*trans*-*N*-retinylidene–*n*-butylamine Schiff bases (**2**). The extent of protonation of **2** by 3-chloropropionic acid (CPA) to give **3** in AOT reverse micelles in heptane was found to depend on the ratio of [CPA] to [**2**], as well as on $[H_2O]/[AOT]$ (i.e., on the ω value). At any given [**2**] and ω values, increasing amounts of CPA increased the protonation and at any given constant [**2**] and [CPA], increasing ω values also increased the protonation. Over a period of 24 hours, there was only 4% decomposition of **2** in AOT reverse micelles in heptane at $\omega = 24$. Conversely, in three hours, 23% of **3** decomposed in the same system. The *trans* to *cis* photoisomerization of **2** in heptane occurred at a much faster rate in the presence of AOT reverse micelles than in their absence. The appearance of carboxylate peaks (FTIR, 1400–1500 cm^{-1}) indicated that the larger the AOT solubilized water pools, the greater the CPA dissociation. **1** also reacted with the α-NH_2 group of *l*-lysine (**4**) in AOT reverse micelles in heptane to give the corresponding Schiff base **6**. Protonation of **6** occurred either intramolecularly or by reaction with unreacted **4**. These results were discussed in terms of rhodopsin protonations.

Key words: retinylidene Schiff bases, reverse micelles, protonation of Schiff bases, *trans* to *cis* photoisomerization.

ANIL K. SINGH, CAMILLE SANDORFY et JANOS H. FENDLER. Can. J. Chem. **68**, 1514 (1990).

Opérant dans des micelles inversées de bis(2-éthylhexyl)sulfosuccinate de sodium (AOT) dans l'heptane, on a fait réagir le rétinal complètement *trans* (**1**) avec la *n*-butylamine pour obtenir la base de Schiff, *N*-rétinylidène–*n*-butylamine complètement *trans* (**2**). Dans des micelles inversées d'AOT dans l'heptane, on a trouvé que le taux de protonation du produit **2** (conduisant à la formation du produit protoné **3**), par l'acide 3-chloropropanoïque (ACP), dépend des rapports de [ACP]/[**2**] et de $[H_2O]/[AOT]$ (c'est à dire de la valeur ω). À des valeurs données de [**2**] et de ω, une augmentation de la quantité d'ACP provoque une augmentation de la protonation; par ailleurs, à des valeurs constantes de [**2**] et de [ACP], une augmentation des valeurs de ω augmente aussi la protonation. En 24 heures, dans des micelles inversées d'AOT dans l'heptane, à une valeur $\omega = 24$, il ne s'est produit que 4% de décomposition du composé **2**. Par ailleurs, dans le même système, 23% du composé **3** s'est décomposé en trois heures. La photoisomérisation *trans* à *cis* du composé **2** dans l'heptane se produit beaucoup plus rapidement en présence de micelles inversées d'AOT qu'en leur absence. L'apparition de bandes carboxylates (FTIR, 1400–1500 cm^{-1}) indique que plus les masses d'eau solubilisées par l'AOT sont grandes, plus l'ACP est dissocié. Dans des micelles inversées d'AOT dans l'heptane, le composé **1** réagit aussi avec le *l*-lysine (**4**) pour donner le base de Schiff correspondante (**6**). La protonation du composé **6** se fait soit d'une façon intramoléculaire ou par réaction avec du produit **4** qui n'a pas réagit. On discute de ces résultats en fonction des protonations de la rhodopsine.

Mots clés : bases de Schiff rétinylidène, micelles inversées, protonation des bases de Schiff, photoisomérisation *trans* à *cis*.

[Traduit par la revue]

Can. J. Chem. Downloaded from www.nrcresearchpress.com by 91.121.58.235 on 09/07/12
For personal use only.

Rhodopsins (1, 2) belong to a major class of membrane-bound proteins and are involved in light-induced bioenergy transduction. The chromophore of rhodopsins is a retinal (**1**) analogue attached to a lysine residue of the apo-protein via a protonated Schiff base (PSB) linkage (Fig. 1). Both polar and apolar microenvironments surrounding the chromophore in the membrane-bound opsins have been suggested to be responsible for the several striking structural and functional features of rhodopsins (3–9). The role of water molecules near the active site of rhodopsin has also been considered (3, 4).

Retinylidene Schiff bases (SB) have been used extensively as rhodopsin models (9, 10). To clarify important chemical and photochemical properties of rhodopsins, in view of the possible polar, as well as nonpolar, nature of the rhodopsin active site, it is desirable to investigate retinylidene SB in a system that has both polar and nonpolar domains. Reverse micellar systems (11–16) mimic the polar pockets in enzymes well and provide unique microenvironments for substrate solubilization and interactions (11). Specifically, they may model the active site of rhodopsin insofar as micropolarity and acidity can be controlled by changing the amount of water solubilized (i.e., the [water]/[surfactant]: the ω value) (12). A bacteriorhodopsin model is presented here in which all-*trans*-retinal–*n*-butylamine SB has been introduced into reverse-micellar sodium bis(2-ethylhexyl)sulfosuccinate (AOT) in *n*-heptane.

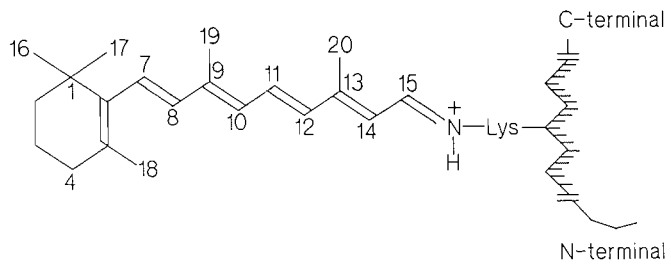

FIG. 1. Retinal attached to lysine via a protonated SB linkage in rhodopsins.

Materials and methods

All-*trans*-retinal, *l*-lysine, and N_α-*tert*-Boc-*l*-lysine were obtained from Sigma Chemical Company, U.S.A. Sodium bis(2-ethylhexyl)-sulfosuccinate (AOT), *n*-butylamine, *n*-heptane (spectrophotometric grade), 3-chloropropionic acid (CPA), trifluoroacetic acid (TFA), and methanesulfonic acid were obtained from Aldrich Chemical Company, U.S.A.

AOT was purified by dissolving in anhydrous, warm (40°C) methanol. The white, milky suspension was centrifuged and the clear supernatant liquid was collected. The methanolic solution was further stirred with activated carbon (Darco G-60 100 mesh) for 3 h. The carbon was separated by filtration and the AOT was recovered by removing the MeOH with a rotary evaporator. The white material was first dried under high vacuum (0.1 Torr; 1 Torr = 133.3 Pa) for 6 h and then over P_2O_5 overnight in an evacuated desiccator. Such purified AOT did not show absorption in the 250–450 nm region. UV–VIS

[1]Author to whom correspondence may be addressed.

Can. J. Chem. Downloaded from www.nrcresearchpress.com by 91.121.58.235 on 09/07/12
For personal use only.

spectrophotometric measurements were made either on a Hewlett–Packard 8450 A diode array or on a Varian Carey 16 spectrophotometer.

All-trans-N-*retinylidene*–n-*butylamine Schiff base (2)*

All-*trans*-*N*-retinylidene–*n*-butylamine (**2**) was prepared by allowing all-*trans*-retinal (**1**) to react with a 3-mol excess of *n*-butylamine (freshly distilled under N_2) in the presence of a small amount of anhydrous sodium sulfate and a few beads of Linde 4A molecular sieves. The reaction mixture was kept under N_2 at 4°C overnight. The dark brown solution was filtered through a small Büchner filter directly into a Schlenk-type storage vessel in which it was carefully evaporated to dryness using high vacuum. The solid residue was redissolved in anhydrous ether and evaporated twice to assure complete removal of excess *n*-butylamine. The brownish-yellow solid melted at 63–64°C and exhibited a UV–VIS absorption band at 357 nm in *n*-heptane.

Micellization of all-trans-N-*retinylidene*–n-*butylamine Schiff base (2) in AOT in heptane*

Micellar solutions of SB **2** ($\sim 1.8 \times 10^{-5}$ M) in 10^{-2} M AOT in *n*-heptane with ω = 0, 8, 24, 48, and 72 ($\omega = [H_2O]/[AOT]$) were prepared by mixing the appropriate amount of the SB in respective AOT solutions. Transparent solutions were obtained up to $\omega = 24$. The solutions with ω exceeding 24 became cloudy. All of the solutions were prepared and stored in the dark to avoid light-induced changes in the SB. Protonation of the micellized SB was done by syringing in an appropriate amount of the acid.

All-trans-N-*retinylidene*–n-*butylamine Schiff base (2) formation in AOT reverse micelles in heptane*

A mixture of all-*trans*-retinal (λ_{max} 368 nm, 1.7×10^{-5} M) and *n*-butylamine (twofold excess) in AOT (1×10^{-2} M, *n*-heptane, H_2O, 0.08 M, ω = 8) solution was sonicated for 2 min. The transparent solution was kept in the dark at room temperature. The formation of SB **2** in the micellar medium was monitored by observing the growth of the absorption band at 357 nm. A control experiment was run by taking the reactants in *n*-heptane only.

Reaction of all-trans-*retinal (1) with* l-*lysine (4)*

l-Lysine (**4**, 0.0350 g) was added to the AOT solution (10 mL, 10^{-2} M in *n*-heptane, 0.08 M H_2O). The suspension was sonicated (90 W, 10 min) or vigorously stirred (Teflon, 30 min). Undissolved lysine was filtered out to obtain a transparent AOT–lysine solution. To this solution was added all-*trans*-retinal ($\sim 5.0 \times 10^{-5}$ M) and the mixture sonicated (90 W, 1 min) in the dark. The resulting solution was kept at room temperature (25°C) in the dark and the progress of the reaction was followed by UV–VIS spectrophotometric measurements. In a control experiment, a mixture of all-*trans*-retinal and *l*-lysine was stirred in *n*-heptane.

Treatment of N_α-tert-*Boc*-l-*lysine (5) with all*-trans-*retinal (1) in AOT micelles in heptane*

N_α-*tert*-Boc-*l*-lysine (**4**) and all-*trans*-retinal (**1**) were mixed in AOT solution (10^{-2} M, *n*-heptane, H_2O, 0.08 M) as described above. The mixture was kept at ambient temperature in the dark and its UV–VIS spectra recorded over a period of time.

Stability of SB (2) and PSB (3) in AOT micelles and heptane

SB (**2**) was constituted in AOT solutions in *n*-heptane/water by sonication. The resulting micellar-SB solutions were kept in the dark at ambient temperature. The UV–VIS spectra of the solutions were measured at different time intervals and changes in the absorbance at 357 nm due to SB **2** were noted. Micellar SB **2** was protonated by adding appropriate amounts of CPA. The solution was shaken and kept in the dark at ambient temperature. Any change in absorbance at 424 nm due to PSB **3** was noted.

Protonation of SB 2 by various acids

Appropriate amounts of different acid solutions in heptane, chloroform, or methanol were added from a microliter syringe to the solutions of **2** in different media of AOT micelles, heptane, chloroform, or methanol. Solutions of **2** turned yellow (depending upon the extent of protonation), giving PSB **3**, which showed a red-shifted absorption band between 420 and 445 nm.

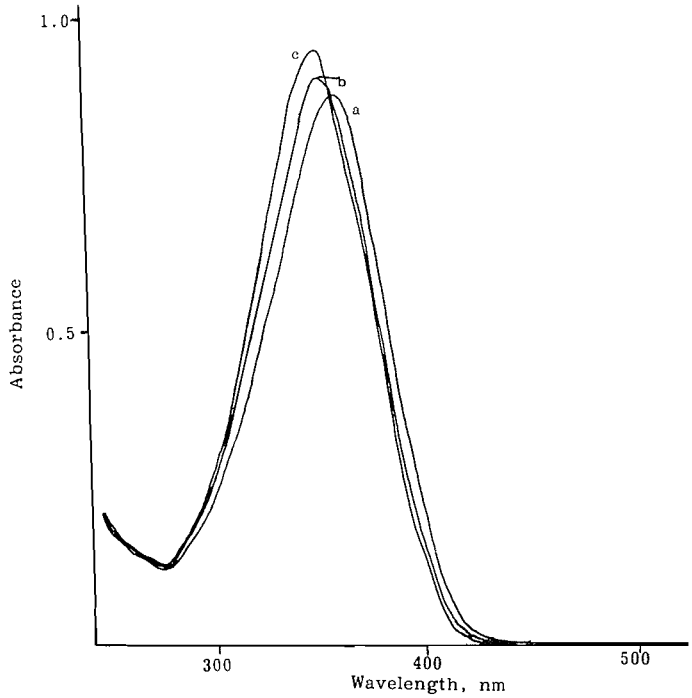

FIG. 2. Absorption spectra of 1.7×10^{-5} M all-*trans*-retinal and 3.4×10^{-5} M *n*-butylamine in 1.0×10^{-2} M AOT in heptane containing 0.08 M H_2O (ω = 8) (a) immediately, (b) 3 h, and (c) 6 h subsequent to mixing the components. The solution was kept in the dark at 22°C.

Irradiation of SB 2

Dilute solutions of SB **2** ($\sim 1.8 \times 10^{-5}$ M) in heptane or AOT micelles in heptane were taken in a quartz cell. The solutions were purged with dry N_2 and septum sealed. Direct irradiation (343 nm; ca. 1 μJ, 2-Hz laser pulses; Lambda-Physik excimer-dye laser) was performed on these samples. The action plots were made by observing the changes in the absorbance at 357 nm for initial-stage and long-time irradiation.

Determination of micellar size

SB **2** ($\sim 1.8 \times 10^{-5}$ M) was micellized in 10^{-1} M AOT in *n*-heptane at ω = 25 by briefly sonicating the sample. The clear solution was subjected to dynamic light scattering experiments using a digital correlator (Brookhaven Instruments Corporation model BI2030 AT) equipped with Microsoft Quick Basic (version 4.0).

FTIR studies on AOT reverse micelles in heptane and SB 2 constituted therein

SB **2** was micellized in AOT solutions as usual. The FTIR spectra were recorded either in 0.25 mM CaF_2 or 0.50 mM IRTRAA-2 liquid cells. Protonation of the micellized SB by CPA was done in an appropriate volumetric flask before taking the sample in the IR cell. All FTIR spectra were measured on a Nicolet 5DXB spectrophotometer with a resolution of 2 cm^{-1}.

Results and discussion

Formation of all-trans-N-*retinylidene*–n-*butylamine (2) in AOT reverse micelles in heptane*

All-*trans*-retinal (**1**) reacted with *n*-butylamine in AOT reverse micelles in heptane to give SB **2** (Fig. 2). The reaction was complete in about 6 h with the appearance of a new peak at 357 nm. The isosbestic point at 364 nm clearly indicated the conversion of retinal (λ_{max} 369 nm) to the corresponding SB. The micellar SB could be completely protonated by the addition of trichloro- or trifluoroacetic acid (λ_{max} PSB, 435–440 nm). The SB showed identical absorption bands in *n*-heptane and

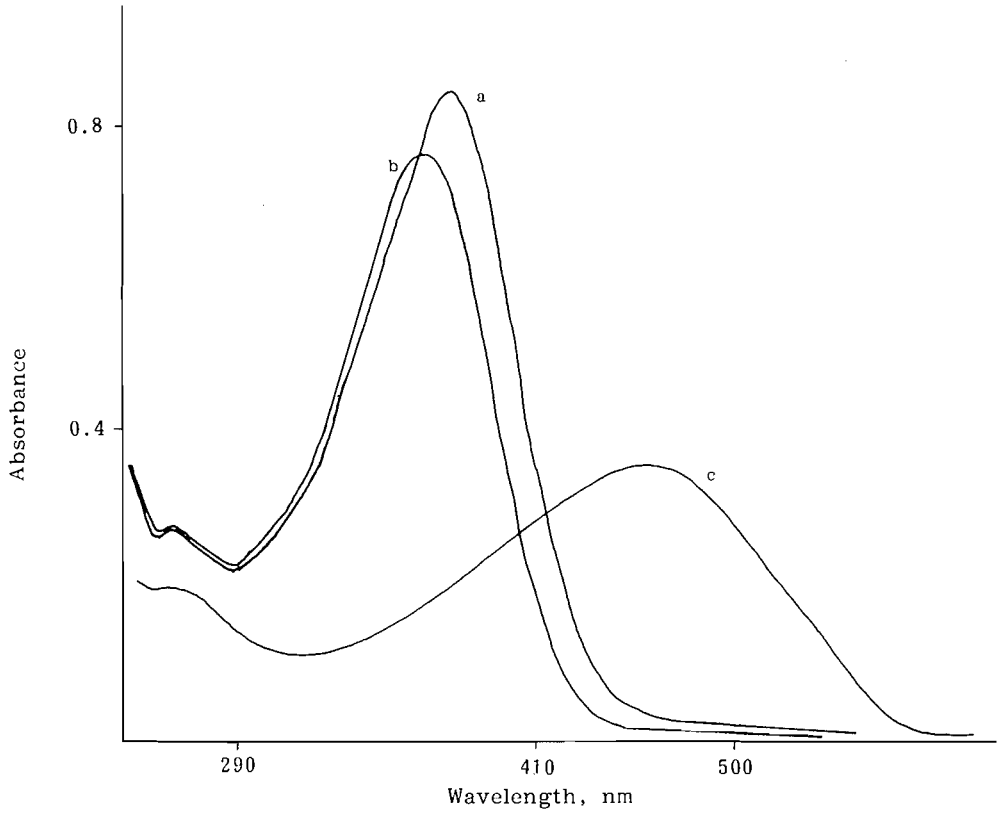

FIG. 3. Absorption spectra of 5.0×10^{-5} M all-*trans*-retinal and lysine (saturated solution) in 1.0×10^{-2} M AOT in heptane containing 0.08 M H_2O ($\omega = 8$) (a) immediately and (b) 5 h subsequent to mixing the components. The solution was kept in the dark at 22°C. Spectrum (c) was obtained subsequent to the addition of excess trifluoroacetic acid.

in AOT reverse micelles in heptane in the range of $\omega = 0$ to $\omega = 72$.

Reaction between l-lysine (4) and retinal (1) in AOT reverse micelles in heptane

l-Lysine (**4**) could be solubilized in AOT micelles in heptane. Cosolubilized all-*trans*-retinal (**1**) reacted with *l*-lysine (**4**), as evident from the appearance of a new UV–VIS peak at 356 nm. However, the retinylidene compounds were not stable, as evidenced by the isosbestic point at 350 nm (Fig. 3). No new peak appeared when *l*-lysine and retinal were stirred in heptane. There was approximately a 23% loss of retinylidene (either retinal or its lysine SB) compounds in AOT–lysine micellar media. Addition of trifluoroacetic acid to the product formed between retinal and *l*-lysine resulted in the formation of a new species with absorption maximum at 430 nm (Fig. 3). These observations indicate that a SB (λ_{max} 356 nm) is formed as a result of reaction between all-*trans* retinal and *l*-lysine in AOT micelles (Scheme 1), which upon protonation of its imine nitrogen exhibits the expected red shift in the absorption spectrum. Protonation of the amine group may also occur, but is not expected to influence the absorption maximum.

To determine which amino group (α or ε, or both) reacts, retinal was treated with N_α-*tert*-Boc-*l*-lysine (**5**) in AOT micellar solution. The only change observed in the absorption behavior of the mixture was a minor reduction (~7%) in the absorbance at the λ_{max} of retinal at 368 nm. Addition of trifluoroacetic acid to this mixture (after keeping it at ambient temperature for 24 h) caused the 368-nm band to shift to 398 nm. Apparently, the ε-amino group of lysine did not react with retinal. Therefore, retinal reacts with the α-NH_2 group of lysine in AOT micelles to give SB **6**.

Retinal–lysine Schiff bases could not be prepared at retinal concentrations higher than 10^{-2} M. The decomposition of the retinylidene compounds was rapid. In addition, correspondingly higher lysine concentrations were found to cause protonation of the retinal–lysine SB. Protonation of retinal–lysine Schiff bases can be caused either by an adjacent carboxyl proton (**6** → **8**) or by carboxylic groups of unreacted lysine (to give **9** or **10**; Scheme 2). The extent of various protonation possibilities will, however, depend upon the acid–base characteristic of the micellar site where the SB and lysine are localized. Self-protonated retinal–lysine Schiff bases showed an absorption band at 440 nm.

In the AOT micellar system, N_α-*tert*-Boc-*l*-lysine ionizes to release its carboxylic proton, which in turn protonates the ε-NH_2 group, rendering it electrophilic. A positively charged nitrogen does not react with the electrophilic retinyl aldehyde group (Scheme 3). Similarly, lysine may also ionize in AOT to release the acidic proton that protonates the more basic ε-NH_2 group (pK_a in H_2O, 10.53) rather than the less basic α-NH_2 group (pK_a in H_2O, 8.95).

It is interesting to note that in rhodopsin the ε-amino group reacts with retinal (α-amino of lysine is in the peptide bond), but in reverse micelles it does not. As indicated in Scheme 3, the ε-N of N_α-*tert*-Boc-*l*-lysine is rendered electrophilic due to its protonation by acidic surroundings. In the protein, however, the same ε-amino group reacts with retinal. Apparently, the acidic protein residues are either incapable of protonating the free ε-amino group of lysine or lie away from it. In other

Can. J. Chem. Downloaded from www.nrcresearchpress.com by 91.121.58.235 on 09/07/12
For personal use only.

Can. J. Chem. Downloaded from www.nrcresearchpress.com by 91.121.58.235 on 09/07/12
For personal use only.

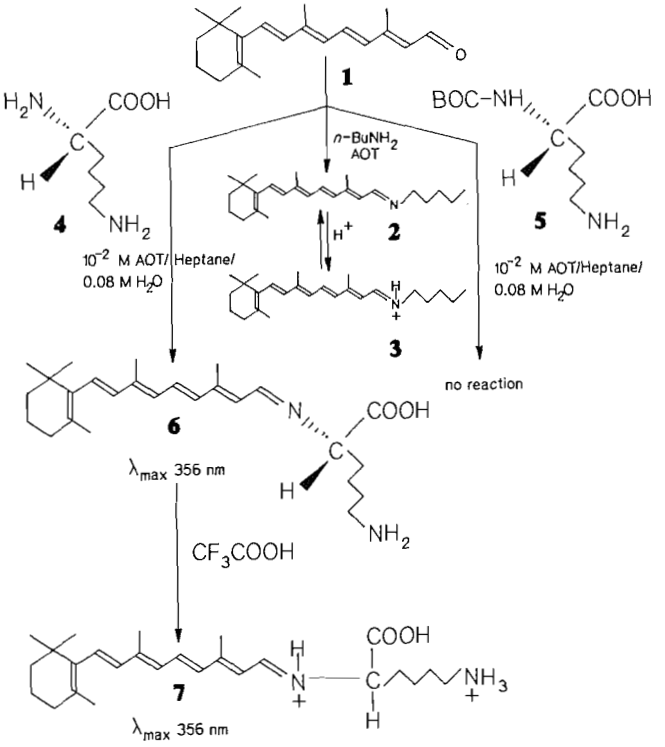

SCHEME 1

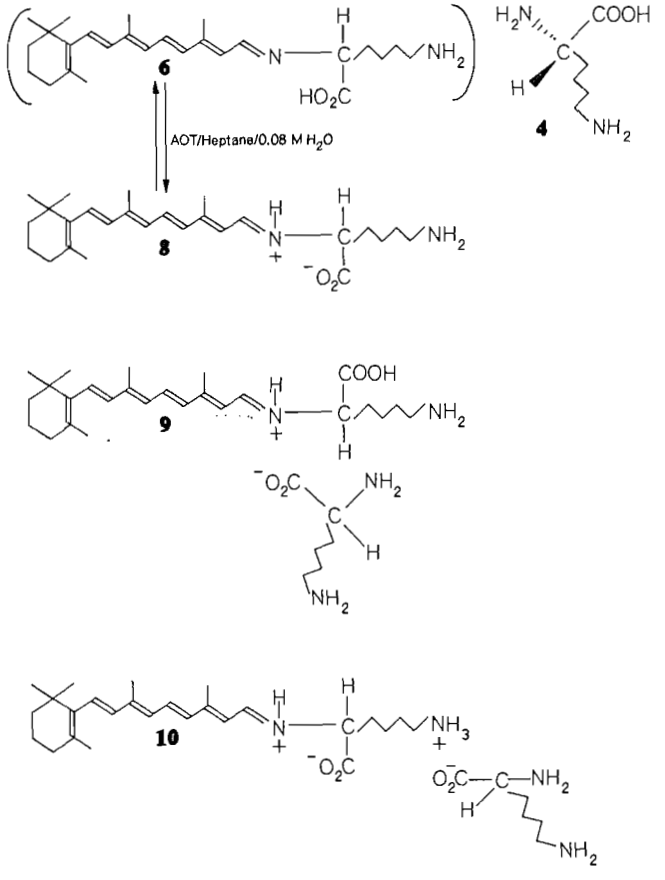

SCHEME 2

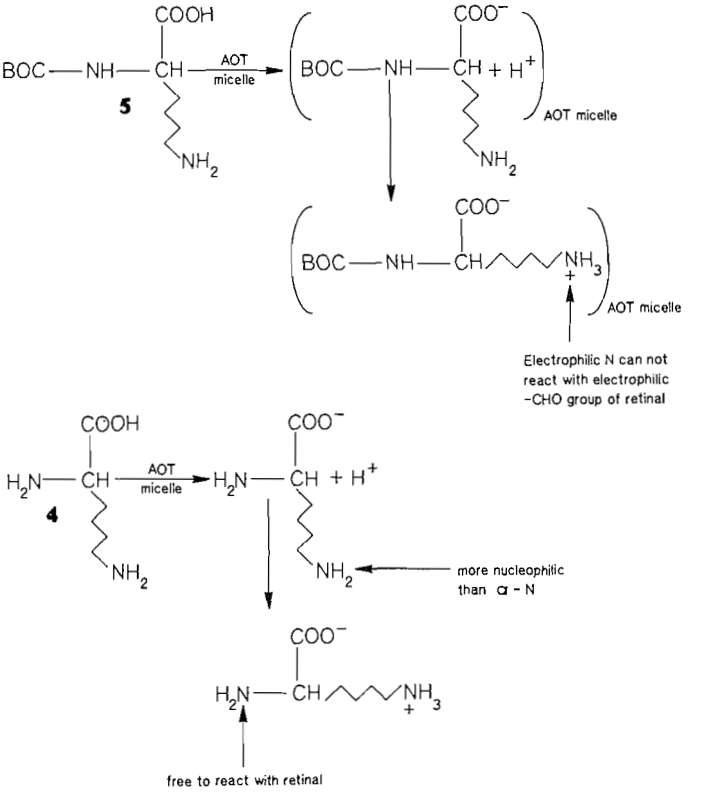

SCHEME 3

words, conformational changes in opsin during regeneration of bleached rhodopsin play important roles. These results also indicate that, prior to or during SB formation, water molecules and the acidic protein residues are at a distance from the lysine group. The SB formation may cause opsin to adapt a conformation that allows the acidic moiety and water to get closer to the imine group. Thus, SB formation between retinal and the ε-amino group of lysine occurs in a totally hydrophobic or nonplanar medium. If the rhodopsin active site has a polar pocket, it must be formed only after generation of the -C=N- chromophore.

Protonation of SB 2 by CPA in heptane

Protonation of 1.8×10^{-5} M SB **2** in *n*-heptane was studied by introducing an appropriate amount of 1.8×10^{-2} M 3-chloropropionic (CPA) acid. There was no appreciable extent of protonation (<0.50%) in an equimolar mixture of SB **2** and CPA. Large excess of CPA (CPA:SB ratio >100) caused ~15% of protonation.

Protonation of SB 2 by CPA in 10^{-2} M AOT reverse micelles in heptane ($\omega = 0$)

Protonation of SB **2** (~1.8×10^{-5} M AOT in *n*-heptane, $\omega = 0$) was done by adding calculated amounts of CPA solution in *n*-heptane. The extent of protonation was measured by monitoring the growth of a red-shifted UV–VIS absorption band at 443 nm. There was ca. 0.50% protonation of the SB in the presence of an equimolar amount of CPA. A maximum protonation of ca. 43% was obtained when the SB:CPA molar ratio reached ~1:180. At this molar ratio, only ca. 19% protonation was observed in the absence of AOT.

Protonation of SB 2 by CPA in AOT reverse micelles in heptane ($\omega = 8$)

A solution of SB **2** (ca. 1.8×10^{-5} M) was prepared in

Can. J. Chem. Downloaded from www.nrcresearchpress.com by 91.121.58.235 on 09/07/12
For personal use only.

TABLE 1. Extent of protonation in a 1:1 mixture of all-*trans*-retinylidene–*n*-butylamine Schiff base (**1**) and 3-chloropropionic acid in different media

Media	% Protonation
n-Heptane	~0.4
AOT/*n*-heptane/	
$\omega = 0$	0.6
$\omega = 5$	6
$\omega = 24$	17
$\omega = 45$	34
$\omega = 72$	67

AOT = 1×10^{-2} M; CPA = SB = 1.8×10^{-5} M.

10^{-2} M AOT–heptane with $\omega = 8$. For the preparation of AOT solutions, it was assumed that the AOT used contained no water. The extent of protonation was enhanced. An equimolar amount of CPA caused ca. 6% protonation, while a maximum of 51% protonation was observed in the presence of ca. 50 mol excess of CPA.

Protonation of SB 2 by CPA in AOT reverse micelles in heptane ($\omega = 24$)

The method of protonation was the same as described above. The extent of protonation was further enhanced. Thus, an equimolar amount of CPA caused 15% protonation. A maximum of 61% protonation could be achieved by only a 6 mol excess of CPA.

Protonation of SB 2 by CPA in AOT reverse micelles in heptane ($\omega = 48$)

Efficient protonation of SB **2** by CPA was observed in AOT in heptane, $\omega = 48$. Thus, at an equimolar amount of CPA, 34% protonation, and a maximum of 69% protonation at a CPA molar excess of 7 was observed.

Protonation of SB 2 by CPA in AOT reverse micelles in heptane ($\omega = 72$)

The appearance of turbidity caused difficulty in measuring the absorption spectra of AOT samples in heptane with $\omega = 72$. However, the solution remained clear for a few minutes, allowing quick measurements. The equimolar amount of CPA caused 67% protonation. As usual, further addition of CPA (ca. 2 mol excess) caused slight enhancement of only about 3%. Thus, most of the SB could be protonated by equimolar CPA only.

The presence of 0.48 or 0.72 M water in the micelles caused some material loss also. Thus, when the ratio of CPA/SB was 6 in AOT micelles having 0.48 M water, there was approximately 8% loss of retinylidene chromophore. The loss of retinylidene chromophores was greater in the presence of 0.72 M water in the micelle. Thus, when the ratio of [CPA] to [SB] was 3 there was approximately 23% loss of retinylidene chromophore.

The extent of protonation of a 1:1 mixture of SB **2** and CPA in AOT micelles with varying amounts of water is shown in Table 1. The extent of protonation depended on the molar ratio of CPA to SB **2** and on the amount of water present in the reverse micelles. At a given ω value, increasing amounts of CPA increased the extent of protonation to a point beyond which the addition of further CPA had no effect. In the absence of water ($\omega = 0.1$), 200-fold excess CPA was needed to reach the equilibrium protonation of **2**, whereas at $\omega = 48$ it took only a sixfold excess to protonate **2** to a much higher extent. It appears thus that availability of protons rather than acid strength is of overriding importance in SB protonation. Proton availability depends on the extent of CPA dissociation. This, in turn, is favored by the availability of water in higher concentrations in the reverse micelles. The extent of protonation is seen to increase linearly with the amounts of water present.

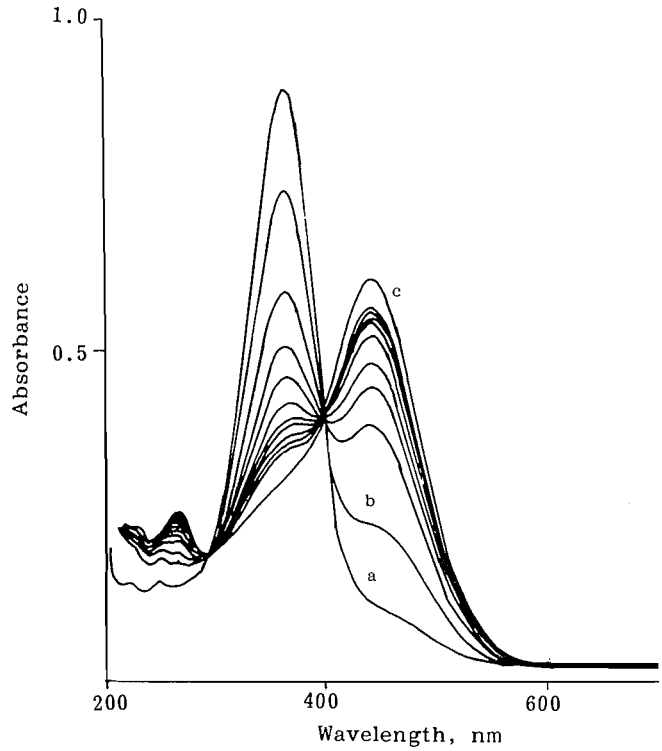

FIG. 4. Absorption spectra of 1.8×10^{-5} M all-*trans*-*N*-retinylidene–*n*-butylamine Schiff base (**2**) in methanol containing 0.24 M H_2O in (a) the absence and (b → c) in the presence of increasing amounts of 3-chloropropionic acid. [3-Chloropropionic acid] = 1.8×10^{-5} M (b) and 1.8×10^{-4} M (c).

Protonation of SB 2 by methanesulfonic acid

AOT has sulfonate groups, which may be competing for CPA protons. The corresponding sulfonic acid may also cause the protonation of SB, though the sulfonic acid generated will be in small quantity as the molar ratio of AOT to CPA is very high (>500). Protonation of SB by methanesulfonic acid was studied in chloroform. Appropriate amounts of methanesulfonic acid in $CHCl_3$ (1.8×10^{-2} M) were added to a chloroform solution of the SB (1.8×10^{-5} M). Approximately 97% protonation was observed in a 1:1 mixture of SB and methanesulfonic acid.

Protonation of SB 2 by CPA in MeOH containing 0.24 M H_2O

The extent of protonation of the SB by CPA in methanol containing 0.24 M H_2O is shown in Fig. 4. A maximum of ~60% protonation occurred when the CPA:SB ratio was 10; when the ratio of CPA to SB was 1, only 17% protonation was observed. The acidity of CPA in methanol with 0.24 M water is found to be very similar to the acidity of the micellar system containing AOT (0.01 M) in *n*-heptane with 0.24 M H_2O and CPA. Clearly, the extent of ionization or, in other words, number of available protons, is important in causing the protonation of the SB. A maximum of 60% protonation occurred only when the CPA:SB ratio exceeded 10.

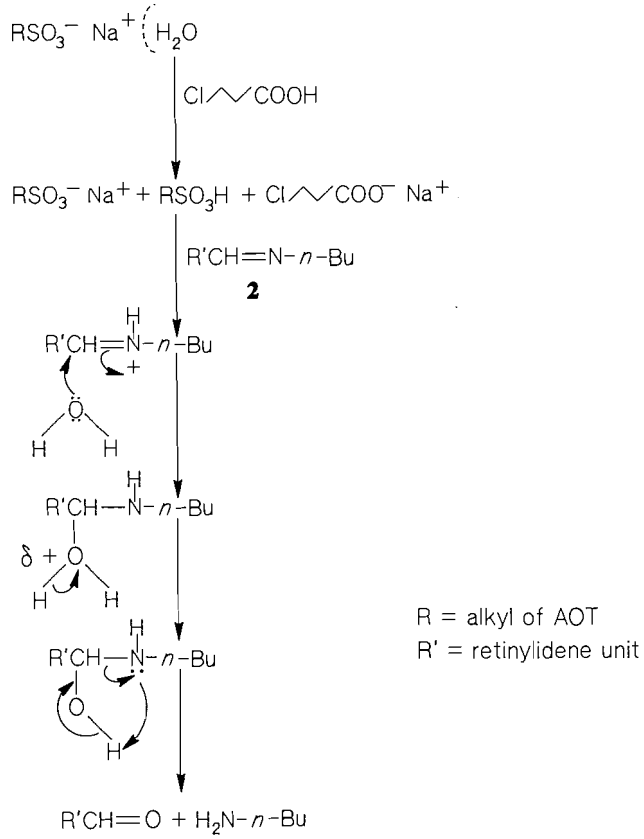

SCHEME 4

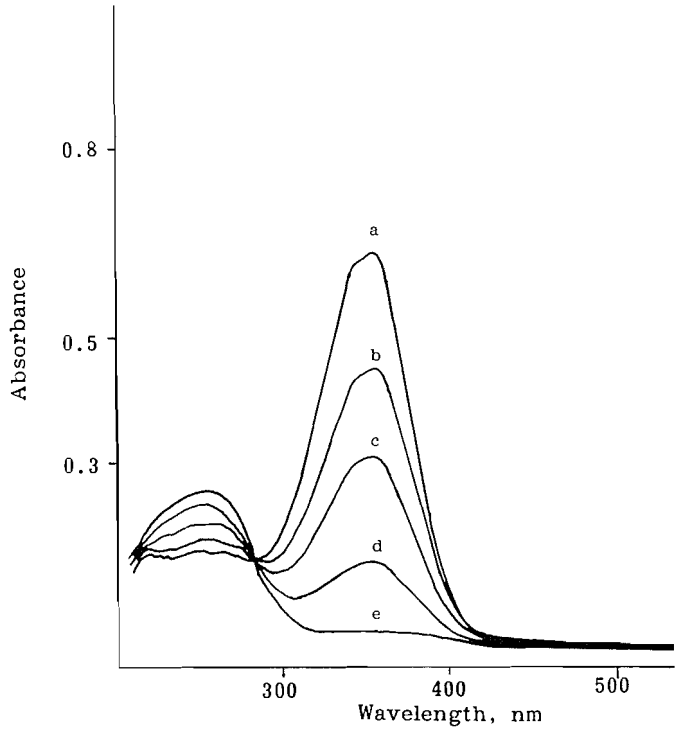

FIG. 5. Absorption spectra of 1.8×10^{-5} M deaerated all-*trans*-*N*-retinylidene–*n*-butylamine Schiff base (**2**) in 1.0×10^{-2} M AOT in heptane in the presence of 0.08 M H_2O ($\omega = 8$) prior (a) and subsequent to 10 (b), 20 (c), 40 (d), and 80 (e) min of irradiation by 343 mm, ca. 1 μJ, 2-Hz laser pulses.

Stability of SB 2 and its protonated form in AOT reverse micelles in heptane

SB **2** ($\sim 1.8 \times 10^{-5}$ M) in AOT–heptane micelles containing 0.24 M water was kept in the dark at ambient temperature and changes in absorbance at 357 nm were monitored at various time intervals. There was ca. 2% loss in the absorbance of SB over a period of 3 h. Over a period of 24 h, there was only ca. 4% loss of SB. Similarly, absorbance changes at 357 and 424 nm were monitored in a 1:1 mixture of SB:CPA in AOT micelles containing 0.24 M water. Addition of CPA caused ~17% protonation of the SB. In 3 h, about 23% of the SB and its protonated form hydrolyzed. After 24 h, 33% of the SB and 65% of PSB hydrolyzed. When CPA was present in sixfold excess over SB, the decomposition of the SB and PSB was faster. Thus during 3 h, about 52% of the SB and PSB hydrolyzed. After 24 h, 85% PSB hydrolyzed. When CPA was present in 20-fold excess over SB, the hydrolysis of PSB was faster and, in about 6 h, 82% of the PSB (λ_{max} 424 nm) hydrolyzed to retinal (λ_{max} 367 nm). The stability of SB and PSB was also studied in AOT micelles of the water pool (ω = 8). The SB was stable. Only ca. 5% loss of the chromophore occurred in 24 h. However, in the presence of CPA (CPA:SB, 1:1) the decomposition was rapid for the protonated SB. Thus, while only ~10% SB was hydrolyzed in about 8 h, ~50% PSB was hydrolyzed in the same period.

The stability of protonated SB **2** in MeOH containing 0.24 M water was also investigated. SB was protonated by adding an excess (20-fold) of CPA. Only ~12% PSB underwent hydrolysis to retinal over a period of 8 h. On the other hand, during the same period, about 52% PSB hydrolyzed in AOT micelles (0.24 M H_2O), even when the ratio of CPA to SB was only 1. Apparently the strong acidity of sulfonic acid formed in the micelle causes rapid decomposition of the SB (Scheme 4). However, the role of micellar catalysis in the hydrolysis reaction cannot be excluded.

Photolysis of SB 2 in AOT reverse micelles in heptane

Direct irradiation (343 nm) of the SB in AOT reverse micelles in heptane at ω = 8 for about 90 min resulted in complete loss of the chromophore at 357 nm (Fig. 5). Photolysis in heptane under similar conditions showed similar behavior but required more than 5 h for complete loss of the SB chromophore (see Fig. 6). Initial-stage irradiation action plots indicated the establishment of a photostationary state. At this point, the absorbance change at 357 nm was ca. 10% in both heptane and micellar media. Assuming that the SB undergoes only *trans* to *cis* photoisomerization during the initial stages of irradiation, it appears that the micellar medium has no significant effect on the photochemical quantum yield of the primary photoreaction. However, it influences the kinetics of this process.

Determination of the hydrodynamic radii of AOT reverse micelles in heptane containing SB 2

The hydrodynamic radii of AOT reverse micelles in heptane (ω = 25) containing $\sim 2 \times 10^{-5}$ M SB **2** were determined by dynamic light scattering to be 44 Å (13).

IR spectra of AOT reverse micelles and micellized SB in heptane

AOT solubilized in *n*-heptane showed the expected ester band at 1739 cm^{-1}. AOT-solubilized water showed -OH stretch and overtone frequencies. Figure 7 shows the IR spectral changes in the 1500–1800 cm^{-1} region as a function of water content in AOT reverse micelles in *n*-heptane. The intensity of the band at 1642 cm^{-1}, due to hydrogen-bonded species (13), increases with increase in water content. A plot of water content

Can. J. Chem. Downloaded from www.nrcresearchpress.com by 91.121.58.235 on 09/07/12
For personal use only.

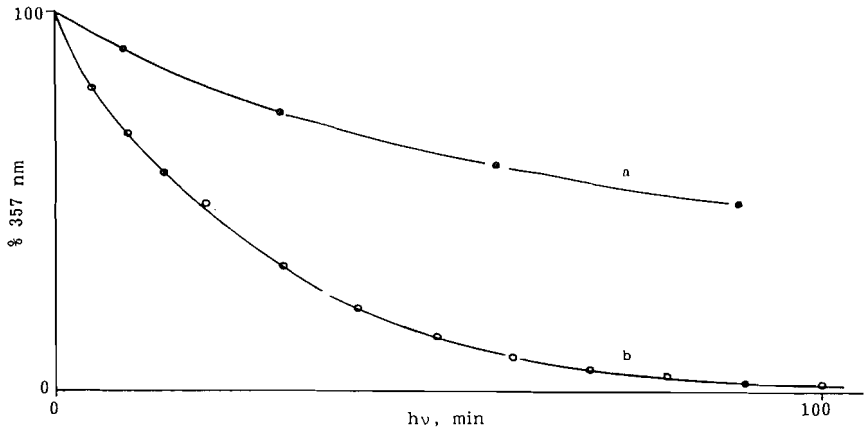

FIG. 6. Changes of concentrations of all-*trans*-*N*-retinylidene–*n*-butylamine (**2**) (a) in heptane and (b) in 1.0×10^{-2} M AOT in heptane in the presence of 0.08 M H_2O ($\omega = 8$) as a function of irradiation time, by repetitive 343 nm, ca. 1 μJ, 2-Hz laser pulses.

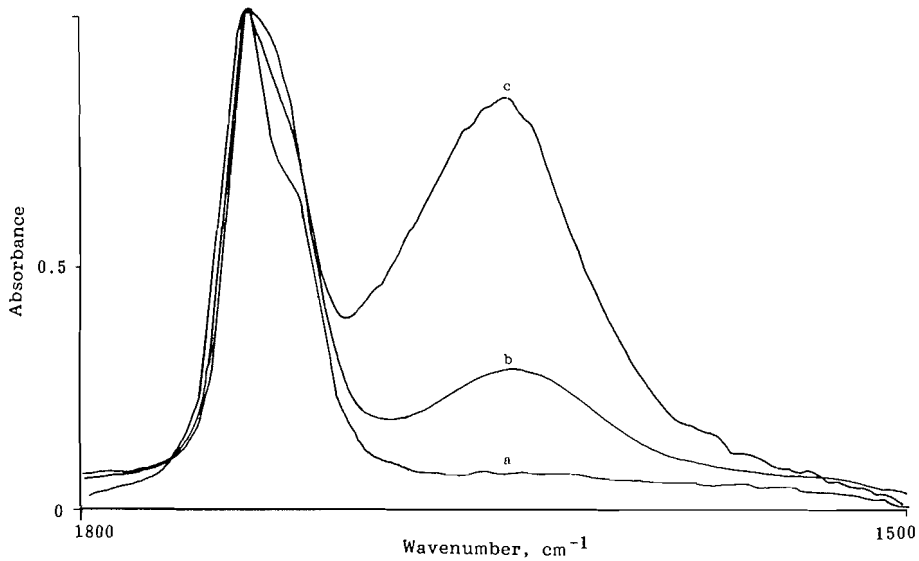

FIG. 7. FTIR difference spectra of 0.3 M AOT in heptane (a) in the absence and (b) in the presence of 1.5 M H_2O, $\omega = 5$, and (c) 7.5 M H_2O, $\omega = 25$ water.

in AOT reverse micelles vs. the intensity of the 1642 cm^{-1} band is shown in Fig. 8. This plot enables the estimation of the exact amount of water present in the AOT reverse micelles. As can be seen, a purified and vacuum-dried sample of AOT contained ~0.8% water ($\omega = 1.5$). AOT micelles containing 0.8% water do not show a band at 1642 cm^{-1}. The band at 1642 cm^{-1} is seen when the ω value is 5 or more. Apparently, water below $\omega = 5$ is used for solvating the AOT ion pair. Once five or more water molecules are present for each AOT molecule, their predominant state corresponds to a hydration shell around the now separated anion and cation. The 1500–1700 cm^{-1} region of the FTIR difference spectrum of SB **2** (1×10^{-1} M) solubilized in AOT reverse micelles in heptane ($\omega < 5$) is shown in Fig. 9. IR frequencies at 1624, 1598, and 1582 cm^{-1}, characteristic of C=N and C=C stretches of the retinylidene chromophore, are observed. Protonation by CPA, however, led to gelification and hydrolysis of the SB as seen from the aldehyde peak (1670.7 cm^{-1}) in Fig. 10. The IR spectrum of SB **2** solubilized in AOT reverse micelles in *n*-heptane with $\omega > 5$ was found to exhibit the C=N stretch, but the spectrum becomes complicated due to the presence of several interacting chromophores. Addition of CPA to a solution of SB **2** (~1×10^{-1} M) in AOT reverse micelles in *n*-heptane (3×10^{-1} M) with $\omega > 5$ led to the hydrolysis of the SB to retinal. The region of interest (1400–1700 cm^{-1}) was very complicated due to the changing nature of the water peaks. The water shows variable IR bands in AOT reverse micelles in *n*-heptane in the presence of SB, PSB, and CPA.

It was found that AOT reverse micelles (10^{-2} M) in *n*-heptane cannot take up more than 2×10^{-5} M SB **2**. The SB was reasonably stable and could be protonated by CPA even in the presence of 0.72 M water. However, it was not possible to record the difference in FTIR spectra of 2×10^{-5} M SB **2** in 1×10^{-2} M AOT reverse micelles in heptane in the range of $\omega =$ 5–50 micelles.

FTIR spectra of CPA solubilized in AOT reverse micelles in heptane

CPA solutions in CCl_4 (1×10^{-1} M) showed an intense IR band at 1718.7 cm^{-1} due to its -COOH group. Weak and broad bands were also present at 1529.6, 1550.5, 1438.4, 1272, 1250, and 1212 cm^{-1}. Different FTIR spectra of CPA (1×10^{-1} M) solubilized in AOT reverse micelles in heptane at $\omega < 2$ (3×10^{-1} M) showed positive bands due to CPA at 1706, 1724,

Can. J. Chem. Downloaded from www.nrcresearchpress.com by 91.121.58.235 on 09/07/12
For personal use only.

Can. J. Chem. Downloaded from www.nrcresearchpress.com by 91.121.58.235 on 09/07/12
For personal use only.

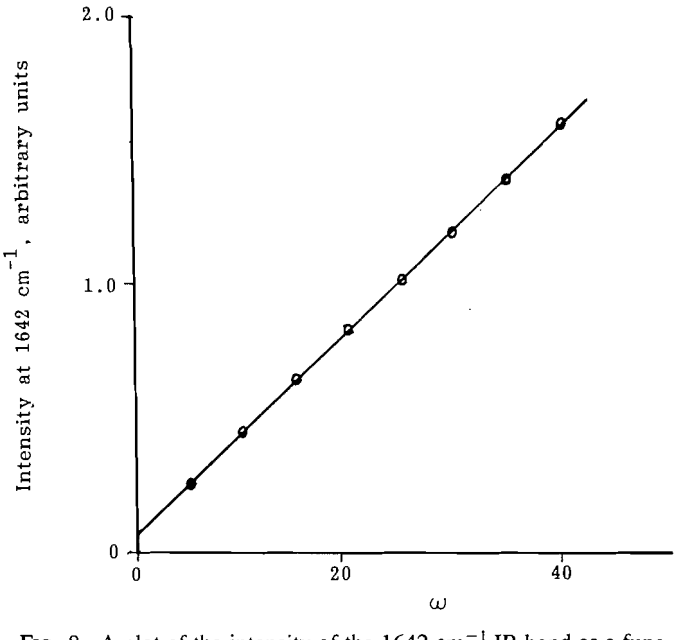

FIG. 8. A plot of the intensity of the 1642 cm^{-1} IR band as a function of water to surfactant ratio (ω) in 1.0×10^{-2} M AOT in heptane.

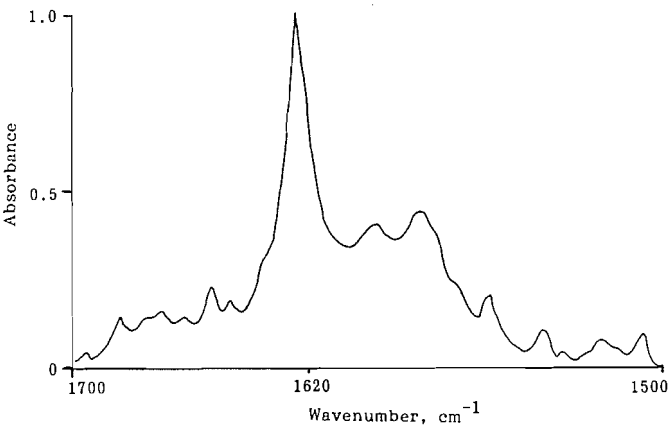

FIG. 9. FTIR difference spectrum (1700–1500 cm^{-1}) of 0.1 M all-*trans*-*N*-retinylidene–*n*-butylamine (**2**) in 0.3 M AOT in heptane ($\omega \approx 0$).

1421, 1396, 1290, 1284, 1278, 1253, 1188, and 1174 cm^{-1}. The intensity of bands at 1706 and 1421 cm^{-1} was almost equal. When CPA (1×10^{-1} M) was solubilized in AOT reverse micelles in heptane (3×10^{-1} M) containing 1.5 M water ($\omega > 5$), positive IR bands were observed at 1741 and 1716, and four strong bands were observed between 1400 and 1500 cm^{-1}. Different FTIR spectra of CPA solubilized in AOT reverse micelles in heptane with water content of more than 1.5 M were very complicated. The appearance of carboxylate peaks (1400–1500 cm^{-1}) indicated that the larger are the water pools, the greater is the dissociation of CPA in AOT reverse micelles. Also, the ionization of CPA occurs when water not directly attached to the hydration shell is available. Water molecules ($\omega < 5$) associated in the AOT hydration shell are not causing dissociation of CPA.

The meaning of pH in the aqueous pools of reversed micelles is somewhat elusive (11, 15, 16). It is only fruitful to report hydrogen ion concentrations as "effective" values defined by a given probe around its immediate environment. Probes used in

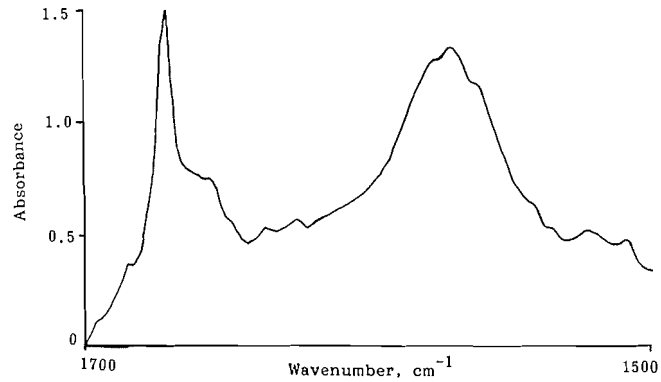

FIG. 10. FTIR difference spectrum (1700–1500 cm^{-1}) of 0.1 M all-*trans*-*N*-retinylidene–*n*-butylamine (**2**) in 0.3 M AOT in heptane ($\omega \approx 0$) in the presence of 0.1 M 3-chloropropionic acid.

reversed micelles undergo absorption (17), infrared (18), and ^{31}P nmr chemical shift (19) changes in response to an alteration of the acidity of their environments. Depending on their position, they report effective pH values in the vicinity of the surfactant headgroups, in the middle of the water pool, or at some intermediate location between these two extremes. Furthermore, the micellar environment may well alter the behavior of the probes. This is a particularly serious problem for indicators whose pK_a values cannot a priori be assumed to be the same in reverse-micelle-entrapped water as in bulk water. Another point of concern is related to the question of exchange of protons between CPA and the sulfonate group of AOT, as shown in eq. [1].

[1] $$(\text{AOT–SO}_3^- \text{ Na}^+)_{\text{H}_2\text{O}} + \text{ClCH}_2\text{CH}_2\text{COOH} \rightarrow (\text{AOT–SO}_3^- \text{ Na}^+)_{\text{H}_2\text{O}} + (\text{AOT–SO}_3\text{H})^{11} + \text{ClCH}_2\text{CH}_2\text{CO}_2^- \text{ Na}^+$$

In such a situation, protonation of the SB can also be caused by the sulfonic acid derivative generated from AOT. The gross micellar structure is not expected to be affected by such exchange if the concentration of AOT is very high as compared to the added CPA. Probably the observed protonation of the SB is due to both the acids (CPA and sulfonic) present in the micelle. Apparently micelles provide an environment for the SB wherein finely tuned interactions and a delicate balance between the right amount and right kind of water influence the stability and protonation of the SB.

Conclusion

The present studies provide some insight into the mechanism of protonation in rhodopsins. It has recently been shown (20) that, in neutral solution, weak acids are incapable of fully protonating the retinylidene SB. In view of these observations, it is important to investigate the mechanism (9) by which weak glutamic (pK_a in H_2O, 3.86) and aspartic (pK_a in H_2O, 4.25) acid residues, present in the vicinity of SB chromophores, cause full protonation of the chromophore of rhodopsins. The driving force behind the shedding of protons by an acid residue in a protein may be provided by the need for the formation of an ion pair, which is required for attaining an appropriate protein conformation. Such ion pairs commonly occur in biologically active proteins. Thus, a positively charged residue in the vicinity of an acid residue can drive the acid and accelerate the proton release process. The released protons can then form hydronium ions with nearby water molecules. Large

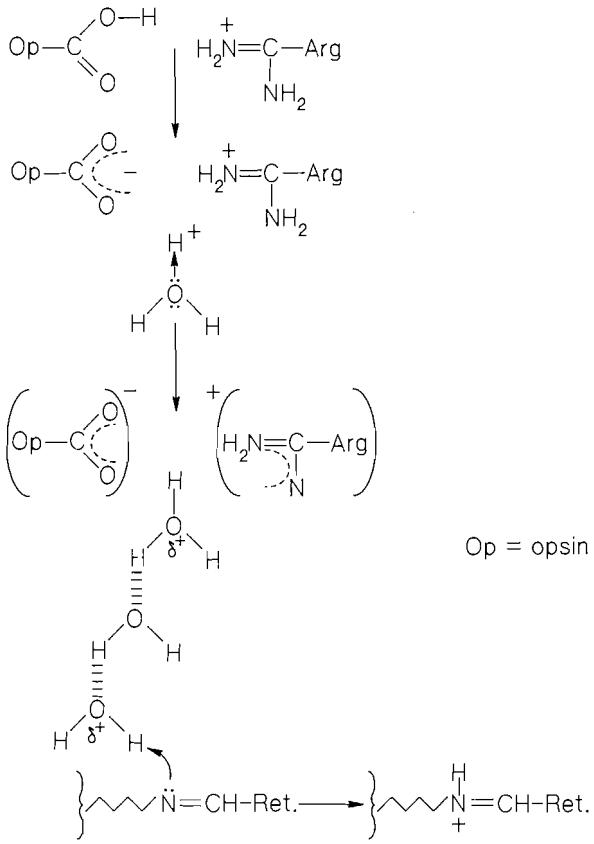

SCHEME 5

numbers of hydronium ions thus generated can protonate the SB (Scheme 5).

Acknowledgments

Support of this work by the Natural Sciences and Engineering Research Council of Canada is gratefully acknowledged. Anil K. Singh thanks the Director of ITT (Bombay, India) for granting him a special leave of absence.

1. G. WALD. Science, **162**, 230 (1967).
2. W. STOECKENIUS and R. A. BOGOMOLINI. Annu. Rev. Biochem. **52**, 587 (1982).
3. N. A. DENCHER, M. B. DRESSELHAUSE, G. PAPADOPOULOS, G. ZACCAI, and G. BUILDT. *In* Proceedings of the Yamada Conference XXI on Molecular Physiology of Retinal Proteins; *Edited by* T. Hara. Yamada Science Foundation, Osaka, Japan. 1988. p. 109.
4. U. M. GANTER, E. D. SCHMID, and F. SIEBERT. J. Photochem. Photobiol. B: **2**, 417 (1988).
5. C. N. RAFFERTY and H. SHICHI. Photochem. Photobiol. **33**, 229 (1981).
6. P. HILDEBRANDT and M. STOCKBURGER. Biochemistry, **23**, 5539 (1984).
7. B. HONIG, T. G. EBREY, R. H. CALLENDER, U. DINUR, and M. OTTOLENGHI. Proc. Natl. Acad. Sci. U.S.A. **76**, 2503 (1979).
8. A. WARSHEL and N. BARBOY. J. Am. Chem. Soc. **104**, 1469 (1982).
9. C. SANDORFY and D. VOCELLE. Can. J. Chem. **64**, 2251 (1986).
10. R. S. BECKER. Photochem. Photobiol. **48**, 369 (1988), and references cited therein.
11. J. H. FENDLER. Membrane mimetic chemistry. Wiley–Interscience, New York. 1982.
12. A. K. SINGH, C. SANDORFY, and J. H. FENDLER. Chem. Commun. 233 (1990).
13. H. F. EICKE and M. ZULAUF. J. Phys. Chem. **83**, 480 (1979).
14. L. M. GIERASCH, K. F. THOMPSON, J. E. LACY, and A. L. ROCKWELL. *In* Reverse micelles. *Edited by* A. L. Luisi and B. E. Straub. Plenum, New York. 1984. p. 265.
15. O. H. EL SEOUD. Adv. Colloid Interface Sci. **30**, 1 (1989).
16. P. L. LUISI, M. GIOMINI, M. P. PILENI, and B. H. ROBINSON. Biochim. Biophys. Acta, **947**, 209 (1988).
17. O. A. EL SEOUD and A. M. CHINELATTO. J. Colloid Interface Sci. **95**, 163 (1983).
18. F. J. NOME, S. A. CHANG, and J. H. FENDLER. J. Chem. Soc. Faraday Trans. 1, **72**, 296 (1976).
19. R. E. SMITH and P. L. LUISI. Helv. Chim. Acta, **63**, 2302 (1980); B. STEINMANN, H. JACKLE, and P. L. LUISI. Biopolymers, **25**, 1133 (1986).
20. L. S. LUSSIER, C. SANDORFY, H. LE-THANH, and D. VOCELLE. J. Phys. Chem. **91**, 2282 (1987).

Can. J. Chem. Downloaded from www.nrcresearchpress.com by 91.121.58.235 on 09/07/12
For personal use only.

Determination of dipole moment values of anisotropic molecules using Brot's formalism

P. BRITO AND M. MECHETTI

Instituto de Física, Facultad de Ciencias Exactas y Tecnología, Universidad Nacional de Tucumán, 4000 Tucumán, R. Argentina

Received June 23, 1989[1]

P. BRITO and M. MECHETTI. Can. J. Chem. **68**, 1523 (1990).

A method for the determination of dipole moment values based on Brot's theory is proposed. It takes into account the influence of the molecular anisotropies of shape and polarizability on the permittivity of a mixture. Starting from measurements performed on dilute solutions and from the knowledge of the molecular structure of some chlorinated derivatives of α-cyanostilbene and 1,3 derivatives of benzene, the best parameters of an ellipsoid used for the representation of a polar anisotropic molecule are determined. The dipole moments obtained, using benzene and tetrachloromethane as solvents, are finally compared to values from the literature.

Key words: dipole moment, Brot's formalism, molecular anisotropy.

P. BRITO et M. MECHETTI. Can. J. Chem. **68**, 1523 (1990).

On propose une méthode, basée sur la théorie de Brot, qui permet de déterminer les valeurs des moments dipolaires; elle tient compte de l'influence des anisotropies moléculaires de la forme ainsi que de la polarisabilité sur la permittivité d'un mélange. En se basant sur des mesures effectuées sur des solutions diluées et sur des connaissances de la structure moléculaire de certains dérivés chlorés de l'α-cyano-stilbène et de dérivés-1,3 du benzène, on a déterminé les meilleurs paramètres d'un ellipsoïde à être utilisés pour représenter une molécule polaire anisotrope. On a finalement comparé les valeurs obtenues pour les moments dipolaires dans le benzène et le tétrachlorométhane avec celles rapportées dans la littérature.

Mots clés : moment dipolaire, formalisme de Brot, anisotropie moléculaire.

[Traduit par la revue]

Can. J. Chem. Downloaded from www.nrcresearchpress.com by 91.121.58.235 on 09/07/12
For personal use only.

Introduction

In this paper we propose a method of evaluating the dipole moment of polar molecules from measurements performed in polar–nonpolar dilute solutions, using results from Brot's theory (1) that take into account the molecular anisotropies of shape and polarizability. This paper follows earlier work (2, 3) in which different theoretical expressions for the permittivity of mixtures were discussed.

To apply this particular formalism using a model in the continuous approach, a previous knowledge of molecular structure is required. This allows the determination of the parameters of the best ellipsoid that must be used for the representation of a polar solute molecule. The proposed method differs from those based on the Debye (4) or Onsager (5) models, as well as from the others traditionally used, in the evaluation of the dipole moment, in spite of the fact that almost the same experimental data are necessary: the variations of the static permittivity and the refractive index of the solution with concentration, the densities of solute and solvent, or the variation of the specific volume of the mixture with concentration. The anisotropy of polarizability can be determined from the Kerr coefficients but if they are not known, as in our case, the ellipsoid can be considered as being composed of a medium characterized by a homogeneous permittivity $\varepsilon_{\infty 2}$ for relating both kinds of molecular anisotropies.

To apply the proposed method we have considered very dilute solutions of seven chlorinated derivatives of α-cyanostilbene and two 1,3 derivatives of benzene in benzene and tetrachloromethane. The dipole moment values obtained are finally compared with those determined by the use of the traditional formulas (6–9), the vectorial sum of bond dipole moments (10), or the CNDO/2 method (11).

Theoretical considerations

An expression for the static permittivity of pure liquids and dilute solutions taking into account the influence of the anisotropies of shape and polarizability was deduced by Brot in 1982. In the case of pure liquids these anisotropies have also been considered by other authors (12, 13).

The result obtained by Brot is

$$[1] \quad \frac{\varepsilon_{12} - \varepsilon_1}{N} = \frac{1}{3\varepsilon_0} \sum_{j=1}^{3} [\alpha_{jj}^* + f_j^2 \mu_j^2 / kT]$$

where ε_{12} and ε_1 are the static permittivities of the solution and the solvent and N is the number of solute molecules per unit volume. Otherwise

$$[2] \quad \alpha_{jj}^* = \{[1 + A_j(\varepsilon_1 - 1)]\alpha_{jj} - v\varepsilon_0(\varepsilon_1 - 1)\} f_j$$

is the effective polarizability increment and

$$[3] \quad f_j = \left\{1 - \frac{\varepsilon_1 - 1}{\varepsilon_1} A_j \left[1 + (1 - A_j)\frac{\alpha_{jj}}{v\varepsilon_0}\right]\right\}^{-1}$$

is the Scholte internal factor.

If a continuous model is used for the solution, the anisotropic solute molecule can be represented by an ellipsoid of half-axis a_j ($j = 1, 2, 3$), having a volume equal to the associated molecular volume in the pure liquid state and depolarizing factors A_j, in order to include shape anisotropy. The anisotropy of polarizability can be estimated by using a theoretical model in which both types of anisotropies are related by considering the ellipsoid made of a homogeneous medium characterized by a permittivity $\varepsilon_{\infty 2}$. In this case the elements of the polarizability tensor are

$$[4] \quad \alpha_{jj} = \frac{a_1 a_2 a_3}{3}(4\pi\varepsilon_0)\frac{(\varepsilon_{\infty 2} - 1)}{[1 + (\varepsilon_{\infty 2} - 1)A_j]}$$

When this result is used in eqs. [2] and [3], the expression for the static permittivity of the polar dilute solution reduces to

$$[5] \quad \frac{\varepsilon_{12} - \varepsilon_1}{\Phi_2} = \frac{\varepsilon_1(\varepsilon_{\infty 2} - \varepsilon_1)}{3} \sum_{j=1}^{3} \frac{1}{\varepsilon_1 + A_j(\varepsilon_{\infty 2} - \varepsilon_1)} + \frac{3}{9}\frac{\varepsilon_1^2}{\varepsilon_0} \sum_{j=1}^{3} \frac{\mu_j^2}{kTv} \left\{\frac{1 + A_j(\varepsilon_{\infty 2} - 1)}{\varepsilon_1 + A_j(\varepsilon_{\infty 2} - \varepsilon_1)}\right\}^2$$

Φ_2 being the solute volume fraction and v its specific volume.

[1]Revision received April 6, 1990.

Can. J. Chem. Downloaded from www.nrcresearchpress.com by 91.121.58.235 on 09/07/12
For personal use only.

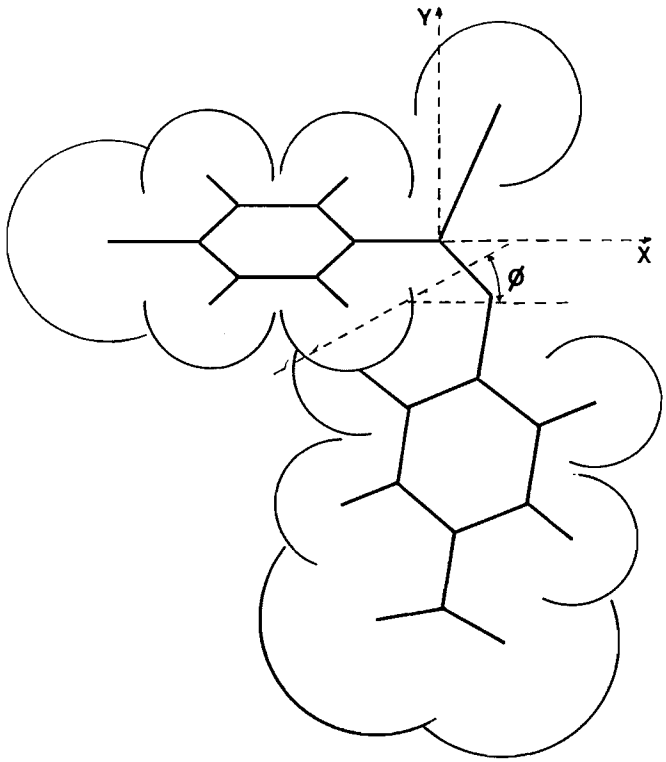

FIG. 1. Projection on the XY-plane of the molecular structure of 4-Cl-4′-*N*,*N*-dimethylamino-α-cyanostilbene. The external atoms are represented by its van der Waals spheres.

Method and results

The dipole moment values can be obtained from eq. [5] when the parameters of the ellipsoid that represents the solute molecule are determined. To do so it is necessary to know the molecular structure, from which it is possible to get the corresponding projections of this structure on three mutually perpendicular planes with the external atoms of the molecule represented by its van der Waals spheres. Then a set of points is chosen on each projection and the initial values of the different parameters of the ellipsoid, which is the geometrical figure leading to the best description of the chosen set of points, are determined. These parameters are the half-axis a_j, the Euler angles with respect to a given reference system, and the coordinates of the center. Due to the symmetry of the molecules considered, the a_3 direction is taken parallel to the Z-axis of the reference system. The projections on the XY-plane corresponding to two of the molecules studied are shown in Figs. 1 and 2. The angle ϕ between a_1 and the X-axis is also indicated.

The initial parameters are then changed by an iteration procedure until the difference between the volumes of ellipsoid and molecule is no greater than 1%. The associated molecular volume is estimated from density data or from the slope of the specific volume vs. concentration curve if the solute density is not known, as in the case of the α-cyanostilbenes. Another condition imposed in the iteration procedure is that the distance between each of the chosen points and the ellipsoid figure be less than 0.1 Å. The last two conditions make the difference between the present procedure and that followed in ref. 14 in which Brot's formalism was also applied for the case of chlorinated derivatives of the α-cyanostilbene. After the iteration procedure is concluded, the depolarizing factors of the molecules are calculated from

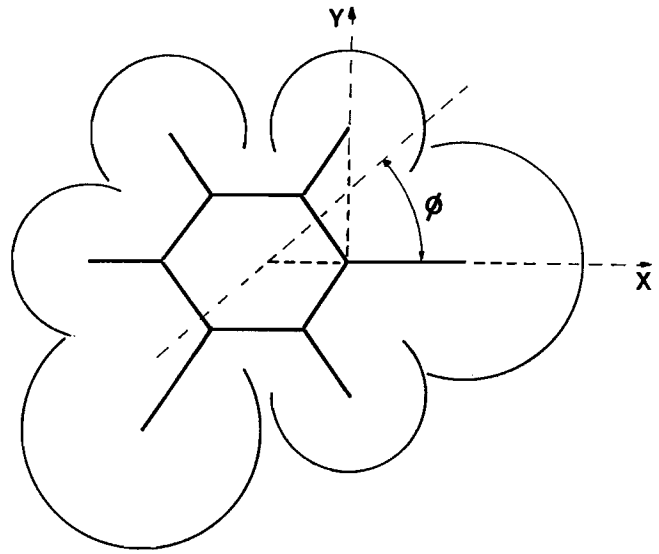

FIG. 2. Projection on the XY-plane of the molecular structure corresponding to 1,3-dibromobenzene. The external atoms are also represented by its van der Waals spheres.

TABLE 1. Depolarizing factors and ellipsoid orientational angles

Substances	A_1	A_2	A_3	φ (deg)
1	0.1974	0.2846	0.5181	−27.50
2	0.2639	0.1855	0.5507	14.32
3	0.2387	0.3254	0.4359	52.14
4	0.3357	0.2057	0.4586	29.79
5	0.2162	0.3142	0.4696	46.40
6	0.3274	0.1832	0.4893	46.03
7	0.3620	0.2180	0.4200	33.04
8	0.1878	0.2212	0.5910	75.82
9	0.1785	0.2823	0.5392	27.02

$$[6]\quad A_j = \tfrac{1}{2}a_1a_2a_3\int_0^\infty \frac{du}{(u+a_j^2)(u+a_1^2)^{1/2}(u+a_2^2)^{1/2}(u+a_3^2)^{1/2}}$$

The values of the angles φ and of the calculated depolarizing factors appear in Table 1. The depolarizing factors found are the same for each substance regardless of which solvent (benzene or tetrachloromethane) is considered.

The value of the high frequency permittivity of the solute, $\varepsilon_{\infty 2}$, is also necessary for calculation of the dipole moment. If this permittivity is not known from relaxation measurements, it is usual to consider it equal to the square of the refractive index multiplied by a factor ranging between 1.0 and 1.1 (3). The permittivity $\varepsilon_{\infty 2}$ can also be estimated from eq. [1], extended to the high frequency limit. This last procedure was also followed in this work.

The available experimental data for the static permittivity, the specific volume, and the refractive index of a very dilute solution are usually written in the following forms (15, 16)

$$[7]\quad \varepsilon_{12} = \varepsilon_1 + \alpha w_2$$

$$[8]\quad v_{12} = v_1 + \beta w_2$$

$$[9]\quad n_{12}^2 = n_1^2 + \tau w_2$$

where ε_1, v_1 and n_1 stand for the solvent and w_2 is the solute

TABLE 2. Values of high frequency permittivity and dipole moments*

Substances	$\varepsilon_{\infty 2}$	μ_{calcd} (D)	$\mu_{lit.}$ (D)
1	2.8490	3.85	3.48–3.69
	2.9195	3.72	3.51–3.64
2	3.5318	6.03	5.56–5.84
	2.9766	5.86	5.45–5.57
3	2.8006	3.48	3.39–3.59
	2.9046	3.52	3.58–3.71
4	3.4399	5.10	4.98–5.27
	3.3567	5.08	5.10–5.28
5	2.9038	3.66	3.65–3.84
	2.7537	3.66	3.71–3.91
6	3.2892	5.76	5.42–5.76
	3.6562	5.27	5.26–5.46
7	3.0594	4.42	4.58–4.85
	3.1172	4.34	4.67–4.83
8	2.3592	1.77	1.39–1.61
	2.2466	1.73	1.42–1.58
			1.68†
9	2.5840	1.48	1.46–1.58
	2.6216	1.44	1.39–1.55

*The first row of values corresponds to C_6H_6 and the second to CCl_4. Substances **1**–**7**, refs. 15 and 16; **8** and **9**, refs. 17 and 18.
†μ_{gas}, ref. 22.

weight fraction. If the static permittivity of the solution and the solvent are replaced by the corresponding refractive index, eq. [1] yields

$$[10]\quad \tau = (1 + \beta d_1)\frac{n_1^2}{3}(\varepsilon_{\infty 2} - n_1^2)\sum_{j=1}^{3}\frac{1}{n_1^2 + A_j(\varepsilon_{\infty 2} - n_1^2)}$$

after expressions [7]–[9] are used. Finally, the dipole moment value can be obtained from eq. [1] as

$$[11]\quad \mu^2 = \frac{S}{\sum_j C_j^2 \cos^2\theta_j}$$

where

$$[12]\quad S = \frac{3\varepsilon_0 kTM_2}{\varepsilon_1^2 N_A}\left\{\frac{\alpha}{d_1} - \left(\frac{1 + \beta d_1}{d_1}\right)\frac{\varepsilon_1(\varepsilon_{\infty 2} - \varepsilon_1)}{3} \times \sum_{j=1}^{3}\frac{1}{\varepsilon_1 + A_j(\varepsilon_{\infty 2} - \varepsilon_1)}\right\}$$

and

$$[13]\quad C_j = \frac{1 + A_j(\varepsilon_{\infty 2} - 1)}{\varepsilon_1 + A_j(\varepsilon_{\infty 2} - \varepsilon_1)}$$

The angle θ_j in eq. [11] is the angle between the dipole vector and the a_j-axis of the ellipsoid and it is evaluated from the vectorial sum of the bond dipole moments. The values of the bond dipole moments used are (17, 18) as follows:

μ_{Cl} = 1.61 D in benzene; 1.60 D in tetrachloromethane.
μ_{CN} = 3.37 D in benzene.
μ_{NDMA} = 1.60 D in benzene; 1.52 D in tetrachloromethane.
μ_{Br} = 1.55 D in benzene; 1.52 D in tetrachloromethane.

The dipole moment values obtained from eq. [11] are shown in Table 2, where the high frequency permittivities and dipole moment values from the literature are also given. It must be pointed out that due to the fact that the benzene rings are in different planes for the α-cyanostilbenes when the *trans* configuration is used, the angle between these planes was taken to be equal to 58° in all cases except for the 2,6-dichloro-4′-*N*,*N*-dimethylamino-α-cyanostilbene, where the value 84° was used (19, 20). The nine polar substances considered in this work are

1 4-Cl-α-cyanostilbene
2 4-Cl-4′-*N*,*N*-dimethylamino-α-cyanostilbene
3 3-Cl-α-cyanostilbene
4 3-Cl-4′-*N*,*N*-dimethylamino-α-cyanostilbene
5 3,4-dichloro-α-cyanostilbene
6 3,4-dichloro-4′-*N*,*N*-dimethylamino-α-cyanostilbene
7 2,6-dichloro-4′-*N*,*N*-dimethylamino-α-cyanostilbene
8 1,3-dichlorobenzene
9 1,3-dibromobenzene

Discussion of results

The method generally employed to determine the dipole moment value of a polar molecule relates it to the static permittivity and the refractive index of a dilute solution through some traditional expressions such as those given by Hedestrand, Le Fevre and Vine, Guggenheim, and Halverstad and Kumler, in which the influence of the molecular anisotropies are not considered.

In this paper, the authors propose a method for evaluating the dipole moment based on the extension of the Onsager model made by Brot for solutions containing anisotropic molecules. The application of this method starts from the knowledge of the molecular structure of the polar molecule as well as of the van der Waals radii (21) of its external atoms. Using an iteration procedure, the parameters of the ellipsoid that represents the molecule are obtained. Calculations show that the depolarizing factors are the same for the two solvents considered. Nevertheless an appreciable difference is observed for the calculated high frequency permittivity values. This fact allows us to interpret any difference in the dipole moment values obtained in benzene and tetrachloromethane as due principally to the influence of polarizability anisotropy.

The results obtained for the dipole moments of the polar molecules considered, in the liquid state, are slightly different from those given in the literature (for the α-cyanostilbenes the range of values obtained from the usual formulas is indicated). The differences can be attributed to the influence of both types of anisotropy. Table 2 shows that in the case of 1,3-dichlorobenzene, the dipole moment of the ellipsoid (characterized by $a > b > c$ and $b/a = 0.88$) is greater than μ_{gas} but is in good agreement with the value 1.72 D given in ref. 23, which was calculated from heat of vaporization data.

Experimentally it is found that for the first six α-cyanostilbenes the dipole vector forms an angle with the *X*-axis greater than 80°, which is reduced to nearly 50° for substance **7**. In almost all cases the dipole has a big *Z*-component. These angles are given in refs. 15 and 16 and show good agreement with those obtained from the vectorial sum of bond dipole moments. For the *m*-dichloro and dibromo, the dipole vector is on the *XY*-plane and directed along the *ortho* position.

In the present work, the variation of the bond angle with the solvent has not been considered. Nevertheless, the results obtained from our method suggest that it is an accurate alternative procedure for evaluating the dipole moment of anisotropic polar molecules.

Can. J. Chem. Downloaded from www.nrcresearchpress.com by 91.121.58.235 on 09/07/12
For personal use only.

1. C. BROT. Mol. Phys. **45**, 543 (1982).
2. C. GROSSE, M. MECHETTI, and P. BRITO. Can. J. Phys. **61**, 1056 (1983).
3. C. GROSSE, M. MECHETTI, and P. BRITO. Can. J. Chem. **63**, 1031 (1985).
4. P. DEBYE. Polar molecules. Dover Publications, New York. 1929.
5. L. ONSAGER. J. Am. Chem. Soc. **58**, 1486 (1936).
6. G. Z. HEDESTRAND. Z. Phys. Chem. **B2**, 428 (1929).
7. R. J. W. LE FEVRE and H. VINE. J. Chem. Soc. 1805 (1937).
8. I. F. HALVERSTADT and W. D. KUMLER. J. Am. Chem. Soc. **64**, 2988 (1942).
9. E. A. GUGGENHEIM. Trans. Faraday Soc. **47**, 573 (1951).
10. M. DIAZ PEÑA and A. ROIG MUNTANER. Quimica Fisica. Vol. I. Alhambra S.A., Madrid, Spain. 1976.
11. J. A. POPLE and D. L. BEVERIDGE. Approximate molecular orbital theory. McGraw–Hill, New York. 1970.
12. T. H. G. SCHÖLTE. Physica, **15**, 437 (1949).
13. C. P. J. HALLOY and M. MECHETTI. An. Asoc. Quím. Argent. **69**, 131 (1981).
14. M. A. ACUÑA DE MOLINA, P. BRITO, and C. GROSSE. An. Asoc. Quim. Argent. **74**, 199 (1986).
15. M. A. ACUÑA DE MOLINA, M. N. LONCHARICH, J. I. GIMENEZ DE PAEZ, A. M. BRU, and P. W. LOBO. An. Asoc. Quim. Argent. **72**, 467 (1984).
16. M. A. ACUÑA DE MOLINA, M. N. LONCHARICH, J. I. GIMENEZ DE PAEZ, and P. W. LOBO. An. Asoc. Quim. Argent. **73**, 455 (1985).
17. A. L. MCCLELLAN. Tables of experimental dipole moments. Vol. 2. Rahara Enterprises, El Cerrito, CA. 1974.
18. J. KOUDELKA and O. EXNER. Collect. Czech. Chem. Commun. **50**, 188 (1985).
19. M. VAN MEERSSCHE and G. LEROY. Bull. Soc. Chim. Belg. **69**, 204 (1960).
20. H. BOIS D'EUGHIEN and M. VAN MEERSSCHE. Bull. Soc. Chim. Belg. **71**, 503 (1962).
21. R. C. WEAST (*Editor*). Handbook of chemistry and physics. 53rd ed. The Chemical Rubber Co., Boca Raton, FL. 1972–1973.
22. L. G. GROVES and S. SUGDEN. J. Chem. Soc. 1782 (1937).
23. C. J. F. BÖTTCHER. Theory of electric polarization. Vol. 1. Elsevier, Amsterdam. 1973.

Can. J. Chem. Downloaded from www.nrcresearchpress.com by 91.121.58.235 on 09/07/12
For personal use only.

Density effects on ion mobilities in electron attaching fluids: CS_2, SF_6, and C_6F_6

NORMAN GEE, G. RAMANAN,[1] AND GORDON R. FREEMAN

Chemistry Department and Radiation Research Centre, University of Alberta, Edmonton, Alta., Canada T6G 2G2

Received March 22, 1990

NORMAN GEE, G. RAMANAN, and GORDON R. FREEMAN. Can. J. Chem. **68**, 1527 (1990).

Ion mobilities μ were measured at densities n ranging from those of the low density gas ($n < 0.01 n_c$, where n_c = critical fluid density) through the dense gas and low-density liquid transition region ($\sim 0.5 n_c$ to $2 n_c$) to the normal liquid ($\sim 3 n_c$). The mobility at a given density was constant over a 10-fold variation of electric field strength, typically in the range $0.1 < E(\mathrm{MV/m}) < 5$. In the gas phase changes in mobility were dominated by changes in gas density. Comparison with neutral molecule transport in SF_6 was used to illustrate the change in the effect of the ion on its local environment from that of molecular cluster formation to that of liquid electrostriction as density was increased. In the liquid, changes in ion mobility are dominated by changes in free volume. Mobilities in the present liquids could be described without reference to the activation energies suggested by the Arrhenius model.

Key words: ion, mobility, fluid, density, electron attaching.

NORMAN GEE, G. RAMANAN et GORDON R. FREEMAN. Can. J. Chem. **68**, 1527 (1990).

On a mesuré les mobilités ioniques μ à des densités allant de celles de gaz de basses densités ($n < 0{,}01 n_c$ où n_c = densité critique du fluide) à celles des gaz denses, puis à la région de transition des liquides de basses densités ($\approx 0{,}5 n_c$ à $2 n_c$) et finalement à celles des liquides normaux ($\approx 3 n_c$). A une densité donnée, la mobilité est constante, même lorsqu'on multiplie par 10 la force du champ électrique (généralement $0{,}1 < E(\mathrm{MV/m}) < 5$). En phase gazeuse, la mobilité est dominée par des changements dans la densité gazeuse. On a utilisé une comparaison avec le transport de molécules neutres dans le SF_6 pour illustrer le changement qui est observé dans l'effet de l'ion sur son environnement local lorsqu'on passe de la formation d'agrégat moléculaire à l'électrostriction du liquide causée par une augmentation de la densité. En phase liquide, les changements dans la mobilité ionique sont dominés par des dans changements dans le volume libre. On peut décrire les mobilités observées dans les liquides sans faire de référence aux énergies d'activation qui sont suggérées par le modèle d'Arrhénius.

Mots clés : ion, mobilité, fluide, densité, attachement d'électron.

[Traduit par la revue]

Introduction

Ion transport in low density gases (1) is largely governed by binary collisions between the ion and gas molecules, so the molecule number density n exerts a major effect. In the liquid phase the ion is in constant contact with fluid molecules; the mobility is often related to the fluid viscosity η (2). In recent years ion transport has been examined as a function of fluid density from that of a normal gas through that of the critical fluid to the density of a normal liquid (3–6): a transition from density control of the mobility to viscosity control occurred at $0.5 \leq n/n_c \leq 1.9$, corresponding to $0.6 \leq \eta/\eta_c \leq 3$ (subscript c denotes a critical fluid property). The bulk of the previous work was done in rare gas and hydrocarbon fluids in which extra electrons are not captured (non electron attaching fluids). As a result mobile electron states can also be observed.

In this work the study of ion transport is extended to the electron attaching fluids carbon disulfide, sulfur hexafluoride, and hexafluorobenzene. The electron capturing properties of these fluids are different from some other electron capturers such as carbon dioxide. In CO_2 extra electrons are not captured at $n < 9 \times 10^{25}$ molecules/m^3 (7). At higher densities electron attachment is stabilized by molecular clusters and capture becomes rapid. By contrast, molecules of CS_2, SF_6, and C_6F_6 at low densities already attach electrons (8–10). They also efficiently attach electrons when they are present as dilute solutes in liquid solvents (11–13). However, in the purified liquids of CS_2 (14) and C_6F_6 (13), electron states that are much more mobile than molecular ions are observed. There is indirect evidence from positronium studies that such might also be the case for purified liquid SF_6 (15). Ion mobilities μ in fluids of CS_2, SF_6, and C_6F_6 are here reported for densities from those of the low density gas, through those of the dense gas/low-density liquid transition region, to those of the normal liquid.

[1]Deceased

Experimental

A. Materials and sample preparation

These were the same as described in refs. 14 and 16.

B. Apparatus and techniques

The high pressure liquid (17) and gas (18) conductance cells were made of 1 cm thick glass and could withstand 6 MPa internal pressure. Diagrams of the cooling (19) and heating (20) setups have been published. Temperature monitoring and measurement at $T < 295$ K is described in ref. 21 and at $T > 295$ K in ref. 14. Four calibrated copper–constantan thermocouples were used, one of which was pushed down a hollow pin to a distance of 2 mm from the electrode outer surface and used to record the fluid temperature. Calibration of the thermocouples at $T < 295$ K is described in ref. 14. To calibrate the thermocouples at $T > 295$ K, they were wrapped snugly about the platinum element temperature probe of a Fluke 2189A Thermometry System. The probe was then immersed into a Dewar containing 710 Silicone fluid, the fluid heated using a Cenco 250W knife heater connected to a variable voltage adjuster, and the temperatures registered by the thermocouples/Fluke 2100A digital thermometer were calibrated to that registered by the 2189A Thermometry System.

The fluid between the plates of the cell was ionized using 0.3 or 1.0 μs pulses of X-rays from a Van de Graaf accelerater delivering (2 or 6) $\times 10^{-5}$ J/kg to the sample (22). The radiation-induced ion current was amplified using a Princeton Applied Research (PAR) 113 preamplifier. The ion mobility μ was obtained from the time t_d needed for the radiation-induced ion current to return to zero (14).

$$[1] \quad \mu = \ell^2 / t_d V$$

where the distance ℓ between the electrodes was measured directly using Do-All, model M-1 minus precision calipers, and the voltage V applied between the plates was obtained using the voltage sources cited in ref. 14. This method measures the mobility of the slowest ion.

Can. J. Chem. Downloaded from www.nrcresearchpress.com by 91.121.58.235 on 09/07/12
For personal use only.

TABLE 1. Summary of results

T (K)	n (10^{25} molecules m^{-3})	μ^a (10^{-7} m^2 V^{-1} s^{-1})	T (K)	n (10^{25} molecules m^{-3})	μ^a (10^{-7} m^2 V^{-1} s^{-1})
		Carbon disulfide[b]			
370.1	909	1.35	500.2	108.0	10.0
408.2	862	1.63	486.0	83.1	12.5
429.2	831	1.81	445.6	37.9	23.9
459.1	791	2.15	406.0	17.9	48
479.4	742	2.35	350.9	5.60	160
499.8	704	2.48	320.2	2.41	384
			295.2	1.05	910
		Sulfur hexafluoride[c]			
224.2	769	0.94	318.0	213	2.66
232.3	749	1.04	316.9	205	3.12
255.6	687	1.38	313.1	154	4.01
274.5	633	1.68	310.8	136	4.37
294.6	558	2.13	295.1	81.9	7.92
302.3	522	2.35	281.6	51.8	11.8
311.5	461	2.69	273.1	39.7	15.2
317.2	404	2.90	257.2	23.5	25.0
318.8	303	2.67	241.6	14.3	43
		Hexafluorobenzene[d]			
294.9	522	0.223	516.9	180	2.73
351.4	481	0.49	517.8	180	2.79
399.4	437	0.85	520.8	180	3.18
422.6	415	1.08	513.1	123	4.3
448.3	387	1.34	499.6	70.5	6.2
476.5	349	1.62	479.0	42.8	9.7
496.4	311	1.99	448.8	23.6	17.1
507.4	270	2.32	399.5	8.55	53
513.4	232	2.55	348.5	1.87	220
516.5	201	2.68	330.0	1.01	410
			294.9	0.24	1810

[a]Cation mobility. In liquid CS_2 $\mu_- = (1.3 \pm 0.1)\,\mu_+$ (ref. 14); in SF_6 $\mu_- \approx \mu_+$; in gaseous C_6F_6 at $n > 40 \times 10^{25}$ molecules/m^3, $\mu_- \approx \mu_+$. For C_6F_6 at $n < 25 \times 10^{25}$ molecules/m^3 μ_- is given in the Results Sect. B.
[b]Ion mobilities at $T < 370$ K are reported in ref. 14. $T_c = 552$ K, $n_c = 354 \times 10^{25}$ molecules/m^3.
[c]$T_c = 318.7$K, $n_c = (303 \pm 4) \times 10^{25}$ molecules/m^3.
[d]$T_c = 516.8$K, $n_c = 180 \times 10^{25}$ molecules/m^3.

Whether this is the cation or anion is discussed further in the Result section.

C. Physical properties

The densities of the liquids and vapors were obtained as described in refs. 14, 16, and 23.

Results

A. Field independence

The ion mobilities in liquids were measured over a 10-fold variation of E, typically in the range $0.1 < E(\mathrm{MV/m}) < 5$. For the lower density gases, field strengths down to 3 kV/m were used. No field dependence was found. The value μ cited at each (n,T) in Table 1 was the average of > 10 measurements, half of which were made with positive and the other half with negative applied voltages. The average deviation of the measured values from the reported mean value in Table 1 was about 2%.

B. Nature of the ions

Absorption of energy from the radiation pulse produced electrons and cations:

[2] $M \rightsquigarrow M^+ + e^-$

The electron can react with all three of the present compounds to form anions.

In general, anions in both liquids and gases move faster than cations (see Figs. 1 and 2 of ref. 24 for extensive demonstration). Hence in CS_2 liquid the slowest ion was assumed to be the cation, and the cation mobility μ_+ was obtained from the time of flight method (eq. [1]). The current–time trace was slightly curved but there was not a separate portion indicating collection of the anions. Combination of the μ_+ values with a total conductance measurement gave the anion mobility $\mu_- = (1.3 \pm 0.1)\mu_+$. In the gas the current–time trace also showed a slight curvature except at $n < 3.8 \times 10^{26}$ molecules/m^3. At those lower densities a single linear decay was observed which indicated that $\mu_+ \approx \mu_-$.

A single linear decay was also observed in SF_6 at all conditions of the present work, in agreement with previous findings in SF_6 dense gas (25) and liquid (26) at 294 ± 2 K. Again the single linearly decaying signal means that $\mu_+ \approx \mu_-$. This is not unexpected since in the gas the ions are likely $SF_5^+(SF_6)_j$ and $SF_6^-(SF_6)_k$, which are the clustered forms of the main cation SF_5^+ (27) and main anion SF_6^- (28) produced in

Can. J. Chem. Downloaded from www.nrcresearchpress.com by 91.121.58.235 on 09/07/12
For personal use only.

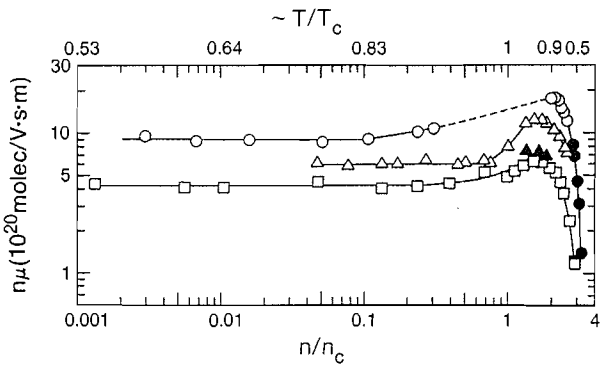

FIG. 1. Density-normalized mobility $n\mu$ as functions of reduced density n/n_c and temperature T/T_c in the liquid and coexisting vapor of CS_2 (○; ●, ref. 14), SF_6 (△; ▲, ref. 26), and C_6F_6 (□; ■, ref. 13). Temperatures and densities are listed in Table 1.

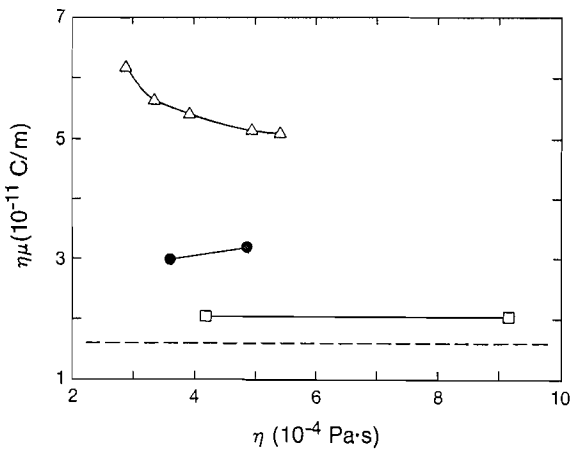

FIG. 2. Viscosity-normalized mobility plotted against liquid viscosity. Symbols as in Fig. 1. The dashed line indicates $\eta\mu_+$ in the hydrocarbon liquids *n*-pentane to *n*-tetradecane (38).

the low density gas. The values of $n\mu$ in low density SF_6 gas at room temperature are 15.6×10^{20} molecules/mV.s for SF_5^+ (29) and 14.6×10^{20} molecules/m.V.s for SF_6^- (27), which are only 7% different from each other. Clustering reduces the mobilities, and in the present system $\mu_+ \approx \mu_- = 6 \times 10^{20}$ molecules/m.V.s (Fig. 1); the extent of clustering of SF_6 molecules around the anion is evidently similar to that around the cation.

In liquid hexafluorobenzene the cations were found to be slower than the anions (13). We assume this to be also true at the conditions of Table 1, so the mobility obtained by eq. [1] is for cations. The signal trace in the liquid was slightly curved. In the gas at $n > 4 \times 10^{26}$ molecules/m^3 a single linear trace was obtained so $\mu_+ \approx \mu_-$. At $n < 2 \times 10^{26}$ molecules/m^3 a separate linear trace indicating collection of anions separate from the slower cations was found ($n/10^{26}$ molecules m^{-3}, $\mu_-/10^{-7}$ m^2 V^{-1} s^{-1}): 2.36, 20.4; 0.86, 71; 0.187, 329; 0.101, 650; 0.024, 2600.

Discussion

A. Effect of density and of viscosity

In liquids and gases the mobility of charged particles is field dependent at appropriately high fields (1). However, theoretical arguments based on the parity invariance of μ when the electric field is reversed indicated that a field-independent mobility must always be found at sufficiently low field strengths (30). The constant mobility found in this work at > 10-fold range of E indicated that the low field limit had been reached.

In low density gases and at a very low ion mole fraction, $n\mu$ at a given temperature is independent of density (1). The value of $n\mu$ can be related to the average ion–molecule momentum transfer cross section σ_{av} by (31):

$$[3] \quad n\mu = \frac{3e}{4M_r < v > \sigma_{av}}$$

In eq. [3] M_r is the ion-molecule reduced mass, e is the protonic charge, and $< v >$ is the average velocity of the ions relative to the molecules. Equation [3] is derivable from eq. [5-3-8] of ref. 1.

The present results are plotted as $n\mu$ against reduced density n/n_c in Fig. 1, along with other available results. The value in liquid C_6F_6 at 295 K agrees with previous work (13). The present values in liquid SF_6 are 1.7 times higher than earlier values (26); no reason for this is apparent.

In the saturated vapors, increasing the density requires increasing the temperature. Equation [3] for simple ions indicates that if σ_{av} were independent of ion temperature (kinetic energy), $n\mu$ would decrease as $T^{-1/2}$. In real systems the energy dependence of σ_{av} usually results in $n\mu$ increasing somewhat with increasing T at constant n, except where charge transfer dominates, in which case $n\mu$ decreases (1, 32, 33). In the present vapors the ions would be clustered with neutral molecules, which would increase their mass and tend to increase σ_{av} and decrease $n\mu$. The approximately constant value of $n\mu$ in the present gases at n/n_c up to 0.5 (Fig. 1) indicates a cancellation of opposing effects. For example, the charge-induced dipole attractions of an ion towards two molecules simultaneously, one on either side of the ion in the dense gas, would decrease the value of σ_{av}.[2] The tendency of multibody attractive interactions to decrease σ_{av} would counteract the tendency of clustering to increase σ_{av} in the dense gas.

In the dense vapor near n_c, $n\mu$ increases as n increases, due to destructive interference of the attractive, long range, charge-induced dipole interactions of the ion with more than one molecule at a time (5). At these high densities the distance between molecules is less than an ion diameter so the concept of a cluster is no longer useful. The continuum concept of electrostriction becomes applicable.

At normal liquid densities ($n/n_c > 2$) $n\mu$ decreases, because mobility is more related to the amount of remaining space between the molecules than to number density itself.

In normal liquids the ion mobility is often compared to the fluid viscosity η (2, 3, 24). Stokes' Law (34) and Walden's Rule suggest that

$$[4] \quad \mu \propto \eta^{-1}$$

so $\eta\mu$ = constant. Available values of η in the present liquids cover only a limited range of conditions (35–37). Values of $\eta\mu$ are shown in Fig. 2. At a given viscosity the ions are considerably more mobile than in the hydrocarbon liquids *n*-pentane to *n*-tetradecane (38). Using Stokes' Law, the effective radius R of the diffusing ion is

$$[5] \quad R = e/\,6\pi\eta\mu$$
$$= 8.5 \times 10^{-21}/\eta\mu, \text{ in SI}$$

[2]Note that destructive interference of attractive interactions does not imply a wave phenomenon.

Can. J. Chem. Downloaded from www.nrcresearchpress.com by 91.121.58.235 on 09/07/12
For personal use only.

TABLE 2. Free volume model parameters[a]

Liquid	E_A[b] (kJ/mol)	$10^6 v_o$ (m^3/mol)	$10^6 A$ ($K^{1/2}$ m^2/V·s)	E (kJ/mol)	E^c/RT_m
CS_2	~6	51.2	11.3	0.83	0.3
SF_6	~7	61	3.9	0.48	0.2
C_6F_6	~14	109.2	6.5	0.02	0.007

[a]Equation [8]. CS_2 values from ref. 14.
[b]Arrhenius activation energy, eq. [9].
[c]T_m = temperature at the middle of the range used to obtain E.

so $R \approx 1.7 \times 10^{-10}$ m in SF_6, 2.7×10^{-10} m in CS_2, and 4.1×10^{-10} m in C_6F_6.

B. Comparison to neutral molecule diffusion

The effect of the charge of the ion on its immediate surroundings can be further examined by comparing its diffusion coefficient D_{ion} to that of the neutral molecule D_M. The value of D_{ion} can be obtained from that of μ using the Nernst–Einstein relation (1),

$$[6] \quad D_{ion} = \mu k_B T/e$$

Diffusion coefficients can be related to R, the effective radius of the diffusing particle by the Stokes–Einstein relation (39),

$$[7] \quad D = k_B T/S\pi R\eta$$

where the constant S has a value near 4 (slip boundary condition) for neutral molecule self diffusion in liquids. For ions in neutral molecular liquids or dense gases the charge particle interacts more strongly with the fluid molecules than does a neutral molecule, so $S \approx 6$ (sticking boundary condition) might apply. The difference in values of S suggests that in dense fluids $D_M/D_{ion} \approx 6/4 = 1.5$ if R is similar for the neutral molecule and ion.

Using available values of D_M (39, 40), D_M/D_{ion} is plotted against reduced density in Fig. 3. The ratio in SF_6 at $n/n_c < 0.5$ is 5.4. This is due to the longer range polarization interaction between ion and molecule compared to that between molecule and molecule, and probably a larger ionic radius because of clustering. At $n/n_c > 0.8$ the ratio decreases. The decrease in D_M/D_{ion} is attributed to (*a*) the ion interacts with several molecules at a time so there is destructive interference of the attractive, charge-induced dipole interactions; (*b*) the ion clustered by molecules becomes a less distinct entity in the denser fluid, as it attracts the many molecules in close proximity to it, which increases the local density and viscosity (electrostriction). This change in the effect of the charge is also responsible for the increase and subsequent decrease in $n\mu$ discussed in the previous section (Fig. 1). Under these circumstances ion transport and neutral molecule transport become similar and $D_M/D_{ion} \approx 1.5$, as expected from eq. [7] for the likely difference in S for ions compared to neutral molecules. The radius of the diffusing ions in liquid SF_6 is hence similar to that of a neutral SF_6 molecule.

This contrasts with the limited results in the liquids CS_2 and C_6F_6 where $D_M/D_{ion} = 2.0$ and 2.7, respectively. Hence the effective ionic radius in liquid CS_2 is likely ~ 1.3 times larger than that of a CS_2 molecule, and in liquid C_6F_6 is ~ 1.8 times larger than that of a C_6F_6 molecule.

C. Free volume model

Arrhenius plots are often used to interpret the temperature

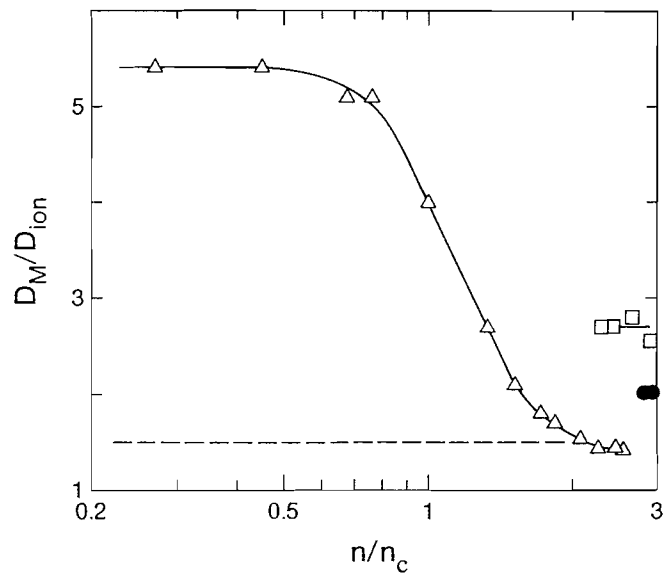

FIG. 3. Ratio of neutral molecule self-diffusion coefficient to ion diffusion coefficient in the same fluid plotted against reduced density n/n_c. Symbols as in Fig. 1. D_M values for SF_6 are from ref. 40 and for C_6F_6 from ref. 39. D_{ion} values were calculated from eq. [6]. The dashed line indicates the value 1.5 expected from eq. [7] between slip and stick boundary conditions.

dependence of diffusion coefficients in the liquid phase (37, 39, 41) and the associated activation energies are then discussed. Alternatively, transport could be described in terms of temperature and molar volume $v = 1/n$ without reference to an energy barrier (37, 39, 42–44). In liquids D_M could be fitted to $T^{1/2}$ $(v - v_0)/v_0$, where v_0 is the molar volume at which the liquid molecules are too crowded for diffusion to occur (5). Then, on the basis of eq. [6], a correlation between μ and $(v - v_0)/v_0T^{1/2}$ was expected and found (14, 38). The value of v_0 was that which gave the best approach of the μ curve to the origin. The lines for the *n*-alkane liquids *n*-hexane to *n*-tetradecane (38) and CS_2 (14) were slightly curved. To fit the results a small exponential coefficient was included:

$$[8] \quad \mu = \frac{A}{T^{1/2}}\left(\frac{v - v_0}{v_0}\right)\exp(-E/RT)$$

where A and E are the fitting parameters.

The liquid phase mobilities are shown as Arrhenius-type plots in Fig. 4. In terms of the Arrhenius model,

$$[9] \quad \mu \approx A_A \exp(-E_A/RT)$$

where A_A is the pre-exponential factor and E_A the activation energy, thermally activated processes over energy barriers

Can. J. Chem. Downloaded from www.nrcresearchpress.com by 91.121.58.235 on 09/07/12
For personal use only.

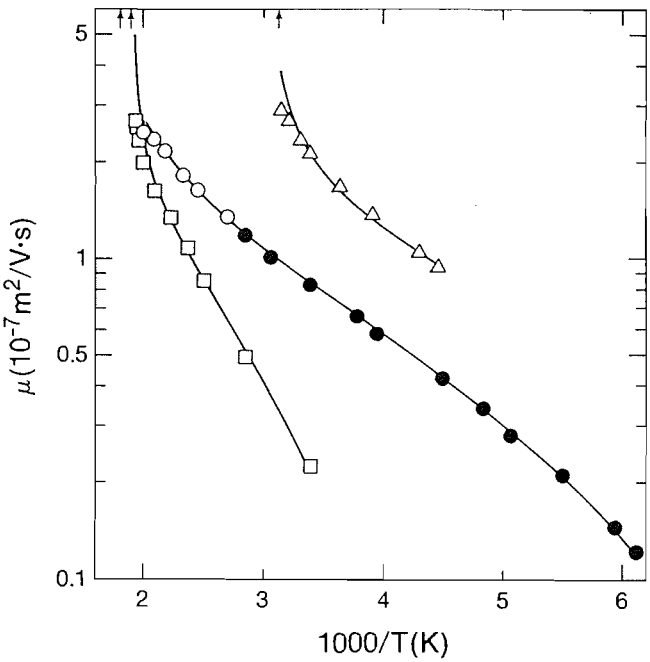

FIG. 4. Arrhenius plot of liquid phase ion mobilities. Symbols as in Fig. 1. The lines were calculated by eq. [8] using the parameter values in Table 2. Arrows indicate T_c.

would be inferred from the values of E_A (Table 2, Arrhenius lines not drawn in Fig. 4). However, the same results are better fitted by the free volume model, eq. [8], with only small values of E, to give the lines drawn in Fig. 4. The largest value of E, 0.8 kJ/mol for CS_2, is only 30% of the average thermal agitation energy RT_m (T_m = temperature at the middle of the range used to obtain E); hence E is considered to be a small exponential correction to the free volume model rather than an "activation energy". The most drastic difference between the models is for C_6F_6, for which E_A = 14 kJ/mol and E = 0.02 kJ/mol. The concept of activation largely disappears once the effect of free volume is accounted for.

Acknowledgements

We thank the Natural Sciences and Engineering Research Council for financial assistance and the Radiation Research Centre for providing and maintaining the experimental facilities.

1. E. W. McDaniel and E. A. Mason. Transport properties of ions in gases. Wiley, New York. 1988.
2. P. Walden and H. Ulich. Z. Phys. Chem. **107**, 219 (1923).
3. N. Gee and G. R. Freeman. Can. J. Chem. (*a*) **59**, 2988 (1981); (*b*) **60**, 1034 (1982).
4. N. Gee, S.-S. Huang, T. Wada, and G. R. Freeman. J. Chem. Phys. **77**, 1411 (1982).
5. I. György, N. Gee, and G. R. Freeman. Can. J. Chem. **63**, 1105 (1985).
6. M. A. Floriano, N. Gee, and G. R. Freeman. Can. J. Chem. **66**, 1872 (1988).
7. F. M. Jacobsen and G. R. Freeman. J. Chem. Phys **84**, 3396 (1986).
8. K. Rohr. J. Phys. B **12**, L185 (1979).
9. A. Chutjian and S. H. Alajajian. J. Phys. B **18**, 4159 (1985).
10. W. C. Wang and L. C. Lee. J. Chem. Phys. **84**, 2675 (1986).
11. E. J. Hart, S. Gordon, and J. K. Thomas. J. Phys. Chem. **68**, 1271 (1964).
12. T. Hirano. J. Appl. Phys. **55**, 9 (1984).
13. C. A. M. van den Ende, L. Nyikos, J. M. Warman, and A. Hummel. Radiat. Phys. Chem. **19**, 297 (1982).
14. N. Gee and G. R. Freeman. J. Chem. Phys. **90**, 5399 (1989).
15. F. M. Jacobsen, M. Eldrup, and O. E. Mogensen. Chem. Phys. **50**, 393 (1980).
16. G. Ramanan, N. Gee, and G. R. Freeman. Can. J. Phys. **68**, Sept. (1990).
17. J.-P. Dodelet and G. R. Freeman. Can. J. Chem. **55**, 2264 (1977).
18. T. Wada and G. R. Freeman. Phys. Rev. Lett. **42**, 715 (1979).
19. M. A. Floriano, N. Gee, and G. R. Freeman. J. Chem. Phys. **84**, 6799 (1986).
20. M. A. Floriano and G. R. Freeman. J. Chem. Phys. **85**, 1603 (1986).
21. M. A. Floriano, N. Gee, and G. R. Freeman. J. Chem. Phys. **87**, 4829 (1987).
22. N. Gee, P. C. Senanayake, and G. R. Freeman. J. Chem. Phys. **89**, 3710 (1988).
23. N. Gee and G. R. Freeman. Can. J. Phys. **68**, Sept. (1990).
24. I. Adamczewski and B. Jachym. Acta Phys. Polon. **30**, 767 (1966).
25. W. F. Schmidt and H. Jungblut. J. Phys. D **12**, L67 (1979).
26. H. Jungblut, W. Döldissen, and W. F. Schmidt. J. Electrostatics, **12**, 59 (1982).
27. I. A. Fleming and J. A. Rees. J. Phys. B, **2**, 777 (1969).
28. F. C. Fehsenfeld. J. Chem. Phys. **53**, 2000 (1970).
29. J. de Urquijo-Carmona, C. Cisneros, and I. Alvarez. J. Phys. D **18**, 2017 (1985).
30. J. K. Baird. J. Chem. Phys. **70**, 1575 (1979); J. Phys. Chem. **84**, 1258 (1980).
31. N. Gee and G. R. Freeman. Can. J. Chem. **61**, 1644 (1983).
32. T. Wada, N. Gee, and G. R. Freeman. Can. J. Chem. **64**, 777 (1986).
33. N. Gee and G. R. Freeman. Rad. Phys. Chem. **32**, 59 (1988).
34. G. G. Stokes. Trans. Cambridge Philos. Soc. **9**, 8 (1850); *In* Mathematical and physical papers. Vol. III. *Edited by* G. G. Stokes. Cambridge University Press, Cambridge. 1901. p. 1.
35. P. Faust. *In* Physico-chemical constants of pure organic compounds. *Edited by* J. Timmerman. Elsevier, Amsterdam. 1950. p. 612.
36. Kirk-Othmer encyclopedia of chemical technology. Vol. 9. Interscience, New York. 1966. p. 666.
37. J. Fischer and A. Weiss. Ber. Bunseg. Phys. Chem. **90**, 896 (1986).
38. N. Gee and G. R. Freeman. Can. J. Chem. **67**, 27 (1989).
39. D. L. Hogenboom, K. Krynicki, and D. W. Sawyer. Mol. Phys. **40**, 823 (1980).
40. J. K. Tisan and E. R. Hunt. J. Chem. Phys. **54**, 1526 (1971).
41. K. Eftaxias and V. Hadjcontis. Philos. Mag. Lett. **58**, 69 (1988).
42. J. H. Dymond and B. J. Alder. J. Chem. Phys. **45**, 2061 (1966).
43. J. H. Hildebrand. Science **174**, 490 (1971).
44. D. Chandler. J. Chem. Phys. **62**, 1358 (1975).

Can. J. Chem. Downloaded from www.nrcresearchpress.com by 91.121.58.235 on 09/07/12
For personal use only.

Liquid–liquid equilibria for the water + ethanol + 2-ethyl-1-hexanol ternary system at several temperatures

HORACIO N. SOLIMO

Laboratorio de Físicoquímica, Instituto de Física, Facultad de Ciencias Exactas y Tecnología, Universidad Nacional de Tucumán Av. Independencia 1800, 4000 San Miguel de Tucumán, Argentina

Received January 5, 1990

HORACIO N. SOLIMO. Can. J. Chem. **68**, 1532 (1990).

Liquid–liquid equilibrium data for the system water + ethanol + 2-ethyl-1-hexanol were obtained at 298.15, 308.15, and 318.15 K. Data for the binodal curves have been determined by cloud-point method and conjugate points on tie-line were obtained by correlating the refractive index of the binodal curves as a function of composition. The tie-line data at each temperatures were satisfactorily correlated using the method of Othmer and Tobias and the plait points coordinates were estimated. The experimental data were also fitted with the UNIFAC group contribution method for the activity coefficients using the isoactivity conditions as restraint equations. From the experimental results, ethanol extraction by 2-ethyl-1-hexanol appears not to depend on temperature and 2-ethyl-1-hexanol could be selected as a promissory solvent for extraction of ethanol from aqueous solutions.

Key words: liquid–liquid equilibria, ethanol extraction, water + ethanol + 2-ethyl-1-hexanol ternary system.

HORACIO N. SOLIMO. Can. J. Chem. **68**, 1532 (1990).

Opérant à des températures de 298,15, 308,15 et 318,15 K, on a déterminé les données d'équilibre liquide-liquide pour le système eau + éthanol + 2-éthyl-hexan-1-ol. On a déterminé les données des courbes binodales à l'aide de la méthode du point de rosée et on a obtenu les points conjugués de la ligne de jonction qui permettent d'établir une corrélation entre les courbes binodales et la composition. Faisant appel à la méthode d'Othmer et de Tobias, on a pu établir une bonne corrélation entre les données relatives aux lignes de jonction pour chacune des températures et on a évalué les coordonnées des points de plissement. En se basant sur la méthode de contribution du groupe UNIFAC et utilisant les conditions d'isoactivité comme équations limites, on a ajusté les données expérimentales et les coefficients d'activité. A partir des données expérimentales, il semble que l'extraction de l'éthanol par le 2-éthyl-hexan-1-ol ne dépend pas de la température et l'on pourrait donc choisir le 2-éthyl-hexan-1-ol comme solvant pour l'extraction de l'éthanol à partir de solutions aqueuses.

Mots clés : équilibre liquide–liquide, extraction de l'éthanol, système tertiaire eau + éthanol + 2-éthyl-hexan-1-ol.

[Traduit par la revue]

Introduction

Liquid–liquid extraction provides an important alternative to distillation for the recovery of ethanol from dilute aqueous solutions. One possible extraction agent is 2-ethyl-1-hexanol (EH) which was selected as a good solvent for ethanol (1, 2). Mutual solubilities of water and EH at several temperatures have been previously measured, but our experimental results are not in agreement with those reported (3) (see Table 2). However, equilibrium data for the ternary system were not found in the literature.

If solvent extraction should be used for ethanol recovery from fermentation broth, a low volatility of the solvent is convenient because the evaporative purification of ethanol would be simpler and accompanied by considerable energy savings. Other requirements are a high distribution coefficient for ethanol, a high selectivity for ethanol compared with water, and a lack of toxicity to microorganism. EH has these characteristics though it is one of the most toxic solvent to ethanol-producing microorganism. This problem could be solved by making a barrier to solvent molecules as a protection against solvent toxicity (1).

To evaluate the potential of EH for the recovery of ethanol from aqueous solutions, the complete phase diagrams for water + ethanol + EH ternary system at 298.15, 308.15, and 318.15 K were obtained. Several tie-lines were determined for each temperature and the correlation of mutual solubility with tie line data (Othmer and Tobias' method) permitted the estimation of the plait point coordinates (4).

The binodal curves, tie-line data, and the plait point coordinates were also fitted by using the UNIFAC group contribution method (5) and the liquid–liquid equilibrium (LLE) interaction parameters reported by Magnussen *et al.* (6).

Experimental

Anhydrous ethanol (Merck, reagent grade) was dried with magnesium activated with iodine under reflux. The product was then fractionally distilled and the middle fraction collected. The last traces of water can be removed by passing the ethanol through a glass column (3 × 200 cm) packed with 0.3 nm molecular sieves.

2-Ethyl-1-hexanol (Sintorgan, commercial grade) was dried over freshly activated CaO and fractionally distilled under reduced pressure. The middle portion with bp 76–78°C at 9 Torr was collected (Purity: 99.9% by GC).

Water was bidistilled in an all-glass apparatus.

All organic purified chemicals were stored over activated molecular sieves to prevent water absorption.

Data for the saturation curves were determined by using the cloud-point method as described earlier (7). Binaries of known composition were shaken in an equilibrium cell equipped with magnetic stirrer and a jacket for circulating the isothermal water at the desired temperatures (±0.05°C). The third component was added from a microburet until the transition point was reached. The contents of the three components yielding a complete binodal curve were determined by weight.

The uncertainty in the observed values was determined by the accuracy of the observation of the transition point since the quantities of the titrating component and the titrated mixtures were accurately determined by weight. The uncertainty through the whole curve was less than 0.05 weight fraction % ethanol at each temperature.

After equilibrium was reached, the refractive index of the ternary mixtures was measured with a Jena Abbe refractometer at each temperature with an accuracy of ±0.0001, and with these values a

Can. J. Chem. Downloaded from www.nrcresearchpress.com by 91.121.58.235 on 09/07/12
For personal use only.

TABLE 1. Experimental density (ρ) and refractive index (n_D) of pure components

Temperature K	Water		Ethanol		2-ethyl-1-hexanol	
	ρ*	n_D†	ρ*	n_D†	ρ*	n_D†
298.15	997.0	1.33285	785.1	1.35939	829.1	1.42900
308.15	994.1	1.33155	776.4	1.35570	822.5	1.42562
318.15	990.3	1.33010	767.3	1.35122	814.1	1.42174

*Measured with a vibrating tube densimeter Anton Paar DMA 45 with an accuracy of ±0.1 kg m^{-3}.
†Measured with a Jena dipping refractometer with an accuracy of ±0.00002.

TABLE 2. Mutual solubility of water (A) and 2-ethyl-1-hexanol (B) at several temperatures

Temperature K	Solubility A in B, wt%		Solubility B in A, wt%		
	Exptl.	Lit.	Exptl.	Lit.	
298.15	1.75	2.44*	0.07	0.107*	0.07†
308.15	2.74	2.62*	0.04	0.101*	
318.15	3.00	2.78*	0.08	0.108*	

*Interpoled from ref. 3.
†At 20°C from ref. 8.

TABLE 3. Binodal curve data for water (1) + ethanol (2) + 2-ethyl-1-hexanol (3) system at 298.15 K*

Water-rich layer			2-Ethyl-1-hexanol-rich layer		
W_{11}%	W_{21}%	W_{31}%	W_{13}%	W_{23}%	W_{33}%
99.93	0.00	0.07	38.18	41.66	20.16
84.68	15.18	0.14	35.24	41.85	22.91
74.30	25.39	0.31	32.11	41.65	26.24
68.66	30.49	0.85	29.77	41.45	28.78
62.96	34.93	2.11	27.33	41.14	31.53
59.29	37.10	3.61	25.41	40.68	33.91
53.48	39.48	7.04	24.40	40.49	35.11
51.19	40.18	8.63	21.45	39.47	39.08
47.12	41.01	11.87	18.76	37.85	43.39
44.41	41.19	14.40	17.13	36.80	46.07
40.91	41.47	17.62	13.33	33.19	53.48
38.96†	41.33†	19.71†	11.36	31.01	57.63
			9.73	27.98	62.29
			8.30	24.85	66.85
			6.88	21.97	71.15
			6.07	19.16	74.77
			4.88	14.46	80.66
			3.58	10.11	86.31
			3.01	6.75	90.24
			1.75	0.00	98.25

*W_{i1}, weight fraction of the component i in aqueous phase; W_{i3}, weight fraction of the component i in organic phase.
†Estimated plait point.

calibrating curve refractive index vs. weight fraction of ethanol was drawn.

Different weighted ternary mixtures with compositions within the heterogeneous region were shaken vigorously in the equilibrium cell for at least 2 h at constant temperature for the tie-line determinations. Preliminary experiments indicated that this time period was sufficient to reach equilibrium. The magnetic stirrer was then turned off and samples of each phase were taken. Samples were analyzed by

TABLE 4. Binodal curve data for water (1) + ethanol (2) + 2-ethyl-1-hexanol (3) system at 308.15 K*

Water-rich layer			2-Ethyl-1-hexanol-rich layer		
W_{11}%	W_{21}%	W_{31}%	W_{13}%	W_{23}%	W_{33}%
99.96	0.00	0.04	38.86	40.33	20.81
80.15	19.71	0.14	35.60	40.63	23.77
74.99	24.69	0.32	32.43	40.45	27.12
69.86	29.39	0.75	30.11	40.40	29.49
65.47	32.80	1.73	27.93	39.92	32.15
57.59	37.25	5.16	25.55	39.43	35.02
52.43	38.52	9.05	23.92	39.00	37.08
49.28	39.51	11.21	22.10	38.13	39.77
44.68	39.93	15.39	19.19	36.90	43.91
41.68	40.29	18.03	17.11	35.15	47.74
40.89†	40.12†	18.99†	13.60	32.03	54.37
			11.10	28.40	60.50
			9.49	25.44	65.07
			8.00	22.47	69.53
			6.68	18.58	74.74
			5.46	14.44	80.10
			4.29	10.00	85.71
			3.06	5.01	91.93
			2.74	0.00	97.26

*W_{i1}, weight fraction of the component i in aqueous phase; W_{i3}, weight fraction of the component i in organic phase.
†Estimated plait point.

measuring their refractive index, and the compositions were obtained with the aid of a calibrating curve. The two end points of a tie-line were thus obtained. An independent material-balance of an equilibrium mixture must lie on a straight line joining the equilibrium layers.

Results and discussion

Densities and refractive indexes of the pure liquids were in good agreement with values published in the literature (8, 9) and are shown in Table 1.

Mutual solubilities of water with EH are listed in Table 2 along with literature values for comparison.

The experimental values for the binodal curves for the three temperatures studied are given in Tables 3, 4, and 5. The tie-line data are given in Table 6.

Figure 1 shows the liquid–liquid equilibrium diagram at 298.15 K containing the binodal curve, tie-lines, and the plait point for the water + ethanol + EH system. Similar plots are obtained at 308.15 and 318.15 K, but are not shown. Predicted LLE data by the UNIFAC method are also shown.

The tie-line data at all the temperatures are satisfactorily correlated by the method of Othmer and Tobias (10). The correlation is shown in Fig. 2 where the dependence of

Can. J. Chem. Downloaded from www.nrcresearchpress.com by 91.121.58.235 on 09/07/12
For personal use only.

TABLE 5. Binodal curve data for water (1) + ethanol (2) + 2-ethyl-1-hexanol (3) system at 318.15 K*

Water-rich layer			2-Ethyl-1-hexanol-rich layer		
W_{11}%	W_{21}%	W_{31}%	W_{13}%	W_{23}%	W_{33}%
99.92	0.00	0.08	39.19	39.28	21.53
79.50	20.34	0.16	36.43	39.62	23.95
74.55	25.00	0.45	32.62	39.35	28.03
68.50	30.03	1.47	30.27	39.36	30.37
64.13	32.98	2.89	28.35	38.96	32.69
56.27	36.63	7.10	26.12	38.37	35.51
52.98	37.62	9.40	24.99	38.19	36.82
49.74	38.18	12.08	22.18	37.40	40.42
45.98	38.76	15.26	19.76	35.92	44.32
42.70	39.07	18.23	17.60	34.36	48.04
42.29†	39.07†	18.64†	14.07	30.93	55.00
			12.00	28.21	59.79
			10.01	25.18	64.81
			7.34	18.90	73.76
			3.92	10.41	85.67
			3.62	4.83	91.55
			3.00	0.00	97.00

*W_{i1}; weight fraction of the component i in aqueous phase; W_{i3}, weight fraction of the component i in organic phase.
†Estimated plait point.

TABLE 6. Tie-line data for water (1) + ethanol (2) + 2-ethyl-1-hexanol system*

Water-rich layer			2-Ethyl-1-hexanol-rich layer		
W_{11}%	W_{21}%	W_{31}%	W_{13}%	W_{23}%	W_{33}%
		298.15 K			
53.50	39.50	7.00	23.20	40.25	36.55
57.99	37.90	4.11	18.13	37.60	44.27
65.30	33.50	1.20	12.25	32.25	55.50
67.50	31.50	1.00	10.50	29.00	60.50
73.40	26.25	0.35	7.60	23.00	69.40
77.50	22.20	0.30	5.90	18.50	75.60
82.20	17.60	0.20	4.90	14.60	80.50
87.90	12.00	0.10	3.20	9.25	87.55
		308.15 K			
53.60	38.60	7.80	26.40	39.60	34.00
59.90	36.00	4.10	20.60	37.50	41.90
65.90	32.50	1.60	14.25	32.75	53.00
69.10	30.20	0.70	11.80	29.70	58.50
72.80	26.85	0.35	9.50	25.60	64.90
77.60	22.10	0.30	6.90	19.00	74.10
81.55	18.15	0.30	5.70	15.00	79.30
85.40	14.35	0.25	4.70	11.00	84.30
90.10	9.75	0.15	3.80	7.50	88.70
94.10	5.75	0.15	3.00	4.50	92.50
		318.15 K			
56.70	36.25	7.05	26.50	38.50	35.00
64.10	33.00	2.90	19.20	35.50	45.30
67.50	30.60	1.90	14.85	31.75	53.40
71.30	27.70	1.00	12.45	28.75	58.80
73.25	26.00	0.75	10.75	26.75	62.50
75.85	23.75	0.40	8.90	23.30	67.80
80.65	19.05	0.30	7.05	18.25	74.70
83.75	16.00	0.25	5.45	14.25	80.30
88.95	10.85	0.20	4.30	9.50	86.20
93.85	6.00	0.15	3.50	4.70	91.80

*W_{i1}, weight fraction of the component i in aqueous phase; W_{i3}, weight fraction of the component i in organic phase.

TABLE 7. Experimental and calculated plait points and linear correlation coefficients for the Othmer and Tobias method for the system water (1) + ethanol (2) + 2-ethyl-1-hexanol (3) at three temperatures

Temperature K	Plait points			Exptl. linear correlation coefficient
	Weight fraction	Exptl.	UNIFAC	
298.15	W_1	0.3896	0.3150	
	W_2	0.4133	0.4720	0.9991
	W_3	0.1971	0.2130	
308.15	W_1	0.4089	0.3157	
	W_2	0.4012	0.4644	0.9992
	W_3	0.1899	0.2199	
318.15	W_1	0.4229	0.3039	
	W_2	0.3907	0.4600	0.9985
	W_3	0.1864	0.2361	

solubility on temperature is clearly shown. Experimental plait points coordinates calculated by using the method of Othmer and Tobias, the UNIFAC plait points coordinates calculated by the same procedure, and the linear correlation coefficients for this method at the three temperatures are given in Table 7.

In selecting solvents, it is necessary to take into account the effect of aqueous ethanol concentration on the ethanol distribution coefficients and the selectivity for ethanol over water.

As shown in Table 8, the ethanol distribution coefficients defined as the ratio of the ethanol concentration (wt%) in organic phase to that in the aqueous phase are not constant, and they have a tendency to increase as ethanol concentration is increased. However, in the low ethanol concentration range the distribution coefficient may be considered to be constant. Similar conclusion can be derived from the distribution coefficient for water (defined as the equilibrium water content in solvent phase, which can be seen in Fig. 1, see also Table 8). The ratio of ethanol distribution coefficient to water distribution coefficient yield the selectivity ratio shown in Table 8.

Zane Egan *et al.* (11) conclude that solvents with experimental distribution coefficients for ethanol greater than 0.15 and a selectivity ratio greater than 10 are potential candidates for extraction process. As shown in Table 8, these extraction properties are largely exceeded by EH, making it a useful alternative for ethanol extraction.

Figure 3 shows a selectivity diagram on a free-solvent basis at all temperatures (12), where ethanol is the distributed substance. As can be seen, the selectivity at 298.15 K is slightly higher than that for the other temperatures studied. Therefore ethanol extraction could be carried out at room temperature, thus saving energy while preserving a fairly important heterogeneous zone. The experimental solubility of this system shows a normal temperature behaviour and similar conclusions are obtained with the UNIFAC method.

At the three temperatures studied the aqueous layer is richer in ethanol than the organic layer (see Figs. 1–3) in the lower ethanol concentration range, which is the most important region for extraction of fermentation broth. However, in the higher ethanol concentration region (above 39% at 298.15 K) an opposite situation is observed. At higher temperatures this situation occurs at lower ethanol concentrations (above 32% at 308.15 K and above 26% at 318.15 K). This is confirmed by the

Can. J. Chem. Downloaded from www.nrcresearchpress.com by 91.121.58.235 on 09/07/12
For personal use only.

Can. J. Chem. Downloaded from www.nrcresearchpress.com by 91.121.58.235 on 09/07/12
For personal use only.

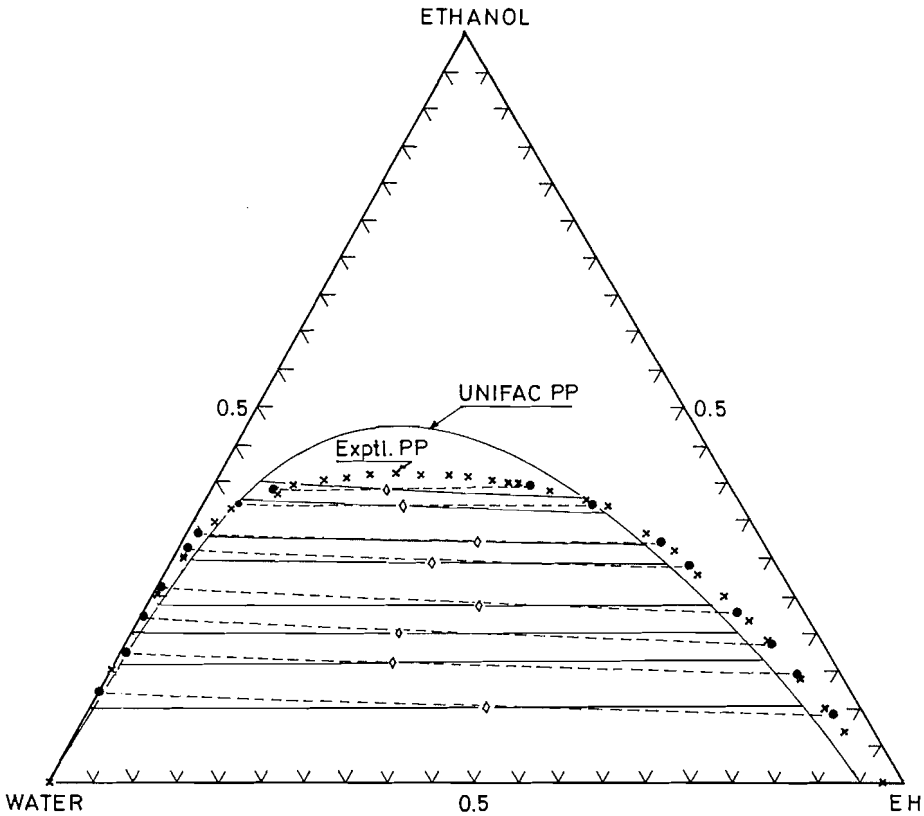

FIG. 1. Liquid–liquid equilibria for the system water (1) + ethanol (2) + 2-ethyl-1-hexanol (3) at 298.15 K. PP = Plait point. Continuous line, LLE predicted by UNIFAC method; ×, experimental binodal points. ●, dashed line: experimental tie-lines; ◇, overall composition for tie-line.

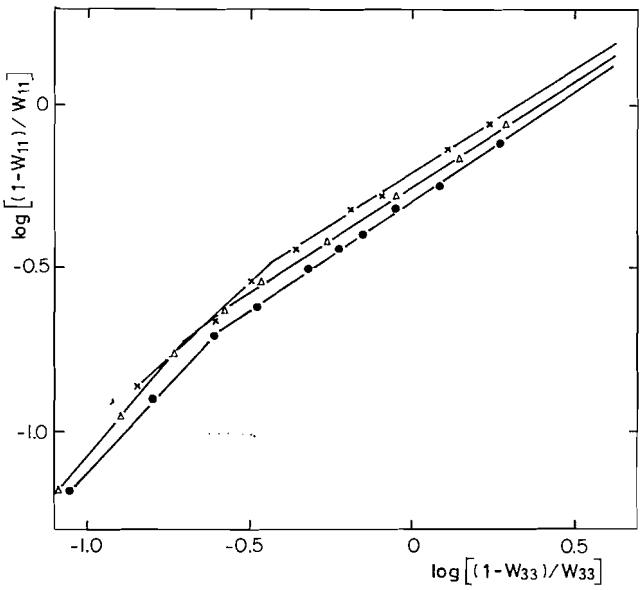

FIG. 2. Correlation of the liquid–liquid equilibrium data at several temperatures by the method of Othmer and Tobias. Straight lines are fitted by least-square method. ×, 298.15 K; △, 308.15 K; ●, 318.15 K.

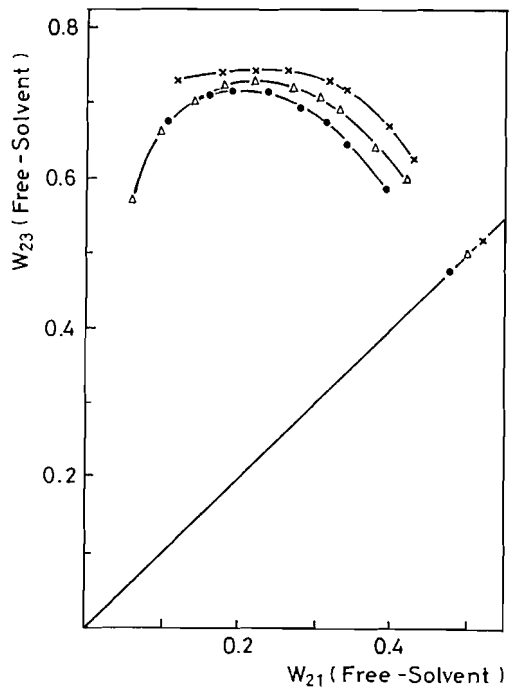

FIG. 3. Selectivity diagram for the system water (1) + ethanol (2) + 2-ethyl-1-hexanol (3) at several temperatures on a free-solvent basis. ×, 298.15 K; △, 308.15 K; ●, 318.15 K.

fact that the ethanol distribution coefficients are higher than that above these ethanol concentrations as can be seen in Table 8.

The liquid–liquid equilibrium data of the ternary system were also predicted using the UNIFAC method (5), which allows the activity coefficients of the three components of both phases to be calculated. The group interaction parameters used were those obtained by Magnussen *et al.* (6) from experimental liquid–liquid equilibrium data and they are shown in Table 9. The equilibrium compositions were calculated using a computer program in which the compositions of the ends of tie-lines are found starting from hypothetical mixtures that give rise to conjugate experimental phases. Figure 1, in which the predicted binodal curve and tie-lines are displayed as continuous lines,

Can. J. Chem. Downloaded from www.nrcresearchpress.com by 91.121.58.235 on 09/07/12
For personal use only.

TABLE 8. Ethanol extraction properties of 2-ethyl-1-hexanol

Temperature K	D_e	D_w	S_w^{EtOH}
298.15	1.02	0.233	4.4
	0.99	0.181	5.5
	0.96	0.122	7.9
	0.92	0.105	8.8
	0.88	0.076	11.6
	0.83	0.060	13.8
	0.83	0.048	17.3
	0.77	0.032	24.1
308.15	1.03	0.265	3.9
	1.04	0.205	5.1
	1.01	0.141	7.2
	0.98	0.117	8.4
	0.95	0.095	10.0
	0.86	0.069	12.5
	0.83	0.057	14.6
	0.77	0.046	16.7
	0.78	0.032	24.4
318.15	1.06	0.265	4.0
	1.08	0.190	5.7
	1.04	0.148	7.0
	1.04	0.124	8.4
	1.03	0.108	9.5
	0.98	0.089	11.0
	0.96	0.069	13.9
	0.89	0.055	16.2
	0.87	0.045	19.3
	0.78	0.032	24.3

*D_e, ethanol distribution coefficient ($D_e = W_{23}/W_{21}$); Dw, water distribution coefficient ($D_w = W_{13}$); S_w^{EtOH}, selectivity ratio ($S_w^{EtOH} = D_e/D_w$).

TABLE 9. UNIFAC interaction parameters*

Main group	1	5	8
1 CH_2	0.0	644.6	1300.0
5 OH	328.2	0.0	28.73
8 H_2O	342.4	−122.4	0.0

*From ref. 6.

shows that the UNIFAC method predicts an immiscibility region larger than that experimentally observed. The inaccuracy of the predictions as measured by the function

$$[1] \quad F_p = 100 \sqrt{\Sigma \Sigma \Sigma (W_{ijk} - \hat{W}_{ijk)2}/6M}$$

was 2.64% at 298.15 K, 2.66% at 308.15 K, and 2.46% at 318.15 K (wt%) where W_{ijk} is the experimental weight fraction of the component i in the phase j for tie-line k; $\hat{W}_{ijk}$ is the UNIFAC calculated weight fraction of the component i in the same phase and tie-line; and M is the number of tie-lines.

Conclusions

Liquid–liquid equilibrium data for the ternary mixture water + ethanol + EH were determined at 298.15, 308.15, and 318.15 K. Comparison of the experimental data for the three temperatures studied here shows that the immiscibility region becomes rather smaller as the temperature rises.

Figure 1, and the residuals of the UNIFAC predictions (F_p) of liquid–liquid equilibrium data for this system (2.64% at 298.15 K, 2.66% at 308.15 K, and 2.46% at 318.15 K), show a correct qualitative behaviour regarding mutual solubilities, but gave a poor quantitative agreement with the experimental data. This could probably be due to inappropriate values for the interaction parameters used for the calculation and the fact that the UNIFAC method had not taken into account the interaction between the OH group of both alcohols in the solution for LLE calculation.

From the analysis of the ethanol extraction properties of EH (see Table 8) it is possible to conclude that this solvent should be considered a potential extractant of ethanol from their aqueous solutions at room temperature.

Acknowledgments

This work was partially supported by a grant from Consejo de Investigaciones de la Universidad Nacional de Tucumán (CIUNT), Argentina. The author thanks Dr. José Lino Zurita for his valuable assistance in computation programming.

1. M. MATSUMURA and H. MARKL. App. Microbiol. Biotechnol. **20**, 371 (1984).
2. J. W. RODDY. Ind. Eng. Chem. Process Des. Dev. **20**, 104 (1981).
3. R. STEPHENSON, J. STUART, and M. TABAK. J. Chem. Eng. Data. **29**, 287 (1984).
4. D. F. OTHMER, R. E. WHITE, and E. TRUEGER. Ind. Eng. Chem. **33**, 1240 (1941).
5. AA. FREDENSLUND, J. GMEHLING, and P. RASMUSSEN. Vapor–liquid equilibria using UNIFAC. Elsevier, Amsterdam. 1977. pp. 27–64 and 243–249.
6. T. MAGNUSSEN, P. RASMUSSEN, and AA. FREDENSLUND. Ind. Eng. Chem. Process Des. Dev. **20**, 331 (1981).
7. H. N. SÓLIMO, H. E. MARTINEZ, and R. RIGGIO. J. Chem. Eng. Data, **34**, 179 (1989).
8. J. A. RIDDICK, W. B. BUNGER, and T. K. SAKANO. Organic solvents. 4th ed. *Edited by* A. Weissberger. Wiley and Sons, New York, Chichester, Brisbane, Toronto, and Singapore. 1986.
9. R. C. WEAST. CRC handbook of chemistry and physics. 69th ed. CRC Press, Boca Raton, FL. 1988–1989.
10. D. F. OTHMER and P. E. TOBIAS. Ind. Eng. Chem. **34**, 690 (1942).
11. B. ZANE EGAN, D. D. LEE, and D. A. MCWHIRTER. Ind. Eng. Chem. Res. **27**, 1330 (1988).
12. R. E. TREYBAL. Liquid extraction. McGraw-Hill, New York, San Francisco, Toronto, and London. 1963. pp. 122–127.

Stabilization of iron-catalysed hydrogen peroxide decomposition by magnesium

JOHN ABBOT AND DOUGLAS G. BROWN
Chemistry Department, University of Tasmania, Hobart, Tasmania, Australia

Received January 5, 1990

JOHN ABBOT and DOUGLAS G. BROWN. Can. J. Chem. **68**, 1537 (1990).

Catalytic decomposition of alkaline hydrogen peroxide by iron can be retarded by introduction of magnesium ions. This effect has been studied to evaluate the possibility of stabilization via formation of an iron–magnesium complex species. Under alkaline conditions, magnesium reacts with initial hydrolysis products of Fe^{3+} to produce a colourless complex species, in which the metal centres are probably linked through oxy or hydroxy bridges. This species is produced when the Mg:Fe molar ratio exceeds 6:1, and this ratio is also significant when magnesium is introduced during peroxide decomposition experiments. The evidence suggests that complex formation is an important factor in producing stabilization, and cannot be disregarded in favour of an alternative explanation where superoxide radicals combine with Mg^{2+} to produce magnesium dioxide.

Key words: hydrogen peroxide, kinetics, iron, magnesium, stabilization.

JOHN ABBOT et DOUGLAS G. BROWN. Can. J. Chem. **68**, 1537 (1990).

L'introduction d'ions magnésium peut retarder la décomposition catalytique du peroxyde d'hydrogène alcalin par le fer. On a étudié cet effet dans le but d'évaluer la possibilité de le stabiliser par le biais de la formation d'un complexe fer–magnésium. Dans des conditions alcalines, le magnésium réagit avec les produits initiaux d'hydrolyse du Fe^{3+} pour donner un complexe incolore dans lequel les centres métalliques sont probablement liés par des ponts oxy ou hydroxy. Il y a production de cette espèce lorsque le rapport molaire Mg:Fe est supérieur à 6:1; ce rapport est aussi important lorsqu'on introduit du magnésium lors des expériences de décomposition du peroxyde. Les données suggèrent que la formation du complexe est un facteur important dans la stabilisation du produit et qu'on ne peut pas l'éliminer en faveur d'une explication alternative qui impliquerait une combinaison des radicaux superoxydes avec le Mg^{2+} pour donner du dioxyde de magnésium.

Mots clés: peroxyde d'hydrogène, cinétique, fer, magnésium, stabilisation.

[Traduit par la revue]

Introduction

The decomposition of hydrogen peroxide in the presence of iron has been studied for many years, particularly under acidic conditions (1–3), where iron is believed to act as a redox catalyst, participating in free radical processes. Although this catalytic process has been studied to a lesser extent at higher pH levels, there is also strong evidence for free radical processes under alkaline conditions (4, 5). At pH levels 10–13, this reaction is of particular interest as hydrogen peroxide is used as an industrial bleaching reagent under these conditions. Loss of hydrogen peroxide due to catalytic decomposition reactions in the presence of transition metals, particularly iron, copper, and manganese, has been a problem in the bleaching of mechanical pulps for manufacture of newsprint, as these metals are often found as trace elements in wood (6). It has been estimated that as much as 30% of the initial hydrogen peroxide charge introduced may be decomposed in these undesirable side reactions (7).

A wide range of chemicals have been tested as stabilizing agents for alkaline hydrogen peroxide systems (8). Complexing agents such as DTPA and EDTA are known to inhibit the catalytic decomposition by iron (4, 9, 10). Other reagents such as sodium silicate and magnesium salts also have proven stabilizing effects, and have widespread industrial application (5, 11). The mechanisms by which stabilization occurs is, however, not clear. The influence of magnesium on the iron-induced decomposition of hydrogen peroxide has been reported by a number of investigators (5, 12). There is some evidence that magnesium forms a "complex" with iron, bonding through hydroxy or oxy bridges. In the presence of carbohydrates, a complex with a Mg:Fe molar ratio of 6:1 has been reported (12, 13), and reduction of peroxide decomposition has been associated with the catalytic inactivity of this species.

Degradation of carbohydrates under alkaline conditions is also retarded by addition of magnesium salts (12, 14, 15). This process is found to be catalysed by the presence of iron, proceeding through a chain reaction involving free radical species (13). Stabilization under these conditions has been attributed to interruption of the chain reaction, through combination of magnesium ions and O_2^- to produce MgO_2 (13). A recent study concluded that this process also occurs during stabilization of peroxide decomposition, and complex formation between iron and magnesium was discounted (5). In the present study we have looked for further evidence for the formation of an iron–magnesium complex, and examined its influence on the peroxide decomposition reaction.

TABLE 1. Trace metal analysis of chemicals used in this study

Metal	Milli-Q (mg/L)	Peroxide* (mg/L)	$Fe(NO_3)_3$ (ppm)	KOH (ppm)	$Mg(NO_3)_2$ (ppm)
Ag	—	—	—	7	—
Ca	—	—	3	0.9	5
Cd	0.00	0.15	—	—	—
Co	0.7	0.6	—	—	—
Cr	0.2	2.6	25	—	—
Cu	0.2	3.3	7	—	—
Fe	0.4	9.8	—	0.7	—
Mg	—	—	0.6	0.08	—
Mn	0.2	1.0	20	0.7	1
Na	—	—	—	250	—
Ni	0.3	4.0	—	—	—
Pb	0.0	2.8	—	—	—
Zn	0.6	5.5	6	3	2

*The levels given are for an undiluted sample.

Experimental

Hydrogen peroxide was obtained from BDH Chemicals. Trace metal analyses of the peroxide and also Milli-Q deionized water were carried out by the CSIRO Marine Laboratories in Hobart, Tasmania, using atomic absorption, and the results are shown in Table 1. Levels of

Can. J. Chem. Downloaded from www.nrcresearchpress.com by 91.121.58.235 on 09/07/12
For personal use only.

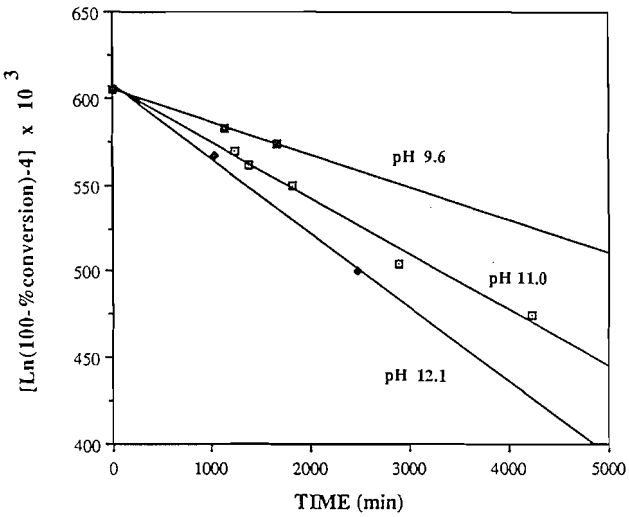

FIG. 1. First order plots for decomposition of hydrogen peroxide in the absence of added iron. Initial hydrogen peroxide concentration 0.10 M.

metallic impurities in the peroxide are comparable to other reported analyses (16). Ferric nitrate (99.99 + %), potassium hydroxide (99.99%) of semiconductor purity and magnesium nitrate (99.99%) were supplied by Aldrich Chemicals and the manufacturers trace analyses are also given in Table 1.

All peroxide decomposition experiments were carried out at a constant temperature of 20°C in capped polyethylene bottles. The bottles were cleaned between experiments using warm dilute sulphuric acid, rinsed with water, dilute potassium hydroxide solution, and finally multiple washings with Milli-Q water.

Decomposition experiments were carried out in hydrogen peroxide solution with initial concentration 0.10 M prepared by addition of 5.0 mL concentrated hydrogen peroxide, ferric nitrate, and potassium hydroxide to an appropriate volume of Milli-Q water. The total volume of solution used was 500 mL. The initial amount of iron introduced was 9.71×10^{-5} mol in all experiments. Aged iron samples were prepared by allowing the solutions to stand at 20°C prior to addition of hydrogen peroxide. The extent of reaction was monitored by titrimetric determination of 10 mL samples withdrawn at intervals. Samples were acidified with sulphuric acid and excess potassium iodide added with a few drops of ammonium molybdate solution. The liberated iodine was titrated against standardized sodium thiosulfate solution (17).

Ultraviolet–visible spectra were recorded using a Varian DMS 100 spectrophotometer.

Results and discussion

Peroxide decomposition in the absence of iron

Hydrogen peroxide decomposition without introduction of ferric nitrate was found to depend on the pH of the alkaline solution. Figure 1 shows that, for a given pH level in the range pH 9–13, the decomposition reaction is first-order with respect to total peroxide concentration. The pH of these solutions was not observed to vary significantly during the initial course of reaction, up to 5% conversion. Table 2 shows the calculated first-order rate constants at each pH level studied.

Under alkaline conditions, the decomposition of hydrogen peroxide has been attributed to an uncatalysed, homogeneous bimolecular reaction involving the perhydroxy anion, HO_2^- (18, 19), and accounts for residual decomposition observed when complexing agents such as EDTA and DTPA are introduced (4). This "spontaneous" decomposition has been shown to be second-order with respect to peroxide concentration (4, 20).

TABLE 2. First-order rate constants for hydrogen peroxide* decomposition in the absence of added iron at 20°C

pH	First-order rate constant $min^{-1} \times 10^3$
9.6	0.0174
11.0	0.0299
12.1	0.0400

*Initial hydrogen peroxide concentration 0.10 M.

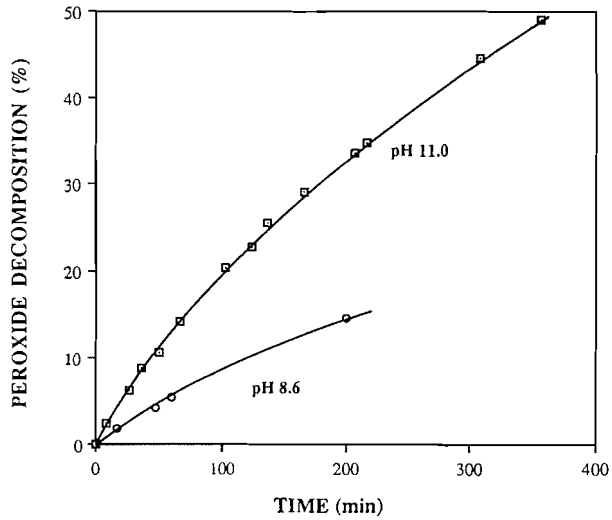

FIG. 2. Decomposition of hydrogen peroxide by alkaline ferric nitrate solutions at 20°C with pH 11.0 and pH 8.6. Initial hydrogen peroxide concentration 0.10 M; initial Fe^{3+} concentration 1.84×10^{-4} M.

Many previous investigations on alkaline peroxide decomposition have noted the importance of purification of the alkali, as this is usually the source of metallic impurities (4, 21). Semiconductor grades of sodium and potassium hydroxide containing very low levels of trace metals are now commercially available, and are well suited for this type of investigation. The very low residual levels of metallic impurities (Table 1) appear to catalyse the first-order peroxide decomposition reactions shown in Fig. 1.

Iron-catalysed decomposition of peroxide

Figure 2 shows the variation in hydrogen peroxide concentration at two pH levels for initial addition of ferric ions at 20°C. It is apparent that the initial rate of peroxide decomposition increases with alkalinity of the solution in the range pH 8–11. It has been reported (22, 23) that, under alkaline conditions, decomposition in the presence of iron can be represented by a first-order kinetic expression with respect to hydrogen peroxide concentration. Figure 3*a* shows that, for results at pH 11.0, there is a non-linear relationship between time and the logarithm of peroxide concentration, unless only the initial reaction period is considered. Other studies have also recognized that this system is indeed more complex than can be represented by a simple first-order process (21, 24). One analysis of kinetic data was interpreted on the basis of two parallel decomposition pathways (21). The first route was reported to depend on the concentration of undissociated hydrogen peroxide and the

Can. J. Chem. Downloaded from www.nrcresearchpress.com by 91.121.58.235 on 09/07/12
For personal use only.

Can. J. Chem. Downloaded from www.nrcresearchpress.com by 91.121.58.235 on 09/07/12
For personal use only.

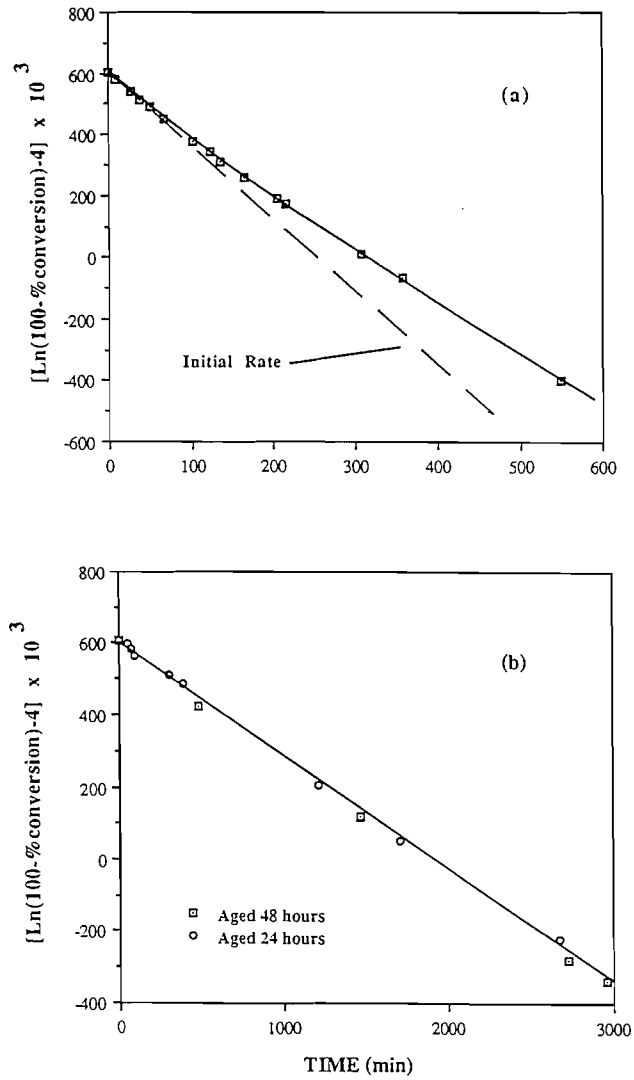

FIG. 3. Logarithmic plots for hydrogen peroxide decomposition at pH 11.0; (*a*) fresh solution, (*b*) after aging of iron for 24 h and 48 h.

alkalinity of the solution for a given metal ion concentration, while the second was independent of the concentration of molecular hydrogen peroxide (21).

An alternative, and probably more fruitful approach, is to recognize that the catalytic species itself evolves with time, and this will be reflected in any kinetic analysis which examines the relationship between decomposition rate and peroxide concentration, as time progresses.[1] Indeed, a declining concentration of the active catalytic species may explain why apparent orders of reaction in the range 1.8–2.0 with respect to peroxide have been reported (24).

It is well known that aqueous solutions of Fe^{3+} undergo hydrolysis to give complex mixtures of species (25), dependent on both pH and time. Hydrolysis products range from simple monomeric species such as $FeOH^{2+}$, through dimers and trimers including $Fe_2(OH)_2^{4+}$, to polymeric species represented by $[Fe(OH)_x(NO_3)_{3-x}]_n$ where $n \sim 900$ (26). The behaviour of such systems has been studied in detail at low pH (27–31), where attainment of equilibrium can occur very slowly, even requiring weeks or months. The evolution of iron species in strongly alkaline media appears to be less well defined, although

[1]J. Abbot and D. G. Brown. Int. J. Chem. Kinet. To be published.

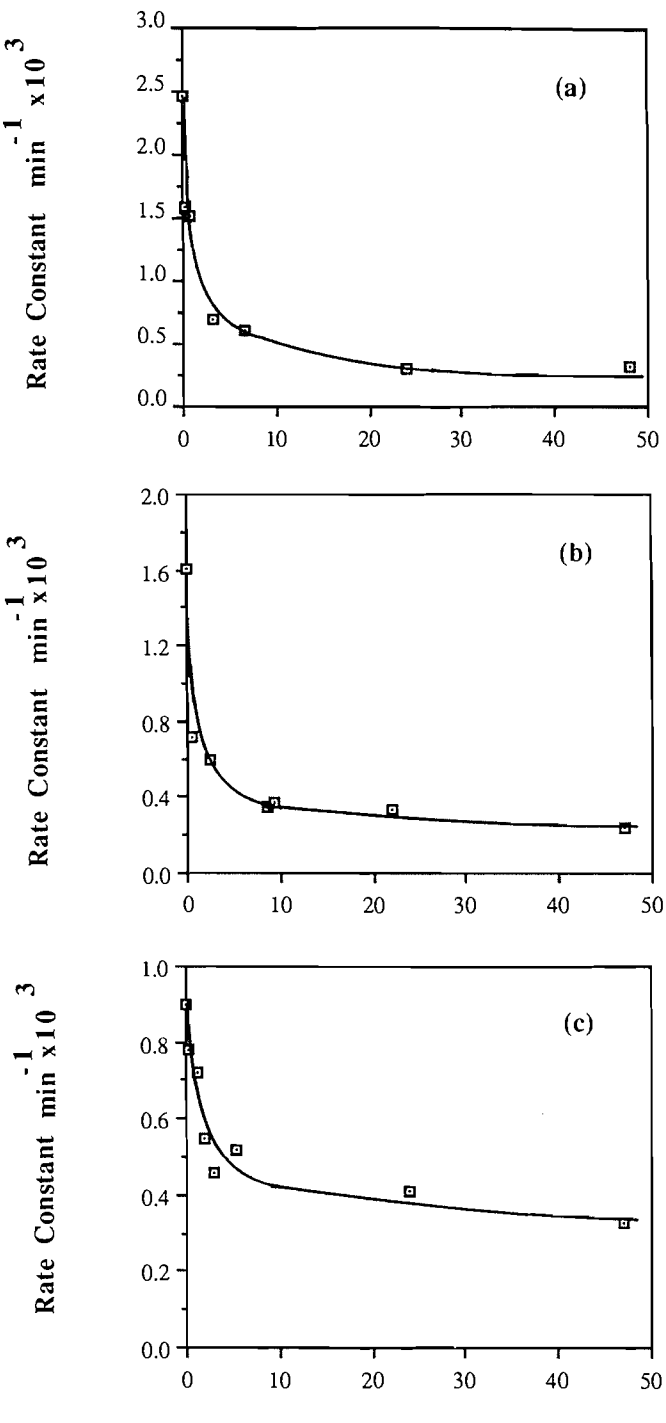

FIG. 4. Effect of aging of iron on initial reaction rates for an iron-catalysed peroxide decomposition at (*a*) pH 11.0, (*b*) pH 9.6, (*c*) pH 8.6.

it is established that the solutions "age" with time, and the aged iron species are less active towards decomposition of hydrogen peroxide (32). Aging of these iron solutions appears to be accompanied not only by an increased degree of polymerization, but replacement of hydroxyl bridges by oxy bridges in the polynuclear iron species (33, 34).

Figure 4*a* shows the variation in initial first-order rate constant for peroxide decomposition at pH 11.0 as the solution is allowed to age prior to addition of hydrogen peroxide. These

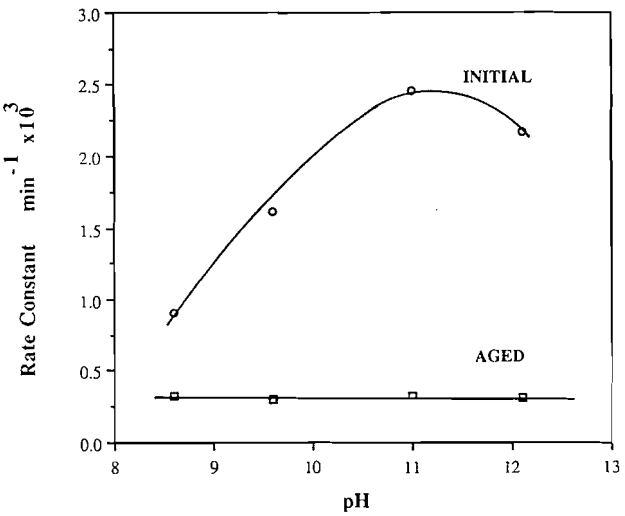

FIG. 5. Effect of pH on initial reaction rate and rate for aged systems (48 h) for iron-catalysed decomposition of hydrogen peroxide.

values have been calculated by subtracting the first-order rate constant for the reaction in the absence of iron (Table 2) from the observed total rate constant. It is apparent that, under the conditions used, the contribution to peroxide decomposition from the "blank" experiments is small compared to that due to the introduced iron. Aging of these solutions took place at pH 12.1, and addition of hydrogen peroxide was accompanied by a reduction in the pH of the solution. It is apparent that aging of the solution is accompanied by an initial rapid decline in catalytic activity of the species present. After about 20 h a constant level of activity is reached. This is also illustrated in Fig. 3*b*, which shows a first-order plot for results obtained after aging the catalysts for 24 and 48 h, respectively.

Figures 4*b* and *c* show that similar trends are observed for peroxide decomposition at pH 9.6 and 8.6, corresponding to aging of the solution at pH 11.0 and 10.2, respectively. The limiting value of the rate constant is observed to be almost independent of pH, as shown in Fig. 5. This figure also shows that the first-order rate constant for initial decomposition of hydrogen peroxide does, however, depend on the pH of the solution and exhibits a maximum at pH ~11. In calculating these values, the rate constants for the corresponding "blank" reactions have again been subtracted from the overall first-order rate constant for peroxide decomposition. A maximum in decomposition at pH ~11 in the presence of iron has been reported previously (24).

Formation of the iron–magnesium complex

Addition of magnesium nitrate to alkaline solutions at 20°C, with ferric nitrate initially introduced, caused precipitation within a few minutes. For systems with pH above 9 and a molar ratio for Mg:Fe in excess of 6:1, the precipitate dissolved on standing to produce a clear, colourless solution. Addition of magnesium to produce molar ratios less than 6:1 also caused precipitation, but complete dissolution did not occur even after standing for 24 h. For solutions with pH <9, the initially formed precipitate also did not dissolve to produce a clear, colourless solution, even when the molar ratio for Mg:Fe was in excess of 6:1. Dispersion of these precipitates by rapid stirring produced solutions containing a coloured colloidal suspension.

Figure 6 shows uv–visible spectra for alkaline iron solutions immediately after addition of ferric ions at pH 12.1, and after allowing the resulting solutions to stand for 24 h. Aging of the

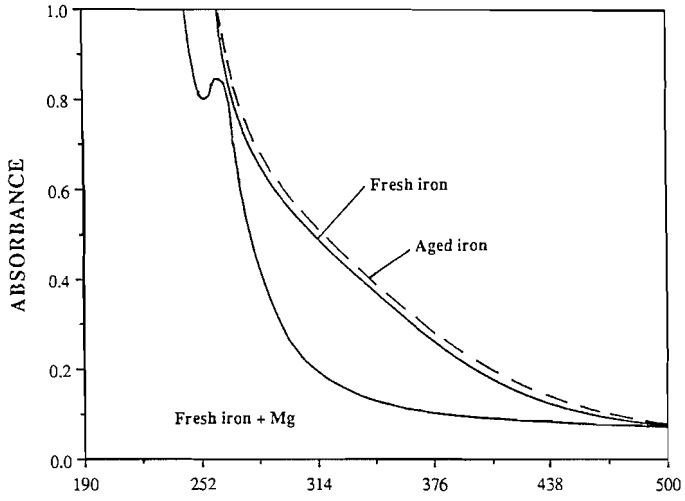

FIG. 6. Ultraviolet–visible spectrum for (*a*) alkaline solution of ferric nitrate at pH 12.1, (*b*) alkaline ferric nitrate with magnesium nitrate added.

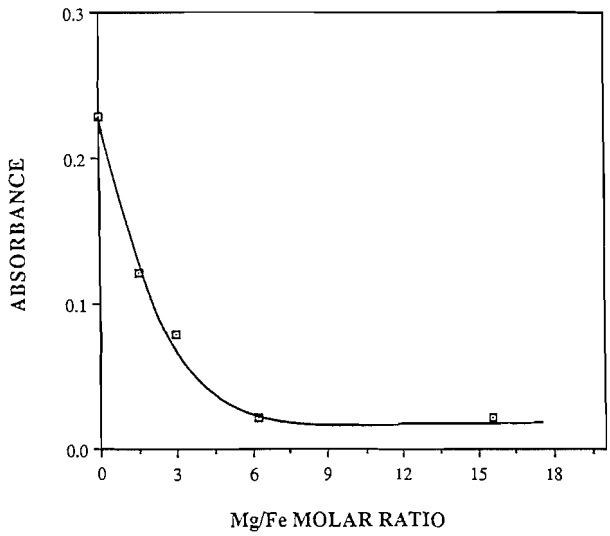

FIG. 7. Effect of Mg:Fe molar ratio on the absorbance at 376 nm.

system does not appear to have a significant influence in the visible region of the spectrum. Figure 6 also shows the corresponding spectrum for the alkaline magnesium-iron system (6:1 molar ratio) at the same total concentration of iron, after standing for about one hour at pH 12.1. The clear solution has an absorbance maximum at 255 nm. Little change in this spectrum was detected on further standing at 20°C.

The change in absorbance in the visible region can be used to follow the effect of Mg:Fe molar ratio on a freshly prepared alkaline solution at pH 12.1. Previously reported studies have shown a discontinuity in the visible absorbance spectrum corresponding to a molar ratio of ~6:1 for Mg:Fe for solutions containing gluconic acid (12). Selecting an arbitrary value of wavelength at 376 nm, Fig. 7 shows the influence of the Mg:Fe molar ratio on absorbance. For samples with Mg:Fe less than 6:1, the solution was stirred vigorously to obtain a homogeneous colloidal suspension prior to measurement of the absorbance. It is clear from Fig. 7 that, in the absence of gluconic

Can. J. Chem. Downloaded from www.nrcresearchpress.com by 91.121.58.235 on 09/07/12
For personal use only.

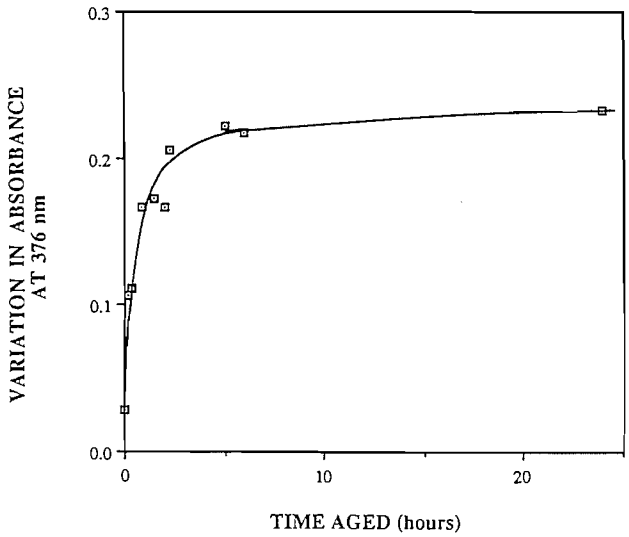

FIG. 8. Variation in absorbance at 376 nm with aging of alkaline ferric nitrate solution at pH 12.1 followed by addition of magnesium nitrate (Mg:Fe molar ratio 15:1).

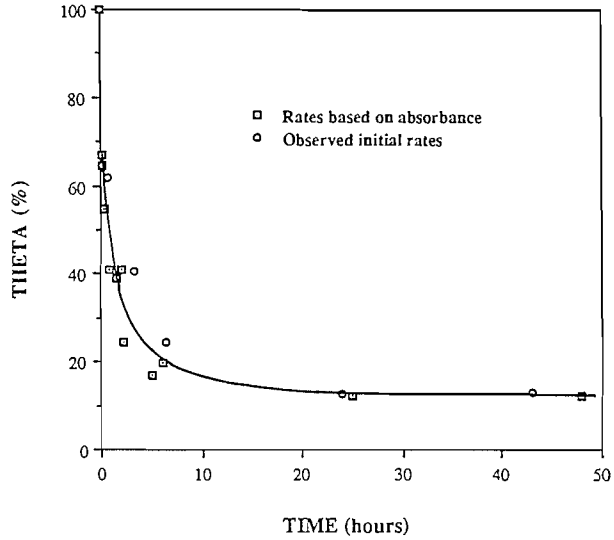

FIG. 9. Correlation between observed initial rate of peroxide decomposition, and rates calculated from absorbance measurements.

acid, there is also a marked discontinuity in absorbance at the 6:1 molar ratio.

Aging phenomena and the iron–magnesium complex

Addition of magnesium to freshly prepared alkaline iron solutions with pH > 10 and Mg:Fe > 6:1 were observed to give clear colourless solutions after dissolution of initially formed precipitates. In contrast, addition of magnesium to iron solutions aged for 24 h at similar pH levels produced no significant change in the absorbance spectra in the visible range. Addition of magnesium to the fully aged iron systems caused precipitation within a few minutes, and the solutions were vigorously stirred, as before, prior to absorbance measurements. It can be concluded that magnesium interacts only with initially produced hydrolysis products from Fe^{3+} to form the colourless complex. Although magnesium may also interact with the aged species, the products formed do not give rise to observable changes in the visible absorbance spectra. This property can be used to follow the progress of the aging process.

Iron solutions at pH 12.1 were allowed to age for various periods, after which magnesium nitrate was added to give a Mg:Fe ratio of 15:1, to provide a large excess of magnesium. The resulting mixtures were allowed to stand for at least an hour, vigorously stirred, and the absorbance spectrum measured in the visible region. The resulting series of spectra were intermediate between those obtained for the freshly prepared and the fully aged (24 h) samples. Figure 8 shows the difference in the measured absorbance at 376 nm between freshly prepared and aged iron after addition of magnesium as the duration of aging was increased. This shows that the absorbance at this wavelength decreases rapidly during the initial aging period, after addition of magnesium, reaching a constant value after an aging period of ~10 h, following the general behaviour of the activity profile in Fig. 4*a*.

The correlation between the activity of the iron species present at various times and the formation of the iron–magnesium complex as reflected by the absorbance measurements can be considered further. Figure 9 shows the change in initial activity of the iron species present, plotted as a percentage (θ) of initial activity, as aging progresses. These values can be compared with those for θ_{Abs}, calculated according to the expression

$$\theta_{Abs} = \left[\frac{k_F (A_A - A_S)}{(A_A - A_F)} + \frac{k_A (A_S - A_F)}{(A_A - A_F)} \right] \times 100\%$$

where k_F and k_A are the first-order rate constants for peroxide decomposition by the fresh and fully aged iron respectively; A_F, A_A, and A_S are the absorption values for fresh, fully aged, and partially aged samples respectively.

This expression assumes that the iron is either present as the more active, initially formed species, which complexes with magnesium, or a second less active species, and that the former is converted directly to the latter. This will almost certainly represent a simplification, as there are likely to be more than two hydrolysis products present at any particular time (25). However, Fig. 9 demonstrates that there is a reasonable correlation between θ and θ_{Abs}. This indicates that there is a direct relationship between peroxide decomposition rate and the presence of highly active initial hydrolysis products of Fe^{3+}, which can react with magnesium to produce the colourless complex.

Figure 10 shows the effect of increasing the molar ratio of Mg:Fe initially introduced on decomposition of hydrogen peroxide at pH 11.0. Increasing the amount of magnesium present inhibits peroxide decomposition up to the point where a 6:1 molar ratio is present. Further increases in this ratio appear to have little influence on the reaction. A significant increase in decomposition rate corresponding to an Fe/Mg molar ratio of 0.167 has been previously reported (5). These authors, however, discounted the significance of this ratio as evidence for complex formation in favour of stabilization through reaction between magnesium ions and superoxide radicals to produce magnesium dioxide and oxygen (5).

The existence of complex species formed between iron and magnesium with 6:1 stoichiometry in the presence of gluconic acid under alkaline conditions has been reported previously (12). Structures for this type of complex have been proposed, which involve oxy or hydroxy bridges between the metal centres. Structures of this type are well known for a wide variety of metals and have been extensively studied as hydrolysis products of individual metal ions (31, 35–37). Much less seems to be known about species containing mixed metal centres.

Can. J. Chem. Downloaded from www.nrcresearchpress.com by 91.121.58.235 on 09/07/12
For personal use only.

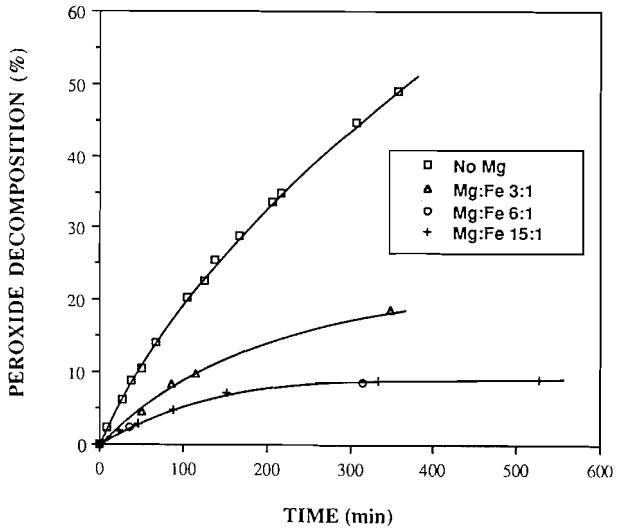

FIG. 10. The influence of magnesium addition on freshly prepared ferric nitrate solutions during peroxide decomposition at pH 11.0.

Iron–scandium and iron–zirconium complexes have been reported (38), and addition of tin salts to iron systems has been shown to stabilize peroxide decomposition under alkaline conditions (8).

The effect of a particular metal additive such as magnesium may not, however, be universal when used in conjunction with catalytically active ions such as iron, manganese, and copper. Addition of magnesium ions to alkaline systems containing manganese ions is reported to produce a rapid acceleration in the rate of peroxide decomposition (5, 39). Recent investigations[2] have confirmed this effect, again showing a correlation between complex formation followed by absorbance measurements, and catalytic activity of the species formed. Evidence for complex formation and structural details has also been provided for the alkaline Mn/Mg system through esr studies (39). These investigations showed that the manganese centres are well separated in the presence of magnesium, so that their environment does not permit significant interaction between Mn^{2+} centres (39). It would appear that the catalytic effects of combinations of hydrolysable metal ions are very specific, and simple explanations such as disruption of the free radical chain process by combination of free Mg^{2+} with intermediate species such as O_2^- are unlikely, particularly as this cannot explain an acceleration of decomposition.

The studies by Colodette *et al.* (5) have shown that the concentration profiles for superoxide anion radical species are perturbed by the addition of magnesium to the iron – alkaline peroxide system. We would infer that this reflects the activity of Fe—O—Mg bridged complex species, as opposed to Fe—O—Fe species, rather than a disruption of the free radical chain reaction by isolated Mg^{2+} ions. Further studies will be required to elucidate the role of the iron–magnesium complex species in producing a stabilization effect, and whether complex formation in other systems such as manganese–magnesium can give rise to species in which the catalytic activity is enhanced rather than suppressed.

The present study has provided additional evidence for complex formation leading to bridged species containing both iron and magnesium centres, thereby modifying the catalytic activity towards peroxide decomposition. These studies were carried out at 20°C, rather than at higher temperatures (50–70°C) usually encountered in commerical bleaching operations. Studies at the lower temperature facilitate measurement of the initial rapid aging process as well as the absorbance of the species present, and we believe that similar phenomena are likely to be observed at raised temperatures. It has also been noted that iron species present in water used for commercial bleaching processes are more likely to resemble "aged" rather than "fresh" iron (5, 32). The extent of interaction between magnesium ions and aged iron species is not clear from the present studies and further investigations will be needed to show whether alternative mechanisms for stabilization through introduction of magnesium are applicable in this situation.

Conclusion

Our studies confirm the existence of complex formation between magnesium and iron species in alkaline solutions above pH 9. Absorbance measurements indicate a stoichiometry of 6:1. The complex is formed through interaction of Mg^{2+} with initially formed hydrolysis products from ferric ions, and dissolves to give a colourless solution. Iron species produced by aging do not undergo reaction to give the colourless complex. These phenomena can be used to follow the progress of the aging process, and provide correlations between activity in peroxide decomposition and complex formation. The rapid peroxide decomposition rates observed for freshly prepared solutions of Fe^{3+} can be directly linked to the presence of initial hydrolysis species which can undergo complexation with magnesium. In the presence of hydrogen peroxide, under alkaline conditions, the Mg:Fe molar ratio of 6:1 is also significant, and suggests that formation of the complex under these conditions reduces the activity of iron towards peroxide decomposition.

Acknowledgement

Financial support for this work was provided by Australian Newsprint Mills Limited.

1. M. L. KREMER. Int. J. Chem. Kinet. **17**, 1299 (1985).
2. F. HABER and J. WEISS. Proc. R. Soc. A, **147**, 332 (1934).
3. W. G. BARB, J. H. BAXENDALE, P. GEORGE, and K. R. HARGRAVE. Trans. Faraday Soc. **47**, 591 (1951).
4. L. J. CSANYI, N. NAGY, Z. M. GALBACS, and L. HORVATH. Z. Phys. Chem. **138**, 107 (1983).
5. J. L. COLODETTE, S. ROTHENBERG, and C. W. DENCE. J. Pulp Paper Sci. **15**, J45 (1989).
6. R. W. ALLISON and K. L. GRAHAM. J. Pulp Paper Sci. **15**, J145 (1989).
7. M. MARTIN. Tappi, **40**, 65 (1957).
8. G. W. KUTNEY. Pulp Paper Can. **86**, 182 (1985).
9. D. R. BAMBRICK. Tappi J. **68**, 96 (1985).
10. P. WHITING, J. M. PITCHER, and D. F. MANCHESTER. J. Pulp Paper Sci. J119 (1984).
11. T. ALI, D. MCARTHUR, D. STOTT, M. FAIRBANK, and P. WHITING. J. Pulp Paper Sci. **12**, J166 (1986).
12. A. F. GILBERT, E. PAVLOVOVA, and W. H. RAPSON. Tappi, **56**, 95 (1973).
13. H. S. ISBELL, E. PARKS, and R. G. NAVES. Carbohydrate Res. **45**, 197 (1975).
14. E. SJOSTROM and O. VATTILA. Pap. ja Puu, 37 (1978).
15. E. SJOSTROM and O. VATTILA. Pap. ja Puu, 695 (1972).
16. S. S. H. TAN and M. K. BALAZS. Semiconductor Int. **11**, 100 (1988).
17. F. KRAFT. *In* Pulp and paper manufacture. Vol. 1. *Edited by*

[2]J. Abbot. J. Pulp Paper Sci. To be published.

Can. J. Chem. Downloaded from www.nrcresearchpress.com by 91.121.58.235 on 09/07/12
For personal use only.

R. G. McDonald. 2nd ed. McGraw-Hill Book Company, New York. 1967. p. 724.
18. F. R. Duke and T. W. Haas. J. Phys. Chem. **95**, 304 (1961).
19. E. Koubek, M. L. Haggett, C. J. Battaglia, K. M. Ibne-rasa, H. Y. Pyun, and J. O. Edwards. J. Am. Chem. Soc. **85**, 2263 (1963).
20. D. F. Evans and M. W. Upton. J. Chem. Soc. Dalton Trans. 2525 (1985).
21. O. Spalek, J. Balej, and I. Paseka. J. Chem. Soc. Faraday Trans. 1, **78**, 2349 (1982).
22. P. K. Smith and T. J. McDonough. Svensk Papperstidning, R106 (1985).
23. R. Agnemo and G. Gellerstedt. Acta. Chem. Scand. **B33**, 337 (1979).
24. Z. M. Galbacs and L. J. Csanyi. J. Chem. Soc. Dalton Trans. 2353 (1983).
25. R. N. Sylva. Rev. Pure Appl. Chem. **22**, 115 (1972).
26. P. R. Danesi, R. Chiarizia, G. Scibona, and R. Riccardi. Inorg. Chem. **12**, 2089 (1973).
27. P. J. Murphy, A. M. Posner, and J. P. Quirk. J. Colloid Interface Sci. **56**, 298 (1976).
28. P. J. Murphy, A. M. Posner, and J. P. Quirk. J. Colloid Interface Sci. **56**, 270 (1976).
29. I. V. Melikhov, E. D. Kozlovskaya, L. B. Beliner, and M. A. Prokofiev. J. Colloid Interface Sci. **117**, 1 (1987).
30. M. Ohyabu and Y. Ujihira. J. Inorg. Nucl. Chem. **43**, 1948 (1981).
31. G. H. Khoe, P. L. Brown, R. N. Sylva, and R. G. Robins. J. Chem. Soc. Dalton Trans. 1901 (1986).
32. J. L. Colodette, S. Rothenberg, and C. W. Dence. J. Pulp Paper Sci. **15**, J3 (1989).
33. O. P. Krivorvchko, B. P. Zolotvskii, R. A. Buyanov, V. I. Zaikovskii, and G. B. Sulima. Kinet. Katal. **18**, 207 (1977).
34. C. F. Wells and M. A. Salam. J. Inorg. Nucl. Chem. **31**, 1083 (1969).
35. P. L. Brown, M. E. Shying, and R. N. Sylva. J. Chem. Soc. Dalton Trans. 2149 (1987).
36. P. L. Brown, R. N. Sylva, G. E. Batley, and J. Ellis. J. Chem. Soc. Dalton Trans. 1967 (1985).
37. P. L. Brown, J. Ellis, and R. N. Sylva. J. Chem. Soc. Dalton Trans. 2001 (1983).
38. V. I. Plotnikov, I. I. Safonov, and V. M. Efemenkov. Vestn. Akad. Nauk. Kaz. SSR. **5**, 28 (1983).
39. R. I. Razouk, G. M. Habashy, and N. P. Kelada. J. Catal. **25**, 183 (1872).

Can. J. Chem. Downloaded from www.nrcresearchpress.com by 91.121.58.235 on 09/07/12
For personal use only.

Oxidative coupling of amines and carbon monoxide catalyzed by palladium complexes. Mono- and double carbonylation reactions promoted by iodine compounds

ILAN PRI-BAR AND HOWARD ALPER[1]

Department of Chemistry, University of Ottawa, Ottawa, Ont., Canada K1N 6N5

Received November 28, 1989

ILAN PRI-BAR and HOWARD ALPER. Can. J. Chem. **68**, 1544 (1990).

Iodine is an effective promoter for the carbonylation of primary and secondary amines to ureas using palladium acetate as the catalyst and a base (e.g. K_2CO_3) in acetonitrile (3 h at 95°C and 2.7 atm). Oxamides are formed in excellent yields when secondary amines are carbonylated in the presence of iodide ion and oxygen, while primary amines give ureas as the principal product at 95°C, and oxamide at room temperature.

Key words: oxamides, ureas, double carbonylation, amines.

ILAN PRI-BAR et HOWARD ALPER. Can. J. Chem. **68**, 1544 (1990).

L'iode est un promoteur efficace de la réaction de carbonylation des amines primaires et secondaires qui les transforme en urées sous l'action de l'acétate de palladium qui agit comme catalyseur et d'une base (comme le K_2CO_3) dans l'acétonitrile (pendant 3 h à 95°C et à 2,7 atm). Il se forme des oxamides avec d'excellents rendements lorsqu'on effectue la carbonylation d'amines secondaires en présence d'ions iodures et d'oxygène; par ailleurs, les amines primaires conduisent principalement à des urées lorsqu'on effectue les réactions à 95°C et à des oxamides lorsqu'on effectue les réactions à la température ambiante.

Mots clés : oxamides, urées, double carbonylation, amines.

[Traduit par la revue]

One of the principal areas in homogeneous catalysis is metal-catalyzed carbonylation reactions. The carbonylation of nitrogen-containing compounds, in particular amines, has attracted considerable interest in recent years (1). For example, early studies on the conversion of amines to ureas, catalyzed by various transition metal complexes, often were carried out using stringent conditions and afforded products in low chemoselectivity and modest yields. A focus of the more recent investigations on the palladium-catalyzed carbonylation of amines to ureas has been on the application of Wacker type conditions (copper salt and oxygen) (2). In some instances, the reported yields are based on the amount of reactant consumed, which may be low, rather than on the actual quantity of amine used (2*b*). Also, the copper salt can participate in secondary oxidation reactions, resulting in low chemoselectivity (2*c*).

The double carbonylation of amines to oxamides can also be catalyzed by palladium compounds, using molecular oxygen as oxidant and cuprous iodide as the co-catalyst (3). For example, piperidine reacts in methanol, but at high pressure of carbon monoxide, to give 1,1′-oxalyldipiperidine in 44% yield and

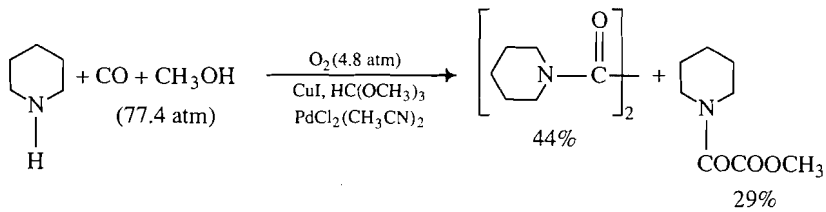

an oxamate in 29% yield. Mixtures of products, including oxamides, result in the absence of a co-catalyst (4).

Iodine compounds (e.g. iodine, potassium iodide) have been employed in recent years as promoters for a number of reactions including the Monsanto acetic acid process, and rhodium-catalyzed carbonylation of benzyl chlorides with borate (5) or formate (6) esters. It is generally assumed that, in the Pd/Cu catalytic system, the main role of copper is to reoxidize *in situ* generated palladium(0) to palladium(II). However, it is conceivable that bimetallic palladium–copper complexes are involved in such processes (7). The use of iodine compounds instead of copper would, of course, rule out the possibility of heterobimetallic intermediates. We now wish to report that iodine and potassium iodide are effective promoters for the palladium catalyzed conversion of amines to ureas and oxamides under mild conditions. It should be noted that a heterogeneous iodide promoted oxidative carbonylation of amines to carbamate esters has been described by Fukuoka and co-workers (8). Elevated temperatures and pressures are required, and the role of the halide is unknown. Also, Chaudhari (9) has reported on the heterogeneous carbonylation of aniline using I^-/O_2. Not only is the process apparently limited to aromatic amines, but no double carbonylation occurs and much higher pressures are required.

Results and discussion

Treatment of primary or secondary amines (**1**, R′ = alkyl or aryl, R^2 = H, alkyl) with carbon monoxide in acetonitrile, in the presence of iodine, potassium carbonate, and a catalytic amount of palladium acetate, for 3 h at 95°C and 2.7 atm, affords di- and tetrasubstituted ureas (**2**). With the exception of diethylamine and di-*n*-butylamine, amines gave ureas in

$$2R'R^2NH + CO + I_2 \xrightarrow[CH_3CN,\ 95°C]{Pd(OAc)_2,\ K_2CO_3} (R'R^2N)_2CO + 2HI$$

(**1**) 2.7 atm (**2**)

reasonable to excellent yields (see Table 1 for results). The

[1]To whom correspondence should be addressed.

Can. J. Chem. Downloaded from www.nrcresearchpress.com by 91.121.58.235 on 09/07/12
For personal use only.

Can. J. Chem. Downloaded from www.nrcresearchpress.com by 91.121.58.235 on 09/07/12
For personal use only.

TABLE 1. Iodine promoted carbonylation of amines to ureas[a]

1, R′ =, R² =	Yield of 2, %[b]
C_2H_5, H	75
n-C_3H_7, H	89
CH_2=$CHCH_2$, H	74
n-C_4H_9, H	98
t-C_4H_9, H	80[c]
Cyclohexyl, H	57[c]
Ph, H	46[c]
CH_3, CH_3	40
$PhCH_2$, CH_3	67
—$(CH_2)_5$—	60[c]
C_2H_5, C_2H_5	8
C_4H_9, C_4H_9	2

[a]Reaction conditions: amine (1.5 mmol), I_2 (0.8 mmol), K_2CO_3 (1.6 mmol), and $Pd(OAc)_2$ (0.1 mmol) were reacted in CH_3CN (10 mL) for 3 h at 95°C and 2.7 atm CO.
[b]Yields determined by gas chromatography, and based on **1**.
[c]Isolated yields.

TABLE 2. Mono and double carbonylation of amines in the presence of KI and O_2[a]

1, R² =, R² =	% 2[b]	% 3[b]
CH_3, CH_3	0	68
C_2H_5, C_2H_5	0	69
n-C_4H_9, n-C_4H_9	0	96
—$(CH_2)_5$—	0	98 (87)[c]
—$(CH_2)_2O(CH_2)_2$—	0	92 (80)[c]
C_2H_5, H	71	12
n-C_3H_7, H	87	12
n-C_4H_9, H	80	8
t-C_4H_9, H	74	4
n-C_4H_9, H[d]	35	0
n-C_4H_9, H[e]	25	66

[a]Reaction conditions: amine (1.5 mmol), KI (0.8 mmol), K_2CO_3 (1.5 mmol), $Pd(OAc)_2$ (0.1 mmol), and oxygen (20 mL) were reacted in CH_3CN (10 mL) for 3 h at 95°C and 2.7 atm CO.
[b]Yields determined by gas chromatography, and based on **1**.
[c]Isolated yield.
[d]Stoichiometric reaction using 0.8 mmol $Pd(OAc)_2$.
[e]Reaction at room temperature for 16 h.

ratio of substrate/iodine/$Pd(OAc)_2$ was 1.5/0.8/0.1 in these reactions.

The influence of several parameters on this reaction was examined using piperidine as the amine. No reaction occurs in the absence of either the palladium catalyst or iodine. A base is not required, but yields are low in its absence, presumably due to the partial conversion of the amine by HI to the ammonium salt. Other bases can be used including pyridine and calcium hydroxide. The yield of urea is dependent on the polarity of the solvent decreasing in the solvent order $CH_3CN > CH_2Cl_2 > THF > C_6H_6$. The addition of a small quantity of air or oxygen to the reaction mixture results in the formation of an oxamide, a product of double carbonylation, in addition to the monocarbonylation species (urea). In principle, a stoichiometric amount of water should also be formed in the reaction (not determined). The relative ratio of mono versus double carbonylation products depends on the proportion of oxygen to palladium. Higher yields of oxamides were realized by increasing the amount of oxygen, decreasing the palladium concentration, or increasing the reaction time. Superior results are attained for secondary amines by using potassium iodide as a promoter, and both carbon monoxide and oxygen.

$$R'R^2NH + CO + O_2 \quad (1)$$

$$\xrightarrow[\text{KI, } CH_3CN]{Pd(OAc)_2,\ K_2CO_3} [R'R^2NCO]_2 + [R'R^2N]_2CO + H_2O$$

95°C, 2.7 atm (3) (2)

As the results in Table 2 indicate, oxamides (**3**) are obtained in fine yields as the sole product from secondary amines, while ureas are the principal products formed in the case of primary amines. It is interesting to note that while di-n-butylamine gave only 2% urea on carbonylation in the presence of iodine (Table 1), carbonylation with potassium iodide and oxygen afforded the oxamide in 96% yield (Table 2). It is possible to increase the proportion of oxamide in the case of primary amines by effecting the reaction at lower temperature. Thus reacting n-butylamine for 16 h at room temperature (instead of 3 h at 95°C) gave the oxamide in 66% yield with the urea formed in 25% yield (compare entries 8 and 11 of Table 2).

As in the case of urea generation, piperidine was used as a probe to learn about factors which influence oxamide formation (Table 3). The conversion of piperidine to the oxamide is sluggish in the absence of iodide ion (Table 3, entry 1). As long as the iodide/$Pd(OAc_2)$ ratio is at least 2/1, increasing the proportion of potassium or tetra-n-butylammonium iodide has only a modest effect on product yields (entries 2–4, 8–9). The addition of potassium carbonate enhances the yield of oxamide (entries 5, 6).

Replacement of an inorganic iodide salt (KI) by a quaternary ammonium iodide has a significant effect on the reaction rate enabling one to perform the reaction at room temperature (entries 7, 8) and in a variety of solvents of which tetrahydrofuran is the most suitable (entries 8, 11–13). In these reactions, an unidentified black precipitate forms several minutes after addition of the reagents, suggesting that heterogeneous palladium species may play a role here. However, substitution of $Pd(OAc)_2$ by a heterogeneous palladium catalyst (Pd/C, Pd black, palladium oxide) results in low catalytic activity (entries 14–16). To ensure homogeneity of the catalytic system, the reaction was effected in the presence of triphenylphosphine with a 2:1 ratio of $PPh_3/Pd(OAc)_2$ affording oxamide in the highest yield (Table 3, entries 17, 18). Tetrabutylammonium iodide is still of value (entries 18, 19) and THF again is the preferred solvent (entries 18, 20, 21). Use of bidentate phosphine as the added ligand is not fruitful in terms of product formation (entries 22, 23).

Let us consider possible mechanisms for the iodine and iodide-oxygen promoted mono and double carbonylation reactions (Scheme 1). The results indicate that the mechanism of the oxidative dicarbonylation promoted by iodide differs from that of the iodine promoted monocarbonylation. For instance, the solvent effects are different in the two processes. In addition, while di-n-butylamine is readily converted to oxamide, the

Can. J. Chem. Downloaded from www.nrcresearchpress.com by 91.121.58.235 on 09/07/12
For personal use only.

TABLE 3. Carbonylation of piperidine promoted by iodide and oxygen

Entry	Catalyst, mmol	Base, mmol	Solvent	Iodide, mmol	Added ligand, mmol	Reaction conditions[a]	Oxamide,[b] %
1	$Pd(OAc)_2$, 0.1	—	CH_3CN	—	—	A	18
2	$Pd(OAc)_2$, 0.1	—	CH_3CN	KI, 0.4	—	A	74
3	$Pd(OAc)_2$, 0.1	—	CH_3CN	KI, 0.8	—	A	85
4	$Pd(OAc)_2$, 0.1	—	CH_3CN	KI, 1.6	—	A	80
5	$Pd(OAc)_2$, 0.1	K_2CO_3, 0.8	CH_3CN	KI, 0.8	—	A	93
6	$Pd(OAc)_2$, 0.1	K_2CO_3, 1.6	CH_3CN	KI, 0.8	—	A	98
7	$Pd(OAc)_2$, 0.1	K_2CO_3, 0.8	THF	KI, 0.8	—	B	8
8	$Pd(OAc)_2$, 0.1	K_2CO_3, 0.8	THF	Bu_4NI, 0.8	—	B	45
9	$Pd(OAc)_2$, 0.1	K_2CO_3, 0.2	THF	Bu_4NI, 0.2	—	B	38
10	$Pd(OAc)_2$, 0.1	K_2CO_3, 0.8	THF	Bu_4NI, 0.8	—	C	75
11	$Pd(OAc)_2$, 0.1	K_2CO_3, 0.8	CH_3CN	Bu_4NI, 0.8	—	B	19
12	$Pd(OAc)_2$, 0.1	K_2CO_3, 0.8	Dioxane	Bu_4NI, 0.8	—	B	13
13	$Pd(OAc)_2$, 0.1	K_2CO_3, 0.8	C_6H_6	Bu_4NI, 0.8	—	B	8
14	Pd/C(10%), 0.1	K_2CO_3, 0.8	THF	Bu_4NI, 0.8	—	B	12
15	Pd(black), 0.1	K_2CO_3, 0.8	THF	Bu_4NI, 0.8	—	B	17
16	PdO, 0.1	K_2CO_3, 0.8	THF	Bu_4NI, 0.8	—	B	2
17	$Pd(OAc)_2$, 0.1	K_2CO_3, 0.2	THF	Bu_4NI, 0.2	Ph_3P, 0.1	B	42
18	$Pd(OAc)_2$, 0.1	K_2CO_3, 0.2	THF	Bu_4NI, 0.2	Ph_3P, 0.2	B	88
19	$Pd(OAc)_2$, 0.1	K_2CO_3, 0.2	THF	—	Ph_3P, 0.2	B	24
20	$Pd(OAc)_2$, 0.1	K_2CO_3, 0.2	CH_3CN	Bu_4NI, 0.2	Ph_3P, 0.2	B	52
21	$Pd(OAc)_2$, 0.1	K_2CO_3, 0.2	C_6H_6	Bu_4NI, 0.2	Ph_3P, 0.2	B	36
22	$Pd(OAc)_2$, 0.1	K_2CO_3, 0.2	THF	Bu_4NI, 0.2	$Ph_2PCH{=}CHPPh_2$, 0.2	B	10
23	$Pd(OAc)_2$, 0.1	K_2CO_3, 0.2	THF	Bu_4NI, 0.2	Diphos, 0.2	B	17

[a]All reactions effected at 2.7 atm CO. A, 95°C for 3 h; B, ambient temperature for 3 h; C, ambient temperature for 22 h.
[b]Yield by gas chromatography and based on piperidine.

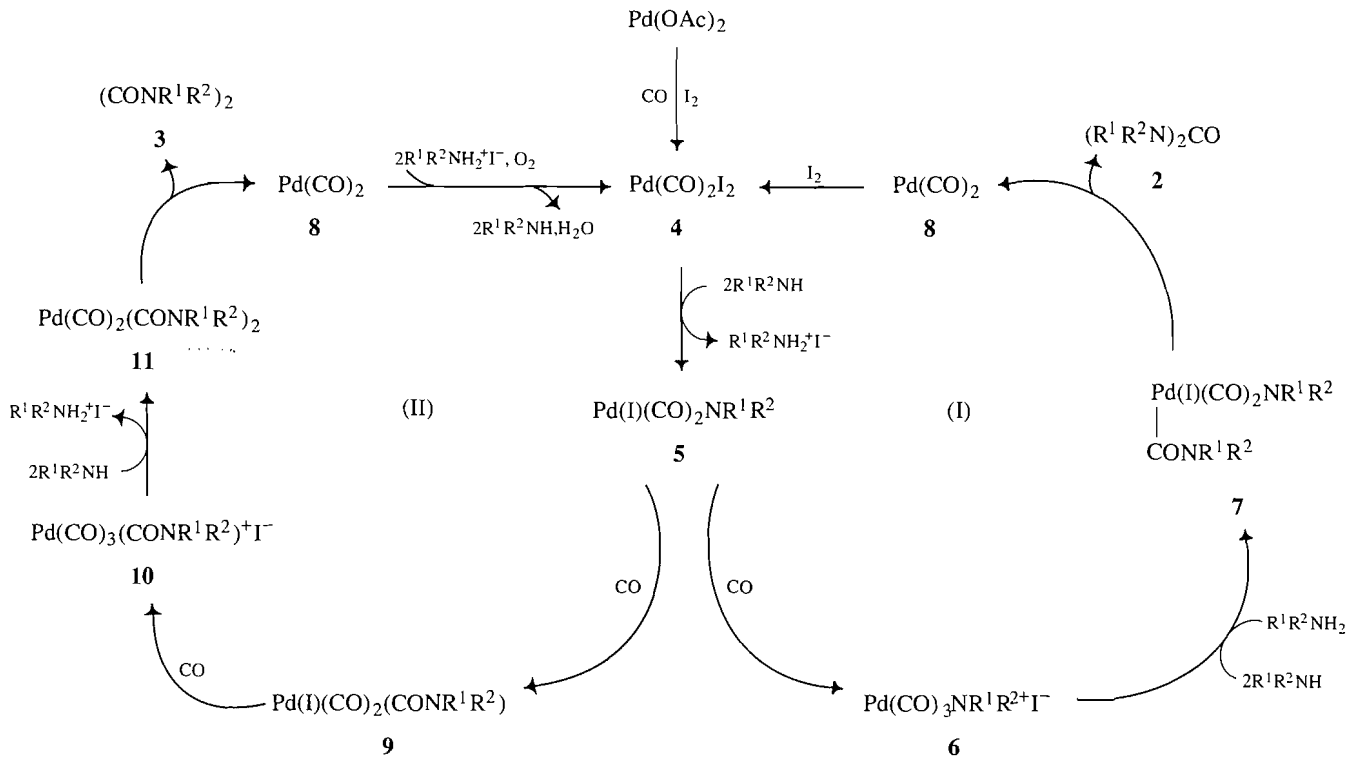

SCHEME 1

Can. J. Chem. Downloaded from www.nrcresearchpress.com by 91.121.58.235 on 09/07/12
For personal use only.

generation of the urea is a sluggish reaction. Consequently, two separate catalytic cycles can be considered to rationalize these reactions (Scheme 1). Palladium acetate can react with carbon monoxide and iodine to form diiododicarbonylpalladium (**4**) (the formation of $(R'R^2NH)_2PdI_2$ by initial reaction of $Pd(OAc)_2$ with amine and iodine is also possible. Nevertheless, the end result in terms of formation of **2** and **3** is the same). Displacement of one of the iodo ligands by amine would give **5**. The latter can react in one of several ways. Reaction with carbon monoxide may afford the cationic palladium complex **6**. Amine addition to one of the carbonyl carbons of **6** may form **7** (Cycle I). The urea can then arise by reductive elimination and the by-product, palladium dicarbonyl (**8**) can undergo oxidative addition of iodine regenerating **4**. Alternatively, complex **5** can experience ligand migration, with addition of carbon monoxide to the vacant coordination site, to give **9** (Cycle II). Addition of another carbon monoxide unit would generate the ionic complex **10**. Amine addition to give **11**, followed by reductive elimination affords the oxamide and **8**. Reoxidation of the latter by oxygen and an ammonium iodide would regenerate **4**. Several of the proposed intermediates are analogous to those postulated in the palladium catalyzed carbonylation of halides to amides and α-ketoamides (10).

In conclusion, this research has demonstrated that amines can be converted to ureas in fine yields using iodine as a promoter for the palladium(II) catalyzed reaction. Also, oxamides are formed in good yields from secondary amines, and ureas from primary amines, when iodide and oxygen are used to induce the reaction. The experiment with *n*-butylamine at room temperature (last entry of Table 2) shows that primary amines can give oxamides as the principal product under appropriate conditions. Attractive features of these processes include the remarkably mild conditions, as well as the efficiency, ease of execution and work-up of the reactions.

Experimental

General data

A Perkin-Elmer 783 spectrometer was used for infrared spectral determinations, a VG7070E micromass spectrometer for mass spectra, and Varian EM-360 and XL-300 instruments were used to record nuclear magnetic resonance spectra. Gas chromatographic determinations were performed on a Varian 3400 instrument equipped with a OV-17 packed glass column, and a DB-1 capillary column.

Amines were purchased from commercial sources and were distilled prior to use. Solvents were dried by standard techniques. Reactions were carried out in a glass pressure vessel containing a magnetic stirring bar. The ureas and oxamides were characterized by comparison of infrared, nuclear magnetic resonance, and mass spectral data with those for authentic materials. Spiking of products with authentic samples, and analysis by gas chromatography, was also used to confirm the structures of the products. Standards of disubstituted ureas which were not commercially available were prepared by treatment of the corresponding isocyanate with a primary amine. Oxamides were prepared independently by reaction of oxalyl chloride with the appropriate amine.

General procedure for the iodine-promoted synthesis of ureas

Palladium acetate (0.022 g, 0.10 mmol), iodine (0.38 g, 1.5 mmol), and potassium carbonate (0.220 g, 1.6 mmol) were placed in a glass autoclave (85 mL). The reaction vessel was sealed and flushed three times with carbon monoxide. A 10 mL solution of acetonitrile containing the amine (1.5 mmol) and biphenyl (gc internal standard) was added by syringe using a rubber septum. The glass autoclave was pressurized to 2.7 atm (with CO) at ambient temperature, sealed, and heated in an oil bath at 95°C for 3 h. During this period, the color of the solution changed from red to pink. The autoclave was cooled to room temperature, the solution was filtered (precipitated inorganic salts), and the filtrate was analyzed by gas chromatography. Isolation of the urea was attained by concentration of the filtrate (rotary evaporation), followed by silica gel thin-layer chromatography, recrystallization or distillation. The ureas were characterized by comparison of infrared, nuclear magnetic resonance, and mass spectra with those for authentic materials and literature data. Disubstituted ureas which were not commercially available were independently prepared by treatment of a primary amine with the corresponding isocyanate.

General procedure for the carbonylation of amines in the presence of iodide ion and oxygen

To a mixture of $Pd(OAc)_2$ (0.022 g, 0.10 mmol), KI or $(C_4H_9)_4N^+I^-$ (0.2–0.8 mmol), K_2CO_3 (1.5 mmol) and triphenylphosphine (0.052 g, 0.20 mmol — if used) was added, under carbon monoxide, 10 mL of a THF solution containing 1.5 mmol of an amine and biphenyl (gc internal standard). Oxygen (20 mL, 1 atm) was added, and the autoclave (85 mL) was pressurized to 2.7 atm with carbon monoxide. The reaction mixture was stirred at 95°C for 3 h, cooled to room temperature, and then filtered. The filtrate (subjected to gc analysis) was concentrated by rotary evaporation, and the oxamide and/or urea were purified by crystallization or silica gel preparative thin-layer chromatography (9:1 petroleum ether – ethyl acetate). Oxamides were characterized by comparison of physical and spectral data with oxamides which were not commercially available were independently synthesized from oxalyl chloride and the appropriate amine.

Acknowledgements

We are grateful to British Petroleum and to the Natural Sciences and Engineering Research Council of Canada for support of this research.

1. R. A. SHELDON. Chemicals from synthesis gas. D. Reidel Publ. Co. Dordrecht, Holland. 1983. Chap. 8.
2. (*a*) H. ALPER, G. VASAPOLLO, F. HARTSTOCK, M. MLEKUZ, D. J. H. SMITH, and G. E. MORRIS. Organometallics, **6**, 2391 (1987); (*b*) P. GIANNOCARRO. J. Organomet. Chem. **336**, 277 (1987); (*c*) N. I. DESAI, J. B. BUTT, and J. S. DRANOFF. J. Catal. **79**, 95 (1983).
3. S. I. MURAHASHI, Y. MITSUE, and K. IKE. J. Chem. Soc. Chem. Commun. 125 (1987).
4. J. TSUJI and N. IWAMOTO. J. Chem. Soc. Chem. Commun. 380 (1966).
5. H. ALPER, N. HAMEL, D. J. H. SMITH, and J. B. WOELL. Tetrahedron Lett. **26**, 2273 (1985).
6. C. BUCHAN, N. HAMEL, J. WOELL, and H. ALPER. J. Chem. Soc. Chem. Commun. 167 (1986).
7. T. HOSOKAWA, T. UNO, S. INUI, and S. I. MURAHASHI. J. Am. Chem. Soc. **103**, 2318 (1981).
8. S. FUKUOKA, M. CHORO, and M. KOHNO. J. Org. Chem. **49**, 1458 (1984); S. FUKUOKA, M. CHORO, and M. KOHNO. J. Chem. Soc. Chem. Commun. 399 (1984).
9. R. V. CHAUDHARI. J. Catal. **114**, 246 (1988).
10. J. COLLIN. Bull. Soc. Chim. Fr. 976 (1988) and references therein.

Molecular orbital computations and ^1H nuclear magnetic resonance measurements of the bending motion of xanthene in the gas and in solution

TED SCHAEFER AND RUDY SEBASTIAN
Department of Chemistry, University of Manitoba, Winnipeg, Man., Canada R3T 2N2

Received January 19, 1990

TED SCHAEFER and RUDY SEBASTIAN. Can. J. Chem. **68**, 1548 (1990).

STO-3G and 4-31G MO computations are reported for a range of values of the folding angle in xanthene, the dihedral angle between the benzene planes. Unlike 9,10-dihydroanthracene but like dibenzo-p-dioxin, its "parent" molecules, the inversion or puckering potential for xanthene is calculated to be rather flat. The molecular energies between a folding angle of 180° (planar molecule) and 120° are reproduced by analytical functions of $\phi = \theta - 180°$, θ being the folding angle. The long-range spin–spin coupling constants between the methylene protons and the aromatic protons at 300 K are reported for xanthene dissolved in a CS_2/C_6D_{12} solvent mixture and in acetone-d_6 solution. These conformationally sensitive coupling constants are consistent with the theoretical puckering potentials and therefore with substantial "butterfly" motion at ambient temperatures. The computed geometries of xanthene are also given and briefly discussed.

Key words: xanthene, MO computations on inversion; xanthene, long-range spin–spin coupling constants; xanthene, internal motion; xanthene, inversion potentials.

TED SCHAEFER et RUDY SEBASTIAN. Can. J. Chem. **68**, 1548 (1990).

On a effectué des calculs d'OM aux niveaux STO-3G et 4-31G pour un ensemble de valeurs de l'angle de plissement du xanthène, l'angle dièdre entre les plans des deux noyaux benzéniques. Contrairement à ce qui a été observé avec le 9,10-dihydroanthracène, mais en accord avec ce qui a été observé avec la dibenzo-p-dioxine, ses molécules «parentes», on a calculé que le potentiel d'inversion ou de gauchissement du xanthène est relativement plat. On peut reproduire les énergies moléculaires calculées par des angles de plissement allant de 180° (molécule plane) à 120° à l'aide des fonctions analytiques $\phi = \theta - 180°$ dans lesquelles θ est l'angle de plissement. Opérant à 300 K, dans des solutions dans l'acétone-d_6 ou dans un mélange de CS_2/C_6D_{12}, on a mesuré les constantes de couplage spin–spin à longue distance entre les protons méthyléniques et les protons aromatiques. À la température ambiante, ces constantes de couplage qui sont sensibles à la conformation sont en accord avec les potentiels théoriques pour le gauchissement et donc avec un mouvement important du type «papillon». On rapporte aussi les géométries calculées pour le xanthène et on les discute brièvement.

Mots clés : xanthène, calculs d'OM pour l'inversion; xanthène, constantes de couplage spin–spin à longue distance; xanthène, mouvement interne; xanthène, potentiels pour l'inversion.

[Traduit par la revue]

Introduction

While 9,10-dihydroanthracene (X = CH_2 = Y in **1**) has a folded structure, the dihedral (folding) angle between the aromatic planes being 144.7° in the crystal (1), dibenzo-p-dioxin (X = Y = O in **1**) is apparently planar in such a state (2);

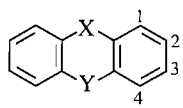

1

diffuse scattering suggests disorder which *may* arise (3) from inversion. Molecular orbital calculations with STO-3G and 4-31G basis sets (4) yield a folding angle of 141° and an inversion barrier of near 8 kJ/mol for 9,10-dihydroanthracene. The latter is consistent with the available experimental data for solutions. The computed geometries (4) also agree reasonably well with experiment. Again, the STO-3G MO computations for the dibenzo-p-dioxin (5) molecule predict a minimum energy at a folding angle of 180°, with a flat puckering potential near this angle. At ambient temperatures, nonplanar populations are appreciable for this potential. The expectation value of the folding angle is 168.3° at 300 K for this potential, in good agreement with values derived for static models from dipole moments (6) and from intramolecular nuclear dipole coupling constants in a nematic solvent (7), for example.

Xanthene (X = CH_2, Y = O), a structural hybrid of the two molecules above, does not appear to have been investigated in the crystalline form. In CCl_4 and benzene solutions at 298 K, the molar Kerr constants (8) indicate a folding angle of 160 ± 6°. Dipole moments, variously reported as 1.29, 1.09, 1.13, 1.14, and 1.43 D (8–10), apparently are consistent with a planar or a rapidly inverting nonplanar conformation (10). The dielectric relaxation times of xanthene in benzene solution at 293 K (11) have been interpreted tentatively in terms of an empirical (molecular mechanics) inversion potential of 0.8 kJ/mol. It seems that the puckering behaviour of xanthene may well approximate to that of the dioxin instead of to 9,10-dihydroanthracene.

Because the STO-3G and 4-31G bases provide reasonably accurate descriptions of the first two molecules above, it appears sensible to apply them to xanthene. Such computations are reported here. In addition, the long-range coupling constants between the methylene and ring protons are reported for CS_2 and acetone-d_6 solutions. These coupling constants are in principle sensitive to the folding angle in xanthene.

Experimental

Solutions, at a concentration of 3.9 mol% of xanthene in CS_2/C_6D_{12}/TMS and acetone-d_6/TMS solvent mixtures, were filtered into 5 mm o.d. nmr sample tubes. These were degassed by the freeze–pump–thaw procedure and were then flame-sealed to yield symmetrical tops. The ^1H nmr spectra were obtained from a Bruker AM 300 nmr spectrometer at a probe temperature of 300 K, just as described previously (12).

Molecular orbital calculations employed the computer program GAUSSIAN 86 (13) on an Amdahl 5870. The constraints on the optimization of bond angles and bond lengths included a mirror plane containing the oxygen atom and the carbon atom of the methylene

Can. J. Chem. Downloaded from www.nrcresearchpress.com by 91.121.58.235 on 09/07/12
For personal use only.

TABLE 1. Computed energies, dipole moments, and dihedral angles for the methylene protons for various folding angles of xanthene

	E (kJ/mol)[b]		μ (Debye)		ψ (H_a)[c]		ψ (H_b)[c]	
θ[a]	STO-3G	4-31G	STO-3G	4-31G	STO-3G	4-31G	STO-3G	4-31G
180	0.067	0.000	1.107	1.611	58.1	58.1	−58.1	−58.1
170	0.002	0.269	1.111	1.624	67.4	67.2	−49.0	−49.0
169.96	0.000	—	1.111	—	67.4	—	−49.0	—
160	0.066	1.248	1.121	1.661	76.7	76.6	−40.0	−39.9
150	1.143	3.651	1.137	1.719	86.2	86.3	−31.2	−30.7
140	5.077	9.325	1.161	1.799	95.9	96.3	−22.5	−21.8
130	15.268	22.180	1.191	1.900	105.7	106.1	−14.4	−13.6
120	37.634	49.120	1.219	2.023	115.1	115.3	−7.2	−7.0
110	82.210	—	1.230	—	122.9	—	−2.7	—

[a]The folding angle, θ, being 180° for the planar molecule.
[b]Relative energies, the total energy being −565.939 776 au for the STO-3G basis at θ = 169.96° and −572.163 613 au for the 4-31G basis at θ = 180°.
[c]These are the dihedral angles for the methylene protons, a value of 0° for ψ meaning that the C—H_a or C—H_b bond lies in the planes of the benzene moieties.

group, as well as planarity of the two benzene fragments. Computations were done for nine values of the folding angle, θ, with the STO-3G basis and for seven values of θ with the 4-31G basis.

Results and discussion

Molecular orbital calculations

Table 1 presents the energies for a range of folding angles. Immediately apparent is the very flat puckering potential near 180°, unlike that computed for 9,10-dihydroanthracene (4) but reminiscent of that for dibenzo-p-dioxin (5). The computations therefore suggest the likelihood of disorder in the crystal of xanthene, arising from a degree of butterfly motion. They are also consistent with the experimental data in solution, as described above.

The relative STO-3G MO energies between 120° and 180° are reproduced by eq. [1], where $\phi = \theta - 180°$. The stated errors are those at the 95% confidence interval.

$$[1]\quad V(\phi)/\text{kJ mol}^{-1} = (-1.65 \pm 0.20) \times 10^{-3}\phi^2 + (2.71 \pm 0.07) \times 10^{-6}\phi^4 + (0.142 \pm 0.060) \exp((1.14 \pm 0.10) \times 10^{-3}\phi^2)$$

The double-minimum potential, if present at all, is very shallow indeed, the planar form being computed as only 0.07 kJ/mol higher in energy than that corresponding to a folding angle of 169.96°. The expectation value of θ is computed as 163.0° at 300 K, in agreement with those of 160 ± 6° deduced from Kerr constant data for CCl_4 and benzene solutions (8).

The 4-31G MO energies can be fit by eq. [2], the indicated

$$[2]\quad V(\phi)/\text{kJ mol}^{-1} = (1.09 \pm 0.45) \times 10^{-3}\phi^2 + (2.59 \pm 0.17) \times 10^{-6}\phi^4 + (0.171 \pm 0.154) \exp((1.17 \pm 0.21) \times 10^{-3}\phi^2)$$

errors again being those at the 95% confidence level. Figure 1 compares the MO energies with the curve represented by eq. [2]. The theoretical potential has a single minimum, that at θ = 180°, and is rather steeper than that given by the STO-3G basis at the larger puckering amplitudes. Nevertheless, at 300 K, the expectation value of θ is computed as 165.4°, not much different than the 163.0° given by the minimal basis set.

Figures 2 and 3 display the computed geometries at the energy minimum for the STO-3G and 4-31G basis sets,

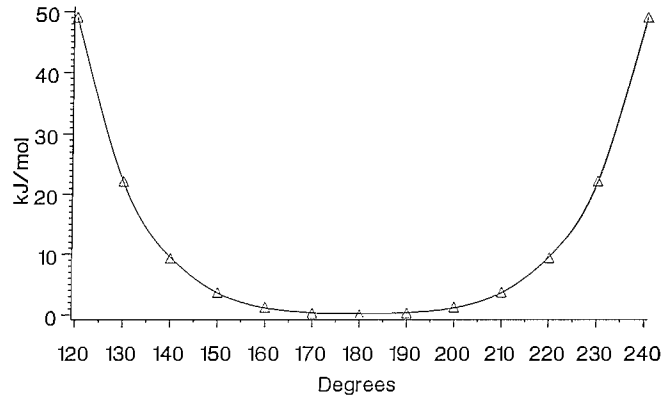

FIG. 1. The triangles represent the relative 4-31G MO energies of xanthene, the planar form with a folding angle of 180° being computed as most stable. The potential function, eq. [2] of the text, is given by the solid curve. The expectation value of the folding angle is 165.4° at 300 K.

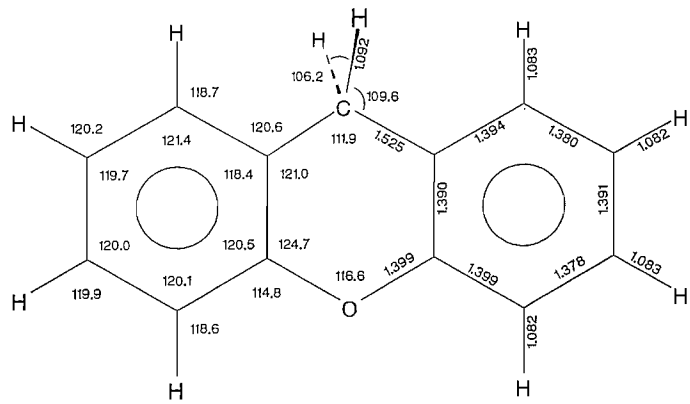

FIG. 2. The computed geometry of xanthene, based on the STO-3G basis set, is displayed for the folding angle of 170°, corresponding to the lowest energy. Bond angles are given in degrees and bond lengths in angstrom units.

respectively. In view of previous comparisons between computed and experimental geometries for the "parent" compounds (4, 5), it appears likely that an eventual structure determination will yield bond angles and lengths very similar to those in Figs. 2 and 3, with the following exception. The COC angle will likely be

Can. J. Chem. Downloaded from www.nrcresearchpress.com by 91.121.58.235 on 09/07/12
For personal use only.

TABLE 2. The ^{1}H nmr spectral parameters for xanthene in CS_2/C_6D_{12} and acetone-d_6 at 300 K

Parameter	CS_2[a]	Acetone-d_6	Parameter	CS_2[a]	Acetone-d_6[b]
$\nu(CH_2)$	1176.00	1204.75	^4J(H-1,CH_2)	−0.986(1)	−0.993(1)
ν_1	2097.772(1)[c]	2160.263(1)	^5J(H-2,CH_2)[d]	0.283(1)	0.287(1)
ν_2	2062.734(1)	2108.166(1)	^5J(H-4,CH_2)	0.410(1)	0.422(1)
ν_3	2113.396(1)	2159.600(1)	^6J(H-3,CH_2)	−0.748(1)	−0.758(1)
ν_4	2065.458(1)	2107.343(1)	Calculated transitions	145	179
$^3J_{12}$[e]	7.558(2)	7.582(1)	Assigned transitions	130	162
$^3J_{23}$	7.322(1)	7.343(1)	Peaks observed	102	113
$^3J_{34}$	8.162(2)	8.178(1)	Largest difference	0.015	0.011
$^4J_{13}$	1.655(1)	1.662(1)	Root-mean-square deviation	0.005	0.004
$^4J_{24}$	1.229(2)	1.219(1)			
$^5J_{14}$	0.408(2)	0.416(1)			

[a]3.9 mol% in CS_2 containing also 10.0 mol% of C_6D_{12} and 0.5 mol% TMS.
[b]3.9 mol% in acetone-d_6 containing also 0.5 mol% TMS.
[c]In hertz at 300.135$_2$ MHz to high frequency of internal TMS, numbers in parentheses being standard deviations in the last significant figure.
[d]The numbering of the aromatic protons is that in **1** of the text; note that H-1 is *ortho* to the methylene group and H-4 is *ortho* to the oxygen atom.
[e]No evidence was found for the existence of coupling constants between protons on different benzene moieties. The generally somewhat larger magnitudes of the coupling constants within the aromatic ring in acetone-d_6 solution relative to those in CS_2 solution are a common observation in this laboratory. The spectral data come from analyses with the computer program NUMARIT (22).

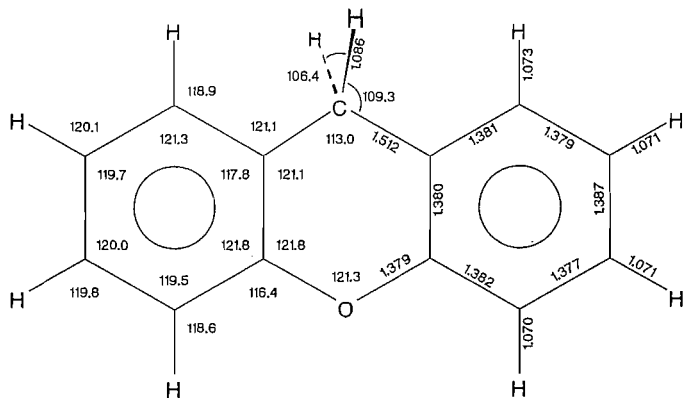

FIG. 3. The computed geometry of planar xanthene is shown as obtained with the 4-31G basis. The text discussed the reliability of the bond parameters.

close to the average of the two computed values. These values for dibenzo-p-dioxin have a mean of 115.9°, the experimental angle being 116.4(5)°.

The dipole moment of xanthene, as computed with the minimal basis set (Table 1) is very close to the lowest and most frequent experimental values (see above). The computed numbers also imply an insensitivity of the dipole moment to the folding angles of highest probability at ambient temperatures. The 4-31G basis yields dipole moments rather higher than those from experiment. A recent comparison (14) of minimal with split-valence basis sets, as to their reproduction of correct electron distributions in monosubstituted benzenes, should be consulted in this connection.

The long-range coupling constants

While the molecular orbital calculations refer to the free molecule, and while the theoretical puckering potentials are both in apparent agreement with experimental data in solution, it was thought desirable to provide a further experimental test of the internal motion of xanthene in solution. Such a test might well be provided by the long-range coupling constants for the methylene protons. Table 2 presents the spectral parameters for xanthene in solution and Fig. 4 displays some experimental and theoretical ^{1}H nmr spectra for this compound.

It is known (12, 15, 16) that ^6J(H,CH_2) in toluene derivatives is proportional to $\sin^2\psi$, where ψ is the angle by which the C—H bond of the side chain twists out of the benzene plane. If the value of ^6J at $\psi = 90°$ can be ascertained, then a measurement of ^6J yields $\langle\sin^2\psi\rangle$, the expectation value of $\sin^2\psi$. In toluene, for example, $^6J_{90}$ is −1.20 Hz (12). In benzyl X compounds, experience shows how $^6J_{90}$ depends on the electronegativity of X. Furthermore, ^5J(H,CH_2) depends (12) on $\langle\sin^2\psi\rangle$ and on $\langle\sin^2\psi/2\rangle$, so that ^5J for xanthene should be rather different for H-2 and H-4. Also, the ψ dependence of ^4J(H,CH_2) is known approximately (17).

In Table 1 the ψ values are given for various folding angles of xanthene. The theoretical potentials can be used to find $\langle\sin^2\psi\rangle$ and give 0.694 and 0.689 at 300 K for the 4-31G and STO-3G bases, respectively, and 0.245 and 0.248 for $\langle\sin^2(\psi/2)\rangle$. It is perhaps unfortunate that these numbers are very little different from those, 0.75 and 0.25, to be expected for rigid planar conformers with a regular tetrahedral geometry at the methylene site. Nevertheless, the following comparisons may be made.

The value of $^6J_{90}$ in benzyl X compounds is fairly reliably given in hertz (Hz) by 0.224 iota (ι) minus 1.653 (18), where the ι value, an inductive parameter, is taken from extensive tabulations (19). The ι value of the phenyl group is 2.295 (19), implying $^6J_{90}$ as −1.14 Hz in, say, diphenylmethane. On the somewhat questionable assumption that this number is applicable to xanthene (the second benzene moiety is, after all, not a phenyl group, among other criticisms), it follows that the ^6J of −0.748(1) in CS_2 solution yields 0.656 for $\langle\sin^2\psi\rangle$ while the −0.758(1) Hz in acetone-d_6 solution gives 0.665. The theoretical assessments of $\langle\sin^2\psi\rangle$ in the free molecule are 0.69. Were the molecule planar and rigid, a ^6J of about −0.85 Hz should have been observed, corresponding to a $\langle\sin^2\psi\rangle$ near 0.75. Again, were the molecule rigid with a folding angle of 145°, that in 9,10-dihydroanthracene, then $\langle\sin^2\psi\rangle$ would be near 0.60, corresponding to a ^6J of −0.68 Hz. These two extremes are therefore unlikely, in agreement with the theoreti-

Can. J. Chem. Downloaded from www.nrcresearchpress.com by 91.121.58.235 on 09/07/12
For personal use only.

Can. J. Chem. Downloaded from www.nrcresearchpress.com by 91.121.58.235 on 09/07/12
For personal use only.

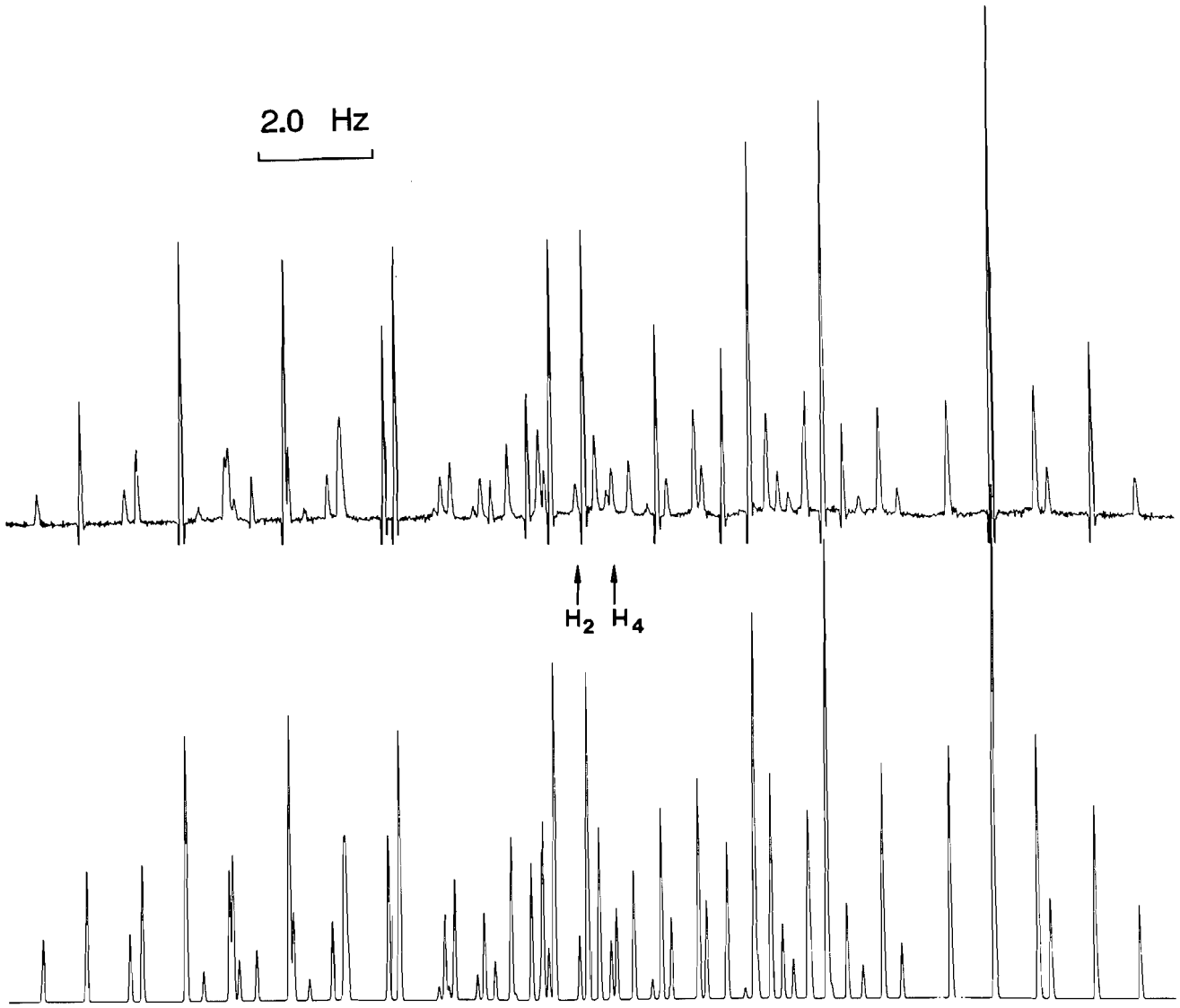

FIG. 4. The ^{1}H nmr spectrum is shown for the protons placed *ortho* and *para* to the methylene protons of xanthene in acetone-d_6 solution at 300 K. The chemical shifts of the two protons differ by 0.66 Hz at 300 MHz. The theoretical spectrum is based on the spectral parameters in Table 2 and assumes a linewidth at half-height of 0.04 Hz. There is no evidence for significant coupling interactions between protons situated on different benzene moieties.

cal results for the free molecule. The measured value of ^6J suggests a somewhat larger amplitude of puckering than that given by the computations because $\langle\sin^2\psi\rangle$ decreases as the folding angle increases. In view of the uncertainty in $^6J_{90}$, it is probably best to conclude that ^6J is consistent with a flat puckering potential in polar and nonpolar media, not unlike those computed with STO-3G and 4-31G basis sets.

Turning to $^5J(\mathrm{H,CH_2})$, in toluene (12) it is given in hertz by $0.336\langle\sin^2\psi\rangle + 0.322\langle\sin^2(\psi/2)\rangle$. For xanthene, the multiplier of $\langle\sin^2\psi\rangle$, representing the $\sigma-\pi$ electron contribution to ^5J, should be reduced by the factor 1.14/1.20, just as the $\sigma-\pi$ contribution to ^6J has been reduced above. If the theoretical values of $\langle\sin^2\psi\rangle$ and $\langle\sin^2(\psi/2)\rangle$ are employed, then $^5J(\mathrm{H\text{-}2,CH_2})$ is calculated as 0.300(1) Hz for both potentials, to be compared with the experimental numbers, 0.283(1) and 0.287(1) Hz in CS_2 and acetone-d_6 solutions, respectively. $^5J(\mathrm{H\text{-}4,CH_2})$ is then calculated as 0.461 Hz (the $\langle\sin^2(\psi/2)\rangle$ values sum to unity for H-2 and H-4), as compared with the measured values of 0.410(1) and 0.422(1) Hz (Table 2). Alternatively, if the $\langle\sin^2\psi\rangle$ values derived from the measured ^6J are used, then $^5J(\mathrm{H\text{-}2,CH_2})$ becomes 0.287 Hz, very close to those measured, and $^5J(\mathrm{H\text{-}4,CH_2})$ becomes 0.451 Hz, still 0.03–0.04 Hz larger than the measured values. However, it is reasonable that a comparison of calculated and observed numbers is more appropriate for $^5J(\mathrm{H\text{-}2,CH_2})$ than for $^5J(\mathrm{H\text{-}4,CH_2})$ because the oxygen atom is attached to the carbon atom in the coupling path for $^5J(\mathrm{H\text{-}4,CH_2})$ and can perturb the coupling magnitude. It is known that ^5J is more sensitive to ring substitution in toluene derivatives than is ^6J (20). Accordingly, it is probable that the ^5J values for xanthene are again consistent with the theoretical puckering potentials.

$^4J(\mathrm{H\text{-}1,CH_2})$ for xanthene presents an interesting problem. A thorough investigation of orthobenzylic coupling constants in a wide variety of compounds (17) recommends the relationship $^4J/\mathrm{Hz} = -1.08\sin^2\psi - 0.32\cos^2\psi$. However (examine Fig. 3 of ref. 17), in the range of ψ between about 30 and 60°, this relationship appreciably underestimates the magnitude of ^4J. A good example is **2**, for which ^4J values of −0.84 and −1.11 Hz are measured, corresponding to ψ's of 45° and 75°, respectively (17), showing also that **2** does not invert on the time

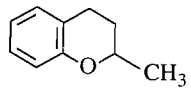

2

scale defined by the difference between the two ^4J numbers. The mean value of the $\sin^2\psi$ values is 0.71_7 and the mean of the ^4J values is -0.97_5 Hz. The latter is very close to the $-0.986(1)$ and $-0.993(1)$ Hz measured for xanthene in CS_2 and acetone-d_6 solutions (Table 2), for which the theoretical potentials yield $\langle\sin^2\psi\rangle$ as 0.692(3) at 300 K. The relationship above, however, after adjustment of the multiplier of $\langle\sin^2\psi\rangle$ by a factor of 1.14/1.20 (reduced $\sigma-\pi$ contribution) would yield -0.81 Hz for ^4J in xanthene, as expected by examination of Fig. 3 in ref. 17; arc sin $(0.692)^{1/2} \sim 56°$, and for that ψ the relationship above underestimates the magnitude of ^4J by about 0.2 Hz. Accordingly, it may be concluded that ^4J(H-1,CH_2) in xanthene is consistent with a large amplitude motion in solution.

The results of the present investigation lend support to the interpretation of the rotational barriers measured for 9-arylxanthyl derivatives (21). One assumption in that interpretation was the facile puckering motion of the xanthene moiety.

Finally, it must be noted that, very likely, puckering potentials other than those discussed here will also be compatible with the magnitudes of the long-range coupling constants in Table 2. The discussion above does not, of course, claim a unique correspondence between experiment and theory.

Acknowledgments

We are grateful to the Natural Sciences and Engineering Research Council of Canada for a grant-in-aid of research and to the referees for constructive criticism.

1. F. H. Herbstein, M. Kapon, and G. M. Reisner. Acta Crystallogr. Sect. B: Struct. Sci. **42**, 181 (1986).
2. P. Singh and J. D. McKinney. Acta Crystallogr. Sect. B: Struct. Crystallogr. Cryst. Chem. **34**, 2956 (1978).
3. J. D. Dunitz, V. Schomaker, and K. N. Trueblood. J. Phys. Chem. **92**, 856 (1988); footnote 5.
4. T. Schaefer and R. Sebastian. J. Mol. Struct. (Theochem), **153**, 55 (1987).
5. T. Schaefer and R. Sebastian. J. Mol. Struct. (Theochem), **204**, 41 (1990).
6. F. P. Colonna, G. Distefano, V. Galasso, K. J. Irgolic, C. E. King, and G. C. Pappalardo. J. Organomet. Chem. **146**, 235 (1978).
7. G. Fronza and E. Ragg. J. Chem. Soc. Perkin Trans. 2, 291 (1982).
8. M. J. Aroney, G. M. Hoskins, and R. J. W. Le Fèvre. J. Chem. Soc. London, Part B, 980 (1969).
9. E. Bergmann and A. Weizmann. Trans. Faraday Soc. **32**, 1318 (1936).
10. Z. Aizenshtat, E. Klein, H. Weiler-Feilchenfeld, and E. D. Bergmann. Isr. J. Chem. **40**, 753 (1972).
11. Y. Koga, H. Takahashi, and K. Higasi. Bull. Chem. Soc. Jpn. **46**, 3359 (1973).
12. T. Schaefer, R. Sebastian, and G. H. Penner. Can. J. Chem. **63**, 2597 (1985).
13. M. J. Frisch, J. S. Binkley, H. B. Schlegel, K. Raghavachari, C. F. Melius, R. L. Martin, J. J. P. Steward, F. W. Bobrowicz, C. F. Rohlfing, L. R. Kahn, D. J. Defrees, R. Seeger, R. A. Whiteside, D. J. Fox, E. M. Fluder, and J. A. Pople. Carnegie–Mellon Quantum Publishing Unit, Pittsburgh, PA. 1984.
14. S. Marriott, A. Silvestro, and R. D. Topsom. J. Chem. Soc. Perkin Trans. 2, 457 (1988).
15. R. Wasylishen and T. Schaefer. Can. J. Chem. **50**, 1852 (1972).
16. W. J. E. Parr and T. Schaefer. Acc. Chem. Res. **13**, 400 (1980).
17. M. Barfield, C. J. Fallick, K. Hata, S. Sternhell, and P. W. Westerman. J. Am. Chem. Soc. **105**, 2178 (1983).
18. T. Schaefer, G. H. Penner, C. S. Takeuchi, and C. Beaulieu. Can. J. Chem. **67**, 1283 (1989).
19. N. Inamoto and S. Masuda. Chem. Lett. 1007 (1982).
20. T. Schaefer and R. Laatikainen. Can. J. Chem. **61**, 2785 (1983).
21. S. V. McKinley, P. A. Grieco, A. E. Young, and H. H. Freedman. J. Am. Chem. Soc. **92**, 5900 (1970).
22. J. S. Martin, A. R. Quirt, and K. E. Worvill. The NMR program library. Daresbury Laboratory, Daresbury, U.K.

Can. J. Chem. Downloaded from www.nrcresearchpress.com by 91.121.58.235 on 09/07/12
For personal use only.

Motion about the C_{sp^2}—C_{sp^3} bond in benzyl OR ($R = CH_3$, CH_2CH_3, $CH(CH_3)_2$, $C(CH_3)_3$). Solvent and substituent dependence

TED SCHAEFER, KERRY J. COX,[1] CHERRIE L. MORIER,[1] CHRISTIAN BEAULIEU,[1] RUDY SEBASTIAN, AND GLENN H. PENNER[2]

Department of Chemistry, University of Manitoba, Winnipeg, Man., Canada R3T 2N2

Received December 12, 1989

TED SCHAEFER, KERRY J. COX, CHERRIE L. MORIER, CHRISTIAN BEAULIEU, RUDY SEBASTIAN, and GLENN H. PENNER. Can. J. Chem. **68**, 1553 (1990).

The ^1H nuclear magnetic resonance spectral parameters of benzyl alkyl ethers (CH_3, CH_2CH_3, $CH(CH_3)_2$, and $C(CH_3)_3$) in CS_2 and acetone-d_6 solutions are obtained, as are those for the 3,5-dichloro derivatives (CH_3, CH_2CH_3, and $CH(CH_3)_3$) in acetone-d_6 solution. The long-range coupling constants between the methylene and *para* ring protons show that the apparent twofold barrier to rotation about the C_{sp^2}—C_{sp^3} bond is solvent and ring-substituent dependent. The apparent twofold barrier ranges from a vanishing value for benzyl methyl ether in CS_2 solution to as much as 4.6 kJ/mol for 3,5-dichlorobenzyl isopropyl ether in acetone-d_6 solution. The data imply that, for the free molecules, the conformation of highest energy has the CH_2—O bond in a plane perpendicular to that of the phenyl group. Molecular orbital computations with a minimal Gaussian basis set agree that, for benzyl methyl ether in the *exo* form (the methyl group pointing away from the phenyl moiety), this conformation is the least stable. However, geometry optimization procedures imply that the CH_2—O bond is twisted out of the ring plane by 30.3° in the most stable geometry of the *exo* form. Such procedures for the (distorted) *endo* form locate another stable conformer, in which the CH_2—O bond is twisted out of the phenyl plane by 45°, only 0.25 kJ/mol less stable than the most stable conformer of the *exo* form. These results, together with some computations for the *tert*-butyl derivative, are discussed in terms of the theoretical potentials for rotation about the C_{sp^2}—C_{sp^3} bond. The approximate potential surface is rather flat compared to kT at ambient temperatures for the free molecules, consistent with its sensitivity to the medium and to ring substituents.

Key words: ^1H NMR, benzyl alkyl ethers; long-range coupling constants in benzyl alkyl ethers; conformations, benzyl alkyl ethers; internal motion, benzyl alkyl ethers; MO computations on benzyl methyl ether.

TED SCHAEFER, KERRY J. COX, CHERRIE L. MORIER, CHRISTIAN BEAULIEU, RUDY SEBASTIAN et GLENN H. PENNER. Can. J. Chem. **68**, 1553 (1990).

On a déterminé les paramètres spectraux de la résonance magnétique nucléaire du ^1H des éthers $C_6H_5CH_2OR$ ($R = CH_3$, CH_2CH_3, $CH(CH_3)_2$ et $C(CH_3)_3$) dans des solutions dans le CS_2 et dans l'acétone-d_6 ainsi que ceux des dérivés 3,5-dichlorés ($R = CH_3$, CH_2CH_3, $CH(CH_3)_2$) dans des solutions dans l'acétone-d_6. Les constantes de couplage à longue distance entre les protons méthyléniques et les protons en position *para* du cycle montrent que la barrière binaire apparente à la rotation autour de la liaison C_{sp^2}—C_{sp^3} dépend à la fois du solvant et de la nature des substituants sur le cycle. La barrière binaire apparente varie d'une valeur pratiquement nulle pour le méthoxyméthylbenzène en solution dans le CS_2 à une valeur de près de 4,6 kJ/mol pour le 3,5-dichloro-1-isopropoxyméthylbenzène en solution dans l'acétone-d_6. Ces données impliquent que, pour les molécules libres, la conformation de plus haute énergie comporte une liaison CH_2—O qui est dans un plan perpendiculaire à celui du groupement phényle. Des calculs d'orbitales moléculaires, réalisés avec des ensembles de base Gaussienne minimale, suggèrent que le méthoxyméthylbenzène dans la forme *exo* (le groupement méthyle s'éloignant de la portion phényle) est la conformation la moins stable. Toutefois, si on fait appel à des méthodes impliquant une optimisation de la géométrie, on arrive à la conclusion que dans la géométrie la plus stable de la forme *exo* la liaison CH_2—O est déplacée de 30,3° par rapport au plan du cycle. Des telles méthodes appliquées à la forme *endo* (déformée) permettent de localiser un autre conformère stable dans lequel la liaison CH_2—O est déplacée de 45° par rapport au plan du noyau phényle; cette conformation n'est que 0,25 kJ/mol moins stable que le conformère le plus stable de la forme *exo*. Ces résultats utilisés de concert avec des calculs effectués sur le dérivé *tert*-butyle sont discutés en fonction des potentiels théoriques pour la rotation autour de la liaison C_{sp^2}—C_{sp^3}. La surface de potentiel approximative est assez plane si on la compare à kT aux températures ambiantes pour les molécules libres; cette observation est en accord avec sa sensibilité au milieu et aux substituants présents sur le cycle.

Mots clés : RMN ^1H, éthers benzylalkyle; constantes de couplage à longue distance, éthers benzylalkyle; conformations, éthers benzylalkyle; déplacement intérieur, éthers benzylalkyle; calculs d'OM, méthoxyméthylbenzène.

[Traduit par la revue]

Introduction

The barriers to rotation about the C_{sp^2}—C_{sp^3} bonds in benzyl fluoride and in benzyl chloride are solvent dependent and are also sensitive to the presence of *meta* substituents. In benzyl fluoride (1, 2) the internal rotational potential is very likely twofold and conformer **1** (X = F) is stabilized by about 2 kJ/mol in passing from a relatively nonpolar CS_2/C_6D_{12} medium to a polar acetone-d_6 environment. Qualitatively, this can be understood as a stabilization of the more polar form **1** by the polar medium or, perhaps, by a reduction of the attractive

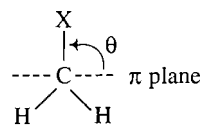

1 $\psi = 30°$, $\theta = 90°$

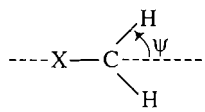

2 $\psi = 60°$, $\theta = 0°$

interaction between the *ortho* C^-—H^+ bonds in the ring and the C^+—F^- bond (3) upon dissolution in the medium of higher dielectric constant. Again, two *meta* chlorine substituents stabilize conformation **2** by at least 2 kJ/mol relative to the parent molecule, possibly via an enhancement of the polarity of the *ortho* C—H bonds (1). Benzyl chloride behaves similarly, except that **1** (X = Cl) is the most stable conformer in each

[1]Undergraduate research participants, 1988–1989.

[2]Present address: Department of Chemistry and Biochemistry, University of Guelph, Guelph, Ont., Canada.

Can. J. Chem. Downloaded from www.nrcresearchpress.com by 91.121.58.235 on 09/07/12
For personal use only.

TABLE 1. The ^{1}H nmr spectral parameters for benzyl isopropyl ether at 300 K

Parameter	Value CS_2[a,g]	Value Acetone-d_6[b,h]	Parameter	Value CS_2[a]	Value Acetone-d_6[b]
$\nu(CH_2)$	1319.5[c]	1345.0	$^5J_{25}$	0.595(1)	0.611(0)
ν_2	2156.213(2)[d]	2201.068(1)	$^4J(H,CH_2)$	−0.719(2)	−0.704(1)
ν_3	2152.686(2)	2194.413(1)	$^5J(H,CH_2)$	0.323(2)	0.316(1)
ν_4	2132.070(1)	2172.302(1)	$^6J(H,CH_2)$	−0.543(1)	−0.524(1)
$^3J_{23}$	7.687(2)	7.694(1)	Calc. transitions	285[e]	269[e]
$^3J_{34}$	7.436(4)	7.438(1)	Peaks observed	255	255
$^4J_{26}$	1.844(2)	1.847(1)	Assigned transitions	217	225
$^4J_{24}$	1.286(4)	1.298(1)	Largest difference	0.021	0.014
$^4J_{35}$	1.399(2)	1.405(1)	Root-mean-square deviation	0.007[f]	0.004[f]

[a]4.0 mol% in CS_2, containing also 10 mol% of C_6D_{12} and 0.5 mol% of TMS.
[b]4.0 mol% in acetone-d_6, containing also 0.5 mol% of TMS.
[c]In hertz at 300.135$_2$ MHz to high frequency of internal TMS.
[d]Numbers in parentheses are standard deviations in the last significant figure.
[e]For the ring protons only.
[f]There occur large correlations between chemical shifts and the coupling constants within the ring, but $^6J(H,CH_2)$ does not correlate significantly with other parameters.
[g]$\nu(CH)$ is 1070.3 Hz, $^3J(H,H)$ is 6.06(3) Hz.
[h]$\nu(CH)$ is 1097.5 Hz, $^3J(H,H)$ is 6.03(5) Hz, and $\nu(CH_3)$ is 347.6 Hz.

situation, so that the barrier to internal rotation increases in the polar solvent but decreases in the presence of *meta* chlorine substituents (4). Of course, in benzyl chloride the internal barrier is relatively large, about 11 kJ/mol in acetone-d_6 solution. The small barrier in benzyl fluoride (1, 2), probably less than 3 kJ/mol in the polar solvent, has the consequence that the most stable conformer can change from **2** to **1** under the appropriate conditions of solvent or *meta* substituent.

By way of contrast, the internal rotational potential in ethyl benzene is strikingly insensitive to solvent (5), perhaps as a consequence of its small polarity, and, tentatively, is a good approximation to its magnitude in the vapor phase (5, 6).

In benzyl alcohol the internal motion about the exocyclic C—C bond is also facile (7–9) but is complicated in principle by the possibility of attractive O—H...π interactions (10) or, alternatively, by repulsion between the lone-pair electrons on the oxygen atom and the π electrons of the ring (11, 12). The *exo* conformer, that with the O—H bond pointing away from the benzene moiety, is present to the extent of, at most, 25% in nonpolar solvents (9) and perhaps 30% in the gas phase at 422 K.

In the presence of groups larger than hydroxyl, that is, for the title compounds, simple steric considerations suggest that the endo form, **3**, would have a large barrier to rotation about the C_{sp^2}—C_{sp^3} bond, that with $\theta = 0°$ having a substantial repulsive energy between R and the *ortho* C—H bonds. The repulsion is absent in the *exo* form, **4**. Measurement of ^6J(H-4,CH_2) for the alkyl groups, R, indicates the freedom of motion about this bond. In this work, the ^{1}H nmr spectral parameters are determined for benzyl OR (R = CH_3, CH_2CH_3, $CH(CH_3)_2$ and R = $C(CH_3)_3$) in polar and nonpolar solvents, as well as for the 3,5-dichloro derivatives (R = CH_3, CH_2CH_3, $CH(CH_3)_2$). STO-3G computations for the motion about the exocyclic C—C bond are also reported for benzyl methyl ether. It appears that the barrier to rotation about this bond is small in the gas phase and in solution, although solvent and *meta* substituent perturbations are rather similar to those known for benzyl fluoride.

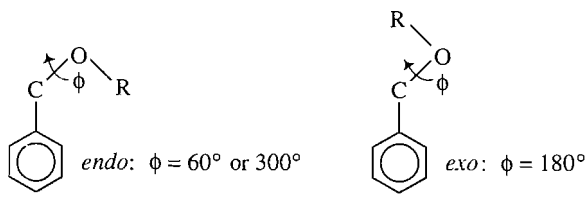

3 **4**

Experimental

The benzyl ethers were prepared from the corresponding benzyl bromides by the standard Williamson procedure, the reflux time for R = $C(CH_3)_3$, however, being raised to 1 week (13). Solutions of the ethers in CS_2/C_6D_{12} and acetone-d_6 (Tables 1 and 2) were filtered into 5 mm o.d. nmr sample tubes and were degassed by the freeze–pump–thaw procedure (minimum of four cycles). The 3,5-dichloro compounds (R = CH_3, CH_2CH_3, $CH(CH_3)_2$) were prepared as acetone-d_6 solutions.

The ^{1}H nmr spectra were obtained at a probe temperature of 300 K on an AM300 Bruker spectrometer in a way previously described in detail (1).

STO-3G MO computations (14), employing MONSTERGAUSS (15), were performed on an Amdahl 5870 system. The geometries of the various conformers of benzyl methyl ether were optimized with the constraint that the phenyl moiety remain planar.

Results and discussion

Spectral analyses

The ^{1}H nmr spectra were analyzed with the computer program NUMARIT (16), as reworked by R. Sebastian in this laboratory. The complete set of ^{1}H nmr spectral parameters for R = $CH(CH_3)_3$ are presented in Table 1. The occasionally larger magnitudes, in the polar relative to the nonpolar solvent, of the proton–proton coupling constants within the ring are a general result in this laboratory and most likely not an artifact. Because the intraring coupling constants vary very little among the compounds for different R, they are not presented for all R. Instead, Table 2 presents the chemical shifts and the long-range coupling constants between the methylene and ring protons. The latter are of immediate interest in the discussion below.

Can. J. Chem. Downloaded from www.nrcresearchpress.com by 91.121.58.235 on 09/07/12
For personal use only.

TABLE 2. The ^{1}H nmr chemical shifts and coupling constants between methylene and ring protons at 300 K for benzyl OR (R = CH_3, CH_2CH_3, $C(CH_3)_3$) in CS_2 and acetone-d_6 solutions

Parameter	CH_3		CH_2CH_3		$C(CH_3)_3$	
$\nu(CH_2)$	1297.3[a,e]	1324.3[b,f]	1311.8[a,e]	1340.5[b,f]	1332.4[a,e]	1367.6[b,f]
ν_2	2151.619(2)[c]	2196.734(4)	2153.872(2)	2199.291(1)	2166.754(3)	2212.669(1)
ν_3	2156.956(2)	2198.333(4)	2154.549(2)	2196.906(2)	2163.083(3)	2202.681(2)
ν_4	2138.496(1)	2178.804(1)	2134.838(1)	2176.044(1)	2144.263(1)	2182.208(1)
$^4J(H,CH_2)$	−0.682(1)[d]	−0.660(3)	−0.702(2)	−0.680(1)	−0.676(2)	−0.664(2)
$^5J(H,CH_2)$	0.316(2)	0.308(3)	0.313(3)	0.310(2)	0.327(3)	0.312(2)
$^6J(H,CH_2)$	−0.511(2)	−0.489(2)	−0.518(2)	−0.504(1)	−0.506(2)	−0.490(2)

[a]4.0 mol% in CS_2, containing also 10.0 mol% C_6D_{12} and 0.5 mol% TMS.
[b]4.0 mol% in acetone-d_6, containing also 0.5 mol% TMS.
[c]In hertz at 300.135$_2$ MHz to high frequency of internal TMS.
[d]Numbers in parentheses are standard deviations in the last significant figure.
[e]$\nu(CH_3)$ is 977.1 for R = CH_3, 351.6 for R = CH_2CH_3, and 344.9 Hz for R = $C(CH_3)_3$; $\nu(CH_2)$ for the ethyl group is 1025.4 Hz.
[f]$\nu(CH_3)$ is 993.9 for R = CH_3, 352.2 for R = CH_2CH_3, and 355.5 Hz for R = $C(CH_3)_3$; $\nu(CH_2)$ for the ethyl group is 1050.0 Hz.

TABLE 3. Conformational results for benzyl OR and 3,5-dichlorobenzyl OR

R	^6J[a]		$\langle\sin^2\psi\rangle$[b]		Apparent V_2[c]		Stable conformer[d]	
CH_3	−0.511(2)[e]	−0.489(2)[f]	0.501[e]	0.479[f]	0.0[e]	0.8[f]	—[e]	**1**[f]
CH_2CH_3	−0.518(2)	−0.504(1)	0.508	0.494	−0.3[h]	0.3	**2**	**1**
$CH(CH_3)_2$	−0.543(1)	−0.524(1)	0.532	0.514	−1.3	−0.5	**2**	**2**
$C(CH_3)_3$	−0.506(2)	−0.490(2)	0.496	0.480	0.2	0.8	**1**	**1**
3,5-diCl-(CH_3)	—	−0.568(1)	—	0.557	—	−2.4	—	**2**
3,5-diCl-CH_2CH_3	—	−0.588(1)	—	0.576	—	−3.3	—	**2**
3,5-diCl-$CH(CH_3)_2$	—	−0.615(5)	—	0.603	—	−4.6	—	**2**

[a]In hertz from Tables 1 and 2.
[b]Because $^6J_{90}$ is −1.02 Hz (see text).
[c]In kJ/mol, perhaps with an error of 0.1 kJ/mol.
[d]See structures in text.
[e]In the CS_2/C_6D_{12}/TMS mixture (Tables 1 and 2).
[f]In the acetone-d_6/TMS solvent (Tables 1 and 2).
[g]Negative values of the apparent V_2 mean that **2** is the conformer of greater stability.

$^6J(H,CH_2)$ values for the 3,5-dichloro derivatives are found in Table 3.

Mobility about the C_{sp^2}—C_{sp^3} bond in the benzyl ethers

(i) Apparent V_2

Apparent twofold barriers to rotation about the C_{sp^2}—C_{sp^3} bond in the ethers can be found on the basis of the relationship $^6J(H,CH_2) = {}^6J_{90}\langle\sin^2\psi\rangle$. Here $^6J_{90}$ is the value of this σ–π coupling constant when ψ is 90° in **1** or **2**, and is known to be −1.02 Hz (17, 18). The expectation value, $\langle\sin^2\psi\rangle$, follows from the measured values of $^6J(H,CH_2)$ and can be related to an assumed twofold barrier by a hindered rotor model (19) or can also be computed classically for various potentials. Table 3 gives $\langle\sin^2\psi\rangle$ at 300 K for the ethers in the polar and nonpolar solvents, as well as the apparent twofold barriers to rotation about the exocyclic C—C bond.

It is clear that the barriers are small for all alkyl groups, implying that at least the larger groups are oriented to avoid the phenyl group during the rotation. In this way the size of the alkyl group will have a minor effect on the apparent V_2. The conformation with the oxygen atom in the plane of the phenyl group is stabilized in going from R = CH_3 to R = $CH(CH_3)_2$. For benzyl fluoride the analogous conformation appears (3) to be stabilized by attractive electrostatic forces between the C^+—F^- and *ortho* C^-—H^+ dipoles. Perhaps the C^+—O^- dipole increases in magnitude in the sequence CH_3, CH_2CH_3, $CH(CH_3)_2$, possibly because the group polarizabilities will increase in this order. The *tert*-butyl group, however, destabilizes the in-plane conformer, perhaps understandable if it is noted that torsional oscillations about both C—O bonds do occur and will be least hindered in the perpendicular conformer for this, the largest of the four alkyl groups.

While this rationalization of the observed sequence is speculative, the solvent effect on the conformer stabilities is unequivocal. The polar solvent stabilizes the perpendicular conformer, **1**, just as it does for benzyl fluoride (1) and benzyl chloride (4). The magnitude of this stabilization, at about 0.6 kJ/mol for the benzyl ethers, is only about 30% of that found for the benzyl halides (see further discussion below).

Again, the *meta* chlorine substituents enhance the stability of the in-plane conformer, **2**, by as much as 4 kJ/mol for R = $CH(CH_3)_2$ and as little as 3 kJ/mol for R = CH_3. The latter number is very similar to that (1) established for benzyl fluoride and its 3,5-dichloro derivative.

The apparent barriers in Table 3 strongly imply that the perpendicular form, **1**, will be the least stable in the free molecule for all the benzyl ethers. This implication follows from the data in Table 3 and from the reaction field model

Can. J. Chem. Downloaded from www.nrcresearchpress.com by 91.121.58.235 on 09/07/12
For personal use only.

Can. J. Chem. Downloaded from www.nrcresearchpress.com by 91.121.58.235 on 09/07/12
For personal use only.

(20) in which the energy difference between the conformers is roughly proportional (see eq. 13.18 and p. 562 of ref. 20) to $(\epsilon - 1)/(2\epsilon + 1)$; ϵ is the static dielectric constant of the medium. Because the change in the energy difference between the conformers in passing from the vapor to CS_2 solution is roughly the same as in going from the latter to an acetone solution (p. 562 of ref. 20), an estimate for benzyl methyl ether is that **2** is more stable than **1** by 0.8(2) kJ/mol in the vapor.

The discussion in this section assumes a twofold barrier, as is found for benzyl fluoride and benzyl chloride on the basis of MO computations (1, 4). However, the local symmetry of benzyl ethers is rather lower than that of the halides, so that the assumption of a twofold barrier is probably a first approximation. Accordingly, geometry-optimized STO-3G MO computations for benzyl methyl ether are also of interest.

(ii) Theoretical barriers in benzyl methyl ether

The STO-3G MO energies in Table 4 confirm the low barrier to rotation about the C_{sp^2}—C_{sp^3} bond in the *exo* form but also imply that the fourfold component is nearly as large as, and of opposite sign to, the twofold component (see caption to Fig. 1 for the potential). The minimum energy corresponds to a θ of 30.3°, the maximum to the perpendicular conformer, **1**, at θ = 90°. The latter is calculated to be 0.73 kJ/mol less stable than the in-plane conformer, **2**, in coincidental agreement with the value extrapolated from solution using the apparent V_2 values.

The theoretical potential has $\langle \sin^2 \psi \rangle$ as 0.515 at 300 K, whereas the extrapolated V_2 of 0.8(2) kJ/mol yields $\langle \sin^2 \psi \rangle$ as 0.520(6) at this temperature. The present experimental data cannot discriminate between a purely twofold and the theoretical, composite potential.

Furthermore, the theoretical data in Table 4 for the *endo* form indicate that, for θ values near those corresponding to minimum energies for the *exo* form, appreciable proportions of the *endo* form can exist at 300 K. Thus, at θ = 45°, the *endo* form is only 0.16 kJ/mol less stable than the *exo* form. Of course, the ^6J values do not distinguish between the *exo* and *endo* forms, being sensitive to θ and, presumably, not to ϕ. Thus, were benzyl methyl ether to exist exclusively in the *endo* form, the energies in Table 4 would imply a $\langle \sin^2 \psi \rangle$ of 0.486 at 300 K, a value less compatible with the extrapolated value of 0.520(6) above than is the value of 0.516 obtained from the theoretical potential for the *exo* form. But it would be unwise to attempt to estimate the population of the *endo* form on the basis of ^6J.

Figure 1 displays the theoretical potentials for rotation about the C_{sp^2}—C_{sp^3} bond for both forms of benzyl methyl ether. A semiquantitative description of the internal motion about this bond then implies that the molecule exists predominantly as the *exo* form near the extremes of the twist angle. However, for a large range of intermediate θ values, particularly near the minimum energies of the *exo* form, it is joined by comparable populations of the *endo* form. The somewhat higher energies of the latter for, say, $30° \leq \theta \leq 75°$, are substantially offset by its twofold degeneracy relative to the *exo* form, so that at 300 K the *endo* population is larger than the *exo* in parts of this range of θ.

The lower stability of the *endo* form at θ = 0° presumably arises from steric repulsion between the methyl and phenyl moieties. It is noted that both the *exo* and *endo* forms maintain a "dimethyl-ether-like" conformation about the C—O bonds for all θ values. More precisely, the methyl group is staggered about the opposite C—O bond to within a few degrees; deviation from exact staggering for a given θ is nearly the same for *exo* and *endo* forms. The repulsion between the methyl and phenyl moieties is reflected in the large ϕ values (Table 4) at low θ ranges. As θ increases, ϕ relaxes towards, but does not reach, the value of 60° defining a "pure" *endo* form. For $30° \leq \theta \leq 60°$, the methyl group is situated relatively far from the phenyl plane and the stability of the *endo* form approaches that of the *exo*. As θ increases further, towards 90°, the methyl group is again approaching a repulsive region of the phenyl group and *endo* stability decreases once more.

TABLE 4. Relative STO-3G MO energies[a] for rotation about the C_{sp^2}—C_{sp^3} bond in the *exo* and *endo* forms of benzyl methyl ether

θ/deg[b]	E_{exo}/kJ mol^{-1}	ϕ/deg[c]	E_{endo}/kJ mol^{-1}
0	0.00[d,e]	88.9	5.80
15	−0.12	80.8	2.50
30	−0.26	74.9	0.53
45	−0.18	71.4	−0.02
60	0.12	70.1	0.37
75	0.41	69.8	1.58
90	0.73	70.5	4.37

[a]All bond lengths and angles are optimized with the constraint that the phenyl group remain planar.

[b]This column refers to the energies of both *exo* and *endo* forms for rotation about the C_{sp^2}—C_{sp^3} bond, a zero value corresponding to the oxygen atom lying in the phenyl plane.

[c]This column refers to the *endo* form only (ϕ being 180° for the *exo* form), the deviation from 60° being a measure of the distortion of the "pure" *endo* form. See **1** and **2** of the text and note that a value greater than 60° for ϕ means that the methyl group "twists" away from the phenyl region.

[d]The total energy of this conformer is −378.885 498 au.

[e]The symmetry near the C—O bonds is C_{2v}-like for the *exo* form, as in dimethyl ether (22). If the methyl group is rotated about its O—C bond by 60°, computations give the energies as about 12.2 kJ/mol higher for all θ values of the *exo* form. In other words, the threefold barrier to rotation of the methyl group is near the value of 11.3 kJ/mol in dimethyl ether (24).

The stability of the *exo* form for low θ values is qualitatively understood by an argument similar to that for benzyl fluoride in which **1** is also of highest energy (1), the stability of the planar form, **2**, being attributed to electrostatic attraction between the C^+—F^- and the *ortho* C^-—H^+ dipoles.[3] The detailed electron distribution about the oxygen atom will be somewhat different than about fluorine, so the minimum in energy of the *exo* form need not occur exactly at θ = 0°. The greater stability of the in-plane conformer for the 3,5-dichloro derivative of benzyl methyl ether, relative to the parent compound (Table 3), would then follow from polarization of the σ electron framework by the electronegative substituents placed *ortho* to the ring C—H bonds in question. The latter acquire increased polarity, entailing a larger electrostatic stabilization of conformers having small θ values.

The computed dipole moments of benzyl methyl ether are rather insensitive to θ and ϕ. For example, they are 1.29 and 1.27 D for the *exo* form at θ = 0° and θ = 90°, respectively, and 1.27 D at both of these θ values for the *endo* form. The dipole moment of benzyl methyl ether is apparently unknown. That of dimethyl ether is 1.31 D (23). The present computations do not indicate a simple electrostatic interpretation of the observed solvent effects on the barrier.

An STO-3G computation for benzyl *tert*-butyl ether in the

[3]Discussion (21, 22) of the C—H dipole in various molecules are available.

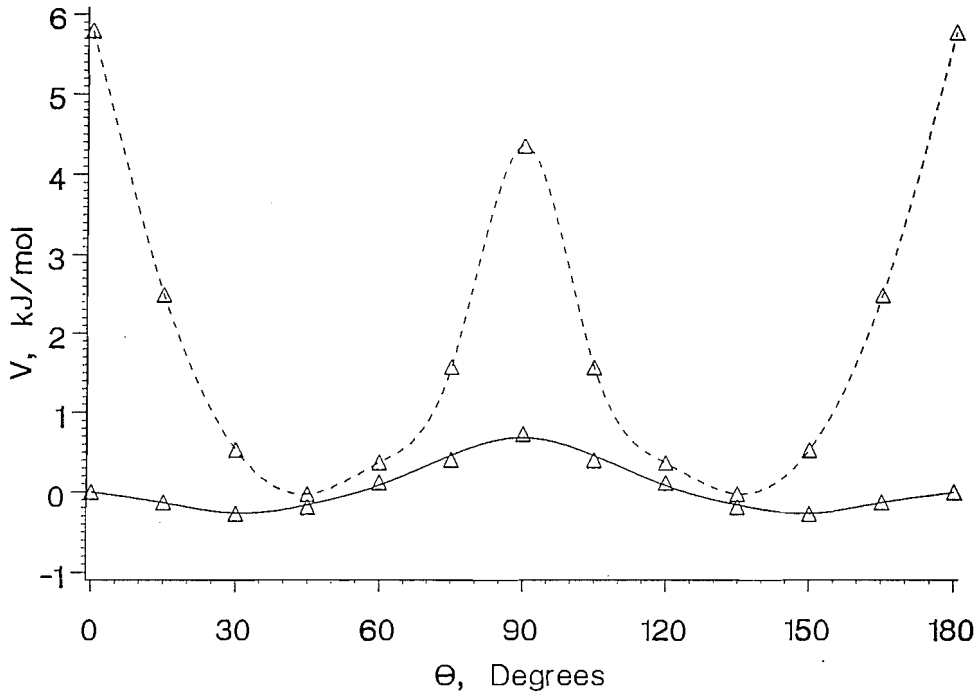

FIG. 1. The STO-3G MO relative energies (Table 4) of the *exo* and *endo* forms of benzyl methyl ether are plotted as a function of the angle, θ, by which the CH_2O—O bond twists away from the phenyl plane. The solid line (*exo*) is represented by the potential $V(\theta)/\text{kJ mol}^{-1} = 0.69 \sin^2\theta - 0.50 \sin^2 2\theta - 0.01 \sin^2 3\theta - 0.07 \sin^2 4\theta$, the standard error of the fit to the energies in Table 4 being 0.02 kJ/mol for each of the terms. The internal potential is dominated by the twofold, in $\sin^2\theta$, and the fourfold, in $\sin^2 2\theta$, terms. The dashed line (*endo*) has the potential $V(\theta)/\text{kJ mol}^{-1} = 5.80 - 1.06 \sin^2\theta - 4.46 \sin^2 2\theta - 0.37 \sin^2 3\theta - 1.72 \sin^2 4\theta - 0.64 \sin^2 6\theta$.

exo form, again wtih geometry optimization as for the benzyl methyl ether, gave a conformer of minimum energy at θ = 30.0°. In other words (see caption to Fig. 1), the conformation of lowest energy for the *exo* form does not depend on the size of the alkyl group, as expected. A fit of the computed energies gave the internal potential as $V(\theta)/\text{kJ mol}^{-1} = 0.58 \sin^2\theta - 0.48 \sin^2 2\theta - 0.22 \sin^2 3\theta - 0.00 \sin^2 4\theta - 0.10 \sin^2 6\theta$, with a standard error of 0.02 kJ/mol in each term. The leading terms in this expression are not very different from those for benzyl methyl ether, but the sixfold term, in $\sin^2 3\theta$, reduces the barrier at θ = 90° to 0.4 kJ/mol, smaller by 0.3 kJ/mol than that for the methyl compound. However, at 300 K, $\langle\sin^2\theta\rangle$ is 0.472 for the *tert*-butyl derivative, very close to that of 0.467 for the *exo* form of the methyl derivative. Qualitatively, the lower theoretical barrier for the larger alkyl group, surely existing predominantly in the *exo* orientation in the ether, is in agreement with the indications from $^6J(H,CH_2)$, discussed in a previous section as a relative destabilization of the in-plane conformer by the *tert*-butyl group.

Of course, the discussion in this section is based on the minimal basis set. It is conceivable that larger basis sets will alter the description; they are also much more demanding of computer time.

Summary and conclusions

The present discussion of the experimental data, in terms of an apparent twofold barrier to rotation about the C_{sp^2}—C_{sp^3} bond in various benzyl alkyl ethers in solution and in terms of theoretical potentials for this motion in the *exo* and *endo* forms of the free benzyl methyl ether molecule, is clearly a simplification of what is no doubt a rather convoluted potential surface defining the internal motion. A large number of conformers, as defined by different combinations of θ and ψ values, are most likely appreciably populated at ambient temperatures in the vapor and in solution. The solution data imply a solvent dependence of the potential surface, but also agree semiquantitatively with the theoretical potential for the *exo* form in that they indicate the perpendicular conformer as least stable in the vapor phase and, also, in that they are in reasonable, perhaps coincidental, agreement with the theoretical values of $\langle\sin^2\psi\rangle$. These, being near 0.5 at 300 K, suggest that the molecule samples a large variety of θ and ψ values, consistent with the somewhat flat (compared to kT) theoretical surface. Ideally, given computing time, this surface should be calculated with a larger basis set and its curvature used to calculate the thermodynamic functions at, say, 300 K.

The essentially equal computed stabilities of the *exo* and *endo* forms of benzyl methyl ether near a θ of 45° (Table 4) contrast sharply with the results for benzyl alcohol (9) using the same basis set. In the latter, the *endo* is 3.8 kJ/mol more stable than the *exo* form, this number changing very little as θ increases to 90°. In the ether, however, the *endo* form is 3.6 kJ/mol less stable than the *exo* for this θ value. If, as has been cogently argued (11, 12), the stability of the *endo* form of benzyl alcohol originates in repulsive interactions between the π system and the lone-pair electrons on the oxygen atom, then the relative stabilities of the *endo* and *exo* forms of the ether for this range of θ values may well imply repulsive $CH_3 \ldots \pi$ forces in the *endo* form. Alternatively, if the *endo* form of benzyl alcohol is being favored by attractive O—H...π forces, then the corresponding $CH_3 \ldots \pi$ attractions in the ether are considerably smaller near θ = 45° and become repulsions near θ = 90°. The ambiguities connected with the question of weak $CH_3 \ldots \pi$ hydrogen bonds are exemplified in a recent paper by Ōki and co-workers (25).

Can. J. Chem. Downloaded from www.nrcresearchpress.com by 91.121.58.235 on 09/07/12
For personal use only.

Acknowledgments

We thank the University of Manitoba for allocations of computing time and the Natural Sciences and Engineering Research Council of Canada for financial assistance.

1. T. SCHAEFER, J. PEELING, and R. SEBASTIAN. Can. J. Chem. **63**, 3219 (1985).
2. G. CELEBRE, G. DELUCA, M. LONGERI, and J. W. EMSLEY. Mol. Phys. **67**, 239 (1989).
3. G. H. PENNER, T. SCHAEFER, R. SEBASTIAN, and S. WOLFE. Can. J. Chem. **65**, 1845 (1987).
4. T. SCHAEFER, R. SEBASTIAN, and G. H. PENNER. Can. J. Chem. **64**, 1372 (1986).
5. T. SCHAEFER, G. H. PENNER, and R. SEBASTIAN. Can. J. Chem. **65**, 873 (1987).
6. A. MILLER and D. W. SCOTT. J. Chem. Phys. **68**, 1317 (1978).
7. M. TRAETTEBERG, H. OSTENSEN, and R. SEIP. Acta Chem. Scand. Part A, **34**, 449 (1980).
8. R. J. ABRAHAM and J. M. BAKKE. Tetrahedron, **34**, 2947 (1978).
9. T. SCHAEFER, R. SEBASTIAN, J. PEELING, G. H. PENNER, and K. KOH. Can. J. Chem. **67**, 1015 (1989).
10. T. VISSER and J. H. VAN DER MAAS. Spectrochim. Acta, Part A, **42**, 599 (1986), and references therein.
11. R. J. ABRAHAM, J. M. BAKKE, and T. SKJETNE. Acta Chem. Scand. Part B, **38**, 547 (1984).
12. J. M. BAKKE, A. M. SCHIE, and T. SKJETNE. Acta Chem. Scand. Part B, **40**, 703 (1986).
13. A. I. VOGEL. Elementary practical organic chemistry. Longman, London. 1966. Part 1. p. 193.
14. W. J. HEHRE, R. DITCHFIELD, R. F. STEWART, and J. A. POPLE. J. Chem. Phys. **52**, 2769 (1970).
15. M. R. PETERSEN and R. A. POIRIER. MONSTERGAUSS, Department of Chemistry, University of Toronto, Toronto, Ontario. 1981.
16. J. S. MARTIN, A. R. QUIRT, and K. E. WORVILL. The nmr program library. Daresbury Laboratory, Daresbury, U.K.
17. R. LAATIKAINEN. Magn. Reson. Chem. **28**, 588 (1986).
18. R. LAATIKAINEN and K. TUPPURAINEN. J. Chem. Soc. Perkin Trans. 2, 121 (1987).
19. W. J. E. PARR and T. SCHAEFER. Acc. Chem. Res. **13**, 400 (1980).
20. R. J. ABRAHAM and E. BRETSCHNEIDER. *In* Internal rotation in molecules. *Edited by* W. J. Orville-Thomas. Wiley and Sons, New York. 1974. Chap. 13.
21. C. HUISZOON. J. Chem. Soc. Faraday Trans. 2, **85**, 727 (1989).
22. C. CASTIGLIONI, M. GUSSONI, and G. ZERBI. J. Mol. Struct. **198**, 475 (1989).
23. U. BLUKIS, P. H. KASAI, and R. J. MYERS. J. Chem. Phys. **38**, 2753 (1963).
24. P. GRONER and J. DURIG. J. Chem. Phys. **66**, 1856 (1977).
25. Y. NAKAI, K. INOUE, G. YAMAMOTO, and M. ŌKI. Bull. Chem. Soc. Jpn. **62**, 2923 (1989).

Can. J. Chem. Downloaded from www.nrcresearchpress.com by 91.121.58.235 on 09/07/12
For personal use only.

Optically pure (*S*)-cyclopent-2-en-1-ol and (*S*)-3-methoxycyclopentene

AMAL WAHHAB, DONALD F. TAVARES, AND ARVI RAUK[1]

Department of Chemistry, The University of Calgary, Calgary, Alta., Canada T2N 1N4

Received February 20, 1990

AMAL WAHHAB, DONALD F. TAVARES, and ARVI RAUK. Can. J. Chem. **68**, 1559 (1990).

Optically pure (*S*)-cyclopent-2-en-1-ol, $[\alpha]_D^{20}$ −137.9° (*c* 1.1, $CHCl_3$), and (*S*)-3-methoxycyclopentene, $[\alpha]_D^{20}$ −116.9° (*c* 3.86, *n*-hexane), were prepared from ethyl (1*R*,2*S*)-2-hydroxycyclopentanecarboxylate, which is readily available by yeast reduction of ethyl 2-oxocyclopentanecarboxylate. The optical purity of the alcohol was determined from its Mosher ester, and that of the ether by gas chromatography using a Ni-4-Pin column.

Key words: (*S*)-cyclopent-2-en-1-ol, (*S*)-3-methoxycyclopentene.

AMAL WAHHAB, DONALD F. TAVARES et ARVI RAUK. Can. J. Chem. **68**, 1559 (1990).

On a préparé du (*S*)-cyclopent-2-èn-1-ol, $[\alpha]_D^{20}$ −137,9° (*c* 1,1, $CHCl_3$), et du (*S*)-3-méthoxycyclopentène, $[\alpha]_D^{20}$ −116,9° (*c* 3,86, *n*-hexane), optiquement purs à partir du (1*R*,2*S*)-2-hydroxycyclopentanecarboxylate d'éthyle qui est facilement accessible par le biais d'une réduction du 2-oxocyclopentanecarboxylate d'éthyle à l'aide de levures. On a déterminé la pureté optique de l'alcool en se basant sur la chromatographie gazeuse (utilisant une colonne de Ni-4-Pin) de son ester de Mosher ainsi que de son éther.

Mots clés : (*S*)-cyclopent-2-èn-1-ol, (*S*)-3-méthoxycyclopentène.

[Traduit par la revue]

Can. J. Chem. Downloaded from www.nrcresearchpress.com by 91.121.58.235 on 09/07/12
For personal use only.

Introduction

Our interest in the chiroptical and the spectroscopic characteristics of cyclic allylic alcohols and ethers created a need for chemically and enantiomerically pure 2-cyclopenten-1-ol **1** and 3-methoxycyclopentene **2**. Previously reported synthetic procedures for the preparation of the alcohol **1** fail in this respect. There are no reports of the preparation of the optically active ether **2** and it is not clear that the allylic alcohol could be converted to the ether without some racemization. Hill and Edwards (1) converted racemic **1** to the acid succinate, and partially resolved it with (+)-α-(1-naphthyl)-ethylamine. After eight recrystallizations and regeneration of the succinate, followed by $LiAlH_4$ reduction, the specific rotation of **1** was $[\alpha]_D^{21}$ +22.8° (*c* 5, CCl_4), corresponding to about 15% ee. Denney *et al.* (2) achieved partial asymmetric induction in the reaction of cyclopentadiene with *tert*-butylhydroperoxide and the cupric salt of (+)-α-ethyl camphorate, and obtained α-ethyl-β-Δ^2-cyclopentenyl camphorate, which upon $LiAlH_4$ reduction yielded **1**, $[\alpha]_D^{26}$ −13.6° (*c* 8.9, $CHCl_3$). Asami and Kirihara (3) reported that the asymmetric transformation of cyclopentene oxide with lithium (*S*)-2-[(pyrrolidin-1-yl)-methyl]pyrrolidide gave **1** in 49% yield and 31% ee, $[\alpha]_D^{30}$ −55° (*c* 1.35, CCl_4). In the work of Sharpless and co-workers (4) introducing kinetic resolution of allylic alcohols by enantioselective epoxidation, the reaction of racemic **1** was not reported. It failed to give satisfactory results in our hands.[2] Sato *et al.* (5) obtained **1** in 77% yield and 82% ee, $[\alpha]_D^{23}$ −105.8° (*c* 1.14, $CHCl_3$), by asymmetric reduction of 2-cyclopenten-1-one **3** with chiral aluminium hydride reagents. More recently, Kitamura *et al.* (6) reported that the BINAP–ruthenium(II)-catalyzed hydrogenation of **3** gave **1** in 50% yield and 79% ee.

Although the optically active ether **2** has not been reported, a few reports have appeared for racemic **2**. Alder and Flock (7*a*) prepared **2** by the reaction of 3-chlorocyclopentene with methanol, while Fleming and Thomas (7*b*) and Ishiyama *et al.* (7*c*) obtained **2** by methylation of **1**.

Inspired by the high enantioselectivity and the good yields of yeast reductions of ketones (8), we chose ethyl (1*R*,2*S*)-2-hydroxycyclopentanecarboxylate **5**, which is easily obtainable by yeast reduction of ethyl 2-oxocyclopentanecarboxylate **4**, as our starting point. Scheme 1 depicts our strategy to prepare the chemically and optically pure compounds **1** and **2**.

Results and discussion

The baker's yeast reduction of ethyl 2-oxocyclopentanecarboxylate **4** by a slight modification of the procedure of Tsuboi *et al.* (9) gave chemically and enantiomerically pure ethyl (1*R*,2*S*)-2-hydroxycyclopentanecarboxylate **5** in 80.3% yield. The more laborious procedure of Deol *et al.* (10) for the reduction of **4**, which involved the preparation of freshly cultivated batches of a sterile mutant of *Saccharomyces cerevisiae*, baker's yeast, under strictly controlled conditions, failed to give satisfactory reduction in our hands. The absolute configuration of **5** was assumed (and subsequently verified) to be the same as that of the product of Deol *et al.* Hence, the absolute configuration of the alcohol belongs to the *S* series.[3] This configuration is maintained all through the reaction sequence and will yield the (*S*)-2-cyclopenten-1-ol **1**. The specific rotation of **5**, $[\alpha]_D^{20}$ +15.1°, was slightly higher than that of the product obtained by Deol *et al.*, $[\alpha]_D^{20}$ +14.1°. ^1H and ^{13}C NMR analysis of the Mosher ester of **5** showed it to consist of one isomer only.

Hydrolysis of the hydroxy ester **5** with 25% NaOH, similar to the reported hydrolysis of ethyl (1*R*,2*S*)-hydroxycyclohexanecarboxylate (10), gave (1*R*,2*S*)-2-hydroxycyclopentanecarboxylic acid **6** in 74.2% yield, $[\alpha]_D^{20}$ +28.0°. ^1H and ^{13}C NMR and the specific rotation of **6** indicated that racemization under the hydrolysis conditions did not occur. Attempts to selectively protect the alcohol of **5** as the silyl ether in the presence of the acid functionality gave a mixture of protected alcohol and protected acid; therefore, excess *tert*-butyldimethylchlorosilane and increased reaction times were required to fully protect both functionalities. The *tert*-butyldimethylsilyl (1*R*,2*S*)-2-*tert*-

[1]Author to whom correspondence may be addressed.

[2]A. Rauk and D. F. Tavares, unpublished results.

[3]Enzymes generally transform ketones into products possessing the *S*-configuration (where steric bulk determines the relative priorities) at the newly formed secondary alcohol unit. See K. Kieslich. Microbial transformations of chemical compounds excluding steroids and non-cyclic structures. G. Thieme, Stuttgart. 1976.

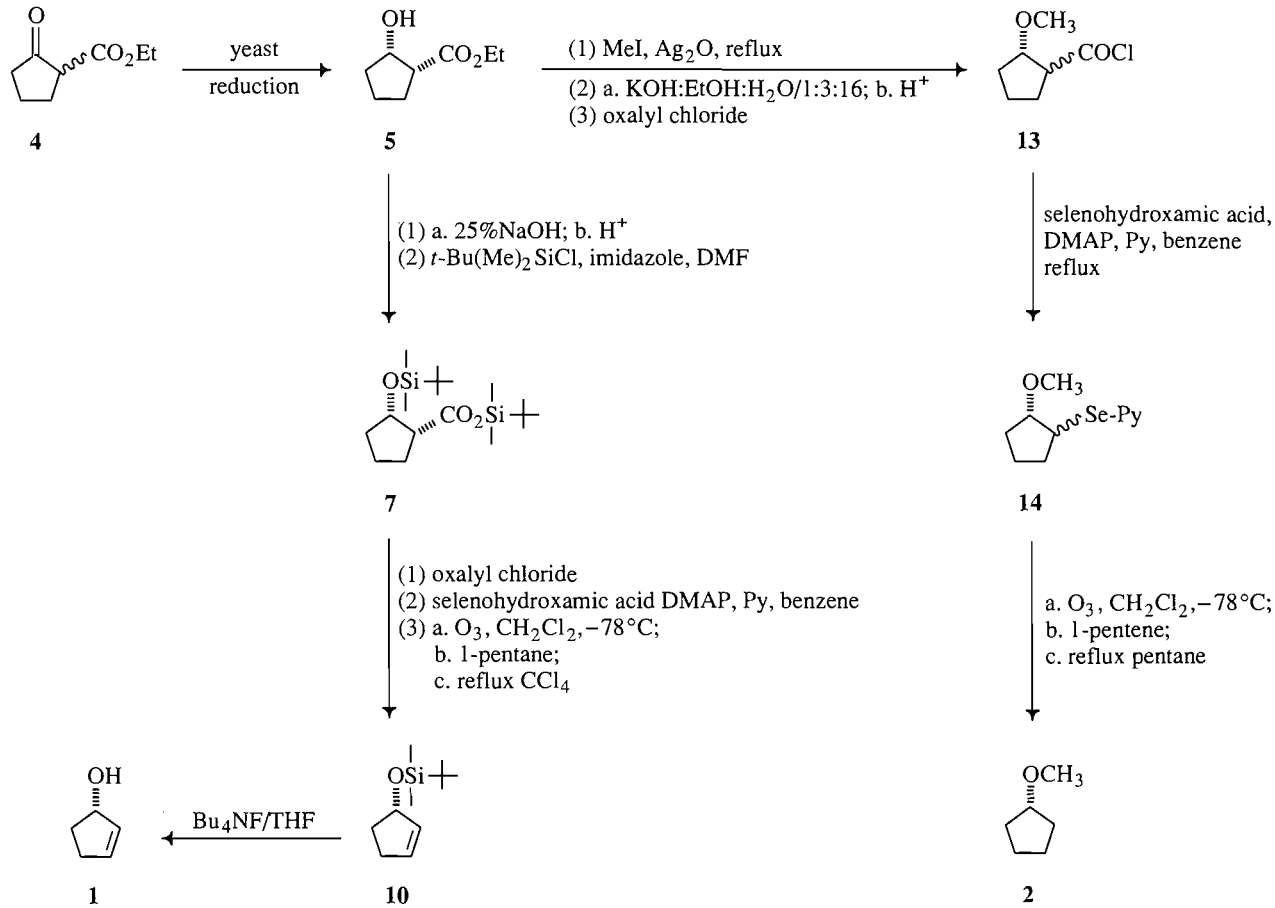

SCHEME 1

butyldimethylsiloxycyclopentanecarboxylate **7** obtained in 80% yield, $[\alpha]_D^{20}$ +24.6°, was reacted with oxalyl chloride following the procedure of Wissner and Grudzinskas (11) to give (1*R*,2*S*)-*tert*-butyldimethylsiloxycyclopentanecarbonyl chloride **8** quantitatively. The decarboxylative selenination of **8** according to the procedure of Barton *et al.* (12) gave 1-*tert*-butyldimethylsiloxy-2-(2′-pyridylseleno)cyclopentane **9** in 85.8% yield as a 7:1 mixture of two diastereomers. The epimerization at carbon 2 of **9** was expected, since the decarboxylative selenination proceeds via a radical mechanism (12). The major isomer is inferred to be the *trans* from the chemical shift of the alkoxy carbon, CH—O-, in the ^{13}C NMR spectrum, which appeared at 79.7 ppm compared to the minor at 75.8 ppm (13). The diastereomers of **9** were not separated, and were ozonized to give 1-*tert*-butyldimethylsiloxycyclopent-2-ene **10** in 77.2% yield. Deprotection of **10** gave (*S*)-2-cyclopenten-1-ol **1** in 46% isolated yield after chromatography and vacuum distillation. The specific rotation of **1**, $[\alpha]_D^{20}$ −137.9°, and the ^1H and ^{13}C NMR spectra of the MPTA ester of **1** and that of the racemic alcohol indicated that **1** was indeed enantiomerically pure.

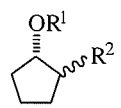

6 (1*R*)R^1 = H, R^2 = -CO_2H
8 (1*R*)R^1 = *t*-Bu(Me)$_2$Si-, R^2 = -COCl
9 R^1 = *t*-Bu(Me)$_2$Si-, R^2 = -SePy
11 (1*R*)R^1 = -CH_3, R^2 = -CO_2Et
12 R^1 = -CH_3, R^2 = -CO_2H
Py = 2-pyridyl

It is worth noting that attempts to prepare optically active 2-phenylselenocyclopentanol by yeast reduction of 2-phenylselenocyclopentanone were not fruitful. The seleno moiety was unstable to the reduction conditions and was recovered as diphenyldiselenide. The α-seleno ketone without the yeast was stable in different buffered solutions, which leads us to think that the fermenting yeast is somehow interacting with the seleno moiety.[4] To our knowledge, this is the first report of such an observation, since α-dithianyl ketones and β-thianyl ketones have been reduced with yeast without reported troubles (8, 14).

The allylic ether **2** was synthesized by a parallel route starting from **5**. The reaction of **5** with a large excess of silver(I) oxide and methyl iodide gave ethyl (1*R*,2*S*)-2-methoxycyclopentanecarboxylate **11** in 86.4% yield, $[\alpha]_D^{20}$ +20.0°. Of several methods attempted for the hydrolysis of **11**, the most satisfactory were Ba(OH)$_2$:ethanol:H_2O (1:4:25), and KOH:ethanol:H_2O (1:3:16) with the former giving a 3.4:1 and the latter a 3:1 mixture of two diastereomers of (2*S*)-2-methoxycyclopentanecarboxylic acid **12**. The chemical shift, in the ^{13}C NMR spectrum, of the alkoxy carbon, C2, of the major isomer appeared at 83.8 ppm, and that of the minor at 85.4 ppm, indicating that the major isomer is most likely the *cis* diastereo-

[4] V. Kaija, H. Kai, E. Kari, and K. Matti. Chem. Abstr. **100**, 153628u (1984), reported that Se is incorporated into analogs of S-containing amino acids if yeast is grown in the presence of a source of inorganic Se.

Can. J. Chem. Downloaded from www.nrcresearchpress.com by 91.121.58.235 on 09/07/12
For personal use only.

Can. J. Chem. Downloaded from www.nrcresearchpress.com by 91.121.58.235 on 09/07/12
For personal use only.

mer[5] (13). The two diastereomers of **12** with oxalyl chloride in refluxing hexanes gave (2*S*)-2-methoxycyclopentanecarbonyl chloride **13** in 93% yield. Decarboxylative selenination of **13** gave (1*S*)-1-methoxy-2-(2-pyridylseleno)cyclopentane **14** in half the yield obtained from the same reaction with **8**. The ozonolysis of **14** and thermal decomposition of the selenoxide by pouring over refluxing pentane produced (*S*)-3-methoxycyclopentene **2** in 68% isolated yield, $[\alpha]_D^{20}$ −116.9°. To our knowledge, this is the first report of the synthesis of optically active **2**. The optical purity of **2** was determined by GC using a chiral column, Ni-4-Pin, and found to be 98.3%, i.e., approximately 97% ee.

A sample of **2** prepared by methylation of optically active **1** by silver(I) oxide/methyl iodide was found to be >99% optically pure by chiral GC analysis as described above. This result verifies that the methylation of **1** under these conditions proceeds without epimerization, and also confirms the optical purity of the allylic alcohol **1**.

Experimental

General information

Infrared spectra (IR) of liquids were recorded using KBr cells on a Nicolet 5-DX FT-IR prism grating spectrophotometer. Gas–liquid chromatography (GC) was accomplished with a Varian model 3700 gas chromatograph fitted with a DB-5, 30 m × 0.249 mm, fused silica column, 0.25 μm film thickness. Proton (^{1}H) and carbon (^{13}C) nuclear magnetic resonance (NMR) spectra were recorded on a 200 MHz Bruker AC-200 spectrometer and signal positions are given in ppm (δ). Flash column chromatography was done on 230–400 mesh silica gel. Rotations were measured on a Rudolph Autopol III automatic polarimeter. Ozone for ozonolysis was generated from a Welsbach ozonator model T-23. Solvents were purified and dried using standard methods. Baker's yeast, *Saccharomyces cerevisiae* type II, was purchased from Sigma. The chiral column was an OV-1 (25 m × 0.25 mm fused silica) coated with 0.25 μm Ni-4-Pin.

Yeast reduction of ethyl 2-oxocyclopentanecarboxylate

A suspension of baker's yeast (12.0 g), sugar (152 g), $MgSO_4$ (1.0 g), KH_2PO_4 (2.0 g), $NH_4H_2PO_4$ (2.0 g), and $CaCO_3$ (5.0 g) in deionized H_2O (1 L) was placed in a water bath at 35°C and allowed to ferment for 45 min (shaken occasionally). Ethyl 2-oxocyclopentanecarboxylate (10.2 g) was added dropwise and the last amount was transferred with the minimum volume of ethanol (1.5 mL). The mixture was magnetically stirred at room temperature for 18 h. A sample analysed by GC showed the disappearance of the starting material. The mixture was transferred to a separatory funnel and extracted with ether (5 × 250 mL). The combined ether extracts were washed with saturated NaCl solution and dried over anhydrous $MgSO_4$ and filtered. Evaporation of the solvent and fractional distillation of the residue under reduced pressure gave (1*R*,2*S*)-2-hydroxycyclopentanecarboxylate **5** in 80.3% yield, bp 59–61°C/0.4 Torr (1 Torr = 133.3 Pa), >98% pure;[6] $[\alpha]_D^{20}$ +15.1° (*c* 1.57, $CHCl_3$) (lit. (10) $[\alpha]_D^{20}$ +14.1° (*c* 1.7, $CHCl_3$)). ^{1}H NMR agreed well with reported data (10). ^{13}C NMR, δ: 174.6 (C=O), 73.6 (CH—O), 60.4 (CH_2—O), 49.5, 33.9, 26.1, 21.9, 14.0.

The Mosher ester of **5** (MTPA ester) was prepared using (*R*)-α-methoxy-α-trifluoromethylphenylacetic acid according to literature procedures (15). ^{1}H NMR ($CDCl_3$), δ: 7.55–7.35 (m, 5H, aromatic), 5.69–5.63 (m, 1H, CH—O), 4.2–3.89 (m, ABX_3, 2H, O—CH_2), 3.495 (d, *J* = 1.1 Hz, 3H, O—CH_3), 3.0–2.89 (8 lines, 1H, CH—CO_2), 1.2 (t, *J* = 7.6 Hz, 3H, CH_2—CH_3). ^{13}C NMR ($CDCl_3$), δ: 170.9 (C=O), 166.0 (C=O), 129.5, 128.3, 127.5, 126.1, 120.0, 79.8 (CH—O), 60.7 (O—CH_3), 55.2, 49.1, 32.3, 25.1, 21.6, 13.9.

Hydrolysis of hydroxy ester 5

The hydroxy ester **5** (17.14 g, 0.103 mol) was stirred with 25% NaOH aqueous solution (85.7 mL) at room temperature according to the procedure in ref. 10. The hydroxy acid **6** was obtained in 74.2% yield, $[\alpha]_D^{20}$ +28.0° (*c* 1.866, $CHCl_3$), as an oil that solidified on standing. IR (thin film): 3676–2291, 1711 cm^{-1}. ^{1}H NMR, δ: 6.8 (br, 2H, -OH and -CO_2H, exchange with D_2O), 4.50 (dd, 1H, *J* = 2.4, 4.6 Hz, CH—O), 2.77 (dt, 1H, *J* = 4.6, 9.2 Hz, CH—CO_2), 2.11–1.61 (m, 6H, ring CH_2's). ^{13}C NMR, δ: 178.7 (CO_2H), 73.9 (CH—OH), 49.6 (CH—CO_2H), 33.9, 25.9, 21.9.

Silylation of hydroxy acid 6

Following the procedure of Wissner and Grudzinskas (11), the hydroxy acid **6** (18.0 g, 0.135 mol), *tert*-butyldimethylchlorosilane (50.0 g, 0.332 mol), and imidazole (45.17 g, 0.663 mol) in DMF (80 mL) were stirred at room temperature. After 44 h, 50% of **6** had reacted. *tert*-Butyldimethylchlorosilane (25.0 g) and imidazole (22.5 g) were added and the reaction mixture was stirred a further 26 h. The reaction mixture was diluted with ether and washed three times with H_2O, then once with saturated NaCl solution. The solvent was removed by fractional distillation and the residue was distilled under reduced pressure to give the disilyl derivative of **7** in 80% yield, bp 120–124°C/0.7 Torr, as a colorless oil; $[\alpha]_D^{20}$ +24.6° (*c* 1.698, $CHCl_3$). ^{1}H NMR, δ: 4.35 (m, 1H, CH—O—Si), 2.7 (m, 1H, CH—CO_2), 2.2–1.5 (multiplets, 6H, ring CH_2's), 0.94 (s, 9H, *t*-Bu-Si), 0.92 (s, 9H, *t*-Bu-Si), 0.27, 0.25, 0.04, 0.03 (singlets, 3H each, CH_3—Si). ^{13}C NMR, δ: 172.9 (CO_2—Si), 75.6 (CH—O—Si), 53.0 (CH—CO_2Si), 34.9, 25.8, 25.6, 25.2, 21.6, 18.0, 17.6, −4.57, −4.61, −4.69, −4.84. Anal. calcd. for $C_{18}H_{38}O_3Si_2$: C 60.28, H 10.68; found: C 60.09, H 10.56.

Reaction of disilyl 7 with oxalyl chloride

Oxalyl chloride (2.3 mL, 26.2 mmol) was added dropwise to a mixture of disilyl **7** (7.56 g, 21.1 mmol) and 3 drops of DMF in CH_2Cl_2 (21 mL) cooled in an ice bath according to the procedure of Wissner and Grudzinskas (11). After work-up and evaporation of the solvent, the residue was connected to a vacuum pump and the by-product, *tert*-butyldimethylchlorosilane, was trapped. The acid chloride **8** (5.6 g, 100% yield) was used in the next step without distillation. IR (thin film): 1811 cm^{-1}. ^{1}H NMR ($CDCl_3$), δ: 4.70 (m, 1H, HC—O—Si), 3.24 (m, 1H, HC—COCl), 2.35–1.57 (m, 6H, ring CH_2's), 0.86 (s, 9H, *t*-Bu-Si), 0.11 (s, 3H, CH_3—Si), 0.08 (s, 3H, Si—CH_3). ^{13}C NMR ($CDCl_3$), δ: 172.2 (C=O), 75.8 (HC—O—Si), 63.7 (HC—COCl), 34.9, 25.6, 25.1, 22.2, 17.9, −4.4 (CH_3—Si), −5.2 (Si—CH_3).

Reaction of acid chloride 8 with selenohydroxamic acid

The acid chloride **8** (5.5 g, 20.9 mmol) in benzene (110 mL) was added dropwise over 30 min to a refluxing solution of selenohydroxamic acid (4.84 g, 27.6 mmol), pyridine (5.5 mL), and DMAP (0.264 g) in benzene (220 mL) under argon according to the procedure of Barton *et al.* (12). The crude product upon chromatography over silica (eluting with 3% EtOAc: pet. ether) gave the selenide **9** in 85.8% yield as a 7:1 mixture of two diastereomers. $[\alpha]_D^{20}$ −15.0° (*c* 1.093, $CHCl_3$). ^{1}H NMR ($CDCl_3$), δ: major 8.41 (m, 1H), 7.38 (m, 2H), 6.99 (m, 1H), 4.30 (m, 1H, HC—O), 3.9 (m, < 1H, HC—Se), 2.5–1.5 (multiplets, 6H, ring CH_2's), 0.85 (s, 9H, *t*-Bu-Si), 0.029 (s, 3H, CH_3—Si), 0.019 (s, 3H, Si—CH_3). ^{13}C NMR ($CDCl_3$), δ: major 156.5, 149.9, 135.7, 125.7, 120.1 (pyridyl carbons), 79.7 (HC—O—Si), 48.6, 33.8, 30.6, 25.7 (*t*-Bu-Si), 22.4, 17.9, −4.7 (CH_3—Si), −4.8 (Si—CH_3); minor 75.8 (CH—O). Anal. calcd. for $C_{16}H_{27}NOSeSi$: C 53.92, H 7.64, N 3.93; found: C 54.26, H 7.78, N 3.74.

Ozonolysis of selenide 9

The selenide **9** (6.4 g) in CH_2Cl_2 was cooled in a Dry Ice – acetone bath and ozone (2.5% O_3) was bubbled through the solution until the

[5] J. Pascual and J. Vinas. Chem. Abstr. **55**, 4383e (1961), reported that the saponification of methyl *cis*-2-methoxycyclopentanecarboxylate with $Ba(OH)_2$ gave 87% *cis*-2-methoxycyclopentanecarboxylic acid.

[6] NOTE ADDED IN PROOF: Noyori *et al.* (J. Am. Chem. Soc. **111**, 9134 (1989)) reported that the hydrogenation of the methyl esters of **4** by (*R*)-BINAP–Ru complex gave a 99:1 mixture of the *trans* hydroxy ester (92% ee) and its C2 epimer (93% ee).

Can. J. Chem. Downloaded from www.nrcresearchpress.com by 91.121.58.235 on 09/07/12
For personal use only.

blue color persisted. Oxygen was passed through the solution to drive off excess ozone and, very cautiously, 1-pentene (37 mL) was added to the cold mixture, and the reaction mixture was added over refluxing CCl_4 (177 mL) at a rate to maintain reflux. After completion of addition, the mixture was refluxed for a further 30 min, then the solvents were removed under reduced pressure. The allylic silyl ether **10** was obtained by vacuum distillation of the residue in 77.2% yield, 35°C/0.5 Torr); $[\alpha]_D^{20}$ −84.9° (*c* 0.855, $CHCl_3$). ^1H NMR ($CDCl_3$), δ: 5.92 (m, 1H, HC=), 5.7 (m, 1H, =CH), 4.94 (m, 1H, HC—O), 2.6–2.21 (m, 3H), 1.67 (m, 1H), 0.84 (s, 9H, *t*-Bu-Si), 0.02 (s, 6H, CH_3—Si—CH_3). ^{13}C NMR ($CDCl_3$), δ: 133.9 (HC=), 133.4 (=CH), 78.1 (HC—O), 33.5, 31.0, 26.0 (*t*-Bu-Si), 18.3, −4.6 (CH_3—Si—CH_3). Exact Mass calcd. for $C_{11}H_{22}OSi$: 198.3822; found: 198.3828.

(S)-2-Cyclopenten-1-ol ***1***

Tetrabutylammonium fluoride (47.9 mL, 1.0 M solution in THF) was added via a syringe to the silyl ether **10** (9.5 g, 47.9 mmol) under argon. After stirring the reaction mixture at room temperature for 90 min, the mixture was transferred to a separatory funnel, and the organic layer was washed with a saturated solution of NaCl and dried over anhydrous $MgSO_4$. The solvent was removed by fractional distillation and the residue was subjected to flash column chromatography to remove the by-product, *t*-Bu-Si(CH_3)$_2$—O—Si(CH_3)$_2$-*t*-Bu, eluting with 10% ether:pentane, then with 25% ether:pentane. Alcohol **1** was obtained in 46% isolated yield, bp 51.5–53°C/aspirator (lit. (16) bp 78°C/59 Torr); $[\alpha]_D^{20}$ −137.9° (*c* 1.10, $CHCl_3$); $[\alpha]_D^{20}$ −113.1° (*c* 1.045, *n*-hexane). IR (thin film): 3325 (O—H), 3058 (H—C=), 1615 (C=C), 1047 (C—O). ^1H NMR ($CDCl_3$), δ: 5.88 (m, 1H, HC=), 5.75 (m, 1H, =HC), 4.77 (m, 1H, CH—O), 3.1 (bs, 1H, -O—H), 2.42 (m, 1H), 2.16 (m, 2H), 1.6 (m, 1H). ^{13}C NMR ($CDCl_3$), δ: 134.4 (CH=), 133.2 (=CH), 77.0 (HC—OH), 32.9, 30.7. The MTPA ester exhibited the following spectroscopic properties: ^1H NMR ($CDCl_3$), δ: 7.57–7.52 (m, 2H), 6.2–6.17 (m, 1H, CH—O), 5.96–5.91 (m, 2H, HC=CH), 3.56 (d, J = 1.2 Hz, 3H, O—CH_3), 2.62–2.22 (m, 3H), 1.97–1.8 (m, 1H). ^{13}C NMR ($CDCl_3$), δ: 166.3 (C=O), 139.08 (CH=), 129.4, 128.3, 128.0 (=CH), 127.35, 126.2, 120.4, 83.03 (CH—O), 55.3 (O—CH_3), 31.0, 29.48. The MTPA ester of the racemic alcohol had the following: ^{13}C NMR ($CDCl_3$), δ: 166.3 (C=O), 139.21, 139.08, 132.46, 132.32, 129.4, 128.3, 128.0, 127.35, 127.26, 126.2, 120.4, 83.12, 83.03, 55.3, 31.0, 29.48, 29.35.

Methylation of hydroxy ester ***5***

A mixture of hydroxy ester **5** (0.5 g, 3.16 mmol), methyl iodide (0.8 mL, 12.6 mmol), and Ag_2O (0.73 g, 3.15 mmol) was refluxed according to the procedure of Mislow (17). After 18 h, 14.2% of **5** remained unreacted. Methyl iodide (1 mL) and Ag_2O (0.8 g) were added and the mixture was refluxed for a further 6 h (progress of the reaction was followed by GC). Ether was added and the mixture was filtered through Celite, and the solvent was removed by fractional distillation. Chromatography of the residue over flash silica (eluting with 15% ether:pet. ether) yielded methoxy ester **11** in 86.4% yield, $[\alpha]_D^{20}$ +20° (*c* 1.311, $CHCl_3$). ^1H NMR ($CDCl_3$), δ: 4.24–4.0 (16 lines ABX_3, 2H, O—CH_2), 3.97–3.88 (m, 1H, CH—O), 3.25 (s, 3H, O—CH_3), 2.9–2.74 (8 lines, 1H, CH—CO_2), 2.2–1.47 (m, 6H, ring CH_2's), 1.22 (t, J = 17.5 Hz, 3H, -CH_3). ^{13}C NMR ($CDCl_3$), δ: 172.6 (C=O), 84.0 (CH—O), 60.0 (O—CH_2), 57.0 (O—CH_3), 49.4, 30.4, 25.2, 22.5, 21.9, 14.2. Anal. calcd. for $C_9H_{16}O_3$: C 62.77, H 9.36; found: C 62.40, H 9.38.

Hydrolysis of methoxy ester ***11***

A mixture of methoxy ester **11** (4.186 g, 24.3 mmol), KOH (11.63 g, 207 mmol), ethanol (34.9 mL), and H_2O (186 mL) was refluxed for 45 min, then it was cooled and extracted with ether. The aqueous layer was carefully acidified with ice-cold 8% H_2SO_4 and extracted with ether. Evaporation of ether gave the methoxy acid **12** in 95% yield as a 3:1 mixture of diastereomers accompanied by 1.5% of 1-cyclopentenecarboxalic acid as a by-product. Hydrolysis of **11** (0.5 g) with $Ba(OH)_2$ (2.0 g) and ethanol (8 mL) in H_2O (50 mL), stirring at room temperature overnight, gave a 3.4:1 mixture of diastereomers, with the major being the same as above. ^1H NMR ($CDCl_3$), δ: 11.48 (br s, 1H, CO_2H), 4.03 (m, 1H, CH—O), 3.339 and 3.334 (two singlets), 2.87 (m, 1H, CH—CO_2), 2.2–1.55 (m, 6H, ring CH_2's). ^{13}C NMR ($CDCl_3$), δ: major 177.9 (C=O), 83.8 (CH—O), 60.0 (O—CH_3), 49.3, 30.3, 25.6, 21.8; minor 181.0 (C=O), 85.4 (CH—O), 56.9 (O—CH_3), 50.3, 32.1, 28.5, 23.4.

Methoxy acid chloride ***13***

A mixture of methoxy acid **12** (3.34 g, 23.2 mmol) and oxalyl chloride (2.7 mL) in hexane (20 mL) was refluxed overnight. Evaporation of the solvent and excess oxalyl chloride gave acid chloride **13** in 93% yield, pure enough to use in the next step. IR (thin film): 1797, 1791 cm^{-1}. ^1H NMR ($CDCl_3$), δ: 4.12 (m, 1H, CH—O), 3.34 (s, 3H, O—CH_3), 3.28–3.17 (8 lines, 1H, CH—COCl), 2.25–1.62 (m, 6H, ring CH_2's). ^{13}C NMR ($CDCl_3$), δ: 175.6 (C=O), 84.8 (CH—O), 62.2 (O—CH_3), 57.1, 32.0, 29.1, 23.2.

Decarboxylative selenination of acid chloride ***13***

The acid chloride **13** (2.29 g, 14.1 mmol) in benzene (70 mL) was added dropwise to a refluxing solution of selenohydroxamic acid (3.0 g, 17.4 mmol), DMAP (0.168 g), and pyridine (3.5 mL) in benzene (140 mL) as described for acid chloride **8**. After work-up, the methoxy selenide **14** was obtained in 42% yield as a 4.8:1 mixture of two diastereomers. ^1H NMR ($CDCl_3$), δ: major diastereomer 8.42 (m, 1H), 7.41 (m, 2H), 7.0 (m, 1H), 4.14 (m, 1H, CH—O), 3.88 (m, 1H, CH—Se), 3.35 (s, 3H, O—CH_3), 2.37 (m, 1H), 2.1–1.6 (multiplets, 5H). ^{13}C NMR ($CDCl_3$), δ: major diastereomer 150.0 (Se—C=N), 135.9, 125.8, 120.3 (pyridyl carbons), 88.4 (CH—O), 44.9 (CH—Se), 31.4, 30.9, 23.1. Anal. calcd. for $C_{11}H_{15}NOSe$: C 51.57, H 5.90, N 5.47; found: C 51.66, H 5.99, N 5.42.

Ozonolysis of methoxy selenide ***14***

Methoxy selenide **14** (3.06 g, 11.9 mmol) in CH_2Cl_2 (75 mL) was ozonized at −78°C (2.5% ozone) as described for **9**. 1-Pentene (24.6 mL) in CH_2Cl_2 (20 mL) was added cautiously to the cold solution and the mixture was added to refluxing pentane. The solvents were removed by fractional distillation and the residue was distilled under reduced pressure to yield 3-methoxycyclopentene **2** (68%); $[\alpha]_D^{20}$ −116.9° (*c* 3.86, *n*-hexane). ^1H NMR ($CDCl_3$), δ: 6.06–6.01 (m, 1H, CH=), 5.92–5.86 (m, 1H, =CH), 4.51–4.43 (m, 1H, CH—O), 3.33 (s, 3H, O—CH_3), 2.56–1.68 (multiplets, 4H, ring CH_2's). ^{13}C NMR ($CDCl_3$), δ: 135.7, 130.5 (CH=CH), 86.1 (CH—O), 55.7 (O—CH_3), 31.0, 29.3. Chromatography of **2** using a Ni-4-Pin chiral column, isothermal at 60°C and 20 psi (1 psi = 6.9 kPa), showed it to be 98.3% optically pure (97% ee). A sample of **2** prepared by an overnight reflux of a mixture of (*S*)-**1** (200 mg), Ag_2O (400 mg), and methyl iodide (8 mL) was >99% optically pure.

Acknowledgements

The financial support of this work by the Natural Sciences and Engineering Research Council of Canada is gratefully acknowledged.

1. R. K. Hill and A. G. Edwards. Tetrahedron Lett. 3239 (1964).
2. D. B. Denney, R. Napier, and A. Cammarata. J. Org. Chem. **30**, 3151 (1965).
3. M. Asami and H. Kirihara. Chem. Lett. 389 (1987).
4. V. S. Martin, S. S. Woodard, T. Katsuki, Y. Yamada, M. Ikeda, and K. B. Sharpless. J. Am. Chem. Soc. **103**, 6237 (1981).
5. T. Sato, Y. Gotoh, Y. Wakabayashi, and T. Fujisawa. Tetrahedron Lett. 4123 (1983).
6. M. Kitamura, I. Kasahara, K. Manabe, R. Noyori, and H. Takaya. J. Org. Chem. **53**, 708 (1988).
7. (*a*) K. Alder and F. H. Flock. Chem. Ber. **89**, 1732 (1956); (*b*) I. Fleming and E. J. Thomas. Tetrahedron, **28**, 5003 (1972); (*c*) J. Ishiyama, Y. Senda, and S. Imaizumi. J. Chem. Soc. Perkin Trans. 2, 71 (1982).

8. K. MORI, H. MORI, and T. SUGAI. Tetrahedron, **41**, 919 (1985), and references cited.
9. S. TSUBOI, E. NISHIYAMA, M. UTAKA, and A. TAKEDA. Tetrahedron Lett. 1915 (1986).
10. B. S. DEOL, D. D. RIDLEY, and G. W. SIMPSON. Aust. J Chem. **29**, 2459 (1976).
11. A. WISSNER and C. V. GRUDZINSKAS. J. Org. Chem. **43**, 3972 (1978).
12. D. H. R. BARTON, D. CRICH, and Y. HERVE. Tetrahedron, **41**, 4347 (1985).
13. E. BREITMAIER and W. VOELTER. Carbon-13 NMR spectroscopy, high resolution methods and applications in organic chemistry and biochemistry. 3rd ed. VCH, Weinheim. 1987. p. 210.
14. G. GUARTI, L. BANFI, and E. NARISANO. Tetrahedron Lett. 3547 (1986).
15. (*a*) J. A. DALE, D. L. DULL, and H. S. MOSHER. J. Org. Chem. **34**, 2543 (1969); (*b*) M. A. KHAN, D. F. TAVARES, and A. RAUK. Can. J. Chem. **60**, 2451 (1982).
16. S. KRISHNAMURTHY and H. C. BROWN. J. Org. Chem. **42**, 1197 (1977).
17. K. MISLOW. J. Am. Chem. Soc. **73**, 4043 (1951).

Can. J. Chem. Downloaded from www.nrcresearchpress.com by 91.121.58.235 on 09/07/12
For personal use only.

A deuterium labelling study into the insertion of diphenylacetylenes into iron–aryl bonds

IAN R. BUTLER,[1] JOANNE L. ELLIOT, AND JEAN HOUDE, JR.
Chemistry Department, The University of Ottawa, Ottawa, Ont., Canada K1N 6N5

Received January 23, 1990

IAN R. BUTLER, JOANNE L. ELLIOT, and JEAN HOUDE, JR. Can. J. Chem. **68**, 1564 (1990).

The mechanism of the reaction of dicarbonyl(η^5-cyclopentadienyl)phenyliron, **1**, with diphenylacetylene to give 2,3-diphenyl-[1*H*]-inden-1-one has been investigated using a partially deuterated **1**. The mechanistic pathway of the reaction is discussed in terms of the labelling of the indenones obtained. The reaction of phenylacetylene with **1** gives a mixture of products including 2,4,6-triphenyl-4′-methylbenzophenone and C-4,C-6a-dihydro-4-(4′-methylphenyl)-2-phenylpentalene(1-*r*-3a*H*)one.

Key words: indenones, acetylenes, iron, carbonyl.

IAN R. BUTLER, JOANNE L. ELLIOT et JEAN HOUDE, JR. Can. J. Chem. **68**, 1564 (1990).

Utilisant un composé **1** partiellement deutéré, on a examiné le mécanisme de la réaction du dicarbonyl(η^5-cyclopentadiényl)phénylfer, **1**, avec le diphénylacétylène qui conduit à la 2,3-diphényl-[1*H*]-indèn-1-one. On discute des diverses voies mécanistiques de la réaction en fonction de la position des marqueurs dans les indénones obtenues. La réaction du phénylacétylène avec le composé **1** conduit à un mélange de produits incluant la 2,4,6-triphényl-4′-méthylbenzophénone et la C-4,C-6a-dihydro-4-(4′-méthylphényl)-2-phénylpentalène(1-*r*-3a*H*)one.

Mots clés : indénones, acétylènes, fer, carbonyl.

[Traduit par la revue]

Introduction

The reactions of iron carbonyls and their derivatives with acetylenes have been studied extensively (1–10), since the initial discoveries and pioneering work of Reppe (1, 2). Some typical organic products obtained from such reactions are substituted quinones and cyclopentadienones or their metal complexes arising from multiple insertion of acetylenes and carbon monoxide into iron–carbon bonds, Scheme 1 (3, 4).

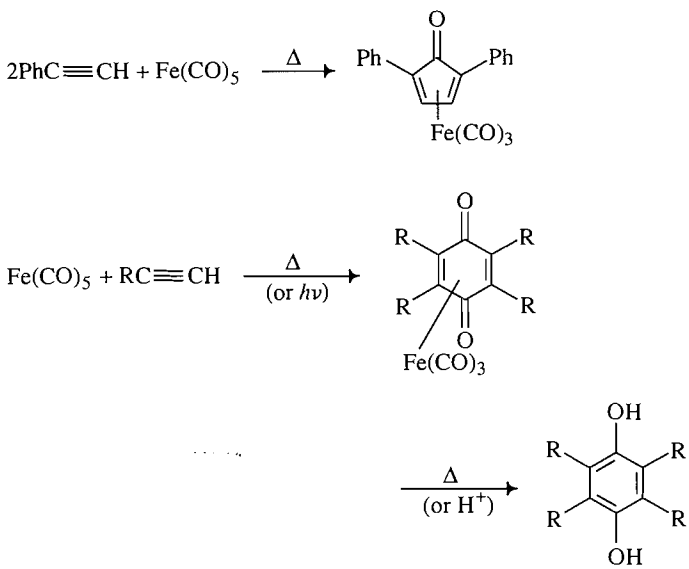

SCHEME 1

In 1971, Nesmeyanov *et al.* (11) reported interesting thermal and photolytic reactions of Fp-($SnAr_3$), **1** (Fp = dicarbonyl(η^5-cyclopentadienyl)iron, Ar = phenyl, *p*-tolyl), with diphenylacetylene to give 2,3-diaryl-[1*H*]-inden-1-ones, **2**, in yields of 10–67%. Their proposed mechanism for this reaction included the suggestion of an iron–benzyne intermediate, Scheme 2.

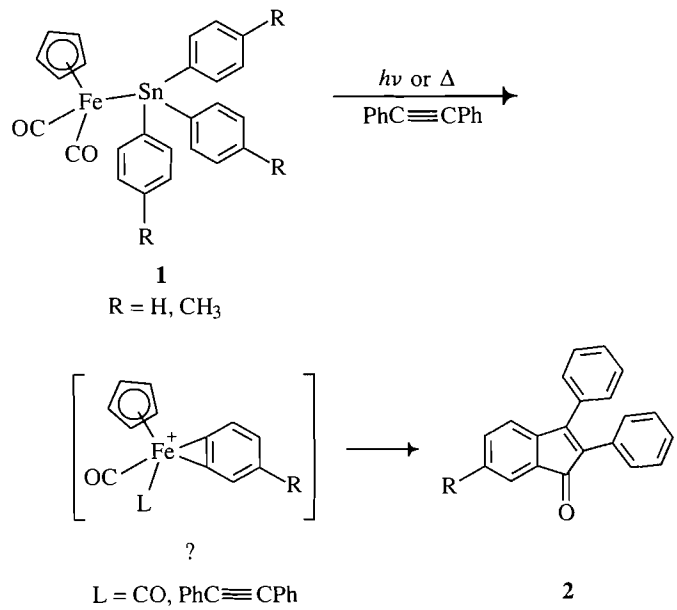

SCHEME 2

This mechanism is unlikely, however, since a mixture of **2***a* and **2***b* would be expected on this basis, whereas only **2***a* was observed.

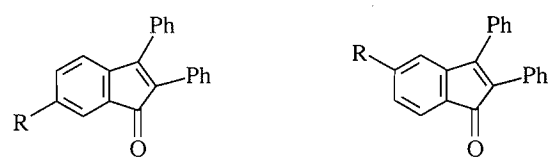

2*a* **2***b*

Later, in 1979, Kolobova and Goncharenko reported a series of photochemical reactions including the reaction of Fp-(2-thienoyl) and Fp-(2-furanoyl) with diphenylacetylene to give thienyl and furanyl indenone isosteres (Scheme 3) (12). The structural identification of **4***a* was made on the basis of a comparison with related isomers prepared from the reaction of diphenylacetylene with the 2-thienoylchloride·aluminum

[1]Author to whom correspondence may be addressed at the Department of Chemistry, University of North Wales, Bangor, Gwynedd, U.K. LL57 2UW.

Can. J. Chem. Downloaded from www.nrcresearchpress.com by 91.121.58.235 on 09/07/12
For personal use only.

Can. J. Chem. Downloaded from www.nrcresearchpress.com by 91.121.58.235 on 09/07/12
For personal use only.

trichloride complex. We have recently completed a study in this area and our results indicate the product assignments to be in error (13).

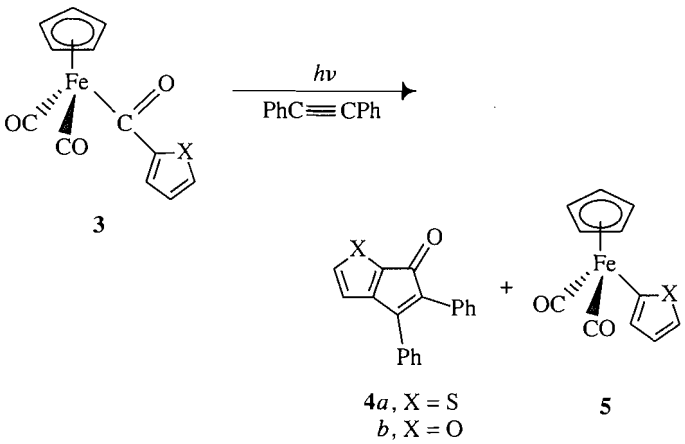

SCHEME 3

In our own work, we have carried out several investigations to clarify the mechanistic details of these reactions as well as to exploit their synthetic utility (14–16). The thermal and photochemical reactions of Fp-(1- and 2-naphthoyls) with diphenylacetylene and 1-phenylprop-2-yne were found to give the products **6** and **7** respectively, in addition to a substantial number of by-products including mono and 1,1′-bis-naphthyl ferrocenes (16) (Scheme 4). These results indicate that the

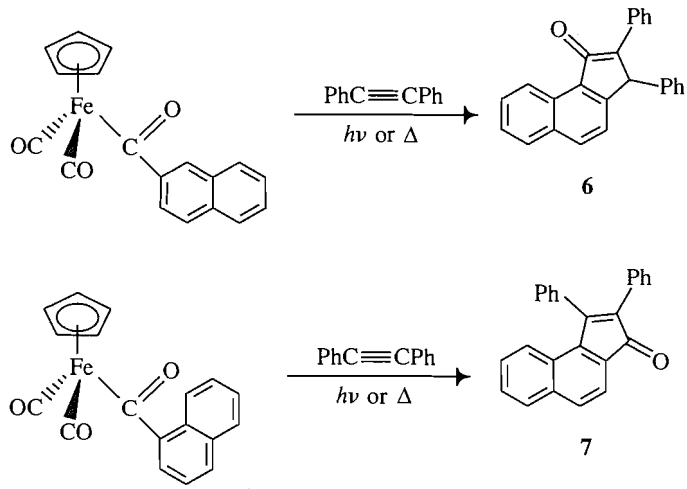

SCHEME 4

insertion of diphenylacetylene precedes that of carbon monoxide. Further work was done to show that indenones could be obtained directly from Fp-(1,2,2-triarylvinyl) derivatives, Scheme 5 (15), which we proposed as reaction intermediates.

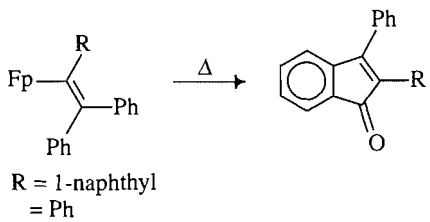

SCHEME 5

To integrate all the available information into a complete plausible mechanism for these processes, we decided to investigate the prototype reaction of all those documented, namely the reaction of Fp-phenyl with diphenylacetylene.

Experimental

All solvents used were predried and were freshly distilled prior to use, with the exception of decalins, which were used as received (Aldrich). Column chromatography was carried out using neutral Alumina (Brockman Grade I) using columns of 5 cm (diam.) × 15 cm (length). Mass spectra were recorded using a VG-Analytical-1000 instrument (operating at 70 eV with a probe temperature of 150°C). The ^{1}H nmr and ^{13}C nmr spectra were obtained using a Varian XL-300 instrument using $CDCl_3$ in each case as solvent, unless otherwise stated (terminology used: d = doublet, t = triplet, ABd = ABdoublet, m = multiplet, bs = broad singlet, s = singlet, ddd = doublet of doublets, dt = doublet of triplets).

*Preparation of (η^5-cyclopentadienyl)dicarbonyl(benzoyl-d$_5$)iron (**15**)*

Benzoyl chloride-d_5 was prepared from commercially available bromobenzene-d_5 via benzoic acid-d_5 using standard synthetic procedures. A solution of sodium dicarbonyl-(η^5-cyclopentadienyl)ferrate in THF (100 mL) prepared from tetracarbonyl-bis(η^5-cyclopentadienyl)di-iron (7.08 g, 20.0 mmol) (17) and a 3% sodium amalgam (1.0 g, 43.5 mmol Na) was added to a solution of benzoylchloride-d_5 (6.55 g, 45.0 mmol) in THF (100 mL) cooled to −70°C. Following solvent removal under vacuum, the product was extracted with dichloromethane and chromatographed, eluting with diethyl ether to give initially Fp_2 (1.2 g) followed by the product Fp-benzoyl-d_5, which, following solvent reduction, was precipitated from solution by addition of hexanes to yield 6.10 g, 53%. IR, ν_{CO}: 2020, 1967, 1618 cm^{-1}; ^{1}H nmr, δ: 4.90 (s); mass spectrum, *m/e* (rel. intensity): 259 (18.6); $M^{+\cdot}$ − CO, 232 (7.1); 231 (47.3); 204 (13.3); 203 (100.0); 201 (12.7); 200 (133); 147 (24.1); 146 (12.5); 138 (5.7); 121 (29.6).

*Reaction of Fp-benzoyl-d$_5$ with diphenylacetylene (**9**)*

A mixture of Fp-benzoyl-d_5 (2.87 g, 10 mmol) and diphenylacetylene (3.56 g, 20 mmol) was refluxed in decalins (25 mL) under a nitrogen atmosphere for 10 min. After cooling, the reaction mixture was chromatographed on a neutral alumina column and the following fractions collected, eluting with progressively more polar mixtures of hexanes and diethyl ether commencing with neat hexane: (i) 1,1′-bis-(phenyl-d_5)ferrocene (0.35 g, 28%); ^{1}H nmr: 4.24 (t, 4), 4.48 (t, 4); mass spectrum, *m/e* (rel. int.): 350 (4.8); 349 (28.8); 348 (100.0), $M^{+\cdot}$; 347 (6.3); 346 (7.8); 267 (4.1); 202 (10.3); 174 (3.9); 146 (22.8); 120 (5.4); 119 (6.2); (ii) phenyl-d_5-ferrocene; ^{1}H nmr: 4.00 (s, 5), 4.24 (t, 2), 4.60 (t, 2); mass spectrum, *m/e* (rel. int.): 268 (10.3); 267 (45.4), ($M^{+\cdot}$); 180 (37.4); (iii) deuterated 2,3-diphenyl-[1*H*]-inden-1-one; mass spectrum, (accurate masses, rel. int.): 289.1397 (5.19); 288.1392 (20.66); 287.1351 (96.46); 286.1294 (100.0); 285.1283 (50.65); 284.1143 (10.15); 284.1324 (2.95); 283.1143 (10.15); 283.0758 (2.83). The ratio of d_4- to d_5-indenone was calculated to be approximately 63:37 by mass spectroscopy (calculated by averaging a number of spectra by comparison with pure undeuterated sample to obtain normal peak distributions), and by ^{1}H nmr was estimated at 61:39 by integration and with respect to an undeuterated sample and mixtures of the two; ^{13}C nmr: 196.34 (CO), 155.20, 145.17, 133.35, 132.69, 132.34, 130.68, 129.91, 128.88, 128.71, 128.52, 128.43, 128.35, 128.21, 128.00, 127.77, 127.67, 122.91, 121.19.

Reaction of Fp-benzoyl-d$_5$ with p-tolyl(phenyl)acetylene

A mixture of *p*-tolyl(phenyl)acetylene (0.55 g, 2.86 mmol) and Fp-benzoyl-d_5 (0.8 g, 2.80 mmol) was heated in decalin (10 mL) to reflux, and maintained at reflux for 5 min. The cooled sample was poured directly onto a neutral alumina column as described in the general experimental section. Following elution with hexanes to remove decalins, the following fractions were isolated: (i) yellow band (120 mg) eluted with hexane/diethyl ether (90:10), identified as a

Can. J. Chem. Downloaded from www.nrcresearchpress.com by 91.121.58.235 on 09/07/12
For personal use only.

mixture of ferrocene (trace), phenyl-d_5-ferrocene; (ii) orange band (170 mg), eluted with hexane/diethyl ether (90:10), identified as 1,1′-bis-(phenyl-d_5)ferrocene by mass and ^{1}H nmr spectroscopy; (iii) bright orange (0.25 g), eluted with hexane/diethyl ether (50:50), identified initially by mass spectroscopy, parent ions at *m/e* 300/301 as the indenone-containing fraction; and (iv) red/brown, Fp_2, eluted with diethyl ether. Comparison of ^{1}H nmr spectra of the indenone-containing fraction with those of authentic sample of non-deuterated indenones prepared from the similar reaction of Fp-*p*-tolyl with diphenylacetylene (4) indicated the mixture to be composed of **22***d* and **23***d* (unable to distinguish by ^{1}H nmr) and **25***d* in the approximate ratio of 64:36 (total 31%). A tlc indicated the presence of a fourth orange product, with parent ion at *m/e* 300 present in only trace quantity.

22*d*, **23***d*, and **25***d* (mixed isomers); mass spectrum, *m/e* (rel. int.): 302 (35.5); 301 (100.0); 300 (88.4); 299 (7.7); 287 (97.9); 286 (38.9); 285 (24.2); 284 (13.0); 283 (9.4); 272 (5.7); 270 (7.2); 269 (8.0); 261 (5.9); 267 (5.6); 258 (12.3); 257 (26.1). A sample free of **25***d* was obtained by fractional crystallization and the ^{1}H nmr spectrum is shown in Fig. 5. The ^{1}H nmr spectrum of **25***d* is similar to that of **25** (undeuterated) obtained from the reaction of Fp-toloyl with diphenylacetylene (11) with the exception of the absence of peaks due to the 3-phenyl group at ~δ 7.4. Chromatography using the chromatoron of mixtures of **22***d*, **23***d*, and **25***d* gave initial separation, by hexane, of **22***d*, **23***d* from **25***d* but, on increasing the polarity slightly to augment band removal, resulted in the mergence of the bands into one diffuse band.

*Reaction of Fp-benzoyl with bis-*p*-tolyacetylene*

The thermal reaction of Fp-benzoyl (1.42 g, 5.0 mmol) with bis-*p*-tolylacetylene (2.06 g, 10 mmol) in refluxing decalins according to the procedure outlined above gives, on isolation of the red/orange fraction following column chromatography, the indenones **26** (7%) and **27** (28%), which were identified by ^{1}H nmr and mass spectroscopy. **26**: ^{1}H nmr: 2.31 (s, 3), 2.34 (s, 3), 7.03 (s, 1), 7.10–7.39 (m's, 10), 7.52 (ddd, 1); mass spectrum, *m/e* (rel. int.): 311 (24.3); 310 (100.0); $M^{+\cdot}$, 309 (18.2); 296 (10.6); 295 (43.4); 294 (5.8); 293 (7.8); 282 (3.0); 281 (4.7); 280 (5.1); 279 (5.8); 267 (9.4); 266 (12.1); 265 (19.1); 252 (17.5). **27**: ^{1}H nmr: 2.30 (s, 3), 2.36 (s, 3), 6.99 (ABd, 1), 7.13 (ABd, 1), 7.14 (ABd, 2), 7.38 (bs, 5); mass spectrum *m/e* (rel. int.): 311 (25.3); 310 (100.0); $M^{+\cdot}$, 309 (18.3); 296 (10.0); 295 (41.0); 294 (5.5); 293 (7.6); 282 (3.2); 281 (4.9); 279 (3.8); 267 (9.5); 266 (12.6); 263 (20.3); 253 (4.8); 252 (18.3). Other products obtained were 1,1′-bis(*p*-tolyl)ferrocene and hexa(4-methylphenyl)benzene (identified by spectral comparison with previously prepared samples).

*Reaction of Fp-*p*-toloyl with phenyl acetylene*

A mixture of Fp-*p*-toloyl (2.0 g, 6.8 mmol) and phenylacetylene (2.5 g, 24.5 mmol) in decalins was gently refluxed for 15 min. Thereafter the reaction mixture was examined by tlc (eluant hexanes/diethyl ether, 70:30) and was shown to contain a large number (>10) of compounds. Subsequent chromatography on a neutral alumina support gave the following fractions, which were initially examined by mass spectroscopy to establish which compounds had not been previously characterized. In addition to the usual bands containing ferrocene and Fp-*p*-tolyl and Fp-*p*-toloyl, several new compounds were observed, which had the following parent ions: (i) 276, identified as *p*-tolylferrocene; (ii) 286 (18%), obtained as a white crystalline substance identified as C-3,C-4,C-6a-trihydro,4-(4′-methylphenyl)-2-phenyl(1-*r*-3a*H*)one, **28**; ^{1}H nmr: 2.35 (s, 3), 3.75 (dd, 1), 3.85 (ddd, 1), 4.37 (dd, 1), 5.78 (dd, 1), 6.03 (dd, 1), 6.85 (d, 1), 7.00 (d, 2), 7.13 (d, 2), 7.30 (m, 3), 7.48 (d, 2); mass spectrum, *m/e* (rel. int.): 287 (22.4); 286.1366 (accurate mass), $M^{+\cdot}$ (100.0); 285 (15.0); 271 (17.3); 258 (13.9); 257 (15.1); 243 (31.2); 242 (16.3); 241 (18.0); 240 (7.3); 229 (13.9); 228 (21.7). The proton nmr of this compound is shown in Fig. 1, together with that of C-3,C-4,C-6a-trihydro,4-(1-naphthyl)-2,3-phenyl(1-*r*-3a*H*)one; (iii) 424 (26%), **29**, isolated as an off-white solid and identified as 2,4,6-triphenyl,4′-methylbenzophenone; ^{1}H nmr: 2.30 (s, 3), 6.98–7.83 (m's, 21); mass spectrum, *m/e* (rel. int.): 425 (31.7); 424.1820 (accurate mass), $M^{+\cdot}$ (100.0); 423 (38.8); 347 (31.5); 334 (10.2); 333 (37.7); 305 (10.6); 304 (17.0); 203 (17.7); 302 (21.7). The red-brown bands containing Fp_2 were shown by mass spectroscopy to contain *p*-tolyl substituted cyclopentadienyls, parent ions *m/e* 444, in addition to the parent Fp_2, parent ion at *m/e* 354.

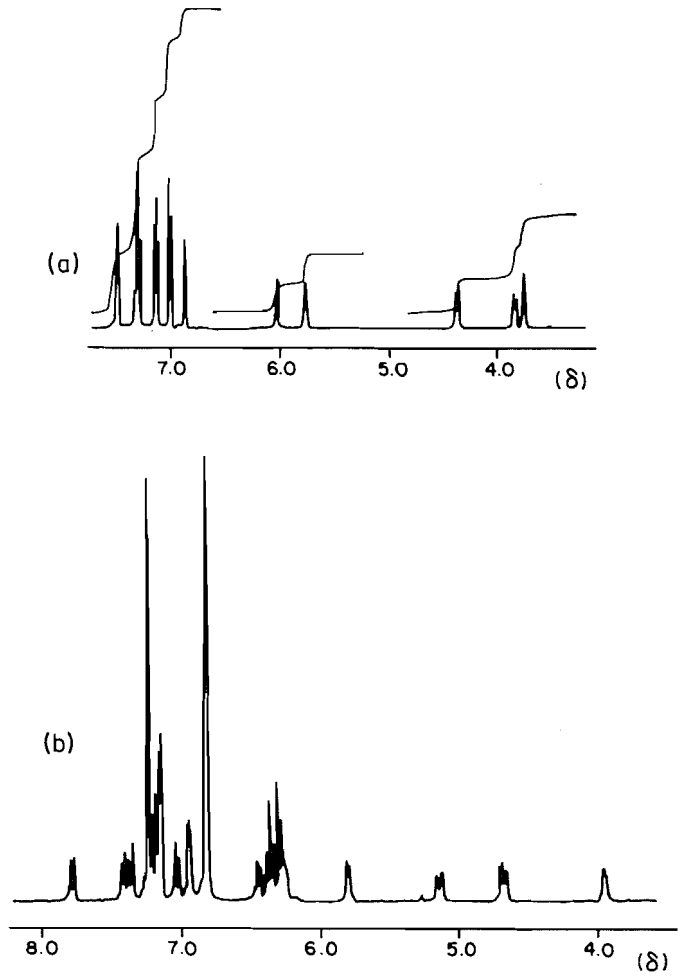

FIG. 1. The ^{1}H nmr spectra (aromatic region) of (a) **28**; (b) C-3,C-4,C-6a-trihydro,4-(1-naphthyl)-2,3-phenyl(1-*r*-3a*H*)one. (δ 4–9).

*Reaction of Fp-*m*-toloyl with bis(*m*-tolyl)acetylene*

A mixture of Fp-*m*-toloyl (296 mg, 1.0 mmol) with bis(*m*-tolyl)-acetylene (206 mg, 1.0 mmol), prepared by the palladium-catalyzed reaction of acetylene with *m*-iodotoluene, was refluxed for 5 min. The cooled reaction mixture was chromatographed on a neutral alumina column to give the following fractions: (i) a pale yellow band shown by mass spectroscopy to be composed mainly of the starting acetylene; (ii) a diffuse orange band shown by mass spectroscopy and ^{1}H nmr to contain a mixture of Fp-*m*-tolyl and *m*-tolylferrocene with parent masses at *m/e* 268 (14%) and 276 (100%), respectively; (iii) a bright orange band, identified as 2,3-(3-methylphenyl),5-methyl-[1*H*]-inden-1-one, **32** (37 mg, 11%); ^{1}H nmr: 2.27 (s, 3), 2.33 (s, 3), 2.60 (s, 3), 6.73 (d, 1), 6.89 (t, 1), 6.93–7.28 (series of m's, 9); mass spectrum, *m/e* (rel. int.): 326 (4.2); 325 (26.8); 324 (100.0), $M^{+\cdot}$; 323 (11.8); 310 (10.7); 309 (45.5); 307 (6.5); 295 (5.1); 266 (11.0); 265 (14.9); 263 (5.9); (iv) a bright orange band identified as 2,3-(3-methylphenyl),7-methyl-[1*H*]-inden-1-one, **33** (91 mg, 28%); ^{1}H nmr: 2.25 (s, 3), 2.33 (s, 3), 2.33 (s, 3), 6.70 (bs, 1), 7.00 (dt, 1), 7.03 (bs, 1), 7.05–7.30 (series of m's, 7), 7.44 (d, 1); mass spectrum, *m/e* (rel. int.): 326 (4.4); 325 (26.1); 324 (100.0), $M^{+\cdot}$; 323 (11.7); 310 (11.9); 309 (44.7); 266 (10.2); 265 (11.6); (v) Fp_2; (vi) a faint brown band subsequently shown by mass spectroscopy, parent ion at *m/e* 618, to contain the trimerized acetylene.

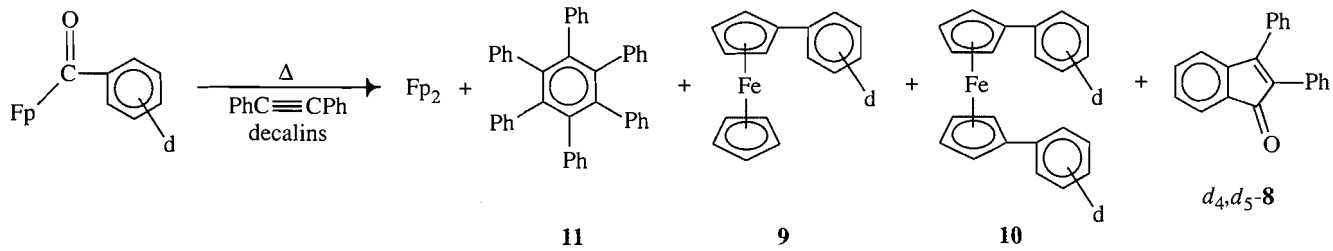

SCHEME 6

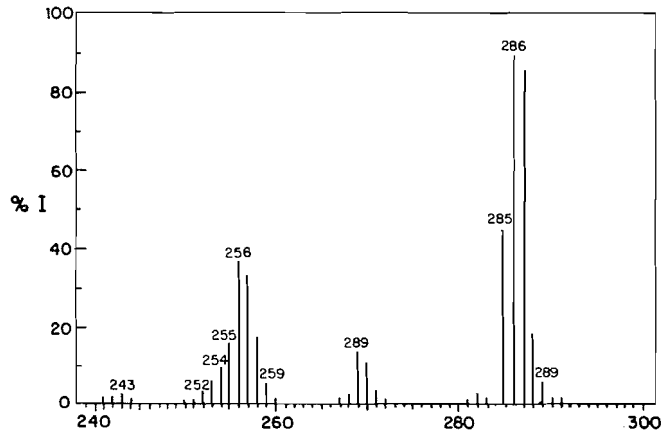

FIG. 2. The mass spectrum illustrating the relative proportions of d_4- and d_5-2,3-diphenylindene-1-one.

Results and discussion

It was decided to investigate the reaction of Fp–Ph with diphenylacetylene, using deuterium labelled Fp–Ph, since this reaction may be considered as the prototype of the more general reaction of Fp–aryls with diaryl acetylenes. One of the standard methods of preparation of Fp–Ph is via the photochemical deinsertion (reverse aryl migration) of carbon monoxide from the Fp–benzoyl derivative (18). Since such reactions also occur thermally (19), the Fp–aroyl derivatives can be used as alternate reactants generating the desired Fp–aryl compound *in situ*. Fp–(benzoyl-d_5) was thus reacted with diphenylacetylene in decalins at reflux for 10 min, under an inert atmosphere. Following column chromatography, 2,3-diphenylinden-1-one(-d_4 and -d_5), **8**, was obtained in 36% yield with smaller quantities of (d_5-phenyl)ferrocene, **9**; bis-1,1′-(d_5-phenyl)ferrocene, **10**; hexaphenylbenzene, **11**; and Fp_2 (Scheme 6).

The mass spectrum obtained of the indenone indicated a mixture (approx. 61:39) of the d_4- and d_5-indenones (Fig. 2). This result was verified using ^{1}H nmr, by comparison of the spectrum with that of an undeuterated sample, although the exact positions of the labels were found to be difficult to establish. ^{13}C spectroscopy at 75 MHz indicated no distinguishable differences in the chemical shift of deuterated and undeuterated samples of **8**; however, there were distinct differences in the relative peak heights of the resonances (Fig. 3). By carrying out ^{13}C/^{1}H heteronuclear correlation experiments,

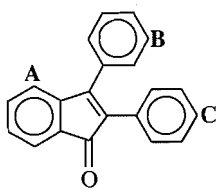

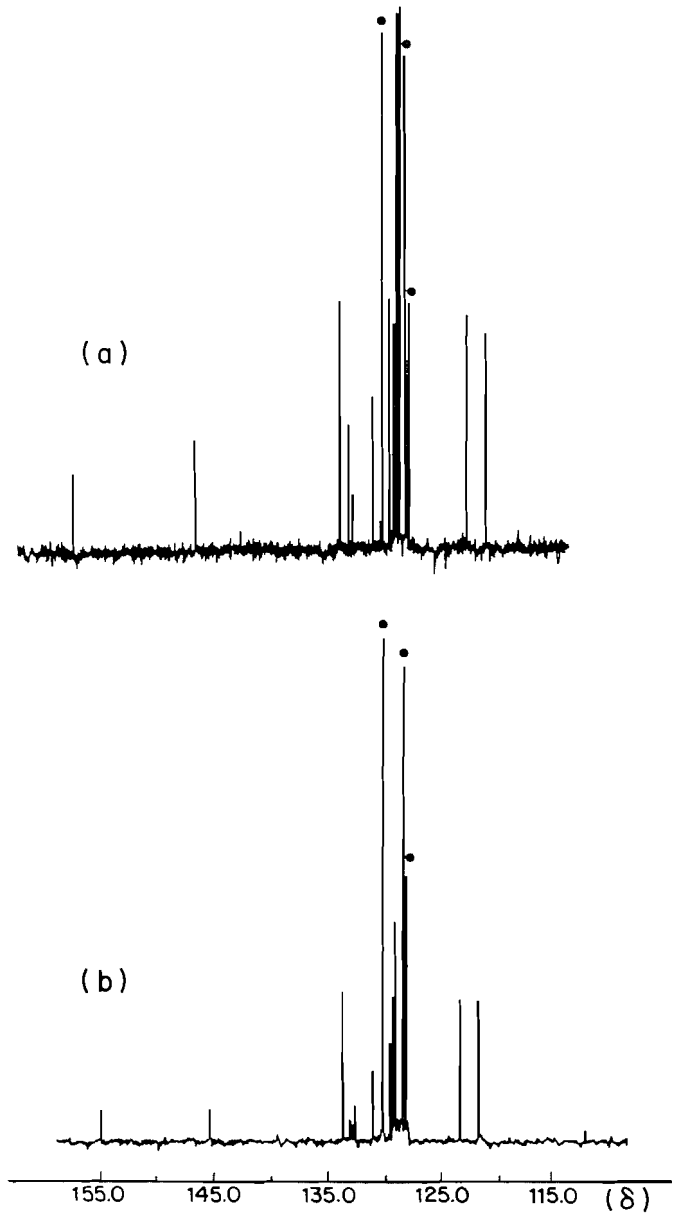

FIG. 3a. The ^{13}C spectrum of (a) non-deuterated and (b) deuterated 2,3-diphenylindene-1-one. The 3-phenyl position carbon resonances are unaffected by deuteration.

we were able to assign the individual resonances in the ^{13}C spectrum. The most important feature of the spectra was that ^{13}C resonances in ring C, when compared to the spectrum of the undeuterated sample, were observed to be much more intense than those in rings A and B. This is indicative of partial deuteration of rings A and B, since deuteration would give rise

Can. J. Chem. Downloaded from www.nrcresearchpress.com by 91.121.58.235 on 09/07/12
For personal use only.

Can. J. Chem. Downloaded from www.nrcresearchpress.com by 91.121.58.235 on 09/07/12
For personal use only.

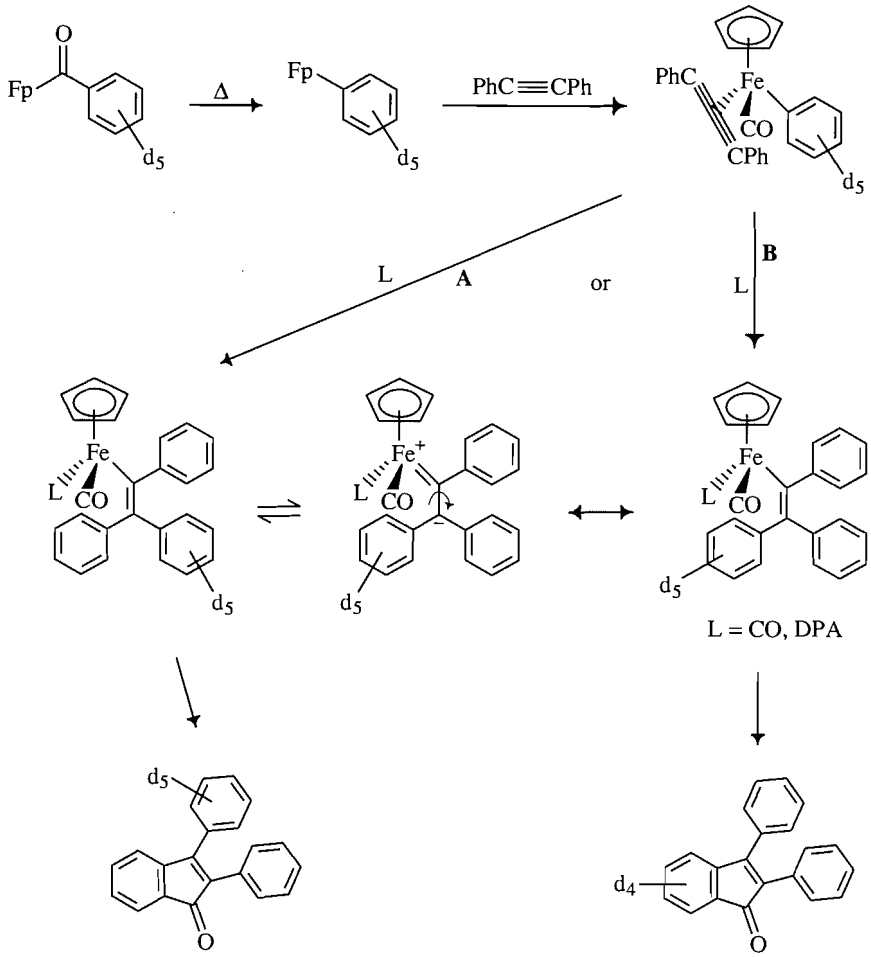

SCHEME 7

to lower peak intensities due to coupling into three lines as well as a loss in nOe. Confirmation of these results was obtained using deuterium nmr, which showed that deuteration had occurred in rings A and B mutually exclusively. These observations are consistent with a reaction mechanism involving insertion of the acetylene into the iron–carbon sigma (σ) bond followed by a *cis–trans* isomerization of the σ-alkene obtained. A simplified mechanism is shown in Scheme 7. It should be noted that there are two alternate modes of insertion of the acetylene. Based on existing experimental reports (20), path B is more likely. The postulated rearrangement step is similar to that observed by Green and co-workers (21) as an intermediate in the synthesis of the molybdenum cyclic alkylidene complex, Scheme 8.

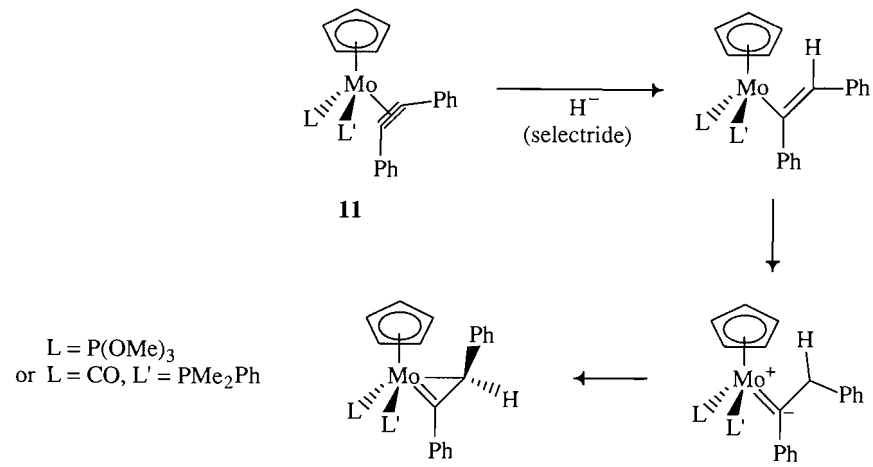

SCHEME 8

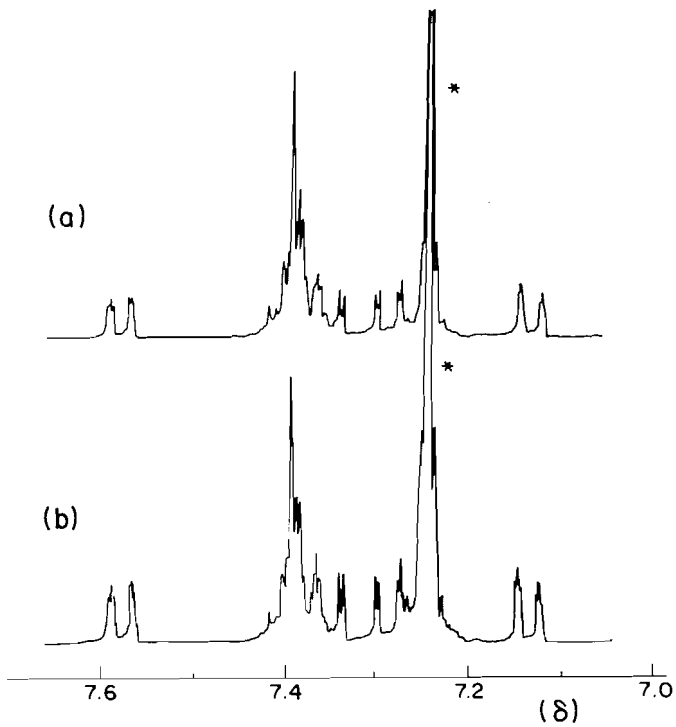

FIG. 3b. The ^1H spectrum of (a) non-deuterated and (b) deuterated 2,3-diphenylindene-1-one.

Similarly, related rearrangements have been reported by a number of workers, the most notable of these being that of Bergman and Huggins (22), Scheme 9, and Reger *et al.* (23–33), Scheme 10.

In the reaction shown in Scheme 9, Bergman observed the initial methyl migration to give the *E* isomer, which underwent a slower equilibration to give a mixture of *E* and *Z* isomers. In a series of papers, Reger and co-workers examined the reactions of cationic iron complexes with a range of nucleophiles. The products of such reactions are identical to the proposed reaction intermediates reported here. For example, the reaction of the cationic acetylene complex (Scheme 10.1) undergoes nucleophilic attack to give the σ alkenyl complex; complexes of this type can equilibrate in the presence of trace oxidants such as ferricinium salts, alumina, or ceric salts, Scheme 10.2. They have also shown that such complexes undergo facile carbonyl insertion to give mixtures of isomers under similar conditions (Scheme 10.3). In addition, they have been able to develop a simple set of rules for assignment of the correct stereochemistry of the iron–alkenyl complexes in which the ligand L is a phosphine or phosphite. In our work, we have shown that alkenyl iron complexes (Scheme 5) decompose cleanly to give indenone products on thermolysis (15).

To further test the mechanism proposed, we decided to carry out further related reactions. A similar reaction of d_5-benzoyl Fp with phenyl(*p*-tolyl)acetylene again gave a complex product mixture from which the indenone mixture containing **22***d*–**25***d*

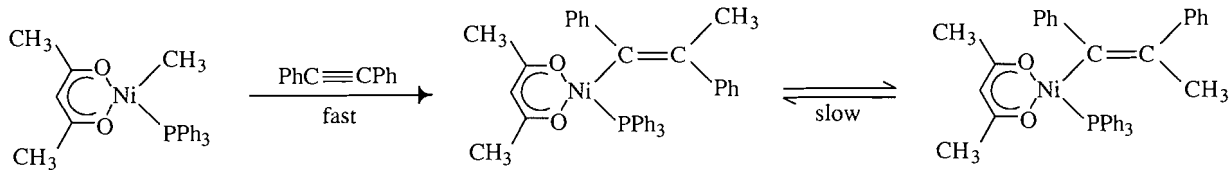

13 **14***a* **14***b*

SCHEME 9

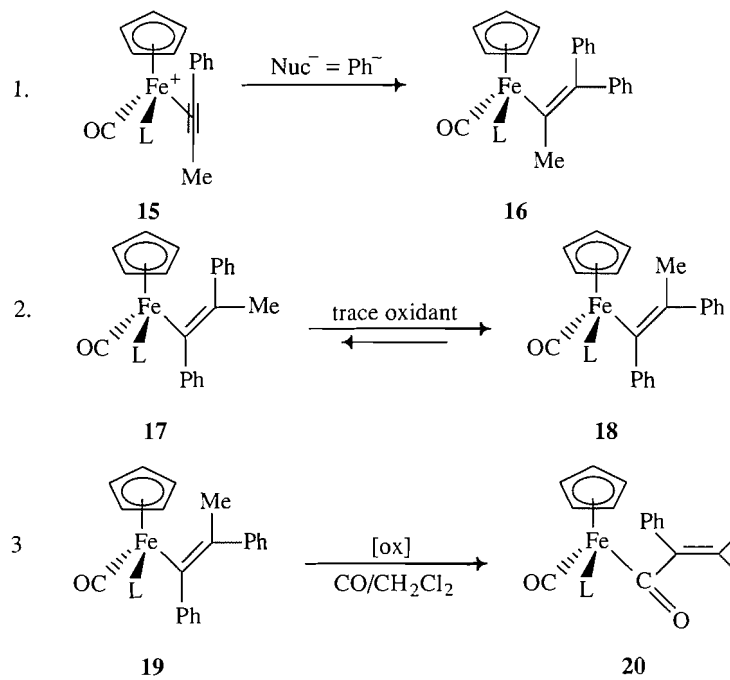

15 **16** **17** **18** **19** **20**

SCHEME 10

Can. J. Chem. Downloaded from www.nrcresearchpress.com by 91.121.58.235 on 09/07/12
For personal use only.

was separated, in 31% combined yield (Scheme 11). These were identified by ^{1}H nmr and mass spectroscopy. On attempted separation, two major indenone fractions were noted. These were identified as **25***d* and a mixture of **22***d* and **23***d* (major products) (not separable by column chromatography). Only a trace of the last indenone, assumed to be **24***d*, was obtained. The individual characterizations were carried out by ^{1}H nmr using comparison of spectra of authentic undeuterated samples (11, 14). The ratio of **22***d* + **23***d* to **25***d* is approximately 64:36, obtained by integration of the methyl singlets in the ^{1}H nmr specturm. Based on the results obtained in the reaction of Fp–benzoyl by Nesmeyanov *et al.* (11) and us, a higher proportion of **25***d* may have been expected. The result demonstrates that insertion of the acetylene into the Fe–C bond gives predominantly the intermediates **22I** and **23I** as opposed to **24I** and **25I** (Scheme 11).

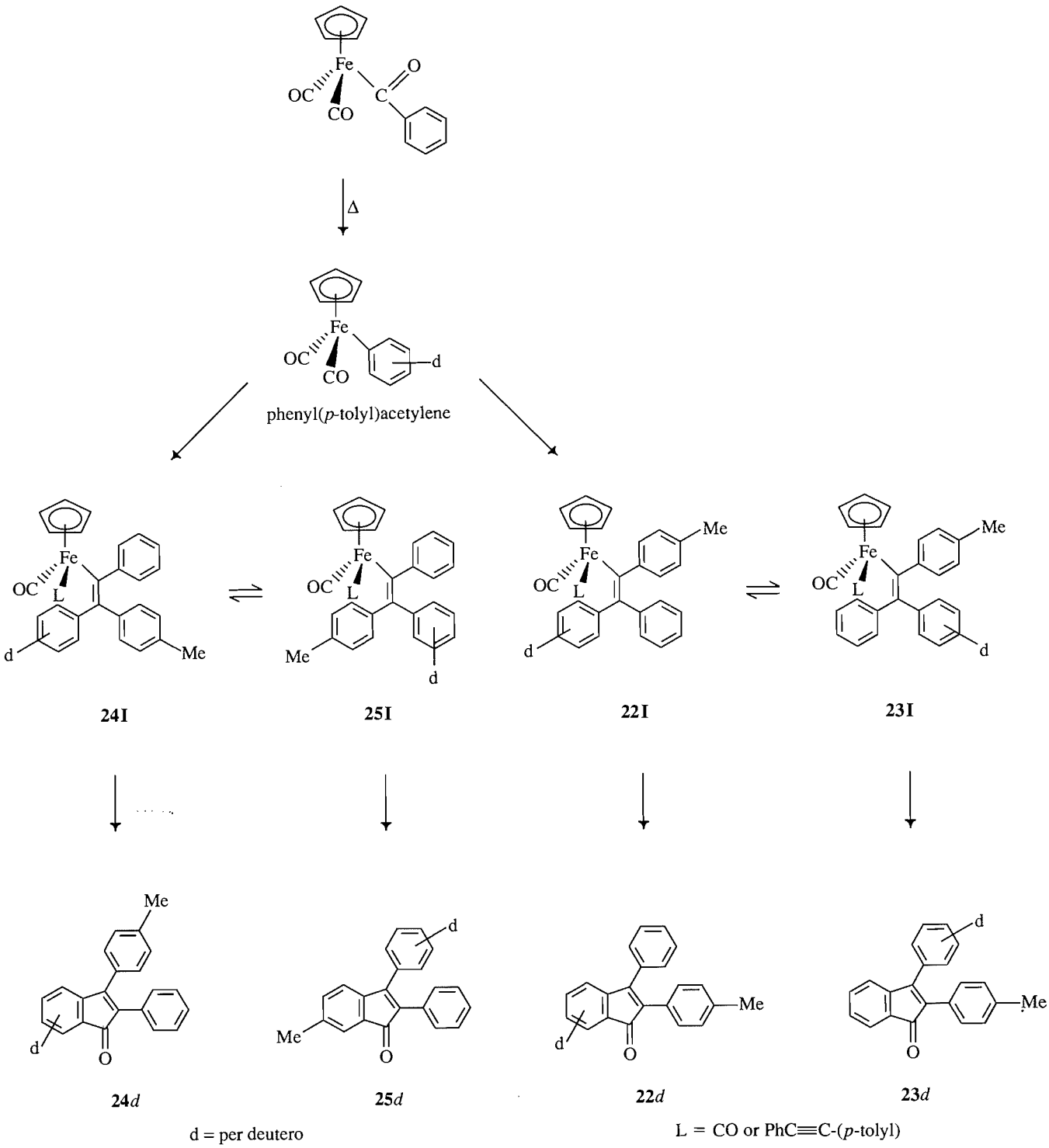

SCHEME 11

Can. J. Chem. Downloaded from www.nrcresearchpress.com by 91.121.58.235 on 09/07/12
For personal use only.

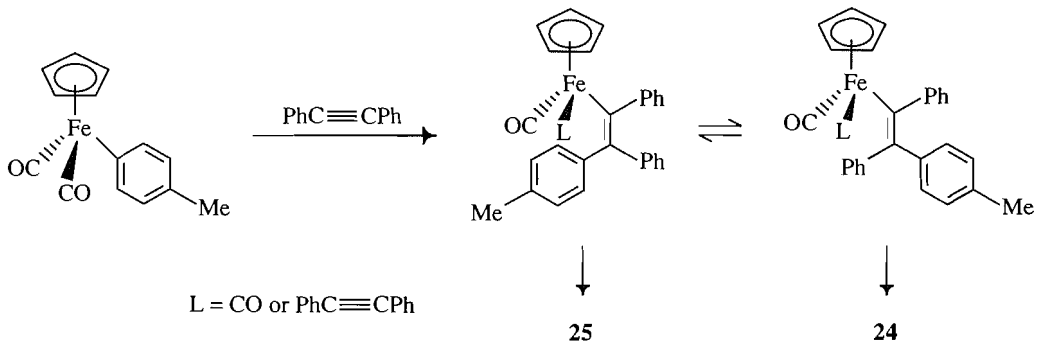

SCHEME 12

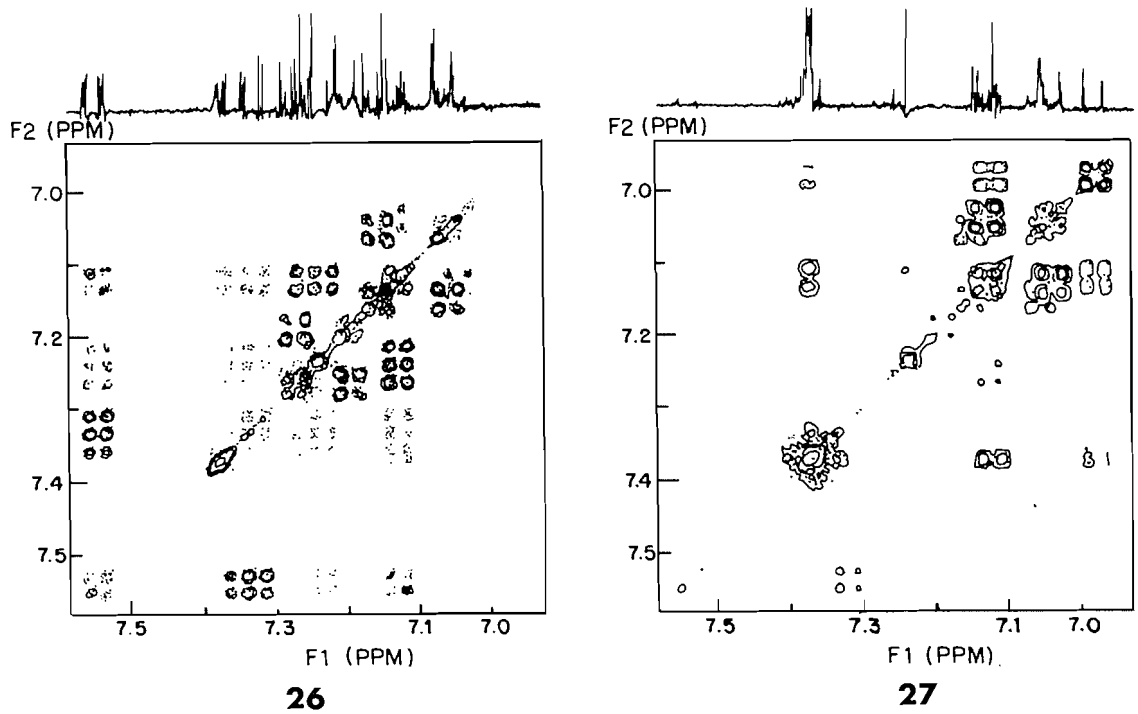

FIG. 4. The ^{1}H COSY spectra of **26** and **27** (aromatic region).

Based on our proposed mechanism, the reaction of Fp-*p*-tolyl with diphenylacetylene would give the intermediates **24I** and **25I** (undeuterated). Nesmeyanov (11) isolated only **25** and no **24**. The finding here that **24***d* is only a minor product indicates that the **25I** is either favoured in the equilibrium and (or) it is kinetically more reactive towards the metallation reaction (Scheme 12).

The reaction of benzoyl–Fp with bis-*p*-tolylacetylene again gave a mixture of two indenones (combined yield 29%), which were separated by preparative plate tlc. These were identified as **26** and **27** using 2D ^{1}H nmr spectroscopy (Fig. 4).

In all the foregoing reactions, mono- and bis-substituted ferrocenes, Fp_2, and trimerized arylacetylenes were isolated as by-products. To test the scope of the reaction with other acetylene derivatives the reaction of Fp-*p*-tolyl with phenylacetylene was carried out. In this reaction a range of products was also observed; however, the indenone products are not the dominant ones. The major products isolated were two colourless compounds **28** and **29**. The former is similar to one in

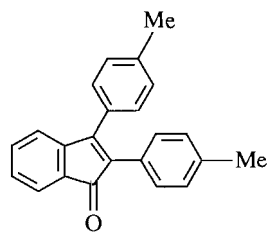

26

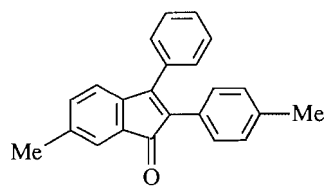

27

the reaction of Fp–Me with trifluoromethylacetylene, reported by Green and co-workers (34) obtained via the photolytic decomposition of the metal complex **30**, and also to the decarbonylated product obtained by us in the reaction of Fp–*o*-F-phenyl with 2-ethynylpyridine (14), **31**, while the latter is an analogue of the compounds we have previously observed to be found in the case of the Fp–naphthoyl reactions with diphenylacetylene (16). We have conducted preliminary experiments on a substantial variety of Fp–aryl groups such as

Can. J. Chem. Downloaded from www.nrcresearchpress.com by 91.121.58.235 on 09/07/12
For personal use only.

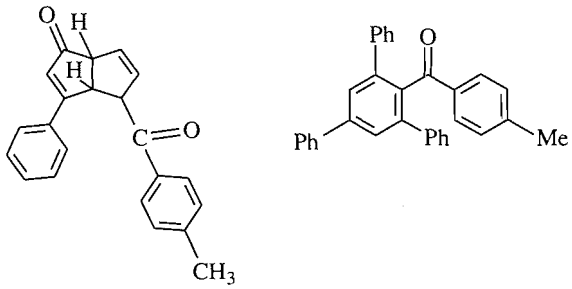

28

29

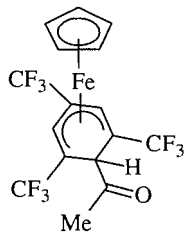

30

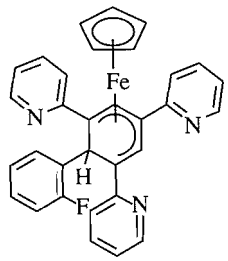

31

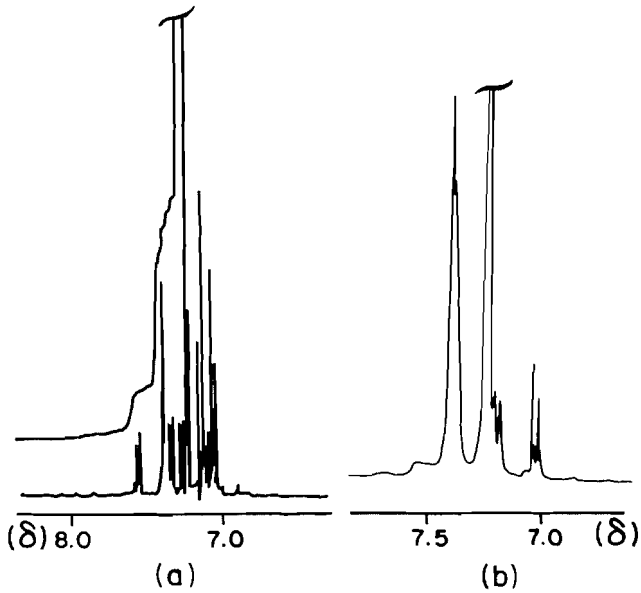

FIG. 5. The ^{1}H nmr spectra of **22***d*, **23***d*, and **25**.

anisoyl, *o*-toloyl, 2-nicotinoyl, 2-quinoloyl, *o*-biphenyl, and in addition have carried out reactions of Fp–benzoyl with phenyl-(aryl)acetylenes (aryl = anisyl, *o*-tolyl, nicotinyl, 2-quinolyl, *o*-biphenyl, triphenylsilyl), and observe that in each case the predicted cyclopentenones are formed, although the yields in some cases are very low.

In general it is now possible to predict the expected cyclopentenones that will be formed in the reaction of Fp–aryls with acetylenes, Scheme 13; however, the ratio of isomers obtained will be determined by the nature of the aryl group. We have tested this hypothesis by carrying out the reaction of Fp–*m*-tolyl with bis-*m*-tolylacetylene, in which we predicted

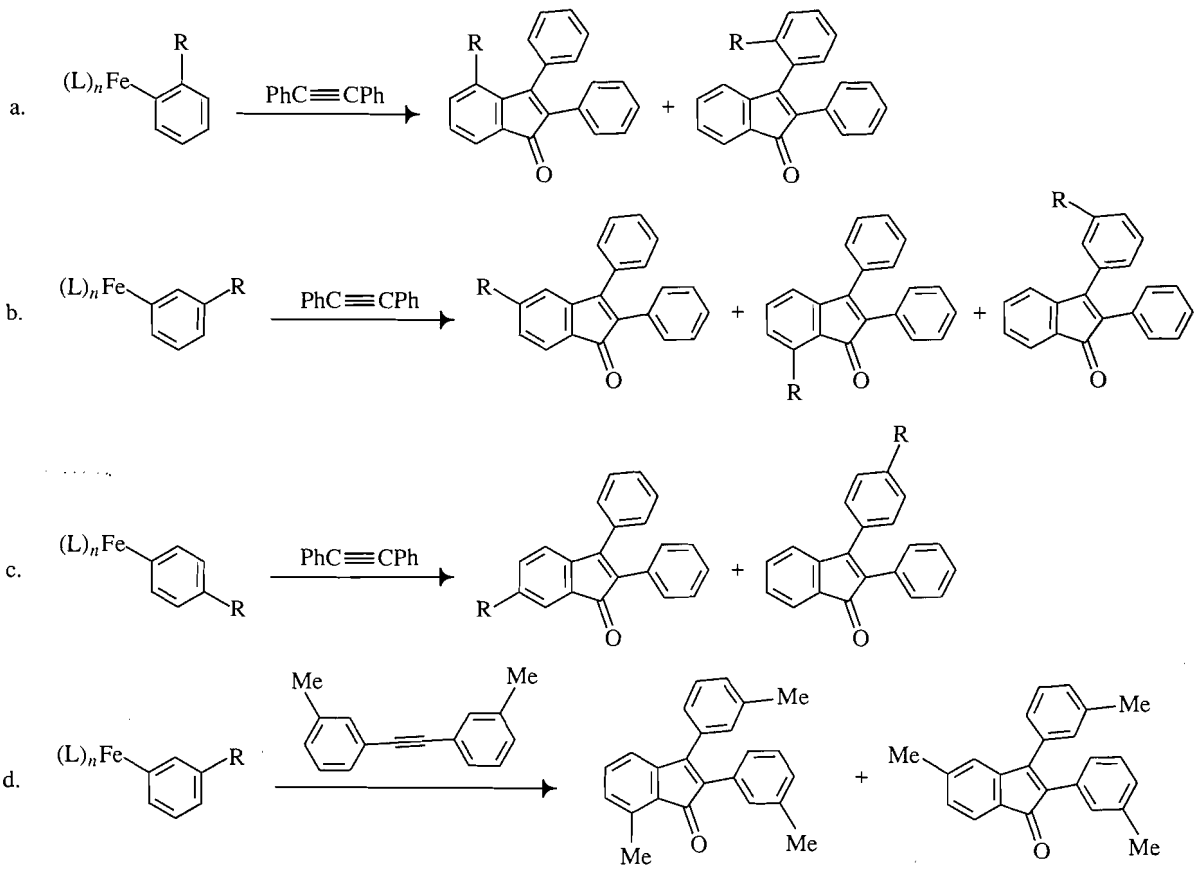

32 **33**

SCHEME 13

Can. J. Chem. Downloaded from www.nrcresearchpress.com by 91.121.58.235 on 09/07/12
For personal use only.

that two isomeric indenones (Scheme 13d) would be formed (the *meta*-substituted acetylene was used to limit the number of possible isomers). Indeed two such indenones are formed: **32** and **33**, in the approximate ratio of 1:2.5. This experiment also gives an indication of the preference for metallation at a position *para* to the methyl group versus metallation at the position *ortho* to the methyl.

Acknowledgements

The authors would like to acknowledge useful discussions with Dr. R. Bergman, and funding in the form of an operating grant from the Natural Sciences and Engineering Research Council of Canada. We express our sincere gratitude to Dr. Clem Kazakoff of the University of Ottawa, who recorded the several hundred mass spectra used during this and related investigations.

1. W. Reppe. Ger. Patent 873,910 (1951).
2. W. Reppe and H. Vetter. Liebigs Ann. Chem. **582**, 133 (1953).
3. W. Hubel and E. H. Braye. J. Inorg. Nucl. Chem. **10**, 250 (1959).
4. J. R. Leto and F. A. Cotton. J. Am. Chem. Soc. **81**, 2970 (1959).
5. F. L. Bowden and A. B. P. Lever. Organomet. Chem. Rev. **3**, 227 (1968).
6. W. Hubel. *In* Organic synthesis via metal complexes. Vol. 1. *Edited by* I. Wender and P. Pino. Interscience, New York. 1969. p. 273.
7. G. N. Shrauzer. Chem. Ind. (London), 1404 (1958).
8. H. W. Steinberg, R. Markby, and I. Wender. J. Am. Chem. Soc. **81**, 2339 (1959).
9. J. Falbe. *In* Carbon monoxide in organic synthesis. Springer-Verlag, New York. 1967. p. 94.
10. H. W. Sternberg, R. Markby, and I. Wender. J. Am. Chem. Soc. **80**, 1009 (1958).
11. A. N. Nesmeyanov, N. E. Kolobova, V. V. Shripkin, and K. N. Anisimov. Dokl. Akad. Nauk S.S.S.R. 196 (1971).
12. N. E. Kolobova and L. V. Goncharenko. Khim. Geterosikl. Soedin. 1461 (1979).
13. I. R. Butler. Can. J. Chem. In press.
14. I. R. Butler, W. R. Cullen, W. E. Lindsell, P. N. Preston, and S. J. Rettig. J. Chem. Soc. Chem. Commun. 439 (1987).
15. I. R. Butler, J. L. Elliot, and J. Houde, Jr. Can. J. Chem. **67**, 1308 (1989).
16. I. R. Butler, J.-P. Charland, J. L. Elliot, J. Houde, Jr., W. E. Lindsell, K. J. McCullough, P. N. Preston, and A. B. Rettie. J. Chem. Soc. Perkin Trans. 2. In press.
17. R. B. King. *In* Transition metal synthesis. Vol. 1. Wiley, New York. 1968, and references therein.
18. R. B. King and M. B. Bisnette. J. Organomet. Chem. **2**, 15 (1964).
19. A. N. Nesmeyanov, N. E. Kolobova, L. V. Goncharenko, and K. N. Anisimov. Izv. Akad. Nauk S.S.S.R. Ser. Khim. 153 (1976).
20. S. Otsuka and A. Nakamaura. Adv. Organomet. Chem. **14**, 245 (1976), and references therein.
21. M. Bottril, M. Green, E. O. O'Brien, L. E. Smart, and P. Woodward. J. Chem. Soc. Dalton Trans. 292 (1980).
22. J. M. Huggins and R. G. Bergman. J. Am. Chem. Soc. **103**, 302 (1981).
23. D. L. Reger, S. A. Klaeron, J. E. Babin, and R. D. Adams. Organometallics, **7**, 181 (1988).
24. D. L. Reger and C. J. Coleman. J. Am. Chem. Soc. **98**, 3155 (1979).
25. D. L. Reger and P. J. McElligott. J. Am. Chem. Soc. **102**, 5424 (1980).
26. D. L. Reger and K. A. Belmore. Organometallics, **4**, 305 (1985).
27. D. L. Reger, S. A. Klaeron, and L. Lebioda. Organometallics, **7**, 189 (1988).
28. D. L. Reger, S. A. Klaeron, and L. Lebioda. Organometallics, **5**, 1072 (1986).
29. D. L. Reger, K. A. Belmore, E. Mintz, and P. J. McElligott. Organometallics, **3**, 134 (1984).
30. D. L. Reger, K. A. Belmore, E. Mintz, W. G. Charles, E. A. H. Griffith, and E. L. Amma. Organometallics, **2**, 101 (1983).
31. D. L. Reger and E. Mintz. Organometallics, **3**, 1759 (1984).
32. D. L. Reger and K. A. Belmore. J. Am. Chem. Soc. **105**, 5710 (1983).
33. D. L. Reger, C. J. Clemm, and P. J. McElligott. J. Organomet. Chem. **171**, 73 (1979).
34. M. Bottrill, M. Green, E. O. O'Brien, L. E. Smart, and P. Woodward. J. Chem. Soc. Dalton Trans. 292 (1980).

Can. J. Chem. Downloaded from www.nrcresearchpress.com by 91.121.58.235 on 09/07/12
For personal use only.

Determination of the structure and absolute configuration of the glycerolphosphate-containing capsular polysaccharide of *Pasteurella haemolytica* serotype T3 by high-resolution nuclear magnetic resonance spectroscopy[1]

JAMES C. RICHARDS[2] AND ROBERT A. LEITCH

Division of Biological Sciences, National Research Council of Canada, Ottawa, Ont., Canada K1A 0R6

Received February 7, 1990

JAMES C. RICHARDS and ROBERT A. LEITCH. Can. J. Chem. **68**, 1574 (1990).

The specific capsular polysaccharide antigen produced by *Pasteurella haemolytica* serotype T3 was found to be a high molecular weight teichoic acid composed of equal molar amounts of D-galactose, glycerol, and phosphate and a nonstoichiometric amount of *O*-acetate. Structural analysis of the polymer employed a combination of one- and two-dimensional ^{1}H and ^{13}C nuclear magnetic resonance methods at high field. Homo- and heteronuclear chemical shift correlation techniques, together with *J*-resolved and nuclear Overhauser effect (nOe) difference experiments led to the unambiguous assignments of the ^{1}H and ^{13}C resonances corresponding to the D-galactose and glycerol structural units and established that the repeating unit of the polysaccharide antigen was composed of →4)-α-D-Gal*p*-(1→1)-L-glycerol-(3→ units joined by phosphate diester groups. The chirality of the glycerol moiety was established by conformational analysis of a 1-*O*-α-D-galactopyranosyl-*S*-glycerol fragment (**2**) obtained from the teichoic acid by depolymerization with HF, from which the stereochemistry of the glycerol methine carbon centre was related to that of the D-glycose from $^{1}H-^{1}H$ nOe and ^{3}J values. The chirality was confirmed by gas–liquid chromatographic and mass spectral analysis of the (−)-camphanate ester of 2,3-di-*O*-methylglycerol derived from permethylated **2**. The D-galactosyl residues are partially mono-*O*-acetylated at C-2 and C-3.

Key words: *Pasteurella haemolytica*, capsular polysaccharide, NMR analysis.

JAMES C. RICHARDS et ROBERT A. LEITCH. Can. J. Chem. **68**, 1574 (1990).

On a trouvé que le polysaccharide capsulaire de l'antigène spécifique produit par la *Pasteurella haemolytica* du sérotype T3 est un acide teichoïque de poids moléculaire élevé et composé de quantités équimolaires de D-galactose, de glycérol et de phosphate et d'une quantité non stoechiométrique de *O*-acétate. L'analyse structurale du polymère est basée sur une combinaison de méthodes mono- et bi-dimensionnelles de la résonance magnétique nucléaire du ^{1}H et du ^{13}C à haut champ. Les techniques de corrélation de déplacements chimiques homo- et hétéro-nucléaires combinées à des expériences de différences d'effet Overhauser nucléaire (eOn) ou résolues pour le *J* ont permis d'attribuer sans ambiguités les bandes des spectres du ^{1}H et du ^{13}C des unités structurales de D-galactose et de glycérol et ont permis d'établir que pour le polysaccharide de l'antigène l'unité de base est →4)-α-D-Gal*p*-(1→1)-L-glycerol-(3→ qui est jointe par des groupements diesters phosphates. On a établi la chiralité de l'unité glycérol en se basant sur une analyse conformationnelle d'un fragment 1-*O*-α-D-galactopyranosyl-*S*-glycérol (**2**), obtenu à partir de l'acide teichoïque par dépolymérisation à l'aide de HF, dont la stéréochimie du carbone méthinique du glycérol a été reliée à celle du D-glycose sur la base des valeurs de l'eOn et des ^{3}J. La chiralité a été confirmée par une analyse par chromatographie en phase gaseuse et spectres de masse de l'ester (−)-camphanate du 2,3-di-*O*-méthylglycérol obtenu à partir du produit **2** perméthylé. Les résidus D-galactosyles sont partiellement mono-*O*-acétylés aux positions C-2 et C-3.

Mots clés : *Pasteurella haemolytica*, polysaccharide capsulaire, analyse RMN.

[Traduit par la revue]

Introduction

Pasteurella haemolytica is a Gram-negative, encapsulated bacterium that is associated with several diseases of domestic animals. The organism has been differentiated into two distinct biotypes, designated A and T, and 16 serotypes are presently recognized (1). Serotypes belonging to biotype A are associated with pneumonia in cattle in sheep of all ages, while serotypes belonging to biotype T cause acute systemic disease in young adult sheep (2). Serotype specificity is thought to be related to the polysaccharide capsular antigens (3) and considerable chemical and immunological information has been recently acquired on these antigens (4). In addition, *P. haemolytica* cell wall lipopolysaccharide (LPS) is antigenic (5) and the LPS of several serotypes has been reported to be chemically (6, 7) and immunologically related (8).

The structures of the specific capsular polysaccharide antigens from several *P. haemolytica* serotypes have been recently reported by Adlam *et al.* (3, 9–12). These antigens were found to be high molecular weight polymers composed of repeating oligosaccharide units containing glycosyl residues only (serotypes A1 and A2) (3, 12), or either phosphate or glycerolphosphate diester linkages (serotypes A7, T4, and T15) (9–11) to form teichoic acid-like structures (13). *Pasteurella haemolytica* serotypes T4 and T15 produce chemically similar but antigenically unique capsular polysaccharides composed of repeating, partially *O*-acetylated, →6)-α-D-Gal*p*-(1→2)-glycerol-(1→ (ref. 9) or →4)-α-D-Gal*p*-(1→2)-glycerol-(1→ (ref. 10) units joined by phosphate diester groups, respectively. This paper records the application of nmr techniques to the structural analysis of the *P. haemolytica* serotype T3 specific capsular polysaccharide antigen, which also has a teichoic acid-like structure.

Results and discussion

Isolation and characterization

Pasteurella haemolytica serotype T3 specific capsular polysaccharide was obtained from the bacterial cell growth by extraction into aqueous sodium chloride solution followed by purification as its insoluble cetyltrimethylammonium salt (14). Extraction of saline washed cells by the modified aqueous phenol method (15) afforded an additional amount of capsular polysaccharide following removal of LPS (16) by ultracentrifugation. Ion-exchange chromatography of the latter material on

[1]Issued as NRCC No. 31716.

[2]Author to whom correspondence may be addressed.

Can. J. Chem. Downloaded from www.nrcresearchpress.com by 91.121.58.235 on 09/07/12
For personal use only.

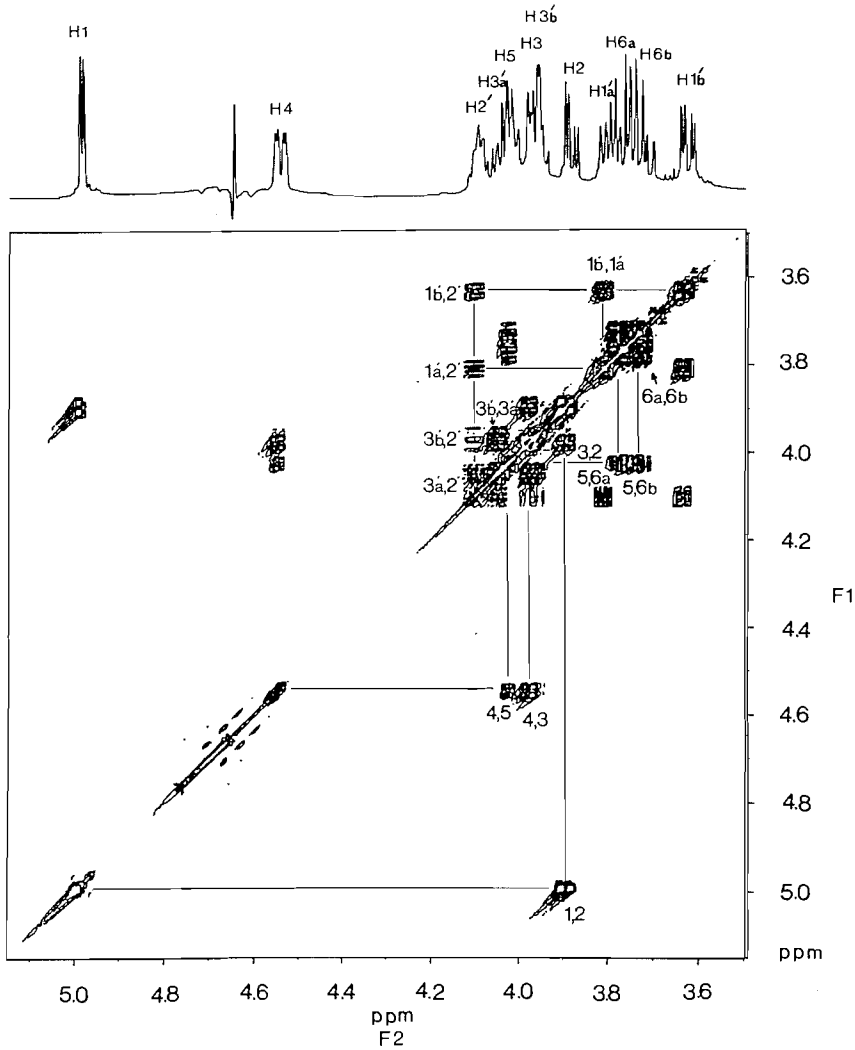

FIG. 1. Contour plot of the 2D COSY spectrum of the *O*-deacetylated *P. haemolytica* serotype T3 capsular polysaccharide at 310 K. Assignments of the cross-peaks are shown and the connectivity pathways corresponding to the D-galactopyranosyl (H-1–H-6b) and the glycerol (H-1a′–H-3b′) subspectra are indicated by the solid lines below and above the diagonal, respectively.

DEAE–Sephacel gave a single peak, which eluted at the beginning of the sodium chloride gradient and which was homogeneous with respect to neutral glycose and phosphate.

The purified polysaccharide had a high molecular weight as evidenced by its elution point (K_{av} 0.1) on a Sephacryl S300 gel filtration system and gave a positive precipitin reaction in immunodiffusion against mouse antiserum to *P. haemolytica* serotype T3 cells. The polymer was freely soluble in water and gave $[\alpha]_D$ 53.0° (*c* 0.46, water). Complete acid hydrolysis of the capsular polysaccharide afforded D-galactose as the only detectable glycose, glycerol, and phosphate. The absolute configuration of the galactosyl residues was established by glc analysis of the corresponding trimethylsilylated *R*-2-butyl glycoside derivatives (17). Quantitative analysis of the acid hydrolysis products by glc–ms of the peracetylated alditol derivatives indicated D-galactose and glycerol to be present in equal molar amounts. The phosphate content of the polymer was determined colorimetrically (18) to be 22% (as PO_4).

The ^{1}H nmr spectrum of the capsular polysaccharide was complex owing to partial substitution (0.68 mole equivalents) by ester-linked acetyl groups. Removal of the *O*-acetyl substituents with dilute aqueous ammonia led to considerable simplification of the ^{1}H nmr spectrum, revealing that the polysaccharide was composed of regular repeating monomeric units: whereas the original polysaccharide showed complex spectral patterns in the low-field region (4.8–5.2 ppm) of the spectrum, the *O*-deacetylated polysaccharide showed only a single anomeric ^{1}H resonance (4.99 ppm).

Examination of the ^{31}P nmr spectrum of the *O*-deacetylated polysaccharide (Na^+ salt, pD ≈ 7.8) revealed a single ^{31}P resonance at 0.86 ppm, which could be attributed to phosphodiester groups (19).

The combined analytical results indicated that the polysaccharide has a regular structure composed of D-galactose, glycerol, phosphate, and ester-linked acetate in the molar ratio of 1.0:1.0:1.0:0.7.

Nuclear magnetic resonance analysis of the O*-deacetylated polysaccharide*

The structure of the chemical repeating unit of the capsular polysaccharide was determined by high resolution one- and two-dimensional ^{1}H and ^{13}C nmr techniques (6). Structural analysis by nmr methods requires unequivocal assignment of the ^{1}H and ^{13}C resonances. The overall strategy was to assign

Can. J. Chem. Downloaded from www.nrcresearchpress.com by 91.121.58.235 on 09/07/12
For personal use only.

Can. J. Chem. Downloaded from www.nrcresearchpress.com by 91.121.58.235 on 09/07/12
For personal use only.

TABLE 1. Proton chemical shifts and coupling contants for the *O*-deacetylated *P. haemolytica* serotype T3 capsular polysaccharide and for the phosphate-free depolymerized product (**2**)

Saccharide	α-D-Galactopyranosyl unit							Glycerol unit				
	H-1 ($J_{1,2}$)	H-2 ($J_{2,3}$)	H-3 ($J_{3,4}$)	H-4 ($J_{4,5}$)	H-5	H-6a ($J_{5,6a}$)	H-6b ($J_{5,6b}$, $J_{6a,6b}$)	H-1a′ ($J_{1a',2'}$)	H-1b′ ($J_{1b',2'}$, $J_{1a',1b'}$)	H-2′	H-3a′ ($J_{2',3a'}$)	H-3b′ ($J_{2',3b'}$, ($J_{3a',3b'}$)
O-deactylated polysaccharide (**1**)[a]	4.989 (3.8)	3.890 (10.4)	3.972 (3.1)	4.542 (0.8) (9.0)[b]	4.022	3.771 (4.9)	3.728 (7.7,11.9)	3.806 (5.6)	3.629 (3.9, 10.7)	4.100	4.046 (4.4) (7.1)[b]	3.967 (6.6, 10.6) (6.8)[b]
α-D-Gal*p*-(1→1)-glycerol (**2**)[c]	4.951 (3.9)	3.818 (10.4)	3.885 (3.4)	3.981 (~1)	3.932	3.74 (6.4)	3.74 (6.4, —[d])	3.762 (5.9)	3.571 (3.9, 10.6)	~3.96	3.684 (4.4)	3.628 (6.8, 11.7)

[a]Data refined by spectral simulation.
[b]$^3J_{H,P}$ value, Hz.
[c]Observed first-order coupling constants.
[d]Unresolved.

fully the ^{1}H nmr spectrum of the *O*-deacetylated polysaccharide using two-dimensional homonuclear chemical shift correlation (COSY) and *J*-resolved experiments, followed by subsequent assignment of the carbon-13 resonances from a 2D heteronuclear ^{1}H–^{13}C chemical shift correlation map. It was to be expected that the nmr parameters would lead to the identification of the monomeric components, including the relative stereochemisty, ring form, and anomeric configuration of the glycose residues and the position of phosphate groups. The arrangement of monomeric components within the repeating unit would then be determined from ^{1}H–^{1}H nOe measurements. Finally, the positions of the ester-linked acetyl groups could be deduced from a comparison of the ^{1}H nmr spectra of the original and *O*-deacetylated polysaccharides.

Examination of the connectivities defined by the cross-peaks observed in the COSY contour plot (Fig. 1) led to the identification of the two independent networks of scalar coupled protons representing subspectra corresponding to the galactosyl ring system and the glycerol moiety. The characteristic chemical shift value (4.989 ppm) and the single vicinal ^{1}H–^{1}H coupling ($J_{1,2}$ = 3.8 Hz) of the anomeric proton resonance of the galactosyl residue provided a convenient starting point for delineation of the connectivity pathway of the corresponding subspectrum (H-1 to H-6b). The seven ^{1}H resonances associated with the residue were well resolved and were readily assigned from the appropriate cross-peaks (Table 1). The methylene proton double doublet (^3J = 3.9 Hz, ^2J = 10.7 Hz) observed in the high-field region of the spectrum (3.629 ppm) provided easy access into the spin system associated with the glycerol moiety (Fig. 1). The connectivity relationships between the two methylene proton resonances at 3.629 ppm (H-1b′) and 3.806 ppm (H-1a′) and between each of these resonances and the methine resonance at 4.100 ppm (H-2′) were readily established from the appropriate cross-peaks in the COSY contour plot. Cross-peaks relating all five ^{1}H resonances belonging to this subspectrum were apparent along the line parallel to the F1 axis at the chemical shift value of the central methine proton (4.100 ppm), leading to the assignment of the resonances corresponding to H-3a′ (4.046 ppm) and H-3b′ (3.967 ppm).

Many of the ^{1}H–^{1}H coupling constants could be measured directly from the 1D ^{1}H nmr spectrum using resolution enhancement techniques (20) or from the appropriate cross-peaks in the COSY spectrum. On the basis of the magnitude of the ring proton coupling constants (Table 1), it was evident that the D-galactosyl residues are present as α-pyranosyl units having the $^4C_1$ ring conformation (21). The H-4 resonance (4.542 ppm) of the galactosyl residues showed, in addition to homonuclear coupling to H-3 ($J_{3,4}$ = 3.1 Hz) and H-5 ($J_{4,5} \approx$ 1 Hz), heteronuclear coupling to phosphorus-31 ($^3J_{H,P}$ = 9 Hz), which indicated C-4 to be the site of phosphate substitution. This was evident from the *J*-resolved spectrum of the *O*-deacetylated polysaccharide (Fig. 2), which permitted a distinction to be made between homo- and heteronuclear coupling (22, 23).

Considerable resonance overlap combined with heteronuclear ^{1}H–^{31}P coupling precluded the direct measurement of the coupling constants associated with the glycerol H-3a′ and H-3b′ resonances. These coupling constants were determined from the 2D *J*-resolved spectrum, which clearly revealed the occurrence of heteronculear coupling to phosphorus-31 of the glycerol H-3 resonances ($J_{H,P} \approx$ 7 Hz), establishing the presence of 3-phosphoglycerol units in the capsular polysaccharide.

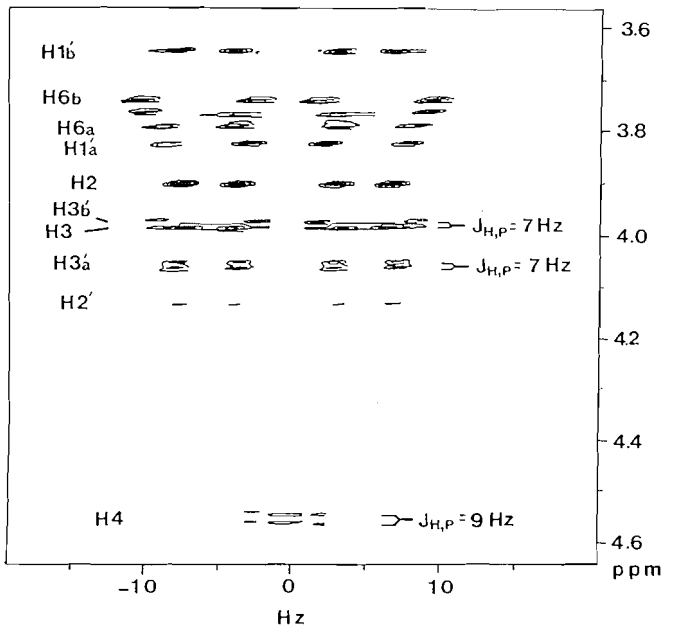

FIG. 2. Contour plot of part of the 2D *J*-resolved spectrum of the *O*-deacetylated *P. haemolytica* serotype T3 capsular polysaccharide at 310 K. Proton resonance assignments and the phosphorus-31 coupled doublets are indicated. Signals due to H-5 were weak and are not visible at the indicated contour level.

The subspectra corresponding to the 4-phospho-α-D-galactopyranosyl and the 3-phosphoglycerol residues could be exactly calculated by computer simulation employing the proton and phosphorus-31 coupling constant values determined from the *J*-resolved spectrum (Fig. 2). The composite simulated ^{1}H nmr spectrum of the *O*-deacetylated polysaccharide is in complete agreement with the experimental spectrum (Fig. 3).

Since only a single phosphate group was indicated by ^{31}P nmr, it follows from the foregoing ^{1}H nmr analysis that the repeating unit of the capsular polysaccharide is composed of monophosphate diester units. The phosphoglycerol moiety could be present either as a side chain phosphate diester substituent on a repeating galactan chain or as an integral part of a linear repeating unit to form a teichoic acid-type (13) structure. A distinction between these two arrangements was made from ^{1}H–^{1}H nOe measurements, which established connectivities between the anomeric and aglyconic protons of adjacent residues (24, 25). The nOe difference spectrum (26) obtained on the *O*-deacetylated polymer is shown in Fig. 4.

Saturation of the anomeric proton resonance (4.989 ppm) of the D-galactopyranosyl residues showed a nOe at H-2 (3.890 ppm) within the pyranosyl ring system together with a nOe of similar magnitude at one of the terminal methylene protons, H-1b′ (3.629 ppm), of the 3-phosphoglycerol moiety, establishing that the D-galactosyl residues are α-linked to the terminal position of the polyolphosphate. It follows that the repeating unit of the capsular polysaccharide of *P. haemolytica* serotype T3 is composed of →4)-α-D-Gal*p*-(1→1)-glycerol-(3→ units joined by phosphate diester groups.

These structural conclusions were reinforced from a detailed analysis of the ^{13}C nmr data. The ^{13}C nmr spectrum of the *O*-deacetylated capsular polysaccharide showed nine well-resolved resonances that were unambiguously assigned (Table 2) by correlation with resonances of the directly attached protons from a 2D heteronuclear ^{1}H–^{13}C chemical shift correlation map (Fig. 5). As expected, the resonances corresponding to C-4, C-3, and C-5 of the α-D-galactopyranosyl residue and to C-2′ and C-3′ of the glycerol moiety were split or broadened (C-3) due to phosphorus coupling. Unequivocal identification of the ^{13}C resonances arising from the three methylene carbon atoms was made from a DEPT experiment (27). The signal at 61.72 ppm, observed in the region of the spectrum characteristic of primary hydroxyl carbons (60–64 ppm) (28), was assigned from the corresponding ^{1}H–^{13}C correlation to C-6 of the α-D-galactopyranosyl residue, while the downfield shifted methylene resonances at 69.25 (s) and 67.60 ppm (d, $J_{C,P}$ = 6.1 Hz) could be attributed to C-1′ and C-3′ of the 3-phosphoglycerol moiety, respectively. The relatively deshielded value of the methylene singlet at 69.25 ppm is consistent with substitution at that position (28).

Depolymerization of the polysaccharide

Depolymerization of the *O*-deacetylated capsular polysaccharide (**1**) with aqueous HF afforded the phosphate-free disaccharide **2**, which was obtained chromatographically pure by gel filtration on Sephadex G15. The disaccharide was identified as 1-*O*-α-D-galactopyranosyl-glycerol from its ^{1}H and ^{13}C nmr spectra. Assignment of the ^{1}H nmr spectrum of the disaccharide was made from selective decoupling experiments (Table 1). The ^{13}C nmr spectrum showed nine signals that could be readily assigned (Table 2) by comparison with data reported for methyl α-D-galactopyranoside (29) and glycerol (28), and was consistent with substitution at one of the terminal methylene carbons (C-1′) of glycerol. The ^{13}C chemical shifts of the oligosaccharide were similar to those observed for the *O*-deactylated polysaccharide except that the phosphate-substituted carbon atoms, C-4 and C-3′, were downfield shifted (5.6 and 4.5 ppm, respectively) in the spectrum of the latter (Table 2).

Saturation of H-1 of the D-galactopyranosyl residue of **2** produced positive nOe at H-2 (~10%) and at the high-field methylene proton (3.571 ppm), H-1b′ (~6%), of the glycerol unit, confirming the position of the glycosidic linkage at C-1′.

In agreement with its proposed structure, the permethylated derivative of disaccharide **2** gave a protonated molecular ion in its ci ms at *m/z* 339, together with characteristic fragment ions (30) at *m/z* 219 (A_1), 187 (A_2), and 161 (J_1).

Absolute configuration of the glycerol-3-phosphate residues

The remaining structural feature of the *O*-deacetylated polysaccharide to be determined is the absolute configuration of the 3-phosphoglycerol moiety. L-Glycerol-3-phosphate (as its cytidine diphosphate derivative) has been implicated in the biosynthesis of the cell wall teichoic acids of Gram-positive bacteria and its stereochemical integrity is maintained in the derived poly(glycosyl-glycerolphosphates) (13, 31, 32). It would be tempting to assume that L-glycerol-3-phosphate is also the precursor of the glycerol-containing extracellular teichoic acid-like capsular antigens (33). Indeed, in one instance the 3-phosphoglycerol component of a teichoic acid-like capsular polysaccharide antigen, that from *Escherichia coli* K2, has been shown (34) to have the L-configuration. However, the membrane bound teichoic acid (lipoteichoic acid) from *Streptococcus lactis* has been found to be composed of D-glycerol-3-phosphate residues (35). It was therefore mandatory to establish the absolute configuration of the 3-phosphoglycerol moiety present in the *P. haemolytica* T3 antigen and this was accomplished by examination of the conformational dependence of the vicinal ^{1}H–^{1}H coupling constants $J_{1a',2'}$ and $J_{1b',2'}$ in the disaccharide **2**.

Can. J. Chem. Downloaded from www.nrcresearchpress.com by 91.121.58.235 on 09/07/12
For personal use only.

Can. J. Chem. Downloaded from www.nrcresearchpress.com by 91.121.58.235 on 09/07/12
For personal use only.

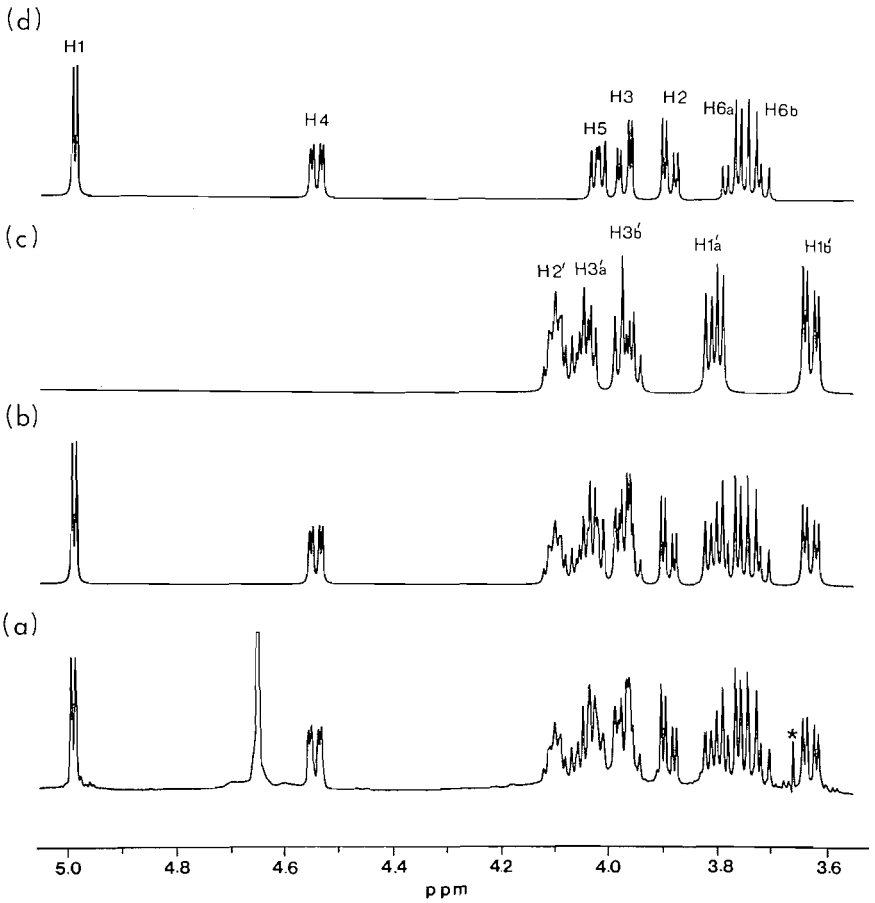

FIG. 3. The ^{1}H nmr spectrum of the *O*-deacetylated *P. haemolytica* serotype T3 capsular polysaccharide at 310 K. (a) Observed spectrum. (b) Simulated spectrum using experimental σ and J values. (c) Subspectrum of the contribution to the simulated spectrum from the glycerol residues. (d) Subspectrum of the contribution to the simulated spectrum from the D-galactopyranosyl residues. The low intensity peaks observed in (a) are due to incomplete *O*-deacetylation and the signal denoted by an asterisk is from a minor impurity of tris(hydroxymethyl)methylamine.

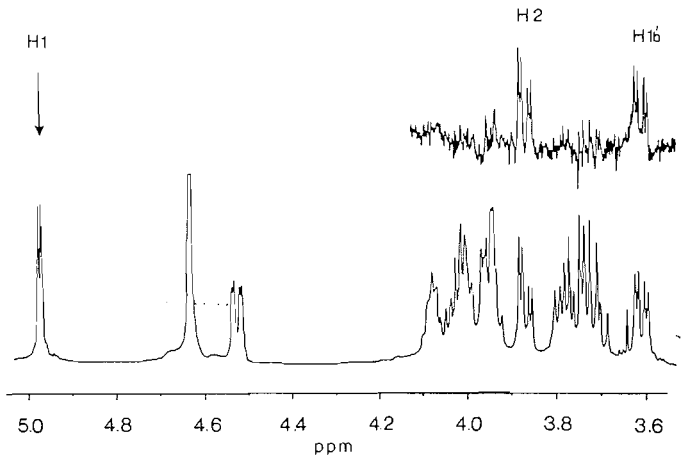

FIG. 4. The ^{1}H nmr spectrum of the *O*-deacetylated *P. haemolytica* serotype T3 capsular polysaccharide at 310 K. Inset shows nOe difference spectrum obtained by saturation of the H-1 resonance of the α-D-galactopyranosyl residues.

Stereochemical assignment of the ^{1}H resonances from the C-1′ methylene protons was essential for configurational analysis. The observation that saturation of the anomeric proton of the α-D-galactopyranosyl residue imparts an nOe at only one of the diastereomeric methylene protons, H-1b′ of the *O*-1 linked glycerol moiety, led to the required stereochemical assignments. In addition, the conformation of the 1-*O*-α-D-galactopyranosyl-glycerol fragment (**2**) was probed by potential energy calculations.

Since the conformation about the glycosidic linkage is to a large extent governed by the *exo*-anomeric effect (36), the minimum energy conformation of the disaccharide **2** was calculated using the HSEA method (36, 37).[3] Interproton distances calculated for the molecule were consistent with the nOe data (Table 3). The ^{1}H–^{1}H nOe are generally observed when interproton distances are less than ca. 2.8 Å (38). Thus, a nOe would be anticipated between the anomeric and the 1′-*pro-S* protons, which are separated by 2.5 Å in the minimum energy conformation, but not between H-1 and the 1′-*pro-R* hydrogen, which have an internuclear separation of 3.0 Å. Since saturation of H-1 of the α-D-galactopyranosyl residue in **2** produced a nOe at only the high-field methylene proton (3.571 ppm), H-1b′ of the glycerol moiety, and no detectable nOe was observed for the low-field methylene proton (3.762 ppm), H-1a′, the two diastereotopic methylene protons were assigned to the 1′-*pro-S* and the 1′-*pro-R* hydrogen atoms, respectively (Table 3). Furthermore, since specific deshielding effects are known (39) to be correlated to short oxygen-to-proton distances, the observed deshielding of H-1a′ relative to H-1b′

[3]The HSEA minimum energy molecule gives a shallow energy well for the range of torsional angles, Φ, −60–−45° and ψ, 15–95° with a minimum energy at Φ = −55° and ψ = 65°. The torsion angles are defined as follows: Φ, H-1—C-1—O-1—C-1′; ψ, C-1—O-1—C-1′—H-1*R*′.

TABLE 2. Carbon-13 chemical shift assignments for the *O*-deacetylated *P. haemolytica* serotype T3 capsular polysaccharide and for the phosphate-free depolymerized product (**2**)

Saccharide	α-D-Galactopyranosyl unit						Glycerol unit		
	C-1	C-2	C-3	C-4	C-5	C-6	C-1′	C-2′	C-3′
O-deacetylated polysaccharide (**1**)[a]	99.33	69.36	69.88 (*ur*)[b]	75.50 (5.9)[c]	71.64 (4.4)[b]	61.72	69.25	70.05 (7.7)[b]	67.60 (6.1)[c]
α-D-Gal*p*-(1→1)-glycerol (**2**)[d]	99.09	69.08[e]	70.10	69.91	71.64	61.85	69.22[e]	71.13	63.13

[a]Assignments made via $^1H-^{13}C$ chemical shift correlation.
[b]$^3J_{C,P}$ value, Hz.
[c]$^2J_{C,P}$ value, Hz.
[d]Assignments made by comparison with reference compounds (cf. refs. 28, 29).
[e]Distinction made from DEPT experiment.

TABLE 3. Proton nmr data[a] and calculated internuclear distances[b] for the α-D-Gal*p*-(1→1)-glycerol unit related to the stereochemical assignments of H-1′

	^1H nmr data			Calculated internuclear distance		
	H-1′ (ppm)	$^3J_{1',2'}$ (Hz)	nOe {H-1} (%)	H-1′/H-1 (Å)	H-1′/O-5 (Å)	Assignment
α-D-Gal*p*-(1→1)-glycerol (**2**)	3.571[c]	3.9	6	2.5	3.3	1′-*pro-S*
	3.762[d]	5.9	—[e]	3.0	2.5	1′-*pro-R*
O-deacetylated polysaccharide (**1**)	3.629[c]	3.9	+			1′-*pro-S*
	3.806[d]	5.6	—[e]			1′-*pro-R*

[a]Chemical shifts and coupling constants are taken from Table 1.
[b]Calculated for **2** using the HSEA method (refs. 36, 37).
[c]Value for H-1b′.
[d]Value for H-1a′.
[e]No detectable nOe observed.

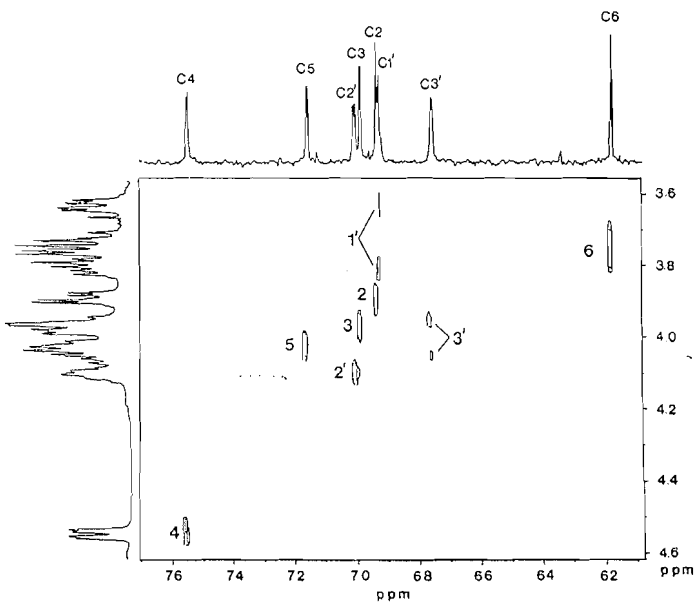

FIG. 5. Part of the heteronuclear $^1H-^{13}C$ nmr chemical shift correlation map of the *O*-deactylated *P. haemolytica* serotype T3 capsular polysaccharide at 310 K. The respective ^{13}C and ^1H 1D projections are displayed above and at the side and the correlated resonances are labelled.

(~0.2 ppm) can be related to the close proximity of the former hydrogen atom to the D-galactopyranosyl ring oxygen, O-5. This is evident in the minimum energy conformation where the H-1R′ to O-5 internuclear distance is 2.5 Å, while the H-1S′ to O-5 separation is greater than 3 A (Table 3). Analogously, in α-(1-6)-linked D-glycopyranosyl disaccharides the glycosylated C-6 *pro-R* hydrogen has been observed (40, 41) to be shifted to lower field than the corresponding *pro-S* hydrogen.

A comparison of chemical shift and nOe values from the *O*-deacetylated polysaccharide with those from oligosaccharide **2** (Table 3) would suggest that the average conformation about the glycosidic linkages of the α-D-galactopyranosyl-(1→1)-L-glycerol units within the intact polymer (**1**) is similar to that of the free disaccharide.

The three staggered conformations about the C-1′—C-2′ bond for the two stereoisomers at C-2′ of the glycerol moiety of 1-*O*-α-D-galactopyranosyl-glycerol are shown in Fig. 6. Substantial experimental evidence from the conformational analysis of polyols in solution (42–44) would suggest that conformers in which the vicinal oxygen atoms adopt a *gauche* rotational orientation (*O*e and *O*g) are most heavily populated, while those in which the vicinal oxygen atoms have a *trans* disposition (*O*t) are considerably less populated. The tendency of the vicinal oxygen atoms to preferentially adopt a *gauche* rotational arrangement has been observed in a number of instances (attractive "*gauche* effect") (45–47).

If it is assumed that the *O*t rotamer does not make a significant contribution to the conformation about the C-1′—C-2′ bond in the disaccharide **2**, then the chirality at C-2′ can be assigned from the magnitude of the observed vicinal coupling constants ($^3J_{1',2'}$).[4] In this case, the $^3J_{1',2'}$ values can be considered as the

[4]A similar assumption has been invoked for the analysis of the rotameric populations about the C-5—C-6 bond in 1,6-linked disaccharides (48, 49).

Can. J. Chem. Downloaded from www.nrcresearchpress.com by 91.121.58.235 on 09/07/12
For personal use only.

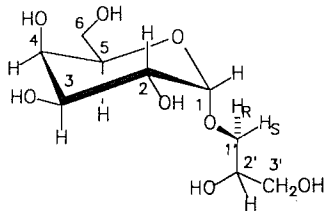

Chirality at C-2′	O_e	Conformation O_g	O_t
S	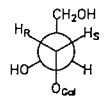	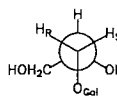	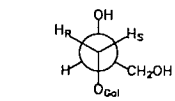
	$J_{1R',2'} > J_{1S',2'}$	$J_{1R',2'} = J_{1S',2'}$	$J_{1R',2'} < J_{1S',2'}$
R	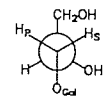	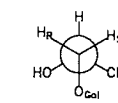	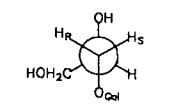
	$J_{1S',2'} > J_{1R',2'}$	$J_{1S',2'} = J_{1R',2'}$	$J_{1S',2'} < J_{1R',2'}$

FIG. 6. Staggered conformations about the C-1′—C-2′ bond of 1-*O*-α-D-galactopyranosyl-glycerol related to the chirality at C-2′. Designation of the rotamers is according to ref. 42 and relative $^3J_{1',2'}$ values are indicated for each conformation.

weighted average of the individual coupling constants from the *O*e and *O*g conformers, which can be described in terms of a Karplus relationship (50): if C-2′ has *S* chirality, $J_{1R',2'} \geq J_{1S',2'}$; whereas, if C-2′ has *R* chirality, $J_{1S',2'} \geq J_{1R',2'}$ (Fig. 6). Since $J_{1R',2'}$ (i.e., $J_{1a',2'} = 5.9$ Hz) was found to be greater than $J_{1S',2'}$ (i.e., $J_{1b',2'} = 3.9$ Hz), it follows that 1-*O*-α-D-galactopyranosly-glycerol (**2**) has *S* chirality at C-2′ and that the glycerol-3-phosphate component in the capsular polysaccharide has the L-configuration.

The foregoing result was also rigorously confirmed by degradation of the disaccharide **2** to a glycerol derivative of known chirality (Scheme 1).[5] Thus, methanolysis of permethylated 1-*O*-α-D-galactopyranosyl-glycerol afforded, without loss of the chiral integrity at C-2′, 2,3-di-*O*-methyl glycerol, which was converted to the corresponding (−)-camphanate ester having 2′*S*-chirality (**3**) as determined by comparison of its glc retention time and ms with those of an authentic standard.

Positions of O*-acetyl substituents*

A detailed analysis of the COSY spectrum of the native polysaccharide led to the location of the *O*-acetyl substituents. Subspectra corresponding to three distinct 4-phospho-α-D-galactopyranosyl ring systems were delineated, which could be assigned to galactosyl residues exclusively mono-substituted at either O-3 (~50%) or O-2 (~20%), and to unsubstituted galactosyl residues (~30%). The substitution pattern was evident from the low-field position of resonances of the protons attached to the carbons bearing the acetate esters (Table 4) (51): 5.10 ppm from H-3 of the 3-substituted residues and 5.04 ppm from H-2 of the 2-substituted residues.

Similar complex *O*-acetyl substitution patterns have been identified for the *P. haemolytica* serotypes T4 (9) and T15 (10) antigens as well as for the *E. coli* K62 (52) and *Neisseria*

[5]J. C. Richards. Manuscript in preparation.

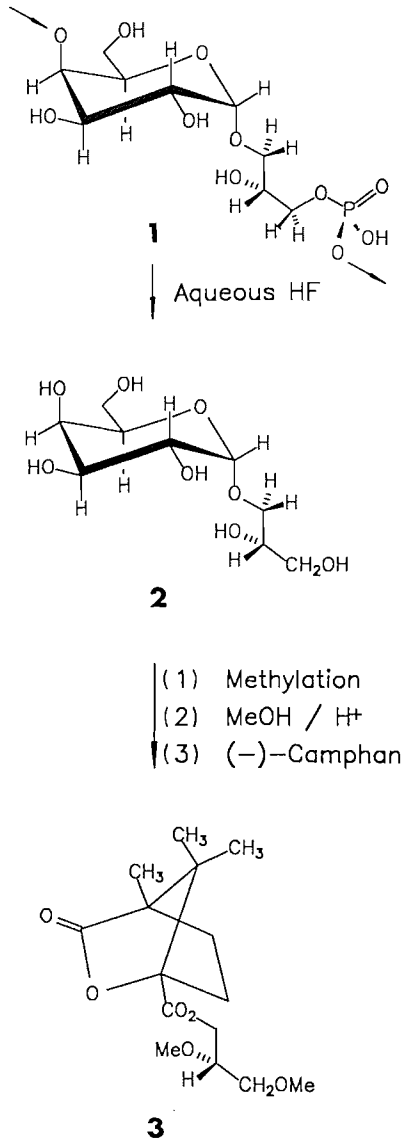

SCHEME 1. Conversion of the *O*-deacetylated polysaccharide (**1**) into 2,3-di-*O*-methyl-L-glycerol camphanate (**3**).

meningitidis group H (53, 54) polysaccharides, with the latter three antigens having essentially the same structure.

The *P. haemolytica* biotype T capsular antigens (serotypes T3, T4, and T15) form a group of structurally related poly(galactosyl-glycerolphosphates) (Table 5) where the T3 and T15 antigens appear to differ only in the mode of substitution at the 3-phosphoglycerol units. The stereochemistry of the 2-substituted 3-phosphoglycerol units of the T15 antigen has not been established, although it too probably has the L-configuration since the T15 polysaccharide is reported (10) to react similarly with both *P. haemolytica* T15 and *E. coli* K62 specific antisera. The 3-phosphoglycerol released from the *O*-deactylated K62 polymer (the K2 antigen) has been shown (34) to have the L-configuration by enzymic oxidation mediated by L-glycerol-3-phosphate dehydrogenase.

Conclusion

In the present study, a combination of 1D and 2D high-resolution nmr techniques was employed for the structural analysis of a glycerolphosphate-containing teichoic acid. Nuclear magnetic resonance techniques were used to probe the

Can. J. Chem. Downloaded from www.nrcresearchpress.com by 91.121.58.235 on 09/07/12
For personal use only.

TABLE 4. Proton chemical shift assignments for α-D-galactopyranosyl residues present in the native *P. haemolytica* serotype T3 capsular polysaccharide[a] and for corresponding *O*-acetylated methyl glycosides[b]

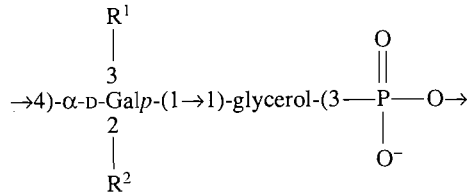

α-D-Galactopyranoside	R^1	R^2	Mol%[c]	H-1	H-2	H-3	H-4	H-5	H-6
Unsubstituted residue	H	H	30	4.99	3.89	3.97	4.54	4.02	~3.75
3-*O*-acetyl residue	Ac	H	50	5.06	4.13	5.10	4.67	4.09	~3.75
2-*O*-acetyl residue	H	Ac	20	5.16	5.04	4.21	4.62	—[d]	—[d]
Methyl 3-*O*-acetyl[b]				4.91	4.07	5.03	4.15	3.98	~3.75
Methyl 2-*O*-acetyl[b]				~5.00	~5.00	4.04	4.04	3.94	~3.78

[a]Measured at 310 K relative to internal acetone.
[b]Data from ref. 51.
[c]Measured from ^{1}H signal areas.
[d]Not determined.

TABLE 5. Structures of the glycerol containing teichoic acid-like capsular antigens of *P. haemolytica*

Serotype	Repeating unit	Ref.
T3	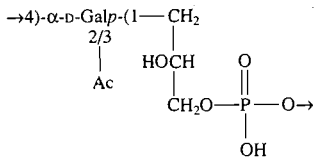	
T4	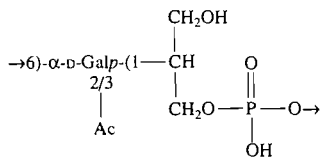	9
T15	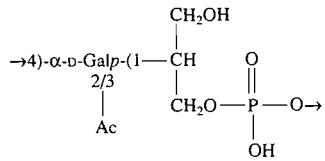	10

stereochemisty of the glycerol moiety within the structure by relating the chirality of the glycerol methine carbon centre to that of D-galactopyranose by ^{1}H–^{1}H nOe and ^3J-values. The absolute configuration of the galactose was readily established by a chemical method. This technique would also be applicable for stereochemical assignment of other 1-*O*-glycosylglycerol derivatives provided stereoselective nOe are observed between the glycosyl anomeric and glycerol C-1 methylene protons.

Experimental

Pasteurella haemolytica *serotype T3 capsular polysaccharide*

Bacterial culture

Pasteurella haemolytica serotype T3 (NRCC 4015) was obtained from the Veterinary Infectious Disease Organization (VIDO), Saskatoon, Sask., and the cells were grown in 4-L baffled conical flasks as previously described (16) (yield, ca. 8 g wet weight/L).

Isolation and purification

The bacterial growth was suspended in aqueous sodium chloride (2.5%, w/v) solution and, after stirring at 22°C overnight, the cellular material was removed by low speed centrifugation. The supernatant was dialysed against running tap water (2 days), digested with ribonuclease, deoxyribonuclease, and proteinase K, and, following further dialysis against distilled water, crude capsular polysaccharide was obtained by precipitation with three volumes of 95% ethanol. The crude capsular polysaccharide material was redissolved in water and purified by precipitation with cetyltrimethylammonium bromide (1%, w/v, final concentration). After keeping the solution at 4°C overnight, the precipitated complex was collected by centrifugation and then dissolved in 2 M sodium chloride solution. After extensive dialysis against distilled water, pure capsular polysaccharide was recovered by lyophilization.

An additional yield of capsular polysaccharide was obtained by extraction of the cellular material using the modified hot phenol – water extraction method (15, 16). The aqueous phase was extensively dialysed against running tap water until phenol free and then lyophilized. The lyophilyzate was taken up in aqueous saline (2.5%, w/v) and subjected to ultracentrifugation (4°C, 105 000 × *g*, 10 h) to remove lipopolysaccharide. The supernatant was dialysed until salt free and lyophilized to afford capsular polysaccharide. which was purified by ion-exchange chromatography on a column of DEAE–Sephacel.

O-*Deacetylation*

Capsular polysaccharide (25 mg) in aqueous ammonia (5%, v/v, 1 mL) was stirred at 35°C for 3 h. Excess ammonia was removed by flushing with nitrogen and the solution was lyophilized (yield, 22 mg). The *O*-deacetylated polymer was converted to its sodium salt by passing an aqueous solution through a column (0.5 × 2 cm) containing Rexyn 101 (Na^+ form) cation exchange resin.

Chromatography

Capsular polysaccharide (15 mg) in water (0.5 mL) was applied to a column (1.2 × 40 cm) of DEAE–Sephacel (Pharmacia) equilibrated with 0.05 M Tris-HCl buffer (pH 7.2). The column was eluted with the same buffer (25 mL), followed by a 0–1.0 M sodium chloride gradient in the same buffer, and fractions (1 mL) were collected and assayed for neutral glycose (55) and phosphate (18).

Gel filtration of polysaccharide samples (25 mg) was carried out on a column (2.5 × 50 cm) of Sephacryl S300 (Pharmacia) using 0.05 M pyridinium acetate (pH 4.5) as the eluant. The column eluant was continuously monitored for changes in refractive index using a Waters

Can. J. Chem. Downloaded from www.nrcresearchpress.com by 91.121.58.235 on 09/07/12
For personal use only.

Can. J. Chem. Downloaded from www.nrcresearchpress.com by 91.121.58.235 on 09/07/12
For personal use only.

R403 differential refractometer, and fractions were analyzed for aldose and phosphate.

Immunodiffusion

Double diffusion studies (56) were made at 4°C in 1% sodium chloride agarose gels using capsular polysaccharide concentrations of 1 mg/mL. Precipitin lines were allowed to develop over 2 days. Antiserum to *P. haemolytica* serotype T3 was prepared by immunization of mice with formalin-killed cells of the bacterium.

Analytical methods

Quantitative colorimetric methods used were phenol – sulfuric acid for neutral glycoses (55) and the method of Chen *et al.* (18) for phosphate.

Glycoses were determined by glc of their alditol acetate derivatives (57) using inositol as internal standard. Samples (2 mg) were hydrolyzed in sealed glass tubes with 3 M hydrochloric acid (1 mL) for 3 h at 100°C or with 1 M sulfuric acid (1 mL) for 12 h at 100°C followed by neutralization (Ag_2CO_3 or $BaCO_3$, respectively) and concentration to dryness *in vacuo*. The liberated free glycoses were reduced ($NaBH_4$) and acetylated as previously described (58).

Gas–liquid chromatography employed a Hewlett Packard model 5710A gas chromatograph fitted with a hydrogen flame-ionization detector, a model 3380A electronic integrator, and a fused silica capillary column (0.3 mm × 25 m) containing 3% (w/w) OV17, using the temperature program, 180°C (for 2 min) to 240°C at 2°C/min. Development was made with nitrogen at 25 mL/min and retention times are quoted relative to D-glucitol hexaacetate (T_{GA}).

The glc–ms measurements were performed with a Hewlett Packard 5985B system employing the aforementioned glc conditions by electron impact (ei) with an ionization potential of 70 eV or by chemical ionization (ci) with methane as the reagent gas.

Absolute configurations of glycoses were established by conversion to the corresponding trimethylsilyated *R*-2-butylglycoside derivatives (17) followed by comparison of the glc retention times and mass spectra with those of authentic reference compounds.

Nuclear magnetic resonance measurements

All spectra were obtained on a Bruker AM-500 spectrometer equipped with an Aspect 3000 computer, using standard Bruker software. Samples were twice lyophilized from deuterium oxide and dissolved at concentrations of 15–45 mg/mL.

Proton and carbon-13 measurements were made on polysaccharide (sodium salt, pD ≈ 7.8) or oligosaccharide samples in 5-mm tubes at 310 K or 300 K, respectively. Proton spectra, recorded at 500 MHz, were obtained using a spectral width of 1.8 kHz, a 8 or 16 K data block, and a 90° pulse. Resolution enhancement was implemented using a Gaussian line shape transformation (20) with values of −3.0 Hz and +0.1 for the line and Gaussian broadening factors, respectively. Chemical shifts are expressed relative to internal acetone (δ 2.225 ppm). The nOe difference spectra were obtained by sequential irradiation of each line in a multiplet (26) for a total irradiation time of either 200 ms for polysaccharide samples or 400 ms for oligosaccharide samples.

Broadband proton-decoupled ^{13}C nmr spectra were obtained at 125 MHz using a spectral width of 25 kHz, a 32 K data block, and a 90° pulse employing WALTZ decoupling (59). Heteronuclear $^1J_{C,H}$ coupling constants were measured using gated decoupling (60). DEPT spectra (27) were obtained with broadband proton decoupling, a 135° proton pulse, and 3.3 ms delay between pulses. Chemical shifts are referenced to that of external 1,4-dioxane (δ 67.40 ppm).

Two-dimensional homonuclear proton chemical shift correlation (COSY) (61) and *J*-resolved (62) experiments were measured by employing the conventional pulse sequences. The COSY spectra were obtained using a data set ($t_1 \times t_2$) of 512 × 2048 points for a spectral width of 830 Hz. The data matrix was zero-filled to 1024 × 2048 points and, following resolution enhancement in both dimensions by a non-shifted sine bell function, the data were processed to give magnitude spectra with symmetrization. The *J*-resolved spectrum was obtained using a data matrix of 64 × 2048 points and spectral widths of 1859 and ±29.1 Hz in the chemical shift (F_2) and coupling constant (F_1) dimensions, respectively. Following zero-filling in t_1 to give 128 × 2048 points, a non-shifted sine bell function was applied in both time domains, and the transformed data were tilted 45° and symmetrized. For both experiments, a recycle delay (T) of 1.6 s was used, and 32 transients were collected for each t_1 value.

Two-dimensional heteronuclear carbon–proton chemical shift correlations were carried out with quadrature detection in F_1 (63) using a data matrix of 128 × 2048 points and spectral widths of 6945 and 451 Hz for the respective carbon-13 (F_2) and proton (F_1) chemical shift domains. A recycle delay of 1.5 s was employed and the fixed delays, τ_1 and τ_2, were set at 3.2 and 1.6 ms, respectively, to select for all multiplicities. Composite broadband proton decoupling was carried out during the acquisition of 1000 transients for each of the 128 t_1 increments. The data matrix was zero-filled in t_1 to 256 × 2048 points and, following resolution enhancement in both dimensions by means of a Lorentz-to-Gauss transformation, the data were processed to give a power spectrum.

Phosphorus-31 spectra were measured at 202 MHz on solutions (ca. 2 mL) in 10-mm sample tubes by employing a spectral width of 10 kHz, a 16 K data set, and 90° pulse. Chemical shifts are referenced to that of an external sample of 85% phosphoric acid.

Spectral simulations were performed using the Bruker Panic program. The spin systems corresponding to the galactosyl and the glycerol moieties were simulated separately, and were then co-added, employing line widths of 3.0 Hz, to give a composite simulated spectrum.

Potential energy calculations

Semi-empirical potential energy calculations were performed by the HSEA method (36, 37) to estimate the minimum energy conformation about the glycosidic bond of disaccharide **2**. Calculations were performed in five-degree steps across the Φ and ψ ranges and the glycosidic bond angle was set at 117°. Atomic coordinates for the α-D-galactopyranose unit were taken from neutron diffraction data of Takagi and Jeffery (64). The heavy atom coordinates for the glycerol moiety were generated by bond modification (65) of D-glucitol X-ray diffraction data (66); the central C—C bond of D-glucitol was replaced by a C—H bond, in which the H atom was positioned along the C—C bond vector, to generate the C-1′—C-2′—C-3′ skeleton of glycerol. Coordinates for hydrogen atoms were generated as previously described (67) using a C—H bond length of 1.10 Å. The torsion angles, Φ and ψ, are defined according to Bock (65).

Depolymerization of the capsular polysaccharide

O-Deacetylated capsular polysaccharide (5 mg) was dissolved in 48% (w/v) aqueous hydrofluoric acid (0.2 mL) and, after the reaction mixture was kept at 4°C for 60 h, excess hydrogen fluoride was removed by evaporation by passing a stream of nitrogen over the solution. The residue was dried over sodium hydroxide *in vacuo* and the phosphate-free product (4 mg) was obtained by gel filtration on a column (1.7 × 95 cm) of Sephadex G-15 eluted with 0.05 M pyridinium acetate (pH 4.5). The product, 1-*O*-α-D-galactopyranosyl-L-glycerol (**2**), showed a single spot on tlc (silica gel) developed with ethyl acetate – acetic acid – methanol–water (12:3:3:5) having R_f 0.36, and gave $[\alpha]_D$ 78.8° (*c* 0.26, water) and the ^1H and ^{13}C nmr data recorded in Tables 1 and 2. A sample (1 mg) of the disaccharide **2** was permethylated as previously described (58). The permethylated derivative eluted as a single peak on glc: ms (ci) *m/z*: 339 (M+1, 1.7%), 219 (67.2), 187 (100.0), 163 (8.3), 103 (23.9).

Degradation of 1-O-α-D-galactopyranosyl-L-glycerol (2)

The permethlyated sample of **2** was treated with methanolic hydrogen chloride (3%, w/v, 1 mL) in a sealed glass tube at 90°C for 14 h and the excess methanolic HCl was removed under a stream of nitrogen. To the residue in dry pyridine (0.5 mL) was added an excess of (1*S*)-(−)-camphanoyl chloride (Aldrich) (ca. 10 mg) and the solution was stirred at room temperature for 3 h. The reaction was quenched by

addition of dilute aqueous sodium carbonate (5%, w/v, 1 mL) and the product, 2,3-di-*O*-methyl-L-glycerol camphanate (**3**), was extracted into methylene chloride (1 mL). The methylene chloride extract was washed with water (3 × 1 mL) and dried over anhydrous sodium sulfate prior to glc–ms analysis using the aforementioned conditions. The glc retention time (T_{GA} 0.74) and ms were identical to those of an authentic sample obtained from L-glyceric acid.[5]

General methods

Commerical reagents and solvents were analytical grade. Concentrations were made under reduced pressure at bath temperatures below 40°C. Optical rotations were determined at 22°C in 10-cm microtubes using a Perkin–Elmer model 243 polarimeter.

Acknowledgments

We thank Dr. D. R. Bundle for helpful discussions, Mr. F. P. Cooper for glc–ms analyses, and Mr. D. W. Griffith for the large-scale production of cells.

1. L. Fodor, J. Varga, J. Hajtos, W. Donachie, and N. J. L. Gilmour. Vet. Rec. **121**, 155 (1987); Res. Vet. Sci. **44**, 399 (1988).
2. G. R. Carter. Essentials of veterinary bacteriology and mycology. 3rd ed. Lea and Febiger, Philadelphia, Pa. 1986. p. 160.
3. C. Adlam, J. M. Knights, A. Mugridge, J. C. Lindon, P. R. W. Baker, J. E. Beesley, B. Spacey, G. R. Craig, and L. K. Nagy. J. Gen. Microbiol. **130**, 2415 (1984).
4. C. Adlam. *In* Pasteurella and Pasteurellosis. *Edited by* C. Adlam and J. M. Rutter. Academic Press, London. 1989.
5. A. W. Confer, R. J. Panciera, and D. A. Mosier. Am. J. Vet. Res. **47**, 1134 (1986).
6. J. C. Richards and R. A. Leitch. Carbohydr. Res. **186**, 275 (1989).
7. J. C. Richards and R. A. Leitch. Abstr. International Conference on the *Haemophilus, Actinobacillus, Pasteurella* group of organisms. University of Guelph, Guelph, Ontario, Canada, June 21–24, 1989.
8. J. A. Durham, S. M. Antone, M. W. Cunningham, and A. W. Confer. J. Clin. Microbiol. **26**, 885 (1989).
9. C. Adlam, J. M. Knights, A. Mugridge, J. C. Lindon, and J. M. Williams. J. Gen. Microbiol. **131**, 387 (1985).
10. C. Adlam, J. M. Knights, A. Mugridge, J. C. Lindon, J. M. Williams, and J. C. Beesley. J. Gen. Microbiol. **131**, 1963 (1985).
11. C. Adlam, J. M. Knights, A. Mugridge, J. C. Lindon, J. M. Williams, and J. C. Beesley. J. Gen. Microbiol. **132**, 1079 (1986).
12. C. Adlam, J. M. Knights, A. Mugridge, J. M. Williams, and J. C. Lindon. FEMS Microbiol. Lett. **42**, 23 (1987).
13. J. Baddiley. Acc. Chem. Res. **3**, 98 (1970).
14. J. E. Scott. Methods Biochem. Anal. **8**, 145 (1960).
15. K. G. Johnson and M. B. Perry. Can. J. Microbiol. **22**, 29 (1976).
16. R. A. Leitch and J. C. Richards. Biochem. Cell Biol. **66**, 1055 (1988).
17. G. J. Gerwig, J. P. Kamerling, and J. F. G. Vliegenthart. Carbohydr. Res. **62**, 349 (1978).
18. P. S. Chen, Jr., T. J. Toribara, and H. Warner. Anal. Chem. **28**, 1756 (1956).
19. D. G. Gorenstein. J. Am. Chem. Soc. **97**, 989 (1975).
20. A. G. Ferrige and J. C. Lindon. J. Magn. Reson. **31**, 337 (1978).
21. C. Altona and C. A. G. Haasnoot. Org. Magn. Reson. **13**, 417 (1980).
22. L. D. Hall and S. Sukumar. J. Am. Chem. Soc. **101**, 3120 (1979).
23. J. R. Everett, D. W. Hughes, A. D. Bain and R. A. Bell. J. Am. Chem. Soc. **101**, 6776 (1979).
24. J. M. Prestegard, T. A. W. Koerner, P. C. Demon, and R. K. Yu. J. Am. Chem. Soc. **104**, 4993 (1982).
25. M. A. Bernstein and L. D. Hall. J. Am. Chem. Soc. **104**, 5553 (1982).
26. M. Kinns and J. K. M. Sanders. J. Magn. Reson. **56**, 518 (1984).
27. D. M. Doddrell, D. J. Pegg, and M. R. Bendall. J. Magn. Reson. **48**, 323 (1982).
28. K. Bock and C. Pedersen. Adv. Carbohydr. Chem. Biochem. **41**, 27 (1983).
29. P. A. J. Gorin and M. Mazurek. Can. J. Chem. **53**, 1212 (1975).
30. N. K. Kochetkov and O. S. Chizov. Adv. Carbohydr. Chem. Biochem. **21**, 39 (1966).
31. M. Burger and L. Glaser. J. Biol. Chem. **239**, 3168 (1964).
32. A. R. Archbald and H. E. Coapes. Biochem. J. **124**, 449 (1971).
33. L. Kenne and B. Lindberg. Polysaccharides, **2**, 287 (1983).
34. W. Fischer, M. A. Schmidt, B. Jann, and K. Jann. Biochemistry, **21**, 1279 (1982).
35. K. U. Koch and W. Fischer. Biochemistry, **17**, 5275 (1978).
36. H. Thøgersen, R. U. Lemieux, K. Bock, and B. Meyer. Can. J. Chem. **60**, 44 (1982).
37. R. U. Lemieux, K. Bock, L. T. J. Delbaere, S. Koto, and V. S. Rao. Can. J. Chem. **58**, 631 (1981).
38. J. P. Carver and J.-R. Brisson. *In* Biology of carbohydrates. Vol. 2. *Edited by* V. Ginsberg and P. W. Robbins. John Wiley and Sons, New York, NY. 1984.
39. R. U. Lemieux and K. Bock. Arch. Biochem. Biophys. **221**, 125 (1983).
40. Y. Nishida, H. Ohrui, and H. Meguro. Tetrahedron Lett. **25**, 1575 (1984).
41. M. Ohrui, Y. Nishida, M. Watanabe, H. Hori, and H. Meguro. Tetrahedron Lett. **26**, 3251 (1985).
42. G. E. Hawkes and D. Lewis. J. Chem. Soc. Perkin Trans. 2, 2073 (1984).
43. D. G. Gillies and D. Lewis. J. Chem. Soc. Perkin Trans. 2, 1155 (1985).
44. Y. Nishida, H. Uzawa, S. Hanada, M. Ohrui, and H. Meguro. Agric. Biol. Chem. **53**, 2319 (1989).
45. S. Wolfe, Acc. Chem. Res. **5**, 102 (1972).
46. N. S. Zefirov, V. V. Samoshin, O. H. Subbotin, V. I. Baranenkov, and S. Wolfe. Tetrahedron, **34**, 2953 (1978).
47. M. Van Duin, J. M. A. Baas, and B. Van de Graaf. J. Org. Chem. **51**, 1298 (1986).
48. J.-R. Brisson and J. P. Carver. Can. J. Biochem. Cell Biol. **61**, 1067 (1983).
49. J.-R. Brisson and J. P. Carver. Biochemistry, **22**, 1362 (1983).
50. C. A. G. Haasnoot, F. D. A. M. De Leeuw, and C. Altona. Tetrahedron, **36**, 2783 (1980).
51. P. E. Jansson, L. Kenne, and E. Schweda. J. Chem. Soc. Perkin Trans. 1, 377 (1987).
52. K. Jann and M. A. Schmidt. FEMS Microbiol. Lett. **7**, 79 (1980).
53. F. Michon, R. Roy, H. J. Jennings, and F. E. Ashton. Can. J. Chem. **62**, 1519 (1984).
54. A. Van Der Kaaden, J. I. M. Van Doorn-Van Wakeren, J. P. Kamerling, J. F. G. Vliegenthart, and R. H. Tiesjema. Eur. J. Biochem. **141**, 513 (1984).
55. M. Dubois, K. A. Gilles, J. K. Hamilton, P. A. Rebers, and F. Smith. Anal. Chem. **28**, 350 (1956).
56. O. Ouchterlony. Acta. Pathol. Microbiol. Scand. **25**, 186 (1958).
57. S. W. Gunner, J. K. N. Jones, and M. B. Perry. Can. J. Chem. **39**, 1892 (1961).
58. J. C. Richards, M. B. Perry, and P. J. Kniskern. Can. J. Biochem. Cell Biol. **62**, 1309 (1984).

Can. J. Chem. Downloaded from www.nrcresearchpress.com by 91.121.58.235 on 09/07/12
For personal use only.

59. A. J. SHAKA, J. KELLER, F. FRENKIEL, and R. FREEMAN. J. Magn. Reson. **52**, 335 (1983).
60. O. A. GANSOW and W. SCHITTENHELM. J. Am. Chem. Soc. **93**, 4294 (1971).
61. A. BAX, R. FREEMAN, and G. MORRIS. J. Magn. Reson. **42**, 164 (1981).
62. W. P. AUE, J. KARHAN, and R. R. ERNST. J. Chem. Phys. **64**, 4226 (1976).
63. A. BAX and G. A. MORRIS. J. Magn. Reson. **42**, 501 (1981).
64. S. TAKAGI and G. A. JEFFREY. Acta. Crystallogr. Sect. B: Struct. Crystallogr. Cryst. Chem. **35**, 902 (1979).
65. K. BOCK. Pure Appl. Chem. **55**, 605 (1983).
66. F. W. LICHTENTHALER and H. J. LINDER. Liebigs Ann. Chem. 2372 (1981).
67. H. PAULSEN, J. PETERS, V. SINNWELL, R. LEBUHN, and B. MEYER. Liebigs Ann. Chem. 489 (1985).

Can. J. Chem. Downloaded from www.nrcresearchpress.com by 91.121.58.235 on 09/07/12
For personal use only.

Calculation of the second electron affinities of atoms

YUFEI GUO[1] AND M. A. WHITEHEAD

Theoretical Chemistry Group, Department of Chemistry, McGill University, 801 Sherbrooke Street West, Montreal, P.Q., Canada H3A 2K6

Received February 6, 1990

YUFEI GUO and M. A. WHITEHEAD. Can. J. Chem. **68**, 1585 (1990).

The second electron affinities of the atoms helium to krypton are calculated using the self-interaction corrected generalized exchange local-spin-density functional theory with the correlation energy functional. The dependence of the second electron affinities of the elements O, S, and Se on the Watson sphere radius is discussed. The present results are compared with other theoretical values and experimental data for the elements helium through krypton.

Key words: second electron affinity, density functional theory.

YUFEI GUO et M. A. WHITEHEAD. Can. J. Chem. **68**, 1585 (1990).

Faisant appel à une combinaison de la théorie fonctionnelle de la densité locale de spin avec échanges généralisés, corrigée pour les auto-interactions et de la corrélation d'énergie fonctionnelle, on a calculé les deuxièmes affinités électroniques des atomes des éléments allant de l'hélium au krypton. On discute de la relation qui existe entre les deuxièmes affinités électroniques du O, du S et du Se et le rayon de la sphère de Watson. On compare ces résultats avec les valeurs calculées à l'aide d'autres théories ainsi qu'avec les données expérimentales des éléments allant de l'hélium au krypton.

Mots clés : deuxième affinité électronique, théorie fonctionnelle de la densité.

[Traduit par la revue]

I. Introduction

Theoretical and experimental investigation of the electron affinities (EA) of atoms has attracted much attention (1–12), because the electron affinity not only leads to understanding microscopic electron structure and the stability of macroscopic matter (13), but tests the reliability of the theory itself. The first electron affinities of atoms can be reproduced very well in the self-consistent-field (SCF) calculation by either the correlation-corrected accurate Hartree–Fock (HF) theory (2, 4–6, 12), or the correlation and self-interaction corrected approximate local-spin-density functional (SIC–LSD) theory (7–11), in agreement with experiment (1,3).

Since Fischer *et al.* (2) reported the electron affinity for the alkaline-earth element Ca from a multi-configuration Hartree–Fock (MCHF) calculation in almost perfect agreement with the measured electron affinity from an elegant experiment by Pegg *et al.* (3), many publications evaluating electron affinities for the alkaline-earth elements, noble gases, and actinides have been published (4, 5, 10–12). The theoretical calculations show that the singly charged negative ions for most atoms in the periodic table are stable, even for alkaline-earth elements, noble gases, and actinides.

Some doubly charged negative ions have been found in nature. For example, the doubly charged negative ion of oxygen, O^{2-}, has been found in oxide crystals during the study of their magnetic properties (14). Other doubly charged negative ions of atoms, like N^{2-}, S^{2-}, Se^{2-}, etc., also exist in solids (15–18). The investigation of doubly charged negative ions is interesting. Furthermore, chemists need the second electron affinities of atoms in their calculation of molecular properties. For example, in Orsky and Whitehead's definition of hardness for an acid and a base (19),

$$\eta_A = 1/4\ (I_{A^+} - A_{A0})$$

and

$$\eta_B = 1/4\ (I_{B0} - A_{B^-})$$

where η_A and η_B are the hardness for the acid A and base B, I_{B0} and I_{A^+} are the first and second ionization potentials, and A_{A0} and A_{B^-} the first and second electron affinities for atom A, respectively. This theory was developed and used in molecular calculations (20),[2,3] and it becomes essential to know the second electron affinities of atoms to evaluate the hardnesses for a base of the atom or group.

Baughan (21) calculated the first, second, and third electron affinities of atoms using the lattice-energy data of some ionic crystals and the spectroscopic data of the corresponding molecules; he also estimated the values of the second electron affinities for elements O, S, and Se and the third electron affinity for N by extrapolation, starting from the first, second, and third ionization potentials of the corresponding atom.

HF calculations of doubly charged negative ions in a crystal have been performed by Gásper and Csavinszky (22), who presented the solution for O^{2-}, and Watson (14), who published the analytic form of wave functions, the one-electron eigenvalues, the two-electron integrals, and the total energy for the doubly charged negative ion, O^{2-}. The SCF calculation for a doubly charged negative ion is much more difficult than that for a neutral atom, a positive ion, or even a singly charged negative ion, since the asymptotic form of the potential function becomes positive when the atomic radial variable r approaches infinity.

The generalized exchange local-spin-density functional (LSD–GX) theory derived by Manoli and Whitehead (23) with the self-interaction correction (SIC) (24) and the Vosko, Wilk, and Nusair (VWN) (25) correlation energy functional has been very successful in predicting the ionization potentials and first electron affinities of atoms (8–10) and as reliable as HF theory, because the LSD–GX–SIC statistical total energy of an atom is very close to the HF value. Therefore, this theory is expected to be as reliable as HF in calculating the second electron affinities of atoms, and very much more convenient.

The second electron affinities in LSD–GX–SIC theory are obtained using the Watson sphere to simulate the environment of the doubly charged negative ion in the crystal and adjusting

[1]Permanent address: Department of Applied Physics, National University of Defense Technology, Shangsha, Hunan, People's Republic of China.

[2]D. Berard and M. A. Whitehead. To be published.

[3]G. Barrie and M. A. Whitehead. To be published.

Can. J. Chem. Downloaded from www.nrcresearchpress.com by 91.121.58.235 on 09/07/12
For personal use only.

TABLE 1. The statistical total energies (Ry) for the singly and doubly charged negative ions of oxygen in the Watson sphere aided LSD–GX–SIC theory with correlation correction

	Without Watson sphere energy charge on sphere			With Watson sphere energy charge on sphere		
Ionicity	+2	+1	0	+2	+1	0
−1	−150.0894	−150.1131	−150.1310	−163.5258	−156.8166	−150.1310
−2	−149.4502	−149.5549	—	−164.2259	−156.8741	—
EA(2)	−0.6392	−0.5582		+0.7001	+0.0575	

the Watson sphere radius to make the calculated values fit experiment for O, S, and Se. The best second electron affinities occur with a Watson sphere radius of about 3.0 au for these three elements. This Watson sphere radius is assumed suitable for other elements, and is applied to estimate the second electron affinities of the elements helium to krypton.

II. Method

In SIC–LSD theory, the asymptotic form of the potential is

$$[1] \quad V(r) = -\frac{Z - N + 1}{r}$$

as r approaches infinity; Z and N are the atomic number and the number of electrons in an atom. For the doubly charged negative ion, $N = Z + 2$, and eq. [1] becomes

$$[2] \quad V(r) = \frac{1}{r}$$

This is a repulsive interaction. Physically, the second extra electron is not bound by a singly charged negative ion in its free state because of the repulsive potential surrounding the isolated negative ion. Numerically, there is a continuous solution of the Schrödinger equation with the asymptotic potential of eq. [2], instead of a bound wave function.

Stable doubly charged negative ions exist in crystals, because of the surrounding environment. To simulate such an environment for the doubly charged negative ions in the crystals and to ensure a bound solution to the Schrödinger equation, Watson proposed a sphere of charge +1 or +2 with a defined radius surrounding the free singly or doubly charged negative ion. The charged sphere forces the asymptotic form of the potential to be negative and the Schrödinger equation to give a bound solution.

The extra potential generated by a Watson sphere with charge +1 or +2 (the environment of the doubly charged negative ion in the crystal) is combined within LSD–GX–SIC theory. The details of this theory and VWM correlation energy functional can be found in the literature (9, 23–25).

III. Results and discussion

The calculation of the doubly charged negative ion of oxygen, O^{2-}, was carried out using LSD–GX–SIC theory with the VWN correlation energy functional, the Gopinathan, Whitehead, and Bogdanovic (GWB) (26) Fermi-hole parameters, and a Watson sphere of charge +1 and +2. The calculated LSD–GX–SIC statistical total energy (including the energy contribution of the Watson sphere but excluding the VWN correlation energy correction) for O^{2-} was −156.2137 Ry for the +1 Watson sphere and −163.5574 Ry for the +2 Watson sphere, compared to Watson's HF calculation (14) in which the total ionic energy (including Watson sphere energy) was −156.1194 Ry for the +1 Watson sphere and −163.4968 Ry for the +2 Watson sphere. The same radius (1.4 Å or 2.66 au) of Watson sphere (14) was used in both calculations. The excellent agreement of the total energies for the doubly charged negative ion from LSD–GX–SIC theory and from HF theory parallels that for the neutral atoms, positive ions, and the singly charged negative ions (8, 27). Therefore LSD–GX–SIC theory predicts doubly charged negative ions as reliably as HF theory.

The statistical total energy of a negative ion from Watson-sphere-aided LSD–GX–SIC theory is dependent on the charge on the Watson sphere. There are several choices for this charge, +2, +1, or 0 for singly and doubly charged negative ions. Calculation shows that there is no difficulty in getting convergent results for singly and doubly charged negative ions with a Watson sphere of charge +1 and +2, but, as mentioned in Sect. II, it is impossible to obtain a convergent value for a doubly charged negative ion using a Watson sphere of charge 0, which is equivalent to a calculation without a Watson sphere.

Table 1 summarizes the VWN correlation energy corrected statistical total energies without and with the energy contribution of the Watson sphere for the singly and doubly charged negative ions of oxygen, O^- and O^{2-}, in LSD–GX–SIC theory with the Watson sphere of charge +2, +1, and 0 and radius 2.66 au. The last line gives the corresponding energy differences of the singly and doubly charged negative ions, that is,

$$[3] \quad \mathrm{EA} = E_{\mathrm{tot}}{}^{-} - E_{\mathrm{tot}}{}^{2-}$$

the second electron affinity of O, where $E_{\mathrm{tot}}{}^{-}$ and $E_{\mathrm{tot}}{}^{2-}$ are the statistical total energy excluding the Watson sphere energy (corresponding to columns 2, 3, and 4 in Table 1) or the statistical total energy including the Watson sphere energy (columns 5, 6, and 7), respectively. Compared to the experimental second electron affinity, −0.61 Ry for O, it is clear that the difference of the statistical total energies (excluding the Watson sphere energy) with both +1 and +2 charges for the singly and doubly charged negative ions (columns 2 and 3) can be used to fit the experimental value of the second electron affinity for O by slightly adjusting the radius of the Watson sphere. However, the difference of the statistical total energy including the Watson sphere energy (columns 5 and 6) cannot be fitted to experiment. The best prediction of the second electron affinity for O is with the Watson sphere of charge +2.

The difference in the statistical total energies between the singly charged negative ion O^- with the Watson sphere of charge +1 and the doubly charged negative ion O^{2-} with the Watson sphere of charge +2 is −0.6629 Ry, close to experiment. It can be used to fit the experimental value by adjusting the radius of the Watson sphere. However, this method was not used to predict any other second electron affinity because (i) the best fit of the second electron affinity is obtained from the

Can. J. Chem. Downloaded from www.nrcresearchpress.com by 91.121.58.235 on 09/07/12
For personal use only.

Can. J. Chem. Downloaded from www.nrcresearchpress.com by 91.121.58.235 on 09/07/12
For personal use only.

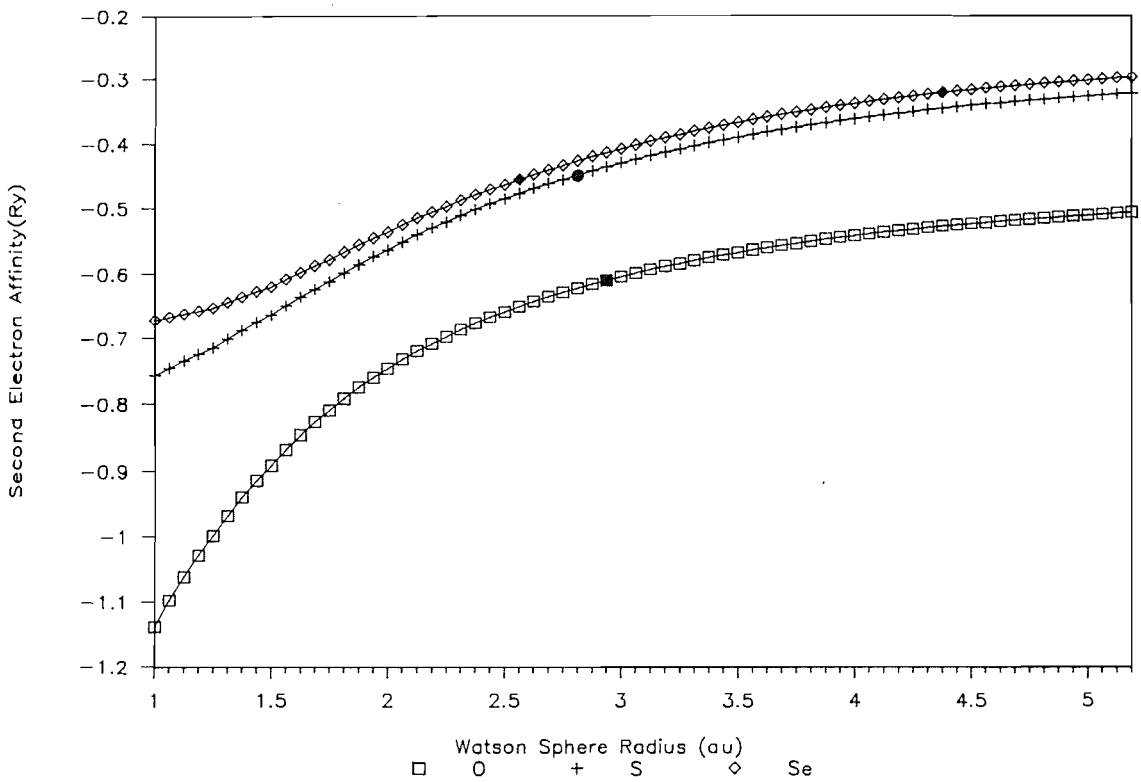

FIG. 1. The second electron affinities of O, S, and Se vs. the radius of the Watson sphere with charge +2.

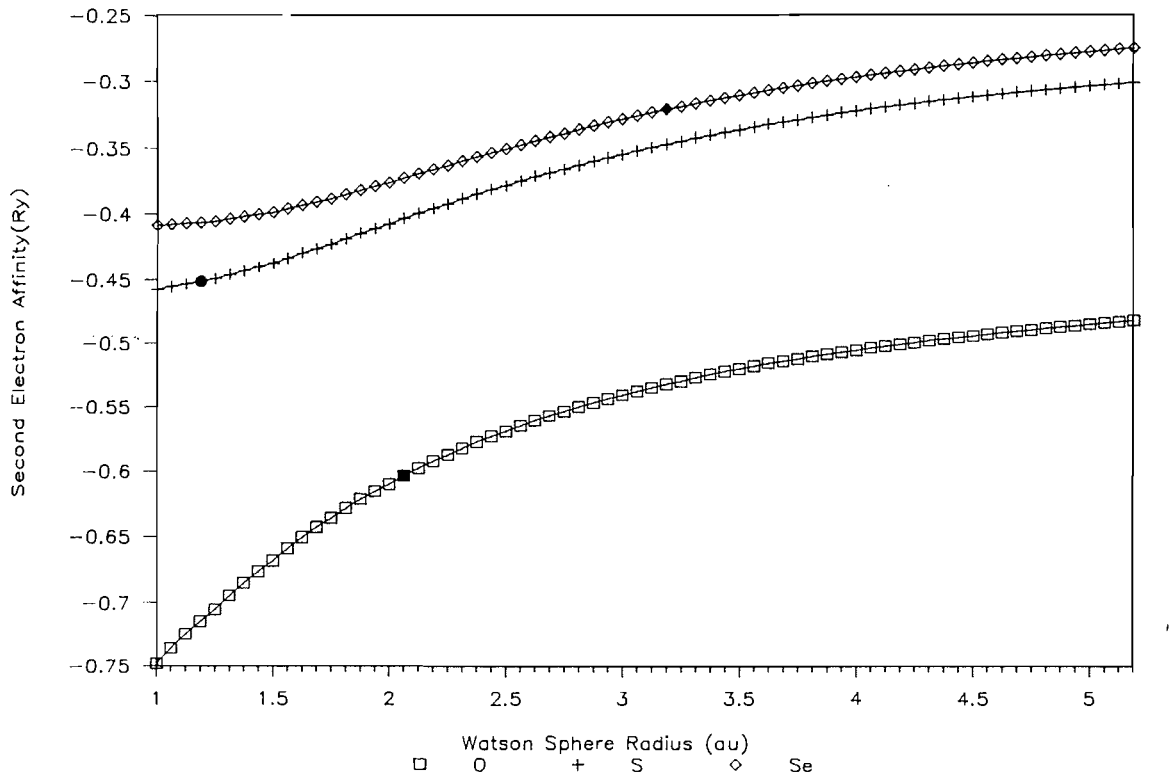

FIG. 2. The second electron affinities of O, S, and Se vs. the radius of the Watson sphere with charge +1.

TABLE 2. The negative of the second electron affinities EA(2) (Ry) of the atoms helium to krypton in the LSD–GX–SIC theory with VWN correlation energy functional, compared with other calculations and experiment

Z	Atom	Electron configuration		LSD–GX–SIC		Other calculations	Experiment
		M^-	M^{2-}	Without VWN	With VWN		
1	H	$1s^2$	$1s^22s^1$	0.4373	0.4303		
2	He	$1s^22s^1$	$1s^22s^2$	0.5092	0.4583		
3	Li	$2s^2$	$2s^22p^1$	0.5977	0.5712		
4	Be	$2s^22p^1$	$2s^22p^2$	0.5754	0.5564		
5	B	$2s^22p^2$	$2s^22p^3$	0.5573	0.5428		
6	C	$2s^22p^3$	$2s^22p^4$	0.7431	0.6635		
7	N	$2s^22p^4$	$2s^22p^5$	0.6993	0.6383	0.61[a]	
8	O	$2s^22p^5$	$2s^22p^6$	0.6534	0.6041	0.61[b]	0.60[b] 0.59[c]
9	F	$2p^6$	$2p^63s^1$	0.5754	0.5649		
10	Ne	$2p^63s^1$	$2p^63s^2$	0.5561	0.5048		
11	Na	$3s^2$	$3s^23p^1$	0.5721	0.5478		
12	Mg	$3s^23p^1$	$3s^23p^2$	0.5376	0.5196		
13	Al	$3s^23p^2$	$3s^23p^3$	0.4992	0.4846		
14	Si	$3s^23p^3$	$3s^23p^4$	0.6077	0.5312		
15	P	$3s^23p^4$	$3s^23p^5$	0.5414	0.4828		
16	S	$3s^23p^5$	$3s^23p^6$	0.4769	0.4282	0.40[b]	0.45[b] 0.45[a]
17	Cl	$3p^6$	$3p^64s^1$	0.5190	0.5054		
18	Ar	$3p^64s^1$	$3p^64s^2$	0.5048	0.4589		
19	K	$4s^2$	$3d^14s^2$	0.5049	0.4814		
20	Ca	$3d^14s^2$	$3d^24s^2$	0.4741	0.4558		
21	Sc	$3d^24s^2$	$3d^34s^2$	0.6282	0.6034		
22	Ti	$3d^34s^2$	$3d^54s^1$	0.6908	0.7546		
23	V	$3d^54s^1$	$3d^54s^2$	0.5781	0.4844		
24	Cr	$3d^54s^2$	$3d^64s^2$	0.8363	0.7657		
25	Mn	$3d^64s^2$	$3d^74s^2$	0.7978	0.7343		
26	Fe	$3d^74s^2$	$3d^84s^2$	0.7635	0.7053		
27	Co	$3d^84s^2$	$3d^{10}4s^1$	1.0075	0.9570		
28	Ni	$3d^{10}4s^1$	$3d^{10}4s^2$	0.5352	0.4877		
29	Cu	$4s^2$	$4s^24p^1$	0.6316	0.6058		
30	Zn	$4s^24p^1$	$4s^24p^2$	0.5665	0.5478		
31	Ga	$4s^24p^2$	$4s^24p^3$	0.5106	0.4957		
32	Ge	$4s^24p^3$	$4s^24p^4$	0.5986	0.5235		
33	As	$4s^24p^4$	$4s^24p^5$	0.5246	0.4669		
34	Se	$4s^24p^5$	$4s^24p^6$	0.4549	0.4066		0.46[b] 0.32[a]
35	Br	$4p^6$	$4p^65s^1$	0.5004	0.4861		
36	Kr	$4p^65s^1$	$4p^65s^2$	0.4839	0.4397		

[a]Reference 15.
[b]Reference 21.
[c]Reference 16.

difference of the statistical total energies, with Watson spheres of charge +2 and radius 2.66 au (which is interestingly close to the lattice distance); (ii) physically, the second electron affinity should be the total energy difference between the singly and doubly charged negative ions in the same environment; it is possible to obtain a positive second electron affinity for an atom by using a different environment for the singly and doubly charged negative ions.

The statistical total energy of the negative ion in Watson-sphere-aided LSD–GX–SIC theory depends on the Watson sphere radius. Therefore the difference between the statistical total energies of the singly and doubly charged ions, eq. [3], depends on the choice of Watson sphere radius. Watson suggested using the ionic radius of the doubly charged negative ion for the artificial charged sphere. This suggestion was tested in the present work for O, S, and Se using a Watson sphere of charge +2. The second electron affinity in LSD–GX–SIC theory with VWN correlation energy correction is −0.6655 Ry for O, −0.3858 Ry for S, and −0.3462 Ry for Se, compared to the averaged experimental values, which are −0.595 Ry for O, −0.45 Ry for S, and −0.39 Ry for Se. Obviously, the agreement between the calculated and experimental values is not consistent for these three elements; the second electron affinity is underestimated for O and overestimated for S and Se using the ionic radii of the doubly charged negative ions for the Watson spheres.

To find the Watson sphere radius that is best for calculating the second electron affinity of an atom, the second electron affinities, the difference of the statistical total energies (including the VWN correlation energy correction but excluding the

Can. J. Chem. Downloaded from www.nrcresearchpress.com by 91.121.58.235 on 09/07/12
For personal use only.

Can. J. Chem. Downloaded from www.nrcresearchpress.com by 91.121.58.235 on 09/07/12
For personal use only.

Watson sphere energy) between the singly and doubly charged negative ions, with a Watson sphere of charge +2 are plotted in Fig. 1 against the radius of Watson sphere for O, S, and Se in LSD–GX–SIC theory with VWN correlation energy functional and GWB Fermi-hole parameters. Figure 2 has a Watson sphere of charge +1. The experimental values of the second electron affinities for O (16, 21), S, and Se (15, 21) are also marked on the corresponding curves of these figures. From Figs. 1 and 2, it is obvious that the calculated second electron affinities of O, S, and Se are much less negative with a Watson sphere of charge +1 than with a sphere of charge +2 for the same Watson sphere radius. Physically, a Watson sphere of charge +2 is more reasonable, because the net charge provided by the remainder of a crystal would be +2 for an equilibrium situation. The Watson sphere has to be very small to give an acceptable second electron affinity with a +1 charge sphere so that it is far from the lattice distance found in the crystal.

Figure 1 illustrates the calculated second electron affinity for O equal to experiment at a Watson sphere radius of approximately 3.0 au: approximately 2.8 au for S and 2.6 au for Se or 4.37 au, since two different experimental values of the second electron affinity for Se are given (15, 21). The "best" Watson sphere radius, suitable for the three doubly charged negative ions to give correct second electron affinities, compared to experiment, is approximately 3.0 au.

Table 2 lists the negative of the second electron affinities for atoms helium to krypton calculated using eq. [3], in which the total energies are the statistical total energies (including VWN correlation energy correction and excluding the energy generated by the Watson sphere) with a Watson sphere of charge +2 and radius 3.0 au using LSD–GX–SIC theory with VWN correlation energy functional and GWB Fermi-hole parameters. These results are compared with other estimations (15, 21), for which extrapolation was used, and with experiment (15, 16, 21). Columns 3 and 4 give the electron configurations of the singly and doubly charged negative ions, chosen according to the ground-state electron configuration of the atom, in which the total number of electrons is the same as in the negative ion. Columns 5 and 6 give the present results without and with VWN correlation energy correction.

Table 2 shows that all the doubly charged negative ions are unstable (the negative values of the second electron affinities), which supports the physical fact that they exist only in crystals (Sect. II). The statistical total energy of the singly charged negative ion is lower than that of the doubly charged negative ion for all these elements.

It may be seen that the second electron affinities for the same group elements become less negative as the atomic number Z increases, except for the first row elements, H and He, where the average Watson sphere radius of 3.0 au is too far from the ideal for these atoms. The second electron affinities, EA(2), of the same row elements in which the outermost orbitals are $2p$ also become less negative as the occupation number of their spin quantum number m_s increases, that is,

$$\mathrm{EA(2)_{Li}} < \mathrm{EA(2)_{Be}} < \mathrm{EA(2)_{B}}$$

and

$$\mathrm{EA(2)_{C}} < \mathrm{EA(2)_{N}} < \mathrm{EA(2)_{O}}$$

etc., as is true for the elements in which the outermost orbitals are $3p$ and $4p$. The calculated results parallel experiment. These trends are reasonable; as the total number of electrons increases, the exchange correlation, which is approximately proportional to the number of electrons, also increases. The existence of stable negative ions of atoms in nature is mainly caused by the quantum effect, which is the negative contribution of the exchange-correlation effect of the electrons to the energy functional; therefore the results should parallel the exchange correlation.

Conclusion

It has been shown that the Watson sphere is an effective technique for calculating the doubly charged negative ions, which normally cause non-convergent problems (28, 29). The second electron affinities of atoms are acceptable when a correct radius of Watson sphere is chosen; the method has been illustrated and the trends established using a fairly accurate average Watson sphere radius of 3.0 au. Specific choice of radius would yield slightly more accurate numerical results but would not alter the trends. This method can be extended to estimate values for the high-Z atoms.

Acknowledgments

This research was partly supported by Natural Sciences and Engineering Research Council of Canada. The authors wish to thank Mr. G. Barrie for useful discussion.

1. H. Hotop and W. C. Lineberger. J. Phys. Chem. Ref. Data, **4**, 539 (1975); **14**, 731 (1985).
2. C. F. Fischer, J. B. Lagowski, and S. H. Vosko. Phys. Rev. Lett. **59**, 2263 (1987).
3. D. J. Pegg, J. S. Thompson, R. N. Compton, and G. D. Alton. Phys. Rev. Lett. **59**, 2267 (1987).
4. S. H. Vosko, J. B. Lagowski, and I. L. Mayer. Phys. Rev. A, **39**, 446 (1989).
5. C. F. Fischer. Phys. Rev. A, **39**, 963 (1989).
6. Z. Cai and D. R. Beck. Phys. Rev. A, **40**, 1657 (1989).
7. J. G. Harrison. J. Chem. Phys. **86**, 2849 (1987).
8. Y. Guo, S. Manoli, and M. A. Whitehead. Phys. Rev. A, **38**, 1120 (1988).
9. Y. Guo and M. A. Whitehead. Phys. Rev. A, **38**, 3166 (1988); **39**, 28 (1989); **39**, 2317 (1989).
10. Y. Guo and M. A. Whitehead. Phys. Rev. A, **40**, 28 (1989).
11. Y. Guo, M. Wrinn, and M. A. Whitehead. Phys. Rev. A, **40**, 6685 (1989).
12. P. Fuentealba, A. Savin, H. Stoll, and H. Preuss. Phys. Rev. A, **40**, 2163 (1989).
13. E. H. Lieb. Phys. Rev. A, **29**, 3018 (1984).
14. R. E. Watson. Phys. Rev. **111**, 1108 (1958).
15. J. E. Huheey. Inorganic chemistry. 3rd ed. Harper and Row, New York. 1983.
16. A. P. Ginsberg and J. M. Miller. J. Inorg. Nucl. Chem. **7**, 351 (1958).
17. R. S. Berry. Chem. Rev. **69**, 533 (1969).
18. H. Massey. Negative ions. 3rd ed. Cambridge, London. 1976.
19. A. R. Orsky and M. A. Whitehead. Can. J. Chem. **65**, 1970 (1987).
20. J. Todd and M. A. Whitehead. Theo. Chem. **202**, 99 (1989).
21. E. C. Baughan. Trans. Faraday Soc. **55**, 736 (1959); 2025 (1959); **57**, 1863 (1963).
22. R. Gásper and P. Csavinszky. Acta Phys. Acad. Sci. Hung. **4**, 125 (1956).
23. S. Manoli and M. A. Whitehead. Phys. Rev. A, **34**, 4629 (1986).
24. S. Manoli and M. A. Whitehead. Phys. Rev. A, **38**, 630 (1988).
25. S. H. Vosko, L. Wilk, and M. Nusair. Can. J. Phys. **58**, 1200 (1980).
26. M. S. Gopinathan, M. A. Whitehead, and R. Bogdanovic. Phys. Rev. A, **14**, 1 (1976).
27. Y. Guo and M. A. Whitehead. Can. J. Chem. **68**, 989 (1990).
28. J. P. Perdew and A. Zunger. Phys. Rev. B, **23**, 5048 (1981).
29. J. P. Perdew and L. A. Cole. Phys. Rev. A, **25**, 1265 (1982).

FOR ERRATA SEE
68 1990 P. 2122

Radical clocks as probes of 1,4-biradical intermediates in the photochemical cycloaddition reactions of 2-cyclopentenone with alkenes[1]

ANDREAS RUDOLPH AND ALAN C. WEEDON[2]

The Photochemistry Unit, Department of Chemistry, The University of Western Ontario, London, Ont., Canada N6A 5B7

Received February 28, 1990

ANDREAS RUDOLPH and ALAN C. WEEDON. Can. J. Chem. **68**, 1590 (1990).

The products of the photochemical reaction of 2-cyclopentenone with 1,6-heptadiene and with vinylcyclopropane have been examined. With 1,6-heptadiene the products were cyclobutanes, which arise from 2 + 2 photocycloaddition between the cyclopentenone carbon–carbon double bond and one of the two terminal double bonds of the heptadiene. The 1,4-biradical that is an intermediate in this reaction contains a derivative of a 1-hexenyl radical; no products derived from cyclization of this intermediate to a cyclopentylmethyl radical were observed. With vinylcyclopropane some of the products isolated also arose from 2 + 2 photocycloaddition; in addition, comparable quantities of products resulting from rearrangement of the intermediate 1,4-biradical were obtained. In this case the initially produced intermediate 1,4-biradical contains a cyclopropylmethyl radical that can rearrange to a homoallylic radical; the products isolated were derived from intramolecular disproportionation in the new 1,7-biradical containing the homoallylic radical. The rate constant for the rearrangement of the cyclopropylmethyl radical to the homoallylic radical is known and was used as a clock to estimate the lifetime of the initially produced 1,4-biradical. The value estimated is of the order of 50 ns. The structures of the products indicate that the initial bonding between the excited cyclopentenone and vinylcyclopropane takes place at both the α-position and the β-position of the enone and not exclusively at the α-position as a recent report claims.

Key words: enone photocycloaddition, 1,4-biradicals, radical clocks.

ANDREAS RUDOLPH et ALAN C. WEEDON. Can. J. Chem. **68**, 1590 (1990).

On a examiné la nature des produits de la réaction photochimique de la cyclopent-2-ènone avec l'hepta-1,6-diène et avec le vinylcyclopropane. Avec l'hepta-1,6-diène, les produits sont des cyclobutanes qui proviennent d'une photocycloaddition 2 + 2 entre la double liaison carbone–carbone de la cyclopenténone et l'une des deux doubles liaisons terminales de l'heptadiène. Le 1,4-diradical intermédiaire dans cette réaction contient un dérivé d'un radical hex-1-ènyle; on n'a pas observé la formation de produits provenant de la cyclisation de cet intermédiaire en un radical cyclopentylméthyle. Avec le vinylcyclopropane, quelques produits isolés provenaient aussi d'une photocycloaddition 2 + 2; de plus, on a obtenu des quantités comparables de produits provenant d'une transposition du 1,4-biradical intermédiaire. Dans ce cas, l'intermédiaire 1,4-biradical qui se forme initialement contient un radical cyclopropylméthyle qui se transpose en un radical homoallylique; les produits isolés proviennent d'une disproportionation intramoléculaire en un nouveau 1,7-biradical qui contient le radical homoallylique. La constante de vitesse pour la transposition du radical cyclopropylméthyle en radical homoallylique est connue et on l'a utilisée comme horloge pour évaluer le temps de vie du 1,4-biradical produit initialement. La valeur estimée est de l'ordre de 50 ns. Les structures des produits indiquent que la liaison initiale entre la cyclopenténone excitée et le vinylcylopropane se produit autant en position α qu'en position β de l'énone et non pas uniquement en position α comme il avait été suggéré récemment.

Mots clés : photocycloaddition d'énone, 1,4-biradicaux, radicaux agissant comme horloge.

[Traduit par la revue]

Introduction

The photochemical cycloaddition reaction of enones with alkenes to give cyclobutane products (e.g., Scheme 1) has been the subject of many reports over the last 30 years and numerous examples of the application of this reaction to the synthesis of natural products and of novel carbon skeletons have appeared (1). The synthetic application of the reaction has made necessary an understanding of the factors that control the stereochemistry and regiochemistry of the alkene addition and this has stimulated a large amount of work aimed towards the determination of the reaction mechanism. It has been proposed by Loutfy and de Mayo (2) that the reaction proceeds as shown in Scheme 2. In this scheme the triplet excited state of the enone, $^3E^*$, forms an exciplex, $^3EA^*$, with the alkene, A. Bond formation in the exciplex between one terminus of the alkene and either the α-position or the β-position of the enone leads to a triplet 1,4-biradical species, BIR. The major fates of the biradical are reversion to ground state enone and alkene, or closure to the

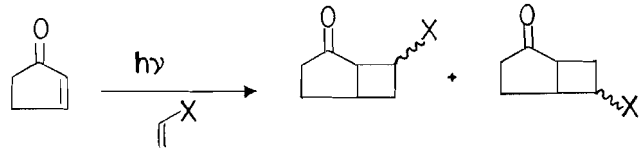

SCHEME 1

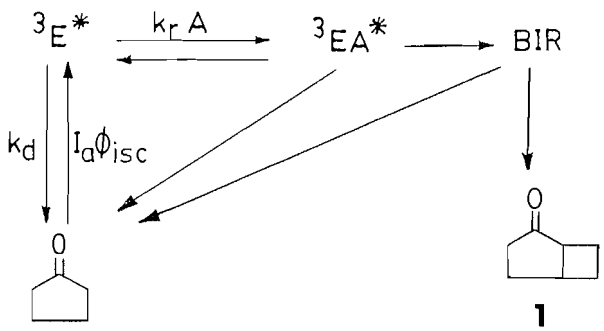

SCHEME 2

[1]Contribution number 430 from the Photochemistry Unit, University of Western Ontario.

[2]Author to whom correspondence may be addressed.

Can. J. Chem. Downloaded from www.nrcresearchpress.com by 91.121.58.235 on 09/07/12
For personal use only.

cyclobutane-containing product **1**, although intramolecular disproportionation is occasionally competitive (1).

Elements of this cycloaddition mechanism remain controversial; for example, there is still no general agreement concerning the site of initial bonding of the alkene to the enone and hence the structure of the intermediate 1,4-biradical (see for, example, ref. 3). Thus for the reaction of cyclopentenone with ethylene to give **1** the biradical could, in principle, have either structure **2** or structure **3**, which correspond to initial bonding to the enone

α-position or β-position, respectively. In addition, while the intermediacy of biradicals in the photocycloaddition reaction is well established from indirect kinetic evidence (1, 2) and from product studies (1), it has not yet been observed directly and no value of the biradical lifetime has been determined.

The work described here was designed to allow an estimate to be made of the biradical lifetime and also to determine whether the initial bonding between the enone and the alkene in the biradical is via the α-position or the β-position of the enone. The approach adopted was to perform the photocycloaddition reaction using alkenes that yield biradicals that, in competition with ring closure to normal cyclobutane products, are capable of undergoing a rearrangement leading to alternative products. The rearrangement reaction can then be used as a probe of both the structure of the biradical and, if the rate of the rearrangement reaction is known, as a clock (4) to measure its lifetime.

The alkenes chosen for this study were 1,6-heptadiene and vinylcyclopropane.

Scheme 3 shows the anticipated outcome of the reaction between cyclopentenone and vinylcyclopropane. Interaction of the triplet excited enone and the alkene can in principle lead to the biradicals **4**–**7**, although **4** and **7** might be expected to dominate over **5** and **6** because the latter pair contain primary radical centres. Biradicals **4** and **5** can cyclize to **8** while **6** and **7** can close to **9**. The biradicals **4** and **7** contain a cyclopropylalkyl radical that is known (5) to ring open rapidly to a homoallylic radical as shown for the formation of **10** and **11** from **4** and **7**, respectively. If double bond geometry is correct in **10** and **11** then they can close to **12** and **13**, respectively. The rate of the rearrangement of the cyclopropyl methyl radical to the homoallylic radical is known (5); therefore, the quantities of **12** and **13** formed relative to the amounts of **8** and **9** can be used to infer the rate of formation of **8** and **9** from **4** and **7**, and hence the lifetime of **4** and **7**. In addition, since **13** is only formed from **7**, and **12** is only formed from **4**, the question of whether the products are formed by initial bonding between the alkene and either the α-position or the β-position of the enone can be answered by determining which of **12** and **13** is produced.

In Scheme 4 the expected outcome of the reaction between cyclopentenone and 1,6-heptadiene is shown. The expected biradicals are **14**–**17**, although **14** and **17** may dominate since **15** and **16** contain primary radical centres. Cyclization of **14** and **15** gives **18** while cyclization of **16** and **17** gives **19**. However, **14** and **17** contain derivatives of 1-hexenyl radicals, which are known (6) to be capable of cyclization to cyclopentylmethyl radicals. If this occurs here then species **20** and **21** will be formed, which can proceed to the various stereoisomers of **22**. Since the rate of the cyclization of 1-hexenyl radicals to cyclopentylmethyl radicals is known (6), the proportions of **18** and **19** relative to **22** formed can be used to define the lifetime of the biradicals **14** and **17**.

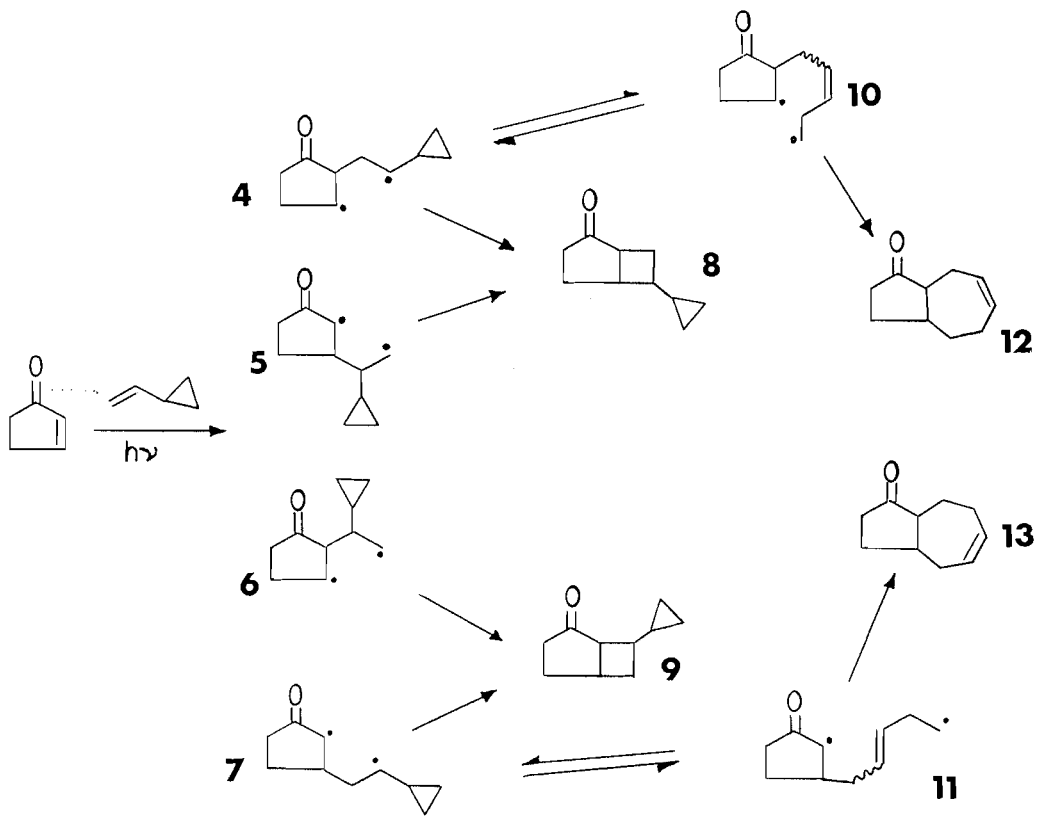

SCHEME 3

Can. J. Chem. Downloaded from www.nrcresearchpress.com by 91.121.58.235 on 09/07/12
For personal use only.

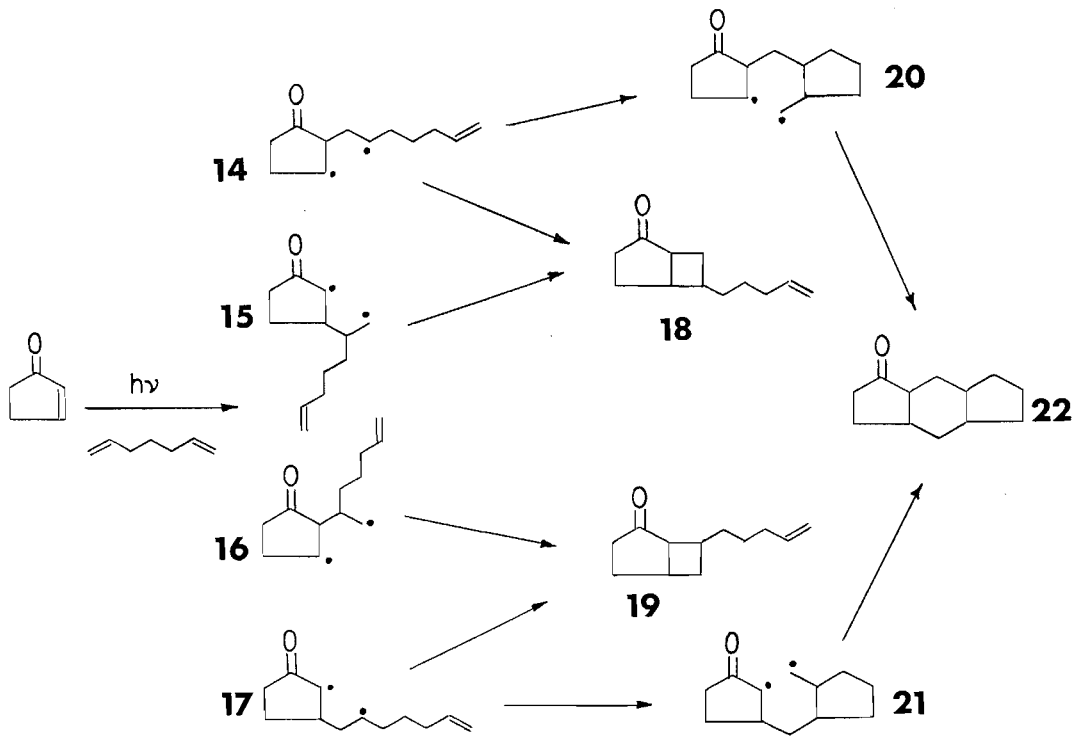

SCHEME 4

Results

Irradiation of cyclopentenone with vinylcyclopropane

Irradiation with UV light of a cyclohexane solution of cyclopentenone and vinylcyclopropane gave the previously described

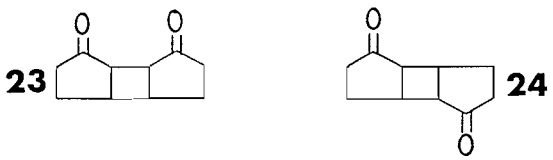

cyclopentenone dimers **23** and **24** (7) along with a mixture of four 1:1 adducts of the cyclopentenone and vinylcyclopropane.

The ^{1}H NMR spectrum of the product mixture after removal of solvent and excess reactants indicated the presence of compounds possessing cyclopropyl rings (signals at 0.1–0.8 ppm). In addition, olefinic signals (at 5.5 ppm) were observed, indicative of non-conjugated 1,2-dialkyl substituted alkenes. This was in accord with expectations since it was anticipated that the mixture would contain adducts of the type **8** and **9**, and **12** and **13**. However, the ^{1}H NMR spectrum of the reaction mixture also contained signals corresponding to the olefinic protons on a cyclopentenone ring (resonances at 6.1 and 7.2 ppm) even though all unreacted cyclopentenone had been removed.

It was possible to separate the adducts from the cyclopentenone dimers by preparative thin-layer chromatography (PLC) and this technique also allowed partial separation of the adducts into two groups. The ^{1}H NMR spectrum of the more polar group of adducts indicated the absence of olefinic signals and the presence of signals in the region 0.1–0.8 ppm. Consequently it was tentatively concluded that this fraction contained the expected 2 + 2 cycloadducts **8** and **9**. The ^{1}H NMR spectrum of the less polar material revealed that this contained the species possessing the olefinic hydrogens and none of the cyclopropyl ring containing species.

The more polar fraction (i.e., that containing the 2 + 2 adducts **8** and **9**) was further separated by preparative gas chromatography. We were not able to obtain the separate adducts entirely free from each other and so full characterization of the structures was not possible. Consequently no conclusions could be drawn as to the stereochemistry and regiochemistry of these compounds. The general structures **8** and **9** were, however, confirmed by the ^{1}H NMR and mass spectra of the partially separated components.

The mixture of compounds present in the less polar fraction from PLC was further separated by preparative GC and yielded comparable amounts of two major components each consisting of a single compound, and a very minor component consisting mainly of a mixture of two compounds. The two major components were identified as single geometrical isomers of the pentenyl substituted cyclopentenones **25** and **26**. The mixture of minor components was identified as the two alternative geometrical isomers of **25** and **26**. No trace of the expected rearrangement products **12** and **13** was found.

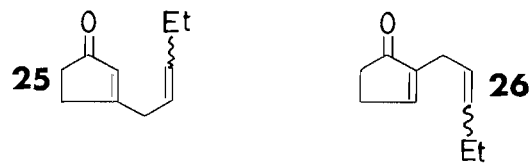

The structures of the two major isomers of **25** and **26** were deduced primarily from their ^{1}H NMR spectra. The ethyl group of both compounds appeared as a three-proton triplet at ca. 0.9 ppm coupled to two protons at 2 ppm, which appeared as a pentuplet showing evidence of further allylic coupling. The allylic coupling and part of the vicinal coupling in the latter signal arose from the adjacent pair of olefinic protons that appeared at ca. 5.3 and 5.5 ppm; these in turn were coupled to the adjacent methylene, which was found at 2.9 ppm. The single cyclopentenone olefinic proton in these compounds appeared in

Can. J. Chem. Downloaded from www.nrcresearchpress.com by 91.121.58.235 on 09/07/12
For personal use only.

Can. J. Chem. Downloaded from www.nrcresearchpress.com by 91.121.58.235 on 09/07/12
For personal use only.

one at 6.05 and in the other at 7.29 ppm. The chemical shifts of these protons allowed the point of attachment of the pentenyl side chain to be established since the α and β hydrogens of cyclopentenone come at 6.22 and 7.76 ppm, respectively; thus the product with a signal at 7.29 was identified as one of the geometrical isomers of **26** and that with the signal at 6.05 was identified as one of the geometrical isomers of **25**. The results of two-dimensional homonuclear ^{1}H correlation experiments showed the expected coupling between all the protons in the spectra of the two major isomers and confirmed the assignments. An attempt was made to assign the stereochemistry of the double bond of the pentenyl side chain by measurement of the coupling constants of the olefinic protons. However, in both compounds the olefinic protons were at very similar chemical shifts and this, along with the fact that they are further coupled both vicinally and allylically, made measurement of the coupling constants difficult. However, in the case of **25** it was possible to measure the desired coupling constant by recording the two-dimensional *J*-resolved ^{1}H NMR spectrum, from which a value of 9 Hz was obtained, indicative of *cis* stereochemistry (8).

The assignment of structure to the two minor geometrical isomers of **25** and **26**, which were isolated as a mixture in very small amounts, was based upon the mass spectral and ^{1}H NMR spectral data, which appeared as a composite of spectra very similar to those of the purified major isomers. In view of the very small amounts of these minor reaction products obtained, no further attempts were made to separate and characterize this mixture.

Comparison of the ^{1}H NMR spectra of the isolated samples of **8** and **9**, and **25** and **26**, with that of the crude reaction mixture indicated that these were the major components of the mixture and that no further products, such as **12** and **13**, had escaped notice. This was confirmed by GC comparison, which also allowed the ratio of (**8** + **9**) to (**25** + **26**) in the reaction mixture to be estimated as approximately 3.7:1.

Irradiation of cyclopentenone with 1,6-heptadiene

The reaction mixture obtained from irradiation of cyclopentenone (0.08 M) with 1,6-heptadiene (0.17 M) in cyclohexane was found to contain five major products by GC. The molecular ions in the mass spectra of the five products obtained by GC–MS of the reaction mixture indicated that two of them were dimers of cyclopentenone while the other three were 1:1 adducts of cyclopentenone with the diene. The fragmentation patterns of the three adducts were similar and showed characteristic $M^+ - 41$ peaks assigned to cleavage of an allyl fragment. This suggested that the adducts are stereoisomers of the expected cyclobutane products **18** and **19**, as did the observation of fragments corresponding to retro 2 + 2 cleavage of the cyclobutane ring. The cyclopentenone/1,6-heptadiene adducts were separated from the other components of the reaction mixture by PLC, although the adducts could not be separated from one another. The ^{1}H NMR spectrum of the adduct mixture contained the expected signals at 4.9 and 5.7 ppm corresponding to the terminal alkene of **18** and **19**. To confirm that none of the rearranged adduct **22** was present but masked by **18** and **19**, the entire reaction mixture was hydrogenated to reduce all alkene double bonds present. Inspection of the hydrogenated mixture by GC-MS revealed that while the cyclopentenone dimers were unchanged, all the other products, assigned to **18** and **19**, had moved to longer retention time and had increased in mass by two units. Thus it was concluded that none of the rearranged adduct **22** had been formed.

Discussion

Irradiation of cyclopentenone with 1,6-heptadiene gave none of the rearranged adduct **22** and no other products derived from the rearranged biradicals **20** or **21** were found. Apart from cyclopentenone dimers, only adducts assigned structures **18** and **19** were found. This must mean that the biradicals **14** and **17** close to the products **18** and **19** much faster than rearrangement of the 1-hexenyl radical to a cyclopentylmethyl radical. The rate constant for the latter rearrangement is at most 1.0×10^5 s^{-1} (6) and so it can be concluded that the biradicals **14** and **17** have lifetimes substantially shorter than 10 μs.

Irradiation of cyclopentenone with vinylcyclopropane gave a mixture of the 2 + 2 adducts **8** and **9** along with comparable amounts of the products **25** and **26**, which presumably result from disproportionation of the biradicals **10** and **11**. The latter are formed by opening the cyclopropyl alkyl radicals **4** and **7**. The cyclopropyl methyl radical has been estimated to open with a rate constant of 2.1×10^8 s^{-1} at room temperature (4, 5). If the methyl group is substituted, as in the cyclopropylethyl radical, then the extra stabilization slows the rate of opening to a value estimated as 2×10^7 s^{-1} (9, 10). If **4** and **7** open at a similar rate to the latter then the sum of their rate constants for ring closure to the cyclobutane products **8** and **9** plus their rate constants for reversion to the starting materials must be comparable with the rate constant for rearrangement of the secondary cyclopropylethyl radical. Hence the lifetimes of the biradicals **4** and **7** must be of the order of 50 ns.

The above arguments assume that none of the products **8**, **9**, **18**, and **19** are formed from biradicals **5**, **6**, **15**, and **16**, respectively, and that the observed products are predominantly derived from **4**, **7**, **14**, and **17**. While reaction via **5**, **6**, **15**, and **16** may represent a minor reaction pathway it is highly unlikely that the enone triplet excited state would react with the more hindered terminus of the mono-substituted alkenes to give the less stable biradical intermediates.This assumption is supported by the observed regioselectivity of the reaction of alkyl radicals with non-symmetrically substituted alkenes where the major product of addition is always that derived from attack at the less substituted end of the alkene (11). However, alkyl radicals are not perfect models of enone triplet excited states and better evidence for the regiochemistry of addition of an enone to an alkene can be found in the observed products of photoaddition between cyclohexenones and 2-methylpropene (12). In addition to cyclobutane-containing products, this reaction yields substantial quantities of compounds derived from intramolecular disproportionation of the intermediate biradicals. For example, the photochemical reaction between 3-methylcyclohexene and 2-methylpropene (Scheme 5) gives **27**–**30** in the yields shown (12*a*–*c*). These must be formed from the biradicals **31**–**34**, with **27** derived exclusively from **31**, and **30** exclusively from **34**. Of the isolated products, at most 14% (i.e., **29**) can have their origin in a biradical resulting from addition of the enone triplet excited state to the more substituted end of the alkene (i.e., **33**).

The value of 50 ns estimated for the lifetime of the 1,4-biradicals produced in the cycloaddition of cyclopentenone to vinylcyclopropane is towards the lower end of the range of lifetimes reported for other 1,4-biradicals such as those generated in the Norrish Type II reaction (13) and the Paterno–Buchi reaction (13c, 14), which have been reported to have lifetimes anywhere in the range of 1–2000 ns. It has been proposed that the lifetime of these biradicals at room temperature depends largely upon the rate of inter-system crossing from the triplet biradical to the singlet biradical, and less upon structural effects in the biradical

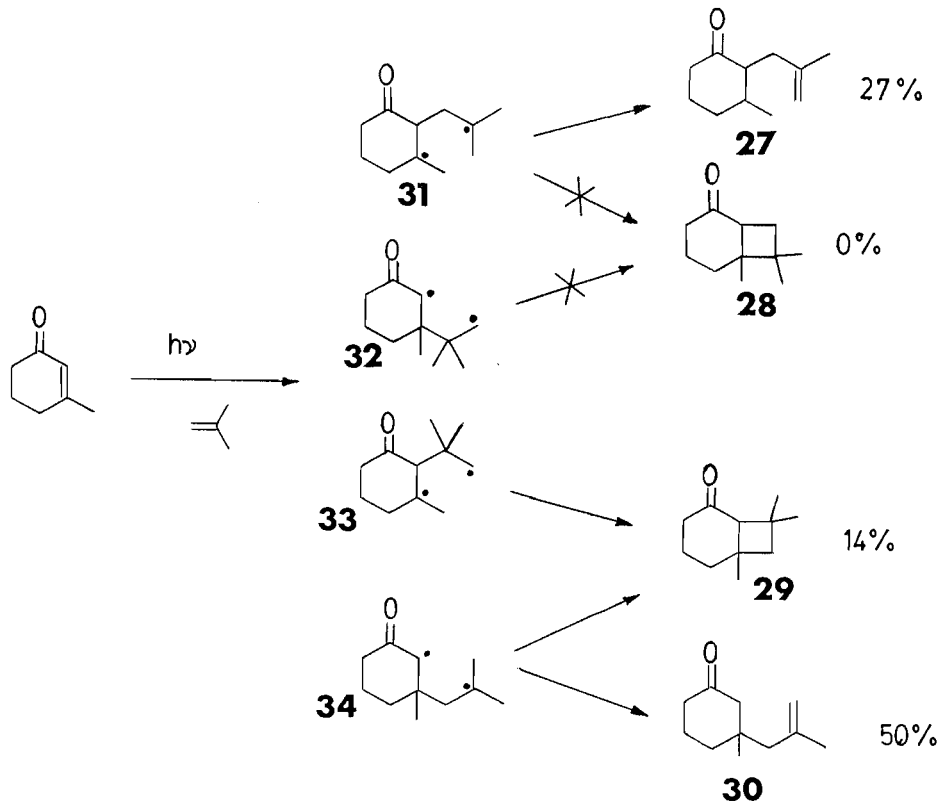

SCHEME 5

(15). The fact that the estimated lifetimes of **4** and **7** are in this range supports this idea.

The formation of similar quantities of **25** and **26** in the reaction between cyclopentenone and vinylcyclopropane indicates that the initial bond formation between the enone and the alkene occurs at both the α-position and the β-position of the cyclopentenone. This has not previously been demonstrated for cyclopentenones, although for cyclohexenones the same would also seem to apply since the products of biradical disproportionation in the reaction between 2-methylpropene and cyclohexenones (e.g., **27** and **30** in Scheme 5) must also be derived from initial bonding to both the α-position and the β-position of the enone (12).

The formation of disproportionation products **25** and **26** rather than the expected bicyclic adducts **12** and **13** requires some comment. Biradicals and radical pairs that contain cyclopropyl alkyl radicals have been generated in a number of photochemical reactions but these mainly involve intermediates produced from the excited states of cyclopropyl ketones. Examples include Norrish Type II reactions (9, 16) and intermolecular hydrogen abstraction reactions (17) of cyclopropyl ketones, as well as Norrish Type I reactions of α-cyclopropyl ketones (18). In general, because of the structures of the biradicals or radical pairs that are formed as intermediates in these reactions, the disproportionation process implicated in the production of **25** and **26** from **10** and **11** is not usually observed. The use of vinylcyclopropane derivatives as precursors of cyclopropyl alkyl radicals in photochemical reactions has been applied to the Paterno–Buchi reactions of aryl ketones and aldehydes (19). The triplet excited states of these carbonyl compounds interact with vinylcycloproprane (19*a*) to give a 1,4-biradical that contains a cyclopropyl alkyl radical capable of rearranging to a homoallylic radical. The isolated products are the unrearranged 2 + 2 adducts **35** (or their decomposition products) and the tetrahydro-oxepins **36** derived from closure of the biradicals formed from ring openings of the intermediate cyclopropyl alkyl radicals, as shown in Scheme 6. Two aspects of this reaction are especially pertinent to the results described in this paper. First, only the adducts with the regiochemistry exhibited by **35** are formed and none of the regioisomers **39** are obtained. This is consistent with the formation of a 1,4-biradical by bonding of the ketone oxygen to the terminus of the alkene to give the more stable secondary radical **37** rather than the primary radical **38**. This supports the argument given above for the preferential formation of biradicals **4** and **7** rather than **5** and **6** in the reaction between vinylcycloproprane and cyclopentenone. Second, the biradical **40** closed to the tetrahydro-oxepin **36** rather than undergoing an intramolecular disproportionation reaction analogous to that observed here for **10** and **11**, which gave **25** and **26**. The preference for closure over disproportionation shown by **40** presumably reflects the absence of an abstractable hydrogen atom adjacent to the ketyl radical in **40**.

Following the completion of this manuscript we became aware of a recent preliminary report describing the intramolecular addition of a 1,6-diene and a vinylcyclopropane to a cyclohexenone (20). The compounds examined were **41** and **42**. The former gave a mixture of compounds identified as cyclobutane-containing adducts while the latter also gave a mixture of species identified as cyclobutane-containing adducts along with a mixture of products assigned structures **43**. The latter are presumed to be formed by rearrangement of the intermediate **44** (which contains a cyclopropylmethyl radical) to **45** and subsequent closure to **43**. No disproportionation products corresponding to **25** and **26** were isolated, presumably because a suitable hydrogen is not present for abstraction by the terminal methylene radical in **45**.

Can. J. Chem. Downloaded from www.nrcresearchpress.com by 91.121.58.235 on 09/07/12
For personal use only.

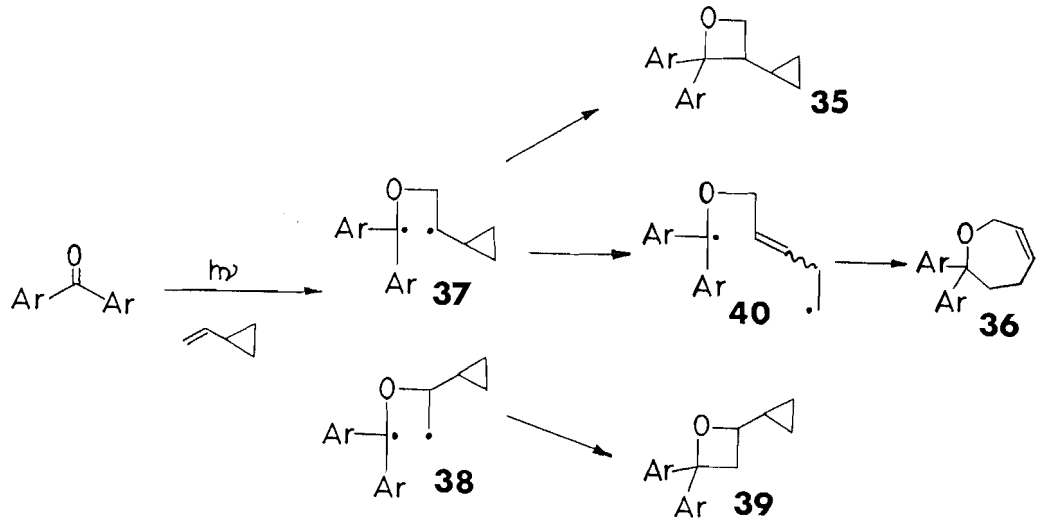

SCHEME 6

These results for the intramolecular 2 + 2 addition to a cyclohexenone complement ours for the intermolecular 2 + 2 addition to cyclopentenone. They imply that the intermediate 1,4-biradicals have similar lifetimes in both systems and decay with rate constants comparable with that of the cyclopropylmethyl radical ring-opening reaction. However, the results obtained for **42** are also used to support the idea that the first-formed bond in enone–alkene 2 + 2 photo-cycloaddition is formed between the alkene and the β-position of the enone. Our results suggest otherwise since we observe rearrangement products from both of the regioisomeric biradicals **4** and **7**. In fact, **42** is not a good probe of the site of initial bonding since the well-known "rule of five" (1) predicts that none of the alternative biradicals **46–48** should be formed in the intramolecular cycloaddition reaction of **42**, but rather that product formation via **44** should be favoured. Indeed, in a yet more recent report from the same laboratory (21) the products of intramolecular photochemical cycloaddition of 2-(4-pentenyl)-2-cyclohexenone and 3-(4-pentenyl)-2-cyclopentenone have been examined and the authors find no conclusive evidence that initial bonding occurs exclusively at any one position.

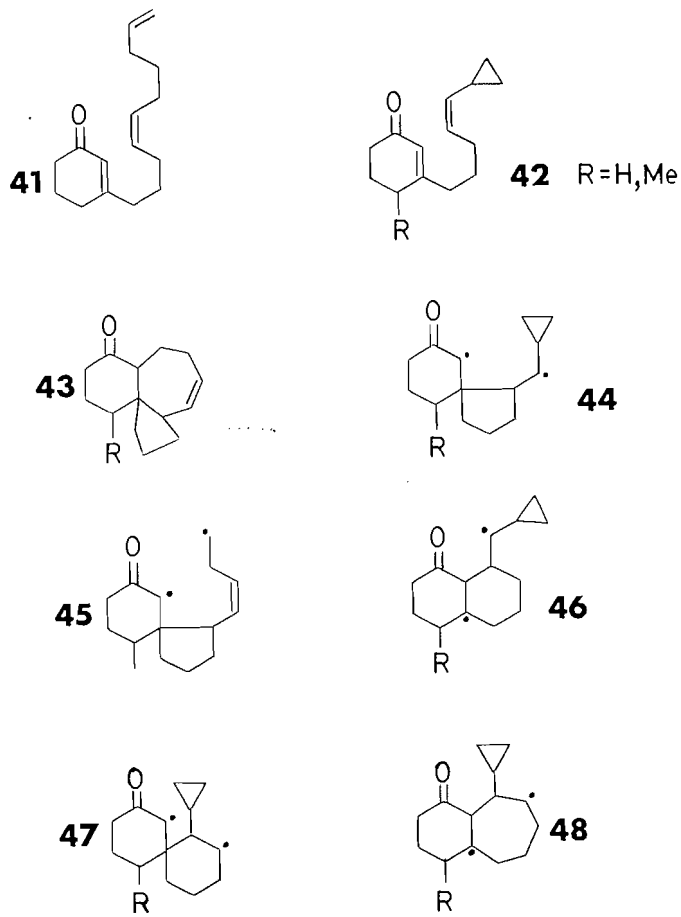

Conclusions

Two conclusions about the mechanism of enone photocycloaddition with alkenes can be drawn from the work described here. First, the formation of a product mixture containing the rearranged adducts **25** and **26** from the photochemical reaction of vinylcyclopropane with 2-cyclopentenone is good evidence that the initial bonding between the alkene and the enone is to both the α-position and the β-position of the enone and not exclusively at the β-position as recently proposed (20). Second, the formation of the rearranged adducts **25** and **26** in addition to the 2 + 2 adducts **8** and **9** suggests that cyclopropane ring opening in the initially formed biradicals occurs at a similar rate to their ring closure to cyclobutane-containing adducts. Using the known rate of the ring-opening reaction as a clock it is possible to assign a rate constant to cyclobutane formation and so arrive at a value of the biradical lifetime that is of the order of 50 ns.

Experimental

Cyclopentenone was prepared from singlet oxygen oxidation of cyclopentene using the method of Mihelich and Eickhoff (22). Vinylcyclopropane was most conveniently prepared in larger quantities by Bamford Stevens reaction of the tosyl hydrazone of cyclopropyl methyl ketone using a modification of a method described by Kirmse *et al.* (23) as outline below. A commerical sample of 1,6-heptadiene was used. ^{1}H NMR spectra were recorded at 200 MHz in $CDCl_3$ on a Varian XL 200 instrument. Coupled gas chromatography–mass spectroscopy (GC–MS) was performed using a Varian 3400 gas chromatograph equipped with a 30-m DB-5 capillary column attached to a Finnegan MAT 8230 mass spectrometer. ^{13}C NMR spectra were recorded at 75 MHz in $CDCl_3$ on a Varian XL 300 instrument. Routine GC was performed on a Hewlett-Packard 5880 instrument equipped with an 18-m methyl silicone capillary column using one of the following temperature programs: (a) 3 min at 35°C then 10°/min to 150°C; (b) 90°C to 150°C at 1°/min.

Can. J. Chem. Downloaded from www.nrcresearchpress.com by 91.121.58.235 on 09/07/12
For personal use only.

Can. J. Chem. Downloaded from www.nrcresearchpress.com by 91.121.58.235 on 09/07/12
For personal use only.

Preparation of vinylcyclopropane

Cyclopropyl methyl ketone was prepared from acid hydrolysis of α-acetyl-γ-butyrolactone and was converted to its tosyl hydrazone by the literature procedures (24). A suspension of sodamide in liquid ammonia was prepared by dissolution of sodium (6.6 g, 287 mmol) in liquid ammonia (200 mL) containing ferric nitrate (0.6 g). Decalin (200 mL) was added and the ammonia was allowed to evaporate. The tosyl hydrazone of cyclopropyl methyl ketone (10 g, 40 mmol) was added and the mixture heated to 190°C. The colourless liquid that distilled out of the reaction mixture was collected using an efficient Dry Ice condenser and redistilled (bp ca. 40°C) to give a mixture of vinylcyclopropane and 1-methylcyclobutene (1.38 g, 50%) in a ratio of 97:3 as determined by ^{1}H NMR spectroscopy. Attempts to use sodium hydride as the base, as described in the literature, gave much higher (up to 28%) proportions of 1-methylcyclobutene. For vinylcyclopropane, ^{1}H NMR: 0.38 (m, 2H), 0.68 (m, 2H), 1.38 (m, 1H), 4.76 (dd, 1H, J = 10, 2 Hz), 4.97 (dd, 1H, J = 17, 2 Hz), 5.25 (ddd, 1H, J = 17, 10, 2 Hz) ppm; ^{13}C NMR: 6.67, 14.76, 111.50, 142.61 ppm. For 1-methylcyclobutene, ^{1}H NMR: 1.64 (m, 3H), 2.27 (m, 2H), 2.36 (m, 2H), 5.55 (m, 1H) ppm; ^{13}C NMR: 16.88, 26.45, 32.67, 146.47 ppm.

Irradiation of cyclopentenone

A solution of cyclopentenone (43 mg) in cyclohexane (4 mL) was purged with nitrogen to remove oxygen and irradiated at room temperature for 5 h with Pyrex and water filtered light from a medium pressure mercury lamp. Gas chromatography showed the formation of three major products in the ratio 1:3:6, which were shown to be cyclopentenone dimers by GC–MS: 164 (M^+, 90%) 82 (100%), 54 (70%). Other minor products were cyclopentanone and a photoreduction product of the dimers (M^+ 166).

Irradiation of cyclopentenone with 1,6-heptadiene

A solution of freshly distilled cyclopentenone (303 mg, 3.7 mmol) and 1,6-heptadiene (730 mg, 7.6 mmol) in cyclohexane was deoxygenated by purging with nitrogen and irradiated at room temperature using water and Pyrex filtered light from a medium pressure mercury lamp for 7 h at which time GC indicated almost 100% conversion of the cyclopentenone. Five products were observed by GC in relative amounts in order of increasing retention time of 1:6:6.5:2.3:2.5. GC–MS indicated the first three of these to be adducts of cyclopentenone and the diene (M^+ = 178) and the latter two to be dimers of cyclopentenone. The retention times and mass spectra of the dimers were identical with those obtained by irradiation of a cyclohexane solution of cyclopentenone in the absence of alkene. The solvent and excess reactants were removed under reduced pressure to give a colourless oil (297 mg) whose ^{1}H NMR spectrum showed multiplets at 4.9 and 5.7 ppm. A portion of the mixture was separated by preparative thin-layer chromatography on silica gel (2 elutions with ether–hexanes, 1:9) to give three major fractions; the most polar was identified as the dimers **23** and **24** (20.5 mg) and the two less polar (23 mg and 5.3 mg) were identified by ^{1}H NMR and mass spectroscopy as mixtures of the adducts **18** and **19**. The ^{1}H NMR spectra of the adducts showed the expected signals in the range 1–2 ppm as well as olefinic signals at 4.9 and 5.7 ppm. The mass spectrum showed : 178 (M^+, 6%), 149 (3%), 137 (5%), 121 (5%), 95 (16%), 83 (100%).

A portion of the reaction mixture was hydrogenated in methanol at atmospheric pressure using PtO_2 as catalyst, as were the isolated adducts. GC indicated loss of all of the adducts and their replacement by peaks at slightly longer retention times but no loss of the dimer products. GC–MS of the hydrogenated reaction mixture and MS of the hydrogenated adducts showed that the adducts had increased in mass by two units, while the ^{1}H NMR spectra showed the loss of olefinic signals. The mass spectrum of the adducts showed: 180 (M^+, 10%), 151 (2%), 123 (6%), 83 (100%).

Irradiation of cyclopentenone with vinylcyclopropane

A procedure was adopted in which the reaction was interrupted at partial conversion, and unconverted starting material was recycled following its separation from photoadducts. This procedure was followed in order to avoid secondary photochemistry of the adducts and yet to ensure maximum conversion of the cyclopentenone and vinylcyclopropane. A solution of cyclopentenone (556 mg, 6.8 mmol) and vinylcyclopropane (1.38 g, 20 mmol) in cyclohexane (40 mL) was deoxygenated by purging with nitrogen and irradiated at room temperature with water and Pyrex filtered light from a medium pressure mercury lamp for 2 h. The solvent and unconverted starting materials were distilled off under reduced pressure to leave a residue containing the photoadducts. The distillate was irradiated for a further 2 h; the solvent and unconverted starting materials were again distilled off under reduced pressure to give a residue containing adducts. More cyclopentenone (202 mg) was added to the distillate and the irradiation was resumed; after 2 h unconverted starting materials were removed by distillation under reduced pressure leaving a third residue containing adducts. The distillate was irradiated for a further 2 h and again distilled; the four residues containing adducts were combined to give a product mixture (1.18 g) that was shown by GC-MS to be predominantly a mixture of four 1:1 adducts of cyclopentenone and vinylcyclopropane (M^+ = 150) in the ratio (in order of elution) 1:0.7:1:2, along with a small amount of cyclopentenone dimers (M^+ = 164). Treatment of a portion of the mixture with bromine resulted in strong depletion of the adduct eluted first and slight depletion of the last adduct eluted. The mixture was separated by PLC on silica gel (two elutions with ether:hexanes, 1:6, one elution with ether:hexanes 1:9) to give three major fractions, I, II, III, in order of increasing polarity. Fraction III contained the cyclopentenone dimers.

Fraction I was further separated by preparative GC (5% SE30 on Chromosorb W: column length 8 ft, diameter 0.25 in., temperature 125°C: carrier gas, helium; flow rate 50 mL/min) to give three fractions, Ia, Ib, and Ic.

Fraction Ia was identified as 3-(*cis*-2-pentenyl)-2-cyclopentenone, **25**. ^{1}H NMR: 0.94 (3H, t, J = 7.4) 1.96 (2H, m), 2.11 (2H, m), 2.40 (2H, m), 2.85 (2H, m), 5.30 (1H, m), 5.45 (1H, m), 6.05 (1H, m); MS: 150 (M^+, 2%), 122 (1%), 121 (1%), 107 (1%), 91 (10%), 82 (100%), 60 (30%), 53 (22%).

Fraction Ic was identified as a single geometrical isomer of 2-(2-pentenyl)-2-cyclopentenone, **26**. ^{1}H NMR: 0.99 (3H, t, J = 7.4), 2.05 (2H, m), 2.43 (2H, m), 2.58 (2H, m), 2.88 (2H, m), 5.50 (2H, m), 7.29 (1H, m); MS: 150 (M^+, 64%), 135 (30%), 121 (62%), 106 (21%), 96 (38%), 93 (40%), 91 (48%), 79 (100%).

Fraction Ib was a mixture of the remaining geometrical isomers of **25** and **26** and possessed ^{1}H NMR and mass spectra that were composites of those given for fractions Ia and Ic.

Fraction II was further separated by preparative GC (10% SE30 on Chromosorb W: column length 8 ft, diameter 0.25 in., temperature 90°C: carrier gas, helium; flow rate 50 mL/min) to give three fractions all of which contained stereo- and regioisomers of adducts **8** and **9**. Their ^{1}H NMR spectra contained multiplets in the range 0.1–0.5 ppm (cyclopropyl) and 1.7–2.8 ppm (cyclobutane and cyclopentenone) and no olefinic protons. The MS showed: 150 (M^+, 8%), 121 (16%), 91 (20%), 79 (38%), 68 (100%), 53 (78%).

1. A. C. Weedon. *In* Synthetic organic chemistry. *Edited by* W. M. Horspool. Plenum, New York. 1984.
2. R. O. Loutfy and P. de Mayo. J. Am. Chem. Soc. **99**, 3559 (1977).
3. (*a*) W. L. Dilling, D. E. Tabor, F. P. Boer, and P. P. North. J. Am. Chem. Soc. **92**, 1399 (1970); (*b*) R. O. Loutfy and P. de Mayo. Can. J. Chem. **50**, 3465 (1972).
4. D. Griller and K. U. Ingold. Acc. Chem. Res. **13**, 317 (1980).
5. L. Mathew and J. Warkentin. J. Am. Chem. Soc. **108**, 7981 (1986).
6. J. Lusztyk, B. Maillard, S. Deycard, D. A. Lindsay, and K. U. Ingold. J. Org. Chem. **52**, 3509 (1987).
7. P. J. Wagner and D. J. Bucheck. J. Am. Chem. Soc. **91**, 5090 (1969).
8. E. Pretsch, J. Seibl, W. Simon, and T. Clerc. Spectral data for structure determination of organic compounds. Springer-Verlag, Berlin. 1983.

9. P. J. WAGNER, K.-C. LIU, and Y. NOGUCHI. J. Am. Chem. Soc. **103**, 3837 (1981).
10. A. J. CASTELLINO and T. C. BRUICE. J. Am. Chem. Soc. **110**, 7512 (1988).
11. J. M. TEDDER and J. C. WALTON. Acc. Chem. Res. **9**, 183 (1976).
12. (*a*) E. J. COREY, J. D. BASS, R. LE MAHIEU, and R. B. MITRA. J. Am. Chem. Soc. **86**, 5570 (1964); (*b*) T. S. CANTRELL, W. S. HALLER, and J. C. WILLIAMS. J. Org. Chem. **34**, 3465 (1969); (*c*) A. J. WEXLER, J. A. HYATT, P. W. REYNOLDS, C. CANTRELL, and J. S. SWENTON. J. Am. Chem. Soc. **100**, 512 (1978); (d) I. ALTMEYER and P. MARGARETHA. Helv. Chim. Acta, **60**, 874 (1977); (*e*) M. L. GREENLEE, E. L. FRITZEN, and J. S. SWENTON. J. Org. Chem. **43**, 4512 (1978).
13. (*a*) P. J. WAGNER. *In* Rearrangements in ground and excited states. Vol. 3. *Edited by* P. de Mayo. Academic, New York. 1980. Essay 20; (*b*) J. C. SCAIANO. Acc. Chem. Res. **15**, 252 (1982); (*c*) R. A. CALDWELL, T. MAJIMA, and C. PAC. J. Am. Chem. Soc. **104**, 629 (1982).
14. S. C. FREILICH and K. S. PETERS. J. Am. Chem. Soc. **107**, 3819 (1985).
15. M. B. ZIMMT, C. DOUBLEDAY, and N. J. TURRO. J. Am. Chem. Soc. **108**, 3618 (1986).
16. (*a*) W. G. DAUBEN, L. SCHUTTE, and R. E. WOLF. J. Org. Chem. **34**, 1849 (1969); (*b*) D. L. GARIN. J. Org. Chem. **35**, 2830 (1970); (*c*) A. OSUKA, H. SHIMIZU, and H. SUZUKI. Chem. Lett. 329 (1982).
17. (*a*) L. A. PAQUETTE and R. F. EIZEMBER. J. Am. Chem. Soc. **91**, (7108); (*b*) W. G. DAUBEN, L. SCHUTTE, R. E. WOLF, and E. J. DEVINY. J. Org. Chem. **34**, 2512 (1969); (*c*) M. S. CARSON, W. COCKER, S. M. EVANS, and P. V. R. SHANNON. J. Chem. Soc. C, 1447 (1970); (*d*) W. G. DAUBEN, L. SCHUTTE, and E. J. DEVINY. J. Org. Chem. **37**, 2047 (1972); (*e*) G. W. SCHAFFER. J. Org. Chem. **38**, 2842 (1973).
18. (*a*) D. C. HECKERT and P. J. KROPP. J. Am. Chem. Soc. **90**, 4911 (1968); (*b*) M. S. CARSON, W. COCKER, S. M. EVANS, and P. V. R. SHANON. Tetrahedron Lett. 6153 (1968); (*c*) R. G. CARLSON and E. L. BIERSMITH. J. Chem. Soc. Chem. Commun. 1049 (1969); (*d*) J. K. CRANDALL, J. P. ARRINGTON, and C. F. MAYER. J. Org. Chem. **36**, 1428 (1971); (*e*) S. MOON and H. BOHM. J. Org. Chem. **36**, 1434 (1971); (*f*) A. SONODA, I. MORITANI, J. MIKI, T. TSUJI, and S. NISHIDA. Bull. Chem. Soc. Jpn. **45**, 1777 (1972); (*g*) R. G. CARLSON and W. S. MARDIS. J. Org. Chem. **40**, 817 (1975); (*h*) A. B. SMITH, L. BRODSKY, S. WOLFF, and W. C. AGOSTA. J. Chem. Soc. Chem. Commun. 509 (1975); (*i*) H. R. SONAWENE, B. S. NANJUNDIAH, and P. C. PUROHIT. Tetrahedron Lett. **24**, 3917 (1983); (*j*) I. M. TAKAKIS and W. C. AGOSTA. J. Am. Chem. Soc. **101**, 2383 (1979); (*k*) P. S. MARIANO, E. BAY, D. G. WATSON, T. ROSE, and C. BRACKEN. J. Org. Chem. **45**, 1753 (1980); (*l*) R. K. MURRAY and T. M. FORD. J. Am. Chem. Soc. **102**, 3194 (1980); (*m*) R. S. COOKE and G. D. LYON. J. Am. Chem. Soc. **103**, 7317 (1981).
19. (*a*) N. SHIMIZU, M. ISHIKAWA, K. ISHIKURA, and S. NISHIDA. J. Am. Chem. Soc. **96**, 6456 (1974); (*b*) M. NITTA and H. SUGIYAMA. Bull Chem. Soc. Jpn. **55**, 1127 (1982).
20. D. BECKER, N. HADDAD, and Y. SAHALI. Tetrahedron Lett. **30**, 2661 (1989).
21. D. BECKER, N, HADDA, and Y. SAHALI. Tetrahedron Lett. **30**, 4429 (1989).
22. E. D. MILELICH and D. J. EICKHOFF. J. Org. Chem. **48**, 4135 (1983).
23. W. KIRMSE, B.-G. VON BULOW, and H. SCHEPP. Ann. Chem. **691**, 41 (1969).
24. G. W. CANNON, R. C. ELLIS, and J. R. LEAL. *In* Organic syntheses. Coll. Vol. IV, 597, (1963).

Can. J. Chem. Downloaded from www.nrcresearchpress.com by 91.121.58.235 on 09/07/12
For personal use only.

The direct electrochemical synthesis of some metal derivatives of 3-hydroxy-2-methyl-4-pyrone

THEODORE A. ANNAN, CLOVIS PEPPE,[1] AND DENNIS G. TUCK

Department of Chemistry and Biochemistry, University of Windsor, Windsor, Ont., Canada N9B 3P4

Received January 30, 1990

THEODORE A. ANNAN, CLOVIS PEPPE, and DENNIS G. TUCK. Can. J. Chem. **68**, 1598 (1990).

The electrochemical oxidation of a metallic sacrificial anode (M = Zn, Cd, Sn, In, Cu) in a non-aqueous solution of 3-hydroxy-2-methyl-4-pyrone (= HL) yields the ML_n complexes (M = Zn, Cd, Sn, Cu, $n = 2$; M = In, $n = 3$). Adducts of the type $ML_2.B$ (M = Zn, Cd, B = *N,N,N′,N′*-tetramethylethylenediamine (tmen); M = Cu, B = triphenylphosphine) were obtained by the reaction between the appropriate ligand (B) and the previously synthesized complexes (M = Zn, Cd), or by arranging for the initial electrolytic phase to include the base (M = Cu). The tin(II) compound shows the typical reactions of such low oxidation state species by reacting with iodine and *ortho*-quinones by oxidative addition. All compounds were characterized by elemental analysis and by IR, ^1H and ^{13}C nmr spectroscopy. The structure of CdL_2.tmen was determined by X-ray crystallography, which identified the CdO_4N_2 kernel, and partial electron delocalization within the pyronate ring.

Key words: electrochemical synthesis, cadmium complexes, zinc complexes, tin(II) oxidation, 3-hydroxy-2-methyl-4-pyrone.

THEODORE A. ANNAN, CLOVIS PEPPE et DENNIS G. TUCK. Can. J. Chem. **68**, 1598 (1990).

L'oxydation électrochimique, dans une solution non-aqueuse de 3 hydroxy-2-méthyl-4-pyrone (= HL), d'une anode métallique qui est sacrifiée (M = Zn, Cd, Sn, In, Cu) fournit des complexes ML_n (M = Zn, Cd, Sn, Cu avec $n = 2$; M = In avec $n = 3$). On a pu obtenir les adduits du type $ML_2.B$ (M = Zn, Cd avec B = *N,N,N′,N′*-tétraméthyléthylènediamine (tmen); M = Cu avec B = triphénylphosphine) en faisant réagir les ligands (B) appropriés avec les complexes (M = Zn et Cd) synthétisés antérieurement ou en s'assurant que la phase initiale de l'électrolyse contenait de la base (M = Cu). Le composé de l'étain(II) présente les réactions typiqués des espèces dont l'état d'oxydation est faible; il réagit donc avec l'iode et les *ortho*-quinones par des réactions d'additions oxydatives. Tous les composés ont été caractérisés par analyse élémentaire et par spectroscopies IR et rmn du ^1H et du ^{13}C. La structure du complexe CdL_2.tmen a été déterminée par diffraction des rayons-X; il a été possible d'identifier la noyau de CdO_4N_2 et la délocalisation partielle des électrons dans le cycle pyronate.

Mots clés: synthèse électrochimique, complexes du cadmium, complexes du zinc, oxydation du Zn(II), 3-hydroxy-2-méthyl-4-pyrone.

[Traduit par la revue]

Introduction

A number of papers from this laboratory have demonstrated that the method of direct electrochemical synthesis is a simple, efficient one-step route to the preparation of a wide range of metal complexes, including metal thiolates (1–5), diphenylphosphides (6), carboxylates (7), catecholates (8, 9), and dipyridylamides (10). The method consists simply in the reduction of the selected substrate at an inert platinum cathode in a non-aqueous solution, followed by the oxidation of a sacrificial metal anode. The desired metal complex frequently precipitates in the electrochemical cell, or is readily isolated from the solution phase.

We have recently investigated the application of this method to the preparation of complexes of anionic bidentate oxygen donors, beginning with substrates containing a carbonyl group *ortho* to a phenolic OH group. These experiments resulted in the one-step synthesis of metallic acetonaphthonates and flavonates (11). We now report the successful application of this method to the direct high yield synthesis of metal pyronates.

Experimental section

General

Zn, Cd, Sn, In, and Tl were in the form of rods (Aldrich); Cu shot was flattened to give discs, ca. 1 cm diameter and 1 mm thick. All metals were washed with nitric acid, distilled water, and acetone, dried, and then abraded with fine sandpaper and polished with tissue. 3-Hydroxy-2-methyl-4-pyrone (maltol, HL) tetrachloro-*ortho*-benzoquinone and di-*tert*-butyl-*ortho*-benzoquinone were used as supplied (Aldrich). Acetonitrile and methylene chloride were freshly distilled from calcium hydride; toluene and diethyl ether were dried over sodium and distilled before use. All other reagents were used as supplied.

Analysis and spectroscopy

Metal analyses were by atomic absorption spectrophotometry, using an IL-251 instrument. Iodine was determined by the Volhard method. Microanalysis was by Guelph Chemical Laboratories Ltd. Infrared spectra were recorded on a Nicolet 5 DX instrument, using KBr discs; ^1H and ^{13}C nuclear magnetic resonance spectra were run on a Bruker AC 300L instrument.

Electrochemical procedures

The electrochemical procedures were essentially those described in earlier papers (1–11). The electrochemical cell was a 100 mL round-bottomed flask with a Schlenk arm containing the solution phase; the sacrificial metal electrode suspended by a platinum wire through the rubber septum was the anode of the cell and a second platinum wire similarly supported was the cathode. All operations were carried out under dry nitrogen, using standard vacuum line techniques. The details of cell composition, electrical conditions, and electrochemical efficiency are given in Table 1.

The solution phase was degassed by pumping on a vacuum line for 3 min with continuous stirring, and the cell was purged with dry nitrogen gas throughout the electrolysis. As soon as current flowed in the cell, bubbles of H_2 gas were visible at the cathode, and the colourless solution began to turn yellow. The electrolysis was conducted for a period of 1–2 h, after which the anode was removed, washed, dried and weighed to obtain the quantity dissolved (and hence the electrochemical efficiency (see below)). The electrode was re-introduced into the cell, and the electrolysis continued until ca. 80–90% of the initial quantity of pyrone was consumed; we frequently observed a significant drop in the current towards the end of the electrolysis. At this stage some small deposition of metal occurred at

[1]Permanent address: Departamento de Quimica, Centro de Ciencias Exatas e da Natureza, Universidade Federal da Paraiba, Cidade Universitaria, Joao Pessoa PB, Brazil.

Can. J. Chem. Downloaded from www.nrcresearchpress.com by 91.121.58.235 on 09/07/12
For personal use only.

TABLE 1. Experimental conditions for the electrochemical synthesis of derivatives of 3-hydroxy-2-methyl-4-pyrone (= HL)

Metal anode	Mass HL (g)[a]	Initial Voltage (V)	Initial Current (mA)	Mass of M dissolved (mg)	E_F (mol F^{-1})	Product	Mass of product (mg)	Yield (%)
Zn	1.02	22	30	190	0.53	ZnL_2	750	82
Cd	1.00	22	30	361	0.52	CdL_2	960	82
Sn	1.00	20	30	232	0.53	SnL_2	682	95
In	0.96	22	30	446	[c]	InL_3	630	[c]
Cu	0.96[b]	16	50	241	1.01	$CuL_2 \cdot PPh_3$	890	82[d]

[a]Dissolved in 40 mL CH_3CN: toluene (1:1) containing ca. 100 mg Et_4NC10_4.
[b]Dissolved in 30 mL CH_3CN containing 1.0 g PPh_3.
[c]Results not reproducible.
[d]Calculation of % yield allows for disproportionation of CuL (see text).

TABLE 2. Analytical results for derivatives of 3-hydroxy-2-methyl-4-pyrone (=HL)

Compound	Colour	M (%) Found	M (%) Calcd.
ZnL_2	Yellow	20.7	20.7
$ZnL_2 \cdot$tmen	Yellow	15.1	15.1
CdL_2	Yellow	31.0	31.0
$CdL_2 \cdot$tmen	Yellow	23.5	23.5
SnL_2	Yellow	[a]	
$SnI_2L_2 \cdot 0.5\ C_4H_{10}O$	Yellow	[b]	
$L_2Sn\ (O_2C_6Cl_4)$	Yellow	19.4	19.3
$L_2Sn\ (O_2C_{14}H_{20}) \cdot CH_3CN$	Yellow	19.0	18.8
InL_3	Yellow	23.0	23.4
$CuL_2 \cdot PPh_3$	Green	10.6	11.0

[a]Solid incompletely digested for atomic absorption analysis; found C 39.5, H 2.77; calcd. C 39.1, H 2.73.
[b]Solid incompletely digested for atomic absorption analysis; found C 24.3, H 1.88, I 38.0; Calcd. C 25.5, H 2.29, I 38.5.

the cathode, and this was followed by mechanical separation which resulted by small quantities of metal contaminating an insoluble ML_n product. These difficulties can be eliminated either by restricting the period of electrolysis or by placing a small beaker (1 cm diameter, 1 cm height) under the electrode to collect any solid residue, since the desired insoluble product tends to fall well away from the electrode. Details of the synthesis and isolation of the compounds investigated are given below.

Zinc(II) derivarives

The electrochemical oxidation of zinc in a solution of HL occurred smoothly, with the solution becoming yellow, and finally yellow–red, in colour. After ca. 1 h of electrolysis, ZnL_2 began to precipitate in the cell as an amorphous yellow powder, which was subsequently collected and dried under vacuum; ZnL_2 is insoluble in common organic solvents (e.g., acetone, chloroform, or acetonitrile) but soluble in strong donors such as dimethylsulphoxide. This is undoubtedly due to solvation, and in keeping with this, ZnL_2 complexes with other donor ligands, as demonstrated by its reaction with *N,N,N′,N′* -tetramethylethylenediamine (tmen). A suspension of ZnL_2 (246 mg, 0.78 mmol) in CH_3CN (15 mL) was treated with tmen (0.5 mL, 385 mg, 3.31 mmol). The reaction was brought to the boiling point of CH_3CN (82°C) and the resultant solution quickly filtered; the filtrate deposited 295 mg (0.68 mmol) of ZnL_2.tmen spontaneously on cooling, in the form of yellow crystals (yield: 88%). Analytical results for these and other products are given in Table 2.

Cadmium(II) derivatives

The oxidation of cadmium to produce CdL_2 followed the same course as for zinc. The solubilities of CdL_2 are also similar to those of ZnL_2, and it reacts with tmen under essentially identical conditions, to produce CdL_2.tmen as a yellow crystalline material in 86% yield.

Tin derivatives

The electrolysis proceeded as above, except that in this case the product (SnL_2) is soluble in the electrochemical phase, and also that towards the end of the electrolysis, a small amount of Sn metal deposited at the cathode. After filtration, the solution was reduced in volume by ca. 10%, and cooled in the freezer, when 232 mg of SnL_2 precipitated in the form of yellow crystals, which lost their crystallinity when filtered and dried *in vacuo*. The residual solution was taken to dryness, and the yellow solid so obtained washed with absolute ethanol (2 × 15 mL) to remove excess HL and the supporting electrolyte; the additional SnL_2 (450 mg) was collected and dried *in vacuo*. This substance is soluble in CH_2Cl_2, $CHCl_3$, and dimethylsulphoxide. There is no reaction between SnL_2 and tmen in CH_2Cl_2 under the conditions used for ZnL_2, since unreacted SnL_2 was isolated quantitatively.

This tin(II) compound can be oxidized to SnI_2L_2 by I_2. A solution of I_2 (392 mg, 1.54 mmol) in diethyl ether (20 mL) was added to a suspension of SnL_2 (569 mg, 1.54 mmol) in the same solvent (15 mL) over a period of 30 min. The colour of I_2 was discharged after the addition of each drop. When all the I_2 had been added, the reaction mixture was stirred at room temperature for 4 h, after which the solid was collected, washed with diethyl ether, dried, and recrystallized from CH_2Cl_2/Et_2O to give $SnI_2L_2.0.5Et_2O$ (904 mg, 1.37 mmol) in 89% yield. This compound is soluble in CH_2Cl_2, $CHCl_3$, acetone, or dmso. SnL_2 can also be oxidized to a tin(IV)-catecholate complex by either tetrachloro-*ortho*-benzoquinone or 3,5-di-*tert*-butyl-*ortho*-benzoquinone. A solution of $Cl_4C_6O_2$-*o* (472 mg, 1.92 mmol) in CH_3CN (20 mL) was added dropwise to a suspension of SnL_2 (709 mg, 1.92 mmol) in the same solvent (20 mL) over a period of 30 min. The red colour of the quinone was discharged, giving a clear yellow solution. When the volume was reduced to ca. 5 mL, a yellow solid was thrown down, and further solid appeared on leaving the mixture overnight at 0°C; this solid was collected and dried *in vacuo*. The yield of bis(3-hydroxy-2-methyl-4-pyronato)-tetrachlorocatecholato-tin(IV), $L_2Sn(O_2C_6Cl_4)$, was 925 mg (78%). The same procedure lead to the synthesis of the analogous di-3,5-*tert*-butylcatecholato compound as the acetonitrile solvate, $L_2SnO_2C_{14}H_{20}.CH_3CN$, in 90% yield from SnL_2 and 3,5-di-*tert*-butyl-*ortho*-benzoquinone.

Indium(III) derivative

As soon as the current flowed in a cell with an indium anode, metal deposited below the anode, and the solution assumed the characteristic yellow–red coloration. At the end of the electrolysis, the deposited metal was collected and weighed (215 mg, 1.87 mmol). The mass of indium lost from the anode was 446 mg (3.88 mmol). The solution was

Can. J. Chem. Downloaded from www.nrcresearchpress.com by 91.121.58.235 on 09/07/12
For personal use only.

pumped to dryness, and the resultant solid collected, washed with ethanol (3 × 10 mL), and dried under vacuum; yield of InL_3 743 mg (1.51 mmol). The compound is soluble in CH_2Cl_2, $CHCl_3$, acetone and dimethylsulphoxide. Like SnL_2, InL_3 is coordinatively saturated, and attempts to coordinate it with tmen in CH_3CN lead to the eventual recovery of unreacted InL_3.

Copper(II) derivative

As in the electrochemical oxidation of indium just described, the oxidation of copper leads to a disproportionation reaction. During the electrolysis, a solid precipitates at the anode, and metallic copper deposited in the cell, mainly on the walls. The green–grey solid formed during electrolysis was collected by filtration, but attempts to extract a pure product with hot CH_3CN, toluene, methanol, or ethanol all failed. The electrolysis was then conducted with triphenylphosphine in the solution, when the same disproportionation to copper metal was observed; in this case we observed only metallic copper precipitating in the cell, which at the end of the experiment contained a dark green–brown solution. The metal was collected (104 mg, 1.64 mmol), and compared to an amount of Cu dissolved from the electrode of 241 mg (3.79 mmol); $CuL_2.PPh_3$ was isolated as a green solid by concentrating the solution phase.

Thallium

An attempt to prepare TlL_n complexes by using solutions of HL in CH_3CN in the usual way was unsuccessful. No current flow was observed, and we attribute this to the formation of insoluble $TlClO_4$ on the anode surface. When solutions containing Et_4NPF_6 were used, thallium was simply transported from anode to cathode, and these systems were not invesigated further.

Crystallographic analysis

A single crystal of CdL_2.tmen was sealed in a capillary tube and mounted in a Syntex $P2_1$ diffractometer along its largest dimension. The cell parameters were obtained from 35 strong reflections in the range $15<2\theta<30°$. The data were collected following the procedures described previously (12). The intensities of three reference reflections were measured every 200 reflections to monitor stability and crystal decomposition, and it was found that the intensity of these reflections did not change significantly during the data collection. The results were then corrected for Lorentz and polarization effects; no absorption corrections were applied because of the low absorption coefficient. The systematic absences suggested the space group *Ibca*, which was later confirmed by the successful refinement. The unit cell contains 16 molecules of CdL_2.tmen, with the asymmetric unit containing two crystallographically non-equivalent molecules. Details of the cell parameters, data collection, and structural refinement are given in Table 3. The positions of the two cadmium atoms were obtained from a sharpened Patterson synthesis, using the SHELX-76 program, and Fourier synthesis gave the positions of the remaining non-hydrogen atoms. Refinement was carried out using full matrix least squares methods, with scattering factors taken from ref. 13.

The initial identification of two non-equivalent molecules appeared to arise from disorder in the tmen ligand of one of these structures, and mainly from the carbon atom C(29). The position of this atom was therefore fixed, with a thermal parameter equal to the average value of the neighbouring carbons. The refinement then proceeded smoothly; in the final cycles of the least-squares refinement, the Cd, O, and N atoms were refined with anisotropic thermal coefficients, while all the remaining carbon atoms were refined isotropically. This refinement converged on a pair of closely related structures at $R = 0.0562$ and $R_w = 0.0658$. All hydrogen atoms were then included in idealized positions (r(C–H) = 0.95A°; ∠CCH = ∠HCH = 109.5°), and their isotropic thermal parameters were assigned values 0.01 U(Å^2) greater than those for the bonded carbon atoms. The structure was further refined until convergence was achieved with the final $R = 0.0428$ and $R_w = 0.0514$. The final atomic coordinates for non-hydrogen atoms are given in Table 4, and the bond distances and angles for the two molecules are in Table 5. Tables of structure factors, anisotropic

TABLE 3. Summary of crystal data, intensity collection and structural refinement for Cd $(O_3C_6H_5)_2$·tmen

Parameter	Value
a (Å)	16.329 (10)
b (Å)	15.911 (8)
c (Å)	32.183 (18)
α (deg) = β = γ	90.0
V (Å^3)	8362
Crystal system	Orthorhombic
Space group	*Ibca*
Mol. wt.	478.62
Z	16
ρ_c (g cm^{-3})	1.52
ρ_o (g cm^{-3})	1.56
Crystal dimensions (mm)	0.15 × 0.23 × 0.28
Radiation	Mo-K$_\alpha$, λ = 0.71069 Å
Monochromator	highly oriented graphite
Temperature (°C)	21
Absorption coefficient, μ (cm^{-1})	9.75
2 θ angle (deg)	4–45
Scan type	Coupled θ (crystal)/2 θ (counter)
Scan width	Kα_1 − 1° to Kα_2 + 1°
Scan speed (deg min^{-1})	variable, 2.02–4.88
Bkgd time/scan time	0.5
Total reflections measured	1659
Unique data used	929 ($I > 3\sigma$ (I))
No. of parameters (NP)	152
R	0.0428
R_w	0.0514

TABLE 4. Final fractional coordinates and isotropic thermal parameters[a] for non-hydrogen atoms of $Cd(O_3C_6H_5)_2$·tmen with standard deviations in parentheses

Atom	X	Y	Z	U_{eq} (×10^3)
Cd(1)	0.0000	0.2500	0.2056(5)	43(1)
Cd(2)	0.0000	0.2500	−0.0377(5)	47(1)
O(11)	0.0915(5)	−0.0477(5)	0.1451(4)	58(6)
O(12)	0.0958(5)	0.1507(5)	0.1979(4)	41(5)
O(13)	−0.0561(5)	0.1511(6)	0.1613(4)	50(6)
O(21)	−0.2852(5)	0.1571(6)	−0.1066(4)	52(6)
O(22)	−0.0986(5)	0.1573(6)	−0.0456(3)	38(5)
O(23)	−0.0930(5)	0.3106(6)	−0.0845(4)	55(6)
N(11)	0.0721(5)	0.3041(7)	0.2629(6)	50(8)
N(21)	0.0602(7)	0.1809(8)	0.0192(7)	83(10)
C(11)	0.1998(8)	0.0029(9)	0.1884(6)	86(5)
C(12)	0.1171(7)	0.0192(8)	0.1688(5)	47(3)
C(13)	0.0719(6)	0.0883(8)	0.1743(5)	44(4)
C(14)	−0.0101(7)	0.0901(9)	0.1552(4)	47(3)
C(15)	−0.0276(8)	0.0182(8)	0.1299(5)	63(4)
C(16)	0.0208(7)	−0.0478(10)	0.1263(6)	66(4)
C(17)	0.0561(8)	0.3953(9)	0.2676(6)	91(6)
C(18)	0.1610(6)	0.2930(8)	0.2587(5)	68(4)
C(19)	0.0444(8)	0.2585(11)	0.3007(7)	88(6)
C(21)	−0.2408(9)	0.0503(9)	−0.0607(6)	91(5)
C(22)	−0.2239(7)	0.1323(8)	−0.0790(5)	51(4)
C(23)	−0.1572(7)	0.1804(8)	−0.0710(4)	46(3)
C(24)	−0.1537(7)	0.2631(8)	−0.0906(4)	45(3)
C(25)	−0.2180(7)	0.2844(9)	−0.1185(5)	55(3)
C(26)	−0.2789(8)	0.2289(9)	−0.1249(6)	64(4)
C(27)	0.0395(9)	0.0908(10)	0.0179(6)	111(6)
C(28)	0.1479(8)	0.1887(10)	0.0204(6)	93(6)
C(29)	0.0184(10)	0.2069(9)	0.0547(7)	90

[a] $U_{eq} = \frac{2}{3}[\Sigma_i \Sigma_j U_{ij} a_i^* a_j^* a_i \cdot a_j]$ (Å^2).

Can. J. Chem. Downloaded from www.nrcresearchpress.com by 91.121.58.235 on 09/07/12
For personal use only.

TABLE 5. Important interatomic distances (Å) and angles (deg) for $Cd(O_3C_6H_5)_2 \cdot tmen$ with standard deviations in parentheses[a]

Atoms	Distance	Atoms	Distance
Cd(1)—O(12)	2.237(8)	Cd(2)—O(22)	2.198(8)
Cd(1)—O(13)	2.312(9)	Cd(2)—O(23)	2.346(10)
Cd(1)—N(11)	2.351(15)	Cd(2)—N(21)	2.352(15)
C(13)—O(12)	1.309(14)	C(23)—O(22)	1.311(15)
C(14)—O(13)	1.242(13)	C(24)—O(23)	1.262(12)
C(17)—N(11)	1.482(15)	C(27)—N(21)	1.474(16)
C(18)—N(11)	1.468(15)	C(28)—N(21)	1.438(15)
C(19)—N(11)	1.488(20)	C(29)—N(21)	1.393(22)
C(12)—O(11)	1.375(15)	C(22)—O(21)	1.395(15)
C(16)—O(11)	1.303(14)	C(26)—O(21)	1.302(15)
C(12)—C(11)	1.513(15)	C(22)—C(21)	1.458(16)
C(13)—C(12)	1.357(14)	C(23)—C(22)	1.355(15)
C(14)—C(13)	1.472(15)	C(24)—C(23)	1.459(15)
C(14)—C(15)	1.434(17)	C(24)—C(25)	1.424(17)
C(15)—C(16)	1.318(19)	C(25)—C(26)	1.336(20)
C(19)—C(19)*	1.474(28)	C(29)—C(29)*	1.497(31)

Bonds	Angles	Bonds	Angle
O(12)—Cd(1)—O(13)	74.2(3)	O(22)—Cd(2)—O(23)	74.2(3)
O(12)—Cd(1)—O(13)*	97.8(3)	O(22)—Cd(2)—O(23)*	96.6(3)
O(12)—Cd(1)—O(12)*	167.5(3)	O(22)—Cd(2)—O(22)*	166.4(3)
O(13)—Cd(1)—O(13)*	103.8(3)	O(23)—Cd(2)—O(23)*	100.3(3)
N(11)—Cd(1)—O(12)	90.0(3)	N(21)—Cd(2)—O(22)	94.5(4)
N(11)—Cd(1)—O(12)*	99.7(3)	N(21)—Cd(2)—O(22)*	96.3(4)
N(11)*—Cd(1)—O(13)	92.3(3)	N(21)*—Cd(2)—O(23)	93.4(4)
N(11)*—Cd(1)—O(13)*	158.7(3)	N(21)*—Cd(2)—O(23)*	163.2(4)
N(11)—Cd(1)—N(11)*	76.0(8)	N(21)—Cd(2)—N(21)*	75.0(8)
C(13)—O(12)—Cd(1)	113.0(7)	C(23)—O(22)—Cd(2)	114.7(8)
C(14)—O(13)—Cd(1)	112.9(7)	C(24)—O(23)—Cd(2)	111.2(8)
C(17)—N(11)—Cd(1)	110.5(10)	C(27)—N(21)—Cd(2)	109.6(13)
C(18)—N(11)—Cd(1)	112.4(11)	C(28)—N(21)—Cd(2)	111.5(12)
C(19)—N(11)—Cd(1)	110.0(8)	C(29)—N(21)—Cd(2)	107.1(11)
C(19)—N(11)—C(17)	109.9(16)	C(29)—N(21)—C(27)	108.2(12)
C(19)—N(11)—C(18)	108.5(12)	C(29)—N(21)—C(28)	116.1(18)
C(12)—O(11)—C(16)	121.8(11)	C(22)—O(21)—C(16)	118.8(11)
O(11)—C(12)—C(11)	111.8(12)	O(21)—C(12)—C(21)	112.1(12)
C(13)—C(12)—O(11)	122.9(12)	O(23)—C(22)—O(21)	122.5(13)
C(13)—C(12)—C(11)	125.3(14)	O(23)—C(22)—C(21)	125.5(15)
C(12)—C(13)—O(12)	122.4(12)	C(22)—O(23)—O(22)	123.1(13)
C(14)—C(13)—O(12)	119.9(12)	C(24)—C(23)—O(22)	119.6(10)
C(14)—C(13)—C(12)	117.6(13)	C(24)—C(23)—C(22)	117.3(12)
C(13)—C(14)—O(13)	119.9(13)	C(23)—C(24)—O(23)	120.3(11)
C(15)—C(14)—O(13)	126.4(12)	C(25)—C(24)—O(23)	122.3(13)
C(15)—C(14)—C(13)	113.7(12)	C(25)—C(24)—C(23)	117.3(11)
C(15)—C(16)—O(11)	119.3(16)	C(25)—C(26)—O(21)	124.5(17)
C(16)—C(15)—C(14)	124.5(15)	C(26)—C(25)—C(24)	119.5(16)

[a]An asterisk denotes a two-fold symmetry related atom within the molecule, symmetry position: $-X, 0.5 - Y, Z$.

thermal parameters, and fractional coordinates for hydrogen atoms and the unit cell diagram are available as deposited material.[2]

Results and discussion

Preparative electrochemistry

Complexes of the type ML_n involving 3-hydroxy-2-methyl-4-pyrone and various d^{10} metal ions can now be readily prepared in high yield by the electrochemical technique in a convenient single step process. This work extends some earlier investigations of such synthetic methods (14). The preparation of ZnL_2, a potential agent for the treatment of anaemia, has been carried out via the reaction of $ZnCl_2$ with maltol in chloroform (15); InL_3 has also been synthesized from $InCl_3$ and maltol in acetone–methanol (16), and other boron, aluminum, and gallium analogues were obtained in a similar manner (17–19), but there seem to be no reports of the preparation of these pyronates starting from the metallic element other than by this electrochemical route.

[2]A complete set of material may be purchased from the Depository of Unpublished Data, CISTI, National Research Council of Canada, Ottawa, Ont., Canada K1A OS2.

Can. J. Chem. Downloaded from www.nrcresearchpress.com by 91.121.58.235 on 09/07/12
For personal use only.

Following our standard procedure, we measured the electrochemical efficiency, E_f, defined as moles of metal dissolved per Faraday of charge, for each system (see Table 1). For Zn, Cd, and Sn, for which ML_2 complexes were obtained, the value of ca. 0.5 mol F^{-1} corresponds to the reaction sequence

Cathode
[1] $2HL + 2\,e^- \rightarrow 2\,L^- + H_2(g)$

Anode
[2] $2\,L^- + M \rightarrow ML_2$

For copper, the value of 1.01 mol F^{-1} indicates the formation of CuL as the primary product, which disproportionates to the element and CuL_2 according to

[3] $2\,CuL \rightarrow Cu + CuL_2$

In keeping with this, we isolated 105 mg (1.64 mol) of metallic copper from an experiment in which 241 mg (3.79 mol) of copper was lost from the electrode, corresponding to a yield of 87% on the basis of the above reaction.

When indium was used as a sacrificial anode, we observed an irreproducible electrochemical efficiency, with values in the range 0.50–0.73 mol F^{-1}. No direct reaction between maltol and indium metal was detected, establishing the absence of any competing chemical reaction at the anode, but we did observe that some of the metal which was thrown down in the cell during electrolysis could become mechanically reattached to the anode when the reaction mixture was shaken, and such processes may account for the observed non-reproducibility in E_F. The product recovered from the solution was identified as InL_3, and in terms of the known chemistry of this element, one would predict the sequence

Cathode
[4] $HL + e \rightarrow 1/2\,H_2(g) + L^-$

Anode
[5] $In + L^- \rightarrow InL + e$

Solution phase
[6] $3InL \rightarrow 2\,In^\circ + InL_3$

so that the overall stoichiometry is

[7] $3In \rightarrow 2\,In + InL_3$: observed (mmol) 3.88, 1.87, 1.51

In view of the experimental observations reported above, we suspect that the loss of indium from the anode is underestimated, and that the quantity of indium metal collected at the end of the experiment is also too low, partly because of adherence to the anode and partly because of the difficulty of quantitatively recovering this finely divided material.

Adduct formation

The reaction between the ML_n complexes and the bidentate ligand tmen were investigated. The results indicate that adduct formation

[8] $ML_n + B \rightarrow ML_n.\,B$

occurs only in the case of M = Cd and Zn. Attempts ro react SnL_2 and InL_3 with tmen resulted in the complete recovery of the unreacted ML_n compounds. As demonstrated below, the pyrone ligand acts as a bidentate donor, and expansion of the coordination numbers beyond five (Sn) or six (In) in these complexes is not expected to occur.

We should also note here that in the case of copper, the only product which could be isolated from electrochemical experiments was the copper(II) adduct $CuL_2.PPh_3$. The reasons for the apparent instability of the uncomplexed CuL and CuL_2 are not clear at this point.

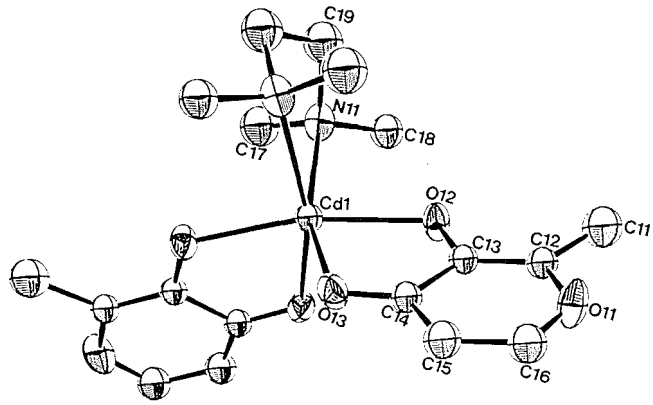

FIG. 1. The molecular structure of one of the forms of $Cd(O_3C_3H_5)_2$.tmen as an ORTEP diagram with 50%-probability ellipsoids. Hydrogen atoms have been omitted for clarity. The second molecular form has essentially the same stereochemistry.

*The structure of $Cd(O_3C_6H_5)_2$.tmen (**1**)*

The structure of the tmen adduct of CdL_2 (Fig. 1) confirms the suggestion that this is a six-coordinate complex with a pseudo-octahedral CdO_4N_2 kernel, in which the cadmium atom is constrained by symmetry requirements to occupy a special position on a two-fold axis. There are a number of interesting features about the structure of this molecule. The Cd–tmen interaction involves a crystallographically imposed symmetrical CdN_2C_2 ring, with Cd—N bond distances similar to those ina number of related molecules (20). The C—C and C—N distances and angles are close to those recently reported for a zinc(II)–tmen adduct (11), except that the N—CH_3 bonds appear to be significantly shorter in that species (1.450(2), 1.462(2) Å) than in **1** (1.482(15), 1.468(15) Å).

The Cd—O bond distances to the γ-pyronate ligand establish a significant difference between that to the keto-oxygen (Cd—0(13), 2.312(9), 2.346(10) Å) and the Cd-hydroxo oxygen (Cd—O(12), 2.237(8), 2.198(8) Å). These values are similar to those reported recently for $Cd(O_2C_{12}H_9)_2$.bpy (**2**) ($C_{12}H_9O_2^-$ = 1′-hydroxo-2′-acetonaphthonate anion) (11), and to relevant compounds discussed in that context. The bite angle at the cadmium atom (O(12)—Cd—O(13)) of 74.2(3)° is also close to those reported for **2** (76.8(2), 78.8(2)°).

There are some closely related molecules with which the present results can be compared, and especially Ph_2BL (18) and AlL_3 (17, 18). The first point is that as the ligated atom increases in size, so the M—O bond becomes longer and the bite angle decreases accordingly (B, 99.49(13)°; Al, 90 ± 5.5°; Cd, 74.2(3)°). There are concomitant changes in the MO_2C_2 ring, in that both the M—O—C and O—C—C angles increase as the bite angles decrease, but the sum of the angles within the MO_2C_2 ring is remarkably constant at 539°. Another interesting and almost constant factor is that although the M—O and C—O distances depend on M, as would be expected, the differences between these bond lengths within the ring do not vary substantially. The actual values, expressed as r(M—O(13)) − r(M—O(12)) are 0.067 (B), 0.055 (Al), and 0.059 Å (Cd); the values for A1 are for the two non-disordered ligands (17). The r(O(12)—C(13)) − r(O(13)—C(14)) differences are 0.055 (B). 0.060 (Al), and 0.067 Å (Cd). Given that the C(13)—C(14) distances also depend on the central atom, in the order B

Can. J. Chem. Downloaded from www.nrcresearchpress.com by 91.121.58.235 on 09/07/12
For personal use only.

TABLE 6. Nuclear magnetic resonance spectra for derivatives of 3-hydroxy-2-methyl-4-pyrone[a] (in ppm from Me_4Si = 0)

Atom	Chemical shift							
	HL	ZnL_2[b]	ZnL_2·tmen	CdL_2[b]	CdL_2·tmen	SnL_2	SnI_2L_2·1/2Et_2O[d]*	InL_3
H(11)	2.32 (s, 3)	2.32 (s, 3)	2.37(s, 3)	2.29 (s, 3)	2.38 (s)[c]	2.36 (s, 3)	2.53 (s, 6)	2.48 (s, 3)
H(15)	6.40 (d, 1)	6.50 (d, 1)	6.38 (d, 1)	6.38 (d, 1)	6.37 (d, 1)	6.67 (d, 1)	6.78 (br, 2)	6.62 (d, 1)
H(16)	7.65 (d, 1)	8.10 (d, 1)	7.53 (d, 1)	8.00 (d, 1)	7.53 (d, 1)	7.73 (d, 1)	8.05 (d, 2)	7.79 (d, 1)
H(17, 18)			2.30 (s, 6)		2.36 (s)[c]			
H(19)			2.50 (s, 2)		2.50 (s, 2)			
C(11)	14.2	14.5	14.8	14.3	15.1	15.0	15.9	15.5
C(15)	113.2	109.7	110.3	112.7	111.3	111.8	110.0	110.8
C(16)	154.0	149.6	150.5	153.9	149.9	152.7	154.6	152.3
C(12, 13)	149.5	153.6	153.3	149.6	153.7	154.3	156.1	154.3
	143.3	151.6	149.8	145.8	151.9	151.8	147.1	150.6
C(14)	173.1	177.4	178.2	174.1	178.4	177.7	171.8	176.5
C(17, 18)			56.6		56.6			
C(19)			46.4		46.4			

[a]In $CDCl_3$ solution unless otherwise noted. Numbering system for C atoms as in Fig. 1; H atoms numbered by bonded C atoms.
[b]In dmso-d_6 solution.
[c]Joint integration of both peaks = 9H.
[d]Et_2O resonances H: 3.45 (q, 2); CH_2: 1.12 (t, 3) CH_3; C: 65.75 (CH_2), 15.21 (CH_3).

(1.394(3)) < Al (1.423(9)) < Cd (1.472(15) Å), it is clear that this five-membered ring has a remarkable facility to accommodate different metals by internal adjustment of both bond distances and angles.

The question of the C—C and C—O bond distances within the C_5O ring has been discussed in detail for Ph_2BL and AlL_3 (18). Given the changes in r(C(13)—C(14)) discussed above, one would expect minor differences in the other distances in the planar ring, as are found, but the conclusion for each of these three compounds is that C(15)—C(16) and C(12)—C(13) are in the range 1.31–1.37 Å, indicating significant double bond character. Together with the differences in length for C(14)—O(13) (1.249(12)) and C(13)—O(12) (1.306(14) Å). it is clear that the metal–ring interaction involves a substantial contribution from form **I** rather than the delocalized structure **II**.

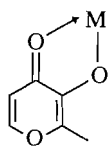

I

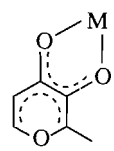

II

Spectroscopic studies

Both nmr and infrared spectroscopy provide useful confirmation that the structure of each of the compounds prepared is the same as CdL_2.tmen as far as the M—L interaction is concerned.

Table 6 gives the nmr spectra (^1H and ^{13}C) for the derivatives of 3-hydroxy-2-methyl-4-pyrone, except for the copper(II) complex, which is paramagnetic. The assignment of the proton spectra follows earlier work on the HL and InL_3 (16), and more recent studies by Orvig and co-workers (19) on aluminum and gallium tris(3-hydroxy-2-methyl-4-pyronates), and does not require detailed comment. The broad-band decoupled ^{13}C spectra of 3-hydroxy-2-methyl-4-pyrone and its metallic complexes show in every case a number of peaks corresponding to the number of non-equivalent carbons required by the molecular formulae, but the assignment of the carbon resonances from the pyrone ring is not a simple matter. The pattern observed for the ring carbons is a set of two intense peaks, one at 109.7–113.2 ppm and the second at lower field (149.6–154.6 ppm), plus two very weak signals which appear in the range 143.3–156.1. Carbon atoms 15 and 16 would be expected to have shorter relaxation times than carbons 12 and 13, and should therefore be more easily detected and give rise to the most intense peaks. Following this argument, we assign the peak at higher field (ca. 110 ppm) to C(15), and that at low field (149.6–154.6 ppm) to C(16). This leaves the two weak resonance signals at 143.3–156.1 ppm, which we attribute to carbons 12 and 13. Other resonances from tmen and diethyl ether are readily assigned in Table 3, and call for no further comment. The most striking feature of the ^{13}C nmr spectra of these complexes is the significant shift of the carbonyl resonance of the pyrone ligand, found at 173.1 ppm in HL, to lower field in the ML_n complexes, in agreement with the coordination of the carbonyl oxygen to the metal, as observed in the crystallographic studies discussed above.

The important features of the ir spectra of HL and its ML_n complexes are given in Table 7. The tentative assignments follow the general work by Katritzky and Jones (21) on γ-pyrone derivatives, and more recent studies on ML_3 compounds (M = Al, Ga, In) (16, 19). The first important point is that ν(O—H), found at 3262 cm^{-1} in 3-hydroxy-2-methyl-4-pyrone, is absent in the spectra of all the complexes prepared. Other absorptions of the pyronate ligand, such as ν(CH)(ring), ν(CH(CH_3)) and δ(CH)(ring) are almost unaffected on complex formation. The most prominent feature in the spectra of HL and its complexes is the set of four strong absorptions in the region 1660–1460 cm^{-1}, attributed to mixed C=O and C=C stretching modes of the pyrone, with the higher frequency band at 1656 cm^{-1} in the parent compound involving mainly ν(C=O) (21). This pattern of strong absorptions is retained in the spectra of the complexes, with a significant bathochromic shift of the order 40–70 cm^{-1} in the two higher frequency absorptions. The weakening of these C=O and C=C bonds is clearly associated with electron donation from the ring to the metal, and we conclude from these results that the coordination of the pyrone ligand to the metal

Can. J. Chem. Downloaded from www.nrcresearchpress.com by 91.121.58.235 on 09/07/12
For personal use only.

TABLE 7. Important features in the infrared spectra of derivatives of 3-hydroxy-2-methyl-4-pyrone

Species	Infrared spectra (cm^{-1})								
	HL	ZnL_2	$ZnL_2 \cdot$tmen	CdL_2	$CdL_2 \cdot$tmen	SnL_2	$SnI_2L_2 \cdot 1/2Et_2O$	InL_3	$CuL_2 \cdot PPh_3$[b]
(OH) (ring)	3262								
(CH) (ring)	3065 (m)	3072 (m)	[a]	3065 (m)	[a]	3086 (m)	3065 (m)	3072 (m)	3051 (m)
(CH) (CH_3)	2924 (vw)	2917 (vw)	[a]	2917 (vw)	[a]	2931 (vw)		2917 (vw)	2917 (vw)
(CH) (tmen)			[a]		[a]				
(C=O)	1656	1609	1591 (sh)	1614	1593	1609	1608	1603	1593
+	1620	1577	1579	1570	1565	1570	1552 (br)	1568	1568
(C=C)	1557	1522	1514	1520	1504	1505	1504	1502	1507
	1460	1461	1456	1459	1452	1459	1461	1460	1478
(CH) (ring) in-plane	918	920		920	914	916	928	923	917
(CH) (ring) out-of-plane	848	845	844	848	842	838	844	846	848

[a]Complicated pattern in the range 3065–2797 cm^{-1} (Zn) and 3072–2791 cm^{-1} (Cd).
[b]Important absorptions related to the PPh_3 ligand: 747 and 697 cm^{-1} ((CH) aromatic o.o.p.); 1438 and 1286 cm^{-1} (unassigned).

involves the same bidentate mode in all the compounds examined.

The oxidation of $Sn(O_3C_6H_5)_2$

As reported in the Experimental section, SnL_2 is readily oxidized by iodine to SnI_2L_2. This reaction, which is clearly similar to that recently reported for a number of tin(II) derivatives of aromatic 1,2-diols (22), causes only minor quantitative changes in the nmr or infrared spectra (see Tables 6 and 7). Following this work, and other studies in this laboratory of the oxidation of tin(II) compounds by *ortho*-quinones (23, 24), we also established that the reaction

$$SnL_2 + Q \rightarrow L_2Sn(Cat)$$

(Q = $Cl_4C_8O_2$-*o*, *t*-$Bu_2H_2C_6O_2$-*o*; Cat^{2-} = corresponding 1,2-diolate dianion) occurs smoothly to give six-coordinate tin(IV) compounds with SnO_6 kernels.

The nmr spectra of these two compounds gave the following resonances (in ppm from Me_4Si = 0):

$L_2Sn(O_2C_6Cl_4)$ (in d_6-dmso)

^{1}H: 2.56(s, 3H). 7.35(d,1H), 8.73(d,1H).

^{13}C: 15.6, 110.0, 116.4, 118.2, 145.6, 147.2, 158.4, 158.9, 171.9.

$L_2Sn(O_2C_{14}H_{20}).CH_3CN$ (in $CDCl_3$)

^{1}H: 1.97(s. 3H), 1.29(s, 9H), 1.40(s, 9H), 2.50(s, 6H), 6.64(d, 1H), 6.82(d, 2H), 6.90(d, 1H), 7.60(d, 2H).

^{13}C: 1.76, 15.6, 29.6, 31.8, 34.2, 34.9, 109.8, 110.3, 110.7, 111.9, 134.1, 138.5, 145.9, 147.6, 149.0, 155.3, 156.7, 173.4.

The proton nmr spectrum of $L_2Sn(O_2C_6Cl_4)$ is analogous to those of other pyronates (see Table 6) and calls for no comment. In the proton spectrum of $L_2Sn(O_2C_{14}H_{20}) \cdot CH_3CN$, the resonances at 6.82, 7.60 and 2 50 ppm are assigned to H(15), (16) and (11) respectively (see Table 6) of the pyronate ligand, so that the resonances of the catecholate ligand are at 1.29 and 1.40 (*t*-C_4H_9) and 6.64 and 6.90 ppm (aromatic protons); the signal at 1.97 ppm is due to the acetonitrile. Certain resonances in the ^{13}C spectra of these compounds are readily assigned. The methyl group of the pyronate ligand appears at 15.6 ppm in both derivatives, and the C(14) resonances are at 171.9 and 173.4 ppm, respectively. Resonances from the *tert*-butyl substituent groups are at 29.6 and 31.8 (CH_3 groups), and 34.2 and 34.9 ppm (CMe_3), and the signal at 1.76 ppm is assigned to the methyl carbon of the acetonitrile. The correct assignment of the resonances in the aromatic region of either catecholate is a difficult matter because of the presence of pyronate resonances in the same region, but we certainly detect resonances corresponding to the number of carbons required by the molecular formulae. Finally, we note that the C=O resonances in the parent quinones, at 168.8 ppm ($Cl_4C_6O_2$-*o*), and 180.5 and 179.7 ppm ($Bu_2H_2C_6O_2$-*o*), disappear following the formation of the tin(IV) catecholates, evidence which unambiguously supports the reduction of the quinones.

The vibrational spectra of the tin(IV) catecholato derivatives also show evidence of the reduction of the quinone to the corresponding catecholate. The strong absorptions at 1670 and 1641 cm^{-1} ($Cl_4C_6O_2$-*o*), and 1661 and 1662 cm^{-1} ($Bu_2H_2C_6O_2$-*o*) disappear. One would expect to find new C—O stretching modes, as were observed in earlier work (23, 24) on tin(IV) catecholates, in the region 1414–1468 cm^{-1}, but unfortunately this region is obscured in the present compounds by the strong absorptions from 1460–1660 cm^{-1} due to mixed C=O and C=C, and C—O stretching modes of the pyronate ligand.

Acknowledgement

This work was supported in part by a Strategic Grant (to D.G.T.) from the Natural Sciences and Engineering Research Council of Canada.

1. F. F. SAID and D. G. TUCK. Inorg. Chim. Acta, **59**, 1 (1982).
2. J. L. HENCHER, M. A. KHAN, F. F. SAID, and D. G. TUCK. Polyhedron, **4**, 1263 (1985).
3. R. K. CHADHA, R. KUMAR, and D. G. TUCK. Can. J. Chem. **65**, 1336 (1987).
4. R. K. CHADHA, R. KUMAR, J. R. LOPEZ-GRADO, and D. G. TUCK. Can. J. Chem. **66**, 2151 (1988).
5. J. H. GREEN, R. KUMAR, N. SEUDEAL, and D. G. TUCK. Inorg. Chem. **28**, 123 (1989).
6. T. A. ANNAN, R. KUMAR, and D. G. TUCK. J. Chem. Soc. Chem. Commun. 446 (1988).
7. N. KUMAR, D. G. TUCK, and K. D. WATSON. Can. J. Chem. **65**, 740 (1987).
8. H. E. MABROUK, D. G. TUCK, and M. A. KHAN. Inorg. Chim. Acta, **129**, 75 (1987).
9. H. E. MABROUK, and D. G. TUCK. J. Chem. Soc. Dalton Trans. 2539 (1988).

Can. J. Chem. Downloaded from www.nrcresearchpress.com by 91.121.58.235 on 09/07/12
For personal use only.

10. R. KUMAR and D. G. TUCK. Inorg. Chim. Acta, **157**, 51 (1989).
11. T. A. ANNAN, C. PEPPE, and D. G. TUCK. Can. J. Chem. **68**, 423 (1990).
12. M. A. KHAN, R. C. STEEVENSZ, D. G. TUCK, J. G. NOLTES, and P. W. R. CORFIELD. Inorg. Chem. **19**, 3407 (1980).
13. International tables for X-ray crystallography. Vol. IV. Kynoch Press, Birmingham 1974.
14. J. J. HABEEB, D. G. TUCK, and F. H. WALTERS. J. Coord. Chem. **8**, 27 (1978).
15. R. C. HIDER, G. KONTOGHIORGHES, J. SILVER, and M. A. STOCKHAM. U. K. Patent Appl. 2, **148**, 896 (1985); Chem. Abstr. **103**, 200877 (1985).
16. D. G. TUCK and M. K. YANG. J. Chem. Soc. A 3100 (1971).
17. M. M. FINNEGAN, S. J. RETTIG, and C. ORVIG. J. Am. Chem. Soc. **108**, 5033 (1986).
18. C. ORVIG, S. J. RETTIG, and J. TROTTER. Can. J. Chem. **65**, 590 (1987).
19. M. M. FINNEGAN, T. G. LUTZ, W. O. NELSON, A. SMITH, and C. ORVIG. Inorg. Chem. **26**, 2171 (1987).
20. D. G. TUCK. Rev. Inorg. Chem. **1**, 209 (1979).
21. A. R. KATRITZKY and R. A. JONES. Spectrochim. Acta, **17**, 64 (1961).
22. H. E. MABROUK and D. G. TUCK. J. Chem. Soc. Dalton Trans. 2539 (1988).
23. T. A. ANNAN, R. K. CHADHA, D. G. TUCK, and K. D. WATSON. Can. J. Chem. **65**, 2670 (1987).
24. T. A. ANNAN, R. K. CHADHA, B. R. MCGARVEY, A. OZAROWSKI, and D. G. TUCK. J. Chem. Soc. Dalton Trans. 439 (1989).

Can. J. Chem. Downloaded from www.nrcresearchpress.com by 91.121.58.235 on 09/07/12
For personal use only.

The crystal structure and chemistry of the "red salt" α-trisilver-amidoselenate, Ag_3NSeO_3

VLADIMIR KOCMAN[1]
Domtar Research Centre, Senneville, P.Q., Canada H9X 3L7

AND

JAN T. SZYMAŃSKI
CANMET, Department of Energy, Mines, and Resources, 555 Booth St., Ottawa, Ont., Canada K1A 0G1

Received August 29, 1989[2]

VLADIMIR KOCMAN and JAN T. SZYMAŃSKI. Can. J. Chem. **68**, 1606 (1990).

The crystal structure of the α-modification of the "red salt" of trisilver amidoselenate, Ag_3NSeO_3 has been determined from Mo$K\alpha$ X-ray diffraction data, and refined to $R = 3.19\%$ from 337 unique absorption-corrected observed reflections. The structure is rhombohedral, $R3c$ (No. 161), with (hexagonal) $a = 8.462(4)$, $c = 11.372(6)$ Å. The formula unit has point symmetry 3 (C_3), with Se and N on the threefold axis, each approximately tetrahedrally coordinated; Se by three oxygen atoms (at 1.651(8) Å) and N (at 1.70(2) Å), and N by Se and three silver atoms (at 2.164(8) Å). The bond of 1.70(2) Å between Se and N is particularly short. The Ag_3NSeO_3 structural unit bridges to three adjacent units via short Ag...O contacts of 2.23(1) Å to form a three-dimensional network.

Key words: trisilver amidoselenate, selenium–nitrogen bond, X-ray structure.

VLADIMIR KOCMAN et JAN T. SZYMAŃSKI. Can. J. Chem. **68**, 1606 (1990).

La structure cristalline de la modification α du «sel rouge» d'amidosélénate d'argent, Ag_3NSeo_3 a été déterminée et affinée à un résidu de $R = 3{,}19\%$ utilisant 337 réflections uniques mesurées à l'aide de la radiation Mo$K\alpha$. La structure est rhomboédrique de groupe spatial $R3c$ (No. 161) avec a (hex.) = 8,462(4) Å, c = 11,372(6) Å. L'unité structurale possède une symétrie d'ordre 3 (C_3), Se et N étant situés sur l'axe ternaire, chacun d'eux ayant une coordination approximativement tétraédrique. Le Se est lié à 3 atomes d'oxygène à 1,651(8) Å et un atome d'azote à 1,70(2) Å, et l'azote est lié à 3 atomes d'argent à 2,164(8) Å et un Se. La liaison de 1,70(2) Å entre Se et N est particulièrement courte. Le groupe Ag_3NSeO_3 est relié à trois autres groupes adjacents par des contacts courts de 2,23(1) Å entre Ag et O, et forme un réseau tridimensionnel.

Mots clés : amidosélénate d'argent, liaison sélénium–azote, structure cristalline.

Introduction

The formation of an orange–red precipitate, during the reaction of ammonium amidoselenate $NH_4SeO_3NH_2$ with silver nitrate in dilute NH_4OH, was first observed by Dostál and Krejčí (1) in 1958. Later, Engelbrecht and Clementi (2) described this reaction in their work on Se—N compounds. They suggested that the formation of the title compound most probably proceeds via substitution of the amino-group hydrogens by silver. Further studies of the compounds of the type Ag—N—X (where X is S or Se) were carried out by Dostál and Růžička (3), Růžička (4), and Paetzold, Dostál, and Růžička (5). It was Dostál and Růžička (3) who first confirmed the existence of two different modifications of Ag_3NSeO_3, and named them α and β. The α-modification results from the reaction given in ref. 3, while the β-modification results when the orange–red precipitate is kept at room temperature in the mother liquor for several days. The β-form can also be obtained as a product of the hydrolysis of $Ag_3NSeO_3.3NH_3.2H_2O$. Both modifications are highly explosive, and can be distinguished easily by their different X-ray powder patterns.

Paetzold, Růžička, and Dostál (5) studied a number of silver compounds containing NXO_3 groups (X = S, Se) by means of IR spectroscopy. They proposed possible structural models for the α and β forms of Ag_3NSeO_3. For the α form, the authors suggested a chain polymer structure with $NSeO_3$ groups bridged through linear O...Ag—N bonds, and a point symmetry C_{3v} for the Ag_3NSeO_3 structural unit. Although many other compounds containing Se—N bonds have been synthesized and characterized in the past (1–7), the structures of only a few compounds with Se—N bonds have been determined by single-crystal diffraction. Among these is the subject of a preliminary short communication by one of us (8) on the title compound, and the full structural report on potassium triselenylimide $K_3(NSeO_3)_3$ by Kocman and Rucklidge (9). The latter compound contains cyclic anions in a "chair" configuration, where the ring consists of three $NSeO_3$ units with Se—N bond lengths ranging from 1.75 to 1.79 Å. Structural studies have been done on nitrogen-containing organic molecules bonded to selenium; in all cases the Se—N bonds are in the range 1.80–1.85 Å. A review of these compounds was done by Roesky *et al.* (10), including the X-ray structural investigations of four selenium-containing compounds by the same authors. Two other X-ray structural determinations of novel compounds with Se—N, S—N, and Se—N—P rings have been recently completed by Chivers *et al.* (11, 12). As structural evidence for a Se—N double (or triple) bond is not available for Se—N acyclic compounds (as opposed to the extensive data available on S—N multiple bonds), we decided to complete the X-ray crystal structure analysis of α-Ag_3NSeO_3.

The original brief communication on the title compound (8) was based on Cu$K\alpha$ data, and had some shortcomings in the refined thermal parameters, probably as a result of inaccuracies in the very large absorption corrections performed on the data ($\mu = 1120\ cm^{-1}$). The present structure determination is based on Mo$K\alpha$ data ($\mu = 198.3\ cm^{-1}$), and will serve to establish the short Se—N bond in this compound.

Experimental

Crystals of the title compound were obtained as described above; they are dark-red, transparent, and quite hard. They crystallize as regular hexagonal prisms $\{11\bar{2}0\}$, capped on one end with a trigonal pyramid of form $\{10\bar{1}1\}$. They are insoluble in water, but dissolve

[1]To whom correspondence should be addressed.
[2]Revision received May 8, 1990.

Can. J. Chem. Downloaded from www.nrcresearchpress.com by 91.121.58.235 on 09/07/12
For personal use only.

Can. J. Chem. Downloaded from www.nrcresearchpress.com by 91.121.58.235 on 09/07/12
For personal use only.

TABLE 1. Crystal data and refinement

Formula	Ag_3NSeO_3
Formula weight	464.6 daltons
Crystal system	Rhombohedral (hexagonal axes)
Space group	$R\bar{3}c$ or $R3c$ from systematic absences $R3c$ determined from structure analysis
Cell dimensions	a = 8.462(4) Å c = 11.372(6) Å Z = 6
Crystal dimensions	0.154 mm between $\{11\bar{2}0\}$ faces, 0.20 mm between {0001} faces
Absorption coefficient	μ(Mo$K\alpha$) = 198.3 cm^{-1} D_{measd} = 6.63 g cm^{-3} D_{calcd} = 6.56 g cm^{-3}
X-ray data	collected with Mo$K\alpha$ ($\lambda(K\alpha_1)$ = 0.70932 Å) to 2θ = 70°, 360 reflections measured, 337 observed with $I > 3\sigma(I)$
Collection mode	θ–2θ scan at 1°(2θ)/min, 2 × 20 background counts, 2 standards every 30 reflections, no decay, variation < 1%
Absorption correction	Gaussian, with 24 × 24 × 24 grid
Refinement	Full matrix least-squares, anisotropic thermal parameters, extinction coefficient, chirality parameter (to define enantiomorph)
Residual	R = 3.19%, R_w = 4.65%

TABLE 2. Positional and anisotropic thermal parameters (×100)[a]

Atom	x	y	z	B_{iso} (Å^2)
Ag	0.26030(16)	0.05443(19)	0.5(0)	1.86(5)
Se	0.0 (0)	0.0 (0)	0.2804(4)	0.88(5)
N	0.0 (0)	0.0 (0)	0.4299(19)	1.11(43)
O	0.2085(15)	0.0798(15)	0.2238(9)	1.36(40)

Atom	U_{11}	U_{22}	U_{33}	U_{12}	U_{13}	U_{23}
Ag	1.76(5)	2.54(6)	2.57(5)	0.94(5)	−0.66(5)	−0.14(5)
Se	0.96(5)	0.96(0)	1.44(8)	0.48(0)	0.00(0)	0.00(0)
N	1.13(45)	1.13(0)	1.96(84)	0.56(0)	0.00(0)	0.00(0)
O	1.89(46)	1.83(46)	1.56(40)	1.01(38)	0.13(37)	0.07(37)

[a]Temp = $\exp\{-2\pi^2(U_{11}h^2a^{*2} .. + .. + 2U_{12}hka^*b^* ..)\}$; B_{iso} is the mean of the principal axes of the thermal ellipsoid.

readily in aquaeous ammonia and acids. The crystal selected was cut with a scalpel parallel to (0001) to remove the pyramidal faces, and this resulted in a hexagonal prism, 0.154 mm between faces, and 0.2 mm long. Weissenberg and precession photographs indicated rhombohedral symmetry, and absences that conformed to space groups $R3c$ and $R\bar{3}c$. The former (non-centric) was selected on the basis of previous IR studies (5), morphology, and the E-distribution.

The cell dimensions and their standard deviations were obtained by a least-squares fit of 15 high-angle carefully centred reflections. A total of 360 unique reflections were collected to a limit of 2θ = 70°, using Mo$K\alpha$ radiation with a scan rate of 1°/min in 2θ, and 20 s background counts on either side of the peak. Standard reflections were monitored, but showed no decay and less than 1% variation. The data set contained 337 observed reflections with $I > 3\sigma(I)$, and these were corrected for absorption using a Gaussian integration procedure and a grid of 24 × 24 × 24 points. The crystal data are summarized in Table 1.

X-ray structure refinement

The earlier structure determination of this compound by Kocman *et al.* (8) using copper radiation provided starting parameters for the refinement. Real $\Delta f'$ and imaginary $\Delta f''$ components of the scattering factors were included for all atoms; the scattering curves for the neutral atomic species were taken from International Tables, Vol. IV (13). Anisotropic thermal parameters were refined, as was an extinction parameter and a chirality parameter. The latter defines the enantiomorph in a non-centric molecular structure (14). The final full-matrix residual was R = 3.19%. The programs used were the PC version of the NRCVAX system (15). The positional and thermal parameters are included in Table 2. All the thermal parameters refined to acceptable values, although the spheroids for Se and especially N are somewhat prolate with the major axis along z. This may be a coupled (riding) motion on the part of the N atom, as there is really no reason for the larger thermal parameter in this direction. There was no evidence of disorder around the N sites, nor any reason to suspect partial interchange between O and N atoms between their assigned positions. However, to confirm this, the population parameters of O and N were varied simultaneously at the end of the refinement. The population parameters of O and N refined to 1.09(10) and 1.02(5) respectively; the differences from unity are not significant, and with *both* increasing, this seems to rule out any possibility of O–N interchange. The list of observed and calculated structure factors has been deposited, and is available from the Depository of Unpublished Data.[3]

[3]Photocopies of the structure factor tables may be purchased from the Depository of Unpublished Data, CISTI, National Research Council of Canada, Ottawa, Ont., Canada K1A 0S2.

Can. J. Chem. Downloaded from www.nrcresearchpress.com by 91.121.58.235 on 09/07/12
For personal use only.

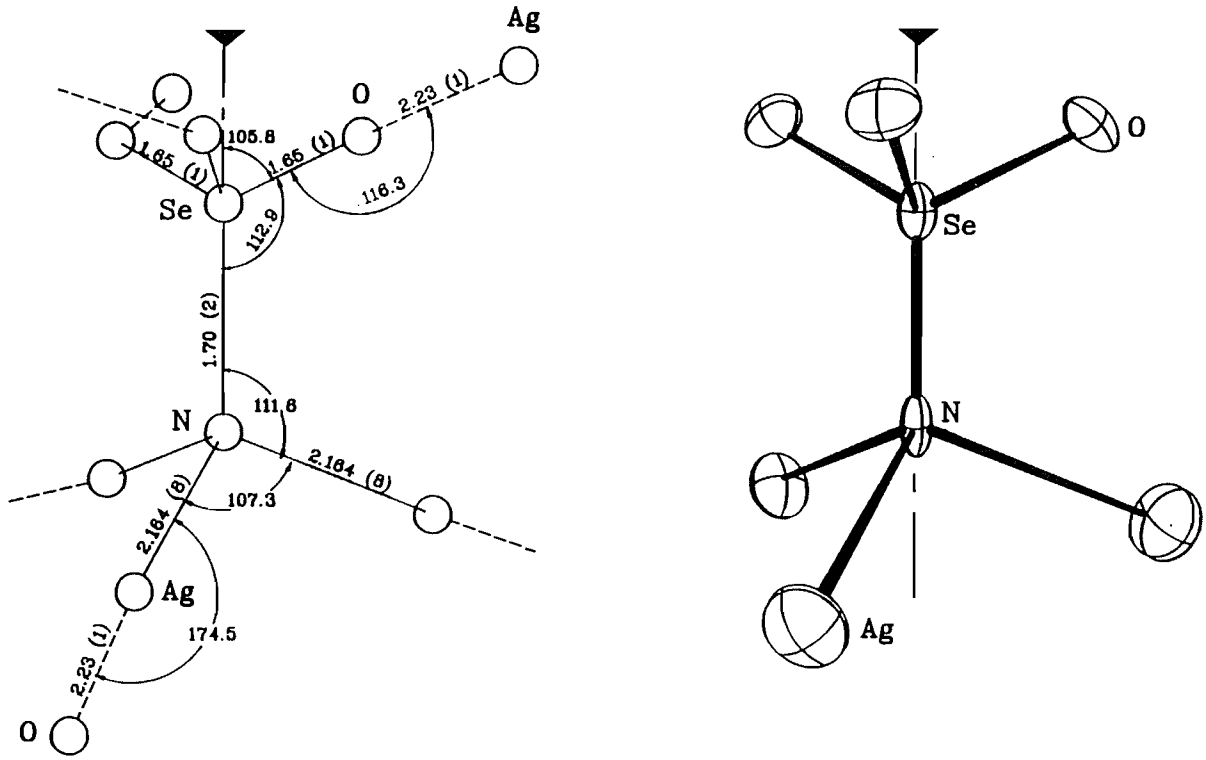

FIG. 1. (*left*) Selected bond lengths and angles in α-Ag_3NSeO_3; (*right*) the structural unit drawn with thermal vibration ellipsoids at 50% probability.

Results and discussion

Figure 1 shows one Ag_3NSeO_3 unit of the polymeric network, with selected bond lengths and angles. The right side of the figure shows a perspective view of the same unit with thermal vibration ellipsoids. Major interatomic distances and angles are summarized in Table 3.

The threefold symmetry of the monomeric unit within the structure is a consequence of the space group. The symmetry of the unit is close to the C_{3v} point group originally predicted for this compound by Paetzold *et al.* (5). Within the monomeric repeat unit, the Se and N atoms (1.70(2) Å apart) are located on a threefold axis, and each atom is approximately tetrahedrally coordinated. The Se atom is bonded to three O atoms and N to three Ag atoms. The Se—O and N—Ag bonds are nearly eclipsed in projection, there being a rotational offset of 11° between the two (Fig. 2). The intermolecular packing is helical, each monomer being bonded via N...Ag...O bridges to three other units. In these bridges, the Ag^+ ion is linearly coordinated, with the N...Ag distances of 2.164(8) Å being slightly shorter than the O...Ag distance of 2.23(1) Å. The polymeric units are arranged in double helices, coaxial with the 3_1 screw axis of the $R3c$ space group. The separation between the helices is $\frac{1}{2}$ in the z-direction as shown in Fig. 3, where two strands of the helices are depicted in perspective. In the polymeric structure, the nearly tetrahedral $NSeO_3$ group acts as a hexadentate bridging group, with N coordinated to three and each O to one Ag-metal centre.

The bonding within this unit and the relatively short Se—N bond length of 1.70(2) Å in this compound is of primary interest. Based on the sum of the single-bond radii (16) of 1.87 Å for Se—N and 1.83 Å for Se—O bonds, it is apparent that appreciable multiple-bond character is suggested for both the Se—N and Se—O bonds in the bridging $NSeO_3$ moiety. The latter with d = 1.651 Å is well within the range reported for metal selenates of 1.60 to 1.70 Å (17), while the slightly longer Se—N bond of 1.70 Å reflects almost precisely the difference in the covalent single-bond radii for N and O of 0.70 and 0.66 Å, respectively (16). This suggests approximately identical

TABLE 3. Bond lengths (Å) and angles (deg)[a]

Bond	Length	Bond	Length
Ag—N	2.164(8)	Se—O(c)	1.651(8)
Ag—O(a)	2.229(12)	N—Ag(b)	2.164(8)
Se—N	1.701(22)	N—Ag(c)	2.164(8)
Se—O	1.651(8)	O—Ag(d)	2.229(12)
Se—O(b)	1.651(8)		

Bonds	Angle	Bonds	Angle
N—Ag—O(a)	174.5(5)	Ag—N—Ag(b)	107.3(6)
N—Se—O	112.9(4)	Ag—N—Ag(c)	107.3(6)
N—Se—O(b)	112.9(4)	Ag—N—Se	111.6(5)
N—Se—O(c)	112.9(4)	Ag(b)—N—Ag(c)	107.3(6)
O—Se—O(b)	105.8(5)	Ag(b)—N—Se	111.6(5)
O—Se—O(c)	105.8(5)	Ag(c)—N—Se	111.6(5)
O(b)—Se—O(c)	105.8(5)	Ag(d)—O—Se	116.3(6)

[a]Coordinates of unlabelled atoms are listed in Table 2. The symmetry equivalents referred to above represent the atoms at the following coordinates

Name	x	y	z			
O(a)	0.54071	0.12754	0.55716	$\frac{2}{3}-x+y$	$\frac{1}{3}-x$	$\frac{1}{3}+z$
O(b)	−0.07983	0.12596	0.22383	$-y$	$x-y$	z
O(c)	−0.12596	−0.20579	0.22383	$-x+y$	$-x$	z
Ag(b)	−0.05443	0.20587	0.50000	$-y$	$x-y$	z
Ag(c)	−0.20587	−0.26030	0.50000	$-x+y$	$-x$	z
Ag(d)	0.27890	−0.12747	0.16667	$\frac{1}{3}-y$	$-\frac{1}{3}+x-y$	$-\frac{1}{3}+z$

Can. J. Chem. Downloaded from www.nrcresearchpress.com by 91.121.58.235 on 09/07/12
For personal use only.

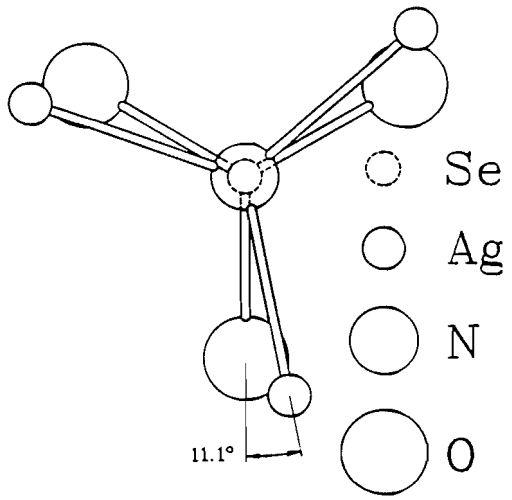

FIG. 2. The almost eclipsed Ag and O atoms of α-Ag_3NSeO_3 viewed down the hexagonal *c*-axis.

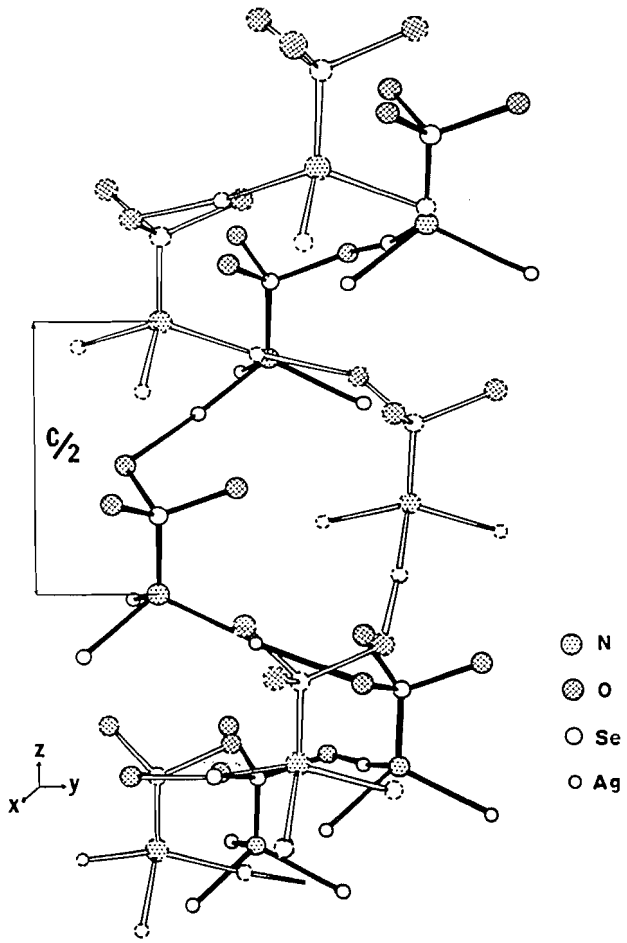

FIG. 3. Two independent strands of helices which represent the dense packing of α-Ag_3NSeO_3 in the hexagonal unit cell.

π-contributions to all four bonds formed by selenium(VI) in this compound. Hence, it seems appropriate to describe the bonding within the approximately tetrahedral $NSeO_3$ group by the three permutations of each of the following two resonance forms

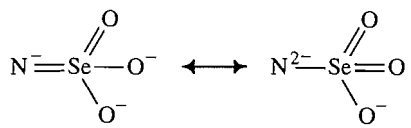

which make identical contributions to the overall structure, resulting in an average bond order of 1.5 for all four bonds, and a π-bond order of 2.0 for this group. This approach follows closely similar ideas developed some time ago by Cruickshank (18) for sulphur–oxygen compounds, invoking $p\pi \rightarrow d\pi$ bonding. The average formal charge on nitrogen of −1.5, suggested by the two resonance forms above, can also explain readily the slightly shorter Ag—N distances compared to the Ag...O contacts: N coordinates to three Ag^+, while O coordinates to one Ag^+ each. The average formal charge on oxygen of −0.5 suggests a lower donor ability towards Ag^+ in agreement with general observations (19). The Ag—N distances of 2.164 Å are slightly longer than distances observed for the linear cation $[Ag(NH_3)_2]^+$, where depending on the type of counter-anion, values of 2.11 and 1.89 Å are reported (19). This in turn suggests a bonding description for the NAg_3 moiety in terms of ionic-covalent resonance

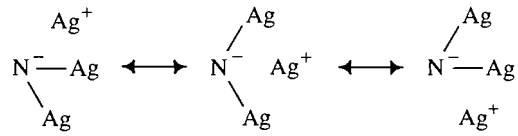

rather than in terms of three distinct N—Ag coordinate bonds, which would certainly imply pentacovalent nitrogen in at least two of the resonance forms. A similar approach is applicable to the description of the Ag—O contacts. It is apparent, in particular from the short Se—N bond observed here, that the bonding in the Se—N moiety is distinctly different from that observed in the zwitterion form of sulfamic acid $[H_3N^+\ SO_3^-]$ studied by Sass (20), and the approach described above appears to be more appropriate for interpreting the bonding in Ag_3NSeO_3.

Other aspects of the structure, its bond lengths and angles conform to values found by X-ray methods in other similar compounds (9, 21, 22). The Ag—N bond length of 2.164(8) Å and the Ag—O distance of 2.229(12) Å do not show any unusual departures from values found in the literature (23). In summary, it appears that the "red salt" of α-trisilveramido-selenate is best viewed as a "coordination polymer", with a double-helix structure, weakly and near-linearly coordinated Ag(I) centres and bridging $NSeO_3$ moieties, with strong Se—N and Se—O bonds and tetrahedrally coordinated N and Se atoms. Even though the amido-selenate anion $H_2NSeO_3^-$ is known (17), there appears to be no precedent for the $NSeO_3^{3-}$ anion, which is isoelectronic with the well-known selenate anion SeO_4^{2-}. Finally, it should be pointed out that the interpretation presented here is totally consistent with the IR absorption spectrum of α-Ag_3NSeO_3 (5), and that the crystal structure confirms most of the structural predictions reported in the same publication.

Only very recently (February 1990), we have obtained information on the newly-completed single-crystal structure determination of the "parent compound" related to the "red salt", namely $Ag_3NSeO_3.3NH_3.2H_2O$ (24). Although full details are not yet available, it appears that the $NSeO_3$ moiety has a very similar geometry to that reported here for α-Ag_3NSeO_3. There is a non-crystallographic pseudo-threefold axis along the Se—N bond, although in this case the Ag_3N and SeO_3 groups appear to be staggered by about 30°. For comparison, the bond lengths are Se—N = 1.73 Å, Se—O = 1.64 Å, Ag—N = 2.11 Å.

Acknowledgements

We would like to thank Dr. A. Růžička and Professor K. Dostál of the University of J. E. Purkyně, Brno, Czechoslo-

vakia for supplying the original crystals, and for their interest in this work. Dr. Z. Žák of the same university is gratefully acknowledged for providing us with details of the still-unfinished structure of the parent salt ($Ag_3NSeO_3.3NH_3.2H_2O$). We are greatly indebted to the two referees for their suggestions.

1. K. Dostál and J. Krejčí. Z. Anorg. Allg. Chem. **269**, 29 (1958).
2. A. Engelbrecht and F. Clementi. Mh. Chem. **92**, 570 (1961).
3. K. Dostál and A. Růžička. Z. Anorg. Allg. Chem. **337**, 325 (1965).
4. A. Růžička. Dr. Sc. Thesis, Univ. J. E. Purkyně, Brno, Czechoslovakia, 1966.
5. R. Paetzold, K. Dostál, and A. Růžička. Z. Anorg. Allg. Chem. **348**, 1 (1966).
6. G. Kempe, M. Lorentz, and H. T. Schneider. Z. Chem. **4**, 184 (1964).
7. K. Dostál, A. Růžička, and M. Sochorcová. Mh. Chem. **101**, 208 (1970).
8. J. K. Fawcett, V. Kocman, S. C. Nyburg, and R. J. O'Brien. Chem. Commun. 1198 (1968).
9. V. Kocman and J. Rucklidge. Acta Crystallogr. B**30**, 6 (1974).
10. H. W. Roesky, K.-L. Weber, U. Seseke, W. Pinkert, M. Noltemeyer, W. Clegg, and G. M. Sheldrick. J. Chem. Soc. Dalton Trans. 565 (1985).
11. A. Apblett, T. Chivers, and J. F. Fait. J. Chem. Soc. Chem. Commun. 1598 (1989).
12. T. Chivers, D. D. Doxsee, and J. F. Fait. J. Chem. Soc. Chem. Commun. 1703 (1989).
13. J. A. Ibers and W. C. Hamilton (*Editors*). International tables for X-ray crystallography. Vol. IV. Kynoch Press, Birmingham, England. 1974.
14. H. D. Flack. Acta Crystallogr. A**39**, 876 (1983).
15. E. J. Gabe, Y. Le Page, J.-P. Charland, F. L. Lee, and P. S. White. J. Appl. Crystallogr. **22**, 384 (1989).
16. L. Pauling. The nature of the chemical bond. 2nd ed. Cornell University Press, Ithaca, New York. 1948. p. 164.
17. Gmelin Handbook. Se supplement B1, Springer Verlag, Berlin. 1981. pp. 300–303 and references therein.
18. D. W. J. Cruickshank. J. Chem. Soc. 5468 (1961).
19. R. J. Lancashire. *In* Comprehensive coordination chemistry. Vol. 5. *Edited by* G. Wilkison, Pergamon Press, Oxford. 1987. p. 775.
20. R. L. Sass. Acta Crystallogr. B**13**, 320 (1960).
21. A. Kalman. J. Chem. Soc. A, 1857 (1971).
22. A. Kalman, A. Stephens, and D. W. J. Cruickshank. Acta Crystallogr. B**26**, 1451 (1970).
23. I. D. Brown, M. C. Brown, M. C. Brown, and F. C. Hawthorne (*Editors*). BIDICS, Bond Index to the Determination of Inorganic Crystal Structures Published during 1969–1981. Institute for Materials Research, McMaster University, Hamilton, Ont., Canada L8S 4M1.
24. Z. Žák and A. Růžička. University of J. E. Purkyně, Brno, Czechoslovakia. Private communication. 1990.

Can. J. Chem. Downloaded from www.nrcresearchpress.com by 91.121.58.235 on 09/07/12
For personal use only.

Tracer diffusion in aqueous sucrose and urea solutions

ALLAN J. EASTEAL
Department of Chemistry, University of Auckland, Auckland, New Zealand

Received November 30, 1989[1]

ALLAN J. EASTEAL. Can. J. Chem. **68**, 1611 (1990).

Tracer diffusion coefficients for water (as HTO), methanol ($^{14}CH_3OH$), and acetonitrile (CT_3CN) in aqueous sucrose (10–25% w/w) and urea (0.25–4 mol L^{-1}) solutions at 298 K have been determined using the diaphragm cell technique. For sucrose solutions tracer diffusion coefficients vary with the 2/3 power of the relative viscosity and the viscosity dependence is the same for the above tracers as for sucrose and oxygen. In urea solutions tracer diffusion coefficients appear to have a solute-specific viscosity dependence, but the solute specificity is largely removed when the effects of proton exchange and urea dimerisation are considered.

Key words: diffusion, water, methanol, acetonitrile, sucrose, urea.

ALLAN J. EASTEAL. Can. J. Chem. **68**, 1611 (1990).

Opérant à 298 K et utilisant la technique de la cellule à diaphragme, on a déterminé les coefficients de diffusion des marqueurs de l'eau (sous la forme de HTO), du méthanol ($^{14}CH_3OH$) et de l'acétonitrile (CT_3CN) dans des solutions aqueuses de sucrose (de 10 à 25% p/p) et d'urée (0,25 à 4 mol L^{-1}). Pour les solutions de sucrose, les coefficients de diffusion des marqueurs varient avec les 2/3 de la puissance de la viscosité relative; la relation avec la viscosité est la même pour les marqueurs mentionnés plus haut. Il semble que, dans les solutions d'urée, la variation des coefficients de diffusion des marqueurs avec la viscosité soit spécifique pour chaque soluté; toutefois, cette spécificité disparaît lorsque les effets de l'échange de proton et de la dimérisation de l'urée sont pris en considération.

Mots clés : diffusion, eau, méthanol, acétonitrile, sucrose, urée.

[Traduit par la revue]

Introduction

The effect of the viscosity (η) on tracer- and self-diffusion coefficients (D) for species in liquid media has been a matter of considerable interest. For example, there is a substantial body of experimental diffusion data for volatile components in concentrated carbohydrate solutions. The dependence of D on carbohydrate concentration and hence medium viscosity simulates the variation in D of "flavour constituents", to be expected in the course of the water content decrease which occurs in spray drying of liquid foods. In another context, the effect of viscosity on diffusion coefficients is central to the correlation between solvent viscosity and the rates of diffusion-controlled reactions. The viscosity dependence of D for a wide variety of solutes in numerous aqueous and non-aqueous solvents has been investigated; the results of such studies (prior to 1973) have been discussed at length by Hiss and Cussler (1).

The Stokes–Einstein equation, in the form

$$[1] \quad D\eta/T = \text{constant}$$

(T = temperature) has been used as the starting point for most attempts to develop predictive methods for D, based on correlations of known values of D with solvent properties. Empirical correlations of that kind have been critically reviewed by Reid and co-workers (2) who concluded that over wide temperature or viscosity ranges simple empirical correlations are inadequate and the viscosity dependence of (tracer- or self-) diffusion coefficients is expressed by (at constant temperature)

$$[2] \quad D \propto \eta^{\alpha}; \; -1 \leq \alpha \leq -0.5$$

According to Hiss and Cussler (1), α in eq. [2] depends on the solute/solvent size ratio (R_D). They postulated that $\alpha = -1$ for $R_D > 5$; α tends to the value $-2/3$ for $R_D < 5$ in high viscosity solvents; $\alpha = 0$ in extremely high viscosity media. The situation regarding diffusion of a variety of solutes in a given solvent is unclear. Oosting and co-workers (3) concluded that α may change for one solute in different carbohydrate solutions or for different solutes in the same carbohydrate solution. However, they found that for 1-hexanol and 2-butanone diffusing in a carbohydrate solution at 60, 75, and 90°C, the single value $\alpha = -0.5$ gave an acceptable representation of the experimental data.

The objective of the present study was to obtain accurate tracer diffusion data for a variety of solutes in aqueous solvents with varying viscosity, to (*a*) investigate the applicability of a relationship of the form of eq. [2]; (*b*) determine the extent to which α varies with solute. Aqueous solutions of sucrose and urea at 298 K were selected as solvents because the diffusion coefficients of sucrose (4) and urea (5) in their solutions have been accurately measured, and the viscosities are known as functions of concentration for both sucrose (6) and urea (7–9) solutions. Furthermore, sucrose and urea provide a contrast in their effects on the viscosity of water. Whereas a very large increase in viscosity can be achieved at small sucrose concentrations, high concentrations of urea are needed to significantly increase the viscosity of water. The solutes (tracers) chosen for initial study were water, methanol, and acetonitrile, all of which were available in suitably labelled form (HTO, $^{14}CH_3OH$ and CT_3CN).

Experimental

Sucrose solutions containing 10, 15, 20, and 25% w/w were made up from AnalaR grade sucrose. Urea solutions of concentration 0.25, 0.5, 1, 2, 3, and 4 mol L^{-1} were made up from AnalaR grade urea.

Tracer diffusion coefficients were measured at 298.15 ± 0.01 K for HTO, $^{14}CH_3OH$ and CT_3CN in each sucrose and urea solution using the (glass) diaphragm cell technique and associated procedures (10). In several cases, diffusion coefficient measurements for a particular tracer and solution were replicated with two independently calibrated diaphragm cells, in order to check that systematic errors in the cell constants were not significant. In all such cases replicated determinations agreed to within a few tenths %, and the accuracy of the values of D is believed to be ±0.5% for the measurements with $^{14}CH_3OH$ and ±1% for the HTO and CT_3CN data.

[1]Revision received May 23, 1990.

Can. J. Chem. Downloaded from www.nrcresearchpress.com by 91.121.58.235 on 09/07/12
For personal use only.

TABLE 1. Experimental data for sucrose solutions at 298.15 K

c/mol L^{-1}	m/mol kg^{-1}	η/η_0	$10^9\ D$/m^2 s^{-1} HTO[a]	$^{14}CH_3OH$[b]	CT_3CN[c]
0.2698	0.2871	1.287	1.903	1.329	1.363
0.4652	0.5178	1.589	1.659	1.165	1.176
0.6321	0.7325	1.932	1.452	1.003	1.031
0.8075	0.9780	2.214	1.252	0.876	0.889

[a] $D_0 = 2.235 \times 10^{-9}$ m^2 s^{-1} (ref. 21).
[b] $D_0 = 1.563 \times 10^{-9}$ m^2 s^{-1}.
[c] $D_0 = 1.632 \times 10^{-9}$ m^2 s^{-1}.

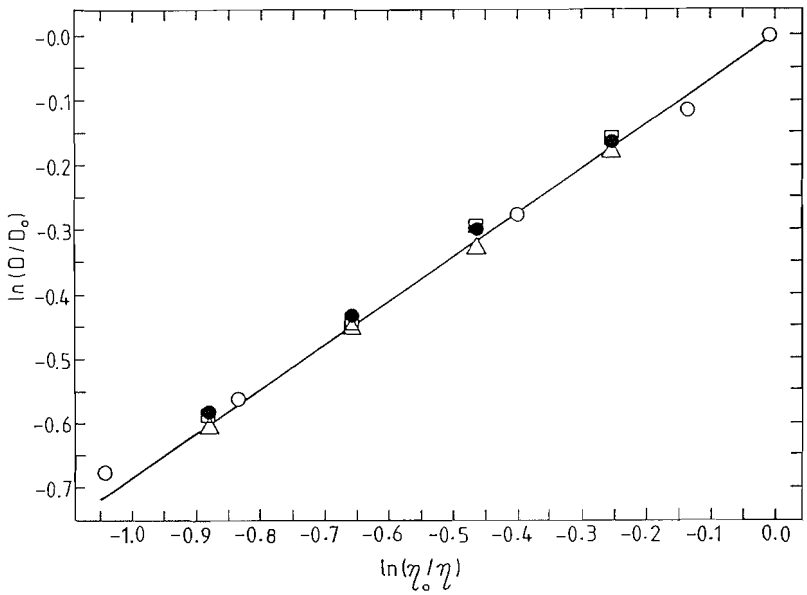

FIG. 1. Viscosity dependence of tracer diffusion coefficients in sucrose solutions at 298.15 K. ○, sucrose; ●, HTO; △, CT_3CN; □, $^{14}CH_3OH$.

Density (ρ) and relative viscosity (η/η_0, where η_0 is the viscosity of water) data were obtained from the literature. The source of data for the sucrose solutions was the critical compilation by Stokes and Mills (6). For urea solutions the density data of Gucker and co-workers (11) were used to interconvert molarities and molalities, and the viscosity data of Dunstan and Mussell (7), Chadwell and Asnes (8), and Jones and Talley (9) combined into a single data set were interpolated at the concentrations of interest.

Results and discussion

1. *Sucrose solutions*

The experimental data are given in Table 1 which includes the values of η/η_0 for the solutions investigated. For a constant temperature eq. [2] can be written in the form

$$[3] \quad D/D_0 \propto (\eta_0/\eta)^{\alpha}$$

where D_0 is the limiting tracer diffusion coefficient at vanishingly low concentration of tracer in water. Figure 1 shows the variation of D/D_0 with η_0/η in the form of a log–log plot, and includes the tracer data for sucrose (4). It is apparent that to within the experimental uncertainty the four solutes obey a relationship of the form of eq. [3]. The values of α which fit the data for the individual tracer molecules are sucrose, 0.65; CH_3OH, 0.66; HTO, 0.66; CT_3CN, 0.69; and the whole data set can be represented to within the experimental uncertainty by eq. [3] with $\alpha = 0.67$. In Fig. 2, the tracer data are compared with data for oxygen diffusion (12) in sucrose solutions. The $D(O_2)$ values plotted were measured at atmospheric pressure and about 300 K, and sucrose concentrations up to 1.96 mol L^{-1}. They can be fitted with a function of the form of eq. [3] with $\alpha = 0.69$ and are collinear within uncertainty with the data for sucrose, HTO, CH_3OH, and CT_3CN.

Also shown in Fig. 2 are tracer data (13) at 298 K for esters (CH_3COOR, where R = ethyl, *n*-propyl, *n*-butyl, and *n*-pentyl) diffusing in 15% w/w and 30% w/w sucrose. The D/D_0 (ester) values for the less concentrated sucrose solution are in accordance with the other tracer data plotted. For the more concentrated sucrose solution, however, the ester data are in substantial disagreement with the other tracer data. Even though the precision of the ester data is not high (±10% at the higher sucrose concentration, according to the authors) the ca. 25% discrepancy is difficult to account for. If all of the D/D_0 values (including ester data at 318 K (13)) are plotted against % w/w sucrose, the data lie close to a smooth curve except for the ester values for 30% sucrose at 298 K. It is possible, therefore, that the latter data are significantly in error. On the other hand, it may be the case that at 298 K in 30% w/w sucrose the esters have a tendency to form clusters. If that were so, the ester diffusion coefficient should be significantly smaller than for non-clustered molecules, leading to an apparent discrepancy qualitatively similar to that in Fig. 2, in the ester diffusion coefficient under these conditons.

Can. J. Chem. Downloaded from www.nrcresearchpress.com by 91.121.58.235 on 09/07/12
For personal use only.

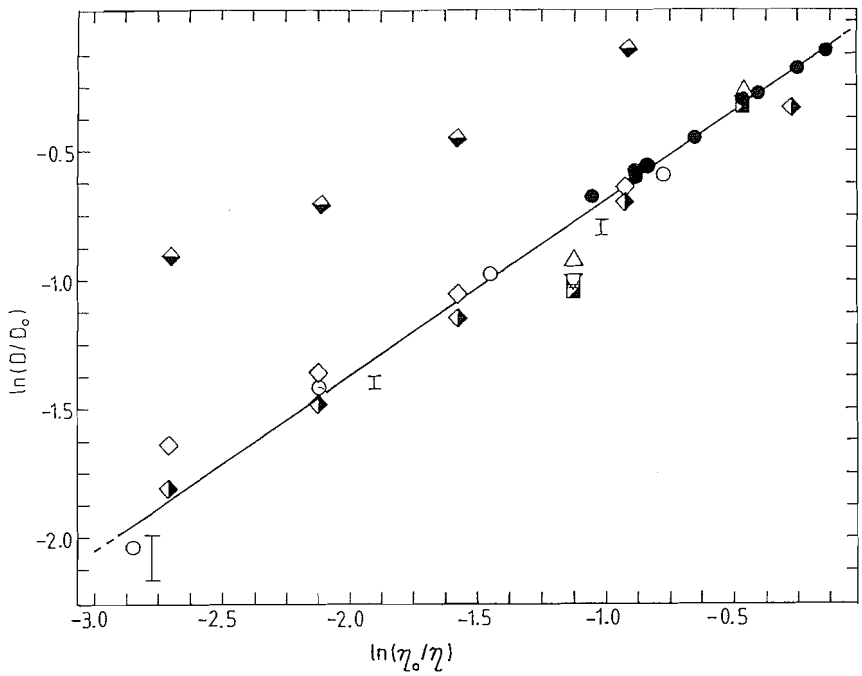

FIG. 2. Viscosity dependence of tracer and mutual diffusion coefficients in sucrose solutions at 298.15 K. Tracer diffusion coefficients are denoted by ●, sucrose, HTO, CH_3OH, CT_3CN; ○, O_2; △, ethylacetate; □, *n*-propylacetate; ▽, *n*-butylacetate; ◪, *n*-pentylacetate. The vertical bars denote ester data at 318 K. Mutual diffusion coefficients are denoted by ◆, uncorrected; ◇, including an activity coefficient correction (eq. [4]); ◈, using eq. [5].

With the exception of the ester data at the higher sucrose concentration at 298 K, the diffusion coefficients for a variety of different solutes with a range of molecular sizes (the extremes being O_2 and sucrose) have virtually identical ($D \propto \eta^{-2/3}$) dependence. This observation is contrary to the selective diffusion concept postulated by Thijssen (14). The $D \propto \eta^{-2/3}$ dependence was also found by Hiss and Cussler (1) for tracer diffusion of *n*-hexane and naphthalene in liquid hydrocarbons with a four decade range of viscosities. Evans and co-workers (15, 16) have observed, on the other hand, for a variety of tetraalkyltins, rare gases, methanes, and substituted methanes diffusing in hydrocarbons, acetone, and alcohols at 298 K, that while eq. [2] is obeyed with $\alpha > -1$ the exponent varies inversely with the solute radius. It is interesting to note that relative tracer diffusion coefficients for esters at 318 K (13) (shown in Fig. 2 as vertical bars) have the same viscosity dependence, to within experimental uncertainty, as that of the tracers at 298 K. The exponent α in eq. [3] is evidently independent of the tracer species, and is temperature invariant within the restricted temperature range for which data are available for sucrose solutions.

Since sucrose contains hydroxylic protons which can exchange with water protons, the effect of tritium exchange between HTO and sucrose on the diffusion coefficient of HTO should be considered. For a solute with p exchangeable protons per molecule, provided that tritium exchange between the solute and HTO is sufficiently rapid, a statistical distribution of the tritium label between solute and solvent water will be attained. The observed diffusion coefficient for tritium (in all forms) is then given by the weighted average, D_T, defined by

$$D_T = (pcD + 2c_W D_W)/(pc + 2cw)$$

where c and D are the concentration and diffusion coefficient of the solute, and c_W and D_W are the corresponding quantities for water. Since c_W is of the order 55 mol L^{-1}, the equation for D_T reduces to

$$[4] \quad D_T = (pcD + 110D_W)(pc + 110)$$

Sucrose has at most eight exchangeable protons per molecule. Substitution in eq. [6] for the values of D_T, c, and D for the most dilute and most concentrated sucrose solutions studied, and solving for D_W gives $D_W = 1.93 \times 10^{-9}$ m^2 s^{-1} for $c = 0.27$ mol L^{-1}, and $D_W = 1.31 \times 10^{-9}$ m^2 s^{-1} for $c = 0.81$ mol L^{-1}. The correction to D_T for tritium exchange is thus no larger than between about 2% and 4% over the concentration range investigated, and does not significantly affect the viscosity dependence of D_T.

The viscosity dependence of mutual diffusion coefficients in sucrose and other solutions has been a matter of interest for a considerable time. Mutual diffusion coefficients, D_{12}, reported by Henrion (17) for sucrose solutions at 298 K are shown in Fig. 2. The values of D_{12} have been reduced by the limiting tracer diffusion coefficient of sucrose (0.523×10^{-9} m^2 s^{-1}) (4, 18, 19) but are othewise unadjusted, and they have a very different viscosity dependence from that of the tracer diffusion coefficients. If the relative mutual diffusion coefficients are divided by the thermodynamic factor

$$[5] \quad Q = \mathrm{d} \ln a / \mathrm{d} \ln x$$

(x = mol fraction of sucrose) as suggested by the Gordon equation (20), they lie close to the line representing the tracer values for concentrations up to about 1.8 mol kg^{-1}. If the values of D_{12} are reduced by the limiting diffusion coefficient given by

$$[6] \quad D_0 = x_W D_{0,S} + x_S D_W$$

where x_W and x_S are mol fractions of water and sucrose, $D_{0,S}$ is

Can. J. Chem. Downloaded from www.nrcresearchpress.com by 91.121.58.235 on 09/07/12
For personal use only.

TABLE 2. Experimental data for urea solutions at 298.15 K[a]

c/mol L^{-1}	m/mol kg^{-1}	η/η_0	$10^9\ D$/m^2 s^{-1}		
			HTO	$^{14}CH_3OH$	CT_3CN
0.25	0.2535	1.010	2.200	1.549	1.617
0.5	0.5128	1.020	2.197	1.542	1.621
1.0	1.0495	1.042	2.165	1.519	1.568
2.0	2.2018	1.091	2.061	1.468	1.507
3.0	3.4738	1.148	1.919	1.412	1.409
4.0	4.8861	1.215	1.821	1.355	1.355

[a]For limiting values of D see footnotes to Table 1.

the limiting tracer diffusion coefficient for sucrose in water and D_W is the self-diffusion coefficient of water (2.299×10^{-9} m^2 s^{-1}) (21) and divided by Q, as in the Hartley–Crank equation (22), they lie close to the line representing the tracer diffusion coefficients up to about 3 mol kg^{-1}. The implication is that up to moderate concentrations corrected relative mutual diffusion coefficients show to a good approximation the same dependence on viscosity as do the tracer diffusion coefficients.

2. Urea solutions

The experimental data are given in Table 2, which includes the values of η/η_0 for the solutions investigated. In marked contrast to sucrose solutions for which the concentration dependence of relative tracer diffusion coefficients can be represented by a single (almost linear) function, for urea solutions D/D_0 for urea (5) and HTO, $^{14}CH_3OH$ and CT_3CN cannot be represented by a single function of concentration.

The viscosity dependence of D/D_0 is shown in Fig. 3. At one extreme, the behaviour of CH_3OH is well represented by a function of the form of eq. [3] with $\alpha \approx 3/4$. At the other extreme, the graph for urea is linear at low concentrations, with slope $\approx 4/3$, but the slope decreases with increasing concentration above about 1 mol L^{-1} to ca. 3/4 at 4 mol L^{-1}. CT_3CN and HTO behave similarly to each other, and approach CH_3OH-type behaviour at low concentrations and urea-type behaviour at high concentrations of urea.

Urea has at most four exchangeable protons per molecule. Calculation of corrected values of D_T, using eq. [4], reveals a correction which is negligibly small at the lowest concentration, increasing to about 5% for the most concentrated solution. The effect of tritium exchange between urea and HTO is therefore to lessen the viscosity dependence of D_T, and the correction gives values of D/D_0 for HTO which are close to those for CH_3OH in Fig. 3.

It should be noted that urea is partially dimerised in aqueous solution, and the effect of dimerisation on the tracer diffusion coefficient of urea has been analyzed in detail by Stokes (24). Stokes concluded that the viscosity dependence of the tracer diffusion coefficient could be accounted for using values for the degree of dimerisation calculated from experimental activity coefficient data, a relationship of the form of eq. [3] with $\alpha = 0.8$, and the value of 0.615 for the ratio, D_R^0, of the limiting tracer diffusion coefficients of dimer to monomer. (It must be borne in mind, however, that other combinations of values of α and D_R^0 are also satisfactory (24).)

When the effects of (*a*) tritium exchange between HTO and urea and (*b*), dimerisation of urea are taken into account, therefore, in the urea solutions the tracer diffusion coefficients of CH_3OH, HTO, and urea have approximately the same viscosity dependence, and the viscosity dependence is consistent with eq. [3] with $\alpha \sim 0.75$. The remaining tracer in the urea solutions, CT_3CN, exhibits qualitatively similar behaviour except that the value of α is close to 1. The different behaviour of CT_3CN cannot be accounted for by tritium exchange with urea or water because the tritium atoms in CT_3CN are non-exchangeable (under the conditions of the diffusion coefficient measurements). It is possible that the diffusive motion of CT_3CN is slowed by a weak association of CT_3CN with urea, since although CT_3CN does not have a hydrogen bond acceptor site it has, like urea, a large dipole moment, and dipole–dipole interactions may be strong enough to lead to the observed viscosity dependence of D.

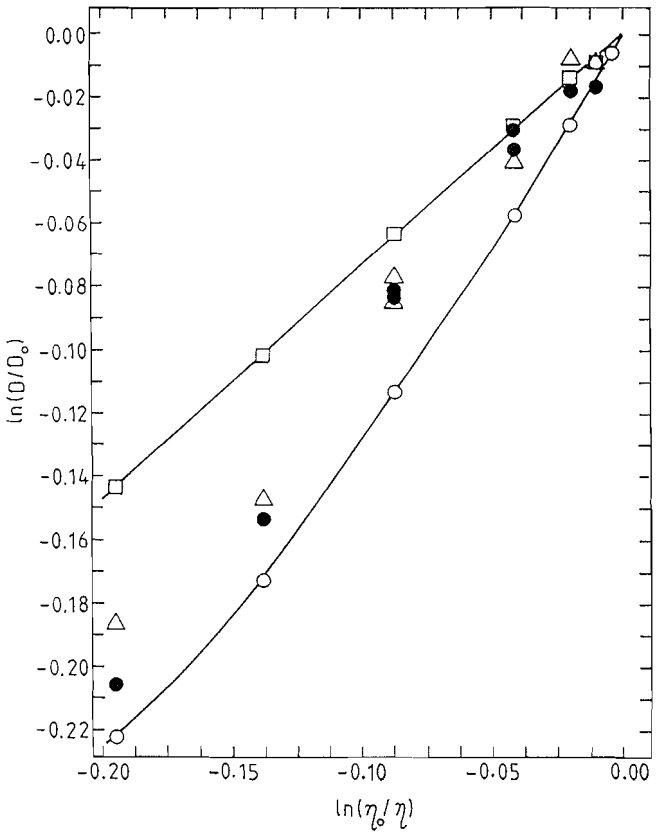

FIG. 3. Viscosity dependence of tracer diffusion coefficients in urea solutions at 298.15 K. ○, urea; ●, HTO; □, CH_3OH; △, CT_3CN.

Mutual diffusion coefficients for urea solutions, relative to the limiting tracer diffusion coefficient for urea (5, 23) and either unadjusted or adjusted as per the Gordon equation, lie

Can. J. Chem. Downloaded from www.nrcresearchpress.com by 91.121.58.235 on 09/07/12
For personal use only.

between the curves for urea and CH_3OH in Fig. 3, and likewise if the mutual diffusion coefficients are reduced according to the Hartley–Crank equation. The viscosity dependence of D_{12} cannot be described by an equation of the form of eq. [3] with a concentration-independent exponent. However, the effect of dimerisation of urea on the mutual diffusion coefficient has not been taken into account. Aspects of the general problem of the effect of solute association on mutual diffusion coefficients have been discussed by several authors (25–28). In particular, Schönert (28) has extended Stokes' analysis (24) of tracer diffusion in urea solutions to mutual diffusion, and concluded, in effect, that the experimental diffusion coefficients can be accounted for using a relative viscosity exponent (α in eq. [3]) of 1.

Acknowledgements

The experimental work reported herein was done at the Atomic and Molecular Physics Laboratories, in the Research School of Physical Sciences of the Australian National University. The author is indebted to Dr. L. A. Woolf for his support and to the Research School of Physical Sciences for a Visiting Fellowship.

Helpful comments by referees are gratefully acknowledged.

1. T. G. Hiss and E. L. Cussler. AIChEJ. **19**, 698 (1973).
2. R. C. Reid, J. M. Prausnitz, and T. K. Sherwood. The properties of gases and liquids. 3rd ed. McGraw-Hill, New York. 1977.
3. E. M. Oosting, J. I. Gray, and E. A. Grulke. AIChEJ. **31**, 773 (1985).
4. J. F. Tilley and R. Mills. J. Phys. Chem. **71**, 2756 (1967).
5. J. G. Albright and R. Mills. J. Phys. Chem. **69**, 3120 (1965).
6. R. H. Stokes and R. Mills. Viscosity of electrolytes and related properties. Pergamon Press, Oxford. 1965.
7. A. E. Dunstan and A. G. Mussell. J. Chem. Soc. **97**, 1935 (1910).
8. H. M. Chadwell and B. Asnes. J. Am. Chem. Soc. **52**, 3507 (1930).
9. G. Jones and S. K. Talley. J. Am. Chem. Soc. **55**, 624 (1933).
10. R. Mills and L. A. Woolf. The diaphragm cell. A.N.U. Press, Canberra. 1968.
11. F. T. Gucker, F. W. Gage, and C. E. Moser. J. Am. Chem. Soc. **60**, 2582 (1938).
12. H. Hikita, S. Asai, and Y. Azuma. Can. J. Chem. Eng. **56**, 371 (1978).
13. D. D. Frey and C. J. King. J. Chem. Eng. Data, **27**, 419 (1982).
14. H. A. C. Thijssen. J. Appl. Chem. Biotechnol. **21**, 373 (1971).
15. D. F. Evans, T. Tominaga, and C. Chen. J. Solution Chem. **8**, 461 (1979).
16. H. T. Davis, T. Tominaga, and D. F. Evans. AIChEJ. **26**, 313 (1980).
17. P. Henrion. Trans. Faraday Soc. **60**, 72 (1964).
18. L. J. Gosting and M. S. Morris. J. Am. Chem. Soc. **71**, 1998 (1949).
19. O. Bryngdahl. Acta Chem. Scand. **11**, 1017 (1957).
20. A. R. Gordon. J. Chem. Phys. **5**, 522 (1937).
21. R. Mills. J. Phys. Chem. **77**, 685 (1973).
22. G. S. Hartley and J. Crank. Trans. Faraday Soc. **45**, 801 (1945).
23. L. J. Gosting and D. F. Akeley. J. Am. Chem. Soc. **74**, 2058 (1952).
24. R. H. Stokes. J. Phys. Chem. **69**, 4012 (1965).
25. L. A. Dunn and R. H. Stokes. Aust. J. Chem. **18**, 285 (1965).
26. L. G. Longsworth. J. Coll. Interf. Sci. **22**, 3 (1966).
27. P. C. Carman. J. Phys. Chem. **71**, 2565 (1967).
28. H. Schönert. Z. phys. Chem. Neue Folge, **119**, 53 (1980).

Can. J. Chem. Downloaded from www.nrcresearchpress.com by 91.121.58.235 on 09/07/12
For personal use only.

Intercalation of cations into niobyl-vanadyl phosphate by redox reactions

A. JIMENEZ-LOPEZ,[1] A. L. GARCIA-PONCE, AND L. MORENO-REAL

Departamento de Química Inorgánica, Cristalografía y Mineralogía, Facultad de Ciencias, Universidad de Málaga, Ap. 59, 29071 Málaga, Spain

Received January 31, 1990

A. JIMENEZ-LOPEZ, A. L. GARCIA-PONCE, and L. MORENO-REAL. Can. J. Chem. **68**, 1616 (1990).

Mixed niobyl-vanadyl phosphate, $Nb_{0.86}V_{0.14}OPO_4 \cdot 2.7H_2O$, intercalates various alkali, NH_4^+ alkaline earth, Zn^{2+}, Cd^{2+}, transition metal, and H^+ cations by topotactic redox reactions. All the intercalates thus obtained are tetragonal ($a = b = 6.44$ Å, c lower than in the precursor solid). The degree of hydrolysis of the mixed phosphate in the intercalate in the redox reactions is always lower than 1%. Upon reduction, the cation exchange capacity (CEC) of the intercalates is 71 mequiv. per 100 g of solid calcined at 1000°C.

Key words: mixed niobyl-vanadyl phosphate, layered compounds, redox intercalation.

A. JIMENEZ-LOPEZ, A. L. GARCIA-PONCE et L. MORENO-REAL. Can. J. Chem. **68**, 1616 (1990).

Utilisant des réactions rédox topotactiques, il est possible d'intercaler les ions H^+ ou NH_4^+ ainsi que des ions de divers métaux alcalins, alcalino-terreux (Zn^{2+}, Cd^{2+}) ou de transition dans un phosphate mixte de niobyle et de vanadyle, $Nb_{0,86}V_{0,14}OPO_4$. Tous les produits intercalés ainsi obtenus sont tétragonaux ($a = b = 6,44$ Å alors que c = est plus courte que dans le solide précurseur). Le degré d'hydrolyse du phosphate mixte présent dans le produit intercalé des réactions rédox est toujours inférieur à 1%. Après réduction, le CEC des produits intercalés est égal à 71 mequiv. par 100 g de solide calciné à 1000°C.

Mots clés : phosphate mixte de niobyle et de vanadyle, composés en couches, intercalation rédox.

[Traduit par la revue]

Introduction

Vanadyl phosphate, α-$VOPO_4 \cdot 2H_2O$, is a layered substance typically undergoing two types of reaction: (a) intercalation of neutral species such as amines, amides, pyridine, etc. (1–3), and (b) electron transfer between the lattice and a reductant, in the presence of a guest species, resulting in the reduction of vanadium to V(IV) (4, 5). This second type of reaction is subject to the high degree of hydrolysis of the reduced phases obtained, so that some authors use small volumes of hydroalcoholic mixtures (4) or acetone (5) as reaction media. The search for a phase that would withstand hydrolysis led to the synthesis of mixed niobyl-vanadyl phosphates, which proved to be solid solutions of the two phosphates of formula $(Nb_{1-x}V_x)OPO_4 \cdot 2.7H_2O$, where x can take a maximum value of 0.21 (6). The mixed phosphates also intercalate neutral substances such as amines (7), pyridine (8), and amides (9) in reactions evidencing the mild acidic nature of the water molecule coordinated to the metal.

This paper reports a study on the intercalation of alkali, alkaline earth, transition, and other cations such as Zn^{2+}, Cd^{2+}, and H^+ into the mixed phosphate of formula $(Nb_{0.86}V_{0.14})OPO_4 \cdot 2.7H_2O$ (NbVP) by a redox reaction from the corresponding iodides in aqueous medium. The redox reaction of NbVP was also carried out with isobutyl alcohol. Each experiment involved the determination of the extent of reaction and the degree of hydrolysis undergone by the intercalates isolated.

Experimental

The intercalation of the inorganic cations into NbVP was carried out by a method reported elsewhere (4) and based on reacting the solid with a solution of the iodide of the cation. To optimize the reaction conditions, we studied the influence of the reaction time and reductant concentration on the extent of reduction. This involved performing two preliminary experiments. In the first, 0.1 g of NbVP was brought into contact with 25 mL of KI solution so that $[I^-] = 5[V^{5+}]$. The suspensions obtained were centrifuged at preset intervals, after which the potassium concentration in the supernatants was measured. The reaction was quite fast: the extent of reduction was 70% after 30 min and 90% after 1 h. Nevertheless, all the intercalation reactions were allowed to develop for 24 h.

The second of the above-mentioned experiments involved studying the influence of the iodide concentration on the intercalation reaction. Thus, 0.3 g of NbVP was suspended at 25°C in 25 mL of solution with $[I^-]/[V^{5+}]$ ratios between 0.1 and 10. After 24 h, the solids were isolated by centrifugation and washed with deionized water. The supernatants and the solids were analyzed for potassium and V^{4+}, respectively. The maximum extent of reduction was reached at a $[I^-]/[V^{5+}]$ ratio of 5, which was chosen for all subsequent experiments.

The different ions intercalated into NbVP phosphate were as follows: alkali (Li^+,Na^+, K^+, and Cs^+) and ammonium; alkaline earth (Mg^{2+} and Ca^{2+}); post-transition (Zn^{2+} and Cd^{2+}), and transition (Mn^{2+}, Fe^{2+}, Co^{2+} and Ni^{2+}). All the reactions were conducted under the above-described conditions. The metallic iodides used were either commercially available or synthesized by the authors. The extent of reduction was measured from the cation content of the isolated solids. In most cases, these values are in good agreement with those found by V^{4+} redox titration.

The synthesis of the H^+ intercalates involved two experiments. In the first, NbVP was brought into contact with an HI solution under the same conditions used in preparing the intercalates of the metal ions; in the second, 0.4 g of NbVP was suspended in 25 mL of isobutyl alcohol and refluxed for 10 days. The resultant solid product was then isolated and washed with acetone.

Finally, as the reduction potential of the Fe^{3+}/Fe^{2+} pair is lower than that of the V^{5+}/V^{4+} pair, the redox intercalation of Fe^{2+} ions was effected by bringing the solid into contact with 25 mL of a $FeSO_4$ solution with an $[Fe^{2+}]/[V^{5+}]$ ratio of 5.

The solids obtained in these reactions were characterized by chemical and TD–TG analyses, X-ray diffraction, and IR and UV–vis–nIR spectroscopy.

The extent of hydrolysis undergone by NbVP in the redox intercalation reaction was determined by measuring the phosphorus content in the supernatants. It was always very low (below 1% in all cases).

Thermogravimetric and differential thermal analyses were carried out on a Rigaku Thermoflex instrument using calcined alumina as internal reference and heating at a rate of 10 K/min. Platinum crucibles and Pt/Pt–Rh thermocouples were used throughout.

Powder X-ray diffraction patterns were recorded on a Siemens

[1]Author to whom correspondence may be addressed.

Printed in Canada / Imprimé au Canada

Can. J. Chem. Downloaded from www.nrcresearchpress.com by 91.121.58.235 on 09/07/12
For personal use only.

Can. J. Chem. Downloaded from www.nrcresearchpress.com by 91.121.58.235 on 09/07/12
For personal use only.

TABLE 1. Chemical composition, degree of reduction of vanadium, and basal spacing (Å) of the monovalent cation intercalates M_x ($V_{0.14}$ $Nb_{0.86}$) $OPO_4 \cdot y\ H_2O$

Cation	% Reduction	x	y	d_{002}
—	—	—	2.7	7.90
Li^+	72.8	0.102	2.5	7.35
Na^+	73.6	0.103	2.3	6.99
K^+	78.6	0.110	2.2	6.95
Cs^+	83.6	0.117	2.0	7.13
NH_4^+	87.1	0.122	2.2	6.99

D-501 automatic diffractometer using graphite-monochromated CuK_α radiation.

Infrared spectra were obtained on a Perkin–Elmer 883 spectrophotometer using KBr pellets (2%), while UV–vis–nIR spectra were recorded on a Shimadzu UV 3100 spectrophotometer using pressed $BaSO_4$ tablets as references.

Results and discussion

Niobyl-vanadyl phosphate, NbVP, is highly stable to hydrolysis; in fact, after undergoing a redox reaction, the degree of hydrolysis of the resultant product is never higher than 1%; in contrast, vanadyl phosphate is hydrolyzed to an extent of 20% under the same conditions. This high hydrolytic stability allowed us to use aqueous solutions to study the intercalation reactions.

Redox intercalation of monovalent ions

The monovalent cations intercalated into NbVP were Li^+, Na^+, K^+, Cs^+, and NH_4^+. Table 1 lists the chemical composition, extent of reduction of V^{5+}, and basal spacings of the compounds isolated. As a rule, and despite the high $[I^-]/[V^{5+}]$ ratios used, the extent of reduction of V^{5+} was not too great; in fact, the maximum was 87%. On the other hand, the extent of reduction increased with the atomic number of the alkali cation. This might be related to the hydrated radii of these ions; as the $Li(H_2O)_n^+$ cation features the largest radius, the narrowing of the basal space brought about by the reduction–intercalation hinders the uptake of further ions.

The smallest extent of intercalation of the Li^+ into NbVP contrasts with the findings of other authors (4) for vanadyl phosphate, which was found to be reduced by 100%. On the other hand, this intercalate features the highest water content, which decreases with decreasing ionic potential along the series. The composition and basal spacing of the NH_4^+ intercalate are similar to those of the K^+ intercalate on account of the similarity of their sizes.

The Li^+ intercalate has the largest basal spacing, consistent with its highest water content; the other intercalates have d_{002} spacings of about 7 Å, smaller than that of the original matrix (7.90 Å) as a result of the electrostatic interactions between the charged layers and the intercalated cations, and lower water contents. The diffractograms of these solids resemble that of the original matrix, although they contain fewer reflections; however, they show higher degrees of crystallinity than organic intercalates (7–9). The (200) reflection appears quite sharp at 3.22 Å, thereby indicating the preservation of the layered structure. The reflections can be indexed in the tetragonal system, with $a = b = 6.44$ Å and c between 13.94 and 14.78 Å, although the corresponding basal spacings (6.99–7.35 Å) are half the value of the c parameter (6). Only a single phase is observed under the experimental conditions used ($[I^+]/[V^{5+}] = 5$);

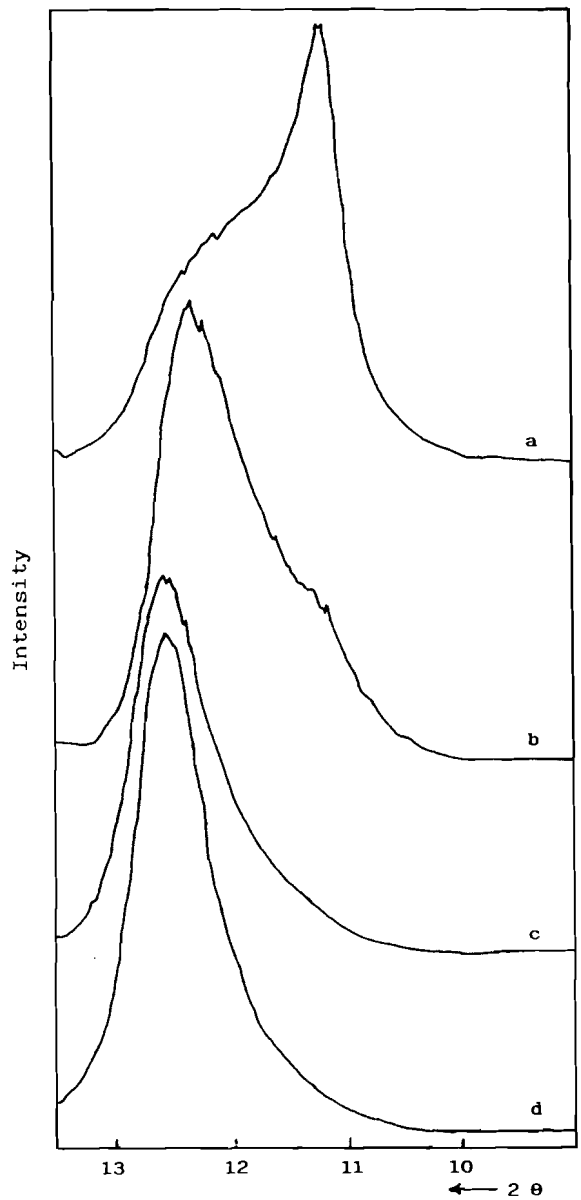

FIG. 1. Basal spacing evolution with the degree of reduction of vanadium of the potassium–NbVP intercalates: (a) 7%, (b) 21%, (c) 43%, (d) 64%.

however, extents of reduction below 43% result in a mixture of the reduced phase with others arising from partial dehydration of the original matrix (Fig. 1).

The thermograms of the intercalates of the monovalent ions are very similar to one another and to that of NbVP, with the exception of that of NH_4^+, which also shows two small exothermal effects at 305 and 435°C, corresponding to the elimination of intercalated ammonium. Figure 2 shows the diagrams of various K^+ intercalates and that of NbVP. As can be seen, all show two endothermal effects similar to NbVP, with two corresponding weight losses in the TG curves that can be assigned to two dehydration stages. The first effect is centred between 83 and 90°C and corresponds to the loss of 1.2 mol of water weakly retained by the solid. The second is influenced by the extent of reduction, as it tends to split with increase in this variable, as does the interval over which coordinated water is removed (1 mol per mol of phosphate); thus, the peak is centred

Can. J. Chem. Downloaded from www.nrcresearchpress.com by 91.121.58.235 on 09/07/12
For personal use only.

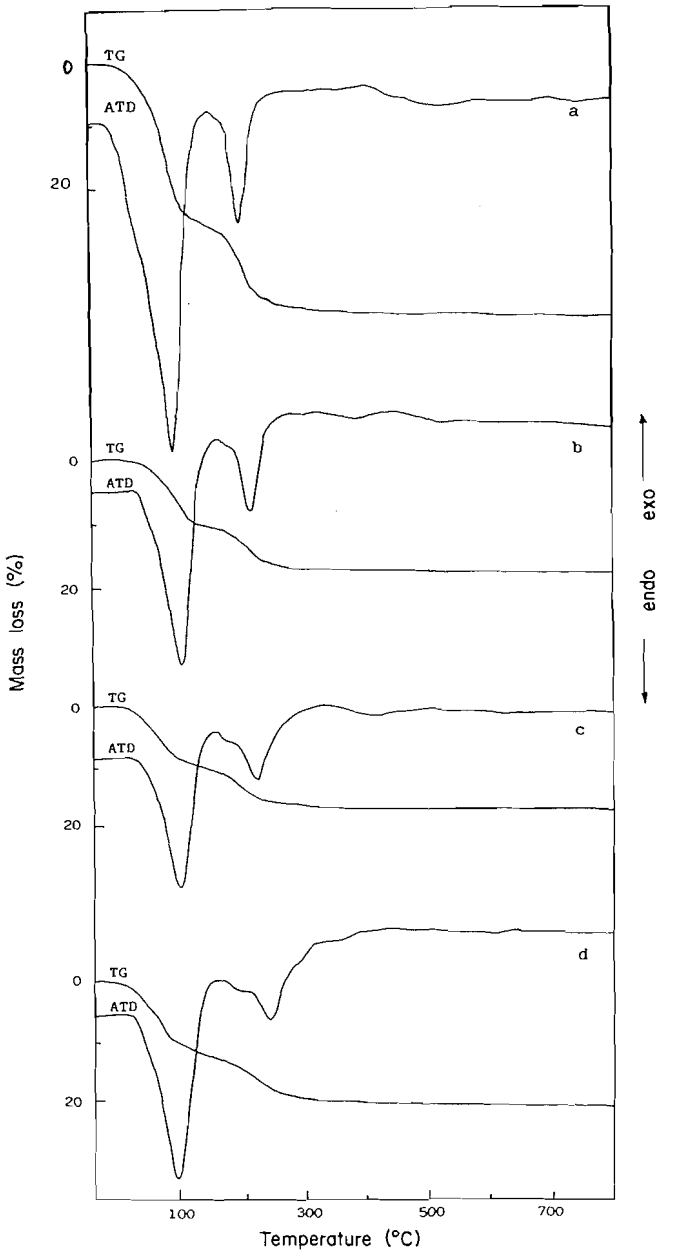

FIG. 2. DTA curves of potassium–NbVP intercalates with different degrees of reduction of vanadium: (a) NbVP, (b) 7%, (c) 43%, (d) 79%.

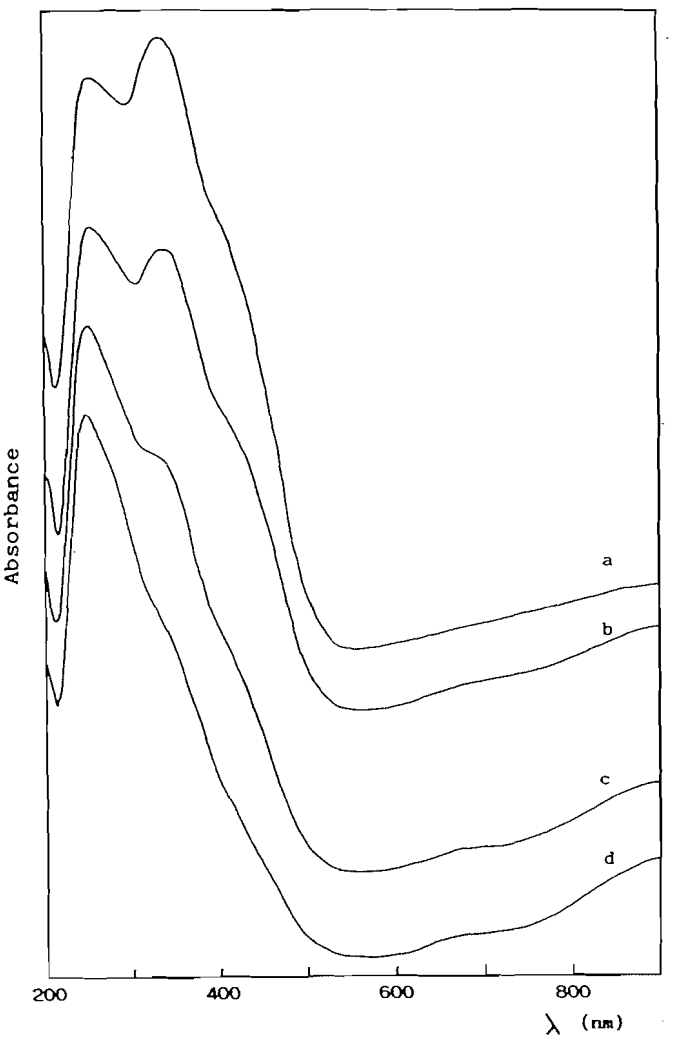

FIG. 3. Diffuse reflectance spectra of potassium–NbVP intercalates with different degrees of reduction of vanadium: (a) 7%, (b) 43%, (c) 64%, (d) 79%.

at 196°C and 228°C for an extent of reduction of 9% and 79%, respectively. This shift appears to arise from the negative charge localized in the $(O_5VH_2O)^-$ octahedron, which exerts a strong attraction on the K^+ ion, so that the water molecule lying between both ion species is strongly retained and hence more difficult to remove.

This phenomenon rules out the possibility of the intercalation taking place via the same mechanism as that proposed by other authors (10) for the intercalation of Na^+ into vanadyl phosphate; the water content and extent of intercalation of the Na^+ ions are supposed to be interrelated as the (O_5VH_2O) octahedron becomes an (O_5V) square pyramid and the Na^+ ion occupies the former position of water. Obviously, if this were also the case with our intercalates, the remaining coordinated water would not be affected by the extent of intercalation as stated above.

The diffuse reflectance spectra of the intercalates of these ions also vary with the extent of reduction as the charge transfer bands of vanadium at 335 nm and the shoulder at 400 nm are shifted to the UV region (where the charge transfer band of niobium is observed (6)) with increasing reduction. Figure 3 is illustrative of this behaviour. The reduction results in a concomitant adoption of a d^1 configuration by V^{4+}, which yields three absorptions, namely $E \leftarrow B_2$ (930–840 nm), $B_1 \leftarrow B_2$ (660 nm), and $A_1 \leftarrow B_2$ (overlapped with the charge transfer bands) in its distorted octahedral environment. The UV–vis–nIR of the K^+ intercalate is presented in Fig. 4, which also shows the bands at 1424 nm corresponding to combinations of ν(OH) and $\delta(H_2O)$, and at 1925 nm, corresponding to the first harmonic of ν(OH).

Redox intercalation of divalent ions

The chemical composition, extent of reduction of vanadium, and basal spacings of the intercalates of divalent ions obtained are listed in Table 2.

The extent of reduction of V^{5+} in these intercalates is greater than in those of the monovalent cations; in some cases, the host matrix was almost completely reduced. The Mg^{2+} intercalate was an exception in this respect since, as a result of its higher

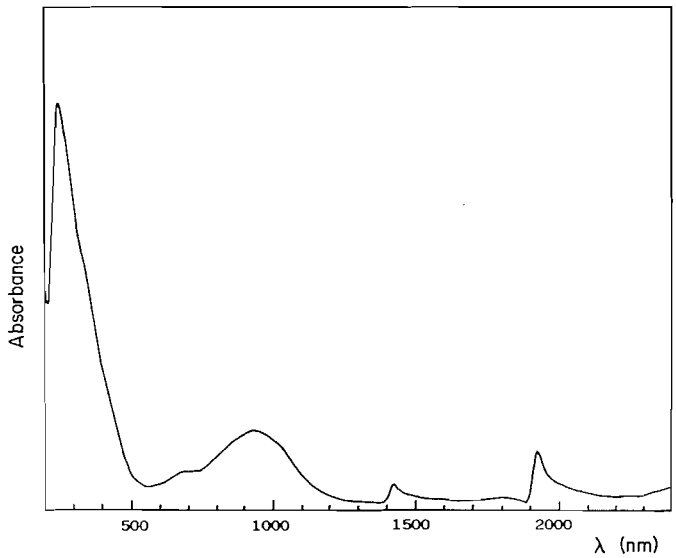

FIG. 4. Diffuse reflectance spectrum (UV–vis–nIR) of potassium–NbVP intercalate (79% reduction).

TABLE 2. Chemical composition, degree of reduction of vanadium, and basal spacing (Å) of the divalent cation intercalates M_x ($V_{0.14}$ $Nb_{0.86}$) $OPO_4 \cdot y\ H_2O$

Cation	% Reduction	x	y	d_{002}
Mg^{2+}	74.3	0.052	2.8	7.76
Ca^{2+}	91.4	0.064	2.3	7.14
Zn^{2+}	94.3	0.066	2.4	7.17
Cd^{2+}	95.7	0.067	2.4	7.17
Mn^{2+}	100	0.070	2.4	7.17
Fe^{2+}	95.7	0.067	2.5	7.47
Co^{2+}	92.8	0.065	2.3	7.30
Ni^{2+}	98.6	0.069	2.5	7.50

ionic potential, it behaved similarly to Li^+: it showed the highest water content as a result of the hindered intercalation of so strongly hydrated a cation, which in turn resulted in the smallest extent of reduction.

As far as the transition metal cations are concerned, the vanadium in the host is reduced in virtually 100% in all cases; their extents of reduction were thus greater than those found by other authors (4, 11) for $VOPO_4 \cdot 2H_2O$.

As one would expect, the water content was higher for the intercalates of these divalent cations than for those of the monovalent ions, so much so that the content of the Mg^{2+} intercalate was equal to or even higher than that of the host matrix.

The unit cell volumes calculated for $Li_{0.10}$ $NbVP \cdot 2.5H_2O$ and $Mg_{0.05}$ $NbVP \cdot 2.8H_2O$ with equivalent extents of reduction were 610 and 644 Å^3, respectively. The difference in the volumes results from the uptake of $4 \times (2.8-2.5)$ water molecules per unit cell ($Z = 4$). This results in a volume of 28.3 Å^3 per water molecule, i.e., very close to that calculated for a liquid water molecule (30 Å^3), which indicates that the interlayer space is fully occupied by the cations and water molecules.

The DTA diagrams of these intercalates are all equivalent and show two endothermal effects, the first centred between 90 and 100°C, depending on the cation, and corresponding to the

TABLE 3. Chemical composition, degree of reduction of vanadium, and basal spacing (Å) of Fe^{2+} and H^+ intercalates M_x ($V_{0.14}$ $Nb_{0.86}$) $OPO_4 \cdot y\ H_2O$

Reductant	% Reduction	x	y	d_{002}
$FeSO_4$	98.6	0.069	2.5	7.31
HI	85.7	0.120	2.5	7.14
Isobutyl alcohol	100	0.140	2.4	7.08

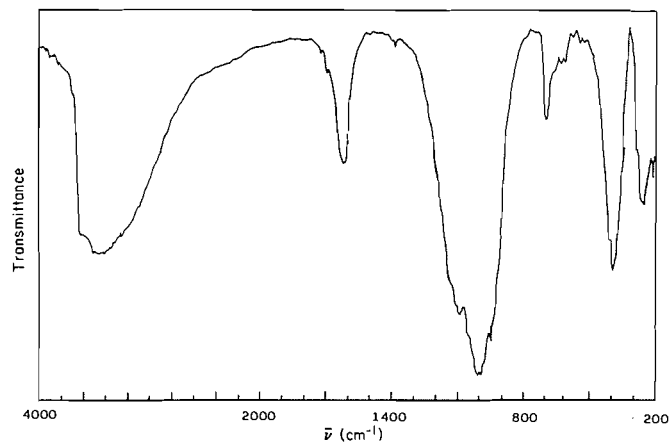

FIG. 5. IR spectrum of H^+–NbVP intercalate.

removal of water not coordinated to vanadium-niobium, and the second, at a higher temperature (213–227°C), corresponding to the loss of that coordinated water.

The diffuse reflectance spectra of the intercalates of the divalent transition metals show none of their typical bands in the visible regions as they are masked by those of V(IV), which is also present at higher concentrations.

Redox reactions with other reductants

A number of reductants have been used by other authors (4) to reduce V^{5+} to V^{4+}; we chose Fe^{2+} to obtain the intercalate of a trivalent metal. On the other hand, some authors have prepared intercalates of the H^+ ion (12, 13) by using 2-propanol or 2-butanol under reflux to reduce vanadyl phosphate to an orthorhombic compound of formula $VO(HPO_4) \cdot 0.5H_2O$ (14). This method has also been used with NbVP, as has the reduction with HI under the same conditions used with the metal ions. Table 3 lists the chemical composition, extent of reduction of vanadium(V), and basal spacings of the intercalates obtained.

The reaction with Fe^{2+} is quite fast, and the extent of reduction is identical with that found in the intercalation with FeI_2, which leads us to think that, although Fe^{2+} is oxidized to Fe^{3+}, the cation actually compensating for the layer charge is Fe^{2+}. In addition to the fact that the layer charge is markedly localized, it would be rather difficult to neutralize by trivalent ions. Moreover, both iron intercalates have the same magnetic susceptibility at 290°C, namely 3.5×10^{-6} μcgs.

The intercalate prepared from HI was only reduced by 85.7%; in this respect, the H^+ ion behaved in much the same way as the more polarizing Li^+ and Mg^{2+} ions. However, the intercalate obtained under reflux with isobutyl alcohol was reduced by 100%. The diffractograms of the two intercalates are identical and can be indexed in the tetragonal system ($a = b = 6.44$ Å; $c = 14.2$ Å), which indicates the preservation of the *ab* plane. The fact that the V^{5+} is evenly distributed throughout the

Can. J. Chem. Downloaded from www.nrcresearchpress.com by 91.121.58.235 on 09/07/12
For personal use only.

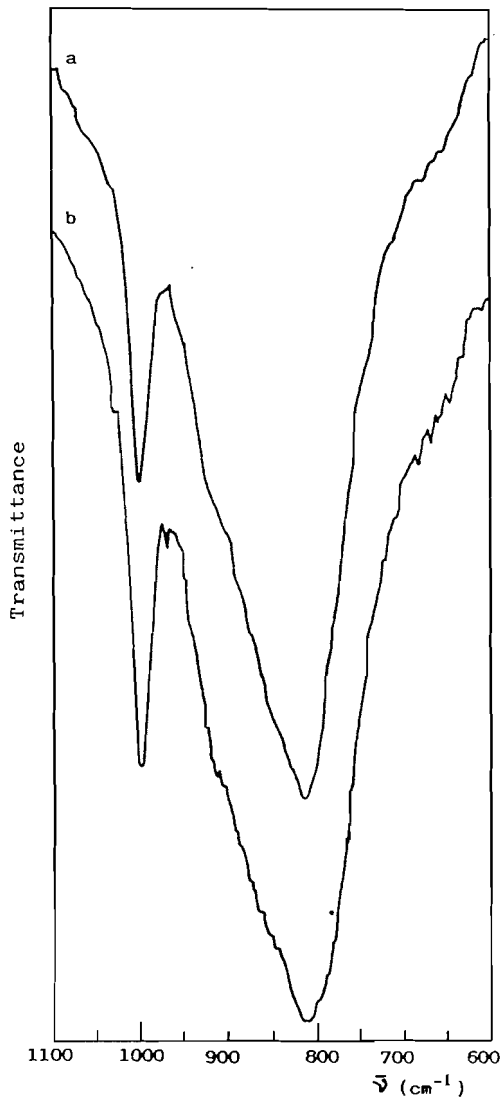

FIG. 6. IR spectra of mixed niobium–vanadium arsenate (a) and its reduced intercalate of potassium (b).

$NbOPO_4$ lattice prevents the reduction from yielding the orthorhombic compound found in reducing $VOPO_4$ with the same reductant.

The IR spectra of the H^+ intercalates (Fig. 5) show small bands at 1700 and 1730 cm^{-1} corresponding to the $\delta_a(H_3O^+)$ of the hydrated protons occurring at the interlayer (15), although their symmetric and asymmetric vibration bands (2940 and 2870 cm^{-1}, respectively) are masked by the broad absorption band of the OH stretching vibrations of the water contained in these compounds.

The reduction of vanadium is also evidenced by the IR spectrum, where the ν(VO) band is shifted to lower frequencies as a result of the relaxation of the double bond. As this band is masked in NbVP by the broad bands of the phosphate groups, it was studied in a mixed arsenate, NbVAs containing only 7% vanadium and prepared by the same method as the mixed phosphate (6). Figure 6 shows a band centred at 998 cm^{-1} and corresponding to the ν(MO) vibration of the mixed arsenate; the reduction yields a small band at 970 cm^{-1} corresponding to the V^{IV}=O stretching vibration (4, 5).

Conclusions

Mixed niobyl-vanadyl phosphate undergoes topotactic redox reactions by intercalating various alkali, alkaline earth, post-transition and transition cations and protons, with preservation of the tetragonal structure of the host solid. Because vanadyl phosphate forms a 14% solid solution in niobyl phosphate, it is substantially stabilized against hydrolysis; the maximum degree of hydrolysis found was only 1%. The intercalates obtained have a cation exchange capacity (CEC) for the maximum reduction of 71 mequiv. referred to 100 g of phosphate calcined at 1000°C.

Acknowledgment

The authors thank CICYT of Spain (Project PB86-0244) for financial support.

1. J. W. JOHNSON, A. J. JACOBSON, J. F. BRODY, and S. M. RICH. Inorg. Chem. **21**, 3820 (1982).
2. K. BENEKE and G. LAGALY. Inorg. Chem. **22**, 1503 (1983).
3. M. MARTÍNEZ-LARA, L. MORENO-REAL, A. JIMÉNEZ-LÓPEZ, S. BRUQUE-GÁMEZ, and A. RODRÍGUEZ. Mater. Res. Bull. **21**, 13 (1986).
4. A. J. JACOBSON, J. W. JOHNSON, J. F. BRODY, J. C. SCANLON, and J. T. LEWANDOWSKI. Inorg. Chem. **24**, 1782 (1985).
5. M. MARTÍNEZ-LARA, A. JIMÉNEZ-LÓPEZ, L. MORENO-REAL, S. BRUQUE, B. CASAL-PIGA, and E. RUIZ-HITZKY. Mater. Res. Bull. **20**, 549 (1985).
6. A. L. GARCÍA-PONCE, L. MORENO-REAL, and A. JIMÉNEZ-LÓPEZ. Inorg. Chem. **27**, 3372 (1988).
7. A. L. GARCÍA-PONCE, L. MORENO-REAL, and A. JIMÉNEZ-LÓPEZ. J. Solid State Chem. In press.
8. A. L. GARCÍA-PONCE, L. MORENO-REAL, and A. JIMÉNEZ-LÓPEZ. Can. J. Chem. **68**, 592 (1990).
9. A. L. GARCÍA-PONCE, L. MORENO-REAL, and A. JIMÉNEZ-LÓPEZ. J. Inclusion Phenom. In press.
10. N. CASAÑ, P. AMOROS, R. IBAÑEZ, E. MÁRTINEZ-TAMAYO, A. BELTRAN-PORTER, and D. BELTRAN-PORTER. J. Inclusion Phenom. **6**, 193 (1988).
11. M. R. ANTONIO, R. L. BARBOUR, and P. R. BLUM. Inorg. Chem. **26**, 1235 (1987).
12. C. C. TORARDI and J. C. CALABRESE. Inorg. Chem. **23**, 1308 (1984).
13. J. W. JOHNSON, D. C. JONSTON, A. J. JACOBSON, and J. F. BRODY. J. Am. Chem. Soc. **106**, 8123 (1984).
14. M. E. LEONOWICZ, J. W. JOHNSON, J. F. BRODY, H. F. SHANNON, JR., and J. M. NEWSAN. J. Solid State Chem. **56**, 370 (1985).
15. A. CORMA, A. LÓPEZ AGUDO, and V. FORNES. J. Chem. Soc. Chem. Commun. 924 (1983).

Can. J. Chem. Downloaded from www.nrcresearchpress.com by 91.121.58.235 on 09/07/12
For personal use only.

Antineoplastic agents. 168. Isolation and structure of axinohydantoin[1]

GEORGE R. PETTIT,[2] CHERRY L. HERALD, JOHN E. LEET, RAJESH GUPTA, DANIEL E. SCHAUFELBERGER, ROBERT B. BATES,[3] PAUL J. CLEWLOW, DENNIS L. DOUBEK, KIRK P. MANFREDI, KLAUS RÜTZLER,[4] JEAN M. SCHMIDT, LARRY P. TACKETT, FRANKLIN B. WARD, MICHAEL BRUCK,[3] AND FERNANDO CAMOU[3]

Cancer Research Institute and Department of Chemistry, Arizona State University, Tempe, AZ 85287, U.S.A.

Received July 4, 1989[5]

GEORGE R. PETTIT, CHERRY L. HERALD, JOHN E. LEET, RAJESH GUPTA, DANIEL E. SCHAUFELBERGER, ROBERT B. BATES, PAUL J. CLEWLOW, DENNIS L. DOUBEK, KIRK P. MANFREDI, KLAUS RÜTZLER, JEAN M. SCHMIDT, LARRY P. TACKETT, FRANKLIN B. WARD, MICHAEL BRUCK, and FERNANDO CAMOU. Can. J. Chem. **68**, 1621 (1990).

Western (Palau) and Eastern (State of Truk) Caroline Islands and Papua New Guinea sponges of the genera *Axinella* and *Hymeniacidon* were found to contain the cytostatic (PS ED_{50} 2.5 and 2.0 μg/mL) and antineoplastic (PS T/C 143 at 3.6 mg/kg and T/C 138 at 3.6 mg/kg) pyrrologuanidines **1***a* and **1***b*. The related hydantoin **2**, designated axinohydantoin, was also isolated from an *Axinella* sp. and its structure was assigned by X-ray crystallographic techniques. Present experience with sponges in the *Axinella* and *Hymeniacidon* genera suggests that the previously known hymenialdisine (**1***b*) and analogous imidazole derivatives may be widely distributed among these and related orange colored Porifera.

Key words: axinohydantoin, hymenialdisine, *Axinella, Hymeniacidon,* cystostatic.

GEORGE R. PETTIT, CHERRY L. HERALD, JOHN E. LEET, RAJESH GUPTA, DANIEL E. SCHAUFELBERGER, ROBERT B. BATES, PAUL J. CLEWLOW, DENNIS L. DOUBEK, KIRK P. MANFREDI, KLAUS RÜTZLER, JEAN M. SCHMIDT, LARRY P. TACKETT, FRANKLIN B. WARD, MICHAEL BRUCK et FERNANDO CAMOU. Can. J. Chem. **68**, 1621 (1990).

On a trouvé que les éponges du genera *Axinella* et du *Hymeniacidon* des iles Caroline occidentale (Palau) et orientale (État de Truk) ainsi que de la Nouvelle Guinée contiennent des pyrrologuanidines **1***a* et **1***b* qui sont des cytostatiques (PS ED_{50} 2,5 et 2,0 μg/mL) et des antinéoplasiques (PS T/C 143 à 3,6 mg/kg et T/C 138 à 3,6 mg/kg). À partir d'un *Axinella* sp., on a aussi isolé l'hydantoïne apparentée **2**, appelée axinohydantoïne, et on a déterminé sa structure à l'aide de la diffraction des rayons-X. L'expérience acquise avec les éponges de l'*Axinella* et de l'*Hymeniacidon* genera suggère que l'hyménialdisine (**1***b*), qui était connue antérieurement, ainsi que les dérivés imidazoles analogues sont peut-être très répandus dans ces éponges et dans les Porifera apparentés de couleur orange.

Mots clés : axinohydantoïne, hyménialdisine, *Axinella, Hymeniacidon,* cytostatique.

[Traduit par la revue]

Introduction

Early (2) in our evaluation of marine animals as new sources of potentially useful anticancer drugs, good leads were uncovered among the Porifera, and this initial (1966–1968) promise is now being amply realized (3, 4). In 1979 in Palau we collected a *Hymeniacidon* species (at −40 m) and an *Axinella* sp. that provided extracts with confirmed levels of activity against the U.S. National Cancer Institute's (NCI) murine P388 lymphocytic leukemia (PS system). Other PS active sponge collections were completed in 1981 (Papua New Guinea) and 1985 (Truk, Federated States of Micronesia) that included *Axinella carteri* (Dendy) and a *Hymeniacidon* species.

Initial extracts of each sponge were found to provide a confirmed level of activity against the PS system. By means of PS (*in vitro*) bioassay guided separation procedures, these sponge species led to two cytostatic and antineoplastic alkaloids (**1***a*,*b*) accompanied in the case of *Axinella* sp. by a closely related, but marginally (PS ED_{50} 18 μg/mL) inactive, component (**2**). The PS active marine alkaloids proved to be identical[6] with the known (5–7) hymenialdisine (**1***b*, ref. 6, PS ED_{50} 2.0 μg/mL and T/C 138 at 3.6 mg/kg)[7] and its debromo derivative **1***a* (refs. 5–7, PS ED_{50} 2.5 μg/mL and T/C 143 at 3.6 mg/kg).

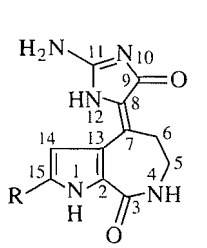

1*a*, R = H debromohymenialdisine
1*b*, R = Br hymenialdisine

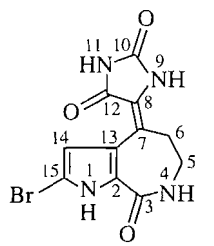

2
axinohydantoin

The unequivocal X-ray crystal structure of hymenialdisine was nicely established by Cimino *et al.* (5) and reconfirmed in the following year by the Kitagawa group (6). In turn, these advances simplified characterization of the companion substance from *Axinella* sp., herein named axinohydantoin (**2**), as a closely related compound. But establishing the exact geometrical configuration for its hydantoin–lactam sp^2 bond required the following crystal structure determination.

Axinohydantoin (**2**) crystallized from methanol as yellow prisms, which corresponded to $C_{11}H_9BrN_4O_3$ (by hreims) and with one mole of methanol. The structure was solved using

---

[1]For contribution 167 refer to ref. 1.

[2]Author to whom correspondence may be addressed.

[3]Department of Chemistry, University of Arizona, Tucson, AZ 85721, U.S.A.

[4]National Museum of Natural History, Smithsonian Institution, Washington, DC 20560, U.S.A.

[5]Revision received March 27, 1990.

[6]By comparison with authentic specimens provided by Dr. I. Kitagawa (see ref. 6).

[7]Interestingly, hymenialdisine was previously active in the KB cell line, but *in*active employing the P388 leukemia: cf. ref. 5. Perhaps the initial negative results were due to the sparingly soluble properties of this pyrrologuanidine.

Printed in Canada / Imprimé au Canada

Can. J. Chem. Downloaded from www.nrcresearchpress.com by 91.121.58.235 on 09/07/12
For personal use only.

Can. J. Chem. Downloaded from www.nrcresearchpress.com by 91.121.58.235 on 09/07/12
For personal use only.

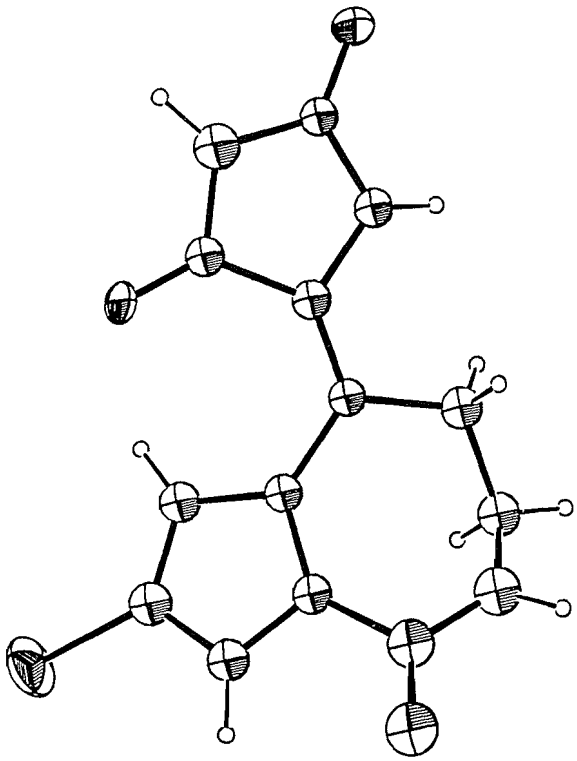

FIG. 1. ORTEP view of a single molecule of **2**, with 50% thermal ellipsoids.

MULTAN (8) and refined to $R = 0.054$ using anisotropic temperature factors for Br and oxygens other than O-3, and isotropic temperature factors for the other non-hydrogens and for hydrogens (unrefined) in calculated positions. HN-1, HN-11, and HN-9 were calculated to be 0.95 Å along a line to the respective oxygen. These positions differed very little from those calculated assuming bonding to trigonal atoms. HN-4 has been shown at the calculated position assuming a trigonal N-4 that is too far (2.4 Å) from the closest O-10 for significant hydrogen bonding; it may actually bend somewhat toward this O-10.

The structure deduced for axinohydantoin (**2**, Fig. 1) was found to be closely related to that of hymenialdisine (**1***b*), with reversal of configuration at the C7—C8 double bond being the most interesting difference. In turn, this suggested that axinohydantoin was not simply a hydrolysis product of guanidine **1***b*. The most prominent bond length difference between the two structures occurs at C10—O10, with 1.23 Å in hydantoin **2** compared to 1.33 Å for C11—N11 in **1***b*. No significant differences in bond angles were observed. An angle of 36° was observed between the least-squares planes of the two nearly planar five-membered rings in hydantoin **2**, compared to 43.8° in guanidine **1***b*. In both cases, the seven-membered ring has adopted a boat conformation with C-5 at the prow, and similar torsion angles except for C2—C3—N4—C5 expanding from −10.5° in **1***b* to −15° in **2**, and C2—C13—C7—C6 contracting from 41.1° in **1***b* to 31° in **2**. The twist angle C13–C7—C8—C12 about the carbon–carbon double bond increases from 0.5° in **1***b* to 10° in **2**, presumably to relieve the steric interaction between O-12 and HC-14.

The arrangement of intermolecular hydrogen bonds governing the packing in hydantoin **2** (see supplementary material)[8] was found to be completely different than that in guanidine **1***b* (6). The hydantoin ring in each molecule was found linked to the hydantoin rings of two other molecules via base-pairing interactions across centers of symmetry. The pyrrole NH proved to be hydrogen bonded to the methanol solvate oxygen and in turn to O-3. Only a few substances (9–12) with a hydantoin system have been isolated from sponges, and one of these, midpacamide, found by Scheuer and co-workers (9) in an unidentified Marshall Island sponge, may be biogenetically related to axinohydantoin. From evidence now in hand, pyrroles **1** and **2** and related substances may prove to be ubiquitous Porifera biosynthetic products.

Experimental

General methods

Marine sponge taxonomic identification was performed in the Smithsonian Institution where voucher specimens are deposited in the collections of the Department of Invertebrate Zoology, National Museum of Natural History. All solvents employed were redistilled. Size exclusion chromatography was accomplished with Sephadex LH-20 (particle size: 25–100 μm) suppled by Pharmacia Fine Chemicals, Uppsala, Sweden. Thin-layer chromatography was carried out with silica gel GHLF Uniplates (Analtech Inc.) and with RP-8 precoated plates (layer thickness: 0.25 mm) from E. Merck, Darmstadt, Germany. High-speed countercurrent chromatography was accomplished with an Ito multilayer coil extractor–separator (P.C. Inc., Potomac, MD) using 2.6 mm i.d. tubing, and an FMI Lab Pump.

Melting points are uncorrected and were determined on a Kofler-type hot-stage apparatus. Ultraviolet spectra were recorded employing a Hewlett–Packard model 8450 uv/vis spectrophotometer and ir spectra with a Nicolet ft-ir model MX-1 instrument. The nmr spectra were measured in DMSO-d_6 using a Bruker AM-400 instrument and are recorded in ppm downfield to TMS (assignments bearing the same superscript may be reversed). The ^{13}C nmr multiplicities were determined with APT experiments based on an average coupling constant of 135 Hz. The eims spectra were recorded with a Kratos AEI 5076 spectrometer at the NSF Regional Facility, University of Nebraska, Lincoln, Nebraska.

Palau Porifera (Axinella *sp. and* Hymeniacidon *sp.) collection and extraction.*

The initial collection of *Axinella* sp. (Demospongiae class, Axinellida order, Axinellidae family) in Palau, Western Caroline Islands, was conducted in May, 1979. The sponge displayed a brownish-yellow exterior of irregular mass. A 2-propanol–$CHCl_3$ extract gave confirmatory in vivo activity with PS T/C 201 at 100 mg/kg, PS ED_{50} = 2.5 μg/mL. A scale-up re-collection (220 kg wet wt.) of this sponge was completed in March, 1985, and preserved in 2-propanol. The preserving solution was separated from the sponge, concentrated to an aqueous slurry, and extracted with CH_2Cl_2 (13). The remaining sponge material was re-extracted with 2-propanol–CH_2Cl_2 (1:1); the extract was separated, solvent removed, and the residue partitioned between CH_2Cl_2 and H_2O. At this early stage a solid precipitate appeared at the CH_2Cl_2–H_2O interface. The precipitate was separated and amounted to

[8]Tables of observed and calculated structure factor amplitudes, calculated hydrogen coordinates, isotropic temperature factors, bond lengths and angles, torsion angles, and a packing diagram may be purchased from the Depository of Unpublished Data, CISTI, National Research Council of Canada, Ottawa, Ont., Canada K1A 0S2.

Tables of positional parameters and bond distances have also been deposited with the Cambridge Crystallographic Data Centre, and can be obtained on request from The Director, Cambridge Crystallographic Data Centre, University Chemical Laboratory, Lensfield Road, Cambridge CB2 1EW, U.K.

Can. J. Chem. Downloaded from www.nrcresearchpress.com by 91.121.58.235 on 09/07/12
For personal use only.

1.8 kg (PS T/C 227 at 294 mg/kg, ED_{50} 2.8 μg/mL). Analogous solid fractions were also obtained at this initial CH_2Cl_2 step during separations of the sponge extracts summarized below.

The orange sponge *Hymeniacidon* sp. (Demospongiae class, Halichondrida order, Hymeniacidonidae family) was collected (1979), re-collected (in 1985, 218 kg wet wt.), and extracted (2-propanol extract showed PS T/C 130 at 5.5 mg/kg and ED_{50} 27 μg/mL) as summarized above. Removal of solvent from the initial 2-propanol extract led to an aqueous concentrate that contained 1.2 kg of a solid fraction with PS ED_{50} = 3.7 μg/mL.

*Isolation of hymenialdisine (**1**b) and axinohydantoin (**2**)*

A 10 g aliquot from the 1.8 kg of solid precipitate noted above was dissolved in CH_3OH (400 mL) and separated by size exclusion chromatography on a column of Sephadex LH-20 (100 × 10 cm) to yield two major marine alkaloid fractions. When fraction 1 (elution volume: 12.0–12.6 L) was allowed to stand for 24 h at room temperature, axinohydantoin (**2**) slowly crystallized as yellow needles (30 mg): mp >350°C; tlc on silica gel R_f = 0.83, 1-BuOH–AcOH 50% (95:5); tlc on RP-8 R_f = 0.51, CH_3OH–AcOH 5% (1:1); uv (CH_3OH) λ_{max}: 264sh (log ε = 3.88), 345 (log ε = 4.16) nm; ir (KBr) ν_{max}: 1740, 1702, 1638, 1480, 1425, 1407 cm^{-1}; ^1H nmr (DMSO-d_6) δ: 2.67 (2H, m, H-6), 3.22 (2H, m, H-5), 6.66 (1H, s, H-14), 7.89 (1H, t, HN-4), 9.83, 10.91 (2 × 1H, s, HN-9, HN-11), 12.35 (1H, s, HN-1); ^{13}C nmr (DMSO-d_6) δ: 36.2 (t, C-6), 38.5 (t, C-5), 101.6 (s, C-15), 113.9 (d, C-14), 120.0 (s, C-13), 121.2 (s, C-7), 125.5 (s, C-2), 126.5 (s, C-8), 153.8 (s, C-10), 162.7 (s, C-3), 163.3 (s, C-12); hreims *m/z*: 325.9842 and 323.9834 ($C_{11}H_9N_4O_3Br$ requires 325.9836).

Fraction 2 (elution volume: 12.9–13.5 L) yielded a crystalline precipitate (100 mg), which was identified as hymenialdisine (**1***b*) by comparison (uv, ir, ^1H nmr, eims) with an authentic sample (6).

*Truk Porifera (*Axinella carteri*) collection and extraction*

In May 1985, approximately 1 kg of an orange-yellow sponge subsequently identified as *Axinella carteri* (Dendy), was collected in the Truk Lagoon, Federated States of Micronesia, at −13 to −24 m. The preserving solution (2-propanol) was removed and this extract proved toxic down to 50 mg/kg against the PS leukemia. The 2-propanol extract was partitioned between CH_2Cl_2 and H_2O and the resulting CH_2Cl_2 extract was successively partitioned (13) between 9:1–4:1–1:1 MeOH:H_2O with hexane–CCl_4–CH_2Cl_2. The final CH_2Cl_2 extract showed PS T/C 135 at 100 mg/kg and PS cell line ED_{50} = 1.2 μg/mL.

In October 1985, approximately 148 kg (wet wt.) of the sponge was recollected and preserved in MeOH. The MeOH solution was decanted, and the sponge was ground and extracted with MeOH:CH_2Cl_2 (1:1). The original MeOH solution was concentrated to an aqueous phase and extracted with CH_2Cl_2 (3×) followed by 1-BuOH. Study of this 1-BuOH fraction was discontinued when PS results showed minimal activity.

When the ambient temperature extraction of the sponge with MeOH:CH_2Cl_2 was completed, the aqueous MeOH phase was separated and concentrated to an aqueous phase, which was extracted with 1-BuOH (15 L). The 1-BuOH phase was concentrated, redissolved in MeOH (1.5 L), and dried to give a 232 g fraction (PS ED_{50} 1.4 μg/mL). A 97 g aliquot of the MeOH soluble fraction was treated with 1-BuOH (800 mL, 50°C, 12 h) and the relatively insoluble part (50 g, PS ED_{50} 1.5 μg/mL) was collected. The MeOH (600 mL) sparingly soluble portion weighed 4.26 g (PS ED_{50} 0.11 μg/mL).

*Papua New Guinea Porifera (*Hymeniacidon *sp.) collection and extraction*

The collection (May 1981, near Motapure Island, Papua New Guinea) and recollection (October 1983, 44 kg wet wt.) of an orange *Hymeniacidon* sp. as well as the large scale extraction (crude extract PS T/C 136 at 100 mg/kg and ED_{50} 24 μg/mL) and solvent partitioning were performed as described above for *A. carteri*. In this case, when the 934 g initial CH_2Cl_2 fraction was subjected to further separation by MeOH:H_2O with the hexane → CCl_4 → CH_2Cl_2 sequence, a total of 135 g (PS ED_{50} 14 μg/mL) of a solid interfacial fraction was collected and used to isolate hymenialdisines **1***a* and **1***b*.

TABLE 1. Positional and thermal parameters

Atom	*x*	*y*	*z*	*B* (Å^2)
Br	0.56111(6)	0.0097(2)	0.18172(7)	4.40(3)
O3	0.7915(4)	−0.210(1)	0.0865(4)	3.4(2)*
O12	0.7371(3)	−0.194(1)	0.4049(4)	3.0(2)
O10	0.9511(3)	−0.093(1)	0.5586(3)	3.3(2)
OM	0.6407(4)	−0.152(2)	0.0121(5)	7.3(3)
N1	0.6929(4)	−0.069(1)	0.1562(4)	2.3(2)*
N4	0.8760(4)	−0.055(1)	0.1624(5)	2.9(2)*
N11	0.8375(4)	−0.161(1)	0.4951(4)	2.5(2)*
N9	0.9106(4)	−0.056(1)	0.4357(4)	2.0(2)*
C15	0.6581(5)	−0.024(2)	0.2056(5)	2.5(2)*
C14	0.7046(4)	−0.000(2)	0.2706(5)	2.2(2)*
C13	0.7725(4)	−0.036(1)	0.2599(5)	1.8(2)*
C2	0.7630(5)	−0.073(1)	0.1875(5)	2.0(2)*
C3	0.8108(5)	−0.120(2)	0.1407(6)	2.8(2)*
C5	0.8961(5)	0.083(2)	0.2145(5)	2.6(2)*
C6	0.9053(4)	0.024(2)	0.2915(5)	2.4(2)*
C7	0.8393(4)	−0.031(1)	0.3144(5)	1.8(2)*
C8	0.8468(5)	−0.069(1)	0.3839(5)	1.9(2)*
C12	0.7982(5)	−0.147(1)	0.4248(5)	2.0(2)*
C10	0.9045(5)	−0.104(2)	0.5026(5)	1.9(2)*
CM	0.5809(8)	−0.093(2)	−0.0359(8)	6.3(4)*

*Starred atoms were refined isotropically.

Anisotropically refined atoms are given in the form of the isotropic equivalent thermal parameter, defined as $8\pi^2(U_{11} + U_{22} + U_{33})/3$.

*Isolation of hymenialdisines **1**a and **1**b—Procedure A*

An aliquot (250 mL) of the preceding *Axinella carteri* MeOH (600 mL) solution was applied to a column of Sephadex LH-20 (1.9 kg in MeOH). A total of 460 fractions of 20 mL each were collected and a fraction weighing 0.73 g (PS ED_{50} 2.2 μg/mL) was further separated using high speed countercurrent distribution with an Ito coil. A 50 mg aliquot was applied (6 mL) in 1-BuOH:HOAc:H_2O (4:1:5) to the coil with the 1-BuOH phase as stationary (upper) and the aqueous part as mobile (lower) phase. Fractions (120) of 6.5 mL each were collected; fractionation was monitored with ultraviolet detection (254 nm). The fractions were neutralized (pH 7) with aqueous NaOH and refrigerated. Debromohymenialdisine **1***a*, 9 mg, PS ED_{50} = 3.0 μg/mL, crystallized from fractions 28–33 and was identical (tlc, ms, nmr) with an authentic sample (6).

The MeOH less soluble fraction (4.26 g) described above was extracted with MeOH (5 × 25 mL) at 40°C and the solution filtered to give 3.73 g of residue. A 0.90 g portion was triturated with DMSO (10 mL). The soluble portion (0.25 g) was chromatographed on a column of Sephadex LH-20 in MeOH to provide 0.13 g of hymenialdisine (**1***b*) as yellow crystals (PS ED_{50} 0.62 μg/mL), identical (tlc and ms comparisons) with an authentic sample (6).

Procedure B

The 1.2 kg fraction (see above) from the Palau *Hymeniacidon* sp. was further separated by successive Soxhlet extraction (20 g aliquot) with CH_2Cl_2 (6 × 5 L), EtOH (6 × 5 L), and 1-BuOH (6 × 5 L) to give respectively 35 g (PS ED_{50} 26 μg/mL), 500 g (PS ED_{50} 8.6 μg/mL), and 106 g (PS ED_{50} 2.6 μg/mL) fractions. A 10 g sample of the 1-BuOH fraction in MeOH was subjected to chromatography on a column of Sephadex LH-20 (500 g) to give 26 individual (by tlc comparisons) fractions using 4:1 CH_2Cl_2:MeOH. Of these, 56 mg proved to be largely debromohymenialdisine **1***a* (PS ED_{50} 1.4 μg/mL) and hymenialdisine (5.5 mg, **1***b*, PS ED_{50} 7.5 μg/mL) by comparison nmr and tlc.

Procedure C

The 135 g fraction from the Papua New Guinea *Hymeniacidon* sp.

was extracted (Soxhlet procedure with two stainless steel 1-gallon extractors) with EtOH to yield a 22 g alcohol soluble fraction. Treatment of this fraction with CH_2Cl_2:CH_3OH (1:1) yielded a precipitate (4.3 g, PS ED_{50} 8.5 μg/mL), which was extracted with hot 1-BuOH. The 1.5 g 1-BuOH soluble fraction was preabsorbed onto silica gel and separated by chromatography on a column (3 × 62 cm) of silica gel (180 g). Gradient elution with 95:5 CH_2Cl_2:CH_3OH with increments of MeOH provided fractions that yielded (0.17 g and 0.06 g respectively) debromohymenialdisine (**1***a*, PS T/C 143 at 3.6 mg/kg and ED_{50} 2.5μg/mL) and hymenialdisine (**1***b*, PS T/C 138 at 3.6 mg/kg and ED_{50} 2.7 μg/mL). Both **1***a* and **1***b* were identified by direct comparison with authentic samples (6) employing tlc, ^{13}C and ^1H nmr, ms, uv, and ir spectral data.

X-ray structure of axinohydantoin (2)

$C_{11}H_8BrN_4O_3 \cdot CH_3OH$ fw = 357.17

Monoclinic, $C2/c$, a = 19.558(2), b = 7.505(1), c = 19.092(3) Å, β = 103.78(1)°, V = 2754.3 Å^3, Z = 8, ρ_c = 1.72; Nicolet $P2_1$ diffractometer, crystal 0.17 × 0.13 × 0.08 mm, 23°C, MoK_{α_1}, λ = 0.71073 Å, 2θ/θ scans, $2\theta_{max}$ 50°; 836 of 2446 reflections with $F_o^2 > 3\sigma(F_o^2)$ used; solved by direct methods; R = 0.053, R_w = 0.055 excluding unobserved reflections. Coordinates and isotropic temperature factors of non-hydrogens are given in Table 1.[8]

Acknowledgments

We are pleased to acknowledge the very necessary financial assistance provided by the Fannie E. Rippel Foundation, the Arizona Disease Control Research Commission, Outstanding Investigator Grant CA 44344-01A1 and PHS Grants CA-16049-07-12 awarded by the National Cancer Institute, DHHS, the Robert B. Dalton Endowment Fund, Virginia Piper, Polly Trautman, Eleanor W. Libby, the Donald Ware Waddell Foundation, Herbert and Dianne Cummings (The Nathan Cummings Foundation, Inc.) Mary Dell Pritzlaff, the Olin Foundation (Spencer T. and Ann W.), and by the U.S. Army Medical Research and Development Command under Grant No. DAMD17-89-Z-9021.

Other helpful assistance was provided by the Governments of Papua New Guinea (N. Kwapena, A. Richards, and Drs. John L. Munro, J. M. Lock, and N. Polunin), the Federated States of Micronesia (Truk, D. E. Aten, R. Killion, and A. Amaraich), and Palau (Dr. T. Paulis and K. B. Batcheller), Singapore Airlines Ltd. (M. Theam Kong), Blue Lagoon Dive Shop (MOEN, Truk), Drs. C. G. Bass, C. Dufresne, Mr. G. R. Pettit III, Mrs. D. N. Tackett, S. Taylor, and T. N. Trautman, the Smithsonian Institution Oceanographic Sorting Center, The U.S. National Science Foundation (Grant CHE-8409644), The Swiss National Science Foundation (to D.E.S.), and the NSF Regional Instrumentation Facility in Nebraska (Grant CHE-8620177).

1. J. A. McBain, G. R. Pettit, and G. C. Mueller. Cell Growth and Differentiation, **1**, 281 (1990).
2. G. R. Pettit, J. F. Day, J. L. Hartwell, and H. B. Wood. Nature, **227**, 962 (1970).
3. Y. Kato, N. Fusetani, S. Matsunaga, and K. Hashimoto. J. Org. Chem. **53**, 3930 (1988).
4. Y. Hirata and D. Uemura. Pure Appl. Chem. **58**, 701 (1986).
5. G. Cimino, S. DeRosa, S. DeStefano, L. Mazzarella, R. Puliti, and G. Sodano. Tetrahedron Lett. **23**, 767 (1982).
6. I. Kitagawa, M. Kobayashi, K. Kitanaka, M. Kido, and Y. Kyogoku. Chem. Pharm. Bull. **31**, 2321 (1983).
7. F. J. Schmitz, S. P. Gunasekera, V. Lakshmi, and L. M. V. Tillekeratne. J. Nat. Prod. **48**, 47 (1985).
8. P. Main, S. J. Fiske, S. E. Hull, L. Lessinger, G. Germain, J. P. Declerq, and M. M. Woolfson. MULTAN 80. A system of computer programs for the automatic solution of crystal structures from X-ray diffraction data. University of York, England, and Louvain, Belgium. 1980.
9. L. Chevolot, S. Padua, B. N. Ravi, P. C. Blyth, and P. J. Scheuer. Heterocycles, **7**, 891 (1977).
10. R. Kazlauskas, P. T. Murphy, R. J. Quinn, and R. J. Wells. Tetrahedron Lett. **1**, 61 (1977).
11. P. Djura, D. B. Stierle, B. Sullivan, D. J. Faulkner, E. Arnold and J. Clardy. J. Org. Chem. **45**, 1435 (1980).
12. D. J. Faulkner. Nat. Prod. Rep. **3**, 1 (1986).
13. G. R. Pettit, Y. Kamano, R. Aoyagi, C. L. Herald, D. L. Doubek, J. M. Schmidt, and J. J. Rudloe. Tetrahedron, **41**, 985 (1985).

Can. J. Chem. Downloaded from www.nrcresearchpress.com by 91.121.58.235 on 09/07/12
For personal use only.

The thermal isomerization of bicyclic oxazines into epoxyepimines. A preliminary theoretical study

MICHEL SANA,[1] GEORGES LEROY, JEAN-LUC VAERMAN, AND HEINZ GUNTER VIEHE

Laboratoire de Chimie Quantique et Laboratoire de Chimie Organique, Université Catholique de Louvain, Bâtiment Lavoisier, Place Louis Pasteur, 1, Bte 35, B-1348 Louvain-la-Neuve, Belgium

Received September 20, 1989[2]

MICHEL SANA, GEORGES LEROY, JEAN-LUC VAERMAN, and HEINZ GUNTER VIEHE. Can. J. Chem. **68**, 1625 (1990).

The thermal isomerization of bicyclic oxazines **1** to epoxyepimines **2** depends on the *N*-substituent. BDE calculations on model systems agree with the mechanistic picture. The rate-determining step in N—O bond homolysis is facilitated by *N*-vinyl substituents.

Key words: oxazines, BDE, NO bond, substituent effect.

MICHEL SANA, GEORGES LEROY, JEAN-LUC VAERMAN et HEINZ GUNTER VIEHE. Can. J. Chem. **68**, 1625 (1990).

L'isomérisation thermique des oxazines bicycliques **1** en époxyépimines **2** dépend de la nature des substituants présents sur le N. Des calculs de BDE réalisés sur des systèmes modèles sont en accord avec ce mécanisme réactionnel. L'homolyse de la liaison N—O qui se produit dans l'étape déterminante de la réaction est facilitée par la présence de substituants *N*-vinyles.

Mots clés : oxazines, BDE, liaison NO, la effet de substituant.

[Traduit par la revue]

Introduction

The nature of the *N*-substituent as well as the size of the bicyclic system of substituted oxazines **1** affect their thermal reactivity (1). Thus some oxazines decompose by cycloreversion reaction (2) whereas others isomerize via Cope rearrangement (3). Generally they are comparatively thermally stable.

We have found that bicyclic oxazines **1** with vinylic captodative substitution (4) isomerize into epoxyepimines **2** (5). Mechanistic studies suggest that this "epoxyepimination" reaction proceeds by a biradical pathway (6) with the rate-determining step being the homolytic cleavage of nitrogen–oxygen bond in oxazine.

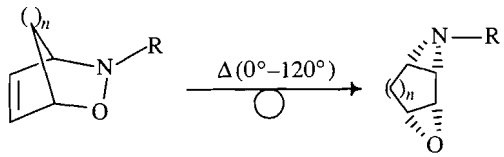

1 **2**

Homolytic breaking of the N—O bond is an endothermic process. According to Hammond's postulate, the structure of the epoxyepimination transition state must be closer to the intermediate biradical **3** than to the starting oxazine **1**. Therefore, knowledge of the energy difference between oxazine and its corresponding biradical (which is the bond dissociation energy: BDE(N—O)) would be an indication of the activation energy for the rate-determining step.

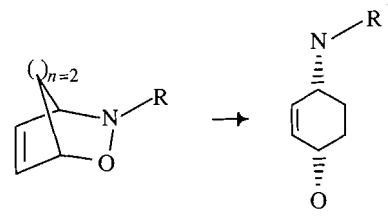

1 **3**

In this preliminary theoretical study we calculate the influence of *N*-substituents on the N—O bond strength in a simple model system without the cyclic structure. According to Leffler's relation (7) (also known as Marcus's relation (8)), a connection exists between the heat of reaction and the activation energy for any chemical process. In some cases, the quadratic Leffler's relation (in ΔH_r) is approximated by a simple linear expression (9, 10): $E_a \approx a + b\Delta E_r$. According to this very simple relationship, the smallest activation energies should correspond to the largest heats of reaction (BDE). Therefore one can modify the bond strengths by using appropriate substituents; large variations in BDE are possible depending on the nature of the groups considered (see Fig. 1): CC bonds with BDE between 22 [$(NC)_3C—C(CN)_3$] and 121 ($CH_3—CN$) kcal mol^{-1} are known. As BDE's are heats of reaction, they can be negative as well as positive. Negative BDE's occurs when bond breaking involves very unstabilized molecules (11)

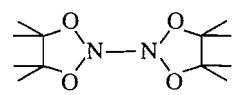

and (or) largely stabilized radicals ($(NH_2)_2N\cdot$ (12)). Thus BDE(NN) varies from −5 [$(NH_2)_2N—N(NH_2)_2$] to 70 ($NHF—NH_2$) kcal mol^{-1} (Fig. 1). Accordingly, the study of the weakness points in a molecule corresponds to an evaluation of BDE's. Unfortunately, thermochemical data (especially for radicals) are not often available for this evaluation. However, quantum chemical calculations are now accurate enough to give reliable heats of formation. The isodesmic procedure of Pople *et al.* (13) attains this goal even for large molecules (14). To estimate the effect of substituents on bond strength (independent of ring nature) we have chosen to apply this procedure to the following model molecules:

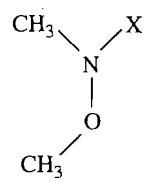

where X stands for CH_3, $CH=CH_2$, CH=O, NH_2, or $CH=C(CN)(NH_2)$.

Methods of calculation

The equilibrium geometry of these molecules and related

[1]Research Director, National Fund for Scientific Research, Belgium. To whom correspondence should be addressed.

[2]Revision received March 23, 1990.

Printed in Canada / Imprimé au Canada

Can. J. Chem. Downloaded from www.nrcresearchpress.com by 91.121.58.235 on 09/07/12
For personal use only.

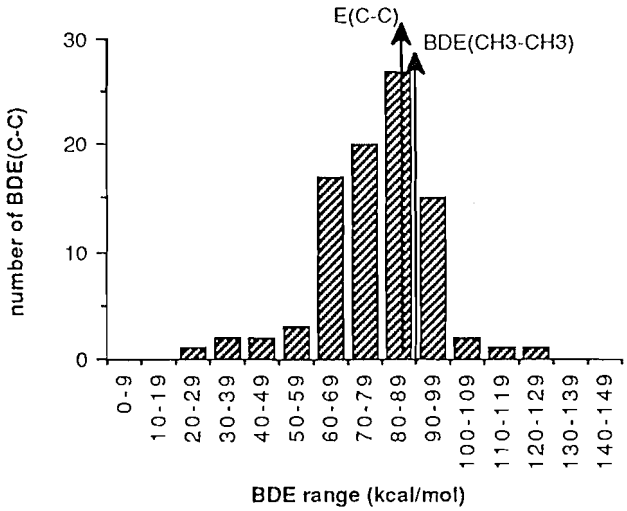

FIG. 1. C—C bond as an example of the domain of variation for bond dissociation energies.

radicals has been determined at the Hartree–Fock level (LCAO-SCF-MO RHF and UHF) (15), using the 6-31G basis set of Pople and co-workers (16). In Table 1 we report their total energies and heats of formation. The chosen isodesmic reactions and other necessary data are commonly available in the literature or can be obtained on request from the authors.

Results and discussion

Figure 2 shows rather large variations in BDE depending on the *N*-substituent. It is interesting to note that the order in BDE's does not correspond to the standard bond energies (standard bond energies are selected from ref. 17). The following sequences are normal (in kcal mol^{-1}):

E(C—O)	$\gg$	E(C—N)	$\gg$	E(N—O)	$>$	E(N—N)	
91	$\gg$	77	$\gg$	52 (ref. 18)	$>$	48	

and

BDE(CH_3—OH)	$>$	BDE(CH_3—NH_2)	$\gg$	BDE(NH_2—NH_2)	$>$	BDE(NH_2—OH)	
93	$>$	86	$\gg$	68	$>$	64	

In CH_3—NX—O—CH_3 compounds, we find unusually weak C—O bonds (53 to 68 kcal mol^{-1} depending on X). Nevertheless, in all cases, the N—O bond is the weakest one. Its strength is particularly small in *N*-vinyl derivatives, but larger in *N*-formyl species. Comparison of BDE modification in various cases is shown in Fig. 3. The first line shows that even methyl groups have a non-negligible effect on the NO single bond energy; substitution on oxygen in particular produces an important lowering of BDE. It is also seen that the substituents considered here produce similar but smaller effects on C—O as well as on O—O bonds.

For analysing bond strengths in terms of stabilization energies (SE), we use the definition of SE introduced by one of us (20): the SE is simply the deviation between the atomization energy (ΔH_a) and the sum of standard bond energies: $\Delta H_a = \Sigma E_b$ + SE. This means that the BDE is mainly dependent on the standard energy of the breaking bond on the one side and on the difference in SE between the radicals and the parent molecule on the other side. For lowering a bond strength, one may destabilize (SE < 0) the parent molecule and/or stabilize (SE > 0) the radicals derived from the homolytic dissociation. As shown in Table 1, one observes negligible SE's for vinilic parent molecules. In these cases, the lowering of BDE can only be induced by large stabilization energies of the radicals

TABLE 1. Total energies (au), heats of formation (kcal mol^{-1}), and stabilization energies (SE) (kcal mol^{-1}) for the compounds of interest

Compounds	E(6-31G)	ΔH_f	SE
$(CH_3)_2NOCH_3$	−247.95758	−9.42	−1.22
CH_3NOCH_3	−208.35113	22.32	6.70
CH_3NCH_3	−133.56545	38.39	−4.71
$(CH_3)_2NO$	−208.36938	12.60	28.47
$CH_2CHN(CH_3)OCH_3$	−285.79146	14.67	−1.16
$CH_2CHNOCH_3$	−246.20185	35.85	17.32
CH_2CHNCH_3	−171.42514	44.36	13.47
$CH_2CHN(CH_3)O$	−246.21046	32.18	33.04
$CHON(CH_3)OCH_3$	−321.62970	−38.58	12.05
$CHONOCH_3$	−282.00772	2.55	10.58
$CHONCH_3$	−207.23441	11.15	6.64
$CHON(CH_3)O$	−282.02841	−6.06	31.24
$NH_2N(CH_3)OCH_3$	−263.92369	10.60	6.38
NH_2NOCH_3	−224.31937	41.01	15.63
NH_2NCH_3	−149.53938	50.92	10.38
$NH_2N(CH_3)O$	−224.32761	37.58	31.11
$(CN)(NH_2)CCHN(CH_3)OCH_3$	−432.48400	50.43	−0.26
$(CN)(NH_2)CCHNOCH_3$	−392.89346	72.18	17.65
$(CN)(NH_2)CCHNCH_3$	−318.11548	81.49	13.00
$(CN)(NH_2)CCHN(CH_3)O$	−392.89830	70.88	31.00

(±13 kcal mol^{-1}). With CHO and NH_2 substituents, the radicals remain stabilized but the parent molecules now also become stabilized. For $NH_2N(CH_3)OCH_3$ the stabilization of the aminyl radical is larger than that of the molecule. It follows a global lowering of the BDE(N—O). For $CHON(CH_3)OCH_3$ the parent molecule has so large an effect the BDE is increased. Nevertheless, in conjunction with the parent molecules, one finds large lowering in the BDE(N—O) only with the vinyl substituents. In the case of formyl derivatives, one has an increase in BDE(NO). An another interesting point, which appears in Fig. 2, is the very low BDE for the C—O bonds (50–70 kcal mol^{-1} compared to the standard value of 93 kcal mol^{-1}). The large stabilization energies of the nitroxide radicals (in the range 28–33 kcal mol^{-1}) lead to these weak C—O bonds. As explained below, the origin of the stabilization energy can be found in the electronic structure of the nitroxyl radicals. The methoxy aminyl radicals have SE values between 14 and 23 kcal mol^{-1}. If we take into account the stabilization energies of the parent molecules, one obtains, except for the formyl derivatives, BDE values ten or more kcal mol^{-1} lower than the usual standard C—N energy. Let us now summarize our observations: one has to retain that the N—O bond is significantly modified by the vinyl substituent. The BDE(N—O) decreases to 34 kcal mol^{-1}. The C—N bonds exhibit small to

Can. J. Chem. Downloaded from www.nrcresearchpress.com by 91.121.58.235 on 09/07/12
For personal use only.

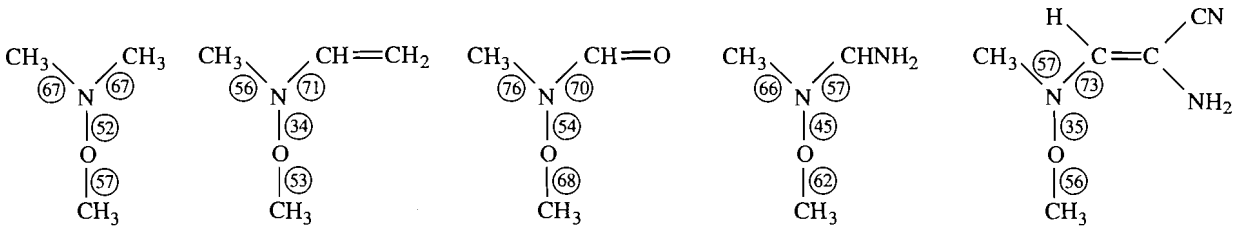

FIG. 2. Bond dissociation energies (kcal mol^{-1}) of the model molecules; all values are obtained from theoretical heats of formation.

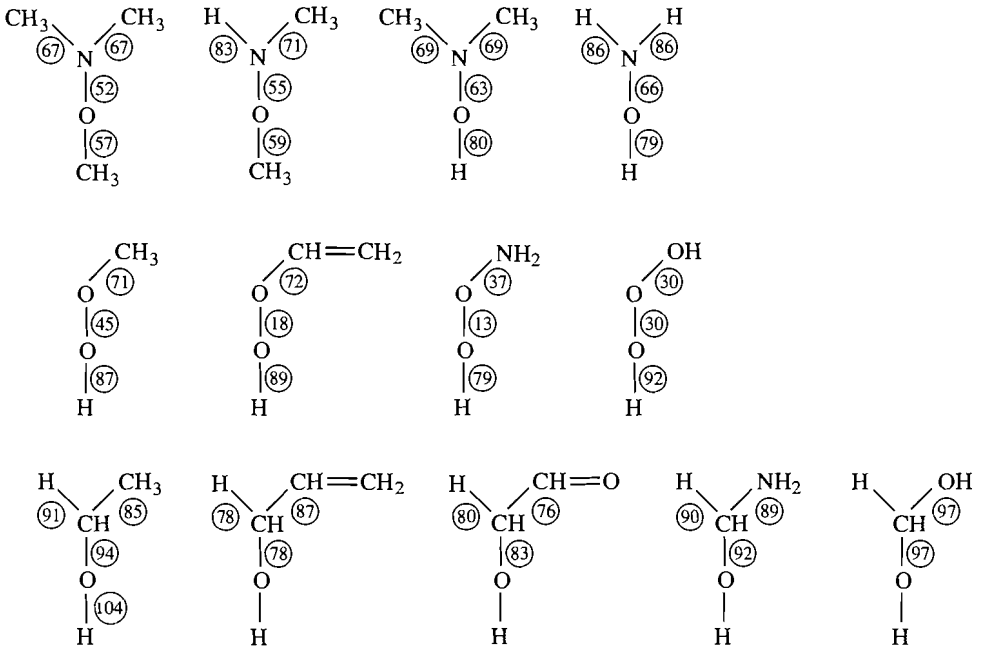

FIG. 3. Bond dissociation energies for various NO, CO, and OO single bonds (in kcal mol^{-1}); the heats of formations are taken from ref. 19.

Can. J. Chem. Downloaded from www.nrcresearchpress.com by 91.121.58.235 on 09/07/12
For personal use only.

medium weakening of strength. The remaining C—O bonds are always weak, but their minimum values remain equal to or larger than 53 kcal mol^{-1}. The

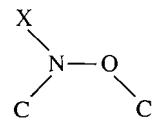

frame exhibits weak bonds. Ring structure connecting the two carbon atoms can enhance the weakness of this frame, as is observed experimentally. The variations in the heats of formations are large enough compared to the usual reliability of the calculations that our conclusions are at least not qualitatively suspicious. The theoretical method we use is known to give heats of formations with a target accuracy of 3 kcal mol^{-1} (21).

Large stabilization energies correspond to the occurrence of non-standard electronic organization or to long range interaction (21) (through the molecular chain or with some polysubstitution). The large SE within the parent molecules (in the case of NH_2 and CHO substitution) are of the second type. For the radicals considered in this work, the first explanation is the only valid one. All the heavy atoms in the radicals lie in the same plane, thus avoiding the usual tetrahedral electronic organization. The Boys' localization of the wave function allows the generation of conventional electronic pictures of any chemical compound (22). Using this technique, one can represent the electron distribution in radicals of interest. Figure 3 shows in a conventional manner the Boys' electronic pictures of some radicals. In those Linnett formulas for the aminyl radicals we have three electrons on the nitrogen atom. Distinction between σ and π type electrons represents a more formal than a physical view. Those electrons or part of them can be delocalized when appropriate groups are attached to the nitrogen atom: i.e. CH_2=CH, CHO, or NH_2. This stabilizes the radical. The large stabilization energies in the nitroxide radicals (and consequently the small BDE of the C—O bonds) can be explained in terms of an electronic description of the compounds. As shown in Fig. 4, the N—O bond in nitroxide derivatives appear as a three-electron two-center bond. This electronic delocalization gives stronger NO bond in the radical which becomes stabilized.

Conclusion

The stabilization energies of radicals and in a lesser way of parent molecules gives large variation in bond dissociation energies depending on the nature of the substituent in $XN(CH_3)OCH_3$ compounds. In each case the BDE(N—O) is the smallest; the vinyl group (with captodative substitution or without) leads to BDE(N—O) close to 30 kcal mol^{-1}. This is not the largest observed variation, but it gives the lowest BDE in those compounds. Those stabilization energies can be explained in terms of electronic Boy's picture. Although the relationship between BDE and E_a is still unknown for such type of bonds,

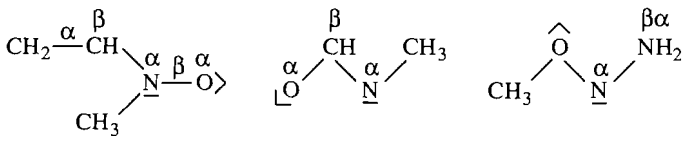

FIG. 4. Conventional representation of the map of charge centroids obtained using the Boys' localization procedure.

one can suppose that these values are small enough for easy bond breaking, especially in bicyclic compounds such as **1** which must be destabilized due to a non-negligible ring strain.

Acknowledgements

G.L. and M.S. thank the National Fund for Scientific Research, Belgium, for permanent support in access to computers.

1. E. FRANCOTTE, R. MERÉNYI, B. VANDENBULCKE-COYETTE, and H. G. VIEHE. Helv. Chim. Acta, **64**, 4, 1208 (1981).
2. M. AHMAD and J. HAMER. J. Org. Chem. **31**, 2831 (1966).
3. G. W. KIRBY and J. W. M. MACKINNON. J. Chem. Soc. Perkin I, 887 (1985).
4. H. G. VIEHE, Z. JANOUSEK, R. MERÉNYI, and L. STELLA. Acc. Chem. Res. **18**, 148 (1985).
5. H. G. VIEHE and J.-L. VAERMAN. J. Prakt. Chem. Band 330, Heft 5, S. 814 (1988).
6. J.-L. VAERMAN and H. G. VIEHE. Tetrahedron, **45**, 3183 (1989).
7. T. W. NEWTON. J. Chem. Educ. **45**, 571 (1968); J. R. MURDOCH. J. Am. Chem. Soc. **94**, 4410 (1972); **105**, 2159 (1983).
8. R. A. MARCUS. J. Chem. Phys. **43**, 679 (1965); **72**, 891 (1968).
9. M. G. EVANS and M. POLANYI. Trans. Faraday Soc. **34**, 11 (1938); G. LEROY. Adv. Quantum Chem. **17**, 1 (1985); M. SANA and G. LEROY. Ann. Soc. Sci. Bruxelles, **101**, 23 (1987).
10. G. LEROY, D. PEETERS, M. SANA, and C. WILANTE. *In* Substituent effects in radical chemistry. *Edited by* H. G. Viehe. D. Reidel (Dordrecht), 1 (1986).
11. G. LEROY, M. SANA, and C. WILANTE. J. Mol. Struct. (Theochem). **207**, 85 (1990).
12. M. SANA, G. LEROY, L. K. VINSON, and J. J. DANNENBERG. J. Mol. Struct. (Theochem), **205**, 89 (1990); M. SANA and G. LEROY. Ann. Soc. Sci. Bruxelles, **101**, 23 (1987); G. LEROY and M. SANA. J. Mol. Struct. (Theochem), **179**, 237 (1988).
13. W. J. HEHRE, R. DITCHFIELD, L. RADOM, and J. A. POPLE. J. Am. Chem. Soc. **92**, 4796 (1970).
14. M. SANA, G. LEROY, D. PEETERS, and C. WILANTE. J. Mol. Struct. (Theochem), **164**, 249 (1988).
15. GAUSSIAN 82 programs have been used in any of the calculations: J. S. BINKLEY, R. A. WHITESIDE, K. RAGHAVACHARI, R. SEEGER, D. J. DEFREES, H. B. SCHLEGEL, M. J. FRISCH, and J. A. POPLE. Gaussian 82. Carnegie-Mellon University, Pittsburgh PA. 1982. Data General implementation. D. Peeters. Université Catholique de Louvain (Belgium).
16. W. J. HEHRE, R. DITCHFIELD, and J. A. POPLE. J. Chem. Phys. **56**, 2257 (1972).
17. G. LEROY. Int. J. Quantum Chem. **XXIII**, 271 (1983).
18. G. LEROY, M. SANA, C. WILANTE, and M.-J. VANZIELEGHEM. J. Mol. Struct. (Theochem). In press.
19. G. LEROY, M. SANA, and C. WILANTE. Thermochemical table of Quantum Chemistry Laboratorium. Place Louis Pasteur 1, B1348 Louvain-la-Neuve, Belgium. 1989.
20. G. LEROY. Adv. Quantum Chem. **17**, 1 (1985).
21. M. SANA, G. LEROY, D. PEETERS, and C. WILANTE. J. Mol. Struct. (Theochem). **200**, 575 (1989).
22. G. LEROY, D. PEETERS, A. DEPLUS, and M. TIHANGE. Nouv. J. Chim. **4**, 403 (1980); M. SANA and G. LEROY. J. Mol. Struct. (Theochem), **109**, 251 (1984); M. SANA. *In* Structure and dynamics of molecular systems. *Edited by* R. Daudel. D. Reidel, Dordrecht. 1985. pp. 1–22.

Can. J. Chem. Downloaded from www.nrcresearchpress.com by 91.121.58.235 on 09/07/12
For personal use only.

Carbocationic polymerization in the gas phase: polymerization of acetylene induced by BF_2^+

LEONARD FORTE, MIN H. LIEN, ALAN C. HOPKINSON, AND DIETHARD K. BOHME
Department of Chemistry, York University, North York, Ont., Canada M3J 1P3

Received August 30, 1989[1]

LEONARD FORTE, MIN H. LIEN, ALAN C. HOPKINSON, and DIETHARD K. BOHME. Can. J. Chem. **68**, 1629 (1990).

Gas-phase measurements for the primary reaction of BF_2^+ with acetylene and the ensuing higher-order reactions with acetylene have been performed at 296 ± 2 K in helium at 0.35 torr using the Selected-Ion Flow Tube (SIFT) technique. The primary reaction was observed to be rapid and to produce two species which both initiated rapid polymerization of acetylene. The major primary product, C_2HBF^+, was observed to initiate the sequential addition of four molecules of acetylene, most likely by termolecular association reactions. The first few steps in this polymerization were also followed using *ab initio* molecular orbital theory. The calculations and measurements provide structural, energetic, and kinetic information and, in combination, reveal several intrinsic features of the initial steps of the cationic polymerization of acetylene initiated by BF_2^+.

Key words: polymerization, acetylene, aromaticity.

LEONARD FORTE, MIN H. LIEN, ALAN C. HOPKINSON et DIETHARD K. BOHME. Can. J. Chem. **68**, 1629 (1990).

Opérant à 296 ± 2 K, à une pression de 0,35 torr d'hélium et faisant appel à la technique du tube à écoulement ionique sélectif (SIFT), on a effectué des mesures en phase gazeuse sur la réaction primaire du BF_2^+ avec l'acétylène et sur les réactions subséquentes d'ordre plus élevées avec l'acétylène. On a observé que la réaction primaire est rapide et qu'elle conduit à deux espèces qui initient chacune une polymérisation rapide de l'acétylène. On a observé que le produit primaire majeur, le C_2HBF^+, initie une addition séquentielle de quatre molécules d'acétylène qui se produisent probablement par des réactions d'association termoléculaires. On a aussi suivi les premières étapes de cette polymérisation à l'aide de la théorie des orbitales moléculaires *ab initio*. Les calculs et les mesures fournissent des informations sur la structure, sur les énergies et sur le cinétique de la réaction et, lorsqu'on les combine, ils révèlent plusieurs caractéristiques intrinsèques des étapes initiales de la polymérisation cationique de l'acétylène initiée par le BF_2^+.

Mots clés : polymérisation, acétylène, aromaticité.

[Traduit par la revue]

Introduction

Our recent observations of the "clean" gas-phase polymerization of ethylene and other olefinic monomers initiated by BF_2^+ (1, 2) prompted us to study the related ion-induced gas-phase polymerization of acetylene. Acetylene has been polymerized in solution by Friedel–Crafts or Lewis acid catalysts such as $AlCl_3$ and BF_3 (3), but the mechanism of the initiation of polymerization remains a matter of speculation.

For the polymerization of olefins in solution, one theory attributes initiation to the ionized form of the initiator resulting from self-dissociation (4, 5). For example, in the polymerization of isobutene by $AlCl_3$, the $AlCl_2^+$ cation formed by self-dissociation could add to the double bond to give an equivalent concentration of propagating carbenium ions (4, 5). Indirect evidence for such a mechanism has been given (5, 6), but direct identification of the initiating and propagating species in solution is lacking. However, we have recently shown that the intrinsic nature and reactivity of these species can be revealed with measurements of the polymerization of isobutene induced by BF_2^+ in the gas phase (2). The gas-phase polymerization of several other olefinic monomers was also investigated (2).

It is reasonable to assume that a similar initiation mechanism can apply to the polymerization of alkynes by Lewis acids. To test this assumption we chose to investigate the polymerization of acetylene initiated by the BF_2^+ cation in the gas phase, both experimentally and theoretically. In our experimental study, mass-selected BF_2^+ ions were allowed to react with acetylene in a flowing helium buffer gas and the primary and higher-order ions evolving in the polymerization chemistry were monitored downstream with a second mass spectrometer. The first few steps of this polymerization also were followed theoretically using *ab initio* molecular orbital calculations. In combination, the measurements and the calculations reveal a number of the intrinsic features of this cationic polymerization by providing kinetic, energetic, and structural information. Such insight is not accessible to measurements made in solution.

Experimental

The selected-ion flow tube (SIFT) apparatus was used to perform the measurements. The apparatus and technique have been described in detail elsewhere (7). BF_2^+ was generated from a mixture of BF_3 (Matheson C.P. grade) and helium (about 30 mol%) by electron impact at 55–80 eV. BF_2^+ was then selected using a quadrupole mass filter and injected into a flow tube containing helium at ca. 0.33 torr. We have seen that $FBOH^+$ arises from the reaction of BF_2^+ with water vapour impurity in the carrier gas (2). All measurements were performed at a room temperature of 296 ± 2 K and a total pressure of ca. 0.33 torr. Helium (Matheson, high purity 99.995 mol%) was used as the carrier gas and acetylene (Matheson, prepurified 99.6 mol%) as the reactant gas.

Table 1 includes a summary of the measured rate coefficients. At least two measurements were made for each determination of a rate coefficient. Sources of uncertainty have been discussed previously (7). The rate coefficient for the reaction for BF_2^+, which was determined from 11 measurements, was derived from a fit to the semilogarithmic decay of this ion and has an estimated accuracy of less than ±30%. The rate coefficients for the secondary and higher-order reactions were derived from a double-exponential computer fit to the profile of the corresponding reactant ion and have an estimated accuracy of less than ±40%.

Figure 1 shows that BF_2^+ reacts rapidly with acetylene to produce two primary products according to reaction [1]. The semilogarithmic

$$[1]\quad BF_2^+ + HC{\equiv}CH \xrightarrow{0.95} C_2HBF^+ + HF$$
$$\xrightarrow{0.05} C_2H_2{\cdot}BF_2^+$$

[1]Revision received May 4, 1990.

Can. J. Chem. Downloaded from www.nrcresearchpress.com by 91.121.58.235 on 09/07/12
For personal use only.

Can. J. Chem. Downloaded from www.nrcresearchpress.com by 91.121.58.235 on 09/07/12
For personal use only.

TABLE 1. Effective bimolecular rate coefficients (in units of 10^{-10} cm^3 molecule^{-1} s^{-1}) for initiating and propagating reactions in the BF_2^+-induced gas-phase polymerization of acetylene at 296 ± 2 K in helium buffer gas at 0.35 torr

Reactant ion	k_{exp}[a]	k_c[b]	k_{exp}/k_c
BF_2^+	4.5	11.0	0.41
C_2HBF^+	3.8	10.8	0.35
$C_4H_3BF^+$	5.5	10.2	0.54
$C_6H_5BF^+$	3.2	9.9	0.32
$C_8H_7BF^+$	0.92	9.7	0.09
$C_2H_2 \cdot BF_2^+$	8.4	10.3	0.82
$C_4H_4 \cdot BF_2^+$	0.57	10.0	0.06

[a]Deduced from data of the type shown in Fig. 1 with computer-fitting techniques using single (for BF_2^+) or double exponentials (for the remaining ions). The estimated accuracies are less than ±30% for the reaction of BF_2^+ and less than ±40% for the remaining reactions.

[b]Collision-rate coefficients were derived using the Average Quadrupole Orientation theory (8) with $\alpha(C_2H_2) = 3.3$ Å^3 (9) and $Q = 3.6 \times 10^{-26}$ esu cm^2 (10).

decay of BF_2^+ provides a rate coefficient of (4.1 ± 1.6) × 10^{-10} cm^3 molecule^{-1} s^{-1}. The adduct ion presumably is formed in a termolecular reaction with helium as the stabilizing third body. The C_2HBF^+ product ion was seen to undergo a rapid sequential addition of four acetylene molecules as shown in reaction [2], again presumably in a termolecular fashion.

$$[2]\quad C_2HBF^+ \xrightarrow[k_2]{C_2H_2} C_4H_3BF^+ \xrightarrow[k_3]{C_2H_2} C_6H_5BF^+ \xrightarrow[k_4]{C_2H_2} C_8H_7BF^+ \xrightarrow[k_5]{C_2H_2} C_{10}H_9BF^+$$

Figure 1 also shows clearly the occurrence of the first three propagation steps indicated by reaction [2]. The fourth was observed in a separate experiment.

Table 1 shows that the acetylene additions in reaction [2] proceed with a slight overall decrease in efficiency, where efficiency is defined as the ratio of the experimental reaction rate coefficient, k_{exp}, to the computed collision rate coefficient, k_c. Collision rate coefficients were computed with the Average Quadrupole Orientation theory (8) taking the polarizability and rotation-averaged quadrupole moment (one-half of the static quadrupole moment) to be 3.33 Å^3 (9) and 3.6 × 10^{-26} esu cm^2 (10)), respectively. The effective bimolecular rate coefficients for the addition reactions were found to be 3.8, 5.5, 3.2, and 0.92 × 10^{-10} cm^3 molecule^{-1} s^{-1}. It is interesting to note that the rate coefficient and efficiency maximize for the addition of the second molecule of acetylene.

The adduct ion, $C_2H_2 \cdot BF_2^+$, also reacted further with two sequential additions of acetylene being observed, as shown in Fig. 1 and reaction [3], with helium presumably acting as the stabilizing third body.

$$[3]\quad C_2H_2BF_2^+ \xrightarrow[k_2']{C_2H_2} C_4H_4BF_2^+ \xrightarrow[k_3']{C_2H_2} \text{products}$$

The effective bimolecular rate coefficients for reaction [3] were found to be 8.4 and 0.57 × 10^{-10} cm^3 molecule^{-1} s^{-1} (Table 1). Here we note a sharp decrease in rate coefficient for the addition of a second molecule of acetylene.

Theory

The reaction sequences for the first three reactions with acetylene were examined using *ab initio* molecular orbital calculations at the HF 3-21G level of theory (11) and for the smaller ions also at the HF 6-31G* level (12). All Hartree–Fock calculations were performed with the MONSTERGAUSS program (13) and single-point MP2 calculations (14) were performed with the Gaussian 82 program (15).

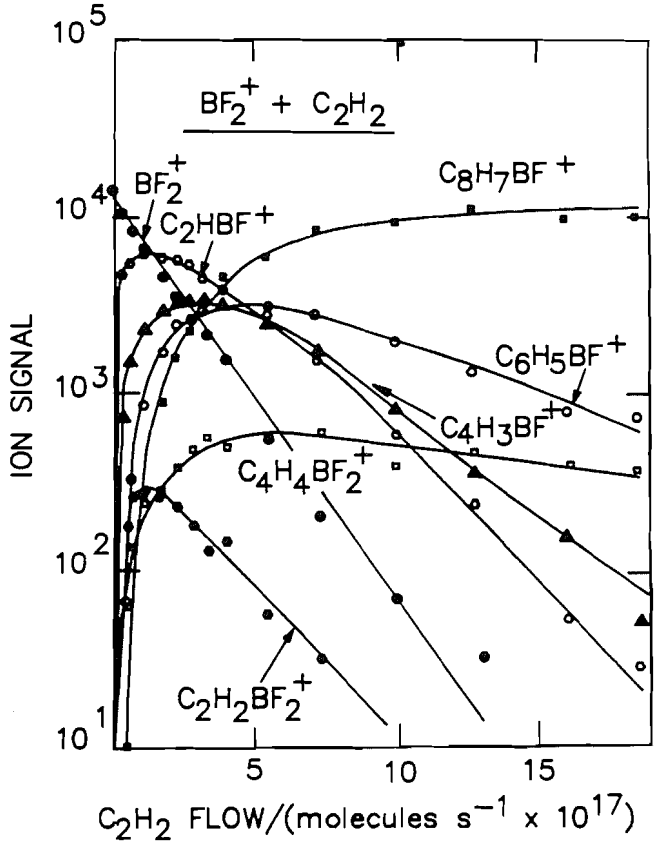

FIG. 1. Observed variation in ion signals upon addition of C_2H_2 into the reaction region in which the reacting ion BF_2^+ has been established with the SIFT technique. $P = 0.35$ torr, $T = 295$ K, [He] = 1.13 × 10^{16} atoms cm^{-3}, $\bar{v} = 6.6 \times 10^3$ cm s^{-1}, $L = 46$ cm.

The energy differences as calculated at the HF 3-21G level for the first three reactions of BF_2^+ with acetylene are shown in Fig. 2. Structures for the small ions, **1**, **3**, **5**, **6**, **7**, **8**, and **9** were optimized at both the HF 3-21G and HF 6-31G* levels of theory and the results of the higher level calculations are given in Fig. 3. For the larger ions, **4**, **10**, **11**, **12**, and **13**, several conformers were optimized at the HF 3-21G level and for each ion the main structural features of the lowest energy conformer are given in Fig. 4. The total energies as calculated at the HF 3-21G//3-21G and HF 6-31G*//6-31G* levels are recorded in Tables 2 and 3.

Reaction profile at the 3-21G level of theory

(a) The major channel

The gas-phase addition of BF_2^+ to acetylene has a large exothermicity, and in the dominant channel, much of this excess energy is used to fragment the initial complex into HF and C_2HBF^+ (**1**). The calculated ΔE for this reaction is −9.9 kcal mol^{-1}. Ion **1** can be represented by two valence tautomers, **1***a* and **1***b*. At the 3-21G level the C—C bond is 1.199 Å

$$F—B^+—C{\equiv}C—H \leftrightarrow F—B{=}C{=}C^+—H$$
$$\mathbf{1}a \qquad\qquad \mathbf{1}b$$

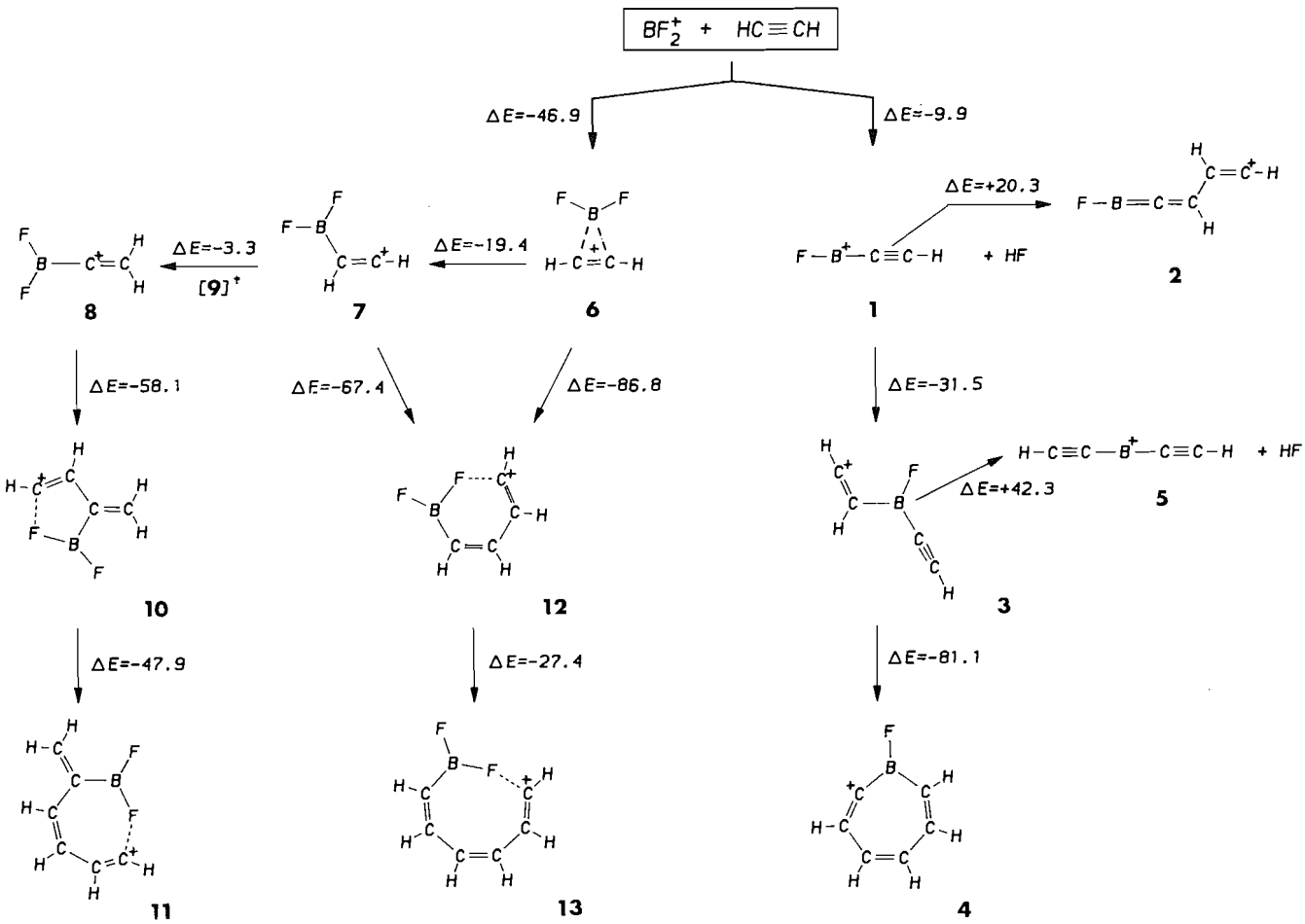

FIG. 2. Differences in total energy, ΔE (in kcal mol^{-1}), computed at 3-21G, for the first three steps in the reaction of BF_2^+ with C_2H_2.

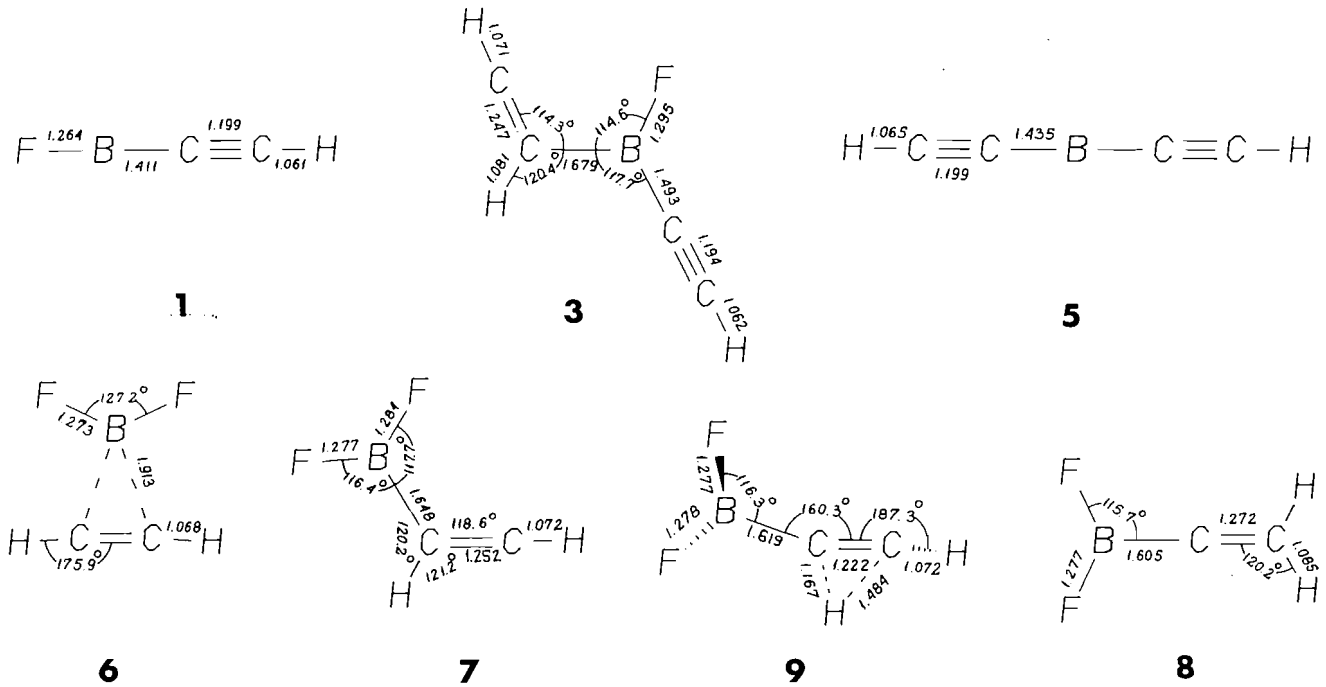

FIG. 3. Structures from HF 6-31G* optimization studies on ions **1**, **3**, **5**, **6**, **7**, **8**, and **9**. Bond lengths are in Ångstroms and bond angles in degrees. Based on the results of optimizations at the HF 3-21G level, ions **1** and **5** were assumed to be linear ($C_{\infty v}$ and $D_{\infty h}$), **6** and **8** were taken to have C_{2v} symmetry, and angles in acetylenes and at cationic carbons in vinyl cations were assumed to be 180°. In transition structure **9** both fluorines and both hydrogens are out of the plane defined by BCC, but all dihedral angles are less than 2°.

Can. J. Chem. Downloaded from www.nrcresearchpress.com by 91.121.58.235 on 09/07/12
For personal use only.

Can. J. Chem. Downloaded from www.nrcresearchpress.com by 91.121.58.235 on 09/07/12
For personal use only.

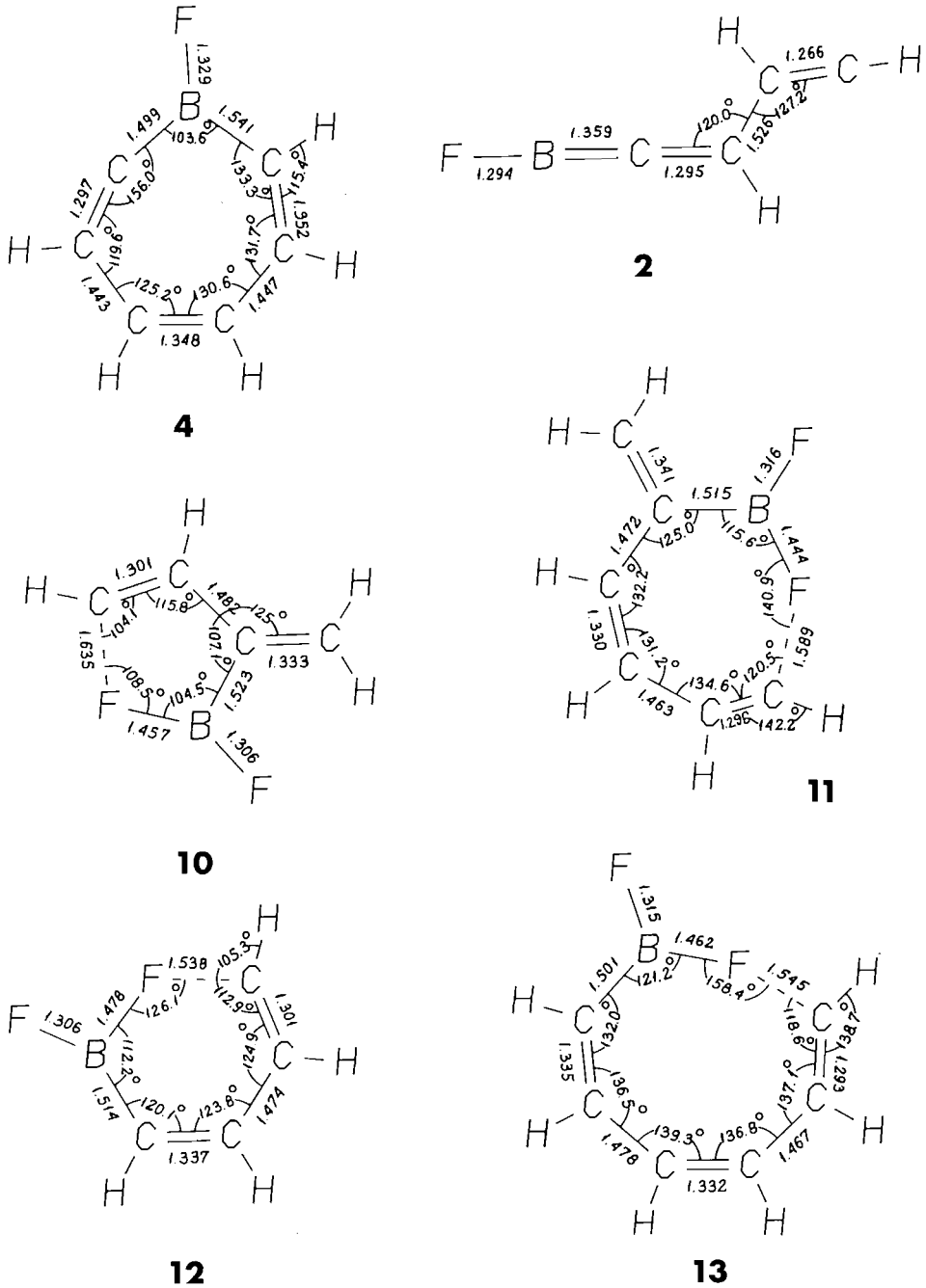

FIG. 4. Structural parameters for planar ions **2**, **4**, **10**, **11**, **12**, and **13** as obtained from HF 3-21G level calculations. Bond lengths are in Ångstroms and bond angles in degrees.

and C—B bond is 1.411 Å, indicating that structure **1***a* is the better representation. Structures **1***a* and **1***b* formally localize the positive charge on boron and the terminal carbon, respectively, and, in principle, nucleophilic attack by acetylene could occur at either of these atoms. However, addition at the carbon leads to ion **2** which is higher in energy than the initial reactants and the only energetically allowed pathway results in formation of **3**, a vinyl cation with a substituent on the β-carbon atom. We studied the profile to rotation about the C—B bond and found the conformation with the fluorine eclipsing the double bond (Figs. 2 and 3) to have the lowest energy. In this structure the positive charge is localized on the cationic carbon, with little participation from the substituent. Rotation by 180° about the C—B bond results in the triple bond eclipsing the double bond, a structure which might be expected to be stabilized by through-space π-donation from the triple bond to the cationic carbon (**3***a*). However, the product formed by collapsing this internal complex is a five-membered ring, **3***b*, which has anti-aromatic character (4π electrons in the ring) and is a vinyl cation with badly distorted geometry at the cationic carbon (bending at the α carbon of vinyl cations is a high energy process (16)). These destabilising interactions result in the structure with fluorine eclipsing the double bond being 2 kcal mol^{-1} lower in energy than **3***a*.

TABLE 2. Total energies of ions and relative energies of products shown in Fig. 2

Products	Total energy of ion[a]	Relative energy[b]
1 + HF	−199.03755	−9.9
2 + HF	−275.40120	+10.4
3 + HF	−275.48363	−41.4
4 + HF	−352.00849	−122.2
5 + 2HF	−175.95598	+0.9
6	−298.55678	−46.9
7	−298.58772	−66.4
8	−298.59292	−69.6
9	−298.55944	−48.6
10	−375.08150	−127.7
11	−451.55376	−175.6
12	−375.09107	−133.7
13	−451.53074	−161.1

[a]Total energy in hartrees computed at the HF/3-21G//HF/3-21G level.

[b]Energy (in kcal mol^{-1}) relative to the reactants $BF_2^+ + nC_2H_2$. Total energies for BF_2^+, C_2H_2, and HF are −222.08601, −76.39596, and −99.46022 hartrees, respectively.

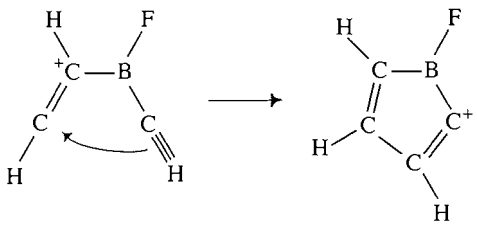

3a *3b*

Addition of a further acetylene molecule to the cationic carbon of **3** results in the vinyl cation

$$HC^+{=}CH{-}CH{=}CH{-}B(F){-}C{\equiv}C{-}H$$

Assuming that this ion is planar, then rotation about the HC—B, HC=CH, and HC—CH bonds lead to eight possible structures. Two of these structures permit formation of cyclic ions both with 6π electrons and these two aromatic ions have the lowest energies. The *trans,cis,cis* arrangement, **4***a*, permits stabilization of the cationic carbon by through-space π-donation from the alkynyl group. This structure, which is the lowest energy conformer, has a distance of 1.443 Å between the terminal carbon atoms, and is best regarded as a seven-membered ring with alternating single and double C—C bonds (Fig. 4, structure **4**). The bond angle of 156° at the α-carbon is far from ideal, but is similar to that calculated for the 1-cyclohexenyl cation (16).

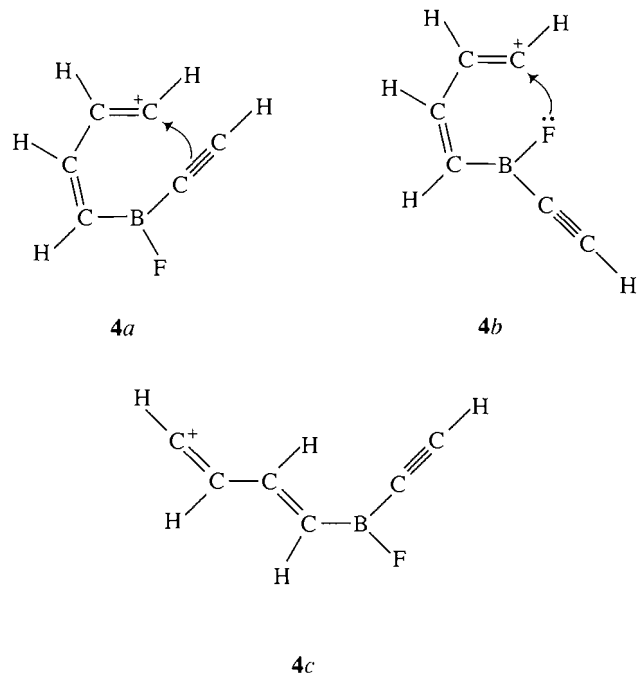

4a *4b*

4c

The *cis,cis,cis* structure **4***b* permits through-space donation from fluorine to the cationic carbon. The $^+$C—F distance is 1.506 Å and the ∠C—C—H at the cationic carbon is 139.7°, showing considerable $^+$C—F interaction. This structure is 16 kcal mol^{-1} higher in energy than **4***a*. All other structures are higher in energy and the *trans,trans,trans* structure **4***c*, where the positive charge is further from the unsaturated bonds and lone pairs, is 47 kcal mol^{-1} above **4***a*. Addition of acetylene to **3** gives the aromatic ion **4** in the most exothermic reaction in the major pathway (ΔE is −80.8 kcal mol^{-1}). Elimination of HF from **3** to form **5**, an analogous reaction to the major pathway

TABLE 3. Total and relative energies for structures shown in Fig. 3

	HF/6-31G*//HF/6-31G*		HF/MP2/6-31G*//HF/6-31G*	
Ion[a]	Total energy of ion[b]	Relative energy[c]	Total energy of ion[b]	Relative energy[c]
1 ($C_{\infty v}$) + HF	−200.12709	−0.8	−200.59836	−2.2
3 (C_s) + HF	−276.98776	−27.7		
5 ($D_{\infty h}$) + 2HF	−176.92115	+12.3		
6 (C_{2v})	−300.20554	−48.2	−300.85686	−50.4
7 (C_s)	−300.21451	−53.8	−300.84870	−45.3
8 (C_{2v})	−300.22232	−58.7	−300.84823	−45.0
9 (C_s)	−300.20596	−48.5	−300.84819	−45.0

[a]Molecular point group used in calculations is given in parentheses.

[b]Total energy in hartrees.

[c]Energy (in kcal mol^{-1}) relative to reactants $BF_2^+ + nC_2H_2$. Total energies for BF_2^+, C_2H_2, and HF are −223.31088, −76.81783, and −100.00291 hartrees, respectively, at the HF/6-31G*//HF/6-31G* level and −223.71188, −77.06463, and −100.181583 hartrees, respectively, at the MP2/6-31G*//HF/6-31G* level.

Can. J. Chem. Downloaded from www.nrcresearchpress.com by 91.121.58.235 on 09/07/12
For personal use only.

Can. J. Chem. Downloaded from www.nrcresearchpress.com by 91.121.58.235 on 09/07/12
For personal use only.

in the initial step, requires 10.8 kcal mol^{-1} more energy than the maximum available in the formation of **3** from **1**, and does not occur.

(b) The minor channel

Adduct $C_2H_2BF_2^+$ is a minor product in the gas-phase addition of BF_2^+ to acetylene. As BF_2^+ and acetylene approach, the initial long-range interaction is expected to be π-donation from the triple bond to the empty *p*-orbital on the boron atom. Similar π-complexes are believed to be intermediates in electrophilic addition to alkynes in solution (17). π-Complexes are stabilized by two interactions, π-donation from the alkyne to a vacant orbital on X^+ and back-donation usually from a lone pair on the electrophile to π* of the alkyne. In the reaction between BF_2^+ and acetylene, the electrophile is a good acceptor but back-donation is minimal and the C—B bonds are effectively one-electron bonds. The π-complex, **6**, has the anti Van't Hoff planar structure and is 19.5 kcal mol^{-1} higher in energy than the β-substituted vinyl cation, **7**. By analogy with profiles to interconversion between the open and cyclic $C_2H_2X^+$ ions (18), there is likely to be little or no barrier to interconversion of **6** and **7**. The planar α-substituted ion, **8**, has the lowest energy 3.2 kcal mol^{-1} below **7** and the barrier to interconversion of **7** and **8** via transition structure **9** is 17.8 kcal mol^{-1} above **7** (Table 1). Structure **8** is 69.6 kcal mol^{-1} below the reactants, C_2H_2 and BF_2^+, and structures **6** to **9** are all easily accessible on this reaction path.

We have calculated structures for the polymerization of acetylene starting with structures **6**, **7**, and **8**. For the larger ions where a multiple carbon–carbon bond or a fluorine atom is at one end of the molecule and the other terminus is a vinyl cation, there is a through-space interaction between the terminal groups and the ion is cyclic. Addition reactions which produce cyclic ions formally containing π electrons in the ring (ions **11** and **12**) are highly exothermic, a fact which we attribute to the aromaticity of the product.

Addition of acetylene to **8** occurs at the cationic carbon and gives ion **10**. This is formally a vinyl cation but there is considerable through-space interaction with the fluorine atom, as shown by the C...F distance of 1.635 Å, the long B—F bond and the bending at the cationic carbon (Fig. 4). Further addition yields the cyclic ion, **11**, in which the C—F distance of 1.589 Å is approximately 0.2 Å longer than a normal C—F bond. Formally there are six π electrons in the cross-conjugated ring in structure **11** and this ion is 14.4 kcal mol^{-1} lower in energy than the isomeric eight-membered ring, **12**, which formally contains eight π electrons in the ring.

Addition of acetylene to **6** and **7** is highly exothermic and leads to structure **12**, a six-membered ring which formally contains six π electrons. Ion **12** is 6.0 kcal mol^{-1} lower in energy than the isomeric ion, **10**. The aromaticity of **12** is destroyed by addition of a further acetylene molecule and ΔE for formation of **13**, which is an eight-membered ring formally carrying eight π electrons in the ring, is small.

Higher level calculations

Ab initio calculations with small gaussian basis sets favour classical structures like **7** and **8** over bridged structures like **6** and transition states like **9**. These ions are sufficiently small that inclusion of polarisation functions in the basis set used in structure optimisation is feasible. We have used the HF/6-31G* level of theory to reoptimize some of the smaller structures and have then used these structures to test the effect of inclusion of correlation energy on the calculated ΔE for the initial step of the reaction sequence. The results of these calculations are included in Table 3 and Fig. 3.

For the major channel, addition followed by elimination of HF, ΔE is −0.8 kcal mol^{-1} at the HF/6-31G* level and −2.2 kcal mol^{-1} at the MP2/6-31G*//HF/6-31G* level. These are much closer to thermoneutral than ΔE calculated at the HF/3-21G level (−9.9 kcal mol^{-1}). The subsequent addition reaction of acetylene to form the adduct **3** is calculated to have ΔE = −26.9 kcal mol^{-1} at the HF/6-31G* level, i.e. it is slightly less exothermic than at the HF/3-21G level. Formation of $B(C{\equiv}CH)_2^+$ by loss of HF from **3** is calculated to require 12.3 kcal mol^{-1} more energy than is available in the initial reactants. To summarise, then, for the major reaction pathway, increasing the basis set size has the effect of decreasing the relative energies of the products but does not change the overall mechanistic conclusions.

For the initial ions in the minor channel, extension of the basis set and inclusion of correlation energy both result in significant stabilisation of the cyclic ions **6** and **9**. At the HF/6-31G* level the non-classical bridged ion, **6**, has the highest energy but is only 5.6 kcal mol^{-1} above the open ion **7**, and the transition structure **9** is only 5.3 kcal above **7**. Inclusion of correlation energy at the MP2 level (valence electrons only) has the dramatic effect of making the bridged ion **6** the lowest energy isomer, with structures **7**, **8**, and **9** all having similar energies 5 kcal mol^{-1} higher than **6**. The highest level calculations then show that, although BF_2^+ is ineffective as a back-donor, nevertheless $C_2H_2BF_2^+$ is a symmetrically bridged ion. Previous theoretical studies have found that the parent vinyl cation to have the open $H_2C{=}C^+H$ structure at the Hartree–Fock level but to have the symmetrically bridged structure when correlation is included (19, 20). A recent experimental study has shown the vinyl cation to be symmetrically bridged (21).

Discussion and conclusions

We have characterized the intrinsic chemistry of the initial steps in the polymerization of acetylene by BF_2^+ in the gas phase experimentally using the SIFT technique. The measurements provide a quantitative measure of the intrinsic reaction kinetics. The initiation reaction is quite rapid (k = 4.1×10^{-10} cm^3 $molecule^{-1}$ s^{-1}) with the major channel being the formation of C_2HBF^+ ion and the elimination of HF. Some addition product is also formed, most likely in a termolecular reaction at our operating pressures. Polymerization occurs mainly via the C_2HBF^+ ion followed by four additions of acetylene. The rate coefficient exhibits a maximum early in the reaction sequence. Two sequential addition reactions were observed with the addition product, $C_2H_2 \cdot BF_2^+$.

The *ab initio* molecular orbital calculations provide insight into the structures and energetics of several of the intermediates in the polymerization chemistry. The energetics of the first few steps in the polymerization reaction involving the major initial product ion, C_2HBF^+, are of interest. Formation of C_2HBF^+ is fast, but the reaction of this ion to form **3** is somewhat slower and is less exothermic than most of the addition reactions in Fig. 2. Ion **3** is unusual in that, unlike other vinyl cations containing unsaturated linkages, it does not adopt the s-*cis* conformation which permits delocalization of the charge through space onto the triple bond. This may be attributed to the antiaromatic character of such a five-membered ring containing four π electrons. The reaction of **3** to form **4** is the fastest reaction in this channel and the product is a seven-membered

Can. J. Chem. Downloaded from www.nrcresearchpress.com by 91.121.58.235 on 09/07/12
For personal use only.

ring with six π electrons (excluding the lone pair on fluorine). It therefore appears that the rates and energetics of reactions in the gas-phase polymerization are dictated by the aromaticity of the product ion.

In solution the major reaction pathway might be addition rather than elimination of HF since solvation of BF_2^+ would make it less reactive. Assuming that the solvent does not act to prevent ring formation, then structure **13** and probably **11** are likely to be major intermediates in the solution-phase polymerization. The highest level calculations show the adduct $C_2H_2BF_2^+$ to have the planar bridged structure **6**. Reaction of ion **6** with acetylene produces cyclic ion **12** which has six π electrons in the ring. This reaction has the largest calculated exothermicity in the two reaction schemes in Fig. 2 and the observed rate constant is the largest in Table 1. Further reaction of **12** with acetylene produces an eight-membered ring with eight π electrons. ΔE for this last step is small (-27.4 kcal mol^{-1}) and the experimental rate coefficient (5.7×10^{-11} cm^3 molecule^{-1} s^{-1}) is the smallest in Table 1. Here again the rates of formation and reaction of the aromatic ion **12** correlate with their calculated exothermicities.

The π-bonds of acetylene are stronger than that of ethylene (the ionization energies are 11.4 and 10.5 eV, respectively) (22). In general then, in reactions in which π-donation is dominant (e.g. electrophilic addition and formation of π-complexes with metals) alkenes react faster than alkynes. Previous results have been for solution reactions, but now we find that the gas-phase reaction of BF_2^+ with ethylene has a larger rate coefficient (7.3×10^{-10} cm^3 molecule^{-1} s^{-1}) than that for the reaction of BF_2^+ with acetylene (4.5×10^{-10} cm^3 molecule^{-1} s^{-1}). In both gas-phase reactions the major pathway is elimination of HF to produce the propagating species $C_2H_3BF^+$ in the ethylene reaction and C_2HBF^+ in the acetylene reaction. In the reaction with ethylene, loss of HF is the only reaction channel. In the reaction with acetylene some addition product is observed (5%) but the dominant pathway is loss of HF. The observation of an addition product in the reaction with acetylene and non-observation in the reaction with ethylene may be explained by the difference in the exothermicity of HF elimination. Elimination of HF in the ethylene reaction is more exothermic (5 kcal mol^{-1} at HF/6-31G*) than elimination in the acetylene reaction (1 kcal mol^{-1} at HF/6-31G*). Thus the initial acetylene adduct can persist for a longer time and can be more easily deactivated by collision with helium buffer atoms before HF is eliminated.

With the SIFT experiments in combination with theoretical calculations we have characterized the intrinsic features of the initial steps of the BF_2^+ ion induced polymerization of acetylene in the gas phase. Such a combined approach should have general applications in the elucidation of intrinsic features of cationic polymerization in the gas phase.

Acknowledgment

We thank the Natural Sciences and Engineering Research Council of Canada for financial support.

1. L. Forte, M. H. Lien, A. C. Hopkinson, and D. K. Bohme. Makromol. Chem. Rapid Commun. **8**, 87 (1987).
2. L. Forte, M. H. Lien, A. C. Hopkinson, and D. K. Bohme. Can. J. Chem. **67**, 1576 (1989).
3. F. Steegmuller. Monde Ind. **74**, 11 (1948).
4. P. H. Plesch. Makromol. Chem. **175**, 1065 (1974).
5. D. W. Grattan and P. H. Plesch. Makromol. Chem. **181**, 751 (1980).
6. D. W. Grattan and P. H. Plesch. J. Chem. Soc. Dalton Trans. 1734 (1977).
7. D. K. Bohme, R. S. Hemsworth, H. W. Rundle, and H. I. Schiff. J. Chem. Phys. **58**, 3504 (1973); G. I. Mackay, G. D. Vlachos, D. K. Bohme, and H. I. Schiff. Int. J. Mass Spectrom. Ion Phys. **36**, 259 (1980); A. B. Raksit and D. K. Bohme. Int. J. Mass Spectrom. Ion Phys. **55**, 69 (1983).
8. T. Su and M. T. Bowers. Int. J. Mass Spectrom. Ion Phys. **17**, 309 (1975); **21**, 424 (1976).
9. E. W. Rothe and R. B. Bernstein. J. Chem. Phys. **31**, 1619 (1959).
10. T. D. Gierke, H. L. Tigelaar, and W. H. Flygare. J. Am. Chem. Soc. **94**, 330 (1972).
11. J. S. Binkley, J. A. Pople, and W. J. Hehre. J. Am. Chem. Soc. **102**, 939 (1980).
12. P. C. Hariharan and J. A. Pople. Theor. Chim. Acta, **28**, 213 (1978).
13. M. R. Peterson and R. A. Poirier. Monstergauss program. University of Toronto, Toronto, Ont., Canada.
14. C. Moller and M. S. Plesset. Phys. Rev. **46**, 618 (1934); J. A. Pople, J. S. Binkley, and R. Seeger. Int. J. Quantum Chem. Symp. **10**, 1 (1976); R. Krishnan and J. A. Pople. Int. J. Quantum Chem. **14**, 91 (1978); R. Krishnan, M. J. Frisch, and J. A. Pople. J. Chem. Phys. **72**, 4244 (1970).
15. J. S. Binkley, M. Frisch, K. Raghavachari, D. Defrees, H. B. Schlegel, R. Whiteside, E. Fluder, R. Seeger, and J. A. Pople. Gaussian 82, Release A, Carnegie-Mellon University, Pittsburgh, PA.
16. H. Mayr, R. Schneider, D. Wilhelm, and P. v. R. Schleyer. J. Org. Chem. **46**, 5336 (1989).
17. H. Hanack. Acc. Chem. Res. **3**, 209 (1970); G. Modena and U. Tonnellato. Adv. Phys. Org. Chem. **9**, 185 (1971); P. J. Stang. Prog. Phys. Org. Chem. **10**, 276 (1973).
18. V. Lucchini and G. Modena. Progress in theoretical organic chemistry. Vol. 2. *Edited by* I. G. Csizmadia. Elsevier. p. 268.
19. B. Zurawski, R. Ahlrichs, and W. Kutzelnigg. Chem. Phys. Lett. **21**, 309 (1973).
20. K. Raghavachari, R. A. Whiteside, J. A. Pople, and P. v. R. Schleyer. J. Am. Chem. Soc. **103**, 5649 (1981).
21. E. P. Kanter, Z. Vager, G. Both, and D. Zajfman. J. Chem. Phys. **85**, 12 (1986).
22. M. J. S. Dewar. The molecular orbital theory of organic chemistry. McGraw-Hill. 1969. p. 147.

The consecutive cyclization–elimination reaction of a radical generated from an epoxide: stereospecific formation of an exocyclic alkene

TIMOTHY B. LOWINGER AND LARRY WEILER[1]

Department of Chemistry, University of British Columbia, 2036 Main Mall, Vancouver, B.C., Canada V6T 1Y6

Received March 23, 1990

TIMOTHY B. LOWINGER and LARRY WEILER. Can. J. Chem. **68**, 1636 (1990).

A titanium(III) mediated radical cyclization–elimination reaction is reported, which allows for the efficient generation of functionalized cyclopentane derivatives. The reaction is highly stereospecific, giving excellent control over the geometry of the resulting exocyclic alkene. In addition, functionality at both reacting termini is retained for subsequent transformations.

Key words: stereospecific, radical cyclization–elimination, exocyclic alkene.

TIMOTHY B. LOWINGER et LARRY WEILER. Can. J. Chem. **68**, 1636 (1990).

On rapporte l'observation d'une réaction radicalaire de cyclisation/élimination promuée par le titane(III) qui permet une génération efficace de dérivés cyclopentaniques fonctionnalisés. La réaction est hautement stéréospécifique et elle permet un contrôle efficace sur la géométrie des alcènes exocycliques qui en résultent. De plus, les fonctions présentes aux deux extrémités de la chaîne sont conservées et permettent d'effectuer des transformations subséquentes.

Mots clés : stéréospécifique, cyclisation/élimination radicalaire, alcène exocyclique.

[Traduit par la revue]

Can. J. Chem. Downloaded from www.nrcresearchpress.com by 91.121.58.235 on 09/07/12
For personal use only.

Following the pioneering work of Beckwith and Schliesser on radical cyclizations (1), the application of these reactions in synthesis has been well established, as illustrated in several recent reviews (2–4). In particular, 5-hexenyl radical cyclizations have emerged as a powerful method for the construction of cyclopentane derivatives. The usual synthetic procedure involves the reaction of a radical precursor, typically an alkyl halide, with tri-*n*-butyltin hydride to generate an alkyl radical that then adds to the alkene in a 5-*exo* fashion. However, one significant drawback of this procedure is the concomitant loss of two functional groups — the halide and the alkene. A novel partial solution to this problem, which allows the synthesis of cyclopentane derivatives, has recently been reported by Nugent and RajanBabu (5). They showed that the reaction of an epoxide with a titanium(III) reagent results in the homolytic cleavage of the C—O bond, resulting in the formation of a secondary carbon-centered radical. This radical undergoes cyclization in the usual fashion and, after hydrolytic work-up, a cyclopentane derivative bearing a hydroxymethylene unit is obtained. We would like to report the extension of this methodology to the stereospecific formation of exocyclic alkenes.

Recently, we reported a stereospecific synthesis of exocyclic alkenes by a radical cyclization in which only the alkene unit of the product is functionalized (6). In 1985, Russell and Ngoviwatchai demonstrated that radicals can undergo a stereospecific vinyl substitution by an addition–elimination sequence (7*a*). In a later study, it was shown that the stereospecificity depends on the substituents on the alkene and the attacking radical (7*b*). In these studies, the radical addition–elimination reactions occur with retention of the geometry of the alkene. Curran and van Elberg have reported a radical annulation, also involving an addition–elimination step, which occurs with inversion of geometry about the alkene (8). The stereochemical outcome of the reaction appears to be controlled by the substituents α to the alkene (8).

The ω-alkenyl acetylenic esters **1** and **2** were prepared as illustrated in Scheme 1. These compounds were then converted to the corresponding *E* and *Z* vinyl stannanes **3**–**6** with high stereoselectivity following the procedure of Piers *et al.* (9). Epoxidation of **3**–**6** with *meta*-chloroperbenzoic acid (MCPBA) in dichloromethane afforded the ω-epoxy vinylstannanes **7**–**10** in good yield. The compounds **7**–**10** were then reacted with chlorobis(η^5-cyclopentadienyl)titanium(III) (10). In a typical reaction, 1.2 molar equivalents of chlorobis(η^5-cyclopentadienyl)titanium(III) in THF were added dropwise to a THF solution of the ω-epoxy vinylstannane at room temperature under argon. When thin-layer chromatography indicated an absence of starting material the reaction was quenched. The crude product was extracted and purified by centrifugal chromatography.

The results of the cyclizations of compounds **7** and **8** are summarized in Table 1. These cyclizations were found to be highly stereospecific, and result from an addition–elimination sequence that involves "retention" of the stereochemistry of the double bond. The reactions proceed smoothly at room temperature and are typically complete in 30 min. In contrast, reaction of compounds **9** and **10** under identical conditions did not yield any of the desired cyclic compounds, even after prolonged reaction times. Instead, the only product obtained at room temperature was the corresponding acyclic alcohol resulting from reduction of the intermediate secondary radical. In an effort to promote cyclization, the reaction was performed in refluxing benzene. However, no cyclic products were formed under these conditions. Instead, the product obtained from reaction at higher temperature was the corresponding alkene (**5** or **6**), resulting from deoxygenation.

These later results are not completely unexpected. Beckwith has shown that the rate of 6-heptenyl radical cyclization is considerably slower than that of 5-hexenyl radical cyclization (1). Consequently, the intermediate radical generated from **9** or **10**, being slow to cyclize, preferentially follows a different, competing reaction pathway.

[1]Author to whom correspondence may be addressed.

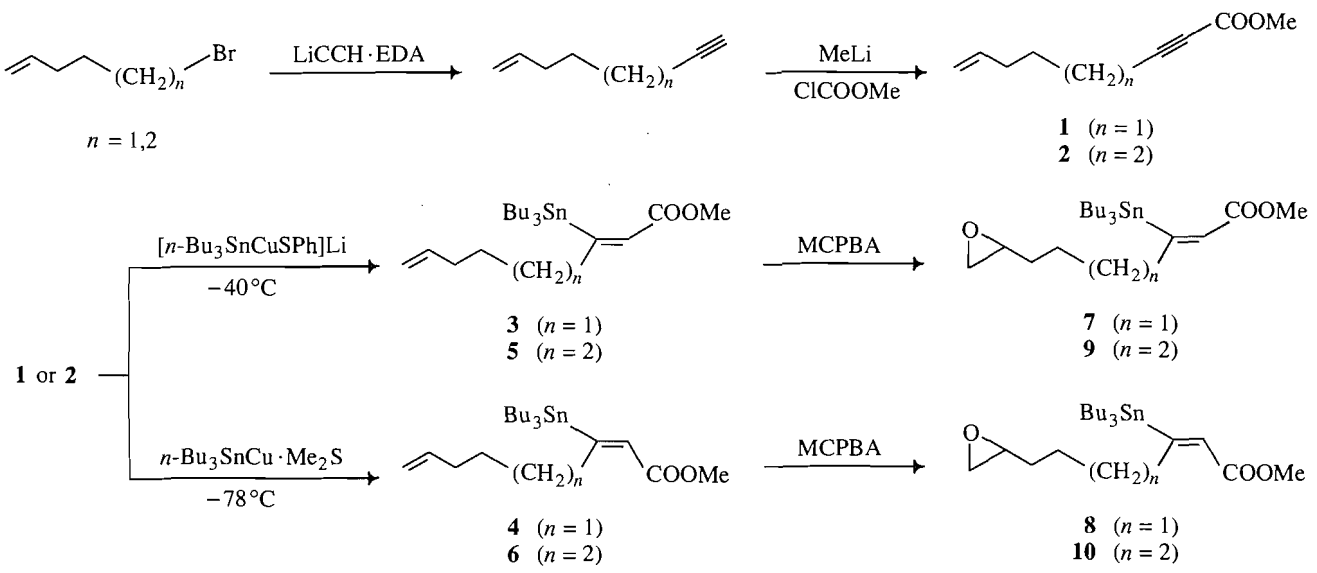

SCHEME 1

TABLE 1. Cyclization of **7** and **8**

Precursor	Product	Yield	*Z*:*E* Ratio*
7	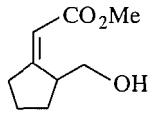	83%	>98:2
8	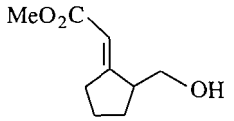	86%	<2:98

*Determined by capillary gas chromatography.

The intramolecular cyclization–elimination reaction of radicals generated from epoxides is a useful method to synthesize cyclopentane derivatives, offering excellent control over the geometry of the exocyclic alkene. In this cyclization functional groups at both termini are retained for subsequent transformations. The use of other radical precursors to form different functionalized exocyclic alkenes, as well as methods to improve cyclization of 6-heptenyl systems via an addition–elimination pathway, is being investigated.

Acknowledgements

We are grateful to the Natural Sciences and Engineering Research Council of Canada for financial support of this work and to Jesse Ng for assistance in the preparation of chlorobis(η^5-cyclopentadienyl)titanium(III).

1. (*a*) A. L. J. BECKWITH. Tetrahedron, **37**, 3073 (1981); (*b*) A. L. J. BECKWITH and C. H. SCHLIESSER. Tetrahedron, **41**, 3925 (1985).
2. B. GIESE. Radicals in organic synthesis: formation of carbon–carbon bonds. Pergamon Press, Oxford. 1986.
3. D. P. CURRAN. Synthesis, **6**, 417 (1988).
4. M. RAMAIAH. Tetrahedron, **43**, 3541 (1987).
5. W. A. NUGENT and T. V. RAJANBABU. J. Am. Chem. Soc. **110**, 8561 (1988).
6. F. L. HARRIS and L. WEILER. Tetrahedron Lett. **28**, 2941 (1987).
7. (*a*) G. A. RUSSELL and P. NGOVIWATCHAI. Tetrahedron Lett. **26**, 4975 (1985); (*b*) G. A. RUSSELL, P. NGOVIWATCHAI, and H. I. TASHTOUSH. Organometallics, **7**, 696 (1988).
8. D. P. CURRAN and P. A. VAN ELBURG. Tetrahedron Lett. **30**, 2501 (1989).
9. (*a*) E. PIERS and H. E. MORTON. J. Org. Chem. **45**, 4263 (1980); (*b*) E. PIERS, J. M. CHONG, and H. E. MORTON. Tetrahedron Lett. **22**, 4905 (1981).
10. L. E. MANZER. Inorg. Synth. **21**, 84 (1982).

Can. J. Chem. Downloaded from www.nrcresearchpress.com by 91.121.58.235 on 09/07/12
For personal use only.

Evidence for stereoregulation in the polymerization of phenylsilane by bis(indenyl)dimethylzirconium complexes

F. GAUVIN AND J. F. HARROD

Chemistry Department, McGill University, 801 Sherbrooke Street West, Montreal, P.Q., Canada H3A 2K6

Received April 11, 1990

F. GAUVIN and J. F. HARROD. Can. J. Chem. **68**, 1638 (1990).

Bis(indenyl)dimethylzirconocene, **1**, and [1,2-bis(indenyl)ethane]dimethylzirconocene, **2**, both catalyze the dehydropolymerization of phenylsilane to a mixture of low molecular weight cyclic oligosilanes $(PhSiH)_n$ (n = 6–9). The limited number of sharp resonances in the ^{29}Si and ^1H NMR spectra of the polymer produced with **2** as catalyst indicates that the catalyst exerts a significant stereoregulating influence on the polymerization.

Key words: polysilanes, catalytic dehydrocoupling, stereoregulation, bis(indenyl)zirconium complexes.

F. GAUVIN et J. F. HARROD. Can. J. Chem. **68**, 1638 (1990).

Le bis(indényl)diméthylzirconocène, **1**, ainsi que le [1,2-bis(indényl)éthane]diméthylzirconocène, **2**, catalysent tous les deux la déshydropolymérisation du phénylsilane pour donner un mélange d'oligosilanes cycliques de bas poids moléculaire $(PhSiH)_n$ (n = 6–9). Le nombre restreint de résonances fines que l'on observe dans les spectres RMN du ^{29}Si et du ^1H du polymère produit sous l'influence du catalyseur **2** indique que ce dernier exerce une grande influence sur la polymérisation et donne naissance à un produit hautement stéréorégulier.

Mots clés : polysilanes, déshydrocouplage catalytique, stéréorégularité, complexes du bis(indényl)zirconium.

[Traduit par la revue]

Can. J. Chem. Downloaded from www.nrcresearchpress.com by 91.121.58.235 on 09/07/12
For personal use only.

Polyorganosilanes have recently attracted a great deal of attention because of their unusual electronic and optical properties (for an excellent review, see ref. 1). These properties are strongly dependent on polymer backbone conformation and, consequently, control of backbone conformation in tactic polyorganosilanes is an important objective. Such control is not likely to be achieved using the Wurtz–Fittig type coupling, which presently is the only synthetic route to high molecular weight polysilanes. In principle, such control could be achieved using syntheses based on coordination catalysis.

In earlier reports we have described the use of a variety of bis(cyclopentadienyl) complexes of titanium and zirconium as catalysts for the polymerization of primary silanes by dehydrocoupling (2–6). Other workers have since made important contributions to our understanding of the mechanisms of such reactions and to extending their scope (7–9).

One of the interesting aspects of primary silane dehydrocoupling is the tactic character of the resulting polymers. With bis(cyclopentadienyl) catalysts there seems to be no stereoregulation in the polymer chain propagation step and the products are essentially atactic. Since chiral bis(indenyl) complexes of titanium and zirconium have been used with considerable success for the stereoregular polymerization of olefins (10), we have also used them for silane polymerization.

Bis(indenyl)dimethyltitanium(IV) proved to be ineffective as a catalyst for the dehydrocoupling of phenylsilane beyond dimer and trimer. On the other hand, the zirconium analogue, **1**, was quite active and, at catalyst concentrations of 1–5 mol%, converted phenylsilane quantitatively to an oligomer in about 24 h. A similar activity was observed for [1,2-bis(indenyl)ethane] dimethylzirconium, **2**. The catalysts were prepared as racemic mixtures by modifications of a literature procedure (11) involving reaction of two equivalents of methyl lithium with the dichloro complexes in diethyl ether. The dichloro precursor to **1** was prepared by the method of Rausch *et al.* (12) and that of **2** by the method of Collins *et al.* (13). Typical polymerization reactions were run at room temperature in toluene with a catalyst concentration of 0.10 M and an initial phenylsilane concentration of 3.2 M.

The ^1H NMR spectra (see Fig. 1) of the polymers, particularly that of the polymer produced with **2** as catalyst, were significantly different from those of similar polymers produced with bis(cyclopentadienyl) complexes. The latter polymers give spectra resembling the lower spectrum in Fig. 1, but without any sign of fine structure. The difference was even more evident in ^{29}Si NMR spectra using a DEPT pulse sequence (see Fig. 2). These spectra show the products to be free of SiH_2 units, i.e., to be entirely free of linear species. Since complete methanolysis of the polymers gives phenyltrimethoxysilane as the sole product, the polymers only contain PhSiH units.

The sharp, relatively well-resolved, resonances for the polymer produced with **2** indicate a dramatic reduction in the number of magnetically distinct stereocenters relative to polymers produced with other catalysts. This could be due to the selective production of a single ring size (e.g., the cyclohexasilane has 9 isomers with a total of 23 different stereocenters). Alternatively, it could be due to stereoselection. Since the mass spectra of the oligomers produced with both **1** and **2** are very similar (see Table 1), and clearly show the presence of Si_n rings (n = 6–9) in both cases, the evidence is strongly in favour of stereoselection. The presence of some fine structure, albeit an extremely complicated one, in the polymer produced with **1** is attributable to the statistical distribution of stereocenters of a mixture of rings. Addition of the further resonances of linear species would result in the relatively featureless massifs typically observed with the bis(cyclopentadienyl) catalysts.

The mechanism whereby stereoselection occurs in these systems is not evident from the present results. Growth of a chain at a single chiral center by repetitive addition of monomer could lead to stereoregulation in a similar manner to Ziegler–Natta type polymerization of olefins. However, since primary silanes are not prochiral, the stereochemistry of the entering silicon atom must be determined entirely by interactions between the chiral metal center and the polymer chain end.

Can. J. Chem. Downloaded from www.nrcresearchpress.com by 91.121.58.235 on 09/07/12
For personal use only.

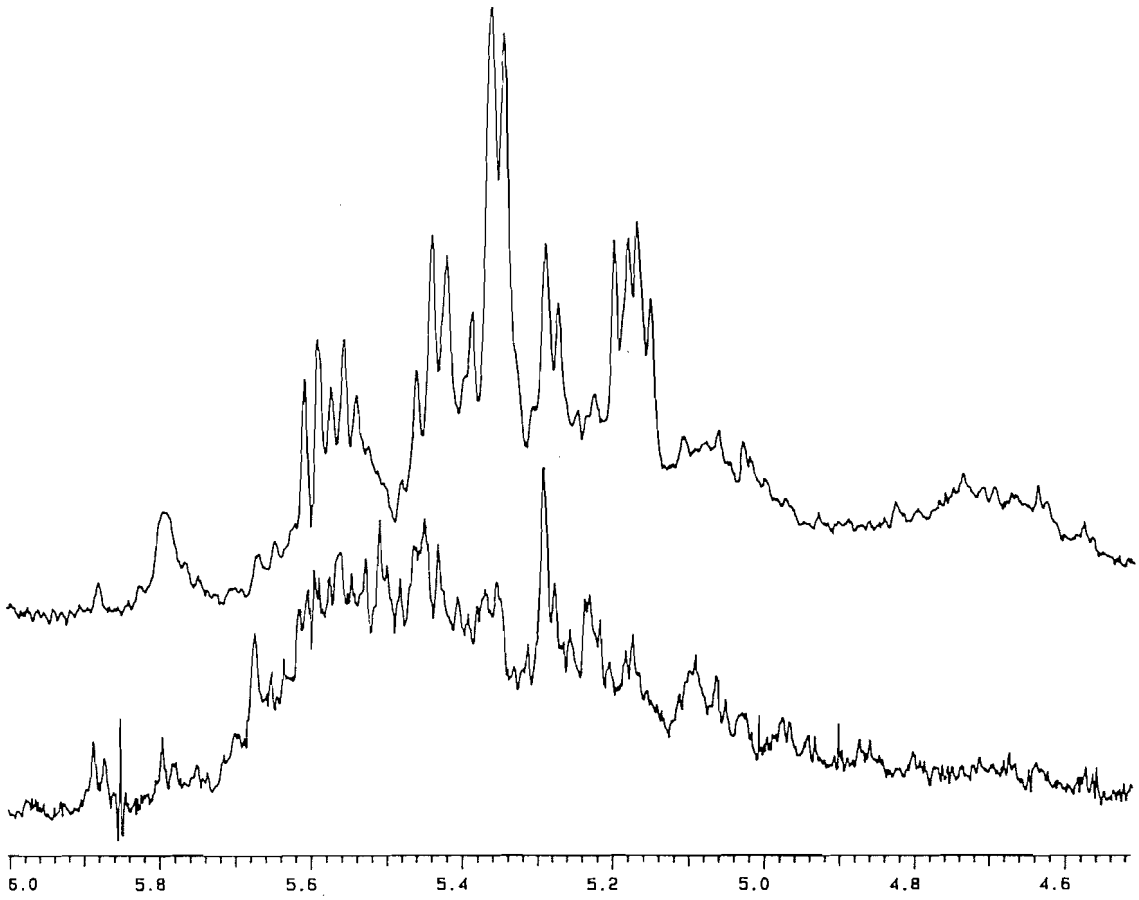

FIG. 1. ^{1}H NMR spectra, in the Si-H region, of polyphenylsilanes produced with **1** (lower) and **2** (upper) as catalysts.

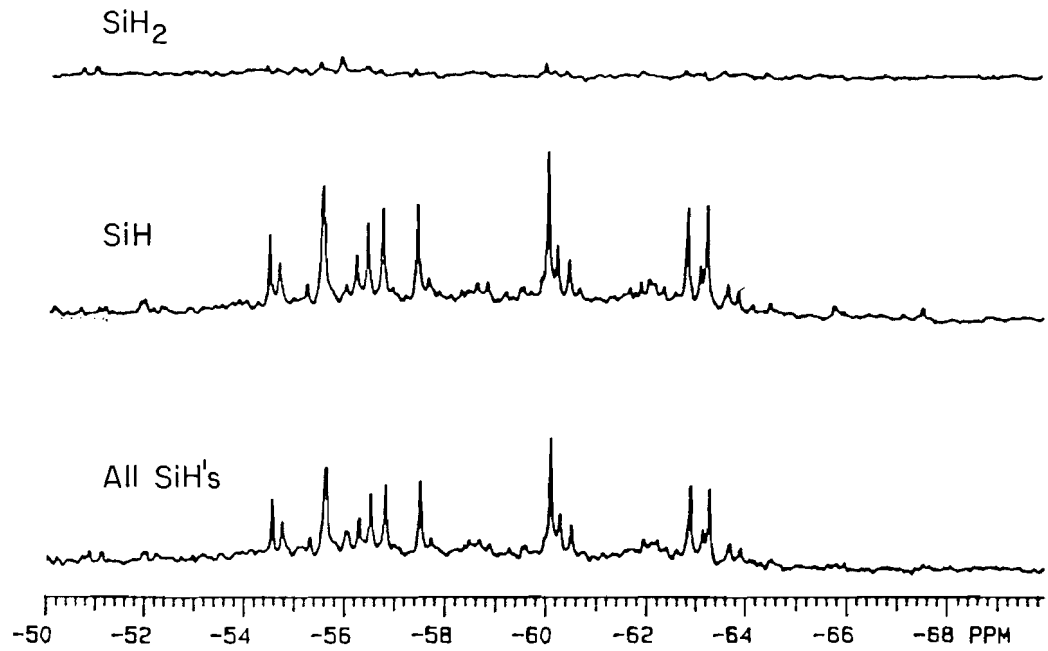

FIG. 2. ^{29}Si DEPT spectra of polyphenylsilanes produced with **2** as catalyst.

TABLE 1. Comparison of mass spectra of oligomers obtained with catalysts **1** and **2**[a]

Source molecule[b]	m/e	Abundance (%) 1	2	Fragments lost
$(PhSiH)_9$	952	0.8	1.5	2H
$(PhSiH)_9$	875	0.4	0.5	C_6H_6, H
$(PhSiH)_8$	846	0.8	1.2	2H
$(PhSiH)_8$	768	1.9	5.0	C_6H_6, 2H
$(PhSiH)_7$	740	6.0	10	2H
$(PhSiH)_7$	662	11	20	C_6H_6, 2H
$(PhSiH)_6$	632	7	5	4H
$(PhSiH)_7$	586	9	12	$2C_6H_6$, 2H
$(PhSiH)_6$	556	36	30	C_6H_6, 2H
$(PhSiH)_5$	525	24	15	5H
$(PhSiH)_7$	482	10	7	$(C_6H_5)_3SiH$
$(PhSiH)_5$	449	49	10	C_6H_6, 3H
$(PhSiH)_4$	420	12	10	4H
$(PhSiH)_5$	372	40	10	$2C_6H_6$, 2H
$(PhSiH)_4$	343	18	3	C_6H_6, 3H
Ph_3Si	259	100	95	—

[a]The cited masses are the major peaks in a given cluster.
[b]Any peak corresponding to $(PhSiH)_n$ may contain contributions from species of higher n that have lost PhSiH units.

Since the rate of catalytic dehydrocoupling is known to be very sensitive to steric effects (4), an alternative mechanism involving diastereoselection between a chiral catalyst complex and an approaching chiral oligomer could lead to stereoregulation in a stepwise growth mechanism.

Further studies involving bis(tetrahydroindenyl) complexes and enantiomerically pure **2** are presently in progress.

Acknowledgements

We thank the Natural Sciences and Engineering Research Council of Canada and the Fonds FCAR de Quebec for financial support.

1. R. D. MILLER and J. MICHL. Chem. Rev. **89**, 1359 (1989).
2. C. T. AITKEN, J. F. HARROD, and E. SAMUEL. J. Organomet. Chem. **279**, C11 (1985).
3. C. T. AITKEN, J. F. HARROD, and E. SAMUEL. Can. J. Chem. **64**, 1677 (1986).
4. J. F. HARROD. *In* Inorganic and organometallic polymers. *Edited by* M. Zeldin, K. J. Wynne, and H. R. Allcock. ACS Symposium Series **360**: American Chemical Society, Washington, DC. 1988. Chap. 7.
5. J. F. HARROD. *In* Transformation of organometallics into common and exotic materials: design and activation. *Edited by* R. M. Laine. NATO ASI Ser., Ser. E: **141**. Martinus Nijhoff, Amsterdam. 1988. p. 103.
6. C. T. AITKEN, J.-P. BARRY, F. GAUVIN, J. F. HARROD, A. MALEK, and D. ROUSSEAU. Organometallics, **8**, 1732 (1989).
7. (*a*) J. Y. COREY, L. S. CHANG, and E. R. COREY. Organometallics, **6**, 1595 (1987); (*b*) L. S. CHANG and J. Y. COREY. Organometallics, **8**, 1885 (1989).
8. W. H. CAMPBELL, T. K. HILTY, and L. YURGA. Organometallics, **8**, 2615 (1989).
9. (*a*) H.-G. WOO and T. D. TILLEY. J. Am. Chem. Soc. **111**, 8043 (1989); (*b*) J. Am. Chem. Soc. **111**, 3757 (1989).
10. (*a*) J. A. EWEN. J. Am. Chem. Soc. **106**, 6355 (1984); (*b*) W. KAMINSKY, K. KULPER, H. BRINTZINGER, and F. R. W. P. WILD. Angew. Chem. Int. Ed. Engl. **24**, 507 (1985).
11. E. SAMUEL and M. D. RAUSCH. J. Am. Chem. Soc. **95**, 6263 (1973).
12. M. D. RAUSCH, K. J. MORIARTY, J. L. ATWOOD, W. E. HUNTER, and E. SAMUEL. J. Organomet. Chem. **327**, 39 (1987).
13. S. COLLINS, B. A. KUNTZ, N. J. TAYLOR, and D. G. WARD. J. Organomet. Chem. **342**, 21 (1988).

Can. J. Chem. Downloaded from www.nrcresearchpress.com by 91.121.58.235 on 09/07/12
For personal use only.

Alkaline cleavage of trihaloacetophenones

J. PETER GUTHRIE[1] AND JOHN COSSAR
Department of Chemistry, University of Western Ontario, London, Ont., Canada N6A 5B7

Received March 2, 1990

J. PETER GUTHRIE and JOHN COSSAR. Can. J. Chem. **68**, 1640 (1990).

Rate constants for haloform cleavage of trifluoro-, trichloro-, and tribromoacetophenone have been measured in aqueous solution; apparent second-order rate constants for reaction by the monoanion are in the ratio $1 : 5.3 \times 10^{10} : 2.2 \times 10^{13}$.

Key words: haloform cleavage, reactivity, trihalomethide leaving groups.

J. PETER GUTHRIE et JOHN COSSAR. Can. J. Chem. **68**, 1640 (1990).

Opérant en solution aqueuse, on a mesuré les constantes de vitesse de clivage des haloformes à partir des trifluoro-, trichloro- et tribromo-acétophénones; les constantes de vitesse apparentes du deuxième ordre pour les réactions des monoanions sont dans le rapport $1 : 5{,}3 \times 10^{10} : 2{,}2 \times 10^{13}$.

Mots clés : coupure haloformique, réactivité, anion trihalogénométhanure comme groupe partant.

[Traduit par la revue]

Trihalomethylketones undergo ready cleavage in alkali: this is the basis of the well-known iodoform test. Astonishingly enough, the rates of these reactions have not been reported, except for some qualitative observations (1) and one related example of chloral (2). It has been reported (3) that, unlike other trihaloacetophenones, trifluooracetophenone dissolves readily in aqueous alkali but undergoes only slow haloform cleavage. The alkaline cleavage of trichloro- and tribromoacetophenones

[1]Author to whom correspondence may be addressed.

TABLE 1. Comparison of mass spectra of oligomers obtained with catalysts **1** and **2**[a]

Source molecule[b]	m/e	Abundance (%) 1	2	Fragments lost
$(PhSiH)_9$	952	0.8	1.5	2H
$(PhSiH)_9$	875	0.4	0.5	C_6H_6, H
$(PhSiH)_8$	846	0.8	1.2	2H
$(PhSiH)_8$	768	1.9	5.0	C_6H_6, 2H
$(PhSiH)_7$	740	6.0	10	2H
$(PhSiH)_7$	662	11	20	C_6H_6, 2H
$(PhSiH)_6$	632	7	5	4H
$(PhSiH)_7$	586	9	12	$2C_6H_6$, 2H
$(PhSiH)_6$	556	36	30	C_6H_6, 2H
$(PhSiH)_5$	525	24	15	5H
$(PhSiH)_7$	482	10	7	$(C_6H_5)_3SiH$
$(PhSiH)_5$	449	49	10	C_6H_6, 3H
$(PhSiH)_4$	420	12	10	4H
$(PhSiH)_5$	372	40	10	$2C_6H_6$, 2H
$(PhSiH)_4$	343	18	3	C_6H_6, 3H
Ph_3Si	259	100	95	—

[a]The cited masses are the major peaks in a given cluster.
[b]Any peak corresponding to $(PhSiH)_n$ may contain contributions from species of higher n that have lost PhSiH units.

Since the rate of catalytic dehydrocoupling is known to be very sensitive to steric effects (4), an alternative mechanism involving diastereoselection between a chiral catalyst complex and an approaching chiral oligomer could lead to stereoregulation in a stepwise growth mechanism.

Further studies involving bis(tetrahydroindenyl) complexes and enantiomerically pure **2** are presently in progress.

Acknowledgements

We thank the Natural Sciences and Engineering Research Council of Canada and the Fonds FCAR de Quebec for financial support.

1. R. D. MILLER and J. MICHL. Chem. Rev. **89**, 1359 (1989).
2. C. T. AITKEN, J. F. HARROD, and E. SAMUEL. J. Organomet. Chem. **279**, C11 (1985).
3. C. T. AITKEN, J. F. HARROD, and E. SAMUEL. Can. J. Chem. **64**, 1677 (1986).
4. J. F. HARROD. *In* Inorganic and organometallic polymers. *Edited by* M. Zeldin, K. J. Wynne, and H. R. Allcock. ACS Symposium Series **360**: American Chemical Society, Washington, DC. 1988. Chap. 7.
5. J. F. HARROD. *In* Transformation of organometallics into common and exotic materials: design and activation. *Edited by* R. M. Laine. NATO ASI Ser., Ser. E: **141**. Martinus Nijhoff, Amsterdam. 1988. p. 103.
6. C. T. AITKEN, J.-P. BARRY, F. GAUVIN, J. F. HARROD, A. MALEK, and D. ROUSSEAU. Organometallics, **8**, 1732 (1989).
7. (*a*) J. Y. COREY, L. S. CHANG, and E. R. COREY. Organometallics, **6**, 1595 (1987); (*b*) L. S. CHANG and J. Y. COREY. Organometallics, **8**, 1885 (1989).
8. W. H. CAMPBELL, T. K. HILTY, and L. YURGA. Organometallics, **8**, 2615 (1989).
9. (*a*) H.-G. WOO and T. D. TILLEY. J. Am. Chem. Soc. **111**, 8043 (1989); (*b*) J. Am. Chem. Soc. **111**, 3757 (1989).
10. (*a*) J. A. EWEN. J. Am. Chem. Soc. **106**, 6355 (1984); (*b*) W. KAMINSKY, K. KULPER, H. BRINTZINGER, and F. R. W. P. WILD. Angew. Chem. Int. Ed. Engl. **24**, 507 (1985).
11. E. SAMUEL and M. D. RAUSCH. J. Am. Chem. Soc. **95**, 6263 (1973).
12. M. D. RAUSCH, K. J. MORIARTY, J. L. ATWOOD, W. E. HUNTER, and E. SAMUEL. J. Organomet. Chem. **327**, 39 (1987).
13. S. COLLINS, B. A. KUNTZ, N. J. TAYLOR, and D. G. WARD. J. Organomet. Chem. **342**, 21 (1988).

Can. J. Chem. Downloaded from www.nrcresearchpress.com by 91.121.58.235 on 09/07/12
For personal use only.

Alkaline cleavage of trihaloacetophenones

J. PETER GUTHRIE[1] AND JOHN COSSAR
Department of Chemistry, University of Western Ontario, London, Ont., Canada N6A 5B7

Received March 2, 1990

J. PETER GUTHRIE and JOHN COSSAR. Can. J. Chem. **68**, 1640 (1990).

Rate constants for haloform cleavage of trifluoro-, trichloro-, and tribromoacetophenone have been measured in aqueous solution; apparent second-order rate constants for reaction by the monoanion are in the ratio $1 : 5.3 \times 10^{10} : 2.2 \times 10^{13}$.

Key words: haloform cleavage, reactivity, trihalomethide leaving groups.

J. PETER GUTHRIE et JOHN COSSAR. Can. J. Chem. **68**, 1640 (1990).

Opérant en solution aqueuse, on a mesuré les constantes de vitesse de clivage des haloformes à partir des trifluoro-, trichloro- et tribromo-acétophénones; les constantes de vitesse apparentes du deuxième ordre pour les réactions des monoanions sont dans le rapport $1 : 5{,}3 \times 10^{10} : 2{,}2 \times 10^{13}$.

Mots clés : coupure haloformique, réactivité, anion trihalogénométhanure comme groupe partant.

[Traduit par la revue]

Trihalomethylketones undergo ready cleavage in alkali: this is the basis of the well-known iodoform test. Astonishingly enough, the rates of these reactions have not been reported, except for some qualitative observations (1) and one related example of chloral (2). It has been reported (3) that, unlike other trihaloacetophenones, trifluooracetophenone dissolves readily in aqueous alkali but undergoes only slow haloform cleavage. The alkaline cleavage of trichloro- and tribromoacetophenones

[1]Author to whom correspondence may be addressed.

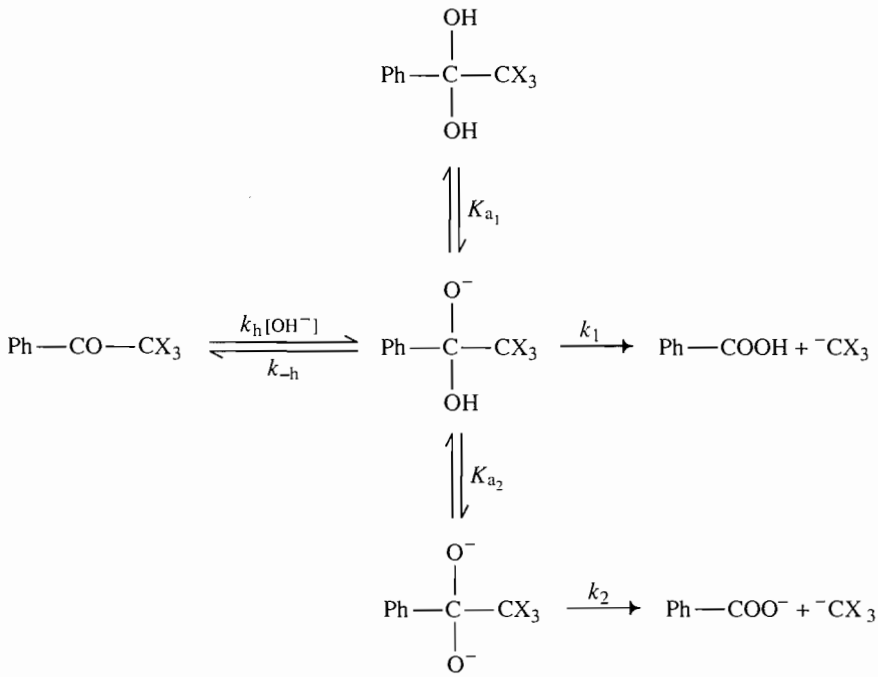

SCHEME 1

TABLE 1. Kinetics of haloform cleavage of α,α,α-trihaloacetophenones[a]

[Ketone] (10^3 M)	[OH^-] (M)	k_ψ (10^4 s^{-1})	k_ψ/[OH^-] (10^{-3} M^{-1} s^{-1})
Trifluoro			
0.11	1.02	0.0816	
0.22	1.02	0.0834	
0.23	0.98	0.0777	
0.23	0.101	0.0120[b]	
Trichloro			
0.0305	1.58×10^{-9}	0.126	7.98
0.0305	1.26×10^{-8}	0.976	7.75
0.0305	1.86×10^{-7}	15.55	8.36
0.0305	8.51×10^{-6}	657.2	7.72
0.0305	8.51×10^{-6}	662.5	7.79
		Ave.	7.92
Tribromo			
0.005	2.09×10^{-11}	0.692	3310
0.005	8.51×10^{-11}	2.743	3220
0.005	4.17×10^{-10}	13.98	3350
0.005	6.17×10^{-9}	201.8	3270
		Ave.	3.29×10^3

[a]In aqueous solution at 25°C, ionic strength 1.0 M (KCl). Hydroxide concentrations determined by titration (trifluoro) or calculated from the pH of buffers (acetate, phosphate, or carbonate) using $pK_w = 14$. k_ψ is the observed pseudo-first-order rate constant.

[b]Initial rate, assuming the same absorbance change as for reaction at 1 M hydroxide with the same initial concentration of ketone.

is very rapid in solution[2] but can be slow if the trihaloacetophenone is simply added to aqueous base because of the insolubility and slow dissolution of the ketone (1).

We now wish to report rate contants for the alkaline cleavage of trifluoro-, trichloro-, and tribromoacetophenone: see Table 1. There is a dramatic effect of the nature of the halogen, which demonstrates quite vividly that electronegativity can be far less important than size-related factors in determining the carbanion stabilizing power of an atom.

For trifluoroacetophenone, 1 N NaOH solution was used to get reasonable reaction rates for the slow cleavage; for the other two it was necessary to use buffer solutions to give reactions slow enough to be followed conveniently. The kinetics are interpreted in terms of the mechanism shown in Scheme 1, for which the pseudo-first-order rate constant, k_ψ, is given by:

$$[1] \quad k_\psi = (k_1K_hK_{a1}K_w[OH^-] + k_2K_{a1}K_{a2}K_h[OH^-]^2)/(K_{a1}K_w + K_hK_w^2 + K_{a1}K_hK_w[OH^-] + K_{a1}K_{a2}K_h[OH^-]^2)$$

Trifluoroacetophenone is fully hydrated in water (4) and is completely converted to its hydrate anion in 1 N NaOH: the pK_a of the ketone hydrate is 10.00 (4). In 0.1 N NaOH the reaction was 0.15 as fast as in 1.0 N NaOH. Since the observed rate constant is approximately proportional to [OH^-], reaction is mainly occurring via the dianion. On the other hand, the rate in 0.1 N NaOH is clearly faster than one tenth the rate in 1.0 N NaOH. It is most likely that what is observed is the beginning of the levelling off corresponding to conversion of trifluoroacetophenone hydrate to its dianion, with $k_2 = 2.1 \times 10^{-5}$ s^{-1}, and $pK_{a2} = 14.2$.[3] Pauling's rules (5) suggest that the second pK_a of trifluoroacetophenone hydrate should be approximately 15, so this is plausible. The monoanion rate would then be an unknown amount slower. A reasonable model would be cleavage of phenyl propargaldehyde (6) for which the leaving group is a localized carbanion of basicity ($pK_a = 20$ (7)) similar to that of CF_3^- ($pK_a = 27$ (8)). For phenylpropargaldehyde, Hine and Koser (6) suggest $k_2/k_1 = 2.0 \times 10^6$ M^{-1}. If a similar ratio

[2]An organic cosolvent is required to increase the solubility of the trihaloketone.

[3]If the term in the numerator and the first two terms in the denominator of eq. [1] are negligible, then k_2 and K_{a2} can be evaluated from the observed rate constants.

Can. J. Chem. Downloaded from www.nrcresearchpress.com by 91.121.58.235 on 09/07/12
For personal use only.

applies to trifluoroacetophenone, k_1 would be 1.33×10^{-11} s^{-1}, and the apparent second-order rate constant at pH 7 would be 1.3×10^{-7} M^{-1} s^{-1}. We note that this is only two orders of magnitude slower than the apparent second-order rate constant at pH 14. Experimental confirmation will be difficult because of the very slow reactions involved.

For the trichloro and tribromo derivatives the observed rates are first order in hydroxide, and the pH used is less than any plausible value for the pK_a of the adduct, so this must be reaction via the monoanion.

There is also a problem of rate-determining step, since it is possible that the trichloro and (or) tribromo compounds react with rate-determining hydroxide addition; if this were the case then the actual rate constants for cleavage would be even larger. This is particularly so for tribromoacetophenone, for which the second-order rate constant is 3.3×10^6 M^{-1} s^{-1}. This value is larger than the rate constant for hydroxide-catalyzed hydration of trifluoroacetophenone, log $k = 5.70$ in 10:1 water/acetonitrile (9). That the rate constant for attack of hydroxide on tribromoacetophenone would be much larger than 10^6 M^{-1} s^{-1} seems highly unlikely. This argument implies that attack of hydroxide is rate limiting, and that the actual cleavage step is much faster. Thus our measures for the effect of halogen on the rate constants for haloform cleavage may be lower limits.

In nmr experiments in partly aqueous solvent[4] (CD_3CN–D_2O) we found that trifluoroacetophenone was completely hydrated, trichloroacetophenone was partly hydrated, and tribromoacetophenone was completely in the carbonyl form.

The breakdown of chloral is much slower than that of trichloroacetophenone, the apparent second-order rate constants at low pH being 2.19 M^{-1} s^{-1} and 7.9×10^3 M^{-1} s^{-1} respectively. This can reasonably be ascribed to the less favorable equilibrium for expulsion to generate formaldehyde vs. acetophenone, by analogy with dehydration of the covalent hydrates for which the equilibrum constants are 0.024 M and 8.3×10^6 M respectively (10).

Our results to date suggest that the relative rates for cleavage of the monoanions are in the ratio $PhCOCF_3$: $PhCOCCl_3$: $PhCOCBr_3$ = 1 : 5.3×10^{10} : 2.2×10^{13}. Although these results appear surprising if one relies on electronegativity arguments to estimate the stability of the trihalomethylcarbanions, they are quite in line with the results of studies of exchange in trihalomethanes. The rate constants for hydroxide-catalyzed reaction at 0°C for CF_3H (8), CCl_3H (11), and CBr_3H (11) are in the ratio 1 : 2.1×10^6 : 2.6×10^8.

[4]The organic cosolvent was needed to get sufficiently concentrated solutions for nmr spectroscopy.

Acknowledgments

We gratefully acknowledge financial support of this work by the Natural Sciences and Engineering Research Council of Canada, and thank Mr. J. Lu for some preliminary kinetics.

1. J. G. Aston, J. D. Newkirk, J. Dorsky, and D. M. Jenkins. J. Am. Chem. Soc. **64**, 1413 (1942).
2. C. Gustafsson and M. Johanson. Acta Chim. Scand. **2**, 42 (1948).
3. J. H. Simons and E. O. Ramler. J. Am. Chem. Soc. **65**, 389 (1943).
4. R. Stewart and R. van der Linden. Can. J. Chem. **38**, 399 (1960).
5. L. Pauling. General chemistry. Freeman and Co., San Francisco. 1947. p. 394.
6. J. Hine and G. F. Koser. J. Org. Chem. **36**, 1348 (1971).
7. A. C. Lin, Y. Chiang, D. B. Dahlberg, and A. J. Kresge. J. Am. Chem. Soc. **105**, 5380 (1983).
8. E. A. Symons and M. J. Clermont. J. Am. Chem. Soc. **103**, 3127 (1981).
9. C. D. Ritchie. J. Am. Chem. Soc. **106**, 7187 (1984).
10. J. P. Guthrie. Can. J. Chem. **56**, 962 (1978).
11. J. Hine. Physical organic chemistry. 2nd ed. McGraw–Hill, New York. 1962. p, 487.

Can. J. Chem. Downloaded from www.nrcresearchpress.com by 91.121.58.235 on 09/07/12
For personal use only.

Concertedness and E2 elimination reactions: prediction of transition state position and reaction rates using two-dimensional reaction surfaces based on quadratic and quartic approximations

J. PETER GUTHRIE

Department of Chemistry, University of Western Ontario, London, Ont., Canada N6A 5B7

Received November 14, 1989

This paper is dedicated to Professor Ross Stewart on the occasion of his 65th birthday

J. PETER GUTHRIE. Can. J. Chem. **68**, 1643 (1990).

An analytical expression for the two-dimensional reaction surface appropriate for discussing a concerted reaction has been derived for the quartic approximation to a reaction coordinate, and shown to be consistent with Marcus theory. By analysis of literature data for S_N1 solvolyses and carbanion formation we have been able to reproduce the qualitative behavior of eliminations involving *t*BuBr, *i*PrBr, and EtBr in EtOH/EtO^-, and to predict the rates of these reactions within the uncertainties of the input data.

Key words: concerted reactions, Marcus theory, eliminations, reaction surfaces.

J. PETER GUTHRIE. Can. J. Chem. **68**, 1643 (1990).

On a développé une expression analytique pour la surface réactionnelle bidimensionnelle qui est appropriée pour discuter une réaction concertée et qui peut être utilisée pour l'approximation quartique d'une coordonnée réactionnelle; on a démontré que cette expression est en accord avec la théorie de Marcus. En se basant sur une analyse des données de la littérature pour des solvolyses S_N1 et pour la formation de carbanions, on a été capable de reproduire le comportement qualitatif des éliminations impliquant le *t*BuBr, *i*PrBr et EtBr dans EtOH/EtO^- et de prédire les vitesses de ces réactions à l'intérieur des limites d'incertitude des données utilisées.

Mots clés : réactions concertées, théorie de Marcus, éliminations, surfaces réactionnelles.

[Traduit par la revue]

Can. J. Chem. Downloaded from www.nrcresearchpress.com by 91.121.58.235 on 09/07/12
For personal use only.

Introduction

We have recently reported an equation for the energy surface for the situation where two reaction progress variables are required to describe a reaction (1). The equation, which was a generalization of the inverted parabola model for the reaction coordinate of a simple reaction, was shown to be consistent with Marcus theory (2–4) for the edge reactions. It provides a basis for predicting when a reaction will be concerted and when it will be stepwise in terms of the thermodynamics and intrinsic barriers of the edge reactions. A logical consequence of the simple theory used is that the intrinsic barriers are the same for each pair of parallel edge reactions.

There has been considerable interest in the use of various energy surfaces to analyze concerted reactions (1, 5–18). We wish now to report that, using information from the literature, it is possible to predict which of a set of simple β-elimination reactions are concerted, and to make semiquantitative predictions of the rate constants, with no adjustable parameters.

We (8) and others (19, 20) have discussed the advantages of a quartic equation as an approximation to a reaction coordinate diagram, since it has the correct shape at the extrema. We have now devised an analogous equation with two reaction coordinate dimensions, which provides the simplest generalized surface in the quartic approximation with the correct behavior for the edge reactions, and which satisfies Marcus theory for all sections through it.

Results

The equation which we used (1), eq. [1], is based on a hyperbolic paraboloid, which gives an inverted parabola for each edge reaction:

$$[1] \quad G = \alpha x + \beta x^2 + \gamma y + \delta y^2 + \epsilon xy$$

This equation can be solved analytically to give the conditions for the transition state

$$x^{\ddagger} = (2\alpha\delta - \gamma\epsilon)/(\epsilon^2 - 4\beta\delta)$$

$$[2] \quad y^{\ddagger} = (2\beta\gamma - \alpha\epsilon)/(\epsilon^2 - 4\beta\delta)$$

$$\Delta G^{\ddagger} = (\alpha^2\delta + \beta\gamma^2 - \alpha\gamma\epsilon)/(\epsilon^2 - 4\beta\delta)$$

If the edge reactions are described by a quartic reaction profile, then the analogous energy surface is given by eq. [3], which provides a basis for examining questions of concertedness. In this equation, as in eq. [1], we have chosen to express all free energies relative to the level of the $x = 0$, $y = 0$ corner of the reaction coordinate diagram, in order to avoid having an additional constant term. This corner corresponds to the reactive encounter complex, at an energy higher than the free reagents by the "work term". We estimate the work term following Hine (21) by assuming that the equilibrium constant for encounter complex formation in the absence of special interactions is the probability of the reactive atom of a second molecule being in a sphere of radius 1.5 Å adjacent to the first molecule. This works out to be $0.0085n$ where n is the number of equivalent positions.[1,2] Corrections for desolvation or electrostatic interactions must be made where appropriate.

$$[3] \quad G = a_1x^2 + a_2y^2 + a_3x^3 + a_4y^3 + a_5x^4 + a_6y^4 + a_7x^2y^3 + a_8x^3y^2 + a_9x^3y^3 + a_{10}x^2y^2$$

We will first show that this equation has the minimum number of terms needed to satisfy the constraints placed upon it. We must first interpret the one-dimensional quartic equation in terms of Marcus theory. For the quartic

[1] See Appendix for details.

[2] Copies of the Supplementary Tables may be purchased from the Depository of Unpublished Data, CISTI, National Research Council of Canada, Ottawa, Ont., Canada K1A 0S2.

$$G = ax^4 + bx^3 + cx^2$$

it may be shown (20) that:

$$c = -2a - 3b/2$$

$$\Delta G^0 = -a - b/2$$

$$x^{\ddagger} = -1 - 3b/4a$$

We observe that when $\Delta G^0 = 0$, $x^{\ddagger} = 0.5$, and $\Delta G^{\ddagger} = a/16$. By definition, the intrinsic barrier is the free energy of activation when the thermodynamic barrier is zero. Thus we can define "a" in terms of the intrinsic barrier, $\tilde{G}$, as

$$a = 16\tilde{G}$$

and it then follows that

$$b = -32\tilde{G} - 2\Delta G^0$$

$$c = 16\tilde{G} + 3\Delta G^0$$

[4] $$\Delta G^{\ddagger} = \tilde{G}(1 + 8y + 18y^2 - 27y^3)$$

where $y = \Delta G^0/16\tilde{G}$. This expression for $\Delta G^{\ddagger}$ is very closely analogous to the corresponding expression for $\Delta G^{\ddagger}$ derived from the quadratic approximation to the reaction profile, namely

[5] $$\Delta G^{\ddagger} = \tilde{G}(1 + 8y + 16y^2)$$

which is equivalent to the more usual form of the Marcus equation,

$$\Delta G^{\ddagger} = \tilde{G}(1 + \Delta G^0/\tilde{G})^2$$

and leads to the commonly employed expression (22) for the intrinsic barrier $\tilde{G}$ in terms of the equilibrium free energy change and the free energy of activation

[6] $$\tilde{G} = \tfrac{1}{2}\{\Delta G^{\ddagger} - \tfrac{1}{2}\Delta G^0 + [(\Delta G^{\ddagger})^2 - \Delta G^{\ddagger}\Delta G^0]^{1/2}\}$$

It is not feasible to derive a corresponding analytical expression for $\tilde{G}$ based on eq. [4], but numerical solution is straightforward.

For the quartic surface, the pairs of edge reactions ($x = 0$ and $x = 1$, $y = 0$ and $y = 1$) must have different equations, thus at least some cross terms are essential. A logical consequence of eq. [1] was that the intrinsic barriers for both of a pair of edge reactions had to be the same. This condition could be relaxed in the quartic approximation, but we will in general have no means to evaluate the intrinsic barriers for some of the edge reactions; to be able to evaluate intrinsic barriers for two reactions is generally difficult enough. Consequently for the moment we continue to impose the constraint that both of a pair of edge reactions must have the same intrinsic barrier. This immediately demands that there be no cross terms involving x^4 or y^4, because the coefficients of these terms are dependent only on the intrinsic barriers; thus any cross terms would imply different intrinsic barriers. Let us rewrite eq. [3] to express the section through the surface at some arbitrary value of x

$$G_x = (a_1x^2 + a_3x^3 + a_5x^4) + (a_2 + a_8x^3 + a_{10}x^2)y^2 + (a_4 + a_7x^2 + a_9x^3)y^3 + a_6y^4$$

The y^2 and y^3 coefficients depend on the intrinsic barrier, which we assume is independent of x, and on the thermodynamic barrier, which will in general be a function of x. Thus at least some of the cross terms must be non-zero.

For this section through the surface, the equilibrium free energy change is

$$\Delta G_x^0 = a_2 + a_4 + (a_{10} + a_7)x^2 + (a_8 + a_9)x^3$$

So long as not all of a_7, a_8, a_9, and a_{10} are zero, then the coefficients of y^2 and y^3 in the expression for G_x, and the coefficients of x^2 and x^3 in the analogous expression for G_y, must include three terms, one independent of the fixed coordinate, one second order, and one third order, or the expressions will not be self-consistent. The parameters can be solved for in terms of the thermodynamic and intrinsic barriers as:

$$a_1 = 16\tilde{G}_x + 3(G_{10} - G_{00})$$

$$a_2 = 16\tilde{G}_y + 3(G_{01} - G_{00})$$

$$a_3 = -32\tilde{G}_x - 2(G_{10} - G_{00})$$

$$a_4 = -32\tilde{G}_y - 2(G_{01} - G_{00})$$

$$a_5 = 16\tilde{G}_x$$

$$a_6 = 16\tilde{G}_y$$

$$a_7 = a_8 = -6(G_{11} - G_{10} - G_{01} + G_{00})$$

$$a_9 = 4(G_{11} - G_{10} - G_{01} + G_{00})$$

$$a_{10} = 9(G_{11} - G_{10} - G_{01} + G_{00})$$

The condition for a transition state that represents a maximum along both coordinates is:

$$\partial G/\partial x = 0 = \partial G/\partial y$$

$$0 = \{2a_5\}(x^{\ddagger})^2 + (3/2)\{a_3 + a_8(y^{\ddagger})^2 + a_9(y^{\ddagger})^3\}x^{\ddagger} + \{a_1 + a_{10}\{y^{\ddagger})^2 + a_7(y^{\ddagger})^3\}$$

$$0 = \{2a_6\}(y^{\ddagger})^2 + (3/2)\{a_4 + a_7(x^{\ddagger})^2 + a_9(x^{\ddagger})^3\}y^{\ddagger} + \{a_1 + a_{10}\{x^{\ddagger})^2 + a_8(x^{\ddagger})^3\}$$

Unfortunately, these equations are intractably difficult to solve analytically, although they could readily be solved numerically. We have found that in many cases the transition state for a concerted reaction is not at a maximum for one of the coordinates; it is more general to find the transition state by calculating contour maps of the reaction surface, and by calculating more detailed maps of the region containing the transition state.

For the quadratic approximation we can use error analysis to deduce the sensitivity of the value assigned to $\tilde{G}$ to errors in ΔG^0, which will be the most uncertain value in the cases of interest here.

$$\partial\tilde{G}/\partial\Delta G^0 = (1/4)(1 + 1/\sqrt{(1 - \Delta G^0/\Delta G^{\ddagger})}$$

$$\sigma_{\tilde{G}} = |\partial\tilde{G}/\partial\Delta G^0|\sigma_{\Delta G^0}$$

For ionization of *t*BuBr, this leads to $\sigma_{\tilde{G}} = 0.8\sigma_{\Delta G^0}$.

Test of the approach

We will consider the examples of ethoxide-induced eliminations of *tert*-butyl bromide, isopropyl bromide, and ethyl bromide in ethanol.

The first example to be considered is the elimination reaction of *tert*-butyl bromide with ethoxide in ethanol. The edge reactions are the ionization of an encounter complex of *tert*-butyl bromide and ethoxide to the ethoxide *tert*-butylium bromide ion triplet, and the reaction of ethoxide ion with *tert*-butyl bromide to give 2-bromo-2-methylpropyl anion hydrogen bonded to ethanol. We must evaluate the free energy change for each edge reaction, and the intrinsic barrier for it.

Thermodynamics of ion triplet formation

For the ionization of *tert*-butyl bromide to the ion pair in ethanol, Abraham gives a value for the equilibrium free energy

Can. J. Chem. Downloaded from www.nrcresearchpress.com by 91.121.58.235 on 09/07/12
For personal use only.

Can. J. Chem. Downloaded from www.nrcresearchpress.com by 91.121.58.235 on 09/07/12
For personal use only.

change (by a careful estimation procedure) as 20.1 kcal/mol (23).

The free energy change for the dissociation of *tert*-butyl bromide to free ions estimated by Abraham (23) is consistent with recent estimates of tertiary carbocation stability by Kresge and co-workers (24, 25). Kresge (24) estimated that for *tert*-butylium ion the rate constant for nucleophilic attack by water at 25°C was $6 \times 10^9\ s^{-1}$. The rate constant for protonation of isobutylene is known to be $3.7 \times 10^{-4}\ M^{-1}\ s^{-1}$ (26, 27). The reaction of *tert*-butylium ion with water as nucleophile is 29 times faster than loss of a proton (28), so the rate constant for deprotonation is $2.1 \times 10^8\ s^{-1}$. Thus the equilibrium constant for deprotonation of the tertiary carbocation to give the alkene is $K_a = 5.6 \times 10^{11}$ M, or $\Delta G^0 = -16.0$ kcal/mol. Abraham (23) gives −16.5 kcal/mol for the same process, in excellent agreement.

We assume that the free energy of ionization of *t*BuBr is only affected by the presence of an EtO^- next to *t*BuBr by the additional electrostatic interaction of ion triplet formation. A crude estimate of the magnitude of this interaction can be calculated by using an oversimplified model where a cation is symmetrically disposed between two anions, with all three ions in a line. The electrostatic energy for a point charge arrangement:

$$-\frac{r}{} + \frac{r}{} -$$

will be given by $E_{el} \propto 2/r_{-+} - 1/r_{--}$. Now $r_{--} = 2r_{+-}$, so $E_{el} \propto 3/2r_{+-}$, while for a simple ion pair, $E_{el} \propto 1/r_{+-}$. The stabilizing electrostatic interaction for this arrangement will be 1.5 times that for an ion pair of two opposite charges at the same distance. We used an ion pair interaction energy based on an estimated ion pair association constant of −2.9 kcal/mol. This will be the sum of the non-electrostatic contribution, +2.8 kcal/mol, and the electrostatic contribution, which is then −5.7 kcal/mol. For the ion triplet, the electrostatic contribution would be $1.5 \times (-5.7) = -8.6$ kcal/mol, and the non-electrostatic contribution would be $+2.2 + 2.8 = 5.0$ kcal/mol. (There are three possible sites for association of the EtO^-, but only one for Br^-). The expected free energy change on formation of the ion triplet is then −3.6 kcal/mol. The free energy for encounter complex formation from EtO^- and *t*BuBr, allowing for loss of one hydrogen bonded solvent molecule, is estimated below (in the section on Equilibria for C—H ionization) as 8.3 kcal/mol.

For the formation of the ion triplet from an ethoxide – *tert*-butyl bromide encounter pair, we calculate:

$t\text{BuBr} \rightleftharpoons t\text{Bu}^+ + \text{Br}^-$	$\Delta G = 23.0$ (23)
$\text{EtO}^-, t\text{BuBr} \rightleftharpoons \text{EtO}^- + t\text{BuBr}$	$\Delta G = -8.3$
$t\text{Bu}^+ + \text{Br}^- + \text{EtO}^- \rightleftharpoons \text{EtO}^-, t\text{Bu}^+, \text{Br}^-$	$\Delta G = -3.6$
$\text{EtO}^-, t\text{BuBr} \rightleftharpoons \text{EtO}^-, t\text{Bu}^+, \text{Br}^-$	$\Delta G = 11.1$

The free energy changes upon ion triplet formation from the encounter complexes of EtO^- and *i*PrBr or EtBr are calculated analogously, following Abraham (23). The calculations are summarized in Tables 1 and 2.

For all of the alkyl bromides we assign an uncertainty of ±5 kcal/mol in the free energy level of the ion triplet corner.[1]

Intrinsic barrier for S_N1 solvolysis

Abraham gives a value for the free energy of activation as 24.7 kcal/mol (23, 29, 30). From this value and the equilibrium free energy change for ionization we can derive the intrinsic barrier as 12.66 kcal/mol in terms of the quadratic model, or 12.39 in terms of the quartic model.

Initially we assume, for lack of information allowing a different estimate, that the intrinsic barriers for ionization of *i*PrBr and EtBr to the contact ion pairs are the same as for *t*BuBr.

We will now attempt to estimate the intrinsic barrier for the ionization process in *t*BuBr in an encounter complex with EtO^-. A possible way to do this is to assume that there is a linear change in the interaction energy along the reaction coordinate as the C—Br bond cleaves. The initial state then has an interaction energy of +8.3 kcal/mol, while the free energy cost of bringing an EtO^- into contact with the $t\text{Bu}^+\text{Br}^-$ ion pair is 2.2 (for encounter) + (−2.9) (for electrostatics) = −0.7 kcal/mol. Thus the interaction energy at the transition state (which is at $x^* = 0.65$ in the quartic approximation) would be $2.2 + 0.65 \times (-2.9) = 0.31$ kcal/mol. This leads to an activation energy of $24.7 + 0.3 - 8.3 = 16.7$ kcal/mol relative to the encounter complex of EtO^- and *t*BuBr. These values lead to an intrinsic barrier of 10.5 in the quadratic approximation, and 10.38 in the quartic approximation, i.e., somewhat smaller than the value derived from the data for the process without EtO^-.

For the simple solvolysis of *t*BuBr, the free energy of ionization is reasonably well defined, as shown by the agreement of estimated (23) and quasi-experimental values (24, 25), and the rate is known (23, 29, 30) so the intrinsic barrier should also be reasonably well defined, and the uncertainty should be $0.8\sigma_{\Delta G^0}$. The free energy changes for the special ionization process of interest here, which take place in the presence of a perturbing EtO^-, are clearly less well defined. We have assigned an uncertainty of ±5 kcal/mol to the free energies of ionization, and clearly the uncertainty in the intrinsic barrier is at least 0.8 times this, as indicated by simple error analysis, leading to an uncertainty of ±4 kcal/mol.

Equilibria for C—H ionization

For the proton transfer reaction we must first estimate the equilibrium free energy change. One possible set of starting points are the acidities of methane and isobutane reported by Breslow and co-workers, based on electrochemical measurements (31). The value which they calculated for methane, by a reasonable extrapolation procedure, was $pK_a = 60.3$–62, which we will take as 61. This value refers to THF as solvent, with some added HMPA, and 0.2 M $LiClO_4$. Very similar electrode potentials were reported by Griller and co-workers (32, 33), who used acetonitrile with 0.1 M tetrabutylammonium perchlorate as the solvent. These solvents are both of enhanced polarity because of the supporting electrolyte. Since the potentials are very similar for both systems we will assume the same potentials, and hence the same relative pK_a values in DMSO. It has been suggested (33) that $\Delta G_{tr}(R^-)$ for benzylic carbanions is small for transfer from acetonitrile to DMSO. Absolute pK_a values are available for triphenylmethane and diphenylmethane in DMSO as 30.6 and 32.2 respectively (34). Following Breslow's procedure, but using the absolute pK_a for triphenylmethane in DMSO as an anchor, we obtain a pK_a of 43.9 for toluene in DMSO. Then by extrapolating a plot of pK_a vs. BDE ($r = 0.9987$) we estimate $pK_a = 60.5$ for methane. Table S2 summarizes our calculations.[2]

For isobutane in acetonitrile containing 0.1 M tetrabutylammonium perchlorate, Breslow and Grant have reported a pK_a of 71 (35). This was based on Streitwieser's pK_a for triphenylmethane, which referred to cesium ion pair equilibria in cyclohexylamine solution (36). If we assume as before that the

TABLE 1. Free energies of dissociation to give ion triplets[a]

Alkyl bromide	$\Delta G^{H_2O}_{diss}$[b]	$\Delta G_t(RBr)$[c]	$\Delta G_t(R^+)$[c]	ΔG^{EtOH}_{diss}[d]	ΔG^{EtOH}_{ip}[e]	ΔG^{EtOH}_{ion}[f]	ΔG^{EtOH}_{ec}[g]	ΔG^{EtOH}_{it}[h]	ΔG^{EtOH}_{ion}[i]
*t*BuBr	11.4[j]	−4.24[k]	2.87[l]	23.0[m]	−2.9[n]	20.1[o]	−8.3[p]	−3.6[q]	11.1[r]
*i*PrBr	27.4[j]	−3.70[k]	3.16[l]	38.7[m]	−3.1[n]	35.1[o]	−8.5[p]	−3.7[q]	26.5[r]
EtBr	42.4[j]	−3.20[k]	3.46[l]	53.4[m]	−3.1[n]	50.3[o]	−8.9[p]	−3.3[q]	41.3[r]

[a]At 25°C; all energies in kcal/mol.
[b]Free energy of dissociation to free ions in water.
[c]Free energy of transfer from water to ethanol.
[d]Free energy of dissociation to free ions in ethanol.
[e]Free energy of ion pair formation from free ions in ethanol.
[f]Free energy of ionization to the ion pair in ethanol.
[g]Free energy of encounter complex formation in ethanol.
[h]Free energy of ion triplet formation from free ions in ethanol.
[i]Free energy of ionization from encounter complex to ion triplet in ethanol.
[j]Calculated after ref. 23.
[k]Estimated by taking advantage of Abraham's finding (64) that for non-polar molecules free energies of transfer from water to alcohol depend only on molecular volume; since isopropyl bromide has a molar volume (94 mL/mol, calculated from data in ref. 65) intermediate between propane and isobutane, we can estimate the required free energy of transfer from the corresponding values for propane and isobutane: see Table 2.
[l]Estimated (23) from a plot of free energy of transfer (66) for Na^+, K^+, Rb^+, Cs^+, Me_4N^+, and Et_4N^+ vs. molar volume (64); see Table S1.[2]
[m]Calculated from other values in this table and the free energy of transfer from water to ethanol for Br^-, taken as 4.35 kcal/mol (66).
[n]Estimated by Abraham's procedure (23) from plots of K_A vs. the molar volume of the cation for tetraalkylammonium bromides in ethanol (67).
[o]Estimated as described in the text for *t*BuBr.
[p]Calculated from other values in this table.

TABLE 2. Free energies of transfer at 25°C for neutral molecules

Compound	*V* (mL/mol)	ΔG_t^c (g, water) (kcal/mol)	ΔG_t^c (g, EtOH) (kcal/mol)	ΔG_t^c (water, EtOH) (kcal/mol)
CH_4	39[a]	2.27[b]	3.90[b]	−1.63[c]
C_2H_4	50[a]			−2.18[d]
C_2H_6	55[a]	1.30[b]	3.73[b]	−2.43[c]
$CH_3CH{=}CH_2$	69[g]	3.17[i]		−2.97[d]
C_3H_8	75[e]	0.65[b]	3.85[b]	−3.20[c]
$(CH_3)_2CHBr$	94[e]	1.42[i]		−3.70[d]
$(CH_3)_2C{=}CH_2$	95[f]			−3.71[d]
$(CH_3)_3CH$	104[f]	4.21[b]	0.25[b]	−3.96[c]
$(CH_3)_3CBr$	113[a]	2.67[g]	−1.63[g]	−4.24[g]
$(CH_3)_4C$	123[a]	4.40[b]	−0.17[b]	−4.57[c]

[a]Reference 64.
[b]Calculated from values in ref. 68.
[c]Calculated from other values in this table.
[d]Calculated by interpolation, assuming linearity of ΔG_t in *V* over short ranges in *V* (64).
[e]Calculated from the molecular weight and the density at the boiling point (65).
[f]Calculated from the molecular weight and the density at the boiling point (69).
[g]Calculated as described in ref. 23. Raoult's law coefficient for methanol as solvent is $\gamma^\infty = (P/P_0N)_{N\to 0} = 13$; $P_0 = 135.3$ Torr (70); ΔG_t^x (g→MeOH) = 0.50; ΔG_t^x (MeOH→water) = 4.55 (71); ΔG_t^x (g→water) = 5.05; ΔG_t^c (g→water) = 2.67; from the data in ref. 71, ΔG_t^x (w→EtOH) = −4.94, and ΔG_t^c (water→EtOH) = −4.24; hence ΔG_t^c (g→EtOH) = −1.63 kcal/mol.

electrode potential would be the same in DMSO, and use the absolute pK_a of triphenylmethane in DMSO as anchor value, we obtain a pK_a value of 69.1. These calculations are also summarized in Table S2.

Given values for methane and a tertiary alkane, we estimate a pK_a for a primary alkane by linear interpolation, assuming the effect of each methyl on the pK_a is the same. We further assume that all simple primary alkanes will be the same and take the pK_a of a primary hydrogen in isobutane as 60.5 + (69.1 − 60.5)/3 = 63.4 in DMSO.

The problem with these values is that the solvent is ill defined, and the extrapolation procedure employed to get a pK_a for methane uses triphenylmethane, which is clearly a delocalized anion, and toluene, which will be semilocalized, to extrapolate to methane where the anion is fully localized. The ion pairing is unlikely to be equivalent over this series.

An alternative starting point is the set of kinetic acidities determined by Streitwieser. These values refer to cesium ion pairs in cyclohexylamine as solvent. The anchor is the equilibrium ion pair acidity for benzene determined as 43.0 (37). Cyclohexane was shown to exchange at a rate 1.1×10^{-8} times that of benzene, and isotope effects showed that internal return is not important (38). Finally, the exchange rate for methane was shown to be 2.2×10^3 times as large as that for

Can. J. Chem. Downloaded from www.nrcresearchpress.com by 91.121.58.235 on 09/07/12
For personal use only.

TABLE 3. Effect of hydrogen bonding on pK_a in DMSO[a]

Acid	pK_a^{DMSO}	pK_a^{water}	ΔpK_a	n_{hb}[b]	ΔpK_a/n_{hb}
ArOH					
H	18.03[c]	9.95[d]	8.08	3	2.69
*p*Me	18.86[c]	10.19[d]	8.67	3	2.89
*m*Me	18.23[c]	10.08[d]	8.15	3	2.71
*p*Cl	16.74[c]	9.38[d]	7.36	3	2.45
*m*F	15.88[c]	9.28[d]	6.60	3	2.20
*m*Cl	15.83[c]	9.02[d]	6.81	3	2.27
*m*CN	14.76[c]	8.61[d]	6.15	3	2.05
mNO_2	14.39[c]	8.35[d]	6.04	3	2.01
MeOH	29.0[e]	15.54[d]	13.5	3	4.5
MeCOOH	11.6[f]	4.76[d]	6.8	4	1.7
PhCOOH	11.0[f]	4.17[d]	6.8	4	1.7
pNO_2	8.9[f]	3.44[d]	4.5	4	1.1
*p*Cl	10.1[f]	3.99[d]	6.1	4	1.5
*m*Me	11.0[f]	4.24[d]	6.8	4	1.7
HCN	12.9[f]	9.40[d]	3.5	2	1.75

For all the data the least-squares line is $\Delta pK_a/n_{hb} = -0.222 \pm 0.100 + (0.161 \pm 0.0054)pK_a^{DMSO}$

[a]At 25°C.
[b]Number of hydrogen bonds, assuming one per lone pair.
[c]Reference 73.
[d]Reference 74.
[e]Reference 75.
[f]Reference 45.

cyclohexane, which in turn means that methane is 2.4×10^{-5} times as reactive as benzene (39). If it is assumed that the Brønsted slope is unity, then the pK_a for methane is 48. Streitwieser has argued that for localized carbanions the cesium ion pair pK values in cyclohexylamine should be very close to pK_a values in methanol, and has shown that for a series of compounds giving localized carbanions the Brønsted slope is approximately unity (40). Streitwieser states that ethane and other compounds with only primary hydrogens are 10^2–10^3 times less reactive than methane (39); this would lead to a pK_a for a primary hydrogen of about 50 in methanol.

A third starting point is the value estimated by Bordwell and Algrim (41) by extrapolation based on measured pK_a values of hydrocarbons in DMSO. The estimate so obtained was pK_a = 56 for methane in DMSO. Following the procedure used above, we estimate that the pK_a for a primary hydrogen of isobutane on this scale would be 59 in DMSO.

A fourth starting point is the theoretical pK_a for ethane in aqueous solution reported by Jorgensen and Briggs (42). This value is based on *ab initio* molecular orbital calculations for gas phase energies and intermolecular potentials, and Monte Carlo calculations for solvation energies. The value so obtained is pK_a = 52 ± 2.

The effect of the neighboring bromine on the pK_a of the primary CH will be estimated by assuming that polar effects have the same magnitude as for the analogous alcohols, i.e., the linear free energy relation for X-CH_2-OH will be used for X-C-CH_2-H. ρ^* for alcohols is −1.32 (43). σ^* for Br^- is 2.84 (44). Thus ΔpK_a for introducing a bromine is 3.75. The pK_a predicted for *tert*-butyl bromide is therefore 63.4 − 3.75 = 59.6 in DMSO on Breslow's scale, 59 − 3.75 = 55 in DMSO on Bordwell's scale, 50 − 3.75 = 46 in methanol on Streitwieser's scale, and 52 − 3.75 = 48 in water on Jorgensen's scale.

For an acid with a simple localized anion the major effect on the pK_a upon transfer from water to DMSO is expected to be the loss of hydrogen bonding solvation (45). The effect of this hydrogen bonding can be estimated from the pK_a differences observed for simple oxygen acids from water to DMSO; using the data in Table 3, we plot $\Delta pK_a/n_{hb}$ vs. pK_a^{DMSO} and obtain $\Delta pK_a/n_{hb} = -0.222 \pm 0.100 + (0.161 \pm 0.005)pK_a^{DMSO}$, which predicts a hydrogen bond effect of 9.4 pK units for an acid with $pK_a^{DMSO} = 59.6$. This leads to a predicted pK_a for *tert*-butyl bromide, on the Breslow scale, of 50.2 in water. From water to ethanol the pK_a difference for simple oxygen acids, where dispersion effects are likely to be small, is 5.7; see Table S3.[2] This leads to a pK_a for *tert*-butyl bromide of 55.7 in ethanol. Similarly we estimated pK_a values for *tert*-butyl bromide, on the Bordwell scale, of 45 in water and 51 in ethanol. Based on measurements in aqueous solution, Stahl and Jencks (46) found $\alpha = 0.15$ and $\beta = 0.10$ for hydrogen bond formation between phenoxide ions and ammonium ions; these values are in approximate agreement with the slope suggested here for the effect of pK_a on hydrogen bond strength.

The net result of our estimations is an increase in acidity of 4 pK_a units for *t*BuBr on transfer from DMSO to ethanol. Highly delocalized carbanions are more basic in methanol or ethanol than in DMSO (47). This is attributed to the effects of dispersion interactions. In the present case the dominating effect is that of hydrogen bond formation, which should be very strong for the highly localized and strongly basic carbanions.

The change in pK_a from water to methanol for a series of OH acids was 4.9 ± 0.2 (48). The change in pK_a from water to ethanol is 5.7 ± 0.5 based on the data in Table S3. The change in pK_a from methanol to ethanol for a series of acids is then +0.82; thus the pK_a for *tert*-butyl bromide in ethanol, on Streitwieser's scale, is 47. The pK_a for *tert*-butyl bromide in ethanol, on Jorgensen's scale, is 48 + 5.7 = 54.

Our four estimates of the pK_a for *tert*-butyl bromide in ethanol are: 56, 54, 51, and 47. We will work principally with the value based on Streitwieser's scale, which is based most directly on measurements on the compounds of interest, but will use the other values to test the sensitivity of our conclusions to the assumptions made.

The ion product of ethanol in ethanol as solvent is 19.1 (49). Thus for the proton transfer reaction:

$$t\text{BuBr} + \text{EtO}^- \rightleftharpoons \text{Me}_2\text{BrC—CH}_2^-\text{,HOEt}$$

log K = −37 and ΔG = 51 kcal/mol (Breslow scale), or log K = −33 and ΔG^0 = 45 kcal/mol (Bordwell scale), or log K = −28 and ΔG = 38.2 kcal/mol (Streitwieser scale), or log K = −35 and ΔG = 48 kcal/mol (Jorgensen scale). Since we take the hydrogen bonding effect on pK_a for ROH as 4.5 pK_a units per hydrogen bond, the cost of desolvating an EtO^- is log K = −4.5, ΔG = 6.1 kcal/mol. The equilibrium constant for bringing a desolvated EtO^- up to one of the antiperiplanar hydrogens of *t*BuBr will then be $3 \times 0.0085 = 0.026\ M^{-1}$, for ΔG = 2.2 kcal/mol. Then the total ΔG for encounter complex formation will be 6.1 + 2.2 = 8.3 kcal/mol. Then:

$$t\text{BuBr} + \text{EtO}^- \rightleftharpoons t\text{BuBr,EtO}^- \qquad \Delta G = 8.3$$

$$t\text{BuBr,EtO}^- \rightleftharpoons \text{Me}_2\text{BrC—CH}_2^-\text{,HOEt} \qquad \Delta G = 30 \text{ (or 43 or 42 or 40)}$$

For lack of any information allowing us to estimate the effect of the methyl groups on the neighboring carbon, we will assume that the acidity of the methyl C—H bonds of isopropyl bromide and ethyl bromide are the same as for *tert*-butyl bromide.

Can. J. Chem. Downloaded from www.nrcresearchpress.com by 91.121.58.235 on 09/07/12
For personal use only.

Can. J. Chem. Downloaded from www.nrcresearchpress.com by 91.121.58.235 on 09/07/12
For personal use only.

Although the various estimates for the pK_a of *tert*-butyl bromide vary by 9 pK_a units, and we have chosen the more acidic of the four, we feel that the Streitwieser scale is the most directly tied to experiments on the class of compounds of interest. As we will argue in the discussion, it is also consistent with patterns of substituent effects on pK_a. We assign an uncertainty of ±5 kcal/mol to the free energy level of the solvated carbanion.[1]

Intrinsic barrier for proton transfer

A possible starting point for estimating the intrinsic barrier for C—H ionization is the investigation by Bednar and Jencks (50) of proton transfer rates for HCN, which is a carbon acid and seems to give a hydrogen bonded species with HCN hydrogen bonded to the base that is to abstract the proton. They give the rate for no thermodynamic barrier as log $k = 9.1$, using a three-step model for the proton transfer reaction, with diffusional encounter and separation (51). This leads to an intrinsic barrier, $\tilde{G} = 5.0$. However HCN is not an ideal model because there may be a considerable change in solvation at N upon ionization. One would expect hydrogen bonding to N of cyanide to be far superior to hydrogen bonding to N of HCN because of

$$^-{:}C{\equiv}N \leftrightarrow {:}C{=}N{::}^-$$

This means that the observed intrinsic barrier for proton transfer to HCN may be an upper limit on the desired barrier for proton abstraction to give a simple alkyl carbanion. From studies with $CHCl_3$, admittedly for conditions well away from $\Delta pK = 0$, Kresge and Lin (52) concluded that these were "normal" acids, with any deviations from "normal" behavior being due to the cost of desolvating strong bases before proton abstraction could take place. This implies a *small* intrinsic barrier.

As we have argued above, the value of 5 kcal/mol for the intrinsic barrier derived from studies of HCN may be an upper bound. Following Kresge (53) we use 1 kcal/mol, the value appropriate to a diffusion controlled proton transfer involving O or N, as the lower bound, and assign an uncertainty of ±4 kcal/mol to this intrinsic barrier. We will use both 5 and 1 kcal/mol in our calculations.

Free energy change for the overall reaction

The overall free energy change for the elimination will be calculated from the standard free energies of reactants and products in ethanol solution. The quantities needed are found in Table 4. From these values we calculate that for

$$t\text{BuBr} \rightleftharpoons Me_2C{=}CH_2 + H^+ + Br^- \qquad \Delta G = 2.86$$

for

$$i\text{PrBr} \rightarrow MeCH{=}CH_2 + H^+ + Br^- \qquad \Delta G = 6.13$$

and for

$$\text{EtBr} \rightarrow CH_2{=}CH_2 + H^+ + Br^- \qquad \Delta G = 7.72$$

From the free energy change for the neutral species and the ion product of ethanol we calculate

$$EtO^- + t\text{BuBr} \rightleftharpoons Me_2C{=}CH_2 + Br^- \qquad \Delta G = -23.2$$
$$EtO^- + i\text{PrBr} \rightleftharpoons CH_3CH{=}CH_2 + Br^- \qquad \Delta G = -20.0$$
$$EtO^- + \text{EtBr} \rightleftharpoons CH_2{=}CH_2 + Br^- \qquad \Delta G = -18.4$$

and allowing for desolvation and product complex formation as described above,

$$EtO^-,t\text{BuBr} \rightleftharpoons Me_2C{=}CH_2,Br^- \qquad \Delta G = -29.3$$
$$EtO^-,i\text{PrBr} \rightleftharpoons CH_3CH{=}CH_2,Br^- \qquad \Delta G = -26.1$$
$$EtO^-,\text{EtBr} \rightleftharpoons CH_2{=}CH_2,Br^- \qquad \Delta G = -24.5$$

Observed rate constants

The rate of the E2 elimination of *t*BuBr with ethoxide in ethanol at 25°C is 3×10^{-5} M^{-1} s^{-1} (54, 55); $\Delta G^{\ddagger} = 23.63$ kcal/mol; the analogous activation energy calculated starting from the EtO^-,*t*BuBr complex is 17.5 kcal/mol. The rate of the E2 elimination of *i*PrBr with ethoxide in ethanol at 25°C is 2.4×10^{-6} M^{-1} s^{-1} (54); $\Delta G^{\ddagger} = 25.13$ kcal/mol starting from separate reagents, and 19.0 starting with the encounter complex. The rate of the E2 elimination of EtBr with ethoxide in ethanol at 25°C is 2.5×10^{-7} M^{-1} s^{-1} (54); $\Delta G^{\ddagger} = 26.46$ kcal/mol starting from separate reagents, and 20.3 kcal/mol starting with the encounter complex.

Calculated rate constants

The energies for the three-dimensional diagram for ethoxide-catalyzed reactions are now as shown in Fig. 1. Calculations using eq. [2], with $\tilde{G} = 5$ kcal/mol, lead to predicted transition state parameters as follows:

*t*BuBr/OEt^-	$x^* = 0.63 \pm 0.25$,	$y^* = 0.00$,	$\Delta G^* = 16.7 \pm 4.9$	edge
*i*PrBr/OEt^-	$x^* = 0.40 \pm 0.14$,	$y^* = 0.42 \pm 0.19$,	$\Delta G^* = 24.3 \pm 5.7$	
EtBr/EtO^-	$x^* = 0.25 \pm 0.12$,	$y^* = 0.65 \pm 0.19$,	$\Delta G^* = 26.8 \pm 5.3$	

For *t*BuBr and *i*PrBr the calculated free energies of activation are within their uncertainty limits of the experimental values.

If we examine the effect of assuming an intrinsic barrier of 1 for the C—H bond breaking, then we obtain:

*t*BuBr/OEt^-	$x^{\ddagger} = 0.46 \pm 0.17$,	$y^{\ddagger} = 0.20 \pm 0.23$,	$\Delta G^{\ddagger} = 15.7 \pm 5.1$
*i*PrBr/OEt^-	$x^{\ddagger} = 0.37 \pm 0.06$,	$y^{\ddagger} = 0.46 \pm 0.11$,	$\Delta G^{\ddagger} = 20.4 \pm 5.7$
EtBr/EtO^-	$x^{\ddagger} = 0.31 \pm 0.06$,	$y^{\ddagger} = 0.60 \pm 0.11$,	$\Delta G^{\ddagger} = 23.0 \pm 5.5$

With this assumed intrinsic barrier for proton abstraction, all three reactions have calculated free energies of activation within their uncertainty limits of the experimental values.

Similarly, using the quartic model, we find, for $\tilde{G}_{C-H} = 5$:

*t*BuBr/OEt^-	$x^{\ddagger} = 0.60$,	$y^{\ddagger} = 0.00$,	$\Delta G^{\ddagger} = 16.8 \pm 4.9$
*i*PrBr/OEt^-	$x^{\ddagger} = 0.44$,	$y^{\ddagger} = 0.44$,	$\Delta G^{\ddagger} = 24.4 \pm 5.7$
EtBr/EtO^-	$x^{\ddagger} = 0.35$,	$y^{\ddagger} = 0.58$,	$\Delta G^{\ddagger} = 27.0 \pm 5.5$

TABLE 4. Thermodynamic quantities needed for equilibrium calculations[a]

Compound	ΔG_f(g)[b]	ΔG_t(g,aq)[c]	ΔG_t(g,e)[d]	ΔG_t(aq,e)[e]	ΔG_f(aq)[f]	ΔG_f(EtOH)[g]
*t*BuBr	−6.73[h]		−1.63[j]			−8.36[l]
$Me_2C{=}CH_2$	12.88[h]	3.18[i]		−3.71[n]	16.06[l]	12.35[l]
HBr				7.00[k]	−24.85[m]	−17.85[l]
*i*PrBr	−6.51[h]	1.42[i]		−3.70[n]	−5.09[l]	−8.79[l]
$MeCH{=}CH_2$	14.99[h]	3.17[i]		−2.97[n]	18.16[l]	15.19[l]
EtBr	−6.29[h]	1.20[i]	−2.00[l]	−3.20[j]	17.48[l]	−8.29[l]
$CH_2{=}CH_2$	16.28[h]	3.18[i]	1.00[l]	−2.18[n]	−3.11[l]	17.28[l]

[a]All at 25°C; standard states are ideal gas at 1 atm (101.3 kPa) and 1 M solutions with an infinitely dilute reference state. All free energies are in kcal/mol.
[b]Free energy of formation of the species in the gas phase.
[c]Free energy of transfer from the gas at 1 atm to 1 M aqueous solution.
[d]Free energy of transfer from the gas at 1 atm to 1 M solution in ethanol.
[e]Free energy of transfer from the 1 M aqueous solution to 1 M solution in ethanol.
[f]Free energy of formation of the species in 1 M aqueous solution.
[g]Free energy of formation of the species in 1 M ethanolic solution.
[h]Reference 76.
[i]Reference 72.
[j]Calculated as described in ref. 23. The Raoult's law coefficient with methanol as solvent is $\gamma^{\infty} = (P/P_0N)_{N\to 0} = 13$; $P_0 = 135.3$ Torr (70); ΔG_t^x (g→MeOH) = 0.50; ΔG_t^x (MeOH→water) = 4.55 (71); ΔG_t^x (g→water) = 5.05; ΔG_t^c (g→water) = 2.67; from the data in ref. 71, ΔG_t^x (w→EtOH) = −4.94, and ΔG_t^c (water→EtOH) = −4.24; hence ΔG_t^c (g→EtOH) = −1.63 kcal/mol.
[k]From the single ion free energies of transfer quoted in ref. 66.
[l]Calculated from other values in this table.
[m]Reference 77.
[n]Interpolated assuming that ΔG_t is approximately linear in V over a narrow range; see Table S6.

TABLE 5. Values of the intrinsic barrier for C—Br cleavage that give the best fit to the experimental free energies of activation, and coordinates of the corresponding transition state[a]

		Quadratic model				Quartic model	
$\Delta G_{EtOH,RBr}$		30		43		30	
$\tilde{G}_{CH}$		5	1	5	1	5	1
*t*BuBr	$\tilde{G}_{CBr}$	11.3	12.3	11.3	11.4	11.2	11.8
	$x^{\ddagger}$	0.62	0.46	0.62	0.56	0.59	0.47
	$y^{\ddagger}$	0.00	0.22	0.00	0.07	0.00	0.30
*i*PrBr	$\tilde{G}_{CBr}$	5.2	9.1	3.2	6.4	11.2	12.5
	$x^{\ddagger}$	0.43	0.37	0.55	0.47	0.45	0.41
	$y^{\ddagger}$	0.35	0.44	0.26	0.29	0.40	0.55
EtBr	$\tilde{G}_{CBr}$	2.7	7.3	<1	3.0	2.7	7.1
	$x^{\ddagger}$	0.33	0.31		0.40	0.37	0.38
	$y^{\ddagger}$	0.47	0.55		0.40	0.48	0.52

[a]In ethanol at 25°C; all energies in kcal/mol.

and for $\tilde{G}_{C-H} = 1$:

*t*BuBr/OEt$^-$	$x^{\ddagger} = 0.48$,	$y^{\ddagger} = 0.29$,	$\Delta G^{\ddagger} = 15.7 \pm 5.2$
*i*PrBr/OEt$^-$	$x^{\ddagger} = 0.42$,	$y^{\ddagger} = 0.46$,	$\Delta G^{\ddagger} = 20.4 \pm 5.7$
EtBr/EtO$^-$	$x^{\ddagger} = 0.37$,	$y^{\ddagger} = 0.56$,	$\Delta G^{\ddagger} = 23.2 \pm 5.6$

These values are very similar to those obtained with the quadratic model. We consider this reassuring because the quadratic model has been extensively used. The present results show that the quartic model, which seems intuitively to be a better approximation to what we believe to be the true shape of the reaction profile, gives results very similar to the quadratic model. The quartic model is less easily worked with but should have advantages in that it can model more complex behavior. We plan to continue the investigation of both models.

Although we consider it very important that we have been able to calculate, at least approximately, the free energies of activation of these concerted reactions using only input parameters for the edge reactions, it is of interest to ask what values for the intrinsic barriers would give exact matches to each of the experimental values. It is also of interest to explore the effect of using the highest of the pK_a values for alkyl bromides, which we deduced above from literature data. We have carried out a series of such calculations, leading to the results in Table 5.

These numerical explorations show that: (1) for the highest pK_a values for the alkyl bromides that could be derived from literature results, it is possible to fit the data, but only if the intrinsic barrier for proton abstraction is very low, and then only with quite low intrinsic barriers for C—Br bond breaking in EtBr. (2) For the lower pK_a values for the alkyl bromides, which we prefer, the best fit is obtained if the intrinsic barrier for C—Br bond cleavage is significantly lower for EtBr than for *t*BuBr.

Discussion

The key result of the present investigation is that a simple model for concertedness, based on analytical expressions for the energy surface, gives qualitative predictions in accord with our expectations for these simple model reactions and semiquantitative predictions of the rates of the concerted reactions, even when these are quite significantly faster than the rates of the simple edge reactions used as inputs. We have also shown that the quartic approximation to the reaction profile can be extended to two reaction coordinate dimensions, and that it can be simply interpreted in terms of Marcus theory.

There has been criticism directed at the use of Marcus theory for electrophile–nucleophile combination reactions (56), but there is a strong empirical basis for using the equation because so many reactions are described by it (21, 57, 58).

A source of concern might be that we have used the lowest of the possible pK_a estimates for CH ionization of the simple alkyl bromides in order to carry out our calculations. The higher values that have been proposed give the same qualitative results,

Can. J. Chem. Downloaded from www.nrcresearchpress.com by 91.121.58.235 on 09/07/12
For personal use only.

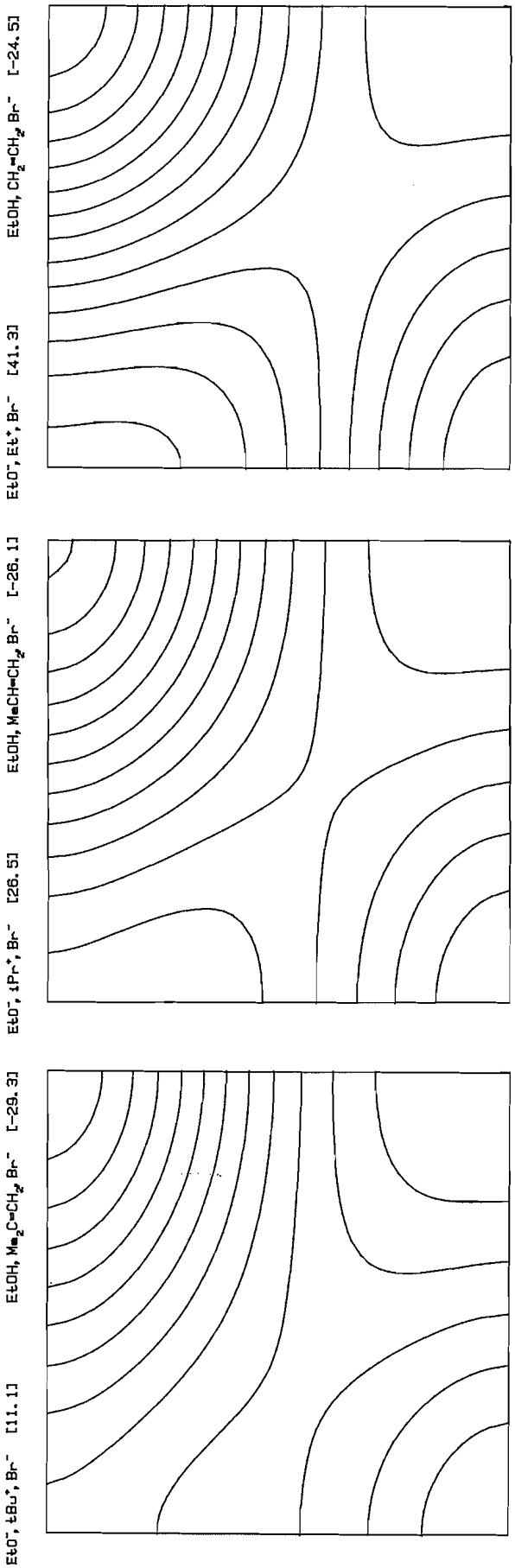

FIG. 1. Energy level contours for the three elimination reactions considered in this work. The energies of the corners were derived as described in the text. The contours are drawn using the quartic model, with $\tilde{G}_{CH} = 1$ and $\tilde{G}_{CBr} = 10.5$.

TABLE 6. Effect of a phenyl substituent on acidity[a]

	Solution			Gas phase[b]	
Compound	pK_a		ΔpK_a	$\Delta\Delta G$	ΔpK_a
R-XH_n	R = H	R = Ph			
X = O	16[c,d]	10[d,e]	6	28[f]	20.5[f]
X = N	35[c,d]	28[c,d]	7	35.9[f]	26.3[f]
X = C	48[g,h]	41[h,i]	7	35.9[f]	26[f]

[a]All at 25°C.
[b]For replacement of R = Me by R = Ph.
[c]Reference 78.
[d]In aqueous solution.
[e]Reference 74.
[f]Reference 79.
[g]Reference 80.
[h]In methanol.
[i]Reference 81.

of transition states changing from essentially S_N1-like for *t*BuBr to highly concerted and rather carbanion-like for EtBr. They do not give calculated $\Delta G^{\neq}$ values matching the experimental values unless very low intrinsic barriers for both processes are postulated. As a justification for the relatively high acidity for methane that we recommend, we point out that there is a consistent pattern to the effects of replacing H by phenyl in RXH_n, as shown by the data in Table 6. There seems to be no basis for concluding that the pK_a of methane proposed by Streitwieser is out of line relative to toluene, which has a generally accepted pK_a of about 41.

The intrinsic barriers for ionization of *i*PrBr and EtBr are not experimentally accessible because the solvolyses of these molecules are S_N2 processes (23, 59). There is a basis for expecting $\tilde{G}$ to be less for the less substituted alkyl bromides. Mitchell *et al.* (60) have reported that $\tilde{G}$ is proportional to the deformation energy for CH_3—X. They were considering S_N2 reactions but it appears likely that similar effects would apply to S_N1 reactions. A crude calculation supports the conclusion that the deformation energy would be less for EtBr than for *t*BuBr, so that $\tilde{G}$ would be smaller as well. It is not possible to estimate how much less the intrinsic barrier should be.

Bordwell (61) challenged the generality of the concerted E2 mechanism for β-eliminations, and proposed that a large fraction of such eliminations proceed by a stepwise path. Saunders (62) reviewed the evidence that there are indeed concerted E2 reactions for suitable reactants. In the present investigation, our calculations led to the conclusion that the elimination reaction of *t*BuBr has a transition state essentially the same as that for solvolysis, although there is no barrier at any stage after the transition state to the proton transfer component of the elimination. For *i*PrBr and EtBr, which would lead to less desirable carbocations, the reactions are predicted to be concerted with significant progress along both coordinates at the transition states.

Clearly the method described in this paper gives only very crude predictions of rates, but it does allow a qualitative prediction of when a reaction will be concerted, and semi-quantitative predictions of rate constants.

The major limitations on the use, or even the thorough testing, of the model is the lack of information about the intrinsic barriers of simple "edge" reactions. We hope that reaction surfaces may prove to be a general way of interpolating

Can. J. Chem. Downloaded from www.nrcresearchpress.com by 91.121.58.235 on 09/07/12
For personal use only.

from simple edge reactions to the wide range of concerted reactions possible for modest changes in structure or conditions.

One major virtue of the equations we have used for surfaces of reaction energy diagrams is that once the input data (corner energies and intrinsic barriers) are specified, the energy surface is unambiguously specified, so that cleaner and more explicit statement and testing of mechanistic hypotheses becomes possible.

Acknowledgments

We thank the Natural Sciences and Engineering Research Council of Canada for financial support of this work.

1. J. P. GUTHRIE and D. C. PIKE. Can. J. Chem. **65**, 1951 (1987).
2. A. O. COHEN and R. A. MARCUS. J. Phys. Chem. **72**, 4249 (1968).
3. R. A. MARCUS. J. Am. Chem. Soc. **91**, 7224 (1969).
4. R. A. MARCUS. Annu. Rev. Phys. Chem. **15**, 155 (1964), and references cited therein.
5. W. J. ALBERY. Prog. React. Kinet. **4**, 355 (1967).
6. W. J. ALBERY. J. Chem. Soc. Faraday Trans. 1, **78**, 1579 (1982).
7. C. L. PERRIN. J. Phys. Chem. **88**, 3611 (1984).
8. J. P. GUTHRIE. J. Am. Chem. Soc. **102**, 5286 (1980).
9. B. A. MILLER and D. L. LEUSSING. J. Am. Chem. Soc. **107**, 7146 (1985).
10. W. P. JENCKS. Acc. Chem. Res. **9**, 425 (1976).
11. D. A. JENCKS and W. P. JENCKS. J. Am. Chem. Soc. **99**, 7948 (1977).
12. W. P. JENCKS. Chem. Rev. **72**, 705 (1972).
13. W. P. JENCKS. Chem. Rev. **85**, 511 (1985).
14. R. A. MORE O'FERRALL. J. Chem. Soc. (B), 274 (1970).
15. J. R. MURDOCH. J. Am. Chem. Soc. **105**, 2660 (1983).
16. G. LAMATY and C. MENUT. Pure Appl. Chem. **54**, 1837 (1982).
17. E. GRUNWALD. J. Am. Chem. Soc. **107**, 125 (1985).
18. J. J. GAJEWSKI. Acc. Chem. Res. **13**, 142 (1980).
19. B. M. DUNN. Int. J. Chem. Kinet. **6**, 143 (1974).
20. W. J. LENOBLE, A. R. MILLER, and S. D. HAMMANN. J. Org. Chem. **42**, 338 (1977).
21. J. HINE. J. Am. Chem. Soc. **93**, 3701 (1971).
22. W. J. ALBERY. Annu. Rev. Phys. Chem. **31**, 227 (1980).
23. M. H. ABRAHAM. J. Chem. Soc. Perkin Trans. 2, 1893 (1973).
24. Y. CHIANG, W. K. CHWANG, A. J. KRESGE, M. F. POWELL, and S. SZILAGYI. J. Org. Chem. **49**, 5218 (1984).
25. Y. CHIANG and A. J. KRESGE. J. Am. Chem. Soc. **107**, 6363 (1985).
26. H. J. LUCAS and W. F. EBERZ. J. Am. Chem. Soc. **56**, 460 (1934).
27. F. G. CIAPETTA and M. KILPATRICK. J. Am. Chem. Soc. **70**, 639 (1948).
28. R. H. BOYD, R. W. TAFT, JR., A. P. WOLF, and D. R. CHIRSTMAN. J. Am. Chem. Soc. **82**, 4729 (1960).
29. P. O. I. VIRTANEN. Suom. Kemistil. B, **40**, 179 (1967).
30. R. A. CLEMENT and M. R. RICE. J. Am. Chem. Soc. **81**, 326 (1959).
31. B. JAUN, J. SCHWARZ, and R. BRESLOW. J. Am. Chem. Soc. **102**, 5741 (1980).
32. D. D. M. WAYNER and D. GRILLER. J. Am. Chem. Soc. **107**, 7764 (1985).
33. B. A. SIM, D. GRILLER, and D. D. M. WAYNER. J. Am. Chem. Soc. **111**, 754 (1989).
34. F. G. BORDWELL, G. E. DRUCKER, N. H. ANDERSEN, and A. D. DENNISTON. J. Am. Chem. Soc. **108**, 7310 (1986).
35. R. BRESLOW and J. L. GRANT. J. Am. Chem. Soc. **99**, 7745 (1977).
36. A. STREITWIESER, J. R. MURDOCH, G. HAFELINGER, and C. J. CHANG. J. Am. Chem. Soc. **95**, 4248 (1973).
37. A. STREITWIESER, JR., P. J. SCANNON, and H. M. NIEMEYER. J. Am. Chem. Soc. **94**, 7936 (1972).
38. A. STREITWIESER, JR., W. R. YOUNG, and R. A. CALDWELL. J. Am. Chem. Soc. **91**, 527 (1969).
39. A. STREITWIESER, JR. and D. R. TAYLOR. Chem. Commun. 1248 (1970).
40. A. STREITWIESER, JR., D. HOLTZ, G. R. ZIEGLER, J. O. STOFFER, M. L. BROKAW, and F. GUIBE. J. Am. Chem. Soc. **98**, 5229 (1976).
41. F. G. BORDWELL and D. J. ALGRIM. J. Am. Chem. Soc. **110**, 2964 (1988).
42. W. L. JORGENSEN and J. M. BRIGGS. J. Am. Chem. Soc. **111**, 4190 (1989).
43. S. TAKAHASHI, L. A. COHEN, H. K. MILLER, and E. G. PEAKE. J. Org. Chem. **36**, 1205 (1971).
44. D. D. PERRIN, B. DEMPSEY, and E. P. SERJEANT. pK_a prediction for organic acids and bases. Chapman and Hall, London. 1981.
45. C. D. RITCHIE. *In* Solute–solvent interactions. *Edited by* J. F. Coetzee and C. D. Ritchie. Dekker, New York. 1969. p. 230.
46. N. STAHL and W. P. JENCKS. J. Am. Chem. Soc. **108**, 4196 (1986).
47. C. D. RITCHIE and R. E. USCHOLD. J. Am. Chem. Soc. **90**, 2821 (1968).
48. J. P. GUTHRIE. Can. J. Chem. **54**, 202 (1976).
49. R. G. BATES. *In* Solute–solvent interactions. *Edited by* J. F. Coetzee and C. D. Ritchie. Dekker, New York. 1969. p. 52.
50. R. P. BEDNAR and W. P. JENCKS. J. Am. Chem. Soc. **107**, 7117 (1985).
51. M. EIGEN. Angew. Chem. Int. Ed. Engl. **3**, 1 (1964).
52. A. J. KRESGE and A. C. LIN. J. Chem. Soc. Chem. Commun. 761 (1973).
53. A. J. KRESGE. Chem. Soc. Rev. **2**, 475 (1973).
54. C. K. INGOLD. Structure and mechanism in organic chemistry. Cornell Univ. Press, Ithaca, NY. 1953. p. 426.
55. M. L. DHAR, E. D. HUGHES, and C. K. INGOLD. J. Chem. Soc. 2065 (1948).
56. C. D. RITCHIE, C. KUBISTY, and G. Y. TING. J. Am. Chem. Soc. **105**, 279 (1983).
57. J. P. GUTHRIE. J. Am. Chem. Soc. **100**, 5892 (1978).
58. J. P. GUTHRIE and P. A. CULLIMORE. Can. J. Chem. **58**, 1281 (1980).
59. P. E. DIETZE, R. HARARI, and J. KHATTAK. J. Org. Chem. **54**, 3317 (1989).
60. D. J. MITCHELL, H. B. SCHLEGEL, S. S. SHAIK, and S. WOLFE. Can. J. Chem. **63**, 1642 (1985).
61. F. G. BORDWELL. Acc. Chem. Res. **5**, 374 (1972).
62. W. H. SAUNDERS, JR. Acc. Chem. Res. **9**, 19 (1976).
63. P. R. BEVINGTON. Data reduction and error analysis for the physical sciences. McGraw–Hill, New York. 1969.
64. M. H. ABRAHAM. J. Chem. Soc. (A), 1610 (1971).
65. R. C. WEAST (*Editor*). Handbook of chemistry and physics. 48th ed. Chemical Rubber Co., Cleveland, OH. 1967.
66. Y. MARCUS. Ion solvation. Wiley, New York. 1985. p. 166.
67. D. F. EVANS and P. GARDAM. J. Phys. Chem. **72**, 3281 (1968).
68. M. H. ABRAHAM. J. Am. Chem. Soc. **104**, 2085 (1982).
69. J. A. DEAN (*Editor*). Lange's handbook of chemistry. 12th ed. McGraw–Hill, New York, NY. 1979.
70. J. TIMMERMANS. Physico-chemical constants of pure organic compounds. Vol. II. Elsevier, Amsterdam. 1965. p. 210.
71. M. H. ABRAHAM. J. Chem. Soc. Perkin Trans. 2, 1343 (1972).
72. J. HINE and P. K. MOOKERJEE. J. Org. Chem. **40**, 292 (1975).
73. F. G. BORDWELL, R. J. MCCALLUM, and W. N. OLMSTEAD. J. Org. Chem. **49**, 1424 (1984).
74. W. P. JENCKS and J. REGENSTEIN. *In* Handbook of biochemistry. 1st ed. *Edited by* H. A. Sober. Chemical Rubber Publishing Co., Cleveland, OH. 1968.
75. W. N. OLMSTEAD, Z. MARGOLIN, and F. G. BORDWELL. J. Org. Chem. **45**, 3295 (1980).

Can. J. Chem. Downloaded from www.nrcresearchpress.com by 91.121.58.235 on 09/07/12
For personal use only.

76. D. R. STULL, E. F. WESTRUM, JR., and G. C. SINKE. The chemical thermodynamics of organic compounds. Wiley, New York. 1967.
77. D. D. WAGMAN, W. H. EVANS, V. B. PARKER, R. H. SCHUMM, I. HALOW, S. M. BAILEY, K. L. CHURNEY, and R. L. NUTTALL. J. Phys. Chem. Ref. Data, **11**, Suppl. 2 (1982).
78. R. STEWART. The proton: applications in organic chemistry. Academic Press, New York. 1985.
79. J. E. BARTMESS, J. A. SCOTT, and R. T. MCIVER, JR. J. Am. Chem. Soc. **101**, 6056 (1979).
80. A. STREITWIESER, JR., R. A. CALDWELL, and W. R. YOUNG. J. Am. Chem. Soc. **91**, 529 (1969).
81. A. STREITWIESER, JR. and F. GUIBE. J. Am. Chem. Soc. **100**, 4532 (1978).

Appendix

Details concerning various calculations

Free energy for encounter complex formation

Hine (21) defined the encounter complex as having the nucleus of the basic atom within either of two spherical regions with the van der Waals radius of oxygen (1.5 Å) on either side of a planar carbon acid. We have generalized this to apply to n spherical regions in contact with the carbon acid. Following Hine, we assume that the basic atom is equally likely to be anywhere in solution, and so calculate the equilibrium constant for encounter formation as the ratio of the volume of the region(s) defining the encounter complex for one molar reagent to the total volume of solution (1 L). This calculation gives $K = 0.0085$ for $n = 1$.

Uncertainty in the free energy of ion triplet formation

Abraham (23) suggests an uncertainty of 3–4 kcal/mol for free energies of ionization estimated by his method. We will use the larger value as a conservative estimate of absolute uncertainty. For the desolvation and encounter we estimate an uncertainty of ±2 kcal/mol; although we believe that the estimation procedure that we used for this process is plausible, to assume anything better than 20% errors in free energy seems rash. The free energy of formation of the ion triplet from the three ions is the small difference between two larger contributions; a prudent estimate of uncertainty begins with 20% uncertainties in both the electrostatic and non-electrostatic contributions. Standard error propagation calculations (63) lead to an overall uncertainty in the free energy of ion triplet formation of 2 kcal/mol. These values for the three contributory processes lead to an uncertainty of ±5 kcal/mol for ionization of an encounter complex of ethoxide and *tert*-butyl bromide to the ion triplet.

$t\text{BuBr} \rightleftharpoons t\text{Bu}^+ + \text{Br}^-$	$\Delta G = 23.0 \pm 4$ (23)
$\text{EtO}^-, t\text{BuBr} \rightleftharpoons \text{EtO}^- + t\text{BuBr}$	$\Delta G = -8.3 \pm 2$
$t\text{Bu}^+ + \text{Br}^- + \text{EtO}^- \rightleftharpoons \text{EtO}^-, t\text{Bu}^+, \text{Br}^-$	$\Delta G = -3.6 \pm 2$
$\text{EtO}^-, t\text{BuBr} \rightleftharpoons \text{EtO}^-, \text{Br}^-$	$\Delta G = 11.1 \pm 5$

Uncertainty in the free energy level of the solvated carbanion

For reasons given in the text, we believe that the estimate based on Streitwieser's approach (37–40) is the most likely to be correct, and have used this value. Prudence dictates that our error estimates should include all current plausible estimates within the 95% confidence bounds. Assigning an estimated standard deviation of ±5 kcal/mol achieves this, since the highest pK_a is then within two standard deviations of our preferred value.

Can. J. Chem. Downloaded from www.nrcresearchpress.com by 91.121.58.235 on 09/07/12
For personal use only.

The ketonization of acetophenone enol in concentrated aqueous sulfuric and perchloric acid solutions. Implication on *X* acidity function correlations of the enolization reaction and determination of the keto–enol equilibrium constant as a function of acidity

Y. CHIANG AND A. J. KRESGE[1]
Department of Chemistry, University of Toronto, Toronto, Ont., Canada M5S 1A1
R. A. MORE O'FERRALL AND B. A. MURRAY
Department of Chemistry, University College, Dublin 4, Ireland
AND
N. P. SCHEPP AND J. WIRZ
Institut für Physikalische Chemie der Universität Basel, CH-4056 Basel, Switzerland

Received December 8, 1989

This paper is dedicated to Professor Ross Stewart on the occasion of his 65th birthday

Y. CHIANG, A. J. KRESGE, R. A. MORE O'FERRALL, B. A. MURRAY, N. P. SCHEPP, and J. WIRZ. Can. J. Chem. **68**, 1653 (1990).

Rates of ketonization of the enol of acetophenone, generated by flash photolytic photohydration of phenylacetylene, were measured in aqueous sulfuric and perchloric acid solutions over the concentration range 1–50 wt.% acid; rates of enolization of acetophenone, monitored by bromine scavenging, were also measured in aqueous perchloric acid solutions over the same concentration range. The results suggest that the curvature observed in a previous *X* acidity function correlation of the rate of enolization in sulfuric acid solutions was an artifact produced by insufficiently efficient scavenging, and that introduction of the activity of water in the correlating expression, used previously to eliminate the curvature and believed to reflect covalent involvement of water in the enolization reaction, is unnecessary. The present results also show that the keto–enol equilibrium constant for acetophenone decreases with increasing acidity in these concentrated sulfuric and perchloric acid solutions.

Key words: acetophenone, enolization, ketonization, keto–enol equilibrium, concentrated acid solutions.

Y. CHIANG, A. J. KRESGE, R. A. MORE O'FERRALL, B. A. MURRAY, N. P. SCHEPP et J. WIRZ. Can. J. Chem. **68**, 1653 (1990).

Opérant dans des solutions aqueuses d'acides perchlorique et sulfurique, à des concentrations allant de 1 à 50%, on a mesuré les vitesses de cétonisation de l'énol de l'acétophénone produit par unc photohydratation (par photolyse éclair) du phénylacétylène; opérant dans des solutions aqueuses d'acide phosphorique aux mêmes concentrations, on a aussi mesuré les vitesses d'énolisation de l'acétophénone, telles que détectées par un piégeage avec du brome. Les résultats obtenus suggèrent que la courbe observée antérieurement dans la corrélation entre la fonction d'acidité *X* et la vitesse d'énolisation des solutions d'acide sulfurique (a) était le produit d'un artefact résultant d'un piégeage qui n'était pas suffisamment efficace et (b) que, contrairement à ce qui a été suggéré antérieurement, il n'est pas nécessaire d'introduire l'activité de l'eau dans l'expresssion de la corrélation pour éliminer la courbe qui avait été considérée comme un reflet d'une implication covalente de l'eau dans la réaction d'énolisation. Les résultats actuels démontrent aussi que, dans ces solutions concentrées d'acides sulfurique et perchlorique, la constante d'équilibre céto–énol de l'acétophénone diminue avec une augmentation de l'acidité.

Mots clés : acétophénone, énolisation, cétonisation, équilibre céto–énol, solutions concentrées d'acides.

[Traduit par la revue]

Introduction

The enolization of acetophenone is one of the reactions used by Hammett in his pioneering investigation of reaction rates in concentrated acid solutions (1), and that work stimulated much other study of strong acids that eventually led to our present-day good understanding of phenomena in these media. A more recent examination of the enolization of acetophenone in concentrated sulfuric acid solutions (2) found that the rate data gave a curved rather than linear correlation with the *X* acidity function (3), but that linearity could be achieved by including the activity of water in the correlating relationship, consistent with the expected mechanistic role of water in the enolization process.

Curvature of the kind observed in this more recent study might also be induced by a change in rate-determining step from enolization, eq. [1], to reaction of enol with the bromine

[1] 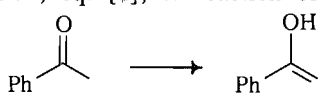

scavenger used to monitor the process, eq. [2]. This scavenging reaction is not catalyzed by acids, whereas reketonization of the enol is (4). As the acidity of the medium is increased, reketonization will therefore speed up while bromination will not, and the two processes might then begin to occur at comparable rates. This would produce a progressive lowering of observed rate constants and lead to a curved acidity function correlation.

[2] 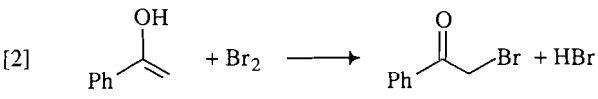

To determine whether or not this was so, we have measured rates of ketonization of acetophenone enol in concentrated acid solutions, using enol generated by flash photolytic hydration of phenylacetylene (5), eq. [3]. Comparison of these rates with rates of enol bromination calculated using the recently determined specific rate of this reaction (6) suggests that such a

[3] 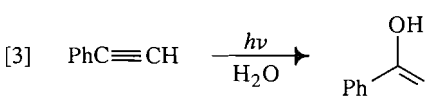

[1]Author to whom correspondence may be addressed.

Printed in Canada / Imprimé au Canada

Can. J. Chem. Downloaded from www.nrcresearchpress.com by 91.121.58.235 on 09/07/12
For personal use only.

change in rate-determining step did indeed take place. Our results, in combination with the enolization data, also provide keto–enol equilibrium constants that show a marked reduction in the enol content of acetophenone with increasing medium acidity.

Experimental

Materials

Phenylacetylene and acetophenone were purified by distillation. All other materials were best available commerical grades and were used as received. Acid solutions were prepared with distilled water and concentrations were determined by titration of weighed amounts.

Kinetics

Ketonization

Two different flash photolysis systems were used: (1) a conventional apparatus with excitation flash produced by capacitor discharge through a pair of xenon flash lamps, 50 μs pulse width, and (2) a laser system using a KrF excimer laser, λ_{excit} = 248 nm, 25 ns pulse width, 200 mJ/pulse. The enol transient was monitored at λ = 270 nm; its decay adhered well to the first-order rate law, and rate constants were calculated by least-squares fitting to a single-exponential function.

Enolization

Rates of enolization were measured by bromine scavenging under zero-order conditions using a ca. 100-fold excess of acetophenone over bromine. Initial bromine concentrations were ca. 1×10^{-4} M. The solutions also contained 0.2 M Br^-, which complexed 77% of the Br_2 as Br_3^-. Reactions were monitored at λ = 320 nm using the operational extinction coefficient ε = 3600 M^{-1} cm^{-1} determined here. Traces of absorbance vs. time were linear over most of their course, and zero-order rate constants were calculated from the slopes of these linear portions.

Results and discussion

Ketonization

Rates of ketonization of acetophenone enol were measured in aqueous solutions of perchloric and sulfuric acid over the concentration range 1–50 wt.% acid. The results are summarized in Table 1.

Figure 1 shows that the data give linear correlations with the X acidity function; least-squares analysis gives $\log(k/C_{H^+}) = (3.08 \pm 0.02) + (0.668 \pm 0.014)X$ for perchloric acid solutions and $\log(k/C_{H^+}) = (3.20 \pm 0.01) + (0.833 \pm 0.008)X$ for sulfuric acid solutions. The intercept of the perchloric acid correlation corresponds to $k_{H^+} = (1.20 \pm 0.05) \times 10^3$ M^{-1} s^{-1}, which agrees well with the catalytic coefficient $k_{H^+} = (1.25 \pm 0.02) \times 10^3$ M^{-1} s^{-1} determined previously in dilute hydrochloric acid solutions (4*a*).

The intercept of the sulfuric acid correlation gives a somewhat greater rate constant, $k = (1.58 \pm 0.03) \times 10^3$ M^{-1} s^{-1}, but this reflects catalysis by bisulfate ion in addition to hydronium ion. A bisulfate ion catalytic coefficient may be estimated on the assumption that the X correlation obtained in perchloric acid solution, where hydronium ion is the only catalytic species, can be used to calculate hydronium ion contributions to observed rates in sulfuric acid solutions. Excess rate constants, k_{xs}, equal to the difference between observed rate constants and these hydronium ion contributions, are a reasonably good linear function of bisulfate ion concentrations for the six least concentrated sulfuric acid solutions used here (Fig. 2). Least-squares analysis gives the relationship $k_{xs} = (5.26 \pm 5.67) \times 10^1 + (5.42 \pm 1.18) \times 10^2[HSO_4^-]$. The intercept of this relationship is zero within its experimental uncertainty, as expected since bisulfate ion is the only catalytically active species present in these solutions in addition to hydronium ion, and the slope gives a bisulfate-ion catalytic coefficient, $k_{HSO_4^-} = 540$ M^{-1} s^{-1}, whose value is reasonable in relation to the hydronium ion catalytic coefficient, $k_{H^+} = 1250$ M^{-1} s^{-1}.

TABLE 1. Rate data for ketonization of acetophenone enol in concentrated aqueous acid solutions at 25°C

Wt.% acid	$k_{obs}/10^3$ s^{-1}
H_2SO_4:	
1.82	0.393, 0.389, 0.372, 0.420
3.58	0.792, 0.832, 0.849, 0.744
4.46	1.08, 1.05, 1.13, 1.02, 1.23, 1.07
5.32	1.20, 1.26, 1.24, 1.13, 1.17
7.01	1.69, 1.81, 1.71, 1.87
8.67	2.21, 2.09, 2.26, 2.37
24.7	26.7, 33.3, 28.3, 30.3, 25.0, 29.7
29.3	52.8, 54.3, 57.2
34.5	108., 104., 95.8
39.6	250., 280., 230.
44.3	410., 460., 450.
49.8	1300., 1100., 1070., 1060.
$HClO_4$:	
1.00	0.108, 0.110, 0.107, 0.110, 0.105, 0.116
2.00	0.215, 0.238, 0.192, 0.210, 0.214, 0.218
3.90	0.512, 0.513, 0.549, 0.514, 0.549, 0.454
5.80	0.767, 0.786, 0.835, 0.828, 0.728, 0.734, 0.812
7.60	1.26, 1.56, 1.30, 1.19, 1.13, 1.26, 1.34, 1.25
9.40	1.78, 1.69, 1.77, 1.60, 1.69, 1.63, 1.87
13.8	3.27, 3.01, 2.88, 3.24, 3.40, 3.17, 3.40
17.9	4.94, 5.98, 4.68, 6.19, 5.29, 4.99, 5.15, 5.76
21.8	8.63, 8.25, 9.60, 8.48, 8.35, 7.92, 9.05
29.7	25.8, 25.9, 25.5
37.5	72.5, 71.9, 70.9, 73.0
44.0	171., 210., 179., 182.
50.0	862., 685., 690., 813., 800., 820., 746

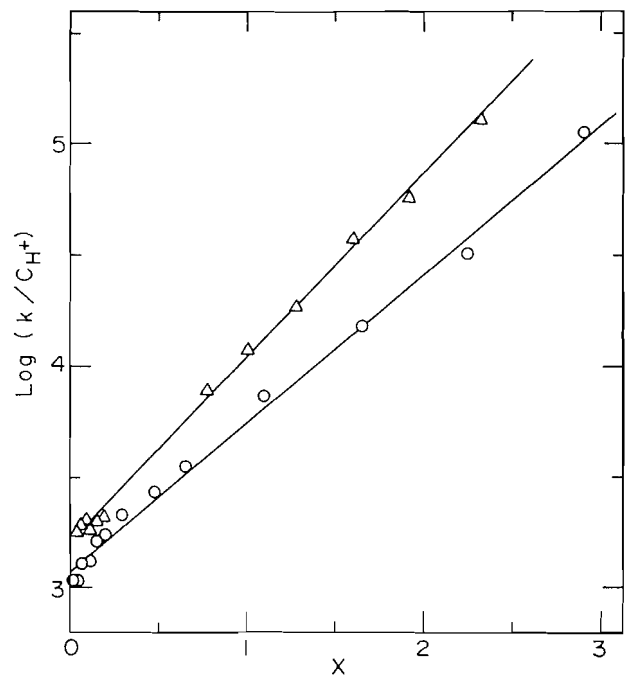

FIG. 1. Acidity function correlations for rates of ketonization of acetophenone enol in aqueous perchloric (○) and sulfuric (△) acid solutions.

Can. J. Chem. Downloaded from www.nrcresearchpress.com by 91.121.58.235 on 09/07/12
For personal use only.

TABLE 2. Comparison of rates of ketonization and bromination of acetophenone enol in sulfuric acid solutions

Wt.% H_2SO_4	$k^K/20^6\ s^{-1}$ [a]	$k^E_{obs}/10^{-4}\ s^{-1}$ [b]	k^K/k^{Br} [c]	$k^E/10^{-4}\ s^{-1}$
17.8	0.0101	0.818	0.00306	0.821
28.1	0.0413	1.95	0.0125	1.97
33.3	0.0878	2.54	0.0266	2.61
38.3	0.186	4.14	0.0563	4.37
43.5	0.420	6.06	0.127	6.83
48.3	0.934	7.71	0.283	9.89
53.3	2.28	8.86	0.690	15.0

[a]Calculated using the X function correlation determined here.
[b]Reference 2.
[c]For $[Br_2] = 10^{-3}$ M.

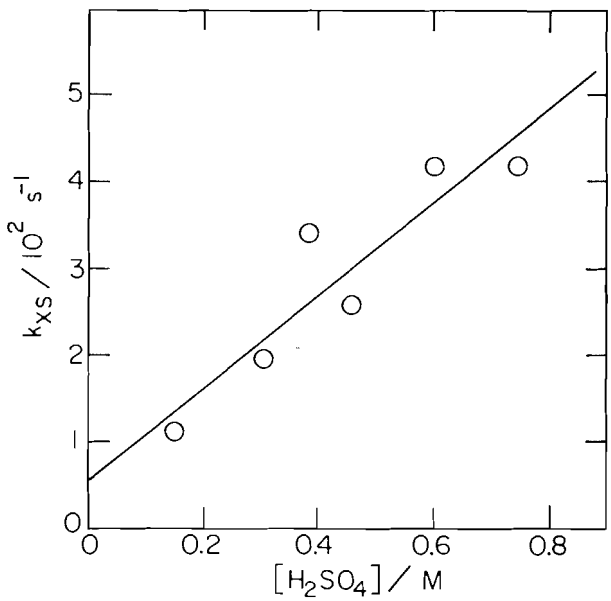

FIG. 2. Relationship between excess rate constants, k_{xs} (= $k_{obs} - k_{H^+}[H^+]$) for the ketonization of acetophenone enol and bisulfate ion concentration in moderately concentrated sulfuric acid solutions.

In the more concentrated sulfuric acid solutions, on the other hand, k_{xs} increases much more rapidly with increasing $[HSO_4^-]$ than required by this correlation. Such differences have been observed before in analyses of rates of other reactions in concentrated sulfuric acid solution (7); they might be the result of salt effects on the bisulfate-ion catalyzed reaction or incursion of catalysis by undissociated sulfuric acid.

Enolization

The rate law that governs the enolization of acetophenone when the process is monitored by bromine scavenging is given by eq. [4]. Here k^E_{obs} is the observed rate constant for the overall process and k^E, k^K, and k^{Br} are rate constants for the enol-forming step (eq. [1], forward direction), the reketonization step (eq. [1], reverse direction), and the enol-bromination step (eq. [2]) respectively. These rate constants are all defined as first-order specific rates, i.e., they contain the effect of acid catalyst or bromine reactant concentration. When bromination is sufficiently more rapid than reketonization, this expression reduces to eq. [5], and observed rate constants provide a true measure of rates of enolization. On the other hand, when bromination and reketonization occur at comparable rates, the full expression applies, and rearrangement of eq. [4] into eq. [6] shows that observed rate constants are reduced from rates of enolization by the fraction $1/(1 + k^K/k^{Br})$.

$$[4]\quad k^E_{obs} = k^E k^{Br}/(k^K + k^{Br})$$

$$[5]\quad k^E_{obs} = k^E$$

$$[6]\quad k^E_{obs} = k^E/(1 + k^K/k^{Br})$$

The critical quantity is therefore the ratio of reketonization to bromination rate constants, k^K/k^{Br}: only when this is small does eq. [5] apply. This ratio may be evaluated for the conditions of the study described in ref. 2 by using the X acidity function correlation established here for rates of ketonization of acetophenone enol in sulfuric acid solutions and the recently determined rate constant for the reaction of acetophenone enol with bromine, $k = 3.3 \times 10^9\ M^{-1}\ s^{-1}$ (6).[2] Evaluation of this ratio also requires knowledge of the bromine concentrations employed. This is not known with certainty, inasmuch as ref. 2 as well as the thesis upon which this reference is based (8) specify only that the range $[Br_2] = 10^{-2}$–10^{-3} M was used for acetophenone and several other substrates. The ratio k^K/K^{Br} was therefore evaluated here using both ends of this range. The results for $[Br_2] = 10^{-3}$ M are listed in Table 2; those for $[Br_2] = 10^{-2}$ M are a factor of 10 less.

It may be seen that k^K/k^{Br} is negligibly small at low acidities, but at higher acidities, especially in the most concentrated acid solution used, it does become significant. Observed rate constants were therefore corrected, i.e., converted into values of k^E, by multiplication by $(1 + k^K/k^{Br})$. The results for $[Br_2] = 10^{-3}$ M are listed in Table 2 and are also displayed in Fig. 3 (open circles) along with the values for $[Br_2] = 10^{-2}$ M (triangles).

Figure 3 shows that, whereas the X function correlation using values of K^E based upon $[Br_2] = 10^{-2}$ M is still curved, the one using values based on $[Br_2] = 10^{-3}$ M is linear. It is likely that the latter is the better representation of the true situation, inasmuch as it provides better agreement with rates of enolization of acetophenone measured by Hammett using iodine scavenging (1); these are shown in Fig. 3 as filled circles. Hammett realized that iodine was not a sufficiently efficient scavenger in the more acidic solutions that he used, and he allowed for this in calculating his rate constants; his results therefore pertain to the enolization step only. The combined data, those of Hammett plus those of ref. 2 corrected using $[Br_2] = 10^{-3}$ M, provide the relationship $\log(k^E/C_{H^+}) = -(4.66 \pm 0.01) + (0.328 \pm 0.008)X$.

These arguments suggest that rates of enolization of aceto-

[2]This reaction is a very nearly diffusion-controlled process whose rate will be independent of medium acidity.

Can. J. Chem. Downloaded from www.nrcresearchpress.com by 91.121.58.235 on 09/07/12
For personal use only.

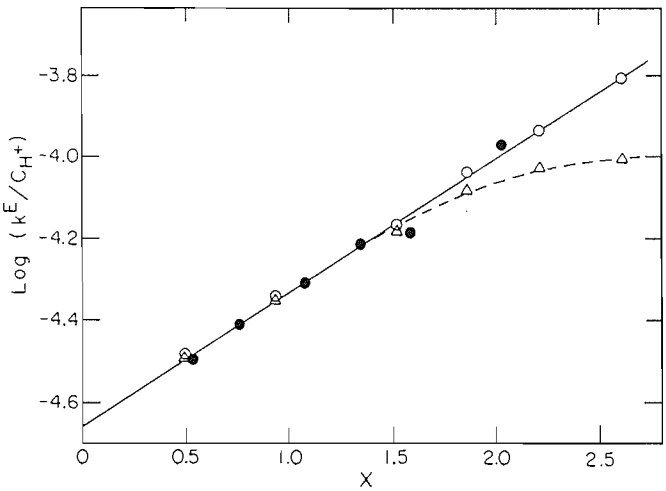

FIG. 3. Acidity function correlation of rates of enolization of acetophenone enol in aqueous sulfuric acid solutions: ○ and △, ref. 8 corrected as described in text using $[Br_2] = 10^{-3}$ and 10^{-2} M respectively; ●, ref. 1.

phenone could give a linear X function correlation without the incorporation of the activity of water in the correlating expression. Water is undoubtedly involved in the enolization process, as the base that receives the proton being transferred from carbon, but to a good approximation this covalent involvement would then already be reflected in a normal, linear X function dependence, and it would not need to be included explicitly. We will return to the role of water in a later paper.

Keto–enol equilibrium

Keto–enol equilibrium constants may be evaluated as ratios of enolization to ketonization rate constants, $K^E = k^E/k^K$. Combination of the X function correlations for enolization and ketonization described above therefore gives an expression relating K^E to X for acetophenone in sulfuric acid solutions: log $K^E = -(7.86 \pm 0.02) - (0.506 \pm 0.012)X$. The intercept of this relationship is consistent with the value determined previously in dilute solution, log $K^E = -7.96 \pm 0.04$ (4*b*), and the slope shows that enol content decreases with increasing acidity.

It is of interest to determine whether this decrease in K^E is specific to sulfuric acid or whether it also occurs in other concentrated acids as well, and we therefore measured rates of enolization of acetophenone in perchloric acid solutions in order to combine these with the ketonization data and provide a K^E–X relationship for this medium also. Enolization was again monitored by bromine scavenging and allowance was made for insufficiently efficient scavenging wherever necessary. The results are summarized in Table 3; it may be seen that only minor adjustments to k^E_{obs} were on the whole necessary.

Hammett also measured rates of enolization in perchloric acid solutions (1), and his values of k^E, again obtained allowing for insufficiently efficient scavenging, are in good agreement with ours. The combined data give the linear correlation: $\log(k^E/C_{H^+}) = -(4.86 \pm 0.01) + (0.086 \pm 0.001)X$. The intercept of this relationship corresponds to the hydronium-ion catalytic coefficient, $k_{H^+} = (1.38 \pm 0.04) \times 10^{-5}\ M^{-1}\ s^{-1}$, which is in reasonable agreement with the value measured previously in dilute acid solutions, $k_{H^+} = (1.21 \pm 0.01) \times 10^{-5}\ M^{-1}\ s^{-1}$ (4*b*).

TABLE 3. Rate data for enolization of acetophenone monitored by bromine scavenging in aqueous perchloric acid solutions at 25°C

Wt.% $HClO_4$	$k_{obs}/10^{-6}\ s^{-1}$	$k^E/10^{-6}\ s^{-1}$
0.40	0.576, 0.589	0.576, 0.589
1.18	1.81	1.81
3.17	5.34	5.35
3.49	5.01	5.02
7.92	11.3, 13.0	11.4, 13.1
20.0	39.5	40.7
29.3	58.2	63.5
37.9	127.	133.
46.3	140.	145.

Combination of the enolization and ketonization correlations for perchloric acid solutions gives log $K^E = -(7.94 \pm 0.02) - (0.581 \pm 0.013)X$. The intercept of this relationship agrees very well with the previously determined value, log $K^E = -7.96 \pm 0.04$ (4*b*), and the slope shows that the enol content decreases with increasing acidity in concentrated perchloric acid solution just as it does in concentrated sulfuric acid.

It is interesting that this change in K^E with increasing medium acidity may be modelled using phenol as a substitute for acetophenone enol. Activity coefficient measurements show that phenol is salted out of concentrated sulfuric acid quite markedly whereas acetophenone is not affected very much at all (9). The ratio of activity coefficients of acetophenone to phenol in 50% H_2SO_4 relative to pure water, $f(PhCOCH_3)/f(PhOH) = 11$, is in fact remarkably similar to the change in keto–enol equilibrium constant for acetophenone in going from water to 50% H_2SO_4, $\delta K^E = 12 \pm 1$.

Acknowledgements

We are grateful to Dr. R. A. Cox for valuable discussion and to the Natural Sciences and Engineering Research Council of Canada and the donors of the Petroleum Research Fund, administered by the American Chemical Society, for financial support of this research.

1. L. ZUCKER and L. P. HAMMETT. J. Am. Chem. Soc. **61**, 2791 (1939).
2. R. A. COX, C. R. SMITH, and K. YATES. Can. J. Chem. **57**, 2952 (1979).
3. R. A. COX and K. YATES. J. Am. Chem. Soc. **100**, 3861 (1978).
4. (*a*) Y. CHIANG, A. J. KRESGE, and J. WIRZ. J. Am. Chem. Soc. **106**, 6392 (1984); (*b*) J. R. KEEFFE, A. J. KRESGE, and J. TOULLEC. Can. J. Chem. **64**, 1224 (1986).
5. Y. CHIANG, A. J. KRESGE, M. CAPPONI, and J. WIRZ. Helv. Chim. Acta, **69**, 1331 (1986).
6. R. HOCHSTRASSER, A. J. KRESGE, N. P. SCHEPP, and J. WIRZ. J. Am. Chem. Soc. **110**, 7875 (1988).
7. A. J. KRESGE, L. E. HAKKA, S. MYLONAKIS, and S. SATO. Disc. Faraday Soc. **39**, 75 (1965); A. J. KRESGE, S. G. MYLONAKIS, and L. E. HAKKA. J. Am. Chem. Soc. **94**, 4197 (1972).
8. C. R. SMITH. M. Sc. Thesis, University of Toronto, 1968.
9. K. YATES and R. A. MCCLELLAND. Prog. Phys. Org. Chem. **11**, 323 (1974).

Can. J. Chem. Downloaded from www.nrcresearchpress.com by 91.121.58.235 on 09/07/12
For personal use only.

Proton transfer reactions between 4-nitrophenylphenylcyanomethanes and cyclic nitrogen bases in acetonitrile solvent

MIROSLAW DWORNICZAK[1] AND KENNETH T. LEFFEK
Department of Chemistry, Dalhousie University, Halifax, N.S., Canada B3H 4H6

Received November 28, 1989

This paper is dedicated to Professor Ross Stewart on the occasion of his 65th birthday

MIROSLAW DWORNICZAK and KENNETH T. LEFFEK. Can. J. Chem. **68**, 1657 (1990).

3,3,6,9,9-Pentamethyl-2,10-diazabicyclo[4.4.0]dec-1-ene has been synthesized and its proton transfer reactions, together with those of the bases 2,2,6,6-tetramethylpiperidine and 1,2,2,6,6-pentamethylpiperidine, have been studied with the carbon acids 4-nitrophenylphenylcyanomethane and 2-methyl-4-nitrophenylphenylcyanomethane. Equilibrium constants, rate constants, primary deuterium isotope effects, and activation parameters are reported for the reactions in acetonitrile solvent. Values of the pK_a in acetonitrile have been measured for the conjugate acid of each base and the Brønsted β value of 0.56 in acetonitrile has been determined for the proton transfer from 4-nitrophenylphenylcyanomethane.

Key words: proton transfer reactions, kinetic isotope effects, cyclic nitrogen bases.

MIROSLAW DWORNICZAK et KENNETH T. LEFFEK. Can. J. Chem. **68**, 1657 (1990).

On a synthétisé le 3,3,6,9,9-pentaméthyl-2,10-diazabicyclo[4,4,0]déc-1-ène et, utilisant les acides carbonés 4-nitrophénylphénylcyanométhane et 2-méthyl-4-nitrophénylphénylcyanométhane, on a étudié ses réactions de transfert de proton avec ceux des bases 2,2,6,6,-tétraméthyl- et 1,2,2,6,6-pentaméthyl-pipéridines. On a déterminé les constantes d'équilibre, les constantes de vitesse, les effets isotopiques primaires du deutérium et les paramètres d'activation de ces réactions dans l'acétonitrile. On a mesuré la valeur du pK_a, dans l'acétonitrile, pour chaque acide conjugué de chaque base et on a déterminé que, dans l'acetonitrile, la valeur β de Brønsted pour le transfert de proton à partir du 4-nitrophénylphénylcyanométhane est égale à 0,56.

Mots clés : réactions de transfert de proton, effets isotopiques cinétiques, bases cycliques d'azote.

[Traduit par la revue]

Introduction

This work continues the study of proton transfer reactions and primary deuterium isotope effects in the reactions of cyanomethane carbon acids and nitrogen bases in acetonitrile solvent. Previous studies have investigated the effects of substituents in the carbon acid with respect to electronic effects (1) and steric effects (2). In this paper, structural changes in the nitrogen base are studied using two carbon acids, 4-nitrophenylphenylcyanomethane **1** and 2-methyl-4-nitrophenylphenylcyanomethane **2**. The base 3,3,6,9,9-pentamethyl-2,10-diazabicyclo[4.4.0]dec-1-ene (PMDBD) **3** has been synthesized in order to study the steric effect on the reactivity of the basic centre and its relation with the isotope effects on deuteron transfer. For comparison, the bases 2,2,6,6-tetramethylpiperidine (**4**) and 1,2,2,6,6-pentamethylpiperidine (**5**) were also studied.

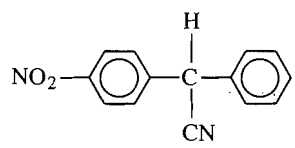

1

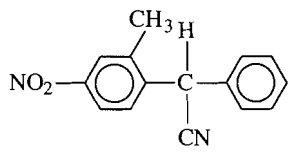

2

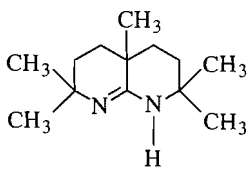

3

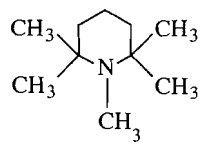

4

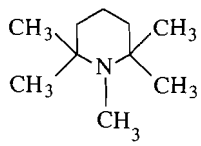

5

The proposition put forward by Sugimoto and Sasaki (3) that increased steric hindrance at the basic centre decreases the extent of proton tunnelling in the proton transfer reaction could also be tested, if the reactions exhibit a significant tunnelling contribution.

[1]Postdoctorate Fellow 1988–1989.

TABLE 1. Equilibrium constants for proton transfer reactions in acetonitrile at 25°C

Acid	Base	pK_a	ε	K(dm^3 mol^{-1})
1	5	18.7±0.2	9 300	440±30
1	4	18.8±0.2	11 900	200±15
1	3	21.4±0.2	28 500	1290±25
1	TMG	23.3*	40 000	6000
2	3	21.4±0.2	21 600	66±2
2	TMG	23.3*	24 000	300±60
2	DBU	23.9±0.1†	37 000	3500±700

*Reference 10.
†Reference 6.

Directly measured pK_a values for the conjugate acids of these bases in acetonitrile solvent allows the determination of the Brønsted β value for the proton transfer reactions. Previously most β values were determined in water or in other mixed solvents using pK_a values measured in water, although some β values based on pK_a measurements in nonaqueous solvents, e.g., DMSO, have been reported (4).

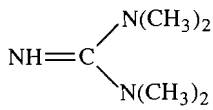

TMG

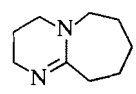

DBU

Results and discussion

Equilibrium constants

The Hildebrand–Benesi method (5) was used to determine the equilibrium constants for each of the bases **3**, **4**, and **5** reacting with carbon acid **1**, and for the base **3** reacting with the

Can. J. Chem. Downloaded from www.nrcresearchpress.com by 91.121.58.235 on 09/07/12
For personal use only.

Can. J. Chem. Downloaded from www.nrcresearchpress.com by 91.121.58.235 on 09/07/12
For personal use only.

TABLE 2. Rate constants and primary deuterium isotope effects for proton transfer reactions in acetonitrile solvent

Transfer	Temp. (°C)	10^3[Base](M)	k_{obs} (s^{-1})	k_2($dm^3\,mol^{-1}\,s^{-1}$)	k_b (s^{-1})	k_H/k_D
(i) 4-Nitrophenylphenylcyanomethane and 1,2,2,6,6-pentamethylpiperidine						
H	10.0	2.22–22.2	0.108–0.570	23.0±0.2	0.06	
H	15.0	2.22–22.2	0.143–0.680	26.6±0.3	0.09	
H	20.0	2.22–22.2	0.187–0.801	30.9±0.3	0.11	
H	25.0	2.22–22.2	0.240–0.954	35.4±0.7	0.16	
H	30.0	2.22–22.2	0.319–1.15	40.9±1.6	0.23	
D	10.0	2.85–28.5	0.0154–0.0822	2.58±0.07	0.008	8.9±0.2
D	15.0	2.85–28.5	0.0209–0.0992	3.02±0.07	0.012	8.8±0.2
D	20.0	2.85–28.5	0.0279–0.120	3.58±0.10	0.018	8.6±0.2
D	25.0	2.85–28.5	0.0367–0.146	4.22±0.09	0.025	8.4±0.2
D	30.0	2.85–28.5	0.0501–0.180	5.00±0.18	0.035	8.2±0.4
(ii) 4-Nitrophenylphenylcyanomethane and 2,2,6,6-tetramethylpiperidine						
H	10.0	4.31–43.1	0.279–1.37	28.1±0.3	0.16	
H	15.0	4.31–43.1	0.32–1.67	35.4±0.6	0.14	
H	20.0	4.31–43.1	0.329–1.93	41.6±1.2	0.155	
H	25.0	4.31–43.1	0.409–2.28	48.1±0.2	0.20	
H	30.0	4.31–43.1	0.643–2.80	55.2±0.7	0.42	
D	10.0	4.82–48.2	0.039–0.194	3.56±0.04	0.021	7.9±0.1
D	15.0	4.82–48.2	0.041–0.238	4.54±0.13	0.022	7.8±0.3
D	20.0	4.82–48.2	0.052–0.285	5.39±0.18	0.028	7.7±0.3
D	25.0	4.82–48.2	0.065–0.355	6.75±0.14	0.031	7.1±0.2
D	30.0	4.82–48.2	0.079–0.425	7.98±0.08	0.041	6.9±0.1
(iii) 4-Nitrophenylphenylcyanomethane and 3,3,6,9,9-pentamethyl-2,10-diazobicyclo[4.4.0]dec-1-ene (PMDBD)						
H	10.0	5.08–25.4	10.1–44.5	1690±30	1.44	
H	15.0	5.08–25.4	10.9–49.0	1880±30	1.46	
H	20.0	5.08–25.4	12.7–56.2	2140±70	1.73	
H	25.0	5.08–25.4	15.1–65.1	2490±80	2.31	
H	30.0	5.08–25.4	17.6–74.3	2750±90	4.46	
D	10.0	5.08–25.4	0.95–3.94	148±5	0.18	11.4±0.4
D	15.0	5.08–25.4	1.06–4.68	177±4	0.17	10.6±0.3
D	20.0	5.08–25.4	1.23–5.34	205±6	0.16	10.4±0.4
D	25.0	5.08–25.4	1.47–6.22	241±8	0.17	10.3±0.5
D	30.0	5.08–25.4	1.71–7.28	272±6	0.35	10.1±0.4
(iv) 4-Nitrophenylphenylcyanomethane and TMG*						
H	25.0	0.49–1.97	5.4–16.9	7860±200	1.5	
D	25.0	1.10–4.40	1.3–3.7	730±30	0.44	10.7
(v) 2-Methyl-4-nitrophenylphenylcyanomethane and 3,3,6,9,9-pentamethyl-2,10-diazabicyclo[4.4.0]dec-1-ene (PMDBD)						
H	10.0	1.28–12.8	1.15–3.14	174±2	0.9	
H	15.0	1.28–12.8	2.58–4.96	205±2	2.3	
H	20.0	1.28–12.8	3.66–6.40	237±2	3.4	
H	25.0	1.28–12.8	5.85–8.96	269±5	5.5	
H	30.0	1.28–12.8	9.08–12.7	317±6	8.6	
H	35.0	1.28–12.8	12.6–14.7	339±3	12.1	
D	10.0	2.54–25.4	0.0441–0.431	16.8±0.2	0.0017	10.4±0.2
D	15.0	2.54–25.4	0.0612–0.530	20.5±0.3	0.0010	10.0±0.2
D	20.0	2.54–25.4	0.0747–0.625	24.1±0.1	0.0011	9.8±0.1
D	25.0	2.54–25.4	0.081–0.726	28.2±0.1	0.0011	9.5±0.2
D	30.0	2.54–25.4	0.097–0.880	34.4±0.2	0.0060	9.2±0.2
D	35.0	2.54–25.4	0.112–0.969	37.6±0.4	0.0021	9.0±0.1
(vi) 2-Methyl-4-nitrophenylphenylcyanomethane and TMG†						
H	25.0	6.5–32.3	4.7–16.1	440±7	2.0	
D	25.0	5.0–50.0	0.28–2.15	43.8±1.9	0.004	10.0±0.5

100±0.5

TABLE 2 (*concluded*)

Transfer	Temp. (°C)	10^3[Base](M)	k_{obs} (s^{-1})	k_2($dm^3\ mol^{-1}\ s^{-1}$)	k_b (s^{-1})	k_H/k_D
(vii) 2-Methyl-4-nitrophenylphenylcyanomethane and DBU†						
H	25.0	0.5–3.0	27.7–103.5	29,300±900	14.6	
D	25.0	1.04–5.2	2.8–15.5	3,050±30	0.30	9.6±0.3

*Reference 11.
†Reference 12.

carbon acid **2**, in accordance with eq. [1].

[1] $AH + B \rightleftharpoons A^-BH^+$

In acetonitrile solvent these reactions gave a product with a single broad strong absorption band at 580 nm for acid **1** and 597 nm for acid **2**. The absorbance values for a series of base concentrations at a constant acid concentration were fitted to eq. [2] for an ion-pair product, where a and b are the initial concentrations of acid and base respectively and A is the equilibrium absorbance

[2] $$a/A = \frac{1}{Kb\varepsilon} + \frac{1}{\varepsilon}$$

The equilibrium constant K and the molar absorptivity ϵ were derived from a plot of a/A vs. $1/b$. A good linear fit, correlation coefficients 0.997–0.9999, verified that the product was an ion-pair. The results are summarized in Table 1, together with those for TMG and DBU from earlier work (2).

The pK_a values of the conjugate acids of the bases **3**, **4**, and **5** were determined by the method described by Leffek *et al.* (6), based on the methods of Coetzee and Padmanabhan (7, 8) and Kolthoff and Chantooni (9, 10), and are included in Table 1.

Despite the good correlation coefficients found for the fit to eq. [2], the values of K are derived from the intercept and the slope of the plot and are subject to larger errors than those indicated by the standard deviations. However, the logarithms of these equilibrium constants correlate with the pK_a except for DBU, which gives an equilibrium constant for the abstraction of the proton from carbon acid **2** about 10 times larger than would be expected from the other equilibrium constants in Table 1. The Hildebrand-Benesi method does not yield highly precise equilibrium constants, particularly when they are large. However, even when a minimum value of 2100 $dm^3\ mol^{-1}$ is assumed for DBU, i.e., 3500 $dm^3\ mol^{-1}$ minus twice the standard deviation, which is close to the equilibrium constant of 2000 ± 200 $dm^3\ mol^{-1}$ determined (2) from the kinetics of the reaction between DBU and carbon acid **2**, the discrepancy between this value and the other equilibrium constants in Table 1 is still well beyond experimental error. Thus DBU is acting as a stronger base in this proton transfer reaction than would be expected from pK_a of 23.9 in acetonitrile (6).

Kinetic measurements

Using the base in large excess, pseudo-first-order rate constants, k_{obs}, were fitted to eq. [3], which may be derived for an equilibrium yielding a single ion-pair product as in eq. [1]. The results obtained at 25°C are shown in Table 2, together with those from previous work (2, 11) with TMG and DBU bases for comparison.

[3] $k_{obs} = k_2[\text{Base}] + k_b$

The equilibrium constants calculated from k_2/k_b in Table 2 are in satisfactory agreement with those listed in Table 1 and, again, log K values from the kinetic data correlate with the pK_a of the conjugate acid of the base, with the exception of DBU noted above.

A Brønsted plot of log k_H against the pK_a of the base for 4-nitrophenylphenylcyanomethane reacting with the four bases listed in Table 2 gives $\beta = 0.53 \pm 0.07$. This is the first β value determined in acetonitrile solvent using pK_a values measured in that solvent and it is remarkably similar to the β value of 0.55 reported by Bordwell and Boyle (12) for several arylnitromethane acids reacting with similar bases in water. The log k_D vs. pK_a plot shows a very similar correlation, with $\beta = 0.50 \pm 0.07$. However, the k_H/k_D values, being much more sensitive measures of the transition state structure, show a reversal in the magnitude of the effect for the two piperidine bases. The smallest isotope effect of 7.1 ± 0.2 at 25°C is found with 2,2,6,6-tetramethylpiperidine **4**, and the *N*-methyl analogue **5**, which is a slightly weaker base, gives $k_H/k_D = 8.4 \pm 0.2$ at 25°C. This difference, well beyond the experimental error of ±(twice the standard deviations), is attributed to the increased steric hindrance in **5** relative to **4**, even though the steric effect is not large enough to be apparent in the Brønsted plots.

For the reaction with the 2-methyl-4-nitrophenylphenylcyanomethane **2** the rate constants are much smaller due to the inhibition of the reaction by the *ortho*-methyl group. The PMDBD base reacts about nine times more slowly at 25°C with the acid **2** than with acid **1**, and the kinetic isotope effect is also smaller although the difference is not much larger than the experimental error. This base is less sensitive to the *ortho*-methyl group than is TMG, which reacts about 18 times more slowly with acid **2** than it does with acid **1**, and the isotope effects with TMG are again diminished slightly from 10.7 to 10.0. The absence of an increase in the isotope effect when the steric hindrance to proton transfer is increased indicates that proton tunnelling is not an important contributor to the rate of this reaction.

The isotope effects on the activation parameters are summarized in Table 3. None of the isotope effects on the enthalpies of activation are beyond the semiclassical limit of 1.1–1.2 kcal mol^{-1}, confirming that there is no significant contribution from proton tunnelling to the reaction rate. These results show that the larger isotope effect found when the nitrogen atom of the piperidine base is methylated results from an entropy of activation effect rather than an enthalpy effect. This indicates that the difference in the isotope effect between the piperidine **4** and the *N*-methylpiperidine **5** probably lies in the difference between the solvent–base interactions for the =N—H and =N—CH_3 groups.

The isotope effects on the activation parameters for PMDBD reacting with the *ortho*-substituted acid **2** are very similar to those for DBU reacting with the same acid (2), i.e., enthalpy isotope effects at about the semiclassical limit of 1.2 kcal mol^{-1} and entropy isotope effects close to zero. Thus, there is no evidence of proton tunnelling and, although PMDBD is a

Can. J. Chem. Downloaded from www.nrcresearchpress.com by 91.121.58.235 on 09/07/12
For personal use only.

TABLE 3. Activation parameters for the proton and deuteron transfer reactions in acetonitrile solvent at 25°C

Parameter	H-transfer		D-transfer
(a) 4-Nitrophenylphenylcyanomethane and 2,2,6,6-tetramethylpiperidine			
$\Delta H‡$ (kcal mol^{-1})	5.1±0.3		6.4±0.2
$\Delta S‡$ (cal mol^{-1} deg^{-1})	−33.8±1.0		−33.4±0.8
$(\Delta H_D‡ - \Delta H_H‡)$		1.3±0.4	
$(\Delta S_D‡ - \Delta S_H‡)$		+0.4±1.3	
(b) 4-Nitrophenylphenylcyanomethane and 1,2,2,6,6-pentamethylpiperidine			
$\Delta H‡$ (kcal mol^{-1})	4.3±0.1		5.1±0.1
$\Delta S‡$ (cal mol^{-1} deg^{-1})	−36.9±0.1		−38.6±0.3
$(\Delta H_D‡ - \Delta H_H‡)$		0.8±0.1	
$(\Delta S_D‡ - \Delta S_H‡)$		−1.7±0.4	
(c) 4-Nitrophenylphenylcyanomethane and PMDBD			
$\Delta H‡$ (kcal mol^{-1})	3.7±0.2		4.6±0.1
$\Delta S‡$ (cal mol^{-1} deg^{-1})	−30.7±0.6		−32.1±0.5
$(\Delta H_D‡ - \Delta H_H‡)$		0.9±0.2	
$(\Delta S_D‡ - \Delta S_H‡)$		−1.4±0.8	
(d) 2-Methyl-4-nitrophenylphenylcyanomethane and PMDBD			
$\Delta H‡$ (kcal mol^{-1})	4.2±0.2		5.4±0.2
$\Delta S‡$ (cal mol^{-1} deg^{-1})	−33.5±0.6		−33.8±0.6
$(\Delta H_D‡ - \Delta H_H‡)$		1.2±0.3	
$(\Delta S_D‡ - \Delta S_H‡)$		−0.3±0.8	

weaker base than DBU and more sterically hindered, the width of the barrier to proton transfer must be very similar for both bases.

In general, the results show that there is no direct relationship between extensive steric hindrance and proton tunnelling and that isotope effects may be increased beyond the semiclassical limit of $k_H/k_D = 7$ at 25°C by entropy of activation effects, so that rate ratios alone may not be used as evidence for proton tunnelling.

Experimental

Materials

4-Nitrophenylphenylcyanomethane and (2-methyl-4-nitrophenyl)-phenylcyanomethane and their deuterated analogues were prepared following the procedure previously described (11).

3,3,6,9-Pentamethyl-2,10-diazabicyclo[4.4.0]dec-1-ene was synthesized according to the procedure described by Heinzer *et al.* (13) with minor modifications.

A mixture of 21 mL 10 M BuLi solution in hexanes and 250 mL of dry ether was cooled to −65°C. To this solution, 28.3 mL of freshly distilled diisopropylamine was added dropwise with stirring. The temperature remained below −60°C. After about 5 min 7.2 mL (5.5 g) of freshly distilled propionitrile was added dropwise. The resulting mixture was stirred for another 30 min. Then 30 g of isoprene hydrobromide was added, keeping the temperature below −50°C. The reaction mixture was stirred for 1.5 h at −65°C followed by an additional 1 h of stirring at room temperature. The flask contents were poured onto ice and acidified with 100 mL of 10% H_2SO_4.

The organic phase was separated, and the water phase was extracted three times with 80-mL portions of diethyl ether. The combined ethereal extracts were washed with $NaHCO_3$ and NaCl and dried overnight with $MgSO_4$. After evaporating the solvent, the product, 5-cyano-2,5,8-trimethylnona-2,7-diene, was used for the next step of synthesis without further purification.

This compound (20 g) was dissolved in 75 mL of dry benzene (distilled from calcium hydride) and 28 mL of a 50% suspension of sodium amide in toluene was added at once. The resulting mixture was refluxed and the progress of the reaction checked by TLC (eluent hexanes:ether 9:1, silica gel). The reaction was completed after 8 h. Then, small portions of ice were added to decompose the remaining $NaNH_2$, and the mixture was stirred with gentle heating to cause liberation of ammonia. This could be facilitated by passing nitrogen through the mixture.

The organic layer was separated and the water phase extracted three times with ether. The combined organic extracts were acidified with four portions of 2 N H_2SO_4. The acidic water was cooled in an ice bath and made alkaline with NaOH pellets to reach pH > 12. The liberated base was separated and the water phase extracted three times with 50-mL portions of ether. The combined extracts were dried over anhydrous K_2CO_3. The purity of the product, 5-amidino-2,5,8-trimethylnona-2,7-diene, was checked by means of NMR and GC-MS.

Ten grams of the product were dissolved in 80 mL of freshly distilled methylene chloride and cooled to 0°C. Gaseous dry HCl was passed through the solution until the pH reached 2. Then the solvent was evaporated and remaining oily substance dried *in vacuo* until a constant mass was reached. A round-bottom flask containing the hydrochloride was provided with a $CaCl_2$ drying tube and heated at 200°C. After the evolution of gaseous HCl had stopped, the flask was closed with a stopcock and heated for an additional 20 h. After cooling, the mixture was dissolved in 100 mL of water and acidified with 30 mL of 2 N H_2SO_4.

The water phase was extracted three times with ether, cooled to 0°C, and NaOH pellets added to reach pH > 12. The alkaline solution was then extracted with ether and the combined extracts dried overnight with anhydrous K_2CO_3. The product was vacuum-distilled to give a dense colourless oil (bp 110°C/3 Torr (1 Torr = 133.3 Pa) (lit. (13) bp 65°C/0.07 Torr). The NMR spectrum of 3,3,6,9,9-pentamethyl-2,10-diazabicyclo[4.4.0]dec-1-ene (CCl_4/TMS) showed 1.06/1.12 (s/s, 6H), 1.19 (s, 3H), 1.21–2.0 (m, 8H), 3.38 (s, NH). The latter signal

Can. J. Chem. Downloaded from www.nrcresearchpress.com by 91.121.58.235 on 09/07/12
For personal use only.

disappeared when the NMR spectrum was run in $CDCl_3$. Picrate: mp 233–234°C.

2,2,6,6-Tetramethylpiperidine and 1,2,2,6,6-pentamethylpiperdine (Aldrich) were dried over KOH and distilled fractionally under vacuum immediately before use. Picrate mp's: 230–231°C and 239–241°C respectively.

Reagent grade acetonitrile was purified by the method of O'Donnell (14) followed by distillation from calcium hydride and final fractional distillation from P_2O_5.

pK_a measurements

These measurements were made using the potentiometric procedure described by Leffek *et al.* (6).

Equilibrium measurements

The absorbance at equilibrium was measured using a Cary 219 spectrometer with a thermostating device. Acid concentrations of 1×10^{-5} and 2×10^{-5} M were used; base concentrations were in excess by factors ranging from 20 to 2000.

Kinetic measurements

Pseudo-first-order rate constants were measured using a Durrum–Gibson stopped-flow spectrometer. Acid and base concentrations are shown in Table 2. Calculations of the rate constants were made using the Guggenheim method (15). The activation parameters were calculated by a least-squares fit to the transition state theory equation.

1. M. Hojatti and K. T. Leffek. Can. J. Chem. **62**, 2653 (1984).
2. K. T. Leffek and P. Pruszynski. Can. J. Chem. **66**, 1454 (1988).
3. N. Sugimoto and M. Sasaki. J. Chem. Soc. Faraday Trans. **81**, 1441 (1985).
4. F. G. Bordwell and D. L. Hughes. J. Am. Chem. Soc. **107**, 4737 (1985).
5. H. A. Benesi and H. H. Hildebrand. J. Am. Chem. Soc. **71**, 2703 (1943).
6. K. T. Leffek, P. Pruszynski, and K. Thanapaalasingham. Can. J. Chem. **67**, 590 (1989).
7. J. F. Coetzee and G. R. Padmanabhan. J. Phys. Chem. **66**, 1708 (1962).
8. J. F. Coetzee and G. R. Padmanabhan. J. Am. Chem. Soc. **87**, 5005 (1965).
9. I. M. Kolthoff and M. K. Chantooni, Jr. J. Am. Chem. Soc. **87**, 4428 (1965).
10. I. M. Kolthoff, M. K. Chantooni, Jr., and S. Bhowmik, J. Am. Chem. Soc. **90**, 23 (1968).
11. A. Jarczewski, P. Pruszynski, and K. T. Leffek. Can, J. Chem. **61**, 2029 (1983).
12. F. G. Bordwell and W. J. Boyle, Jr. J. Am. Chem. Soc. **94**, 3907 (1972).
13. F. Heinzer, M. Soukup, and A. Eschenmoser. Helv. Chim. Acta, **61**, 2851 (1978).
14. J. F. O'Donnell, J. T. Ayers, and C. K. Mann. Anal. Chem. **37**, 1161 (1965).
15. E. A. Guggenheim. Philos. Mag. **2**, 538 (1926).

Can. J. Chem. Downloaded from www.nrcresearchpress.com by 91.121.58.235 on 09/07/12
For personal use only.

On the electron transfer and hydrogen atom abstraction mechanism for 1-benzyl-1,4-dihydronicotinamide reduction of benzoquinones

DENNIS D. TANNER,[1] ABDELMAJID KHARRAT,[2] AND H. OUMAR-MAHAMAT[3]

The Department of Chemistry, The University of Alberta, Edmonton, Alberta, Canada T6G 2G2

Received September 5, 1989

This paper is dedicated to Professor Ross Stewart on the occasion of his 65th birthday

DENNIS D. TANNER, ABDELMAJID KHARRAT, and H. OUMAR-MAHAMAT. Can. J. Chem. **68**, 1662 (1990).

The reduction of *p*-benzoquinone (BQ) by 1-benzyl-1,4-dihydronicotinamide (BNAH) proceeds by a free-radical chain mechanism initiated by single electron transfer (SET). In dry deoxygenated acetonitrile, the chain, whose propagation steps contain a SET–hydrogen atom transfer sequence, could be inhibited by dinitrobenzene and initiated by di-*tert*-butylperoxyoxalate. The reduction does not follow second-order reaction kinetics. The fractional order of each reactant was found to be 0.80 and 1.36 for BNAH and BQ, respectively. The ΔG^0 values for both the initiation and the propagation steps were evaluated electrochemically (CV) and were found to be of a reasonable magnitude to sustain a free-radical chain process.

Key words: 1-benzyl-1,4-dihydronicotinamide, *p*-benzoquinone, free radical, reduction.

DENNIS D. TANNER, ABDELMAJID KHARRAT et H. OUMAR-MAHAMAT. Can. J. Chem. **68**, 1662 (1990).

La réduction de la *p*-benzoquinone (BQ) par la 1-benzyl-1,4-dihydronicotinamide (BNAH) se produit par un mécanisme radicalaire en chaîne qui est initié par un transfert d'électron unique (TEU). Dans de l'acétonitrile désoxygéné, la chaîne, dont les étapes de propagation comportent une séquence de transfert d'atome d'hydrogène par un TEU, peut être inhibée par le dinitrobenzène et initiée par le peroxyoxalate de di-*tert*-butyle. La réduction ne suit pas une cinétique d'ordre deux. On a trouvé que l'ordre fractionnaire pour chacun des réactifs est de 0,80 et de 1,36 respectivement pour la BNAH et la BQ. Faisant appel à des méthodes électrochimiques (CV), on a évalué les ΔG^0 des étapes d'initiation et de propagation et on a trouvé qu'ils sont d'une amplitude telle qu'ils permettent un processus radicalaire en chaîne.

Mots clés : 1-benzyl-1,4-dihydronicotinamide, *p*-benzoquinone, radical libre, réduction.

[Traduit par la revue]

Can. J. Chem. Downloaded from www.nrcresearchpress.com by 91.121.58.235 on 09/07/12
For personal use only.

Introduction

A recent communication (1) has prompted us to report the results of our investigation of the mechanism of the reduction of benzoquinone by the NADH model compound, 1-benzyl-1,4-dihydronicotinamide (BNAH). Previously we reported that the reductions by BNAH and a series of substituted dihydronicotinamides (DHN's) reacted with a variety of substrates via a free-radical chain process (2–4). Both the initiation and propagation sequences contained an electron transfer reaction, see Scheme 1. The mechanistic path followed during these reductions, however, is substrate specific, since under the same reaction conditions the reduction of *N*-methyl acridinium iodide proceeds by a hydride transfer process (Scheme 2) (3).

During the course of our studies the electron transfer initiation process was substantiated for substrates with high electron affinities by the observation that 2,6-di-*tert*-butyl benzoquinone gives strong EPR signals for the 2,6-di-*tert*-butyl benzoquinone radical anion. Since a rate-limiting step in the chain reduction of the quinone would be the single electron transfer (SET) initiation (3), it was suprising to learn from the report of the studies of the BNAH reduction of benzoquinone, a substrate that is more reactive than 2,6-di-*tert*-butylbenzoquinone, that the authors had concluded that the reduction proceeds by a hydride transfer mechanism (1).

Results

Several mechanisms have been proposed to rationalize the reduction reactions of a hydride equivalent acceptor with BNAH. Besides a heterolytic hydride transfer, three homolytic processes have been suggested: SET–proton–SET (5) or a SET – hydrogen atom transfer, both from a geminate caged pair (6), and a SET – hydrogen atom abstraction radical chain (2–4). A kinetic analysis of the progress of the reaction requires second-order kinetics for both the heterolytic process and the homolytic reactions involving caged species. In the case of the radical chain process initiated by SET, only a chain terminated solely by cross termination shows second-order kinetics (3), eq. [11] (Scheme 3).

The reduction of *p*-benzoquinone (BQ) with BNAH was carried out in dry acetonitrile (23°C). Contrary to the previous report by Tanaka and co-workers (7), when equal concentrations (10^{-3} M) of each reactant are used, a plot of the second-order reaction rate ($1/(A_\infty - A)$ vs. time) is not found to be linear (see Fig. 1).

The kinetics of the reduction reaction with DHN's have been studied in water or in a mixed aqueous–organic solvent (6, 8–10). In the reduction of methyl acridinium iodide by NADH models (3) we had observed that the addition of a small amount of water (1–5%) increased the curvature of the second-order plot with a decrease in the instantaneous rate at $t = 0$. In this study the addition of small amounts of water (1%) produced a linear second-order plot, see Fig. 2, but with an increase in the rate of reaction. Since the presence of a small amount of water changed the kinetics, and undoubtedly the mechanism of the reaction, the solvent of choice was dry acetonitrile.

The rate of reduction in dry acetonitrile could be inhibited by the addition of small amounts of DNB (5–10%) and initiated by di-*tert*-butylperoxyoxalate, see Fig. 3.

The kinetic behaviour of the BQ reduction is consistent with a free-radical chain mechanism. As proposed previously (2–4), the electron transfer takes place in both the initiation and propagation steps (Scheme 4).

Tanaka and co-workers (7) reported a kinetic isotope effect for the reduction of BQ with 4-deutero-*N*-benzyldihydronicotinamide. The isotope effect indicates that the rate-determining

[1]Author to whom correspondence may be addressed.
[2]Postdoctorate Fellow, University of Alberta, 1986–1988.
[3]Postdoctorate Fellow, University of Alberta, 1988–1989.

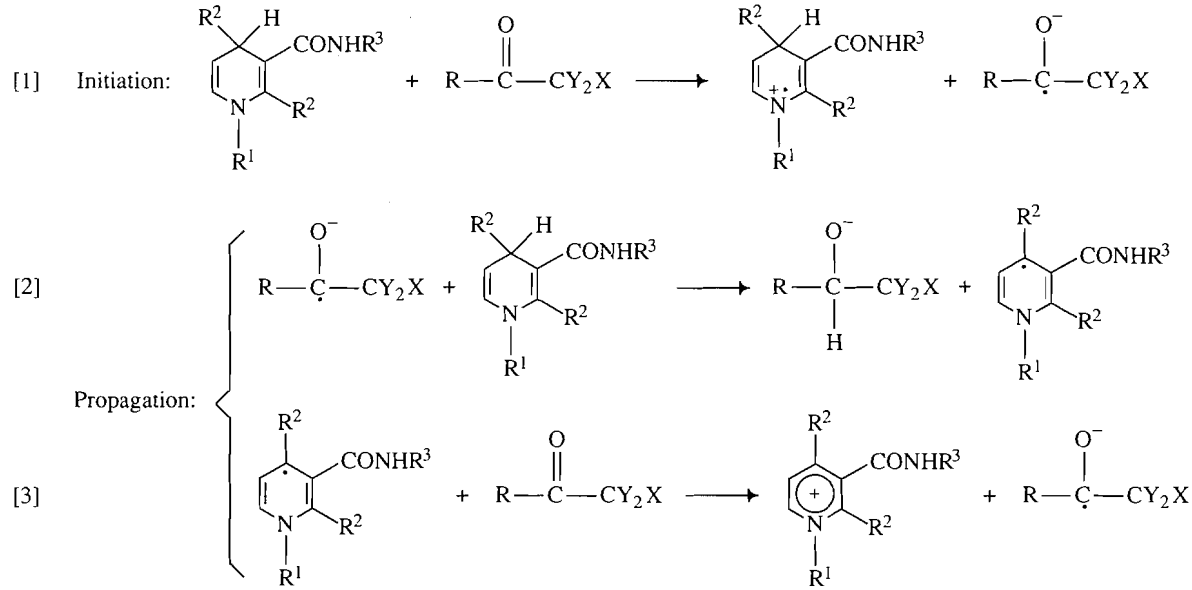

SCHEME 1

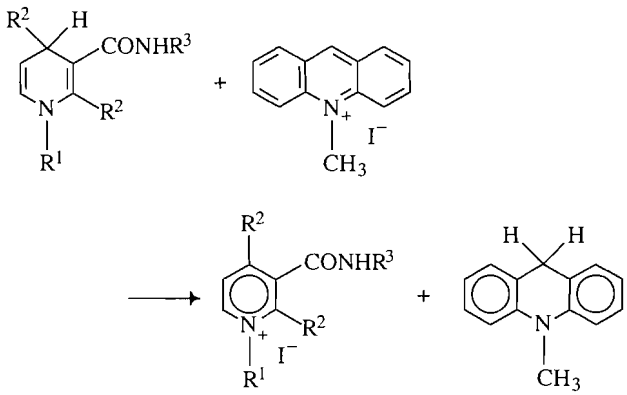

SCHEME 2

[5] Initiation: $AH + B \xrightarrow{k_i} AH^{+\bullet} + B^{-\bullet}$

[6] Propagation: $AH + B^{-\bullet} \xrightarrow{k_1} A^{\bullet} + BH^{-}$

[7] Propagation: $A^{\bullet} + B \xrightarrow{k_2} A^{+} + B^{-\bullet}$

[8] Termination: $2A^{\bullet} \xrightarrow{2k_3} P_1$

[9] Termination: $A^{\bullet} + B^{-\bullet} \xrightarrow{k_4} P_2$

[10] Termination: $2B^{-\bullet} \xrightarrow{2k_5} P_3$

[11] $$\frac{-d[AH]}{dt} = k_i[AH][B]\left[2+\left(\frac{k_1k_2}{k_4k_i}\right)^{1/2} + k_1\left(\frac{[AH]}{2k_ik_5[B]}\right)^{1/2} + k_2\left(\frac{[B]}{2k_3k_i[AH]}\right)^{1/2}\right]$$

SCHEME 3

step is the hydrogen atom abstraction, eq. [13]. The hydrogen atom abstraction mechanism had been discarded by Tanaka (11) since it was thought to be inconsistent with their linear kinetic data. Carlson and Miller (10) conceded that the hydrogen atom abstraction mechanism process proposed was possible; however, this was not investigated further.

The kinetic expression for the free-radical chain processes when cross termination is not the sole termination step can be formulated as

[18] $$\text{rate} = k_{obs}[BQ]^a[BNAH]^b$$

where a and b are the fractional order of BQ and BNAH, respectively.

To evaluate a and b in eq. [18], the difference in the log of the initial rate of reaction was determined at several values of ratios of concentration for the reactants (r):

[19] $$a \text{ or } b = \left[\log\left(\frac{dx}{dt}\right)_{0,I} - \log\left(\frac{dx}{dt}\right)_{0,II}\right] \Big/ \log r$$

where $(dx/dt)_0$ is the initial rate at concentration I or II, which can be evaluated graphically using the plot of absorbance versus time (12). Table 1 summarizes the results.

We have reported (3) that the kinetic expression for a free-radical chain process depends upon the termination step. Equation [11] can be transformed into the general expression for a kinetic chain, in which cross termination may not be the sole termination process:

[20] $$\begin{aligned}\text{rate} = &\left(2+\left(\frac{k_1k_2}{k_4k_i}\right)^{1/2}\right)k_i[BNAH][BQ] \\ &+ \frac{k_1k_i}{(2k_ik5)^{1/2}}[BNAH][BQ]\frac{[BNAH]^{1/2}}{[BQ]^{1/2}} \\ &+ \frac{k_4k_i}{(2k_3k_i)^{1/2}}[BNAH][BQ]\frac{[BQ]^{1/2}}{[BNAH]^{1/2}} \\ &= k_1[BNAH][BQ] + k_2[BNAH]^{3/2}[BQ]^{1/2} \\ &+ k_3[BNAH]^{1/2}[BQ]^{3/2}\end{aligned}$$

From the initial rate data we have shown that the reaction has a

Can. J. Chem. Downloaded from www.nrcresearchpress.com by 91.121.58.235 on 09/07/12
For personal use only.

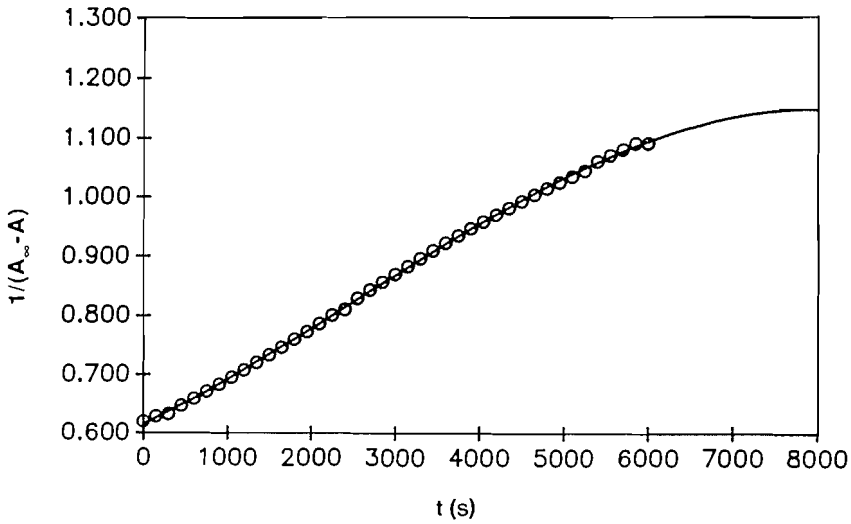

FIG. 1. Plot of the second-order rate of reaction; [BQ] and [BNAH] = 1.00×10^{-3} M.

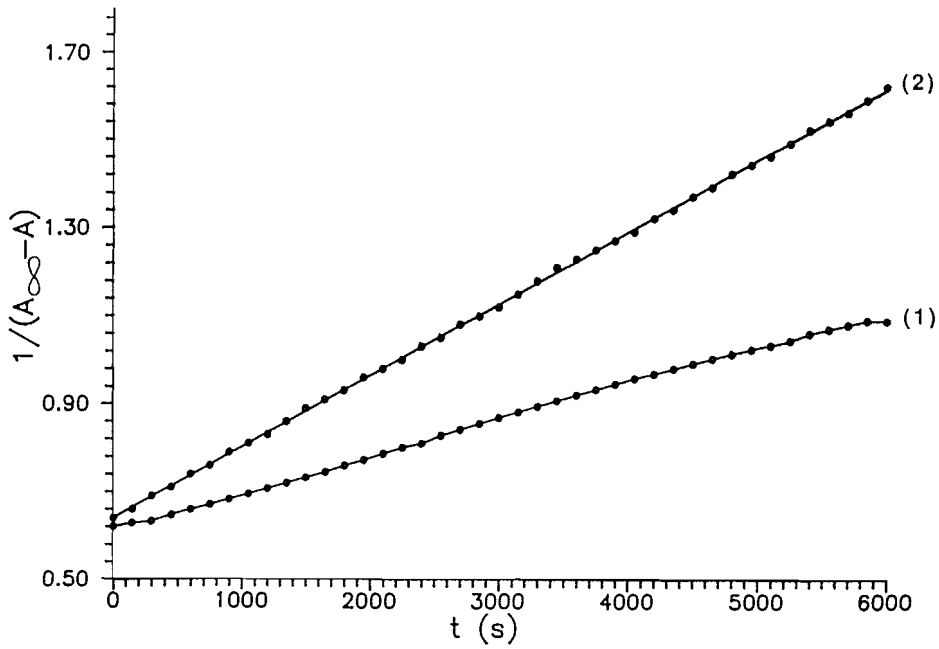

FIG. 2. Comparison plots of second-order rates of reaction [BQ] and [BNAH], 1.00×10^{-3} M, in dry acetonitrile (1), and in 1% water–acetonitrile (2).

fractional order (rate = k_{obs}[BNAH]$^{0.80}$[BQ]$^{1.36}$). The rate expression suggests that several termination steps are involved, and that cross termination, eq. [16], is not the dominant process.

The plots for the pseudo first-order reaction of either reactant are not linear; however, when the solutions were not deoxygenated a straight line was observed and the second-order rate constant obtained was similar to the value reported by Tanaka (7). The radical chain appears to be inihibited by atmospheric oxygen.

Tanaka and co-workers (7) reported that plots of the observed rate constant versus the concentration of [BQ] or [BNAH] are linear, and that the [BNAH] plot had a larger slope than the plot of [BQ] vs. k_{obs}. They argued that the difference in the slopes was due to the stoichiometry of the reaction. When our data were plotted in this manner two curves were obtained (Fig. 4), and although the BNAH plot does have the larger slope at concentrations $>1.5 \times 10^{-3}$, neither plot was linear.

Thermochemical aspects for the reduction

The value of the redox potential of *p*-benzoquinone (−0.50 V vs. SCE in acetonitrile) has previously been reported (1). For BNAH, several values for the redox potential in acetonitrile have been reported (13).[4] We have chosen +0.57 V vs. SCE (13) because the CV technique used in these studies was similar to those used to determine the E^0 for *p*-benzoquinone. The ΔG^0 for the initiation step using these redox potentials is equal to 24.7 kcal mol^{-1}, and although it is rather high it is not an unreasonable value for the initiation of a free-radical chain process. Supporting evidence was obtained for the electron transfer initiation reaction when solutions of [BQ], 3×10^{-3} M, and [BNAH], 3×10^{-3} M, were degassed and mixed in an EPR tube, and the ESR spectrum was taken. The spectrum appeared

[4]A value by the same authors (13) using a fluorescence quenching technique gave quite similar results, 0.60 V vs. SCE.

Can. J. Chem. Downloaded from www.nrcresearchpress.com by 91.121.58.235 on 09/07/12
For personal use only.

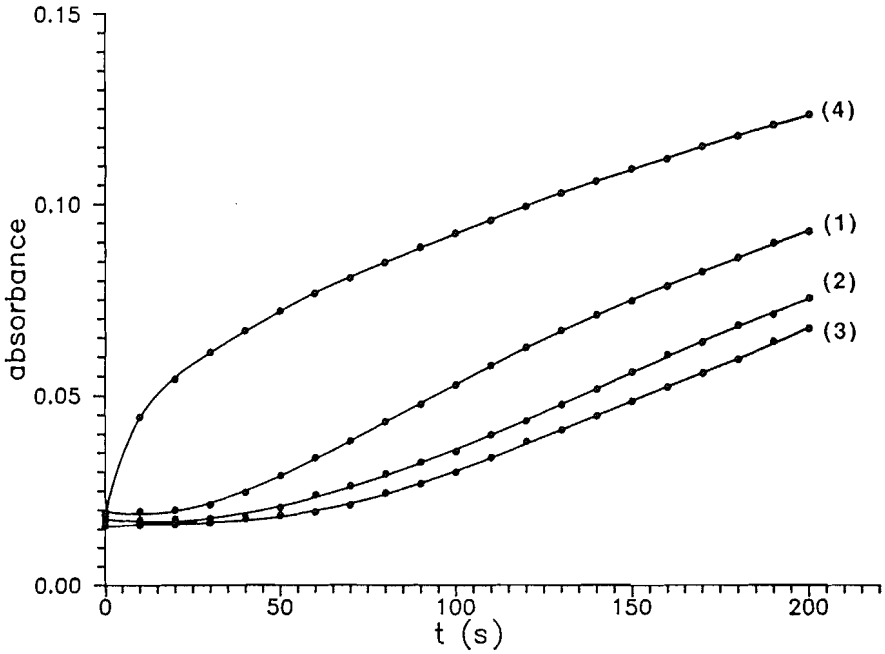

FIG. 3. Absorbance vs. time observed for [BQ] and [BNAH], 1.00×10^{-3} M: (1) without additives; (2) with 5% DNB; (3) with 10% DNB; (4) with 10% DTBPO.

Can. J. Chem. Downloaded from www.nrcresearchpress.com by 91.121.58.235 on 09/07/12
For personal use only.

[12] Initiation:

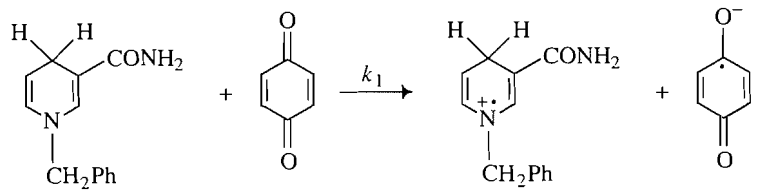

BNAH BQ

Propagation:

[13]

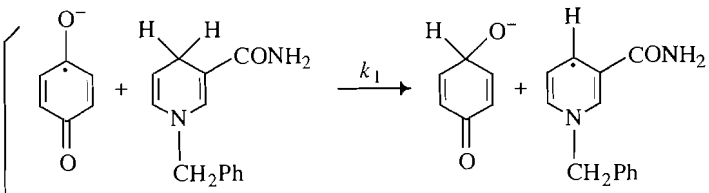

[14]

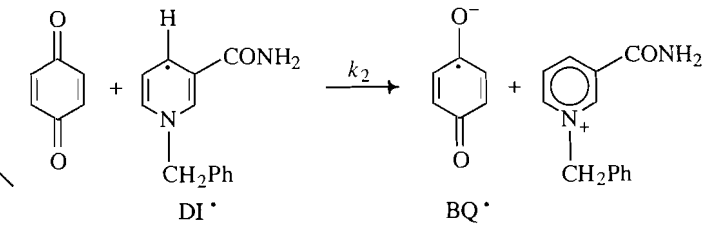

DI• BQ•

Termination:

[15] $2DI^{\bullet} \xrightarrow{2k_3} P_1$

[16] $DI^{\bullet} + BQ^{\bullet} \xrightarrow{k_4} P_2$

[17] $2BQ^{\bullet} \xrightarrow{2k_5} P_3$

SCHEME 4

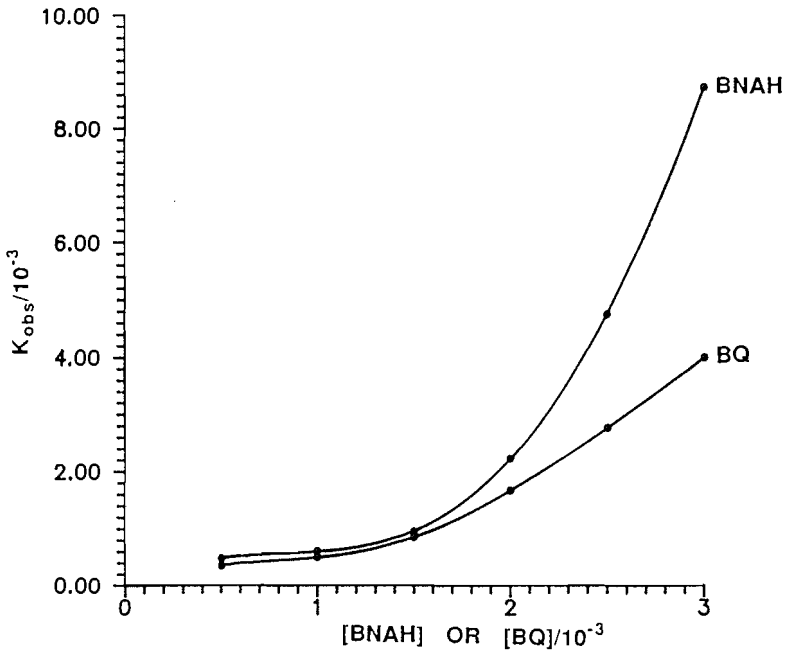

FIG. 4. Pseudo first-order rate constant, K_{obs}, vs. [BQ] and [BNAH] in deoxygenated dry acetonitrile.

TABLE 1. Determination of the fractional order by changing the concentration of BQ and BNAH using eq. [19]

[BQ]	[BNAH]	r	a	b
2×10^{-3}	10^{-3}	2	1.34	
1.8×10^{-3}	10^{-3}	1.8	1.34	
1.3×10^{-3}	10^{-3}	1.3	1.4	
10^{-3}	2×10^{-3}	2		0.79
10^{-3}	1.8×10^{-3}	1.8		0.79
10^{-3}	1.5×10^{-3}	1.5		0.81
		Average	1.36±0.02	0.80±0.01

immediately, showing the five lines of the *p*-benzoquinone radical anion. The spectrum observed is completely consistent with the observed formation of the charge transfer complexes between BNAH and *p*-benzoquinone derivatives reported by Tanaka and co-workers (7, 11, 14).

The feasibility of the electron transfer step in the propagation sequence could be evaluated electrochemically. The redox potential for BNA^+ is determined to be −0.94 V vs. SCE in acetonitrile (glassy carbon electrode). ΔG^0 for the electron transfer, in eq. [14], is evaluated to be exergonic, −10.1 kcal mol^{-1}. The thermochemical data are consistent with the proposed free-radical chain mechanism.

Conclusion

The *N*-benzyl-1,4-dihydronicotinamide used as a biomimetic model for enzyme-controlled reductions by NADH reduces *p*-benzoquinone by a free-radical chain mechanism in dry and deoxygenated acetonitrile. Kinetic studies show that the reduction is not a second-order reaction.

Since a free-radical chain process could not take place in the enzyme-controlled reaction, the model studies when run under these conditions cannot be extended to the biological systems.

Experimental

Materials

Reagent acetonitrile (Caledon, HPLC grade) was purified by successive distillations over potassium permanganate and sodium carbonate. The distillate was treated with several drops of concentrated sulfuric acid and redistilled. Finally it was distilled again from calcium hydride.

1-Benzyl-1,4-dihydronicotinamide was described in an earlier paper (2). *p*-Benzoquinone (Matheson Coleman and Bell) was dried under vacuum over P_2O_5, mp 113°C (lit. (15) mp 113–115°C). *m*-Dinitrobenzene (Fisher) was recrystallized from ethanol, mp 89°C (lit. (16) mp 80–90°C). Di-*tert*-butyl peroxyoxalate was prepared according to the literature procedure (17).

General procedure for determination of the kinetics of the reduction p-*benzoquinone by BNAH*

Acetonitrile solution containing 3×10^{-3} M of *p*-benzoquinone or 3×10^{-3} M BNAH was deoxygenated by bubbling dry argon for 15 min through each solution, protected from the atmosphere with a septum. After the solutions were deoxygenated the concentration of each solution was readjusted by the syringe addition of a few drops of previously deoxygenated acetonitrile.

An aliquot of each solution with the corresponding concentration (with or without additives) was transferred by syringe to the ultraviolet cell, protected by a septum at room temperature. When the reaction was initiated a stop-flow apparatus was used.

The kinetics were investigated as described in the literature (7) using an ultraviolet HP 8450A diode array spectrophotometer connected to an HP 7470A plotter and an HP 82901 M flexible disc drive.

The pseudo first-order rates were investigated by using 10-fold excess BNAH or *p*-benzoquinone. For the determination of the fractional order of each reactant, three ratios (r) of concentration were used: 1.5, 1.8, and 2. The order given is the mean value of three determinations (see text).

The kinetic data were investigated by least-squares curve fitting.

ESR spectroscopy

The ESR spectra were obtained for the radical anion of *p*-benzoquinone by mixing a 3×10^{-3} M solution of the quinone and 3×10^{-3} M BNAH in acetonitrile at room temperature. A Brucker ER 200 E/D spectrometer was used to record the spectra.

Can. J. Chem. Downloaded from www.nrcresearchpress.com by 91.121.58.235 on 09/07/12
For personal use only.

Cyclic voltammetry

The electrochemistry of BNA^+ was studied as previously described (18), using a glassy carbon electrode. The reversible wave was observed at a scan rate equal to 50 V/s.

1. L. L. MILLER and J. R. VALENTINE. J. Am. Chem. Soc. **110**, 3982 (1988).
2. D. D. TANNER, H. K. SINGH, A. KHARRAT, and A. R. STEIN. J. Org. Chem. **52**, 2142 (1987).
3. D. D. TANNER and A. KHARRAT. J. Org. Chem. **53**, 1646 (1988).
4. D. D. TANNER and A. KHARRAT. J. Am. Chem. Soc. **110**, 2968 (1988).
5. A. OHNO, T. SHIO, H. YAMAMOTO, and S. OKA. J. Am. Chem. Soc. **103**, 2041 (1981); **108** 2045 (1981).
6. J. W. BUNTING, V. S. F. CHEW, G. CHU, N. P. FITZGERALD, A. GUNASEKARA, and H. T. P. OH. Bioorg. Chem. **12**, 141 (1984).
7. S. FUKUZUMI, N. NISHIZAWA, and T. TANAKA. J. Org. Chem. **49**, 3571 (1984).
8. D. J. CREIGHTON, J. HAJDU, G. MOOSER, and D. S. SIGMAN. J. Am. Chem. Soc. **95**, 6855 (1973).
9. A. VAN. LAAR, H. J. VAN RAMESDONK, and J. W. VERHOEVEN. Recl: J. R. Neth. Chem. Soc. **102**, 158 (1983).
10. B. W. CARLSON and L. L. MILLER. J. Am. Chem. Soc. **107**, 479 (1985).
11. S. FUKUZUMI, S. KOUMITSOU, K. HIRONAKA, and T. TANAKA. J. Am. Chem. Soc. **109**, 305 (1987).
12. R. LIVINGSTON. *In* Investigation of rates and mechanisms of reaction. *Edited by* S. L. Friess, E. S. Lewis, and A. Weissberger. Interscience, New York. 1961. Chap. V. p. 124.
13. S. FUKUZUMI, K. HIRONAKA, N. NISHIZAWA, and T. TANAKA. Bull. Soc. Chem. Jpn. **56**, 2220 (1983).
14. S. FUKUZUMI, N. NISHIZAWA, and T. TANAKA. J. Chem. Soc. Perkin Trans. 2, 371 (1985); Chem. Lett. 1755 (1983).
15. O. HESSE. Liebigs Ann. Chem. **114**, 300 (1860).
16. T. S. PATTERSON. J. Chem. Soc. **93**, 1855 (1908).
17. P. D. BARTLETT, E. P. BENZING, and R. E. PINCOCK. J. Am. Chem. Soc. **82**, 1762 (1960).
18. D. D. TANNER, N. DEONARIAN, and A. KHARRAT. Can. J. Chem. **67**, 171 (1989).

Can. J. Chem. Downloaded from www.nrcresearchpress.com by 91.121.58.235 on 09/07/12
For personal use only.

The chain carriers of intermolecular hydrogen abstraction in the photobromination with *N*-bromosuccinimide; modifications of the chain carriers

YU-HUANG ZHANG, MING-HUA DONG, XI-KUI JIANG, AND YUAN L. CHOW[1]

Shanghai Institute of Organic Chemistry, Academia Sinica, 345, Ling-Ling Lu, Shanghai, The People's Republic of China

Received January 26, 1990

This paper is dedicated to Professor Ross Stewart on the occasion of his 65th birthday

YU-HUANG ZHANG, MING-HUA DONG, XI-KUI JIANG, and YUAN L. CHOW. Can. J. Chem. **68**, 1668 (1990).

The photoinitiated bromination of 1-chloropentane with *N*-bromosuccinimide (NBS) in the presence of Br_2 is compared with that of NBS and 1,1-dichloroethene to generate the succinimidyl radical (S$^\bullet$) and with that of $Br_2 + K_2CO_3$ to generate the bromine atom (Br$^\bullet$) as the chain carriers. The relative reactivities of intermolecular H-abstraction (*r*-values) shown by the NBS + Br_2 system decrease to levels lower than those shown by either S$^\bullet$ or Br$^\bullet$ chain propagations at lower temperatures under appropriate conditions: these observations indicate the presence of a new chain propagating species that is assumed to be the bromine radical complex (BRC) modified from S$^\bullet$ or Br$^\bullet$ reversibly under the experimental conditions. Supporting evidence for the equilibria of S$^\bullet$, Br$^\bullet$, and BRC in the photodecomposition of NBS + Br_2 is discussed. The unusual H-abstraction reactivity of Br$^\bullet$ toward the methyl hydrogens of 1-chloropentane was noted; this serves as independent support for the presence of a new radical propagation species.

Key words: *N*-bromosuccinimide, succinimidyl radical, photobromination, bromine radical complex.

YU-HUANG ZHANG, MING-HUA DONG, XI-KUI JIANG et YUAN L. CHOW. Can. J. Chem. **68**, 1668 (1990).

On a comparé la bromation photoinitiée du 1-chloropentane par la *N*-bromosuccinimide (NBS) en présence de Br_2 avec celles réalisées par la NBS et le 1,1-dichloroéthène pour générer les radicaux succinimidyles (S$^\bullet$) et par le $Br_2 + K_2CO_3$ pour générer l'atome de brome (Br$^\bullet$) comme propagateur de la chaîne. On a démontré que les réactivités relatives d'enlèvement intermoléculaires d'hydrogène (valeurs-*r*) pour le système NBS + Br_2 diminue jusqu'à des valeurs qui sont plus basses que celles observées avec les propagations de chaîne à l'aide de S$^\bullet$ ou de Br$^\bullet$, à des températures plus basses et des conditions appropriées : ces observations suggèrent l'apparition d'une nouvelle espèce pour propager la chaîne et on fait l'hypothèse qu'il s'agit d'un complexe radicalaire de brome (CRB) qui a été modifié d'une façon réversible à partir du S$^\bullet$ ou du Br$^\bullet$, dans les conditions expérimentales. On discute des données suggérant l'existence de l'équilibre S$^\bullet$, Br$^\bullet$ et CRB dans la photodécomposition du NBS + Br_2. On a noté la réactivité inhabituelle du Br$^\bullet$ dans l'enlèvement d'hydrogènes des groupements méthyles du 1-chloropentane; ce résultat sert de support indépendant pour la présence d'une nouvelle espèce pour la propagation des radicaux.

Mots clés : *N*-bromosuccinimide, radical succinimidyle, photobromination, complexe radicalaire de brome.

[Traduit par la revue]

Introduction

Mechanistic studies of the photodecomposition of *N*-bromosuccinimide (NBS) under various conditions have caused many controversies over the number and nature of the chain propagating species (1–8). The claim (4–7) of "the generation and identification of excited state and ground state Σ–Π succinimidyl radicals" appears to arise from experimental artefacts and has been withdrawn (3). Recently it was shown (9, 10) that the photoexcitation of NBS in the presence of 1,1-dichloroethene (DCE) causes the enhanced ring-opening reaction to form extra amounts of β-bromopropionyl isocyanate (BPI) from the excited state *NBS directly or via a vibrationally "hot" succinimidyl radical (†S$^\bullet$) (Scheme 1); this observation has led to the discussion of probable sources of previous controversies (1–8). Reviews of the NBS photodecomposition and details of the controversies are described in recent publications (1–3) and will not be repeated here.

There exists another controversy, namely the type of chain carriers involved in photobromination with NBS in the presence of Br_2. In a recent paper Skell *et al.* (3) reiterated the previous claim that the photodecomposition of 2,2-dimethyl-*N*-bromosuccinimide (or NBS) in the presence of bromine must involve a third propagating radical in addition to Br$^\bullet$ and the succinimidyl radicals (S$^\bullet$). While this paper (3) reports some evidence for the claim, the line of arguments has been questioned since it compares the percentage yields of the ring-opened product under different photolysis conditions as a criterion for judging the reaction pattern; such comparisons may cause serious errors because of the presence of two parallel channels for the formation of the ring-opened product in direct excitation of NBS. Results from Tanner's and Walling's groups (1, 2, 8) indicate that simple competing S$^\bullet$ and Br$^\bullet$ propagation processes can adequately explain this photobromination system with the exception of some experiments that imply the presence of a third propagating radical. Indeed in the photodecomposition of NBS + Br_2, using either neopentane (1, 4, 8) or cyclohexane (9) as a substrate in CH_2Cl_2, the patterns of relative reactivities (*r*-values) do not require proposing a third chain propagating intermediate in intermolecular H-abstraction. Controlled photolysis of the NBS + Br_2 system or of NBS without the addition of DCE to scavenge Br_2 or Br$^\bullet$ shows that these photobromination systems can be explained by reactions involving S$^\bullet$ and Br$^\bullet$ as the chain propagating species, which are interrelated by the fast equilibria (9, 11, 12) shown in Scheme 2. A crucial question in the radical equilibria of Scheme 2 is whether the bromine radical complex (BRC), the intermediate formed either from Br$^\bullet$ + NBS or from S$^\bullet$ + Br_2, will be stable enough to act independently as a chain propagating radical to show its own reactivity (11). In other words, the reactivity of the S$^\bullet$ and $Br_2^\bullet$

[1]Visiting Professor from Simon Fraser University, Burnaby, B.C., Canada, 1985 and 1986.

Printed in Canada / Imprimé au Canada

Can. J. Chem. Downloaded from www.nrcresearchpress.com by 91.121.58.235 on 09/07/12
For personal use only.

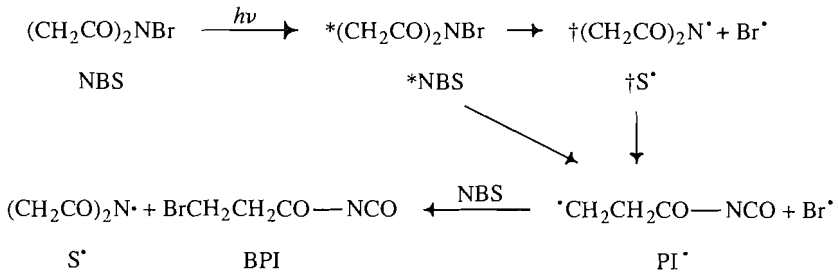

SCHEME 1

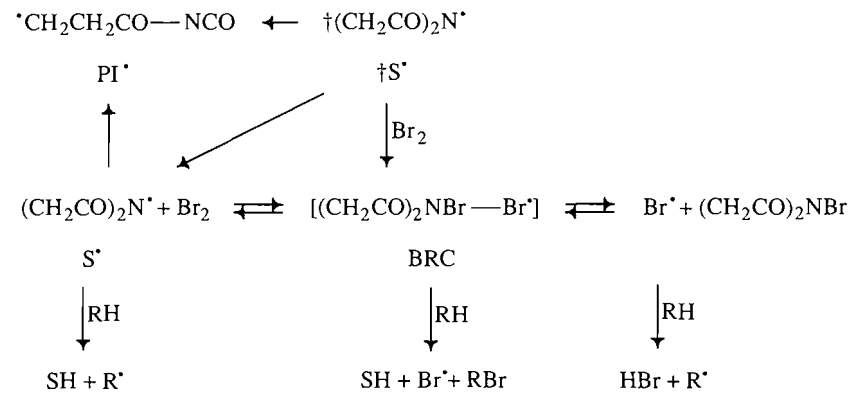

SCHEME 2

propagation species might be modified somewhat under the NBS + Br_2 conditions. In a photodecomposition of a tricyclic *N*-bromoimide, it is demonstrated that such a BRC exists, acting as a distinctive intermediate in intramolecular H-abstraction and bromination (12).

Simple radicals form complexes, most commonly with those electron-donating solvent molecules (13), and modify the reactivity of the radicals significantly (13–15) as recently shown in a selective chlorination of steroidal molecules (16). In this report, we wish to provide more evidence in support of the presence of the equilibria and BRC, as shown in Scheme 2, that modify the propagating species in the photodecomposition of NBS and its tetrafluoro derivative.

Results

The photodecomposition of NBS was carried out in CH_2Cl_2 in the presence of 1-chloropentane as the substrate, under four types of conditions that have evolved over the years through contributions from various groups (1–9); in this study the experimental conditions described in ref. 9 were adapted in order to avoid ambiguity on the excited species. Firstly, a solution of NBS in CH_2Cl_2 is photolysed through a Pyrex filter in the presence of DCE to scavenge Br_2 and Br• (Type I); these are the typical conditions in which the succinimidyl radical is the only chain carrier, as has been agreed by various groups (1–9). Secondly, NBS is photolysed under the same conditions without the presence of DCE (Type II); it is known that Br_2 is generated as the photodecomposition progresses (9). Thirdly, a mixture of NBS + Br_2 is decomposed by irradiation of Br_2 using a filter transparent >400 nm (Type III); photolytically generated Br• initiated the decomposition of NBS as shown in Scheme 2. Finally, Br_2 and K_2CO_3 are photodecomposed to generate Br• under the same conditions as above in the absence of NBS (Type IV); this system is designed to examine the reactivity of Br•, and K_2CO_3 is present to scavenge HBr generated as the by-product in the system (5, 6).

The bromination of 1-chloropentane in CH_2Cl_2 was carried out at 20°C to a low monobromination yield (5–8%) according to the procedures defined for the four types of conditions. From these photolysates the brominated products, 1-chloro-*x*-bromopentanes and $CHBrCl_2$, were isolated and their corresponding factors with respect to bromobenzene (the internal standard) in GC peaks were determined. These factors were used to do quantitative determinations of the brominated products by GC analysis. The structures of these chlorobromopentanes were determined from their MS and NMR spectra (Table 4). Since the yield of 1-chloro-5-bromopentane was low, this compound was identified by direct comparison with an authentic sample obtained from a commercial source by GC–MS. The percentages of β-bromopropionyl isocyanate (BPI) were determined by ^1H NMR spectroscopy using the intensity of the triplet at 3.63 and 2.81 ppm according to the method described by Tanner's and Walling's groups (1, 8). From the photolysate of NBS + DCE, we isolated the addition product **1**, $(CH_2CO)_2NCH_2CCl_2Br$, which was characterized from its spectroscopic data; the percentage yield of this compound was determined from the intensity of ^1H NMR singlets at 2.9 (4H) and 3.85 ppm (2H). This adduct has been detected in comparable reactions in the presence of high DCE concentrations (8).

In each series, two or more experiments were carried out under the same bromination conditions and the yields of the products were determined using bromobenzene as the internal standard; the average yields of these experiments were used to represent the series. The yields were used to calculate the

Can. J. Chem. Downloaded from www.nrcresearchpress.com by 91.121.58.235 on 09/07/12
For personal use only.

TABLE 1. The photobromination of 1-chloropentane with NBS in CH_2Cl_2[a]

Expt. no.	Type	Conditions (mmol)	Temp. (°C)	% Yields[b] SH	% Yields[b] BPI	Relative reactivities (r-value) r_1	r_2	r_3	r_4	r_5	r_t
1	I	[NBS] = 0.06 [DCE] = 0.13	20	74.5[c]	7.7	24.8±0.0	55.8±1.1	108±2	168±2	<0.2	63.2
2	I	[NBS] = 0.07 [DCE] = 0.13	20	84.3[c]	5.7	21.4	47.9	92	143	<0.2	55.4
3	II	[NBS] = 0.07	20	83.5	3.9	10.0±0.0	18.6±0.0	23.1±0.1	59.8±0.2	<0.2	20.1
4	II	[NBS] = 0.06	20	82.0	3.8	10.0±0.0	18.0±0.3	27.6±0.3	56.9±0.4	<0.2	19.5
5	III	[NBS] = 0.07 [Br_2] = 0.02	20	92.9	2.4	9.2±0.1	16.0±0.0	14.6±0.6	48.0±0.0	<0.2	16.0
6	III	[NBS] = 0.06 [Br_2] = 0.02	20	96.6	0.8	9.1±0.1	14.9±0.3	14.0±0.2	46.6±1.8	<0.2	15.4
7	IV	[Br_2] = 0.04 [K_2CO_3] = 0.18	20	—	—	8.3±0.2	12.5±0.4	13.4±0.0	39.9±0.2	1.1	13.5
8	IV	[Br_2] = 0.04 [K_2CO_3] = 0.16	20	—	—	8.5±0.0	12.9±0.0	14.1±0.2	41.7±0.2	1.1	14.1
9	III	[NBS] = 0.06 [Br_2] = 0.02	10	94.4	[d]	7.9±0.6	11.8±0.6	10.2±0.0	32.7±0.6	<0.2	11.7
10	IV	[Br_2] = 0.04 [K_2CO_3] = 0.15	10	—	—	9.0±0.0	14.7±0.0	13.5±0.0	37.8±0.6	1.1	13.6
11	III	[NBS] = 0.06 [Br_2] = 0.02	0	88.0	[d]	7.3±0.6	13.5±0.6	11.3±0.6	33.8±0.6	<0.2	11.9
12	IV	[Br_2] = 0.04 [K_2CO_3] = 0.15	0	—	—	8.8±0.0	15.2±0.0	13.8±0.6	38.2±0.6	1.1	13.8

[a]Experiments were carried out in an NMR tube containing the amounts of reagents indicated, in CH_2Cl_2 (0.4 mL) and 1-chloropentane (0.11 mmol) in a thermostated bath. For Types I and II conditions, a Pyrex filter was used; for Types III and IV conditions, a JB-400 filter (cutoff <400 nm) was used. The duration of irradiation was 10 min at 17 ± 1°C, 45 minutes at 10 ± 1°C, and 58 minutes at 0 ± 3°C.

[b]The yields were determined by GC analysis.

[c]These data contain the percentage of the addition product to DCE, compound **1**; the values of which are 26.5% in expt. 1 and 30.2% in expt. 2.

[d]The % yield is low.

relative reactivities per hydrogen of each group of chemically identical hydrogens in 1-chloropentane with respect to the hydrogen of CH_2Cl_2 as shown in eqs. [1] and [2]; this is defined as the r-value (Table 1). In eq. [2], $[C_5H_{10}ClBr]_t$ represents the yield of the all monobrominated products, which is used to calculate the overall relative reactivity of 1-chloropentane (r_t) with respect to CH_2Cl_2.

$$[1] \quad r_x = \frac{[CH_2Cl_2][1\text{-Cl-}x\text{-Br-}C_5H_{10}]}{[1\text{-}ClC_5H_{11}][CHBrCl_2]}$$

$$[2] \quad r_t = \frac{2[CH_2Cl_2][C_5H_{10}ClBr]_t}{11[1\text{-}ClC_5H_{11}][CHBrCl_2]}$$

$$[3] \quad q_x = \frac{[1\text{-Cl-}x\text{-Br-}C_5H_{10}]}{[1\text{-Cl-1-Br-}C_5H_{10}]}$$

Alternatively, the relative reactivity of H-abstraction for each position with respect to the first position in 1-chloropentane, defined as the q-value, could be calculated as in eq. [3]; calculated q-values of typical experiments for each type of condition are given in Table 2. For the calculation of r_5 and q_5, the multiplication of a factor of 2/3 in eqs. [1] and [3] is required. All the experiments in Table 1 used the same apparatus and a set of standard conditions.

Similar experiments were carried out using *N*-bromotetrafluorosuccinimide (4F-NBS) as the brominating agent under the four types of reaction conditions. Both tetrafluorosuccinimide (4F-SH) and 4F-NBS were sensitive to moisture and light; reactions with water led to the rapid formation of tetrafluorosuccinic acid as the final product. Therefore, the preparation of the starting solutions was carried out inside a darkened dry box. While the bromination products, 1-chloro-*x*-bromopentane and $CHBrCl_2$, were the same as those obtained above, $BrCF_2CF_2CONH_2$ (**2**) was isolated in the photolysis of 4F-NBS alone, and $Br(CCl_2CH_2)_nCF_2CF_2CONH_2$ (**3**), where n = 1 and 2, was obtained in the photolysis of 4F-NBS + DCE. It should be mentioned that the addition product of 4F-NBS and DCE, the compound corresponding to **1**, was not obtained. The latter products **3** were obtained as a mixture of the products with n = 1 and 2 and were derived (17) from the reaction of the ring-opened radical $^{\bullet}CF_2CF_2CONCO$ (4F-PI$^{\bullet}$) (see eq. [5]). Both amides **2** and **3** were isolated since the corresponding isocyanates rapidly underwent hydrolysis and decarboxylation. The structures of these new products were assigned on the basis of their MS and ^{19}F NMR spectra (Table 5). By analogy with the NBS cases, the same apparatus and processes were maintained and the yields of the products were determined from several experiments in each series; their q-values and r-values were calculated (Tables 2 and 3).

It should be noted that 1-chloro-5-bromopentane was formed in insignificant amounts except in the bromination by Br$^{\bullet}$ atom chain processes (Br_2 + K_2CO_3) under Type IV conditions as

Can. J. Chem. Downloaded from www.nrcresearchpress.com by 91.121.58.235 on 09/07/12
For personal use only.

TABLE 2. Relative reactivities of C—H bonds in 1-chloropentane (q-values) toward photobromination[a]

Expt. no.	Condition type	Temp. (°C)	$ClCH_2$--- CH_2--- CH_2--- CH_2--- CH_3 q_1	q_2	q_3	q_4	q_5	q_3/q_2
1	I	20	1	2.26	4.35	6.61	<0.03	1.9
2	I	20	1	2.22	4.30	6.70	<0.03	1.9
3	II	20	1	1.79	2.24	5.88	<0.03	1.3
4	II	20	1	1.79	2.23	5.70	<0.03	1.3
5	III	20	1	1.74	1.58	5.20	<0.03	0.9
6	III	20	1	1.64	1.54	5.13	<0.03	0.9
7	IV	20	1	1.51	1.62	4.83	0.14	1.1
8	IV	20	1	1.52	1.67	4.91	0.13	1.1
9	III	10	1	1.56	1.35	4.30	<0.02	0.9
10	IV	10	1	1.56	1.45	4.10	0.09	0.9
11	III	0	1	1.56	1.41	4.10	<0.02	0.9
12	IV	0	1	1.60	1.51	4.09	0.09	0.9
13	I	20	1	1.85	4.44	6.12	<0.03	2.4
14	I	20	1	1.86	4.19	5.71	<0.03	2.3
15	II	20	1	1.79	2.16	5.15	<0.03	1.2
16	II	20	1	1.80	2.08	5.19	<0.03	1.2
17	III	20	1	1.76	1.96	4.85	<0.03	1.1
18	III	20	1	1.74	1.85	4.77	<0.03	1.1
19	IV	20	1	1.41	1.46	4.15	0.17	1.0
20	IV	20	1	1.43	1.49	4.20	0.13	1.0
21	III	10	1	1.75	1.55	4.54	<0.02	0.9
22	III	0	1	1.77	1.52	4.38	<0.02	0.9

[a]The experimental numbers (and the conditions) are the same as those given in Tables 1 and 3; the footnotes cited also apply.

TABLE 3. The photobromination of 1-chloropentane with tetrafluoro-*N*-bromosuccinimide (4F-NBS) in CH_2Cl_2[a]

Expt. no.	Type	Conditions (mmol)	Temp. (°C)	% Yields[b] 4F-SH	4F-BPI	Relative reactivities (r-value) r_1	r_2	r_3	r_4	r_5	r_t
13	I	[4F-NBS] = 0.04 [DCE] = 0.13	20	21.8	53.2[b]	33.3±0.0	61.4±1.1	147±1	291±1	<0.2	80.9
14	I	[4F-NBS] = 0.04 [DCE] = 0.13	20	20.9	53.1[b]	35.0±1.7	64.3±0.0	145±1	197±5	<0.2	80.1
15	II	[4F-NBS] = 0.04	20	60.4	39.0	9.0±0.6	16.9±0.6	20.3±0.6	48.5±1.1	<0.2	17.5
16	II	[4F-NBS] = 0.04	20	62.3	37.0	9.6±0.6	16.9±0.6	19.7±0.6	47.9±0.6	<0.2	17.0
17	III	[4F-NBS] = 0.04 [Br_2] = 0.02	20	79.1	10.4	9.0±0.6	15.2±0.6	16.9±0.0	41.7±0.6	<0.2	14.9
18	III	[4F-NBS] = 0.04 [Br_2] = 0.02	20	77.9	9.8	9.0±0.6	15.2±0.6	16.4±0.6	42.3±0.6	<0.2	15.1
19	IV	[Br_2] = 0.04 [K_2CO_3] = 0.15	20	—	—	9.6±0.0	14.1±0.0	14.7±0.0	40.6±0.0	1.7	14.7
20	IV	[Br_2] = 0.04 [K_2CO_3] = 0.15	20	—	—	9.6±0.0	13.5±0.6	14.1±0.6	38.9±0.6	1.1	13.9
21	III	[4F-NBS] = 0.06 [Br_2] = 0.02	10	81.7	15	7.9±0.0	14.1±0.6	11.8±0.6	36.1±0.6	<0.2	12.7
10	IV	[Br_2] = 0.04 [K_2CO_3] = 0.15	10	—	—	9.0±0.0	14.7±0.0	13.5±0.6	37.8±0.6	1.1	13.6
22	III	[4F-NBS] = 0.06 [Br_2] = 0.02	0	78.3	16.7	8.5±0.0	15.2±0.0	13.0±0.0	36.6±0.6	<0.2	13.2
12	IV	[Br_2] = 0.04 [K_2CO_3] = 0.15	0	—	—	8.8±0.0	15.2±0.0	13.8±0.0	38.2±0.6	1.1	13.8

[a]The reaction conditions were the same as those shown in footnote *a* of Table 1, except that the duration of irradiation was 25 min for expt. 21 and 40 min for expt. 23.

[b]These data include 44.2% (for expt. 13) and 46.1% (for expt. 14) of **3** (where n = 1 and 2); these two amides appeared as a single peak in GC analysis.

Can. J. Chem. Downloaded from www.nrcresearchpress.com by 91.121.58.235 on 09/07/12
For personal use only.

TABLE 4. The spectral data of *x*-bromo-1-chloropentanes

	MS	^{1}H NMR
$ClCHBrCH_2CH_2CH_2CH_3$	151 (0.12, M − Cl), 149 (0.12, M − Cl), 143 (0.01, M − C_3H_7), 141 (0.01, M − C_3H_7), 107 (8, M − Br), 105 (20, M − Br), 70 (8, M − Br − Cl), 69 (100, M − Br − Cl − 1)	1.18 (t, 3H, J = 7.2 Hz), 1.55–1.80 (m, 4H), 2.44–2.52 (m, 2H), 5.92 (t, 1H, J = 6.2 Hz)
$ClCH_2CHBrCH_2CH_2CH_3$	150 (1, M − HCl), 148 (1.7, M − HCl), 137 (0.8, M − Cl − 14), 135 (0.7, M − Cl − 14), 107 (4, M − Br), 106 (3, M − HBr), 105 (2, M − Br), 104 (8, M − HBr), 104 (8, M − HBr), 69 (100, M − Br − Cl − 1)	1.22 (t, 3H, J = 7.4 Hz), 1.75–2.29 (m, 4H), 4.1 (m, 2H, J_{AB} = 10.9 Hz, J_{AX} = 10.9 Hz, J_{BX} = 4.4 Hz), 4.27 (m, 1H)
$ClCH_2CH_2CHBrCH_2CH_3$	187 (8, M − 1), 185 (31, M − 1), 183 (22, M − 1), 149 (34, M − HCl − 1), 147 (28, M − HCl − 1), 123 (3, M − C_2H_4Cl), 121 (8, M − C_2H_4Cl)	1.18 (t, 3H, J = 7.2 Hz), 2.0 (m, 2H), 3.77 (t, 2H, J = 5 Hz), 4.72 (m, 1H)
$ClCH_2CH_2CH_2CHBrCH_3$	188 (0.24, M^+), 186 (1.7, M^+), 184 (1.6, M^+), 149 (26, M − HCl − 1), 147 (29, M − HCl − 1), 107 (11), 105 (31), 67 (100)	1.93 (d, 3H, J = 6.6 Hz), 2.1 (m, 4H), 3.72 (t, 2H, J = 5.3 Hz), 4.27 (m, 1H)
$ClCH_2CH_2CH_2CH_2CH_2Br$	188 (2, M^+), 186 (16, M^+), 187 (13, M^+), 150 (7, M − Cl), 148 (7, M − Cl), 107 (4, M − Br), 106 (8, M − HBr), 105 (11, M − Br), 104 (22, M − HBr), 68 (22), 69 (100), 55 (42)	1.6 (m, 2H), 1.8 (m, 4H), 3.42 (t, 2H, J = 6.7 Hz), 3.55 (t, 2H, J = 6.5 Hz)

TABLE 5. Products of NBS and 4F-NBS photodecomposition

$BrCCl_2CH_2N(COCH_2)_2$ (**1**)[a]

MS	275 (18, M^+), 273 (18), 197 (6, M − HBr), 195 (14), 193 (23), 183 (8, CH_2CCl_2Br), 181 (14), 179 (43), 177 (87), 175 (57), 167 (6, CCl_2Br), 165 (9), 163 (16), 161 (12), 112 (20), 98 (20), 63 (38), 61 (100)
^{1}H NMR	δ 2.90 (s, 4H), 3.85 (s, 2H)

$BrCF_2CF_2CONH_2$ (**2**)

MS	226 (0.14, M^+ + 1), 225 (0.05, M^+), 224 (0.16, M^+ + 1), 223 (0.04, M^+), 181 (0.19, M − 44), 179 (0.22, M − 44), 162 (0.49, M − 19 − 44), 160 (0.56, M − 19 − 44), 144 (1.08), 131 (1.36), 129 (1.56), 100 (4.03), 44 (100)
^{19}F NMR	δ 13.69 (t, 2F), −36.86 (t, 2F)

$Br(CCl_2CH_2)_2CF_2CF_2CONH_2$ (**3**, n = 2)[b]

MS	421 (3.19, M^+), 419 (4.52), 417 (3.78), 415 (2.52), 405 (2.46, M − 18), 403 (13.75), 401 (42.90), 399 (37.52), 397 (18.79), 379 (2.52, M − 44), 377 (2.12), 375 (3.65), 373 (7.44), 371 (4.78), 327 (6.44, M − HBr − 16), 325 (13.15), 323 (25.90), 321 (50.0), 319 (52.12), 2.80 (12.62, M − 79 − 44 − 20), 278 (12.68), 276 (43.76), 274 (83.27), 272 (100), 144 (36.25)
^{19}F NMR	δ −33.5 (t, 2F), −43.04 (t, 2F)

$BrCCl_2CH_2CF_2CF_2CONH_2$ (**3**, n = 1)[b]

MS	325 (13.15, M^+), 323 (25.90), 321 (50.00), 319 (52.12), 307 (2.72, M − 18), 305 (3.98), 303 (6.31), 301 (6.97), 281 (24.44, M − 44), 279 (16.80), 277 (14.43), 275 (16.80), 272 (100, M − Cl − 16), 270 (53.25), 268 (2.06), 144 (36.25), 142 (29.55, M − $BrCCl_2$ − 16)
^{19}F NMR	δ −33.5 (t, 2F), −43.04 (t, 2F)

[a]The sample is contaminated by about 10% of succinimide.
[b]These two compounds were isolated as a mixture.

in expts. 7, 8 and 19, 20; the r_5-values in these experiments are small but reproducible. In view of reports (3, 8) that the corresponding r-value of the Br$^\bullet$ chain process toward neopentane and CH_2Cl_2 is 0.02–0.1, the r_5-value of about 1.1 must indicate an unusual reactivity of the methyl group of 1-chloropentane toward Br$^\bullet$; this anomaly is worthy of investigation in future. The pattern of r-values obtained at 20°C (except that of r_5-values) is characteristically similar to those of the previous publications using other substrates (1–3, 9); the relative reactivities are highest with the S$^\bullet$ reaction (Type I conditions) and lowest with the Br$^\bullet$ reactions (Type IV conditions), and those from the NBS + Br_2 system (Type III or II conditions) are in between these two extremes but closer to the latter (9). Previously this reactivity pattern was interpreted as a simple

Can. J. Chem. Downloaded from www.nrcresearchpress.com by 91.121.58.235 on 09/07/12
For personal use only.

Can. J. Chem. Downloaded from www.nrcresearchpress.com by 91.121.58.235 on 09/07/12
For personal use only.

competition of S• and Br• propagation processes (1, 2), and led to the suspicion that an additional propagating radical in the NBS + Br_2 system is not required. The relative reactivities (Tables 1–3) show that S• preferentially abstracts hydrogens from the methylene groups, but not from the terminal methyl group, of 1-chloropentane over those of CH_2Cl_2, and does so more selectively from the CH_2 at the C4 and C3 (in that order) positions than does Br•.

The brominations with Br_2 + K_2CO_3 (Type IV) and with NBS (or 4F-NBS) + Br_2 (Type III) were also investigated at 10° and 0°C. The data were treated as usual to give the *r*-values and *q*-values that are shown in Tables 1 and 2 for NBS experiments and in Tables 3 and 2 for 4F-NBS experiments. It is noteworthy that at 10°C the *r*-values of the NBS + Br_2 system under Type III conditions dramatically decrease to levels below the *r*-values of the Br• reaction, although the corresponding *q*-values do not show such drastic changes. However, at 0°C the decrease of the *r*-values is abruptly attenuated and they even show slight increases in some cases, although all *r*- and *q*-values are still far below these levels at 20°C. This trend hints that a counterbalancing factor starts to operate at 0°C; this factor is believed to arise from rapid changes of viscosity around this temperature range. The experiments at 10°C and 0°C were repeated several times and average values are shown in Tables 1 and 3.

Discussion

The results shown in Tables 1–3 for the photodecomposition of either NBS or 4F-NBS in the presence of 1-chloropentane as a substrate under four different types of conditions at 20°C are generally comparable with those using neopentane or cyclohexane as a substrate (1–9) but differ somewhat in the pattern of the reaction with DCE. As the percentage yields of 4F-BPI are higher than those of BPI under comparable conditions in the corresponding reactions (Tables 1 and 3), undoubtedly 4F-S• ring-opens to form 4F-PI• considerably faster than does S• to give PI•. Thus, **3** is derived from the addition of 4F-PI• to DCE (17) as in eq. [5], but **1** is formed from that of S• to DCE as in eq. [4]. The addition of PI• to DCE is probably much slower

[4] $CCl_2{=}CH_2 + (CH_2CO)_2N^{\bullet} \rightarrow {}^{\bullet}CCl_2CH_2{-}N(COCH_2)_2 \rightarrow \mathbf{1}$
S•

[5] $CCl_2{=}CH_2 + {}^{\bullet}CF_2CF_2CONCO$
4F-PI•
$\rightarrow {}^{\bullet}CCl_2CH_2CF_2CF_2CONCO \rightarrow \mathbf{3}$

than the reaction of PI• with Br_2 or NBS. In the present cases, the formation of **1** and **3** is undoubtedly facilitated by a high concentration of DCE. The low %BPI in expts. 1 and 2 (Table 1) under Type I conditions no doubt shows that S• is efficiently scavenged by DCE at a concentration >0.25 M; this pattern is analogous to the scavenging of S• with a high concentration of benzene (10, 18).

The results (Tables 1 and 3), however, share a number of similarities with those of NBS photodecompositions using cyclohexane as the substrate (9). First of all, the photolysis of NBS or 4F-NBS in the presence of a Br_2 and Br• scavenger (Type I conditions) yields the highest amount of ring-opened products, obviously arising from the enhanced ring opening upon direct excitation (9, 10) of NBS (or 4F-NBS). It should be mentioned that the %BPI in expts. 1 and 2 is considerably higher if **1** is not formed. Secondly, the direct photolysis of NBS (or 4F-NBS) in the absence of DCE (Type II conditions) yields a lesser amount of BPI (or 4F-BPI) than that in the presence of DCE (Type I conditions). This has been shown to arise from the formation of Br_2 during the photolysis (9) of NBS alone, in which Br_2 intercepts S• to prevent the ring opening. Thirdly, Br• induces decomposition of NBS (or 4F-NBS) under Type III conditions (expts. 5, 6 and 17, 18), to cause the formation of BPI (or 4F-BPI), indicating the generation of S• (or 4F-S•) and subsequent ring-opening in the process. The last two conclusions both support the previous proposal, of equilibria (9–12) that can be approached either from S• + Br_2 or Br• + NBS as shown in Scheme 2. In the ensuing discussion, NBS, SH, S•, PI•, and BPI are used on the understanding that they also represent their tetrafluoro analogues, unless specified otherwise.

The examination of the relative reactivities per hydrogen, *r*-values, provides information on the nature of propagation processes under different conditions; in particular, those in the presence of Br_2 are of great interest to us. The r_1–r_4 values in the Br• initiated photodecomposition of NBS under Type III conditions at lower temperatures (expts. 9, 11, 21, and 22) exhibit levels lower than the corresponding *r*-values of Br• H-abstraction under Type IV conditions (expts. 10 and 12). The observations clearly rule out the propagation by simple competition of S• and Br• chain processes, and *indicate the presence of another propagating radical in addition to S• and Br• radicals under Type III conditions*. Secondly, the anomalous bromination reactivity of Br• at the C5 position of 1-chloropentane under Type IV conditions provides independent support for this claim. The insignificant r_5-values under Type III conditions in comparison to low but reproducible r_5-values under Type IV conditions (Tables 1 and 3) *unambiguously show that Br• is not the major propagating radical under Type III conditions, and that the* r_1–r_4*-values in the cases under Type III conditions do not represent the Br• reactivities*; this conclusion is significant since only Br• is generated by the photoexcitation of Br_2 under Type III conditions. Thirdly, in the photolysis of NBS alone under Type II conditions, in spite of the fact that both S• and Br• are generated by photoexcitation, the *r*-values in expts. 3, 4 and 15, 16 are clearly inconsistent with those arising from a mixture of S• and Br• chain propagations determined under Type I and IV conditions respectively. A simple competition of propagation processes by S• and Br•, even after subtraction of the S• ring-opening reaction, would give higher estimated *r*-values than these observed values. A similar trend of *r*-values has been noted in the photodecomposition of NBS in the presence of cyclohexane under Type II conditions during which the formation of Br_2 has been established (9).

The three conclusions drawn from the *r*-values in Tables 1 and 3 uniquely indicate that S• and Br• generated in the photobromination with NBS in the presence of Br_2 under Type II and III conditions must be rapidly modified in their nature and reactivities, leading to the appearance of a new radical chain carrier. We advocate the equilibria and reactions proposed previously (9) as shown in Scheme 2, and suggest that the modified chain carrier is BRC derived from either S• or Br• in the equilibria under these conditions. It should be mentioned that the basic concept of the equilibria has been proposed before (11, 12) and that in the NBS + Br_2 reaction system a simple competition of Br• and S• processes was shown to pose difficulties in explaining certain experiments, in recent publications from Walling's and Tanner's groups (1, 8).

It follows that the *r*-values under Type II and III conditions (Tables 1 and 3) consist mainly of the intermolecular relative reactivities of BRC toward 1-chloropentane and CH_2Cl_2; the *r*-values of expts. 9, 11, 21, and 23 should closely represent those of BRC at these same temperatures. It is noted that these

Can. J. Chem. Downloaded from www.nrcresearchpress.com by 91.121.58.235 on 09/07/12
For personal use only.

r-values of BRC are very similar to those of Br• H-abstraction under Type IV conditions. We assume that the structure of BRC is somewhat similar to that proposed by Walling *et al.* (8) in having two non-equivalent bromine atoms, one of which may have a pentavalent configuration. The bromination of a substrate (RH) by BRC may be represented by an overall reaction as shown in Scheme 2. It is reasonable to expect that a BRC is more stabilized and possesses a longer lifetime in which to show its reactivities at a lower temperature; at a higher temperature, the dissociation of BRC is faster, to show more of S• and Br• reactivities. It is very fortunate indeed that the *r*-values of the intermolecular H-abstraction by BRC from 1-chloropentane under the present conditions are lower than those by Br• under comparable conditions, and the inversion of *r*-values occurs in the experimentally readily accessible region of 0–20°C. In the photobromination of cyclohexane with NBS + Br_2 in CH_2Cl_2, it is shown that such an *r*-value inversion does not occur even at −20°C. In an intramolecular H-abstraction, the corresponding BRC reactivities can be detected even at room temperature (12) because an activation energy for such intramolecular reactions is generally small and is probably much smaller than the barriers of BRC dissociations.

As shown by its *r*-values (expts. 13 and 14), the tetrafluorosuccinimidyl radical (4F-S•) abstracts H-atoms more vigorously from 1-chloropentane than does S• (expts. 1 and 2). However, 4F-S• is undoubtedly more electrophilic than S•, as shown by the higher q_2/q_3 ratio (expts. 1, 2 and 13, 14 in Table 2). It appears that the electron-withdrawing properties of fluorine atoms may also contribute to the facile ring opening of 4F-S•; undoubtedly, it is these same properties that make 4F-PI• attack DCE more vigorously. The present results have clearly established the presence of a new chain carrier derived from a modification of Br• or S• in intermolecular H-abstraction; an analogous case in intramolecular H-abstraction has been published by us (12). Indeed, such phenomena appear to be fairly common in radical reactions (13). In the present case, no doubt both NBS and Br_2 can participate in the complex formations that make the reactions of this system unusually complicated. Even in simple radical reactions, one should be aware of a possible participation of solvent molecules, in a complex formation, that may not be totally innocent in terms of mechanistic effects.

Experimental

General conditions and chemicals

The ultraviolet spectra were taken with a Perkin–Elmer 559 spectrophotometer and GC–MS with a Finigan 4021 or a Shimadzu QP 1000 mass spectrometer; GC analysis was carried out with a Shangfen model 102GD gas chromatograph equipped with a glass column (0.3 cm × 300 cm) with a packing of 10% polyethylene glycol (PEG). ^1H NMR spectra were taken with a Varian EM-360 (at 60 MHz) or a Varian XL-200 (at 200 MHz) using TMS as the internal standard, and ^{19}F NMR spectra with a Perkin–Elmer R-32 (at 90 MHz) using CF_3CO_2H as the internal standard.

NBS was recrystallized from hot water and kept in a desiccator over P_2O_5. Br_2 was redistilled. 1-Chloro-5-bromopentane was purchased from Aldrich Chemical Co., Milwaukee, U.S.A. Both CH_2Cl_2 and 1-chloropentane were purified according to the published method (19). Argon was successively passed through 5A molecular sieves, Ag molecular sieves, and Pd molecular sieves to remove O_2 and moisture.

Preparation of N*-bromotetrafluorosuccimide (4F-NBS)*

Tetrafluorosuccinic diamide, $NH_2COCF_2CF_2CONH_2$ ((9.6 g, Fluorocarbon Group, Shanghai Institute of Organic Chemistry), mp 258–260°C (lit. (20) mp 259.8–260.3°C); ^{19}F NMR −42 ppm (s)), and concentrated H_2SO_4 were treated according to Henne's method (20) to give tetrafluorosuccinimide (4F-SH, 5 g). The crude product was redistilled at bp 82°C/15 Torr (1 Torr = 133.3 Pa) to afford a white solid; mp 66°C in a capillary tube (lit. (20) mp 66.0–66.5°C); ^{19}F NMR −49 ppm. This product (7.5 g) was brominated with bromine (10 g) and AgO (8 g) according to the published method (21) to give 4F-NBS (79% yield), which was sublimed; mp 51–52°C in a capillary tube; UV λ_{max} 231.2 nm (log ε, 3.2); ^{19}F NMR −45 ppm. Owing to the great sensitivity to light and moisture, both 4F-NS and 4F-NBS were handled in a darkened dry box.

Photobromination

CH_2Cl_2 or its solution containing a suitable concentration of Br_2 or DCE, followed by 1-chloropentane, was added to an NMR tube containing the desired amount of NBS (or 4F-NBS). The tube was wrapped with aluminum foil and capped with a septum. The solution was purged with deoxygenated and dried argon through a needle inserted through the septum; the use of either a stainless steel needle or a Teflon needle caused no difference in the results. The light source was a Hanovia medium pressure mercury lamp (200 W) filtered through a Pyrex filter or a JB-400 filter (cutoff <400 nm, Shanghai Color Glass Works). The lamp was placed in a cooling sleeve, which was placed in a thermostated bath. The NMR spectrum of the solution was recorded at 200 MHz before and after photolysis and the % yields of NBS (singlet at 3.0 ppm), SH (singlet at 2.80 ppm), BPI (triplet at 3.20 ppm), and **1** (singlet at 2.9 ppm) were calculated from the integration of the characteristic peaks according to the method described by Walling's and Tanner's groups (1, 8). To the photolysate was added an exact amount of a solution containing bromobenzene as the internal standard in CH_2Cl_2. The solution was treated with an aqueous $NaHSO_3$ solution (5%) and was washed with water twice. The CH_2Cl_2 solution was dried over Na_2SO_4 for GC analysis. At least three injections were made under comparable GC conditions and the ratios of peak area to internal standard area were averaged to give the yields of the particular experiments. For each series, two or more tubes were photolysed, and the average yields were used to calculate *r*-values as shown in Tables 1 and 3.

For experiments using 4F-NBS, ^{19}F NMR spectra were recorded with a Perkin–Elmer R-32 spectrophotometer in a different type of NMR tube and the characteristic ^{19}F peaks at δ −45 ppm (s, 4F-NBS), −49 ppm (s, 4F-SH), −36.86 ppm (t, **2**), and −43.04 ppm (t, **3**) were used to determine the % yields before and after the photolysis. Both 4F-NBS and 4F-SH decomposed rapidly during washings with $NaHSO_3$ solution to give tetrafluorosuccinic acid, which was washed with water; the products, chlorobromopentanes, in the organic phase were analysed by GC.

Isolation of products

For the preparative run, photolysis was carried out in a test tube without NMR monitors. For the photolysis of Br_2 + K_2CO_3 in the presence of 1-chloropentane, the solution, after treatment with $NaHSO_3$ solution, was injected into a preparative GC to separate chlorobromopentanes. 1-Chloro-5-bromopentane was produced in too small yield and was not isolated; it was identified by coinjection into GC analysis with an authentic sample from the commercial source. In the photolysis of NBS in the presence of DCE (0.5 M), the crude products in pentane were filtered through a silica gel column to give fractions containing **1** contaminated by some succinimide. In the photolysis of 4F-NBS in CH_2Cl_2, the photolysate was washed with 5% aqueous $NaHSO_3$ solution and twice with water to decompose 4F-BPI, 4F-NBS, and 4F-SH. Pure β-bromotetrafluoropropionamide (**2**) derived from 4F-BPI was obtained from the organic phase after evaporation of solvent. In the photolysis of 4F-NBS in the presence of DCE (0.5 M), the photolysate was treated as above and the crude product was chromatographed on a silica gel column; **3** was obtained as a mixture of the compounds with n = 1 and 2 and was contaminated with a trace amount of **2**. Both **2** and **3** were derived from the hydrolysis and decarboxylation of the corresponding isocyanates.

Acknowledgement

Support of this work by the National Natural Science Foundation of China, Beijing, is gratefully acknowledged.

1. D. D. TANNER, D. W. REED, S. L. TAN, C. P. MEINTZER, C. WALLING, and A. SOPCHIK. J. Am. Chem. Soc. **107**, 6576 (1985).
2. D. D. TANNER and C. P. MEINTZER. J. Am. Chem. Soc. **107**, 6584 (1985).
3. P. S. SKELL, U. LÜNING, D. S. MCBAIN, and J. M. TANKO. J. Am. Chem. Soc. **108**, 121 (1986).
4. J. C. DAYS, M. G. KATSAROS, W. D. KOCHER, A. E. SCOTT, and P. S. SKELL. J. Am. Chem. Soc. **100**, 1950 (1978).
5. R. L. TLUMAK, J. C. DAY, J. P. SLANGA, and P. S. SKELL. J. Am. Chem. Soc. **104**, 7257 (1982).
6. R. L. TLUMAK and P. S. SKELL. J. Am. Chem. Soc. **104**, 7267 (1982).
7. P. S. SKELL and J. C. DAY. Acc. Chem. Res. **11**, 381 (1978).
8. C. WALLING, G. M. EL-TALIAWI, and C. X. ZHAO. J. Am. Chem. Soc. **105**, 5119 (1983).
9. Y. L. CHOW and D. C. ZHAO. J. Org. Chem. **52**, 1931 (1987).
10. Y. L. CHOW and D. C. ZHAO. J. Org. Chem. **54**, 530 (1989).
11. Y. L. CHOW and Y. M. A. NAGUIB. Rev. Chem. Intermed. **5**, 325 (1984).
12. Y. L. CHOW and Y. M. A. NAGUIB. J. Am. Chem. Soc. **106**, 7557 (1984).
13. G. A. RUSSELL. *In* Free radicals. Vol. I. *Edited by* J. Kochi. Wiley, New York. 1973. Chap. 7.
14. N. J. BUNCE, K. U. INGOLD, J. P. LANDERS, J. LUSZTY, and J. C. SCAIANO. J. Am. Chem. Soc. **107**, 5464 (1985).
15. P. S. SKELL, H. N. BAXTER, J. M. TANKO, and J. CHEVOLU. J. Am. Chem. Soc. **108**, 6300 (1986).
16. (*a*) R. BRESLOW, M. BRANDL, J. HUNGER, and A. D. ADAMS. J. Am. Chem. Soc. **109**, 3799 (1987); (*b*) R. BRESLOW, R. J. CORCORAN, B. B. SNIDER, R. J. DOLL, P. L. KHANNA, and R. KELEYA. J. Am. Chem. Soc. **99**, 905 (1977); (*c*) R. BRESLOW. *In* Advances in enzymology and related areas of molecular biology. Vol. 58. *Edited by* A. Meister. Wiley, New York. 1986. pp. 1–60.
17. Fluorocarbon Group, Shanghai Institute of Organic Chemistry. Sci. Sin. (Engl. Ed.), **20**, 353 (1977).
18. F. L. YU, Y. M. A. NAGUIB, M. KITADANI, and Y. L. CHOW. Can. J. Chem. **57**, 1967 (1979).
19. D. D. PERRIN. Purification of laboratory chemicals. 2nd ed. Pergamon Press, Oxford. 1980.
20. A. L. HENNE and W. F. ZIMMER. J. Am. Chem. Soc. **73**, 1103 (1951).
21. R. E. PEARSON and J. C. MARTIN. J. Am. Chem. Soc. **85**, 3142 (1963).

Can. J. Chem. Downloaded from www.nrcresearchpress.com by 91.121.58.235 on 09/07/12
For personal use only.

β-Ureido acids and dihydrouracils.[1] The kinetics and mechanism of the reversible ring closure of 3-(3′-methylureido)-propanoic acid and 3-(3[1]-phenylureido)-2-methylpropanoic acid in sulfuric acid solutions

VETKA RACHINA
Higher Institute of Medicine, Pleven, Bulgaria

IVA B. BLAGOEVA AND IVAN G. POJARLIEFF
Institute of Organic Chemistry, Bulgarian Academy of Sciences, Sofia, Bulgaria

AND

KEITH YATES
Department of Chemistry, University of Toronto, Toronto, Ont., Canada M5S IAI

Received October 23, 1989

This paper is dedicated to Professor Ross Stewart on the occasion of his 65th birthday

VETKA RACHINA, IVA B. BLAGOEVA, IVAN G. POJARLIEFF, and KEITH YATES. Can. J. Chem. **68**, 1676 (1990).

The pK_{BH^+} values for protonation of the ureido groups of the title acids, and for protonation at the 2-carbonyl groups of the product hexahydropyrimidine-2,4-diones, have been determined by standard UV and NMR methods. A bell-shaped dependence of the observed rate constants on H_2SO_4 concentration was found for both the ring-closure and ring-opening directions. This medium dependence is satisfactorily reproduced by means of rate equations based on the excess acidity treatment, providing account is taken of unproductive protonation equilibria. The derived slope parameters (m^+) for the ring-closure direction indicate that the slow step involves proton transfer from nitrogen rather than to oxygen. For the ring-opening or hydrolysis reactions, the corresponding slope parameters (m^+m^*) are characteristic of similar reactions known to proceed with slow C—N scission concerted with proton transfer.

Key words: mechanism, hydrolysis, cyclization, acid catalysis.

VETKA RACHINA, IVA B. BLAGOEVA, IVAN G. POJARLIEFF et KEITH YATES. Can. J. Chem. **68**, 1676 (1990).

Faisant appel à des méthodes RMN et UV standard, on a déterminé les valeurs de pK_{BH^+} pour la protonation des groupements uréido des acides mentionnés dans le titre ainsi que pour la protonation des groupements carbonyles en position 2 des hexahydropyrimidine-2,4-diones. Tant pour la fermeture que pour l'ouverture du cycle, on a observé une relation en forme de cloche entre les constantes de vitesse et la concentration en H_2SO_4. Si on tient compte de l'équilibre de protonation qui n'est pas productif, on peut assez bien reproduire cette relation avec le milieu à l'aide d'équations de vitesse basées sur un d'excès d'acidité. Les paramètres de pente (m^+) que l'on dérive pour la direction de la fermeture de cycle indiquent que l'étape lente implique un transfert de proton à partir de l'azote plutôt qu'à l'oxygène. Pour les réactions d'hydrolyse ou d'ouverture de cycle, les paramètres de pente correspondants (m^+m) sont caractéristiques de réactions semblables qui sont connues et qui procèdent avec une scission lente de la liaison C—N, concertée avec un transfert de proton.

Mots clés : mécanisme, hydrolyse, cyclisation, catalyse acide.

[Traduit par la revue]

Introduction

The ring closure of 3-ureidopropanoic acid to dihydrouracil was found previously (2) to be reversible to aqueous HCl solutions, and from acidity function criteria (3) and other evidence it was concluded that the reverse, ring-opening reaction proceeds with slow attack of water on the protonated form of the dihydrouracil. This is analogous to the currently accepted mechanism of acid-catalyzed amide hydrolysis (4). Subsequently, a similar conclusion was drawn for the closely related reactions of acetylthiourea and thiohydantoin (4). More recently, however, Guler and Moodie (5), on the basis of ^{18}O-exchange experiments, have shown that the slow step in the cyclization of 5-methylhydantoic acid to the corresponding hydantoin is the formation of the C—N bond and not the breakdown of the tetrahedral intermediate, which is inconsistent with the above conclusions with respect to the ring-opening step in related systems. In the pH region, these authors (5) observed general acid catalysis and proposed a concerted mechanism, illustrated by the transition state **A**.

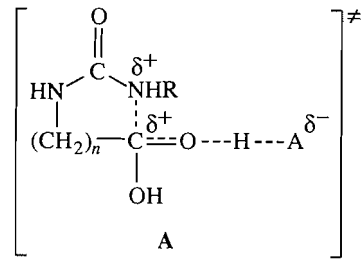

A

Subsequent studies (6) with strained hydantoic acids, which react rapidly at room temperature, also demonstrated general acid catalysis with Brønsted α values of 0.3 and 0.6 for 5-methyl and 5-phenyl substitution respectively, thus confirming the concertedness of heavy atom reorganization with proton transfer. Considerations of the effect of structure on the basicity of the nitrogen atom, in terms of its effect on Jencks – More O'Ferrall type diagrams (7), were all in agreement with the direction of change of α with structure expected for transition state **A**, and that which was observed experimentally (6).

However, for cyclization reactions in H_2SO_4 solutions, where a similar mechanism presumably operates, the m^+m^*

[1]Part XXI. For Part XX, see ref. 1.

Printed in Canada / Imprimé au Canada

Can. J. Chem. Downloaded from www.nrcresearchpress.com by 91.121.58.235 on 09/07/12
For personal use only.

values obtained from an X-function treatment (5, 8) were 0.64 and 0.4 for the 5-methyl- and 5-phenylhydantoic acids respectively. If these parameters are interpreted in a similar way to Brønsted α values, this indicates the alternative and kinetically equivalent process of specific acid – general base catalysis, going through the more likely transition state **B**, especially where a very weakly basic ureido nucleophile is involved.

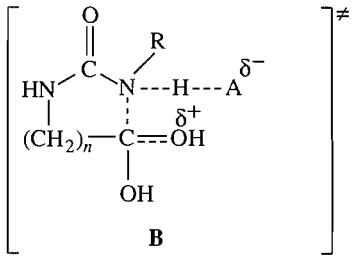

B

The above discrepancy posed a number of questions as to its origin, particularly: is the same mechanism operative in moderately concentrated H_2SO_4 solutions as in HCl, and can acidity function treatments be successfully applied to differentiate between possible concerted reactions where slow proton transfers between heteroatoms are involved? We now wish to report on ring-closure reactions of β-ureido acids in dilute to 70% sulfuric acid solutions, as shown in Scheme 1. The ring

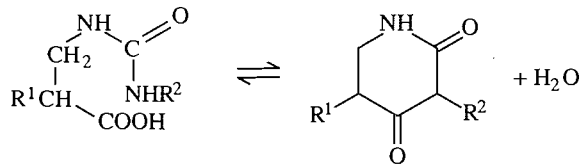

1,3 **2,4**

1 R^1 = H, R^2 = Me; **3** R^1 = Me, R^2 = Ph

1 R^1 = H, R^2 = Me; **3** R^1 = Me, R^2 = Ph

SCHEME 1

closures of 3-ureidopropanoic acids such as **1** and **3** have the advantage of being measurably reversible, unlike hydantoic acids where the equilibria lie far on the hydantoin side, and hence can be studied kinetically in both directions. Also the hydrolysis reactions of **2** and **4** can be compared with the better

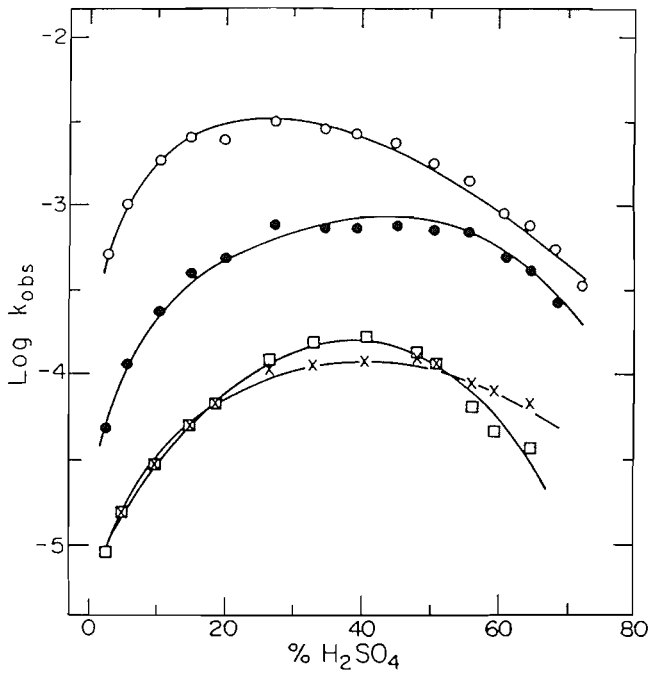

FIG. 1. Rate profiles for ring closure of **1** (○) and **3** (●) and for ring opening of **2** (□) and **4** (×) in H_2SO_4 solutions at 70°C. The points are experimental values of log k_{obs} and the solid curves are calculated (see text).

known amide hydrolysis mechanism. The effect of changing the N-substitution from methyl to phenyl was again intended to give information on the effect of N-basicity on transition-state structure. The 2-methyl derivatives **3** and **4** were chosen because the apparent equilibrium constant for this reaction is close to unity.

Results

Rate measurements

Plots of the observed first-order rate constants for both ring closure (k_f) and ring opening (k_r) versus % H_2SO_4 (w/w) are shown in Fig. 1. In the acidity range studied (0–70% H_2SO_4), both reactions are accompanied by the unproductive (and thermodynamically favoured) protonations shown in Scheme 2.

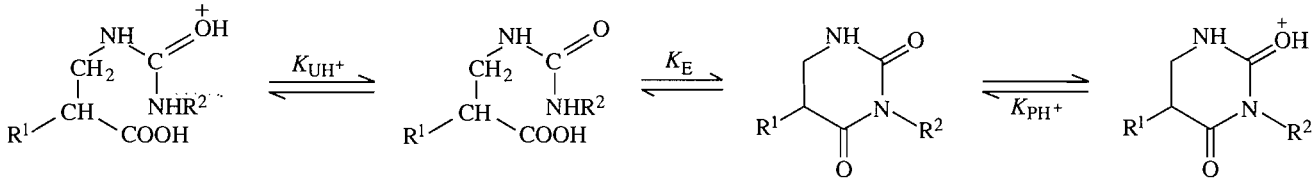

UH^+ U P PH^+

SCHEME 2

Therefore the observed rates of cyclization (V_f) and ring opening (V_r), and overall equilibrium constant are given by

$$V_f = k_f^{obs}([U] + [UH^+])$$

$$V_r = k_r^{obs}([P] + [PH^+])$$

$$K_e^{obs} = \frac{([P] + [PH^+])}{([U] + [UH^+])}$$

Thus corrections are needed for these unproductive ionizations.

pK determinations

The pK values of **1**–**4** listed in Table 1 were obtained using the excess acidity treatment of Cox and Yates (9). This has recently been shown (10) to be equivalent to the Bunnett–Olsen method (11), provided correct values of C_{H^+} are used in the latter treatment. The pK values are the thermodynamic values extrapolated to $X = 0$, obtained from the expression

$$\log [BH^+]/[B] - \log C_{H^+} = m^*X + pK_{BH^+}$$

Can. J. Chem. Downloaded from www.nrcresearchpress.com by 91.121.58.235 on 09/07/12
For personal use only.

TABLE 1. Protonation equilibrium constants and statistical parameters from excess acidity treatment

Compound	T(K)	pK_{BH^+}	pK^a	m^*	δ^a	r^b	δy^c
1	292	−0.85	0.01	1.02	0.02	0.998	0.019
2	303	−2.60	0.004	0.48	0.003	0.999	0.028
3	298	−1.83	0.01	0.73	0.008	0.994	0.048
4	298	−3.56	0.003	0.57	0.003	0.996	0.058

[a]Standard deviations of quantities indicated.
[b]Least-squares correlation coefficient.
[c]Standard deviation on y-axis (log K_{BH^+} axis).

Can. J. Chem. Downloaded from www.nrcresearchpress.com by 91.121.58.235 on 09/07/12
For personal use only.

These pK values, because of the extrapolation involved, are frequently sensitive to errors in determining m^* and the ionization ratio terms $[BH^+]/[B]$. However, the bases studied here are not very weak, so that the extrapolations involved are not that long. The *N*-methyl compounds **1** and **2** were studied via ^1H and ^{13}C NMR spectroscopy since the only changes observed in UV spectra with acidity were at the short wavelength (ca. 200 nm) end of the spectrum where accurate measurements are difficult. The variation in ^{13}C chemical shift of the 2-carbon gave reasonable sigmoidal behaviour with acidity, and thus was used to determine pK (see experimental section).

The *N*-phenyl compounds **3** and **4** were studied by standard UV measurements (see experimental section), using the procedure of Katritzky *et al.* (12) to account for spectral solvent dependencies, as described in detail in ref. 8.

We have used three criteria for the reliability of the pK values obtained: linearity of the Cox–Yates plots; the derived statistical parameters for m^*; and the fit of the recalculated to the observed spectral changes with acidity. In addition, the changes in basicity shown in Table 1 as a function of structure are very reasonable, either in terms of *N*-methyl versus *N*-phenyl substitution, or acyclic urea versus uracil formation.

Acidity dependence of the rate constants

The reactions (cyclization and ring opening) were sufficiently slow that they could be conveniently followed kinetically at 70°C. The observed rate constants were corrected for the unproductive ionizations discussed in the previous section, as in

$$k_{corr} = k_{obs}(1 + [BH^+]/[B])$$

where

$$[BH^+]/[B] = \text{antilog}\,(m^*X + pK_{BH^+} + \log C_{H^+})$$

The X-function and pK_{BH^+} values were temperature corrected to 70°C as recommended by Cox *et al.* (13). Values of log C_{H^+} at 25°C were used unchanged, since it has been shown that temperature corrections over the range studied would be very small or negligible (9).

The rate constants for the cyclization direction (k_f), which are the more important in terms of the present mechanistic comparisons, were treated by both the Cox–Yates (C–Y) (14) and Bunnett–Olsen (B—O) (15) treatments, as in eqs. [1] and [2] respectively.

[1] $\log k_f^{corr} - \log C_{H^+}$

[2] $\log k_f^{corr} + H_0 = \phi(H_0 + \log C_{H^+})$

In both cases linear plots were obtained (see Fig. 2), without including any water activity terms as is reasonable in terms of

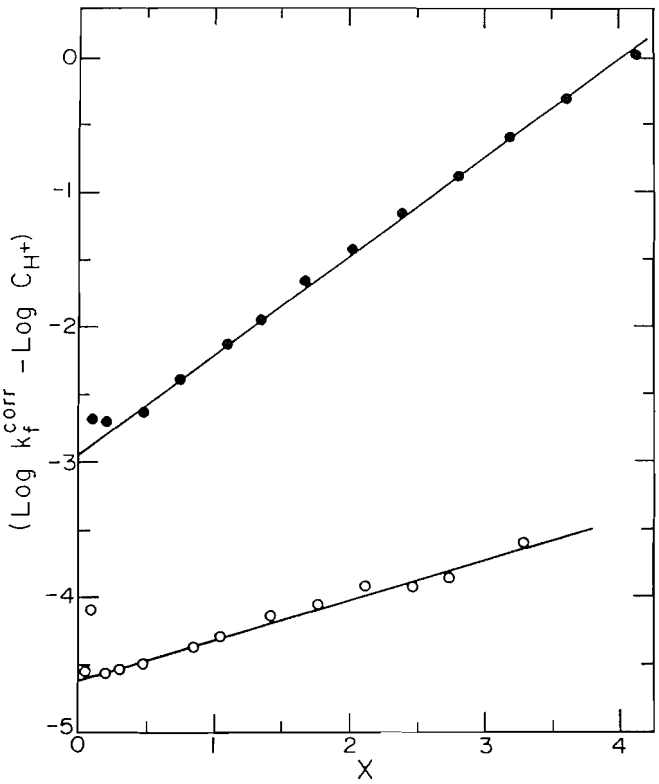

FIG. 2. Plots of (log k_f^{corr} − log C_{H^+}) versus the X-function for the ring closure of **1** (●) and **3** (○).

Scheme 1 for reaction in the forward direction. The medium-independent rate constants k_2^0 and the slope parameters ($m^*m^\ddagger$ or ϕ) are given in Table 2, along with the appropriate statistical parameters. Given the previously demonstrated (14) equivalence between $m^*m^\ddagger$ and $(1 - \phi)$, the two kinetic treatments give essentially the same results for both k_f and k_r. Since the former is somewhat easier to interpret mechanistically, only $m^*m^\ddagger$ will be used in subsequent discussion.

The rate constants in the ring-opening direction (k_r) were also treated by both the C–Y and B–O approaches, but the correlations were less clear-cut. The unmodified eqs. [1] and [2] led to downward curving plots, which is not reasonable either in terms of the negative $m^*m^\ddagger$ values implied or in terms of the stoichiometry of Scheme 1. Incorporation of explicit water activity terms as in eqs. [3] or [4]

[3] $\log k_+^{corr} - \log C_{H^+} + n \log aH_2O = m^*m^\ddagger X$

[4] $\log k_r^{corr} + H_0 + n \log aH_2O = \phi(H_0 + \log C_{H^+})$

improved the fit in some, but not all, cases. Also, although the

Can. J. Chem. Downloaded from www.nrcresearchpress.com by 91.121.58.235 on 09/07/12
For personal use only.

TABLE 2. Rate constants and associated parameters from acidity function treatment

Treatment	Rate constant	n^a	log $k_2^{0\,b}$	Slope parameter[c]	r^d	δy^e
	3-(3′-Methylureido)-propanoic acid (**1**)					
C–Y[f]	log k_f^{corr}	0	−2.851	0.70	0.998	0.06
	log k_f^{corr}	0	−3.702	−0.10	0.915	0.06
		1	−3.809	0.196	0.949	0.088
		2	−3.916	0.422	0.968	0.172
B–O[g]	log k_f^{corr}	0	−2.808	0.35	0.987	0.082
	log k_f^{corr}	0	−3.707	0.09	0.999	0.059
		1	−3.800	0.82	0.998	0.075
		2	−3.893	0.54	0.982	0.151
	3-(3′-Phenyl)-2-methylpropanoic acid (**3**)					
C–Y	log k_f^{corr}	0	−4.616	0.29	0.992	0.041
	log k_f^{corr}	0	−4.526	−0.16	0.974	0.041
		1	−4.588	0.09	0.927	0.038
		2	−4.649	0.336	0.977	0.080
B–O	log k_f^{corr}	0	−4.609	0.72	0.999	0.043
	log k_f^{corr}	0	−4.528	1.16	0.999	0.072
		1	−4.584	0.92	0.999	0.048
		2	−4.641	0.68	0.994	0.085

[a]Number of log aH_2O included in eqs. [3] and [4].
[b]Medium-independent bimolecular rate constant from extrapolation to $X = 0$ or $(H_0 + \log C_{H^+}) = 0$.
[c]$m^*m^{\neq}$ (C–Y) or ϕ (B–O).
[d]Correlation coefficient.
[e]Standard deviation on y-axis (log k axis).
[f]Cox–Yates treatment, eqs. [1] or [3].
[g]Bunnett–Olsen treatment, eqs. [2] or [4].

slope parameters $m^*m^{\neq}$ became positive using eq. [3], there was no significant difference in linearity[2] between the cases of $n = 1$ and $n = 2$, as shown in Table 2. It therefore seems to be the case that, although a water activity term should be included, there is no clear-cut answer as to the molecularity of the ring-opening reaction in terms of water, unlike the situation found with ester and related hydrolysis reactions. The problem can be illustrated using the Yates r-parameter (17) modification of the original Bunnett w-parameter treatment (18) as shown in Fig. 3, where (log $k_r - H_s$) is plotted against log α_{H_2O}. The plots are again curved, as found in r-plots for amide hydrolysis (17*b*, 19), and there is a clear indication of a sharp break in water–activity dependence between reactions in dilute ($r \sim 4$) and more concentrated ($r \sim 1.5$) acid solutions. This again is reminiscent of amide hydrolysis, where, as the availability of water is strongly decreased in more concentrated acids, the mechanism changes from $r = 3$ to $r = 1$ in terms of its water dependence. Since the emphasis in the present paper is on comparisons of five- and six-membered ureido derivatives, and k_r cannot be studied kinetically in the former case, the kinetic treatment of these hydrolysis rate constants was not pursued further.

Acidity dependence of the equilibrium constants

The effect of changing acidity on the observed equilibrium constants is not very pronounced, as shown in Fig. 4. The equilibrium between the *N*-methyl compounds (**1** ⇄ **2**) shifts towards **1** with increasing acid concentration, as observed previously for dihydrouracil itself (2), and is explainable in terms of the protonation of the relatively basic methylureido group. A similar effect is observed for the equilibrium **3** ⇄ **4**, but is only exhibited at higher acidity because of the weaker basicity of the phenyl-ureido group. However, in both cases log K_{obs} changes by less than one unit over the entire range 0–70% H_2SO_4. The problem is that the equilibria of interest (Scheme 1) are complicated by the two unproductive protonations of Scheme 2. Taking these into account leads to the following expression for K_{obs}:

[2]This is due in part to the approximate linearity of the excess acidity function, X, with log aH_2O (slope ca. 0.3) in the region of acidities studied.

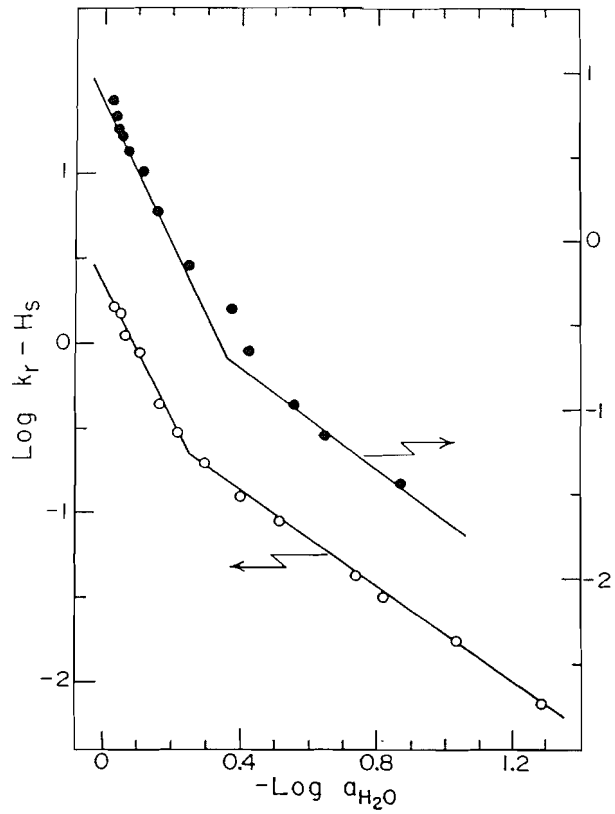

FIG. 3. Yates r-plots for the hydrolysis of **2** (●) and **4** (○).

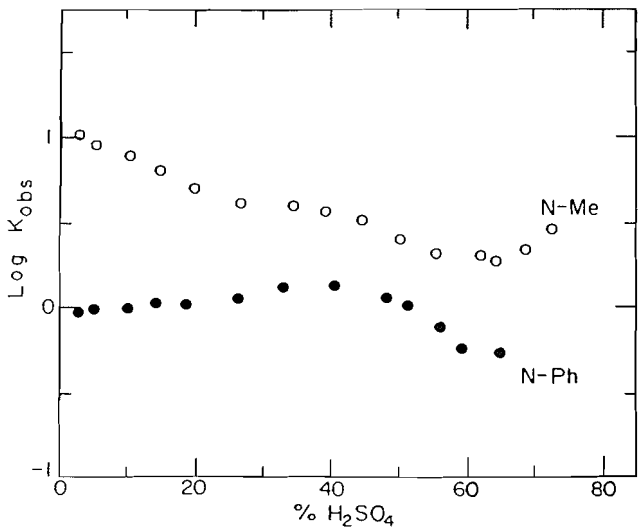

FIG. 4. Medium dependence of the equilibrium constants (log k_{obs}) on acid concentration. **1** ⇄ **2** (○); **3** ⇄ **4** (●).

$$[5] \quad K_{obs} = \left(\frac{(h_3{}^{P} + K_{PH^+})K_{UH^+}}{(h_s{}^{u} + K_{UH^+})K_{PH^+}}\right) \cdot \left(\frac{K_e f_u}{f_p a_{H_2O}}\right)$$

where the h and f terms refer to the relevant acidity functions and activity coefficients for the neutral species. The last term on the right of eq. [5] is the apparent equilibrium constant for the unprotonated species (as shown in Scheme 1), i.e., U ⇄ P, as given by eq. [6].

$$[6] \quad K_{app} = K_{obs}\frac{(1 + I_p)}{(1 + I_u)} = \frac{K_e f_u}{f_p a_{H_2O}}$$

Thus a plot of (log K_{app} + log aH_2O) versus X should give as slope the acidity dependence of log f_u/f_p and as intercept log K_e. The correlations are reasonable, as shown in Table 3. The slopes, which are equal to m_e, are positive in both cases, as expected because of the greater hydration requirements of the ureido acids than the uracils. The m_e values obtained should be equal to the difference between the kinetic $m^*m^{\ddagger}$ values for k_f and k_r given in Table 1, which is found to be the case.

TABLE 3. Equilibrium constants and associated parameters from acidity function treatment

Equilibrium[a]	log K_c[b]	m_c[c]	r[d]	δy[e]
1 ⇄ **2**	0.96	0.51	0.987	0.114
3 ⇄ **4**	−0.04	0.20	0.991	0.029

[a]Equilibrium of unprotonated species, as in Scheme 1.
[b]Based on eq. [6] and plot of (log K_{app} + log aH_2O) versus X-function.
[c]Medium-dependent slope parameter from Cox–Yates treatment.
[d]Correlation coefficient.
[e]Standard deviation on y-axis (log K_{app} + log aH_2O).

Discussion

The pK_{BH^+} value of **1** (−0.85) is close to that reported for 5-methylhydantoic acid (5), if the latter is corrected by 0.3 units because of the mis-anchoring of the original H_A scale (20) (−1.06). Both values are significantly lower than the kinetically determined pK value of −0.25 reported for 3-ureidopropanoic acid (2), which is probably due to some loss of planarity in 1,3-disubstituted ureas. A similar effect is found when the pK_{BH^+} of the phenylureido acid **3** (−1.83) is compared with that for phenylurea (−1.22) (21). No reliable pK_{BH^+} values have been reported for the corresponding uracil derivatives. An H_0 value of −4.7 for the half-protonation of dihydrouracil has been reported (26) in $HClO_4$, and from somewhat uncertain ionization ratio determinations the Bunnett–Olsen treatment had given a pK_{BH^+} value of −2.54 (ϕ = 0.55) (2). The latter values are close to the values obtained in this work for **2** (pK_{BH^+} = −2.6, ϕ = 0.48). The value for **4** is significantly more negative (pK_{BH^+} = −3.56), as expected for the base-weakening effect of *N*-phenyl, rather than *N*-methyl substitution. It is interesting that effects of ring closure on the basicity of **1** and **3** are practically identical, as shown in Table 1. In addition, the decreases in $m^{\ddagger}$ for both **1** → **2** and **3** → **4** are in the expected direction, because of the higher hydration requirements of the ureido acid form. The m^* values for the protonation of the pyrimidinediones **2** and **4** fall in the usual range observed for amides (22).

Because of their structural similarities to amides and ureas, it is instructive first to consider possible hydrolysis mechanisms for pyrimidinediones (such as **2** and **4**) before examining the reaction in the ring-closure direction. The overall scheme including all reasonable intermediates is shown in Scheme 3.

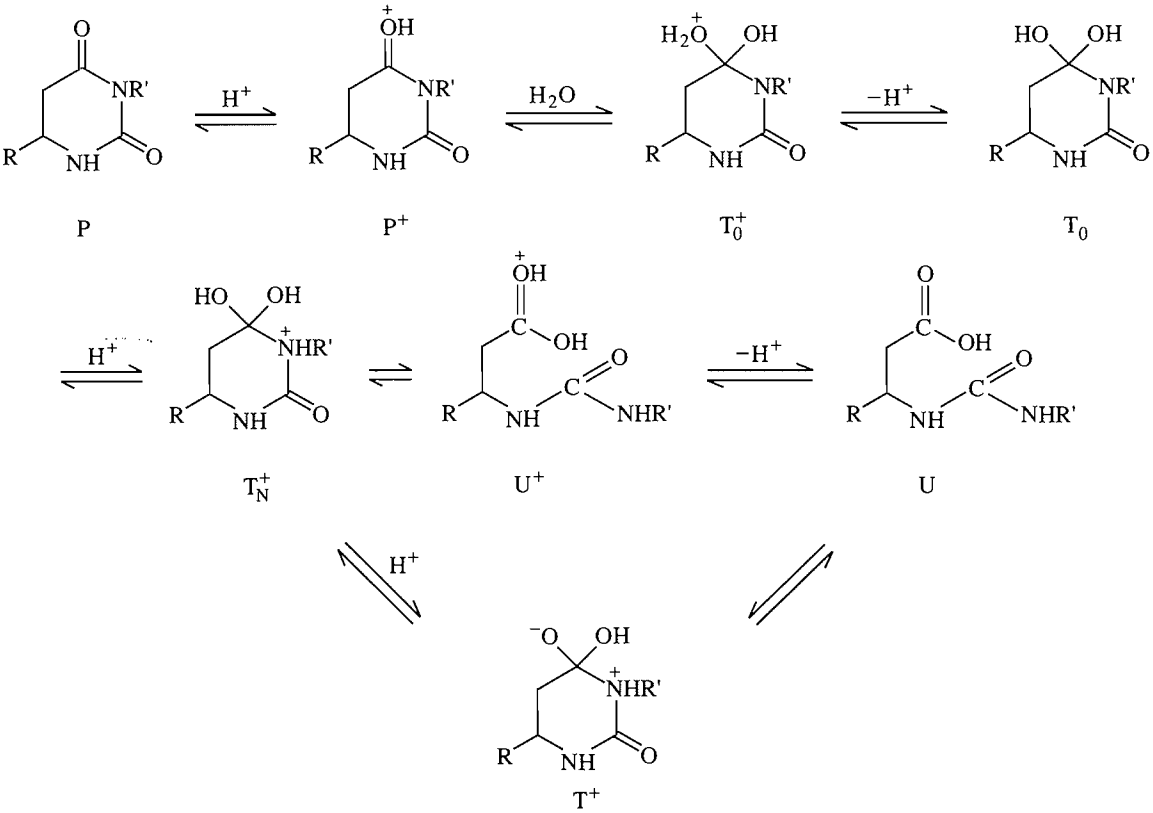

SCHEME 3

Can. J. Chem. Downloaded from www.nrcresearchpress.com by 91.121.58.235 on 09/07/12
For personal use only.

Can. J. Chem. Downloaded from www.nrcresearchpress.com by 91.121.58.235 on 09/07/12
For personal use only.

Currently it is considered that in $A_{AC}2$ type ester (13) and amide hydrolysis (3), although T_0^+ can be formed by rate-determining attack of water on the protonated substrate, its presence can be avoided in dilute to moderately concentrated acids by the further participation of water (as a base) in a one-step process leading directly to T_0.

The parameters obtained from acidity function treatment of **2** and **4** are not very different from those observed for acid-catalyzed amide hydrolysis ($A_{AC}2$) (3) and, as previously mentioned, dihydrouracil (2) and acylthiourea (4) hydrolyses also behave similarly: with the latter, the interpretation of rate-determining water attack on the protonated substrate was consistent with other evidence, such as high negative $\Delta S^{\neq}$ values, inverse solvent isotope effect, and substituent effects in the acyl moiety (2, 4).

However, there is evidence for an alternate mechanism in the case of 3-methylhydantoin, where Guler and Moodie (5) observed that ^{18}O-exchange is at least 10 times faster than ring opening.[3] This strongly supports the idea that C—N bond breaking or formation is involved in the rate-determining steps of acid-catalyzed ring opening and ring closing. Furthermore, the same authors (5) observed general acid catalysis, whereas typical $A_{AC}2$ amide hydrolysis is specific acid catalyzed (3). In addition, one of us (2) has found that cyclization of sterically strained hydantoic acids showed general acid catalysis with Brønsted coefficients $0 < \alpha < 1$. This is generally believed to indicate proton transfer concerted with heavy atom reorganization.

An important question at this point is, how likely is it that the above five-membered ring compounds (hydantoins) hydrolyse by a different mechanism from the six-membered rings (uracils) of the present study? Five-membered rings are usually more difficult to open, and this can make ring formation rate determining on changing from six- to five-membered ring compounds, as shown previously for 3-(2′-aminophenyl) propanoic (24) and 2-aminophenylacetic acids (25). However, decreased basicity of the amino group in the hydrolysis direction tends to shift the rate-determining step in Scheme 3 from formation of T_0 or T_0^+ to one of the subsequent steps. Since anilines are a borderline case (26), then the much more weakly basic amino group of the present ureido systems is most unlikely to be affected by ring size.

Hydrolysis of **2** in ^{18}O-enriched 0.5 M HCl solutions showed that its rate of ^{18}O-exchange is 7.85 times faster than the rate of hydrolysis (**2** → **1**). This demonstrates that the process T → U occurs about 16 times faster than T → P, thus proving that C—N bond scission is also rate determining for the six-membered ring compounds.

Since the mechanism of hydrolysis of both hydantoin and uracil derivatives involves rate-determining C—N bond breaking, as opposed to the standard $A_{AC}2$ mechanism for amide hydrolysis, then are the acidity function parameters $m^*m^{\neq}$ or ϕ able to distinguish between such processes? The answer is certainly no, since the $m^*m^{\neq}$ or ϕ parameters listed in Table 2 fall within the range observed (3) for various types of amide hydrolysis, as do the m^* for the protonation step itself (see Table 1). A major problem, alluded to earlier, is that amide-type hydrolyses are more complex in terms of their medium dependence than other types of hydrolysis, as shown earlier by Cox and Yates (3*a*), and as illustrated by Fig. 3. One thing seems clear, however, from all the evidence; that is, in Scheme 3 the transition state in the ring-opening direction is almost certainly at T_0 or to the right of T_0. Therefore the transition state in the ring-closure direction must lie between T_0 and the starting ureido acid.

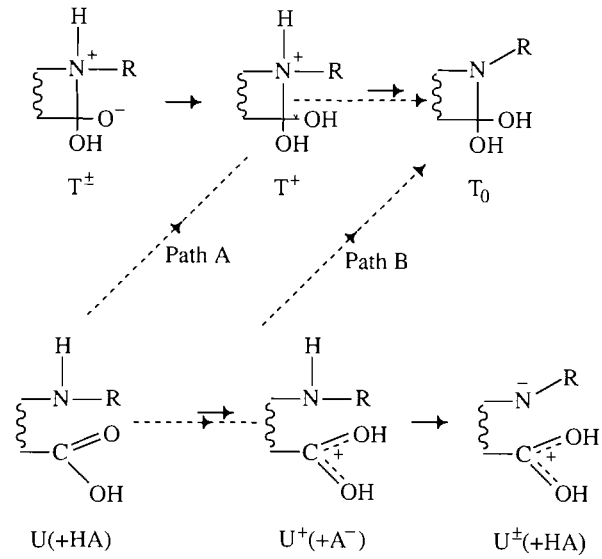

SCHEME 4

The possible pathways for ring closure are as shown in Scheme 4, since this approach will allow clearer consideration of alternate route diagrams of the Albery–Jencks – More O'Ferrall type (7).

First of all, pathways leading through $T^{\pm}$ can be neglected. Since the ureido nitrogen is very weakly, and the O^- group very strongly basic, this will represent a very high energy species. Similarly, the species $U^{\pm}$ will probably be even higher in energy than $T^{\pm}$ and can also be neglected. This means that the only two viable pathways will be paths A and B (see Scheme 4). Path A represents true general acid catalysis, and path B specific acid – general base catalysis, both being concerted with C—N bond formation. Since these two pathways are kinetically indistinguishable, there are two approaches to try to resolve the problem. One is to consider the effects of N-substitution on the basicity or acidity of the various intermediates. It is clear from Fig. 2 that the ring closure of the *N*-methyl derivative **1** has a substantially higher value of $m^*m^{\neq}$ than that of the *N*-phenyl derivative **3** (0.7 versus 0.3), similar to the situation reported (8) for five-membered ring analogues. On the highly probable assumption that N-substitution will have very little effect on the m^* value for proton transfer to the remote carboxyl group, this means that the $m^{\neq}$ value for proton transfer, following Kresge's interpretation (29) of the slope parameters obtained from the rate–acidity profiles, corresponds to the Brønsted α. This means that **1** will have a higher α, or later transition state, than **3**. As can be seen from Scheme 4 for path A, decreased basicity of N-Ph versus N-Me will increase the degree of proton transfer to nitrogen at the transition state and hence increase α, which is opposite to what is observed. For path B, a similar decrease of N-basicity (or increase of NH-acidity) will increase proton transfer from nitrogen to H_2O at the transition state and hence increase β for this step. Experimentally, this will be detected as a decrease in the observed α, which is what is observed experimentally. Thus path B is clearly favoured by this argument.

A second approach is to construct a three-dimensional Albery–Jencks – More O'Ferrall diagram (7) as shown in Fig. 5. This shows both pathways A and B as in Scheme 4, with the

[3]Dr. Moodie has kindly drawn attention to an error of 4 in the published estimate.

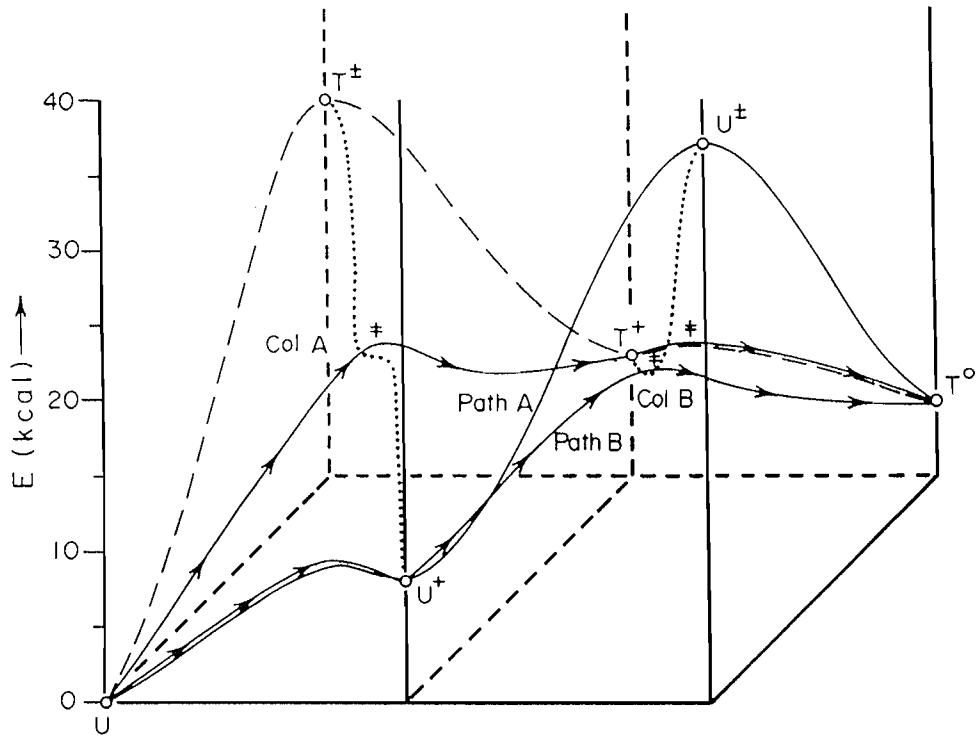

FIG. 5. Energy–reaction coordinate profiles for the ring closure of ureido acid (**U**) to form the neutral tetrahedral intermediate ($\mathbf{T_0}$). See text for description of intermediates and pathways.

heights of the various intermediates in energy terms, relative to that of the substrate, taken as the zero reference point. Estimates of these relative energies were based on p*K* values for related model compounds and on standard bond energy values, as described in the experimental section. It seems clear from the diagram that the saddle-point for path B (denoted Col. B) will be close in energy to, and probably lower than, that of the intermediate T^+, which lies on path A. As far as the saddle-point on path A is concerned (denoted by Col. A), this will either be higher than T^+ (and hence higher than Col. B), which would mean simple general acid catalysis, or it is lower than T^+, which would mean that the transition state for path A would lie between T^+ and T_0. The latter would imply that proton transfer from nitrogen would be rate determining, *after* the acid-catalyzed formation of the C—N bond, which seems most improbable, although it would lead to observed general acid catalysis. In the former, more probable case, if Col. A is higher than T^+, which in turn is equal to or higher in energy than Col. B, this indicates that path B would be the favoured mechanism, as already concluded from comparison of the *N*-methyl and *N*-phenyl derivatives' response to changing acidity. It should be emphasized that the conclusions based on Fig. 5 do not depend on the precise energy values calculated for the various intermediates, but only on the general features of the diagram.

Thus, overall, it seems probable that both six- and five-membered ring formation take place by rate-determining proton transfer from nitrogen, concerted with C—N bond formation, and not slow proton transfer to oxygen as previously assumed. As already mentioned, the variation of Brønsted α values observed for buffer catalysis with strained hydantoic acids, upon replacing N-Me for N-Ph, favour the alternate mechanism, path A. The reasons for this difference are at the present not clearly understood.

Experimental

Spectra

UV spectra were taken on a Carl Zeiss, Jena, Specord UV–VIS spectrophotometer and the NMR spectra on a Bruker WM 250 instrument.

Materials

3-(3[1]-Methylureido)-propanoic acid, **1**, was prepared by adding 0.033 mol of methyl isocyanate to an ice-cooled solution of 0.03 mol of 3-aminopropanoic acid in 15 mL of 2 M NaOH under vigorous stirring. The mixture was heated to ambient temperature for 5–10 min and, after a further 5 min, the pH of the solution was brought to 2 by adding cation-exchanger Dowex W in H^+-form. The resin was filtered and the filtrate evaporated to dryness to yield 1.68 g (38%) of **1**. The pure compound was obtained after repeated crystallization from acetone, mp 132–134°C (dec.). Anal. calcd. for $C_5H_8N_2O_2$: C 41.69, H 6.90, N 19.17; found: C 40.86, H 6.64, N 18.87%. 3-Methylhexahydropyrimidine-2,4-dione was obtained by evaporating to dryness a solution of **1** in 1:1 HCl at 100°C, extracting the residue with hot dioxane, and recrystallizing from ethanol; mp 128.5–129°C (lit. (30) mp 128–129°C). 3-(Phenylureido)-2-methylpropanoic acid, **3**, and 5-methyl-3-phenylhexahydropyrimidine-2,4-dione have been described previously (31).

Sulfuric acid solutions were prepared from analytical grade H_2SO_4 (Riedel de Haen) and distilled water, and the concentrations determined by titration.

pK_{BH^+} determinations; NMR measurements

These were carried out at 19°C and 30°C for **1** and **2** respectively. The p*K* value of **1** was determined from the changes in the ^1H chemical shifts at 250 MHz of the methyl protons with the concentration of the sulfuric acid. The shifts varied from 1.917 to 2.013 ppm for the unprotonated and protonated form respectively. Solutions (2%) of **1** in aqueous H_2SO_4 were used with acetone-d_6 and TMS as external lock and standard respectively. Care was taken to use the same capillaries throughout the series of measurements. The p*K* value of **2** was determined from the changes in the ^{13}C chemical shifts of the 2-CO carbon at 62.7 MHz, using 2% (w/v) solutions of **2** in aqueous H_2SO_4

Can. J. Chem. Downloaded from www.nrcresearchpress.com by 91.121.58.235 on 09/07/12
For personal use only.

Can. J. Chem. Downloaded from www.nrcresearchpress.com by 91.121.58.235 on 09/07/12
For personal use only.

and D_2O and TMS as external lock and standard respectively. The shifts varied from 135.7 for the unprotonated form to 159.3 for the protonated form.

UV measurements

The pK values of **3** and **4** were determined from the changes in absorbance at 238 nm with sulfuric acid concentration (24 solutions from 2.5 to 78%) at 25.0°C in a temperature controlled cell holder. Stock solutions of **3** and **4** (2×10^{-3} M) in ethanol were used and the final solutions prepared by adding 0.085 mL of **3** or 0.17 mL of **4** to 2.75 mL of the sulfuric acid solution. The changes in the total spectra did not show isosbestic points and were treated as described in Calculations.

Kinetic runs

In the case of **1** and **2** these were carried out in the temperature-controlled cell holder of the spectrometer at 70.0 ± 0.1°C in 10-nm stoppered cells. The reaction was initiated by adding 0.05–0.1 mL of a 2.2×10^{-2} M ethanolic solution of **1** or **2** to 2.75 mL of the H_2SO_4 solution at 70.0°C and monitored at 232 nm where **2** has a higher absorbance than **1**. The reaction of **3** or **4** was carried out in sealed ampoules in a thermostat bath at 70.0°C. The solutions were prepared by making up to 100 mL, 3 mL of an ethanolic 2×10^{-3} M solution of the substrate, with the sulfuric acid solution. The reaction was monitored at 238 nm by the decrease of the absorbance of **3** or the increase of that of **4**. In all cases good isosbestic points were obtained. With all sulfuric acid concentrations the reactions were carried out in both directions and the spectra obtained at $10t_{1/2}$, A_∞, were found to be identical within experimental error. The observed first-order rate constants $k^{obs} = k_f + k_r$, where k_f and k_r are the rate constants for the forward and reverse reactions, were calculated by the least-squares procedure from the linear dependence of $\ln(A_t - A_\infty)$ or $\ln(A_\infty - A_t)$ against time. The apparent equilibrium constant, $K_e^{obs} = k_f/k_r$ was obtained from

$$K_e^{obs} = \frac{A_\infty - A^0_u}{A^0_p - A_\infty}$$

where A^0_u and A^0_p are the initial absorbances of the ureido acid or pyrimidine, respectively, at a particular sulfuric acid concentration. The rate and equilibrium constants were obtained as averages from 2–3 runs. The differences between separate determinations did not exceed 5%. k_f and k_r were derived from the two equations above.

Kinetics of ^{18}O-exchange of 2

These were carried out in 0.5 M HCl at 50.0°C. In a separate experiment, K_e^{obs} and k^{obs} were determined as described above, to be 15.3 and 2.20×10^{-4} s^{-1}, respectively, yielding $k_f = 2.06 \times 10^{-4}$ s^{-1} and $k_r = 1.35 \times 10^{-5}$ s^{-1}.

A 0.5 M solution of HCl in water 20% enriched in ^{18}O was prepared by volume with concentrated HCl and the concentration checked by titration; 11.6 mg (10^{-4} mol) of **2** was dissolved in 0.9 mL of the HCl solution in a stoppered UV cell at 50.0°C in the temperature controlled cell holder. Aliquots of 0.1 or 0.05 mL were withdrawn and quenched in a small flask containing 0.5 mL of water and 0.4 (or 0.2) mL of 0.1 M KOH. The pH was adjusted to 7 with KOH solution and the contents evaporated to dryness. The residue was extracted three times with a total of 4 mL of methylene chloride. The extract was filtered and evaporated and the dry residue analysed on a JEOL JMS-D300 mass spectrometer, electron impact mode, ionization potential 70 eV, ionization current 300 μA, and ion source temperature 170°C. A separate experiment showed that no ureido acid is extracted under these conditions. The extent of exchange was monitored by the ratio of the M^+ to ($M^+ + 2$) peaks, averaged from several determinations and corrected for the natural content of ^{18}O. The rate constant of exchange, $k = 1.06 \times 10^{-4}$ s^{-1}, was calculated from the integrated first-order rate equation after accounting for rapid exchange via the ureido acid.[4]

[4]The hydrolysis of **2** is appreciably reversible, $K_e = 15.3$, so that the exchange can occur via the free acid. From the data in ref. 28 on ^{18}O-exchange in acetic acid, a rate of 0.002 s^{-1} can be calculated at the temperature at which the exchange rate of **2** was measured. Because of this rather high estimate for the exchange of the free carboxy group, the exchange data for **2** were corrected by assuming that every molecule of **1** exchanged before recycling. The ratio P*/P, for the exchange along this pathway, was found by means of the integrated rate equation for consecutive irreversible first-order reactions. The results obtained indicated that this was probably an "over-correction"; plots of ln (% of exchange) against time of the uncorrected data were linear for ca. 70% conversion; however, the rate constants before and after correction differed by less than 20%.

Calculations

*p*K *values*

These were obtained using the Cox–Yates (9) treatment outlined in the results section. In the case of **1** this method was applied in a straightforward fashion to the variation of ^1H chemical shift of the *N*-methyl group with acidity. For compound **2** the ^{13}C chemical shifts of the 2-CO group varied in the expected way up to 79% H_2SO_4, then decreased slightly (i.e., points at 83.5 and 88% H_2SO_4). That this is not due to a medium effect but rather is due to the onset of a second protonation at 4-CO was evidenced by the chemical shift behavior of the latter carbon. The chemical shifts decreased in parallel to the protonation of 2-CO (ca. 70 Hz up to $H_A = -3.5$), and then increased rapidly (by ca. 110 Hz up to $H_A = -5$). Since too few data were available in the high acidity region, no quantitative treatment of this second protonation was attempted. The ionization ratios for the first protonation were obtained by assuring that the maximum chemical shift is ΔBH^+. For compound **3**, the variation in UV spectra with acidity showed no isosbestic point, similar to the cases of arylureas (21, 32) and 5-arylhydantoic acids (8). Following previous experience the ionization ratios were obtained by assuming (12, 33) linear dependence of A(B) and $A(BH^+)$ on H_A. The latter values were obtained by plotting the absorbance (A) at 238 nm versus H_A, and extrapolating the linear portions of each end of the sigmoid curve obtained.

The 3-phenyldihydrouracil **4** showed only end UV absorption, which increased with acid concentration, but did not level off at high acidity. When plotted against H_0, however, an inflection point around $H_0 = -7$ was observed, indicating the completion of the first protonation and beginning of the second, as indicated by the ^{13}C NMR spectra of **2**. Usually with weaker bases, only A(B) is significantly medium dependent (33), and thus the ionization ratios for **4** were calculated by assuming linear dependence of A(B) on H_0 and by adjusting $A(BH^+)$ iteratively until the best fit was obtained for the total variation of A.

Rate constants

The medium independent bimolecular rate constants and equilibrium constants were obtained by means of eqs. [1]–[6] (see Results). The values for X and pK were corrected as recommended (13); log C_{H^+} values for 25°C were used. In the Bunnett–Olsen treatment H_0 values interpolated for 70°C from the data in ref. 34 were used together with log C_{H^+} instead of the acid molarity. The log aH_2O values at 70°C are from ref. 35; values for solutions more concentrated than 63% H_2SO_4 were obtained by extrapolation of a plot log aH_2O^{25} vs. log aH_2O^{70} (36).

Energy–reaction coordinate profiles

For the change in free energy for $U^+ \rightarrow U$, a pK value of approximately −4 was used, based on values obtained (37) for aromatic and α,β-unsaturated acids, using the Bunnett–Olsen

treatment. To the best of our knowledge, no pK values have been reported for simple aliphatic carboxylic acids. Recently, however, Edward and Wong (38) have determined $pK_{BH^+} = -4.7$ ($m^* = 0.56$) for benzoic acid. For the change $U^+ \rightarrow U^{\pm}$, we have used the reported pK values of 18.3 (39) for the equilibrium $H_2NCONHCH_3 \rightleftarrows H_2NCON^- CH_3 + H^+$, and 16.3 and 16.6 for the ionizations of $PhNHCONHCH_2COO^-$ and $PhNHCON(CH_3)CH_2COO^-$ respectively (40).

For the tetrahedral intermediates shown below, the following pK values are estimated using the approach of Fox and Jencks (41): $pK_1 = -8.1$, $pK_2 = 8.2$, $pK_3 = 12.8$, $pK_4 = -3.3$. These are based on a pK_{BH^+} of -3.9 reported (39) for the *N*-methyl nitrogen in methylurea and a suitable LFER recommended by Fox and Jencks (41), assuming that a unit charge changes the pK by 4.8 units.

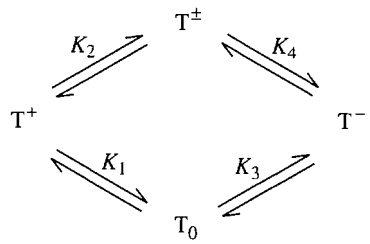

The most difficult term to estimate reliably was the energy difference between U and T_0. Using representative average bond energies (16), T_0 was estimated to be only 2 kcal higher in energy than U. However, using group contributions from two sources (16, 23), based on somewhat dubious analogies, higher values of 9.5–11.8 kcal were obtained. Finally, heats of formation for U and T_0 based on AM1 calculations (27) gave $\Delta\Delta H_f$ of 7.2 kcal. We have therefore used an average value of ~6 kcal for this difference. The absolute accuracy is not, however, critical in comparing the relative energy changes of paths A and B from U to T_0.

Acknowledgements

The continued financial support of NSERC of Canada and the Committee of Science of Bulgaria is acknowledged. We are also very grateful to Dr. Alexander Dyulgerov for carrying out the mass-spectral measurements for the ^{18}O-exchange studies, and to Dr. Jose Kaneti for the AM-1 calculations.

1. I. B. Blagoeva, A. H. Koedjikov, and I. G. Pojarlieff. Izv. Khim. **21**, No. 2, 208 (1988).
2. I. G. Pojarlieff. Tetrahedron, **23**, 4307 (1967).
3. (*a*) R. A. Cox and K. Yates. Can. J. Chem. **59**, 2853 (1981); (*b*) L. M. Druet and K. Yates. Can. J. Chem. **62**, 2401 (1984).
4. W. I. Congdon and J. T. Edward. J. Am. Chem. Soc. **94**, 6099 (1972).
5. G. F. Guler and R. Moodie. J. Chem. Soc. Perkin Trans. 2, 1752 (1980).
6. (*a*) I. B. Blagoeva. J. Chem. Soc. Perkin Trans. 2, 245 (1984); (*b*) I. B. Blagoeva, I. G. Pojarlieff, D. T. Tashev, and A. J. Kirby. J. Chem. Soc. Perkin Trans. 2, 347 (1989).
7. R. A. More O'Ferrall. J. Chem. Soc. Perkin Trans. 2, 274 (1970); W. P. Jencks. Chem. Rev. **72**, 705 (1972); Chem. Rev. **85**, 511 (1985).
8. I. B. Blagoeva, I. G. Pojarlieff, and V. T. Rachina. Izv. Khim. **20**, No. 1, 119 (1987).
9. R. A. Cox and K. Yates. J. Am. Chem. Soc. **100**, 3861 (1978).
10. V. Lucchini, G. Modena, G. Scorrano, R. A. Cox, and K. Yates. J. Am. Chem. Soc. **104**, 1958 (1982).
11. J. F. Bunnett and F. P. Olsen. Can. J. Chem. **44**, 1899 (1966).
12. A. R. Katritzky, A. J. Waring, and K. Yates. Tetrahedron, **19**, 465 (1966).
13. R. A. Cox, M. F. Goldman, and K. Yates. Can. J. Chem. **57**, 2960 (1979).
14. R. A. Cox and K. Yates. Can. J. Chem. **57**, 2944 (1979).
15. J. F. Bunnett and F. P. Olsen. Can. J. Chem. **44**, 1917 (1966).
16. T. H. Lowry and K. S. Richardson. Mechanism and theory in organic chemistry. 2nd ed. Harper and Row, New York. 1981. pp. 146–147.
17. (*a*) K. Yates. Acc. Chem. Res. **4**, 136 (1971); (*b*) K. Yates and J. B. Stevens. Can. J. Chem. **43**, 529 (1965); K. Yates and J. C. Riordan. Can. J. Chem. **43**, 2328 (1965).
18. J. F. Bunnett. J. Am. Chem. Soc. **83**, 4956 (1961); **83**, 4968 (1961); **83**, 4973 (1961); **83**, 4978 (1961).
19. L. M. Druet and K. Yates. Can. J. Chem. **62**, 2401 (1984).
20. J. T. Edward and S. C. Wong. Can. J. Chem. **55**, 2492 (1977).
21. C. J. Giffney and C. J. O'Connor. J. Chem. Soc. Perkin Trans. 2, 1206 (1975).
22. R. A. Cox, L. M. Druet, A. D. Klausner, P. Wan, and K. Yates. Can. J. Chem. **59**, 1969 (1981).
23. S. W. Benson, F. R. Cruickshank, D. M. Golden, G. R. Hagen, H. E. O'Neal, A. S. Rodgers, R. Shaw, and R. Walsh. Chem. Rev. **69**, 279 (1969).
24. A. J. Kirby, T. G. Mujahad, and P. Camilleri. J. Chem. Soc. Perkin Trans. 2, 1610 (1979).
25. T. H. Fife and N. W. Duddy. J. Am. Chem. Soc. **105**, 74 (1983).
26. J. M. Abdallah and R. B. Moodie. J. Chem. Soc. Perkin Trans. 2, 1243 (1983).
27. M. J. S. Dewar, E. G. Zoebisch, E. F. Healey, and J. J. P. Stewart. J. Am. Chem. Soc. **107**, 3902 (1985).
28. D. R. Llewellyn and C. J. O'Connor. J. Chem. Soc. 545 (1964).
29. A. J. Kresge, R. A. More O'Ferrall, L. E. Hakka, and V. P. Vitullo. Chem. Commun. 46 (1965); A. J. Kresge, S. G. Mylonakis, Y. Sato, and V. P. Vitullo. J. Am. Chem. Soc. **93**, 6181 (1971).
30. E. G. Sander. J. Am. Chem. Soc. **93**, 3629 (1967).
31. I. B. Blagoeva, V. T. Rachina, and I. G. Pojarlieff. Dokl. Bolg. Akad. Nauk, **35**, 1499 (1982).
32. J. W. Barnett and C. J. O'Connor. J. Chem. Soc. Perkin Trans. 2, 1331 (1973).
33. R. A. Cox and K. Yates. Can. J. Chem. **59**, 1560 (1981).
34. C. D. Johnson, A. R. Katritzky, and S. A. Shapiro. J. Am. Chem. Soc. **91**, 6654 (1969).
35. C. R. Smith and K. Yates. J. Am. Chem. Soc. **93**, 6758 (1971).
36. W. C. Giaugue, E. W. Horning, J. E. Kunzler, and T. R. Rubin. J. Am. Chem. Soc. **82**, 62 (1960).
37. R. I. Zalewski and G. E. Dunn. Can. J. Chem. **46**, 2471 (1968).
38. J. T. Edward and S. C. Wong. J. Am. Chem. Soc. **99**, 4229 (1977).
39. R. S. Molday and R. G. Kallen. J. Am. Chem. Soc. **94**, 6739 (1972).
40. M. Bergon and J.-P. Calmon. J. Chem. Soc. Perkin Trans. 2, 493 (1978).
41. J. P. Fox and W. P. Jencks. J. Am. Chem. Soc. **96**, 1436 (1974).

Can. J. Chem. Downloaded from www.nrcresearchpress.com by 91.121.58.235 on 09/07/12
For personal use only.

The mechanism of the photochemical cycloaddition reaction of *N*-benzoylindole with cyclopentene[1]

BIMSARA W. DISANAYAKA AND ALAN C. WEEDON[2]

The Photochemistry Unit, Department of Chemistry, University of Western Ontario, London, Ont., Canada N6A 5B7

Received March 28, 1990

This paper is dedicated to Professor Ross Stewart on the occasion of his 65th birthday

BIMSARA W. DISANAYAKA and ALAN C. WEEDON. Can. J. Chem. **68**, 1685 (1990).

The mechanism of the photochemical cycloaddition reaction between *N*-benzoylindole, **1**, and cyclopentene to give cyclobutane adducts **2** and **3** has been examined. The triplet excited state lifetime and quantum yield of intersystem crossing were determined for **1** as $(2.8 \pm 0.3) \times 10^{-8}$ s and 0.39 ± 0.01, respectively, using the triplet counting procedure. In addition, the dependence of the quantum yield of cycloadduct formation upon the concentration of cyclopentene and upon the concentration of excited state quenchers has been determined. The results are used to propose a mechanistic model in which the triplet excited state of **1** reacts with cyclopentene to give a triplet 1,4-biradical intermediate. Following spin inversion the biradical intermediate reverts to the ground state starting materials or proceeds to the products **2** and **3**; this partitioning, along with the quantum yield of intersystem crossing, gives rise to a limiting quantum yield of cycloaddition at infinite alkene concentration of 0.061. It is calculated that 84% of the biradical intermediates revert to the starting materials and 16% proceed to cycloadducts. The quantum yield data are also used to calculate two independent values of the rate constant for reaction of the triplet excited **1** with alkene; the values are $(1.8 \pm 0.1) \times 10^7\ M^{-1}\ s^{-1}$ and $(4.0 \pm 0.8) \times 10^6\ M^{-1}\ s^{-1}$. Some evidence for self quenching of the triplet excited state of **1** by ground state **1** was also observed. The quantum yield of intersystem crossing and the triplet excited state lifetime of **1** were found to vary with the solvent used; this is discussed in terms of the possible existence of a charge transfer triplet excited state.

Key words: indole, photocycloaddition, mechanism.

BIMSARA W. DISANAYAKA et ALAN C. WEEDON. Can. J. Chem. **68**, 1685 (1990).

On a étudié le mécanisme de la réaction de cycloaddition photochimique entre le *N*-benzoylindole, **1**, et le cyclopentène qui conduit aux adduits cyclobutaniques **2** et **3**. Utilisant la technique de comptage des états triplets, on a établi que le temps de vie de l'état triplet excité et le rendement quantique du croisement intersystème du composé **1** sont respectivement de $(2,3 \pm 0,3) \times 10^{-9}$ s et $0,39 \pm 0,01$. De plus, on a déterminé la relation qui existe entre le rendement quantique pour la formation du cycloadduit et, d'une part, la concentration de cyclopentène et, d'autre part, la concentration des pièges des états excités. On a utilisé les résultats obtenus pour proposer un modèle mécanistique dans lequel l'état triplet excité du produit **1** réagit avec le cyclopentène pour donner un intermédiaire triplet 1,4-biradicalaire. Après une inversion de spin, l'intermédiaire biradicalaire retourne à l'état fondamental des produits réactionnels ou il se transforme pour donner les produits **2** et **3**; cette répartition prise de concert avec le rendement quantique du croisement intersystème placent à 0,061, la limite du rendement quantique de la cycloaddition à une concentration infinie d'alcène. On a calculé que 84% des intermédiaires biradicalaires retournent aux produits de départ et que 16% donnent des produits de cycloadditions. On a aussi utilisé les rendements quantiques pour calculer deux valeurs indépendantes de la constante de vitesse de la réaction du triplet excité du produit **1** avec l'alcène; ces valeurs sont $(1,8 \pm 0,1) \times 10^7\ M^{-1}\ s^{-1}$ et $(4,0 \pm 0,8) \times 10^6\ M^{-1}\ s^{-1}$. On a aussi obtenu quelques données suggérant l'existence d'un auto-piégeage de l'état triplet excité du produit **1** par l'état fondamental du produit **1**. On a trouvé que le rendement quantique du croisement intersystème ainsi que le temps de vie de l'état triplet excité du produit **1** varient avec le solvant utilisé; on discute de ces données en fonction de l'existence possible d'un état triplet excité de transfert de charge.

Mots clés : indole, photocycloaddition, mécanisme.

[Traduit par la revue]

Introduction

The indole chromophore is a common component of alkaloids and also of proteins where it occurs as part of the amino acid tryptophan. The latter is one of the few naturally occurring amino acids that absorbs light in the near uv region and is responsible for the major part of the accessible absorption spectra of proteins. Possibly because of its ubiquitous presence in living organisms the photophysics of the indole system has received much attention (1). Fortunately for those life-forms exposed to sunlight the simple indole chromophore has relatively low photochemical reactivity and fluorescence is a major fate of the excited state initially formed by light absorption (2). The few photochemical reactions that have been reported include the formation of 3-(1-cyanoethyl)indole from irradiation of indole in the presence of acrylonitrile (3), and the photoaddition of alkynes across the indole 2,3 double bond to give cyclobutenes, which then open thermally to give benzazepines (4). The low photochemical reactivity of the indole chromophore contrasts with the properties of the analogous heterocycles benzofuran and benzothiophene, which have an extensive photochemistry (5). This includes photodimerization by 2 + 2 addition of the 2,3 double bond of an excited heterocycle to the same bond in a ground state partner. The 2 + 2 addition of alkenes across the 2,3 double bond of the excited states of these heterocycles to form cyclobutanes is also well known (5).

The photochemical and photophysical properties of the indole chromophore are dramatically altered if the nitrogen atom is substituted by an electron-withdrawing group such as acetyl, benzoyl, or toluenesulfonyl (6–9). It has been shown in this laboratory for various *N*-benzoylindoles that the excited state initially formed by light absorption is non-fluorescent; rather it undergoes intersystem crossing to the triplet excited state in competition with relaxation to a charge transfer singlet

[1]Contribution No. 431 from the Photochemistry Unit, University of Western Ontario.

[2]Author to whom correspondence may be addressed.

Can. J. Chem. Downloaded from www.nrcresearchpress.com by 91.121.58.235 on 09/07/12
For personal use only.

Can. J. Chem. Downloaded from www.nrcresearchpress.com by 91.121.58.235 on 09/07/12
For personal use only.

excited state that is weakly fluorescent (9). It has also been reported that ultraviolet irradiation of these N-substituted indoles in the presence of ketones and alkenes can lead to the formation of good chemical yields of oxetanes (7) and cyclobutanes (6, 8), respectively, by addition of the ketone or alkene π-system across the 2,3 double bond of the indole derivative. If the nitrogen substituent is absent then no cycloaddition occurs. The reaction with alkenes offers a potentially powerful route for the preparation of 2- or 3-substituted indoles if selective methods for the cleavage of the cyclobutane ring can be developed, and if the limitations of the photochemical cycloaddition reaction are known. The latter requires a knowledge of the mechanism of the cycloaddition reaction so that the stereochemistry and regiochemistry of the reaction can be understood and predicted. This paper describes a study in which the mechanism of the photochemical cycloaddition reaction between *N*-benzoylindole, **1**, and cyclopentene was investigated.

Results

Spectroscopic properties of N-*benzoylindole, 1, in the presence and absence of cyclopentene*

The ultraviolet absorption spectrum of indole shows two maxima, one at 225 nm (extinction coefficient 25 000) and the other at 270 nm (extinction coefficient 6000). The latter possesses vibrational structure and the position of the whole spectrum is somewhat dependent upon solvent polarity (1). In contrast, the absorption spectrum of *N*-benzoylindole possesses maxima at 247 nm (extinction coefficient 24 000) and 302 nm (extinction coefficient 8000), neither of which has any obvious vibrational structure. The position of these bands is not affected by changes in solvent polarity (9). At room temperature weak fluorescent emission from **1** has been observed (9) with a quantum yield in hexanes of 0.041. This emission is structureless and occurs with a very large Stokes' shift. The magnitude of the Stokes' shift increases with increasing solvent polarity and this has been used to assign the emission to a charge transfer singlet excited state that is formed from the initially produced singlet excited state (9).

The absorption spectrum of **1** suggests that the first singlet excited state formed from direct excitation has an energy of 95 kcal/mol, while the charge transfer state formed from it has an energy varying from 65 kcal/mol in hexane to 53 kcal/mol in acetonitrile. Time-resolved fluorescence measurements obtained by the single photon counting technique indicate that the lifetime of the fluorescing state is ca. 0.5 ns. At 77 K *N*-benzoylindole was found to phosphoresce strongly and this completely masked the weak fluorescence. The position of the O–O band of the phosphorescence (422 nm) was not solvent dependent and corresponds to a relaxed triplet excited state energy of 68 kcal/mol.

The positions and intensities of the absorption and emission spectra of **1** were not affected by the presence of high concentrations of cyclopentene.

Characterization of photoadducts from ultraviolet irradiation of N-*benzoylindole with cyclopentene*

Ultraviolet light irradiation of a benzene solution of *N*-benzoylindole containing cyclopentene resulted in the apparent formation of a single product, as indicated by gas chromatography. At low conversions the rate of formation of this product and the rate of disappearance of *N*-benzoylindole were zero order; however, at high conversions the formation of insoluble matter became evident and the reaction slowed down. The insoluble matter is assumed to be cyclopentene polymers and it is light scattering by these which is the most likely cause of the slowing of the reaction. The ^{13}C NMR and ^{1}H NMR spectra of the isolated product indicated the presence of two compounds in approximately equal amounts, even though both gas and liquid chromatography indicated the presence of a single component. One of the two products was crystalline and this allowed their separation. Mass spectroscopy confirmed that the two compounds were 1:1 adducts of *N*-benzoylindole and cyclopentene, and the ^{1}H NMR spectra were consistent with the structures **2** and **3**. The stereochemistries of the cyclopentane–cyclobutane and indoline–cyclobutane ring fusions were assumed to be *cis* in each compound, and the coupling constants of cyclobutane methine protons support this assignment. Thus J_{ab} and J_{cd} were ca. 8 Hz for both compounds. The crystalline isomer was assigned the *cis-anti-cis* stereochemistry shown in **2**, which results from *exo* addition of the alkene to the indole. This assignment was made on the basis of the coupling constants observed between protons a and d (J = 2.9 Hz) and between protons b and c (J = 2.9 Hz). The non-crystalline isomer was assigned the *cis-syn-cis* stereochemistry shown in **3**, which results from *endo* addition, and the coupling constants observed support this (J_{ad} = 7.7 Hz; J_{bc} = 8.0 Hz). Further details of the assignment of stereochemistry to these and other alkene adducts will be described elsewhere.[3]

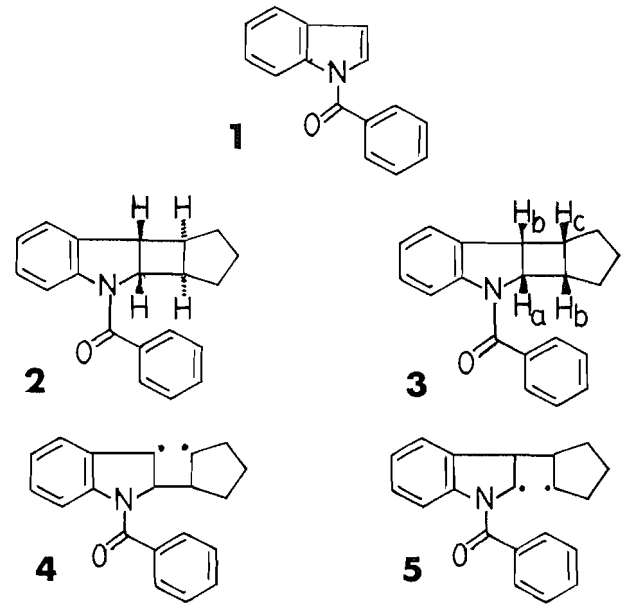

Relative quantum yields of formation of adducts 2 and 3 in the presence of varying concentrations of quenchers and cyclopentene

Qualitative experiments revealed that the rate of the photochemical cycloaddition reaction between *N*-benzoylindole and cyclopentene was diminished when the alkene concentration was lowered or when typical triplet excited state quenchers such as cyclohexadiene, *trans*-piperylene, or isoprene were present in the solution during the irradiation. This was quantified by measurement of the relative amounts of the adducts **2** and **3** formed when *N*-benzoylindole (0.02 M in benzene) was irradiated in the presence of varying concentrations of cyclopentene and cyclohexadiene in a merry-go-round apparatus (10). Under these conditions the relative amounts of the adducts produced are a direct measure of their relative quantum yields of

[3]D. J. Hastings and A. C. Weedon. Unpublished work.

TABLE 1. Stern–Volmer quenching data for the reaction of *N*-benzoylindole, **1**, with cyclopentene[a]

	ϕ^0/ϕ						
[Q][b]	[A][c] 156	[A] 0.303	[A] 0.550	[A] 0.820	[A] 1.073	[A] 1.336	[A] 1.55
2.5×10^{-4}	1.80	1.35	1.25	1.31	1.25	1.03	1.09
5.0×10^{-4}	2.32	2.20	1.65	1.51	1.42	1.26	1.29
10×10^{-4}	3.00	3.15	2.30	2.09	1.80	1.56	1.62
15×10^{-4}	4.90	4.64	3.15	2.20	2.20	1.83	1.90
20×10^{-4}	7.40	6.57	3.85	2.88	2.52	2.16	2.13
25×10^{-4}	9.00	7.60	4.50	3.34	2.90	2.35	2.39
M[d]	3200 ±200	2700 ±100	1440 ±20	900 ±40	750 ±10	570 ±20	570 ±15

[a]Solvent: benzene. [**1**] = 2.04×10^{-2}. ϕ^0/ϕ is the quantum yield of adduct formation in the absence of quencher divided by the same quantum yield in the presence of quencher at concentrations [Q] and [A].

[b]Concentration of quencher (cyclohexadiene).

[c]Concentration of alkene (cyclopentene).

[d]Gradient of the line in the plot of ϕ^0/ϕ against [Q]. The uncertainty was calculated from the goodness of the least-squares fit.

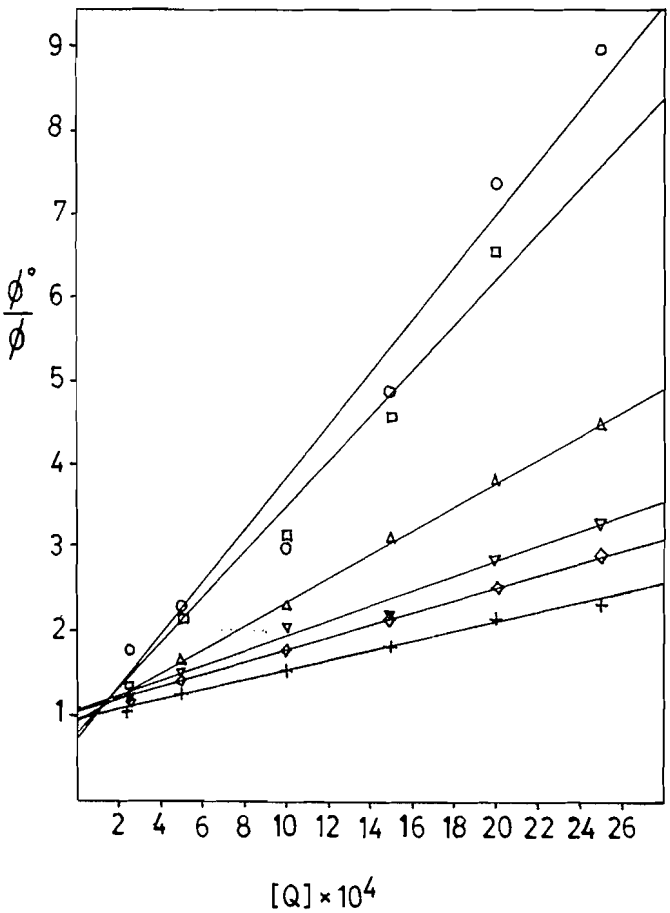

FIG. 1. Stern–Volmer plot for the photochemical cycloaddition of **1** to cyclopentene quenched by cyclohexadiene (Q). ϕ^0/ϕ is quantum yield of formation of **2** and **3** in the absence of cyclohexadiene relative to that in the presence of cyclohexadiene at concentration [Q]. Each line represents a different concentration of cyclopentene: ⊥, 0.156 M; □, 0.303 M; △, 0.55 M; ▽, 0.82 M; ◇, 1.073 M; +, 1.336 and 1.55 M.

formation. Conversions were kept low so that the yields were recorded in the region where the reaction followed zero-order kinetics. The results are given in Table 1 and are shown graphically in Fig. 1 as Stern–Volmer plots in which the quantum yield of adduct formation in the absence of quencher, ϕ^0, relative to the quantum yield of adduct formation in the presence of cyclohexadiene quencher, ϕ, is plotted against quencher concentration for various values of cyclopentene concentration.

Absolute quantum yield of N-*benzoylindole cycloaddition in the presence of varying concentrations of cyclopentene and* N-*benzoylindole*

The absolute quantum yields of adduct formation were determined for benzene solutions containing various concentrations of cyclopentene. The results are shown in Table 2 and indicate a nonlinear increase in quantum yield with increasing cyclopentene concentration. The quantum yield of adduct formation was found to decline very slightly with increasing *N*-benzoylindole concentration when the cyclopentene concentration was held constant; these data are shown in Table 3.

Quantum yield of intersystem crossing and triplet excited state lifetime of N-*benzoylindole from triplet counting*

The quantum yield of intersystem crossing of *N*-benzoylindole, ϕ_{isc}, was determined in three solvents utilizing the triplet counting method of Lamola and Hammond (11). In this procedure *trans*-piperylene is used to quench *all* of the *N*-benzoylindole triplet excited states produced by a known number of photons; the amount of *cis*-piperylene produced by relaxation of the triplet excited state of piperylene is then determined and this yields an apparent value of the quantum yield for *trans* → *cis* isomerization of piperylene, $\phi_{t\rightarrow c}$. This is used to count the number of triplet excited states of *N*-benzoylindole quenched by comparison with the actual value of the quantum yield of *trans* → *cis* isomerization of piperylene via the triplet excited state. To ensure that the value of $\phi_{t\rightarrow c}$ determined corresponds to the condition that all *N*-benzoylindole triplet excited states are quenched, the apparent piperylene

Can. J. Chem. Downloaded from www.nrcresearchpress.com by 91.121.58.235 on 09/07/12
For personal use only.

TABLE 2. Variation of quantum yield of adduct formation, ϕ, with alkene concentration in the photochemical cycloaddition of cyclopentene to *N*-benzoylindole, **1**[a]

[Cyclopentene]	ϕ
1.14	0.0068
1.40	0.0082
2.28	0.013
3.41	0.0175
4.55	0.019
5.69	0.023

[a]Solvent: benzene. [**1**] = 0.027 M.

TABLE 3. Quantum yield of formation of cycloadducts, ϕ, as a function of concentration of *N*-benzoylindole, **1**, in the photochemical cycloaddition reaction of **1** with cyclopentene in benzene solution[a]

[**1**]	ϕ
0.027	0.0518
0.054	0.0501
0.082	0.0491
0.108	0.0484
0.136	0.0481

[a][Cyclopentene] = 2.276 M.

isomerization quantum yield is measured as a function of piperylene concentration and fitted to eq. [1] (11). In eq. [1],

$$[1] \quad \frac{0.44}{\phi_{t\rightarrow c}} = \frac{1}{\phi_{isc}}\left\{1 + \frac{1}{k_q\tau[Q]}\right\}$$

k_q is the rate constant for quenching of the triplet excited state of **1** by piperylene, τ is the lifetime of the *N*-benzoylindole triplet excited state, and [Q] is the concentration of the quencher piperylene. The quantity 0.44 is the experimentally determined value of $\phi_{t\rightarrow c}$ for complete quenching when benzophenone (for which ϕ_{isc} is known to be unity) is used as a sensitizer instead of **1**.

The fit of the data to eq. [1] gives the quantum yield of intersystem crossing, ϕ_{isc}, for **1** as well as a value of the triplet excited state lifetime of **1** if the quenching rate constant k_q is assumed to be equal to the rate constant for diffusion, k_{diff}. This assumption is based upon the fact that energy transfer from triplet excited **1** (triplet excited state energy 68 kcal/mol) to piperylene (triplet excited state energy 59 kcal/mol) is sufficiently exothermic for every collision to result in energy transfer. The values obtained are shown in Table 4 and the data plotted to fit eq. [1] are shown in Fig. 2.

Discussion

In their paper on the photochemical cycloaddition of alkenes to *N*-benzoylindole Julian and Foster reported qualitative results which indicated that the reaction could be sensitized by acetophenone and quenched by naphthalene (6), and they interpreted this to mean that the reaction proceeded via the triplet excited state of *N*-benzoylindole. Their results do not, however, exclude the possibility that the singlet excited state

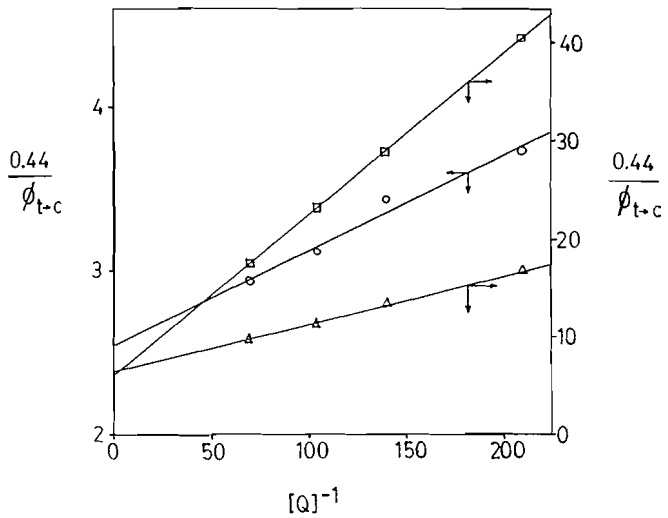

FIG. 2. Plot of $0.44/\phi_{t\rightarrow c}$ against reciprocal piperylene concentration, where $\phi_{t\rightarrow c}$ is the apparent quantum yield of *trans* to *cis* isomerization of *trans*-piperylene in benzene solvent (○), acetonitrile solvent (□), and dichloromethane solvent (△).

can also undergo cycloaddition. In the work reported here it was found that the fluorescence of the charge transfer singlet excited state of **1** was not quenched when high concentrations of cyclopentene were present. This indicates that the charge transfer singlet excited state of **1** is unreactive with cyclopentene and also indicates that the singlet excited state formed initially by light absorption, from which the charge transfer state is derived, is also unreactive with cyclopentene and so is not involved in the cycloaddition reaction. In addition, the Stern–Volmer plots shown in Fig. 1 are linear; if more than one excited state were involved in the cycloaddition reaction then the plots would be curved unless the lifetimes of the states were identical, which is unlikely.

If it is assumed that the singlet excited state of **1** is unreactive and that photocycloaddition occurs through the triplet excited state exclusively, then the simplest reaction mechanism that can be envisaged is as shown in Scheme 1. In the scheme, light absorption (rate I_a einstein/s) and intersystem crossing lead to the triplet excited state of **1**, which either decays to the ground state (rate constant k_d) or reacts with alkene to give the adducts (rate constant k_a).

The efficiency of population of the triplet excited state of **1** is given by the quantum yield of intersystem crossing, ϕ_{isc}, which was determined in this work by triplet counting to be 0.39 ± 0.1 in benzene. The triplet counting procedure leads to a value of the triplet excited state lifetime for **1** in benzene of $(2.8 \pm 0.3) \times 10^{-8}$ s, which corresponds to a triplet decay rate constant, k_d, of $(3.6 \pm 0.4) \times 10^7\ s^{-1}$. The value of the triplet excited state lifetime is extracted from the gradient of the plot for benzene solvent in Fig. 2 assuming that k_q is equal to k_{diff} and adopting a value of $1.6 \times 10^{10}\ M^{-1}\ s^{-1}$ for the latter.

Application of the steady state approximation to the sequence shown in Scheme 1 yields an expression relating the quantum yield of adduct formation, ϕ, to the rate constants defined in the scheme and to alkene concentration; this expression is shown in eq. [2], where [A] is the alkene concentration. Equation [2]

$$[2] \quad \phi = \frac{k_a[A]\phi_{isc}}{k_a[A] + k_d}$$

predicts that at high alkene concentrations the value of k_d

Can. J. Chem. Downloaded from www.nrcresearchpress.com by 91.121.58.235 on 09/07/12
For personal use only.

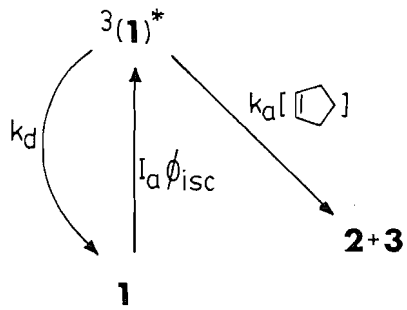

SCHEME 1

becomes negligible and that ϕ becomes identical to ϕ_{isc}. This corresponds to interception of all of the triplet excited states of **1** by the alkene and their conversion into the product. In addition, eq. [2] predicts a linear relationship between $1/\phi$ and $1/[A]$ with an intercept at high [A] equal to $1/\phi_{isc}$. The plot of the data obtained in this work (Table 2) is shown in Fig. 3 and is linear, although the intercept yields a value of ϕ_{isc} of 0.061, which is in very poor agreement with the value of 0.39 determined by triplet counting (Table 4). The value of 0.061 should represent the limiting quantum yield of photocycloaddition at infinite alkene concentration, under which circumstances the triplet excited state of **1** is completely intercepted by alkene. Therefore, to account for the inefficient quantum yield there must be a step following interception that prevents the formation of the products and regenerates the starting materials.

A similar state of affairs has been found to obtain in the photochemical cycloaddition of alkenes to 2-cyclopentenones and 2-cyclohexenones (12). In these cases the intermediacy of a triplet 1,4-biradical intermediate between the triplet excited state and the products has been demonstrated. This biradical intermediate partitions between the products and the starting materials and accounts for a quantum yield of product formation that is lower than the quantum yield of intersystem crossing at infinite alkene concentration (12).

For the reaction between *N*-benzoylindole and cyclopentene the appropriate biradical intermediates would be stereoisomers of **4** and **5**; these are the triplet 1,4-biradicals produced by bonding of the alkene to either the 2-position or 3-position of the indole nucleus, respectively. Such biradicals are logical intermediates in a triplet excited state reaction. If the production of the adducts **2** and **3** were a singlet excited state process then the two new bonds of the cyclobutane rings could be formed concertedly. However, for a triplet reaction, spin inversion must occur at some point along the reaction pathway and, since this is normally a relatively slow process, a biradical intermediate in which only one of the new cyclobutane bonds has been formed provides an opportunity for spin inversion to take place.

If it is assumed that a biradical species is an intermediate in the formation of **2** and **3** then the mechanism shown in Scheme 1 can be modified to that shown in Scheme 2. In this scheme a biradical intermediate is introduced which partitions to the starting materials (rate constant k_r) and the adducts (rate constant k_c); also two additional processes for decay of the triplet excited state have been incorporated. These are self quenching of the triplet by ground state **1** (rate constant k_{sq}) and quenching of the triplet by an added quenching species Q (rate constant k_q). The introduction of these species will be discussed further below. Adaptation of eq. [2] to take into account the extra processes in Scheme 2 gives eq. [3], which

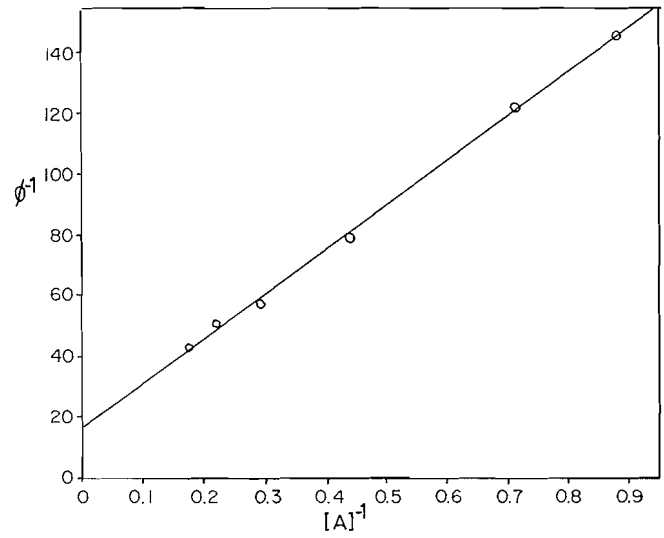

FIG. 3. Plot of reciprocal quantum yield of cycloadduct formation against reciprocal of alkene concentration ([A]) for the photochemical cycloaddition of cyclopentene to **1** in benzene solution.

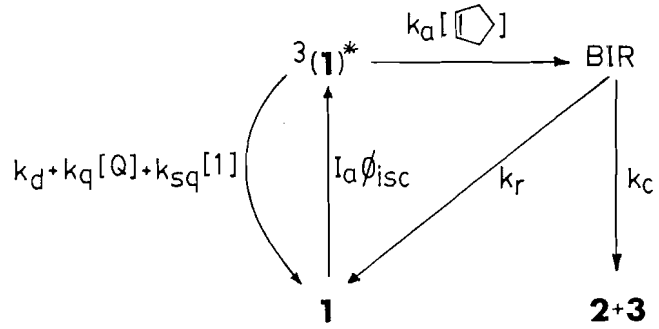

SCHEME 2

can be cast into reciprocal form to give eq. [4].

$$[3]\quad \phi = \left\{\frac{k_c}{k_r + k_c}\right\}\left\{\frac{k_a[A]\phi_{isc}}{k_a[A] + k_d + k_q[Q] + k_{sq}[\mathbf{1}]}\right\}$$

$$[4]\quad \frac{1}{\phi} = \frac{1}{\phi_{isc}}\left\{\frac{k_c}{k_r + k_c}\right\}^{-1}\left\{1 + \frac{(k_d + k_q[Q] + k_{sq}[\mathbf{1}])}{k_a[A]}\right\}$$

Equation [4] predicts that the inverse of the quantum yield of adduct formation should vary linearly with the inverse of the alkene concentration, as did eq. [2]; however, eq. [4] requires that the intercept corresponding to infinite alkene concentration should have a value equal to the reciprocal of $\phi_{isc}k_c/(k_c + k_r)$ where $k_c/(k_c + k_r)$ is the fraction of biradical intermediates that proceed to the adducts. From the plot of the data obtained in this work (Table 2, Fig. 3), combination of the intercept with the value of ϕ_{isc} in benzene (determined by triplet counting as 0.39 ± 0.01) gives a value of $k_c/(k_c + k_r)$ of 0.16 ± 0.02, indicating that 84% of the biradicals revert to the starting materials and only 16% close to the products.

It was found in this work that the quantum yield of adduct formation was reduced when the concentration of **1** was increased. This can be ascribed to self quenching of the triplet excited state of **1** by ground state **1** and is the reason for the incorporation of the k_{sq} term in eqs. [3] and [4]. Self quenching of triplets has been observed previously in photocycloaddition chemistry (13). To determine the importance of self quenching, the inverse of the quantum yield of adduct formation, ϕ, was

Can. J. Chem. Downloaded from www.nrcresearchpress.com by 91.121.58.235 on 09/07/12
For personal use only.

TABLE 4. Observed quantum yields of *trans* → *cis* isomerization of *trans*-1,3-pentadiene sensitized by *N*-benzoylindole, **1**

	$0.44/\phi_{t\rightarrow c}$		
[Pentadiene]$^{-1}$	Solvent: C_6H_6	Solvent: CH_3CN	Solvent: CH_2Cl_2
69.4	2.94	17.5	9.84
104	3.12	23.1	11.3
139	3.44	28.8	13.3
208	3.73	40.4	16.4
Intercept[a]	2.55 ± 0.07	5.9 ± 0.1	6.5 ± 0.2
Gradient[a]	0.0058 ± 0.0005	0.1656 ± 0.0007	0.048 ± 0.001
ϕ_{isc}	0.39 ± 0.01	0.169 ± 0.003	0.155 ± 0.005
$k_q\tau$ (M^{-1})	440 ± 50	35.6 ± 0.8	135 ± 7
τ (ns)	28 ± 3	1.23 ± 0.03	5.9 ± 0.3

[a]Intercept and gradient calculated from the plot of [pentadiene]$^{-1}$ against $0.44/\phi_{t\rightarrow c}$.

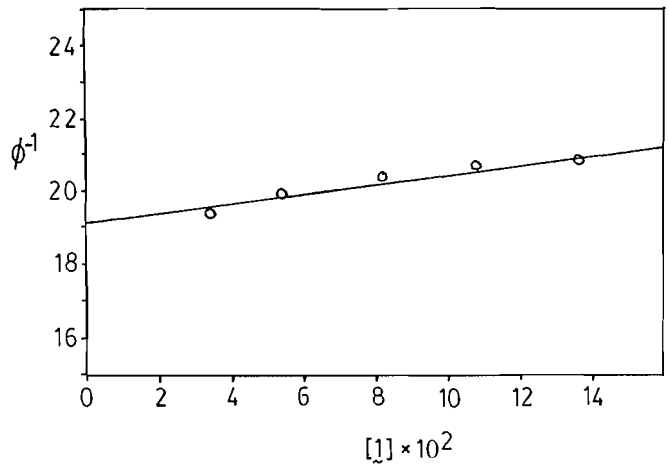

FIG. 4. Plot of reciprocal quantum yield of cycloadduct formation against concentration of **1** for the photochemical cycloaddition of cyclopentene to **1** in benzene solution.

plotted against [**1**] to get the line predicted by eq. [4]. The result is shown in Fig. 4; the gradient, M, of this line is 13.6 ± 1.7 and is given by eq. [5] if [Q] is put to zero. Using the values

$$[5]\quad M = \frac{1}{\phi_{isc}}\left\{\frac{k_c}{k_c + k_r}\right\}^{-1}\frac{k_{sq}[\mathbf{1}]}{k_a[A]}$$

already determined for ϕ_{isc} and $k_c/(k_c + k_r)$ gives a value for $k_{sq}/k_a[A]$ of 0.8 ± 0.4. The concentration of alkene used in this experiment was 2.276 M. Therefore, k_{sq}/k_a is estimated to be 1.8 ± 0.4. The more accurate values of k_a estimated in this work are described below and are (1.8 ± 0.1) × 10^7 M^{-1} s^{-1} and (4.0 ± 0.8) × 10^6 M^{-1} s^{-1}; consequently, k_{sq} is estimated to be (3.2 ± 0.9) × 10^7 M^{-1} s^{-1} or (7 ± 3) × 10^6 M^{-1} s^{-1}, depending upon which number is chosen for k_a. In the experiments in which the data in Tables 1 and 2 were determined, the concentration of **1** used was 0.02 and 0.027 M, respectively. Therefore, the value of $k_{sq}[\mathbf{1}]$ is small compared with the value of k_d and so can be ignored in eq. [4]. In effect this means that self quenching does not contribute greatly to triplet excited state decay under the conditions used in this work for the determination of ϕ as a function of alkene concentration.

The intercept in Fig. 4 is given by eq. [6], which can be used

$$[6]\quad C = \frac{1}{\phi_{isc}}\left\{\frac{k_c}{k_r + k_c}\right\}\left\{1 + \frac{(k_d + k_q[Q])}{k_a[A]}\right\}$$

for the estimation of a very inaccurate value for k_a, the rate constant for reaction of the triplet excited state of **1** with the alkene, if the value of k_d obtained from the triplet counting experiments is used and if $k_q[Q]$ is set to zero. The value of k_a so calculated is (10 ± 7) × 10^7 M^{-1} s^{-1}.

A more accurate estimate of k_a can be obtained from the data for the variation of ϕ with cyclopentene concentration (Table 2). Assuming that no triplet quencher is present then the plot of this data fitted to eq. [4] (Fig. 3) yields a line whose gradient, $M^{\mathbf{1}}$, should be given by eq. [7]. Using the value of

$$[7]\quad M^{\mathbf{1}} = \frac{1}{\phi_{isc}}\left\{\frac{k_c}{k_r + k_c}\right\}^{-1}\left\{\frac{(k_d + k_{sq}[\mathbf{1}])}{k_a}\right\}$$

$\phi_{isc}k_c/(k_c + k_r)$ obtained from the reciprocal of the intercept of the line in Fig. 3 along with the value of k_{sq} just determined and the value of k_d obtained from triplet counting gives a value of k_s of (4.0 ± 0.8) × 10^6 M^{-1} s^{-1}.

Independent values of k_a and k_d were obtained from the relative quantum yield data given in Table 1. The quantum yield of adduct formation in the absence of a quencher can be represented by ϕ^0 and is defined by eq. [3] if the validity of Scheme 2 is assumed and if [Q] is put to zero. Division of ϕ^0 by ϕ (as defined by eq. [3]) then gives the Stern–Volmer expression shown in eq. [8], which relates the relative quantum

$$[8]\quad \frac{\phi^0}{\phi} = 1 + \frac{k_q[Q]}{(k_a[A] + k_d + k_{sq}[\mathbf{1}])}$$

yield ϕ^0/ϕ to the concentration of quencher, [Q], in a linear manner if the concentration of alkene **1** is held constant.

The plots of the data in Table 1 are shown for various [A] in Fig. 1; the concentrations of A and Q were held approximately constant by keeping conversions low. If the gradients of the lines in Fig. 1 are denoted by M^{II}, then the inverse of M^{II} can be obtained from eq. [8] and is given by eq. [9]. This equation

$$[9]\quad \frac{1}{M^{II}} = \frac{k_a}{k_q}[A] + \frac{(k_d + k_{sq}[\mathbf{1}])}{k_q}$$

predicts that a plot of $1/M^{II}$ against [A] should be linear and

Can. J. Chem. Downloaded from www.nrcresearchpress.com by 91.121.58.235 on 09/07/12
For personal use only.

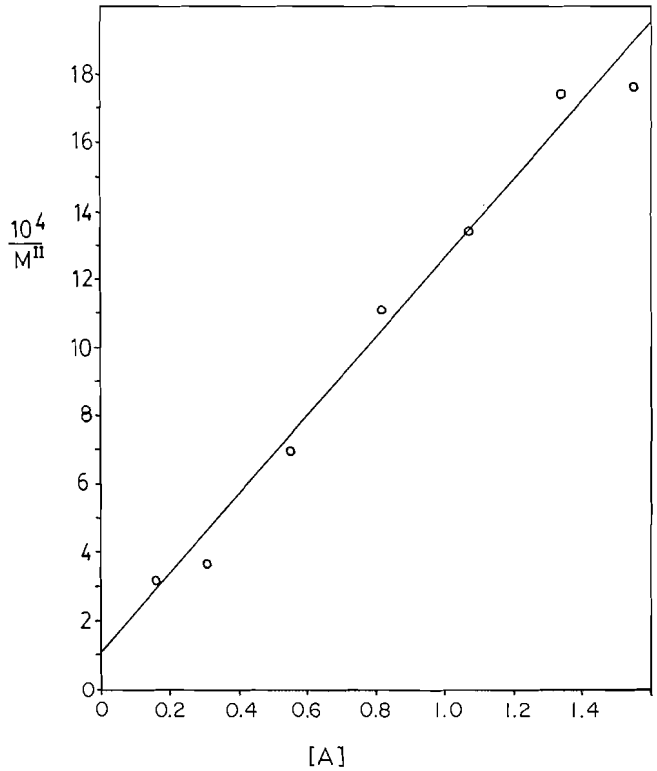

FIG. 5. Plot of reciprocal of the gradients of the lines in Fig. 1 against cyclopentene concentration ([A]).

yield a value of k_a if k_q is known. As long as quenching is appreciably exothermic then the quenching rate constant k_q can be equated with the rate constant for diffusion, which can be calculated from the Debye equation. In benzene at 25°C this value is $1.6 \times 10^{10}\ M^{-1}\ s^{-1}$ (10). The plot of $1/M^{11}$ against [A] is shown in Fig. 5. The gradient of the line is $(1.15 \pm 0.06) \times 10^{-3}$ and this yields a value of k_a of $(1.8 \pm 0.1) \times 10^7\ M^{-1}\ s^{-1}$. The intercept of the plot is equal to k_d/k_q if self quenching is ignored. This yields a new but inaccurate value of k_d of $(1.6 \pm 0.9) \times 10^6\ s^{-1}$.

The value of the rate constant for triplet excited state decay of $(1.6 \pm 0.9) \times 10^6\ s^{-1}$ obtained from the Stern–Volmer plot is appreciably different from that obtained by the triplet counting procedure, which gave $k_d = (3.6 \pm 0.4) \times 10^7\ s^{-1}$. Similarly, the value of k_a obtained by measurement of relative quantum yields in the Stern–Volmer determination of $(1.8 \pm 0.1) \times 10^7\ M^{-1}\ s^{-1}$ is different from that obtained from the plot of reciprocal quantum yield against reciprocal alkene concentration, which was $(4.0 \pm 0.8) \times 10^6\ M^{-1}\ s^{-1}$. These differences may reflect the greater magnitude of the errors in the Stern–Volmer determination. An additional and likely major source of the differences is that some of the rate constants are estimated using the assumption that the rate constant for quenching by piperylene in the triplet counting experiment and by cyclohexadiene in the Stern–Volmer experiments can be equated with the calculated rate constant for diffusion in benzene. While both quenching rate constants are expected to approach the value for diffusion, the value of one or the other may fall slightly below it.

The triplet counting procedure was used to measure the triplet excited state lifetime and quantum yield of intersystem crossing of **1** in several solvents. The results are given in Table 4

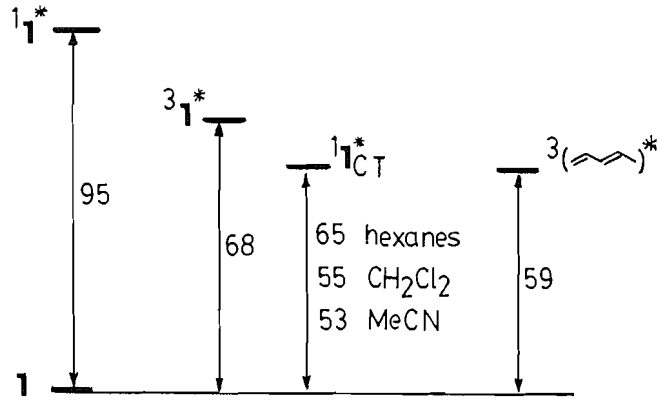

FIG. 6. Diagram showing relative energies of various electronic states of **1** and 1,3-pentadiene. All energies are in kcal mol^{-1}.

and indicate a remarkable solvent effect that translates into a lowering of the values of ϕ_{isc} and the triplet excited state lifetime, τ, in the more polar solvents dichloromethane and acetonitrile, as compared with benzene. To explain this unusual effect we postulate the existence of a lower energy triplet excited state possessing charge transfer character. It was mentioned above that we have previously shown that the singlet excited state of **1** produced by light absorption relaxes to a weakly fluorescent state possessing charge transfer character (9) in competition with intersystem crossing. The energy of this state is highly solvent dependent and varies from 65 kcal mol^{-1} in nonpolar solvents such as pentane or hexanes to 55 kcal mol^{-1} in dichloromethane and 53 kcal mol^{-1} in acetonitrile. The energy of the state in these solvents was determined from the wavelength of the fluorescent emission. It could not be determined in benzene because this solvent absorbs and fluoresces too efficiently; however, the state's energy depends largely upon solvent polarity and the value in benzene is not expected to be very different from that in alkane solvents. The energies of the known states of **1** are shown diagrammatically in Fig. 6 along with the energy of the triplet excited state of *trans*-pentadiene; if it is assumed that the triplet excited state of **1** can also relax to a charge transfer state of similar energy to the singlet analogue, then it can be seen that energy transfer from this state to the pentadiene will become endergonic in the more polar solvents. The consequence of this will be that in polar solvents the pentadiene will be able to quench only the non-charge transfer triplet state and the latter will have a shorter lifetime because it has an extra mode of decay (to the charge transfer triplet). If the charge transfer triplet excited state is not populated from the singlet excited state, then the number determined for ϕ_{isc} should be unaffected by the existence of a charge transfer triplet state. Consequently, the lower values of ϕ_{isc} determined in the more polar solvents must reflect less efficient intersystem crossing in singlet excited **1**. This is reasonable since in polar solvents relaxation of singlet excited **1** to the charge transfer singlet excited state becomes more exergonic and hence possibly faster, thus reducing the efficiency of intersystem crossing.

Conclusions

The work described indicates that the photochemical cycloaddition of cyclopentene to *N*-benzoylindole in benzene solution proceeds via a short-lived triplet excited state of the indole derivative (τ = 28 ns by triplet counting), which reacts with

Can. J. Chem. Downloaded from www.nrcresearchpress.com by 91.121.58.235 on 09/07/12
For personal use only.

cyclopentene (rate constant in the range of 4×10^6 to 1.8×10^7 M^{-1} s^{-1}) to give biradical intermediates, 16% of which proceed to cycloadducts with the remainder returning to the starting materials.

Experimental

Irradiation of N-*benzoylindole,* **1**, *in benzene containing cyclopentene*

N-Benzoylindole (1.63 g) was dissolved in benzene (300 mL) and purged with nitrogen. Cyclopentene (7.8 g) was added and the solution was irradiated with light from a Pyrex and water filtered medium pressure mercury lamp for 89 h. The reaction solution was evaporated to yield 2.13 g of a brown oil, which was purified by column chromatography to yield unreacted **1** (0.53 g) and a yellow oil (0.49 g), which partially crystallized. The crystals were separated from the oil by washing with hexanes to yield the *cis-anti-cis* adduct **2** (0.3 g), mp 123–126°C. The hexanes solution was evaporated to yield the *cis-syn-cis* adduct **3** (0.18 g) contaminated with small amounts of **2**. For **2**: ^{1}H NMR ($CDCl_3$, 200 MHz): 8.3 (br s, 1H), 7.44 (m, 5H), 7.4–7.0 (m, 3H), 3.94 (br s, 1H), 3.32 (dd, J = 7.5, 2.9 Hz, 1H), 2.84 (m, 1H), 2.66 (m, 1H), 1.80 (m, 2H), 1.62 (m, 2H), 1.31 (m, 2H) ppm; ^{13}C NMR ($CDCl_3$) CH_2 signals: 25.4, 30.9, 32.4; CH signals: 45.1, 46.2, 47.9, 63.7; aryl signals: 110.5, 118.3, 124.7, 126.4, 126.8, 127.6, 128.3, 128.4, 130.0, 137.5; carbonyl: 193.8. MS *m/e*: 289 (4.1%), 221 (46), 105 (100%), 77 (20). Exact Mass calcd. for $C_{20}H_{19}NO$: 289.14666; found: 289.14654. For **3**: ^{1}H NMR ($CDCl_3$, 200 MHz): 8.3 (br s, 1H), 7.44 (m, 5H), 7.4–7.7 (3, 5H), 4.70 (br s, 1H), 4.05 (br dd, J = 7.5, 8.0 Hz, 1H), 3.08 (br m, 2H), 1.80 (m, 2H), 1.31 (m, 2H) ppm; ^{13}C NMR ($CDCl_3$) CH_2 signals: 27.1, 27.9, 28.9; CH signals: 42.2, 43.4, 45.5, 61.7; aryl signals: 110.5, 118.3, 125.7, 126.4, 126.8, 127.3, 128.3, 128.4, 130.5, 137.5; carbonyl signal: 195.0. Exact Mass calcd. for $C_{20}H_{19}NO$: 289.14666; found: 289.14656.

Procedure for determination of relative quantum yields

A series of nitrogen-purged benzene solutions containing **1** (0.0156 M), octacosane (2.74 mg/mL), cyclopentene (0.156–1.55 M), and 1,3-cyclohexadiene ($(0–2.5) \times 10^{-3}$ M) were prepared, and identical volumes (4.0 mL) placed in Pyrex tubes. These were then irradiated in a merry-go-round apparatus using light from a Pyrex and water filtered medium pressure mercury lamp. This apparatus ensures that all of the tubes receive the same dose of ultraviolet light. After the irradiation the amount of cycloadducts formed in each sample relative to the internal standard octacosane was determined by GC. For a given concentration of cyclopentene, the relative amount of cycloadduct formed in each tube containing cyclohexadiene divided by the relative amount of cycloadduct formed in the tube containing no cyclohexadiene is equal to the ratio of quantum yields ϕ^0/ϕ. The results for each concentration of cyclopentene are given in Table 1 and shown graphically in Fig. 1.

Procedure for the determination of absolute quantum yields

The quantum yield of cycloaddition between **1** and cyclopentene in nitrogen-purged benzene solution was determined for various concentrations of **1** and cyclopentene by measuring the total amount of cycloadducts produced following the absorption of a known quantity of photons. Light from a high pressure mercury lamp was used and a wavelength of 313 ± 2 nm was selected using a monochromator. Its intensity was determined by potassium ferrioxalate actinometry. The conversions were kept low (<5%) and the total amount of cycloadducts produced in the irradiations was determined by GC relative to a previously calibrated octacosane internal standard. The results are shown in Tables 2 and 3.

Determination of the quantum yield of intersystem crossing and the triplet excited state lifetime of **1** *by triplet counting*

The quantum yield of isomerization of *trans*-piperylene to *cis*-piperylene sensitized by benzophenone was determined in benzene, acetonitrile, and dichloromethane by measuring the amount of *cis*-piperylene produced when a known number of photons were absorbed by the benzophenone. The concentrations used were *trans*-piperylene, 0.0144 M; benzophenone, 0.0247 M. Under these conditions all of the benzophenone triplets should be quenched by the piperylene. Light of wavelength 213 ± 2 nm was used and its intensity was determined by potassium ferrioxalate actinometry. Conversions were kept low (<4%) and the amount of *cis*-piperylene produced was determined by GC relative to a previously calibrated cycloheptane internal standard. The value of $\phi_{t\rightarrow c}$ determined was 0.440 ± 0.003.

The above procedure was repeated using 0.0267 M **1** as the sensitizer instead of benzophenone, and various concentrations of *trans*-piperylene ranging from 0.0048 to 0.0144 M. The apparent values of $\phi_{t\rightarrow c}$ determined were used to give the data shown in Table 4 and Fig. 2. Values of ϕ_{isc} and the triplet lifetime are extracted from these data as described in the results and discussion sections above.

1. R. LUMRY and M. HERSHBERGER. Photochem. Photobiol. **27**, 818 (1978).
2. O. BUCHARDT. Photochemistry of heterocyclic compounds. Wiley, New York. 1976.
3. K. YAMASALI, T. MATSUURA, and I. SAITO. J. Chem. Soc. Chem. Commun. 944 (1974).
4. P. D. DAVIS and D. C. NECKERS. J. Org. Chem. **45**, 456 (1980); P. D. DAVIS, D. C. NECKERS, and J. R. BLOUNT. J. Org. Chem. **45**, 462 (1980).
5. D. C. NECKERS and A. TINNEMANS. *In* Synthetic organic photochemistry. *Edited by* W. H. Horspool. Plenum, New York. 1984.
6. D. R. JULIAN and R. FOSTER. J. Chem. Soc. Chem. Commun. 311 (1973).
7. D. R. JULIAN and G. D. TRINGHAM. J. Chem. Soc. Chem. Commun. 13 (1973).
8. H. TAKECHI, M. TAKAHASHI, and Y. TAMURA. J. Chem. Soc. Perkin Trans. 1, 405 (1984).
9. B. W. DISANAYAKA and A. C. WEEDON. Can. J. Chem. **65**, 245 (1987).
10. S. L. MUROV. *In* handbook of photochemistry. Dekker, New York. 1973.
11. A. A. LAMOLA and G. S. HAMMOND. J. Chem. Phys. **43**, 2129 (1965).
12. R. O. LOUTFY and P. DE MAYO. J. Am. Chem. Soc. **99**, 3559 (1977).
13. P. J. WAGNER and D. J. BUCHECK. J. Am. Chem. Soc. **91**, 5090 (1969).

Can. J. Chem. Downloaded from www.nrcresearchpress.com by 91.121.58.235 on 09/07/12
For personal use only.

Phosphorescence quenching studies of bromoacetonaphthones in solution

ZDENEK HRUSKA,[1] MARK C. PITON, AND MITCHELL A. WINNIK[2]

Department of Chemistry and Erindale College, University of Toronto, Toronto, Ont., Canada M5S 1A1

Received April 3, 1990

This paper is dedicated to Professor Ross Stewart on the occasion of his 65th birthday

ZDENEK HRUSKA, MARK C. PITON, and MITCHELL A. WINNIK. Can. J. Chem. **68**, 1693 (1990).

4′-Bromo-1′-acetonaphthone (BAN) and 4′-bromo-1′-(1-dodecano)naphthone (BLN) exhibit strong phosphorescence in degassed solutions in benzene. We report rate constants (k_q) for phosphorescence quenching determined by phosphorescence quenching measurements for the following series of quenchers: pyrene, anthracene, tetracyanoethylene, *p*-dicyanobenzene, *N,N*-dimethylaniline (DMA), and *N,N*-dimethylamino-4-toluidine (DMAT). The first three quenchers quench at the diffusion-controlled rate. DMAT is 20-fold more effective as a quencher than DMA ($k_q = 1.4 \times 10^6$ M^{-1} s^{-1}), but what is noteworthy is that both activation energies are very small, and quenching by DMAT is favoured over DMA mainly by entropic effects ($\triangle S^{\neq} = -105$ vs. -120 J mol^{-1} K^{-1}, respectively).

Key words: aromatic ketone photochemistry, triplet exciplex.

ZDENEK HRUSKA, MARK C. PITON et MITCHELL A. WINNIK. Can. J. Chem. **68**, 1693 (1990).

En solution dans du benzène dégazé, les 4′-bromo-1′-acétonaphtone (BAN) et 4′-bromo-1′-(1-dodécano)naphtone (BLN) présentent une forte phosphorescence. On a mesuré l'extinction de la phosphorescence par des pièges comme le pyrène, l'anthracène, le tétracyanoéthylène, le *p*-dicyanobenzène, la *N,N*-diméthylaniline (DMA) et la *N,N*-diméthylamino-4-toluidine (DMAT) et on en a déduit les constantes de vitesse (k_q) de l'extinction de la phosphorescence. Avec les trois premiers pièges, les constantes de vitesse d'extinction de la phosphorescence sont limitées par la diffusion. La DMAT est un piège 20 fois plus efficace que la DMA ($k_q = 1{,}4 \times 10^6$ M^{-1} s^{-1}); il est toutefois remarquable que les énergies d'activation de ces réactions sont toutes les deux très faibles et que l'efficacité de la DMAT par rapport à celle de la DMA est principalement due à des effets entropiques ($\triangle S^{\neq} = -105$ vs. -120 J mol^{-1} K^{-1}, respectivement).

Mots clés : photochimie de cétones aromatiques, triplet exciplex.

[Traduit par la revue]

Introduction

For many years we have been interested in the reactivity of the triplet states of aromatic ketones as measured by phosphorescence quenching in solution (1, 2). Our own particular interest stems from the idea that when such chromophores are attached to flexible molecules (or polymers) the quenching kinetics can be used as a tool to study issues of conformation and dynamics in these molecules (3, 4). Such applications require a rather detailed understanding of chromophore reactivity and quenching kinetics. As a consequence we have expended a significant effort studying these processes for the particular chromophores of interest to us, and paid considerable attention to the large and ever-growing body of literature on triplet quenching processes in general. Lissi and Encinas have recently done a tremendous service for the entire photochemistry community with an excellent review of this field (5).

Our early experiments involved benzophenone derivatives (1–3). To enlarge the scope of our experiments we needed a different chromophore with easily detected phosphorescence in solution, with a triplet lifetime τ on the order of 100–300 μs, and with very low reactivity toward hydrogen abstraction. A useful candidate is 4′-bromo-1′-acetonaphthone as well as its longer chain alkylnaphthone homologues. These derivatives have been cleverly exploited by Turro and co-workers (6) in their study of aqueous surfactant micelles. Since little has been reported on the triplet reactivity of this chromophore in solution in isotropic solvents, we undertook a study of the phosphorescence quenching kinetics of 4′-bromo-1′-acetonaphthone itself, and 4′-bromo-1′-(1-dodecano)naphthone in benzene solution.

[1]On leave from the Institute of Macromolecular Chemistry, Czechoslovak Academy of Sciences, Prague, Czechoslovakia.

[2]Author to whom correspondence may be addressed.

Experimental

Sample preparation

The quenchers *N,N*-dimethylaniline and *N,N*-dimethylamino-*p*-toluidine were purchased from Eastman. Pyrene (PY), *p*-dicyanobenzene (DCB), tetracyanoethylene (TCNE), and anthracene (ANT) were purchased from Aldrich. The quenchers were further purified just prior to use by the following methods: *N,N*-dimethylaniline and *N,N*-dimethylamino-*p*-toluidine by refluxing several hours with an excess of acetic anhydride, and then fractional distillation; *p*-dicyanobenzene by recrystallization from methanol; tetracyanoethylene, pyrene, and anthracene by vacuum sublimation. Benzene, 99+ %, thiophene free (Aldrich), was distilled prior to use. For the synthetic work, lauroyl chloride, acetyl chloride, and aluminum trichloride were purchased from Aldrich, 1-bromonaphthalene and carbon disulfide from Eastman.

The ketones were prepared by a standard Friedel-Crafts reaction of 1-bromonaphthalene with the appropriate acyl chloride in carbon disulfide in the presence of aluminum trichloride.

4′-Bromo-1′-acetonaphthone (BAN) was prepared according to ref. 7. The crude product was isolated in 75% yield as a pale yellow oil that crystallized on standing for several days at 0°C. The ketone was further purified by recrystallization from hexane, mp 47–48°C (lit. (7) mp 47–47.5°C).

4′-Bromo-1′-(1-dodecano)naphthone (BLN), to the best of our knowledge, has not been reported previously. It was prepared according to the following procedure. Into a 250-mL flask were placed 20.7 g (0.1 mol) of 1-bromonaphthalene, 24.1 g (0.11 mol) of lauroyl chloride, and 80 mL of carbon disulfide. The solution was cooled to 0°C and 17.3 g (0.13 mol) of aluminum trichloride was added in small portions. The reaction was maintained at this temperature for 5 h and stirred overnight at room temperature. The reaction mixture was then decomposed with concentrated hydrochloric acid and extracted with ether. The organic layer was washed with water until neutral, dried over $MgSO_4$, and the ether evaporated. Recrystallization of the residue from isopropanol yielded 22.2 g (57%) of white crystals, mp 41°C. 200 MHz proton NMR ($CDCl_3$) δ (ppm): 0.85 (t, 3H, CH_3, J =

Can. J. Chem. Downloaded from www.nrcresearchpress.com by 91.121.58.235 on 09/07/12
For personal use only.

TABLE 1. Rate and thermodynamic constants for the quenching of 4′-bromo-1′-acetonaphthone triplet ($BAN^{3}*$) and 4′-bromo-1′-(1-dodecano)naphthone triplet ($BLN^{3}*$) in benzene

Donor/ quencher	k_q ($M^{-1}s^{-1}$)	A ($M^{-1}s^{-1}$)	E_a (kJ mol^{-1})	$\Delta H^{\neq}$ (kJ mol^{-1})	$\Delta S^{\neq}$ (J mol^{-1} K^{-1})
BAN/DMA	1.41×10^6 (22°C)	6.74×10^6	3.5	0.91	−120
BAN/DMAT	3.00×10^7 (25.5°C)	6.21×10^7	1.6	−0.91	−105
BAN/DCB	1.11×10^6 (21.1°C)	3.44×10^7	8.3	5.7	−110
BAN/TCNE	3.21×10^9 (24.5°C)	3.94×10^{11}	11.8	9.2	−32
BAN/ANT	8.99×10^9 (24.8°C)	5.45×10^{11}	10.2	7.6	−29
BAN/PY	7.29×10^9 (24.6°C)	4.70×10^{11}	10.2	7.6	−30
BLN/DMA	3.60×10^6 (23.8°C)	4.5×10^6	0.60	−2.1	−127

6.35 Hz), 1.23 (m,18H, $9CH_2$), 2.99 (t, 2H, $COCH_2$, J = 7.8 Hz), 7.59–8.50 (m, 6H, aromatic). Mass spectrum: 390 and 388 (M^+), 309, 250, 248, 235, 233, 207, 205, 126.

UV–VIS absorption spectra were obtained using a Hewlett Packard 8465A diode array spectrophotometer. Acquisition and analysis were performed using an IBM XT personal computer running software purchased from Hewlett Packard.

Steady-state Stern–Volmer analyses were performed for BAN and BLN using the quenchers listed above. The results are summarized in Table 1. Phosphorescence spectra were recorded on a Spex Fluorolog 2 spectrometer controlled by an AT-type personal computer using Spex DMB 3000 acquisition software. Sample excitation was at 340 nm, and the emission spectra were measured between 400 and 670 nm using a right-angle alignment. The slit openings were 0.5 mm on both the excitation and emission monochromators in all cases.

Ketone phosphorescence is notoriously sensitive to the presence of oxygen. To minimize this effect, freeze–pump–thaw techniques have classically been employed to eliminate the bulk of the dissolved oxygen from solution. To avoid this tedious procedure, which typically takes several hours for a species of samples, we employed a special technique for preparing samples for the purposes of obtaining preliminary results. A quartz fluorescence cell equipped with Teflon stopcock and rubber septum was filled with 2–3 mL of sample solution and then, using a 22-gauge syringe needle, was vigorously purged with nitrogen (Canox, less than 3 ppm of oxygen) presaturated with solvent, for 15 min. Quencher was added by injection of small volumes (10–50 μL) of concentrated solution (prepurged with nitrogen) through the septum cap and stopcock. After each addition the stopcock was closed, the cell shaken, and the spectrum recorded. Volume changes due to quencher addition were assumed to be additive, but in fact were negligible in calculating final concentrations.

For the lifetime measurements, solutions containing 1×10^{-3} M of the ketones with the varying concentrations of quenchers in benzene were prepared by serial dilution. The range of concentrations for each quencher was chosen so that the highest concentration reduced the observed lifetimes of the ketones by a factor of 10–20. The samples were placed in Pyrex cells constructed from 6.1 mm o.d. tubing (approx. 0.5 mL), thoroughly degassed by five freeze–pump–thaw cycles, and sealed under vacuum. Sample temperatures for Arrhenius studies were controlled using a circulating water/ethylene glycol bath and monitored using a copper–constantan thermocouple.

Lifetimes were measured by monitoring phosphorescence decays using a conventional laser flash-photolysis apparatus. Samples were placed in a temperature-controlled cell holder and allowed to attain the desired temperature prior to analysis. Sample excitation was performed using 355-nm pulses from a Quanta-Ray DCR3 Nd:YAG laser fitted with a harmonic generator and separator. Pulses were attenuated using neutral density filters, thereby eliminating distortions in the shape of the observed decay traces due to triplet–triplet annihilation.

The emission from the samples was monitored using a Schott 530-nm cutoff filter in front of a gated photomultiplier tube (PMT) (8). Decay signals were acquired using a Tektronix 7912AD transient digitizer interfaced to an AT-type personal computer. The PMT was gated on 150 ns after the laser pulse to protect it from short bursts of intense light (possibly scattered light and prompt fluorescence), which was a recurring problem in these experiments. Signal averaging of 64 traces and the addition of three signal-averaged "files" gave decays that were exponential over at least two decades. These yielded lifetime values with a precision better than 3% from duplicate samples.

Steady-state spectra

In steady-state experiments, the emission intensities at 570 nm were recorded from the spectra. The ratios $(I_o/I)_{570}$ were calculated, where I_o represents the emission intensity at 570 nm prior to the addition of any quencher. The intensities at 540 nm (first peak) were not reliable enough. The Stern–Volmer plots were constructed according to eq. [1].

$$[1] \quad (I_o/I)_{570} = 1 + k_q\tau_o[\text{quencher}]$$

Here we assume no singlet quenching. With estimated or measured values of τ_o, approximate values of k_q for each quencher allowed us to calculate the best concentration of the quencher for lifetime measurements, where sample preparation by vacuum degassing is more reproducible but much more time consuming.

Lifetime measurements

The rate constants for quenching of the triplet ketone, k_q, were obtained from the slope of the linear Stern–Volmer relation between the measured lifetime and the quencher concentration (eq. [2]).

$$[2] \quad 1/\tau = 1/\tau_o + k_q[\text{quencher}]$$

Here τ and τ_o are the observed lifetimes obtained in the presence and absence of quencher, respectively. Stern–Volmer plots constructed from these results provided k_q with correlation coefficients better than 0.99. The quenching rate constants, determined at various temperatures between 5 and 90°C and corrected for solvent density changes at each temperature (9), were analyzed using the Arrhenius equation

$$[3] \quad k_q = A \exp(-E_a/RT)$$

The activation energy (E_a) and preexponential factor A were calculated from the plot of log k_q versus $1/T$. The activation parameters such as molar enthalpy of activation ($\Delta H^{\neq}$) and molar entropy of activation ($\Delta S^{\neq}$) were obtained directly from Eyring plots of $\ln(k_q/T)$ versus $1/T$

Can. J. Chem. Downloaded from www.nrcresearchpress.com by 91.121.58.235 on 09/07/12
For personal use only.

according to relationship [4]. Here, k_B and h are the Boltzmann and Planck constants respectively.

$$[4] \quad \ln(k_q/T) = \ln(k_B/h) + \Delta S^{\neq}/R - \Delta H^{\neq}/RT$$

Results and discussion

BAN and BLN have identical UV–VIS absorption spectra. These in turn are essentially the same as in the similar molecule 10-(4-bromo-1-naphthoyl)decyltrimethyl-ammonium bromide, BND-10, reported by Turro (6). All 4-bromo-1-naphthoyl

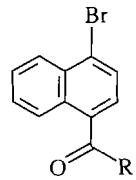

R	Name
$CH_2(CH_2)_9N^+(CH_3)_3Br^-$	BND-10
CH_3	BAN
$CH_2(CH_2)_9CH_3$	BLN

spectra exhibit a broad absorption from approximately 265 nm to 355 nm. For BLN the maxima occurs at 304 nm with an extinction coefficient of 8500 M^{-1} cm^{-1} in cyclohexane. Our studies confirm previous work (*6a*) on the effect of solvent polarity on the position of this maxima. These show a bathochromic shift with increasing solvent polarity. This, together with the observed magnitude of the extinction coefficient, is consistent with the assignment of this band as a π,π^* transition.

The excitation and emission spectra for BAN in benzene at room temperature are shown in Fig. 1. The emission spectrum is characterized by a broad intense peak with maxima at 540 and 570 nm. A minor emission occurs in the region 360–400 nm for all samples. In aerated solutions, the 540/570 nm peak is quenched while the 360–400 nm emission remains. This is consistent with the assignment of phosphorescence to the former and fluorescence to the latter. To further confirm these assignments, spectra of BAN in CCl_4 show little or no emission around 400 nm and enhanced phosphorescence emission (540 and 570 nm).

The emission spectra of BAN in the presence of TCNE and DMA are presented in Figs. 2a and 2b, respectively. Both quench BAN^{3*}, but the quenching by DMA is accompanied by a new broad emission in the 400–500 nm region. We are currently examining this quenching behaviour in the presence of DMA, and hope to be able to assign this emission in a future publication.

All phosphorescence decay measurements gave exponential decay profiles, whose lifetimes fit very well to eq. [3]. For example, in the case of pyrene as a quencher, we show in Fig. 3 a series of plots of reciprocal phosphorescence lifetimes versus pyrene concentration at various temperatures. Excellent linearity is observed, allowing the rate constants to be calculated from the slopes. Values of k_q at various temperatures were used to construct Arrhenius plots for the quenching of BAN^{3*} and BLN^{3*} phosphorescence (Figs. 4 and 5). The diffusion-controlled rate constant, k_{diff}, was calculated from the Debye equation [5] as a function of T using literature values (10) for viscosity η.

$$[5] \quad k_{diff} = 8\pi RT/3000\eta$$

Diffusion-controlled processes

4′-Bromo-1′-acetonaphthone triplets (BAN^{3*}) are quenched by pyrene, anthracene, and tetracyanoethylene with rate constants near the diffusional limit (see Table 1). For anthracene at 25°C ($k_q = 9.0 \times 10^9$ M^{-1} s^{-1}) and for pyrene at 25°C ($k_q = 7.3 \times 10^9$ M^{-1} s^{-1}) the rate constants are very similar in magnitude to other examples reported by Lissi (5) involving triplet energy transfer from $\pi-\pi^*$ triplet states to lower energy acceptors. In the case of tetracyanoethylene, the rate constant is somewhat smaller, and the quenching mechanism may well involve electron transfer.

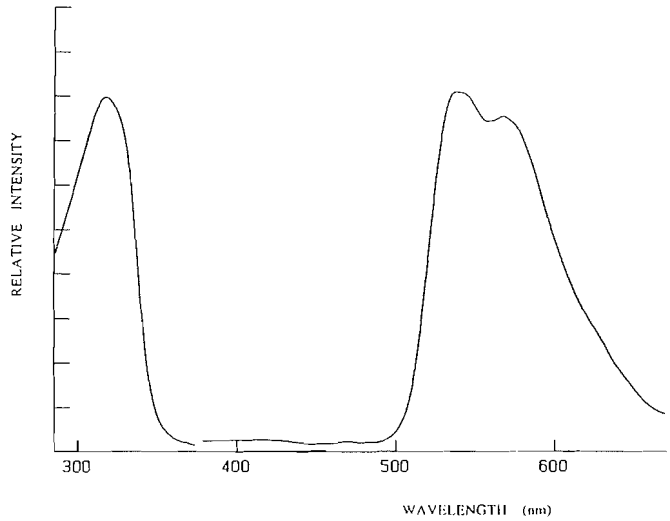

FIG. 1. Phosphorescence excitation (λ_{em} = 570 nm) and emission (λ_{exc} = 318 nm) spectra of 4′-bromo-1′-acetonaphthone for concentrations of 1×10^{-4} M in benzene at room temperature.

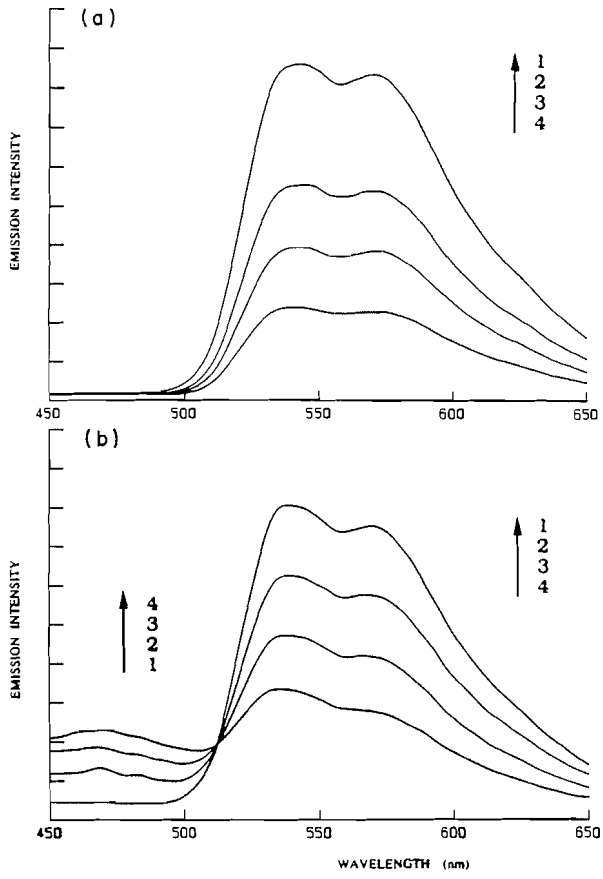

FIG. 2. Emission spectra of BAN^{3*} quenched by TCNE (a) and by DMA (b). Concentration of TCNE: (1) 0; (2) 8.8×10^{-7} M; (3) 2.2×10^{-6} M; (4) 4.8×10^{-6} M; concentration of DMA: (1) 0; (2) 0.001 M; (3) 0.01 M; (4) 0.0192 M. λ_{exc} = 340 nm.

Can. J. Chem. Downloaded from www.nrcresearchpress.com by 91.121.58.235 on 09/07/12
For personal use only.

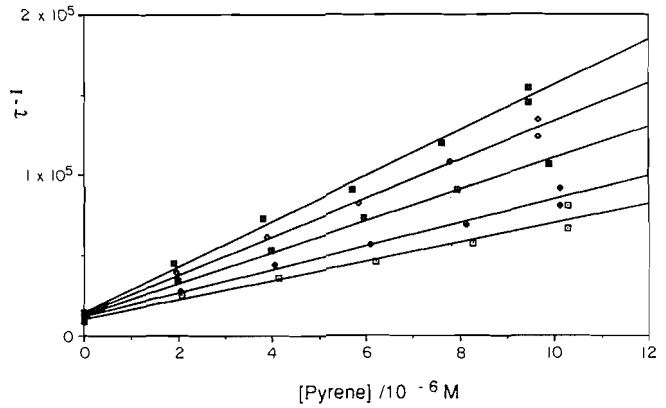

FIG. 3. Pyrene quenching of phosphorescence of BAN^3*, 1×10^{-3} M in benzene. Decay rate, τ^{-1} (s^{-1}), versus pyrene concentration at five different temperatures: (⊡) 9.9°C; (◆) 24.6°C; (■) 44.6°C; (◇)61.8°C; (■) 81.4°C.

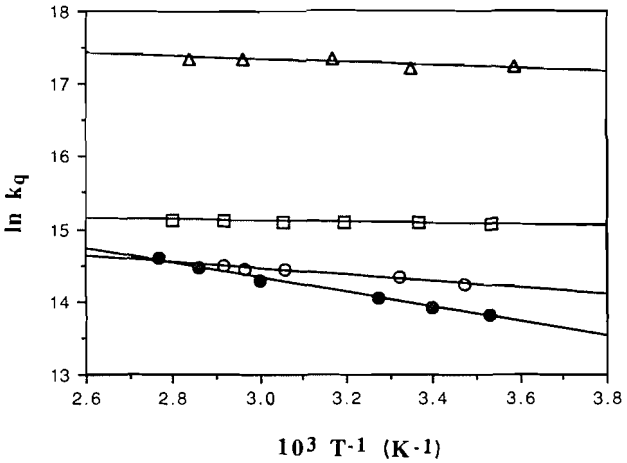

FIG. 4. Arrhenius plots of the quenching of aromatic ketones by various quenchers: BAN^3* quenched by DMA (○); DMAT (△); and DCB (●); BLN^3* quenched by DMA (□).

Non-diffusion-controlled processes

N,N-Dimethylaniline, *N,N*-dimethylamio-*p*-toluidine, and *p*-dicyanobenzene quench the BAN and BLN triplets with considerably lower rate constants. Observed values of k_q were in these cases almost four orders of magnitude lower than in diffusion-controlled processes. These molecules all have triplet energies much larger than that of BAN. Here the quenching mechanism almost certainly involves charge transfer interactions (11).

Table 1 also presents some important thermodynamic parameters for the quenching of bromonaphthoyl triplets in benzene. For pyrene, anthracene, and tetracyanoethylene, the Arrhenius parameters are entirely consistent with diffusion-controlled quenching, i.e., A values on the order of $(4–5) \times 10^{11}$ M^{-1} s^{-1} and apparent activation energies (10–12 kJ mol^{-1}) close to that for diffusion in benzene (12.8 kJ mol^{-1}).

This situation is very different for DCB, DMA, and DMAT. Here we find very low activation energies. In the case of the aromatic amines, the E_a values are close to zero, corresponding to quenching rate constants that do not increase significantly with temperature (Fig. 4). The activation entropies, on the other hand, are typical for bimolecular reactions. Relatively slow quenching, coupled with very low apparent activation energies,

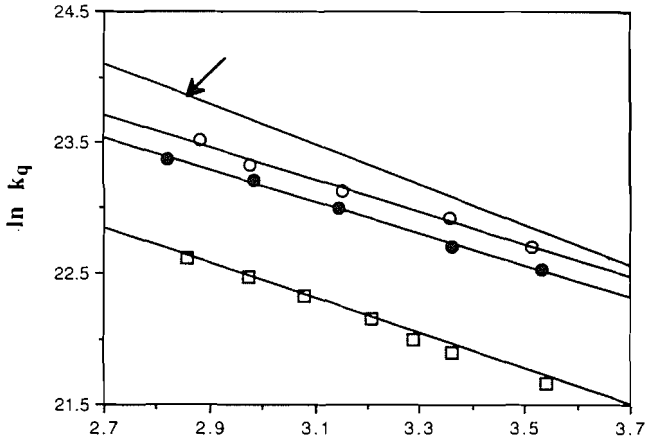

FIG. 5. Arrhenius plots of the quenching of BAN^3* phosphorescence by TCNE (□); ANT (○); and PY (●). Arrow denotes the curve for the diffusion-controlled rate constant.

often points to involvement of a bound complex (an exciplex) along the reaction pathway. Increasing temperature promotes dissociation of the complex to regenerate the excited state, compensating in part for the true activation energy for the quenching reaction. The photoreduction of ketones by amines has been studied extensively (11). In these reactions there is good evidence that the triplet ketones form an exciplex with the amine and that the quenching mechanism has charge transfer character. This explains, for example, very low E_a and negative $\Delta H^{\neq}$ values for quenching BLN by DMA.

There are two particular results that require special comment. One is that DMAT is almost 20 times more efficient as a quencher than is DMA. In one sense, this result is not so surprising, since it is well known (11) that triplet quenching by electron-rich species is sensitive to the presence of additional electron-donating substituents on the quencher. For fluorenone, for example, introduction of a methyl group to an aromatic amine increases the quenching efficiency by a factor of six. What is special here is that the difference in quenching efficiency between DMA and DMAT is almost entirely entropic in origin.

The final point concerns the remarkable difference in activation parameters for DMA quenching BAN^3* and BLN^3*. Here the activation entropies are rather similar, but E_a for BLN reactivity is nearly 3 kJ mol^{-1} lower than that for BAN. In absolute terms, the effect is small, but because the E_a values are so close to zero, this difference seems to be well outside experimental error. We have no unambiguous explanation for this difference. Further experiments are in progress. We hope to be able to comment further on these differences in a future publication.

Acknowledgements

We thank NSERC Canada for their support of this research. MCP thanks the University of Toronto for a Fellowship.

1. (*a*) U. MAHARAJ and M. A. WINNIK. J. Am. Chem. Soc. **103**, 2328 (1981); (*b*) M. A. WINNIK and U. MAHARAJ. Macromolecules, **10**, 902 (1979); (*c*) U. MAHARAJ, M. A. WINNIK, B. DORS, and H. J. SCHAFER. Macromolecules, **10**, 905 (1979).
2. A. MAR, S. FRASER, and M. A. WINNIK. J. Am. Chem. Soc. **103**, 491 (1981).

Can. J. Chem. Downloaded from www.nrcresearchpress.com by 91.121.58.235 on 09/07/12
For personal use only.

3. M. A. WINNIK. Acc. Chem. Res. **10**, 173 (1977).
4. (*a*) K. HORIE, W. SCHNABEL, I. MITA, and H. USHIKI. Macromolecules, **14**, 1422 (1981); (*b*) K. HORIE and I. MITA. Macromolecules, **11**, 1175 (1978).
5. E. A. LISSI and M. V. ENCINAS. CRC handbook of organic photochemistry. Vol. 2. *Edited by* J. C. Scaiano. CRC Press, Boca Raton, FL. 1989. Chap. 7.
6. (*a*) J. D. BOLT and N. J. TURRO. Photochem. Photobiol. **35**, 305 (1982); (*b*) N. J. TURRO and T. OKUBO. J. Phys. Chem. **86**, 1535 (1982); (*c*) T. OKUBO and N. J. TURRO. J. Phys. Chem. **85**, 4034 (1981); (*d*) J. D. BOLT and N. J. TURRO. J. Phys. Chem. **85**, 4029 (1981).
7. T. L. JACOBS, S. WINSTEIN, J. W. RALLS, and J. H. ROBSON. J. Org. Chem. **11**, 27 (1946).
8. M. C. PITON, W. PANNING and M. A. WINNIK. Rev. Sci. Instr. In press.
9. J. A. RIDDICK, W. B. BUNGER and T. K. SAKANO. Techniques of chemistry. Vol. II. Organic solvents. 4th ed. J. Wiley & Sons, New York. 1986.
10. R. C. WEAST (*Editor*). Handbook of chemistry and physics. 60th ed. Chemical Rubber Publishing Co., Cleveland, OH. 1980.
11. (*a*) S. G. COHEN, A. PAROLA and G. H. PARSONS. Chem. Rev. **73**, 141 (1973); (*b*) A. A. GORMAN, C. T. PAREKH, M. A. J. RODGERS, and P. G. SMITH. J. Photochem. **9**, 11 (1978); (*c*) S. G. COHEN, G. A. DAVIS, and W. D. K. CLARK. J. Am. Chem. Soc. **94**, 869 (1972); (*d*) S. G. COHEN and G. H. PARSONS. J. Am. Chem. Soc. **92**, 7603 (1970).

Can. J. Chem. Downloaded from www.nrcresearchpress.com by 91.121.58.235 on 09/07/12
For personal use only.

The chemistry of thujone. XV.[1] A versatile route to antifeedants of the polygodial family

JAMES P. KUTNEY,[2] KRYSTYNA PIOTROWSKA, YONG-HUANG CHEN, KWOK-PING NORMAN CHENG, ZHENYONG GAO, AND STEVEN J. RETTIG

Department of Chemistry, University of British Columbia, 2036 Main Mall, Vancouver, B.C., Canada V6T 1Y6

Received March 16, 1990

This paper is dedicated to Professor Ross Stewart on the occasion of his 65th birthday

JAMES P. KUTNEY, KRYSTYNA PIOTROWSKA, YONG-HUANG CHEN, KWOK-PING NORMAN CHENG, ZHENYONG GAO, and STEVEN J. RETTIG. Can. J. Chem. **68**, 1698 (1990).

Utilizing thujone-derived intermediates, efficient routes to the natural polygodial family of antifeedants as well as novel analogues within this family are described. One of the key features of this study involves the insertion of an oxygen function into a tertiary carbon center adjacent to a cyclopropane ring system thus providing convenient intermediates for subsequent elaboration. An interesting ring expansion of five-membered to six-membered ring systems by means of tri-*n*-butyltin hydride is also described.

Key words: antifeedants, polygodial, thujone.

JAMES P. KUTNEY, KRYSTYNA PIOTROWSKA, YONG-HUANG CHEN, KWOK-PING NORMAN CHENG, ZHENYONG GAO et STEVEN J. RETTIG. Can. J. Chem. **68**, 1698 (1990).

Utilisant des intermédiaires dérivés de la thujone, on a développé des méthodes efficaces pour préparer les produits de la famille du polygodial, un anti-nutrition naturel, ainsi que de nouveaux analogues de cette famille. L'une des caractéristiques principales de cette étude implique l'insertion d'une fonction oxygénée sur un carbone tertiaire adjacent d'un système cyclopropanique; cette méthode fournit des intermédiaires précieux pour le reste de la synthèse. On décrit aussi une intéressante extension d'un cycle à cinq chaînons en système à six chaînons qui se produit sous l'influence de l'hydrure de tri-*n*-butyl-étain.

Mots clés : anti-nutrition, polygodial, thujone.

[Traduit par la revue]

Can. J. Chem. Downloaded from www.nrcresearchpress.com by 91.121.58.235 on 09/07/12
For personal use only.

The naturally occurring sesquiterpenoid dialdehydes of the drimane series exemplified by polygodial (**1**), warburganal (**2**), and cinnamodial (**3**) have been thoroughly investigated for

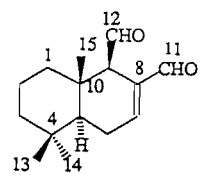

1

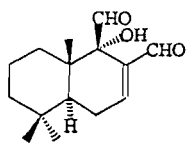

2

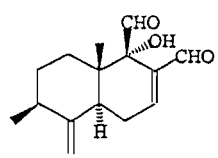

3

their strong antifeedant activities, and considerable efforts have been devoted to syntheses of these compounds. Extensive reviews (2, 3) summarize the various studies in this area. In our program directed at the utilization of the readily available and inexpensive chiral monoterpene thujone (**7**) in the synthesis of biologically active substances, we became interested in developing a versatile route to this family of compounds. The utilization of a chiral starting material would afford chiral end products, an obvious advantage in any subsequent commercial application *if* evaluation of antifeedant activity should reveal that only one optimal isomer possesses optimum activity. Hopefully the developed strategy would also entail the synthesis of polygodial analogues, not previously studied, so as to establish a proper structure–activity relationship within this area. This publication presents results that satisfy a number of these objectives.

It was clear from the previously published syntheses (2, 3) that bicyclic intermediates such as **4** and **5** were most ideal for our further studies, the former providing a route to novel ring A monomethyl analogues of polygodial while **5** would allow an entry directly to the natural products. With ready access to tricyclic intermediates such as **6**, via Robinson annelation of thujone (4), it was now appropriate to develop methods for converting the "cyclopropyl ring – isopropyl side chain component" of **6** into the ketone functionality portrayed in **4** and **5**. The overall strategy for this process is summarized in the sequence **7** → **8** → **9** → **10**. Thujone (**7**) was used in the initial studies, with X representing a leaving group and N an appropriate nucleophile.

It is known that ozone reacts slowly with saturated hydrocarbons with oxygen insertion into the C—H bond. Insertion occurs preferentially at the tertiary carbon atoms, resulting in alcohols and ketones. This type of reaction had been little

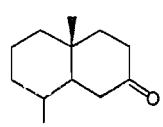

4

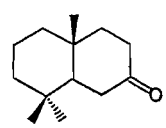

5

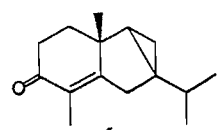

6

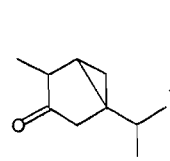

7

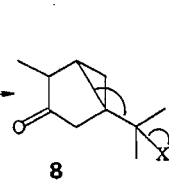

8

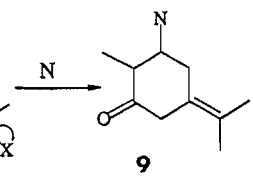

9

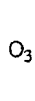

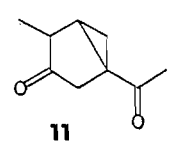

11

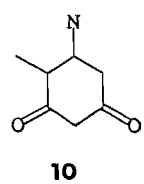

10

[1]For Part XIV, see ref. 1.

[2]Author to whom correspondence may be addressed.

used until 1975 when it was reported (5) that a dry ozonation method allows introduction of hydroxyl groups into saturated compounds. The main idea was to use silica gel as the reaction matrix based on the fact that silica gel absorbs ozone efficiently at low temperature (its concentration being about 4.5% by weight at −78°C). In practice, the silica gel is preabsorbed with the organic substrate, cooled to −78°C, and then saturated with ozone; it is then allowed to warm slowly to room temperature and the product is eluted in the normal fashion. It has also been observed (6) that ozone cleaves not only C—H bonds, but also C—CH_3 bonds, the reaction involving a direct insertion of ozone into these bonds. Application of this reaction to thujone (**7**) afforded a mixture of the alcohol **8** (X = OH) and the ketone **11** in a 3:1 ratio respectively, and an overall combined yield of 70% based on recovery of starting material. Since **11**, after hydride reaction, can also afford the necessary functionality for the ring-opening process (**8** → **9**), *both* compounds (**8** and **11**) could be useful for our objective. Extension of this ozonation process to the tricyclic ketone **12**, available from other studies in our laboratory, similarly provided **13** and **14**. Although this

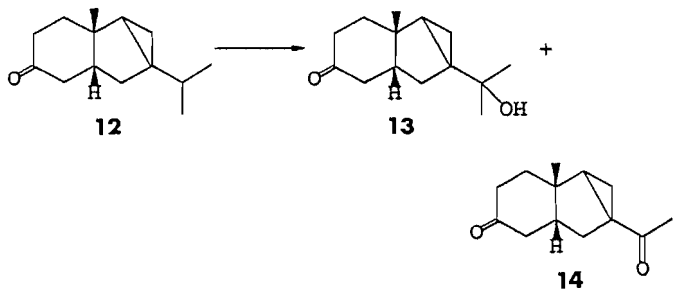

method offered some potential in our overall strategy, the difficulties with scale-up and substantial recovery of starting materials discouraged further development. However, these results stimulated the approach to perform ozonation reactions in solution with thujone and other thujone-derived intermediates. Indeed when **7**, dissolved in anhydrous ethyl acetate at −25°C, is treated with a stream of ozone over a 10 h period, the alcohol **8** (X = OH, 50% yield) and ketone **11** (20% yield) were obtained. As will be seen later, both types of products are indeed useful in the cyclopropyl ring-opening reaction (e.g., **8** → **9**) and this reaction became sufficiently attractive for future applications.

With the above data on hand, the synthetic route to novel ring A monomethyl polygodial analogues was undertaken. For this purpose, the previously synthesized tricyclic ketone **15** (4) (Scheme 1) was reduced, in quantitative yield, to the saturated ketone **16**. The stereochemistry of **16** at C4 and C5 was first investigated by a detailed proton nmr study. The C4 and C5 methine protons appeared as multiplets at 2.59 and 1.70 ppm respectively, while the C4 methyl group revealed a doublet at 0.94 ppm. These assignments were established from the following decoupling studies. There are three multiplets, each integrating for one proton, resonating at 2.15, 2.42, and 2.59 ppm in the spectrum. On the basis of their chemical shifts, they must be attached to C2 and C4. Irradiation of the signal at 2.59 ppm resulted in the three-proton doublet at 0.94 ppm collapsing into a singlet, thereby implying that the multiplet at 2.59 ppm was due to the proton at C4, and the doublet at 0.94 ppm was, in turn, due to the C14 methyl group. Conversely, irradiation of the signal at 0.94 ppm changed the splitting pattern at 2.59 ppm from a multiplet to a poorly resolved doublet. Also as a result of irradiation of the C4 proton signal at 2.59 ppm, the multiplet at 1.70 ppm, integrating for one proton, became a doublet of doublets, thereby allowing assignment of the multiplet at 1.70 ppm to be that of the C5 proton. The C15 methyl signal was then easily recognized at 1.23 ppm since it is the only three-proton singlet in the spectrum.

Having located these key protons in the nmr spectrum, the stereochemistry at C4 and C5 could be investigated in a nuclear Overhauser effect (nOe) difference experiment. Examination of a molecular model of **16** showed that the distances between the C14 methyl group and the C5 proton, and also the C15 methyl group and the C5 proton are small if these nuclei are on the same side of the molecule. Therefore irradiation of the β-oriented C15 methyl or C14 methyl signals should enable determination of the configurations at C4 and C5.

Irradiation at 1.23 ppm (C15 methyl) resulted in the enhancement of the multiplet at 2.59 ppm due to the C4 proton, but revealed no effect on the multiplet at 1.70 ppm due to the C5 proton. Irradiation at 0.94 ppm (C14 methyl) gave only a very small enhancement at 1.70 ppm. These observations indicated that the C4 proton is on the same side as the C15 methyl group, namely, the C14 methyl group is α-oriented; however, the nature of the ring A/B fusion (*cis* or *trans*) remained unclear.

To settle this question and to allow assignments in subsequent synthetic intermediates, as outlined in Scheme 1, a suitable crystalline compound for X-ray analysis was required. Fortunately compound **26**, obtained from ozonation of **16**, provided satisfactory crystals and the subsequent X-ray analysis of **26** clearly revealed the C14α-methyl orientation and *cis* A/B ring fusion as shown in Scheme 1 and Fig. 1. As a result, it is possible to assign *cis* A/B ring fusion to all compounds arising from **16**.

Employing the classical Huang–Minlon modification of the Wolff–Kishner reduction, **16** was converted to the required intermediate **17** (87% yield) for subsequent ozonation studies according to the earlier developed conditions. Treatment of a cooled (−40°C) ethyl acetate solution of **17** with a stream of ozone over a 10 h period provided a 1:1 ratio of the expected products **18** and **19** (combined yield 70%), which were easily separated by silica gel chromatography. Control of temperature during ozonization was important in that a complex mixture was obtained if the reaction was conducted at 0°C while only a slow reaction was noted with **17** at −50°C.

The ketone **19**, upon reduction with sodium borohydride, yielded the expected alcohol **24** (93% yield). Both alcohols **18** and **24** can be utilized to provide the crucial intermediate **25** (see Scheme 1).

Cyclopropyl ring opening of **18** was then evaluated under acidic conditions similar to those employed in our earlier study (4). Thus treatment of **18** with concentrated hydrochloric acid at 0°C afforded a highly unstable oily product with spectroscopic properties consistent with the structure **20**. The mass spectrum with fragments at *m/z* 240 and 242 was consistent with the formulae $C_{15}H_{25}{}^{35}Cl$ and $C_{15}H_{25}{}^{37}Cl$ respectively, and the ^1H nmr spectrum was particularly informative, revealing a typical ABX coupling pattern, that is, two well-resolved doublets of doublets at 3.45 ppm (1H, dd, J = 11 Hz) and 3.61 ppm (1H, dd, J = 11 Hz), consistent with methylene protons on a carbon atom attached to the chlorine. It was thus clear that cyclopropyl ring opening to the five-membered ring intermediate **20** was occurring, in contrast to the mode of cyclopropyl ring opening to a six-membered ring B intermediate observed in another series studied previously (4). Further studies of the ring opening of **18** were performed with 48%

Can. J. Chem. Downloaded from www.nrcresearchpress.com by 91.121.58.235 on 09/07/12
For personal use only.

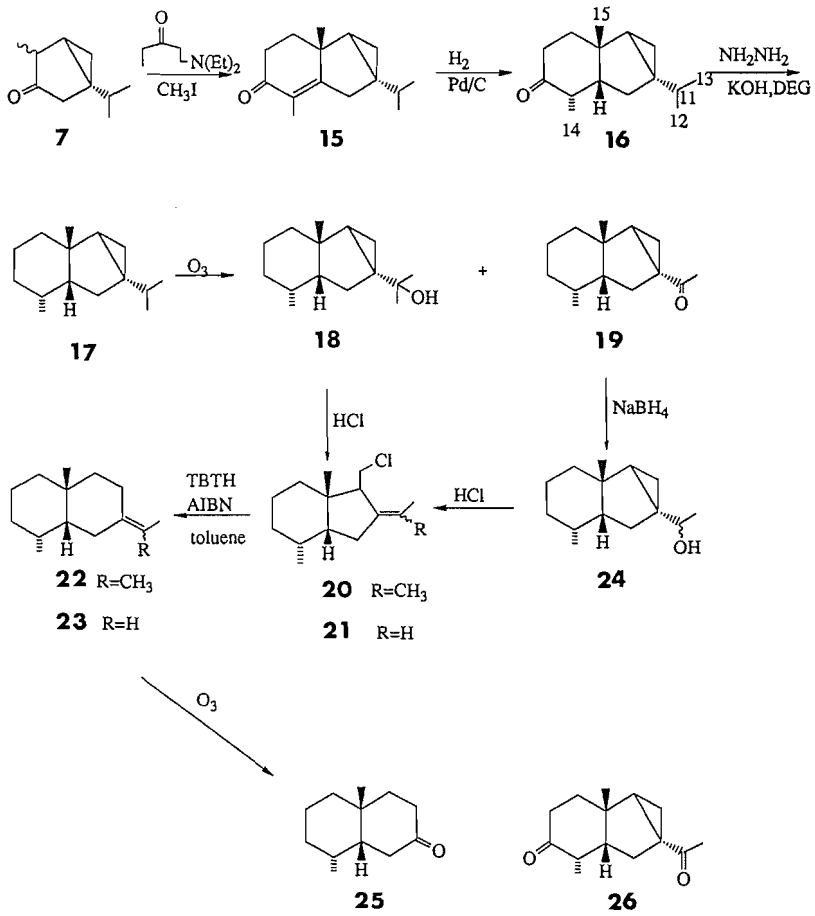

SCHEME 1. Conversion of thujone to the carbonyl intermediate **25**.

hydrobromic acid and magnesium bromide or iodide in refluxing anhydrous ether employing the conditions of McCormick *et al.* (7, 8) and a combination of magnesium and zinc halides (9), but, in each instance, more complex reaction mixtures and lower overall yields of products were obtained.

Interestingly the five-membered ring intermediate **20** was converted to the desired bicyclic intermediate **22** when **20** was treated with an excess of tri-*n*-butyltin hydride in refluxing toluene employing azobisisobutyronitrile as radical initiator. In similar fashion, the chloride **21**, obtained after acid treatment of **24**, afforded **23**. In fact, for preparative purposes, the entire sequence **17** → **18** + **19** → → **20**, **21** → **22**, **23** could be conducted without isolation of intermediates. Thus the reaction mixture containing **18** and **19** resulting from ozonolysis of **17** is treated directly with borohydride to afford a mixture of alcohols **18** and **24**, and the latter, without purification, is subjected to the acidic treatment. The resulting mixture of **20**, **21** is treated with the tin hydride to afford **22**, **23** in an overall yield ot 45%. As is noted below, a mixture of **22** and **23** can be subsequently converted to the common intermediate **25**.

The six-membered ring structure of **22** was supported by the ^{1}H nmr spectrum, which clearly revealed four methyl signals at 0.88 (3H, d, J = 6.6 Hz, C14-CH_3), 0.94 (3H, s, C15-CH_3), 1.65 (3H, s, C12-CH_3), and 1.66 ppm (3H, s, C13-CH_3). If ring B in the structure was five-membered, one more methyl signal, occurring as a doublet, would be observed.

There is little doubt that the above conversion of **20** to **22** involves a radical process. Thus homolytic fission of the carbon–halogen bond, initiated by the tri-*n*-butyltin radical,

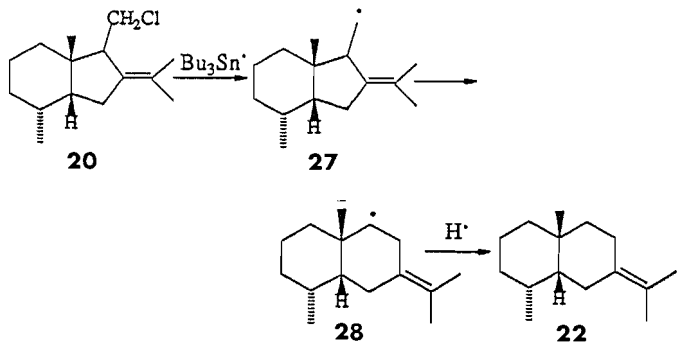

generates intermediate **27**. Rearrangement of **27** affords **28**, which is finally converted to **22**. It is logical to assume that the rearrangement, **27** → **28**, could involve a concerted 1,2-shift although mechanistic studies were not performed here.

With the alkenes **22** and **23** in hand, the important intermediate decalone **25** was readily available. Alkene **22** or **23** (or the mixture) was treated with ozone at −60°C, followed by decomposition of the resultant intermediate ozonide under reductive conditions employing dimethyl sulfide, and decalone **25** was thus obtained in 90–93% yield. In summary, the majority of the reactions outlined in Scheme 1 can be conducted without isolation of intermediates, thereby affording an overall efficient route to **25** from thujone.

For the functionalization of ring B in decalone **25** so as to provide a synthetic route to ring A monomethylated A/B *cis* fused drimane dialdehydes (see **38**, Scheme 2) for subsequent evaluation as antifeedants, it was considered appropriate to

Can. J. Chem. Downloaded from www.nrcresearchpress.com by 91.121.58.235 on 09/07/12
For personal use only.

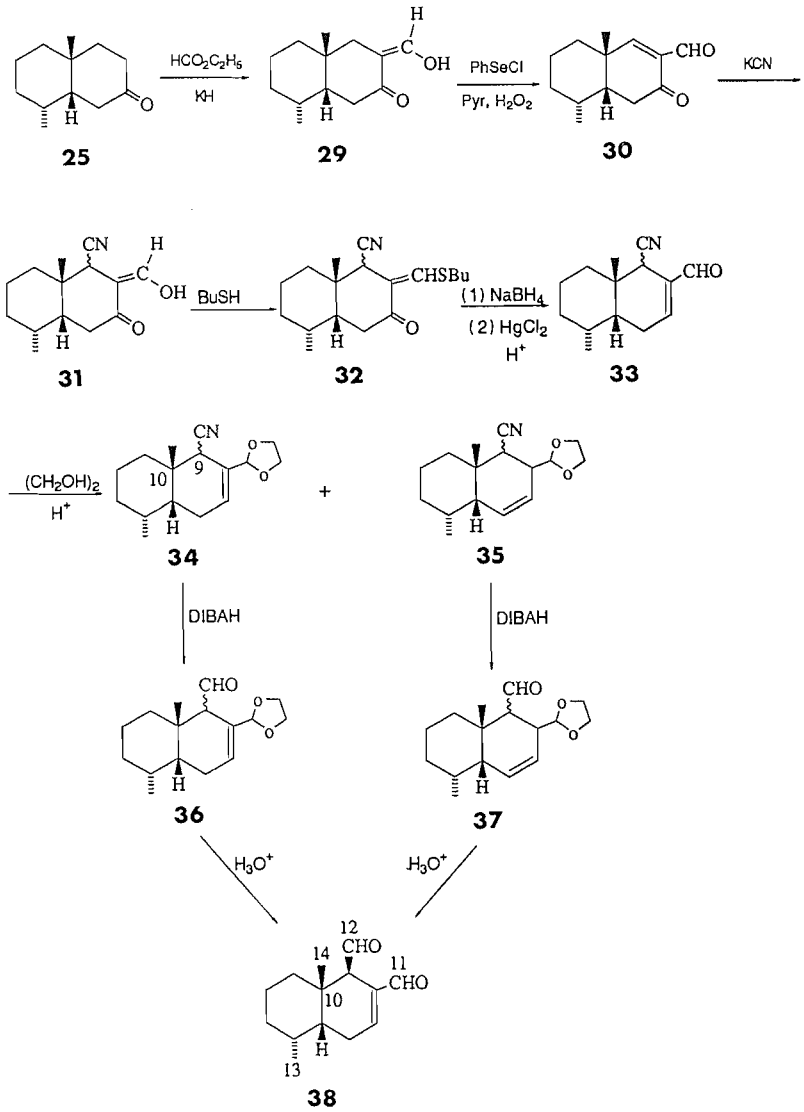

SCHEME 2. Conversion of the carbonyl intermediate **25** into the monomethylated A/B *cis* fused drimane aldehyde **38**.

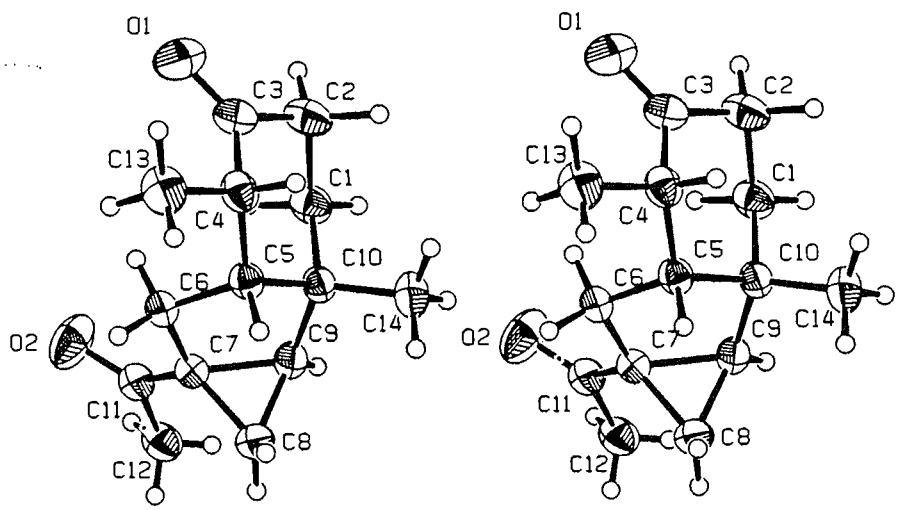

FIG. 1. Stereoview of **26**; 50% probability thermal ellipsoids are shown for the non-hydrogen atoms.

Can. J. Chem. Downloaded from www.nrcresearchpress.com by 91.121.58.235 on 09/07/12
For personal use only.

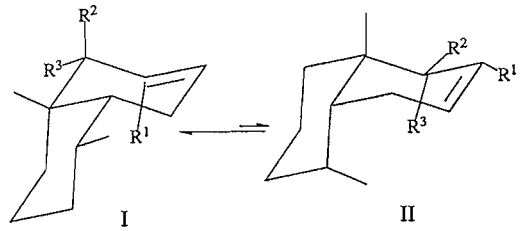

I II

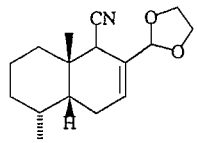

34

34 I R^1= R^2=H R^3=CN

34 II R^1= R^2=CN R^3=H

consider methodology developed earlier by de Groot and co-workers (10) for a related series of compounds. Thus introduction of the C8 aldehyde function was attempted initially with ethyl formate and sodium hydride in the manner described (10) but no reaction occurred. However, the use of stronger base (KH) was successful and a high yield (89%) of **29** was obtained. The latter compound, although easily purified by silica gel chromatography, was somewhat unstable and it was best to perform the next reaction without delay.

The olefinic bond in **30** was introduced via a selenylation–deselenylation reaction with **29**. Liotta *et al.* reported (11) that the rate of selenation with PhSeCl/pyridine can be roughly correlated with the percent enolic character of the starting β-dicarbonyl compound. When the substrate in question exists to a substantial extent in its enol form, selenation is instantaneous at room temperature. In our case, **29** exists entirely in the enol form, as supported by two singlets shown in the ^{1}H nmr spectrum at 8.56 and 14.29 ppm. Compound **29** was therefore readily converted to the corresponding unsaturated derivative **30** by (a) selenation using a 1:1 complex of phenylselenenyl chloride/pyridine and (b) *in situ* oxidation with 30% H_2O_2. The isolated yield of **30** was 86%.

The unsaturated keto aldehyde **30** was reacted with cyanide to afford the expected nitrile **31** as an unstable yellow oil that could not be purified due to rapid decomposition. However, the characteristic nitrile absorption (2236 cm^{-1}) in its infrared spectrum and the ^{1}H nmr spectrum with singlets at 4.01, 8.98, and 15.04 ppm clearly supported the assigned structure. Further characterization could be achieved, however, when the crystalline *n*-butylthio derivative **32**, obtained by treatment of **31** with 1-butanethiol under acidic conditions, was obtained. The stereochemistry of the nitrile group in **32** is uncertain and NMR data (see below) were inconclusive.

Borohydride reduction of **32** followed by treatment of the product (not isolated) with mercuric chloride and hydrochloric acid afforded the unsaturated aldehyde **33** as a crystalline product. For preparative purposes, isolation of intermediates **31** and **32** was not essential and the overall yield in the conversion **30** → → **33** was 52%.

To convert the nitrile function in **33** to the required aldehyde, initial protection of the aldehyde group in **33** by ketalization was considered. Thus, reaction of **33** with ethylene glycol catalyzed by *p*-toluenesulfonic acid afforded, somewhat surprisingly, a mixture of the expected ketal **34** (71% yield, one olefinic proton at 6.05 ppm) and the isomeric ketal **35** (18% yield, two olefinic protons at 5.53 and 6.62 ppm). Since it was expected that the double bond in **35** would migrate into conjugation with the aldehyde function on subsequent deprotection, it could be also utilized in the preparation of **38** (see Scheme 2).

A comment concerning the stereochemistry of the nitrile function at C9 in **34** is appropriate and nmr data were considered for this purpose. Examination of the ^{1}H nmr spectrum of **34** revealed a one-proton singlet (2.79 ppm) for the C9 proton and a three-proton singlet at 1.24 ppm for the methyl group at C10. Irradiation of this methyl proton resonance resulted in an nOe enhancement of the C9 proton signal thereby establishing their close proximity to each other. However, conformational analysis suggests that in the most stable conformation (I) for the two possible C9 epimers (**34**I and **34**II), the distances between the C9 protons and the corresponding methyl protons are very similar, thereby preventing a definitive conclusion to be drawn from the nOe experiment.

Nitrile **34** was conveniently reduced to the corresponding aldehyde **36** (85% yield) by treatment with diisobutyl aluminum hydride at low temperature. In a similar manner, **35** was also converted to **37**.

Removal of the ketal group in **36** was achieved under acidic conditions to afford the target compound **38** in 93% yield. As was expected, deketalization of the minor isomer **37** also afforded **38**. Again, for preparative purposes, the cyano compounds **34** and **35** obtained as a mixture in the ketalization reaction of **33** can be directly reduced to **36** and **37** and the mixture then treated directly with acid. In this manner, the overall yield in the conversion **34**, **35** → → **38** is 77%. The dialdehyde functionality in **38** was clearly established by infrared (1718 and 1665 cm^{-1}) and ^{1}H nmr (9.44 and 9.79 ppm) spectroscopy.

Another nOe difference experiment was applied to **38**. Irradiation at the C14 methyl protons resonance (1.26 ppm) resulted in the enhancement of the C9 proton (3.33 ppm) and the C9 aldehyde proton (9.79 ppm). Similar arguments to those presented above for **34**, concerning nOe results and stereochemistry at C9, apply in this case and therefore nOe data cannot conclusively establish the C9 configuration in the final product **38**. However, it is logical to assume that the acidic treatment employed in the deketalization process leading to **38** may well provide the C9β orientation (equatorial) for the aldehyde function in **38**.

Can. J. Chem. Downloaded from www.nrcresearchpress.com by 91.121.58.235 on 09/07/12
For personal use only.

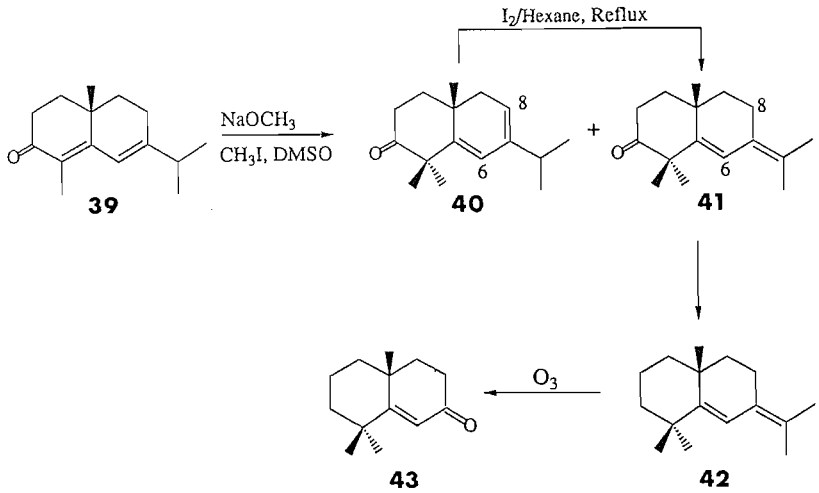

In conclusion, the sequence of reactions as summarized in Schemes 1 and 2, particularly since many of them can be conducted without isolation of intermediates, affords efficient routes to novel polygodial analogues. Subsequent evaluation will determine their antifeedant properties, if any.

As was noted earlier, the naturally occurring drimane antifeedants possess a *trans* A/B ring fusion and a *gem* dimethyl functionality in ring A. It was therefore desirable to establish an efficient route to the natural series employing thujone-derived intermediates. For this purpose, the previously synthesized β-cyperone molecule (**39**) (4) was considered as an appropriate starting material. Alkylation of **39** with methyl iodide and sodium methoxide in dimethyl sulfoxide yielded an inseparable mixture of the dienes **40** (5.38, m, C8-H; 5.80, s, C6-H) and **41** (6.41, s, C6-H) in an approximate ratio of 2:1 respectively, as determined by the relative intensity ratios of the olefinic signals in the ^{1}H nmr spectrum. Direct treatment of this mixture with iodine in refluxing hexane afforded pure **41** for further elaboration.

Wolff–Kishner reduction of **41** provided **42**, and the latter on low temperature ozonolysis (−78°C) afforded the conjugated ketone **43**. Since the latter, synthesized previously in racemic form by de Groot and co-workers (10), has been converted to (±)-polygodial (**1**) and (±)-warburganal (**2**), the present study with thujone-derived intermediates allows a synthetic entry to the natural series of antifeedants.

Experimental

Melting points were determined on a Nalge melting point apparatus and are uncorrected. The infrared spectra were recorded on Perkin–Elmer 710B and 1710 (Fourier Transform IR) spectrometers either in chloroform solution (using sodium chloride cells of 0.1-mm path length) or as a neat liquid film. The ultraviolet spectra were recorded on a Cary 15 spectrometer, the extinction coefficients (log ε_{max}) are given in parentheses, and the wavelength(s) of the maxima in nanometers. The mass spectra were recorded on AEI-MS-9 (low resolution) or Kratos-MS-50 (high resolution) spectrometers. The ^{1}H nmr spectra were recorded on either Bruker WH-400 or Varian XL-300 spectrometers in $CDCl_3$ solution and the chemical shifts are reported in ppm relative to tetramethylsilane (internal standard). The optical rotations were recorded on a Perkin–Elmer 141 automatic polarimeter in a 10-cm cell at ambient temperature using the solvent and concentrations (g/100 mL) indicated in parentheses following the recorded rotation values. The elemental analyses were determined by Mr. P. Borda, Microanalytical Laboratory, The University of British Columbia. The X-ray diffraction analysis was performed by Dr. S. Rettig on a Rigaku AFC6 diffractometer. Column chromatography was performed using 230–400 mesh silica gel supplied by E. Merck Co. Gas–liquid chromatography was performed on a Hewlett Packard model 5890 gas chromatograph, using a flame ionization detector and a 25 m × 0.21 mm fused silica capillary column: DB1701.

"Wet" ozonation of thujone

A solution of thujone **7** (10 g, 66 mmol) in ethyl acetate (100 mL) was cooled to −25°C and a stream of ozone was passed through with the employment of a gas dispersion tube for 10 h. While the ozonizer was turned off, the oxygen flow was continued for the next 15 min to remove an excess of ozone and the reaction mixture was allowed to warm up slowly to room temperature. Then 5 mL of dimethyl sulfide was added and stirred for 15 min. The reaction mixture was washed with a saturated solution of sodium bicarbonate and water and dried with sodium sulfate. After evaporation of solvent, the resulting oil was chromatographed on 250–400 mesh silica gel with the employment of a mixture of isopropanol and hexane (2:8) to yield alcohol **8** (4.7 g, 47%) and ketone **11** (2.3 g, 23%) with a combined yield of 70%.

"Dry" ozonation of thujone

To the solution of thujone **7** (350 mg, 2.3 mmol) in 50 mL of methyl chloride, 35 mg of silica gel was added and the solvent was removed under vacuum. The flask containing silica gel impregnated with thujone was equipped with a rotating mechanism, placed in a cooling bath (−78°C), and the stream of ozone was passed continuously for the period of 8 h. Then the mixture was allowed to warm up slowly from −78°C to room temperature. The elution with an organic solvent followed by chromatographic separation of the crude product yielded 195 mg of unreacted thujone and 115 mg (70% yield) of a mixture of alcohol **8** and ketone **11** in 3:1 ratio. Repeated column chromatography gave pure **8** and **11**.

Alcohol **8**: ir ν_{max} (neat): 3500, 1730 cm^{-1}; ^{1}Hmr δ: 0.11 (1H, t, J = 4.8), 1.13 (1H, m), 1.18 (3H, d, J = 7.6), 1.22 (3H, s), 1.32 (3H, s), 1.35 (1H, dd, J = 4.0, 8.0), 1.60 (1H, bs, OH), 2.19 (1H, d, J = 16.4), 2.29 (1H, q, J = 7.6), 2.79 (1H, dm, J = 16.4); ms m/z: 168 (M^+, 10%), 150 (4%), 107 (69%), 43 (100%). High resolution molecular weight determination calcd. for $C_{10}H_{16}O_2$: 168.1150; found: 168.1146.

Ketone **11**: ir ν_{max} (neat): 1740, 1685 cm^{-1}; ^{1}Hmr δ: 0.75 (1H, t, J = 4.8), 1.22 (3H, d, J = 8.4), 1.86–1.98 (2H, m), 2.09 (3H, s), 2.30–2.41 (2H, m), 3.25 (1H, m); ms m/z: 152 (M^+, 35%), 137 (11%), 124 (32%), 109 (100%). High resolution molecular weight determination calcd. for $C_9H_{12}O_2$: 152.0837; found: 152.0839.

*Dry ozonation of (5β)-7α-isopropyl-10β-methyltricyclo[4.4.0^{5,10}.0^{7,9}]-dec-3-one (**12**)*

To the solution of ketone **12** (500 mg, 2.5 mmol) in methylene dichloride (100 mL), silica gel (50 g) was added. After evaporation of solvent, the flask containing silica gel impregnated with ketone **12** was

Can. J. Chem. Downloaded from www.nrcresearchpress.com by 91.121.58.235 on 09/07/12
For personal use only.

Can. J. Chem. Downloaded from www.nrcresearchpress.com by 91.121.58.235 on 09/07/12
For personal use only.

equipped with a rotating mechanism, placed in a cooling bath, and a stream of ozone was passed continuously for 8 h at the temperature of −78°C. Then the mixture was allowed to warm up slowly to room temperature. Silica gel was washed with methylene chloride and ethyl acetate. Evaporation of solvents gave 470 mg of oil, which after first chromatography yielded 310 mg of unreacted starting material and 132 mg of a 3:1 mixture of alcohol **13** and ketone **14** respectively. Repeated chromatography yielded pure **13** and **14**.

Alcohol **13**: ir ν_{max} (neat): 3459, 1690 cm^{-1}; ^{1}Hmr δ: 0.45 (1H, m), 0.63 (1H, m), 1.14 (3H, s), 1.15 (1H, m), 1.21 (3H, s), 1.24 (3H, s), 1.41 (1H, s, b, OH), 1.57–1.83 (5H, m), 2.09–2.25 (2H, m), 2.31–2.52 (2H, m); ms *m/z*: 222 (M^+), 204, 189.

Ketone **14**: ir ν_{max} (neat): 1705, 1680 cm^{-1}; ^{1}Hmr δ: 1.06 (1H, t), 1.25 (3H, s), 1.39 (1H, d, d), 1.69–1.89 (5H, m), 2.05 (3H, s), 2.12–2.25 (3H, m), 2.36–2.48 (2H, m); ms *m/z*: 206 (M^+), 191, 147.

*(5β)-4α,10β-Dimethyl-7α-isopropyltricyclo[4.4.0^{5,10}.0^{7,9}]dec-3-one (**16**)*

A mixture of tricyclic enone **15** (8.00 g, 36.7 mmol), potassium hydroxide (1 g, 17.8 mmol), and 10% palladium on active charcoal (2 g) in ethanol (800 mL) was hydrogenated at room temperature and atmospheric pressure. Hydrogen absorption ceased after 3.5 h. The mixture was filtered through a Celite plug and the filtrate evaporated. Water (100 mL) was added to the residue, and the mixture was extracted with methylene chloride (2 × 100 mL) and dried over sodium sulfate. Evaporation of the solvent at reduced pressure afforded the saturated ketone **16** as a colorless oil (7.99 g, 99%); ir ν_{max} (neat): 2942, 2846, 1702 cm^{-1}; ^{1}Hmr δ: 0.20 (1H, dd, *J* = 9, 4, C8), 0.43 (1H, dd, *J* = 6, 4, C8), 0.85 (3H, d, *J* = 8), 0.91 (3H, d, *J* = 8), 0.94 (3H, d, *J* = 7), 1.18 (1H, t, *J* = 11), 1.23 (3H, s), 1.33 (1H, h, *J* = 8), 1.61–1.83 (5H, m), 2.15 (1H, m, C2), 2.42 (1H, m, C2), 2.59 (1H, m, C4); ms *m/z*: 220 (M^+, 8%), 205 (5%), 177 (25%), 136 (32%), 124 (35%), 105 (51%), 93 (75%), 86 (100%), 82 (32%), 67 (26%), 55 (41%), 41 (54%). High resolution molecular weight determination calcd. for $C_{15}H_{24}O$: 220.1821; found: 220.1815. Anal. calcd. for $C_{15}H_{24}O$: C 81.76, H 10.98; found: C 81.67, H 11.00.

*(5β)-4α,10β-Dimethyl-7α-isopropyltricyclo[4.4.0^{5,10}.0^{7,9}]decane (**17**)*

A mixture of **16** (30 g, 136.4 mmol) and hydrazine (21.8 g, 681.8 mmol) in diethylene glycol (300 mL) was heated from 100 to 130°C for 1.5 h (water and excess hydrazine were distilled). After cooling, potassium hydroxide (45.8 g, 818.4 mmol) was added to the reaction mixture and heating was continued at 200–210°C for 6 h. The cooled reaction mixture was added to water (300 mL), extracted with ether (2 × 250 mL), washed with brine, and dried over sodium sulfate. The solvent was removed and the residue was purified on a silica gel column using petroleum ether as eluant to give the ketone-free compound **17** (24.5 g, 87%) as a colorless oil; ir ν_{max} (neat): 3035, 2995, 2925, 2860, 1470, 1385 cm^{-1}; ^{1}Hmr δ: 0.07 (1H, dd, *J* = 8, 5, C8), 0.40 (1H, dd, *J* = 10, 5, C8), 0.81 (3H, d, *J* = 7), 0.89 (3H, d, *J* = 7), 0.96 (3H, d, *J* = 7, C13), 0.95 (3H, s), 1.10–1.63 (12H, m); ms *m/z*: 206 (M^+, 15%), 191 (35%), 163 (100%), 123 (40%), 110 (24%), 95 (32%), 81 (41%), 55 (60%). High resolution molecular weight determination calcd. for $C_{15}H_{26}$: 206.2034; found: 206.2033. Anal. calcd. for $C_{15}H_{26}$: C 87.30, H 12.70; found: C 87.24, H 12.75.

*(5β)-4α,10β-Dimethyl-7α-isopropinoltricyclo[4.4.0^{5,10}.0^{7,9}]decane (**18**) and (5β)-7α-acetyl-4α,10β-dimethyltricyclo[4.4.0^{5,0}.0^{7,9}]-decane (**19**)*

Ozone was bubbled through a solution of **17** (24 g, 116.5 mmol) in ethyl acetate (500 mL) containing sodium bicarbonate (9.8 g) at −40°C (acetonitrile/Dry Ice bath) for 8 h. The excess ozone was removed under a stream of argon and then dimethyl sulfide (5 mL) was added to the solution. The reaction mixture was allowed to warm to room temperature and stirred for 1 h. Filtration and concentration, followed by flash chromatography on a silica gel column (hexanes–ethyl acetate as eluant, 17:3, v/v), provided alcohol **18** (10 g, 38.7%), ketone **19** (7.7 g, 32.3%), and starting material **17** (6.9 g, 28.7%). The total yield was 71% based on the recovered starting material. Alcohol **18**: ir ν_{max} (neat): 3405, 3050, 2903, 2850, 1140 cm^{-1}; ^{1}Hmr δ: 0.43 (1H, dd, *J* = 5, 4, C8), 0.48 (1H, dd, *J* = 6, 4, C8), 0.83 (3H, d, *J* = 6), 0.98 (3H, s), 1.18 (3H, s), 1.27 (3H, s), 1.00–1.51 (10H, m), 1.62 (1H, O-H), 1.75 (1H, t, *J* = 12); ms *m/z*: 222 (M^+, 2.1%), 204 ($M^+ - H_2O$, 17%), 189 (18%), 161 (28%), 133 (30%), 119 (13%), 105 (49%), 95 (100%), 91 (57%), 81 (59%), 67 (37%), 59 (27%), 55 (37%), 41 (63%), 32 (30%). High resolution molecular weight determination calcd. for $C_{15}H_{26}O$: 222.1984; found: 222.1982. Anal. calcd. for $C_{15}H_{26}O$: C 81.02, H 11.78; found: C 80.80, H 11.53.

For ketone **19**: ir ν_{max} (neat): 3000, 2925, 2859, 1680 cm^{-1}; ^{1}Hmr δ: 0.86 (3H, d, *J* = 6), 1.03 (3H, s), 1.04–1.73 (12H, m), 2.03 (3H, s), 2.10 (1H, t, *J* = 12); ms *m/z*: 206 (M^+, 17%), 191 (10%), 177 (2%), 163 (19%), 95 (25%), 81 (42%), 43 (100%). High resolution molecular weight determination calcd. for $C_{14}H_{22}O$: 206.1671; found: 206.1662. Anal. calcd. for $C_{14}H_{22}O$: C 81.50, H 10.75; found: C 81.56, H 10.90.

*(5β)-4α,10β-Dimethyl-7α-(1'-hydroxyethyl)-tricyclo[4.4.0^{5,10}.0^{7,9}]-decane (**24**)*

To a solution of ketone **19** (5.2 g, 25 mmol) in methanol (70 mL) was added sodium borohydride (0.58 g, 15 mmol) at 0°C. The reaction mixture was stirred at 0°C for 20 min, then the methanol was evaporated. Ether was added to the residue and the solution was washed with water and brine. The solvent was removed under reduced pressure and the residue was purified by chromatography on a silica gel column (ether/pet. ether as eluant, 1:1, v/v) to afford alcohol **24** (4.8 g, 93%) as a colorless oil; ir ν_{max} (neat): 3325, 3050, 2900, 1100 cm^{-1}; ^{1}Hmr δ: 0.24 (1H, dd, *J* = 9, 5, C8), 0.56 (1H, dd, *J* = 6, 5, C8), 0.82 (3H, d, *J* = 7), 0.98 (3H, s), 1.21 (3H, d, *J* = 7), 0.88–1.67 (11H, m), 1.72 (1H, t, *J* = 11), 3.42 (1H, q, *J* = 7).

*(5β)-8-Chloromethyl-4α,9β-dimethyl-7α-isopropylidenebicyclo-[4.3.0^{5,9}]nonane (**20**)*

Compound **18** (6.08 g, 27.4 mmol) was dissolved in dichloromethane (150 mL) and added to ice-cold concentrated hydrochloric acid (150 mL). The mixture was stirred rapidly at 0°C for 2 h. The mixture was poured into water (200 mL), and the aqueous layer was extracted with dichloromethane (3 × 70 mL). The combined organic extracts were washed with saturated aqueous sodium bicarbonate solution (2 × 70 mL), dried over sodium sulfate, and the solvent was evaporated. The yellow oil was carried over to the next step without purification; ir ν_{max} (neat): 2905, 2850, 1654, 718 cm^{-1}; ^{1}Hmr δ: 0.87 (3H, d, *J* = 7), 1.14 (3H, s), 1.65 (3H, s), 1.73 (3H, s), 0.89–1.59 (7H, m), 1.90 (1H, m), 2.11 (2H, d, *J* = 10, C6), 2.50 (1H, m, C8), 3.45 (1H, dd, *J* = 11, 4, C10), 3.61 (1H, dd, *J* = 11, 8, C10); ms *m/z*: 242/240 (M^+, 3/11%), 227/225 (1/5%), 204 (45%), 197 (20%), 189 (52%), 161 (100%), 147 (25%), 133 (44%), 119 (60%), 105 (52%), 95 (57%), 91 (58%), 83 (24%), 79 (35%), 61, 55 (45%), 41 (84%). High resolution molecular weight determination calcd. for $C_{15}H_{25}{}^{35}Cl$: 240.1656; found: 240.1650.

Compound **21** was prepared from **24** as described for **20**. The crude oily product was carried over to the next step without purification.

*(5β)-4α,10β-Dimethyl-7-isopropylidenebicyclo[4.4.0^{5,10}]decane (**22**)*

To a solution of crude **20** in dry toluene (250 mL) under argon was added tri-*n*-butyltin hydride (11.9 g, 41.1 mmol). AIBN (300 mg, 1.9 mmol) was then added and the reaction mixture was heated at reflux under argon for 2 h. A further portion of AIBN (300 mg) was added and the reaction maintained at gentle reflux for an additional 6 h. The solvent was evaporated and the residue chromatographed on silica gel with hexanes to give **22** (3.16 g, 56%, calculated from **18**), as a colorless oil; ir ν_{max} (neat): 2920, 1660 cm^{-1}; ^{1}Hmr δ: 0.88 (3H, d, *J* = 7), 0.94 (3H, s), 1.11–1.62 (10H, m), 1.65 (3H, s), 1.66 (3H, s), 1.83–1.98 (2H, m), 2.41 (2H, m); ms *m/z*: 206 (M^+, 3%), 191 (2%), 163 (6%), 109 (9%), 95 (7%), 81 (22%), 67 (10%), 55 (11%), 41 (17%), 17 (100%). High resolution molecular weight determination calcd. for $C_{15}H_{26}$: 206.2034; found: 206.2037. Anal. calcd. for $C_{15}H_{26}$: C 87.30, H 12.70; found: C 87.05, H 12.60.

Compound **23** was prepared from **21** as described for **22**. The total

Can. J. Chem. Downloaded from www.nrcresearchpress.com by 91.121.58.235 on 09/07/12
For personal use only.

yield from **24** to **23** was 53%; ir ν_{max} (neat): 2950, 2930, 2859, 1660, 829 cm^{-1}. Partial ^{1}Hmr (1:1 C11 isomer) δ: 0.83, 0.87 (3H, two sets, d, J = 6), 0.95 (3H, two sets, s), 1.56 (3H, two sets, d, J = 4, C12), 5.13 (1H, two sets, m, C11); ms m/z: 192 (M^+, 42%), 177 (28%), 163 (39%), 109 (100%), 95 (41%), 81 (58%), 67 (38%), 55 (27%), 41 (34%). High resolution molecular weight determination for $C_{14}H_{24}$: 192.1878; found: 192.1870.

(5β)-4α,10β-Dimethyl-octahydro-7-(6H)-naphthalenone (25)

Ozone was bubbled through a solution of **22** (2.30 g, 11.2 mmol) in ethyl acetate (70 mL) at −60°C. After 20 min, the system was flushed with argon until there was no blue color in the solution, and dimethyl sulfide (1.12 mL, 15.2 mmol) was added. The solution was then allowed to warm up slowly to 0°C in 1 h, then stirred at ice bath temperature for 1 h, and finally at room temperature for 1 h. The solvent was removed and the residue was purified by flash chromatography (ether/pet. ether, 2:8, v/v) to give decalone **25** (1.83 g, 91%) as a colorless oil.

23 provided **25** in the same way to give a yield of 90%; $[\alpha]_D^{18}$ +12.9° (*c* 0.940, methanol); ir ν_{max} (neat): 2900, 2845, 1705 cm^{-1}; ^{1}Hmr δ: 0.80 (3H, d, J = 7, C11), 1.05 (3H, s, C12), 1.06–2.03 (10H, m), 2.12–2.56 (4H, m); ms m/z: 180 (M^+, 10%), 123 (9%), 109 (23%), 95 (17%), 81 (14%), 69 (14%), 55 (13%), 41 (15%), 31 (100%). High resolution molecular weight determination calcd. for $C_{12}H_{20}O$: 180.1514; found: 180.1514. Anal. calcd. for $C_{12}H_{20}O$: C 79.94, H 11.18; found: C 80.00, H 11.30.

(5β)-7α-Acetyl-4α,10β-dimethyltricyclo[4.4.0^{5,10}.0^{7,9}]dec-3-one (26)

Diketone **26** was obtained in the process of "wet" ozonation as described earlier ("wet" ozonation of thujone); ir ν_{max} ($CHCl_3$): 1713, 1680 cm^{-1}; ^{1}Hmr δ: 0.98 (3H, d, J = 6.4), 1.06 (1H, t, J = 4.8), 1.33 (3H, s), 1.38 (1H, dd, J = 4.8, 8.0), 1.65–2.00 (6H, m), 2.07 (3H, s), 2.46 (1H, m), 2.64 (1H, m); ms m/z: 220 (M^+, 15.3%), 205 (3.2%), 177 (10.4%), 43 (100%). High resolution molecular weight determination calcd. for $C_{14}H_{20}O_2$: 220.1463; found: 220.1461. Anal. calcd. for $C_{14}H_{20}O_2$: C 76.33, H 9.15; found: C 76.28, H 9.13.

*4α,10β-Dimethyl-*cis*-perhydro-7-oxonaphthalene-8-carboxaldehyde (29)*

The formylation of **25** was performed by suspending potassium hydride (1.33 g, 33.3 mmol) in dry THF (120 mL). To this suspension was added a mixture of **25** (6.00 g, 33.3 mmol) and ethyl formate (5.00 g, 66.6 mmol) in dry THF (10 mL) over 5 min. After stirring at room temperature for 20 min, the solvent was evaporated and ether (100 mL) was added to the residue. The ethereal solution was extracted twice with 4 N potassium hydroxide (50 mL). The combined alkaline solution was acidified with concentrated hydrochloric acid and extracted with ether. The ethereal solution was washed with brine and dried. Evaporation of ether gave **29** (6.17 g, 89%) as a light yellow liquid; $[\alpha]_D^{23}$ 0.575° (*c* 1.980, methanol); ir ν_{max} (neat): 3350, 2920, 2850, 1650, 1600 cm^{-1}; ^{1}Hmr δ: 0.85 (3H, d, J = 6), 1.09 (3H, s), 0.88–1.63 (8H, m), 2.05 (2H, d, J = 15, C9), 2.28 (2H, dd, J = 8.4, C6), 8.56 (1H, s, olefin-H), 14.29 (1H, s, O-H); ms m/z: 208 (M^+, 31%), 190 (5%), 178 (6%), 110 (50%), 95 (100%). High resolution molecular weight determination calcd. for $C_{13}H_{20}O_2$: 208.1463; found: 208.1462.

4α,10β-Dimethyl-1,2,3,4,5β,6,7,10-octahydro-7-oxonaphthalene-8-carboaldehyde (30)

To an ice-cooled solution of benzene selenenyl chloride (5.68 g, 29.7 mmol) in dichloromethane (300 mL) were added pyridine (2.58 g, 32.6 mmol) and **29** (6.17 g, 29.7 mmol) in dichloromethane (25 mL). The reaction mixture was stirred for 1 h and washed with 4 N hydrochloric acid (25 mL) and brine (25 mL). The dichloromethane solution was cooled to 0°C, 30% hydrogen peroxide (4.5 mL) was added in three portions with intervals of 20 min, and the reaction was stirred at 0°C for another 30 min. The solvent was then evaporated and the residue was purified by column chromatography on silica gel using pet. ether/ether (4:1 v/v) as eluant to give **30** (5.26 g, 86%) as a colorless oil; $[\alpha]_D^{20}$ 96.16° (*c* 1.016, methanol); uv λ_{max}: 238, (3.836); ir ν_{max} (neat): 2920, 2856, 1680, 1617 cm^{-1}; ^{1}Hmr δ: 0.91 (3H, d, J = 7), 1.21 (3H, s), 1.07–2.05 (8H, m), 2.42 (2H, m, C6), 7.45 (1H, s, C9), 10.09 (1H, s, aldehyde-H); ms m/z: 206 (M^+, 26%), 191 (29%), 178 (70%), 110 (87%), 95 (100%), 55 (13%), 41 (20%). High resolution molecular weight determination calcd. for $C_{13}H_{18}O_2$: 206.1307; found: 206.1303. Anal. calcd. for $C_{13}H_{18}O_2$: C 75.67, H 8.79; found: C 75.55, H 8.94.

*4α,10β-Dimethyl-8-(hydroxymethylene)-*cis*-perhydro-7-oxonaphthalene-9-carbonitrile (31)*

To a solution of **30** (3.00 g, 14.6 mmol) in dioxane (43 mL) and water (4.3 mL) was added a solution of potassium cyanide (0.949 g, 14.6 mmol) in dioxane (4.3 mL) and water (1 mL). The reaction mixture was stirred at room temperature for 30 min, and then the dioxane was evaporated. The residue was treated with 4 N potassium hydroxide (20 mL) and extracted with ether. The basic solution was acidified with concentrated hydrochloric acid (5 mL) and washed with ether. The ethereal solution was washed with brine and dried. The ether was evaporated to give crude **31** (2.41 g, 71%) as a yellow oil; ir ν_{max} (neat): 3621, 3019, 2964, 2933, 2236, 1220 cm^{-1}. ^{1}Hmr δ: 0.91 (3H, d, J = 5), 1.15 (3H, s), 1.22–2.00 (8H, m), 2.53 (1H, d, J = 20, C6), 2.56 (1H, dd, J = 20, 5, C6), 4.01 (1H, s, C9), 8.98 (1H, s, olefin-H), 15.04 (1H, s, O-H); ms m/z: 233 (M^+, 8%), 215 (1%), 206 (5%), 178 (21%), 110 (78%), 95 (100%), 81 (26%), 77 (30%), 67 (31%), 53 (36%), 41. High resolution molecular weight determination calcd. for $C_{14}H_{19}NO_2$: 233.1415; found: 233.1415.

*8-[(Butylthio)methylene]-4α,8aβ-dimethyl-*cis*-perhydro-7-oxonaphthalene-9-carbonitrile (32)*

A solution of **31** (2.41 g, 10.4 mmol), 1-butanethiol (1.0 mL), and *p*-toluenesulfonic acid (14 mg) in dry benzene (60 mL) was refluxed for 3 h in a Dean–Stark apparatus. After cooling, the reaction mixture was washed with saturated sodium bicarbonate solution (10 mL), water (10 mL), and brine (10 mL), and dried. The benzene was evaporated and the residue was purified by column chromatography on silica gel using ether/pet. ether (3:7 v/v) as eluant to give compound **32** (2.77 g, 88%) as white crystals; mp 85–86°C, ir ν_{max} ($CHCl_3$): 2990, 2950, 2933, 2852, 2220, 1660, 1545 cm^{-1}; ^{1}Hmr δ: 0.85 (3H, d, J = 6), 0.95 (3H, t, J = 8), 1.38 (3H, s), 1.02–2.25 (12H, m), 2.32 (1H, dd, J = 20, 10, C6), 2.43 (1H, dd, J = 20, 8, C6), 2.94 (2H, t, J = 8, S-CH_2), 3.37 (1H, s, C9), 7.89 (1H, s, olefin-H); ms m/z: 305 (M^+, 17%), 248 (38%), 217 (20%), 109 (100%), 89 (32%), 67 (29%), 55 (50%), 44 (12%). High resolution molecular weight determination calcd. for $C_{18}H_{27}NOS$: 305.1805; found: 305.1809. Anal. calcd. for $C_{18}H_{27}NOS$: C 70.77, H 8.91, N 4.59, S 10.50; found: C 70.63, H 8.72, N 4.41, S 10.39.

4α,10β-Dimethyl-8-formyl-1,2,3,4,5β,6,9,10-octahydronaphthalene-9-carbonitrile (33)

To a solution of **32** (1.623 g, 5.3 mmol) in methanol (15 mL) was added sodium borohydride (62 mg, 1.6 mmol) at 0°C. The reaction mixture was stirred for 15 min, and then the methanol was evaporated. Ether was added to the residue, and the solution was washed with water and brine. The ether was evaporated and the residue was dissolved in methanol (25 mL). Mercuric chloride (2.44 g, 9.0 mmol) and 4 N hydrochloric acid (7.5 mL) were added to this solution. The reaction mixture was stirred at room temperature for 16 h, and then filtered. The methanol was evaporated, and ether (100 mL) was added. The ethereal solution was washed with saturated sodium bicarbonate solution and with brine, and dried. The ether was evaporated, and the residue was purified by column chromatography on silica gel using ether/pet. ether (3:7 v/v) as eluant to give **33** (0.712 g, 84%) as white crystals; mp 103–104.5°C; $[\alpha]_D^{15}$ 149.8° (*c* 0.990, methanol); uv λ_{max}: 224, (4.129); ir ν_{max} ($CHCl_3$): 2915, 2850, 2220, 1683, 1659 cm^{-1}; ^{1}Hmr δ: 0.91 (3H, d, J = 5), 1.36 (3H, s), 1.05–2.13 (8H, m), 2.31 (1H, ddd, J = 20, 9, 4, C6), 2.45 (1H, ddd, J = 20, 8, 4, C6), 3.30 (1H, s, C9), 7.05 (1H, dd, J = 4, 4, C7), 9.51 (1H, s, aldehyde-H); ms m/z: 217 (M^+, 12%), 200 (10%), 190 (30%), 146 (21%), 110 (98%), 105 (39%), 95 (100%), 81 (23%), 77 (21%), 55 (31%), 41 (50%). High resolution molecular weight determination calcd. for $C_{14}H_{19}NO$: 217.1471; found: 217.1469.

Can. J. Chem. Downloaded from www.nrcresearchpress.com by 91.121.58.235 on 09/07/12
For personal use only.

*4α,10β-Dimethyl-8-(1,3-dioxolan-2-yl)-1,2,3,4,5β,6,9,10-octahydronaphthalene-9-carbonitrile (**34**) and 4α,10β-dimethyl-8-(1,3-dioxolan-2-yl)-1,2,3,4,5β,8,9,10-octahydro-naphthalene-9-carbonitrile (**35**)*

A solution of **33** (712 mg, 3.3 mmol), ethylene glycol (0.83 mL), and *p*-toluenesulfonic acid (5 mg) in benzene (9 mL) was refluxed for 3 h in a Dean–Stark apparatus. The reaction mixture was cooled, ether (50 mL) was added, and the solution was washed with saturated sodium bicarbonate solution and dried. The solvent was evaporated and the residue was purified by column chromatography on silica gel using ether/pet. ether (3:7 v/v) as eluant to give **34** (615 mg, 71%) and **35** (156 mg, 18%).

Compound **34**: $[\alpha]_D^{15}$ 109.6° (*c* 0.920, methanol); ir ν_{max} (neat): 2950, 2900, 2220, 1680 cm^{-1}; ^{1}Hmr δ: 0.79 (3H, d, *J* = 7), 1.24 (3H, s), 0.85–2.14 (10H, m), 2.79 (1H, s, C9), 3.85–4.04 (4H, m), 5.19 (1H, s), 6.05 (1H, dd, *J* = 4, 4, C7); ms *m/z*: 261 (M^+, 12%), 246 (6%), 221 (3%), 138 (21%), 110 (47%), 95 (73%), 86 (100%), 73 (84%), 55 (18%), 41 (23%). High resolution molecular weight determination calcd. for $C_{16}H_{23}NO_2$: 261.1729; found: 261.1724. Anal. calcd. for $C_{16}H_{23}NO_2$: C 73.53, H 8.87, N 5.36; found: C 73.31, H 8.98, N 5.36.

Compound **35**: ^{1}Hmr δ: 0.84 (3H, d, *J* = 7), 1.30 (3H, s), 1.19–2.32 (9H, m), 2.85 (1H, d, *J* = 4, C9), 3.83–4.05 (4H, m), 5.14 (1H, d, *J* = 6, C8), 5.53 (1H, dd, *J* = 10, 2, olefin-H), 6.02 (1H, dd, *J* = 10, 2, olefin-H).

*4α,10β-Dimethyl-8-(1,3-dioxolan-2-yl)-1,2,3,4,5β,6,9,10-octahydronaphthalene-9-carboxaldehyde (**36**) and 4α,10β-dimethyl-8-(1,3-dioxolan-2-yl)-1,2,3,4,5β,8,9,10-octahydronaphthalene-9-carboxaldehyde (**37**)*

A solution of **34** (250 mg, 0.96 mmol) in dry toluene (19 mL) was cooled to −60°C under argon, and a solution of diisobutylaluminum hydride (1.0 M, hexane solution) (1.80 mL) was added. The reaction mixture was stirred at −60°C for 3 h and then poured into saturated ammonium chloride solution (15 mL). The layers were separated and the aqueous layer was extracted 5 times with ether (100 mL). The combined organic solutions were dried, and the solvent was evaporated. The residue was purified by column chromatography on silica gel using ether/pet. ether (3:7 v/v) as eluant to give **36** (215 mg, 85%) as a colorless oil; $[\alpha]_D^{21}$ 311° (*c* 0.820, methanol); ir ν_{max} (neat): 2900, 2835, 2690, 1705, 1655 cm^{-1}; ^{1}Hmr δ: 0.84 (3H, d, *J* = 7), 1.10 (3H, s), 0.93–2.25 (10H, m), 2.67 (1H, d, *J* = 5, C9), 3.80–4.10 (4H, m), 5.16 (1H, s, C11), 6.20 (1H, dd, *J* = 4, 4, C7), 9.50 (1H, d, *J* = 5, aldehyde-H); ms *m/z*: 264 (M^+, 1%), 249 (0.5%), 235 (44%), 73 (100%), 55 (23%), 45 (40%), 41 (34%). High resolution molecular weight determination calcd. for $C_{16}H_{24}O_3$: 264.1726; found: 264.1723. Anal. calcd. for $C_{16}H_{24}O_3$: C 72.70, H 9.15; found: C 73.00, H 9.30.

Compound **35** (188 mg, 0.72 mmol) in toluene (15 mL) was reduced by DIBAH (toluene solution, 1.5 M) (1.3 mL) at −78°C in 2 h by the above procedure to give **37**. The crude product was hydrolyzed in the next reaction without further purification.

*4α,10β-Dimethyl-1,2,3,4,5β,6,9,10-octahydronaphthalene-9,8-dicarboxaldehyde (**38**)*

A solution of **36** (92 mg, 0.35 mmol) and *p*-toluenesulfonic acid (8 mg) in acetone (7 mL) and water (1.7 mL) was stirred for 2 h at room temperature. The acetone was evaporated, and water/ether were added. The aqueous layer was extracted with ether, and the combined ethereal solution was washed with saturated sodium bicarbonate solution, with water, and brine, and then dried. The ether was evaporated and the residue was chromatographed on silica gel using ether/pet. ether (3:7 v/v) as eluant to give **38** (71 mg, 93%) as a colorless oil; $[\alpha]_D^{16}$ 393° (*c* 0.700, methanol); uv λ_{max}: 229 (4.026); ir ν_{max} (neat): 2920, 2860, 2820, 2715, 1718, 1665, 1300 cm^{-1}; ^{1}Hmr δ: 0.86 (3H, d, *J* = 7), 1.26 (3H, s), 1.05–2.50 (10H, m), 3.33 (1H, d, *J* = 3, C9), 7.09 (1H, dd, *J* = 4, 4, C7), 9.44 (1H, s, C8-aldehyde-H), 9.79 (1H, d, *J* = 3, C9-aldehyde-H); ms *m/z*: 220 (M^+, 1%), 202 (2%), 192 (70%), 177 (20%), 121 (42%), 109 (44%), 95 (100%), 91 (67%), 81 (56%), 77 (57%), 67 (45%), 55 (46%), 41 (50%). High resolution molecular weight determination calcd. for $C_{14}H_{20}O_2$: 220.1461; found: 220.1462. Anal. calcd. for $C_{14}H_{20}O_2$: C 76.33, H 9.15; found: C 76.38, H 9.20.

Crude **37** from last step in acetone (15 mL), water (3.6 mL), and 1 N hydrochloric acid (2 mL) was refluxed for 6 h to give **38** (121 mg, 77% from **35**).

*7-Isopropyl-4,4,10β-trimethyl-1,4,9,10-tetrahydro-3-(2H)-naphthalenone (**40**) and 7-isopropenyl-4,4,10β-trimethyl-1,4,7,8,9,10-hexahydro-3-(2H)naphthalenone (**41**)*

To a mixture of β-cyperone (11.7 g) and dry DMSO (90 mL) at room temperature and under argon atmosphere, was added sodium methoxide (8.5 g). After stirring for 1 h, methyl iodide (15 mL) was added. The reaction mixture was stirred for 0.5 h. It was then poured into 1 N HCl (400 mL) and extracted with ether (3 × 500 mL). The combined ethereal layers were washed with water, dried over sodium sulfate, filtered, and evaporated to give an oil, which was chromatographed on silica gel to give a mixture of **40** and **41** (4.82 g, 39% isolated yield or 61% based on recovered starting material) and starting material **39** (4.22 g, 36%).

Analytical samples of **40** and **41** were obtained by subjecting the mixture to preparative tlc (2% ethyl ether in petroleum ether as eluting solvent, eight developments). In this manner, pure **40** was isolated as the more mobile compound. Compound **40**: ir ν_{max} ($CHCl_3$): 1710, 1660 (w), 1605 (w) cm^{-1}; uv (methanol) λ_{max}: 266 nm (ε 5 600); ^{1}Hmr δ: 1.01 (3H, s), 1.02 (3H, d, *J* = 7.2), 1.03 (3H, d, *J* = 7.2), 1.31 (6H, s), 5.38 (1H, br d, *J* = 5.8), 5.80 (1H, s); ms *m/z*: 232 (M^+, 58%), 217 (13%), 189 (35.5%), 175 (100%). High resolution molecular weight determination calcd. for $C_{16}H_{24}O$: 232.1829; found: 232.1827. Anal. calcd. for $C_{16}H_{24}O$: C 82.71, H 10.41; found: 82.91, H 10.40.

Compound **41**: ir ν_{max} ($CHCl_3$): 1710, 1605 (w) cm^{-1}; uv (methanol) λ_{max}: 251 nm (ε 18 000); ^{1}Hmr δ: 1.04 (3H, s), 1.31 (6H, s), 1.77 (3H, s), 1.82 (3H, s), 6.40 (1H, s); ms *m/z*: 232 (M^+, 100%), 217 (64%), 189 (78%), 175 (19%). High resolution molecular weight determination calcd. for $C_{16}H_{24}O$: 232.1829; found: 232.1828. Anal. calcd. for $C_{16}H_{24}O$: C 82.71, H 10.41; found: C 82.90, H 10.45.

*7-Isopropenyl-4,4,10β-trimethyl-1,4,7,8,9,10-hexahydro-3-(2H)-naphthalenone (**41**) by isomerization of a mixture of **40** and **41***

A mixture of **40** and **41** (5.38 g), iodine (550 mg), and hexane (110 mL) was heated under reflux for 1 h. The mixture was poured into saturated sodium thiosulfate (300 mL) and then extracted with ether (3 × 500 mL). The combined organic layers were washed with water, dried over sodium sulfate, filtered, and evaporated to give an oil, which was purified on a silica gel column to afford **41** (4.6 g, 86%) as a slightly yellow oil.

*7-Isopropenyl-4,4,10β-trimethyl-1,2,3,4,7,8,9,10-octahydronaphthalene (**42**)*

A mixture of **41** (4.94 g), hydrazine monohydrate (5 mL), potassium hydroxide (3.2 g), and diethylene glycol (40 mL) was heated under reflux at 135°C for 1 h. Then the temperature of the reaction mixture was slowly raised to 205–210°C. Volatile materials were removed with a Dean–Stark trap. After stirring for 1 h at 205–210°C, the mixture was cooled, poured into water (200 mL), and extracted with petroleum ether (3 × 200 mL). The combined organic layers were washed with water, dried over sodium sulfate, filtered, and evaporated to leave an oil, which was chromatographed on a silica gel column to afford **42** (3.94 g, 85%) as a colorless oil; uv (methanol) λ_{max}: 250 nm (ε 20 000); ^{1}Hmr δ: 1.13 (3H, s), 1.15 (3H, s), 1.16 (3H, s), 1.73 (3H, s), 1.81 (3H, d, *J* = 2.0), 6.35 (1H, s); ms *m/z*: 218 (M^+, 100%), 203 (96%), 175 (21%). High resolution molecular weight determination calcd. for $C_{16}H_{26}$: 218.2035; found: 218.2037. Anal. calcd. for $C_{16}H_{26}$: C 88.00, H 12.00; found: 87.99, H 12.10.

*4,4,10β-Trimethyl-1,2,3,4,9,10-hexahydro-7-(8H)-naphthalenone (**43**)*

Diene **42** (3.94 g) in a mixture of dichloromethane–methanol (9:1, 500 mL) was ozonized at −78°C for 20 min. Then dimethyl sulfide

(20 mL) was added. The reaction mixture was allowed to warm up to room temperature and stirred at room temperature for 3 h. Removal of solvents followed by chromatography on a silica gel column afforded recovered starting material (475 mg) and enone **43** (2.14 g, 70% based on recovered starting material) as a yellow oil; ir ν_{max}: 1660, 1600 cm^{-1}; uv (methanol) λ_{max}: 241 nm (ε 13 200); ^{1}Hmr δ: 1.15 (3H, s), 1.19 (3H, s), 1.34 (3H, s), 5.96 (1H, s); ms *m/z*: 192 (M^+, 86%), 177 (14%), 164 (30%), 149 (51%), 136 (75%), 123 (100%). High resolution molecular weight determination calcd. for $C_{13}H_{20}O$: 192.1514; found: 192.1507.

Acknowledgements

Financial aid from the Natural Sciences and Engineering Research Council of Canada, Intrinsic Research and Development Inc., and the National Research Council of Canada (IRAP Program) is gratefully acknowledged.

1. C. CARVALHO, W. R. CULLEN, M. D. FRYZUK, H. JACOBS, B. R. JAMES, J. P. KUTNEY, K. PIOTROWSKA, and V. K. SINGH. Helv. Chim. Acta, **72**, 205 (1989).
2. T. A. VAN BEEK and A. DE GROOT. Recl. Trav. Chim. Pays-Bas, **105**, 513 (1986).
3. A. DE GROOT and T. A. VAN BEEK. Recl. Trav. Chim. Pays-Bas, **106**, 1 (1987).
4. J. P. KUTNEY, J. BALSEVICH, and P. GRICE. Can. J. Chem. **58**, 2641 (1980).
5. Z. COHEN, E. KEINAN, Y. MAZUR, and T. H. VARKONY. J. Org. Chem. **40**, 2141 (1975).
6. D. TAL, E. KEINAN, and Y. MAZUR. J. Am. Chem. Soc. **101**, 502 (1979).
7. J. P. MCCORMICK and D. L. BARTON. J. Chem. Soc. Chem. Commun. 303 (1975).
8. J. P. MCCORMICK, A. S. FITTERMAN, and D. L. BARTON. J. Org. Chem. **46**, 4708 (1981).
9. J. P. MCCORMICK and D. L. BARTON. J. Org. Chem. **45**, 2566 (1980).
10. B. J. M. JANSEN, H. H. W. J. M. SENGERS, H. J. T. BOS, and A. DE GROOT. J. Org. Chem. **53**, 855 (1988).
11. D. LIOTTA, C. BARNUM, R. PULEO, G. ZIMA, C. BAYER, and H. S. KEZAR. J. Org. Chem. **46**, 2920 (1981).
12. International tables for X-ray crystallography. Vol. IV. Kynoch Press, Birmingham, U.K. 1974. pp. 99–102 and 149.

Appendix

X-ray crystallographic analysis of ***26***

A crystal ca. 0.10 × 0.25 × 0.33 mm in size was mounted in a general orientation. Unit-cell parameters were refined by least squares on setting angles for 25 reflections (2θ = 50.1–94.2°) measured on a diffractometer with Cu-K_α radiation (λ = 1.54178 Å). Crystal data at 21°C are as follows:

$C_{14}H_{20}O_2$ f.w. = 220.31

Orthorhombic, a = 6.165(2), b = 12.649(1), c = 15.997(1) Å, V = 1247.5(4) Å^3, Z = 4, ρ_c = 1.173 Mg m^{-3}, $F(000)$ = 480, μ(Cu-K_α) = 5.70 cm^{-1}. Absent reflections ($h00$, h odd; $0k0$, k odd; and $00l$, l odd) uniquely indicate the space group $P2_12_12_1$.

Intensities were measured with graphite-monochromated Cu-K_α radiation on a Rigaku AFC6S diffractometer. An ω–2θ scan at 8° min^{-1} over a range of (1.25 + 0.30 tan θ)° in ω (with up to eight rescans, background/scan time ratio = 0.5) was employed. Data were measured to 2θ = 150°. The intensities of three check reflections, measured every 150 reflections throughout the data collection, showed only small random fluctuations. After data reduction,[3] an empirical absorption correction, based on azimuthal scans for three reflections, was applied, which resulted in transmission factors ranging from 0.95 to 1.00. Of the 1307 independent reflections measured, 1083 (82.9%) had intensities greater than or equal to $3\sigma(F^2)$ above background where $\sigma^2(F^2) = [S^2(C + 4B) + (0.04F^2)^2]/(Lp)^2$ with S = scan rate, C = scan count, B = total background count, and Lp = Lorentz polarization factor.

The structure was solved by direct methods, the coordinates of all 16 non-hydrogen atoms being determined from an E-map. Hydrogen atoms were positioned from a subsequent difference Fourier synthesis. The non-hydrogen atoms were refined with anisotropic thermal parameters and the hydrogen atoms with isotropic thermal parameters. Scattering factors for all atoms and anomalous dispersion corrections for the non-hydrogen atoms were taken from ref. 12. The weighting scheme $w = 4F_o^2/\sigma^2(F_o^2)$ gave uniform average values of $w(|F_o| - |F_c|)^2$ over ranges of both $|F_o|$ and sin θ/λ and was employed in the final stages of full-matrix least-squares refinement of 226 variables. Reflections with $I < 3\sigma(I)$ were not included in the refinement. Convergence was reached at R = 0.032 and R_w = 0.047 for 1083 reflections with $I \geq 3\sigma(I)$. The

TABLE 1. Final atomic coordinates (fractional) and B_{eq}

Atom	*x*	*y*	*z*	B_{eq}
O(1)	−0.0396(5)	0.1597(2)	0.4315(2)	7.3(1)
O(2)	−0.1521(5)	0.2163(2)	0.0926(2)	8.0(1)
C(1)	−0.0083(5)	0.3978(3)	0.3234(2)	4.8(1)
C(2)	−0.0179(6)	0.3454(3)	0.4098(2)	5.8(1)
C(3)	0.0637(5)	0.2337(3)	0.4052(2)	5.2(1)
C(4)	0.2869(5)	0.2228(2)	0.3693(2)	4.4(1)
C(5)	0.3025(4)	0.2787(2)	0.2839(1)	3.7(1)
C(6)	0.1824(5)	0.2227(2)	0.2123(1)	4.0(1)
C(7)	0.1422(4)	0.3072(2)	0.1471(1)	3.8(1)
C(8)	0.3372(5)	0.3758(2)	0.1259(2)	4.6(1)
C(9)	0.1799(4)	0.4148(2)	0.1895(1)	3.9(1)
C(10)	0.2170(4)	0.3939(2)	0.2824(1)	3.7(1)
C(11)	−0.0379(5)	0.2924(2)	0.0872(2)	4.6(1)
C(12)	−0.0791(6)	0.3723(3)	0.0202(2)	5.1(1)
C(13)	0.3679(7)	0.1104(3)	0.3662(2)	5.8(2)
C(14)	0.3739(6)	0.4709(3)	0.3226(2)	5.1(1)

TABLE 2. Bond lengths (Å) with estimated standard deviations in parentheses

Atom–atom	Distance	Atom–atom	Distance
O(1)—C(3)	1.208(4)	C(5)—C(10)	1.550(3)
O(2)—C(11)	1.196(3)	C(6)—C(7)	1.513(3)
C(1)—C(2)	1.534(4)	C(7)—C(8)	1.521(3)
C(1)—C(10)	1.537(4)	C(7)—C(9)	1.539(3)
C(2)—C(3)	1.502(5)	C(7)—C(11)	1.478(4)
C(3)—C(4)	1.497(4)	C(8)—C(9)	1.490(4)
C(4)—C(5)	1.541(3)	C(9)—C(10)	1.525(3)
C(4)—C(13)	1.508(4)	C(10)—C(14)	1.517(4)
C(5)—C(6)	1.536(3)	C(11)—C(12)	1.495(4)

[3]TEXSAN/TEXRAY structure analysis package which includes versions of the following: MITHRIL, integrated direct methods, by C. J. Gilmore; DIRDIF, direct methods for difference structures, by P. T. Beurskens; ORFLS, full-matrix least squares, and ORFFE, function and errors, by W. R. Busing, K. O. Martin, and H. A. Levy; ORTEP II, illustrations, by C. K. Johnson.

Can. J. Chem. Downloaded from www.nrcresearchpress.com by 91.121.58.235 on 09/07/12
For personal use only.

TABLE 3. Bond angles (deg) with estimated standard deviations in parentheses

Bonds	Angle	Bonds	Angle
C(2)—C(1)—C(10)	113.9(2)	C(8)—C(7)—C(11)	121.5(2)
C(1)—C(2)—C(3)	110.4(2)	C(9)—C(7)—C(11)	120.8(2)
O(1)—C(3)—C(2)	122.4(3)	C(7)—C(8)—C(9)	61.5(2)
O(1)—C(3)—C(4)	123.1(3)	C(7)—C(9)—C(8)	60.3(2)
C(2)—C(3)—C(4)	114.4(3)	C(7)—C(9)—C(10)	107.4(2)
C(3)—C(4)—C(5)	110.8(2)	C(8)—C(9)—C(10)	120.7(2)
C(3)—C(4)—C(13)	113.8(3)	C(1)—C(10)—C(5)	109.3(2)
C(5)—C(4)—C(13)	112.5(2)	C(1)—C(10)—C(9)	105.9(2)
C(4)—C(5)—C(6)	114.8(2)	C(1)—C(10)—C(14)	112.0(2)
C(4)—C(5)—C(10)	115.1(2)	C(5)—C(10)—C(9)	103.2(2)
C(6)—C(5)—C(10)	104.9(2)	C(5)—C(10)—C(14)	112.4(2)
C(5)—C(6)—C(7)	105.5(2)	C(9)—C(10)—C(14)	113.4(2)
C(6)—C(7)—C(8)	115.3(2)	O(2)—C(11)—C(7)	119.8(2)
C(6)—C(7)—C(9)	107.2(2)	O(2)—C(11)—C(12)	119.7(3)
C(6)—C(7)—C(11)	118.7(2)	C(7)—C(11)—C(12)	120.5(2)
C(8)—C(7)—C(9)	58.3(2)		

function minimized was $\Sigma w(|F_o| - |F_c|)^2$, $R = \Sigma||F_o| - |F_c||/\Sigma|F_o|$, $R_w = (\Sigma w(|F_o| - |F_c|)^2/\Sigma w|F_o|^2)^{1/2}$.

On the final cycle of refinement the maximum parameter shift corresponded to 0.04σ. The mean error in an observation of unit weight was 1.95. The final difference map showed maximum fluctuations of $-0.09 - +0.12$ e Å^{-3}. The absolute configuration was based on that known for C(10). A parallel refinement of the opposite enantiomer resulted in marginally higher residuals (R_w ratio = 1.002). The final positional and (equivalent) isotropic thermal parameters for the non-hydrogen atoms appear in Table 1. Bond lengths and angles are given in Tables 2 and 3. Hydrogen atoms parameters, anisotropic thermal parameters, torsion angles, intermolecular contacts, least-squares planes, bond lengths and angles involving hydrogen, and structure factors have been deposited.[4]

Discussion

Compound **26** has the structure and absolute configuration shown in Fig. 1. Both ring junctions are *cis*. The six- and five-membered rings have chair and flattened C(5)-envelope conformations, respectively. Bond lengths and angles (Tables 2 and 3) are normal. All intermolecular distances correspond to normal van der Waals interactions, the shortest intermolecular distance between non-hydrogen atoms being O(2)···C(12) = 3.383(5) Å.

[4]Supplementary material mentioned in the text may be purchased from the Depository of Unpublished Data, CISTI, National Research Council of Canada, Ottawa, Ont., Canada K1A 0R6.

Tables of atomic coordinates, bond lengths and angles, hydrogen atom coordinates, and intramolecular distances and bond angles involving the H-atoms have also been deposited with the Cambridge Crystallographic Data Centre and can be obtained on request from The Director, Cambridge Crystallographic Data Centre, University Chemical Laboratory, Lensfield Road, Cambridge CB2 1EW, U.K.

Can. J. Chem. Downloaded from www.nrcresearchpress.com by 91.121.58.235 on 09/07/12
For personal use only.

Formation and reactivity of 1-pyrrolyl-2,2,2-trifluoroethyl cations[1]

ANNETTE D. ALLEN, JEAN-MARC KWONG-CHIP, WING CHEUNG LIN, PAUL NGUYEN, AND THOMAS T. TIDWELL[2]

Department of Chemistry, University of Toronto, Scarborough Campus, Scarborough, Ont., Canada M1C 1A4

Received March 14, 1990

This paper is dedicated to Professor Ross Stewart on the occasion of his 65th birthday

ANNETTE D. ALLEN, JEAN-MARC KWONG-CHIP, WING CHEUNG LIN, PAUL NGUYEN, and THOMAS T. TIDWELL. Can. J. Chem. **68**, 1709 (1990).

1-(1-Methyl-2-pyrrolyl)-2,2,2-trifluoroethyl *p*-nitrobenzoate (**3**) reacts by carbocation formation with an *m* value for the dependence of rate on the solvent polarity parameter Y_{OTs} of 0.56, and a rate 41 times slower than (1-methyl-2-pyrrolyl)methyl *p*-nitrobenzoate. The products from **3** include significant amounts of material derived from solvent attack at the 5-position of the pyrrole ring. The results indicate a high degree of charge delocalization by the strongly donating pyrrolyl group, resulting in a low $k(H)/k(CF_3)$ rate ratio and nucleophilic attack on the ring. 1,1,1-Trifluoro-2-(1-methyl-2-pyrrolyl)propan-2-ol (**10**) reacted with CF_3CO_2H via a tertiary carbocation, which led to dimeric products resulting from electrophilic substitution on the pyrrole ring.

Key words: pyrrole, trifluoromethyl substituents, carbocations.

ANNETTE D. ALLEN, JEAN-MARC KWONG-CHIP, WING CHEUNG LIN, PAUL NGUYEN et THOMAS T. TIDWELL. Can. J. Chem. **68**, 1709 (1990).

Le *p*-nitrobenzoate de 1-(1-méthyl-2-pyrrolyl)-2,2,2-trifluoroéthyle (**3**) réagit par formation de carbocation avec une valeur *m*, pour la dépendance de la vitesse de réaction sur le paramètre de polarité du solvant Y_{OTs}, de 0,56 et avec une vitesse de réaction qui est 41 fois moindre que celle du *p*-nitrobenzoate de (1-méthyl-2-pyrrolyl)méthyle. Les produits obtenus à partir du composé **3** comprennent des quantités importantes de matériaux provenant d'une attaque de la position 5 du noyau pyrrole par le solvant. Les résultats indiquent que le groupement pyrrolyle fortement donneur provoque une grande délocalisation de charge qui a comme conséquence que le rapport des vitesses $k(H)/k(CF_3)$ est faible et qu'il se produit une attaque nucléophile sur le cycle. Le 1,1,1-trifluoro-2-(1-méthyl-2-pyrrolyl)propan-2-ol (**10**) réagit avec le CF_3CO_2H par le biais d'un carbocation tertiaire qui conduit à la formation de produits dimères provenant d'une substitution électrophile sur le noyau pyrrole.

Mots clés : pyrrole, substituants trifluorométhyles, carbocations.

[Traduit par la revue]

Introduction

The CF_3 group ordinarily has a powerful destabilizing effect on the formation of an adjacent carbocation, resulting in rate ratios $k(H)/k(CF_3)$ of 10^6 or more (2). In certain circumstances the ratio can be significantly less, in particular the values of 1.4–2.8 for 2-trifluoromethyl-2-adamantyl tosylate (2*b*), those of 2.4–5.2 for the doubly destabilized system 4-$CH_3OC_6H_4$-$CR(CF_3)$OTs (2*c*), and that of 4×10^3 for 4-$CH_3OC_6H_4CH$-(OTs)R (2*d*). These reduced ratios are attributed (2) to delocalization of the positive charge away from the CF_3 group in every case, and also to steric effects in the adamantyl derivative.

The pyrrolyl group is known to be an extraordinarily strong electron donor, as shown by the high reactivity of pyrrole in electrophilic aromatic substitution (3) and by the facility of side-chain carbocation formation adjacent to the pyrrolyl group (4). The present report deals with the generation and further reactions of carbocations substituted with both the strongly electron-withdrawing CF_3 group and the strongly donating 1-methyl-2-pyrrolyl group.

Results

Reaction of 1-methylpyrrole with trifluoroacetic anhydride gave 1-methyl-2-trifluoroacetylpyrrole **1** (5), which was reduced with $NaBH_4$ to the alcohol **2**, which was converted to the *p*-nitrobenzoate **3** by reaction with triethylamine and *p*-nitrobenzoyl chloride.

Solvolysis rates for the reaction of **3** in various solvents were measured by uv, and the derived rate constants are given in Table 1. For the correlation of the reactivity of **3** with solvent polarity the Y_{OTs} scale (6*a*) was used, as there is no reported scale of solvent polarities for carbocation generation based on the *p*-nitrobenzoate leaving group. The correlation obtained, $\log k = 0.56\ Y_{OTs} - 3.36$, $r = 0.990$, is surprisingly good considering that scales of solvent polarity are generally leaving group dependent (6). Other examples of the successful correlation of carbocation-forming reactions of *p*-nitrobenzoates have been reported (2*c*).

The products of the reaction of **3** in CH_3OH and EtOH at 40°C were mixtures of a 1-(1-methyl-2-pyrrolyl)-2,2,2-trifluoroethyl

TABLE 1. Solvolytic rate constants for **3** at 25°C

Solvent[a]	Y_{OTs}[b]	$k_{obs}(s^{-1})$[c]
97 HFIP	3.61	5.27×10^{-2}
97 TFE	1.83	4.36×10^{-3}
70 TFE	2.00	3.68×10^{-3}
50 TFE	2.14	4.63×10^{-3}
HCO_2H	3.04	3.23×10^{-2}
80 EtOH	0.00	4.40×10^{-4}
60 EtOH	0.92	1.17×10^{-3}
CH_3CO_2H	−0.61	2.69×10^{-4}
MeOH	−0.92	1.32×10^{-4}[d]
80 MeOH	0.47	6.54×10^{-4}
60 MeOH	1.52	3.33×10^{-3}

[a]Solvents are v/v mixtures with H_2O, HFIP is $(CF_3)_2CHOH$, TFE is CF_3CH_2OH.
[b]Reference 6*a*.
[c]Average of at least two runs in each case, ±2%, unless noted.
[d]Five runs, ±10%.

[1]Reported in part as a preliminary communication, ref. 1.
[2]Author to whom correspondence may be addressed.

Can. J. Chem. Downloaded from www.nrcresearchpress.com by 91.121.58.235 on 09/07/12
For personal use only.

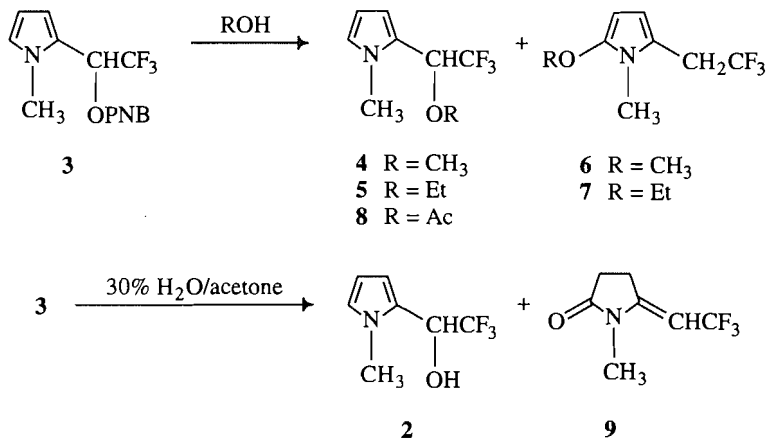

ether (**4** or **5**) and a 1-methyl-2-(2,2,2-trifluoroethyl)-5-alkoxypyrrole (**6** or **7**), with product ratios **4**/**6** and **5**/**7** of 2:1 and 3:2, respectively. The reaction of **3** in acetic acid gave the acetate **8** while reaction in 70% acetone/30% H_2O at 25°C gave the alcohol **2** and 1-methyl-5-(2,2,2-trifluoroethylidene)-2-pyrrolidinone (**9**). The structures of **4**–**9** follow from their ^1H nmr, ir, and mass spectral properties. Reported data (7) for similar compounds are particularly helpful in establishing the structure of **9**.

Reaction of **1** with methylmagnesium iodide gave the alcohol **10**, which on reaction with 0.1 M CF_3CO_2H in CCl_4 for 18 h gave a complex mixture of products from which **10**–**14** were isolated by gas chromatography, with relative peak heights of 7, 4, 7, 8, and 74, respectively. A proposed mechanism for formation of these products is shown in Scheme 1. The structures were readily established by their ^1H nmr, ir, and mass spectral properties. The mass spectrum of the crude reaction product also showed peaks corresponding to trimeric and tetrameric products, but these were not isolated and positively identified.

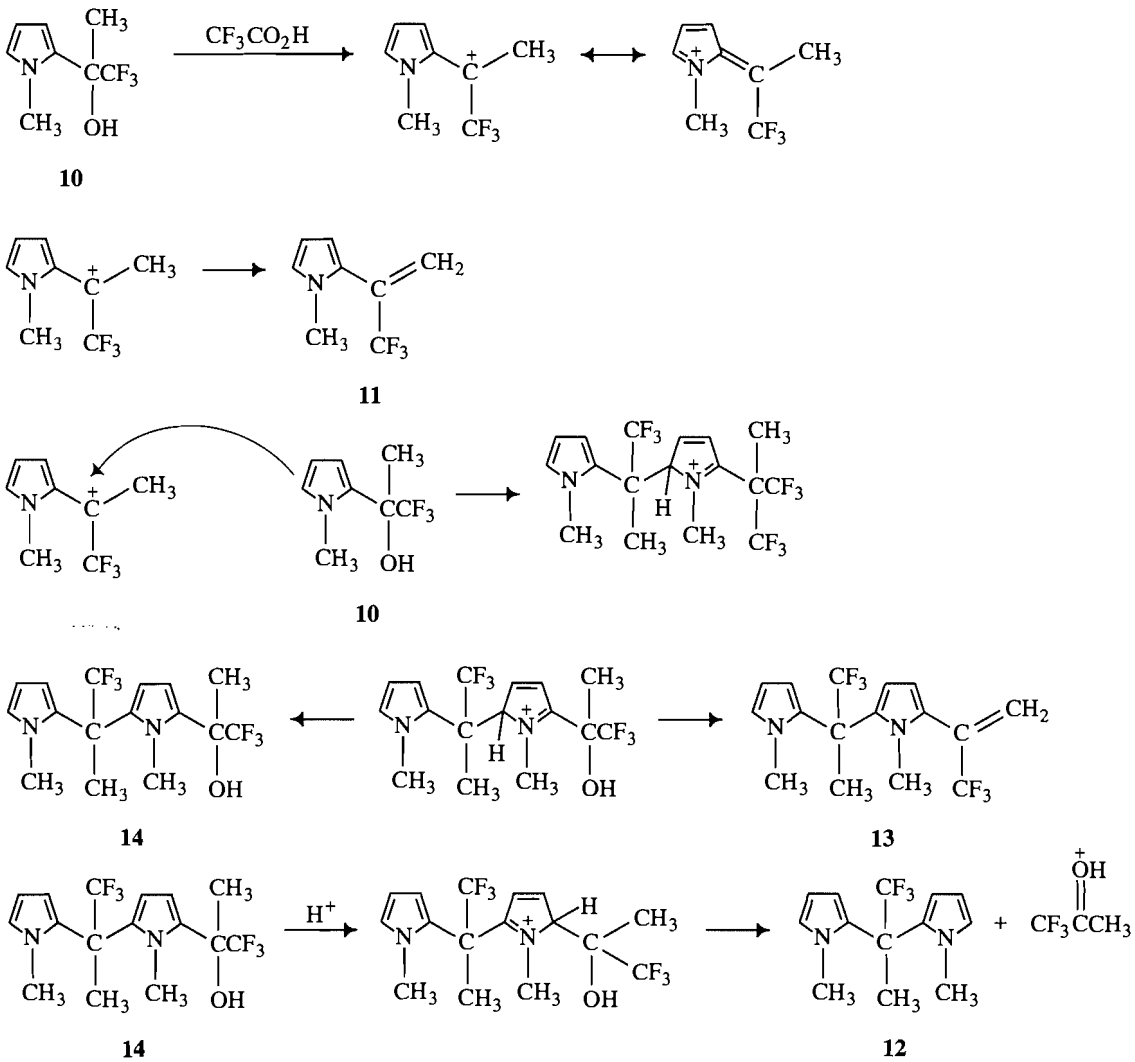

SCHEME 1

Can. J. Chem. Downloaded from www.nrcresearchpress.com by 91.121.58.235 on 09/07/12
For personal use only.

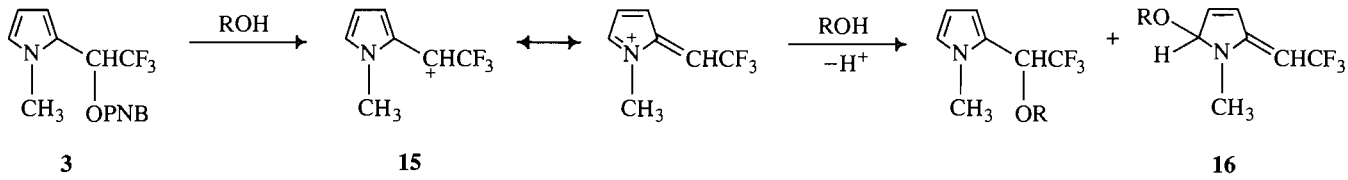

SCHEME 2

Discussion

The reactivity of **3** and the formation of mixtures of ring and side-chain substitution products for the reactions in methanol, ethanol, and aqueous acetone are strong evidence for the occurrence of reactions proceeding through carbocation intermediates with a high degree of positive charge delocalization, as shown in Scheme 2. In the case of methanol and ethanol the intermediate **16** rearranges to the alkoxypyrroles **6** and **7**, respectively, whereas for H_2O the pyrrolidinone **9** is favored. The *m* value of 0.56 for the correlation of the reactivity of **3** with Y_{OTs} is significantly less than unity, and this is typical of the behaviour we have observed for highly delocalized benzylic cations (2*a*, *c*, *d*; 8*a*).

Nucleophilic attack on the aromatic ring of benzylic carbocations with α-CF_3 substituents has been observed before (2*c*, 8), and appears to reflect the high degree of charge delocalization into the ring induced by the electron-withdrawing group.

Further evidence for the carbocationic nature of the reaction of **3** comes from the results of Noyce and Fraser[3] on the solvolysis of (1-methyl-2-pyrrolyl)methyl *p*-nitrobenzoate (**17**) and ring-substituted analogues. These compounds showed high reactivity in carbocation formation with a strong dependence of the rate on the electron-donor ability of the ring substituent, and were interpreted[3] as proceeding through carbocations as shown.

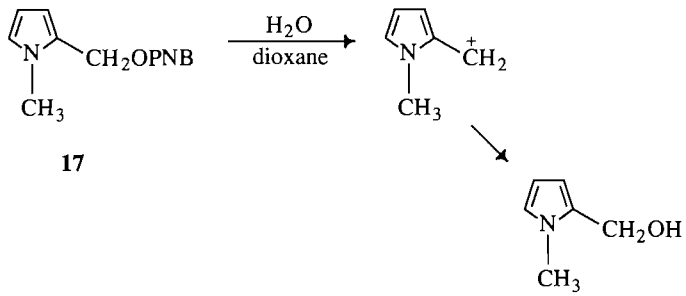

The value of k_{obs} for **17** in 70% H_2O/dioxane was 1.82×10^{-2} s^{-1} at 25°C. The Y_{Cl} parameter for this solvent is 0.01 (6*a*), which is essentially the same as that of 0.00 defined for 80% ethanol. Thus the rate constant of 4.40×10^{-4} s^{-1} observed here for **3** in 80% ethanol can be compared to that for **17** to give a rate ratio $k(H)/k(CF_3) = 41$. This ranks with other low values that have been observed for this ratio as cited in the introduction (2*b*,*c*,*d*). In the 1-aryl-2,2,2-trifluroethyl systems these ratios are attributed to diminution of the effect of the CF_3 group due to delocalization of the charge to a remote location in the ring (2*a*).

The value of σ^+_{Ar} for the 1-methyl-2-pyrrolyl group has been measured as −1.90 (4*a*) from a correlation of the reactivity of 1-arylethyl acetates in 30% ethanol. Such σ^+_{Ar} constants consider the aryl group as equivalent to a substituted phenyl ring. The rate ratio k(1-methyl-2-pyrrolyl)/k(4-$Me_2NC_6H_4$) in the above series was 9.0 (4*a*), whereas the value of $k_{obs} = 8.56 \times 10^{-4}$ for 4-$Me_2NC_6H_4CH_2OPNB$ in 70% aqueous dioxane at 25°C[3] leads to a comparable value of 21 for the same ratio. Thus the substituent effect of the 1-methyl-2-pyrrolyl group on carbocation formation in these two systems is mutually consistent, and the value of −1.90 proposed (4*a*) for σ^+_{Ar} for the 1-methyl-2-pyrrolyl group is reasonable in view of the value of −1.74 for σ^+_p for Me_2N derived from solvolytic data (9).

The reaction of (1-methyl-2-pyrrolyl)methyl *p*-nitrobenzoate (**17**) in 70% dioxane leads to the carbinol as the only observed product,[3] together with polymeric material. The apparent greater propensity of **3** to form ring-substituted products is expected on the basis of the known (2*a*) barriers to substitution in 2,2,2-trifluoroethyl systems.

The formation of the products from the reaction of **10** with CF_3CO_2H may be readily rationalized by the pathway shown in Scheme 1. The details of this pathway have not been tested and variants of this scheme may be equally plausible.

The oligomerization of pyrroles by electrophilic attack on the α-ring carbons of pyrroles by the side-chain carbon of 2-pyrrolylcarbinyl derivatives is well documented (10). There was evidence for the presence of trimeric and tetrameric products in the mass spectra of the crude reaction products from **10** so this type of chemistry promises to serve as a preparative route to such materials and to fluorinated porphyrin-like materials.

In summary, the side-chain carbocations generated from the pyrrolyl derivatives **3** and **10** both dislay the consequences of extensive charge delocalization into the strongly electron-donating pyrrolyl ring. The formation of 2,5-substituted pyrrole systems occurs in each series, with the formation of fluorinated dipyrrolylmethanes in the latter.

Experimental

Fluorinated solvents and reagents were obtained from Aldrich, and the solvent purification was described previously (2*c*). All reactions were carried out under N_2 in dry glassware. Liquid chromatographic separations were carried out using a Chromatotron centrifugal radial thin-layer chromatograph from Harrison Research. Spectra were measured using Varian T-60 and Gemini 200 nmr spectrometers and a Nicolet Ftir spectrometer.

1-Methyl-2-trifluoroacetylpyrrole (1)

To a stirred solution of 12.2 mL (0.0864 mol) of trifluoroacetic anhydride in 23 mL ether cooled in an ice bath was added dropwise *N*-methylpyrrole (7.00 g, 0.0863 mol) in 25 mL ether over 2 h. After 4 h further stirring, water was added and the aqueous layer extracted twice with ether. The combined ether layers were extracted three times each with saturated $NaHCO_3$ and NaCl solutions and dried over $MgSO_4$. The solvent was evaporated and the product distilled at 59°C and 6.5 Torr (1 Torr = 133.3 Pa) to give **1** (9.58 g, 0.0541 mol, 63%) as a colorless liquid; ir (CCl_4): 1680 (C=O) cm^{-1}; ^1H nmr (CCl_4) δ: 3.96 (s, 3, CH_3), 6.18 (m, 1, H-4), 6.92 (m, 1, H-5), 7.12 (m, 1, H-3); ms, *m*/*z* (rel. intensity): 177 (69, M^+), 163 (7), 108 (100, $M^+ - CF_3$), 94 (13), 80 (23, $M^+ - CF_3CO$), 69 (17, CF_3^+); hrms, *m*/*z* calcd. for $C_7H_6F_3NO$ (M^+): 177.0401; found: 177.0408.

1-(1-Methyl-2-pyrrolyl)-2,2,2-trifluoroethanol (2)

To a stirred solution of **1** (4.0 g, 0.023 mol) in 15 mL methanol

[3]D. S. Noyce and G. M. Fraser, Department of Chemistry, University of California, Berkeley, unpublished results privately communicated.

Can. J. Chem. Downloaded from www.nrcresearchpress.com by 91.121.58.235 on 09/07/12
For personal use only.

Can. J. Chem. Downloaded from www.nrcresearchpress.com by 91.121.58.235 on 09/07/12
For personal use only.

cooled in an ice bath was carefully added $NaBH_4$ (2.0 g, 0.053 mol). After 4 h stirring, saturated $NaHCO_3$ was added and the solution was extracted three times with ether, and the combined ether layers were extracted twice each with saturated $NaHCO_3$ and NaCl and dried over $MgSO_4$. Evaporation of the solvent gave a thick oil that crystallized on standing. Distillation at 60°C (2 Torr) gave **2** (2.89 g, 0.016 mol, 70%); ir (CCl_4): 3200–3550 (associated OH) cm^{-1}; ^1H nmr (CCl_4) δ: 2.35 (s, 1, OH), 3.63 (s, 3, CH_3), 4.82 (q, 1, J_{HF} = 7 Hz, $CHCF_3$), 5.96 (m, 1, H-4), 6.14 (m, 1, H-3), 6.52 (m, 1, H-5); ms, *m/z* (rel. intensity): 179 (100, M^+), 162 (47, M^+ −OH), 110 (89, $M^+ - CF_3$), 82 (69); hrms, *m/z* calcd. for $C_7H_8F_3NO$ (M^+): 179.0558; found: 179.0542.

1-(1-Methyl-2-pyrrolyl)-2,2,2-trifluoroethyl p*-nitrobenzoate (**3**)*

To a solution of **2** (2.89 g, 0.0161 mol) and 3 mL triethylamine in 25 mL ether cooled in an ice bath was slowly added *p*-nitrobenzoyl chloride (3.1 g, 0.0167 mol) dissolved in 25 mL ether. After 3 h stirring at room temperature water was added and, after extraction and drying as previously, **3** was obtained as a yellow solid (3.19 g, 0.0097 mol, 60%) that, after recrystallization from pentane, gave mp 78–79°C; ir (CCl_4): 1741 (C=O) cm^{-1}; ^1H nmr (CCl_4) δ: 3.78 (s, 3, CH_3), 6.0 (m, 1, H-4), 6.4 (m, 2, H-3 and $CHCF_3$), 6.6 (m, 1, H-5), 8.19 (s, 4, $C_6H_4NO_2$); ms, *m/z* (rel. intensity): 328 (66, M^+), 259 (25, $M^+ - CF_3$), 178 (28, M^+ − PNB), 162 (97, M^+ − OPNB), 150 (100, PNB^+), 104 (26); hrms, *m/z* calcd. for $C_{14}H_{11}F_3N_2O_4$ (M^+): 328.0670; found: 328.0677.

Solvolysis studies of 3

A solution of **3** (0.50 g, 1.5 mmol) in 65 mL CH_3OH was kept 14 h at 40°C, then was poured into H_2O and extracted as above. Separation of the crude product by gc (20% OV-17 column, flow rate 110 mL/min, 130°C) gave two significant peaks in the ratio 1:2. The peak at 6.6 min was identified as 1-(1-methyl-2-pyrrolyl)-2,2,2-trifluoroethyl methyl ether (**4**) by its spectral properties; ir (CCl_4): 2800–3015 (C—H) cm^{-1}; ^1H nmr (CCl_4) δ: 3.34 (s, 3, OCH_3), 3.68 (s, 3, NCH_3) 4.53 (q, 1, J_{HF} = 7 Hz, $CHCF_3$), 5.9 (m, 1, H-4), 6.1 (m, 1, H-3), 6.45 (t, 1, $J_{4,5}$ = 2 Hz, H-5); ms, *m/z* (rel. intensity): 193 (48, M^+), 179 (20, $M^+ - CH_2$), 162 (68, $M^+ - OCH_3$), 124 (100, $M^+ - CF_3$); hrms, *m/z* calcd. for $C_8H_{10}F_3NO$ (M^+): 193.0714; found: 193.0725.

The smaller peak at 8.2 min was a yellow solid identified as 1-methyl-2-(2,2,2-trifluoroethyl)-5-methoxypyrrole (**6**); ir (CCl_4): 3015–2800 (CH) cm^{-1}; ^1H nmr (CCl_4) δ: 3.20 (q, 2, J_{HF} = 10 Hz, CH_2CF_3), 3.32 (s, 3, OCH_3), 3.78 (s, 3, NCH_3), 5.02 (d, 1, $J_{3,4}$ = Hz, H-4), 5.78 (d, 1, $J_{3,4}$ = 4 Hz, H-3); ms, *m/z* (rel. intensity): 193 (73, M^+), 179 (20, $M^+ - CH_2$), 178 (100, $M^+ - CH_3$), 124 (50, $M^+ - CF_3$), 67 (17, $M^+ - C_4H_5F_3O$); hrms, *m/z* calcd. for $C_8H_{10}F_3NO$ (M^+): 193.0714; found: 193.0708.

Ethanolysis of **2** was carried out similarly to give a product that showed two components collected by gc with a 2:3 ratio of peak heights. The larger peak at 9.8 min was an oil identified as 1-(1-methyl-2-pyrrolyl)-2,2,2-trifluoroethyl ethyl ether (**5**); ^1H nmr (CCl_4) δ: 1.24 (t, 3, *J* = 7 Hz, OCH_2CH_3), 3.50 (q, 2, *J* = 7 Hz, OCH_2CH_3), 3.68 (s, 3, NCH_3), 4.62 (q, 1, J_{HF} = 7.5 Hz, $CHCF_3$), 5.98 (m, 1, H-4), 6.10 (m, 1, H-3), 6.52 (m, 1, H-5). The ms showed a major peak at *m/z* 207 as expected for M^+ but also signals at higher *m/z*, and had apparently decomposed. The smaller peak at 12.8 min was identified as 1-methyl-2-(2,2,2-trifluoroethyl)-5-ethoxy pyrrole (**7**); ir (CCl_4): 2800–3000 (CH) cm^{-1}; ^1H nmr (CCl_4) δ: 1.40 (t, 3, *J* = 7 Hz, OCH_2CH_3), 3.22 (q, 2, J_{HF} = 10 Hz, CH_2CF_3), 3.34 (s, 3, NCH_3), 3.97 (q, 2, *J* = 7 Hz, OCH_2CH_3), 5.04 (d, 1, $J_{4,5}$ = 4 Hz, H-4), 5.82 (d, 1, $J_{4,5}$ = 4 Hz, H-3); ms, *m/z* (rel. intensity): 207 (46, M^+), 179 (18, $M^+ - C_2H_4$), 178 (100, $M^+ - C_2H_5$), 110 (31, $M^+ - C_3H_4F_3$); hrms, *m/z* calcd. for $C_9H_{12}F_3NO$ (M^+): 207.0871; found: 207.0881.

Acetolysis of **3** (0.60 g, 1.83 mmol) in 5 mL acetic acid for 20 h at 25°C was followed by removal of precipitated *p*-nitrobenzoic acid by filtration, partitioning between water and ether, drying, and evaporation. Radial chromatography (10% ethyl acetate/petroleum ether) gave **8**; ir (CCl_4); 1757 (C=O) cm^{-1}; ^1H nmr (CCl_4) δ: 2.10 (s, 3, $COCH_3$), 3.68 (s, 3, NCH_3), 6.1 (m, 2, $CHCF_3$ and H-4), 6.30 (m, 1, H-3), 6.53 (m, 1, H-5); ms, *m/z* (rel. intensity); 221 (78, M^+), 162 (93, M^+ − AcO), 110 ($M^+ - CF_3$, C_2H_2O); hrms, *m/z* calcd. for $C_9H_{10}F_3NO_2$ (M^+): 221.0663; found: 221.0662.

Hydrolysis was carried out with **3** (1.0 g, 3 mmol) in 33 mL of 30% H_2O/acetone for 16 h at 25°C. The mixture was worked up as before and separated by gc (30% Carbowax 20 M, 120 mL/min, 200°C) to give two peaks in a 1:1 ratio. The peak at 4.2 min was identified as **2** by a comparison of spectral properties, whereas that at 2.8 min was identified as *1-methyl-5-(2,2,2-trifluoroethylidene)-2-pyrrolidinone* (**9**): ir (CCl_4); 1749 (C=O), 1666 (C=C) cm^{-1}; ^1H nmr (CCl_4) δ: 2.57 (m, 2, H-4), 2.96 (s, 3, NCH_3), 2.96 (m, 2, H-3), 4.89 (q, 1, *J* = 8 Hz, $CHCF_3$); ms, *m/z* (rel. intensity): 179 (78, M^+), 160 (15), 150 (38), 123 (27), 104 (27), 82 (28), 68 (23); hrms, *m/z* calcd. for $C_7H_8F_3NO$ (M^+): 179.0558; found: 179.0542.

*1,1,1-Trifluoro-2-(1-methyl-2-pyrrolyl)propan-2-ol (**10**)*

A solution of 1-methyl-2-trifluoroacetylpyrrole (**1**, 0.50 g, 3.0 mmol) in 10 mL ether was added dropwise to methylmagnesium iodide (6.0 mmol) in 20 mL ether. After stirring overnight 25 mL of saturated NH_4Cl solution was added, the layers were separated, and the aqueous layer was extracted with ether. The combined ether layers were extracted with water followed by saturated NaCl, dried over Drierite, and evaporated. The residue was purified on the Chromatotron (10% ethyl acetate in petroleum ether) to yield **10** (0.385 g, 2.1 mmol, 70%); ir (CCl_4): 3480 (OH) cm^{-1}; ^1H nmr ($CDCl_3$) δ: 1.80 (s, 3, CCH_3), 2.40 (s, 1, OH), 3.83 (s, 3, NCH_3), 6.07 (q, 1, $J_{3,4}$ = 3.8 Hz, $J_{4,5}$ = 2.7 Hz, H-4), 6.20 (m, 1, H-3), 6.63 (t, 1, $J_{3,5}$ = 1.8 Hz, $J_{4,5}$ = 2.6 Hz, H-5); ms, *m/z*: 193 (93, M^+), 176 (13, M^+ − OH), 124 (100, $M^+ - CF_3$), 69 (13, CF_3^+); hrms, *m/z* calcd. for $C_8H_{10}F_3NO$ (M^+): 193.0714; found: 193.0718.

*Reaction of 1,1,1-trifluoro-2-(1-methyl-2-pyrrolyl)propan-2-ol (**10**) with trifluoroacetic acid*: To a solution of **10** (1.47 g, 7.62 mmol) in 40 mL carbon tetrachloride was added 0.6 mL of trifluoroacetic acid. The reaction mixture was stirred at room temperature 18 h, was then poured over 40 mL of saturated $NaHCO_3$ solution and extracted three times with ether. The combined ethereal solution was washed successively with water and saturated NaCl solution, then dried over anhydrous $CaSO_4$. Evaporation of the solvent gave 0.9 g of a brown, sticky oil. The sample was tested with tlc using petroleum ether (40–60°C) – ethyl acetate (97:3) as the solvent, and gave R_f values of 0.27, 0.38, 0.52, 0.45, and 0.18; it was separated by gc (OV-17, 165°C) with retention times 3.0, 0.5, 18.4, 21.2, and 68 min for **10**–**14**, respectively.

Separation of the reaction products by gc gave **10**–**14** in 7, 4, 7, 8, and 74% relative yields as determined by the relative areas of the gc peaks. The compounds were identified by their spectral properties:

*3,3,3-Trifluoro-2-(1-methyl-2-pyrrolyl)propene (**11**)*: ir (CCl_4): 1740 (C=C) cm^{-1}; ^1H nmr (CCl_4) δ: 3.60 (s, 3, NCH_3), 5.47 (d, 1, *J* = 1.3 Hz, *syn*-CF_3C=CH), 6.00 (t, 2, *anti*-CF_3C=CH and H-4), 6.20 (m, 1, H-3), 6.55 (t, 1, $J_{3,5}$ = 2.2 Hz, H-5); ms, *m/z* (rel. intensity): 175 (100, M^+), 156 (13, M^+ − F), 106 (96, $M^+ - CF_3$); hrms, *m/z* calcd. for $C_8H_8F_3N$ (M^+): 175.0609; found: 175.0611.

*1,1,1-Trifluoro-2,2-bis(1-methyl-2-pyrrolyl)propane (**12**)*: ir (CCl_4): 2960–3000 (aromatic C—H) cm^{-1}; ^1H nmr ($CDCl_3$) δ: 1.89 (s, 3, CCH_3), 2.98 (s, 6, NCH_3), 6.10 (q, 2, $J_{3,4}$ = 3.8 Hz, $J_{4,5}$ = 2.7 Hz, H-4), 6.30 (m, 2, H-3), 6.55 (t, 2, $J_{4,5}$ = 2.7 Hz, H-5); ms, *m/z* (rel. intensity): 256 (81, M^+), 187 (100, $M^+ - CF_3$), 106 (34, $C_7H_8N^+$), 94 (17, $C_3HF_3^+$); hrms, *m/z* calcd. for $C_{13}H_{15}F_3N_2$ (M^+): 256.1187; found: 256.1202.

*3,3,3-Trifluoro-2-(1-methyl-5-[1,1,1-trifluoro-2-(1-methyl-2-pyrrolyl)propyl]-2-pyrrolyl)propene (**13**)*: ir (CCl_4): 2960–3000 (aromatic C-H) cm^{-1}; ^1H nmr ($CDCl_3$) δ: 1.92 (s, 3, CCH_3), 2.92 (s, 3, NCH_3), 2.98 (s, 3, NCH_3), 5.57 (d, 1, *J* = 1.3 Hz, *syn*-CF_3C=CH), 6.10 (q, 1, $J_{3',4'}$ = 3.2 Hz, $J_{4',5'}$ = 2.2 Hz, H-4'), 6.15 (d, 1, *J* = 1.3 Hz, *anti*-CF_3C=CH), 6.24 (d, 1, $J_{3,4}$ = 3.3 Hz, H-4), 6.35 (m, 2, H-3, H-3'), 6.56 (t, 1, *J* = 2.2 Hz, H-5'); ms, *m/z* (rel. intensity): 350 (62, M^+), 281 (100, $M^+ - CF_3$), 200 (12, $C_{10}H_9F_3N^+$), 106 (16, $C_7H_8N^+$), 94 (17, $C_3HF_3^+$); hrms, *m/z* calcd. for $C_{16}H_{16}F_6N_2$ (M^+): 350.1217; found: 350.1215.

*1,1,1-Trifluoro-2-(1-methyl-5-[1,1,1-trifluoro-2-(1-methyl-2-pyrrolyl)propyl]-2-pyrrolyl)propan-2-ol (**14**)*: ir (CCl_4): 3600 (O-H) cm^{-1}; ^1H nmr ($CDCl_3$) δ: 1.79 (s, 3, CCH_3), 1.91 (s, 3, CCH_3), 2.27 (s, 1, OH), 2.96 (s, 3, NCH_3), 3.23 (s, 3, NCH_3), 6.09 (m, 1, H-4'), 6.19 (d, 1, $J_{3,4}$ = 3.8 Hz, H-4), 6.27 (m, 2, H-3, H-3'), 6.53 (m, 1, H-5'); ms, *m/z* (rel. intensity): 368 (32, M^+), 299 (65, $M^+ - CF_3$),

218 (20, $M^+ - C_6H_7F_3N$); hrms, m/z calcd. for $C_{16}H_{18}F_6N_2O$ (M^+): 368.1323; found: 368.1315.

Kinetic studies were carried out by injecting 4-mL aliquots of 0.03 M solutions of **3** into 1.2 mL of the solvent in 1 cm pathlength quartz cells and observing the decrease in uv absorption with time. Wavelengths used were 264 nm (HFIP), 236 nm (TFE), and 240 nm (EtOH). Constant final absorbances were obtained, and plots of log ($A - A_\infty$) versus time gave good first-order rate constants (correlation coefficients greater than 0.999 in all cases), which were reproducible to ±2%.

Acknowledgements

The financial support of the Natural Sciences and Engineering Research Council of Canada is gratefully acknowledged, and our thanks are due to Professor D. S. Noyce for kindly supplying unpublished data on the reactivity of **17**.

1. J.-M. KWONG-CHIP and T. T. TIDWELL. Tetrahedron Lett. **30**, 1319 (1989).
2. (*a*) T. T. TIDWELL. Adv. Carbocation Chem. **1**, 1 (1989); (*b*) A. D. ALLEN, R. KRISHNAMURTI, G. K. S. PRAKASH, and T. T. TIDWELL. J. Am. Chem. Soc. **112**, 1291 (1990); (*c*) A. D. ALLEN, V. M. KANAGASABAPATHY, and T. T. TIDWELL. J. Am. Chem. Soc. **108**, 3470 (1986); (*d*) A. D. ALLEN, I. C. AMBIDGE, C. CHE, H. MICHEAL, R. J. MUIR, and T. T. TIDWELL. J. Am. Chem. Soc. **105**, 2343 (1983); (*e*) A. D. ALLEN, F. SHAHIDI, and T. T. TIDWELL. J. Am. Chem. Soc. **104**, 2516 (1982).
3. (*a*) S. CLEMENTI and G. MARINO. Tetrahedron, **25**, 4599 (1969); (*b*) G. MARINO. Adv. Heterocycl. Chem. **13**, 235 (1971); (*c*) R. A. JONES. *In* Comprehensive heterocyclic chemistry. Vol. 4. Part 3. *Edited by* A. R. Katritzky and C. W. Rees. Pergamon Press, New York, NY. 1984. pp. 201–312.
4. (*a*) E. A. HILL, M. L. GROSS, M. STASIEWICZ, and M. MANION. J. Am. Chem. Soc. **91**, 7381 (1969); (*b*) M. C. HARSANYI and R. K. NORRIS. Aust. J. Chem. **40**, 2063 (1987); (*c*) M. V. SIGALOV, E. YU. SCHMIDT, and B. A. TROFIMOV. Izv. Akad. Nauk SSSR, Ser. Khim. 1146 (1987).
5. (*a*) W. D. COOPER. J. Org. Chem. **23**, 1382 (1958); (*b*) D. J. CHADWICK, G. D. MEAKINS, and C. A. RHODES. J. Chem. Research (S), **42**, (1980).
6. (*a*) F. L. SCHADT, T. W. BENTLEY, and P.v.R. SCHLEYER. J. Am. Chem. Soc. **98**, 7667 (1976); (*b*) T. W. BENTLEY and G. E. CARTER. J. Am. Chem. Soc. **104**, 5741 (1982); (*c*) T. W. BENTLEY, G. E. CARTER, and K. ROBERTS. J. Org. Chem. **49**, 5183 (1984); (*d*) X. CREARY and S. R. MCDONALD. J. Org. Chem. **50**, 474 (1985); (*e*) D. N. KEVILL and S. W. ANDERSEN. J. Org. Chem. **50**, 3330 (1985); (*f*) J. B. LAMBERT, G. WANG, and D. H. TERAMURA. J. Org. Chem. **53**, 5422 (1988).
7. (*a*) L. F. CANNIZZO and R. H. GRUBBS. J. Org. Chem. **50**, 2316 (1985); (*b*) W. FLITSCH and F. KAPPENBERG. Chem. Ber. **111**, 2401 (1978); (*c*) The Sadtler standard spectra: nuclear magnetic resonance spectra. Vol. 1-86, 2829OM. Sadtler Research Lab., Philadelphia, PA.
8. (*a*) A. D. ALLEN, R. GIRDHAR, M. P. JANSEN, J. D. MAYO, and T. T. TIDWELL, J. Org. Chem. **51**, 1324 (1986); (*b*) J. P. RICHARD. J. Am. Chem. Soc. **111**, 1455 (1989); (*c*) J. P. RICHARD. Tetrahedron Lett. **30**, 23 (1989).
9. H. C. BROWN, C. G. RAO, and M. RAVINDRANATHAN. J. Am. Chem. Soc. **100**, 7946 (1978).
10. R. A. JONES and G. P. BEAN. The chemistry of pyrroles. Academic Press, New York, NY. 1977. pp. 356–357.

Can. J. Chem. Downloaded from www.nrcresearchpress.com by 91.121.58.235 on 09/07/12
For personal use only.

Acidities and homolytic bond dissociation energies of the α C—H bonds in ketones in DMSO

FREDERICK G. BORDWELL[1] AND JOHN A. HARRELSON, JR.
Department of Chemistry, Northwestern University, Evanston, IL 60208-3113, U.S.A.

Received March 28, 1990

This paper is dedicated to Professor Ross Stewart on the occasion of his 65th birthday

FREDERICK G. BORDWELL and JOHN A. HARRELSON, JR. Can. J. Chem. **68**, 1714 (1990).

Equilibrium acidities in DMSO are reported for nine cycloalkanones, acetone, acetophenone, and 19 of their α-substituted derivatives. Oxidation potentials in DMSO for the conjugate bases of most of these ketones are also reported. Combination of these $E_{OX}(A^-)$ and pK_{HA} values gives estimates of the homolytic bond dissociation energies (BDEs) of the acidic C—H bonds in the ketones. The ΔBDEs, relative to the BDE of CH_3-H, or a parent ketone, provide a measure of the radical stabilization energies (RSEs) of the corresponding radicals. The effects of successive α-Me and α-Ph substitutions on RSEs, relative to those of CH_3COCH_2-H or $PhCOCH_2$-H, are similar to those reported in the gas phase for methane. The RSE for the $MeCHCOPh$ radical, relative to CH_3• is 17 kcal/mol, which is smaller than the sum of the RSEs of the $MeCH_2$• and $PhCOCH_2$• radicals relative to CH_3• (7 + 12 = 19), contrary to the prediction of the captodative postulate. When G in $PhCOCH_2G$ is PhCO, CH_3CO, or CN the ΔBDEs (relative to $PhCOCH_2$-H) are 0, 1, and 3 respectively; for $MeCOCH_2SO_2Ph$, $PhCOCH_2SO_2Ph$, and $PhCOCH_2NMe_3^+$ the ΔBDEs are −5, −2, and −4, respectively. The BDEs in C_5, C_6, C_7, C_8, C_{10}, and C_{12} cycloalkanones are within ±2.5 kcal/mol of that of 3-pentanone. Acetophenones bearing *meta* or *para* substituents all have BDEs of 93–94 kcal/mol. Ketone radical cations, $[RCOR']^{+\bullet}$, appear to be superacids with estimated $pK_{HA}{}^{+\bullet}$ values below −25.

Key words: acidities, bond dissociation energies, ketones.

FREDERICK G. BORDWELL et JOHN A. HARRELSON, JR. Can. J. Chem. **68**, 1714 (1990).

On a déterminé les acidités à l'équilibre dans le DMSO de neuf cycloalcanones, de l'acétone, de l'acétophéone et de 19 de leurs dérivés substitués en α. On a aussi déterminé les potentiels d'oxydation dans le DMSO des bases conjuguées de la plupart de ces cétones. En combinant les valeurs de ces E_{OX} (A^-) et de ces pK_{HA}, on a évalué les énergies de dissociation homolytique des liaisons (EDL) C—H acides de ces cétones. Les valeurs des ΔEDL, relatives à l'EDL du CH_3-H ou d'une cétone parente, sont des mesures des énergies de stabilisation radicalaire (ESR) des radicaux correspondants. Les substitutions successives de la CH_3COCH_2-H ou de la $PhCOCH_2$-H par des α-Me ou des α-Ph provoquent des effets sur les ESR qui sont semblables à ceux qui sont observés avec le méthane en phase gazeuse. L'ESR du radical $MeC•HCOPh$, relative à celle du radical CH_3•, est égale à 17 kcal/mol; celle valeur est inférieure à la somme des ESR, relatives au CH_3•, des radicaux $MeCH_2$• et $PhCOCH_2$• (7 + 12 = 19) et ce résultat est contraire à ce que prédit le postulat captodatif. Lorsque le groupement G de la molécule $PhCOCH_2G$ est égal à PhCO, CH_3CO ou CN, les valeurs des ΔEDL (relatives à celle de la $PhCOCH_2$-H) sont respectivement 0, 1 et 3; pour les composés $MeCOCH_2SO_2Ph$, $PhCOCH_2SO_2Ph$ et $PhCOCH_2NMe_3^+$, les valeurs de ΔEDL sont respectivement −5, −2 et −4. Les valeurs des EDL des cycloalcanones en C_5, C_6, C_7, C_8, C_{10} et C_{12} sont égales à celle de la 3-pentanone, à ±2,5 kcal/mol. Les EDL des acétophénones portant des substituents en positions *méta* ou *para* sont toutes égales à 93–95 kcal/mol. Il semble que les cations radicaux des cétones, $[RCOR']^{+\bullet}$, sont des superacides; les valeurs de leurs $pK_{HA}{}^{+\bullet}$ seraient inférieures à −25.

Mots clés : acidités, énergies de dissociation de liaison, cétones.

[Traduit par la revue]

Introduction

Although ketonic functions abound in nature, and base-catalyzed condensation reactions with ketones are commonly used in syntheses, relatively little information on the acidity of ketones occurs in the literature. The reason is, of course, that ketones are too weakly acidic for direct measurements of their acidities to be made in hydroxylic solvents. Numerous measurements of the rates of deuterium exchange have been made, however, and equilibrium acidities for a few ketones have been determined therefrom, or by other methods. For example, numerous indirect determinations of the equilibrium acidity of acetone in aqueous solution have been made, the most accurate of which gives the pK_a as 19.16 ± 0.04 (1).

Establishment of an acidity scale in dimethyl sulfoxide (DMSO) solution has provided a large number of pK_{HA} values of weak acids, including ketones, in that solvent (2). Furthermore, combination of these pK_a values with ketone oxidation potentials and those of their conjugate bases has made possible estimates of (a) the acidities of the radical cations formed by removing an electron from the parent acids (3), and (b) the homolytic bond dissociation energies (BDEs) of their acidic C—H bonds (4). Equations [1] and [2] are used to estimate these $pK_{HA}{}^{+\bullet}$ and BDE values.

$$[1]\quad pK_{HA}{}^{+\bullet} = pK_{HA} + [E_{OX}(A^-) - E_{OX}(HA)]\ 23.06/1.37$$

$$[2]\quad BDE = 1.37\ pK_{HA} + 23.06\ E_{OX}(A^-) + 56$$

In eqs. [1] and [2], both of which are based on thermodynamic cycles, the factors 1.37 and 23.06 are used to convert pK_{HA} units and oxidation potential eV units to kcal/mol. The number 56 is a constant made up of the free energy of formation of the hydrogen atom, $\Delta G_f^0(H•)_g$, together with estimates of $\Delta G_{sol}^0(H•)$, $\Delta G_{tr}^0(H^+)$, and $T\Delta S^0$, which are needed to relate the free energies in solution to gas phase $\Delta H°$ values. The constant used (56) is semiempirical in the sense that some of these conversion factors are difficult to evaluate. Nevertheless, the BDEs obtained by use of eq. [2] agree to within ±3 kcal/mol, for the most part, with the best gas phase values that have been obtained for six hydrocarbons, phenol, thiophenol, aniline, and acetone (4*a*). In a family of compounds such as the ketones, the relative BDEs are believed to be accurate to about ±1 kcal/mol

In this paper we will present pK_{HA} data for a variety of ketones in DMSO, and compare the effects of structural changes on their acidities, BDEs, and radical cation acidities.

[1]Author to whom correspondence may be addressed.

Printed in Canada / Imprimé au Canada

Can. J. Chem. Downloaded from www.nrcresearchpress.com by 91.121.58.235 on 09/07/12
For personal use only.

Can. J. Chem. Downloaded from www.nrcresearchpress.com by 91.121.58.235 on 09/07/12
For personal use only.

TABLE 1. Acidities of α-substituted acetones and acetophenones and oxidation potentials of their conjugate bases in DMSO

Ketone	pK_{HA}[a]	E_{OX} (A^-)[c]	BDE[d]	ΔBDE
CH_3COCH_3	26.5	0.076	94	(0.0)
$MeCH_2COCH_2Me$	27.1	−0.203	88	6
$Me_2CHCOCHMe_2$	28.2	−0.417	85	9
t-$BuCOCH_3$	27.7	0.000	94	0
$PhCH_2COCH_3$	19.8	−0.003	83	11
$PhCH_2COCH_2Ph$	18.7	+0.072	83	11
$Ph_2CHCOCH_3$	19.4[b]	−0.016	82	12
$PhCOCH_3$	24.7	0.143	93	(0.0)
$PhCOCH_2CH_2Ph$	23.5	0.024[b]	88.5	4.5
$PhCOCH_2Me$	24.4	−0.065	88	5
$PhCOCHMe_2$	26.3	−0.253	86	7
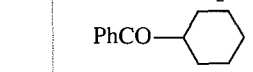	26.7	−0.199[b]	88	5
$PhCOCH_2OMe$	22.85	−0.175	81	12
$PhCOCH_2NMe_2$	23.55	−0.572	72	21
$PhCOCH_2Ph$	17.7	0.105	82.5	10.5
$PhCOCHPh_2$	18.75	0.059[b]	83	10
$PhCOCH_2COPh$	13.4	0.820	93	0
$PhCOCH_2COMe$	14.2	0.720	92	1
$PhCOCH_2CN$	10.2	0.861	90	3
$MeCOCH_2SO_2Ph$	12.5	1.146	99	−5
$PhCOCH_2SO_2Ph$	11.4	1.029	95	−2
$PhCOCH_2NMe_3^+$	14.6	0.903	97	−4

[a]Measured in DMSO against two or more indicators as described in earlier papers.
[b]Measured by X.-M. Zhang.
[c]Measured by cyclic voltammetry under the conditions previously described and referenced to the standard hydrogen electrode (3, 4).
[d]Estimated by eq. [2].

Results and discussion

Acidities of ketones

Table 1 presents data that allow one to discern the effects on acidities (pK_{HA}) and BDEs of substitution of alkyl, phenyl, or electron-withdrawing groups for α-hydrogen atoms in acetone and acetophenone.

In DMSO, acetone has a pK_{HA} of 26.5, which is 7.3 units higher than the value determined in aqueous solution (1). This difference in DMSO vs. aqueous acidities (ΔpK_{HA}) is almost the same as for the CH_3NO_2 ($\Delta pK_{HA} = 7.2$), where the negative charge in the anion is also delocalized to oxygen, but is much greater than those for carbon acids wherein the negative charge in the anion is localized primarily on carbon, such as malononitrile ($\Delta pK_{HA} = 0$) or $(Me_2SO)_2CH_2$ ($\Delta pK_{HA} = 2.3$).[2]

Substitution of an α- and an α′-hydrogen atom in acetone by methyl groups causes a 0.4 unit decrease in acidity (statistically corrected for the number of acidic hydrogen atoms). A second such substitution causes a further 0.8 decrease in acidity (Table 1). These small decreases in acidity can be attributed to increases in steric inhibition of solvation in the anion, which overshadow the stabilizing effect of Me on the C=C bond in the enolate ion. Note in this connection that replacement of one of the methyl groups in acetone by a *tert*-butyl group also causes a small (0.9 unit) decrease in acidity. On the other hand, replacement of one of the methyl groups by phenyl causes a 1.5 unit increase in acidity because the field/inductive (*F*) effect of the phenyl group on the anion overshadows the steric effect.

[2]Table I in ref. 2.

Substitution of a methyl group for an α-hydrogen atom in acetophenone causes a 0.1 unit *increase* in acidity, but a second methyl substitution causes a 1.6 unit decrease. Two effects are evidently operative here, namely, an acid-strengthening stabilization of the π-bond in the enolate ion by methyl, which is dominant in **1**, and an acid-weakening steric inhibition of solvation by methyl in the enolate ion, which is dominant in **2**. We have seen previously that α-OR and α-NR_2 groups cause slight increases in acidity (4*c*). For these, the acidifying *F* and *R* effects in the enolate ions are opposed by lone pair – lone pair repulsions (Z-isomer) (5) and (or) steric inhibition of solvation.

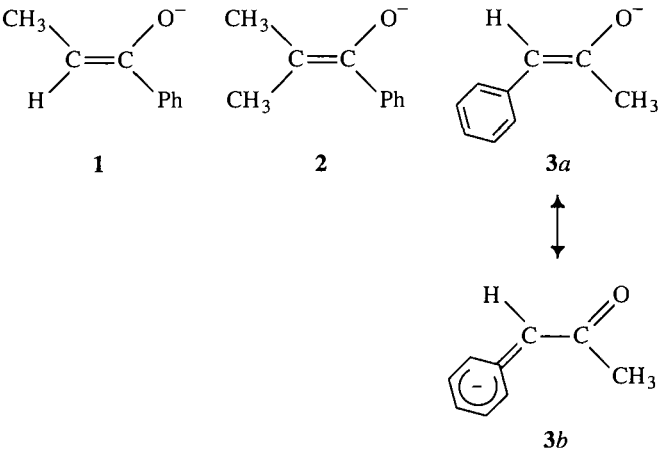

1 **2** **3*a***

3*b*

Substitution of a phenyl group for an α-hydrogen atom in acetone causes a 6.4 pK_a unit increase in acidity. A similar effect is observed for phenyl substitution into acetophenone (a 6.8 increase) (6). Extensive delocalization of the negative charge in the anion (*R* effect), as illustrated in **3*b***, is responsible for these changes. Introduction of a second α-phenyl group into acetone and into acetophenone causes a 0.7 unit acidity *increase* and an 0.8 unit acidity *decrease*, respectively. Evidently the second phenyl substituent introduces severe steric inhibition of resonance and of solvation effects, which are sufficient to cause the acidity decrease in $Ph_2CHCOPh$.

Homolytic bond dissociation energies (BDEs) for open-chain ketones

The BDE estimated from eq. [2] for the C—H bond in acetone of 94 kcal/mol (4*a*) is 4 kcal/mol below the "best" gas phase value (7), but is 2 kcal/mol higher than a more recent corrected value (8). The only other estimates of BDEs for the acidic C—H bonds in ketones of which we are aware is that for $PhCOCH_2$-H of 95 kcal/mol[3] and that for the secondary C—H bond in $CH_3CH_2COCH_3$ of 92 kcal/mol (9). In the series $(CH_3)_2C{=}O$, $(MeCH_2)_2C{=}O$, $(Me_2CH)_2C{=}O$, the first α-Me substitution lowers the BDE of the α C—H bonds by 6 kcal/mol, and the second by an additional 3 kcal/mol (Table 1). These ΔBDE values are close to those reported for the gas phase ΔBDEs for successive methyl substitution into CH_4 (7 and 3.5 kcal/mol, respectively (7)), as are those for α-methyl substitution into acetophenone (5 and 2 kcal/mol, respectively). On the other hand, the decrease in BDE caused by substituting an α-phenyl substituent into acetone or acetophenone, although large (10–11 kcal/mol), is much smaller than that into methane (17 kcal/mol). The smaller effect in the ketones is probably due primarily to a larger steric effect (**4*a*** ↔ **4*b***).

[3]From the thermodynamic cycle $DH(HA) = \Delta H_{HA} + IP(H\cdot) - EA(A^-)$ given in a list compiled by J. E. Bartmess.

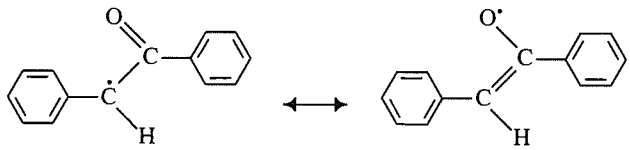

4a 4b

The effect on BDE of a second α-phenyl substitution into either acetone or acetophenone is negligible, whereas a second α-Ph substitution into methane causes a further 14 kcal/mol decrease in BDE (7). The zero decrease in BDE for the second α-Ph substitution into acetone or acetophenone should be compared, however, with the *third* α-Ph substitution into methane (ΔBDE = 1 kcal/mol (4*a*)). Steric effects have also been found to cause sizable decreases in ΔBDEs in other trisubstituted systems (4*d*).

In substituted acetophenones $PhCOCH_2G$, where G is a donor group, Me, MeO, or Me_2N, the ΔBDE (or RSEs) are 5, 12, and 21 kcal/mol, respectively, relative to G = H. In terms of RSEs, we can account for the effects of the methyl group as a hyperconjugative interaction with the orbital holding the odd electron, and for MeO and Me_2N groups as lone pair conjugative interactions (**5***a* ↔ **5***b* ↔ **5***c*). Since extended

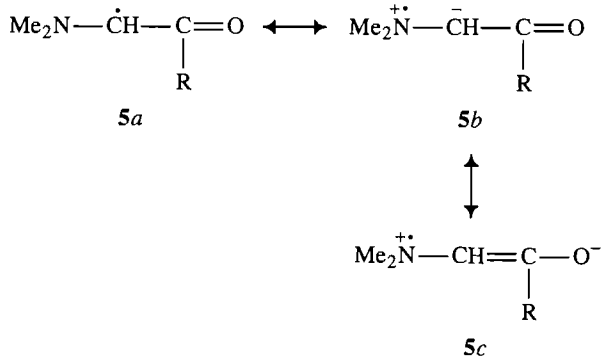

5a 5b 5c

conjugation is possible between the donor and acceptor groups in these radicals, e.g., as in **5***c*, several authors have suggested that extra (more than additive) stabilization should be present (10). The effects with COR acceptors and MeO or Me_2N donors are no more than additive, however (4*c*). The same is true for the $MeCHCOCH_3$ and MeCHCOPh radicals where the observed RSEs (or ΔBDEs), relative to CH_3-H (BDE = 105 kcal/mol) (7) are 17 and 16 kcal/mol, respectively, compared to (7 + 12 = 19) and (7 + 11 = 18), respectively, for the individual effects. Also, the combined RSE for $PhCH_2$• and $PhCOCH_2$• is 29 (17 + 12) whereas the RSE for the PhCHCOPh radical is only 22.5 (Table 1). These data support our recent conclusion that the presence of both donor and acceptor functions attached to a carbon or nitrogen-centered radical results in little or no synergism (11).

Examination of Table 1 shows that, when G in $PhCOCH_2G$ is PhCO, MeCO, or CN, the ΔBDEs are 0, 1, and 3 kcal/mol, respectively. Apparently electron acceptor groups play a dual role toward the radical, stabilizing it by virtue of their delocalizing ability, but destabilizing it by virtue of their *F* effects. When G is SO_2Ph or Me_3N^+ the *F* effects on the radical are dominant, and are destabilizing by 2 and 4 kcal/mol, respectively, in the $PhCOCH_2G$ systems. Radical destabilizing (bond strengthening) effects by these electron-withdrawing groups have been observed previously in other systems (3*d*, 3*e*).

Acidities and BDEs for cyclic ketones

In Table 2 we present acidity and oxidation potential data for a number of cyclic ketones and open-chain analogues.

Examination of Table 2 shows that the acidities of the cycloalkanones in DMSO are remarkably similar to that of the open-chain analogue, 3-pentanone. Cyclobutanone, cyclopentanone, and cyclohexanone are 1–2.5 kcal/mol more acidic than 3-pentanone, and the C_7, C_8, C_{10}, and C_{12} cycloalkanones have acidities within ±0.4 kcal/mol of 3-pentanone. The peaks for the cyclic voltammograms (CVs) for the enolate ions derived from cycloalkanones, as well as from open-chain ketones, are relatively narrow and are reproducible. For the cycloalkanones and 3-pentanone the BDEs estimated for the acidic C—H bonds are all identical (88 kcal/mol). For comparison, the C—H bonds in C_4, C_5, C_6, and C_7 cycloalkanes are all 94.5 ± 2 (7).

1-Indanone was found to be 1.9 kcal/mol more acidic than its open-chain analogue, propiophenone, and its BDE is estimated to be 1 kcal/mol higher. 2-Indanone is 2.5 kcal/mol more acidic than its open-chain analogue 1,3-diphenylacetone, and its BDE is estimated to be 3 kcal/mol lower. The pK_{HA} and BDE of 2-indanone are 8 and 10 kcal/mol lower, respectively, than that of 1-indanone, as expected for benzylic vs. non-benzylic α-hydrogens.

Radical cation acidities of ketones

Radical cation acidities for the acidic C—H bonds in fluorene, cyclopentadiene, phenylacetonitrile, benzyl phenyl sulfone, and a number of their derivatives have been estimated previously by eq. [1] (3). The validity of this method has been supported by the observation of a linear plot for $pK_{HA^{+\cdot}}$ in the gas phase vs. $pK_{HA^{+\cdot}}$ in DMSO solution for radical cations derived from $PhCH_2CN$, Ph_2CH_2, $PhCH_3$, cylopentadiene, fluorene, thiophenol, phenol, and aniline (3*h*). There appears to be no previous report of the radical cation acidity of a ketone. Examination of Table 2 shows that the ketone radical cations are all super acids with $pK_{HA^{+\cdot}}$ values in the −24 to −31 range. There is no obvious trend in acidity caused by structural changes in the ketones. The oxidation potentials of the ketones are all strongly positive, which necessitated a change in the solvent from DMSO to CH_3CN. (DMSO itself has an E_{OX} (HA) of about 1.5.) The radical cation acidities of *p*-substituted acetophenones in the series H, *p*-Me, *p*-MeO (−24, −20, −12) follow the same trend as in the series $GC_6H_4CH_2SO_2Ph$ (−25, −18, and −12) (12*a*) and in the series $GC_6H_4CH_2CN$ (−32, −28, −19) (12*b*). This suggests that in all three series the electron is being removed from the GC_6H_4 moiety to form the radical cation.

Remote substituent effects on acidities and BDEs of acetophenones

In an earlier paper we presented a Hammett plot for the acidities in DMSO of 14 *m*- and *p*-substituted acetophenones with a ρ = 3.55 and a correlation coefficient, R^2 = 0.998 (13). Oxidation potentials for ten of these acetophenones and their conjugate bases, along with their pK_{HA}'s are given in Table 3.

Examination of Table 3 shows that remote electron-accepting groups (*p*-CN, *p*-Cl, *m*-Cl, and *m*-Br) acidify acetophenone by 2–3.7 kcal/mol, but these effects on BDE are offset in eq. [1] by shifts of E_{OX} (A^-) to more positive potentials by 1.1–3.9 kcal/mol. As a consequence, there is no change in BDE. On the other hand, the donor groups (*p*-CH_3, *m*-CH_3, *p*-NH_2, *p*-MeO) decrease the acidity of acetophenone by 0.4–1.37 kcal/mol, and these effects are for the most part *augmented* by small positive shifts in E_{OX} (A^-) values in eq. [2]. The result is about

Can. J. Chem. Downloaded from www.nrcresearchpress.com by 91.121.58.235 on 09/07/12
For personal use only.

TABLE 2. Equilibrium acidity and oxidation potential data for cyclic ketones and open-chain ketone models in DMSO

Ketone	pK_{HA}[a]	E_{OX} (A^-)[b]	BDE[c]	E_{OX} (HA)[d]	$pK_{HA^{+\bullet}}$[e]
Acetone	26.5	+0.076	94	3.299	−28
		(100)		(170)	
3-Pentanone	27.1	−0.203	88	3.203	−30
		(70)		(170)	
Cyclobutanone	25.3				
Cyclopentanone	25.8	−0.151	88	3.088	−29
		(70)		(130)	
Cyclohexanone	26.4	−0.191	88	2.945	−26
		(60)		(170)	
Cycloheptanone	27.8	−0.246	88	3.102	−29
		(70)		(160)	
Cyclooctanone	27.4				
Cyclodecanone	26.7				
Cyclododecanone	26.9	−0.183	88	3.245	−31
		(90)		(180)	
Propiophenone	24.4	−0.065	88	3.096	−29
		(60)		(150)	
1-Indanone	23.0	+0.065	89	2.880	−24
		(70)		(90)	
1,3-Diphenylacetone	18.7	+0.059	82	2.802	−27
		(60)		(170)	
2-Indanone	16.9	0.000	79	2.573	−26
	(60)		(100)		

[a]Measured in DMSO against two or more indicators as described in earlier papers.
[b]Measured by cyclic voltammetry under the conditions previously described and referenced to the standard hydrogen electrode (3, 4). Numbers in parentheses are wave widths in mV.
[c]Estimated by eq. [2].
[d]Measured in acetonitrile under the conditions previously described.
[e]Estimated by eq. [1].

TABLE 3. Acidities and oxidation potentials for acetophenones, *m*- and *p*-$GC_6H_4COCH_3$, in DMSO

G	pK_{HA}[a]	E_{OX} (A^-)[b]	BDE[d]	E_{OX} (HA)[e]	$pK_{HA^{+\bullet}}$[f]
p-CN	22.0	0.314	93	3.448	−31
		(60)		(180)	
		0.302[c]			
p-Cl	23.8	0.192[c]	93	3.096	−25
m-Cl	23.2	0.232[c]	93	3.151	−26
m-Br	23.2	0.237[c]	93		
H	24.7	0.143	93	3.062	−24
		(60)		(190)	
		0.133[c]			
p-CH_3	25.2	0.145	94	2.836	−20
		(70)		(190)	
m-CH_3	25.0	0.152[c]	94		
p-NH_2	25.3	0.153	94		
		(70)			
p-MeO	25.7	0.092	93	2.329	−12
		(60)			
m-MeO	24.5	0.192[c]	94		

[a]Reference 11.
[b]Measured by cyclic voltammetry under the conditions previously described, and referenced to the standard hydrogen electrode. Numbers in parentheses are wave widths in mV.
[c]Measured by C. A. Wilson.
[d]Estimated by eq. [2].
[e]Measured in acetonitrile.
[f]Estimated by eq. [1].

a 1 kcal/mol increase in BDE for the acidic C—H bonds in these acetophenones. The E_{OX} (A^-) values for remote *p*-donor substituents in arylacetonitriles (12*b*, 14), and benzyl phenyl sulfones (12*a*), have been shown to become more negative as their donor properties increase along the series *p*-Me, *p*-MeO, *p*-NH_2. Although these effects are offset in eq. [2] to some extent by small increases in pK_{HA}, the net result for *p*-Me and *p*-NH_2 groups is a small *decrease* in BDE, relative to G = H. The difference in the present instance is that the acidic site is separated from the ring by the carbonyl group and the donor groups such as *p*-Me and *p*-NH_2 cannot interact directly to stabilize the incipient radical. Their major effect is apparently to stabilize the parent acetophenone. The lowered ground state energy raises the pK_{HA} and also leads to a small increase in BDE.

Experimental

The ketones were for the most part commercial samples that were carefully purified prior to pK_{HA} or oxidation potential measurements.

Strongly basic indicators, such as 9-phenylxanthenide ion (pK_{HA} = 27.9) have been shown to add to the carbonyl group of ketones lacking α-hydrogen atoms, such as benzophenones. Addition of acetone to a DMSO solution containing fluorenide ion (pK_{HA} = 22.6) caused no change in absorbance, other than that caused by dilution, however. Experiments such as this, together with the consistency of the E_{OX} (A^-) measurements, indicate that addition to the carbonyl group does not compete with proton transfer reactions in the formation of these enolate ions.

Can. J. Chem. Downloaded from www.nrcresearchpress.com by 91.121.58.235 on 09/07/12
For personal use only.

Equilibrium acidities in DMSO were measured by an overlapping indicator method (2). Cyclic voltammograms were measured by the method described earlier (4*b*). The oxidation potentials of the enolate ions gave irreversible waves that were, however, narrow and reproducible. Some gave small shoulders at more negative potentials, prior to the much stronger main peak. The oxidation peaks for the ketones themselves were strong and broad, but not so readily reproduced.

Acknowledgments

We are grateful to Craig A. Wilson for some of the cyclic voltammetric measurements on *m*- and *p*-substituted acetophenone enolate ions, and to Frederick J. Cornforth, Walter S. Matthews, and Noel R. Vanier for the pK_{HA} measurements of the ketones. This work was supported by the National Science Foundation.

1. Y. CHIANG, A. J. KRESGE, and P. A. WALSH. J. Am. Chem. Soc. **108**, 6314 (1986), and references cited therein.
2. F. G. BORDWELL. Acc. Chem. Res. **21**, 456 (1988).
3. (*a*) F. G. BORDWELL and M. J. BAUSCH. J. Am. Chem. Soc. **108**, 2473 (1986). (*b*) F. G. BORDWELL, J.-P. CHENG, and M. J. BAUSCH. J. Am. Chem. Soc. **110**, 2869 (1988); J. Am. Chem. Soc. **110**, 2872 (1988); (*d*) J. Phys. Org. Chem. **1**, 209 (1988); (*e*) F. G. BORDWELL, M. J. BAUSCH, J. C. BRANCA, and J. A. HARRELSON, JR. J. Phys. Org. Chem. **1**, 225 (1988); (*f*) F. G. BORDWELL, D. J. ALGRIM, and J. A. HARRELSON, JR. J. Am. Chem. Soc. **110**, 5904 (1988); (*g*) F. G. BORDWELL, J.-P. CHENG, S. E. SEYEDREZAI, and C. A. WILSON. J. Am. Chem. Soc. **110**, 8178 (1988); (*h*) F. G. BORDWELL and J.-P. CHENG. J. Am. Chem. Soc. **111**, 1793 (1989).
4. (*a*) F. G. BORDWELL, J.-P. CHENG, and J. A. HARRELSON, JR. J. Am. Chem. Soc. **110**, 1229 (1988); (*b*) F. G. BORDWELL, J. A. HARRELSON, JR., and A. V. SATISH. J. Org. Chem. **54**, 3101 (1989); (*c*) F. G. BORDWELL and T.-Y. LYNCH. J. Am. Chem. Soc. **111**, 7558 (1989); (*d*) F. G. BORDWELL, M. J. BAUSCH, J.-P. CHENG, T. A. CRIPE, and M. E. MUELLER. J. Org. Chem. **55**, 58 (1990).
5. R. W. TAFT and F. G. BORDWELL. Acc. Chem. Res. **21**, 463 (1988).
6. F. G. BORDWELL, J. E. BARES, J. E. BARTMESS, G. J. MCCOLLUM, M. VAN DER PUY, N. R. VANIER, and W. S. MATTHEWS. J. Org. Chem. **42**, 321 (1977).
7. D. F. MCMILLEN and D. M. GOLDEN. Annu. Rev. Phys. Chem. **33**, 473 (1982).
8. J. L. HOLMES, F. P. LOSSING, and J. K. TERLOUW. J. Am. Chem. Soc. **108**, 1086 (1986).
9. R. K. SOLLY, D. M. GOLDEN, and S. W. BENSON. Int. J. Chem. Kinet. **2**, 381 (1970).
10. A. T. BALABAN. Rev. Roum. Chim. **16**, 725 (1971); (*b*) R. W. BALDOCK, P. HUDSON, A. R. KATRITZKY, and F. SATI. J. Chem. Soc. Perkin Trans. 1, 1422 (1974); (*c*) H. G. VIEHE, Z. JANOUSEK, R. MERÉNYI, and L. STELLA. Acc. Chem. Res. **18**, 148 (1985).
11. F. G. BORDWELL, J. A. HARRELSON, JR., and T.-Y. LYNCH. J. Org. Chem. **55**, 3337 (1990).
12. (*a*) F. G. BORDWELL, M. J. BAUSCH, J. C. BRANCA, and J. A. HARRELSON, JR. J. Phys. Org. Chem. **1**, 225 (1988); (*b*) F. G. BORDWELL, J.-P. CHENG, M. J. BAUSCH, and J. E. BARES. J. Phys. Org. Chem. **1**, 209 (1988).
13. F. G. BORDWELL and F. J. CORNFORTH. J. Org. Chem. **43**, 1763 (1978).
14. F. G. BORDWELL and M. J. BAUSCH. J. Am. Chem. Soc. **108**, 1979 (1986).

Can. J. Chem. Downloaded from www.nrcresearchpress.com by 91.121.58.235 on 09/07/12
For personal use only.

Isotope effects in solution: contrasts between muonium and hydrogen in reactions with acetone

DAVID C. WALKER
Chemistry Department and TRIUMF, University of British Columbia, Vancouver, B.C., Canada V6T 1C6

Received March 7, 1990

This paper is dedicated to Professor Ross Stewart on the occasion of his 65th birthday

DAVID C. WALKER. Can. J. Chem. **68**, 1719 (1990).

Munonium atoms are hydrogen isotopes with positive muons rather than protons, deuterons, or tritons as nuclei. Thus, they have one ninth the mass of ^{1}H, and microsecond lifetimes. By using nuclear physics counting techniques, muonium can be studied in a wide variety of media and its chemical and physical properties used to appraise hydrogen. Results are described for the interaction of muonium with acetone, showing two types of kinetic isotope effects, formation of free radicals, evidence for intermolecular "muonium bonding", and micelle-induced enhancements of reaction rate constants.

Key words: isotope effects, muonium atoms, muonium bonding, thiyl radicals, micelles.

DAVID C. WALKER. Can. J. Chem. **68**, 1719 (1990).

Les atomes de muonium sont des isotopes de l'hydrogène incorporant des muons positifs pluôt que des protons, des deutérons ou des tritons comme noyaux. Ils ont donc une masse qui est neuf fois plus faible que celle du ^{1}H et des temps de vie de l'ordre de la microseconde. Utilisant des techniques de comptage issues de la physique nucléaire, on peut étudier le muonium dans un grand nombre de milieux et on peut utiliser ses propriétés physiques et chimiques pour évaluer l'hydrogène. On décrit les résultats obtenus lors de l'interaction entre le muonium et l'acétone; ces résultats permettent de mettre en évidence deux types d'effets isotopiques cinétiques, la formation de radicaux libres, des données suggérant l'existence de liaisons muonium intermoléculaires ainsi que des accélérations des constantes des vitesses de réactions induites par des micelles.

Mots clés : effets isotopiques, atomes de muonium, liaisons muonium, radicaux thiyles, micelles.

[Traduit par la revue]

Can. J. Chem. Downloaded from www.nrcresearchpress.com by 91.121.58.235 on 09/07/12
For personal use only.

Introduction

(a) Muonium

The proton is a unique chemical species (1), being a bare nucleon, while the positive muon is unique in being a lepton acting as a nucleus. When given orbital electrons these two "elementary" particles form a pair of atoms whose comparisons show some of the best isotope effects, and some surprises.

Muons are formed as decay products of pions (lifetime 26 ns) and live for 2 μs before decaying to positrons, as in [1].

[1] $\pi^+ \rightarrow \mu^+ + \nu_\mu \qquad \mu^+ \rightarrow e^+ + \nu_e + \bar{\nu}_\mu$

Table 1 gives the basic physical properties of ^{1}H, ^{2}H(D), ^{3}H(T) compared to muonium (Mu, the atom with a positive muon as its nucleus). Mu has virtually the same size and shape of electron orbital as the others, therefore it has almost the same ionization energy, van der Waals radius, polarizability, etc. Any "chemical" difference between Mu and the other H-isotopes should arise primarily from their diverse atomic masses, which differ by factors of 9, 18, and 27. They also differ from each other in nuclear magnetic moments, so this confers on them distinguishable hyperfine interactions and magnetic resonance phenomena.

(b) Kinetic isotope effects, k_M/k_H

For bimolecular reactions in solution, there are three mass-dependent factors that enter into the simple empirical analysis of a rate constant: (i) the encounter frequency, (ii) the activation barrier, and (iii) the quantum mechanical tunneling coefficient.

For (i), the muonium rate constant, k_M, should be greater than that of H, k_H, by a factor of three, the inverse ratio of the square roots of the masses, based on mean thermal velocities. This seems to apply for simple gas phase reactions (2), but not for Mu reactions in solution (3). In water, both Mu and H reactions reach the same maximum rate constants at the diffusion-controlled limit, and show a temperature dependence characteristic of water's viscosity ($E \sim 17$ kJ/mol, as in the top line of Fig. 1(b)). Consequently, the diffusion of both Mu and H must be governed by the structure of water rather than by their intrinsic velocities (4). This was a surprise, but it has been rationalized by simulation studies that indicate the atoms are significantly clathrated in water (5).

For (ii), the popular rule-of-thumb "lighter isotope reacts faster" does not apply when the isotopes react as atoms. This is because only the isotopic differences in the zero point energies of the transition states affect the activation barrier (see Fig. 1(a)), whereas the "rule" applies to the breaking of C—H compared with C—D, where zero point energy differences are larger in the reactants than in the transition states. Thus, for reactions with large energy barriers, Mu is expected to be slower that H if this term dominates, and there are examples in both gaseous (2, 6) and liquid phases (3) where it evidently applies. For example, the reaction of Mu with HCO_2^- in water (lowest line of Fig. 1(b)) has an activation energy of 33 kJ/mol and k_M/k_H is 0.03 (3), so it looks like a zero point energy effect on the transition states.

For (iii), muonium is so light that even at room temperature there is evidence of significant tunneling. This should strongly favour Mu over H, even though the width and height of the barriers are somewhat larger, because quantum mechanical barrier penetration has an inverse exponential mass dependence. The best example here is Mu + $F_2 \rightarrow$ MuF + F (7), and is confirmed by theory (8). An example in water seems to be the Mu + NO_3^- reaction, where the measured pre-exponential factor ($A = 7 \times 10^{10}$ M^{-1} s^{-1}) and activation energy ($E_a = 6$ kJ/mol) are both remarkably small (3). These data suggest the type of behaviour indicated by the middle line of Fig. 1(b), where an activation-controlled reaction is subsumed by its tunneling component in the lower temperature range.

Kinetic isotope effects have been found to range from >100 to <0.01 for Mu versus H, in water, as seen in the sample of data quoted in Table 2. Dividing them up into various combina-

TABLE 1. Basic physical properties of Mu compared with H, D, and T

Property	Mu	^{1}H	^{2}H(D)	^{3}H(T)
Atomic mass/$m_{(e)}$	207.7	1837	3675	5498
Reduced mass ($Mm/(M + m)$)	0.9952	0.9994	0.9997	0.9998
Bohr radius/pm	53.17	52.95	52.93	52.93
Ionization energy/eV	13.54	13.597	13.602	13.603
Nuclear spin	½	½	1	½
Nuclear magnetic moment/BM	8.886	2.793	0.8574	2.979
Mean nuclear lifetime/s	2.2×10^{-6}	$>3 \times 10^{40}$	$>10^{38}$	5.6×10^{8}

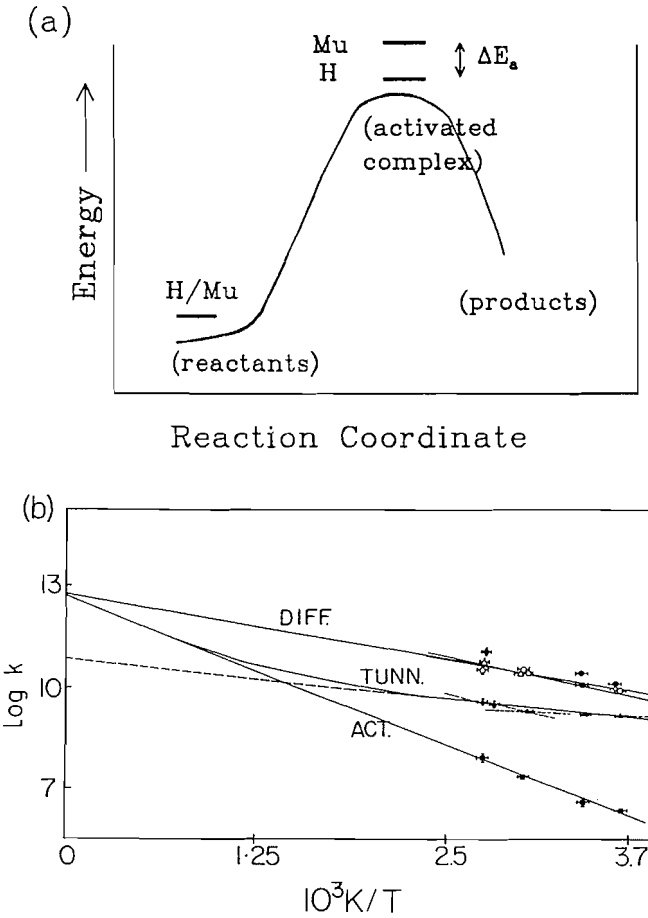

FIG. 1. Schematic illustrations of (a) zero point energy effects for reactions of atoms, showing the origin of the difference in activation barriers (ΔE_a) of Mu compared to H, and (b) Arrhenius plots with quantum mechanical tunneling (TUNN) contributing significantly to an activation-controlled reaction (ACT) so that its rate approaches that of a diffusion-limited rate (DIFF). The right-hand side of this figure shows actual data obtained in water (3, 4). The middle line represents reaction of Mu with NO_3^-. Its slope and intercept, obtained from the region of observation, both *appear* to be much smaller than the others. This is characteristic of tunneling.

tions of the above three components is impossible, and there are solvation and "cage" effects to include as well. Thus, at best, one can suppose that tunneling makes a substantial contribution when Mu is strongly favoured, and that transition state energy differences dominate when H is favoured. For the two reactions of Mu with acetone both extremes may be present (see later).

Muonium may not be the physical-organic chemists' choice reagent, but it readily attacks the benzene ring to form muonated cyclohexadienyl radicals (which live for at least a microsecond),

TABLE 2. Sample of observed kinetic isotope effects (k_M/k_H) in water at ~295 K

Solute	$k_M/M^{-1}\,s^{-1}$	k_M/k_H^a	Type of reaction (conjectured)
NO_3^-	1.5×10^9	150	?
Acetone	9×10^7	34	Addition (to O)
CH_3CSNH_2	3×10^{10}	5	Addition (to C)
O_2	2.4×10^{10}	~2	Combination or spin exchange
I_2	1.7×10^{10}	~1	Abstraction (−MuI + I)
Ni^{2+}	1.7×10^{10}	—	Spin exchange
MnO_4^-	2.5×10^{10}	1	Reduction
Ag^+	1.6×10^{10}	0.5	Reduction
Acrylamide	1.9×10^{10}	1	Addition
Styrene	2×10^{10}	—	Addition to side chain
Benzene	3×10^9	—	Addition into ring
OH^-	1.7×10^7	1	Proton (μ^+) transfer
HCO_2^-	8×10^6	0.03	Abstraction of H
2-propanol	1.0×10^6	0.01	Abstraction of inner H
CH_3CONH_2	$<10^5$	—	No reaction

[a]Muonium rate constants, k_M, taken from tables in refs. 4 and 11; hydrogen rate constants, k_H, taken from tables in ref. 12.

and the tools available for studying it reveal how much addition actually occurs at each *ortho, meta,* and *para* position, for any substituent or pairs of substituents. It means one can calculate *absolute* rate constants for each directional isomer. This has been done for single substituents and for substituted benzoic acids in water (9). When plotted against Hammett σ-parameters, these results show muonium to be weakly nucleophilic, with $\rho \sim +0.3$. This is opposite to H, which is reported to be electrophilic for ring additions, with $\rho \sim -0.5$ (10).

Perhaps ρ is more often used in conjunction with equilibrium data than with absolute rate constants (as here) but, regardless of whether it is kinetic or thermodynamic in orgin, the question arises as to whether the difference between Mu and H stems primarily from their small differences in atomic ionization energies (see Table 1). Another question raised is whether this nucleophilic character of Mu may have bearing on the fact that (i) it adds to a carbonyl group much faster than does H, and (ii) that Mu adds to the O of a C=O group but to the C of a C=S group (as discussed below).

2. Experimental

Reaction rate constants are most directly measured by using a short impulse of energy to produce the reactive species, and then following its concentration by kinetic spectrometry. H-atoms can be produced from hydrated electrons by pulse radiolysis of strongly acidic water, and have their concentrations monitored by ESR spectroscopy or VUV photometry. Substantial tables of k_H values have become available by these techniques (12). Muonium, on the other hand, needs a muon beam, such as is available at the TRIUMF cyclotron, and fast nuclear

Can. J. Chem. Downloaded from www.nrcresearchpress.com by 91.121.58.235 on 09/07/12
For personal use only.

Can. J. Chem. Downloaded from www.nrcresearchpress.com by 91.121.58.235 on 09/07/12
For personal use only.

physics counting equipment. Given those facilities, however, Mu can be studied with better time resolution, without the need for an acidified water medium, and with greater versatility than can H.

The basic principles of the two techniques used for Mu studies will be outlined briefly here. They were both developed for physics but quickly applied in chemistry. Muon Spin Rotation (μSR) is used for muonium rate constants, fractional muon yields (P-values), and muon hyperfine coupling constants ($A\mu$), whereas Level Crossing Resonance (LCR) provides information on muonated free radicals, their structure, yields, and occasionally their rate and mode of formation.

(a) Muon spin rotation (μSR) studies

Details of this technique are available elsewhere (13). It is a single particle counting method in which each muon is timed as it arrives at the sample and its decay position is timed when it is emitted. A lifetime histogram is then composed from 5–50 million such events.

It transpires that there is a breakdown of the parity-invariance principle in both steps of eq. [1], which results in the muon being formed as a spin-polarized particle, then decaying by emitting its positron along its instantaneous spin direction. Use is made of both these asymmetries in the spin rotation method. The sample is placed in a fixed transverse magnetic field so that each muon's spin precesses at a frequency characteristic of that muon's chemical state. A small detector for positrons in the plane of precession sees an oscillation at this frequency superposed on its ordinary muon lifetime histogram. In pure water the oscillation that corresponds to muonium lasts for several microseconds, but as a reactive solute is added it is damped accordingly. Figure 2 shows typical histograms in a field of 8 G with muonium observable as the small ripple. An eight-parameter MINUIT χ^2- minimization fitting procedure gives the munonium relaxation as one of these parameters. The experiment is repeated at different solute concentrations, so that a plot of relaxation against solute concentration produces the bimolecular rate constant k_M.

Muonium-containing free radicals can also be detected at precession frequencies related to their hyperfine coupling constants and split by the various protons present. In the high field limit, as used in ENDOR, these merge to just a pair of frequencies whose sum equals A_μ (14). In all μSR studies the state to be observed has to be formed rapidly enough that there is no precession in a prior muon state, in order for the spins to all precess coherently. For radical formation in solution this is a serious disadvantage.

The μSR technique allows different initial types of chemical states of muons to be determined. These are presented as fractional yields (P) and appear in four forms: as muonium atoms, P_M, as free radicals, P_R, and as diamagnetic species, P_D. When these sum to less than 1.0 the deficit is described as the missing fraction and designated P_L.

(b) Level crossing resonance (LCR) studies

In the LCR technique (15), the sample is held in a longitudinal magnetic field and the total number of muons emitting their positrons in the forward direction is compared with those going backwards. The integrated forward-to-backward difference is studied as a function of field. There are resonance fields (B_R) where the Zeeman-split levels of the muon and a proton of the radical cross. At this field, spin polarization is transferred from muon to proton via their mutual hyperfine couplings in the radical. This results in some loss of the intrinsic polarization of the muon, and hence a decrease of the forward-to-backward asymmetry. A small modulation field of ~50 G is usually applied to maximize the signal-to-noise ratio, and this gives the plots a "differential" appearance. Figure 3 shows typical LCR spectra. Fitting programs allow for the "best" values to be obtained for B_R, and for intensity. The former is related to A_μ and to any proton hyperfine coupling constants of the radical, A_H, by eq. [2] (15)

$$[2] \qquad B_R = \frac{1}{2}\left[\frac{A_\mu - A_H}{\gamma_\mu - \gamma_H} - \frac{A_\mu^2 - 2MA_H^2}{\gamma_e(A_\mu - A_H)}\right]$$

where the γ's are magnetogyric ratios of muon, proton, and electron and M is the sum of the quantum numbers at the resonance.

The intensity can be used to evalutate the yield of that particular radical (P_R) by eq. [3] (16)

$$[3] \qquad P_R = \frac{(\Delta B)^2 \mathrm{ampl}(\gamma_\mu - \gamma_H)^2}{A_{bf}\nu_R^2}$$

where ΔB and "ampl" are the fitted width and amplitude of the LCR spectra, A_{bf} is the experimental asymmetry, and ν_R the LCR frequency.

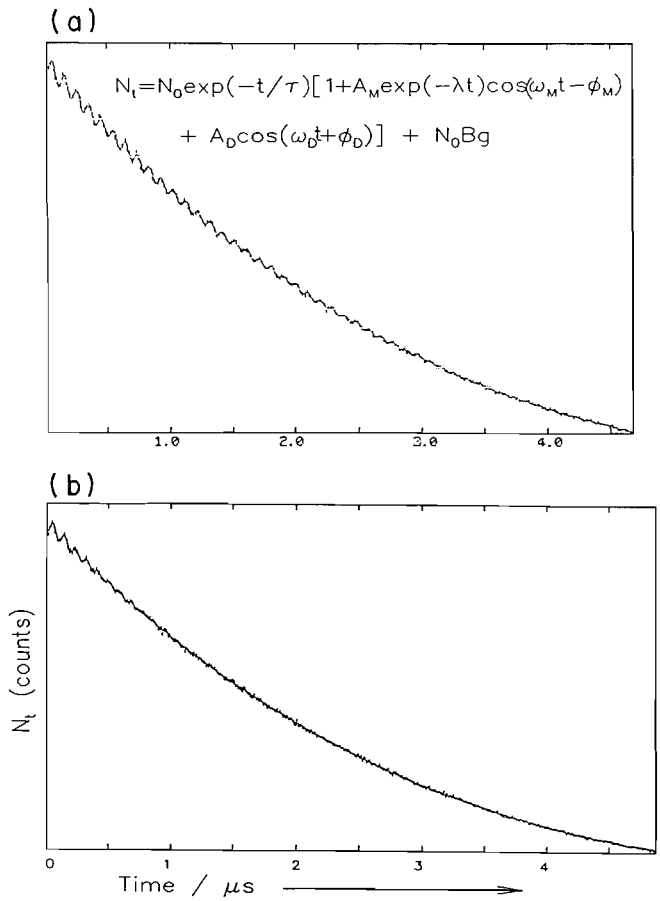

FIG. 2. Typical μSR lifetime histograms in transverse fields of 8 G for (a) pure water, showing a long-lived muonium signal as the ~10 MHz oscillation, and (b) a dilute aqueous solution of a reactive solute like acetone, showing damping of the superposed muonium oscillation due to chemical reaction. (The μSR "fitting" equation is given in (a), with λ as the muonium relaxation parameter.)

(c) Reactions in micelles

Addition of amphiphilic "surfactant" molecules to water at concentrations above their critical micelle concentration causes them to coalesce into micelles. These have hydrocarbon cores capable of solubilizing organic molecules that would otherwise be insoluble in water. This micellization of a solute can change k_M markedly (17). Such changes have been interpreted through a kinetic model (18) that is based on steady-state and pre-equilibrium conditions, arising from the much shorter mean residence time of Mu at a micelle (~2 ns (19)) than either its lifetime (2 μs) or the time to diffuse between micelles ($1/k_d$[micelle]). In the presence of added micelles the muonium rate constant is designated k_M(mic), and the ratio k_M(mic)/k_M changes markedly with *type* of reaction (17).

LCR can be used to observe the free radicals produced by reaction of Mu with unsaturated organic solutes solubilized in water by micelles. For benzene, styrene, vinyl acetate, acrylonitrile, and others, in dilute aqueous micelles, the same Mu radical is found as in these pure organic liquids, with its yield corresponding to the yield of muonium in water (20). But for acetone it is different.

Can. J. Chem. Downloaded from www.nrcresearchpress.com by 91.121.58.235 on 09/07/12
For personal use only.

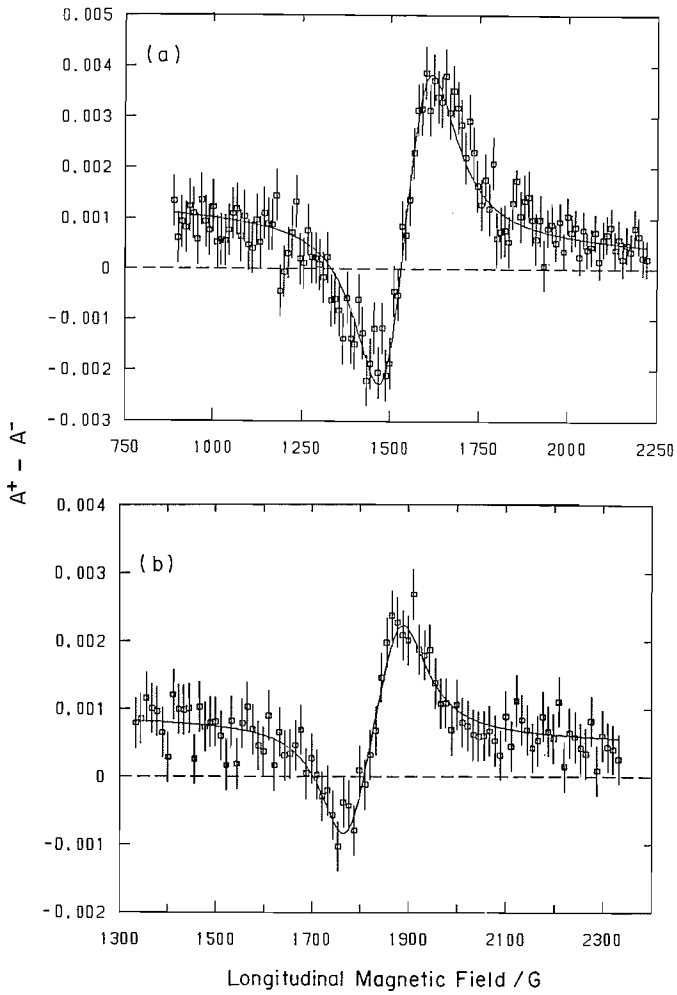

FIG. 3. The LCR spectra of (a) pure acetone, and (b) 0.1 M acetone in water, given as $A^+ - A^-$ (ordinate) against applied longitudinal magnetic field (abscissa) in gauss. A^+ is the normalized difference between forward-to-backward count rates with a positive modulation field, and A^- with the modulation field negative. These are typical LCR plots, showing transfer of muon spin polarization from the muon to a proton at a resonant level crossing field. In (a) the resonance field is centred at 1.540 kG, in (b) at 1.820 kG.

3. Results obtained for acetone

Table 3 summarizes most of the LCR and μSR data obtained for acetone, both as a solute in solution and as a pure liquid. Interactions between muons and acetone show quite a variety of results.

When a pure liquid is studied by either of these techniques, the high-energy charged particle (μ^+) may undergo chemical reactions in that state before reaching thermal energy, so that the muonated products observed can have *ionic* or *hot* precursors. These are "direct" effects. When acetone is present as a dilute solute in an inert solvent like water or hexane, however, the muon initially interacts mainly with solvent and some of them form muonium. Such Mu-atoms then undergo "secondary" reactions with solutes. It is in these dilute solutions that contrasts with reactions of H-atoms are evident.

The extent to which acetone's overall muon chemistry is representative of compounds containing carbonyl groups remains to be fully explored, but it certainly reacts much faster than acetamide and much slower than thioacetamide (see Table 2).

(a) Reaction rate constants in water

From the measured rates of disappearance of Mu and H in dilute acetone solutions at pH = 1 the overall isotope effect is seen to favour Mu by a factor of 34. There is almost no pH dependence on the Mu reaction, so it can probably also be ignored for the H reaction. Product analysis of the H reaction has shown there are two channels (21), with addition via reaction [3] being only half as fast as abstraction via reaction [4].

[3] $(CH_3)_2CO + H \rightarrow (CH_3)_2\dot{C}OH, \quad k_3 = 9 \times 10^5$ (21)

[4] $(CH_3)_2CO + H \rightarrow CH_3C\dot{O}CH_2 + H_2, \quad k_4 = 1.9 \times 19^6$ (21)

Mu, on the other hand, reacts predominantly via the addition pathway [5].

[5] $(CH_3)_2CO + Mu \rightarrow (CH_3)_2\dot{C}OMu, \quad k_5 = 9 \times 10^7$ (22)

The reason for this conclusion is that the yields of radicals show complete conversion of all muonium to radicals, and the fact that k_M equals the radical formation rate constants, k_f. Both are detailed below. It means that an abstraction reaction analogous to [4] involving Mu (reaction [6])

[6] $(CH_3)_2CO + Mu \rightarrow CH_3C\dot{O}CH_2 + MuH, \quad k_6 < 9 \times 10^6$

cannot be detected, though it could easily be there at the 10% level.

With two reaction paths we have two kinetic isotope effects. (a) For the addition reaction, $k_{M[5]}/k_{H[3]}$ equals $9 \times 10^7/9 \times 10^5$, i.e., 100. (b) For the abstraction of a hydrogen atom from acetone, $k_{M[6]}/k_{H[4]}$ must be less than $9 \times 10^6/1.9 \times 10^6$, i.e., <5. The latter is based on the presumption that the abstraction reaction [6] with Mu is *at most* 10% of the addition reaction [5]. In fact, most abstraction reactions favour H over Mu by about 10^2 (4), as with 2-propanol and formate (Table 2), so this may well be too large, even by two or three orders of magnitude.

(b) Muonated free radicals in acetone

The LCR spectra obtained in pure acetone and in 0.1 M acetone in water are shown in Figs. 3 (a) and (b). They undoubtedly arise from the same radical, but there is a shift in B_R of 280 MHz and a large change in amplitude.

The spectral shift can be attributed to a change in A_μ, rather than to the A_H of eq. [2], because a similar shift was found in A_μ by transverse field μSR (23). It is interpreted as a change in the degree of hydrogen bonding, here muonium bonding, between the Mu of the free radical and O-atoms of the molecules composing its microenvironment (23). In a pure acetone environment hydrogen bonding will be much weaker than it will be in an aqueous medium. The shift is such that A_μ is smaller when Mu has more restricted rotation around the C—O bond axis (the C—O—Mu angle is expected to be ~120 degrees). This corroborates an earlier suggestion that the hyperfine coupling constant of -O-Mu relative to -O-H is much larger than normal isotope effects, due to it being a difference in moments of inertia, rather than simply differences in vibrational modes (24). Acetone was the first example in which there was an isotope effect greater than twice the ratio of nuclear magnetic moments, and it differs from other radicals in having Mu attached to O. Table 3 gives the ratio of muon-to-proton hyperfine coupling constants for this radical formed by addition of Mu and H to the C=O group of acetone, and the ratio of 9 has already been compensated for the factor of 3.18 in nuclear magnetic moments.

The muonated free radical yield in pure acetone has been

TABLE 3. μSR and LCR data for acetone as the reactive ingredient

Parameter	Values and conditions	Reference
k_M	9×10^7 at pH = 1; 1.1×10^8 at pH = 7	4, 27
k_f[a]	8.5×10^7 (±25%)	22
k_M/k_H	34 (overall); 100 (for addition)	
k_M(mic)	2.5×10^{10} in CTAB (3 solutes/micelle)	27
k_M(mic)/k_M	290 (overall); >2700 (for abstraction)	
B_R	1.540 kG in pure acetone	22
	1.425 kG in hexane	22
	1.820 kG in water	22
A_{H_β}[b]	55.5 MHz in all three media	22
A_μ	26.1 MHz in pure acetone	14
	29.4 MHz in hexane	22
	22.0 MHz in water	23
A_μ/A_p[c]	9.1[d]	11
P_R	0.41 (in pure acetone)	24
	0.27 (in 5 M acetone in water)	22
	0.16 (at 0.1 M); 0.11 (at 0.01M)	22

[a] k_f is the rate constant for the formation of radicals.
[b] This is the hyperfine coupling constant of the six hydrogens in the $(CH_3)_2COMu$ radical.
[c] The muon-to-proton isotope ratio of hyperfine coupling constants for the radicals formed when Mu and H add to the O of acetone.
[d] Actual ratio is 29; but this is divided by 3.18, due to the muon's nuclear magnetic moment being that much bigger, in order to separate out the genuine isotope effect.

estimated from transverse field μSR to be 0.45 ± 0.03 (24). Also, the diamagnetic yield is known to be 0.54 (4), so all muons in acetone are accounted for. They either form diamagnetic species directly or they produce the radical of reaction [5]. Therefore there is no "missing fraction" on the μSR timescale, as there would have been with a slow abstraction reaction, because Mu would be dephased in the transverse field of a P_D measurement. This is the first of the reasons leading us to conclude that reaction [5] completely dominates over reaction [6].

For the 0.1 M acetone solution in water the free radical yield is much smaller than in pure acetone, and has been evaluated using eq. [3] to be 0.16 (22) (equal to the scavengable muonium yield in water for those conditions). In experiments with 0.01 M acetone, the yield was found to be smaller still (0.11) (22), as given in Table 3. This difference is due to significant radioactive decay of the muon in muonium *prior* to it being scavenged by acetone, particularly at the lowest concentration. (One can see this from the *overlap* of the timescale for reaction ($1/k_M(0.01)$ = 1.1 μs) with the intrinsic muon lifetime (2 μs).) From the ratio of these yields (0.16/0.11) one then calculates a rate constant for the *formation* of radicals in reaction [5] to be $8.5(\pm 2) \times 10^7$. This is indistinguishable from k_M, as determined for the total rate of loss of muonium by μSR, and therefore is a second reason why reaction [5] can be taken as the dominant reaction path.

(c) Micelle-mediated muonium reactions

No free radicals were found for acetone solutions in water to which micelles were added, even after scanning 500 G both sides of the signal shown in Fig. 3. The implication is that muonium undergoes reaction [6] rather than reaction [5] *when* it is within the micelle. If this is so, it is an example in which one reaction, the abstraction, is enhanced much more than the other, the addition, with the result that micelles have actually changed the dominant reaction channel. It means that the abstraction reaction has been enhanced from $<9 \times 10^6$ to 2.5×10^{10} M^{-1} s^{-1}, an enhancement factor of >2700. This is not inconsistent with enchancement factors specific to abstraction, which were found to be as high as 20 000 for molecules like 2-propanol and ethyl formate (17).

(d) Comparison with thiocarbonyls

Because of the instability of thioacetone, it was not possible to directly compare the exchange of acetone's C=O for C=S; however, in thioacetamide (and dimethylthioformamide) an LCR study produced a radical that had muonium attached to the C, and which was therefore a thiyl radical R-S• (25). Such radicals are not seen by ESR because of line-broadening effects. This one is quite evident here, however, at least on the LCR and μSR timescales. It is positively identified as an S• radical, and not C•, by its enormous muon hyperfine coupling (380 MHz) (26) compared with acetone (26 MHz) and non-aromatic C-centred radicals (100–150 MHz) (4, 14).

Muonium reacts with thioacetamide on first encounter (k_M = 3×10^{10} M^{-1} s^{-1} (27), which is the diffusion-controlled limit (4)). This is 3000 times more efficient than the acetone reaction. It is also faster than the corresponding H-atom reaction (12), but only by a factor of ~6. There was no micelle-induced enchancement of the Mu + thioacetamide reaction, but this is not surprising since it is already diffusion limited, and is an addition reaction rather than an abstraction (17).

Summary

Muonium is proving to be a probe of hitherto hidden kinetic isotope effects. Just from these studies with acetone as solute in water it has shown a number of surprises. It adds across a carbonyl group 100 times faster than does H, but it probably

Can. J. Chem. Downloaded from www.nrcresearchpress.com by 91.121.58.235 on 09/07/12
For personal use only.

abstracts a hydrogen from a methyl group more slowly than H does. It attaches to the oxygen atom when it adds to a carbonyl, but to the carbon of a thiocarbonyl. It reacts with thiocarbonyls three orders of magnitude faster than with carbonyls. Its abstraction reaction seems to be enhanced more than its addition reaction when incorporated in micelles, so there is a switch in the dominant reaction channel. Its thiyl radicals are sufficiently stable to be observed, and have large coupling constants. Hyperfine coupling constants can be determined for all protons, and for other nuclei with non-zero magnetic moments, in radicals produced from muonium; for the six β hydrogens of acetone the value is 55.5 MHz. There is intermolecular muonium bonding, analogous to hydrogen bonding, seen as a decrease in the muon coupling constant when water is exchanged for acetone as the radical's microenvironment. Mu shows the opposite directional effect to H when adding into substituted benzene rings, which is its major reaction path with most aromatics. Yet it diffuses in water at the same rate as H, despite its mass being only one ninth that of H.

Accordingly, if muonium is to usurp H as the leading hydronium isotope, there is still much to be learned about isotope effects!

Acknowledgments

The author is most grateful to his colleagues in the work reviewed here: particularly Drs. Mary Barnabas, Krishnan Venkateswaran, John Stadlbauer, Bill Ng, and Mr. Zhennan Wu. Many enjoyable "working" lunches with Ross Stewart also contributed to these studies. NSERC provided some of the funds needed.

1. R. Stewart. The proton: applications to organic chemistry. Academic Press, New York. 1985.
2. D. G. Fleming, D. M. Garner, and J. R. Mikula. Hyperfine Interact. **8**, 337 (1981).
3. B. W. Ng, Y. C. Jean, Y. Ito, T. Suzuki, J. H. Brewer, D. G. Fleming, and D. C. Walker. J. Phys. Chen. **85**, 454 (1981).
4. D. C. Walker. Muon and muonium chemistry. Cambridge University Press, Cambridge. 1983. pp. 115–119 and 166–174.
5. J. S. Tse and M. L. Klein. J. Phys. Chem. **87**, 5055 (1983).
6. D. G. Fleming, D. M. Garner, L. C. Vaz, D. C. Walker, J. H. Brewer, and K. M. Crowe. Adv. Chem. Ser. **175**, 279 (1979).
7. D. M. Garner, D. G. Fleming, and J. H. Brewer. Chem. Phys. Lett. **55**, 163 (1978).
8. J. N. L. Connor, W. Jakubetz, and J. Manz. Chem. Phys. Lett. **45**, 265 (1977).
9. (*a*) J. M. Stadlbauer, B. W. Ng, R. Ganti, and D. C. Walker. J. Am. Chem. Soc. **106**, 3151 (1984); (*b*) J. M. Stadlbauer, B. W. Ng, and D. C. Walker. Hyperfine Interact. **32**, 721 (1986).
10. R. A. Witter and P. Neta. J. Org. Chem. **38**, 484 (1973).
11. M. V. Barnabas. Ph.D. Thesis, University of British Columbia (1989).
12. G. V. Buxton, C. L. Greenstock, W. P. Helman, and A. B. Ross. Critical Reviews, NSRDS-NBS, Washington, DC. (1988).
13. (*a*) J. H. Brewer, K. M. Crowe, F. N. Gygax, and A. Schenck. *In* Muon physics. Vol. 3. *Edited by* V. W. Hughes and C. S. Wu. Academic Press, New York. 1975. p. 3;(*b*) V. W. Hughes. Annu. Rev. Nucl. Part. Sci. **16**, 445 (1966); (*c*) J. H. Brewer and K. M. Crowe. Annu. Rev. Nucl. Part. Sci. **28**, 239 (1978); (*d*) D. C. Walker. Acc. Chem. Res. **18**, 167 (1985); (*e*) S. F. J. Cox. J. Phys. C, **20**, 3187 (1987).
14. (*a*) E. Roduner, P. W. Percival, D. G. Fleming, J. Hochmann, and H. Fischer. Chem. Phys. Lett. **57**, 37 (1978); (*b*) E. Roduner and H. Fischer. Chem. Phys. Lett. **65**, 582 (1979).
15. (*a*) R. F. Kiefl. Hyperfine Interact. **32**, 707 (1986); (*b*) R. F. Kiefl, S. R. Kreitzman, M. Celio, R. Keitel, J. H. Brewer, G. M. Luke, D. R. Noakes, P. W. Percival, T. Matsuzaki and K. Nishiyama. Phys. Rev. A, **34**, 681 (1986); (*c*) P. W. Percival, R. F. Kiefl, S. R. Kreitzman, D. M. Garner, S. F. J. Cox, G. M. Luke, J. H. Brewer, K. Nishiyama, and K. Venkateswaran. Chem. Phys. Lett. **133**, 465 (1987).
16. K. Venkateswaran, M. V. Barnabas, R. F. Kiefl, J. M. Stadlbauer, and D. C. Walker. J. Phys. Chem. **93**, 388 (1989).
17. K. Venkateswaran, M. V. Barnabas, Z. Wu, J. M. Stadlbauer, B. W. Ng, and D. C. Walker. Chem. Phys. Lett. **143**, 313 (1988).
18. K. Venkateswaran, M. V. Barnabas, J. M. Stadlbauer, and D. C. Walker. Can. J. Phys. In press.
19. K. Venkateswaran, M. V. Barnabas, B. W. Ng, and D. C. Walker. Can. J. Chem. **66**, 1979 (1988).
20. M. V. Barnabas, K. Venkateswaran, J. M. Stadlbauer, B. W. Ng. Z. Wu, A. Gonzalez, and D. C. Walker. Hyperfine Interact. In press.
21. P. Neta and R. H. Schuler. J. Phys. Chem. **77**, 1368 (1973).
22. K. Venkateswaran, R. F. Kiefl, M. V. Barnabas, J. M. Stadlbauer, B. W. Ng, Z. Wu, and D. C. Walker. Chem. Phys. Lett. **145**, 289 (1988).
23. (*a*) A. Hill, M. C. R. Symons, S. F. J. Cox, R. De Renzi, and C. A. Scott. J. Chem. Soc. Faraday Trans. 1, **81**, 433 (1985); (*b*) S. F. J. Cox and M. C. R. Symons. Radiat. Phys. Chem. **27**, 53 (1986).
24. E. Roduner. Radiat. Phys. Chem. **28**, 75 (1986).
25. M. V. Barnabas and D. C. Walker. Chem. Phys. Lett. **168**, 9 (1990).
26. C. J. Rhodes, M. C. R. Symons, and E. Roduner. J. Chem. Soc. Chem. Commun. 3 (1988).
27. M. V. Barnabas, K. Venkateswaran, and D. C. Walker. Can. J. Chem. **67**, 120 (1989).

Can. J. Chem. Downloaded from www.nrcresearchpress.com by 91.121.58.235 on 09/07/12
For personal use only.

Photosolvolysis of 11*H*-benzo[*b*]fluoren-11-ol in aqueous solution

ERIK KROGH AND PETER WAN[1]

Department of Chemistry, University of Victoria, Victoria, B.C., Canada V8W 2Y2

Received March 14, 1990

This paper is dedicated to Professor Ross Stewart on the occasion of his 65th birthday

ERIK KROGH and PETER WAN. Can. J. Chem. **68**, 1725 (1990).

The photosolvolysis of 11*H*-benzo[*b*]fluoren-11-ol (**2**), a 9-fluorenol derivative, has been studied in aqueous solution to test the hypothesis of enhanced photosolvolytic reactivity of these compounds. It is found that compared to the model compound, α-phenyl-2-naphthalenemethanol (**3**), **2** exhibited enhanced photosolvolytic reactivity. Quantum yields for photosolvolysis in aqueous alcohol solutions and steady-state and transient fluorescence studies are reported in neutral and acid solutions. The results further support the notion that an intrinsically accelerated *photo*dehydroxylation step is associated with the formation of a 9-fluorenyl type carbocation intermediate (formally $4n\pi$ electrons).

Key words: photosolvolysis, photodehydroxylation, carbocation.

ERIK KROGH et PETER WAN. Can. J. Chem. **68**, 1725 (1990).

Afin de vérifier l'hypothèse selon laquelle ces composés présentent une réactivité photosolvolytique accrue, on a étudié la photosolvolyse du 11*H*-benzo[*b*]fluorèn-11-ol (**2**), un dérivé du 9-fluorénol, en solution aqueuse. On a trouvé que, si on compare sa réactivité avec celle du composé modèle, le α-phényl-2-naphtalèneméthanol (**3**), le composé **2** présente une réactivité photosolvolytique accrue. On rapporte les rendements quantiques pour les photosolvolyses en solutions aqueuses d'alcool; on a aussi étudié la fluorescence des états stationnaires et de transition dans des solutions neutres et acides. Les résultats obtenus apportent un nouveau support à l'hypothèse selon laquelle une étape de *photo*déhydroxylation intrinsèquement accélérée est associée à la formation d'un carbocation intermédiaire de type 9-fluorényle qui contient formellement $4n\pi$ électrons.

Mots clés : photosolvolyse, photodéhydroxylation, carbocation.

[Traduit par la revue]

Can. J. Chem. Downloaded from www.nrcresearchpress.com by 91.121.58.235 on 09/07/12
For personal use only.

Continued interest in photosolvolytic reactions stems partly from the fact that these reactions generate ion pairs, which are much less common intermediates than radicals or radical pairs in organic photochemistry (1). In addition, recent studies by McClelland *et al.* (2–6) have utilized these types of reactions for photogenerating carbocation intermediates for study by flash photolysis, from which new insights into structure–reactivity of the *photogenerated* carbocations in aqueous solutions have been obtained. We have been exploring structure–reactivity effects of the *initial* photochemical step for a number of systems (7–11) and have discovered that 9-fluorenols **1** are particularly prone to photosolvolyze (10, 11). It has been proposed (10, 11) that the reaction proceeds from the singlet state via primary benzylic C—OH bond heterolysis (photodehydroxylation), to generate a 9-fluorenylium ion intermediate, which is rapidly trapped by nucleophiles in the system. The 9-fluorenylium ion is an antiaromatic species in the ground state (12, 13) and is therefore very difficult to generate and characterize thermally. This instability, compared to $4n + 2$ π systems or molecules lacking the cyclic array altogether, is commonly employed to explain the marked reduced solvolytic reactivity of fluorenol derivatives in the ground state. The photochemical method is therefore significant by providing $\mathbf{1}^+$ and related cations. In particular it provides a potential means of studying these elusive antiaromatic cations via laser flash photolysis. That a 9-fluorenylium ion is an intermediate in these reactions is supported by recent flash photolysis studies (14, 15). We proposed (11) that photodehydroxylation leading to a 4π electron cation in the Internal Cyclic Array (ICA; defined as the carbocyclic array immediately surrounding the cation on solvolysis) is a favourable arrangement, suggesting that such species have an enhanced stability in the excited singlet state, when compared to similar systems lacking the 4π ICA (11). Calculations by us[2] and others (16) support the suggestion that $4n\pi$ systems adopt pseudo-aromatic characteristics in the S_1 state. Several features of the original 9-fluorenol system (11) made the study of its photochemical reaction mechanism difficult. Most notably, 9-fluorenols, **1**, are very weakly fluorescent ($\Phi_f < 0.01$) and have very short fluorescence lifetimes (typically $\tau < 100$ ps) (11) in aqueous solution. Secondly, they failed to exhibit acid-catalyzed photosolvolysis, a feature that we have used often (7, 9) to rule out electron transfer and homolytic pathways. We report here a study of the photosolvolysis of a benzannelated derivative of 9-fluorenol, 11*H*-benzo[*b*]fluoren-11-ol (**2**). Like 9-fluorenol, **2** is very reactive towards photosolvolysis. We have also studied a reference compound, α-phenyl-2-naphthalenemethanol (**3**), and find it to be much less reactive with respect to photosolvolysis. Furthermore, **2** allows us to probe steady-state and transient fluorescence behaviour in detail, as well as providing the first example of acid catalysis in the photosolvolysis of 9-fluorenol type systems.

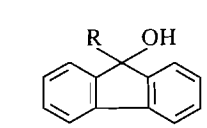

1

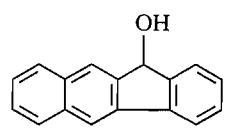

2

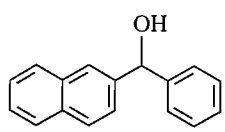

3

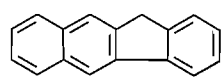

4

Results

Materials

The compound of interest, 11*H*-benzo[*b*]fluoren-11-ol (**2**), was made from $NaBH_4$ reduction of the corresponding ketone **5**, which was in turn prepared from a base-catalyzed aldol con-

[1]Author to whom correspondence may be addressed.

[2]B. Chak, T. W. Dingle, and P. Wan. Unpublished results.

Can. J. Chem. Downloaded from www.nrcresearchpress.com by 91.121.58.235 on 09/07/12
For personal use only.

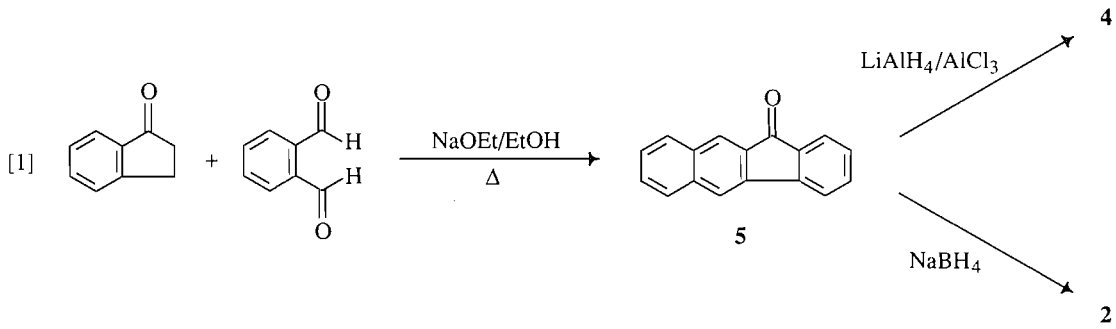

densation of 1-indanone with *o*-phthaldehyde, according to the procedure of Streitwieser *et al.* (17) (eq. [1]). The reference alcohol **3** was studied because it lacks an ICA, but possesses a chromophore similar to **2**. It was made via the addition of phenyllithium to 2-napthaldehyde. The corresponding hydrocarbon **4** was of interest for comparison purposes (steady-state and transient fluoresence studies) since it is known to be inert to photosolvolysis and other photochemical pathways in the absence of oxygen. It was made via reduction of **5** using $LiAlH_4/AlCl_3$ (eq. [1]).

Product studies

Photolysis of either **3** or **4** (typical conditions: 10^{-3} M substrate, 50% (v/v) MeOH–H_2O, neutral water; Rayonet RPR 100 photochemical reactor; 254-nm lamps; argon-purged solutions; 5–60 min irradiation) resulted in no observable photoreaction. However, a 2 min photolysis of **2** under the same conditions resulted in high yields (>50%) of the corresponding methyl ether product **6** (eq. [2]). Extended photolysis results in

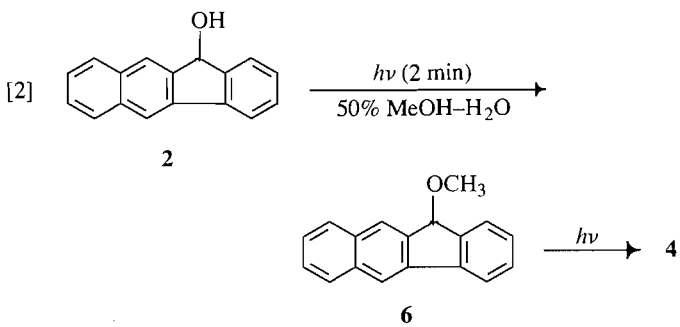

the formation of **4**, which arises from the secondary photolysis of **6**. This was confirmed by independent photolysis of **6** in the same solvent, and from the dependence of product formation on the photolysis time as shown in Fig. 1. The efficient photoreduction of **6** to **4** is analogous to the photoreduction of 9-methoxyfluorene to fluorene, which we (11) and Tomioka *et al.* (18) have shown to occur via initial C—OMe homolysis, to give the radical pair, followed by disproportionation. Photolysis of **2** in a variety of alcohol–water mixtures also gave the corresponding ethers in good yields (Table 1). However, photolysis (10–60 min) in either 0.25 M NaCN or NaBr (50% acetonitrile cosolvent) failed to produce significant quantities of the corresponding cyano or bromo derivatives. This may in part be due to the inherent photolability of the initially formed products. In all of the above reactions control experiments showed no reaction in the absence of irradiation.

To investigate the possibility of acid catalysis in the photosolvolysis reaction, **2** and **3** were irradiated in methanol – aqueous sulfuric acid mixtures. When **3** was photolyzed in a 50% MeOH–H_2O (0.1 M H_2SO_4) solution for 20 min, it was converted to its corresponding methyl ether, **7**, in 25% yield (eq. [3]). Furthermore, **2** demonstrated an increased reactivity under acidic conditions. The conversion to methyl ether, after a 1 min photolysis, rose from 20% in neutral solution to 35% when the water portion was replaced by 0.1 M H_2SO_4. In both cases, no reactions were observed in the absence of light, thus clearly indicating that acid catalysis of photosolvolysis was taking place (*vide infra*). Compounds **2** and **3** will thermally solvolyze under the reaction conditions at sulfuric acid concentrations above 1.5 M and 0.5 M, respectively. Photolyses were not studied at these higher acidities.

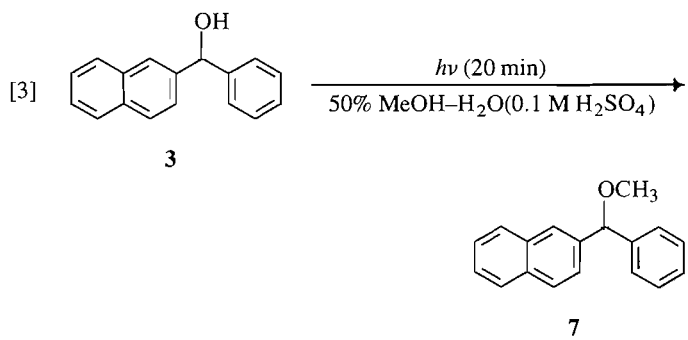

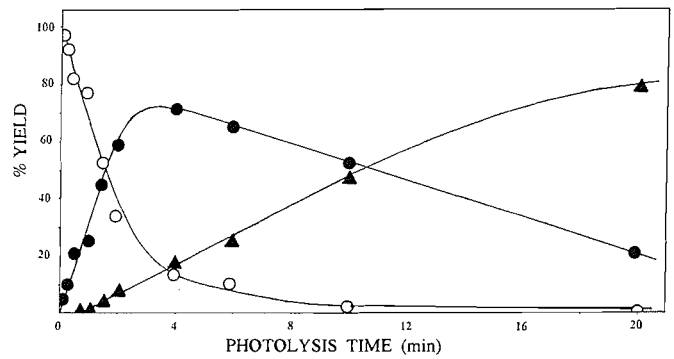

FIG. 1. Time-dependent product formation for the photosolvolysis of **2** in 50% MeOH–H_2O. Open circles represent **2**, filled circles represent primary photoproduct **6**, and triangles represent secondary photoproduct **4**.

Product quantum yields

Quantum yields for product formation (Φ_p) were measured using GC to analyze the extent of conversion and potassium ferrioxalate actinometry (19) for light intensity measurements. Photolyses were carried out under a stream of argon in quartz cuvettes (10^{-3} M substrate) and irradiated on an optical bench with an Oriel 200-W Hg source and an Applied Photophysics monochromator (λ_{ex} = 280 nm, 5-nm band width). Table 1 summarizes quantum yields of ether formation in different solvent systems. Quantum yields in MeOH–H_2O solution as a

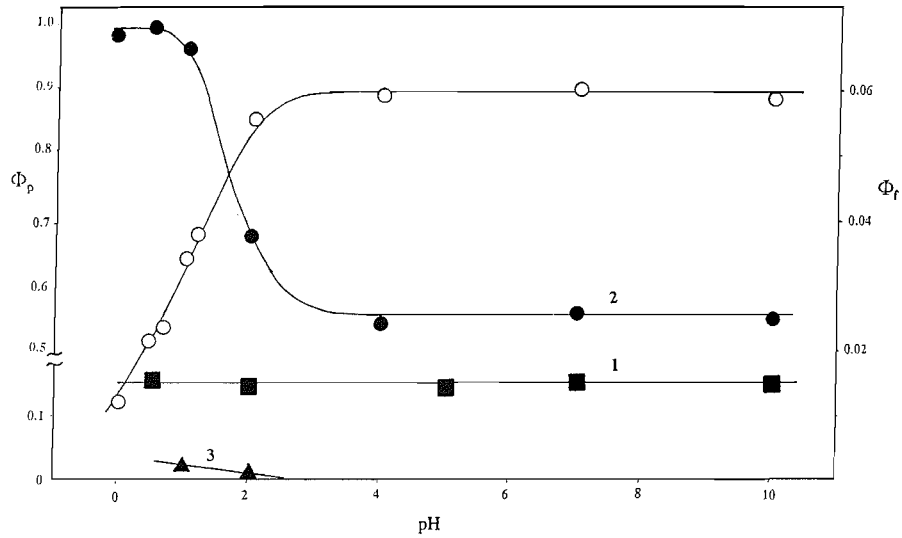

FIG. 2. Plot of product quantum yield for methyl ether formation (Φ_p) for compounds **1** (R = H), **2**, and **3** as a function of pH (or H_0), solid points. Also included is the pH dependence of fluorescence quantum yield (Φ_f) for **2** (open circles). The quoted pH (or H_0) value is for the aqueous portion of the solvent mixture.

TABLE 1. Product quantum yields (Φ_p) for photosolvolysis of **2**

Solvent system	Φ_p
100% MeOH	0.27±0.05[a]
50% MeOH–H_2O	0.56±0.04[a]
50% MeOD–D_2O	0.53±0.04[a]
50% MeOH–H_2O (0.10 M H_2SO_4)	1.0±0.05[a]
EtOH–H_2O[b]	0.32±0.1[c]
1-PrOH–H_2O[b]	0.26±0.1[c]
2-PrOH–H_2O[b]	0.22±0.1[c]

[a]Measured using an optical bench setup at λ_{ex} = 280 nm; substrate concentration, 10^{-3} M; conversions determined by GC analysis and light intensity measurements by potassium ferrioxalate actinometry (19).

[b]Experiments were carried out using 50 mg of substrate dissolved in 60 mL ROH and 40 mL H_2O (pH 7) and photolyzed at 254 nm for 4 min.

[c]Quantum yields were calculated by ^{1}H NMR integration using the value in 50% MeOH–H_2O as a secondary standard.

function of acidity of the *aqueous portion* are plotted in Fig. 2, with the results for the parent 9-fluorenol (**1**, R = H) shown for comparison purposes. It is evident from this plot that **3** has appreciable reactivity only in the presence of acid, with measurable Φ_p only below pH 2. From a previous study (11), the parent 9-fluorenol (**1**, R = H) did not display acid catalysis. However, it is clear that the reactivity of **2** is enhanced below pH 2, with Φ_p reaching a limit close to unity below pH 1.

Steady-state and transient fluorescence studies

The fluorescence excitation and corrected emission spectra of **2–4** are shown in Fig. 3. The absorption spectra of **2** and **4** are similar, with a long wavelength band $\lambda_{max} \approx 340$ nm. On the other hand, **3** does not possess this longer wavelength absorption, and its absorption spectrum resembles that of naphthalene. The emission intensity of **2** showed a marked solvent dependence whereas the intensity of **4** was invariant with a change in solvent, consistent with a similar trend in the fluorescence lifetimes (*vide infra*). The reference alcohol **3** displayed a reduced emission intensity only in acidic MeOH–H_2O solutions, concurrent with its increased reactivity in this solvent system. Fluorescence quantum yields in aqueous CH_3CN and 50% MeOH–H_2O are shown in Table 2. The nonreactive parent compound **4** was the most strongly fluorescent, with $\Phi_f \approx 0.85$ in either solvent; **2** has a fluorescence quantum yield of 0.26 in the inert solvent CH_3CN, and 0.06 in MeOH–H_2O solutions where efficient photosolvolysis occurs. The fluorescence quantum yield was further diminished with decreasing pH (H_0) (Fig. 2). Fluorescence lifetimes of **2–4** were measured using time-correlated single photon counting, on a Photon Technology instrument, using a hydrogen spark lamp as the excitation source. All lifetimes were obtained using fresh samples and a minimum exposure to the excitation source light. Solutions were exhaustively purged with a stream of a argon prior to data collection. The results are shown in Table 3, and are consistent with the above observations of the fluorescence emisison intensity. The decrease in the fluorescent lifetime of **2** with increasing acid concentration is consistent with the interception of the excited state by protons. A Stern–Volmer plot for **2** (Fig. 4) displays the linear dependence of (τ_0/τ) on the proton concentration at moderate acidities ($\leq$0.2 M). The slope provides a measure of k_q, the quenching rate constant, which can be equated with the acid-catalyzed rate coefficient, k_H, assuming a dynamic quenching mechanism. We calculate values of k_H for **2** to be $(4.0 \pm 0.3) \times 10^9$ M^{-1} s^{-1} and $(3.4 \pm 0.4) \times 10^9$ M^{-1} s^{-1}, in 20% CH_3CN–H_2O and 50% MeOH– H_2O, respectively. A similar treatment of the steady-state quenching (Φ^0_f/Φ_f), 20% CH_3CN–H_2O, also gave a value of $(3.7 \pm 0.2) \times 10^9$ M^{-1} s^{-1}.

The fact that the values in the different mixed solvent systems are in relative agreement suggests that a simple treatment of correcting the proton concentration by a dilution factor is adequate at these low proton concentrations. Plots of the fluorescence (Φ_f) and product (Φ_p) quantum yields as a function of pH are shown in Fig. 2 for **2** (open and solid circles respectively). The complementary behaviour of the acid-catalyzed photosolvolysis and the acid quenching of fluorescence strongly suggests a reactive singlet excited state for these substrates.

Solvent isotope effects

Solvent isotope effects for the quantum yield of photosolvoly-

Can. J. Chem. Downloaded from www.nrcresearchpress.com by 91.121.58.235 on 09/07/12
For personal use only.

Can. J. Chem. Downloaded from www.nrcresearchpress.com by 91.121.58.235 on 09/07/12
For personal use only.

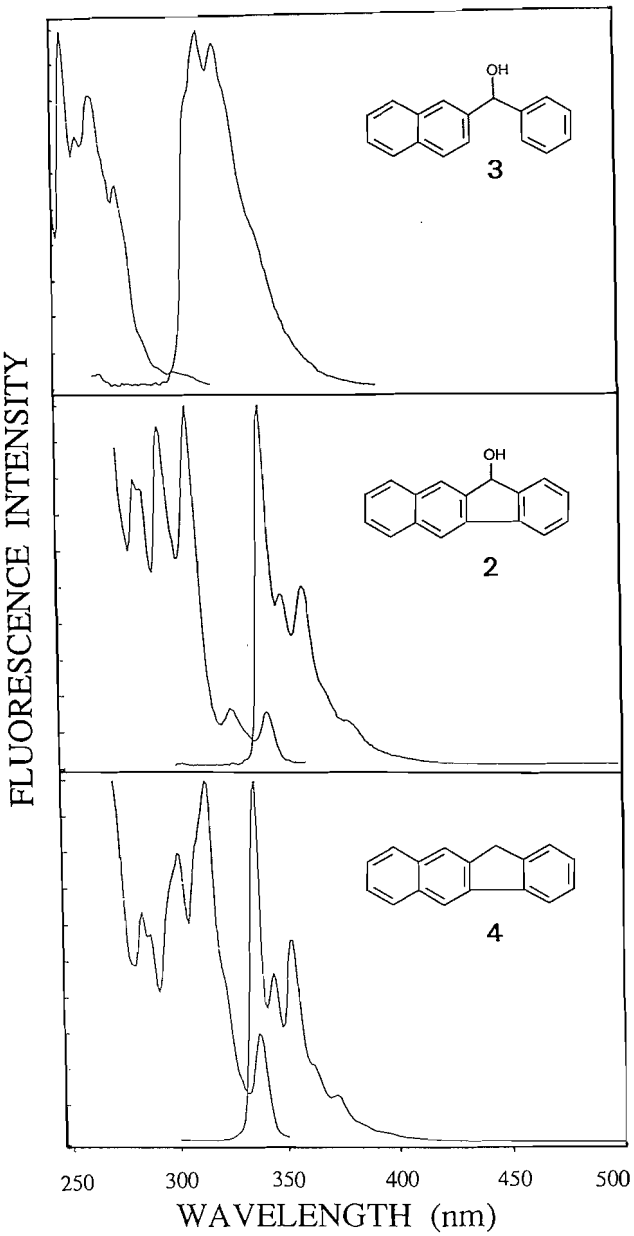

FIG. 3. Overlay of the fluorescence excitation and corrected emission spectra of **2**–**4** in 100% CH_3CN (λ_{ex} = 300 nm for **2** and **4**, λ_{ex} = 260 nm for **3**).

sis of **2** were measured in 50% MeOH–H_2O (Φ_{H_2O}) and compared to 50% MeOD–D_2O (Φ_{D_2O}). The observed value was $\Phi_{H_2O}/\Phi_{D_2O} = 1.1 \pm 0.1$. The fluorescence lifetimes of **2** were also measured in the deuterated solvents and the values of τ_{D_2O}/τ_{H_2O} are 1.24 ± 0.04 and 1.21 ± 0.04 for 50% MeOL–L_2O and 20% CH_3CN–L_2O, respectively. The unreactive compounds **3** and **4** displayed no solvent isotope effect. Using the relation, $k = \Phi_p/\tau$, the ratio of the rate constant k_{H_2O}/k_{D_2O} was determined to be 1.3 ± 0.1. This value is consistent with a mechanism involving a solvent-assisted bond cleavage step, and supports our mechanism of heterolytic bond cleavage as the primary photochemical event.

Triplet sensitization

Both steady-state and transient fluorescence studies indicate that the photosolvolysis of **2** and **3** occurs via the excited single state. Triplet sensitization experiments, carried out for **2**, in

TABLE 2. Fluorescence quantum yields (Φ_f) for **2**–**4**[a]

Solvent	Φ_f		
	2[b]	**3**[c]	**4**[b]
CH_3CN	0.26±0.03	0.10±0.01	0.82±0.06
50% MeOH–H_2O	0.06±0.01	0.10±0.01	0.85±0.06

[a]Determined by comparing the integrated emission areas of absorbance matched solutions using a Photon Technologies LS-1 spectrofluorimeter with recommended standards (25).
[b]Secondary standard was 2-aminopyridine in 0.05 M H_2SO_4, Φ_f = 0.60 (25).
[c]Secondary standard was naphthalene in cyclohexane, Φ_f = 0.23 (25).

TABLE 3. Fluorescence lifetimes (τ) for **2**–**4** in various solvent systems

Solvent system	Lifetime τ (ns)[a]		
	2[b]	**3**[b]	**4**[b]
100% CH_3CN	19	39	26
100% MeOH	13	36	27
20% CH_3CN–H_2O	3.8	36	25
50% MeOH–H_2O	4.6	36	26
50% MeOD–D_2O	5.7	36	26
10% MeOH–H_2O	1.5	36	26
50% MeOH–H_2O (pH 1)	2.6	35	26
50% MeOH – 20% H_2SO_4	0.25	26	24

[a]Errors are estimated to be less than 4% of the quoted value, except for lifetimes less than 1 ns, where they may be larger. The absorbance at the excitation wavelength was less than 0.3 in all cases.
[b]Excitation wavelength was 295 nm for **2** and **4** and 265 nm for **3**. Monitoring wavelength was 355 nm for **2** and **4** and 340 nm for **3**.

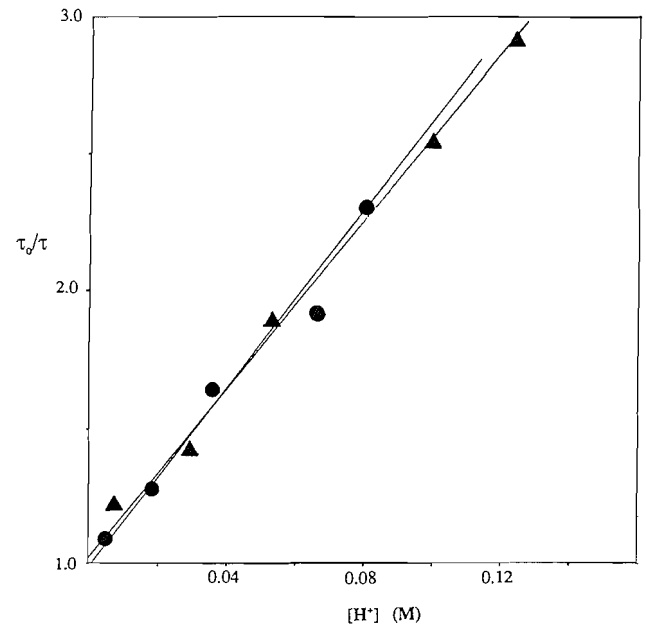

FIG. 4. Stern–Volmer plot of (τ_0/τ) versus [H_3O^+] for **2**. Triangles represent measurements in 20% CH_3CN–H_2O, slope = 15.3 ± 0.4 M^{-1}; circles represent measurements in 50% MeOH–H_2O, slope = 15.6 ± 0.8 M^{-1}.

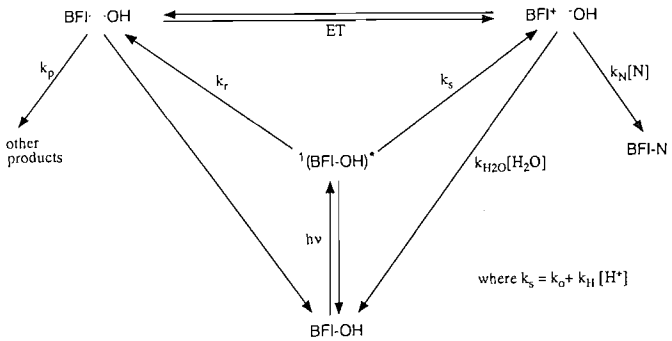

SCHEME 1

60% MeOH–H_2O (pH ≈ 10, λ_{ex} = 350 nm) using sodium benzophenone-2-carboxylate (100 molar excess) as the sensitizer lead to no photosolvolysis products. Thus, the photodehydroxylation appears to be an exclusively singlet state reaction. It was not possible to carry out the same sensitization studies with **3** since this compound had measurable solvolytic reactivity only at low pH, a solvent system where insufficient amounts of the sensitizer could be dissolved. However, the similar behaviour observed so far between **2** and **3** would suggest that **3** also reacts exclusively via S_1.

Discussion

Mechanism and rate constants

The photosolvolytic behaviour of **2** and **3** closely resembles that observed for other benzylic alcohols studied in our laboratory, all of which are known to proceed via heterolysis (photodehydroxylation) from S_1 to generate ion pairs. Our working mechanism of photosolvolysis of dibenzannelated systems has been proposed previously (11) and is shown in Scheme 1 (where BF1-OH represents **2**). Preparatory photolysis and laser flash photolysis studies of 9-fluorenol (11, 14, 15) have shown that a competing homolytic reaction pathway, k_r, contributed to the loss of the excited state, particularly in low dielectric solvents. The possibility of radical intermediates and electron transfer processes has therefore been included in this scheme, although we have no evidence that these steps are important in the present study. The very high product quantum yields for **2** necessarily relegate competing pathways to minor processes. The solvent isotope effect, k_{H_2O}/k_{D_2O} = 1.3, and the observed acid catalysis provide convincing evidence for the heterolytic bond cleavage step. The rate constant associated with this step, k_s, can be separated into two components: one, k_0, associated with the solvent assisted cleavage that is dominant in neutral solution, and another, k_H[H^+], associated with acid catalysis that contributes at higher proton concentrations. Use of the Stern–Volmer relation above established a value of $k_H = (3.7 \pm 0.4) \times 10^9\ M^{-1}\ s^{-1}$, for **2**. Because the other alcohols **1** and **3** did not display significant acid catalysis in a suitable pH region, they could not be treated in a similar manner to yield comparative values. However, the overall rate constants, k_s, could be evaluated in all cases using the relation $k_s = (\Phi_p/\tau)\cdot\{(k_{H_2O}[H_2O] + k_N[N])/k_N[N]\}$, where the term in brackets arises from the competition for the intermediate cation by the two nucleophiles in mixed solvent environments. These values are summarized in Table 4 under neutral and acid conditions. The rate constant for the heterolysis of **2**, leading to the 4π intermediate, is at least three orders of magnitude greater than that for **3**, which does not contain the ICA. This order of reactivity is the opposite to that observed in the ground state. The rate constant, k_s, for **2** is about an order of magnitude less than the value we estimated for **1** in neutral MeOH–H_2O. The annelation effect of the added benzene ring understandably decreases the reactivity of benzofluorenol by reducing the electron density in the vicinity of the incipient cyclopentadienyl cation. Thus, in terms of their rate constants, the 9-fluorenols are still the most photosolvolytically reactive molecules of which we are aware to date. Presumably, the lack of acid catalysis for 9-fluorenol can be explained by its very high reactivity in neutral solution, which would necessitate the use of much stronger acid media to observe the onset of catalysis. Our attempts to trap the photogenerated cations of **1** and **2** with added nucleophiles (i.e., Br^-, CN^-) in aqueous solvents have been unsuccessful. We have attributed this observation to an extremely short lifetime associated with the intermediate cation, which would therefore preclude cage escape and ensuing bimolecular reaction. Recent assignments by Mecklenburg and Hilinski (15) confirm this proposal. They have estimated the lifetime of $\mathbf{1}^+$ to be around 20 ps in aqueous methanol solutions.

TABLE 4. Values of k_s for **1–3** in 50% MeOH–H_2O

Solvent system	k_s[a] (s^{-1}) **1**[b]	**2**	**3**
50% MeOH–H_2O (pH 7)	$\approx 5 \times 10^9$	1.2×10^8	$\leq 5.5 \times 10^4$[c]
50% MeOH–H_2O (pH 1)	—	3.6×10^8	5.7×10^5

[a]Rate constants calculated by the relation $k_s = \Phi_p/\tau$.
[b]Based on a lifetime of ≈30 ps in this solvent (11).
[c]Estimated upper limit.

Quantum yields

The surprisingly high product quantum yields for **2** seem to indicate a strong preference for methanol attack. In the absence of quantitative data to the contrary (at least for excited states), we have previously assumed the rates of MeOH and H_2O attack to be similar. The results of this study severely question this assumption. Ritchie (20) has reported relative nucleophilicity values, $N+$, for H_2O and MeOH of 0.0 and 0.5, respectively. These are log values, so MeOH sould be ≈3.2 times more reactive than H_2O. When this reactivity difference is combined with the fact that the mole fraction of MeOH in a 50% (v/v) solution is 0.31, we are still unable to accommodate quantum yields approaching unity. The unusually high selectivity of the intermediate carbocation is not fully understood at this time. We provide two possible explanations here. Firstly, the $N+$ values measured with relatively stable ground state cations may not be appropriate for short-lived photogenerated intermediates. However, based on reactivity–selectivity arguments one might expect even less of a difference in the nucleophilic properties of MeOH and H_2O. A second possibility is that the arrangement of the solvent cage predisposes the MeOH molecules to solvolyze the incipient cation once it is formed. We know that the solvolytic step is very rapid, probably involving little more than the collapse of the solvent cage once the cation is formed. 11*H*-Benzo[*b*]fluoren-11-ol (**2**) is quite hydrophobic and it may not be unreasonable to expect that the microscopic environment immediately surrounding it is methanol enriched. We await laser flash photolysis studies to comment further on this phenomena.

Can. J. Chem. Downloaded from www.nrcresearchpress.com by 91.121.58.235 on 09/07/12
For personal use only.

Can. J. Chem. Downloaded from www.nrcresearchpress.com by 91.121.58.235 on 09/07/12
For personal use only.

Conclusion

The study of the photosolvolysis of **2** has brought additional insights into the details of the reaction pathway for these types of compounds. Since **2** has a close structural resemblance to the parent 9-fluorenol systems, its photochemical behaviour was expected to parallel that of 9-fluorenol. This indeed was observed, as demonstrated by the high reactivity of **2**, compared to a closely related compound **3** that lacks a 4π ICA. However, unlike the situation encountered in **1** (11), it was possible to measure several important experimental parameters, which strengthens the proposed mechanism offered in the previous study (11). In addition, the availability of measurable fluorescence lifetimes and acid catalysis observed in **2** allows for the calculation of primary rate constants of reaction.

Experimental

General

^{1}H NMR spectra were recorded on a Perkin–Elmer R32 instrument in $CDCl_3$ or acetone-d_6 (TMS internal standard). UV spectra were obtained on a Perkin–Elmer Lamda 4B or a Pye–Unicam 800 spectrophotometer. Fluorescence spectra were taken on a Perkin–Elmer MPF66 spectrofluorimeter or the Photon Technologies LS-1 in steady-state mode. Fluorescence lifetimes were measured using time-correlated single photon counting on a Photon Technologies LS-1 instrument in lifetime mode. Mass spectra were taken on a Finnigan 3300 instrument. Melting points were obtained on a Koefler hot stage microscope and are uncorrected. Gas chromatography (GC) was performed on a Varian 3700 instrument with a Hewlett–Packard 3390A integrator. Photolyses were carried out in Suprasil quartz cuvettes or 100-mL quartz tubes using a Rayonet RPR 100 photochemical reactor. An Oriel 200-W Hg light source and an Applied Photophysics monochromator on an optical bench were used for the quantum yield determinations.

Materials

Naphthalene and 2-aminopyridine (99%+) were purchased from Aldrich Chemical Co. The naphthalene sample was recrystallized twice from ethanol and then sublimed before use as a secondary quantum yield reference. 2-Aminopyridine was used as received. All solvents were of spectral grade and checked for spurious emission prior use. β-Napthylaldehyde, 1-indanone, and *o*-phthaldehyde were used as received from Aldrich Chemical Co. in the synthesis of **2** and **3**.

11H-Benzo[b]fluorenone (5)

This compound was synthesized in 53% yield according to the method in ref. 17; mp 153°C (lit. (21) mp 153–154.5°C).

11H-Benzo[b]fluoren-11-ol (2)

A solution of 5.0 g (22 mmol) of benzo[*b*]fluorenone in 100 mL of MeOH and 50 mL of THF was cooled while a suspension of 0.80 g (11 mmol) of $NaBH_4$ in 20 mL of MeOH was added dropwise. The reaction was warmed to ambient temperature and then refluxed for 12 h. The product was worked up by concentrating the mixture of 20 mL, diluting with CH_2Cl_2, and then washing with aqueous NH_4Cl and H_2O. The organic fraction was dried over $MgSO_4$, and evaporated to yield 4.6 g (90% yield) of a light yellow solid, which was recrystallized from ligroin to give white plates; mp 184°C (lit. (22) mp 185°C); ^{1}H NMR δ: 1.9 (d, J = 6 Hz, 1H), 5.75 (d, J = 6 Hz, 1H), 7.3–8.1 (arom., 10H); mass spectrum (EI) (m/z): 232 (M^+).

11H-Benzo[b]fluorene (4)

To a stirred suspension of 0.30 g (8 mmol) $LiAlH_4$ in 150 mL of dry THF was added 2.4 g (18 mmol) of $AlCl_3$ in small portions. The mixture was heated to reflux and 1.0 g (4.4 mmol) of **5** was extracted from the thimble of a Soxhlet extractor into the reaction vessel over a 6 h period. The reaction was worked up by reducing the THF to 10 mL, diluting with 100 mL CH_2Cl_2, and pouring onto 50 g of ice acidified with 5% H_2SO_4. The organic layer was separated, washed with H_2O, dried over $MgSO_4$, and evaporated to yield 0.88 g of a white solid (90% yield), which was recrystallized from MeOH and sublimed; mp 209–211°C (lit. (23) mp 208.5–209.5°C); ^{1}H NMR δ: 4.05 (s, 2H), 7.3–8.2 (arom., 10H); mass spectrum (EI) (m/z): 216 (M^+).

α-Phenyl-2-naphthalenemethanol (3)

To a solution of 5.0 g (32 mmol) of β-napthaldehyde (32 mmol) in dry THF was added via syringe 20 mL of PhLi (1.8 M, 35 mmol), under nitrogen. The solution was refluxed for 4 h and worked up as follows. The solution was concentrated to about 20 mL, diluted with 200 mL CH_2Cl_2, and washed with H_2O (2 × 200 mL). The combined organic fractions were dried over $MgSO_4$, and evaporated to yield 6.5 g (85% yield) of a white solid, which was recrystallized from petroleum ether; mp 87–88°C (lit. (24) mp 87–88°C); ^{1}H NMR δ: 2.45 (d, J = 5 Hz, 1H), 5.92 (d, J = 5 Hz, 1H), 7.2–7.9 (arom., 12H); mass spectrum (EI)(m/z): 232 (M^+).

Product studies. Dark reactions

The photosolvolytic behaviour of alcohols **2** and **3** was investigated at acidities (0.10 M H_2SO_4) where there were no concurrent dark reactions. In more concentrated sulfuric acid solutions, 1.5 M for **2** and 0.5 M for **3**, thermal solvolysis reactions became significant. A typical experimental procedure for a preparative dark reaction follows. A solution of 50 mg of compound in 50 mL of MeOH was diluted with 50 mL of aqueous sulfuric acid. The solution was stirred in the dark with a cold water circulator (≈12°C) for the appropriate irradiation time (usually 5–30 min). The reactions were worked up by saturating the aqueous solution with NaCl and extracting with CH_2Cl_2. The isolated materials were then analyzed by ^{1}H NMR spectroscopy.

Preparatory photolysis

In a typical photolsysis, 50 mg of substrate was dissolved in 50 mL of MeOH and diluted with 50 mL of H_2O. (Due to its low solubility in aqueous solutions, 60% MeOH–H_2O was often employed in the preparatory photolysis of **2**.) The solution was placed in a quartz tube fitted with a cold finger (≈12°C) and deaerated with a continuous stream of argon. The solution was then irradiated at 254 nm. After photolysis, the solution was worked up by saturating with NaCl, followed by extraction (2 × 100 mL) with CH_2Cl_2. The identity and yields of the photosolyate products were determined by ^{1}H NMR and gas chromatography. Product mixtures were separated by preparative TLC. The ethers of **2** and **3** were characterized by ^{1}H NMR and mass spectroscopy, as presented below.

11-Methoxy-11*H*-benzo[*b*]fluorene (**6**): mp 90–92°C; ^{1}H NMR δ: 3.05 (s, 3H), 5.75 (s, 1H), 7.3–8.1 (arom., 10H); mass spectrum (EI) (m/z): 246 (M^+).

α-(Methoxy)-α-(phenyl)-2-methylnapthalene (**7**): ^{1}H NMR δ: 3.38 (s, 3H), 5.38 (s, 1H), 7.2–7.5 (m, 8H), 7.7–7.9 (m, 4H); mass spectrum (EI) (m/z): 248 (M^+).

11-Ethoxy-11*H*-benzo[*b*]fluorene: ^{1}H NMR δ: 1.18 (t, 3H), 3.35 (q, 2H), 5.85 (s, 1H), 7.2–8.1 (arom., 10H).

11-(*n*-Propyloxy)-11*H*-benzo[*b*]fluorene: ^{1}H NMR δ: 0.90 (t, 3H), 1.56 (sextet, 2H), 3.20 (t, 2H), 5.85 (s, 1H), 7.2–8.1 (arom., 10H).

11-(2-Propyloxy)-11*H*-benzo[*b*]fluorene: ^{1}H NMR δ: 1.24 (d, 6H), 3.94 (septet, 1H), 5.80 (s, 1H), 7.2–8.1 (arom., 10H).

Steady-state fluorescence and lifetime measurements

Fluorescence spectra and lifetimes were recorded on a Photon Technologies LS-1 instrument in 1.00-cm Suprasil quartz cuvettes at 10^{-5} M. Solutions were purged with argon for 10 min prior to measurement.

Quantum yields and pH effects

Quantum yields for methyl ether formation of **2** and **3** were carried out in a variety of solvent systems. In a typical experiment, 0.50 mL of a stock solution of substrate in MeOH (4×10^{-3} M) was transferred to a quartz cuvette, and diluted with 1.0 mL of MeOH followed by 1.5 mL of H_2O. The solutions were argon purged for 10 min prior to and during the photolysis (usually 2–20 min, at 280 nm). After irradiation the photosolyate was transferred to a test tube, saturated with NaCl, and extracted with CH_2Cl_2 (3 × 3 mL). The organic fractions were separated using a pipette, and then dried over $MgSO_4$, filtered, and evaporated to ca. 100 μL before being injected onto a capillary column

(220°C) for analysis. Control experiments indicated that material is not lost during the work-up procedures. Conversions were determined by the relative peak areas of ether and alcohol, using a Hewlett–Packard integrator. Conversions determined this way are in agreement with those obtained from integration of ^{1}H NMR signals. Light intensity measurements were determined by irradiating a 0.006 M aqueous solution of potassium ferrioxalate under identical conditions and working up according to the method of Hatchard and Parker (19).

Fluorescence quantum yields

Fluorescence quantum yields for **2**–**4** were obtained on a Photon Technologies LS-1 instrument using secondary standards and recommended procedures (25). Naphthalene was the standard of choice for **3** whereas 2-aminopyridine provided a better overlap of the emission bands for **2** and **4**.

Registry No.: **2**, 110334-50-4; **3**, 35060-38-9P; **4**, 243-17-4; **5**, 96575-40-5P.

Acknowledgments

The authors thank the Natural Sciences and Engineering Research Council of Canada for support of this research and for a postgraduate scholarship (to E.K.). Additional support was provided by the University of Victoria.

1. S. J. Cristol and T. H. Bindel. Org. Photochem. **6**, 327 (1983).
2. R. A. McClelland, N. Banait, and S. Steenken. J. Am. Chem. Soc. **108**, 7023 (1986).
3. R. A. McClelland, V. M. Kanagasabapathy, and S. Steenken. J. Am. Chem. Soc. **110**, 6913 (1988).
4. R. A. McClelland, N. Banait, and S. Steenken. J. Am. Chem. Soc. **111**, 2929 (1989).
5. R. A. McClelland, V. M. Kanagasabapathy, N. S. Banait, and S. Steenken. J. Am. Chem. Soc. **111**, 3966 (1989).
6. S. Steenken and R. A. McClelland. J. Am. Chem. Soc. **111**, 4967 (1989).
7. N. J. Turro and P. Wan. J. Photochem. **28**, 93 (1985).
8. P. Wan, K. Yates, and M. K. Boyd. J. Org. Chem. **50**, 2881 (1985).
9. P. Wan and B. Chak. J. Chem. Soc. Perkin Trans. 2, 1751 (1986).
10. P. Wan and E. Krogh. J. Chem. Soc. Chem. Commun. 1027 (1985).
11. P. Wan and E. Krogh. J. Am. Chem. Soc. **111**, 4887 (1989).
12. D. Lloyd. Non-benzenoid conjugated carbocyclic compounds. Elsevier, Amsterdam. 1984.
13. G. A. Olah, G. K. S. Prakash, G. Liang, P. W. Westerman, K. Kunde, J. Chandrasekhar, and P. v. R. Schleyer. J. Am. Chem. Soc. **102**, 4485 (1980).
14. E. Gaillard, M. A. Fox, and P. Wan. J. Am. Chem. Soc. **111**, 2180 (1989).
15. S. L. Mecklenburg and E. F. Hilinski. J. Am. Chem. Soc. **111**, 5471 (1989).
16. E. J. Padma Malar and K. Jug. Tetrahedron, **42**, 417 (1986).
17. A. Streitwieser, Jr. and S. M. Brown. J. Org. Chem. **53**, 904, (1988).
18. H. Tomioka, H. Nakamura, and Y. Izawa. J. Chem. Soc. Chem. Commun. 1070 (1983).
19. C. G. Hatchard and C. A. Parker. Proc. R. Soc. (London), **A235**, 518, (1958).
20. C. D. Ritchie. Acc. Chem. Res. **5**, 348 (1972).
21. J. Blum, M. Ashenasy, and Y. Pickholtz. Synthesis, 352 (1974).
22. F. G. Baddar, A. M. Fleifel, and S. Sherif. J. Chem. Soc. 1009 (1959).
23. A. Streitwieser, Jr., J. H. Hammons, E. Cuiffarin, and J. I. Brauman. J. Am. Chem. Soc. **89**, 59 (1967).
24. A. M. Osman, M. Z. A. Badr, M. M. Aly, and H. A. H. El-Sherief. J. Appl. Chem. Biotechnol. **24**, 319 (1974).
25. D. F. Eaton. Pure Appl. Chem. **60**, 1107 (1988).

Can. J. Chem. Downloaded from www.nrcresearchpress.com by 91.121.58.235 on 09/07/12
For personal use only.

Distorted amides as models for activated peptide N-C=O units. 2. The synthesis, hydrolytic profile, and molecular structure of 3,4-dihydro-2-oxo-1,4-propanoquinoline

QINGPING WANG, A. J. BENNET, AND R. S. BROWN[1]
Department of Chemistry, University of Alberta, Edmonton, Alta., Canada T6G 2G2

AND

B. D. SANTARSIERO
Structure Determination Laboratory, Department of Chemistry, University of Alberta, Edmonton, Alta., Canada T6G 2G2

Received November 21, 1989

This paper is dedicated to Professor Ross Stewart on the occasion of his 65th birthday

QINGPING WANG, A. J. BENNET, R. S. BROWN, and B. D. SANTARSIERO. Can. J. Chem. **68**, 1732 (1990).

A distorted anilide (3,4-dihydro-2-oxo-1,4-propanoquinoline (**3**)) has been synthesized, its structure determined by X-ray diffraction, and its hydrolysis profile from pH 0–13 investigated. The amide unit in **3** is distorted in that the N lone pair is twisted 35° and tilted 15° out of optimum conjugation with the C=O Π system. Due to this distortion, **3** hydrolyses rapidly in H_2O at 25°C. The pH/rate constant profile exhibits domains consistent with OH^- attack on **3** (k_{OH^-} = 17.2 M^{-1} s^{-1}) and H_2O attack on a protonated form of **3** ($k_{H_3O^+}$ = 8.26 s^{-1}; pK_a (**3**-H^+) = 0.56). The kinetic pK_a is most consistent with an N-protonated form. It is also shown that this mechanism of hydrolysis is common to the series of bridged anilides consisting of **3**, 3,4-dihydro-2-oxo-1,4-ethanoquinoline (**1**), and 2,3,4,5-tetrahydro-2-oxo-1,5-ethanobenzazepine (**2**).

Key words: distorted amide, hydrolysis, X-ray structure.

QINGPING WANG, A. J. BENNET, R. S. BROWN et B. D. SANTARSIERO. Can. J. Chem. **68**, 1732 (1990).

On a synthétisé un anilide déformé (3,4-dihydro-2-oxo-1,4-propanoquinoléine (**3**)), on a déterminé sa structure par diffraction des rayons-X et on a étudié son profil d'hydrolyse en fonction du pH (de 0 à 13). L'unité amide du composé **3** est déformée; la paire d'électrons non partagée forme un angle de torsion de 35° et une inclinaison de 15° par rapport au plan de conjugaison optimale du C=O avec le système Π. À cause de cette distorsion, l'hydrolyse du produit **3** se fait rapidement dans l'eau, à 25°C. Le profil de la constante de vitesse vs. le pH est en accord avec une attaque d'un OH^- sur le composé **3** (k_{OH^-} = 17,2 M^{-1} s^{-1}) et d'une attaque de H_2O sur la forme protonée du composé **3** ($k_{H_3O^+}$ = 8,26 s^{-1}; pK_a (**3**-H^+) = 0,56). Le pK_a cinétique est principalement en accord avec une forme N-protonée. On démontre aussi que ce mécanisme d'hydrolyse est commun dans la série d'anilides pontés formée du produit **3**, de la 3,4-dihydro-2-oxo-1,4-éthanoquinoléine (**1**) et de la 2,3,4,5-tétrahydro-2-oxo-1,5-éthanobenzazépine (**2**).

Mots clés : amide déformé, hydrolyse, structure par rayons-X.

[Traduit par la revue]

Introduction

As part of an ongoing program in understanding the detailed mechanism of hydrolysis of strained amides (1) we have embarked on the syntheses and physicochemical studies of a series of anilides **1**–**4**. The synthesis and hydrolysis of amide

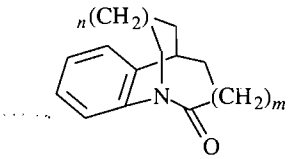

1 $n = m = 0$
2 $n = 0$; $m = 1$
3 $n = 1$; $m = 0$
4 $n = m = 1$

1 had originally been reported by Blackburn *et al.* (2) and molecular models indicate that the N "lone pair" of the N-C=O unit is essentially orthogonal to the C=O Π-system. This geometric constraint leads to a large hydrolytic reactivity of **1** in both acid and base (1, 2). Amide **2**, in which the geometry allows more conjugation of the N-C=O system (3), is similarly prone to accelerated hydrolysis. Moreover, **2** shows a remarkable activation toward attack by bifunctional nucleophiles such as β-aminoalcohols (3–5) and diacids capable of forming cyclic anhydrides (6, 7) in a way that is reminiscent of the serine proteases and aspartate proteinases respectively.

To probe more completely the manner in which amide hydrolytic reactivity can be influenced by distortion within the anilide series, we have synthesized **3**. Herein we report the synthetic procedure as well as the hydrolytic profile and details of the crystal structure.

Experimental

(a) Synthesis

The synthesis of 3,4-dihydro-2-oxo-1,4-propanoquinoline (**3**) was accomplished according to the route outlined in Scheme 1 starting with the known keto *N*-tosylate **5** (8).

*5-(Ethoxycarbonylmethyl)-5-hydroxy-*N*-tosyl-2,3,4,5-tetrahydrobenzazepine (**6**)*

To a 500-mL 3-necked flask equipped with a 250-mL dropping funnel (charged with 16.6 g (0.053 mol) of 5-oxo-*N*-tosylbenzazepine (**5**, (8)), 6.45 mL (0.058 mol, d = 1.506) of ethyl-α-bromoacetate, and 210 mL of dry benzene), a reflux condenser, and magnetic stir bar, was added 4.56 g (0.070 mol) of zinc powder and 210 mL of dry ether. The contents of the dropping funnel were added dropwise to the stirred Zn suspension, after which time the mixture was heated at reflux overnight under an Ar atmosphere. By morning a white suspension had formed and the mixture was cooled (ice bath) and treated with 210 mL of 10% H_2SO_4. The phases were separated and the organic phase washed with 5 × 140 mL of 10% H_2SO_4, the combined extracts being saved. The organic layer was then extracted with 5 × 100 mL of 5% KOH and 5 × 100 mL of saturated NaCl, and subsequently dried ($MgSO_4$), filtered,

[1]Author to whom correspondence may be addressed.

Can. J. Chem. Downloaded from www.nrcresearchpress.com by 91.121.58.235 on 09/07/12
For personal use only.

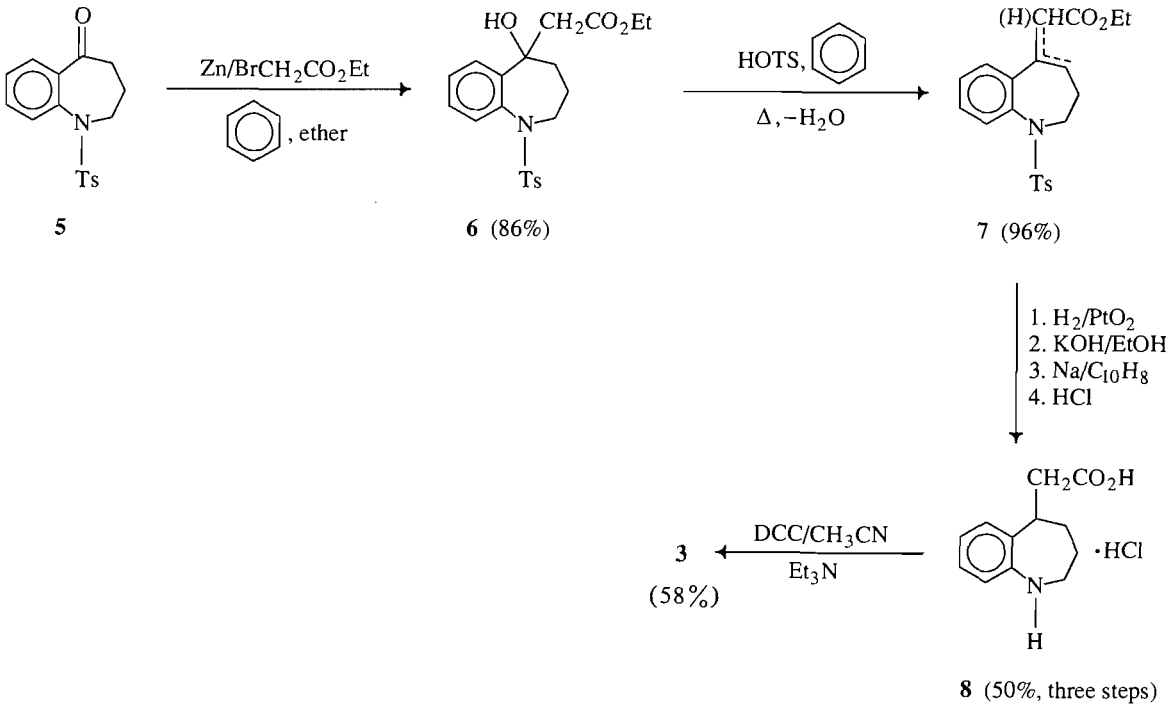

SCHEME 1

and stripped of volatiles to give crude **6**. The combined acid extracts were reextracted with 3 × 100 mL of $CHCl_3$, these extracts being combined, dried ($MgSO_4$), filtered, and stripped of volatiles. The crude product thus obtained was combined with that above, and recrystallized from 95% EtOH to yield 18.3 g (86.3%) of pure **6**, mp 149.0–150.0°C; ^{1}H NMR (200 MHz, $CDCl_3$) δ: 7.80 (2H, m), 6.9–7.35 (6H, m), 4.08 (4H, q, J = 7 Hz), 3.15 (2H, s), 2.90 (1H, br t), 2.45 (3H, s), 2.15 (2H, br), 1.80 (2H, br t), 1.20 (3H, t, J = 7 Hz). Exact mass calcd. for $C_{21}H_{25}NO_5S$: 403.1453; found: 403.1445. Anal. calcd. for $C_{21}H_{25}NO_5S$: C 62.51, H 6.25, N 3.47; found: C 62.24, H 6.44, N 3.44.

*(5-Ethoxycarbonylmethyl)-2,3-dihydro-*N*-tosylbenzazepine and (5-ethoxycarbonylmethylidene)-2,3,4,5-tetrahydro-*N*-tosylbenzazepine (7)*

Into a 500-mL round-bottom flask was placed 250 mL of benzene, 0.7 g of *p*-toluenesulfonic acid, and 36.0 g (0.0892 mol) of alcohol **6**. The mixture was heated at reflux for 16 h and 1.5 mL of H_2O was removed via a Dean–Stark apparatus. The benzene was extracted with 2 × 200 mL of saturated $NaHCO_3$ and 2 × 200 mL of H_2O, after which it was dried ($MgSO_4$), filtered, and the volatiles removed by rotary evaporation. The crude residue was recrystallized from 95% EtOH after it had been decolorized with charcoal to yield 33.0 g (96%) of 7 as a mixture of isomers, mp 126.5–128.5°C; ^{1}H NMR (200 MHz, $CDCl_3$) of the *exo* methylene derivative, δ: 7.6–7.4 (8H, m), 5.28 (1H, s), 4.06 (2H, q, J = 7 Hz), 3.77 (2H, t, J = 5 Hz), 2.75 (2H, br t), 2.35 (3H, s), 1.80 (2H, m), 1.28 (3H, t, J = 7 Hz); of the ethoxycarbonylmethyl isomer, δ: 7.64–7.12 (8H, m), 5.75 (1H, t, J = 6 Hz), 4.08 (2H, q, J = 7 Hz), 3.93 (2H, m), 2.78 (2H, s), 2.35 (3H, s), 2.20 (2H, m), 1.22 (3H, t, J = 7 Hz). Exact mass calcd. for $C_{21}H_{23}NO_4S$: 385.1348; found: 385.1351. Anal. calcd. for $C_{21}H_{23}NO_4S$: C 65.43, H 6.01, N 3.63; found: C 65.39, H 6.22, N 3.58.

(5-Ethoxycarbonylmethyl)-2,3,4,5-tetrahydrobenzazepine

This was made by catalytic hydrogenation (30 psi; 1 psi = 6.9 kPa) of 17.4 g (0.045 mol) of 7 in 150 mL THF containing 0.5 g of PtO_2. After 36 h, the mixture was filtered and the volatiles removed to yield 17.4 g (100%) of hydrogenated product, mp 97.5–98.5°C; ^{1}H NMR (200 MHz, $CDCl_3$) δ: 7.65 (2H, m), 7.10 (6H, m), 4.05 (2H, q, J = 7 Hz), 3.2–3.0 (2H, br), 2.64 (2H, br), 2.34 (3H, s), 1.4–1.8 (4H, br m), 1.18 (3H, t, J = 7 Hz). Exact mass calcd. for $C_{21}H_{25}NO_4S$: 387.1504; found: 387.1504. Anal. calcd. for $C_{21}H_{25}NO_4S$: C 65.09, H 6.50, N 3.62; found: C 65.12, H 6.51, N 3.56.

2[5'(2,3,4,5-Tetrahydrobenzazepinyl)]acetic acid (8)

To a 100-mL round-bottom flask containing 16 mL of 20% KOH and 24 mL of 95% EtOH was added 3.614 g (9.33 mmol) of the hydrogenated ester (above). The contents were heated at reflux for 5 h, and then the mixture was poured into an ice–HCl mixture at pH 1. The mixture was then extracted with 3 × 50 mL of $CHCl_3$, and the combined extracts dried ($MgSO_4$), filtered, and the volatiles removed. The acid so obtained was not purified further, but taken immediately on to the next step. Removal of the *N*-tosyl protecting group was effected by a modification of a reported (9) procedure. Into a 500-mL 3-necked round-bottom flask equipped with serum stoppers, magnetic stirbar, and Ar inlet was placed the crude acid product from above, 10 mL of dry DME, and 720 mg (30 mmol) of NaH (prepared from 1.2 g of 60% NaH in oil, which was freed from the oil by washing with heptane).

In a separate 200-mL 3-necked round-bottom flask equipped with serum stoppers, magnetic stirbar, and Ar inlet was placed 16.8 g (0.13 mol) of naphthalene and 40 mL of dry DME. To this solution was added 2.7 g (0.12 mol) of Na^0, upon which the solution turned deep green. This was allowed to stir at room temperature for 15 min and then it was taken up via syringe, and injected into the first flask. As the $Na/C_{10}H_8$ solution was injected, the green colour immediately disappeared, and enough was then added so that the colour persisted. This resulting mixture was allowed to stir at room temperature overnight. In the morning, the DME was removed by rotary evaporation, and H_2O/benzene was added to the residue. The H_2O layer was extracted with 3 × 100 mL of benzene and then the pH of the aqueous layer was adjusted to 1 by addition of concentrated HCl. Solid Na_3PO_4 was added to adjust the pH to 5–6, and then the solution was extracted with 50 mL of EtOAc, followed by 2 × 25 mL of CH_2Cl_2. The organic layers were combined, dried ($MgSO_4$), filtered, and the volatiles removed to yield 1.5 g of crude product **8**. Purification was effected by dissolving this material in a small amount of 95% EtOH containing a few drops of concentrated HCl and then adding ether to turbidity. After refrigeration, a yellow crystalline material was removed by filtration. This was dissolved in H_2O, treated with charcoal to decolorize it, filtered, and the H_2O removed to give a solid. The solid was dissolved

Can. J. Chem. Downloaded from www.nrcresearchpress.com by 91.121.58.235 on 09/07/12
For personal use only.

Can. J. Chem. Downloaded from www.nrcresearchpress.com by 91.121.58.235 on 09/07/12
For personal use only.

again in the above EtOH/HCl solution and ether added to turbidity. Refrigeration yielded 1.1 g (50%) of the HCl salt of **8**, mp >200°C (dec.). ^{1}H NMR (200 MHz, DMSO-d_6) δ: 6.75 (1H, m), 6.30–6.40 (3H, m), 3.70 (1H, m), 3.50 (1H, m), 2.70–3.10 (3H, m), 2.55 (2H, m), 1.90–2.22 (3H, br m), 1.4–1.6 (1H, br). Exact mass calcd. for $C_{12}H_{15}NO_2$: 205.1103; found: 205.1099. Anal. calcd. for $C_{12}H_{15}NO_2 \cdot HCl$: C 59.63, H 6.67, N 5.79, Cl 14.67; found: C 59.53, H 6.66, N 5.76, Cl 14.76.

3,4-Dihydro-2-oxo-1,4-propanoquinoline (3)

To a 500-mL 3-necked round-bottom flask was added 220 mL of dry CH_3CN (distilled from P_2O_5), 1.0 g of the HCl salt of **8** (4.14 mmol), and 0.58 mL (d = 0.726, 4.17 mmol) of triethylamine. The mixture was stirred under a blanket of Ar until everything dissolved, and then 0.86 g (4.17 mmol) of dicyclohexylcarbodiimide in 4.2 mL of dry CH_3CN was added via syringe. The solution was periodically monitored by IR to observe the progress by the appearance of a 1711 cm^{-1} C=O bond. The mixture was allowed to stand overnight, filtered, and the volatiles removed by rotary evaporation. The solid residue was redissolved in dry benzene, filtered to remove traces of the dicyclohexyl urea, and evaporated to dryness with a vacuum pump. The solid so obtained was recrystallized from octane to give 0.45 g (58%) of **3**, which was filtered in a cold room (4°C); mp 36.0–37.0°C; IR ($CHCl_3$): 1711.50 cm^{-1}; ^{1}H NMR (200 MHz, $CDCl_3$) δ: 7.15 (4H, m), 3.90 (1H, m), 3.15 (2H, m), 2.68 (2H, d, J = 2 Hz), 2.05 (1H, br), 1.3–1.7 (3H, m); ^{13}C NMR (40 MHz, $CDCl_3$) δ: 200.5, 129.7, 128.7, 127.8, 126.9, 125.4, 54.9, 44.6, 33.7, 28.4, 24.8. Exact mass calcd. for $C_{12}H_{13}NO$: 187.0997; found: 187.1001. Anal. calcd. for $C_{12}H_{13}NO$: C 76.98, N 7.48, H 7.00; found: C 76.62, N 7.37, H 6.99.

(b) Kinetics

Triply distilled water was used throughout. Kinetic data at 25°C were obtained by monitoring the rate of change of absorbance of 3×10^{-4} M aqueous solutions of **3** at the wavelength of maximum change (260 nm, pH <5; 280 nm, pH >5) with an HP8451A diode array UV–VIS spectrophotometer. Buffered solutions at four concentrations from 0.05 to 0.20 M were employed, μ = 1.0 KCl. The buffers used were HCl (pH ≤2); formate (3.0–4.0); acetate (4.0–5.0); MES (2-(*N*-morpholino)ethane sulfonic acid) (5.1–6.5); MOPS (3-*N*-(morpholino)propanesulfonic acid) (6.7–7.6); EPPS (*N*-(2-hydroxyethyl)-piperazine-*N'*-(3-propanesulfonic acid) (8.0–8.7); CHES (2-(*N*-cyclohexylamino)-ethanesulfonic acid) (9.0–9.8); CAPS (3-(cyclohexylamino)-1-propanesulfonic acid) (9.8–11.1); NaOH (>11). Slower reactions were initiated by injecting 10 μL of a stock solution of **3** (0.015 g (0.080 mmol) in 1.0 mL CH_3CN) into 3.0 mL of the buffer in a 10-cm quartz cuvette that had thermally equilibrated in the spectrophotometer cell holder for 30 min at 25.0 ± 0.2°C. All reactions were followed in triplicate and monitored for at least three half-lives. Pseudo-first-order rate constants were evaluated by non-linear least-squares fitting of the absorption vs. time data to a standard exponential model. Plots of k_{obsd} data vs. buffer concentration for a given pH were extrapolated back to zero buffer concentration in order to yield the k_{hyd} values given in the text. Primary data are given as Supplementary Material.[2]

Faster reactions (k_{obsd} > 0.1 s^{-1}) were obtained using a Durrum–Gibson 115 stopped-flow kinetics system thermostated at 25°C. Into one drive syringe was placed the main buffer solution, μ = 1.0 (KCl), while the second syringe contained a 2.7×10^{-4} M solution of **3** in 10 mL of 1 M KCl along with one drop of a MOPS buffer (0.05 M) to set the pH at the value corresponding to the slowest hydrolysis. Both solutions were thermostated at 25°C for 20 min, and then rapidly mixed. Four runs were made at each pH. pH measurements were made on the effluent from the mixing chamber and it is assumed that the pH was instantly equilibrated on mixing. When the pH was <2 or >12, $[H_3O^+]$ or $[OH^-]$ was determined by titration using bromothymol blue as the indicator. In general, pH measurements were made with a Radiometer TTT2 titration unit and Radiometer GK-2321C combination electrode. The electrode was standardized prior to use using Fisher Certified pH 4.00, 7.00, and 10.00 buffers.

TABLE 1. Experimental details of the crystal of **3**

$C_{12}H_{13}NO$
FW = 187.24
Crystal dimensions: 0.13 × 0.13 × 0.35 mm
Monoclinic space group $P2_1/c$
a = 6.686(4) Å
b = 10.508(4) Å
c = 28.397(9) Å
β = 102.80(5)°
V = 1945 Å^3
D_c = 1.278 g cm^{-3}
μ = 0.50 cm^{-1}

(c) Product analysis

Into a 3.0-mL sample of pH 7.93 CHES buffer was injected 20 μL of 20 mM **3** in CH_3CN. The UV spectrum (330–250 nm) was continuously scanned using a Cary 210 UV–VIS spectrophotometer. An isosbestic point at λ = 265 nm was observed during the run. At the completion of the kinetic event the spectrum indicated a λ_{max} of 278 nm (ε = 1015 M^{-1} cm^{-1}), which was superimposable upon the spectrum of a solution of authentic amino acid at the same concentration in a pH 7.93 CHES buffer.

(d) Crystal structure

Crystals were grown by dissolving **3** in a small amount of pentane, and placing the solution in a sealed disposable pipette in the freezer compartment of a refrigerator.

(i) Data collection

A clear, colorless crystal of $C_{12}H_{13}NO$, with the approximate dimensions of 0.13 × 0.13 × 0.35 mm, was mounted on a glass fiber with a thin coat of viscous oil, and placed in a stream of cold air. The crystal was cooled to roughly −80°C, and all measurements were made at this temperature. The crystal was optically centered in the X-ray beam of an Enraf–Nonius CAD4 automated diffractometer with graphite monochromator and Mo radiation (λ = 0.7107 Å).

The automatic peak search and reflection indexing programs[3] suggested a unit cell with monoclinic symmetry. The systematic absences of $h0l$, l odd and $0k0$, k odd and the magnitude of the unit cell volume led to the unique choice of space group as $P2_1/c$ (No. 14 (ref. 10)), with two independent molecules in the asymmetric unit. The cell constants and orientation matrix were obtained from a least-squares refinement of the setting angles of 25 reflections in the range 11.8 < θ < 19.9°. The unit cell parameters and other crystallographic information are given in Table 1.

The intensity data were collected with θ–2θ scans of fixed speed, 5.0° min^{-1} (in θ) for the low-angle shell (θ <20°) and 2.0° min^{-1} for the remaining data. The scan range was varied as a function of θ to compensate for α_1–α_2 wavelength dispersion: ω scan width = 0.800 + 0.347 tan θ. The backgrounds for the peaks were measured by extending the scan 25% on each side of the calculated range; this gave a peak-to-background counting time ratio of 2:1. Intensity measurements were made out to a maximum 2θ of 50°. One reflection was chosen as a standard reflection and was remeasured after every 120 min of exposure time to check on crystal and electronic stability over the course of data collection. There was no unusual variation in the intensities of this standard reflection. A total of 8277 reflections, (h, ±k, ±l), was collected and reduced to intensities.

[2]These data may be purchased from the Depository of Unpublished Data, CISTI, National Research Council of Canada, Ottawa, Ont., Canada K1A 0S2.

[3]The diffractometer programs are those supplied by Enraf–Nonius for operating the CAD4F diffractometer with some local modifications made by Dr. R. G. Ball.

TABLE 2. Table of atomic coordinates ($\times 10^4$) and isotropic Gaussian ($\times 10^3$) parameters[a]

Atom	x	y	z	U_{eq} (Å^2)	Atom	x	y	z	U_{eq} (Å^2)
N1	1332(8)	2461(6)	2547(2)	21(2)	N2	282(8)	2696(6)	5595(2)	29(2)
C1	778(10)	3712(7)	2387(2)	26(2)	C21	69(11)	1390(9)	5700(3)	39(3)
O1	−908(7)	3900(5)	2122(2)	36(2)	O2	1367(8)	627(6)	5627(2)	53(2)
C2	2468(10)	4708(7)	2480(3)	28(2)	C22	−1873(11)	1002(8)	5843(3)	40(3)
C3	4368(10)	3941(7)	2385(2)	24(2)	C23	−3556(11)	1865(8)	5532(3)	39(3)
C4	4932(9)	3062(7)	2805(2)	24(2)	C24	−3113(10)	3173(7)	5734(2)	28(2)
C5	6848(10)	2879(7)	3114(2)	26(2)	C25	−4480(11)	4002(9)	5880(3)	40(3)
C6	7089(10)	2025(7)	3491(2)	28(2)	C26	−3853(12)	5195(8)	6058(3)	43(3)
C7	5444(10)	1333(8)	3575(2)	31(3)	C27	−1840(11)	5602(8)	6081(3)	32(3)
C8	3493(10)	1499(7)	3272(2)	27(2)	C28	−453(11)	4769(8)	5937(2)	33(3)
C9	3272(9)	2325(7)	2899(2)	17(2)	C29	−1103(10)	3573(8)	5769(2)	26(2)
C10	3858(10)	3240(7)	1895(2)	28(2)	C30	−3543(12)	1819(9)	4985(3)	45(3)
C11	3145(9)	1837(7)	1903(2)	23(2)	C31	−2211(11)	2832(8)	4807(3)	43(3)
C12	1261(10)	1611(7)	2127(2)	26(2)	C32	65(12)	2846(9)	5065(3)	44(3)

[a]The equivalent isotropic Gaussian parameter U_{eq} is $\frac{1}{3}\Sigma_{i=1}^{3} r_i^2$, where r_i are the root-mean-square amplitudes of the anisotropic Gaussian displacement parameter.

Can. J. Chem. Downloaded from www.nrcresearchpress.com by 91.121.58.235 on 09/07/12
For personal use only.

(ii) Structure solution and refinement

All of the non-hydrogen atoms of the two molecules were evident in an electron density map calculated from a set of phases generated by the direct methods program MITHRIL (11). Adjustment[4] of atomic parameters was carried out by full-matrix least-squares refinement on F_o minimizing the function $\Sigma w(|F_o| - |F_c|)^2$, where $|F_o|$ and $|F_c|$ are the observed and calculated structure factor amplitudes and the weight w is $4F_o^2/\sigma^2(F_o^2)$. The neutral atom scattering factors were calculated from the analytical expression for the scattering factor curves (12). The f' and f'' components of anomalous dispersion (13) were included in the calculations of all non-hydrogen atoms.

The hydrogen atoms were generated at idealized calculated positions by assuming a C—H bond length of 1.00 Å and the appropriate sp^2 or sp^3 geometry. These atoms were then included in the calculations with an isotropic U = 0.013 Å^2 and constrained to "ride" on the attached atom.

The refinement of the coordinates and isotropic U's for all non-hydrogen atoms was continued to convergence. At that stage the data were corrected for absorption using an empirical scheme based on the absorption surface (Fourier filtering) method of Walker and Stuart (14). The maximum and minimum correction factors applied to F_o were 1.4617 and 0.7850. After averaging over $2/m$ symmetry (R-merge on F is 0.148, high due to the dominance of weak intensities) and deleting the systematic absences, there were 3590 averaged observations, 1212 with $I > 3\sigma(I)$. The refinement was continued with use of anisotropic Gaussian displacement parameters for the non-hydrogen atoms. In the final cycle, 253 parameters were refined using the 1212 reflections with $I > 3\sigma(I)$, and the largest and average shift/error ratio was less than 0.01. As a result, the final goodness-of-fit was 1.66, and

$$R_1 = \Sigma||F_o| - |F_c||/\Sigma|F_o| = 0.065$$

$$R_2 = (\Sigma w(|F_o| - |F_c|)^2/\Sigma wF_o^2)^{1/2} = 0.070$$

An analysis of R_2 in terms of F_o, $\sin\theta/\lambda$, and various combinations of (h, k, l) indicated no unusual trends. No substantial differences in the model were evident from a refinement with more of the intensity data; there were 1871 reflections with $I > \sigma(I)$, and the resultant goodness-of-fit was 1.52. Adjustment of the hydrogen atom coordinates with the other variables also indicated no substantial differences, resultant goodness-of-fit to 1.59. The highest peak in the final difference Fourier map has a density of 0.26(7) e Å^{-3}.[2,5] A listing of atomic coordinates and isotropic Gaussian parameters is given in Table 2.

[4]The computer programs used in this analysis include the Enraf–Nonius Structure Determination Package, Version 3 (1985, Delft, The Netherlands) adapted for a Sun Microsystems 3/160 computer, and several locally written programs by Dr. R. G. Ball.

Results and discussion

Amide **3** can be prepared in 24% purified yield in six steps (Scheme 1) from the known ketone **5** (8). The most notable spectroscopic feature of **3** is its C=O stretch appearing at 1711 cm^{-1}, which can be compared with values of 1755 cm^{-1} and 1705 cm^{-1} for **1** and **2** respectively (1).

(a) Molecular and crystal structure of 3

Similar views of the two independent molecules are given in Fig. 1a,b. Because it is the source of the enhanced hydrolytic reactivity, the distortion imposed by the bridged structure on the amidic N-C=O unit is the unique feature of interest in these molecules. The geometrical details of the amide section in each are not significantly different ($>3\sigma$) from those found for amide **2** (Tables 3–5).[2,5] The degree of pyramidalization at N and C(=O) is also similar for amides **2** and **3**. For amide **2**, the displacement of C1 from the NCO (N1—O1—C2) plane is 0.064 Å, and the displacement of N1 from the attached-carbon-atom (C1—C9—C12) plane is 0.436 Å. The corresponding values for amide **3** are 0.079 and 0.408 Å in molecule 1, and 0.048 and 0.430 Å in molecule 2. It is important to note that the environment around molecules 1 and 2 is substantially different. Very roughly, there are eight molecules in contact with molecule 1, but only six molecules in contact with molecule 2. This is somewhat evident from the stereoview of the unit cell projection shown in Fig. 2. One effect of this different packing

[5]A full summary of crystallographic information, the complete listings of anisotropic Gaussian displacement parameters for the non-hydrogen atoms, hydrogen atom coordinates, interatomic bond lengths, angles, and least-squares plane information, and a listing of structure factor amplitudes have been deposited as Supplementary Material. These data may be purchased from the Depository of Unpublished Data, CISTI, National Research Council of Canada, Ottawa, Ont., Canada K1A 0S2.

The crystallographic data, hydrogen atom coordinates, and interatomic bond lengths and angles have also been deposited with the Cambridge Crystallographic Data Centre, and can be obtained on request from The Director, Cambridge Crystallographic Data Centre, University Chemical Laboratory, Lensfield Road, Cambridge CB2 1EW, U.K.

TABLE 3. Table of selected bond lengths (Å)[a]

Molecule 1	Length	Molecule 2	Length	Average[b]	Amide **2**[c]
N1—C1	1.413 (10)	N2—C21	1.419 (11)	1.416	1.401 (2)
N1—C9	1.459 (7)	N2—C29	1.467 (10)	1.462	1.452 (2)
N1—C12	1.482 (9)	N2—C32	1.488 (9)	1.485	1.490 (2)
C1—O1	1.225 (7)	C21—O2	1.233 (10)	1.228	1.216 (2)
C1—C2	1.521 (10)	C21—C22	1.500 (11)	1.511	1.507 (2)

[a]Numbers in parentheses represent standard deviations of the least significant digit. Atom numbering from Fig. 1a,b.
[b]The weighted average I from the population I_i with esd's σ_i is $(\Sigma I_i/\sigma_i^2)/(\Sigma 1/\sigma_i^2)$.
[c]Corresponding values determined from the molecular structure of **2** (3).

TABLE 4. Table of selected interatomic angles (degrees)

Molecule 1	Angle	Molecule 2	Angle	Amide **2**[a]
C1—N1—C9	116.2 (5)	C21—N2—C29	115.8 (6)	116.5 (1)
C1—N1—C12	110.0 (5)	C21—N2—C32	108.9 (6)	109.3 (1)
C9—N1—C12	110.9 (5)	C29—N2—C32	110.3 (6)	108.0 (1)
N1—C1—O1	119.2 (6)	N2—C21—O2	119.1 (7)	119.8 (2)
N1—C1—C2	116.9 (5)	N2—C21—C22	117.0 (7)	116.1 (1)
O1—C1—C2	122.9 (7)	O2—C21—C22	123.6 (8)	123.4 (2)

[a]Corresponding values determined for molecular structure of **2** (3).

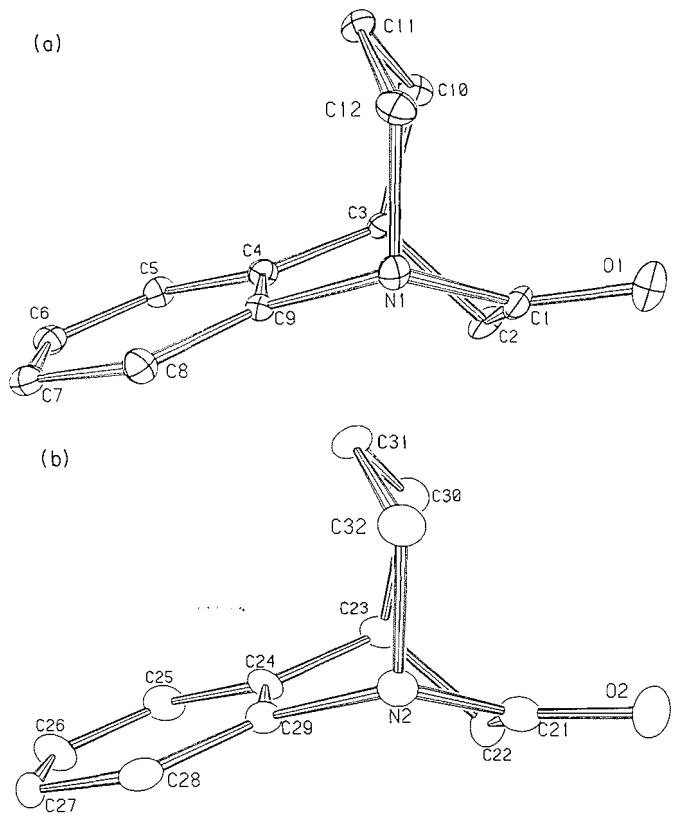

FIG. 1. Perspective view of (a) molecule 1 (atoms N1–C14) and (b) molecule 2 (atoms N2–C32) showing the labelling scheme. Atoms are represented as Gaussian ellipsoids at the 30% probability level.

arrangement is that the U_{eq}'s for the non-hydrogen atoms in molecule 1 are approximately 50% smaller than the corresponding values in molecule 2; the average U_{eq} of the 14 atoms is 0.025 Å^2 in molecule 1 and 0.038 Å^2 in molecule 2. Surprisingly, the conformations of the two molecules are not significantly different (*vide infra*), suggesting that the observed conformation in each represents a ground state configuration unperturbed by crystal packing forces.

TABLE 5. Table of torsional angles (degrees)

Atom 1	Atom 2	Atom 3	Atom 4	Angle (°)	Amide **2**[a]
C9	N1	C1	O1	−174.1 (6)	177.5 (2)
C29	N2	C21	O2	−169.7 (6)	
C9	N1	C1	C2	16.9 (8)	−11.5 (2)
C29	N2	C21	C22	17.0 (9)	
C12	N1	C1	O1	58.8 (8)	−59.7 (2)
C32	N2	C21	O2	65.4 (8)	
C12	N1	C1	C2	−110.3	111.3 (2)
C32	N2	C21	C22	−107.9 (7)	

[a]Corresponding values for amide **2** (3). Difference in sign arises from amide **2** being originally reported in the opposite absolute configuration to **3**.

We have previously described the distortion in amide **2** in terms of a twist angle (ϕ) and tilt angle (θ) of the N "lone pair" away from optimum conjugation with the C=O Π system (1, 3). For **2**, the N pair of electrons was located as a peak in the difference Fourier map lying ~1.2 Å away from the N in a position expected on geometric grounds. Using the centre of this electron density, the respective twist and tilt angles are ϕ = 30–35° and θ = 18° (3). In **3**, the corresponding peak cannot be located, so a geometric position for the N lone pair was assigned on the basis of a perpendicular drawn through N1 from the plane defined by C1, C9, and C12. On this basis, the twist and tilt angles (visualized in Fig. 3) are 35° and 15° respectively. With reference to the deformation of the amide group, we note that Winkler and Dunitz (15) have studied the distortions of amides in closed-ring systems. For **3**, the values of the bending and twisting coordinates are χ_C = 11.0°, χ_N = 52.8°, and τ' = 75.6°. Although the N-C=O units in **2** and **3** are nearly superimposable, there is a substantial difference in the disposition of the aromatic ring, evident from a comparison of the lone pair–N1—C9—C4 torsion angle in **3**, 27°, and the corresponding angle in **2**, −3°.

Can. J. Chem. Downloaded from www.nrcresearchpress.com by 91.121.58.235 on 09/07/12
For personal use only.

Can. J. Chem. Downloaded from www.nrcresearchpress.com by 91.121.58.235 on 09/07/12
For personal use only.

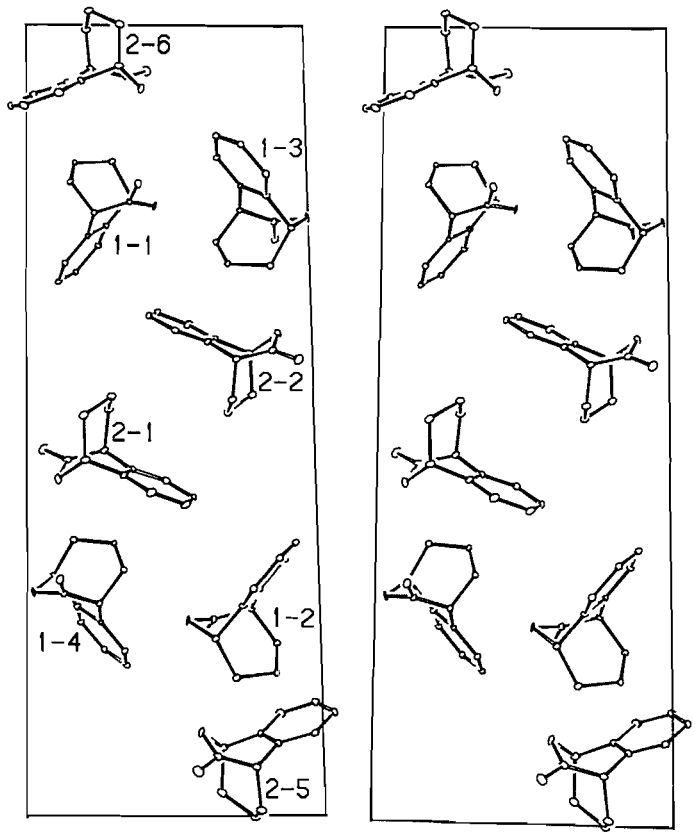

FIG. 2. Stereoview of the unit cell viewed up a with b to the left and c down the page. The labels identify the specific molecule, with the first digit indicating molecule 1 or 2, and the second digit indicating the symmetry operation (1–6). The symmetry operation, $\boldsymbol{Rx} + \boldsymbol{t}$, is described by use of a rotation matrix $\boldsymbol{R}$ and a translation matrix $\boldsymbol{t}$, and operates on the atomic coordinates $\boldsymbol{x}$. The specific symmetry operations are:

$$R_1 = \begin{pmatrix} 1 & 0 & 0 \\ 0 & 1 & 0 \\ 0 & 0 & 1 \end{pmatrix}, \; t_1 = \begin{pmatrix} 0 \\ 0 \\ 0 \end{pmatrix}; \quad R_2 = \begin{pmatrix} -1 & 0 & 0 \\ 0 & -1 & 0 \\ 0 & 0 & -1 \end{pmatrix}, \; t_2 = \begin{pmatrix} 0 \\ 1 \\ 1 \end{pmatrix}$$

$$R_3 = \begin{pmatrix} -1 & 0 & 0 \\ 0 & 1 & 0 \\ 0 & 0 & -1 \end{pmatrix}, \; t_3 = \begin{pmatrix} 0 \\ \frac{1}{2} \\ \frac{1}{2} \end{pmatrix}; \quad R_4 = \begin{pmatrix} 1 & 0 & 0 \\ 0 & -1 & 0 \\ 0 & 0 & 1 \end{pmatrix}, \; t_4 = \begin{pmatrix} 0 \\ \frac{1}{2} \\ \frac{1}{2} \end{pmatrix}$$

$$R_5 = \begin{pmatrix} -1 & 0 & 0 \\ 0 & 1 & 0 \\ 0 & 0 & -1 \end{pmatrix}, \; t_5 = \begin{pmatrix} 0 \\ \frac{1}{2} \\ \frac{3}{2} \end{pmatrix}; \quad R_6 = \begin{pmatrix} 1 & 0 & 0 \\ 0 & -1 & 0 \\ 0 & 0 & 1 \end{pmatrix}, \; t_6 = \begin{pmatrix} 0 \\ \frac{1}{2} \\ -\frac{1}{2} \end{pmatrix}$$

(b) Kinetics of hydrolysis

Given in Table 6 are the pseudo-first-order rate constants (k_{hyd}) for hydrolysis of **3** at 25°C, μ = 1.0 (KCl), extrapolated to zero buffer concentration. Given as Supplementary Material[2] are the primary kinetic constants for each buffer concentration. The pH/rate profile given in Fig. 4 shows three domains: one first order in $[OH^-]$, and a second, first order in $[H_3O^+]$, which gives way at low pH to a pH-independent domain. The appearance of the profile is consistent with the mechanism given in eq. [1] from

$$[1] \quad \mathrm{P} \underset{H_2O}{\overset{k_{H_3O^+}}{\longleftarrow}} \mathbf{3}\text{-}H^+ \overset{K_a}{\rightleftharpoons} H_3O^+ + \mathbf{3} \xrightarrow{k_{OH^-}[OH^-]}$$

for which can be derived the kinetic expression in eq. [2].

$$[2] \quad k_{hyd} = k_{H_3O^+}[H_3O^+]/(K_a + [H_3O^+]) + k_{OH^-}K_w/[H_3O^+]$$

Non-linear least-squares (NLLSQ) fitting of the k_{hyd} and

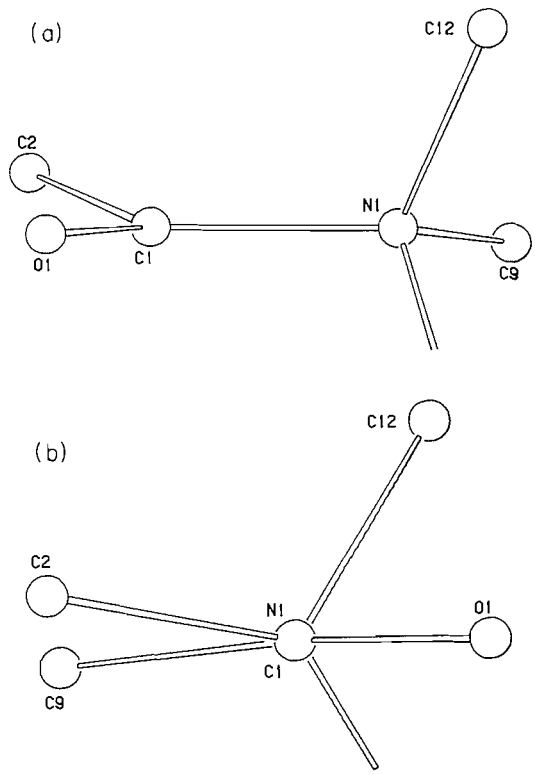

FIG. 3. Views of the amidic section of amide **3** (a) down the N-C=O bond showing the twist angle ϕ, and (b) perpendicular to the O=C-N plane showing the tilt angle θ. Position of the N lone pair represented by line having no terminal atom.

TABLE 6. Pseudo-first-order hydrolysis rate constants (k_{hyd}) for **3** at [buffer] = 0, T = 25°C, μ = 1.0 (KCl)[a]

pH	Buffer	k_{hyd} (s^{-1})[b]
0.01	HCl	6.47 (0.15)
0.30	HCl	5.71 (0.06)
0.60	HCl	3.86 (0.02)
1.00	HCl	2.14 (0.09)
1.95	HCl	0.23 (0.01)[c]
3.10	Formate	$2.33\,(0.05) \times 10^{-2}$
3.55	Formate	$8.34\,(0.18) \times 10^{-3}$
4.20	Acetate	$2.44\,(0.03) \times 10^{-3}$
4.60	Acetate	$8.21\,(0.05) \times 10^{-4}$
5.56	MES	$9.18\,(0.08) \times 10^{-5}$
6.25	MES	$1.19\,(0.03) \times 10^{-5}$
6.75	MOPS	$8.26\,(0.09) \times 10^{-6}$
7.22	MOPS	$5.87\,(0.04) \times 10^{-6}$
7.60	MOPS	$7.92\,(0.17) \times 10^{-6}$
8.06	EPPS	$3.56\,(0.27) \times 10^{-5}$
9.35	CHES	$3.98\,(0.11) \times 10^{-4}$
10.45	CAPS	$5.40\,(0.05) \times 10^{-3}$
12.94	NaOH	1.080 (0.004)[c]

[a]pH 0.01–4.60, kinetics followed at 260 nm; pH 5.56–12.94, kinetics followed at 280 nm.

[b]Numbers in parentheses are standard deviation of the mean of at least three separate determinations.

[c]Calculated from Eyring plot of k_{obsd} vs. T (5°C < T < 48°C) at pH indicated.

Can. J. Chem. Downloaded from www.nrcresearchpress.com by 91.121.58.235 on 09/07/12
For personal use only.

$[H_3O^+]$ data of Table 5 to eq. [2] yields values of $k_{H_3O^+}$ = 8.26 (1.7) s^{-1}, k_{OH^-} = 17.2 (1.7) M^{-1} s^{-1}, and K_a = 0.28 (0.07) (pK_a = 0.56), assuming $K_w = 10^{-14}$: the line drawn through the data points in Fig. 4 is that computed on the basis of the NLLSQ fit. Also given in Fig. 4 are the hydrolytic profiles for amides **1** and **2** (1).

The kinetic profile for **3** invites comparison with those for **1** and **2**. The base domains for **1–3** show a striking similarity, which suggests that in this region, **3**, like **1** and **2** (1), suffers rate-limiting irreversible attack of OH^-. Normal acetanilides (16), trifluoromethyl acetanilides (17, 18), and formanilides (19) show base domains for log k_{hyd} vs. pH of slopes 1, >1, and 1 in passing from low to high pH. This is analyzable in terms of eqs. [3] and [4] where the intermediate (Tl^-), in competition

[3] $$OH^- + R{-}\overset{\overset{O}{\|}}{C}NRAr \underset{k_{-1}}{\overset{k_1}{\rightleftharpoons}} R{-}\overset{\overset{O^-}{|}}{\underset{\underset{OH}{|}}{C}}{-}NRAr \quad (Tl^-)$$

$$\xrightarrow[k_3'[OH]]{k_2} P$$

[4] $$k_{hyd} + k_1[OH^-](k_2 + k_3[OH^-])/(k_{-1} + k_2 + k_3[OH^-])$$

with reversion to starting materials or uncatalyzed breakdown to product, can be intercepted by a second OH^- and driven forward. The inherent distortion in anilides **1–3** obviously facilitates the forward pathway since the corresponding Tl^-, once formed, has little tendency to reverse because amidic resonance (which accelerates k_{-1} in the normal anilides (16–19) is substantially eliminated in **1–3**.

By way of comparison, the values of the second-order rate constants for OH^- attack on **1**, **2**, and **3** are 262 (1), 60 (1), and 17.2 M^{-1} s^{-1} respectively at 25°C while the apparent ones for acetanilide (0.957 M, NaOH) and *N*-methylacetanilide (0.89 M NaOH) are 7.55 × 10^{-6} M^{-1} s^{-1} (16)[6] and 1.5 × 10^{-5} M^{-1} s^{-1} respectively. Although the structure of **1** is unknown, its amide unit must certainly be more strained (with respect to orthogonality of the N: and C=O Π system arising from rotation around the C—N bond) than those of **2** (3) and **3** (*vide infra*). On the surface, it would be anticipated that the attack rate constant would be related to the carbonyl electrophilicity, which by these simple geometric arguments is anticipated to be **1** > **2** ≈ **3**. Surprisingly, the rate constant differences for OH^- attack are small (16:4:1 respectively), suggesting that beyond a certain point, rotation about the O=C—N bond produces little additional kinetic benefit. We note that each of **1–3** has an additional nearly equivalent distortion, namely that of N pyramidalization, which has also been shown to accelerate dramatically nucleophilic OH^- attack (20). Perhaps that distortion dominates the kinetics in this series, but in the absence of activation parameter studies with **1–3** (currently in progress), little additional comment on the relationship between OH^- attack and twisting can be offered at this time.

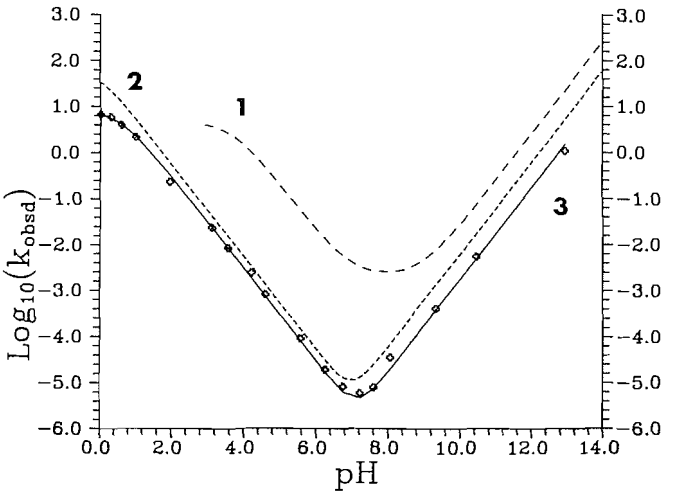

FIG. 4. A plot of log k_{hyd} vs. pH for the hydrolysis of amide **3**, T = 25°C, μ = 1.0 (KCl); line through the data points calculated on the basis of eq. [2]; kinetic profiles for amide **1** (———) and **2** (- - -) (1). Data for **2** from pH 0–2 determined in present study.

The observation of kinetic pK_a values of 3.7 (1) for **1** and 0.6 for **3** prompted a reinvestigation of the hydrolysis kinetics for **2** at low pH. We had originally failed to detect the onset of plateauing for **2**, but the structural similarity to **3** suggested that both might hydrolyze by common mechanisms. Indeed, as shown in Fig. 4 the new data[7] from pH 0–2 give evidence of plateauing for **2** and NLLSQ fitting provides a K_a of 1.8 (pK_a −0.28 ± 0.03) and $k_{H_3O^+}$ of 101 ± 7 s^{-1}. These latter values are considered as less accurate than the corresponding ones for **1** and **3** since at the lowest pH (0) attainable,[7] substantially less than half of the material is protonated.

The distinction between N- and O-protonation sites can be made by comparison of the kinetic pK_a's of **1–3** with those for normal amides. Typical amides have N-H^+ and O-H^+ pK_a values of −6 to −8 (21) and 0 to −2 (21*b–e*) respectively. In **1**, and to a lesser extent **2** and **3**, favorable resonance effects that stabilize the O-protonation of amides are precluded. Thus, the N and C=O in **1** should tend to behave independently, as amino and ketonic units, but exert mutual inductive effects that destabilize the other's protonated form. Thus, the pK_a of the C=O—H^+ unit in **1** is anticipated to be even lower than that of a ketone (normally −7 to −5 for acetone, cyclohexanone, etc. (21*d*)) so that the observed kinetic pK_a must be attributable to the N-H^+ form. By way of comparison, the pK_a of 3.7 for the conjugate acid of **1** (1) is ~4 units lower than the pK_a of benzoquinuclidine (7.79 (22)), in line with the inductive destabilization of N-H^+ by an adjacent orthogonal C=O.

As pointed out above, the structures of **2** and **3** do not completely inhibit N-C=O delocalization, and this leads to a drop in the N-H^+ pK_a relative to **1**. Correspondingly, the N-C=OH^+ forms of **2**, **3** are more stable than O-protonated **1**,

[6]It is known that acetanilide exhibits a large amount of ^{18}O-exchange concurrent with its hydrolysis in base and that reversal of Tl^- tends to slow the hydrolysis markedly. The second-order rate constants quoted above are termed apparent ones because in the NaOH concentration range used (16), the kinetics contain terms second order in [NaOH]. From a graphical analysis of the exchange/hydrolysis ratios vs. $[OH^-]$ values quoted in ref. 16 it can be shown that k_2/k_{-1} = 0.047; k_3/k_{-1} = 0.097. On this basis, one can calculate that for acetanilide at 25°C, the true rate constant for OH^- attack, namely, $k_1 = (1.3 \pm 0.2) \times 10^{-4}$ M^{-1} s^{-1}.

[7]k_{hyd}(pH) data for **2** at T = 25°C, μ = 1.0 KCl in units of s^{-1}: 0.59 ± 0.1 (1.95); 5.78 ± 0.04 (1); 14.50 ± 0.18 (0.60); 26.15 ± 0.22 (0.30); 42.8 ± 1.1 (0.01). These data were fit to a standard titration model to yield the values quoted in the text. Unfortunately, $[H_3O^+]$ in excess of 1 M was not accessible due to the timescale of the reaction and problems in stopped-flow mixing of solutions of widely different ionic strengths.

but they cannot be as stable as that of a normal amide where full delocalization is permitted. Thus we are forced to conclude that the observed kinetic pK_a values of -0.3 (**2**) and 0.6 (**3**) are most consistent with the N-H^+ forms. It must be pointed out that the kinetics do not provide information as to which of the N-H^+ or O-H^+ forms is attacked by H_2O although we favor the former. Thus although the N-H^+ form is arguably the most thermodynamically stable, it could be kinetically less reactive toward nucleophilic attack than the O-H^+ form. In that event, the N-H^+ form would be not considered to be on the reaction pathway.

Conclusions

The strained amides **1–3** hydrolyze rapidly in both acid and base. X-ray crystallographic structural comparison can be made between **2** and **3**, and the amidic unit in each is structurally similar with respect to bond lengths and angles. In both cases, the N is essentially sp^3 hybridized with the N "lone pair" being twisted some 30–35° out of optimum alignment with the C=O Π system.

Acknowledgements

The authors gratefully acknowledge the financial assistance of the University of Alberta and the Natural Sciences and Engineering Research Council of Canada.

1. V. Somayaji and R. S. Brown. J. Org. Chem. **51**, 2676 (1986).
2. G. M. Blackburn, C. J. Skaife, and I. T. Kay. J. Chem. Res. Miniprint, 3650 (1980).
3. V. Somayaji, K. I. Skorey, R. S. Brown, and R. G. Ball. J. Org. Chem. **51**, 4866 (1986).
4. V. Somayaji, K. I. Skorey, and R. S. Brown. J. Am. Chem. Soc. **110**, 5205 (1988).
5. K. I. Skorey, V. Somayaji, and R. S. Brown. J. Am. Chem. Soc. **111**, 1445 (1989).
6. V. Somayaji and R. S. Brown. J. Am. Chem. Soc. **109**, 4738 (1987).
7. V. Somayaji, J. Keillor, and R. S. Brown. J. Am. Chem. Soc. **110**, 2625 (1988).
8. (*a*) G. R. Proctor. J. Chem. Soc. 3989 (1961); (*b*) I. McCall, G. R. Proctor, and L. Purdie. J. Chem. Soc. (C), 1126 (1970).
9. S. Ji, L. B. Gortler, A. Waring, A. Battisti, S. Bank, W. D. Closson, and P. Wriede. J. Am. Chem. Soc. **89**, 5311 (1967).
10. International tables for X-ray crystallography. Vol. 1. The Kynoch Press, Birmingham, England. 1969.
11. C. J. Gilmore. MITHRIL 83. A multiple solution direct methods program. University of Glasgow, Scotland. 1983.
12. International tables for X-ray crystallography. Vol. IV. Table 2.2B. The Kynoch Press, Birmingham, England. 1974.
13. International tables for X-ray crystallography. Vol. IV. Table 2.3.1. The Kynoch Press, Birmingham, England. 1974.
14. N. Walker and D. Stuart. Acta Crystallogr. Sect. A: Found. Crystallogr. **A39**, 158 (1983).
15. F. K. Winkler and J. D. Dunitz. J. Mol. Biol. **59**, 169 (1971).
16. M. L. Bender and R. J. Thomas. J. Am. Chem. Soc. **83**, 4183 (1961).
17. (*a*) R. L. Schowen and G. W. Zuorich. J. Am. Chem. Soc. **88**, 1223 (1966); (*b*) R. L. Schowen, H. Jayaraman, and L. D. Kershner. J. Am. Chem. Soc. **88**, 3373 (1966); (*c*) L. D. Kershner and R. L. Schowen. J. Am. Chem. Soc. **93**, 2014 (1971); (*d*) J. K. Young, S. Pazhanisamy, and R. L. Schowen. J. Org. Chem. **49**, 4148 (1984).
18. (*a*) S. O. Ericksson. Acta Chem. Scand. **22**, 892 (1968); (*b*) S. O. Ericksson and C. Holst. Acta Chem. Scand. **20**, 1892 (1966); (*c*) S. O. Ericksson and L. Bratt. Acta Chem. Scand. **21**, 1812 (1967).
19. R. H. De Wolfe and R. C. Newcomb. J. Org. Chem. **36**, 3870 (1971).
20. H. Slebocka-Tilk and R. S. Brown. J. Org. Chem. **52**, 805 (1987).
21. (*a*) A. Williams. J. Am. Chem. Soc. **98**, 5645 (1976); (*b*) E. M. Arnett. Prog. Phys. Org. Chem. **1**, 223 (1963); (*c*) J. P. Guthrie. J. Am. Chem. Soc. **96**, 3608 (1974); (*d*) E. M. Arnett, R. P. Quick, and J. W. Larsen. J. Am. Chem. Soc. **92**, 3977 (1970); (*e*) A. Fersht. J. Am. Chem. Soc. **93**, 3504 (1971).
22. B. M. Wepster. Recl. Trav. Chim. Pays-Bas, **71**, 1171 (1952).

Can. J. Chem. Downloaded from www.nrcresearchpress.com by 91.121.58.235 on 09/07/12
For personal use only.

Observations on cation-binding characteristics and nuclear magnetic resonance spectra of the *N*-carboxymethyl and *N*-acetyl analogs of heparin

RABINDRA N. REJ, KEVIN R. HOLME, AND ARTHUR S. PERLIN
Department of Chemistry, McGill University, Montreal, P.Q., Canada H3A 2A7

Received March 30, 1990

This paper is dedicated to Professor Ross Stewart on the occasion of his 65th birthday

RABINDRA N. REJ, KEVIN R. HOLME, and ARTHUR S. PERLIN. Can. J. Chem. **68**, 1740 (1990).

Based on the observed paramagnetic relaxation effects of Cu^{2+} and Fe^{3+} ions and the chemical shift displacements induced by Ca^{2+} ions, nuclear resonance spectroscopy has been used to compare cation-binding characteristics of heparin with those of its *N*-carboxymethyl and *N*-acetyl analogs and related polyanions. Heparin is unique in exhibiting a high affinity for all three cations. Among the other polymers, binding selectivities differ notably. Such factors as the incidence and distribution of anionic charges are discussed. The preparation of the *N*-carboxymethyl analog of heparin is described, and ^1H and ^{13}C nuclear magnetic resonance spectroscopic data are reported for it, as well as for the *N*-acetyl analog.

Key words: heparin, *N*-carboxymethyl analog, *N*-acetyl analog, cation binding, ion-selectivity, anionic charge distribution.

RABINDRA N. REJ, KEVIN R. HOLME et ARTHUR S. PERLIN. Can. J. Chem. **68**, 1740 (1990).

En se basant sur les effets de relaxation paramagnétique observés pour les ions Cu^{2+} et Fe^{3+} ainsi que les variations des déplacements chimiques induite par les ions Ca^{2+}, on a utilisé la résonance magnétique nucléaire pour comparer les caractéristiques de capture de cation de l'héparine avec celles de ses analogues *N*-carboxyméthyle et *N*-acyle et celles des polyanions apparentés. L'héparine est le seul produit à présenter une grande affinité pour les trois cations. Parmi les autres polymères, les sélectivités de capture diffèrent beaucoup. On discute de fracteurs comme l'incidence et la distribution des charges anioniques. On décrit la préparation de l'analogue *N*-carboxyméthyle de l'héparine et on rapporte des données relatives à ses spectres de résonance magnétique nucléaire du ^1H et du ^{18}C ainsi qu'à ceux de son analogue *N*-acétylé.

Mots clés : héparine, analogue *N*-carboxyméthyle, analogue *N*-acétyle, affinité pour les cations, sélectivité ionique, distribution des charges ioniques.

[Traduit par la revue]

Introduction

The binding of cations by heparin, which has been studied extensively (1, 2) in relation to its clinical importance as a blood anticoagulant, is attributable to the polymer's strongly anionic character, as represented in the major disaccharide repeating unit (**1**→**2**) shown. Not only are there marked differences among cations (3–10) in their affinity for heparin, depending upon such factors as the valence of the cation and (or) its ionic radius, but also in their specificity for modified forms of the polymer (11–15) that contain fewer negative charges and differing distributions of those residual charges.

Recently, we reported (16) that the binding of cupric ion (Cu^{2+}) by heparin is detectable by nmr spectroscopy through highly sensitive paramagnetic relaxation effects. The effects on ^1H and ^{13}C nuclei were observed even when the proportion of the cation was several orders of magnitude lower than that of the polymer. By contrast, no comparable interaction was detected between Cu^{2+} and a variety of other anionic polymers, including the chondroitin sulfates and several modified forms of heparin. As these non-binding substances contain fewer anionic charges than does heparin, total charge density is likely to be a highly important factor. Nevertheless, a single exception was encountered. That is, the 2-acetamido-2-deoxy (*N*-acetyl) analog of heparin (**1**→**3**), which also is less strongly anionic, does respond to the paramagnetic relaxation influence of Cu^{2+} ion. This appeared to be consistent with an earlier suggestion (14) that although an overall high charge density may be necessary for binding, the geometric arrangement of the anionic groups is critical as well.

Results and discussion

The N-*carboxymethyl analog of heparin*

In this context, we have prepared the *N*-carboxymethyl analog (**1**→**4**) of heparin, which, to our knowledge, has not previously been described.[1] In addition to having the three anionic groups that the *N*-acetyl derivative contains, this derivative carries a total of four negative charges per disaccharide unit, as does heparin itself, and, at least superficially, the spatial distribution of the anionic groups is similar in both polymers. The *N*-carboxymethyl substituent of **4** was introduced by the reaction of selectively *N*-desulfated heparin (**1**→**5**) with bromoacetic acid in aqueous sodium carbonate, conditions analogous to those conventionally used for selective *N*-sulfation of residues of **5**. The ^1H nmr spectrum (Fig. 1C), following two successive treatments with bromoacetic acid, indicated that >80% of *N*-substitution had occurred, and had not been accompanied by other detectable modifications. That is, there is a major H-2 signal (δ 2.70) attributable to the *N*-carboxymethylated residue (**4**), although the minor peak at δ ~3.0 suggests that a small proportion of amine **5** remained unsubstituted. A high level of conversion into **4** was confirmed by the ^{13}C spectrum of the new polymer, which is composed essentially of the 14 resonances expected (Table 1). It is noteworthy that both the ^1H-1 and ^{13}C-1 resonances of residue **4** are well upfield of the corresponding signals in heparin, whereas ^1H-2 and ^{13}C-2 are, respectively, upfield and downfield (δ 2.7 vs. δ 3.3, and δ 63.3 vs. δ 60.0).

To test for the effect of Cu^{2+} on the *N*-carboxymethyl derivative, the solution of the derivative was adjusted to pD ~5.8, at which heparin has been found (16) to respond to the paramagnetic effect of the cation more strongly than at neutrality. This change in pD, in the absence of the metal ion, caused (Fig. 1B) several resonances of the aminohexose residue (**4**) to be displaced downfield relative to those in Fig. 1C, most strikingly A-1, A-2, and the methylene doublets of the carboxymethyl

[1]As determined by assays of anti-XA potency, neither this polymer nor the *N*-acetyl analog of heparin exhibits significant anticoagulant activity.

Can. J. Chem. Downloaded from www.nrcresearchpress.com by 91.121.58.235 on 09/07/12
For personal use only.

Can. J. Chem. Downloaded from www.nrcresearchpress.com by 91.121.58.235 on 09/07/12
For personal use only.

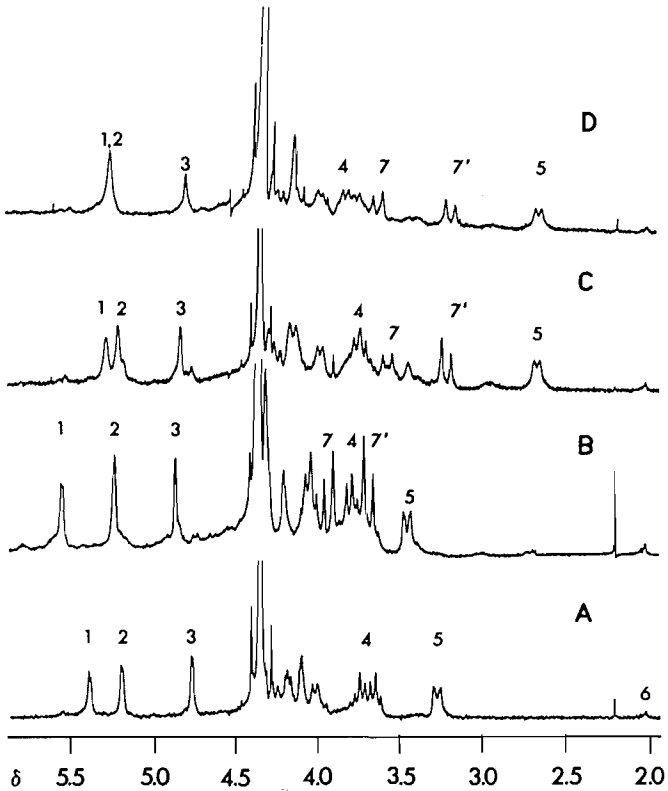

FIG. 1. The ^{1}H nmr spectra (300 MHz; 65°C) of (A) beef lung heparin (**1**→**2**, sodium salt) in D_2O; (C) the *N*-carboxymethyl analog (**1**→**4**, sodium salt) in D_2O; (B) solution in (C) adjusted to pD ~5.8; (D) solution in (C) following the introduction of 2 moles of Ca^{2+} per mole (643) of disaccharide. Signal designations: 1, 4, and 5 are for H-1, H-3 and (or) H-4, and H-2, respectively, of both residues **2** and **4**; 2 and 3 are for H-1 and H-5, respectively, of residue **1**; 7 and 7′ are for the methylene (CH_2) protons of residue **4**.

TABLE 1. ^{13}C chemical shifts for *N*-carboxymethyl and *N*-acetyl analogs of heparin[a]

Carbon	Heparin[b]	*N*-Carboxymethyl heparin	*N*-Carboxymethyl modified heparin	*N*-Acetyl heparin
I-1	101.4	101.9	105.0 (104.5)[c]	101.9
I-2	78.3	76.6	72.1 (72.0)	76.5
I-3	71.4	68.9	72.8 (72.0)	69.2
I-4	78.2	74.1	79.0 (77.5)	74.0
I-5	71.7	70.6	72.1 (72.5)	70.7
I-6	176.2	178.0	177.6 (177.0)	178.1
A-1	99.0	94.0	94.2 (98.5)	96.4
A-2	60.0	63.3	63.2 (60.0)	56.2
A-3	71.9	71.3	71.2 (71.9)	72.7
A-4	78.6	78.2	76.5 (79.6)	79.1
A-5	71.3	72.4	71.2 (71.3)	72.0
A-6	68.6	67.6	68.9 (68.6)	67.0
CH_2		51.2	50.8	
COO		174.0	173.8	
COMe				177.5
Me				25.0

Based on assignments obtained by a combination of ^{1}H–^{1}H (COSY) and ^{13}C–^{1}H (HETCOR) correlation spectra.

[b]Data from ref. 27.

[c]Data in parentheses are for the corresponding 2-sulfamino analog (**6**→**2**), from ref. 19.

group. By comparing these spectra and the accompanying spectrum of heparin itself (Fig. 1A), the signals (I-1 and I-5) for H-1 and H-5 of the uronic acid residue (**1**) are found to remain largely unaffected throughout, which suggests that this conformationally unstable (2, 17) type of residue is not appreciably altered by the changes to the aminodeoxyhexose residues (**2** and **4**). The I-1 and I-5 nuclei of **1** are of particular concern in copper binding because, in the ^{1}H nmr spectrum of heparin, their resonances undergo (16) the most marked broadening in the presence of Cu^{2+} (as also do the signals for ^{13}C-1, ^{13}C-5, and ^{13}COOH). However, the introduction of Cu^{2+} (10^{-3} moles/disaccharide unit) into the solution represented by Fig. 1B caused essentially no change, and this evidence of unreactivity persisted when the cation level was increased threefold.

Hence, despite the high charge density of the *N*-carboxymethyl derivative, and its (seemingly) closer structural resemblance to heparin than all of the other polymers tested, it showed no paramagnetic response to Cu^{2+} analogous to that exhibited by heparin and its *N*-acetyl analog. The possible influence of varying the pD of the measurements, so as to allow for pK_a differences between this polyanion and heparin, was not examined, nor was the possibility that binding may occur when the proportion of Cu^{2+} is *equal* to that of the polymer (or higher), i.e., conditions that others (5, 18) have described in detail for heparin itself.

Many studies already mentioned, including some of our own, have dealt with characteristics of complex formation between heparin and calcium ion (Ca^{2+}). Consequently, the *N*-carboxymethyl derivative was tested with this cation as well, under conditions similar to those used previously (13, 14, 16) with the parent polymer. In this instance, evidence for the binding of Ca^{2+} is given by the ^{1}H nmr spectrum in Fig. 1D, which shows the changes occurring relative to Fig. 1C, following the introduction of 2 moles of Ca^{2+} per mole of disaccharide. The displacements in chemical shift for resonances A-1, I-1, and I-5, respectively, attributable to the binding of the cation, are compared in Table 2 with values of the corresponding resonances of heparin. There also is a large downfield displacement of the doublet of one of the diastereotopic methylene protons by 21 Hz. It is worth noting that although the *N*-carboxymethyl derivative interacts with Ca^{2+}, which leads to ^{1}H chemical shift displacements not unlike those (13, 14) exhibited by heparin, the amino derivative (**1** plus **5**) from which it was derived is incapable of binding either Ca^{2+} or Cu^{2+}.

The N*-carboxymethyl analog of modified heparin* (**6**→**2**)

A second *N*-carboxymethyl derivative based on heparin was prepared from a recently described (19) modified form of the polymer, represented by the disaccharide sequence, **6**→**2**. This material was obtained from heparin by a selective base-catalysed displacement of the 2-*O*-sulfo group of its L-iduronic acid residue (**1**). In the absence of this sulfate group, the anomeric proton of **6** resonates ~0.2 ppm upfield of that of **1** (see Fig. 2A). By selective hydrolysis of the *N*-sulfo group of the pyridinium salt of the polymer in 19:1 dimethyl sulfoxide/water, the procedure (20) employed to generate residue **5** (above), the corresponding amine derivative (**6**→**5**) was prepared, and analogously converted into the *N*-carboxymethyl derivative (**6**→**4**). That the latter was of relatively high purity was evident from the structural homogeneity implicit in its ^{1}H nmr spectra at pD 5.8 and 7.0, respectively (Figs. 2B and 2C), as well as the fact that its ^{13}C spectrum consisted essentially of the 14 resonances (Table 1) required by the formula shown.

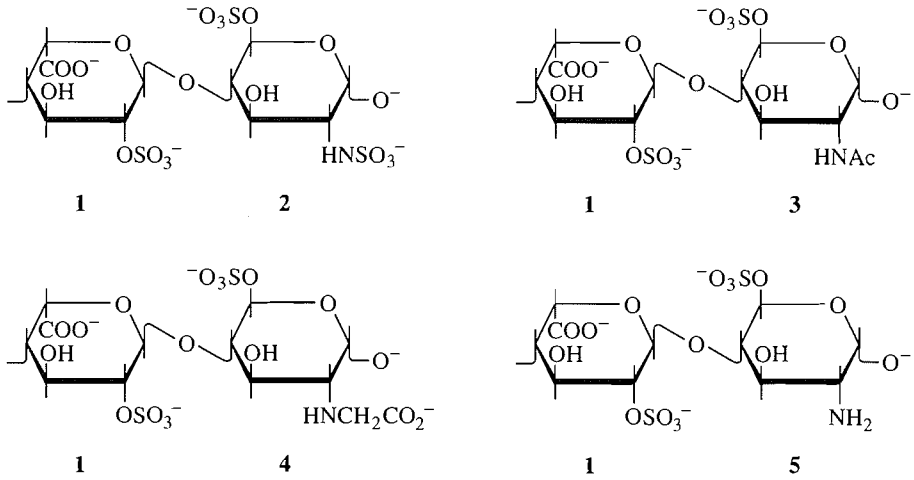

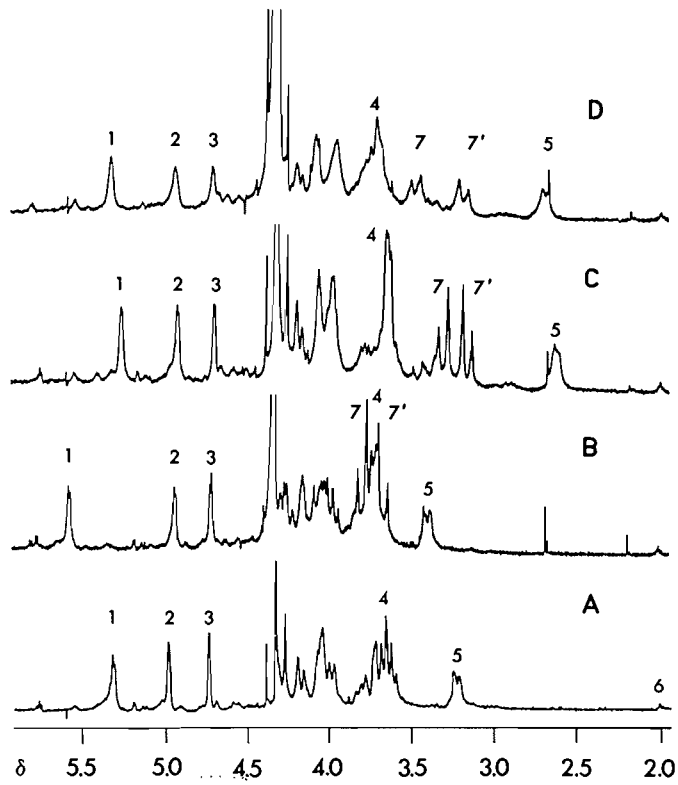

FIG. 2. The ^{1}H nmr spectra (300 MHz; 65°C) of (A) modified heparin (**6**→**2**, sodium salt) in D_2O; (C) the *N*-carboxymethyl analog (**6**→**4**, sodium salt) in D_2O; (B) solution in (C) adjusted to pD ~5.8; (D) solution in (C) following the introduction of 2 moles of Ca^{2+} per mole (541) of disaccharide. Signal designations: 1, 4, and 5 are for H-1, H-3 and (or) H-4, and H-2, respectively, of both residues **2** and **4**; 2 and 3 are for H-1 and H-5, respectively, of residue **6**; 7 and 7′ are for the methylene (CH_2) protons of residue **4**.

TABLE 2. Displacement (Δ Hz) of ^{1}H nmr signals of *N*-carboxymethyl heparin and *N*-carboxymethyl modified heparin (**6**→**4**) by Ca^{2+}[a,b]

Proton	*N*-Carboxymethyl heparin[c]	*N*-Carboxymethyl modified heparin[d]
A-1	−4.1 (−2.4)	+20.3 (−10)
A-2	+0.7 (0)	+22.4 (0)
I-1	+18.8 (+29)	+5.7 (+45)
I-5	−4.7 (+25)	+4.5 (+32)
CH	+21.1	+50.1
CH^1	−3.3	+8.5

[a]At 2.0 mol of Ca^{2+}/repeating unit (**1**→**4** and **6**→**4**, respectively); − denotes upfield shift, and + denotes downfield shift.
[b]At 65°C.
[c]The values in parentheses are those obtained (16) for heparin under comparable conditions.
[d]The values in parentheses are those obtained (16) for the corresponding 2-sulfamino analog (**6**→**2**).

A close correspondence in the chemical shifts of protons 1–4 and CH_2 of residue 4, in this *N*-carboxymethyl derivative and that of heparin, is seen by comparing Figs. 2B and 2C with Figs. 1B and 1C, including the marked downfield displacements of the H-1, H-2, and CH_2 signals of residue 4 that accompanied the drop in pD. Data for the ^{13}C spectrum are listed in Table 1.

As polymer **6**→**2** does not bind Cu^{2+} (16), perhaps it is not surprising that this *N*-carboxymethyl derivative was also found to be unreactive towards Cu^{2+} at pD 5.8. That is, in the presence of the cation its spectrum was virtually indistinguishable from that in Fig. 2B. It proved to be highly sensitive, however, to Ca^{2+} (at pD 7.0), as shown in Fig. 2D from the occurrence of major alterations with respect to the spectrum in Fig. 2C; the most substantial displacement (Table 2) was the downfield shift by 50 Hz of the methylene doublet at δ 3.3. Nevertheless, the influence of the cation appears to be more selective for the *N*-carboxymethyl aminodeoxyhexose than the uronic acid residue, whereas the data for heparin (13, 14) and its *N*-carboxymethyl analog correspond to a relatively greater impact by Ca^{2+} on their L-iduronic acid 2-sulfate residues. The 2-*O*-sulfo substituent cannot account solely for the differences in signal displacement, because the modified heparin precursor (**6**→**2**) lacking this substituent shows Ca^{2+}-binding nmr characteristics (see Table 2) similar to that of heparin itself. Hence, it is apparent that a simple replacement of one anionic function (SO_3^-) on the amino group by another (CH_2COO^-), although maintaining a total negative charge of three, cannot ensure a retention of metal-binding characteristics.

The 2-acetamido-N-acetyl) analog of heparin

As already mentioned, and now supplemented by the *N*-carboxymethyl examples just described, the only glycosami-

Can. J. Chem. Downloaded from www.nrcresearchpress.com by 91.121.58.235 on 09/07/12
For personal use only.

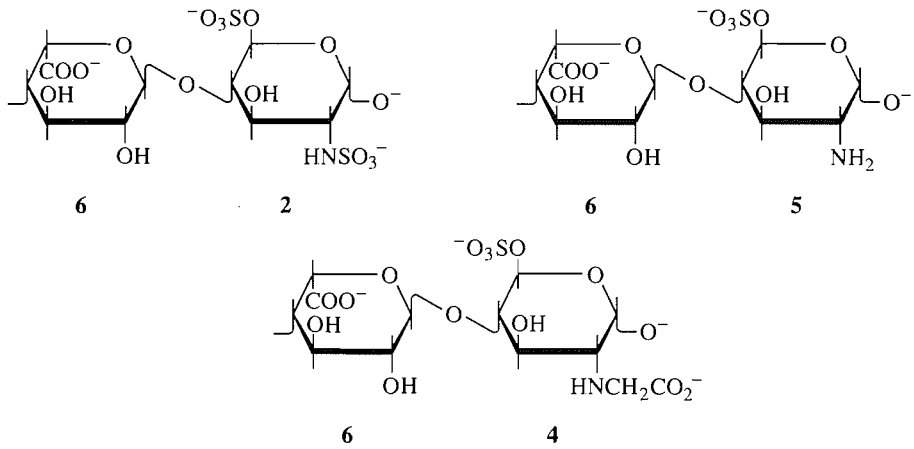

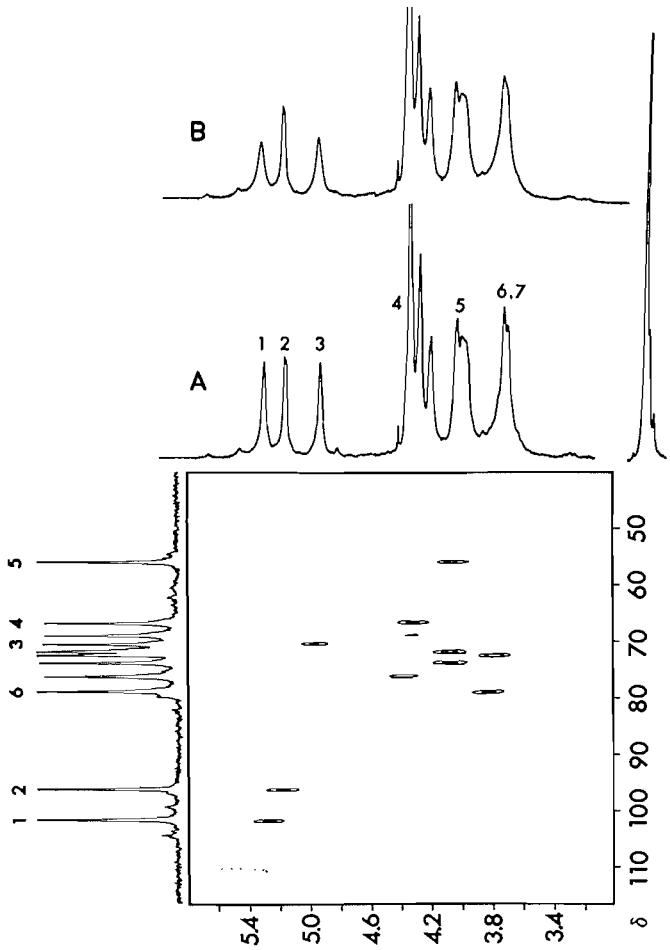

FIG. 3. (A) The ^1H and ^{13}C nmr heterocorrelation spectrum (300/75 MHz) of the *N*-acetyl analog (**1**→**3**, sodium salt) in D_2O; although the correlation data were obtained at 25°C, the ^1H spectrum shown was actually recorded at 65°C. Signal designations: 1 and 3 are for H-1 and H-5, respectively, of residue **1**; 2, 4, 5, 6, and 7 are for H-1, H-6, 6′, H-2, H-3, and H-4, respectively, of residue **3**; (B) the ^1H nmr spectrum (300 MHz; 65°C) of the *N*-acetyl analog (**1**→**3**) in D_2O (pD ~5.8) following the introduction of 1×10^{-3} moles of Cu^{2+} per mole (605) of disaccharide.

noglycan-type polymer that we have found (16), similar to heparin in its ability to bind Cu^{2+}, is the *N*-acetyl derivative (**1**→**3**). In the present study, nmr spectra of this derivative have been examined in greater detail than previously, and are more fully described. Also, the strong paramagnetic effect of Cu^{2+} on

TABLE 3. Effect of Cu^{2+} on some ^1H spin-lattice relaxation times (in s) of the *N*-acetyl analog of heparin[a]

Proton	*N*-Acetyl analog	$+Cu^{2+}$ [b]	Heparin[c]	$-Cu^{2+}$ [b,c]
A-1	0.83	0.46	1.12	0.57
A-2	0.61	0.25	1.22	0.56
A-3, A-4	0.67	0.20	—	—
I-1	0.49	0.11	0.82	0.15
I-5	0.60	0.12	1.21	0.21
CH_3	0.93	0.69	—	—

[a]For solutions in D_2O; error ±0.02 s.
[b]1.1×10^{-3} mol per disaccharide repeating unit.
[c]Data from ref. 16, for solutions 0.8 M with respect to NaCl.

spin-lattice relaxation times is now illustrated (Fig. 3), and described quantitatively by the data in Table 3. By analogy with the response of heparin to the cation, the T_1 values for resonances I-1 and I-5 of the uronic acid residue (**1**) (Fig. 3A) are notably broadened in the presence of the cation (Fig. 3B), whereas the other signals are less strongly perturbed. These differences are a reflection of the fact that the T_1 values for I-1 and I-5 are reduced by a value of ~4, whereas those of A-1 and A-2 of the aminodeoxyhexose residue (**3**) are affected to a lesser extent, i.e., by a factor of 2–3 (Table 3).

In marked contrast to this rare capacity it shares with heparin in binding Cu^{2+}, the *N*-acetyl derivative does not (11) form a complex with Ca^{2+}, despite the fact that most other modified forms of heparin bind that cation to a greater or lesser extent. Hence, the *N*-acetyl analog possesses a unique combination of characteristics, which further emphasizes the wide range of selectivities found among the interactions of anionic polymers with cations.

Although we previously described (13) a preparation of the *N*-acetyl derivative, that particular material has been found in the interim to have been incompletely *N*-acetylated. A newly synthesized specimen (see Experimental), which was used in the cation-binding tests, has the characteristics of a far more fully *N*-substituted derivative. This follows from its ^1H and ^{13}C spectra, shown in Fig. 3A together with the corresponding ^{13}C–^1H correlation (HETCOR) spectrum; the ^1H signal assignments were confirmed by reference to a COSY version of the ^1H spectrum. One striking difference between the present data and those reported earlier is the location of the A-2 signal for residue **3**. Here it is far downfield of its location in the spectrum (13) of the incompletely *N*-acetylated sample, its chemical shift (δ 3.95) being close to that (δ 3.92) reported (21, 22) for the A-2 signal of residues of **3** in the spectra of hog mucosal heparin. It is

Can. J. Chem. Downloaded from www.nrcresearchpress.com by 91.121.58.235 on 09/07/12
For personal use only.

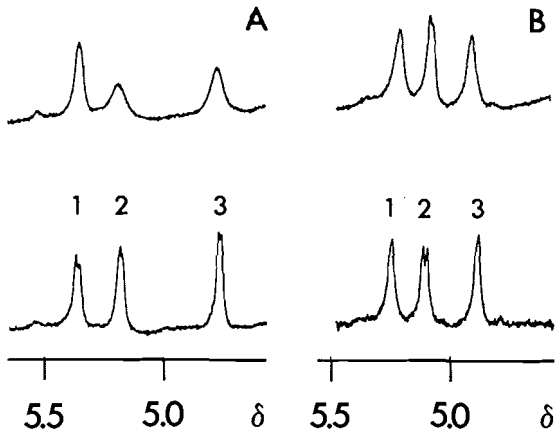

FIG. 4. Partial ^1H nmr spectra (200 MHz; 65°C) of (A) heparin (**1**→**2**, sodium salt) and (B) *N*-acetyl analog (**1**→**3**, sodium salt) in D_2O at pD ~5.8 (lower tracings); following the introduction of 1×10^{-3} moles of Fe^{3+} per mole of disaccharide (upper tracings). Signal designations: (A) 1, 2, and 3 are for H-1 of residue **2**, and H-1 and H-5 of residue **1**, respectively; (B) 2, 1, and 3 are for H-1 of residue **3**, and H-1 and H-5 of residue **1**, respectively.

TABLE 4. Comparative selectivity in the binding of cations by heparin and analogs

Polymer	Binding affinity for Cu^{2+}	Ca^{2+}	Fe^{3+}
Heparin (**1**→**2**)	+	+	+
Heparin (**1**→**3**)	+	–	[a]
Heparin (**1**→**4**)	–	+	–
Heparin (**1**→**5**)	–	–	[b]
Heparin (**6**→**4**)	–	+	[b]

[a]Weak response.
[b]Not tested.

noteworthy that the chemical shift (δ 5.1) of the anomeric proton (A-1) of the *N*-acetyl analog shows it to be more strongly shielded than is that of the aminodeoxyhexose residue of all other heparin-derived polymers of which we are aware. Also unaccounted for is the fact that in the ^{13}C spectrum (Fig. 3A) the I-4 signal for residue **1** of the *N*-acetyl analog is substantially upfield from that of ^{13}C nucleus I-4 in heparin, i.e., δ 74.0 as compared with δ 78.2, respectively. Contributing factors may be the magnetic anisotropy of the *N*-acetyl group and orientational differences about the glycosidic bonds. As to the latter possibility, however, infrared spectroscopic data (23) emphasize a similarity, rather than a difference, between conformational states of the two polymers.

Paramagnetic effect of ferric ion on the nmr spectra of heparin and its analogs

In addition to Cu^{2+} (16) and Gd^{3+} (24), other metal ions may be utilized (25) as paramagnetic probes. Among these is ferric ion (Fe^{3+}), which has now been tested for effects that it may have on the nmr spectra of heparin and derivatives. At the very low metal/polymer ratio used with Cu^{2+}, it was found (Fig. 4) that Fe^{3+} makes an equally marked impact on the relaxation characteristics of the L-iduronic acid residue (**1**) of heparin, as shown by the pronounced line-broadening of its I-1 and I-5 signals (Fig. 4A). The *N*-acetyl analog is affected to a lesser extent (Fig. 4B) and, in addition, its response is noticeably weaker than that observable (Fig. 3) in the binding of Cu^{2+}. Under comparable conditions, *N*-carboxymethyl heparin showed no interaction with Fe^{3+}. Hence, the degree of sensitivity of heparin towards the paramagnetic relaxation effects of transition metal ions appears to be uniquely high among the various glycosaminoglycan-type polymers examined.

Overall, for the group of polymers dealt with here, the variations in cation-binding selectivity are summarized in Table 4.

Summary

The current study supplements earlier observations designed to identify structural elements of the heparin molecule that determine its properties as a polyanion. Its high charge density readily accommodates strong interactions with a host of cations, including proteins. Many of these cations show little or no affinity for the other glycosaminoglycans and various modified forms of heparin, which contain fewer anionic groups per disaccharide unit than the four present in sequence **1** → **2**. Consistent with this comparison is the finding that whereas both the *N*-desulfated polymer (**1**→**5**), and that produced by acetylation of its amino group (**1**→**3**), do not interact with Ca^{2+}, binding does occur with the *N*-carboxymethyl analog (**1**→**4**), which represents the restoration of a *total* of four anionic groups. An appropriate spatial configuration of the negative charges must also be highly significant because polymer **6**→**2**, for example, formed by selective removal of the 2′-*O*-sulfo group of heparin, has the capacity to bind Ca^{2+} despite its reduced overall charge density. As this is also true for its *N*-carboxymethyl analog (**6**→**4**), prepared for comparison with that of heparin, it appears that the $N\text{-}SO_3^-$ and $N\text{-}CH_2COO^-$ functions are (qualitatively) interchangeable as anionic components when Ca^{2+} is the counterion.

Cupric ion does not elicit the same response, however, because heparin binds this cation whereas its *N*-carboxymethyl analog does not. That a fourth negative charge does not ensure binding is confirmed by the fact that the *N*-acetyl analog of heparin also binds Cu^{2+} — the only other polymer to do so under the experimental conditions used. It appears that if the total charge density is not the preponderant factor, neither is there an obvious relationship as to how the charges are distributed. That is, all three polymers contain the two anionic groups of the residue of L-iduronic acid 2-sulfate (**1**), *plus* that of the 6-sulfate group of the aminodeoxyhexose residue (**2**, **3**, or **4**), whereas only two of the polymers bind Cu^{2+}. Furthermore, the paramagnetic effects observed are largely confined to the uronide residues, which, based on their similar chemical shifts, appear to have analogous conformations. As noted for the *N*-acetyl analog, however, such parameters as the torsion angles of the various inter-residue linkages may differ significantly. This is suggested by the chemical shift data in Table 1, showing that the change from $N\text{-}SO_3^-$ to $N\text{-}CH_2CO_2^-$ (or $N\text{-}COCH_3$) has a greater impact on the shielding of ^{13}C nuclei of the neighbouring uronic acid residue **1** than those of **6** (i.e., compare the values for the I nuclei in column 1 with those in 2 (or 5), and 3 with 4).

Overall, many more of the polyelectrolytes in this series bind Ca^{2+} than Cu^{2+}. This suggests that the types of interaction are different. The binding of Ca^{2+} by heparin is a delocalized process (14), involving relatively long-range electrostatic interactions that are characterized by the counterion condensation model of Manning (26). Although this requires a charge density value that exceeds some substantial minimum value, it appears that the Ca^{2+} ion is able to accommodate a relatively broad

Can. J. Chem. Downloaded from www.nrcresearchpress.com by 91.121.58.235 on 09/07/12
For personal use only.

range of spatial dispositions among the anionic groups. By contrast, the restricted selectivity of Cu^{2+}, as well as its localized effects on relaxation, suggests that the interaction of this cation with a polyelectrolyte entails a more specific type of complex formation. The binding of Fe^{3+} by heparin may be categorized in the same way.

Experimental

Beef lung heparin was furnished by the Upjohn Company of Canada. Modified heparins **1→5** and **6→2** were available from earlier studies. Nuclear magnetic resonance spectra were recorded with a Varian XL-300 spectrometer operating at 300 MHz for ^1H and 75 MHz for ^{13}C, or with a Varian XL-200 spectrometer (^1H at 200 MHz). Chemical shifts are given with respect to the signal for internal sodium 4,4-dimethyl-4-silapentane-1-sulfonate (δ 0.0). The poylsaccharide solutions consisted of approximately 20 mg per 0.5 mL of D_2O, and the appropriate quantity of a given cation was introduced into the nmr tube as a solution (generally 2–10 μL) of either $CuSO_4 \cdot 5H_2O$, $FeCl_3$, or $CaCl_2 \cdot 2H_2O$ of the required molarity in D_2O. The adjustment of pH was carried out initially with an aqueous solution of the polymer sample, which was then evaporated. Deuterium exchange was carried out subsequently by repeatedly dissolving the residue in D_2O, followed by distillation of the solvent under reduced pressure.

N-Carboxymethyl analog of heparin

A sample (40 mg) of polymer **1→5**, prepared from beef lung heparin by selective hydrolysis (20) of the 2-*N*-sulfo group, was dissolved in water (9 mL). Sodium carbonate (70 mg) was introduced, followed by bromoacetic acid (60 mg); the mixture was held at 55–60°C for 20 h, then neutralized with acetic acid, and the solution was dialysed against water for 18 h. Chelex ion-exchange resin was added to the solution, then filtered off, and the filtrate was concentrated and subjected to D_2O exchange. As the ^1H nmr spectrum of the powdery residue indicated that *N*-substitution was incomplete (from the presence of a strong residual signal for $CHND_2$ at δ 3.0, at pD 9), the reaction with bromoacetic acid was repeated (as above). The 300 MHz ^1H nmr spectrum (Figs. 1B, C) of the solid product (32 mg), recovered following dialysis, indicated that >80% *N*-carboxymethylation had been effected. In a second experiment, which involved two successive additions of the bromoacetic acid without interruption, the product was indistinguishable (nmr evidence) from the initial one; $[\alpha]_D$ +34° (*c* 1.5, D_2O) (in comparison with +40° for the beef lung heparin).

N-Carboxymethyl analog of modified heparin (**6→2**)

A sample (50 mg) of modified heparin (**6→2**) was converted into the pyridium salt form by dissolution in water (5 mL), by acidification with Amberlite IR-120 ion-exchange resin, neutralization with pyridine, followed by concentration to dryness. A solution of the residue in 1:19 water/methyl sulfoxide (20) (5 mL) was heated at 60°C for 2h, diluted with water (10 mL), adjusted to pH 9 with 0.1 N sodium hydroxide, dialysed against water, and concentrated. The powdery residue (44 mg) was found by ^1H nmr spectroscopy (δ 3.0, $CHND_2$ at pD 9) to consist essentially of the 2-amino derivative (**6→5**). By reaction of the product (40 mg) in water (9 mL) with bromoacetic acid (85 mg) and sodium carbonate (100 mg) at 55–60°C for 22 h, and recovery as above, the *N*-carboxymethyl derivative (**6→4**) (25 mg) was obtained, as evidenced by its 300 MHz ^1H nmr spectrum (Figs. 2B, C).

N-Acetyl analog of heparin

A sample (120 mg) of polymer **1→5**, prepared from beef lung heparin by selective hydrolysis of the 2-*N*-sulfo group (also see preceding paragraph), was dissolved in sodium bicarbonate solution (5%, 10 mL). Acetic anhydride (0.2 mL) and methanol (0.2 mL) were added with stirring, and successive additions were made at 4 and 16 h, respectively. Following each addition of these reagents, the pH of the solution was monitored for 1 h and, when necessary, 5% sodium bicarbonate solution was introduced to ensure that the pH did not fall below 7. After 24 h the solution was dialysed exhaustively against distilled water, and lyophilized, giving a white solid (130 mg); $[\alpha]_D$ +41° (*c* 1.5, D_2O). The ^1H and ^{13}C nmr spectra of the product are shown, and correlated, in Fig. 3.

Acknowledgements

Generous support was provided by the Natural Sciences and Engineering Research Council of Canada and by McGill University. The assays of anti-XA activity were kindly conducted by Karla Ludwig-Baxter.

1. L. B. JAQUES. Pharmacol. Rev. **31**, 99 (1980).
2. B. CASU. Adv. Carbohydr. Chem. Biochem. **43**: 51 (1985).
3. J. R. DUNSTONE. Biochem. J. **85**, 336 (1962).
4. S. E. LASKER and S. S. STIVALA. Arch. Biochem. Biophys. **115**, 360 (1966).
5. B. LAGES and S. S. STIVALA. Biopolymers, **12**, 127 (1973).
6. L. HERWATS, P. LASZLO, and P. GENARD. Nouv. J. Chem. **1**, 173 (1977).
7. D. C. MUKHERJEE, J. W. PARK, and B. CHAKRABARTI. Arch. Biochem. Biophys. **191**, 393 (1978).
8. C. BRAUD, C. VILLIERS, and M. VERT. Carbohydr. Res. **86**, 165 (1980).
9. J. MATTAI and J. C. T. KWAK. Biochem. Biophys. Acta, **677**, 303 (1981).
10. P. DAIS, K. R. HOLME, and A. S. PERLIN. Can. J. Chem. **66**, 2601 (1988).
11. J. N. LIANG, B. CHAKRABARTI, L. AYOTTE, and A. S. PERLIN. Carbohydr. Res. **106**, 101 (1982).
12. C. BRAUD and M. VERT. Macromolecules, **18**, 856 (1985).
13. L. AYOTTE and A. S. PERLIN. Carbohydr. Res. **145**, 267 (1986).
14. P. DAIS, Q. J. PENG, and A. S. PERLIN. Carbohydr. Res. **168**, 163 (1987).
15. C. BRAUD, M. VERT, and P. GRANGER. Int. J. Biol. Macromol. **10**, 2 (1988).
16. R. N. REJ, K. R. HOLME, and A. S. PERLIN. Carbohydr. Res. **207**, 143 (1990).
17. A. S. PERLIN, B. CASU, G. R. SANDERSON, and J. TSE. Carbohydr. Res. **21**, 123 (1972).
18. S. S. STIVALA and P. A. LIBERTI. Arch. Biochem. Biophys. **122**, 40 (1967).
19. M. JASEJA, R. N. REJ, F. SAURIOL, and A. S. PERLIN. Can. J. Chem. **67**, 1449 (1989).
20. Y. INOUE and K. NAGASAWA. Carbohydr. Res. **46**, 87 (1976).
21. T. N. HUCKERBY and I. A. NIEDUSZYNSKI. Carbohydr. Res. **138**, 141 (1986).
22. B. MULLOY and E. A. JOHNSON. Carbohydr. Res. **170**, 151 (1987).
23. D. GRANT, W. F. LONG, C. F. MOFFAT, and F. B. WILLIAMSON. Biochem. J. **261**, 1035 (1989).
24. B. CASU, G. GATTI, N. CYR, and A. S. PERLIN. Carbohydr. Res. **41**, C6 (1975).
25. I. D. CAMPBELL, C. M. DOBSON, R. J. P. WILLIAMS, and A. V. XAVIER. J. Magn. Reson. **11**, 172 (1973).
26. G. S. MANNING. Acc. Chem. Res. **12**, 443 (1979).
27. K. R. HOLME and A. S. PERLIN. Carbohydr. Res. **186**, 301 (1989).

Can. J. Chem. Downloaded from www.nrcresearchpress.com by 91.121.58.235 on 09/07/12
For personal use only.

Thermodynamics of protonation of *N,N*-dimethylthioamides in aqueous sulfuric acid

ALESSANDRO BAGNO[1]

Centro CNR Meccanismi di Reazioni Organiche, Dipartimento di Chimica Organica, via Marzolo 1, 35131 Padova, Italy

VITTORIO LUCCHINI

Dipartimento di Scienze Ambientali, Universita' di Venezia, Dorsoduro 2137, 30123 Venezia, Italy

AND

GIANFRANCO SCORRANO[1]

Centro CNR Meccanismi di Reazioni Organiche, Dipartimento di Chimica Organica, via Marzolo 1, 35131 Padova, Italy

Received February 8, 1990

This paper is dedicated to Professor Ross Stewart on the occasion of his 65th birthday.

ALESSANDRO BAGNO, VITTORIO LUCCHINI, and GIANFRANCO SCORRANO. Can. J. Chem. **68**, 1746 (1990).

The protonation (m^* and pK_{BH^+}) and thermodynamic ($\Delta G°$, $\Delta H°$, $\Delta S°$) parameters of ionization of four thioamides $RCSNMe_2$ (R = Me, Et, *i*-Pr, *t*-Bu) have been determined in aqueous sulfuric acid in the 25–60°C temperature range with a UV technique. The title compounds are relatively strong bases; 100% protonation is reached in 47% H_2SO_4. Their solvation is lower than for primary thioamides and sulfides, as indicated by the higher values of m^*, and close to the range of carbon bases. Base strengths are discussed in terms of the competition between internal and external stabilization.

Key words: basicity, protonation, solvation, thermodynamics, thioamides.

ALESSANDRO BAGNO, VITTORIO LUCCHINI et GIANFRANCO SCORRANO. Can. J. Chem. **68**, 1746 (1990).

Faisant appel à une technique UV et opérant dans de l'acide sulfurique aqueux, à des températures allant de 25 à 60°C, on a déterminé les paramètres de protonation (m^* et pK_{BH^+}) et thermodynamiques ($\Delta G°$, $\Delta H°$ et $\Delta S°$) pour l'ionisation de 4 thioamides $RCSNMe_2$ (R = Me, Et, *i*-Pr, *t*-Bu). Les composés mentionnés dans le titre sont des bases relativement fortes; on atteint 100% de protonation dans du H_2SO_4 à 47%. Comme l'indique leurs valeurs plus élevées de m* qui se rapprochent de celles des bases carbonées, leur solvatation est plus faible que celle des thioamides primaires ou des sulfures. On discute des forces des bases en fonction de la compétition entre les stabilisations interne et externe.

Mots clés : basicité, protonation, solvatation, thermodynamique, thioamides.

[Traduit par la revue]

Introduction

In contrast to the widely studied acid–base properties of the carbonyl group (1–5), analogous thiocarbonyl compounds have received little attention. While this is in part due to the lack of stability of many such derivatives, there are nonetheless some which exhibit sufficient stability towards acids. Among these, thioamides R—CS—NR_2' are probably the best suited, and have been the object of a number of studies (6–8). An acidity function (H_T) for thiocarbonyl bases has been constructed (7, 8*a*, 9) and protonation data for a wide variety of the same have been reported (7, 8). p*K* data obtained by the Hammett acidity function, Bunnett–Olsen and Marziano–Cimino–Passerini methods have been compared (7, 8) and found to be rather similar. Moreover, the values of the φ parameter (8) indicate that the solvation requirements of these compounds are low (1) and little dependent on structure. Thus, unlike their oxygen analogs (1), thiocarbonyl bases from a homogeneous family of bases, well suited for defining an acidity function. The above data, and studies in superacid media (10), indicate that thioamides are *S*-protonated.

The comparison between analogous families of bases with *O* or *S* as the basic site has proved very informative in other cases (11). Thus a comparison with amides, whose acid–base properties are well established (1, 2, 12), is certainly interesting. In order to completely characterize the acid–base behavior of thioamides, we undertook the study of the protonation equilibria of four *N,N*-dimethylthioamides $RCSNMe_2$ (R = Me (**1**), Et (**2**), *i*-Pr (**3**), *t*-Bu (**4**)) at various temperatures. This enabled us to obtain enthalpies and entropies (as well as free energies) of ionization in solution, which contributes information for the eventual determination of their hydration energies.

Experimental

The thioamides **2, 3** and **4** were prepared from the corresponding acid chlorides and dimethylammonium chloride with P_2S_5 in anhydrous pyridine; **1** was prepared directly from the corresponding amide (13). **1** and **4** were purified by vacuum sublimation or recrystallization from toluene/ligroin; **2** and **3** by distillation. Physical constants and spectral data for **1** (14*a*), **2** (14*a, b*), **3** (14*c*), **4** (14*d*) agreed with literature values.

Preparation of sulfuric acid solutions and data processing were carried out as previously described (3). Ultraviolet spectra were run on a Varian Cary 214A instrument with a thermostatted cell compartment; the actual temperature in the cell was measured with a thermocouple. NMR spectra were run on a Bruker WP-60 operating at 1.4 T.

Results

We have studied the protonation equilibria of the thioamides **1–4** in aqueous sulfuric acid at 25, 40, and 60°C. All compounds had strong UV absorptions in a convenient spectral range (see Table 1). The spectra defined good isosbestic points, thus indicating a very small solvent effect. This was probably due to the narrow acidity range in which these bases are protonated. Ultraviolet spectra were subjected to Principal Component Analysis (PCA), as suggested by Edward and Wong (15); this treatment should enable one to separate the spectral changes due to protonation from those due to other (including solvent) effects into orthogonal components (vectors) (3, 15). In all cases, the spectra were reproduced to >99.5% accuracy with a single vector, thus ensuring that no relevant phenomenon other than protonation was taking place. The spectra were recalculated from that vector, and absorbances at a single

[1]To whom correspondence should be addressed.

Printed in Canada / Imprimé au Canada

Can. J. Chem. Downloaded from www.nrcresearchpress.com by 91.121.58.235 on 09/07/12
For personal use only.

TABLE 1. Spectral data,[a] protonation,[b, c] and thermodynamic parameters[c, d] of *N,N*-dialkylthioamides

T	λ_B^{max}	$\lambda_{BH^+}^{max}$	m^*	pK	$\Delta G°$	$\Delta H°$	$\Delta S°$
$MeCSNMe_2$ (**1**)							
25.4	263	235	1.67(0.01)	−2.25(0.01)	−3.07(0.01)	−4.7(0.2)	−5.4(0.7)
41.4			1.64(0.02)	−2.08(0.02)			
60.5			1.59(0.01)	−1.89(0.01)			
$EtCSNMe_2$ (**2**)							
25.4	264	238	1.69(0.01)	−2.26(0.01)	−3.09(0.01)	−5.0(0.2)	−6.7(0.7)
41.4			1.62(0.01)	−2.08(0.01)			
61.3			1.56(0.02)	−1.86(0.02)			
i-$PrCSNMe_2$ (**3**)							
25.2	265	239	1.73(0.03)	−2.48(0.04)	−3.39(0.05)	−4.3(0.6)	−3.1(2.0)
39.9			1.70(0.02)	−2.33(0.03)			
60.0			1.69(0.03)	−2.15(0.03)			
t-$BuCSNMe_2$ (**4**)							
25.4	268	243	1.78(0.01)	−2.32(0.02)	−3.17(0.03)	−3.9(0.2)	−2.2(0.7)
41.4			1.81(0.02)	−2.20(0.02)			
60.0			1.77(0.01)	−2.03(0.01)			

[a]Wavelengths in nm; log ϵ = 4.2 for B and 4.0 for BH^+. Data for B were determined in water or 5% H_2SO_4, and those for BH^+ in 50% H_2SO_4. For all compounds, an additional weaker band of the free base was present at 211 nm (log ϵ = 1.5).
[b]See eq. [2].
[c]Errors (in parentheses) from linear weighted least-squares fitting.
[d]Energies in kcal mol^{-1}; entropies in cal mol^{-1} K^{-1}.

wavelength were used for calculating ionization ratios; as implied by the method, the results were within experimental error at any wavelength (15).

Ionization ratios I were calculated as

$$[1] \quad I = [BH^+]/[B] = (A - A_B)/(A_{BH^+} - A)$$

The protonation parameters were obtained using an excess acidity function (X) (1, 16) based on nitroaniline indicators, for which $X = -(H_0 + \log c_{H^+})$ and $m^* = 1 - \varphi$ (1, 9, 16, 17). log I values were fitted to eq. [2] (1, 3, 16):

$$[2] \quad \log I - \log c_{H^+} = m^*X + pK$$

where log c_{H^+} and X for the H_2SO_4/H_2O system were calculated as previously described (3). Ultraviolet absorbances *vs.* the H_0 acidity function defined very good sigmoid plots with random differences from the calculated curve from eqs. [1] and [2]; the values of m^* and pK at the various temperatures are reported in Table 1.

Enthalpies and entropies of ionization were obtained as slopes and intercepts, respectively, of pK *vs.* $10^3/T$ plots (see Table 1).

The protonation of **4** was also followed by NMR, monitoring the chemical shift changes with acidity of the *t*-Bu and *N*-Me protons relative to trimethylammonium sulfate (3). The resulting sigmoid curves showed a very small chemical shift change ($\nu_{BH^+} - \nu_B$ = 7–10 Hz at 60 MHz), even lower than for carboxamides (12); protonation occured in a very narrow acidity range (15–40% H_2SO_4). Some peculiar features were observed: (*a*) at acidities below *ca.* 36% H_2SO_4, the *N*-methyl groups were observed as a single sharp resonance; above this value, the rotation around the C—N bond slowed down, until above 57% acid two sharp distinct resonances were observed. The line broadening occurring in this range introduces some inaccuracy in the chemical shifts measurements. (*b*) Within the same acidity range (about a half of the extremely steep protonation curve), a medium effect amounting to *ca.* 10% of the total shift was present, thus making measurements questionable in a large portion of the acidity range in which protonation takes place (unlike carboxamides, for which points affected by medium effects can be safely eliminated (12)).

The dynamic NMR data are consistent only with *S*-protonation, thus confirming earlier observations. On the other hand, a detailed analysis is prevented by the very low accuracy of chemical shifts. The apparent protonation parameters so obtained (m^* = 2.43, pK = −2.91) will obviously need correction for the other processes (rotation and medium effect). For these reasons, in this paper we will only discuss UV data, which do not appreciably suffer from medium effects and yield very accurate protonation parameters.

Discussion

An examination of the available data for primary thioamides (7, 8, 18) indicates that m^* values for a wide variety of compounds containing the —$CSNH_2$ group (and also some thioureas, thioesters, and related compounds) span only a very limited range (1.4 ± 0.1), so that these bases meet the suggested requirements for constructing an acidity function (16*a*).

On the other hand, our values for *N,N*-dimethyl derivatives (1.6–1.8) are higher by an amount outside the experimental error, thus showing that m^*'s for thiocarbonyl bases show a structural dependence if appropriately substituted. Consequently, these compounds may not be used for the building of H_T, nor is their protonation accurately described by that acidity function.

While the need for individual acidity functions can be overcome by the Bunnett–Olsen, Marziano–Cimino–Passerini, or Cox–Yates methods (1, 9), the use of an excess acidity function based on nitroanilines allows one to give a physical meaning to the slope parameter m^* (1). In fact, with the excess acidity function being defined as $X = \log (\gamma_{B^*}\gamma_{H^+}/\gamma_{B^*H^+})$ (1, 9, 16,

Can. J. Chem. Downloaded from www.nrcresearchpress.com by 91.121.58.235 on 09/07/12
For personal use only.

TABLE 2. Thermodynamic data[a] at 25°C

Base	m^*	pK	$\Delta G°$	$\Delta H°$	$\Delta S°$	Reference
$MeCONMe_2$	0.62	−0.21	−0.3	−2.4	−7.0	12, 20
$MeCSNMe_2$	1.67	−2.25	−3.1	−4.7	−5.4	
Me_2O	0.18	−2.48	−3.4	0.6	13.3	19
Me_2CO	0.35	−3.06	−4.2	−0.3	13.1	5
Me_2SO	0.42	−1.54	−2.1	−2.3	−0.7	19
Me_2S	1.27	−6.99	−9.5	−6.9	9.0	19

[a]Energies in kcal mol^{-1}; entropies in cal mol^{-1} K^{-1}.

17), where B* is the nitroaniline taken as reference, the activity coefficient term for another base B will be linearly related to X according to eq. [3] (1):

[3] $\log (\gamma_B\gamma_{H^+}/\gamma_{BH^+}) = m^* \log (\gamma_{B^*}\gamma_{H^+}/\gamma_{B^*H^+})$

Such activity coefficients represent free energies of transfer from the standard state to the non-ideal acidic solutions, and are dominated by solvation effects (1). It is easy to show that, if $\gamma_{BH^+}/\gamma_B \gg 1$, then $0 < m^* < 1$ and, conversely, $m^* > 1$ when $\gamma_{BH^+}/\gamma_B \approx 1$. The first case applies when there is a large difference of solvation between B and BH^+, on a scale referred to B^*/B^*H^+ (an aniline), and the second when the solvation of B and BH^+ are similar (1, 18, 19). However, since solvation energies of charged species are higher than for neutrals (1, 20), m^* essentially measures the hydrogen bonding solvation of the protonated base. Thus, as we might expect, m^* increases in the series $ROH < R_2O < R_2CO < R_2SO < ArNH_2 < R_2S < Ar_3C^+$ (1).

Both the m^* values and the dynamic NMR behavior confirm that thioamides are sulfur bases. The solvation requirements of thioamides are lower than those of sulfides, as shown by the m^* of the latter (*ca.* 1.3) (1). In fact, charge stabilization in protonated thioamides is provided by the polarizable sulfur atom and by delocalization into the amide group, which effectively reduces the interactions with the solvent; the latter accounts for the decreased solvation relative to sulfides. It is then evident that this parameter is directly affected by *N*-substitution, as in amides (2, 12), and will increase with alkyl substitution. For example, CH_3CSNH_2 and *t*-$BuCSNH_2$ studied by Edward *et al.* (8*b*) ($m^* = 1.44$ and 1.49, respectively) can be compared with their *N,N*-dimethyl derivatives (1.67 and 1.78).

These values are among the highest known, being only lower than those for carbon bases (1). These bases are also peculiar in that, unlike most others (1), they feature a rather high aqueous basicity accompanied by a very low solvation, which corresponds to a very steep protonation curve (3). These two factors make thioamides readily protonated; in fact, 100% protonation is reached at *ca.* 47% H_2SO_4 (amides are fully protonated at *ca.* 55% H_2SO_4, despite their pK's being *ca.* 2 units higher (12)).

Within many families of bases in which substituents change around the basic site, substitution with electron-releasing groups usually causes an increase in m^* and a decrease in pK (1, 3–5). This has been explained with the consideration that the substituent stabilizes the protonated base, thus decreasing the interactions with the solvent (higher m^*) and therefore its overall stabilization in water (lower pK). For thioamides, there is very little stabilization by solvation; since internal stabilization is the major factor involved, we might expect a better electron-releasing substituent to increase the aqueous basicity. However, while changing from Me to *t*-Bu does increase m^*, as expected, the pK's remain practically identical suggesting that the two effects are compensating.

Because of the very small range spanned by these thermodynamic parameters, it is pointless to discuss their values in detail. However, we can compare these values with those for other classes of bases, and attempt an investigation of the origin of the relative basicities of thioamides and their oxygen analogues carboxamides, which behave rather differently (see Table 2). The order of basicity in water is $MeCSNMe_2 < MeCONMe_2$. This difference arises from both enthalpic and entropic effects; amide protonation is less endothermic and entropically more favored. The trend for enthalpies is consistent with the expectation that protonation on a less solvated site gives rise to a weaker hydrogen bonding stabilization and therefore makes protonation more endothermic. With regard to the entropy change for the process $BH^+ \rightarrow B + H^+$, besides the purely statistical term (positive), the other major contribution comes from the difference in solvation of H^+ and BH^+, which causes an ordering of the water molecules involved in hydrogen bonding and thus makes a negative contribution depending on the solvation of BH^+. The balance between these two factors determines the size of $\Delta S°$, if the solvation of B makes a minor contribution.

Despite the large difference in solvation, the two bases have very similar entropies of ionization. This discrepancy probably stems from a negative contribution coming from the strong hydrogen bonds existing in the free amide, thus making $\Delta S°$ for $MeCONMe_2$ more negative than expected. A similar situation is found in the dimethyl derivatives listed in Table 2; dimethyl sulfoxide has a lower $\Delta S°$ than expected because of a peculiar solvation of the free base (19).

Acknowledgement

Financial assistance from the Ministero della Pubblica Istruzione (Finanziamento 40% and Finanziamento 60%) is gratefully acknowledged.

1. A. BAGNO, G. SCORRANO, and R. A. MORE O'FERRALL. Rev. Chem. Interm. **7**, 313 (1987).
2. (*a*) R. A. Cox and K. YATES. Can. J. Chem. **59**, 1560 (1981); (*b*) R. A. Cox, L. M. Druet, A. E. Klausner, T. A. Modro, P. Wan, and K. YATES. Can. J. Chem. **59**, 1568 (1981).
3. A. BAGNO, V. LUCCHINI, and G. Scorrano. Bull. Soc. Chim. Fr. 563 (1987).
4. A. BAGNO, G. SCORRANO, and V. LUCCHINI. Gazz. Chim. Ital. **117**, 475 (1987).
5. A. BAGNO, V. LUCCHINI, and G. SCORRANO. J. Phys. Chem. In press.
6. R. STEWART. The proton: applications to organic chemistry. Academic Press, New York, 1985.
7. C. TISSIER and M. TISSIER. Bull. Soc. Chim. Fr. 2109 (1972).
8. (*a*) J. T. EDWARD, I. LANTOS, G. D. DERDALL, and S. C. WONG. Can. J. Chem. **55**, 812 (1977); (*b*) J. T. Edward, G. D. Derdall, and S. C. WONG. Can. J. Chem. **55**, 2331 (1977); (*c*) M. PAVENTI, F. HEIRTZLER, and J. T. EDWARD. Can. J. Chem. **64**, 2310 (1986).
9. R. A. COX and K. YATES. Can. J. Chem. **61**, 2225 (1983).
10. (*a*) T. Birchall and R. J. GILLESPIE. Can. J. Chem. **41**, 2642 (1963); (*b*) G. A. OLAH and A. T. KU. J. Org. Chem. **35**, 331 (1970); (*c*) W. WALTER, M. F. SIEVEKING, and E. SCHAUMANN. Tetrahedron Lett. 839 (1974).
11. P. BONVICINI, A. LEVI, V. LUCCHINI, G. MODENA, and G. SCORRANO. J. Am. Chem. Soc. **95**, 5960 (1973).
12. A. BAGNO and G. SCORRANO. J. Am. Chem. Soc. **110**, 4577 (1988).

Can. J. Chem. Downloaded from www.nrcresearchpress.com by 91.121.58.235 on 09/07/12
For personal use only.

13. J. Voss and W. Walter. Liebigs Ann. Chem. **716**, 209 (1968).
14. (*a*) P. Reynaud, R. C. Moreau and J. P. Samama. Bull. Soc. Chim. Fr. 3623 (1965); (*b*) J. Meijers, H. E. Wijers, and L. Brandsma. Recl. Trav. Chim. Pays-Bas, **91**, 1423 (1972); (*c*) J. Perregaard and S.-O. Lawesson. Acta Chem. Scand. Ser. B. **29**, 604 (1975); (*d*) J. Perregaard, I. Thomsen, and S.-O. Lawesson. Bull. Soc. Chim. Belg. **86**, 321 (1977).
15. J. T. Edward and S. C. Wong. J. Am. Chem. Soc. **99**, 4229 (1977).
16. (*a*) R. A. Cox and K. Yates. J. Am. Chem. Soc. **100**, 3861 (1978); (*b*) R. A. Cox and K. Yates. Can. J. Chem. **59**, 2116 (1981).
17. V. Lucchini, G. Modena, G. Scorrano, R. A. Cox, and K. Yates. J. Am. Chem. Soc. **104**, 1958 (1982).
18. A. Levi, G. Modena and G. Scorrano. J. Am. Chem. Soc. **96**, 6585 (1974).
19. G. Perdoncin and G. Scorrano. J. Am. Chem. Soc. **99**, 6983 (1977).
20. R. W. Taft, J. F. Wolf, J. L. Beauchamp, G. Scorrano, and E. M. Arnett. J. Am. Chem. Soc. **100**, 1240 (1978).

Can. J. Chem. Downloaded from www.nrcresearchpress.com by 91.121.58.235 on 09/07/12
For personal use only.

Spectrophotometric determination of peroxydisulphate with *o*-dianisidine by flow injection

PAUL M. SHIUNDU AND ADRIAN P. WADE

Laboratory for Automated Chemical Analysis, Department of Chemistry, University of British Columbia, Vancouver, B.C., Canada V6T 1Y6

AND

S. B. JONNALAGADDA

Department of Chemistry, University of Nairobi, P.O. Box 30197, Nairobi, Kenya

Received January 2, 1990

This paper is dedicated to Professor Ross Stewart on the occasion of his 65th birthday

PAUL M. SHIUNDU, ADRIAN P. WADE, and S. B. JONNALAGADDA. Can. J. Chem. **68**, 1750 (1990).

Precise and accurate knowledge of peroxydisulfate ion concentration is critical in industrial polymer production, where it is extensively used as an activator. Its ability to oxidize in either acidic, neutral, or alkali media also makes it widely applicable in many other areas of chemistry.

In this paper we present an optimized spectrophotometric flow injection method for determination of peroxydisulfate. The analyte oxidizes *o*-dianisidine to form a stable product which has a convenient absorbance maximum at 450 nm. This provides a simple and sensitive alternative to present methods which are more costly, tedious, or complex.

Key words: spectrophotometric method, peroxydisulphate.

PAUL M. SHIUNDU, ADRIAN P. WADE et S. B. JONNALAGADDA. Can. J. Chem. **68**, 1750 (1990).

Une connaissance exacte et précise de la concentration en ions peroxydisulfates est critique dans la production industrielle de polymères où il est utilisé d'une façon extensive comme activant. Comme il peut provoquer des oxydations en milieux acide, basique ou neutre, on peut l'utiliser dans plusieurs autres domaines de la chimie.

Dans ce travail, on présente une méthode spectrophotométrique optimisée pour déterminer la concentration en ion peroxydisulfate. Le produit à analyser oxyde l'*o*-dianisidine pour former un produit stable qui possède une bande d'absorption maximale à 450 nm. Cette procédure fournit une alternative simple et sensible aux méthodes actuelles qui sont plus couteuses, plus embêtantes ou plus complexes.

Mots clés : méthode spectrophotométrique, peroxydisulfate.

[Traduit par la revue]

Introduction

The peroxydisulphate (persulphate) ion is a strong two-electron oxidizing agent

$$S_2O_8^{2-} + 2e^- \rightarrow 2SO_4^{2-}$$

with a standard redox potential of -2.01 V in either neutral or alkaline solution (1). Its utility as an oxidizing agent for various substrates is derived from its ability to oxidize in acidic, neutral, and alkaline media (2). It has industrial importance as a polymerization activator, e.g., in production of polystyrene (3).

The literature provides a number of methods for the determination of persulphate. Kolthoff and Carr (4) reported several reductometric methods for the volumetric determination of persulphate ions. Of these, the iodometric and ferrometric (titrimetric) methods were the most practicable from the points of view of rate of reaction, accuracy, and simplicity (4). However, both procedures involve a back-titration step after the redox reactions with persulphate and thus are tedious to perform in any number. They also require reaction times of at least 15–30 min. Amin and Hareez (5) reported a procedure using a combination of titrimetry with alternating current (a.c.) polarography. This method is likewise tedious and complex. Amin (6) later reported an indirect amplification method by a.c. polarography which enabled measurement of persulphate concentrations as low as 2.6×10^{-6} M with reasonable accuracy. This method, however, involves an extraction step followed by a back-titration. Ion-exchangers are also required to remove metal ions which form water-insoluble iodides that would otherwise interfere. Kolthoff and Woods (7) reported an alternating-current polarographic method by which persulphate concentrations in the range (10^{-4}–10^{-3} M) could be measured. This method was found to be highly temperature dependent. Substances that have wave potentials close to that of the iodate are known to interfere (6) (for example, Zn(II) in alkali media or Mo(IV), Cu(II), and Bi(II) under acidic conditions). These examples show that development of rapid selective methods for determination of persulphate has proven a difficult analytical problem.

The reaction between persulphate ions and aromatic amines, now known as the Boyland–Sims oxidation, was first reported in 1953 (8). A literature survey found that the reaction of persulphate with the substituted aromatic amine, *o*-dianisidine (ODA) has not previously been used for quantitative analysis of persulphate. However, persulphate ion has been used as a spray reagent for detection of aromatic amines and related compounds in thin layer chromatography (9), and the kinetics of the reaction of ODA with oxidizing agents such as H_2O_2 are well known (10, 11).

This paper reports the automated development of a simple flow injection procedure to determine persulphate ions at low concentrations, and is based on reaction with ODA. Flow injection (FI) is a versatile form of microflow analysis (12). Typical FI methods are fast, dependable, semi-automated, and use colorimetric or electrochemical detection in low volume flow-through cells. Samples are typically 30–100 μL in volume and throughput rates of 120 samples h^{-1} are commonly reported.

Printed in Canada / Imprimé au Canada

Can. J. Chem. Downloaded from www.nrcresearchpress.com by 91.121.58.235 on 09/07/12
For personal use only.

Can. J. Chem. Downloaded from www.nrcresearchpress.com by 91.121.58.235 on 09/07/12
For personal use only.

Many manual procedures have been adapted to flow injection (12). Advantages of this include decreased reagent consumption and improved precision.

The present work has been carried out on an automated flow injection methods development system, which has been reported elsewhere (13). Such computer-controlled units have much to offer analytical chemistry. Reaction conditions may be specified from the keyboard and automatically adjusted. This is achieved by mixing streams of the required composition (reagent(s), solvent(s), buffer, diluent) using variable speed pumps and stock solutions. Sample introduction is via computer-controlled injection valves or stream switching valves. Optimization of such systems requires that operating conditions be found which maximize some measure of performance (e.g. extent of reaction) whilst limiting unnecessary sample dispersion. This is typically a highly multivariate problem, as flow conditions must be optimized in addition to the chemical parameters.

Simplex optimization (14–16) and automated response surface mapping (13, 17) have been implemented on these systems. The former provides a rapid means to find the optimum conditions for analysis. The latter seeks to establish the effects of system variables such as flow rates, sample size, pH, and ionic strength. Together or separately these facilitate essentially operator-unassisted methods development, in a matter of a few hours.

Experimental

Reagents

A stock solution of persulphate (1.00×10^{-2} M) was prepared by dissolving 0.676 g of potassium persulphate (Fisher Scientific, Fairlawn, NJ), in 250 mL of distilled water. Standard solutions were prepared from this by appropriate dilution. A 1.0×10^{-2} M ODA solution (2.443 g L^{-1}) (Aldrich, Milwaukee, WI) was freshly prepared daily in a 40% v/v mixture of acetone in water. Solutions of ODA were freshly prepared every day. A buffer solution was prepared from 100 mL of 0.1 M 3,3-dimethylglutaric acid (Aldrich, Milwaukee, WI) in 1 M sodium chloride (18). Sodium chloride was present to minimize the effect of changes in ionic strength of the reaction media. Various reaction pHs for the batch method experiments were obtained by adding appropriate volumes of 0.1 M sodium hydroxide to the buffer.

Apparatus

The automated flow injection analyzer used was the same as in previous methods development (16, 17) and is discussed in detail elsewhere (13). The options used in this work included a custom-built variable speed peristaltic pump unit containing five independent pump heads, a high precision variable speed peristaltic pump (Models C-4V or C-6V, Alitea USA, Seattle, WA), and a six-port air-driven solenoid-actuated injection valve (Rheodyne 5020P, Cotati, CA) equipped with a 100 μL sample loop. A diode array spectrophotometer (Hewlett Packard 8452A) with a standard 1 cm quartz cell was used for absorption measurements. This was interfaced to the control computer, an IBM PC/AT compatible computer (NORA Systems, Vancouver, B.C.), via an IEEE-488 instrumentation interface. All the other units were controlled by the same microcomputer as described elsewhere (13). For the flow injection studies, a 30 μL, 1 cm path length quartz flow cell was used. The pH of reaction mixtures was determined on-line using a flow through electrode cell, a Ag/AgCl electrode (Radiometer America Electrodes Inc., GK473901), and a laboratory pH meter (Model 119, Fisher Scientific, Richmond, B.C.). Polytetrafluoroethylene (PTFE) tubing of 0.5 mm i.d. was used throughout. Software was written in Microsoft QuickBASIC^R version 4.0, as was the code used for nonlinear curve fitting and other data processing tasks. The optimization algorithm used was the composite modified simplex method (14, 19, 20). Response surface plots were generated using a commercial scientific graphics program (SURFER^R v. 3.0, Golden Software, Golden, CO).

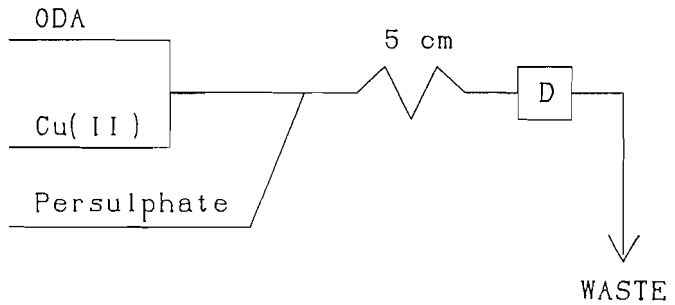

FIG. 1. Continuous flow manifold used for stopped flow kinetic studies for the reaction between ODA and persulphate. The reagent stream was of ODA in 40% v/v acetone in DMGA buffer at pH 7.0. A 1.0×10^{-4} M Cu(II) stream was used to catalyze the reaction. Absorbance measurements were made using the spectrophotometer, D.

Procedures

Batch kinetics studies

A series of preliminary batch kinetics experiments were performed to investigate the suitability of ODA as a reagent for the determination of persulphate ions.

A standard reaction was first obtained by adding 5.0 mL of 1.0×10^{-4} M persulphate solution to a mixture containing 5.0 mL of 1.0×10^{-2} M ODA solution and 10.0 mL distilled water. After thorough mixing an appropriate reaction mixture volume was transferred to a standard 1 cm cell in the spectrophotometer. Absorbance measurements at 450 nm were initiated 30 s after the start of the reaction and acquired at 10 s intervals for a period of 900 s. The effect of pH on this reaction for the above ODA concentration was then established by adding 10.0 mL of buffer solution at a known pH in place of the distilled water. The pH was varied from 3.00 to 9.00.

Stopped flow kinetic studies

Once the optimum reaction pH was identified, stopped-flow experiments were conducted to determine the kinetic parameters (i.e. final amount of product formed, order of reaction, and rate constant, K'). The flow configuration used for the stopped flow experiments is as shown in Fig. 1. A single Alitea pump was run at maximum speed to merge the reagents and then rapidly transport the reaction mixture to the cell (in less than $\frac{1}{2}$ s from the tee to observation window). The flow was then stopped and absorbance measurements were made at 1 s intervals at 450 nm for a period of 400 s.

The effect of various metal ions on the kinetics at pH 7 was then established by adding dilute metal ion solutions in place of the 10.0 mL distilled water. A similar procedure was followed using neutral salts to determine the effect of ionic strength on the reaction. Finally, the effect of other possible solvents and solvent mixture composition on the ODA solution and product stability was determined.

Flow injection studies

The flow injection configuration used for both the automated simplex optimization and response surface mapping studies is shown in Fig. 2*a*. The reagent stream, R, consisted of ODA merged with distilled water to give a total flow rate of 1.00 mL min^{-1} and maximum ODA concentration of 1.0×10^{-2} M. The buffer stream, B, comprised 0.10 M 3,3-dimethylglutaric acid in 0.10 M NaCl merged with a 0.10 M sodium hydroxide stream to give a total flow rate of 1.0 mL min^{-1} and a maximum NaOH concentration of 0.10 M. The carrier stream was made up of 5.00×10^{-4} M Cu(II) solution as a catalyst, flowing at a fixed rate of 2.00 mL min^{-1}. By allowing the NaOH flow rate to vary from (0.00–1.00) mL min^{-1}, the pH was varied from about 3.50–10.00. The flow at the detector was kept at a constant total rate of 3.00 mL min^{-1}. This ensured a constant sample residence time in the system. Separate pumps were used for each solution. The internal diameter (i.d.) of reaction coils was 0.5 mm for all sets of experimental conditions. Before any sample injection was made, the system was allowed to equilibrate to a steady baseline reading.

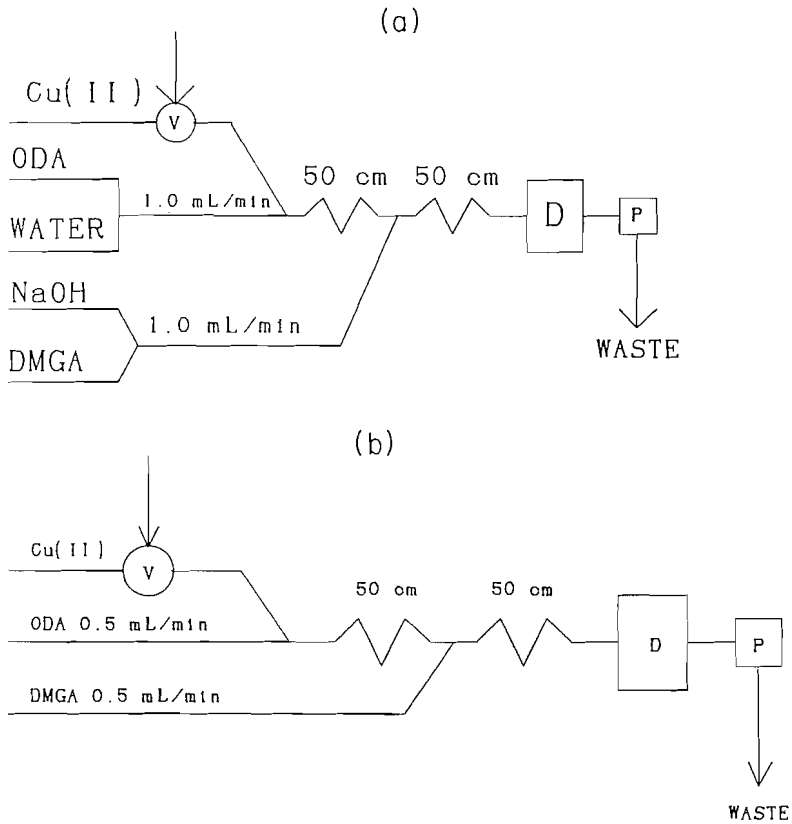

FIG. 2. (*a*) Flow injection manifold used for automated optimization and response surface mapping studies. This comprised a 5.0×10^{-4} M Cu(II) carrier stream flowing at a constant flow rate of 2.0 mL min^{-1}, an injection valve with 100 μL loop (V), reagent and water streams buddied at 1.0 mL min^{-1}, a buffer stream consisting of NaOH and DMGA buddied at 1.0 mL min^{-1}, a spectrophotometer (D), and a pH electrode cell (P). (*b*) Flow injection manifold used for the calibration studies and investigation of the effect of organic substances. This is comprised of a 5.0×10^{-4} M Cu(II) carrier stream flowing at a constant flow rate of 1.5 mL min^{-1}, an injection valve with 100 μL loop (V), an 1.0×10^{-2} M ODA reagent stream flowing at 0.5 mL min^{-1}, a DMGA buffer stream at pH 7.0 flowing at a constant 0.5 mL min^{-1}, a spectrophotometer (D), and a pH electrode cell (P).

TABLE 1. The response, pH, and the relative standard deviation (RSD) of the initial (expt. #1) and the five best simplex experimental conditions (total number of experimental points, 20)

Expt. #	Variable #1 (ODA)/mL min^{-1}	Variable #2 NaOH/mL min^{-1}	Response[a]	pH	(RSD)/%
1	0.400	0.400	0.071	4.42	1.5
4	0.840	0.672	0.198	5.75	0.3
5	1.000	0.807	0.198	7.5	1.6
7	1.000	0.664	0.211	6.67	0.7
8	0.763	0.775	0.190	7.12	1.0
12	1.000	0.585	0.189	5.26	0.6

[a]Responses were measured as peak absorbance.

A 100 μL sample of 1.00×10^{-4} M persulphate was then injected into the carrier stream and absorbances measured at 450 nm. The pH of the reaction mixture was measured simultaneously in a simple-flow through cell placed 5 cm after the spectrophotometric detector.

Automated simplex optimization

During automated simplex optimization, the flow rates of all streams save for the carrier stream were automatically adjusted. This was to determine the optimum flow rates for the reagent and NaOH streams (optimum pH from flow rate of NaOH and the buffer stream).

The initial experimental conditions and the best experimental conditions established during the simplex optimization procedure are summarized in Table 1. The best conditions obtained correspond to those of experimental point number 7, i.e. ODA and NaOH flow rates of 1.00 and 0.66 mL min^{-1} respectively, with the pH of the reaction mixture equal to 6.67 as recorded by the pH meter.

Once the optimum conditions were established, these were implemented on a simpler flow injection system shown in Fig. 2*b*, comprising two pumps, three pump tubes, and a single injection valve. This was used for subsequent routine analysis, calibration, and studies on the effect of organic substances. Alternatively, a single pump could have been employed with the carrier stream channel having a pump tubing which could provide a flow rate that is three times higher than that of the other channels.

Automated response surface mapping

A more thorough investigation of the ODA–persulphate response surface was then achieved by carrying out triplicate experiments at

Can. J. Chem. Downloaded from www.nrcresearchpress.com by 91.121.58.235 on 09/07/12
For personal use only.

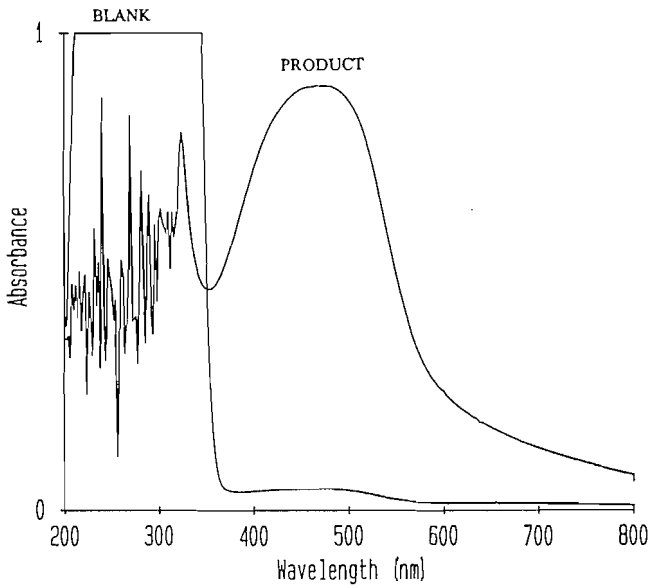

FIG. 3. UV–visible absorption spectra of the ODA–persulphate reaction product: (*1*) reagent blank with water as reference; (*2*) ODA–persulphate mixture after 300 s with the reagent blank as reference.

TABLE 2. Effect of metal ions on the ODA–persulphate reaction; absorbance measurements taken 5 min after initiation

M^{n+}	$[M^{n+}]$/mol L^{-1}	Absorbance	Enhancement factor[a]
Blank	—	0.747	0.63 (300 s)
Mo^{6+}	1×10^{-3}	0.779	0.66 (300 s)
Mn^{2+}	1×10^{-3}	0.946	0.80 (300 s)
Ni^{2+}	1×10^{-3}	1.040	0.88 (215 s)
Co^{2+}	1×10^{-3}	1.038	0.88 (200 s)
Zn^{2+}	1×10^{-3}	1.108	0.94 (245 s)
Pb^{2+}	1×10^{-3}	1.133	0.96 (245 s)
Cu^{2+}	1×10^{-3}	1.181	1.00 (85 s)
Fe^{3+}	1×10^{-3}	Interferes	—
Ag^{+}	1×10^{-3}	Interferes	—

[a]Enhancement factor is calculated relative to 10^{-3} M Cu^{2+} ions and the values in brackets show the times at which maximum absorbance were recorded with [ODA] = 5.0×10^{-3} M, $[S_2O_8^{2-}] = 1.0\times10^{-4}$ M, buffered at pH = 7.0.

each of the 64 sets of reaction conditions. These were regularly spaced across the search space in the pattern of an 8 × 8 square lattice. The average absorbance at each set of conditions was taken as the height of the response surface at that point.

Results and discussion

Selection of analytical wavelength

The absorption spectra of 5.0×10^{-3} M ODA in 40% v/v acetone–water mixture and that of the reaction product formed from the reaction between 5.0×10^{-3} M ODA in 40% v/v aqueous acetone and 1.0×10^{-4} M persulphate after 5 min as reaction time are shown in Fig. 3. This reveals that absorbance measurements due to formation of product can be made at 450 nm without interference from the reagent matrix.

Batch kinetic studies

Effect of metal ions

A number of metal ions are known to catalyze reactions involving persulphate ions. The metal ions studied are given in Table 2. Most showed catalytic activity to varying degrees.

TABLE 3. Effect of neutral salts on rate of formation of product; reaction conditions: [ODA] = 1.0×10^{-3} M, $[S_2O_8^{2-}] = 5.0\times10^{-5}$ M

Salt	Concentration mol L^{-1}	Absorbance after 600 s	Relative increase (%)
Blank	0.0	0.0932	0
NaCl	1.0×10^{-4}	0.1479	58.69
	4.0×10^{-3}	0.1488	59.66
KCl	1.0×10^{-4}	0.1401	50.32
	4.0×10^{-3}	0.1495	60.41
KNO_3	1.0×10^{-4}	0.1040	11.59
	4.0×10^{-3}	0.1323	41.95

Both Fe(II) and Cu(II) showed remarkable catalytic activity even at concentrations as low as 10^{-5} M. Reactions catalyzed by Fe(II), however, yielded very unstable products. This was not surprising since the reaction mechanism is thought to be via a free radical species (4) producing Fe(III), which in itself formed a colored complex with ODA. A substantial catalytic effect was also observed for Pb(II). The catalytic activities of Mn(II), Co(III), Ni(II), Zn(II), and Mo(VI) were much less than that of Cu(II). About a 100-fold concentration (10^{-1} M) of these metal ions had a comparable catalytic effect as that of the Cu(II) (10^{-3} M). Both Ag(I) and Fe(III) formed colored complexes with ODA and thus interfered.

Further investigation of the suitability of Cu(II) as a catalyst in the ODA–persulphate reaction was then performed. The concentration of Cu(II) was varied from 10^{-7} to 10^{-1} M. At concentrations below 10^{-6} M, the reaction rate was slightly increased relative to the uncatalyzed reaction. For concentrations between 10^{-6} and 10^{-4} M, equilibrium of the reaction mixture was reached between 240 and 90 s, respectively, while with concentrations between 5.0×10^{-4} and 10^{-1} M, equilibrium was attained within 60 s. A Cu(II) concentration in the range 10^{-3} to 10^{-2} M is recommended. This is a compromise between the rate of attaining equilibrium and product instability, since at concentrations above 10^{-2} M Cu(II) instability became more apparent.

Effect of neutral salts

Ionic strength often varies from sample to sample and so the effects of NaCl, KCl, and KNO_3 concentrations on the ODA–persulphate reaction was investigated. Table 3 summarizes the effect of various concentrations of these neutral salts on the rate of reaction. The reported absorbances were measured 300 s after initiating the reactions. All these neutral salts showed a positive effect on the rate of the reaction with increase in concentration. KCl and NaCl showed approximately equal effects which were greater than that observed with KNO_3 (Table 3).

Effect of % v/v composition of acetone in water as solvent

The % v/v composition of acetone in water was varied from 20 to 100%. The lower limit was chosen because of the limited solubility of ODA in water. The results showed a general increase in rate of the reaction with increase in mole fraction of acetone, but product stability decreased. In the presence of 10^{-4} M Cu(II) as catalyst, equilibrium was attained in less than 60 s with compositions above 40%. Product stability, however, decreased with increase in % composition above 40%. Under similar conditions with 20–40% acetone, equilibrium was achieved between 60 and 90 s, respectively, with product stability times greater than 300 s (product stability times = time

Can. J. Chem. Downloaded from www.nrcresearchpress.com by 91.121.58.235 on 09/07/12
For personal use only.

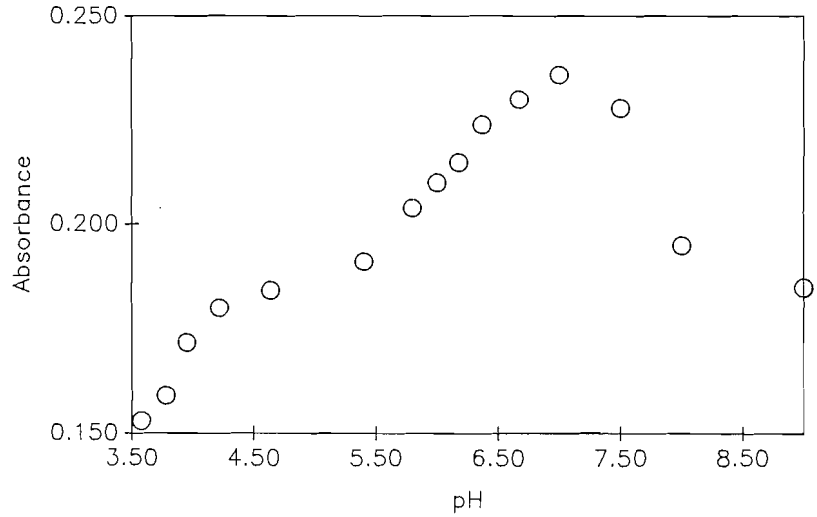

FIG. 4. Absorbance at 450 nm for the ODA–persulphate reaction mixture as a function of pH.

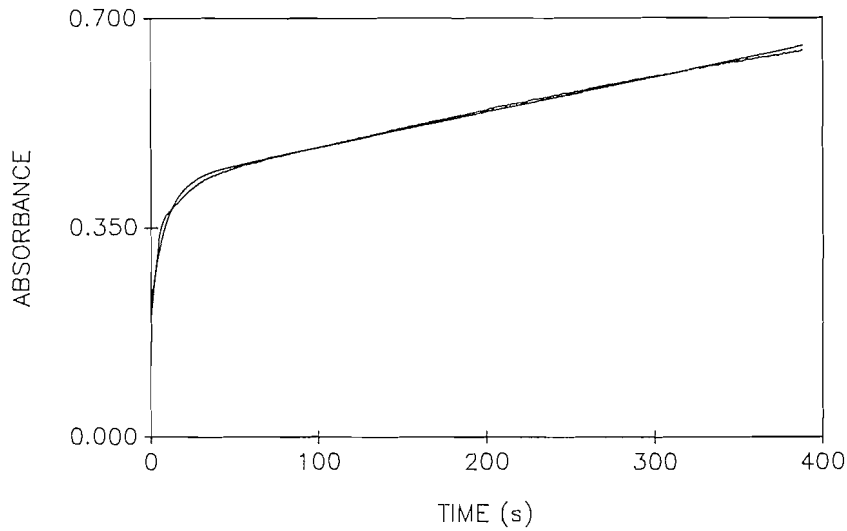

FIG. 5. Fit of a pseudo-first order reaction model to data collected for the reaction between ODA and persulphate at pH 7.0.

period over which absorbance readings were recorded within ±0.05 absorbance units). Thus a composition of between 20 and 40% is recommended.

Effect of reaction mixture pH

3,3-Dimethylglutaric acid (0.1 M) in 1 M NaCl and 0.1 M NaOH was used to vary the pH of the reaction mixtures from 3.5 to 10.0. A high concentration of NaCl was employed to keep the ionic strength of reaction medium constant. Figure 4 shows the responses obtained from reaction mixtures at various pH values. Absorbance was measured after 300 s of reaction time. From these batch reactions, the maximum response obtained corresponded to neutral conditions; however, acceptable sensitivity was obtained between pH 6.5 and 7.5.

Reaction kinetics studies

Reaction kinetics were investigated at neutral pH conditions under pseudo-first order conditions, with ODA in excess. Expressing the reaction as

$$S_2O_8^{2-} + n\text{ODA} \rightarrow \text{Product}$$

the reaction rate can be written as

$$\text{Rate} = K'[S_2O_8^{2-}]$$

where K' is the pseudo-first order rate constant.

A non-linear curve fitting program was used to extract the pseudo-first rate constant from the stopped-flow experimental data. The equation fit to the data was

$$A_t = A_0[1 - \exp(-K't)] + C$$

where A_t is the absorbance at time t, A_0 is the final solution absorbance due to product, and C is a constant background term. The flow through cell was thermostated at 25°C. Figure 5 is representative of the fits of the model to the data. Excellent fits were obtained for each of the solutions tested. The pseudo-first order rate constant obtained from the fitting routine was 0.06 ± 0.01 s^{-1}. The final equilibrium absorbance due to the product remained unchanged within ±0.01 absorbance units for ODA concentrations in the range 0.001 to 0.01 M, an indication that reaction was going to completion. The reaction is essentially finished in less than 90 s.

Can. J. Chem. Downloaded from www.nrcresearchpress.com by 91.121.58.235 on 09/07/12
For personal use only.

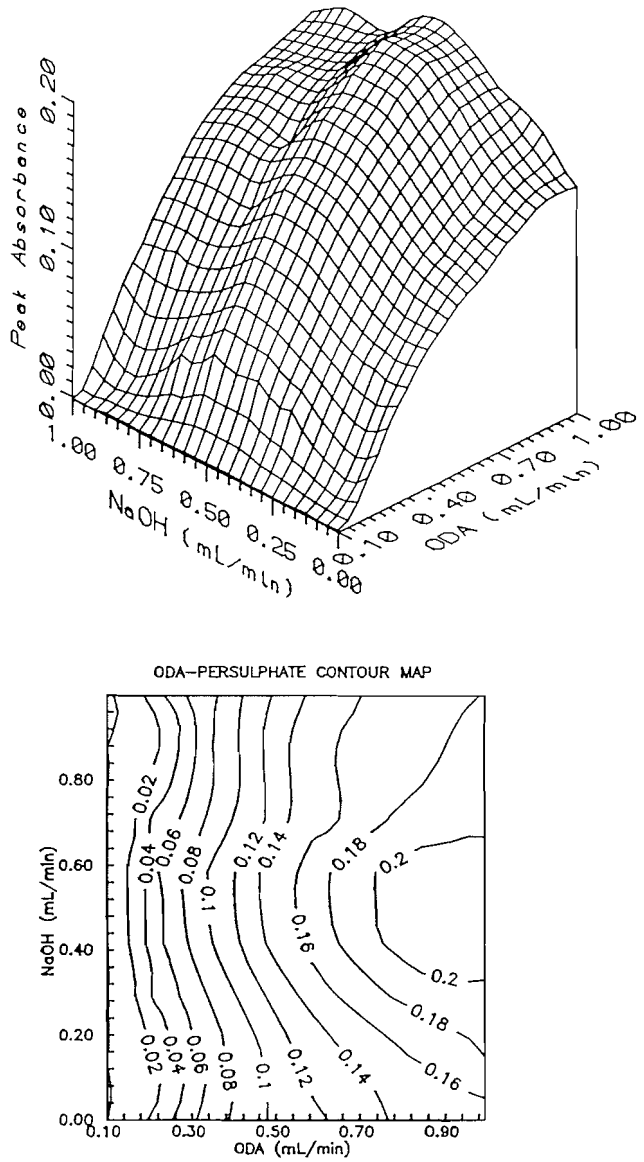

FIG. 6. The ODA–persulphate response surface shown as a 3D plot and its corresponding contour map. The response shown is the peak absorbance at 450 nm. ODA and NaOH flow rates are in mL min^{-1}.

Automated optimization of the flow injection system

Both simplex optimization and response surface mapping were employed. The results are compared. Simplex optimization was chosen as an optimization procedure because it rapidly optimizes chemical and flow conditions in flow injection systems (12). While this approach adequately locates the maximum, it gives little information about the global nature of the response surface (13). Some workers have advocated carrying out an additional set of experiments around the best conditions found by an experimental optimization to confirm that the true optimum has indeed been located and establish the effect of changes in experimental variables in this region (21). This provides the experimentalist with evidence of the stability and therefore experimental repeatability of the analytical method. This was not done here as the same function was achieved globally by the response surface mapping experiments.

With three replicate runs at every experimental condition, the total time taken to achieve the optimum conditions by simplex optimization was 2.0 h. This was for about 20 sets of experimental conditions. For the automated response surface mapping, a factorial design consisting of 64 experiments each with three replicates, was used. This optimization process took about 4 h.

TABLE 4. Optimization of coil length for ODA–$S_2O_8^{2-}$ reaction

Coil length/cm	Peak maximum (AU)	Relative performance (%)
55	0.391	77.4
60	0.423	83.8
80	0.466	92.3
90	0.477	94.5
100	0.505	100
110	0.477	94.5
120	0.446	88.3

The results of the response surface mapping study are shown in Fig. 6. The ideal pH for this reaction was established as 7.0, however the pH range 6.0 to 7.5 could be used without great loss in sensitivity. This range corresponded to NaOH stream flow rates in the range 0.30–0.80 mL min^{-1} for the FIA manifold of Fig. 2*a*. Thus the whole pH range 6.0–7.5 is recommended. These results were in good agreement with those from the simplex optimization procedure. As shown in Table 1, the optimum flow rate conditions obtained from simplex experiments fall in the region considered optimum from the response surface studies. Also the pH's corresponding to the five best simplex experimental conditions are within the pH range established as optimum from the response surface studies. The optimum conditions established by the simplex procedure were thus confirmed by the automated response surface mapping studies at the expense of more experiments and somewhat less information about the region of the optimum.

The effect of reaction coil length on the sensitivity of the system was determined by performing 10 replicate experiments under the optimum conditions obtained from the first simplex optimization experiment with different reaction coil lengths. A 100 cm coil length was established as optimum. Results of these studies are summarized in Table 4. Since this value was (fortuitously) as used in the previous automated chemical flow optimization, no further optimization experiments were warranted. The automated analyzer used does not presently have the capability of automatically adjusting coil length.

Interference studies

In polymerization studies with persulphate as activator, persulphate must often be determined in the presence of various organic substances. Thus the effect of methanol, ethanol, allyl acetate, formaldehyde, ethyl acetate, and allyl alcohol on the ODA–persulphate reaction was investigated. Of these substances, methanol and ethanol showed the least effect even at concentrations as high as 1.0 M. Solutions containing 2.5 M methanol and 1.0 M ethanol caused an error of about +0.22% in the determination of 2.0×10^{-4} M persulphate ions. At 0.25 M concentrations of both allyl alcohol and allyl acetate errors of +0.50% and −6.98% respectively were recorded. The worst acceptable interference was obtained with 0.5 M ethyl acetate which gave an error of +11.80. Reaction in the presence of formaldehyde resulted in a turbid mixture which then formed a pinkly colored precipitate. Formaldehyde thus strongly interferes, and should not be present.

Can. J. Chem. Downloaded from www.nrcresearchpress.com by 91.121.58.235 on 09/07/12
For personal use only.

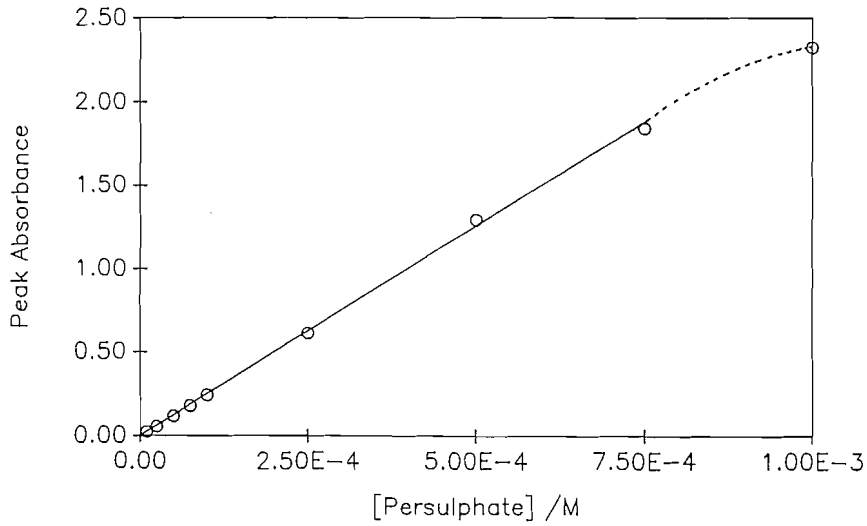

FIG. 7. Calibration curve for developed method of persulphate determination. The solid line represents the linear dynamic range.

Analytical implications

The calibration curve obtained with the flow geometry of Fig. 2*b* is shown in Fig. 7. This indicates a linear dynamic range of 2.50×10^{-5} M to 7.5×10^{-4} M, with a sensitivity of 2.4×10^3 Abs M^{-1}. The detection limit (3 × standard deviation of the baseline noise) with this system was 5.0×10^{-7} M. The lower limit of the linear dynamic range was detected with a relative standard deviation of 1.5% from 10 replicates.

Conclusions

The analytical method developed is both simple and sensitive. Other advantages generic to flow injection techniques include high precission, high sample throughput rate, and low sample and reagent consumption rates. Together these give the analytical procedure reported here many advantages over previous classical (4, 9), titrimetric (4), and the polarographic methods (6, 7). While a few organic species and metal ions do interfere, either the extent of their effects is tolerable, or the interference is usually obvious in the reaction mixture.

Acknowledgements

The authors wish to thank Peter D. Wentzell for his assistance with computer programming and modifications to the hardware which have made this and previous work possible. This work was supported by NSERC operating grant 5-80246 and UBC-NSERC grant 5-80085. P.M.S. acknowledges support from the UBC-University Graduate Fellowship research program.

1. W. M. LATIMER. The oxidation states of the elements and their potentials in aqueous solution. Prentice-Hall, Englewood Cliffs, NJ. 1952. p. 78.
2. W. K. WILMARTH and A. HAIM. *In* Peroxide reaction mechanisms. *Edited by* J. O. Edwards. Wiley Inter-Science, New York. 1962. pp. 175–222.
3. R. B. SEYMOUR. *In* An introduction to polymer chemistry. International student edition. McGraw-Hill, Kogukusha, Ltd-Tokyo. 1956. p. 157.
4. I. M. KOLTHOFF and E. M. CARR. Anal. Chem. **25**, 298 (1953).
5. D. AMIN and A. K. HAREEZ. Analyst, **106**, 1221 (1981).
6. D. AMIN. Analyst, **106**, 1217 (1981).
7. I. M. KOLTHOFF and R. J. WOODS. J. Am. Chem. Soc. **88**, 13 (1966).
8. E. BOYLAND, D. MANSON, and P. SIMS. J. Chem. Soc. 3623 (1953).
9. K. C. KHULBE and R. S. MANN. Chromatogr. **150**, 554 (1978).
10. H. MULLU, J. MATTUSCH, and G. WERNER. Mikrochim. Acta, **II**, 349 (1980).
11. K. B. YATSIMIRSKI. Kinetics methods of analysis. Pergamon Press, London. 1966.
12. J. RUZICKA and E. H. HANSEN. Flow injection analysis. 2nd ed. Wiley, New York. 1988.
13. P. D. WENTZELL, M. J. HATTON, P. M. SHIUNDU, R. M. REE, A. P. WADE, D. BETTERIDGE, and T. J. SLY. J. Automatic Chem. **11**, 227 (1989).
14. D. BETTERIDGE, T. J. SLY, A. P. WADE, and J. E. W. TILMAN. Anal. Chem. **55**, 1292 (1983).
15. D. BETTERIDGE, T. J. SLY, A. P. WADE, and D. G. PORTER. Anal. Chem. **58**, 2258 (1986).
16. P. M. SHIUNDU, P. D. WENTZELL, and A. P. WADE. Talanta, **37**, 329 (1990).
17. P. M. SHIUNDU, P. D. WENTZELL, and A. P. WADE. Anal. Chim. Acta. In press.
18. D. D. PERRIN and B. DEMPSEY. Buffers for pH and metal ion control. Chapman-Hill, London. 1974. p. 133.
19. D. BETTERIDGE, A. G. HOWARD, and A. P. WADE. Talanta, **32**(8B), 709 (1985).
20. D. BETTERIDGE, A. G. HOWARD, and A. P. WADE. Talanta, **32**(8B), 723 (1985).
21. S. L. MORGAN and S. N. DEMING. Anal. Chem. **46**, 1170 (1974).

Can. J. Chem. Downloaded from www.nrcresearchpress.com by 91.121.58.235 on 09/07/12
For personal use only.

Evaluation of K_{BH^+} constants for weak organic bases

W. David Chandler and Donald G. Lee
Department of Chemistry, University of Regina, Regina, Sask., Canada S4S 0A2

Received February 9, 1990

This paper is dedicated to Professor Ross Stewart on the occasion of his 65th birthday

W. David Chandler and Donald G. Lee. Can. J. Chem. **68**, 1757 (1990).

A non-linear regression procedure has been developed to analyze simgoidal plots even when data at or near the plateaus are missing. The method was used to fit relative C-13 nmr chemical shifts (Δ) of five alcohols to sigmoidal functions of the excess acidity (X). With two of the functions, the regression gives Δ_{BH^+}, the relative chemical shift of the protonated alcohol. That parameter permits calculation of the ratio, $[BH^+]/[B]$, necessary for an additional linear regression to determine pK_{BH^+} and m^*. With a third function, regression gives Δ_{BH^+}, pK_{BH^+} and m^* directly. Comparison of pK_{BH^+} values obtained from these methods with those estimated previously suggests that the sigmoidal regressions are reliable, and can be of considerable use in handling titration-type curves generally.

Key words: basicities, alcohols, regression, sulfuric aid.

W. David Chandler et Donald G. Lee. Can. J. Chem. **68**, 1757 (1990).

On a mis au point une proédure de régression non-linéaire qui permet d'analyser des courbes sigmoïdales, même lorsqu'il manque des données près de ou au niveau des plateaux. On a utilisé cette méthode pour ajuster les déplacements chimiques relatifs (Δ) de la rmn du ^{13}C de cinq alcools avec les fonctions sigmoïdales de l'excès d'acidité (X). Avec deux de ces fonctions, la régression fournit la valeur de Δ_{BH^+}, le déplacement chimique relatif de l'alcool protoné. Ce paramètre permet de calculer la valeur du rapport $[BH^+]/[B]$ qu'il est nécessaire de connaître pour effectuer une régression linéaire additionnelle dans le but de déterminer les valeurs de pK_{BH^+} et de m^*. Avec une troisième fonction, la régression fournit directement les valeurs de Δ_{BH^+}, pK_{BH^+} et m^*. Une comparaison des valeurs de pK_{BH^+} obtenues par ces méthodes avec celles évaluées antérieurement suggère que les régressions simoïdales sont fiables et qu'elles peuvent être très utiles pour traiter d'une façon générale des courbes du type "titration".

Mots clés : basicités, alcools, régression, acide sulfurique.

[Traduit par la revue]

Introduction

An ability to accurately measure dissociation constants (K_{BH^+}, eq. [1]) for the conjugate acids, BH^+, of weak bases, B, is essential to a quantitative understanding of reactions that are subject to acid catalysis. Because of the number and importance of such reactions in organic chemistry and biochemistry it is not surprising that the literature contains descriptions of attempts that have been made to estimate K_{BH^+} values for many weak bases including alcohols (1–4), ketones and aldehydes (3–9), carboxylic acids and esters (7–11), ethers (3, 4, 12, 13), and sulfur-containing compounds (3, 13, 14).

$$[1] \quad BH^+ \overset{K_{BH^+}}{\rightleftharpoons} B + H^+$$

In the absence of a reliable value for the dissociation constant it is impossible to quantitatively analyze the kinetics of reactions that are catalyzed by acid (15).

Three requirements must be met before K_{BH^+} values can be determined accurately: (*i*) a suitable acidity function must exist (15); (*ii*) it must be possible to measure some physical property that accurately determines the ratio $[BH^+]/[B]$ (16), and (*iii*) methods must be available to analyze a plot of a function of $[BH^+]/[B]$ against the acidity of the solution.

Extensive studies based on the pioneering work of Hammett led, eventually, to the development of acidity functions that can be used with confidence (17). The most general of these (the excess acidity function, X) utilizes a plot of $\log [BH^+]/[B] - \log [H^+]$ vs. X (eq. [2]) (18).

$$[2] \quad \log [BH^+]/[B] - \log [H^+] = m^*X + pK_{BH^+}$$

Two physical properties have been used extensively to measure the ratio $[BH^+]/[B]$ – UV absorption intensities (18) and nmr chemical shifts (2, 3, 12). The former is useful if the base contains a chromophore that undergoes a change of either position or intensity on protonation. If ϵ_B and ϵ_{BH^+} are extinction coefficients of the base and its conjugate acid at a particular wavelength and ϵ is the observed extinction coefficient at the same wavelength when the base is dissolved in an acidic solution, $[BH^+]/[B]$ is equivalent to $(\epsilon_B - \epsilon)/(\epsilon - \epsilon_{BH^+})$ (16). The reliability of this method rests on the assumption that the extinction coefficients are not subject to solvent effects and that no other reactions are occurring. Figure 1 illustrates a typical curve that may be obtained when ultraviolet spectroscopy is used to monitor the protonation of a weak base.

The use of nuclear magnetic resonance to estimate $[BH^+]/[B]$ relies on the *position* of the chemical shifts rather than the intensities of the signals (2, 12). If Δ_B and Δ_{BH^+} are the proton or carbon-13 chemical shifts for particular atoms of the base and its conjugate acid and Δ is the observed chemical shift when the base is dissolved in an acidic solution, $[BH^+]/[B]$ is equivalent to $(\Delta_B - \Delta)/(\Delta - \Delta_{BH^+})$ (2, 12). This method has the advantage that the occurrence of side reactions does not necessarily invalidate the measurement. It suffers, however, from the disadvantage that high concentrations of base, which are often required in order to obtain a measurable signal, may alter the properties of the solution. Figure 2 illustrates a curve typical of those that may be obtained by using nmr signals.

While it is usually quite straightforward to analyze the plots obtained when all of the properties (ϵ_B, ϵ_{BH^+}, and ϵ, or Δ_B, Δ_{BH^+}, and Δ) can be accurately measured, it is unfortunately true that for some of the most interesting and important reactions reliable direct measurements of either ϵ_{BH^+} or Δ_{BH^+} are impossible to obtain. For example, if the base is sufficiently weak, conditions may not exist under which it is both fully protonated *and* stable. In such cases one is faced with the challenge of analyzing a partial curve as in Fig. 3.

Can. J. Chem. Downloaded from www.nrcresearchpress.com by 91.121.58.235 on 09/07/12
For personal use only.

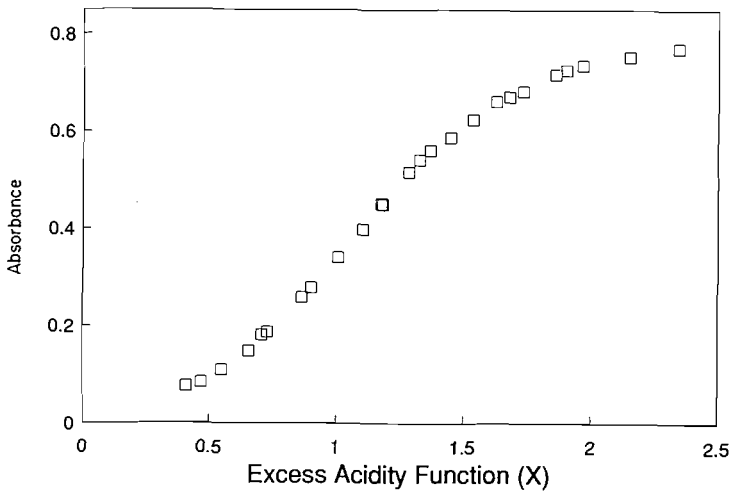

FIG. 1. Absorbance of a weak base as a function of the acidity of the medium.

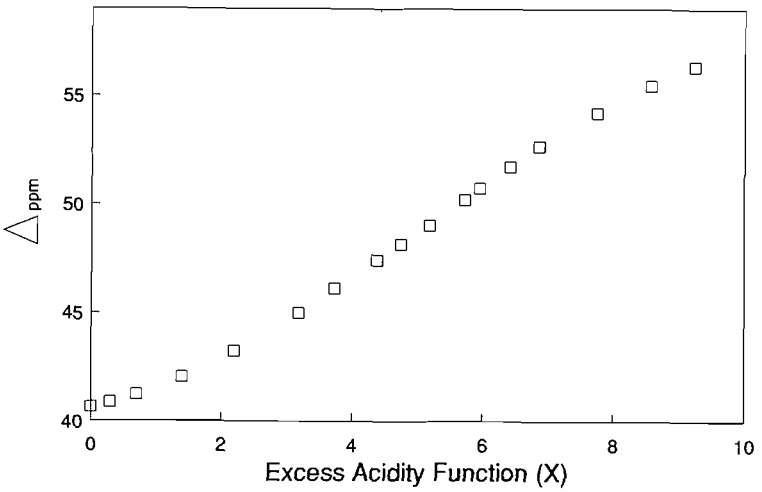

FIG. 2. Difference in C-13 chemical shifts (Δ) at C1 and C2 of an alcohol as a function of the acidity of the medium. Data up to near Δ_{BH^+} are available.

Several approaches may be considered when complete sigmoidal curves are not available. For example, attempts have been made to estimate Δ_{BH^+} by selecting the value that gives the best straight line when log $(\Delta_B - \Delta)/(\Delta - \Delta_{BH^+})$ is plotted against a known acidity function (2, 3, 6, 13). Alternatively, one may attempt to fit experimental values of Δ or absorbance to a known function of acidity and then determine the position of the inflection point (which will correspond to the situation where $[BH^+] = [B]$). If the sigmoidal curve is symmetrical, the vertical distance from the inflection point to Δ_{BH^+} should then be the same as that from Δ_B to the inflection point. In theory, the inflection point may be obtained by setting the second derivative of the function equal to zero and solving for acidity.

The most obvious type of function to use is a polynomial in excess acidity, X (eq. [3]). Such a function

$$[3] \quad \Delta = a_0 + a_1X + a_2X^2 + a_3X^3 + \cdots + a_nX^n$$

is easily fitted to experimental data and, for orders three or four, produces a simple second derivative (20).

An alternative is a function that is known to be sigmoidal. Examples are the hyperbolic tangent of [4] and the exponential ratio of [5].

$$[4] \quad \Delta = A \tanh (BX - C) + D$$

$$[5] \quad \Delta = \frac{A + BX\exp(CX + D)}{1 + X\exp(CX + D)}$$

Both of these can give Δ_{BH^+}) directly without the necessity of finding an inflection point. With [4], $\Delta_{BH^+} = A + D$, $\Delta_B = D - A$, and $\Delta_{inf} = D$. In the case of [5], $\Delta_{BH^+} = B$ and $\Delta_B = A$. Fitting these functions to the data is more complex than fitting [3] since they are not linear in the variable parameters A, B, C, and D. However, gradient techniques are available so that, with modern microcomputers, regression analysis is achievable (20, 21).

The principal goal of finding Δ_{BH^+} (or ϵ_{BH^+}) in this and earlier work was to find K_{BH^+} for a weak base such as an alcohol. With Δ_{BH^+} in hand, log $[BH^+]/[B]$ may be calculated, and the linear regression of [2] carried out. Determining K_{BH^+} and m^* then requires two regressions; one produces Δ_{BH^+} while the second gives pK_{BH^+} as the intercept of a straight line (eq. [2]). It would seem preferable to combine the two regressions into one.

Recognizing that $[BH^+]/[B]$ is equivalent to $(\Delta_B - \Delta)/(\Delta - \Delta_{BH^+})$, [2] can be rewritten in exponential form, [6],

$$[6] \quad \Delta = \frac{A + B[H^+]\exp(CX + D)}{1 + [H^+]\exp(CX + D)}$$

Can. J. Chem. Downloaded from www.nrcresearchpress.com by 91.121.58.235 on 09/07/12
For personal use only.

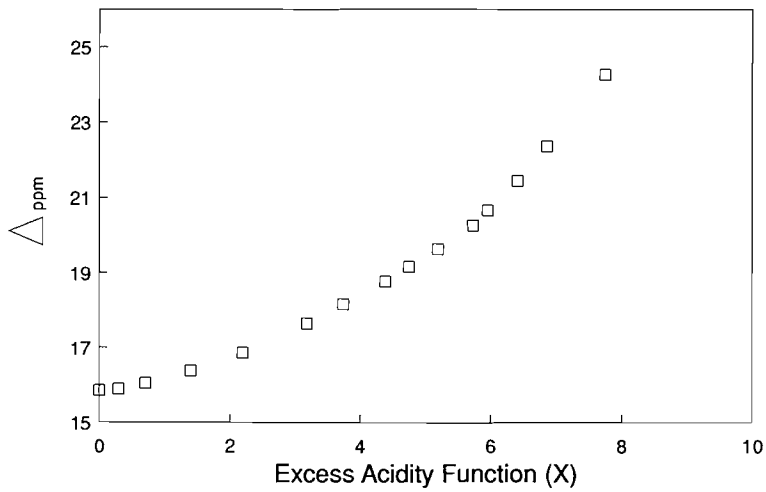

FIG. 3. Difference in C-13 chemical shifts (Δ) at C1 and C2 of an alcohol as a function of the acidity of the medium. Data near Δ_{BH^+} are not available.

TABLE 1. C-13 Δ_B and Δ_{BH^+} values for some aliphatic alcohols[a]

	Δ_B		Δ_{BH^+}		
Alcohol	Eq. [4]	Eq. [5]	Eq. [4]	Eq. [5]	Ref. 2
Ethanol	38.70±0.24	40.64±0.04	59.8±0.24	59.10±0.46	60
1-Propanol	36.54±0.35	39.04±0.03	57.59±0.35	59.10±0.46	57
2-Propanol	36.04±0.41	40.48±0.04	66.43±0.41	67.62±0.28	65
2-Phenoxyethanol	−9.91±0.41	−8.95±0.03	−4.56±0.41	−4.32±0.38	−4

[a]Shifts in ppm using experimental data from ref. 2.

where $A = \Delta_B$, $B = \Delta_{BH^+}$, $C = 2.303m^*$, and $D = 2.303pK_{BH^+}$. All four of the desired basicity parameters are readily extractable from a regression involving only the experimental or derivable quantities Δ, X, and $[H^+]$.

This paper describes the successes we have had using the various functions to fit previously reported C-13 nmr data for some alcohols in sulphuric acid (2) and to obtain pK_{BH^+} values.

Experimental

The C-13 chemical shift (Δ) data for a series of aliphatic alcohols have been correlated with the excess acidity (X) using four functions (eqs. [3]–[6]). Values of X and $[H^+]$ for H_2SO_4 were taken from the work of Cox and Yates (18). Using gradient, least-squares algorithms (20, 21) discussed previously, computer programs were written in BASIC, C, or Pascal to handle all regressions on an MS-DOS computer; the basic gradient technique proved to be far faster and more reliable than simplex algorithms (6). Aside from the experimental data, only a preliminary guess for pK_{BH^+} was required. Initial values for the other variable parameters were then calculated from the appropriate equations using two data parts. Output included the final values of each variable and its uncertainty. While an 80×87 math coprocessor was not necessary its presence greatly accelerated the non-linear calculations.

Results

A fourth-order polynomial (eq. [3]) was successful in locating Δ_{BH^+} only if data were available well past the inflection point and nearly up to the Δ_{BH^+} plateau. Since such a function is useful only within the region of X spanned by experimental data; extrapolation is not possible. In several cases the second derivative either found a false inflection point or was unable to locate one at all. As a result the polynomial turned out to be an unreliable function when applied to real data of the type available.

Better success accompanied the use of the two sigmoidal functions (eqs. [4] and [5]). As Table 1 shows, these two give values for Δ_{BH^+} that are comparable with each other as well as with previously published results. Moreover, not only are the sigmoidal regressions faster than for other methods (2), the reported Δ_{BH^+} values are expected to be more reliable; plots of correlation coefficients vs. Δ_{BH^+} values usually have imprecise broad maxima. The hyperbolic tangent does not equate Δ_B to Δ ($X = 0$) since tanh is symmetric about the inflection point, and Δ_{BH^+} is between 2 and 5% lower than that obtained from the regression using [5]. Figure 4 illustrates how well the two functions correlate with experimental data, and how they can be extrapolated to give Δ_{BH^+}. Both regressions work even when experimental data are available only up to (or nearly up to) the inflection point, provided these data are reliable. Some of the alcohols reported earlier did not have enough sufficiently good data to allow analysis by either sigmoidal function (2).

Using the Δ_{BH^+} values obtained, the relationship defined by [2] was used to determine pK_{BH^+} and m^* (Table 2). Within the estimated error, the results of this and previous work are identical. The errors quoted for this work in Table 2 include both the uncertainty in Δ_{BH^+} and the error inherent in the linear regression. Those quoted by Lee and Demchuk (2) are for the linear regression alone.

The use of [6] obviates the need to estimate Δ_{BH^+} before obtaining m^* and pK_{BH^+}. In addition, there is less reason to limit data to $\log [BH^+]/[B] < 1.0$, or to use only acidity data below 84% H_2SO_4 where the dramatic decrease in $[H^+]$ at high acid concentration is avoided. To test this particular sigmoidal

Can. J. Chem. Downloaded from www.nrcresearchpress.com by 91.121.58.235 on 09/07/12
For personal use only.

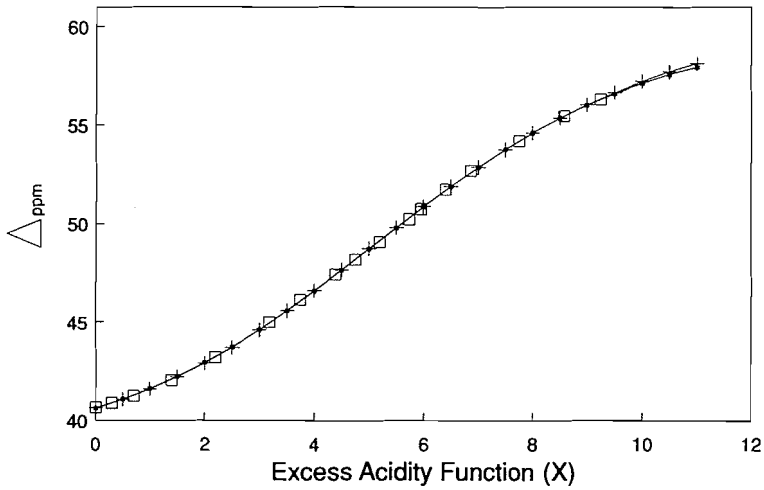

FIG. 4. Difference in C-13 chemical shifts (Δ) at C1 and C2 of ethanol as a function of the acidity of the medium. (□) Experimental data. (●) Regression curve from equation [4]. (+) Regression curve from eq. [5].

TABLE 2. Basicity data for some aliphatic alcohols obtained by applying eq. [5] to C-13 nmr shifts[a]

Alcohol	pK_{BH^+}		m^*	
	This work[b]	Ref. 2	This work[b]	Ref. 2
Ethanol	−2.12±0.02	−2.12±0.02	0.169±0.004	0.17±0.02
1-Propanol	−2.14±0.02	−2.12±0.02	0.157±0.003	0.16±0.02
2-Propanol	−2.02±0.02	−2.02±0.02	0.167±0.005	0.18±0.02
2-Phenoxyethanol	−1.85±0.04	−1.87±0.09	0.197±0.010	0.18±0.07

[a]Data taken from ref. 2. Only those data for which $0.1 < [BH^+]/[B] < 10$ and for which % H_2SO_4 <84 were used.
[b]Δ_{BH^+} obtained from sigmoidal regression using eq. [4].

TABLE 3. Basicity and spectroscopic parameters for 2,5-dichloro-4-nitroaniline in H_2SO_4

Source	Abs_B	Abs_{BH^+}	pK_{BH^+}	m^*	r
This work[a]	0.009±0.016	0.795±0.011	−1.78±0.08	0.993±0.066	0.991
Ref. 17[b]	(0)[c]	(0.8)[c]	−1.72±0.03	0.94±0.02	0.994

[a]26 data points from ref. 18 and references cited therein. Data were fitted to eq. [6].
[b]25 data points.
[c]Estimated from reported data.

TABLE 4. Basicity data for some aliphatic alcohols obtained from C-13 nmr chemical shifts[a]

Alcohol	Δ_{BH^+}		pK_{BH^+}		m^*	
	Eq. [6]	Ref. 2	Eq. [6]	Ref. 2	Eq. [6]	Ref. 2
Ethanol	61.0±1.3	60	−2.11±0.01	−2.12±0.12	0.162±0.008	0.17±0.02
1-Propanol	59.4±1.5	57	−2.13±0.02	−2.12±0.02	0.148±0.007	0.16±0.02
2-Propanol	65.3±0.9	65	−2.01±0.01	−2.02±0.02	0.176±0.007	0.18±0.02
2-Phenoxyethanol	−4.81±0.2	−4	−1.82±0.03	−1.87±0.09	0.188±0.002	0.28±0.07
2-Nitroethanol	−12.1±2.1	−12	−2.06±0.09	−2.09±0.08	0.120±0.018	0.12±0.03
2-Chloroethanol	[b]	31	−2.58±0.32	−2.45±0.03	0.142±0.029	0.17±0.01
2-Bromoethanol	[b]	43	−2.94±1.11	−2.45±0.03	0.123±0.027	0.17±0.01

[a]Data taken from ref. 2. Only those data for which % H_2SO_4<84 were used.
[b]Error in Δ_{BH^+} exceeds estimated value.

regression, absorbance data for 2,5-dichloro-4-nitroaniline were used (18, 19). The results shown in Table 3 indicate that, even without calculating $[BH^+]/[B]$, quite acceptable values of pK_{BH^+} are obtained. As an added bonus, absorbances for the aniline and anilinium ion become available in spite of their not being measured directly.

Table 4 presents results from the use of [6] to analyze nmr data for seven alcohols. Of these, five — ethanol, 1-propanol,

Can. J. Chem. Downloaded from www.nrcresearchpress.com by 91.121.58.235 on 09/07/12
For personal use only.

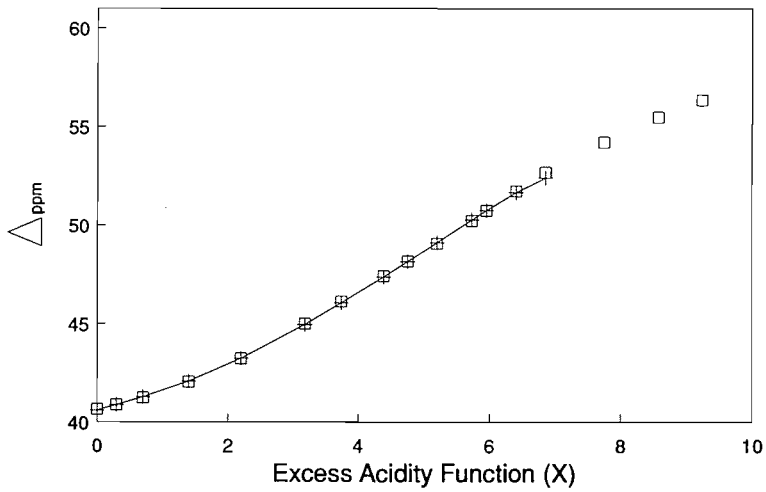

FIG. 5. Difference in C-13 chemical shifts (Δ) at C1 and C2 of ethanol as a function of the acidity of the medium. (□) Experimental data. (+) Regression curve from eq. [6].

2-propanol, 2-phenoxyethanol, and 2-nitroethanol — have values for Δ_{BH^+}, pK_{BH^+} and m^* that are virtually identical to those of previous work and those reported earlier in this paper. The apparently low errors quoted by Lee and Demchuk (2) are misleading because they refer only to the linear regression part of the analysis and assign no uncertainty to Δ_{BH^+}. 2-Chloroethanol and 2-bromoethanol did not give good regressions although they did not fall as when using the hyperbolic tangent (eq. [5]).

Conclusions

K_{BH^+} constants for weak bases such as alcohols and amines can be evaluated from nmr chemical shifts or from absorbance data for the bases in a strong acid if a non-linear regression is used to fit the data to the sigmoidal function of [6]. Alternatively, the property of the fully protonated conjugate acid (ϵ_{BH^+} or Δ_{BH^+}) can be obtained from sigmoidal functions like those of [4] or [5], and that property used in the standard way (eq. [2]) to calculate pK_{BH^+}. Sigmoidal regression offers a straightforward way of analyzing titration curves in general. It is especially useful when data are unavailable over the complete curve.

Acknowledgements

The authors are grateful for financial support from the Natural Sciences and Engineering Research Council of Canada.

1. E. M. ARNETT, J. J. BURKE, J. V. CARTER, and C. F. DOUTY. J. Am. Chem. Soc. **94**, 7837 (1972).
2. D. G. LEE and R. CAMERON. J. Am. Chem. Soc. **93**, 4724 (1971); D. G. LEE and K. J. DEMCHUK. Can. J. Chem. **65**, 1769 (1987).
3. G. PERDONCIN and G. SCORRANO. J. Am. Chem. Soc. **99**, 6983 (1977).
4. V. GOLD, K. LAALI, K. P. MORRIS, and L. Z. ZDUNCK. J. Chem. Soc. Perkin Trans. II, 865 (1988).
5. K. YATES and R. STEWART. Can J. Chem. **37**, 664 (1959); H. J. CAMPBELL and J. T. EDWARD. Can. J. Chem. **38**, 2109 (1960); T. G. BONNER and J. PHILLIPS. J. Chem. Soc. (B) 650 (1966); R. STEWART, M. R. GRANGER, R. B. MOODIE, and L. J. MUENSTER. Can. J. Chem. **41**, 1065 (1963); R. I. ZALEWSKI and G. E. DUNN. Can. J. Chem. **47**, 2263 (1969); **48**, 2538 (1970); G. C. LEVY, J. D. CARGIOLI, and W. RACELA. J. Am. Chem. Soc. **92**, 6238 (1970); N. K. SKVORTSOV, V. P. LIZINA, A. U. STEPANYANTS, G. F. TERESCHENKO, and B. I. IONIN. J. Org. Chem. USSR, **44**, 2249 (1974); D. G. LEE. Can. J. Chem. **48**, 1919 (1970); S. GERIBALDI, A. GREC-LUCIANO, P. C. MARIA, and M. AZZARO. J. Chim. Phys. **79**, 103 (1982); H. ROTH, W. FREIBERG, and C. F. KROGER. J. Prakt. Chem. **330**, 89 (1988); J. T. EDWARD and S. C. WONG. J. Am. Chem. Soc. **99**, 4429 (1977).
6. A. BAGNO, V. LUCCHINI, and G. SCORRANO. Bull. Soc. Chim. Fr. 563 (1987).
7. A. LEVI, G. MODENA, and G. SCORRANO. J. Am. Chem. Soc. **96**, 6585 (1974).
8. E. M. ARNETT, R. P. QUIRK, and J. W. LARSEN. J. Am. Chem. Soc. **92**, 3977 (1970).
9. M. BERTHELOT, J. F. GAL, M. HELBERT, C. LAURENCE, and P. C. MARIA. J. Chim. Phys. Phys.-Chim. Biol. **82**, 427 (1985).
10. A. BAGNO, G. SCORRANO, and V. LUCCHINI. Gazz. Chim. Ital. **117**, 475 (1987).
11. J. T. EDWARD and I. C. WANG. Can. J. Chem. **40**, 966 (1962); J. SIIGUR and U. HALDNA. Org. Reactivity, **7**, 197 (1970); D. G. LEE and M. H. SADAR. Can. J. Chem. **54**, 3464 (1976); J. Am. Chem. Soc. **96**, 2862 (1974); J. R. SIIGUR and U. L. HALDNA. Org. Reactivity, **7**, 211 (1970).
12. J. T. EDWARD, J. B. LEANE, and I. C. WANG. Can. J. Chem. **40**, 1521 (1962); D. G. LEE and R. CAMERON. Can. J. Chem. **50**, 445 (1972).
13. P. BONVICINI, A. LEVI, V. LUCCHINI, G. MODENA, and G. SCORRANO. J. Am. Chem. Soc. **95**, 5960 (1973).
14. G. SCORRANO and G. PERDONCIN. J. Am. Chem. Soc. **99**, 6983 (1977); G. SCORRANO. Acc. Chem. Res. **6**, 132 (1973); D. LANDINI, G. MODENA, G. SCORRANO, and F. TADDEI. J. Am. Chem. Soc. **91**, 6703 (1969).
15. M. LILER. Reaction mechanisms in sulfuric acid. Academic Press, New York. 1971.
16. M. A. PAUL and F. A. LONG. Chem. Rev. **57**, 1 (1957).
17. L. P. HAMMETT. Physical organic chemistry. McGraw-Hill, New York. 1940
18. R. A. COX and K. YATES. Can. J. Chem. **61**, 2225 (1983).
19. M. J. JORGENSON and D. R. HARTTER. J. Am. Chem. Soc. **85**, 878 (1963).
20. W. D. CHANDLER, E. J. LEE, and D. G. LEE. J. Chem. Ed. **64**, 878 (1987).
21. E. PRINCE. Mathematical techniques in crystallography and materials science. Springer-Verlag, New York. 1982. Chapt. 6.

Can. J. Chem. Downloaded from www.nrcresearchpress.com by 91.121.58.235 on 09/07/12
For personal use only.

Rate constants for the addition of the enolate ion of acetone to quinolinium and acridinium cations

JOHN W. BUNTING, CYNTHIA FU,[1] AND JAMES W. TAM[2]

Department of Chemistry, University of Toronto, Toronto, Ont., Canada M5S 1A1

Received February 16, 1990

This paper is dedicated to Professor Ross Stewart on the occasion of his 65th birthday

JOHN W. BUNTING, CYNTHIA FU, and JAMES W. TAM. Can. J. Chem. **68**, 1762 (1990).

The reaction of acetone with four heteroaromatic cations (10-methylacridinium (**1**), 3-aminocarbonyl-1-methylquinolinium (**2***a*), 3-cyano-1-methylquinolinium (**2***b*), and 3-bromo-1-methylquinolinium (**2***c*)) has been investigated in basic aqueous solutions (pH 9–12, ionic strength 0.1, 25°C). For each of **2***a* and **2***b*, the kinetically controlled product is a 35:65 mixture of the C-2 and C-4 enolate ion adducts; the C-2 adduct subsequently isomerizes to give the C-4 adduct as the only observable species under thermodynamic control. For **2***c*, the C-2 enolate adduct appears to be favoured both kinetically and thermodynamically. Under kinetic control, the pH-dependence of adduct formation from each cation is consistent with rate-determining attack of the enolate ion upon the heterocyclic cation. Comparisons of regiochemical control of acetone enolate ion attack with hydroxide ion attack upon these same cations indicate that acetone enolate ion shows a more pronounced preference for C-4 attack over C-2 attack than does hydroxide ion. The thermodynamically controlled regiochemistry is similar for each of these two nucleophiles.

Key words: nucleophilic addition, regioselectivity, kinetic control, thermodynamic control, quinolinium cations.

JOHN W. BUNTING, CYNTHIA FU et JAMES W. TAM. Can. J. Chem. **68**, 1762 (1990).

Opérant dans des solutions aqueuses basiques (pH de 9 à 12, force ionique de 0,1 et température de 25°C), on a examiné la réaction de l'acétone avec quatre cations hétéroaromatiques (10-méthylacridinium (**1**), 3-aminocarbonyl-1-méthylquinolinium (**2***a*), 3-cyano-1-méthylquinolinium (**2***b*) et 3-bromo-1-méthylquinolinium (**2***c*)). Pour les cations **2***a* ainsi que **2***b*, le produit de contrôle cinétique est un mélange 35:65 des adduits des ions énolates C-2 et C-4; l'adduit C-2 s'isomérise ultérieurement pour donner l'adduit C-4, la seule espèce observée sous contrôle thermodynamique. Pour le cation **2***c*, il semble que l'adduit énolate C-2 est favorisé tant d'un point de vue cinétique que thermodynamique. Sous contrôle cinétique, la relation entre le pH et la nature de l'adduit qui se forme à partir de chaque cation est en accord avec une étape déterminant la vitesse de la réaction qui implique l'attaque de l'ion énolate sur le cation hétérocyclique. Des comparaisons du contrôle régiochimique de l'attaque de ces cations par l'ion énolate de l'acétone avec celui de l'attaque par l'ion hydroxyde permet de montrer que, par comparaison avec ce qui est observé avec l'ion hydroxyde, l'ion énolate de l'acétone offre une nette préférence pour une attaque en C-4 plutôt qu'en C-2. Sous contrôle thermodynamique, la régiochimie des réactions de ces deux nucléophiles est très semblable.

Mots clés : addition nucléophile, régiosélectivité, contrôle cinétique, contrôle thermodynamique, cations quinolinium.

[Traduit par la revue]

Can. J. Chem. Downloaded from www.nrcresearchpress.com by 91.121.58.235 on 09/07/12
For personal use only.

The addition of carbanionic nucleophiles to cationic heteroaromatic species is commonly used as a synthetic method for the introduction of side chains onto heterocyclic rings (1–5). Such additions to quinolinium cations are influenced by the usual C-2 vs. C-4 regiochemical considerations that complicate all such nucleophilic additions to these cations. Substituent effects, and considerations of kinetic and thermodynamic control, also constrain attempts to reliably predict the regiochemical outcomes of such processes. Quantitative investigations (6) of the addition of hydroxide ion to quinolinium cations in aqueous solutions have clarified these latter considerations for this one nucleophile. However, the general applicability of the results for hydroxide ion to other nucleophilic species remains an area of uncertainty.

We have demonstrated (7) that the rates and equilibria for the addition of the enolate ion of acetone to the 2-methyl-5-nitroisoquinolinium cation can be readily measured in aqueous solution. As a follow up, we have now investigated the addition of this nucleophile to the 10-methylacridinium cation (**1**) and also to several C-3 substituted 1-methylquinolinium cations (**2**). These data allow the first quantitative insight into many of the regiochemical considerations mentioned above for the reaction of a carbanionic nucleophile with quinolinium cations. In addition, these data, together with our earlier studies, provide further insight into the relative reactivities of acridinium, quinolinium, and isoquinolinium cations in their reactions with nucleophilic addends.

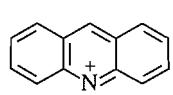

1

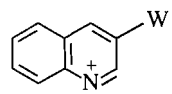

2*a*: W = $CONH_2$
b: W = CN
c: W = Br

Experimental

Bromide salts of the *N*-methyl quinolinium cations (**2**.Br^-) and 10-methylacridinium chloride (**1**.Cl^-) were available from earlier studies in our laboratories (6, 8). Acetone was HPLC Grade (99.9 + %) supplied by Aldrich Chemical Co. Buffer solutions were prepared using $NaHCO_3/Na_2CO_3$ for pH 9.0–10.8 and standard solutions of KOH adjusted to ionic strength 0.1 with KCl for pH ≥ 11.0. The pH values of all solutions were measured at the end of each kinetic run with a Radiometer PHM82 pH meter equipped with a GK2401B combination electrode.

All kinetic studies were done in buffered aqueous solutions of ionic strength 0.1 at 25°C. All reactions were followed spectrophotometrically under pseudo-first-order conditions on a Varian Cary 210 spectrophotometer, with digitized absorbance data being recorded on a Commodore 4048 computer. Data were collected for at least 95%

[1]Recipient of a 1988 NSERC Summer Bursary for Undergraduate Research.

[2]Recipient of a 1985 NSERC Summer Bursary for Undergraduate Research.

of each reaction, and were accurately first-order for at least three half-times. Pseudo-first-order rate constants were calculated by fitting the absorbance (A) at time (t) to the relationship:

$$A = A_f + (A_i - A_f) \exp(-k_{obs}t)$$

via the Marquardt algorithm, treating the initial absorbance (A_i), the final absorbance (A_f), and the pseudo-first-order rate constant as parameters to be evaluated. Data at each pH were collected for at least five acetone concentrations in the range 0.09–0.50 M. Analytical wavelengths and concentrations used for kinetic studies on each cation were: **1** — 420 nm, 0.17 mM; **2***a* — 355 nm, 0.060 mM; **2***b* — 345 nm, 0.05 mM; **2***c* — 370 nm, 0.40 mM.

Results

*10-Methylacridinium cation (**1**)*

We have isolated a colourless oil upon prolonged treatment of an aqueous solution (pH 8.5) of 10-methylacridinium chloride with a large excess of acetone. This product displayed an ^{1}H nmr spectrum that is consistent with the structure of the adduct (**3**) from the addition of the enolate ion of acetone to C-9 of the 10-methylacridinium cation: δ 1.87 (s, 3H, CH_3CO), 2.64 (d, J = 7 Hz, 2H, CH_2), 3.40 (s, 3H, N-CH_3), 4.42 (t, J = 7 Hz, 1H, C(9)—H), 6.7–7.4 (m, 8H, aromatic H) (in $CDCl_3$). The electronic absorption spectrum of this product showed an intense maximum at 284 nm (log ε = 4.09) (in acetonitrile) which is similar to the spectrum of related 9,10-dihydroacridine derivatives (9–11); e.g., 9,10-dihydroacridine, itself, has λ_{max} = 289 nm (log ε = 4.14) (in ethanol (9)).

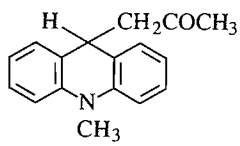

3

The conversion of the 10-methylacridinium cation into its acetone adduct could be conveniently monitored from the time-dependence of the characteristic absorption spectrum of this cation in the range 320–450 nm. The spectrum of this cation in the presence of a large excess of acetone gradually decayed in the vicinity of pH 9–10, and was replaced by an intense increase in absorption in the vicinity of 290 nm. The strong background absorption from the relatively high concentrations of acetone required in these experiments prevented the direct observation of the absorption maximum of the adduct produced. The time-dependence of the absorbance at 420 nm proved to be cleanly first-order in acridinium cation concentration. Pseudo-first-order rate constants (k_{obs}) were evaluated at a number of acetone concentrations in the range 0.1–0.5 M at pH 9.13, 9.57, and 10.12. In less basic solutions, the addition reaction became too slow for convenient rate measurements, while experiments in more basic solutions were precluded by the competition from C-9 pseudobase formation by hydroxide ion addition to the 10-methylacridinium cation (pK_{R^+} = 10.01 at 25°C, ionic strength 0.1 (12)).

The pseudo-first-order rate constants proved to be linear in acetone concentration with ordinate intercepts being zero within experimental error. Apparent second-order rate constants (k_f), calculated from the slopes of k_{obs} vs. [acetone], are given in Table 1.

*3-Aminocarbonyl-1-methylquinolinium cation (**2**a)*

The electronic absorption spectrum of this cation in aqueous base (pH 9–12) undergoes a dramatic time-dependent change in the presence of acetone (0.05–0.5 M). The major observation is the growth of an absorption maximum at 348 nm which is accompanied by a much less intense shoulder in the vicinity of 410 nm. This long wavelength absorbance eventually reaches a maximum value having an apparent extinction coefficient of ≈1000, which is independent of both pH and acetone concentration. At this stage, the apparent extinction coefficient at λ_{max} = 348 nm is ≈10000. The shoulder near 410 nm subsequently disappears in a much slower process, and this change is accompanied by a further intensifying of the absorption maximum at 348 nm which approaches a final ε ≈ 15000.

We have investigated the rates of the initial reaction described above as a function of both pH and acetone concentration, but have not attempted a quantitative investigation of the second, much slower, reaction in the present work. The rate of initial increase in absorbance at 348 nm proved to be cleanly first-order in quinolinium cation concentration. Pseudo-first-order rate constants were linear in acetone concentration with ordinate intercepts that were experimentally indistinguishable from zero. Second-order rate constants (k_f) were evaluated from the slopes of such plots, and are included in Table 1 at various pH.

Several 3-aminocarbonyl-1,4-dihydroquinolines have been well characterized and in general have intense absorption maxima in the vicinity of 340 nm (13–17); for instance, 3-aminocarbonyl-1-benzyl-1,4-dihydroquinoline has λ_{max} = 343 nm (ε = 13100) in water (15). The assignment of the product species displaying λ_{max} = 348 nm (ε ≈ 15000) as the adduct (**4**) that is formed by the addition of the enolate ion of acetone to C-4 of **2***a* appears quite reasonable. The shoulder appearing near 410 nm is most likely due to the presence of the isomeric C-2 adduct (**5**). We have been unable to locate a well characterized example of a 3-aminocarbonyl-1,2-dihydroquinoline in the literature for comparison, however it is known that related 3-ethoxycarbonyl- and 3-cyano-1,2-dihydroquino-

TABLE 1. Apparent second-order rate constants (k_f) for the reaction of acetone with acridinium and quinolinium cations[a]

Cation	pH	k_f (M^{-1} s^{-1})	k_d (s^{-1})
1	9.13	$3.6(\pm0.1)\times10^{-4}$	
	9.57	$5.4(\pm0.4)\times10^{-4}$	
	10.12	$14.3(\pm0.5)\times10^{-4}$	
2*a*	9.31	$2.8(\pm0.3)\times10^{-4}$	
	9.85	$9.0(\pm0.5)\times10^{-4}$	
	10.31	$2.7(\pm0.3)\times10^{-3}$	
	10.72	$8.7(\pm0.5)\times10^{-3}$	
	11.49	$4.9(\pm0.4)\times10^{-2}$	
2*b*	9.35	$3.2(\pm0.2)\times10^{-3}$	
	9.84	$4.3(\pm0.2)\times10^{-3}$	
	10.32	$5.0(\pm0.2)\times10^{-3}$	
	10.58	$4.9(\pm0.2)\times10^{-3}$	
	11.48	$4.8(\pm0.2)\times10^{-3}$	
2*c*	9.92	$4.5(\pm0.5)\times10^{-3}$	$4.2(\pm0.1)\times10^{-3}$
	10.21	$9.1(\pm0.5)\times10^{-3}$	$4.4(\pm0.2)\times10^{-3}$
	10.83	$2.4(\pm0.2)\times10^{-2}$	$4.4(\pm0.4)\times10^{-3}$
	11.31	$7.7(\pm0.4)\times10^{-2}$	
	12.18	$0.17(\pm0.01)$	

[a]In aqueous solution at 25°C, ionic strength 0.1. k_f and k_d are defined by eq. [1]. Missing values of k_d indicate that $k_d \ll k_f$[acetone] in these experiments.

Can. J. Chem. Downloaded from www.nrcresearchpress.com by 91.121.58.235 on 09/07/12
For personal use only.

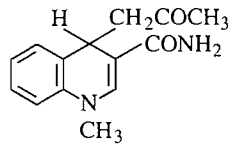

4

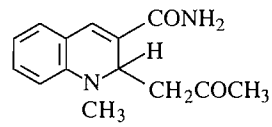

5

lines do display absorption maxima in the 400–420 nm range (13, 18).

3-Cyano-1-methylquinolinium cation (2b)

In basic aqueous solutions, this cation exists in equilibrium with a mixture of its C-2 and C-4 pseudobases, with the C-4 hydroxide adduct (λ_{max} = 304 nm) predominating in a 26:1 ratio over its C-2 isomer (6). Addition of acetone to basic solutions (pH 8–11) of this cation produces a species which has maximum absorbance at 402 nm. The increasing concentration of this species can be readily followed in successive spectrophotometric scans (Fig. 1). The absorbance in this region reaches a maximum value with an apparent extinction coefficient ≈ 1000. The intensity of this maximum value is independent of pH and acetone concentration (0.1–0.5 M). At much longer reaction times, this long wavelength absorbance slowly decays. The initial increase in absorbance in the vicinity of 400 nm is accompanied by a significant decrease in the range 300–320 nm, while the following decrease in absorbance near 400 nm is accompanied by an increase in the region 300–320 nm. Unfortunately, the background absorption due to the high concentrations of acetone that are required in these reactions obscures accurate spectral observations in the vicinity of 300 nm.

The long wavelength absorption of λ_{max} = 402 nm is typical of that of a 3-cyano-1,2-dihydroquinoline derivative; for instance, 3-cyano-1,2-dihydro-1-methylquinoline is reported to have λ_{max} = 410 nm in ethanol (13) and 416 nm in 4:1 2-propanol–water (16). We therefore assign the species having λ_{max} = 402 nm as the product (7) of the addition of the acetone enolate ion to C-2 of the 3-cyano-1-methylquinolinium cation. The isomeric 3-cyano-1,4-dihydroquinoline (**6**) is expected to have λ_{max} in the vicinity of 320–330 nm as do related species bearing this same chromophore; e.g. 3-cyano-1,4-dihydroquinoline has λ_{max} = 325 or 327 nm in ethanol (13, 19), while its N-methyl derivative displays λ_{max} = 333 nm in methanol (19) and 334 nm in 4:1 2-propanol–water (18).

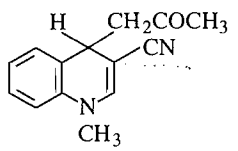

6

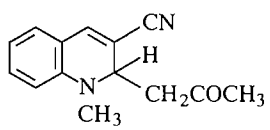

7

Rates of the reaction of acetone with **2***b* were most conveniently monitored at 345 nm. In the presence of excess acetone (0.1–0.5 M), these reactions were strictly first-order in quinolinium cation concentration, and values of k_{obs} and k_f (see Table 1) were evaluated as described above for **2***a*.

3-Bromo-1-methylquinolinium cation (2c)

This cation reacts with acetone in aqueous base to give a product having an absorption maximum near 330 nm. Successive spectral scans of this ongoing reaction show a clean isosbestic point at 333 nm. There is no increase in absorbance in the vicinity of 400 nm as reported above for **2***a* and **2***b*. These

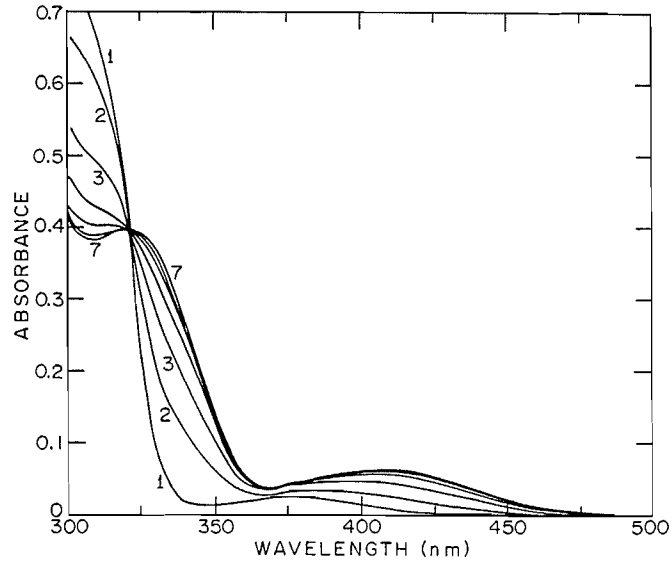

FIG. 1. Time-dependence of the electronic absorption spectrum of **2***b* (0.05 mM) in the presence of acetone (0.55 M) at pH 11.55 (cell path = 1 cm). Curves 1–7 are at 0, 2, 6, 12, 18, 24, and 36 min, respectively after mixing. The subsequent much slower decay of the absorbance in the vicinity of 400 nm is not shown.

observations indicate a simple equilibration of **2***c* with a single acetone enolate adduct in this case. We assign this product as the C-2 adduct (**8**) by analogy with absorption maxima in the range 333–344 nm for other 3-bromo-1,2-dihydroquinolines (6).

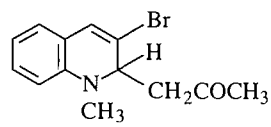

8

The 3-bromo-1-methylquinolinium cation (**2***c*) was unique in the current study in that plots of k_{obs} vs. [acetone] display significant ordinate intercepts at low pH (Fig. 2). Such plots are described by eq. [1]. Values of k_f and k_d for **2***c* are included in Table 1. Cation **2***c* was also the only cation in the current study to display an equilibrium absorbance which increased with both acetone concentration and solution pH. Such observations are consistent with equilibrated solutions of **2***c* with acetone containing significant amounts of both **2***c* and **8**.

$$[1] \quad k_{obs} = k_f[\text{acetone}] + k_d$$

Extensive attempts to characterize the acetone adducts from **2***a*, **2***b*, and **2***c* by ^{1}H nmr spectroscopy were unfruitful. Complex multi-component spectra were obtained both for isolated products, and also for in situ observations (in D_2O + CD_3COCD_3 containing Na_2CO_3), from the reactions of these cations with acetone in aqueous base. The presence of pseudobase species, and also disproportionation products of these pseudobase species, extensively contaminated the acetone adducts from reactions at high concentrations of these quinolinium cations in aqueous base. The presence of time-dependent ratios of the isomeric 1,2-dihydro- and 1,4-dihydro-quinoline acetone adducts, which are indicated by electronic absorption spectroscopy for **2***a* and **2***b*, even further complicates attempts at ^{1}H nmr spectral observations in these systems.

No reaction between acetone and the 1-methylquinolinium cation (**2**: W = H) was observed by electronic absorption

Can. J. Chem. Downloaded from www.nrcresearchpress.com by 91.121.58.235 on 09/07/12
For personal use only.

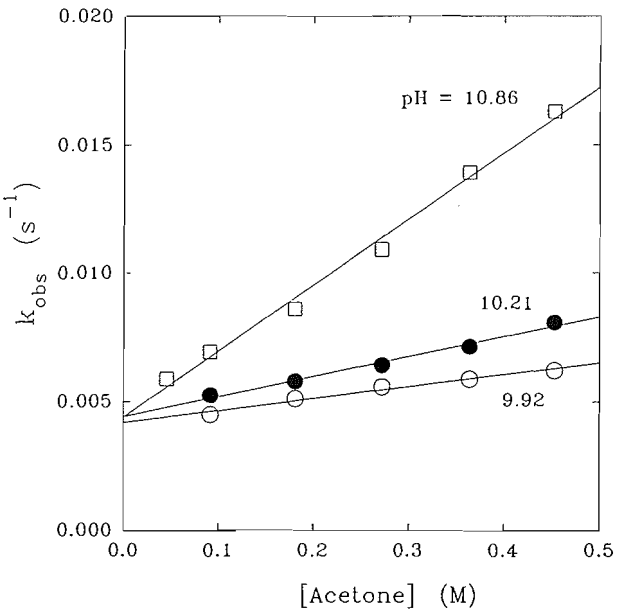

FIG. 2. The dependence of k_{obs} upon acetone concentration for the reaction of **2***c* at various pH (ionic strength 0.1, 25°C).

spectroscopy in basic aqueous solutions. We attribute this result to an unfavourable equilibrium constant under the current experimental conditions.

Discussion

There are many claims in the literature for the isolation of addition products from the reaction of nitrogen heteroaromatic cations with acetone and related carbon acids (20–41). However, there do not seem to have been any attempts to investigate such reactions in a systematic manner, and in cases where isomeric adducts are possible, such as for pyridinium and quinolinium cations, it is usually unclear whether the reported products are obtained under kinetic or thermodynamic control. In such cases, even the structure assignments are sometimes uncertain. We have been unable to locate any report of a quantitative study of rate or equilibrium constants for such reactions, other than our own earlier report (7) for the addition of the acetone enolate ion to the 2-methyl-5-nitroisoquinolinium cation.

The addition of the anionic conjugate bases of many carbon acids to C-9 of acridinium cations has been reported (26, 27). Although we could find no report of the addition of the enolate ion of acetone to the *N*-methyl acridinium cation, the 9,10-dihydroacridine addition products have been isolated from the reaction of the enolate ion of acetophenone and related ketones with this acridinium cation in basic media (27). Interestingly, acetone and many related ketones have been added to acridine, itself, in basic methanol to give 9-substituted 9,10-dihydroacridines in good yield (10, 11). The adduct (**3**) has been isolated in the current work, and was unambiguously characterized by ^{1}H nmr spectroscopy as the product from the reaction of **1** with acetone in aqueous base.

Products have been isolated from the addition of the conjugate bases of many carbon acids to a number of *N*-substituted quinolinium cations (20–22, 25, 28–33). The structures of these products have usually been assumed to be 1,2-dihydroquinolines, although 1,4-dihydroquinoline structures have occasionally been established. The products obtained from the reactions of the *N*-(2,6-dichlorobenzyl) quinolinium cation in basic ethanol have been unambiguously established as the C-2 adduct from the addition of the enolate ion of acetone, but the C-4 adduct from the enolate ion of 4-nitroacetophenone (31). The addition of the enolate ion of acetone to the *N*-methyl quinolinium cation in basic ethanol has been claimed (30) to occur at C-4, however, the reported λ_{max} = 350 nm for this product clearly indicates (42, 43) that it must be a 1,2-dihydroquinoline rather than a 1,4-dihydroquinoline.

We could locate no previous reports of the addition of the conjugate base of a carbon acid to **2***a*, **2***b*, or **2***c*. The C-4 adducts have been isolated from reactions of the conjugate bases of a variety of strongly activated carbon acids with the 1-methyl-3-nitroquinolinium cation (32). It seems likely that these C-4 adducts are the thermodynamic products of these reactions since the C-4 hydroxide adduct of this same cation predominates over its C-2 isomer at equilibrium by 180:1 (6). We have shown above that the electronic absorption spectra of the equilibrium products from the reaction of both **2***a* and **2***b* with acetone enolate ion are predominantly 1,4-dihydroquinolines, and this observation is also consistent with the thermodynamic preference that is found for hydroxide ion addition to these two cations (6). 3-Cyano-1,2-dihydro-1-methylquinoline has also been shown to be thermodynamically less stable than its 1,4-dihydro isomer (18). The C-2 addition of the enolate ion to **2***c* is also similar to the observed thermodynamic preference for hydroxide ion addition at C-2 of the 3-bromoquinolinium cation.

The uv–visible spectral observations for the reactions of each of **2***a* and **2***b* with acetone are consistent with the competitive addition of the enolate ion at C-2 and C-4 under the initial kinetic control, with the C-2 adduct being subsequently slowly converted into its C-4 isomer. The general appearance of the spectra of the kinetic products is somewhat misleading as a guide to the relative amounts of C-2 and C-4 addition products, because of the very large difference in magnitude of the extinction coefficients of these isomeric species. For instance, 3-cyano-1,4-dihydro-1-methylquinoline has ϵ = 12000 at 334 nm whereas its 1,2-dihydroquinoline isomer has ϵ = 2800 at 416 nm (18). Thus the absorption maximum in the vicinity of 400 nm for the 3-substituted 1,2-dihydroquinolines has only about 25% of the intensity of the long wavelength maximum near 350 nm for their 1,4-dihydro isomers.

The observations reported in the Results section allow at least an approximate estimation of the ratio of the concentrations of the C-2 and C-4 adducts from each of **2***a* and **2***b* when the initial addition is complete. This ratio will represent the kinetically controlled product mixture, and can be used as described below to estimate individual rate constants for nucleophilic attack by the enolate ion at C-2 and C-4 from the observed second-order rate constants.

On the assumption that ϵ = 2800 at λ_{max} = 416 nm that was reported (18) for 3-cyano-1-methyl-1,2-dihydroquinoline is typical of the intensity of the long wavelength absorption maximum of such species, we can use $\epsilon \approx 1000$ at λ_{max} = 402 nm to estimate that the kinetically controlled product mixture from **2***b* and acetone contains 35% of the C-2 adduct (**7**) and 65% of the C-4 adduct (**6**). The initial decrease in absorbance that we report in the vicinity of 300–320 nm at the start of this reaction then represents the conversion of some of the predominant C-4 hydroxide adduct of **2***b* into the C-2 acetone adduct. The subsequent increase in absorbance at 300–320 nm that is concomitant with the decay in absorbance at 402 nm then represents the increase in concentration of **6** at

Can. J. Chem. Downloaded from www.nrcresearchpress.com by 91.121.58.235 on 09/07/12
For personal use only.

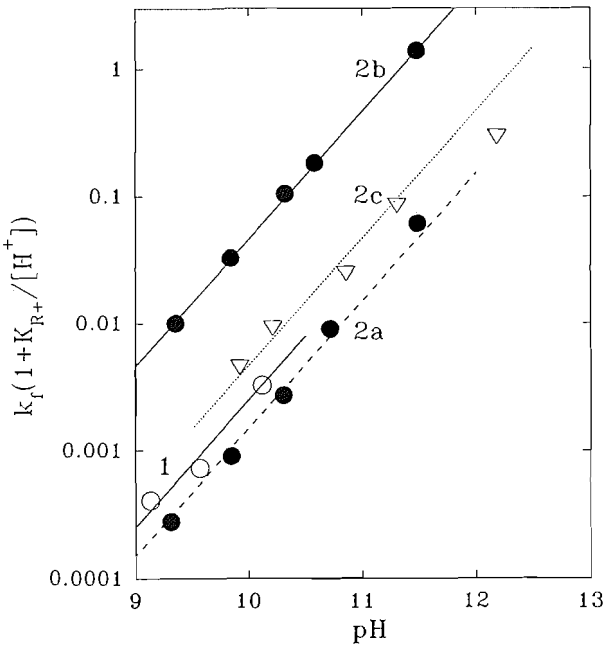

FIG. 3. pH dependence of $k_f(1 + K_{R^+}/[H^+])$ for each of **1**, **2***a*, **2***b*, and **2***c*. Lines are drawn with slope = 1.

the expense of **7** as the final equilibrium mixture is reached. A similar ratio of 35% of the C-2 adduct (**5**) and 65% of **4** in the kinetically controlled product from **2***a* may also be made from the kinetic product and final product absorbances at 348 nm, if it is assumed that **5** does not make a large contribution to the absorbance at this wavelength. We have been unable to locate accurate extinction coefficients for any 3-aminocarbonyl-1,2-dihydroquinolines in the literature. However, this approximate estimate of the product ratio is also supported by the similar intensity of the shoulder at 410 nm in the kinetic product from **2***a* to that of the maximum at 402 nm in the spectrum of the kinetic product from **2***b*.

Kinetic analysis

The equilibration of the cations (R^+) with their acetone enolate ion adducts (RC) can be represented by eq. [2].

[2] $R^+ + CH \rightleftharpoons RC + H^+$

Kinetic studies of all cations, with the exception of **2***c*, were under conditions in which this equilibrium heavily favours the adduct. Under these conditions, the experimentally measured rate constants, k_{obs} and k_f, are defined by eqs. [3] and [4], where ROH is the hydroxide adduct (pseudobase) which is in equilibrium with R^+ in these basic solutions.

$$[3]\quad \frac{d[RC]}{dt} = k_{obs}([R^+] + [ROH])$$

$$[4]\quad = k_f[CH]([R^+] + [ROH])$$

$$[5]\quad = k_f[CH][R^+](1 + K_{R^+}/[H^+])$$

The pH-dependence of the second-order rate constant, k_f, after correction for the presence of ROH, is shown for each cation in Fig. 3. From this figure, it is clear that $k_f(1 + K_{R^+}/[H^+])$ is proportional to hydroxide ion concentration, and eq. [5] can be rewritten as eq. [6]. Values of k_3 were evaluated for each cation from the data in Fig. 3, and are listed in Table 2. The third-order rate constants were converted to second-order rate constants (k_2 in Table 2) for the attack of the enolate ion on the heterocyclic cation according to eq. [7], where $pK_a = 19.16$ for acetone in aqueous solution (44), and K_w is the ionic product of water.

TABLE 2. Values of k_3 and k_2 for the reaction of heterocyclic cations with acetone[a]

Cation	k_3 (M^{-2} s^{-1})	k_2 (M^{-1} s^{-1})
1	25 (±5)	3.6×10^6
2*a*	15 (±3)	2.2×10^6
2*b*	460 (±50)	6.6×10^7
2*c*	47 (±10)	6.8×10^6
9[b]	38	5.5×10^6

[a]In aqueous solution at 25°C, ionic strength 0.1. k_2 and k_3 are defined by eqs. [6] and [7].
[b]Data from ref. 7.

$$[6]\quad \frac{d[RC]}{dt} = k_3[^-OH][CH][R^+]$$

$$= (k_3K_w/K_a)[C^-][R^+]$$

$$[7]\quad = k_2[C^-][R^+]$$

For **2***a* and **2***b*, k_2 is the sum of the individual second-order rate constants for enolate ion attack at C-2 and C-4 to give the kinetically controlled product mixture. For these two cations, k_2 can be apportioned using the ratio of 35% of C-2 adduct to 65% of C-4 adduct that is estimated above for these two cations. The true second-order rate constants (k_{Nu}) for enolate ion attack at individual sites in each of the cations under study are listed in Table 3, along with literature data for the related hydroxide ion reactions, and also data from our earlier study (7) of acetone addition to the 2-methyl-5-nitroisoquinolinium cation (**9**).

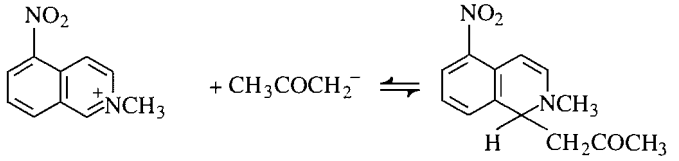

9

The 3-bromo-1-methylquinolinium cation is the only electrophile in the current study for which we were able to observe an equilibrium mixture containing significant amounts of both RC and R^+. In this case the pH-independent (see Table 1) k_d of eq. [1] represents the first-order rate constant for the uncatalyzed expulsion of the enolate ion from adduct **8**. This value $k_d = 0.0043\ s^{-1}$ allows the calculation of the pH-independent equilibrium constant $K_{HNu} = [H^+][RC]/[R^+][CH] = k_2K_a/k_d = 1.1 \times 10^{-10}$ for reaction [2]. The values of k_{Nu}, k_d, and K_{HNu} that are found in the current study for C-2 attack of acetone enolate ion on **2***c*, are all quite similar to the values of these parameters that were found (7) for the same reaction at C-1 of (**9**) ($k_{Nu} = 5.5 \times 10^6\ M^{-1}\ s^{-1}$, $k_d = 1.9 \times 10^{-3}\ s^{-1}$, $K_{HNu} = 2.0 \times 10^{-10}$). These observations seem to be a reflection of the similar pK_{R^+} values for hydroxide ion addition to these two cations ($pK_{R^+} = 12.34$ for **2***c* (6) and 11.7 for **9** (45)).

Table 3 presents detailed comparisons of the rate constants for hydroxide ion and acetone enolate ion attack upon the five heteroaromatic cations for which quantitative data are now available. The k_{Nu}/k_{OH} ratio is similar for C-2 attack in quinolinium cations (**2**) and C-1 attack in the isoquinolinium cation (**9**). We suspect that the somewhat smaller values for this ratio for **2***a* and **2***b* are possibly influenced by steric interactions

Can. J. Chem. Downloaded from www.nrcresearchpress.com by 91.121.58.235 on 09/07/12
For personal use only.

TABLE 3. Second-order rate constants (M^{-1} s^{-1}) for acetone enolate ion and hydroxide ion addition to heteroaromatic cations

	C-4[a]			C-2[b]		
Cation	k_{Nu}	k_{OH}	k_{Nu}/k_{OH}	k_{Nu}	k_{OH}	k_{Nu}/k_{OH}
1	3.6×10^6	550[c]	6500			
2*a*	1.4×10^6	450[d]	3100	7.6×10^5	1.7×10^4[e]	45
2*b*	4.3×10^7	1.6×10^4[d]	2700	2.3×10^7	7.7×10^5[d]	30
2*c*				6.8×10^6	2.8×10^4[e]	240
9[f]				5.5×10^6	4.2×10^4	130

[a]For reaction at C-4 of the quinolinium cations and at C-9 of the acridinium cation.
[b]For reaction at C-2 of the quinolinium cations and at C-1 of the isoquinolinium cation.
[c]From ref. 12.
[d]From ref. 6.
[e]Calculated from $\log k_{OH} = -0.45\ pK_{R^+} + 10.0$ for hydroxide ion attack at C-2 of quinolinium cations (47), using pK_{R^+} data from ref. 6.
[f]Data from ref. 7.

between the enolate ion and the C-3 substituents in **2***a* and **2***b*. Of particular interest are the enhanced k_{Nu}/k_{OH} ratios that are observed for C-4 attack on quinolinium cations and C-9 attack on the acridinium cation in comparison with these ratios for C-2 attack upon the quinolinium cations. This 100-fold enhancement in the relative rates of formation of 1,4-dihydro derivatives when compared with the formation of their 1,2-dihydro isomers is reminiscent, at least qualitatively, of similar rate enhancements for C-4 attack over C-2 attack that are found (16, 46) in the formal hydride transfer from 1,4-dihydronicotinamides to quinolinium cations.

These regiochemical differences in relative rates of hydroxide ion and acetone enolate ion attack upon quinolinium cations are determined by different regioselectivities for these two nucleophiles in the formation of C-2 and C-4 adducts under kinetic control. Whereas reactions of hydroxide ion with **2***a* and **2***b* show approximately a 40-fold preference for C-2 attack over C-4 attack under kinetic control, the nucleophilic attack of the acetone enolate ion upon these two cations occurs approximately twice as fast at C-4 as at C-2. With both nucleophiles, thermodynamic control favours the 1,4-dihydro derivatives from both **2***a* and **2***b*.

Although in principle the acetone enolate ion is an ambident nucleophile, it is clear from the data in Table 3 that the formal oxyanion is unlikely to be able to compete effectively with the carbanionic centre as the attacking nucleophile. In all cases the enolate ion is more reactive than hydroxide ion ($k_{Nu} > k_{OH}$). This observation can only be interpreted as nucleophilic attack by carbon, since the oxyanion of the enolate ion is less basic than hydroxide ion ($pK_a = 10.96$ for the enol of acetone in aqueous solution (44)) and should therefore also be less nucleophilic than hydroxide ion.

The current study provides the first quantitative data of which we are aware for the regiochemical preferences of a carbanion in its nucleophilic addition to quinolinium cations. These data should provide a reasonable guide for the analysis of reactions of related carbanionic species with these cations until such time as a more comprehensive rate and equilibrium analysis of such reactions becomes available.

Acknowledgement

We appreciate the support of this work by the Natural Scienees and Engineering Research Council of Canada.

1. M. N. PATTREYMAN and K. R. H. WOOLDRIDGE. J. Chem. Soc. Perkin Trans. **1**, 57 (1974).
2. M. J. WANNER, G. J. KOOMEN, and U. K. PANDIT. Tetrahedron, **38**, 2741 (1982).
3. M. J. WANNER, G. J. KOOMEN, and U. K. PANDIT. Tetrahedron, **39**, 3673 (1983).
4. E. WENKERT, E. C. ANGELL, J. DREXLER, P. D. R. MOELLER, J. T. PYREK, Y. SHI, M. SULTANA, and Y. D. VANKAR. J. Org. Chem. **51**, 5328 (1986).
5. H. BIERAUGEL, K. M. J. BRANDS, and U. K. PANDIT. Heterocycles, **27**, 1589 (1988).
6. J. W. BUNTING and N. P. FITZGERALD. Can. J. Chem. **62**, 1301 (1984).
7. J. W. BUNTING and J. W. TAM. Can. J. Chem. **64**, 973 (1986).
8. J. W. BUNTING and M. L. LUSCHER. Can. J. Chem. **66**, 2524 (1988).
9. A. ALBERT. The acridines. 2nd ed. Edward Arnold Ltd., London. 1966. p. 200.
10. F. KROHNKE and H. L. HONIG. Liebigs Ann. Chem. **624**, 97 (1959).
11. E. HAYASHI and T. NAKURA. Yakugaku Zasshi, **87**, 570 (1967).
12. J. W. BUNTING and W. G. MEATHREL. Can. J. Chem. **51**, 1965 (1973).
13. Y. KIKUGAWA, M. KURAMOTO, I. SAITO, and S. YAMADA. Chem. Pharm. Bull. **21**, 1914 (1973).
14. J. F. MUNSHI and M. M. JOULLIE. Tetrahedron, **24**, 1923 (1968).
15. S. SHINKAI, H. HAMADA, Y. KUSANO, and O. MANABE. Bull. Chem. Soc. Jpn. **52**, 2600 (1979).
16. J. W. BUNTING and N. P. FITZGERALD. Can. J. Chem. **63**, 655 (1985).
17. T. T. ROMOFF, N. S. SAMPSON, and P. VAN EIKEREN. J. Org. Chem. **52**, 4454 (1987).
18. R. M. G. ROBERTS, D. OSTOVIC, and M. M. KREEVOY. J. Org. Chem. **48**, 2053 (1983).
19. M. FERLES and O. KOCIAN. Coll. Czech. Comm. Commun. **44**, 2238 (1979).
20. N. J. LEONARD, A. A. DE WALT, JR., and G. W. LEUBNER. J. Am. Chem. Soc. **73**, 3325 (1951).
21. N. J. LEONARD and R. L. FOSTER. J. Am. Chem. Soc. **74**, 2110 (1952).
22. N. J. LEONARD and R. L. FOSTER. J. Am. Chem. Soc. **74**, 3671 (1952).
23. F. KROHNKE and K. ELLEGAST. Liebigs Ann. Chem. **600**, 176 (1956).
24. F. KROHNKE and I. VOGT. Liebigs Ann. Chem. **600**, 211 (1956).
25. F. KROHNKE and I. VOGT. Liebigs Ann. Chem. **600**, 228 (1956).
26. O. DIMROTH and R. CRIEGEE. Chem. Ber. **90**, 2207 (1957).

Can. J. Chem. Downloaded from www.nrcresearchpress.com by 91.121.58.235 on 09/07/12
For personal use only.

27. F. KROHNKE and H. L. HONIG. Chem. Ber. **90**, 2215 (1957).
28. F. KROHNKE and I. VOGT. Chem. Ber. **90**, 2227 (1957).
29. H. VON DOBENECK and W. GOLTZSCHE. Chem. Ber. **95**, 1484 (1962).
30. J. METZGER, H. LARIVE, R. DENNILAULER, R. BARALLE, and C. GAURAT. Bull. Soc. Chim. Fr. 30 (1967).
31. H. AHLBRECHT and F. KROHNKE. Liebigs Ann. Chem. **717**, 96 (1968).
32. T. SEVERIN, D. BATZ, and H. LERCHE. Chem. Ber. **101**, 2731 (1968).
33. J. D. BATY, C. MOORE, and G. JONES. J. Org. Chem. **34**, 3295 (1969).
34. J. LUDOWIEG, N. BHACCA, and A. LEVY. Biochem. Biophys. Res. Commun. **14**, 431 (1964).
35. M. I. DOLIN and K. B. JACOBSON. J. Biol. Chem. **239**, 3007 (1964).
36. R. F. OZOLS and G. V. MARINETTI. Biochem. Biophys. Res. Commun. **34**, 712 (1969).
37. R. M. WILSON and F. DININNO, JR. Tetrahedron Lett. 289 (1970).
38. J. EVERSE, E. C. ZOLL, L. KAHAN, and N. O. KAPLAN. Bioorg. Chem. **1**, 207 (1971).
39. L. J. ARNOLD, JR. and N. O. KAPLAN. J. Biol. Chem. **249**, 652 (1974).
40. J. KAVALEK, A. LYCKA, V. MACHACEK, and V. STERBA. Coll. Czech. Chem. Commun. **41**, 67 (1976).
41. S. W. H. DAMJI, C. A. FYFE, D. SMITH, and F. J. SHAROM. J. Org. Chem. **44**, 1761 (1979).
42. W. S. JOHNSON and B. G. BUELL. J. Am. Chem. Soc. **74**, 4517 (1952).
43. J. W. BUNTING and W. G. MEATHREL. Tetrahedron Lett. 133 (1971).
44. Y. CHIANG, A. J. KRESGE, Y. S. TANG, and J. WIRZ. J. Am. Chem. Soc. **106**, 460 (1984).
45. J. W. BUNTING and W. G. MEATHREL. Can. J. Chem. **52**, 972 (1974).
46. J. W. BUNTING and J. L. BOLTON. Tetrahedron, **42**, 1007 (1986).
47. J. W. BUNTING and D. J. NORRIS. J. Am. Chem. Soc. **99**, 1189 (1977).

Can. J. Chem. Downloaded from www.nrcresearchpress.com by 91.121.58.235 on 09/07/12
For personal use only.

Kinetics and mechanism of the bromination of phenols in aqueous solution. Evidence of general base catalysis of bromine attack

OSWALD S. TEE[1] AND N. RANI IYENGAR

Department of Chemistry and Biochemistry, Concordia University, Montreal, P.Q., Canada H3G 1M8

Received April 5, 1990

This paper is dedicated to Professor Ross Stewart on the occasion of his 65th birthday

OSWALD S. TEE and N. RANI IYENGAR. Can. J. Chem. **68**, 1769 (1990).

The reactions of bromine with phenol, 4-bromophenol, and 4-methylphenol (*p*-cresol) in aqueous solution are catalyzed by carboxylate anions, confirming the suggestions of earlier work. The results are consistent with deprotonation of the phenol hydroxyl group by a general base occurring at more or less the same time as electrophilic attack by molecular bromine. Possible origins of the general base catalysis are discussed. Combined with earlier results, the present findings suggest that a *protonated* cyclohexadienone is not a mandatory intermediate in phenol bromination; it can be avoided in both the formation of and enolization of the cyclohexadienone intermediate by general catalysis.

Key words: bromination, phenol, mechanism, catalysis, kinetics.

OSWALD S. TEE et N. RANI IYENGAR. Can. J. Chem. **68**, 1769 (1990).

Les réactions du brome avec le phénol, le 4-bromophénol et le 4-méthylphénol (*p*-crésol), en solution aqueuse, sont catalysées par les anions carboxylates; cette observation confirme les suggestions faites antérieurement. Les résultats sont en accord avec un mécanisme impliquant une déprotonation du groupement hydroxyle du phénol par une base générale qui se produirait pratiquement en même temps que l'attaque électrophile par le brome moléculaire. On discute des origines possible de la catalyse basique générale. Si l'on combine les résultats actuels avec ceux obtenus antérieurement, on peut suggérer qu'une cyclohexadiènone *protonée* n'est pas un intermédiaire nécessaire dans la bromation du phénol; cet intermédiaire peut être évité par la formation et par l'énolisation de l'intermédiaire cyclohexadiènone par une catalyse générale.

Mots clés : bromation, phénol, mécanisme, catalyse, cinétique.

[Traduit par la revue]

Can. J. Chem. Downloaded from www.nrcresearchpress.com by 91.121.58.235 on 09/07/12
For personal use only.

The importance of acid–base catalysis for a large number of reactions occurring in aqueous solution is firmly established (1). Many reactions which are sluggish or non-existent in other media are facilitated by the ease of proton transfers in water, thereby allowing highly unfavorable intermediates to be stabilized or avoided (1, 2). As reported herein, such may be the case with phenol bromination in aqueous solution.

Several recent studies in this laboratory have been concerned with the mechanism of bromination of phenol derivatives in aqueous solution (3–9). Some of these studies dealt mainly with electrophilic bromine attack (3, 4), while others were devoted to the enolization or debromination of transient bromocyclohexadienones (5–9). Three studies, in particular, suggested that bromine attack may be catalyzed by general bases.

Firstly, we found that salicylate (*o*-hydroxybenzoate) anions (**1**) have an enhanced reactivity towards bromine and a reduced selectivity (less negative ρ^+), when compared to analogous, monosubstituted phenols (3*b*). As a result, we argued that the attack of bromine on salicylate anions is intramolecularly catalyzed by their *ortho* carboxylate groups (reaction [1]).

[1] 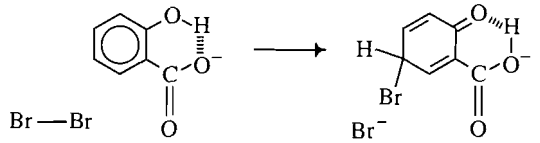

1 **2**

Secondly, it was observed that the bromide ion-induced debromination of labile 4-bromo-4-alkyl-2,5-cyclohexadienones (*ipso*-dienones) (**3**, reaction [2]) is catalyzed by general acids (6). This observation, through the Principles of Microscopic Reversibility and of Detailed Balance (10*a*), implies that the reverse reaction, bromine attack *ipso* to the alkyl group of the *p*-alkylphenol (**4**), is catalyzed by general bases (reaction [2]).

[2] 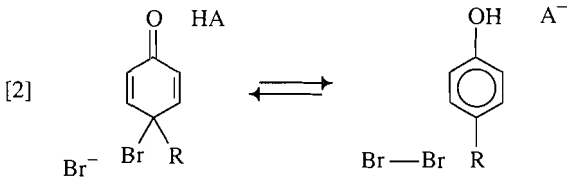

3 **4**

Complementary to these conclusions, we also found that debromination of the *ipso*-dienone **5** by bromide ion is strongly catalyzed by the internal carboxyl group (reaction [3]) (3*b*, 6, 9).[2]

[3] 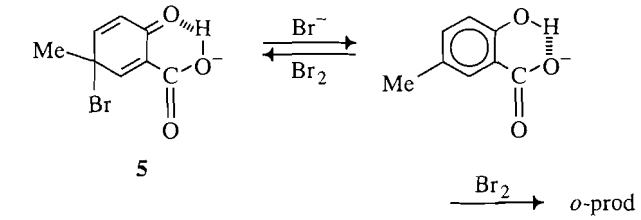

5

Since three, quite distinct studies strongly suggested that the attack of bromine on phenols is catalyzed by general bases, we have looked for buffer catalysis in the aqueous bromination of phenol and two derivatives.

Results

The fast reactions of phenols with bromine in aqueous

[1]Author to whom correspondence may be addressed.

[2]Debrominations of the *ipso*-dienones **3** are also strongly catalyzed by α-cyclodextrin (7), as is that of the salicylate derivative **5** (9). In the latter case, the combination of the two types of catalysis results in an overall rate enhancement of about 12 million (9).

Can. J. Chem. Downloaded from www.nrcresearchpress.com by 91.121.58.235 on 09/07/12
For personal use only.

TABLE 1. Effect of acetate buffer concentration on the rate of bromination of anisole and 2-pyridine[a]

[Buffer], M	k_1^{obsd}, s^{-1}	k_2^{obsd}, M^{-1} s^{-1}
Anisole	(at pH = 4.32)[b]	
0.025	2.10	42 000
0.050	2.14	42 800
0.100	2.09	41 800
2-Pyridine	(at pH = 4.90)[c]	
0.01	1.41	28 200
0.05	1.39	27 800
0.15	1.40	28 000

[a][Substrate]$_0$ = 0.50 mM, [Br_2]$_0$ = 0.05 mM, total I = 1.00 M = NaOAc + NaCl + 0.50 M KBr.
[b]Experiments by J. M. Bennett (cf. ref. 14*b*).
[c]Experiments by B. K. Takasaki (cf. ref. 15).

TABLE 2. Effect of buffers on the rate of the bromination of phenol[a,b]

[Buffer], M		k_1^{obsd}, s^{-1}	
Acetate:	pH = 4.26	4.86	5.36
0.025	28.2	34.7	53.8
0.050	28.7	35.8	57.3
0.075	30.8	38.6	61.0
0.100	32.6	40.7	63.7
Slope (M^{-1} s^{-1}) =	61 ± 9	83 ± 9	134 ± 6
r =	0.9752	0.9878	0.9979
Propionate:	pH = 4.28	4.53	5.06
0.010	25.6	27.1	38.5
0.025	26.8	29.1	39.6
0.050	28.9	31.3	43.2
0.075	31.5	35.3	
0.100	34.1	37.8	50.3
Slope (M^{-1} s^{-1}) =	95 ± 3	120 ± 6	135 ± 7
r =	0.9984	0.9963	0.9971

[a]At 25°C, [phenol]$_0$ = 0.50 mM, [Br_2]$_0$ = 0.05 mM, and total I = 1.00 M = [NaCl] + [buffer salt] + 0.50 M KBr. The "slope" is from a least squares analysis of k_1^{obsd} vs. [buffer], its error is its standard deviation; r is the correlation coefficient.
[b]The data for acetate buffers are presented in Fig. 1. Buffer catalysis was also observed with succinate, methoxyacetate, and chloroacetate buffers.

solution follow second-order rate laws: first-order in substrate and in bromine (3, 4, 11, 12). For the present work rates were measured as the first-order disappearance of bromine, in the presence of an excess of the substrate and a large excess of bromide ion.[3] In some cases observed first-order rate constants (k_1^{obsd}) were converted to second-order constants (k_2^{obsd}), assuming there is no reaction with tribromide ion (13), which is true for phenols but not always true for very reactive phenoxide anions (4). For comparative purposes, we also studied the rates of bromination of anisole (methoxybenzene) and of 2-pyridone, which also show second-order kinetics in their reactions with bromine (14, 15). Depending on the pH of the medium, phenols react with bromine either as such or by way of their anions (3, 4, 11, 12); the same is true of 2-pyridone (15). Therefore, in order to maximise our chances of observing general base catalysis,

[3]The practical reasons for using high concentrations of bromide ion have been given previously (13).

TABLE 3. Effect of buffers on the rate of bromination of 4-methylphenol and 4-bromophenol[a]

Buffer	pH	[Buffer], M	r	Slope, M^{-1} s^{-1}
4-Methylphenol:				
cyanoacetate	2.52	0.025–0.10	0.9997	59 ± 1
chloroacetate	3.11	0.025–0.10	0.9975	51 ± 4
acetate	4.83	0.025–0.10	0.9968	92 ± 5
acetate	5.35	0.025–0.10	0.9998	104 ± 2
4-Bromophenol:[b]				
chloroacetate	2.65	0.050–0.20	0.9822	0.5 ± 0.06
succinate	4.29	0.025–0.10	0.9971	2.6 ± 0.2
acetate	4.85	0.025–0.10	0.9997	20 ± 0.5

[a]As in Table 2.
[b][Substrate]$_0$ = 0.1 mM; [Br_2]$_0$ = 0.01 mM.

we carried out experiments at pHs near the changeover between the two reaction modes (e.g. see Fig. 1, ref. 4*b*).

The rates of bromination of anisole and of 2-pyridone are *not* affected by the concentration of an acetate buffer, at fixed pH (Table 1). In sharp contrast, the values of k_1^{obsd} for the bromination of phenol, 4-methylphenol (*p*-cresol), and 4-bromophenol all show linear dependences on the concentration of several carboxylate buffers (Tables 2 and 3). Some examples are plotted in Fig. 1. Note that the slopes of the plots in Fig. 1 (and Table 2) increase with pH, so that the active form of the buffer is the anion, implying that bromine attack occurs with general base catalysis. From the buffer slopes, and assuming that water functions in the same way, we estimate a Brønsted β (1) of ~0.4 for this catalysis.[4]

Discussion

The absence of any buffer catalysis in the case of the bromination of anisole and of 2-pyridone (Table 1) rules out the possibility that bromine reacts with the buffer anion to produce another, more reactive electrophile. Such has been postulated from time to time in the literature, and has been cited by some textbooks and reviews. In particular, it has been proposed that an acyl hypobromite, formed from bromine and the buffer anion [4], might be the brominating agent.[5] Certainly, on the basis

[4] $RCCO^- + Br_2 \rightleftharpoons RCOOBr + Br^-$

of leaving group abilities, one expects Br—Br to be a much more reactive brominating agent than an acyl hypobromite, RCOO—Br (16).[6]

The bromination of the three phenols studied here (Tables 2 and 3) show catalysis by buffer anions. This is *not* due to the known buffer catalysis of the enolization of bromocyclohexadienone intermediates (5). Under the chosen reaction conditions,

[4]From the slopes in Table 2 the estimated catalytic coefficients are acetate, 185 M^{-1} s^{-1}; propionate, 290 M^{-1} s^{-1}. Converting these to third-order rate constants gives 3.7 × 10^6 and 5.8 × 10^6 M^{-2} s^{-1}, respectively. Using these and a value of 7400 M^{-2} s^{-1} (= 4.1 × 10^5 M^{-1} s^{-1}/55.5 M) for water (4*b*) leads to β ~ 0.43.

[5]The observations which led to such proposals may well have been due to buffer catalysis in a later stage of the reaction. Such is not the case in the present work, as discussed later.

[6]The involvement of the equilibrium [4] is ruled out on other grounds also: it would lead to an inverse dependence on [Br^-], over and above that due to the formation of tribromide ion, which is not observed in any of the large number of brominations that we and others have studied (3, 4, 11, 12, 14–16).

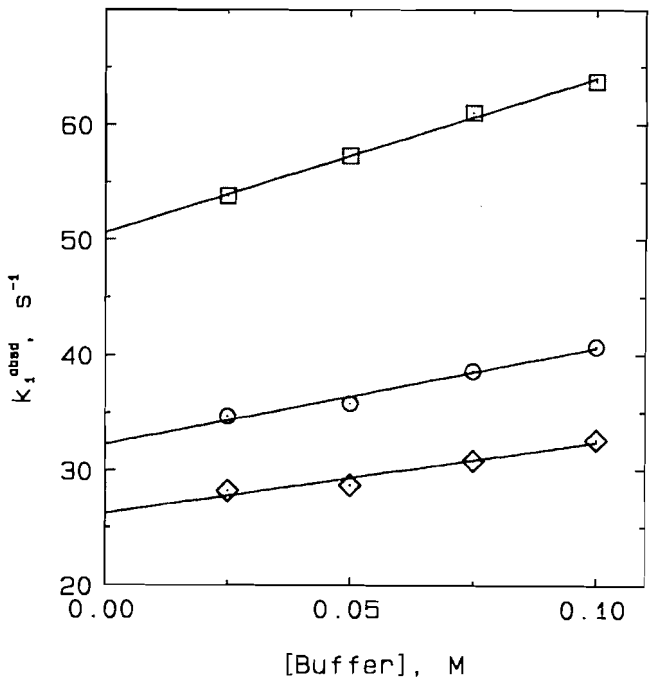

FIG. 1. Effect of acetate buffers on the rate of bromination of phenol. Data taken from Table 2, as follows: diamonds, pH 4.26; circles, pH 4.86; squares, pH 5.36. Note the slopes increase with pH. The intercepts also increase with pH due to the onset of reaction on phenoxide ion (4*b*).

enolization of the intermediate in the *para* bromination of phenol is slower than bromine attack (5), as is debromination of the *ipso*-dienone derived from 4-methylphenol (5–7).[7] In any event, we monitored bromine disappearance at a wavelength longer than that where the enolizations are observable. Further, the Brønsted β values for cyclohexadienone enolization is 0.54 (5*b*), higher than the value of 0.4 suggested by the present data. In the case of 4-bromophenol no cyclohexadienone is observable (5*b*). We conclude, therefore, that the attack of bromine on phenols is subject to general base catalysis, as presaged by earlier work (3*b*, 6, 9).

The simplest interpretation of the anion catalysis is that a general base abstracts the phenolic proton more or less in synchrony with the electrophilic attack by bromine [5]. As to the origins of this catalysis, they probably lie in the instability and high reactivity of potential intermediates (2), such as the bromocyclohexadienone conjugate acid, the phenoxide anion, or the phenol cation-radical.

[5]

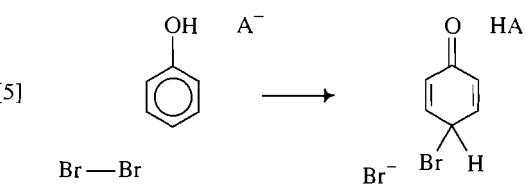

Electrophilic attack by bromine on phenol would lead to the protonated cyclohexadienone ($BrCh{=}OH^+$) [6]. The oxygen-bound proton of this intermediate must be very acidic ($pK_a < -3$ (3*b*, 5*b*)), so that proton transfer to an adjacent water molecule would be favorable and quite fast. If bromine attack took place within an encounter complex (10*b*, 17) also containing a carboxylate anion (A^-),[8] proton transfer would be even more favorable, so much so that it could occur faster than diffusional departure (18) of the bromide ion [7]. In this event,

[6] $Br_2 + Ph{-}OH \rightarrow Br^- + BrCh{=}OH^+ \rightarrow Br^- + BrCh{=}O + H^+(H_2O)$

[7] $\{Br_2.Ph{-}OH.A^-\} \rightarrow \{Br^-.BrCh{=}OH^+.A^-\} \rightarrow \{Br^-.BrCh{=}O.HA\}$

the reaction would exhibit catalysis by the buffer anion.

A possibility which does not involve actual proton transfer is that the protonated dienone and the transition state leading to it are stabilized by the buffer anion through hydrogen-bonding. However, such a mechanism should give rise to a fairly small Brønsted β value 0.1–0.2 (19), smaller than the value suggested by the present data.

A quite different mechanism to that shown in [7] reverses the sequence of bromine attack and proton transfer; it recognizes the high reactivity of Br_2 towards phenoxide ions. The attack of molecular bromine on simple phenoxide ions is diffusion-controlled (3, 4, 11, 12), and so the reaction of Br_2 with the phenoxide ion within the encounter complex $\{Br_2.Ph{-}O^-\}$ must be much faster than diffusional separation of the two reactants ($\sim 10^{10}\ s^{-1}$) (18). Thus, one can imagine that proton transfer within the encounter complex $\{Br_2.Ph{-}OH.A^-\}$

[8] $\{Br_2.Ph{-}OH.A^-\} \rightarrow \{Br_2.Ph{-}O^-.HA\} \rightarrow \{Br^-.BrCh{=}O.HA\}$

leads to a highly reactive ternary complex $\{Br_2.Ph{-}O^-.HA\}$ in which bromine and phenoxide ion react to give Br^- and the bromocyclohexadienone ($BrCh{=}O$) faster than diffusional separation of any of the partners. Estimation of a value of β for this mechanism is difficult since it would be composite, being due to the formation of the initial complex and to the proton transfer step. However, as a referee has rightly pointed out, mechanism [8] should have a positive ρ value (due to the substituent effect on phenol acidity), whereas the observed value is −5.21 (3*a*). Also, for the bromination of salicylate ions, where the proton transfer is intramolecular, ρ is −2.7 (3*b*). These observations strongly militate against the operation of mechanism [8].

In recent years, evidence has been accumulating for the involvement of charge-transfer (CT) complexes in aromatic halogenation carried out in non-aqueous solution (20). From such CT complexes reaction may ensue by single electron transfer (SET) rather than by conventional electrophilic attack, a two-electron process. In the present case, an SET process within the encounter complex formed between Br_2 and phenol would led to the phenol cation-radical.

[9] $\{Br_2.Ph{-}OH\} \rightarrow \{Br^-.Br\cdot.Ph{-}OH\cdot^+\} \rightarrow \{Br^-.BrCh{=}OH^+\}$

Combination of the bromine atom with the cation-radical would give the dienone conjugate acid, $BrCh{=}OH^+$ [9]. However, bearing in mind the high acidity of cation-radicals (21), it is unlikely that the phenol cation-radical would survive very long, particularly adjacent to a buffer anion: thermodynamically favorable proton transfer should be very rapid. If this proton transfer is faster than the Br atom/cation-radical combination, a phenoxy radical will be formed adjacent to the bromine atom;

[7] Thus, in these two cases intermediates build up significantly (5–7). In no cases have the bromocyclohexadienones involved in *ortho* bromination been observed in aqueous solution; apparently, they enolize too rapidly (5–9).

[8] How this ternary encounter complex might arise is considered later.

Can. J. Chem. Downloaded from www.nrcresearchpress.com by 91.121.58.235 on 09/07/12
For personal use only.

these should rapidly combine to give the dienone (BrCh=O), without the prior formation of its conjugate acid. Operation of this mechanism, [10], would also explain the observed buffer catalysis.

[10] $\{Br_2.Ph—OH.A^-\} \rightarrow \{Br^-.Br\cdot.Ph—OH\cdot^+.A^-\}$
$\rightarrow \{Br^-.Br\cdot.Ph—O\cdot.HA\} \rightarrow \{Br^-.BrCh=O.HA\}$

The ternary complex $\{Br_2.Ph—OH.A^-\}$ is implicated in all of the mechanisms outlined above. This complex would most likely arise from the encounter of $Br_2$with a hydrogen-bonded complex of phenol and the buffer anion, [11]:

[11] $Br_2 + Ph—OH + A^- \rightleftharpoons Br_2 + Ph—OH.A^- \rightleftharpoons \{Br_2.Ph—OH.A^-\}$

For the hydrogen-bonded complex between phenol and acetate ion Stahl and Jencks (19) have estimated a formation constant of $0.06\ M^{-1}$ implying very weak hydrogen-bonding. Nevertheless, it could be kinetically significant.

Without much more extensive data from a range of substrates and several buffers distinguishing between the mechanisms for bromine attack (above) is not possible.

Conclusions

The combination of the present findings and those from earlier studies (3–9) provide a reasonably detailed picture of the course of bromination of simple phenols, as it occurs in aqueous solution (Scheme 1).

Previous work has shown that bromocyclohexadienones can be observed in phenol bromination (5–9). The general acid-catalyzed enolization of these intermediates does not appear to involve the dienone conjugate acid (5*b*, 8*a*). If, through general base catalysis, the protonated bromocyclohexadienone is also avoided in bromine attack (*vide supra*), then this putative intermediate is not mandatory in the aqueous bromination of phenol (4*b*).

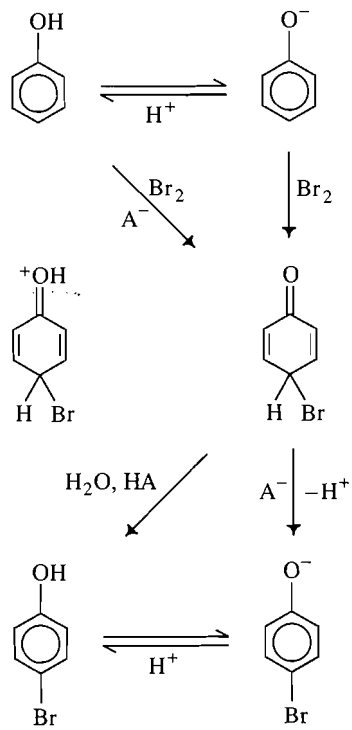

SCHEME 1

Experimental

The phenols used were obtained from commercial sources and purified by distillation or recrystallization, where necessary. All buffer components and inorganic reagents were of the highest purity available. In the main, the procedures for making up solutions and measuring the kinetics followed normal practice (3–9). *Fresh* stock solutions of bromine (0.1 M in 1.0 M aqueous KBr) were made up by weight and then a small volume was diluted with the desired electrolyte solution, just before use. For the phenols stock solutions were prepared in HPLC grade methanol and small volumes of these were diluted with the desired buffer medium. The actual concentrations of the phenols used in the experiments are given in the tables. Final solutions had a total ionic strength of 1.0 M (= [KBr] + [NaCl] + buffer salt).

Rates were measured at 25.0 ± 0.1°C by monitoring the disappearance of bromine using an Aminco-Morrow stopped-flow apparatus + Aminco DW-2 spectrophotometer interfaced to an Apple II microcomputer (22). Normally, bromination reactions are monitored at the tribromide ion maximum at 265 nm (13). In the present case, we used 275 nm to minimize any interference from the enolization of bromocyclohexadienones, which is apparent at shorter wavelengths (5–7).

For a ten (or more)-fold excess of substrate over bromine the absorbance decrease exhibited good first-order behavior. From the traces pseudo first-order rate constants (k_1^{obsd}) were calculated from data covering about 90% reaction. Reported values were the averages of 4–5 determinations. In some cases values of k_1^{obsd} was converted to second-order constants (k_2^{obsd}) by correction for the substrate concentration and the fraction of free bromine in equilibrium with tribromide ion (13). The dissociation constant of tribromide ion was taken as 0.0625 M (I = 1.0 M) (23).

Acknowledgements

The authors thank the Natural Sciences and Engineering Research Council of Canada for an operating grant to O.S.T. and Professor W. P. Jencks for a preprint of ref. 19. The results in Table 1 were obtained by Ms. J. M. Bennett and Mr. B. K. Takasaki.

1. R. STEWART. The proton: applications to organic chemistry. Academic Press, Orlando, FL. 1985; R. P. BELL. The proton in chemistry. 2nd ed. Chapman and Hall, London. 1973; E. CALDIN and V. GOLD. Proton transfer reactions. Chapman and Hall, London. 1975.
2. W. P. JENCKS. Acc. Chem. Res. **9**, 425 (1976); **13**, 161 (1980); Chem. Rev. **72**, 705 (1972); **85**, 511 (1985); J. P. GUTHRIE. J. Am. Chem. Soc. **102**, 5286 (1980).
3. (*a*) O. S. TEE, N. R. IYENGAR, and B. KRAUS. J. Org. Chem. **50**, 973 (1985); (*b*) O. S. TEE and N. R. IYENGAR. J. Org. Chem. **50**, 4468 (1985).
4. (*a*) O. S. TEE and J. M. BENNETT. J. Am. Chem. Soc. **110**, 269 (1988); (*b*) O. S. TEE, M. PAVENTI, and J. M. BENNETT. J. Am. Chem. Soc. **111**, 2233 (1989).
5. O. S. TEE, N. R. IYENGAR, and M. PAVENTI. J. Org. Chem. **48**, 759 (1983); O. S. TEE and N. R. IYENGAR. J. Am. Chem. Soc. **107**, 455 (1985).
6. O. S. TEE, N. R. IYENGAR, and J. M. BENNETT. J. Org. Chem. **51**, 2585 (1986).
7. O. S. TEE and J. M. BENNETT. J. Am. Chem. Soc. **110**, 3226 (1988).
8. (*a*) O. S. TEE and N. R. IYENGAR. Can. J. Chem. **65**, 1714 (1987); (*b*) Can. J. Chem. **66**, 1194 (1988).
9. B. K. TAKASAKI and O. S. TEE. Can. J. Chem. **67**, 193 (1989).
10. K. J. LAIDLER. Chemical kinetics. 3rd ed. Harper and Row, New York. 1987. (*a*) pp. 129, 130; (*b*) pp. 212–222.
11. R. P. BELL and D. J. RAWLINSON. J. Chem. Soc. 63 (1961).
12. J. KULIC and M. VECERA. Collect. Czech. Chem. Commun. **39**, 71 (1974).
13. O. S. TEE and C. G. BERKS. J. Org. Chem. **45**, 830 (1980).

Can. J. Chem. Downloaded from www.nrcresearchpress.com by 91.121.58.235 on 09/07/12
For personal use only.

14. (*a*) J.-J. AARON and J.-E. DUBOIS. Bull. Soc. Chim. Fr. 603 (1971); (*b*) O. S. TEE and J. M. BENNETT. Can. J. Chem. **62**, 1585 (1984).
15. O. S. TEE and M. PAVENTI. J. Am. Chem. Soc. **104**, 4142 (1982).
16. P. B. D. DE LA MARE. Electrophilic halogenation. Cambridge University Press, Cambridge, England, 1976.
17. J. H. RIDD. Adv. Phys. Org. Chem. **16**, 1 (1978).
18. I. AMDUR and G. G. HAMMES. Chemical kinetics. McGraw-Hill, New York. 1966. p. 63.
19. N. STAHL and W. P. JENCKS. J. Am. Chem. Soc. **108**, 4196 (1986).
20. S. FUKUZUMI and J. K. KOCHI. J. Am. Chem. Soc. **103**, 7240 (1981); S. SANKARARAMAN, W. A. HANEY, and J. K. KOCHI. J. Am. Chem. Soc. **109**, 5235 (1987); **109**, 7824 (1987) and references therein.
21. F. G. BORDWELL, J.-P. CHENG, and M. J. BAUSCH. J. Am. Chem. Soc. **110**, 2867 (1988); **110**, 2872 (1988); F. G. BORDWELL and J.-P. CHENG. J. Am. Chem. Soc. **111**, 1792 (1989) and references therein.
22. O. S. TEE, M. TRANI, R. A. MCCLELLAND, and N. E. SEAMAN. J. Am. Chem. Soc. **104**, 7219 (1982); O. S. TEE and B. K. TAKASAKI. Can. J. Chem. **65**, 3540 (1985).
23. G. JONES and S. BAECKSTROM. J. Am. Chem. Soc. **56**, 1517 (1936).

Can. J. Chem. Downloaded from www.nrcresearchpress.com by 91.121.58.235 on 09/07/12
For personal use only.

Kinetics and mechanism of the oxidation of alcohols by ruthenate and perruthenate ions

DONALD G. LEE AND LIGAYA N. CONGSON
Department of Chemistry, University of Regina, Regina, Sask., Canada S4S 0A2

Received February 8, 1990

This paper is dedicated to Professor Ross Stewart on the occasion of his 65th birthday

DONALD G. LEE and LIGAYA N. CONGSON. Can. J. Chem. **68**, 1774 (1990).

In addition to being important synthetic reagents, ruthenate and perruthenate are of interest because they are representative of a number of high valent transition metal ions that can be used as oxidants in organic chemistry. In their reactions with alcohols both ions exhibit several striking similarities — concave Hammett plots, primary deuterium isotope effects, small enthalpies of activation, and large negative entropies of activation. The most likely explanation of the concave upward Hammett plots is the involvement of free radical-like transition states that could be formed by the decomposition of organometallic intermediates.

Key words: oxidation, ruthenate, perruthenate, alcohols, mandelic acid.

DONALD G. LEE et LIGAYA N. CONGSON. Can. J. Chem. **68**, 1774 (1990).

En plus d'être des réactifs de synthèse importants, le ruthénate et le perruthénate présentent de l'intérêt parce qu'ils sont représentatifs d'un certain nombre d'ions de métaux de transition polyvalents qui peuvent être utilisés comme oxydants en chimie organique. Dans leurs réactions avec les alcools, ces deux ions présentent plusieurs similarités frappantes — courbes de Hammett concaves, effets isotopique primaires du deutérium, petites enthalpies d'activation et importantes entropies négatives d'activation. La cause la plus probable de la concavité des courbes de Hammett serait une implication d'états de transition ressemblant à des radicaux libres qui se formeraient par la décomposition d'intermédiaires organométalliques.

Mots clés : oxydation, ruthénate, perruthénate, alcools, acide mandélique.

[Traduit par la revue]

Introduction

Ruthenate (RuO_4^{2-}) and perruthenate (RuO_4^-) ions have both been employed as oxidants in various synthetic procedures. Ruthenate, because it reacts very slowly with carbon–carbon double bonds (1), has found extensive use as a selective oxidant for unsaturated alcohols (2), while perruthenate has been used for the oxidative cleavage of carbon–carbon double bonds (3), the oxidation of secondary alcohols to ketones (4), and the conversion of primary alcohols to carboxylic acids (4). Ruthenate also oxidizes saturated secondary alcohols to ketones in good yields (5). Both ions are stable only under basic conditions (6), thus limiting their use as oxidants to organic compounds that are both stable *and* soluble in aqueous solutions of high pH.

Burke and Healy at one time suggested that ruthenate oxidations actually proceed via perruthenate (7). However, a careful study of the reactions of these two oxy-anions has shown this contention to be false (8). Perruthenate is not involved when ruthenate is used as an oxidant.

In addition to being important synthetic reagents, ruthenate and perruthenate are of interest because of their possible involvement as intermediates in ruthenium tetroxide oxidations and the fact that they are representative of a number of high valent transition metal ions that are used as oxidants in organic chemistry. It is likely that knowledge of the mechanisms of these reactions will also aid in an understanding of the reactions of other more common high valent transition metal oxidants such as permanganate which has been investigated extensively by Stewart and co-workers (9).

Experimental

Reagents and substrates

Sodium ruthenate and perruthenate were prepared by the reduction of ruthenium tetroxide in sodium hydroxide solutions. Sodium perruthenate solutions were obtained when ruthenium tetroxide (prepared by the oxidation of hydrated ruthenium dioxide with periodate (10)) was distilled on a stream of nitrogen into 0.3 M NaOH at 0°C. After standing at 5°C overnight this solution exhibited an absorption spectrum that was identical with that previously reported for sodium perruthenate (11).

Sodium ruthenate was obtained by the reduction of ruthenium tetroxide in 1 M NaOH at 23°C for 24 h. Spectroscopic analysis of the resulting solution showed that it did not contain detectable amounts of either RuO_4 or RuO_4^-.

2-Propanol, obtained commercially, was distilled from calcium oxide and a middle fraction (bp 81–82°C) was collected for use in the kinetic experiments.

2-Propanol-2-*d* was prepared following the procedure of Leo and Westheimer (12). Dry acetone (86 mmol) in 20 mL of anhydrous ether was added dropwise to a stirred solution of lithium aluminum deuteride (25 mmol) in 50 mL of anhydrous ether at −80°C. The mixture was allowed to warm slowly to room temperature and the complex decomposed with dilute sulfuric acid. The heterogeneous reaction mixture was then distilled and an azeotrope of 2-propanol-2-*d* and water collected at 70–90°C. The azeotrope was dissolved in ether, dried over anhydrous magnesium sulfate and after evaporation of the ether, the resulting clear solution was distilled from calcium oxide to give 2-propanol-2-*d* (bp = 81–82°C). The purity of the compound was further verified by means of gas chromatographic analysis and the deuterium incorporation was checked by proton NMR spectroscopy.

THF was refluxed over LAH and fractionally distilled just prior to use. The mandelic acids were obtained commercially and purified by Soxhlet extraction using benzene as the solvent (13). When the hot benzene extract was allowed to cool, crystallization occurred. The product was then collected on a Buchner funnel and air dried. Melting points (14) and NMR spectra were used to verify the purity of these acids. The observed melting points were: *p*-methoxymandelic acid, 108–109°C (lit. 108–111°C); *p*-methylmandelic acid, 139–140°C; mandelic acid, 119–120°C (lit. 120–122°C); mandelic acid-α-*d*, 119–121°C; *p*-fluoromandelic acid, 137–138°C; *p*-chloromandelic acid, 119–120°C (lit. 119–122°C); *p*-bromomandelic acid, 118–120°C (lit. 118–120°C).

Kinetic methods

All kinetic measurements were done under pseudo first order conditions with a substrate concentration at least ten times that of the oxidant. A minimum of three kinetic measurements were performed for each experiment.

The kinetics of the oxidations by sodium perruthenate were studied

Can. J. Chem. Downloaded from www.nrcresearchpress.com by 91.121.58.235 on 09/07/12
For personal use only.

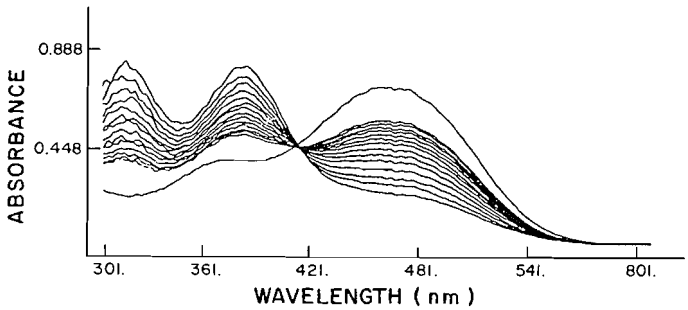

FIG. 1. Sequential scans for the oxidation of 2-propanol by sodium perruthenate. Spectra taken at 30 ms intervals, top to bottom at 385 nm. The lowest trace at this wavelength was obtained about 1 min after completion of the reaction.

using a Tracor Northern System 777 Rapid Scanning Stopped-Flow Spectrophotometer. Stock solutions of RuO_4^- and reductant, both in 0.3 M NaOH, were first thermostated at 25.0°C for 15 min. The sample syringes were then filled, one with perruthenate and the other with reductant solution, and equal volumes of the two reactants forced into the observation cell. Spectra of the reaction solutions were collected at preset intervals (5 to 200 ms), stored in a multichannel analyzer, displayed on a CRT as smooth curves, and recorded as shown in Fig. 1. The reaction rate was followed by monitoring the disappearance of the absorption band at 385 nm ($\epsilon = 2275\ M^{-1}\ cm^{-1}$).

Pseudo first order rate constants were then obtained from plots of $-\ln(A - A_\infty)$ against time (which exhibited good linearity through at least two half lives).

For ruthenate oxidations, stock solutions of RuO_4^{2-} and 2-propanol, THF, or mandelic acid in 1.0 M NaOH were first thermostated at 25°C for 30 min. Then 2.0 mL of the oxidant solution was transferred to a quartz cuvette which was in turn placed in the thermostated cell compartment of the HP 8450A spectrophotometer. An excess of reductant solution (100 μL) was added using a microlitre syringe and the progress of the reaction monitored by following the formation of RuO_2 spectrophotometrically.

Under these conditions it is impossible to directly measure the concentration of ruthenate remaining in solution. However, if the reaction is carried out in a flask and aliquots are centrifuged to remove suspended ruthenium dioxide, a transparent solution of sodium ruthenate is obtained. The concentration of this solution can then be determined by measuring the absorbance at 464 nm ($\epsilon = 1960\ M^{-1}\ cm^{-1}$). A plot of ln (Absorbance) versus time was linear, thus indicating that the reaction is first order in ruthenate.

Measuring the reaction rates by this method is slow, cumbersome, and susceptible to error because the solutions cannot be thermostated during centrifugation. Consequently, the rates of reaction were usually determined by following the increase in absorbance at 320 nm as the reaction progressed. This approach, based on the assumption that the rate of formation of RuO_2 is equal to the rate of disappearance of RuO_4^{2-}, is consistent with previous work which indicated ruthenate is a two-electron oxidant (15). Both kinetic methods gave very similar values for the rate constants.

When the increase in absorbance at 320 nm is monitored, the concentration of ruthenate ion can be calculated using eq. [1], where A is the absorbance at time t, A_∞ is the final absorbance, and $\Delta\epsilon$ is the difference in the extinction coefficients of ruthenium dioxide and ruthenate ion (16).

$$[1] \quad [RuO_4^{2-}] = (A_\infty - A)/\Delta\epsilon$$

The general rate law is then given by eq. [2], or by eq. [3] under pseudo first order conditions.

$$[2] \quad -d(A_\infty - A)/dt = k_2[RuO_4^{2-}]^x[ROH]^y$$

$$[3] \quad -d(A_\infty - A)/dt = k_1[RuO_4^{2-}]^x$$

TABLE 1. Order of perruthenate oxidations with respect to reductants[a]

[Reductant] (M)	k_1 (s^{-1})	k_2 ($M^{-1}\ s^{-1}$)
2-Propanol		
4.64×10^{-3}	1.88 ± 0.04	405 ± 9
1.28×10^{-2}	5.21 ± 0.04	407 ± 3
1.69×10^{-2}	7.14 ± 0.29	422 ± 18
3.39×10^{-2}	13.4 ± 0.4	395 ± 12
Mandelic acid		
4.95×10^{-3}	3.67 ± 0.06	741 ± 12
7.23×10^{-3}	5.49 ± 0.09	759 ± 12
1.03×10^{-2}	7.74 ± 0.09	751 ± 9

[a]Temperature = 25.0 ± 0.1°C, [NaOH] = 0.30 ± 0.01 M.

TABLE 2. Kinetic isotope effects[a]

Reductant	Oxidant	k_2 ($M^{-1}\ s^{-1}$)	k_H/k_D
2-Propanol	Perruthenate	404 ± 11	
2-Propanol-2-*d*	Perruthenate	155 ± 12	2.6 ± 0.3
2-Propanol	Ruthenate	0.11 ± 0.01	
2-Propanol-2-*d*	Ruthenate	0.048 ± 0.004	2.4 ± 0.3

[a]Temperature = 25.0 ± 0.1°C; perruthenate oxidations in 0.31 M NaOH; ruthenate oxidations in 1.02 M NaOH.

Since A_∞ is a constant, the rate, $-d(A_\infty - A)/dt$, is equivalent to dA/dt and the rate law can then be rewritten in its simplest form:

$$[4] \quad dA/dt = k_1[RuO_4^{2-}]^x$$

In order to obtain dA/dt, the absorbance/time data was first fitted to eq. [5] using a program described in a previous publication (17).

$$[5] \quad A = a_0 + a_1t + a_2t^2 + a_3t^3 + a_4t^4 + a_5t^5$$

Differentiation of eq. [5] with respect to time gives eq. [6] from which the initial reaction rate, $(dA/dt)_i$, can be obtained by setting $t = 0$.

$$[6] \quad dA/dt = a_1 + 2a_2t + 3a_3t^2 + 4a_4t^3 + 5a_5t^4$$

Products

Acetone, isolated as the 2,4-dinitrophenylhydrazone, was the only product obtained from the oxidation of 2-propanol. The oxidation of mandelic acid by sodium perruthenate in 0.3 M NaOH or by sodium ruthenate in 1.0 M NaOH gave benzoic acid (isolated by acidification, extraction with ether, and evaporation of the solvent) in 98–99% yields. This result, however, does not preclude the involvement of an intermediate such as phenylglyoxylic acid that would be susceptible to oxidative decarbonylation under these conditions.

Results

Perruthenate oxidations

Linear plots of $-\ln(A - A_\infty)$ against time indicated that these reactions are first order with respect to oxidant. Since the pseudo first order rate constants so obtained are proportional to the concentrations of 2-propanol or mandelic acid (Table 1) it is clear that the reaction is also first order with respect to reductant.

Primary kinetic isotope effects were observed when the rate of oxidation of 2-propanol-2-*d* was compared with the corresponding unlabelled compound (Table 2).

Can. J. Chem. Downloaded from www.nrcresearchpress.com by 91.121.58.235 on 09/07/12
For personal use only.

TABLE 3. Rate constants for the oxidation of substituted mandelic acids by ruthenate and perruthenate ions[a]

Substituent	Oxidant	k_2 (M^{-1} s^{-1})
p-Methoxy	Ruthenate	4.67 ± 0.43
p-Methyl	Ruthenate	3.97 ± 0.53
Hydrogen	Ruthenate	3.65 ± 0.34
p-Fluoro	Ruthenate	3.93 ± 0.22
p-Chloro	Ruthenate	5.85 ± 0.38
p-Bromo	Ruthenate	6.44 ± 0.52
p-Methoxy	Perruthenate	943 ± 24
p-Methyl	Perruthenate	816 ± 7
Hydrogen	Perruthenate	750 ± 14
p-Fluoro	Perruthenate	765 ± 8
p-Chloro	Perruthenate	856 ± 10
p-Bromo	Perruthenate	865 ± 18

[a]Temperature = 25.0 ± 0.1°C; ruthenate oxidations in 1.02 ± 0.01 M NaOH, perruthenate in 0.30 ± 0.01 M NaOH.

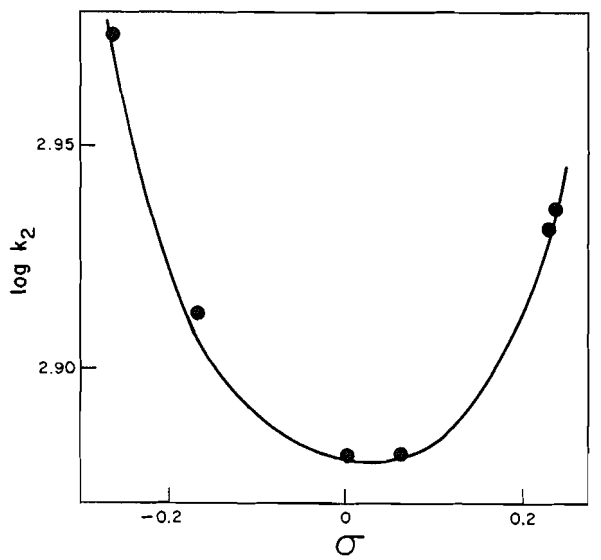

FIG. 2. Hammett plot for the oxidation of substituted mandelic acids by perruthenate. Substituents are (from left to right) *p*-methoxy, *p*-methyl, hydrogen, *p*-fluoro, *p*-chloro, *p*-bromo.

The rate constants for the oxidation of a series of substituted mandelic acids (Table 3) gave a concave Hammett plot (Fig. 2). Activation parameters calculated from plots of ln (k_2/T) against $1/T$, are summarized in Table 4.

Ruthenate oxidations

As indicated by the typical plots in Figs. 3 and 4, the orders of the reaction with respect to oxidant and reductant are both unity.

Primary isotope effects were observed for the oxidation of 2-propanol-2-*d* (Table 2) and the activation parameters were calculated from rate constants obtained at different temperatures (Table 4). A concave Hammett plot was obtained when the rate constants for the oxidation of substituted mandelic acids (Table 3) were plotted against the corresponding σ values (18) as in Fig. 5.

The rate of oxidation of 2-propanol decreases as the basicity of the solution increases (Table 5). This decrease in rate could be a consequence of reaction [10] since it is expected that

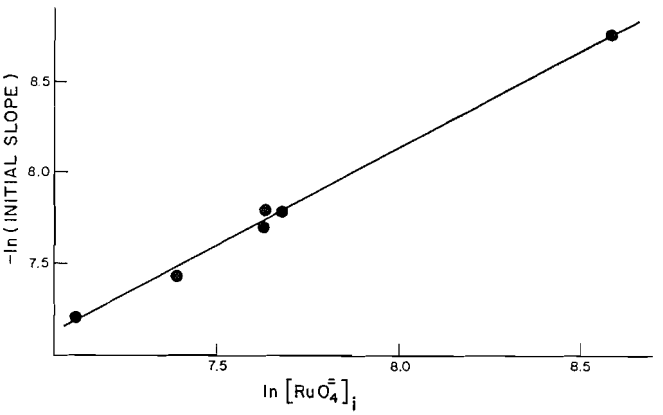

FIG. 3. Determination of the order with respect to ruthenate. [2-Propanol] = 5.15×10^{-3} M; [NaOH] = 1.02 M; T = 25.0 ± 0.1°C; r = 0.999; slope = 1.0.

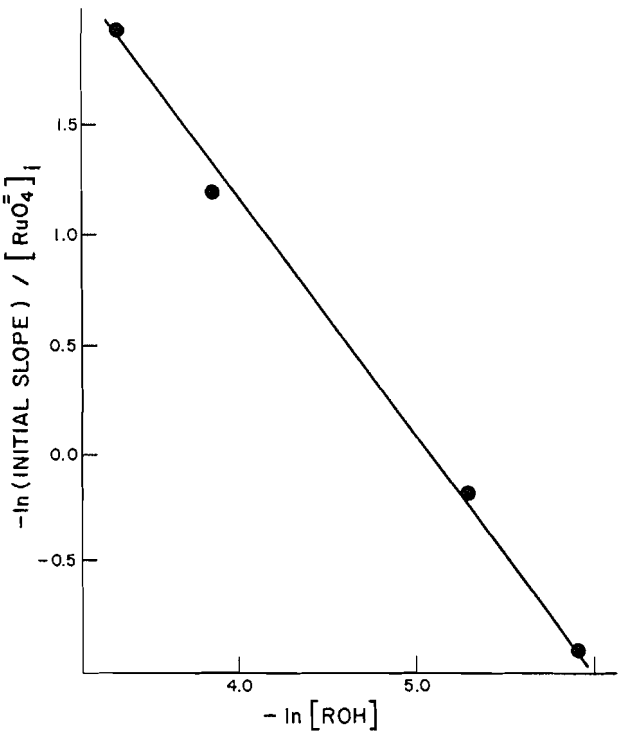

FIG. 4. Determination of the order with respect to 2-propanol for ruthenate oxidations. [NaOH] = 1.02 M; T = 25.0 ± 0.1°C; r = 0.999; slope = 1.0.

hydrogen ruthenate ion ($HRuO_4^-$) would be a more reactive oxidant than ruthenate ion (RuO_4^{2-}) (9, 19).

[10] $HRuO_4^- + OH^- \rightleftharpoons RuO_4^{2-} + H_2O$

Discussion

The reactions of ruthenate and perruthenate exhibit several striking similarities — concave Hammett plots, primary deuterium isotope effects, small enthalpies of activation, and large negative entropies of activation — that suggest some common mechanistic features. However, it must also be remembered that the two reagents give different products with certain substrates. For example, the oxidation of cyclobutanol by ruthenate gives quantitative yields of cyclobutanone, but the use of perruthenate produces only acyclic products (8).

Can. J. Chem. Downloaded from www.nrcresearchpress.com by 91.121.58.235 on 09/07/12
For personal use only.

TABLE 4. Activation parameters

Reductant	Oxidant	$\Delta H^{\ddagger}$ (kcal/mol)	$\Delta S^{\ddagger}$ (eu)	Temperature range (°C)
2-Propanol	Perruthenate	2.0±0.2	−40±1	5–35
2-Propanol	Ruthenate	12.2±0.2	−23±1	15–35
Tetrahydrofuran	Ruthenate	10.9±0.2	−28±2	15–45
Mandelic acid	Perruthenate	0.95±0.02	−42±1	5–40
Mandelic acid	Ruthenate	3.2±0.2	−45±1	10–30

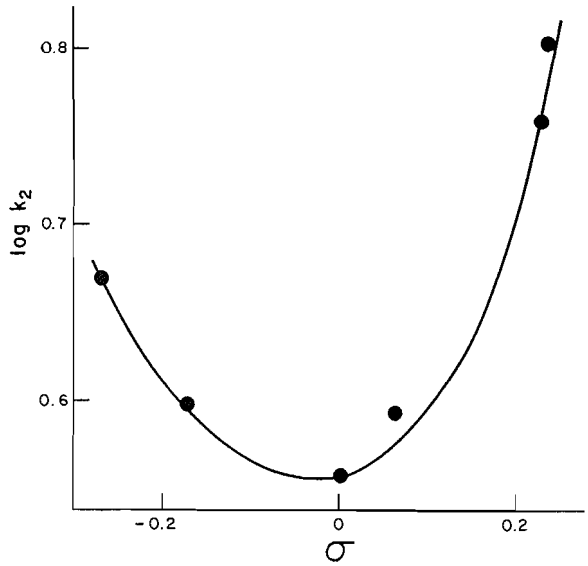

FIG. 5. Hammett plot for the oxidation of substituted mandelic acids by ruthenate. Substituents are (from left to right) *p*-methoxy, *p*-methyl, hydrogen, *p*-fluoro, *p*-chloro, *p*-bromo.

TABLE 5. Effect of basicity on the rate of oxidation of 2-propanol by RuO_4^{2-} [a]

[NaOH] (M)	k_2 (M^{-1} s^{-1})
0.544	0.2291±0.006
1.020	0.0737±0.013
1.075	0.0959±0.011
1.620	0.0753±0.004
2.168	0.0292±0.003

[a] [2-Propanol] = 5.15×10^{-3} M, temperature = 25.0 ± 0.1°C.

Concave upward Hammett plots have previously been observed when the introduction of substituents caused a change in mechanism (20, 21) or when free radicals were formed in the rate-limiting step (20, 22). It may be noted, however, that a change of the rate-limiting step of a multi-step mechanism causes a concave downward Hammett plot and is, therefore, not a possible explanation for the substituent effects observed in these reactions (20, 21).

An explanation based on a change in reaction mechanism would require the oxidants to be ambiphilic — reacting as electrophiles when electron-donating substituents are present and as nucleophiles when electron-withdrawing substituents are present. This seems unlikely, especially in light of the most recent theoretical studies which suggest that all transition metal oxides are electrophiles (23).

The involvement of free radicals seems more likely. It is known, for example, that perruthenate effects single electron-transfer oxidations (8), and free radicals have been detected by use of esr during ruthenium tetroxide oxidations (24). Consequently, the most likely explanation for the concave upward Hammett plots is the formation of free radical-like transition states which can be stabilized by both electron-withdrawing and electron-donating substituents (20, 21).

Ruthenate oxidations

The most direct way in which neutral free radicals could be formed would be by transfer of a hydrogen atom to the oxidant as in reaction [11].

[11] $RCH_2OH + RuO_4^{2-} \rightarrow R\dot{C}HOH + HRuO_4^{2-}$

However, this mechanism, despite its apparent simplicity, is not consistent with recent theoretical predictions. Molecular orbital calculation by Goddard and Rappe' (23) indicate that the reactions between alcohols and transition metal oxides are initiated by an oxidative addition of an O—H or C—H bond to an oxo metal bond (M=O) to give intermediate products as indicated in reactions [12] and [13].

[12] 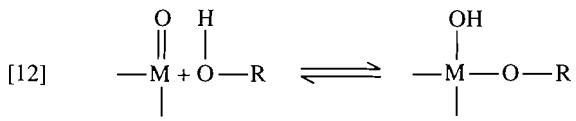

[13] 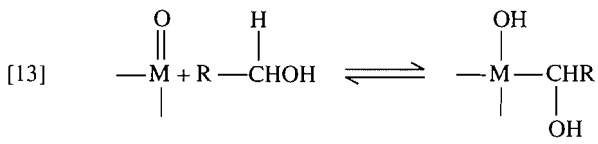

Addition to an O—H bond (as in reaction [12]) leads to formation of esters, intermediates that have been proposed for several reactions, the most well known being the oxidation of alcohols by chromic acid (25).

Addition to a C—H bond (the α-C—H being most reactive) as in reaction [13] leads to formation of an organometallic compound. These intermediates are most likely for those elements that form strong metal–carbon bonds (26).

Fortunately it is possible to experimentally distinguish between the possibilities shown in reactions [12] and [13]. If a reaction occurs by addition to an O—H bond it is expected that the oxidant would not react as readily with ethers as with alcohols. For example, chromic acid reacts about 1500 times faster with isopropyl alcohol than with isopropyl ether (27), thus confirming (along with other evidence (28)) that esters are intermediates in chromic acid oxidations. However, if the reaction proceeds by way of reaction [13] it is to be expected

Can. J. Chem. Downloaded from www.nrcresearchpress.com by 91.121.58.235 on 09/07/12
For personal use only.

that alcohols and ethers would be oxidized with approximately equal ease. Such an observation has been made for ruthenium tetroxide (29) and it is also the case for ruthenate as indicated by the data in Table 4. Consequently, it appears likely that ruthenate reacts with 2-propanol by addition to the α-C—H bond giving the intermediate depicted in reaction [14].

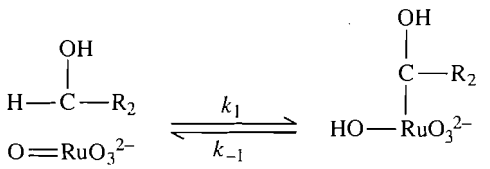

[14]

1

In agreement with these theoretical predictions, Behari *et al.* (30) have shown that the kinetics obtained when cyclohexanol is oxidized by RuO_4^{2-} (using hexacyanoferrate(III) ion as a cooxidant) indicate the reaction mechanism involves formation of an alcohol/RuO_4^{2-} "complex" in a rapid equilibrium step, followed by a rate-limiting decomposition of the complex to give products. Although these authors did not speculate on a possible structure for the intermediate, it seems clear from the aforementioned theoretical calculations that their "complex" is likely the adduct, **1**. A rate-limiting decomposition of this intermediate by homolytic cleavage of the Ru—C bond (reaction [15]) would then be consistent with the observation of a concave Hammett plot.

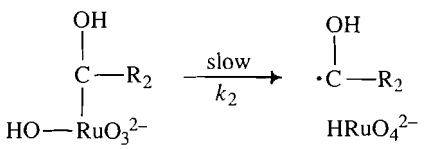

[15]

1

Since the oxo-ruthenium species formed in reaction [15] ($HRuO_4^{2-}$) is in the reactive 5+ oxidation state, a subsequent single electron transfer (reaction [16]) would probably occur before the radical could diffuse out of the solvent cage.

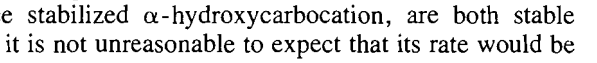

[16]

Because the products of this reaction, ruthenium(IV) and a resonance stabilized α-hydroxycarbocation, are both stable moieties it is not unreasonable to expect that its rate would be rapid.

Deprotonation of the carbocation and hydrolysis of the ruthenium(IV) ion (reactions [17] and [18]) would give the observed products — a ketone and RuO_2.

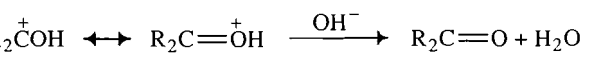

[17]

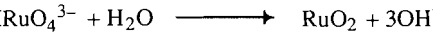

[18]

Application of the steady-state approximation (31) to the intermediate **1** in reactions [14] and [15] indicates why the reaction mechanism would produce an isotope effect in spite of the fact that the α-C—H bond is cleaved prior to the rate-limiting step.

$$[19]\quad -d[RuO_4^{2-}]/dt = k_1[R_2CHOH][RuO_4^{2-}] - k_{-1}[\mathbf{1}]$$

$$[20]\quad = k_1k_2/(k_{-1}+k_2)[R_2CHOH][RuO_4^{2-}]$$

Because the values of the observed rate constant depend directly on the magnitude of k_1 (which would, in turn, be reduced by deuterium substitution at the α-hydrogen) a primary isotope effect results.

The negative entropy of activation, $\Delta S^{\ddagger} = -23 \pm 1$ eu, observed for the oxidation of 2-propanol by ruthenate, indicates that the rate-limiting step, in common with most second order reactions, involves an increase in organization of the transition state as compared to the ground state.

Perruthenate oxidations

A concave Hammett plot suggests that perruthenate oxidations also involve the formation of free radical intermediates which, if the MO calculations of Goddard and Rappe' (23) are correct, would be formed by the homolytic decomposition of the complex **2** as in reactions [21] and [22].

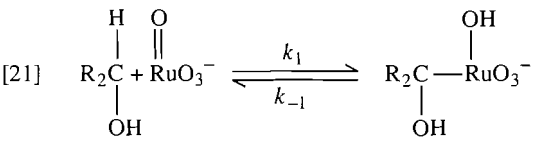

[21]

2

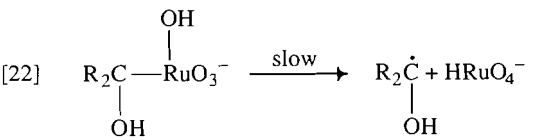

[22]

The very negative entropy of activation for this reaction ($\Delta S^{\ddagger} = -40 \pm 1$ eu) is consistent with a highly organized transition state.

There appears to be one substantial difference between this reaction and the one previously described for ruthenate. Because the hydrogen ruthenate(VI) ion formed in reaction [22] would be less reactive than the hydrogen ruthenate(V) ion formed in reaction [15], it is more likely that the products of reaction [22] will move out of the solvent cage before undergoing further reaction. It is to be expected, therefore, that the radicals will diffuse into the bulk of the solution and undergo further reaction with a second molecule of perruthenate (reaction [23]). Reaction within the solvent cage would undoubtedly result in the eventual formation of RuO_2, a possibility that is not consistent with the experimental evidence.

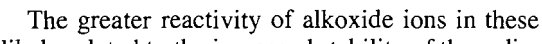

[23]

The greater reactivity of alkoxide ions in these reactions is likely related to the increased stability of the radical anion, **3** in reaction [24], as compared to an uncharged radical (9).

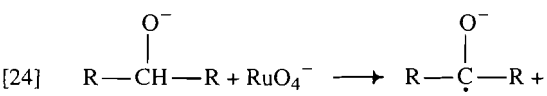

[24]

3

This understanding of the reaction mechanism also accounts for the different products obtained when cyclobutanol is oxidized by ruthenate and perruthenate ions. As indicated in Scheme 1, transfer of a second electron (to the ruthenium(V) ion, $HRuO_4^{2-}$) would likely occur very rapidly when ruthenate is used as an oxidant. Assuming that the free radical never escapes the solvent cage, it is to be expected that the product will be cyclobutanone. However, in the case of perruthenate ion (Scheme 2), transfer of a second electron would be much slower (because of the lower reactivity of $HRuO_4^-$) and the free radical

Can. J. Chem. Downloaded from www.nrcresearchpress.com by 91.121.58.235 on 09/07/12
For personal use only.

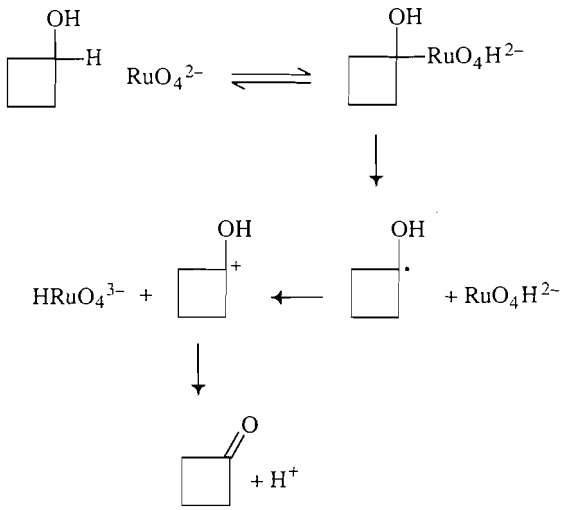

SCHEME 1

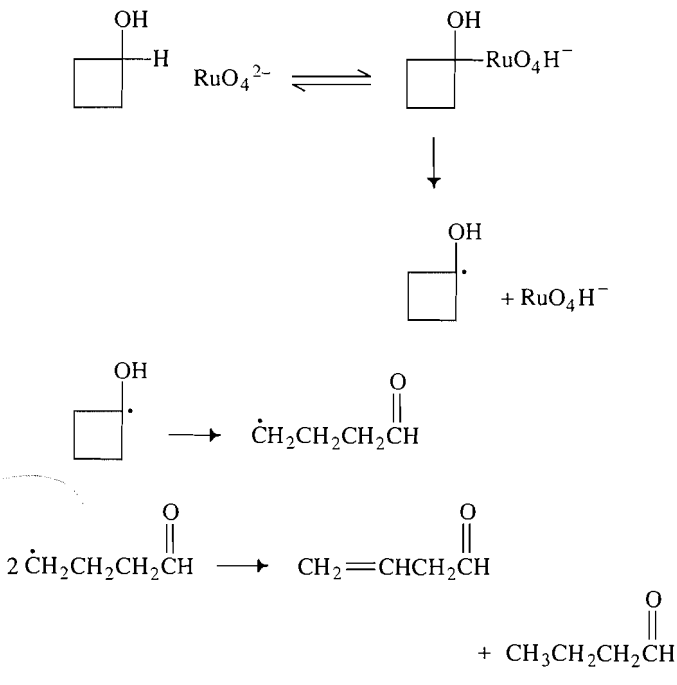

SCHEME 2

could diffuse into the solution and undergo α-scission with the consequent formation of acyclic products (32).

Acknowledgement

The authors are grateful for financial support from the Natural Sciences and Engineering Research Council of Canada.

1. D. G. LEE and S. HELLIWELL. Can. J. Chem. **62**, 1085 (1984).
2. W. G. DAUBEN and A. F. CUNNINGHAM, JR. J. Org. Chem. **48**, 2842 (1983); R. M. COATS, P. D. SENTER, and W. R. BAKER. J. Org. Chem. **47**, 3597 (1982); E. J. COREY, R. L. DANHEISER, S. CHANDRASEKARAN, G. E. KECK, B. GOPALAN, S. D. LARSEN, P. SIRET, and J. L. GRAS. J. Am. Chem. Soc. **100**, 8034 (1978).
3. Y. NAKANO and T. A. FOGLIA. J. Am. Oil Chem. Soc. **59**, 163 (1982).
4. G. GREEN, W. P. GRIFFITH, D. M. HOLLINSHED, S. V. LEVY, and M. SCHRODER. J. Chem. Soc. Perkin Trans. 1, 681 (1984).
5. D. G. LEE, D. T. HALL, and J. H. CLELAND. Can. J. Chem. **50**, 3741 (1972).
6. J. L. HOWE and F. H. MERCER. J. Am. Chem. Soc. **47**, 2926 (1925).
7. L. D. BURKE and J. F. HEALY. J. Chem. Soc. Dalton Trans. 1091 (1982).
8. D. G. LEE, L. N. CONGSON, U. A. SPITZER, and M. E. OLSON. Can. J. Chem. **62**, 1835 (1984).
9. R. STEWART. Oxidation in organic chemistry. Part A. *Edited by* K. B. Wiberg. Academic Press, New York. 1965; R. STEWART. Oxidation mechanisms. W. A. Benjamin, New York. 1964. Chap. 5.
10. D. G. LEE and M. VAN DEN ENGH. *In* Oxidation in organic chemistry. Part B. *Edited by* W. S. Trahanovsky. Academic Press, New York. 1973. p. 177.
11. R. C. CONNICK and C. R. HURLEY. J. Am. Chem. Soc. **74**, 5012 (1952).
12. A. LEO and F. H. WESTHEIMER. J. Am. Chem. Soc. **74**, 4383 (1952).
13. A. VOGEL. A textbook of practical organic chemistry. 4th ed. Longmans, London. 1978. p. 534.
14. Catalog handbook of fine chemicals. Aldrich Chemical Company, Inc. 1990; Organic and inorganic chemicals for research. Pfaltz and Bauer, Inc. 1988.
15. D. G. LEE, U. A. SPITZER, J. CLELAND, and M. E. OLSON. Can. J. Chem. **54**, 2124 (1976).
16. K. B. WIBERG. Physical organic chemistry. Part 3. Wiley, New York. 1964.
17. W. D. CHANDLER, E. J. LEE, and D. G. LEE. J. Chem. Ed. **64**, 878 (1987).
18. J. MARCH. Advanced organic chemistry. 3rd ed. Wiley, New York. p. 244.
19. F. H. WESTHEIMER and A. NOVICK. J. Chem. Phys. **11**, 506 (1943).
20. O. EXNER. Advances in linear free energy relationships. *Edited by* N. B. Chapman and J. Shorter. Plenum Press, New York. 1972. p. 12.
21. D. SCHULTE-FROHLINDE. Ann. Chem. **612**, 138 (1958).
22. J. HINE. Structural effects on equilibria in organic chemistry. Wiley-Interscience, New York. 1975. Chap. 10.
23. A. K. RAPPE' and W. A. GODDARD III. J. Am. Chem. Soc. **104**, 448 (1982); **104**, 3287 (1982).
24. D. C. AYRES and R. GOPALAN. J. Chem. Soc. Chem. Commun. 890 (1976).
25. F. H. WESTHEIMER. Chem. Rev. **45**, 419 (1949).
26. J. P. COLLMAN, L. S. HEGEDUS, J. R. NORTON, and R. G. FINKE. Principles and applications of organotransion metal chemistry. University Science Books, Mill Valley, CA. 1986. p. 100.
27. R. BROWNELL, A. LEO, Y. W. CHANG, and F. H. WESTHEIMER. J. Am. Chem. Soc. **82**, 406 (1960).
28. J. ROCEK, F. H. WESTHEIMER, A. ESCHENMOSER, L. MOLDOVANYI, and J. SCHREIBER. Helv. Chem. Acta, **45**, 2554 (1962).
29. D. G. LEE and M. VAN DEN ENGH. Can. J. Chem. **50**, 2000 (1972); **50**, 3129 (1972).
30. K. BEHARI, H. NARAYAN, R. S. SHUKLA, and K. C. GUPTA. Int. J. Chem. Kinet. **16**, 195 (1984).
31. A. FROST and R. PEARSON. Kinetics and mechanism. Wiley, New York. 1953. p. 172.
32. K. MEYER and J. ROCEK. J. Am. Chem. Soc. **94**, 1209 (1972); J. ROCEK and A. E. RADKOWSKI. J. Am. Chem. Soc. **95**, 7123 (1973); J. ROCEK and D. E. AYLWARD. J. Am. Chem. Soc. **97**, 5452 (1975).

Can. J. Chem. Downloaded from www.nrcresearchpress.com by 91.121.58.235 on 09/07/12
For personal use only.

Stereoelectronic effects in ring closure reactions: the 2′-hydroxychalcone – flavanone equilibrium, and related systems

COLIN M. BRENNAN, IAN HUNT, TERENCE C. JARVIS, C. DAVID JOHNSON,[1] AND PETER D. MCDONNELL
School of Chemical Sciences, University of East Anglia, Norwich, Norfolk, NR4 7TJ, U.K.

Received March 30, 1990

This paper is dedicated to Professor Ross Stewart on the occasion of his 65th birthday

COLIN M. BRENNAN, IAN HUNT, TERENCE C. JARVIS, C. DAVID JOHNSON, and PETER D. MCDONNELL. Can. J. Chem. **68**, 1780 (1990).

The 2′-hydroxychalcone (2-$HOC_6H_4COCH{=}CHC_6H_4X$)–flavanone equilibrium in trifluoroacetic acid (TFA) has been examined. The influence of substituents X on the rate of attainment of equilibrium shows that the 6-*endo*-trig mode of ring closure by Michael addition is disallowed, by demonstrating a negative ρ value for the reaction rate when X is varied. Reaction therefore proceeds either on the carbonyl-protonated form, which allows twisting about the 2,3 bond, its double bond character being reduced by resonance, or through direct rate-limiting protonation on the 2,3 double bond. Either pathway permits the allowed 6-*exo*-trig mode of ring closure to be followed. Alternative mechanisms involving intermolecular Michael addition of trifluoroacetate, followed by intramolecular 6-*exo*-tet displacement are considered. Such Michael adducts can be detected in the ring closures of 2-crotonyl-4-methylphenol and 4,4-dimethyl-1-(2-hydroxyphenyl)-2-penten-1-one in TFA, but they do not appear to lie on the main pathway, because the reactions proceed with equal facility in methanesulphonic acid/chloroform medium, which does not contain a suitable nucleophile for such a mechanism. Further important mechanistic information is given by studying the reactions in TFA-*d*, together with measurements on the (*E*)-2-methyl-3-oxo-5-arylpent-4-en-2-ol and 3′-methoxychalcone systems. These isotope effect studies, which yield k_H/k_D values of about 3, indicate that the proton is in flight during the rate-limiting step, and provide evidence against the mechanism involving a preequilibrium carbonyl protonation, such as in the Nazarov rearrangement of 3′-methoxychalcones, where k_H/k_D is ca. 0.7. Some results are also reported for ring closure of the 2-aminochalcones in TFA.

Key words: 2′-hydroxychalcones, flavanones, 3′methoxychalcones, 3-aryl-6-methoxyindanones, 2′-aminochalcones, 2-aryl-1, 2, 3, 4-tetrahydroquinolines, Baldwin's rules.

COLIN M. BRENNAN, IAN HUNT, TERENCE C. JARVIS, C. DAVID JOHNSON et PETER D. MCDONNELL. Can. J. Chem. **68**, 1780 (1990).

On a étudié l'équilibre de la 2′-hydroxychalcone (2-$HOC_6H_4COCH{=}CHC_6H_4X$)–flavone dans l'acide trifluoroacétique (TFA). L'influence des substituants X sur le temps qu'il faut pour atteindre l'équilibre, exprimée par la valeur négative de ρ sur la vitesse de la réaction, démontre que le mode 6-*endo*-trig de fermeture du cycle par addition de Michael n'est pas permis. La réaction se produit donc soit par une attaque sur la forme protonée du carbonyle, qui permet une torsion autour de la liaison 2,3 puisque son caractère de liaison double est réduit par résonance, soit par une protonation directe de la double liaison 2,3 qui limite la vitesse. On considère aussi d'autres mécanismes impliquant une addition de Michael intramoléculaire de l'ion trifluoroacétate, suivie par des déplacements 6-*exo*-tet. On peut détecter de tels adduits de Michael dans les cyclisations du 2-crotonyl-4-méthylphénol et de la 4,4-diméthyl-1-(2-hydroxyphényl)-2-pentèn-1-one dans l'acide TFA; toutefois, ils ne semblent pas faire partie du mécanisme principal puisque les réactions se produisent avec une facilité similaire dans un milieu comme l'acide méthanesulfonique/chloroforme qui ne contient pas de nucléophile susceptible de participer à un tel mécanisme. On a obtenu d'autres informations importantes d'un point de vue mécanistique en étudiant les réactions dans le TFA-*d* et en faisant des mesures sur les systèmes (*E*)-2-méthyl-3-oxo-5-aryl pent-4-ène-2-ol et 3′-méthoxychalcone. Ces études d'effets isotopiques, qui nous permettent d'évaluer le k_H/k_D à environ 3, indiquent que le proton se déplace au cours de l'étape qui détermine la vitesse de la réaction; ces données s'opposent à un mécanisme impliquant un prééquilibre pour la protonation du carbonyle puisque dans la transposition de Nazarov des 3′-méthoxychalcones k_H/k_D = environ 0,7. On rapporte aussi quelques données relatives à la cyclisation des 2-aminochalcones dans l'acide TFA.

Mots clés : 2′-hydroxychalcones, flavanones, 3′-méthoxychalcones, 3-aryl-6-méthoxyindanones, 2′-aminochalcones, 2-aryl-1,2,3,4-tétrahydroquinolines, règles de Baldwin.

[Traduit par la revue]

Introduction

Baldwin's rules offer assistance to the rationalisation of organic synthesis (1). As an added bonus, they also provide valuable signposts to important perspectives in physical and mechanistic organic chemistry, and it is this aspect of the rules that has taken our attention (2–6). Experiments on (*E*)-2-methyl-3-oxo-5-phenylpent-4-en-2-ol and its phenyl substituted derivatives **1** were interpreted as showing that the ring closure to give 2,2-dimethyl-5-aryltetrahydro-3-furanone **2** in TFA proceeds via the protonation form **3**, in which the double bond character of the 4,5 linkage is reduced by the participation of canonical form **4** in the resonance hybrid. This permits more facile twisting to allow the 5-*exo*-trig mode to occur (2, 4, 7). Such a process can be detected by a "reverse substituent effect" (2, 4), in which the usual role of electron-withdrawing groups (EWG's) substituted in the phenyl ring of compounds (2–6), in accelerating the rate of reaction for a Michael addition, is not observed. Instead, a reverse effect, whereby electron-donating substitutents (EDG's) speed the reaction, is found.

According to Baldwin's rules, 6-*endo*-trig reactions are allowed (8), but are slower than the corresponding *exo* process when a choice is available (9). In such a critical case, the "allowedness" of the 6-*endo*-trig reaction may be further reduced by the nature of the connection between the two reacting centres.

A suitable case to investigate this situation appears to be the biologically important (10, 11) 2′-hydroxychalcone **5** – flavanone **6** system. Here models reveal the hydroxyl group to be

[1]Author to whom correspondence may be addressed.

Printed in Canada / Imprimé au Canada

Can. J. Chem. Downloaded from www.nrcresearchpress.com by 91.121.58.235 on 09/07/12
For personal use only.

TABLE 1. Rate constants for ring closure of 2′-hydroxychalcones **5** in TFA and TFA-*d* at 35°C

Substrate (X)	Solvent	[**6**]/[**5**][a]	$10^6 k_{obs}$[b] (s^{-1})	$10^6 k_f$[b] (s^{-1})	$10^6 k_r$[b] (s^{-1})	r[c]	k_H/k_D[d]
5*a* (H)	TFA	5.6	1.92±0.07	1.63	0.29	0.995	2.2
	TFA-*d*	3.5	0.95±0.03	0.74	0.21	0.997	
5*b* (*p*-OCH_3)	TFA	7.1	269±6	236	33.1	0.994	3.4
	TFA-*d*	4.6	83.6±4	68.7	14.9	0.985	
5*c* (*p*-CH_3)	TFA	6.1	8.14±0.24	6.99	1.15	0.997	3.3
	TFA-*d*	3.8	2.72±0.38	2.15	0.567	0.996	
5*d* (*p*-Cl)	TFA	7.2	0.72±0.11	0.628	0.087	0.973	2.2
	TFA-*d*	4.7	0.35±0.01	0.289	0.061	0.981	

[a]At equilibrium.
[b]k_{obs}, observed rate constant; k_f, forward reaction rate constant; k_r, backward reaction rate constant.
[c]Correlation coefficient.
[d]k_f(TFA)/k_f(TFA-*d*).

well off-line for a 109° approach of its lone pairs in the plane of the *p*-orbitals of the double bond, the optimum trajectory for the fastest reaction (12). This arises, in part at least, from the increased bond angle of the sp^2 hybridised connecting chain compared to that of a chain of sp^3 hybridised carbons, and must be accentuated by the tendency of conjugated systems to stay in plane.

Results and discussion

Table 1 gives the results of rate and equilibrium studies on the 2-hydroxychalcone **5** – flavanone **6** system in TFA and TFA-*d*, and Table 2 gives the corresponding results for ring closure of compounds **1** in TFA and TFA-*d*.

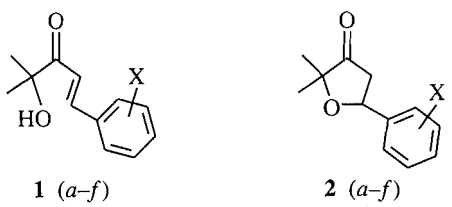

1 (*a–f*) **2** (*a–f*)

a X = H *d* X = *m*-CH
b X = *p*-OCH_3 *e* X = *p*-Cl
c X = *p*-CH *f* X = *m*-Cl

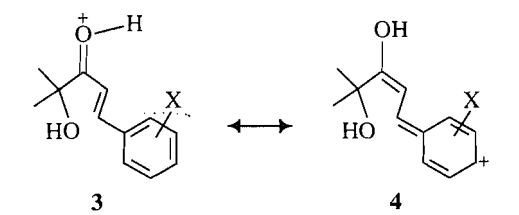

3 **4**

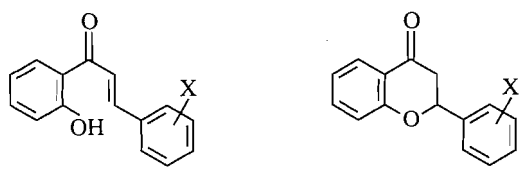

5 (*a–j*) **6** (*a–j*)

a X = H *f* X = *p*-CN
b X = *p*-OCH_3 *g* X = *m*-OCH_3
c X = *p*-CH_3 *h* X = *m*-CH_3
d X = *p*-Cl *i* X = *m*-Cl
e X = *p*-F *j* X = *m*-F

The logarithmic rates for the ring closure of compounds **5** using log k_{obs} values give the ρ value of −2.55 against σ^+ values[2] (correlation coefficient 0.991). Measurements on a more extended series (**5***a–j*) give ρ = −2.43 (0.963). Plots using log k_f give essentially the same result. Thus in this latter case ρ becomes −2.42 (0.960). The similar size and sign of ρ to that for the closures of **1** in the same media suggest that the two systems go via the same mechanism, i.e., through *exo* closure onto the protonated forms **3** and **7** utilising canonical forms **4** and **8**. A complicating factor in our studies of compounds **1** was the reversible formation of trifluoroesters (4). With the phenolic hydroxy group in compounds **5**, however, no such esterification can be seen.

Another possible mechanism involves the nucleophilic attack of trifluoroacetic acid on protonated systems **3** and **7**, in an intermolecular Michael type addition, to yield **9** and **10** followed by *exo*-tet displacement to give the ring-closed products. The substituent effect for such a process would be expected to be positive if the attack of the nucleophile is rate determining, but the possibility exists that this step might be fast, and the subsequent displacement the slow step. Examination of the nmr spectra used to determine the rates of conversion of **1** to **2** and **5** to **6** showed no indication of any buildup of detectable quantities of **9** or **10**. Moreover, we found that the initial nmr spectra of 2′-methoxychalcone, 2′-methoxy-4-methylchalone, and 2′,4-dimethoxychalcone in TFA, indicative of these compounds, remained unchanged over several weeks: no evidence for formation of double bond addition compounds could be seen. We were, however, able to show that aliphatic derivatives **11** did give, in TFA, appreciable amounts of such adducts, judging from the appearance of the nmr spectra as they changed with time. A relevant spectrum is shown in Fig. 1. It was thus necessary to find out if such adducts could lie on the reaction pathway. We therefore examined the reactions in a 3% v/v solution of methanesulfonic acid in $CDCl_3$. These results are recorded in Table 3. This solution contains a weaker nucleophile than TFA. If no reaction occurred, a reasonable assumption might be that the nucleophilic addition–displacement mechanism did particpate to a significant or predominant extent in TFA. If, however, the rates were not significantly reduced, this fact, together with the substituent effect observed, would serve to suggest the absence of such a mechanism to any significant degree. Comparison of the results given in Tables 1 and 2 with

[2]All substituent constants were taken from ref. 13.

Can. J. Chem. Downloaded from www.nrcresearchpress.com by 91.121.58.235 on 09/07/12
For personal use only.

TABLE 2. Rate constants for ring closure of (*E*)-2-methyl-3-oxo-5-aryl pent-4-en-2-ols **1** in TFA and TFA-*d* at 35°C

Substrate (X)	Solvent	[2]/[1][a]	$10^6 k_{obs}$[b](s^{-1})	$10^6 k_f$[b](s^{-1})	$10^6 k_r$[b](s^{-1})	r[c]	k_H/k_D[d]
1*a* (H)	TFA	3.6	7.94±1.07	6.20	1.74	0.985	3.7
	TFA-*d*	2.1	2.46±0.27	1.67	0.79	0.983	
1*b*(*p*-OCH_3)	TFA	2.1	488±18	331	157	0.994	4.3
	TFA-*d*	1.7	125±4	77.8	47.2	0.982	
1*c* (*p*-CH_3)	TFA	2.5	35.0±4.0	24.9	10.1	0.976	4.2
	TFA-*d*	1.8	9.32±0.88	5.94	3.38	0.976	
1*d* (*m*-CH_3)	TFA	3.2	12.4±0.13	9.48	2.95	1.000	2.9
	TFA-*d*	1.9	5.02±0.08	3.32	1.71	1.000	

[a,b,c,d]See footnotes to Table 1.

those in Table 3 show that in the $MeSO_3H$ medium, the rates observed are very similar to those in TFA and, further, that in both media EDG's X accelerate the reaction.

We therefore consider it unlikely that the intermolecular nucleophilic addition pathway plays a large part in the overall mechanism. A further mechanistic variation must also be considered as a possibility. In this, protonation occurs directly on the carbon–carbon double bond conjugated with the carbonyl group

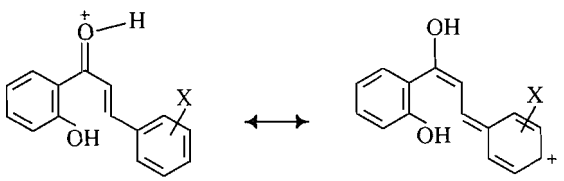

7 ⟷ **8**

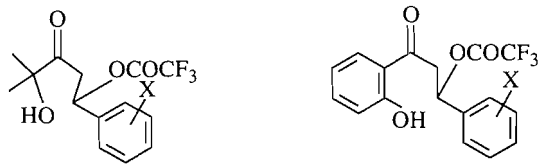

9 **10**

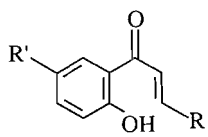

11 *a* R = R' = CH_3 *b* R = $C(CH_3)_3$, R' = H

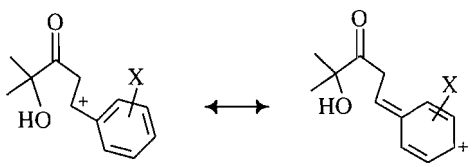

12 ⟷ **13**

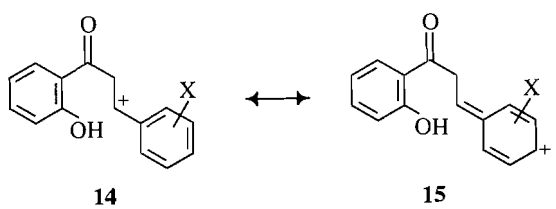

14 ⟷ **15**

in structures **1** and **5** to give the carbocations **12**↔**13** and **14**↔**15**, which are tautomers of carbonyl protonated forms **3** and **7** respectively. To shed some light on this possibility, we measured the solvent kinetic isotope effect (SKIE) observed in going from TFA to TFA-*d* as solvent. The results are given in Table 1. We do not believe that the variation of k_H/k_D is experimentally significant (see discussion of errors in the experimental section), but the values are considerably greater than unity, and in the range that suggests the proton is in flight in the rate-limiting step. Similarly, SKIE values have been reported for rate-limiting proton addition to CC double and triple bonds (6, 14), and these suggest the predominant mechanism is the rate-limiting protonation of the carbon–carbon double bond.

The alternative mechanism involving a preequilibrium protonation on the carbonyl group is predicted to have a value of k_H/k_D of less than unity (15–18). The situation in TFA has not been experimentally verified, however, and to our knowledge results confirming this are not readily found in the literature. We therefore examined the solvent isotope effect on the TFA-catalysed rates of ring closure reaction of 3′-methoxychalcones **16** to give 1-indanones **17**, a reaction believed to go via an electrocyclic Nazarov reaction initiated by a preequilibrium carbonyl protonation (19, 20). The results are given in Table 4. The logarithmic rates afford a ρ value of −0.7 using σ^+ values, and the k_H/k_D values are all consistently less than unity. This supports the notion that if compounds **1**, **5**, and **11** had cyclised in TFA by a preequilibrium protonation at the carbonyl group, k_H/k_D would also be less than unity. We therefore favour a mechanism for ring closure of these compounds in which the proton is in flight in the rate-limiting step, that is, rate-determining protonation of the carbon–carbon double bond. Usually, however, ρ values for such reactions are much more negative than the −2.4 observed for cyclisation of **1** and **5**; values observed are usually about double this for acid-catalysed hydration involving rate-limiting proton transfer to CC double or triple bonds (6, 21). It may be that in these cases the attack of the intramolecular nucleophile commences before carbocation formation is complete, so that it intrudes to a certain extent in the rate-limiting step, and therefore the substituents are not called upon to stabilise the positive charge to the same extent that they are in the case of intermolecular attack.

We also investigated the ring closure of 2′-aminochalcones **18** to 2-aryl-1,2,3,4-tetrahydroquinolines **19**, which appears to be a closely analogous case to the 2′-hydroxychalcone ring closure. The pseudo-first-order rate constants ($k/10^{-6}$ s^{-1}) were as follows: **18***a*, 25; **18***b*, 41; **18***c*, 127; **18***d*, 4.9. The final nmr spectrum in all cases showed no indication of residual 2′-aminochalcone. Cyclisation of **18***e* was observed in TFA, but the nmr was complicated by the formation of what appeared to

Can. J. Chem. Downloaded from www.nrcresearchpress.com by 91.121.58.235 on 09/07/12
For personal use only.

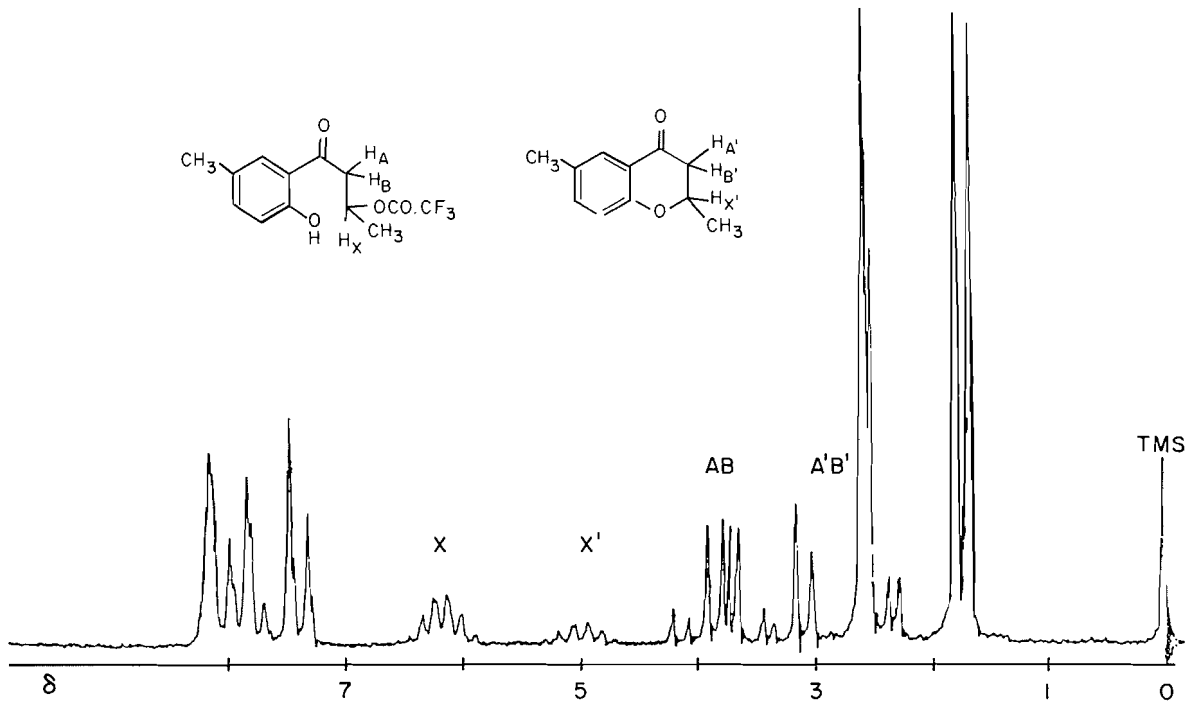

FIG. 1. The nmr spectrum of **11***a* in TFA at 35°C, 9 h after preparation of the solution. X and AB refer to the ABX pattern of the TFA adduct of **11***a*; X′ and AB′ to the ABX pattern of the ring closed product from **11***a*.

TABLE 3. Rate constants for ring closures of **5**, **1**, and **11** in 3% $MeSO_3H/CDCl_3$ at 35°C

Substrate (X or R and R′)	[RC]/[RO][a]	10^6k_{obs}[b](s^{-1})	10^6k_f[b](s^{-1})	10^6k_r[b](s^{-1})	r[c]
5*b* (OCH_3)	2.5	195±50	139	55.6	0.995
5*c* (CH_3)	1.2	10.6±0.2	5.85	4.75	0.999
1*b* (OCH_3)	2.6	1490±30	1080	414	0.991
1*c* (CH_3)	3.9	103±8	82.4	21.0	0.989
11*a* (CH_3, CH_3)		22.2 ± 2.1			0.995
11*b* ^{t}Bu, H)		11.9±1.5			0.985

[a][Ring Closed form]/[Ring Open form].
[b,c]See footnotes to Table 1.

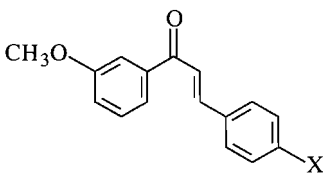

16 (*a–e*)

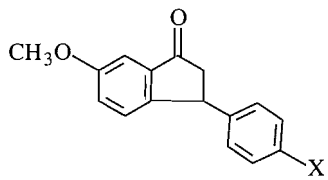

17 (*a–e*)

a X = H
b X = CH_3
c X = OCH_3
d X = Cl
e X = NO_2

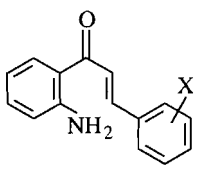

18 (*a–e*)

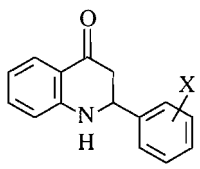

19 (*a–e*)

a X = H
b X = *p*-CH_3
c X = *p*-OCH_3
d X = *m*-Br
e X = *p*-NO_2

TABLE 4. Rate constants for Nazarov ring closures of 3′-methoxychalcones **16**→**17** in TFA and TFA-*d* at 35°C

Substrate (X)	Solvent	10^6k(s^{-1})	r	k_H/k_D
16*a* (H)	TFA	2.19±0.25	0.994	0.73
	TFA-*d*	3.01±0.28	0.990	
16*b* (CH_3)	TFA	3.57±0.27	0.989	0.78
	TFA-*d*	4.55±0.35	0.989	
16*c* (OCH_3)	TFA	8[a]		0.8
	TFA-*d*	10[a]		
16*d* (Cl)	TFA	1.93±0.18	0.982	0.71
	TFA-*d*	2.73±0.20	0.992	
16*e* (NO_2)	TFA	0.57±0.03	0.993	0.88
	TFA-*d*	0.65±0.03	0.992	

[a]Only approximate due to overlap of H_A and H_B protons of ABX system of indanone **17***c* with the methoxy peak; some side reactions also observed.

be a TFA adduct. These rate constants give a ρ value of −2.1 against σ^+, but the SKIE found by measuring rates for **18***b* and **18***d* in TFA-*d* was in both cases indistinguishable from unity. One has here the added complication that the majority species in TFA is protonated on the amino nitrogen, so that the situation is

Can. J. Chem. Downloaded from www.nrcresearchpress.com by 91.121.58.235 on 09/07/12
For personal use only.

TABLE 5. Treatment of data for the ring closure of 2′-hydroxy-4-methoxychalcone (**5***b*) in TFA at 35°C

				Normalised figures					
				X		AB		ln([*C*] − [C_∞])	
t (min)	X (mm)	AB (mm)	Me (mm)	*C*[a]	*F*[b]	*C*[a]	*F*[b]	X	AB
15	2	6	50	0.880	0.120	0.820	0.180	−0.273	−0.355
25	5	11	58	0.741	0.259	0.716	0.284	−0.475	−0.516
38	10.5	20	79	0.601	0.399	0.620	0.380	−0.730	−0.691
45	13	24	85	0.541	0.459	0.576	0.424	−0.863	−0.783
55	18	35	95	0.432	0.568	0.447	0.553	−1.162	−1.115
60	19	36	96	0.406	0.594	0.437	0.563	−1.248	−1.146
70	21	38	101	0.376	0.624	0.436	0.564	−1.359	−1.149
80	16	31	74	0.351	0.649	0.372	0.628	−1.461	−1.374
85	16	31	73	0.342	0.658	0.363	0.637	−1.501	−1.411
90	17	33	75	0.320	0.680	0.340	0.660	−1.605	−1.510
95	18	35	76	0.289	0.711	0.329	0.671	−1.772	−1.561
100	19	36	80	0.287	0.713	0.315	0.675	−1.784	−1.580
105	20	37	81	0.259	0.741	0.315	0.685	−1.966	−1.630
110	14	26	55	0.236	0.764	0.291	0.709	−2.146	−1.760
115	14	26	54	0.222	0.778	0.278	0.772	−2.273	−1.839

Xk = 310 × 10^{-6} s^{-1} (0.992);[c] AB k = 241 × 10^{-6} s^{-1} (0.992)[c]

[a]*C* represents the mole fraction of chalcone at time *t*.
[b]*F* represents the mole fraction of flavanone at time *t*.
[c]Correlation coefficient for plot of ln([*C*] − [C_∞]) against *t*.

more complex than that for the 2′-hydroxychalcone–flavanone system: we are in the course of further experimental investigations, and full details will be reported later.

The ring closure of **5** and **18** in TFA to give flavanones and 2-aryl-1,2,3,4-tetrahydroquinolines respectively appears to be a good method for the preparation of such compounds in reasonable yields (22). We are currently preparing a paper to describe these synthetic routes in detail.

Conclusion

The evidence presented here makes it seem more likely that ring closure of **1** and **5** involves rate-limiting protonation at carbon rather than a carbonyl preequilibrium protonation. In other words the reaction proceeds via **12** and **14** rather than through the alternative tautomeric systems **3** and **7**, respectively. The extent to which these systems eschew the intramolecular Michael addition on the majority species free base forms **1** and **5** because of operation of Baldwin's rules is a matter for debate: base catalysis might be very different (11), and Baldwin's rules could be more important here.

Experimental

TFA and TFA-*d* were reagent grade and used as received. Proton nmr spectra were recorded on a Perkin–Elmer R12 60-MHz instrument. Methanesulphonic acid was dried and distilled as described by Schofield and co-workers (23). (*E*)-2-Methyl-3-oxo-5-arylpent-4-en-2-ols were prepared as described previously (4).

2′-Hydroxy-, 2′-methoxy-, and 2′-aminochalcones were prepared by condensation of 2-hydroxy-, 2-methoxy-, or 2-aminoacetophenone with the appropriately substituted benzaldehydes in aqueous ethanolic sodium hydroxide. 3′-Methoxychalcones were prepared in the same manner using 3-methoxy acetophenone. Melting points agreed with literature values.

Flavonones were prepared in good yield by refluxing the appropriate 2′-hydroxychalcone in TFA, evaporating the bulk of the solvent under vacuum, chromatographing the residue on alumina, and recrystallising. 2-Aryl-1,2,3,4-tetrahydroquinolin-4-ones and 6-methoxy-3-arylindan-1-ones were prepared similarly. Melting points agreed with literature values. Where the compounds had not been prepared before (**6***c*, **6***g*, **6***h*, **17***b*, **17***c*, **17***d*, and **17***e*, **18***b–e*, **19***b–e*), satisfactory elemental analyses were obtained (22). These procedures form an efficient mode of synthesis of these compounds, in reasonable to high yields, and their description will form a further publication.

2-Crotonyl-4-methylphenol **11***a* was prepared by the procedure of von Auwers and Lammerhirt (24), which involves a Friedel–Crafts reaction between *p*-methylanisole and crotonyl chloride.

4,4-Dimethyl-1-(2-hydroxyphenyl)-2-penten-1-one **11***b*: Pivaldehyde (4.31 g, 50 mmol) was added to a solution of *o*-hydroxyacetophenone (6.8 g, 50 mmol) in dry THF (20 mL) under nitrogen, and then, portionwise, sodium hydride (4.0 g, 60% dispersion in mineral oil, washed with hexane, 100 mmol). The mixture was stirred at room temperature for 36 h, acidified to pH 3 with 5% v/v hydrochloric acid, diluted with water (100 mL), and extracted with ether (addition of water before acidification gives high yields of the cyclised product **12***b*). The combined ethereal extract was washed three times with water and dried with $MgSO_4$. The solvent was removed *in vacuo* to give an orange oil, which on distillation under reduced pressure gave **11***b* as a mobile yellow oil (5.85 g, 57%); bp 106°C/0.6 Torr (1 Torr = 133.3 Pa); H nmr δ($CDCl_3$): 1.15 (s, 9H, $C(CH_3)_3$, 6.62–7.80 (m, 6H, aromatic and vinyl); ms, *m/z*: 204 (M^+, 4%), 147 (M^+ ^tBu, 100%). Anal. calcd. for $C_{13}H_{16}O_2$: C 76.42, H 7.91; found: C 76.12, H 8.08.

Kinetic measurements

The kinetics of ring closure of enones **1** were measured by monitoring the change in proton nmr spectra with time as described previously (4).

The kinetics of cyclisation of 2′-hydroxy- and 2′-aminochalcones **5** and **18** respectively were determined using nmr integral measurements for the ABX signals due to the C-2 and C-3 protons of the flavonones **6** and the tetrahydroquinolones **19**. Solutions of the chalcones were prepared as 10% w/v solutions in TFA or TFA-*d*, tetramethylsilane was added, and the tubes stoppered or, in cases of longer reactions, sealed, then shaken, and maintained at 35°C in a water bath when not being measured.

Integrals were usually measured three times in each direction and the mean value calculated for the AB and X proton signals. Similar measurements were made on an internal methyl peak for normalisation purpose or, where no such peak was available, on 1,4-dioxan added as

Can. J. Chem. Downloaded from www.nrcresearchpress.com by 91.121.58.235 on 09/07/12
For personal use only.

an internal standard, which gives a sharp singlet close to δ 4.0 in TFA and thus falls between the AB and X resonances. The 1,4-dioxan is nonvolatile and no decomposition was observed in the stock solution in TFA over 4 months. In the case of the 2′-aminochalcones, cyclohexane was used, because the dioxan peak overlapped with other peaks.

A representative treatment of data is given in Table 5. The kinetics of cyclisation of the 3′-methoxychalcones were examined in an analogous fashion, by following the appearance of the ABX peaks.

Kinetics for cyclisation of the 2′-hydroxychalcones in 3% methanesulphonic acid were also measured in this fashion. This approach gave good first-order kinetics for the results in Table 3; however, for less reactive compounds, increasing decomposition with the passage of time was observed.

Errors

The accuracy of nmr integrals on a 60-MHz machine is not very high, probably at best within ±5%. Consequently, in some of the longer kinetic runs, some scatter is observed in the calculated concentration terms. This is because of the problems associated with measuring small integrals or small changes in integrals at the start and end of a run.

This means that evaluation of the [**6**]/[**5**] ratios is particularly dependent on this variation. The ratios in TFA vary between 5.6 and 7.2 (Table 1), which implies that the percentage of flavonone **6** varies from 85 to 88% respectively, indicating that the variation is within the limits of the accuracy of the nmr integrals. As a consequence, it appears that [**6**]/[**5**] ratios are approximately constant across the series. In TFA, determination of the rate constants is based upon the ABX pattern in the nmr, using the integrals of these two sets of peaks to obtain an average value. In TFA-*d* this is not possible due to incorporation of deuterium at C3, α to the carbonyl group. This suggests that the results in TFA-*d* will be more susceptible to accuracy of the integrals and hence *k* in TFA-*d* are probably less reliable than those in TFA. We are, however, convinced that the accuracy of our measurements is amply sufficient to draw the mechanistic conclusions given in the discussion.

Acknowledgements

The authors gratefully acknowledge the support of this work by the Science and Engineering Research Council. They also thank a referee for helpful comments.

1. R. K. MACKIE and D. M. SMITH. Guidebook to organic synthesis. Longman, London. 1982. pp. 129–131.
2. G. W. L. ELLIS, C. D. JOHNSON, and D. N. ROGERS. J. Chem. Soc. Chem. Commun. 36 (1982).
3. J. P. BRADLEY, T. C. JARVIS, C. D. JOHNSON, P. D. MCDONNELL, and T. A. P. WEATHERSTONE. Tetrahedron Lett. **24**, 2851 (1983).
4. G. W. L. ELLIS, C. D. JOHNSON, and D. N. ROGERS. J. Am. Chem. Soc. **105**, 5090 (1983).
5. M. E. A. ASTUDILLO, N. C. J. CHOKOTHO, T. C. JARVIS, C. D. JOHNSON, C. C. LEWIS, and P. D. MCDONNELL. Tetrahedron, **41**, 5919 (1985).
6. C. M. BRENNAN, C. D. JOHNSON, and P. D. MCDONNELL. J. Chem. Soc. Perkin Trans. 2, 957 (1989).
7. J. E. BALDWIN, R. C. THOMAS, L. I. KRUSE, and L. SILBERMAN. J. Org. Chem. **42**, 3846 (1977).
8. J. E. BALDWIN. J. Chem. Soc. Chem. Commun. 734 (1976).
9. J. E. BALDWIN and J. A. REISS. J. Chem. Soc. Chem. Commun 77 (1977).
10. P. MANITTO. Biosynthesis of natural products. Ellis Horwood, Chichester. 1981. p. 404.
11. C. O. MILES and L. MAIN. J. Chem. Soc. Perkin Trans. 2, 1623 (1989).
12. H. B. BURGI and J. D. DUNITZ. Acc. Chem. Res. **16**, 153 (1983).
13. C. D. JOHNSON. The Hammett equation, Cambridge University Press, London. 1980.
14. J. J. DANNENBERG, B. J. GOLDBERG, J. K. BARTON, K. DILL, D. H. WEIRWURZEL, and M. O. LOGAN. J. Am. Chem. Soc. **103**, 7764 (1981); R. H. SUMMERVILLE and P. R. SCHLEYER. J. Am. Chem. Soc. **94**, 3629 (1972); **96**, 1110 (1974).
15. D. S. NOYCE and M. J. JORGENSON. J. Am. Chem. Soc. **83**, 2525 (1961).
16. D. S. NOYCE and M. J. JORGENSON. J. Am. Chem. Soc. **85**, 2420 (1963).
17. B. CAPON and F. C. KWOK. Tetrahedron, **43**, 69 (1987).
18. A. V. WILLI. *In* Chemical kinetics. Vol. 8. *Edited by* C. H. Bamford and C. F. H. Tipper. Elsevier, Amsterdam. 1977. p. 21.
19. S. E. DENMARK and R. C. KLIX. Tetrahedron, **44**, 4043 (1988).
20. C. SANTELLI-ROUVIER and M. SANTELLI. Synthesis, 429 (1983).
21. A. D. ALLEN, M. ROSENBAUM, N. O. L. SETO, and T. T. TIDWELL. J. Org. Chem. **47**, 4234 (1982).
22. P. D. MCDONNELL. Ph.D. Thesis, University of East Anglia. 1987; C. M. BRENNAN. Ph.D. Thesis, University of East Anglia. 1988.
23. R. B. MOODIE, K. SCHOFIELD, and P. G. TAYLOR. J. Chem. Soc. Perkin Trans. 2, 133 (1979); J. W. BARRETT, R. B. MOODIE, K. SCHOFIELD, P. G. TAYLOR, and J. W. WESTON. J. Chem. Soc. Perkin Trans 2, 747 (1979).
24. K. VON AUWERS and E. LAMMERHIRT. Justus Liebigs Ann. Chem. **421**, 1 (1920).

Can. J. Chem. Downloaded from www.nrcresearchpress.com by 91.121.58.235 on 09/07/12
For personal use only.

Acid-catalyzed hydrolysis of tetramethoxyethene in aqueous solution. Initial state stabilization by the methoxy groups

A. J. KRESGE[1] AND M. LEIBOVITCH
Department of Chemistry, University of Toronto, Toronto, Ont., Canada M5S 1A1
AND
K. R. KOPECKY
Department of Chemistry, University of Alberta, Edmonton, Alta., Canada T6G 2G2

Received January 26, 1990

This paper is dedicated to Professor Ross Stewart on the occasion of his 65th birthday

A. J. KRESGE, M. LEIBOVITCH, and K. R. KOPECKY. Can. J. Chem. **68**, 1786 (1990).

The acid-catalyzed hydrolysis of tetramethoxyethene to methyl dimethoxyacetate in aqueous solution at 25°C was found to occur with the hydronium-ion catalytic coefficient $k_{H^+} = 0.454\ M^{-1}\ s^{-1}$, to give the solvent isotope effect $k_{H^+}/k_{D^+} = 3.15$, and to provide a Brønsted relation based upon six carboxylic acids with the exponent $\alpha = 0.42$. These data indicate that the reaction proceeds via rate-determining proton transfer from the catalyzing acid to an olefinic carbon atom of the substrate. They also show tetramethoxyethene to be 1.0×10^6 times less reactive than 1,1-dimethoxyethene (ketene dimethyl acetal), a rate retardation 600 times greater than that expected from initial state stabilization by the two additional methoxy groups in tetramethoxyethene; possible causes of this disparity are discussed.

Key words: tetramethoxyethene, carbon–carbon double bond reactivity, ketene acetal, vinyl ether hydrolysis.

A. J. KRESGE, M. LEIBOVITCH et K. R. KOPECKY. Can. J. Chem. **68**, 1786 (1990).

On a trouvé que l'hydrolyse acido-catalysée du tétraméthoxyéthène en diméthoxyacétate de méthyle, en solution aqueuse, à 25°C, se produit avec un coefficient catalytique de l'ion hydronium $k_{H^+} = 0{,}454\ M^{-1}\ s^{-1}$ et un effet isotopique du solvant $k_{H^+}/k_{D^+} = 3{,}15$ et qu'elle donne lieu à une relation de Brønsted, basée sur six acides carboxyliques, avec un exposant $\alpha = 0{,}42$. Ces données indiquent que la réaction se produit par le biais d'un transfert de proton du catalyseur acide avec un atome de carbone oléfique et que ce transfert limite la vitesse de la réaction. Ces données démontrent aussi que le tétraméthoxyéthène est $1{,}0 \times 10^6$ fois moins réactif que le 1,1-diméthoxyéthène (diméthyl acétal du cétène); ce ralentissement est 600 fois plus grand que celui attendu sur la base d'une stabilisation de l'état initial du tétraméthoxyéthène par deux groupements méthoxyles additionnels: on discute des causes possibles de cette disparité.

Mots clés: tétraméthoxyéthène, réactivité de la double liaison carbone-carbone, acétal du cétène, hydrolyse de l'éther vinylique.

[Traduit par la revue]

Introduction

Alkoxy substituents raise the reactivity of carbon-carbon double bonds to electrophilic addition by impressively large amounts. Methyl vinyl ether (1), **2**, for example, is protonated on carbon fifteen orders of magnitude more rapidly than is ethylene (2), **1**, and ketene dimethyl acetal, **3**, is another five orders of

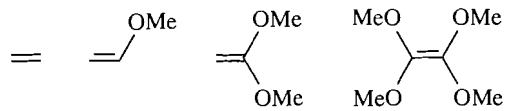

1 **2** **3** **4**

magnitude more reactive than the mono-ether (3). These rate accelerations can be understood in terms of resonance stabilization of the alkoxy carbocation product of these reactions, as shown for example in reaction [1].

[1]

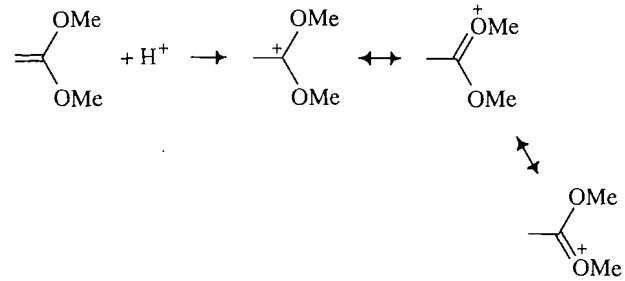

Further methoxy substitution, however, as in tetramethoxyethene, **4**, is likely to lead to a decrease rather than to a further increase in reactivity. This is because the additional substituents will be unable to interact conjugatively with the positive charge being generated on the substrate in the reaction's transition state, but they will be able to lower the energy of the initial state of the reaction by stabilizing the substrate through the well-known carbon–carbon double bond stabilizing effect of methoxyl (4), and this will raise the reaction barrier and exert a retarding effect on the reaction rate.

We have now substantiated this expectation by measuring rates of acid-catalyzed hydrolysis of tetramethoxyethene.

Experimental section

Materials

Tetramethoxyethene was prepared by treating dimethoxy-*p*-chlorophenoxymethane with sodium hydride (5) and was purified by recrystallization from isopentane followed by distillation. All other materials were best available commercial grades. Solutions were prepared using deionized H_2O purified further by distillation or D_2O (Merck, Sharp & Dohme 99.8%) as received.

Kinetics

Rates of hydrolysis of tetramethoxyethene were measured spectroscopically by monitoring the decrease in absorbance at $\lambda = 205$ nm (mineral acid solutions) or $\lambda = 225$ nm (carboxylic acid buffers). Measurements were made with Cary Model 118 and Model 2200 spectrophotometers whose cell compartments were thermostatted at 25.0 ± 0.1°C. Reactions were initiated by injecting 5 μL of a solution of tetramethoxyethene in tetrahydrofuran into a cuvette containing 3 mL

[1]Author to whom correspondence should be addressed.

Can. J. Chem. Downloaded from www.nrcresearchpress.com by 91.121.58.235 on 09/07/12
For personal use only.

TABLE 1. Rate data for the hydrolysis of tetramethoxyethene in aqueous perchloric acid at 25°C[a]

[Acid]/10^{-2} M	$k_{obs}/10^{-2}$ s^{-1}
H_2O solution	
10.1	4.51, 4.55, 4.63, 4.59, 4.68, 4.69, 4.31, 4.37, 4.48, 4.55, 4.55
8.04	3.96, 3.74, 3.83, 3.86, 3.91, 3.89
6.03	2.94, 2.79, 2.86, 2.84
4.02	1.86, 1.88, 1.98, 1.83, 1.76
1.01	0.458, 0.453, 0.447, 0.482
0.603	0.319, 0.280, 0.296, 0.289
$k_{obs}/s^{-1} = (4.90\pm4.12) \times 10^{-4} + (4.54\pm0.06) \times 10^{-1}[HClO_4]$	
D_2O solution	
10.2	1.44, 1.46, 1.51, 1.46
6.11	0.884, 0.866, 0.890, 0.918
2.04	0.298, 0.284, 0.289, 0.291
$k_{obs}/s^{-1} = -(0.07\pm1.22) \times 10^{-4} + (1.44\pm0.02) \times 10^{-1}[DClO_4]$	

[a]Ionic strength = 0.10 M ($NaClO_4$).

of acid or buffer solution which had been allowed to come to temperature equilibrium with the spectrometer cell compartment; the concentration of tetramethoxyethene in the reaction mixture was *ca.* 1×10^{-3} M. The reactions followed the first-order rate law accurately, and observed first-order rate constants were calculated from slopes of appropriate linear expressions and/or by least-squares fitting to an exponential function.

Results

Rates of hydrolysis of tetramethoxyethene were measured in dilute solutions of perchloric acid in H_2O and in D_2O over a range of acid concentrations; the data are summarized in Table 1. Observed first-order rate constants obtained in both solvents were accurately proportional to acid concentration (Fig. 1), and linear least-squares analysis gave the catalytic coefficients k_{H+} = 0.454 ± 0.006 M^{-1} s^{-1} and k_{D+} = 0.144 ± 0.002 M^{-1} s^{-1}; these provide the solvent isotope effect k_{H+}/k_{D+} = 3.15 ± 0.06.

Rates of hydrolysis of tetramethoxyethene were also measured in buffer solutions of six different carboxylic acids. These data are summarized in Table 2. It may be seen that measurements were made in sets of solutions of varying buffer concentrations but constant buffer ratio and constant ionic strength. This served to keep hydronium-ion concentrations constant in the less acidic buffers (acetic and hydroxyacetic acids) and thus facilitated assessment of catalysis by buffer species by keeping hydronium-ion contributions to observed rates constant. In the more acidic buffers, however, "buffer failure" (6*a*) occurred and hydronium ion concentrations dropped significantly with decreasing buffer concentration. These changes were compensated for by adjusting observed rate constants where necessary using the hydronium-ion catalytic coefficient measured in perchloric acid solutions. Hydronium-ion concentrations needed for this purpose were obtained by calculation using literature pK_a values for the buffer acids and activity coefficients recommended by Bates (7).

Strong buffer catalysis was found in all of the buffer systems examined, with rates of disappearance of tetramethoxyethene accurately proportional to buffer concentration. Measurements made in acetic acid buffers at two different buffer ratios showed this catalysis to be of the general acid type. The data were therefore fitted by linear least-squares analysis to the rate law given in eq. [2]; the general acid catalyic coefficients so evaluated are listed in Table 3.

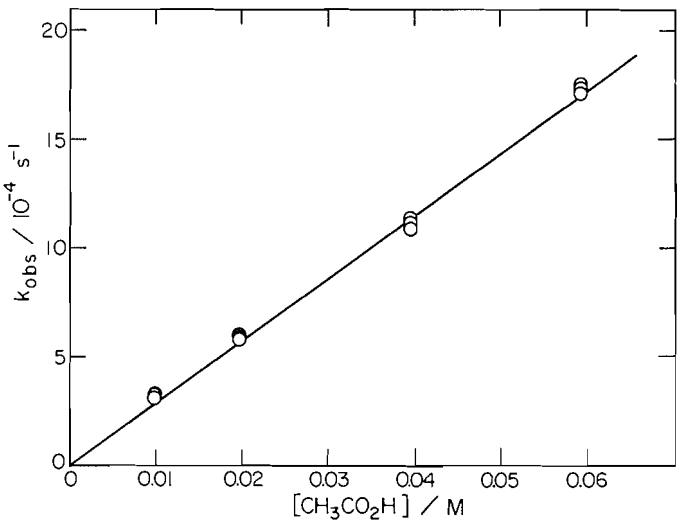

FIG. 1. Relationship between acid concentration and observed first-order rate constants for the hydrolysis of tetramethoxyethene in aqueous solution at 25°C; ○, H_2O; △, D_2O.

$$[2] \quad k_{obs} = k_{H+}[H^+] + k_{HA}[HA]$$

Hydronium-ion catalytic coefficients were also determined from the buffer solution data using the terms $k_{H+}[H^+]$ of the rate law (eq. [2]) and the known hydrogen ion concentrations of the buffers. These results are also listed in Table 3. It may be seen that, whereas all k_{H+} values so obtained are consistent with k_{H+} = 0.454 measured directly in perchloric acid solutions, uncertainties in these results increase with decreasing buffer solution acidity and eventually become greater than the values of k_{H+} themselves. This is because general acid catalysis in these solutions is very strong and hydronium-ion contributions to observed rates are correspondingly small, as seen, for example, in Fig. 2. Situations such as this arise in reactions with small Brønsted exponents and/or hydronium-ion catalytic coefficients that fall markedly below the Brønsted line (6*b*); both of these factors were operative in the present case (*vide infra*).

Can. J. Chem. Downloaded from www.nrcresearchpress.com by 91.121.58.235 on 09/07/12
For personal use only.

TABLE 2. Rate data for the hydrolysis of tetramethoxyethene in aqueous buffer solutions at 25°C[a]

$[HA]/10^{-2}$ M	$k_{obs}/10^{-3}$ s^{-1}
HA = $CNCH_2CO_2H$; [HA]/[NaA] = 0.980	
3.92	9.29, 9.51, 9.57, 9.64
2.75	6.95, 7.19, 7.16, 7.10, 7.09
1.96	4.91, 4.94, 4.98, 4.85, 4.87
0.980	2.72, 2.68, 2.76, 2.65, 2.71, 2.75
0.588	1.70, 1.75, 1.71, 1.73, 1.72
$k_{adj}/s^{-1} = (1.76\pm0.05) \times 10^{-3} + (2.23\pm0.03) \times 10^{-1}$[HA]	
$k_{H+} = (4.21\pm0.12) \times 10^{-1}$ M^{-1} s^{-1}	
HA = $ClCH_2CO_2H$; [HA]/[NaA] = 0.967	
3.87	8.38, 8.30, 8.36, 8.31, 8.46, 8.23
3.09	6.85, 6.88, 6.84, 6.82, 6.81
1.93	4.51, 4.53, 4.51, 4.53
1.16	2.73, 2.69, 2.71, 2.71
$k_{adj}/s^{-1} = (8.98\pm0.51) \times 10^{-4} + (2.03\pm0.02) \times 10^{-1}$[HA]	
$k_{H+} = (4.87\pm0.28) \times 10^{-1}$ M^{-1} s^{-1}	
HA = $CH_3OCH_2CO_2H$; [HA]/[NaA] = 1.19	
4.74	4.91, 4.98, 4.99, 4.89, 4.95, 5.07, 4.88
3.80	4.00, 4.05, 4.03, 4.16, 4.01
2.85	3.13, 3.12, 3.14, 3.12
1.90	2.08, 2.07, 2.08, 2.07
0.949	1.13, 1.13, 1.13, 1.12
$k_{adj}/s^{-1} = (2.36\pm0.24) \times 10^{-4} + (1.01\pm0.01) \times 10^{-1}$[HA]	
$k_{H+} = (4.86\pm0.50) \times 10^{-1}$ M^{-1} s^{-1}	
HA = HCO_2H; [HA]/[NaA] = 1.08	
4.32	2.10, 2.10, 2.12, 2.13, 2.09
3.46	1.75, 1.79, 1.74, 1.71
2.30	1.20, 1.22, 1.21, 1.14
1.30	0.715, 0.709, 0.712, 0.702
$k_{adj}/s^{-1} = (1.39\pm0.18) \times 10^{-4} + (4.63\pm0.06) \times 10^{-2}$[HA]	
$k_{H+} = (4.65\pm0.59) \times 10^{-1}$ M^{-1} s^{-1}	
HA = $HOCH_2CO_2H$; [HA]/[NaA] = 1.01	
5.63	3.84, 3.80, 3.87, 3.89, 3.75
4.02	2.79, 2.81, 2.81, 2.78, 2.79, 2.82, 2.88
3.22	2.26, 2.24, 2.26, 2.26, 2.25
2.01	1.40, 1.41, 1.40, 1.40, 1.35
$k_{obs}/s^{-1} = (6.98\pm3.04) \times 10^{-5} + (6.74\pm0.08) \times 10^{-2}$[HA]	
$k_{H+} = (3.04\pm1.33) \times 10^{-1}$ M^{-1} s^{-1}	
HA = CH_3CO_2H; [HA]/[NaA] = 1.79	
7.16	1.98, 1.94, 1.93, 1.97, 1.99
5.73	1.66, 1.55, 1.55, 1.65, 1.56
3.58	0.990, 0.980, 0.992, 0.990
2.15	0.602, 0.606, 0.612, 0.614
$k_{obs}/s^{-1} = (2.28\pm2.08) \times 10^{-5} + (2.72\pm0.04) \times 10^{-2}$[HA]	
$k_{H+} = (4.69\pm4.28) \times 10^{-1}$ M^{-1} s^{-1}	
HA = CH_3CO_2H; [HA]/[NaA] = 0.988	
5.93	1.74, 1.74, 1.76, 1.72
3.95	1.09, 1.09, 1.13, 1.14
1.98	0.586, 0.584, 0.589
0.988	0.309, 0.312, 0.309
$k_{obs}/s^{-1} = (1.03\pm1.65) \times 10^{-5} + (2.88\pm0.05) \times 10^{-2}$[HA]	
$k_{H+} = (3.85\pm6.16) \times 10^{-1}$ M^{-1} s^{-1}	

[a]Ionic strength = 0.10 M ($NaClO_4$).

The Brønsted plot constructed with the seven carboxylic acid catalytic coefficients determined here is shown in Fig. 3. Linear least-squares analysis gave the exponent $\alpha = 0.42 \pm 0.05$ and predicted a value for the hydronium-ion catalytic coefficient which is greater than the experimentally determined value, $k_{H+} = 0.454$ M^{-1} s^{-1} by a factor of 45. The presently determined Brønsted exponent is similar to values obtained before for

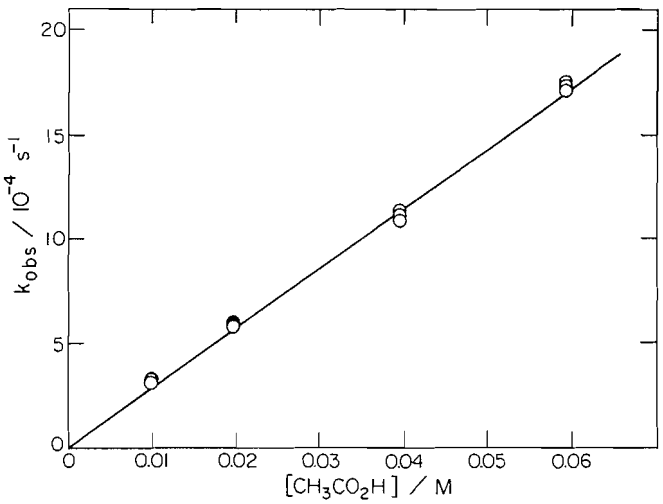

FIG. 2. Relationship between buffer acid concentration and observed first-order rate constants for the hydrolysis of tetramethoxyethene in aqueous acetic acid buffer solutions at 25°C; buffer ratio ([HA]/[NaA]) = 0.99, ionic strength = 0.10 M.

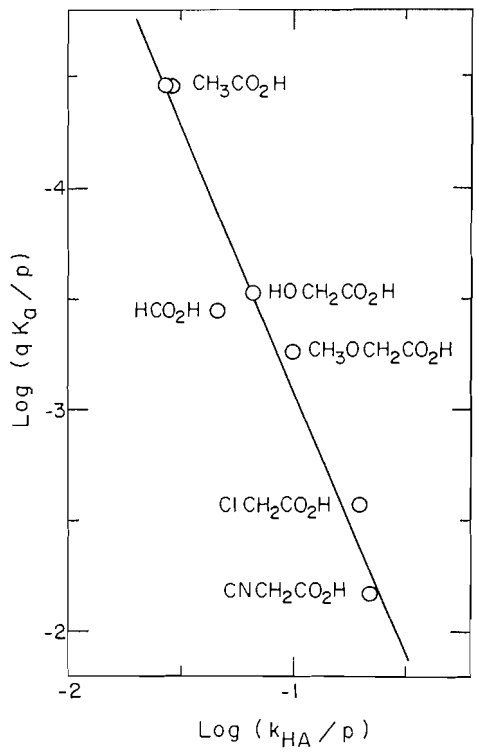

FIG. 3. Brønsted relation for the hydrolysis of tetramethoxyethene catalyzed by carboxylic acids in aqueous solution at 25°C.

the hydrolysis of ketene acetals (8), and the present hydronium-ion deviation is typical of reactions undergoing rate-determing proton transfer to carbon (9). The present Brønsted relation also shows carboxylic acid deviations which are strikingly similar to characteristic deviations for individual carboxylic acids found before in other ketene acetal hydrolysis reactions (8): formic acid is consistently low and chloro- and methoxyacetic acid are consistently high, while cyano-, hydroxy-, and acetic acid itself lie on the Brønsted line. It was pointed out before (8) that these deviations seem to be related to the size of the catalysts involved and may therefore be caused by London dispersion interactions between catalyst and substrate.

Can. J. Chem. Downloaded from www.nrcresearchpress.com by 91.121.58.235 on 09/07/12
For personal use only.

TABLE 3. Summary of rate data obtained for the hydrolysis of tetramethoxyethene in aqueous buffer solutions at 25°C[a]

HA	pK_a	[HA]/[NaA]	$k_{HA}/10^{-2}\,M^{-1}\,s^{-1}$	$k_{H+}/10^{-1}\,M^{-1}\,s^{-1}$
$CNCH_2CO_2H$	2.47	0.98	22.3±0.3	4.21±0.12
$ClCH_2CO_2H$	2.87	0.97	20.3±0.2	4.87±0.28
$CH_3OCH_2CO_2H$	3.57	1.19	10.1±0.1	4.86±0.50
HCO_2H	3.75	1.08	4.63±0.06	4.65±0.59
$HOCH_2CO_2H$	3.83	1.01	6.74±0.08	3.04±1.33
CH_3CO_2H	4.76	1.79	2.72±0.04	4.69±4.28
CH_3CO_2H	4.76	0.99	2.88±0.05	3.85±6.16

[a]Ionic strength = 0.10 M ($NaClO_4$).

Discussion

Reaction mechanism

The product of hydrolysis of tetramethoxyethene in dilute aqueous acid is reported to be methyl dimethoxyacetate, reaction [3] (10).

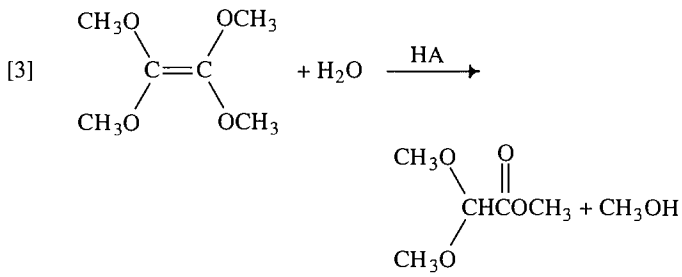

This was confirmed in the present study by the changes that occurred in the proton NMR spectrum of a reacting solution tetramethoxyethene in D_2O containing approximately 0.1 M DCl: the signal of tetramethoxyethene at δ = 3.42 ppm quickly diminished as three new peaks, at δ = 3.61, 3.22, and 3.13 ppm in the intensity ratio 1:2:1, grew in; the first two of these new resonances are consistent with expectation for the methyl proton signals of the ester and acetal groups of methyl dimethoxyacetate, respectively, and the third was identified as the signal from the methyl group of methanol by adding a small sample of this alcohol to the reaction mixture. These changes were complete in 10 min, and they were then followed by very much slower decreases of the ester and acetal signals and increase of the methanol signal as further hydrolysis of methyl dimethoxyacetate took place.

The analog of the accepted mechanism for vinyl ether or ketene acetal hydrolysis (8, 11) which applies in the present case consists of protonation of tetramethoxyethene on carbon, reaction [4], followed by hydration of the dialkoxycation so formed, reaction [5], and decomposition of the ensuing hydrogen ortho ester, reaction [6]. This reaction scheme is consistent

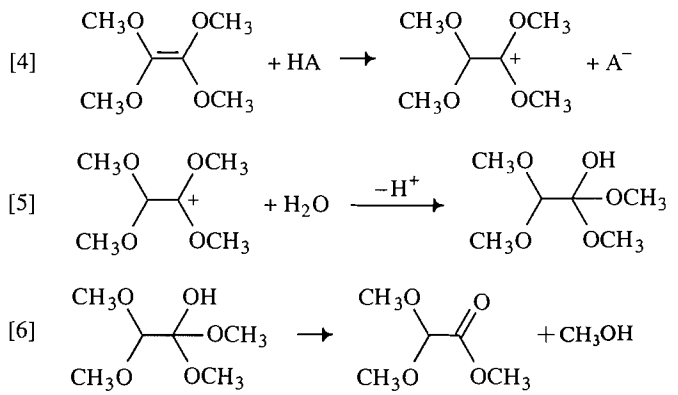

with all of the evidence presented here. The large hydrogen ion isotope effect found, moreover (k_{H+}/k_{D+} = 3.15), indicates that the first step is rate-determining, for reversible carbon protonation with some subsequent step rate-determining would have produced an inverse isotope effect, $k_{H+}/k_{D+} < 1$ (6c). This assignment is supported by the observation of general acid catalysis, though such catalysis is also consistent with rate-determining hydration of the dialkoxy cation, reaction [5], assisted by general-base promoted removal of a proton from the attacking water molecule.

This assignment of a rate-determining, non-reversible role to the carbon protonation step is also consistent with the fact that the subsequent steps are expected to be very fast. A rate constant of $3 \times 10^6\ s^{-1}$ can be estimated for the hydration reaction [5] from $k = 1.8 \times 10^5\ s^{-1}$ for the hydration of the α,α-dimethoxyethyl cation (12), **5**, plus an accelerating effect of 4 for each of the β-methoxy substituents introduced in going from **5** to the substrate of reaction [5]; this accelerating effect is based upon the difference in hydration rate constants for the α-methyl-α-methoxyethyl cation, **6**, $k = 1 \times 10^9\ s^{-1}$, and the α-methoxymethyl-α-methoxyethyl cation, **7**, $k = 4 \times 10^9\ s^{-1}$ (13). Decomposition of the hydrogen ortho ester, reaction [6], will also be rapid inasmuch as such processes are well-known to be fast reactions (14); for example, the hydronium-ion catalytic coefficient for decomposition of dimethyl hydrogen orthoacetate, **8**,

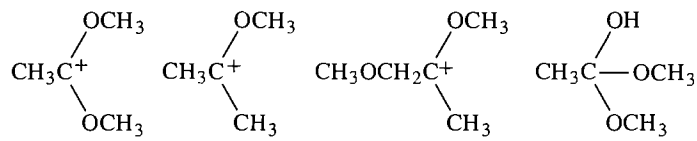

5 **6** **7** **8**

has been estimated to be greater than $7 \times 10^4\ M^{-1}\ s^{-1}$ (15).

Reactivity

The hydronium-ion catalytic coefficient determined here for tetramethoxyethene, k_{H+} = 0.454 $M^{-1}\ s^{-1}$, is considerably smaller than that for 1,1-dimethoxyethene (ketene dimethyl acetal, **3**), $k_{H+} = 2.3 \times 10^5\ M^{-1}\ s^{-1}$ (3). The two additional methoxy groups introduced in going from 1,1-dimethoxyethene to tetramethoxyethene thus decrease rather than increase the reactivity of the carbon–carbon double bond to electrophilic addition of a proton. This, of course, is consistent with expectation based upon the double-bond stabilizing effect of methoxy groups.

Some additional insight into the nature of this retarding effect may be gained from a quantitative comparison of the rate reduction observed with that expected from the double-bond stabilizing effect of the additional methoxy groups. This effect has been evaluated as $\delta\Delta G$ = 5.2 kcal mol^{-1} per methoxy

Can. J. Chem. Downloaded from www.nrcresearchpress.com by 91.121.58.235 on 09/07/12
For personal use only.

group (4). If all of this stabilization were present in the initial state of the reaction and were absent from its transition state, a rate retardation corresponding to $2 \times 5.2 = 10.4$ kcal mol^{-1} would be realized. However, some of the stabilizing effect will still be present in the transition state because this state still contains a partial double bond. On the assumption that the Brønsted exponent, α, for the system measures the resemblance of the transition state to the final state, and $1 - \alpha$ therefore measures its resemblance to the initial state, $(1 - \alpha)$ $(5.2) = (1 - 0.42)$ $(5.2) = 3.0$ kcal mol^{-1} double-bond stabilization should still be present in the transition state. Two methoxy groups will contribute twice this amount, and the difference between that and the initial state stabilization corresponds to a rate retardation of 1.7×10^3. The experimentally observed value, based on the difference in rate between 1,1-dimethoxyethene and tetramethoxyethene, calculated taking into account the fact that tetramethoxyethene has two equivalent carbon-protonation sites, is 1.0×10^6. Tetramethoxyethene is thus 600 times less reactive than it should be on the basis of the effect of double bond stabilization by methoxy groups estimated in this way.

A similar disparity between an estimate made in the same way and the experimental value for the hydronium-ion catalyzed hydrolysis of dihydro-1,4,-dioxin, **9**, has been ascribed to an

9

additional, destabilizing inductive effect of the second oxygen on the positive charge being generated on the substrate in the transition state (16). This explanation could apply here, but there is also another possibility: the disparity might be due to imperfect synchronization of the changes that occur as the system moves from initial state through the transition state to the final state (17). If, for example, changes in conjugation of the methoxy groups with the carbon–carbon double bond run ahead of proton transfer, then $1 - \alpha$ will overestimate the methoxy-group double-bond stabilization left at the transition state, and the rate retardation calculated on this basis will consequently be too low. Such a disparity between changes in conjugation and the extent of proton transfer is believed to occur in the ionization of nitroalkanes (18).

Acknowledgements

We are grateful to the Natural Sciences and Engineering Research Council of Canada and the Donors of the Petroleum Research Fund, administered by the American Chemical Society, for financial support of this research.

1. A. J. KRESGE, D. S. SAGATYS, and H. L. CHEN. J. Am. Chem. Soc. **99**, 7228 (1977).
2. W. K. CHWANG, V. J. NOWLAN, and T. T. TIDWELL. J. Am. Chem. Soc. **99**, 7233 (1977).
3. A. J. KRESGE and T. I. YOUSAF. Unpublished work.
4. J. HINE. Structural effects on equilibria in organic chemistry. Wiley, New York. 1973. pp. 270–276.
5. J. W. SCHEEREN, R. J. E. M. STRAPS, and R. J. F. NIVARD. Recl. Trav. Chim. Pays-Bas, **92**, 11 (1973); K. R. KOPECKY, J. MOLINA, and R. RICO. Can. J. Chem. **66**, 2234 (1988).
6. J. R. KEEFFE and A. J. KRESGE. *In* Techniques of chemistry. Vol. VI. Investigation of rates and mechanisms of reactions. *Edited by* C. F. Bernasconi, Wiley-Interscience, New York. 1986. (*a*) pp. 776, 777; (*b*) pp. 777–783; (*c*) pp. 763–764.
7. R. G. BATES. Determination of pH, theory and practice. Wiley, New York. 1973. p. 49.
8. A. J. KRESGE and T. S. STRAUB. J. Am. Chem. Soc. **105**, 3957 (1983).
9. A. J. KRESGE. Chem. Soc. Rev. **2**, 475 (1973).
10. D. M. LEMAL, E. P. GOSSELINK, and S. D. MCGREGOR. J. Am. Soc. **88**, 582 (1966).
11. A. J. KRESGE. Acc. Chem. Res. **20**, 365 (1987).
12. S. STEENKEN and R. A. MCCLELLAND. J. Am. Chem. Soc. **111**, 4967 (1989).
13. T. L. AMYES and W. P. JENCKS. J. Am. Chem. Soc. **111**, 3677 (1989).
14. R. A. MCCLELLAND and L. J. SANTRY. Acc. Chem. Res. **16**, 394 (1983); B. CAPON, M. I. DOSUNMU, and M. DE N. DE MATOS SANCHEZ. Adv. Phys. Org. Chem. **21**, 37 (1985).
15. Y. CHIANG, A. J. KRESGE, M. O. LAHTI, and D. P. WEEKS. J. Am. Chem. Soc. **105**, 6852 (1983).
16. A. J. KRESGE and Y. YIN. J. Phys. Org. Chem. **2**, 43 (1989).
17. C. F. BERNASCONI. Tetrahedron, **41**, 3219 (1985); Acc. Chem. Res. **20**, 301 (1987).
18. A. J. KRESGE. Can. J. Chem. **52**, 1897 (1974).

Can. J. Chem. Downloaded from www.nrcresearchpress.com by 91.121.58.235 on 09/07/12
For personal use only.

Structural studies of organoboron compounds. XXXIX.[1] 1,4-Bis(2,2-diethoxyethyl)-6,8-diphenyl-5,7,9-trioxa-4-aza-1-azonia-8-bora-6-boratabicyclo[4.3.0]nonane

HENNING AMT AND WOLFGANG KLIEGEL

Institut für Pharmazeutische Chemie, der Technischen Universität Braunschweig, Beethovenstraße 55, 3300 Braunschweig, Bundesrepublik Deutschland

AND

STEVEN J. RETTIG AND JAMES TROTTER

Department of Chemistry, University of British Columbia, 2036 Main Mall, Vancouver, B.C., Canada V6T 1Y6

Received March 12, 1990

This paper is dedicated to Professor Ross Stewart on the occasion of his 65th birthday

HENNING AMT, WOLFGANG KLIEGEL, STEVEN J. RETTIG, and JAMES TROTTER. Can. J. Chem. **68**, 1791 (1990).

Reaction of *N,N'*-1,2-ethanediylidenebis(2,2-diethoxyethanamine)-*N,N'*-dioxide and phenylboronic acid yields the title compound. Crystals of 1,4-bis(2,2-diethoxyethyl)-6,8-diphenyl-5,7,9-trioxa-4-aza-1-azonia-8-bora-6-boratabicyclo[4.3.0]-nonane are triclinic, $a = 12.625(2)$, $b = 13.962(2)$, $c = 9.273(1)$ Å, $\alpha = 104.81(1)$, $\beta = 98.61(1)$, $\gamma = 106.52(1)°$, $Z = 2$, space group $P\bar{1}$. The structure was solved by direct methods and was refined by full-matrix least-squares procedures to $R = 0.058$ and $R_w = 0.081$ for 3677 reflections with $I \geq 3\sigma(I)$. The molecule has a bicyclo[4.3.0]nonane structure containing one transannular N—B bond. Important bond lengths are sp^3-boron, N—B = 1.759(3), O—B = 1.435(3) and 1.454(3), C—B = 1.579(4); sp^2-boron, O—B = 1.335(3) and 1.404(3), C—B = 1.557(4) Å. The (sp^3)B—C(phenyl) bond is the shortest yet reported for this type of compound.

Key words: crystal structure, boron compound, organoboron compound.

HENNING AMT, WOLFGANG KLIEGEL, STEVEN J. RETTIG et JAMES TROTTER. Can. J. Chem. **68**, 1791 (1990).

La réaction de la *N,N'*-dioxyde de *N,N'*-1,2-éthanediylidène bis(2,2-diéthoxy-éthanamine) avec l'acide phénylboronique fournit le composé mentionné dans le titre. Les cristaux du 1,4-bis(2,2-diéthoxyéthyl)-6,8-diphényl-5,7,9-trioxa-4-aza-1-azonia-8-bora-6-boratabicyclo[4.3.0]nonane sont tricliniques avec $a = 12,625(2)$, $b = 13,962(2)$ et $c = 9,273(1)$ Å, $\alpha = 104,81(1)$, $\beta = 98,61(1)$ et $\gamma = 106,52(1)°$, $Z = 2$, groupe d'espace $P\bar{1}$. On a résolu la structure par des méthodes directes et on l'a affinée par la méthode des moindres carrés jusqu'à des valeurs respectives de $R = 0,058$ et $R_w = 0,081$ pour 3677 réflexions avec $I \geq 3\sigma(I)$. La molécule possède une structure bicyclo[4.3.0]nonane contenant une liaison transannulaire N—B. Les longueurs de liaisons importantes sont : sp^3-bore, N—B = 1,759(3), O—B = 1,435(2) et 1,454(3), C—B = 1,579(4); sp^2-bore, O—B = 1,335(3) et 1,404(3), C—B = 1,557(4) Å. La longueur de la liaison (sp^3)B—C(phényle) est la plus courte à avoir été observée jusqu'à maintenant pour ce type de composé.

Mots clés : structure cristalline, composé du bore, composé du organobore.

[Traduit par la revue]

Introduction

Reduction of glyoxalbisnitrone **1** with potassium tetrahydroborate gives the *N,N'*-dihydroxy-1,2-ethanediamine derivative **2** which was then reacted with phenylboronic acid. We expected a condensation leading to the tricyclo[5.4.0.$0^{3,9}$]undecane **3** with the "4-homotwistane" ring skeleton which has recently been structurally characterized for the *N*-methyl derivative **2** (R = Me) (1). Surprisingly the crystalline reaction product of **2** (R = $CH_2CH(OEt)_2$) and phenylboronic acid showed the quantitative elemental analysis and nmr spectral data consistent with a 1:2 condensate, regardless of the molar ratio of the reactants (1:3 or 1:2). Chemical and spectroscopic data were not sufficient to allow for an unambiguous decision between the possible isomeric structures of **4** which include structures having both bicyclic (**A–C**) and tricyclic ring systems (**D**, **E**). The cyclononane **A** with transannular N—B coordination represents a ring-enlarged homolog of bicyclic compounds of the type **5** (2) which have been structurally characterized by X-ray crystallographic analysis (3). Similar ring systems, containing a pyroboronate —OB(Ph)OB(Ph)O— partial structure cyclized with one hydroxylamine function to form a BOBON ring, have already been found for the compounds **6** (4) and **7** (5). The bicyclo[3.3.0]octane type structure **B** would also possess a transannular N—B bond but would have an *N*-oxide function with its nitrogen atom bound to tetracoordinated boron, an unstable grouping expected to rearrange to the more stable structure **A**. The third bicyclic variation **C** could be formed by an N—O—B bridge within an isomeric cyclononane system.

All three transannular mono-coordinated ring systems, **A**, **B**, and **C**, could undergo fluxional intramolecular coordination exchange because of the additional sp^2-boron atom and electron-donating N/O groups present in each of these systems. As an alternative, in the structures **D** and **E**, two transannular coordinative interactions could give rise to the tricyclic systems, **D** being formed from **A** by an additional N—B bond and **E** being formed from **B** or **C** by additional O—B or N—B bonds, respectively. Structures **D** and **E** represent symmetric heterocyclanes with "nortwistane" and "norisotwistane" skeletons, respectively.

An X-ray crystallographic analysis has been carried out to determine the solid state structure of **4** definitively.

Experimental

N,N'-1,2-Ethanediylidenebis(2,2-diethoxyethanamine)-N,N'-dioxide, ***1***

N-Hydroxy-2,2-diethoxyethanamine (6) (2.98 g, 20 mmol) and gyloxal (0.58 g, 10 mmol, applied as the hydrate) are heated in 30 mL

[1]Previous paper in the series: ref. 14.

Printed in Canada / Imprimé au Canada

Can. J. Chem. Downloaded from www.nrcresearchpress.com by 91.121.58.235 on 09/07/12
For personal use only.

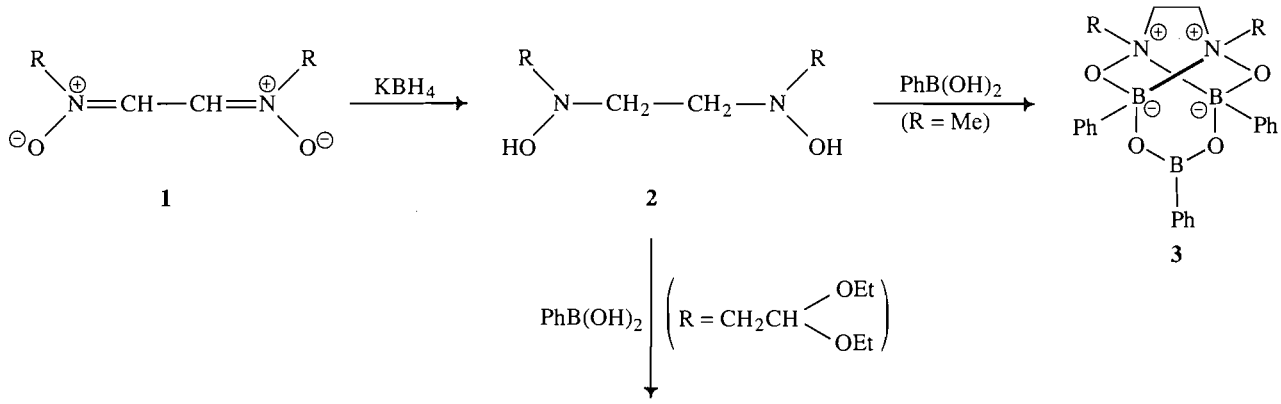

1 2 3

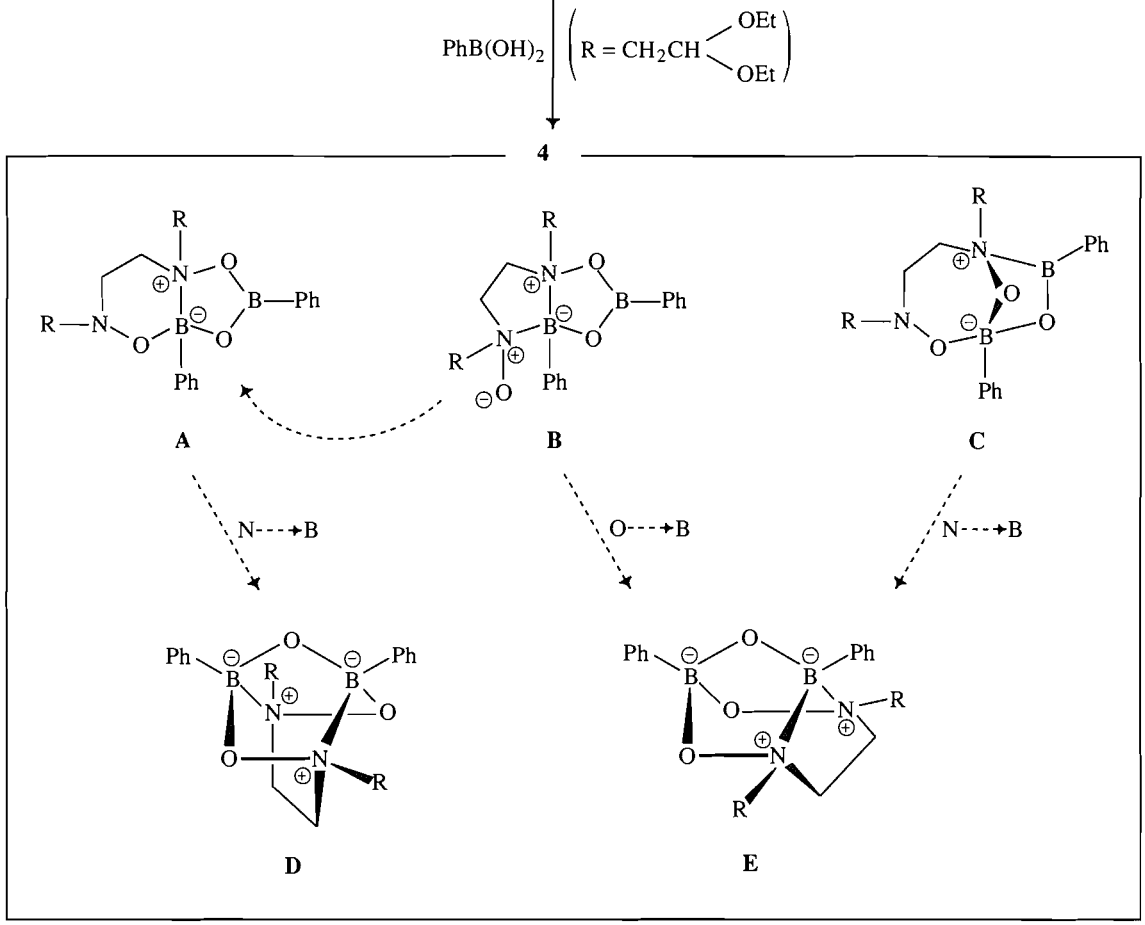

4 A B C D E

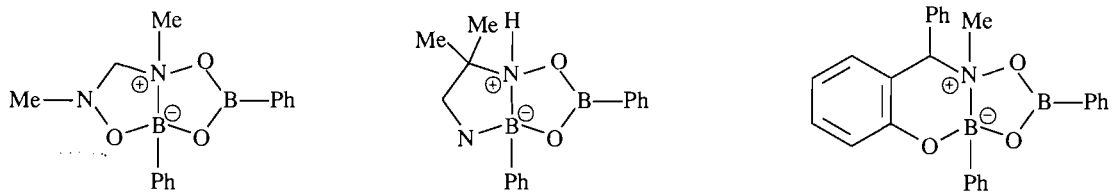

5 6 7

ethanol under reflux conditions for 10 min. After evaporating the solvent to 1/3 of its initial volume, the solution is cooled down and stored at −18°C for 24 h yielding 2.50 g (78%) of colorless crystals. Melting point 163°C (from ethanol). *Anal.* calcd. for $C_{14}H_{28}N_2O_6$: C 52.48, H 8.81, N 8.74; found: C 52.11, H 8.87, N 8.40. Infrared (KBr): 1540 cm^{-1} (C=N). ^1H nmr ($CDCl_3$/TMS): δ (ppm) = 1.19 (t, J = 7 Hz, 4 CH_3), 3.58 and 3.68 (q, q, J = 7 Hz, 4 O—CH_2), 3.90 (d, J = 5 Hz, 2 N—CH_2), 4.59 (t, J = 5 Hz, 2 C—CH(O)O), 7.70 (s, =CH—CH=).

N,N′-*bis(2,2-Diethoxyethyl)*-N,N′-*dihydroxy-1,2-ethanediamine, 2*

N,N′-1,2-Ethanediylidenebis(2,2-diethoxyethanamine)-*N,N′*-dioxide (1.60 g, 5 mmol) is dissolved in 150 mL methanol at 40°C. A solution of KBH_4 (1.08 g, 20 mmol) in 20 mL water is added dropwise with stirring which is continued for 24 h at room temperature. The solution is evaporated *in vacuo*, and the residue dissolved in water. Extraction with chloroform, drying of the solution with $NaSO_4$, and evaporation *in vacuo* lead to **2** which is recrystallized from chloroform/ether (1:1). Yield: 1.02 g (63%). Melting point: 94°C ($CHCl_3$/Et_2O). *Anal.* calcd. for $C_{14}H_{32}N_2O_6$: C 51.83, H 9.94, N 8.64; found: C 51.88, H 10.12, N 8.50. Infrared (KBr): 3500–2700 cm^{-1} (O—H, broad). ^1H nmr ($CDCl_3$/TMS): δ (ppm) = 1.18 (t, J = 7 Hz, 4 CH_3), 2.83 (d, J = 5 Hz, 2 $CH_2C(O)O$), 2.94 (s, N—CH_2—CH_2—N), 3.50 and 3.60 (q, q, J = 7 Hz, 4 O—CH_2), 4.73 (t, J = 5 Hz, 2 CH(O)O), 6.69 (s, broad, exchangeable, OH).

1,4-bis(2,2-Diethoxyethyl)-6,8-diphenyl-5,7,9-trioxa-4-aza-1-azonia-8-bora-6-boratabicyclo[4.3.0]nonane, 4A

N,N′-bis(2,2-Diethoxyethyl)-*N,N′*-dihydroxy-1,2-ethanediamine (0.65 g, 2 mmol) and phenylboronic acid (procedure [*a*]: 0.71 g,

Can. J. Chem. Downloaded from www.nrcresearchpress.com by 91.121.58.235 on 09/07/12
For personal use only.

Can. J. Chem. Downloaded from www.nrcresearchpress.com by 91.121.58.235 on 09/07/12
For personal use only.

6 mmol; procedure [*b*]: 0.49 g, 4 mmol) are heated in 80 mL absolute ethanol under reflux for 1 h. After evaporation of the solvent *in vacuo* the remaining oil is diluted with ether/petroleum ether (1:1) and cooled 24 h for crystallization. Yields: procedure [*a*]: 0.71 g (69%), procedure [*b*]: 0.68 g (66%). Melting point: 95°C (ether/petroleum ether). *Anal.* calcd. for $C_{26}H_{40}B_2N_2O_7$: C 60.73, H 7.84, B 4.21, N 5.45; found: C 60.74, H 8.07, B 4.34, N 5.24. Infrared (KBr): 1605 cm^{-1} (phenyl C=C). ^1H nmr ($CDCl_3$/TMS): δ (ppm) = 0.90 and 1.09 (t, t, J = 7 Hz, 4 CH_3), 2.79 (d, J = 5 Hz, 2 $CH_2C(O)O$), 3.08–3.62 (m, 4 O—CH_2), 4.61 (t, J = 5 Hz, 2 CH(O)O), 7.20–7.42 (m, 6 aromatic H), 7.70–7.89 (m, 4 aromatic H). Crystals suitable for X-ray analysis were obtained by recrystallization from absolute diethylether.

X-ray crystallographic analysis of 1,4-bis(2,2-diethoxyethyl)-6,8-diphenyl-5,7,9-trioxa-4-aza-1-azonia-8-bora-6-boratabicyclo-[4.3.0]nonane

A crystal *ca.* 0.24 × 0.25 × 0.35 mm in size was mounted in a general orientation. Unit-cell parameters were refined by least-squares on setting angles for 25 reflections (2θ = 54–80°) measured on a diffractometer with Cu-$K\alpha$ radiation (λ = 1.54178 Å). Crystal data at 21°C are as follows:

$C_{26}H_{40}B_2N_2O_7$ f.w. = 514.23

Triclinic, a = 12.625(2), b = 13.962(2), c = 9.273(1) Å, α = 104.81(1), β = 98.61(1), γ = 106.52(1)°, V = 1470.8(4) $Å^3$, Z = 2, ρ_c = 1.161 Mg m^{-3}, $F(000)$ = 552, μ(Cu-$K\alpha$) = 6.36 cm^{-1}. Absent reflections: none, space group $P\bar{1}$ (reduced cell, Donnay convention) from structure analysis.

Intensities were measured with graphite-monochromated Cu-$K\alpha$ radiation on a Rigaku AFC6S diffractometer. An ω–2θ scan at 32° min^{-1} over a range of (1.25 + 0.30 tan θ) degrees in ω (with up to eight rescans, background/scan time ratio = 0.5) was employed. Data were measured to 2θ = 151.6°. The intensities of three check reflections, measured every 150 reflections throughout the data collection, showed only small random variations. After data reduction,[2] an empirical absorption correction based on azimuthal scans for four reflections was applied, resulting in relative transmission factors ranging from 0.94 to 1.00. Of the 6200 reflections measured, 5811 were unique (R_{int} = 0.009) and 3677 (63.3%) of these had intensities greater than or equal to $3\sigma(F^2)$ above background where $\sigma^2(F^2) = (S^2(C + 4B) + (0.04(F_o^2))^2)/Lp^2$ with S = scan speed, C = scan count, B = total background count, and Lp = Lorentz-polarization factor.

The structure was solved by direct methods, 29 of the 37 non-hydrogen atoms being positioned from an E-map. The remaining non-hydrogen atoms were positioned from subsequent difference Fourier syntheses. The non-hydrogen atoms were refined with anisotropic thermal parameters and the hydrogen atoms were fixed in calculated positions (C—H = 0.98 Å, $B_H = 1.2B_{bonded\ atom}$). The peripheral atoms C(9) and C(10) show a high degree of thermal motion that results in anomalous bond lengths and angles. The fact that the thermal motion of atom C(9) is nearly isotropic suggested that a simple disordered model would not be adequate in this case, thus no attempt to refine a disordered model for this ethyl group was made. Scattering factors for all atoms and anomalous dispersion corrections for the non-hydrogen atoms were taken from ref. 7. The weighting scheme $w = 4F_o^2/\sigma^2(F_o^2)$ gave uniform average values of $w(|F_o| - |F_c|)^2$ over ranges of both $|F_o|$ and sin θ/λ and was employed in the final stages of full-matrix refinement of 335 variables. Reflections with $I < 3\sigma(I)$ were not included in the refinement. An extinction correction was applied, the final value of the extinction parameter being 1.63 × 10^{-5}. Convergence was reached at R = 0.058 and R_w = 0.081 for

[2]All computations performed using the TEXSAN – TEXRAY Structure Analysis Package which includes versions of the following: MITHRIL, Integrated direct methods, by C. J. Gilmore; AGNOST, absorption corrections, by J. A. Ibers; ORFLS, full-matrix least-squares, and ORFFE, function and errors, by W. R. Busing, K. O. Martin, and H. A. Levy; DIRDIF, phase extension and refinement of difference structures, by P. T. Beurskens; ORTEP II, illustrations, by C. K. Johnson.

TABLE 1. Final atomic coordinates (fractional) and B (eq)

Atom	x	y	z	B (eq)
O(1)	0.3468(1)	0.4700(1)	0.1294(2)	5.60(6)
O(2)	0.2505(1)	0.3896(1)	0.4024(2)	5.30(6)
O(3)	0.1946(1)	0.4885(1)	0.2586(2)	5.24(6)
O(4)	0.4846(2)	0.7291(2)	0.4614(3)	8.1(1)
O(5)	0.5539(3)	0.7674(2)	0.2616(4)	10.5(1)
O(6)	0.1961(2)	0.0941(1)	0.2367(3)	7.58(8)
O(7)	0.0386(2)	0.1236(2)	0.3195(3)	8.1(1)
N(1)	0.4247(2)	0.5042(2)	0.2800(2)	5.56(7)
N(2)	0.2487(2)	0.3350(1)	0.2456(2)	5.01(7)
C(1)	0.4604(2)	0.4149(2)	0.2857(3)	6.2(1)
C(2)	0.3579(2)	0.3148(2)	0.2450(3)	5.8(1)
C(3)	0.5182(2)	0.5951(2)	0.2804(4)	6.5(1)
C(4)	0.4800(3)	0.6900(2)	0.3053(4)	7.0(1)
C(5)	0.1477(2)	0.2374(2)	0.1968(3)	5.6(1)
C(6)	0.1479(3)	0.1690(2)	0.2991(3)	6.5(1)
C(7)	0.4145(4)	0.7888(4)	0.4979(5)	10.0(2)
C(8)	0.4211(4)	0.8185(3)	0.6636(6)	10.8(2)
C(9)	0.511(1)	0.788(1)	0.143(1)	23.1(7)
C(10)	0.507(1)	0.8565(7)	0.099(1)	20.2(5)
C(11)	0.2232(4)	0.0379(3)	0.3380(6)	11.5(2)
C(12)	0.2655(5)	−0.0429(4)	0.257(1)	16.3(3)
C(13)	−0.0392(4)	0.0523(3)	0.1874(5)	9.6(2)
C(14)	−0.1536(4)	0.0098(4)	0.2230(7)	13.0(2)
C(15)	0.1480(2)	0.3636(2)	−0.0174(3)	5.27(9)
C(16)	0.0398(3)	0.3706(2)	−0.0459(3)	6.2(1)
C(17)	−0.0371(3)	0.3175(3)	−0.1856(4)	8.0(1)
C(18)	−0.0087(4)	0.2555(3)	−0.3007(4)	8.4(1)
C(19)	0.0984(4)	0.2464(3)	−0.2798(3)	8.0(1)
C(20)	0.1771(3)	0.3019(2)	−0.1381(3)	6.7(1)
C(21)	0.1930(2)	0.5406(2)	0.5452(3)	5.24(9)
C(22)	0.1378(3)	0.6121(2)	0.5365(4)	6.9(1)
C(23)	0.1186(3)	0.6737(3)	0.6644(5)	8.4(1)
C(24)	0.1551(3)	0.6642(3)	0.8056(4)	8.3(1)
C(25)	0.2066(3)	0.5914(3)	0.8181(3)	7.3(1)
C(26)	0.2249(2)	0.5292(2)	0.6880(3)	6.0(1)
B(1)	0.2339(3)	0.4233(2)	0.1449(3)	5.1(1)
B(2)	0.2138(2)	0.4747(2)	0.3961(3)	5.1(1)

TABLE 2. Bond lengths (Å) with estimated standard deviations in parentheses

Atom	Atom	Distance	Atom	Atom	Distance
O(1)	N(1)	1.458(3)	C(3)	C(4)	1.510(4)
O(1)	B(1)	1.435(3)	C(5)	C(6)	1.508(4)
O(2)	N(2)	1.453(2)	C(7)	C(8)	1.468(6)
O(2)	B(2)	1.404(3)	C(9)	C(10)	1.143(9)
O(3)	B(1)	1.454(3)	C(11)	C(12)	1.466(7)
O(3)	B(2)	1.335(3)	C(13)	C(14)	1.517(6)
O(4)	C(4)	1.396(4)	C(15)	C(16)	1.388(4)
O(4)	C(7)	1.399(4)	C(15)	C(20)	1.393(4)
O(5)	C(4)	1.402(4)	C(15)	B(1)	1.579(4)
O(5)	C(9)	1.286(8)	C(16)	C(17)	1.376(4)
O(6)	C(6)	1.399(3)	C(17)	C(18)	1.355(5)
O(6)	C(11)	1.431(4)	C(18)	C(19)	1.384(5)
O(7)	C(6)	1.408(4)	C(19)	C(20)	1.402(4)
O(7)	C(13)	1.385(4)	C(21)	C(22)	1.381(3)
N(1)	C(1)	1.450(3)	C(21)	C(26)	1.388(4)
N(1)	C(3)	1.466(4)	C(21)	B(2)	1.557(4)
N(2)	C(2)	1.484(3)	C(22)	C(23)	1.374(4)
N(2)	C(5)	1.487(3)	C(23)	C(24)	1.373(5)
N(2)	B(1)	1.759(3)	C(24)	C(25)	1.372(5)
C(1)	C(2)	1.525(4)	C(25)	C(26)	1.387(4)

Can. J. Chem. Downloaded from www.nrcresearchpress.com by 91.121.58.235 on 09/07/12
For personal use only.

TABLE 3. Bond angles (deg) with estimated standard deviations in parentheses

Atom	Atom	Atom	Angle	Atom	Atom	Atom	Angle
N(1)	O(1)	B(1)	108.0(2)	O(4)	C(7)	C(8)	110.3(3)
N(2)	O(2)	B(2)	106.3(2)	O(5)	C(9)	C(10)	142(1)
B(1)	O(3)	B(2)	113.4(2)	O(6)	C(11)	C(12)	108.9(4)
C(4)	O(4)	C(7)	115.8(3)	O(7)	C(13)	C(14)	109.9(4)
C(4)	O(5)	C(9)	116.1(5)	C(16)	C(15)	C(20)	117.1(3)
C(6)	O(6)	C(11)	113.6(3)	C(16)	C(15)	B(1)	121.2(2)
C(6)	O(7)	C(13)	114.6(3)	C(20)	C(15)	B(1)	121.7(2)
O(1)	N(1)	C(1)	105.0(2)	C(15)	C(16)	C(17)	122.1(3)
O(1)	N(1)	C(3)	105.0(2)	C(16)	C(17)	C(18)	120.2(3)
C(1)	N(1)	C(3)	112.7(2)	C(17)	C(18)	C(19)	120.4(3)
O(2)	N(2)	C(2)	108.5(2)	C(18)	C(19)	C(20)	119.2(3)
O(2)	N(2)	C(5)	105.2(2)	C(15)	C(20)	C(19)	121.0(3)
O(2)	N(2)	B(1)	104.1(1)	C(22)	C(21)	C(26)	117.7(2)
C(2)	N(2)	C(5)	113.5(2)	C(22)	C(21)	B(2)	119.3(2)
C(2)	N(2)	B(1)	111.8(2)	C(26)	C(21)	B(2)	122.9(2)
C(5)	N(2)	B(1)	112.9(2)	C(21)	C(22)	C(23)	122.0(3)
N(1)	C(1)	C(2)	111.0(2)	C(22)	C(23)	C(24)	119.3(3)
N(2)	C(2)	C(1)	113.3(2)	C(23)	C(24)	C(25)	120.3(3)
N(1)	C(3)	C(4)	109.2(2)	C(24)	C(25)	C(26)	119.8(3)
O(4)	C(4)	O(5)	109.3(3)	C(21)	C(26)	C(25)	120.7(3)
O(4)	C(4)	C(3)	108.3(3)	O(1)	B(1)	O(3)	116.2(2)
O(5)	C(4)	C(3)	109.2(3)	O(1)	B(1)	N(2)	103.8(2)
N(2)	C(5)	C(6)	114.4(2)	O(1)	B(1)	C(15)	111.2(2)
O(6)	C(6)	O(7)	112.9(2)	O(3)	B(1)	N(2)	96.7(2)
O(6)	C(6)	C(5)	107.8(2)	O(3)	B(1)	C(15)	116.1(2)
O(7)	C(6)	C(5)	112.2(3)	N(2)	B(1)	C(15)	111.1(2)
O(2)	B(2)	O(3)	116.1(2)				
O(2)	B(2)	C(21)	118.2(2)				
O(3)	B(2)	C(21)	125.7(2)				

3677 reflections with $I \geq 3\sigma(I)$. For all 5811 reflections $R = 0.094$. The function minimized was $\Sigma w(|F_o| - |F_c|)^2$, $R = \Sigma||F_o| - |F_c||/\Sigma|F_o|$ and $R_w = (\Sigma w(|F_o| - |F_c|)^2/\Sigma w|F_o|^2)^{1/2}$.

On the final cycle of refinement the maximum parameter shift corresponded to 0.11σ. The mean error in an observation of unit weight was 3.04. The final difference map showed maximum fluctuations of -0.29 to 0.37 e $Å^{-3}$. The final positional and equivalent isotropic thermal parameters for the non-hydrogen atoms appear in Table 1. Bond lengths and angles are listed in Tables 2 and 3, and intra-annular torsion angles in Table 4. Hydrogen parameters, anisotropic thermal parameters, torsion angles, intermolecular contacts, least-squares planes, and structure factors have been deposited.[3]

Results and discussion

The structure analysis confirms the bicyclic formulation **4***A*, with one transannular N—B bond dividing the heterononane system into a six-membered BONCCN ring and a five-membered BOBON ring containing the pyroboronate moiety. The BOBON ring is axially fused to the side of the BONCCN boat, while the *N*- and *B*-substituents (—$CH_2CH_2(OEt)_2$ and phenyl groups, respectively) occupy equatorial positions (see Fig. 1).

The B(2) phenyl group is not exactly coplanar with the O(2)—B(2)—O(3) plane of the BOBON ring (dihedral angle between normals to the mean planes = 9.2°), but the shortened B(2)—C(21) distance is indicative of some π-interaction between the phenyl group and the sp^2-boron atom. The bond length of 1.557(4) Å is comparable to similar bond distances in

TABLE 4. Intra-annular torsion angles (deg) standard deviations in parentheses

Atoms	Value (deg)
B(1)—O(1)—N(1)—C(1)	90.6(2)
O(1)—N(1)—C(1)—C(2)	−52.0(3)
N(1)—C(1)—C(2)—N(2)	−13.6(3)
C(1)—C(2)—N(2)—B(1)	47.3(3)
C(2)—N(2)—B(1)—O(1)	−15.3(2)
N(2)—B(1)—O(1)—N(1)	−48.8(2)
B(2)—O(2)—N(2)—B(1)	13.3(2)
O(2)—N(2)—B(1)—O(3)	−17.5(2)
N(2)—B(1)—O(3)—B(2)	16.1(3)
B(1)—O(3)—B(2)—O(2)	−10.0(3)
O(3)—B(2)—O(2)—N(2)	−4.0(3)

the related bicyclic systems **5** (1.548 Å) (3), **6** (1.557 Å) (4), and **7** (1.555 Å) (5). As in compounds **5–7** there is evidence of O—B $pp(\pi)$ back-donation in the O—(sp^2)B—O portion of the BOBON ring, the partial π-bond character causing short O—B bonds, especially at the anhydridic O(3)—B(2) bond. The bond lengths of 1.454(3), 1.335(3), and 1.404(3) Å in the (sp^3)B—O—(sp^2)B—O moiety are similar to corresponding distances of 1.466, 1.339, 1.406 Å in **5** (3); 1.467, 1.334, 1.404 Å in **6** (4); 1.458, 1.331, 1.404 Å in **7** (5); 1.487, 1.329, 1.422 Å in **8** (8); and 1.495, 1.332, 1.418 Å in **9** (9).

The (sp^3)B—phenyl distance (B(1)—C(15) = 1.579(4) Å) is the shortest yet observed for a compound having a "$PhBO_2N$" ligand set; the bonds in **3** (1), **5** (3), **6** (4), **7** (5), and **10–12**

[3]Supplementary material mentioned in the text may be purchased from the Depository of Unpublished Data, CISTI, National Research Council of Canada, Ottawa, Ont., Canada K1A 0S2.

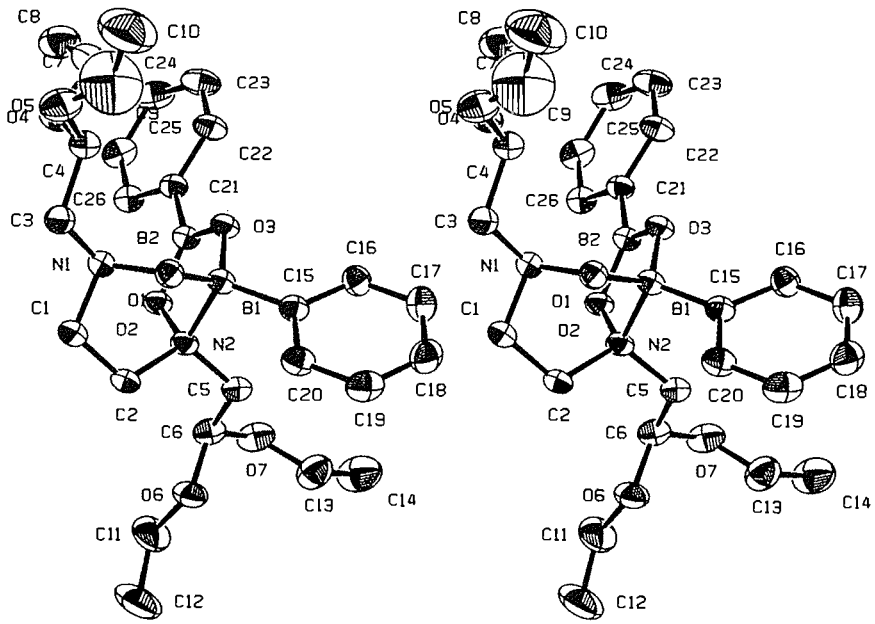

FIG. 1. Stereoscopic view of 1,4-bis(2,2-diethoxyethyl)-6,8-diphenyl-5,7,9-trioxa-4-aza-1-azonia-8-bora-6-boratabicyclo[4.3.0]nonane; 25% probability thermal ellipsoids are shown for the non-hydrogen atoms.

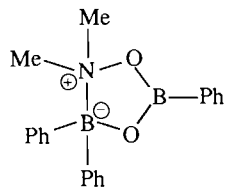

8

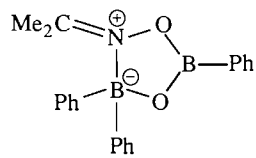

9

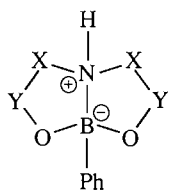

10*a* —X—Y— = —CH_2CH_2—

b —X—Y— =

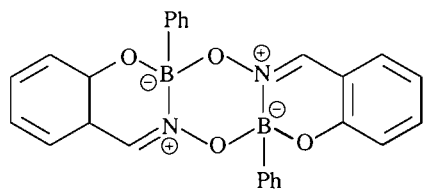

11

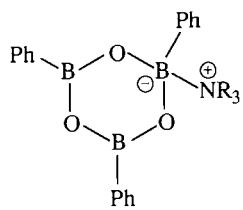

12

(10–13) range from 1.582 Å in **5** to 1.633 Å in **12** with an average value of 1.601 Å. The B(1)—phenyl bond in **4***A* is nearly as short as some (sp^2)B—phenyl bond lengths such as one of the (sp^2)B—C bonds in the phenylboroxin ring of **12** (13) at 1.575 Å and the (sp^2)B—C bond length of 1.574 Å in **3** (1). It is possible that some degree of π-interaction may be occurring between the phenyl substituent and the boron atom involved in the transannular coordinative bond. The shortening of the (sp^3)B—phenyl bond is balanced by the relatively long transannular N(2)—B(1) bond (1.759(3) Å), similar in length to those observed for compounds **5** (1.742 Å) (3) and **7** (1.754 Å) (5). While weaker basicity of the hydroxylamine function could be invoked as a possible cause of the lengthening of the N—B coordinative bond, the most important factor is steric with the

Can. J. Chem. Downloaded from www.nrcresearchpress.com by 91.121.58.235 on 09/07/12
For personal use only.

ring fusion forcing an eclipsed configuration about the N—B bond as noted earlier for **5** and **7**. The N—B bonds in **3** are about 1.66 Å in length (1) and that in **11** is only 1.59 Å (12) in spite of the low basicity at the oxime nitrogen atom. The intramolecular contact N(1)···B(2) = 2.981(4) Å is shorter than the sum of the van der Waals radii (~3.15 Å), but not short enough to form the second intramolecular N—B coordinative interaction required to produce the "nortwistane" structure ***4D***.

Within the ethylenediamine portion of the ring system, the difference between the N(2)—C(2) and N(1)—C(1) distances is striking: the bond at the quaternized nitrogen atom is about 0.03 Å longer than that at the trivalent nitrogen atom (1.484(3) vs. 1.450(3) Å, the latter being a very short N—C single bond). The difference between the other N—C bonds, N(2)—C(5) = 1.487(3) Å and N(1)—C(3) = 1.466(3) Å, is close to that normally observed between N—C bonds at tetravalent and trivalent nitrogen, e.g. compound **5** N—C(methyl): 1.476 and 1.465 Å (3). Surprisingly the two N—O bond lengths are equal to within experimental error (1.458(3) and 1.453(2) Å). In compound **5** a difference of 0.015 Å between the N—O bonds was noted (3).

The five-membered BOBON ring containing the trigonal planar (sp^2)-boron atom has a nearly planar, flattened B(1)—envelope conformation (see Table 4). The geometry of this ring is very similar to that observed for **5** (3) and is comparable to that observed for corresponding BOBON rings in compounds **6–9** (4, 5, 8, 9) which exhibit varying degrees of non-planarity (most pronounced in **8** (8)).

Can. J. Chem. Downloaded from www.nrcresearchpress.com by 91.121.58.235 on 09/07/12
For personal use only.

Acknowledgments

We thank the Natural Sciences and Engineering Research Council of Canada and the Fonds der Chemischen Industrie, Frankfurt am Main, for financial support.

1. H. Amt, W. Kliegel, S. J. Rettig, and J. Trotter. Can. J. Chem. **66**, 1117 (1988).
2. W. Kliegel. J. Organomet. Chem. **253**, 9 (1983).
3. W. Kliegel, S. J. Rettig, and J. Trotter. Can. J. Chem. **62**, 515 (1984).
4. S. J. Rettig, J. Trotter, W. Kliegel, and H. Becker. Can. J. Chem. **54**, 3142 (1976).
5. W. Kliegel, D. Nanninga, S. J. Rettig, and J. Trotter. Can. J. Chem. **62**, 845 (1984).
6. E. Gehrer, W. Klotzer, N. Singewald, and J. Stadlwieser. Synthesis, 633 (1987).
7. International tables for X-ray crystallography. Vol. IV. Kynoch Press, Birmingham. 1974. pp. 99–102 and 149.
8. W. Kliegel, H.-W. Motzkus, S. J. Rettig, and J. Trotter. Can. J. Chem. **62**, 838 (1984).
9. W. Kliegel, D. Nanninga, S. J. Rettig, and J. Trotter. Can. J. Chem. **61**, 2329 (1983).
10. S. J. Rettig and J. Trotter. Can. J. Chem. **53**, 1393 (1975).
11. N. Farfan, P. Joseph-Nathan, L. M. Chiquete, and R. Contreras. J. Organomet. Chem. **348**, 149 (1988).
12. S. J. Rettig and J. Trotter. Can. J. Chem. **61**, 206 (1983).
13. M. Yalpani and R. Boese. Chem. Ber. **116**, 3347 (1983).
14. W. Kliegel, M. Tajerbashi, S. J. Rettig, and J. Trotter. Can. J. Chem. **68**, 69 (1990).

Structural studies of organoboron compounds XL.[1] 4,7-Dicyclohexyl-2,2,5,6-tetraphenyl- 1,3-dioxa-4-aza-7-azonia-2-boratacycloheptane

HENNING AMT AND WOLFGANG KLIEGEL

Institut für Pharmazeutische Chemie, der Technischen Universität Braunschweig, Beethovenstrasse 55, 3300 Braunschweig, Bundesrepublik Deutschland

AND

STEVEN J. RETTIG and JAMES TROTTER

Department of Chemistry, University of British Columbia, 2036 Main Mall, Vancouver, B.C., Canada V6T 1Y6

Received March 13, 1990

This paper is dedicated to Professor Ross Stewart on the occasion of his 65th birthday

HENNING AMT, WOLFGANG KLIEGEL, STEVEN J. RETTIG, and JAMES TROTTER. Can. J. Chem. **68**, 1797 (1990).

The synthesis of 4,7-dicyclohexyl-2,2,5,6-tetraphenyl-1,3-dioxa-4-aza-7-azonia-2-boratacycloheptane is reported. Crystals of the compound are orthorhombic, $a = 10.893(1)$, $b = 28.072(1)$, $c = 10.596(1)$ Å, $Z = 4$, space group $P2_12_12_1$. The structure was solved by direct methods and was refined by full-matrix least-squares procedures to $R = 0.036$ and $R_w = 0.043$ for 2480 reflections with $I \geq 3\sigma(I)$. The molecule has a seven-membered chelate structure. The seven-membered ring, which has a twisted chair conformation, is stabilized by an intramolecular N—H···O hydrogen bond. Bond lengths O—B = 1.468(4) and 1.554(4), C—B = 1.621(5) and 1.626(4) Å are consistent with moderately strong binding of the diphenylboron moiety by the *O,O*-chelating ligand.

Key words: crystal structure, organoboron compound, boron compound.

HENNING AMT, WOLFGANG KLIEGEL, STEVEN J. RETTIG et JAMES TROTTER. Can. J. Chem. **68**, 1797 (1990).

On décrit la synthèse du 4,7-dicyclohexyl-2,2,5,6-tétraphényl-1,3-dioxa-4-aza-7-azonia-2-boratacycloheptane. Les cristaux de ce composé sont orthorhombiques et ils appartiennent au groupe d'espace $P2_12_12_1$, avec $a = 10,893(1)$, $b = 28,072(1)$, $c = 10,596(1)$ Å et $Z = 4$; on a résolu la structure par les méthodes directes et on l'affiné par la méthode des moindres carrés jusqu'à des valeurs respectives de $R = 0,036$ et $R_w = 0,043$ pour 2480 réflexions avec $I \geq 3\sigma(I)$. La molécule possède une structure chélatée à sept chaînons. Le cycle à sept chaînons, qui possède une conformation chaise déformée, est stabilisé par une liaison hydrogène intramoléculaire N—H...O. Les longueurs des liaisons O—B = 1,468 (4) et 1,554(4), C—B = 1,621(5) et 1,626(4) Å sont en accord avec une liaison relativement forte de la portion diphénylbore par le ligand *O,O*-chélatant.

Mots clès : structure cristalline, composé du organobore, composé du bore.

[Traduit par la revue]

Introduction

The addition of 2 mol of phenylmagnesium bromide to glyoxalbisnitrone **1** led to the substituted bishydroxylamine **2** which was reacted with diphenylborinic acid anhydride in ethanol at room temperature. The crystalline reaction product was shown to be a mono-acylation product of the reaction of bishydroxylamine with diphenylborinic acid using quantitative elemental analysis. The presence of an intact diphenylboron moiety was substantiated by the color reaction with diphenylcarbazone (1). The ^{1}H nmr spectrum confirmed the elemental analysis but no signal for an exchangeable proton (OH or NH) was detectable up to $\delta = 20$ ppm. The OH protons of **2**, for instance, give a broad singlet at 4.70 ppm. In the infrared spectrum of the diphenylborinic acid derivative a distinct absorption band at 3100 cm^{-1} is conspicuous, this could correspond to the N—H stretching frequency of an ammonium grouping. Similar values (3050–3150 cm^{-1}) have been reported for N—H vibrations in hydroxylamine derivatives with quaternized nitrogen (2). The O—H absorption of **2** is found as a broadened band between 3200 and 3600 cm^{-1} with a sharp peak at 3580 cm^{-1}. Thus an open-chain acylation derivative **3** or its BONBON-cyclic dimer seemed less reasonable than chelate structures like the seven-membered species **4** or its intramolecular hydrogen bridged variants **4***A* and **4***B*. Although seven-membered boron chelates are rare in the literature (3–6), both the fact that they can be stable compounds and the high affinity of oxygen ligands to boron strongly support a type **4** structure. The six-membered isomer **5** resembles the diphenylboron chelates of 3-aminoalkanols (7, 8) or 2-aminooxyalkanols (9) and could not be definitely precluded, nor could we preclude the hydrogen-bridged derivatives **5***A* and **5***B*. The least probable isomer considered is the five-membered chelate **6** and its hydrogen-bridged derivative **6***A*. Even though five-membered boron chelates with two nitrogen atoms are well known (10) the molecular arrangement of an N—B coordinated *N*-oxide function seems very unfavorable even if stablized by an intramolecular hydrogen bond as in **6***A*. Formally, an intramolecular exchange of the *O,O*-chelated proton in **6***A* for the *N,N*-chelated diphenylborenium (Ph_2B^+) ion would lead to structure **4***A*. The same relationship exists between **5***B* and **4***B*. For clarity an X-ray crystallographic analysis has been undertaken.

Experimental

Synthesis

N,N′-*Dicyclohexyl*-N,N′-*dihydroxy-1,2-diphenyl-1,2-ethanediamine, 2*

N,N′-1,2-Ethanediylidenebis(cyclohexanamine)-*N,N′*-dioxide, **1**[2] (5.05 g, 20 mmol) is suspended in 150 mL dry ether. Under vigorous stirring a Grignard solution of bromobenzene (25.12 g, 160 mmol) and magnesium (3.89 g, 160 mmol) in 150 mL dry ether is added over a period of 10 min. After refluxing for 1 h, the solution is cooled and hydrolysis carried out by the addition of water and then 2 N hydrochloric acid until the magnesium hydroxide is dissolved. The aqueous phase

[1]Previous paper in this series: ref. 22.

[2]Compound **1** has been synthesized by condensation of glyoxal and *N*-cyclohexylhydroxylamine. Melting point 214°C (from ethanol) (11).

Printed in Canada / Imprimé au Canada

Can. J. Chem. Downloaded from www.nrcresearchpress.com by 91.121.58.235 on 09/07/12
For personal use only.

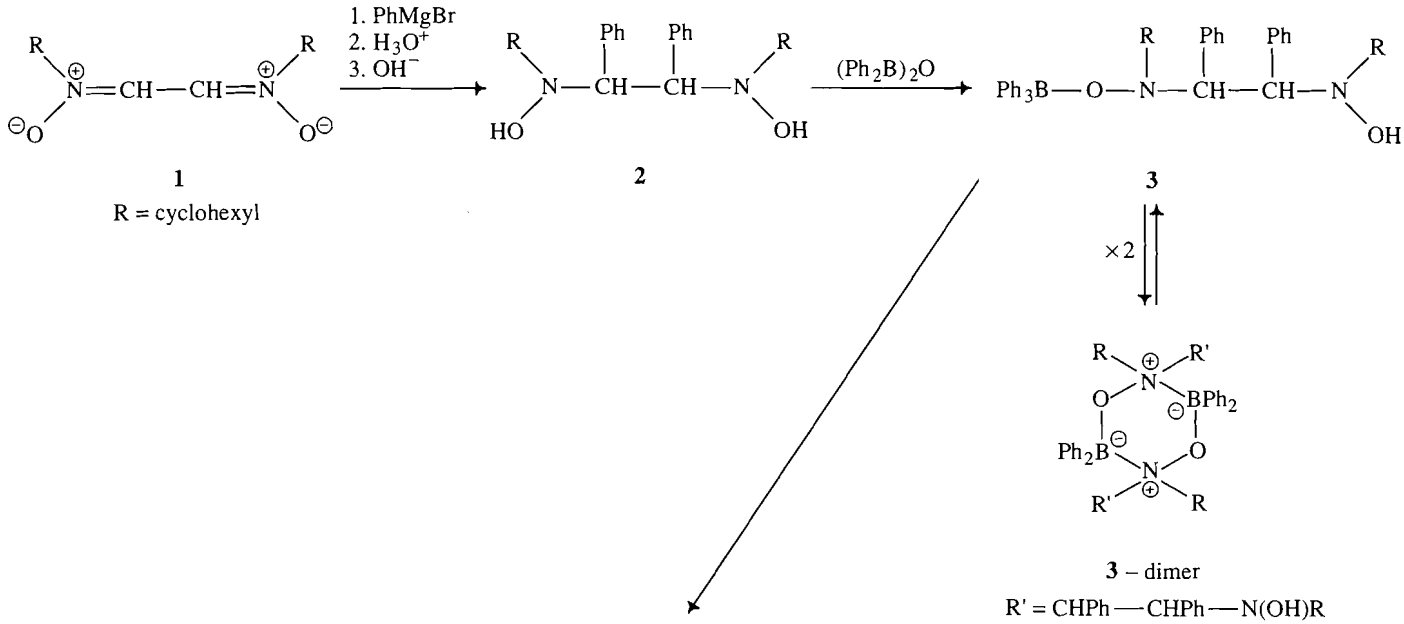

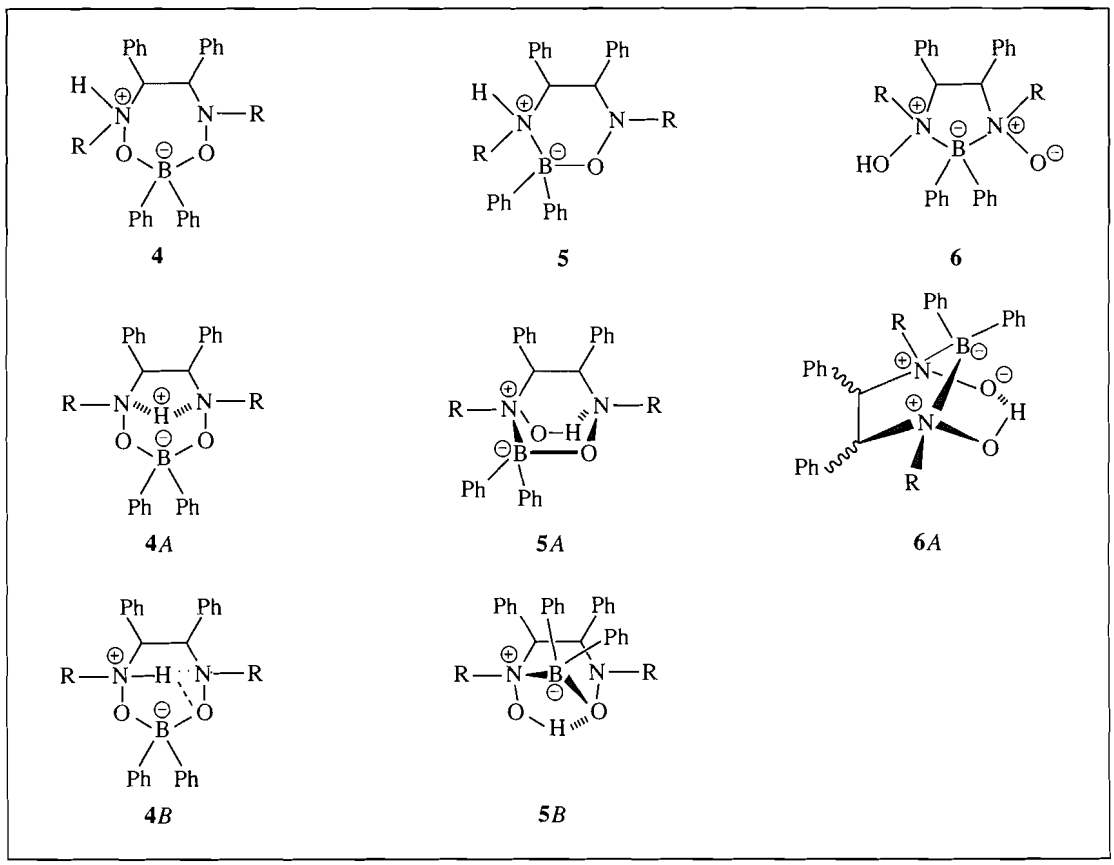

is neutralized with $NaHCO_3$, the pH being brought up to 7–8, and the ether phase separated and dried with Na_2SO_4. After evaporation *in vacuo* the remaining oil is dissolved in a small amount of ether, and crystallization from this solution yields 4.38 g (54%) of a colorless substance. Melting point 139–141°C (from ether). *Anal.* calcd. for $C_{26}H_{36}N_2O_2$: C 76.43, H 8.88, N 6.86; found: C 76.35, H 8.96, N 6.99. Infrared (KBr): 3200–3600 (broad, O—H, H-bonded), 3580 cm^{-1} (O—H, sharp, free O—H?). ^1H nmr ($CDCl_3$/TMS): δ(ppm) = 0.80–1.95 (m, 2 $—CH_2)_5—$), 2.16–2.45 (m, 2 N—CH(cyclohexyl)), 4.62 (s, N—CH—CH—N), 4.70 (s, broad, exchangeable, 2 OH), 7.20 (s, 2 C_6H_5).

4,7,Dicyclohexyl-2,2,5,6-tetraphenyl-1,3-dioxa-4-aza-7-azonia-2-boratacycloheptane, 4

2 (0.82 g, 2 mmol) is dissolved in 20 mL absolute ethanol and mixed with a solution of oxybis(diphenylborane) (0.35 g, 1 mmol) in 10 mL absolute ethanol at room temperature.[3] Crystallization starts after a few minutes and is complete after cooling at −18°C for 6 h. Yield: 0.94 g (82%) of analytically pure material. Recrystallization from ethanol involves heavy losses of the compound. Diethyl ether is the best solvent

[3]Higher temperatures cause dephenylation and rearrangement of the compound (12).

Can. J. Chem. Downloaded from www.nrcresearchpress.com by 91.121.58.235 on 09/07/12
For personal use only.

Can. J. Chem. Downloaded from www.nrcresearchpress.com by 91.121.58.235 on 09/07/12
For personal use only.

for recrystallization but loss of material still occurs.[3] Melting point (decomp.): 114°C (from ether). *Anal.* calcd. for $C_{38}H_{45}BN_2O_2$: C 79.71, H 7.92, B 1.89, N 4.89; found: C 79.72, H 7.83, B 1.96, N 4.88. Infrared (KBr): 3100 cm^{-1} (N—H). ^1H nmr ($CDCl_3$/TMS): δ(ppm) = 0.74–2.20 (m, 2 —$(CH_2)_5$—), 2.40 and 2.56 (m, m, 2 N—CH(cyclohexyl)), 4.40 and 4.58 (s, s, N—CH—CH—N), 7.1–8.0 (m, 4 C_6H_5).

The substance gave a blue color reaction (1) with diphenylcarbazone in methanolic solution, indicating the presence of a diphenylboron moiety. Crystals suitable for X-ray analysis were obtained by recrystallization from ethanol after 14 days at −18°C.

X-ray crystallographic analysis of ***4***

A crystal ca. 0.20 × 0.20 × 0.25 mm in size was mounted on a glass fiber. Unit-cell parameters were refined by least-squares on setting angles for 25 reflections (2θ = 50.2–91.9°) measured on a diffractometer with Cu-K_α radiation (λ = 1.54178 Å). Crystal data at 21°C are as follows:

$C_{38}H_{45}BN_2O_2$ f.w. = 572.60

Orthorhombic, a = 10.893(1), b = 28.072(1), c = 10.596(1) Å, V = 3240.0(5) $Å^3$, Z = 4, ρ_c = 1.174 Mg m^{-3}, $F(000)$ = 1232, μ(Cu-K_α) = 5.16 cm^{-1}. Absent reflections: $h00$, h odd, $0k0$, k odd, and $00l$, l odd, uniquely indicate the space group $P2_12_12_1$ (No. 19).

Intensities were measured with graphite-monochromated Cu-K_α radiation on a Rigaku AFC6S diffractometer. An ω–2θ scan at 16° min^{-1} over a range of (1.05 + 0.30 tan θ)° in ω (with up to eight rescans, background/scan time ratio = 0.5) was employed. Data were measured to 2θ = 155°. The intensities of three check reflections, measured every 150 reflections throughout data collection, showed only small random variations. After data reduction,[4] an empirical absorption correction based on azimuthal scans for three reflections was applied. Transmission factors range from 0.98 to 1.00. Of the 3807 independent reflections measured, 2480 (65.1%) had intensities greater than or equal to 3σ(F^2) above background where $\sigma^2(F^2) = [S^2(C + 4B) + (0.035F^2)^2]/Lp^2$ with S = scan rate, C = scan count, B = total background count, and Lp = Lorentz-polarization factor.

The structure was solved by direct methods, the coordinates of all non-hydrogen atoms being determined from an E-map. The non-hydrogen atoms were refined with anisotropic thermal parameters and the hydrogen atoms (with the exception of the N—H hydrogen atom which was refined with an isotropic thermal parameter) were fixed in idealized positions (C—H = 0.98 Å, $B_H = 1.2B_{bonded\ atom}$). A correction for secondary extinction was applied, the final value of the extinction coefficient being 1.73 × 10^{-4}. Scattering factors for all atoms and anomalous dispersion corrections for the non-hydrogen atoms were taken from ref. 13. The weighting scheme $w = 4F_o^2/\sigma^2(F_o^2)$ gave uniform average values of $w(|F_o| - |F_c|)^2$ over ranges of both $|F_o|$ and sin θ/λ and was employed in the final stages of full-matrix least-squares refinement of 393 variables. Reflections with $I < 3\sigma(I)$ were not included in the refinement. Convergence was reached at R = 0.036 and R_w = 0.043 for 2480 reflections with $I \geq 3\sigma(I)$. A parallel refinement of the mirror-image structure gave slightly higher residuals, the R_w ratio being 1.002. The function minimized was $\Sigma w(|F_o| - |F_c|)^2$, $R = \Sigma||F_o| - |F_c||/\Sigma|F_o|$, $R_w = (\Sigma w(|F_o| - |F_c|)^2/\Sigma w|F_o|^2)^{1/2}$.

On the final cycle of refinement the maximum parameter shift corresponded to 0.01σ. The mean error in an observation of unit weight was 1.44. The final difference map showed maximum fluctuations of −0.12 +0.14 e $Å^{-3}$. The final positional and (equivalent) isotropic thermal parameters for the non-hydrogen atoms appear in Table 1. Bond lengths and angles are given in Tables 2 and 3 and intra-annular torsion angles in Table 4. Hydrogen atom parameters, anisotropic thermal parameters, torsion angles, intermolecular contacts, least-squares planes, bond lengths and angles involving hydrogen, and structure factors have been deposited.[5]

TABLE 1. Final atomic coordinates (fractional) and B_{eq}

Atom	x	y	z	B_{eq}
O(1)	0.1919(2)	0.40303(7)	0.4171(2)	3.05
O(2)	0.1837(2)	0.33464(6)	0.2761(2)	3.02
N(1)	0.2873(2)	0.37550(8)	0.4702(2)	2.8
N(2)	0.1143(2)	0.30278(8)	0.3591(2)	2.9
C(1)	0.2301(3)	0.3349(1)	0.5488(3)	3.0
C(2)	0.2020(2)	0.2920(1)	0.4622(3)	2.9
C(3)	0.3729(3)	0.4087(1)	0.5411(3)	3.2
C(4)	0.4736(3)	0.3814(1)	0.6091(3)	3.8
C(5)	0.5657(3)	0.4158(1)	0.6671(4)	4.7
C(6)	0.6216(3)	0.4479(1)	0.5691(4)	4.6
C(7)	0.5217(3)	0.4764(1)	0.5053(4)	4.9
C(8)	0.4253(3)	0.4439(1)	0.4464(3)	4.2
C(9)	0.0920(3)	0.2597(1)	0.2782(3)	3.6
C(10)	0.2053(3)	0.2380(1)	0.2176(3)	4.5
C(11)	0.1744(5)	0.1972(1)	0.1294(4)	6.2
C(12)	0.0812(5)	0.2121(1)	0.0308(4)	7.0
C(13)	−0.0329(5)	0.2304(1)	0.0932(4)	6.7
C(14)	−0.0026(4)	0.2726(1)	0.1791(3)	4.6
C(15)	0.1318(3)	0.3553(1)	0.6334(3)	3.3
C(16)	0.1618(4)	0.3671(2)	0.7576(3)	5.5
C(17)	0.0776(5)	0.3890(2)	0.8353(4)	8.0
C(18)	−0.0389(5)	0.3974(2)	0.7933(5)	7.4
C(19)	−0.0717(4)	0.3854(1)	0.6714(4)	5.4
C(20)	0.0144(3)	0.3648(1)	0.5919(3)	3.7
C(21)	0.1658(3)	0.2496(1)	0.5430(3)	2.9
C(22)	0.0559(3)	0.2465(1)	0.6082(3)	3.2
C(23)	0.0312(3)	0.2076(1)	0.6853(3)	3.6
C(24)	0.1147(3)	0.1711(1)	0.6973(3)	3.7
C(25)	0.2235(3)	0.1735(1)	0.6332(3)	4.1
C(26)	0.2488(3)	0.2124(1)	0.5570(3)	3.7
C(27)	0.2512(3)	0.4095(1)	0.1808(3)	3.1
C(28)	0.3261(3)	0.3835(1)	0.1006(3)	4.4
C(29)	0.4072(4)	0.4047(1)	0.0178(4)	6.1
C(30)	0.4159(4)	0.4536(1)	0.0128(4)	6.1
C(31)	0.3430(4)	0.4807(1)	0.0900(4)	5.3
C(32)	0.2617(3)	0.4592(1)	0.1717(3)	4.1
C(33)	0.0183(3)	0.4052(1)	0.2630(3)	3.2
C(34)	−0.0371(3)	0.4376(1)	0.3445(3)	3.8
C(35)	−0.1532(3)	0.4567(1)	0.3231(4)	4.5
C(36)	−0.2192(3)	0.4428(1)	0.2178(4)	5.1
C(37)	−0.1673(3)	0.4110(1)	0.1346(3)	4.8
C(38)	−0.0502(3)	0.3932(1)	0.1558(3)	3.9
B	0.1572(3)	0.3859(1)	0.2822(3)	3.0

Results and discussion

The X-ray analysis confirms a seven-membered chelate structure having a twisted chair conformation (see Fig. 1 and Table 4). If an idealized C_2 symmetry, distorted in ***4B***, is taken as a basis for the twisted chair conformation of the seven-membered chelate ring the boron atom would lie on the two-fold axis to offer the most favorable position for geminal disubstitution. The conformation of the seven-membered ring along with the substitution pattern — the C(1) phenyl group is positioned (pseudo)axial while the C(2)—phenyl and the N-cyclohexyl residues occupy (pseudo)equatorial positions — forces H(1) into a (pseudo)axial position at the quaternized nitrogen atom N(1). This particular arrangement only allows the formation of

[4]TEXSAN/TEXRAY structure analysis package which includes versions of the following: MITHRIL, integrated direct methods, by C. J. Gilmore; DIRDIF, direct methods for difference structures, by P. T. Beurskens; ORFLS, full-matrix least-squares, and ORFFE, function and errors, by W. R. Busing, K. O. Martin, and H. A. Levy; ORTEP II, illustrations, by C. K. Johnson.

[5]Supplementary material mentioned in the text may be purchased from the Depository of Unpublished Data, CISTI, National Research Council of Canada, Ottawa, Ont., Canada K1A 0S6.

Can. J. Chem. Downloaded from www.nrcresearchpress.com by 91.121.58.235 on 09/07/12
For personal use only.

TABLE 2. Bond lengths (Å) with estimated standard deviations in parentheses

Atom	Atom	Distance	Atom	Atom	distance
O(1)	N(1)	1.412(3)	C(16)	C(17)	1.377(6)
O(1)	B	1.554(4)	C(17)	C(18)	1.366(6)
O(2)	N(2)	1.464(3)	C(18)	C(19)	1.382(6)
O(2)	B	1.468(4)	C(19)	C(20)	1.388(5)
N(1)	C(3)	1.517(3)	C(21)	C(22)	1.385(4)
N(1)	C(1)	1.543(3)	C(21)	C(26)	1.389(4)
N(2)	C(2)	1.482(4)	C(22)	C(23)	1.390(4)
N(2)	C(9)	1.502(4)	C(23)	C(24)	1.376(4)
C(1)	C(15)	1.510(4)	C(24)	C(25)	1.368(4)
C(1)	C(2)	1.543(4)	C(25)	C(26)	1.386(4)
C(2)	C(21)	1.519(4)	C(27)	C(28)	1.387(4)
C(3)	C(8)	1.520(4)	C(27)	C(32)	1.403(4)
C(3)	C(4)	1.521(4)	C(27)	B	1.626(4)
C(4)	C(5)	1.523(4)	C(28)	C(29)	1.380(5)
C(5)	C(6)	1.503(5)	C(29)	C(30)	1.378(5)
C(6)	C(7)	1.511(5)	C(30)	C(31)	1.370(5)
C(7)	C(8)	1.524(4)	C(31)	C(32)	1.377(5)
C(9)	C(14)	1.515(4)	C(33)	C(34)	1.391(4)
C(9)	C(10)	1.518(5)	C(33)	C(38)	1.400(4)
C(10)	C(11)	1.516(5)	C(33)	B	1.621(5)
C(11)	C(12)	1.515(6)	C(34)	C(35)	1.392(5)
C(12)	C(13)	1.499(6)	C(35)	C(36)	1.383(5)
C(13)	C(14)	1.529(5)	C(36)	C(37)	1.375(5)
C(15)	C(20)	1.378(4)	C(37)	C(38)	1.389(5)
C(15)	C(16)	1.396(4)			

TABLE 3. Bond angles (deg) with estimated standard deviations in parentheses

Atom	Atom	Atom	Angle	Atom	Atom	Atom	Angle
N(1)	O(1)	B	112.1(2)	C(18)	C(17)	C(16)	120.1(4)
N(2)	O(2)	B	118.1(2)	C(17)	C(18)	C(19)	120.1(4)
O(1)	N(1)	C(3)	108.2(2)	C(18)	C(19)	C(20)	119.6(4)
O(1)	N(1)	C(1)	108.8(2)	C(15)	C(20)	C(19)	120.9(3)
C(3)	N(1)	C(1)	115.8(2)	C(22)	C(21)	C(26)	117.5(3)
O(2)	N(2)	C(2)	103.6(2)	C(22)	C(21)	C(2)	123.7(2)
O(2)	N(2)	C(9)	103.4(2)	C(26)	C(21)	C(2)	118.7(3)
C(2)	N(2)	C(9)	111.2(2)	C(21)	C(22)	C(23)	120.6(3)
C(15)	C(1)	N(1)	109.1(2)	C(24)	C(23)	C(22)	120.8(3)
C(15)	C(1)	C(2)	120.5(2)	C(25)	C(24)	C(23)	119.3(3)
N(1)	C(1)	C(2)	109.6(2)	C(24)	C(25)	C(26)	120.0(3)
N(2)	C(2)	C(21)	114.1(2)	C(25)	C(26)	C(21)	121.7(3)
N(2)	C(2)	C(1)	114.0(2)	C(28)	C(27)	C(32)	115.7(3)
C(21)	C(2)	C(1)	109.2(2)	C(28)	C(27)	B	124.1(3)
N(1)	C(3)	C(8)	107.7(2)	C(32)	C(27)	B	120.2(3)
N(1)	C(3)	C(4)	111.5(2)	C(29)	C(28)	C(27)	122.6(3)
C(8)	C(3)	C(4)	111.7(3)	C(30)	C(29)	C(28)	119.9(3)
C(3)	C(4)	C(5)	110.2(3)	C(31)	C(30)	C(29)	119.4(3)
C(6)	C(5)	C(4)	111.6(3)	C(30)	C(31)	C(32)	120.4(3)
C(5)	C(6)	C(7)	109.5(3)	C(31)	C(32)	C(27)	122.0(3)
C(6)	C(7)	C(8)	111.3(3)	C(34)	C(33)	C(38)	115.4(3)
C(3)	C(8)	C(7)	112.2(3)	C(34)	C(33)	B	123.1(3)
N(2)	C(9)	C(14)	108.3(2)	C(38)	C(33)	B	121.3(3)
N(2)	C(9)	C(10)	115.6(3)	C(33)	C(34)	C(35)	123.0(3)
C(14)	C(9)	C(10)	110.8(3)	C(36)	C(35)	C(34)	119.6(3)
C(11)	C(10)	C(9)	112.5(3)	C(37)	C(36)	C(35)	119.2(3)
C(12)	C(11)	C(10)	111.4(3)	C(36)	C(37)	C(38)	120.5(3)
C(13)	C(12)	C(11)	110.3(3)	C(37)	C(38)	C(33)	122.3(3)
C(12)	C(13)	C(14)	110.4(4)	O(2)	B	O(1)	107.3(2)
C(9)	C(14)	C(13)	112.0(3)	O(2)	B	C(33)	120.4(3)
C(20)	C(15)	C(16)	118.2(3)	O(2)	B	C(27)	104.4(2)
C(20)	C(15)	C(1)	122.8(3)	O(1)	B	C(33)	103.8(2)
C(16)	C(15)	C(1)	118.9(3)	O(1)	B	C(27)	109.1(2)
C(17)	C(16)	C(15)	120.9(4)	C(33)	B	C(27)	111.6(2)

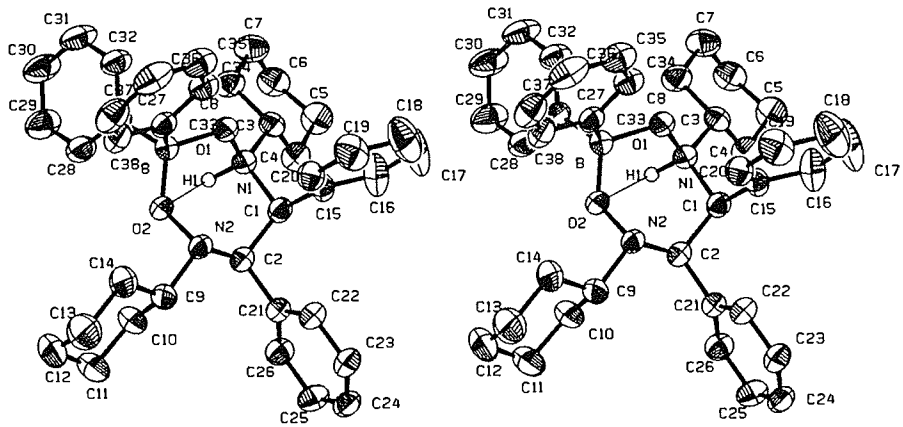

FIG. 1. Stereoview of the 4,7-dicyclohexyl-2,2,5,6-tetraphenyl-1,3-dioxa-4-aza-7-azonia- 2-boratacycloheptane molecule; 50% probability thermal ellipsoids are shown for the non-hydrogen atoms.

TABLE 4. Intra-annualr torsion angles

Atoms	Value
B—O(1)—N(1)—C(1)	−93.1(2)
O(1)—N(1)—C(1)—C(2)	85.8(3)
N(1)—C(1)—C(2)—N(2)	−60.4(3)
C(1)—C(2)—N(2)—O(2)	69.1(3)
C(2)—N(2)—O(2)—B	−102.3(3)
N(2)—O(2)—B—O(1)	63.4(3)
O(2)—B—O(1)—N(1)	29.0(3)
C(8)—C(3)—C(4)—C(5)	53.2(3)
C(3)—C(4)—C(5)—C(6)	−57.9(4)
C(4)—C(5)—C(6)—C(7)	59.7(4)
C(5)—C(6)—C(7)—C(8)	−57.2(4)
C(6)—C(7)—C(8)—C(3)	54.1(4)
C(7)—C(8)—C(3)—C(4)	−52.1(4)
C(14)—C(9)—C(10)—C(11)	−51.8(4)
C(9)—C(10)—C(11)—C(12)	54.2(4)
C(10)—C(11)—C(12)—C(13)	−57.1(5)
C(11)—C(12)—C(13)—C(14)	58.2(5)
C(12)—C(13)—C(14)—C(9)	−57.2(4)
C(13)—C(14)—C(9)—C(10)	53.2(4)

an intramolecular N—H···O(2) hydrogen bond, resulting in the H-bridged structure **4***B*. The N(1)···O(2) distance (2.612(3) Å) is shorter than the alternative N(2)···O(1) distance (3.002(3) Å). The H(1)···O(2) contact of 2.18(3) Å is similar to those reported for intermolecular N—H···O hydrogen bonds in the solid state structures of compounds **7** (2.11(5) Å) (14), **8** (1.97(2) Å) (2*a*), and **9** (2.15(4) Å) (15). These types of *N*-monoprotonated boron chelate compounds all show relatively sharp N—H stretching frequencies at about 3100 cm^{-1} in their infrared spectra (2, 16, 17), indicating weak N—H···O hydrogen bonding, as does the bent (102(2)°) intramolecular N(1)—H(1)···O(2) hydrogen bridge in **4***B* with an infrared band at 3100 cm^{-1}. A strong intramolecular N—H···N hydrogen bond, as proposed in formula **4***A*, cannot be formed for steric reasons (ring conformation). The presence of such a hydrogen bridge would be indicated by broad association bands in the infrared spectrum and signals in the ^1H nmr spectrum such as those reported for "proton cryptates" or "proton sponges" (18).

The mono-protonation and H-bridging in **4***B* introduces asymmetry into the basically symmetric ring skeleton. The N—C bonds of the ethylenediamine portion of the ring differ by about 0.06 Å: N(1)—C(1) = 1.543(3) Å and N(2)—C(2) = 1.482(4) Å. The O(1)—B bond (1.554(4) Å) is markedly longer than the O(2)—B bond (1.468(4) Å). This difference is larger than that between the O—B bonds in the asymmetric six-membered diphenylboron chelate **10** with values of 1.552 and 1.493 Å (19). The N—O bond length within the quaternized hydroxylamine group (N(1)—O(1) = 1.412(3) Å) is about 0.05 Å shorter than that involving the trivalent nitrogen atom (N(2)—O(2) = 1.464(3) Å). A similar, but less pronounced, difference has been observed for the N—O bonds in compound **11** (20) which also contains both tri- and tetravalent hydroxylamine nitrogen atoms. The asymmetry of **4***B* is also reflected by the ^1H nmr spectrum which displays separate signals for the methine protons of C(1) and C(2), and also for those of C(3) and C(9). Both geminal *B*-phenyl substituents display nearly equal C—B distances of normal magnitude (1.621(5) and 1.626(5) Å), comparable to those in **10** which average 1.623 Å (19).

The mean C—B/mean O—B bond length ratio of 1.074 for **4***B* is indicative of fairly strong overall binding of the *O,O*-chelating ligand to the diphenylboron moiety (21). The two cyclohexane rings have essentially undistorted chair conformations (see Table 4). The remaining molecular geometry (Tables 2 and 3) is as expected. Molecules are well separated in the crystal lattice, the shortest intermolecular contact between non-hydrogen atoms being C(6)···C(35) (1 + *x*, *y*, *z*) = 3.587(5) Å.

Acknowledgements

We thank the Natural Sciences and Engineering Research Council of Canada and the Fonds der Chemischen Industrie, Frankfurt am Main, for financial support.

Can. J. Chem. Downloaded from www.nrcresearchpress.com by 91.121.58.235 on 09/07/12
For personal use only.

1. R. NEU. Z. Anal. Chem. **176**, 334 (1960).
2. (*a*) S. J. RETTIG, J. TROTTER, W. KLIEGEL, and H. BECKER. Can. J. Chem. **54**, 3142 (1976); (*b*) W. KLIEGEL, B. ENDERS, and H. BECKER. Liebigs Ann. Chem. 1712 (1982); (*c*) W. KLIEGEL and J. GRAUMANN. Chemiker-Ztg. **106**, 378 (1982).
3. M. FINKELSTEIN, E. A. MAYEDA, and S. D. ROSS. J. Org. Chem. **40**, 804 (1975); G. SAICHEK *et al.* (Chemie Linz A.G.-Lentia G. m.b.H.). Europ. Pat. 0 005 497 (1979); Chem. Abstr. **93**, 46174*h* (1980).
4. W. KLIEGEL and D. NANNINGA. J. Organomet. Chem. **243**, 373 (1985) and references therein.
5. W. KLIEGEL, U. LAUTERBACH, S. J. RETTIG, and J. TROTTER. Can. J. Chem. **65**, 1457 (1987).
6. W. KLIEGEL, M. TAJERBASHI, S. J. RETTIG, and J. TROTTER. Can. J. Chem. **66**, 2621 (1988).
7. J.-L. DELARUE and R. L. FALLARD (Laboratoires Toraude). French Pat. 3036 M (1965); Chem. Abstr. **62**, 13179*e* (1965).
8. H. WEIDMANN and H. K. ZIMMERMAN. Liebigs Ann. Chem. **619**, 28 (1958); S. J. RETTIG and J. TROTTER. Can. J. Chem. **61**, 2334 (1983).
9. K. DRÜCKLER, W. KLIEGEL, S. J. RETTIG, and J. TROTTER. Can. J. Chem. **67**, 2218 (1989).
10. R. KOSTER. *In* Houben-Weyl, Methoden der organischen chemie. Vol. 13, part 3 b, Organobor-Verbindungen II. Stuttgart. 1983.
11. W. KLIEGEL and H. BECKER. Unpublished results; H. Becker. Ph.D. Dissertation, Braunschweig. 1975.
12. W. KLIEGEL and H. AMT. Unpublished results.
13. International tables for X-ray crystallography Vol. IV. Kynoch Press, Birmingham, U.K. (present distributor Kluwer Academic Publishers:Dordrecht, The Netherlands), 1974; pp. 99–102, 149.
14. S. J. RETTIG and J. TROTTER. Can. J. Chem. **53**, 1393 (1975).
15. S. J. RETTIG and J. TROTTER. Can. J. Chem. **55**, 958 (1977).
16. O. C. MUSGRAVE and T. O. PARK. Chem. Ind. (London) **26**, 1552 (1955).
17. F. DALLACKER, E. M. BOTH-POLLMANN, and W. MÜLLNERS. Chemiker-Ztg. **108**, 287 (1984).
18. J. CHENEY and J. M. LEHN. J. Chem. Soc. Chem. Commun. 487 (1972); R. W. ALDER, R. E. MOSS, and R. B. SESSIONS. J. Chem. Soc. Chem. Commun. 1000 (1983); H. A. STAAB and T. SAUPE. Angew. Chem. **100**, 895 (1988).
19. E. EBELING, W. KLIEGEL, S. J. RETTIG, and J. TROTTER. Can. J. Chem. **67**, 933 (1989).
20. W. KLIEGEL, S. J. RETTIG, and J. TROTTER. Can. J. Chem. **62**, 515 (1984).
21. W. CULLEN, S. J. RETTIG, J. TROTTER, and E. B. WICKENHEISER. Can. J. Chem. **66**, 2007 (1988) and references therein.
22. H. AMT, W. KLIEGEL, S. J. RETTIG, and J. TROTTER. Can. J. Chem. **68**, 1791 (1990).

Can. J. Chem. Downloaded from www.nrcresearchpress.com by 91.121.58.235 on 09/07/12
For personal use only.

Structural studies of organoboron compounds. XLI. (3-Hydroxy-2-methyl-1-(*p*-tolyl)-4-pyridinonato)diphenylboron

CHRIS ORVIG, STEVEN J. RETTIG, JAMES TROTTER, AND ZAIHUI ZHANG
Department of Chemistry, University of British Columbia, 2036 Main Mall, Vancouver, B.C., Canada V6T 1Y6

Received March 26, 1990

This paper is dedicated to Professor Ross Stewart on the occasion of his 65th birthday

CHRIS ORVIG, STEVEN J. RETTIG, JAMES TROTTER, and ZAIHUI ZHANG. Can. J. Chem. **68**, 1803 (1990).

(3-Hydroxy-2-methyl-1-(*p*-tolyl)-4-pyridinonato)diphenylboron has been prepared in high yield by the reaction of 3-hydroxy-2-methyl-1-(*p*-tolyl)-4-pyridinone with diphenylborinic acid. Crystals of the hemi-acetone solvate are triclinic, a = 15.119(2), b = 16.528(1), c = 9.5802(9) Å, α = 98.721(6), β = 93.344(8), γ = 102.443(6)°, Z = 4, space group $P\bar{1}$. The structure was solved by direct methods and was refined by full-matrix least-squares procedures to R = 0.050 and R_w = 0.065 for 4330 reflections with $I \geq 3\sigma(I)$. The five-membered chelate rings in both of the two crystallographically independent molecules have flattened *B*-envelope conformations (maximum deviations from the mean planes = 0.114(4) and 0.065(5) Å). Mean bond lengths O—B = 1.553 and C—B = 1.599 Å are consistent with intermediate strength binding of the diphenylboron moiety by the *O,O*-chelating ligand.

Key words: crystal structure, organoboron compound.

CHRIS ORVIG, STEVEN J. RETTIG, JAMES TROTTER et ZAIHUI ZHANG. Can. J. Chem. **68**, 1803 (1990).

On a préparé le (3-hydroxy-2-méthyl-1-(*p*-tolyl)-4-pyridinato)diphénylbore avec un excellent rendement en faisant réagir de la 3-hydroxy-2-méthyl-1-(*p*-tolyl)-4-pyridinone avec de l'acide diphénylborinique. Les cristaux solvatés par une demi-molécule d'acétone sont tricliniques et ils appartiennent au groupe d'espace $P\bar{1}$ avec a = 15,119(2), b = 16,528(1), et c = 9,5802(9) Å, α = 98,721(6), β = 93,344(8), et γ = 102,443(6)°, et Z = 4. On a résolu la structure par les méthodes directes et on l'a affinée par la méthode des moindres carrés jusqu'à des valeurs respectives de R = 0,050 et R_w = 0,065 pour 4330 réflexions avec $I \geq 3\sigma(I)$. Les cycles chélatés à cinq chainons des deux molécules cristallographiquement indépendantes possèdent une conformation enveloppe-B (déviations maximales du plan moyen = 0,114(4) et 0,065(5) Å). Les longueurs moyennes des liaisons O—B et C—B (1,553 et 1,599 Å) sont en accord avec une liaison de force moyenne entre la portion diphénylbore et le ligand chélatant-*O,O*.

Mots clés : structure cristalline, composé du organobore.

[Traduit par la revue]

Introduction

The title compound **1** has been prepared as part of a continuing investigation of the structures of organoboron compounds (1) (including 3-hydroxy-4-pyrone **4** (2) and 3-hydroxy-4-pyridinone (3) complexes **2** and **3**) and in parallel with chemical and biological studies of neutral 3-hydroxy-4-pyridinone complexes (of variable lipophilicity) of the other group 13 metal ions Al^{3+}, Ga^{3+}, and In^{3+} (4, 5).

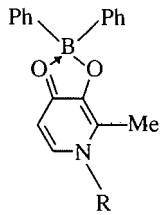

1, R = *p*-tolyl
2, R = H
3, R = Me

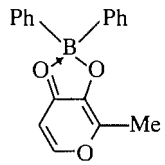

4

Experimental

*(3-Hydroxy-2-methyl-1-(*p*-tolyl)-4-pyridinonato)diphenylboron*

A solution of diphenylborinic acid was prepared by the acid hydrolysis (60 mL 0.10 *M* HCl) of (2-aminoethanolato)diphenylboron (0.658 g, 2.92 mmol, Aldrich Chemical) and was extracted with diethyl ether (4 × 50 mL). To the organic layer was added a solution of (3-hydroxy-2-methyl-1-(*p*-tolyl)-4-pyridinone (0.620 g, 2.88 mmol, prepared according to ref. 5) in 50 mL ethanol. The solution was stirred for 1 h, reduced in volume to 120 mL, and kept at 4°C overnight. A white crystalline product was isolated by filtration and dried *in vacuo* (yield 0.892 g, 82%). Analytically pure flakes were obtained by recrystallization from acetone/water, mp 160–161°C (uncorrected). *Anal.* calcd. for $C_{25}H_{22}BNO_2$: C 79.13, H 5.85, N 3.69; found: C 79.31, H 5.83, N 3.62. Infrared (KBr, all strong, cm^{-1}): 1635 ($\nu_{C=O}$); 1580, 1570, 1530, 1480 ($\nu_{C=C}$, pyridinone ring). ^1H NMR (d_6-acetone, 25°C, 300 MHz): δ 2.19 (s, 3H, NC(CH_3)); 2.48 (s, 3H, $C_6H_4(CH_3)$); 6.82 (d, 6.7 Hz, 1H, C*H*C(O)); 7.1–7.5 (m, 14H, $2C_6H_5$ and C_6H_4); 7.83 (d, 6.7 Hz, 1H, CHC*H*N).

The infrared spectrum was recorded on a Perkin-Elmer 783 from 4000–200 cm^{-1} and the ^1H NMR spectrum on a Varian XL-300. Crystals used for the X-ray analysis were obtained by slow evaporation of an acetone solution.

X-ray crystallographic analysis

A crystal *ca.* 0.12 × 0.15 × 0.35 mm in size was mounted on a glass fiber. Unit-cell parameters were refined by least-squares on setting angles for 25 reflections (2θ = 50.1–82.8°C) measured on a diffractometer with Cu-K_α radiation (λ = 1.54178 Å). Crystal data at 21°C are as follows:

$C_{25}H_{22}BNO_2 \cdot (1/2)\ C_3H_6O$ f.w. = 408.30

Triclinic, a = 15.119(2), b = 16.528(1), c = 9.5802(9) Å, α = 98.721(6), β = 93.344(8), γ = 102.443(6)°, V = 2300.4(4) Å^3, Z = 4, ρ_c = 1.179 Mg m^{-3}, $F(000)$ = 864, μ(Cu-K_α) = 5.53 cm^{-1}. Absent reflections: none, space group $P\bar{1}$ (reduced cell, Donnay convention) from structure analysis.

Intensities were measured with graphite-monochromated Cu-K_α radiation on a Rigaku AFC6S diffractometer. An ω–2θscan at 16° min^{-1} over a range of (1.00 + 0.25 tan θ)° in ω (with up to eight rescans, background/scan time ratio = 0.5) was employed. Data were measured to 2θ = 155°. The intensities of three check reflections, measured every 200 reflections throughout the data collection, re-

Can. J. Chem. Downloaded from www.nrcresearchpress.com by 91.121.58.235 on 09/07/12
For personal use only.

Can. J. Chem. Downloaded from www.nrcresearchpress.com by 91.121.58.235 on 09/07/12
For personal use only.

TABLE 1. Final atomic coordinates (fractional) and B_{eq}

Atom	x	y	z	B_{eq}
O(1)	0.5032(1)	0.2704(1)	0.4040(2)	3.96(8)
O(2)	0.3983(1)	0.3495(1)	0.3342(2)	4.55(9)
O(3)	0.3050(1)	0.7488(1)	0.1974(2)	5.2(1)
O(4)	0.3115(1)	0.7047(1)	−0.0508(2)	5.05(9)
O(5)	0.9399(4)	0.0355(4)	0.6195(6)	15.1(3)
N(1)	0.6649(2)	0.4609(1)	0.3749(3)	4.0(1)
N(2)	0.5206(2)	0.8835(1)	0.1578(3)	3.9(1)
C(1)	0.7027(2)	0.3355(2)	0.4562(4)	5.3(1)
C(2)	0.6361(2)	0.3811(2)	0.4054(3)	3.7(1)
C(3)	0.5449(2)	0.3478(2)	0.3854(3)	3.5(1)
C(4)	0.4825(2)	0.3925(2)	0.3411(3)	3.9(1)
C(5)	0.5146(2)	0.4724(2)	0.3116(4)	4.9(1)
C(6)	0.6060(2)	0.5041(2)	0.3289(4)	4.6(1)
C(7)	0.7610(2)	0.5020(2)	0.3946(3)	4.1(1)
C(8)	0.7980(3)	0.5445(3)	0.5241(4)	7.2(2)
C(9)	0.8887(3)	0.5852(3)	0.5416(4)	8.1(2)
C(10)	0.9424(2)	0.5844(2)	0.4327(4)	5.4(1)
C(11)	0.9025(2)	0.5418(3)	0.3032(4)	6.6(2)
C(12)	0.8117(2)	0.5003(2)	0.2836(4)	5.9(2)
C(13)	1.0416(3)	0.6293(3)	0.4525(5)	8.3(2)
C(14)	0.3454(2)	0.1873(2)	0.2814(3)	4.1(1)
C(15)	0.3509(3)	0.1058(2)	0.2955(4)	5.7(2)
C(16)	0.3025(3)	0.0363(2)	0.2019(5)	7.1(2)
C(17)	0.2468(3)	0.0455(3)	0.0902(5)	6.9(2)
C(18)	0.2402(3)	0.1244(3)	0.0728(5)	7.0(2)
C(19)	0.2883(2)	0.1936(2)	0.1671(4)	5.6(2)
C(20)	0.3666(2)	0.2749(2)	0.5484(4)	4.4(1)
C(21)	0.4258(3)	0.2922(2)	0.6709(4)	5.2(2)
C(22)	0.3967(4)	0.3010(3)	0.8048(5)	7.3(2)
C(23)	0.3066(5)	0.2933(3)	0.8193(6)	8.5(3)
C(24)	0.2449(4)	0.2773(3)	0.7016(7)	8.1(2)
C(25)	0.2752(3)	0.2671(2)	0.5668(4)	6.0(2)
C(26)	0.4417(2)	0.8836(2)	0.3805(4)	5.1(1)
C(27)	0.4473(2)	0.8511(2)	0.2281(3)	3.9(1)
C(28)	0.3805(2)	0.7898(2)	0.1501(3)	3.9(1)
C(29)	0.3840(2)	0.7622(2)	0.0043(3)	4.0(1)
C(30)	0.4586(2)	0.7955(2)	−0.0615(3)	4.2(1)
C(31)	0.5257(2)	0.8556(2)	0.0186(3)	4.3(1)
C(32)	0.5952(2)	0.9504(2)	0.2311(3)	4.1(1)
C(33)	0.6576(2)	0.9337(2)	0.3230(4)	5.3(1)
C(34)	0.7281(2)	0.9987(2)	0.3900(4)	5.7(2)
C(35)	0.7372(2)	1.0789(2)	0.3641(4)	4.8(1)
C(36)	0.6737(3)	1.0934(2)	0.2691(5)	6.8(2)
C(37)	0.6019(3)	1.0301(2)	0.2026(4)	6.6(2)
C(38)	0.8128(3)	1.1492(2)	0.4392(5)	7.0(2)
C(39)	0.1585(2)	0.7280(2)	0.0326(4)	4.9(1)
C(40)	0.1134(4)	0.7629(3)	0.1386(5)	8.9(3)
C(41)	0.0354(4)	0.7909(4)	0.1099(7)	11.0(3)
C(42)	0.0007(4)	0.7850(3)	−0.0255(8)	8.8(3)
C(43)	0.0427(3)	0.7505(3)	−0.1328(5)	7.7(2)
C(44)	0.1194(3)	0.7220(3)	−0.1028(4)	6.5(2)
C(45)	0.2259(2)	0.5951(2)	0.0880(3)	4.4(1)
C(46)	0.2964(2)	0.5541(3)	0.1005(4)	6.0(2)
C(47)	0.2814(3)	0.4689(3)	0.1065(4)	6.6(2)
C(48)	0.1940(3)	0.4227(2)	0.1005(4)	6.3(2)
C(49)	0.1228(3)	0.4605(2)	0.0899(4)	5.8(2)
C(50)	0.1386(2)	0.5458(2)	0.0842(4)	5.0(1)
C(51)	0.9645(5)	−0.0227(5)	0.6704(7)	10.5(4)
C(52)	0.9196(5)	−0.1076(5)	0.6187(9)	13.7(4)
C(53)	1.0376(5)	−0.0013(5)	0.7812(8)	15.2(4)
B(1)	0.4003(2)	0.2665(2)	0.3928(4)	4.0(1)
B(2)	0.2454(3)	0.6922(3)	0.0691(4)	4.8(2)

TABLE 2. Bond lengths (Å) with estimated standard deviations in parentheses

Atom	Atom	Distance	Atom	Atom	Distance
O(1)	C(3)	1.342(3)	C(20)	C(25)	1.384(5)
O(1)	B(1)	1.540(4)	C(20)	B(1)	1.599(5)
O(2)	C(4)	1.310(3)	C(21)	C(22)	1.377(5)
O(2)	B(1)	1.564(4)	C(22)	C(23)	1.357(7)
O(3)	C(28)	1.337(4)	C(23)	C(24)	1.376(7)
O(3)	B(2)	1.535(4)	C(24)	C(25)	1.394(6)
O(4)	C(29)	1.309(3)	C(26)	C(27)	1.491(4)
O(4)	B(2)	1.574(4)	C(27)	C(28)	1.359(4)
O(5)	C(51)	1.255(7)	C(28)	C(29)	1.410(4)
N(1)	C(2)	1.379(4)	C(29)	C(30)	1.377(4)
N(1)	C(6)	1.349(4)	C(30)	C(31)	1.360(4)
N(1)	C(7)	1.453(4)	C(32)	C(33)	1.353(4)
N(2)	C(27)	1.382(4)	C(32)	C(37)	1.369(4)
N(2)	C(31)	1.356(4)	C(33)	C(34)	1.386(4)
N(2)	C(32)	1.457(4)	C(34)	C(35)	1.364(5)
C(1)	C(2)	1.482(4)	C(35)	C(36)	1.367(5)
C(2)	C(3)	1.361(4)	C(35)	C(38)	1.501(5)
C(3)	C(4)	1.401(4)	C(36)	C(37)	1.380(5)
C(4)	C(5)	1.383(4)	C(39)	C(40)	1.379(5)
C(5)	C(6)	1.359(4)	C(39)	C(44)	1.374(5)
C(7)	C(8)	1.353(4)	C(39)	B(2)	1.594(5)
C(7)	C(12)	1.347(4)	C(40)	C(41)	1.385(7)
C(8)	C(9)	1.379(5)	C(41)	C(42)	1.351(7)
C(9)	C(10)	1.359(5)	C(42)	C(43)	1.357(7)
C(10)	C(11)	1.365(5)	C(43)	C(44)	1.373(6)
C(10)	C(13)	1.510(5)	C(45)	C(46)	1.388(5)
C(11)	C(12)	1.384(5)	C(45)	C(50)	1.390(4)
C(14)	C(15)	1.394(4)	C(45)	B(2)	1.609(5)
C(14)	C(19)	1.385(4)	C(46)	C(47)	1.389(5)
C(14)	B(1)	1.595(5)	C(47)	C(48)	1.369(5)
C(15)	C(16)	1.381(5)	C(48)	C(49)	1.362(5)
C(16)	C(17)	1.371(6)	C(49)	C(50)	1.388(5)
C(17)	C(18)	1.362(6)	C(51)	C(52)	1.420(8)
C(18)	C(19)	1.380(5)	C(51)	C(53)	1.432(8)
C(20)	C(21)	1.388(5)			

mained essentially constant. After data reduction,[1] an empirical absorption correction (based on azimuthal scans for four reflections) was applied. Transmission factors range from 0.96 to 1.00. Of the 10304 reflections measured, 9377 were unique ($R_{int} = 0.020$) and 4330 (46.2%) of these had intensities greater than or equal to $3\sigma(F^2)$ above background where $\sigma^2(F^2) = [S^2(C + 4B) + (0.045F^2)^2]/Lp^2$ with S = scan rate, C = scan count, B = total background count, and Lp = Lorentz-polarization factor.

The structure analysis was initiated in the centrosymmetric space group $P\bar{1}$ on the basis of the E-statistics, the choice being verified by the subsequent successful solution and refinement of the structure. The structure was solved by direct methods, the coordinates of all non-hydrogen atoms being determined from the E-map or from subsequent difference Fourier syntheses. The non-hydrogen atoms were refined with anisotropic thermal parameters and the hydrogen atoms were fixed in idealized positions (methyl group orientations based on difference Fourier peaks, C—H = 0.98 Å, $B_H = 1.2B_{bonded\ atom}$). A correction for secondary extinction was applied, the final value of the extinction coefficient being 3.68×10^{-4}. Scattering factors for all atoms

[1]TEXSAN/TEXRAY structure analysis package which includes versions of the following: MITHRIL, integrated direct methods, by C. J. Gilmore; DIRDIF, direct methods for difference structures, by P. T. Beurskens; ORFLS, full-matrix least-squares, and ORFFE, function and errors, by W. R. Busing, K. O. Martin, and H. A. Levy; ORTEP II, illustrations, by C. K. Johnson.

TABLE 3. Bond angles (deg) with estimated standard deviations in parentheses

Atom	Atom	Atom	Angle	Atom	Atom	Atom	Angle
C(3)	O(1)	B(1)	106.9(2)	O(3)	C(28)	C(27)	126.2(3)
C(4)	O(2)	B(1)	107.5(2)	O(3)	C(28)	C(29)	111.6(3)
C(28)	O(3)	B(2)	107.7(2)	C(27)	C(28)	C(29)	122.2(3)
C(29)	O(4)	B(2)	107.6(2)	O(4)	C(29)	C(28)	112.0(3)
C(2)	N(1)	C(6)	122.0(2)	O(4)	C(29)	C(30)	128.4(3)
C(2)	N(1)	C(7)	120.2(3)	C(28)	C(29)	C(30)	119.7(3)
C(6)	N(1)	C(7)	117.8(3)	C(29)	C(30)	C(31)	117.5(3)
C(27)	N(2)	C(31)	121.8(2)	N(2)	C(31)	C(30)	122.4(3)
C(27)	N(2)	C(32)	120.8(2)	N(2)	C(32)	C(33)	120.6(3)
C(31)	N(2)	C(32)	117.4(2)	N(2)	C(32)	C(37)	118.5(3)
N(1)	C(2)	C(1)	120.6(3)	C(33)	C(32)	C(37)	120.8(3)
N(1)	C(2)	C(3)	116.3(3)	C(32)	C(33)	C(34)	119.0(3)
C(1)	C(2)	C(3)	123.1(3)	C(33)	C(34)	C(35)	121.8(3)
O(1)	C(3)	C(2)	125.8(3)	C(34)	C(35)	C(36)	117.6(3)
O(1)	C(3)	C(4)	111.6(2)	C(34)	C(35)	C(38)	121.4(3)
C(2)	C(3)	C(4)	122.5(3)	C(36)	C(35)	C(38)	121.0(3)
O(2)	C(4)	C(3)	112.1(3)	C(35)	C(36)	C(37)	121.9(3)
O(2)	C(4)	C(5)	128.9(3)	C(32)	C(37)	C(36)	118.9(3)
C(3)	C(4)	C(5)	119.1(3)	C(40)	C(39)	C(44)	115.0(4)
C(4)	C(5)	C(6)	117.8(3)	C(40)	C(39)	B(2)	121.1(4)
N(1)	C(6)	C(5)	122.3(3)	C(44)	C(39)	B(2)	123.8(3)
N(1)	C(7)	C(8)	119.3(3)	C(39)	C(40)	C(41)	122.2(5)
N(1)	C(7)	C(12)	120.1(3)	C(40)	C(41)	C(42)	120.5(5)
C(8)	C(7)	C(12)	120.5(3)	C(41)	C(42)	C(43)	119.1(5)
C(7)	C(8)	C(9)	119.2(3)	C(42)	C(43)	C(44)	119.9(5)
C(8)	C(9)	C(10)	122.2(3)	C(39)	C(44)	C(43)	123.3(4)
C(9)	C(10)	C(11)	116.9(3)	C(46)	C(45)	C(50)	115.9(3)
C(9)	C(10)	C(13)	122.0(3)	C(46)	C(45)	B(2)	121.3(3)
C(11)	C(10)	C(13)	121.1(4)	C(50)	C(45)	B(2)	122.7(3)
C(10)	C(11)	C(12)	121.7(3)	C(45)	C(46)	C(47)	122.7(3)
C(7)	C(12)	C(11)	119.4(3)	C(46)	C(47)	C(48)	119.2(4)
C(15)	C(14)	C(19)	115.3(3)	C(47)	C(48)	C(49)	120.1(4)
C(15)	C(14)	B(1)	121.2(3)	C(48)	C(49)	C(50)	120.1(3)
C(19)	C(14)	B(1)	123.5(3)	C(45)	C(50)	C(49)	121.9(3)
C(14)	C(15)	C(16)	122.2(3)	O(5)	C(51)	C(52)	119.9(7)
C(15)	C(16)	C(17)	120.5(4)	O(5)	C(51)	C(53)	118.7(7)
C(16)	C(17)	C(18)	118.9(4)	C(52)	C(51)	C(53)	121.4(7)
C(17)	C(18)	C(19)	120.4(4)	O(1)	B(1)	O(2)	100.6(2)
C(14)	C(19)	C(18)	122.8(4)	O(1)	B(1)	C(14)	111.6(3)
C(21)	C(20)	C(25)	116.5(3)	O(1)	B(1)	C(20)	109.3(3)
C(21)	C(20)	B(1)	122.9(3)	O(2)	B(1)	C(14)	110.0(3)
C(25)	C(20)	B(1)	120.6(3)	O(2)	B(1)	C(20)	108.5(3)
C(20)	C(21)	C(22)	122.7(4)	C(14)	B(1)	C(20)	115.8(3)
C(21)	C(22)	C(23)	119.4(5)	O(3)	B(2)	O(4)	100.7(2)
C(22)	C(23)	C(24)	120.4(4)	O(3)	B(2)	C(39)	110.5(3)
C(23)	C(24)	C(25)	119.5(5)	O(3)	B(2)	C(45)	111.1(3)
C(20)	C(25)	C(24)	121.5(4)	O(4)	B(2)	C(39)	108.9(3)
N(2)	C(27)	C(26)	121.3(3)	O(4)	B(2)	C(45)	108.2(3)
N(2)	C(27)	C(28)	116.4(3)	C(39)	B(2)	C(45)	116.3(3)
C(26)	C(27)	C(28)	122.4(3)				

and anomalous disperson corrections for the non-hydrogen atoms were taken from ref. 6. The weighting scheme $w = 4F_o^2/\sigma^2(F_o^2)$ gave uniform average values of $w(|F_o| - |F_c|)^2$ over ranges of both $|F_o|$ and sin θ/λ and was employed in the final stages of full-matrix least-squares refinement of 560 variables. Reflections with $I < 3\sigma(I)$ were not included in the refinement. Convergence was reached at $R = 0.050$ and $R_w = 0.065$ for 4330 reflections with $I \geq 3\sigma(I)$. The function minimized was $\Sigma w(|F_o| - |F_c|)^2$, $R = \Sigma||F_o| - |F_c||/\Sigma|F_o|$, $R_w = (\Sigma w(|F_o| - |F_c|)^2/\Sigma w|F_o|^2)^{1/2}$.

On the final cycle of refinement the maximum parameter shift corresponded to 0.003σ. The mean error in an observation of unit weight was 1.80. The final difference map showed maximum fluctuations of -0.22 to $+0.21$ e Å^{-3}. The final positional and (equivalent) isotropic thermal parameters for the non-hydrogen atoms appear in Table 1. Bond lengths and angles are given in Tables 2 and 3 and intra-annular torsion angles in Table 4. Hydrogen atom parameters, anisotropic thermal parameters, torsion angles, intermolecular contacts, least-squares planes, bond lengths and angles involving hydrogen, and structure factors have been deposited.[2]

[2]Supplementary material mentioned in the text may be purchased from the Depository of Unpublished Data, CISTI, National Research Council of Canada, Ottawa, Ont., Canada K1A 0S2.

Can. J. Chem. Downloaded from www.nrcresearchpress.com by 91.121.58.235 on 09/07/12
For personal use only.

Can. J. Chem. Downloaded from www.nrcresearchpress.com by 91.121.58.235 on 09/07/12
For personal use only.

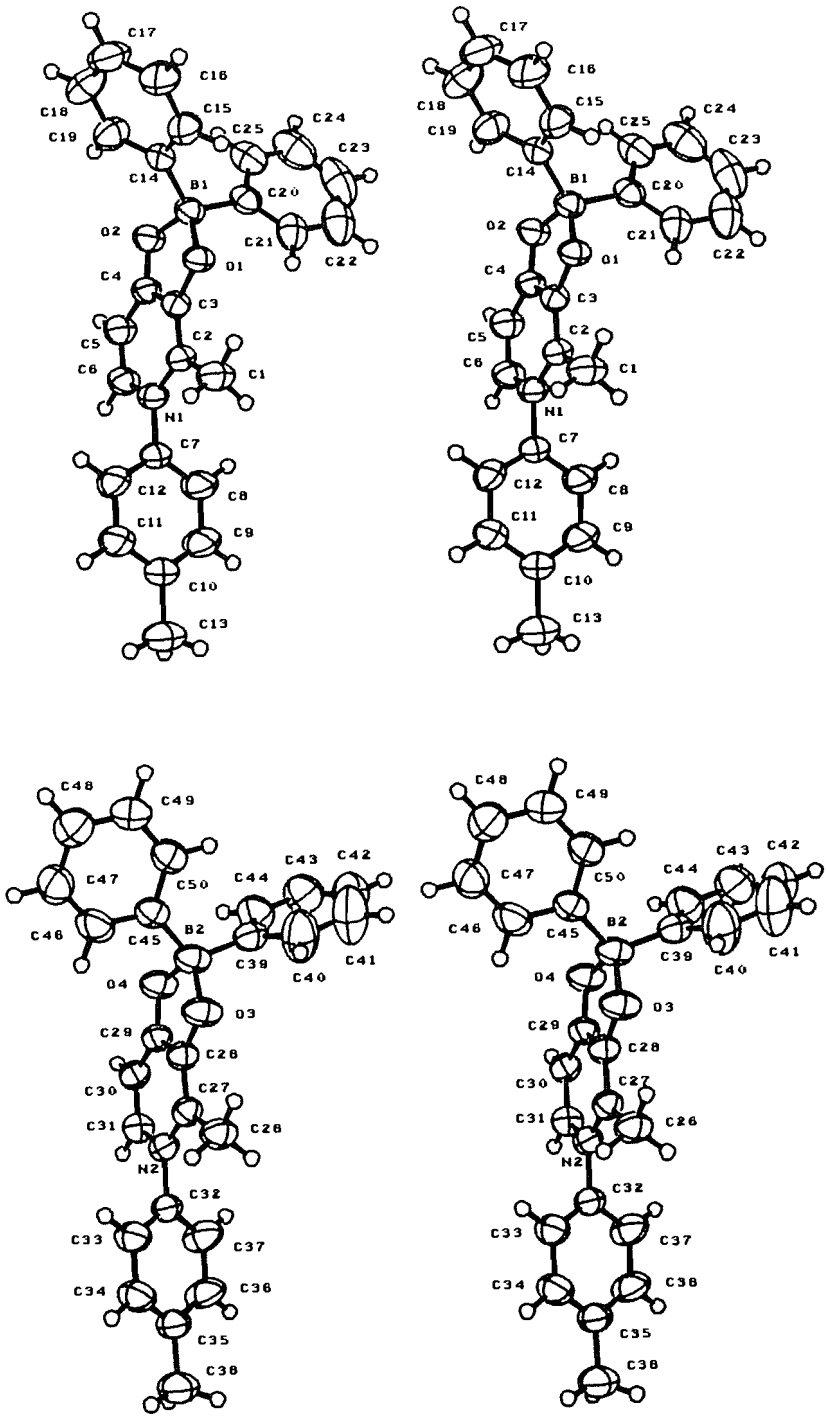

FIG. 1. Stereoviews of the two crystallographically independent (3-hydroxy-2-methyl-1-(*p*-tolyl)-4-pyridinonato)diphenylboron molecules; 50% probability thermal ellipsoids are shown for the non-hydrogen atoms.

Results and discussion

The crystal structure of **1**·0.5 Me_2CO consists of molecules of **1** and acetone separated mainly by van der Waals distances. There is one weak C—H···O interaction between molecules of **1** (C(30)—H(26)···O(1)(1 − *x*, 1 − *y*, −*z*), C···O = 3.419(4), H···O = 2.45 Å). The shortest contact between non-hydrogen atoms occurs between a pair of acetone molecules (O(5)···C(51) (2 − *x*, −*y*, 1 − *z*) = 3.205(8) Å). The two crystallographically independent molecules of **1** are shown in Fig. 1. The central fused-ring systems are planar to within 0.150(4) and 0.085(5) Å in the two independent molecules, these deviations from planarity being larger than the corresponding values of 0.067, 0.015, and 0.054 Å for **2, 3**, and **4** respectively (2, 3). The C_2O_2B five-membered rings in both molecules of **1** are significantly non-planar and have flattened *B*-envelope conformations (see Table 4), that containing B(1) showing a greater deviation from planarity (deviations of the boron atoms from the mean planes = 0.114(4) Å for B(1) and 0.065(5) Å for B(2)). The six-membered heterocyclic rings are both slightly but significantly non-planar (maximum deviations from the mean

TABLE 4. Intra-annular torsion angles (deg) with estimated standard deviations in parentheses

Atoms	Value
B(1)—O(1)—C(3)—C(4)	−9.4(3)
O(1)—C(3)—C(4)—O(2)	2.7(4)
C(3)—C(4)—O(2)—B(1)	5.2(3)
C(4)—O(2)—B(1)—O(1)	−9.9(3)
O(2)—B(1)—O(1)—C(3)	11.3(3)
B(2)—O(3)—C(28)—C(29)	−5.5(4)
O(3)—C(28)—C(29)—O(4)	1.7(4)
C(28)—C(29)—O(4)—B(2)	2.8(4)
C(29)—O(4)—B(2)—O(3)	−5.5(3)
O(4)—B(2)—O(3)—C(28)	6.5(3)

planes = 0.012(3) and 0.013(3) Å for the two independent molecules), as noted earlier for compounds **2**–**4** (2, 3) as well as for the free ligands 3-hydroxy-2-methyl-4-pyridinone and 3-hydroxy-1,2-dimethyl-4-pyridinone (7). The *B*-phenyl and *N*-tolyl rings are all planar to within experimental error and show normal geometry (8).

The mean C—B/mean O—B bond length ratios, indicative of the overall binding strength of the *O,O*-chelating ligand with respect to the diphenylboron moiety (9), are 1.029 and 1.030 for the B(1) and B(2) molecules of **1**, respectively. These values are consistent with intermediate ligand binding strength. The bond length ratios for other "Ph_2BO_2" compounds containing five-membered chelate rings range from 1.016 to 1.066 with an average value of 1.033 (ref. 2 and references therein, refs. 3, 10). The average bond length ratio of 1.030 for **1** is intermediate between the values of 1.016 for **2** and 1.034 for **3**, and greater than the value of 1.023 for **4**. The slightly stronger ligand binding in **3** relative to **1** is consistent with the fact that the chelate ring in the former is more nearly planar than that in the latter. It has been noted that the O—B binding in diphenylboron complexes having unsaturated five-membered chelate rings is strongest when these rings are planar (3, 11). The differing values of the ligand binding strength for compounds **1**–**3** reflect both the electronic effects of *N*-substitution and packing forces for this system.

The pattern of bond lengths within the pyridinone ring of **1** differs from those observed for the complexes **2**–**4**. The most noticeable feature is the fact that in each of compounds **2**–**4** the longest bond in the six-membered heterocyclic ring is C(4)—C(5) while in the present structure the C(3)—C(4) (C(28)—C(29)) bond is the longest (see Table 2). The significant bond length alternation observed for **2**–**4** (most pronounced for **3**) gives way to a more delocalized structure which also involves the oxyen atoms in **1**. The average difference between the C—O bond lengths in each molecule of **1** is 0.030 Å compared to corresponding values of 0.051, 0.081, and 0.055 Å for **2**–**4** respectively. The C=O stretching frequency of 1635 cm^{-1} for **1** in the solid state is consistent with the longer C=O bond in **1** than in **3** ($\nu_{C=O}$ = 1640 cm^{-1}). A combination of steric and inductive effects is probably responsible for the differences in pyridinone ring geometry. In the other *N*-substituted molecule, **3**, the N—C(2) bond is short (1.349 Å), but a shortening of the same bond in **1** is sterically unfavorable due to the bulk of the *N*-*p*-tolyl substituent. The tolyl rings are oriented roughly at right angles to pyridinone rings (the angles between the normals to the mean planes are 85.0 and 73.7° for the two molecules) to minimize steric interactions with the adjacent C(1) and C(26) methyl groups. There is no evidence for any conjugative interaction between the ring nitrogen atom and the tolyl substituent, the difference between the N–C(tolyl) distances in **1** (mean 1.455 Å) and the N—Me distance in **3** (1.465 Å) being explicable in terms of hybridization effects alone; thus the electronic differences between the substituents must be inductive in nature.

Acknowledgements

This work was supported by operating grants from the U.S. National Institutes of Health (CA 48964) (C.O) and the Natural Sciences and Engineering Research Council of Canada (C.O., J.T.). We thank Mr. P. Borda for the C, H, N analysis and U.B.C. for a University Graduate Fellowship (Z.Z.).

1. H. AMT, W. KLIEGEL, S. J. RETTIG, and J. TROTTER. Can. J. Chem. **68**, 1797 (1990).
2. C. ORVIG, S. J. RETTIG, and J. TROTTER. Can. J. Chem. **65**, 590 (1987).
3. W. O. NELSON, C. ORVIG, S. J. RETTIG, and J. TROTTER. Can. J. Chem. **66**, 132 (1988).
4. D. J. CLEVETTE, D. M. LYSTER, W. O. NELSON, T. RIHELA, G. A. WEBB, and C. ORVIG. Inorg. Chem. In press, and references therein.
5. Z. ZHANG, D. M. LYSTER, S. J. RETTIG, and C. ORVIG. To be published.
6. International tables for X-ray crystallography. Kynoch Press: Birmingham, U.K. (present distributor Kluwer Academic Publishers: Dordrecht, The Netherlands). Vol. IV. 1974, pp. 99–102 and 149.
7. W. O. NELSON, T. KARPISHIN, S. J. RETTIG, and C. ORVIG. Can. J. Chem. **66**, 123 (1988).
8. A. DOMENICANO, P. MURRAY-RUST, and A. VICIAGO. Acta Crystallogr. Sect. B, **39**, 457 (1983) and references therein.
9. W. R. CULLEN, S. J. RETTIG, J. TROTTER, and E. B. WICKENHEISER. Can. J. Chem. **66**, 2007 (1988).
10. W. KLIEGEL, M. TAJERBASHI, S. J. RETTIG, and J. TROTTER. Can. J. Chem. **68**, 69 (1990).
11. W. KLIEGEL, D. NANNINGA, S. J. RETTIG, and J. TROTTER. Can. J. Chem. **61**, 2493 (1983).

Can. J. Chem. Downloaded from www.nrcresearchpress.com by 91.121.58.235 on 09/07/12
For personal use only.

Ruthenium(III) complexes containing dimethylsulfoxide or dimethylsulfide ligands, and a new route to *trans*-dichlorotetrakis(dimethylsulfoxide)ruthenium(II)

JASWINDER S. JASWAL, STEVEN J. RETTIG, AND BRIAN R. JAMES

Department of Chemistry, University of British Columbia, 2036 Main Mall, Vancouver, B.C., Canada V6T 1Y6

Received March 19, 1990

This paper is dedicated to Professor Ross Stewart on the occasion of his 65th birthday

JASWINDER S. JASWAL, STEVEN J. RETTIG, and BRIAN R. JAMES. Can. J. Chem. **68**, 1808 (1990).

The new Ru(III) complex *trans*-$[(dmso)_2H]^+[RuCl_4(dmso)_2]^-$ (**1**) (dmso = S-bonded dimethylsulfoxide) has been synthesized. New synthetic routes are reported for *mer*-$RuX_3(dms)_3$ complexes (dms = dimethylsulfide, X = Cl (**2**) and Br (**3**)) and for *trans*-$RuCl_2(dmso)_4$ (**4**). The complexes have been studied spectroscopically while **1**, **2** and **4** have also been characterized crystallographically. Crystals of **1** are monoclinic, $P2/n$, $a = 9.280(3)$, $b = 16.518(4)$, $c = 14.034(3)$ Å, $\beta = 100.78(2)°$, $Z = 4$, $\rho_c = 1.75$ g cm^{-3}. Crystals of **2** are orthorhombic, $Pca2_1$, $a = 10.764(2)$, $b = 11.375(1)$, $c = 12.243(1)$ Å, $Z = 4$, $\rho_c = 1.74$ g cm^{-3}. Crystals of **4** are tetragonal, $I4/m$, $a = 9.1256(8)$, $c = 11.184(2)$ Å, $Z = 2$, $\rho_c = 1.73$ g cm^{-3}. The structures were determined by heavy atom methods and were refined by full-matrix least-squares procedures to R (R_w) values of 0.030 (0.036), 0.025 (0.032), and 0.051 (0.071) for 3051, 3354, and 1205 reflections with $I \geq 3\sigma(I)$, respectively. The ionic complex **1** contains the protonated dmso cation $[(dmso)_2H]^+$, with the proton asymmetrically bonded between the two O atoms (O(3)—H(1) = 1.30(6); O(4)—H(1) = 1.12(6) Å), and the $[RuCl_4(dmso)_2]^-$ octahedral anion with *trans*-disposed S-bonded dmso ligands. The structure determined for **4** duplicates one reported recently in the literature (E. Alessio *et al.* Inorg. Chem. **27**, 4099 (1988)), and reveals all S-bonded dmso ligands; the Ru—Cl distance, 2.432(1) Å, is significantly longer than that reported, 2.402(2) Å. The dms complexes **2** and **3** were isolated unexpectedly from reaction of Ru salts with acidic dmso solutions.

Key words: ruthenium complexes, dimethylsulfoxide, dimethylsulfide, hydrogen bonding.

JASWINDER S. JASWAL, STEVEN J. RETTIG et BRIAN R. JAMES. Can. J. Chem. **68**, 1808 (1990).

On a synthétisé un nouveau complexe du Ru(III), le *trans*-$[(dmso)_2H]^+[RuCl_4(dmso)_2]^-$ (**1**) (dmso = diméthylsulfoxyde lié par le S). On a développé de nouvelles voies de synthèse des complexes *mer*-$RuX_3(dms)_3$ (dms = diméthylsulfure, X = Cl (**2**) et Br (**3**) et *trans*-$RuCl_2(dmso)_4$ (**4**). On a étudié les complexes par diverses méthodes spectroscopiques alors que l'on a caractérisé les composés **1**, **2** et **4** par diffraction des rayons-X. Les cristaux du produit **1** sont monocliniques et ils appartiennent au groupe d'espace $P2/n$, avec $a = 9,280(3)$, $b = 16,518(4)$, et $c = 14,034(3)$ Å, $\beta = 100,78(2)°$, $Z = 4$, et $\rho_c = 1,75$ g cm^{-3}. Les cristaux du produit **2** sont orthorhombiques et ils appartiennent au groupe d'espace $Pca2_1$ avec $a = 10,764(2)$, $b = 11,375(1)$, et $c = 12,243(1)$ Å, $Z = 4$, $\rho_c = 1,74$ g cm^{-3}. Les cristaux du produit **4** sont tétragonaux et ils appartiennent au groupe d'espace $I4/m$ avec $a = 9,1256(8)$, et $c = 11,184(2)$ Å, $Z = 2$, $\rho_c = 1,73$ g cm^{-3}. On a déterminé les structures par la méthod des atomes lourds et on les a affinées par la méthode des moindres carrés jusqu'à des valeurs de R (R_w) de 0,030 (0,036), 0,025 (0,032) et 0,051 (0,071) pour respectivement 3051, 3354 et 1205 réflexions avec $I \geq 3\sigma(I)$. Le complexe ionique **1** contient le cation du dmso protoné $[(dmso)_2H]^+$ dans lequel le proton est lié d'une façon asymétrique entre les deux atomes de O [O)3)—H(1) = 1,30(6); O(4)—H(1) = 1,12(6) Å] et l'anion octaédrique $[RuCl_4(dmso)_2]^-$ portant des ligands dmso liés par le S et disposés en *trans*. La structure du composé **4** une réplique de celle rapportée récemment dans la littérature (E. Alessio *et al.* Inorg. Chem. **27**, 4099 (1988)) et elle révèle tous les ligands dmso liés par le S; la distance Ru—Cl, 2,432(1) Å est beaucoup plus longue que celle rapportée, 2,402(2) Å. On a été surpris de pouvoir isoler les complexes **2** et **3** du dms provenant de la réaction de sels du Ru avec des solutions acides de dmso.

Mots clés : complexes de ruthénium, diméthylsulfoxide, diméthylsulfure, liaison hydrogène.

[Traduit par la revue]

Introduction

Earlier studies from this laboratory focussed on the potential of sulfoxide complexes of ruthenium(II) as catalysts for homogeneous hydrogenation, including asymmetric catalysis using chiral sulfoxides (1). Some years later, Italian workers from Trieste (Alessio, Mestroni, Monti-Bragadin, and co-workers) reported that *cis*-$RuCl_2(dmso)_4$ possesses mutagenic properties, exhibits antitumour activity, and interacts with nucleobases of DNA (2); and recently, the Trieste group has reported on the synthesis of *trans*-$RuCl_2(dmso)_4$ and its antitumour activity (3), while its interaction with nucleic acid components has also been studied (4). Concurrent with developments in the antitumour properties of Ru(II)–dmso complexes, a joint program between this laboratory and the B.C. Cancer Research Centre in Vancouver (Skov and co-workers) has led to the effective use *in vitro* and *in vivo* of Ru(II)–sulfoxide-nitroimidazole complexes as radiosensitizers, the work also requiring complementary studies on genotoxicity and DNA-binding (5); these nitroimidazole complexes are formed via Ru(II)–sulfoxide precursors.

A potentially important parameter in all of the applications outlined above is the oxidation state of the metal, although the chemistry described thus far is restricted to that of Ru(II). Extension of the synthetic methods for the isolation of Ru(III)–sulfoxides was an obvious goal and, during our attempts to accomplish this using chemical oxidants with $RuX_2(dmso)_4$ precursors (X = Cl, Br) (6), reports by Poddar and co-workers (7, 8) appeared, describing apparently simple routes to Ru(III)–dmso complexes via the commercially available $RuCl_3 \cdot 3H_2O$; some of the complexes reported were *fac*- and *mer*-$RuCl_3(dmso)_3$,[1] $RuBr_3(dmso)_3$, and a chloro-bridged dimer $Ru_2Cl_6(dmso)_4$. We repeated the synthetic procedures reported for these four complexes, but isolated instead, following the respective recipes, *trans*-$[(dmso)_2H]^+[RuCl_4(dmso)_2]^-$ (**1**), *mer*-$RuCl_3(dms)_3$ (**2**), *mer*-$RuBr_3(dms)_3$ (**3**) (**2** and **3** both containing coordinated *dimethylsulfide*), and *trans*-$RuCl_2(dmso)_4$ (**4**).[2]

[1] A complex of formula $RuCl_3(dmso)_3$ was first reported by Wilkinson's group (J. Chem. Soc. A. 2765 (1970)), but the work was later retracted by the same group (J. Chem. Soc. Dalton Trans. 204 (1973)).

[2] dmso and dmso refer to S- and O-bonded dmso, respectively.

Can. J. Chem. Downloaded from www.nrcresearchpress.com by 91.121.58.235 on 09/07/12
For personal use only.

Can. J. Chem. Downloaded from www.nrcresearchpress.com by 91.121.58.235 on 09/07/12
For personal use only.

This present paper reports on the isolation and characterization of **1**–**4**, including crystallographic analyses of **1**, **2** and **4**, and comments on the uncertainties in the literature regarding Ru(III) sulfoxide complexes. An account of this work, dedicated to Ross Stewart, seems particularly appropriate in that it incorporates data on the protonated dmso cation $[(dmso)_2H]^+$, and Ross has done pioneering research on acidity function measurements in dmso, even though his interests have focussed on the acidic properties of this solvent.

Experimental

Materials and methods

Analytical grade dmso (BDH), acetone, *n*-hexane, and CCl_4 were used without further purification; CH_2Cl_2 was refluxed for 3 h over P_2O_5, and MeOH over Mg powder for 2 h, prior to distillation, Ruthenium was obtained as $RuCl_3 \cdot 3H_2O$ (43.96% Ru) on loan from Johnson, Matthey Ltd.

Electronic and ir spectra (KBr) were recorded on Perkin Elmer 552A and Nicolet 5DX-FT spectrometers, respectively. ^1H nmr spectra were recorded in $CDCl_3$ on a Varian XL-300 (FT mode) instrument, with shifts in ppm relative to internal TMS, downfield shifts being positive. Equivalent conductivities were measured at 25°C at $\sim 10^{-3}$ M concentration using a Thomas Serfass conductivity bridge and a cell from Yellow Springs Instrument Co.

The synthesis reactions, including isolation of the complexes, did not require inert atmosphere techniques and the procedures described below were all carried out in air; complexes **1**–**4** are not air-sensitive in the solid state or in solution, and physical measurements on the complexes were also carried out in air. TLC was done using Merck Kieselgel 60 F254 plates/CH_2Cl_2, and for column chromatography Merck silica gel 60 (mesh 70-230) was used.

Bis(dimethylsulfoxide)hydrogen trans*-tetrachlorobis(S-dimethylsulfoxide)ruthenate(III), $[(dmso)_2H]^+[RuCl_4(dmso)_2]^-$ (1)*

Concentrated HCl (5 mL) was added to a solution of $RuCl_3 \cdot 3H_2O$ (0.25 g, 1.0 mmol) in dmso (1.5 mL), and the mixture heated at 85°C for 30 min; the solution was then concentrated to ~1 mL under reduced pressure at 85°C, and left at room temperature. Orange–yellow needle-like crystals, suitable for X-ray analysis, separated out over 2 days. **1** could be isolated in powder form by adding acetone (5 mL) to the concentrated solution. Yield 0.30 g, 55%. *Anal.* calcd. for $C_8H_{25}Cl_4O_4RuS_4$: C 17.27, H 4.49; found: C 17.25, H 4.4. λ_{max} nm (log ϵ), MeCN: 485 (2.76), 408 (3.67). Infrared: ν_{SO} 1082 cm^{-1}, and see text. Λ_0, in MeOH 115, in MeCN 9 ohm^{-1} cm^2 mol^{-1}.

mer*-Trichlorotris(dimethylsulfide)ruthenium(III), $RuCl_3(dms)_3$ (2)*

Concentrated HCl (5 mL) was added to a solution of $RuCl_3 \cdot 3H_2O$ (0.25 g, 1.0 mmol) in dmso (1.5 mL), and the mixture refluxed at 130–140°C for 1.5 h. The red complex that separated out on cooling the solution to room temperature was collected, washed 3 times with CCl_4, and dried *in vacuo*. TLC revealed a minor impurity that was removed by column chromatography using CH_2Cl_2/MeOH (100:1 v/v); the major component was collected and solvent removed by Rotovap. Yield 0.31 g (80%). *Anal.* calcd. for $C_6H_{18}Cl_3RuS_3$: C 18.29, H 4.82; found: C 18.3, H 4.6. λ_{max} nm (log ϵ), MeCN: 433 (3.20), 377 (3.26); $CHCl_3$: 433 (3.36), 377 (3.39). Needle-like crystals for X-ray analysis were obtained by recrystallization from acetone/*n*-hexane (1:1 v/v).

mer*-Tribromotris(dimethylsulfide)ruthenium(III), $RuBr_3(dms)_3$ (3)*

$RuCl_3 \cdot 3H_2O$ (0.25 g, 1.0 mmol) was dissolved in concentrated HBr (5 mL) containing LiBr (1 g). The mixture was warmed to give a clear solution to which dmso (1.5 mL) was added. The solution was then refluxed for 5 min at ~130°C, and left to cool at room temperature. The dark violet crystals that separated out were collected, washed 3 times with small amounts of water followed by ethanol, and dried *in vacuo*. Yield 0.45 g (86%). *Anal.* calcd. for $C_6H_{18}Br_3RuS_3$: C 13.66, H 3.42; found: C 13.7, H 3.4. λ_{max} nm (log ϵ), $CHCl_3$: 620 (3.0), 540 (3.44), 395 (3.00).

trans*-Dichlorotetrakis(S-dimethylsulfoxide)ruthenium(II), $RuCl_2(dmso)_4$ (4)*

$RuCl_3 \cdot 3H_2O$ (0.25 g, 1.0 mmol) was dissolved in dmso (1.5 mL) by warming the mixture to 70°C for ~15 min. The solution was cooled to room temperature and acetone (30 mL) added with continuous stirring until a red complex separated out. This red solid was collected, washed with acetone, and dried *in vacuo*, while the mother liquor on standing for 3 days deposited orange crystals (60 mg) that were shown by X-ray diffraction and elemental analysis to be pure *trans*-$RuCl_2(dmso)_4$, **4**. *Anal.* calcd. for $C_8H_{24}Cl_2O_4RuS_4$: C 19.83, H 4.99; found: C 19.8, H 4.9. λ_{max} nm (log ϵ), $CHCl_3$: 441(2.39), 286(3.13). Infrared: ν_{SO} 1086 cm^{-1}. TLC of the red solid revealed two components, one being **4** but the major one was not identified; recrystallization of the red solid from dmso/acetone (1:10 v/v) yields further crystals of **4**. Total yield of **4** was 0.35 g (75%).

X-ray crystallographic analyses of 1, 2 and 4

Crystallographic data for the three compounds appear in Table 1. The final unit-cell parameters were obtained by least-squares on the setting angles for 25 reflections with 2θ = 35.8–40.5° for **1**, 53.0–62.8° for **2**, and 40.5–50.3° for **4**. The intensities of three standard reflections, measured every 200 reflections throughout the data collections, decayed uniformly by 29.0% for **1** and were essentially constant for **2** and **4**. The data were processed[3] and corrected for Lorentz and polarization effects, decay (for **1**), and absorption (empirical, based on azimuthal scans for four reflections).

The structure analysis of **1** was initiated in the centrosymmetric space group $P2/n$ on the basis of *E*-statistics and the Patterson function, the choice being confirmed by subsequent calculations. The structure analyses of **2** and **4** were initiated in the noncentrosymmetric space groups $Pca2_1$ and $I4$, respectively, based on *E*-statistics. The choice of space group $Pca2_1$ for **2** was confirmed by the subsequent successful solution and refinement of the structure. In the case of **4**, originally thought to be a different complex, both the presence of additional symmetry elements and the identification of the material as *trans*-$RuCl_2(dmso)_4$ verified the space group $I4/m$, as reported for the earlier structure analysis of this compound (3). The structures were solved by conventional heavy atom methods, the coordinates of the Ru, Cl, and S atoms being determined from the Patterson functions and those of the remaining non-hydrogen atoms from subsequent difference Fourier syntheses. The asymmetric unit of **1** contains two crystallographically distinct *trans*-$[RuCl_4(dmso)_2]^-$ anions, both situated on crystallographic two-fold rotation axes, and a $[(dmso)_2H]^+$ cation. The chlorine atoms of one of the anions in **1** were found to be disordered, a (1:1) two-fold disordered model being refined. All non-hydrogen atoms were refined with anisotropic thermal parameters. Hydrogen atoms were fixed in idealized positions (d_{C-H} = 0.98 Å, B_H = 1.2 $B_{bonded\ atom}$) except for the bridging hydrogen atom of the cation in **1** which was refined with an isotropic thermal parameter. Neutral atom scattering factors and anomalous dispersion corrections for the non-hydrogen atoms were taken from the International tables for X-ray crystallography (9). A parallel refinement of the structure of **2** having the opposite polarity gave higher residuals, the R_w factor ratio being 1.037. Final atomic coordinates and equivalent isotropic thermal parameters ($B_{eq} = 4/3\Sigma_i\Sigma_j\beta_{ij}(\mathbf{a}_i \cdot \mathbf{a}_j)$), bond lengths, and bond angles appear in Tables 2–4, respectively. Hydrogen atom parameters, anisotropic thermal parameters, torsion angles, intermolecular contacts, least-squares planes, and measured and calculated structure factor amplitudes for the three structures are included as supplementary material.[4]

[3]TEXSAN/TEXRAY structure analysis package which includes versions of the following: MITHRIL, integrated direct methods, by C. J. Gilmore; DIRDIF, direct methods for difference structures, by P. T. Beurskens; ORFLS, full-matrix least-squares, and ORFFE, function and errors, by W. R. Busing, K. O. Martin, and H. A. Levy; ORTEP II, illustrations, by C. K. Johnson.

[4]Supplementary material mentioned in the text may be purchased from the Depository of Unpublished Data, CISTI, National Research Council of Canada, Ottawa, Ont., Canada K1A 0S6.

Can. J. Chem. Downloaded from www.nrcresearchpress.com by 91.121.58.235 on 09/07/12
For personal use only.

TABLE 1. Crystallographic data[a]

Compound	**1**	**2**	**4**
Formula	$C_8H_{25}Cl_4O_4RuS_4$	$C_6H_{18}Cl_3RuS_3$	$C_8H_{24}Cl_2O_4RuS_4$
fw	556.41	393.82	484.49
Crystal size, mm	0.12 × 0.25 × 0.45	0.25 × 0.30 × 0.30	0.20 × 0.20 × 0.35
Crystal system	Monoclinic	Orthorhombic	Tetragonal
Space group	$P2/n$	$Pca2_1$	$I4/m$
a, Å	9.280(3)	10.764(2)	9.1256(8)
b, Å	16.518(4)	11.375(1)	9.1256(8)
c, Å	14.034(3)	12.243(1)	11.184(2)
β, deg	100.78(2)	90	90
V, Å^3	2113.3(9)	1499.1(6)	931.4(2)
Z	4	4	2
ρ_{calc}, g/cm^3	1.75	1.74	1.73
$F(000)$	1124	788	492
$\mu(MoK_\alpha)$, cm^{-1}	16.26	19.34	15.51
Transmission factors	0.863–1.00	0.738–1.00	0.886–1.00
Scan type	ω–2θ	ω–2θ	ω–2θ
Scan range, deg in ω	1.00 + 0.35 tan θ	1.40 + 0.35 tan θ	1.25 + 0.35 tanθ
Scan speed, deg/min	16	32	32
Data collected	$+h, +k, \pm l$	$+h, +k, +l$	$+h, +k, +l$
$2\theta_{max}$, deg	55	80	80
Crystal decay	29.0%	Negligible	Negligible
Total no. of reflections	5309	5157	1630
No. of unique reflections	5011	5157	1500
R_{merge}	0.025		0.020
No. of reflcns with $I \geq 3\sigma(I)$	3051	3354	1205
No. of variables	214	118	27
R	0.030	0.025	0.051
R_w	0.036	0.032	0.071
gof	1.36	1.45	1.80
Maximum Δ/σ (final cycle)	0.03	0.08	0.09
Residual density e/Å^3	0.92 (near Ru)	0.52 (near Ru)	3.21 (near Ru)

[a]Temperature 294 K, Rigaku AFC6S diffractometer, Mo K_α radiation (λ = 0.71069 Å), graphite monochromator, takeoff angle 6.0°, aperture 6.0 × 6.0 mm at a distance of 285 mm from the crystal, stationary background counts at each end of the scan (scan/background time ratio 2:1), $\sigma^2(F^2) = [S^2(C + 4B) + (pF^2)^2]/Lp^2$ (S = scan rate, C = scan count, B = normalized background count, $p = 0.035$ for **1**, 0.028 for **2**, and 0.040 for **4**), function minimized $\Sigma w(|F_o| - |F_c|)^2$ where $w = 4F_o^2/\sigma^2(F_o^2)$, $R = \Sigma||F_o| - |F_c||/\Sigma|F_o|$, $R_w = (\Sigma w(|F_o| - |F_c|)^2/\Sigma w|F_o|^2)^{1/2}$, and gof = $[\Sigma(|F_o| - |F_c|)^2/(m - n)]^{1/2}$. Values given for R, R_w, and gof are based on those reflections with $I \geq 3\sigma(I)$.

Results and discussion

Synthetic procedures, and characterization of the Ru-containing species, excluding crystallographic data

The synthetic procedures used for obtaining **1–4** follow as closely as possible those given by Poddar and co-workers (7, 8) for reported isolation, respectively, of *fac*-$RuCl_3(dmso)_3$, *mer*-$RuCl_3(dmso)_3$, $RuBr_3(dmso)_3$ (of unspecified configuration) and $Ru_2Cl_6(dmso)_4$. In each case, we isolate a different complex and, of the four **1**, **2** and **4** are identified crystallographically. No crystal data were given in Poddar's reports.

Complex 1

We isolate $[(dmso)_2H]^+[RuCl_4(dmso)_2]^-$ (**1**) after heating $RuCl_3 \cdot 3H_2O$ in dmso in the presence of concentrated HCl for 30 min at 85°C, and then concentrating the solution and cooling (or by precipitation with acetone). The two procedures were described by Poddar's group (7) to give correspondingly yellow needle-like crystals or a powder, respectively, the material being characterized as *fac*-$RuCl_3(dmso)_3$ with all S-bonded sulfoxides; the ν(S=O) of *S*-bonded dmso was seen at 1087 cm^{-1}, close to that (1082 cm^{-1}) of **1** which does have all S-bonded sulfoxides, and the Poddar complex, like **1**, is a Ru(III) species (μ_{eff} = 1.7 BM). The major distinction is in elemental analyses: $RuCl_3(dmso)_3$ requires C 16.3, H 4.1, Cl 24.6; while **1** requires C 17.27, H 4.43, Cl 25.5, and Poddar's reported data are closer to those of the neutral compound (the *fac*- geometry was inferred from ν(Ru-Cl) ir data).

Of interest, **1** is conducting in MeOH, but is weakly conducting in MeCN, Λ_0 9 = ohm^{-1} cm^2 mol^{-1} (Poddar's group reported a Λ_0 value of 8 in MeCN for this compound). It seems likely that the H-bonded cation "breaks down" in MeCN, and that HCl is formed, with concomitant generation of $RuCl_3(dmso)_3$ and a molecule of dmso. Corresponding behavior has been noted for the rhodium(III) complex $[(dmso)_2H]^+[RhCl_4(dmso)_2]^-$ (10). Complex **1** in MeCN shows electronic absorption maxima at 485 and 408 nm; Poddar's group report maxima at 468 and 405 nm for "*fac*-$RuCl_3(dmso)_3$". The ir data for the cation of **1** will be discussed following consideration of the crystallographic data. The $[RuCl_4(dmso)_2]^-$ anion has been isolated previously as the Na^+ and Bu_4N^+ salts using as precursor $[Ru(dmso)_6]Cl_3$ (11, 12).

Complexes 2 and 3

The synthetic procedure for *mer*-$RuCl_3(dms)_3$ (**2**) follows that for **1** except that a higher temperature (130–140°C) is required, and the product separates out merely on cooling. The observations appear identical to those noted by Poddar and co-workers (7), although this group formulates the product as *mer*-$RuCl_3(dmso)_2(dmso)$, the arrangement and types of ligands being inferred from ir data (ν(S=O): S-bonded, 1113, 1093;

TABLE 2. Final atomic coordinates (fractional) and B(eq)

Atom	x	y	z	B(eq)
		trans-[(dmso)$_2$H] [RuCl$_4$(dmso)$_2$], **1**		
Ru(1)	1/4	0.08277(2)	1/4	2.09(2)
Ru(2)	1/4	0.50624(2)	3/4	1.97(1)
Cl(1)	0.2187(1)	0.08377(7)	0.07976(6)	4.02(5)
Cl(2)	1/4	0.22516(8)	1/4	5.17(7)
Cl(3)	1/4	−0.05869(8)	1/4	3.82(6)
Cl(4)[a]	0.2099(5)	0.4821(2)	0.5809(3)	4.3(1)
Cl(4A)[a]	0.2140(5)	0.5256(2)	0.5844(3)	5.0(2)
Cl(5)	0.2417(5)	0.3651(1)	0.7732(2)	4.2(1)
Cl(6)	0.2512(6)	0.6457(1)	0.7213(2)	5.3(1)
S(1)	−0.0064(1)	0.08084(5)	0.23341(6)	2.70(4)
S(2)	0.50582(9)	0.50621(5)	0.76130(6)	2.39(3)
S(3)	0.0352(1)	0.18834(6)	0.59773(8)	3.92(4)
S(4)	−0.4188(1)	0.30275(6)	0.59714(7)	3.76(4)
O(1)	−0.0664(3)	0.0723(2)	0.3222(2)	4.7(1)
O(2)	0.5625(3)	0.5013(2)	0.6705(2)	4.0(1)
O(3)	−0.0743(3)	0.2272(2)	0.6536(2)	4.2(1)
O(4)	−0.3121(4)	0.2492(2)	0.5531(2)	6.1(2)
C(1)	−0.0904(4)	0.1667(3)	0.1712(4)	5.2(2)
C(2)	−0.0878(5)	0.0031(3)	0.1526(4)	5.7(2)
C(3)	0.5908(4)	0.4278(2)	0.8378(3)	3.3(2)
C(4)	0.5897(4)	0.5904(2)	0.8282(3)	4.1(2)
C(5)	−0.0538(5)	0.1014(3)	0.5429(3)	4.6(2)
C(6)	0.0324(6)	0.2497(3)	0.4941(4)	5.6(2)
C(7)	−0.5039(7)	0.3611(3)	0.4980(4)	6.9(3)
C(8)	−0.5578(6)	0.2344(4)	0.6092(4)	7.7(3)
		mer-RuCl$_3$(dms)$_3$, **2**		
Ru	0.46114(2)	0.25181(2)	0	2.083(5)
Cl(1)	0.33227(7)	0.14772(7)	0.12101(8)	3.78(3)
Cl(2)	0.59565(7)	0.33342(7)	−0.12945(7)	3.41(3)
Cl(3)	0.43755(8)	0.43471(6)	0.08529(8)	3.57(3)
S(1)	0.28298(7)	0.28942(7)	−0.11032(8)	3.17(3)
S(2)	0.63009(7)	0.20691(8)	0.12118(8)	3.31(3)
S(3)	0.48481(8)	0.06767(6)	−0.09414(8)	3.25(3)
C(1)	0.1606(3)	0.3442(4)	−0.0245(4)	4.9(2)
C(2)	0.3097(4)	0.4182(4)	−0.1909(4)	5.6(2)
C(3)	0.5838(5)	0.2552(3)	0.2567(4)	4.5(2)
C(4)	0.7533(4)	0.3122(4)	0.0976(4)	5.8(2)
C(5)	0.4648(4)	0.0919(3)	−0.2389(3)	4.6(2)
C(6)	0.6448(4)	0.0249(4)	−0.0950(4)	5.5(2)
		trans-RuCl$_2$(dmso)$_4$, **4**		
Ru(1)	0	0	1/2	1.67(1)
Cl(1)	0	0	0.2826(1)	2.72(3)
S(1)	0.2551(1)	0.0379(1)	1/2	2.51(3)
O(1)	0.3403(4)	−0.1017(4)	1/2	4.4(2)
C(1)	0.3240(4)	0.1436(5)	0.3763(3)	3.6(1)
H(1)	0.2826	0.1059	0.3015	4.3
H(2)	0.4311	0.1359	0.3737	4.3
H(3)	0.2959	0.2465	0.3864	4.3

[a]Occupancy factor 0.50.

O-bonded, 981 cm^{-1}. ν(Ru—Cl): 340, 326, 313 cm^{-1}). Complex **2** shows strong ir bands at 1030 and 973 cm^{-1}, both of which can be attributed to CH_3 rocking modes (13), strong and medium bands at 340, 320 cm^{-1}, respectively, which are likely due to ν(Ru–Cl), and also a medium band at 270 cm^{-1} which could be the third required ν(Ru—Cl) band for a *mer*-configuration. The electronic spectrum of **2** in $CHCl_3$ (see Experimental section) is close to that reported by Poddar's group: λ_{max} nm (log ϵ), 435 (3.41), 380 (3.46). It seems more probable that the complex reported by Poddar's group is, in fact, the tris(dimethylsulfide), although their analytical data (C 16.6, H 4.3, Cl 24.0) are much closer to those required for the sulfoxide complex (C 16.3, H 4.1, Cl 24.1). Complex **2** that initially separated out did contain a minor impurity that we removed by chromatography on silica gel.

That the structure revealed coordinated thioether certainly surprised us, but the formulation accommodated our analytical data well. A corresponding higher temperature procedure, but using a concentrated HBr/LiBr medium, again identical to that used by Poddar and co-workers (8), generated a dark violet

Can. J. Chem. Downloaded from www.nrcresearchpress.com by 91.121.58.235 on 09/07/12
For personal use only.

Can. J. Chem. Downloaded from www.nrcresearchpress.com by 91.121.58.235 on 09/07/12
For personal use only.

TABLE 3. Intramolecular distances[a]

Atom	Atom	Distance	Atom	Atom	Distance
		trans-[(dmso)$_2$H] [RuCl$_4$(dmso)$_2$], **1**			
Ru(1)	Cl(3)	2.337(2)	S(1)	C(2)	1.785(4)
Ru(1)	S(1)	2.347(1)	S(2)	O(2)	1.469(3)
Ru(1)	Cl(2)	2.352(2)	S(2)	C(3)	1.771(4)
Ru(1)	Cl(1)	2.352(1)	S(2)	C(4)	1.775(4)
Ru(2)	Cl(4A)	2.308(4)	S(3)	O(3)	1.536(3)
Ru(2)	Cl(6)	2.339(2)	S(3)	C(5)	1.761(5)
Ru(2)	S(2)	2.349(1)	S(3)	C(6)	1.769(5)
Ru(2)	Cl(5)	2.357(2)	S(4)	O(4)	1.541(3)
Ru(2)	Cl(4)	2.366(4)	S(4)	C(8)	1.747(5)
S(1)	O(1)	1.464(3)	S(4)	C(7)	1.754(5)
S(1)	C(1)	1.769(4)			
O(3)	H(1)	1.30(6)	O(4)	H(1)	1.12(6)
		mer-RuCl$_3$(dms)$_3$, **2**			
Ru	Cl(2)	2.3388(8)	S(1)	C(2)	1.789(4)
Ru	Cl(3)	2.3417(8)	S(1)	C(1)	1.797(4)
Ru	Cl(1)	2.3497(8)	S(2)	C(4)	1.811(4)
Ru	S(1)	2.3843(8)	S(2)	C(3)	1.818(5)
Ru	S(2)	2.4020(8)	S(3)	C(6)	1.790(4)
Ru	S(3)	2.4043(8)	S(3)	C(5)	1.806(4)
		trans-RuCl$_2$(dmso)$_4$, **4**			
Ru(1)	S(1)	2.3534(9)	S(1)	O(1)	1.492(4)
Ru(1)	Cl(1)	2.432(1)	S(1)	C(1)	1.800(4)

[a]Distances are in angstroms. Estimated standard deviations in the least significant figure are given in parentheses.

crystalline compound that we formulate as *mer*-RuBr$_3$(dms)$_3$, **3**, again a thioether complex. Poddar's group formulate the complex as RuBr$_3$(dmso)$_3$ containing only *O*-bonded dmso (ρ_r(CH$_3$) 1030, ν(S=O) 970 cm^{-1}), but could not assign the *mer*- or *fac*-geometry. The ir of **3** showed strong ir bands at 1028 and 968 cm^{-1}, which we believe are both due to ρ_r(CH$_3$). Further, the electronic spectrum of **3** in CHCl$_3$ (see Experimental section) corresponds to that reported in Poddar's paper (8). The analytical data given by Poddar's group, however, again match better those required for the sulfoxide (C 12.5, H 3.1, Br 41.7). We assign the *mer*-configuration to **3** based on its almost superimposable ir spectrum (from 3000–450 cm^{-1}) with that of **2**.

It appears that strongly acidic solutions of RuCl$_3$·3H$_2$O containing dmso, when heated to ~130°C, generate dms species. Indeed, this provides a convenient route to the Ru(III)-dms complexes and avoids the use of the obnoxious thioether itself; the RuCl$_3$(dms)$_3$ complex, synthesized previously by refluxing RuCl$_3$·3H$_2$O with dms in alcohol (14, 15), has been assigned the *mer*-configuration based on esr (14) and ν(Ru—Cl) data (15), the latter (345, 330, 280 cm^{-1}) agreeing well with those found for **2**. The bromo analogue, **3**, to our knowledge, has not been reported previously, although both RuX$_3$(Et$_2$S)$_3$ complexes (X = Cl, Br), tentatively assigned the *fac*-configuration based on ν(Ru—X) data, have been made previously, again using the thioether ligand as a reactant (16, 17). Whether use of the sulfoxide at higher temperatures in acid solution provides a general preparative method for the sulfide complexes needs to be explored. The complex RuCl$_3$(^{n}Bu$_2$SO)$_3$ is reportedly formed on refluxing RuCl$_3$·3H$_2$O with the sulfoxide in MeOH, although the characterization data are minimal (17); the analytical data are poor, and are only marginally more satisfactory for the sulfoxide than for a corresponding tris-(dibutylsulfide) complex. We have found recently that use of tetramethylenesulfoxide (tmso) instead of dmso, under acid conditions similar to those used for the synthesis of RuBr$_3$(dms)$_3$, also gives generation of the corresponding thioether complex RuBr$_3$(tms)$_3$ (6).

The redox chemistry of Ru in sulfoxides deserves comment. It should be noted first that the commercially available compound RuCl$_3$·3H$_2$O consists, in fact, of a mixture of Ru(III) and Ru(IV), the latter probably being present as a hydroxo species (18). Work from this laboratory first reported the synthesis of *cis*-RuCl$_2$(dmso)$_4$ from the commercial trichloride in a method where H$_2$ was used as the reductant (1*a*, 19). Wilkinson's group later synthesized the same Ru(II) complex by simply refluxing RuCl$_3$·3H$_2$O in dmso under N$_2$ (20), and this method has been widely used since (2–5, 11). However, whether the reductant is dmso (itself being oxidized to the sulfone Me$_2$SO$_2$) or perhaps dms impurity (giving dmso as oxidized product) has not been determined. The former has been implied by Ledlie *et al.* (17) but with no evidence, for example reaction [1], while the same group has presented evidence for the reversible equilibrium shown in reaction [2] (17)

[1] $2\,Ru^{III} + Me_2SO + H_2O \rightarrow 2\,Ru^{II} + Me_2SO_2 + 2\,H^+$

[2] $2\,Ru^{III} + {}^nBu_2S + H_2O \rightleftharpoons 2\,Ru^{II} + {}^nBu_2SO + 2\,H^+$

Further, more careful studies are required on the dmso redox chemistry of well-defined Ru(III) and Ru(II) complexes (rather than RuCl$_3$·3H$_2$O) before our new route to thioether complexes is understood mechanistically. However, the dms almost certainly comes via reduction of dmso in acid solution (*cf.* the reverse of reaction [2]); the reductant is probably Ru(II) formed via reaction [1], although the ligand sets coordinated at Ru(II) and Ru(III) are ill-defined. A relative lower solubility of the RuX$_3$(dms)$_3$ (X = Cl, Br) complexes at lower temperatures could shift the relevant equilibria and allow for isolation of these species.

The isolation of the thioether complexes is important in that Poddar and co-workers (7, 8) have used their complexes formulated as *mer*-RuCl$_3$(dmso)$_2$(dmso) and RuBr$_3$(dmso)$_3$ as precursors for the synthesis of a range of other Ru(III) species, which includes: RuCl$_3$L$_2$(dmso) (L = MeCN, py; L$_2$ = phen, bipy), RuCl$_2$(acac)(dmso)$_2$, RuBr$_3$L(dmso)$_2$ (L = py, 4-Mepy), RuBr$_3$L$_2$(dmso) (L = PPh$_3$, AsPh$_3$), [RuBr$_2$(pda)$_2$(dmso)$_2$]Br, RuBr$_2$(pda)(dmso)$_2$, and RuBr$_2$(Et$_2$NCS$_2$)(dmso)$_2$; where py = pyridine, phen = *o*-phenanthroline, bipy = 2,2′-bipyridyl, Hacac = acetylacetone, and pda = *o*-phenylenediamine. The theoretical elemental analyses for the corresponding dms complexes are little different from those of the sulfoxides and, as noted above, ir data, the other major criteria used by Poddar's group, are not unequivocal.

Complex 4

The *trans*-RuCl$_2$(dmso)$_4$ complex (**4**) was isolated in good yield as orange crystals by addition of acetone to a dmso solution of RuCl$_3$·3H$_2$O, the dissolution of the trichloride being effected by warming. The initially precipitated solid contained a red, major component that was converted to **4** during recrystallization from dmso/acetone. The method follows closely that reported by Poddar *et al.* for synthesis of a brown–red compound formulated as Ru$_2$Cl$_6$(dmso)$_4$, which from elemental analysis and ir data was considered to be a chloride-bridged dimer containing both O- and S-bonded dmso (7); their reported dimer, which was obtained following a simple washing of the precipitated solid with acetone, is clearly different from **4** in

TABLE 4. Intramolecular bond angles[a]

Atom	Atom	Atom	Angle	Atom	Atom	Atom	Angle
			trans-[(dmso)$_2$H] [RuCl$_4$(dm*so*)$_2$], **1**				
Cl(3)	Ru(1)	S(1)	89.22(2)	S(2)	Ru(2)	Cl(4)	92.0(1)
Cl(3)	Ru(1)	Cl(2)	180.00	S(2)	Ru(2)	Cl(4)″	88.0(1)
Cl(3)	Ru(1)	Cl(1)	90.40(3)	Cl(5)	Ru(2)	Cl(4)	88.2(1)
S(1)	Ru(1)	S(1)′	178.44(4)	O(1)	S(1)	C(1)	107.2(2)
S(1)	Ru(1)	Cl(2)	90.78(2)	O(1)	S(1)	C(2)	106.8(2)
S(1)	Ru(1)	Cl(1)	88.23(4)	O(1)	S(1)	Ru(1)	117.2(1)
S(1)	Ru(1)	Cl(1)′	91.78(4)	C(1)	S(1)	C(2)	99.7(3)
Cl(2)	Ru(1)	Cl(1)	89.60(3)	C(1)	S(1)	Ru(1)	112.5(1)
Cl(1)	Ru(1)	Cl(1)′	179.20(6)	C(2)	S(1)	Ru(1)	111.9(2)
Cl(4A)	Ru(2)	Cl(6)″	91.9(1)	O(2)	S(2)	C(3)	107.1(2)
Cl(4A)	Ru(2)	S(2)	91.3(1)	O(2)	S(2)	C(4)	108.1(2)
Cl(4A)	Ru(2)	S(2)″	88.7(1)	O(2)	S(2)	Ru(2)	117.5(1)
Cl(4A)	Ru(2)	Cl(5)″	90.0(1)	C(3)	S(2)	C(4)	98.7(2)
Cl(4A)	Ru(2)	Cl(4)″	178.1(2)	C(3)	S(2)	Ru(2)	111.8(1)
Cl(6)	Ru(2)	S(2)	88.5(1)	C(4)	S(2)	Ru(2)	111.9(1)
Cl(6)	Ru(2)	S(2)″	91.5(1)	O(3)	S(3)	C(5)	105.3(2)
Cl(6)	Ru(2)	Cl(5)	177.7(1)	O(3)	S(3)	C(6)	105.8(2)
Cl(6)	Ru(2)	Cl(4)	89.9(1)	C(5)	S(3)	C(6)	100.1(2)
S(2)	Ru(2)	S(2)″	180.00	O(4)	S(4)	C(8)	102.1(3)
S(2)	Ru(2)	Cl(5)	92.8(1)	O(4)	S(4)	C(7)	103.0(2)
S(2)	Ru(2)	Cl(5)″	87.2(1)	C(8)	S(4)	C(7)	101.6(3)
O(3)	H(1)	O(4)	177(5)				
			mer-RuCl$_3$(dms)$_3$, **2**				
Cl(2)	Ru	Cl(3)	90.95(3)	S(1)	Ru	S(2)	175.58(3)
Cl(2)	Ru	Cl(1)	173.10(4)	S(1)	Ru	S(3)	88.28(3)
Cl(2)	Ru	S(1)	92.46(3)	S(2)	Ru	S(3)	91.75(3)
Cl(2)	Ru	S(2)	91.96(3)	C(2)	S(1)	C(1)	99.0(2)
Cl(2)	Ru	S(3)	87.44(3)	C(2)	S(1)	Ru	109.3(2)
Cl(3)	Ru	Cl(1)	95.89(3)	C(1)	S(1)	Ru	108.7(1)
Cl(3)	Ru	S(1)	90.34(3)	C(4)	S(2)	C(3)	98.4(2)
Cl(3)	Ru	S(2)	89.75(3)	C(4)	S(2)	Ru	108.4(2)
Cl(3)	Ru	S(3)	177.84(4)	C(3)	S(2)	Ru	107.0(1)
Cl(1)	Ru	S(1)	88.44(3)	C(6)	S(3)	C(5)	98.6(2)
Cl(1)	Ru	S(2)	87.16(3)	C(6)	S(3)	Ru	110.0(1)
Cl(1)	Ru	S(3)	85.75(3)	C(5)	S(3)	Ru	108.9(1)
			trans-RuCl$_2$(dm*so*)$_4$, **4**				
O(1)	S(1)	C(1)	106.0(2)	C(1)	S(1)	C(1)	100.5(3)
O(1)	S(1)	Ru(1)	112.9(1)	C(1)	S(1)	Ru(1)	115.1(1)

[a]Angles are in degrees. Estimated standard deviations in the least significant figure are given in parentheses. Primes and double primes refer to the symmetry operations: $1/2 - x$, y, $1/2 - z$; and $1/2 - x$, y, $3/2 - z$; respectively.

terms of analytical and ir data, and solubility characteristics (e.g. **4** does not dissolve in MeCN whereas the dimer does). The dimer was also paramagnetic, consistent with a Ru(III) formulation (7). Of interest, Poddar's group were actually attempting to prepare RuCl$_3$(dmso)$_3$ species following a route reported earlier by Antonov *et al.* (21)!

The identity of **4** was established by crystallographic analysis as well as ir data: ν(S=O) 1086 cm^{-1}, ^{1}H nmr data ($CDCl_3$): δ 3.4 (S-bonded dmso), 2.62 (free dmso), and UV/vis spectra ($CHCl_3$): λ_{max} 441, 286, 246 nm. During the course of our studies, a paper by Alessio *et al.* reported the synthesis and structure of **4**, made via photolysis, under an inert atmosphere, of the thermodynamically more stable *cis*-RuCl$_2$(dmso)$_4$ compound (3); our spectroscopic and structural data are generally in good agreement with those of the Italian workers (see below). Our synthesis of **4** is remarkably simple, and may be of benefit considering its promising pharmacological properties (3).

Crystallographic data on the Ru moieties

The relevant bond lengths and angles for complexes **1**, **2**, and **4** are given in Tables 2 and 3.

The complex *trans*-[(dmso)$_2$H]$^+$[RuCl$_4$(dm*so*)$_2$]$^-$ (**1**) is isomorphous and isostructural with the corresponding rhodium complex *trans*-[(dmso)$_2$H]$^+$[RhCl$_4$(dm*so*)$_2$]$^-$, synthesized earlier in this laboratory (10).[5] Both complexes contain in the asymmetric unit two essentially octahedral anions (both having exact C_2 symmetry), one of which is disordered and exists in two possible orientations of a square planar arrangement of chlorides, and in **1**, one is related to the other by a 17.6° rotation about the S—Ru—S axis (see Fig. 1). If there were substantial double bond character in the Ru—S bonds due to Ru $d_\pi \rightarrow S$ d_π backbonding, only one mutual orientation of dmso and chloride

[5]The space group in ref. 10 was incorrectly given as $P2_1/n$, instead of $P2/n$.

Can. J. Chem. Downloaded from www.nrcresearchpress.com by 91.121.58.235 on 09/07/12
For personal use only.

Can. J. Chem. Downloaded from www.nrcresearchpress.com by 91.121.58.235 on 09/07/12
For personal use only.

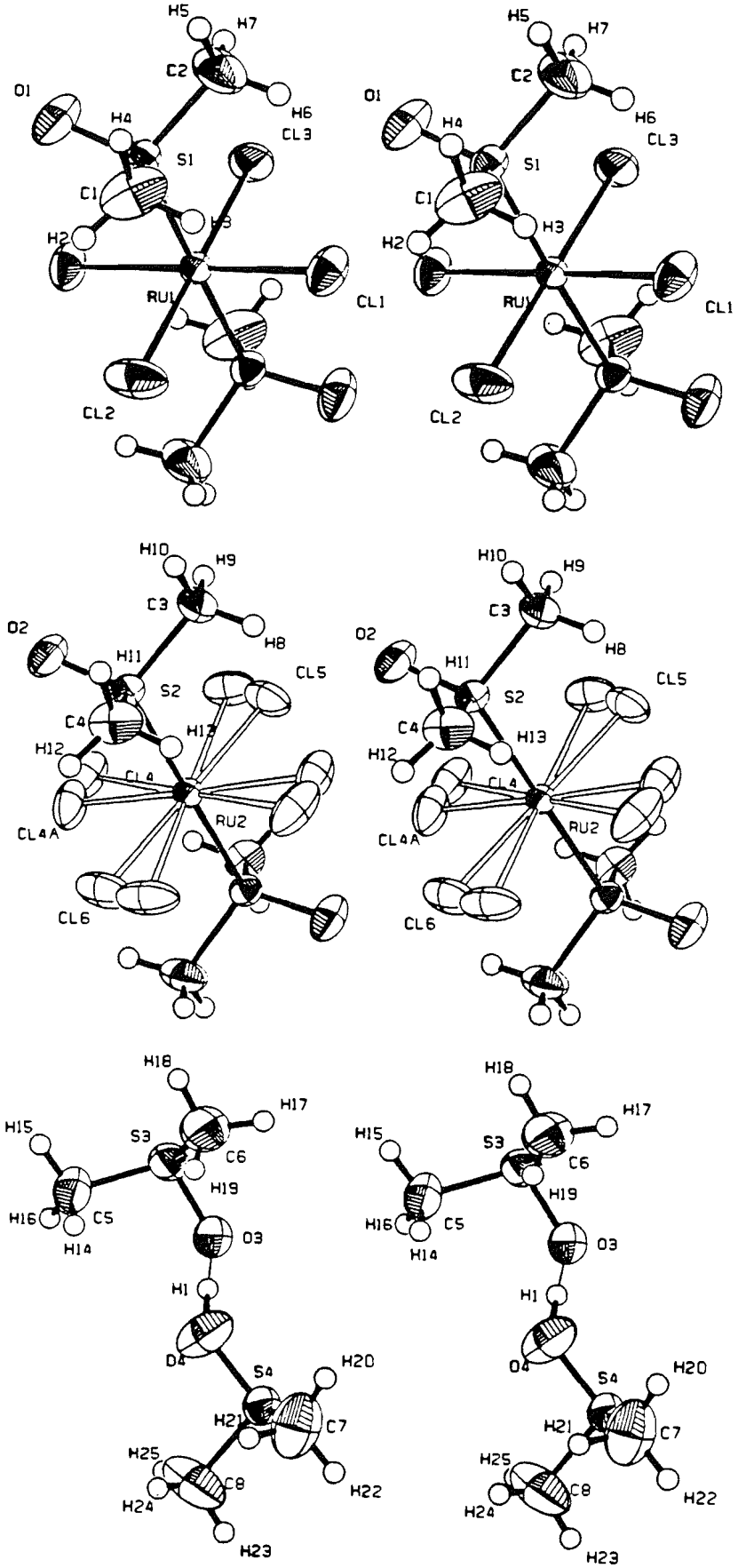

FIG. 1. Stereoviews of the two independent *trans*-$[RuCl_4(dmso_2]^-$ anions (top, middle) and the $[(dmso)_2H]^+$ cation (bottom) in **1**; 50% probability thermal ellipsoids are shown for the non-hydrogen atoms.

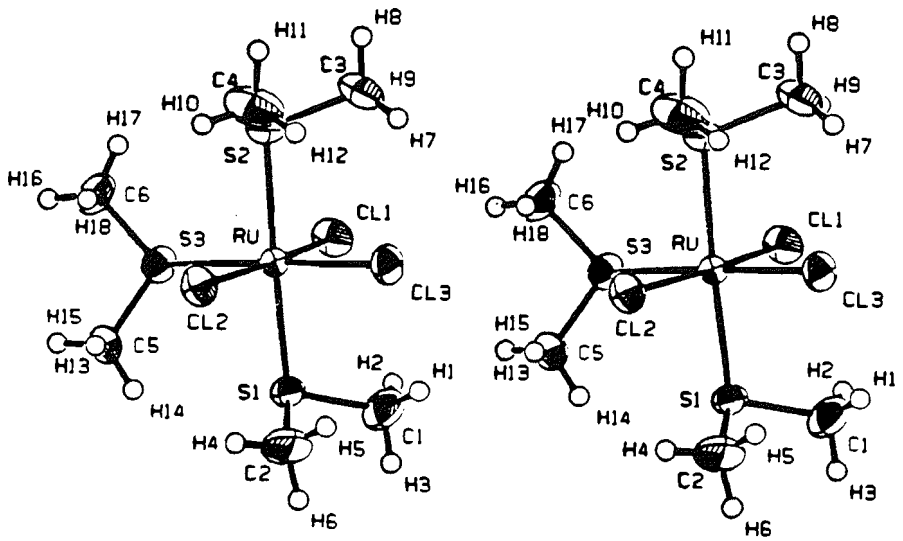

FIG. 2. Stereoview of *mer*-$RuCl_3(dms)_3$, **2**; 50% probability thermal ellipsoids are shown for the non-hydrogen atoms.

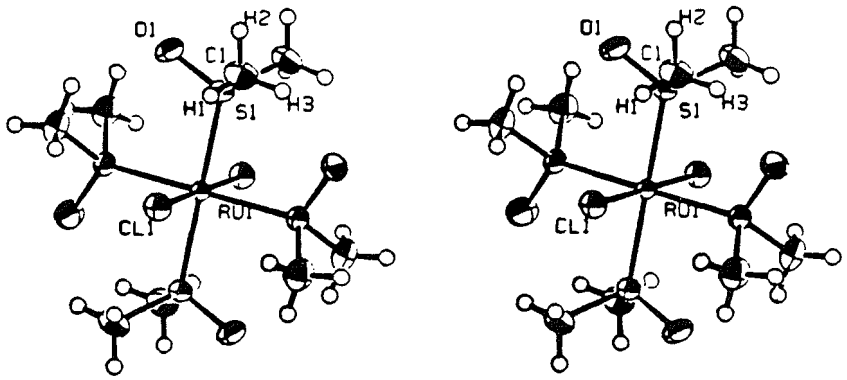

FIG. 3. Stereoview of *trans*-$RuCl_2(dmso)_4$, **4**; 50% probability thermal ellipsoids are shown for the non-hydrogen atoms.

ligands might be expected, this giving optimum overlap of such orbitals. Thus, any *trans* influence (see below) of the mutually *trans* dmso ligands is possibly exerted by way of σ-bonding orbitals (22). Alternatively, intermolecular forces in the crystal might prevail over the rotational barrier of a partial Ru—S double bond and determine the observed disorder. The *trans* dmso ligands in the non-disordered and disordered anions are related by a C_2 axis of symmetry along a Cl—Ru—Cl axis, or along a line bisecting the two Cl—Ru—Cl orientations, respectively.

The average Ru—Cl distance in **1** is 2.35 Å which is shorter than that found (2.43 Å) for the *trans*-chlorides in *trans*-$RuCl_2(dmso)_4$ (**4**, Fig. 3) or that found (2.42 Å) for the *cis*-chlorides in *cis*-$RuCl_2(dmso)_4$ (3). The shorter bond length seems reasonable for the low-spin d^5 Ru(III) complex compared to the low-spin d^6 Ru(II) species. The average Ru—Cl bond length of 2.34 Å in *mer*-$RuCl_3(dms)_3$ (**2**), again close to octahedral, also follows this trend. Of note, however, the average Ru—S bond lengths within **1** and **4**, both for mutually *trans* sulfoxide ligands, are essentially the same (2.35 Å); the significant increase compared to those in *cis*-$RuCl_2(dmso)_4$ (ave 2.27 Å. with two sulfurs being *trans* to chloride, and one being *trans* to O-bonded sulfoxide) is attributed to the *trans* influence of the S ligands and, although this is usually thought to result from π-backbonding competition between the *trans* dmso ligands (1*a*, 1*d*, 3), the disorder effect discussed above perhaps argues for a σ-directed *trans* influence. This must dominate over any decrease in Ru—S bond length that might arise from a change to the higher oxidation state. The average S—O bond lengths within the anions of **1** (1.46 Å) — as for the Rh analogue (10) — and within **4** (1.46 Å) are, as usually in S-bonded dmso metal complexes, shorter than in crystalline dmso, 1.51 Å (23), because of a resonance contribution from $M \leftarrow S^- \equiv O^+$ (24).

The structure of **1** has been mentioned in a review but no crystal data were presented by the authors (25).[6] The same group has recently published structural data on **4** (3); the data are in good agreement generally although our Ru—Cl distance of 2.432(1) Å is significantly longer than that reported, 2.402(2) Å. The Italian group rationalized the shortness of this bond relative to that of the Ru—Cl bond in the three forms of *cis*-$RuCl_2(dmso)_4$ (2.435(1), 2.42(1), 2.422(3) Å) in terms of the greater *trans* influence of S-bonded dmso compared to chloride (3). Our structural data imply that such an effect is not evidenced within the Ru—Cl bond lengths of these *cis* and *trans* isomers. It should be noted that although the published *R* factors for structure **4** (3) are somewhat smaller than in the

[6]We have learned from this group via M. Calligaris (private communication) that the determined cell parameters are in excellent agreement with those reported in Table 1.

Can. J. Chem. Downloaded from www.nrcresearchpress.com by 91.121.58.235 on 09/07/12
For personal use only.

Can. J. Chem. Downloaded from www.nrcresearchpress.com by 91.121.58.235 on 09/07/12
For personal use only.

present work, we collected significantly more data over a wider 2θ angle range and obtained, for example, more accurately determined cell parameters.

The Ru—S bond lengths in *mer*-$RuCl_3(dms)_3$ (**2**, Fig. 2) are 2.40 Å for S *trans* to Cl, and 2.38 and 2.40 Å for the mutually *trans* S atoms; the "constant" values imply the absence of any significant *trans* influence of the thioether ligand. We have been unable to find any literature data on Ru(III) thioether complexes, while structural data on Ru(II) saturated thioether complexes first appeared in 1982 (26), and now appear with increasing frequency, particularly for systems with multidentate ligands including crown thioethers (e.g. refs. 27–34); incidentally, a paper published in 1988 (30) incorrectly claims the first structurally characterized Ru(II) thioether complex. The Ru(II)—S bond lengths are in the range 2.26–2.40 Å, most commonly 2.32–2.37 Å, and in the higher range 2.37–2.40 Å when the thioether links are mutually *trans* (33, 34). The generally shorter distances compared to those found in **2** could be rationalized in terms of some π-backbonding to S from the strongly π-basic Ru(II) (26).

*The $[(dmso)_2H]^+$ cation of complex **1** (and the Rh analogue)*

To our knowledge, the only other report describing crystallographic data on the hydrogen-bonded cation (Fig. 1) is that noted above on the analogous $[(dmso)_2H]^+[RhCl_4(dmso)_2]^-$ complex (10); a somewhat more detailed discussion, taken also in part from ref. 35, is presented here.

The short O···O distance of 2.42 Å is observed in both **1** and the Rh analogue, consistent with the presence of a strong hydrogen bond (36, 37); within **1**, the H position is now somewhat better defined: O(3)—H(1), 1.30(6); H(1)—O(4), 1.12(6) Å, and perhaps implies an asymmetric H position with a closely spaced double minimum potential for the proton (36). The average S—O bond length (1.539 Å) is somewhat larger than the corresponding value in crystalline dmso (see above), and is consistent with protonation at oxygen; similar, small increases in S—O bond length are seen on coordination of metals to the oxygen of dmso (1*d*, 3, 24). The asymmetry of the O(4)···H···O(3) is more convincingly reflected by the two sets of C—S—O angles: 102.5° (ave) on the O(4) side, and 105.5° (ave) on the O(3) side. The significant decrease in the C—S—O angles from those in free dmso, 107° (23), is observed also in O-bonded dmso at transition metal centres (1*d*, 3, 24, 38). The C—S—C angles and C—S bond lengths are typical of those in free or coordinated dmso (100°, 1.78 Å, respectively).

The ir spectrum of the $[(dmso)_2H]^+$ cation has been discussed previously in some detail in our earlier papers describing the $[RhCl_4(dmso)_2]^-$ complex (10, 13), and the data obtained for the new ruthenate(III) complex are essentially identical: there is a "background", medium intensity, broad band from 1600–1100 cm^{-1}, and an intense broad band at 900–600 cm^{-1} centered at 730 cm^{-1}. This type of spectrum is typical of O···H···O systems (10, 36), and indeed the correct structure of protonated dmso was first predicted in 1967 from ir data on dmso containing methanesulfonic acid (39).

Attempts to detect by ^1H nmr in $CDCl_3$ or D_2O the proton of the $[(dmso)_2H]^+$ cation within **1** were unsuccessful; the dmso associated with the cation appeared at the chemical shift for free dmso in the respective solvents (δ 2.6–2.7), suggesting that the HCl is eliminated when the tetrachloro salt is dissolved. The same phenomenon was observed with the Rh system, the product being *mer*-$RhCl_3(dmso)_3$ which, being diamagnetic, was readily detected in the ^1H nmr spectrum (10, 13). The expected *in situ* Ru product would be the "elusive" paramagnetic $RuCl_3(dmso)_3$; several weak, broad resonances were observed in the ^1H nmr, and such solutions might well provide a source of this Ru(III) complex.

Acknowledgements

We thank the Natural Sciences and Engineering Research Council of Canada for financial support, Professor J. Trotter for the use of crystallographic facilities, Johnson Matthey Ltd. for the loan of ruthenium, and a reviewer for some constructive comments.

1. (*a*) R. S. McMillan, A. Mercer, B. R. James, and J. Trotter. J. Chem. Soc. Dalton Trans. 1006 (1975); (*b*) B. R. James, R. S. McMillan, and K. J. Reimer. J. Mol. Catal. **1**, 439 (1976); (*c*) B. R. James and R. S. McMillan. Can. J. Chem. **55**, 3927 (1977); (*d*) A. R. Davies, F. W. B. Einstein, N. P. Farrell, B. R. James, and R. S. McMillan. Inorg. Chem. **17**, 1965 (1978); (*e*) B. R. James, R. S. McMillan, R. H. Morris, and D. K. W. Wang. Adv. Chem. Ser. No. 167. Am. Chem. Soc. Washington. 1978. p. 122.
2. (*a*) G. Sava, S. Zorzet, T. Giraldi, G. Mestroni, and G. Zassinovich. Eur. J. Caner Clin. Oncol. **20**, 841 (1984); (*b*) C. Monti-Bragadin, M. Giacca, L. Dolzani, and M. Tamaro. Inorg. Chim. Acta, **137**, 31 (1987); (*c*) S. Cauci, E. Alessio, G. Mestroni, and F. Quadrifoglio. Inorg. Chim. Acta, **137**, 19 (1987).
3. E. Alessio, G. Mestroni, G. Nardin, W. M. Attia, M. Calligaris, G. Sava, and S. Zorzet. Inorg. Chem. **27**, 4099 (1988).
4. E. Alesio, Y. Xu, S. Cauci, G. Mestroni, F. Quadrifoglio, P. Viglino, and L. G. Marzilli. J. Am. Chem. Soc. **111**, 7068 (1989).
5. (*a*) P. K. L. Chan, P. K. H. Chan, D. C. Frost, B. R. James, and K. A. Skov. Can. J. Chem. **66**, 117 (1988); (*b*) P. K. L. Chan, B. R. James, D. C. Frost, P. K. H. Chan, H.-L. Hu, and K. A. Skov. Can. J. Chem. **67**, 508 (1989) and references therein.
6. J. S. Jaswinder and B. R. James. To be published.
7. U. C. Sarma, K. P. Sarma, and R. K. Poddar. Polyhedron, **7**, 1727 (1988).
8. U. C. Sarma and R. K. Poddar. Polyhedron, **7**, 1737 (1988).
9. International tables for X-ray crystallography. Kynoch Press, Birmingham, U.K. Vol. IV. 1974. pp. 99–102 and 149 (present distributor Kluwer Academic Publishers. Dordrecht, The Netherlands).
10. B. R. James, R. H. Morris, F. W. B. Einstein, and A. Willis. J. Chem. Soc. Chem. Commun. 31 (1980).
11. T. Bora and M. M. Singh. J. Inorg. Nucl. Chem. **38**, 1815 (1976).
12. T. Bora and M. M. Singh. Trans. Met. Chem. **3**, 27 (1978).
13. B. R. James and R. H. Morris. Can. J. Chem. **58**, 399 (1980).
14. J. Chatt, G. J. Leigh, and A. P. Storace. J. Chem. Soc. A, 1380 (1971).
15. J. E. Fergusson, J. D. Karran, and S. Seevaratram. J. Chem. Soc. A, 2627 (1965).
16. B. E. Aires, J. E. Fergusson, D. T. Howarth, and J. M. Miller. J. Chem. Soc. A, 1144 (1971).
17. M. A. Ledlie, K. G. Allum, I. V. Howell, and C. R. Pitkethly. J. Chem. Soc. Perkin I, 1734 (1976).
18. J. Halpern and B. R. James. Can. J. Chem. **44**, 495 (1966); B. C. Hui and B. R. James. Can. J. Chem. **52**, 348 (1974).
19. B. R. James, E. Ochiai, and G. L. Rempel. Inorg. Nucl. Chem. Lett. **7**, 781 (1971).
20. I. P. Evans, A. Spencer, and G. Wilkinson. J. Chem. Soc. Dalton Trans. 204 (1973).
21. P. G. Antonov, Y. N. Kukushkin, V. I. Konnov, and B. I. Ionin. Russ. J. Inorg. Chem. **23**, 245 (1978).
22. T. G. Appleton, H. C. Clark, and L. E. Maijer. Coord. Chem. Rev. **10**, 335 (1973).

23. R. THOMAS, C. B. SHOEMAKER, and K. ERIKS. Acta Crystallogr. **21**, 12 (1966).
24. J. A. DAVIES. Adv. Inorg. Chem. Radiochem. **24**, 115 (1981).
25. G. MESTRONI, E. ALESSIO, M. CALLIGARIS, W. M. ATTIA, F. QUADRIFOGLIO, S. CAUCI, G. SAVA, S. ZORZET, S. PACOR, C. MONTI-BRAGADIN, M. TAMARO, and L. DOLZANI. *In* Progress in clinical biochemistry and medicine. Vol. 10. Springer-Verlag, Berlin–Heidelberg. 1989. p. 71.
26. T. F. LAI and C. K. POON. J. Chem. Soc. Dalton Trans. 1465 (1982).
27. J. AMARASEKERA, T. B. RAUCHFUSS, and S. R. WILSON. J. Am. Chem. Soc. **110**, 2332 (1988).
28. B. R. JAMES, A. PACHECO, S. J. RETTIG, and J. A. IBERS. Inorg. Chem. **27**, 2414 (1988).
29. S. R. COOPER. Acc. Chem. Res. **21**, 141 (1988).
30. R. KROENER, M. J. HEEG, and E. DEUTSCH. Inorg. Chem. **27**, 558 (1988).
31. S. C. RAWLE, T. J. SEWELL, and S. R. COOPER. Inorg. Chem. **26**, 3769 (1987).
32. M. N. BELL, A. J. BLAKE, M. SCHRODER. H.-J. KÜPPERS, and K. WEIGHARDT. Angew. Chem. Int. Ed. Engl. **26**, 250 (1987).
33. D. SELLMANN, G. BIRKER, M. MOLL, and C. E. CAMPANA. Inorg. Chim. Acta, **130**, 221 (1987).
34. D. P. RILEY and J. D. OLIVER. Inorg. Chem. **25**, 1814 (1986); **25**, 1821 (1986); **25**, 1825 (1986).
35. R. H. MORRIS. Ph.D. Dissertation. University of British Columbia, Vancouver, B.C. 1978.
36. J. EMSLEY. Chem. Soc. Rev. **9**,91 (1980).
37. L. K. KEEFER, J. A. HRABIE, L. OHANNESIAN, J. L. FLIPPEN-ANDERSON, and C. GEORGE. J. Am. Chem. Soc. **110**, 3701 (1988).
38. M. J. BENNETT, F. A. COTTON, and D. L. WEAVER. Acta Crystallogr. **23**, 581 (1967).
39. J. M. WILLIAMS and M. KREEVOY. J. Am. Chem. Soc. **89**, 5499 (1967).

Can. J. Chem. Downloaded from www.nrcresearchpress.com by 91.121.58.235 on 09/07/12
For personal use only.

Kinetics of the detritiation of [10,10-^3H] mianserin and related compounds in highly basic media

JOHN R. JONES AND DAVID A. WICKENDEN

Chemistry Department, University of Surrey, Guildford, GU2 5XH England

FOR ERRATA SEE
69 1991 P. 912

AND

CAREL W. FUNKE AND FRANS M. KASPERSEN

Scientific Development Group, Organon International B.V., P.O. Box 20, 5340 BH Oss, The Netherlands

Received January 26, 1990

This paper is dedicated to Professor Ross Stewart on the occasion of his 65th birthday

JOHN R. JONES, DAVID A. WICKENDEN, CAREL W. FUNKE, and FRANS M. KASPERSEN. Can. J. Chem. **68**, 1818 (1990).

A recently developed procedure (Buist *et al.*, J. Chem. Soc. Perkins II, 169 (1990)) has been used to study the kinetics of detritiation of [10,10-^3H] mianserin and two other structurally related compounds in highly basic media. Over the H_- range 16–20 the stereoselectivity of the exchange process k_{eq}/k_{ax} for all three compounds is virtually constant (5 ± 1). The apparent increase at still higher basicities is associated with distinct curvature in the log k vs. H_- plots, indicating the onset of another mechanism. Partial detritiation studies at higher levels of radioactivity, when combined with ^3H nmr spectroscopic analysis, confirms the greater lability of the C-10 (or C-9) equatorial hydrogen.

Key words: detritiation, high basic media, mianserin.

JOHN R. JONES, DAVID A. WICKENDEN, CAREL W. FUNKE et FRANS M. KASPERSEN. Can. J. Chem. **68**, 1818 (1990).

On a utilisé une méthode développée récemment (Buist *et al.*, J. Chem. Soc. Perkins II, 169 (1990)) pour étudier la cinétique de la détritiation, dans des milieux fortement basiques, de la [10,10-^3H] miansérine et de deux autres composés de structures apparentées. À des H_- allant de 16 à 20, la stéréosélectivité du processus d'échange, k_{eq}/k_{ax}, pour les trois composés est virtuellement constante (5 ± 1). L'augmentation apparente qui est observée à des basicités encore plus élevées est associée à une inflexion distincte dans les courbes de log k vs. H_- qui indique le début d'un autre mécanisme. Lorsqu'on combine des études de détritiation partielle à des niveaux plus élevés de radioactivité avec des analyses spectroscopiques par rmn du ^3H, on peut confirmer la labilité plus grande de l'hydrogène équatorial en C-10 (ou C-9).

Mots clés : détritiation, milieux fortement basiques, miansérine.

[Traduit par la revue]

Can. J. Chem. Downloaded from www.nrcresearchpress.com by 91.121.58.235 on 09/07/12
For personal use only.

The challenge of designing organic compounds with unusual reactivity can only be tackled when one has a good appreciation of the many factors that affect reactivity. One of the least well understood is stereoelectronic in nature (2) and so far most of the studies in this area have been concerned with the hydrolysis of esters, acetals, and amides. It is clearly desirable to widen the range of compounds that can be investigated and this can only be done when one can apply another widely encountered reaction; hydrogen isotope exchange is ideal for such a purpose.

In the few examples of base-catalysed hydrogen isotope exchange reactions so far studied the emphasis has been on using ketones. Thus in one of the earliest cases, that of 4-*t*-butylcyclohexanone (3) $k_{ax}/k_{eq} \sim 5$, but *ab initio* calculations (4) suggest that much higher selectivities should be possible. This has been borne out in some recent results, e.g., for 4′,1″-dimethyl-1,2,3,4-dibenzcyclohepta-1,3-diene-6-one (**1**) hydrogen–deuterium exchange (5) of the methylene protons in MeOD–OMe^- proceeds with a stereoselectivity of 73:1 whilst a kinetic selectivity of 290:1 was witnessed (6) in the base-catalysed exchange of the diastereotopic protons α to the carbonyl group in twistan-4-one (**2**).

There are many other types of carbon acids of lower acidity than these ketones and for which highly basic media need to be employed in order that hydrogen isotope exchange takes place at a measurable rate. Such an example is mianserin (1,2,3,4,10,14*b*-hexahydro-2-methyldibenzo[*c.f*]pyrazino-[1,2-*A*]azepine (**3**)), a tetracyclic antidepressant initially developed as an antihistamine and antiserotonin compound. Although it has been the subject of extensive pharmacological studies (7) its chemistry has received scant attention. Various deuterated mianserins (8) have been prepared as part of a project to assign the ^1H nmr spectra; the C-10 hydrogens were found to undergo deuteration when sodium deuteroxide was used in hexamethylphosphoric triamide.

One of the many advantages of using mianserin as a model for studying the importance of stereoelectronic effects is the ready availability of structurally similar compounds. We have therefore taken advantage of this in the present study by carrying out parallel investigations on two other compounds, 1,2,3,4,10,14*b*-hexahydro-2-methylpyrazino[2,1-*A*]pyrido-[2,3-*C*](2)benzazapine (**4**, or Org 3770) and 1,2,3,13*b*-tetrahydro-2-methyl-9*H*-dibenzo[*c.f*]imidazo[1,5-*A*]azepine (**5**, or Org 2249).

Experimental

Synthesis and purification of compounds

Compounds **4** and **5** were supplied chromatographically pure. Mianserin itself was provided as the hydrochloride of which 200 mg was dissolved in approximately 20 mL of distilled water and the solution saturated with anhydrous Na_2CO_3. The precipitated mianserin was extracted into diethyl ether (3 × 50 mL), the solution dried over anhydrous Na_2SO_4 before the solvent was removed by rotary evaporation to give the crude product. The latter was further purified by preparative thin layer chromatography (silica gel plates 200 × 200 × 1 mm, solvent system ethyl acetate – methanol 4:1).

Tritiation procedure

Typically some 150–200 mg of compound was dissolved in the minimum amount of freshly distilled hexamethylphosphoric triamide and transferred to a thick-walled glass tube containing a small quantity of powdered solid sodium hydroxide. Tritiated water (5 μL, 50 Ci mL^{-1}) was added and the tube sealed under vacuum before being

kept in a thermostat at 95°C for 2 days. The tritiated substrate was then extracted into diethyl ether, the solution washed with water to remove any labile tritium, and dried over anhydrous Na_2SO_4; after further filtration the solvent was removed by rotary evaporation to give a product which typically had a specific activity in the range 16–45 mCi mmol^{-1}.

^3H nmr analysis

The procedure was the same as that described previously (1).

Kinetic procedure

To a mixture of dimethyl sulphoxide in water (of known mole fraction) was added a few crystals of the tritiated substrate. Some 100 mL of this solution was transferred to a round-bottom flask and thermostatted at 95°C. A 2 mL portion was withdrawn, added to 5 mL of scintillator and 5 mL of water, shaken and allowed to settle before pipetting off most of the non-aqueous layer, drying over anhydrous Na_2SO_4, and counting 2 mL to give the N_0 value. The reaction was initiated by adding an aliquot of a stock sodium hydroxide solution to give a solution of known H_. Samples were subsequently withdrawn at fixed time intervals so as to cover over 90% of the reaction. As well as some 30 N_t values a value of N_∞ was also obtained in order to calculate the experimental extent of detritiation P_{obs} ($= (N_0 - N_t)/(N_0 - N_\infty)$), which increases from $0 \rightarrow 1$ as the detritiation proceeds.

The theoretical extent of detritiation is given by

$$P_{cal} = x_{ax}[1 - \exp(-k_{ax}t)] + x_{eq}[1 - \exp(-k_{eq}t)]$$

where x_{ax} and x_{eq} are the tritium atom fractions and k_{ax} and k_{eq} the unknown first-order rate constants for exchange from the axial and equatorial positions, respectively. The ^3H nmr results give values of x_{ax} and x_{eq} and a computer programme allows one to determine the optimum values of k_{ax} and k_{eq} when the "least squares error" criterion

$$S\left[= \sum_i^n (P^i_{cal} - P^i_{obs})^2 \right]$$

is employed. The results can be supplemented by a graphical procedure when the ratio k_{eq}/k_{ax} are very high, e.g., >10.

Partial detritiation experiments

On at least one occasion for each of the three compounds studied an experiment was carried out using much higher levels of radioactivity (usually 7–10 mCi) than usual so that a partially detritiated sample could be withdrawn and its ^3H nmr spectrum recorded. In this way one was able to confirm that for all three compounds the equatorial triton exchanged faster than the axial triton.

Results and discussion

The kinetic data are summarised in Table 1 and, taken together with the nmr results, give a consistent picture for all three compounds. Previous nmr studies (9) have shown that mianserin has the same conformation in solution as in the solid state (10) — the piperazine ring is chair formed, with an equatorial N—CH_3 and the piperazine–dihydroazepine junction is *trans*. The difference between H(14b) and the N(5) lone pair results in both sides of the dihydroazepine ring being non-equivalent: the C(10) bridge twists to the side of the N(5) lone pair. Selective irradiation experiments of the H(10) signal at δ 4.82 and 3.30 followed by nOe experiments allows one to identify the former as axial and the latter as equatorial. The ^3H nmr (^1H decoupled) spectrum of tritiated mianserin merely gives rise to these two signals and the results for the partially detritiated compound shows that the equatorial triton is the more reactive of the two.

This stereoselectivity can be rationalised in terms of stabilisation of the intermediate carbanions. β-Halocarbanions have been shown to be stabilised by through-bond interaction (11), the lone pair of the carbanion being delocalised to the anti-bonding σ* (C—X) orbital. This delocalisation is maximal for conformations with a planar lone-pair —C—C—C—X path. In mianserin (and Org 2249 and 3770) a similar situation exists: abstraction of the equatorial ^3H (10) yields a carbanion with a planar lone-pair —C—C—N (5) path, *i.e.*, with optimal through-bond stabilisation. Abstraction of the axial ^3H (10) yields a carbanion in which the lone-pair is roughly perpendicular to the C(10)—C—C—C—N (5) plane, *i.e.*, with less stabilisation.

Table 1. Kinetic data for the detritiation of [10,10-^3H] mianserin, [10,10-^3H] Org 3770, and [9,9-^3H] Org 2249 in highly basic media (CH_3SOCH_3–H_2O–OH^-) at 95.0°C

x_{DMSO}	[NaOH]/M	H_	$10^3 k_{eq}$/M^{-1} s^{-1}	k_{eq}/k_{ax}
		[10,10-^3H] mianserin		
0.50	0.040	18.10	0.055	4.2±0.4
0.60	0.060	19.28	0.820	5.5±0.2
0.70	0.043	20.12	5.00	4.7±0.3
0.80	0.021	20.82	25.7	5.5±0.5
0.82_5	0.019	21.08	41.0	6.7±0.2
0.85	0.015	21.28	63.0	10.0±0.5
0.90	0.021	22.32	74.0	18.8±2.5
		[10,10-^3H] Org 3770		
0.30	0.059	16.32	0.18_5	4.1±0.2
0.40	0.040	17.10	0.62	3.7±0.1
0.50	0.040	18.10	6.69	7.2±0.2
0.60	0.020	18.80	18.3	5.2±0.4
0.70	0.010	19.50	43.3	9.0±0.3
0.80	0.010	20.50	105	19.0±1.4
0.85	0.010	21.10	100	23.7±1.2
0.90	0.010	22.00	123	23.1±1.0
		[9,9-^3H] Org 2249		
0.30	0.063	16.35	0.098	4.0±0.2
0.40	0.041	17.11	0.51	4.6±0.2
0.50	0.019	17.78	4.60	5.8±0.2
0.60	0.024	18.85	59.7	3.6±0.1
0.70	0.020	19.80	157	4.0±0.1
0.80	0.010	20.50	323	5.3±0.1
0.90	0.010	22.00	613	9.4±0.2

Although the pK_a of the benzylic protons of mianserin (or Org 3770 and 2249) has not been measured, the fact that one has to use highly basic media and an elevated temperature to induce hydrogen isotope exchange to proceed at a measurable rate suggests that it is in the 27–30 range. For such compounds the log k – H_ plots are usually linear with slopes approaching unity and this is the case for all three compounds studied here (Fig. 1) with the difference that at the higher basicities deviations from linearity occur. For mianserin itself in the H_ range 18–21 the stereoselectivity is effectively constant ($k_{eq}/k_{ax} = 5 \pm 0.5$) with a log k – H_ slope of 0.94. For Org 3770 in the H_ range 16–19 $k_{eq}/k_{ax} = 4.6 \pm 1$ with a log k – H_ slope of 0.65 and for Org 2249 in the H_ range 16–20.5 $k_{eq}/k_{ax} = 4.6 \pm 0.8$ with a log k – H_ slope of 0.90. The stereoselectivity for all three compounds is therefore effectively constant. This of course assumes that internal return is either absent or its contribution to the rates is effectively constant.

The deviation in the linearity of the log k – H_ plots for all three compounds suggests that at the higher basicities we are witnessing the onset of another mechanism. Three possibilities emerge, namely demethylation of the N-methyl group, hydroxide-ion addition to the substrate or oxidation of the

Can. J. Chem. Downloaded from www.nrcresearchpress.com by 91.121.58.235 on 09/07/12
For personal use only.

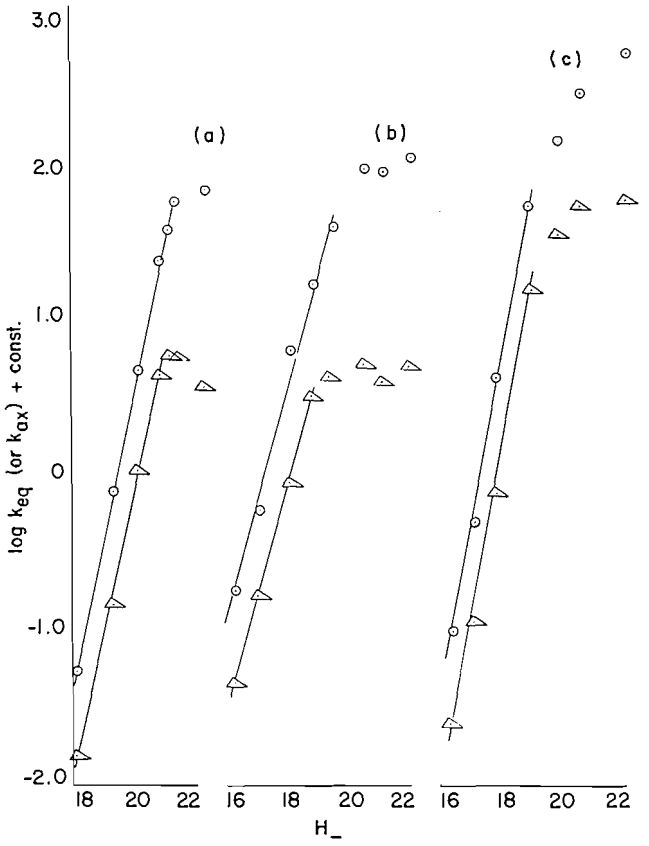

FIG. 1. Plot of log k_{eq} (or log k_{ax}) against H_ for (*a*) mianserin, (*b*) Org 3770, and (*c*) Org 2249. ○ k_{eq}, △ k_{ax}.

benzylic methylene hydrogens by dimethyl sulphoxide, the latter being the more likely (as illustrated by the isolation of 10-hydroxymianserin); however, more work is required before firmer conclusions can be drawn.

We may therefore conclude that studies of hydrogen isotope exchange processes in highly basis media, besides providing a route to stereospecifically tritiated (or deuterated) compounds, also allow one to determine the true stereoselectivity especially in circumstances where the onset of another mechanism can introduce an element of uncertainty.

Acknowledgements

We are grateful to Organon International B.V. for financial support and Professor Dr. J. W. Verhoeven (Laboratory of Organic Chemistry, University of Amsterdam) for discussions concerning the stereoselectivity of the carbanion stabilisation.

1. G. J. BUIST, E. BUNCEL, J. P. DAVEY, J. R. JONES, and K. D. PERRING. J. Chem. Soc. Perkins II, 169 (1990).
2. P. DESLONGCHAMPS. Stereoelectronic effects in organic chemistry. Pergamon Press, Oxford. 1983.
3. G. B. TRIMITSIS and E. M. VAN DAM. J. Chem. Soc. Chem. Commun. 610 (1974).
4. S. WOLFE, H. B. SCHLEGEL, I. G. CZISMADIA, and E. BERNARDI. Can. J. Chem. **53**, 3365 (1975).
5. R. R. FRASER and P. J. CHAMPAGNE. Can. J. Chem. **54**, 3809 (1976); **58**, 72 (1980).
6. R. R. FRASER and P. J. CHAMPAGNE. J. Am. Chem. Soc. **100**, 657 (1978).
7. H. VAN RIEZEN, R. M. PINDER, V. J. NICKOLSON, P. HOBBELEN, I. ZAYED, and F. VAN DER VEEN. Pharmacological and biochemical properties of drug substances. Vol. 3. Mianserin. *Edited by* M. E. Goldberg. American Pharmaceutical Association, Washington. 1981. p. 56.
8. F. M. KASPERSEN, J. S. FAVIER, G. WAGENAARS, J. WALLAART, and C. W. FUNKE. Recl. Trav. Chim. Pays-Bas, **103**, 32 (1984).
9. C. W. FUNKE. Recl. Trav. Chim. Pays-Bas, **101**, 437 (1982).
10. M. VAN MEERSCHE and J. P. DECLERQ. Bull. Soc. Chim. Belg. **92**, 342 (1983).
11. J. M. LEHN and G. WIPFF. Tetrahedron Lett. 159 (1980).

Can. J. Chem. Downloaded from www.nrcresearchpress.com by 91.121.58.235 on 09/07/12
For personal use only.

Formation of synthetically useful camphor derivatives: mechanistic aspects

WILLIAM M. DADSON, JOHN H. HUTCHINSON,[1] AND THOMAS MONEY[2]

Chemistry Department, University of British Columbia, 2036 Main Mall, Vancouver, B.C., Canada V6T 1Y6

Received March 21, 1990

This paper is dedicated to Professor Ross Stewart on the occasion of his 65th birthday

WILLIAM M. DADSON, JOHN H. HUTCHINSON, and THOMAS MONEY. Can. J. Chem. **68**, 1821 (1990).

Evidence is presented to support the occurrence of a 3,2-*endo*-methyl shift during the C(8)-bromination of 3,3-dibromocamphor. The mechanism proposed for the rearrangement of (+)-3-bromocamphor to (−)-6-bromocamphor is also supported by experimental evidence.

Key words: 8-bromocamphor, 6-bromocamphor, 3,2-*endo* methyl shifts.

WILLIAM M. DADSON, JOHN H. HUTCHINSON et THOMAS MONEY. Can. J. Chem. **68**, 1821 (1990).

On présente des données qui supportent le mécanisme selon lequel il se produit un déplacement 3,2-*endo* de groupement méthyle au cours de la bromation en C(8) du 3,3-dibromocamphre Le mécanisme proposé pour la transposition du (+)-3-bromocamphre en (−)-6-bromocamphre est aussi supporté par les données expérimentales.

Mots clés : 8-bromocamphre, 6-bromocamphre, transposition 3,2-*endo* de groupements méthyles.

[Traduit par la revue]

Introduction

A variety of camphor derivatives (**2**–**5**, Scheme 1) have been used successfully as optically pure intermediates in natural product synthesis (1). Other interesting derivatives, **6** (2*a*), **7** (2*b*), and **8** (2*c*, *d*), are currently being evaluated. In all cases these camphor derivatives have been prepared by reactions in which the basic camphor framework undergoes rearrangement to provide intermediates that react with electrophiles (SO_3, Br_2) and then rearrange to the original camphor framework or its enantiomer. The rearrangements that form the basis of the transformations outlined in Scheme 1 can be considered as extensions or modifications of the fundamental rearrangement mechanism (Scheme 2), which has been proposed (3) to explain the acid-catalysed partial racemization of camphor. As shown in Scheme 2 this involves Wagner–Meerwein rearrangements, 3,2-*exo*-methyl shifts, and 6,2-hydride shifts and provides intermediates (e.g., **9***b*, **10***b*) in which the original C(10) and C(9) methyl groups have become electrophilic *exo*-methylene groups. Thus to explain C(10) sulfonation of (+)-camphor (**1**) it is assumed that intermediate **9***b* reacts with SO_3 or equivalent to provide an intermediate that can then undergo Wagner–Meerwein rearrangement to regenerate the camphor framework and provide (+)-camphor-10-sulfonic acid (**5**). Similarly, to explain C(9) bromination of camphor, it is assumed that bromine reacts with intermediates **10***b* and *ent*-**10***b* to provide brominated intermediates, which can then undergo Wagner–Meerwein rearrangement to regenerate the camphor framework and provide a mixture of (+)-9-bromocamphor and (−)-9-bromocamphor (cf. references 1*a*, *b* for a detailed description of these transformations).

To explain the C(9)-bromination reaction that converts (+)-*endo*-3-bromocamphor (**12**) to (+)-*endo*-3,9-dibromocamphor (**17**) (4) (Scheme 3), it is assumed that the *exo*-methylene intermediate (**14**) reacts with bromine to provide a carbocation (**15**) (or bromonium ion) intermediate, which then rearranges back to the camphor framework. The product of this reaction, (+)-*endo*-3,9-dibromocamphor (**17**), can then be debrominated regioselectively to provide optically pure (+)-9-bromocamphor

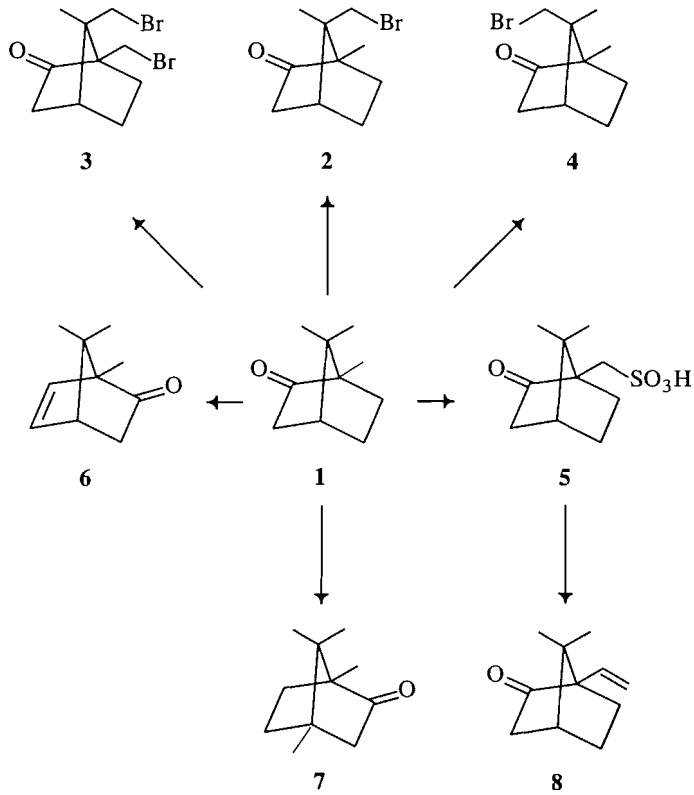

SCHEME 1

(**2**). The mechanism outlined in Scheme 3 is supported by appropriate labelling experiments using 3-bromo-[8-^{2}H]-camphor (**19**) as substrate (5*b*). The results of this investigation (5*b*) demonstrated that, during the C(9)-bromination process, the methyl groups retain their positional integrity.

Synthesis of 8-bromocamphor (4): evidence for 3,2-*endo* methyl shifts

Examination of the mechanism proposed (Scheme 3) for the C(9) bromination of (+)-*endo*-3-bromocamphor (**12**) (or (+)-camphor) led us to conclude (6) that C(8)-bromination could

[1]Merck Frosst, Canada, Inc., Pointe Claire–Dorval, P.Q.

[2]Author to whom correspondence may be addressed.

Can. J. Chem. Downloaded from www.nrcresearchpress.com by 91.121.58.235 on 09/07/12
For personal use only.

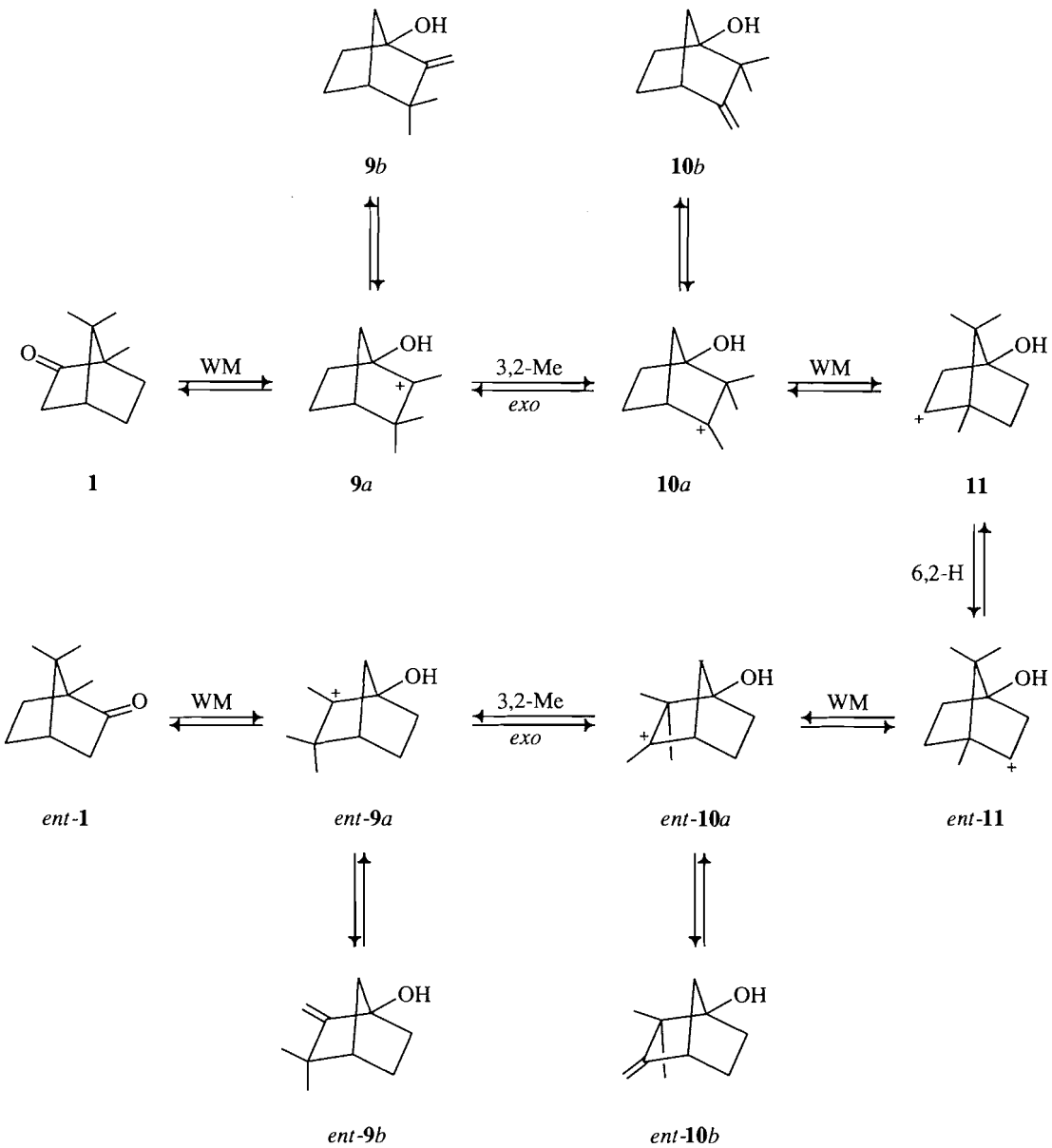

WM = Wagner–Meerwein rearrangement; 3,2-Me-*exo* = 3,2-*exo*-methyl shift; 6,2-H = 6,2-hydride shift

SCHEME 2

only occur if an intermediate similar to **15** (Scheme 3) underwent a 3,2-*endo*-methyl shift. Authentic examples of 3,2-*endo*-methyl shifts are exceedingly rare (7, 8), and indeed, in the absence of special structural features, molecules will tend to rearrange by a circuitous route involving 3,2-*exo*-methyl shifts rather than by a more direct route involving *endo*-methyl shifts (cf. transformation of longifolene to isolongifolene (9) and albene structure and synthesis (10)).

In spite of these reservations, we considered (6) the possibility of reversing the normal preference (9–17) for 3,2-*exo*-methyl over 3,2-*endo*-methyl shifts in bicyclo[2.2.1]heptyl systems by having a bulky group (i.e., a bromine atom) in the 7-*syn*-position of intermediate **15** (Scheme 3). This led us previously (6) to synthesize (+)-3,3-dibromocamphor (**27**) (Scheme 4) and subject it to the conditions ($Br_2/ClSO_3H$) that are used normally to accomplish C(9)-bromination. The product of this reaction was (+)-3,3,8-tribromocamphor (**42**) and subsequent regiospecific debromination provided optically pure (+)-8-bromocamphor (**4**).[3] In spite of its poor overall yield (30–40%) (1*c*) the simplicity of our route (1*c*, 6) compared to the 12-step procedures previously used (3*b*, 18) makes it the most convenient way of preparing optically pure 8-bromocamphor. However, the successful outcome of these previous synthetic studies (6) could not be considered as evidence for the occurrence of a 3,2-*endo*-methyl shift. Evidence in support of the C(8)-bromination mechanism outlined in Scheme 4 was obtained by using 9-deuterio-3,3-dibromocamphor[4] (**28**; 99 mol% deuterium) and 8-deuterio-3,3-dibromocamphor[4] (**29**; 94–

[3]The optical purity of (+)-8-bromocamphor (**4**) was established (6) by hydrogenolysis (Bu_3SnH) to (+)-camphor (**1**).

[4]9-Deuteriocamphor (**26**) (16, 19, 24–26) and 8-deuteriocamphor (**18**) (19, 26, 27) were synthesized by reducing 9-bromocamphor (**2**) and 8-bromocamphor (**4**), respectively, with Bu_3SnD/AIBN. Subsequent bromination (1*c*) then provided the corresponding 3,3-dibromo derivatives.

Can. J. Chem. Downloaded from www.nrcresearchpress.com by 91.121.58.235 on 09/07/12
For personal use only.

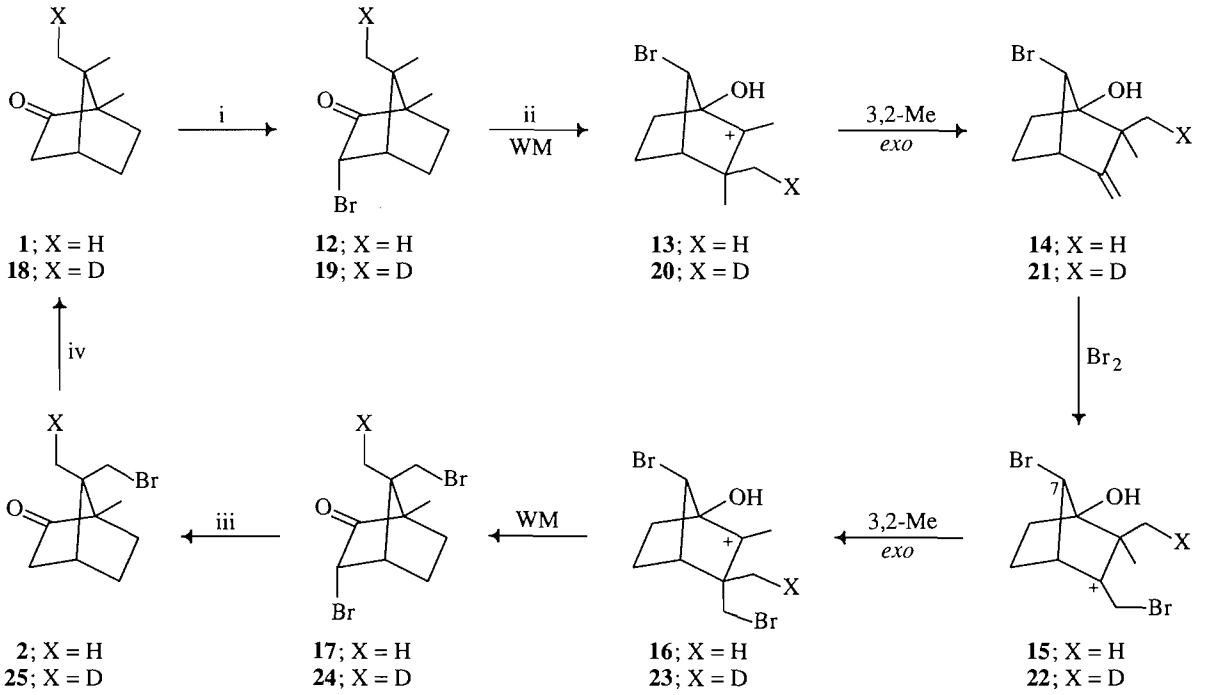

1; X = H
18; X = D

12; X = H
19; X = D

13; X = H
20; X = D

14; X = H
21; X = D

2; X = H
25; X = D

17; X = H
24; X = D

16; X = H
23; X = D

15; X = H
22; X = D

WM = Wagner–Meerwein rearrangement; 3,2-*exo*-Me = 3,2-*exo*-methyl shift;
i, Br_2, HOAc; ii, Br_2, $ClSO_3H$, 1 h; iii, Zn, HOAc; iv, Bu_3SnH, AIBN, C_6H_6

SCHEME 3

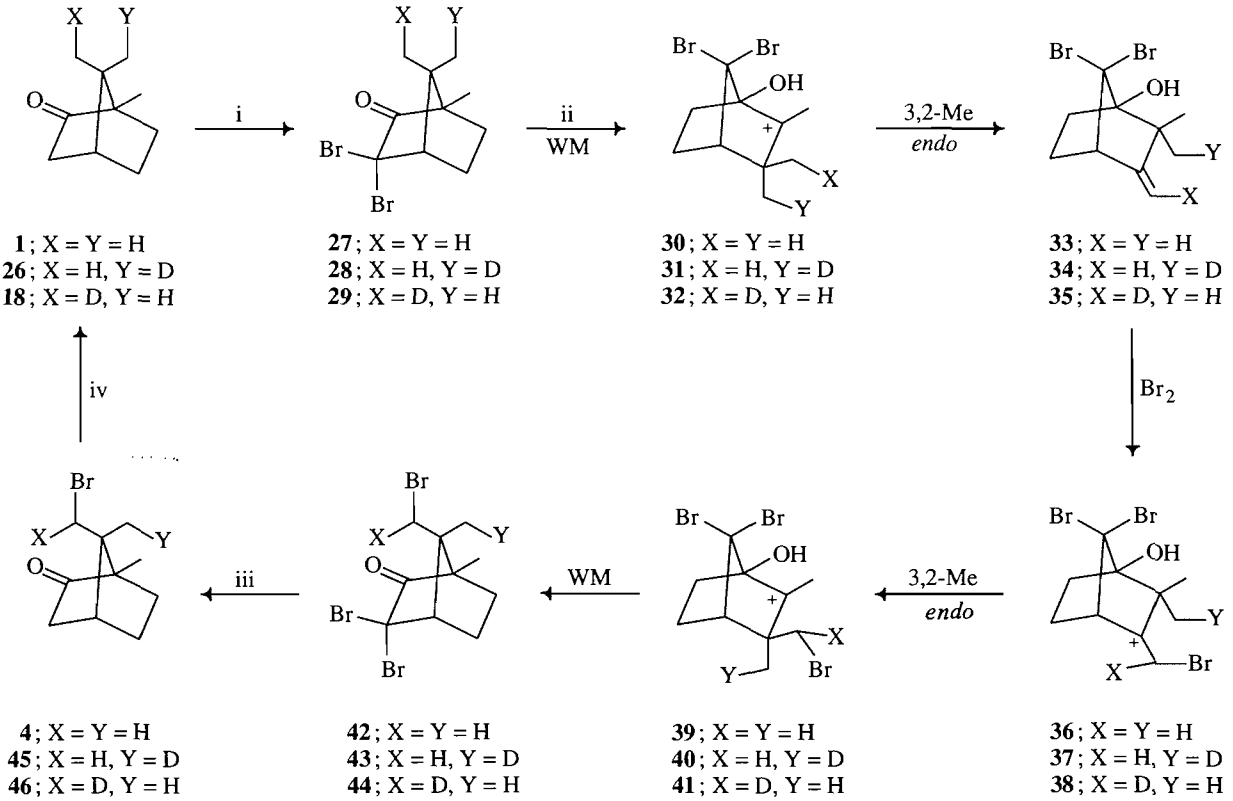

1; X = Y = H
26; X = H, Y = D
18; X = D, Y = H

27; X = Y = H
28; X = H, Y = D
29; X = D, Y = H

30; X = Y = H
31; X = H, Y = D
32; X = D, Y = H

33; X = Y = H
34; X = H, Y = D
35; X = D, Y = H

4; X = Y = H
45; X = H, Y = D
46; X = D, Y = H

42; X = Y = H
43; X = H, Y = D
44; X = D, Y = H

39; X = Y = H
40; X = H, Y = D
41; X = D, Y = H

36; X = Y = H
37; X = H, Y = D
38; X = D, Y = H

WM = Wagner–Meerwein rearrangement; 3,2-Me *endo* = 3,2-*endo*-methyl shift;
i, Br_2, HOAc; ii, Br_2, $ClSO_3H$, 4 h; iii, Zn, HOAc, Et_2O; iv, Bu_3SnH, AIBN, C_6H_6

SCHEME 4

Can. J. Chem. Downloaded from www.nrcresearchpress.com by 91.121.58.235 on 09/07/12
For personal use only.

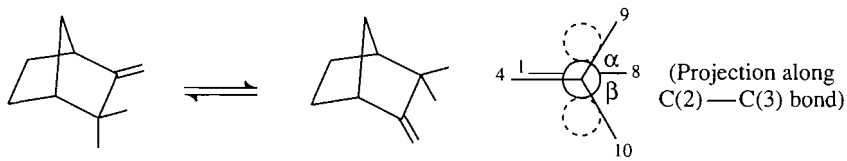

47 *ent*-**47**

FIG. 1

96 mol% deuterium) as substrates in the C(8)-bromination reaction (19). The ^{1}H nmr spectrum (δ ($CDCl_3$, 250 MHz): 0.90 (3H,s), 1.13 (2H, t), 3.08(1H, d, J = 11.0 Hz), and 3.14 (1H, d, J = 11.0 Hz)) of the deuterated 8-bromocamphor (**45**) (Scheme 4) derived from 9-deuterio-3,3-dibromocamphor (**28**) indicated that the deuterium was exclusively located in the C(9) position and this was confirmed when hydrogenolysis (Bu_3SnH) provided 9-deuteriocamphor (**26**; 98 mol% deuterium) (δ (CCl_4, 250 MHz): 0.83 (3H, s), 0.87 (3H, s), 0.94 (2H, t, J = 2 Hz); δ (^{13}C, $CDCl_3$, 20 MHz): 9.3, 18.9 (t, J = 19 Hz), 19.8). In a similar fashion the ^{1}H nmr spectrum (δ (CCl_4, 400 MHz): 0.90 (3H, s) 1.14 (3H, s), and 3.12 (1H, m)) of deuterated 8-bromocamphor (**46**) derived from 8-deuterio-3,3-dibromocamphor (**29**; 94–96 mol% deuterium) (Scheme 4) indicated that the deuterium was located in the C(8) position. This was confirmed by subsequent transformation of **46** to 8-deuteriocamphor (**18**; 84–86 mol% deuterium) (δ ($CDCl_3$, 250 MHz): 0.82 (2H, t, J = 2 Hz), 0.84 (s), 0.91 (3H, s), 0.96 (3H, s); δ (^{13}C, $CDCl_3$, 20 MHz): 9.2, 19.1, and 19.4 (t, J = 19 Hz)). The lower deuterium content revealed by mass spectroscopic analysis and the presence of a weak sharp singlet at δ 0.84 in the ^{1}H nmr spectrum clearly indicated that there was some undeuterated camphor in this product. The partial loss of deuterium from the C(8) position of 8-deuterio-3,3-dibromocamphor (**29**) during its conversion to 3,3,8-tribromocamphor (**44**) provides some additional support for the intervention of intermediates **35** and **38** (Scheme 4) in the C(8) bromination process.[5]

The almost exclusive occurrence of 3,2-*exo* rather than 3,2-*endo* methyl shifts in rearrangements involving bornyl or norbornyl carbocations has been thoroughly documented by several research groups (9–17), and a stereoelectronic effect (8, 20, 21) has been proposed to account for this stereoselectivity. The stereoelectronic effect can be illustrated in the case of camphene (**47**) racemization (cf. **47** = *ent*-**47**, Fig. 1) where it has been proposed (8, 20) that the preferred migration of the *exo*-methyl group could possibly be due to unequal dihedral angles (α and β; cf. Fig. 1) between the C(3)—C(9), C(3)—C(10) bonds and the C(2)—C(8) bond. If α > β, the *exo*-methyl group will be closer than the *endo*-methyl group to the ideal coplanar relationship with the developing *p*-orbitals at C(2) and will therefore migrate preferentially. The converse, β > α, would of course result in a 3,2-*endo*-methyl shift.

Although this proposal has not been tested with camphene, an X-ray cyrstallographic analysis of camphene-8-carboxylic acid (**48**), (20*b*, *c*) has shown that this molecule is twisted and that the dihedral angle α is greater than β (see Table 1). This distortion is also reflected in a decreased C(3)—C(9)/C(4)—C(7) dihedral angle and a corresponding increase in the C(3)—C(10)/C(4)—C(5) angle (Table 1).

[5]In addition, the complete retention of deuterium during the conversion of 9-deuterio-3,3-dibromocamphor (cf. **28**; Scheme 4) to 9-deuterio-8-bromocamphor (**45**) indirectly supports intervention of intermediates **30**–**41** in the C(8) bromination process.

If a 3,2-*endo*-methyl shift is occurring during the formation of 3,3,8-tribromocamphor (**42**) (cf. Scheme 4), then according to the Sorensen–Vaughan proposal (8, 20) this could be due to distortion of the postulated intermediates **30** and **36** (Scheme 4) in such a way as to increase the dihedral angle β at the expense of α. This explanation could not be tested directly, but indirect evidence for its validity was obtained from the structure of dibromoketone **49**, a compound that could be regarded as a reasonably close structural analog of the hypothetical intermediate, **30**. Dibromoketone **49** (6) is formed during the bromination of 3,3-dibromocamphor (**27**) and reexamination of the previously reported X-ray crystallographic data (22) for this compound revealed that the dihedral angle C(3)—C(8)/C(2)—O (α) is less than the angle C(3)—C(9)/C(2)—O (β) (cf. Table 1). In addition the expected relationship between the angles C(3)—C(8)/C(4)—C(7) and C(3)—C(9)/C(4)—C(5) is also evident (cf. Table 1).

However, the small difference in α and β angles in **49** is not a

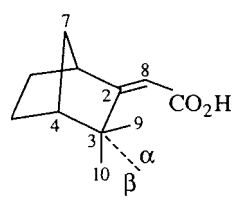

48

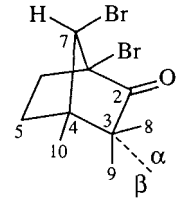

49

sufficiently convincing explanation for the exclusive occurrence of 3,2-*endo*-methyl shifts in **30** and **36**. Indeed it seems more likely that our original explanation (6) for the occurrence of 3,2-*endo*-methyl shifts during the C(8)-bromination of 3,3-dibromocamphor (**27**) has greater validity, i.e., the C(7)-*syn* bromine substituents in the proposed intermediates, **30** and **36**, sterically inhibit 3,2-*exo*-methyl shifts and, hence, the alternative 3,2-*endo*-methyl shifts occur.

Synthesis of 6-bromocamphor: mechanistic aspects

Recent investigations (2*a*) in our laboratory have established that (+)-5,6-dehydrocamphor (**6**) has considerable potential as an optically pure intermediate in terpenoid synthesis. One of the routes (Scheme 5) we have developed to this compound involves acid-catalysed rearrangement of (+)-*endo*-3-bromocamphor (**12**) to (−)-*endo*-6-bromocamphor (**63**) followed by dehydrohalogenation with base. The remarkable transformation of **12** to **63** is an extension of a previous report by Nishikawa and co-workers (23), which described the rearrangement of (+)-3,9-dibromocamphor (**17**) to (−)-6,9-dibromocamphor (**65**) in fuming sulfuric acid (Scheme 5). It was also reported (23) that the corresponding reaction with (+)-3-bromocamphor (**12**) resulted only in C(9)-sulfonation.

Our investigations have shown that treatment of (+)-*endo*-3-bromocamphor (**12**) with chlorosulfonic acid at 55°C for 15 min produces (−)-*endo*-6-bromocamphor (**63**) in 35–40% yield. The structure of this product was established by its ^{1}H nmr

Can. J. Chem. Downloaded from www.nrcresearchpress.com by 91.121.58.235 on 09/07/12
For personal use only.

TABLE 1. Dihedral angles for compounds **48** and **49**

Compound **48**		Compound **49**	
C(3)—C(9)/C(2)—C(8) (α)	~64°	C(3)—C(8)/C(2)—O (α)	~57°
C(3)—C(10)/C(2)—C(8) (β)	~56°	C(3)—C(9)/C(2)—O (β)	~61°
C(3)—C(9)/C(4)—C(7)	~78°	C(3)—C(8)/C(4)—C(7)	~88°
C(3)—C(10)/C(4)—C(5)	~52°	C(3)—C(9)/C(4)—C(5)	~42°

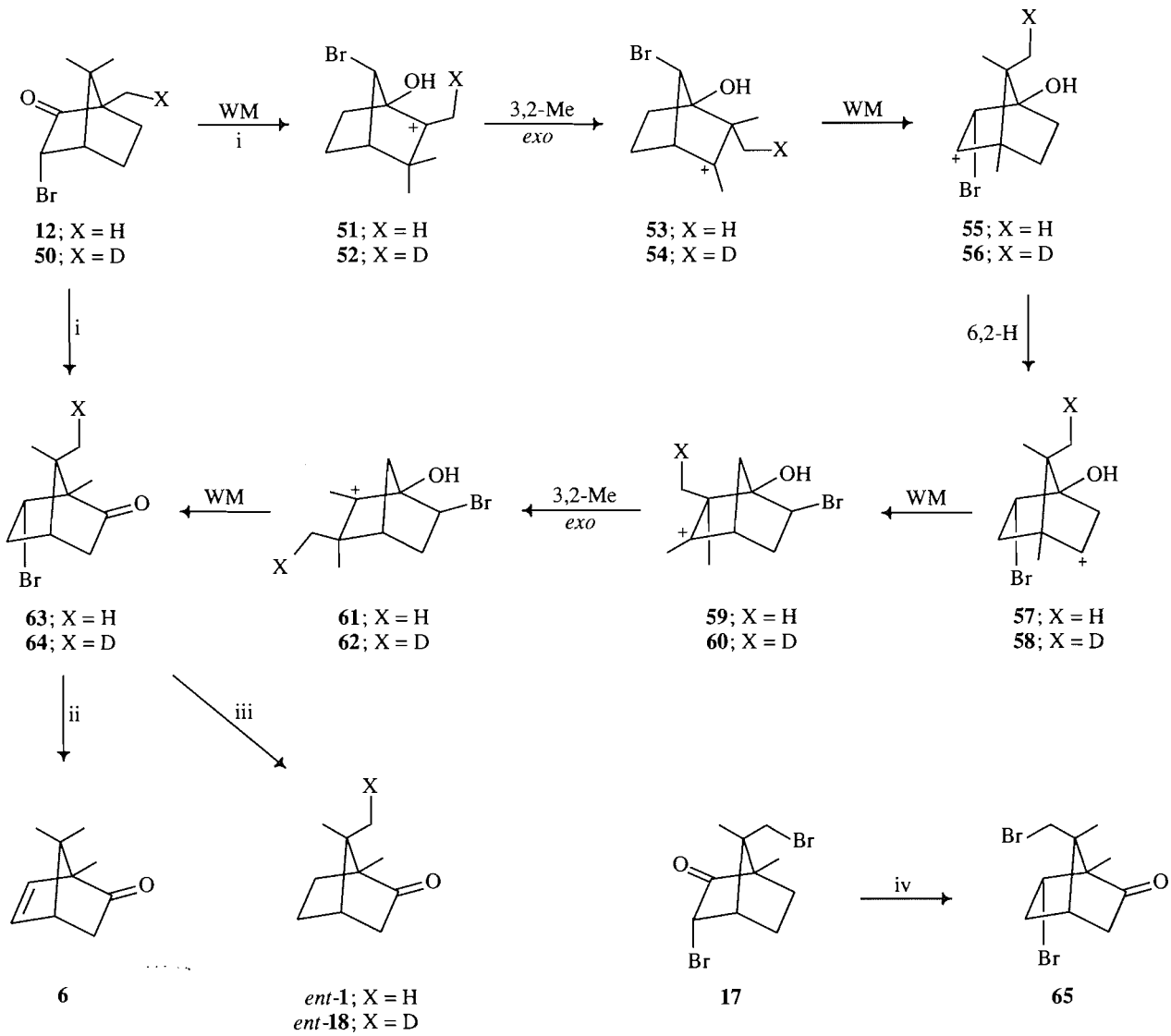

WM = Wagner–Meerwein rearrangement; 3,2-Me-*exo* = 3,2-*exo*-methyl shift;
6,2-H = 6,2-hydride shift
i, $ClSO_3H$, 55 °C, 15 min; ii, KOH, DMSO:H_2O (6:1); iii, Bu_3SnH, AIBN, C_6H_6;
iv, $ClSO_3H$, 55 °C, 45 min

SCHEME 5

spectrum (400 MHz) and by reduction (Bu_3SnH) to optically pure (−)-camphor (*ent*-**1**) ($[\alpha]_D$ −44.75 (c 0.4, EtOH)). Later studies revealed that (+)-3,9-dibromocamphor (**17**), under similar conditions, rearranges to (−)-6,9-dibromocamphor (**65**) in ~50% yield.

During the transformation of (+)-*endo*-3-bromocamphor (**12**) to (−)-*endo*-6-bromocamphor (**63**) the basic camphor framework is inverted and this probably occurs by a mechanism (Scheme 5) that is analogous to that proposed for the acid-catalysed transformation of (+)-camphor (**1**) to (−)-camphor (*ent*-**1**) (Scheme 2). Experimental support for the proposed mechanism (Scheme 5) is provided by the fact that (+)-*endo*-3-bromo-10-deuteriocamphor (**50**) rearranges to (−)-*endo*-6-bromo-8-deuteriocamphor (**64**). The structure of the latter

Can. J. Chem. Downloaded from www.nrcresearchpress.com by 91.121.58.235 on 09/07/12
For personal use only.

compound was confirmed by hydrogenolysis (Bu_3SnH/C_6H_6) to (−)-8-deuteriocamphor (*ent*-**18**; Scheme 5).

Experimental

Low resolution mass spectra were determined on a Varian MAT CH-4B spectrometer and high resolution spectra on a Kratos MS-50 spectrometer. Mass spectroscopic deuterium analyses were determined by Dr. Jim Yergey (Merck Frosst, Canada Inc., Pointe Claire – Dorval, Quebec). Infrared spectra were recorded on a Perkin–Elmer 710B spectrometer and ^1H nmr spectra were taken on Bruker WH-400 and Bruker AM-250 spectrometers. Elemental analyses were performed by Mr. P. Borda, Microanalytical Laboratory, Chemistry Department, U.B.C.

*8-Deuteriocamphor (**18**) (19, 26, 27)*

A solution of 8-bromocamphor (**4**) (1*c*) (1.0 g, 4.3 mmol), tri-*n*-butyltin deuteride (2.0 mL, 7.4 mmol), and AIBN (100 mg, 0.43 mmol) in dry benzene (10 mL) was heated to reflux under nitrogen. After 3 h the solution was cooled, the solvent removed, and the residue chromatographed (silica gel; hexane/ethyl acetate 19:1) to yield 8-deuteriocamphor (**18**) (19, 26, 27) (560 mg, 85%) as a waxy solid; δ ($CDCl_3$, 250 MHz): 0.82 (2H, t, J = 1.8 Hz), 0.90 (3H, s), 0.94 (3H, s), 1.30–1.46 (2H, m), 1.68 (1H, m), 1.83 (1H, d, J = 18 Hz) 1.94 (1H, m), 2.07 (1H, dd, J = 4.5 Hz, 4.5 Hz), 2.33 (1H, ddd, J = 18 Hz, 5 Hz, 4.5 Hz); δ (^{13}C, $CDCl_3$, 20 MHz): 9.2, 19.1, 19.4 (t, J = 19 Hz). Mass spectroscopic analysis[6] showed this material to contain 94–96 mol% deuterium. Exact mass calcd. for $C_{10}H_{15}DO$: 153.1264; found: 153.1265.

*8-Deuterio-3,3-dibromocamphor (**29**)*

Hydrogen bromide was passed through a solution of 8-deuteriocamphor (**18**) (433 mg, 2.8 mmol) and bromine (1.25 mL, 24 mmol) in acetic acid (3 mL). The solution was heated to 100°C for 5 h, then cooled and poured into water. After extraction with ether (3×) the combined organic layers were washed with saturated $NaHCO_3$ solution, then twice with water, dried, and evaporated. The crude product was purified by flash chromatography (hexane/ethyl acetate 19:1) to yield 8-deuterio-3,3-dibromocamphor (**29**) (565 mg, 65%), mp 57.5–59°C; δ ($CDCl_3$, 250 MHz): 1.01 (3H, s), 1.10 (3H, s), 1.22 (2H, bs), 1.60–1.68 (2H, m), 2.08 (1H, m), 2.32 (1H, m), 2.81 (1H, d, J = 4.2 Hz). Exact mass calcd. for $C_{10}H_{13}Br_2DO$: 308.9473/310.9453/312.9433; found: 308.9423/310.9449/312.9416.

*8-Bromo-8-deuteriocamphor (**46**)*

8-Deuterio-3,3-dibromocamphor (**29**) (550 mg, 1.77 mmol) was added to a solution of bromine (0.3 mL) and chlorosulfonic acid (1.2 mL). The mixture was stirred at room temperature for 3 h, then poured onto ice and solid $NaHSO_3$. Water was added and the mixture was extracted with ether (3×). The combined ether layers were washed with saturated $NaHCO_3$ solution, then with water (2×), and dried. Removal of the solvent gave impure 8-deuterio-3,3,8-tribromocamphor (**44**) as a brown oil, which was dissolved in ether (2.0 mL) and acetic acid (2.0 mL) and cooled in a water bath. Zinc dust (170 mg, 2.6 mmol) was added (vigorous reaction) and after 30 min the solution was poured into water. After extraction with ether (3×) the combined ether extracts were washed with saturated $NaHCO_3$ solution, water (2×), dried, and evaporated. Column chromatography of the resulting oil (hexane/ethyl acetate 20:1) gave 8-bromo-8-deuteriocamphor (**46**) (127 mg) as a waxy solid; δ ($CDCl_3$, 250 MHz): 0.92 (3H, s), 1.14 (3H, s), 1.39 (1H, m), 1.58 (1H, m), 1.82 (1H, m), 1.95 (1H, m), 1.96 (1H, d, J = 18 Hz), 2.30–2.47 (2H, m), 3.15 (~1H, m). Exact mass calcd. for $C_{10}H_{14}BrDO$: 231.0369/233.0349; found: 231.0364/233.0331.

*Conversion of 8-bromo-8-deuteriocamphor (**46**) to 8-deuteriocamphor (**18**)*

A solution of 8-bromo-8-deuteriocamphor (**46**) (109 mg, 0.47 mmol), tri-*n*-butyltin hydride (0.19 mL, 0.7 mmol), and AIBN (10 mg, 0.047 mmol) in dry benzene (3 mL) was heated at reflux under a nitrogen atmosphere for 1.5 h. The solution was cooled, solvent removed, and the resulting oil purified by flash chromatography (hexane/ethyl acetate 20:1) to give 8-deuteriocamphor (**18**) (37 mg, 51%) as a waxy solid. Mass spectroscopic analysis showed this material to contain 85–87 mol% deuterium. Comparison of the ^1H nmr spectrum (δ ($CDCl_3$, 250 MHz): 0.82 (2H, t, J = 2 Hz), 0.84 (s), 0.91 (3H, s), 0.96 (3H, s)) of this compound with that of authentic 8-deuteriocamphor (prepared, as described above, from 8-bromocamphor by reduction with tri-*n*-butyltin deuteride) also indicated that approximately 10–20% loss of deuterium had occurred.

*9-Deuteriocamphor (**26**) (16, 19, 24–26)*

A solution of 9-bromocamphor (**2**) (4) (1.0 g, 4.3 mmol), tri-*n*-butyltin deuteride (2.0 mL, 7.4 mmol), and AIBN (200 mg, 0.86 mmol) in dry benzene (20 mL) was heated to reflux under nitrogen. After 8 h the solution was cooled, the solvent removed, and the residue chromatographed (silica gel; hexane/ethyl acetate 19:1) to yield 9-deuteriocamphor (**26**) (480 mg, 73%; 99 mol% deuterium) as a waxy solid; δ ($CDCl_3$, 250 MHz): 0.82 (3H, s), 0.90 (3H, s), 0.93 (2H, t, J = 2 Hz), 1.30–1.47 (2H, m), 1.68 (1H, m), 1.83 (1H, d, J = 18 Hz), 1.94 (1H, m), 2.07 (1H, dd, J = 4.5 Hz, 4.5 Hz), 2.33 (1H, ddd, J = 18 Hz, 5 Hz, 4.5 Hz); δ (^{13}C, $CDCl_3$, 20 MHz): 9.3, 18.9 (t, J = 19 Hz), 19.8. Exact mass calcd. for $C_{10}H_{15}DO$: 153.1264; found: 153.1272.

*9-Deuterio-3,3-dibromocamphor (**28**)*

Hydrogen bromide was passed through a solution of 9-deuteriocamphor (**26**) (373 mg, 2.4 mmol) and bromine (1.1 mL, 20.7, mmol) in acetic acid (2 mL). The solution was heated to 100°C for 5 h, then cooled and poured into water. After extraction with ether (3×) the combined organic layers were washed with saturated $NaHCO_3$ solution, water (2×), dried, and evaporated. The crude product was purified by flash chromatography (hexane/ethyl acetate 19:1) to yield 9-deuterio-3,3-dibromocamphor (**28**) (512 mg, 69%), mp 57–58°C; δ ($CDCl_3$, 250 MHz): 1.01 (3H, s), 1.08 (2H, t, J = 2 Hz), 1.23 (3H, s), 1.60–1.68 (2H, m), 2.08 (1H, m), 2.32 (1H, m), 2.81 (1H, d, 4.2 Hz). Exact mass calcd. for $C_{10}H_{13}Br_2DO$: 308.9473/310.9453/312.9433; found: 308.9491/310.9445/312.9412.

*8-Bromo-9-deuteriocamphor (**45**)*

9-Deuterio-3,3-dibromocamphor (**28**) (470 mg, 1.51 mmol) was added to a solution of bromine (0.3 mL) and chlorosulfonic acid (1.2 mL). The mixture was stirred at room temperature for 3 h, then poured onto ice and solid $NaHSO_3$. Water was added and this was then extracted with ether (3×). The combined ether layers were washed with saturated $NaHCO_3$ solution, then with water (2×), and dried. Removal of the solvent *in vacuo* gave a brown oil, which was used without purification. The impure 9-deuterio-3,3,8-tribromocamphor (**43**) was dissolved in ether (1.5 mL) and acetic acid (1.5 mL) and cooled in a water bath. Zinc dust (160 mg, 2.5 mmol) was added in one lot (vigorous reaction) and after 30 min the solution was poured onto water. After extraction with ether (3×) the combined ether layers were washed with saturated $NaHCO_3$ solution, then twice with water, dried, and evaporated. Column chromatography of the resulting oil (hexane/ethyl acetate 20:1) gave 8-bromo-9-deuteriocamphor (**45**) (80 mg, 23%) as a waxy solid; δ ($CDCl_3$, 250 MHz): 0.93 (3H, s), 1.14 (2H, t, J = 2 Hz), 1.39 (1H, m), 1.58 (1H, m), 1.82 (1H, m), 1.94 (1H, m), 1.95 (1H, d, J = 18 Hz), 2.31–2.48 (2H, m), 3.10 and 3.17 (AB quartet; 2H, J = 11 Hz). Exact mass calcd. for $C_{10}H_{14}BrDO$: 231.0369/233.0349; found 231.0367/233.0325.

*Conversion of 8-bromo-9-deuteriocamphor (**45**) to 9-deuteriocamphor (**26**)*

A solution of 8-bromo-9-deuteriocamphor (**45**) (77 mg, 0.33 mmol), tri-*n*-butyltin hydride (0.13 mL, 0.5 mmol), and AIBN (7 mg, 0.033 mmol) in dry benzene (2 mL) was heated to reflux under a nitrogen atmosphere for 1.5 h. The solution was cooled, solvent removed, and the resulting oil purified by flash chromatography (hexane/ethyl acetate 20:1) to give 9-deuteriocamphor (**26**) (32 mg, 635) as a waxy solid. Mass spectroscopic analysis showed this material to contain 98–100 mol% deuterium. This compound was identical to

[6]We are grateful to Dr. Jim Yergey (Merck-Frosst Inc.) for the quantitative deuterium analyses.

Can. J. Chem. Downloaded from www.nrcresearchpress.com by 91.121.58.235 on 09/07/12
For personal use only.

Can. J. Chem. Downloaded from www.nrcresearchpress.com by 91.121.58.235 on 09/07/12
For personal use only.

9-deuteriocamphor (**26**) prepared, as described above, by reduction of 9-bromocamphor with tri-*n*-butyltin deuteride.

*Rearrangement of (+)-3-*endo*-bromocamphor (**12**) to (−)-*endo*-6-bromocamphor (**63**)*

(+)-3-*endo*-Bromocamphor (**12**) (7.5 g) (Aldrich Chemical Co.) in chlorosulfonic acid (30 mL) was stirred at 50°C for 15 min, then poured onto ice. After extraction with ether (3×), the ether layers were washed with sodium bicarbonate solution, then twice with water, and finally dried over $MgSO_4$. Removal of the solvent under reduced pressure gave a light yellow crystalline solid (3.51 g). Column chromatography (silica gel; petroleum ether/ether 9:1) gave the 7-*anti*-bromofenchone (75 mg, 1%) as a cyrstalline solid, mp 49–50°C (sealed tube); $[\alpha]_D$ −133.15° (*c* 0.19, CH_2Cl_2); ν_{max} (film): 1745 cm^{-1}; δ ($CDCl_3$, 400 MHz): 1.09 (3H, s), 1.13 (3H, s), 1.16 (3H, s), 1.38 (1H, m), 1.75–1.90 (2H, m), 2.22 (1H, m), 2.34 (1H, br d, J = 4 Hz; C-4 proton), 4.26 (1H, br s; C-7 *syn* proton); *m/e* (relative intensity): 232/230 (M^+, 1/0.6), 151 (8), 123 (60), 81 (100). Exact mass calcd. for $C_{10}H_{15}OBr$: 232.0286/230.0306; found: 232.0291/230.0312.

Further elution provided a mixture of unidentified compounds (186 mg) that decomposed spontaneously and this was followed by (−)-*endo*-6-bromocamphor (**63**) (34), (2.67 g, 36%) as a white crystalline solid, $[\alpha]_D$ −51.77° (*c* 4.96, CH_2Cl_2); ν_{max} ($CHCl_3$): 1745 cm^{-1}; δ ($CDCl_3$, 400 MHz): 0.92 (3H, s), 0.97 (3H, s), 1.00 (3H, s) 1.90 (1H, dd, J = 15 Hz, 3.5 Hz; C-5 *endo* proton), 2.05 (1H, d, J = 18 Hz; C-3 *endo* proton), 2.22 (1H, dd, J = 4 Hz, 4 Hz; C-4 proton), 2.44 (1H, ddd, J = 18 Hz, 4 Hz, 4 Hz; C-3 *exo* proton), 2.85 (1H, dddd, J = 15 Hz, 10 Hz, 4 Hz, 4 Hz; C-5 *exo* proton), 4.22 (1H, dd, J = 10 Hz, 3.5 Hz; C-6 *exo* proton); *m/e* (relative intensity): 232/230 (M^+, 1.2/1.8), 167 (11), 151 (39), 149 (30), 109 (100), 108 (34), 107 (43). Exact mass calcd. for $C_{10}H_{15}$ OBr: 232.0286/230.0306; found: 232.0274/230.0303. Anal calcd. for $C_{10}H_{15}OBr$: C 51.97, H 6.54, Br 34.57: found: C 51.93, H 6.45, Br 34.68.

*Conversion of (−)-*endo*-6-bromocamphor (**63**) to (−)-camphor (*ent*-**1**)*

To a solution of (−)-6-*endo*-bromocamphor (**63**) (107 mg, 0.46 mmol) and azobisisobutyronitrile (20 mg) in benzene (4 mL) was added tri-*n*-butyltin hydride (29) (0.2 mL, 0.74 mmol) and the mixture refluxed under argon for 16 h. After cooling the solution, it was poured into 10% aqueous potassium fluoride solution (28) and extracted twice with ether. The ether layers were washed twice with the postassium fluoride solution, dried ($MgSO_4$), and evaporated to yield a colourless oil (377 mg). Column chromatography (silica gel; petroleum ether/ether 20:1), gave (−)-camphor (*ent*-**1**) (33.4 mg, 47%), $[\alpha]_D$ −44.75° (*c* 0.40, 95% EtOH); authentic (−)-camphor (Aldrich Chemical Co.) had $[\alpha]_D$ −40.15° (*c* 0.396, 95% EtOH) and authentic (+)-camphor (Aldrich Chemical Co.) had $(\alpha]_D$ +44.80° (*c* 0.386, 95% EtOH). The synthetic (−)-camphor was identical (ir; ^1H nmr, tlc, glc) to authentic material.

*(+)-*endo*-3-Bromo-10-deuteriocamphor (**50**)*

Bromination of (+)-10-deuteriocamphor (24, 30–33) with bromine/acetic acid according to the procedure reported by Meyer *et al.* (5) provided (+)-*endo*-3-bromo-10-deuteriocamphor (**50**), mp 74.5–76°C; δ ($CDCl_3$, 400 MHz): 0.93 (3H, s), 0.96 (2H, t, J = 2 Hz), 1.08 (3H, s), 1.43 (1H, ddd, J = 14 Hz, 9 Hz, 5 Hz), 1.69 (1H, m), 1.88 (1H, m), 2.09 (1H, ddd, J = 13 Hz, 9 Hz, 4 Hz), 1.30 (1H, dd, J = 4.5 Hz, 4.5 Hz; C-4 proton), 4.62 (1H, br d, J = 4.5 Hz). Exact mass calcd. for $C_{10}H_{14}DOBr$: 233.0349/231.0369; found: 233.0348/231.0369.

*Rearrangement of (+)-*endo*-3-bromo-10-deuteriocamphor (**50**) to (−)-6-endo-*bromo-8-deuteriocamphor (**64**)*

Rearrangement of (+)-*endo*-3-bromo-10-deuteriocamphor (**50**), as described above for *endo*-3-bromocamphor, provided (−)-*endo*-6-bromo-8-deuteriocamphor (**64**), mp 55–56°C; δ ($CDCl_3$, 400 MHz): 0.90 (2H, bs), 0.97 (3H, s), 0.99 (3H, s), 1.90 (1H, dd, J = 14.5 Hz, 3 Hz), 2.05 (1H, d, J = 18.5 Hz), 2.21 (1H, dd, J = 4.5 Hz, 4.5 Hz), 2.44 (1H, ddd, J = 18.5 Hz, 5 Hz, 4.5 Hz), 2.85 (1H, m), 4.22 (1H, dd, J = 10 Hz, 3.5 Hz). Exact mass calcd. for $C_{10}H_{14}DOBr$: 233.0349/231.0369; found: 233.0346/231.0374.

*Conversion of (−)-*endo*-6-bromo-8-deuteriocamphor (**64**) to (−)-8-deuteriocamphor (*ent*-**18**)*

(−)-*endo*-6-Bromo-8-deuteriocamphor (**64**) was reduced by the tri-*n*-butyltin hydride method (above) to provide (−)-8-deuteriocamphor (*ent*-**18**) (19, 25–27) in 60% yield; ν_{max} ($CHCl_3$): 1740 cm^{-1}; δ ($CDCl_3$, 400 MHz): 0.83 (2H, t, J = 1.8 Hz; C-8 methyl), 0.93 (3H, s; C-10 methyl), 0.97 (3H, s; C-9 methyl); *m/e* (relative intensity): 153 (M^+, 49), 109 (72), 96 (100), 84 (44), 81 (84). Exact mass calcd. for $C_{10}H_{15}DO$: 153.1264; found: 153.1264. This compound was identical (400 MHz ^1H nmr) to an authentic sample prepared from (+)-8-bromocamphor (1*c*).

*Rearrangement of (+)-*endo*-3,9-dibromocamphor (**17**) to (−)-*endo*-6,9-dibromocamphor (**65**)*

(+)-*endo*-3,9-Dibromocamphor (**17**), (4) (2.13 g) was stirred in chlorosulfonic acid (7.5 mL) at 55°C for 45 min. The mixture was carefully added to ice-cold brine and extracted with ether (3×). The combined ether layers were washed with aqueous postassium hydroxide/brine (emulsion formed), then twice with brine before being dried over $MgSO_4$. Removal of the solvent gave a waxy orange solid (1.73 g), which was recrystallized from ether to yield (−)-*endo*-6,9-dibromocamphor (**65**) (23) (1.01 g). Chromatography (silica gel; petroleum ether/ether 13:1) of the mother liquors provided a further quantity (144 mg) of **65** (total yield, 54%); mp 153.5–154°C (lit. (23) mp 152°C); $[\alpha]_D$ −98.3° (*c* 0.402, CH_2Cl_2) (lit. (23) $[\alpha]_D$ −81° (EtOH)); δ ($CDCl_3$, 270 MHz): 1.02 (3H, s), 1.07 (3H, s), 1.99 (1H, dd, J = 14 Hz, 3 Hz; C-5 *endo* proton), 2.13 (1H, d, J = 19 Hz; C-3 *endo* proton), 2.46 (1H, ddd, J = 19 Hz, 5 Hz, 4 Hz; C-3 *exo* proton), 2.64 (1H, dd, J = 4 Hz, 4 Hz; C-4 proton), 2.83 (1H, m), 3.26 (1H, d, J = 10 Hz), 3.54 (1H, d, J = 10 Hz), 4.27 (1H, dd, J = 10 Hz, 3 Hz; C-6 *exo* proton); *m/e* (relative intensity): 312/310/308 (M^+, 2/5/2), 231/229 (67/67), 217/215 (24/24), 175/173 (24/25), 149 (34), 121 (26), 107 (100). Exact mass calcd. for $C_{10}H_{14}OBr_2$: 311.9371/309.9391/307.9411; found: 311.9381/309.9393/307.9422. Anal. calcd. for $C_{10}H_{14}OBr_2$: C 38.74, H 4.55, Br 51.55; found: C 38.68, H 4.54, Br 51.49.

Acknowledgement

We are grateful to Dr. Jim Yergey (Merck Frosst, Pointe Claire – Dorval, Quebec) for mass spectroscopic deuterium analysis and to N.S.E.R.C. for financial support.

1. (*a*) T. Money. Nat. Prod. Rep. **2**, 253 (1985); (*b*) T. Money. *In* Studies in natural products chemistry. Vol. 4. Part C. *Edited by* Atta-ur Rahman. Elsevier, Amsterdam. 1989; (*c*) D. L. Kuo and T. Money. Can. J. Chem. **66**, 1794 (1988), and references cited.
2. (*a*) J. H. Hutchinson, D. L. Kuo, T. Money, and B. Yokoyama. J. Chem. Soc. Chem. Commun. 1281 (1988); (*b*) J. A. Clase, D. L. F. Li, L. Lo, and T. Money. Can. J. Chem. **68**, 000 (1990); (*c*) L. A. Paquette, D. T. DeRussy, N. A. Pegg, R. T. Taylor, and T. M. Zydowsky. J. Org. Chem. **54**, 4576 (1989); (*d*) L. A. Paquette, N. A. Pegg, D. Toops, G. D. Maynard, and R. D. Rogers. J. Am. Chem. Soc. **112**, 277 (1990).
3. (*a*) W. F. Erman. *In* Chemistry of monoterpenes. Part B. *Edited by* P. G. Gassman. Marcel Dekker, New York. 1985. p. 1173; (*b*) A. M. T. Finch and W. R. Vaughan. J. Am. Chem. Soc. **91**, 1416 (1969); (*c*) T. Miki, M. Nishkawa, and H. Hagiwara. Proc. Jpn. Acad. (Tokyo), **31**, 718 (1955); Chem Abstr. **50**, 13819d (1956); (*d*) Y. Asahina. Proc. Imp. Acad. **13**, 38 (1937); (*e*) O. R. Rodig and R. J. Sysko. J. Am. Chem. Soc. **94**, 6475 (1972).
4. (*a*) H. Nishimitsu, M. Nishikawa, and H. Hagiwara. Proc. Jpn. Acad. **27**, 285 (1951); Chem. Abstr. **46**, 6112a (1952); (*b*) E. J. Corey, S. W. Chow, and R. A. Scherrer. J. Am. Chem. Soc. **79**, 5773 (1957).
5. (*a*) W. L. Meyer, A. P. Lobo, and R. N. McCarty. J. Org. Chem. **32**, 1754 (1967); (*b*) J. H. Johnson. Diss. Abstr. Int. B, **35**, 2657 (1974).
6. (*a*) C. R. Eck, R. W. Mills, and T. Money. J. Chem. Soc. Chem. Commun. 911 (1973); J. Chem. Soc. Perkin Trans. I, 251

(1975); (*b*) P. CACCIA, N. DARBY, C. R. ECK, and T. MONEY. J. Chem. Soc. Perkin Trans. I, 359 (1976).
7. S. RENGARAJU and K. D. BERLIN. Tetrahedron, **27**, 2399 (1971).
8. (*a*) R. P. HASELTINE and T. S. SORENSEN. Can. J. Chem. **53**, 1067 (1975); (*b*) T. S. SORENSEN. Acc. Chem. Res. **9**, 257 (1976).
9. (*a*) J. A. BERSON, J. H. HAMMONS, A. W. MCROWE, R. G. BERGMAN, A. REMANICK, and D. HOUSTON. J. Am. Chem. Soc. **89**, 2590 (1967), and references cited therein; (*b*) J. A. BERSON. *In* Molecular rearrangements. Part 1. *Edited by* P. de Mayo. Interscience, New York. 1963. pp. 111–131; (*c*) J. S. YADAV, U. R. NAYAK, and S. DEV. Tetrahedron, **36**, 309 (1980); (*d*) J. S. YADAV, R. SOMAN, R. R. SOBTI, U. R. NAYAK, and S. DEV. Tetrahedron, **36**, 2105 (1980).
10. (*a*) T. MONEY. *In* Terpenoids and steroids. Vol. 9. The Chemical Society, London. 1979. p. 94; (*b*) J. S. ROBERTS. *In* Terpenoids and steroids. Vol. 10. The Chemical Society, London. 1981. p. 20; (*c*) J. E. BALDWIN and T. C. BARDEN. J. Am. Chem. Soc. **105**, 6656 (1983), and references cited; (*d*) J. E. BALDWIN, T. C. BARDEN, and S. J. CIANCIOSI. J. Org. Chem. **51**, 1133 (1986); (*e*) W. KREISER and L. JANITSCHKE. Chem. Ber. **112**, 408 (1979), and references cited; (*f*) P. T. LANSBURY and R. M. BODEN. Tetrahedron Lett. 5017 (1973).
11. J. D. ROBERTS and J. A. YANCEY. J. Am. Chem. Soc. **75**, 3165 (1953).
12. (*a*) W. R. VAUGHAN and R. PERRY. J. Am. Chem. Soc. **75**, 3168 (1953); (*b*) W. R. VAUGHAN, C. T. GOETSCHEL, M. H. GOODROW, and C. L. WARREN. J. Am. Chem. Soc. **85**, 2282 (1963); (*c*) C. W. DAVID, B. W. EVERLING, R. J. KILLIAN, J. B. STOTHERS, and W. R. VAUGHAN. J. Am. Chem. Soc. **95**, 1265 (1973).
13. C. J. COLLINS and M. H. LIETZKE. J. Am. Chem. Soc. **95**, 6842 (1973).
14. (*a*) G. E. GREAM and D. WEGE. Tetrahedron, **22**, 2583 (1966); (*b*) G. C. GREAM. Rev. Pure Appl. Chem. **16**, 25 (1966).
15. P. HIRSJARVI, K. HEINANEN, and L. PIRILA. Suomen Kemi, **B37**, 5520 (1964).
16. D. R. DIMMEL and W. Y. FU. J. Org. Chem. **38**, 3782 (1973).
17. W. F. ERMAN. *In* Chemistry of monoterpenes. Part B. *Edited by* P. G. Gassman. Marcel Dekker, New York. 1985. pp. 1120, 1178.
18. (*a*) O. R. RODIG and R. J. SYSKO. J. Org. Chem. **36**, 2324 (1971); (*b*) C. R. ECK, G. L. HODGSON, D. F. MACSWEENEY, R. W. MILLS, and T. MONEY, J. Chem. Soc. Perkin Trans. 1, 1938 (1974); (*c*) W. L. MEYER, C. E. CAPSHEW, J. H. JOHNSON, A. R. KLUSENER, A. P. LOBO and R. N. MCCARTY. J. Org. Chem. **42**, 527 (1977).
19. W. M. DADSON and T. MONEY. J. Chem. Soc. Chem. Commun. 112 (1982).
20. (*a*) W. R. VAUGHAN and D. M. TEEGARDEN. J. Am. Chem. Soc. **96**, 4902 (1974); (*b*) P. C. MOEWS, J. R. KNOX, and W. R. VAUGHAN. Tetrahedron Lett. 359 (1977); (*c*) J. Am. Chem. Soc. **100**, 260 (1978), and references cited.
21. A. NICKON and R. C. WEGLEIN. Tetrahedron Lett. **27**, 2675 (1986), and references cited.
22. C. A. BEAR and J. TROTTER. Acta Crystallogr. Sect. B: Struct. Crystallogr. Cryst. Chem. **B31**, 904 (1975).
23. (*a*) A. PELTER and S. H. HARPER. *In* Rodd's chemistry of carbon compounds. Vol. IIc. *Edited by* S. Coffey. Elsevier, Amsterdam. 1969; (*b*) T. MIKI, M. NISHIKAWA, and H. HAGIWARA. Proc. Jpn. Acad. (Tokyo), **31**, 718 (1955); Chem. Abstr. **50**, 13819d (1956); (*c*) M. NISHIKAWA. Yakugako Zasshi, **72**, 634 (1952); **72**, 637 (1952); **72**, 643 (1952); Chem Abstr. **47**, 6379h (1953); **47**, 6380a, b (1953); (*d*) M. NISHIKAWA. Yakugaku Zasshi, **76**, 309 (1956); Chem. Abstr. **50**, 13818 (1956).
24. G. C. JOSHI and E. W. WARNHOFF. J. Org. Chem. **37**, 2383 (1972).
25. W. L. MEYER, C. E. CAPSHEW, J. H. JOHNSON, A. R. KLUSENER, A. P. LOBO, and R. N. MCCARTY. J. Org. Chem. **42**, 527 (1977).
26. T. M. ATLAY. M.Sc. Thesis, University of B.C., Vancouver (1983).
27. W. M. DADSON and T. MONEY. Can. J. Chem. **58**, 2524 (1980).
28. J. E. LIEBNER and J. J. JACOBUS. J. Org. Chem. **44**, 449 (1979).
29. H. G. KUIVILA. Synthesis, 499 (1970).
30. A. NICKON, J. L. LAMBERT, J. E. OLIVER, D. F. COVEY, and J. MORGAN. J. Am. Chem. Soc. **98**, 2593 (1976).
31. C. C. HINCKLEY. J. Org. Chem. **35**, 2834 (1970).
32. D. R. DIMMEL and J. WOLINSKY. J. Org. Chem. **32**, 410 (1967).
33. J. D. CONNOLLY and R. MCCRINDLE. Chem. Ind. (London), 379 (1965).
34. L. A. HEITANIEMI and P. J. MALKONEN. Dev. Biochem. **23**, 477 (1982); Chem. Abstr. **98**, 156960x (1983).

Can. J. Chem. Downloaded from www.nrcresearchpress.com by 91.121.58.235 on 09/07/12
For personal use only.

A simple synthetic route to 4-methylcamphor: mechanistic aspects

J. Andrew Clase, Diana L. F. Li, Linda Lo, and Thomas Money[1]

Chemistry Department, University of British Columbia, 2036 Main Mall, Vancouver, B.C., Canada V6T 1Y6

Received March 28, 1990

This paper is dedicated to Professor Ross Stewart on the occasion of his 65th birthday

J. Andrew Clase, Diana L. F. Li, Linda Lo, and Thomas Money. Can. J. Chem. **68**, 1829 (1990).

A mechanism proposed for the rearrangement of (+)-2-methylenebornane (**8**) to a mixture of (+)-4-methylisobornyl acetate (**5**) and its enantiomer (*ent*-**5**) is supported by evidence obtained by investigating the rearrangement of deuterated 2-methylenebornane.

Key words: 4-methylcamphor, Wagner–Meerwein rearrangement, 6,2-hydride shift, 9-bromo-4-bromomethylcamphor.

J. Andrew Clase, Diana L. F. Li, Linda Lo et Thomas Money. Can. J. Chem. **68**, 1829 (1990).

En examinant la transposition du 2-méthylènebornane deutéré, on a obtenu des données supportant le mécanisme qui a été proposé antérieurement pour la transposition du (+)-2-méthylènebornane (**8**) en un mélange d'acétate de (+)-4-méthylisobornyle (**5**) et de son énantiomère (*ent*-**5**).

Mots clés : 4-méthylcamphre, transposition de Wagner–Meerwein, déplacement 6,2 d'hydrure, 9-bromo-4-bromométhylcamphre.

[Traduit par la revue]

Can. J. Chem. Downloaded from www.nrcresearchpress.com by 91.121.58.235 on 09/07/12
For personal use only.

In connection with our general synthetic objective of using camphor derivatives as enantiomerically pure intermediates in terpenoid synthesis (1), we required an enantiospecific procedure for the conversion of camphor to 4-methylcamphor. Literature procedures (2) (Scheme 1) for the synthesis of (−)-4-methylcamphor (**7**) generally involve initial conversion of (+)-camphor (**1**) to (−)-2-methylisoborneol (**2**) or 1-methylcamphene (**3**) followed by acid-catalysed rearrangement to (+)-4-methylisoborneol (**4**) (2*c*,*g*), (+)-4-methylisobornyl acetate (**5**) (2*h*,*i*), or (+)-4-methylisobornyl nitrate (**6**) (2*d*,*f*). In no case was the optical purity of these products or the derived (−)-4-methylcamphor (**7**) determined and, hence, only an estimate of relative enantiomeric purity can be gauged from literature values of specific rotations listed in Table 1.

Since the conversion of (+)-camphor (**1**) to (−)-2-methylisoborneol (**2**) does not occur in high yield (3), we recently devised an alternative and potentially enantiospecific route to 4-methylcamphor that involves direct acid-catalysed rearrangement of (+)-2-methylenebornane (**8**) (Scheme 1) or its enantiomer (*ent*-**8**). The latter compounds are readily prepared (4, 5) in high yield (>90%) from (+)- and (−)-camphor, respectively, and we have discovered that treatment of **8** with $HOAc/H_2SO_4$ (conc.) (40:1 v/v) for 30 min at room temperature provides (+)-4-methylisobornyl acetate (**5**) ($[\alpha]_D^{20}$ +39.2 (*c* 2.20, EtOH)) in ~70% yield. Subsequent conversion of **5** to (+)-4-methylisoborneol (**4**) ($[\alpha]_D^{30}$ +19.5 (*c* 10.00, EtOH)) and (−)-4-methylcamphor (**7**) ($[\alpha]_D^{21}$ −16.0 (*c* 2.00, EtOH)) was then accomplished in ~90% overall yield.

Although the specific rotations (see above) of 4-methylisobornyl acetate, 4-methylisoborneol, and 4-methylcamphor prepared in this way were comparable to those recorded in the literature (cf. Table 1), the optical purity of our compounds or those described in the literature had not been established. Accordingly, the optical purity of our synthetic 4-methylisobornyl acetate was determined by measuring the ^1H nmr spectrum in the presence of a chiral shift reagent (6), $Eu(hfc)_3$. Three methyl groups in **5** (presumably C(8), C(10), and C(11)) appeared as a pair of signals, and their integration indicated that the enantiomeric ratio (**5**: *ent*-**5**) was ~4.5:1, i.e., an optical purity of ~64%. Authentic (±)-isobornyl acetate and (−)-isobornyl acetate were used as standards to establish the accuracy of this method of estimating optical purity. In a similar fashion, the optical purity of (−)-4-methylcamphor (**7**), derived from (+)-4-methylisobornyl acetate (**5**), was also estimated by recording the ^1H nmr spectrum in the presence of $Eu(hfc)_3$. In this case, one of the methyl groups (presumably C(10), see below) was clearly discernible as two signals with relative area ~4.3:1. Attempts to determine the optical purity of our synthetic (+)-4-methylisoborneol (**5**, or **5** + *ent*-**5**), by measuring the ^{31}P nmr spectrum (121.421 MHz) in the presence of Anderson–Shapiro reagent (7), clearly showed that the compound was not enantiomerically pure. However, the difference in chemical shift (0.04 ppm) between the two diastereomeric phosphate esters was too small to provide a reliable estimate of optical purity.

A comparison of the specific rotations quoted in the literature (cf. Table 1) and those recorded in our laboratory (*vide infra*) leads to the conclusion that all of the current methods of preparing 4-methylisobornyl acetate (**5**) provide material that is not enantiomerically pure. A plausible mechanism for the conversion of 2-methylisoborneol (**2**) (2*f*,*i*), 1-methylcamphene (**3**) (2*g*,*h*,*j*,*k*), and (+)-2-methylenebornane (**8**) to (+)-4-methylisobornyl acetate (**5**) and its enantiomer (*ent*-**5**) is shown in Scheme 2 and involves a combination of Wagner–Meerwein rearrangements, 3,2-*exo*-methyl shifts, and 6,2-hydride shifts. The validity of this mechanism can be evaluated by tracing the fate of deuterium when deuterated 2-methylenebornane (**8**) is rearranged to deuterated 4-methylisobornyl acetate (**5**). To accomplish this objective, however, it was necessary to assign chemical shifts to each of the four methyl groups in 4-methylcamphor (**7**).

The assignment of chemical shifts to the C(8), C(9), and C(10) methyl groups in camphor (**1**) was made by Connolly and McCrindle (8) by comparing the nmr spectra recorded in deuteriochloroform and benzene. Benzene-induced upfield shifts were noted for the C(8) and C(9) methyl groups ($\Delta\delta$ 0.23 and 0.32 ppm) while the C(10) methyl group absorption had almost the same chemical shift in deuteriochloroform and benzene ($\Delta\delta \sim 0.02$ ppm). Connolly and McCrindle suggested (8) that benzene-induced shifts of methyl group nmr absorptions

[1]Author to whom correspondence may be addressed.

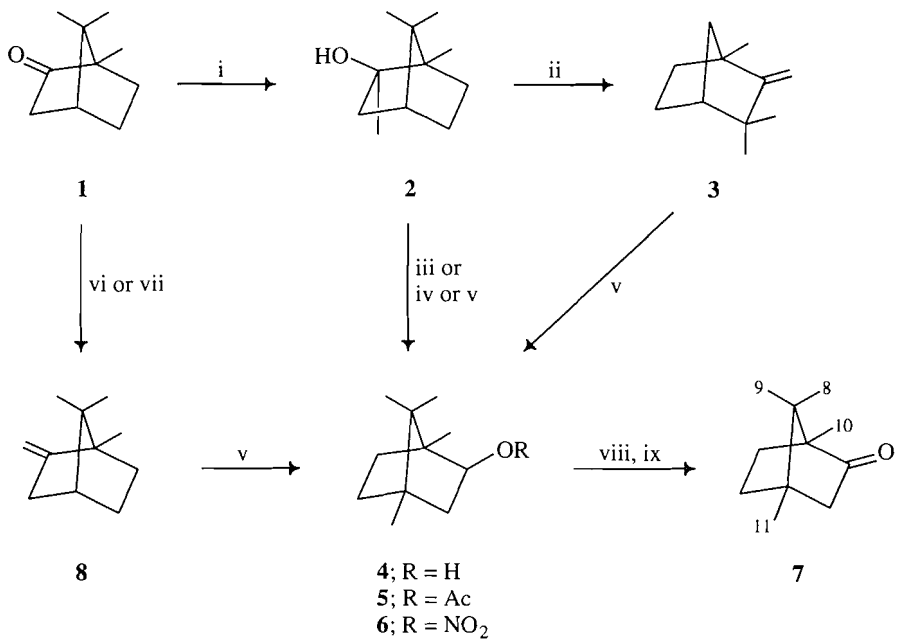

i, MeMgI, Et_2O; ii, $KHSO_4$, heat; iii, H_2SO_4, H_2O; iv 65% HNO_3;
v, HOAc, H_2SO_4; vi, $TiCl_4$, Zn, CH_2Br_2, THF; vii, CH_3PPh_3Br, BuLi, THF;
viii, $LiAlH_4$, Et_2O; ix, PCC, CH_2Cl_2

SCHEME 1

TABLE 1. Literature values of the specific rotation of 4-methylisoborneol (**4**), 4-methylisobornyl acetate (**5**), and 4-methylcamphor (**7**)

Compound	Specific rotation $[\alpha]_D^{20}$	Reference
4	+14.8°	2*a*
	+22.69° (EtOH)	2*g*
	+25.20° (*c* 10.0, EtOH)	2*c*,*f*
5	+18.90°	2*a*
	+35.84°	2*g*,*i*
7	−14.5° (*c* 10.0, EtOH)	2*c*,*f*

in cyclic ketones could be predicted by considering the position of the methyl group with respect to a reference plane passing through the carbon of the carbonyl group and perpendicular to its axis. Methyl groups that lie close to but behind this plane experience small upfield benzene-induced shifts (>0.1 ppm) while those some distance behind the plane show larger upfield shifts (~0.25–0.55 ppm).

Comparing the nmr spectra of 4-methylcamphor (**7**) in $CDCl_3$ (δ 0.71, 0.83, 0.92, and 1.04) and benzene-d_6 (δ 0.47, 0.51, 0.70, and 0.92) clearly reveals that one methyl group signal (δ 0.92) does not undergo an upfield shift in benzene-d_6 and, by analogy with camphor, this absorption (δ 0.92) was assigned to the C(10) methyl group. The assignment of chemical shifts to the C(9) and C(11) methyl groups (δ ($CDCl_3$) 0.83 and 1.04) was deduced from the nmr spectrum of 9-deuterio-4-deuteriomethylcamphor (**30**) (δ: 0.71 (s), 0.85 (t, J = 2 Hz), 0.92 (s), and 1.02 (t, J = 2 Hz)). This compound was prepared (Scheme 3) by reduction (Bu_3SnD) of 9-bromo-4-bromomethylcamphor (**29**) (9) and, since this structure has been confirmed by X-ray crystallographic analysis[2] of its synthetic precursor (**28**), the assignment of signals to C(9) and C(11) methyl groups rests on secure experimental evidence. The assignment of the signal at 0.83 ppm to the C(9) methyl group was deduced from an nOe difference experiment; irradiation at this frequency results in enhancement of the signals for the C(5) and C(6) *exo*-protons (δ 1.59–1.77). Thus the signal at δ 1.04 ppm was assigned to the C(11) methyl group protons. The remaining unassigned signal at δ 0.71 in the spectrum of 4-methylcamphor (**7**) was, of course, assigned to the C(8) methyl group and confirmatory evidence for this assignment was obtained from nOe difference experiments. Thus, irradiation at the C(8) methyl group resonance frequency resulted in enhancement of the C(3)-*exo*-hydrogen signal (δ 2.08, dd, J = 18 and 3 Hz).

General support for the mechanism outlined in Scheme 2 was obtained by rearranging 2-(dideuteriomethylene)bornane (**21**), derived from (+)-camphor (**1**), to deuterated 4-methylisobornyl acetate (**25** + *ent*-**25**). The ^1H nmr spectrum (δ ($CDCl_3$, 400 MHz): 0.69 (3H, s, C(8) methyl), 0.83 (3H, s, C(9) methyl), 0.86 (3H, s, C(10) methyl), 0.88 (m, C(11) deuteriomethyl + C(11) dideuteriomethyl), 0.90 (3H, s, C(11) methyl), 2.01 (3H, s, CH_3CO), 4.65 (1H, dd, J = 9 and 3.5 Hz, C(2) H)) of this compound demonstrated that considerable loss of deuterium had occurred during its formation from 2-(dideuteriomethylene)bornane (**21**). When the rearrangement of 2-(dideuteriomethylene)bornane (**21**) was carried out in CH_3CO_2D/H_2SO_4 (catalytic) the ^1H nmr (400 MHz) spectrum (δ: 0.71 (3H, s, C(8) methyl), 0.83 (3H, s, C(9) methyl), 0.92 (3H, s, C(10) methyl), 1.01 (m, C(11) dideuteriomethyl)) of the derived 4-methylcamphor (**26**) indicated that the C(11) methyl group signal was very weak and weak multiplets appeared at δ 0.82 and 0.90, upfield from the normal C(9) and C(10) methyl signals. According to the mechanism outlined in Scheme 2, the C(9) and C(10) methyl groups (but not the C(8) methyl group) of 2-methylenebornane (**8**) can become *exo*-methylene groups and, hence, incorporate deuterium.

[2]S. Rettig and J. Trotter, unpublished results.

Can. J. Chem. Downloaded from www.nrcresearchpress.com by 91.121.58.235 on 09/07/12
For personal use only.

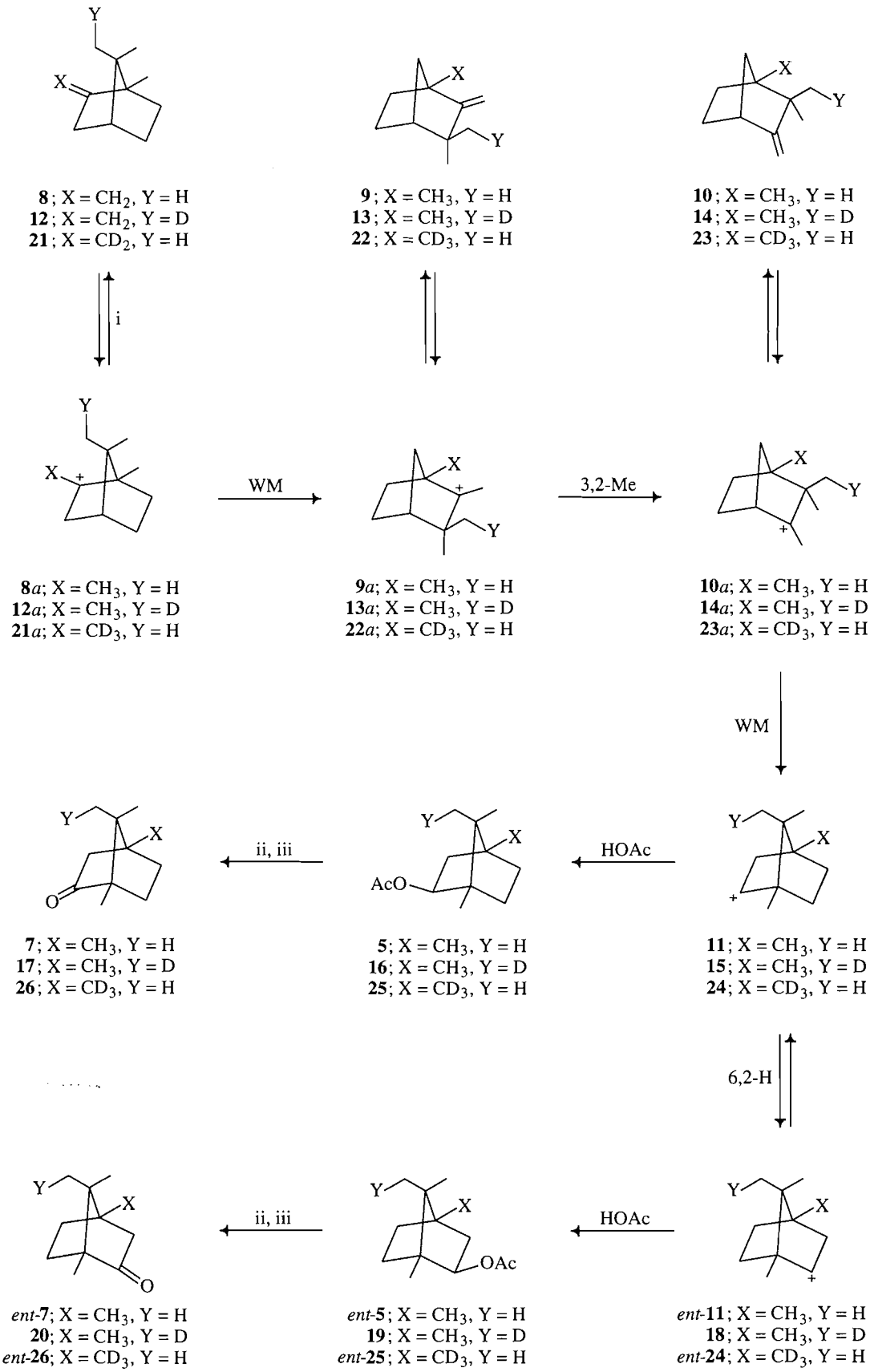

WM = Wagner–Meerwein rearrangement; 3,2-Me = 3,2-*exo*-methyl shift;
6,2-H = 6,2-hydride shift
i, HOAc, H_2SO_4 (cat.); ii, $LiAlH_4$, THF; iii, PCC, CH_2Cl_2

SCHEME 2

Can. J. Chem. Downloaded from www.nrcresearchpress.com by 91.121.58.235 on 09/07/12
For personal use only.

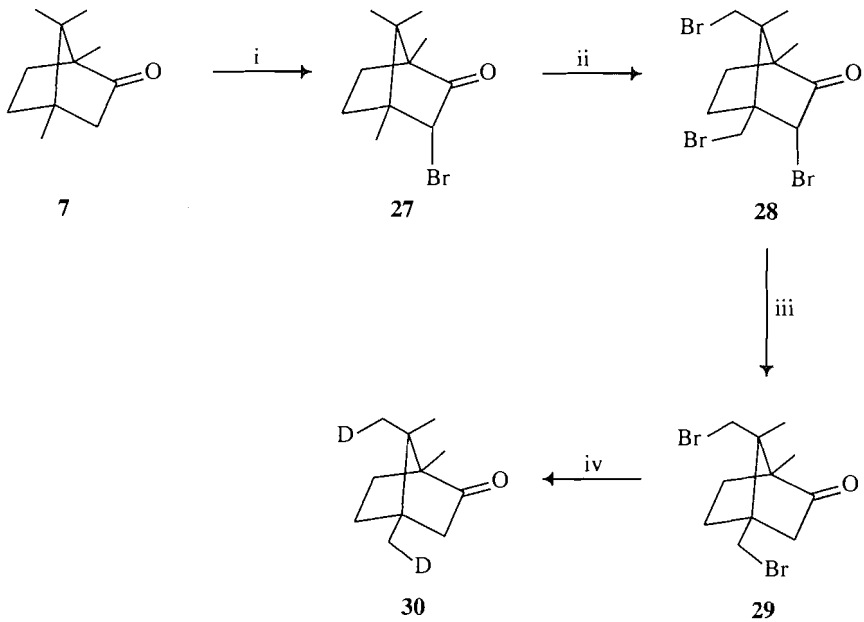

i, Br_2, HOAc; ii, Br_2, $ClSO_3H$, 18 h; iii, Zn, HOAc, 0°C; iv, Bu_3SnD, AIBN, C_6H_6

SCHEME 3

Support for the operation of a 6,2-hydride shift[3] (Scheme 2) to explain the formation of *ent*-**5** was obtained by converting 8-deuterio-2-methylenebornane (**12**) (Scheme 2), derived from 8-deuteriocamphor (10), to deuterium-labelled 4-methylisobornyl acetate (**16** + **19**). The ^1H nmr spectrum (δ ($CDCl_3$, 400 MHz): 0.70 (2H, 1:1:1 t, J = 2 Hz, C(8) dideuteriomethyl), 0.71 (s, C(8) methyl), 0.81 (sh, C(9) dideuteriomethyl), 0.83 (3H, s, C(9) methyl), 0.92 (3H, s, C(10) methyl), 1.04 (3H, s, C(11) methyl)) of 4-methylcamphor (**17** + **20**) derived from this sample of 4-methylisobornyl acetate (**16** + **19**) showed that deuterium was located primarily in the C(8) methyl group with a small amount present in the C(9) methyl group. This evidence is consistent with the proposal (Scheme 2) that partial racemization is due to the occurrence of a 6,2-hydride shift, and the relative amount of deuterium present in the C(8) and C(9) methyl groups, although not estimated accurately, is consistent with the ratio of enantiomers, (**5** + *ent*-**5**) or (**7** + *ent*-**7**), determined by the chiral shift reagent method (cf. above).

From the mechanism proposed for the conversion of (+)-2-methylenebornane (**8**) to (+)-4-methylisobornyl acetate (**5**) and its enantiomer (*ent*-**5**) (Scheme 2), it is obvious that optically pure 4-methylisobornyl acetate can only be obtained if intermediate **11** reacts exclusively with solvent (HOAc) rather than undergoing a 6,2-hydride shift. Suppression of the 6,2-hydride shift could be accomplished perhaps by introducing a removable functional group into an appropriate position (e.g., C(3) or C(5)) in 2-methylenebornane, and we are currently investigating this possibility.

[3]It is worth noting that the intermediate **11** in Scheme 2 could be converted to *ent*-**11** by the occurrence of a 3,2-hydride shift rather than (or in addition to) the proposed 6,2-hydride shift. In general, however, 6,2-hydride shifts are generally preferred over 3,2 hydride shifts in bicyclo[2,2,1]heptyl carbocations (11). Also, it has been established (12) that when hydride shifts occur in carbocations of this type they are almost exclusively *exo* (12) and, hence, the product would be 4-methylbornyl acetate, i.e., the C(2) epimer of **5**. The chemical shift (δ 4.65) and multiplicity of the C(2) hydrogen of **5** formed by rearrangement of 2-methylenebornane (**8**) is almost identical to that of isobornyl acetate (δ 4.67) and, therefore, inconsistent with the *endo* epimer.

Experimental

Infrared (ir) spectra were recorded on a Perkin–Elmer model 710B spectrophotometer and were calibrated using the 1601 cm^{-1} band of polystyrene. Optical rotations ($[\alpha]_D$) were measured on a Perkin–Elmer 141 polarimeter at room temperature. The proton nuclear magnetic resonance spectra were recorded in deuteriochloroform at 400 MHz on a Bruker WH-400 spectrometer. The ^{31}P nmr spectra were recorded in benzene at 121.421 MHz using a Varian XL-300 spectrometer. Signal positions are given in ppm downfield from H_3PO_4 (used as an external reference standard) with an internal benzene-d_6 lock. Low-resolution mass spectra were obtained using a Varian MAT CH-4B spectrometer, and exact masses were obtained by high-resolution mass spectroscopy on a Kratos MS-50 mass spectrometer. All compounds characterized by high-resolution mass spectrometry exhibited one spot on a tlc (thin-layer chromatography) plate. Low-resolution gas liquid chromatography/mass spectra (gc/ms) were obtained on a Carlo Erba 41 60/Kratos MS 80 RFA instrument using a 0.25 mm × 15 m column with helium as the carrier gas. Gas–liquid chromatography (glc) was performed on either a Hewlett Packard model 5830A gas chromatograph with a 6 ft × 1/8 in. column of 3% OV-17 (carrier gas nitrogen) or a Hewlett Packard model 5880A gas chromatograph using a 50 m or 12 m × 0.2 mm column of Carbowax 10 M or a 12 m × 0.2 mm column of OV-101 (carrier gas helium). X-ray crystallographic analysis was carried out by Dr. S. Rettig and microanalyses were performed by Mr. P. Borda, Microanalytical Laboratory, University of British Columbia.

All reactions involving moisture-sensitive reagents were performed under an atmosphere of dry argon using either oven- or flame-dried glassware. All reaction products were dried by allowing the solutions to stand over anhydrous magnesium sulfate. The solvents and reagents used were purified as follows: tetrahydrofuran (THF) was distilled from calcium hydride, lithium aluminum hydride (LAH), and sodium/benzophenone. Diethyl ether was distilled from LAH. Benzene, dichloromethane, triethylamine, and pyridine were distilled from

Can. J. Chem. Downloaded from www.nrcresearchpress.com by 91.121.58.235 on 09/07/12
For personal use only.

Can. J. Chem. Downloaded from www.nrcresearchpress.com by 91.121.58.235 on 09/07/12
For personal use only.

calcium hydride. Methanol was distilled from dry magnesium and iodine following reflux. Petroleum ether (bp 30–60°C) was distilled prior to use.

Flash chromatography was performed using Merck silica gel 60, 230–400 mesh, and tlc using Merck silica gel 60 F_{254} sheets.

(−)-2-Methylenebornane (8) (4, 5b)

(i) Method A (4)

Methyltriphenylphosphonium bromide (154.73 g, 0.43 mol) was vacuum pumped for 3 h to remove any trace of moisture before it was dissolved in dry THF (400 mL). *n*-Butyllithium (0.43 mol, 270.7 mL of a 1.6 M solution) was added dropwise at room temperature and the resultant mixture was stirred at 50°C for 2 h under argon. (+)-Camphor (**1**) (41.21 g, 0.27 mol) in dry THF (160 mL) was then added dropwise to the Wittig reagent and the reaction mixture was refluxed for 15 h under argon. Upon completion of the reaction, the THF solution was reduced to half volume by rotary evaporation, diluted with water, and extracted with pentane. The pentane extracts were combined, washed with water, and dried over anhydrous magnesium sulfate. Evaporation of the solvent yielded a viscous yellow oil that was purified by column chromatography (230–400 mesh silica; elution with 100% petroleum ether) to provide (−)-2-methylenebornane (**8**) as a white crystalline solid (35.5 g, 87%), mp 70–71°C (sealed tube) (lit. (4*a*) mp 68–70°C); $[\alpha]_D^{23}$ −52.88 (*c* 2.67, benzene) (lit. (4*c*) $[\alpha]_D^{26}$ −48.5 (*c* 2.12, benzene)); ν_{max} ($CHCl_3$): 1650, 885 cm^{-1}; δ ($CDCl_3$, 400 MHz): 0.76 (3H, s, C(8)H_3), 0.89 (3H, s, C(10)H_3), 0.92 (3H, s, C(9)H_3), 1.16–1.30 (2H, m, C(5) and C(6) *endo* protons), 1.64 (1H, ddd, *J* = 12, 12, and 4 Hz, C(6) *exo* proton), 1.73 (1H, dd, *J* = 8 and 4 Hz, C(4) proton), 1.78 (1H, m, C(5) *exo* proton), 1.91 (1H, bd, *J* = 16 Hz, C(3) *endo* proton), 2.38 (1H, bd, *J* = 16 Hz, C(3) *exo* proton), 4.63 (d) and 4.69 (d) (2H, AB quartet, *J* = 22 Hz, *exo*-methylene protons); *m/e* (relative intensity): 150 (M^+, 10.2), 135 (8.6), 69 (80.6), 55 (26.9), 41 (52.4). Exact mass calcd. for $C_{11}H_{18}$: 150.1409; found: 150.1413. Anal. calcd. for $C_{11}H_{18}$: C 87.93, H 12.07; found: C 87.71, H 12.10.

(ii) Method B (5)

Titanium tetrachloride (0.48 mL, 4.37 mmol) was added dropwise to a stirred suspension of zinc dust (1.18 g, 18.0 mmol) and dibromomethane (1.04 g, 0.42 mL, 6.0 mmol) in THF (20 mL) at −40°C. The reaction mixture was allowed to warm to 5°C and kept in the refrigerator for 3 days to give a thick brown slurry (5*a*). The ice-cold slurry was added portionwise to a stirred solution of (+)-camphor (**1**) (0.30 g, 2.0 mmol) in dichloromethane (2.0 mL) and the resultant mixture was stirred at room temperature for 18 h under argon. The reaction mixture was then quenched with saturated sodium bicarbonate solution, extracted with ether, the combined ether extracts washed with water, and dried over anhydrous magnesium sulfate. Evaporation of the solvent yielded pure (−)-2-methylenebornane (**8**) as a white crystalline solid (0.30 g, 99%) exhibiting spectral data comparable to those above.

(+)-Methylisobornyl acetate (5) (2)

Concentrated sulfuric acid (1.31 mL, 0.016 mol) was added dropwise to (−)-2-methylenebornane (**8**) (12.64 g, 0.084 mmol) in glacial acetic acid (54.4 mL). The reaction mixture was stirred at 0°C for 30 min, quenched in water, and extracted with ether. The ether extracts were combined, washed with saturated sodium bicarbonate solution, then with water, and dried over anhydrous magnesium sulfate. Evaporation yielded a light-yellow oil (12.58 g) that was purified by column chromatography (silica gel 230–400 mesh). Elution with petroleum ether/ether (98:2) provided pure (+)-4-methylisobornyl acetate (**5**) as a clear colorless oil (9.54 g, 73%); $[\alpha]_D^{20}$ +39.2 (*c* 2.20, 95% ethanol) (lit. (2*j*) $[\alpha]_D$ +35.84); ν_{max} (film): 1740, 1250, 1040 cm^{-1}; δ ($CDCl_3$, 400 MHz): 0.69 (3H, s, C(9)H_3), 0.83 (3H, s, C(8)H_3), 0.86 (3H, s, C(10)H_3), 0.90 (3H, s, C(11)H_3), 1.10–1.19 (2H, m, C(5) and C(6) *endo* protons), 1.36–1.54 (3H, m, C(6) *exo*, C(3) *endo*, and C(5) *exo* protons), 1.82 (1H, dd, *J* = 14 and 8 Hz, C(3) *exo* proton), 2.01 (3H, s, CH_3CO), 4.65 (1H, dd, *J* = 9 and 3.5 Hz, C(2) proton); *m/e* (relative intensity): 210 (M^+, 2.0), 150 (50.9), 135 (48.3), 109 (82.3), 43 (100.0). Exact mass calcd. for $C_{13}H_{22}O_2$: 210.1620; found: 210.1622. Anal. calcd. for $C_{13}H_{22}O_2$: C 74.24, H 10.54; found: C 74.82, H 10.70.

(+)-4-Methylisoborneol (4) (2)

Lithium aluminum hydride (3.1 g, 0.082 mol) was added to a solution of (+)-4-methylisobornyl acetate (**5**) (9.54 g, 0.045 mol) in dry THF (160 mL) and the reaction mixture was stirred at 0°C for 4 h. The reaction mixture was then quenched in water, extracted with ether, and the ether extracts washed with 1 M HCl solution, brine, and water, and dried over anhydrous magnesium sulfate. Evaporation of the ether yielded (+)-4-methylisoborneol (**4**) as white needles (7.56 g, 99%), mp 193–194°C (sealed tube) (lit. (2*f*) mp 195–196.5°C; lit (2*i*) mp 193–194°C); $[\alpha]_D^{30}$ +19.5 (*c* 10.0, 95% ethanol) (lit. (2*f*) $[\alpha]_D$ +25.2 (*c* 10.0, EtOH); lit. (2*j*) $[\alpha]_D$ +22.69 (EtOH); lit. (2*b*) $[\alpha]_D$ +18.9° (EtOH)); ν_{max} ($CHCl_3$): 3600, 1210 cm^{-1}; δ ($CDCl_3$, 400 MHz): 0.67 (3H, s, C(9)H_3), 0.87 (3H, s, C(8)H_3), 0.90 (3H, s, C(10)H_3), 0.93 (3H, s, C(11)H_3), 0.94–1.11 (2H, m, C(5) and C(6) *endo* protons), 1.34–1.46 (2H, m, C(6) *exo* and C(3) *endo* protons), 1.51 (1H, ddd, *J* = 8, 8, and 4 Hz, C(5) *exo* proton), 1.74 (1H, dd, *J* = 14 and 8 Hz, C(3) *exo* proton), 3.52 (1H, dd, *J* = 8 and 4 Hz, C(2) proton); *m/e* (relative intensity): 168 (M^+, 2.1), 150 (14.4), 109 (100.0), 41 (70.6). Exact mass calcd. for $C_{11}H_{20}O$: 168.1514; found: 168.1514. Anal. calcd. for $C_{11}H_{20}O$: C 78.51, H 11.98; found: C 78.57, H 11.99.

(−)-4-Methylcamphor (7) (2)

(+)-4-Methylisoborneol (**4**) (7.50 g, 0.045 mol) was dissolved in dichloromethane (150 mL) and the solution was added dropwise to pyridinium chlorochromate (PCC) (14.4 g, 0.067 mol) in methylene chloride (150 mL). After stirring at room temperature for 3.5 h, the reaction mixture was filtered through a layer of silica gel and anhydrous magnesium sulfate and washed with ether. Evaporation of the solvent provided (−)-4-methylcamphor (**7**) as a white crystalline solid (7.45 g, 99%), mp 150–151°C (sealed tube) (lit. (2*c*,*f*) mp 167–168°C); $[\alpha]_D^{21}$ −16.0 (*c* 2.04, 95% ethanol) (lit. (2*c*,*f*) $[\alpha]_D$ −14.50 (*c* 10.0, EtOH)); ν_{max} ($CHCl_3$): 1730 cm^{-1}; δ ($CDCl_3$, 400 MHz): 0.71 (3H, s, C(8)H_3), 0.83 (3H, s, C(9)H_3), 0.92 (3H, s, C(10)H_3), 1.04 (3H, s, C(11)H_3), 1.35–1.43 (2H, m, C(5) and C(6) *endo* protons), 1.57–1.75 (2H, m, C(5) and C(6) *exo* protons), 1.87 (1H, d, *J* = 18 Hz, C(3) *endo* proton), 2.08 (1H, dd, *J* = 18 and 3 Hz, C(3) *exo* proton); δ (C_6D_6, 400 MHz): 0.48 (3H, s, C(8)H_3), 0.51 (3H, s, C(9)H_3), 0.71 (3H, s, C(11)H_3), 0.92 (3H, s, C(10)H_3); *m/e* (relative intensity): 166 (M^+, 39.8), 138 (13.9), 109 (94.8), 83 (19.6), 82 (100.0). Exact mass calcd. for $C_{11}H_{18}O$: 166.1358; found: 166.1360. Anal. calcd. for $C_{11}H_{18}O$: C 79.47, H 10.91; found: C 79.67, H 11.03.

Determination of optical purity using tris[3-(heptafluoropropylhydroxymethylene)-d-camphorato]europium(III), Eu(hfc)$_3$

(i) (+)-4-Methylisobornyl acetate (**5**) (21.03 mg, 0.10 mmol) was dissolved in $CDCl_3$ (1 mL) and a series of four 400-MHz ^1H nmr spectra were recorded in the presence of different amounts of $Eu(hfc)_3$ (cf. Table 2).

(ii) (−)-4-Methylcamphor (**7**) (16.63 mg, 0.10 mmol) was dissolved in $CDCl_3$ (1 mL) and a series of ^1H nmr spectra (400 MHz) were recorded before addition of $Eu(hfc)_3$ and after sequential addition of 11.94 mg (0.01 mmol), 23.87 mg (0.02 mmol), and 35.81 mg (0.03 mmol) of $Eu(hfc)_3$ (cf. Table 3).

Determination of optical purity using the Anderson–Shapiro reagent (7)((4R,5R)-2-chloro-4,5-dimethyl-1,3,2-dioxaphospholane-2-oxide)

Anderson–Shapiro reagent (7) (358 mg, 2.10 mmol) was added to (+)-4-methylisoborneol (**4**) ($[\alpha]_D^{30.5}$ +19.47 (*c* 10.0, 95% ethanol) (334.5 mg, 2.0 mmol)), dry triethylamine (0.42 mL, 0.20 mmol), and 4-(dimethylamino)pyridine in dry benzene (2.0 mL). After 15 min a small amount of C_6D_6 was added and the mixture was filtered through a cotton plug. The ^{31}P nmr spectrum of this solution was recorded at 121.4 MHz using H_3PO_4 as internal standard; δ: 13.667, 13.628 (relative intensity ~2:1, Δδ 4.86 Hz).

8-Deuterio-2-methylenebornane (12)

Methylenation of 8-deuteriocamphor (10) by the method B described

TABLE 2. The ^{1}H nmr spectra of (+)-4-methylisobornyl acetate (**5**) in presence of Eu(hfc)$_3$

Molar equiv. of Eu(hfc)$_3$	δ (ppm)				Δδ (Hz)			
	C(9)Me	C(8)Me	C(10)Me	C(11)Me	C(9)Me	C(8)Me	C(10)Me	C(11)Me
0	s, 0.70	s, 0.85	s, 0.88	s, 0.91	0	0	0	0
0.10	s, 0.79	s, 0.95	s, 1.04	s, 1.14	0	0	0	0
0.25	s, 0.92	1.02	1.36	1.54	0	4	6	8
		1.03	1.37	1.56				
0.50	s, 1.14	1.16	1.91	2.24[a]	0	4	12	16
		1.17	1.94	2.28				

[a]Integrated ratio, ~4.5:1.

TABLE 3. The ^{1}H nmr spectra of (−)-4-methylcamphor (**7**) in presence of Eu(hfc)$_3$

Molar equiv. of Eu(hfc)$_3$	δ (ppm)				Δδ (Hz)			
	C(9)Me	C(8)Me	C(10)Me	C(4)Me	C(9)Me	C(8)Me	C(10)Me	C(4)Me
0	s, 0.72	s, 0.84	s, 1.05	0	0	0	0	0
0.10	s, 1.04	1.06	s, 1.18	s, 1.46	0	7	0	0
		1.08						
0.30	s, 1.41	1.42	1.66	s, 2.39	0	2	18	0
		1.43	1.71					
0.60	s, 1.89	1.73	2.45[a]	s, 3.60	0	8	32	0
		1.75	2.53					

[a]Integrated ratio, ~4.3:1.

above provided 8-deuterio-2-methylenebornane (**12**) as a white solid, mp 170–171°C; ν_{max} ($CHCl_3$): 3075, 1660, 880 cm^{-1}; δ (400 MHz, $CDCl_3$): 0.74 (2H, t, J = 2 Hz, C(8)H_2D), 0.88 (3H, s, C(10)H_3), 0.91 (3H, s, C(9)H_3), 1.15–1.30 (2H, m, C(5) and C(6) *endo*-H), 1.63 (1H, td, J = 11.5, 4 Hz, C(6) *exo*-H), 1.71–1.83 (2H, m, C(4) H and C(5) *exo*-H), 1.93 (1H, dt, J = 16, 2 Hz, C(3) *endo*-H), 2.40 (1H, dm, J = 16 Hz, C(3) *exo*-H), 4.65 (1H, bs) and 4.70 (1H, bs) (=CH_2); *m/e* (relative intensity): 151 (M^+, 22.9), 136 (42.6), 79 (100.0). Exact mass calcd. for $C_{11}H_{17}D$: 151.1470; found: 151.1470.

Rearrangement of 8-deuterio-2-methylenebornane (12)

Rearrangement of 8-deuterio-2-methylenebornane (**12**) by the procedure described above provided 8-deuterio-4-methylisobornyl acetate (**16**) as a colourless mobile oil; ν_{max} (neat): 2195, 1740, 1240, 1025 cm^{-1}; δ (400 MHz, $CDCl_3$): 0.68 (3H, s, C(9)H_3), 0.81 (2H, br s, C(8)H_2D), 0.86 (3H, s, C(10)H_3), 0.90 (3H, s, C(11)H_3), 1.11–1.21 (2H, m, C(5) and C(6) *endo*-H), 1.37–1.47 (2H, m, C(5) and C(6) *exo*-H), 1.50 (1H, dt, J = 14, 3.5 Hz, C(3) *exo*-H), 1.84 (1H, dd, J = 14, 8.5 Hz, C(3) *endo*-H), 2.03 (3H, s, CH_3CO-), 4.65 (1H, dd, J = 8.5, 3.5 Hz, CHOAc). The spectrum also shows a small broad peak at 0.67 ppm, and a small sharp singlet at 0.83 ppm, which are assigned respectively to C(9)H_2D and C(8)H_3 of 9-deuterio-4-methylisobornyl acetate (**19**), a minor coproduct. Mass spectrum, *m/e* (relative intensity): 211 (M^+, 7.7), 169 (16.5), 151 (85.5), 43 (100.0). Exact mass calcd. for $C_{13}H_{21}DO_2$: 211.1681; found: 211.1681.

8-Deuterio-4-methylcamphor (17)

Conversion of 8-deuterio-4-methylisobornyl acetate (**16**) to 8-deuterio-4-methylcamphor (**17**) was accomplished by reductive removal of the acetyl group followed by oxidation as described above. This afforded 8-deuterio-4-methylcamphor (**17**) as white crystals; 54%; mp 150–151°C; ν_{max} ($CHCl_3$): 3020, 2980, 2900, 1740 cm^{-1}; δ (400 MHz, $CDCl_3$): 0.70 (2H, 1:1:1 t, J = 1.8 Hz, C(8)H_2D), 0.83 (3H, s, C(9)H_3), 0.92 (3H, s, C(10)H_3), 1.04 (3H, s, C(11)H_3), 1.35–1.45 (2H, m, C(5) and C(6) *endo*-H), 1.59–1.77 (2H, m, C(5) and C(6) *exo*-H), 1.88 (1H, d_{AB}, J = 18 Hz, C(3) *endo*-H), 2.09 (1H, dd_{AB}, J = 18, 3 Hz, C(3) *exo*-H). The spectrum also exhibits a small singlet at 0.71 ppm and a shoulder at 0.81 ppm that were assigned respectively to C(8)H_3 and C(9)H_2D of 9-deuterio-4-methylcamphor (**20**). δ (C_6D_6): 0.45 (2H, 1:1:1 t, J = 7 Hz, C(8)H_2D), 0.51 (3H, s, C(9)H_3), 0.71 (3H, s, C(11)H_3), 0.91 (3H, s, C(10)H_3), 1.03 (1H, br t, J = 10 Hz, C(5) *endo*-H), 1.20 (1H, td, J = 10, 5 Hz, C(6) *endo*-H), 1.24–1.40 (2H, m, C(5) and C(6) *exo*-H), 1.62 (1H, d_{AB}, J = 18 Hz, C(3) *endo*-H), 1.81 (1H, br d_{AB}, J = 18 Hz, C(3) *exo*-H); *m/e* (relative intensity): 167 (M^+, 95.0), 152 (3.2), 139 (47.8), 110 (100.0). Exact mass calcd. for $C_{11}H_{17}DO$: 167.1420; found: 167.1425.

2-(Dideuteriomethylene)bornane (21)

Methylenation of (+)-camphor (**1**) with freshly distilled dideuteriomethylene bromide using method B described above provided a pale yellow liquid, which was purified by column chromatography (70–230 mesh SiO_2), eluting with petroleum ether to provide 2-(dideuteriomethylene)bornane (**21**) as a white solid, mp 69–71°C; ν_{max} ($CHCl_3$): 2300, 1610, 700 cm^{-1}; δ (400 MHz, $CDCl_3$): 0.76 (3H, s, C(8)H_3), 0.89 (3H, s, C(10)H_3), 0.92 (3H, s, C(9)H_3), 1.15–1.30 (2H, m, C(5) and C(6) *endo*-H), 1.64 (1H, td, J = 13, 5 Hz, C(6) *exo*-H), 1.74 (1H, m, C(4)H), 1.78 (1H, m, C(5) *exo*-H), 1.92 (1H, d, J = 16 Hz, C(3) *endo*-H), 2.40 (1H, dt, J = 16, 4 Hz, C(3) *exo*-H); *m/e* (relative intensity): 152 (M^+, 14.6), 137 (25.8), 41 (100.0). Exact mass calcd. for $C_{11}H_{16}D_2$: 152.1532; found: 152.1541.

Rearrangement of 2-(deuteriomethylene)bornane (21)

Concentrated sulfuric acid (1 drop) was added to a solution of 2-(dideuteriomethylene)bornane (**21**) (39.2 mg, 0.257 mmol) in CH_3CO_2D (1 mL) and the solution was stirred for 4 h at 25°C. The mixture was diluted with ether and water and the aqueous layer was extracted with ether. The combined organics were washed with water, saturated $NaHCO_3$, and brine, and dried over anhydrous magnesium sulfate. Evaporation of the solvent produced a colourless oil that was purified by column chromatography (230–400 mesh SiO_2). Elution with petroleum ether provided 4-(trideuteriomethyl)isobornyl acetate (**25**) as a colourless mobile liquid; ν_{max} (neat): 2220, 1740, 1220, 1020 cm^{-1}; δ (400 MHz, $CDCl_3$): 0.69 (3H, s, C(9)H_3), 0.83 (3H, s, C(8)H_3), 0.86 (3H, s, C(10)H_3), 1.11–1.20 (2H, m, C(5) and C(6)

Can. J. Chem. Downloaded from www.nrcresearchpress.com by 91.121.58.235 on 09/07/12
For personal use only.

Can. J. Chem. Downloaded from www.nrcresearchpress.com by 91.121.58.235 on 09/07/12
For personal use only.

endo-H), 1.37–1.55 (3H, m, C(5) and C(6) *exo*-H, and C(3)-*exo*-H), 1.83 (1H, dd, J = 14, 8.5 Hz, C(3)-*endo*-H), 2.02 (3H, s, CH_3CO), 4.66 (1H, dd, J = 8.5, 3.5 Hz, CHOAc). The ^{1}H nmr spectrum also exhibits small peaks at 0.67 and 0.85 ppm due respectively to deuterium exchange into the C(9) and C(10) methyl groups. Mass spectrum, m/e (relative intensity):[4] 213 (M^+, 0.8), 170 (2.4), 153 (29.2), 43 (100.0). Exact mass calcd. for $C_{13}H_{19}D_3O$: 213.1808; found: 213.1777.

*4-(Trideuteriomethyl)camphor (**26**)*

Sequential reduction and oxidation of 4-(trideuteriomethyl)isobornyl acetate (**25**) by the procedures described above provided 4-(trideuteriomethyl)camphor (**26**) as white crystals, mp 150–151°C; ν_{max} ($CHCl_3$): 2210, 1735 cm^{-1}; δ ($CDCl_3$).[5] 0.71 (3H, s, C(8)H_3), 0.83 (3H, s, C(9)H_3), 0.92 (3H, s, C(10)H_3), 1.35–1.45 (2H, m, C(5) and C(6) *endo*-H), 1.58–1.77 (2H, m, C(5) and C(6) *exo*-H), 1.88 (1H, d_{AB}, J = 18 Hz, C(3) *endo*-H), 2.08 (1H, dd_{AB}, J = 18, 3 Hz, C(3) *exo*-H); m/e (relative intensity):[6] 169 (M^+, 20.8), 141 (9.2), 85 (100.0). Exact mass calcd. for $C_{11}H_{15}D_3O$: 169.1546; found: 169.1543.

endo-*3-Bromo-4-methylcamphor (**27**)*

A solution of (−)-4-methylcamphor (**7**) (6.37 g, 0.038 mol) in glacial acetic acid (28 mL) was warmed to 80°C, and bromine (2.29 mL, 6.87 g, 76.6 mmol) in glacial acetic acid (2.29 mL) was added dropwise. The mixture was stirred at 80°C for 24 h, then cooled, and poured into ice-water. The resulting solid was filtered and washed with water to yield *endo*-3-bromo-4-methylcamphor (**27**) as a white crystalline solid (9.30 g, 99%), mp 119.5–120.5°C (sealed tube); ν_{max} ($CHCl_3$): 1700 cm^{-1}; δ ($CDCl_3$, 400 MHz): 0.81 (3H, s, C(8)H_3), 0.98 (3H, s, C(9)H_3), 1.00 (3H, s, C(10)H_3), 1.06 (3H, s, C(11)H_3), 1.40 (1H, m, C(6) *endo* proton), 1.55–1.67 (2H, m, C(5) *endo* and C(6) *exo* protons), 2.07 (1H, m, C(5) *exo* proton), 4.31 (1H, d, J = 1.5 Hz, C(3) proton); m/e (relative intensity): 246/244 (M^+, 5.0/4.9), 165 (48.1), 137 (52.1), 123 (45.0), 109 (75.7), 83 (100.0). Exact mass calcd. for $C_{11}H_{17}OBr$: 246.0442/244.0462; found: 246.0439/244.0467. Anal. calcd. for $C_{11}H_{17}OBr$: C 53.89, H 6.99, Br 32.59; found: C 53.81, H 6.86, Br 32.80.

endo-*3,9-Dibromo-4-(bromomethyl)camphor (**28**)*

endo-3-Bromo-4-methylcamphor (**27**) (7.36 g, 0.030 mol) and bromine (3.47 mL, 0.069 mol) were added to a single-neck flask. Chlorosulfonic acid (5.48 mL, 0.082 mol) was added slowly to the reaction mixture. After being stirred at room temperature for 19 h, the reaction mixture was added to ice-cold bisulfite solution and extracted with ether. The ether extracts were combined, washed with saturated sodium bicarbonate solution and water, and dried over anhydrous magnesium sulfate. Evaporation of the solvent yielded a yellow solid, which was triturated with ice-cold ether to provide *endo*-3,9-dibromo-4-(bromomethyl)camphor (**28**) as a white crystalline solid (6.20 g, 51%), mp 142.5–143.5°C (sealed tube); ν_{max} ($CHCl_3$): 1750 cm^{-1}; δ ($CDCl_3$, 400 MHz): 1.07 (3H, s, C(8)H_3), 1.27 (3H, s, C(10)H_3), 1.53 (1H, ddd, J = 14, 9, and 4 Hz, C(6) *endo* proton), 1.72 (1H, td, J = 14 and 4 Hz, C(5) *endo* proton), 1.85 (1H, tdd, J = 14, 4, and 2.5 Hz, C(5) *exo* proton), 2.22 (1H, ddd, J = 14, 9, and 4 Hz, C(6) *exo* proton), 3.45 and 3.74 (2H, AB quartet, J = 11 Hz, C(9) methylene), 3.52 and 4.05 (2H, AB quartet, J = 11.5 Hz C(11) methylene), 4.92 (1H, d, J = 2.5 Hz, C(3) proton); m/e (relative intensity): 406/404/402/400 (M^+, 0.4/1.8/2.0/0.7), 325/323/321 (17.1/41.7/18.8), 245/243 (14.0/18.8), 201/199 (28.7/22.2), 163 (16.9), 121 (36.3), 107 (50.8), 105 (37.8), 93 (66.7), 91 (69.2). Exact mass calcd. for $C_{11}H_{15}OBr_3$: 405.8612/403.8632/401.8652/399.8672; found: 405.8605/403.8637/401.8667/399.8675. Anal. calcd. for $C_{11}H_{15}OBr_3$: C 32.79, H 3.75, Br 59.49; found: C 33.05, H 3.78, Br 59.22. The structure of this compound was confirmed by X-ray analysis.[2]

*9-Bromo-4-(bromomethyl)camphor (**29**)*

A solution of 3,9-dibromo-4-(bromomethyl)camphor (580 mg, 1.44 mmol) in 1:1 Et_2O/AcOH was cooled to 0°C. While stirring vigorously, zinc (294 mg, 4.50 mmol) was added in portions over 30 min. Stirring was continued for a further 15 min before Celite (500 mg) was added and the mixture was filtered. The solution was diluted with ether and washed with water, saturated sodium bicarbonate, and brine, and dried over magnesium sulfate. Evaporation of the solvents yielded a pale yellow slushy solid, which was recrystallized from methanol to afford 9-bromo-4-(bromomethyl)camphor as white crystals; yield: 283 mg, 61%; mp 53–55°C.

The mother liquor was concentrated and the residue purified by column chromatography (230–400 mesh SiO_2), eluting with 19:1 petroleum ether/ether to provide a further 146 mg; total yield: 429 mg, 92%; ν_{max} ($CHCl_3$): 3025, 2980, 1745 cm^{-1}; δ (400 MHz, $CDCl_3$): 0.99, 1.03 (3H each, 2 s, C(8)H_3 and C(10)H_3), 1.50–1.59 and 1.70–1.79 (1H each, 2 m, C(5) and C(6) *endo*-H), 1.87–2.03 (2H, m, C(5) and C(6) *exo*-H), 2.32 (1H, d_{AB}, J = 18 Hz, C(3) *endo*-H), 2.35 (1H, dd_{AB}, J = 18, 3 Hz, C(3) *exo*-H), 3.36 and 3.66, 3.62 and 4.02 (2H each, $2q_{AB}$, J = 11, 10 Hz, C(9)H_2Br and C(11)H_2Br); m/e (relative intensity): 326/324/322 (M^+, 11.4/23.9/12.7), 245/243 (56.2/56.2), 217/215 (35.5/35.2), 201/199 (83.9/76.6), 163 (50.3), 135 (85.8), 121 (77.8), 107 (69.6), 93 (90.0), 81 (97.4), 41 (100.0). Exact mass calcd. for $C_{11}H_{16}OBr_2$: 325.9527/323.9547/321.9567; found: 325.9532/323.9543/321.9585. Anal. calcd. for $C_{11}H_{16}Br_2O$: C 40.77, H 4.98, Br 49.31; found: C 40.99, H 5.04, Br 49.09.

*9-Deuterio-4-(deuteriomethyl)camphor (**30**)*

9-Bromo-4-(bromomethyl)camphor (**29**) (384 mg, 1.25 mmol) was dissolved in dry benzene (7 mL) and AIBN (cat.) and tributyltin deuteride (1.0 mL, 1.1 g, 3.7 mmol) were added. The solution was refluxed for 18 h. The solvent was evaporated to provide a yellow oil, which was purified by column chromatography (70–230 mesh SiO_2), eluting with petroleum ether and increasing polarity to 9:1 petroleum ether/ether to afford a mixture of 9-deuterio-4-(deuteriomethyl)camphor (**30**) and tributyltin bromide. Further purification by sublimation provided pure 9-deuterio-4-(deuteriomethyl)camphor (**30**) as a white crystalline solid; yield: 121 mg, 58%; mp 149–150°C; ν_{max} ($CHCl_3$): 2200, 1735 cm^{-1}; δ ($CDCl_3$): 0.71 (3H, s, C(8)H_3), 0.82 (2H, 1:1:1 t, J = 2 Hz, C(9)H_2D), 0.92 (3H, s, C(10)H_3), 1.03 (2H, 1:1:1 t, J = 2 Hz, C(11)H_2D), 1.35–1.43 (2H, m, C(5) and C(6) *endo*-H), 1.57–1.77 (2H, m, C(5) and C(6) *exo*-H), 1.88 (1H, d_{AB}, J = 18 Hz, C(3) *endo*-H), 2.08 (1H, dd_{AB}, J = 18, 3.5 Hz, C(3) *exo*-H); δ (C_6D_6): 0.48 (3H, s, C(8)H_3), 0.495 (2H, br s, C(9) H_2D), 0.69 (2H, br s, C(11) H_2D), 0.92 (3H, s, C(10) H_3), 1.03 (1H, br t, J = 10 Hz, C(5) *endo*-H), 1.15–1.40 (3H, m, C(6) *endo*-H, C(5) and C(6) *exo*-H), 1.62 (1H, d_{AB}, J = 18 Hz, C(3) *endo*-H), 1.86 (1H, dd_{AB}, J = 18, 3 Hz, C(3) *exo*-H); m/e (relative intensity): 168 (M^+, 62.0), 140 (23.9), 84 (100.0). Exact mass calcd. for $C_{11}H_{16}D_2O$: 168.1483; found: 168.1483.

[4]The masses listed are only those for the trideuterio compound. The low resolution ms also exhibits peaks at m/e (%) = 216 (0.5), 215 (0.8), 214 (0.5), and 212 (0.1), presumably due to the picking up of up to three additional deuterons or, in the latter case, a proton during the rearrangement. The measured masses support these assignments.

[5]The signals quoted are only those for 4-(trideuteriomethyl)camphor. The ^{1}H nmr also exhibits a broad shoulder at 0.82 ppm, a 1:1:1 triplet at 0.90 ppm, and a multiplet at 1.01 ppm, corresponding to C(9)H_2D, C(10)H_2D, and C(11)HD_2 respectively.

[6]The masses quoted are only those for the trideuterated compound. The low resolution ms also exhibits peaks at m/e (%) = 172 (28.2), 171 (33.6), 170 (30.6), and 168 (8.7), corresponding to the uptake of up to three more deuterons or, in the latter case, a proton during the rearrangement. The exact masses measured for these peaks support this assignment.

1. (*a*) T. MONEY. Nat. Prod. Rep. **2**, 253 (1985); (*b*) T. MONEY. Studies in natural products chemistry. Vol. 4. Part C. *Edited by* Atta-ur-Rahman. Elsevier, Amsterdam. 1989; (*c*) D. L. KUO and T. MONEY. Can. J. Chem. **66**, 1794 (1988), and references cited.
2. (*a*) J. L. SIMONSEN and L. N. OWEN. The terpenes. Vol. II. Cambridge University Press, 1957. pp. 447, 579; (*b*) E. JOSEPHY and F. RADT (*Editors*). Elsevier's encyclopaedia of organic

chemistry. Vol. 12A. Elsevier Scientific Publishing Co., Amsterdam. 1948. pp. 572, 696, 791; (*c*) M. F. ANSELL (*Editor*). Rodd's Chemistry of Carbon Compounds. Suppl. Vol. IIc. Elsevier Scientific Publishing Co., Amsterdam. 1974. p. 83; (*d*) S. COFFEY (*Editor*). Rodd's chemistry of carbon compounds. Suppl., Vol. II. Elsevier Scientific Publishing Co., Amsterdam. 1969. p. 165; (*e*) P. DE MAYO (*Editor*). Molecular rearrangements. Part I. Interscience, New York. 1963. pp. 130–150; (*f*) H. TOIVONEN. Tetrahedron Lett. 3041 (1968), and references cited; (*g*) S. NAMETKIN and L. BRUSSOF. Justus Liebigs Ann. Chem. **459**, 144 (1927); J. Prakt. Chem. [2] **135**, 155 (1932); (*h*) J. WOLINSKY, D. R. DIMMEL, and T. W. GIBSON. J. Org. Chem. **32**, 2087 (1967); (*i*) D. R. DIMMEL and W. Y. FU. J. Org. Chem. **38**, 3778 (1973); (*j*) A. I. SHAVRYGIN. J. Gen. Chem. (U.S.S.R.), **18**, 499 (1948); Chem. Abstr. **42**, 7276h (1948); (*k*) M. BREDT-SAVELSBERG and J. BUEHKREMER. Ber. Dtsch. Chem. Ges. **64**, 600 (1931).

3. W. F. ERMAN. *In* Chemistry of the monoterpenes. Part B. *Edited by* P. G. Gassmann. Marcel Dekker, New York. 1985. p. 1073, and references cited.
4. (*a*) R. GREENWALD, M. CHAYKOVSKY, and E. J. COREY. J. Org. Chem. **28**, 1128 (1963); (*b*) J. M. CONIA and J. C. LIMASSET. Bull. Soc. Chim. Fr. 1936 (1967); (*c*) G. GREAM, C. PINCOMBE, and D. WEGE. Aust. J. Chem. **27**, 624 (1974); (*d*) L. FITJER and U. QUABECK. Synth. Commun. **15**, 855 (1985).
5. (*a*) L. LOMBARDO. Tetrahedron Lett. **23**, 4293 (1982); (*b*) K. TAKAI, Y. HOTTA, K. OSHIMA, and H. NOZAKI. Tetrahedron Lett. **19**, 2417 (1978); Bull. Chem. Soc. Jpn. **53**, 1698 (1980); (*c*) J. HIBINO, T. OKAZOE, K. TAKAI, and H. NOZAKI. Tetrahedron Lett. **26**, 2579 (1985).
6. (*a*) G. R. SULLIVAN. Topics in stereochemistry. Vol. 10. *Edited by* E. L. Eliel and N. L. Allinger. John Wiley & Sons, New York. 1978. p. 287; (*b*) K. A. KIME and R. E. SIEVERS. Aldrichimica Acta, **10**, 54 (1977); (*c*) S. YAMAGUCHI. Asymmetric synthesis. Vol. 1. *Edited by* J. D. Morrison. Academic Press, New York. 1983. pp. 125–152; (*d*) C. C. HINCKLEY. J. Org. Chem. **35**, 2384 (1970); (*e*) R. H. NEWMAN. Tetrahedron, **30**, 969 (1974).
7. R. C. ANDERSON and M. J. SHAPIRO. J. Org. Chem. **49**, 1304 (1984).
8. J. D. CONNOLLY and R. MCCRINDLE. J. Chem. Soc. (C), 1613 (1966); Chem. Ind. 379 (1965).
9. D. L. F. LI. M.Sc. Thesis, University of B.C., Vancouver (1988).
10. (*a*) W. M. DADSON and T. MONEY. Can. J. Chem. **58**, 2524 (1980); (*b*) T. M. ATLAY. M.Sc. Thesis, University of B.C., Vancouver (1983); (*c*) W. M. DADSON and T. MONEY. J. Chem. Soc. Chem. Commun. 112 (1982).
11. (*a*) P. VON R. SCHLEYER, W. E. WATTS, R. C. FORT, JR., M. B. COMISAROW, and G. A. OLAH. J. Am. Chem. Soc. **86**, 5679 (1964); (*b*) M. SAUNDERS, P. VON R. SCHLEYER, and G. A. OLAH. J. Am. Chem. Soc. **86**, 5680 (1964); (*c*) C. C. LEE and L. K. M. LAM. J. Am. Chem. Soc. **88**, 5355 (1966); (*d*) F. A. CAREY and R. J. SUNDBERG. Advanced organic chemistry. 2nd ed. Part A. Plenum Press, New York. 1984. p. 309.
12. (*a*) J. A. BERSON. *In* Molecular rearrangements. Part I. *Edited by* P. de Mayo. Interscience Publishers, New York. 1963. p. 145; (*b*) J. A. BERSON, J. H. HAMMONS, A. W. MCROWE, R. G. BERGMANN, A. REMANICK, and D. HOUSTON. J. Am. Chem. Soc. **89**, 2950 (1967), and references cited; (*c*) H. C. KRETSCHMAR, Z. BARNEIS, and W. F. ERMAN. Tetrahedron Lett. 37 (1970).

Can. J. Chem. Downloaded from www.nrcresearchpress.com by 91.121.58.235 on 09/07/12
For personal use only.

Metal ion catalysis in nucleophilic displacement reactions at carbon, phosphorus, and sulfur centers. II. Metal ion catalysis in the reaction of *p*-nitrophenyl diphenylphosphinate with alkali metal phenoxides in ethanol

EDWARD J. DUNN, ROBERT Y. MOIR, AND ERWIN BUNCEL[1]
Department of Chemistry, Queen's University, Kingston, Ont., Canada K7L 3N6

AND

J. GARFIELD PURDON[2] AND ROBERT A. B. BANNARD
Chemical Detection and Decontamination Section, Protective Sciences Division, Defence Research Establishment Ottawa, Ottawa, Ont., Canada K1A 0Z4

Received November 1, 1989

This paper is dedicated to Professor Ross Stewart on the occasion of his 65th birthday

EDWARD J. DUNN, ROBERT Y. MOIR, ERWIN BUNCEL, J. GARFIELD PURDON, and ROBERT A. B. BANNARD. Can. J. Chem. **68**, 1837 (1990).

The reactions of *p*-nitrophenyl diphenylphosphinate (**1**) with lithium, sodium, potassium, and benzyltrimethylammonium phenoxides (BTMAOPh) have been studied by spectrophotometric techniques in anhydrous ethanol at 25°C. The reactivity (k_{obs}) of the alkali metal phenoxides increases in the order BTMAOPh < KOPh < NaOPh < LiOPh. The rate of reaction of **1** with LiOPh is enhanced when lithium salts (LiSCN, $LiNO_3$, $LiClO_4$, LiOAc) are added to the reaction media. The addition of the alkali metal complexing agents dicyclohexyl-18-crown-6 ether or [2.2.2]cryptand for Na^+, and [2.1.1]cryptand for Li^+, to each of the alkali metal phenoxide reactions resulted in a decrease in rate, indicating catalysis by the alkali metal ions. The kinetic data are analyzed to obtain specific rate coefficients of reactions of phenoxide and ethoxide as the dissociated ions and as alkali metal – phenoxide ion pairs. Reactivities follow the order $k_{PhOM} > k_{PhO^-}$; $k_{EtOM} > k_{EtO^-}$; $k_{EtO^-} > k_{PhO^-}$; $k_{EtOM} > k_{PhOM}$. A mechanism is proposed in which the ion-paired metal phenoxide is more reactive towards the substrate than is the dissociated phenoxide. Analysis of the data in terms of initial state and transition state interactions with metal ions indicates that the increased reactivity of the ion-paired species results from greater stabilization of the negatively charged transition state relative to stabilization of the ion-paired nucleophile.

Key words: nucleophilic displacement at phosphorus by phenoxide, alkali-metal-ion catalysis.

EDWARD J. DUNN, ROBERT Y. MOIR, ERWIN BUNCEL, J. GARFIELD PURDON et ROBERT A. B. BANNARD. Can. J. Chem. **68**, 1837 (1990).

Faisant appel à des techniques spectrophotométriques et opérant dans de l'éthanol anhydre, à 25°C, on a étudié les réactions du diphénylphosphinate de *p*-nitrophényle (**1**) avec les phénolates de lithium, de sodium, de potassium et de benzyltriméthylammonium (BTMAOPh). La réactivite (k_{obs}) des phénolates des métaux alcalins augmente dans l'ordre : BTMAOPh < KOPh < NaOPh < LiOPh. Lorsqu'on ajoute des sels de lithium (LiSCN, $LiNO_3$, $LiClO_4$, LiOAc) au milieu réactionnel, il y a une augmentation de la vitesse de réaction du composé **1** avec le LiOPh. Lorsqu'on ajoute des agents complexants des métaux alcalins, comme l'éther dicyclohexyl-18-couronne-6 ou le cryptand[2.2.2] pour le Na^+ et le cryptand[2.1.1] pour le Li^+, à chacune des réactions des phénolates de métaux alcalins, les vitesses de réaction sont abaissées; ces résultats indiquent qu'il y a catalyse par les ions des métaux alcalins. On a analysé les données cinétiques pour obtenir les coefficients spécifiques des vitesses de réactions du phénolate et de l'éthylate comme ions dissociés ainsi que sous la forme de paires l'ions phénolate – métal alcalin. Les réactivités sont dans l'ordre suivant : $k_{PhOM} > k_{PhO^-}$; $k_{EtOM} > k_{EtO^-}$; $k_{EtO^-} > k_{PhO^-}$; $k_{EtOM} > k_{PhOM}$. On propose un mécanisme selon lequel, par rapport à chaque substrat, chaque phénolate existant sous la forme d'une paire d'ions est plus réactif que le phénolate qui n'est pas dissocié. Une analyse des données en fonction de l'état initial et des interactions avec les ions métalliques dans l'état de transition indique que la réactivité accrue des espèces existant sous la forme de paires d'ions provient d'une plus grande stabilisation de l'état de transition portant une charge négative par rapport à la stabilisation du nucléophile existant sous la forme de paire d'ions.

Mots clés : déplacement nucléophile à phosphore par phenoxide, catalyse par les ions des métaux alcalins.

[Traduit par la revue]

Introduction

A number of cases demonstrating catalysis of nucleophilic displacement reactions by divalent metal ions have been reported for substrates containing phosphoryl centers (1–4). In our own studies we have shown previously (5) that the reaction of *p*-nitrophenyl diphenylphosphinate (**1**) with ethoxide ion in ethanol at 25°C is catalysed by alkali metal ions (Li^+, Na^+, K^+). Catalysis by the alkali metal ions in this system is believed to result from lowering of the free energy of activation for formation of a negatively charged transition state, which is stabilized by association with the alkali metal cation. It was not clear, however, if this stabilization occurred by interaction of dissociated ions with the substrate in a pre-equilibrium step, or whether alkali metal ion pairs were involved. Participation of

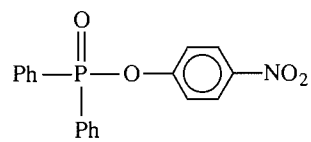

1

[1]Author to whom correspondence may be addressed.

[2]Present address: CB Defence Section, Defence Sciences Division, Defence Research Establishment Suffield, Box 4000, Medicine Hat, Alta., Canada T1A 8K6.

Can. J. Chem. Downloaded from www.nrcresearchpress.com by 91.121.58.235 on 09/07/12
For personal use only.

TABLE 1. Kinetic data for the reaction of **1** with LiOPh, NaOPh, KOPh, and BTMAOPh in EtOH at 25°C

Nucleophile	10^3 [PhO^-] (M)	10^3 k_{obs} (s^{-1})
BTMAOPh	4.935	0.8828
	9.774	1.605
	14.52	2.231
	19.18	2.900
	23.74	3.493
KOPh	5.445	1.944
	11.09	3.398
	16.60	4.744
	21.93	6.127
	27.15	7.255
NaOPh	4.686	2.492
	9.280	4.129
	13.79	5.453
	18.20	6.758
	22.54	8.080
LiOPh	3.748	2.921
	7.422	4.786
	11.03	6.214
	14.56	7.490
	18.03	8.682

the ion-paired species was chosen as the more probable explanation of these observations.

To gain more information regarding metal ion catalysis in this and related systems, it was desirable to extend the study to other nucleophiles and substrates. The results of a study of the reaction of **1** with lithium, sodium, potassium, and benzyltrimethylammonium phenoxides in ethanol are presented herein.

Results

The kinetic data for the reaction of *p*-nitrophenyl diphenylphosphinate (**1**) with lithium phenoxide (LiOPh), sodium phenoxide (NaOPh), potassium phenoxide (KOPh), and benzyltrimethylammonium phenoxide (BTMAOPh) in ethanol at 25°C are given in Table 1. It can be seen from the plots of k_{obs} vs. $[MOPh]_0$ (Fig. 1) that the apparent reactivity of these nucleophiles towards **1** increases in the order BTMAOPh < KOPh < NaOPh < LiOPh. These results imply that the reaction of **1** with PhO^- in EtOH is catalysed by the alkali metal ions.

In our study of metal ion catalysis in the reaction of *p*-nitrophenyl diphenylphosphinate with ethoxide ion in ethanol at 25°C (5), the plots of k_{obs} vs. [EtO^-] displayed an *upward* curvature, which was attributed to differences in reactivities of the free ethoxide and the metal–ethoxide ion pair. However, the observed rate constants for the reaction of **1** with KOPh, NaOPh, LiOPh, and BTMAOPh in EtOH give rise to plots with a *downward* curvature (Fig. 1), that is, opposite to the behaviour observed with the ethoxide ion.

Catalysis by metal ions in the present system is also evident in that addition of Li^+ ions, in the form of an unreactive salt, to the reaction of **1** with LiOPh causes an initial increase in rate (Table 2). However, after the initial rapid increase the plots level off at a value of ca. 1.0 M^{-1} s^{-1} (Fig. 2).

Further evidence of catalysis by metal ions is observed through addition of macrocyclic complexing agents to the reaction system (Table 3). Figure 3 demonstrates that addition of

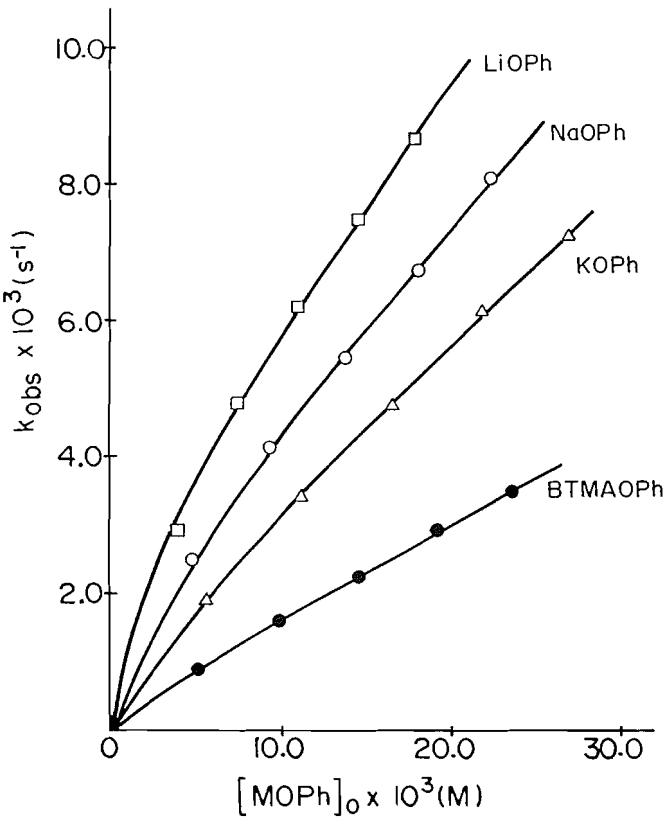

FIG. 1. Reaction of *p*-nitrophenyl diphenylphosphinate (**1**) with LiOPh (□), NaOPh (○), KOPh (△), and BTMAOPh (●) in EtOH at 25°C.

complexing agent causes a rapid initial decrease in reaction rate to a value of ca. 0.19 M^{-1} s^{-1}. The plots, however, do not level off at a minimum value, as was observed in the reaction of **1** with MOEt (5). Instead, after the initial decrease, the rates began to increase slowly as the concentration of complexing agent was increased. The reason for this rate increase is not clear at present. It can be concluded, however, that the initial decrease in the rate with added complexing agent is consistent with catalysis of nucleophilic displacement by the metal ions.

Discussion

Metal ion catalysis

It can be seen from Fig. 1 that the alkali metal phenoxides and benzyltrimethylammonium phenoxide (BTMAOPh) all have different reactivities towards **1**. The observation that the observed rate constants are greater for the alkali metal phenoxides, relative to BTMAOPh, implies involvement of the metal ion in the nucleophilic displacement. The decrease in rate constants with added complexing agent, and their increase on addition of metal ions, also supports a mechanism in which the nucleophilic displacement reaction of **1** by phenoxide ion is catalysed by the alkali metal ions. Possible mechanisms to account for catalysis by alkali metal ions have been described in some detail previously (5) and will be reviewed only briefly here.

First, one can consider the basic reaction of the substrate with phenoxide as proceeding by rate-determining attack of the free nucleophile at the phosphorus center of **1** to form a pentacoordinate intermediate, **2**, followed by expulsion of the leaving group in a subsequent fast step, eq. [1].

Can. J. Chem. Downloaded from www.nrcresearchpress.com by 91.121.58.235 on 09/07/12
For personal use only.

TABLE 2. Kinetic data on the effect of adding unreactive lithium metal salts (LiX) to the reaction of **1** with LiOPh in EtOH at 25°C

Reaction system	10^2 [LiOPh] (M)	10^3 k_{obs} (s^{-1})	k_2 (M^{-1} s^{-1})[a]	[LiX]/[LiOPh]
LiOPh + LiSCN	0.923	5.688	0.616	0.00
	0.914	6.597	0.722	1.20
	0.906	7.315	0.808	2.40
	0.897	7.734	0.862	3.60
	0.889	7.784	0.876	4.80
	0.881	7.936	0.901	5.99
	0.842	8.157	0.969	12.0
	0.806	8.035	0.997	18.0
	0.773	7.702	0.996	24.0
LiOPh + LiOAc	0.881	6.392	0.726	1.11
	0.842	6.756	0.803	2.23
	0.806	6.889	0.855	3.34
	0.773	6.961	0.900	4.45
	0.743	7.130	0.960	5.56
LiOPh + $LiNO_3$	0.914	7.052	0.771	1.08
	0.906	7.764	0.857	2.15
	0.897	8.399	0.936	3.23
	0.889	8.643	0.972	4.30
	0.881	8.713	0.989	5.38
	0.842	8.774	1.042	10.8
	0.806	8.812	1.093	16.1
	0.773	8.572	1.109	21.5
LiOPh + $LiClO_4$	0.914	7.042	0.770	1.28
	0.906	7.604	0.840	2.56
	0.897	7.918	0.882	3.84
	0.889	8.023	0.903	5.13
	0.881	8.030	0.912	6.39
	0.842	8.033	0.954	12.8
	0.806	7.238	0.898	19.8
	0.773	6.622	0.856	25.6

[a] $k_2 = k_{obs}/[LiOPh]$.

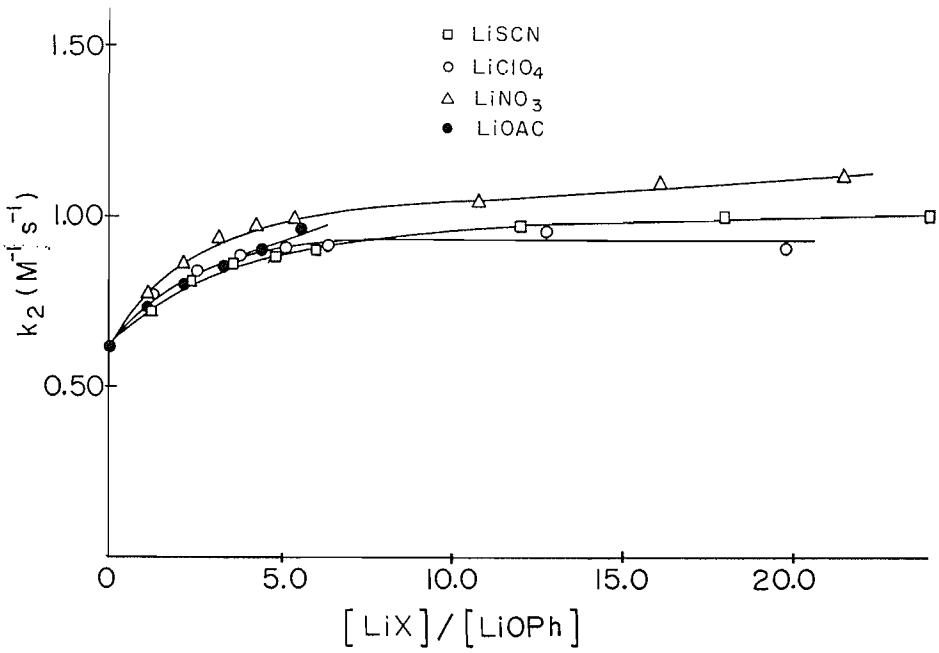

FIG. 2. Effect of added LiSCN (□), $LiClO_4$ (○), $LiNO_3$ (△), and LiOAc (●) on the reaction of **1** with LiOPh in EtOH.

Can. J. Chem. Downloaded from www.nrcresearchpress.com by 91.121.58.235 on 09/07/12
For personal use only.

TABLE 3. Kinetic data on the effect of adding complexing agents to the reaction of **1** with NaOPh and LiOPh in EtOH

Reaction system	10^2 [Base] (M)	10^3 k_{obs} (s^{-1})	k_2 (M^{-1} s^{-1})[a]	[Complexing agent] / [Base]
NaOPh + DC18C6	1.154	5.119	0.444	0.00
	1.149	4.094	0.356	0.44
	1.141	2.543	0.223	1.10
	1.127	2.316	0.206	2.21
	1.101	2.301	0.210	4.41
	1.076	2.258	0.210	6.62
	1.052	2.274	0.216	8.83
	1.029	2.286	0.222	11.1
	0.967	2.314	0.239	17.6
	0.929	2.274	0.248	22.1
NaOPh + [2.2.2]	1.149	4.443	0.387	0.22
	1.127	2.265	0.201	1.12
	1.101	2.278	0.207	2.23
	1.052	2.218	0.211	4.46
	1.008	2.168	0.215	6.69
	0.967	2.072	0.214	8.93
LiOPh + [2.1.1]	0.923	5.658	0.613	0.00
	0.912	4.272	0.468	0.40
	0.904	2.466	0.273	0.80
	0.901	1.664	0.185	1.99
	0.881	1.659	0.188	3.98
	0.861	1.612	0.187	5.96
	0.842	1.616	0.192	7.95
	0.823	1.605	0.195	9.94
	0.806	1.597	0.198	11.9
	0.773	1.570	0.203	15.9
	0.743	1.534	0.206	19.9

[a] $k_2 = k_{obs}$/[Base].

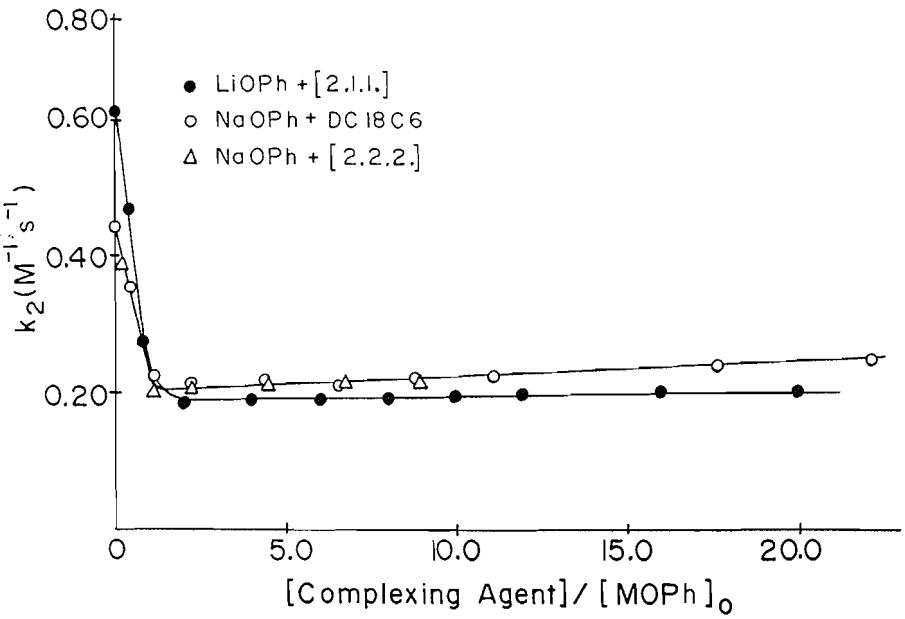

FIG. 3. Effect of added [2.1.1]cryptand (●) on the reaction of **1** with LiOPh; effect of added DC18C6 (○) and [2.2.2]cryptand (△) on the reaction of **1** with NaOPh in EtOH.

Can. J. Chem. Downloaded from www.nrcresearchpress.com by 91.121.58.235 on 09/07/12
For personal use only.

Can. J. Chem. Downloaded from www.nrcresearchpress.com by 91.121.58.235 on 09/07/12
For personal use only.

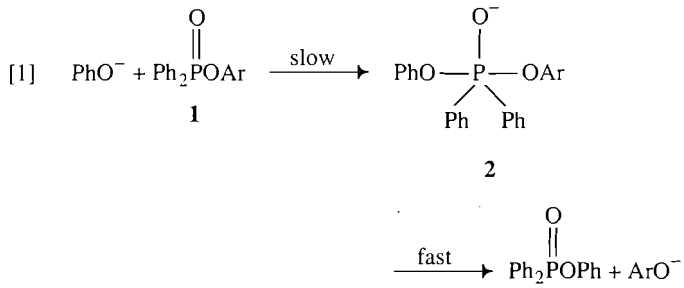

Formation of a pentacoordinate intermediate has been proposed in the alkaline hydrolysis reaction of aryl diphenylphosphinothioates, based on the correlation of rate constants with Hammett σ values rather than σ^- values, and on the magnitude of the Hammett ρ value (6). We have studied the reaction of substituted aryl diphenylphosphinates with ethoxide, phenoxide, and other nucleophiles and, based on the observed Hammett ρ values and correlation of rates with σ^0 constants, similarly propose the formation of a pentacoordinate intermediate. The results of these experiments will be presented subsequently in this series.

Explanations for rate accelerations by metal ions include the situation in which the metal ion coordinates to the substrate, likely at the phosphoryl oxygen, making the phosphorus atom more electrophilic, eq. [2]. This gives rise to an intermediate (**3**), which is stabilized by association with the metal ion. Preassociation of M^+ with the oxygen of the aryloxy leaving group is considered to be less likely since cleavage of the P—OAr bond does not occur to a significant extent in the rate-determining step.

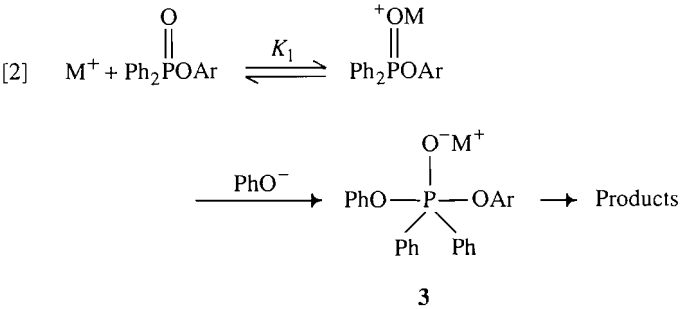

Alternatively, the metal ion may be associated with the base as an ion pair, which would react with the substrate giving rise to intermediate **3**. The rate law for the mechanisms according to eqs. [2] and [3] would be identical.

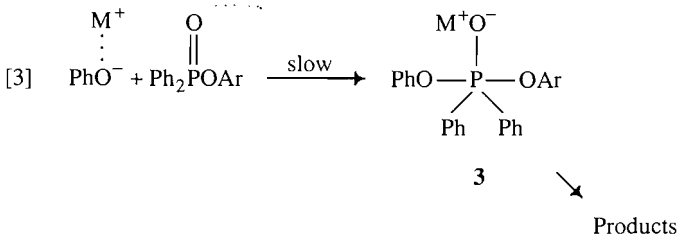

Assuming that ion pairs and free ions are both capable of reacting with the substrate gives rise to a kinetically complex system. Thus, there is the possibility of four species capable of reacting with the substrate, namely free and ion-paired phenoxide, and free and ion-paired ethoxide, generated through solvolysis of phenoxide. The overall pseudo-first-order rate equation, which would describe reaction by all species, can be given as eq. [4].

$$[4]\quad k_{obs} = k_{PhO^-}[PhO^-] + k_{PhOM}[PhOM] + k_{EtO^-}[EtO^-] + k_{EtOM}[EtOM]$$

These reactive species are related by a number of equilibria as shown in Scheme 1, where E refers to the ester **1**. In this scheme there are four rate constants and three equilibrium constants that must be reconciled. These are k_{EtO^-}, the rate constant for the reaction of free ethoxide; k_{EtOM}, the rate constant for the reaction of the ethoxide ion pair; k_{PhO^-}, the rate constant of the free phenoxide; k_{PhOM}, the rate constant of the phenoxide ion pair; K_d, the dissociation constant of the ethoxide ion pair; K'_d, the dissociation constant of the phenoxide ion pair; and K_s, the solvolysis constant of phenoxide in ethanol.

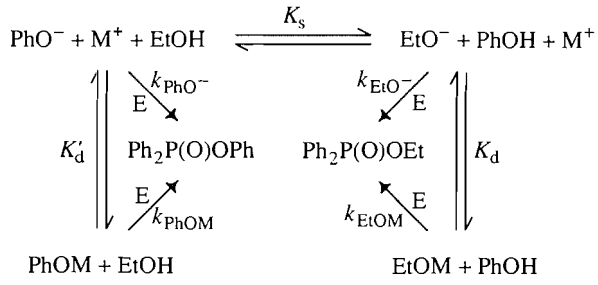

SCHEME 1

The rate constants for the reactions of free ethoxide (k_{EtO^-}) and the ion pair (k_{EtOM}) with **1** have been determined previously (5), while the value of K_d is known from conductivity studies (7). K_s and k_{PhO^-} can be determined from the reaction of **1** with BTMAOPh in EtOH, by dissecting the rate data into contributions by EtO^- and PhO^- as described below.

Phenoxide ion reactivity

In the reaction of **1** with the benzyltrimethylammonium salt of phenoxide, it is assumed that the large benzyltrimethylammonium ion has no effect on the reaction, that is, the ammonium ion acts neither as catalyst nor as rate inhibitor. In the absence of alkali metal ions to influence the reaction, a simple pseudo-first-order rate equation can be written:

$$[5]\quad k_{obs} = k_{EtO^-}[EtO^-]_{eq} + k_{PhO^-}[PhO^-]_{eq}$$

The equilibrium concentrations of phenoxide and ethoxide are related via K_s (eq. [6], which is a combination of the dissociation constant of PhOH in EtOH (eq. [7]) and the autoprotolysis constant of EtOH (eq. [8]), from which eq. [9] follows:

$$[6]\quad PhO^- + EtOH \overset{K_s}{\rightleftharpoons} PhOH + EtO^-$$

$$[7]\quad PhOH + EtOH \overset{K_{PhOH}}{\rightleftharpoons} PhO^- + EtOH_2^+$$

$$[8]\quad EtOH + EtOH \overset{K_{auto}}{\rightleftharpoons} EtO^- + EtOH_2^+$$

$$[9]\quad K_s = \frac{[EtO^-]_{eq}[PhOH]_{eq}}{[PhO^-]_{eq}} = \frac{K_{auto}}{K_{PhOH}}$$

A value for K_s (5.01×10^{-4} M) can be determined using the literature values of 15.8 for pK_{PhOH} (8, 9) and of 19.1 for pK_{auto} (9, 10). The equilibrium concentrations of phenoxide ($[PhO^-]_{eq}$) and ethoxide ($[EtO^-]_{eq}$) can then be calculated from eq. [10],

TABLE 4. Modified pseudo-first-order rate constants, k_ψ, and equilibrium concentrations of phenoxide ion, $[PhO^-]_{eq}$, for the reaction of **1** with BTMAOPh used in determination of k_{PhO^-}

$[BTMAOPh]_0$ (M)	k_{obs} (s^{-1})	$[EtO^-]_{eq}$ (M)	$[PhO^-]_{eq}$ (M)	k_ψ (s^{-1})
0.004935	0.0008828	0.0004221	0.004513	0.0004693
0.009774	0.001605	0.0004564	0.009318	0.001158
0.01452	0.002231	0.0004697	0.01405	0.001771
0.01918	0.002900	0.0004768	0.01870	0.002433
0.02374	0.003493	0.0004812	0.02326	0.003021

TABLE 5. Summary of rate and equilibrium constants for the reaction of **1** with free and ion-paired ethoxide and phenoxide in ethanol at 25°C

Reactant	k (M^{-1} s^{-1})	K_d (M)	K_s (M)	K'_d (M)	K_a (M^{-1})	K_a^{ts} (M^{-1})
EtO^-	0.980[a]	—	—	—	—	—
LiOEt	24.0[a]	0.00472[d]	—	—	212	5188
NaOEt	11.6[a]	0.009802[d]	—	—	102	1207
KOEt	4.84[a]	0.0111[d]	—	—	90	445
PhO^-	0.14[b], 0.13[c]	—	0.000501	—	—	—
LiOPh	0.37[c]	—	—	0.0018[c]	570	1700
NaOPh	0.26[c]	—	—	0.014[c]	74	140
KOPh	0.14[c]	—	—	0.090[c]	11	12

[a]Reference 6.
[b]Calculated using linear least-squares analysis.
[c]Calculated using differential least-squares analysis.
[d]Reference 7.

noting that $[PhOM]_0$ is the initial stoichiometric concentration of phenoxide and that the initial concentrations of phenoxide and phenol are equivalent ($[PhOM]_0 = [PhOH]_0$).

$$[10]\quad [EtO^-]_{eq} = -\{([PhOM]_0 + K_s) + (([PhOM]_0 + K_s)^2 + 4K_s[PhOM]_0)^{1/2}\}/2$$

$$[11]\quad [PhO^-]_{eq} = [PhOM]_0 - [EtO^-]_{eq}$$

The equilibrium concentration of EtO^- can be calculated according to eq. [10] and since k_{EtO^-} is known from the previous study ($k_{EtO^-} = 0.980\ M^{-1}\ s^{-1}$) (5), the ethoxide term of eq. [5] ($k_{EtO^-}[EtO^-]$) can be evaluated and subtracted from k_{obs} to give a modified pseudo-first-order rate constant k_ψ:

$$[12]\quad k_\psi = k_{obs} - k_{EtO^-}[EtO^-]_{eq} = k_{PhO^-}[PhO^-]_{eq}$$

The values of k_ψ and $[PhO^-]_{eq}$ for the reaction of **1** with BTMAOPh are presented in Table 4. The rate constant for the phenoxide ion ($k_{PhO^-} = 0.14\ M^{-1}\ s^{-1}$: $r = 0.9998$) was calculated from these data by linear regression analysis. The rate constant for the phenoxide ion was also determined from a non-linear differential least-squares (DLS) fitting of the experimental data to eq. [5].[3] This treatment yields a value for k_{PhO^-} of $0.13\ M^{-1}\ s^{-1}$. Two-parameter DLS fitting of the BTMAOPh data gave a value for k_{PhO^-} of $0.14\ M^{-1}\ s^{-1}$ and a value for K_s of 3.0×10^{-4} M, which is in good agreement with the value of K_s derived from the literature pK_a values. It follows that phenoxide ion is approximately an order of magnitude less reactive than ethoxide ion, since $k_{EtO^-} = 0.980\ M^{-1}\ s^{-1}$ (5).

[3]A description of the DLS treatment has been deposited as supplementary material. Copies may be purchased from the Depository of Unpublished Data, CISTI, National Research Council, Ottawa, Ont., Canada K1A 0S2.

Phenoxide ion-pair reactivity

Having determined the rate constant for the reaction of **1** with free phenoxide ion, two constants in Scheme 1, i.e., K'_d and k_{PhOM}, still require evaluation. These constants were determined for the reaction of **1** with LiOPh, NaOPh, and KOPh using differential least-squares (DLS) curve fitting of the experimental data to eq. [4]. The calculated plots are shown in Fig. 1 as solid lines, while the experimental points are shown as open symbols. It can be seen from Fig. 1 that the DLS fitting produces a good simulation of the experimental data with very little deviation from the curve. The values of k_{PhOM} and K'_d determined by this method are given in Table 5. It follows that the rate constants for the alkali metal phenoxides increase in the order $k_{PhOK} < k_{PhONa} < k_{PhOLi}$. These results are similar to those obtained for the reaction of **1** with alkali metal ethoxides (5) where rate constants increased in the order $k_{EtO^-} < k_{EtOK} < k_{EtONa} < k_{EtOLi}$ (Table 5).

The values of K'_d calculated using the DLS fitting (Table 5) similarly show that association of the metal ion with phenoxide ion decreases on going from LiOPh to KOPh. This again corresponds to the trend in dissociation constants (K_d) observed for the alkali metal ethoxides (Table 5), indicating that the smaller metal cations are associated more strongly with the anions than are the larger cations (5).

The accuracy of the values of k_{PhOM} and K'_d derived from the DLS fitting is difficult to assess since they are derived using constants from various sources. While the standard deviation of the experimental points from the calculated curves may be very small, the true error in the calculated constants will be a combination of all errors associated with all of the parameters used in their derivation. For this reason the equilibrium and rate constants determined by the DLS fitting for the reaction of **1** with PhOM are reported only to two significant figures.

Can. J. Chem. Downloaded from www.nrcresearchpress.com by 91.121.58.235 on 09/07/12
For personal use only.

TABLE 6. Dissection of rate data for the reaction of **1** with phenoxide into contributions of dissociated and ion-paired nucleophiles

Reactant	$[PhOM]_0$ (M)	k_{obs} (s^{-1})	Calcd. k_{obs} (s^{-1})	% Contribution to rate			
				EtO^-	EtOM	PhO^-	PhOM
BTMAOPh	0.004935	0.0008828	0.0009934	41.6	—	58.4	—
	0.009774	0.001605	0.001644	27.2	—	72.8	—
	0.01452	0.002231	0.002265	20.3	—	79.7	—
	0.01918	0.002900	0.002870	16.3	—	83.7	—
	0.02374	0.003493	0.003459	13.6	—	86.4	—
LiOPh	0.003748	0.002921	0.003053	6.6	64.7	7.0	21.7
	0.007422	0.004786	0.004726	3.6	54.4	7.3	34.7
	0.01103	0.006214	0.006149	2.5	46.5	7.3	43.7
	0.01456	0.007490	0.007470	1.8	40.8	7.1	50.3
	0.01803	0.008682	0.008736	1.4	36.4	6.9	55.3
NaOPh	0.004686	0.002492	0.002396	13.3	59.0	17.9	9.8
	0.009280	0.004129	0.004088	7.4	56.0	18.9	17.7
	0.01379	0.005453	0.005521	5.1	51.8	19.0	24.1
	0.01820	0.006758	0.006813	3.9	48.0	18.9	29.2
	0.02254	0.008080	0.008025	3.1	44.7	18.7	33.5
KOPh	0.005445	0.001944	0.001853	20.4	45.5	32.1	2.0
	0.01109	0.003398	0.003408	11.4	49.2	35.2	4.2
	0.01660	0.004744	0.004807	8.0	49.4	36.3	6.3
	0.02193	0.006127	0.006079	6.2	48.8	36.9	8.1
	0.02715	0.007255	0.007264	5.0	47.9	37.2	9.9

Can. J. Chem. Downloaded from www.nrcresearchpress.com by 91.121.58.235 on 09/07/12
For personal use only.

The main conclusion of the DLS treatment is that the qualitative trends and the relative magnitudes of k_{PhOM} and K_d' values can be considered as valid and are in fact mutually supportive of the behaviour observed in our previous study (5). The derived values are also fully consistent with the observed experimental kinetic data, i.e., $k_{LiOPh} > k_{NaOPh} > k_{KOPh}$ (Fig. 1).

Dissection of nucleophilic reactivities of free ions and ion pairs

It is now possible to calculate the relative contribution of each nucleophile to the overall rate (Table 6) using the calculated values for the rate constants, k_{EtO^-}, k_{PhO^-}, k_{EtOM}, and k_{PhOM}, and the equilibrium solvolysis constant, K_s.

First, consider only the reaction of **1** with BTMAOPh. It can be shown that at the lowest concentration studied the contributions of EtO^- and PhO^- to the overall reaction are 41.6 and 58.4% respectively. However, at the highest concentration studied the contributions of EtO^- and PhO^- change to 13.6 and 86.4% respectively. This change, coupled with the fact that EtO^- is ca. 10 times more reactive than PhO^-, leads to the downward curvature observed in Fig. 1. In dilute solutions of base, a large fraction of phenoxide ion will be converted to ethoxide ion; as the initial base concentration is increased, the amount of ethoxide ion produced, as a fraction of the total amount of base present, becomes relatively small. Since $k_{EtO^-} > k_{PhO^-}$, the reaction of **1** with EtO^- will predominate at low initial phenoxide concentration ($[PhOM]_0$). As the PhO^- concentration ($[PhO^-]_{eq}$) increases relative to that of $[EtO^-]_{eq}$, the reaction of **1** with PhO^- will take precedence. In this region the rate will exhibit a decrease and become proportional to the initial BTMAOPh concentration, thus giving rise to the observed downward curvature.

Proceeding to the reactions of **1** with the alkali metal phenoxides, downward curvature is similarly observed in the plots of k_{obs} vs. LiOPh, NaOPh, and KOPh (Fig. 1). This is in contrast to the upward curvature observed in similar plots for the reaction of **1** with KOEt, NaOEt, and LiOEt (5). The upward curvature in these plots was explained as arising from an increase in ion pairing of the nucleophile at higher base concentrations, leading to an increase in rate due to the reaction of the more reactive ion-paired species.

Table 6 shows the percentage contribution of each nucleophile to the overall rate calculated using the derived rate and equilibrium constants for each nucleophile system. For the reaction **1** with LiOPh it is seen that the relative contributions of EtO^- and PhO^- remain relatively constant. In contrast, the contribution of EtOM decreases while that of PhOM increases over the range of base concentrations studied. This situation is similar to that of the benzyltrimethylammonium phenoxide system described above, where the change from nucleophilic attack of the more reactive EtOLi to the less reactive PhOLi results in downward curvature of the plots. This also holds true for the reaction of **1** with PhONa, though the change is more gradual and the curvature less pronounced. In the PhOK system the situation is a little different. The contributions of EtOK and PhO^- remain constant and dominant while the downward curvature arises from a decrease in EtO^- contribution and increase in PhOK contribution.

Transition state vs. ground state stabilization

The above analysis of the kinetic data has led to the conclusion that the alkali metal ion paired nucleophile is more reactive than the corresponding free nucleophile. This conclusion may seem contrary to the conventional wisdom that predicts a decrease in reactivity due to stabilization of the anion by pairing to the cation. This apparent contradiction can be resolved, however, if one considers that the metal ion catalysis can occur in this system as a result of either an interaction of M^+ with the ground state of the nucleophile, the substrate, or with the transition state of reaction. Since no appreciable

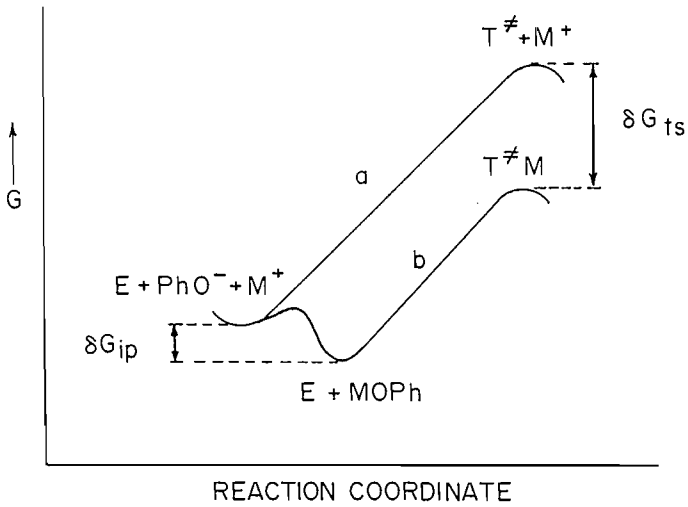

FIG. 4. Reaction coordinate diagram illustrating the uncatalysed reation of the phosphinate ester (E) with PhO^- (path a) and the alkali metal ion catalysed reaction of E with MOPh (path b).

interaction between M^+ and the substrate has yet been observed, the interaction of M^+ with the ground state of the nucleophile and the transition state of the reaction remain to be considered as the main interactions.

These two interactions can be illustrated in Fig. 4. Path a illustrates the uncatalysed reaction of **1** (E) with PhO^-, whereas path b describes the reaction of E with the ion-paired phenoxide. Since the association constants ($K_a = 1/K_d'$) for the ion-paired phenoxides are greater than unity, the ion-paired nucleophile must lie at a lower free energy than the free nucleophile, the difference being shown as δG_{ip} in Fig. 4.

Similarly, it is expected that the ion pairing of the transition state ($T^{\neq}$) will result in a lowering of its free energy. This stabilization is shown as δG_{ts} in Fig. 4. Therefore, if the difference in free energy between $T^{\neq}M$ and $T^{\neq}$ (δG_{ts}) is greater than the stabilization of the ion-paired nucleophile (δG_{ip}), catalysis will be observed in the system.

Association constants for the interaction of M^+ with the transition state (Scheme 2) were determined as described by Kurz (11) and are given in Table 5.

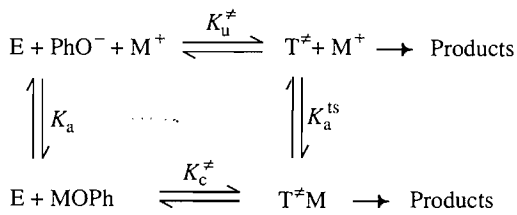

SCHEME 2

Here, E is the phosphinate ester, $K_u^{\neq}$ and $K_c^{\neq}$ are the equilibrium constants for the formation of the uncatalysed and catalysed transition states ($T^{\neq}$ and $T^{\neq}M$), while K_a and K_a^{ts} are the equilibrium association constants of M^+ with PhO^- and the transition state, respectively. From transition state theory eq. [13] can be derived.

$$[13] \quad K_a^{ts} = \frac{k_{PhOM}\, K_a}{k_{PhO^-}} = \frac{k_{EtO^-}}{k_{PhO^-}\, K_d'}$$

These equilibrium constants are given in Table 5.

The trend in K_a^{ts} values follows the same order for the reaction of **1** with EtOM and with PhOM in that the constants increase in the order $K^+ < Na^+ < Li^+$. It can also be seen from the data in Table 5 that the magnitude of K_a^{ts} is typically much greater than that of K_a. The larger values of K_a^{ts} relative to K_a find explanation in a chelation effect of the metal ion by nucleophile and substrate, as illustrated in structure **4**. The greater association of the metal ion with the transition state resulting from this chelation effect would account for its increased stability relative to the ground state, and hence the observed catalysis by the metal ion.

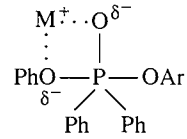

4

Although the kinetic data cannot distinguish between pre-association and the ion-pair mechanism, the latter is more attractive since the rate increases with increasing base concentration and hence with increasing ion-pair concentration. A mechanistic model for the transfer of the metal ion from the ion pair to the transition state, with the inclusion of solvent molecules, has been proposed for the reaction of **1** with the EtOM ion pair (5). A similar model can be proposed for the reaction of **1** with the PhOM ion pair.

It is also interesting to note that the magnitudes of the K_a^{ts} values for the phenoxide reactions are substantially lower than the corresponding values for the ethoxide reactions. This may be due to an increase in delocalization of negative charge in the transition state on the phenoxy moiety. The net overall charge on the phosphoryl oxygen for reaction with phenoxide may therefore be less than that in the reaction with the charge-localized ethoxide ion. Further studies concerning the association of M^+ with the transition state of nucleophilic displacement reactions of different carbon, phosphorus, and sulfur systems will be reported in subsequent papers in this series (12).

Experimental

The *p*-nitrophenyl diphenylphosphinate, ethanol, alkali metal ethoxides, and lithium salts used in this study were prepared as described previously (5). The preparation of solutions and the kinetic methods have also been described previously (5). No attempt was made to isolate and analyze the reaction products due to the complexity of the system, since the phenoxide product is capable of reacting further to give the ethoxide product. This reaction will be reported on subsequently. Also, no correction of the data was made for ionic strength effects. The equilibrium constants used in this study can therefore be considered as apparent equilibrium constants that change nominally over the relatively small range of concentrations used.

Preparation of LiOPh, NaOPh, and KOPh solutions

The alkali metal phenoxide solutions were prepared by addition of the corresponding alkali metal ethoxide solution in ethanol of known concentration to solid phenol in the inert atmosphere of a Dri-Lab (Vacuum Atmospheres Co.) glove box. Generally, 10 mL of a ca. 0.05 M ethoxide solution was added to 0.01 mol of PhOH. This produced a solution in which the initial concentrations of phenoxide and phenol were equivalent.

Preparation of BTMAOPh solutions

Benzyltrimethylammonium phenoxide (BTMAOPh, mp 114–116°C) was prepared by the following general method. Benzyltrimethylammonium hydroxide (57.7 g of a 40% methanolic solution) was added to sublimed phenol (13.0 g) dissolved in methanol. The mixture

Can. J. Chem. Downloaded from www.nrcresearchpress.com by 91.121.58.235 on 09/07/12
For personal use only.

was stirred for 3 h at room temperature, the bulk of the solvent removed on a rotary evaporator, and the residue dried overnight under high vacuum (< 0.001 Torr; 1 Torr = 133.3 Pa). The resulting solid was dissolved in acetone, filtered to remove impurities, and the product was precipitated with ether.

A solution containing equimolar proportions of BTMAOPh and phenol was obtained by first preparing a solution of PhOH in EtOH in the Dri-Lab. The BTMAOPh was then weighed into a volumetric flask, again in the Dri-Lab, and diluted to the mark with the phenol solution.

Acknowledgments

This research was supported by the Department of National Defence and by the Natural Sciences and Engineering Research Council of Canada. The award of a Queen's University Graduate Student Fellowship to E.J.D. is also acknowledged. The authors wish to thank Dr. J. W. Bovenkamp (DREO) for supplying the benzyltrimethylammonium phenoxide.

1. J. EPSTEIN and W. A. MOSHER. J. Phys. Chem. **72**, 622 (1968).
2. J. EPSTEIN and D. H. ROSENBLATT. J. Chem. Soc. **80**, 3590 (1958).
3. J. J. STEFFENS, E. J. SAMPSON, I. J. SIEWERS, and S. J. BENKOVIC. J. Am. Chem. Soc. **95**, 936 (1973).
4. W. S. WADSWORTH, JR. J. Org. Chem. **46**, 4080 (1981).
5. E. BUNCEL, E. J. DUNN, R. A. B. BANNARD, and J. G. PURDON. J. Chem. Soc. Chem. Commun. 162 (1984); E. J. Dunn and E. BUNCEL. Can. J. Chem. **67**, 1440 (1989).
6. R. D. COOK and L. RAHHAL-ARABI. Tetrahedron Lett. 3147 (1985).
7. J. BARTHEL, R. WACHTER, and M. KNERR. Electrochim. Acta, **16**, 723 (1971).
8. R. G. BATES. *In* Solute–solvent interactions, Vol I. *Edited by* J. F. Coetzee and C. D. Ritchie. Marcel Dekker, New York, NY. 1969.
9. B. D. ENGLAND and D. A. HOUSE. J. Chem. Soc. 4421 (1962).
10. R. P. BELL. The proton in chemistry. Cornell University Press, Ithaca, NY. 1959.
11. J. L. KURZ. J. Am. Chem. Soc. **85**, 987 (1963).
12. E. BUNCEL and M. J. PREGEL. J. Chem. Soc. Chem. Commun. 1566 (1989).

Can. J. Chem. Downloaded from www.nrcresearchpress.com by 91.121.58.235 on 09/07/12
For personal use only.

Metal ion catalysis in nucleophilic displacement reactions at carbon, phosphorus, and sulfur centers.[1] III. Catalysis vs. inhibition by metal ions in the reaction of *p*-nitrophenyl benzenesulfonate with ethoxide

MARKO J. PREGEL, EDWARD J. DUNN, AND ERWIN BUNCEL[2]
Department of Chemistry, Queen's University, Kingston, Ont., Canada K7L 3N6

Received March 16, 1990

This paper is dedicated to Professor Ross Stewart on the occasion of his 65th birthday

MARKO J. PREGEL, EDWARD J. DUNN, and ERWIN BUNCEL. Can. J. Chem. **68**, 1846 (1990).

The rate of the nucleophilic displacement reaction of *p*-nitrophenyl benzenesulfonate (**1**) with alkali metal ethoxides in ethanol at 25°C has been studied by spectrophotometric techniques. For lithium ethoxide, sodium ethoxide, potassium ethoxide, and cesium ethoxide, the observed rate constants increase in the order LiOEt < NaOEt < CsOEt < KOEt. The effect of added crown ether and cryptand complexing agents was also investigated. Addition of complexing agent to the reaction of KOEt results in the rate *decreasing* to a minimum value corresponding to the reaction of free ethoxide. Conversely, addition of complexing agent to the reaction of LiOEt results in the rate *increasing* to a maximum value that is identical to the minimum value seen in the reaction of KOEt in the presence of excess complexing agent. In complementary experiments, alkali metal ions were added in the form of unreactive salts. Addition of a K^+ salt to the reaction of KOEt increases the reaction rate, while addition of a Li^+ salt to the reaction of LiOEt decreases the rate. The involvement of metal ions in the reaction of **1** is proposed to occur via reactive alkali metal – ethoxide ion pairs. The kinetic data are analyzed in terms of an ion pairing treatment that allows the calculation of second-order rate constants for free ethoxide and metal–ethoxide ion pairs; the rate constants increase in the order LiOEt < EtO^- < NaOEt < CsOEt < KOEt. *Thus, Li^+ is an inhibitor of the reaction of ethoxide with **1**, while the other metals ions studied are all catalysts.* Equilibrium constants for the association of the various metal ions with the transition state are calculated using a thermodynamic cycle, and are compared to association constants in the ground state. Consistent with the observed kinetic results, Li^+ is found to stabilize the ground state more than the transition state, while Na^+, K^+, and Cs^+ all stabilize the transition state more than the ground state. The trend in the magnitude of the transition state stabilization is interpreted in terms of interactions of the transition state with bare or solvated metal ions. It is concluded that the transition state for the reaction of **1** with ethoxide forms solvent separated ion pairs with alkali metal ions. Analogous data were available for the reaction of *p*-nitrophenyl diphenylphosphinate (**2**) with ethoxides, where Li^+, Na^+, K^+, and Cs^+ all function as catalysts, and the results are analyzed as above. In contrast to the sulfonate system, it is proposed that the phosphinate transition state forms contact ion pairs with alkali metal ions. The difference is attributed to a greater localization of negative charge in the phosphinate transition state, leading to stronger interactions with metal ions, which overcome metal ion – solvent interactions.

Key words: nucleophilic substitution at sulfur, alkali metal ion catalysis.

MARKO J. PREGEL, EDWARD J. DUNN et ERWIN BUNCEL. Can. J. Chem. **68**, 1846 (1990).

Utilisant des techniques spectrophotométriques et opérant à 25°C, on a déterminé les vitesses de réactions nucléophiles du benzénesulfonate de *p*-nitrophényle avec les alcoolates des métaux alcalins, en solution dans l'éthanol. Pour les éthylates de lithium, de sodium, de potassium et de césium, les constantes de vitesse observées augmentent dans l'ordre LiOEt < NaOEt < CsOEt < KOEt. On a aussi examiné l'effet de l'addition d'éther couronne et de cryptand comme agents complexants. L'addition d'agents complexants à la réaction avec le KOEt provoque une diminution de la vitesse jusqu'à une valeur minimale correspondant à la réaction de l'alcoolate libre. Par ailleurs, l'addition d'un agent complexant à la réaction avec le LiOEt provoque une augmentation de la vitesse jusqu'à une valeur maximale qui est identique à la valeur minimale observée dans la réaction du KOEt en présence d'un excès d'agent complexant. Au cours d'expériences complémentaires, on a ajouté des ions métalliques sous la forme de sels non-réactifs. L'addition d'un sel de K^+ à la réaction du KOEt provoque une augmentation de la vitesse alors que l'addition d'un sel de Li^+ à la réaction de LiOEt provoque une diminution de la vitesse. On suggère que l'implication des ions métalliques dans la réaction du composé **1** se produit par le biais de paires d'ions formées de métal alcalin et d'éthylate. On a analysé les données cinétiques en fonction d'un traitement de couplage ionique qui permet de calculer les constantes de vitesse du deuxième ordre pour l'éthylate libre et pour les paires d'ions métal–éthylate; les constantes de vitesse augmentent dans l'ordre LiOEt < EtO^- < NaOEt < CsOEt < KOEt. *Le Li^+ est donc un inhibiteur de la réaction de l'éthylate avec **1** alors que les autres ions métalliques étudiés sont des catalyseurs.* Utilisant un cycle thermodynamique, on calcule les constantes d'équilibre pour l'association des divers ions métalliques avec l'état de transition et on les compare avec les constantes d'association de l'état fondamental. En accord avec les résultats cinétiques observés, on a trouvé que le Li^+ stabilise plus l'état fondamental que l'état de transition alors que le Na^+, le K^+ et le Cs^+ stabilisent tous plus l'état de transition que l'état fondamental. On interprète cette variation de l'amplitude de la stabilisation de l'état de transition en fonction d'interactions de l'état de transition avec des ions métalliques nus ou solvatés. On en conclut que l'état de transition pour la réaction du produit **1** avec l'éthylate forme des paires d'ions où les ions des métaux alcalins sont séparés par le solvant. Des données analogues sont disponibles pour la réaction du diphénylphosphinate de *p*-nitrophényle (**2**) avec les éthylates où Li^+, Na^+, K^+ et Cs^+ agissent tous comme catalyseurs et pour lesquels on a analysé les résultats comme précédemment. Par opposition avec ce qui a été observé avec le système sulfonate, on propose que l'état de transition du phosphinate forme des pairs d'ions de contact avec les ions des métaux alcalins. La différence est attribuée à une plus grande localisation de la charge négative dans l'état de transition du phosphinate qui provoquerait de plus grandes interactions avec les ions métalliques et permettrait de surmonter les interactions ion métallique–solvant.

Mots clés : substitution nucléophile à soufre, catalyse par les ions des métaux alcalins.

[Traduit par la revue]

[1]This paper is an extension of our series on Bond Scission in Sulfur Compounds. For previous papers in this series, see ref. 1.
[2]Author to whom correspondence may be addressed.

Can. J. Chem. Downloaded from www.nrcresearchpress.com by 91.121.58.235 on 09/07/12
For personal use only.

Can. J. Chem. Downloaded from www.nrcresearchpress.com by 91.121.58.235 on 09/07/12
For personal use only.

Introduction

Subtle differences in the physical and chemical properties of alkali metal ions, particularly Na^+ and K^+, have been exploited in living systems to discriminate between the various ions and to develop markedly different roles for each (2). Studies of the mechanism of discrimination between alkali metal ions in organic reactions would provide a bridge between observations on selectivity between alkali metal ions in biological and nonbiological systems and bring further evidence to bear on the underlying mechanism. However, this area has not been extensively investigated.

We have initiated systematic studies into the influence of alkali metal ions on nucleophilic substitution/addition reactions at carbon, phosphorus, and sulfur centers. The present study deals with the effects of alkali metal ions on nucleophilic substitution reactions of sulfonate esters, specifically, the reaction of alkali metal ethoxides with *p*-nitrophenyl benzenesulfonates (**1**). Alkali metal ions are expected to behave similarly, but surprisingly, we have found that in this case, *the ions Na^+, K^+, and Cs^+ cause a rate acceleration, while Li^+ causes a rate retardation.* A previous report outlined the observation of alkali metal ion catalysis in the reaction of ethoxide with *p*-nitrophenyl diphenylphosphinate (**2**), in which *Li^+, Na^+, K^+, and Cs^+ all acted as catalysts* (1*c*).

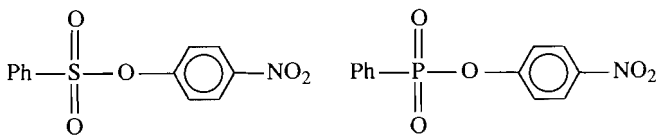

1 **2**

The alkaline hydrolysis reactions of benzenesulfonate and tosylate esters have been studied in a number of different media: water (3), aqueous ethanol (4), aqueous DMSO (4), aqueous acetonitrile (5), aqueous DME (5), aqueous dioxane (6), and aqueous acetone (6). However, no studies have used single solvent systems other than water. In particular, no studies of the reaction in anhydrous ethanol have been reported.

Ion pairing is important to the understanding of the behavior of alkali metal ethoxides in ethanol, as it is for the behaviour of other ionizable species in solvents of moderate polarity (7, 8). In ethanol, stabilization of the metal ion through electrostatic interactions with anions becomes significant and ion pairs are formed to an appreciable extent. Ion pairing of alkali metal ethoxides is well known and can have interesting effects on reactivity. For instance, downward plots of rate constant versus base concentration were obtained in the reaction of ethoxides in ethanol with benzyl chloride (9), methyl iodide (10), and phenyl acetate (11) and were attributed to ion pairing effects. Consequently, ion pairing will be considered in relation to the experimental results on the effects of alkali metal ions on the reaction of **1** with ethoxide ion in ethanol.

The kinetic data will be analyzed in terms of stabilization/destabilization of the ground state and transition state by metal ions. In the ground state, the metal ion is known to ion pair to the ethoxide ion and may also complex the ester. In the transition state, chelation of the sulfonyl oxygens is conceivable. Thus, ground state and transition state interactions will be the focus of our discussion (12).

Results

Reactions of alkali metal ethoxides

We have studied the reactions of *p*-nitrophenyl benzenesulfonate (**1**) with lithium ethoxide, sodium ethoxide, potassium ethoxide, and cesium ethoxide in anhydrous ethanol at 25°C. Reaction rates were measured spectrophotometrically by following the appearance of the absorption due to released *p*-nitrophenoxide ion. Plots of $\log(A_\infty - A_t)$ versus time were linear for more than three half-lives, the slopes yielding the pseudo-first-order rate constants, k_{obs}.

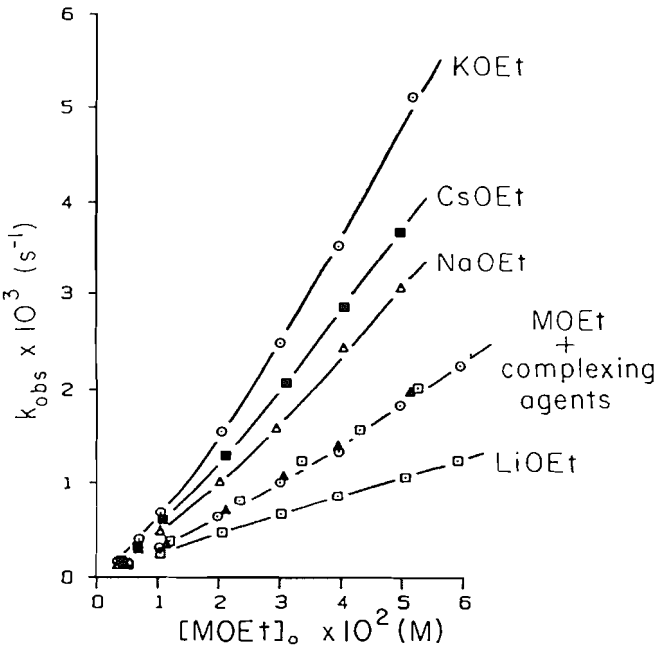

FIG. 1. Kinetic data for reaction of **1** with LiOEt, NaOEt, KOEt, CsOEt, and MOEt in the presence of excess complexing agents in EtOH at 25°C in the 10^{-2} M concentration range. The line labelled "MOEt + complexing agents" is made up of data for KOEt in the presence of excess 18C6 (⊙), KOEt with excess 2.2.2 (▲), and LiOEt with excess 2.1.1 (⊡).

The variation of k_{obs} with the concentration of alkali metal ethoxide is shown in Fig. 1 and Table 1. It is significant that the ethoxides appear to have different reactivities, which follow the order LiOEt < NaOEt < CsOEt < KOEt. Furthermore, the dependence of k_{obs} on $[MOEt]_0$, the total base concencentration, is nonlinear in some cases. Sharp upward curvature is seen for KOEt, while CsOEt and NaOEt display slight upward curvature, and the plot for LiOEt is apparently linear.

Effect of added complexing agents

Complexing agents such as crown ethers and cryptands eliminate interactions between metal ions and their counterions (13, 14). Consequently, coronate and cryptate formation has been a powerful tool in the determination of the role of metal ions in reaction mechanisms (13, 15).

The effects of added cryptands on the reactions of KOEt and LiOEt with **1** are shown in Fig. 2. As increasing amounts of 2.2.2 cryptand are added to the KOEt reaction, the rate *decreases* until one equivalent of complexing agent has been added, at which point further addition of cryptand has no effect. When 2.1.1 is added to the reaction of LiOEt with **1**, the rate constant *increases* until one equivalent of cryptand has been added, then levels off to a constant value. The plots for KOEt + 2.2.2 and LiOEt + 2.1.1 reach a common plateau. This is assumed to correspond to the reaction of free ethoxide since all metal ions should be complexed at these concentrations of added cryptands.

The dependence of k_{obs} on the ethoxide concentrations for the reaction of KOEt in the presence of excess 18C6 is shown in Fig. 1, which also shows that the kinetic behavior for KOEt in the presence of excess 18C6 is identical to the behavior of KOEt

TABLE 1. Kinetic data for the reaction of **1** with alkali metal ethoxides in the presence and absence of excess complexing agents in EtOH at 25°C

	$[MOEt]_0 \times 10^3$ (M)	$k_{obs} \times 10^4$ (s^{-1})
KOEt	1.19	0.402
	2.06	0.732
	2.93	1.20
	4.05	1.85
	5.16	2.56
	6.25	3.19
LiOEt	2.14	0.489
	2.97	0.736
	4.18	0.930
	5.36	1.23
	6.13	1.40
	7.25	1.63
KOEt + 18C6	2.31	0.552
$[18C6]/[KOEt]_0 = 3.2$	3.39	0.954
	4.95	1.28
	6.00	1.70
	7.05	2.00
	$[MOEt]_0 \times 10^2$ (M)	$k_{obs} \times 10^3$ (s^{-1})
KOEt	0.349	0.165
	0.695	0.393
	1.04	0.668
	2.04	1.55
	3.02	2.48
	3.97	3.51
	5.20	5.08
LiOEt	0.526	0.130
	1.04	0.252
	2.04	0.459
	3.01	0.657
	3.94	0.845
	5.05	1.06
	5.91	1.24
NaOEt	0.347	0.134
	0.688	0.296
	1.03	0.480
	2.01	1.01
	2.94	1.58
	4.04	2.43
	4.99	3.04
CsOEt	0.408	0.177
	0.677	0.320
	1.08	0.594
	2.11	1.30
	3.11	2.07
	4.07	2.85
	4.99	3.66
LiOEt + 2.1.1	1.19	0.374
$[2.1.1]/[LiOEt]_0 = 1.5$	2.33	0.800
	3.36	1.23
	4.31	1.56
	5.26	2.01
KOEt + 18C6	0.517	0.152
$[18C6]/[KOEt]_0 = 1.9–2.0$	1.02	0.310
	1.97	0.624
	3.00	1.00
	3.96	1.33
	4.97	1.82
	5.96	2.23
KOEt + 2.2.2	1.13	0.350
$[2.2.2]/[KOEt]_0 = 1.5$	2.10	0.696
	3.05	1.08
	3.94	1.40
	5.13	1.97
	6.07	2.36
	7.17	2.85

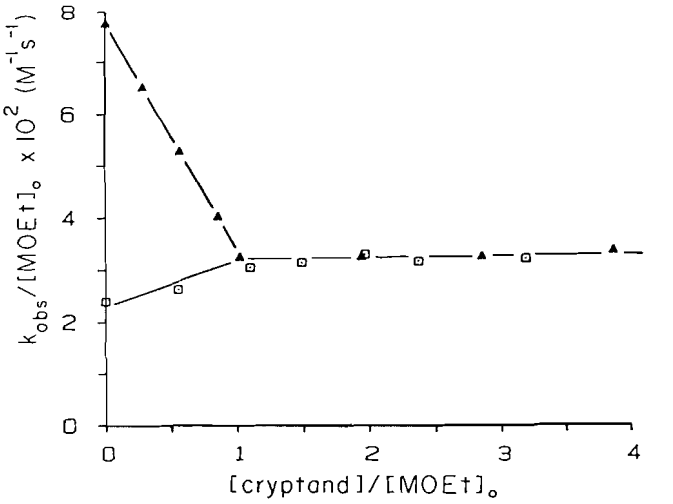

FIG. 2. Effects of added 2.2.2 on the reaction of **1** with KOEt (▲), and of added 2.1.1 on the reaction of **1** with LiOEt (⊡) in EtOH at 25°C at constant base concentration.

in the presence of excess 2.2.2, and LiOEt in the presence of excess 2.1.1, i.e., all of the data points fall on a common line. These data are also found in Table 1. Reactions in the presence of excess complexing agents are thought to represent the reaction of free ethoxide, so it is evident that EtO^- is more reactive than LiOEt, but less reactive than NaOEt. The order of reactivity is: LiOEt < EtO^- < NaOEt < CsOEt < KOEt.

Effect of added metal ions

Since removal of metal ions by complexation had a marked effect on the rate of reaction, it was also of interest to look at the effect of the addition of metal ions in the form of unreactive salts.

The effect of added potassium iodide on the reaction of potassium ethoxide with **1** is shown in Fig. 3. When the K^+ salt is added at a constant concentration of KOEt, the observed rate constant *increases* asymptotically to a maximum value.

The effect of added LiCl on the reaction of LiOEt with **1** is shown in Fig. 4. Addition of a Li^+ salt to a constant concentration of LiOEt causes a *decrease* in rate, with the rate constant approaching a minimum value asymptotically. Similarly, when $LiNO_3$ is added to the reaction of LiOEt with **1**, the rate decreases, approaching a limiting minimum value.

It should be noted that when increasing amounts of $NaBPh_4$ are added to the reaction of NaOEt with **1** at a constant concentration of NaOEt, the reaction rate increases, approaching a limiting maximum value. However, further additions cause a significant decrease in rate. The reasons for the rate decrease after the maximum are not fully understood at present.

Can. J. Chem. Downloaded from www.nrcresearchpress.com by 91.121.58.235 on 09/07/12
For personal use only.

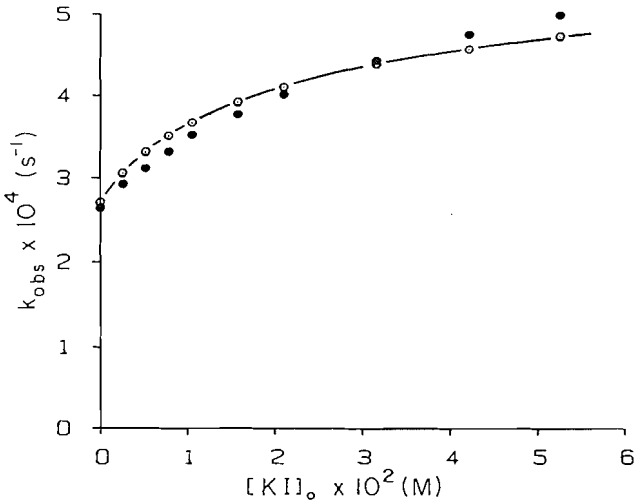

FIG. 3. Effect of added KI on the reaction of **1** with KOEt in EtOH at 25°C at constant base concentration and comparison of calculated (⊙) and observed (●) rate constants.

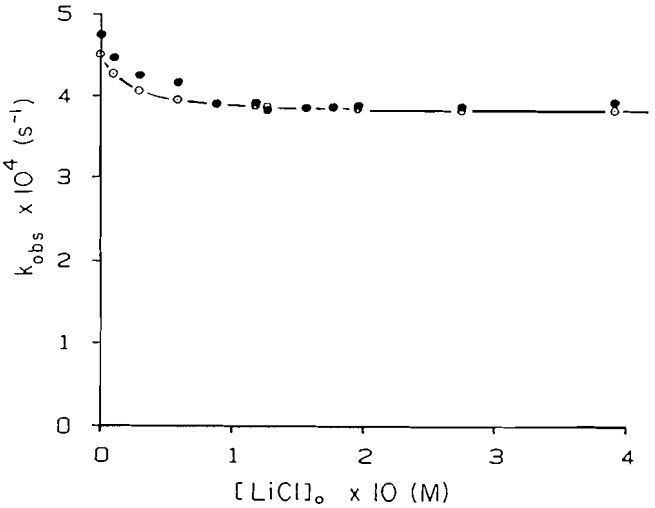

FIG. 4. Effect of added LICl on the reaction of **1** with LiOEt in EtOH at 25°C at constant base concentration and comparison of calculated (⊙) and observed (●) rate constants.

Kinetic data on the effect of added salts have been deposited as Supplementary Material.[3] The effects of added KI on the reaction of KOEt, of added $LiNO_3$ and LiCl on the reaction of LiOEt, and of added $NaBPh_4$ on the reaction of NaOEt are reported. The Supplementary Material also includes data on the effects of increasing amounts of added 18C6 and 2.2.2 on the reaction of KOEt and the effects of increasing amounts of added 2.1.1 on the reaction of LiOEt with **1**.

Discussion

The behaviour of the observed rate constants for the reaction of **1** with alkali metal ethoxides, and the effects of both added complexing agents and added metal salts, indicate significant and differing involvement of metal ions in the reaction mechanism. Certain metal ions, e.g., K^+, act as *catalysts*, i.e., the rate increases when they are added as inert salts and decreases when they are removed by complexing agents. One metal ion studied, Li^+, acts as an *inhibitor*, i.e., the rate decreases when it is added and increases when it is complexed.

In the following discussion, we consider the involvement of alkali metal ions via association with either the ester or the ethoxide ion. Interaction with the transition state will be considered subsequently. The reaction is depicted as an addition–elimination mechanism with nucleophilic attack as the rate-limiting step. This is consistent with the results of our investigations into the mechanism of these reactions, which include Hammett σ–ρ treatment of leaving group effects. These results will be reported subsequently in this series of articles. However, a concerted $S_N2(S)$ mechanism is also conceivable, and the discussion would apply equally to this mechanism.[4]

In the absence of metal ions, the mechanism in eq. [1] is assumed, i.e., the nucleophile attacks the substrate in a slow step, forming a pentacoordinate intermediate, and the leaving group is expelled in a subsequent fast step. The rate law in eq. [2] will apply (E denotes the substrate ester).

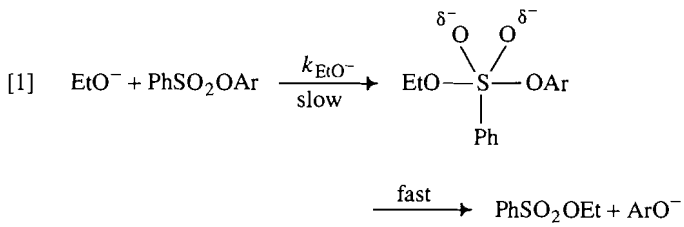

[2] rate = k_{EtO^-}[EtO$^-$][E]

Catalysis via alkali metal ethoxide ion pairs

Ion pairing is known to occur in solutions of alkali metal ethoxides in ethanol. Other associated species, such as dimers and aggregates, may also exist. Zavada and co-workers have measured the degree of association in lithium, sodium, and potasium ethoxide solutions by ebulliometry (17), and concluded that at relatively low concentrations (<0.1 M), the main species present were free ions and ion pairs. Because the present study involves lower total base concentrations, only free ions and ion pairs will be considered in the following discussion.

The association of alkali metal ions with ethoxide ion is governed by an ion pair association constant, K_a (eq. [3]). Since free ions and ion pairs are in equilibrium, two reaction pathways should be possible. The substrate can in principle react with either free ethoxide or an alkali metal – ethoxide ion pair, as shown in eq. [3]. Therefore, the overall rate law and the observed pseudo-first-order rate constant will both be sums of terms corresponding to reaction of free ions and ion pairs (eqs. [4], [5]).

[3]This material may be purchased from the Depository of Unpublished Data, CISTI, National Research Council of Canada, Ottawa, Ont., Canada K1A 0S2.

[4]In further studies, Hammett treatment of leaving group effects in the reaction of substituted aryl benzenesulfonates with ethoxide was found to yield a best correlation with σ^0 substituent constants.[5] These results imply that the transition state is characterized by well-advanced EtO—S bond formation, but negligible S—OAr bond breakage. However, this conclusion is at variance with that of Williams concerning the reaction of aryloxides with substituted 2-hydroxyphenylmethanesulfonic acid sultones (16), in which a concerted process and a symmetrical transition state were inferred. Efforts are currently underway to address the origin of this variance.

[5]M. J. Pregel and E. Buncel. Manuscript in preparation.

Can. J. Chem. Downloaded from www.nrcresearchpress.com by 91.121.58.235 on 09/07/12
For personal use only.

Can. J. Chem. Downloaded from www.nrcresearchpress.com by 91.121.58.235 on 09/07/12
For personal use only.

$$M^+ + EtO^- + PhSO_2OAr \xrightarrow{k_{EtO^-}} \text{products}$$

[3] K_a

$$MOEt + PhSO_2OAr \xrightarrow{k_{MOEt}} \text{products}$$

[4] $\text{rate} = k_{EtO^-}[EtO^-][E] + k_{MOEt}[MOEt][E]$

[5] $k_{obs} = k_{EtO^-}[EtO^-] + k_{MOEt}[MOEt]$

As the total base concentration increases, the ion pair equilibrum shifts, leading to a greater proportion of ion pairs to free ions. This is consistent with the curvature observed in plots of k_{obs} versus $[MOEt]_0$ (Fig. 1). If the ion pair model applies, upward curvature for NaOEt, KOEt, and CsOEt would imply that for these bases, *the ion pair is more reactive than the free anion*. The absence of observable curvature for LiOEt may be due to changes in activity coefficients with concentration. A small accelerating activity coefficient effect could counterbalance downward curvature due to ion pairing effects.

The ion pair model has been applied to the reactions of alkali metal ethoxides in ethanol with various substrates. Kinetic data for the attack of sodium ethoxide on benzyl chloride (9) and methyl iodide (10), and the attack of lithium, potassium, and cesium ethoxides on phenyl acetate (11) were all analyzed in terms of the reactivity of free ions and ion pairs *only*. In the case of the S_N2 reactions, ion pairs had measurable reactivity and were less reactive than free ions (9, 10), but in the reaction of phenyl acetate, ion pairs were found to be more reactive than free ions (11), as in the present case.

The idea that ion pairs could be more reactive than free ions seems to be contrary to chemical intuition. Association of a metal ion to an anionic nucleophile would result in neutralization of negative charge, producing a less basic nucleophile, which would be expected to have lesser reactivity. In fact, this is just what is observed in the case of typical S_N2 reactions, such as the examples given above and the exchange reaction of alkali metal iodides and methyl iodide in ethanol (18). In all three cases, ion pairing to the nucleophile caused a *decrease in rate* and plots of the observed rate constant versus concentration of nucleophile curved *downwards*. This behavior is expected when the metal ion interacts with the nucleophile predominantly in the ground state. In S_N2 reactions, this occurs because the charges in the transition state are delocalized over the nucleophile, reacting center, and leaving group, leading to weak interactions of the transition state with metal ions.

However, when the charge on the transition state is localized (or if effective chelation of the transition state by the metal ion is possible), the metal ion may be able to stabilize the transition state to a greater extent than the ground state, and if metal ion involvement occurs through ion pairing to the nucleophile, then ion pairs could be more reactive than free ions. This is seen in the reaction of alkali metal ethoxides with phenyl acetate in ethanol, where ion pairs are more reactive than free ethoxide (11). Reactive ion pairs have also been proposed to account for metal ion involvement in the reaction of KOEt and LiOEt with aryl diphenylphosphinates in anhydrous ethanol (1*c*), and in the reaction of barium and strontium methoxides with phenyl acetates in methanol (19). As well, attack of a metal–methoxide ion pair on a metal-complexed ester has been inferred in the reaction of lithium methoxide with phenyl acetate in methanol (20). Therefore, a number of literature precedents support the application of the ion pair model to the present work: ion pairs are known to be present and are known to be reactive in reactions of alkali metal alkoxides with esters.

Catalysis by preassociation of metal ion with substrate

It is also conceivable that metal ions may be involved in the reaction by complexing the substrate in a pre-equilibrium step (21, 22). Coordination to the sulfonate oxygen(s) of the substrate would polarize the S—O bond(s), making the sulfur center more electrophilic. The possibility of metal ion catalysis by preassociation is inferred from infrared spectroscopic studies of carboxylic acid esters, which have demonstrated the existence of Li^+ and Ba^{2+} complexes in methanol (23), as well as kinetic studies of the reactions of alkoxides with carboxylate esters which were interpreted in terms of a preassociation mechanism (19, 23). There are no reports, to our knowledge, of significant interactions between sulfonate esters and alkali metal ions in alcoholic solution.

Preassociation would result in the reaction pathway shown in eq. [6]. Since ethoxide can in principle react with both free and metal-complexed substrates as well as in the form of an ion pair, as illustrated below, the observed rate law would be eq. [7]. The observed pseudo-first-order rate constant is now given by eq. [8], which is identical in form to eq. [4] in the discussion of the ion pair model.

$$MOEt + PhSO_2OAr \xrightarrow{k_{MOEt}} \text{products}$$

K_a

[6] $$EtO^- + M^+ + PhSO_2OAr \xrightarrow{k_{EtO^-}} \text{products}$$

K_c

$$EtO^- + PhSO_2OAr \,.\, M^+ \xrightarrow{k_{M^+}} \text{products}$$

[7] $\text{rate} = k_{EtO^-}[EtO^-][E] + k_{M^+}[EtO^-][E.M^+] + k_{MOEt}[MOEt][E]$

[8] $k_{obs} = k_{EtO^-}[EtO^-] + (k_{MOEt} + (k_{M^+}K_c)/K_a)[MOEt]$

If ion pairs are assumed to be unreactive, eq. [8] simplifies to:

[9] $k_{obs} = k_{EtO^-}[EtO^-] + ((k_{M^+}K_c)/K_a)[MOEt]$

Comparing eq. [9] to eq. [5], one observes that the equations are identical except that the coefficient for [MOEt] is k_{MOEt} in eq. [5], while the coefficient is $(k_{M^+}K_c)/K_a$ in eq. [9]. The following section assumes the ion pair mechanism (eq. [5]) and calculates k_{MOEt}. However, if the preassociation mechanism is assumed instead, the product $k_{M^+}K_c$ can be calculated ($k_{M^+}K_c = k_{MOEt}K_a$) since K_a values are known. This results in $k_{M^+}K_c$ values of 3.82, LiOEt; 8.16, NaOEt; 12.3, KOEt; and 11.7, CsOEt. Since K_c is expected to be much less than unity (esters are poor ligands), k_{M^+} can be calculated using fixed values of K_c (1, 0.1, and 0.01 M^{-1}). The results are summarized in Table 2.

When these values are compared to the free ion rate constant ($k_{EtO^-} = 0.0287\ M^{-1}\ s^{-1}$), it is clear that for the preassociation

Can. J. Chem. Downloaded from www.nrcresearchpress.com by 91.121.58.235 on 09/07/12
For personal use only.

TABLE 2. Values of k_{M^+} (M^{-1} s^{-1}) derived from fixed values of K_c (M^{-1}) if the preassociation mechanism of eq. [6] is assumed

	K_c	k_{M^+}		K_c	k_{M^+}
KOEt			LiOEt		
	1	12.3		1	3.82
	0.1	123		0.1	38.2
	0.01	1230		0.01	382
NaOEt			CsOEt		
	1	8.16		1	11.7
	0.1	81.6		0.1	117
	0.01	816		0.01	1170

model to apply, the complexed ester must be extraordinarily reactive when compared to the uncomplexed ester, which does not appear to be reasonable. This suggests that *p*-nitrophenyl benzenesulfonate does not react via the preassociation mechanism. Unfortunately, rate constants or association constants for sulfonate ester – metal ion complexes are not available for comparison to the values presented above and this conclusion must therefore be a tentative one at present.

In summary, metals ions may in principle be involved in reactions of **1** with ethoxide either via metal ethoxide ion pairs or by preassociation to the ester. Kinetic experiments cannot distinguish between the two possibilities since the two mechanisms give rate laws with identical forms. In this respect, the present study illustrates a drawback inherent in all kinetic studies, which can give information on the composition of a transition state, but not its structure.

Following previous treatments (1*c*, 9–11, 19), the results are discussed below in terms of the ion pair mechanism. This is done because ion pairs are known to be present, while there is no evidence for the existence of sulfonate ester – metal ion complexes. The ion pair model is the simplest mechanism that at the same time involves only those species known to be present and completely accounts for all of the kinetic data. Also, fitting of the kinetic data to the preassociation mechanism with reasonable values of K_c implied that the putative complexed ester must be extraordinarily reactive, and this is considered unlikely, as discussed above.

Reactivities of free ions and ion pairs

The discussion in this section is based on the assumption that free ions and ion pairs are the only reactive species in reactions of alkali metal ethoxides with *p*-nitrophenyl benzenesulfonate. When both free ions and ion pairs can react with the substrate, the observed rate is the sum of the rates of reaction of the free and associated ions (24), as shown by eq. [5]. The equilibrium concentrations of free and ion-paired ethoxide can be calculated if the association constant, K_a, is known since the total base concentration, $[MOEt]_0$, is known and $[M^+] = [EtO^-]$ at equilibrium. Once the concentration of free ethoxide has been calculated, the observed rate constants can be dissected into rate constants for the reaction of free ethoxide and alkali metal – ethoxide ion pairs using eq. [10].

$$[10] \quad \frac{k_{obs}}{[EtO^-]} = k_{EtO^-} + k_{MOEt}K_a[EtO^-]$$

It is apparent from eq. [10] that a plot of $k_{obs}/[EtO^-]$ vs. $[EtO^-]$ should be linear with slope $k_{MOEt}K_a$ and intercept k_{EtO^-}. Therefore, the second-order rate constants for the reaction of

TABLE 3. Second-order rate constants (at 25°C) for various ethoxide species from ion pairing treatment of kinetic data

Ethoxide	$k_2 \times 10^2$ ($M^{-1}s^{-1}$)
KOEt	13.7
CsOEt	9.7
NaOEt	8.0
LiOEt	1.80
EtO^-	2.87

free and ion-paired ethoxide can be calculated from the kinetic data. K_a values for alkali metal ethoxides in anhydrous ethanol at 25°C have been determined by Barthel *et al.* (25). They are as follows: LiOEt, 212 M^{-1}; NaOEt, 102 M^{-1}; KOEt, 90 M^{-1}; CsOEt, 121 M^{-1}. Plots of $k_{obs}/[EtO^-]$ vs. $[EtO^-]$ were linear for all ethoxide species, and yielded k_{MOEt} and k_{EtO^-} values. However, better values for k_{EtO^-} were obtained by taking the intercept of a plot of $k_{obs}/[KOEt]_0$ vs. $[KOEt]_0$ for the reaction of KOEt in the presence of excess 18C6. These results generally had smaller error limits than the values of k_{EtO^-} that were obtained from the intercept of plots of $k_{obs}/[EtO^-]$ vs. $[EtO^-]$. k_{EtO^-} was not obtained from the slope of plots of k_{obs} vs. $[KOEt]_0$ in the presence of excess 18C6 because of the slight curvature in these plots. Data for ion pairing treatment plots of $k_{obs}/[EtO^-]$ vs. $[EtO^-]$ for KOEt and LiOEt, as well as data used in the calculation of k_{EtO^-} are given in the Supplementary Material.[3]

The ion pair rate constants of the various species that resulted from the calculations described above are listed in Table 3. Consistent with the observed kinetic results, these follow the order LiOEt < EtO^- < NaOEt < CsOEt < KOEt. The values range from LiOEt, which is 1.6 times less reactive than free ethoxide, to KOEt, which is 4.8 times more reactive.

The curvature in plots of k_{obs} vs. $[KOEt]_0$ in the presence of excess 18C6 may have its origin in weak ion pairing between the complexed metal ions and ethoxide ion. According to Lehn, the crown-complexed cation is accessible from above and below the plane of the crown ether in alkali metal – crown ether complexes (15). Ion pairing of the complexed cation to an anion is considered to be possible. Similarly, alkali metal – cryptand complexes may interact with anions through a face of the cryptand, especially when the face is an 18-membered ring, as in 2.2.2 (15).

Abraham *et al.* have studied the conductivity of 2.2.2 complexes of alkali metal halides in methanol and obtained evidence for association of halide ions with complexed cations (eq. [11]) with ion pair association constants ranging from 20 to 68 for the various halide ions (26).

$$[11] \quad [M.2.2.2]^+ + X^- \rightleftarrows [M.2.2.2]^+X^-$$

There are numerous other examples of formation of crown- and cryptand-complexed ion pairs in nonpolar (27) and dipolar aprotic solvents (28), as well as in the solid state (29).

Given that weak ion pairing of ethoxide ion to the complexed metal ion may be occurring, the complexed ion pair thus formed could be slightly more reactive than free ethoxide due to interaction of the complexed metal ion with the substrate or transition state, leading to slight upward curvature in plots of observed rate constant versus base concentration. Alternatively, changes in activity coefficients with base concentration could be

TABLE 4. Ion pair association constants for alkali metal salts in ethanol at 25°C

Salt	K_a (M^{-1})	Reference
KI	68.4	30
$NaBPh_4$	31	31
$LiNO_3$	19.2	32
LiCl	27	33

exerting a slight rate-accelerating effect which could be responsible for the observed curvature.

Since the ion pair association constants for both alkali metal ethoxides and alkali metal salts are known, the equilibrium concentrations of free ions and ion pairs can be calculated as follows. Values of the association constants for the various salts are presented in Table 4, and the kinetic scheme for reactions in the presence of added metal salts is presented below:

[12] $$M^+ + X^- \underset{}{\overset{K_a(MX)}{\rightleftharpoons}} MX$$

$$MOEt + PhSO_2OAr + X^- \xrightarrow{k_{MOEt}} \text{products}$$

$$K_a(MOEt) \uparrow\downarrow$$

[13] $$EtO^- + M^+ + X^- + PhSO_2OAr \xrightarrow{k_{EtO^-}} \text{products}$$

$$K_a(MX) \uparrow\downarrow$$

$$EtO^- + MX + PhSO_2OAr$$

K_a(MOEt), K_a(MX), k_{EtO^-}, and k_{MOEt} are all known, so the rate constant can be predicted from the pseudo-first-order rate equation (eq. [5]) once the equilibrium concentrations of EtO^- and MOEt are calculated. These concentrations were obtained through combining expressions for K_a(MOEt), K_a(MX), charge balance, and mass balance. Details of the calculation and the equilibrum concentrations of free ions and ion pairs, as well as a comparison of calculated and observed rate constants are reported in the Supplementary Material.[3]

Thus, the results for the effect of added salts can be predicted since k_{EtO^-} and k_{MOEt} are known. The agreement between calculated and observed rate constants is good for KI and LiCl, as shown in Figs. 3 and 4, as well as for $LiNO_3$. $NaBPh_4$ shows very poor agreement, but this salt also shows unusual downward curvature in plots of k_{obs} vs. [added salt]. Therefore, factors such as salt effects, ionic strength effects, and changes in activity coefficients apparently do not significantly affect the reaction rate, at least for KI, LiCl, and $LiNO_3$, and the ion pair mechanism adequately describes the observed behavior.

Interaction of metal ions with ground state and transition state

The kinetic data can be dissected into ground state and transition state contributions to catalysis and inhibition to give greater insight into the roles of metal ions in the reaction. As above, involvement of metal ions is assumed to occur through ion pairing to the nucleophile, rather than the alternative preassociation mechanism, because this is the simplest explanation consistent with all of the data.

Catalysis results from greater stabilization of the transition state by the metal ion relative to stabilization of the ground state. Conversely, inhibition is due to greater stabilization of the ground state relative to the transition state. The degree of transition state stabilization can be evaluated using a method developed by Kurz (34), and applied subsequently by Wolfenden (35) and Lienhard (36).

In the present system, the reaction mechanism is described as a set of equilibria among the various reactants and transition states for catalyzed and uncatalyzed pathways (Scheme 1):

$$E + EtO^- + M^+ \underset{}{\overset{K^{\neq}}{\rightleftharpoons}} A^{\neq} + M^+ \longrightarrow \text{products}$$

$$K_a \uparrow\downarrow \qquad\qquad K_a' \uparrow\downarrow$$

$$E + EtOM \underset{}{\overset{K^{\neq\prime}}{\rightleftharpoons}} A^{\neq} M^+ \longrightarrow \text{products}$$

SCHEME 1

In this scheme, $K^{\neq}$ and $K^{\neq\prime}$ are the equilibrium constants for formation of the uncatalyzed and catalyzed transition states; K_a and K_a' are the association constants for ion pairing of M^+ with EtO^- and the transition state, respectively.

If the transition states are assumed to be in equilibrium with their respective reactants, the equilibrium constant for the association of M^+ with the transition state, K_a', can be calculated even though there is no direct equilibrium between the two transition states (34). This value is obtained from the kinetic data using eq. [14].

[14] $$K_a' = \frac{k_{MOEt} K_a}{k_{EtO^-}}$$

K_a' values for the various metal ions were calculated and are presented in Table 5. Analogous data were available for the reaction of *p*-nitrophenyl diphenylphosphinate, **2**, with alkali metal ethoxides in anhydrous ethanol at 25°C (1*d*). K_a' values for this system are also included in Table 5. These data clearly show that Li^+, an inhibitor in the reaction of **1**, has a stronger association with the ground state than the transition state. Conversely, the other metal ions, which are all catalysts, have values of K_a' greater than K_a. In the phosphinate system, all metal ions act as catalysts. It is interesting and significant to note that the trends in K_a' values are different in the two systems, and, with the exception of Cs^+, are inverted relative to each other. This observation will be discussed in the following section.

The effects of metal ions on the ground and transition states can be discussed with reference to the free energies shown in Fig. 5 (37). In this diagram, $\Delta G_u^{\neq}$ and $\Delta G_c^{\neq}$ are the free energies of activation of the uncatalyzed and catalyzed reactions, respectively. δG_{ip} and δG_{ts} refer to the free energies for association of a metal ion to ethoxide ion and the transition state, respectively. The net catalytic effect of the metal ion is given by ΔG_{cat}, the difference in free energies of activation between the catalyzed and uncatalyzed reactions. From the diagram, the following relationships can be written:

[15] $$\Delta G_u^{\neq} = G_u^{ts} - G_u^{gs}$$

[16] $$\Delta G_c^{\neq} = G_c^{ts} - G_c^{gs}$$

Can. J. Chem. Downloaded from www.nrcresearchpress.com by 91.121.58.235 on 09/07/12
For personal use only.

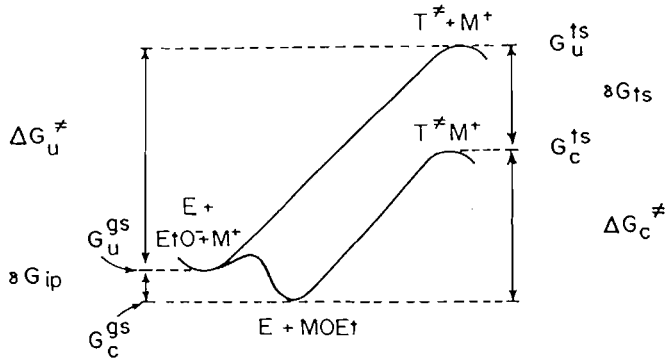

FIG. 5. Free energies involved in the uncatalyzed and metal ion catalyzed reactions of an ester, E, with an alkali metal ethoxide, MOEt. $\Delta G_u^{\neq}$ and $\Delta G_c^{\neq}$ are the activation energies for the uncatalyzed and catalyzed reactions, respectively. δG_{ip} and δG_{ts} refer to the stabilization of the ground state and transition state of the reaction by the metal ion, respectively.

TABLE 5. Association constants for the interaction of various metal ions with the transition states (K_a') and ground state (EtO^-, K_a) of the reaction of EtO^- with **1** and **2** at 25°C (K_a values from ref. 25). All values are in M^{-1}

Ion	K_a	K_a' (**1**)	K_a' (**2**)
Li^+	212	133	5188
Na^+	102	284	1207
K^+	90	430	347
Cs^+	121	409	266

$$\delta G_{ip} = G_c^{gs} - G_u^{gs} \quad [17]$$

$$\delta G_{ts} = G_c^{ts} - G_u^{ts} \quad [18]$$

$$-\delta G_{ip} + \Delta G_u^{\neq} = \Delta G_c^{\neq} - \delta G_{ts} \quad [19]$$

$$\Delta G_{cat} = \Delta G_c^{\neq} - \Delta G_u^{\neq} = \delta G_{ts} - \delta G_{ip} \quad [20]$$

The previously calculated association constants are presented as free energies of association in Table 6. Comparing δG_{ts} and δG_{ip} values helps explain the variation in catalytic efficiency among metal ions. Thus, δG_{ts} measures the stabilization of the transition state by the metal ion (which is its maximum catalytic potential), while δG_{ip} measures the stabilization of the nucleophile by the metal ion (which detracts from its catalytic effect) (37). ΔG_{cat} is the difference between δG_{ts} and δG_{ip} and is a measure of the net catalytic effect of the metal ion. A positive value of ΔG_{cat} implies that the transition state stabilization is a smaller negative number than the ground state stabilization and the net effect of the metal ion is to act as an *inhibitor*. A negative value of ΔG_{cat} means that the metal ion is acting as a *catalyst*.

Thus, it is seen from the data that Li^+ associates more strongly with the ground state than with the transition state, so the net effect is inhibition of the reaction ($\Delta G_{cat} > 0$). The other metal ions all stabilize the transition state to a greater extent than the ground state, and act as catalysts ($\Delta G_{cat} < 0$). Since K^+ has the strongest association with the transition state and the weakest association with the ground state, it is the best catalyst and has the largest negative value of ΔG_{cat}.

Given this quantitative description of catalysis and inhibition, some chemical insight into how and why metal ions bind the ground state and transition state more or less strongly is required. In particular, an explanation of how metal ions could bind to the transition state more strongly than to ethoxide ion, which has a more localized negative charge, is needed. Structure **3** depicts a *proposed* structure for the transition state for the attack of ethoxide on the sulfonate ester, which resembles the intermediate in the addition–elimination mechanism. The negative charge is therefore expected to reside predominantly on the sulfonyl oxygens, with only a small charge on the ethoxide oxygen.

TABLE 6. Free energies of metal ion stabilization of ethoxide (δG_{ip}) and the transition states (δG_{ts}) for the reaction of ethoxide with **1** at 25°C. The net catalytic effect of the metal ion (ΔG_{cat}) is also given. All values are in kJ mol^{-1}

Ion	δG_{ip}	δG_{ts}	ΔG_{cat}
Li^+	−13.3	−12.1	+1.2
Na^+	−11.5	−14.0	−2.5
K^+	−11.2	−15.0	−3.8
Cs^+	−11.9	−14.9	−3.0

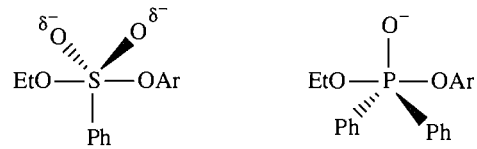

3 **5**

Chelation of the metal ion to two or three negatively charged oxygens, as shown in structures ***4a*** and ***4b***, may result in the transition state binding the metal ion more strongly than ethoxide. Chelation, therefore, would allow the sulfonate transition state to bind metal ions more strongly than ethoxide ion.

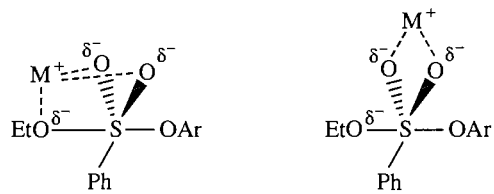

4a ***4b***

Interactions of metal ions in the phosphinate system will be considered subsequently.

Trends in the degree of transition state stabilization by metal ions

Data on the interactions of metal ions with the phosphinate and sulfonate transition states can now be compared. Table 7 summarizes the degree of stabilization of the sulfonate and phosphinate transition states by various metal ions. In the case of the phosphinate transition state, the ordering of δG_{ts} values is $Li^+ < Na^+ < K^+ < Cs^+$. For the sulfonate transition state, the order is $K^+ < Cs^+ < Na^+ < Li^+$. The two sets of reactions were carried out under identical conditions and the two esters are believed to react by similar mechanisms. However, the way in which the metal ion interacts with the transition state is apparently not the same in both cases. It is expected that the explanation underlying these differing results arises from

Can. J. Chem. Downloaded from www.nrcresearchpress.com by 91.121.58.235 on 09/07/12
For personal use only.

Can. J. Chem. Downloaded from www.nrcresearchpress.com by 91.121.58.235 on 09/07/12
For personal use only.

TABLE 7. Free energies of metal ion stabilization of ethoxide (δG_{ip}) and of the transition states for the reaction of ethoxide with **1** (δG_{ts} (**1**)) and **2** (δG_{ts} (**2**)) at 25°C (kJ mol^{-1})

Ion	δG_{ip}	δG_{ts} (**1**)	δG_{ts} (**2**)
Li^+	−13.3	−12.1	−21.2
Na^+	−11.5	−14.0	−17.6
K^+	−11.2	−15.0	−14.5
Cs^+	−11.9	−14.9	−13.8

differences in the geometric and electronic structures of the two transition states.

One obvious difference between the two transition states is that they do not contain the same number of potential ligand oxygens. Assuming that both transition states are intermediate-like, the sulfonate transition state contains two ligand oxygens with a significant negative charge (structure **3**), while the phosphinate has only one (structure **5**). With a single oxygen, simple cation–anion electrostatic interactions are expected to result in stronger association for smaller cations for the phosphinate transition state, as observed.

In the sulfonate transition state, the situation is more complex. Attractive interactions with two negatively charged oxygens as well as repulsive interactions with a positively charged sulfur center are possible. If the oxygens are far enough apart, chelation of a small metal ion to the sulfonyl oxygens may be possible, but this would be counterbalanced in part by repulsive interactions with the sulfur center. Larger cations would be further from the sulfur, but would be less effective at chelating the sulfonyl oxygens. The optimum balance between attractive forces to the negatively charged oxygens and repulsive forces from the positively charged sulfur may be achieved by metal ions of intermediate size, accounting for the observed size selectivity of the sulfonate transition state.

As a test of the above hypothesis, electrostatic metal ion – transition state interactions were modeled in a preliminary manner using MNDO calculations. The limitations of the application of semiempirical calculations to compounds containing SO and SO_2 groups have been noted for MNDO (38). However, these drawbacks can be reduced by fixing the geometry of the sulfonate and by considering relative energies only.

A model for the pentacoordinate intermediate resulting from the attack of methoxide on methyl methanesulfonate was constructed (structure **6**). Bond lengths and angles about the sulfur center from the crystal structure of pentacoordinate sulfur compound (39) were used to define a reasonable starting geometry for the intermediate, whose structure was then optimized using MNDO, giving a structure with partial negative charges on oxygens and a substantial positive charge on the sulfur center (as expected).

The optimized geometry of the intermediate was then fixed and the energies of complexes with alkali metal ions (Li^+-, Na^+-, and K^+-like sparkles in MNDO) were minimized. The resulting complexes had similar geometries, with the metal ion interacting with the equatorial sulfonyl oxygens, but with one sulfonyl oxygen to a greater extent than with the other, as shown in **6**. The sparkles in MNDO do not have an intrinsic heat of formation, so the heats of formation of the complexes give the heat of association. These fell in the order $Li^+ < Na^+ < K^+$, i.e., Li^+ gave the largest heat of association, which is opposite to the observed ordering in the experimental data for **1**.

Therefore, calculations on the interaction of the modelled intermediate with metal-ion-like "sparkles" suggested that a simple electrostatic model involving interactions of the metal ion, negatively charged oxygens, and a positively charged sulfur probably does not account for the observed ordering in the association constants for the various metal ions.

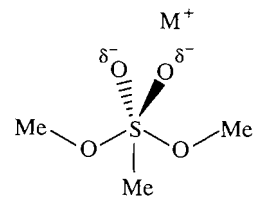

6

Another difference between the two transition states is the extent of charge delocalization. In the phosphinate transition state (**5**), the charge is localized mainly on the phosphoryl oxygen. There is evidence to suggest that the P=O bond is highly polarized, resembling $P^+—O^-$, even in the ground state (40). This means that a relatively strong interaction with metal ions is possible since the negative charge is highly localized. In a solvent of moderate polarity, such as ethanol, the stabilizing effect of solvent on metal ions, i.e., solvation, is reduced in comparison to solvation in water, so it is reasonable to suppose that the energy of the electrostatic interaction of M^+ with the transition state ($M^+ + ts^- \rightarrow M^+ts^-$) could be greater than the energy of solvation of the metal ion ($M^+ + n.\text{solvent} \rightarrow M(\text{solvent})_n^+$) in certain instances. This being the case, contact ion pairing between the transition state and the metal ion would be the result. Here, association would involve the interaction of the transition state with bare metal ions, which increase in size in the order $Li^+ < Na^+ < K^+ < Cs^+$ (41). Since the smaller cations should interact more strongly with the anionic transition state, this would lead to δG_{ts} values increasing in the order $Li^+ < Na^+ < K^+ < Cs^+$, which is identical to the observed ordering for reactions with **2** (Table 7). Furthermore, contact ion pairing is known to cause spectral shifts that show a correlation with the reciprocal of the cation crystal radius (42, 43). This is because the metal ion affects the energy levels of its counterion in inverse relation to its electrostatic potential. We observe that the stabilization of the phosphinate transition state by metal ions (δG_{ts}) does in fact increase with the reciprocal of the cation crystal radius (r_c). Thus, a plot of δG_{ts} versus $1/r_c$ is linear and has a negative slope (Fig. 6), as expected for contact ion pairs.

In contrast, the sulfonate transition state, which has its charge delocalized over two (or more) oxygens, is expected to have weaker interactions with metal ions and may not be able to displace a solvent molecule from the coordinate sphere of the metal ion. Hence, the transition state would interact with solvated metal ions. The magnitudes of solvated radii now follow a trend opposite to crystal radii ($Cs^+ > K^+ > Na^+ > Li^+$) because the metal ions with smaller crystal radii, having a greater electrostatic potential, attract more solvent molecules. Values of crystal and solvated radii are listed in Table 8. The solvated radii of the alkali metal ions in ethanol were calculated using the Stokes equation from the data of Kay and Evans (44). Since it is known that the Stokes equation underestimates the solvated radii of ions, the values were corrected by the method of Della Monica and Senatore (45) using data from ref. 46. These calculations are described in the Supplementary Material.[3]

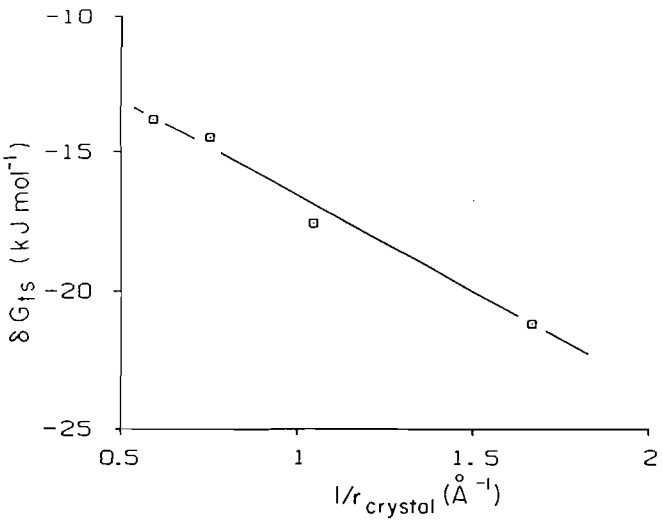

FIG. 6. Plot of δG_{ts} versus the reciprocal of the crystal radius of the metal ion for the reaction of *p*-nitrophenyl diphenylphosphinate with alkali metal ethoxides in EtOH at 25°C ($r = -0.9920$).

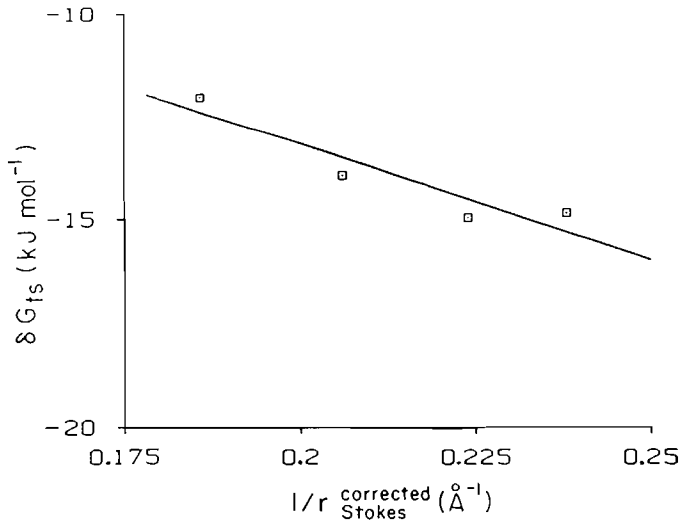

FIG. 7. Plot of δG_{ts} versus the reciprocal of the corrected Stokes radius of the metal ion for the reaction of *p*-nitrophenyl benzenesulfonate with alkali metal ethoxides in EtOH at 25°C ($r = -0.9334$).

TABLE 8. Crystal radii, Stokes radii, and corrected Stokes radii for alkali metal ions in ethanol (in Å). See text for details on calculation of Stokes and corrected Stokes radii

Radius	Li^+	Na^+	K^+	Cs^+
Cation crystal radius (Pauling)	0.60	0.95	1.33	1.69
Stokes radius	4.43	3.73	3.21	2.86
Corrected Stokes radius	5.39	4.86	4.47	4.20

Association with solvated metal ions would result in δG_{ts} values increasing in the order $Cs^+ < K^+ < Na^+ < Li^+$, which is similar to the observed order, $K^+ \leq Cs^+ < Na^+ < Li^+$ for **1** (Table 7). In this situation, one might still expect a relationship between the free energy of association and the size of the metal ion, but now the size of the ion is given by its solvated or Stokes radius. A plot of δG_{ts} versus the reciprocal of the corrected Stokes radius gives a linear relationship that shows that the free energy of association increases with the electrostatic potential of the metal ion, as given by its solvated radius (Fig. 7). However, the plot is not as linear as in the case of the phosphinate transition state. One of the reasons for this may be that the solvated ions are probably not exactly spherical, so the corrected Stokes radii are only an approximate measure of their sizes. Furthermore, it is worth noting that the δG_{ts} values in the sulfonate system are, in general, smaller than in the phosphinate system. This is consistent with the present explanation because the solvated radii are all much greater than the crystal radii of the ions. The larger ions have a lesser electrostatic potential, which results in lower association constants.

Parallel arguments have been advanced by Eisenman to explain selectivity among alkali metal ions by ion exchange resins (47). As above, two types of interaction were considered: (a) electrostatic interaction between the anionic group and its alkali metal counterion, and (b) rearrangement of solvent molecules to permit the anion and counterion to come into direct contact. The anion and solvent are said to compete for the metal ion (48). Anionic groups with high electric strengths win the contest and attract cations away from solvent. The smallest cations are attracted most strongly, so the affinity sequence is $Li^+ > Na^+ > K^+ > Cs^+$. This ordering is found in practice for carboxylate ion exchange resins and is consistent with the small size and high field strength of the carboxylate group (47). This ordering is also seen in δG_{ts} values for the phosphinate transition state, indicating a high electric field strength.

Conversely, anionic groups with low electric field strengths lose the contest with solvent for association with the metal ion. The cations remain solvated, leaving the ions with the smaller solvated radii to be bound most strongly (48). The affinity sequence in this case is $Cs^+ > K^+ > Na^+ > Li^+$. The sulfonate group is believed to have a low field strength and, in fact, many different types of ion exchange resins containing sulfonate groups have displayed the affinity sequence described above (47).

From the above arguments, it is clear that, as the field strength of the anion is increased, the affinity sequence must change from $Cs^+ > K^+ > Na^+ > Li^+$ (the order of solvated radii) to $Li^+ > Na^+ > K^+ > Cs^+$ (the order of crystal radii) with a number of different sequences as intermediates. Eisenman's theory predicts that the first change will be from $Cs^+ > K^+ > Na^+ > Li^+$ to $K^+ > Cs^+ > Na^+ > Li^+$ (47). Thus, the observed ordering of δG_{ts} values for the sulfonate transition state is quite consistent with an anion with low to intermediate field strength as the transition state.

The discussion presented here can be summarized in a scheme which is an extension of the Kurz approach and is reminiscent of solvolysis schemes involving different types of ion pairs (Fig. 8) (49). In the ground state, free ions, solvent separated ion pairs, and contact ion pairs are all in equilibrium. It is not known whether alkali metal ethoxides prefer to form contact or solvent separated ion pairs. However, each species has the potential to react with the substrate to form a transition state, which may not be associated with metal ions, or, alternatively, which may form a contact or solvent separated ion pair with a metal ion, as in the ground state. Because it is possible for solvent reorganization to occur along the reaction coordinate (50), a contact ion paired ethoxide, for example, need not react with substrate to form a contact ion paired transition state. In this scheme, solvent separated ion pairs

Can. J. Chem. Downloaded from www.nrcresearchpress.com by 91.121.58.235 on 09/07/12
For personal use only.

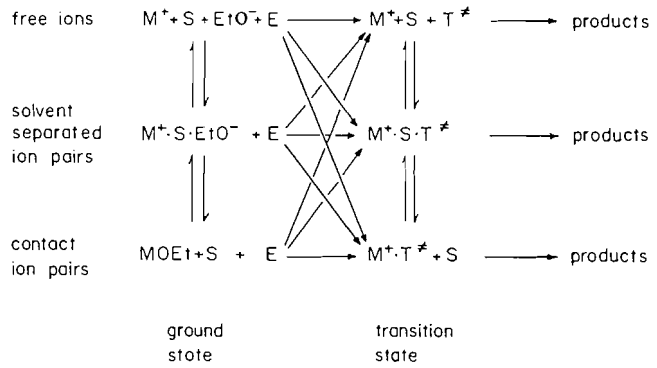

FIG. 8. Scheme showing equilibria between free ions, solvent-separated ion pairs, and contact ion pairs in the ground state and transition state for the reaction of alkali metal ethoxides with an ester, E. $T^{\neq}$ represents the transition state formed by reaction of ethoxide ion with the ester.

would be favoured for the sulfonate transition state, while contact ion pairs would be favored for the phosphinate transition state.

The above discussion has omitted consideration of differences in solvation of the two transition states in the absence of metal ions. The phosphinate transition state, with a greater charge density on oxygen, is expected to benefit more from solvation than the sulfonate transition state. Thus, stronger solvation of the transition state might be expected to result in a greater tendency to form solvent separated ion pairs with metal ions for the phosphinate, in opposition to the predictions above. However, since the experimental results show that the phosphinate transition state prefers to form contact ion pairs with alkali metal ions, it follows that electrostatic interactions of metal ions with these transition states are stronger than solvation effects.

Therefore, the trends in δG_{ts} values can be rationalized by considering differences in solvation of ion pairs of the transition states of the two systems studied. An alternative explanation based on a simple electrostatic model appears less likely. Consequently, it is concluded that the effects of alkali metal ions on nucleophilic displacement reactions are determined in part by the extent of charge delocalization in the transition state for the reaction. It is proposed that the transition state for reaction of alkali metal ethoxides with *p*-nitrophenyl benzenesulfonate exists as a species analogous to a solvent separated ion pair. On the other hand, the transition state for the reaction of *p*-nitrophenyl diphenylphosphinate forms a species that may be described as a contact ion pair with alkali metal ions. The difference in behavior between the two systems is consistent with a greater delocalization of charge in the sulfonate transition state.

To investigate the influence of the degree of charge delocalization on the association of the transition state with metal ions, further work is in progress on metal ion effects in related systems, including other esters containing phosphoryl and carbonyl centers. The results of these studies as well as investigations of the mechanisms of these reactions will be presented in subsequent papers.

Conclusions

These studies have allowed significant insight into the role of alkali metal ions in nuleophilic displacement reactions of sulfonate and phosphinate esters (**1** and **2**, respectively). Some of the main conclusions that we have reached are as follows:

1. In the reaction of **1**, certain metal ions, e.g., K^+, act as *catalysts*, i.e., the rate increases when they are added as inert salts and decreases when they are removed by complexing agents. One metal ion studied, Li^+, acts as an *inhibitor*, i.e., the rate decreases when it is added and increases when it is complexed.

2. Metal ions are assumed to be involved in the reaction of **1** via reactive alkali metal – ethoxide ion pairs. Metal–ethoxide ion pairs are known to be present in ethanol solutions of alkali metal ethoxides and assumption of the alternative mechanism involving preassociation of metal ions to the ester led to unrealistically large rate constants for reaction of the putative ester – metal ion complexes.

3. The catalytic or inhibitory effects of metal ions have been discussed in terms of ground state (δG_{ip}) and transition state (δG_{ts}) stabilizations. The overall catalytic effect (ΔG_{cat}) has also been calculated for each metal ion. ΔG_{cat} values quantitate the catalytic or inhibitory effects. The values are -3.8, -3.0, -2.5, and $+1.2$ kJ mol^{-1} for K^+, Cs^+, Na^+, and Li^+, respectively, indicating that K^+ is the best catalyst, Cs^+ and Na^+ are less effective catalysts, and that Li^+ is an inhibitor of the reaction of **1**.

4. Trends in δG_{ts} values for systems **1** and **2** were compared and the results rationalized in terms of the extent of charge delocalization in the two transition states and the role of metal ion solvation. It is concluded that the negative charge in the sulfonate transition state is significantly delocalized and that consequently solvent separated ion pairs are formed with alkali metal ions. The phosphinate transition state, with a more localized negative charge, forms contact ion pairs. These conclusions are supported by the linear relationships between δG_{ts} and $1/r_{Stokes}^{corrected}$ and $1/r_{crystal}$ in the case of reactions of **1** and **2**, respectively.

5. The balance in equilibrium between contact and solvent separated ion pairs is governed by two competing effects. The cation and anion can be stabilized by organization of solvent molecules around themselves (solvation) and by electrostatic interaction with each other. When the energy gained by solvation is greater than the energy of cation–anion electrostatic interaction, solvent separated ion pairs are favored (sulfonate transition state). When the reverse is true, contact ion pairs are favored (phosphinate transition state).

Experimental

Materials

Anhydrous ethanol was obtained by refluxing absolute ethanol (2 L) with magnesium turnings (10 g, BDH) and iodine (1 g, BDH) followed by fractional distillation (51).

18-Crown-6 (Parish and Aldrich) was recrystallized from acetonitrile, then dried over P_2O_5 under vacuum (<1 Torr (133.3 Pa)) before use. 2.2.2 Cryptand (Fluka) was recrystallized from hexanes, then dried over P_2O_5 under vacuum; 2.2.2 and 2.1.1 cryptands (E. Merck) were used without further purification; 2.2.2 was dried over P_2O_5 *in vacuo*.

Sodium tetraphenylborate (Aldrich, Gold label) was dried at 76°C under vacuum before use. Anhydrous lithium chloride (Aldrich, Gold label) was used as received. Lithium nitrate (Merck, Suprapur) and potassium iodide (BDH, Analar) were dried under vacuum with P_2O_5 before use.

Sodium, potassium, and cesium ethoxides were prepared as follows. Dry ethanol (200 mL) was collected in a round-bottom flask equipped

Can. J. Chem. Downloaded from www.nrcresearchpress.com by 91.121.58.235 on 09/07/12
For personal use only.

with a nitrogen inlet and magnetic stirrer. The solvent was cooled under nitrogen using an ice-water bath. The alkali metal (0.2 mol of Na (BDH Assured ACS), K (BDH or Alfa 99.95%), or Cs (Alfa, 99.95%)) was cut under petroleum ether and added in small portions to the stirred, cooled ethanol under nitrogen. Liquid Cs was added to ethanol that had been cooled in a Dry Ice – isopropanol bath and the solution allowed to warm slowly. When the reaction was complete, the flask was stoppered, sealed, and stored in a freezer.

Lithium ethoxide was prepared by adding lithium hydride (Aldrich, 95% or Alfa, 98%) to dry ethanol. The powder was added gradually from a glass bulb to a stirred, ice-cooled ethanol solution under nitrogen. In some cases, all of the LiH did not react and the excess was filtered off in a Vacuum Atmospheres Co. dry box. The LiOEt solution was sealed and stored in a freezer. Ethoxide solutions were standardized against 0.1 M HCl, which was in turn standardized against trishydroxymethylaminomethane (THAM, Fisher primary standard) (52).

p-Nitrophenyl benzenesulfonate was prepared following the procedure of Davy *et al.* (53).

Kinetic measurements

Reaction rates were measured by following ultraviolet–visible absorbance changes using Beckman DU-8 and Perkin–Elmer λ-5 spectrophotometers. All reactions were carried out under pseudo-first-order conditions with the base concentration usually at least 20 times greater than the substrate concentration. UV cells were equilibrated to 25.0°C in the thermostatted cell block of the spectrophotometer.

Rate constants were measured by following the appearance of the product continuously at fixed wavelength. Absorbance readings were made at the λ_{max} of the product, *p*-nitrophenoxide (400 nm).

Rate constants were calculated from at least 30 absorbance readings spanning three half-lives. An infinity absorbance reading was taken after at least 10 half-lives. Rate constants were calculated as the slope of a plot of $\ln(A_\infty - A_t)$ vs. time. It is estimated that the measured rate constants have errors of no more than ±3% (95% confidence interval).

Acknowledgements

This research was supported by the Natural Sciences and Engineering Research Council of Canada (NSERC). The awards to M.J.P. of a Postgraduate Scholarship by NSERC and a Graduate Award by Queen's University are gratefully acknowledged, as are discussions with Professors S. Hoz and R. Y. Moir.

1. (*a*) E. Buncel, H. Wilson, and C. Chuaqui. J. Am. Chem. Soc. **104**, 4896 (1982); (*b*) E. Buncel, C. Chuaqui, and H. Wilson. J. Org. Chem. **45**, 2825 (1980); (*c*) E. Buncel, E. J. Dunn, R. A. B. Bannard, and J. G. Purdon. Chem. Commun. 162 (1984); (*d*) E. J. Dunn and E. Buncel. Can. J. Chem. **67**, 1440 (1989); (*e*) E. J. Dunn, R. Y. Moir, E. Buncel, J. G. Purdon, and R. A. B. Bannard. Can. J. Chem. **68**, 1837 (1990).
2. C. H. Suelter. *In* Metal ions in biological systems. Vol. 3. *Edited by* H. Sigel. Marcel Dekker, New York. 1976. Chapt. 7.
3. R. V. Vizgert. J. Gen. Chem. USSR, **28**, 1917 (1958).
4. P. Krishnan, S. Sundaram, and N. Venkatasubramanian. Ind. J. Chem. **20B**, 731 (1981).
5. J. L. Kice, C. Walters, and S. Burton. J. Org. Chem. **39**, 346 (1974).
6. R. V. Vizgert. Russ. Chem. Rev. **32**, 1 (1963).
7. M. Szwarc. *In* Ions and ion pairs in organic reactions. Vol. 1. *Edited by* M. Szwarc. Wiley Interscience, New York. 1972. Chap. 1.
8. (*a*) B. C. Menon, H. F. Shurvell, J. P. Colpa, and E. Buncel. J. Mol. Struct. **78**, 29 (1982); (*b*) E. Buncel and B. C. Menon. J. Org. Chem. **44**, 317 (1979); (*c*) E. Buncel, B. C. Menon, and J. P. Colpa. Can. J. Chem. **57**, 999 (1979).
9. P. Cayzergues, C. Georgoulis, and G. Mathieu. J. Chim. Phys. **84**, 55 (1987).
10. A. Papoutsis, G. Papanastasiou, D. Jannakoudakis, and C. Georgoulis. J. Chim. Phys. **82**, 913 (1985).
11. J. Barthel, G. Bader, and M. Raach-Lenz. Z. Phys. Chem. **103**, 135 (1976).
12. (*a*) E. Buncel and H. Wilson. J. Chem. Educ. **9**, 629 (1980); (*b*) Acc. Chem. Res. **12**, 42 (1979).
13. J.-M. Lehn. Acc. Chem. Res. **11**, 49 (1978).
14. A. Knipe. J. Chem. Educ. **53**, 618 (1976).
15. J.-M. Lehn. Pure Appl. Chem. **52**, 2303 (1980).
16. T. Deacon, C. R. Farrar, B. J. Sikkel, and A. Williams. J. Am. Chem. Soc. **100**, 2525 (1978).
17. V. Pechanec, O. Kocian, and J. Zavada. Collect. Czech. Chem. Commun. **47**, 3405 (1982).
18. L. Pataki and P. Beronius. Radiochem. Radioanal. Lett. **31**, 303 (1977).
19. G. Ercolani and L. Mandolini. J. Am. Chem. Soc. **112**, 423 (1990).
20. A. Loupy, G. Meyer, and B. Tchoubar. Tetrahedron, **34**, 1333 (1978).
21. A. Mildvan and C. Grisham. *In* Structure and bonding. Vol. 20. *Edited by* J. D. Dunitz, P. Hemmerich, R. H. Holm, J. A. Ibers, C. K. Jorgensen, J. B. Nielands, D. Reiner, and R. J. P Williams. Springer Verlag, New York. 1974.
22. B. Cooperman. *In* Metal ions in biological systems. Vol. 5. *Edited by* H. Sigel. Marcel Dekker, New York. 1974.
23. R. Moravie, J. Corset, M. Josien, G. Nee, G. Levy, and B. Tchoubar. Tetrahedron, **32**, 693 (1976).
24. J. Gordon. The organic chemistry of electrolyte solutions. Wiley and Sons, New York. 1975.
25. J. Barthel, J. Justice, and R. Wachter. Z. Phys. Chem. N. F. **84**, 100 (1973).
26. M. H. Abraham, A. Danil de Namor, W. Lee, and R. Wheaton. Acta Chem. Scand. **A34**, 621 (1980).
27. J. Smid, A. Varma, and S. Shah. J. Am. Chem. Soc. **101**, 5764 (1979).
28. (*a*) J. Smid. Pure and Appl. Chem. **48**, 343 (1976); (*b*) C. Cambillau, G. Bram, J. Corset, C. Riche, and C. Paschard-Billy. Tetrahedron, **34**, 6765 (1978); (*c*) C. Chen, W. Wallace, E. Eyring, and S. petrucci. J. Phys. Chem. **88**, 5445 (1984).
29. C. Cambillau, G. Bram, J. Corset, and C. Riche. Can. J. Chem. **60**, 2554 (1982).
30. P. Beronius and L. Pataki. Acta Chem. Scand. **A33**, 675 (1979).
31. S. Schiavo and G. Marrosu. Z. Phys. Chemie N. F. **105**, 157 (1977).
32. G. Parfitt and A. Smith. Trans. Faraday Soc. **59**, 257 (1963).
33. R. L. Kay. J. Am. Chem. Soc. **82**, 2099 (1960).
34. J. L. Kurz. J. Am. Chem. Soc. **85**, 987 (1963).
35. R. Wolfenden. Acc. Chem. Res. **5**, 10 (1972).
36. G. Lienhard. Science, **180**, 149 (1973).
37. R. L. Schowen. *In* Transition states of biochemical processes. *Edited by* R. D. Gandour and R. L. Schowen. Plenum, New York and London. 1978.
38. T. Clark. A handbook of computational chemistry. John Wiley and Sons, New York. 1985.
39. R. A. Hayes and J. C. Martin. Stud. Org. Chem. **19**, 408 (1985).
40. A. Streitweiser, Jr., A. Rajca, R. S. McDowell, and R. Glaser. J. Am. Chem. Soc. **109**, 4184 (1987); **109**, 4189 (1987).
41. F. A. Cotton and G. Wilkinson. Advanced inorganic chemistry. Wiley and Sons, New York. 1980.
42. J. Smid. Angew. Chemie Int. Ed. Engl. **11**, 112 (1972).
43. E. M. Arnett and V. DePalma. J. Am. Chem. Soc. **98**, 7447 (1976).
44. R. L. Kay and D. J. Evans. J.Phys. Chem. **70**, 2325 (1966).
45. M. Della Monica and L. Senatore. J. Phys. Chem. **74**, 205 (1970).

Can. J. Chem. Downloaded from www.nrcresearchpress.com by 91.121.58.235 on 09/07/12
For personal use only.

46. (*a*) D. F. EVANS, C. ZAWOJSKI, and R. L. KAY. J. Phys. Chem. **69**, 3878 (1965); (*b*) D. ARRINGTON and E. J. GRISWOLD. J. Phys. Chem. **74**, 123 (1970).
47. G. EISENMAN. Biophys. J. Suppl. **2**, 259 (1962).
48(*a*). D. Reichenberg. *In* Ion exchange. Vol. 1. *Edited by* J. A. Marinsky. Marcel Dekker, New York. 1966. Chap. 7; (*b*) W. RIEMAN and H. F. WALTON. *In* Ion exchange in analytical chemistry. Pergamon Press, Oxford. 1970.
49. D. J. RABER, J. M. HARRIS, and P. v. R. SCHLEYER. *In* Ions and ion pairs in organic reactions. Vol. 2., *Edited by* M. Szwarc. Wiley and Sons, New York. 1974. Chap. 3.
50. C. F. BERNASCONI. Acc. Chem. Res. **20**, 301 (1987).
51. A. I. VOGEL. *In* Practical organic chemistry. 5th ed. Longman and Green, London. 1989.
52. R. BELCHER and C. WILSON. New methods of analytical chemistry. Chapman and Hall, London. 1964.
53. M. B. DAVY, K. T. DOUGLAS, J. S. LORAN, A. STELTNER, and A. WILLIAMS. J. Am. Chem. Soc. **99**, 1196 (1977).

Can. J. Chem. Downloaded from www.nrcresearchpress.com by 91.121.58.235 on 09/07/12
For personal use only.

The base-catalysed anomerization of dinitrophenyl glycosides: evidence for a novel reaction mechanism

LEISE A. BERVEN, DAVID DOLPHIN, AND STEPHEN G. WITHERS[1]

Department of Chemistry, University of British Columbia, Vancouver, B.C., Canada V6T 1Y6

Received April 17, 1990

This paper is dedicated to Professor Ross Stewart on the occasion of his 65th birthday

LEISE A. BERVEN, DAVID DOLPHIN, and STEPHEN G. WITHERS. Can. J. Chem. **68**, 1859 (1990).

The mechanism of base-catalysed anomerization of per-*O*-acetylated 2,4-dinitrophenyl-β-D-glucopyranoside in dimethylsulfoxide has been investigated using a variety of techniques. A mechanism involving proton abstraction at C-1 was eliminated by the absence of proton exchange at that center and the measurement of a secondary deuterium kinetic isotope effect for the 1-deuterio substrate. A mechanism involving phenolate departure and recombination is rendered unlikely on the basis of remote substituent effects on the reaction rate and by the absence of any exchange of the phenyl moiety with added phenolate. A mechanism involving nucleophilic aromatic substitution initiated by an attack of the dimethylsulfinyl anion to generate a glucosyl oxyanion intermediate that anomerizes and recombines with the reactive aryl intermediate is consistent with the observations. This mechanism is further supported by the observation of a purple Meisenheimer complex intermediate and by the observed exchange between the substrate containing a labelled sugar moiety and added unlabelled 2,3,4,6-tetra-*O*-acetyl-β-D-glucopyranose.

Key words: glycoside, anomerization, reaction mechanism.

LEISE A. BERVEN, DAVID DOLPHIN et STEPHEN G. WITHERS. Can. J. Chem. **68**, 1859 (1990).

Faisant appel à diverses techniques, on a examiné le mécanisme de l'anomérisation catalysée par les bases du β-D-glucopyranoside de 2,4-dinitrophényle per-*O*-acétylé en solution dans le diméthylsulfoxyde. En se basant sur le fait qu'il n'y a pas d'échange de proton dans cette position et sur la mesure d'un effet isotopique cinétique secondaire du deutérium pour le substrat 1-deutéré on a éliminé un mécanisme impliquant l'enlèvement d'un proton de la position C-1. En se basant sur l'existence d'effets des substituants éloignés sur la vitesse de la réaction et sur l'absence de tout échange de la portion phénylée lorsqu'on ajoute des ions phénolates, on peut déduire qu'un mécanisme impliquant un départ et une recombinaison du phénolate est improbable. Un mécanisme impliquant une substitution aromatique nucléophile, initiée par une attaque de l'anion diméthylsulfinyle pour générer l'intermédiaire oxyanion glucosyle qui s'anomérise et se recombine avec l'intermédiaire aryle réactif, est en accord avec les données expérimentales. Ce mécanisme est aussi supporté par l'observation d'un complexe intermédiaire de Meisenheimer violet et par l'observation d'un échange entre le substrat contenant une portion sucrée marquée et du 2,3,4,6-tétra-*O*-acétyl-β-D-glucopyranose qui n'est pas marqué.

Mots clés : glycoside, anomérisation, mécanisme de réaction.

[Traduit par la revue]

Introduction

There are many examples of acid-catalysed glycoside anomerization and their mechanisms are reasonably well understood (1–7). In all cases studied to date, including simple alkyl glycosides (1–3), protected alkyl glycosides (4), or fully acetylated sugars (5–7), the mechanism has involved oxocarbonium ion intermediates, whether catalysed by a Lewis or a Brønsted acid. Usually, reaction proceeds via cleavage of the exocyclic carbon–oxygen bond, though in some cases it is suggested that the preferred mode involves endocyclic bond cleavage. Base-catalysed reactions involving the glycosidic linkage are less common and, consequently, little is known about the mechanisms of such reactions. The anomerization of 1,2,3,4,6-penta-*O*-acetyl-β-D-glucopyranose and 2′,4′-dinitrophenyl 2,3,4,6-tetra-*O*-acetyl-β-D-glucopyranoside (β-2,4-DNPG)[2] has been reported using sodium hydroxide in anhydrous pyridine (8). Although yields were low, this reaction was one of the first methods used to transform a β- to the α-phenyl glycoside. Interestingly, anomerization of the β-glucosides of phenol, 2-nitrophenol, and 4-nitrophenol were unsuccessful. More recent studies (9) have shown that treatment of β-2,4-DNPG with potassium carbonate in dimethylsulfoxide (DMSO) afforded an equilibrium mixture of the α and β anomers (80:20, respectively) in good yield. Reaction of 2′,4′-dinitrophenyl 2,3,4,6-tetra-*O*-benzyl-β-D-glucopyranoside, however, was found to proceed approximately 70 times more slowly than the acetylated glycoside, leading to the suggestion that the acetyl group at C-2 may participate in the reaction.

Very little is known concerning the mechanism of this base-catalysed anomerization. The only published suggestion for a mechanism is that (10) involving initial abstraction of the proton from the anomeric centre, generating a glycoside anion that can then reprotonate from either side. However, there has been no published evidence in support of this, or any other mechanism. We have considered four possible mechanisms for the carbonate catalysed anomerization of 2′,4′-dinitrophenyl 2,3,4,6-tetra-*O*-acetyl-β-D-glucopyranoside (Scheme 1). The first (i) involves proton abstraction at C-1 as suggested by Ferrier (10), forming a carbanion intermediate that can reprotonate from either face. The second (ii) is initiated by phenolate departure, forming an oxocarbonium ion intermediate with possible neighboring group assistance of the C-2 acetoxy group. The phenolate and oxocarbonium ions then recombine to give α or β product. The third mechanism (iii) also involves phenolate departure, but is in this case an elimination reaction initiated by proton abstraction from C-2 with formation of an acetoxyglucal intermediate that subsequently recombines with phenolate. The

[1]Author to whom correspondence may be addressed.

[2]Abbreviations: α-2,4-DNPG = 2′,4′-dinitrophenyl 2,3,4,6-tetra-*O*-acetyl-α-D-glucopyranoside; β-2,4-DNPG = 2′,4′-dinitrophenyl 2,3,4,6-tetra-*O*-acetyl-β-D-glucopyranoside; β-2,6-DNPG = 2′,6′-dinitrophenyl 2,3,4,6-tetra-*O*-acetyl-β-D-glucopyranoside; DMSO = dimethylsulfoxide.

Can. J. Chem. Downloaded from www.nrcresearchpress.com by 91.121.58.235 on 09/07/12
For personal use only.

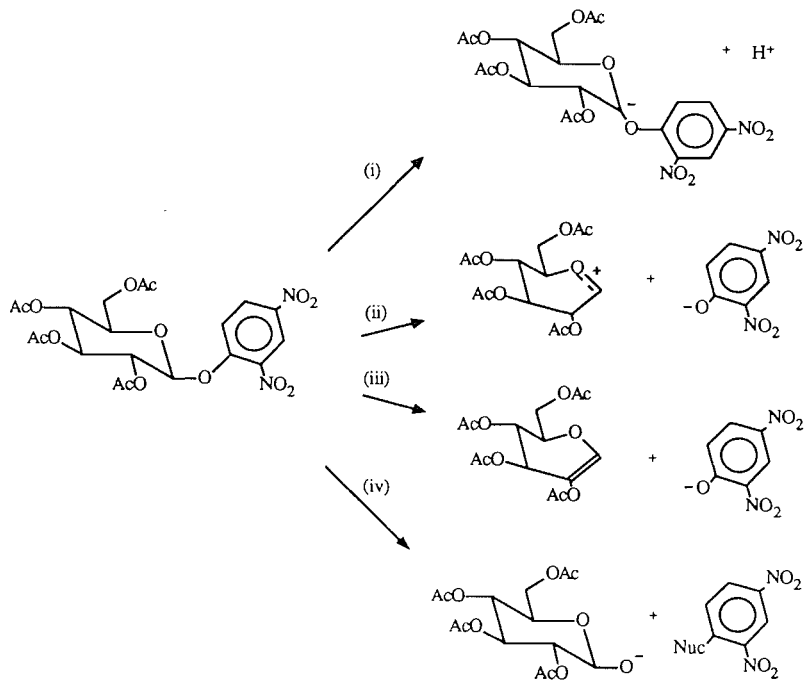

SCHEME 1

fourth mechanism (iv) involves an initial nucleophilic substitution reaction at C-1′ of the aromatic ring by an added, or generated, nucleophile (most likely dimethylsulfinyl anion in the present work), displacing a glycosyl oxyanion and forming an activated aromatic intermediate. This glycosyl oxyanion then anomerizes by the usual mechanism (1, 2) under the basic conditions and subsequently recombines with the reactive aromatic species (see also Scheme 2 for mechanism (iv)). Each of these mechanisms has some attractive and unattractive features. Mechanism (i) is certainly consistent with the basic conditions of the reaction, but involves a most unusual deprotonation of the anomeric carbon. However, this would be consistent with the earlier observations (8) that only glycosides of extremely electron-deficient phenols undergo the anomerization. Mechanism (ii) is consistent with known carbohydrate chemistry and with the requirement for electron-deficient phenol leaving groups, and with the greater reaction rate for glycosides with potential participating groups at C-2. However, it is difficult to envisage a role for the base in such a reaction. Mechanism (iii) is also reasonably consistent with known carbohydrate chemistry and with the requirement for reactive leaving groups. In addition, it does suggest a clear role for the base. However, it seems doubtful that the glycal intermediate would be reactive enough to recombine with such a poor nucleophile as dinitrophenolate. Additional problems also arise concerning retention of stereochemistry at C-2 in the product. Mechanism (iv) is consistent with the requirement for an electron-deficient aromatic ring and suggests a role for the base either as the nucleophile or in generating the dimethylsulfinyl anion nucleophile. However, it suffers from a paucity of precedence since nucleophilic aromatic substitution reactions are rare in aryl glycoside chemistry. Nonetheless, an important precedent for this exists in the base-catalysed hydrolysis of nitrophenyl glycosides (11, 12). In this case reaction is initiated by base-catalysed intramolecular attack of the sugar 2-hydroxyl upon C-1′ of the aromatic moiety, resulting in migration of the nitrophenyl group to O-2. Subsequent further migration of the aromatic group to O-3 is followed by elimination, yielding nitrophenolate and saccharinic acids.

This paper describes our approaches to identifying the mechanism through a combination of kinetic and product identification studies. A preliminary account of this work has been published previously (13).

Results and discussion

Investigation of solvents, catalysts, and substrates

The first factors to be investigated were the solvents and the catalysts capable of effecting the transformation. This was of particular interest not only in terms of providing clues to the mechanism itself, but also in terms of finding a totally homogeneous system that would be suitable for kinetic studies. For these initial investigations β-2,4-DNPG was used as the substrate and potassium carbonate as the catalyst while thin-layer chromatography was used to determine whether or not reaction had occurred. The substrate, β-2,4-DNPG, was soluble in all the solvents tested, while the potassium carbonate was, at best, only sparingly soluble. Reaction failed to occur only in the least polar of the solvents tested, namely toluene, diethyl ether, and dichloromethane, while reaction was successful in a range of more polar solvents including dimethylsulfoxide, *N*,*N*-dimethylformamide, propylene carbonate, tetrahydrofuran, pyridine, chloroform, and acetonitrile. The reaction does not therefore appear to be especially solvent dependent. Indeed, the absence of reaction in the least polar solvents may simply reflect poor solubility of the catalyst. On the basis of these results dimethylsulfoxide (DMSO) was chosen as the solvent for subsequent studies due to the ease of reactions therein and due to its stability to bases.

A variety of other bases was tested for their ability to catalyse the anomerization of β-2,4-DNPG in DMSO. All the carbonate salts tested (potassium, barium, cesium, tetramethyl-, tetraethyl-, and tetrabutyl-ammonium) were effective, along with

Can. J. Chem. Downloaded from www.nrcresearchpress.com by 91.121.58.235 on 09/07/12
For personal use only.

Can. J. Chem. Downloaded from www.nrcresearchpress.com by 91.121.58.235 on 09/07/12
For personal use only.

other dianions or trianions such as trisodium phosphate and bis-tetramethylammonium hydrogen phosphate. The very weakly basic dianion potassium sulfate and the monoanion potassium perchlorate were ineffective. Neutral bases of comparable basicity[3] to carbonate (triethylamine and 1,8-bis(dimethylamino)naphthalene) were unable to support the reaction. However, relatively strong monoanionic bases such as potassium *tert*-butoxide, dimethylsulfinyl anion, and sodium hydride were quite effective at promoting anomerization. These observations were initially confusing since there appeared to be no clear correlation with base strength until it was realized that anionic bases, and particularly dianionic bases, are *much* stronger bases in DMSO than in water (14–16) while neutral bases are of comparable basicity in the two solvents. Indeed potassium *tert*-butoxide was shown previously (14) to be capable of generating a high concentration of dimethylsulfinyl anion when dissolved in DMSO, and it is probable that the carbonate dianion has a comparable basicity. It therefore appears that a strong base is required to bring about anomerization, possibly strong enough to generate significant quantities of dimethylsulfinyl anion. The fact that dimethylsulfinyl anion itself promotes anomerization supports this contention. The search for different catalysts also revealed several that were soluble in DMSO, these being the bis(tetra-alkylammonium) carbonates and dimethylsulfinyl anion. This finding is particularly relevant not only in terms of providing a completely soluble homogeneous system for kinetic studies, but also because it disproves an earlier hypothesis (8) that the reaction requires heterogeneous catalysis.

The previous assertion (8) that the only aryl glycosides to undergo this transformation are those with aglycone moieties of low pK_a was investigated further by synthesis and testing of a series of protected aryl glycosides to see which underwent anomerization. Thus the per-*O*-acetylated β-D-glucopyranosides of the following phenols were synthesized: phenol, 4-nitrophenol, pentafluorophenol, 3,4-dinitrophenol, 2,3-dinitrophenol, 2,5-dinitrophenol, 2,6-dinitrophenol, and 2,6-dichloro-4-nitrophenol. These glycosides were dissolved in DMSO containing potassium carbonate and stirred for several days. Analysis of reaction products by tlc and nmr revealed that only the 2,6-dinitrophenyl and 2,6-dichloro-4-nitrophenyl glucosides anomerized at a comparable rate to β-2,4-DNPG. These are the only three phenols that have pK_a's less than 4.0 (17, 18), confirming that the reaction depends on the electron-withdrawing effects of substituents on the aryl ring.

The search for intermediates. Exchange reactions

All four possible mechanisms proposed for the anomerization reaction occur via bond cleavage at either C-1—H-1 (proton abstraction), C-1—O-1 (phenolate departure), or O-1—C-1′ (nucleophilic aromatic substitution). In all cases, the intermediates generated by bond cleavage should be exchangeable with appropriate equivalent substances added to the reaction mixture. Therefore a series of exchange reactions was performed to determine which bond is cleaved during anomerization.

Proton abstraction (mechanisms (i) or (iii)) was investigated by anomerizing [1-^{2}H]-β-2,4-DNPG (19) in DMSO-d_6 containing tetramethylammonium carbonate in the presence of *tert*-butanol as a proton source (100-fold mole excess). The ^{1}H nmr analysis of the isolated product mixture indicated that although complete anomerization had occurred, there had been no exchange of the deuteron at C-1 since no resonance due to an anomeric proton was observed. Similarly, anomerization of non-labelled β-2,4-DNPG in the presence of a deuteron source (^{2}H-*tert*-butanol) showed no exchange at either C-1 or C-2. These observations are strong evidence against mechanisms (i) or (iii).

Demonstration of a dinitrophenolate intermediate was attempted by looking for exchange of added dinitrophenolate anion with that which might be generated during the reaction. Ideally this could be achieved using appropriately labelled (e.g., deuterated), 2,4-dinitrophenolate in the presence of β-2,6-DNPG. However, since such material was not readily available, and since β-2,6-DNPG had also been shown to undergo anomerization, experiments were performed in which β-2,4-DNPG was anomerized in the presence of added potassium 2,6-dinitrophenolate and β-2,6-DNPG in the presence of potassium 2,4-dinitrophenolate. In both cases, ^{1}H nmr analysis of the product mixture indicated that no exchange had occurred. The lack of phenolate exchange is significant evidence against mechanisms (ii) and (iii). However, it is just possible, though unlikely, that exchange might not occur if the phenolate was not released from the immediate solvent shell before recombining with the sugar moiety.

To test mechanism (iv), a third exchange reaction was performed in which [1-^{2}H]-β-2,4-DNPG was anomerized in the presence of one equivalent of 2,3,4,6-tetra-*O*-acetyl-β-D-glucopyranose. In the presence of base, 2,3,4,6-tetra-*O*-acetyl-β-D-glucopyranose is deprotonated to produce the glycosyl oxyanion intermediate proposed in the nucleophilic aromatic substitution mechanism (Scheme 2). If this is indeed an intermediate in the reaction, then the added, unlabelled, 2,3,4,6-tetra-*O*-acetyl-β-D-glucopyranose should be capable of exchanging with the deuterated species generated from the substrate during reaction. The ^{1}H nmr spectrum of the isolated α-2,4-DNPG revealed that exchange had indeed occurred since an anomeric proton resonance integrating to approximately half a proton was evident in the spectrum (Fig. 1). Had there been no exchange, no anomeric proton resonance whatsoever would have been seen. The glycosyl oxyanion must therefore be an intermediate in the reaction mechanism, and this strongly supports mechanism (iv).

A final experiment performed to probe mechanism (iii) involved the independent synthesis of 2,3,4,6-tetra-*O*-acetyl-D-glucal, the postulated intermediate, and attempted reaction of this with potassium 2,4-dinitrophenolate in DMSO in the presence of potassium carbonate. No dinitrophenyl glycoside product was observed, providing additional evidence against mechanism (iii).

Kinetic studies

Two kinds of kinetic studies were performed to attempt to distinguish between mechanisms. One of these involved measurement of the kinetic isotope effect associated with the anomerization of 1-[^{2}H]-β-2,4-DNPG in an attempt to distinguish between the anomeric proton abstraction mechanism (i), which should show a primary kinetic isotope effect, and the other mechanisms, which would likely be subject to a secondary deuterium kinetic isotope effect. The second study involved comparison of the rates of anomerization of a series of remotely substituted 2′,4′-dinitrophenyl glycosides in an attempt to distinguish between cationic and anionic mechanisms. At-

[3]Basicity in H_2O.

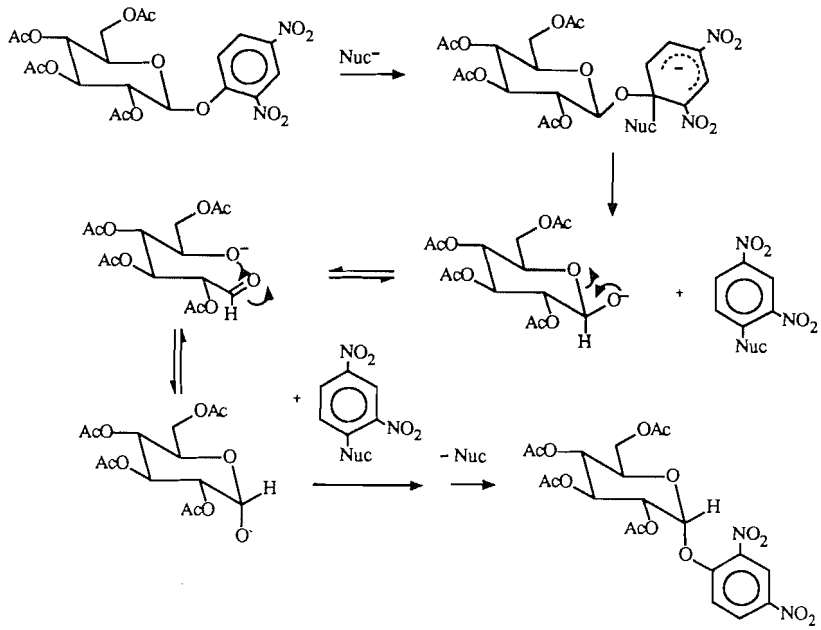

SCHEME 2

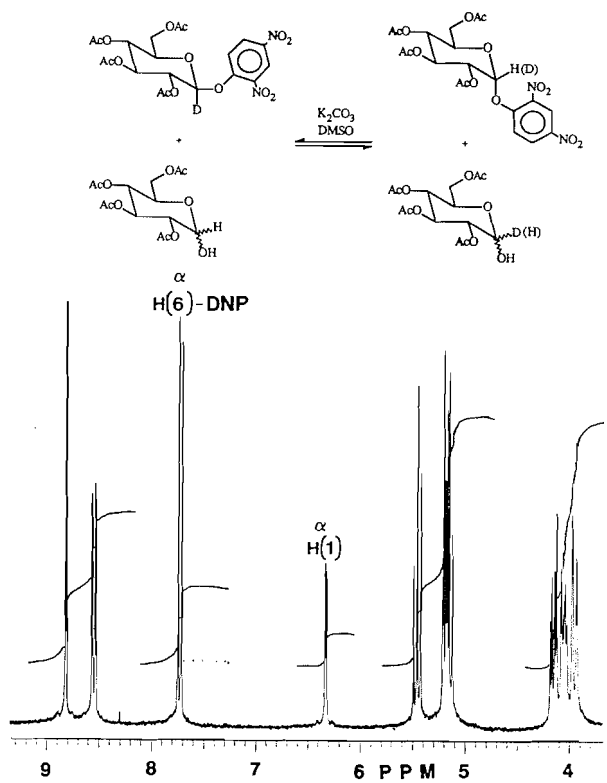

FIG. 1. The ^{1}H nmr spectrum of α-2,4-DNPG isolated from the reaction mixture shown. Integration of the anomeric proton resonance reveals that exchange has occurred.

tempts were made initially to monitor the reaction by use of a polarimeter since there is a significant difference in optical rotation between β-2,4-DNPG and α-2,4-DNPG. Unfortunately all such attempts were unsuccessful because of the relatively rapid appearance of small amounts of a highly chromophoric by-product, identified as 2,4-dinitrophenolate, even under anhydrous conditions. This rendered the use of polarimetry unreliable and forced the use of ^{1}H nmr to follow the reaction. This was more suitable since the reaction could be followed directly using sealed tubes under scrupulously anhydrous conditions. The quantity of 2,4-dinitrophenolate formed was too small to be observable by ^{1}H nmr, and hence it did not interfere with this technique. Direct monitoring by ^{1}H nmr allowed determination of the amounts of product and starting materials at any time by careful integration of the appropriate resonances. It should also allow the observation of any intermediate species generated if they are formed at significant concentrations.

Deuterium kinetic isotope effects

The deuterium kinetic isotope effect measured for the anomerization of 1-substituted β-2,4-DNPG was $k_H/k_D = 1.09 \pm 0.06$. This is a small, but real, isotope effect, but is clearly not a primary kinetic isotope effect since much larger values (up to 7) might have been expected. This finding argues strongly against the proton abstraction mechanism (i) since it is reasonable to assume that the initial proton abstraction step would be rate determining for this mechanism, and thus a primary kinetic isotope effect would be expected. The value measured is, however, in the range expected for a secondary (α or β) deuterium kinetic isotope effect. Either of the other three mechanisms (ii, iii, or iv) could be expected to show such an effect.

Remote substituent effects

It has long been known that substitution of sugar ring hydroxyl groups by hydrogen or other substituents can have a pronounced effect upon the rate of hydrolysis of such substituted glycosides when reaction proceeds via an oxocarbonium ion mechanism (2, 20–22). These changes in rate have generally been considered to be the result of some combination of steric and electronic effects that affects the stability of the transition state. More recent studies on the hydrolysis rates of a complete series of deoxy- and deoxyfluoro-α-D-glucopyranosyl phosphates (23, 24) have suggested that, in these cases at least, the effect is entirely electronic in origin, with the deoxysugars hydrolysing faster than the parent compound and the deoxyfluorosugars hydrolys-

Can. J. Chem. Downloaded from www.nrcresearchpress.com by 91.121.58.235 on 09/07/12
For personal use only.

TABLE 1. Substituent effects on anomerization rate

β-2,4-DNPG Substrate	[DNPG] (M)	$[(Me_4N)_2CO_3]$ (M)	Rel. Rate (disappearance of β-anomer)
β-2,4-DNPG	0.0138	0.0167	1.00*
2,3,6-Tri-*O*-acetyl-4-deoxy	0.0138	0.0167	0.13
2,3,4-Tri-*O*-acetyl-6-deoxy	0.0153	0.0167	0.40
2,3,6-Tri-*O*-acetyl-4-deoxy-4-fluoro	0.0136	0.0167	1.05
β-2,4-DNPG	0.0121	0.0182	1.00
3,4,6-Tri-*O*-acetyl-2-deoxy-2-fluoro	0.0134	0.0182	0.90

*Apparent first-order rate constant at 25°C = 3.63×10^{-3} min^{-1}.

ing more slowly. It should therefore be possible to measure anomerization rates for several deoxy- and deoxyfluoro-β-2,4-DNPG substrates and determine whether the reaction proceeds via an anionic mechanism or a cationic mechanism. Such data are presented in Table 1. As can be seen, the two deoxy-β-2,4-DNPG substrates anomerize considerably more slowly than the parent substrate while the two fluorinated substrates anomerize at comparable rates to β-2,4-DNPG. This supports an anionic rather than a cationic mechanism and is therefore inconsistent with mechanism (ii) involving phenolate departure from an oxocarbonium ion.

Conclusion

The only mechanism to emerge unscathed from this investigation is the nucleophilic aromatic substitution mechanism (iv), Scheme 2. The kinetic studies are consistent with a mechanism such as this, which involves anionic intermediates and exhibits a secondary deuterium kinetic isotope effect. In this case the isotope effect would be a β-kinetic isotope effect if the nucleophilic attack is rate limiting (most likely) and an α-kinetic isotope effect if the anomerization of the hemiacetal anion is rate limiting. Either could be consistent with the observed effect of $k_H/k_D = 1.09$. The best evidence, however, is the observation of exchange between [1-^{2}H]-β-2,4-DNPG and added unlabelled 2,3,4,6-tetra-*O*-acetyl-β-D-glucopyranose. This provides unequivocal evidence for the intermediacy of the protected sugar oxyanion. Additional support for this mechanism comes from the observation that when the anomerization is performed under scrupulously anhydrous conditions a deep purple coloration ($\lambda_{max} = 574$ nm) is observed initially in the reaction mixture. Similar observations have been described previously in nucleophilic aromatic substitution reactions and attributed to the formation of Meisenheimer complexes (25); thus it seems likely that the colored species generated in this reaction is the initial adduct formed upon attack o sthe nucleophile onto β-2,4-DNPG.

The identity of the nucleophile and therefore of the activated aryl intermediate is, as yet, unproven. Likely candidates are the added nucleophile itself (carbonate or phosphate) or dimethylsulfinyl anion generated in the solution by addition of the anionic base. Clearly, in the reaction where dimethylsulfinyl anion is used as the base, there is no other candidate. In all the other cases studied, as stated previously, it is either known, or at least probable, that the bases employed are strong enough to generate significant quantities of dimethylsulfinyl anion *in situ*.

The possibility that phosphate is the nucleophile was eliminated by independent synthesis (26) of 2,4-dinitrophenyl phosphate, the putative intermediate in that case, and reacting it with 2,3,4,6-tetra-*O*-acetyl-β-D-glucopyranose in DMSO in the presence of trisodium phosphate. No dinitrophenyl glucoside product was observed. Attempts to synthesize 2,4-dinitrophenyl carbonate were, not surprisingly, unsuccessful. Such an intermediate would be extremely unstable and subject to rapid spontaneous decarboxylation, liberating 2,4-dinitrophenolate. This could explain formation of dinitrophenolate, even under strictly anhydrous conditions. Such an intermediate therefore remains a possibility.

There are two likely candidates for the intermediate if dimethylsulfinyl anion is the nucleophile, either **1** or **2**.

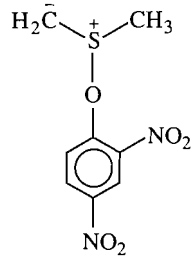

1

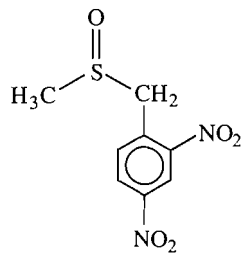

2

Compound **2** was synthesized by an independent route involving oxidation of the methyl dinitrobenzyl thioether formed by reaction of methane thiol with 2,4-dinitrobenzyl chloride (27, 28). Reaction of this with 2,3,4,6-tetra-*O*-acetyl-β-D-glucopyranose in DMSO in the presence of bis(tetramethylammonium) carbonate yielded no dinitrophenyl glucoside product, thus eliminating compound **2** as a possible candidate.

All of our attempts to synthesize compound **1** have been unsuccessful. The most promising approach, involving direct substitution of fluoro-2,4-dinitrobenzene with dimethylsulfinyl anion in DMSO failed as the reaction proved difficult to control and products formed decomposed upon work-up and purification. Interestingly, the same compound was suggested to be an intermediate in the reaction of chloro-2,4-dinitrobenzene with DMSO at high temperature (29), as well as in the reaction of 2,4-dinitrophenol with dicyclohexylcarbodiimide and DMSO in the presence of acid/base catalysts (30, 31). Considerable effort was expended by these authors in attempts to isolate and characterize this intermediate, but without success. Suggestive evidence for the identity of the intermediate as compound **1** is provided by the observation that, even under anhydrous conditions, some 2,4-dinitrophenolate by-product is formed in these reactions. This could be explained readily by the collapse of **1**, yielding 2,4-dinitrophenolate and the sulfonium derivative. It was of concern to us initially that the generation of this type of intermediate had previously been shown to be accompanied by *ortho*-alkylation of the aromatic ring, yet no such reaction has been observed in our hands. However, it has

Can. J. Chem. Downloaded from www.nrcresearchpress.com by 91.121.58.235 on 09/07/12
For personal use only.

Can. J. Chem. Downloaded from www.nrcresearchpress.com by 91.121.58.235 on 09/07/12
For personal use only.

been shown (31) that no such reaction occurs with the 2,4-dinitrophenyl derivative, presumably because of the electron-deficient nature of the system.

In summary, the anomerization of protected 2,4-dinitrophenyl-β-D-glucopyranosides has been shown to proceed via a novel mechanism involving an initial nucleophilic aromatic substitution reaction. The identity of the aromatic intermediate involved has not been proven, but is in all likelihood the aryldimethylsulfinyl species generated by attack of dimethylsulfinyl anion on the substrate. It also suggests that a likely mechanism for the pyridine-catalysed anomerization of per-*O*-acylated sugars (8) involves initial attack of the pyridine on the acyl carbon of the anomeric substituent, resulting in formation of the acyl pyridinium species and the protected sugar oxyanion. This could then mutarotate and react with the acyl pyridinum salt by an entirely analogous process to that described in this work.

Experimental

Thin-layer chromatography (tlc) was performed on Merck Silica Gel 60 F_{254} aluminum backed plates using a solvent system of 1:1 (v/v) ethyl acetate/petroleum ether unless otherwise stated. Chromatograms were visualized by uv irradiation or by charring with 10% sulfuric acid in methanol. Flash chromatography was carried out on Merck Silica Gel (180–230 mesh). The ^{1}H nmr spectra were recorded on a 300 MHz Varian XL-300 instrument using $CDCl_3$ solutions and tetramethylsilane as an internal standard. Chemical shifts are expressed in ppm and coupling constants (J) are given in hertz (s = singlet, d = doublet, t = triplet, m = multiplet). Kinetic measurements were carried out in DMSO-d_6 solutions using residual proton resonances from DMSO (δ = 2.49) as a reference.

Syntheses

With the exception of the 2,4-dinitrophenyl glycosides, commercially unavailable acetylated phenyl glycosides were prepared by condensation of the sodium salt of the phenol with 2,3,4,6-tetra-*O*-acetyl-α-D-glucopyranosyl bromide (32). Protected 2,4-dinitrophenyl glucosides were prepared from the corresponding protected glycoside hemiacetals using fluoro 2,4-dinitrobenzene according to the method of van Boom *et al.* (9). Physical properties were in agreement with those previously reported (32, 33).

The following new compounds were prepared.

*Pentafluorophenyl 2,3,4,6-tetra-*O*-acetyl-β-D-glucopyranoside:* mp 144–145°C; ^{1}H nmr data: δ ($CDCl_3$) 5.34–5.12 (m, 3H, H-2, H-3, H-4), 4.97 (d, 1H, $J_{1,2}$ 8 Hz, H-1), 4.25–4.10 (2 dd, $J_{6,5}$ 4, $J_{6',5}$ 2, $J_{6,6'}$ 12 Hz, H-6, H-6'), 3.70 (m, 1H, H-5), 2.10–2.02 (4 s, 12H, 4 × CH_3CO). Anal. calcd. for $C_{20}H_{17}F_5O_{10}$: C 46.71, H 3.72; found: C 45.90, H 3.56.

*2'3'-Dinitrophenyl 2,3,4,6-tetra-*O*-acetyl-β-D-glucopyranoside:* mp 191–192°C; ^{1}H nmr data: δ ($CDCl_3$) 7.96 (dd, 1H, $J_{4',5'}$ 8, $J_{4'6'}$ 2 Hz, H-4), 7.68 (dd, 1H, $J_{6',5'}$ 8, $J_{6',4'}$ 2 Hz, H-6), 7.62 (dd, 1H, $J_{5',4'}$ 8, $J_{5',6'}$ 8 Hz, H-5), 5.32–5.05 (m, 4H, H-1, H-2, H-3, H-4), 4.24 (d, 2H, $J_{6,5'} = J_{6',5}$ 4 Hz, H-6, H-6'), 3.86 (dt, 1H, $J_{5,4}$ 10, $J_{5,6'}$ 4 Hz, H-5), 2.14–2.03 (4 s, 12H, 4 CH_3CO). Anal. calcd. for $C_{20}H_{22}N_2O_{14}$: C 46.69, H 4.31, N 5.47; found: C 46.32, H 4.51, N 5.42.

*2'5'-Dinitrophenyl 2,3,4,6-tetra-*O*-acetyl-β-D-glucopyranoside:* mp 145–147°C; ^{1}H nmr data: δ ($CDCl_3$) 8.23 (d, 1H, $J_{6',4'}$ 2 Hz, H-6), 8.06 (dd, 1H, $J_{4',3'}$ 9, $J_{4',6'}$ 2 Hz, H-4'), 7.89 (d, 1H, $J_{3',4'}$ 9 Hz, H-3'), 5.37–5.06 (m, 4H, H-1, H-2, H-3, H-4), 4.30 (dd, 1H, $J_{6',6}$ 12, $J_{6',5}$ 3 Hz, H-6'), 4.19 (dd, 1H, $J_{6,6'}$ 12, $J_{6,5}$ 6 Hz, H-6), 4.02 (m, 1H, H-5), 2.13–2.02 (4 s, 12H, 4 CH_3CO).

*2'6'-Dichloro-4'-nitrophenyl 2,3,4,6-tetra-*O*-acetyl-β-D-glucopyranoside:* mp 181–182°C; ^{1}H nmr data: δ $CDCl_3$) 8.20 (s, 2H, H-3', H-5'), 5.46–5.13 (m, 4H, H-1, H-2, H-3, H-4), 4.18 (dd, 1H, $J_{6,6'}$ 11 Hz, H-6), 4.07 (dd, 1H, $J_{6',6}$ 11, $J_{6',5'}$ 2 Hz, H-6'), 3.65 (m, 1H, H-5), 2.09–2.02 (3 s, 12H, 4 CH_3CO). Anal. calcd. for $C_{20}H_{21}Cl_2NO_8$: C 44.62, H 3.93, N 2.61; found: C 44.39, H 4.06, N 2.79.

*2'6'-Dinitrophenyl 2,3,4,6-tetra-*O*-acetyl-β-D-glucopyranoside:* mp 190–191°C; ^{1}H nmr data: δ ($CDCl_3$) 7.98 (d, 2H, $J_{3',5'}$ 8 Hz, H-3', H-5'), 7.47 (t, 1H, $J_{4',5'} = J_{4',3'}$ 8 Hz, H-4'), 5.36–5.08 (m, 4H, H-1, H-2, H-3, H-4), 4.03 (d, 2H, $J_{6,5} = J_{6',5}$ 4 Hz, H-6'), 3.62 (dt, 1H, $J_{5,4}$ 10, $J_{5,6} = J_{5,6'}$ 4 Hz, H-5), 2.13–2.00 (4 s, 12H, CH_3CO). Anal. calcd. for $C_{20}H_{22}N_2O_{14}$: C 46.69, H 4.31, N 5.47, found: C 46.45, H 4.23; N 5.29.

*2',4'-Dinitrophenyl 2,3,6-tri-*O*-acetyl-4-deoxy-4-fluoro-β-D-glucopyranoside*

A solution of 1,2,3,6-tetra-*O*-acetyl-4-deoxy-4-fluoro-β-D-glucopyranose (23) (0.100 g, 0.29 mmol) in 45% HBr/HOAc (3.0 mL) and acetic anhydride (0.30 mL) was stirred for 2 h at room temperature, then cooled to 0°C, diluted with dichloromethane (30 mL), washed five times with ice-cold water, and the organic phase dried with sodium sulfate. Removal of the solvent produced 2,3,6-tri-*O*-acetyl-4-deoxy-4-fluoro-α-D-glucopyranosyl bromide as a colourless syrup, which was crystallized from diethyl ether/hexanes; 90 mg, 0.24 mmol, 85%.

A solution of 2,3,6-tri-*O*-acetyl-4-deoxy-4-fluoro-α-D-glucopyranosyl bromide (90 mg, 0.24 mmol) was dissolved in acetone (0.20 mL) and cooled to 0°C. Water (10 μL) was added, followed by addition of silver carbonate (0.10 g, 0.36 mmol) in small portions. The solution was stirred for 20 h at room temperature in the dark, warmed to 50°C, filtered, and washed with two portions of warm acetone. The solvent was removed from the combined filtrates to produce a brown syrup of 2,3,6-tri-*O*-acetyl-4-deoxy-4-fluoro-D-glucopyranose (64 mg, 0.21 mmol).

Derivatization of 2,3,6-tri-*O*-acetyl-4-deoxy-4-fluoro-D-glucopyranose was performed according to van Boom *et al.* (9) giving the title compound as yellow needles (45 mg, 0.091 mmol); mp 171–173°C; ^{1}H nmr data: δ ($CDCl_3$) 8.72 (d, 1H, $J_{3',5'}$ 3 Hz, H-3'), 8.44 (dd, 1H, $J_{5',6'}$ 10, $J_{5',3'}$ 3 Hz, H-5'), 7.47 (d, 1H, $J_{6',5'}$ 10 Hz, H-6'), 5.50–5.23 (m, 3H, H-1, H-2, H-4), 4.68 (dt, 1H, $J_{F,4}$ 50, $J_{3,4} = J_{4,5}$ 9 Hz, H-4), 4.55 (dd, 1H, $J_{6,6'}$ 12 Hz, H-6), 4.28 (dd, 1H, $J_{6',6}$ 12 Hz, H-6'), 4.20 (m, 1H, H-5), 2.14 (s, 6H, 2CH_3CO), 2.09 (s, 3H, CH_3CO). Anal. calcd. for $C_{18}H_{19}FN_2O_{12}$: C 45.57, H 4.04, N 5.93; found: C 45.50, H 3.82, N 6.01

*2',4'-Dinitrophenyl 2,3,6-tri-*O*-acetyl-4-deoxy-β-D-glucopyranoside*

To a suspension of methyl 2,3,6-tri-*O*-benzoyl-4-deoxy-α-D-glucopyranoside (24) (0.20 g, 0.41 mmol) in methanol (1.0 mL) was added 1 M sodium methoxide in methanol (0.010 mL). The mixture was stirred for 2 days at room temperature, neutralized with Dowex 50W-X8 (H^+) ion exchange resin, and the suspension filtered. The filtrate was concentrated *in vacuo* and the concentrate was purified by column chromatography (9:1 v/v ethyl acetate/methanol). The resulting syrup (72 mg, 88%) was immediately acetylated by addition of a cold (0°C) solution of acetic anhydride (0.37 mL, 3.9 mmol) and pyridine (0.47 mL), warmed to room temperature, and stirred overnight. This was cooled to 0°C, then quenched by addition of methanol and stirred at 0°C for 1 h. The solution was diluted with dichloromethane, washed three times with ice-cold water, and the organic phase was dried with sodium sulfate. Removal of the solvent *in vacuo* afforded methyl 2,3,6-tri-*O*-acetyl-4-deoxy-α-D-glucopyranoside as a colourless syrup, which was crystallized from diethyl ether (87 mg, 0.29 mmol, 71%).

Methyl 2,3,6-tri-*O*-acetyl-4-deoxy-α-D-glucopyranoside was dissolved in dichloromethyl methyl ether (0.40 mL) and a catalytic amount of freshly fused zinc chloride was added. The solution was stirred at 65–70°C for 1 h, then concentrated *in vacuo*, diluted with chloroform, and washed twice with 10 mL of cold saturated aqueous sodium bicarbonate. The organic phase was dried with sodium sulfate and removal of the solvent produced a brown syrup of 2,3,6-tri-*O*-acetyl-4-deoxy-α-D-glucopyranosyl chloride (65 mg).

2,3,6-Tri-*O*-acetyl-4-deoxy-α-D-glucopyranosyl chloride was hydrolysed exactly as described previously for the 4-fluoro derivative to yield a yellow syrup, which was reacted directly with fluoro-2,4-dinitrobenzene according to van Boom *et al.* (9) to yield the title compound as a yellow crystalline solid; mp 180–181°C; ^{1}H nmr data:

Can. J. Chem. Downloaded from www.nrcresearchpress.com by 91.121.58.235 on 09/07/12
For personal use only.

δ ($CDCl_3$) 8.71 (d, 1H, $J_{3',5'}$ 3 Hz, H-3'), 8.42 (dd, 1H, $J_{5',6'}$ 10, $J_{5',3'}$ 3 Hz, H-5'), 7.48 (d, 1H, $J_{6',5'}$ 10 Hz, H-6'), 5.32–5.05 (m, 3H, H-1, H-2, H-3), 4.22 (d, 2H, $J_{6,6'}$ 7 Hz, H-6, H-6'), 4.40 (m, 1H, H-5). Anal. calcd. for $C_{18}H_{20}N_2O_{12}$: C 47.36, H 4.42, N 6.16; found: C 47.27, H 4.40, N 6.18.

*2',4'-Dinitrophenyl 2,3,4-tri-*O*-acetyl-6-deoxy-β-*D*-glucopyranoside*

1,2,3,4-Tetra-*O*-acetyl-6-deoxy-D-glucopyranose (24) (0.40 g, 1.2 mmol) was brominated at the anomeric centre as described previously for the 4-deoxy sugar. The product was isolated as a white solid (420 mg, 1.06 mmol, 99%), and directly hydrolysed as described previously, using silver carbonate, yielding 2,3,4-tri-*O*-acetyl-6-deoxy-D-glucopyranose as a colourless gum (306 mg, 1.05 mmol). This was derivatized using fluoro-2,4-dinitrobenzene by the general method to afford 2'4'-dinitrophenyl 2,3,4-tri-*O*-acetyl-6-deoxy-β-D-glucopyranoside as white needles (424 mg, 0.93 mmol); mp 198–199°C (lit. (34) mp 152–156°C); ^{1}H nmr data: δ ($CDCl_3$) 8.70 (d, 1H, $J_{3',5'}$ 3 Hz, H-3'), 8.43 (dd, 1H, $J_{5',6'}$ 10, $J_{5',3'}$ 3 Hz, H-5'), 7.45 (d, 1H, $J_{6',5'}$ 10 Hz, H-6'), 5.46–5.20 (m, 3H, H-1, H-2, H-3), 4.95 (m, 1H, H-5), 2.12, 2.08, 2.05 (3 s, 9H, CH_3CO), 1.35 (d, 3H, $J_{6,5}$ 4 Hz, 3 × H-6). Anal. calcd. for $C_{18}H_{20}N_2O_{12}$: C 47.36, H 4.42, N 6.16; found: C 47.34, H 4.35, N 6.10.

*2',4'-Dinitrophenyl 3,4,6-tri-*O*-acetyl-2-deoxy-2-fluoro-β-*D*-glucopyranoside*

3,4,6-Tri-*O*-acetyl-2-deoxy-2-fluoro-α-D-glucopyranosyl bromide (35) (1.4 g) was hydrolysed using silver carbonate, as described previously, yielding 3,4,6-tri-*O*-acetyl-2-deoxy-2-fluoro-D-glucopyranose as a colourless gum. This was dissolved in DMF (10 mL) containing DABCO (1.5 g), stirred over 4A molecular sieves for 15 min, then a solution of fluoro-2,4-dinitrobenzene (0.9 g) in DMF (5 mL) added. After 1.5 h the solution was filtered, and the solvent removed by evaporation under vacuum. The residual oil was redissolved in chloroform, washed twice with saturated aqueous sodium bicarbonate, then twice with water, and dried over sodium sulfate. Evaporation of the solvent yielded an oil, which crystallized spontaneously upon addition of ethanol giving a mixture of the α(20%)- and β(80%)-glycosides (0.99 g). This solid was dissolved in a minimal volume of hot ethyl acetate and, upon cooling to room temperature, the pure α-glucoside crystallized out. After filtration, petroleum ether was added to induce crystallization of the β-glycoside. This process was repeated twice, giving a mixture of the α(5%)- and β(95%)-glycosides as a crystalline solid. Pure β-glycoside was obtained by preparative thin-layer chromatography (silica; 1.2:1 ethyl acetate/petroleum ether) and recrystallized from ethyl acetate/petroleum ether; mp 145–147°C; ^{1}H nmr data: δ ($CDCl_3$) 8.77 (d, 1H, $J_{3',5'}$ 2.6 Hz, H-3'), 8.50 (dd, 1H, $J_{5',6'}$ 9.3, $J_{5',3'}$ 2.5 Hz, H-5'), 7.41 (d, 1H, $J_{6',5'}$ 9.3 Hz, H-6'), 5.52–5.39 (m, 2H, H-3, H-1), 5.15 (t, 1H, $J_{4,3} = J_{4,5}$ 9.7 Hz, H-4), 4.73 (ddd, 1H, $J_{2,F}$ 49.5, $J_{2,3}$ 8.9, $J_{2,1}$ 7.4 Hz, H-2), 4.28 (dd, 1H, $J_{6,6'}$ 14.6, $J_{6,5}$ 5.4 Hz, H-6), 4.20 (dd, 1H, $J_{6',6}$ 14.6, $J_{6',5}$ 2.9 Hz, H-6'), 3.95 (ddd, 1H, $J_{5,4}$ 9.7, $J_{5,6}$ 5.4, $J_{5,6'}$ 2.9 Hz, H-5), 2.14 (s, 3H, CH_3CO), 2.08 (s, 6H, CH_3CO). Anal. calcd. for $C_{18}H_{19}N_2O_{12}F$: C 45.48, H 4.04, N 5.91; found: C 45.10, H 4.18, N 5.69.

2,4-Dinitrobenzylchloride

A mixture of nitric acid (7 mL) and sulfuric acid (12 mL) was added with stirring to a suspension of 4-nitrobenzylchloride (11.4 g, 55 mmol) in sulfuric acid (52 mL) at 0°C, stirred at 0°C for 30 min, then at room temperature for 1 h. The mixture was poured onto ice and extracted with chloroform; the combined chloroform extracts were washed with cold water until the aqueous layer was neutral to pH paper, then dried with sodium sulfate and the chloroform removed *in vacuo*, producing a red oil. The oil was purified by flash chromatography (silica; 3:1 petroleum ether/ethyl acetate) to afford the product as a yellow oil, which solidified upon cooling (11.6 g, 43 mmol, 81%); ^{1}H nmr data: δ ($CDCl_3$) 8.91 (d, 1H, H-3), 8.53 (dd, 1H, H-5), 8.05 (d, 1H, H-6), 5.10 (s, 2H, $-CH_2-$).

2,4-Dinitrobenzylmethyl sulfide

The sulfide was prepared by the method of Russell and Pecoraro (27) as follows. 2,4-Dinitrobenzylchloride (8.02 g, 37 mmol) in methanol (100 mL) was added slowly, under nitrogen, to a 2.5 M solution of sodium (70 mmol) and methyl mercaptan in methanol (28 mL) at 0°C (28). After stirring for 15 min, the mixture was acidified with 1 M hydrochloric acid, diluted with water, and extracted with ether. The combined ether extracts were washed with water until the aqueous layer was neutral, dried with magnesium sulfate, and concentrated *in vacuo* to produce a red solid. Purification by flash chromatography (silica; 5:1 petroleum ether/ethyl acetate) afforded 2,4-dinitrobenzylmethyl sulfide as yellow crystals (5.78 g, 25 mmol, 68%); ^{1}H nmr data: δ ($CDCl_3$) 8.83 (d, 1H, H-3), 8.41 (dd, 1H, H-5), 7.72 (d, 1H, H-6), 4.11 (s, 1H, $-CH_2-$), 2.05 (s, 3H, $-CH_3$).

2,4-Dinitrobenzylmethyl sulfoxide

2,4-Dinitrobenzylmethyl sulfide (0.830 g, 3.64 mmol) in methylene chloride (1.0 mL) was cooled to −20°C and a solution of *m*-chloroperbenzoic acid (0.628 g, 3.64 mmol) in methylene chloride (6.0 mL) was added under nitrogen. The mixture was stirred for 20 h, at which time tlc (silica; ethyl acetate) showed one major product (R_f = 0.14) plus a very small amount of a component later identified as 2,4-dinitrobenzylmethyl sulfone (R_f = 0.54). The sulfoxide product was separated by flash chromatography, eluting first with ethyl acetate to remove the sulfone by-product and any residual starting material, then with methanol. The sulfoxide was isolated as a yellow solid, which was crystallized from warm ethanol (0.650 g, 2.66 mmol, 73%); mp 125–127°C; ir data: (KBr pellet) 1049 cm^{-1} (S=O stretch); ^{1}H nmr data: δ ($CDCl_3$) 9.02 (d, 1H, H-3), 8.54 (dd, 1H, H-5), 7.80 (d, 1H, H-6), 4.48 (m, 2H, $-CH_2-$), 2.73 (s, 3H, $-CH_3$); ms data: *m/z* 244, M^+ for $C_8H_8N_2O_5S$. Anal. calcd. for $C_8H_8N_2O_5S$: C 39.32, H 3.31, N 11.52; found: C 39.85, H 3.28, N 11.40.

Anomerization reactions

Tests for anomerization of substrates were performed by dissolving the aryl β-glycoside (0.036 mmol) over 3A molecular sieves in anhydrous DMSO (0.2 mL) containing anhydrous potassium carbonate (0.10 mmol). Reaction was monitored by tlc (1:1 ethyl acetate/petroleum ether) and product composition was confirmed by ^{1}H nmr of the isolated product mixture. Typically, anomerization was complete in approximately 20 h. Exchange reactions were also carried out by this method, but with the addition of appropriate potentially exchangeable compounds.

Isolation of the product α-2,4-DNPG, when necessary, was achieved by the following method. The reaction mixture was diluted with chloroform, filtered, and concentrated *in vacuo* to a red syrup, which was redissolved in chloroform, washed twice with 10% aqueous sodium bicarbonate, and twice with water. The organic phase was dried over magnesium sulfate, concentrated to a yellow syrup, dissolved in warm 95% ethanol, and allowed to cool to room temperature when the α-2,4-DNPG crystallized out. Further cooling yielded a mixture of α and β anomers. If necessary, separation of the anomers could be achieved readily by flash chromatography (silica; 97:3 chloroform/acetone).

Kinetic studies

All kinetic studies were performed by using ^{1}H nmr to follow the reaction. Reactions were performed in DMSO-d_6 solutions containing bis(tetramethylammonium) carbonate as catalyst. Solutions of both the aryl glycoside and the carbonate catalyst were prepared separately under anhydrous conditions. The solution of carbonate was introduced into the 5-mm nmr tube and frozen at −70°C, then the solution of glycoside was layered on top and frozen. Samples were stored in sealed tubes at −70°C until needed, then reaction initiated by warming to 25°C and mixing. The ^{1}H nmr spectra were recorded at 25°C at appropriate time intervals. Rates of disappearance of the β-glycoside and appearance of the α-glycoside were estimated by integration of both the anomeric proton resonances and the aromatic proton H-6' resonance. The total integral measured for the acetate resonances (δ 2.2–2.0) was used for standardization. Rate constants were calculated using a plot of log ($B_t - B_e$) against time, where B_t is the con-

centration of β anomer remaining at time t and B_e is the concentration of β anomer at equilibrium. Such plots were linear ($p > 0.98$) for at least two half-lives. A linear regression analysis was used to extract rate constants. Errors in reported values are ± 5% on single runs. The kinetic isotope effect reported was measured in the same manner, using four pairs of substrates (protiated and deuterated). The value reported is calculated from the average of the four rate constants determined for protiated material and the four rate constants for the deuterated material.

Acknowledgements

We thank the Natural Sciences and Engineering Research Council of Canada for financial support. We also wish to thank Professor Ross Stewart and Professor Gary Gray for helpful discussions.

1. W. G. OVEREND. *In* The carbohydrates. Vol. 1. *Edited by* W. Pigman and D. Horton. Academic Press, New York, NY. 1972. pp. 310–316.
2. B. CAPON. Chem. Rev. **69**, 407 (1969).
3. L. L. JENSEN, S. C. TSUANG, and A. H. USHAN. J. Org. Chem. **51**, 816 (1986).
4. B. LINDBERG. Acta Chem. Scand. **2**, 534 (1948).
5. R. U. LEMIEUX and C. BRICE. Can. J. Chem. **30**, 295 (1952).
6. R. U. LEMIEUX, C. BRICE, and G. HUBER. Can. J. Chem. **33**, 134 (1955).
7. W. A. BONNER. J. Am. Chem. Soc. **83**, 962 (1961).
8. B. LINDBERG. Acta Chem. Scand. **4**, 49 (1950).
9. J. H. VAN BOOM, H. J. KOENERS, A. J. DE KOK, and C. ROMERS. Recl. Trav. Chim. Pays-Bas, **99**, 355 (1980).
10. R. J. FERRIER. Fortschr. Chem. Forsch. **14**, 389 (1970).
11. D. HORTON and A. E. LEUTZOW. J. Chem. Soc. Chem. Commun. 79 (1971).
12. S. ROSENBERG and J. F. KIRSCH. Biochemistry, **20**, 3196 (1981).
13. L. A. BERVEN, D. H. DOLPHIN, and S. G. WITHERS. J. Am. Chem. Soc. **110**, 4864 (1988).
14. J. I. BRAUMAN, J. A. BRYSON, D. G. KAHL, and N. J. NELSON. J. Am. Chem. Soc. **92**, 6679 (1970).
15. F. G. BORDWELL. Pure Appl. Chem. **49**, 963 (1977).
16. F. G. BORDWELL. Acc. Chem. Res. **21**, 456 (1988).
17. J. R. A. POLLOCK and R. STEVENS (*Editors*). Dictionary of organic compounds. Eyre and Spottiswood, London, 1965.
18. M. M. DAVIS. Acid–base behavior in aprotic organic solvents. NBS Monograph. **105**. (1968).
19. L. A. BERVEN and S. G. WITHERS. Carbohydr. Res. **156**, 282 (1986).
20. W. G. OVEREND, C. W. REES, and J. S. SEQUIERA. J. Chem. Soc. 3429 (1962).
21. T. MEGA and Y. MATSUSHIMA. J. Biochem. (Tokyo), **94**, 1637 (1983).
22. E. BUNCEL and P. R. BRADLEY. Can. J. Chem. **45**, 515 (1967).
23. S. G. WITHERS, D. J. MACLENNAN, and I. P. STREET. Carbohydr. Res. **154**, 127 (1986).
24. S. G. WITHERS, M. D. PERCIVAL, and I. P. STREET. Carbohydr. Res. **187**, 43 (1989).
25. K. BOWDEN and N. S. NADVI. J. Chem. Soc. Perkin Trans. 2, 189 (1987).
26. F. RAMIREZ and J. F. MARECEK. Synthesis, 601 (1978).
27. G. A. RUSSELL and J. M. PECORARO. J. Am. Chem. Soc. **101**, 3331 (1979).
28. L. A. PLIENINGER. Chem. Ber. **83**, 264 (1950).
29. M. E. C. BIFFIN and D. B. PAUL. Aust. J. Chem. **27**, 777 (1974).
30. M. G. BURDON and J. G. MOFFATT. J. Am. Chem. Soc. **88**, 5855 (1966).
31. J. P. MARINO, K. R. PFITZNER, and R. A. OLOFSON. Tetrahedron, **27**, 4181 (1971).
32. R. U. LEMIEUX. Methods Carbohydr. Chem. **2**, 22 (1963).
33. B. CAPON and J. W. THOMSON. Bioorg. Chem. **8**, 147 (1979).
34. F. BALLARDIE, B. CAPON, J. D. G. SUTHERLAND, D. COCKER, and M. L. SINNOTT. J. Chem. Soc. Perkin Trans. 1, 2418 (1973).
35. J. G. SHELLING, D. DOLPHIN, P. WIRZ, R. E. COBBLEDICK, and F. W. B. EINSTEIN. Carbohydr. Res. **132**, 241 (1984).

Can. J. Chem. Downloaded from www.nrcresearchpress.com by 91.121.58.235 on 09/07/12
For personal use only.

An efficient route to vinylporphyrins

PAUL YON-HIN, TILAK WIJESEKERA, AND DAVID DOLPHIN[1]

Department of Chemistry, University of British Columbia, 2036 Main Mall, Vancouver, B.C., Canada V6T 1Y6

Received April 3, 1990

This paper is dedicated to Professor Ross Stewart on the occasion of his 65th birthday

PAUL YON-HIN, TILAK WIJESEKERA, and DAVID DOLPHIN. Can. J. Chem. **68**, 1867 (1990).

The use of 1-bromo-19-methylbiladienes-ac in the synthesis of vinylporphyrins is described. The effect of the vinyl precursors on the reactions of the dipyrromethene intermediates and the construction of the linear tetrapyrrole are discussed. High-yield syntheses of a methylvinylporphyrin, an H-vinyl analogue, as well as two A,C-divinylporphyrins are presented.

Key words: pyrrole, dipyrromethene, acetoxyethylpyrrole, chloroethylpyrrole, biladiene-ac, porphyrin, vinylporphryin, benzoporphyrin, decarboxylation, transesterification.

PAUL YON-HIN, TILAK WIJESEKERA et DAVID DOLPHIN. Can. J. Chem. **68**, 1867 (1990).

On décrit l'utilisation des 1-bromo-19-méthylbiladiènes-ac dans la synthèse des vinylporphyrines. On discute de l'effet des précurseurs vinyles sur les réactions des intermédiaires dipyrrométhènes et sur la construction du tétrapyrrole linéaire. On rapporte des synthèses avec rendements élevés d'une méthylvinylporphyrine, d'un analogue H-vinyle ainsi que de deux A,C-divinylporphyrines.

Mots clés: pyrrole, dipyrrométhène, acétoxyéthylpyrrole, chloroéthylpyrrole, biladiène-ac, porphyrine, vinylporphyrine, benzoporphyrine, dicarboxylation, transesterification.

[Traduit par la revue]

Can. J. Chem. Downloaded from www.nrcresearchpress.com by 91.121.58.235 on 09/07/12
For personal use only.

Introduction

Porphyrins and related macrocycles bearing peripheral vinyl substituents play an important role in the vital functioning of living organisms (1). Of particular interest is heme, the iron(II) complex of protoporphyrin IX (**1**), which is the prosthetic group of hemoglobin, myoglobin, and several heme enzymes. Because of their biological significance, synthesis of vinylporphyrins has received special attention, particularly in structure/function (2–6) and isotopic labelling studies (7–9). In addition, the vinyl and cross-conjugated porphyrinic β,β′ double bonds of protoporphyrin IX (**1**) have been shown (10, 11) to undergo [4+2] cycloaddition reactions with electron-deficient dienophiles to give compounds (**3**) having essentially a *chlorin* chromophore (Scheme 1). With alkynes (**2**), the initially formed cycloadducts, under certain reaction conditions, undergo aromatization (12) with the concomitant loss of the angular methyl group to give benzoporphyrins (**4**). To study this cycloaddition reaction further, we have developed, and describe here, an efficient synthesis of vinylporphyrins.

Although peripheral substituent manipulations of protoporphyrin IX have been used to prepare several useful porphyrins (13), synthesis of a totally unsymmetrical porphyrin involves the stepwise coupling of individual pyrroles, leading to a linear tetrapyrrole, which is cyclized in the final step. Two of the most commonly used tetrapyrrolic precursors are 1,19-dimethylbilenes-b and 1,19-dimethylbiladienes-ac (14), which are converted to the porphyrin using cupric salts in refluxing solvents (e.g., dimethylformamide). This method, originally developed by Johnson and Kay (15), has since been successfully modified for the synthesis of several vinylporphyrins (2–9) and other unsymmetrically substituted porphyrins. However, the varying yields (20–50%) of porphyrin produced and the harsh acidic conditions required (H_2SO_4–CF_3CO_2H) to remove coordinated Cu after cyclization are notable disadvantages of this method.

Our approach to unsymmetrical porphyrins has been via 1-bromo-19-methylbiladienes-ac (**7**), which are prepared by the stannic chloride mediated coupling of a 5′-unsubstituted

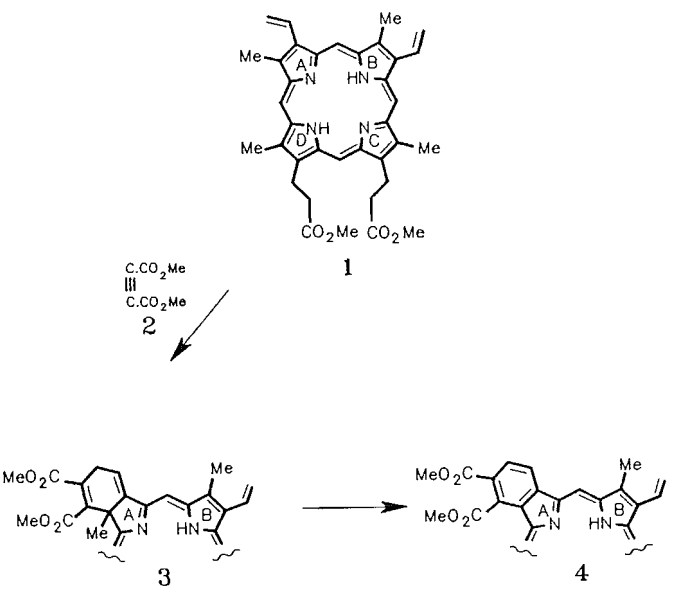

SCHEME 1

5-methyldipyrromethene (**5**) with a 5-bromo-5′-bromomethyldipyrromethene (**6**) and cyclized to the porphyrin (**8**) in DMSO–pyridine at room temperature, each reaction producing a greater than 80% yield (Scheme 2). This method, originally described by Johnson and co-workers (16, 17), suffered from a major drawback, viz. the traditional preparation of dipyrromethene **6** by the bromination of dipyrromethene **5** in hot anhydrous acetic or formic acid produced varying results, with yields of 50% being considered exceptional. However, the mild room temperature bromination procedure developed by us (18) (bromine in 10–15% TFA–1,2-dichloroethane) increased the accessibility of this important dipyrrolic intermediate and thereby made this route more versatile (19). We report here the syntheses of four vinylporphyrins using this method: a methylvinyl and an H-vinyl analogue (**8***a* and **8***b*), which have been used to study the regio- and stereochemistry of Diels–Alder additions as well as transformation to benzoporphyrins, and, in

[1]Author to whom correspondence may be addressed.

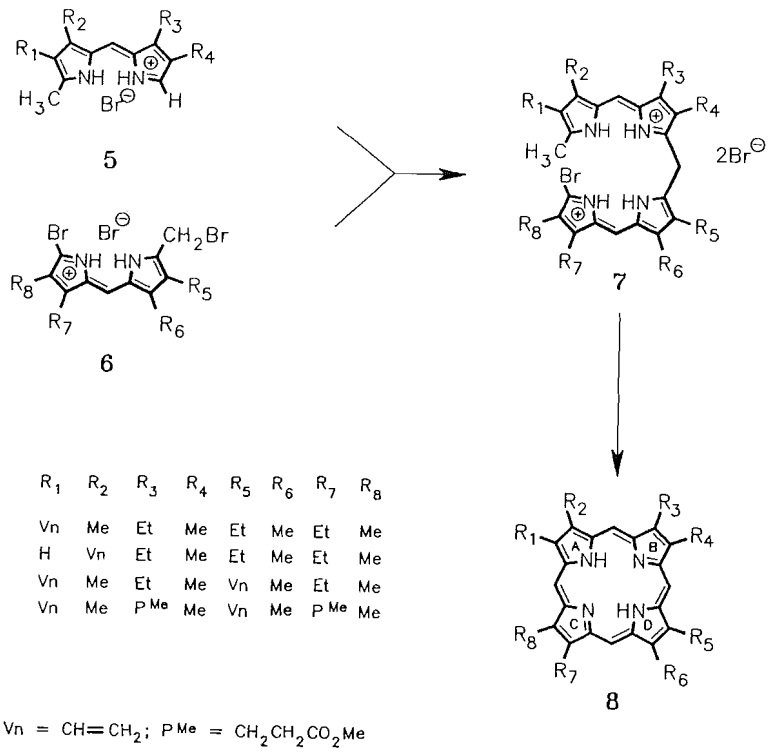

8	R_1	R_2	R_3	R_4	R_5	R_6	R_7	R_8
a.	Vn	Me	Et	Me	Et	Me	Et	Me
b.	H	Vn	Et	Me	Et	Me	Et	Me
c.	Vn	Me	Et	Me	Vn	Me	Et	Me
d.	Vn	Me	P^{Me}	Me	Vn	Me	P^{Me}	Me

SCHEME 2

addition, ring A,C-divinylporphyrins (**8***c* and **8***d*) have been prepared and used for a high yield synthesis of bacteriochlorins via two simultaneous Diels–Alder reactions.

Results and discussion

The sensitive nature of the vinyl substituent requires that a two-carbon vinyl precursor be carried through most of the synthetic sequence, with generation of the vinyl group being delayed until the final stages. The two most commonly used precursors are the 2-chloroethyl group (20) (derived from methoxycarbonylmethyl) and the acetyl group (21), the latter being transformed to the vinyl via the 1-hydroxyethyl moiety. Scheme 3 outlines the synthesis of the unsymmetrical porphyrins **8***a* and **8***b*; the cycloaddition reactions of the latter leading to benzoporphyrins have already been reported (22). Retrosynthetic analysis of the target porphyrins clearly indicated that the northern half carrying the reactive centres should constitute the 5′-unsubstituted 5-methyldipyrromethene components **20** and **21**. Of the two monopyrrolic precursors required for each synthesis, the common 5-unsubstituted 2-formylpyrrole (**19**) was prepared in high yield as reported earlier (23). The dipyrromethene **20** was obtained in 90% yield by coupling pyrrole **19** with 4-(methoxycarbonyl)methyl-3,5-dimethylpyrrole-2-carboxylic acid (**10**) (24) in the presence of 48% aqueous hydrobromic acid, the decarboxylation occurring *in situ*.

The α,β-diunsubstituted pyrrole **18** necessary for the synthesis of the dipyrromethene **21** was obtained from pyrrole **11** (Scheme 3), which in turn was prepared from benzyl acetoacetate and diethyl 3-oxopentanedioate as described earlier (25). Following catalytic debenzylation using 10% Pd–C, the resulting pyrrole-4-carboxylic acid (**12**) was decarboxylated by an indirect iodinative–deiodinative procedure (the electron-withdrawing 2-ethoxycarbonyl group prevents direct decarboxylation) to give the β-unsubstituted pyrrole (**14**) in 60% overall yield (from **11**). To manipulate the α-ester for pyrrole coupling, compound **14** was transbenzylated to the bis-benzyl ester **15** and preferentially transmethylated with sodium methoxide in methanol–THF at room temperature to give benzyl 3-(methoxycarbonyl)methyl-5-methylpyrrole-2-carboxylate (**16**) in 77% overall yield. Debenzylation of **16** to pyrrole-2-carboxylic acid **17** and coupling with the formylpyrrole **19** in the usual manner resulted in a low yield of the dipyrromethene **21**, suggesting that the replacement of an alkyl group at the 4-position by a hydrogen atom deactivated the ring towards electrophilic substitution. To overcome this problem, **17** was first decarboxylated to the diunsubstituted pyrrole **18** with trifluoroacetic acid at room temperature. Removal of the electron-withdrawing carboxyl group increased the nucleophilicity of the ring system and the coupling with **19** proceeded smoothly.

The dipyrromethenes **20** and **21** in dichloromethane were condensed separately with the 5-bromo-5′-bromomethyldipyrromethene **22** (18) using stannic chloride as the catalyst to give the biladienes **23** and **24** respectively in over 90% yield. They in turn, when treated with DMSO–pyridine, cyclized to the porphyrins **25** and **28** in over 80% yield. The transformation of the methoxycarbonylmethyl to the required vinyl substituent was effected via 2-hydroxyethyl and 2-chloroethyl groups. For best results, the porphyrins **25** and **28** were metalated (Zn) prior to reduction with lithium aluminum hydride and subsequently demetalated; this avoids any complications that may arise due to the possible irreversible insertion of aluminum. The porphyrins **26** and **29** so obtained (>95% yield) were converted to the 2-chloroethyl analogs **27** and **30** using thionyl chloride (95% yield) and dehydrochlorinated (aqueous NaOH in pyridine) to the vinylporphyrins **8***a* and **8***b* in 85% yield.

The substituents in the ring A,C-divinylporphyrins **8***c* and **8***d* (Scheme 2) were arranged to give the molecules a twofold axis of symmetry so that the 5-bromo-5′-bromomethyldipyrromethene (**6**) could be obtained by the direct bromination of 5′-unsubstituted 5-methyldipyrromethene (**5**). However, bro-

Can. J. Chem. Downloaded from www.nrcresearchpress.com by 91.121.58.235 on 09/07/12
For personal use only.

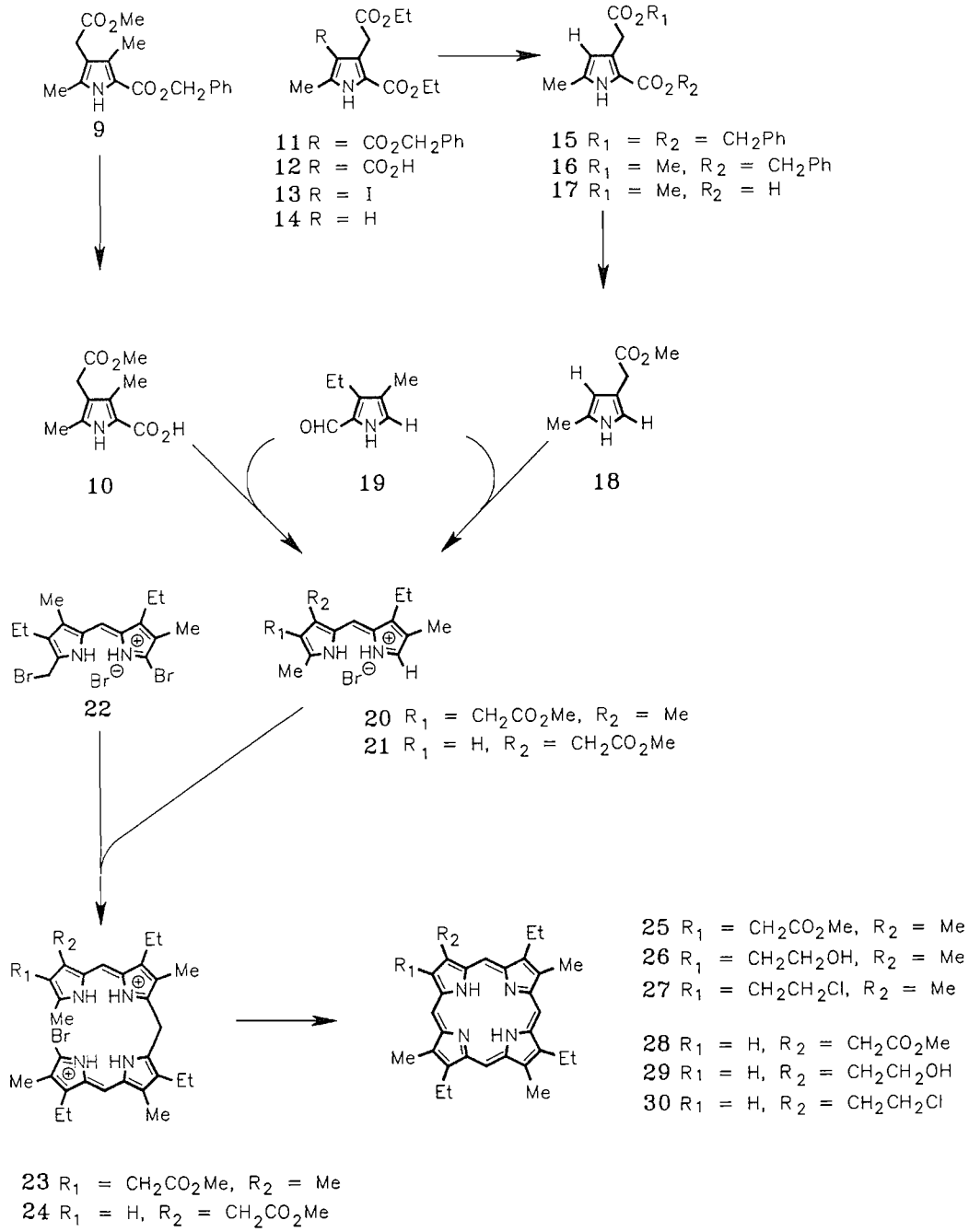

SCHEME 3

mination of the dipyrromethene **20** (Scheme 3), using bromine in 10–15% trifluoroacetic acid/1,2-dichloroethane turned out to be rather slow, giving at best a 70% yield of the bromomethyl derivative in 2 weeks. This required that the vinyl precursor be modified prior to bromination.

Scheme 4 outlines the synthetic sequence used. The common monopyrrolic precursor **33** was prepared starting from 4-(methoxycarbonyl)methylpyrrole **9**, by diborane reduction to 4-(2-hydroxyethyl)pyrrole **31**, protecting as the 4-(2-acetoxyethyl) derivative (**32**) followed by catalytic debenzylation of the α-ester group. 2-Formyl-3-ethyl-4-methylpyrrole (**19**) (23) and 2-formyl-3-(2-methoxycarbonyl)ethylpyrrole (**38**) (25) were synthesized according to literature procedures. Acid-catalyzed condensation of the pyrrole pairs **19, 33** and **38, 33** afforded the dipyrromethenes **39** and **40** in high yield. The former was successfully brominated (85% yield) with bromine in 10–15% TFA–1,2-dichloroethane, and the product, 5-bromo-5′-bromomethyldipyrromethene (**41**), coupled with **39** itself in the presence of anhydrous stannic chloride to give the biladiene-ac **43** in 79% yield. However, the bromination of the 2-(methoxycarbonyl)ethyl analog **40** under the same conditions was incomplete after 1 week, with the isolated material exhibiting approximately 80% reaction at the α-methyl group. To maximize the yield of the biladiene-ac **44**, the brominated product **42** was coupled, *without isolation* (after removal of excess bromine), with the α-unsubstituted dipyrromethene **40** to give an overall yield of 59% (from **40**). The biladienes **43** and **44** were subsequently cyclized in DMSO–pyridine to give the bis(2-acetoxyethyl)porphyrins **45** and **48** in over 85% yield. Removal of the acetoxy protection using 5% H_2SO_4 – methanol,

Can. J. Chem. Downloaded from www.nrcresearchpress.com by 91.121.58.235 on 09/07/12
For personal use only.

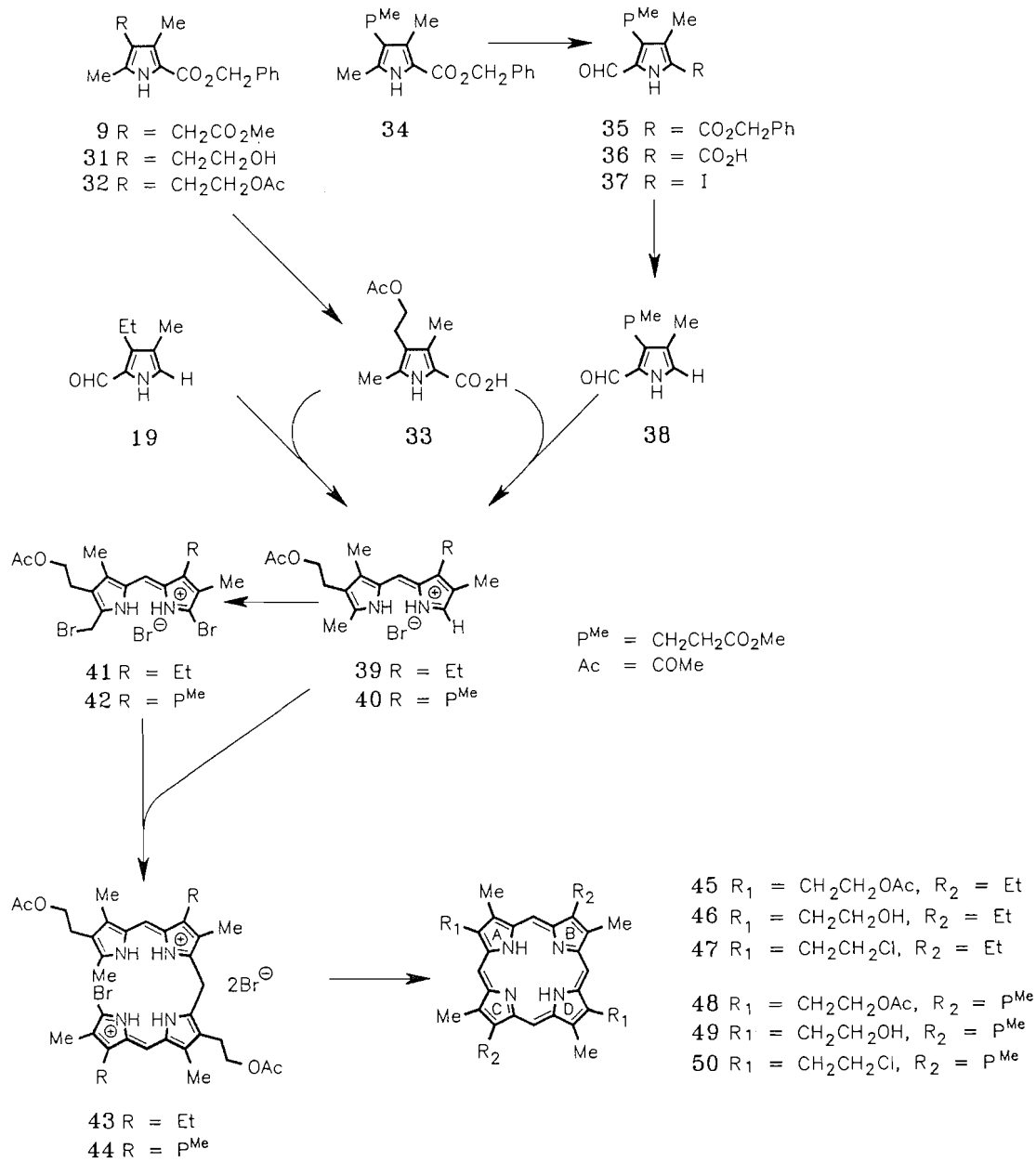

SCHEME 4

chlorination with thionyl chloride, and dehydrochlorination with aqueous NaOH in pyridine afforded the ring A,C-divinyl porphyrins **8***c* and **8***d* in high yield.

Experimental

The ^{1}H nmr spectra were recorded in the indicated solvents on a Varian XL-300 or a Bruker WH-400 spectrometer. Low resolution mass spectra were recorded on either a Varian MAT CH4B or a Kratos-AEI MS-50 instrument while high resolution measurements were obtained on the latter instrument. Melting points were determined using a Thomas Kofler Micro Hot Stage apparatus (dipyrromethenes and biladienes decompose rather than melt cleanly).

*Ethyl 4-carboxy-3-(ethoxycarbonyl)methyl-5-methylpyrrole-2-carboxylate (**12**)*

Ethyl-4-benzyloxycarbonyl-3-ethoxycarbonylmethyl-5-methylpyrrole-2-carboxylate (**11**) (37.3 g, 0.10 mol) in THF (500 mL) containing triethylamine (5 drops) and 10% Pd–C (1.5 g) was hydrogenated to completion at room temperature and atmospheric pressure. The catalyst was filtered, the filtrate evaporated to dryness, and the residue redissolved in hot ethanol (300 mL) and crystallized by the addition of water. The product, a white powder, was collected by filtration, washed with water, and dried. Yield 25.0 g (88%), mp 244–246°C; ^{1}H nmr (DMSO-d_6) δ: 1.25 (t, 3H, OCH_2CH_3), 1.32 (t, 3H, OCH_2CH_3), 4.10 (q, 2H, OCH_2CH_3), 4.15 (s, 2H, $CH_2CO_2C_2H_5$), 4.30 (q, 2H, OCH_2CH_3), 8.00 (s, 1H, NH), 11.80 (s, 1H, CO_2H); ms (*m/z*); 283 (M^+), 265, 236. Anal. calcd. for $C_{13}H_{17}NO_6$: C 55.12, H 6.05, N 4.94; found: C 55.07, H 6.10, N 4.85.

*Ethyl 3-(ethoxycarbonyl)methyl-4-iodo-5-methylpyrrole-2-carboxylate (**13**)*

To a hot solution of $NaHCO_3$ (35.0 g) in water (150 mL) was added the carboxypyrrole **12** (23.0 g, 81.3 mmol), and 1,2-dichloroethane (150 mL) added with stirring. A solution of I_2 (25 g) and NaI (30 g) in water (150 mL) was carefully added over 5 min and the reaction mixture refluxed for 15 min. The excess I_2 was destroyed by cautious

Can. J. Chem. Downloaded from www.nrcresearchpress.com by 91.121.58.235 on 09/07/12
For personal use only.

addition of aqueous $NaHSO_3$ and the reaction mixture extracted with dichloromethane. The organic phase was filtered, the solvent removed under reduced pressure, and the residual yellowish-brown oil dissolved in warm ethanol. Water was added until the solution turned turbid and, on cooling, the iodopyrrole crystallized out as pale yellow crystals that were filtered, washed with 65% aqueous ethanol, and air dried. Yield 25.6 g (86%), mp 110–111°C; ^{1}H nmr ($CDCl_3$) δ: 1.30 (2t, overlapping, 6H, 2 × OCH_2CH_3), 2.30 (s, 3H, CH_3), 3.80 (s, 2H, $CH_2CO_2C_2H_5$), 4.20 (q, 2H, OCH_2CH_3), 4.30 (q, 2H, OCH_2CH_3), 9.50 (br s, 1H, NH); ms (*m/z*): 365 (M^+), 320, 319, 292. Exact mass calcd. for $C_{12}H_{16}NO_4I$: 365.0123; found: 365.0123.

*Ethyl 3-(ethoxycarbonyl)methyl-5-methylpyrrole-2-carboxylate (**14**)*

The iodopyrrole **13** (21.3 g, 58 mmol) was dissolved in boiling methanol (150 mL) and treated with a solution of NaI (18 g) in water (20 mL), followed immediately by concentrated HCl (10 mL). The solution turned dark brown with liberation of iodine. The mixture was refluxed for 10 min, cooled to room temperature, and solid $NaHSO_3$ was added to destroy the iodine. Water (150 mL) was added to dissolve the excess bisulfite and the mixture extracted with dichloromethane (3 × 100 mL). The combined organic layers were washed with saturated $NaHCO_3$ (2 × 200 mL) and water (200 mL), dried over anhydrous $MgSO_4$, and concentrated to give a pale yellow oil. The oil was dissolved in ether (30 mL) and *n*-hexane added dropwise to induce crystallization. The white crystals were collected by filtration, washed with *n*-hexane, and air dried. Yield 11.0 g (79%), mp 80–81°C; ^{1}H nmr ($CDCl_3$) δ: 1.28 (t, 3H, OCH_2CH_3), 1.35 (t, 3H, OCH_2CH_3), 2.30 (s, 3H, CH_3), 3.82 (s, 2H, $CH_2CO_2C_2H_5$), 4.18 (q, 2H, OCH_2CH_3), 4.30 (q, 2H, OCH_2CH_3), 5.95 (s, 1H, pyr-H), 8.92 (br s, 1H, NH); ms (*m/z*): 239 (M^+), 193, 166. Exact mass calcd. for $C_{12}H_{17}NO_4$: 239.1158; found: 239.1155.

*Benzyl 3-(benzyloxycarbonyl)methyl-5-methylpyrrole-2-carboxylate (**15**)*

The pyrrole (**14**) (6.0 g, 25.2 mmol) in refluxing benzyl alcohol (150 mL) was treated, under nitrogen, with 1-mL portions of a concentrated solution of sodium benzyloxide (prepared from freshly cut sodium in benzyl alcohol) until no further evolution of ethanol vapors occurred. The hot solution was poured into a stirred solution of methanol (100 mL) and acetic acid (10 mL), diluted with water, and cooled. The precipitated solid was collected by filtration, washed with 50% aqueous methanol, then with water, and air dried to give the desired product as colourless crystals. Yield 7.78 g (85%), mp 92–93°C; ^{1}H nmr ($CDCl_3$) δ: 2.24 (s, 3H, CH_3), 2.86 (s, 2H, $CH_2CO_2CH_2C_6H_5$), 5.08 (s, 2H, $CH_2C_6H_5$), 5.21 (s, 2H, $CH_2C_6H_5$), 5.92 (s, 1H, pyr-H), 7.32 (m, 10H, 2 × C_6H_5), 8.70 (br s, 1H, NH); ms (*m/z*): 363 (M^+), 228, 91. Exact mass calcd. for $C_{22}H_{21}NO_4$: 363.1471; found: 363.1470.

*Benzyl 3-(methoxycarbonyl)methyl-5-methylpyrrole-2-carboxylate (**16**)*

A solution of the pyrrole **15** (6.0 g, 17 mmol) in dry tetrahydrofuran (20 mL) and anhydrous methanol (25 mL) was stirred at room temperature under argon with a solution of sodium methoxide (63.3 mg of sodium in 5 mL of methanol). When tlc indicated that no starting material remained, the reaction was quenched with acetic acid (10 mL) and the solution concentrated to a pale yellowish-brown oil, which was dissolved in a minimum of methanol and treated with water to afford a precipitate of tan crystals. The solid was recrystallized from ether–hexane to give the product as colourless crystals (4.30 g, 91%), mp 82–84°C; ^{1}H nmr ($CDCl_3$) δ: 2.25 (s, 3H, CH_3), 3.65 (s, 3H, CO_2CH_3), 3.82 (s, 2H, CH_2CO_2CH3), 5.30 (s, 2H, $CH_2C_6H_5$), 5.95 (s, 1H, pyr-H), 7.40 (m, 5H, C_6H_5), 8.90 (br s, 1H, NH); ms (*m/z*): 287 (M^+), 196, 153, 91. Anal. calcd. for $C_{16}H_{17}NO_4$: C 66.89, H 5.96, N 4.88; found: C 66.69, H 5.95, N 4.84.

*3-(Methoxycarbonyl)methyl-5-methylpyrrole-2-carboxylate (**17**)*

The pyrrole **16** (4.0 g, 14 mmol) in THF (400 mL) containing triethylamine (0.1 mL) and 10% Pd–C (0.4 g) was hydrogenated as described earlier and the resulting pale yellow oil was crystallized from THF–hexane to give the desired product as a white powder (2.6 g, 95%), mp 190°C (dec.); ^{1}H nmr (DMSO-d_6) δ: 2.10 (s, 3H, CH_3), 3.60 (s, 3H, OCH_3), 3.76 (s, 2H, $CH_2CO_2CH_3$), 5.80 (s, 1H, pyr-H), 11.22 (br s, 1H, NH), CO_2H too broad to be observed; ms (*m/z*): 153 ($M^+ - CO_2$), 94. Exact mass calcd. for $C_8H_{11}NO_2$: 153.0790; found: 153.0791.

*4-Methoxycarbonylmethyl-2-methylpyrrole (**18**)*

The foregoing pyrrolecarboxylic acid **17** (2.50 g, 12.7 mmol) was stirred in trifluoroacetic acid (20 mL) under nitrogen for 30 min (reaction monitored by tlc). The trifluoroacetic acid was evaporated *in vacuo*, the residual oil dissolved in dichloromethane (50 mL), washed twice with aqueous $NaHCO_3$, and dried ($MgSO_4$). The filtered solution was evaporated to a yellow oil, which was purified by column chromatography (silica gel 60, dichloromethane eluent) to give the product as a colourless oil (1.85 g, 95%) that could not be induced to crystallize; ^{1}H nmr ($CDCl_3$) δ: 2.30 (s, 3H, CH_3), 3.50 (s, 2H, $CH_2CO_2CH_3$), 3.70 (s, 3H, CO_2CH_3), 5.85 (s, 1H, 4-H), 6.56 (s, 1H, 2-H), 7.86 (br s, 1H, NH); ms (*m/z*): 153 (M^+), 94. Exact mass calcd. for $C_8H_{11}NO_2$: 153.0790; found: 153.0796.

*3′-Ethyl-4-(methoxycarbonyl)methyl-3,4′,5-trimethyl-2,2′-dipyrromethene hydrobromide (**20**)*

3-Ethyl-2-formyl-4-methylpyrrole (**19**) (23) (3.01 g, 21 mmol) and 2-carboxy-4-methoxycarbonylmethyl-3,5-dimethylpyrrole (**10**) (25) (4.22 g, 20 mmol) were dissolved in THF (110 mL) and treated with aqueous HBr (48%, 5 mL). The colour of the solution changed from yellow to dark orange. The solvent was replaced under reduced pressure by adding methanol at regular intervals. The reaction mixture was cooled in an ice bath, the precipitated product filtered, washed with 10% methanol – ether, then with ether, and air dried. Yield 5.15 g (90%), mp 160°C (dec.); ^{1}H nmr ($CDCl_3$) δ: 1.17 (t, 3H, J = 7.5 Hz, CH_2CH_3), 2.10 (s, 3H, CH_3), 2.35 (s, 3H, CH_3), 2.70 (q, 2H, CH_2CH_3), 2.75 (s, 3H, CH_3), 3.67 (s, 3H, OCH_3), 3.71 (s, 2H, CH_2CO), 7.17 (s, 1H, bridge CH), 7.57 (d, 1H, J = 4.0 Hz, pyr-H), 13.23 (br s, 2H, 2 × NH); ms (*m/z*): 286 ($M^+ - HBr$), 271. Exact mass calcd. for $C_{17}H_{22}N_2O_2$: 286.1681; found: 286.1685.

*3′-Ethyl-3-(methoxycarbonyl)methyl-4′,5-dimethyl-2,2′-dipyrromethene hydrobromide (**21**)*

3-Ethyl-2-formyl-4-methylpyrrole (**19**) (1.66 g, 12.1 mmol) and 4-(methoxycarbonyl)methyl-2-methylpyrrole (**18**) in methanol were cooled to 0°C and treated with aqueous HBr (48%, 2 mL). The mixture was stirred for 30 min, when the solution darkened and the product crystallized. The crystals were collected, washed successively with cold methanol, ether, and hexane, and air dried. Yield 3.22 g in three crops (75%), mp 120–121°C; ^{1}H nmr ($CDCl_3$) δ: 1.22 (t, 3H, CH_2CH_3), 2.15 (s, 3H, CH_3), 2.76 (q, 2H, CH_2CH_3), 2.80 (s, 3H, CH_3), 3.80 (s, 3H, OCH_3), 3.82 (s, 2H, CH_2CO), 6.40 (s, 1H, 4-H), 7.30 (s, 1H, bridge CH), 7.62 (d, 1H, J = 3.0 Hz, 5-H), 13.50 (br s, 2H, 2 × NH); ms (*m/z*): 272 ($M^+ - HBr$), 257, 243. Exact mass calcd. for $C_{16}H_{20}N_2O_2$: 272.1725; found: 272.1728.

*4-(2-Acetoxyethyl)-3′-ethyl-3,4′,5-trimethyl-2,2′-dipyrromethene hydrobromide (**39**)*

Benzyl-4-(2-acetoxyethyl)-3,5-dimethylpyrrole-2-carboxylate (**32**) (20 g, 63 mmol) in THF (300 mL) containing triethylamine (5 drops) and 10% Pd–C (2.0 g) was hydrogenated at room temperature and atmospheric pressure. The catalyst was filtered, and the filtrate treated with a solution of pyrrole **19** (9.6 g, 70 mmol) in THF (75 mL) followed by aqueous HBr (48%, 70 mL). The solvent was slowly replaced with methanol under reduced pressure until crystallization occurred. The orange crystals were filtered, washed with methanol, and air dried. Yield 19 g in two crops (79%), mp 146°C (dec.); ^{1}H nmr ($CDCl_3$/TFA) δ: 1.18 (t, 3H, J = 7.5 Hz, CH_2CH_3), 2.00 (s, 3H, CH_3), 2.04 (s, 3H, CH_3), 2.35 (s, 3H, $COCH_3$), 2.65 (s, 3H, CH_3), 2.75 (m, overlap, 4H, CH_2CH_3 and CH_2CH_2O-), 4.10 (t, 2H, J = 6.5 Hz, CH_2CH_2O-), 6.80 (s, 1H, bridge CH), 7.45 (d, 1H, J = 3.2 Hz, pyr-H), 12.80 (br s, 1H, NH), 13.00 (br s, 1H, NH). Anal. calcd. for $C_{19}H_{27}N_2BrO_2$: C 57.22, H 6.88, N 7.09; found: C 57.68, H 6.85, N 7.05.

Can. J. Chem. Downloaded from www.nrcresearchpress.com by 91.121.58.235 on 09/07/12
For personal use only.

Can. J. Chem. Downloaded from www.nrcresearchpress.com by 91.121.58.235 on 09/07/12
For personal use only.

*4-(2-Acetoxyethyl)-3'-[(methoxycarbonyl)ethyl]-3,4',5-trimethyl-2,2'-dipyrromethene hydrobromide (**40**)*

The pyrrole **32** (25), (1.35 g, 4.3 mmol) in THF (35 mL) containing triethylamine (5 drops) and 10% Pd–C (140 mg) was hydrogenated as described above. The 2-formylpyrrole **38** (24) (0.85 g, 4.4 mmol) was added, the catalyst filtered, and the volume reduced to 15 mL. Methanol (35 mL) was added, the solution warmed on a water bath and treated with aqueous HBr (1 mL). Following 5 min of heating, trimethyl orthoformate (1 mL) was added and heating was continued for a further 5 min. The solution was concentrated *in vacuo* (ca. 15 mL), diluted with diethyl ether (50 mL), and cooled. The solid was collected by filtration, washed with 5% methanol – diethyl ether, then with ether, and dried in air. Yield 1.67 g (89%), mp 157–159°C; ^{1}H nmr ($CDCl_3$/TFA) δ: 2.05 (s, 3H, CH_3), 2.11 (s, 3H, CH_3), 2.40 (s, 3H, $COCH_3$), 2.57 (t, 2H, CH_2), 2.75 (s, 3H, CH_3), 2.79 (t, 2H, CH_2), 3.02 (t, 2H, CH_2), 3.63 (s, 3H, OCH_3), 4.13 (t, 2H, OCH_2), 7.43 (s, 1H, bridge CH), 7.61 (d, 1H, pyr-H), 13.17 (br s, 1H, NH), 13.35 (br s, 1H, NH); ms (*m/z*): 358 ($M^+ - HBr$), 284, 223, 211. Exact mass calcd. for $C_{20}H_{26}H_2O_4$: 358.1892; found: 358.1891.

*4-(2-Acetoxyethyl)-5'-bromo-5-bromomethyl-3'-ethyl-3,4'-dimethyl-2,2'-dipyrromethene hydrobromide (**41**)*

4-(2-Acetoxyethyl)-3'-ethyl-3,4',5-trimethyl-2,2'-dipyrromethene hydrobromide **39** (1.5 g, 4 mmol), trifluoroacetic acid (1.5 mL), and bromine (1.9 g, 12 mmol) were stirred in 1,2-dichloroethane (12 mL) at room temperature with exclusion of moisture for 1 week. The solution was cooled and ether (20 mL) added with stirring until crystallization occurred. The crystals were collected, washed with ether, redissolved in dichloromethane (70 mL), and treated with cyclohexene (6 mL). The dichloromethane was replaced by ethyl acetate under reduced pressure, the resulting red crystals were collected, washed with ethyl acetate, then with hexane, and air dried. Yield 1.81 g (85%), mp 175°C (dec.); ^{1}H nmr ($CDCl_3$/TFA) δ: 1.25 (t, 3H, J = 7.5 Hz, CH_2CH_3), 2.10 (s, 3H, CH_3), 2.18 (s, 3H, $COCH_3$), 2.40 (s, 3H, CH_3), 2.75 (q, 2H, J = 7.5 Hz, CH_2CH_3), 3.00 (t, 2H, J = 6.5 Hz, CH_2CH_2O-), 4.50 (t, 2H, J = 6.5 Hz, CH_2CH_2O-), 4.95 (s, 2H, CH_2Br), 7.20 (s, 1H, bridge CH), 13.00 (br 2s, 2H, 2 × NH). Anal. calcd. for $C_{18}H_{23}N_2Br_3O_2$: C 40.10, H 4.30, N 5.20; found: C 39.45, H 4.15, N 4.85.

*1-Bromo-3,8,13-triethyl-18-(methoxycarbonyl)methyl-2,7,12,17,19-pentamethylbiladiene-ac dihydrobromide (**23**)*

The dipyrromethenes **20** (917 mg, 2.5 mmol) and **22** (1.202 g, 2.5 mmol) in dichloromethane (200 mL) were treated with stannic chloride (4 mL) and the mixture stirred for 1.5 h with exclusion of moisture. The reaction was quenched with aqueous HBr (4 mL of 48% HBr in 50 mL of water), the organic phase was poured into a mixture of methanol (100 mL) and aqueous HBr (48%, 25 mL), concentrated *in vacuo*, and allowed to stand in the refrigerator. The desired biladiene was collected by filtration, washed with ethyl acetate, then with *n*-hexane, and air dried. Yield 1.92 g (99%), mp 190°C (dec.); ^{1}H nmr ($CDCl_3$) δ: 0.67, 1.12, 1.22 (3t, 3H each, 3 × CH_2CH_3), 1.98, 2.09, 2.29, 2.35 (4s, 3H each, 4 × CH_3), 2.52 (q, 2H, CH_2CH_3), 2.64 (q, 2H, CH_2CH_3), 2.75 (s, overlap, 3H, CH_3), 2.75 (q, overlap, 2H, CH_2CH_3), 3.48 (s, 2H, CH_2CO), 3.72 (s, 3H, OCH_3), 5.25 (s, 2H, bridge CH_2), 7.12, 7.15 (2s, 1H each, 2 × bridge CH), 13.35, 13.52, 13.70, 13.92 (4 br s, 1H each, 4 × NH); ms (*m/z*): 522 (M^+; cyclized porphyrin product). Exact mass calcd. for $C_{33}H_{38}N_4O_2$: 522.2995; found: 522.2996.

*1-Bromo-3,8,13-triethyl-17-(methoxycarbonyl)methyl-2,7,12,19-tetramethylbiladiene-ac dihydrobromide (**24**)*

This biladiene was similarly prepared from the dipyrromethenes **21** (1.26 g, 3.56 mmol) and **22** (1.72 g, 3.56 mmol) and afforded 2.41 g (90%) of dark reddish-brown crystals, mp 182°C (dec.); ^{1}H nmr ($CDCl_3$) δ: 0.75, 0.92, 1.14 (3t, 3H each, 3 × CH_2CH_3); 1.99, 2.30, 2.31 (3s, 3H each, 3 × CH_3) 3.50 (q, 2H, CH_2CH_3), 2.65 (s, 3H, CH_3), 2.75 (2q, overlap, 2H each, 2 × CH_2CH_3), 3.59 (s, 3H, OCH_3), 3.95 s, 2H, CH_2CO), 5.18 (s, 2H, bridge CH_2), 7.14, 7.15 (2s, 1H each, 2 × bridge CH), 7.32 (s, 1H, β-H), 13.57, 13.65, 13.73, 13.79 (4 br s, 1H each, 4 × NH); ms (*m/z*): 508 (M^+; cyclized porphyrin product). Exact mass calcd. for $C_{32}H_{36}N_4O_2$: 508.2828; found: 508.2838.

*1-Bromo-8,18-bis(2-acetoxyethyl)-3,13-diethyl-2,7,12,17,19-pentamethylbiladiene-ac dihydrobromide (**43**)*

This biladiene was similarly prepared from the dipyrromethenes **39** (0.9 g, 2.4 mmol) and **41** (1.3 g, 2.4 mmol) to give 1.60 g (79%) of product, mp 195°C (dec.); ^{1}H nmr ($CDCl_3$) δ: 1.20 (2t, overlap, 6H, 2 × CH_2CH_3), 2.15 (s, 3H, CH_3), 2.16 (s, 3H, CH_3), 2.37 (s, 6H, 2 × $COCH_3$), 2.60–3.00 (m, overlap, 4H, 2 × CH_2CH_3), 2.65, 2.68, 2.70 (3s, 3H each, CH_3), 3.80 (2t, overlap, 4H, 2 × CH_2CH_2O-), 4.40 (2t, overlap, 4H, 2 × CH_2CH_2O-), 4.50 (s, 2H, bridge CH_2), 7.20, 7.26 (2s, 1H each, bridge CH), 11.70–12.60 (4s, 1H each, 4 × NH); ms (*m/z*): 594 (M^+; cyclized porphyrin product). Exact mass calcd. for $C_{32}H_{42}N_4O_4$: 594.3206; found: 594.3208.

*1-Bromo-8,18-bis(2-acetoxyethyl)-3,13-bis[(methoxycarbonyl)ethyl]-2,7,12,17,19-pentamethylbiladiene-ac dihydrobromide (**44**)*

The dipyrromethene **40** (355 mg; 0.81 mmol), trifluoroacetic acid (2.5 mL), bromine (390 mg; 2.4 mmol), and dichloromethane (10 mL) were stirred at room temperature for 2 weeks, protected from moisture. The solvent was removed *in vacuo*, the residue taken into dichloromethane and treated with cyclohexene. The solution was evaporated to dryness, redissolved in dichloromethane (20 mL), stirred in the dipyrromethene **40** (290 mg; 0.66 mmol), and treated with $SnCl_4$ (1 mL) in dichloromethane (1 mL). The solution was allowed to stand at room temperature for 2.5 h and quenched with a mixture of methanol (10 mL) and 48% aqueous HBr (1.5 mL). Dichloromethane (60 mL) was added, the solution extracted with water (2 × 30 mL) and concentrated to ca. 15 mL. Slow addition of diethyl ether resulted in the crystallization of the product, which was filtered, washed with 10% methanol – diethyl ether, and dried in air. Yield 456 mg; 59% overall for 2 steps; ^{1}H nmr ($CDCl_3$) δ: 1.86, 2.00, 2.06, 2.09, 2.37, 2.40 (6s, 3H each, 6 × CH_3), 2.53 (t, 2H, CH_2), 2.60 (t, 2H, CH_2), 2.75 (s, 3H, CH_3), 2.80 (t, 2H, CH_2), 2.96 (2t, overlap, 4H, 2 × CH_2), 3.07 (t, 2H, CH_2), 3.52 (t, 2H, CH_2), 3.62, 3.65, (2s, 3H each, 2 × OCH_3, 4.13 (t, 2H, CH_2), 5.25 (s, 2H, bridge CH_2), 7.35, 7.37, (2s, 1H each, bridge CH), 13.41, 13.54, 13.88, 14.12 (4s, 1H each, NH); ms (*m/z*): 710, (M^+; cyclized porphyrin product), 696, 651, 637. Exact mass calcd. for $C_{40}H_{46}N_4O_8$: 710.3316; found: 710.3322.

*7,12,17-Triethyl-2-(methoxycarbonyl)methyl-3,8,13,18-tetramethylporphyrin (**25**)*

The biladiene **23** (1.60 g, 2.08 mmols) dissolved in DMSO (200 mL) was treated with pyridine (10 mL) and allowed to stand in the dark at room temperature for 5 days. The porphyrin crystals were collected by filtration, washed with methanol, and air dried. Yield 0.89 g in two crops (82%), mp 289–290°C; visible spectrum (CH_2Cl_2) λ_{max} (nm) (relative intensities): 400 (18.5), 498 (2.00), 534 (1.57), 568 (1.08), 620 (1.00); ^{1}H nmr ($CDCl_3$) δ: −3.73 (br s, 2H, 2 × NH), 1.86 (3t, 3H each, 3 × CH_2CH_3), 3.60 (s, 3H, CH_3), 3.65 (s, 9H, 3 × CH_3), 3.76 (s, 3H, OCH_3), 4.03–4.14 (3q, overlap, 2H each, 3 × CH_2CH_3), 5.05 (s, 2H, CH_2CO), 10.07 (s, 2H, 2 × *meso*-H), 11.01, 11.04 (2s, 1H each, 2 × *meso*-H; ms (*m/z*): 522 (M^+). Anal. calcd. for $C_{33}H_{38}N_4O_2$: C 75.83, H 7.33, N 10.72; found: C 75.67, H 7.39, N 10.68.

*7,12,17-Triethyl-2-(2-hydroxyethyl)-3,8,13,18-tetramethylporphyrin (**26**)*

A solution of the porphyrin **25** (200 mg, 0.38 mmol) in dichloromethane (60 mL) was stirred with a saturated solution of zinc acetate in methanol (2 mL) and the metal insertion was monitored by ultraviolet–visible spectroscopy. More dichloromethane (100 mL) was added, the organic phase washed twice with water, and the solvent removed to afford the zinc complex (0.20 g, 90%), which was dried and used without further purification.

In a cooled 250-mL two-necked round-bottomed flask equipped with a magnetic stirring bar and an argon gas inlet was placed a slurry of

Can. J. Chem. Downloaded from www.nrcresearchpress.com by 91.121.58.235 on 09/07/12
For personal use only.

lithium aluminum hydride (49.0 mg, 1.28 mmol) in THF (30 mL), which was treated, dropwise, with a solution of the zinc complex (150 mg, 0.26 mmol) in THF. The reaction mixture was allowed to warm to room temperature and stirred for 2 h (progress monitored by tlc). Cold water was carefully added to quench the reaction (H_2 evolved), the mixture was extracted with dichloromethane, and the organic phase shaken with trifluoroacetic acid (3 mL) to demetalate the zinc complex. The excess acid was removed by washing the dichloromethane solution with 5% aqueous $NaHCO_3$, followed by water, and dried ($MgSO_4$). Evaporation of the solvent *in vacuo* afforded the desired porphyrin. Yield 122 mg (95%). A sample was recrystallized from chloroform–ether to give fine purple crystals, mp 275°C (dec.); visible spectrum (CH_2Cl_2) λ_{max} (nm) (relative intensities): 400 (25.2), 498 (2.78), 532 (2.24), 566 (1.65), 620 (1.00); ^{1}H nmr ($CDCl_3$) δ: −3.76 (br s, 2H, 2 × NH), 1.87 (3t, overlap, 9H, 3 × CH_2CH_3), 3.61, 3.64, 3.65, 3.66 (4s, 3H each, 4 × CH_3), 4.10 (3q, overlap, 6H, 3 × CH_2CH_3), 4.35 (t, 2H, CH_2CH_2OH), 4.48 (t, 2H, CH_2CH_2OH), 10.08 (s, 1H, *meso*-H), 10.09, (s, 2H, 2 × *meso*-H), 11.01 (s, 1H, *meso*-H); ms (*m/z*): 494 (M^+), 463. Exact mass calcd. for $C_{32}H_{38}N_4O$: 494. 3046; found: 494.3051.

*2-(2-Chloroethyl)-7,12,17-triethyl-3,8,13,18-tetramethylporphyrin (**27**)*

A mixture of the porphyrin (**26**) (200 mg, 0.405 mmol), dichloromethane (100 mL), DMF (20 mL), and K_2CO_3 (6 g) was stirred at room temperature and treated with thionyl chloride (6 mL). On completion of the reaction (monitored by tlc), water was added, the organic phase washed with $NaHCO_3$, followed by water, and dried ($MgSO_4$). After filtration, removal of solvent under reduced pressure gave a purple-brown solid, which was purified by chromatography (silica gel 70–230 mesh, dichloromethane eluent) and recrystallized from chloroform–methanol. Yield 180.4 mg (86%), mp 250°C (dec.); visible spectrum (CH_2Cl_2) λ_{max} (nm) (relative intensities): 398 (34.1), 498 (2.35), 534 (1.82), 566 (1.35), 620 (1.00); ^{1}H nmr ($CDCl_3$) δ: −3.75 (br s, 2H, 2 × NH), 1.88 (2t, overlap, 9H, 3 × CH_2CH_3), 3.61 (s, 3H, CH_3), 3.66 (s, 9H, 3 × CH_3), 4.04–4.14 (3q, overlap, 6H, 3 × CH_2CH_3), 4.32 (t, 2H, CH_2CH_2Cl), 4.52 (t, 2H, CH_2CH_2Cl), 10.01, 10.08, 10.09, 10.11 (4s 1H each, 4 × *meso*-H); ms (*m/z*): 512 (M^+), 497, 478, 463. Exact mass calcd. for $C_{32}H_{37}N_4Cl$: 512.2707; found: 512.2715.

*7,12,17-Triethyl-3,8,13,18-tetramethyl-2-vinylporphyrin (**8**a)*

The porphyrin **27** (150 mg, 0.293 mmol) in pyridine (100 mL) was heated at reflux under nitrogen for 10 min and treated with a 10% aqueous NaOH solution (10 mL). Heating was continued for an additional 2 h (completion of reaction shown by tlc), 50% aqueous acetic acid (40 mL) was added, and the mixture was extracted with dichloromethane (200 mL). The organic layer was washed with 5% aqueous $NaHCO_3$ (3 × 200 mL), followed by water (2 × 200 mL), dried ($MgSO_4$), and evaporated to dryness. The residue was chromatographed (silica gel 60, dichloromethane eluent) to give a pink residue after solvent evaporation. Recrystallization from chloroform–methanol gave the title porphyrin as purple prisms. Yield 121.3 mg (87%), mp 220°C (dec.); visible spectrum (CH_2Cl_2) λ_{max} (nm) (relative intensities): 400 (18.6), 502 (2.04), 538 (1.93), 570 (1.40), 624 (1.00); ^{1}H nmr ($CDCl_3$) δ: −3.68 (br s, 2H, 2 × NH), 1.90 (3t, overlap, 3H each, 3 × CH_2CH_3) 6.15 (dd, 1H, J = 1.5, 11.5 Hz, CH=CH_2), 6.36 (dd, 1H, J = 1.5, 17.5 Hz, CH=CH_2), 8.32 (dd, 1H, J = 11.5, 17.5 Hz, CH=CH_2), 10.07 (s, 2H, 2 × *meso*-H), 10.15, 10.23 (2s, 1H each, 2 × *meso*-H); ms (*m/z*): 476 (M^+), 461, 446. Exact mass calcd. for $C_{32}H_{36}H_4$: 476.2940; found: 476.2940. Anal. calcd. for $C_{32}H_{36}N_4$: C 80.63, H 7.61, N 11.76; found: C 80.54, H 7.63, N 11.74.

*7,12,17-Triethyl-3-(methoxycarbonyl)methyl-8,13,18-trimethylporphyrin (**28**)*

The biladiene **24** (2.00 g, 2.66 mmol) was cyclized in DMSO (300 mL) and pyridine (10 mL) as described earlier to afford 1.12 g (83%) of the pure product after chromatography and recrystallization; mp 228–230°C; visible spectrum (CH_2Cl_2) λ_{max} (nm) (relative intensities): 398 (29.9), 498 (3.00), 534 (2.37), 566 (1.80), 620 (1.00); ^{1}H nmr ($CDCl_3$) δ: −3.88 (br s, 2H, 2 × NH), 1.85 (3t, overlap, 9H, J = 7.5 Hz, 3 × CH_2CH_3), 3.55, 3.58, 3.62 (3s, 9H, 3 × CH_3), 3.85 (s, 3H, OCH_3), 3.97–4.11 (3q, overlap, 6H, J = 7.5 Hz, 3 × CH_2CH_3), 5.16 (s, 2H, $CH_2CO_2CH_3$), 9.24 (s, 1H, β-H), 10.00–10.12 (4s, 1H each, 4 × *meso*-H); ms (*m/z*): 508 (M^+), 493, 478, 449. Anal. calcd. for $C_{32}H_{36}N_4O_2$: C 75.56, H 7.13, N 11.01; found: C 75.40, H 7.25, N 10.86.

*7,12,17-Triethyl-3-(2-hydroxyethyl)-8,13,18-trimethylporphyrin (**29**)*

This was prepared in 95% yield from the porphyrin **28** as described earlier; mp 273–274°C; visible spectrum (CH_2Cl_2) λ_{max} (nm) (relative intensities): 400 (28.17), 498 (2.29), 532 (2.05), 568 (1.78), 620 (1.00); ^{1}H nmr ($CDCl_3$) δ: −3.75 (br s, 2H, 2 × NH), 1.88 (2t, overlap, 9H, 3 × CH_2CH_3), 3.62, 3.65, 3.69 (3s, 3H each, 3 × CH_3), 4.10 (3q, 6H, 3 × CH_2CH_3), 4.45 (t, 2H, CH_2CH_2OH), 4.62 (t, 2H, CH_2CH_2OH), 9.19 (s, 1H, β-H), 10.08–10.16 (4s, 1H each, 4 × *meso*-H); ms (*m/z*): 480 (M^+), 465, 449. Exact mass calcd. for $C_{31}H_{36}N_4O$: 480.2889; found: 480.2892.

*3-(2-Chloroethyl)-7,12,17-triethyl-8,13,18-trimethylporphyrin (**30**)*

This was prepared in 95% yield from 2-hydroxyethylporphyrin **29** as described earlier; mp 230–232°C; visible spectrum (CH_2Cl_2) λ_{max} (nm) (relative intensities): 400 (30.1), 502 (2.52), 542 (2.42), 570 (1.73), 626 (1.00); ^{1}H nmr ($CDCl_3$) δ: −3.80 (br s, 2H, 2 × NH), 1.08 (3t, overlap, 9H, 3 × CH_2CH_3), 3.61, 3.65, 3.69 (3s, 3H each, 3 × CH_3), 4.02–4.17 (3q, overlap, 6H, 3 × CH_2CH_3), 4.51 (t, 2H, CH_2CH_2Cl), 4.67 (t, 2H, CH_2CH_2Cl), 9.20 (s, 1H, β-H), 10.10–10.14 (4s, 1H each, 4 × *meso*-H); ms (*m/z*): 498 (M^+), 483, 462. Exact mass calcd. for $C_{31}H_{35}N_4Cl$: 498.2550; found: 498.2552.

*7,12,17-Triethyl-8,13,18-trimethyl-3-vinylporphyrin (**8**b)*

This was prepared in 88% yield by the dehydrochlorination of porphyrin **30** as described earlier; mp 221–222°C; visible spectrum (CH_2Cl_2) λ_{max} (nm) (relative intensities): 402 (22.35), 504 (2.27), 544 (2.51), 570 (1.69), 630 (1.00); ^{1}H nmr ($CDCl_3$) δ: −3.66 (s, 2H, 2 × NH), 1.90 (2t, overlap, 9H, 3 × CH_2CH_3), 3.60, 3,64, 3.66 (3s, 9H, 3 × -CH_3), 4.15 (2q, overlap, 6H, 3 × CH_2CH_3), 6.40 (d, 1H, J = 12.0 Hz, CH=CH_2), 6.63 (d, 1H, J = 17.0 Hz, CH=CH_2), 8.47 (dd, 1H, J = 12.0, 17.0 Hz, CH=CH_2), 9.44 (s, 1H, Ar-H), 10.06, 10.07, 10.10, 10.26 (4s, 1H each, 4 × *meso*-H); ms (*m/z*): 462 (M^+), 447, 432. Exact mass calcd. for $C_{31}H_{34}N_4$: 462.2783; found: 462.2784.

*2,12-Bis(2-acetoxyethyl)-7,17-diethyl-3,8,13,18-tetramethylporphyrin (**45**)*

The biladiene **43** (1.55 g, 1.85 mmol) was cyclized in DMSO–pyridine as described earlier to afford the title porphyrin in 81% yield. A pure sample was obtained for characterization by column chromatography (silica gel 60, 95:5, dichloromethane–methanol eluent); mp 320°C; visible spectrum (CH_2Cl_2) λ_{max} (nm) (relative intensities): 398 (26.81), 498 (2.66), 534 (2.10), 568 (1.52), 620 (1.00); ^{1}H nmr ($CDCl_3$) δ: −3.80 (br s, 2H, 2 × NH), 1.90 (t, 6H, J = 8.0 Hz, 2 × CH_2CH_3), 2.10 (s, 6H, 2 × C(=O)CH_3), 3.65 (s, 6H, 2 × CH3), 3.70 (s, 6H, 2 × CH_3), 4.15 (q, 4H, J = 8.0 Hz, 2 × CH_2CH_3), 4.38 (t, 4H, J = 8.0 Hz, 2 × CH_2CH_2O-), 4.90 (t, 4H, J = 8.0 Hz, 2 × CH_2CH_2O-), 10.10 (s, 2H, 2 × *meso*-H), 10.15 (s, 2H, 2 × *meso*-H); ms (*m/z*): 594 (M^+), 552, 536, 521. Anal. calcd. for $C_{26}H_{42}N_4O_4$: C 72.70, H 7.12, N 9.42; found: C 72.52, H 7.69, N 9.08.

*7,17-Diethyl-2,12-bis(2-hydroxyethyl)-3,8,13,18-tetramethylporphyrin (**46**)*

The bis(acetoxyethyl)porphyrin **45** (600 mg, 1.01 mmol) was dissolved in methanol (150 mL) containing 5% (w/v) concentrated H_2SO_4 and stirred in the dark for 16 h (reaction monitored by tlc). The mixture was poured onto ice (150 g) and the product extracted with dichloromethane. The organic phase was washed with 5% aqueous $NaHCO_3$, dried ($MgSO_4$), and evaporated to dryness to give a purple-red solid, which was recrystallized from chloroform–ether to give the bis(hy-

droxyethyl)porphyrin (505 mg, 98%), mp 240°C (dec.); visible spectrum (CH_2Cl_2) λ_{max} (nm) (relative intensities): 394 (18.41), 496 (2.14), 530 (1.65), 564 (1.28), 618 (1.00); ^{1}H nmr ($CDCl_3$) δ: −3.40 (br s, 2H, 2 × NH), 1.75 (t, 6H, 2 × CH_2CH_3), 3.66 (s, 6H, 2 × CH_3), 3.71 (s, 6H, 2 × CH_3), 4.16 (q, 4H, 2 × CH_2CH_3), 4.56 (t, 4H, 2 × CH_2CH_2OH), 5.04 (t, 4H, 2 × CH_2CH_2OH), 10.65 (s, 2H, 2 × *meso*-H), 10.70 (s, 2H, 2 × *meso*-H); ms (*m/z*): 510 (M^+), 495, 479, 448. Exact mass calcd. for $C_{32}H_{38}N_4O_2$: 510.2995; found: 510.2999.

*2,12-Bis(2-chloroethyl)-7,17-diethyl-3,8,13,18-tetramethylporphyrin (**47**)*

Porphyrin **46** was converted to its bis(chloroethyl) analog **47** in 85% yield as described earlier; mp 324–325°C; visible spectrum (CH_2Cl_2) λ_{max} (nm) (relative intensities): 398 (17.53), 498 (1.69), 534 (1.43), 570 (1.16), 620 (1.00); ^{1}H nmr ($CDCl_3$) δ: −3.75 (br s, 2H, 2 × NH), 1.88 (t, 6H, J = 7.5 Hz, 2 × CH_2CH_3), 3.65 (s, 6H, 2 × CH_3), 3.68 (s, 6H, 2 × CH_3), 4.13 (q, 4H, J = 7.5 Hz, 2 × CH_2CH_3), 4.32 (t, 4H, J = 8.0 Hz, 2 × CH_2CH_2Cl), 4.50 (t, 4H, J = 8.0 Hz, 2 × CH_2CH_2Cl), 10.03 (s, 2H, 2 × *meso*-H), 10.13 (s, 2H, 2 × *meso*-H); Exact mass calcd. for $C_{32}H_{36}N_4Cl_2$: 546.2307; found: 546.2307. Anal. calcd. for $C_{32}H_{36}N_4Cl_2$: C 70.19, H 6.63, N 10.23; found: C 70.25, H 6.58, N 10.20.

*7,17-Diethyl-3,8,13,18-tetramethyl-2,12-divinylporphyrin (**8**c)*

Dehydrochlorination of the porphyrin **47** was carried out as described earlier to afford the title compound in 84% yield; mp 225°C (dec.); visible spectrum (CH_2Cl_2) λ_{max} (nm) (relative intensities): 402 (19.2), 506 (2.05), 546 (2.68), 572 (1.80), 626 (1.00); ^{1}H nmr ($CDCl_3$) δ: −3.66 (br s, 2H, 2 × NH), 1.90 (t, 6H, 2 × CH_2CH_3), 3.68 (s, 6H, 2 × CH_3), 3.72 (s, 6H, 2 × CH_3), 4.15 (q, 4H, 2 × CH_2CH_3), 6.15 (dd, 2H, J = 2.0, 12.0 Hz, CH=CH_2), 6.34 (dd, 2H, J = 2.0, 18.0 Hz, CH=CH_2), 8.32 (dd, J = 12.0, 18.0 Hz, 2H, CH=CH_2), 10.15 (s, 2H, 2 × *meso*-H), 10.23 (s, 2H, 2 × *meso*-H); ^{13}C nmr (10% TFA – $CDCl_3$) δ: 11.71, 12.61 (4C, 4 × -CH_3), 16.18 (2C, 2 × CH_2CH_3); 20.07 (2C, 2 × CH_2CH_3), 99.09, 99.48 (4C, 4 × *meso* carbons); 127.59 (2C, 2 × CH=CH_2), 128.23 (2C, 2 × CH=CH_2), 138.34, 138.60, 140.52, 141.54, 142.82, 145.00, (16C, α- and β-pyrrolic carbons); ms (*m/z*): 474 (M^+) 459, 444. Anal. calcd. for $C_{32}H_{34}N_4$: C 80.98, H 7.22, N 11.80; found: C 80.41, H 7.38, N 11.65.

*2,12-Bis(2-acetoxyethyl)-7,17-[(methoxycarbonyl)ethyl]-3,8,13,18-tetramethylporphyrin (**48**)*

The biladiene **44** (370 mg, 0.39 mmol) dissolved in DMSO (25 mL) was treated with pyridine (1.5 mL) and allowed to stand in the dark at room temperature for 6 days. Methanol (15 mL) was added followed by water (6 mL), the solution was cooled to 0°C, and the porphyrin crystals were filtered and washed with methanol. Yield 194 mg (71%); mp 238–240°C; visible spectrum (CH_2Cl_2) λ_{max} (nm) (relative intensities): 400 (25.6), 498 (2.53), 532 (1.79), 568 (1.35), 620 (1.00); ^{1}H nmr ($CDCl_3$) δ: −3.76 (br s, 2H, 2 × NH), 2.09 (s, 6H, 2 × $COCH_3$), 3.29 (t, 4H, 2 × CH_2CO), 3.67, 3.68, 3.69 (3s, 6H each, 2 × OCH_3, 4 × CH_3), 4.36–4.48 (m, 8H, 2 × CH_2CH_2CO, 2 × CH_2CH_2O), 4.89 (t, 4H, 2 × CH_2O), 10.10, 10.15 (2s, 2H each, 2 × *meso*-H); ms (*m/z*): 710 (M^+), 696, 637, 577. Exact mass calcd. for $C_{40}H_{46}N_4O_8$: 710.3316; found: 710.3320.

*2,12-Bis(2-hydroxyethyl)-7,17-bis[(methoxycarbonyl)ethyl]-3,8,13,18-tetramethylporphyrin (**49**)*

The bis(acetoxyethyl)porphyrin **48** (190 mg, 0.27 mmol) was dissolved in 5% H_2SO_4 – methanol (40 mL) and allowed to stand in the dark for 20 h. Dichloromethane (50 mL) and dilute aqueous sodium acetate (100 mL) were added, the organic phase separated, and was washed with 5% aqueous $NaHCO_3$, then with water, and dried ($NaSO_4$). The product was crystallized by the addition of *n*-hexane. Yield 165 mg (99%); mp 253–255°C; visible spectrum (CH_2Cl_2) λ_{max} (nm) (relative intensities): 400 (20.5), 498 (2.19), 532 (1.63), 568 (1.27), 620 (1.00); ^{1}H nmr ($CDCl_3$/TFA) δ: −3.25 (br s, 2H, 2 × NH), 3.18 (t, 4H, 2 × CH_2CO), 3.66, 3.70, 3.74 (3s, 6H each, 2 × OCH_3, 4 × CH_3), 4.48 (t, 4H, 2 × CH_2CH_2CO), 4.56 (t, 4H, 2 × CH_2CH_2OH), 5.05 (t, 4H, 2 × CH_2OH), 10.73, 10.86 (2s, 2H each, 2 × *meso*-H); ms (*ms/z*): 626 (M^+), 595, 564, 553. Exact mass calcd. for $C_{36}H_{42}N_4O_6$: 626.3104; found: 626.3113.

*2,12-Bis(2-chloroethyl)-7,17-bis[(methoxycarbonyl)ethyl]-3,8,13,18-tetramethylporphyrin (**50**)*

The bis(hydroxyethyl)porphyrin **49** (152 mg, 0.24 mmol) was chlorinated as described earlier. The crude reaction mixture was chromatographed on neutral alumina (4% water added), using dichloromethane as eluent. The product was isolated by crystallization from dichloromethane–*n*-hexane. Yield 143 mg (89%); mp 265–267°C; visible spectrum (CH_2Cl_2) λ_{max} (nm) (relative intensities): 400 (26.8), 498 (2.62), 534 (1.87), 568 (1.40), 622 (1.00); ^{1}H nmr ($CDCl_3$/TFA) δ: −3.15 (t, 4H, 2 × CH_2CO), 3.60, 3.67 3.72 (3s, 6H each 2 × OCH_3, 4 × CH_3), 4.17 (t, 4H, CH_2CH_2CO), 4.43 (t, 4H, CH_2CH_2Cl), 4.56 (t, 4H, CH_2Cl), 10.55, 10.74 (2s, 2H each, 2 × *meso*-H), NH protons not observed; ms (*m/z*): 662 (M^+), 628, 613, 589. Exact mass calcd. for $C_{36}H_{40}N_4O_4Cl_2$: 662.2427; found: 662.2429.

*7,17-Bis[(methoxycarbonyl)ethyl]-3,8,13,18-tetramethyl-2,12-divinylporphyrin (**8**d)*

The bis(chloroethyl)porphyrin **50** (143 mg, 0.22 mmol) in pyridine (30 mL) was heated to reflux and treated with 10% aqueous NaOH (5 mL). Heating was continued for 3 h, the reaction mixture was cooled, 25% aqueous acetic acid (50 mL) and water (25 mL) were added, and the solution concentrated *in vacuo*. The precipitated solid was filtered onto a Celite pad, washed with water, and dried in a vacuum desiccator over KOH.

The product was dissolved in 5% H_2SO_4 – methanol (100 mL), the Celite removed by filtration, and the solution allowed to stand overnight. Dichloromethane (100 mL) was added to the above solution, the organic layer was washed with 5% aqueous $NaHCO_3$, then washed and dried (Na_2SO_4). After filtration, the solution was evaporated to dryness, redissolved in dichloromethane, chromatographed on neutral alumina (4% water added), and the product crystallized from *n*-hexane. Yield 101 mg (79%); mp 268–270°C (lit. (4) mp 270–272°C); visible spectrum (CH_2Cl_2) λ_{max} (nm) (relative intensities): 402 (27.6), 506 (2.57), 544 (2.90), 572 (1.89), 630 (1.00); ^{1}H nmr ($CDCl_3$/TFA) δ: −3.75 (br s, 2H, 2 × NH), 3.27 (t, 4H, 2 × CH_2CO), 3.65, 3.68, 3.71 (3t, 6H each, 2 × OCH_3, 4 × CH_3), 6.18 (dd, 2H, J = 2.0, 12.0 Hz, -CH=CH_2), 6.36 (dd, 2H, J = 2.0, 18.0 Hz, -CH=CH_2), 8.28 (dd, J = 12.0, 18.0 Hz, -CH=CH_2), 10.07, 10.17 (2s, 2H each, *meso*-H); ms (*m/z*): 590 (M^+), 531, 517. Exact mass calcd. for $C_{36}H_{38}N_4O_4$: 590.2893; found: 590.2894.

Acknowledgements

This work was supported by the Natural Sciences and Engineering Research Council of Canada and in part by an IRAP Contribution Arrangement of the National Research Council of Canada. A Killam Predoctoral Fellowship (to P.Y.-H.) is gratefully acknowledged.

1. D. DOLPHIN (*Editor*). The porphyrins. Vol. VII. Academic Press, New York. 1978.
2. A. R. BATTERSBY, E. MCDONALD, M. THOMPSON, I. A. CHAUDHRY, P. S. CLEZY, C. J. R. FOOKES, and T. T. HAI. J. Chem. Soc. Perkin Trans. 1, 135 (1985).
3. P. S. CLEZY and C. J. R. FOOKES. Aust. J. Chem. **34**, 871 (1981).
4. P. S. CLEZY and C. J. R. FOOKES. Aust. J. Chem. **33**, 557 (1980).
5. K. M. SNOW and K. M. SMITH. J. Org. Chem. **54**, 3270 (1989).
6. K. M. SMITH and D. A. GOFF. J. Org. Chem. **51**, 657 (1986).
7. K. M. SMITH, D. W. PARISH, and W. S. INOUYE. J. Org. Chem. **51**, 666 (1986).
8. K. M. SMITH, M. MIURA, and I. K. MORRIS. J. Org. Chem. **51**, 4660 (1986).
9. K. M. SMITH, E. M. FUJINARI, R. K. PANDEY, and H. D. TABBA. J. Org. Chem. **51**, 4667 (1986).
10. R. K. DINELLO and D. DOLPHIN. J. Org. Chem. **45**, 5196 (1980).

Can. J. Chem. Downloaded from www.nrcresearchpress.com by 91.121.58.235 on 09/07/12
For personal use only.

11. V. SCHERRER PANGKA, A. R. MORGAN, and D. DOLPHIN. J. Org. Chem. **51**, 1094 (1986).
12. A. R. MORGAN, V. SCHERRER PANGKA, and D. DOLPHIN. J. Chem. Soc. Chem. Commun. 1047 (1984).
13. K. M. SMITH and J. A. S. CAVALEIRO. Heterocycles, **26**, 1947 (1987).
14. A. W. JOHNSON. *In* The porphyrins. Vol. I. *Edited by* D. Dolphin. Academic Press, New York. 1978. pp. 235–264.
15. A. W. JOHNSON and I. T. KAY. J. Chem. Soc. 2418 (1961).
16. R. L. N. HARRIS, A. W. JOHNSON, and I. T. KAY. J. Chem. Soc. C, 22 (1966).
17. P. BAMFIELD, R. L. N. HARRIS, A. W. JOHNSON, I. T. KAY, and K. W. SHELTON. J. Chem. Soc. C, 1436 (1966).
18. J. B. PAINE III, J. HIOM, and D. DOLPHIN. J. Org. Chem. **53**, 2796 (1988).
19. T. P. WIJESEKERA and D. DOLPHIN. Synlett. 235 (1990).
20. P. S. CLEZY and C. J. R. FOOKES. Aust. J. Chem. **30**, 217 (1977).
21. P. S. CLEZY and C. J. R. FOOKES. Aust. J. Chem. **30**, 609 (1977).
22. P. YON-HIN, T. P. WIJESEKERA, and D. DOLPHIN. Tetrahedron Lett. **30**, 6135 (1989).
23. J. B. PAINE III and D. DOLPHIN. J. Org. Chem. **53**, 2787 (1988).
24. R. P. CARR, A. H. JACKSON, G. W. KENNER, and G. S. SACH. J. Chem. Soc. C, 487 (1971).
25. A. R. BATTERSBY, E. HUNT, E. MCDONALD, J. B. PAINE III, and J. SAUNDERS. J. Chem. Soc. Perkin Trans. 1, 1008 (1976).

Can. J. Chem. Downloaded from www.nrcresearchpress.com by 91.121.58.235 on 09/07/12
For personal use only.

The hydration of 1-aryl-3,3,3-trifluoropropynes and some other phenylacetylenes in sulfuric acid. An excess acidity analysis[1]

ROBIN A. COX,[2] EWART GRANT, TODD WHITAKER, AND THOMAS T. TIDWELL
Department of Chemistry, University of Toronto, 80 St. George St., Toronto, Ont., Canada M5S 1A1

Received March 27, 1990

This paper is dedicated to Professor Ross Stewart on the occasion of his 65th birthday

ROBIN A. COX, EWART GRANT, TODD WHITAKER, and THOMAS T. TIDWELL. Can. J. Chem. **68**, 1876 (1990).

The excess acidity method has been used to analyse the hydration kinetics of the phenylacetylenes Y-C_6H_4-C≡C-Z in aqueous sulfuric acid mixtures; Z = CF_3 (**1**), H (**2**), COC_6H_4-X (**3**), and CO_2H (**4**). All substrates gave acetophenone-type products consistent with the normal hydration mechanism involving rate-determining vinyl cation formation. Standard-state log k_0 intercepts, and $m^{\neq}m^*$ slopes, were both used in linear free energy relationship plots against the substituent σ^+ values. Solvent isotope effects and activation parameters were obtained in some cases. The deactivating Z substituents in **1**, **3**, and **4** all cause reaction to be some 100 times slower than that of the parent phenylacetylene **2**. Compounds **2**, **3**, and **4** all have ρ^+ values of about −3.8, but **1** is more substituent sensitive, with a ρ^+ of −5.3. A σ^+ value of 0.38 is calculated for the $CF_3C{\equiv}C$ substituent. The ρ^+ values were found to be acidity independent for **1** and **2**, and probably for **3**, but not for **4**. Proton transfer at the transition state was found to be most advanced for the fastest reaction, that of **2**, contrary to intuition.

Key words: alkyne hydration, excess acidity, phenylacetylenes, vinyl cations, deactivated carbocations.

ROBIN A. COX, EWART GRANT, TODD WHITAKER et THOMAS T. TIDWELL. Can. J. Chem. **68**, 1876 (1990).

On a utilisé la méthode d'acidité en excès pour analyser la cinétique d'hydratation des phénylacétylènes, Y-C_6H_4-C≡C-Z (Z = CF_3 (**1**), H (**2**), COC_6H_4-X (**3**) et CO_2H (**4**)), dans des solutions aqueuses d'acide sulfurique. Tous les substrats ont donné naissance à des produits du type acétophénone qui correspondent au mécanisme normal d'hydratation impliquant la formation d'un cation vinylique dans l'étape qui détermine la vitesse de la réaction. Dans le but d'obtenir des courbes relation linéaire d'énergie libre, on a utilisé les ordonnées à l'origine du log k_0 ainsi que les pentes $m^{\neq}m^*$ de l'état standard vs. des valeurs σ^+ des substituants. Dans quelques cas, on a aussi obtenu les effets isotopiques du solvant ainsi que les paramètres d'activation. Les vitesses de réaction des composés **1**, **3** et **4** portant des substituants désactivants Z sont environ 100 fois plus lentés que celle du phénylacétylène parent, **2**. Les valeurs de ρ^+ des composés **2**, **3** et **4** sont toutes égales à environ −3,8; toutefois, le composé **1** est plus sensible aux substituants et sa valeur de ρ^+ est égale à −5,3. On a calculé que la valeur σ^+ du substituant $CF_3C{\equiv}C$ est égale à 0,38. On a trouvé que les valeurs de ρ^+ des composés **1** et **2** et probablement du composé **3** sont indépendantes de l'acidité; ce n'est toutefois pas le cas avec le composé **4**. Contrairement à ce que l'on pouvait croire d'une façon intuitive, on a trouvé que le transfert de proton dans l'état de transition est le plus avancé avec la réaction la plus rapide.

Mots clés : hydratation des alcynes, acidité en excès, phénylacétylènes, cations vinyliques, carbocations désactivés.

[Traduit par la revue]

Introduction

The effect of deactivating substituents like CF_3 upon carbocations has become a subject of considerable recent interest (1, 2). The work reported in this paper was initiated as a study of the influence of the β-CF_3 substituent on vinyl cation formation (3). This is conveniently studied by following the rates of hydration of suitably substituted phenylacetylenes in aqueous sulfuric acid, the well-known (4–10) mechanism of which is shown below, Z being CF_3 (3).

[1] $Y{-}C_6H_4{-}C{\equiv}C{-}Z \xrightarrow[\text{slow}]{+H^+}$

$Y{-}C_6H_4{-}\overset{+}{C}{=}CHZ \xrightarrow[\text{fast}]{+H_2O,\ -H^+}$

$Y{-}C_6H_4{-}\overset{OH}{\overset{|}{C}}{=}CHZ \xrightarrow{\text{tautomerization}}$

$Y{-}C_6H_4{-}\overset{OH}{\overset{\|}{C}}{-}CH_2Z$

For comparison purposes, existing hydration rate data for the parent phenylacetylenes (Z = H) (6–14), and for compounds with the deactivating substituents Z = COC_6H_4-X (15) and Z = CO_2H (16), were also analysed, along with those for some aliphatic alkynes (4–6, 13, 17). The major compounds in the study, **1**–**4**, are shown below.

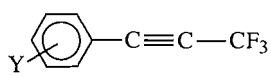

1*a*, Y = 4-OMe
1*b*, Y = 4-Me
1*c*, Y = 3-Me
1*d*, Y = H
1*e*, Y = 4-Cl
1*f*, Y = 3-Cl
1*g*, Y = 4-$CF_3C{\equiv}C$
1*h*, Y = 4-CF_3CH_2CO

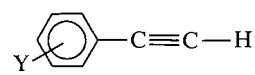

2*a*, Y = 4-OMe
2*b*, Y = 4-Me
2*c*, Y = 3-Me
2*d*, Y = H
2*e*, Y = 4-Cl
2*f*, Y = 4-Br
2*g*, Y = 3-Cl
2*h*, Y = 3-NO_2
2*i*, Y = 4-NO_2

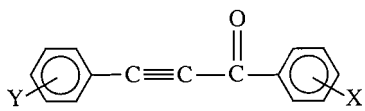

3*a*, Y = 4-OMe, X = H
3*b*, Y = 4-Me, X = H
3*c*, Y = H, X = H
3*d*, Y = H, X = 4-Me
3*e*, Y = H, X = 4-NO_2

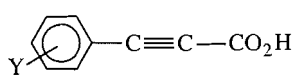

4*a*, Y = 4-OMe
4*b*, Y = 4-Me
4*c*, Y = H
4*d*, Y = 4-Cl
4*e*, Y = 3-Cl
4*f*, Y = 3, 4-Cl_2

[1]Presented in part at the 5th International Conference on the Mechanisms of Reaction in Solution, Canterbury, England, July 1990.
[2]Author to whom correspondence may be addressed.

Can. J. Chem. Downloaded from www.nrcresearchpress.com by 91.121.58.235 on 09/07/12
For personal use only.

TABLE 1. Standard-state hydration rate constants and slopes for **1**

Substrate	$m^{\neq}m^{*a}$	log $k_0{}^a$	k_{H^+}
1*a*	1.13±0.06	−4.52±0.08	3.0×10^{-5}
1*b*	1.26±0.04	−7.15±0.14	7.1×10^{-8}
1*c*	1.17±0.04	−8.46±0.16	3.5×10^{-9}
1*d*	1.39±0.04	−9.49±0.14	3.2×10^{-10}
1*e*	1.14±0.02	−8.95±0.09	1.1×10^{-9}
1*f*	1.18±0.03	−10.60±0.18	2.5×10^{-11}
1*g*[b]	1.08±0.14	−10.70±0.82	2.0×10^{-11}
1*h*[b]	0.62±0.06[c]	−9.35±0.54[c]	4.5×10^{-10c}

[a]Slopes and intercepts of the lines in Fig. 1.
[b]Not included in the LFER in Fig. 2.
[c]Not directly comparable with the other table entries; see text.

The rate data were analysed using the excess acidity method (18), which was successfully used previously in the analysis of alkenyl ester hydration data (19). It has also been used in the analysis of rate data for enolizations and aldol condensations (20), acylhydrazine hydrolyses (21), amide hydrolyses (22), and many other reactions (18) in aqueous sulfuric acid. The excess acidity equation applicable to the rate-determining proton transfer of eq. [1] is eq. [2] (18). In eq. [2] the k_ψ are the

$$[2] \quad \log k_\psi - \log C_{H^+} = m^{\neq}m^*X + \log k_0$$

observed pseudo-first-order rate constants. C_{H^+} is the proton concentration and X is the excess acidity; these take the place of an acidity function in the excess acidity method (18, 23). The slope parameter m^* refers to equilibrium protonation of the substrate; $m^* = 1.0$ for primary aromatic amines, 0.6 for carbonyl compounds, 1.3 for tertiary aromatic amines, etc. (23). The term $m^{\neq}$ refers to the transition state; $m^{\neq} > 1$ for A-1 reactions, $m^{\neq} < 1$ for A-S_E2 reactions, such as the one in eq. [1], and $m^{\neq} \cong 1$, with additional water activity terms, etc., necessary in eq. [2], for A-2 reactions (18). The intercept gives k_0, the medium-independent rate constant for the reaction, i.e., the value in the hypothetical ideal 1 M acid solution which is the standard state (18, 23); these are directly comparable with values obtained in aqueous buffer media. For the mechanism of eq. [1] these are rate constants for proton transfer from the acid "H^+", commonly symbolized k_{H^+}.

Experimental

The 1-aryl-3,3,3-trifluoropropyne substrates **1***a–g* were synthesized by a Wittig procedure (24*a*), purified by GLC (all but **1***g* are oils), and their purity and identity confirmed by comparison of their spectra with published spectral data (24*a–e*).

Compound **1***g* is new: colourless needles, mp 92–93°C; IR (CCl_4): 2256 (C≡C) cm^{-1}; ^1H NMR ($CDCl_3$) δ: 7.60 (s, 4); ^{19}F NMR (C_6D_6) δ: −54.3 (6); ^{13}C NMR (C_6D_6) δ: 78.0 (q, 2, J_{CCF} = 52.7 Hz, CCF_3), 85.6 (q, 2, J_{CCCF} = 6.4 Hz, $CCCF_3$), 115.4 (q, 2, J_{CF} = 257.2 Hz, CF_3), 120.5 (2, quarternary C), 132.4 (4); MS *m/z* (rel. intensity): 262 (100, M^+), 243 (55, $M^+ - F$), 193 (35, $M^+ - CF_3$), 69 (49, CF_3^+); HRMS *m/z*: 262.0208 (M^+), $C_{12}H_{14}F_6$ requires 262.0217. Preparation according to ref. 24*a* gave a yield of 10%.

Compounds **1***c*, **1***f*, and **1***h* are also new. **1***c*: IR (CCl_4): 2266, 2233 (C≡C) cm^{-1}; ^1H NMR (CCl_4) δ: 2.34 (s, 1, CH_3), 7.1 (m, 4, Ar). **1***f*: IR (CCl_4): 2261 (C≡C) cm^{-1}; ^1H NMR ($CDCl_3$) δ: 7.3–7.5 (m, 4); MS *m/z* (rel. intensity): 206 (46, M^+), 204 (100, M^+), 185 (46, $M^+ - F$), 169 (69), 154 (21), 125 (38); HRMS *m/z*: 203.9954, $C_9H_4ClF_3$ requires 203.9954. Compound **1***h* was not isolated but was generated *in situ* from the reaction of **1***g* in acid.

The 3,3,3-trifluoropropiophenone products Y-$C_6H_4COCH_2CF_3$ have been reported previously (24*f*) for Y = 4-OMe, 4-Me, H, and 4-Cl.

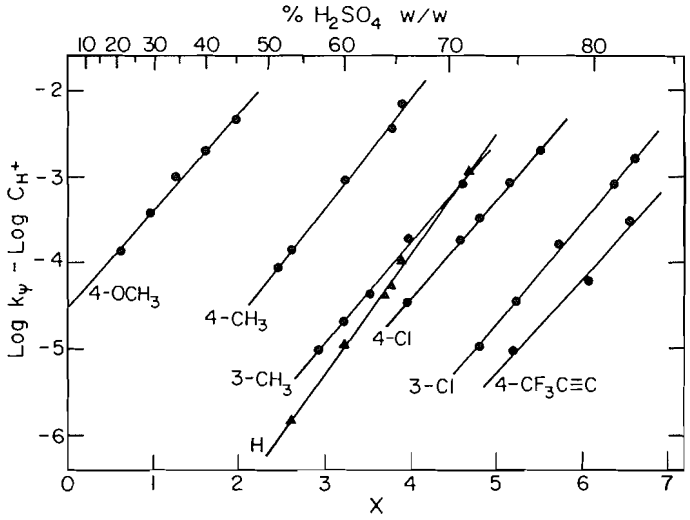

FIG. 1. Excess acidity plots according to eq. [2], for the hydration of various 1-aryl-3,3,3-trifluoropropynes **1** in aqueous sulfuric acid mixtures.

The formation of the ketone from **1***c*, Y = 3-Me, was confirmed by neutralizing the product of the reaction of 5 mg of **1***c* in 2 mL of concentrated H_2SO_4 with 10% aqueous KOH. After extraction into CCl_4 and evaporation, the product showed the characteristic propiophenone IR absorption at 1694 cm^{-1}.

The hydration kinetics were studied at 25°C using a Cary 210 UV–VIS spectrophotometer, following the disappearance of the aryl-acetylene peak at 230–240 nm. Runs were performed in duplicate; agreement was within ±5%. Reaction was initiated by injecting stock substrate solutions in acetonitrile into the aqueous sulfuric acid mixtures. The latter were analysed by titration. The measured rate constants are in Table S1, available from the Depository of Unpublished Data,[3] along with those literature values for **2** which are not readily available otherwise, Table S2.

The rate constants obtained for **1**, and those available in the literature for **2**, **3**, and **4**, were analysed according to the excess acidity procedure as previously described (18–22), using linear regression on eq. [2]. The values of X and log C_{H^+} used are from Cox and Yates (23). In those cases where rate constants at several different temperatures were available they were analysed using standard multiple linear regression or curve-fitting techniques (25) as described in the literature (22, 26), taking into account the variation of X and log C_{H^+} with temperature (25*a*). Rate constants obtained in D_2SO_4 enabled the calculation of solvent isotope effects; Noyce's assumption (27) that medium acidities are equal at equal mole fractions of H_2SO_4 and D_2SO_4 was used so that X and log C_{D^+} could be calculated in D_2SO_4 media, since there are at present no measured values.

All of the derived information, $m^{\neq}m^*$ slopes, log k_0 values and the aqueous standard-state k_{H^+} values that are their antilogs, activation parameters, solvent isotope effects, and certain other information, is collected in Table 1–8. The errors reported in the tables are standard deviations. The σ and σ^+ values used for the LFER's in Figs. 2–5 are from Hammett (28).

Results

The rate constants obtained for **1**, with the exception of those for **1***h*, are plotted according to the excess acidity equation [2] in Fig. 1. As can be seen, the plots are nicely linear and all roughly parallel, with that for the parent phenyl compound **1***d* being somewhat deviant. The slopes, intercepts, and derived k_{H^+}

[3]Tables S1 and S2 are on deposit and may be purchased from the Depository of Unpublished Data, CISTI, National Research Council of Canada, Ottawa, Ont., Canada K1A 0S2.

Can. J. Chem. Downloaded from www.nrcresearchpress.com by 91.121.58.235 on 09/07/12
For personal use only.

Can. J. Chem. Downloaded from www.nrcresearchpress.com by 91.121.58.235 on 09/07/12
For personal use only.

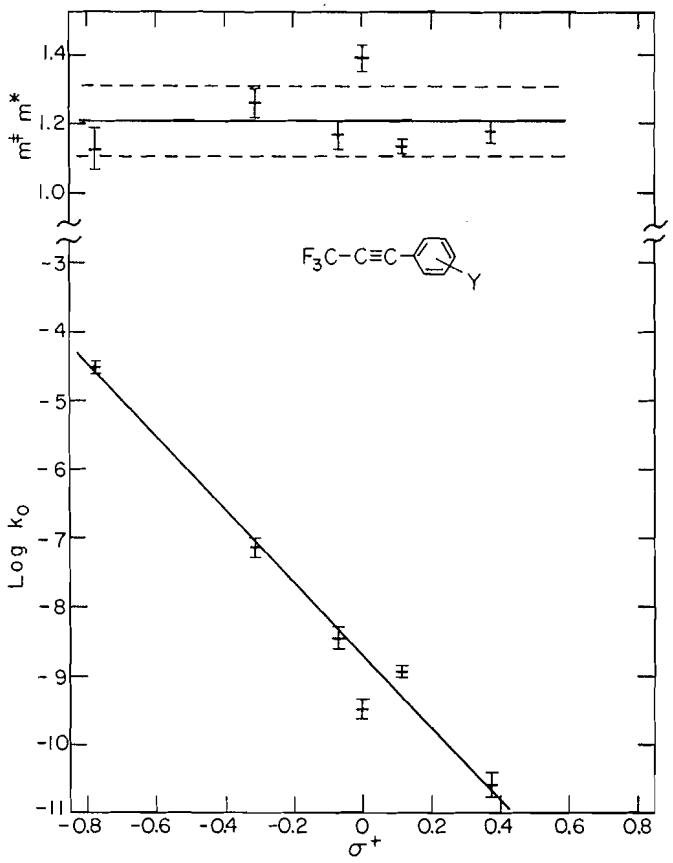

FIG. 2. Linear free energy relationship plots for **1**, as a function of the σ^+ values of the substituents. Lower half: standard-state log k_0 values. Upper half: $m^{\neq}m^*$ slopes. Data from Table 1.

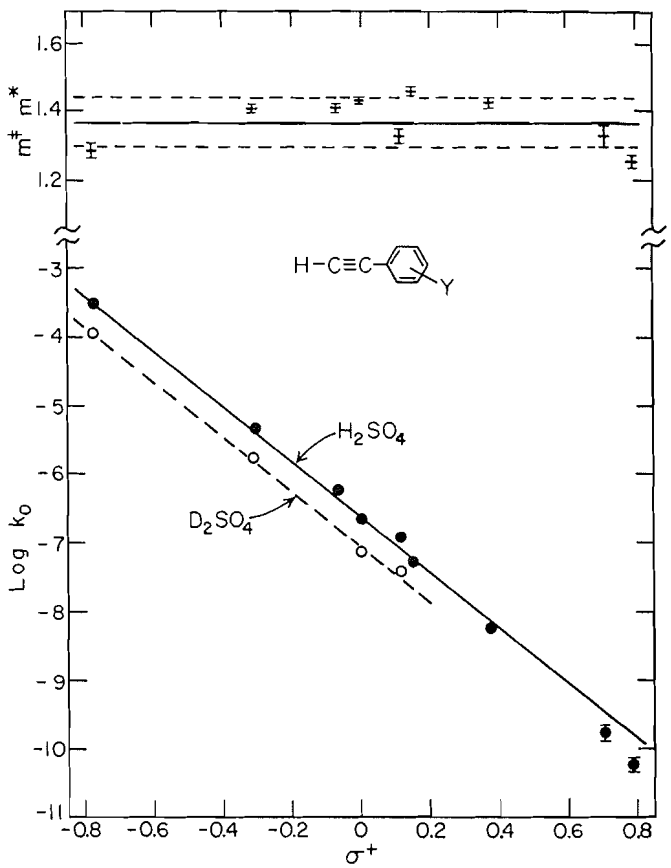

FIG. 3. LFER plots for **2**. Data from Tables 2 and 3. See Fig. 2.

TABLE 2. Standard-state hydration rate constants and slopes for **2**

Substrate	$m^{\neq}m^*$	log k_0	k_{H^+}	Reference
2*a*	1.28±0.02	−3.51±0.01	3.1×10^{-4}	6–8, 11, 13
2*b*	1.40±0.01	−5.34±0.01	4.6×10^{-6}	6, 8, 10, 11, 13
2*c*	1.41±0.01	−6.23±0.02	5.8×10^{-7}	13
2*d*	1.43±0.01	−6.66±0.01	2.2×10^{-7}	6–9, 12–14
2*e*	1.32±0.02	−6.91±0.03	1.2×10^{-7}	6, 8, 11
2*f*	1.46±0.01	−7.29±0.02	5.1×10^{-8}	13
2*g*	1.42±0.02	−8.25±0.04	5.7×10^{-9}	13
2*h*	1.32±0.03	−9.77±0.11	1.7×10^{-10}	13
2*i*	1.25±0.02	−10.24±0.08	5.8×10^{-11}	13

TABLE 3. Activation parameters and solvent isotope effects for **2**[a]

Substrate	$\Delta H^{\neq}$[b]	$\Delta S^{\neq}$[c]	$k_{H^+}^{H_2SO_4}/k_{D^+}^{D_2SO_4}$
2*a*	17.6±0.2	−15.6±0.8	2.8±0.1
2*b*	20.6±0.4	−13.8±1.4	2.7±0.1
2*d*	22.0±0.3	−15.2±1.1	3.0±0.2[d]
2*e*	19.3±0.5	−25.6±1.7	3.2±0.3

[a]Data reference given in Table 2.
[b]Units: kcal mol^{-1}.
[c]Units: cal mol^{-1} deg^{-1}.
[d]Replacing the alkynyl H by D results in a secondary isotope effect of 1.14 ± 0.02.

TABLE 4. Standard-state hydration rate constants and slopes for **3**[a]

Substrate	$m^{\neq}m^*$	log k_0	k_{H^+}
3*a*	1.116±0.017	−6.25±0.02	5.7×10^{-7}
3*b*	1.156±0.008	−8.19±0.03	6.4×10^{-9}
3*c*	0.992±0.004	−9.00±0.02	1.0×10^{-9}
3*d*	1.057±0.010	−9.08±0.04	8.2×10^{-10}
3*e*	0.952±0.017	−9.12±0.08	7.6×10^{-10}

[a]Data from ref. 15.

values are listed in Table 1. Linear free energy relationships (LFER's) for both the log k_0 intercepts and the $m^{\neq}m^*$ slopes as functions of σ^+ are shown in Fig. 2; ρ^+ is −5.28. No σ^+ value is known for the 4-$CF_3C\equiv C$ substituent, but based upon the LFER for the others a value of 0.38 can be calculated from this work. Rate constants obtained for the 4-CF_3CH_2CO substituent, compound **1***h* in Table 1, are not directly comparable with the others because this compound appears to protonate on the substituent carbonyl oxygen (e.g., see the highly deviant slope in Table 1), and as sufficient information to allow for this is not available, the actual reaction rate could not be calculated, as it could be for **3**, see below.

The results of applying eq. [2] to the plenitude of literature information available for **2** (6–14) are listed in Tables 2 and 3. Results obtained by different authors are in complete agreement, and so all data for the same compound were treated together, regardless of source. Table 2 lists the basic $m^{\neq}m^*$, log k_0 and k_{H^+} information, and Table 3 has the activation parameters and solvent isotope effects obtainable for some of

TABLE 5. Activation parameters, solvent isotope effects, and basicities for **3**[a]

Substrate	$\Delta H^{\neq b}$	$\Delta S^{\neq c}$	$k_{H^+}^{H_2SO_4}/k_{D^+}^{D_2SO_4}$	pK_{SH^+}
3*a*	20.9±0.3	−17.2±1.0	2.0±0.2	—
3*b*	21.0±0.5	−25.5±1.8	2.2±0.2	−5.25±0.05[d]
3*c*	27.8±0.2	−6.7±0.7	1.8±0.1	−5.55±0.04[e]
3*d*	—	—	—	−5.14±0.12[f]
3*e*	—	—	—	−7.06±0.12[f]

[a]Data from ref. 15.
[b]Units: kcal mol^{-1}.
[c]Units: cal mol^{-1} deg^{-1}.
[d]$m^* = 0.99 \pm 0.01$.
[e]$m^* = 0.942 \pm 0.007$.
[f]$m^* = 1$ (assumed).

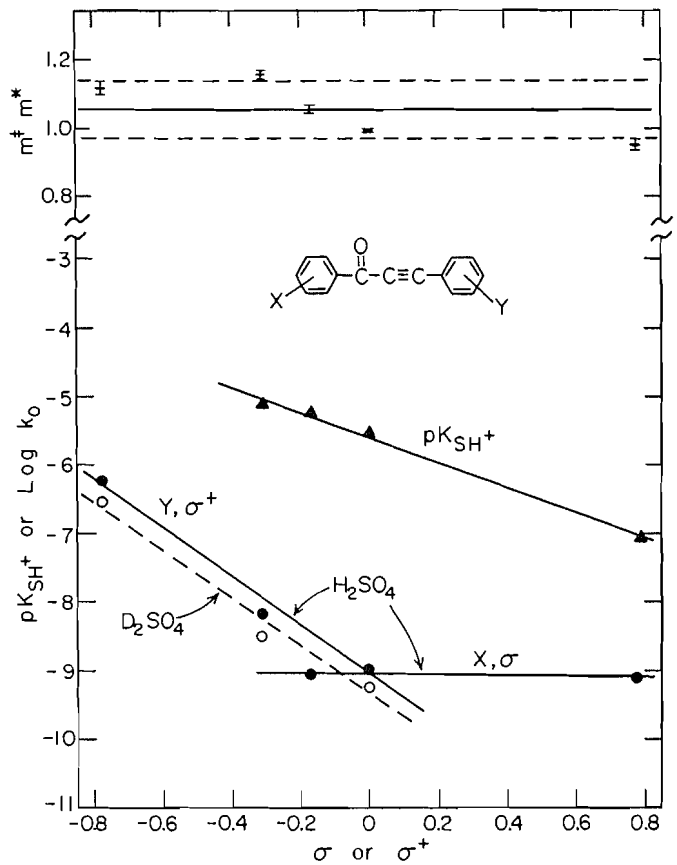

FIG. 4. LFER plots for **3**. Data from Tables 4 and 5. See Fig. 2. The pK_{SH^+} values are carbonyl group basicities; see text. For the remote substituents X, σ values are used; for the ones nearest the vinyl cation centre, Y, σ^+ values.

the phenylacetylenes. An LFER for the Table 2 information is given as Fig. 3; ρ^+ is −4.03.

Compound **3** (15) also protonates on the carbonyl oxygen, and plots according to eq. [2] curve downward because of this. However, the curvature can be accounted for by adding an additional $\log(C_S/(C_S + C_{SH^+}))$ term to eq. [2] (18), and curve-fitting the entire equation to obtain slope, intercept, and pK_{SH^+} (25). Sufficient rate constant data were available to also enable calculation of m^* for carbonyl protonation in two cases; in two more $m^* = 1$ was assumed, based upon the two known ones (Table 5). For **3***a* carbonyl protonation was not a complication. Table 4 lists the basic eq. [2] information, and Table 5 has the pK_{SH^+} values, with activation parameters and solvent isotope effects. Figure 4 has the LFER's; changing Y directly affects the vinyl cation, ρ^+ being −3.54, but changing X on the benzoyl group does not, ρ being essentially zero. The benzoyl pK_{SH^+} values also form a reasonable LFER, the ρ for this being -1.8 ± 0.1.

The phenylpropiolic acids **4** give β-ketoacids as first-formed products, which subsequently decarboxylate (16). However, this is not a problem in obtaining the hydration rates (16), and the excess acidity analysis results are given in Table 6. Figure 5 has the LFER's; ρ^+ is −3.85. Here for the first time it is apparent that the $m^{\neq}m^*$ slopes also vary with substituent; for **1**–**3** (Figs. 2–4) they are invariant.

In Table 7 we have collected together the results of applying eq. [2] to some other 25°C alkyne hydration rate constants, which we had obtained previously (4, 5) or which are available in the literature (6, 13, 17), for comparison and completeness. Table 8 is a summary table, containing the ρ^+ values for **1**–**4**, the intercepts of the LFER's in Figs. 2–5 (the most convenient data for relative rate comparisons), averaged solvent isotope effects, and, except for **4**, averaged $m^{\neq}m^*$ slopes.

Discussion

All of the evidence in the previous section is in favour of the rate-determining vinyl cation formation mechanism for this reaction, given in eq. [1]: the fact of linearity according to eq. [2] (18); the magnitudes of most of the entropies of activation (29); the magnitudes of the $m^{\neq}m^*$ slopes. These latter are all less than the 1.8 that is typical of carbocation formation m^* values (30); unfortunately no m^* value is available for vinyl cation formation. However, it seems likely that all of the $m^{\neq}$ values will be less than 1, the mechanistic criterion for an A-S_E2 process (18).

Having said that, some of the individual numbers are puzzling. The magnitudes of all of the solvent isotope effects lie between the values of 2 and 4, but it is by no means obvious why that for **2** should be 3, intermediate between the value of 2 obtained for **3**, with its deactivating benzoyl group, and the value of 4 obtained for **4**, with its deactivating CO_2H group. There are wide discrepancies between the entropies of activation for **3***a*, **3***b*, and **3***c* in Table 5; however, since these are derived from rate constants obtained at only two temperatures (15) they may not be too reliable. Typical protonation m^* values for the carbonyl group are around 0.6 (23), considerably lower than those of around 1.0 found for **3**.

All of the deactivating substituents do in fact slow the reac-

Can. J. Chem. Downloaded from www.nrcresearchpress.com by 91.121.58.235 on 09/07/12
For personal use only.

Can. J. Chem. Downloaded from www.nrcresearchpress.com by 91.121.58.235 on 09/07/12
For personal use only.

TABLE 6. Standard-state hydration rate constants, slopes, and solvent isotope effects for **4**[a]

Substrate	$m^{\neq}m^*$	log k_0	k_{H^+}	$k_{H^+}^{H_2SO_4}/k_{D^+}^{D_2SO_4}$
4*a*	1.11±0.01	−5.26±0.01	5.4×10^{-6}	4.2±0.2
4*b*	1.06±0.02	−7.29±0.07	5.1×10^{-8}	3.7±0.9
4*c*	0.94±0.02	−8.36±0.07	4.3×10^{-9}	4.0±1.0
4*d*	0.88±0.02	−8.43±0.12[b]	3.7×10^{-9}	3.9±1.5
4*e*	0.86±0.02	−9.64±0.10	2.3×10^{-10}	—
4*f*	0.92±0.01	−10.08±0.07	8.2×10^{-11}	—

[a]Data from ref. 16.
[b]$\Delta H^{\neq} = 24.6 \pm 1.0$ kcal mol^{-1}; $\Delta S^{\neq} = -15 \pm 4$ cal mol^{-1} deg^{-1}.

TABLE 7. Standard-state rate constants and slopes for some other alkynes

Substrate	$m^{\neq}m^*$	log k_0	k_{H^+}	Reference
MeC≡CH	1.59±0.08	−10.16±0.28	6.9×10^{-11}	5
EtC≡CH	1.45±0.06	−9.24±0.21	5.8×10^{-10}	4
^{n}BuC≡CH	1.24±0.01	−8.49±0.01	3.2×10^{-9}	4
^{c}PrC≡CH	1.26±0.02	−3.79±0.03	1.6×10^{-4}	4
MeC≡CMe	1.57±0.02	−9.81±0.06	1.6×10^{-10}	4
EtC≡CEt	1.31±0.04	−8.41±0.10	3.9×10^{-9}	6
PhC≡CMe[a]	1.56±0.02	−8.31±0.06	4.9×10^{-9}	17
^{o}TolC≡CH	1.41±0.04	−5.64±0.06	2.3×10^{-6}	13

[a]Has a solvent isotope effect of 2.1 ± 0.4.

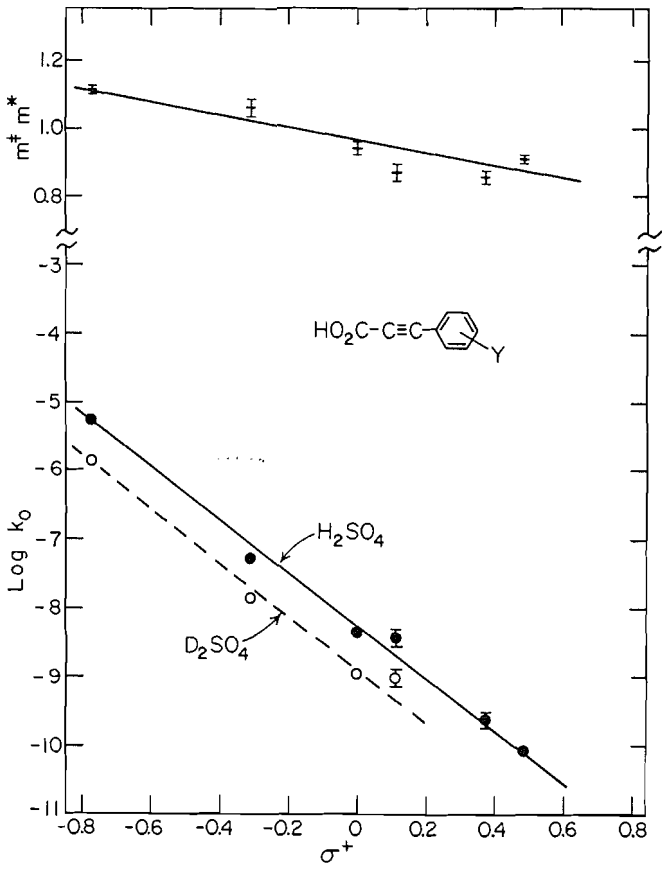

FIG. 5. LFER plots for **4**. Data from Table 6. See Fig. 2.

tion down. Table 8 shows that log k_0 for **2** (Z = H) is at least two log units more positive (factor of 100 times faster) than that for **1** (Z = CF_3), **3** (Z = COC_6H_4-X), and **4** (Z = CO_2H). However, **1** is far more substituent sensitive ($\rho^+ = -5.3$) than **3** ($\rho^+ = -3.5$) and **4** ($\rho^+ = -3.8$); **2** lies between, at −4.0. Electron demand in the transition state must be stronger with a non-polarizable CF_3 substituent present.

Dividing the $m^{\neq}m^*$ slopes in Table 8 by 1.8 should give some idea of the degree of proton transfer at the transition state (18, 31). The fastest reaction is that of **2**, followed by those of **4**, **1**, and **3**; the extents of proton transfer calculated this way are 76%, about 54%, 67%, and 59%. (If m^* for a vinyl cation is not 1.8, the absolute magnitudes will be different, but it is unlikely that the relative magnitudes will change.) Thus the fastest reaction may well have the most advanced transition state. To explain this counter-intuitive result a two-dimensional reaction surface such as the one drawn by Chokotho and Johnson (10) is undoubtedly necessary, rather than a linear reaction profile.

Previously, in a study of acylal and thioacylal hydrolyses (32), we found that the reaction ρ values were dependent upon the acidity at which they were measured. When using the excess acidity method, this is most easily expressed as a variation of the $m^{\neq}m^*$ slopes with substituent; if these are in fact independent of substituent, ρ will not vary with acidity (32). This is the case in this work for **1** and **2**, and probably for **3** (see Figs. 2–4), which agrees with Johnson's conclusion for **2** (9, 10). However, compound **4** certainly does not have a substituent-independent slope (see Fig. 5); in this case ρ^+ measured at high acidities will be *more negative* than the value reported here, extrapolated to the standard state. This is in contrast to the acylal/thioacylal study, which found that ρ at high acidity is usually *more positive*

TABLE 8. Summarized results for **1**–**4**

Substrate	ρ^+	log k_0 for Y = H[a]	$k_{H^+}^{H_2SO_4}/k_{D^+}^{D_2SO_4}$[b]	$m^{\neq}m^*$[b]
1	−5.28±0.41	−8.69±0.19	—	1.21±0.10
2	−4.03±0.06	−6.63±0.03	2.9±0.2	1.37±0.07
3	−3.54±0.21[c]	−9.05±0.09	2.0±0.2	1.06±0.08
4	−3.85±0.09	−8.26±0.07	4.0±0.2	[d]

[a]Intercepts of LFER plots, Figs. 2–5.
[b]Averages of values in Tables 1–6.
[c]Variation of X, Y constant, gives $\rho = -0.1 \pm 0.6$; see Fig. 4.
[d]$(0.97 \pm 0.02) - (0.18 \pm 0.03)\sigma^+$. See Fig. 5.

for those compounds (32). The reason for the difference is, at present, obscure; the slope of the Fig. 5 line is difficult to interpret since $m^{\neq}m^*$ is already an LFER slope parameter (33) and, plotting these in another LFER, while a useful visual illustration, has no readily interpretable theoretical meaning.

We reemphasize here that derived quantities like ρ and $\Delta S^{\neq}$ have maximum mechanistic meaning if obtained in the standard state, as is done in this work by extrapolation to $X = 0$, rather than at some arbitrary acidity. Studies like this have a bearing on the incompatibility of the Hammett equation with the reactivity–selectivity principle (RSP) discussed by Johnson (9, 10, 34), even if this bearing is hard to interpret. The effect for **4** found here would be categorized by Johnson as an anti-RSP effect, whereas **1**, **2**, and **3** show no evidence for the operation of the RSP at all.

Acknowledgements

We would like to thank Dr. C. D. Johnson for discussion and the provision of thesis material, and the referees for helpful comments. Financial support is by the Natural Sciences and Engineering Research Council of Canada, and the Donors of the Petroleum Research Fund.

1. (*a*) A. D. ALLEN and T. T. TIDWELL. Adv. Carbocation Chem. **1**, 1 (1989); (*b*) P. G. GASSMAN and T. T. TIDWELL. Acc. Chem. Res. **16**, 279 (1983); (*c*) T. T. TIDWELL. Angew. Chem. Int. Ed. Engl. **23**, 20 (1984).
2. (*a*) Y. TSUNO, A. MURATA, M. GOTO, and M. FUGIO. Stud. Org. Chem. (Amsterdam), **31**, 167 (1987); Chem. Abstr. **108**, 166764 (1988); (*b*) A. D. ALLEN, J. M. KWONG-CHIP, J. MISTRY, J. F. SAWYER, and T. T. TIDWELL. J. Org. Chem. **52**, 4164 (1987); (*c*) J. P. RICHARD. J. Am. Chem. Soc. **108**, 6819 (1986); (*d*) A. D. ALLEN, V. M. KANAGASABAPATHY, and T. T. TIDWELL. J. Am. Chem. Soc. **108**, 3470 (1986); (*e*) K.-R. GASSEN and W. KIRMSE. Chem. Ber. **119**, 2233 (1986).
3. A. D. ALLEN, G. ANGELINI, C. PARADISI, A. STEVENSON, and T. T. TIDWELL. Tetrahedron Lett. **30**, 1315 (1989).
4. A. D. ALLEN, Y. CHIANG, A. J. KRESGE, and T. T. TIDWELL. J. Org. Chem. **47**, 775 (1982).
5. P. CRAMER and T. T. TIDWELL. J. Org. Chem. **46**, 2683 (1981).
6. G. MODENA, F. RIVETTI, G. SCORRANO, and U. TONELLATO. J. Am. Chem. Soc. **99**, 3392 (1977).
7. D. S. NOYCE and M. D. SCHIAVELLI. J. Am. Chem. Soc. **90**, 1020 (1968).
8. D. S. NOYCE and M. D. SCHIAVELLI. J. Am. Chem. Soc. **90**, 1023 (1968).
9. G. W. L. ELLIS and C. D. JOHNSON. J. Chem. Soc. Perkin Trans. 2, 1025 (1982).
10. N. C. J. CHOKOTHO and C. D. JOHNSON. Isr. J. Chem. **26**, 409 (1985).
11. M. D. SCHIAVELLI. Ph.D. Thesis, University of California, Berkeley. 1967.
12. G. W. L. ELLIS. Ph.D. Thesis, University of East Anglia. 1982.
13. N. C. J. CHOKOTHO. Ph.D. Thesis, University of East Anglia. 1984.
14. N. BANAIT, M. HOJATTI, P. FINDLAY, and A. J. KRESGE. Can. J. Chem. **65**, 441 (1987).
15. D. S. NOYCE and K. E. DEBRUIN. J. Am. Chem. Soc. **90**, 372 (1968).
16. D. S. NOYCE, M. A. MATESICH, and P. E. PETERSON. J. Am. Chem. Soc. **89**, 6225 (1967).
17. D. S. NOYCE and M. D. SCHIAVELLI. J. Org. Chem. **33**, 845 (1968).
18. R. A. COX. Acc. Chem. Res. **20**, 27 (1987).
19. R. A. COX, M. MCALLISTER, K. A. ROBERTS, P. J. STANG, and T. T. TIDWELL. J. Org. Chem. **54**, 4899 (1989).
20. L. M. BAIGRIE, R. A. COX, H. SLEBOCKA-TILK, M. TENCER, and T. T. TIDWELL. J. Am. Chem. Soc. **107**, 3640 (1985).
21. R. A. COX and K. YATES. Can. J. Chem. **62**, 1613 (1984).
22. R. A. COX and K. YATES. Can. J. Chem. **59**, 2853 (1981).
23. R. A. COX and K. YATES. J. Am. Chem. Soc. **100**, 3861 (1978).
24. (*a*) Y. KOBAYASHI, T. YAMASHITA, K. TAKAHASHI, H. KURODA, and I. KUMADAKI. Chem. Pharm. Bull. **32**, 4402 (1984); (*b*) Y. KOBAYASHI, T. YAMASHITA, K. TAKAHASHI, H. KURODA, and I. KUMADAKI. Tetrahedron Lett. **23**, 343 (1982); (*c*) J. E. BUNCH and C. L. BUMGARDNER. J. Fluorine Chem. **36**, 313 (1987); (*d*) G. MEAZZA, L. CAPUZZI, and P. PICCARDI. Synthesis, 331 (1989); (*e*) T. HIYAMA, K. SATO, and M. FUJITA. Bull. Chem. Soc. Jpn. **62**, 1352 (1989); (*f*) Y. KAMITORI, M. HOJO, R. MASUDA, S. OHARA, Y. KAWAMURA, and T. EBISU. Synthesis, 43 (1989).
25. (*a*) R. A. COX and K. YATES. Can. J. Chem. **62**, 2155 (1984); (*b*) P. R. BEVINGTON. Data reduction and error analysis for the physical sciences. McGraw-Hill, New York. 1969.
26. R. A. COX, M. F. GOLDMAN, and K. YATES. Can. J. Chem. **57**, 2960 (1979).
27. D. S. NOYCE, H. S. AVARBOCK, and W. L. REED. J. Am. Chem. Soc. **84**, 1647 (1962).
28. L. P. HAMMETT. Physical organic chemistry, 2nd. ed. McGraw-Hill, New York. 1970. p. 356.
29. (*a*) C. H. ROCHESTER. Acidity functions. Academic Press, London. 1970; (*b*) M. LILER. Reaction mechanisms in sulphuric acid. Academic Press, London. 1971.
30. R. A. COX and K. YATES. Can. J. Chem. **59**, 2116 (1981).
31. R. A. COX and K. YATES. Can. J. Chem. **57**, 2944 (1979).
32. R. A. COX and K. YATES. J. Org. Chem. **51**, 3619 (1986).
33. A. BAGNO, G. SCORRANO, and R. A. MORE O'FERRALL. Rev. Chem. Intermed. **7**, 313 (1987).
34. (*a*) C. D. JOHNSON. The Hammett equation. Cambridge University Press. 1973; (*b*) C. D. JOHNSON. Chem. Rev. **75**, 755 (1975).

Can. J. Chem. Downloaded from www.nrcresearchpress.com by 91.121.58.235 on 09/07/12
For personal use only.

A study on the backbone/side-chain interaction in *N*-formyl-(L)serineamide

ANDRÁS PERCZEL[1] AND RAYMOND DAUDEL
Laboratoire de Chimie Physique, Université de Pierre et Marie Curie, 11 Rue Pierre et Marie Curie, 75005 Paris, France
JÁNOS G. ÁNGYÁN[2]
Laboratoire de Spéctrochimie Moléculaire, Université de Pierre et Marie Curie, 4 Place Jussieu 75252 Paris Cedex 5, France
AND
IMRE G. CSIZMADIA
Department of Chemistry and Protein Structure Research Centre, University of Toronto, Toronto, Ont., Canada M5S 1A1

Received December 5, 1989[3]

This paper is dedicated to Professor Ross Stewart on the occasion of his 65th birthday

ANDRÁS PERCZEL, RAYMOND DAUDEL, JÁNOS G. ÁNGYÁN, and IMRE G. CSIZMADIA. Can. J. Chem. **68**, 1882 (1990).

The *N*-formyl-serineamide (For-Ser-NH_2), a model diamide for the conformational behaviour of the protein backbone at serine residue, has been gradient optimized for selected conformations at the *ab initio* 3-21G level. Previous molecular mechanics ECEPP/2 calculations suggested that the optimal side-chain (χ_1, χ_2) and backbone (ϕ, ψ) conformations are strongly coupled, due to intramolecular H-bonding formed between the side-chain hydroxyl group and the amide moiety. Four different side-chain geometries (I–IV) were considered at each of the four backbone conformations (α, β, β', γ) giving a total 16 different critical points on the coupled (ϕ, ψ)–(χ_1, χ_2) surface. The very fact that upon changing the (ϕ, ψ) values the global minimum of (χ_1, χ_2) surface was shifted indicated clearly that the two subspaces are strongly coupled. The present theoretical results were compared to experimental peptide and protein geometries taken from the Cambridge Structure Database and from the Brookhaven Protein Data Bank, respectively.

Key words: conformation of a serinediamide, backbone side-chain interactions, topological analysis of potential energy surfaces, *ab initio* calculations.

ANDRÁS PERCZEL, RAYMOND DAUDEL, JÁNOS G. ÁNGYÁN et IMRE G. CSIZMADIA. Can. J. Chem. **68**, 1882 (1990).

Opérant au niveau 3-21G et faisant appel à des calculs *ab initio*, on a optimisé des conformations choisies de la *N*-formyl-sérinamide (For-Ser-NH_2), une diamide utilisée comme modèle pour étudier le comportement conformationnel du squelette protéinique au niveau des restes de sérine. Des calculs antérieurs au niveau ECEPP/2 avaient suggéré que les conformations optimales de la chaîne latérale (χ_1, χ_2) et du squelette (ϕ, ψ) sont fortement couplées à cause d'une liaison hydrogène intramoléculaire entre le groupement hydroxyle de la chaîne latérale et la portion amide. On a considéré quatre géométries différentes (I–IV) pour la chaîne latérale, pour chacune des quatre conformations (α, β, β', γ) du squelette, soit 16 points critiques différents sur la surface de couplage (ϕ, ψ)–(χ_1, χ_2). Le fait qu'un changement dans les valeurs de (ϕ, ψ) provoque un déplacement global de la surface (χ_1, χ_2) indique clairement que les deux sous-surfaces sont fortement couplées. On a comparé les résultats géométriques obtenus ici avec les géométries expérimentales de peptides et de protéines telles qu'on peut extraire respectivement de la base de donnée de structures de Cambridge et de la banque de donnée sur les protéines de Brookhaven.

Mots clés: conformation d'une sérindiamide, interactions du squelette avec la chaîne latérale, analyse topologique des surfaces de l'énergie potentielle, calculs *ab initio*.

[Traduit par la revue]

1. Introduction

The quantum chemical study of the conformational behaviour of diamide model systems has been the subject of continuous interest since Pullman's pioneering work at the semiempirical PCILO level (1). During the 80's several papers (2–9) had been published on *ab initio* studies of such systems. Recent calculations on the simplest case (i.e. on *N*-methyl-glycineamide) have raised the question about the reliability of earlier molecular mechanics (10, 11), and semiempirical (1) studies for predicting peptide conformations.

The smallest chiral system, *N*-acetylalanine *N'*-methylamide, is another important model case. *Ab initio* 4-21G calculations by Schäfer and co-workers (6, 7) demonstrated the possibility of interconversion of the most important α, β, and γ conformations through low-energy pathways (7). They found that the β and γ conformations are stabilized by intramolecular H-bonding, which is characteristic to these specific backbone structures. The "intra-backbone" H-bonding may be perturbed by the presence of polar side-chains with H-bonding donor/acceptor ability and a new side-chain/backbone H-bond may eventually be formed. The simplest system modelling this feature is the serine diamide. In the recent calculations by Schäfer and co-workers (6) on the *N*-acetyl-*N'*-methylserineamide, the side-chain conformation was kept fixed in + *syn-clinial* conformation ($\chi_1 = 60°$, $\chi_2 = 60°$) as suggested by their previous studies on the *N*-acetyl-*N'*-methylserineamide (9). This strategy was based on the hypothesis that perturbations coming from different (χ_1, χ_2) side-chain structures can be neglected on the two dimensional (ϕ, ψ) cross-section of the conformational potential energy surface. Unfortunately this assumption is not confirmed by X-ray, NMR, and CD-spectroscopical evidences (12, 13). In effect, the "side-chain/backbone interaction" is a key concept in the interpretation of experimental data (12, 13).

The four possible structures involving H-bonding between the backbone and the serine side-chain have been discussed in a molecular mechanics study by Scheraga and co-workers on

[1]Permanent address: Institute of Organic Chemistry, Roland Eötvös University, Múzeum krt. 4/B, Budapest H-1088, Hungary.

[2]Permanent address: Chinoin Research Centre, Budapest, P.O. Box 110, H-1325, Budapest, Hungary.

[3]Revision received June 7, 1990.

Printed in Canada / Imprimé au Canada

Can. J. Chem. Downloaded from www.nrcresearchpress.com by 91.121.58.235 on 09/07/12
For personal use only.

Can. J. Chem. Downloaded from www.nrcresearchpress.com by 91.121.58.235 on 09/07/12
For personal use only.

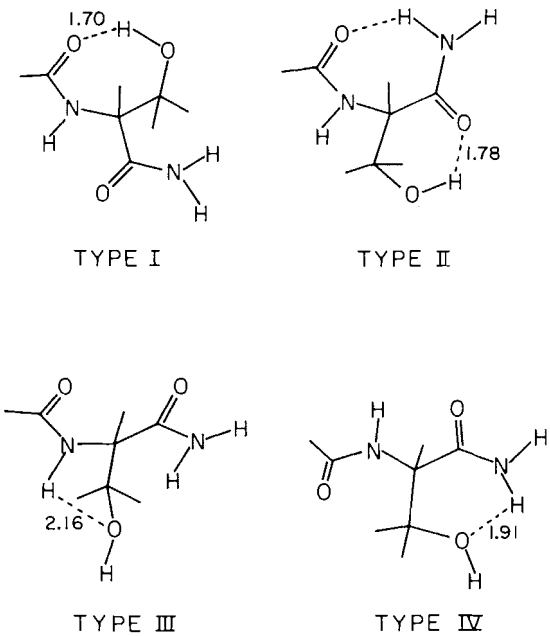

FIG. 1. The four hydrogen bonded conformations of FSA used as starting point for the ab initio SCF-MO computions. The gradient optimized torsional angles are given below in degree: type **I** has $\phi = 174, \psi = 169, \chi_1 = -89, \chi_2 = 52$; type **II** has $\phi = -83, \psi = 72, \chi_1 = 53, \chi_2 = 66$; type **III** has $\phi = -76, \psi = -36, \chi_1 = 49, \chi_2 = 178$; type **IV** has $\phi = -171, \psi = -172, \chi_1 = -172, \chi_2 = 173$. The hydrogen bond distances are given in Angström.

N-acetyl-*N'*-methylserineamide (10). These structures, labelled as **I, II, III,** and **IV,** are illustrated in Fig. 1.

In the present work a systematic study of the coupling between the serine side-chain and the peptide model system was undertaken by calculating the various cross-sections as well as selecting the critical points of the four-dimensional conformational hypersurface $E(\phi, \psi, \chi_1, \chi_2)$. The variables were torsional angles defined according to the IUPAC-IUB convention for peptides.

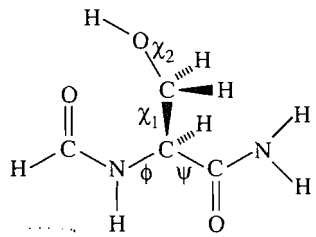

This four-dimensional space has been subdivided into two subspaces:

$$(\phi, \psi, \chi_1, \chi_2) \rightarrow \begin{cases} (\phi, \psi) \\ (\chi_1, \chi_2) \end{cases}$$

Such a subdivision leads to two (regular) potential energy surfaces each having two independent variables. These two variables are parametrically dependent on the other two variables as well as an ensemble of the remaining internal coordinates of the molecules.

$$E(\phi, \psi, \chi_1, \chi_2 \rightarrow \begin{cases} E_{\chi_1, \chi_2}(\phi, \psi) \\ E_{\phi, \psi}(\chi_1, \chi_2) \end{cases}$$

The $E(\phi, \psi)$ surface is expected to have several minima, and some of these should correspond to traditional backbone conformations: α-helix, β-pleated sheet, γ-turn, (i.e. α, β, γ). The interconnection between the three classical conformations (α, β, γ) that exists in peptides and in proteins may be depicted by the following scheme:

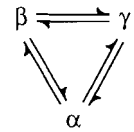

Another possibility is that a common transient structure may be considered. This transient structure was labeled as β' by Schäfer *et al.* (4), and its involvement is illustrated by

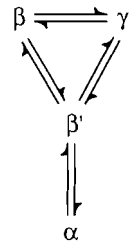

This transient structure, β' has turned out to be a first-order saddle point. To each of the minima (α, β, γ), as well as to the transient structure β' of the $E(\phi,\psi)$ surface one may associate a separate $E(\chi_1, \chi_2)$ surface, with its own minima labelled as **I, II, III, IV** (Fig. 1).

2. Computational method

Due to the large dimensionality of the problem, peptide and protein conformations are usually studied by empirical methods. ECEPP/2 calculations (11) were performed on twenty backbone geometries of various (φ, ψ) values, selected on low-energy pathways, interconnecting the α, β, and γ structures of the model diamide. For each of these backbone conformations a separate $E(\chi_1, \chi_2)$ surface was generated consisting of a 25 × 25 grid.

Four typical backbone conformations (α, β, β', γ) were computed using an *ab initio* SCF-MO method. For each of these four possible backbone structures four side-chain conformations (**I, II, III, IV**) were included in the study yielding a total of sixteen rotamers of FSA. These sixteen structures were gradient-optimized using the MONSTERGAUSS program (14) at the 3-21 G basis set level. All internal degrees of freedom, including bond lengths, bond angles, and torsion angles were optimized, thus energies reported in this paper are for totally relaxed geometries. The extent of optimization was such that the total gradient length was reduced to at least a few hundredths of a mdyn. However, most of the individual gradients were no more than a few thousandths of a mdyn. Further geometry optimization at this level, due to the length of the calculation, can only be performed with an excessive use of computer time.

3. Results and discussion

3.1. Molecular mechanics calculation

The ECEPP/2 potential energy surface is shown in Fig. 2. It can be seen that the low energy paths going from the β-pleated sheet conformation to α may occur via two pathways: either on the way of crossing through γ and β' or via passing directly through β' (see Fig. 2).

One of the reaction coordinates on the $E(\phi, \psi)$ surface is a path connecting points from β (−150, 150) through β' (−150, 80) to α (−50, −50). The other reaction coordinate connects

Can. J. Chem. Downloaded from www.nrcresearchpress.com by 91.121.58.235 on 09/07/12
For personal use only.

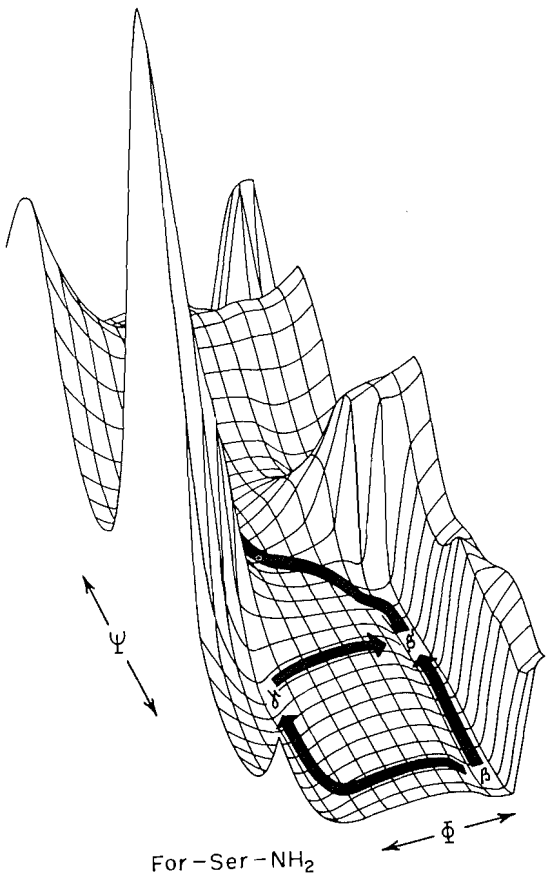

FIG. 2. An enlarged detail of $E(\phi, \psi)$ surface of FSA computed with ECEPP/2 in the range of $-180 < \phi < -50$ and $-180 < \psi < 180$ where the low energy pathways are indicated as $\beta \rightarrow \gamma \rightarrow \beta' \rightarrow \alpha$. (The position of the α conformation is hidden by the high maximum).

points from β through γ $(-75, 75)$ toward β' $(-150, 80)$ with a destination to α $(-50, 50)$. On these paths the β' is a saddle point. At several (ϕ, ψ) points, on or near the path, we performed (χ_1, χ_2) grid searches and obtained $E(\chi_1, \chi_2)$ surfaces with similar general features, as shown in Fig. 3.

3.1.1. The topology of $E(\chi_1, \chi_2)$ *surfaces*

The critical points of cross-sections of the conformational potential energy surfaces $E(\chi_1, \chi_2)$ at all (ϕ, ψ) points were found and the index (λ) of the critical points was evaluated using numerical methods to determine the second derivatives of the energy. The minima ($\lambda = 0$) were labelled as 0_i, the saddle points ($\lambda = 1$) as 1_i and the maxima ($\lambda = 2$) as 2_i. The $E(\chi_1, \chi_2)$ surface, given in Fig. 4, is regarded as "ideal" (15), since the alternating sum rule (16).

$$N_0 + N_1 + N_2 = 0$$

is such that it follows the "κ- rule" (17, 18)

$$N_\lambda = \kappa \binom{n}{\lambda}$$

Note that $N\lambda$ is the total number of critical points of a given type (λ) on the whole surface: $(9 - 18 + 9 = 0)$. The value of κ is the product of the two three-fold rotational axes: $3^2 = 9$ and $n = 2$ is the dimensionality of the conformational space.

Due to the presence of internal attraction or repulsion, all other $E(\chi_1, \chi_2)$ surfaces are more or less distorted but they still could be considered as "ideal". Detailed analysis of the $E(\chi_1, \chi_2)$ surface shows that at all $E(\phi,\psi)$ minima the number of

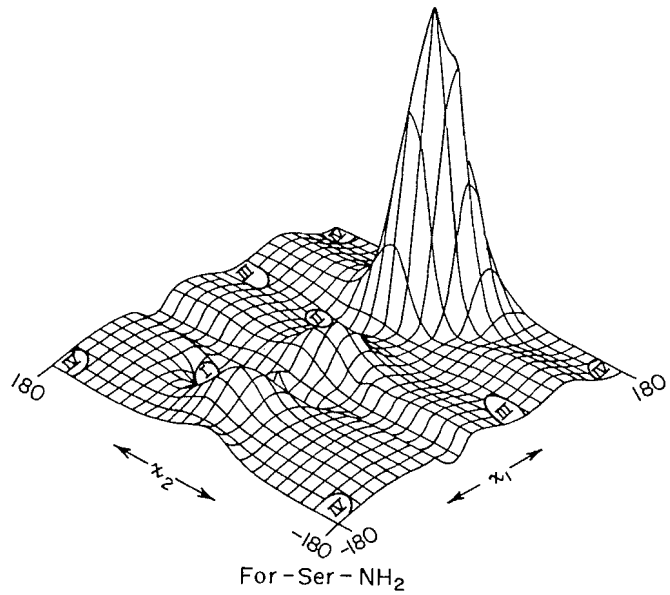

FIG. 3. A typical $E(\chi_1, \chi_2)$ surface of FSA computed with ECEPP/2. Roman numbers indicate the labeled minima associated with the —CH_2OH side-chain conformation.

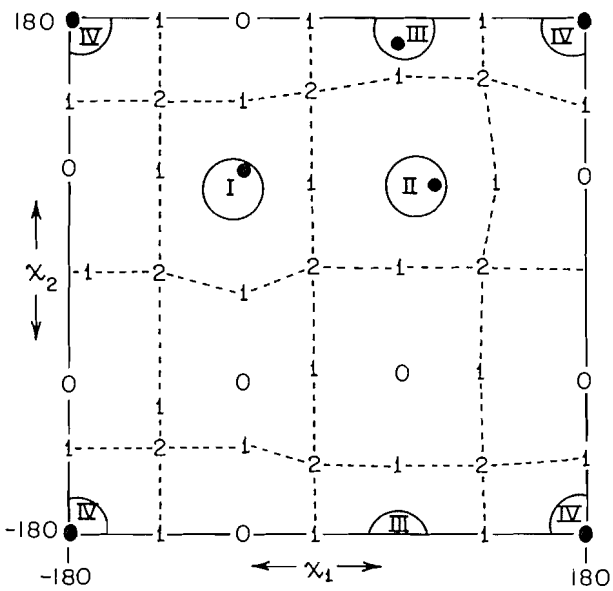

FIG. 4. The topology of an $E(\chi_1, \chi_2)$ surface, where 0's indicate the various minima, 1's symbolize the different saddle points, and 2's are positioned at all the maxima. Roman labeled black spots are the most important minima. The catchment regions associated with each of the minima are located with the four broken lines that are forming the various rectangles. The black spots around the most important minima denote the regions where the actual side-chain minima (**I-IV**) of the four backbone conformations ($\alpha, \beta, \beta', \gamma$) are located (see Table 1 for details).

critical points in $E(\chi_1, \chi_2)$ surfaces are the same. In other words, a displacement on the $E(\phi, \psi)$ surface leaves $E(\chi_1, \chi_2)$ always identical in a topological sense; only the values of the position and height of the critical points are changing but not the overall feature of the $E(\chi_1, \chi_2)$ surfaces. From the given nine minima of the $E(\chi_1, \chi_2)$ surface only four of the minima are stabilized by different types of intramolecular hydrogen bonding (**I, II, III, IV**) as shown in Fig. 3. These four critical points have more significance than the others, as any one of these conformations

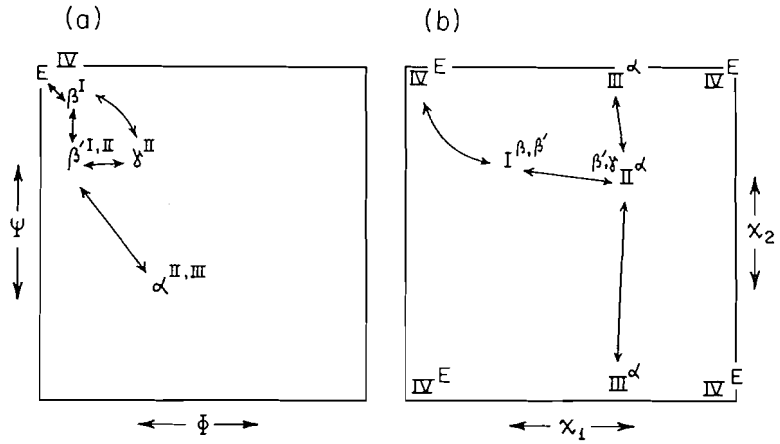

FIG. 5. Coupling effects of the $E(\phi, \psi)$ and $E(\chi_1, \chi_2)$ surfaces. The torsion angles (ϕ, ψ) of backbone and the torsion angles (χ_1, χ_2) of the side-chains mutually determine each other. Each of the symbols used consists of two characters. The main symbol characterizes the critical point on a given surface and its superscript characterizes the minimum on the associated coupled surface.

could be candidates for global minimum in the course of changing (ϕ, ψ) values, corresponding to different backbone conformations (e.g. $\beta \rightarrow \beta' \rightarrow \alpha$ or $\beta \rightarrow \gamma \rightarrow \beta' \rightarrow \alpha$).

3.1.2. Coupling of the (ϕ, ψ) and (χ_1, χ_2) subspaces

It has been already demonstrated (6) that there are several minima both on the $E(\phi, \psi)$ and on the $E(\chi_1, \chi_2)$ surfaces. The most important of them are labelled as α, β, β', γ and **I, II, III, IV**, respectively. The present study of FSA showed that minima on the $E(\phi, \psi)$ and an $E(\chi_1, \chi_2)$ are intimately related to each other. A rigorous interdependence can be demonstrated in the sense that displacement along the minimum energy pathway on $E(\phi, \psi)$ involves a shift of the global minimum on the $E(\chi_1, \chi_2)$ potential energy surface. This is also illustrated in Fig. 5*a* and *b*. The most favourable side-chain conformation can be found at the upper left corner of the $E(\phi, \psi)$ surface, labelled as extended (E) backbone geometry, *i.e.* structure **IV**. In this structure (E–**IV**) all torsion angles are *trans*-like and the six-membered ring involves a hydrogen bond between the side-chain hydroxy group and the amino group of the C-terminal amide (O...HN distance is 1.91 Å). The (E–**IV**) $\rightarrow$ (β-**I**) transition is also illustrated in Fig. 6.

The β-pleated sheet, labelled as the β conformation ($\phi = -150$, $\psi = 150$), slightly differs from the extended (*E*) one ($\phi = -180$, $\psi = 180$) and involves a side-chain conformation participating in a seven-membered intramolecular hydrogen bond. The HO...HN distance has a favourable 1.70 Å value (Fig. 1). Following the pathway from β to β' (Fig. 5*a*) one observes a displacement on the $E(\chi_1, \chi_2)$ surface (Fig. 5*b*) in the horizontal direction from **I** to **II**. The γ backbone conformation ($\phi = -78$, $\psi = 78$) is associated with a $+syn$ clinal ($\chi_1 = 68$, $\chi_2 = 56$) side-chain conformation resulting in two hydrogen bonds. The rigidity of the geometry in structure γ-**II** is produced by locking of the all four tension angles due to the presence of the two hydrogen bonds (Fig. 1). One of these forms a seven-membered ring, where the proton donor is the NH of the *C*-terminal amide and the carbonyl of the *N*-terminal formyl group is the proton acceptor. In the same structure there is also a six-membered hydrogen-bonded ring in which the proton is donated by the hydroxy-methyl group of the side-chain and accepted by the carbonyl group of the serine—CONG—moiety.

Following the pathway from β or from γ towards α through the saddle point β' induced a displacement of the global minimum on the $E(\chi_1, \chi_2)$ surface from **I** or **II** to **III**. On the way from **II** towards **III** there is a saddle point. As it may be seen from Fig. 5*b*, it is only 3 kcal/mol higher in energy than the adjacent minimum previously occupied. Conformation **III** is a five-membered ring resulting from the H-bonding between the serine NH group and the serine hydroxyl group, with an interatomic NH...O distance of 2.16 Å.

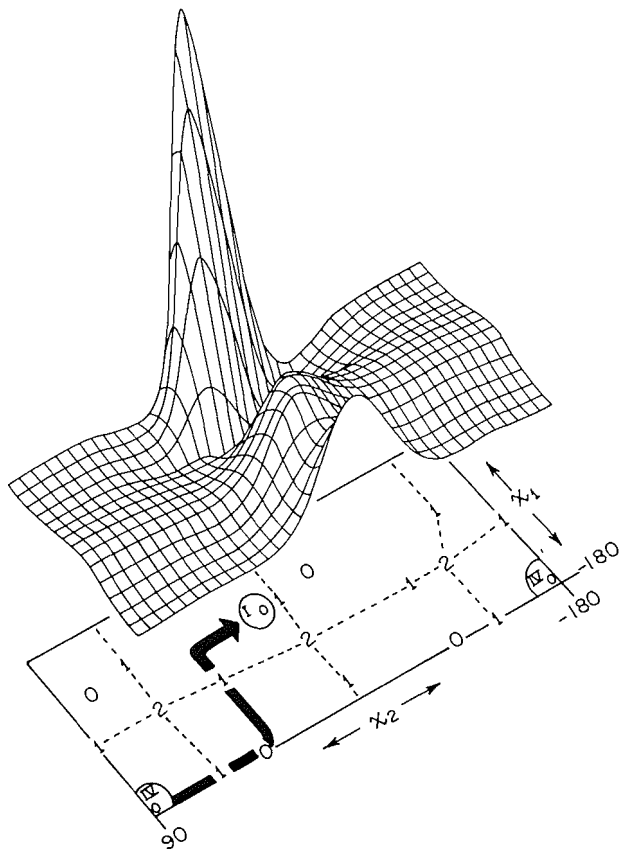

FIG. 6. The low energy pathway related **IV** with **I** on the $E(\chi_1, \chi_2)$ surfaces. The path is directed from minimum **IV** to minimum **I** through an unlabeled minimum and two unlabeled saddle points.

In order to prove thoroughly the hypothesis of "coupling phenomenon" between the (ϕ, ψ) and (χ_1, χ_2) subspaces, *ab initio* calculations were performed on the above sixteen selected geometries. In agreement with the conclusions drawn from the

Can. J. Chem. Downloaded from www.nrcresearchpress.com by 91.121.58.235 on 09/07/12
For personal use only.

TABLE 1. *Ab initio* SCF (3-21G) results of *N*-formyl-(L)serine-amide (FSA) conformations[a]

BB	ϕ	ψ	χ_1	χ_2	E	ΔE_{rel}	ΔE_{abs}	SC
β	−174.4	169.3	−88.5	51.6	−910.416	1.81	5.62	I
	−153.6	150.0	50.5	50.7	−901.623	7.33	11.14	II
	−161.5	171.9	66.3	−176.9	−901.300	7.53	11.34	III
	−171.5	187.4	−171.7	173.0	−913.301	0.00	3.80	IV
β′	−155.0	80.0	55.7	64.1	−903.729	0.00	9.82	II
	−155.0	80.0	−88.0	46.5	−896.321	4.61	14.47	I
	−155.0	80.0	47.1	175.4	−889.239	9.09	18.91	III
	−155.0	80.0	180.0	−177.8	−894.764	5.63	15.45	IV
γ	−83.1	71.8	53.2	65.9	−919.378	0.00	0.00	II
	−85.6	70.7	−66.9	59.9	−902.644	10.50	10.50	I
	−83.0	67.9	40.4	171.1	−908.360	6.91	6.91	III
	−86.1	78.2	−169.3	−169.6	−901.935	10.95	10.95	IV
α	−75.7	−36.0	48.9	177.7	−899.876	0.21	12.24	III
	−78.0	−22.9	−67.2	57.7	−890.698	5.97	18.00	I
	−73.6	−30.4	53.1	78.9	−900.217	0.00	12.02	II
	−68.4	−39.2	178.7	179.7	−885.674	9.11	21.15	IV

[a]Torsion angles ($\phi, \psi, \chi_1, \chi_2$) in degrees, energy ($E = E_{tot} - 486.000$ Hartees) in milihartrees, and energy differences ($\Delta E_{rel}, \Delta E_{abs}$) in kcal/mol units, BB = backbone, SC = side-chain.

Can. J. Chem. Downloaded from www.nrcresearchpress.com by 91.121.58.235 on 09/07/12
For personal use only.

molecular mechanics computations (Table 1) the *ab initio* results (Table 2) confirm the hypothesis and demonstrate clearly that the backbone torsional angles (ϕ, ψ) and the optimal side-chain dihedral angles (χ_1, χ_2) mutually dependent on each other. Thus this coupling enables one to predict the optimum (χ_1, χ_2) values from a given pair of (ϕ, ψ) values and vice versa. Details of this phenomenon are given in the next section.

3.2. *Ab initio SCF results and their comparison with molecular mechanics*

Tables 1 and 2 demonstrate the qualitative agreement of the results obtained by the two methods. In β′ and γ conformations both methods predict the same dihedral angle combinations for the side-chain. Moreover, all conformations having β′ or γ like backbones have the same relative energetic order (ΔE_{ref}).

Note that for the *ab initio* results (Table 2) the minimum, labelled as β-**IV** structure has a backbone conformation ($\phi = -171$, $\psi = -173$), which is in fact quite close to the extended geometry ($\phi = -180$, $\psi = -180$). If we disregard this structure (β-**IV**), we find that the remaining three conformations obtained in molecular mechanics (Table 1) and *ab initio* (Table 2) results are in qualitative agreement in as far as the order of stability is the same.

As far as the α-like backbone torsion angles are concerned one can see that there is only a few tenths of kcal/mol difference between type **II** and type **III** conformations. This means that both minima on the $E(\chi_1, \chi_2)$ surface can be populated approximately to the same extent. However, the *ab initio* calculation predicted a slightly lower energy for type **II** in contrast with ECEPP/2 method. Figure 5 schematically illustrates the topology of the two surfaces. The topology is the same, irrespective of the fact that it is generated by molecular mechanics or by the *ab initio* methods. Consequently the two methods are in good qualitative agreeesnt.

3.3. *Computed conformations versus crystal structures*

X-ray data concerning serine containing peptides and proteins can be obtained from the Cambridge Structural Data Base (19) and from Brookhaven Protein Data Bank (20). It was the pioneering work by Dunitz and co-workers (2) that first

TABLE 2. Molecular mechanics (ECEPP/2) results of N-formyl-(L)serine-amide (FSA) conformations[a]

BB	ϕ	ψ	χ_1	χ_2	ΔE_{rel}	ΔE_{abs}	SC
β	−171.4	155.4	−86.9	51.9	0.00	1.15	I
	−158.7	150.0	55.1	67.8	3.59	4.75	II
	−158.6	157.7	62.0	−77.3	3.30	4.45	III
	−159.8	166.1	−178.6	178.3	2.27	3.41	IV
β′	−154.8	77.5	68.9	56.4	0.00	2.01	II
	−169.4	81.0	−85.0	50.8	0.25	2.26	I
	−156.7	81.0	53.5	177.8	3.55	5.56	III
	−157.0	81.0	−179.5	−177.8	2.92	4.93	IV
γ	−78.4	78.4	67.9	55.9	0.00	0.00	II
	−79.6	76.8	−63.1	61.3	3.47	3.47	I
	−80.0	75.0	52.0	174.9	2.97	2.97	III
	−77.8	79.9	−178.1	−176.1	3.49	3.49	IV
α	−72.3	−38.6	56.6	178.9	0.00	3.33	III
	−75.4	−33.0	−63.6	60.1	1.51	4.84	I
	−72.1	−36.2	56.1	78.3	0.38	3.71	II
	−70.7	−37.8	−178.7	179.1	1.47	4.80	IV

[a]Torsion angles($\phi, \psi, (\chi_1, \chi_2)$ in degrees and energy differences (ΔE_{rel}, ΔE_{abs}) in kcal/mol units, BB = backbone, SC = side-chain.

indicated that the maximum population of a given geometrical arrangement for a particular fragment in various molecular environments, as deduced from crystallographic data bases, outlines the domain, where a minimum lies. This leads to the possibility of a meaningful comparison between experimental and theoretical results. This type of procedure has, for example, been applied recently in our laboratory to the case of pyrrolidone ring puckering (22).

The application of a procedure similar to that suggested by Dunitz and co-workers seemed to be desirable here as well. Due to the relatively small number of serine diamide fragments in CCDB, a statistically significant analysis of the data was difficult. We also have to emphasize that the crystal-phase conformation of a peptide is not necessarily the best choice of a primary standard to be compared with theoretical results. This is

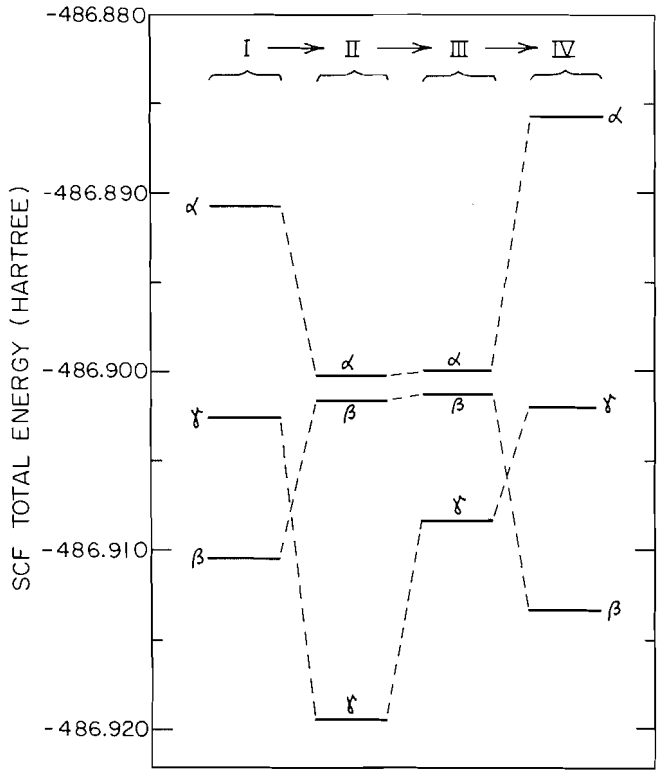

FIG. 7. Energy levels of α, β, and γ backbone conformations (ϕ, ψ) associated with changing sidechain (χ_1, χ_2) conformations: **I → II → III → IV.**

due to the almost always presence of external hydrogen bonds or hydrophobic attractions (23). Nevertheless, a comparison of experimentally determined conformations with surrounding-dependence and the computed environment-free geometries might lead to certain conclusions.

From the few serine-containing structures found in the Cambridge Structure Data Bank only six molecules have features reminiscent of the FSA structure. There are two cyclo-dioxopiperazines (cyclo-(Ser-Ser) and cyclo-(Ser-His)) with distorted backbones due to the six-membered diamide ring that have (ϕ,ψ) torsion angles close to 0 degree. Whereas it is not a typical backbone conformation, it is on a low pathway (Fig. 2) and the coupling correlation predicts type **II** or type **III** side-chain conformation, which happened to be the observed crystallographic combinations of χ_1 and χ_2.

In cyclio(Gly-Pro-Dêr-(D)Ala-Pro) the serine torsion angles are $\phi = -167.4$, $\psi = 114.7$, $\chi_1 = 179.5$, $\chi_2 = 172$, strongly resembling the type E-**IV** which is in good agreement with the present predictions. Furthermore, *t*-butylcarbonyl-L-prolyl-*N*-methyl-L-serine amide represents a conformation of the type α-**III** ($\phi = -75$, $\psi = -11$, $\chi_1 = 50.8$, $\chi_2 = -168.3$) just as well as *t*-butylcarbonyl-L-prolyl-L-serine-*N'*-methylamide fits in the class labeled as type α-**III** ($\phi = -75$, $\psi = -11$, $\chi_1 = 50.9$, $\chi_2 = -167$). The prediction based on FSA stereochemistry is generally good, the only exception is *t*-butylcarbonyl-L-serine-*N'*-methylamide. In this case the side-chain conformation is type **III** ($\chi_1 = 69.7$, $\chi_2 = -88.2$) which does not harmonize with the backbone conformation ($\phi = -90.8$, $\psi = 153.4$) and with the rule deduced from the FSA results. However, we can explain this discrepancy if we allow for geometrical variations due to the strong intermolecular interactions detected in the experimentally determined crystal conformations.

Instead of analyzing the whole set of data coming from several hundred proteins provided by the Brookhaven Protein Data Bank, attention has been paid to a randomly chosen subset consisting of eight proteins: SUBSTILISIN/BPN (E.C.3.4.21.14), LYSOZYME (E.C.3.2.1.17), RIBONUCLEASE (E.C.3.1.4.22), CYTOCHROME C, FERROCYTOCHROME C, TOSYLE-LASTASE (E.C.3.4.21.11), MYOGLOBINE, and ACID PROTEASE (E.C.3.4.23.9). A comprehensive utilization of the information contained in the Brookhaven PDB for the present purposes is difficult because of the lack of hydrogen coordinates, i.e., the absence of χ_2 angles.

The above eight proteins analyzed contained 116 serine units. About 22% of these was α-helix like, 9% was γ-turn like, and 16% was β-pleated sheet like conformations. The remaining 53% belonged to other backbone conformations. In the β backbone conformation only two third of the side-chain geometry was of type **I** or **IV** that obeyed the present coupling rule. In the γ backbone conformation only a tenth was of type **II** and nine tenth was of type **I**. On the other hand, all γ backbone conformations were distorted toward the β conformation, for α-like backbone geometry one fourth was of the expected type **II** or type **III**. These discrepancies can be regarded as a result of long-range intermolecular interactions. In effect, the serine residue are most probably situated in hydrophylic regions of the protein, *i.e.*, where the intramolecular H-bonding is competing with external H-bondings caused by other side-chains or solvent molecules.

4. Conclusions

The present analysis demonstrae s that a strong correlation (coupling rule) exists between the (ϕ, ψ) and the (χ_1, χ_2) subspaces in the four dimensional conformational space (ϕ,ψ, χ_1, χ_2) associated with the stereochemistry of For-Ser-NH. This coupling enables one to predict the optimum χ_1 and χ_2 from a given pair of (ϕ, ψ) values and *vice versa*, as illustrated by Fig. 6. If the energy levels shown on Fig. 6 would reduce or increase along the reaction coordinate associated with the side-chain conformation (**I → II → III → IV**) in a parallel fashion then the $E(\phi, \psi)$ and $E(\chi_1, \chi_2)$ surfaces would be completely independent. A small deviation from such a parallelism would indicate a modest interaction between the (ϕ, ψ) and (χ_1, χ_2) subspaces but the crossing of levels, as shown in Fig. 7, is a clear indication of strong coupling of the two subspaces.

It is found that internal hydrogen bonding is an important feature which influences the overall conformation of the serine-containing peptides as demonstrated by both theoretical calculations and experimental findings.

Acknowledgements

The *ab initio* computations were carried out at CIRCE (Orsay, France). One of us (J.G.A.) thanks IBM-France and CNRS the generous allocation of computer time within the framework of the GS (Groupment Scientifique) "Modélisation Moléculaire". The continued financial support of the NSERC of Canada as well as the Canadian NRC and the CNRS (France) are also gratefully acknowledged.

1. B. PULLMAN. *In* Aspects de la Chimie Quantique Contemporaine. *Edited by* R. Daudel and A. Pullman. CNRS, Paris. 1971. p. 261.
2. B. M. PETTIT and M. KARPLUS. J. Am. Chem. Soc. **107**, 1166 (1985).
3. S. J. WEINER, V. C. SINGH, T. J. O'DONNELL, and P. A. KOLLMAN. J. Am. Chem. Soc. **106**, 6243 (1984).

Can. J. Chem. Downloaded from www.nrcresearchpress.com by 91.121.58.235 on 09/07/12
For personal use only.

4. L. SCHÄFER, C. VAN ALSENOY, and J. N. SCARSDALE. J. Chem. Phys. **76**, 1438 (1982).
5. V. J. KLINKOWSKI, L. SCHÄFER, F. A. MOMANY, and C. VAN ALSENOY. J. Mol. Struct. **124**, 143 (1985).
6. J. N. SCARSDALE, CA. VAN ALSENOY, V. J. KLINKOWSKI, L. SCHÄFER, and F. A. MOMANY. J. Am. Chem. Soc. **105**, 3438 (1983).
7. L. SCHÄFER, V. J. KLINKOWSKI, F. A. MOMANY, H. CHUMAN, and C. VAN ALSENOY. Biopolymers, **23**, 2335 (1984).
8. K. SIAM, S. Q. KLUP, J. D. EWBANK, and L. SCHÄFER. J. Mol. Struct. **184**, 143 (1989).
9. K. SIAM, V. J. KLINKOWSKI, C. VAN ALSENOY, J. D. EWBANK, and L. SCHÄFER. J. Mol. Struct. **152**, 261 (1987).
10. P. N. LEWIS, F. A. MOMANY, and H. A. SCHERAGA. Isr. J. Chem. **11**, 121 (1973).
11. M. VASQUEZ, G. NEMETHY, and H. A. SCHERAGA. Macromolecules, **16**, 1043 (1983).
12. I. L. KARLE. J. Am. Chem. Soc. **181**, 4 (1979).
13. A. AUBRY, N. GHERMAN, and M. MARRAUD. Int. J. Peptide and Protein Res. **23**, 113 (1984).
14. M. R. PETERSON and R. A. POIRIER. MONSTERGAUSS. 1984. Department of Chemistry, University of Toronto, Toronto, Ont., Canada M5S 1A1.
15. J. G. ANGYAN, R. DAUDEL, A. KUCSMAN, and I. G. CSIZMADIA. Chem. Phys. Lett. **136**, 1 (1987).
16. M. R. PETERSON, I. G. CSIZMADIA, and R. W. SHARPE. J. Mol. Struct. (THEOCHEM). **94**, 363 (1983).
17. I. G. CSIZMADIA and J. G. ANGYAN. *In* Applied quantum chemistry, proceedings of the nobel laureate symposium. Honolulu. 16–21 Dec. 1984. 1986. pp. 75.
18. I. G. CSIZMADIA. J. Mol. Struct. (THEOCHEM). **138**, 1 (1986).
19. F. H. ALLEN, S. BELLARD, M. D. BRICE, B. A. CARTWRIGHT, A. DOUBLEDAY, H. HIGGS, T. HUMMELINK, B. J. HUMMELINK-PETERS, O. KENNARD, W. D. S. MOTHERWELL, J. R. RODGERS, and D. G., WATSON. Acta Crystallogr. B, **35**, 2331 (1979).
20. F. C. BERNSTEIN, T. F. KOETZLE, G. J. B. WILLIAMS, E. F. MAYER JR., M. D. BRICE, J. R. RODGERS, O. KENNARD, T. SHIMANOUCHI, and M. TASUMI. J. Mol. Biol. **112**, 535 (1977); E. E. ABOLA, F. G. BERNSTEIN, S. H. BRYANT, T. F. KOETZLE, and J. WENG. *In* Crystallographic database-information content, software system, scientific applications. *Edited by* F. H. Allen, G. Bergerhoff, and R. Sievers. Data Commission of the International Union of Crystallography, Bonn/Cambridge/Chester. 1987. pp. 107–132.
21. R. E. ROSENFIELD JR., R. PARTHASARATHY, and J. D. DUNITZ. J. Am. Chem. Soc. **99**, 4860 (1977).
22. GY. BÁNHEGYI, J. ANGYÁN, and M. KAJTÁR. Coll. Czech. Chem. Commun. **51**, 249 (1986).
23. I. L. KARLE. Biopolymers, **28**, 1 (1989).

Can. J. Chem. Downloaded from www.nrcresearchpress.com by 91.121.58.235 on 09/07/12
For personal use only.

A study of the observable axial- and equatorial-2,4-dimethyl-2-adamantyl cations. Further examples of equilibrating nonclassical structures in "ordinary" tertiary carbocations

D. J. BUFFAM, T. S. SORENSEN,[1] AND S. M. WHITWORTH
The Department of Chemistry, University of Calgary, Calgary, Alta., Canada T2N 1N4

Received April 3, 1990

This paper is dedicated to Professor Ross Stewart on the occasion of his 65th birthday

D. J. BUFFAM, T. S. SORENSEN, and S. M. WHITWORTH. Can. J. Chem. **68**, 1889 (1990).

The title cations have been prepared *in situ* from the corresponding tertiary alcohols, using three different superacid systems. The ^{13}C NMR spectra were measured at a number of different temperatures, using the structurally related ^{13}C peaks of internal 2-methyl-2-adamantyl cation as a reference. Using this protocol, one finds that the ^{13}C chemical shifts of the four β carbons are quite temperature dependent, two of them shifting to higher field and the other two on the opposite face shifting to lower field, or vice versa, as the temperature is increased or decreased. This behavior is uniquely ascribed to a rapid equilibration between two "structures" for each cation system. The two structures in question involve selective C–C hyperconjugative delocalization on one face or the other of the 2-adamantyl skeleton. In the case of the 4-equatorial-methyl isomer, a structure with C–C hyperconjugation on the methyl-substituted face is most stable, while for the 4-axial-methyl cation, the structure with delocalization from the face opposite the substituent is favored. The former preference is regarded as stereoelectronic in origin while the latter is ascribed to steric effects.

Key words: non-planar carbocations, temperature dependent NMR shifts, stereoelectronic effects.

D. J. BUFFAM, T. S. SORENSEN et S. M. WHITWORTH. Can. J. Chem. **68**, 1889 (1990).

Utilisant trois systèmes différents de superacides, on a préparé les cations mentionnés dans le titre *in situ* à partir des alcools tertiaires correspondants. On a mesuré leurs spectres RMN du ^{13}C à diverses températures; comme référence, on a utilisé les bandes internes du cation 2-méthyl-2-adamantyle. Utilisant cette méthode, on trouve que, en RMN du ^{13}C, les déplacements chimiques des quatre carbones β dépendent beaucoup de la température; lorsqu'on augmente la température, deux des déplacements dérivent vers les hauts champs alors que les deux autres qui correspondent aux carbones qui se trouvent sur la face opposée se déplacent vers les bas champs et l'inverse se produit lorsqu'on diminue la température. Ce comportement est attribué uniquement à un équilibre rapide entre deux «structures» pour système cationique. Les deux «structures» en question impliquent une délocalisation sélective par hyperconjugaison C—C sur une face ou l'autre du squelette 2-adamantyle. Dans le cas de l'isomère portant un groupement méthyle en position 4-équatoriale, une structure avec une hyperconjugaison C–C de la face substituée par un méthyle est la plus stable; pour le cation portant un groupement méthyle en position 4-axiale, la structure favorisée est celle avec une délocalisation de la face opposée au substituant. On considère que la première préférence est d'origine stéréoélectronique alors que la dernière est attribuée à des effets stériques.

Mots clés : carbocations non-plans, déplacements RMN qui dépendent de la température, effets stéréoélectroniques.

[Traduit par la revue]

Most tertiary alkyl carbocations, as a class, have been regarded as planar, sp^2-hybridized structures, and there is of course much solvolysis and stable ion work to support this generalization. Increasingly, however, as one looks in more detail at individual systems, one begins to find behavior at odds with this generalization and, furthermore, this often has some chemical reactivity or selectivity considerations. The 2-methyl-2-adamantyl cation **1** is a case in point.

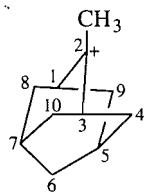

1

The ^1H and ^{13}C NMR spectral data for **1** are normal (1); however, we have recently suggested from a more detailed analysis (2, 3) that **1**, in superacid media, is in fact two structures, degenerate in energy in this case, and each involving C–C hyperconjugation with only one face of the molecule. These conclusions were derived from a study of two substituted derivatives of **1**, the 2,5-dimethyl- and the 2,4,4-trimethyl-2-adamantyl cations **2** and **3**. In each case, the evidence suggested that one had two populated structures for each cation, as shown below:

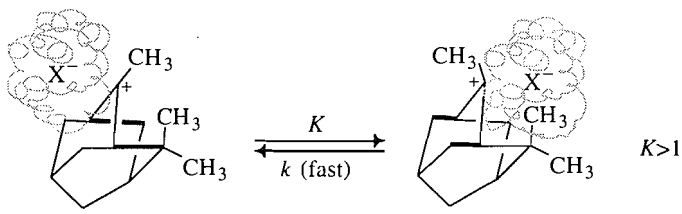

3*a* **3***b*

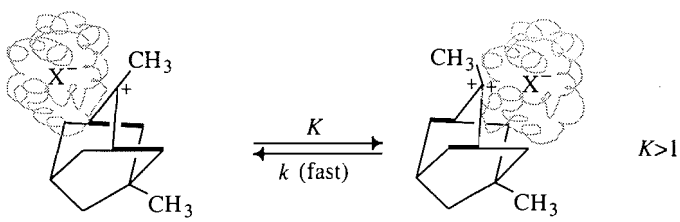

2*a* **2***b*

The heavy lines in these structures are meant to signify C–C hyperconjugative delocalization.

The evidence for these equilibria was indirect, in the sense that one does not see separate NMR peaks for each "*a*" and "*b*"

[1]Author to whom correspondence may be addressed.

Can. J. Chem. Downloaded from www.nrcresearchpress.com by 91.121.58.235 on 09/07/12
For personal use only.

Can. J. Chem. Downloaded from www.nrcresearchpress.com by 91.121.58.235 on 09/07/12
For personal use only.

structure. However, the NMR spectra of cations **2** and **3** each showed several ^{13}C NMR peaks whose chemical shift positions had unusual temperature dependences. These observations were interpreted in terms of a rapid equilibrium of two structures **2***a* ⇄ **2***b* or **3***a* ⇄ **3***b*, resulting in averaged peaks whose positions are temperature dependent because the magnitude of K can change with a change in temperature. However, the interpretation of such temperature dependent chemical shifts is not an easy matter, as Lambert *et al.* (4) have pointed out, and in this paper we would like to report the results of a second study, in which several experimental improvements have been made. As well, the study involves two new unsymmetrical derivatives of **1**: the 2, axial-4- and the 2, equatorial-4-dimethyl-2-adamantyl cations, **4** and **5**, respectively (both depicted at this stage in a traditional way).

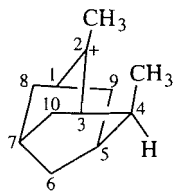

4

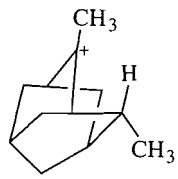

5

Results

Cations **4** and **5** were generated from the corresponding tertiary alcohols **6** and **7**, which were in turn prepared from the known ketones **8** and **9**. Alcohol **6** was essentially a single stereoisomer from ^1H or ^{13}C NMR, whereas **7** was an approximate 60:40 mixture of the two epimers.

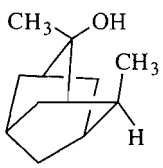

6

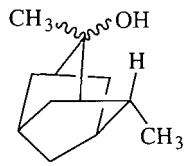

7

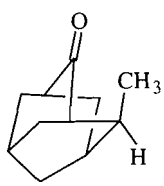

8

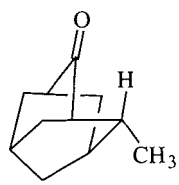

9

In the previous study involving cations **2** and **3**, ^{13}C NMR peaks were referenced relative to internal standards such as $CFCl_3$ or TMS, and in such instances one has to be concerned with the temperature dependence of both the substrate peaks and the reference peaks. In this study, we have used the internal 2-methyl-2-adamantyl cation **1** as a temperature reference, each peak in **4** or **5** being referenced to the corresponding peaks in **1** (except for the 4-methyl peak). In addition, the previous study involving **2** and **3** was carried out at 22.6 MHz and involved only 8K data points (4K real). The present study was carried out at 100 MHz, and up to 512K data points were used, giving a much improved digital resolution in determining the chemical shift positions. In addition, the added chemical shift dispersion at 100 MHz lessens the chances for peak overlaps. The studies were also carried out in three different acid–solvent systems, ROH in 1:1 FSO_3H–SbF_5 and SO_2ClF solvent, ROH in 4:1 FSO_3H–SbF_5, and ROH in 1:1 FSO_3H–SbF_5 and 3:1 SO_2ClF–SO_2F_2 solvent, giving in each case virtually identical results in the temperature regions where there was an overlap.

*Chemical shift assignments for **4** and **5***

At 400 MHz, both **4** and **5** show nearly resolved ^1H NMR spectra. Coupling networks were traced from COSY spectra, although the abundance of W-couplings makes this procedure tricky. The ^{13}C $\{^1H\}$ data were obtained at 100 MHz, and a DEPT spectrum was used to assign the carbon multiplicities. A HETCOR (cation **5**) or an INVERSE HETCOR (cation **4**) was then used to make the more detailed ^{13}C NMR assignments. In the end, the only ambiguity involves the C8–C10 carbons in **4**, where the two peaks have a chemical shift separation of only ca. 0.3 ppm. and the corresponding proton peaks overlap. However, the exact assignment of C8–C10 is immaterial for our purposes. The end result of these assignments is entirely consistent, i.e., the 4-methyl group has the usual effect on nearby ^{13}C resonances, including a significant shielding for carbons δ to an axial methyl group (C2 and C9 in **4**, C6 and C10 in **5**). The NMR assignments for **4** and **5** are listed in the experimental section and these are also entirely consistent with carbon assignments for the related ketones **8** and **9**.

*Temperature dependence of the ^{13}C shifts in **4** and **5***

In 1:1 FSO_3H–SbF_5 in SO_2ClF, usable data were obtained from 157 to 237 K (six temperatures) and in 4:1 FSO_3H–SbF_5, data were obtained from 198 to 280 K (five temperatures). With the mixed 3:1 SO_2ClF–SO_2F_2 solvent, data were obtained from 143 to 183 K (three temperatures), but at 143 K, some of the peaks were rather broad so these data do not in fact usefully extend the temperature range. Only the first two data sets were used in the detailed analysis. At or above 280 K, both **4** and **5** are rapidly transformed into a mixture of the 1,2-dimethyl- and 2,5-dimethyl-2-adamantyl cations (2), the latter the predominant species. The 2-methyl-2-adamantyl cation **1** reference peaks were clear of interference from **4** or **5** peaks, and in fact all three cations can be made up in a single solution and at most temperatures all 30 peaks are base-line resolved.

At each individual temperature, the chemical shift of each carbon was corrected for "intrinsic" temperature effects by using the temperature behavior of the corresponding carbon peak of **1**. There is some arbitrariness in reporting the corrected ^{13}C NMR chemical shifts for **4** and **5** since the corrections can be made in several ways. We have used the data at 200 K as uncorrected, all chemical shifts for higher or lower temperatures being adjusted by the quantity $\delta_1{}^{200}C_X - \delta_1{}^{T}C_X$, i.e., the chemical shift change for an X-type carbon in **1** measured at a temperature T(K), relative to the same measurement at 200 K. The main point is simply that one now has a set of ^{13}C shift vs. T data for which intrinsic temperature effects are hopefully corrected (or partially corrected) for. The validity of this procedure is best evaluated by looking at the resulting data. In Table 1, the temperature-induced changes in the corrected ^{13}C chemical shifts are shown, assuming a linear relationship between temperature and the δ shift change. One notes several things from this table:

1. Carbons 4, 8, 9, and 10 show large chemical shift changes in both cations **4** and **5**.

2. In both cations, several carbons, such as the C2 methyl group and the C6 carbon, show very small chemical shift changes.

Can. J. Chem. Downloaded from www.nrcresearchpress.com by 91.121.58.235 on 09/07/12
For personal use only.

TABLE 1. Corrected temperature shifts[a] of ^{13}C NMR peaks

Carbon	Cation **4**	Cation **5**
1	+24	+13
2	+60	+61
3	−19	+10
4	+409	−390
5	+50	−35
6	+14	−11
7	−38	+31
8	−285 or −298	+333
9	+308	−300
10	−298 or −285	+313
11	~0	~0

[a]Corrected as defined in the text using data from 157 K to 237 K in 1:1 SbF_5–FSO_3H in SO_2ClF solvent, in units of ppm × 10^4/°C. The units are positive when the chemical shifts move upfield with decreasing temperature.

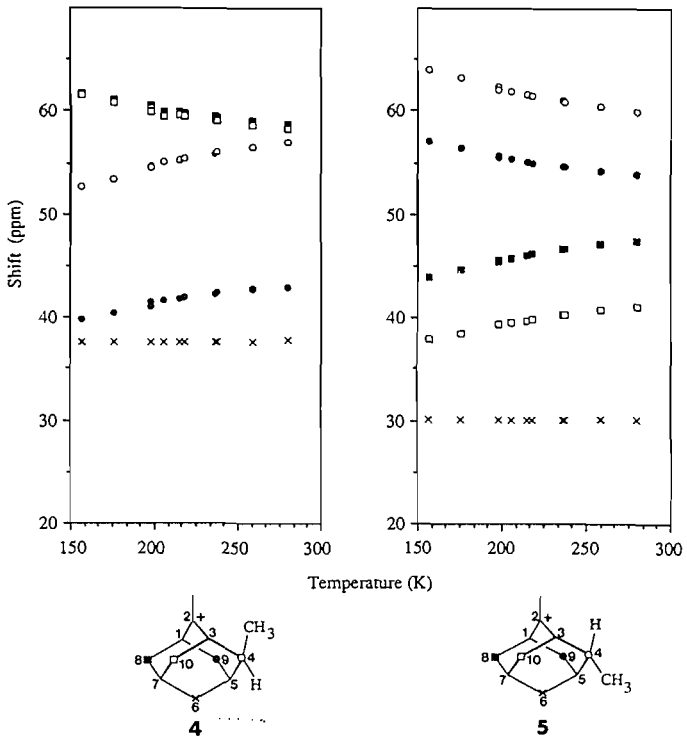

4 5

FIG. 1. Temperature dependence of ^{13}C chemical shifts for carbons 4(○), 6(X), 8(■), 9(●), and 10(□) in cations **4** and **5**.

3. In both cations, the behavior of carbons 4 and 9 is similar, as is the behavior of carbons 8 and 10. Furthermore, these carbon pairs show nearly equal and opposite temperature-induced chemical shift changes.

4. Comparing cations **4** and **5**, one sees completely opposite temperature-induced chemical shift behavior for C4–C9 and for C8–C10.

In Fig. 1, we have plotted the corrected ^{13}C chemical shifts for carbons 4, 8, 9, and 10, as well as for C6, vs. temperature, for both **4** and **5**. It is readily apparent that most of these curves are not strictly linear, as assumed in Table 1. If this data is replotted as a function $1/T$ (K), one still does not see linearity.

Discussion

The temperature-induced chemical shift data for cations **4** and **5**, reported in Table 1, can only be rationalized if one proposes that each is a pair of structures, i.e., consistent with the previous interpretation involving **2** and **3**. Thus, **4** should be written as a rapid equilibrium of two structures **4***a* and **4***b*, and likewise for **5**, **5***a* and **5***b*, where the heavy lines again refer to structures with predominant hyperconjugation on that face of the molecule. Because of this hyperconjugation, carbons 4 and 9 in **4***a* are quite deshielded compared to those on the opposite face (C8 and C10), and an opposite situation applies for **4***b*. The interpretation of structures **5***a* and **5***b* is similar. The large chemical shift difference of carbons 4 and 9 collectively in **4***a* and **4***b*, or for carbons 8 and 10 in these same two structures allows the averaged ^{13}C peaks for these carbons to have unusually large temperature dependences (the van't Hoff equation). A similar situation applies to **5***a*–**5***b*. This analysis uniquely rationalizes why C4–C9 or C8–C10 act in concert, and why one pair shows a positive temperature effect and the other a negative one (or vice versa).

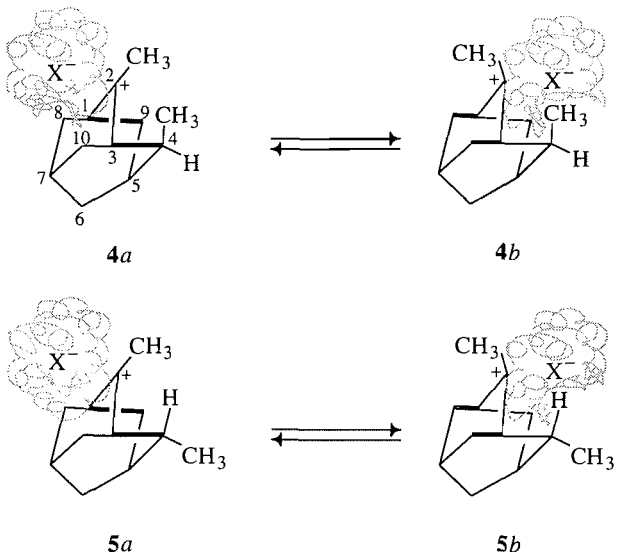

4*a* **4***b*

5*a* **5***b*

For both **4** and **5**, the data require that $\Delta\Delta H = \Delta H_b - \Delta H_a \neq 0$, i.e., that one isomer forms a dominant population in each case. For **4**, the isomer **4***b* is dominant, while for **5**, **5***a* is dominant (as one goes from low to high temperature, $K \rightarrow 1$, so the averaged chemical shift changes observed reflect an increase in the minor isomer in each case).

Besides the temperature dependent ^{13}C shifts observed, one should also note that if **4** or **5** were really a single structure in each case, one would expect C8 to have a virtually identical δ value in both **4** and **5**, as is found in the ketones **8** and **9** (δ 39.5 and 39.4, respectively). In fact, at low temperatures, this C8 carbon is nearly 20 ppm different in **4** and **5**.

The rationale for using 2-methyl-2-adamantyl cation **1** as a reference can now be expanded upon. One presumes that **1** is also an equilibrium of two degenerate structures, for which $K = 1$, $\Delta\Delta H = 0$, and, necessarily, no van't Hoff type temperature dependent chemical shifts would be observed. However, intrinsic temperature dependent chemical shifts for like carbons can be expected to be similar in **1** and **4** or **5**, so one hopes to cancel these out. The results shown in Table 1 bear this out. Thus C6 in both **4***a* and **4***b*, or in **5***a* and **5***b*, is far from the cation centre and is symmetrically located with respect to the distortion on either face. Hence δ C6 should be similar in **4***a* and **4***b* and, since we

Can. J. Chem. Downloaded from www.nrcresearchpress.com by 91.121.58.235 on 09/07/12
For personal use only.

have corrected for intrinsic temperature-derived shifts, this carbon should be fairly insensitive to temperature changes, as is indeed observed. Note also that carbons 1 and 3 in **4***a* and **4***b*, or in **5***a* and **5***b*, also have a nearly identical local environment so that once again one would not expect the respective δ values for these carbons in **4***a* and in **4***b* (or **5***a*–**5***b*) to be very different. Hence, like C6, population changes should not have a large effect on the δ_{AV} value for C1 or C3, again as experimentally observed.

The 4-methyl substituent effect

In work involving simple cyclohexyl cations (3), it was found that equatorial β-alkyl substituents favor C–C hyperconjugation, while γ-alkyl substitution has an opposite effect. In previous work with the adamantyl cations **2** and **3**, one finds in **2** that a 5-methyl substituent (γ) favors C–C hyperconjugation on the unsubstituted face, in agreement with the cyclohexyl cation work, but this same preference is also found for the 4,4-dimethyl substituents (β,β) in ion **3**, in disagreement. In the present work, the equatorial 4-methyl (β) substituent in **5** favors C–C hyperconjugation on the substituted face, also in agreement with the cyclohexyl cation results. However, the axial 4-methyl substituent in **4** causes the opposite behavior. Combined with the previous results for the 4,4-dimethyl cation **3**, one can now show that this axial-4-methyl substituent result in **4** is not a stereoelectronic effect, and is almost certainly steric in origin.

Since the axial and equatorial 4-methyl cations **4** and **5** show opposite population preferences (see next section), one would predict on stereoelectronic grounds that the 4,4-dimethyl cation **3** would show some intermediate behavior. In fact, cation **3** shows an even greater population preference for C–C hyperconjugation on the face opposite the substituents, consistent with a further steric buttressing of the axial 4-methyl group by the equatorial 4-methyl group.

In recently published high level *ab initio* computations, the secondary 2-adamantyl cation has been shown (5) to adopt an unsymmetrical, non-planar C^+ centre, structure (two degenerate structures separated by a very small barrier). We believe that a similar kind of geometric distortion is probable in the case of **4***a* and **4***b* (or **5***a* and **5***b*). Such distortion would in fact enhance the steric interaction between the C2 methyl group and the axial C4 methyl group in **4***a* and help explain why this isomer is not favored in the **4***a*–**4***b* equilibrium.

Possible quantitative treatment of the data

For two species X and Y in rapid equilibrium in an NMR spectrometer, the equilibrium constant K is given by:

$$K = \frac{\delta_X - \delta_{AV}}{\delta_{AV} - \delta_Y} = \frac{[Y]}{[X]}$$

where δ_{AV} is the experimental chemical shift and δ_X and δ_Y are the positions of a given atom in the pure compounds X and Y. In the case at hand, δ_X and δ_Y are unknown. In theory, one can use the van't Hoff equation to solve for these but in practice the linearity of a van't Hoff relationship is fairly insensitive to the choice of δ_X and δ_Y. In the previous work (2), values of δ_X and δ_Y for a carbon such as C8 in **4** or **5** was estimated as δ ca. 65.5 in isomer **4***b* or **5***b*, and δ ca. 36.5 in **4***a* or **5***a*. Our van't Hoff analysis of the present data show that these numbers are still reasonable choices. Using these values gives a K for cation **4**, **4***b*/**4***a* = 3.8, and for **5**, **5***b*/**5***a* = 0.45.

We previously noted that the Fig. 1 data are not linear for δ_{AV} vs. T, nor are they linear for δ_{AV} vs. $1/T$(K). This negative result is consistent with the van't Hoff equation, where δ_{AV} and T involve a more complex relationship.

Significance of the present results

There is a good correlation between solvolysis results involving 5-methyl- or 2,5-dimethyl-2-adamantyl esters (or ethers) (6) and our previous stable ion results (2) for cation **2**. The rate of equilibration of the isomers **2***a* and **2***b* in solvolysis solvents appears to be competitive with the rates for nucleophilic capture, so that one gets both net retention and net inversion of configuration depending upon which stereoisomer is being solvolyzed and the particular solvent being used.

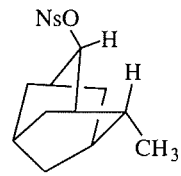

10

Unfortunately, there are no comparable solvolysis data for either the 2,4-dimethyl- or the 4-methyl-2-adamantyl systems. Grob *et al.* (7) have reported that equatorial-4-methyl-2-adamantyl nitrobenzenesulfonate **10** solvolyzes slightly faster than the parent adamantyl compound and shows predominant retention of configuration in the alcohol product (76% vs. 24% inversion). These results are certainly consistent with our results for cation **5**, but they are relatively meaningless without comparison data for the stereoisomeric (at C2) nitrobenzenesulfonate ester. Grob has described the solvolysis intermediate in this reaction as a weakly σ-delocalized, bridged, cation. The C–C hyperconjugative delocalization description given in our work bears some relationship to their ideas. We also note that our structures shown for **4***a*, or for **5***a*, suggest equal C–C delocalization from both the C1—C9 and C3—C4 bonds. If one looks in detail at Table 1, one notes that the substituted C4 carbon is more temperature dependent, suggesting perhaps that the C3—C4 bond contributes slightly more to the cation C–C stabilization than does the C1—C9 bond. If the C4 substituent were a group such as cyano, one can predict that isomer *b* will now dominate the *a* ⇄ *b* equilibrium, and that in the isomer *a*, if present, C–C hyperconjugation will probably predominate from the unsubstituted C1—C9 bond.

The present work concerns a somewhat esoteric dimethyl 2-adamantyl system, but the real significance is that it shows some rather ordinary looking tertiary carbocations to have a detailed structure that is not "classical". In fact, as Schleyer *et al.* (8) have pointed out, at a detailed level of study, whether computational or experimental, there are probably very few classical cations. Moreover, these structural details concern cation properties that lead to chemical reactivity and (or) stereoelectronic consequences.

One would still like to know more about the dynamics of the interconversion of isomers such as **5***a* and **5***b*, since all one can do at present (via NMR spectroscopy) is to put an upper limit of ca. 5 kcal/mol on the transition-state barrier.

Conclusions

In cases such as the present, where one cannot "freeze-out" the equilibrium pair, or even see dynamic NMR line-broadening, one has to be cognizant of alternative interpretations. However, in the present work there are two key experimental observations that do not fit any other explanation:

Can. J. Chem. Downloaded from www.nrcresearchpress.com by 91.121.58.235 on 09/07/12
For personal use only.

1. The temperature dependences of similarly substituted and positioned carbons, such as C8 and C9 in **4** or **5**, show totally opposite shift behavior.

2. For a given carbon, such as C8, the temperature – chemical shift behavior is completely reversed in comparing cation **4** to cation **5**.

We feel therefore that the evidence for two populated structures in both cation **4** and cation **5** is unambiguous.

Experimental

NMR spectra were recorded on a Bruker AM-400 or ACE-200 spectrometer. Preparative GLC was carried out with a Hewlett–Packard model 5890 gas chromatograph, employing a thermal conductivity detector.

Axial-4-methyl- and equatorial-4-methyl-2-adamantanones **8** and **9**, respectively, were prepared as a ca. 60:40 mixture, as described (9). They were separated by preparative GLC, using a 3% OV225-Chromosorb W (80/100) column, 0.4 (i.d.) × 244 cm. The axial isomer elutes first.

2-Equatorial-methyl, 4-axial-methyl-2-adamantanol ***6***

The ketone **8** (13.2 mg, 0.080 mmol) was treated dropwise, under nitrogen, with an excess of methyl lithium solution (1.5 M in ether) at 0°C. After ca. 1 h, the excess methyl lithium was destroyed with water, the phases separated, and the aqueous phase extracted (4 × 5 mL) with ether. After drying ($MgSO_4$), the combined ether layers were evaporated to yield 14.5 mg (0.080 mmol) of a single oily alcohol, assigned the title structure for obvious steric reasons, and which was used without further purification. ^{1}H NMR shows characteristic peaks at δ 1.32 (s, 3H, the C2 methyl), and a doublet at δ 1.26, J = 7, the C4 methyl. ^{13}C NMR: 75.37, 44.61, 41.42, 40.26, 39.17, 37.12, 35.49, 33.15, 29.36, 27.97, 27.29, and 21.67.

Mixture of 2-equatorial-methyl,4-equatorial-methyl- and 2-axial-methyl,4-equatorial-methyl-2-adamantanol ***7***

This preparation was carried out in the same way as for tertiary alcohol **6**, employing 11.9 mg (0.072 mmol) of ketone **9**. ^{1}H NMR spectroscopy shows clearly that the two isomeric alcohols were formed in about a 60:40 ratio; however, the spectra permit no specific assignments. ^{1}H NMR; δ 1.375 (major) and 1.360 (minor), both s, the epimeric C2 methyl group, δ 1.055, d, J = 7 (major), and 1.090, d, J = 7 (minor), the C4 methyl group. The alcohol mixture was used for the cation preparations since the alcohol stereochemistry at C2 is immaterial.

Carbocation preparations and NMR spectra

The cation solutions were made up at −80°C (or lower) directly in 5-mm NMR tubes. Typically, about 13 mg of alcohol **6** or **7** and 7 mg of 2-methyl-2-adamantanol was dissolved in the minimum amount of CD_2Cl_2 and slowly stirred into the pre-prepared superacid solvent mixture (0.4 mL) using syringe techniques. A large molar excess of superacid to alcohol (>5:1) was used. ^{1}H NMR spectra at various low temperatures were measured at 400 MHz for both **4** and **5**, and COSY 2D ^{1}H–^{1}H spectra were also obtained. These ^{1}H NMR spectra were only used for verification of the ^{13}C assignments, via a HETCOR spectrum for **5** and an INVERSE HETCOR for **4**. The ^{1}H NMR data are available on request. The ^{13}C NMR spectra[2] were measured at 100 MHz, employing sweep widths of ca. 36 000 Hz (32K FID) and transforming over 128K data points (up to 512K data points were used in several trial instances to even better define peak shapes, but the end result did not differ significantly from the 128K data). The individual peaks are characterized by data points every 0.0055 ppm. Since chemical shift comparisons are being made to an internal reference with the same uncertainty, the overall uncertainty in chemical shifts should be of the order ±0.01 ppm. DEPT 90 and 135 spectra were used to assign ^{13}C multiplicities.

The ^{13}C NMR shifts for **4** and **5** can be listed in two ways: (1) the actual temperature dependences, given in Table 1, which, as defined in the text, are independent of the actual ^{13}C chemical shifts themselves; and (2) the data in Fig. 1, which were corrected as defined in the text. The absolute ^{13}C chemical shifts at 200 K were referenced to internal CD_2Cl_2, taken as δ 53.80 (middle peak). The data at 200 K are as follows: cation **4**, 325.42 (C2), 72.94 (C3), 66.51 (C1), 60.45 and 60.19 (C8 and C10), 54.46 (C4), 43.70 (C2 methyl), 41.10 (C9), 37.62 (C6), 32.99 (C5), 29.57 (C7), 21.15 (C4 methyl). Cation **5**, 318.21 (C2), 71.19 (C1), 64.44 (C3), 62.35 (C4), 55.70 (C9), 45.45 (C8), 41.22 (C2 methyl), 39.24 (C10), 33.82 (C5), 30.08 (C6), 27.62 (C7), 18.60 (C4 methyl). Cation **1**, 322.33 (C2), 66.07 (C1, 3), 52.32 (C4, 8, 9, 10), 41.15 (C2 methyl), 36.34 (C6), 28.83 (C5, 7).

The temperature of the probe was calibrated using a standard methanol sample (^{1}H), or for temperatures below 173 K, neat 2-chlorobutane (^{13}C) was used for the calibration (10). Internal CD_2Cl_2 was used as a lock and ^{1}H decoupling of the ^{13}C spectra employed the WALTZ procedure.

[2]Tables of chemical shift data for cations **1**, **4**, and **5**, as a function of temperature, have been deposited and may be purchased from the Depository of Unpublished Data, CISTI, National Research Council of Canada, Ottawa, Ont., Canada K1A 0S2.

Acknowledgement

We thank the Natural Sciences and Engineering Research Council for generous financial support.

1. G. A. Olah, G. Liang, and G. D. Mateescu. J. Org. Chem. **39**, 3750 (1974).
2. E. S. Finne, J. R. Gunn, and T. S. Sorensen. J. Am. Chem. Soc. **109**, 7816 (1987).
3. R. P. Kirchen, K. Ranganayakulu, and T. S. Sorensen. J. Am. Chem. Soc. **109**, 7811 (1987).
4. J. B. Lambert, A. R. Vagenas, and S. Somani. J. Am. Chem. Soc. **103**, 6398 (1981).
5. R. Dutler, A. Rauk, T. S. Sorensen, and S. M. Whitworth. J. Am. Chem. Soc. **111**, 9024 (1989).
6. J. A. Bone, J. R. Pritt, and M. C. Whiting. J. Chem. Soc. Perkin Trans 2, 1447 (1975).
7. C. A. Grob, G. Wittwer, and K. Rama Rao. Helv. Chim. Acta **68**, 651 (1985).
8. P. von R. Schleyer, J. W. de M. Carneiro, W. Koch, and K. Raghavachari. J. Am. Chem. Soc. **111**, 5475 (1989).
9. D. A. Lightner and W. M. D. Wijekoon. J. Org. Chem. **47**, 306 (1982).
10. J. R. Lloyd. Ph.D. Thesis, Yale University (1978).

The 1:1 and 2:1 adducts of cyclopentadiene with *p*-benzoquinone

PETER YATES AND KRZYSZTOF SWITLAK

Lash Miller Chemical Laboratories, University of Toronto, Toronto, Ont., Canada, M5S 1A1

Received April 17, 1990

This paper is dedicated to Professor Ross Stewart on the occasion of his 65th birthday

PETER YATES and KRZYSZTOF SWITLAK. Can. J. Chem. **68**, 1894 (1990).

The *exo-cis* isomer (**8**) of the well-known *endo-cis* 1:1 adduct (**4**) of cyclopentadiene and *p*-benzoquinone has been obtained by heating the *endo-cis-anti-cis-endo* 2:1 adduct (**13**) with *p*-benzoquinone and also by heating **4** alone. The *exo-cis* isomer of the 1:1 adduct (**11**) of cyclopentadiene and *p*-toluquinone has also been obtained for the first time. Heating of the 2:1 adduct **13** gives a mixture containing the *endo-anti-exo* isomer **15**, the *exo-anti-exo* isomer **16**, and **13**. The structures of these two new isomers are assigned on the basis of (i) spectroscopic comparison with **13** and the known *endo-syn-endo* and *endo-syn-exo* isomers, **12** and **14**; (ii) spectroscopic comparison of the corresponding tetrahydro compounds; and (iii) the conversion of tetrahydro **15** by oxidation and acetylation to the *syn*-hydroquinone diacetate **28**, which is stereoisomeric with the *anti*-hydroquinone diacetate **25**, prepared by similar treatment of tetrahydro **13**, **14**, and **16**. It is proposed that interconversion of the 1:1 adducts occurs via dissociation–recombination, interconversion of the tetrahydro 2:1 adducts occurs via enolization, while interconversion of the 2:1 adducts themselves can occur by both routes.

Key words: Diels–Alder, benzoquinone, cyclopentadiene, stereoisomerism, cycloaddition.

PETER YATES et KRZYSZTOF SWITLAK. Can. J. Chem. **68**, 1894 (1990).

En faisant chauffer de l'adduit 2:1 *endo-cis-anti-cis-endo* (**13**) en présence de *p*-benzoquinone, on a obtenu l'isomère *exo-cis* (**8**) de l'adduit 1:1 bien connu *endo-cis* (**4**) du cyclopentadiène et de la *p*-benzoquinone; on a aussi obtenu l'isomère **8** par chauffage de l'adduit **4**. On a aussi préparé pour la première fois l'isomère *exo-cis* de l'adduit 1:1 (**11**) du cyclopentadiène et de la *p*-toluquinone. Par chauffage, l'adduit 2:1 (**13**) fournit un mélange contenant l'isomère *endo-anti-exo* (**15**), l'isomère *exo-anti-exo* (**16**) et le produit **13**. On a attribué les structures de ces deux nouveaux isomères en se basant : (i) sur un comparaison de leurs spectres avec ceux du produit **13** et des isomères bien connus *endo-syn-endo* (**12**) et *endo-syn-exo* (**14**); (ii) sur un comparaison spectroscopique des composés tétrahydrogénés correspondants; et (iii) par la conversion du dérivé tétrahydrogéné **15**, par oxydation et acétylation, en diacétate de la *syn*-hydroquinone (**28**) qui est un stéréoisomère du diacétate de l'*anti*-hydroquinone **25**, préparé par une méthode semblable à partir des dérivés tétrahydrogénés **13**, **14** et **16**. On suggère que l'interconversion des adduits 1:1 se produit par une dissociation–recombinaison, que l'interconversion des adduits 2:1 tétrahydrogénés se produit par le biais d'une énolisation et que l'interconversion des adduits 2:1 peut se produire par les deux voies.

Mots clés : Diels–Alder, benzoquinone, cyclopentadiène, stéréoisomérie, cycloaddition.

[Traduit par la revue]

Can. J. Chem. Downloaded from www.nrcresearchpress.com by 91.121.58.235 on 09/07/12
For personal use only.

1:1 Adducts

The reaction of cyclopentadiene and *p*-benzoquinone to give a 1:1 adduct was first reported in 1906 by Albrecht (1). Although the reaction was initially considered to involve Michael addition to give **1** or 1,2-cycloaddition to give **2** (2), it was later shown by Diels and Alder (3) to be a 1,4-cycloaddition reaction giving **3**, and is one of the first reported examples of the reaction that now bears their names.

The stereochemistry of this adduct was established to be *cis-endo* as in **4** on the basis of its photoconversion to the pentacyclic isomer **5** (4); its preferred conformation in solution is considered to be the "open" form **6** rather than the "closed" form **7** (5). The preferred formation of the *cis-endo* stereoisomer under conditions of kinetic control in Diels–Alder reactions is now generally recognized and is enshrined in the *Alder rules* (6). However, in this case, unlike many others (7),[1] the formation of the *cis-exo* isomer, **8**, has not been reported previously. We describe now the preparation of this compound; its availability is of interest because it permits spectroscopic comparison of the two isomers, assists in the assignment of stereochemistry to the 2:1 adducts of cyclopentadiene and *p*-benzoquinone (*vide infra*), and provides a stereochemical variant of **4** for application in synthesis.

Compound **8** was obtained by heating the *initially formed* isomer of the 2:1 adduct of cyclopentadiene and *p*-benzoquinone (**13**: *vide infra*) with *p*-benzoquinone in boiling

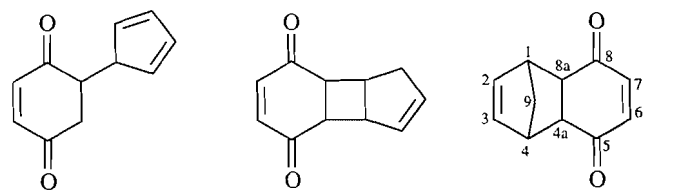

1 **2** **3**

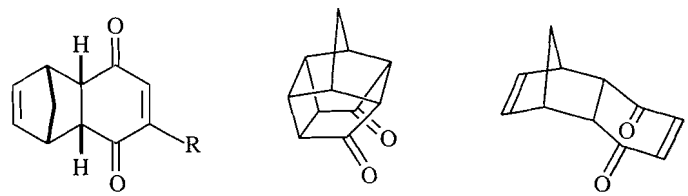

cis-endo
4 R = H
10 R = Me

5 **6**

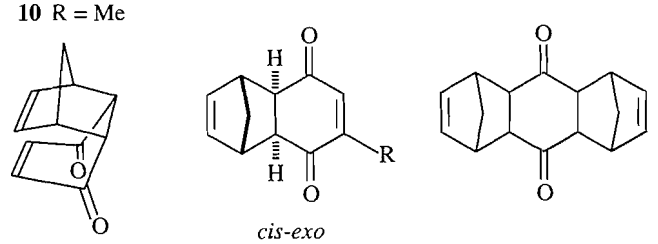

7

cis-exo
8 R = H
11 R = Me

9

[1]For example, both the *cis-endo* and *cis-exo* adducts of cyclopentadiene with maleic anhydride (*vide infra*) have long been known (8).

TABLE 1. The ^{1}H nmr spectra of the 1:1 adducts **4**, **8**, **10**, and **11**[a]

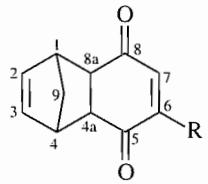

	4 (R = H) *endo*	**8** (R = H) *exo*	**10** (R = CH_3) *endo*	**11** (R = CH_3) *exo*
1,4	3.50 (br s)	3.27 (p, 1.7)	3.51 (m)	3.25 (p, 1.7)
2,3	6.02 (br s)	6.29 (t, 1.9)	6.02 (m)	6.28 (t, 1.9)
4a, 8a	3.17 (d, 1.8)	2.49 (d, 1.5)	3.20 (d, 1.5), 3.21 (d, 1.4)	2.49 (d, 1.5)
6,7	6.52 (s)	6.74 (s)	6.46 (1, 1.4)	6.14 (q, 1.5)
9*anti*	1.49 (dt, 8.8, 1.7)	1.34 (dp, 9.4, 1.6)	1.51 (dt, 8.8, 1.8)	1.32 (dp, 9.3, 1.5)
9*syn*	1.38 (br d, 8.7)	1.25 (dt, 9.4, 1.6)	1.42 (br d, 8.8)	1.23 (dt, 9.3, 1.5)
CH_3	—	—	1.91 (d, 1.5)	2.00 (d, 1.4)

[a]The coupling patterns were not analyzed and the multiplicites and numerical values given in parentheses (apparent coupling constants) are phenomenological and not analytical, except in the case of the one-carbon bridge protons. Pentet (p) is used rather then quintet to avoid confusion with quartet.

xylene for 20 min, when thin-layer chromatography showed that no **13** remained; a 7:3 mixture of the *endo* and *exo* 1:1 adducts, **4** and **8**, was formed. The *exo* isomer **8** was obtained by chromatographic separation of this mixture. It was also formed, but more slowly, by heating the *endo* isomer alone in boiling toluene.

The structure of **8** follows from its elemental composition and its spectra. Its ir spectrum in the 1650 cm^{-1} region is very similar to that of **4** and confirms the presence of the 2-ene-1,4-dione system in **8**. The ^{1}H nmr spectra of **4** and **8**, which are compared in Table 1, resemble one another, but are readily distinguishable, the most striking difference being in the chemical shifts of the C-4a(8a) protons (for numbering, see **3**). The upfield shift ($\Delta\delta$ −0.68) of the signal for the *exo* isomer **8**, where these protons are *endo*, relative to that for the *endo* isomer **4**, where they are *exo*, is in accord with the previously observed upfield shifts of the signals of the corresponding protons in the spectra of other norbornenes and norbornanes (9). Both signals appear as apparent doublets, which are attributable to C-4a(8a) *endo* – C-9 *anti* proton coupling in the *exo* isomer and to C-4a(8a) *exo* – C-1(4) proton coupling in the *endo* isomer. In accord with this interpretation is the relationship of the coupling patterns of the signals assigned to the C-9 *anti* protons, the greater multiplicity shown by the *exo* isomer being attributable to the coupling of the C-9 *anti* proton with the *endo* protons at C-4a and C-8a.

The ^{13}C nmr spectra of **4** and **8** (Table 2) are very similar except for an upfield shift ($\Delta\delta$ −4.5) of the C-9 signal in the *exo* isomer **8** and a downfield shift ($\Delta\delta$ 4.3) of the C-2(3) signal. These differential shifts are interpretable in terms of a γ-effect of C-5(8) at C-9 in **8** and at C-2(3) in **4**. It is unlikely that the effect at C-2(3) stems from electronic interaction between the two ethylenic bonds in **4** (5).

Ultraviolet irradiation of **8** under conditions that convert **4** to the pentacyclic compound **5** does not lead to cyclization, and **8** is recovered largely unchanged. This is to be expected, and provides further evidence favoring assignment of the *cis-endo* structure **4** to the initially formed adduct on photochemical grounds, since it allays the possible fear (10) that this adduct is **8** and undergoes photoisomerization to **4** prior to photocyclization to **5**.

TABLE 2. The ^{13}C nmr spectra of the 1:1 adducts **4**, **8**, **10**, and **11**[a,b]

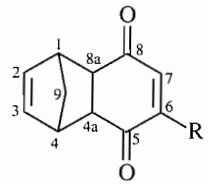

	4 (R = H) *endo*	**8** (R = H) *exo*	**10** (R = CH_3) *endo*	**11** (R = CH_3) *exo*
1,4	48.3*	48.1*	48.1, 48.5*	48.4, 48.9*
2,3	133.1	137.4	134.7, 135.3	137.38, 137.44
4a, 8a	48.7*	49.3*	48.8, 49.3*	49.1, 49.2*
5,8	199.2	199.2	199.0, 199.5	199.0, 199.4
6	141.9	141.7	151.9	151.4
7	141.9	141.7	139.5	139.4
9	48.6	44.1	48.7	44.3
CH_3	—	—	16.2	16.4

[a]The assignments are in accord with APT spectra.
[b]For each compound the assignments of the signals marked with an asterisk are interchangable.

We have also found that the *cis-endo* 1:1 adduct, **10**, of cyclopentadiene and *p*-toluquinone, which is formed exclusively at room temperature or below (11, 12), is converted to a mixture of **10** and its *cis-exo* isomer **11** on being heated in boiling xylene. The structure of the latter follows from its composition and spectra; the latter are compared with those of **10** in Tables 1 and 2. Exclusive formation of *cis-endo* 1:1 adducts from methylcyclopentadiene and *p*-benzoquinone at room temperature has also been reported, although reaction of cyclopentadiene with nitro-*p*-benzoquinone gives a mixture of *endo* and *exo* 1:1 adducts (12). However, it cannot be excluded that formation of the *exo* isomer was catalyzed by species associated with the *in situ* generation of nitro-*p*-benzoquinone from the corresponding hydroquinone and silver oxide.

2:1 Adducts

The adducts of *p*-benzoquinone with two molar equivalents of

Can. J. Chem. Downloaded from www.nrcresearchpress.com by 91.121.58.235 on 09/07/12
For personal use only.

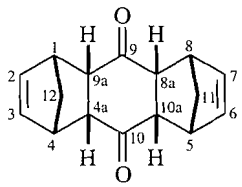

12 (*endo-syn-endo*)

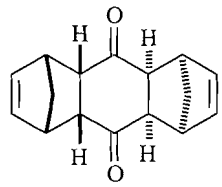

13 (*endo-anti-endo*)

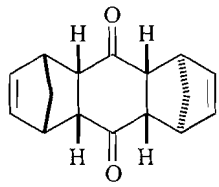

14 (*endo-syn-exo*)

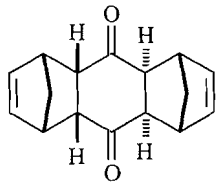

15 (*endo-anti-exo*)

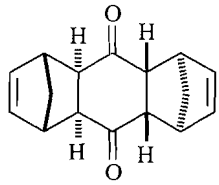

16 (*exo-anti-exo*)

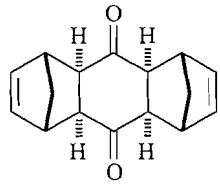

17 (*exo-syn-exo*)

cyclopentadiene have the gross structure **9**. If it is assumed that all are formed by *cis* addition, as has been observed for other 1,4 cycloaddition reactions of cyclopentadiene, six stereoisomers of **9** are possible, viz. compounds **12–17**.

A compound of type **9**, mp 155°C, was first isolated by Albrecht (1) from the reaction of the *endo* 1:1 adduct **4** with cyclopentadiene. It was initially assigned the *endo-syn-endo* structure **12** (13, 14), but was later proved to be the *endo-anti-endo* isomer **13** (11, 15, 16), as confirmed by X-ray crystallography (10). A second stereoisomer, mp 186°C, was prepared by isomerization of **13** with alkali, and was assigned the *endo-syn-exo* structure **14** (15, 16). Very recently the synthesis of a third stereoisomer, mp 184°C, was reported; this is assigned the *endo-syn-endo* structure **12** on the basis of its method of preparation and its reactions (17).

We now report the preparation of two additional stereoisomers, the *endo-anti-exo* compound **15**, mp 153–154°C, and the *exo-anti-exo* isomer **16**, mp 163–164°C. These were obtained by heating the initially formed isomer **13** in xylene in a sealed tube at 120°C; this gave a mixture of **13**, **15**, and **16**, together with the hydroquinone **18**, which was obtained previously (18). The structures of the newly discovered isomers have been established by spectroscopic and chemical means.

Qualitative comparisons of the ^{1}H and ^{13}C nmr spectra of the isomers **12–14** and those of the two newly obtained isomers (Tables 3 and 4) show that these compounds are all compounds of type **9**. As expected, the nmr spectra of the *endo-exo* isomer **14** are more complex than those of the *endo-endo* isomers **12** and **13** because of the lower degree of symmetry of **14**. The nmr spectra of the new isomer, mp 153–154°C, resemble those of **14** in complexity and thus it follows immediately that it is the *endo-anti-exo* compound **15**, since this is the only remaining structure with a degree of symmetry corresponding to that of **14**. It further follows that the new isomer, mp 163–164°C, must have either the *exo-anti-exo* structure **16** or the *exo-syn-exo* structure **17**. This is confirmed by the fact that the nmr spectra of this compound are analogous in complexity to those of **12** and **13**. The choice of the *exo-anti-exo* structure **16** for this compound follows from studies of the chemistry of the tetrahydro derivatives **19** of the compounds of type **9** (*vide infra*).

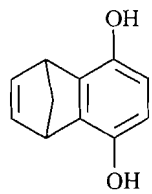

18

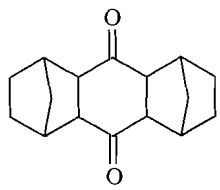

19

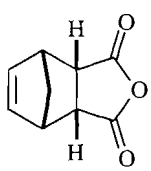

20

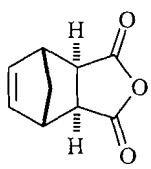

21

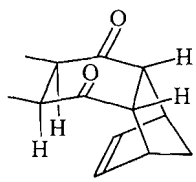

22

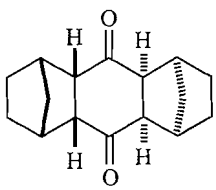

23 (*endo-anti-endo*)

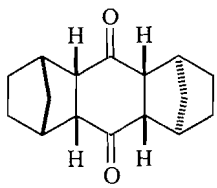

24 (*endo-syn-exo*)

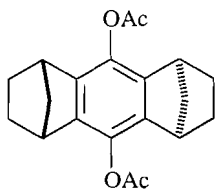

25

Can. J. Chem. Downloaded from www.nrcresearchpress.com by 91.121.58.235 on 09/07/12
For personal use only.

TABLE 3. The ^{1}H nmr spectra of the 2:1 adducts **13–16** and **12**[a]

	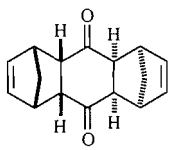 **13** *endo-anti-endo*	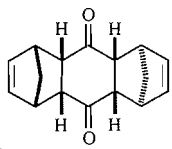 **14** *endo-syn-exo*	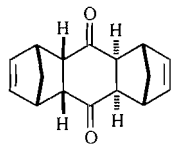 **15** *endo-anti-exo*	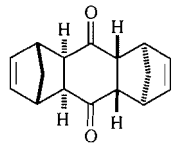 **16** *exo-anti-exo*	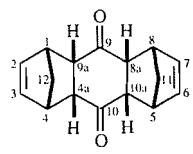 **12**[b] *endo-syn-endo*
1,4	3.30 (d, 1.5)	3.36 (t, 1.6)	3.32 (p, 1.8)	3.34 (t, 1.8)	3.40
5,8		3.36 (t, 1.7)	3.37 (p, 1.7)		
2,3	6.15 (t, 1.8)	6.07 (t, 1.8)	6.17 (t, 2.0)	6.21 (t, 2.0)	5.94
6,7		6.11 (t, 1,9)	6.18 (t, 2.1)		
4a,9a	2.83 (t, 1.7)	3.54 (br s)	3.19 (br s)	2.51 (d, 2.1)	3.24
8a,10a	2.63 (t, 1.4)		2.09 (s)		
11*anti*	1.40 (dt, 8.6, 1.8)	1.42 (d, 8.6)	1.50 (dt, 8.6, 1.7)	1.37 (m)	1.3
12*anti*		1.23 (d, 9.1)	1.27 (dp, 9.2, 1.3)		
11*syn*	1.25 (br d, 8.6)	1.28 (d, 8.6)	1.37 (dt, 8.6, 1.4)	1.37 (m)	
12*syn*		0.51 (br d, 9.1)	1.19 (br d, 9.2)		

[a]See footnote *a* in Table 1.
[b]Reference 17.

TABLE 4. The ^{13}C nmr spectra of the 2:1 adducts **13–16** and **12**[a]

	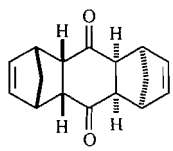 **13** *endo-anti-endo*	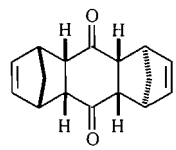 **14** *endo-syn-exo*	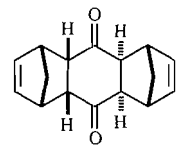 **15** *endo-anti-exo*	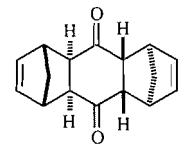 **16** *exo-anti-exo*	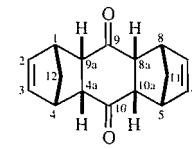 **12**[b] *endo-syn-endo*
1,4	48.1	43.4	47.6	47.8	43.9
5,8		43.9	48.7		
2,3	136.2	137.2	135.9	137.6	136.7
6,7		137.7	137.3		
4a,9a	53.1	52.9	52.4	53.2	54.0
8a,10a		55.4	53.6		
9,10	212.5	210.4	211.9	211.4	209.8
11	49.5	47.6	50.4	45.5	47.0
12		47.4	46.5		

[a]See footnote *a* in Table 2.
[b]Reference 17.

We next discuss quantitative aspects of the ^{1}H nmr spectra of compounds **12–16** and interpret them in structural terms, an exercise whose validity is not compromised by the use of qualitative aspects of these spectra in the structural assignments. The proton signals in the δ 0.5–1.7 and 5.9–6.1 regions (Table 3) can immediately be assigned to the bridge protons at C-11 and C-12 and to the ethylenic protons at C-2(3) and C-6(7), respectively. Distinction can be made between the signals of the two remaining types of protons, the bridgehead protons at C-1(4) and C-5(8) and the ring-fusion protons at C-4a(9a) and C-8a(10a), on the basis of the relative broadness of the signals. The former type are broader than the latter because of the more extensive coupling of the bridgehead protons (19) (cf. the analogous signals in the ^{1}H nmr spectra of the *endo* and *exo* adducts of cyclopentadiene and maleic anhydride, **20** and **21** (20), and of **4** and **8**). The assignments in the case of **13** were confirmed by a COSY spectrum and by the fact that treatment with potassium deuteroxide in deuterium oxide/tetrahydrofuran at room temperature for 0.5 h led to a 65% reduction of the intensity of the δ 2.88 signal relative to all other signals.

The bridgehead proton signals occur in a narrow range (δ 3.3–3.4) and in this respect resemble the ethylenic proton signals with a range of δ 5.9–6.2. The ring-fusion proton signals occur in the much broader range δ 2.1–3.5. This wide variation can be interpreted in terms of the interplay of two factors. First, the variance in the shielding of *endo* vs. *exo* protons in norbornene systems (cf., for example, the cases of the *endo* and *exo* 1:1 adducts discussed above), and second, the shielding of the ring-fusion protons in one norbornene system by the ethylenic group in the other when this group is *syn* with respect to the ring-fusion protons. The latter effect we refer to as interannular ("inter-ann") shielding, in contrast to the intraannular shielding involved in the *endo* vs. *exo* effect. It can be operative only in *anti-endo* isomers (cf. **22**). These effects are codified in Table 5, which it is hoped may serve predictive purposes.

With one exception, the signals of the C-11 and C-12 protons fall in the range δ 1.2–1.6. It is possible to associate these in pairs on the basis of the magnitudes of the geminal coupling constants, but unambiguous assignments to *syn* and *anti* protons are not possible with the data currently available. The exception

Can. J. Chem. Downloaded from www.nrcresearchpress.com by 91.121.58.235 on 09/07/12
For personal use only.

TABLE 5. Factors affecting the chemical shifts of C-4a(9a) and C-5a(8a) in the ^{1}H nmr spectra of the 2:1 adducts **12–16**

Factor(s)	Compound	Chemical shift	Range
exo	**12**	3.24	3.2–3.5
exo	**15**	3.54	
exo	**16**	3.19	
exo + *inter-ann*	**13**	2.83	
endo	**14**	2.63	2.5–2.6
endo	**16**	2.51	
endo + *inter-ann*	**15**	2.09	

is a one-proton signal of **14** that appears at δ 0.51. This effect could be associated with interannular shielding in the preferred conformation by either the ethylenic or carbonyl π electrons. The latter source is more probable since a similar effect is shown in the spectrum of the corresponding tetrahydro compound (see Experimental).

The ^{13}C nmr spectral assignments are given in Table 4. These are based on APT spectra, which distinguish all types of signal other than those of C-1,4(5,8) and C-4a,9a(8a,10a). A HETCOR spectrum in the case of **13** permitted this distinction to be made; assignments for corresponding carbons in the spectra of the other compounds were made by analogy. The ^{13}C nmr spectra are in accord with the gross structural assignments, but are not very useful for making stereochemical distinctions.

Tetrahydro 2:1 adducts

Hydrogenation of the original 2:1 adduct **13** gives a tetrahydro compound **23**, mp 255°C; similar treatment of the isomer **14** gives a tetrahydro compound **24**, mp 188°C (13, 15, 16). Compound **24** could also be obtained by alkaline treatment of **23** in the same fashion that **13** was converted to **14**, or by heating **23** above its melting point (ca. 240°C). More vigorous basic treatment of **23**, e.g., with aluminum *tert*-butoxide at 250°C, gives a mixture of **23** and a third isomer, mp 165°C, in comparable amounts; a similar mixture is formed on analogous treatment of the third isomer. All three of these tetrahydro compounds give the same hydroquinone diacetate **25** on oxidation with bromine in carbon tetrachloride followed by acetylation. The structure of this product follows from its formation from **23** and **24**, which both have an *anti* relationship of their one-carbon bridges. It further follows that the third tetrahydro isomer must possess an analogous *anti* relationship of its one-carbon bridges and must be the *exo-anti-exo* compound **26**, the only remaining isomer with this relationship (16).

Hydrogenation of the two newly obtained stereoisomers **16** and **15** gives **26** and a fourth tetrahydro isomer, mp 200–202°C, respectively. The formation of the former leads to the assignment to **16** of a structure with an *anti* relationship between the one-carbon bridges and thus completes the proof that it is the *exo-anti-exo* isomer. The fourth tetrahydro isomer must have the *endo-anti-exo* structure **27** and, as expected, gives with bromine followed by acetylation the *syn* hydroquinone diacetate **28**, which is different from, although very similar to, the *anti* hydroquinone diacetate **25**.

As expected, the ^{1}H nmr spectra of compounds **24** and **27** are more complex than those of **23** and **26** because of the lower symmetry of the former compounds (see Experimental). However, quantitative comparisons of these four spectra are of less diagnostic value than those for compounds **12–16** because the bridgehead and ring-fusion proton signals overlap in the

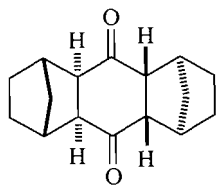

26 (*exo-anti-exo*)

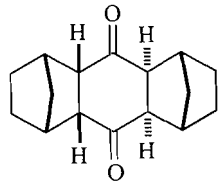

27 (*endo-anti-exo*)

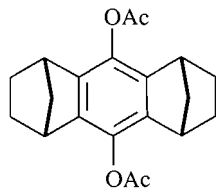

28

narrow range δ 2.5–2.9 and the signals of the one-carbon bridge protons and those of the *exo* and *endo* protons on the two-carbon bridges overlap in the similarly narrow range of δ 1.2–1.6.

Discussion

A number of pathways have been considered for the interconversion of the *endo* and *exo* forms of Diels–Alder adducts related to those investigatged here. These include enolization, dissociation to diene and dienophile followed by recombination, formation of a complex of the diene and dienophile, cleavage of one bond of the adduct followed by rebonding or followed by hydrogen transfer and then rebonding (refs. 21–23 and refs. quoted therein). In most cases the initially formed adduct is the *endo* isomer, formed under kinetic control, and subsequent thermal treatment results in its conversion to the more stable *exo* isomer, with subsequent isomerization leading to the eventual formation of an equilibrium mixture when the reactions are under full thermodynamic control. Thus the formation of the *exo* adduct **8** from the *endo* 1:1 adduct **4** can be represented as in Scheme 1 (the position of equilibrium was not established).

We consider that the present observations can be most simply interpreted in the following terms. The isomerization of the 1:1 adducts occurs via dissociation–recombination as in Scheme 1 (the position of equilibrium was not established). In the cases of **23**, **24**, **26**, and **27**, the tetrahydro derivatives of the 2:1 adducts, the dissociation–recombination pathway is not available for the interconversion of stereoisomers, but such interconversion can occur. This has usually been effected under basic conditions, and in at least one case thermal interconversion has also been observed (**23** → **24**), albeit at a considerably higher temperature than that used for the formation of **8** from **4**. We subscribe to the proposal of Cookson *et al.* (15) that the changes in the tetrahydro series involve enolization of the two carbonyl groups, although the detailed pathway cannot at present be defined. Thus the reaction of **23** to give **24** may proceed via the enolate or enol **30** or via the dienolate or dienol **31** and may or may not involve the

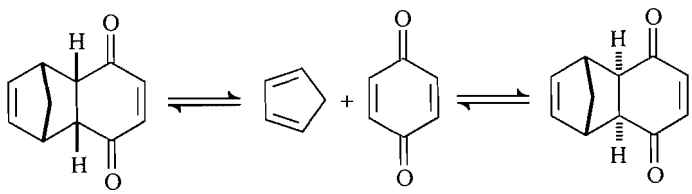

4 **8**

SCHEME 1

Can. J. Chem. Downloaded from www.nrcresearchpress.com by 91.121.58.235 on 09/07/12
For personal use only.

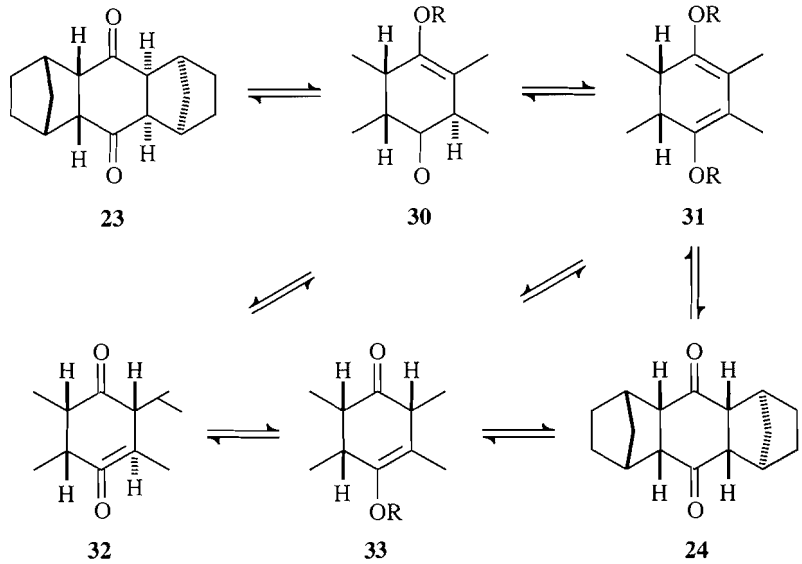

SCHEME 2

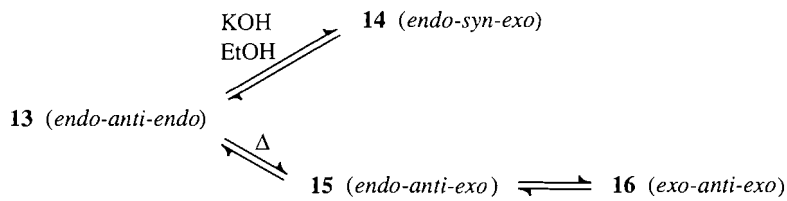

SCHEME 3

transitory formation of the *trans*-fused intermediate **32** (Scheme 2). It may be noted that, whatever the details of the mechanism, each such conversion of an *endo* to an *exo* system, or vice versa, must be accompanied by a change from an *anti* to a *syn* system, or vice versa. This is not the case for interconversion via retro-Diels–Alder reaction and recombination.

A similar type of enolization mechanism is not applicable in the case of the 1:1 adducts, for enolization leads to irreversible aromatization. However, for the 2:1 adducts **12–16** both retro-Diels–Alder and enolization routes are viable and we propose that this duality accounts for our observations in the present work as shown in Scheme 3.

Experimental

Melting points (mp) were measured on a Fisher-Johns melting point apparatus and are uncorrected. Infrared spectra were recorded in chloroform solutions or on potassium bromide discs. ^1H and ^{13}C nuclear magnetic resonance spectra (nmr) were recorded in deuteriochloroform solutions with a Varian Gemini 200 or XL-200 spectrometer.

endo-cis-*1,4,4a,8a-Tetrahydro-1,4-methanonaphthalene-5,8-dione (4)*

Compound **4** was prepared by the procedure of Marchand and Allen (24); mp 76–77°C (lit. (19) mp 75.8–76.2°C, (24) mp 76.0–78.5°C); ν_{max} (CCl_4): 1666 (br, vs), 1650 (infl, m), 1605 (m) cm^{-1} (cf. ref. 15).

exo-cis-*1,4,4a,8a-Tetrahydro-1,4-methanonaphthalene-5,8-dione (8)*

(*i*) *p*-Benzoquinone (3.05 g, 27.8 mmol) was added to a boiling solution of compound **13** (*vide infra*; 4.50 g, 18.7 mmol) in xylene (70 mL). Boiling was continued under reflux for 20 min, when tlc (silica with ethyl acetate/hexanes) showed that all of the **13** had been consumed. The mixture was cooled to room temperature and hexanes (500 mL) were added. The black suspension was filtered and the filtrate was cooled in a Dry Ice/acetone bath. A yellow solid (0.6 g) separated, which was shown by ^1H nmr spectroscopy to contain compounds **4** (95%) and **8** (5%). The mother liquor was stripped of solvent to give a 65:35 mixture of compounds **4** and **8** (3.0 g). Flash chromatography on silica with 1:4 ethyl acetate/hexanes led first to the elution of the oxidation product, 1,4-dihydro-1,4-methanonaphthalene-5,8-dione (11), followed by compound **8** and then **4**. Compound **8** was recrystallized from methanol; mp 80.5–81.5°C; ν_{max} (CCl_4): 1778 (vs), 1667 (s), 1657 (infl, s), 1608 cm^{-1}. Anal. calcd. for $C_{11}H_{10}O_2$: C 75.84, H 5.78; found: C 75.61, H 5.94.

(*ii*) A solution of compound **4** (1.00 g) in toluene (50 mL) was boiled under reflux under argon for 36 h. The product consisted of a 1:9 mixture of compounds **8** and **4** (50%), hydroquinone **18**, and *p*-benzoquinone.

endo-cis-*1,4,4a,8a-Tetrahydro-6-methyl-1,4-methanonaphthalene-5,8-dione (10)*

Compound **10** was prepared by the procedure of Marchand and Allen (24); mp 62–63°C (lit. (11) mp 62°C); ν_{max} (CCl_4): 1675 (s), 1667 (vs), 1652 (s), 1625 (m) cm^{-1}.

exo-cis-*1,4,4a,8a-Tetrahydro-6-methyl-1,4-methanonaphthalene-5,8-dione (11)*

A solution of compound **10** (5.00 g, 26.6 mmol) in xylene (50 mL) was boiled under reflux for 15 h. Removal of the solvent gave a residue that was shown by ^1H nmr spectroscopy to contain compounds **10** (80%) and **11** (15%). Compound **11** (0.60 g) was separated by flash chromatography on silica with 1:4 ethyl acetate/hexanes and recrystallized from methanol; mp 59–60°C; ν_{max} (CCl_4): 1666 (br, vs), 1648 (s), 1627 (m) cm^{-1}. Anal calcd. for $C_{12}H_{12}O_2$: C 76.57, H 6.42; found: C 76.42, H 6.49.

endo-cis-anti-cis-endo-*1,4,4a,5,8,8a,9a,10a-Octahydro-1,4:5,8-dimethanoanthracene-9,10-dione (13)*

Compound **13** was prepared by the method of Alder and Stein (13); mp 153–154°C (dec.) (lit. (13) mp 157–158°C (dec.)).

Can. J. Chem. Downloaded from www.nrcresearchpress.com by 91.121.58.235 on 09/07/12
For personal use only.

Can. J. Chem. Downloaded from www.nrcresearchpress.com by 91.121.58.235 on 09/07/12
For personal use only.

Base-catalyzed stereoisomerization of ***13****. Formation of its* endo-cis-syn-cis-exo *isomer* ***14***

Compound **13** was treated with ethanolic potassium hydroxide to give compound **14** (5); mp 184–185°C (lit. (13) mp 186°C).

Thermal stereoisomerization of compound ***13****. Formation of its* endo-cis-anti-cis-exo *and* exo-cis-anti-cis-exo *isomers* ***15*** *and* ***16***

A solution of compound **13** (10.0 g, 0.42 mmol) in xylene (3 mL) in a sealed tube was heated at 120°C for 15 h. The mixture remaining after removal of the xylene was flash chromatographed on silica with 1:4 ethyl acetate/hexanes and gave five fractions, each ca. 20%.

Crystallization of the first fraction from acetone gave compound **16**, mp 163–164°C; ν_{max}: 1687, 1681 cm^{-1}. Anal. calcd. for $C_{16}H_{16}O_2$: C 79.97, H 6.71; found: C 79.84, H 6.95.

Crystallization of the second fraction from methanol gave compound **15**, mp 153–154°C; ν_{max}: 1686 cm^{-1}. Anal. calcd. for $C_{16}H_{16}O_2$: C 79.97, H 6.71; found: C 79.68, H 6.79.

Crystallization of the third fraction gave compound **13**. The fourth fraction was an unstable mixture, which was not further investigated. The fifth fraction contained the aromatization product, 1,4-dihydro-1,4-methanonaphthalene-5,8-diol (**18**) (25).

Hydrogenation of compounds ***13–16****. Formation of 1,2,3,4,4a,5,6,7,-8,8a,9a,10a-dodecahydro-1,4:5,8-dimethanoanthracene-9,10-diones* ***23****,* ***24****,* ***27****, and* ***26***

The octahydroanthracenedione was dissolved in ethanol (50 mL), 5% palladium/carbon was added, and hydrogenation was carried out at atmospheric pressure and temperature for 2 h. The catalyst was filtered and the solid residue obtained after removal of the solvent was recrystallized from methanol.

Compound **13** gave the *endo-cis-anti-cis-endo* isomer **23**, mp 222–223°C (lit. (13) mp 225°C); ν_{max}: 1686 cm^{-1}; $^{H}\delta$: 2.83 (m, 4H), 2.75 (m, 4H), 1.2–1.6 (m, 12H).

Compound **14** gave the *endo-cis-syn-cis-exo* isomer **24**, mp 250–252°C (lit. (13) mp 255°C); $^{H}\delta$: 3.15 (m, 2H), 3.01 (m, 2H), 2.81 (m, 2H), 2.66 (m, 2H), 1.1–1.6 (m, 11H), 0.71 (m, 1H).

Compound **15** gave the *endo-cis-anti-cis-exo* isomer **27**, mp 200–202°C (dec.); ν_{max}: 1681, 1687 cm^{-1}; $^{H}\delta$: 2.87 (m, 2H), 2.71 (m, 2H), 2.62 (m, 2H), 1.2–1.6 (m, 12H). Exact Mass calcd. for $C_{16}H_{20}O_2$: 244.1463; found: 244.1451.

Compound **16** gave the *exo-cis-anti-cis-exo* isomer **26**, mp 156–157°C; (lit. (16) mp 165–166°C); ν_{max}: 1692 cm^{-1}; $^{H}\delta$: 2.69 (m, 4H), 2.63 (m, 4H), 1.2–1.6 (m, 12H).

Thermal stereoisomerization of compound 23 to 24

Compound **23** was heated at ca. 240°C for 5 min and the resulting mixture, which consisted mainly of compounds **23** and **24**, was flash chromatographed on silica with 1:4 ethyl acetate/hexanes. Compound **24** was isolated in ca. 15% yield; mp 251–252°C (lit. (13) mp 255°C).

*Oxidation of compounds 23, 24, and 26 followed by acetylation. Formation of 9,10-diacetoxy-*anti-1,2,3,4,5,6,7,8-*octahydro-1,4:5,8-dimethanoanthracene (25)*

Compounds **23**, **24**, and **26** were oxidized with bromine in carbon tetrachloride by the procedure of Alder and Stein (13) to give *anti*-1,2,3,4,5,6,7,8-octahydro-1,4:5,8-dimethanoanthracene-9,10-diol. Treatment of the hydroquinone (0.50 g, 2.06 mmol) with acetic anhydride (10 mL) and pyridine (2 mL) at room temperature overnight gave the diacetate **25**, which was purified by chromatography on silica with 1:4 ethyl acetate/hexanes; mp 222–224°C (lit. (13) mp 226°C); ν_{max} (KBr): 1752 cm^{-1}; $^{H}\delta$: 3.27 (m, 4H), 2.30 (m, 6H), 1.7–1.8 (m, 6H), 1.4 (m, 2H), 1.2 (m, 4H); $^{C}\delta$: 169.8 (e), 138.9 (e), 136.3 (e), 49.3 (e), 41.2 (o), 26.3 (e), 20.9 (o).

*Oxidation of compound 27 followed by acetylation. Formation of 9,10-diacetoxy-*syn-*1,2,3,4,5,6,7,8-octahydro-1,4:5,8-dimethanonthracene (28)*

Compound **27** was oxidized and the resulting *syn* hydroquinone was acetylated as above to give compound **28**, mp 206–207°C; mixture mp with **25**, 202–204°C; ν_{max} (KBr): 1757 cm^{-1}; $^{H}\delta$: 3.25 (m, 4H), 2.27 (m, 6H), 1.7–1.8 (m, 6H), 1.4 (m, 2H), 1.2 (m, 4H); $^{C}\delta$: 169.7 (e), 138.9 (e), 136.2 (e), 49.9 (e), 41.0 (o), 26.3 (e), 20.9 (o). Exact Mass calcd. for $C_{20}H_{22}O_4$: 326.1518; found 326.1513.

Acknowledgment

We thank the Natural Sciences and Engineering Research Council of Canada for support of this work.

1. W. ALBRECHT. Ann. Chem. **348**, 31 (1906).
2. H. STAUDINGER. Die keten. Stuttgart, Germany. 1912. p. 39; Ann. Chem. **443**, 73 (1928).
3. O. DIELS, J. H. BLOM, and Y. KOLL. Ann. Chem. **443**, 247 (1925); O. DIELS and K. ALDER. Ann. Chem. **460**, 98 (1928); **478**, 137 (1930).
4. R. C. COOKSON, R. CRUNDWELL, and J. HUDEC. Chem. Ind. (London), 1003 (1958); R. C. COOKSON, R. CRUNDWELL, R. R. HILL, and J. HUDEC. J. Chem. Soc. 3062 (1964).
5. R. L. AL-HAMDANY, J. M. BRUCE, F. HEATLEY, and J. KHALAFY. J. Chem. Soc. Perkin Trans. 2, 1395 (1985).
6. M. C. KLOETZEL. Org. Reactions, **4**, 1 (1948); A. S. ONISHCHENKO. Diene synthesis. Israel Program for Scientific Translations, Jerusalem. 1964. pp. 34–60.
7. J. MARCH. Advanced organic chemistry. 2nd ed. McGraw–Hill, New York. 1977. p. 764.
8. O. DIELS and K. ALDER. Angew. Chem. **50**, 514 (1937); Cf. R. B. Woodward. J. Am. Chem. Soc. **66**, 645 (1944).
9. L. M. JACKMAN and S. STERNHELL. Applications of nuclear magnetic spectroscopy in organic chemistry. 2nd ed. Pergamon Press, New York, NY. 1969. pp. 230–231; B. FRANZUS, W. C. BAIRD, JR., N. F. CHAMBERLAIN, T. HINES, and E. I. SNYDER. J. Am. Chem. Soc. **90**, 3721 (1968); A. P. MARCHAND and J. E. ROSE. J. Am. Chem. Soc. **90**, 3724 (1968); J. L. MARSHALL and S. R. WALTER. J. Am. Chem. Soc. **96**, 6358, (1974).
10. R. BROWN, J. M. BRUCE, D. W. HUDSON, and O. S. MILLS. J. Chem. Soc. Perkin Trans 2, 132 (1974).
11. K. ALDER, F. H. FLOCK, and H. BEUMLING. Chem. Ber. **93**, 1896 (1960).
12. A. P. MARCHAND, S. C. SURI, A. D. EARLYWINE, D. R. POWELL, and D. VANDERHELM. J. Org. Chem. **49**, 670 (1984).
13. K. ALDER and G. STEIN. Ann. Chem. **501**, 247 (1933).
14. S. WINSTEIN. Experientia, Suppl. 2, 137 (1955).
15. R. C. COOKSON, R. R. HILL, and J. HUDEC. J. Chem. Soc. 3043 (1964).
16. L. DE VRIES, A. HECK, R. PICCOLINI, and S. WINSTEIN. Chem. Ind. (London), 1416 (1959).
17. G. MEHTA and S. PADMA. J. Am. Chem. Soc. **109**, 7230 (1989).
18. W. R. VAUGHAN and M. YOSHIMA. J. Org. Chem. **26**, 7 (1957).
19. M. GREEN and E. A. C. LUCKEN. Helv. Chim. Acta, **45**, 1870 (1962).
20. N. KAMEZAWA, K. SAKASHITA, and K. HYAMRU. Org. Magn. Reson. **1**, 405 (1969).
21. D. CRAIG. J. Am. Chem. Soc. **73**, 4889 (1951).
22. J. A. BERSON, R. D. REYNOLDS, and W. M. JONES. J. Am. Chem. Soc. **78**, 6049 (1956).
23. R. B. WOODWARD and T. J. KATZ. Tetrahedron, **5**, 70 (1949).
24. A. P. MARCHAND and R. W. ALLEN. J. Org. Chem. **39**, 1596 (1974).
25. J. MEINWALD and G. A. WILEY. J. Am. Chem. Soc. **80**, 3667 (1958).

Pyrazine and 2,5-dimethylpyrazine complexes of copper(I) trifluoromethanesulfonate. The crystal and molecular structure of poly-μ-2,5-dimethylpyrazine-(2,5-dimethylpyrazine)-(trifluoromethanesulfonato-*O*)copper(I)

TOM OTIENO, STEVEN J. RETTIG, ROBERT C. THOMPSON,[1] AND JAMES TROTTER

Department of Chemistry, University of British Columbia, 2036 Main Mall, Vancouver, B.C., Canada V6T 1Y6

Received April 6, 1990

This paper is dedicated to Professor Ross Stewart on the occasion of his 65th birthday

TOM OTIENO, STEVEN J. RETTIG, ROBERT C. THOMPSON, and JAMES TROTTER. Can. J. Chem. **68**, 1901 (1990).

The complexes $CuL_2(CF_3SO_3)$ where L is pyrazine and 2,5-dimethylpyrazine have been prepared by the reaction of copper(I) triflate with the neutral ligand in methanol. Single crystal X-ray diffraction studies on the 2,5-Me_2pyz complex are reported. Crystals of the compound are triclinic, a = 9.424(4), b = 12.103(4), c = 9.113(4) Å, α = 110.97(3), β = 117.20(3), γ = 80.26(3)°, Z = 2, space group $P\bar{1}$. The structure was solved by heavy atom methods and was refined by full-matrix least-squares procedures to R = 0.033 and R_w = 0.039 for 3326 reflections with $I \geq 3\sigma(I)$. The structure is similar to that of the pyz analogue involving chains of copper ions linked by bridging 2,5-Me_2pyz ligands and monodenate triflate and terminal 2,5-Me_2pyz ligands completing a distorted tetrahedral CuN_3O chromophore. Mono-pyrazine and -2,5-dimethylpyrazine complexes of the type $CuL(CF_3SO_3)$ were obtained by thermolysis of the corresponding bis-ligand complexes. These compounds are assigned a polymeric structure involving bridging neutral ligands and monodenate triflate groups on the basis of infrared spectroscopy studies. Electronic spectroscopy and differential scanning calorimetry studies are also reported.

Key words: pyrazine and 2,5-dimethylpyrazine complexes, copper(I) triflate, crystal structure.

TOM OTIENO, STEVEN J. RETTIG, ROBERT C. THOMPSON et JAMES TROTTER. Can. J. Chem. **68**, 1901 (1990).

On a préparé les complexes $CuL_2(CF_3SO_3)$, dans lesquels L représente la pyrazine et la 2,5-diméthylpyrazine, en faisant réagir le triflate de cuivre(I) avec le ligand neutre, dans le méthanol. On rapporte des études de diffraction des rayons-X sur des cristaux uniques du complex 2,5-Me_2pyz. Les cristaux son tricliniques, avec a = 9,424(4), b = 12,103(4) et c = 9,113(4)Å, α = 110,97(3), β = 117,20(3) et γ = 80,26(3)°, Z = 2 et groupe d'espace $P\bar{1}$. On a résolu la structure par la méthode des atomes lourds et on l'a affinée par la méthode des moindres carrés jusqu'à des valeurs de R = 0,033 et R_w = 0,039 pour 3326 réflexions avec $I \geq 3\sigma(I)$. La structure est semblable à celle de l'analogue pyz impliquant des chaînes d'ions cuivres liés par des ligands 2,5-Me_2pyz qui servent de ponts alors que le triflate monodentate et les ligands 2,5-Me_2pyz complètent un chromophore CuN_3O tétraédrique déformé. On a obtenu les complexes de monopyrazine et de la 2,5-dimethylpyrazine du type $Cu(CF_3SO_3)$ par thermolyse des complexes correspondants portant deux ligands. Sur la base d'études de spectroscopie infrarouge, on a attribué à ces composés une structure polymérique comportant des ligands neutres servant de ponts ainsi que des groupments triflates monodentates. On rapporte aussi des études de spectroscopie électronique et de calorimétrie à balayage différentiel.

Mots clés : complexes de la pyrazine et de la 2,5-diméthylpyrazine, triflate de cuivre(I), structure cristalline.

[Traduit par la revue]

Introduction

The first and, until recently, only reported pyrazine-bridged compounds of copper(I) were some bimetallic complexes of composition Cu_2LX_2 (where L is pyrazine or a methylpyrazine and X is Cl, Br, I, or CN) (1, 2). Recently we reported the serendipitous isolation of a polymeric complex $[Cu(pyz)_2(CF_3SO_3)]_x$, **1**, from the reaction of copper(II) trifluoromethanesulfonate (copper(II) triflate) with pyz in a 1:2 mole ratio in methanol (3). The reaction involves the reduction of copper(II) to copper(I), presumably by the solvent. The present work was aimed primarily at developing a synthetic route to this compound starting with a copper(I) salt and, in addition, at obtaining and characterizing analogous complexes containing substituted pyrazine ligands.

We describe here the synthesis of **1** by the direct reaction of copper(I) triflate (4) with pyz, and the isolation by a similar route, and X-ray crystallographic analysis of the 2,5-dimethylpyrazine analogue, $[Cu(2,5\text{-}Me_2pyz)_2(CF_3SO_3)]_x$, **2**. The structure of **2** is similar to that of **1** in that it is polymeric and contains both bridging and terminal 2,5-Me_2pyz ligands. Compounds **1** and **2** are found to undergo ready thermal dissociation of one mole of neutral ligand to produce materials of composition $Cu(pyz)(CF_3SO_3)$, **3**, and $Cu(2,5\text{-}Me_2pyz)(CF_3SO_3)$, **4**. Spectroscopic studies on **3** and **4** suggest polymeric structures with bridging neutral ligands and monodentate triflate groups.

Experimental

Syntheses

Poly-μ-pyrazine-(pyrazine)(trifluoromethanesulfonato-O)-copper(I), $Cu(pyz)_2(CF_3SO_3)$, 1

Copper(I) trifluoromethanesulfonate, $Cu(CF_3SO_3)$, was prepared by a method similar to that described by Dines (5). To 16.0 g (112 mmol) of red copper(I) oxide was added 50 mL of *n*-octane and 20 mL (~226 mmol) of trifluoromethanesulfonic acid. The mixture was refluxed under nitrogen at about 110°C overnight, filtered, and the precipitate washed with *n*-octane and dried *in vacuo* at room temperature for 6 h, then at 135°C for 6 h. Subsequent reactions involving this copper(I) triflate and manipulation of the products of its reactions were performed using standard dry-box and vacuum-line techniques. To 1.07 g (~5 mmol) of copper(I) triflate was added 10 mL of methanol containing 10% v/v 2,2-dimethoxypropane, and the resulting slurry was stirred for 0.5 h. A solution of 1.63 g (20.4 mmol) of pyrazine in 5 mL of the above solvent was then added and the slurry stirred for an additional 2 h. On filtering and washing with a small amount of solvent, the solid product was found to consist of a mixture of an orange compound and copper(I) oxide. The presence of the latter, which was identified by infrared spectroscopy, indicated incomplete conversion of copper(I) oxide to copper(I) triflate in the initial reaction. The presence of this oxide impurity did not adversely affect subsequent reactions. The orange compound and the oxide were separated by

[1]Author to whom correspondence may be addressed.

Can. J. Chem. Downloaded from www.nrcresearchpress.com by 91.121.58.235 on 09/07/12
For personal use only.

Can. J. Chem. Downloaded from www.nrcresearchpress.com by 91.121.58.235 on 09/07/12
For personal use only.

TABLE 1. Final atomic coordinates (fractional) and equivalent isotropic thermal parameters

Atom	x	y	z	B_{eq}
Cu	0.32664(3)	0.25447(2)	0.15988(3)	3.06(1)
S	0.14852(7)	0.20881(5)	0.41331(8)	3.46(2)
F(1)	−0.0747(3)	0.1201(2)	0.4295(4)	8.4(1)
F(2)	−0.1222(3)	0.1087(2)	0.1735(3)	8.2(1)
F(3)	0.0495(3)	−0.0067(2)	0.3004(4)	8.5(1)
O(1)	0.2020(2)	0.1774(2)	0.2794(3)	4.83(8)
O(2)	0.2617(3)	0.1872(2)	0.5696(3)	5.8(1)
O(3)	0.0672(3)	0.3196(2)	0.4351(3)	5.80(9)
N(1)	0.4310(2)	0.1035(1)	0.0760(2)	2.53(5)
N(2)	0.4374(2)	0.3957(1)	0.3634(2)	2.46(5)
N(3)	0.1164(2)	0.2962(2)	−0.0188(2)	3.24(6)
N(4)	−0.1786(3)	0.3542(3)	−0.2518(3)	5.4(1)
C(1)	−0.0070(4)	0.1017(3)	0.3239(5)	5.1(1)
C(2)	0.4058(3)	0.0653(2)	−0.0967(3)	2.72(7)
C(3)	0.5268(3)	0.0371(2)	0.1695(3)	2.62(6)
C(4)	0.5616(4)	0.0766(3)	0.3578(3)	3.7(1)
C(5)	0.3649(3)	0.4566(2)	0.4650(3)	2.59(6)
C(6)	0.5754(2)	0.4394(2)	0.3993(3)	2.51(6)
C(7)	0.6648(4)	0.3763(3)	0.2946(4)	4.2(1)
C(8)	0.1064(3)	0.3642(2)	−0.1123(3)	3.74(9)
C(9)	−0.0424(4)	0.3903(3)	−0.2274(4)	5.2(1)
C(10)	−0.1685(3)	0.2876(3)	−0.1586(3)	4.3(1)
C(11)	−0.0209(3)	0.2594(2)	−0.0443(3)	3.79(9)
C(12)	0.2565(5)	0.4079(3)	−0.0869(5)	4.9(1)
C(13)	−0.3177(5)	0.2453(5)	−0.1800(6)	6.4(2)

mixing with acetonitrile, in which only the former is soluble, followed by filtration. The filtrate was evaporated to dryness, *in vacuo*, to give an orange powder that was further dried at room temperature *in vacuo*, for about 0.75 h. Anal. calcd. for $CuC_9H_8N_4F_3SO_3$: C 29.00, H 2.16, N 15.03; found: C 28.73, H 2.22, N 15.23. Yield: 82%.

Poly-μ-2,5-dimethylpyrazine-(2,5-dimethylpyrazine)(trifluoromethanesulfonato-O)copper(I), Cu(2,5-Me$_2$pyz)$_2$(CF$_3$SO$_3$), 2

A slurry of copper(I) triflate (1.09 g, ~5 mmol), prepared as above, in methanol containing 10% v/v 2,2-dimethoxypropane (10 mL) was stirred for 0.5 h and then 2,5-dimethylpyrazine (3.0 mL, 27 mmol) was added and the slurry stirred for an additional 2 h. The solid produced was separated by filtration, washed with a small amount of solvent, then treated with acetonitrile to separate insoluble copper(I) oxide from the soluble complex as above. After filtration, the filtrate was allowed to evaporate slowly in a nitrogen atmosphere glove box, yielding a crystalline yellow product. Anal. calcd. for $CuC_{13}H_{16}N_4F_3SO_3$: C 36.41, H 3.76, N 13.06; found: C 36.60, H 3.79, N 12.96. Yield: 55%.

Pyrazinecopper(I) trifluoromethanesulfonate, Cu(pyz)(CF$_3$SO$_3$), 3

A sample of **1** was heated, *in vacuo*, at 140°C for 3.5 h during which time the color changed from orange to yellow. Anal. calcd. for $CuC_5H_4N_2F_3SO_3$: C 20.52, H 1.38, N 9.57; found: C 20.58, H 1.36, N 9.60.

2,5-Dimethylpyrazinecopper(I) trifluoromethanesulfonate, Cu(2,5-Me$_2$pyz)(CF$_3$SO$_3$), 4

A sample of **2** was heated, *in vacuo*, at 85°C for 0.5 h and then at 135°C for a further 6 h to yield the desired product as a yellow powder. Anal. calcd. for $CuC_7H_8N_2F_3SO_3$: C 26.21, H 2.52, N 8.73; found: C 26.32, H 2.59, N 8.84.

Physical measurements

Differential scanning calorimetry (DSC) studies were made using a Mettler DSC20 cell and TC10 TA processor. Infrared spectra in the range 4000–250 cm^{-1} were recorded on a Perkin–Elmer model 598 spectrometer using samples mulled in Nujol and hexachlorobutadiene and pressed between KRS-5 plates (Harshaw Chemical Co.). Calibration was achieved using polystyrene and frequencies are considered accurate to ±3 cm^{-1}. Electronic spectra (360–800 nm) of samples mulled in Nujol and smeared on filter paper were obtained on a Shimadzu UV-2100 spectrometer. Magnetic susceptibilities were measured using a P.A.R. model 155 vibrating sample magnetometer as described previously (6). X-ray powder diffraction patterns were recorded in the range 2θ = 5–60° using a Rigaku Rotaflex rotating anode X-ray powder diffractometer (Ni filtered Cu-K_α radiation). Carbon, hydrogen, and nitrogen were determined by P. Borda of this department.

X-ray crystallographic analysis of 2

A crystal ca. 0.25 × 0.30 × 0.45 mm in size was mounted in a glass capillary. Unit-cell parameters were refined by least squares on setting angles for 25 reflections (2θ = 35.8–40.7°) measured on a diffractometer with Mo-K_α radiation (λ = 0.71069 Å). Crystal data at 21°C are

$C_{13}H_{16}CuF_3N_4O_3S$ f.w. = 428.90

Triclinic, a = 9.424(4), b = 12.103(4), c = 9.113(4) Å, α = 110.97(3), β = 117.20(3), γ = 80.26(3)°, V = 863(1) Å^3, Z = 2, ρ_c = 1.650 Mg m^{-3}, $F(000)$ = 436, μ(Mo-K_α) = 14.32 cm^{-1}. Absent reflections: none, space group $P\bar{1}$ (reduced cell, Donnay convention) from structure analysis.

Intensities were measured with graphite-monochromated Mo-K_α radiation on a Rigaku AFC6S diffractometer. An ω–2θ scan at 32° min^{-1} over a range of (0.94 + 0.35 tan θ)° in ω (with up to 8 rescans, background/scan time ratio = 0.5) was employed. Data were measured to 2θ = 60°. The intensities of three check reflections, measured every 150 reflections throughout the data collection, showed a uniform decay of 3.6%. After data reduction,[2] an empirical absorption correction, based on azimuthal scans for three reflections, and a linear decay correction were applied. Transmission factors range from 0.87 to 1.00. Of the 5320 reflections measured, 5035 were independent (R_{merge} = 0.029) and 3326 (66.1%) of these had intensities greater than or equal to $3\sigma(F^2)$ above background where $\sigma^2(F^2) = [S^2(C + 4B) + (0.03F^2)^2]/Lp^2$ with S = scan speed, C = scan count, B = total background count, and Lp = Lorentz-polarization factor.

The structure was solved by conventional heavy atom methods, the coordinates of the Cu and S atoms being determined from the Patterson function. The remaining atoms (including hydrogen) were positioned from subsequent difference Fourier syntheses. The non-hydrogen atoms were refined with anisotropic thermal parameters and the hydrogen atoms with isotropic thermal parameters. Scattering factors for all atoms and anomalous dispersion corrections for the non-hydrogen atoms were taken from ref. 7. The weighting scheme $w = 4F_o^2/\sigma^2(F_o^2)$ gave uniform average values of $w(|F_o| - |F_c|)^2$ over ranges of both $|F_o|$ and sin θ/λ and was employed in the final stages of full-matrix least-squares refinement of 290 variables. Reflections with $I < 3\sigma(I)$ were not included in the refinement. Convergence was reached at R = 0.033 and R_w = 0.039 for 3326 reflections with $I \geq 3\sigma(I)$. The function minimized was $\Sigma w(|F_o| - |F_c|)^2$, $R = \Sigma||F_o| - |F_c||/\Sigma|F_o|$, $R_w = (\Sigma w(|F_o| - |F_c|)^2/\Sigma w|F_o|^2)^{1/2}$.

On the final cycle of refinement the maximum parameter shift corresponded to 0.19σ. The mean error in an observation of unit weight was 1.57. The final difference map showed maximum fluctuations of −0.23 to +0.42 e Å^{-3}. The final positional and (equivalent) isotropic thermal parameters for the non-hydrogen atoms appear in Table 1. Bond lengths and angles are given in Tables 2 and 3. Hydrogen atom parameters, anisotropic thermal parameters, torsion angles, intermolecular contacts, least-squares planes, bond lengths and angles involving hydrogen, and structure factors have been deposited.[3]

[2]TEXSAN/TEXRAY structure analysis package which includes versions of the following: MITHRIL, integrated direct methods, by C. J. Gilmore; DIRDIF, direct methods for difference structures, by P. T. Beurskens; ORFLS, full-matrix least squares, and ORFFE, function and errors, by W. R. Busing, K. O. Martin, and H. A. Levy; ORTEP II, illustrations, by C. K. Johnson.

[3]Supplementary material mentioned in the text may be purchased from the Depository of Unpublished Data, CISTI, National Research Council of Canada, Ottawa, Ont., Canada K1A 0S2.

Can. J. Chem. Downloaded from www.nrcresearchpress.com by 91.121.58.235 on 09/07/12
For personal use only.

TABLE 2. Bond lengths (Å) with estimated standard deviations in parentheses[a]

Atom	Atom	Distance	Atom	Atom	Distance
Cu	O(1)	2.388(2)	N(2)	C(6)	1.340(3)
Cu	N(1)	2.007(2)	N(3)	C(8)	1.347(3)
Cu	N(2)	2.005(2)	N(3)	C(11)	1.332(3)
Cu	N(3)	2.033(2)	N(4)	C(9)	1.322(4)
S	O(1)	1.433(2)	N(4)	C(10)	1.331(4)
S	O(2)	1.421(2)	C(2)	C(3)′	1.382(3)
S	O(3)	1.424(2)	C(3)	C(4)	1.494(3)
S	C(1)	1.813(3)	C(5)	C(6)″	1.385(3)
F(1)	C(1)	1.319(4)	C(6)	C(7)	1.490(3)
F(2)	C(1)	1.325(4)	C(8)	C(9)	1.382(4)
F(3)	C(1)	1.311(4)	C(8)	C(12)	1.483(4)
N(1)	C(2)	1.341(3)	C(10)	C(11)	1.381(4)
N(1)	C(3)	1.342(3)	C(10)	C(13)	1.483(5)
N(2)	C(5)	1.336(3)			

[a]Primed and double-primed atoms refer to symmetry operations 1-x, -y, -z and 1-x, 1-y, 1-z, respectively.

Results and discussion

Syntheses and thermal studies

$[Cu(pyz)_2(CF_3SO_3)]_x$, **1**, was obtained by the direct reaction of copper(I) triflate with excess pyrazine in methanol. The compound is soluble in acetonitrile, from which it may be obtained in pure form by the removal of the solvent under vacuum. The 2,5-dimethylpyrazine analogue, **2**, was prepared in the same manner; slow evaporation of an acetonitrile solution yielded **2** in crystalline form suitable for X-ray diffraction studies. Attempts to obtain a 2-methylpyrazine complex by the same route failed. Whereas in the preparation of **1** and **2** immediate formation of yellow/orange precipitates was noted on mixing $Cu(CF_3SO_3)$ with ligand in methanol, no such precipitate was obtained with the 2-Mepyz ligand. In this case the reaction produced a mixture of brown and pink solids and a dark brown solution, the latter giving a dark green solid on standing. C, H, and N analysis indicated the green material is non-stoichiometric and a room temperature magnetic susceptibility measurement showed it to be paramagnetic. No further characterization of this material was attempted. These observations suggest that in this reaction the copper(I) complex is not stabilized by polymer formation and in solution disproportionation occurs. This indicates the need for a symmetrically bridging ligand in order to obtain stable copper(I) polymers such as **2**.

Compound **1** prepared as described here exhibits three endothermic events in its DSC thermogram at 80, 107, and 217°C. ΔH for the first two events is 24 kJ mol^{-1} each and for the third event, 55 kJ mol^{-1}. Weight measurements before and after the first two events show a loss of ~6% and corresponding measurements for the third show an additional 15% weight loss. The total loss for the three events agrees well with the 21% loss expected for the dissociation of one mole of pyz. The thermal behavior of this material differs from that of crystalline samples of **1** prepared as described previously (3). In the latter case a single endothermic event occurs at 204°C (ΔH = 61 kJ mol^{-1}) and weight loss measurements confirm the loss of one mole of pyz. We interpret these results as follows. The synthetic procedure described here produces analytically pure samples of composition $Cu(pyz)_2(CF_3SO_3)$. This material, however, consists of a mixture of the extended chain polymer present in the crystalline form of **1**, plus lower oligomers. The latter dissociate pyrazine at lower temperatures than the former. Both types of sample show the onset of exothermic decomposition at temperatures immediately above the ~200°C endothermic event. The presence of the extended chain polymer in the sample of **1** prepared here was confirmed by an X-ray powder diffraction study. A simulated powder X-ray diffraction pattern for **1** was generated using the single crystal data from ref. 3 and the computer program LAZY PULVERIX (8). All of the observed peaks in the powder sample prepared here could be assigned as arising from the polymer and the absence of peaks assignable to other species suggests the lower oligomers are present in an amorphous phase.

The bis(2,5-dimethylpyrazine) complex, **2**, exhibits two closely spaced endothermic events at 182 and 221°C (total ΔH for the two events = 104 kJ mol^{-1}). The weight loss of 24% measured over the two events compares favorably with the value of 25% expected for the loss of one mole of ligand. The onset of exothermic decomposition is observed at temperatures immediately above the 221°C endothermic event.

The thermal analysis results for both **1** and **2** suggested the possibility of obtaining, on a preparative scale, $Cu(pyz)(CF_3SO_3)$, **3**, and $Cu(2,5\text{-}Me_2pyz)(CF_3SO_3)$, **4**, by the thermolysis route. As described in the experimental section, the syntheses of **3** and **4** were achieved by preparative thermolysis by heating **1** and **2** at ~140 and ~135°C respectively, *in vacuo*. The technique of employing, in preparative thermolysis, temperatures well below DSC peak temperatures for ligand dissociation has been used previously (9) and avoids significant thermal decomposition of the product. The DCS thermogram of **3** shows the onset of exothermic decomposition above 200°C with no events below this temperature, thus indicating that the complex does not lose neutral ligand prior to decomposition. The thermogram of **4** shows a small, reversible, endothermic event at 137°C (ΔH ~ 4 kJ mol^{-1}) of unknown origin. This complex also does not dissociate neutral ligand prior to decomposition, the onset of which occurs at about 205°C.

Crystal structure of 2

The crystal structure analysis shows that the structure of the bis(2,5-Me_2pyz) complex **2** is very similar to that of its pyrazine analogue **1** (3). A stereoview of the unit cell is shown in Fig. 1 while the geometry around each copper is given in Fig. 2 together with the atom numbering scheme. The structure consists of spiral chains of copper atoms linked by bidentate bridging 2,5-Me_2pyz ligands. Monodentate neutral ligand and triflate groups complete the coordination around each copper to yield a distorted tetrahedral CuN_3O chromophore.

The triflate anion in **2** is very similar, in regard to internal bonding parameters, to that in **1** (Table 4): it adopts a staggered-ethane configuration about the C—S bond; the O—S—O angles are greater than 109°C while the C—S—O angles are less than this angle, indicating that repulsions between adjacent oxygen atoms are greater than those between oxygen atoms and the trifluoromethyl group; the S—O bond involving the coordinated oxygen atom is longer than those involving the non-coordinated ones.

The 2,5-dimethylpyrazine moieties in **2** are planar to within experimental error and the internal bonding parameters for the three attached to a given copper atom are presented in Table 5. For comparison, data obtained for $Ni(2,5\text{-}Me_2pyz)Br_2$ (10) are included in Table 5. Even though the corresponding parameters for all the 2,5-dimethylpyrazines listed in the table are comparable (indicating lack of substantial distortion of all the rings), it is noteworthy that those for the two bridging ligands in $Cu(2,5\text{-}Me_2pyz)_2(CF_3SO_3)$ are identical within experimental

TABLE 3. Bond angles (deg) with estimated standard deviations in parentheses

Atom	Atom	Atom	Angle	Atom	Atom	Atom	Angle
O(1)	Cu	N(1)	97.35(8)	S	C(1)	F(1)	111.2(2)
O(1)	Cu	N(2)	100.55(8)	S	C(1)	F(2)	111.5(2)
O(1)	Cu	N(3)	93.93(9)	S	C(1)	F(3)	111.6(2)
N(1)	Cu	N(2)	126.28(8)	F(1)	C(1)	F(2)	106.6(3)
N(1)	Cu	N(3)	115.75(8)	F(1)	C(1)	F(3)	107.0(3)
N(2)	Cu	N(3)	112.99(8)	F(2)	C(1)	F(3)	108.7(3)
O(1)	S	O(2)	114.5(1)	N(1)	C(2)	C(3)′	123.3(2)
O(1)	S	O(3)	114.2(1)	N(1)	C(3)	C(2)′	119.6(2)
O(1)	S	C(1)	102.8(1)	N(1)	C(3)	C(4)	119.3(2)
O(2)	S	O(3)	115.6(2)	C(2)′	C(3)	C(4)	121.0(2)
O(2)	S	C(1)	103.9(2)	N(2)	C(5)	C(6)″	123.3(2)
O(3)	S	C(1)	103.7(1)	N(2)	C(6)	C(5)″	120.0(2)
Cu	O(1)	S	143.1(1)	N(2)	C(6)	C(7)	119.3(2)
Cu	N(1)	C(2)	119.2(1)	C(5)″	C(6)	C(7)	120.7(2)
Cu	N(1)	C(3)	123.8(1)	N(3)	C(8)	C(9)	118.9(3)
C(2)	N(1)	C(3)	117.0(2)	N(3)	C(8)	C(12)	118.3(3)
Cu	N(2)	C(5)	118.5(1)	C(9)	C(8)	C(12)	122.8(3)
Cu	N(2)	C(6)	124.7(1)	N(4)	C(9)	C(8)	124.5(3)
C(5)	N(2)	C(6)	116.7(2)	N(4)	C(10)	C(11)	119.9(3)
Cu	N(3)	C(8)	123.2(2)	N(4)	C(10)	C(13)	118.8(3)
Cu	N(3)	C(11)	120.3(2)	C(11)	C(10)	C(13)	121.3(3)
C(8)	N(3)	C(11)	116.5(2)	N(3)	C(11)	C(10)	123.6(3)
C(9)	N(4)	C(10)	116.5(3)				

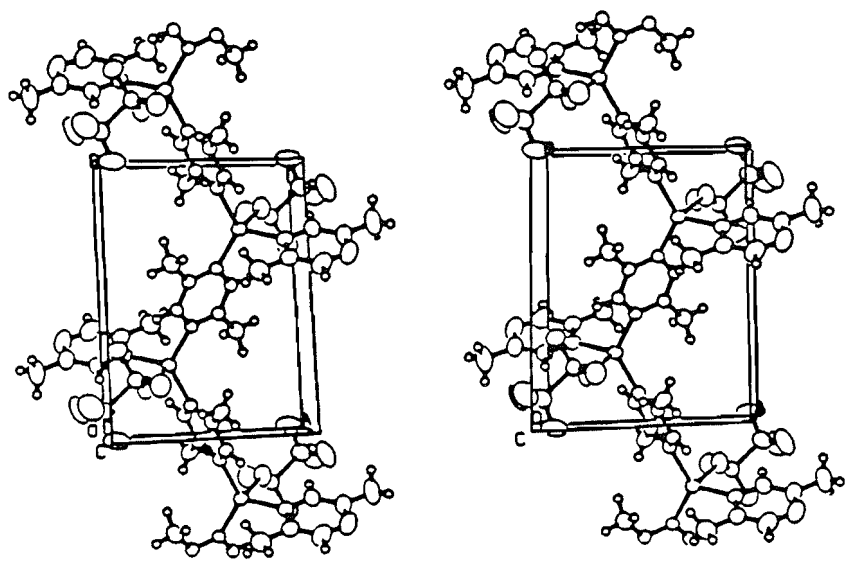

FIG. 1. Stereoview of the unit cell of **2**.

error. The terminal 2,5-dimethylpyrazine ligand is the least symmetrical.

A detailed comparison of the structures of **1** and **2** reveals some interesting differences, however. Attention was drawn previously (3) to the long Cu—O bond in **1** and the fact that the triflate–metal interaction is weak in this compound. The Cu—O distance in **2** is, in fact, ~0.06 Å longer than in **1** (Table 4), indicating even weaker metal–anion interactions in **2**. The observation that the S—O bond associated with the bridging oxygen atom is slightly shorter in **2** than in **1** is also consistent with weaker metal–anion interaction in **2**.

In **1**, two bridging pyrazine groups distinguished by different Cu–N bond distances are present. In contrast, although there are also two crystallographically different bridging ligands in **2**, the two Cu–N bridging distances are equal within experimental error. The mean bridging Cu—N distance of 2.006 Å in **2** is slightly longer than the corresponding value of 1.999 Å in **1**, while the terminal Cu—N distance in **2** (2.033(2) Å) is significantly longer than that in **1** (1.985(2) Å). It is interesting that on average both Cu—O and Cu—N distances are greater in **2** than in **1**, a consequence, presumably, of steric effects imposed by the methyl substituents on the pyrazine ligands of the former.

Steric interactions involving the methyl substituents of the 2,5-Me_2pyz ligand in **2** are responsible for the most obvious structural differences between this compound and the unsubstituted analogue **1**. These differences involve bond angles

Can. J. Chem. Downloaded from www.nrcresearchpress.com by 91.121.58.235 on 09/07/12
For personal use only.

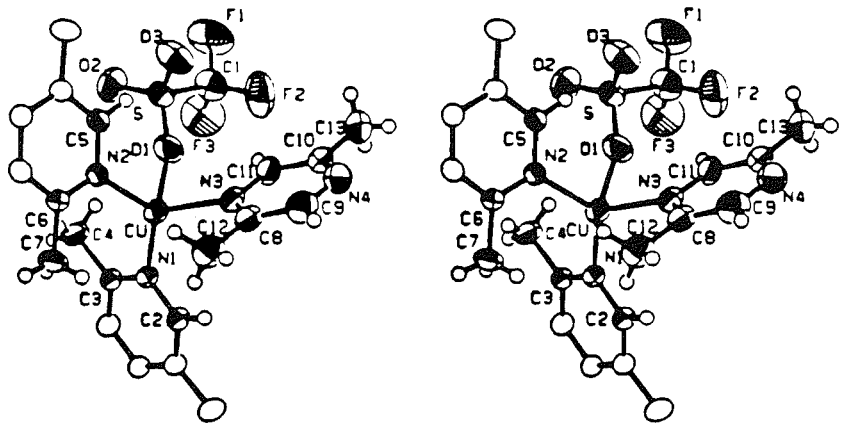

FIG. 2. Stereoview of the coordination about the copper atom in **2**; 50% probability thermal ellipsoids are shown for the non-hydrogen atoms. Shaded atoms make up the asymmetric unit.

TABLE 4. Selected bonding parameters[a,b] for **1** and **2**

	Atoms	2	1
Bond lengths (Å)	Cu—O(1)	2.388(2)	2.331(2)
	Cu—N(1)[c]	2.007(2)	1.971(1)
	Cu—N(2)[c]	2.005(2)	2.027(2)
	Cu—N(3)	2.033(2)	1.985(2)
	S—O(1)[c]	1.433(2)	1.440(2)
	S—O(2)	1.421(2)	1.422(3)
	S—O(3)	1.424(2)	1.432(3)
Mean bond angles (deg)	O—S—O	114.8	114.7
	C—S—O	103.5	103.6
	F—C—S	111.4	111.5
	F—C—F	107.4	107.4

[a]Estimated standard deviations in parentheses.
[b]Data for **1** from ref. 3.
[c]Bridging.

TABLE 5. Internal bonding parameters[a,b] for 2,5-dimethylpyrazine in **2** and in Ni(2,5-Me_2pyz)Br_2, **5**

	2			5
	Bridging[c]		Terminal	
Bond lengths (Å)				
C—C	1.382(3)	1.385(3)	1.381(4)	1.40
			1.382(4)	
N—CH	1.341(3)	1.336(3)	1.332(3)	1.38
			1.322(4)	
N—CH_3	1.342(3)	1.340(3)	1.347(3)	1.32
			1.331(4)	
Bond angles (deg)				
C—N—C	117.0(2)	116.7(2)	116.5(2)	117
			116.5(3)	
N—C—C	123.3(2)	123.3(2)	118.9(3)	121
	119.6(2)	120.0(2)	123.6(3)	
			124.5(3)	
			119.9(3)	

[a]Standard deviations in parentheses.
[b]Data for **5** from ref. 10.
[c]N(1) ligand, first column; N(2) ligand, second column.

TABLE 6. Vibrational spectra (CF_3SO_3 bands)[a,b]

Assignment[c]	1[d]	2	3	4
ν_{as} SO_3, E	1279 s	1281 s	1278 s	1291 s
	1247 s	1264 sh[e]	1237 s	1272 sh
		1243 s		1254 sh[e]
				1240 s
				1234 sh
ν_s CF_3, A_1	1228 m sh	1224 s	1227 s	1219 s
	1222 m sh			
ν_{as} CF_3, E	1160 sh	1163 sh	1168 s	1151 s
	1156 s	1152 s		1165 s[f]
		1175 s[f]		
ν_s SO_3, A_1	1027 s	1029 s	1028 s	1028 s
ν CS, A_1	774 w	762 m	764 w	759 w
δ_s SO_3, A_1	641 s	643 s	636 s	636 s
δ_{as} CF_3, E	584 m	584 m	588 w	584 w
δ_{as} SO_3, E	526 s	526 s	526 m	529 m

[a]Frequencies in cm^{-1}
[b]s = strong, m = medium, w = weak, sh = shoulder.
[c]Assignments (CSO_3 part and SCF_3 part, C_{3v} symmetry) from ref. 3.
[d]Data from ref. 3.
[e]2,5-Me_2pyz absorbs in this region (1255 w, in liquid) and possibly accounts for the shoulders at 1264 and 1254 cm^{-1} in **2** and **4** respectively.
[f]2,5-Me_2pyz absorbs in this region (1165 w, in liquid) and probably accounts for the bands at 1175 and 1165 cm^{-1} in **2** and **4** respectively.

about the copper atom and the relative orientations of the bridging ligands. The N—Cu—N angle involving the bridging pyrazine ligands is substantially larger (126.28(8)°) for the 2,5-Me_2pyz derivative than for the unsubstituted complex (110.6(1)°). In compound **1** the normals to the mean planes of the μ-pyz ligands lie roughly in the plane of the copper atoms of the polymeric chain, while in **2** one μ-2,5-Me_2pyz ligand is oriented as in **1** and the other (that in the center of the unit cell, see Fig. 1) is oriented approximately at a right angle to the first (the normal to the mean plane being roughly orthogonal to the plane of the Cu atoms). Thus adjacent μ-2,5-Me_2pyz ligands along the polymer **2** are mutually orthogonal, minimizing steric interactions between methyl groups on neighboring μ-2,5-Me_2pyz ligands. The orientation of the terminal 2,5-Me_2pyz ligand in **2** also differs from that of the corresponding pyz ligand in **1**, as a result of the rearrangement of the bridging ligands and the more stringent steric requirements of the substituted pyrazine ligands in **2**.

Can. J. Chem. Downloaded from www.nrcresearchpress.com by 91.121.58.235 on 09/07/12
For personal use only.

TABLE 7. Vibrational spectra (2,5-Me_2pyz bands)[a]

Compound	Infrared frequencies (cm^{-1})										
2,5-Me_2pyz	3005 w	2927 w	1531 vw	1449 m br	1328 s	1165 m[b]	1037 s	963 w	883 w	743 w[c]	419 s
Liquid	3085 w	2965 w		1488 s	1380 m	1255 w	1062 w sh				454 w
2	3039 wsh	2927 w		1448 m br	1333 m		1056 m	973 w	885 vw		430 m
	3049 w	2973 vw		1494 s	1378 m		1068 vw	984 vw	900 vw		451 m
	3079 wsh	3001 vw		1504 m sh	1392 w sh	1075 w			913 vw		
	3111 w										
	3115 w										
4	3068 vw	2936 vw		1443 w br	1322 vw		1048 w	975 w	894 w		461 m
	3142 vw	2998 vw		1502 m	1341 w		1089 w				
					1390 w						

[a]v = very, s = strong, m = medium, w = weak, sh = shoulder.
[b]Bands in this region in the complexes obscured by anion vibrations. See footnotes *e* and *f*, Table 6.
[c]Not observed in the complexes; possibly obscured by anion vibrations.

Spectroscopic studies

The electronic spectra of **1, 2, 3**, and **4** show the presence of a single band at 19.0, 21.9, 19.8, and 20.4 kK, respectively. No d–d transitions are expected for these d^{10} complexes. The diamagnetism of **2** was, in fact, confirmed by magnetic susceptibility studies over the temperature range 4.2–80 K. The spectra are assigned to a metal to ligand π^* charge transfer transition. Methyl substituents on the pyrazine ring may be expected to increase the charge density on the ring, making it a poorer π-acceptor (11). This may account for the fact that the charge transfer transition for each of the 2,5-Me_2pyz complexes is higher in energy than that of the corresponding pyz complex.

The bands observed in the infrared spectra of these complexes may be separated as described previously (3) into those due to the triflate anion vibrations and those due to neutral ligand vibrations. Infrared frequencies with assignments are given in Tables 6 and 7. As mentioned previously (3), assignments for the pyrazine complexes in the 1150–1230 cm^{-1} range are tentative due to overlap of anion and pyz bands in this region. A similar problem arises with the 2,5-dimethylpyrazine complexes in this region, as noted in Table 6 and 7.

The infrared spectrum of $Cu(pyz)_2(CF_3SO_3)$ prepared in this work differs only slightly from that of the crystalline form reported earlier (3). The weak band at 774 cm^{-1} is absent and probably arose from an impurity in the earlier sample; in addition, the bands at 1247 and 1279 cm^{-1} assigned to the antisymmetric SO_3 stretching mode are broadened somewhat in the spectrum observed here, resulting in a less distinct splitting. This band broadening may well be a consequence of the presence of lower oligomers in addition to the extended chain polymer in this sample, as suggested above. The remainder of the spectrum agrees within error (±3 cm^{-1}) with that reported previously.

The infrared spectrum of $Cu(pyz)(CF_3SO_3)$, **3**, is, in general, similar to that of its bis(pyrazine) analogue, **1**, with the following notable differences. While **1** exhibits two bands of medium intensity at 452 and 472 cm^{-1}, assigned to terminal and bridging pyrazine respectively (3), **3** exhibits only one band in this region, at 473 cm^{-1}, which we assign to bridging pyrazine. In addition a medium intensity pyz band at 1051 cm^{-1} in **1** (3) is not observed in **3** and is likely a vibration associated with terminal pyz moieties. The anion spectra of **1** and **3** (Table 6) are virtually identical, suggesting that in **3** the mode of anion coordination is the same as in **1**, monodentate via oxygen. The splitting of the antisymmetric SO_3 stretching vibration (E symmetry in C_{3v}) is only slighter greater in **3** than in **1** (41 versus 32 cm^{-1}), suggesting, as discussed previously (3), a similar degree of anion distortion and therefore similar metal–anion bonding interactions in the two compounds. The vibrational spectra, therefore, are consistent with a polymeric structure for **3** involving three-coordinate copper(I) ions bridged by pyz ligands with the coordination around each copper completed by monodentate triflate groups to produce a CuN_2O chromophore.

Considering the 2,5-Me_2pyz complexes, **2** and **4**, it is evident from the data in Table 7 that most of the bands in free 2,5-Me_2pyz are present in the spectra of the complexes, with most bands shifting by a few wavenumbers to higher frequencies on coordination. In addition, band splitting is generally evident in **2** as a consequence, in part at least, of the presence of both bridging and terminal 2,5-Me_2pyz ligands in this compound. The band at 419 cm^{-1} in free 2,5-Me_2pyz, like that at 417 cm^{-1} in liquid pyrazine (3), is of potential diagnostic value to distinguish between monodentate and bidentate ligand coordination. In **2** the band is replaced by two medium intensity bands at 430 and 451 cm^{-1} and in **4** it is replaced by one band at 461 cm^{-1}. Assigning the higher frequency vibrations to bridging ligands would be consistent with the assignments made previously for the pyz analogues and would support the assignment of bridging 2,5-Me_2pyz in **4**. The close correspondence between the spectral bands assigned to triflate vibrations in compounds **1** and **2** (Table 6) is consistent with the X-ray diffraction studies which, as described above, reveal very similar internal bonding parameters for the anions in the two compounds. Apart from the fact that the splitting of the antisymmetric SO_3 stretching vibration in **4** is slightly, but significantly, greater than the corresponding splitting observed for the other three compounds, the anion spectrum of **4** is comparable to those of the other compounds and is consistent with monodentate triflate coordination. We conclude the structure of **4** to be polymeric, and similar to that of its pyz analogue **3**. Finally, we note that for both the pyz and the 2,5-Me_2pyz pairs of complexes the splitting of the infrared band assigned to the antisymmetric SO_3 stretching vibration is slightly, but significantly, greater in the three-coordinate complex than in the corresponding four-coordinate complex. This possibly reflects

Can. J. Chem. Downloaded from www.nrcresearchpress.com by 91.121.58.235 on 09/07/12
For personal use only.

stronger metal–triflate interactions in the former complexes due to fewer steric repulsions associated with a CuN_2O chromophore than with a CuN_3O chromophore.

Acknowledgements

We thank the Natural Sciences and Engineering Research Council of Canada for financial support.

1. A. B. P. LEVER, J. LEWIS, and R. S. NYHOLM. Nature, **189**, 58 (1961).
2. A. B. P. LEVER, J. LEWIS, and R. S. NYHOLM. J. Chem. Soc. 3156 (1963).
3. T. OTIENO, S. J. RETTIG, R. C. THOMPSON, and J. TROTTER. Can. J. Chem. **67**, 1964 (1989).
4. R. D. HOWELLS and J. D. MCCOWN. Chem. Rev. **77**, 69 (1972).
5. M. B. DINES. Sep. Sci. **8**, 661 (1973).
6. J. S. HAYNES, K. W. OLIVER, S. J. RETTIG, R. C. THOMPSON, and J. TROTTER. Can. J. Chem. **62**, 891 (1984).
7. International tables for X-ray crystallography. Vol. IV. Kynoch Press, Birmingham, U.K. (present distributor Kluwer Academic Publishers, Dordrecht, The Netherlands). 1974. pp. 99–102 and 149.
8. K. YVON, W. JEITSCHKO, and E. PARTHE. J. Appl. Crystallogr. **10**, 73 (1977).
9. J. S. HAYNES, J. R. SAMS, and R. C. THOMPSON. Can. J. Chem. **66**, 2079 (1988).
10. F. D. AYRES, P. PAULING, and G. B. ROBERTSON. Inorg. Chem. **3**, 1303 (1964).
11. A. B. P. LEVER, J. LEWIS, and R. S. NYHOLM. J. Chem. Soc. 4761 (1964).

Can. J. Chem. Downloaded from www.nrcresearchpress.com by 91.121.58.235 on 09/07/12
For personal use only.

^{1}H NMR studies of proton transfer in Schiff base and carboxylic acid systems

HOA LE-THANH AND D. VOCELLE[1]

Département de chimie, Université du Québec à Montréal, C.P. 8888, succ. A, Montréal (Québec), Canada H3C 3P8

Received February 6, 1990

HOA LE-THANH and D. VOCELLE. Can. J. Chem. **68**, 1909 (1990).

When the unconjugated Schiff base, isobutylidene isopropylamine (**2**), reacts with acids such as the mineral acids HCl, HBr, and HI, or the carboxylic acids trichloroacetic, monochloroacetic, and propionic acid, in $CDCl_3$, several complexes are formed. In this study, ^{1}H NMR allows us to differentiate between several possibilities. With the mineral acids, only 1:1 structures are seen and the chemical shift of the N---H---X proton varies according to the strength of the hydrogen bond between the protonated Schiff base and its counterion. With the carboxylic acids, 1:1 and 1:2 structures are present in rapid equilibrium. In the presence of an excess of acid, protonation of the Schiff base increases considerably. Extrapolation of the results is given in terms of the molecular mechanism of vision.

Key words: protonation, proton nuclear magnetic resonance, proton transfer, rhodopsins, Schiff base.

HOA LE-THANH et D. VOCELLE. Can. J. Chem. **68**, 1909 (1990).

Quand la base de Schiff non conjuguée, l'isobutylidène isopropylamine (**2**), réagit dans le $CDCl_3$ avec différents acides tels que les acides minéraux HCl, HBr et HI ou les acides carboxyliques comme trichloroacétique, monochloroacétique et propionique, plusieurs complexes sont formés. Dans cette étude, la RMN du proton permet de différencier plusieurs possibilités. Avec les acides minéraux, seules les structures 1:1 sont observées et le déplacement chimique du proton N---H---X varie selon la force de la liaison hydrogène entre la base de Schiff protonée et son contre-ion. Avec les acides carboxyliques, les structures 1:1 et 1:2 sont présentes dans un équilibre rapide. En présence d'un excès d'acide, la protonation de la base de Schiff augmente considérablement. La discussion de ces résultats en fonction du mécanisme moléculaire de la vision est abordée.

Mots clés : protonation, résonance magnétique nucléaire du proton, transfert du proton, rhodopsines, bases de Schiff.

Can. J. Chem. Downloaded from www.nrcresearchpress.com by 91.121.58.235 on 09/07/12
For personal use only.

Introduction

In visual pigments such as rhodopsins, or in related bacterial pigments such as bacteriorhodopsins, the retinylidene Schiff base is protonated or deprotonated depending upon the stage in the photocyclic mechanism of vision, or proton pumping, at which the chromophore is located. As an example, the large blue shift occurring during the formation of metarhodopsin II (or at M_{412} in bacteriorhodopsin) is explained in terms of deprotonation of the preceding intermediate metarhodopsin I (L_{550} for bacteriorhodopsin) (1–5). One is tempted to believe that in such systems there exists an easily polarizable hydrogen bond such as this one:

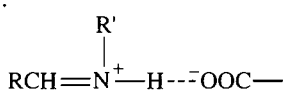

This has been advocated by Zundel and Merz (6, 7) on the basis of continua in IR spectra of model systems of rhodopsins and bacteriorhodopsins. Consequently, protonation or deprotonation of a Schiff base can be summarized by the following equilibrium:

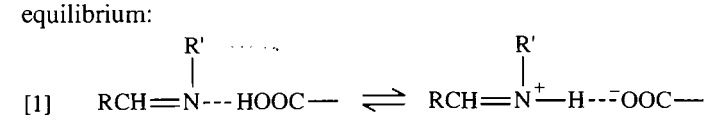

[1]

In such systems, the equilibrium would be quite sensitive to the nature of the environment (in model systems, it will be the solvent) and to a variety of other well-known effects in vision research such as the presence of water molecules (8–10) and of a local electrical field surrounding the chromophore (11).

Most model systems of rhodopsins and bacteriorhodopsins use a mineral acid (usually HCl) as the proton donor. With this acid (HCl), protonation is always complete and the equilibrium:

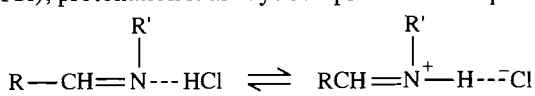

is strongly shifted to the right. For some years now, we have investigated the effects of carboxylic acids on Schiff bases (SB) since aspartic or glutamic acids[2] are reputed to be the proton donor in the pigments (6). This has been done using UV, FTIR at room temperature and at low temperature, and by ^{13}C and ^{15}N NMR spectroscopy (see refs. 5 and 14). Some interesting facts emerged from these studies. In particular, protonation in nonpolar solvents by weak carboxylic acids is incomplete and acids having pK_a's near to those of aspartic and glutamic acids (pK_a's of 3.9 and 4.2 respectively in water) need some additional stabilizing factors to effect 100% protonation. These factors could be of different natures but we are especially interested in the effects of water molecules near the SB and in the presence of several carboxylic acids, which may act as a proton relay transfer (4, 5).

In the present study, we intend to investigate the effects of excess acid on the proton transfer capability of three carboxylic acids of quite different pK_a's: trichloroacetic acid (TCA, pK_a 0.66), monochloroacetic acid (MCA, pK_a 2.85), and propionic acid (PRO, pK_a 4.9). Also, steric effects around the SB will be studied with the help of three different imines: neopentylidene *n*-butylamine (**1**), isobutylidene isopropylamine (**2**), and isobutylidene *tert*-butylamine (**3**).

^{1}H NMR spectroscopy was chosen for this investigation since it is not affected by the presence of excess acid, as is the case for IR studies (because of the proximity of $-CO_2H$, $-CO_2^-$, $-C{=}N^+H$, $-C{=}N$ bands in the 1600–1750 cm^{-1} region). By looking at the behavior of the $-N^+{-}{-}{-}H{-}{-}{-}{}^-O$ proton we can gain a good idea of how much proton transfer has occurred when excess acid is used.

[1]Author to whom correspondence may be addressed.

[2]Quite recently, Sakmar *et al.* (12) and Zhukovsky and Oprian (13) in a most elegant experiment using site-directed mutagenesis of opsin genes were able to show quite convincingly that the protonating agent of the retinyl Schiff base chromophore is glutamic acid-113 in bovine rhodopsin.

Can. J. Chem. Downloaded from www.nrcresearchpress.com by 91.121.58.235 on 09/07/12
For personal use only.

Experimental

The imines **1**, **2**, and **3** were prepared according to a method previously described (15). Their purity was assessed by IR and ^{1}H NMR spectroscopy. The imines were freshly distilled before use. The acids TCA and MCA were dried in a desiccator under vacuum and in the presence of P_2O_5. Propionic acid was dried over activated molecular sieves (3Å). Preparation of the mineral salts has also been described (15). Deuterated chloroform was used as received (Merck, Sharp & Dohme). The concentration of the imines and their salts in $CDCl_3$ was always 0.1 M. All operations concerning the preparation of the samples for NMR spectra were carried out under dry nitrogen atmosphere in a glovebox and the spectra were recorded immediately after. The NMR spectra were taken on a Bruker WH-400/DS (400 MHz) at 293 K and in some cases at 233 K (−40°C).

Results and discussion

To our knowledge, no ^{1}H NMR study of the N---H---O bonds of SB/carboxylic acid systems has been reported before. However, N---H---O bonds in other systems have already been studied. For instance, *syn* and *anti* isomers of di-α-pyridyl ethylene (16), homoconjugated and heteroconjugated amines and amine oxides (17), diamine monosalts (18), trimethylamine oxide and carboxylic acids (19), pyridine dicarboxylic acid *N*-oxide (20), pyridine and several substituted acetic acids (21, 22), 4-methyl pyridine and dichloroacetic acid (23), substituted pyridines and trifluoroacetic acid complexes (24), some Mannich bases and alcohols (25, 26), a phenol derivative with triethylamine (27) and with a disubstituted aniline (28), both at low temperatures, have been studied by NMR.

It is a known fact that proton transfer can be assisted through the participation of solvent molecules (29) and that it is linearly correlated with the difference between the pK_a's of the base (proton acceptor) and the acid (proton donor), ΔpK_a (29, 30). In our study, it is expected that with mineral acids full protonation occurs because of the large ΔpK_a. Full protonation means that the equilibrium (eq. [1]) is shifted completely to the right and consequently implies that 100% proton transfer is also present. From our previous studies carried out in deuterated chloroform (5, 15), imines and acids are expected to form ion pairs and neutral associated species (as in the left hand of eq. [1]). In all the spectra, concentrations of the SB were held constant at 0.1 M while the concentrations of the acids vary from 0.05 M to 1.0 M (2.0 M for PRO). The chemical shift of the OH of the carboxylic acids is sensitive to changes in concentration. Therefore the measurements for the acids alone and for the SB/carboxylic acid systems were done under exactly the same experimental conditions. Results will be first discussed for the mineral acids, then followed by the carboxylic acids.

Schiff bases/mineral acids systems

For isobutylidene isopropylamine (**2**), all three mineral acids were used. That full protonation (and proton transfer) has occurred is indicated by the fact that the N---H---X proton (where X = Cl, Br, I, henceforth abbreviated H_{NX}) is coupled with the α and α′ protons of the SB (Fig. 1) and by IR data (15) that leave no doubt on its state of protonation (presence only of the $\nu_{C=N^+H}$ band).

The chemical shift of the α protons (Table 1) is greater for HI than for HBr than for HCl. It follows the strength of the acids (HI > HBr > HCl). On the contrary, for the H_{NX}, results of Table 2 show an increase in the chemical shifts while going from HI to HBr and to HCl. This indicates that the strength of the hydrogen bonding between the protonated SB and its counterion increases following this order:

$$N^+\text{-H---}Cl^- > N^+\text{-H---}Br^- > N^+\text{-H---}I^-$$

TABLE 1. Chemical shifts of the α, β protons, at 293 K, for the Schiff bases **1**, **2**, **3** interacting with TCA, MCA, PRO, and halogenated mineral acids in $CDCl_3$

System (1:1)	H_α	$H_{\alpha'}$	H_β	$H_{\beta'}$
1 alone	7.48	3.35	—	1.55
2 alone	7.44	3.20	2.37	1.12
3 alone	7.38	—	2.40	1.15
1:TCA	7.82	3.76	—	1.80
2:TCA	7.72	3.99	3.28	1.46
3:TCA	7.66	—	3.41	1.50
1:MCA	7.58	3.52	—	1.62
2:MCA	7.52	3.59	2.82	1.28
3:MCA	7.46	—	2.98	1.32
1:PR	7.48	3.37	—	1.55
2:PR	7.44	3.29	2.49	1.16
3:PR	7.36	—	2.53	1.18
1:HBr	8.72	3.92	—	1.90
2:HBr	8.37	4.25	3.60	1.55
3:HBr	8.16	—	3.79	1.57
2:HI	8.47	4.25	3.85	1.50
2:HCl	8.00	4.11	3.63	1.54

TABLE 2. Chemical shifts of the N---H---O protons for **2** interacting with different acids

Systems[a]		Peak positions				H_d[b]	
		293 K		233 K		293 K	233 K
TCA	1:0.5	17.09	—	16.77	—	10.41	12.04
	1:1	16.91	—	16.67	—	10.87	12.29
	1:2	14.27	14.84	13.53	15.89	11.47	12.58
	1:5	13.02	12.81	12.39	13.58	11.82	12.68
	1:10	12.69	12.20	12.32	12.85	12.05	12.71
MCA	1:0.5	16.51	—	18.14	—	10.32	11.59
	1:1	16.11	—	17.34	—	11.06	12.05
	1:2	14.96	—	15.59	—	11.57	12.40
	1:5	13.15	—	13.91	13.51	11.90	12.55
	1:10	12.62	—	13.47	13.01	12.08	12.45
PR	1:0.5	11.65	—	14.33	—	10.61	11.80
	1:1	11.98	—	14.04	—	11.19	12.13
	1:5	12.19	—	13.13	—	11.94	12.52
	1:10	12.23	—	12.94	—	12.06	12.55
	1:20	12.24	—	12.77	—	12.10	12.54
HCl	1:1	15.83	—	—	—	—	—
HBr	1:1	14.38	—	14.11	—	—	—
HI	1:1	11.95	—	—	—	—	—

[a]Expressed in molar ratio of **2**:acids.

[b]The H_d values at 293 and 233 K refer to the acid alone, in solution, at the same concentrations as those containing SB/acid; see text.

These observations are in good agreement with the previous results obtained in FTIR spectroscopy (15).

It is obvious also that the chemical shifts of H_{NX} taken alone do not indicate full protonation. The variation in the chemical shifts of the three salts indicates that the counterion (X^-) exerts a strong influence on the N^+-H proton. Again this signifies that ion pairs are formed in deuterated chloroform. Because of this, their chemical shifts cannot be used to evaluate the degree of protonation in systems where protonation is incomplete. As we

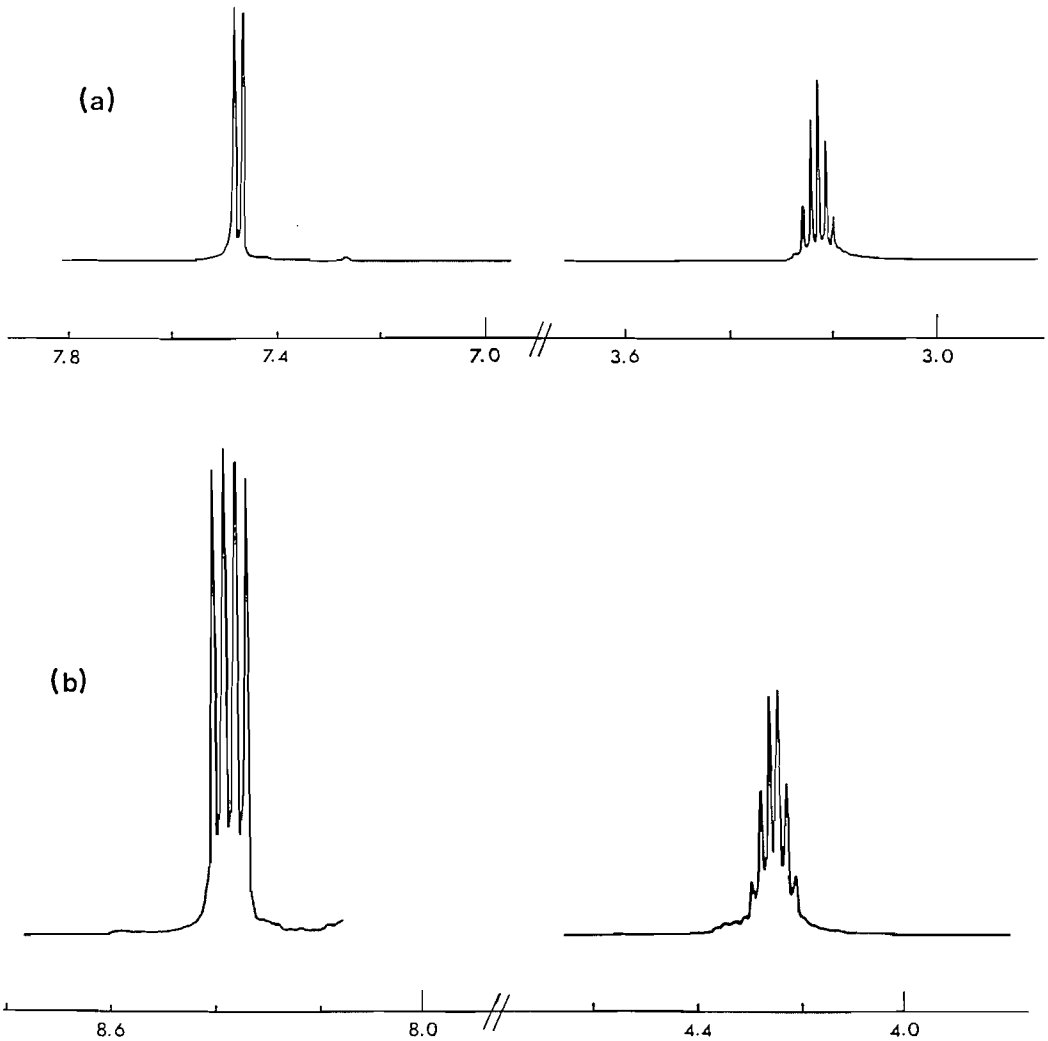

FIG. 1. A part of ^{1}H NMR spectra showing the spin–spin coupling of α and α′ protons, at 293 K: (a) SB **2**; (b) SB **2** + HBr 1:1.

have demonstrated for ^{13}C and ^{15}N NMR (31, 32), chemical shifts for some judiciously chosen nuclei could be used to evaluate the degree of protonation of SB. The data in Table 1 indicate that the β′ protons for **2** and possibly for **3** could be used for that purpose since they are well deshielded upon protonation of the SB but are somewhat insensitive to the presence of the counterion. A value of 1.52 ppm was retained for these protons and will serve later as the 100% protonation reference point. The β′ protons of **1** are more deshielded than those of **2** and **3** since they are methylene protons rather than methyl protons.

Tables 2–4 also show that the chemical shifts of H_{NX} vary according to the degree of branching of the amine residue. Upon branching, H_{NX} is shifted to low field while the aldimine proton is shifted to high field. This could be explained by steric hindrance caused by the bulky isopropyl and *tert*-butyl groups.

Schiff bases/carboxylic acids systems

Let us recall that one of the principal aims of this study is to show the presence and effects, if possible, of several carboxylic acid molecules acting simultaneously on the SB. By stabilizing the negative charge on the carboxylate anion, the presence of two or more molecules of acid should make the acid appear stronger. This resembles the so-called proton relay transfer often mentioned in enzyme chemistry (33). That such complexes do exist has been demonstrated by Barrow (34) and Denisov and Golubev (35) for related systems. In an attempt to show the presence of these complexes, the molar ratios of SB to carboxylic acid were varied from 1:0.5 to 1:10 (1:20 for PRO). The chemical shifts of the N--H--O protons are shown in Tables 2–4.

At first glimpse, inspection of these tables shows that the data appear rather similar for the three SB. As was the case for the mineral acids, imine **1** is the most deshielded by the carboxylic acids, as seen for H_α, while for N--H--O protons it is the most shielded (systems 1:1), and this is true for all the acids used. Furthermore, while spectra for TCA show two peaks in the 10–17 ppm region for molar ratios of 1:2 and up (see Fig. 2c, f and Fig. 4a, b), spectra for MCA present two peaks only for molar ratio 1:5 and up (see Figs. 3, 4c, d), and only one broad peak appears in that same region for PRO (see Fig. 5a–f). Also, the chemical shifts obtained with MCA (as is also the case for TCA) decrease from 16.5 to 12.6 ppm (17.1 to 12.7 ppm for TCA) upon increase in the acid concentration, while for propionic acid the contrary is observed: the chemical shifts increase from 11.65 to 12.24 ppm upon addition of acid. Because of these facts, each acid will be discussed separately.

Trichloroacetic acid

IR results show (15) that this acid is able to protonate SB to a large extent. Data of Table 1 for compound **2** only allow the evaluation of the degree of protonation by considering that when **2** is fully protonated the β′ proton should have a mean value of

Can. J. Chem. Downloaded from www.nrcresearchpress.com by 91.121.58.235 on 09/07/12
For personal use only.

Can. J. Chem. Downloaded from www.nrcresearchpress.com by 91.121.58.235 on 09/07/12
For personal use only.

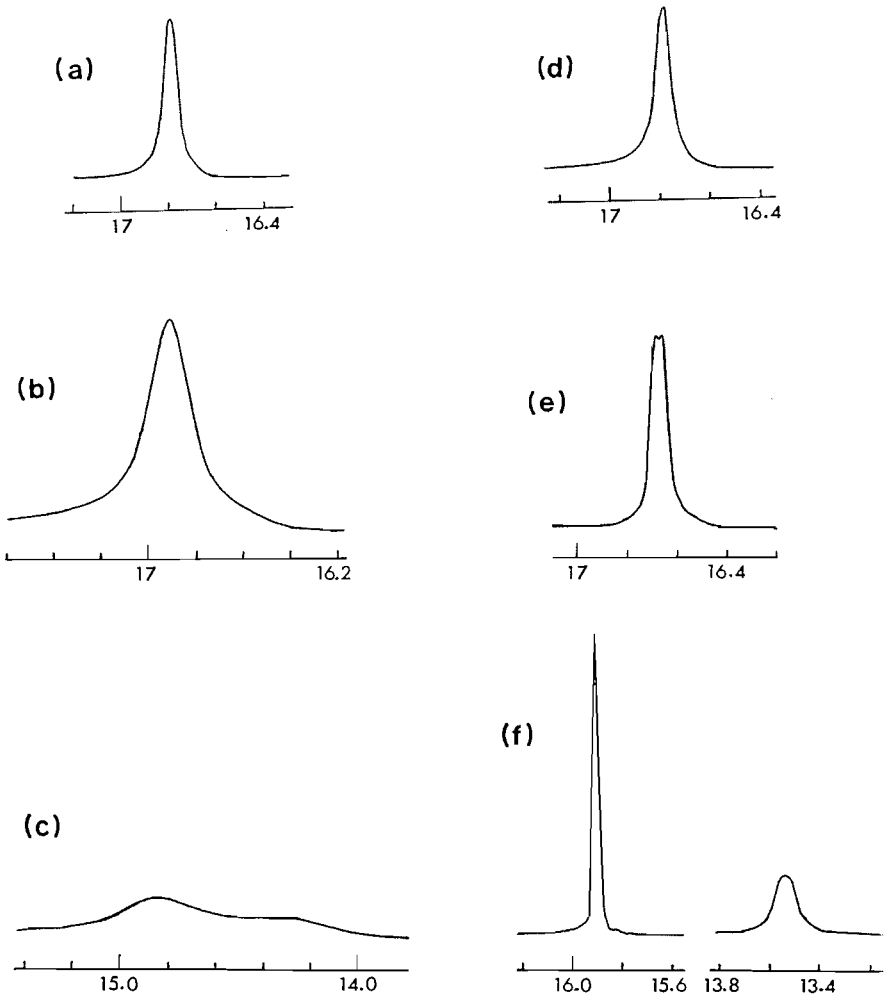

FIG. 2. ^{1}H NMR spectra for N---H---O protons at 293 and 233 K and for different molar ratios of **2**:TCA: At 293 K (a) 1:0.5; (b) 1:1; (c) 1:2. At 233 K (d) 1:0.5; (e) 1:1; (f) 1:2.

TABLE 3. Chemical shifts of the N---H---O protons for **1** interacting with different acids

Systems[a]		Peak positions 293 K		Peak positions 233 K		H_d[b] 293 K	H_d[b] 233 K
TCA	1:0.5	16.59	—	16.17	—	10.41	12.04
	1:1	16.20	—	15.90	—	10.87	12.29
	1:2	14.00	15.60	13.28	16.70	11.47	12.58
	1:5	12.38	12.88	11.94	13.62	11.82	12.68
	1:10	12.05	12.39	11.68	13.08	12.05	12.71
MCA	1:0.5	15.67	—	17.06	—	10.32	11.59
	1:1	15.28	—	16.51	—	11.06	12.05
	1:2	14.47	—	15.26	—	11.57	12.40
	1:5	13.07	—	13.57	—	11.90	12.55
	1:10	12.57	—	12.81	13.05	12.08	12.45
PR	1:0.5	11.44	—	13.74	—	10.61	11.80
	1:1	11.82	—	13.51	—	11.19	12.13
	1:5	12.13	—	12.99	—	11.94	12.52
	1:10	12.19	—	12.86	—	12.10	12.55
	1:20	12.22	—	12.75	—	12.10	12.54
HBr	1:1	13.46	—	13.10	—	—	—

[a]Expressed in molar ratio of **1**:acids.
[b]The H_d values at 293 and 233 K refer to the acid alone, in solution, at the same concentrations as those containing SB/acid; see text.

TABLE 4. Chemical shifts of the N---H---O protons for **3** interacting with different acids

Systems[a]	Peak positions 293 K		Peak positions 233 K		H_d[b] 293 K	H_d[b] 233 K
TCA 1:1	16.74	—	16.44	—	10.87	12.29
MCA 1:1	16.44	—	17.81	—	11.06	12.05
PR 1:1	11.90	—	14.24	—	11.19	12.13
HBr 1:1	14.53	—	—	—	—	—

[a]Expressed in molar ratio of **3**:acids.
[b]The H_d values at 293 and 233 K refer to the acid alone, in solution, at the same concentrations as those containing SB/acid; see text.

1.52 ppm (see before) while, as observed, the value is 1.12 ppm for 0% protonation. With a found value of 1.46, the degree of protonation is calculated to be 85%. With acid concentrations of 0.05 and 0.1 M, only one peak is present at 293 K and the chemical shifts have values near 17 ppm (see Fig. 2a, b). When excess acid is present and the molar ratio changes to 1:2, two rather broad peaks are seen at 293 K (Fig. 2c) while one is sharper than the other at 233 K (Fig. 2f). To assign proper structures for these two N--H--O protons, the possibility of the simultaneous presence of several complexes must be considered and one also cannot forget that, in systems like these, fast

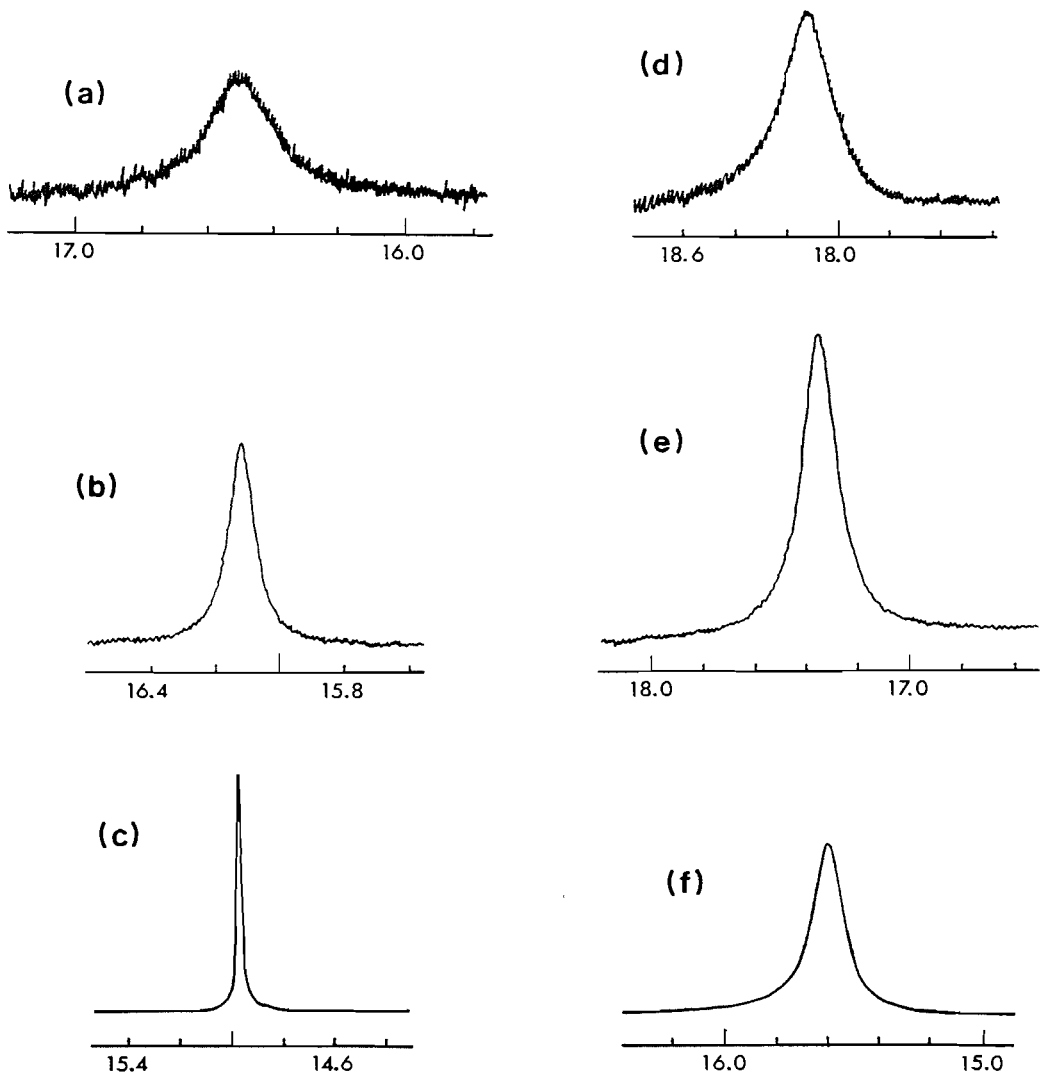

FIG. 3. ^{1}H NMR spectra for N---H---O protons at 293 and 233 K and for different molar ratios of **2**:MCA: At 293 K (a) 1:0.5; (b) 1:1; (c) 1:2. At 233 K (d) 1:0.5; (e) 1:1; (f) 1:2.

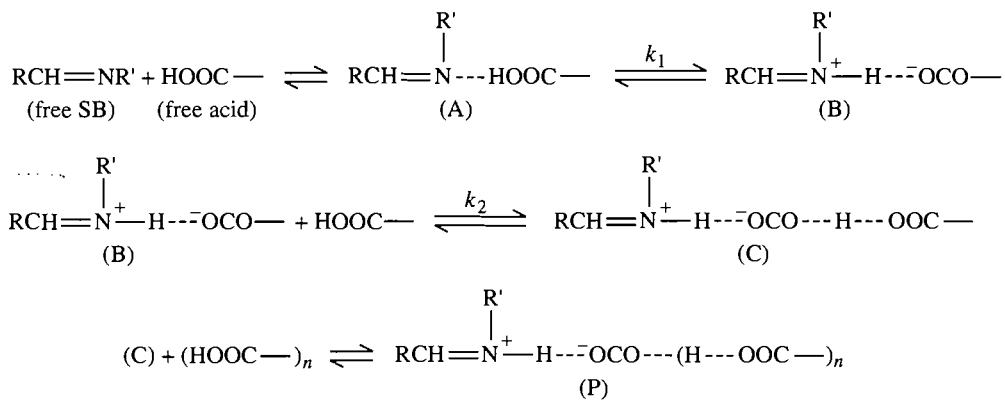

SCHEME 1

intermolecular exchanges could always be present. Scheme 1 (see below) shows some of the complexes that could reasonably be occurring. In this scheme, we see the solvated SB and acid interacting first to form the molecular adduct A, which equilibrates rapidly with the ionic species B. By the addition of more acid, a 1:2 complex (C) can be formed, followed by a polymeric structure such as P. All these structures are in equilibrium.

Also, the presence of an acid dimer cannot be excluded. The RCOOH proton will be abbreviated H_d. It is shown below.

A 2:1 complex is not shown in Scheme 1 since such a structure would only be possible when the amount of acid is low compared to the Schiff base concentration, as for the ratio 1:0.5. However, no peak assignment could be related to such a structure in this work and, furthermore, review of the literature on related systems as discussed before (13–23) shows that such

Can. J. Chem. Downloaded from www.nrcresearchpress.com by 91.121.58.235 on 09/07/12
For personal use only.

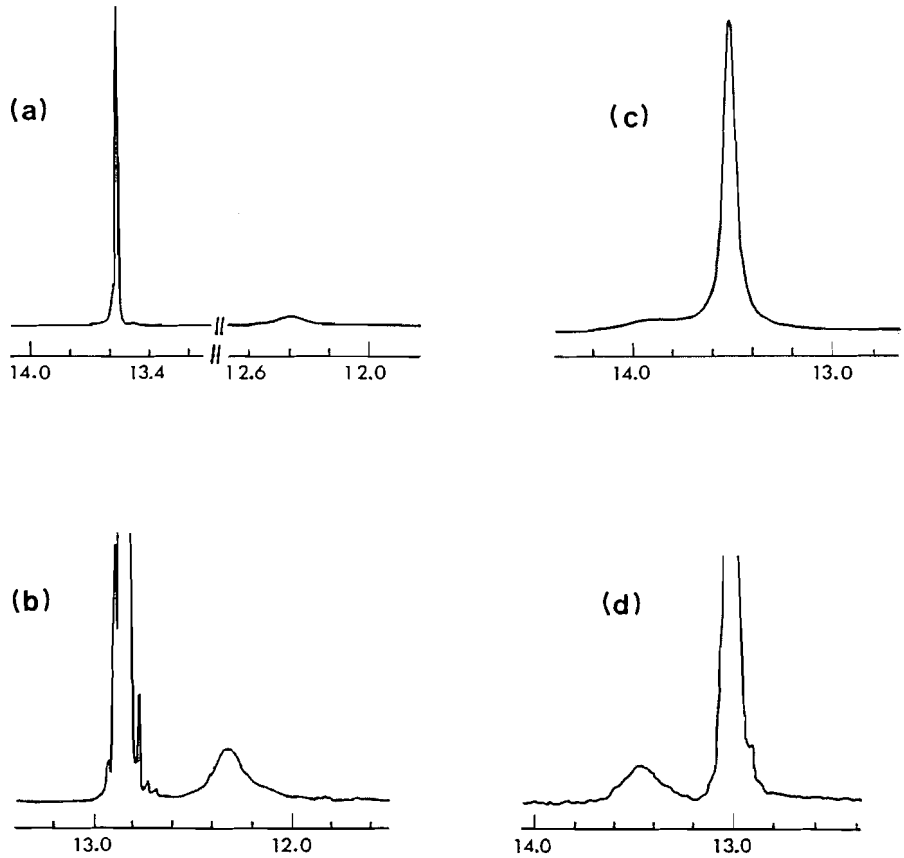

FIG. 4. ^{1}H NMR spectra for N---H---O protons at 233 K and for two molar ratios of **2**:TCA and **2**:MCA. System **2**:TCA (a) 1:5; (b) 1:10. System **2**:MCA (c) 1:5; (d) 1:10.

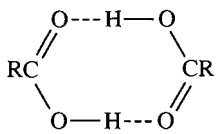

H_d

structures are rarely invoked. Since the location of the peak for samples having molar ratios of 2:1 can readily be explained with 1:1 structures, in this work 2:1 structures will be omitted.

In Scheme 1, the free forms of SB and the acid are probably present only at very low concentration for an acid as strong as TCA, which means that at the rather high concentrations used here (0.1 M) it could be considered absent. This has been confirmed by UV spectroscopy.[3] Furthermore, structures A and B are expected to be in a fast equilibrium (26) and their N--H--O protons are not expected to be differentiable at room temperature. These protons will be abbreviated as H_A and H_B (or H_{AB}). The 1:2 complex must also be in equilibrium with the 1:1 complex and it is reasonable to expect that the equilibrium would not be as fast as between A and B since a second molecule of acid must be added, which is obviously not the case for A and B. Another possibility could arise for the formation of structure C: this could not only be formed as described before but also, conceivably, by direct reaction of the free Schiff base with the dimer complex of the acid as shown in eq. [2]:

[2] $RCH{=}NR' + (HOOC\text{-})2 \rightleftharpoons C$

This is a distinct possibility and it shows the complexity of the question. Nevertheless, in this work it will be neglected on the basis that since 1:1 structures are present, it seems logical to think that the cyclic dimer would be broken in the presence of the Schiff base.

In C, however, there are two highly deshielded protons (N--H--O and O--H--O); they are not expected to be differentiable either at room temperature or at 233 K. These two protons will be abbreviated H_C. Finally, polymeric complexes (n = 2, 3, etc.) might also be present, especially when large excesses of acid are used, but these complexes will be quite difficult to differentiate from C since their structures appear similar.

With molar ratios of 1:0.5 and 1:1 only one broad peak is present and is quite deshielded (Fig. 2a, b). This can be explained in terms of a fast equilibrium between the molecular (A) and the ionic species (B) of Scheme 1 since it is known that protonation is incomplete and that the free forms are unlikely with a strong acid like TCA, as previously discussed. The chemical shifts must represent the mean values of the proportions of each of the two entities. At 233 K no second peak is present and the peak appears more shielded by some 0.3 ppm. At 233 K and with an equimolar concentration of SB and acid (Fig. 2e), the N--H--O proton is now coupled with the α and α' protons of the SB. On the other hand, one can see that H_α appears now as a doublet of doublets and that the coupling of $H_{\alpha'}$ with the N--H--O proton results in an overlapped doublet of a multiplet, similar to those observed in the systems of SB and halogenated mineral acids, as shown in Fig. 1b. This can be explained on the basis that the free energy between the free forms (even at very low concentration) and B is, at 233 K, large enough that the rate of exchange is now sufficiently slow to

[3]D. Cossette and D. Vocelle. To be published.

Can. J. Chem. Downloaded from www.nrcresearchpress.com by 91.121.58.235 on 09/07/12
For personal use only.

Can. J. Chem. Downloaded from www.nrcresearchpress.com by 91.121.58.235 on 09/07/12
For personal use only.

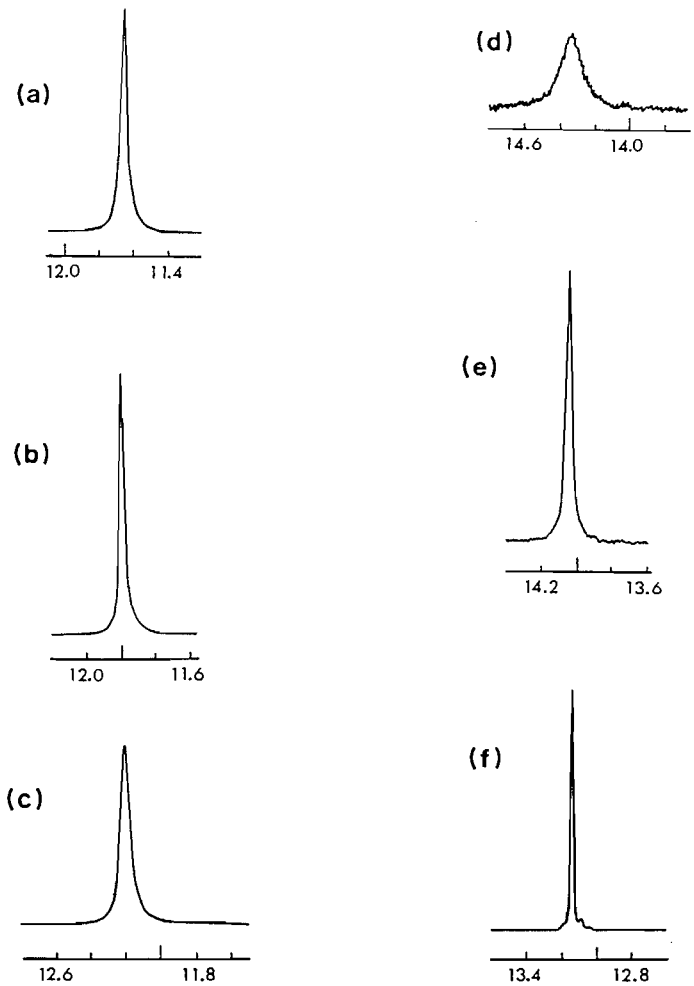

FIG. 5. ^{1}H NMR spectra for N---H---O protons at 293 and 233 K and for different molar ratios of **2**:PRO: At 293 K (a) 1:0.5; (b) 1:1; (c) 1:5. At 233 K (d) 1:0.5; (e) 1:1; (f) 1:5.

make the α protons appear as a doublet of doublets. All these observations signify as expected that, as the concentration of acid increases and with a lowering of the temperature, the equilibrium k_1 is shifted to the right.

When excess acid is added as in the molar ratio of 1:2 at 293 K, the spectrum reveals two peaks located at 14.84 and 14.27 ppm (Fig. 2c). According to Denisov and Golubev (35), the more deshielded peak could be attributed to the two protons of C, which are interchanging rapidly, and the more shielded peak could come from the averaging of the N---H---O protons in A and B, this latter being preponderant for the reasons already stated. This assignment is also supported by the shape of the peaks obtained when the temperature is lowered. This will be discussed later. The proton at 14.27 ppm will then be referred to as H_{AB}. H_{AB} experiences a large shielding effect of more than 2 ppm compared to the value obtained previously at a molar ratio of 1:1. This can be explained by a strong shift of the equilibrium to the right, that is, towards protonation or proton transfer. The presence of a second peak in the NMR spectrum signifies that C is slowly equilibrating with B (compared to the timescale of NMR). How can this be rationalized? Compared to a 1:1 structure, a 1:2 complex is a trimeric structure, which should be quite different in energy from a dimeric one. With TCA, this is the case. (For MCA and PRO, as will be shown, the situation is somewhat different.) At 233 K and with a molar ratio of 1:2 (Table 2 and Fig. 2f), the shapes of the two peaks obtained differ: one is sharper (at 15.89 ppm) than the other (at 13.53 ppm). Peak integration indicates that they are in a 1:1 ratio. As said before, the broader and more shielded one is assigned to the N---H---O proton in A and B (or H_{AB}), which is thought to be in a slower equilibrium than at 293 K, but still fast compared to the NMR timescale. The sharper peak at 15.89 ppm comes from the two protons in C. The peak H_{AB} is broad because of some couplings with the vicinal protons (not always resolved due to the fast equilibria between the different structures) and also because of the nitrogen quadrupolar effect. The more deshielded peak H_C is sharper due to the influence of the O---H---O proton in rapid exchange with the proton N---H---O in structure C (Scheme 1). Incidentally, the H_d peak of the carboxylic acid (that is, the peak of the carboxylic acid taken alone in the solvent: see Experimental) is always sharper than those of B and C. The chemical shift of H_{AB} moves to higher field at 233 K while H_C parallels H_d and goes to lower field. This is not too surprising since H_C must have much in common with H_d (same O---H---O bond). In conclusion then, with a molar ratio of 1:2, the results can be explained in terms of

$$A \overset{k_1}{\rightleftharpoons} B \overset{k_2}{\rightleftharpoons} C$$

where $k_1 \gg k_2$.

For molecular ratios of 1:5 and 1:10, again two peaks are obtained at room temperature as well as at 233 K (Fig. 4a, b). This time the assignments are easy since, for instance, at a molar ratio of 1:5 the peak at 12.81 ppm (see Table 2) integrates for a ratio of 1:5 compared to the aldimine proton. The same situation as described before is maintained except that the proportion of C increases while that of B decreases. At a ratio of 1:10, B now represents around 25% of the mixture while it was 50% for a molar ratio of 1:2 (at 293 K). Also, the N--H--O proton of B has its coupling with adjacent protons resolved, which means that A is not contributing in the overall picture. Furthermore, it is probable that complexes formed by one molecule of imine and several molecules of carboxylic acid (as in P of Scheme 1) do exist, along with the three complexes already proposed (A, B, and C), but NMR is not expected to be able to differentiate C from P since they have quite similar structures. It is interesting also to note that the chemical shift of H_C now approaches that of H_d: at a molar ratio of 1:10, the chemical shifts are at 12.20 and 12.05 ppm respectively (Table 2).

Monochloroacetic acid

With this acid of medium strength, all the spectra at room temperature show only one peak whatever the molar ratio used (Fig. 3a, b, c). At 233 K, one broad peak is present for molar ratios of 1:0.5, 1:1, and 1:2 (Fig. 3d, e, f). Only at molar ratios of 1:5 and 1:10 (Tables 2 and 3) is there a second peak present (Fig. 4c, d). However, the behavior of MCA as judged by the peak's chemical shifts and shapes in Fig. 3 is rather similar to that obtained with TCA (compare Figs. 2a, b and 3a, b), so that MCA seems to act much like TCA except for ratios of 1:2 (compare Figs. 2c and 3c). This difference can be explained by the fact that because MCA is a weaker acid, complexes B and C must have closer free energies so that B and C are rapidly equilibrating (faster than the timescale of NMR). Also, since the SB is now only 40% protonated, structure A is expected to play a more important role. With MCA then, the results can be explained as with TCA, that is, in terms of $A \rightleftharpoons B \rightleftharpoons C$ but where A and B are more populous.

Another fact must be pointed out. When the temperature is lowered to 233 K, the chemical shift of the N--H--O proton varies in a different way depending on the acids used. For

example, with TCA and a molar ratio 1:1, the chemical shift was seen to decrease from 293 to 233 K; with MCA, the contrary is observed, but the values of the chemical shift for the two acids are similar (16–17 ppm). According to Rospenk and Sobczyk (26), these results could suggest that, in the system of SB and TCA, the proton transfer form (B) prevails, while in the system of SB and MCA, the hydrogen-bonding complex (A) is preponderant and, in complex A, the lowering of the temperature enhances the strength of the hydrogen bond, affording an increase of the chemical shift.

Propionic acid

PRO is a very weak acid and data from Table 1 indicate that **2** is only 10% protonated. Data from Tables 2 and 3 show that only one peak is present whatever the molar ratios or temperatures used (Fig. 5a–f). When the temperature is decreased, the chemical shift of H_{AB} increases, similar to the system SB + MCA. This again characterizes the usual behavior of the protons involved in the hydrogen-bonding complexes. Furthermore, the chemical shifts are quite different from those of the other acids: they resemble more the chemical shifts of H_d than anything else. These facts can be explained by now proposing that the free SB and acid are in fast equilibrium with A and B as in the first part of Scheme 1. With a large excess of acid, structure C is probably present but, as with MCA, it must be in rapid equilibrium with B. Since PRO is such a weak acid, C is probably in very low concentration.

Finally, all the results and discussion already presented used data obtained with compound **2**. For imines **1** and **3**, the NMR spectra closely resemble those shown for **2** except that the chemical shifts are somewhat different. Tables 3 and 4 present these results. The chemical shift changes can be attributed to the differences in the branching of the molecules. In point of fact, both **1** and **3** served to double-check our results.

Conclusion

This study demonstrates that two or more carboxylic acid molecules can act simultaneously and that, in consequence, the equilibrium that exists between N--H-O $\rightleftharpoons$ N^+-H---$^-$O is shifted to the right. This means that proton transfer is induced by the cooperative presence of several molecules of acid. Of course, our system is somewhat remote from being a proper model of rhodopsins or bacteriorhodopsins since our SB are not conjugated and the acids are not part of a protein. Notwithstanding these points, our study still indicates that aspartic or glutamic acid, in a nonpolar environment, could not protonate a SB completely without some additional stabilizing factors. This study does indicate that one of these factors could be the presence of several molecules of acid acting simultaneously on the SB, thereby causing a proton transfer.

Acknowledgements

The authors wish to thank Professor C. Sandorfy of the Université de Montréal for very helpful discussions. The NMR spectra were obtained at the Centre régional de RMN de haut champ of the Université de Montréal, whose help we acknowledge here. This study was made possible by grants received from the National Research Council (AO-943) and the Fonds pour la formation de chercheurs et l'aide à la recherche (FCAR) of Québec.

1. W. Stoeckenius, R. H. Lozier, and R. A. Bogomolni. Biochem. Biophys. Acta, **505**, 215 (1979).
2. M. Ottolenghi. Adv. Photochem. **12**, 97 (1980).
3. R. R. Birge. Ann. Rev. Biophys. Bioeng. **10**, 315 (1981).
4. C. Sandorfy and D. Vocelle. Can. J. Chem. **64**, 2251 (1986).
5. C. Sandorfy and D. Vocelle. *In* Molecules in physics, chemistry and biology. Vol. IV. *Edited by* M. Marioni. Kluwer Academic Publishers, Amsterdam. 1989. pp. 195–211.
6. G. Zundel and H. Merz. *In* Information and energy transduction in biological membranes. Alan R. Liss, New York. 1984. pp. 153–164.
7. H. Merz and G. Zundel. Biochem. Biophys. Res. Commun. **138**, 819 (1986).
8. C. N. Rafferty and H. Shichi. Photochem. Photobiol. **33**, 229 (1981).
9. P. Hildebrandt and M. Stockburger. Biochemistry, **23**, 5539 (1984).
10. N. A. A. Dencher and G. Buldt. *In* Molecular retinal protein. *Edited by* T. Hara. Yamada Science Foundation, Osaka, Japan. 1988. p. 109.
11. M. Arnaboldi, M. G. Motto, K. Tsujemoto, V. Balogh-Nair, and K. Nakaniski. J. Am. Chem. Soc. **101**, 7082 (1979).
12. T. P. Sakmar, R. R. Franke, and H. G. Khorana. Proc. Natl. Acad. Sci. U.S.A. **86**, 8309 (1989).
13. E. A. Zhukovsky and D. D. Oprian. Science, **246**, 928 (1989).
14. H. J. M. de Groot, G. S. Harbison, J. Herzfeld, and R. G. Griffin. Biochemistry, **28**, 3346 (1989).
15. L. S. Lussier, A. Dion, C. Sandorfy, H. Le-Thanh, and D. Vocelle. Photochem. Photobiol. **44**, 629 (1986).
16. B. Brzezinski and G. Zundel. Chem. Phys. Lett. **115**, 212 (1985).
17. B. Brzezinski and G. Zundel. J. Magn. Reson. **48**, 361 (1982).
18. B. Brzezinski and G. Zundel. J. Chem. Soc. Faraday Trans. 2, **79**, 1249 (1983).
19. V. Bohner and G. Zundel. J. Phys. Chem. **90**, 964 (1986).
20. B. Brzezinski, G. Zundel, and R. Kramer. Chem. Phys. Lett. **124**, 395 (1986).
21. P. Barczynski, Z. Dega-Szafran, and M. Szafran. J. Chem. Soc. Perkin Trans. 2, 765 (1985).
22. S. E. Odinokov, A. A. Maskovsky, V. P. Glazunov, A. V. Iogansen, and B. V. Rassodin. Spectrochim. Acta, **32A**, 13555 (1976).
23. Z. Dega-Szafran, E. Grech, M. Z. Naskret-Barciszewska, and M. Szafran. J. Chem. Soc. Perkin Trans. 2, 250 (1975).
24. Z. Dega-Szafran and E. Dulewicz. Org. Magn. Reson. **16**, 214 (1981).
25. E. Haslinzer and P. Wolschann. Monatsh. Chem. **111**, 563m (1981).
26. M. Rospenk and L. Sobczyk. Magn. Reson. Chem. **27**, 445 (1989).
27. M. Ilczyszyn, H. Ratajczak, and J. A. Ladd. Chem. Phys. Lett. **153**, 385 (1988).
28. M. Ilczyszyn, H. Ratajczak, and J. A. Ladd. J. Mol. Struct. **198**, 499 (1989).
29. A. I. Kulbida and W. M. Schreiber. Dokl. Akad. Nauk SSSR, **250**, 889 (1980).
30. P. Huyskens and Th. Zeegers-Huyskens. J. Chem. Phys. **61**, 81 (1964).
31. D. Cossette and D. Vocelle. Can. J. Chem. **65**, 1576 (1987).
32. D. Cossette and D. Vocelle. Can. J. Chem. **65**, 661 (1987).
33. L. Streyer. *In* Biochemistry. 2nd ed. W. H. Freeman, San Francisco. 1981. pp. 163–165.
34. G. M. Barrow. J. Am. Chem. Soc. **78**, 5802 (1956).
35. G. S. Denisov and N. S. Golubev. J. Mol. Struct. **75**, 311 (1981).

Can. J. Chem. Downloaded from www.nrcresearchpress.com by 91.121.58.235 on 09/07/12
For personal use only.

Synthesis of 14-hydroxy steroids. Total synthesis of methyl 14β-hydroxy-1,7,17-trioxo-5β,8-androstene-10β-oate and related compounds

RÉJEAN RUEL[1] AND PIERRE DESLONGCHAMPS[2]

Laboratoire de synthèse organique, Département de chimie, Faculté des sciences, Université de Sherbrooke, Sherbrooke (Québec), Canada J1K 2R1

Received April 24, 1990

RÉJEAN RUEL and PIERRE DESLONGCHAMPS. Can. J. Chem. **68**, 1917 (1990).

The total synthesis of the title compound **22** and methyl 14α-hydroxy-5β,13α,8-androstene-1,7,17-trioxo-10β-oate **21** isomer is reported. We also describe the 1,6-Michael addition of 2-methyl-1,3-cyclopentanedione on dienone **14** and the protic ammonium salt catalyzed intramolecular Michael addition of cyclic β-ketoester on the conjugated acetylenic ketone **13**.

Key words: cardenolides, steroid synthesis, aldol, Michael addition.

RÉJEAN RUEL et PIERRE DESLONGCHAMPS. Can. J. Chem. **68**, 1917 (1990).

On rapporte la synthèse totale des isomères 13α,14α **21** et 13β,14β **22** du 14-hydroxy-5β,8-androstene-1,7,17-trioxo-10β-oate de méthyle. Nous décrivons l'addition de Michaël-1,6 de la 2-méthyl cyclopentane-1,3-dione sur la diènone **14** de même que l'addition de Michäel intramoléculaire du β-cétoester cyclique sur la cétone acétylénique conjuguée **13**, cette dernière addition étant catalysée par un sel d'ammonium protique.

Mots clés : cardénolides, synthèse des stéroïdes, aldol, addition de Michaël.

Introduction

We have previously reported the synthesis of 14α-hydroxy steroid **1** (Scheme 1) using a new stereocontrolled anionic polycyclization method (1). Base-catalyzed aldol condensation involving the cesium enolate **3** led to bis-β-ketoester **2**, which was transformed to steroid **1** upon selective decarboxylation of the *tert*-butyl ester (PTSA, C_6H_6, 80°C). A single-crystal X-ray analysis revealed that the 14-hydroxy substituent in steroid **1** had an α configuration. This configuration was, however, opposite to the 14β-hydroxy substituent normally found in cardioactive steroids (2).

It then came to our attention that in Valenta's modified Torgov sequence (3) the closure of ring C effected by base-catalyzed aldol condensation on dienone **4** led to the 14α-hydroxy steroid **5**. On the other hand, when the aldol condensation involved the anion formed from the trienone system in **6** bearing a C9–C11 (steroid numbering) olefin, the 14β-hydroxy steroid **7** was the only product formed. Based on these results, we expected the preferential formation of a 14β-hydroxy steroid from the aldol condensation that would involve an enolate related to **3** but bearing a conjugated double bond between carbons C9 and C11. This account describes the synthesis of this aldol precursor as well as the results observed during the aldol condensation.

Results and discussion

The synthesis of *cis*-bicyclic dienone **14** is depicted in Scheme 2. The β-ketoester **8** was first obtained by treatment of 2-carbomethoxy-2-cyclohexenone (4) with allyltrimethylsilane and titanium tetrachloride (5). The dimethyl ketal **9** was then formed by treatment of **8** with methanol containing *p*-toluenesulfonic acid and methyl orthoformate. Subsequent ozonolysis led to the aldehyde **10** and, like its olefinic precursor **9**, this aldehyde **10** existed as a 2:1 *trans/cis* mixture of isomers that was used without separation. These isomers could be separated and were in fact isolated as pure compounds for the purpose of characterization (see Experimental). The acetylide formed from *n*-butyllithium (THF, −78°C) and the *O*-tosyl derivative of commercially available 3-butyn-1-ol was then added to

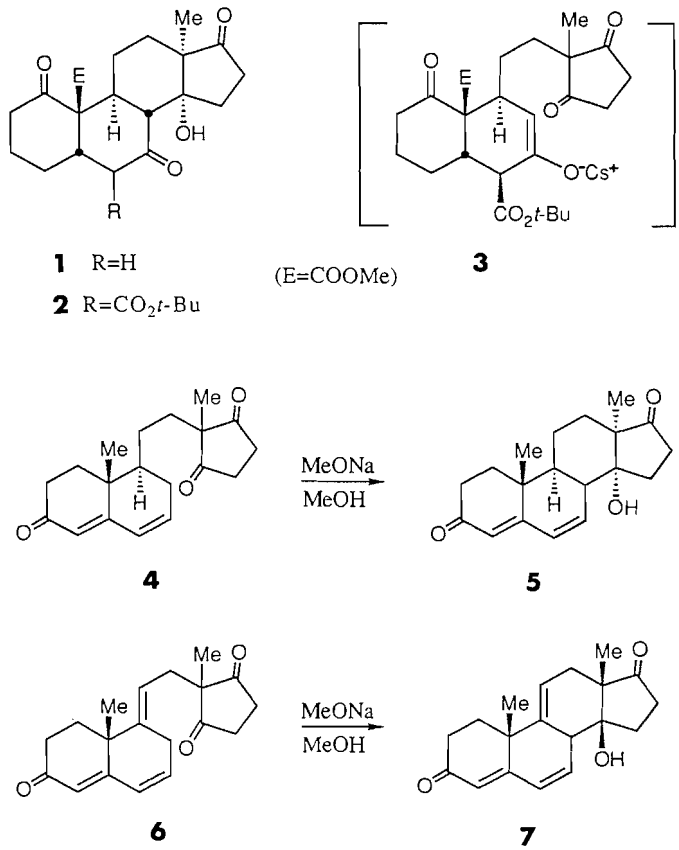

SCHEME 1

aldehyde **10** and the resulting propargylic alcohol **11** was oxidized with Jones reagent (5 min, 0°C, Me_2CO) to the ynone **12**. It should be pointed out here that in these conditions the dimethyl ketal protecting group was not hydrolyzed. Transacetalization of dimethyl ketal **12** (12 h, 23°C, Me_2CO, PTSA) then yielded β-ketoester **13**.

Previous reports from this laboratory described in a systematic study the intramolecular Michael addition of cyclic β-ketoesters on conjugated acetylenic (6) and olefinic (7) ketones. Cesium carbonate was the base used for these stereocontrolled

[1]FCAR predoctoral fellow, 1988–1990.

[2]Author to whom correspondence may be addressed.

Can. J. Chem. Downloaded from www.nrcresearchpress.com by 91.121.58.235 on 09/07/12
For personal use only.

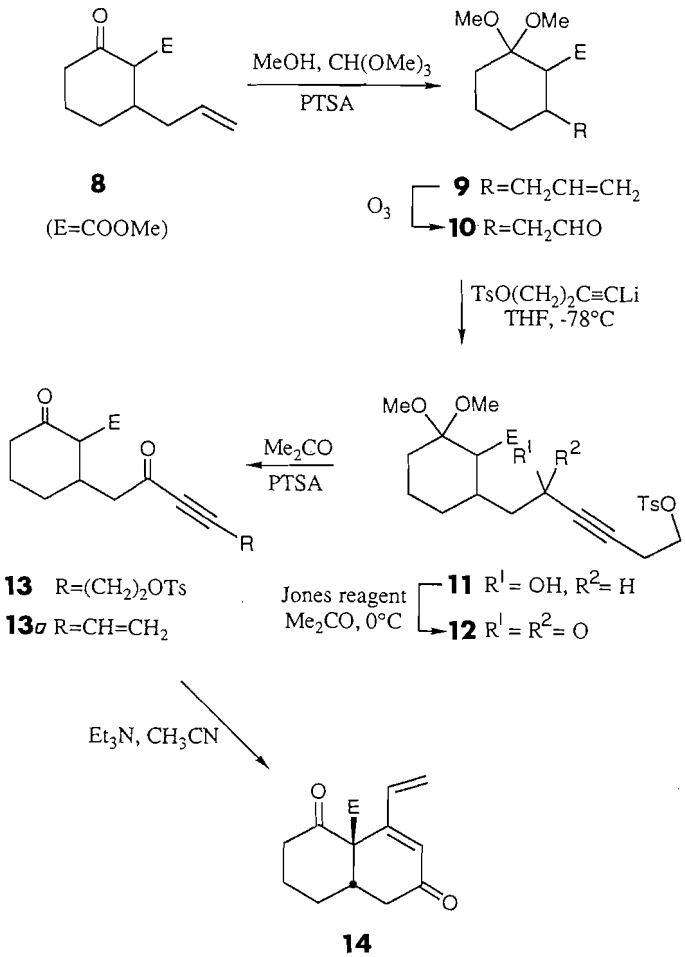

SCHEME 2

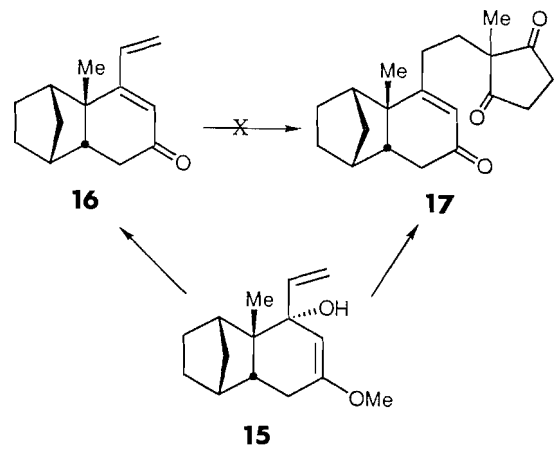

SCHEME 3

processes, which yielded specifically *cis*-decalin products. Using the conditions described (6, 7), we were, however, unable to achieve the Michael addition on acetylenic ketone **13** and obtained mainly decomposition products. This problem was solved when we found complementary experimental conditions very effective for the desired intramolecular Michael addition. When triethylamine (3 equiv.) was indeed added to a solution of β-ketoester **13** in acetonitrile, the *cis*-decalin dienone **14** (74%) was obtained after completion of the reaction. The first intermediate formed in the reaction was the elimination product **13***a*. This β-ketoester **13***a* was in fact spontaneously produced in the reaction mixture and transformed, after 3 h in acetonitrile at room temperature, to the Michael addition product **14**. If, however, acetonitrile was replaced by the less polar solvent methylene chloride (8), only the elimination product **13***a* was obtained from tosylate **13** after the same period of time. This elimination process generated a triethylammonium salt that catalyzed the intramolecular Michael addition, as the following results clearly indicate. When the elimination product **13***a* was submitted to the reaction conditions (Et_3N, CH_3CN) but without any protic ammonium salt, the Michael adduct **14** was formed, but with a modest 50% yield, while completion of the reaction required 2 days. On the other hand, when triethylammonium hydrochloride (1 equiv.) was added to a solution of **13***a* and triethylamine (2 equiv.) in acetonitrile, the formation of the Michael adduct **14** was completed after only 3 h and proceeded with better yield (74%). The synthesis of dienone **14** thus required seven steps and the overall yield was 30%.

Having the dienone **14** in our hands, only the 1,6-Michael addition of 2-methyl-1,3-cyclopentanedione (for a related 1,8-Michael addition, see ref. 9) remained to be done in order to get the requisite aldol condensation precursor of the steroid. Dienone **14** resembles Yates' bridged-ring dienone **16** (Scheme 3), which arose upon attempted purification on silica gel of allylic alcohol **15** (10). Yates *et al.* also reported the synthesis of enone **17**, through their modified Torgov sequence, from allylic alcohol **15**, but attempts to synthesize enone **17** from the Michael addition of 2-methyl-1,3-cyclopentanedione on dienone **16** were uniformly unsuccessful (10). Bearing this in mind, we were pleased to find that the Michael addition of 2-methyl-1,3-cyclopentanedione on our dienone **14** (in CH_3CN) took place cleanly and efficiently (80% yield) to give enone **18** (Scheme 4) when triethylamine was used as the base. It should be pointed out here that since the experimental conditions used (Et_3N, CH_3CN) for this Michael addition are essentially the same as required for the previously described intramolecular Michael addition (**13** → **14**), enone **18** could be synthesized in a "one pot" procedure from ynone tosylate **13** in 65% yield. We have investigated here again whether a protic ammonium salt would enhance the efficiency of this Michael addition, that is, if the reaction **14** → **18** would be also catalyzed by the protic salt as was the case for intramolecular Michael reaction **13***a* → **14**. For the 1,6-Michael addition leading to enone **18**, however, we found no appreciable effect when a protic ammonium salt ($Et_3NH^+Cl^-$) was added to the reaction mixture. The absence of catalysis by the protic ammonium salt may not be surprising if one considers the inherent acidity of the nucleophile 2-methyl-1,3-cyclopentanedione ($pK_a \sim 9$), which could itself catalyze the Michael reaction.

Hydrogenation of enone **18** gave the dihydro compound **19** where hydrogen has approached the less-hindered β face of the cyclohexenone ring. Aldol condensation (*t*-BuOK, *t*-BuOH–THF) of tetraketone **19** then gave 14β-hydroxy steroid **20**. The structure of **20** was predicted, based on related work reported in Professor Yates' elegant synthesis of 1,4-methano bridged steroids (10), and was later confirmed by a single crystal X-ray analysis (11). One should note that steroid **20** has an "unnatural" *syn* relationship between the carbomethoxy group (at C-10) and the C-9 hydrogen atom. Base-catalyzed aldol condensation of enone **18** then led to interesting results. When enone **18** was treated with cesium carbonate in refluxing acetonitrile for 48 h, a 3:2 mixture of 14α- and 14β-hydroxy steroids **21** and **22** was obtained (54% yield). Structures **21** and **22** were also confirmed by single crystal X-ray analysis.[3] No trace of the $\Delta^{9(11)}$-7-keto

[3]A. G. Michel, R. Ruel, and M. Drouin. Unpublished results.

Can. J. Chem. Downloaded from www.nrcresearchpress.com by 91.121.58.235 on 09/07/12
For personal use only.

Can. J. Chem. Downloaded from www.nrcresearchpress.com by 91.121.58.235 on 09/07/12
For personal use only.

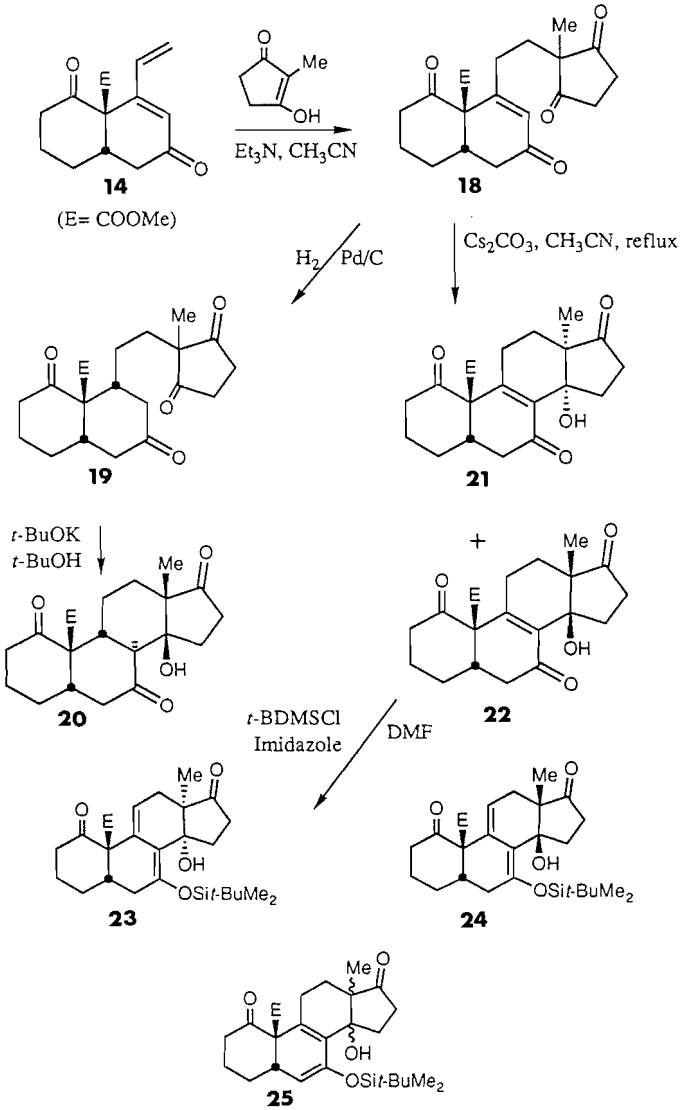

SCHEME 4

steroids corresponding to steroids **21** and **22** could be isolated since, after the aldol condensation, the C9—C11 double bond must rapidly isomerize to the more stable C9—C8 conjugated double bond in **21** (or **22**). This isomerization obviously makes this aldol condensation irreversible.

The 14-hydroxy steroids **21** and **22** could not, however, be separated using low or medium pressure flash chromatography techniques. We could, however, later obtain pure 14-hydroxy steroids **21** and **22** since other quite interesting and unexpected results emerged upon attempted *tert*-butyldimethylsilylation of the tertiary alcohol in **21** or **22**. For example, when *tert*-butyldimethylsilyl chloride was added to a dimethylformamide solution of the 3:2 mixture of steroids **21** and **22** and imidazole, a 19:13:1 mixture of silyl enol ethers **23**, **24**, and **25** was isolated. Whether these silyl enol ethers were formed via an internal S_N2 migration of the "normally expected" silyl ether is not known but none of that silyl ether could be isolated. Technically, this reaction (**21**/**22** → **23**/**24**/**25**) could never be driven to completion but proceeded nevertheless in 67% yield (based upon recovered starting material). We were also pleased to find that 14-hydroxy silyl enol ethers **23** and **24** were easy to separate using flash chromatography techniques. Once the isomers **23** and **24** were separated, regeneration of enone steroids **21** and **22** was the only thing that remained to be done in order to obtain pure steroids. The use of tetrabutylammonium fluoride in THF at −78°C, even for a reaction time as low as 30 s, uniformly led to extensive decomposition. The reasons for this behavior are not quite understood. Among other things, unavoidable traces of hydroxide ions in the ammonium fluoride reagent may, for example, induce retro-Claisen type opening of A-ring β-ketoester. If that process operates, the generated ester enolate would be conjugated with the $\Delta^{8(9)}$-7-keto system of enones **21** and **22** and a complex cascade of reactions could follow. Fortunately, the use of cesium fluoride proved successful. Thus, when silyl enol ether **23** or **24** was treated with cesium fluoride in acetonitrile, the pure hydroxy steroid **21** or **22** was obtained in good yield (73%).

In summary, the enolate derived from the aldol condensation precursor **18** led, although with low selectivity, to the expected 14β-hydroxy steroid **22**. We also found new conditions (Et_3N, $Et_3N^+HCl^-$) for the intramolecular Michael addition of cyclic β-ketoester on acetylenic ketone. Furthermore, our work describes the successful 1,6-Michael addition of 2-methyl-1,3-cyclopentanedione to bicyclic dienone **14** bearing a 9-vinyl-$\Delta^{8(9)}$-7-keto system (steroid numbering).

Experimental

All reactions were carried out under an argon atmosphere unless otherwise noted. Melting points are uncorrected. R_f values were determined by using 5 × 20 cm^2 plates and an equilibrated solvent chamber. Chromatographic separations were made using Merck Kieselgel 60 (230–400 mesh ASTM). The infrared (ir) spectra were taken on a Perkin–Elmer 681 spectrophotometer. The ultraviolet (uv) spectra were registered on a Varian Tecktron 635 spectrophotometer. Mass spectral assays (ms, *m/e*) and peak matching were obtained using a VG Micromass ZAB-1F spectrometer. Proton nmr and carbon nmr spectra were recorded on a Bruker WM-250 instrument. Chemical shifts are reported in δ values relative to chloroform as internal standard. Abbreviations used are m: multiplet, s: singlet, d: doublet, t: triplet, q: quartet, dd: double doublets.

Allyl β-ketoester 8

To a stirred solution of 2-carbomethoxy-2-cyclohexenone (4.13 g, 26.8 mmol) in methylene chloride (55 mL) at −78°C is added titanium tetrachloride (2.8 mL, 28.1 mmol) followed by allyltrimethylsilane (5.8 mL, 37.5 mmol). After stirring for 20 min, aqueous sodium carbonate (20%) is added to the mixture. The aqueous layer is extracted with methylene chloride (3 × 50 mL) and the combined organic layers are washed with brine, dried ($MgSO_4$), filtered, and evaporated to yield 5.3 g of an oil. Flash chromatography of the residue (ethyl acetate/hexane,1:3) yields 4.7 g (90%) of **8** as a colorless oil; R_f 0.26–0.43 (ethyl acetate/hexane,1:4); ir (neat, ν cm^{-1}): 3070, 2935, 2860 (CH), 1745 (C=O ester), 1710 (C=O, ketone) cm^{-1}; ^1H nmr (250 MHz, $CDCl_3$) δ ppm: 5.80–5.68 (1H, m, CH_2=C*H*-), 5.15–4.90 (2H, m, CH_2=CH-), 3.76 (3H, s, CO_2CH_3), 3.16 (1H, d, J = 11.0 Hz, -CO-C*H*-CO_2CH_3), 2.60–1.40 (9H, m, -$(CH_2)_3$-C*H*-CH_2-). Enol form (characteristic signals): 12.36 (>1H, s, enolic H), 3.75 (>3H, s, CO_2CH_3).

Allyl dimethyl ketal 9

To a stirred solution of ketoester **8** (5.1 g, 26.0 mmol) and trimethyl orthoformate (3.7 mL, 33.7 mmol) in methanol (50 mL) at 23°C is added *p*-toluenesulfonic acid (247 mg, 1.3 mmol). After 12 h at 23°C, saturated sodium bicarbonate is added and the mixture is extracted with methylene chloride. The separated aqueous layer is extracted with methylene chloride (3 × 50 mL) and the combined organic layers are washed with brine, dried ($MgSO_4$), filtered, and evaporated to yield 6.3 g of an oil. Flash chromatography of the residue (ethyl acetate/hexane,1:4) yields 5.25 g (84%) of a 2:1 *trans/cis* mixture of dimethyl ketal **9**; R_f 0.36 (**9**-*cis*) and 0.28 (**9**-*trans*) (ethyl acetate/hexane,1:4); ir (neat, ν cm^{-1}): 3070, 2940 (CH), 1740 (C=O ester); ^1H nmr (250 MHz, $CDCl_3$) δ ppm (**9**-*cis*): 5.83–5.72 (1H, m, CH_2=C*H*-), 5.03–4.96 (2H, m, CH_2=CH-), 3.67 (3H, s, -CH_2CH_3),

Can. J. Chem. Downloaded from www.nrcresearchpress.com by 91.121.58.235 on 09/07/12
For personal use only.

3.20, 3.15 (6H, 2s, 2 × -OCH_3), 3.04 (1H, dd, J = 4.4, 1.8 Hz, -CH-CO_2CH_3), 2.03–1.34 (9H, m, -(CH_2)$_3$-CH-CH_2-); (**9**-*trans*): 5.78–5.64 (1H, m, CH_2=CH-), 5.02–4.95 (2H, m, CH_2=CH-), 3.68 (3H, s, -CO_2CH_3), 3.21 (6H, s, 2 × -OCH_3), 2.62 (1H, d, J = 6.7 Hz, -CH-CO_2CH_3), 2.21–1.12 (9H, m, -(CH_2)$_3$-CH-CH_2-); ms *m/e*: 242 (M^+), 227 ($M^+ - CH_3$), 211 ($M^+ - OCH_3$). Exact mass calcd. for $C_{13}H_{22}O_4$ (M^+): 242.1518: found 242.1526.

Aldhyde ***10***

Ozone is bubbled into a cold (−78°C) solution of olefin **9** (5.0 g, 20.7 mmol) in methylene chloride (200 mL) until a blue color persists. Argon is then passed through the solution to lower the concentration of ozone, and triphenylphosphine (7.0 g, 26.9 mmol) is added at −78°C. The resulting mixture is stirred for 2 h at room temperature. Concentration under reduced pressure yields the aldehyde **10**, which can be used without purification in the next step. Pure material may be obtained by means of flash chromatography (ethyl acetate/hexane, 7:13), which yields 4.5 g (89%) of aldehyde **10**; R_f 0.13 (**10**-*cis*) and 0.10 (**10**-*trans*) (ethyl acetate/hexane,1:4); (**10**-*cis*): white needles; mp 124–126°C (heptane); (**10**-*trans*): oil; ir (CH_2Cl_2, ν cm^{-1}): 2940, 2830, 2720 (CH), 1740 (C=O ester), 1720 (C=O aldehyde); ^{1}H nmr (250 MHz, $CDCl_3$) δ ppm: (**3**-*cis*): 9.74 (1H, t, J = 1.4 Hz, -CHO), 3.67 (3H, s, -CO_2CH_3), 3.19 (6H, s, 2 × -OCH_3), 3.07 (1H, dd, J = 4.3, 1.7 Hz, -CH-CO_2CH_3), 2.42–1.39 (9H, m, -(CH_2)$_3$-CH-CH_2-), (**3**-*trans*): 9.71 (1H, t, J = 1.5 Hz, -CHO), 3.69 (3H, s, -CO_2CH_3), 3.20–3.19 (6H, 2s, 2 × -OCH_3), 2.70 (1H, d, J = 6.5 Hz, -CH-CO_2CH_3), 2.63–1.15 (9H, m, -(CH_2)$_3$-CH-CH_2-); ms, *m/e*: 229 ($M^+ - CH_3$), 213 ($M^+ - OCH_3$), 201 ($M^+ - CH_2CHO$). Exact mass calcd. for $C_{11}H_{17}O_5$ ($M^+ - CH_3$): 229.1076; found: 229.1074.

Propargylic alcohol ***11***

To a stirred solution of the tosyl derivative of 3-butyn-1-ol (2.0 g, 8.9 mmol) in THF (20 mL) at −78°C is added dropwise a solution of *n*-butyllithium (1.6 M in hexane, 5.1 mL, 8.2 mmol). After stirring for 45 min at −78°C, the solution is transferred, via cannula, to a solution of aldehyde **3** (1.5 g, 6.2 mmol) in THF (35 mL) at − 78°C. The mixture is stirred at −78°C for 1.5 h and quenched with saturated ammonium chloride (50 mL). The aqueous layer is extracted with (1:1) ether/ethyl acetate (5 × 60 mL) and the combined organic layers are washed with brine, dried ($MgSO_4$), filtered, and evaporated to yield crude propargylic alcohol **11** as an oil. Flash chromatography of the residue (ethyl acetate/hexane,3:2) yields 2.1 g (72%) of alcohol **11**; R_f 0.19 (**11**-*cis*) and 0.15 (**11**-*trans*) (ethyl acetate/hexanes,1:1); ir (neat, ν cm^{-1}): 3460 (OH), 2940 (CH), 1735 (C=O ester); ^{1}H nmr (250 MHz, $CDCl_3$) δ ppm: (**11**-*cis*) (diastereomeric mixture): 7.80, 7.36* (4H, 2m, -CH arom.), 4.42* (1H, m, -CH-OH), 4.08* (2H, t, J = 7.0 Hz, -CH_2-OTs), 3.68, 3.66 (3H, 2s, -CO_2CH_3), 3.19, 3.18, 3.15, 3.13 (6H, 4s, 2 × -OCH_3), 3.06, 2.99 (1H, 2dd, J = 5.0, 1.7 Hz, -CH-CO_2CH_3), 2.58, 2.57 (2H, 2t, J = 7.0 Hz, -CH_2CH_2OTs), 2.45* (3H, s, Ar-CH_3), 2.03–1.380* (9H, m, -(CH_2)$_3$-CH-CH_2-); (**11**-*trans*) (diastereomeric mixture): 7.80, 7.36* (4H, 2m, -CH arom.), 4.36* (1H, m, -CH-OH), 4.10, 4.08 (2H, 2t, J = 7.0 Hz, -CH_2-OTs), 3.68* (3H, s, -CO_2CH_3), 3.20, 3.19* (6H, 2s, 2 × -OCH_3), 2.79, 2.71 (1H, 2d, J = 5.8 Hz, -CH-CO_2CH_3), 2.62–2.54* (2H, m, -CH_2-CH_2OTs), 2.45* (3H, s, Ar-CH_3), 2.21–1.17* (9H, m, -(CH_2)$_3$-CH-CH_2-), (*same signal for both diastereomers); ms, *m/e*: 436 ($M^+ - CH_3OH$), 418 ($M^+ - CH_3OH$-H_2O). Exact mass calcd. for $C_{22}H_{28}SO_7$ ($M^+ - CH_3OH$): 436.1556; found: 436.1545.

Ynone dimethylketal ***12***

To a stirred solution of propargylic alcohol **11** (1.0 g, 2.1 mmol) in acetone (15 mL) at 0°C is added dropwise a solution of Jones reagent until the red color persists. After 5 min at 0°C, isopropanol is added until a green mixture is obtained. The mixture is diluted with water and extracted with methylene chloride (4 × 40 mL). The combined organic layers are washed with brine, dried ($MgSO_4$), filtered, and evaporated to yield 965 mg (97%) of an oil. Flash chromatography of the residue (ethyl acetate/hexanes,1:1) yields 926 mg (93%) of a colorless oil; R_f 0.31 (**12**-*cis*) and 0.27 (**12**-*trans*) (ethyl acetate/hexane,1:1); ir (neat, ν cm^{-1}): 2940 (CH), 2210 (C≡C), 1735 (C=O ester), 1657 (C=O ketone); ^{1}H nmr (250 MHz, $CDCl_3$) δ ppm: (**12**-*cis*): 7.80, 7.37 (4H, 2m, -CH arom.), 4.12 (2H, t, J = 6.8 Hz, -CH_2-OTs), 3.68 (3H, s, -CO_2CH_3), 3.20, 3.18 (6H, 2s, 2 × -OCH_3), 3.06 (1H, m, -CH-CO_2CH_3), 2.74 (2H, t, J = 6.8 Hz, -CH_2-CH_2-OTs), 2.46 (3H, s, Ar-CH_3), 2.39 (2H, m, -CH-CH_2-CO-C≡C-), 2.03–1.30 (7H, m, -CH_2-CH_2-CH_2-CH-); (**12**-*trans*): 7.80, 7.37 (4H, 2m, -CH arom.), 4.06 (2H, t, J = 6.8 Hz, -CH_2-OTs), 3.67 (3H, s, -CO_2CH_3), 3.19, 3.18 (6H, 2s, 2 × OCH_3), 2.69 (2H, t, J = 6.8 Hz, -CH_2-CH_2-OTs), 2.68 (1H, m, -CH-CO_2CH_3), 2.46 (3H, s, Ar-CH_3), 2.33 (2H, m, -CH-CH_2-CO-C≡C-), 2.20–1.18 (7H, m, -CH_2-CH_2-CH_2-CH-); ms, *m/e*: 465 (M^+ − H), 438 (M^+ − CO), 434 ($M^+ - CH_3OH$).

Ynone β*-ketoester* ***13***

p-Toluenesulfonic acid (39 mg, 0.2 mmol) is added at 23°C to a stirred solution of ynone dimethylketal **12** (908 mg, 1.95 mmol) in acetone (20 mL). After 36 h at 23°C, water (20 mL) is added and the mixture is extracted with methylene chloride (5 × 25 mL). The combined organic layers are washed with salted sodium bicarbonate and brine, dried ($MgSO_4$), filtered, and evaporated to yield 820 mg of an oil. Flash chromatography of the residue (ethyl acetate/hexane,1:1) yields 736 mg (90%) of a colorless oil; R_f 0.26–0.32 (ethyl acetate/hexane,1:1); ir (neat, ν cm^{-1}): 2940 (CH), 2125 (C≡C), 1745 (C=O ester), 1715 (C=O ketone), 1670 (C=O ynone); ^{1}H nmr (250 MHz, $CDCl_3$) δ ppm: 7.80, 7.36 (4H, 2m, -CH arom.), 4.14 (2H, t, J = 6.8 Hz, -CH_2-OTs), 3.75 (3H, s, -CO_2CH_3), 3.26 (1H, d, J = 10.8 Hz, -CO-CH-CO_2CH_3), 2.76 (2H, t, J = 6.8 Hz, -CH_2-CH_2OTs), 2.60 (2H, m, -CH_2CO), 2.45 (3H, s, Ar-CH_3), 2.27 (2H, m, -CH_2-CO-C≡C-), 2.02 (1H, m, -CH_2-CH-CH_2-), 1.72–1.42 (4H, m, -CH_2-CH_2-CH-). Enol form (characteristic signals): 12.4 (>1H, s, enolic H), 3.76 (>3H, s, -CO_2CH_3), 3.22 (1H, m, -(OH)C=C(E)-CH-CH_2-CO-); ms, *m/e*: 420 (M^+), 402 ($M^+ - H_2O$), 389 ($M^+ - OCH_3$). Exact mass calcd. for $C_{21}H_4SO_7$ (M^+): 420.1243; found: 420.1238. (^{1}H nmr (250 MHz, $CDCl_3$) of the corresponding enol acetate derivative, δ ppm: 7.78, 7.35 (4H, 2m, -CH arom.), 4.13 (2H, t, J = 6.9 Hz, -CH_2-OTs), 3.69 (3H, s, -CO_2CH_3), 3.35 (1H, m, -(OAc)C=C(E)-CH-CH_2-CO-), 2.74 (2H, t, J = 6.9 Hz, -CH_2-CH_2OTs), 2.73 (1H, dd, J = 16.8, 2.9 Hz, -HCH-CO-C≡C-), 2.55 (1H, dd, J = 16.8, 9.9 Hz, -HCH-CO-C≡C-), 2.45 (3H, s, Ar-CH_3), 2.21 (2H, m, -CH_2-(OAc)C=C-), 2.17 (3H, s, -C-CH_3), 1.75–1.57 (4H, m, -CH_2-CH_2-).)

Dienone ***14*** *(and conjugated ynone* **13**a)

To a stirred solution of ynone-tosylate **13** (2.1 g, 5.0 mmol) in acetonitrile (50 mL) at 23°C is added triethylamine (2.1 mL, 15.0 mmol). (Spontaneous elimination of tosylate then leads to conjugated ynone **13***a*.) After stirring for 3 h at 23°C, the mixture is evaporated and purified by flash chromatography (ethyl acetate/hexanes,1:1) and yields 917 mg (74%) of **14** as a viscous liquid; R_f 0.31 (ethyl acetate/hexane,1:1); ir (CH_2Cl_2, ν cm^{-1}): 2960 (CH), 1740 (C=O ester), 1715 (C=O ketone), 1675 (C=O enone); ^{1}H nmr (250 MHz, $CDCl_3$) δ ppm: 6.30 (1H, s, -C=CH-CO), 6.28 (1H, ddd, J = 17.7, 11.2, 0.8 Hz, -HC=CH_2), 5.72 (1H, dd, J = 17.7, 0.8 Hz, -CH=CH-H), 5.43 (1H, dd, J = 11.2, 0.8 Hz, -CH=CH-H), 3.81 (3H, s, -CO_2CH_3), 3.21 (1H, m, -CH_2-CH-CH_2-), 2.69–1.70 (8H, m, -CH_2-CH_2-CH_2-CH-CH_2); ^{13}C nmr (62.9 MHz, $CDCl_3$) δ ppm: 206.4 (s, C=O ketone), 197.0 (s, C=O enone), 170.0 (s, C=O ester), 151.6 (s, CH_2=CH-C=CH-CO), 134.7 (d, -C=CH-CO), 126.0 (d, -CH=CH_2), 121.6 (t, -CH=CH_2), 66.1 (s, C quat.), 53.0 (q, -COCH_3), 42.2 (d, -CH_2-CH-CH_2-), 40.2 (t, CH_2), 40.0 (t, CH_2), 27.1 (t, CH_2), 24.5 (t, CH_2); ms, *m/e*: 248 (M^+), 220 (M^+ − CO). Exact mass calcd. for $C_{14}H_{16}O_4$ (M^+): 248.1049; found: 248.1051. For **13***a*: ir (neat, ν cm^{-1}): 2950 (CH), 2120 (C≡C), 1745 (C=O ester), 1715 (C=O ketone), 1670 (C=O enone); ^{1}H nmr (250 MHz, $CDCl_3$) δ ppm: 5.88 (3H, m, CH olefin), 3.78 (3H, s, -CO_2CH_3), 3.30 (1H, d, J = 12.5 Hz, -CO-CH-CO_2CH_3), 2.84–1.56 (9H, m, -CH_2-CH_2-CH_2CH-CH_2-). Enol form (characteristic signals): 12.4 (>1H, s, enolic H), 3.77 (>3H, s, CO_2CH_3), 3.25 (>1H, m, (OH)C=C(E)-CH-).

Enone ***18***

Upon completion of the reaction **13** → **14** monitored by tlc, 2-methyl-1,3-cyclopentanedione (840 mg, 7.5 mmol) is added to the

Can. J. Chem. Downloaded from www.nrcresearchpress.com by 91.121.58.235 on 09/07/12
For personal use only.

reaction mixture at 23°C. The mixture temperature is raised to 40°C and stirred for 36 h. After evaporation and purification by flash chromatography (ethyl acetate/hexane,3:2), 1.17 g of enone **18** (65% from ynone **13**) is isolated as a white solid; mp 110–112°C (MeO*t*-Bu); R_f 0.13 (ethyl acetate/hexane,1:1); ir (CH_2Cl_2, ν cm^{-1}): 2930, 2870 (CH), 1740, 1730 (C=O ester and ketone), 1680 (C=O enone); ^1H nmr (250 MHz, $CDCl_3$) δ ppm: 6.04 (1H, s, -C=C*H*-CO-), 3.85 (3H, s, -CO_2CH_3), 3.16 (1H, m, -CH_2-C*H*-CH_2-), 2.89–2.64 (4H, m, OC-CH_2-CH_2-CO-), 2.39 (12H, m, 6 × -CH_2-), 1.13 (3H, s, -CH_3); ^{13}C nmr (62.9 MHz, $CDCl_3$) δ ppm: 215.4, 215.3 (2s, C=O cyclopentanedione), 205.8 (s, C=O ketone), 196.4 (s, C=O enone), 170.2 (s, C=O ester), 157.2 (s, -*C*=CH-CO-), 127.8 (d, -C=*C*H-CO-), 67.5 (s, -OC-*C*(CH_3)-CO-), 56.0 (s, -OC-*C*-CO_2CH_3), 53.1 (q, -CO_2CH_3), 41.5 (d, -CH_2-*C*H-CH_2), 40.2, 39.2, 34.9, 32.0, 28.4, 27.1, 23.2 (7t, 8 × -CH_2- methylenes in cyclopentanedione are equivalent), 19.4 (q, -CH_3); ms, *m/e*: 360 (M^+), 342 ($M^+ - H_2O$). Exact mass calcd. for $C_{20}H_{24}O_6$ (M^+): 360.1573; found: 360.1568.

*Tetraketone **19***

Under an atmosphere of hydrogen, a suspension of enone **18** (590 mg, 1.63 mmol) and 5% palladium on carbon (59 mg, 10% w/w) in methanol (30 mL) is vigorously stirred at 23°C for 3 h. The mixture is filtered on a Celite pad and evaporated. Flash chromatography of the residue (ethyl acetate/hexane,1:1) yields 348 mg (59%) of tetraketone **19** and 83 mg (14%) of 14β-hydroxy steroid **20**. Tetraketone **19**: mp 148–149°C (cyclohexane); R_f 0.16 (ethyl acetate/hexane,1:1); ir (CH_2Cl_2, ν cm^{-1}): 2960 (CH), 1725 (C=O); ^1H nmr (250 MHz, $CDCl_3$) δ ppm: 3.83 (3H, s, -CO_2CH_3), 2.90–1.08 (20H, m, 9 × -CH_2- + 2 × -C*H*-), 1.07 (3H, s, -CH_3); ^{13}C nmr (62.9 MHz, $CDCl_3$) δ ppm: 216.4, 216.0 (2s, C=O cyclopentanedione), 208.3, 207.4 (2s, C=O ketone), 172.6 (s, C=O ester), 64.0 (s, -OC-*C*(CH_3)-CO-), 56.2 (s, -OC-*C*-CO_2CH_3), 52.8 (q, -CO_2CH_3), 41.6 (d, -CH_2-*C*H-CH_2-), 43.7, 41.8, 40.8, 35.1, 33.8, 27.3, 26.0, 21.6 (8t, 9 × -CH_2- methylenes in cyclopentanedione are equivalent), 19.8 (q, -CH_3); ms, *m/e*: 362 (M^+), 344 ($M^+ - H_2O$), 330 ($M^+ - CH_3OH$). Exact mass calcd. for $C_{20}H_{26}O_6$ (M^+): 362.1729; found: 362.1727.

*14β-Hydroxy steroid **20***

To a stirred solution of tetraketone **19** (200 mg, 0.55 mmol) in a 1:1 mixture of tetrahydrofuran and *tert*-butanol (8 mL) is added potassium *tert*-butoxide until pH reaches 8–9. (Approximately 3 equivalents are required.) After 3 h at 23°C, saturated ammonium chloride solution is added and the mixture is extracted with methylene chloride (6 × 30 mL). The combined organic layers are washed with brine, dried ($MgSO_4$), filtered, and evaporated to yield 169 mg of an oil. Flash chromatography of the residue (ethyl acetate/hexane,1:1) yields 109 mg (55%) of 14β-hydroxy steroid **20**; mp 169–171°C (petroleum ether 60–110); R_f 0.25 (ethyl acetate/hexane,1:1); ir (CH_2Cl_2, ν cm^{-1}): 3500 (OH), 2940 (CH), 1740 (C=O ester), 1710, 1700 (C=O ketone) cm^{-1}; ^1H nmr (250 MHz, $CDCl_3$) δ ppm: 4.35 (1H, s, -O*H*), 3.80 (3H, s, -CO_2CH_3), 2.94 (1H, m, -CH_2-C*H*-CH_2-), 2.90 (1H, d, J = 12.2 Hz, -OC-C*H*-CH-), 2.88–1.77 (14H, m), 1.58–1.06 (3H, m), 0.99 (3H, s, -CH_3); ^{13}C nmr (62.9 MHz, $CDCl_3$) δ ppm: 217.7, 213.1, 207.7 (3s, C=O ketone), 172.2 (s, C=O ester), 77.4 (s, -HC-*C*(OH)-CH_2-), 64.1 (s, -OC-*C*-(CH_3)-C-OH), 53.8 (s, -OC-*C*-CO_2CH_3), 52.2 (q, -CO_2-CH_3), 52.6, 45.0, 44.4 (3d, 3 × -CH-), 43.3, 41.3, 34.6, 31.5, 28.3, 27.7, 23.8, 22.4 (8t, 8 × -CH_2-), 19.5 (q, -CH_3); ms, *m/e*: 362 (M^+), 344 ($M^+ - H_2O$). Exact mass calcd. for $C_{20}H_{26}O_6$ (M^+): 362.1729; found: 362.1727.

*14-Hydroxy enone steroids **21** and **22***

Cesium carbonate (63.2 mg, 0.2 mmol) is added to a solution of enone **18** (350 mg, 0.97 mmol) in acetonitrile (15 mL). The mixture is heated at reflux for 48 h and cooled down to 23°C before filtration on silica gel. Evaporation and flash chromatography of the residue yields 189 mg (54%) of a 3:2 mixture of 14-hydroxy steroids **21** and **22**; R_f 0.22 (ethyl acetate/hexane,1:1); uv (CH_3CN) λ_{max}: 246 nm (ε 6700); ir (CH_2Cl_2, ν cm^{-1}): 3500 (OH), 2950 (CH), 1740 (C=O ester), 1715 (C=O ketone), 1660 (C=O enone). For **21**: mp 151–153°C ($CHCl_3$–heptane); ^1H nmr (250 MHz, $CDCl_3$) δ ppm: 4.27 (1H, s, -O*H*), 3.80 (3H, s, -CO_2-CH_3), 3.12 (1H, m, -CH_2-C*H*-CH_2-), 2.69–1.47 (16H, m, 8 × -CH_2), 1.10 (3H, s, -CH_3). For **22**: mp 168–170°C (MeO*t*-Bu); ^1H nmr (250 MHz, $CDCl_3$) δ ppm: 4.39 (1H, s, O*H*), 3.85 (3H, s, -CO_2CH_3), 3.24 (1H, m, -CH_2-C*H*-CH_2-), 2.90–1.20 (16H, m, 8 × -CH_2), 1.05 (3H, s, -CH_3); ms, *m/e*: 360 (M^+), 342 ($M^+ - H_2O$). Exact mass calcd. for $C_{20}H_{24}O_6$ (M^+): 360.1573; found: 360.1568.

*14-Hydroxy silyl enol ether steroids **23, 24, 25***

To a solution of a 3:2 mixture of enones **21** and **22** (100 mg, 0.28 mmol) and imidazole (47 mg, 0.69 mmol) in freshly distilled dimethylformamide (300 μL) is added *tert*-butyldimethylsilylchloride (58 mg, 0.39 mmol). The mixture is stirred at 23°C for 52 h, quenched with saturated ammonium chloride, and diluted with water (5 mL). The mixture is extracted with 1:1 ether–hexane (5 × 10 mL). The combined organic layers are washed with brine, dried ($MgSO_4$), filtered, and evaporated to yield 107 mg of an oil. Flash chromatography of the residue (ethyl acetate/hexane,1:3) yields **23** (25.0 mg) and **24** (16.7 mg) (37% yield, 67% yield based on recovered starting material) as well as **25** (1.3 mg) and recovered starting material (52.4 mg). For **23**: R_f 0.22 (ethyl acetate/hexane,3:7); ^1H nmr (250 MHz, $CDCl_3$) δ ppm: 5.17 (1H, dd, J = 6.3, 2.5 Hz, -C=C*H*-CH_2-), 4.84 (1H, s, -O*H*), 3.73 (3H, s, -CO_2CH_3), 2.80 (1H, m, -CH_2-C*H*-CH_2-), 2.75–1.65 (14H, m, 7 × CH_2), 1.12 (3H, s, -CH_3), 0.97 (9H, s, -Si-C(CH_3)$_3$, 0.27, 0.20 (6H, 2s, 2 × Si-CH_3). For **24**: R_f 0.19 (ethyl acetate/hexanes,3:7); uv (CH_3CN) λ_{max}: 250 nm (ε 20 800); ir ($CHCl_3$, ν cm^{-1}): 3500 (OH), 2930, 2860 (CH), 1740 (C=O ester), 1705 (C=O ketone); ^1H nmr (250 MHz, $CDCl_3$) δ ppm: 5.18 (1H, dd, J = 6.4, 2.5 Hz, -C=C*H*-CH_2-), 4.61 (1H, s, -O*H*), 3.76 (3H, s, -CO_2CH_3), 2.85 (1H, m, -CH_2-C*H*-CH_2-), 2.75–1.60 (14H, m, 7 × -CH_2), 1.11 (3H, s, -CH_3), 0.99 (9H, s, -Si-C(CH_3)$_3$), 0.29 (6H, s, -Si(CH_3)$_2$); ms, *m/e*: 474 (M^+), 456 ($M^+ - H_2O$), 417 ($M^+ - C_4H_9$). Exact mass calcd. for $C_{26}H_{38}SiO_6$ (M^+): 474.2437; found: 474.2444. For **25** (unseparated mixture of isomers): R_f 0.13 (ethyl acetate/hexane,3:7); ^1H nmr (250 MHz, $CDCl_3$) δ ppm: 5.58 (1H, d, J = 6.4 Hz, -CH-C*H*=C-OSi*t*BDM), 5.27 (1H, d, J = 5.0 Hz, -CH-C*H*=C-OSi*t*BDM), 3.92 (1H, s, -O*H*), 3.87 (1H, s, -O*H*), 3.74 (3H, s, -CO_2-CH_3), 3.70 (3H, s, -CO_2CH_3), 3.44 (1H, m, -C*H*-CH=C-OSi*t*BDM), 3.25 (1H, m, -C*H*-CH=C-OSi*t*BDM), 2.90–1.60 (14H, m, 7 × -CH_2), 1.21 (3H, s, -CH_3), 1.18 (3H, s, -CH_3), 0.99 (9H, s, -SiC(CH_3)$_3$), 0.98 (9H, s, -SiC(CH_3)$_3$, 0.28, 0.26 (6H, 2s, 2 × -Si-CH_3), 0.28 (6H, s, -Si(CH_3)$_2$).

*Cleavage of 14-hydroxy silyl enol ether **23** or **24**. Formation of pure 14-hydroxy steroids **21** and **22***

To a solution of silyl enol ether **23** (35.8 mg, 0.08 mmol) in acetonitrile at 23°C is added cesium fluoride (23.0 mg, 0.15 mmol). The mixture is stirred vigorously at 23°C for 15 min, quenched with saturated ammonium chloride, and diluted with water. The mixture is extracted with ethyl acetate and the combined organic layers are washed with brine, dried ($MgSO_4$), filtered, and evaporated to yield 25 mg of an oil. Flash chromatography of the residue (ethyl acetate/hexanes,1:1) yields 19.6 mg (73%) of 14-hydroxy steroid **21**. The same procedure applies for the reaction **24** → **22**.

Acknowledgements

We are grateful to NSERC–Canada and FCAR–Québec for financial support of this work. We also thank NSERCC summer student Dennis Hall (1988) for his technical assistance at an early stage of this work.

1. J.-F. Lavallée and P. Deslongchamps. Tetrahedron Lett. **29**, 6033 (1988).
2. S. Lociuro, T. Y. R. Tsai, and K. Wiesner. Tetrahedron, **44**, 35 (1988).
3. A. R. Daniewski, Z. Valenta, and P. S. White. Bull. Pol. Acad. Sci. Chem. **32**, 29 (1984).
4. D. Liotta, C. Barnum, R. Puleo, G. Zima, C. Bayer, and H. S. Kezar. J. Org. Chem. **46**, 2920 (1981), and references cited therein.

5. H. SAKURAI. Pure Appl. Chem. **54**, 1 (1982).
6. J.-F. LAVALLÉE, G. BERTHIAUME, and P. DESLONGCHAMPS. Tetrahedron Lett. **27**, 5455 (1986).
7. G. BERTHIAUME, J.-F. LAVALLÉE, and P. DESLONGCHAMPS. Tetrahedron Lett. **27**, 5451 (1986).
8. J.-F. LAVALLÉE and P. DESLONGCHAMPS. Tetrahedron Lett. **29**, 5117 (1988).
9. T. B. WINDHOLZ, J. H. FRIED, H. SCHWAM, and A. A. PATCHETT. J. Am. Chem. Soc. **85**, 1707 (1963).
10. P. YATES, S. P. DOUGLAS, S. K. DATTA, and J. J. SAWYER. Can. J. Chem. **66**, 2268 (1988).
11. A. G. MICHEL, R. RUEL, and N. MICHEL-DEWEZ. Acta Crystallogr. Sect. C: Cryst. Struct. Commun. **C45**, 1760 (1989).

Can. J. Chem. Downloaded from www.nrcresearchpress.com by 91.121.58.235 on 09/07/12
For personal use only.

Synthesis, characterization, and dynamic behaviour of pseudoferrocene complexes

MICHAEL D. CLERK AND MICHAEL J. ZAWOROTKO[1]
Department of Chemistry, Saint Mary's University, Halifax, N.S., Canada B3H 3C3
AND
BOZENA BORECKA, T. STANLEY CAMERON,[2] DONALD L. HOOPER, AND ANTHONY LINDEN
Department of Chemistry, Dalhousie University, Halifax, N.S., Canada B3H 4J3

Received April 4, 1990

MICHAEL D. CLERK, MICHAEL J. ZAWOROTKO, BOZENA BORECKA, T. STANLEY CAMERON, DONALD L. HOOPER, and ANTHONY LINDEN. Can. J. Chem. **68**, 1923 (1990).

Carbanion sources (organolithium and Grignard reagents) react with $[(mesitylene)_2Fe]^{2+}$ and $[(mesitylene)(Ch)Fe]^{+}$ cations (Ch = cyclohexadienyl) to afford neutral Ch_2Fe and ChCh'Fe ("pseudoferrocene") complexes, respectively. Addition of R^- (R^- = methyl, phenyl, benzyl, and *t*-butyl) occurs stereospecifically via *exo* addition at an unsubstituted carbon atom of the arene ring. The synthesis and characterization of these complexes is detailed and the structure of bis(η^5-*exo*-6-phenyl-1,3,5-trimethylcyclohexadienyl)iron(II), **3***b*, has been determined by single crystal X-ray diffraction analysis. **3***b* crystallizes in the triclinic space group $P\bar{1}$, with a = 11.947(2), b = 12.784(1), c = 8.865(2), α = 108.59(1)°, β = 108.19(1)°, γ = 84.91(1)°, and D_{calcd} 1.227 g cm^{-3} for Z = 2. Least-squares refinement gave a conventional R value of 0.0452 for 2080 independent observed reflections. The structure reveals that the complex adopts a *gauche*-eclipsed conformation. The variable temperature (vt) ^{1}H NMR spectra of pseudoferrocenes are interpreted in terms of restricted ring rotation around the ligand—metal—ligand axis.

Key words: arene, cyclohexadienyl, pseudoferrocene, variable temperature NMR, X-ray diffraction.

MICHAEL D. CLERK, MICHAEL J. ZAWOROTKO, BOZENA BORECKA, T. STANLEY CAMERON, DONALD L. HOOPER et ANTHONY LINDEN. Can. J. Chem. **68**, 1923 (1990).

Les réactifs pouvant conduire à des carbanions (organolithiens et réactifs de Grignard) réagissent avec les cations $[(mésitylène)_2Fe]^{2+}$ et $[(mésitylène)(Ch)Fe]^{+}$ (dans lesquels Ch = cyclohexadiényl) pour fournir respectivement les complexes neutres ("pseudoferrocène") Ch_2Fe et ChCh'Fe. Les additions des radicaux R^- (R^- = méthyl, phényl, benzyl et *tert*-butyl) se produisent d'une façon stéréospécifique par le biais d'une addition exo sur un atome de carbone non-substitué du noyau arène. On décrit la synthèse et la caractérisation de ces complexes et on a déterminé la structure du bis(η^5-exo-6-phényl-1,3,5-triméthylcyclohexadiényl)fer(II), **3***b*, grâce à une analyse du spectre de diffraction des rayons-X réalisée sur un cristal unique. Les cristaux du produit **3***b* cont tricliniques et ils appartiennent au groupe d'espace $P\bar{1}$, avec a = 11,947(2), b = 12,784(1) et c = 8,865(2) Å, α = 108,59(1), β = 108,19(1) et γ = 84,91(1)°, D_{calcd} = 1.227 g cm^{-3} et Z = 2; on a affiné la structure par la méthode des moindres carrés jusqu'à une valeur de R de 0,0452 pour 2080 réflexions indépendantes observées. La structure révèle que le complexe adopte une conformation *gauche*-éclipsée. Les spectres rmn du ^{1}H à température variable des pseudoferrocènes ont été interprétés en fonction d'une restriction à la rotation du cycle autour de l'axe ligand—métal—ligand.

Mots clés : arène, cyclohexadiényl, pseudoferrocene, rmn à température variable, diffraction des rayons-X.

[Traduit par la revue]

Introduction

Attention has recently concentrated upon cyclohexadienyl (Ch) ligands as possible reaction intermediates for bifunctionalized arenes (1–5), for synthetically applicable cyclohexadienes (6), or for highly substituted arenes (7). However, progress has been impeded by the lack of facile, high yield routes to cyclohexadienyl intermediates via inexpensive and readily available substrates. For example, traditional alkylating reagents such as organolithiums, Grignards, and organocuprates often react to yield undesirable products (5). However, recent work in our laboratory (8, 9) has shown that C—C bond formation in the series $[(arene)_2Fe]^{2+}$ (arene = benzene, *p*-xylene, mesitylene, pentamethylbenzene, and hexamethylbenzene) occurs readily when AlR_3 (R = Me, Et) is employed as the carbanion source. The possibility of synthesizing a wide range of Ch_2Fe and ChCh'Fe "pseudoferrocene" complexes therefore becomes apparent as Ch_2Fe complexes may be prepared from $[(mesitylene)_2Fe]^{2+}$ (10, 11).

There are several reasons for studying pseudoferrocene complexes: (*i*) They have attracted very little attention from organometallic chemists even though they are analogues of ferrocene and bispentadienyl (pd_2Fe), "open ferrocene" complexes, which have received considerable attention in recent years (12). (*ii*) They are potentially useful synthetically, particularly as precursors to substituted cyclohexadienes (6) or arenes (7). (*iii*) It has been shown (11) that Ch_2Fe complexes exhibit temperature dependent ^{1}H NMR spectra with the explanation of the occurrence of a "rocking" of the two rings with respect to the iron atom (Fig. 1). However, a crystallographic paper subsequently published by Palenik and Mathew (13) showed a solid state conformation different from that assumed for the lowest

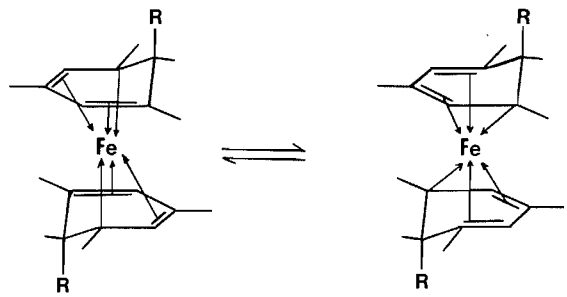

FIG. 1. Proposed "rocking" effect in pseudoferrocenes.

[1]Author to whom correspondence concerning syntheses should be addressed.

[2]Author to whom correspondence concerning crystallography should be addressed.

Can. J. Chem. Downloaded from www.nrcresearchpress.com by 91.121.58.235 on 09/07/12
For personal use only.

Can. J. Chem. Downloaded from www.nrcresearchpress.com by 91.121.58.235 on 09/07/12
For personal use only.

energy conformation in solution by Helling and Braitsch. Furthermore, temperature dependent spectra of pd_2Fe complexes were recently explained in terms of electronically controlled restricted rotation (12).

We have therefore undertaken synthesis of several new pseudoferrocene compounds and report an investigation of their dynamic behaviour in solution via variable temperature ^1H NMR studies.

Experimental

General

The following chemicals were purchased from Aldrich Chemical Company, Inc. and used as supplied: acetone-d_6, ammonium hexafluorophosphate, benzene-d_6, benzylmagnesium chloride, decahydronaphthalene, 1,2-dichloroethane, mesitylene, methyllithium, phenyllithium, *tert*-butyllithium, toluene-d_8. Acetone, hexanes, and tetrahydrofuran were purchased from BDH Chemicals, and were distilled over calcium hydride under a dinitrogen atmosphere prior to use. Anhydrous iron (III) chloride and anhydrous aluminum chloride were purchased from Johnson-Matthey Inc. and stored in desiccators prior to use. Calcium hydride, purchased from the Eastman Kodak Company, potassium iodide, purchased from Fisher Scientific Company, Ltd, and triethylaluminum, purchased from Texas Alkyls Inc., were used as supplied. All manipulations involving neat triethylaluminum were performed in a Vacuum Atmospheres' glove box equipped with a HE-493 dritrain under an argon atmosphere. Manipulations involving lithium reagents and the Grignard reagent were conducted using standard Schlenk and vacuum line techniques under a dinitrogen atmosphere.

Spectroscopy

^1H NMR spectra (60 MHz) were recorded on a Varian EM-360 spectrometer while 360 MHz ^1H NMR, variable temperature ^1H NMR, and 91 MHz ^{13}C NMR studies were conducted on a Nicolet 360NB spectrometer. Infrared spectra were obtained on a Perkin-Elmer 1600 Fourier Transform Infrared Spectrophotometer equipped with a diffuse reflectance accessory. Infrared samples were prepared as 5% mixtures of the compounds in KBr.

$[(\eta^6\text{-mesitylene})_2Fe]^{2+}$

(i) PF_6^- salt, **1***a* — 10.00 g (0.0616 mol) of anhydrous $FeCl_3$ and 24.64 g (0.1848 mol) of anhydrous $AlCl_3$ were stirred in 150 mL of dried, distilled mesitylene for 24 h under ambient conditions. The reaction flask was cooled at 0°C and the contents quenched with 200 mL of H_2O. After filtration the aqueous phase was separated from the organic phase and washed several times with hexanes, affording an orange aqueous solution. The dication was precipitated with saturated aqueous $NH_4^+PF_6^-$ and the resulting orange solid washed with hexanes and dried *in vacuo* yielding 19.16 g (32.69 mmol, 53%) of **1***a*. ^1H NMR ($(CD_3)_2CO$): δ 2.64(s, 9H), 6.50(s, 3H); ^{13}C NMR ($(CD_3)_2CO$): δ 19.7q, 92.0d, 113.3s. Infrared (cm^{-1}): 3117m, 3076m, 2930w, 1548m, 1459s, 1388m, 1036m, 1016m, 842s. In addition to NMR and IR data, **1***a* has been characterized via X-ray crystallography (14).

(ii) I^- salt, **1**b — Prepared as for **1***a* but the dication was precipitated with saturated aqueous K^+I^-. Yield: 16.96 g (30.83 mmol, 50%) of **1***b*. Nuclear magnetic resonance data could not be obtained on the solid due to its limited solubility, however, **1***b* has been characterized via X-ray crystallography (15). Infrared (cm^{-1}): 3078m, 2970s, 2894s, 2827s, 1535s, 1452s, 1429s, 1389s, 1034m, 1013m.

[(mesitylene)(Ch)Fe]$^+$

(i)(η^5-exo-6-Ethyl-1,3,5-trimethylcyclohexadienyl)(η^6-mexitylene)iron(II) hexafluorophosphate, **2**a — 7.00 g (0.0119 mol) of **1***b* was stirred in 150 mL of 1,2-dichloroethane in a 250 mL Erlenmeyer flask to which was added 6.53 mL (0.0476 mol) of neat $AlEt_3$. This resulted in the formation of a deep red reaction mixture within 30 s, which was then stirred at room temperature for 24 h. The mixture was cooled to 0°C and quenched with 50 mL of water. After filtration, the organic phase was separated and concentrated under reduced pressure. The red–orange solid was recrystallized from acetone/H_2O (4.41 g, 9.38 mmol, 77%). ^1H NMR spectroscopy (360 MHz) revealed the crude product to be a mixture of two compounds: **2***a* (80%) and [(η^5-*exo*-6-$CH_2CH_2ClC_6H_3Me_3$)(η^6-$C_6H_3Me_3$)Fe]PF_6 (20%). For **2***a*, ^1H NMR ($(CD_3)_2CO$): δ 5.86(s, 3H), 4.37(s, 2H), 2.76(s, 3H), 2.61(t, 1H), 2.47(s, 9H), 1.70(s, 6H), 0.56(q, 2H), 0.46(t, 3H); ^{13}C NMR ($(CD_3)_2CO$): δ 102.0s, 94.8s, 92.5d, 84.0d, 63.0s, 49.0d, 29.8t, 23.3q, 18.7q, 11.3q, 5.3q. Infrared (cm^{-1}): 3056w, 2975m, 2929m, 1540m, 1452m, 1383m, 1037m, 1012m, 875m, 840s. **2***a* has also been characterized via X-ray crystallography (8).

(ii) (η^5-exo-6-Ethyl-1,3,5-trimethylcyclohexadienyl)(η^6-mesitylene)iron(II) iodide, **2**b — A similar procedure was carried out for the idodide salt affording 2.20 g (4.87 mmol, 38%) of the pure product, **2***b*. ^1H NMR ($(CD_3)_2CO$): δ 5.74(s, 3H), 4.27(s, 2H), 2.74(s, 3H), 2.44(s, 9H), 1.67(s, 6H), 0.51(m, 5H). Infrared (cm^{-1}): 3056w, 3008s, 2954s, 1910s, 1540s, 1540s, 1458s, 1382s, 1169w, 1033s, 1011s.

Ch_2Fe complexes

These complexes were prepared in a manner similar to that described previously (11).

(i)Bis(η^5-1,3,5-exo-6-tetramethylcyclohexadienyl)iron(II), **3**a 1.00 g (1.71 mmol) of **1***b* was suspended in 50 mL of dried, distilled THF in a 150 mL Schlenk tube, and cooled to −95°C via an acetone slush bath. Under a stream of dinitrogen gas, 3.66 mL (5.12 mmol) of a 1.4 M solution of methyllithium in diethyl ether was added via syringe yielding a red–brown reaction mixture within seconds. After removing the acetone slush bath, the reaction mixture was stirred until it came to room temperature, at which point it was quenched with 10 mL of H_2O to remove excess MeLi. The mixture was subsequently filtered and concentrated under reduced pressure to give an orange aqueous suspension. Extraction with distilled hexanes afforded an orange solution which gave an orange oily solid following rotoevaporation. Recrystallization of the solid from hexanes at −20°C afforded 0.36 g (1.10 mmol, 61%) of red–orange crystals of **3***a*. Melting point 72–74°C. ^1H NMR (toluene-d_8, 30°C): δ 3.37(s, 4H), 2.33(q, 2H), 2.06(s, 6H), 1.61(br s, 12H), 0.43(d, 6H).

(ii) Bis(η^5-exo-6-phenyl-1,3,5-trimethylcyclohexadienyl)iron(II), **3**b — 1.00 g (1.82 mmol) of **1***b*, 3.64 mL (7.27 mmol) of a 2.0 M PhLi solution in cyclohexane/diethyl ether, 0.40 g (0.89 mmol, 49%) of orange crystals. Melting point 134–135°C. ^1H NMR (acetone-d_6, 30°C): δ 7.29(m, 10H), 3.71(s, 4H), 3.51(s, 2H), 2.16(s, 6H), 1.57(s, 12H).

(iii) Bis(η^5-exo-6-benzyl-1,3,5-trimethylcyclohexadienyl)iron(II), **3**c — 1.00 g (1.71 mmol) of **1***a*, 5.12 mL (5.12 mmol) of a 1.0 M solution of benzylmagnesium chloride in diethyl ether, 0.74 g (1.55 mmol, 91%) of orange solid. Melting point 82–84°C. ^1H NMR (toluene-d_8, 30°C): δ 6.89(m, 10H), 3.22(s, 4H), 2.52(t, 2H), 1.86(s, 6H), 1.76(d, 4H), 1.29(s, 12H).

(iv) Bis(η^5-exo-6-t-butyl-1,3,5-trimethylcyclohexadienyl)iron(II), **3**d — 1.00 g (1.82 mmol) of **1***b*, 4.28 mL (7.27 mmol) of a 1.7 M *t*-BuLi solution in pentane, 0.63 g (1.53 mmol, 84%) of orange crystals. Melting point 201–203°C. ^1H NMR (toluene-d_8, 70°C): δ 3.57(br s, 2H), 2.96(br s, 2H), 2.19(br s, 6H), 2.16(s, 2H), 1.83(s, 6H), 1.06(br s, 6H), 0.65(s, 18H).

ChCh'Fe complexes

(i) (η^5-exo-6-Ethyl-1,3,5-trimethylcyclohexadienyl)(η^5-1,3,5,exo-6-tetramethylcyclohexadienyl)iron(II), **4**a — 0.500 g (1.11 mmol) of **2***b* was dissolved in 50 mL of THF in a 150 mL Schlenk tube, and cooled to −95°C via an acetone slush bath. Under a stream of dry dinitrogen gas, 3.16 mL (4.42 mmol) of a 1.4 M MeLi solution in diethyl ether was added via syringe affording a red–brown reaction mixture within 1 min. After removing the acetone slush bath, the reaction mixture was stirred until it came to room temperature, at which point it was quenched with 10 mL of H_2O to eliminate excess MeLi. The mixture was filtered and concentrated under reduced pressure to an orange aqueous suspension. Extraction with hexanes afforded an orange solution which was concentrated under reduced pressure yielding 0.28 g (0.82 mmol, 74%) of an orange solid, **4***a*. Melting point 65–67°C. ^1H NMR (toluene-d_8, 20°C): δ 3.22(br s, 4H), 1.87(s, 3H), 1.83(s, 3H), 1.47(s, 6H), 1.42(s, 6H), 0.60(m, 5H), 0.20(d, 3H).

Can. J. Chem. Downloaded from www.nrcresearchpress.com by 91.121.58.235 on 09/07/12
For personal use only.

TABLE 1. Crystallographic data collection and structure refinement parameters for **3***b*

Formula	$FeC_{30}H_{34}$
Formula weight	686.4
Radiation	Mo-K_α
Crystal system	Triclinic
Space group	$P\bar{1}$
a, Å	11.947(2)
b, Å	12.784(1)
c, Å	8.865(2)
α, deg	108.59(1)
β, deg	108.19(1)
γ, deg	84.91(1)
V, Å^3	1218.9
Z	2
D_{calcd} g cm^{-3}	1.227
μ, cm^{-1}	6.51
Crystal dimensions, mm	0.35 × 0.35 × 0.55
Scan type	ω/2θ
2θ range, deg	4–46
Reflections measured	3908
Reflections observed[a]	2087
Parameters refined	314
Ratio data/parameter	6.6
R	0.0452
R_w	0.0429

[a] $I > 3\sigma(I)$.

(ii) (η^5-exo-6-Ethyl-1,3,5-trimethylcyclohexadienyl)(η^5-exo-6-phenyl-1,3,5-trimethylcyclohexadienyl)iron(II), **4**c — 0.500 g (1.11 mmol) of **2***b*, 0.66 mL (1.33 mmol) of a 2.0 M PhLi solution in cyclohexane/diethyl ether, 0.33 g (0.82 mmol, 74%) of an orange oil. ^{1}H NMR (toluene-d_8, 20°C): δ 7.15(m, 5H), 3.58(s, 1H), 3.48 (br s, 4H), 2.33(t, 1H), 2.08(s, 3H), 2.06(s, 3H), 1.63(br s, 12H), 0.85(m, 5H).

(iii) (η^5-exo-6-Ethyl-1,3,5-trimethylcyclohexadienyl)(η^5-exo-6-benzyl-1,3,5-trimethylcyclohexadienyl)iron(II), **4**c — 0.500 g (1.11 mmol) of **2***b*, 3.32 mL (3.32 mmol) of a 1.0 M solution of benzylmagnesium chloride in diethyl ether, 0.33 g (0.79 mmol, 72%) of an orange oil. ^{1}H NMR (toluene-d_8, 40°C): δ 7.02(m, 5H), 3.28(s, 2H), 3.24(s, 2H), 2.60(d, 2H), 2.49(t, 1H), 1.90(s, 3H), 1.88(s, 3H), 1.48(br s, 12H), 0.98(d, 2H), 0.62(m, 5H).

(iv) (η^5-exo-6-Ethyl-1,3,5-trimethylcyclohexadienyl)(η^5-exo-6-t-butyl-1,3,5-trimethylcyclohexadienyl)iron(II), **4**d — 0.500 g (1.11 mmol) of **2***b*, 2.60 mL (4.42 mmol) of a 1.7 M solution of *t*-BuLi in pentane, 0.41 g (1.07 mmol, 97%) of orange–red crystals, mp 50–52°C. ^{1}H NMR (toluene-d_8 at 80°C): δ 3.34(br s, 2H), 3.31 (br s, 2H), 2.23(s, 1H), 2.16(t, 1H), 1.98(s, 3H), 1.85(s, 3H), 1.65(br s, 6H), 1.56(br s, 6H), 0.74(s, 14H).

X-ray crystallography

The crystal used for X-ray diffraction studies was an orange cube obtained by cooling a concentrated hexanes solution of **3***b* to −20°C. The single crystal was sealed in a thin-walled capillary and placed on an Enraf-Nonius Cad-4 four circle diffractometer (graphite-monochromated Mo K_α radiation). Cell dimensions were calculated from 25 reflections with 2θ angles in the range 26–30° and are listed along with other pertinent crystallographic parameters in Table 1. The structure was solved by heavy-atom methods and refined using the SHELX Crystal Structure System (16). Refinement was based on $R = \Sigma||F_o| - |F_c||/\Sigma|F_o|$ and $R_w = [\Sigma(w(F_o - F_c)^2)/\Sigma wF_o^2]^{1/2}$. It converged at $R = 0.0452$ and $R_w = 0.0429$ with all non-hydrogen atoms refined with anisotropic thermal parameters and hydrogen atoms placed geometrically and refined with individual isotropic thermal parameters. Weights were given by $w = 1.3994/[\sigma^2(F) + 0.000375F^2]$. No corrections were made for extinction but an absorption correction was applied (17). Atomic scattering factors and corrections for anomalous dispersion for Fe, C, and H were taken from International tables for X-ray crystallography, Vol. IV (18). Final fractional coordinates and interatomic distances and angles are presented in Tables 2 and 3, respectively.[3]

TABLE 2. Fractional atomic positional parameters and equivalent isotropic temperature factors (Å^2) with esd's in parentheses

Atom	*X*	*Y*	*Z*	*U*(iso)
Fe	0.32498(6)	0.21581(6)	0.29454(8)	0.0416
C1	0.2140(3)	0.0257(3)	0.2232(4)	0.0404
C2	0.1687(3)	0.1414(3)	0.2839(4)	0.0424
C3	0.2282(3)	0.2085(3)	0.4451(4)	0.0468
C4	0.3472(4)	0.1944(3)	0.5219(5)	0.0479
C5	0.4070(4)	0.1126(3)	0.4273(5)	0.0505
C6	0.3454(4)	0.0457(3)	0.2653(5)	0.0525
C7	0.0433(3)	0.1641(4)	0.1993(5)	0.0622
C8	0.4136(4)	0.2686(4)	0.6946(5)	0.0649
C9	0.4104(4)	−0.0344(4)	0.1584(6)	0.0785
C11	0.1817(3)	−0.0618(3)	0.2856(5)	0.0424
C12	0.1521(4)	−0.0355(4)	0.4324(5)	0.0618
C13	0.1237(4)	−0.1158(4)	0.4885(5)	0.0720
C14	0.1249(4)	−0.2255(4)	0.3981(6)	0.0645
C15	0.1550(4)	−0.2541(4)	0.2530(6)	0.0592
C16	0.1822(3)	−0.1729(4)	0.1978(5)	0.0542
C21	0.2220(3)	0.3429(3)	0.1059(4)	0.0408
C22	0.2749(4)	0.2310(3)	0.0498(4)	0.0472
C23	0.3952(4)	0.2180(3)	0.1128(5)	0.0610
C24	0.4628(4)	0.2874(4)	0.2708(6)	0.0610
C25	0.3988(4)	0.3670(4)	0.3594(5)	0.0565
C26	0.2771(4)	0.3785(3)	0.2925(5)	0.0448
C27	0.2048(4)	0.1503(3)	−0.1134(4)	0.0614
C28	0.5926(4)	0.2713(5)	0.3445(7)	0.0942
C29	0.2109(4)	0.4599(3)	0.3966(5)	0.0711
C31	0.2287(3)	0.4253(3)	0.0157(4)	0.0441
C32	0.3299(4)	0.4855(3)	0.0541(5)	0.0582
C33	0.3329(4)	0.5598(4)	−0.0285(5)	0.0672
C34	0.2351(4)	0.5750(4)	−0.1502(6)	0.0723
C35	0.1360(4)	0.5148(4)	−0.1898(6)	0.0823
C36	0.1320(4)	0.4408(4)	−0.1071(4)	0.0702

Since anisotropic vibrations of the atoms in the two organic portions of the molecule showed clear indications of concerted motion, the rigid body motion of the molecule (19) was analyzed with routine "tls" (20) calculations. The results of these calculations are seen in Fig. 2 and the salient details are given in Table 4.

The two organic portions of the molecule are both librating with independent motions and it is not clear from the calculations whether the motion of the two portions is linked or not (see below). In each of the two portions there is little or no concerted translation or screw motion, and the librations of both parts adopt a broadly similar motion which differs more in detail than type.

Both phenyl rings have a major libration about an axis which runs close to the axis of the ring from the *p* carbon through the C—C bond joining the ring to the pseudoferrocene moiety. This libration has an amplitude of 8.9° for ring 1 and of 10.2° for ring 2 (Fig. 2 *a* and *c*) and operates about a centre close to the carbon atoms, C(11) and C(31) respectively, which form the bond to the rest of the molecule. There are smaller, but significant librations which operate at right angles to this major motion and these two have centres close to C(11) or C(31).

There is a second libration of the pseudoferrocene rings and these

[3] Supplementary tables providing hydrogen atom positional parameters for bis(phenylmesitylene)iron, anisotropic temperature factors (Å^2) for bis(phenylmesitylene)iron, torsional angles (deg) for bis(phenylmesitylene)iron, and observed and calculated structure factors for bis(phenylmesitylene)iron may be purchased from the Depository of Unpublished Data, CISTI, National Research Council of Canada, Ottawa, Ont., Canada K2A 0S2.

TABLE 3. Interatomic distances (Å) and interbond angles (deg) for **3***b*

(*i*) distances

Bond	Distance	Bond	Distance
Fe(1)—C(2)	2.133(4)	C(11)—C(16)	1.385(7)
Fe(1)—C(3)	2.046(5)	C(12)—C(13)	1.381(7)
Fe(1)—C(4)	2.053(5)	C(13)—C(14)	1.377(8)
Fe(1)—C(5)	2.032(5)	C(14)—C(15)	1.372(7)
Fe(1)—C(6)	2.107(5)	C(15)—C(16)	1.381(7)
Fe(1)—C(22)	2.131(5)	C(21)—C(22)	1.509(6)
Fe(1)—C(23)	2.044(5)	C(21)—C(26)	1.507(6)
Fe(1)—C(24)	2.049(5)	C(21)—C(31)	1.531(6)
Fe(1)—C(25)	2.030(5)	C(22)—C(23)	1.385(7)
Fe(1)—C(26)	2.112(5)	C(22)—C(27)	1.518(7)
C(1)—C(2)	1.518(6)	C(23)—C(24)	1.425(7)
C(1)—C(6)	1.520(6)	C(24)—C(25)	1.402(7)
C(1)—C(11)	1.519(6)	C(24)—C(28)	1.506(8)
C(2)—C(3)	1.405(6)	C(25)—C(26)	1.402(7)
C(2)—C(7)	1.501(7)	C(26)—C(29)	1.502(7)
C(3)—C(4)	1.395(6)	C(31)—C(32)	1.382(7)
C(4)—C(5)	1.410(7)	C(31)—C(36)	1.369(7)
C(4)—C(8)	1.524(7)	C(32)—C(33)	1.380(7)
C(5)—C(6)	1.416(7)	C(33)—C(34)	1.369(8)
C(6)—C(9)	1.500(7)	C(34)—C(35)	1.359(8)
C(11)—C(12)	1.385(7)	C(35)—C(36)	1.380(8)

(*ii*) angles

Bonds	Angle	Bonds	Angle
C(2)—C(1)—C(6)	102.4(4)	C(22)—C(21)—C(26)	103.0(4)
C(2)—C(1)—C(11)	117.2(4)	C(22)—C(21)—C(31)	116.6(4)
C(6)—C(1)—C(11)	115.3(4)	C(26)—C(21)—C(31)	116.9(4)
C(1)—C(2)—C(3)	118.1(4)	C(21)—C(22)—C(23)	119.1(4)
C(1)—C(2)—C(7)	117.6(4)	C(21)—C(22)—C(27)	117.2(4)
C(3)—C(2)—C(7)	120.7(4)	C(23)—C(22)—C(27)	120.2(4)
C(2)—C(3)—C(4)	122.0(4)	C(22)—C(23)—C(24)	121.9(5)
C(3)—C(4)—C(5)	116.8(4)	C(23)—C(24)—C(25)	115.4(5)
C(3)—C(4)—C(8)	122.4(4)	C(23)—C(24)—C(28)	122.6(5)
C(5)—C(4)—C(8)	120.6(4)	C(25)—C(24)—C(28)	121.8(5)
C(4)—C(5)—C(6)	120.3(4)	C(24)—C(25)—C(26)	121.4(5)
C(1)—C(6)—C(5)	118.9(4)	C(21)—C(26)—C(25)	119.5(4)
C(1)—C(6)—C(9)	117.4(4)	C(21)—C(26)—C(29)	117.5(4)
C(5)—C(6)—C(9)	120.4(4)	C(25)—C(26)—C(29)	119.5(4)
C(1)—C(11)—C(12)	122.4(4)	C(21)—C(31)—C(32)	122.2(4)
C(1)—C(11)—C(16)	120.9(4)	C(21)—C(31)—C(36)	119.6(4)
C(12)—C(11)—C(16)	116.7(4)	C(32)—C(31)—C(36)	118.2(4)
C(11)—C(12)—C(13)	121.9(5)	C(31)—C(32)—C(33)	120.9(5)
C(12)—C(13)—C(14)	120.0(5)	C(32)—C(33)—C(34)	120.3(5)
C(13)—C(14)—C(15)	119.5(5)	C(33)—C(34)—C(35)	119.0(5)
C(14)—C(15)—C(16)	119.8(5)	C(34)—C(35)—C(36)	121.1(5)
C(11)—C(16)—C(15)	122.1(5)	C(31)—C(36)—C(35)	120.6(5)

Can. J. Chem. Downloaded from www.nrcresearchpress.com by 91.121.58.235 on 09/07/12
For personal use only.

have a distinctive difference from one to the other. Both have the major libration about an axis running perpendicular to the general plane of the ring (4.7° for ring 3 and 6.0° for ring 4), but in one case (ring 3) the centre of libration is close to the centre of the ring (Fig. 2*e*) and in the other (ring 4) the centre of libration is close to the end of the ring where the phenyl group is bonded (Fig. 2*f*). Thus in one case (ring 1 + ring 3), the pseudoferrocene moiety is librating about an axis joining the iron atom with the centre of the ring and thus through the connection of C(1)—C(11) causing the phenyl group to librate from side to side about a centre somewhat "above" C(11) (Fig. 2*b*). While independently this phenyl group is librating approximately about the C(11)—C(14) axis. In the other case (ring 2 + ring 4) the pseudoferrocene portion is librating from "side to side" in the general plane of the ring, but about an axis close to the carbon atom bonded to the phenyl group (Fig. 2*f*). This reduces the consequent motion of the bonded phenyl group (ring 2) when it is compared with ring 1. Ring 2 has its own major libration approximately about the C(31)—C(34) axis.

The "tls" calculations for the rigid body motion of the phenyl groups show good correlation between the observed and calculated anisotropic thermal parameters, R = 4.4% and 4.9%, respectively, with rms deviations of the same order as the esd's calculated from the full X-ray structure refinement. The "tls" calculations for the pseudoferrocene fragments are not so good. The "tls" R is 7.5% and 7.7%, respectively and the rms deviations are at least 50% greater than the esd's

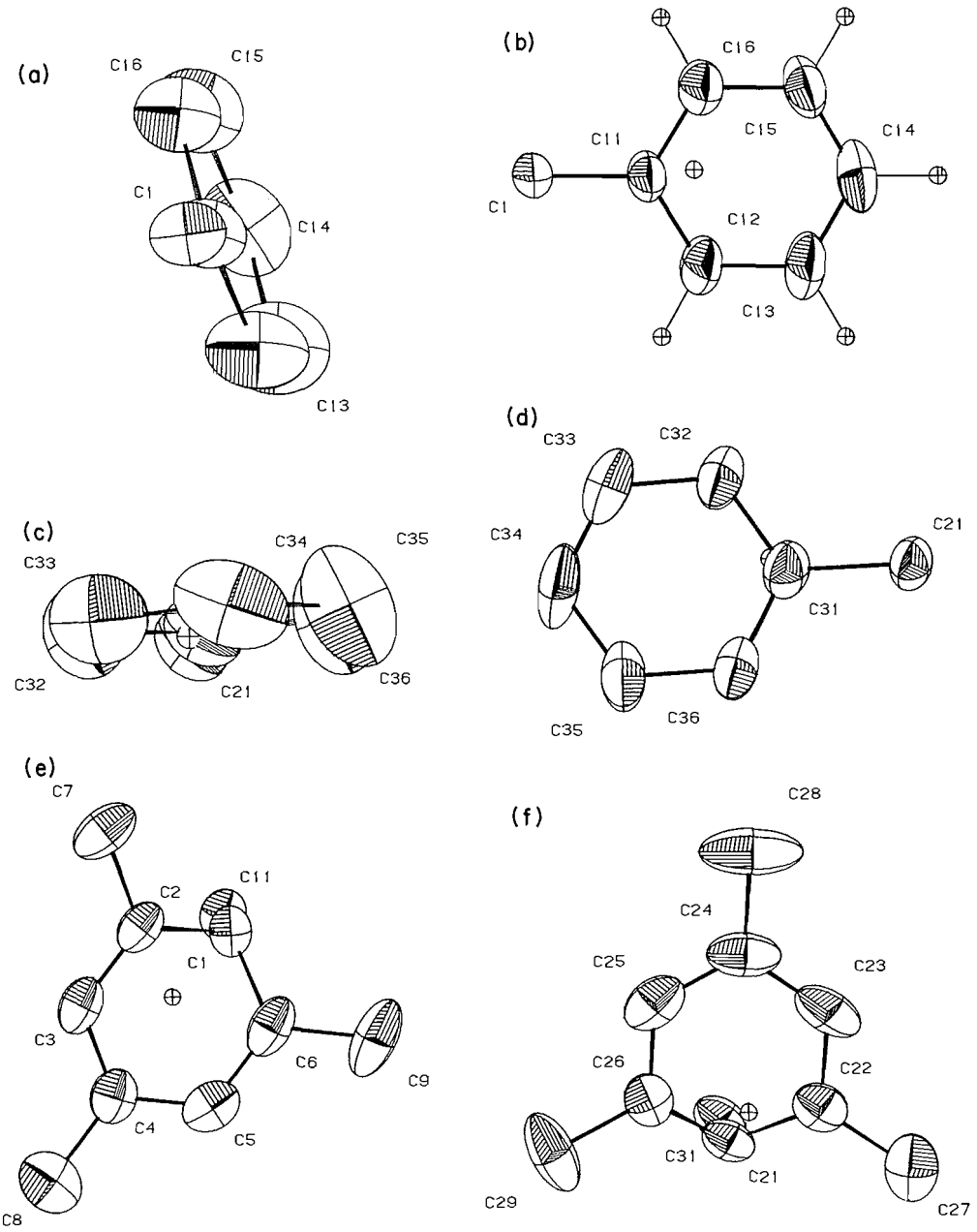

FIG. 2. Libration axes. ⊕ indicates the centre of librations. In (*a*), (*c*), (*e*), and (*f*) the principal libration axis (*Z*″) is perpendicular to the page and the third axis (*X*″) down the page. (*a*) Libration axes for ring 1 (note the centre of libration is hidden between C(11) and C(14) and cannot be seen from either end of the axis). (*b*) Location of the centre of libration for ring 1. (*c*) Libration axes for ring 2. (*d*) Location of the centre of libration for ring 2. (*e*) Libration axes for ring 3. (*f*) Libration axes for ring 4.

determined from the X-ray data refinement. It seems probable that these two groups are more flexible and are not the strictly rigid bodies that have been assumed in the calculation.

Thus the two organic portions of the molecule have broadly similar librations. From the perspective of conservation of angular momentum, it is tempting to suggest that the two systems are linked with one pseudoferrocene librating to the left while the opposite ring is rotating to the right. However, the demonstration of such a motion is beyond the limit of the current structure determination.

Results and discussion

The dications **1***a* and **1***b* and the monocations **2***a* and **2***b* react with excess R^- (R^- = methyl, phenyl, benzyl, *t*-butyl) to afford neutral Ch_2Fe (**3***a*–*d*) and ChCh′Fe (**4***a*–*d*) pseudoferrocene complexes, respectively.

Varible temperature (VT) ^1H NMR studies demonstrate that **3***a*–*d* and **4***a*–*d* are fluxional. Representative spectra for the ChCh′Fe complex, **4***d*, are presented in Fig. 3. The spectra are consistent with the proposed structure of the complex, and, as expected (11), only the peaks corresponding to the 1,5-methyl groups and the 2,4-protons are temperature dependent.

Coalescence temperatures (T_c) and the free energy of rotational barriers, $\Delta G^{\neq}$, were calculated for the 1,5-methyl groups and the 2,4-protons of all compounds and are tabulated in Table 5. An interesting trend evident in Table 5 is that as the R

Can. J. Chem. Downloaded from www.nrcresearchpress.com by 91.121.58.235 on 09/07/12
For personal use only.

TABLE 4. Salient details on **3***b*

Ring	Librations about (X'', Y'', Z'')				R	RMS dev	Centroid (x, y, z)*		
Ring 1	C(11)—C(16)	3.9°	5.2	8.9	4.4%	0.0021	0.1757	−0.1040	0.3065
Ring 2	C(31)—C(36)	3.3	4.3	10.2	4.9	0.0026	0.2431	0.4352	0.0108
Ring 3	C(1)—C(9)	2.7	3.9	4.7	7.5	0.0035	0.2662	0.1539	0.3123
Ring 4	C(21)—C(29)	2.8	3.0	6.0	7.7	0.0038	0.2765	0.2525	0.2086

*The centroid is given in crystal fraction units with respect to the real crystal axes. In the diagram (Fig. 2), the largest libration occurs around the Z'' axis which is perpendicular to the page and passes through the centroid. The X'' and Y'' axes, perpendicular to the Z'' axis, are down and across the page respectively, but do not necessarily intersect either with the Z'' axis or with themselves.

(*b*) Rotation matrices from crystal fractions (x, y, z) to orthogonal libration axes (X'', Y'', Z'')

Ring 1	0.6158	−0.1046	0.5518
	0.6003	−0.4836	−0.5640
	0.5103	0.8690	−0.6143
Ring 2	−0.7722	−0.0836	−0.3287
	−0.5091	0.5653	0.5261
	0.3801	0.8206	−0.7843
Ring 3	0.5709	−0.4232	−0.6441
	−0.7739	−0.1082	−0.3181
	0.2741	0.8995	−0.6957
Ring 4	0.2514	−0.5708	−0.5942
	0.9617	0.1502	−0.0787
	−0.1088	−0.8072	0.8005

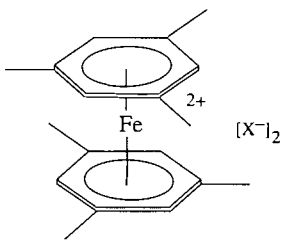

1
a: X = PF_6
b: X = I

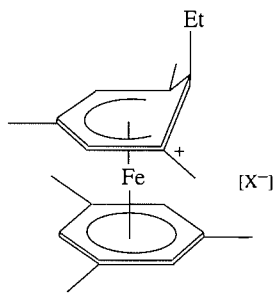

2
a: X = PF_6
b: X = I

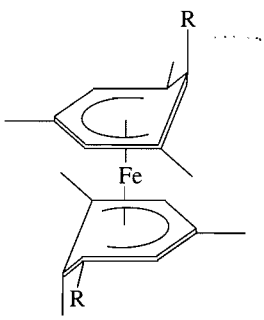

3
a: R = Me
b: R = Ph
c: R = Bz
d: R = *t*-Bu

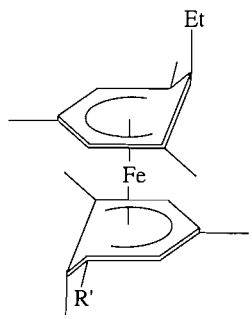

4
a: R' = Me
b: R' = Ph
c: R' = Bz
d: R' = *t*-Bu

substituents increase in size, both T_c and $\Delta G^{\neq}$ increase. This observation indicates that the dynamic behaviour of pseudoferrocene complexes is not purely an electronic effect, as has been suggested for pd_2Fe complexes (12).

The earlier study of pseudoferrocenes conducted by Helling and Braitsch (11) attributed the temperature dependent spectra of Ch_2Fe complexes to a "rocking" effect of the two rings with respect to the iron atom (see Fig. 1). It was suggested that the NMR spectra could be explained by free rotation or lack of rotation but not by restricted rotation. This conclusion was reached assuming the preferred conformation of **3***b* and **3***d* at low temperature to be anti-eclipsed, **I**. However, the possibility of other low energy conformations taking precedence in solution at low temperature or in the solid state was not considered. Two other conformations are, of course, possible: *gauche* (either eclipsed or staggered), **II**, and *syn*-eclipsed, **III**. Subsequent X-ray crystallographic (Ch_2Fe (13), pd_2Fe (12)) and theoretical studies (pd_2Fe (21)) suggest that *gauche*-eclipsed conformations are favoured by $(dienyl)_2Fe$ complexes. This is very important, as a feature of conformation **II** is that a C_2-axis bisecting the angle between the two R groups is present as the Ch_2Fe complexes possess C_2 point-group symmetry, which is observed crystallographically in the case of **3***d*. Adoption of conformation **II** by Ch_2Fe complexes would therefore put the methyl group at position 3 on one ring in the same chemical environment as the symmetry related 3-methyl group on the other ring. One would therefore expect the two methyl groups to appear as a sharp singlet with a relative area of 6, independent of temperature. However, the 1,5-methyl substituents and the 2,4-protons should not be equivalent in conformation **II** and would be expected to split into two peaks each at the low temperature limit. In the case of the ChCh′Fe complexes the C_2 axis is no longer present so at both low and

Can. J. Chem. Downloaded from www.nrcresearchpress.com by 91.121.58.235 on 09/07/12
For personal use only.

Can. J. Chem. Downloaded from www.nrcresearchpress.com by 91.121.58.235 on 09/07/12
For personal use only.

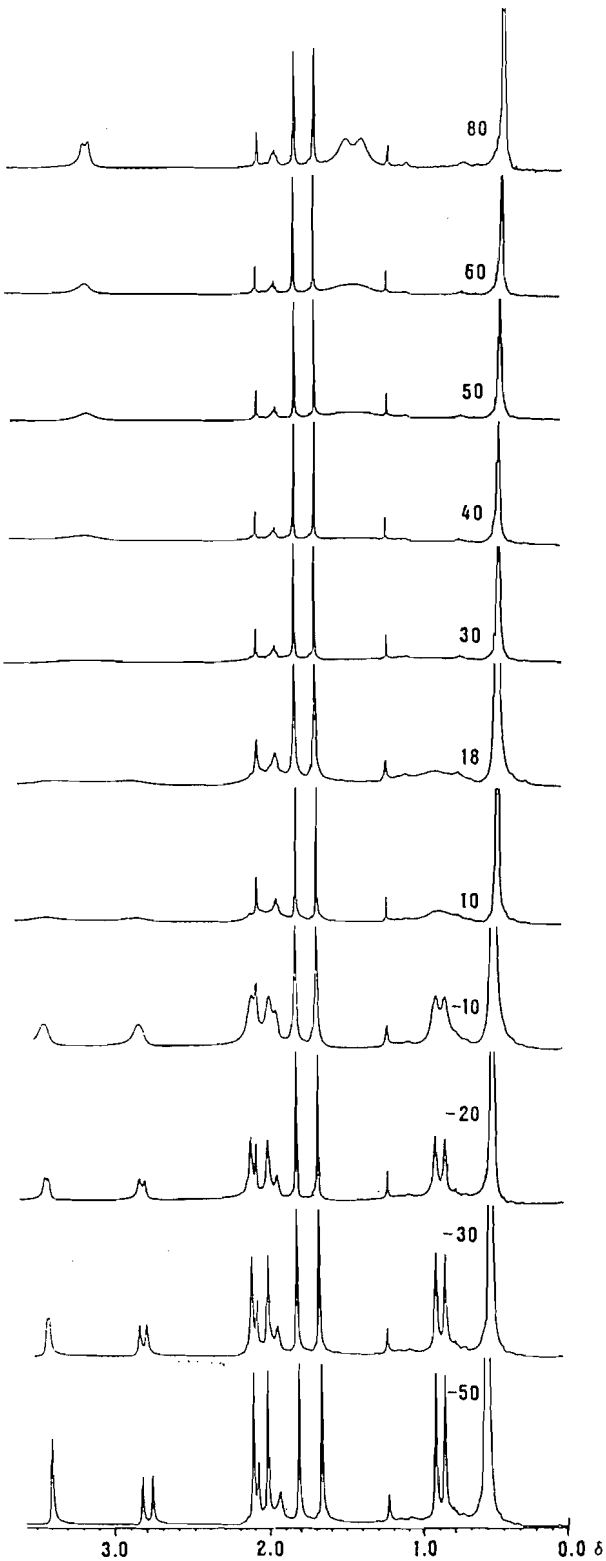

FIG. 3. Representative spectra of ChCh′Fe complex, **4***d*.

high temperature limits the spectra should be more complex. This, of course, corresponds to the observed spectra for both Ch_2Fe and ChCh′Fe complexes. Explanation of the spectra by assuming restricted rotation with adoption of conformation **II** at low temperature therefore appears a reasonable interpretation of our observations; however, they do not fully explain the effect.

TABLE 5. $\Delta G^{\neq a}$ values in kJ/mol, for complexes **3***a–d* and **4***a–d*

Complex	Protons	Coalescence temperature (°C)	$\Delta G^{\neq}$
3*a*	1,5-Me's	−25	46.3
	2,4-H's	−30	46.7
3*b*	1,5-Me's	−28	45.5
	2,4-H's	−35	45.5
3*c*	1,5-Me's	−10	49.2
	2,4-H's	−15	49.9
3*d*	1,5-Me's	[b]	63.3[c]
	2,4-H's	−57	64.8
4*a*	1,5-Me's	−10	50.0[d]
	2,4-H's	−15	47.6
4*b*	1,5-Me's	−10	49.2[d]
	2,4-H's	−20	48.6
4*c*	1,5-Me's	0	51.7[d]
	2,4-H's	−20	49.8[d]
4*d*	1,5-Me's	40	59.1[d]
	2,4-H's	30	58.8[d]

[a] $\Delta G^{\neq} = RT_c[23 + \ln(T_c/\Delta\nu)]$ (25).
[b] Could not be determined, T_c above 90°C.
[c] Average of two calculated values.
[d] Values obtained from work done by Helling and Braitsch (11).

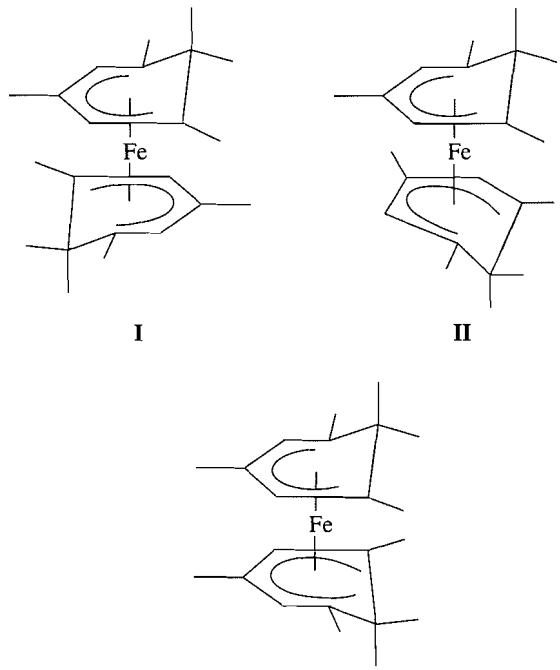

I II III

Electronic and steric factors that favour conformation ***II***

Calculations of rotational barriers for pd_2Fe complexes by Ernst *et al.* (21) suggested two energy minima, one at $\alpha = 0$ (*anti*) and the other at $\alpha \approx 70°$ (*gauche*) ($\Delta G^{\neq}$ = 22 kJ/mol, 29 kJ/mol calculated by the EH and INDO methods, respectively). The X-ray structures of **3***b* and **3***d* reveal torsion angles of 63.0° and 63.2°, respectively, close to the electronic minimum calculated and indeed observed (12) in the solid state for pd_2Fe compounds. According to the calculations this particular minimum should be higher in energy than *anti*-eclipsed, **I**.

Can. J. Chem. Downloaded from www.nrcresearchpress.com by 91.121.58.235 on 09/07/12
For personal use only.

TABLE 6. Structural comparison of metal cyclohexadienyl complexes

R	R′	Average deviation from planarity of 1,5-Me's		Average deviation from planarity of 3-Me's		X (Å)[a]		θ (deg)[a]	
A	B	A		B		A	B	A	B
t-Butyl[b]	*t*-Butyl[b]	0.25,	0.25	0.01,	0.01	0.67,	0.67	43.5,	43.5
t-Butyl[b]	Ethyl[c]	0.25,	0.22	0.01,	0.04	0.67,	0.66	43.5,	44.2
Benzyl[d]	Benzyl[d]	— ,	—	— ,	—	— ,	—	— ,	—
Benzyl[d]	Ethyl[c]	— ,	0.22	— ,	0.04	— ,	0.66	— ,	44.2
Phenyl[e]	Ethyl[c]	0.12,	0.22	0.05,	0.04	0.62,	0.66	40.7,	44.2
Methyl[f]	Methyl[f]	0.21,	0.21	0.04,	0.04	0.59,	0.59	39.9,	39.9
Phenyl[e]	Phenyl[e]	0.13,	0.12	0.04,	0.06	0.64,	0.60	41.8,	39.7
Methyl[f]	Ethyl[c]	0.21,	0.22	0.04,	0.04	0.59,	0.66	39.9,	44.2

[a]Average value given where appropriate. X is the distance of the sp^3 carbon atom from the C_s plane; θ is the angle subtended by the plane of the sp^3 carbon atom and the adjacent dienyl carbon atoms with the C_s plane. Calculations are done using programs in ref. 26.
[b]Value obtained from structure of **3***d* (13).
[c]Value predicted from structure of **2***a* (8).
[d]No experimental values available.
[e]This study.
[f]Value predicted from structure of (η^5-1,3,5,exo-6-tetramethylcyclohexadienyl)$Mn(CO)_3$ (27).

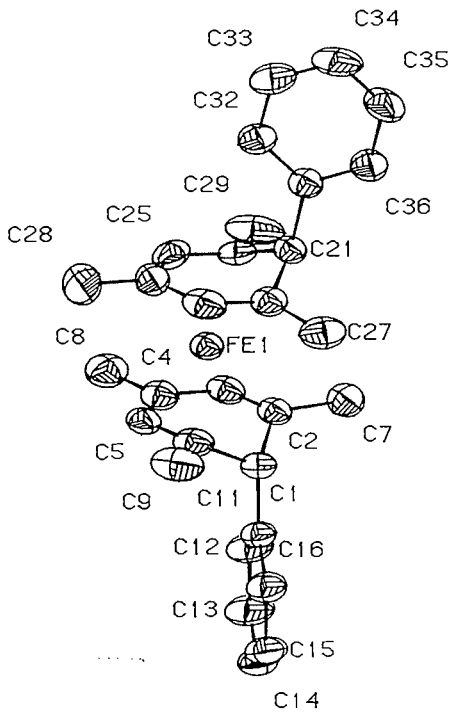

FIG. 4. Perspective view of bis(η^5-exo-6-phenyl-1,3,5-trimethylcyclohexadienyl)iron(II), **3***b*.

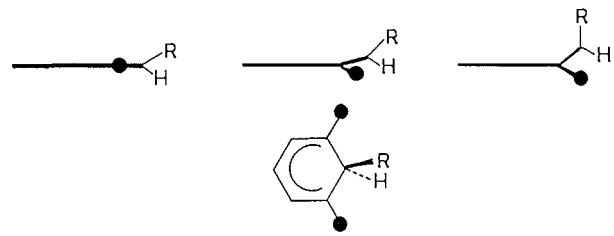

FIG. 5. Steric effect of R group on 1,5-methyl groups.

However, steric factors would be expected to favour the *gauche* conformation, particularly for the compounds described herein, which possess 1,5-methyl substituents that orient down towards the metal atom (see later).

That the size of the R group on carbon 6 of the Ch ring affects the values of $\Delta G^{\neq}$ and T_c suggests that a steric component to the rotational barrier exists. A possible rationalization is that the R group influences the two adjacent methyl groups at positions 1 and 5 by forcing them out of the plane of the ring towards the iron moiety. In order to test this hypothesis and check the apparent anomaly with the data in Table 5 (i.e. **3***b* having lower $\Delta G^{\neq}$ and T_c values than **3***a*) the crystal structure of complex **3***b* was determined.

A perspective view of **3***b* is given in Fig. 4. It reveals that the phenyl groups have added in the expected *exo* fashion and that the Ch rings adopt a *gauche* conformation. The two ligands are not identical in the solid state as the phenyl groups are oriented differently from each other. The deviation from planarity of the 1-methyl and 5-methyl groups averages 0.12 Å, which may be compared with the considerably larger 0.25 Å deviation observed for **3***d*. Indeed, the deviation in **3***b* is small even compared with a range of Ch complexes (Table 6).

The small deviation could be a simple manifestation of the fact that carbon 6 is sp^3 hybridized. Steric pressure from the iron atom forces C6 above the plane of the dienyl fragment of the Ch ring, a feature common to coordinated cyclohexadienyl moieties (8, 9, 13) but not to uncoordinated cyclohexadienylium cations (22–24). The other five carbons atoms in the ring maintain their sp^2 hybridization and planarity, hence the 1,5-methyls are forced below the plane of the ring. The size of R is expected to influence the magnitude of this effect as steric repulsions would increase with the size of R (see Fig. 5).

Summary

Synthesis and characterization of a series of pseudoferrocene complexes has been achieved. Temperature dependent ^{1}H NMR spectra were observed for all compounds studied, restricted rotation about the ring—Fe—ring axis instead of a "rocking" effect being the probable cause of the dynamic behaviour. Both

steric and electronic factors support this claim and a crystal structure of **3***b* has been presented in support.

Acknowledgements

We are grateful to the Natural Sciences and Engineering Research Council of Canada (operating grants to T.S.C. and M.J.Z., undergraduate fellowship to M.D.C.) and the donors of the Petroleum Research Fund, administered by the American Chemical Society (M.J.Z.), for financial support of this work. High field NMR spectra were recorded by the Atlantic Region Magnetic Resonance Centre, Dalhousie University.

1. S. G. Davies, M. L. H. Green, and D. M. P. Mingos. Tetrahedron, **34**, 3047 (1978).
2. J. P. Collman, L. S. Hegedus, J. R. Norton, R. G. Finke. Principles and applications of organotransition metal chemistry. University Science Books, Mill Valley, CA. 1987. pp. 921–940.
3. D. Astruc. Tetrahedron, **39**, 4027 (1983).
4. S. G. Davies. Organotransition metal chemistry: applications to organic synthesis. Pergamon, Oxford. 1982.
5. M. F. Semmelhack, G. R. Clark, J. L. Garcia, J. J. Harrison, Y. Thebtaranonth, W. Wulff, A. Yamashita. Tetrahedron, **37**, 3957 (1981).
6. A. M. Madonik, D. Mandon, P. Michaud, C. Lapinte, and D. Astruc. J. Am. Chem. Soc. **106**, 3381 (1984).
7. F. Moulines, D. Astruc. Angew Chem. Int. Ed. Engl. **27**, 1347 (1988).
8. T. S. Cameroon, M. D. Clerk, A. Linden, K. C. Sturge, and M. J. Zaworotko. Organometallics, **7**, 2571 (1988).
9. M. D. Clerk, P. S. White, K. C. Sturge, and M. J. Zaworotko. J. Organomet. Chem. **368**, C33 (1989).
10. J. F. Helling, D. M. Braitsch. J. Am. Chem. Soc. **92**, 7207 (1970).
11. J. F. Helling and D. M. Braitsch. J. Am. Chem. Soc. **92**, 7209 (1970).
12. R. D. Ernst. Chem. Rev. **88**, 1255 (1988).
13. M. Mathew, G. J. Palenik. Inorg. Chem. **11**, 2809 (1972).
14. T. S. Cameron, A. Linden, K. C. Sturge, and M. J. Zaworotko. Unpublished results.
15. R. D. Rogers and M. J. Zaworotko. Unpublished results.
16. G. M. Sheldrick. SHELX-76, Program for crystal structure determination. University of Cambridge, Cambridge. U.K. 1976.
17. N. Walker and D. Stuart. Acta. Crystallogr. A**39**, 158 (1983).
18. International tables for X-ray crystallography. Vol. IV, Kynoch Press, Birmingham, U.K. 1974.
19. V. Schomaker, K. N. Trueblood. Acta. Crystallogr. B**24**, 63 (1968).
20. J. R. Carruthers, and D. L. Watkins. Crystals, Issue 8 (Revised 1989), Chemical Crystallography Laboratory, Oxford, England. 1984.
21. M. C. Böhm, M. Eckert-Maksić, R. D. Ernst, D. R. Wilson, and R. Gleiter. J. Am. Chem. Soc. **104**, 2699 (1982).
22. N. C. Baenziger and A. D. Nelson. J. Am. Chem. Soc. **90**, 6602 (1968).
23. R. Effenberger, F. Reisinger, K. H. Schonwalder, P. Bauerle, J. J. Stezowski, K. H. Jogun, K. Schollkopf, and W. D. Stohrer. J. Am. Chem. Soc. **109**, 882 (1987).
24. T. S. Cameron, A. Linden, K. C. Sturge, and M. J. Zaworotko. Acta. Crystallogr. C**45**, 996 (1989).
25. D. H. Williams, and I. Flemming. Spectroscopic methods in organic chemistry. 4th ed. McGraw-Hill Book Company (UK) Limited. 1987. p. 103.
26. E. J. Gabe, F. L. Lee, and Y. Le Page. *In* Crystallographic computing 3: data collection, structure determination, proteins and databases. *Edited by* G. M. Sheldrick, C. Kruger, and R. Goddard. Clarendon: Oxford. 1985. pp. 167–174.
27. M. V. Gaudet, A. W. Hanson, P. S. White, and M. J. Zaworotko. Organometallics, **8**, 286 (1989).

Can. J. Chem. Downloaded from www.nrcresearchpress.com by 91.121.58.235 on 09/07/12
For personal use only.

A study of the Ca^{2+} – Arsenazo III system and its application to the spectrophotometric determination of free calcium in solution

BYRON KRATOCHVIL[1] AND XI-WEN HE[2]

Department of Chemistry, University of Alberta, Edmonton, Alta., Canada T6G 2G2

Received February 13, 1990

BYRON KRATOCHVIL and XI-WEN HE. Can. J. Chem. **68**, 1932 (1990).

A two-wavelength method was applied to the determination of free, ionic calcium with Arsenazo III in solutions containing calcium-binding ligands. By this procedure impurities in the indicator can be corrected for, thereby allowing the use of commercial indicator preparations with purities as low as 80%. Only a 1:1 complex with a conditional log stability constant of 4.28 ± 0.13 at pH 4.6 and ionic strength 0.1 was found under the conditions studied.

Key words: free metal ion determination, calcium ion speciation, spectrophotometry, arsenazo III, ion increment method for speciation.

BYRON KRATOCHVIL et XI-WEN HE. Can. J. Chem. **68**, 1932 (1990).

On a utilisé une méthode faisant appel a deux longueurs d'onde pour déterminer le calcium ionique libre dont Arsenazo III dans des solutions contenent des ligands pouvant lier le calcium. Cette procédure permet de corriger la présence d'impuretés dans l'indicateur; on peut ainsi utiliser des préparations d'indicateurs commerciaux dont la pureté ne dépasse pas 80%. Dans les conditions utilisées, on n'a observé que la formation d'un complexe 1:1 dont le log (conditionnel) de la constante de stabilité est égal à 4,28 ± 0,13 à un pH de 4,6 et à une force ionique de 0,1.

Mots clés : détermination d'ions métalliqueslibres, spéciation de l'ion calcium, spectrophotométrie, Arsénazo III, méthode d'augmentation d'ionique pour la spéciation.

[Traduit par la revue]

Can. J. Chem. Downloaded from www.nrcresearchpress.com by 91.121.58.235 on 09/07/12
For personal use only.

The determination of free calcium in solution is important in many biological, clinical, environmental, and agricultural systems. Methods that have been studied include ion selective electrode potentiometry (1), spectrophotometry with indicator dyes (2, 3), and equilibrium calculations (4, 5). When the bound species is chemically inert the free calcium can be separated for measurement by techniques such as filtration (6), solvent extraction (7), chromotography (8), or ion exchange (9). A related specialized problem, the measurement of free calcium in biological cells and tissues, has also received intensive study (10). All these methods suffer interferences from other species or from limited applicability in terms of pH or calcium concentration range.

One of the more widely used techniques is that employing the chelating indicator dye Arsenazo III. This dye is a sensitive and selective reagent for calcium, and has been studied for the determination of calcium both in solution (10*a*, 11–21) and in cells and tissue (10*a*,*b*,*c*, 11). A problem with the system has been uncertainties in combining ratios of calcium with Arsenazo III, which have been measured variously as 1:1 (12, 14); 2:1 (10*d*, 13); 2:2 and 1:1, 1:2, or 2:1 (17). Also, the purified, low-calcium reagent is costly, and interferences from sodium and potassium have been reported (14, 18). Accordingly, we have investigated the effects of pH, ionic strength, and sodium and potassium ion concentrations on the calcium – Arsenazo III system. We have also measured the protonation constants for the dye in water, and the conditional stability constant of the calcium-dye complex at pH 7.25 and 4.60. Finally, we have applied the sample ion increment method to the measurement of free calcium with Arsenazo III in the presence of citrate, and in several urine samples.

Sample ion increment method

Direct spectrophotometric measurements of free calcium ion concentrations have several limitations. The most severe restriction is that only a small fraction of the ionic calcium, usually less than 1%, may be allowed to complex with the indicator if the equilibria existing in the original sample solution are not to be significantly perturbed. This requires a relatively small value for the conditional formation constant(s) of the calcium–indicator complex(es), which limits sensitivity.

These limitations can be overcome by the approach described by Fulton and Kratochvil (21), the Sample Ion Increment Method (SIIM). In this method, a known amount of indicator is added to the sample and the absorbance is measured. Then an accurately known amount of the sample ion to be determined is added and the absorbance is remeasured. The second measurement determines the sample ion buffering capacity of the original solution and permits a correction for the amount of sample ion complexed by the indicator. With this approach close to 100% of the sample ion can be complexed by the indicator before adding the sample ion increment without introducing appreciable determinate error, thereby reducing previous stringent requirements on the magnitude of the conditional formation constant and of the molar absorptivity of the sample ion – indicator complex. It is still necessary that the indicator be of either high or accurately known purity; this requirement may be overcome by measuring the difference between absorbance values of a solution at two wavelengths (22, 23).

Experimental

Reagents and solutions

Stock 1×10^{-3} M solutions of Arsenazo III, either free acid (Aldrich) or the sodium salt (Fluka), were prepared in water. For the free acid three different levels of purity were purchased and assessed. The first was labelled as containing 1 to 5% calcium, the second less than 0.1% calcium, and the third as 98% pure. The degree of purity was screened by measuring the ratio of absorbance at the wavelength of maximum absorbance for the uncomplexed dye, 646 nm, to that for the calcium complex, 548 nm. The first material gave a ratio of 3.0, the second 5.0, and the third 15. For the disodium salt the ratio was 21. Photometric titrations of the first and third free acid material with standard calcium solution at pH 4.6 gave purities of 80% and 98%; the

[1]Author to whom correspondence may be addressed.

[2]On leave from Department of Chemistry, Nankai University, Tianjin, People's Republic of China.

disodium salt also gave a purity of 98%. Stock 5×10^{-3} M solutions of calcium nitrate ($Ca(NO_3)_2 \cdot 4H_2O$) (Baker Analyzed Reagent) were prepared by weight. The purity of the calcium nitrate was determined by titration with EDTA standardized against pure calcium carbonate. A purity of 100.8% was found; this value was used to calculate the concentrations of all calcium solutions. All solutions were prepared with distilled, demineralized water. Other chemicals were analytical or reagent grade.

Instrumentation

All pH measurements were made with a Fisher Accumet Model 525 pH meter and a glass–SCE pair that was calibrated with commercial buffers (Fisher). Spectrophotometric measurements were made on a Hewlett-Packard Model 8451A diode array spectrophotometer in 1-cm silica cells in a constant temperature room held at 25 ± 1°C.

Procedure for calibration plots and spectrophotometric measurements

A series of solutions were prepared in 25-mL volumetric flasks. Varying amounts of calcium and/or Arsenazo III stock solution were added to each flask by Mohr pipet. The ionic strength was adjusted, usually with NaCl but in a few cases with KNO_3, as required, then the solution diluted to near volume and the pH adjusted to the desired value by addition of concentrated HCl. Dilution to volume was then completed. All solutions were measured spectrophotometrically the same day they were prepared.

Results and discussion

Purity of commercial arsenazo III

Spectrophotometric titrations of commercial Arsenazo III as free acid and as the sodium salt with standard calcium solution gave purities ranging from 81% for the lowest grade of free acid to 98% for both the highest grade of free acid and the sodium salt. All subsequent work was done using the less expensive sodium salt.

Dual wavelength method

The difficulty in obtaining Arsenazo III and reagents such as NaOH, NaCl, and KNO_3 with sufficiently low levels of calcium led us to use a dual wavelength procedure (22, 23) to compensate for this contamination. In this method absorbance readings are taken at two wavelengths, chosen so that the absorbance difference changes in a major way with concentration. The advantage of this procedure is that the precise calcium contamination of the dye and reagents need not be known. Wavelengths selected for this work were 458 and 598 nm in water, 458 and 600 nm in NaCl solutions, and 458 and 602 nm in KNO_3 solutions; 458 nm is an isosbestic point.

Effect of pH and ionic strength on absorbance of Arsenazo III (ArIII) and Ca^{2+}–ArIII complex

Plots of absorbance difference as a function of pH for 1×10^{-4} M ArIII (Fluka, sodium salt) with and without 5×10^{-5} M Ca^{2+} present are shown in Fig. 1. The ΔA value ($A_{598} - A_{458}$) for free ArIII is 0 in water and in 0.1 M NaCl over the pH range 4 to 6. THe ΔA value for the Ca^{2+}–ArIII complex is higher in pure water than in 0.1 M sodium chloride because of the effect of ionic strength on the conditional stability constant, K_{cond}, of the Ca^{2+}–ArIII complex over the pH range studied:

$$K_{cond} = \frac{[CaArIII^{2-x}]}{[Ca^{2+}][ArIII^{x-}]}$$

$$K_{th} = \frac{a_{CaArIII}{}^{2-x}}{a_{Ca^{2+}} a_{ArIII}{}^{x-}} = K_{cond} \frac{\gamma_{CaAr}{}^{2-x}}{\gamma_{Ca^{2+}} \gamma_{Ar}{}^{x-}}$$

where x is predominately 3 to 4 over the pH range of 4 to 6 (24). The increase in ΔA with pH is expected if calcium is competing with hydrogen ion for sites on the indicator. Since absorbance changes appeared smallest in the pH range 4.6 to 4.8 in both water and 0.1 M NaCl, a value of 4.6 was arbitrarily chosen for subsequent work. Figure 2 shows spectra of ArIII and the Ca^{2+}–ArIII complex at pH 4.6 for varying concentrations of NaCl. The effect of increasing ionic strength on complex formation is clearly evident.

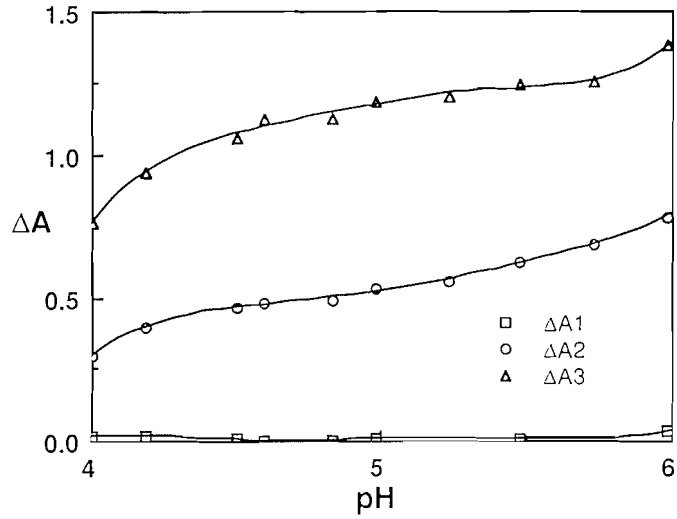

FIG. 1. Plot of ΔA against pH for (*1*) 1×10^{-4} M Arsenazo III in H_2O ($\Delta A = A_{598} - A_{458}$) and in 0.1 M NaCl ($\Delta A = A_{600} - A_{458}$), (*2*) 1×10^{-4} M Arsenazo III + 5×10^{-5} M Ca^{2+} in 0.1 M NaCl ($\Delta A = A_{600} - A_{458}$), and (*3*) same as *2*, but in H_2O ($\Delta A = A_{598} - A_{458}$). H_2O used as reference.

Effect of Na^+ and K^+ on Ca^{2+}–ArIII complex formation

It has been reported that both Na^+ and K^+ interfere with the Ca^{2+}–ArIII reaction (14, 18). This was checked by recording spectra for free ArIII and the Ca^{2+}–ArIII complex as a function of cation at constant ionic strength. Spectra in the presence of Na^+, K^+, and NH_4^+ are shown in Fig. 3. The spectra in NH_4Cl and KNO_3 are superimposable, thereby showing that none of the ions in these salts have a discernible effect upon the absorbance spectrum of the Ca^{2+}–ArIII system. The spectrum in NaCl indicates slightly more Ca^{2+}–ArIII complex formation than in KNO_3 or NH_4Cl; this may be the result of small differences between activity coefficients for Na^+ and K^+ or NH_4^+. We conclude that the effect of Na^+ or K^+ upon Ca^{2+}–ArIII complex formation is not species specific for these ions, but is a function of ionic strength. We also find no specific interaction with chloride, in contrast to the report of Minganti *et al.* (25). Their results also appear to be due to ionic strength changes. The effect of ionic strength is significant, as can be seen from the calibration curves in Fig. 4. Our results confirm the findings of Brown and Rydquist (19).

Determination of combining ratio for Ca^{2+}–ArIII system at pH 4.6

As mentioned in the Introduction, several combining ratios have been reported for the Ca^{2+}–ArIII system. Therefore we remeasured this ratio at pH 4.6 by both the molar ratio and Job methods. A molar ratio plot at 648 nm showed only a break at a 1:1 ratio, and Job's plots of ΔA ($A_{600} - A_{458}$) and of A at 648 nm directly also both showed a maximum at a 1:1 ratio only. Thus at pH 4.6, under the conditions used we observe only a 1:1 combining ratio for Ca^{2+} with ArIII.

A 1:1 ratio does not differentiate between 1:1 and 2:2 species. To determine which was present the method of He and Poe (26)

Can. J. Chem. Downloaded from www.nrcresearchpress.com by 91.121.58.235 on 09/07/12
For personal use only.

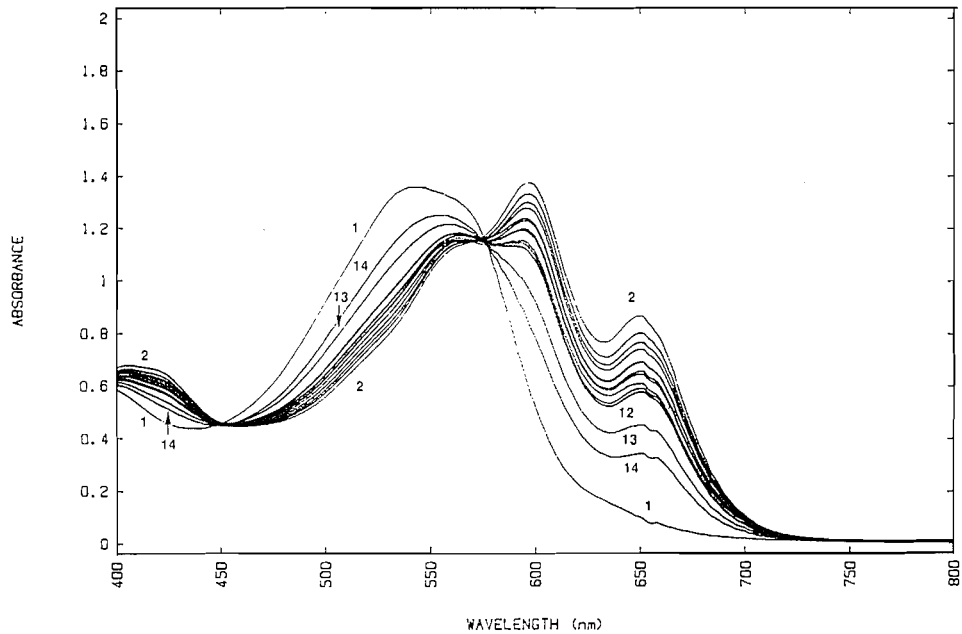

FIG. 2. Effect of ionic strength on spectrum of mixture of Ca^{2+} and ArIII: (*1*) Spectrum of 5×10^{-5} M ArIII in 0.5 M NaCl. Remaining spectra are of 5×10^{-5} M ArIII + 2.5×10^{-5} M Ca^{2+} in (*2*) H_2O, and in NaCl at (*3*) 0.01, (*4*) 0.02, (*5*) 0.03, (*6*) 0.04, (*7*) 0.05, (*8*) 0.06, (*9*) 0.07, (*10*) 0.08, (*11*) 0.09, (*12*) 0.10, (*13*) 0.2, and (*14*) 0.5 M. pH = 4.6 throughout; H_2O used as reference.

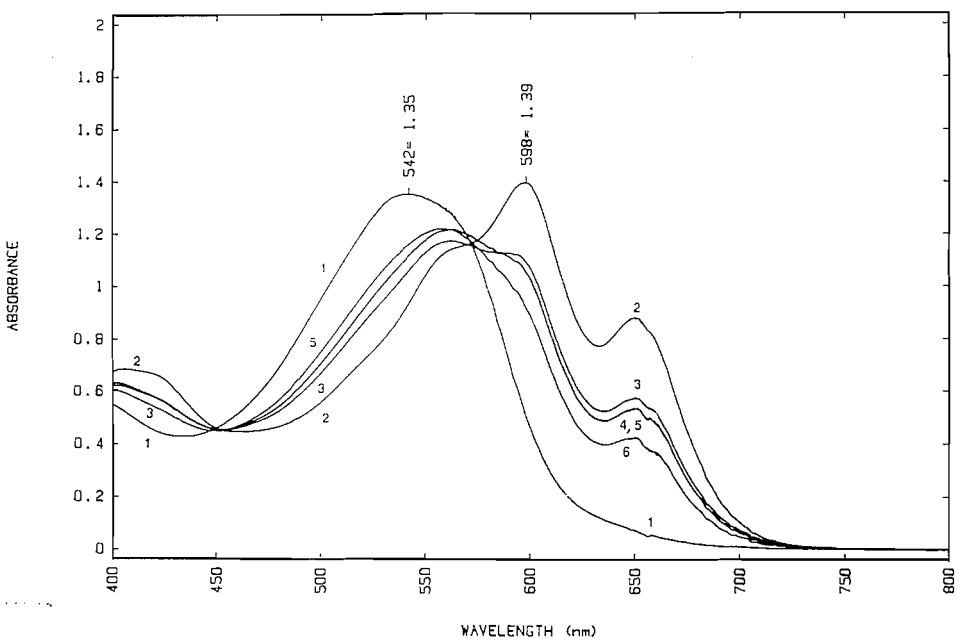

FIG. 3. Spectra of (*1*) 5×10^{-5} M ArIII in H_2O, (*2*) same as (*1*) but 2.5×10^{-4} M Ca^{2+} present, (*3*) same as (*2*) but in 0.1 M NaCl, (*4*) same as (*2*) but in 0.1 M NH_4Cl, (*5*) same as (*2*) but in 0.1 M KNO_3, and (*6*) same as (*2*) but in 0.05 M Na_2SO_4. pH = 4.6 throughout; H_2O used as reference.

was used, with slight changes. Following their procedure, for

$$m\mathrm{Ca}^{2+} + m\mathrm{ArIII} \rightleftharpoons \mathrm{Ca}_m\mathrm{ArIII}_m$$

if $C_{Ca^{2+}} = C_{ArIII}$ initially, then the stability constant expression can be written as

$$[1] \quad K_{cond} = \frac{C_{Ca^{2+}}\alpha_C}{m[C_{Ca^{2+}}]^{2m}(1-\alpha_C)^{2m}}$$

where

$$\alpha_C = \frac{m[Ca_m^{2+}\,ArIII_m]}{C_{Ca^{2+}}} = \frac{\Delta A}{\Delta A_{max}}$$

In this work $\Delta A = A_{598} - A_{458}$.

Taking the logarithm of eq. [1] gives

$$[2] \quad \log \frac{\alpha_C}{(1-\alpha_C)^{2m}} = (2m-1)\log C_{Ca^{2+}} + \log mK_{cond}$$

By plotting $\log (\alpha_C/(1-\alpha_c)^{2m})$ against $\log C_{Ca^{2+}}$, a slope of

Can. J. Chem. Downloaded from www.nrcresearchpress.com by 91.121.58.235 on 09/07/12
For personal use only.

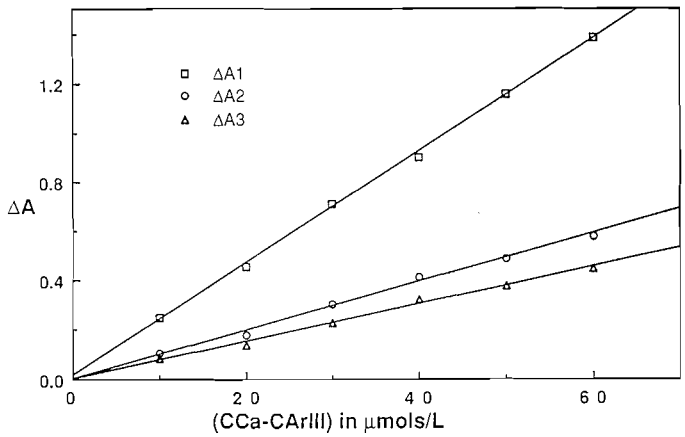

FIG. 4. Calibration plots for Ca^{2+}–ArIII in water and in 0.1 M NaCl and 0.1 M KNO_3 at pH 4.6. Concentration of ArIII = 1×10^{-4} M, H_2O used as reference. Absorbances are ΔA values: (*1*) $\Delta A = A_{598} - A_{458}$ in H_2O; (*2*) $\Delta A = A_{600} - A_{458}$ in 0.1 M NaCl; (*3*) $\Delta A = A_{602} - A_{458}$ in 0.1 M KNO_3.

$(2m - 1)$ and an intercept of log mK_{cond} is obtained. Selection of different integer values of m will yield straight lines with different slopes, but only the true value of m will yield a slope equal to the value predicted by the equation.

For this system, insertion of 1, 2, and 3 for m into eq. [2] gave predicted slope values of 1, 3, and 5, respectively, and experimental slopes from the plots of 1.4, 2.1, and 3.1. Since the experimental value of 1.4 for m is the closest to the corresponding predicted value, we conclude that only a 1:1 complex is present under the conditions studied.

Determination of K_{cond} for the Ca^{2+}–ArIII complex at pH 4.6

The intercept of eq. [2] gives the value of log mK_{cond}. Using $m = 1$, a value for log K_{cond} in water of 6.43 ± 0.08 is obtained by a least-squares fit. This value was measured at a low but variable ionic strength.

A second estimation of K_{cond} at $\mu = 0.1$ (adjusted with NaCl) was made using absorbance data from a series of solutions for which $C_{ArIII} = C_{Ca^{2+}}$ in the range of 3 to 6 × 10^{-5} M. A log K_{cond} value of 4.28 ± 0.13 was obtained for four measurements (Table 1). This value compares reasonably well with literature values, which range for 1:1 complex formation from 3.5 by Thomas (15) to 4.77 by Onishi (14). The sensitivity of the conditional constant to pH and ionic strength is great because of the large number of weak protons on Arsenazo III and the high charge on the ligand anion. This sensitivity may account in part for the range of stability constant values reported in the literature (14–19).

Test of the SIIM method for measurement of free Ca^{2+} in the presence of citrate

To evaluate the applicability of ArIII to the determination of free Ca^{2+} by the SIIM method (21), a series of solutions containing varying amounts of Ca^{2+} and citrate were prepared and the free Ca^{2+} calculated using literature values for the Ca–citrate complex. The experimental conditions and results are given in Table 2. The conventional spectrophotometric indicator method gives good agreement with calculated values of pCa at lower citrate concentrations, but begins to deviate at higher levels. Under these conditions the SIIM may be used to advantage, as can be seen from Table 2.

TABLE 1. Conditional stability constants of the 1:1 calcium-arsenazo III complex at ionic strength 0.1 in NaCl and pH 4.6

$C_{Ca^{2+}} = C_{ArIII}$, M	ΔA $(A_{600} - A_{458})$	ΔA_{max}	α_C	log K_{cond}[a]
3×10^{-5}	0.073	0.295	0.248	4.18
4×10^{-5}	0.116	0.392	0.296	4.17
5×10^{-5}	0.190	0.487	0.387	4.31
6×10^{-5}	0.280	0.578	0.474	4.45
				Av. 4.28 ± 0.13

[a]Literature values: 3.52 (15), 4.3 (19), 4.36 (18), 4.6 (16), 4.77 (14).

TABLE 2. Calculated and experimentally determined values for free Ca^{2+} in solutions containing citrate at pH 4.6. For all solutions C_{ArIII} was 1×10^{-4} M, $C_{Ca^{2+}}$ was 5×10^{-5} M, and the ionic strength was adjusted to 0.1 with NaCl

	Calculation		Regular spectrophotometric method		SIIM[a]	
C_{Cit} (M)	$\alpha_{Ca} = \frac{[Ca^{2+}]}{C_{Ca^{2+}}}$	pCa	α_{Ca}	pCa	α_{Ca}	pCa
1×10^{-4}	0.97	4.31	0.91	4.34		
4×10^{-4}	0.92	4.34	0.89	4.35		
8×10^{-4}	0.84	4.37	0.82	4.39		
2×10^{-3}	0.68	4.47	0.74	4.43		
4×10^{-3}	0.52	4.59	0.58	4.54	0.57	4.55
6×10^{-3}	0.42	4.68	0.55	4.56	0.46	4.64

[a]$\Delta C_{Ca^{2+}} = 2 \times 10^{-5}$ M.

Determination of free Ca^{2+} in urine with ArIII and the SIIM

Several urine samples were analyzed for free Ca^{2+} by the SIIM. The original pH of the urine, about 5.8, was adjusted to 4.6 before measurement. This shift could change the free Ca^{2+} in solution by shifting the equilibria; to avoid this would require K_{cond} to be known at each sample pH. Table 3 gives results along with total calcium values as measured by atomic absorption spectroscopy and some preliminary values obtained on two samples by an ion exchange method under development in this laboratory. It can be seen that the values fall within a reasonable range. We were not able to obtain stable readings on these samples with a calcium ion selective electrode.

In summary, we have found the SIIM method with ArIII as indicator to be useful for the determination of free calcium in solutions containing calcium bound as metal–ligand complexes. The major disadvantage of the method is that the metal-indicator conditional stability constant must be known precisely, otherwise significant error is introduced into the value obtained for the free metal. Also, since K_{cond} varies with ionic strength in all systems, and with pH in most, the scope of applicability is limited to cases where the pH and ionic strength can be adjusted to specified values without shifting the original equilibria to an unacceptable extent. If necessary the pH and ionic strength of the samples under study could be matched, but this would involve additional time and work.

The dual wavelength method was found to be satisfactory over the range of calcium concentrations investigated here. The importance to medicine of knowing free as compared to

Can. J. Chem. Downloaded from www.nrcresearchpress.com by 91.121.58.235 on 09/07/12
For personal use only.

TABLE 3. Values for total and free Ca^{2+} in urine samples from five normal individuals; uncertainties are one standard deviation, number of measurements given in parentheses

Individual	Free Ca^{2+}, μg/mL, this work	Free Ca^{2+}, μg/mL, est. by IE[a]	Total Ca^{2+}, μg/mL[b]
A	76 ± 1.5 (6)	80	84 ± 4
B	124 ± 1 (6)	90	163 ± 4
C	224 ± 1.4 (6)	225 to 250	312 ± 6
D	87 ± 1 (3)	—	165 ± 3
E	169 ± 1 (3)	—	242 ± 3

[a]IE = ion exchange procedure under development in this laboratory. Values approximate only.
[b]Total calcium concentration measured by atomic absorption spectroscopy.

total calcium ion concentrations makes continued evaluation of methods such as the one described here worthwhile.

Acknowledgments

This research was supported by the Natural Sciences and Engineering Research Council of Canada and the University of Alberta. The authors thank Norine Motkosky for the atomic absorption measurements of total calcium, Marei Pflugge Griffith and Iqbal Tabani for preliminary studies on the Ca–ArIII system, and Amitha Hewavitharana for the ion exchange measurements on the urine samples.

1. J. GARDINER. Water Res. **8**, 23 (1974).
2. F. J. BRENLEY, A. SCARPA, and T. TIFFERT. J. Physiol. **266**, 545 (1977).
3. R. Y. TSIEN. Biochemistry, **19**, 2396 (1980).
4. C. Y. C. PAK, E. C. DILLER, G. W. SMITH, and E. S. HOWE. Proc. Soc. Exp. Biol. Med. **130**, 653 (1969).
5. G. LUTWICK, G. WEBSTER, and B. KRATOCHVIL. Can. J. Soil Sci. **68**, 433 (1988).
6. M. R. HOFFMAN, E. C. YOST, S. J. EISENREICH, and W. J. MAIER. Envir. Sci. Technol. **15**, 655 (1981).
7. R. FUKAI, C. N. MURRAY, and L. HUYNH-NGOC. Estuarine Coastal Mar. Sci. **3**, 177 (1975).
8. J. C. VAN LOON. Anal. Chem. **51**, 1139A (1979).
9. T. M. FLORENCE and G. E. BATLEY. Talanta, **24**, 151 (1977).
10. C. C. ASHLEY and A. K. CAMPBELL (*Editors*). Detection and measurement of free calcium in cells. Elsevier/North Holland, Amsterdam. 1979 (*a*) pp. 85–115; (*b*) pp. 269–285; (*c*) pp. 287–308; (*d*) pp. 311–318.
11. R. DIPOLO, J. REQUENA, F. J. BRINLEY, JR., L. J. MULLINS, A. SCARPA, and T. TIFFERT. J. Gen. Physiol. **67**, 433 (1976).
12. W. B. GRATZER and G. H. BEAVEN. Anal. Biochem. **81**, 118 (1977).
13. A. SCARPA, F. J. BRINLEY, JR., T. TIFFERT, and G. R. DUBYAK. Ann. N.Y. Acad. Sci. **307**, 86 (1978).
14. S. T. OHNISHI. Biochim. Biophys. Acta, **586**, 217 (1979).
15. M. V. THOMAS. Biophys. J. **25**, 541 (1979).
16. Z. AHMED, L. KRAGIE, and J. A. CONNOR. Biophys. J. **32**, 907 (1980).
17. P. L. DOROGI and E. NEUMANN. Biophys. Chem. **13**, 125 (1981).
18. P. J. BAUER. Anal. Biochem. **110**, 61 (1981).
19. H. M. BROWN and B. RYDQUIST. Biophys. J. **36**, 117 (1981).
20. P. PALADE and J. VERGARA. Biophys. J. **43**, 355 (1983).
21. R. FULTON and B. KRATOCHVIL. Anal. Chem. **52**, 546 (1980).
22. B. CHANCE. Methods Enzymol. **24**, 322 (1972).
23. S. T. OHNISHI. Anal. Biochem. **85**, 165 (1978).
24. I. TABANI. M.Sc. Thesis, University of Alberta. 1986.
25. C. MINGANTI, B. F. GISIN, and G. W. GOKEL. Anal. Chem. **55**, 383 (1983).
26. X.-W. HE and D. POE. Talanta, **29**, 767 (1982).

Can. J. Chem. Downloaded from www.nrcresearchpress.com by 91.121.58.235 on 09/07/12
For personal use only.

The enthalpy and entropy of cavity formation in liquids and Corresponding States Principle

MADALENA S. DIONÍSIO and JOAQUIM J. MOURA RAMOS[1]
Centro de Química Física Molecular (INIC), Complexo I, IST, Av. Rovisco Pais, 1096 Lisboa Codex, Portugal

AND

RAQUEL M. GONÇALVES
CECUL (INIC), Calçada Bento de Rocha Cabral, 14 1200 Lisboa, Portugal

Received October 13, 1989

MADALENA S. DIONÍSIO, JOAQUIM J. MOURA RAMOS, and RAQUEL M. GONÇALVES. Can. J. Chem. **68**, 1937 (1990).

A new method to calculate the enthalpy and entropy of cavity formation in liquids is proposed. The reference cavity formation process is identified with the vaporization of liquid in the absence of order and Corresponding States Principle is used to eliminate the order contribution to vaporization enthalpy. The proposed method agrees very well with Claverie's modification of the Pierotti's method but strongly disagrees with the Sinanoglu's method, particularly in the context of entropy of cavity formation.

The new method is checked by applying it to the description of solution process in alkane binary mixtures at infinite dilution and is used to study the solvent effect on the solvolysis of *t*-butyl chloride and bromide.

Key words: cavity formation, enthalpy and entropy of cavity formation, Corresponding States Principle, alkanes, intermolecular interactions, acentric factor, solvent effect.

MADALENA S. DIONÍSIO, JOAQUIM J. MOURA RAMOS et RAQUEL M. GONÇALVES. Can. J. Chem. **68**, 1937 (1990).

Dans ce travail nous proposons une rouvelle méthode pour calculer l'enthalpie et l'entropie de formation de cavités microscopiques dans les liquides. Le processus de formation de la cavité de référence est identifié au processus de vaporisation du liquide en absence d'ordre; le Principle des États Correspondants est utilisé pour éliminer de l'enthalpie de vaporisation cette contribution due à l'ordre. La méthode proposée conduit à des résultats qui sont en bon accord avec ceux obtenues par la méthode de Pierotti modifiée par Claverie mais sont en désaccord avec la méthode de Sinanoglu particulièrement en ce qui concerne l'entropie de formation de la cavité.

La nouvelle méthode est testée en l'utilisant pour décrire le processus de dissolution à dilution infinie en mélanges binaires d'alcanes et utilisée pour étudier l'effect de solvent sur la solvolyse d'halogénures de tertio-butyle.

Mots clés : formation de cavité, enthalpie et entropie de formation de cavité, Principle des États Correspondants, alcanes, interactions intermoleculaires, facteur acentrique, effect de solvent.

Introduction

During the past years considerable progress has been made in the theory of liquid mixtures of non-electrolytes. If molecular properties of component molecules are known it is possible to predict the thermodynamic equilibrium properties of mixtures by using appropriate statistical mechanical theories. This is certainly an interesting scientific subject with several important practical applications (1). Nevertheless, the case is less straightforward for mixtures whose components are polyatomic molecules interacting through non-spherically symmetric potentials and several molecular conformations are possible. The latter is usually the case for mixtures of practical importance in chemical engineering or in biochemistry. The major difficulties are associated with insufficient knowledge of many-body effects including short-range molecular order and medium effects on conformational equilibria, and also with the uncertainty of intermolecular potential between unlike molecules. Moreover, these theoretical treatments are very time-consuming, even in the era of supercomputers, so that there is still a need for simple models which, in some cases, can overcome the difficulties of rigorous treatment. The cavity model which has been extensively used to interpret solvent effects on chemical processes (2–6) is an example. In this model it is possible to calcualte the enthalpy, H_c the entropy, S_c, and the Gibbs energy, G_c, needed to create a microscopic (molecular sized) cavity in a pure liquid. The calculated quantities, together with the experimental dissolution thermodynamic quantities, enable us to obtain (without calculation) the solute–solvent interaction energy.

One of the main problems associated with the calculation of the energetics of cavity formation in liquids is a thermodynamic description of the *reference* cavity formation process. A reference cavity is one that has same size and shape as the space occupied by a single molecule in a pure liquid. This reference cavity corresponds to the absence of a molecule in the bulk of the liquid and it is thus characterised by the same correlations with its neighbouring molecules as the "absent" molecule. The calculation of the energetics of formation of a reference cavity was based on the identification of its formation process with that of vaporization of the liquid (3, 5). In recent works (7, 8) we pointed out that these two processes cannot be identified with each other because we have emphasized on their differences. In fact, the formation of a reference cavity is not associated with the changes in molecular order of the liquid, as is the case for vaporization. An alternative method was thus proposed to calculate the enthalpy of formation of a reference cavity and this method was tested using solution enthalpy data at infinite dilution for *n*-alkane binary mixtures. It has also been shown that this method is potentially better than other methods proposed in the literature, namely that based on the Scaled Particle Theory.

In the present work we wish to present a new formulation of this problem. In this new formulation the reference cavity formation process is viewed again as physically different from a vaporization process (it does not imply the destruction of the molecular order of a liquid) and now we will be able to calculate

[1]Author to whom correspondence should be addressed.

Printed in Canada / Imprimé au Canada

Can. J. Chem. Downloaded from www.nrcresearchpress.com by 91.121.58.235 on 09/07/12
For personal use only.

Can. J. Chem. Downloaded from www.nrcresearchpress.com by 91.121.58.235 on 09/07/12
For personal use only.

its energetics from different physical properties of the liquid. We will propose a set of equations to calculate the enthalpy, the entropy, and the Gibbs energy of cavity formation and show that these equations are thermodynamically consistent in that they are related to each other by the Gibbs-Helmholtz relationship. This new semi-empirical method will be used to describe the dissolution of alkane solutes at infinite dilution in alkane solvents and to study the solvent effect on the solvolysis of *t*-butyl halides.

The vaporization of a liquid in the absence of order

Let us first consider simple liquids (monoatomic or apolar and spherical molecular liquids) that comply with the two-parameter Corresponding States Principle (CSP) (9). For these liquids the reduced saturated pressure varies with the reduced temperature in a way that is approximately described by Rowlinson equation:

$$[1] \qquad \ln p_r = 5.365\left(1 - \frac{1}{T_r}\right)$$

If eq. [1] holds in low saturated pressure region, by applying the Clapeyron–Clausius equation,[2] it can be shown that the vaporization enthalpy, H^0_{vs}, is independent of temperature:

$$[2] \qquad H^0_{vs} = 5.365RT_c$$

where T_c is the critical temperature.

For liquids complying with the three-parameter CSP, so-called normal liquids (9, 11), the following equation applies:

$$[3] \qquad \ln p_r = 5.365(1 + \omega)\left(1 - \frac{1}{T_r}\right)$$

where ω is the Pitzer acentric factor. For normal liquids of weak polarity and/or small shape anisotropy, the vaporization enthalpy is also independent of temperature in the low pressure region and is represented by

$$[4] \qquad H^0_{vn} = 5.365(1 + \omega)RT_c$$

Complex liquids composed of polar, associated, and/or anisotropic and flexible molecules deviate from the three-parameter CSP and have temperature-dependent vaporization enthalpies. These liquids show a temperature-dependent molecular order and temperature-dependent molecular degrees of freedom which are changed in the vaporization process and are at the origin of the temperature dependence of vaporization enthalpy. There are different qualitative explanation on their deviations from CPS (12): (*1*) interactions between molecular peripheries; (*2*) non-central forces arising from electric moments (long-range forces) and/or anisotropic shape (short-range forces), leading to ordered local structures at low temperatures; and (*3*) density-dependent rotational and librational degrees of freedom (internal rotation in flexible molecules, hindered overall rotation in anisotropic molecules).

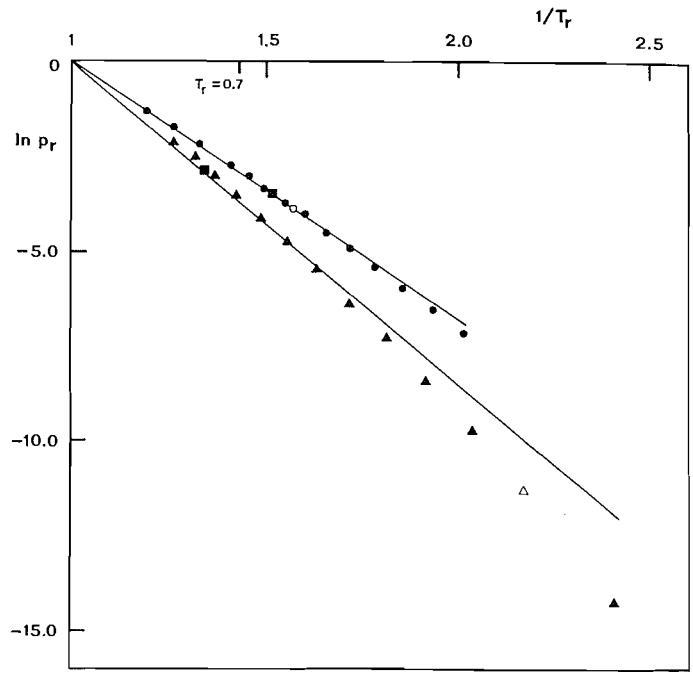

FIG. 1. Reduced saturated vapor pressure as a function of the inverse of reduced temperature for *n*-pentane (circles) and *n*-dodecane (triangles). Empty symbols indicate values at room temperature (25°C). Squares are values at normal boiling point. These data are taken from ref. 24.

For complex liquids we have a bending in the $\ln p_r$ *vs.* $1/T_r$ curve in the low pressure region as shown in Fig. 1 (for pentane and dodecane), 2 (for acetone and methanol), and 3 (for water). Between the critical point and normal boiling point (shown as squares) these curves are nearly linear or have a very elongated S-shape (13). With decreasing temperature the reduced saturated vapor pressure curve shows an increased curvature for ordered liquids. For *n*-pentane the curve is almost linear even at temperatures far below room temperature (empty circle), the deviation from the linearity being apparent only for temperatures lower than -10°C ($1/T_r > 1.78$). On the other hand, the curve for *n*-dodecane, as well as curves for methanol and water, show that deviation from linearity starts near T_b and is quite strong at room temperature. Since the deviation from linearity of the reduced vapor pressure curve is a consequence of the liquid order which decreases rapidly with increasing temperature (14, 15), at normal boiling point liquid order is destroyed and the liquid is expected to obey the three-parameter CSP (in fact, one can eliminate the contribution of order using behaviour at high temperatures). If so, the same must be true for temperature $T_r = 0.7$ at which the acentric factor is measured. In fact, as shown in Table 1, this temperature is generally higher than the normal boiling temperature except for long *n*-alkanes. Even in this case, the temperature $T_r = 0.7$ is not very different from normal boiling temperature and is higher than room temperature. Moreover, we can see from Figs. 1–3 that the points at $T_r = 0.7$ and at normal boiling point are inside the linear region of the curves. This is true for alkanes, acetone, methanol, and even for water. We can thus assume that the straight line defined by the

[2]The fact that the $\ln p_r$ *vs.* $1/T_r$ curve is linear between the critical point and the normal boiling point (high pressure region) does not mean that the vaporization enthalpy is constant and independent of temperature in this region. The Clapeyron–Clausius equation in reduced variables can be written as

$$\frac{d \ln p_r}{d\, 1/T_r} = -\frac{H^0_v}{RT_c}$$

if we assume an ideal gas behaviour. The linearity in the high pressure region is then the result of compensation of errors from assuming a constant vaporization enthalpy and an ideal gas behaviour. Below the normal boiling point, on the other hand, the saturated vapor pressures are small and so are the deviations from the ideal gas behaviour. Thus the linearity of the $\ln p_r$ *vs.* $1/T_r$ curve in this low pressure region indicates that the vaporization enthalpy is independent of the temperature.

TABLE 1. A comparison between normal boiling temperature (T_b) and the temperature at which acentric factor is measured ($0.7T_c$)

Compound	T_c /K	$0.7T_c$ /K	T_b /K
n-Pentane	469.7	329.8	309.2
n-Hexane	507.5	355.3	341.9
n-Decane	617.7	432.4	447.3
n-Dodecane	658.2	460.7	489.5
n-Hexadecane	722	505.4	560.0
Benzene	562.2	393.5	353.2
Acetone	508.1	355.7	329.2
Methanol	512.6	358.8	337.7
Ethanol	513.9	359.7	351.4
Water	647.3	453.1	373.2

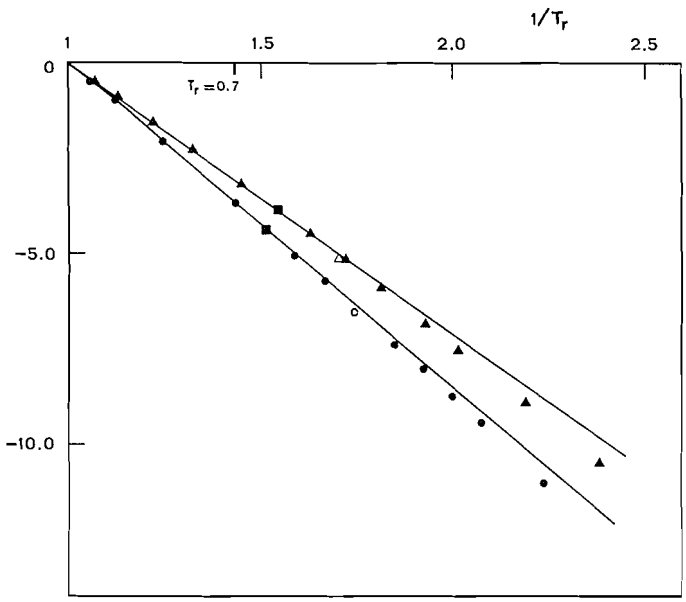

FIG. 2. Reduced saturated vapor pressure as a function of the inverse of reduced temperature for acetone (triangles) and methanol (circles). Empty symbols indicate values at room temperature (25°C). Squares are values at normal boiling point. These data are taken from ref. 24.

critical point and the point at $T_r = 0.7$, or alternatively at normal boiling point, will represent the saturated vapor pressure curve a liquid would have in the absence of order.

We will now show that both definitions are similar. Equation [3] is the straight line which passes through the critical point and the point at $T_r = 0.7$, its slope is $-5.365\,(1 + \omega)$. On the other hand, the equation of the straight line which passes through the critical point and normal boiling point ($p_b = 1$ atm) can be written as:

$$[5] \qquad \ln p_r = \frac{\ln p_c}{T_c/T_b - 1}\left(1 - \frac{1}{T_r}\right)$$

where p_c, critical pressure, is expressed in atmospheres. The slope of $\ln p_r$ *vs.* $1/T_r$ is $-\ln p_c/(T_c/T_b - 1)$. Equations [3] and [5] will be equivalent if their slopes are the same or if

$$[6] \qquad \omega = \frac{T_b}{5.365(T_c - T_b)} \ln p_c - 1$$

for different liquids. In Table 2 experimental values of the

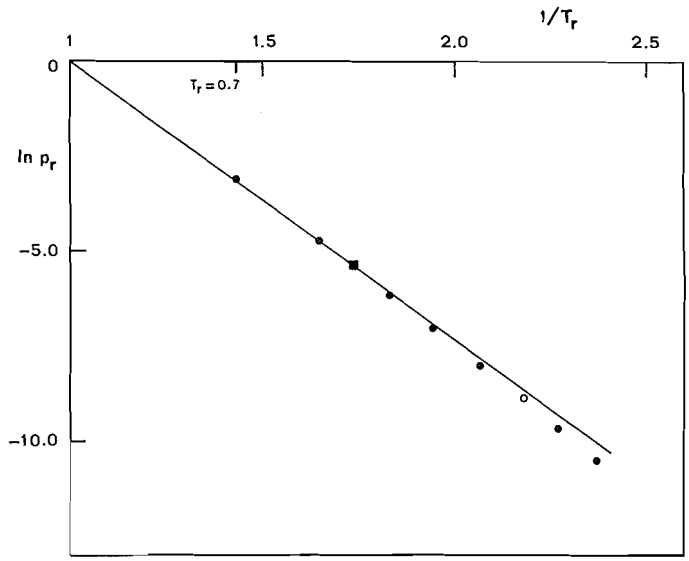

FIG. 3. Reduced saturated vapor pressure as a function of the inverse of reduced temperature for water. Empty symbol indicates value at room temperature (25°C) and square is the value at normal boiling point. These data are taken from ref. 24.

TABLE 2. A comparison between experimental values of acentric factor, ω, and those calculated with eq. [6][a]

Compound	ω Experimental	ω Eq. [6]
n-Pentane	0.251	0.258
n-Hexane	0.296	0.305
n-Decane	0.490	0.488
n-Dodecane	0.562	0.562
n-Hexadecane	0.742	0.697
Benzene	0.212	0.221
Acetone	0.304	0.316
Methanol	0.556	0.567
Ethanol	0.644	0.654
Water	0.344	0.367

[a]Experimental acentric factors, normal boiling temperatures, and critical data are taken from ref. 16.

acentric factor are compared with those calculated from the right-hand side of eq. [6]. That these values are similar, even for complex liquids (alcohols and water), shows that eqs. [3] and [5] are equivalent and suggests that eq. [6] can be used to predict acentric factor values. We can thus assume eq. [3] and eq. [5] both represent the saturated vapor pressure curve a complex liquid would have if order was absent. From eq. [5] we can also obtain the vaporization enthalpy of a normal liquid in the low pressure region:

$$[7] \qquad H^0_{vn} = R\frac{T_c T_b}{T_c - T_b} \ln p_c$$

Since eqs. [3] and [5] are equivalent as indicated by their similar slopes (Table 2), so are eqs. [4] and [7].

The enthalpy of the reference and of the solute cavity formation

We emphasized previously (7, 8) that the reference cavity formation process does not imply molecular order changes in the

Can. J. Chem. Downloaded from www.nrcresearchpress.com by 91.121.58.235 on 09/07/12
For personal use only.

Can. J. Chem. Downloaded from www.nrcresearchpress.com by 91.121.58.235 on 09/07/12
For personal use only.

liquid and that the internal molecular degrees of freedom are maintained in this process. In this context the enthalpy of formation of the reference cavity, H_{c0}, can be identified with the vaporization enthalpy a liquid would have if it was a normal liquid (if it obeyed the three-parameter CSP), i.e., if temperature-dependent contributions to the vaporization enthalpy were absent. From eq. [4] we can thus write

$$[8] \quad H_{c0} = 5.365(1 + \omega)RT_c$$

or, alternatively, from eq. [7]

$$[9] \quad H_{c0} = R\frac{T_cT_b}{T_c - T_b} \ln p_c$$

The enthalpy of the reference cavity, calculated using eqs. [8] and [9] can be compared with the values obtained by our previously proposed method (7) which was based on

$$[10] \quad H_{c0} = \frac{H_v^0}{1 + \omega} - T\Delta C_v$$

where H_v^0 is vaporization enthalpy at working temperature (25°C) and ΔC_v the difference, at the same temperature, between the specific heat at constant volume of gas and that of liquid. Table 3 shows a comparison between the H_{c0} values calculated from eqs. [8] and [10] and we can observe that the two sets of values show, except for water, a similar behaviour. We can also see that the H_{c0} value obtained for water from eq. [10] is greater than the vaporization enthalpy of water at 25°C (44.0 kJ mol^{-1}). For an ordered liquid H_{c0} must always be smaller than the vaporization enthalpy at room temperature since in the reference cavity formation process there is no order destruction as occurs in the vaporization process. The value of H_{c0} obtained for water from eq. [10] is thus inconsistent and we think that the method of calculating H_{c0} from eqs. [8] and [9] has a deeper physical foundation and a clearer physical meaning when compared with that based on eq. [10]. In fact, eq. [10] is the sum of two terms whose physical significance is not very clear. On the one hand, the ΔC_v contains an order contribution; and $H_v/(1 + \omega)$ does not represent, as previously shown, the vaporization enthalpy of a liquid in the absence of order which is most correctly described by eq. [4] or [7]. Equation [10] is thus a semi-empirical equation in which the sum $H_v/(1 + \omega) - T\Delta C_v$ has no overall physical significance. Moreover, the method based on eqs. [8] or [9] is easier to use since the physical properties needed for calculation are easily available in the literature (in particular this method avoids the use of ΔC_v values which are not always available).

It is also interesting to note that the quantity H_{c0}/S_0, where H_{c0} is calculated from eq. [8] or [9] and S_0 is the exposed molecular area (surface of the reference cavity), shows similar values for liquids composed of molecules of similar chemical nature. This was expected since H_{c0} is related to the interaction energy of a molecule with its whole surroundings. Alkane liquids are composed by molecules with similar contact energies and so the molar interaction energy per unit of exposed surface area must be identical for different alkanes. Table 4 shows the H_{c0}/S_0 values for different *n*-alkanes (S_0 was calculated as indicated in the table). The close similarity of these values supports the idea of similar contact energies of those molecules. This behaviour was not observed for other properties such as cohesive energy density or internal pressure which have been used extensively in the theories of solutions (17, 18). The quantity H_{c0}/S_0 is thus potentially a useful property of liquids in liquid–solution thermodynamics and is to be explored in the quantitative study of intermolecular forces.

TABLE 3. A comparison between two different methods of calculating enthalpy of the reference cavity; the third column (the enthalpy of vaporization at 25°C) can be compared with the first column to estimate the order of contribution to the enthalpy of the liquid

Compound	H_{co} /kJ mol^{-1} Eq. [8]	H_{co} /kJ mol^{-1} Eq. [10]	H_v^0(25°C) /kJ mol^{-1}
n-Pentane	25.2	26.3	26.7
n-Hexane	29.4	29.2	31.5
n-Decane	41.0	43.5	51.4
n-Dodecane	46.3	50.1	61.3
n-Hexadecane	56.1	61.4	81.4
Benzene	30.4	34.2	33.9
Acetone	29.6	29.7	30.9
Methanol	35.6	33.0	37.4
Ethanol	37.7	36.8	42.3
Water	38.8	47.4	44.0

The entropy and the Gibbs energy of the reference cavity

From eq. [1] it can be shown that the standard vaporization entropy of a simple liquid is given by

$$[11] \quad S_{vs}^0 = 5.365R + R \ln p_c$$

For a normal liquid, from eq. [3] we will have

$$[12] \quad S_{vn}^0 = 5.365(1 + \omega)R + R \ln p_c$$

and from eq. [5]

$$[13] \quad S_{vn}^0 = R\frac{T_b}{T_c - T_b} \ln p_c + R \ln p_c$$

We recall that the critical pressure in eqs. [11]–[13] must be expressed in atmospheres, and that eqs. [12] and [13] are equivalent as are eqs. [4] and [7].

We will now focus our attention on the entropy of formation of the reference cavity. For a simple liquid (composed of spherical and non-polar molecules) this entropy must be zero since there are no correlations between the reference cavity and the neighbouring molecules. The entropy of cavity formation in those liquids is a configurational entropy (the ideal entropy of mixing) or a cratic entropy in the language of Gurney (19), as opposed to the unitary or contact entropy which reflects contacts or correlations, at the molecular level, between movements and orientations of the reference cavity and those of the neighbouring molecules.[3] The cratic contribution to entropy (or to Gibbs energy) is not measurable, i.e., it is not included in experimental thermodynamic properties such as solution entropies or Gibbs energies. For a normal liquid (complying with the three-parameter CSP), on the other hand, the reference cavity will

[3]Cratic entropy does not depend on the chemical nature of particles taking part in the process. It is only a function of composition. As pointed out by Ben-Naim (20) the unitary entropy, on the other hand, may also depend on the composition of non-ideal solutions of intermediate concentration. In this situation the unitary entropy is not a characteristic of the particles only. We are considering, however, the infinite dilution situation and in this context the unitary entropy is really a characteristic of the contact between particles, and is independent of composition.

Can. J. Chem. Downloaded from www.nrcresearchpress.com by 91.121.58.235 on 09/07/12
For personal use only.

TABLE 4. Molar interaction energy per unit of exposed surface area, H_{c0}/S_0, for *n*-alkane liquids

Compound	$10^8 H_{c0}/S_0$[a] /J cm^{-2}
n-Pentane	269.3[b]
n-Hexane	260.1[d]
n-Heptane	267.8[d]
n-Octane	253.3[c]
n-Nonane	257.1[c]
n-Decane	259.1[c]
n-Undecane	261.7[c]
n-Dodecane	261.7[c]
n-Tridecane	262.6[c]
n-Tetradecane	265.4[c]
n-Pentadecane	262.5[c]
n-Hexadecane	261.8[c]

[a] H_{c0} calculated from eq. [8].

[b] S_0 calculated assuming spherical approximation by using the equation $S_0/\text{cm}^2\ \text{mol}^{-1} = 4.084 \times 10^8 V_0^{2/3}$, where V_0 is the molar volume in cm^3 mol^{-1}. In fact, it is known that long *n*-alkane molecules in the liquid state are in extended conformations so that the cavity occupied by each molecule is much more like cylinders than spheres. For smaller alkane molecules, however, the shape anisotropy is small and the spherical approximation must be used.

[c] S_0 calculated assuming the molecules are cylindrical with $r = 3.5$ Å (see ref. 7) by using the equation $S_0/\text{cm}^2\ \text{mol}^{-1} = 10^8 (46.358 + 0.571\ V_0)$, where V_0 is the molar volume in cm^3 mol^{-1}.

[d] Mean value from footnotes *b* and *c*. As explained in footnote *b* it is logical to consider intermediate sized *n*-alkane molecules as ellipsoidal, a shape which is intermediate between a sphere and a cylinder.

have orientational correlations with neighbouring molecules and so the reference cavity will have a non-zero entropy. This entropy, S_{c0} (which must be negative since the presence of those correlations lowers the entropy), will thus be given by the difference between the entropy of the liquid if it was normal and the entropy of the simple liquid. Otherwise stated, the entropy of the reference cavity will be the difference between the vaporization entropy of the simple liquid (eq. [11]) and the vaporization entropy the liquid under consideration would have if it was a normal liquid (eq. [12] or [13]). For eqs. [11] and [12] we thus have

$$[14] \quad S_{c0} = -5.365\omega R$$

and from [11] and [13]

$$[15] \quad S_{c0} = R\left[5.365 - \frac{T_b}{T_c - T_b} \ln p_c\right]$$

Hence, Gibbs energy of the reference cavity will be given by

$$[16] \quad G_{c0} = 5.365R\,[\,T_c + \omega(T_c + T)]$$

from eqs. [8] and [14] or, alternatively, from eqs. [9] and [15]

$$[17] \quad G_{c0} = R\left[\frac{T_b(T_c + T)}{T_c - T_b} \ln p_c - 5.365\,T\right]$$

where T is the working temperature. We recall again that the critical pressure, p_c, in eqs. [15] and [17] must be expressed in atmospheres.

We thus have two different sets of equivalent equations ([8], [14], and [16] on the one hand — method 1 — and eqs. [9], [15], and [17] on the other — method 2) which enable us to calculate the energetics of the reference cavity from different macroscopic properties of liquids. To use method 1 the experimental values of ω and T_c are needed. To use method 2 we need to know T_c, p_c, and T_b. Since the knowledge of the acentric factor implies the knowledge of the critical pressure, method 2 can be more useful if the critical pressure is known but not the acentric factor (or the vapor pressure at $T_r = 0.7$). Nevertheless in the case where all the experimental data are available, the two methods are equivalent and there is no reason to prefer one or the other. The fact that these properties are generally available in the literature is one advantage of the present method over methods proposed before (the Sinanoglu method (5) needs saturated vapor pressure at 25°C, a statistic not available for liquids of very low volatility, such as hexadecane, and our previous method for calculating H_{c0} (7, 8) needed ΔC_v, the difference between the specific heats at constant volume of the gas and liquid at 25°C, a value not easily available in the literature for many organic liquids). The most important point, however, is that we have now a thermodynamically consistent method to obtain the different quantities associated with the formation of the reference cavity.

Table 5 shows the values of H_{c0}, S_{c0}, and G_{c0} for different liquids and calculated by different methods (the Sinanoglu method (5), the modified SPT (6), and the method we presented based on eqs. [8], [14], and [16]). Table 5 shows that (*a*) the H_{c0} values calculated by all three methods are relatively close for most liquids; (*b*) the S_{c0} values are large and positive when calculated by the Sinanoglu method and are always negative and generally small when calculated by the two other methods. A relatively good agreement exists between the S_{c0} values calculated by Claverie's modification (6) of the Pierotti method and those calculated by the method we propose in the present work (eq. [14]). As argued (6), these values are compatible with the negative values obtained by Ben-Naim (21) for "insertion" entropy, since the cavity contributes most to that entropy. This is not the case with the values obtained by the Sinanoglu method; (*c*) there is a good agreement between the G_{c0} values calculated by modified SPT (6) and by eq. [16]. The Sinanoglu values are substantially lower as a consequence of the large and positive S_{c0} values obtained by this method.

It seems to us that the high S_{c0} and low G_{c0} values obtained by the Sinanoglu method are the result of an incorrect treatment of G_{c0} which is taken as

$$[18] \quad G_{c0} = -RT \ln p + RT \ln (V_g/V)$$

where p is the saturated vapor pressure at 25°C (in atmospheres), V_g the molar volume of the ideal gas at 25°C and 1 atm, and V the volume accessible to the translational motions of the molecules in the liquid (taken as the molar volume of the liquid). We must realize that both terms on the right-hand side of eq. [18] are "purely" entropic terms. In the first one $R \ln p$ describes the entropy change of the vapor when it is compressed from the saturated vapor pressure at 25°C to the standard pressure ($p^0 =$ 1 atm) and is thus a gas phase term. The second term accounts for the change in positional entropy of the molecules as they go from an accessible volume V to the volume of one mole of ideal gas. Since in the cavity formation process all molecules remain

TABLE 5. Enthalpy, H_{c0}, entropy, S_{c0}, and Gibbs energy, G_{c0}, of the reference cavity for different liquids calculated following the Sinanoglu method (line *1*), the modified SPT (line *2*)[a], and eqs. [8], [14], and [16] (line *3*)

Compound	H_{c0} /kJ mol^{-1}	S_{c0} /J K^{-1} mol^{-1}	G_{c0} /kJ mol^{-1}
Cyclohexane	31.44	43.4	18.50
	30.25	−5.3	31.84
	29.92	−9.5	32.74
Benzene	32.27	44.3	19.06
	31.21	−1.4	31.67
	30.39	−9.5	33.21
Toluene	36.30	49.3	21.61
	32.22	−9.0	34.89
	33.34	−11.7	36.84
Acetone	29.57	41.0	17.34
	27.24	−1.1	26.90
	29.55	−13.6	33.60
Carbon tetrachloride	30.83	41.8	18.38
	31.42	−4.5	32.80
	29.61	−8.6	32.18
Chloroform	29.45	39.9	17.54
	29.83	−4.8	31.25
	29.14	−9.7	32.04
Aniline	53.90	75.9	31.29
	41.46	−22.6	48.20
	43.15	−17.1	48.26
Nitromethane	36.69	47.0	22.68
	25.77	−11.7	29.29
	34.36	−13.8	38.48
Dimethylformamide	45.74	61.3	27.47
	32.93	−18.7	38.49
	48.35	−36.4	59.22
Nitorbenzene	50.60	58.6	33.13
	37.24	−18.3	42.68
	44.61	−16.3	49.48

[a]Values taken from ref. 6.

in the liquid phase (they do not undergo any phase transition), it is hard to understand how the terms in eq. [18] are able to describe this process. Another criticism to the Sinanoglu method is that we cannot identify H_{c0} with the vaporization enthalpy of the liquid at 25°C. This does not dramatically affect the liquids presented in Table 5 but is, as previously shown (7, 8), very important when we are dealing with long-chain alkanes where the deviations from the three-parameter CSP are very large at 25°C. These are strong enough arguments which lead us to consider that the Sinanoglu method is not a good method to calculate the energetics of cavity formation, particularly on the entropy and Gibbs energy of cavity formation.

Energetics of the solute cavity formation

From the thermodynamic parameters associated with the formation of the reference cavity in a given solvent we can calculate those parameters for any solute cavity in the same solvent. The method has already been described (7, 8) and we will just briefly refer to it to clarify the text which follows.

If we describe the cavity formation process as work done against the surface forces of the solvent we will have, for molar Gibbs energy of cavity formation,

$$[19] \quad G_c = N_A \sigma_0 S k_g$$

and for molar enthapy

$$[20] \quad H_c = N_A \sigma_0 A_0 S k_h$$

where A_0 is given by

$$[20a] \quad A_0 = 1 - T\left(\frac{1}{\sigma_0}\frac{d\sigma_0}{dT} + \frac{2}{3}\alpha_0\right)$$

In these equations N_A is the Avogadro's constant, σ^0 the solvent surface tension, α_0 the isobaric thermal expansion coefficient of the solvent, S the surface area of the cavity, k_g a correction factor to take into account the influence of the curvature of the cavity surface on its surface tension, and k_h a similar correction factor for the enthalpy part of surface tension. k_g and k_h depend on the size and shape of the cavity and we will consider, as before, (7, 8) two different significant situations. (*1*) *the curvature of the solute cavity is the same as that of the reference cavity* (see ref. (7) for a detailed explanation of the significance of this situation); in this case we will have

$$[21] \quad k_g = k_{g0} \quad \text{and} \quad k_h = k_{h0}$$

where the subscript zero denotes the reference cavity. For this cavity eqs. [19] and [20] take the form

$$[22] \quad G_{c0} = N_A \sigma_0 S_0 k_{g0}$$

and

$$[23] \quad H_{c0} = N_A \sigma_0 A_0 S_0 k_{h0}$$

where S_0 is the surface area of the reference cavity.

Comparing [22] with [19] and [23] with [20] we conclude that

$$[24] \quad G_c = \frac{S}{S_0} G_{c0}$$

and

$$[25] \quad H_c = \frac{S}{S_0} H_{c0}$$

(*2*) *The solute and the reference cavities are spheres of different radii*. In this case k_g and k_h will depend on the size of the cavity according to

$$[26] \quad k = 1 + \frac{S_0}{S}(k_0 - 1)$$

and we obtain

$$[27] \quad G_c = N_A \sigma_0 (S - S_0) + G_{c0}$$

$$[28] \quad H_c = H_A \sigma_0 A_0 (S - S_0) + H_{c0}$$

It is most useful to express eqs. [24]–[27] in terms of the cavity volume instead of its surface area. For spherical cavities we have $S = 4\pi r^2$ and if we consider $V = N_A 4\pi r^3/3$ where V is the molar volume of the liquid, we have

$$[29] \quad S = (4\pi)^{1/3}\left(\frac{3V}{N_A}\right)^{2/3}$$

and substituting [29] in [27] and [28] we will obtain

$$[30] \quad G_c/\text{J mol}^{-1} = 40.840\sigma_0(V^{2/3} - V_0^{2/3}) + G_{c0}$$

Can. J. Chem. Downloaded from www.nrcresearchpress.com by 91.121.58.235 on 09/07/12
For personal use only.

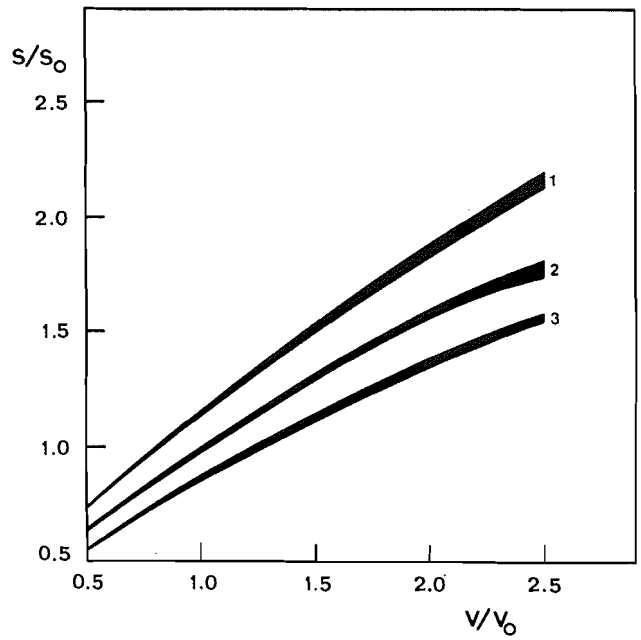

FIG. 4. Qualitative picture of the variation of S/S_0 with the volume of cavity according to eq. [33], curve *1*, eq. [31] or eq. [35], curve *2*, and eq. [34], curve *3*.

and

[31] $$H_c/\text{J mol}^{-1} = 40.840\sigma_0 A_0(V^{2/3} - V_0^{2/3}) + H_{c0}$$

where the factor 40.840 contains constants and unit conversion factors to give G_c and H_c in J mol^{-1} if V is expressed in cm^3 mol^{-1} and σ_0 in dyn cm^{-1}. We would recall that eqs. [30] and [31] can be used if both solute and reference cavities are spherical, in which case k varies according to [26]. If the curvature of those cavities are similar we must use eqs. [24] and [25]. As shown in ref. 7, the quantity S/S_0 in these equations may take different forms according to the shape of the cavities. We will consider here only two kinds of cavity shape: cylindrical cavities of radius 3.5 Å (see footnote 8 in ref. 7) and spherical cavities. We will thus have the following different situations:

(*a*) cylindrical cavity in a cylindrical solvent

[32] $$\frac{S}{S_0} = \frac{0.140V + 11.3509}{0.140V_0 + 11.3509}$$

(*b*) cylindrical cavity in a spherical solvent

[33] $$\frac{S}{S_0} = \frac{0.140V + 11.3509}{V_0^{2/3}}$$

(*c*) spherical cavity in a cylindrical solvent

[34] $$\frac{S}{S_0} = \frac{V^{2/3}}{0.140V_0 + 11.3509}$$

(*d*) spherical cavity in a spherical solvent

[35] $$\frac{S}{S_0} = \left(\frac{V}{V_0}\right)^{2/3}$$

Figure 4 shows qualitatively how S/S_0 depends on the size of the cavity according to eqs. [32]–[35]. Equations [32] and [35] are nearly equivalent, leading to S/S_0 values which never differ more than 5% in the whole V/V_0 range. The results for these two equations are thus presented as a single curve (curve *2*). From Fig. 4 we can see that eq. [33] leads to higher S/S_0 values (curve *1*) and eq. [34] leads to lower values (curve *3*). We can also see that the difference between the S/S_0 values obtained by the different equations is significant and increases when the solute is large compared with the solvent molecule. These conclusions show the need for a realistic description of the shape of the solute and the reference cavities. The appropriate S/S_0 value must thus be introduced in eqs. [24] and [25] in order to calcuate the Gibbs energy and the enthalpy of solute cavity when its curvature is similar to that of the reference cavity. In Table 6 the physical properties for a large number or organic solvents needed for the calculations are presented.

Application to *n*-alkane binary mixtures and discussion

The difficulty with any model for calculating cavity properties is that we cannot verify its validity experimentally. The most straightforward method of verifying the validity of a cavity model is to apply it to the description of the dissolution process of a liquid solute in a solvent at infinite dilution (7). In fact, under such conditions there are no solute–solute interactions and the thermodynamic properties, X_d, associated with the solution process ($X_d = G_d, S_d, H_d$) can be factorized as

[36] $$X_d = X_v + X_{solv} = X_s + X_c + X_i$$

where X_v is the vaporization energy of the solute, X_{solv} is the solvation energy of the solute in the solvent, X_s describes the separation or dispersion of the solute molecules in the solvent, X_c describes the formation of the solute cavity in the solvent, and X_i describes the solute–solvent interaction. For structured solvents a fourth term should be added to eq. [36] to describe the change of the solvent structure around the solute molecule. Nevertheless, as pointed out by Friedman (22) this term would be zero for Gibbs energy since the solute cosphere is in equilibrium with the bulk. Equation [36] can be used to evaluate a cavity model if we calculate the solute–solvent interaction energy and the cavity energy and compare with the experimental solvation energy. This was done by Pierotti (23) to test the method based on the Scaled Particle Theory. Nevertheless, as pointed out in the Introduction, the calculation of the interaction term is a difficult task for complex systems, precisely where the different cavity models diverge. In fact, for simple systems (composed of molecules with moderate shape anisotropy and polarity and without strong directional interactions) the different methods proposed in the literature to calculate the energetics of cavity formation are nearly equivalent. On the other hand, one advantage of the cavity models is, as stated before in the Introduction and in ref. 7, the possibility of obtaining the interaction term and thus avoiding the complex and uncertaint task of its calculation. This is why we prefer to check our cavity model by applying it to systems in which the solute and solvent molecules have similar chemical nature or similar contact energies. In this situation we have $X_c = -X_i/2$, so eq. [36] becomes

[37] $$X_s - X_d = X_c$$

The *n*-alkane molecules have very similar chemical nature, the only difference being the fraction of molecular surface covered by methyl and methylene groups. Since these groups are thermodynamically very similar, the *n*-alkane binary mixtures are certainly the systems most likely to satisfy eq. [37]. As shown before (7, 8), X_s is equivalent to the energy of the solute

Can. J. Chem. Downloaded from www.nrcresearchpress.com by 91.121.58.235 on 09/07/12
For personal use only.

TABLE 6. Physical properties of some organic liquids

Reference number	Compound	V^a /cm^3 mol^{-1}	σ^b /dyne cm^{-1}	A^c	ω^d	T_c^e /K	p_c^f /atm	T_b^g /K
1	*n*-Pentane	116.29	15.48	2.712	0.251	469.7	33.26	309.2
2	*n*-Hexane	131.61	17.91	2.426	0.299	507.5	29.71	341.9
3	*n*-Heptane	147.47	19.80	2.227	0.349	540.3	27.04	371.6
4	*n*-Octane	163.54	21.14	2.111	0.398	568.8	24.57	398.8
5	*n*-Nonane	179.68	22.38	2.032	0.445	594.6	22.60	424.0
6	*n*-Decane	195.92	23.37	1.965	0.489	617.7	20.92	447.3
7	*n*-Undecane	211.23	24.34	1.886	0.535	638.8	19.44	469.1
8	*n*-Dodecane	228.60	24.91	1.864	0.575	658.2	18.00	489.5
9	*n*-Tridecane	244.92	25.69	1.822	0.619	676.0	16.98	508.6
10	*n*-Tetradecane	261.30	26.26	1.793	0.680	693.0	15.99[h]	526.7
11	*n*-Pentadecane	277.69	26.74	1.769	0.706	707.0	15.00	543.8
12	*n*-Hexadecane	294.07	27.22	1.753	0.742	722.0	13.92	560.0
13	Cyclopentane	97.72	21.82	2.371	0.192	511.7	44.51	322.4
14	Cyclohexane	108.75	24.35	2.473	0.212	553.5	40.17	353.8
15	Cyclooctane	134.87	29.30	1.915	0.236	647.2	35.13	422.0
16	Benzene	89.41	28.18	2.236	0.212	562.2	48.26	353.2
17	Chlorobenzene	102.24	32.7	1.899	0.249	632.4	44.61	404.9
18	Cabon tetrachloride	97.09	26.15	2.126	0.193	556.4	45.00	349.9
19	Carbon disulphide	60.63	31.52	2.143	0.109	552.0	77.97	319.0
20	Diethyl ether	104.75	16.50	2.670	0.281	466.7	35.92	307.6
21	Acetone	73.98	22.67	2.296	0.304	508.1	46.39	329.2
22	Chloroform	80.67	26.53	2.166	0.218	536.4	53.00	334.3
23	Acetonitrile	52.86	23.45	2.275	0.327	545.5	47.67	354.8
24	Dimethylformamide	77.43	36.17	1.814	0.817	596.6	51.5	426.2
25	Nitromethane	53.96	36.48	1.919	0.310	588.0	62.27	374.3
26	Nitrobenzene	102.74	42.76	1.742	0.366	732.15	42.9	484.0
27	Aniline	91.53	42.79	1.528	0.384	699.0	52.41	457.6
28	Methanol	40.73	22.20	1.918	0.556	512.6	79.84	337.7
29	Ethanol	58.69	21.85	1.929	0.644	513.9	60.60	351.4
30	1-Propanol	75.17	23.30	1.839	0.623	536.8	51.02	370.3
31	2-Propanol	76.96	21.24	1.561	0.665	508.3	46.98	355.4
32	1-Butanol	91.99	24.16	1.827	0.593	563.1	43.62	390.9
33	*t*-Butanol	97.76	20.02	2.254	0.612	506.2	39.18	355.5
34	Water	18.07	71.97	1.591	0.344	647.3	218.31	373.2

[a]Molar volume at 25°C.
[b]Surface tension at 25°C.
[c]Calculated at 25°C from eq. [20*a*].
[d]Acentric factor from ref. 16.
[e]Critical temperature from ref. 16.
[f]Critical pressure from ref. 16 unless otherwise stated.
[g]Normal boiling temperature.
[h]From ref. 24.

Can. J. Chem. Downloaded from www.nrcresearchpress.com by 91.121.58.235 on 09/07/12
For personal use only.

reference cavity formation, so that we have $X_s = X_{c1}$, where the subscript 1 refers to the solute and [37] takes the form

[38] $$X_{c1} - X_d = X_c$$

To evaluate the validity of the method we propose to calculate the enthalpy and entropy of cavity formation by applying eq. [38] to *n*-alkane binary mixtures. Table 6 shows some physical properties of liquids needed for the calculations. The solution enthalpies at infinite dilution for *n*-alkane binary systems are shown in Table 3 of ref. 7. Table 7 shows a comparison between the quantity $H_{c1} - H_d$ (first member of eq. [38]) and H_c calculated by the method we propose in this work. Our H_c values are also compared with those calculated using the Scaled Particle Theory. From this table we can see that our values are in good agreement with the $H_{c1} - H_d$ values. Moreover, our results show an interesting feature we wish to emphasize. If we consider a given solute in different solvents we would expect to obtain the same H_c value if the interaction potential is the same for different solvents. This is the case for different *n*-alkanes solvents where molecules contain identical segments. In fact, from Table 7 we can see that the *n*-hexane cavity, for example, has nearly the same enthalpy in all *n*-alkane solvents, from *n*-heptane (30.3 kJ mol^{-1}) to *n*-hexadecane (31.0 kJ mol^{-1}). This interesting feature is not observed if we look at the H_c values obtained from the Scaled Particle Theory. We can also conclude that these H_c values are different from those obtained by our model, particularly for systems in which the solute and solvent molecules have different sizes.

The results in Table 7 are graphically presented in Fig. 5. To represent these results we transform eq. [38] by subtracting X_{c0} (a thermodynamic quantity associated with solvent reference cavity formation) to both sides of the equation. We thus have

[39] $$X_{c1} - X_{c0} - X_d = X_c - X_{c0}$$

Can. J. Chem. Downloaded from www.nrcresearchpress.com by 91.121.58.235 on 09/07/12
For personal use only.

TABLE 7. Enthalpy of cavity formation for different *n*-alkane solutes in different *n*-alkane solvents

Solute[a]	Solvent[a]	$H_{c1} - H_d$[b,c] /kJ mol^{-1}	H_c[c,d] /kJ mol^{-1}	H_c[e] /kJ mol^{-1}
1	2	26.4	27.4	28.1
3	2	32.6	31.7	34.1
4	2	35.5	33.9	37.0
6	2	41.0	38.4	42.5
7	2	43.5	40.5	45.4
8	2	45.8	43.0	48.1
12	2	54.1	52.0	57.4
1	3	26.3	28.2	28.5
2	3	29.5	30.3	31.5
4	3	35.5	34.9	37.5
5	3	38.3	37.2	40.5
6	3	41.0	39.5	43.2
8	3	45.8	44.2	48.8
12	3	54.1	53.5	58.2
2	4	29.5	30.9	31.2
8	4	45.8	44.9	48.4
12	4	54.3	54.4	57.8
2	6	29.4	31.5	32.4
8	6	45.9	45.8	50.3
2	7	29.4	31.7	35.3
2	8	28.3	31.5	34.3
3	8	32.5	33.9	37.8
4	8	35.4	36.3	40.9
6	8	41.0	41.1	47.2
1	12	25.1	24.8[f]	31.2
2	12	29.1	31.0	34.5
3	12	32.2	33.3	38.0
4	12	35.2	35.6	41.2
6	12	40.9	40.3	47.4

[a]Reference numbers of solutes and solvents are given in Table 6.
[b]Dissolution enthalpy, H_d, for these systems have been tabulated in ref. 7.
[c]The method used in the calculations was that based on eq. [9].
[d]Unless otherwise stated, eq. [32] was used to describe the molecular shape of both solute and solvent.
[e]H_c values calculated from the SPT using hard spheres diameters from Wilhelm and Battino (Table 4 in ref. 7).
[f]Equation [34] was used to describe the molecular shape of both solute and solvent.

The rationale for the modification is that eq. [39] is more discriminative than eq. [38], since it enables us to distinguish clearly systems composed of a large solute in a small solvent (positive values for both sides of eq. [39]) from those composed of a small solute in a large solvent (negative values for both sides). In Fig. 5 the ordinate represents the right hand side in eq. [39], the abcissa the left hand side, and the straight line means that both sides of eq. [39] are equal. We can see that the calculated points are reasonably close to the line. This observation is not a proof or a demonstration of the correctness of our model but shows that it enables us to make a consistent description of the solution process in terms of enthalpy. We have stated that there are no experimental methods to verify the validity of the model. However, the fact that our model allows for a consistent description of the solution process is a strong indication of its validity.

We will now use eq. [38] to check the validity of our model for Gibbs energy. In Table 8 the experimental Gibbs energies of dissolution for different alkane solutes at infinite dilution in alkane solvents as well as the results of calculations of G_c according to the model based on eq. [16] are presented. From

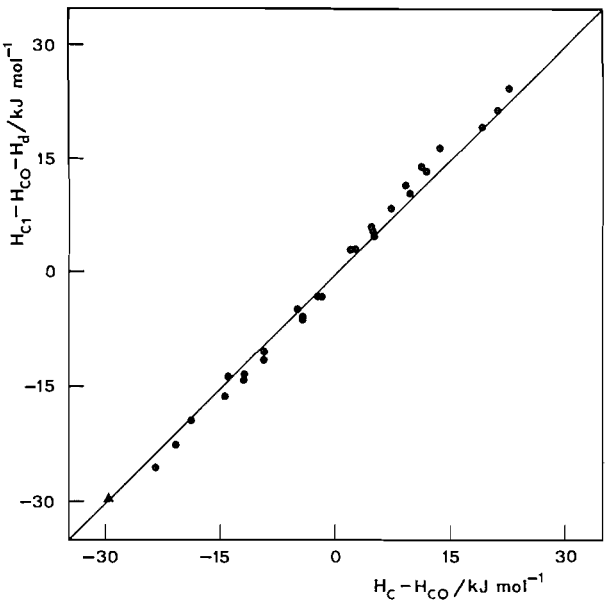

FIG. 5. Comparison between the parameters in eq. [39] for enthalpy. The points correspond to the systems presented in Table 7. To calculate H_c eq. [32] was used for all systems except for system 1/12 (triangle) where eq. [34] was used.

this table we can see that our G_c values compare reasonably well with $G_{c1} - G_d$. This agreement is not so good when the Sinanoglu method is used, as also shown in Table 8. The G_c values obtained using the Sinanoglu method are substantially lower than those obtained using our method. This is expected since, as discussed before, the Sinanoglu method gives high and positive values for the cavity entropy. Moreover, the same interesting feature we pointed out for enthalpy is observed again for Gibbs energy. Indeed we obtain for the cyclohexane cavity a G_c value which is similar in hexane and in hexadecane. The same is observed for the *n*-hexane solute for which G_c is identical in decane, dodecane, and hexadecane (32 kJ mol^{-1}) and also similar to the *n*-hexane reference cavity Gibbs energy, G_{c0} (33 kJ mol^{-1}). This interesting feature is not so clearly observed when the Sinanoglu method is used (the systems containing hexadecane are lacking because its saturated vapor pressure at 25°C is not available), as is not observed at all when the Pierotti method is used to calculate G_c.

As stated before, the fact that our G_c values are close to the $G_{c1} - G_d$ values is not a demonstration of the correctness of our method of calculation of the energetics of cavity formation in liquids. However, the fact that the calculated results follow eq. [38] means that our method allows for a consistent description of the solution process both for enthalpy and Gibbs energy.

The solvent effect on the solvolysis of *tert*-butyl chloride and bromide

To study the influence of solvent on reaction rates two main methods have been developed. One is to make use of multiple linear correlation analysis between rate constants (or Gibbs energies of activation) and a number of solvent parameters. In the second method, the solvent effect, generally in terms of Gibbs energy, is divided into initial-state and transition-state contributions. Further the resulting energies of transfer of the transition-state from one solvent to another are compared with corresponding values from a suitable model of the activated complex. In what concerns the solvolytic reactions of *tert*-butyl

TABLE 8. Gibbs energy of cavity formation for different alkane solutes in different alkane solvents, and a comparison with the Sinanoglu method

			Method based on eq. [16]		Sinanoglu method[h]	
Solute[a]	Solvent[a]	G_d[b] /kJ mol^{-1}	$G_{c1} - G_d$ /kJ mol^{-1}	G_c /kJ mol^{-1}	$G_{c1} - G_d$ /kJ mol^{-1}	G_c /kJ mol^{-1}
14	2	0.22[i]	32.5	31.1[c]	18.3	14.7[c]
6	2	−0.02[j]	47.6	50.2[d]	27.8	25.4[d]
7	2	−0.05[k]	50.9	53.0[d]	30.6	26.8[d]
8	2	−0.08[l]	54.0	56.1[d]	33.2	28.4[d]
12	2	−0.30[m]	66.3	68.0[d]		
14	12	−0.56[n]	33.3	33.4[e]		
2	12	−0.26[m]	33.6	32.5[e]		
2	6	−0.03[j]	33.4	31.7[e]	17.0	18.5[e]
2	7	−0.06[k]	33.4	32.2[e]	17.0	19.3[e]
2	8	−0.09[l]	33.5	32.2[e]	17.0	19.8[e]
2	14	0.37[i]	33.0	35.8[c]	16.6	21.5[g]
4	14	0.17[o]	40.6	39.8[c]	22.1	25.6[c]
10	14	−0.53[n]	61.5	59.1[f]		
12	14	−0.82[n]	66.8	64.7[f]		
13	14	−0.02[p]	29.8	31.2[c]	15.9	16.9[c]
15	14	0.10[p]	38.8	37.8[g]		
14	13	−0.02[p]	32.8	31.2[c]	18.5	17.2[c]
15	13	0.04[q]	38.8	36.0[g]		
14	15	0.10[p]	32.6	33.6[g]		
13	15	−0.02[q]	29.8	31.3[g]		
14	10	−0.39[n]	33.1	33.8[f]		

[a]Reference numbers of solutes and solvents are given in Table 6.
[b]Gibbs energy of dissolution of a solute at infinite dilution in a solvent, G_d, was obtained from the excess function G^E by calculating the limit of G^E/x_0x_1, when the solute mole fraction x_1 approaches zero (and when the solvent mole fraction x_0 approaches unity).
[c]Equation [30] was used to describe the molecular shapes of both solute and solvent.
[d]Equation [33] was used to describe the molecular shapes of both solute and solvent.
[e]Equation [34] was used to describe the molecular shapes of both solute and solvent.
[f]Equation [32] was used to describe the molecular shapes of both solute and solvent.
[g]Equation [35] was used to describe the molecular shapes of both solute and solvent.
[h]Calculations were not peformed on systems containing *n*-hexadecane, tetradecane, and cyclooctane since their saturated pressure at 25°C is not available in the literature.
[i]From ref. 25.
[j]From ref. 26.
[k]From ref. 27.
[l]From ref. 28.
[m]From ref. 29.
[n]From ref. 30.
[o]From ref. 31.
[p]From ref. 32.
[q]From ref. 33.

halides, pertinent properties of the transition state were deduced using the latter method (10, 34).

Some years ago, a different approach to the treatment of solvent effect on the rate of chemical reactions was proposed (4) and illustrated with a study of the solvent effect on the solvolysis of *tert*-butyl chloride. According to this approach the Gibbs energy of transfer of a solute from one solvent to another, δG, can be described as the sum of two contributions:

$$[40] \quad \delta G = \delta G_c + \delta G_i$$

where δG_c is related to energies required to create cavities in the solvents and δG_i is associated with solute–solvent interaction. The Gibbs energies of reorganization of the solvent molecules around the solute was neglected because of the enthalpy–entropy compensation which exists in those phenomena as pointed out before in this paper. Since charge separation in a given solute will only be reflected in δG_i, the calculated δG_i terms, instead of δG, were used as a sensitive probe for charge separation.

In a previous paper (4) the Sinanoglu method was used to give the related cavity terms for the *tert*-butyl chloride transition-state and for the model compound, the $Me_4N^+Cl^-$ ion-pair, in twelve solvents. A good linear correlation between these values was observed and the slope, 0.73, was taken as charge separation in the solvolytic reaction activated complex. The estimated value of δG_i, however, depends on the adopted model to calculate the energetics of cavity formation. Therefore, a comparison of the results from different methods plays an important part in rational selection. To perform comparative analysis we chose the solvolyses of *tert*-butyl chloride (in sixteen solvents) and *tert*-butyl bromide (in eight solvents). Methanol was taken as the reference solvent. The cavity terms were then calculated

Can. J. Chem. Downloaded from www.nrcresearchpress.com by 91.121.58.235 on 09/07/12
For personal use only.

Can. J. Chem. Downloaded from www.nrcresearchpress.com by 91.121.58.235 on 09/07/12
For personal use only.

TABLE 9. Relative Gibbs energies of interaction, δG_i, of the activated complex (≠) and the model solute (MS) for the solvolysis of *t*-BuCl, calculated following the Pierotti method (line *1*),[a] the Sinanoglu method (line *2*), and using eq. [16] (line *3*); methanol was the reference solvent

Solvent	$\delta G_i^{\neq}$/kJ mol^{-1}	δG_i^{MS}/kJ mol^{-1}
Water	−20.9	−25.9
	−51.9	−55.0
	−46.2	−49.3
Ethanol	4.1	6.0
	6.6	8.4
	4.2	6.1
1-Propanol	5.0	7.3
	7.8	10.2
	6.6	9.0
2-Propanol	8.7	10.1
	13.1	14.5
	10.4	11.8
1-Butanol	3.6	6.7
	8.2	11.3
	8.7	11.8
t-Butanol	13.0	18.7
	18.7	24.4
	17.6	23.4
Nitromethane	5.4	7.8
	5.1	8.0
	12.0	14.9
Acetonitrile	13.4	18.8
	14.7	20.2
	21.3	26.8
Dimethylformamide	9.3	12.8
	6.6	10.6
	−2.5	1.5
Acetone	19.2	28.6
	26.3	35.8
	32.7	42.1
Ether	31.0	60.3
	48.7	77.7
	55.6	84.5
Benzene	27.5	51.4
	37.9	62.0
	46.4	70.5
Chlorobenzene	14.1	35.7
	29.9	51.7
	37.9	59.7
Nitrobenzene	11.8	11.3
	5.2	4.2
	−1.1	−2.1
Pentane	59.2	131.6
	69.3	105.7
	76.6	113.1

[a]The hard-sphere diameters of *t*-BuCl$^{\neq}$ and $Me_4N^+Cl^-$ were assumed to be 5.77 and 5.62 Å, respectively.

TABLE 10. Relative Gibbs energies of interaction, δG_i, of the activated complex (≠) and the model solute (MS) for the solvolysis of *t*-BuBr, calculated following the Pierotti method (line *1*),[a] the Sinanoglu method (line *2*), and using eq. [16] (line *3*); methanol was the reference solvent

Solvent	$\delta G_i^{\neq}$/kJ mol^{-1}	δG_i^{MS}/kJ mol^{-1}
Water	−20.0	−22.2
	−51.3	−52.8
	−45.5	−47.1
Ethanol	3.1	5.1
	5.6	7.6
	3.2	5.2
2-Propanol	7.3	9.3
	11.7	13.7
	9.1	11.0
t-Butanol	11.7	18.0
	17.3	23.7
	16.3	22.6
Nitromethane	−0.8	1.4
	−1.2	1.2
	5.6	8.0
Dimethylformamide	1.6	5.9
	−1.3	3.4
	−10.4	−5.7
Acetone	12.8	19.0
	19.8	26.1
	26.2	32.5

[a]Hard-sphere diameters of *t*-BuBr$^{\neq}$ and $Me_4N^+Br^-$ were assumed to be 5.81 and 5.73 Å, respectively.

TABLE 11. Parameters and correlation coefficients (r) of the linear regression analysis between the relative Gibbs energies of interaction, δG_i, of the activated complex (≠) and the model solute (MS), for the solvolytic reactions of *t*-butyl halides, calculated following the Pierotti method (line *1*), the Sinanoglu method (line *2*), and using eq. [16] (line *3*)

	$\delta G_i^{\neq} = a_0 + a_1 \delta G_i^{MS}$		
Reaction	a_0	a_1	r
t-BuCl solvolysis			
16 solvents	1.54	0.47	0.950
	−1.58	0.70	0.972
	−1.31	0.71	0.984
8 solvents[a]	−0.56	0.74	0.993
	−2.06	0.88	0.994
	−1.98	0.87	0.995
t-BuBr solvolysis			
8 solvents	−1.64	0.79	0.987
	−2.52	0.91	0.994
	−2.44	0.91	0.993

[a]The same set of solvents are used in analysing *t*-BuBr solvolysis.

using different methods: the original Pierotti method, the Sinanoglu method, and the new approach proposed here (eq. [16]). Tables 9 and 10 give the relative Gibbs energies of interaction with the solvent of the activated complex and the model for the two mentioned solvolytic reactions. The corresponding linear plots are shown in Figs. 6 and 7. The results confirm the poor results using the Pierotti method in these systems. Not only are correlation coefficients smaller than those obtained by other methods, but the slope for *t*-BuCl solvolysis is only 0.47. Several independent studies give 0.70–0.80 as charge separation in the transition state of this reaction (10, 34).

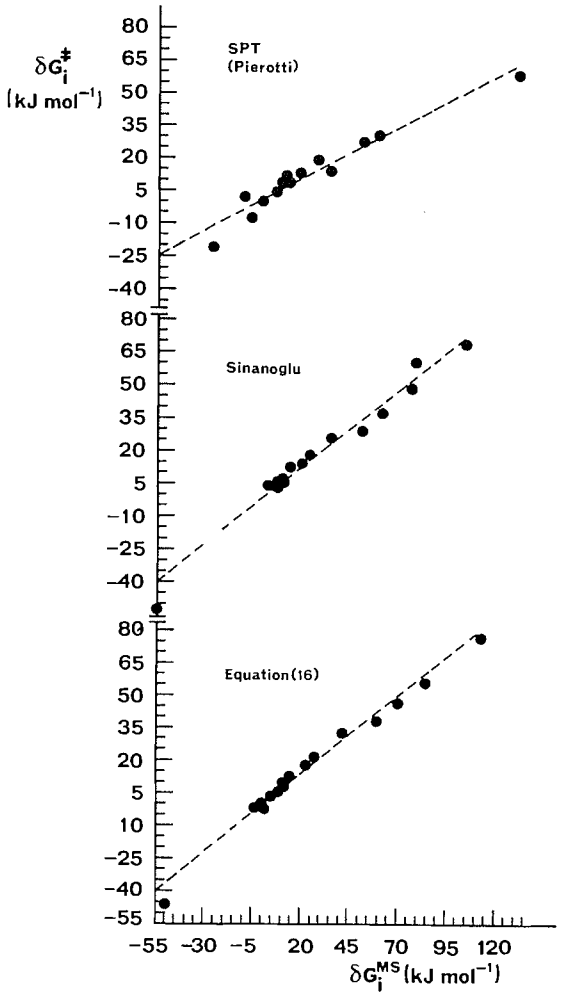

FIG. 6. Correlation between the differential solute–solvent interaction Gibbs energy for the activated complex (‡) and the model solute (MS) in solvolysis of *tert*-butyl chloride.

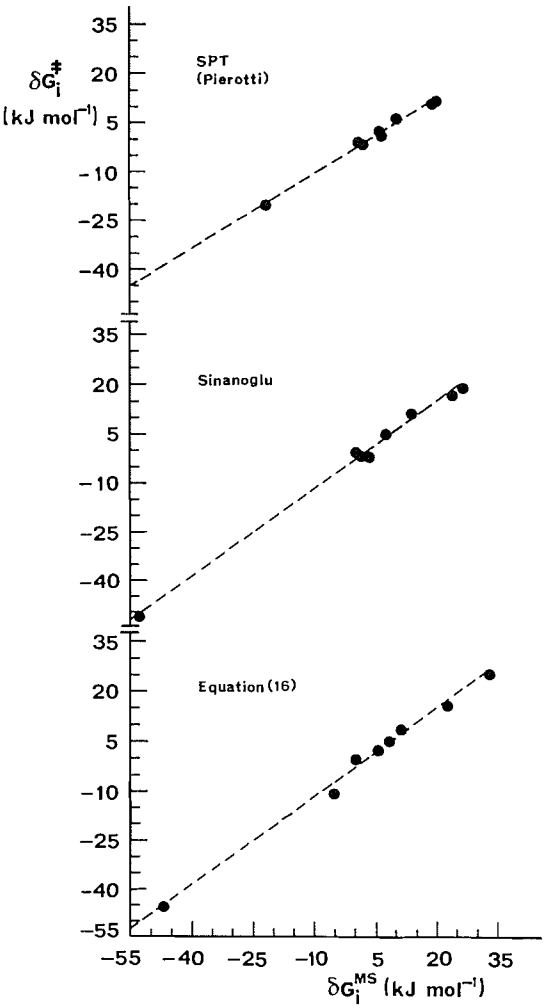

FIG. 7. Correlation between the differential solute–solvent interaction Gibbs energy for the activated complex (‡) and the model solute (MS) in the solvolysis of *tert*-butyl bromide.

On the other hand, the other two approaches give consistent charge separation values. Excellent linear correlations are observed, particularly for the method we proposed in this work. Thus we may conclude that, whatever the structure of the transition-state, charge separation is always quite high.

Although the same straight line is found to be adequate to characterize in general the polar nature of the transition state of the *t*-BuCl solvolysis over all solvents studied, the slope of the line for a smaller set of very polar and associated solvents increases to 0.87. This agrees with previous results when data for the more polar solvents are used: 0.81–0.94 (34). The same set of solvents was also used to analyse the solvolytic reaction of *t*-BuBr (Table 11). No significant differences can be assigned to the solvolysis of both substrates, except that the transition state in *t*-BuBr solvolysis is even more ion-pair like in nature.

Conclusions

In this work we proposed a new method for calculating the energetics of cavity formation in liquids. This method enables the calculation of different thermodynamic properties associated with the cavity formation process. It is consistent from a thermodynamic point of view in the sense that we can relate those properties by using the Gibbs–Helmholtz relationship.

We believe that the proposed method is better than others previously proposed in the literature, namely the Pierotti method and the Sinanoglu method, and several features were pointed out to support this statement. The fact that our method allows a consistent description of the dissolution process of alkane solutes at infinite dilution in alkane solvents (for Gibbs energy as well as for enthalpy and obviously for entropy) is probably the most important feature. Other features to validate our method have been stated in our previous works (7, 8). Our calculated energy of cavity formation is the same for same solute in different alkane solvents. This feature, which has been observed for enthalpy and for Gibbs energy, reinforces the idea of similar contact energies in different *n*-alkane molecules.

Our method of calculating the energetics of cavity formation has been applied to the study of solvent effect on the solvolytic reactions of *tert*-butyl halides. We obtain very good correlations between the relative Gibbs energy of interaction with the solvent for the activated complex and for its ion-pair model. From these correlations the charge separation in the transition state was deduced and our results are in very good agreement with independent studies.

Acknowledgments

We are grateful to the Instituto Nacional de Investigação Científica for financial support. One of us (M.S.D.) also

Can. J. Chem. Downloaded from www.nrcresearchpress.com by 91.121.58.235 on 09/07/12
For personal use only.

gratefully acknowledges the Junta Nacional de Investigação Científica e Tecnológica (JNICT).

1. E. WILHEIM. Thermochim. Acta, **94**, 47 (1985).
2. O. SINANOGLU. *In* Molecular associations in biology. *Edited by* B. Pullman. Academic Press, New York. 1968. p. 427.
3. J. J. MOURA RAMOS, M. LEMMERS, R. OTTINGER, M. L. STIEN, and J. REISSE. J. Chem. Res. (*M*), 655 (1977).
4. J. J. MOURA RAMOS, J. REISSE, and M. H. ABRAHAM. Can. J. Chem. **57**, 500 (1979).
5. O. SINANOGLU. *In* Molecular interactions. Vol. 3. *Edited by* H. Ratajczak and W. J. Orville-Thomas. John Wiley. 1982. p. 283.
6. J. LANGLET, P. CLEVERIE, J. CAILLET, and A. PULLMAN. J. Phys. Chem. **92**, 1617 (1988).
7. J. J. MOURA RAMOS, M. S. DIONÍSIO, R. C. GONÇALVES, and H. P. DIOGO. Can. J. Chem. **66**, 2894 (1988).
8. J. J. MOURA RAMOS. J. Sol. Chem. **18**, 957 (1989).
9. T. W. LELAND, JR. and P. S. CHAPPELEAR. Ind. Eng. Chem. **60**, 15 (1968).
10. M. H. ABRAHAM. Pure Appl. Chem. **57**, 1055 (1985).
11. J. M. SMITH and H. C. VAN NESS. Introduction to chemical engineering thermodynamics. 4th ed. McGraw-Hill, New York. 1988.
12. F. KOHLER. *In* Organic liquids: structure, dynamics, chemical properties. *Edited by* A. D. Buckingham, E. Lippert, and S. Bratos. John Wiley. 1978. p. 245.
13. G. THODOS. Ind. Eng. Chem. **42**, 1514 (1950).
14. M. BARBE and D. PATTERSON. J. Phys. Chem. **82**, 40 (1978).
15. S. N. BATTACHARRYYA and D. PATTERSON. J. Sol. Chem. **9**, 247 (1980).
16. R. C. REID, J. M. PRAUSNITZ, and B. E. POLING. The properties of gases and liquids. 4th ed. McGraw-Hill, New York. 1987.
17. J. H. HILDEBRAND, J. M. PRAUSNITZ, and R. L. SCOTT. Regular and related solutions. Van Nostrand Reinhold Co., New York. 1970.
18. E. B. BAGLEY, T. P. NELSON, and J. M. SCIGLIANO. J. Phys. Chem. **77**, 2794 (1973).
19. R. W. GURNEY. Ionic process in solution. McGraw-Hill, New York. 1953.
20. A. BEN-NAIM. J. Phys. Chem. **82**, 792 (1978).
21. A. BEN-NAIM. J. Chem. Phys. **81**, 2016 (1984).
22. H. L. FRIEDMAN. Chem. Brit. **9**, 300 (1973).
23. R. A. PIEROTTI. Chem. Rev. **76**, 717 (1976).
24. N. B. VARGAFTIK. Tables on the thermophysical properties of liquids and gases. Hemisphere Publishing Co. 1975.
25. J. B. OTT, K. N. MARSH, and R. H. STOKES. J. Chem. Thermodyn. **12**, 1139 (1980).
26. K. N. MARSH, J. B. OTT, and M. J. COSTIGAN. J. Chem. Thermodyn. **12**, 343 (1980).
27. K. N. MARSH, J. B. OTT, and A. E. RICHARDS. J. Chem. Thermodyn. **12**, 897 (1980).
28. J. B. OTT, K. N. MARSH, and R. H. STOKES. J. Chem. Thermodyn. **13**, 371 (1981).
29. M. L. MCGLASHAN and A. G. WILLIAMSON. Trans. Faraday Soc. **57**, 588 (1961).
30. R. L. SNOW, J. B. OTT, J. R. GOATES, K. N. MARSH, S. O'SHEA, and R. H. STOKES. J. Chem. Thermodyn. **18**, 107 (1986).
31. T. E. MAIRS and F. L. SWINTON. J. Chem. Thermodyn. **12**, 575 (1980).
32. M. B. EWING and K. N. MARSH. J. Chem. Thermodyn. **6**, 395 (1974).
33. M. B. EWING, B. V. LEVIEN, K. N. MARSH, and R. N. STOKES. J. Chem. Thermodyn. **2**, 689 (1970).
34. M. H. ABRAHAM. Prog. Phys. Org. Chem. **11**, 1 (1974).

Can. J. Chem. Downloaded from www.nrcresearchpress.com by 91.121.58.235 on 09/07/12
For personal use only.

Benzoxathiete and related structures: experimental and quantum chemical studies

ALI NAGHIPUR, KRZYSZTOF RESZKA,[1] AND J. WILLIAM LOWN[2]
Department of Chemistry, University of Alberta, Edmonton, Alta., Canada T6G 2G2

AND

ANNE-MARIE SAPSE
City University of New York and Rockefeller University, New York, NY 10021, U.S.A.

Received March 29, 1990

Can. J. Chem. Downloaded from www.nrcresearchpress.com by 91.121.58.235 on 09/07/12
For personal use only.

ALI NAGHIPUR, KRZYSZTOF RESZKA, J. WILLIAM LOWN, and ANNE-MARIE SAPSE. Can. J. Chem. **68**, 1950 (1990).

The products, plausible intermediates, and their mechanisms of formation in the aprotic diazotization of 2-[(2-acetoxyethyl)-sulfinyl (and sulfonyl)]anilines with isoamyl nitrate have been investigated by experimental and quantum chemical methods. Oxidation of 1,2,3-benzthiadiazole with hydrogen peroxide in acetic acid affords 1,2,3-benzthiadiazole-1-oxide, **13**. The thermal stability of **13** up to 135°C, together with EPR evidence which disfavors an aryldiazenyl radical precursor, discount **13** as an intermediate in the formation of benzoxathiete **14** or its valence tautomer **17** during aprotic diazotization of the sulfinylanilines. Electron paramagnetic resonance evidence in conjunction with spin trapping indicates an intermediate arylaminyl radical. This evidence, taken together with *ab initio* calculations of optimized geometries energies and energy differences for biradical intermediate **15**, favors a mechanism of formation of benzoxathiete **14** via aryldiazoate anhydride **5** thence to rapid ring closure of carbon-centered radical **8**. Further oxidation of 1,2,3-benzthiadiazole-1-oxide, **13**, with hydrogen peroxide in methanol – acetic acid affords biphenylene and dibenzo-1,4-oxathiane-*S*-oxide, **38**. Rose bengal sensitized photooxidation of 1,2,3-benzthiadiazole affords **13**, biphenylene, and **38**. Formation of the latter, in which one of the original S—O bonds has been broken, requires the formation of benzoxathiete-*S*-oxide, **34**, and its rapid valence tautomerism to ketosulfine **36** and (2+4) cycloaddition of **36** to the simultaneously generated dehydrobenzene to give **38**. Both ring closure of singlet biradical **35** to **34** and valence tautomerism of the latter to **36** are predicted by *ab initio* calculations to be facile and exothermic. In contrast to the aprotic diazotization of 2-[(2-acetoxyethyl)sulfinyl]anilines, the reaction of isoamyl nitrite with the corresponding sulfonyl anilines may plausibly follow a mechanism via 1,2,3-benzthiadiazole-1,1-dioxide **33** owing to the thermal instability of the latter and supported by *ab initio* treatments of the energetics of the processes involved. In addition EPR evidence, in conjunction with spin trapping of carbon centered radicals, support the viability of the pathway via **23**, **25**, **28**, and **16** to biphenylene **20**. The *ab initio* calculations of the energy differences between the reaction intermediates and estimates of the activation energies elucidated several aspects of these novel reactions.

Key words: benzoxathiete, *ab initio* calculations, valence tautomerism.

ALI NAGHIPUR, KRZYSZTOF RESZKA, J. WILLIAM LOWN et ANNE-MARIE SAPSE. Can. J. Chem. **68**, 1950 (1990).

Utilisant des méthodes expérimentales et des méthodes de la chimie quantique, on a étudié la nature des produits, des intermédiaires possibles ainsi que de leurs mécanismes de formation lors de la diazotation aprotique des 2-[(2-acétoxyéthyl)sulfinyl (et sulfonyl)]anilines avec du nitrite d'isoamyle. L'oxydation du 1,2,3-benzthiadiazole par le peroxyde d'hydrogène dans l'acide acétique fournit le 1,2,3-benzthiadiazole-1-oxyde (**13**). La stabilité du produit **13** jusqu'à une température de 135°C ainsi que les données de la rpe qui défavorisent un radical aryldiazényle comme précurseur permettent d'éliminer le produit **13** comme intermédiaire possible dans la formation du benzoxathiète **14** ou de son tautomère de valence **17** lors de la diazotation aprotique des sulfinylanilines. Les données de la rpe et celles du piégeage de spin suggèrent plutôt le radical arylaminyle comme intermédiaire. Ces données, utilisées de concert avec des calculs *ab initio* d'énergies de géométries optimisées et de différences d'énergie de l'intermédiaire biradicalaire **15**, favorisent un mécanisme de formation du benzoxathiète **14** impliquant l'anhydride d'aryldiazoate **5**; ceci expliquerait la fermeture rapide du radical **8** qui est centré sur le carbone. L'oxydation subséquente du 1,2,3-benzthiadiazole-1-oxyde **13** par le peroxyde d'hydrogène dans un mélange de méthanol et d'acide acétique fournit du biphénylène et du dibenzo-1,4-oxathiane-*S*-oxyde, **38**. La photooxydation du 1,2,3-benzthiadiazole, photosensibilisée par le rose du bengale, fournit du produit **13**, du biphénylène et du produit **38**. La formation de ce dernier produit, dans lequel les liaisons S—O originales ont été brisées, implique la formation du benzoxathiète-*S*-oxyde **34** et de sa tautomérie de valence rapide vers la cétosulfine **36** et une cycloaddition (2+4) subséquente du composé **36** sur le déhydrobenzène qui est généré simultanément pour donner le produit **38**. Les calculs *ab initio* prédisent que la cyclisation du biradical singulet **35** en **34** ainsi que la tautomérie de valence de ce dernier en **36** sont deux processus faciles et exothermiques. Par opposition à la diazotation aprotique des 2-[(2-acétoxyéthyl)sulfinyl]anilines, il est possible que la réaction du nitrite d'isoamyle avec les sulfonyl anilines correspondantes puisse se produire par un mécanisme impliquant le 1,2,3-benzthiadiazole-1,1-dioxyde **33**; en effet, ce dernier composé est instable d'un point de vue thermique et ce mécanisme est supporté par les traitements *ab initio* des énergies des processus impliqués. De plus, les données de la rpe, prises de concert avec le piégeage de spin des radicaux centrés sur le carbone, supportent la viabilité d'une voie réactionnelle impliquant les composés **23**, **25**, **28** et **16** pour obtenir le biphénylène **20**. Les calculs *ab initio* des différences d'énergie entre les intermédiaires réactionnels et des évaluations des énergies d'activation ont permis d'élucider plusieurs aspects de ces nouvelles réactions.

Mots clés : benzoxathiète, calculs *ab initio*, tautomérie de valence.

[Traduit par la revue]

[1]Present address: Laboratory of Molecular Biophysics, NIEHS, P.O. Box 12233, Research Triangle Park, NC 27709, U.S.A.
[2]Author to whom correspondence may be addressed.

Printed in Canada / Imprimé au Canada

Can. J. Chem. Downloaded from www.nrcresearchpress.com by 91.121.58.235 on 09/07/12
For personal use only.

Introduction

1,2-Oxathietanes and their derivatives have been identified as intermediates in the spontaneous decomposition of anticancer (2-chloroethyl)sulfinyl nitrosoureas under physiological conditions (1–3). Subsequently means were developed to prepare and isolate these novel reactive heterocycles (2, 4, 5) which are of practical and theoretical interest in their structural similarity to the extensively studied 1,2-dioxetanes (6). Some of the characteristic chemical reactions of 1,2-oxathietanes have been explored (1–3) and, recently, the formation and some reactions of benzoxathiete were examined both experimentally (4) and by quantum chemical methods (5). Among the novel reactions of benzoxathiete uncovered was its valence tautomerism to monothio-*o*-benzoquinone (4) which, while being formally disallowed under thermal conditions (5), nevertheless proceeds under the experimental conditions used and, by trapping with the simultaneously generated dehydrobenzene, affords dibenzo-1,4-thioxane.

A number of questions concerning the alternative mechanisms of formation of benzoxathiete as well as the stability and reactivity of plausible intermediates arose from the previous communications (4, 5). The present report addresses these questions and our results serve to clarify several aspects of the chemical reactivity of these novel heterocycles as well as to uncover some novel chemistry of benzoxathiete-*S*-oxide and its valence tautomer. Since many of the intermediates are amenable to *ab initio* calculations the application of quantum chemical methods (5) permitted greater insight into several aspects of stability, reactivity, and orbital symmetry considerations.

Experimental section

Melting points were determined on a Fisher-Johns apparatus and are uncorrected. IR spectra were recorded on a Nicolet 7199 F.T. spectrophotometer, and only the principal sharply defined peaks are reported. NMR spectra were recorded on Varian HA-100, Bruker WH-200, or WH-400 spectrometers. The spectra were recorded on approximately 5–15% (w/v) solutions, depending upon the spectrometers, in appropriate deuterated solvents with tetramethylsilane as internal standard. EI mass spectra were determined on an Associated Electrical Industries (AEI) MS-9 double focusing high-resolution mass spectrometer with ionization energies at 70 eV. Peak measurements were made by comparison with perfluorotributylamine at a resolving power of 15000 on an AEI-MS-50 mass spectrometer. GC analyses were performed on a Hewlett-Packard 5840A analytical gas chromatograph equipped with a flame ionization detector. GC/MS analyses were performed on an AEI-MS-12 spectrometer. Samples were injected onto a 6–ft, 10% Carbowax 20M 80-100 WAW-DMCS a5830 column with a helium flow rate of 20 mL/min. The column was heated at 60°C for 20 min and was heated further at a rate of 10°C/min up to 150°C for 1 h.

1,2,3-Benzothiadiazole-1-oxide

To a stirred solution of 1,2,3-benzothiadiazole (7) (0.45 g, 3 mmol) in 1:1 methanol – acetic acid (20 mL) was added a 30% solution of hydrogen peroxide (3 g, 88 mmol), and the mixture was stirred at room temperature for 45 days, at which time TLC analysis showed complete disappearance of starting material. The solvent and excess of the reagent were removed *in vacuo*, and the residual solid was purified by column chromatography (silica gel, hexane) to afford first biphenylene as a light yellow solid: mp 110°C (lit. (7) mp 110°C); MS, *m/z* (rel. int.) 153 (12.90), 152 (M^+, 100), 151 (18.77), 126 (7.11), 125 (1.45), 76 (11.87), 51 (3.03). Further elution with hexane – ethyl acetate (2:1) afforded 1,2,3-benzothiadiazole-1-oxide as a yellow crystalline solid: mp 132–134°C; 0.3 g (60% yield); MS, *m/z* (rel. int.) 152 (M^+, 100), 136 ($M^+ - 16$, 9.69), 124 ($M^+ - 28$, 2.63), 122 (40.31), 108 (27.15), 76 (26.55), 75 (13.03), 74 (14.53), 51 (23.55).

Thermal stability of 1,2,3-benzothiadiazole-1-oxide in solution

A solution of 1,2,3-benzothiadiazole-1-oxide (0.1 g, 0.65 mmol) in freshly distilled dry ethylene glycol and dimethyl ether (10 mL) was heated under reflux under a nitrogen atmosphere for 5 h. TLC analysis indicated no decomposition and the solvent was removed *in vacuo*. Recrystallization of the solid residue from 1:1 dichloromethane/hexane afforded only pure unreacted 1,2,3-benzothiadiazole-1-oxide. Similar experiments were performed using successively toluene, *o*-xylene, and *o*-dichlorobenzene as solvents. In no case was any thermal decomposition of 1,2,3-benzothiadiazole-1-oxide detected.

Photooxidation procedure

Photooxidation reactions were carried out in a 20 cm water-cooled square quartz reaction vessel equipped with a gas bubbler which was driven from above the vessel. A slow stream of oxygen gas was passed into the solution during the course of irradiation. The light source consisted of a medium pressure Hanovia mercury lamp with a UV cutoff filter (7910) and the sensitizer was rose bengal polymer supported 0.12 mmol/g.

Photosensitized oxidation of 1,2,3-benzothiadiazole

To a stirred solution of 1,2,3-benzothiadiazole (0.2 g, 1.47 mmol) in dry dichloromethane (100 mL) was added rose bengal, polymer supported ca. 0.12 mmol/g (0.5 g). The reaction mixture was irradiated for 60 h, at which time TLC analysis showed complete disappearance of the starting material. The solution was filtered through celite and washed with methanol. The solvents were removed *in vacuo* and the residual solid was subjected to column chromatography (silica gel, pentane) to afford biphenylene as a light yellow solid, mp 110°C (lit. (8) mp 110°C) trace, MS, *m/z* (rel. int.) 153 (12.27), 152 (M^+, 100), 151 (22.19), 150 (11.95), 126 (4.69), 125 (1.10), 76 (12.98), 51 (1.50).

Further elution with hexane:ethyl acetate (2:1) afforded 1,2,3-benzothiadiazole-1-oxide as a yellow crystalline solid: mp 132–134°C, 0.15 g (67% yield); MS, *m/z* (rel. int.), 153 (7.57), 152 (M^+, 130), 136 (2.70), 122 (39.06), 104 (3.49), 76 (11.38), 51 (9.66).

Further elution with hexane:ethyl acetate (1:1) afforded dibenzo-1,4-oxathiane-*S*-oxide, **38**, as a white crystalline solid mp 153–154°C (lit. (9) mp 152–153°C); MS, *m/z* (rel. int.) 217 (13.96), 216 (M^+, 100), 200 ($M^+ - 16$, 16.64), 188 (19.14), 187 (69.61), 168 ($M^+ - 48$, 86.52), 139 (23.64), 115 (7.31), 79 (2.07), 76 (2.09), 63 (11.04), 51 (5.01).

General procedure for analysis of the products of aprotic diazotization of substituted arylalkylsulfoxide or substituted arylalkylsulfones

A solution of substituted arylalkylsulfoxide (4) or corresponding sulfone (4) (2.5 mmol) and isoamyl nitrite (1 mL, 7.5 mmol) each in glyme (3 mL) were added simultaneously in 1 h to a refluxing solution of trapping agent (1.25 mmol) in glyme (7 mL). After the addition was completed, the mixture was refluxed for 20–30 min and then allowed to cool. Dichloromethane (40 mL) was added and the mixture was evaporated to dryness. The residual solid was purified by column chromatography as described previously (4) to separate the products.

EPR spectroscopy

Isoamyl nitrite, 5,5-dimethyl-1-pyrroline *N*-oxide (DMPO), and benzene were purchased from Aldrich (Milwaukee, WI). Arylalkyl thioethers (**1***a–c*) and sulfoxides (**11***a–b*) were synthesized as previously described (4). DMPO was purified by distillation under reduced pressure. All other compounds were used as received.

Stock solutions of the amines (0.1 M and 0.2 M) of iAmONO (70 mM and 100 mM) and ND (10 mM) were prepared in benzene. Samples were prepared adding 10, 20, or 50 μL of iAmONO to 450 μL of the amine solutions containing DMPO (usually 10–100 mM) or ND (5 mM) in quartz EPR tubes (internal diameter 3 mM). Solutions were saturated with argon of 25 min and sealed tightly. EPR spectra were measured using a Bruker ER-400 spectrometer operating at 9.3 GHz with 100 kHz modulation frequency. The following instrumental settings were generally employed; microwave power, 20 mW; modulation amplitude, 0.5 G; time constant, 0.2 or 0.5 s; scan rate 500 or 1000 s and the appropriate gain level. Magnetic field calibration was

TABLE 1. Electron paramagnetic resonance hf coupling constants (in Gauss) of DMPO spin adducts formed during diazotazation of amines **I–III** in C_6H_6 with *i*AmONO

Amine	X	$^aN1$	$^aN2$	$^a\beta_H$
I*a*	S–OAc			
I*b*	S–OCH_3	13.9[a]	2.9[a]	14.1[a]
I*c*	S–OH	14.0[a]	2.7[a]	15.2[a]
II*a*	S(O)–OAc	13.7[a]	3.2[a]	13.9[a]
III*b*	S(O)–OCH_3	13.7[a]	3.2[a]	13.9[a]
III*a*	$S(O_2)$–OAc	14.1[b]	—	21.2[b]
III*b*	$S(O_2)$–OH	14.5[b]	—	22.2[b]

[a]Hyperfine coupling constants refer to spin adducts (**A**).
[b]Hyperfine coupling constants refer to spin adducts (**B**).

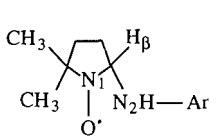

A

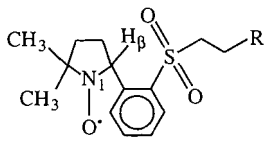

B

achieved using the known distance between the hf components of the EPR spectrum of Fremy salt in 50 mM K_2CO_3. All measurements were performed at room temperature.

Results and discussion

Synthetic and product isolation studies

Attempted oxidation of 1,2,3-benzthiadiazole with *m*-chloroperbenzoic acid, with 30% aqueous hydrogen peroxide, hydrogen peroxide in methylene chloride – acetic acid mixtures, sodium metaperiodate in aqueous dioxane or prolonged photosensitized oxidation using rose bengal on silica gel were unsuccessful. However, treatment of 1,2,3-benzthiadiazole with 30% hydrogen peroxide in a mixture of acetic acid and methanol afforded a product, the physical and spectral data of which are consistent with 1,2,3-benzthiadiazole-1-oxide, **13**, in 60% yield. Compound **13** is a stable pale yellow solid, mp 132–134°C. Solutions of **13** heated under reflux in the following progressively higher boiling solvents were indefinitely stable; 1,2-dimethoxyethane, toluene, *o*-xylene, and *o*-dichlorobenzene.

In the aprotic diazotization of 2-[(2-acetoxyethyl)sulfonyl]-anilines (**21**, X = OAc), analogy with the observed behavior and product distribution from the corresponding 2-[(2-acetoxyethyl)sulfinyl]anilines (**1**, X = OAc), would suggest the possible intermediacy of 1,2,3-benzthiadiazole-1,1-dioxide, **33** (Scheme 2). Although the latter compound has been reported (10), the availability of the novel compound **13** suggested attempted conversion of **13** to **33** by selective oxidation so as to explore the relationship between the two species.

Accordingly further oxidation of **13** was attempted under a variety of conditions. Finally prolonged oxidation of **13** with hydrogen peroxide in acetic acid afforded evidence of conversion to the corresponding 1,1-dioxide in that biphenylene, derived from the dimerization of the intermediate dehydrobenzene and dibenzo-(1,4)-oxathiane-*S*-oxide **38** were identified among the products. Further oxidation of 1,2,3-benzthiadiazole was also effected by rose bengal photosensitized oxidation which afforded **13**, biphenylene, and **38**. Formation of the latter product requires formation of benzoxathiete-*S*-oxide, **34**, its ketosulfine valence tautomer **36**, and cycloaddition of the latter to dehydrobenzene (*vide infra*).

Spin trapping EPR detection of free radical intermediates

The involvement of free radical species in the reaction of 2-[(2-acetoxyethyl)sulfinyl]aniline (**1**, X = OAc) with isoamyl nitrite under aprotic conditions (11) was proven by spin trapping experiments (4, 12*a*, *b*) in conjunction with EPR spectroscopy. However, since EPR spectra are seldom diagnostic for particular species (12*c*, *d*) a more detailed examination was undertaken with a series of model compounds to attempt to delineate the actual types of radicals involved. Treatment of amines **I***a* or **II***a* (Table 1) (0.1 M) with iAmONO (2–7 mM) in the presence of spin trap DMPO (0.1 M) in deaerated benzene at room temperature generated strong and persisted EPR spectra assigned to DMPO adducts of arylaminyl radicals **39** (4, 12*a*, *b*).

Spin adducts can be formed either by trapping arylaminyl radicals by DMPO (reaction [1]), or by oxidation of hydroxylamines (**40**), formed via nucleophilic addition of an amine to DMPO (reaction [2]).

[1] DMPO + $ArNH^{\cdot}$ → 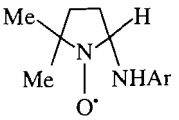

39

[2] DMPO + $ArNH_2$ → 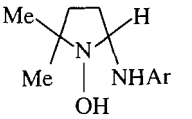 $\xrightarrow{[O_2]}$ **39**

40

For example, *n*-butyl amine is known to add to the nitrone and form a nitroxide radical according to reaction [2] (13*a*). The question, which of these two alternative pathways (or both) contribute to formation of radical **39**, has been discussed separately (12*a*, *b*). Nevertheless, arylaminyl radicals, if formed, do not participate in the main pathways of processes **1** → ... → **12** (Scheme 1) and **21** → ... → **28** (Scheme 2). Treatment of amines such as **21**, or **III***a* (Table 1) (0.1 M) with iAmONO (2–7 mM) in the presence of DMPO (ca. 20 mM) in deaerated benzene produced the spin adduct of a carbon-centered radical assigned to a DMPO–Ar species (12*a*, *b*)

Can. J. Chem. Downloaded from www.nrcresearchpress.com by 91.121.58.235 on 09/07/12
For personal use only.

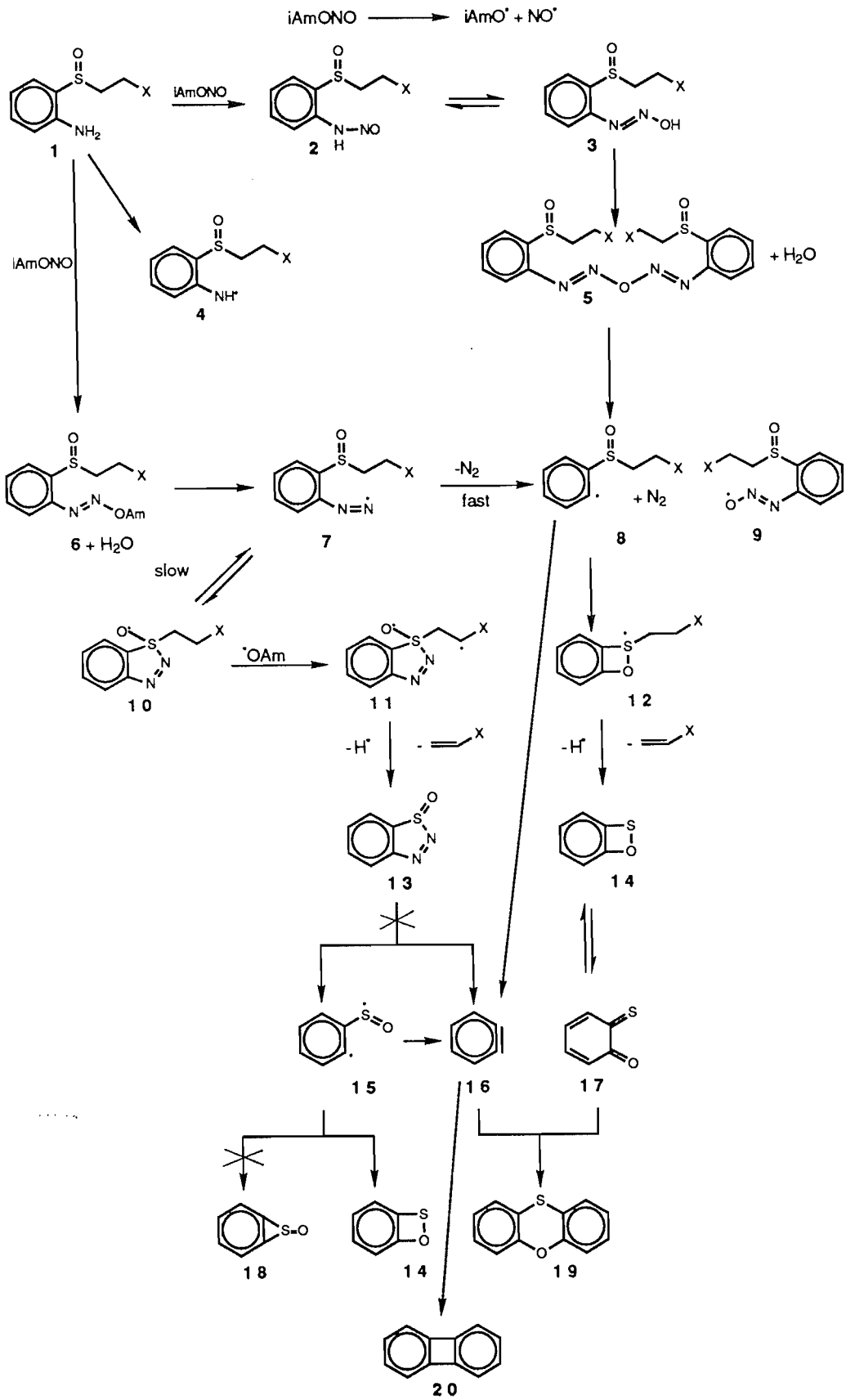

SCHEME 1. Products and alternative pathways of aprotic diazotization of 2-[(2-acetoxyethyl)sulfinyl]aniline with isoamyl nitrite.

Can. J. Chem. Downloaded from www.nrcresearchpress.com by 91.121.58.235 on 09/07/12
For personal use only.

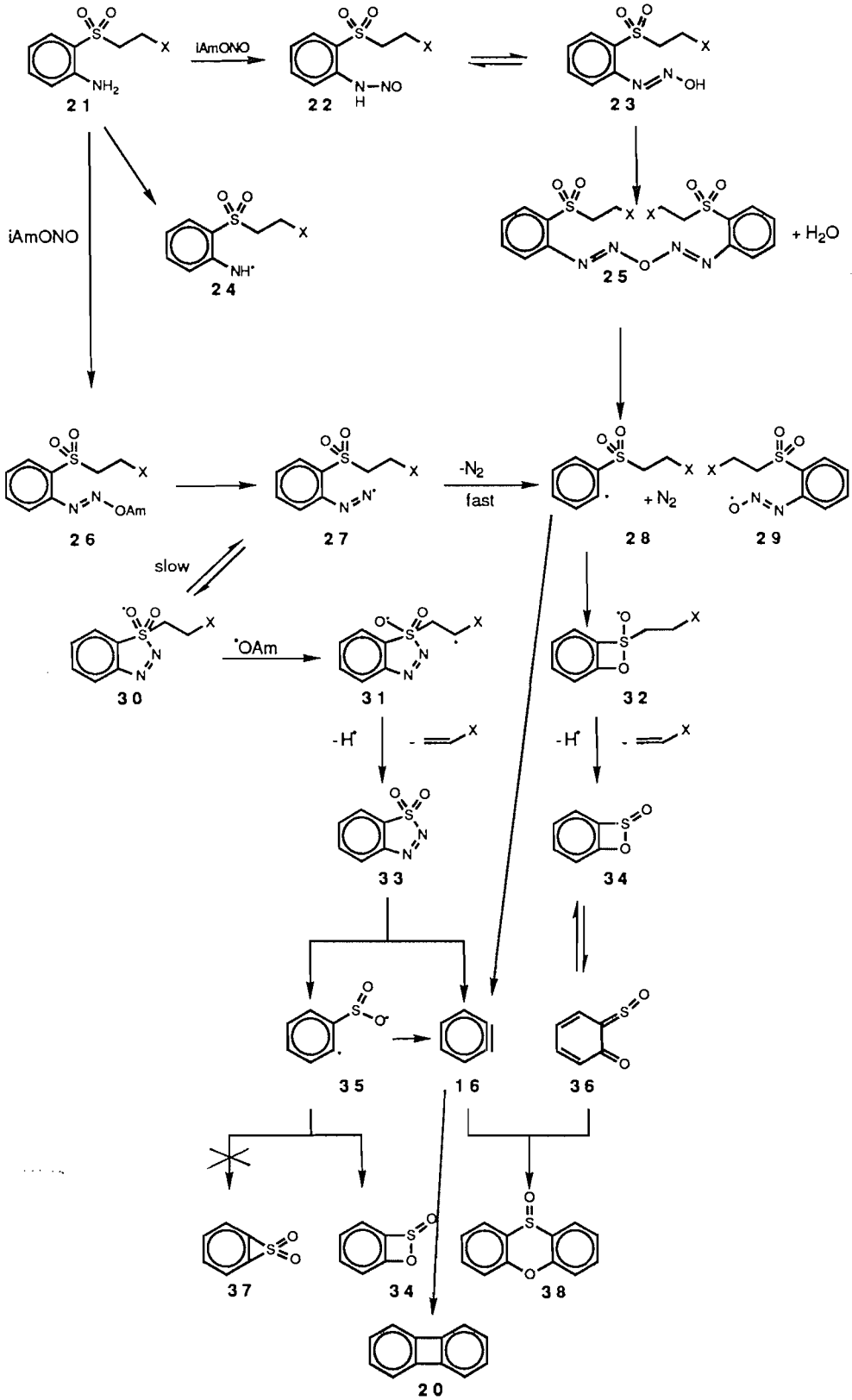

SCHEME 2. Products and alternative pathways of aprotic diazotization of 2-[(2-acetoxyethyl)sulfonyl]aniline with isoamyl nitrite.

where Ar = **28**, *vide infra*) (EPR spectrum is shown in Fig. 1). A similar spectrum was recorded with **III***b*. Evidently, amines **III***a* and **III***b* do not form the intermediate hydroxylamine, similar to **40**, otherwise, upon its oxidation, an EPR spectrum typical for radical **39** would be recorded.

The EPR spectrum of the spin adduct depicted in Fig. 1 does not provide sufficient information to identify the trapped radical unambiguously. This is because hf coupling constants of DMPO adducts with various carbon-centered radicals are very close (13*a*). However, additional evidence in support of the intermediacy of radical species **28** and its discrimination from species **42** was obtained by further spin trapping experiments

Can. J. Chem. Downloaded from www.nrcresearchpress.com by 91.121.58.235 on 09/07/12
For personal use only.

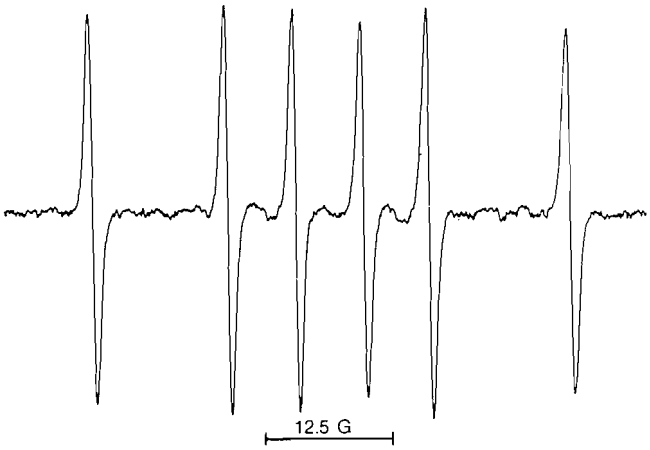

FIG. 1. EPR spectrum derived from a solution of 2-[(2-acetoxyethyl)sulfonyl]aniline (0.1 M), DMPO (10 mM), and isoamyl nitrite (3.5 mM) in deaerated benzene at room temperature. Hyperfine coupling constants are a_N = 14.1 G and $a_{\beta H}$ = 21.2 G.

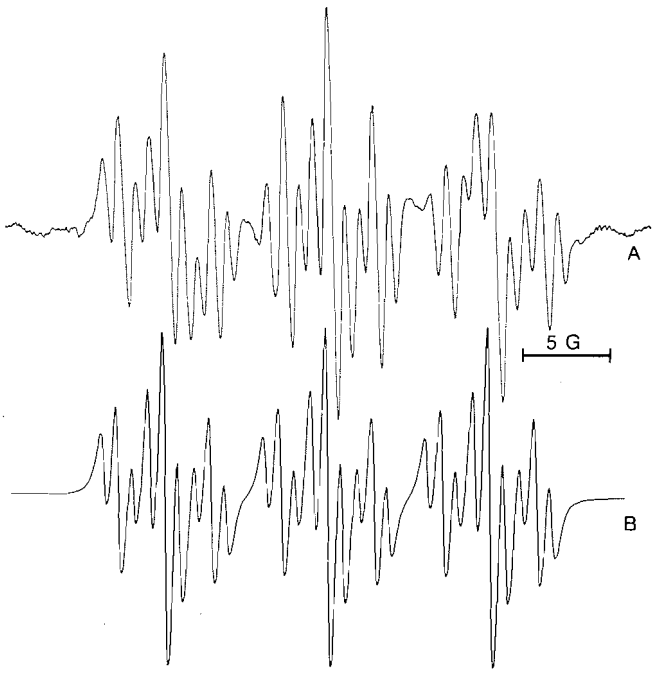

FIG. 2. (*A*) EPR spectrum derived from a solution containing 2-[(2-acetoxyethyl)sulfonyl]aniline (0.1 M), nitrosodurene (5 mM), and isoamyl nitrite (3.5 mM) in deaerated benzene at room temperature. (*B*) Simulated EPR spectrum using the hyperfine coupling constants a_N = 9.6 G, a_H = 2.7 G (2H), a_H = 0.75 G (2H).

using nitrosodurene (ND). In this case the reaction between **21** (**III***a*,*b* Table 1) and iAmONO gave rise to a well resolved and strong EPR signal of an ND adduct with an aryl radical (Fig. 2A). Analysis of the EPR spectrum yielded the following hyperfine splittings: a_N = 9.6 G, a_H = 2.7 G (two equivalent protons), and a_H = 0.75 G (two equivalent protons). Coupling to two pairs of equivalent protons can only arise from the aromatic ring radical **28**. This observation provides support for the assignment of the carbon-centered radical trapped by DMSO to species **28** (*vide supra*). Reaction of **1** with isoamyl nitrite in the presence of ND in benzene produced an EPR spectrum similar to that shown in Fig. 3*A* and was assigned to the ND—Ar (Ar = **8**) spin adduct, for which the following hyperfine coupling constants were determined: a_N = 9.7 G, a_H = 2.99 G (2H), a_H = 1.01 G (2H).

In a control experiment without isoamyl nitrite no spin adduct was obtained. An additional control experiment was performed with aniline, and isoamyl nitrite in benzene which in the presence of nitrosodurene afforded the well resolved EPR spectrum of the phenyl radical spin adduct (12*b*) with hf splittings in agreement with literature reports (12*d*).

Ab initio *calculations of optimized geometries and energies of species implicated in the formation and reactions of benzoxathiete*

Self-consistent field (SCF) *ab initio* calculations were made with full geometry optimization of the energies of relevant species. The *ab initio* calculations at the Hartree–Fock level were performed on products and intermediates using the 3-21G* Gaussian basis set, as implemented in the Gaussian-82 (14) and Gaussian-86 programs (15). The geometry optimizations were performed using the Berny optimization techniques (16). As in our previous studies (4, 5) the inclusion of *d* orbitals is particularly necessary for a good theoretical description of sulfur (17). It may be seen that 1,2,3-benzthiadiazole-1-oxide, **13**, is predicted to be stable relative to the 1,1-dioxide, **33** (Table 2).

Bicyclic species

The energy differences for certain reactions of 1,2,3-benzthiadiazole-1-oxide, **13**, and related structures are given in Table 2. The parent 1,2,3-benzthiadiazole is predicted to be more stable than the *S*-oxide with respect to the oxidation reaction by about 62.8 kJ/mol. Reaction of **13** to give biphenylene **20**, the dimerization product of dehydrobenzene, **16**, nitrogen, and singlet sulfur monoxide is predicted to be mildly exothermic (ΔE = −86.6 kJ/mol). However, the high energy of the transition states (largely due to the high energy of ^{1}SO, as well as of dehydrobenzene) would make **13** very stable relative to this decomposition reaction as is found experimentally. In a related example the high energy of singlet sulfur monoxide resulted in the highly endothermic nature (178.6 kJ/mol) of the orbital symmetry allowed (18) formyl [σ_{2s} + σ_{2a}] cycloreversion of benzoxathiete to singlet sulfur monoxide and the dimer of dehydrobenzene biphenylene (4) (see Table 3). Similar energetic considerations apply to the alternative decomposition of **13** via biradical **15** and thence to dehydrobenzene **16** and biphenylene **20**. Although biradical species **15** (17) may be implicated in alternative pathways (q.v.), its generation via **13** may be discounted since **13** is demonstrably stable under the reaction conditions. The biradical **15**, is, however, a viable intermediate in the pathway from **8** to **16** and **15** is predicted to have substantial stability relative to its decomposition products. The calculated energy of **15** is somewhat artificially low since the triplet also has some quintuplet character mixed in, *i.e.* the spin which has to be perpendicular, so $(\sqrt{s(s+1)})^2 = 2$ is approximately 2.3 for $s(s+1)$.

In contrast the comparable decomposition reaction of 1,2,3-benzthiadiazole-1,1-dioxide, **33**, to biphenylene, sulfur dioxide, and nitrogen is predicted to be highly exothermic with an estimated ΔE = −200 kJ/mol. In this case estimates of the transition state energy are much lower (~148.5 kJ/mol) and may be even lower owing in large part to the stability of SO_2, compared with **13**. This result is in accord with the observed facile generation of biphenylene from **33** formed by further oxidation of the otherwise stable **13**.

In contrast to the situation with **13** where its great stability

Can. J. Chem. Downloaded from www.nrcresearchpress.com by 91.121.58.235 on 09/07/12
For personal use only.

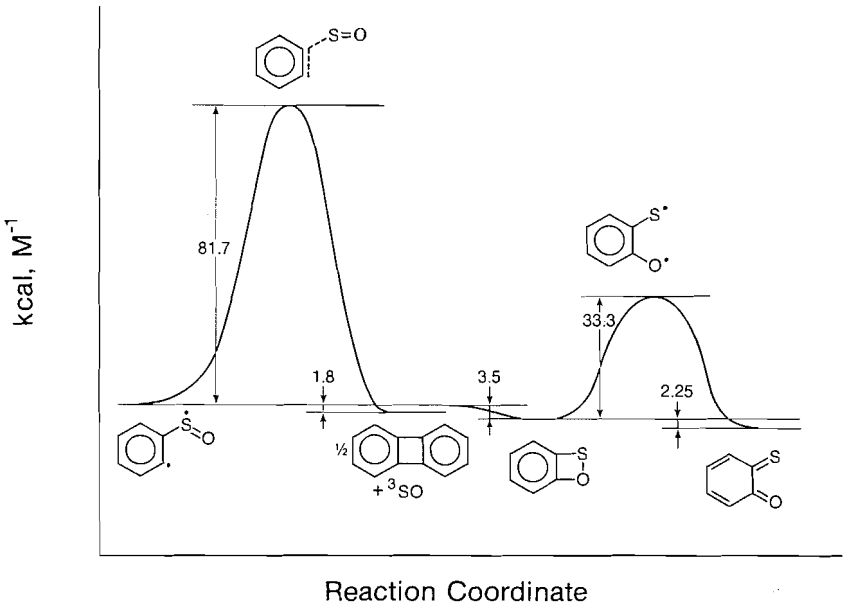

FIG. 3. Depiction of relative energies (derived from *ab initio* calculations) of intermediates and transition states along the reaction coordinate leading to benzoxathiete, **14**, and its valence tautomer monothio-*o*-benzoquinone, **17**.

TABLE 2. Calculated energies and energy differences at 3-21G* for reactions of 1,2,3-benzthiadiazole and related structures

Reactants	Products			ΔE^a
				kJ/mol ($\times 10^{-1}$)
Benzthiadiazole + $(1/2)O_2$ −732.1312 −74.3846	Benzthiadiazole-1-oxide (**13**) −806.4911			6.48
13 + $(1/2)O_2$ −806.4911 −74.3846	Benzthiadiazole-1,1-dioxide (**33**) −880.9420			17.41
13 −806.4911	(1/2)Biphenylene (**20**) + −228.2137	^1SO −470.0094	+ N_2 −108.3010	−8.66
13	Dehydrobenzene (**16**) + −228.0808	^1SO −470.0094	+ $2N_2$ −108.3010	26.2[b]
33 −880.9420	(1/2)Biphenylene + −228.2137	SO_2 −544.5036	+ N_2 −108.3010	−20.0
33	Dehydrobenzene + −228.0808	SO_2 −544.5036	+ $2N_2$ −108.3010	14.85[b]

[a]Difference in energy between products and reactants.
[b]Estimate of transition state energy for the preceding reaction via intermediate dehydrobenzene.

precludes generation of biradical **15** (at least by this pathway) the facile thermolysis of **33** renders generation of the corresponding biradical **35** quite likely. Since **33** is observed experimentally to decompose to dehydrobenzene and biphenylene (10) it is useful to consider alternative pathways. Energy differences predict a highly exothermic conversion of **35** to biphenylene **20** and sulfur dioxide. In this reaction the transition state energy is estimated to be very low (ca. 18.8 kJ/mol) as in the corresponding reaction of **33**, rendering this pathway quite feasible. Compound **18** was predicted not to be stable and there is no experimental evidence for its contribution in the overall reaction scheme.

Biradical species

Free radical species generated in these reactions have been detected and their structures and reactivities investigated by EPR. In addition, certain biradical species are implicated in the alternative pathways of aprotic diazotization of aryl sulfinyl amines and in the generation of benzoxathiete and related structures (1–5). The results of the *ab initio* calculations permit an examination of their properties and an assessment of the contributions. The consensus of opinion following extensive experimental and theoretical studies of dioxetane decomposition favors a biradical intermediate corresponding to cleavage of the O—O bond (6, 19). Similarly experimental and *ab initio* studies favor biradical intermediates in the formal cycloreversion of 1,2-oxathietane (5) and in the valence tautomerism of benzoxathiete **14** to monothio-*o*-benzoquinone **17** (4). Ring closure of biradical **15**, involved in the latter process, to **14** is predicted to be exothermic.

Although the isomeric biradical **15** is not generated from **13**, at least under the present mild experimental conditions, it

Can. J. Chem. Downloaded from www.nrcresearchpress.com by 91.121.58.235 on 09/07/12
For personal use only.

TABLE 3. Calculated energies and energy differences at 3-21G* for reactions of benzoxathiete **14**

Reactant	Products		ΔE^a kJ/mol ($\times 10^{-1}$)
Benzoxathiete (**14**) −698.2911	(1/2)Biphenylene (**20**) + −228.2137	^{1}SO −470.0094	17.86
Benzoxathiete (**14**)	Dehydrobenzene (**16**) + −228.0808	^{1}SO −470.0094	52.76[b]
Benzoxathiete (**14**)	(1/2)Biphenylene (**20**) + −228.2137	^{3}SO −470.0747	0.71
Benzoxathiete (**14**)	Dehydrobenzene (**16**) + −228.0808	^{3}SO −470.0747	35.61[b]

[a]Difference in energy between products and reactants.
[b]Estimate of transition state energy for the preceding overall reaction via intermediate dehydrobenzene.

TABLE 4. Calculated energies and energy differences at 3-21G* for reactions involving biradical species

Reactant	Products		ΔE^a kJ/mol ($\times 10^{-1}$)
I. Biradicals associated with 1,2,3-benzthiadiazole-1-oxide			
Benzthiadiazole-1-oxide (**13**) −806.4911	Biradical **15** + −698.2856	N_2 −108.3010	−25.06
Biradical **15** −698.2856	(1/2)Biphenylene (**20**) + −228.2137	^{1}SO −470.0094	16.40
Biradical **15**	Dehydrobenzene (**16**) + −228.0808	^{1}SO −470.0094	51.30[b]
Biradical **15**	(1/2)Biphenylene (**20**) + −228.2137	^{3}SO −470.0747	−0.736
Biradical **15**	Dehydrobenzene (**16**) + −228.0808	^{3}SO −470.0747	34.18[b]
Biradical **15**	Benzoxathiete (**14**) −698.2911		−1.44
II. Biradicals associated with 1,2,3-benzthiadiazole-1,1-dioxide			
Benzthiadiazole-1,1-dioxide **33** −880.9420	Biradical **33***a* −880.8172		32.76
Benzthiadiazole-1,1-dioxide **33**	Biradical **35** + −772.6368	N_2 −108.3010	1.10
Biradical **35** −772.6368	(1/2)Biphenylene (**20**) + −228.2137	SO_2 −544.5036	−21.13
Biradical **35**	Dehydrobenzene (**16**) + −228.0808	SO_2 −544.5036	13.76[b]

[a]Difference in energy between reactants and products.
[b]Estimate of transition state energy for the preceding reaction via intermediate dehydrobenzene.

is quite likely to be generated from radical **8**. Therefore its characteristics were examined theoretically. Biradical **15** is surprisingly stable quite close in energy to **14** (Table 4, Fig. 3). The conversion of **15** to biphenylene and ^{1}SO would be highly endothermic. If one considers the high transition state energy for this process via dehydrobenzene (ΔE = 513.1 kJ/mol, endothermic), this pathway is even less likely. While the alternative conversion of **15** to biphenylene and ^{3}SO overall is slightly exothermic, consideration of the high transition state energy (ΔE = 341.6 kJ/mol) indicates this is also not a feasible reaction pathway. In contrast the energy difference for ring closure of biradical **15** to benzoxathiete predicts a facile and slightly exothermic process.

Products of aprotic diazotization of 2-[(2-acetoxyethyl)sulfonyl]-anilines benzoxathiete-S-oxide and its valence tautomer

The situation with the aprotic diazotization of 2-[(2-acetoxyethyl)sulfonyl]anilines is somewhat different in that, in contrast to the very stable compound **13**, 1,2,3-benzthiadiazole-1,1-dioxide (**33**) and the attendant species are plausible intermediates en route to the isolated biphenylene, **20**. Azosulfones are generally in equilibrium with diazonium sulfinates and on

Can. J. Chem. Downloaded from www.nrcresearchpress.com by 91.121.58.235 on 09/07/12
For personal use only.

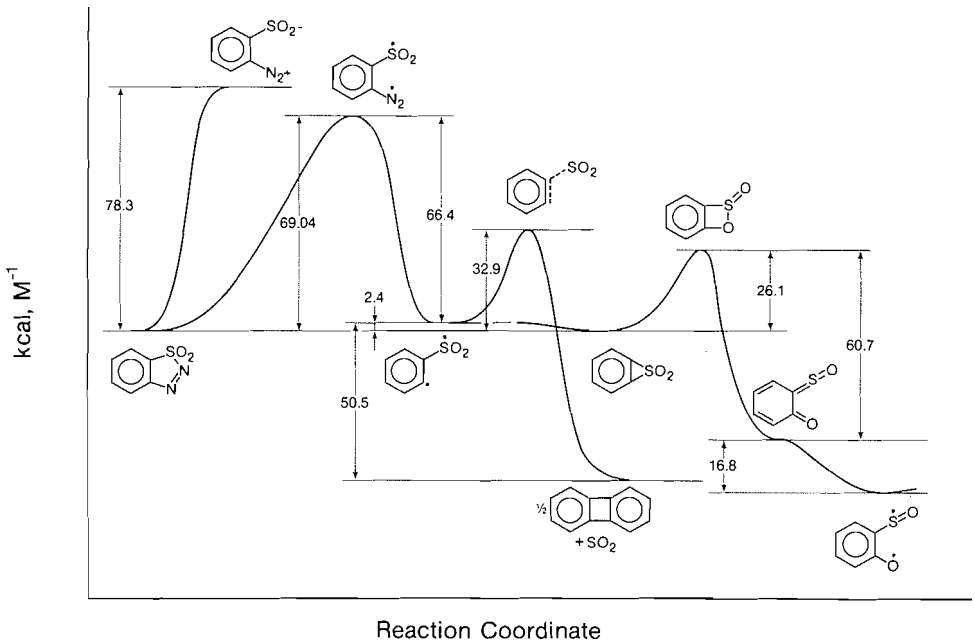

FIG. 4. Depiction of relative energies (derived from *ab initio* calculations) of intermediates and transition states along the reaction coordinate involved in aprotic diazotization of 2-[(2-acetoxyethyl)sulfonyl]aniline and leading to benzoxathiete-*S*-oxide, **34**, and its valence tautomer *o*-benzketosulfine, **36**.

this basis it has been suggested that 1,2,3-benzthiadiazole-1,3-dioxide, **35**, is in equilibrium with *o*-benzenediazonium sulfinate or equivalent biradical species (20). The principle of microscopic reversibility applied to these equilibria provides support for the suggested processes **27** $\rightleftharpoons$ **30** thence to **33**. In addition the isolation of dibenzo-1,4-oxathiane-*S*-oxide, **38**, from further oxidation of **13** and which requires intermediate formation of benzoxathiete-*S*-oxide **34** and its valence tautomer **36** required theoretical examination. Therefore the energetics of these species were examined using quantum chemical methods. Reaction of **33** to give triplet biradical **35** and sulfur dioxide predicts an endothermic reaction with ΔE = 31 kcal/mol. The estimate of the energy of triplet biradical **35** is somewhat low since there is quintuplet character mixed in. However, it is evident that triplet biradical **35** has significant stability.

Alternatively decomposition of **33** to give singlet **35** and sulfur dioxide predicts an even more endothermic process with $\Delta E = 27.8 \times 10^4$ J/mol and, as such, the reaction would not be spontaneous. While generation of biradical **35** is therefore energetically disfavored, compared with spontaneous decomposition of **33** to biphenylene and SO_2 (10), species **35** could reasonably arise by side chain elimination from **28** by analogy with the reaction **8** to **15**. For this reason the energetics of the processes arising from **35** were examined and are summarized in Fig. 4. The behavior of **35** is quite different from that of **15**. Thus the conversion of **35** to biphenylene and SO_2 is predicted to have a ΔE value of -211.3 kJ/mol and the process is expected to be highly exothermic owing largely to the high stability of SO_2. When consideration is taken of the energy of the transition state via dehydrobenzene an estimated activation energy is found to correspond to ΔE = 137.6 kJ/mol.

The corresponding ring closure of biradical **35** to benzoxathiete-*S*-oxide **34** is predicted, like the ring closure of **15** to **14** to be favorable both energetically ($\Delta E = -10.0$ kJ/mol) and entropically. Despite the energetically favored cleavage of **35** to dehydrobenzene and sulfur dioxide, dibenzo-1,4-oxathiane-*S*-oxide, **38**, is obtained from the further oxidation of **13** to **33** and the spontaneous decomposition of the latter. This requires formation of ketosulfine **36** by valence tautomerism of **34** and therefore strongly suggests that ring closure of biradical **35** is rapid.

In view of the precedent of valence tautomerism of benzoxathiete, **14**, to monothio-*o*-benzoquinone, **1** (4), the properties of **34** were examined by *ab initio* treatment. The photochemical generation of the isomeric thiobenzpropiolactone in a solid matrix has been described and its photoelectron spectrum reported and interpreted theoretically (21). Upon optimization, benzoxathiete-*S*-oxide, **34**, has not been found to represent a minimum in energy. A single-point calculation which keeps the SCC and OCC angles frozen at values that insure the formation of the ring leads to an energy value of -772.6064 au (Table 5). An analogy for the suggested valence tautomerism of **14** to **15** and **34** to **36** is that involved in the decomposition of benzenediazonium carboxylate. In this case participation to the incipient unsaturated center gives benzoxetone which is suggested to be in equilibrium with *o*-quinone methide ketene (22). More closely related analogies are those between thiobenzpropiolactone and the corresponding thioketoketene (23), between benzthietekene and the corresponding valence tautomer thioketocumulene (24), and between benzothiete and *o*-quinonemethide (25).

The valence tautomer, **36**, could be optimized to a much lower energy of -772.7012 au, therefore more stable than **34** by 251 kJ/mol. This difference is due to the relief of ring strain (26). As such, valence tautomerism should take place readily (Fig. 5). Species **34** represents a transition state between **35** and **36** since, when SCC and OCC are allowed to relax, **34** reverts to **36**. According to reaction conditions, **34** can revert to biphenylene and SO_2 in a reaction which is predicted to be exothermic. It can be seen from Table 5 that reaction **36** $\rightarrow$ biphenylene and SO_2 is also exothermic. However, a factor that may render observation of **34** or its valence tautomer **36** strongly

Can. J. Chem. Downloaded from www.nrcresearchpress.com by 91.121.58.235 on 09/07/12
For personal use only.

TABLE 5. Calculated energies and energy differences at 3-21G* for reactions of benzoxathiete-*S*-oxide and its valence tautomer

Reactant	Products	ΔE^a kJ/mol ($\times 10^{-1}$)
Benzoxathiete-*S*-oxide (**34**) −772.6044[b]	Ketosulfine (**36**) (singlet) −772.7012[b]	−25.40
Benzoxathiete-*S*-oxide (**34**)	Ketosulfine (**36**) (triplet) −772.7279	−32.43
Benzoxathiete-*S*-oxide (**34**)	(1/2)Biphenylene + −228.2137 SO_2 −544.5036	−29.66
Benzoxathiete-*S*-oxide (**34**)	Dehydrobenzene + −228.0808 SO_2 −544.5036	5.23[c]
Biradical **35** −772.6368	Benzoxathiete-*S*-oxide (**34**) −772.6044	8.49
Benzoxathiete-*S*-oxide (**34**)	Bicyclic species (**37**) −772.6406	−9.50
Bicyclic species **37** −772.6406	(1/2)Biphenylene + −228.2137 SO_2 −544.5036	−20.12
Bicyclic species **37**	Dehydrobenzene + −228.0808 SO_2 −544.5036	14.77[c]

[a]Difference in energy between reactants and products.
[b]The energy corresponding to an SO distance of 1.7 Å (*i.e.* bonding distance).
[c]Estimate of transition state energy for the preceding reaction via intermediate dehydrobenzene.

dependent on reaction conditions is that cycloreversion of **34** to biphenylene and SO_2 is predicted to be highly exothermic and thus favored energetically. This is in complete contrast to the energetically highly disfavored (though orbital symmetry allowed) reaction of benzoxathiete, **14**, to biphenylene and SO (4). The fact that **34** is not a stable species might explain why compound **38** was not detected in the aprotic diazotization of 2-[(2-acetoxyethyl)sulfonyl]aniline.

Conclusions

1,2,3-Benzthiadiazole-1-oxide, **13**, previously considered an intermediate in one pathway of formation of benzoxathiete via the aprotic diazotization of 2-[(2-acetoxyethyl)sulfonyl]anilines (4), has been synthesized by an unambiguous method. This previously unreported compound proved to be indefinitely stable at ambient temperatures so that the possibility of its giving rise to dehydrobenzene spontaneously in solution must be discounted. The marked thermal stability of **13** (up to the temperature of refluxing *o*-dichlorobenzene) is fully in accord with the *ab initio* calculation of its energy and in relation to its putative decomposition products. The more extensive EPR experiments described herein also tend to favor the pathway **1** → **2** → **3** → **5** → **8** → **12** as the principal route to benzoxathiete and disfavor the intermediacy of radical **7**, the logical precursor to **13**. The energetics of the processes from species **15** (derived from **8**) are depicted in Fig. 3. Literature precedents exist for each of the key steps: (*i*) step **1** → **2** (27–29); (*ii*) equilibrium **2** ⇌ **3** (28, 29); (*iii*) formation of the anhydride of diazohydroxide **5** (30); (*iv*) formation of diazotate ester **6** (31); (*v*) generation of the carbon centered radical **8** via rapid dediazionation of **7** (31–34) or homolysis of a diazoanhydride **5** (30); (*vi*) facile ring closure of radical **8** to **12** (13*b*,*c*); (*vii*) free radical abstraction of hydrogen atom from alkyl side chain, e.g., **28** → **42** (13*b*,*c*).

The synthesis of compound **13** afforded an opportunity to attempt further selective oxidation to the corresponding 1,2,3-benzthiadiazole-1,1-dioxide, **33**, which is a possible intermediate in the generation of dehydrobenzene during comparable aprotic diazotization of 2-[(2-acetoxyethyl)sulfonyl]aniline with isoamyl nitrite. 1,2,3-Benzothiadiazole-1,1-dioxide is conventionally generated by treatment of sodium salt of 2-aminobenzenesulfinic acid with sodium nitrite in aqueous sulfuric acid at −15°C (10). It is not normally isolated because of its great instability and tendency to explode spontaneously in the solid state (10).

In the event prolonged treatment of 1,2,3-benzthiadiazole-1-oxide, **13**, with hydrogen peroxide in acetic acid at ambient temperatures or rose bengal sensitized photooxidation afforded, among the products, biphenylene and dibenzo-1,4-oxathiane-*S*-oxide, **38**. Since the monooxide **13** is stable at this temperature this result implies selective S-oxidation to the 1,1-dioxide, **33**, and spontaneous decomposition of the latter with formation of dehydrobenzene **16** and concomitant generation of biradical **35** by loss of nitrogen. Rapid ring closure of **35** gives benzoxathiete-*S*-oxide, **34**, which reverts immediately via valence tautomerism to the ketosulfine **36**. Thus the chemical behavior and products derived from **33** are sensitive to reaction conditions. This may explain why **38** was not detected among the products of the aprotic diazotization of 2-[(2-acetoxyethyl)sulfonyl]anilines. Conceivably radical **28** may decompose directly to **16**, thereby preventing the formation of species **32**. Trapping of **36** from **34** by dehydrobenzene gives **38** and dimerization of **16** affords biphenylene.

EPR evidence in conjunction with spin trapping experiments employing both DMPO and nitrosodurene unambiguously identify an aryl radical intermediate, corresponding to **28**. Since the major product of aprotic diazotization is biphenylene **20** derived from dimerization of dehydrobenzene **16** the experimental evidence suggests radical **28** converts to **35** or **16**

Can. J. Chem. Downloaded from www.nrcresearchpress.com by 91.121.58.235 on 09/07/12
For personal use only.

in preference to species **32**. The energetics of the processes following from the biradical species **35** (and derived from either **28** or **33**) are depicted in Fig. 4.

Acknowledgments

This work was supported by Grant 1R01 CA/GM2 R0121488-12 awarded (to J.W.L.) by the National Cancer Institute, DHHS. We thank Dr. Tom Nakashima and his associates for the NMR experiments and Dr. Alan Hogg and his colleagues for MS, GCMS, and CIMS spectra. A.M.S. thanks the City University of New York for computer time and for grant no. 666275.

1. J. W. LOWN and R. R. KOGANTY. J. Am. Chem. Soc. **105**, 126 (1983).
2. J. W. LOWN and R. R. KOGANTY. J. Am. Chem. Soc. **108**, 3811 (1986).
3. J. W. LOWN, R. R. KOGANTY, and A. NAGHIPUR. J. Org. Chem. **51**, 2112 (1986).
4. A. NAGHIPUR, K. RESZKA, A.-M. SAPSE, and J. W. LOWN. J. Am. Chem. Soc. **111**, 258 (1989).
5. A. NAGHIPUR, J. W. LOWN, D. C. JAIN, and A.-M. SAPSE. Can. J. Chem. **66**, 1890 (1988).
6. (*a*) W. ADAM. *In* Chemical and biological generation of excited states. *Edited by* W. Adam and G. Cilento. Academic Press, New York. 1982. Chap. and references therein; (*b*) N. J. TURO and P. LECHTKEN. J. Am. Chem. Soc. **94**, 2886 (1972); (*c*) W. H. RICHARDSON, F. C. MONTGOMERY, M. B. YELVINGTON, and K. E. O'NEAL. J. Am. Chem. Soc. **96**, 7525 (1974); (*d*) W. H. WHITE, P. D. WILDES, J. WEICKO, H. DOSHAM, and C. C. WEI. J. Am. Chem. Soc. **95**, 7050 (1973); (*e*) K. R. KOPECKY, J. E. FILBY, C. MUMFORD, and P. A. DING. Can. J. Chem. **53**, 1103 (1975).
7. P. JACOBSON. Chem. Ber. **21**, 3014 (1988).
8. L. P. FIESER. Advanced organic chemistry. Reinhold, New York. 1963. p. 920.
9. H. GILMAN and L. ESMAY. J. Am. Chem. Soc. **74**, 202 (1952).
10. G. WITTIG and R. W. HOFFMANN. Org. Synth. **47**, 4 (1962).
11. (*a*) L. FRIEDMANN and J. F. CHLEBOWSKI. J. Org. Chem. **33**, 1633 (1968); (*b*) R. M. PATON and R. U. WEBER. Org. Magn. Res. **9**, 494 (1977); (*c*) H. ZOLLINGER. Azo and diazo chemistry. Interscience, New York. 1961; (*d*) J. W. BENTLEY, J. A. JOHN, R. A. W. JOHNSTONE, P. J. RUSSELL, and L. H. SUTCLIFFE. J. Chem. Soc. Perkin Trans. II, 1039 (1973).
12. (*a*) K. RESZKA, A. NAGHIPUR, and J. W. LOWN. 2nd International Symposium on Spin Trapping and Aminoxyl Radicals, Guelph. 1989; (*b*) K. RESZKA, A. NAGHIPUR, and J. W. LOWN. Free Rad. Res. Commun. In press; (*c*) E. G. JANZEN. Acc. Chem. Res. **4**, 31 (1971); (*d*) M. J. PERKINS. Adv. Phys. Org. Chem. **17**, 1 (1980).
13. (*a*) E. G. JANZEN, C. A. EVANS, and I.-P. J. LIU. J. Magn. Res. **9**, 513 (1973); (*b*) A. L. J. BECKWITH and W. B. GARA. J. Am. Chem. Soc. **91**, 5689 (1969); (*c*) A. L. J. BECKWITH and W. B. GARA. J. Am. Chem. Soc. **91**, 5691 (1969).
14. J. S. BINKLEY, M. J. FRISCH, D. M. DEFREES, K. RAGHAVACHARI, R. A. WHITESIDE, B. SCHLEGEL, E. M. FLUTER, and J. A. POPLE. Gaussian 82. Carnegie-Mellon University, Pittsburgh, PA. 15213.
15. M. J. FRISCH, J. S. BINKLEY, H. B. SCHLEGEL, K. RAGHAVACHARI, C. F. NELIUS, R. L. MARTIN, J. J. P. STEWART, F. W. BOBROWICZ, C. M. ROHIFING, L. R. KAHN, D. J. DEFREES, R. SEEGER, R. A. WHITESIDE, D. J. FOX, E. M. FLEUDER, and J. A. POPLE. GAUSSIAN-86. Carnegie-Mellon Quantum Chemistry Publishing Unit, Pittsburgh, PA. 1984.
16. H. B. SCHLEGEL. J. Comput. Chem. **3**, 214 (1982).
17. J. D. GODDARD. Can. J. Chem. **63**, 1910 (1985).
18. R. B. WOODWARD and R. HOFFMANN. The conservation of orbital symmetry. Verlag Chemie, Weinham. 1970. p. 72.
19. L. B. HARDING and W. A. GODDARD. J. Am. Chem. Soc. **99**, 4520 (1977).
20. R. W. HOFFMANN. Dehydrobenzene and cycloalkynes. Academic Press. 1967. p. 67.
21. R. SCHULTZ and A. SCHWEIG. Tetrahedron Lett. **1**, 59 (1979).
22. (*a*) R. GOMPPER, G. SEYBOLD, and B. SCHMOLKE. Angew Chem. Int. Ed. Engl. **7**, 389 (1968); (*b*) R. W. HOFFMANN, W. SIEBER, and G. GUHN. Angew Chem. Int. Ed. Engl. **4**, 704 (1965).
23. R. SCHULTZ and A. SCHWEIG. Tetrahedron Lett. **20**, 59 (1979).
24. R. SCHULTZ and A. SCHWEIG. Tetrahedron Lett. **21**, 343 (1980).
25. D. JACOB, H. PETER-NIDERMANN, and H. MEIER. Tetrahedron Lett. **27**, 5703 (1986).
26. E. VOGEL. Angew Chem. **72**, 4 (1960).
27. J. I. G. CADOGAN. J. Chem. Soc. 4257 (1962).
28. L. FRIEDMAN and J. F. CHLEBOWSKI. J. Org. Chem. **33**, 1633 (1968).
29. A. F. HEGARTY. *In* The chemistry of diazonium and diazo groups. Pt. 2. *Edited by* S. Patai. Wiley, New York. 1978. pp. 511–590.
30. C. RUCHARDT and E. MERZ. Tetrahedron Lett. **36**, 3431 (1964).
31. (*a*) T. J. BROXTON and M. J. MCLEISH. J. Org. Chem. **48**, 191 (1983); (*b*) J. F. BUNNETT and H. TAKAYAMA. J. Org. Chem. **33**, 1424 (1968); (*c*) C. GALLI. Chem. Res. **88**, 765 (1988).
32. O. BREDE, R. MEHNERT, W. NAUMANN, and H. G. O. BECKER. Ber. Bursgenges Phys. Chem. **54**, 666 (1980).
33. K. C. BROWN and M. P. DOYLE. J. Org. Chem. **53**, 3255 (1988).
34. H. LOEWENSCHUSS, G. H. WAHL, and H. ZOLLINGER. Helv. Chim. Acta, **59**, 1438 (1976).

Can. J. Chem. Downloaded from www.nrcresearchpress.com by 91.121.58.235 on 09/07/12
For personal use only.

The solution-phase photochemistry of 2-trifluoromethylnorbornene

N. NGUYEN, B. E. HARRIS, K. B. CLARK,[1] AND W. J. LEIGH[2]
Department of Chemistry, McMaster University, Hamilton, Ont., Canada L8S 4M1

Received March 28, 1990

N. NGUYEN, B. E. HARRIS, K. B. CLARK, and W. J. LEIGH. Can. J. Chem. **68**, 1961 (1990).

The photochemistry of 2-trifluoromethylnorbornene in pentane solution has been investigated. Direct photolysis with 193 nm light yields 1-trifluoromethyl-2-norcarene in 90% yield, due to formal [1,3]-sigmatropic rearrangement, in addition to three other minor products. Chlorobenzene-sensitized photolysis affords photoreduction products, principally *exo*- and *endo*-2-trifluoromethylnorbornane and decane isomers, in addition to several products of higher molecular weight. On the basis of comparisons of the photochemistry of this compound to that previously reported for norbornene and 2-cyanonorbornene, as well as spectroscopic evidence, it is suggested that the lowest excited singlet state (the photoreactive state in solution) in 2-trifluoromethylnorbornene is the π,π^* state. The results indicate that trifluoromethyl substitution has the effect of significantly raising the energy of the π,R(3*s*) Rydberg state in simple alkenes, without altering the high energy (*ca.* 6.5 eV) or the localized character of the alkene π,π^* state. Furthermore, they lend additional support to the view that the carbene-derived products typically formed upon photolysis of alkenes in solution are derived from π,R(3*s*) excitation.

Key words: Rydberg, photolysis, far-uv, alkene, solution phase, singlet, triplet.

N. NGUYEN, B. E. HARRIS, K. B. CLARK et W. J. LEIGH. Can. J. Chem. **68**, 1961 (1990).

On a étudié la photochime du 2-trifluoromethylnorbornene, en solution dans le pentane. La photolyse directe avec de la lumière à 193 nm fournit du 1-trifluorométhyl-2-norcarène avec un rendement de 90%, en plus de trois autres produits qui sont présents en quantités mineures; le produit principal se forme par le biais d'une transposition formelle [1,3]-sigmatropique. La photolyse sensibilisée par le chlorobenzène fournit des produits de photoréduction, principalement les isomères *exo*- et *endo*-2-trifluorométhylnorbornanes et décanes, en plus de plusieurs produits de poids moléculaires élevés. En se basant sur des données spectroscopiques ainsi que sur une comparaison de la photochimie de ce composé avec celles rapportées antérieurement pour le norbornène et pour le 2-cyanonorbornène, on suggère que l'état excité singulet de plus basse énergie (l'état photoréactif en solution) du 2-trifluorométhylnorbornène est l'état π,π^*. Les résultats indiquent que la substitution par un groupement trifluorométhyle a pour effet d'augmenter considérablement l'énergie de l'état Rydberg π,R(3*s*) des alcènes simples sans toutefois altéré l'énergie élevée (environ 6,5 eV) ou le caractère localisé de l'état π,π^* de l'alcène. De plus, ces résultats ajoutent un poids additionnel à la théorie selon laquelle les produits dérives des carbènes, qui se forment d'une façon typique par photolyse des alcènes, sont dérivés d'une excitation π,R(3*s*).

Mots clés : Rydberg, photolyse, UV lointain, alcène, solution, singulet, triplet.

[Traduit par la revue]

Introduction

The photochemistry of simple alkenes in solution has been a subject of intense interest over the past three decades (1–5). The complex photobehaviour that is frequently observed on direct irradiation of aliphatic olefins in solution has been attributed to the involvement of two singlet excited states of comparable energies, the π,π^* valence and the π,R(3*s*) Rydberg states (1). The π,π^* state is thought to lead to *cis,trans*-isomerization in acyclic and larger-ring cyclic (*i.e.*, $\geq C_6$) alkenes, and hydrogen-abstraction reactions. The π,R(3*s*) Rydberg state has been proposed to be responsible for the products of carbene intermediates derived from [1,2]-hydrogen or -alkyl shifts and in alcohol solvents, the products of nucleophilic addition to the C=C bond (1). Products attributable to formal [1,3]-H or -alkyl migration are also frequently observed in alkene photochemistry (1–4), and their origin has been subject to some discussion (6). In general, these products may arise from either concerted pathways or stepwise ones involving carbene intermediates, and thus may derive from either the π,π^* or π,R(3*s*) state. Inoue and co-workers have suggested that yet a third singlet excited state may in fact be responsible for the formation of [1,3]-hydrogen migration products in solution-phase alkene photolysis, on the basis of their observation of wavelength-dependence in the photochemistry of 2,3-dimethyl-2-butene and *cis*-2-octene (6). In our view, however, the evidence in support of this proposal is not compelling.[3]

The assignment of carbene-derived products as due to π,R(3*s*) excitation in simple alkenes has been made largely on the basis of gas-phase uv absorption (7, 8*a*) and (solution-phase) fluorescence emission studies (9), which indicate that this state is lower in energy than the spectroscopic π,π^* state in most cases. In tri- and tetraalkyl-substituted olefins, the π,R(3*s*) is thought to be lower in energy than the twisted π,π^* singlet state. These studies have further shown that the energy of the π,R(3*s*) state is markedly more sensitive to alkyl substitution than the π,π^* state; increasing the degree of alkyl substitution at the C=C bond results in a lowering of energies of both the π,R(3*s*) and π,π^* states, the former more than the latter (7, 8*a*). A similar effect is observed on alkene π-ionization potentials (IP's) (8*a*, 10). Since the relative yield of carbene- versus π,π^*-derived products from alkene photolysis

[1]Present address: Division of Chemistry, National Research Council of Canada, 100 Sussex Drive, Ottawa, Ont., Canada K1A 0R6.

[2]Natural Sciences and Engineering Research Council of Canada University Research Fellow, 1983–1993. Author to whom correspondence should be addressed.

[3]The evidence for the third photoreactive state in simple alkenes is that longer excitation wavelengths result in reduced yields of 1,3-H migration products relative to carbene-derived (π,R(3*s*)) ones in the photolysis of 2,3-dimethyl-2-butene, and to $E \rightleftarrows Z$ isomerization (π,π^*) in the photolysis of *cis*-2-octene. Strictly speaking though, these experiments demonstrate only that [1,3]-H migration is not Rydberg-derived in the case of 2,3-dimethyl-2-butene, and not π,π^*-derived in the case of *cis*-2-octene. The indication that it is not π,π^*-derived in the latter compound does not preclude it from being so in the former compound. In the case of 2-octene, these products could result from carbenes derived from the π,R(3*s*) state.

Can. J. Chem. Downloaded from www.nrcresearchpress.com by 91.121.58.235 on 09/07/12
For personal use only.

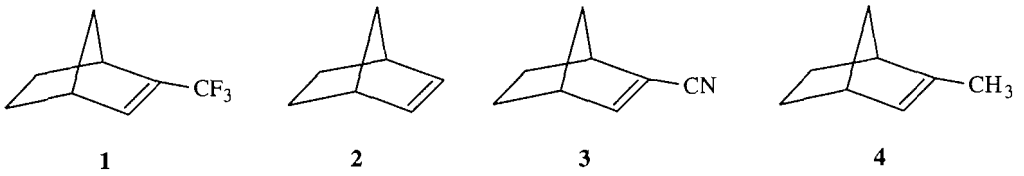

1 2 3 4

in solution also increases with increasing alkyl substitution on the double bond (1), the identification of the $\pi,R(3s)$ state as that responsible for the formation of carbene-derived products seems to be a logical one. In addition, the product distribution from solution-phase photolysis of tetramethylethylene is wavelength dependent, with the yields of carbene-derived products increasing relative to [1,3]-migration product at longer excitation wavelengths (6).

[1,2]-Migrations are also common in the photochemistry of β-alkylstyrene derivatives (11, 12). Hixson and co-workers have demonstrated that these products, as well as those of formal [1,3]-H or -alkyl migration, are in fact formed by complex pathways involving carbenes (12). The state responsible for carbene formation in phenylated alkenes has not been identified, however. In benzenoid systems, the $\pi,R(3s)$ state is higher in energy than the lowest π,π^* state (8*b*).

The photochemistry of simple alkenes is thus often complex, even in monosubstituted systems. As a further aid to the assignment of alkene photoproduct types to the involvement of specific excited states, it is desirable to be able to selectively excite one state or the other. This is usually not possible by simple variation of the excitation wavelength (*cf.* ref. 6, however), so it is necessary to alter the state-separation through substitution on the alkene. As mentioned above, increasing alkyl substitution at the C=C bond can be employed to lower the Rydberg state energy at the expense of that of the π,π^* state. Conjugative substituents can of course be used to lower the energy of the π,π^* state at the expense of the Rydberg, but this also changes the basic character of the chromophore. We wished to develop a means of *raising* the energy of the $\pi,R(3s)$ state so that the π,π^* state would be rendered lower in energy, but still maintain the high energy and localized character of the basic system.

The $\pi,R(3s)$ state can be considered to have radical–cation character at the double bond (7), since the 3*s* orbital is quite diffuse and is approximately of *molecular* size for small alkenes such as tetramethylethylene. With this simple picture in mind, we reasoned that substitution at the C=C bond with nonconjugative electron-withdrawing groups such as trifluoromethyl might have the desired effect of raising the energy of the $\pi,R(3s)$ state without substantially affecting the energy or localized nature of the ethylenic π,π^* singlet state. In this paper, we describe the results of a study of the photochemistry of 2-trifluoromethylnorbornene (**1**) in hydrocarbon solution. This compound was chosen for our initial study because it is easily synthesized and the photochemistry of norbornene (**2**) and 2-cyanonorbornene (**3**) have both been reported (13–15). Compounds **2** and **3** are excellent model compounds with which to compare the behaviour of **1**; direct photolysis of **2** yields predominantly carbene-derived products upon photolysis in solution (13, 14), while **3** affords only products consistent with π,π^* photochemistry (15). We have coupled this study with gas-phase spectroscopic studies of **1**, **2**, and 2-methylnorbornene (**4**), which are reported in a separate paper (16).

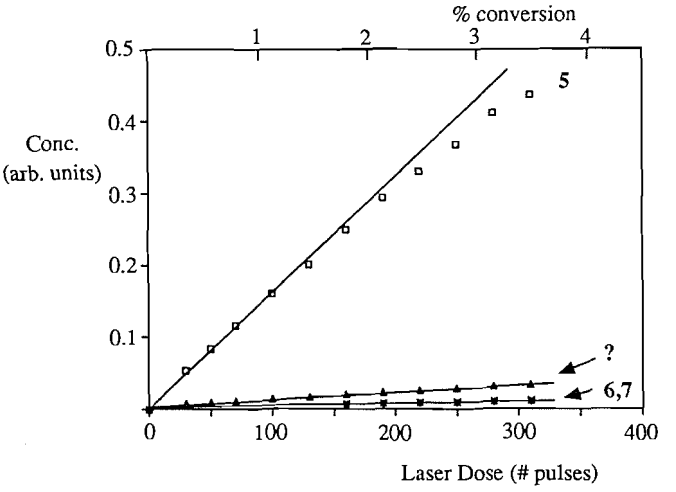

FIG. 1. Plots of product concentration vs. excitation dose from 193 nm photolysis of **1** as a deoxygenated, 0.02 M pentane solution.

Results

Compound **1** was synthesized by free radical addition of trifluoromethyl iodide to norbornene (17), followed by base-catalysed elimination with potassium *tert*-butoxide (18). It was purified by preparative vapour-phase chromatography (vpc) to >99.5% purity.

Photolysis of a deoxygenated, 0.02 M pentane solution of **1** with the pulses (193 nm, *ca.* 40 mJ) from an Ar/F_2 excimer laser led to the product mixture shown in reaction [1].

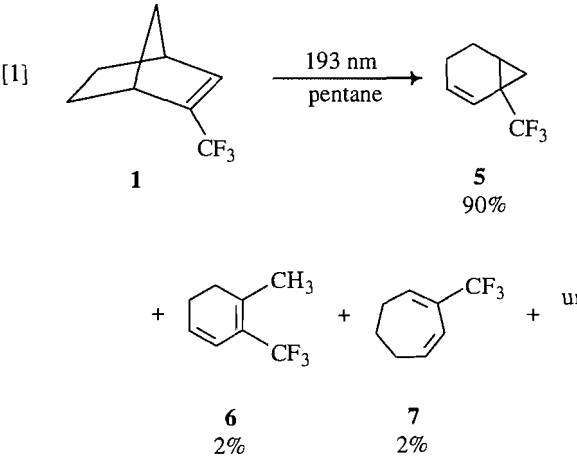

1 → **5** 90%

+ **6** 2% + **7** 2% + 6%

Products **5–7** were isolated by preparative vpc from semi-preparative runs (*ca.* 300 mg scale) carried to *ca.* 40% conversion, and were identified on the basis of their ^1H, ^{13}C, and ^{19}F nmr, infrared, uv absorption, and mass spectra. The photolysate also contained one other component (*ca.* 6%) for which quantities adequate for its identification could not be obtained. A major factor in the identification of **5** was the fact that its ^1H and ^{13}C nmr spectra show very marked similarities to

Can. J. Chem. Downloaded from www.nrcresearchpress.com by 91.121.58.235 on 09/07/12
For personal use only.

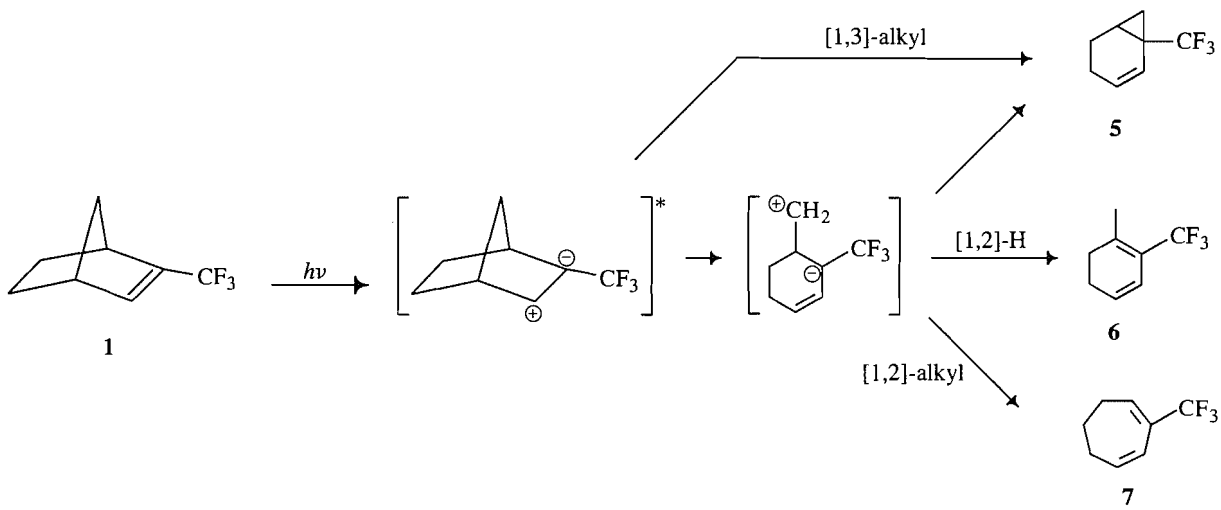

SCHEME 1

those reported for the analogous cyano-substituted derivative (*vide infra*), which is the major product from direct photolysis of **3** in solution (15). The structure of this compound was proven by X-ray crystallography of a derivative.

Product yields listed in reaction [1] were obtained from the slopes of plots of product concentration versus excitation dose, constructed from small scale runs that were monitored between 0.3 and 4% conversion. Typical plots of this type are shown in Fig. 1. The material balance is estimated to be at least 98% at 4% conversion.

To verify that **6** and **7** are primary products from photolysis of **1** and do not arise from secondary photolysis of **5** (products of this type are known to result from direct photolysis of 2-norcarene derivatives (19)), a deoxygenated pentane solution of the latter (0.02 M) was photolysed at 193 nm under similar conditions to those used for the photolysis of **1**. As expected, **6** and **7** are formed from photolysis of **5**, but only as minor products. The major products in this photolysis were not identified, but could not be detected as products from the photolysis of **1** at low (<10%) conversions, within the accuracy limits of our analytical method.

Chlorobenzene- or toluene-sensitized photolysis of a deoxygenated 0.01 M solution of **1** in pentane (containing 0.02 M sensitizer) afforded similar, complex mixtures of products. The major volatile products of chlorobenzene-sensitized photolysis are *exo*- and *endo*-2-trifluoromethylnorbornane (**8**) (formed in roughly equal yields) and three isomers of decane (due presumably to coupling of 2- and 3-pentyl radicals). The structures of *exo*- and *endo*-**8** were assigned on the basis of their ^{1}H nmr, ir, and mass spectra, after isolation from the crude photolysate by semi-preparative vpc. Several products of higher molecular weight were also formed in these photolyses. Gas chromatographic/mass spectroscopic (gc/ms) analysis indicated three of these to have parent ions of 234 amu, corresponding to addition products of **1** with the solvent. In addition, a product of parent ion mass 274 amu was formed in minor yield, and is presumably a cycloaddition product between **1** and the sensitizer. None of the products formed in the direct photolysis of this compound could be detected in the sensitized photolysis.

Discussion

The major product from direct photolysis of **1** is formally the product of a [1,3]-sigmatropic shift, although the formation of all three identified products can be rationalized as arising from a common mechanistic pathway which involves initial heterolytic cleavage of the C_4—C_7 bond in **1** (Scheme 1). Such a cleavage would be expected to be facilitated by zwitterionic character in the singlet excited state of **1**, as depicted in Scheme 1. The zwitterionic intermediate so formed can then collapse to form **5**, undergo [1,2]-H migration to yield **6**, or ring expansion to yield **7**. Naturally, it is not possible to define whether **5** is formed by one or both of these two possible routes.

The products of chlorobenzene- and toluene-sensitized photolysis of **1** are analogous to those observed in the toluene- or xylene-sensitized photolyses of norbornene and other substituted derivatives, and presumably involve the alkene triplet state (20). The absence of **5**–**7** as products of the sensitized photolysis of **1** suggests that in the direct photolysis, these products are formed exclusively via the singlet excited state(s). This is not surprising, since intersystem crossing in alkenes is generally relatively inefficient (1).

The photochemistry of **1** is to be compared to that reported previously for norbornene (**2**; reaction [2] (13, 14)) and 2-cyanonorbornene (**3**; reaction [3] (15)). The main products from

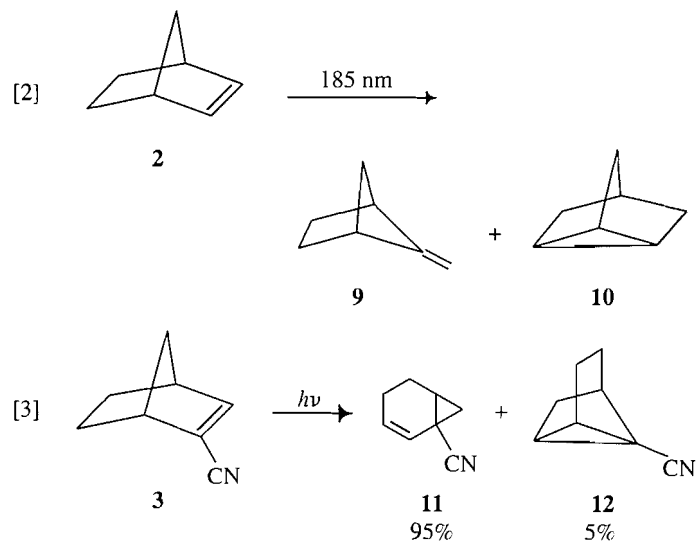

photolysis of **2** (*i.e.*, **9** and **10**) are thought to derive from carbenes formed via [1,2]-alkyl and [1,2]-H migrations, respectively, in the π,R(3*s*) state (reaction [4]). Norbornane,

Can. J. Chem. Downloaded from www.nrcresearchpress.com by 91.121.58.235 on 09/07/12
For personal use only.

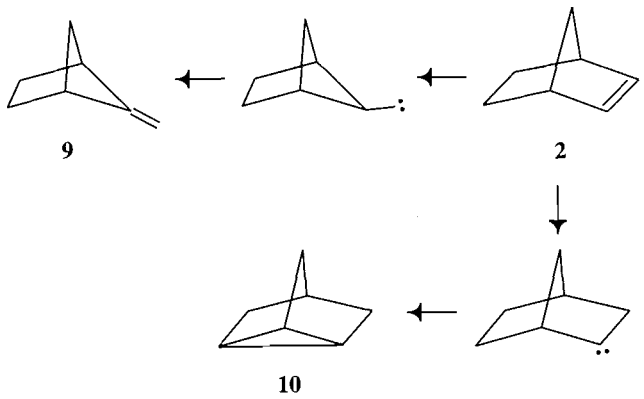

[4]

norbornyl dimers, solvent-addition products, and solvent-derived dimers formed as minor products in the photolysis of **2** presumably arise from H-abstraction from the solvent (14). Carbene-derived products are also the main ones in the photolyses of monocyclic (C_5–C_7) alkenes in solution (1, 13, 14, 21–24). Gas-phase uv absorption studies have identified the π,R(3*s*) state as the lowest energy (vertical) excited singlet state in these systems (8*a*). While the oscillator strengths of Rydberg transitions drop dramatically in the condensed phase and the band is slightly blue-shifted (8), photochemical (6) and spectroscopic (9) results indicate that Rydberg state population in solution is most efficient by direct excitation of the absorption band (as opposed to internal conversion from more intensely absorbing upper states).

In the gas phase, the lowest energy (vertical) excited singlet state of norbornene (**2**) is the π,R(3*s*) state (7, 8*a*, 16), but the 0,0 level appears to be similar in energy to that of the π,π^* state. In solution, the Rydberg levels are shifted to slightly higher energies compared to the valence levels (Rydberg absorptions are not visible in the solution phase uv spectrum of **2** (16)) (7, 8*a*, 16). In the case of **1**, gas-phase optical and energy loss spectroscopies demonstrate that the π,R(3*s*) absorption maximum is shifted to much higher energies than it is in **2** (by *ca.* 0.4 eV), placing it slightly higher in energy than the π,π^* absorption maximum. Thus, the *absence* of carbene-derived products in the direct photolysis of **1** provides additional support for the notion that in the case of **2** and other simple alkenes, such products result from π,R(3*s*) excitation.

The lowest energy singlet excited state in **3** is the π,π^* state (15), which is lowered below the π,R(3*s*) state due presumably to the conjugative effect of the —CN substituent. Furthermore, this substituent should raise the energies of the Rydberg manifold relative to the situation in **2** because of the correlation between Rydberg state energies and π-ionization potential of the alkene (8*a*). Accordingly, the photochemistry of **3** is markedly different from that of **2**, the major product (**11**) being derived from formal (*supra, supra*) [1,3]-migration of the bridgehead carbon from C_4 to C_2. The minor product from photolysis of **3** (*i.e.*, **12**) was formalized by McCullough and co-workers as arising from a ($\sigma_{2a} + \pi_{2a}$) [1,2]-migration pathway analogous to that postulated to account for the photochemistry of β-alkylstyrene derivatives (11, 12).

The main product from photolysis of **1** is the [1,3]-migration product analogous to that obtained from **3**. This suggests that the configuration of the lowest excited singlet states (or at least, the photoreactive singlet states) in these two compounds are identical, although they are very different in energy. It is interesting that the formation of **12** can be viewed in terms of a zwitterionic rearrangement pathway similar to that shown for **1** in Scheme 1, invoking C5-to-C3 migration in the excited state of **3** (instead of C7—C6 bond cleavage). On the basis of our spectroscopic studies of **1** (16), the π,π^* state is very strongly implicated as the primary photoreactive state in the solution-phase photolyses of **1** and **3**.

Conclusions

Trifluoromethyl-substitution has profound effects on the ordering of the lowest Rydberg and π,π^* singlet excited states in simple alkenes. In di-, tri-, and tetraalkyl substituted olefins, the π,R(3*s*) state is similar or lower in energy than the π,π^* state, and the photochemistry in solution is dominated by [1,2]-alkyl and -hydrogen migrations leading to carbene intermediates. Trifluoromethyl-substitution raises the energies of states in the Rydberg manifold due to the strong inductive electron-withdrawing power of the —CF_3 group, without altering the energy or localized character of the π,π^* state. Accordingly, the photoreactivity of such alkenes can be viewed as typical of π,π^* state excitation, and provides a further indication that carbene-derived products from photolysis of simple alkenes result from π,R(3*s*) excitation. The use of trifluoromethyl substituents to delineate "true" π,π^* state reactivity should prove to be of considerable mechanistic value in other simple olefinic systems that exhibit complex photobehaviour. Studies of this type are in progress.

Experimental

The ^{1}H, ^{13}C, and ^{19}F nmr spectra were recorded in $CDCl_3$ solution on a Bruker AM500 (500 MHz) spectrometer and are reported in ppm downfield from tetramethylsilane (^{1}H and ^{13}C) or external fluorotrichloromethane (^{19}F). Infrared spectra were recorded on a Perkin-Elmer 283 spectrometer in $CDCl_3$ solution; spectra are reported in wavenumbers, calibrated against polystyrene. Mass spectra were recorded on a Finnigan 4000 mass spectrometer (Model 4500 ion source), interfaced with a Finnigan gas chromatograph, equipped with a 60 m × 1.0 μm DB1-30W fused silica capillary column (Chromatographic Specialties, Inc.), or a VG7070 mass spectrometer coupled with a Varian 3700 gas chromatograph, equipped with a 60 m × 0.25 mm DB-1701 fused silica capillary column (Chromatographic Specialties, Inc.). Exact masses were determined on a VGH ZABE mass spectrometer, and employed a mass of 12.000 000 for carbon. Ultraviolet absorption spectra were recorded in pentane solution using a Perkin-Elmer Lambda 9 spectrometer equipped with a Model 3600 data station.

Analytical vpc separations were carried out using a Hewlett-Packard 5890 gas chromatograph equipped with a flame ionization detector, a Hewlett-Packard 3396 recording integrator, and a 1.0 μm SPB-1 wide-bore capillary column (30 m × 0.75 mm id borosilicate; Supelco, Inc.). Semi-preparative vpc separations employed a Hewlett-Packard 5750B gas chromatograph equipped with a thermal conductivity detector and one of the following stainless steel columns: (*a*) 3% OV-17 on 80/100 Chromosorb WAW (6′ × 0.25″; Supelco, Inc.); (*b*) 15% Carbowax 20M on 60/80 Chromosorb W (5′ × 0.25″; Supelco, Inc.); (*c*) 3.8% UCW 982 on 80/100 Supelcoport (24′ × 0.25″; Supelco, Inc.); (*d*) 20% tris(cyanoethoxy)propane (TCEP) on 80/100 Chromosorb PNAW (6′ × 0.25″; Supelco, Inc.).

n-Pentane (Baker Photrex), 2,2,4-trimethylpentane (isooctane; Baker Photrex), trifluoromethyl iodide (Columbia), dimethylsulfoxide (Fisher), chlorobenzene (Fisher Reagent), toluene (Fisher Reagent), and potassium *tert*-butoxide (Aldrich) were used as received from the suppliers. Norbornene (Aldrich) was vacuum distilled before use.

2-Trifluoromethylnorbornene (**1**) was prepared using the following typical procedure (17, 18). In a thick-walled Pyrex tube (6″ × 1″ o.d.) fitted at one end with a Rotaflo stopcock was placed norbornene (10 g, 0.106 mmol). The tube was attached to a vacuum line via a rubber hose,

Can. J. Chem. Downloaded from www.nrcresearchpress.com by 91.121.58.235 on 09/07/12
For personal use only.

Can. J. Chem. Downloaded from www.nrcresearchpress.com by 91.121.58.235 on 09/07/12
For personal use only.

and degassed twice by the freeze–pump–thaw method. It was then placed on a balance in a Dewar containing liquid nitrogen, and trifluoromethyl iodide (40.0 g, 0.2 mol) was introduced through a separate stopcock on the vacuum line. The stopcock was closed, and the tube was removed from the vacuum line. After allowing the contents to melt and the norbornene to dissolve, the tube was placed in a quartz Dewar containing Dry Ice/isopropanol at *ca.* −30°C in a Rayonet reactor. The solution was then irradiated with twelve 300 nm Rayonet lamps until it turned yellow (*ca* 6 h), periodically adding Dry Ice to the Dewar to maintain a temperature below *ca.* −30°C. The tube was reattached to the vacuum line and excess trifluoromethyl iodide was separated from the product by distillation into another sealable Pyrex tube (cooled with liquid nitrogen). The slightly yellow liquid that remained (30.5 g) was used without further purification in the following step. On the basis of its 90 MHz ^{1}H nmr spectrum (Varian EM390; $CDCl_3$; δ (ppm) = 1.27 (t, 2H), 1.4–1.9 (m, 4H), 2.1–2.5 (m, 3H), 4.14 (m, 1H)), the major component of the liquid was identified as 2-iodo-3-trifluoromethylbicyclo[2.2.1]heptane (17).

In a large Pyrex tube containing deoxygenated dimethyl sulfoxide (25 mL) and potassium *tert*-butoxide (1.5 g) was placed a portion of the product from the above reaction (2.0 g; 6.8 mmol), resulting in a yellow solution. The tube was placed in a Dry Ice/isopropanol bath, evacuated and sealed, and then heated at 60°C for 12 h. The tube was opened and the deep red reaction mixture was placed in a separatory funnel. Water (25 mL) was added and the resulting mixture was extracted with *n*-pentane (4 × 15 mL). The combined extracts were washed thrice with water, dried over anhydrous sodium sulfate, and filtered. Careful removal of the solvent by distillation afforded a yellow liquid. This was bulb-to-bulb distilled under vacuum to yield a colourless liquid that was shown to consist of 2-trifluoromethylnorbornene (**1**; 0.44 g, 2.7 mmol, 40%) contaminated with a small amount (<5%) of residual *n*-pentane and dimethyl sulfoxide (by vpc analysis). Compound **1** was purified by semi-preparative vpc, using one pass through column a to remove residual DMSO followed by two passes through column b, after which it was > 99.8% pure by vpc. Compound **1** has the following spectral properties:

*2-Trifluoromethylbicyclo[2.2.1]hept-2-ene (**1**).* ^{1}H nmr: δ (ppm) = 1.07 (m, 1H), 1.19 (m, 2H), 1.53 (m, 1H), 1.73 (m, 2H), 2.98 (br s, 1H), 3.08 (br s, 1H), 6.46 (br s, 1H); ^{13}C nmr: δ (ppm) = 24.4, 24.7, 41.3, 42.5, 49.1, 124.2, 137.8, 138.7; ^{19}F nmr: δ (ppm) = −65.3; ir (neat): 3010 (sh, w), 2982 (s), 2881 (m), 1626 (m), 1450 (w), 1356 (s), 1299 (s), 1269 (m), 1233 (m), 1150 (s), 1101 (s), 1037 (s), 876 (m), 843 (m), 831 (w), 730 (w), 688 (m); ms (m/e (I)): 162 (6), 134 (93), 135 (7), 127 (8), 115 (9), 114 (10), 93 (4), 91 (4), 84 (6), 65 (6); Mass calcd. for $C_8H_9F_3$: 162.0656. found: 162.0664; uv (λ_{max} (ε)): 194 nm (3190).

Analytical and preparative-scale photolysis experiments used pulses (193 nm, *ca.* 15 ns, *ca.* 40 mJ) from a Lumonics TE-861M excimer laser filled with an argon/fluorine/helium mixture. Analytical photolyses were carried out at ambient temperature (*ca.* 22°C) in rectangular cells constructed from 10 × 20 mm rectangular Suprasil tubing (Vitro Dynamics), using a 0.5–1 Hz laser pulse repetition rate. Solutions of **1** and isooctane (as internal standard) in *n*-pentane were deoxygenated with argon prior to irradiation, and the sample was agitated during photolysis with a magnetic stirrer. The course of photolysis was monitored between 0.2 and 4% conversion, with aliquots being removed periodically for vpc analysis. Relative product yields were determined from the slopes of concentration vs. laser dose constructed for all components of the mixture relative to the internal standard. The vpc detector was not calibrated for variations in response towards the different products.

Preparative scale (*ca.* 300 mg) photolyses were carried out in 2″ × 2″ cylindrical cells with Suprasil windows (*ca.* 50 mL volume), using a 6 Hz laser pulse repetition rate and vigorous stirring of the predeoxygenated solutions during photolysis to *ca.* 40% conversion (monitoring by vpc). After photolysis, the pentane was carefully distilled from the mixture through a long Vigreux column. The residue from the distillation was bulb-to-bulb distilled under vacuum, and the products were separated by preparative vpc using column *a*. One product (*ca.* 6% yield) could not be isolated in pure form since it eluted just slightly before **1** on all three vpc columns employed in this work. The photolysis products, listed in order of vpc retention time on column, a, had the following spectral characteristics.

*1-Trifluoromethylbicyclo[4.1.0]hept-2-ene (**5**).* ^{1}H nmr: δ (ppm) = 0.92 (t, 1H), 1.21 (m, 1H), 1.57 (m, 1H), 1.74 (m, 2H), 1.93 (m, 1H), 2.03 (m, 1H), 5.64 (m, 1H), 6.02 (dd, 1H); ^{13}C nmr: 14.7, 17.1, 18.1, 20.0, 122.7, 125.7, 127.7 (q); ^{19}F nmr: −65.3; ir: 3050 (w), 2940 (m), 2870 (w), 1442 (w), 1412 (m), 1394 (m), 1354 (s), 1334 (s), 1318 (s), 1181 (m), 1162 (s), 1147 (s), 1134 (s), 1067 (m), 927 (w), 689 (m); ms (*m/e* (I)): 162 (36), 147 (22), 141 (7), 127 (64), 114 (6), 115 (5), 93 (100), 83 (6), 77 (54), 65 (23); Mass calcd. for $C_8H_9F_3$: 162.0656; found: 162.0665; uv (λ_{max} (ε)): 200 nm (830).

*1-Methyl-2-trifluoromethyl-1,3-cyclohexadiene (**6**).* ^{1}H nmr: δ (ppm) = 1.95 (br s, 3H), 2.14 (m, 2H), 2.21 (m, 2H), 5.78 (dt, 1H), 6.00 (tt, 1H); ^{13}C nmr: 20.3, 21.6, 30.7, 120.7, 124.9 (quaternary carbons not detected); ^{19}F nmr: −60.3; ir: 2940 (s), 2880 (w), 2840 (w), 2340 (w), 1650 (w), 1600 (w), 1420 (w), 1410 (w), 1360 (s), 1305 (s), 1160 (s), 1120 (s), 1030 (s), 887 (w), 704 (w), 636 (m); ms (*m/e* (I)): 162 (24), 147 (17), 141 (4), 134 (10), 127 (60), 93 (100), 91 (40), 77 (50), 69 (8), 65 (16); Mass calcd. for $C_8H_9F_3$: 162.0656; found: 162.0662; uv (λ_{max}) = 263 nm (ε unknown).

*2-Trifluoromethyl-1,3-cycloheptadiene (**7**).* ^{1}H nmr: δ (ppm) = 1.86 (m, 2H), 2.37 (m, 4H), 5.84 (d, 1H), 6.04 (dt, 1H), 6.46 (t, 1H); ^{13}C nmr: 25.1, 29.9, 31.5, 119.9, 134.9, 137.0 (quaternary carbons not detected); ^{19}F nmr: −68.0; ir: 2940 (m), 1360 (w), 1305 (s), 1180 (s), 1120 (s); ms (*m/e* (I)): 162 (65), 147 (43), 134 (22), 127 (47), 101 (8), 93 (100), 91 (31), 77 (35), 69 (8), 65 (17); Mass calcd. for $C_8H_9F_3$: 162.0656; found: 162.0651; uv (λ_{max}) = 243 nm (ε unknown).

Chlorobenzene-sensitized photolysis of a deoxygenated pentane solution (70 mL) containing **1** (0.01 M), chlorobenzene (0.02 M), and isooctane (0.001 M) was carried out in a quartz tube with a Rayonet reactor fitted with twelve 253.7 nm lamps. The photolysis was continued until *ca* 60% conversion of **1**, with periodic monitoring by vpc, and final analysis by gc/ms. These analyses showed that the photolysate consisted of four main volatile (C_{10} or less) products, in addition to several products that eluted only at relatively high column temperatures. Gas chromatographic/mass spectroscopic analysis of the volatile components showed that two of the products had molecular weights of 164 amu, while the other two had molecular weights of 142 amu and were tentatively identified as decane isomers on the basis of their fragmentation patterns. The major higher molecular weight products had parent ions of 234 amu, corresponding to the free radical addition product of pentane to **1** (three isomers). A relatively small peak with parent ion mass of 274 eluted at even longer time. This is the correct mass for a cycloaddition product of **1** with chlorobenzene. The first two volatile products were isolated from the photolysate, after removal of the solvent and bulb-to-bulb distillation of the residue under vacuum, by semi-preparative vpc (columns c and d). The structures of the two products, listed below in order of their elution from the SPB-1 megabore capillary column, were identified primarily on the basis of their ^{1}H nmr spectra (25). They exhibit the following spectral characteristics.

*exo-2-Trifluoromethylnorbornane (exo-**8**).* ^{1}H nmr: δ (ppm) = 1.17 (m, 2H), 1.22 (m, 1H), 1.50 (m, 2H), 1.55 (m, 3H), 2.07 (m, 1H), 2.30 (br s, 1H), 2.43 (br s, 1H); ir ($CDCl_3$): 2960 (s), 2880 (w), 1315 (w), 1275 (s), 1265 (w), 1220 (w), 1110 (s), 1040 (w); ms (*m/e* (I)): 164 (11), 149 (30), 136 (40), 122 (13), 103 (8), 95 (50), 77 (21), 68 (96), 67 (100), 55 (19), 44 (77).

*endo-2-Trifluoromethylnorbornane(endo-**8**).* ^{1}H nmr: δ (ppm) = 1.27 (m, 2H), 1.34 (br s, 2H), 1.37 (m, 1H), 1.57 (m, 1H), 1.73 (m, 2H), 2.30 (br s, 1H), 2.44 (br s, 1H), 2.47 (m, 1H); ir ($CDCl_3$): 2960 (s), 2920 (w), 2880 (w), 1380 (br, w), 1320 (m), 1275 (s), 1260 (w), 1220 (w), 1180 (w), 1160 (s), 1130 (m), 1100 (br, w), 1050 (w); ms (*m/e* (I)): 164 (26), 149 (42), 136 (34), 122 (18), 103 (6), 95 (73), 85 (6),77 (23), 68 (90), 67 (86), 55 (23), 44 (100).

Acknowledgements

We thank Dr. D. Hughes (McMaster University) for acquiring the high field ^{1}H, ^{13}C, and ^{19}F nmr spectra, Dr. R. E. Hill (McMaster University) for some of the gc/ms analyses, and the McMaster University Regional Mass Spectrometry Facility for gc/ms analyses and exact mass determinations. The financial support of this work by the Natural Sciences and Engineering Research Council of Canada is gratefully acknowledged.

1. P. J. KROPP. *In* Organic photochemistry. Vol. 4. *Edited by* A. Padwa. Marcel Dekker, Inc., New York 1979. p. 1.
2. W. ADAM and T. OPPENLÄNDER. Angew. Chem. Int. Ed. Engl. **25**, 661 (1986).
3. W. J. LEIGH and R. SRINIVASAN. Acc. Chem. Res. **20**, 107 (1987).
4. M. G. STEINMETZ. *In* Organic photochemistry. Vol. 8. *Edited by* A. Padwa. Marcel Dekker, Inc., New York 1987. p. 67.
5. G. J. COLLIN and G. R. DE MARÉ. J. Photochem. **38**, 205 (1987).
6. Y. INOUE, T. MUKAI, and T. HAKUSHI. Chem. Lett. 1665 (1983).
7. (*a*) A. J. MERER and R. S. MULLIKEN. Chem. Rev. **69**, 639 (1969); (*b*) R. S. MULLIKEN. J. Chem. Phys. **66**, 2448 (1977).
8. M. B. ROBIN. Higher excited states of polyatomic molecules. Vol. II. Academic Press, New York. 1975(*a*) pp. 22–45; (*b*) p. 209.
9. (*a*) F. HIRAYAMA and S. LIPSKY. J. Chem. Phys. **62**, 576 (1975); (*b*) Y. INOUE, Y. DAINO, A. TAI, T. HAKUSHI, and T. OKADA. J. Am. Chem. Soc. **111**, 5584 (1989).
10. P. MOSCLET, D. GROSJEAN, G. MOUVIER, and J. DUBOIS. J. Electron Spectrosc. Related Phenom. **2**, 225 (1973).
11. (*a*) H. KRISTINSSON and G. W. GRIFFIN. J. Am. Chem. Soc. **88**, 378 (1966); (*b*) S. S. HIXSON and T. P. CUTLER. J. Am. Chem. Soc. **95**, 3031 (1973); (*c*) E. C. SANFORD and G. S. HAMMOND. J. Am. Chem. Soc. **92**, 3497 (1970); (*d*) S. S. HIXSON. J. Am. Chem. Soc. **97**, 1981 (1975).
12. S. S. HIXSON, J. C. TAUSTA, and J. BOROVSKY. J. Am. Chem. Soc. **97**, 3230 (1975).
13. R. SRINIVASAN and K. H. BROWN. J. Am. Chem. Soc. **100**, 4602 (1978).
14. Y. INOUE, T. MUKAI and T. HAKUSHI. Chem. Lett. 1045 (1982).
15. I. A. AKHTAR, J. J. MCCULLOUGH, S. VAITEKUNAS, R. FAGGIANI, and C. J. L. LOCK. Can. J. Chem. **60**, 1657 (1982).
16. A. T. WEN, A. P. HITCHCOCK, N. H. WERSTIUK, N. NGUYEN, and W. J. LEIGH. Can. J. Chem. **68**, 1967 (1990).
17. R. N. HASZELDINE and B. R. STEELE. J. Chem. Soc. 1199 (1953).
18. P. G. GASSMAN and J. BREITWEISER-HALL, J. Am. Chem. Soc. **106**, 4267 (1984).
19. (*a*) W. J. LEIGH and R. SRINIVASAN. J. Am. Chem. Soc. **105**, 514 (1983); (*b*) W. J. LEIGH and R. SRINIVASAN. J. Org. Chem. **48**, 3970 (1983).
20. P. J. KROPP. J. Am. Chem. Soc. **91**, 5783 (1969).
21. (*a*) P. J. KROPP, E. J. REARDON, JR., Z. L. F. GAIBEL, K. F. WILLIARD, and J. H. HATTAWAY, JR. J. Am. Chem. Soc. **95**, 7058 (1973); (*b*) T. R. FIELDS and P. J. KROPP. J. Am. Chem. Soc. **96**, 7559 (1974); (*c*) P. J. KROPP, H. G. FRAVEL, JR., and T. R. FIELDS. J. Am. Chem. Soc. **98**, 86 (1976).
22. (*a*) Y. INOUE, S. TAKAMUKU, and H. SAKURAI. J. Chem. Soc. Chem. Commun. 577 (1975); (*b*) Y. INOUE, S. TAKAMUKU, and H. SAKURAI. J. Chem. Soc. Perkin Trans. II 1635 (1977).
23. Y. INOUE, N. MATSUMOTO, T. HAKUSHI, and R. SRINIVASAN. J. Org. Chem. **46**, 2267 (1981).
24. W. ADAM and T. OPPENLÄNDER. J. Am. Chem. Soc. **107**, 3924 (1985).
25. L. M. JACKMAN and S. STERNHELL. Applications of nuclear magnetic resonance spectroscopy in organic chemistry. International Series of Monographs in Organic Chemistry. Vol. 5. Pergamon Press, New York 1969. p. 230–233 and references therein.

Can. J. Chem. Downloaded from www.nrcresearchpress.com by 91.121.58.235 on 09/07/12
For personal use only.

Studies of electronic excited states of substituted norbornenes by UV absorption, electron energy loss, and HeI photoelectron spectroscopy

A. T. WEN, A. P. HITCHCOCK,[1] N. H. WERSTIUK, N. NGUYEN AND W. J. LEIGH[2]
Department of Chemistry, McMaster University, Hamilton, Ont., Canada L8S 4M1

Received March 28, 1990

A. T. WEN, A. P. HITCHCOCK, N. H. WERSTIUK, N. NGUYEN, and W. J. LEIGH. Can. J. Chem. **68**, 1967 (1990).

Valence and inner-shell (C_{1s}) electronic excitation spectra of norbornene, 2-methylnorbornene, and 2-trifluoromethylnorbornene have been measured by electron energy loss spectroscopy. These data have been complemented with gas- and solution-phase UV absorption spectra in the 5–6.7 eV range, HeI UV photoelectron spectra, and AM1 semi-empirical calculations for the three compounds. The valence shell energy loss and UV absorption spectra show marked variations throughout the series of compounds, suggesting the presence of at least three low-lying electronic excited states. The spectral bands have been assigned as due to π,R($3s$), π,π^*, and π,R($3p$) excitations on the basis of their term values and the differences between their intensities in the solution and gas phase absorption spectra. The valence shell spectra indicate that while the vertically-excited π,R($3s$) state is substantially lower in energy than the (vertically-excited) π,π^* state in norbornene and the 2-methyl derivative, they are nearly isoenergetic in 2-trifluoromethylnorbornene. This difference in excited state manifolds is reflected in profound differences between the solution phase photochemistry of norbornene and the 2-trifluoromethyl derivative.

The carbon 1s spectra are even more sensitive to substituent than the valence shell energy loss spectra. An interpretation is proposed which reflects the spatially localized character of inner-shell excitation and a "group orbitals" picture of the unoccupied MO's as accessed by C_{1s} excitation.

Key words: Rydberg, electron energy loss, UV absorption, UV photoelectron spectroscopy, alkene, gas-phase.

A. T. WEN, A. P. HITCHCOCK, N. H. WERSTIUK, N. NGUYEN et W. J. LEIGH. Can. J. Chem. **68**, 1967 (1990).

Faisant appel à la spectroscopie de la perte d'énergie électronique, on a mesuré les spectres d'excitation électronique de valence et de couche interne (C_{1s}) du norbornène, du 2-methylnorbornène et du 2-trifluorométhylnorbornène. On a complété ces données en déterminant aussi les spectres d'absorption UV en solution (énergies de 5 à 6, 7 eV), les spectres photo-électroniques UV HeI et en effectuant des calculs semi-empiriques AM1 pour les trois composés. Pour toute la serie des composés, on a noté d'importantes variations dans les spectres de perte d'énergie de la couche interne et des spectres d'absorption UV; ces résultats suggèrent qu'il existe au moins trois états électroniques excités de basses énergies. En se basant sur les valeurs de leurs termes ainsi que sur les différences entre les intensities de leurs spectres d'absorption en solution et en phase gazeuse, on a attribué les bandes spectrales aux excitations π,R($3s$), π,π^* et π,R($3p$). Les spectres des couches de valences internes indiquent que, même si l'énergie de l'état excité verticalement (π,R($3s$)) du norbornène et de son dérivé méthylé en position 2 est beaucoup plus faible que celle de son état π,π^* (excité verticalement), ils sont pratiquement isoénergétiques dans le 2-trifluorométhylnorbornène. Cette différence dans les états excités se reflète par des différences importantes entre les photochimies en solution du norbornène et du 2-trifluorométhylnorbornène.

Les spectres 1s du carbone sont encore plus sensibles aux substituants que les spectres de perte d'énergie de la couche interne. On propose une interprétation qui est le reflet du caractère orienté dans l'espace de l'excitation de la couche interne ainsi que d'une représentation des orbitales de groups des OM qui ne sont pas ocupées telles qu'elles sont influencées par l'excitation C_{1s}.

Mots clés : Rydberg, perte d'énergie électronique, absorption UV, spectroscopie photo-électronique UV, alcènes, phase gazeuse.

[Traduit par la revue]

Introduction

The far-UV solution phase photochemistry of 2-trifluoromethylnorbornene (**1**) (1) shows significant differences compared to that reported previously for norbornene (**2**) under similar conditions (2). These differences are consistent with a dramatic alteration in the ordering of the lowest electronic excited states that are accessible in the far-UV (6.5–6.7 eV) region in solution, presumably induced by the effects of trifluoromethyl-substitution at the C=C bond. For most simple alkenes (*e.g.* **2**), direct photolysis in solution results in predominant formation of carbene-derived rearrangement products (3). Such products are thought to result from π,R($3s$) excitation, since the π,R($3s$) state is lower in energy than the π,π^* valence excited state in most simple alkenes (4, 5). The photochemical results for **1**, when compared to those previously reported for **2**, are consistent with an inversion of the ordering of the π,R($3s$) and the π,π^* singlet states in these two compounds (1). To investigate this point further, we have recorded the valence electronic excitation spectra of **1, 2**, and 2-methylnorbornene (**3**) by electron energy loss and gas- and solution-phase UV absorption spectroscopy, along with the HeI UV photoelectron spectra (PES) of each compound.

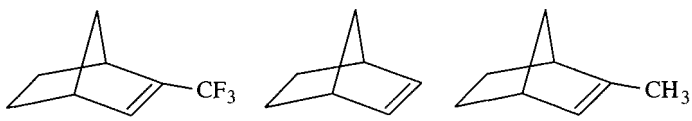

1 **2** **3**

In addition to the valence spectra in the 2–40 eV range, electronic spectra in the region of C_{1s} excitation (275–325 eV) have been recorded. Inner-shell excitation emphasizes the more compact valence component of virtual orbitals. Since the bonding/non-bonding character of photoactive orbitals is dictated by the valence component (6), it is possible that the C_{1s} spectra might also give useful insight into the origins of the differences in the photochemistry of **1** and **2** in solution.

[1]Natural Sciences and Engineering Research Council of Canada University Research Fellow, 1980–1990.

[2]Natural Sciences and Engineering Research Council of Canada University Research Fellow, 1983–1993. Author to whom correspondence should be addressed.

Can. J. Chem. Downloaded from www.nrcresearchpress.com by 91.121.58.235 on 09/07/12
For personal use only.

Can. J. Chem. Downloaded from www.nrcresearchpress.com by 91.121.58.235 on 09/07/12
For personal use only.

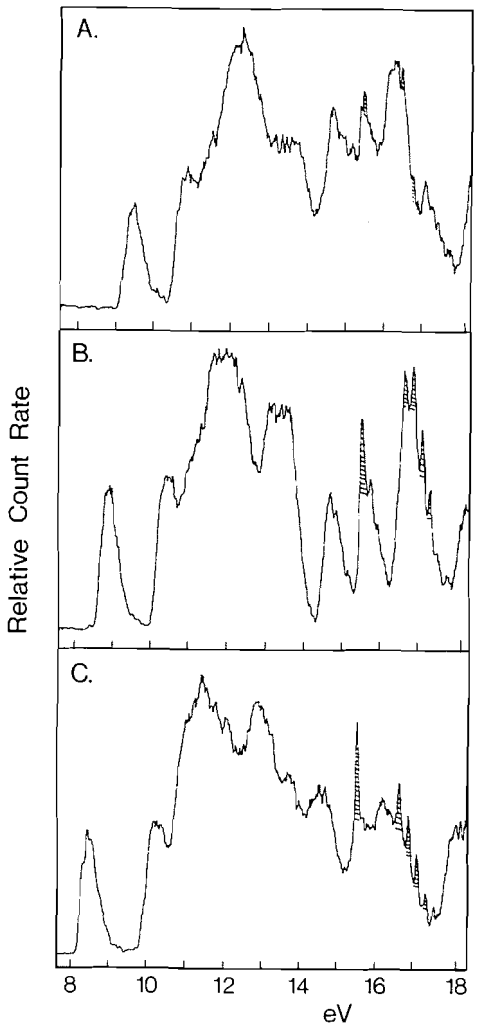

FIG. 1. HeI UV photoelectron spectra of (*A*) 2-trifluoromethylnorbornene (**1**); (*B*) norbornene (**2**); and (*C*) 2-methylnorbornene (**3**). The shaded peaks correspond to N_2 of air, which was used as a calibrant.

Results and discussion

HeI ultraviolet photoelectron spectra

HeI photoelectron spectra (PES) of **1–3** are shown in Fig. 1, and the two lowest vertical ionization potentials, as obtained from the spectra, are listed for each compound in Table 1. The PE spectra reveal the expected trend in π-IP throughout the series, and are more or less unexceptional. The spectrum of **2** is similar to the one reported previously by Heilbronner and co-workers (7). Methyl substitution results in a (0.7 eV) decrease in the π-IP, while trifluoromethyl substitution results in an increase of 0.4 eV. AM1 semi-empirical calculations were carried out for **1–3**, and the calculated π- and σ-eigenvalues are shown in Table 1 along with the experimental ionization energies from PES. These calculations qualitatively reproduce the substituent effect on the experimental π-IP's. Quantitatively though, AM1 underestimates the absolute effects of methyl substitution on the π-IP of norbornene, and overestimates that of trifluoromethyl substitution. AM1 does not reproduce the known effects of methyl substitution on π^*-MO energies (*i.e.*, electron affinities (8)) even on a qualitative level (9), so these eigenvalues have not been included in Table 1.

Optical spectra

Gas-phase UV absorption spectra of **1–3**, recorded on a conventional UV spectrometer with samples of pressures in the 1.5–2 torr range, are presented in Fig. 2. Figure 2 also contains spectra recorded for each compound in deoxygenated *n*-pentane solution with the same system and under identical conditions.

TABLE 1. Ionization energies (PES) and eigenvalues of substituted norbornenes **1–3**

Compound	Ionization energy (eV)[a]		ϵ^b	
	π	σ	π	σ
1	−9.6	−11.1	−10.4	−11.5
2	−9.2	−10.6	− 9.6	−10.9
3	−8.5	−10.3	− 9.2	−10.9

[a]Error estimated at ±0.1 eV.
[b]Computed using AM1.

The optical spectrum of **2** reported here (Fig. 2*b*) can be compared to the vacuum ultraviolet optical absorption spectra previously reported for the same compound (10). The previously reported spectra of **2** show three prominent bands in the region below 7.5 eV, centred at 5.97 eV (208 nm), 6.34 eV (196 nm), and 7.10 eV (175 nm) (10). These have been assigned as due to the π,R(3*s*), π,π^*, π,R(3*p*) transitions, respectively, by Robin and co-workers (4, 10*b*, 11). The Rydberg transitions in the optical spectra are quite sharp and well-defined compared to the valence (π,π^*) transition. The gas-phase spectrum shown in Fig. 2*b* exhibits absorption bands centred at 6.02 and 6.30 eV, in satisfactory agreement with the somewhat better-resolved spectra reported previously for the region below 6.7 eV (the upper energy limit of our spectrometer). The noise appearing in our spectra in the 6.6–6.7 eV region is due to background absorption by oxygen. As expected (4, 5), the 6.02 eV Rydberg absorption is absent in the solution-phase spectrum of **2**, which shows only the valence transition centred at 198 nm (6.26 eV).

The gas-phase optical spectrum of **3** shows weak, but sharp absorption bands centred at 5.62 eV (220.5 nm) and 6.43 eV (193 nm), which can be assigned to the π,R(3*s*) and π,R(3*p*) transitions on the basis of their term values (*vide infra*) and the fact that they are quenched in the solution-phase spectrum (4, 5). The latter is a standard "test" for Rydberg transitions — these bands are severely reduced in intensity and blue-shifted in the condensed phase compared to the gas phase at low pressure (4, 5). The prominent band centred at 6.16 eV (201 nm) is also present in the solution spectrum and can thus be assigned to the π,π^* transition.

The gas-phase spectrum of **1** in the 5.5–6.7 eV region shows a single, symmetrical absorption band centred at 6.46 eV (192 nm) that can be assigned as due to the π,π^* transition. The slight shift of the absorption maximum (to 195 nm) in the solution-phase spectrum is probably due to background absorption by the solvent. The weak feature that appears at 6.37 eV in the gas-phase spectrum may be due to π,R(3*s*) absorption. Because it is so poorly resolved from the prominent, underlying π,π^* absorption, we consider this assignment to be more tentative than the others.

The energies and proposed assignments for the various bands in the gas-phase optical spectra are listed in Table 2. Table 2 also contains term values (*T*) calculated for each transition as the difference between the spectral band maxima and the lowest vertical (π) ionization potentials of the three compounds from PES (4). The term values support our assignments for the various bands in the spectra of **1–3** based on Mulliken's (4) and

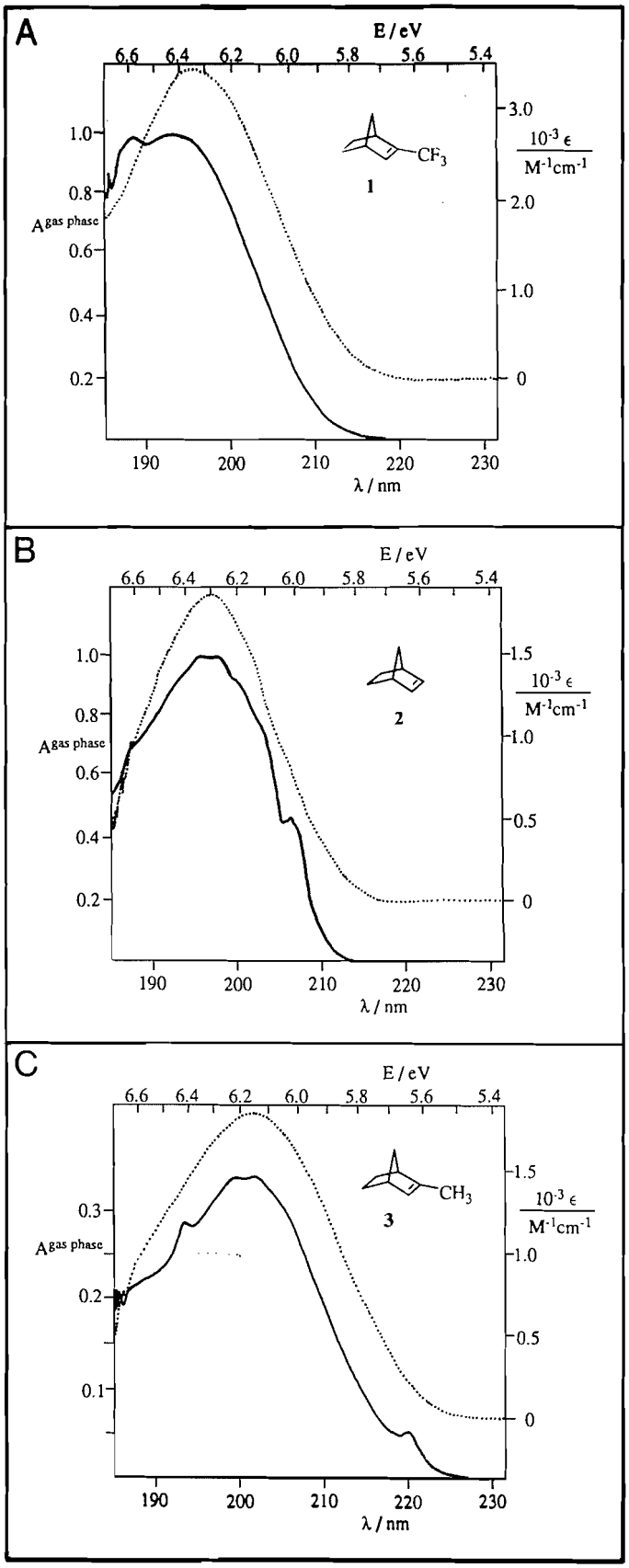

FIG. 2. Ultraviolet absorption spectra of **1–3** in gas phase (——) and in deoxygenated pentane solution (····). Gas phase spectra were recorded at pressures of 1,4, 1.7, and 1.5 torr for **1**, **2**, and **3**, respectively. The left axes refer to gas-phase spectra and right axes refer to solution phase spectra.

TABLE 2. Energies (E; eV), term values (T; eV),[a] and possible assignments for features in the gas-phase UV absorption spectra of **1–3**

	E/eV (T/eV)			
Feature	**1**	**2**	**3**	Assignment
1	6.37(3.2)	6.02(3.2)	5.62(2.9)	π,R(3*s*)
2	6.46(3.1)	6.30(2.9)	6.16(2.3)	π,π*
3	—	—	6.43(2.1)	π,R(3*p*)

[a]Term values calculated as the difference between absorption maxima and the vertical ionization potentials for **1–3**, determined by PES (Table 1).

Robin's (5) extensive generalizations on valence and Rydberg assignments in the optical spectra of alkenes, and the variations in term values with substituent. It is well-known that in alkylethylenes, increasing methyl substitution at the C=C bond results in decreases in the Rydberg transition energies (π,R(3*s*) and especially π,R(3*p*)) that are comparable to those in the π-ionization potentials (4, 5). This is reasonable to the extent that Rydberg excitation can be viewed as involving partial ionization of the molecule. Furthermore, the larger and more diffuse the Rydberg orbital, the better the correlation should be between transition energy and ionization potential. The π,π* transition energies also decrease with increasing alkyl substitution in the same way, but much less dramatically. Thus, the π,π* transitions in **1–3** are assigned as those bands whose term values vary the most with substituent throughout the series (*i.e.*, whose energies are least sensitive to variations in the π-IP), and the π,R(3*s*) transitions as those whose term values vary the least (*i.e.*, whose energies are most senstitive to variations in π-IP).

Valence-shell electron energy loss spectra

The valence-shell energy loss spectra of **1–3** are presented in Fig. 3. Figure 3 also includes expansions of the 4–10 eV region, which is of greatest interest to the solution phase photochemistry of these molecules. The energies, term values, and proposed assignments of the various features in these spectra are listed in Table 3.

The energy loss spectrum of **2** reported by Kupperman and co-workers (12) has been included for comparison with the present one in Fig. 3*b*. The qualitative features of the two spectra agree quite closely. The main difference is in resolution, which is three to four times lower in our spectrometer than in that used for the previously reported spectrum. Also, Kupperman's spectrum exhibits a shoulder at 6.6 eV which is not resolved in ours. The intensity of this feature was found to increase very rapidly with increasing momentum transfer (*i.e.*, scattering angle) relative to the 6.3 eV feature (12). Since the momentum transfer is much smaller under our experimental conditions, it is likely that the relative intensity of the 6.6 eV feature is reduced to the point where we are unable to detect it.

As in the case of Kupperman *et al.* (12), we are not able to resolve the lowest energy Rydberg transition which is observed at 6.02 eV in the optical spectrum of **2**. This band is presumably obscured in the low energy tail of the prominent π,π* absorption centred at 6.53 eV, and our failure to observe it as a discrete feature is due simply to inadequate spectral resolution. We observe a second band, occurring as a shoulder at 7.5 ± 0.1 eV on the rising edge of the diffuse, higher energy absorption above 10 eV. A corresponding feature is also evident in the spectrum of Kupperman *et al.* This band has not been previously assigned, unless it coincides with the 7.10 eV

Can. J. Chem. Downloaded from www.nrcresearchpress.com by 91.121.58.235 on 09/07/12
For personal use only.

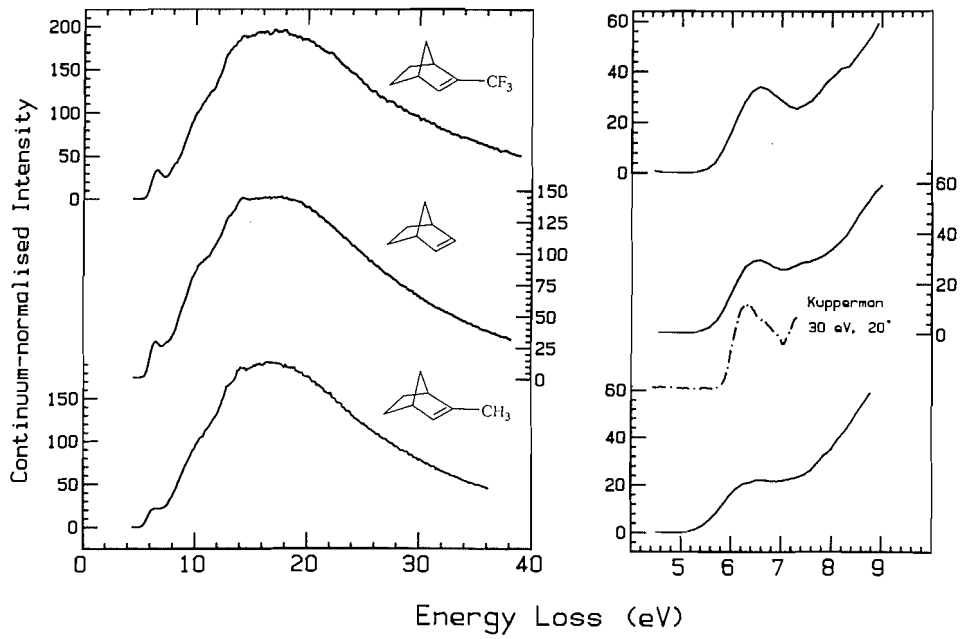

FIG. 3. Energy loss spectra of substituted norbornenes **1**–**3** in the region of valence electronic excitation. For each spectrum, the 4–10 eV region, normalized at 30 eV to an intensity proportional to the total number of electrons in the molecule, has been expanded (left). The previously reported energy loss spectrum of **2** (12) has been superimposed on the present one in (*b*).

TABLE 3. Energies (E; eV),[a] term values (T; eV),[b] and possible assignments for features in the valence shell energy loss spectra of **1**–**3**

	E/eV (T/eV)			
Feature[c]	**1**[d]	**2**[e]	**3**[f]	Assignment
2	6.52(3.0)	6.50(2.7)	6.15(2.3)	π,π^*
3	7.90(1.7)	7.50(1.7)	6.62(1.9)	π,3R(3p)

[a]From absorption band maxima in valence shell energy loss spectra. The uncertainty in the absolute energy is estimated at ±0.05 eV.

[b]Term values calculated as the difference between E-values and the vertical ionization potentials for **1**–**3** determined by PES (Table 1).

[c]Spectral features numbered so as to allow comparison with optical spectra (see Fig. 2 and Table 2).

[d]Additional bands occur at 8.24, 11.53, 13.40, 14.29, and 16.99 eV (see Fig. 3).

[e]Additional bands occur at 10.37, 13.08, and 14.32 eV (see Fig. 3). These can be compared with the high energy features reported previously at 8.25, 8.97, 10.3, 11.9, and 12.8 eV (12).

[f]Additional bands occur at 7.90, 10.65, 13.04, 14.23, and 16.75 eV (see Fig. 3).

(π,R(3p) (5, 10b, 11)) absorption band in the optical spectrum (10). We tentatively assign this band to the π,R(3p) transition on the basis of its term value (*vide infra*).

The energy loss spectra of **1** and **3** show distinct differences compared to that of **2**. The low energy band of **3** is distinctly broader than the corresponding absorption in **2**, and appears to consist of two overlapping transitions with maxima at *ca.* 6.2 and 6.6 eV. Again, we see no discrete evidence for the low energy (5.62 eV) π,R(3s) transition which is observed in the optical spectrum of this compound. In contrast, the low energy region in the spectrum of **1** seems to have a rather symmetric first absorption band, similar to that of **2**. While all three compounds show absorption bands centred at 6.5–6.6 eV, the 7–8 eV regions exhibit distinct shoulder absorptions whose positions vary dramatically throughout the series.

The energy loss spectra of these compounds complement the optical spectra in that they provide evidence for π,R(3p) excitations, which are of too high energy in **1** and **2** to be observed with our absorption spectrometer. We assign the 7.9, 7.5, and 6.6 eV features in the energy loss spectra of **1**, **2**, and **3**, respectively, as due to this transition, since their term values are essentially independent of substituent. The 6.6 eV transition in the energy loss spectrum of **3** is also observed in the optical spectrum at 6.43 eV. The latter energy should be considered more accurate because better resolution is obtained in optical experiments. In fact, the π,R(3p) transition energies from the energy loss spectra of all three compounds should probably be considered to have uncertainties of 0.2–0.3 eV because of the resolution of our spectrometer, which results in the appearance of these bands as shoulders on more intense excitations.

The combination of optical and energy loss spectroscopies bolster our assignment of the weak feature at 6.37 eV in the gas-phase optical spectrum of **1** as due to π,R(3s) absorption, or at least suggest that the π,R(3s) transition should occur at roughly this energy in **1**. It is possible to estimate a probable range of energies for the π,R(3s) transition in **1**, using the term values for the π,R(3p) excitations in **1**–**3** and by taking into account the trends in the *differences* between term values for the two Rydberg transitions in **2**, **3**, and other alkyl-substituted olefins (4, 5). The extensive published data for alkenes show that depending on the structure and the degree of alkyl substitution, the π,R(3s) state is situated between 0.3 and 1.2 eV below the π,R(3p) state (4, 5). For **2**, the reported optical absorption data (10) places the π,R(3s)–π,R(3p) energy gap at *ca.* 1.1 eV, in satisfactory agreement with the 1.0 eV gap given by our energy loss spectrum of this compound. This is similar to the value obtained for **3** (0.8 eV) from its optical spectrum (Fig. 2*c* and Table 2). Assuming a similar π,R(3s)–π,R(3p) energy gap for **1**, we thus estimate the π,R(3s) energy to be in the 6.4–6.9 eV range. The suggestion that the π,R(3s) transition is superposed on the intense π,π^* band is thus a reasonable one, and it can be concluded that the vertically-excited π,R(3s) state

Can. J. Chem. Downloaded from www.nrcresearchpress.com by 91.121.58.235 on 09/07/12
For personal use only.

Can. J. Chem. Downloaded from www.nrcresearchpress.com by 91.121.58.235 on 09/07/12
For personal use only.

is of similar or even higher energy than the vertically-excited π,π^* state in this compound. This difference in the vertical energies of the two states is expected to be magnified in the 0,0 levels, since Rydberg transitions are much sharper than valence transitions (4, 5). Assuming the normal shift to higher energies of Rydberg states in the condensed phase (4, 5), the present data suggest that the π,π^* state should be the lowest energy singlet excited state in solution.

This lowest state assignment for **1** is consistent with its solution-phase 193 nm (6.5 eV) photochemistry (1). Far-UV photolysis of **2** affords carbene-derived rearrangement products consistent with Rydberg state excitation (2, 3). Photolysis of **1** under similar conditions, on the other hand, affords products that are most consistent with valence (π,π^*) excitation; analogous products are formed upon photolysis of 2-cyanonorbornene whose lowest excited state is very clearly of π,π^* configuration (13). While it has been proposed that there may be yet a third photoactive alkene excited singlet state accessible in solution, presumably underlying the intense π,π^* absorption (14), we observe no evidence for such a state in the optical and energy loss spectra of **1**–**3**.

Carbon 1s spectra

The oscillator strengths for C_{1s} excitation of **1**–**3** are presented in Fig. 4 while energies, term values (the differences between the excitation energies and the average CH_xIP) and proposed assignments are summarized in Table 4. The average CH_x C_{1s} ionization potential has been estimated as 290.5 ± 0.4 eV from the measured XPS of similar molecules (15). The C_{1s} IP of the CF_3 carbon is estimated as 299.0 ± 0.5 eV while that of the sp^2 carbon to which the CF_3 group is attached has an estimated IP of 292.0 ± 0.5 eV. These estimates are derived from data for 3,3,3-trifluoropropene, which has IP's of 291.6, 292.0, and 298.7 eV for the 1-, 2-, and 3-carbons, respectively (15).

The C_{1s} spectra exhibit much larger variation with substituent than the valence spectra. This can be attributed to the spatially-localized character of core electronic excitation, which makes these excitations much more sensitive to differences in the structure of these molecules than spatially-delocalized valence excitations. In particular, the second and third peaks in the spectrum of **3**, corresponding to σ(C—H) and σ(C—C) resonances, are more intense than their counterparts in the spectrum of **2**, due simply to the higher carbon-number of **3**. The spectrum of **1** consists of the overlap of transitions originating at the CF_3 and CH_x carbons, which are well-isolated because of the large C_{1s} chemical shift associated with the electronegative fluorines. Thus the CF_3 component of the spectrum of **1** is composed of strong σ*(C—F) and σ*(C—C) resonances, while the CH_x component is similar to that seen in the spectra of the other two molecules. The term values for corresponding transitions in the three compounds are generally similar (see Table 4); indeed the constancy of the term values, based on the similarity of the energies of corresponding virtual orbitals, has guided our assignments.

The C_{1s},π^* excitation energies and term values are of particular interest, from the point of view of comparisons with the π,π^* excitation energies, term values, and the π-IP's discussed earlier. The variation in π,π^* and $C_{1s}\pi^*$ term values and π-ionization potentials throughout the three compounds is depicted in Fig. 5. The slight decrease in the π,π^* term value for **3** relative to **2** is consistent with a slight destabilization of the π^* MO as a result of methyl substitution. The same trend is observed in the electron affinities of simple alkenes (8). In the

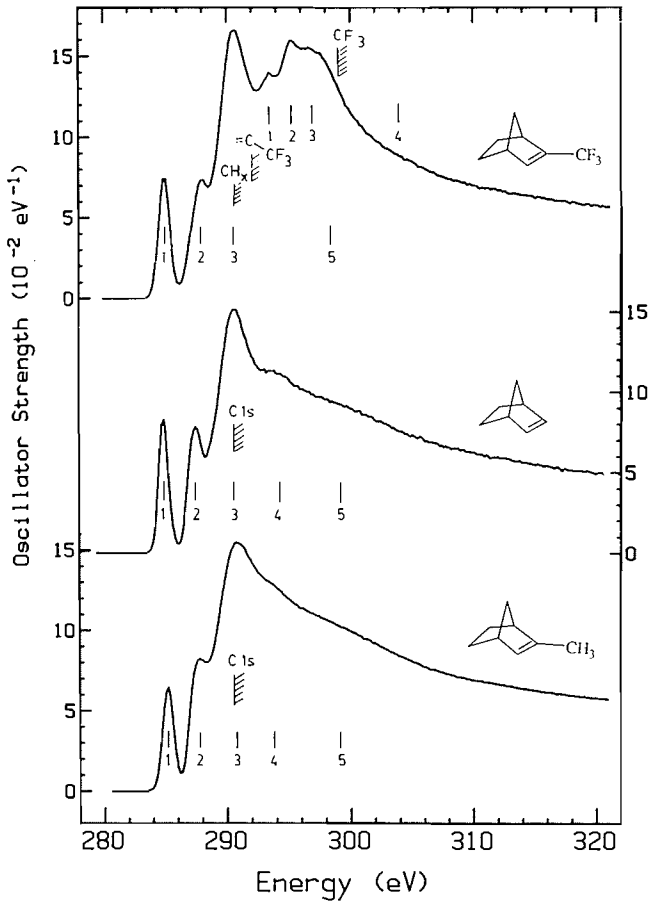

FIG. 4. Oscillator strengths for C_{1s} excitation of substituted norbornenes **1**–**3**, derived from electron energy loss spectra recorded with 2.5 keV final electron energy, 2° scattering angle and 0.6 eV FWHM resolution. The indicated C_{1s} IP's are estimated from XPS values of similar molecules (14).

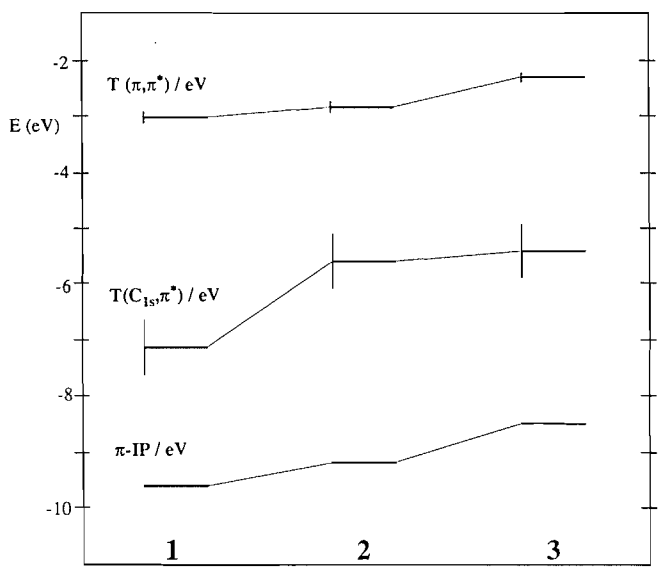

FIG. 5. Histograph showing the variation in π,π^* and C_{1s},π^* term values and π-IP's with substituent in **1**–**3**, from the electron energy loss spectra. Error bars are due to the uncertainty in the associated IP's.

TABLE 4. Energies (T; eV), term values (R; eV), and possible assignments of features in the carbon 1s inner shell energy loss spectra of **1–3**[a]

		1			2		3		Assignment	
Feature[b]	E	$T(C_{sp^3})$	$T(C_{sp^2})$	$T(C_F)$	E	T_{CH}[a]	E	T_{CH}[a]	CH_x	CF_3
1	284.92[c]		7.1		284.91[c]	5.6	285.15[c]	5.4	π*(C═C)	
2	287.9	2.6	(4.1)		287.5	3.0	287.9	2.6	π*(CH_2)	
	290.5_5				290.5		290.5		CH_x IP[c]	
	292.0_5								C═C IP (**1**)	
3	291.1	−0.1			290.6	−0.1	290.8	−0.5	σ*(C—C)	
4 sh					294.0	−3.5	293.7	−3.4	2e-(?)	
F1	293.4			5.6						π*(C═C)
F2	295.2	−4.2		3.8					2e-(?)	σ*(C—F)
F3	297			2						π*(C—C)
5	298	−7.5			299.3	−8.8	299.2	8.9	σ*(C═C)	
	299.2									CF_3 IP[c]
F4	304			5						σ*(C═C)

[a]T = IP − E, where IP is the appropriate C_{1s} ionization energy, estimated from the IP's of similar species (14). Note that there will be at most a 0.2 eV chemical shift between the sp^3 and sp^2 carbons in **2** and **3** . The sp^2 carbons in **1** will have significantly higher IP's than the sp^3 carbons. Bracketed term values indicate that there is likely to be only a small contribution to intensity from this core level.

[b]Entries labelled "F" are features associated with $C_{1s}(CF_3)$ excitation.

[c]Calibration relative to $CO_2(C_{1s},\pi^* = 290.74\,eV)$; $\Delta E = -5.82_4$ (**1**), -5.83_4 (**2**), and -5.59_4 (**3**).

case of **1**, the π-IP and π,π* excitation energies predict that trifluoromethyl substitution should result in stabilization of the π*-MO by *ca.* 0.3 eV relative to **2**. The fact that the C_{1s},π* transition is observed at 285.1 eV in the low energy region of the spectrum of **1**, even though the C_{1s} IP of the 2-carbon (═*C*—CF_3) is clearly going to be 1–2 eV higher in energy than that of the sp^2 carbons in **2** or **3**, indicates that the C_{1s},π* state has an appreciably larger term value. Thus one sees that the C_{1s} spectrum also senses the stabilization of the π*-MO that is reflected in the valence shell π,π* transition energy. In fact, the C_{1s} spectrum appears to predict a stabilization of more than twice that predicted from the valence electronic spectra, although the larger error bars associated with the $C1_s$ (due to the uncertainty in the estimated $C1_s$ IP's) make this a tentative statement.

Conclusions

Previous work has shown that the lowest electronic excited state of norbornene (**2**) is the π,R(3s) Rydberg state (4, 10), which is consistent with the photochemical behaviour of this molecule in solution (2, 3). The present study demonstrates that the valence shell optical and energy loss spectra of **1–3** show significant differences throughout the series. These differences are suggested to be the result of a dramatic substituent effect on the energies of the π,R(3s) and π,R(3p) excited states. Trifluoromethyl substitution at the C═C bond has little effect on the energy of the π,π* state relative to the unsubstituted derivative, but destabilizes the π,R(3p) and π,R(3s) Rydberg states considerably. The effect is large enough that in **1**, the (vertical) π,π* state is *ca.* 1.3 eV lower in energy than the π,R(3p) state, and slightly lower in energy than (or at most, isoenergetic with) the π,R(3s)) Rydberg state. These differences are expected to be magnified in the 0,0 levels so that for **1**, the π,π* valence state appears to be the lowest energy excited singlet state that is accessible in solution. This is consistent with the solution phase photochemistry of this molecule, which leads to products attributable to π,π* excitation exclusively (1).

Experimental

The gas- and solution-phase UV absorption spectra were recorded in single beam mode on a Perkin-Elmer Lambda 9 spectrophotometer equipped with a Model 3600 Data Station. The spectrometer sample compartment was continuously flushed with dry nitrogen. Samples were contained in 1 cm Suprasil UV cells (Hellma) which were fitted with a glass stopcock for gas-phase spectra. Gas-phase samples were prepared by introducing the compound into the cell from a cold finger on a vacuum line whose pressure was measured by a Varian 801 vacuum gauge. A background spectrum, recorded under identical conditions with the empty cell (evacuated to 30 mtorr), was electronically subtracted from the sample spectra. Reference and sample solutions for the solution-phase spectra were deoxygenated with a stream of argon for 10 min prior to recording the spectrum.

The valence and inner-shell energy loss spectra were obtained by inelastic electron scattering with a high velocity incident electron beam (E_0 = 2.5 keV plus the energy loss), using an instrument that has been described in detail previously (16). The valence spectra were recorded with a 0° average scattering angle while the $C1_s$ spectra were obtained using a small scattering angle (~2°) to eliminate an instrumental background associated with scattering of the incident electron beam inside the electron energy analyser. The instrumental resolution was 0.6 eV fwhm. Under these electron scattering conditions only electric dipole transitions are excited, with intensities that are very similar to those in the corresponding optical absorption spectra (17).

The valence energy loss spectra were calibrated with the $1s \rightarrow 2p$ transition of He (21.22 eV). A semiquantitative comparison of the intensities has been achieved by normalizing at 30 eV in the valence ionisation continuum to a value proportional to the number of valence electrons in each molecule. The $C1_s$ spectra were calibrated with the π* feature of CO_2 at 290.74 eV (17), and were converted to absolute optical oscillator strengths (f values) using a procedure described and tested previously (18).

Ultraviolet photoelectron spectra were recorded in conventional mode using a spectrometer which has been described in detail elsewhere (19), and are the averages of 50–100 scans. The spectra were calibrated relative to the peak at 15.67 eV corresponding to the ionization of nitrogen.

Semi-preparative gas chromatographic (vpc) purifications were carried out with a Hewlett-Packard 5750B gas chromatograph, fitted with a thermal conductivity detector and one of the following stainless steel columns: (*a*) 3% OV-17 on 80/100 Chromosorb WAW (6′ × 0.25″ stainless steel; Supelco, Inc.); (*b*) 15% Carbowax 20M on 60/80 Chromosorb W (5′ × 0.25″ stainless steel; Supelco, Inc.); (*c*) 3.8% UCW982 on 80/100 Supelcoport (24′ × 0.25″ stainless steel; Supelco, Inc.).

Analytical vpc separations were carried out with a Hewlett-Packard

Can. J. Chem. Downloaded from www.nrcresearchpress.com by 91.121.58.235 on 09/07/12
For personal use only.

5890 gas chromatograph equipped with a flame ionization detector, a borosilicate megabore capillary column (30 m × 0.75 mm SPB-1; Supelco, Inc.), and a Hewlett-Packard 3396 recording integrator.

2-Trifluoromethylnorbornene (**1**) was prepared by a modification (1) of a reported procedure (20) and purified by semi-preparative vpc (columns b, c). Norbornene (**2**; Aldrich) was purified by distillation followed by semi-preparative gas chromatography (column a). 2-Methylnorbornene was available from an earlier study (21) and was purified by vacuum distillation, followed by semi-preparative vpc (column a). The samples of **1**–**3** used in this work were all of > 99.9% purity as estimated by vpc.

Computational studies were carried out using AM1, Version 2.1, of the general purpose molecular orbital computational package AMPAC (22). Optimizations were carried out using the AM1 default parameters.

Acknowledgment

We thank the Natural Sciences and Engineering Research Council of Canada for its generous financial support of this work.

1. N. NGUYEN, B. E. HARRIS, K. B. CLARK, and W. J. LEIGH. Can. J. Chem. **68**, 1961 (1990).
2. (*a*) R. SRINIVASAN and K. H. BROWN. J. Am. Chem. Soc. **100**, 4602 (1978); (*b*) Y. INOUE, T. MUKAI, and T. HAKUSHI. Chem. Lett. 1045 (1982).
3. P. J. KROPP. *In* Organic photochemistry. Vol. 4. *Edited by* A. Padwa. Marcel Dekker, Inc., New York. 1981. p. 1 and references therein.
4. (*a*) A. J. MERER and R. S. MULLIKEN. Chem. Rev. **69**, 639 (1969); (*b*) R. S. Mulliken. J. Chem. Phys. **66**, 2448 (1977).
5. M. B. ROBIN. Higher excited states of polyatomic molecules. Vol. II. Academic Press, New York. 1975. pp. 22–45.
6. A. P. HITCHCOCK. Phys. Scr. In press.
7. G. BIERI, F. BURGER, E. HEILBRONNER, and J. P. MAIER. Helv. Chim. Acta, **60**, 2213 (1977).
8. K. D. JORDAN and P. D. BURROW. J. Am. Chem. Soc. **102**, 6882 (1980).
9. N. H. WERSTIUK and W. J. LEIGH. Unpublished results.
10. (*a*) S. STOKES and L. W. PICKETT. J. Chem. Phys. **23**, 258 (1955); (*b*) M. B. ROBIN and N. A. KUEBLER. J. Chem. Phys. **44**, 2664 (1966).
11. M. B. ROBIN, R. R. HART, and N. A. KUEBLER. J. Chem. Phys. **44**, 1803 (1966).
12. R. P. FRUEHOLZ, W. M. FLICKER, O. A. MOSHER, and A. KUPPERMAN. J. Chem. Phys. **70**, 1986 (1979).
13. I. A. AKHTAR, J. J. MCCULLOUGH, S. VAITEKUNAS, R. FAGGIANI, and C. J. L. LOCK. Can. J. Chem. **60**, 1657 (1982).
14. Y. INOUE, T. MUKAI, and T. HAKUSHI. Chem. Lett. 1665 (1983).
15. W. L. JOLLY, K. D. BOMBEN, and C. J. EYERMANN. At. Data Nucl. Data Tables, **31**, 433 (1984).
16. A. P. HITCHCOCK, S. BEAULIEU, T. STEEL, J. STÖHR, and F. SETTE. J. Chem. Phys. **80**, 3927 (1984).
17. A. P. HITCHCOCK and I. ISHII. Electron Spectrosc. **42**, 11 (1987).
18. R. MCLAREN, S. A. C. CLARK, I. ISHII, and A. P. HITCHCOCK. Phys. Rev. A, **36**, 1683 (1987).
19. N. H. WERSTIUK, D. N. BUTLER, and E. SHAHID. Can. J. Chem. **65**, 760 (1986).
20. (*a*) R. N. HASZELDINE and B. R. STEELE. J. Chem. Soc. 1199 (1953); (*b*) P. G. GASSMAN and J. BREITWEISER-HALL. J. Am. Chem. Soc. **106**, 4267 (1984).
21. N. H. WERSTIUK and F. P. CAPPELLI. Can. J. Chem. **58**, 1725 (1980).
22. Austin Method 1 Package, 1.0 QCPE 506. Dewar Research Group and J. P. Stewart. QCPE Bull. **6**, 24*a*, *b* (1986).

Can. J. Chem. Downloaded from www.nrcresearchpress.com by 91.121.58.235 on 09/07/12
For personal use only.

Oxidation of tetrahydropterins by azide radical and the spectra of trihydropterin radicals[1,2]

DAVID A. ARMSTRONG[3]
Radiation Laboratory, University of Notre Dame, Notre Dame, IN 46556, U.S.A.

AND

MOHSEN FARAHANI AND PARMINDER S. SURDHAR
Department of Chemistry, University of Calgary, Calgary, Alta., Canada T2N 1N4

Received February 5, 1990

DAVID A. ARMSTRONG, MOHSEN FARAHANI, and PARMINDER S. SURDHAR. Can. J. Chem. **68**, 1974 (1990).

Spectrophotometric titration of tetrahydropterins with incremental amounts of $^{\bullet}N_3$ showed that 6,7-dimethyl-7,8-dihydropterin was an intermediate in the oxidation of 6,7-dimethyltetrahydropterin at the two electron-equivalent oxidation point. The eventual end product at four electron equivalents was 6,7-dimethylpterin. In the case of unsubstituted tetrahydropterin, the dihydro form was clearly not an exclusive product at the two electron equivalent point, and this was attributed to the disproportionation of different forms of dihydropterin to tetrahydropterin and pterin.

The azide radical oxidized tetrahydropterins to trihydropterin radicals, $^{\bullet}PnH_3$, with overall second-order rate constants at pH 7 of 4.1, 3.8, and 2.9×10^9 M^{-1} s^{-1} for tetrahydropterin, 6,7-dimethyltetrahydropterin, and 6-carboxylated tetrahydropterin, respectively. At pH 10 the rate constants are slightly larger due to the presence of the deprotonated enolate forms of tetrahydropterins. Spectra vary somewhat with substitution in the pterin molecule, but all species have a strong peak ($\epsilon \sim 9000$ M^{-1} cm^{-1}) near 320 nm and lower absorption above this, with a tail extending to 580 nm.

Key words: tetrahydropterin oxidation, tetrahydropterin, trihydropterin radical, azide radical, trihydropterin spectrum.

DAVID A. ARMSTRONG, MOHSEN FARAHANI et PARMINDER S. SURDHAR. Can. J. Chem. **68**, 1974 (1990).

Le titrage spectrophotométrique des tétrahydroptérines avec des quantités croissantes de $^{\bullet}N_3$ a permis de démontrer que, au niveau de l'oxydation par deux équivalents d'électron, la 6,7-diméthyl-7,8-dihydroptérine est un intermédiaire dans l'oxydation de la 6,7-diméthyltétrahydroptérine. La 6,7-diméthylptérine est le produit qui se forme éventuellement au niveau de l'oxydation par quatre équivalents d'électron. Dans le cas de la tétrahydroptérine qui n'est pas substituée, il est clair que la forme dihydro n'est pas le produit exclusif au niveau de l'oxydation par deux équivalents d'électron; ce résultat est attribué à la disproportionation des diverses formes de la dihydroptérine en tétrahydroptérine et en ptérine.

A un pH de 7, le radical azoture oxyde les tétrahydroptérines en radicaux trihydroptérines, $^{\bullet}PnH_3$; les constantes de vitesse du deuxième ordre sont respectivement 4,1, 3,8 et $2,9 \times 10^9$ M^{-1} s^{-1} pour la tétrahydroptérine, la 6,7-diméthyltétrahydroptérine et la tétrahydroptérine portant un groupement carboxyle en position 6. A un pH de 10, les constantes de vitesse sont légèrement supérieures à cause de la présence des formes énoliques déprotonées des tétrahydroptérines. Les spectres varient légèrement avec les substituants présents sur la molécule de ptérine; toutefois, toutes les espèces présentent une forte bande ($\epsilon = 9000$ M^{-1} cm^{-1}) près de 320 nm et une absorption moins intense à une longueur d'onde plus grande avec une queue allant jusqu'à 580 nm.

Mots clès : tétrahdroptérine oxidation, tétrahydroptérine, radical trihydroptérine, radical azoture, spectre trihydroptérine.

[Traduit par la revue]

Introduction

Reduced derivatives of folic acid are carriers of activated one-carbon units in the synthesis of nucleic acids (1), and the related unconjugated pterins act as cofactors in the enzymically-catalyzed conversion of phenylalanine to tyrosine and of tyrosine to dihydroxyphenylalanine (1–3). In addition, knowledge of the mechanisms of oxidation of reduced pterin coenzymes is important for the preservation of vitamin activity during the course of food processing (4). For these reasons, there has been extensive interest in the oxidation–reduction reactions by which the biologically relevant di- and tetrahydro forms of folic acid are interconverted. Important studies (5–9) have been conducted with the structurally simpler pterin analogues, PnH_2 and PnH_4 (as shown in Scheme 1) which still posess the heterocyclic ring system essential to the redox chemistry and biological functions.

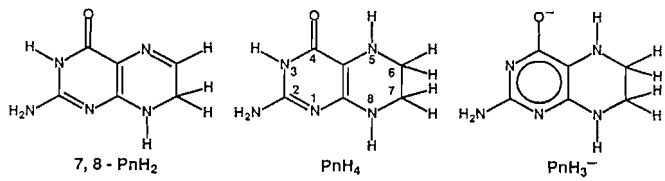

SCHEME 1. Structures of dihydro and tetrahydropterins.

Several authors have postulated the involvement of trihydropterin radicals ($^{\bullet}PnH_3$) as intermediates, for example in the autooxidation of PnH_4 (8, 9). Such radicals have been produced in strongly acid media by chemical oxidizing agents (10, 11) and more recently in acetonitrile by photochemical methods (12). They have been characterized in those systems by esr. However, although frequent reference has been made to the coloration of these solutions (8, 9, 11), definitive investigations of the absorption spectra of $^{\bullet}PnH_3$ radicals appear to be lacking. The main reason for this is that to date only relatively mild oxidizing agents, such as oxygen and $Fe(CN)_6^{3-}$, have been used. These react relatively slowly with PnH_4 and its derivatives, which

[1]The research described herein was supported by the Natural Sciences and Engineering Research Council of Canada under grant A3571 and by the Office of Basic Energy Sciences of the United States Department of Energy. This is Document No. NDRL-3265 from the Notre Dame Radiation Laboratory.

[2]Taken in part from the M.Sc. Thesis of M. Farahani, Department of Chemistry, University of Calgary, 1987.

[3]Visiting Professor at the University of Notre Dame Radiation Laboratory 1989–1990, while on sabbatical leave from the University of Calgary.

Printed in Canada / Imprimé au Canada

Can. J. Chem. Downloaded from www.nrcresearchpress.com by 91.121.58.235 on 09/07/12
For personal use only.

Can. J. Chem. Downloaded from www.nrcresearchpress.com by 91.121.58.235 on 09/07/12
For personal use only.

means that the ambient concentrations of radicals are low and their optical absorbances cannot be properly differentiated from those of parent compounds and the PnH_2 and pterin (Pn) products. The object of this work was to find an alternative one-electron oxidant, which would still sequentially convert PnH_4 to PnH_2 and Pn via a radical mechanism, but at the same time could be used under conditions that would permit the absorption spectrum of $^{\cdot}PnH_3$ to be recorded.

The azide radical, $^{\cdot}N_3$, which normally reacts with aromatic systems specifically by electron transfer (13, 14), was chosen as a suitable oxidant. The radical can be generated conveniently through the oxidation of N_3^- by $^{\cdot}OH$ radicals, produced in the pulse radiolysis of N_2O-saturated solutions. The following relevant reactions (15, 16) take place immediately after the pulse and are complete within 10 ns:

$$[1]\quad 4.36H_2O \rightarrow 2.90\, e_{aq}^- + 2.90\, H^+ + 0.52\, {}^{\cdot}H + 0.47\, H_2 + 0.73\, H_2O_2 + 2.90\, {}^{\cdot}OH$$

$$[2]\quad N_2O + H_2O + e_{aq}^- \rightarrow N_2 + OH^- + {}^{\cdot}OH$$

$$[3]\quad {}^{\cdot}OH + N_3^- \rightarrow OH^- + {}^{\cdot}N_3$$

The coefficients in reaction [1] are moles per 10 MJ of radiation energy absorbed.

Azide has the advantage over several other radicals in that it does not itself absorb significantly above 300 nm, provided complexation with N_3^- is eliminated by keeping the N_3^- concentration below 0.2 M. Also the $^{\cdot}H$ atoms are removed by reaction with N_3^- to form $^{\cdot}HN_3^-$ (14) which is a potential reducing agent and would be inert to PnH_4.

This paper demonstrates that $^{\cdot}N_3$ sequentially oxidizes tetrahydropterins to their dihydro and pterin forms. It also reports the spectra of trihydropterin radicals derived from unsubstituted tetrahydropterin (PnH_4), 6,7-dimethyltetrahydropterin ($Pn(Me)_2H_4$), and 6-carboxylated tetrahydropterin ($Pn(CO_2^-)H_4$). The latter was produced by reaction of $^{\cdot}CO_2^-$ with pterin.[4] Experiments were carried out mainly at neutral pH and pH 10.

Experimental

Pulse radiolysis experiments were conducted at 23 ± 2°C in 1 cm optical path length "supercil" cells on solutions, which were flushed after each radiation pulse. For some experiments, the electron beam source was the 1.5 MeV Van de Graaff accelerator at the University of Calgary, but most of the pulse radiolysis was done with the 8 MeV linear accelerator in the U.S. Department of Energy Radiation Laboratory at the University of Notre Dame. Methods of dosimetry and other experimental details for these two facilities have been given in refs. 17 and 13, respectively. γ-Radiolysis was carried out at room temperature in an Atomic Energy of Canada Gamma Cell, either at Calgary or Notre Dame. Dose rates were checked routinely with the Fricke dosimeter solution (16) with the ferric ion yield taken from the literature as 1.61 mole per MJ of radiation energy absorbed (15).

Absorption spectra of solutions were measured on a Cary 219 Spectrophotometer and absorbance coefficients were used routinely to determine concentrations of tetrahydropterins. For PnH_4 and $Ph(Me)_2H_4$, the first λ_{max} was at 297 nm for both pH 7 and 10. The value of ϵ_{max} was also the same at both pH's and equal to 8200 ± 200 M^{-1} cm^{-1} for the former and 8500 ± 200 M^{-1} cm^{-1} for the latter. It may be noted that these pH coincidences were fortuitous, as some PnH_3^- was present with PnH_4 at pH 10 (pK PnH_4 amide ~ 10.4 (18)) and a trace of PnH_5^+ (pK ~ 5.6 (18)) occurs at pH 7. $Pn(CO_2^-)H_4$ had λ_{max} = 302 nm and ϵ_{max} = 8020 ± 200 M^{-1} cm^{-1} at pH 10.

[4]Details of $^{\cdot}CO_2^-$ reductions will be presented elsewhere (M. Farahani, P. S. Surdhar, R. Allen, C. Schoneich, K.-D. Asmus and D. A. Armstrong. To be published).

All chemicals were the purest available and solutions were made up in triply-distilled or chromatographically-purified deionized water with 10–20 mM phosphate buffer present. They were deaerated by purging with nitrous oxide, nitrogen, or argon before use. Solutions of tetrahydropterins were kept free of air to avoid oxidation by oxygen. Sources of pterin derivatives were tetrahydropterin sulphate, K and K Laboratories; 6,7-dimethyl-5,6,7,8-tetrahydropterin, pterin-6-carboxylic acid, and pterin, Fluka. Pterin obtained from the Sigma Chemical Company gave identical results.

Results and discussion

Two and four electron-equivalent oxidation by $^{\cdot}N_3$

Tetrahydropterin derivatives in N_2O-saturated solutions, containing 0.02 to 0.05 M sodium azide, were subjected to oxidation by $^{\cdot}N_3$ produced by γ radiolysis over measured periods of time (5–15 min). Absorption spectra were taken several minutes after each successive addition of this oxidant, when the radical reactions had ceased. An illustration of one of these spectrophotometric titrations has been given in Fig. 1*a* for 6,7-dimethyltetrahydropterin at pH 10. The observations at pH 7 were similar. The numbers on the curves correspond to the number of minutes of exposure to radiation, and each ten minutes corresponds to the addition of 32 μmol of $^{\cdot}N_3$ per litre. The initial spectrum, very similar to the "ten minute spectrum", was omitted.

At the start of the oxidation, there were isobestic points at 318 and 286 nm, and, as illustrated for 318 nm in the inset, the absorbances at these wavelengths did not change until two equivalents of $^{\cdot}N_3$ had reacted per mole of $Pn(Me)_2H_4$. Beyond this point, two new isobestic points appeared at 267 and 332 nm. Finally there was no change in absorbance at any wavelength for oxidizing equivalents in excess of 4.1 per mole of $Pn(Me)H_4$ initially present, and at that point the spectrum corresponded to that of 6,7-dimethylpterin. The solubility of this compound in 0.02 M phosphate buffer at pH 7 and 10 and 23°C was found to be about 20 μM. A fine precipitate appeared in the latter stages of the oxidative titration, if the initial $Pn(Me)_2H_4$ concentration exceeded this. In separate experiments with unsubstituted pterin, no oxidation by $^{\cdot}N_3$ was seen, and this appeared true for all pterin derivatives examined here.

When $Pn(Me)_2H_4$ was allowed to react with oxygen in an aerated solution and the conversion to 6,7-dimethyl-7,8-dihydro-pterin ($Pn(Me)_2H_2$) was followed spectrophotometrically, as in earlier work (2), isobestic points were observed at the same wavelengths as those seen initially in Fig. 1*a*. Also, the spectrum at the two electron equivalence point in Fig. 1*a* ($e_{oxd}/Pn(Me)_2H_4$ = 2.0) was found to be within experimental error the same as that of $Pn(Me)_2H_2$, produced by oxidation of $Pn(Me)_2H_4$ with two equivalents of $Fe(CN)_6^{3-}$ (6, 7) or by oxidation with air. The results in Fig. 1*a* can therefore be explained on the basis of three major species being present during the titration: (*a*) $Pn(Me)_2H_4$ and $Pn(Me)_2H_2$ from $e_{oxd}/(Pn(Me)_2H_4)_0$ = 0 to 2.1; and (*b*) $Pn(Me)_2H_2$ and $Pn(Me)_2$ from $e_{oxd}/(Pn(Me)_2H_4)_0$ = 2.1 to 4.1. The fact that the titration requires a slight excess of $^{\cdot}N_3$ can be explained by the presence of the reducing entity $^{\cdot}HN_3^-$, which is formed with one tenth the yield of $^{\cdot}N_3$ (see Introduction) and could reconvert some Pn and PnH_2 to their reduced forms.

The effects observed with PnH_4 and $Pn(CO_2^-)H_4$ were different to the extent that there was no clearcut two-electron equivalent end point, although oxidation again ceased at the four-electron equivalent point. This has been illustrated for the case of the carboxylated tetrahydropterin at pH 10 in Fig. 1*b*. The presence of the isobestic point between the absorbances of the

Can. J. Chem. Downloaded from www.nrcresearchpress.com by 91.121.58.235 on 09/07/12
For personal use only.

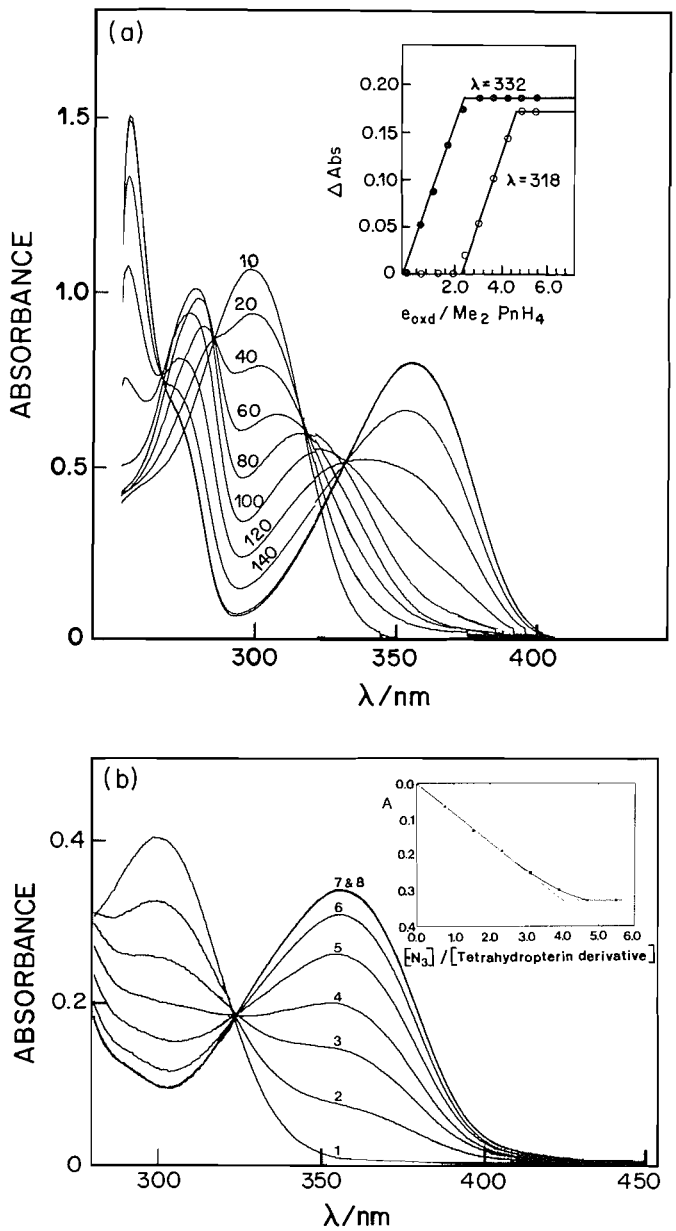

FIG. 1. Spectrophotometric titrations of tetrahydropterins in N_2O-saturated 40 mM NaN_3 solutions at pH 10. (*a*) 62 μM 6,7-dimethyltetrahydropterin. Numbers on curves correspond to minutes of exposure to γ radiation; (*b*) 50 μM 6-carboxylated tetrahydropterin. Numbered curves correspond to 0 (*1*), 8 (*2*), 16 (*3*), 24 (*4*), 32 (*5*), 40 (*6*), 48 (*7*) and 56 min (*8*) of γ radiation. Insets: Changes in absorbance versus moles of oxidant $^{\bullet}N_3$ per mole of initial tetrahydropterin.

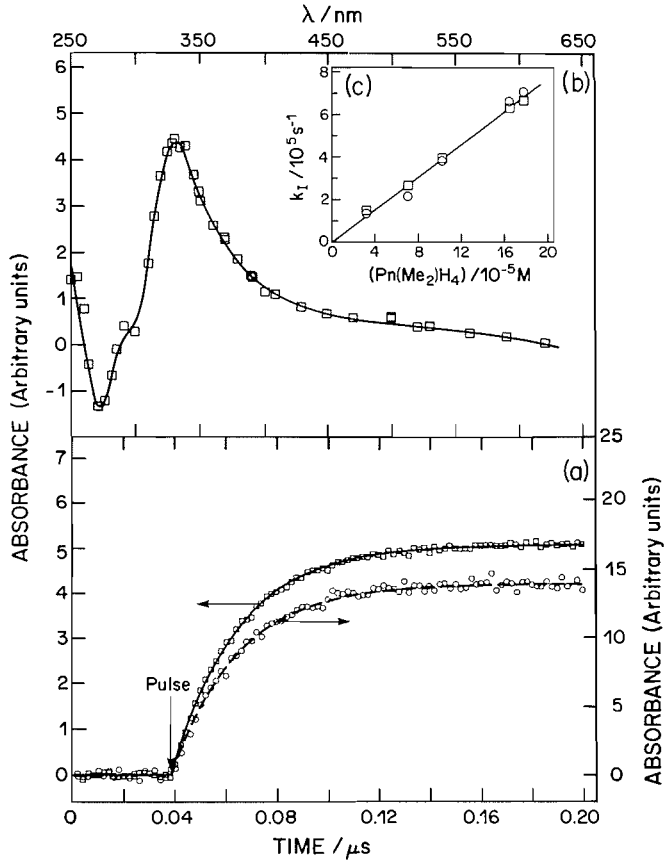

FIG. 2. Growth of absorbance of radicals produced by $^{\bullet}N_3$ oxidation illustrated for 6,7-dimethyltetrahydropterin at pH 7 in 0.05 M NaN_3 solutions. (*a*) Kinetics of growth at 330 nm (□) and 400 nm (○) for 103 μM solutions. Lines are fitted first-order growth curves. (*b*) Differential spectrum—changes in absorbance when radical formation was complete plotted against wavelength—for a 32 μM solution. (*c*) Pseudo first order rate constants for growth at 330 nm (□) and 400 nm (○) plotted against concentration of the tetrahydropterin.

tetrahydropterin and pterin implies that pterin is present right from the start of the titration and that the 7,8-dihydropterin never builds up to a significant concentration.

The earlier research with $Fe(CN)_6^{3-}$ (6, 7) as oxidant showed that the first non-radical product of one electron oxidation was a quinonoid dihydropterin (6, 7). This rearranged to 7,8-dihydropterin in a process, which was on a sub-second time scale for "unhindered" tetrahydropterins, like PnH_4, but could be observed by spectrophotometry for the 6,7-dimethyl derivative. Also, with the exception of this derivative, the quinonoid dihydropterins disproportionated quite rapidly with their 7,8-isomers to yield the PnH_4 and Pn forms. The present observations for unsubstituted PnH_4 are in agreement with this. The finding that $Pn(CO_2^-)H_4$ behaved similarly is consistent with the fact that blocking groups were required at both C-6 and C-7 to fully inhibit the disproportionation. In summary, therefore, the products and stoichiometry observed on the oxidation of tetrahydropterins with $^{\bullet}N_3$ are similar to those seen with $Fe(CN)_6^{3-}$. However, as will be appreciated from the next section, the primary one-electron oxidation step is much faster.

Pulse radiolysis observation of one electron oxidation

Kinetics of $^{\bullet}PnH_3$ Growth:

The reaction of $^{\bullet}N_3$ radicals with tetrahydropterin derivatives was followed by observing the changes in absorption (ΔA) at wavelengths in the region λ = 250 to 650 nm. Examples of the growth of ΔA *with time at* λ = 330 and 400 nm are shown in Fig. 2*a* for 103 μM 6,7-dimethyltetrahydropterin at pH 7. For solutions of a particular tetrahydropterin at a given pH, the growth obeyed pseudo first-order kinetics at all wavelengths with similar rates. Plots of the pseudo first-order rate constants versus concentrations of the tetrahydropterin were linear, as illustrated by the example in Fig. 2*c*. This is consistent with reaction [4].

$$[4] \quad {}^{\bullet}N_3 + PnH_4 \rightarrow N_3^- + \cdot PnH_4^+$$

as the rate-controlling process, the values of k_4 calculated from the slopes of such plots have been summarized in Table 1.

Reference to Table 1 shows that, while the differences are comparable to the ±15% experimental uncertainty, there is a consistent pH dependence of k_4 for each derivative. For the case

TABLE 1. Rate constants for oxidation by $^{\bullet}N_3$

Tetrahydropterin	Rate constants* pH 10	pH 7
PnH_4	5.7	4.1
$Pn(Me)_2H_4$	4.3	3.8
$Pn(CO_2^-)H_4$	4.2	2.9

*Units: 10^9 M^{-1} s^{-1}; uncertainties ±15%.

of $Pn(Me)_2H_4$, Kallen and Jencks (18) have determined the pK of the 3,4-amide group to be 10.4. This means that at pH 10 about 26% of the compound will be in the deprotonated enolate form (see structures in Introduction, Scheme 1). Based on $^{\bullet}N_3$ oxidation rates for model aromatic compounds (13), one would expect a slightly higher rate constant for this species. Allowing for the fractions of enolate (0.26) and amide (0.74) forms and assuming $k_4 = 3.8 \times 10^9$ M^{-1} s^{-1} for the latter, one finds from the pH 10 rate constant $k_{4e} = 5.7 \times 10^9$ M^{-1} s^{-1}

[4e] $^{\bullet}N_3 + PnH_3^- \rightarrow N_3^- + \cdot PnH_3$

for the PnH_3^- form of $Pn(Me)_2H_4$. In accord with this, when the rate constant was determined at pH 11.5 where 95% of the $Pn(Me)_2H_4$ would have been in the PnH_3^- form, the rate constant was found to be 5.8×10^9 M^{-1} s^{-1}. Since the amide ionization constants for the other tetrahydropterins are probably similar to that of $Pn(Me)_2H_4$, the trends with pH for the other compounds in Table 1 can be rationalized on a similar basis. The lower rate constants for the carboxylated derivative suggest that the presence of the CO_2^- group exerts a small inhibitory effect, perhaps by partially blocking access to the N-5 position. The rates at both pH's are also largest for the unsubstituted PnH_4.

The rate constants for the oxidation of the PnH_4 derivatives at pH 7 and for $Pn(Me)_2H_3^-$ are comparable to those for the $^{\bullet}N_3$ oxidation of phenolates (13) and of the dihydroflavin molecule (19), which has a number of structural similarities to tetrahydropterin. They are several orders of magnitude larger than the rate constants for oxidation of tetrahydropterins by $Fe(CN)_6^{3-}$ (~ 10^6 M^{-1} s^{-1} (7)) and oxygen (~ 1 M^{-1} s^{-1} (8)) at the same pH's. This can be attributed primarily to the much higher reduction potential of $^{\bullet}N_3$ (20) ($E^0(^{\bullet}N_3/N_3^-)$ = 1.33 V (21); $E^0(Fe(CN)_6^{3-}/Fe(CN)_6^{4-})$ = 0.36 V (22); E^0 (O_2/O_2^-) = −0.16 (21)).

As shown in Fig. 2*a*, for typical conditions, growth of the radical absorbance was complete at a microsecond or less. The change in absorbance at that point and before significant radical decay has been plotted against λ in Fig. 2*b* for the case of a 32 μM solution of $PnMe_2H_4$ at pH 7. Similar data were obtained for each PnH_4 derivative at neutral pH and pH 10. These "differential spectra" were independent of PnH_4 concentration, apart from expected minor variations in intensity due to the greater losses of $^{\bullet}N_3$ by combination at lower PnH_4 concentration (15).

The lifetimes of the present pterin radicals were surprisingly long and their decays could not be followed quantitatively with present apparatus. However, first half lives were in the region of 0.1 s. This means that rate constants for self reaction are in the region of 10^6 M^{-1} s^{-1} or less, and that $^{\bullet}PnH_3$ radicals are much more stable kinetically than many other biological radicals, such as flavin and nicotinamide radicals.

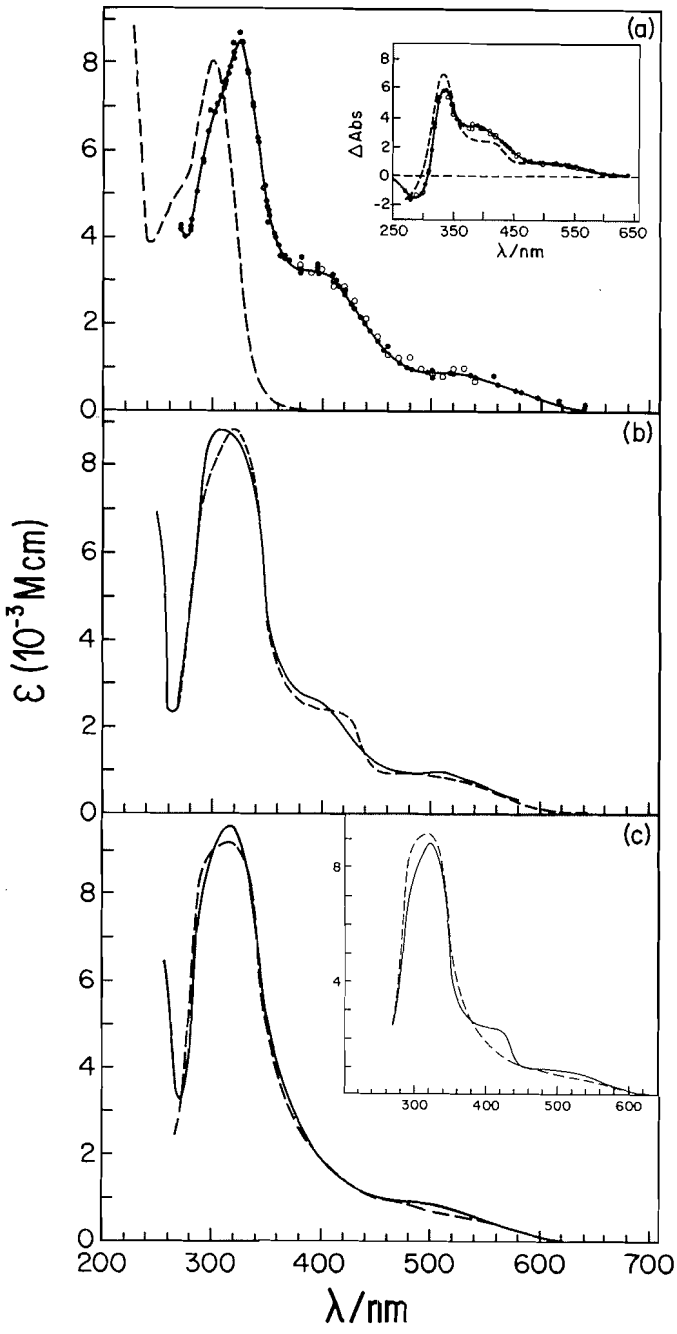

FIG. 3. Absorption spectra of radicals formed by $^{\bullet}N_3$ oxidation of tetrahydropterins. (*a*) 6-Carboxylated tetrahydropterin radical at pH 10 – solid line (filled and open circles were obtained at Notre Dame and Calgary, respectively). The dashed line is the spectrum of the parent compound. Inset: Differential spectra of radicals from: 6-carboxylated tetrahydropterin (solid line and circles) and tetrahydropterin (dashed line). (*b*) Radicals from 6,7-dimethyltetrahydropterin (solid line) and tetrahydropterin (dashed line) at pH 10. (*c*) As for (*b*) at pH 7. Inset: Comparison of the spectra of the radicals formed from PnH_4 at pH 10 (solid line) and pH 7 (dashed line).

Spectra of the radicals

Spectra of the radicals, derived by adding the values of ΔA (divided by the concentration of radicals produced per pulse) to the absorbance coefficient of the PnH_4 derivative determined at each given wavelenth on a Cary 219 spectrophotometer at the same pH, are shown in Fig. 3*a*, *b*, and *c*. The data for the carboxylated derivative, prepared by $^{\bullet}CO_2^-$ reduction of Pn, has been presented in more detail in Fig. 3*a*. The spectrum of this

Can. J. Chem. Downloaded from www.nrcresearchpress.com by 91.121.58.235 on 09/07/12
For personal use only.

tetrahydropterin was typical of those of the tetrahydropterins studied here, which all exhibited peaks near 300 nm and stronger absorption below 240 nm. Further discussion of $Pn(CO_2^-)H_4$ will be given elsewhere,[4] but it may be noted here that no evidence for the previously reported (23) absorbance near 380 nm was seen. It appears that this may have been due to experimental artifacts.

The isobestic point at 318 nm in Fig. 3*a* corresponds with the cross over from gain in absorbance to loss in the differential spectrum in the inset of the same Figure. It is important to note that these ΔA vs. λ plots are characteristic "signatures" of the parent compound and its daughter radical. When a comparison of the data points for the carboxylated tetrahydropterin (the solid line and points) with the corresponding ΔA vs. λ plot for tetrahydropterin, shown by the dashed line, was made on an enhanced scale, the differences of up to 1000 M^{-1} cm^{-1} units at several λ indicated that the radicals were different.[4] This is also shown to some extent by a comparison of the absolute spectra at pH 10 in Fig. 3*a* and *b*.

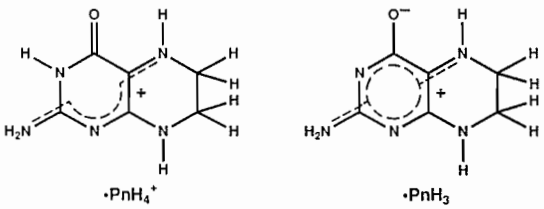

SCHEME 2. Two forms of "PnH" radical.

The structures of the two $^{\bullet}PnH_3$ species formed by removal of electrons from PnH_4 and PnH_3^- in Scheme 1 are shown in Scheme 2. Molecular orbital calculations (9, 11) on these predicted high spin densities on N-5 in both $^{\bullet}PnH_4^+$ and $^{\bullet}PnH_3$, but it was clear that other canonical forms would also contribute significantly, especially in $^{\bullet}PnH_3$ where a relatively large spin density was found (9) on C-4a. For the following reasons the data of the present study also demonstrate that there is significant delocalization of the unpaired electron from N-5 in the $^{\bullet}PnH_3$ radicals. First, recent research (24) has shown that aminyl cation radicals with α-hydrogen are susceptible to deprotonation, viz:

[5] $\quad -\dot{N}\overset{+}{H}-CH(R)- \rightarrow H^+ + -NH-\dot{C}(R)-$

with pK in the region of 8. Had this occurred here the spectrum seen would have been that of an α-carbon radical localized on C-6, and such a species does not absorb strongly above 300 nm (24, 25). Second, the 6-carboxylated tetrahydropterin would be susceptible to reaction [6], which has been shown to proceed on a microsecond or shorter time scale with α-carboxylated aminyl radicals (26). Again this would give a C-6 localized α-carbon radical and an absorption very different from that observed here. It is therefore evident that the radicals are stabilized by electron delocalization to the extent that these processes do not occur or take place on a 0.1 s or longer time scale. This delocalization is clearly reflected in the wavelength at which the absorption occurs and its intensity.

[6[$\quad -\dot{N}\overset{+}{H}-CH(CO_2^-)- \rightarrow CO_2 + -NH-\dot{C}H-$

The exact structures to be associated with the spectra in Fig. 3 remain to be determined. However, the pK of the amide group in the parent molecules is ~ 10.4 (18). In the radical the pK of this group should be the same or less. Since further experiments at pH 11.5 showed no significant change in absorbance from that of the radical form at pH 10, it appears that loss of the amide proton has occurred at that pH. At pH 7 there are some small differences in the absorption spectra, which suggest protonation may take place in that region. These are illustrated for the radicals of unsubstituted PnH_4 in the inset of Fig. 3*c*.

Finally, although this appears to be the first report of a UV/visible spectrum of $^{\bullet}PnH_3$ type radicals, the "tailing" absorbances in Fig. 3*a*, *b* and *c* at wavelengths above 400 nm are consistent with earlier reports of coloration of oxidized solutions of PnH_4 and its derivatives (9–11). The results reported here should stimulate further research on $^{\bullet}PnH_3$ radicals and assist in quantifying data relating to the kinetics of their reactions.

Acknowledgments

The authors are indebted to Dr. S. Mezyk and Mr. R. Allen for helpful discussions and technical assistance in some phases of this work.

1. R. L. BLAKLEY. The biochemistry of folic acid and related pteridines. North-Holland Publishing Co., Amsterdam, 1969. p. 139.
2. S. J. KAUFMAN. Biol. Chem. **234**, 2677 (1959); **236**, 804 (1961); **239**, 332 (1964); **242**, 3934 (1967).
3. S. J. KAUFMAN. Ann. Rev. Biochem. **36**, 171 (1967).
4. L. S. REED and M. C. ARCHER. J. Agr. Food Chem. **28**, 801 (1980).
5. D. J. VONDERSCHMITT and K. G. SCRIMGEOUR. Biochem. Biophys. Res. Commun. **28**, 302 (1967).
6. M. C. ARCHER and K. G. SCRIMGEOUR. Can. J. Biochem. **48**, 278 (1970).
7. M. C. ARCHER, D. J. VONDERSCHMITT, and K. G. SCRIMGEOUR. Can. J. Biochem. **50**, 1174 (1972).
8. J. A. BLAIR and A. J. PEARSON. Tetrahedron Lett. **3**, 203 (1973); J. Chem. Soc. Perkin II 80 (1974).
9. A. J. PEARSON. Chem. Ind. 233 (1974).
10. A. EHRENBERG, P. HEMMERICH, F. MÜLLER, T. OKADA, and M. VISCONTINI. Helv. Chim. Acta, **50**, 411 (1967).
11. A. BOBST. Helv. Chim. Acta, **50**, 2222 (1967); **51**, 607 (1968).
12. S. FUKUZNMI, K. TANII, and T. TANAKA. Chem. Soc. Jpn. Chem. Lett. 35 (1989).
13. Z. B. ALFASSI and R. H. SCHULER. J. Phys. Chem. **89**, 3359 (1985).
14. M. YE, K. P. MADDEN, R. W. FESSENDEN, and R. H. SCHULER. J. Phys. Chem. **90**, 5397 (1986).
15. I. G. DRAGANIĆ and Z. D. DRAGANIĆ. The radiation chemistry of water. Academic Press, New York. 1971.
16. J. W. T. SPINKS and R. J. WOODS. An introduction to radiation chemistry. Wiley, New York. 1976.
17. A. J. ELLIOTT, F. WILKINSON, and D. A. ARMSTRONG. Int. J. Radiat. Biol. Relat. Stud. Phys. Chem. Med. **38**, 1 (1980).
18. R. G. KALLEN and W. P. JENCKS. J. Biol. Chem. **241**, 5845 (1966).
19. P. S. SURDHAR and D. A. ARMSTRONG. J. Phys. Chem. **89**, 5514 (1985).
20. R. A. MARCUS and N. SUTIN. Biochim. Biophys. Acta, **811**, 265 (1985).
21. D. M. STANBURY. Adv. Inorg. Chem. **33**, 69 (1989).
22. A. J. BARD, R. PARSONS, and J. JORDAN. Standard potentials in aqueous solutions. Marcel Dekker, New York. 1985.
23. B. L. O'DELL, J. M. VANDERBELT, E. S. BLOOM, and J. J. PFIFFNER. J. Am. Chem. Soc. **69**, 250 (1947).
24. S. DAS and C. VON SONNTAG. Z. Naturforsh. **41**b, 505 (1986).
25. P. S. SURDHAR and D. A. ARMSTRONG. Can. J. Chem. **66**, 535 (1988).
26. J. MONIG, R. CHAPMAN, and K.-D. ASMUS. J. Phys. Chem. **89**, 3139 (1985).

Can. J. Chem. Downloaded from www.nrcresearchpress.com by 91.121.58.235 on 09/07/12
For personal use only.

The reaction of (η^5-cyclopentadienyl)dicarbonyliron(2-thienoyl) with acetylenes; a mechanistic study using proton nuclear magnetic resonance, and application in synthesis

IAN R. BUTLER[1]

Chemistry Department, University of Ottawa, Ottawa, Ont., Canada K1N 6N5

Received January 23, 1990

IAN R. BUTLER. Can. J. Chem. **68**, 1979 (1990).

The thermal reactions of dicarbonyl-η^5-cyclopentadienyl(2-thienoyl)iron with a series of substituted acetylenes to give indenones and cyclopentathiophenones have been reinvestigated. The results obtained support a reaction mechanism involving initial acetylene insertion followed by that of carbon monoxide, in contradiction to the previously reported results. The reaction products were identified and characterized primarily using 2D ^{1}H nmr spectroscopy.

Key words: acetylene, carbon monoxide, iron, indenone, mechanism, thienyl.

IAN R. BUTLER. Can. J. Chem. **68**, 1979 (1990).

On a réetudié les réactions thermiques du dicarbonyl-η^5-cyclopentadiényl(2-thienoyl)fer avec une série d'acétylènes substituées qui conduisent à des indénones et à des cyclopentathiophénones. Les résultats obtenus sont en accord avec un mécanisme réactionnel impliquant une insertion initiale de l'acétylène, suivie de celle du monoxyde de carbone; ce mécanisme est en contradiction avec les résultats rapportés antérieurement. Pour identifier et pour caractériser les produits réactionnels, on a principalement fait appel à la spectroscopie rmn du ^{1}H en 2D.

Mots clés : acétylène, monoxyde de carbone, fer, indénone, mécanisme, thiényle.

[Traduit par la revue]

Introduction

The insertion of acetylenes into metal–carbon bonds is a synthetically useful procedure, although the mechanistic details of such processes are not fully understood. Recently we have elucidated some of the mechanistic features of one specific type of reaction in this class, namely that of the thermal reaction of dicarbonyl-η^5-cyclopentadienyliron(I)aryls, FPAr, with diarylacetylenes to give [1*H*]-2,3-diarylinden-1-ones, using deuterium labelled samples (1). A summary of the proposed mechanistic results is shown in Scheme 1, for the reaction of Fp(phenyl-d_5) with diphenylacetylene. In addition to the indenone products, ferrocene and mono and 1,1′-bis(phenyl-d_5) ferrocene are observed as by-products, indicating the transfer of the σ bound phenyl group to the η^5-cyclopentadienyl ring. By studying the reactions (photochemical and thermal) of the related Fp(1- and 2-naphthoyl) compounds with diphenylacetylene, we were able to show that the insertion of the diarylacetylene precedes that of carbon monoxide, Scheme 2 (2). Moreover, by independent synthesis of the proposed intermediate, **4** (undeuterated) in Scheme 1, we were able to show that such compounds decompose cleanly to [1*H*]-2,3-diphenylinden-1-one (3).

On surveying the literature, we encountered a report by Kolobova and co-workers documenting a similar reaction of Fp-2-thienoyl, **11**, with diphenylacetylene under photolytic conditions to give indenone isostere **12** as the major reaction product, in addition to Fp-2-thienyl (4, 5), Scheme 3. Product **12** is not what would be predicted if our tentative reaction mechanism is correct, assuming that thermal and photochemical reactions have common reaction intermediates. Moreover, the reaction of Fp-2-thienoyl with (triphenylgermyl)phenylacetylene gives a single indenone product, **13** (6), which has been structurally characterized by the same research group. This result is in apparent contradiction to their earlier findings. For these reasons we decided to investigate a series of reactions of Fp-2-thienoyl with a range of disubstituted acetylenes to establish a mechanistic pathway for the thermal process, and compare the results obtained with those of reported photochemical reactions.

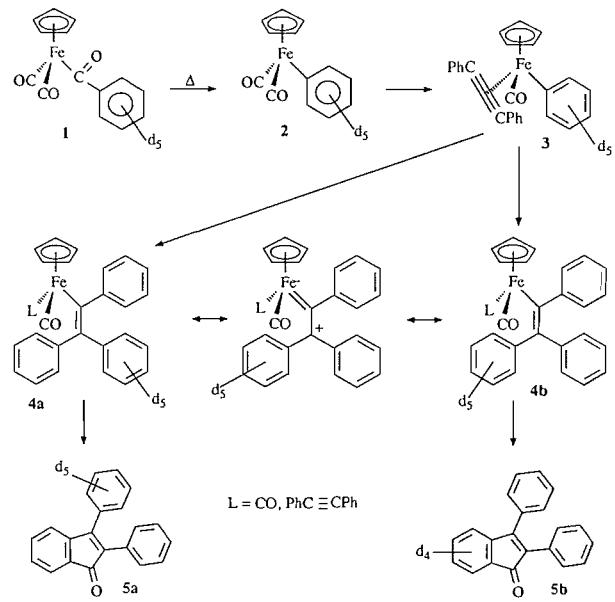

SCHEME 1

Experimental

All reactions were carried out under an atmosphere of dry nitrogen; however subsequent column chromatographic separations were carried out under aerobic conditions. ^{1}H nmr spectra were recorded using a Varian XL-300 spectrometer, using $CDCl_3$ as solvent unless otherwise stated. Mass spectra were obtained, using electron impact ionization on a VG Analytical 7070E instrument (at 70 MeV) at the University of Ottawa Mass Spectroscopy Centre. Neutral alumina (Aldrich Chemical Co.) was used throughout for column chromatographic separations. In addition, a mode 7924 chromatatron supplied by Harrison Research was used with a silica gel support (Merck 7749-60 PF_{254} plates). Substituted acetylenes were prepared by palladium-catalysed coupling reactions of phenylacetylene and the appropriate aryl halide (7). Derivatives of dicarbonyl(η^5-cyclopentadienyl)iron, (Fp), were prepared either by reaction of sodium dicarbonyl(η^5-cyclopentadienyl)

[1]Present address: Department of Chemistry, University College of North Wales, Bangor, Gwynedd, LL57 ZUW, United Kingdom.

Can. J. Chem. Downloaded from www.nrcresearchpress.com by 91.121.58.235 on 09/07/12
For personal use only.

Can. J. Chem. Downloaded from www.nrcresearchpress.com by 91.121.58.235 on 09/07/12
For personal use only.

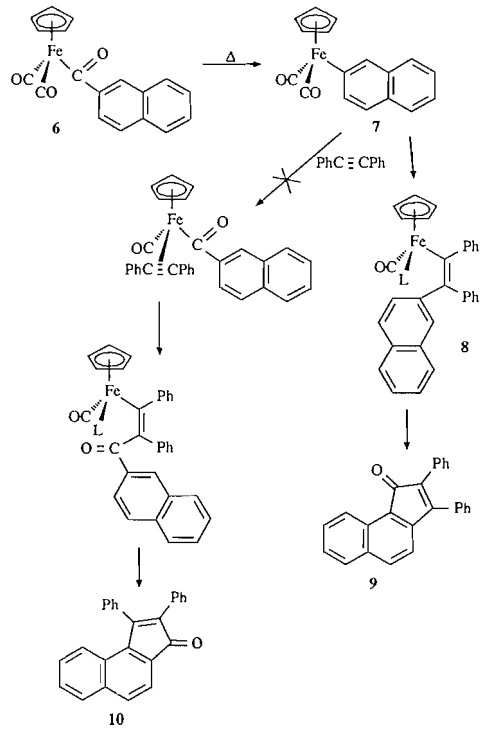

SCHEME 2

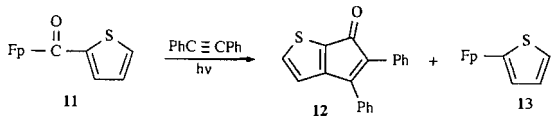

SCHEME 3

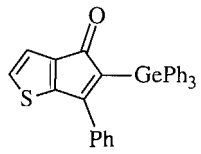

13

ferrate with the appropriate aroyl halide (8), or by reaction of dicarbonyl(η^5-cyclopentadienyl)iron iodide with the appropriate aryllithium (9). The solvent was decalins (mixture of *cis* and *trans* isomers), which was degassed prior to use. The standard procedure was to heat the reaction mixture using an isomantle as heat source, with good agitation. In general the reaction mixtures darken, becoming almost black, with, at reflux, rapid effervescence accompanied by a dense smoke-like vapour above the reaction mixture. The melting points reported are uncorrected. Two dimensional nmr experiments were conducted using conventional experimental parameters; dd = doublet of doublets, m = multiplet, bs = broad singlet, ad = asymmetric doublet. Yields quoted are based on isolated, crystallized samples, unless otherwise stated.

Reaction of Fp-2-thienoyl with diphenylacetylene

A mixture of Fp-2-thienoyl (5.32 g, 18.4 mmol) (4, 5) and diphenylacetylene (7.50 g, 42.1 mmol) was refluxed in decalins (25 mL) for 10 min. The cooled reaction mixture was chromatographed on a neutral alumina (Grade 1) column, (50 cm × 20 cm (diameter)). Initial elution with hexane gave decalins and a pale yellow fraction (subsequently shown to be predominantly diphenylacetylene). Subsequent incremental addition of diethyl ether eluted a series of coloured fractions, followed by a red/brown band of Fp_2. A red fraction (violet on drying), which was bound strongly to the column, was eluted with ethyl acetate. This was combined with the previous mixed coloured solutions. The coloured fractions were reapplied to a second column on which the following fractions, in order of elution, were obtained: (*i*) yellow, identified as ferrocene by mass spectroscopy and nmr; (*ii*) violet (55 mg), ^{1}H nmr: 6.81 (s, 1); 6.88 (d, 1); 6.91 (d, 1); 6.98–7.26 (m's 9). Mass spectrum: parent ion at *m/e* 572 (see below); (*iii*) red (250 mg), obtained as a slightly impure powder. ^{1}H nmr: 4.24 (s, 5); 6.44 (dd, 1); 6.72 (dd, 1); 6.86–7.40 (m's, approx. 14); 7.61 (dd, 1). Attempted recrystallization and purification by further chromatographic steps were unsuccessful in obtaining a pure crystalline sample; (*iv*) violet, identified as 4*H*-cyclopenta-[*b*]-thiophen-4-one-5,6-diphenyl, **14**; (*v*) violet and orange mixture of **14** and **15**; (*vi*) orange, identified as 2-phenyl 3-(2-thienyl)-[1*H*]-inden-1-one, **15**. The mixed fraction (*v*) was further separated twice using the chromatatron to give pure samples of **14** and **15**.

14 (14%), ^{1}H nmr ($CDCl_3$): 7.12 (d, 1, J_{H-H} = 4.8 Hz); 7.17 (d, 1); 7.28 (bs, 3); 7.30–7.35 (m's, 5); 7.48–7.50 (2d, 2). Mass spectrum: *m/e* (rel. int.) 290 (8.1); 289 (20.9); 288 (100.0), $M^{+\bullet}$; 287 (43.3); 273 (2.2); 272 (6.5); 260 (7.9); 259 (20.7); 258 (23.1); 255 (3.8); 226 (5.3); 215 (17.3); 189 (4.5); 179 (11.6). *Anal.* calcd. for $C_{19}H_{12}OS$: C 78.15, H 4.20; found: C 78.65, H 4.64. Melting point 161–162°C, lit. 164–165°C (9).

15 (26%), ^{1}H nmr ($CDCl_3$): 7.12 (dd, 1); J_{H-H} = 3.8, 8.0 Hz; 7.28–7.37 (series of multiplets, 9); 7.46 (dd, 1, J_{H-H} = 1.0, 5.1); 7.56 (ddd, 1). Mass spectrum: *m/e* (rel. int.) 290 (6.9); 289 (24.4); 288 (100.0), $M^{+\bullet}$; 287 (63.8); 272 (4.5); 271 (21.4); 260 (14.3); 259 (38.4); 258 (41.6); 255 (12.5); 226 (12.7); 215 (13.0); 189 (5.3); 129 (19.0); 113 (6.9); 108 (5.9). *Anal.* calcd. for $C_{19}H_{12}OS$: C 78.15, H 4.20; found: C 78.43, H 4.60. Crystalline samples of **15** exist in two forms, (*a*) as orange crystals and (*b*) as deep red crystals. Melting point 118–119°C (colour change at 115°C for orange crystalline samples), lit. 124°C (10).

Reaction of 2-thienoylchloride with diphenylacetylene and aluminum trichloride

To a solution of 2-thienoyl chloride (1.46 g, 10 mmol) and aluminum trichloride (1.33 g, 10 mmol) in dichloromethane (20 mL) maintained at 0°C in an ice bath, was added a solution of diphenylacetylene (1.78 g, 10 mmol) in dichloromethane (10 mL). The mixture was stirred at this temperature for 30 min before being carefully hydrolyzed by the addition of 20 mL of a 6 M solution of HCl. The organic layer was separated, dried over magnesium sulphate, filtered, and reduced in volume to a few mL. The mixture was then chromatographed using the chromatatron. Initial elution with hexane gave unreacted diphenylacetylene and blue 1,2,3-triphenylazulene (210 mg, 5.9 mmol) which was subsequently crystallized from the hexanes. Continued elution gave a colourless ultraviolet-active band and two indenone-containing coloured bands; however, in each of the latter cases, a colourless compound was present as a contaminant. Crystallization of the fractions gave mixtures of colourless crystals of **17***a* and *b* and the violet [6*H*]-cyclopenta-[*b*]-thiopen-6-one-4,5-diphenyl **12** and orange 2-phenyl-3-(2′-thienyl)-[1*H*]-inden-1-one, **15**, respectively. ^{1}H nmr study of the hand-selected violet and red crystals, respectively, indicated that **17** was still present as an impurity, thus the spectra were compared with a series of authentic samples previously prepared. Using this procedure, the violet fraction was shown conclusively not to be **14**, since a 2,3-disubstituted thienyl ring (doublets at 6.98 and 7.68, respectively) was evident. The orange sample was identical (ir, ^{1}H nmr) to that of an authentic sample of **15**.

16 (1,2,3-triphenylazulene, 14%), ^{1}H nmr ($CDCl_3$): 7.00–7.08 (m's, 2), 7.10–7.18 (m's, 4), 7.24–7.41 (m's, 6); 7.55 (t, 1); 8.32 (s, 1); 8.36 (s, 1). Mass spectrum: 357 (24.8); 356 (79.2); 278 (4.7); 277 (3.0); 276 (4.5); 183 (20.5); 111 (100.0); 83 (5.0); 73 (4.4); 58 (20.7); 39 (14.9); 30 (15.3). Melting point 216– 216.5°C, lit. 209–210°C (11), 216–217°C (12).

17 (mixed isomers, 37%), Mass spectrum: *m/e* (rel. int.) 326 (13.0); 325 (11.0); 324 (34.2); 223 (8.1); 289 (15.7); 288 (4.4); 261 (7.7); 179 (14.4); 178 (100.0).

17*a*, ^{1}H nmr: 7.12 (dd, 1, J_{H-H} = 4.9, 3.9); 7.16–7.58 (m's, 10);

Can. J. Chem. Downloaded from www.nrcresearchpress.com by 91.121.58.235 on 09/07/12
For personal use only.

7.69 (dd, 1, J_{H-H} = 1.1, 4.9); 7.77 (dd, 1, J_{H-H} = 1.1, 3.9). **17***b*: 6.93 (dd, 1, J_{H-H} = 4.9, 3.9); 7.16–7.58 (m's, 12, including dd at 7.51, J_{H-H} = 4.9, 1.2, and dd at 7.56, J_{H-H} = 3.9, 1.2).

Reaction of Fpbenzoyl with phenyl(2-thienyl)acetylene

A mixture of Fpbenzoyl (1.41 g, 5.0 mmol) and phenyl(2-thienyl) acetylene (1.38 g, 7.5 mmol) in decalins (60 mL) was refluxed for 15 min. After cooling, the reaction mixture was passed through an alumina precolumn (4 cm depth) to remove insoluble impurities. The alumina was washed with dichloromethane and the washings were combined with the mixture. The mixture was then chromatographed, using conventional chromatography and the standard procedure outlined above to give the following fractions: (*i*) pale yellow identified as residual phenyl(2-thienyl)acetylene; (*ii*) 1,1′-diphenyl ferrocene, parent ion at *m/e* 338, spectroscopically (ir, nmr) identical to an authentic sample; (*iii*) phenyl ferrocene, parent ion at *m/e* 262, identical to an authentic sample; (*iv*) red, identified as 2-(2′-thienyl)3-phenyl-[1*H*]-inden-1-one, **20**, (24%); (*va*) violet + orange (collected as a mixture and rechromatographed using the chromatatron to give (*vb*) violet, **14** (8%), and orange, **15** (10%).

20, ^{1}H nmr ($CDCl_3$): 6.87 (dm, 1); 6.93 (dd, 1, J_{H-H} = 3,7, 5.1); 7.27 (dd, 1, J_{H-H} = 1.1, 5.1); 7.40 (dd, 1, J_{H-H} = 1.1, 3.7); 7.42–7.46 (m's 2); 7.47–7.54 (overlapping m's, 4) Mass spectrum: *m/e* (rel. int.) 290 (6.8); 289 (22.5); 288 (100.0), $M^{+\bullet}$; 287 (44.7); 271 (10.1); 259 (31.9); 258 (37.4); 255 (7.3); 226 (12.2); 215 (11.3); 213 (9.1); 189 (5.3); 129 (17.6). *Anal.* calcd. for $C_{21}H_{14}OS$: C 78.18, H 4.20; found: C 78.43, H 4.60. Melting point 155–156°C.

*Reaction of Fp-2-thienoyl with phenyl(*p*-tolyl)acetylene*

A sample of Fp-2-thienoyl (2.0 g, 6.9 mmol) and phenyl (4-methylphenyl)acetylene (1.0 g, 5.2 mmol) were refluxed in decalins for 10 min. After cooling, the mixture was chromatographed on an alumina support to give, initially, decalins and excess acetylene (eluted with hexane) and, subsequently, a deep orange/red band (eluted with 50/50 hexanes/diethyl ether), followed by Fp_2 (trace, eluted with 90/10 diethyl ether/dichloromethane). Examination of the red/orange fraction by tlc indicated that it contained three coloured compounds: (*i*) pale orange (present in low concentration), (*ii*) violet, (*iii*) orange. The initial pale orange fraction was shown to be a mixture of compounds present in low quantities with parent ions of *m/e* 466, 600, 576, and 665, respectively. Further chromatography using the chromatatron separated the violet, (subsequently shown to be [4*H*]-cyclopenta-[*b*]-thiophen-4-one-5-phenyl-6-(4′-methylphenyl), **21***a*), and a second orange cyclopentenone fraction; however, further examination of the orange fraction by ^{1}H nmr indicated it to be an isomeric mixture of **22***a* and **23***a*, thus a further chromatographic separation, using the chromatatron, eluting with hexane, was attempted. This proved to be unsuccessful also. Final product identification of the mixture was made by ^{1}H nmr spectroscopy. Yields of **21***a*, **22***a*, and **23***a* were 6%, 12%, and 11% respectively, based on the acetylene.

21*a* (violet), ^{1}H nmr: 2.33 (s, 3); 7.08 (ad, 2, part of AB system), 7.12 (ad, 1, J_{H-H} = 4.8 Hz); 7.14 (ad, 1, J_{H-H} = 4.8 Hz); 7.17 (ad, 2, *J*~6.6 Hz); 7.34–7.38 (m's, 3); 7.48–7.52 (m's, 2). Mass spectrum: *m/e* (rel. int.) 303 (24.1); 302 (100.0), $M^{+\bullet}$; 301 (27.2); 287 (39.0); 285 (10.0); 273 (10.1); 272 (5.0); 271 (9.0); 269 (10.8); 259 (28.2); 213 (6.1); 143.5 (7.7); 129 (19.3).

22*a*, **23***a* (ratio of isomers 52:48), ^{1}H nmr: 2.36 (s, 3); 2.38 (s, 3); 7.06–7.59 (m's, 22). Mass spectrum: *m/e* (rel. int.): 303 (23.6); 302 (100.0), $M^{+\bullet}$; 301 (29.0); 288 (11.1); 287 (48.9); 286 (13.9); 285 (14.6); 273 (11.9); 269 (14.2); 259 (27.9); 258 (36.9); 239 (9.8); 226 (10.6).

*Reaction of Fp-2-thienoyl, **11**, with bis-*p*-tolylacetylene*

A solution containing Fp-2-thienoyl, **11** (0.5 g, 1.75 mmol), and bis-*p*-tolylacetylene (0.3 g, 1.46 mmol) in decalins (10 mL) was refluxed for 10 min. The solution mixture was examined by tlc, and two major indenone products were apparent (coloured bands with similar R_f values). Following a short precolumn to remove non-soluble and highly polar fractions, the mixture was chromatographed on a neutral alumina column to give the following fractions: (following ferrocene, hexa(*p*-tolyl)benzene, identical with an authentic sample, and Fp-thienyl) (*i*) violet, identified as a mixture of **21***b* and **22***b* (15%); (*ii*) red/orange, identified as **22***b* (16%). Band (*i*) was rechromatographed using the chromatatron to give additional pure 4*H*-cyclopenta[*b*]-thiophen-4-one-5,6-bis(4′-methylphenyl), **21***b* (8%), and additional 6-methyl-2-(4-methylphenyl)-3-(2-thienyl)-[1*H*]-inden-1-one, **22***b* (7%). Compounds **21***b* and **22***b* were subsequently crystallized from hexanes.

21*b* (violet), ^{1}H nmr: 2.33 (s, 3); 2.36 (s, 3); 7.11 (d, 1, J_{H-H} = 4.7 Hz); 7.09 (d, 2); 7.15 (d, 1, *J* = 4.7 Hz); 7.14 (d, 2); 7.15 (d, 2). Mass spectrum: *m/e* (rel. int.) 318 (10.2); 317 (22.3); 316 (100.0), $M^{+\bullet}$; 315 (9.8); 302 (6.4); 301 (25.9); 273 (5.8); 272 (7.2); 271 (7.7) 258 (7.4); 243 (6.1); 226 (5.6).

22*b* (red), ^{1}H nmr: 2.35 (s, 3); 2.37 (s, 3); 7.08 (dd, 1, J_{H-H} = 3.7, 5.1); (7.14) (ad, 2); 7.17 (d, 1) (overlapped); 7.19 (ad, 2); 7.21 (broad s, 1); 7.35 (dd, 1, *J* = 1.1, 3.7); 7.38–7.41 (2m's, 2); 7.44 (dd, 1, *J* = 1.1, 5.1). Mass spectrum: *m/e* (rel. int.) 318 (8.0); 317 (23.6); 316 (100.0), $M^{+\bullet}$; 315 (13.4); 302 (6.2); 301 (29.0); 300 (5.2); 299 (6.2); 287 (6.2); 283 (5.6); 273 (9.9); 272 (9.6); 271 (9.6); 258 (9.6); 239 (5.3); 151 (5.9); 149 (5.5); 136 (11.7); 129 (12.3); 57 (13.9); 41 (12.7); 34 (12.9).

Reaction of Fp-2-thienoyl with 1-naphthyl(phenyl)acetylene

A mixture containing Fp-2-thienoyl, **11** (1.0 g, 3.5 mmol), and 1-naphthyl(phenyl)acetylene (0.5 g, 2.2 mmol) in decalins (15 mL) was refluxed for 10 min. After cooling, the mixture was analyzed using tlc. In addition to several pale yellow bands, three intensely coloured spots, (red/violet, violet and orange) with similar R_f values characteristic of substituted cyclopentadienones, were observed. The mixture was initially chromatographed on a neutral alumina column, eluting initially with hexanes, then increasing the polarity by gradual incremental addition of diethyl ether. The highly coloured fractions (combined crude yield 37%), were collected as a mixture and, following concentration of the solution by vacuum distillation of the solvent at room temperature, were rechromatographed using the chromatatron. The products were eluted with a 5% solution of diethyl ether in hexanes in the following order: (*i*) red/violet, identified as **25** (5%) following concentration and crystallization from hexanes; (*ii*) violet, identified as **26** (13%), on crystallization from hexanes; (*iii*) orange, identified as **27** (19%) on concentration and crystallization from hexanes.

25 (red violet), ^{1}H nmr: δ 7.19 (m's, 7); 7.38 (td, 1); 7.48 (td, 2); 7.53 (td, 1), 7.90 (broad t's, 3). Mass spectrum: *m/e* (rel. int.) 339 (27.2); 338 (100.00), $M^{+\bullet}$; 337, (27.2); 310 (13.3); 309 (25.9); 308 (34.5); 305 (17.8); 276 (15.5); 263 (12.1); 261 (14.0); 260 (12.4); 154 (13.5); 153 (10.4); 28 (13.8). Melting point 143°C.

26 (violet), ^{1}H nmr: 7.14–7.48 (m's, 11); 7.76 (dd, 1), 7.84 (dd, 2). Mass spectrum: 339 (26.2); 338 (100.00), $M^{+\bullet}$; 337 (23.7); 309 (21.5); 308 (24.7); 305 (10.2); 276 (10.8); 168 (10.2); 167 (10.1); 154 (10.5); 149 (29.8); 57 (18.0); 43 (11.7). Melting point 118°C.

27 (orange), ^{1}H nmr: 6.95 (t, 1), 7.29–7.45 (m's, 6); 7.51 (2Xdd's, 2), 7.66 (t, 2); 7.74 (d, 1); 7.89 (2t's, 2). Mass spectrum: *m/e* (rel. int.) 339 (23.5); 338 (100.00), $M^{+\bullet}$; 337 (19.6); 309 (17.0); 308 (21.1); 305 (27.1); 272 (10.8); 276 (18.0); 154 (12.0); 138 (10.3); 57 (50.5); 56 (34.4); 43 (35.9); 42 (17.2); 41 (36.9); 29 (27.3); 27 (14.8). Melting point 166°C.

Reaction of Fp-2-thienoyl with phenyl(2-thienyl)acetylene

A mixture of Fp-2-thienoyl, **11** (1.44 g, 5 mmol), and phenyl(2-thienyl)acetylene (1.84 g, 10 mmol) in decalin (10 mL) was refluxed for 10 min. After cooling, the reaction was filtered through a short (10 cm) alumina precolumn, thereafter the reconstituted mixture was chromatographed using the chromatatron to give the following fractions, in order of elution: (*i*) orange, identified as ferrocene (8%); (*ii*) violet (14%), identified as **29**; (*iii*) violet (trace) (**30**); (*iv*) deep violet (11%), identified following crystallization from hexanes as **31**; (*v*) orange, unidentified, shown to be a mixture of two compounds by tlc, with parent ions at *m/e* 450 and 584 respectively; (*v*) red/brown, Fp_2 (6%); (*vi*) yellow, Fp-2-thienoyl (11%).

29, ^{1}H nmr ($CDCl_3$): 7.01 (dd, 1, J_{H-H} = 3.7, 5.1); 7.21 (dd,

Can. J. Chem. Downloaded from www.nrcresearchpress.com by 91.121.58.235 on 09/07/12
For personal use only.

1, J_{H-H} = 3.6, 5.1); 7.21 (ddd, 1); 7.32 (dd, 1, J_{H-H} = 1.1, 5.1); 7.34 (ddd, 1); 7.37 (dd, 1, J_{H-H} = 1.1, 3.6); 7.47 (dd, 1, J_{H-H} = 1.1, 3.7); 7.54 (ddd, 1); 7.58 (dd, 1, J_{H-H} = 1.1, 5.8). Mass spectrum: *m/e* (rel. int.) 296 (11.4); 295 (21.1); 294 (100.0), $M^{+\bullet}$, 293 (37.1); 277 (7.3); 267 (4.4); 266 (16.2); 265 (16.6); 261 (13.3); 249 (19.0); 234 (8.5); 232 (7.7); 222 (7.0); 221 (33.8); 189 (8.0); 147 (7.3); 111 (8.1); 110 (9.5). *Anal.* calcd. for $C_{17}H_{11}OS_2$: C 69.38, H 3.42; found: C 69.68, H 3.67. Melting point 127–128°C, lit. 129–130°C (10).

30, trace product mass spectrum parent ion at *m/e* 294.

31, ^{1}H nmr: 7.05 (dd, 1); 7.16 (d, 1); 7.23 (d, 1); 7.36–7.42 (m's, 5); 7.40 (dd, 1); 7.52 (dd, 1). Mass spectrum: *m/e* (rel. int.) 296 (11.4); 295 (21.8); 294 (100.0), $M^{+\bullet}$; 293 (38.1); 266 (16.3); 265 (21.6); 264 (18.9); 261 (14.7); 249 (10.1); 234 (6.9); 233 (4.0); 232 (8.0); 221 (33.6); 221 (33.6); 189 (8.9); 176 (7.2); 163 (4.7); 147 (5.0); 111 (5.4); 57 (29.3); 56 (27.4); 43 (21.6); 42 (11.6). Melting point 147–148°C.

Reaction of Fp-2-thienoyl with bis(trimethylsilyl)acetylene

A mixture of Fp-2- thienoyl (300 mg, 1.04 mmol) and bis(trimethylsilyl)acetylene (1.0 g, 5.88 mmol) was refluxed with decalins (6 mL) for 10 min. The mixture was then chromatographed on a neutral alumina column, eluting initially with hexanes to remove the decalins and unreacted bis(trimethylsilyl)acetylene, followed by the following bands: (*i*) ferrocene; (*ii*) 2-thienylferrocene (16); (*iii*) a mixture containing **32, 33**, and **34** (eluted with diethyl ether); (*iv*) Fp_2. Each of the fractions was initially characterized by mass spectroscopy. The mixed reactions were rechromatographed to give pure samples of **33** and **34**; however, only a trace of impure **32** could be isolated.

32, mass spectrum: parent ion at *m/e* 280.

33 (violet, 26 mg, 17%), ^{1}H nmr: 0.28 (s, 9); 7.02 (d, 1); 7.05 (dd, 1); 7.07 (d, 1); 7.11 (dd, 1); 7.38 (dd, 1). Mass spectrum: *m/e* (rel. int.) 292 (14.4); 291 (22.3); 290 (100.0), $M^{+\bullet}$; 289 (9.0); 277 (12.5); 276 (17.5); 275 (83.0); 268 (14.4); 247 (17.0); 217 (14.0); 216 (18.7); 205 (12.0); 204 (22.6); 203 (16.3); 192 (17.6); 171 (19.3).

34 (orange/red, 11 mg, 7%), ^{1}H nmr: 0.11 (s, 9); 7.02 (d, 1); 7.14 (dd, 1); 7.15 (dd, 1); 7.17 (d, 1); 7.41 (dd, 1). Mass spectrum: *m/e* (rel. int.) 292 (14.8); 291 (23.0); 290 (100.0), $M^{+\bullet}$; 289 (10.2); 278 (19.0); 277 (11.0); 276 (22.0); 275 (74.2); 247 (20.2); 217 (16.6); 216 (18.8); 205 (41.8); 192 (58.6); 191 (31.2).

One other product with parent ion *m/e* 395 was observed but not characterized.

Reaction of Fp-1-naphthoyl with bis-1-naphthylacetylene

Bis-1-naphthylacetylene was prepared from the reaction of naphthyl iodide and acetylene, catalysed by bis(triphenylphosphine)palladium dichloride/copper(I) iodide in diethylamine. The reaction of Fp-1-naphthoyl (1.66 g, 50 mmol) with bis-1-naphthylacetylene (2.78 g, 10.0 mmol) in decalene was carried out according to the general procedure, and the red product chromatographed on neutral alumina to give [1*H*]-[*e*]-benzoinden-1-one 2,3-bis(1-naphthyl) 31%, ^{1}H nmr ($CDCl_3$): δ 6.70–8.10 (series of overlapping multiplets). Mass spectrum: *m/e* (rel. int.) 433 (35.7); 432 (100.0), $M^{+\bullet}$; 431 (12.3); 403 (14.2); 402 (11.1); 400 (16.8); 308 (13.8); 304 (10.4); 276 (17.6); 200 (13.1); 186 (37.6); 177 (11.4); 149 (11.7).

Results and discussion

This investigation is centred on the thermal reactions of dicarbonyl(η^5-cyclopentadienyl)-2-thienoyliron, Fp-2-thienoyl, **11**, with a series of disubstituted acetylenes to compare with the literature results for the similar photochemical reactions. Compound **11** is conveniently prepared in high yield from the metathesis of NaFp with 2-thienoyl chloride in diethyl ether or THF (4, 13). The reactions of **11** with a series of acetylenes were all carried out under an inert atmosphere. However, all subsequent chromatographic steps were carried out aerobically. Although many by-products were obtained in each reaction, we focused on the isolation and characterization of cyclopentenone products.

When Fp-2-thienoyl is reacted with a stoichiometric excess of diphenylacetylene at reflux for 10 min, we observe a number of readily identifiable products such as ferrocene, Fp_2 and 2-thienylferrocene in addition to four unidentified coloured bands. On tlc comparison of these coloured fractions with an authentic sample of [1*H*]-2,3-diphenylinden-1-one, it was established that three of the bands had similar R_f values. Following complete separation by column chromatography, it was established that two of the coloured bands were iron complexes and the other two were isomeric indenone-like products. The latter compounds were positively identified as **14** (violet) and **15** (yellow/orange) by ^{1}H nmr spectroscopy. The identity of **15** was initially established using ^{1}H nmr COSY spectroscopy (Fig. 1*a*). The spectrum of **15** clearly indicates a monosubstituted thienyl ring. The resonances of the thienyl ring protons of **15** are observed as doublets of doublets at 7.09, 7.36, and 7.46 δ, respectively, the low field resonance assigned to the proton which is α to the sulphur atom, and the high field resonance to the proton which is α to the cyclopentalene substituent.

The thienyl ring proton resonances in **14** are observed at 7.13 and 7.18, respectively (Fig. 1*b*). The assignment of structure **14** as opposed to **12** was made on the basis of a spectral comparison with that of 2-thienoyl chloride and phenyl-2-thienyl ketone in which the resonances of the α- and β-thienyl protons are separated considerably, unlike those of **14**. Kolobova *et al.* (4) had reported that **14** is red, in apparent contradiction to our findings here and in contradiction to another documented characterization of the same compound by Ivanov and Mondeshka, who had prepared the compound by the base-catalyzed dehydrative cyclization of 2,3-diphenyl-3-(2′-thienyl)hydroxypropanoic acid (10, 14). It should be noted also that the spectral properties of **12** reported by Kolobova *et al.* are very similar to those reported for **14** by Ivanov and Mondeshka (both compounds dark violet, mp 161–162°C, Ivanov (164–165°C, Kolobova) uv λ_{max}, (e, X10^3): 267 (4.67); 510 (3.10), Ivanov. 261 (25.4); 508 (2.9), Kolobova). It seems fair to conclude that Kolobova and co-workers have misassigned the structures of **12** and **14**. A tlc study of the products derived from photochemical reactions showed that they are identical to those observed in thermal reaction. Our structural results are in agreement with those of Ivanov. The identity of **15** was unequivocally established by us, using X-ray crystallography to corroborate these findings.[2] We decided to probe the reasons for the structural misassignments.

The erroneous literature structural assignments for **12** and **14** had been made partially on the basis of a structural comparison with products obtained from the aluminum trichloride catalyzed reaction of 2-thienoyl chloride with diphenylacetylene. The report documents the formation of several products on a 17 mmol scale from this reaction, including **16** (28%) formed by acetylene dimerization, and indenones **12** (15%) and **14** (19%). In our hands, although we observe two intense coloured spots on tlc corresponding to indenones or their isosteres, we find that the actual indenone yields are very low, due to the formation of

[2]The X-ray structures of **15** and **21b** have been determined **15**: $C_{19}H_{12}OS$, space group $P2_1/n$, cell parameters are as follows: a = 9.532(3), b = 17.096(4), c = 9.577(4), β = 109.54°, V = 1470.8(8) Å^3. **24***b*: $C_{21}H_{16}OS$, space group $P2_1/n$, cell parameters, a = 5.7974(6), b = 19.1044(10), c = 15.0025(15), β = 100.910(9), V = 1631.58(25)-Å^3. Complete crystallographic data will be reported in a forthcoming paper together with that of related derivatives.

Can. J. Chem. Downloaded from www.nrcresearchpress.com by 91.121.58.235 on 09/07/12
For personal use only.

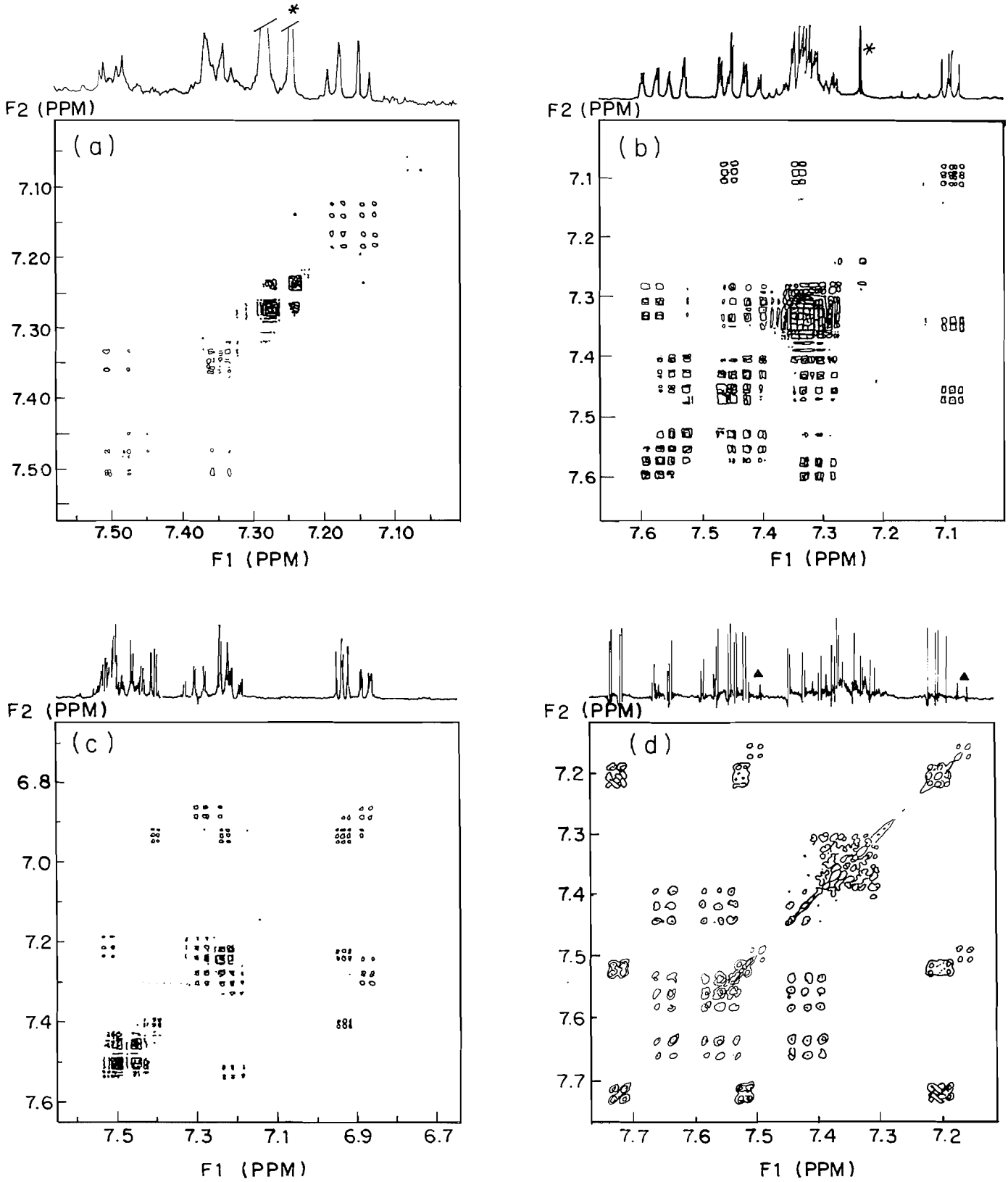

FIG. 1. The ^{1}H COSY nmr spectra of (*a*) **14**, (*b*) **15**, (*c*) **17***a*,*b*, and (*d*) **20**.

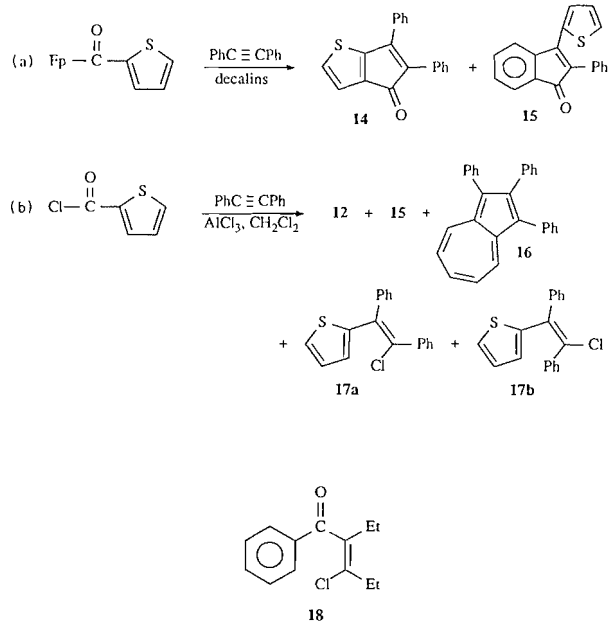

SCHEME 4

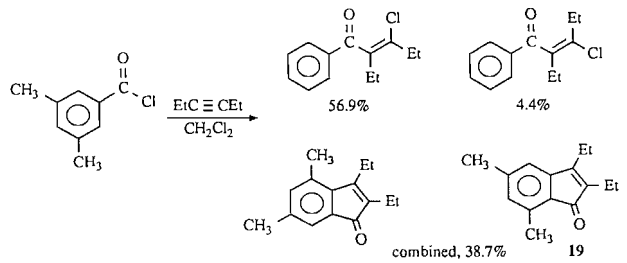

SCHEME 5

large amounts of the colourless **17** (mixture of *cis* and *trans* isomers), which elutes concurrently with the indenone fractions, resulting in mixtures. Attempted isolation of the pure coloured compounds following several chromatographic steps, including preparative plate tlc, was unsuccessful; all samples were contaminated with **17**. However, we were able to identify each of the coloured compounds present by ^{1}H nmr spectral comparison with that of pure samples of **17***a,b* and authentic samples of the indenones (Fig. 1*d*). The orange compound present was identified as **15**, while the violet fraction was identified as **12** (thienyl proton resonances at δ 6.98 (d) and 7.68 (d), respectively, $J_{H-H} = 4.4$ Hz). It should be noted that **14** and **12** are virtually indistinguishable in colour and have identical R_f values on tlc in a range of hexane/diethyl ether mixtures. Our results are in accord with those obtained by Martens and Hoornaert (15), who studied a series of similar reactions, observing, for example, **18** as the major product formed (80%) in the reaction of benzoyl chloride·aluminum trichloride adduct with 3-hexyne. Interestingly, the same authors report the formation of two indenones from the reaction of 3,5-dimethylbenzoyl chloride·aluminum trichloride adduct with 3-hexyne, Scheme 5. To account for the formation of **19**, in which the carbonyl function is no longer *meta* to both methyl groups, they propose a relatively complex mechanism to account for the apparent migration. In the present case, a further complexity is required to account for the formation of **15**, albeit in low yield. This may suggest a similarity between the reaction mechanism, in that the aryl groups are capable of migration with

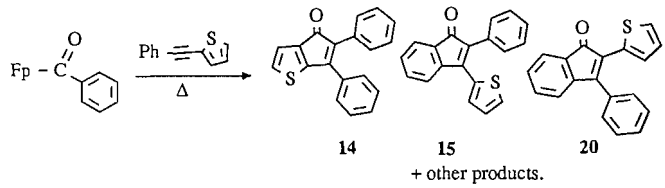

SCHEME 6

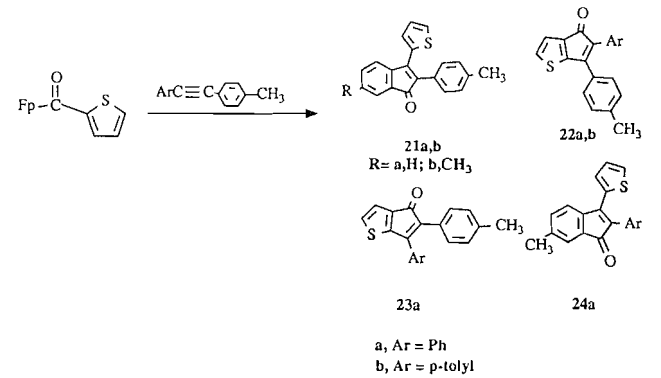

SCHEME 7

respect to the carbonyl group. This result probably warrants an independent mechanistic study of the aluminum trichloride catalyzed reaction. Our conclusion is that, unlike the reactions of benzoyl and naphthoylchlorides with diphenylacetylene in the presence of $AlCl_3$, which give high yields of indenones and benz(*e*)indenones respectively, the reaction of 2-thienoylchloride to give the thienyl isosteres is only of limited applicability.

To further test the proposed mechanism, the reaction of Fpbenzoyl with 2-thienyl(phenyl)acetylene was carried out (Scheme 6). We obtained a mixture of isomeric products including **14**, **15**, and **20**, the latter being the major product (24%), in addition to phenylferrocene and Fp_2. Compound **20** is red, possessing a similar ^{1}H nmr spectrum to that of **15** (Fig. 1*b*), with the exception that the resonances of the *ortho*-disubstituted phenyl group are shifted considerably in comparison (Fig. 1*c*).

The reactions of Fp-2-thienoyl with phenyl(4-methylphenyl) acetylene and bis(4-methylphenyl)acetylene, respectively, were carried out to verify the previous regiochemical results, and, in addition, to examine the electronic effect of substituents. The products obtained were structurally characterized using ^{1}H nmr. Compounds **21***a* and **24***a* were obtained as a mixture, following column chromatography and recrystallization, from the former reaction. Only a trace of the compound assumed to be **22***a* was observed. The results are summarized in Scheme 7. In the latter reaction, only **21***b* and **22***b* are observed with **21***b* predominant. These results are consistent with earlier findings, indicating that preferential metalation takes place in the following order: *p*-tolyl > phenyl > 2-thienyl. The reaction of Fp-2-thienoyl with phenyl(1-naphthyl)acetylene gave three isomeric products as indicated in Scheme 8*a*. In this case the major product is **27**, again consistent with our proposed reaction mechanism. This result contrasts with our previous findings in the case of the reaction of Fp-naphthoyls with diphenylacetylene, in which 1,2-naphthyl disubstituted products predominate (2). In the present case, the formation of products **25** and **28** may be disfavoured because of steric interaction in the reaction intermediate, Fig. 4. The preferred σ alkenyl complex will be the one with a bulky group adjacent to the iron, which at first sight is contrary to normal expectations. However, obviously a secondary influence on the ratio of reaction products will also be the

Can. J. Chem. Downloaded from www.nrcresearchpress.com by 91.121.58.235 on 09/07/12
For personal use only.

Can. J. Chem. Downloaded from www.nrcresearchpress.com by 91.121.58.235 on 09/07/12
For personal use only.

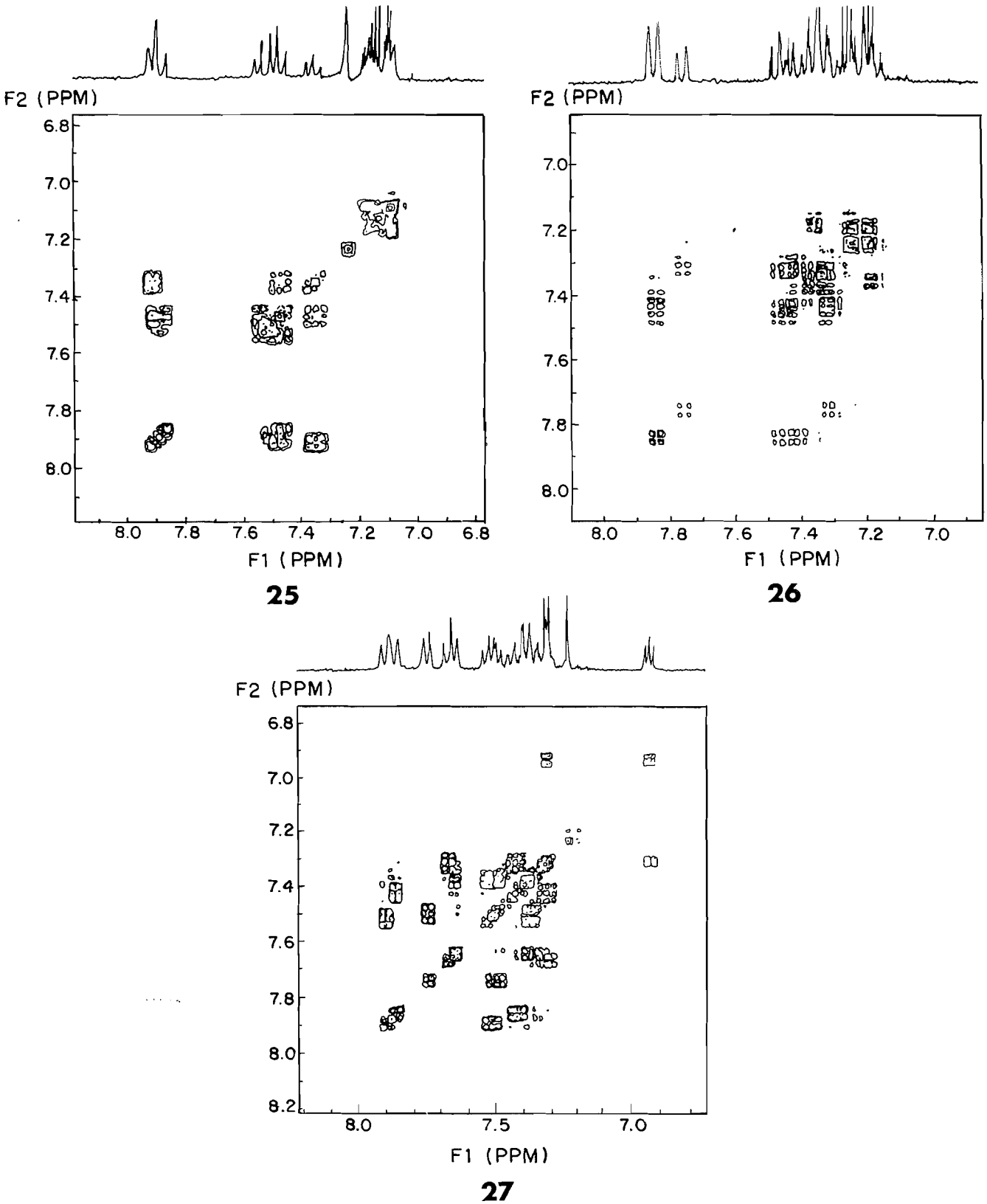

FIG. 2. The ^{1}H COSY nmr spectra of (*a*) **25**, (*b*) **26**, (*c*) **27**.

steric crowding in the resultant σ-alkenyl complex, with maximum significance anticipated near the iron centre. In the present case, since three isomeric products are obtained with traces of a fourth, a balance between these factors and the kinetics of isomerism of individual σ-alkenyl complexes and ring closure steps must exist. In an attempt to test whether a general reaction would be limited to the reactions of acetylenes with at least one non-bulky substituent, we carried out the

Can. J. Chem. Downloaded from www.nrcresearchpress.com by 91.121.58.235 on 09/07/12
For personal use only.

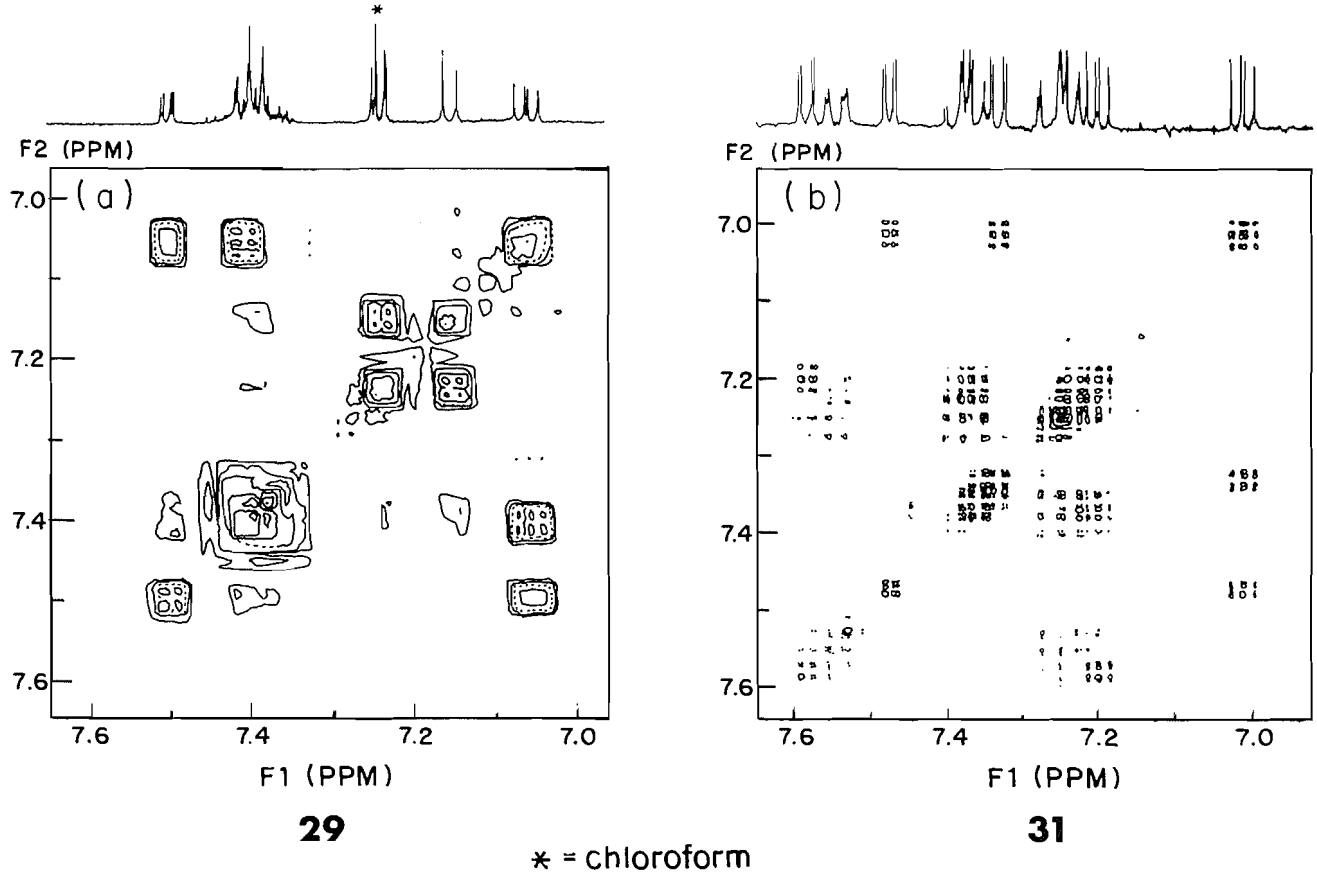

FIG. 3. The ^{1}H COSY nmr spectra of (*a*) **29** and **31**.

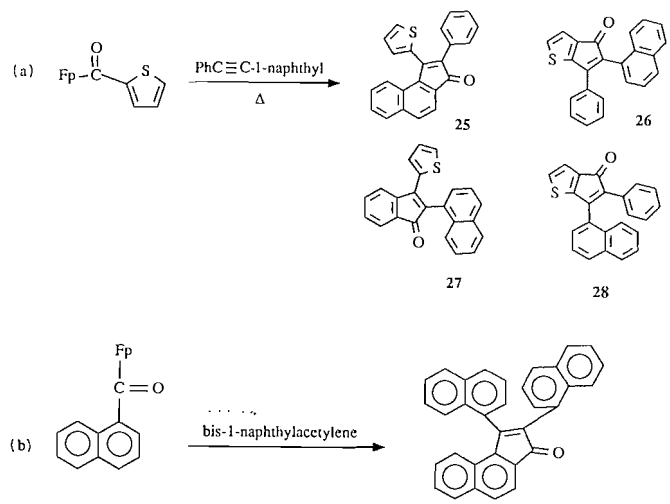

SCHEME 8

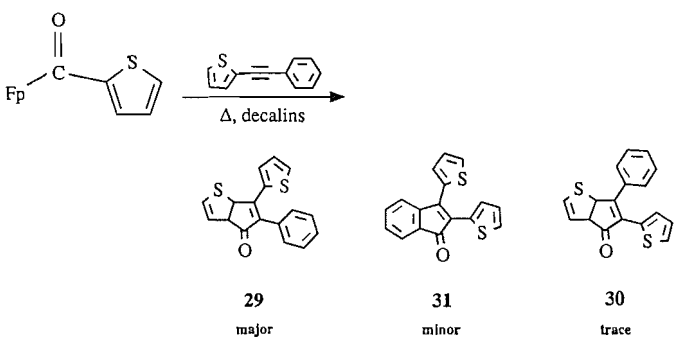

SCHEME 9

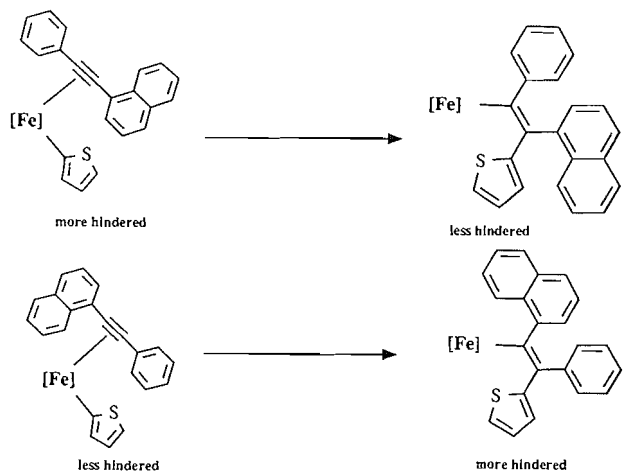

FIG. 4. The more hindered intermediate will give rise to the less hindered product and vice versa.

reaction of Fp-1-napthoyl with bis(1-naphthyl)acetylene. The product [1*H*]-[*e*]-benzoinden-1-one-2,3-bis(1-naphthyl) was observed, although heating for 20 min was required. This indicates that the reaction is still possible with relatively bulky groups on the acetylene and on the iron centre (Scheme 8*b*).

Finally, we carried out the reaction of Fp(2-thienoyl) with phenyl(2-thienyl)acetylene in an attempt to prepare analogues containing more than one thienyl group. Two major products were observed, as indicated in Scheme 9. Only a trace of the product assumed to be **31** was observed. The identification of **30** was made on the basis of a spectral comparison with **14**, **22***a*, **22***b*, and **24***a*.

The reaction of Fp-2-thienoyl with bis(trimethylsilyl)acetylene was attempted; however, following work up, only a low yield of the expected cyclopentenone **32** was obtained, in addition to ferrocene, 2-thienylferrocene, **33** and **34**. The latter are presumably formed by a metal-catalyzed exchange of the 2-thienyl group with one trimethylsilyl group. No evidence for the formation of **35** was observed.

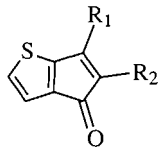

32: $R_1 = R_2 = Si(CH_3)_3$
33: R_1 = 2-thienyl; $R_2 = Si(CH_3)_3$
34: $R_1 = Si(CH_3)_3$; R_2 = 2-thienyl
35: $R_1 = R_2$ = 2-thienyl

Figures 1–3 show representative COSY ^1H nmr spectra used in the assignment of structures. The two dimensional technique allows a simple assignment of thienyl resonances in most cases, readily differentiating mono and 1,2-disubstituted thienyl compounds, even when there is considerable resonance overlap. In Fig. 1, the general differences between isomers **14**, **15** and **20**, which may be taken as representative compounds, can be observed. The position of the thienyl proton resonances is indicative of whether it is present in the 2, 3, or disubstituted position of the indenone or thienyl isostere. In light of the use of photoreactive polythienyl compounds as insecticides, there are similar potential applications for these thienyl derivatives, and a programme of screening is underway.

Acknowledgements

This work was funded by an operating grant to I.R.B. from the Natural Sciences and Engineering Research Council of Canada. Our grateful thanks are due to Dr. Clem Kazakoff of the University of Ottawa for recording the mass spectra and to Raj Capoor who recorded some of the 2D nmr spectra used in product assignment.

1. I. R. BUTLER, J. L. ELLIOT, and J. HOUDE, JR. Can. J. Chem. **68**, 000 (1990).
2. I. R. BUTLER, J-P. CHARLAND, J. L. ELLIOT, J. HOUDE, JR., W. E. LINDSELL, K. J. MCCULLOUGH, P. N. PRESTON, and A. B. RETTIE. J. CHEM. SOC. PERKIN TRANS. 2. In press.
3. I. R. BUTLER, J. L. ELLIOT, and J. HOUDE, JR. Can. J. Chem. **67**, 1308 (1989).
4. N. E. KOLOBOVA and L. V. GONCHARENCO. Khim. Getersikl. Soedin. 1461 (1979).
5. L. V. GONCHARENCHO, N. E. KOLOBOVA, and P. V. PETROUSKII. Izv. Akad. Nauk SSSR, 42 (1982), Eng. Transl. 382 (1982).
6. L. V. GONCHARENKO, N. E. KOLOBOVA, L. G. KUZ'MINA, and YU T. STRUCHKOV. Izv. Akad. Nauk, SSSR, 1162 (1983) (Eng. Trans. 1049) (1983).
7. D. E. AMES, D. BULL, and C. TAKUNDWA. Synthesis, 364 (1981).
8. R. B. KING and M. B. BISNETTE. J. Organomet. Chem. **2**, 15 (1964).
9. I. R. BUTLER, P. N. PRESTON, and W. E. LINDSELL. J. Chem. Res. (S), 185 (1981); (M), 2573 (1981).
10. C. P. IVANOV and D. M. J. MONDESHKA. Rev. Roum. Chim. 20 (1975).
11. R-L. FAN, J. I. DICKSTEIN, and S. I. MILLER. J. Org. Chem. **47**, 2466 (1982).
12. I. G. BUCHI, G. PERRY, and E. W. ROB. J. Org. Chem. **27**, 4106 (1962).
13. A. N. NESMEYANOV, N. E. KOLOBOVA, L. V. GONCHARENKO, and K. N. ANISIMOV. Izv. Akad. Nauk SSSR, Ser. Khim. **153**, 547 (1976).
14. C. P. IVANOV and D. M. MONDESHKA. J. Prakt. Chem. **315(6)**, 993 (1973).
15. H. MARTENS and G. HOORNAERT. Tetrahedron Lett. 1821 (1970).
16. A. N. NESMEYANOV, N. E. KOLOBOVA, V. V. SHRIPKIN, and K. N. ANISIMOV. Dokl. Akad. Nauk SSSR, **196**, 606 (1971).

Can. J. Chem. Downloaded from www.nrcresearchpress.com by 91.121.58.235 on 09/07/12
For personal use only.

Cyclobutene photochemistry. Substituent and wavelength effects on the photochemical ring opening of monocyclic alkylcyclobutenes[1]

WILLIAM J. LEIGH,[2] KANGCHENG ZHENG,[3] AND K. BRADY CLARK[4]
Department of Chemistry, McMaster University, Hamilton, Ont., Canada L8S 4M1

Received March 26, 1990

WILLIAM J. LEIGH, KANGCHENG ZHENG, and K. BRADY CLARK. Can. J. Chem. **68**, 1988 (1990).

The photochemical ring opening of *cis*- and *trans*-3,4-dimethyl-, 1,3,4-trimethyl-, and 1,2,3,4-tetramethylcyclobutene (**1**, **3**, and **4**, respectively) has been investigated in hydrocarbon solution with 193 nm and 214 nm light sources. Ring opening is non-stereospecific in all cases at both wavelengths. The ratio of dienes formed by the formally allowed to formally forbidden pathways in the photolysis of these compounds is highest (ca. 2) for the trimethylcyclobutenes, and approximately 1 for both *cis* and *trans* isomers of the di- and tetramethylcyclobutenes with 193 nm excitation. The diene distributions from photolysis of all compounds but *cis*-**3** show slight wavelength dependence. Gas- and solution-phase UV absorption spectra are reported for **3** and **4**, and indicate that there are at least three singlet excited states accessible in the 185–230 nm region in these molecules. The $\pi,R(3s)$ state is the lowest energy state in the gas phase in **3** and **4**. The results verify that orbital symmetry factors do not play a role (or a consistent one, at least) in controlling the stereochemistry of the reaction, but they do not allow a firm assignment of the excited state(s) responsible for ring opening. Direct photolysis of these compounds also results in fragmentation to yield *Z*-2-butene (from *cis*-**3** and **4**) or *E*-2-butene (from *trans*-**3** and **4**) in addition to propyne or 2-butyne. The 2-butenes are formed with greater than 90% stereospecificity in all cases. The structures of the four 3-methyl-2,4-hexadiene isomers obtained from photolysis of **3** have been assigned on the basis of ^{1}H NMR spectroscopy and the results of thermolysis of the two cyclobutene isomers.

Key words: cyclobutene, photolysis, Rydberg, orbital symmetry, far-UV, solution phase, UV spectra.

WILLIAM J. LEIGH, KANGCHENG ZHENG et K. BRADY CLARK. Can. J. Chem. **68**, 1988 (1990).

Opérant en solution dans les hydrocarbures et utilisant des sources lumineuses de 193 et de 214 nm, on a étudié l'ouverture photochimique du cycle des *cis*- et *trans*-3,4-diméthyl-, 1,3,4- et 1,2,3,4-tétraméthylcyclobutènes (respectivement **1**, **3** et **4**). Dans tous les cas et à toutes les longueurs d'onde, l'ouverture du cycle n'est pas stéréospécifique. Avec une excitation de 193 nm, le rapport des dienes qui se forment par des voies permises/voies interdites est maximal (environ 2) avec les triméthylcyclobutènes alors qu'il est égal à approximativement 1 pour les isomères tant *cis* que *trans* des di- et tétraméthylcyclobutènes. À part le cas du produit *cis*-**3**, la distribution des dienes est insensible à la longueur d'onde. On a déterminé les spectres UV des produits **3** et **4** tant en solution qu'en phase gazeuse; ils indiquent qu'il existe au moins trois états singulets excités accessibles dans la région de 185 à 230 nm de ces molécules. Pour les composés **3** et **4**, en phase gazeuse, l'état $\pi,R(3s)$ possède l'énergie la plus basse. Les résultats confirment que les facteurs de symétrie orbitalaire ne jouent pas un rôle (au moins important) dans le contrôle de la stéréochimie de la réaction; ils ne permettent toutefois pas déterminer avec certitude quel(s) est (sont) le(s) état(s) excité(s) de l'ouverture du cycle. La photolyse directe de ces composés conduit aussi à une fragmentation conduisant au *Z*-2-butène (à partir des composés *cis*-**3** et **4**) ou au *E*-2-butène (à partir des *trans*-**3** et **4**) en plus du propyne ou du 2-butyne. Dans tous les cas, les 2-butènes se forment avec une stéréospécificité supérieure à 90%. Les structures des quatre 3-méthyl-2,4-hexadiènes isomères qui se forment par photolyse du produit **3** ont été attribuées sur la base de leurs spectres RMN du ^{1}H et des résultats de la thermolyse des deux cyclobutènes isomères.

Mots clés : cyclobutène, photolyse, Rydberg, symétrie orbitalaire, UV lointain, solution, spectre UV.

[Traduit par la revue]

Introduction

We have recently reported the initial results of a study of the stereochemistry of the photochemical ring opening of simple alkylcyclobutenes (1). Prior to this study, there existed only one reported example that illustrated the stereochemical course of this reaction in alkylated systems (2), in spite of the fundamental role that the thermal and photochemical interconversions of cyclobutene and butadiene play in pericyclic reaction theory (3). The earlier study indicated that photochemical ring opening proceeds stereospecifically and in disrotatory fashion (2), as the theory predicts (3). The absence of conjugating substituents appears to be a general requisite for ring opening to occur except in rather special systems. Thus, while arylcyclobutenes do not undergo ring opening upon photolysis (4), benzocyclobutenes have been reported to do so non-stereospecifically (5) and Dewar aromatics open adiabatically (6). The photochemical ring opening of cyclobutene itself in solution has been reported by Adam *et al.* (7).

Photolysis of *cis*- and *trans*-3,4-dimethylcyclobutene (*cis*- and *trans*-**1**, respectively) in hydrocarbon solution with 185 nm light (at low conversions and under monochromatic conditions, where only the cyclobutene absorbs the light) leads in both cases to mixtures of all three geometric isomers of 2,4-hexadiene (eq. [1]) (1). The two isomers afford different mixtures of the 2,4-hexadienes, in both cases weighted in favour of the formally forbidden isomers that would be formed by the conrotatory ring-opening pathway. Similarly, 185 nm photolysis of bicyclo-[4.2.0]oct-6-ene yields *cis,cis*- and *cis,trans*-1,3-cyclooctadiene in a ratio of 3:1 (1). An earlier study reported similar results for this compound, but the formation of the *cis,trans* isomer was attributed to secondary diene photolysis by the long-wavelength component of the low pressure Hg lamp that was used as the light source (8). Since our initial study

[1]Part 3 of the series. For Part 2 see ref. 15.

[2]Natural Sciences and Engineering Research Council of Canada University Research Fellow, 1983–1993. Author to whom correspondence should be addressed.

[3]Permanent address: Department of Chemistry, Zhongshan University, Guangzhou, People's Republic of China.

[4]Current address: Division of Chemistry, National Research Council of Canada, 100 Sussex Drive, Ottawa, Ont., Canada K1A 0R6.

Can. J. Chem. Downloaded from www.nrcresearchpress.com by 91.121.58.235 on 09/07/12
For personal use only.

Can. J. Chem. Downloaded from www.nrcresearchpress.com by 91.121.58.235 on 09/07/12
For personal use only.

[1] 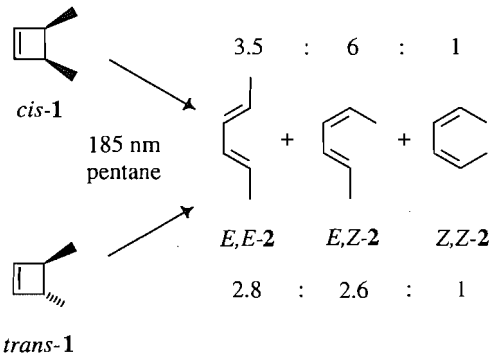

was published, an additional report that illustrates the non-stereospecificity of the process in simple systems has appeared (9).

We now wish to report the results of 193 and 214 nm photolysis of *cis*- and *trans*-1,3,4-trimethylcyclobutene (*cis*-**3** and *trans*-**3**, respectively) and *cis*- and *trans*-1,2,3,4-tetramethylcyclobutene (*cis*-**4** and *trans*-**4**, respectively) in hydrocarbon solution, and the results of 193 nm photolysis of *cis*- and *trans*-**1** under similar conditions. The present study was

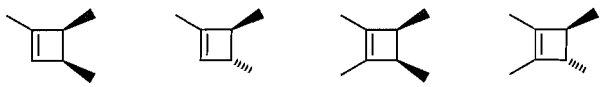

undertaken to obtain additional examples that might illustrate the generality of the process, and investigate the possibility that the non-stereospecificity of the reaction may result from participation of *two* excited states (the π,π^* and $\pi,R(3s)$ Rydberg states) in solution. Rydberg state involvement in alkene photochemistry has been postulated in order to account for the high yields of carbene-derived products that are commonly observed upon photolysis of alkenes in solution (10).[5] The yields of such products are known to increase (at the expense of π,π^*-derived products) with the extent of alkyl substitution at the double bond. There is a similar substituent effect on the relative energies of the π,π^* and $\pi,R(3s)$ states in alkenes, as determined by gas-phase UV absorption (12) and fluorescence emission spectroscopy (13), and the $\pi,R(3s)$ state is the lowest energy state in tri- and tetrasubstituted alkenes (12, 14). We have recently reported evidence for carbene involvement in cyclobutene photochemistry (15). Although we were unable to quantify the extent of carbene involvement in those cases, the results suggest that the $\pi,R(3s)$ state does contribute to the photochemistry of alkylcyclobutenes, as it does in the case of simpler alkenes. Compounds **3** and **4** were chosen for the present study to provide a series of compounds in which the relative π,π^* and $\pi,R(3s)$ state energies might vary systematically, assuming that substituent effects on the excited state manifold in alkylcyclobutenes parallel those known for simple alkenes.

Results

Cyclobutenes **3** and **4** were synthesized as mixtures of *cis* and *trans* isomers by the route shown in eq. [2] (1, 16, 17). The isomeric cyclobutenes were separated and each was purified to >99.9% purity by semi-preparative vapour-phase chromatography (vpc). The preparation of *cis*- and *trans*-**4** by a different

[2] 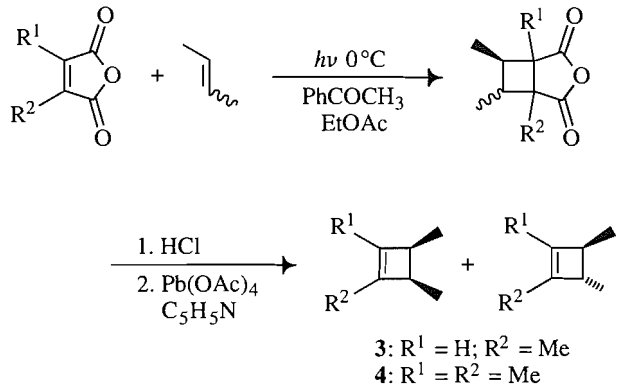

route has been reported previously (18*a*–*c*), while *cis*- and *trans*-**3** are evidently new compounds. The *cis* isomers of **3** and **4** were also prepared stereospecifically by routes analogous to that reported for *cis*-**1** by Brauman and Archie (18*g*).

The *cis* and *trans* isomers of all three cyclobutenes in the series **1**, **3**, and **4** can be differentiated on the basis of their UV absorption (*vide infra*) and ^{1}H NMR spectra. In the ^{1}H NMR spectra of the *trans* isomers, the doublet due to the C_3/C_4 methyl groups is situated at lower field than that in the spectrum of the corresponding *cis* isomer by 0.1–0.2 ppm. Furthermore, the quartet due to the C_3/C_4 protons is situated at ca. 0.6 ppm higher field in the *trans* compared to the *cis* isomers.

Ultraviolet absorption spectra of the *cis* and *trans* isomers of **1**, **3**, and **4** were recorded in deoxygenated pentane solution and are shown as plots of molar extinction coefficient (ϵ) versus wavelength in Fig. 1. Qualitative gas-phase (ca. 2 Torr; 1 Torr = 133.3 Pa) UV absorption spectra were also recorded for **3** and **4**, and are shown along with the solution phase spectra in Fig. 1.

Photolysis of deoxygenated, 0.02 M pentane solutions of **3** and **4** with the unfocussed pulses from an Ar/F_2 excimer laser (193 nm; ca. 20 mJ/pulse) produced mixtures of the isomeric 3-methyl-2,4-hexadienes (**5**; from *cis*- and *trans*-**3**) or 3,4-dimethyl-2,4-hexadienes (**6**; from *cis*- and *trans*-**4**), along with fragmentation products, as shown in eqs. [3] and [4]. The dienes were identified in each case by coinjection of photolysates taken

[3] 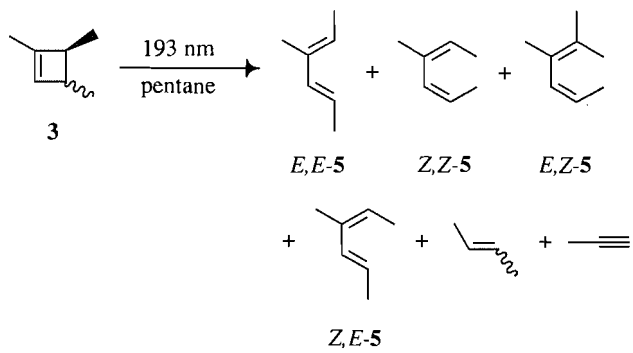

[4] 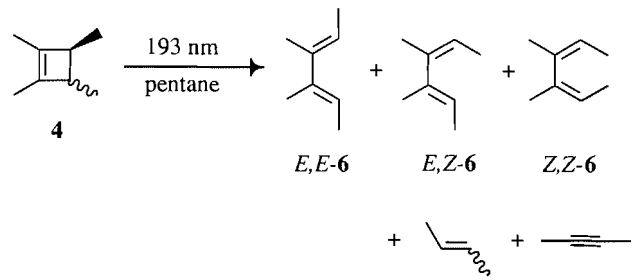

[5] For more recent reviews of alkene photochemistry, see ref. 11.

Can. J. Chem. Downloaded from www.nrcresearchpress.com by 91.121.58.235 on 09/07/12
For personal use only.

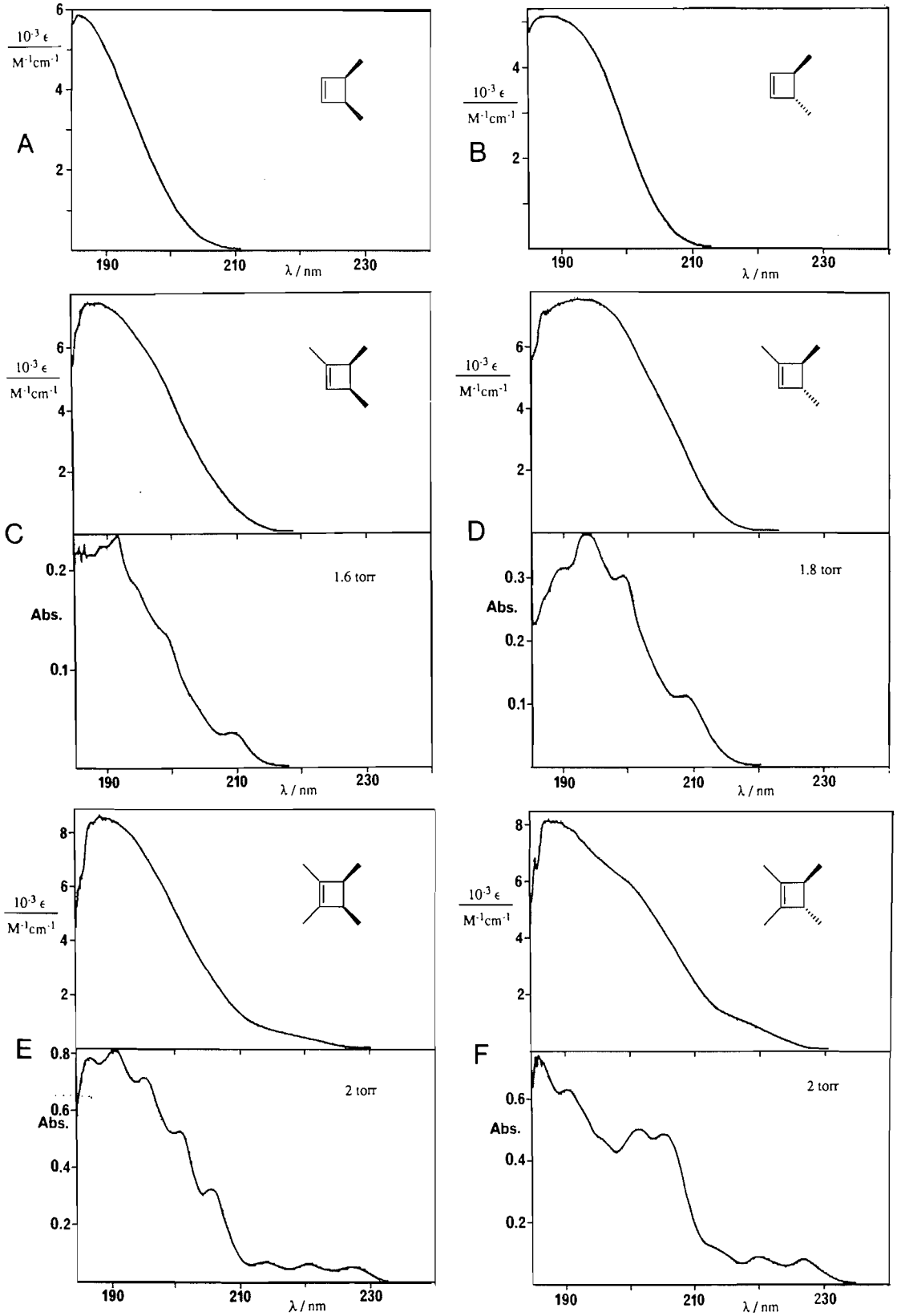

FIG. 1. Ultraviolet absorption spectra of *cis*-**1** (A), *trans*-**1** (B), *cis*-**3** (C), *trans*-**3** (D), *cis*-**4** (E), and *trans*-**4** (F) in deoxygenated pentane solution and in the gas phase (1.6–2.0 Torr; **3** and **4** only) at 22°C. Upper traces: solution-phase spectra. Lower traces: gas-phase spectra.

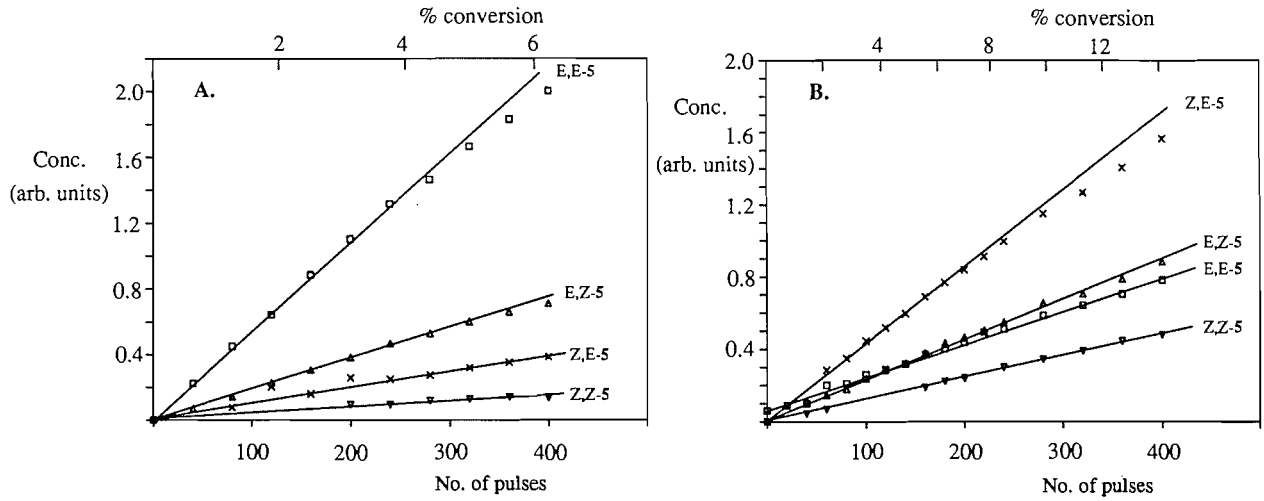

FIG. 2. Plots of product concentration (relative to internal standard) versus excitation dose for 193 nm photolysis of deoxygenated 0.02 M pentane solutions of *cis*-**3** (a) and *trans*-**3** (b).

TABLE 1. Product yields from gas phase thermolysis of *cis*- and *trans*-1,3,4-trimethylcyclobutene (*cis*- and *trans*-**3**) at 180°C[a]

Cyclobutene	*E,E*-**5**	*Z,Z*-**5**	*Z,E*-**5**	*E,Z*-**5**
cis-**3**	1.3±0.3	0.72±0.02	40.7±0.2	53.9±0.3
trans-**3**	99.0±0.1	0.06±0.01	0.08±0.01	0.51±0.02

[a]Yields determined by gas chromatography, after thermolysis of the cyclobutenes in sealed tubes at 180°C for 3 h. Yields represent the average of triplicate analyses.

to ca. 10% conversion with authentic samples of each of the pure materials. In the photolyses of *cis*-**3**, *trans*-**3**, and *cis*-**4**, the isomeric dienes accounted for 93–97% of the detectable products of similar volatility to the starting materials. Photolysis of *trans*-**4** gave four additional products that could not be identified. One of these was formed in ca. 6% yield, while the rest were formed in yields of 4% or less. In this case, the dienes **6** accounted for ca. 84% of the product mixture.

The C_3- and C_4-hydrocarbon products were identified after photolysis (214 nm) of 0.06 M isooctane solutions of **3** and **4**, by VPC spiking experiments with authentic samples. It was determined that the 2-butenes are formed with at least 90% stereospecificity in all cases (i.e., *Z*-2-butene from *cis*-**3** and **4**; *E*-2-butene from *trans*-**3** and **4**). The yields of these products were not determined.

The various isomers of **5** were identified on the basis of ^{1}H NMR spectroscopy (19) and the results of gas-phase thermolysis of *cis*- and *trans*-**3** at 180°C. The latter results are shown in Table 1. The high degree of stereospecificity associated with the thermal ring opening of monocyclic cyclobutenes is well established (3, 18). Thermolysis of *trans*-**3** affords only one of the isomers of **5** as the major product, that with vicinal vinylic (H4–H5) coupling of 15.5 Hz in its ^{1}H NMR spectrum and which can thus be identified as *E,E*-**5** (19). Thermolysis of *cis*-**3** affords two different isomers in highest yield (Table 1), one with H4–H5 coupling of 15.4 Hz and one with H4–H5 coupling of 11.7 Hz. These can be identified as *Z,E*- and *E,Z*-**5**, respectively. The remaining isomer, formed as a minor product in the thermolyses of both *cis*- and *trans*-**3**, exhibits vicinal vinylic coupling of 11.4 Hz and can thus be identified as *Z,Z*-**5**.

The relative yields of isomeric dienes from photolysis of **3** and **4** were determined from the slopes of plots of concentration versus excitation dose (number of pulses), constructed from runs monitored between 0.5 and ca. 5% conversion. Figure 2 shows examples of such plots for photolysis of *cis*- and *trans*-**3** with 193 nm light. The yields of the fragmentation products were not determined. They were shown to be *E*- or *Z*-2-butene and propyne (from **3**) or 2-butyne (from **4**) by GC/MS analysis (see experimental section).

Photolyses of 0.02 M isooctane solution of *cis*- and *trans*-**1** were carried out under similar conditions with the 193 nm laser, and afforded *E,E*-, *E,Z*-, and *Z,Z*-**2** in the relative yields shown in eq. [5].

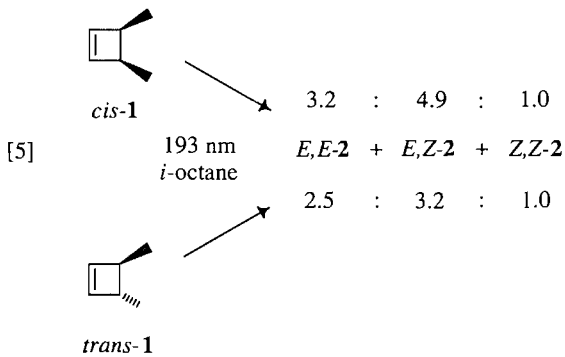

[5]

Compounds **3** and **4** were also photolysed as deoxygenated 0.1 M (**3**) or 0.06 M (**4**) pentane solutions with a Zn resonance lamp (214 nm), and relative isomeric diene yields were determined in similar fashion to the 193 nm runs. Examples of such plots for the 214 nm photolyses of *cis*- and *trans*-**3** are shown in Fig. 3. In these experiments, the accuracy of the VPC integrations for *E,Z*- and *Z,Z*-**5** at low conversions are considerably lower than those for the other two diene isomers, because they elute on the tail of the solvent and (or) cyclobutene. Thus, the yields of these two isomers of **5** in the 214 nm photolyses have been calculated from the slopes of the concentration vs. time plots in the 2.5–4% conversion range. The yields of minor, unidentified products were similar in each case to those obtained from 193 nm photolysis (*vide supra*). Tables 2 and 3 list the relative diene yields from photolysis of **3** and **4**,

Can. J. Chem. Downloaded from www.nrcresearchpress.com by 91.121.58.235 on 09/07/12
For personal use only.

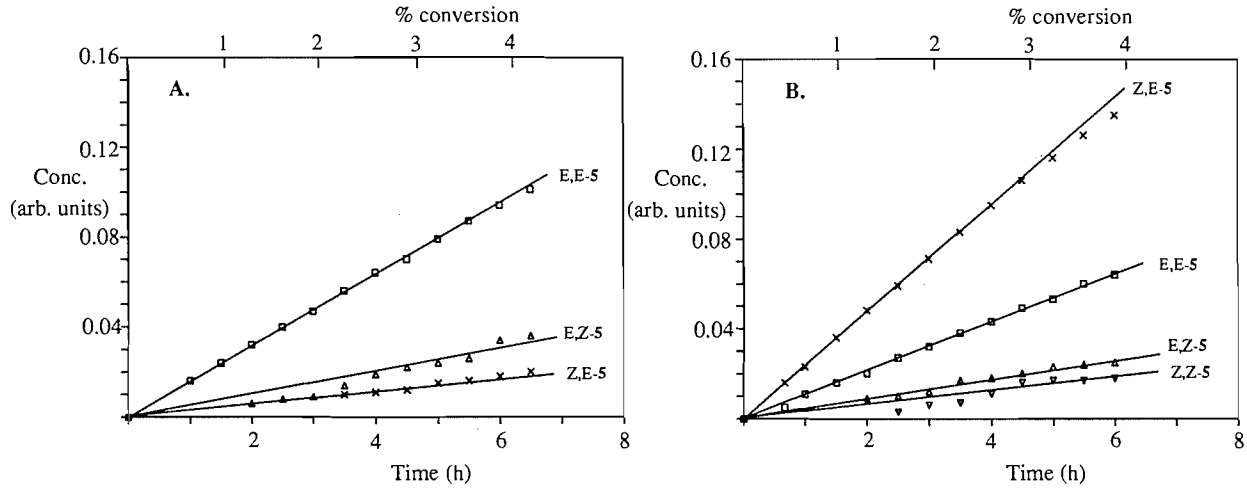

FIG. 3. Plots of product concentration (relative to internal standard) versus irradiation time for 214 nm photolysis of deoxygenated 0.10 M pentane solutions of *cis*-**3** (a) and *trans*-**3** (b). The relative slopes of the lines in these two plots are proportional to the relative quantum yields for formation of each diene.

TABLE 2. Relative isomeric diene yields from photolysis of *cis*- and *trans*-**3** in deoxygenated pentane solution at 193[a] and 214[b] nm at 23°C[c]

Cyclobutene	λ (nm)	*E,E*-**5**	*Z,Z*-**5**	*Z,E*-**5**	*E,Z*-**5**
cis-**3**	193	63	4.0	11.5	22
	214	65	2.1	11.7	21
trans-**3**	193	20	12.3	44	23
	214	26	7.2	57	10.3

[a]Ar/F_2 excimer laser; 0.02 M solutions.
[b]Zn resonance lamp; 0.10 M solutions.
[c]Product yields determined from the slopes of concentration vs. time plots from runs monitored between 0.2 and 4.0% conversion, and normalized to a total of 100%. The yields are not corrected for differences in light intensity between the excitation sources. Errors are ca. 5%. The yields of propyne and 2-butene were not determined.

TABLE 3. Relative isomeric diene yields from photolysis of *cis*- and *trans*-**4** in deoxygenated pentane solution at 193[a] and 214[b] nm at 23°C[c]

Cyclobutene	λ (nm)	*E,E*-**6**	*Z,Z*-**6**	*E,Z*-**6**
cis-**4**	193	55	0.4	44
	214	41	0.3	58
trans-**4**	193	38	11	51
	214	34	16	50

[a]Ar/F_2 excimer laser; 0.02 M solutions.
[b]Zn resonance lamp; 0.06 M solutions.
[c]Product yields determined from the slopes of concentration vs. dose plots from runs monitored between 0.2 and 5.0% conversion, and normalized to a total of 100%. The yields are not corrected for differences in light intensity between the excitation sources. Errors are ca. 5%. The yields of 2-butyne and 2-butene were not determined.

respectively, with the 193 nm and 214 nm light sources. The yields listed in Tables 2 and 3 were calculated from the slopes of the concentration vs. time plots, and normalized to a total of 100%.

The 214 nm photolyses of *cis*- and *trans*-**3** were carried out under nearly identical conditions, so the differences in the slopes of the concentration vs. time plots (Fig. 3) are representative of differences in the quantum yields for diene formation in these cases.

Control experiments were carried out to ensure that the relative product yields reported in Tables 2 and 3 correspond to primary photolysis yields, and suffer no distortion due to secondary photolysis of the dienes (1, 20). To this end, we have photolysed solutions of **3** and **4** containing small amounts of an additional photolabile diene as a control compound, and examined the photolysate after ca. 4% conversion for isomerization of the diene. In this work, 3-ethylidenecyclohexene (**7**) was chosen as the control diene because its VPC retention time under our conditions is much different than those of the various isomers of **3**–**6**. In a typical experiment, a deoxygenated

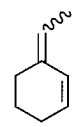

7

pentane solution containing *cis*-**3** (0.10 M) and a mixture of *E*- and *Z*-**7** (enriched in one of the isomers; 0.002 M) was irradiated with the 214 nm light source. Analysis of the photolysate up to ca. 4% conversion of *cis*-**3** showed there to be a change of less than 5% in the relative amounts of *E*- and *Z*-**7** present. The photostationary state for photolysis of **7** alone under similar conditions is $E\text{-}7/Z\text{-}7 \approx 1.0$. Analogous results were obtained from similar experiments carried out for the 214 nm irradiations of *trans*-**3** and *cis*-**4**, and for the 193 nm irradiation of *cis*-**3**.

Toluene-sensitized photolysis of *cis*-**4** was carried out to determine whether the triplet state of the cyclobutene contributes to ring opening. After ca. 15% conversion of *cis*-**4**, VPC analysis of the photolysate showed the presence of one new (unidentified) product that is not formed in the direct photolysis of *cis*-**4**; none of the isomers of **6** could be detected in the photolysate within the sensitivity limits of our VPC method.

Discussion

UV absorption spectroscopy

The solution-phase UV absorption spectra of **1**, **3**, and **4**

Can. J. Chem. Downloaded from www.nrcresearchpress.com by 91.121.58.235 on 09/07/12
For personal use only.

Can. J. Chem. Downloaded from www.nrcresearchpress.com by 91.121.58.235 on 09/07/12
For personal use only.

exhibit minor differences throughout the series, the main general feature being that in all three sets of compounds, the prominent bands in the spectra of the *trans* isomers are broader and more diffuse than those of the *cis* isomers. The source of this relative broadening in the spectra of the *trans* isomers can be better understood, at least qualitatively, from consideration of the gas-phase spectra of **3** and **4**. The gas-phase spectra show regular variations with the stereochemistry at the 3,4 positions, which are washed out in the solution-phase spectra due to broadening of the individual vibronic transitions.

The gas-phase spectra of *cis*- and *trans*-**3** (Fig. 1c,d) consist of at least two absorption bands in the 185–220 nm region. The spectrum of *cis*-**3** is similar to that of 1-methylcyclobutene (**8**) (21). The relatively weak, long-wavelength band (λ_{max} = 209 nm) observed in both spectra can be assigned to $\pi,R(3s)$ absorption (12, 14), by analogy with Robin's assignment of a similarly placed band in the spectrum of **8** (14). This band is reduced in intensity in the solution-phase spectra of *cis*- and *trans*-**3**, consistent with the Rydberg assignment. On the basis of the spectra of *cis*- and *trans*-**4** (*vide infra*), we assign the absorption in the 185–205 nm region as due to overlapping transitions to two electronic states, one centred below 185 nm and the other at 193–200 nm. In the solution-phase spectra, all vibrational fine structure is lost, and the intensity of the longer wavelength (193–200 nm) component seems to be reduced compared to the gas-phase spectra. The reduction in absorption intensity in the condensed phase is consistent with a Rydberg assignment for this band, perhaps $\pi,R(3p)$ (12, 14). The shorter wavelength band should be assigned to π,π^* absorption, by analogy with the spectra of simple alkenes (12, 14). The relative extinction coefficients of the $\pi,R(3s)$ and $\pi,R(3p)$ absorptions are approximately equal in the spectra of *cis*- and *trans*-**3**, while the extinction coefficient of the highest energy transition (relative to those of the lower energy bands) is much higher in *cis*-**3** than it is in the *trans* isomer.

The gas-phase spectra of *cis*- and *trans*-**4** show similar trends to those of the corresponding isomers of **3**, except the various absorptions are better separated and much richer in vibrational fine structure. The three weak bands centred at 214, 221, and 228 nm can be assigned to the $\pi,R(3s)$ progression. The appearance of these three bands, with a separation of ca. 1400 cm^{-1}, is a general feature in the gas-phase spectra of tetraalkyl ethylenes (14). The spectrum of *trans*-**4** clearly demonstrates two additional absorptions at shorter wavelengths. The two bands centred at 203 nm (separation $\approx$ 1000 cm^{-1}), occurring on the rising edge of the higher energy absorption band(s) at wavelengths less than 195 nm, can be assigned to $\pi,R(3p)$ absorption based on their considerably reduced intensity in the solution-phase spectra. In the spectrum of *cis*-**4**, we identify the $\pi,R(3p)$ absorptions as the two vibronic bands at 201 nm and 206 nm; i.e., at the same positions as the two more prominent bands in the spectrum of the *trans* isomer. The shift of both Rydberg bands to longer wavelengths with increasing alkyl substitution at the C=C bond follows the trends observed in simpler alkenes (14). As is the case for **3**, the relative intensities of these two absorptions are similar in the two isomers of **4**, and the high energy absorption (<195 nm) is relatively much stronger in *cis*-**4** than in the *trans* isomer. The high energy (<195 nm) band can be assigned to π,π^* absorption, and is again comparatively more intense in *cis*-**4** than in the *trans* isomer.

It is interesting to note that the two long-wavelength Rydberg progressions in the spectra of *cis*- and (in particular) *trans*-**4** appear to be retained in the solution-phase spectra, although they are shifted somewhat to shorter wavelengths, reduced in intensity relative to the short-wavelength absorptions, and devoid of fine structure. These characteristics are precisely those of Rydberg absorptions, though evidently much less dramatic than should be expected for "pure" Rydberg transitions (12, 14). The fact that these bands are observable in the solution-phase spectra may indicate that the Rydberg transitions are substantially mixed with valence transitions (22). Thus, the valence components are responsible for the sizeable oscillator strengths of these bands in the solution spectra. These components may involve the σ-manifold; Robin has noted that the σ,π^* transition is of fairly low energy in small-ring cycloalkenes (12).

While we are thus unable to completely assign the solution-phase spectra of **3** and **4** with certainty, it is clear that at least *three* singlet excited states are accessible in these compounds upon direct absorption of light in the 185–220 nm region. Based on previous work (12, 14), two of these are presumably assignable to the π,π^* and σ,π^* states, with the latter being the lowest energy (vertical) state in *cis*- and *trans*-**4**.

*Solution-phase photochemistry of **1**, **3**, and **4***

Photolysis of **3** and **4** results in non-stereospecific ring opening, in competition with stereospecific, formal $\sigma_{2s} + \sigma_{2s}$ cycloreversion. The relative contribution of the latter process to overall product yield has not been quantified in the present study. As a general observation, *cis* and *trans* isomers afford different mixtures of isomeric dienes in each case, so the product distributions are not governed by the relative thermodynamic stabilities of the various diene isomers. In the case of **6**, the distribution of the three isomers at 90°C (in HMPA) has recently been reported to be $(E,E):(E,Z):(Z,Z) \approx (1.0):(0.23):(0.21)$ (23), clearly a much different distribution than those obtained from photolysis of **4**, even allowing for the differences in temperature and solvent.

A potential problem of particular significance in studies of this type is the lability of **5** and **6** towards direct photoisomerization (20). Thus, it is particularly important to rule out secondary diene photolysis as a contributor to the apparent non-stereospecificity with which **3** and **4** undergo photochemical ring opening (1). Such problems can be minimized by working with solutions of high optical density at the excitation wavelength, and monitoring the progress of the photolyses at very low conversions, as has been done in the present study. A particularly valuable control experiment to examine secondary diene photolysis involves including a small amount of an additional photolabile diene (such as **7**) in the photolysis mixtures, and monitoring its direct photoisomerization along with the formation of products from cyclobutene photolysis. Control experiments of this type have been carried out for the 193 and 214 nm photolyses of *cis*- and *trans*-**3** and the 214 nm photolysis of *trans*-**4**, and demonstrate that secondary diene photolysis does not contribute significantly to the observed diene distributions from **3** and **4** in any case.

We have previously considered three possible reasons for the non-stereospecificity of the photochemical ring opening of cyclobutenes (1): (i) adiabatic (disrotatory) π,π^*-state ring opening to yield diene(s) in the first excited singlet state; (ii) competitive ring opening from two or more excited states (e.g., π,π^* and $\pi,R(3s)$); and (iii) competitive ring opening from both excited and vibrationally excited ground state surfaces, the latter formed via internal conversion from the excited state. Of

TABLE 4. Substituent and wavelength dependence on the "allowed/forbidden" ratios from far-UV photolysis of alkylcyclobutenes in hydrocarbon solution at 23°C[a]

λ (nm)	*cis*-**1**	*trans*-**1**	*cis*-**3**	*trans*-**3**	*cis*-**4**	*trans*-**4**
193	0.9	0.9	2.0	2.1	1.2	1.1
214	—	—	2.1	2.1	0.6	1.0

[a]Ratio of the yields of formally allowed to formally forbidden diene isomers; e.g., (*E,E*-**5** + *Z,Z*-**5**)/(*E,Z*-**5** + *Z,E*-**5**) or the inverse. Errors are ca. ±10%.

course, a fourth possibility is that excited-state ring opening (from any state) is simply not controlled by orbital symmetry factors. Previously, we ruled out the first possibility (in general) on the basis of the diene distributions from photolysis of *cis*- and *trans*-**1** with 185 nm light; the fact that *both* cyclobutene isomers give diene mixtures weighted in favour of the formally forbidden isomers is incompatible with such a mechanism as the exclusive one for their formation (1). Table 4 summarizes the relative yields of isomeric dienes from **1**, **3**, and **4** as the ratios of formally allowed to formally forbidden diene isomers formed from each compound at the different excitation wavelengths, from which it can be seen that the 193 nm photolyses of *cis*- and *trans*-**3** and **4** all afford diene mixtures weighted in favour of the formally allowed isomers. Thus, the behaviour of these derivatives *is* consistent with partial ring opening by the adiabatic pathway. Of the compounds that we have studied to date, only **1** yields diene mixtures that are incompatible with this mechanism.

The second possibility, and the one that we set about to study in the present work, is that ring opening ensues from *two* (or more) excited states in solution. In favourable circumstances, one would expect that competitive ring opening from two or more excited states should be revealed in the form of a regular trend in the isomeric diene distributions as the separation between the excited states involved is varied through substitution (24). It is well known that the (π,π^*)–$(\pi,R(3s))$ state separation in alkenes can be altered through alkyl substitution at the double bond (10, 14) and, from the spectroscopic results presented earlier for **3** and **4**, it is clear that the same is true in alkylcyclobutenes. Thus, if both these states are involved in ring opening, one should expect an increase in the Rydberg component in *cis*- and *trans*-**4** compared to **3**. With 193 nm excitation, *cis*- and *trans*-**3** both give diene mixtures weighted in favour of the isomers corresponding to formal ring opening by the allowed disrotatory pathway, while from *cis*- and *trans*-**4**, only a slight preference for the allowed products is observed. The product ratios from *cis*- and *trans*-**1** are weighted in favour of the forbidden isomers. Thus, the present results show no evidence for a regular variation in diene distribution (formally allowed vs. formally forbidden) that might be linked to the variation in the (π,π^*)–$(\pi,R(3s))$ state separation that accompanies increasing alkyl substitution at the C=C bond, at least when the results are analysed in this way. It should be recognized, though, that the trend in diene distribution with substituent that is expected according to this mechanism will only be (easily) discernible if reaction from the Rydberg state is either completely stereospecific or completely random. This, of course, may not be the case.

The diene distributions obtained from photolysis of all these compounds except *cis*-**3** are altered slightly by variation of the excitation wavelength. Again, however, no consistent trend is evident in the data. When the diene distributions are analysed according to orbital symmetry selection rules, it can be seen that only *cis*-**4** shows a change in the ratio of formally allowed to formally forbidden dienes. The fact that wavelength dependence is observed in the diene distributions from photolysis of these compounds is consistent with ring opening ensuing from either two (or more) competing excited states or from both the excited state and vibrationally activated ground state surfaces. The absence of diene products in the toluene-sensitized photolysis of *cis*-**4** verifies (16*f*) that the triplet state is not involved in ring opening. If more than one singlet excited state is involved in the reaction, then the absence of a trend in the formally allowed/forbidden diene distributions with substituent (at a single wavelength) indicates at least that orbital symmetry factors do not play a *consistent* role in the photochemical ring opening of simple cyclobutenes. In this regard, it is interesting to note that the nonsymmetric cyclobutene derivatives *cis*- and *trans*-**3** both afford higher yields of the formally allowed diene isomers than do **1** and **4**, which possess a high degree of *molecular* symmetry.

The present study underlines the fact that the non-stereospecificity observed previously for the photochemical ring opening of simple cyclobutenes is quite general. However, it does not allow firm conclusions to be made regarding the reasons for this behaviour. The observation of slight wavelength dependence in the distribution of isomeric dienes from the reaction suggests that two or more excited states may contribute to ring opening in simple systems, but other possibilities could also be consistent with this result. Further mechanistic studies of this reaction, a central issue in photochemical pericyclic reaction theory, are in progress.

Experimental

^{1}H NMR spectra were recorded on Varian EM390 (90 MHz) or Bruker AM500 (500 MHz) spectrometers in carbon tetrachloride (or deuteriochloroform where noted) and ^{13}C NMR spectra were recorded at 125.6 MHz on the Bruker AM500; all are reported in parts per million downfield from tetramethylsilane. Infrared spectra were recorded on a Perkin–Elmer 283 spectrometer in carbon tetrachloride solution or as the neat liquids (where noted); spectra are reported in wavenumbers, calibrated using the 1601.9 cm^{-1} polystyrene absorption. Mass spectra were recorded on a VG7070 mass spectrometer interfaced with a Varian 3700 gas chromatograph, equipped with a 30 m × 0.25 mm DB-1 fused silica capillary column (Chromatographic Specialties, Inc.). Exact masses were determined on a VGH ZABE mass spectrometer, and employed a mass of 12.000000 for carbon.

Ultraviolet absorption spectra were recorded using a Perkin–Elmer Lambda 9 spectrometer equipped with a model 3600 data station. The spectrometer sample compartment was continuously flushed with nitrogen. Spectra were recorded in 1-cm Suprasil UV cells (Hellma) that were fitted with a stopcock for gas phase spectra. For solution-phase spectra, the sample and reference solutions were deoxygenated with argon prior to recording the spectrum. Gas-phase spectra were recorded in single beam mode, after recording the spectrum of the empty, evacuated (to 30 mTorr) cell for background correction. Samples of the cyclobutene were introduced into the cell from a cold finger attached to a high vacuum line, and the system pressure was measured with a Varian 801 vacuum gauge.

Analytical VPC separations were carried out using a Hewlett–Packard 5890 gas chromatograph (injector temperature = 120°C) equipped with a flame ionization detector, a Hewlett–Packard HP-3396 recording integrator, and a 1.0-μm SPB-1 wide-bore capillary column (30 m × 0.75 mm i.d. borosilicate; Supelco, Inc.). The detector response was not calibrated.

Semi-preparative VPC separations employed a Hewlett–Packard 5750B gas chromatograph equipped with a thermal conductivity detector (detector temperature = 120°C) and one of the following

Can. J. Chem. Downloaded from www.nrcresearchpress.com by 91.121.58.235 on 09/07/12
For personal use only.

Can. J. Chem. Downloaded from www.nrcresearchpress.com by 91.121.58.235 on 09/07/12
For personal use only.

stainless steel columns: (a) 3.8% UC W982 on 80/100 Supelcoport (24 ft × 1/4 in.); or (b) 20% oxybis(dipropionitrile) (ODPN) on Chromosorb 80/100 PNAW (20 ft × 1/4 in.).

n-Pentane and 2,2,4-trimethylpentane (isooctane) were Baker Photrex grade and used as received from the supplier, as were toluene (Fisher Reagent) and citraconic anhydride, maleic anhydride, 2-aminopyridine, propionic anhydride, acetophenone, lead tetraacetate, triphenylphosphine, 4-vinylcyclohexene, and potassium *tert*-butoxide, all from Aldrich Chemical Co. 2-Butene (mixture of isomers) was used as received from Canada Liquid Air, Inc. for synthetic purposes. *Cis*- and *trans*-2-butene and propyne were used for VPC analyses as received from Canada Liquid Air, Inc. 2-Butyne for VPC spiking experiments was part of a calibrated mixture of C_2–C_4 alkynes (Scott, Inc.). Cyclobutenes *cis*- and *trans*-**1** were synthesized as part of our earlier study (1). *E* and *Z*-ethylidenecyclohexene (**7**) were synthesized as a mixture according to the published procedure (25). The mixture was enriched in one of the isomers by semi-preparative VPC (column (a)), and exhibited a ^{1}H NMR spectrum that agreed satisfactorily with that previously reported (25).

Synthetic photolyses employed a Hanovia 450-W medium pressure mercury lamp with quartz or Pyrex immersion wells (Ace Glass, Inc.), or a Rayonet photochemical reactor fitted with 12 253.7-nm lamps and a merry-go-round apparatus.

Preparation of compounds

Cis- and *trans*-1,3,4-trimethylcyclobutene (*cis*- and *trans*-**3**) and *cis* and *trans*-1,2,3,4-tetramethylcyclobutene (*cis*- and *trans*-**4**) were prepared by routes similar to those published previously for related methylated cyclobutenes (1, 15), starting with the acetophenone-sensitized photocycloadditions of citraconic anhydride or dimethylmaleic anhydride (prepared by the method of Baumann and Bossard (26)) with 2-butene (17), followed by hydrolysis of the bicyclic anhydrides and bisdecarboxylation of the resulting dicarboxylic acids with lead tetraacetate (27). In both syntheses, the two cyclobutene isomers were obtained in similar yields. They were separated and repeatedly purified by semi-preparative VPC using a combination of columns (a) and (b). Analytical VPC analysis showed them to be of >99.90% purity in every case. They had the following spectral characteristics:

trans-*1,3,4-Trimethylcyclobutene* (trans-*7*): IR (neat): 3030 (m), 2949 (s), 2920 (m), 2880 (m), 2860 (m), 1638 (w), 1449 (m), 1368 (m), 1347 (w), 1299 (m), 1268 (w), 1025 (w), 1000 (w), 970 (w), 811 (m), 778 (w), 572 (w); ^{1}H NMR, δ: 1.05 (d, 6H), 1.62 (br s, 3H), 2.05 (br q, 2H), 5.66 (br s, 1H); MS (*m/e* (I)): 96 (40), 81 (100), 79 (45), 77 (18), 67 (30), 65 (20), 63 (17), 53 (54), 41 (72). Exact Mass calcd. for C_7H_{12}: 96.0960; found: 96.0922.

cis-*1,3,4-Trimethylcyclobutene* (cis-*3*): IR (neat): 3038 (s), 2956 (s), 2933 (s), 2886 (s), 2716 (w), 1641 (s), 1616 (w), 1466 (m), 1442 (s), 1376 (s), 1329 (m), 1316 (m), 1273 (m), 1193 (w), 1091 (m), 1039 (m), 806 (s), 631 (w), 601 (m); ^{1}H NMR, δ: 0.90 (d, 6H), 1.55 (br s, 3H), 2.66 (m, 2H), 5.64 (br s, 1H); MS (*m/e* (I)): 96 (27), 95 (4), 81 (100), 79 (18), 77 (7), 67 (16), 56 (10), 57 (18), 53 (26), 41 (38), 39 (23).

trans-*1,2,3,4-Tetramethylcyclobutene* (trans-*4*): IR (neat): 2952 (s), 2924 (s), 2912 (s), 2874 (s), 1692 (w), 1447 (s), 1367 (m), 1337 (w), 1299 (m), 1279 (w), 1202 (w), 1124 (m), 1068 (w), 1021 (w), 995 (w), 962 (w); ^{1}H NMR, δ: 0.99 (d, 6H), 1.53 (s, 6H), 1.93 (q, 2H); MS (*m/e* (I)): 110 (52), 95 (100), 81 (15), 77 (10), 67 (50), 55 (45), 53 (21), 51 (8), 41 (34). Exact Mass calcd. for C_8H_{14}: 110.1120; found: 110.1102.

cis-*1,2,3,4-Tetramethylcyclobutene* (cis-*4*): IR (neat): 2953 (s), 2929 (s), 2906 (s), 2866 (s), 1688 (w), 1461 (m), 1435 (s), 1374 (s), 1326 (w), 1316 (m), 1289 (m), 1211 (w), 1133 (m), 1096 (m), 1024 (m), 996 (m), 976 (w), 658 (m), 628 (m); ^{1}H NMR, δ: 0.90 (d, 6H), 1.48 (s, 6H), 2.58 (br q, 2H); MS (*m/e* (I)): 110 (37), 109 (3), 95 (100), 91 (5), 81 (14), 79 (9), 77 (7), 67 (48), 56 (14), 55 (37), 53 (18), 51 (7), 41 (29), 39 (20).

3-Methyl-2,4-hexadienes (Z,Z-, Z,E-, E,Z-, *and* E,E-*5*) (19)

Authentic samples of *Z,E*-**5** and *E,E*-**5** as a mixture of isomers were prepared by iodine-catalysed dehydration of *E*-4-hexen-3-ol, which was synthesized by 1,2-addition of ethyllithium to *E*-3-penten-2-one (28). A mixture of lithium (1.5 g, 0.21 g-atom) and bromoethane (13 g, 0.12 mol) was refluxed in anhydrous ether (30 mL) for 0.5 h. A solution of *E*-3-penten-2-one (2.5 g, 0.03 mol; prepared by the method of House *et al.* (28)) in anhydrous ether (10 mL) was then added dropwise over 0.5 h, with vigorous stirring and cooling to 1–5°C. Stirring was continued for a further 4 h at 5°C. Ice water (20 mL) was added, and the resulting mixture was acidified with 5% hydrochloric acid (10 mL) and then stirred for 0.5 h at room temperature. The ether layer was separated, and the aqueous fraction remaining was extracted with ether (2 × 10 mL). The combined ether fractions were washed with saturated bicarbonate, dried over anhydrous sodium sulfate, and filtered. The solvent was removed on the rotary evaporator to yield a slightly yellow oil (2.3 g, 75%); the major component of this product was identified as *E*-4-hexen-3-ol on the basis of its ^{1}H NMR spectrum (δ(CCl_4): 0.84 (t, 3H), 1.17 (s, 3H), 1.43 (q, 2H), 1.67 (d, 3H), 2.63 (br, 1H), 5.46 (s, 1H), 5.49 (q, 1H).

The crude alkenol from above was combined with propionic anhydride (10 mL) and a crystal of iodine in a 25-mL round-bottom flask fitted with a reflux condenser and magnetic stirrer (29). After the initial frothing had subsided, the mixture was stirred at 130°C for 1 h. After cooling to room temperature, the mixture was poured into ether (30 mL) and the solution was washed with saturated aqueous bicarbonate (3 × 40 mL) and water (2 × 20 mL), and then dried over anhydrous sodium sulfate. The bulk of the solvent was removed by careful distillation, and the resulting liquid was then bulb-to-bulb distilled with gentle heating under vacuum. VPC analysis of the distillate (1.2 g) showed it to consist predominantly of ether, *Z,E*-**5** (*vide infra*), and *E,E*-**5** in a ratio of ca. 3:2:4. Pure samples of the two isomeric dienes were isolated by semi-preparative VPC (column (b)) and had the following spectral characteristics:

Z,E-*3-Methyl-2,4-hexadiene* (Z,E-*5*): IR: 3040 (m), 3000 (m), 2968 (s), 2920 (s), 2882 (m), 2860 (m), 1652 (w), 1540 (w), 1449 (s), 1380 (m), 1110 (w), 1070 (w), 1035 (w), 960 (s), 922 (m), 828 (w), 770 (w); ^{1}H NMR, δ: 1.69 (d, *J* = 7.0 Hz, 3H), 1.74 (br s, 3H), 1.80 (d, *J* = 6.6 Hz, 3H), 5.22 (q, *J* = 7.0 Hz, 1H), 5.59 (dq, *J* = 15.4, 6.6 Hz, 1H), 6.36 (d, *J* = 15.4 Hz, 1H); MS (*m/e* (I)): 96 (25), 81 (62), 79 (15), 77 (6), 67 (12), 55 (12), 53 (17), 44 (73), 41 (20), 39 (17).

E,E-*3-Methyl-2,4-hexadiene* (E,E-*5*): IR: 3036 (s), 2998 (m), 2958 (s), 2918 (s), 2878 (m), 2858 (s), 1629 (m), 1518 (w), 1446 (s), 1379 (m), 1108 (w), 1078 (w), 1059 (w), 1022 (m), 960 (s), 920 (m), 834 (w), 788 (w), 720 (w); ^{1}H NMR, δ: 1.67 (s, 3H), 1.69 (d, *J* = 7.0 Hz, 3H), 1.74 (d, *J* = 6.6 Hz, 3H), 5.32 (q, *J* = 7.0 Hz, 1H), 5.45 (dq, *J* = 15.5, 6.7 Hz, 1H), 5.95 (d, *J* = 15.5 Hz, 1H); MS (*m/e* (I)): 96 (15), 81 (28), 79 (6), 67 (5), 55 (6), 53 (8), 44 (75), 41 (8), 40 (10), 39 (6).

The former isomer is one of two major products in the thermolysis of *cis*-**3**, while the latter is formed as the major product in the thermolysis of *trans*-**3** (*vide infra*). The ^{1}H NMR spectrum of *E,E*-**5** matches that reported previously and assigned to this isomer (19*b*).

A portion of the mixture of *Z,E*- and *E,E*-**5** (0.3 g) and acetophenone (0.05 g) was dissolved in pentane, placed in a quartz tube, and deoxygenated by bubbling dry nitrogen through the solution for 15 min. The solution was then irradiated in a Rayonet reactor (300 nm) for 6 h, producing a mixture of all four isomers of **5** in relative amounts (*Z,Z*):(*E,Z*):(*Z,E*):(*E,E*) ≈ 2:1:3.5:4 (by VPC analysis). The solvent was removed by careful distillation, and the isomeric dienes were separated from acetophenone and a small amount of polymeric material by bulb-to-bulb distillation under vacuum. The four dienes were isolated by semi-preparative VPC (column (b)), eluting in the order (*Z,Z*) < (*E,Z*) < (*Z,E*) < (*E,E*) (they elute in the same order from the SPB-1 column). The second isomer is one of two major products from thermolysis of *cis*-**3** (*vide infra*). The first two dienes that eluted exhibit the following spectral characteristics:

Z,Z-*3-Methyl-2,4-hexadiene* (Z,Z-*5*): IR: 3020 (s), 2968 (s), 2936 (s), 2920 (s), 2876 (m), 2860 (s), 1645 (w), 1540 (w), 1450 (s), 1375 (m), 1035 (m), 910 (m), 800 (w), 715 (w); ^{1}H NMR, δ: 1.51

Can. J. Chem. Downloaded from www.nrcresearchpress.com by 91.121.58.235 on 09/07/12
For personal use only.

(d, J = 6.8 Hz, 3H), 1.59 (dd, J = 6.9, 1.6 Hz, 3H), 1.75 (s, 3H), 5.27 (q, J = 6.7 Hz, 1H), 5.46 (dq, J = 11.5, 6.9 Hz, 1H), 5.76 (d, J = 11.5 Hz, 1H); MS (*m/e* (I)): 96 (12), 81 (25), 79 (7), 67 (5), 55 (5), 53 (6), 44 (83), 41 (8), 40 (9), 39 (8).

E,Z-*3-Methyl-2,4-hexadiene* (E,Z-**5**): IR: 3010 (s), 2962 (s), 2926 (s), 2858 (m), 1643 (w), 1536 (w), 1444 (s), 1412 (w), 1378 (m), 1366 (w), 1000 (w), 958 (m), 908 (w), 893 (w), 798 (w), 708 (w); ^{1}H NMR, δ: 1.67 (d, J = 6.6 Hz, 3H), 1.74 (s, 3H), 1.76 (dd, J = 7.3, 1.4 Hz, 3H), 5.28 (dq, J = 11.7, 7.2 Hz, 1H), 5.33 (q, J = 6.6 Hz, 1H), 5.72 (d, J = 11.7 Hz, 1H); MS (*m/e* (I)): 96 (5), 81 (10), 79 (3), 67 (3), 55 (3), 53 (3), 44 (90), 41 (3), 40 (10), 39 (3).

3,4-Dimethyl-2,4-hexadienes (E,E-, E,Z-, *and* Z,Z-*6*)

Authentic samples of *E,E*- and *E,Z*-**6** were prepared by dehydration of 3,4-dimethyl-3,4-hexanediol with iodine and propionic anhydride (29), and isolated from the reaction mixture by semi-preparative VPC (column (a)). The *Z,Z* isomer was prepared from *E,E*-**6** by direct photoisomerization (20). A deoxygenated solution of *E,E*-**6** (0.030 g) in pentane (30 mL) in a quartz tube was irradiated in the Rayonet reactor (254 nm) for 12 h, affording a mixture of *Z,Z*-, *E,Z*-, and *E,E*-**6** in a ratio of 2.5:6:1 (by VPC). The solvent was removed on the rotary evaporator, the residue was bulb-to-bulb distilled under vacuum, and the dienes were isolated by semi-preparative VPC (column (b)). They were identified on the basis of comparisons of their ^{1}H NMR spectra to those previously published (29). The three isomers elute from the SPB-1 column in the order (*Z,Z*) < (*E,Z*) < (*E,E*).

Thermolysis of cis- *and* trans-*3*

Samples of *cis*- and *trans*-**3** (ca. 5 mg) were placed in 7-mm Pyrex tubes, attached to a vacuum line, cooled with liquid nitrogen, evacuated, and finally sealed. They were then pyrolysed in an oil bath at 180°C for 3 h. The tubes were opened and analysed by VPC, which indicated thermal ring opening to be complete and afforded the relative yields of the isomeric 3-methyl-2,4-hexadienes (**5**) listed in Table 1. The values listed are the average of three runs for each compound, each analysed in triplicate.

Photolysis of 1, 3, and 4

Quantitative cyclobutene photolyses employed the pulses (193 nm, ca. 10 ns, 20–30 mJ, 1 Hz repetition rate) from a Lumonics TE-861M excimer laser filled with an argon/fluorine/helium mixture, or a 16-W Philips 93106E zinc resonance lamp (214 nm). The Zn resonance lamp was surrounded by a metal case, which incorporates a 1-in. port to contain the sample cell. The lamp was given a 20 min warm-up period before each experiment and cooled with a stream of dry nitrogen.

The photolyses were carried out at ambient temperature (ca. 23°C) in 10 × 25 mm cylindrical Suprasil UV cells (Hellma). Solutions of **3** or **4** in pentane (0.02 M for the 193 nm photolysis; 0.06 M (**4**) or 0.10 M (**3**) for the 214 nm photolyses), with 0.001 M isooctane as internal standard, were deoxygenated with a stream of dry nitrogen in an ice bath for ca. 10 min prior to photolysis. The photolyses were monitored between 0.5 and 5–10% conversion by withdrawing aliquots at suitable time intervals for VPC analysis. Relative product yields were determined from the slopes of concentration versus time plots constructed for all components of the mixture relative to internal standard. The concentration vs. time plots were linear up to at least 3% conversion in each case. Figures 2 and 3 show examples of such plots for the photolyses of *cis*- and *trans*-**3** with 193 nm and 214 nm light. The integrals for *Z,Z*- and *E,Z*-**5** are less accurate than those for the other two isomers of **5**, particularly at low conversions of **3**, because these dienes elute on the tails of the solvent and (or) cyclobutene peaks under our VPC conditions. The isomeric dienes **5** and **6** were identified by VPC coinjection of 193 nm photolysates (carried to ca. 10% conversion) with each of the authentic diene samples on the SPB-1 capillary column.

The photolyses of **3** and **4** were also carried out as 0.06 M solutions in deoxygenated isooctane with the 214 nm lamp to ca. 15% conversion, in order to identify the C_3 and C_4 hydrocarbons. These products were identified by VPC spiking experiments using authentic samples with the SPB-1 megabore column. This column is capable of resolving propyne, 2-butyne, *E*-2-butene, and *Z*-2-butene to baseline at 30°C with low (ca. 8 mL/min) flow rates. Propyne and 2-butyne were identified as products from photolysis of **3** and **4**, respectively. *Z*-2-Butene was identified in the photolysates from the *cis* isomers of **3** and **4**; the yield of *E*-2-butene from these two compounds was estimated to be <10% that of the *Z* isomer. Similarly, the *trans* isomers of **3** and **4** were shown to afford *E*-2-butene with >90% stereospecificity. The yields of the C_3 and C_4 products were not determined.

In the photolyses of *cis*-**3**, *trans*-**3**, and *cis*-**4**, the corresponding isomeric dienes accounted for 93–97% of the detectable products of similar volatility to the starting materials, for both excitation wavelengths. In these three cases, the photolysates each contained one or two additional products formed in yields (<3%) too small to enable isolation. Photolysis of *trans*-**4** at both wavelengths gave four products in addition to those shown in eq. [3]; one of these was formed in ca. 6% yield, while the rest were formed in yields of 4% or less. In this case, the isomeric **6** accounted for 84% of the product mixture.

Control experiments

A few control experiments were carried out in order to rule out secondary isomerization of the initially formed dienes due to their direct photoisomerization in the 193 nm and 214 nm cyclobutene photolyses. In these experiments, deoxygenated pentane solutions of the cyclobutene, containing internal standard (isooctane; 0.001 M) and a mixture of *E*- and *Z*-**7** (0.002 M; $E/Z = 2.59 \pm 0.05$) were irradiated with the 193 or 214 nm light sources to ca. 4% conversion of the cyclobutene, with the photolysate being monitored periodically by VPC for the formation of isomeric diene products and for *cis,trans* photoisomerization of **7**. For example, after photolysis of a pentane solution of cis-**4** (0.06 M), *E*-/*Z*-**7** (0.002 M), and isooctane (0.001 M) with 214 nm light to 4% conversion, the relative amounts of *E*- and *Z*-**7** present after 4% conversion was $E/Z = 2.49 \pm 0.05$. The relative yields of *E,E*-, *E,Z*-, and *Z,Z*-**6** (from concentration vs. time plots) were identical to those from the photolysis without added **7**. The photostationary state for **7**, determined by separate irradiation of a 0.002 M solution of the dienes at 214 nm, was determined to be E/Z = 1.0. Similar experiments were carried out with the 193 nm photolysis of *cis*-**3** (0.02 M + 0.002 M **7** in pentane), and the 214 nm photolyses of both *cis*- and *trans*-**3** (0.1 M **3** + 0.002 M **7**). The change in the relative amounts of *E*- and *Z*-**7** present at 4–6% conversion was negligible in all cases, and the relative yields of the isomers of **5** were identical to those from the photolyses in the absence of **7**.

Irradiation of a deoxygenated pentane solution of *cis*-**4** (0.01 M) and toluene (0.02 M) in a Rayonet reactor fitted with 12 253.7-nm lamps resulted in the formation of only one volatile product, which eluted before *cis*-**4** on the SPB-1 capillary column but was not identified. Dienes *E,E*-, *E,Z*-, and *Z,Z*-**6** could not be detected in the photolysate after ca. 15% conversion of *cis*-**4**, within the detection limits of our analytical method.

Acknowledgments

We thank Dr. D. Hughes (McMaster University) for acquiring the high field ^{1}H NMR spectra, and the McMaster University Regional Mass Spectrometry Facility for the mass spectra and exact mass determinations. Acknowledgment is made to the Natural Sciences and Engineering Research Council of Canada and to the donors of The Petroleum Research Fund, administered by the American Chemical Society, for support of this research.

1. K. B. Clark and W. J. Leigh. J. Am. Chem. Soc. **109**, 6086 (1987).
2. J. Saltiel and L.-S. Ng Lim. J. Am. Chem. Soc. **91**, 5404 (1969).
3. R. B. Woodward and R. Hoffmann. The conservation of orbital symmetry. Verlag Chemie, Weinheim. 1970.
4. (*a*) C. D. DeBoer and R. H. Schlessinger. J. Am. Chem. Soc. **90**, 803 (1968); (*b*) M. Sakuragi and M. Hasegawa. Chem.

Lett. 29 (1974); (*c*) G. KAUPP and M. STARK. Chem. Ber. **111**, 3608 (1978).
5. G. QUINKERT, M. FINKE, J. PALMOWSKI, and W.-W. WIERSDORFF. Mol. Photochem. **1**, 433 (1969).
6. (*a*) N. C. YANG, R. V. CARR, E. LI, J. K. MCVEY, and S. A. RICE. J. Am. Chem. Soc. **96**, 2297 (1974); (*b*) R. V. CARR, B. KIM, J. K. MCVEY, N. C. YANG, W. GERHARTZ, and J. MICHL. Chem. Phys. Lett. **39**, 57 (1976).
7. W. ADAM, T. OPPENLANDER, and G. ZANG. J. Am. Chem. Soc. **107**, 3921 (1985).
8. Y. INOUE, M. SAKAE, and T. HAKUSHI. Chem. Lett. 1495 (1983).
9. W. G. DAUBEN and J. E. HAUBRICH. J. Org. Chem. **53**, 600 (1988).
10. P. J. KROPP. Org. Photochem. **4**, 1 (1979), and references cited therein.
11. (*a*) W. J. LEIGH and R. SRINIVASAN. Acc. Chem. Res. **20**, 107 (1987); (*b*) W. ADAM and T. OPPENLANDER. Angew. Chem. Int. Ed. Engl. **25**, 661 (1986); (*c*) M. G. STEINMETZ. Org. Photochem. **8**, 1 (1987).
12. (*a*) A. J. MERER and R. S. MULLIKEN. Chem. Rev. **69**, 639 (1969); (*b*) R. S. MULLIKEN. J. Chem. Phys. **66**, 2448 (1977).
13. (*a*) F. HIRAYAMA and S. LIPSKY. J. Chem. Phys. **62**, 576 (1975); (*b*) Y. INOUE, Y. DAINO, A. TAI, T. HAKUSHI, and T. OKADA. J. Am. Chem. Soc. **111**, 5584 (1989).
14. M. B. ROBIN. Higher excited states of polyatomic molecules. Vol. II. Academic Press, New York. 1975. Chap. 4.
15. K. B. CLARK and W. J. LEIGH. Can. J. Chem. **66**, 1571 (1988).
16. K. B. CLARK. Ph.D. Thesis, McMaster University. 1988.
17. D. C. OWSLEY and J. J. BLOOMFIELD. J. Org. Chem. **36**, 3768 (1971).
18. (*a*) R. CRIEGEE and K. NOLL. Justus Liebigs Ann. Chem. **627**, 1 (1959); (*b*) R. CRIEGEE, U. ZIRNGIBL, H. FURRER, D. SEEBACH, and G. FREUND. Chem. Ber. **97**, 2942 (1964); (*c*) G. R. BRANTON, H. M. FREY, and R. F. SKINNER. Trans. Faraday Soc. **62**, 1546 (1966); (*d*) R. E. K. WINTER. Tetrahedron Lett. 1207 (1965); (*e*) J. I. BRAUMAN and D. M. GOLDEN. J. Am. Chem. Soc. **90**, 1920 (1968); (*f*) R. SRINIVASAN. J. Am. Chem. Soc. **91**, 7557 (1969); (*g*) J. I. BRAUMAN and W. C. ARCHIE. J. Am. Chem. Soc. **94**, 4262 (1972).
19. (*a*) P. G. GASSMAN, T. J. ATKINS, and F. J. WILLIAMS. J. Am. Chem. Soc. **93**, 1812 (1971); (*b*) J. M. MCINTOSH and G. M. MASSE. J. Org. Chem. **40**, 1294 (1975).
20. J. SALTIEL, L. METTS, and M. WRIGHTON. J. Am. Chem. Soc. **92**, 3227 (1970).
21. B. B. LOEFFLER, E. EBERLIN, and L. W. PICKETT. J. Chem. Phys. **28**, 345 (1958).
22. M. B. ROBIN. Higher excited states of polyatomic molecules. Vol. III. Academic Press, New York. 1985. pp. 35–47.
23. W. R. ROTH, H.-W. LENNARTZ, W. VON E. DOERING, W. R. DOLBIER, JR., and J. C. SCHMIDHAUSER. J. Am. Chem. Soc. **110**, 1883 (1988).
24. Y. INOUE, T. MUKAI, and T. HAKUSHI. Chem. Lett. 1655 (1983).
25. S. BANK, C. A. ROWE, JR., A. SCHRIESHEIM, and L. A. NASLUND. J. Org. Chem. **33**, 221 (1968).
26. M. E. BAUMANN and H. BOSSARD. Helv. Chim. Acta, **61**, 2751 (1978).
27. C. M. CIMARUSTI and J. WOLINSKY. J. Am. Chem. Soc. **90**, 113 (1968).
28. H. O. HOUSE, W. L. RESPESS, and G. M. WHITESIDES. J. Org. Chem. **31**, 3128 (1966).
29. W. REEVE and D. M. REICHEL. J. Org. Chem. **37**, 68 (1972).

Can. J. Chem. Downloaded from www.nrcresearchpress.com by 91.121.58.235 on 09/07/12
For personal use only.

Lithium aluminium hydride reduction of some triarylvinyl bromides and acetates catalyzed by some transition metal chlorides

CRAIG A. OBAFEMI AND CHOI CHUCK LEE[1]

Department of Chemistry, Obafemi Awolowo University, ILE–IFE, Nigeria

Received January 3, 1990

CRAIG A. OBAFEMI and CHOI CHUCK LEE. Can. J. Chem. **68**, 1998 (1990).

A number of triarylvinyl halides and acetates were reduced with lithium aluminium hydride using various transition metal chlorides as catalysts. The vinylic halides were reduced to the corresponding alkenes while the vinylic acetates were reduced to mixtures of triarylketones and alcohols. The reduction of labeled vinylic halides did not result in any scrambling of the label from C-2 to C-1. The reactions took place under mild conditions and relatively fast reaction times.

Key words: triarylvinyl chlorides, triarylvinyl acetates, lithium aluminium hydride reduction, 1,2,2-triarylethanol, 1,1,2-tri-*p*-tolyl[1-^{13}C]ethane.

CRAIG A. OBAFEMI et CHOI CHUCK LEE. Can. J. Chem. **68**, 1998 (1990).

On a réduit un certain nombre d'acétates et d'halogénures de triarylvinyle à l'aide de l'hydrure double de lithium et d'aluminium, utilisant divers chlorures de métaux de transition comme catalyseurs. Les halogénures de vinyle sont réduits en alcanes correspondants alors que les acétates vinyliques sont réduits en des mélanges de triarylcétones et de triarylalcools. La réduction d'halogénures vinyliques marqués ne conduit à aucun brouillage du marqueur de la position C-2 à C-1. Les réactions sont conduites dans des conditions douces et elles se réalisent relativement rapidement.

Mots clés : chlorures de triarylvinyle, acétates de triarylvinyle, réduction à l'aide de l'hydrure double de lithium et d'aluminium, 1,2,2-triaryléthanol, 1,1,2-tri-*p*-tolyl[1-^{13}C]éthane.

[Traduit par la revue]

Can. J. Chem. Downloaded from www.nrcresearchpress.com by 91.121.58.235 on 09/07/12
For personal use only.

The conversion of organic halides to the corresponding hydrocarbons, which is an important synthetic procedure, has been accomplished with organolithium–copper complexes, titanium chloride – magnesium complexes (1–4), and by the combination of lithium aluminium hydride (LAH) and transition metal chlorides (5). The results with the latter system indicate that $LiAlH_4/NiCl_2$, in particular, is capable of reducing primary, cyclic, and aromatic halides in quantitative yields.

However, by comparison, little has been reported regarding the $LiAlH_4$ reduction of triarylvinyl halides and acetates, without transition metal halides as catalysts (6).

In a report of Lee and Weber (6), triarylvinyl bromides were reduced to the corresponding olefins by $LiAlH_4$, by refluxing for 12 h. On the other hand, reduction of triarylvinyl acetates required refluxing with $LiAlH_4$ for 5 h, twice (7).

This paper reports the reduction of some ^{13}C-labeled and unlabeled triarylvinyl halides and acetates using lithium aluminium hydride catalyzed by some transition metal chlorides.

Results and discussion

The general reaction procedure involved mixing the appropriate vinyl halide or acetate with the transition metal chloride (1 mole equivalent) in tetrahydrofuran (THF) followed by the addition of lithium aluminium hydride in THF (10 mole equivalents) slowly at temperatures well below 0°C. The reduction results are summarized in Table 1. Generally, the various vinyl halides **1** were completely reduced to the corresponding alkenes, **2**, within 15 min (reactions monitored by ^{1}H nmr and ir), while the various vinyl acetates gave mixtures of ketones, **4**, and alcohols, **5**. A second further reduction of the mixture **4** and **5** gave only **5**.

The two types of reductions, of halides and acetates, are of different natures. The acetates are, presumably, being reduced as normal ester reductions, with lithium aluminium hydride,

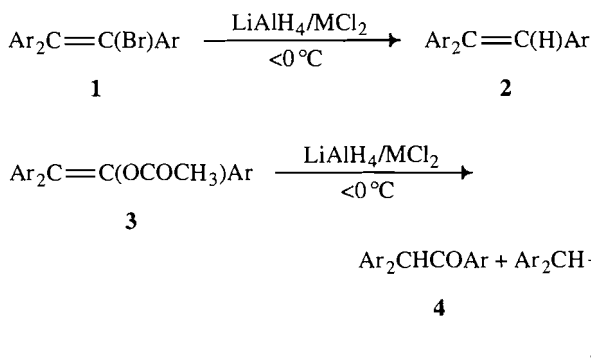

to enolates, some of which are converted to the enol, in equilibrium with the ketone form, and reduced to the alcohol via the keto form. The part remaining as the enolate affords the ketone upon work-up:

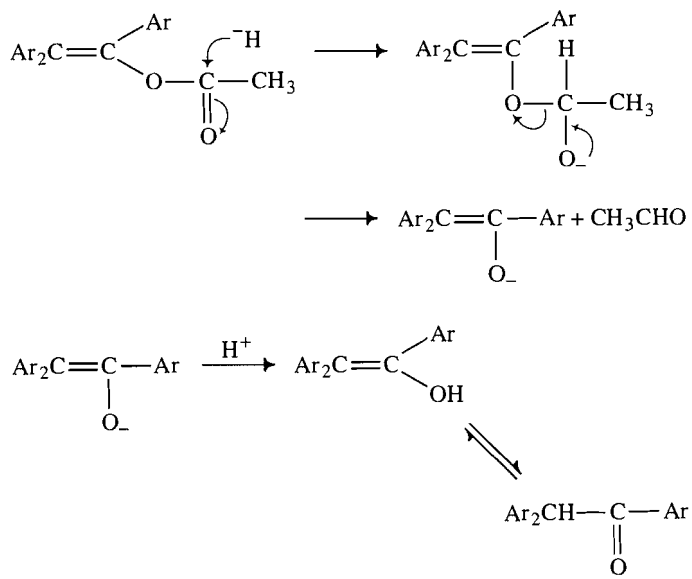

[1]Department of Chemistry, University of Saskatchewan, Saskatoon, Sask., Canada S7N 0W0.

Printed in Canada / Imprimé au Canada

Can. J. Chem. Downloaded from www.nrcresearchpress.com by 91.121.58.235 on 09/07/12
For personal use only.

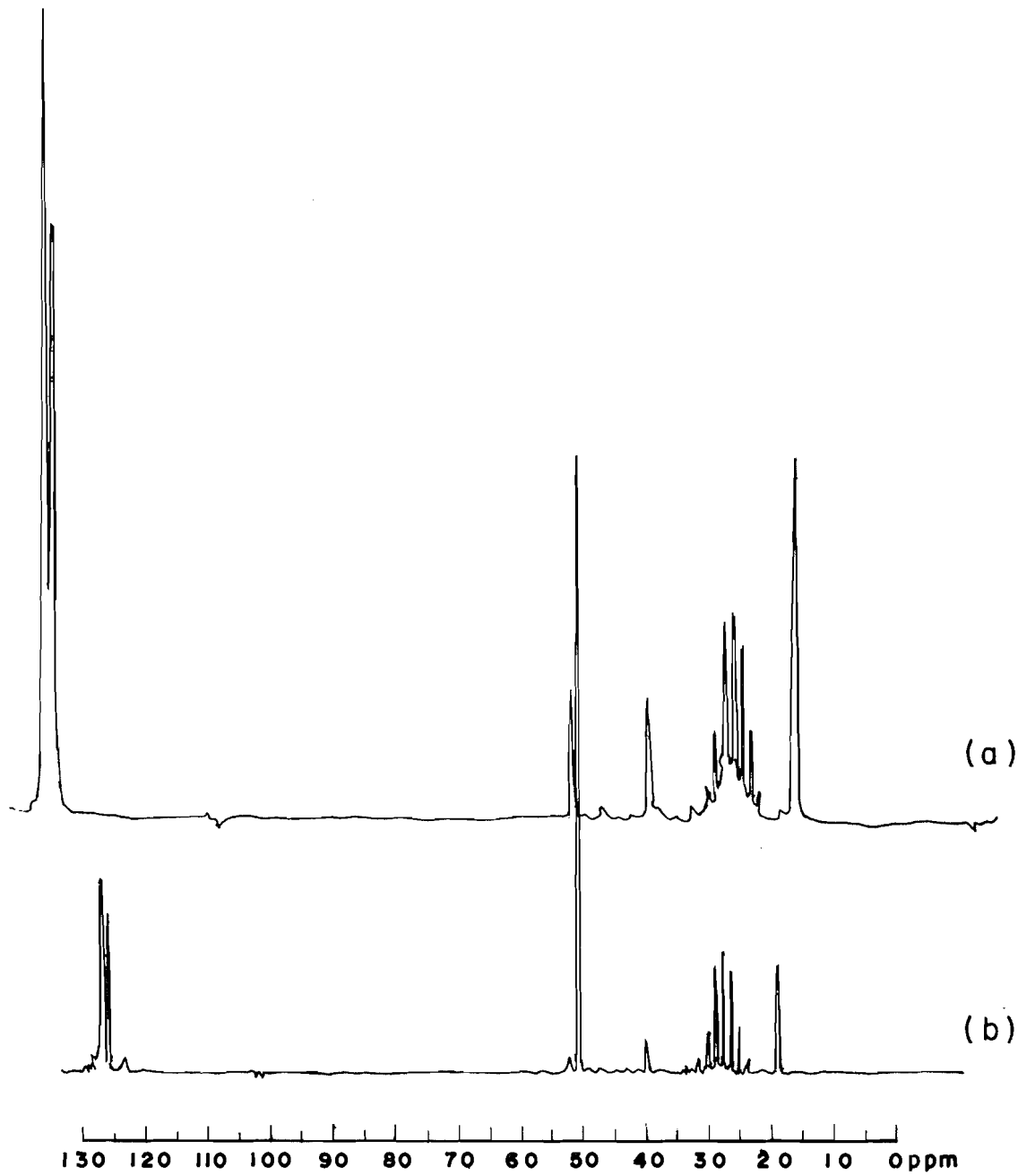

FIG. 1. The ^{13}C nmr spectrum of (a) ordinary 1,1,2-tritolylethane; (b) 1,1,2-tritolyl[1-^{13}C]ethane.

The halides, on the other hand, are possibly reduced via an initial electron-transfer process or metallation reaction. A direct S_N2 displacement process is eliminated, since starting with either the *E* or *Z* isomer (experiment 10) affords the *E* and *Z* alkenes in equimolar amounts.

Experiments were also carried out with carbon-13 labeled trianisylvinyl bromide and tri-*p*-tolylvinyl bromide (trianisyl-[2-^{13}C]vinyl bromide and tri-*p*-tolyl[2-^{13}C]vinyl bromide), prepared as already described in the literature (7, 8). They were reduced under conditions similar to those used for unlabeled vinyl substrates. The alkene products were hydrogenated catalytically to the corresponding triarylalkanes and then subjected to ^{13}C nmr analysis (7, 9). The ^{13}C enrichment was found to be located on C-1 of each alkane, indicating that no rearrangement occurred during the reduction processes:

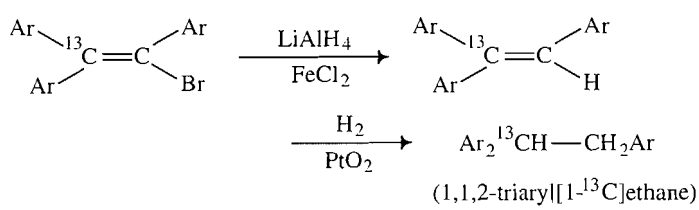

Ar = 4-$CH_3OC_6H_4$〰
= 4-$CH_3C_6H_4$〰

Figure 1 shows the ^1H-decoupled ^{13}C nmr in acetone-d_6 for unenriched 1,1,2-tri-*p*-tolylethane and 1,1,2-tri-*p*-tolyl[1-^{13}C]-ethane, respectively.

TABLE 1. The results of reduction of vinylic substrates

Expt. no.	Vinylic substrates	Transition metal halide	Product	Isolated yield (%)
1	$Ph_2C{=}C(Br)Ph$	$FeCl_2$	$Ph_2C{=}C(H)Ph$	92
2	$Ph_2C{=}C(Br)Ph$	$NiCl_2$	$Ph_2C{=}C(H)Ph$	95
3	$Tol_2C{=}C(Br)Tol$	$FeCl_2$	$Tol_2C{=}C(H)Tol$	96
4	$An_2C{=}C(Br)An$	$FeCl_2$	$An_2C{=}C(H)An$	91
5	$Tol_2{}^{13}C{=}C(Br)Tol$	$FeCl_2$	$Tol_2{}^{13}C{=}C(H)Tol$	94
6	$An_2{}^{13}C{=}C(Br)An$	$NiCl_2$	$An_2{}^{13}C{=}C(H)An$	92
7	$An_2C{=}C(Cl)An$	$NiCl_2$	$An_2C{=}C(H)An$	95
8	$An_2C{=}C(Br)An$	$CoCl_2$	$An_2C{=}C(H)An$	95
9	$An_2C{=}C(I)An$	$NiCl_2$	$An_2C{=}C(H)An$	96
10	$An(Ph)C{=}C(Br)An$ *E* or *Z* isomer	$FeCl_2$	$An(Ph)C{=}C(H)An$[a] *E*/*Z* 1.0	90
11	$Ph_2C{=}C(OAc)Ph$	$FeCl_2$	Ph CHCOPh + $Ph_2CHCH(OH)Ph$[b]	
12	$Tol_2C{=}C(OAc)Tol$	$NiCl_2$	$Tol_2CHCOTol + Tol_2CHCH(OH)Tol$[b]	
13	$An_2C{=}C(OAc)An$	$FeCl_2$	$AnCHCOAn + An_2CHCH(OH)An$[b]	
14	$An_2C{=}C(OAc)An$	$FeCl_2$	$An_2CHCH(OH)An$[c]	89
15	$An(Ph)C{=}C(OAc)An$	$FeCl_2$	$An(Ph)CHCH(OH)An$[c] *erythro* and *threo* (ref. 7)	83

[a] $E/Z = 1.0$ eliminates the direct S_N2 displacement process (6).
[b] Mixture of ketone and alcohol when treated only once with LAH.
[c] Products when reduced twice with LAH.

Experimental

The various vinylic substrates were prepared according to literature procedures (7–13). The reactions were performed as illustrated by the following typical procedures.

Reduction of trianisylvinyl bromide

Trianisylvinyl bromide (0.50 g, 1.18 mmol) in tetrahydrofuran (20 mL) was added to ferrous chloride (anhydrous, 0.15 g, 1.18 mmol in a 100-mL round-bottomed flask. The flask was cooled in liquid nitrogen and lithium aluminium hydride (0.45 g, 1.18 mmol) in THF (20 mL) was added slowly. There was an immediate black coloration and gas evolution. The reaction mixture was then kept for 5–15 min with occasional swirling. The excess $LiAlH_4$ was destroyed with cold water (2 mL) and the THF solution separated. The black residue was further extracted with THF or ether and the combined organic layer dried over anhydrous magnesium sulfate. The solvent was evaporated to afford the trianisylethene, identical with an authentic sample via mp, mixture mp, nmr, and mass spectrum (0.37 g, after recrystallization from acetone/methanol, 91% yield).

Reduction of trianisylvinyl acetate

Trianisylvinyl acetate (0.50 g, 1.24 mmol) was reduced as above (acetate/$FeCl_2$/$LiAlH_4$ = 1:1:10). After extraction and evaporation of THF, the ^1H nmr of the product showed it to be a mixture of 1,2,2-trianisylethanol and the corresponding ketone derivative (**4**). A second treatment under similar conditions afforded the pure alcohol, 1,2,2-trianisyl ethanol (mp 112–114°C, nmr, and ms) (0.4 g, 89% yield).

Platinum oxide catalyzed reduction of trianisyl[x-^{13}C]ethene

Trianisyl[x-^{13}C]ethene (300 mg, 0.87 mmol), obtained from $NiCl_2$-catalyzed $LiAlH_4$ reduction of trianisyl[2-^{13}C]vinyl bromide as described above, was dissolved in ethyl acetate (20 mL) and hydrogenated catalytically (PtO_2) under 40 psi (1 psi = 6.9 kPa) pressure for 15 h, after which the solvent was removed under reduced pressure. The crude 1,1,2-trianisyl[x-^{13}C]ethane was purified by column chromatography, using an alumina column and eluting with petroleum ether (bp 40–60°C)/diethyl ether (20:1) to give the pure hydrocarbon (260 mg, 86%), mp 88–89°C (lit. (13) mp 86–87°C).

The carbon-13 labeled trianisylethane was subjected to ^{13}C nmr analysis. The analysis showed that the ^{13}C-label was at the C-2 position of the original trianisylvinyl bromide; that is, there was no scrambling of the label during either the $LiAlH_4$ reduction or the catalytic hydrogenation, and the product was, in fact, 1,1,2-trianisyl[1-^{13}C]ethane.

1. S. MASAMUNE, P. A. RUSSY, and G. S. BATES. J. Am. Chem. Soc. **95**, 6452 (1973).
2. S. MASAMUNE, G. S. BATES, and P. E. GEORGHION. J. Am. Chem. Soc. **96**, 3686 (1974).
3. S. TYRLIK and I. WOLOCHOWICZ. J. Chem. Soc. Chem. Commun. 781 (1975).
4. T. R. NELSEN and J. J. TUFARIELLO. J. Org. Chem. **40**, 3159 (1975).
5. E. C. ASHBY and J. J. LIN. J. Org. Chem. **43**, 1263 (1978).
6. C. C. LEE and U. WEBER. J. Org. Chem. **43**, 2721 (1978).
7. C. A. OBAFEMI. Ph.D. Thesis, University of Saskatchewan. 1981.
8. C. C. LEE, A. J. PAINE, and E. C. F. KO. Can. J. Chem. **55**, 2310 (1977).
9. C. C. LEE, C. A. OBAFEMI, J. W. QUAIL, and Z. RAPPOPORT. Can. J. Chem. **59**, 2342 (1981).
10. C. C. LEE, A. J. CESSNA, B. A. DAVIES, and M. OKA. Can. J. Chem. **52**, 2679 (1974).
11. M. OKA and C. C. LEE. Can. J. Chem. **53**, 320 (1975).
12. C. C. LEE and E. C. F. KO. Can. J. Chem. **54**, 3041 (1976).
13. R. S. SHELTON, M. G. VAN CAMPEN, JR., D. F. MEISUER, S. M. PARAMETER, E. R. ANDREWS, R. E. ALLEN, and K. K. WYKOFF. J. Am. Chem. Soc. **75**, 5491 (1953).

Can. J. Chem. Downloaded from www.nrcresearchpress.com by 91.121.58.235 on 09/07/12
For personal use only.

Some reactions of ferrocenyl phosphines with $M_3(CO)_{12}$ (M = Fe, Ru). The structures of $Ru_3(CO)_{11}(PFcPh_2)$ and $Ru_3(CO)_{10}\{(PPh_2\text{-}\eta\text{-}C_5H_4)_2Fe\}$

STEPHANIE T. CHACON AND WILLIAM R. CULLEN[1]
Department of Chemistry, University of British Columbia, Vancouver, B.C., Canada V6T 1Y6
MICHAEL I. BRUCE AND OMAR BIN SHAWKATALY
Department of Physical and Inorganic Chemistry, University of Adelaide, Adelaide, South Australia
AND
FREDERICK W. B. EINSTEIN, RICHARD H. JONES, AND ANTHONY C. WILLIS
Department of Chemistry, Simon Fraser University, Burnaby, B.C., Canada V5A 1S6

Received February 21, 1990

STEPHANIE T. CHACON, WILLIAM R. CULLEN, MICHAEL I. BRUCE, OMAR BIN SHAWKATALY, FREDERICK W. B. EINSTEIN, RICHARD H. JONES, and ANTHONY C. WILLIS. Can. J. Chem. **68**, 2001 (1990).

Substitution reactions of $M_3(CO)_{12}$ (M = Fe, Ru) and $Ru_4(\mu\text{-}H)_4(CO)_{12}$ involving a range of ferrocenyl phosphines are described. Compounds isolated and characterized include $Fe_3(CO)_{11}PFcPh_2$, $Fe_3(CO)_{10}(PBuFcPh)_2$, $Fe(CO)_4L$ (L = PFc_2Ph, PFc_3), $Ru_3(CO)_{11}L$ (L = PFc_3, PFc_2Ph, $PFcPh_2$), $Ru_3(CO)_{10}L_2$ (L = PFc_2Ph, $PFcPh_2$), and $Ru(CO)_4PFc_3$. $Ru_4(\mu\text{-}H)_4(CO)_{10}$(L—L) and $Ru_3(CO)_{10}$(L—L) result from reactions with L—L = $(Ph_2PC_5H_4)_2Fe$. The structure of two derivatives are described. Crystals of $Ru_3(CO)_{11}(PFcPh_2)$ are triclinic, space group $P\text{-}1$, a = 8.576(1), b = 11.150(2), c = 9.160(3) Å, α = 76.65(1), β = 80.75(1), γ = 72.02(1)°, Z = 2, final R_W = 0.027 from 3144 observed reflections. $Ru_3(CO)_{10}(Ph_2PC_5H_4)_2Fe$, monoclinic crystals, space group $C\ 2/c$, a = 17.005(2), b = 18.411(1), c = 14.961(1) Å, β = 117.112(8)°, Z = 4, final R_W = 0.023 from 2395 observed reflections.

Key words: ferrocenylphosphines, ruthenium carbonyl derivatives, structures, synthesis, iron carbonyl derivatives.

STEPHANIE T. CHACON, WILLIAM R. CULLEN, MICHAEL I. BRUCE, OMAR BIN SHAWKATALY, FREDERICK W. B. EINSTEIN, RICHARD H. JONES et ANTHONY C. WILLIS. Can. J. Chem. **68**, 2001 (1990).

On décrit les réactions de substitutions des $M_3(CO)_{12}$ (M = Fe et Ru) et $Ru_4(\mu\text{-}H)_4(CO)_{12}$ avec une série de ferrocénylphosphines. Les composés isolés et caractérisés sont: $Fe_3(CO)_{11}PFcPh_2$, $Fe_3(CO)_{10}(PBuFcPh)_2$, $Fe(CO)_4L$ (L = PFc_2Ph, PFc_3), $Ru_3(CO)_{11}L$ (L = PFc_3, PFc_2Ph, $PFcPh_2$), $Ru_3(CO)_{10}L_2$ (L = PFc_2Ph, $PFcPh_2$), et $Ru(CO)_4PFc_3$. Les produits $Ru_4(\mu\text{-}H)_4(CO)_{10}$(L—L) et $Ru_3(CO)_{10}$(L—L) se forment par réaction avec L—L = $(Ph_2PC_5H_4)_2Fe$. On décrit les structures de deux dérivés. Les cristaux de $Ru_3(CO)_{11}(PFcPh_2)$ sont tricliniques et ils appartiennent au groupe d'espace $P\text{-}1$, avec a = 8,576(1), b = 11,150(2) et c = 9,160(3) Å, α = 76,65(1), β = 80,75(1), et γ = 72,02(1)°, Z = 2, R_W = 0,027 pour 3144 réflexions. Les cristaux de $Ru_3(CO)_{10}(Ph_2PC_5H_4)_2Fc$ sont monocliniques et ils appartiennent au groupe d'espace $C\ 2/c$, avec a = 17,005(2), b = 18,411(1) et c = 14,961(1) Å, β = 117,112(8)°, Z = 4 et R_W = 0,023 pour 2395 réflexions.

Mots clés : ferrocénylphosphines, dérivés du ruthénium carbonyl, structures, synthèses, dérivés du Fe carbonyl.
[Traduit par la revue]

Tertiary phosphine substituted metal carbonyl complexes are generally very well known (1) although there have been only a few studies in this area involving ferrocenylphosphines such as PFc_nPh_{3-n}, n = 1–3 (2–8) (FcH = $Fe(\eta\text{–}C_5H_5)_2$), and 1,1′-disubstituted ferrocene derivatives such as dppf, 1,1′-bis(diphenylphosphino)ferrocene (2, 9, 10). Phosphine derivatives are generally prepared by direct reaction of the phosphine with the metal carbonyl. Sometimes, and especially in the case of $Fe_3(CO)_{12}$, cluster breakdown is found so that the isolated products are phosphine derivatives of mononuclear carbonyls, e.g. $Fe(CO)_4(PR_3)$ and $Fe(CO)_3(PR_3)_2$ (3, 5, 8, 11–16). Reactions of this type involving $Ru_3(CO)_{12}$ usually afford trinuclear products (17–20). Photosubstitution of $Ru_3(CO)_{12}$ seems to occur largely from higher energy states whereas photofragmentation involves the lowest excited state (20). The use of the radical anion, sodium diphenylketyl, as a catalyst has recently greatly facilitated the preparation of a wide range of derivatives $Ru_3(CO)_{12-n}L_n$, n = 1–4, because the reactions are essentially stoichiometric (21). The method is also useful for the synthesis of derivatives of $Fe_3(CO)_{12}$. Salts of the bis(triphenylphosphine)iminium ion, ppn^+, are also effective catalysts (22).

In view of the success in trapping a benzyne fragment on a metal cluster from reactions of arylphosphines with $M_3(CO)_{12}$ (M = Ru, Os) (23–25) directly or stepwise, we have initiated a study of the corresponding reactions of ferrocenylphosphines in the hope that this will lead to the trapping of a ferrocyne fragment. The present paper describes the synthesis of some derivatives of $Fe_3(CO)_{12}$ and $Ru_3(CO)_{12}$, because of our interest in their pyrolysis products, and the crystal structures of $Ru_3(CO)_{11}(PFcPh_2)$ and $Ru_3(CO)_{10}(\mu\text{-dppf})$. The thermal decomposition of $Ru_3(CO)_{10}(PFcPh_2)_2$ to a benzyne complex has been reported (25).

Experimental section

Reactions were carried out in a nitrogen atmosphere by using standard Schlenk procedures. Solvents were dried and distilled before use. Separation of products was usually achieved by column chromatography on Florisil or neutral alumina (activity I) by using petroleum ether (35–60°C bp fraction)/diethyl ether mixtures as eluent. ^1H NMR spectra were recorded from $CDCl_3$ solutions by using Bruker WH400 or WP80 and Varian XL300 instruments. Infrared spectra, usually of C_6H_{12} solutions, were run on a Bowman Fourier Transform or a Perkin Elmer 589 spectrometer. Mass spectra were obtained from a Kratos MS 50 instrument; only peaks with high m/e values are listed and electron impact ionization was used unless otherwise stated. Elemental analyses were determined by Mr. P. Borda of the Chemistry Department, University of British Columbia. Melting points were measured by using a Kofler microheating stage and are uncorrected. A Hanovia 100W lamp (903A-1) was used for UV irradiations. To minimize

[1]Author to whom correspondence may be addressed.

Printed in Canada / Imprimé au Canada

Can. J. Chem. Downloaded from www.nrcresearchpress.com by 91.121.58.235 on 09/07/12
For personal use only.

Can. J. Chem. Downloaded from www.nrcresearchpress.com by 91.121.58.235 on 09/07/12
For personal use only.

thermal reactions the irradiated solution was kept cold by means of a Dry Ice/cold-finger inserted into the closed reaction vessel which was held 10 cm from the lamp.

Preparation of n-*butylferrocenylphenylphosphine, PBuFcPh.*

A hexane solution of *n*-BuLi (0.20 mol) was added to ferrocene (25 g, 0.13 mol) in diethyl ether (150 mL). The solution was stirred (20 h) at 20°C after which it was cooled to −78°C and $PhPCl_2$ (15 g, 0.08 mol) was added dropwise. The stirred solution was allowed to warm to 20°C. After 2 h, water (100 mL) was added. The ether layer was separated, reduced in volume, and chromatographed on alumina. Ferrocene eluted with a petroleum ether/diethyl ether mixture (20:1); PBuFcPh eluted with a 9:1 mixture of solvents and was isolated as as yellow orange solid, mp 38–39°C, ~40% yield. ^{1}H NMR δ 0.94–0.88 (m, 3), 1.50–1.38 (m, 4), 1.99–1.91 (m, 2), 4.14 (s, 5), 4.30–4.27 (m, 2), 4.35–4.32 (m, 2), 7.31–7.28 (m, 3), 7.50–7.45 (m, 2). Mass spec. *m/z* 350 (P^+), 293 ($P - Bu^+$), 216 ($P - Ph - Bu^+$), 186 (Fc^+), 121 ($CpFe^+$), 77 (Ph^+).

Anal. calcd. for $C_{20}H_{23}FeP$: C 68.58, H 6.63; found: C 68.41, H 6.60.

1. Reaction of triferrocenylphosphine with $Fe_3(CO)_{12}$ The phosphine (26–28) (90 mg, 0.20 mmol) and $Fe_3(CO)_{12}$ (100 mg, 0.20 mmol) in THF (10 mL) were gently refluxed for 10 min. Cyclohexane (10 mL) was added to the reaction mixture and the THF removed under vacuum. The residual solution was chromatographed on alumina. The only significant product, the known compound $Fe(CO)_4(PFc_3)$, eluted with petroleum ether. It was isolated as an orange solid in 80% yield mp 225–230°C dec. (lit (4) 225–230°C dec.). The mass spectrum showed a parent peak at *m/z* 754 and others associated with stepwise loss of CO.

2. Reaction of PFc_2Ph *with* $Fe_3(CO)_{12}$

(*a*) Bisferrocenylphenylphosphine (29) (190 mg, 0.40 mmol) and $Fe_3(CO)_{12}$ (200 mg, 0.40 mmol) were reacted as in experiment 1. The only product $Fe(CO)_4(PFc_2Ph)$, an orange red solid, mp 165°C, was isolated following chromatographic work-up on Florisil (~80% yield. ^{1}H NMR δ 3.98 (s, 10), 4.48–4.40 (m, 6), 4.60–4.52 (m, 2), 7.52–7.38 (m, 3), 8.23–7.95 (m, 2). Mass spec. (probe temperature 100°C) *m/z* 646 (M^+), 618, 590, 562, 534, 478. Infrared ν(CO) 2040s, 1970s, 1937vs, 1932vs cm^{-1}.

Anal. calcd. for $C_{30}H_{23}Fe_3O_4P$: C 55.77, H 3.60, O 9.91; found: C 55.79, H 3.70, O 9.92.

(*b*) A stirred solution of the phosphine (80 mg, 0.20 mmol) and $Fe_3(CO)_{12}$ (100 mg, 0.20 mmol) in THF (10 mL) at 20°C was treated with 1 mL of a solution of sodium diphenylketyl in THF (~0.025 M). After 10 min the reaction mixture was worked up to give a low yield of $Fe(CO)_4(PFc_2Ph)$.

3. Reaction of $PFcPh_2$ *with* $Fe_3(CO)_{12}$. Ferrocenyldiphenylphosphine (29–30) (73.4 mg, 0.20 mmol) and $Fe_3(CO)_{12}$ (100 mg, 0.20 mmol) were reacted as follows.

(*a*) The same condition as in experiment 2(*b*) afforded $Fe_3(CO)_{11}(PFcPh_2)$ as an unstable dark green solid, mp 95–100°C dec., in high yield (~80%) following chromatographic work-up on Florisil (diethyl ether/dichloromethane 4:1). ^{1}H NMR δ 3.93 (s, 5), 4.18–4.08 (m, 2), 4.55–4.40 (m, 2), 7.75–7.53 (m, 10). The mass spectrum was essentially that of $Fe(CO)_4(PFcPh_2)$ (q.v). Infrared ν(CO) 2085m, 2033s, 2012s, 2002sh cm^{-1}.

Anal. calcd. for $C_{33}H_{10}Fe_4O_{11}P$: C 58.02, H 3.57, O 11.89; found: C 57.79, H 3.63, O 12.20.

(*b*) The same conditions as in experiment 1 afforded $Fe_3(CO)_{11}(PFcPh_2)$, (~40% yield) and $Fe(CO)_4(PFcPh_2)$, an orange solid mp 169–173°C dec. (~20% yield) following separation on Florisil. The $Fe(CO)_4$ derivative eluted with petroleum ether. ^{1}H NMR δ 3.78 (s, 5), 4.56–4.45 (m, 4), 7.70–7.33 (m, 10). Mass spec. (probe temperature 140°C) *m/z* 538 (m^+), 510, 482, 454, 426, 370. Infrared ν(CO) 2050s, 1977m, 1947s, 1936s cm^{-1}.

Anal. calcd. for $C_{26}H_{10}Fe_2O_4P$: C 58.02, H 3.57, O 11.89; found: C 57.79, H 3.62, O 12.20.

(*c*) The reagents were dissolved in hexanes (10 mL) and irradiated for 60 min. Chromatographic work-up afforded $Fe_3(CO)_{11}(PPh_2Fc)$ in ~40% yield.

4. Reaction of $Fe_3(CO)_{12}$ *with PBuFcPh.* The carbonyl (100 mg, 0.20 mmol) and the phosphine (70 mg, 0.20 mmol) in hexanes (10 mL) were irradiated for 45 min. The solvent was reduced in volume and the residue chromatographed on alumina. A 1:1 mixture of petroleum ether/diethyl ether eluted a dark green solid which is probably $Fe_3(CO)_{11}$(PBuFcPh). Infrared ν(CO) 2083w, 2030m, 2010m, 2007m cm^{-1}. Another olive green band was eluted with diethyl ether. This was identified as $Fe_3(CO)_{10}(PBuFcPh)_2$, mp 59–62°C dec., moderate yield. Infrared ν(CO) FT 2053s, 2029w, 2007vs, 1980s, 1959sh, 1945sh, 1930w, 1816m, 1794 m cm^{-1}. ^{1}H NMR δ 2.40–0.70 (m(br), 9), 4.60–2.95(m(br), 9), 7.88–7.15 (m)br), 5).

Anal. calcd. for $C_{50}H_{46}Fe_5O_{10}P_2$: C 52.30, H 4.05, O 13.94; found: C 51.88, H 4.00, O 14.09.

Attempts to purify $Fe_3(CO)_{11}$(PBuFcPh) by recrystallization resulted in decomposition and the production of $Fe(CO)_4$(PBuFcPh), a yellow solid, mp 73–75°C. ^{1}H NMR δ 0.70–1.70 (m, 9), 4.00 (s, 5), 4.33–4.22 (m, 1), 4.50–4.33 (m, 3), 7.55–7.40 (m, 3), 7.93–7.65 (m, 2). Mass spec. (probe temperature 110°C *m/z* 518 (M^+), 490, 482, 434, 406, 350, 293. Infrared ν(CO) 2050s, 1975s, 1943vs, 1936vs cm^{-1}.

5. Reaction of PFc_3 *with* $Ru_3(CO)_{12}$. A stirred solution of $Ru_3(CO)_{12}$ (117 mg, 0.18 mmol) and PFc_3 (107 mg, 0.18 mmol) in THF (5 mL) was treated dropwise with sodium diphenylketyl in THF as described for experiment 2(*b*). After 10 min the reaction mixture was chromatographed on Florisil. Elution with diethyl ether gave $Ru_3(CO)_{11}(PFc_3)$ as an orange solid, 80% yield, mp 115–116°C dec., R_F 0.56 in 7:1 petroleum ether/diethyl ether. Infrared ν(CO) 2097(m), 2044(s), 1981(sh), 1960(sh) cm^{-1}. Mass spec. (probe temperature 210°C) *m/z* 640, 612, 586, 529, 500, 472, 444, 415, 389.

Anal. calcd. for $C_{41}H_{27}Fe_3O_{11}P_3Ru_3$: C 41.13, H 2.27; found: C 41.45, H 2.47.

6. Preparation of $Ru(CO)_4(PFc_3)$

(*a*) $Ru_3(CO)_{11}(PFc_3)$ (25 mg) in hexane (15 mL) was irradiated for 40 min with the 100 W lamp as described above. The yield of $Ru(CO)_4(PFc_3)$ was 45% as judged from the ^{1}H NMR spectrum of the mixture that contained $Ru(CO)_4(PFc_3)$, $Ru_3(CO)_{11}(PFc_3)$, and $Ru_3(CO)_{12}$. The phosphine derivatives were not separable by column chromatography, although $Ru_3(CO)_{12}$ was isolated as a pure fraction.

(*b*) A solution of pure $Ru_3(CO)_{11}(PFc_3)$ in hexane/diethyl ether slowly deposited a few orange crystals of $Ru(CO)_4(PFc_3)$ on standing. ^{1}H NMR δ 4.74–4.69 (m, 1), 4.65–4.56 (m, 3), 4.52 (s, 5), Infrared (FT) ν(CO) 2061(s), 1981(w), 1943(s) cm^{-1}.

7. Reaction of PFc_2Ph *with* $Ru_3(CO)_{12}$.

(*a*) The carbonyl (100 mg, 0.16 mmol) and phosphine (74.8 mg, 0.16 mmol) were treated with ketyl as in experiment 2(*b*). An orange solid $Ru_3(CO)_{11}(PFc_2Ph)$, mp 147–150°C dec., was the main product (~80% yield) isolated following chromatography on alumina (petroleum ether/diethyl ether 1:2) R_f 0.53, 7:1 petroleum ether/diethyl ether. ^{1}H NMR δ 4.15–4.05 (m, 2), 4.20 (s, 5), 4.40–4.31 (m, 2), 4.55–4.42 (m, 4), 7.43–7.27 (m, 3), 7.90–7.60 (m, 2). Mass spec. (FAB) *m/z* 1089 (M^+), 1061, 1033, 1005, 977, 949, 921, 893, 876, 865, 848, 837, 820, 809, 781. Infrared (FT) ν(CO), 2096w, 2045s, 2028m, 2015s, 1955w, 1984s, 1966vw, 1958vw cm^{-1}.

Anal. calcd. for $C_{37}H_{23}Fe_2O_{11}PRu_3$: C 40.79, H 2.13, O 16.15; found: C 41.11, H 2.20, O 16.0.

A second fraction $Ru_3(CO)_{10}(PFc_2Ph)_2$, a dark red solid, mp 117–119°C dec., was eluted, in low yield, with diethyl ether/dichloromethane 18:1. ^{1}H NMR δ 4.13 (m, 2), 41.9 (s, 10), 4.40 (m, 2), 4.45 (m, 2), 4.49 (m, 2), 7.36–7.29 (m, 3), 7.81–7.67 (m, 2). Mass spec. (FAB) *m/z* 889, 815, 714. Infrared (FT) ν(CO) (CH_2Cl_2), 2075w, 2044w, 2029s, 2005sh, 1988s, 1974vw, 1957vw, 1948vw cm^{-1}.

Anal. calcd. for $C_{62}H_{46}Fe_4O_{10}P_2Ru_3.1.5CH_2Cl_2$: C 45.75, H 2.97, O 9.60; found: C 45.75, H 3.21, O 10.34.

Can. J. Chem. Downloaded from www.nrcresearchpress.com by 91.121.58.235 on 09/07/12
For personal use only.

TABLE 1. Crystal data [a]

Formula	$Ru_3(CO)_{11}(PFcPh_2)$ $C_{33}H_{19}FeO_{11}PRu_3$	$Ru_3(CO)_{10}(dppf)$ $C_{44}H_{28}FeO_{10}P_2Ru_3$
fw	981.54	1137.80
Crystal system	Triclinic	Monoclinic
Space group	*P-1*	*C* 2/*c*
a	8.576(1) Å	17.005(2) Å
b	11.150(2) Å	18.411(1) Å
c	19.160(3) Å	14.961(1) Å
α	76.65(1)°	—
β	80.75(1)°	117.112(8)°
γ	72.02(1)°	—
V	1687.7 Å^3	4169.3 Å^3
Z	2	4
ρ_{calcd}	1.931 gm cm^{-3}	1.812 g cm^{-3}
$\rho_{obsvd.}$[b]	—	1.80 g cm^{-3}
μ	18.18 cm^{-1}	15.20 cm^{-1}
Radiation	MoKα	MoKα
λ	0.70930 Å(α_1) 0.71359 Å(α_2)	0.70930 Å(α_1) 0.71359 Å(α_2)
Scan mode	coupled ω–2θ	coupled ω–2θ
Scan width	0.7° in ω	0.6° in ω
Scan speed	5.0–0.56° in ω	5.0–0.56° in ω
Background	Extended 25% on each side	Extended 25% on each side
2θ range	3–45°	3–45°
Crystal size	0.19 × 0.26 × 0.10 mm	0.14 × 0.15 × 0.41 mm
Total no. unique Reflection	4398	2729
Observed reflections[c]	3144	2395
Number of variables	442	315
Final R_f	0.022	0.017
Final R_w	0.027	0.023
Goodness of fit	1.02	1.06

[a]At 18 ± 1°C Enraf-Nonius CAD4F diffractometer.
[b]Density by flotation in $ZnBr_2$ solution.
[c]$I > 2.3\delta(I)$.

(*b*) The carbonyl (251 mg, 0.39 mmol) and phosphine (3.76 mg, 0.79 mmol) were treated with the ketyl as in experiment 2(*b*). $Ru_3(CO)_{10}(PFc_2Ph)_2$ was eluted from an alumina column with 18:1 diethyl ether/dichloromethane and was isolated as a dark red solid, 251 mg (86% yield), R_f 0.22, petroleum ether/diethyl ether 7:1.

(*c*) Both substitution products were isolated in low yield after the reactants, 1:1 mole ratio, were refluxed in THF for 10 min.

8. Reaction of $PFcPh_2$ with $Ru_3(CO)_{12}$

(*a*) The phosphine (57.9 mg, 0.16 mmol) and $Ru_3(CO)_{12}$ (100 mg, 0.16 mmol) were treated with the ketyl as in experiment 2(*b*). Chromatography on alumina with diethyl ether/$CHCl_3$, 1:1, eluted $Ru_3(CO)_{11}(PFcPh_2)$ as the only product, orange solid, mp 112–115°C dec. R_f 0.52, petroleum ether/diethyl ether, 7:1. ^{1}H NMR δ 3.97 (s, 5), 4.21–4.18 (m, 2), 4.52–4.49 (m, 2), 7.43–7.40 (m, 6), 8.03–7.48 (m, 4). Mass spec. (FAB) *m/z* 981 (M^+), 953, 925, 897, 869, 841, 813, 785, 757, 740, 729, 712, 701, 684, 673, 656, 628, 600, 572. Infrared (FT) ν(CO) 2099sh, 2095m, 2060sh, 2046s, 2028sh, 2015s, 2003sh, 1997sh, 1986m, 1970w, 1964w cm^{-1}.

Anal. calcd. for $C_{33}H_{19}FeO_{11}PRu_3$: C 40.38, H 1.96, O 17.93; found: C 40.78, H 2.15, O 17.97.

(*b*) The same quantities of reagents were refluxed gently in THF for 10 min. Chromatography on alumina afforded $Ru_3(CO)_{11}(PFcPh_2)$ as in (*a*), in low yield, together with a second fraction which also eluted with 1:1 diethyl ether/$CHCl_3$. This was identified as $Ru_3(CO)_{10}(PFcPh_2)_2$, a dark purple solid. mp 103–107°C dec. R_F 0.20, petroleum ether/ diethyl ether (7:1). ^{1}H NMR δ 3.93 (s, 5), 4.20 (m, 2), 4.45 (m, 2), 7.75–7.35 (m, 10). Infrared (FT) ν(CO) 2075s, 2063s, 2045vs, 2019m, 1998s, 1990sh, 1976m, 1960m, 1921w cm^{-1}.

Anal. calcd. for $C_{54}H_{38}Fe_2O_{10}P_2Ru_3$: C 48.99, H 2.90, O 12.07; found: C 49.24, H 3.00, O 12.25.

(*c*) The carbonyl (360 mg, 0.56 mmol) and phosphine (412 mg, 1.11 mmol) were treated with the ketyl as in experiment 2(*b*). $Ru_3(CO)_{10}(PFcPh_2)_2$ was eluted from an alumina column with 1:1 diethyl ether/chloroform. The yield of dark purple solid was 593 mg (80%).

9. Reaction of $Ru_3(CO)_{12}$ with dppf.

(*a*) A mixture of $Ru_3(CO)_{12}$ (100 mg, 0.156 mmol) and Fe(η-$C_5H_4PPh_2)_2$, dppf (9) was dissolved in dry THF (20 mL). The catalyst [ppn][OAc] (15 mg) was added to the reaction mixture and the colour changed immediately to dark red. The reaction mixture was left stirring for 5 min, after which time solvent was removed *in vacuo*. The residue was redissolved in the minimum amount of dichloromethane and purified by preparative TLC. (Kieselgel GF_{254}, developing with 3/1/1 light petroleum/diethyl ether/acetone). The following bands were obtained: band 1 (orange, R_f 0.92) identified (IR) as $Ru_3(CO)_{12}$; band 2 (orange, R_f 0.83) trace, identified as dppf by comparison with an authentic sample; band 3 (dark red, R_f 0.71) was recrystallized from CH_2Cl_2/cyclohexane at −30°C to give dark red crystals of $Ru_3(CO)_{10}$(μ-dppf). $2C_6H_{12}$ (146 mg. 76.5% yield), mp 205°C dec. Infrared ν(CO) 2086s, 2020(sh), 2010vs, 1972(sh), 1967w cm^{-1}. ^{1}H NMR ($CDCl_3$) δ 1.43 (s, 24), 4.36 (m, 4), 4.47 (m, 4), 7.43 (m, 20). ^{13}C NMR ($CDCl_3$) δ 28.7 (s, C_6H_{12}), 73.7 (d, *J*(CP) = 7 Hz, C(1))

Can. J. Chem. Downloaded from www.nrcresearchpress.com by 91.121.58.235 on 09/07/12
For personal use only.

TABLE 2. Final positional parameters for the non-hydrogen atoms in $Ru_3(CO)_{11}(PFcPh_2)$ esd's refer to the last digit printed

Atom	x	y	z
Ru(1)	0.35109(4)	0.84941(3)	0.25425(2)
Ru(2)	0.43057(5)	1.04110(4)	0.30748(2)
Ru(3)	0.54248(5)	0.77775(4)	0.37681(2)
Fe	0.26747(8)	0.74979(7)	0.03993(4)
P	0.34807(14)	0.65305(11)	0.22754(6)
O(1)	0.1365(5)	1.0496(4)	0.1473(2)
O(2)	0.6510(5)	0.8619(4)	0.1450(2)
O(3)	0.0357(5)	0.8493(4)	0.3559(2)
O(4)	0.2987(5)	1.2579(4)	0.1837(2)
O(5)	0.5293(6)	1.1800(5)	0.4052(2)
O(6)	0.7809(5)	1.0042(4)	0.2320(2)
O(7)	0.0848(6)	1.0860(4)	0.3894(3)
O(8)	0.7375(6)	0.8546(5)	0.4709(2)
O(9)	0.6293(5)	0.4889(4)	0.4318(3)
O(10)	0.8385(5)	0.7130(4)	0.2666(2)
O(11)	0.2304(5)	0.8142(5)	0.4836(2)
C(1)	0.2160(6)	0.9700(5)	0.1861(3)
C(2)	0.5429(6)	0.8565(5)	0.1890(3)
C(3)	0.1570(6)	0.8483(5)	0.3219(3)
C(4)	0.3453(6)	1.1781(5)	0.2303(3)
C(5)	0.4919(7)	1.1276(6)	0.3698(3)
C(6)	0.6524(7)	1.0095(5)	0.2594(3)
C(7)	0.2123(8)	1.0619(5)	0.3600(3)
C(8)	0.6654(7)	0.8262(6)	0.4363(3)
C(9)	0.5930(7)	0.5969(6)	0.4107(3)
C(10)	0.7237(7)	0.7423(5)	0.3045(3)
C(11)	0.3410(7)	0.8071(5)	0.4412(3)
C(21)	0.2545(5)	0.6641(4)	0.1469(2)
C(22)	0.0987(6)	0.7492(5)	0.1278(3)
C(23)	0.0486(6)	0.7088(5)	0.0729(3)
C(24)	0.1706(7)	0.5991(5)	0.0569(3)
C(25)	0.2988(6)	0.5698(4)	0.1017(3)
C(26)	0.4266(10)	0.8609(7)	0.0123(3)
C(27)	0.2680(10)	0.9335(6)	−0.0051(3)
C(28)	0.2255(8)	0.8770(7)	−0.0548(3)
C(29)	0.3548(9)	0.7697(7)	−0.0661(3)
C(30)	0.4779(7)	0.7607(7)	−0.0251(3)
C(31)	0.2337(5)	0.5568(4)	0.2959(2)
C(32)	0.1437(6)	0.4883(4)	0.2768(3)
C(33)	0.0638(6)	0.4144(5)	0.3286(3)
C(34)	0.0727(6)	0.4062(5)	0.4005(3)
C(35)	0.1612(7)	0.4743(5)	0.4202(3)
C(36)	0.2416(6)	0.5490(5)	0.3686(3)
C(41)	0.5482(6)	0.5353(4)	0.2139(3)
C(42)	0.5960(6)	0.4187(5)	0.2610(3)
C(43)	0.7458(7)	0.3301(5)	0.2480(4)
C(44)	0.8506(6)	0.3582(6)	0.1883(4)
C(45)	0.8075(7)	0.4736(6)	0.1421(3)
C(46)	0.6578(6)	0.5614(5)	0.1544(3)

76.8. 77.4 (2s, C(2, 5), C(3, 4)), 129.8–134.3 (m, Ph), 214.3 (m, CO).

Anal. calcd. for $C_{56}H_{52}FeO_{10}P_2Ru_3$: C 51.98, H 4.05; found: C 51.39, H 4.00.

(*b*) *Preparation of* $Ru_3(CO)_8(\mu\text{-}dppf)_2$. A mixture of $Ru_3(CO)_{12}$ (50 mg, 0.078 mmol) and dppf (88 mg, 0.158 mmol) was dissolved in dry THF (40 mL). The reaction mixture was heated at reflux point for 1 h, after which time the reaction, which was monitored by TLC, was judged to be complete. After cooling, the solvent was removed *in vacuo* and the mixture was separated by using column chromatography on silica. Light petroleum eluted a trace amount of dppf; acetone eluted $Ru_3(CO)_8(dppf)_2$ which was recrystallized from CH_2Cl_2/heptane; mp 160°C dec. (67% yield). Infrared (CH_2Cl_2) ν(CO) 2052m, 1980vs (br), 1910w cm^{-1}. ^1H NMR ($CDCl_3$) δ 7.73 (m, 40), 4.21–3.90 (m, 16). Mass spec. (FAB) m/z 1636 $(P\text{-}1)^{+\ -1}$.

Anal. calcd. for $C_{76}H_{56}O_8Fe_2P_4Ru_3$: C 55.78, H 3.45; found: C 54.78, H 3.76.

10. Hydrogenation of $Ru_3(CO)_{10}(\mu\text{-}dppf)$. The complex (100 mg, 0.09 mol) was dissolved in cyclohexane and the solution was placed in the glass liner of a small autoclave which was then charged with hydrogen (225 psi). The reactants were heated (80°C, 18 h), cooled, and the solvent was removed. The solid residue given gave seven bands on a preparative TLC plate. Only band 6 (R_f = 0.50, 3/1/1 light petroleum/acetone/diethyl ether) contained a significant amount of material which was identified as $Ru_4(\mu\text{-}H)_4(CO)_{10}(\mu\text{-}dppf)$ (50 mg, 46% yield) by comparison with an authentic ample.

11. Preparation of $Ru_4(\mu\text{-}H)_4(CO)_{10}(\mu\text{-}dppf)$. A mixture of $Ru_4(\mu\text{-}H)_4(CO)_{12}$ (100 mg, 0.134 mmol) and dppf (78 mg, 0.14 mmol) was dissolved in THF (25 mL). A THF solution of the ketyl was added (0.2 mL) and the reaction solution darkened immediately. The solvent was removed *in vacuo*, the residue redissolved in the minimum volume of dichloromethane and purified by preparative TLC (3/1/1 petroleum ether/diethyl ether/acetone). Only band 5 (R_f = 0.50), of six, contained sufficient material for characterization. This solid was recrystallized from dichloromethane/methanol at −30°C to give dark red crystals of $Ru_4(\mu\text{-}H)_4(CO)_{10}(dppf)$ (80 mg, 48% yield) mp 160°C (dec.). ^1H NMR ($CDCl_3$) δ 4.4 (m, 8), 7.4(m, 20), −16.9 (s, 4). Mass spec. (FAB) m/e 1244 (P^+). Infrared ν(CO) 2088w(sh), 2076s, 2054s, 2036vs, 2016s, 1990m, 1985m, 1977s cm^{-1}.

Anal. calcd. for $C_{44}H_{32}FeO_{10}P_2Ru_4$: C 41.43, H 2.54; found: C 42.53, H 2.60.

Crystal structure analysis of $Ru_3(CO)_{10}(\mu\text{-}dppf)$[2]

A single crystal of $Ru_3(CO)_{10}Fe[C_5H_4P(C_6H_5)_2]_2$ was selected and affixed to the end of a glass fibre and mounted on the diffractometer. Unit cell dimensions and the orientation matrix were determined by least-squares analysis of the setting angles of 25 reflections, widely distributed in reciprocal space ($23° < 2\theta < 31°$), which were accurately centred. Crystal data are given in Table 1.

The intensities of a unique data set ($\pm h$, k, l) were measured as outlined in Table 1. Two standards, measured at regular intervals, showed small fluctuations in intensity (all < ±2%) and data were scaled accordingly. All data were corrected for absorption (T range 0.779–0.840) (31). The structure was solved by heavy-atom techniques. Refinement of the non-hydrogen atoms with isotropic temperature factors converged at R_F 0.056. Subsequently these atoms were refined with anisotropic temperature factors. Hydrogen atom coordinates were calculated (d(C—H) =0.95 Å) and their isotropic temperature factors were set equal to U_{iso} of the C atoms to which they were attached. Refinement (hydrogen atom parameters invariant) led to R_F = 0.018. Hydrogen atoms parameters were recalculated and their positional parameters were allowed to refine and an extinction parameter (32) was added. The structure was refined to completeness (all shift-to-error ratios < 0.01). Final R_F = 0.017. All features in a final difference map were < 0.24(5) e $Å^{-3}$.

Refinement throughout was by least-squares analysis minimizing the function $\Sigma w(|F_o| - |F_c|)^2$. The weighting scheme, w, was unity in the early stages of refinement and $1/[\sigma(F))^2 + 0.0003F^2)]$ in the final cycles. Neutral scattering factors with anomalous dispersion corrections were used (33). Computer programs were run on a VAX 11/750 computer (34). Atomic coordinates are listed in Table 4, selected bond lengths and angles in Table 5, and a PLUTO plot (34) of the molecule is shown in Fig. 2.

Crystal structure analysis of $Ru_3(CO)_{11}(PFcPh_2)$[2]

Dark red–purple crystals of the complex were obtained from

[2]Full listings of interatomic distances and angles; hydrogen atom positions; thermal parameters; observed and calculated structure factors have been deposited and may be purchased from the Depository of Unpublished Data, CISTI, National Research Council of Canada, Ontario, Canada, K1A 0S2.

TABLE 3. Selected interatomic distances (Å) and angles (deg) for $Ru_3(CO)_{11}(PFcPh_2)$

Atoms	Distance	Atoms	Distance
Ru(1)—Ru(2)	2.8641(6)	P—C(21)	1.816(4)
Ru(1)—Ru(3)	2.9000(6)	P—C(31)	1.849(4)
Ru(2)—Ru(3)	2.8560(7)	P—C(41)	1.833(5)
Ru(1)—P	2.369(1)	C(1)—O(1)	1.136(7)
Ru(1)—C(1)	1.889(5)	C(2)—O(2)	1.155(6)
Ru(1)—C(2)	1.910(5)	C(3)—O(3)	1.133(7)
Ru(1)—C(3)	1.940(6)	C(4)—O(4)	1.131(7)
Ru(2)—C(4)	1.915(6)	C(5)—O(5)	1.128(7)
Ru(2)—C(5)	1.919(6)	C(6)—O(6)	1.132(7)
Ru(2)—C(6)	1.940(6)	C(7)—O(7)	1.130(8)
Ru(2)—C(7)	1.950(6)	C(8)—O(8)	1.126(7)
Ru(3)—C(8)	1.931(6)	C(9)—O(9)	1.137(7)
Ru(3)—C(9)	1.904(6)	C(10)—O(10)	1.134(7)
Ru(3)—C(10)	1.917(6)	C(11)—O(11)	1.142(7)
Ru(3)—C(11)	1.941(6)		

Bonds	Angle	Bonds	Angle
Ru(2)—Ru(1)—Ru(3)	59.48(2)	Ru(3)—Ru(2)—C(6)	83.9(2)
Ru(1)—Ru(2)—Ru(3)	60.89(2)	Ru(3)—Ru(2)—C(7)	92.4(2)
Ru(2)—Ru(3)—Ru(1)	59.63(2)	C(4)—Ru(2)—C(5)	102.9(2)
Ru(2)—Ru(1)—P	164.09(3)	C(4)—Ru(2)—C(6)	92.2(2)
Ru(2)—Ru(1)—C(1)	94.1(1)	C(4)—Ru(2)—C(7)	91.5(2)
Ru(2)—Ru(1)—C(2)	83.2(1)	C(5)—Ru(2)—C(6)	89.2(2)
Ru(2)—Ru(1)—C(3)	94.5(1)	C(5)—Ru(2)—C(7)	91.0(2)
Ru(3)—Ru(1)—P	105.49(3)	C(6)—Ru(2)—C(7)	176.2(2)
Ru(3)—Ru(1)—C(1)	153.1(1)	Ru(1)—Ru(3)—C(8)	148.5(2)
Ru(3)—Ru(1)—C(2)	91.1(2)	Ru(1)—Ru(3)—C(9)	109.5(2)
Ru(3)—Ru(1)—C(3)	88.0(2)	Ru(1)—Ru(3)—C(10)	82.7(2)
P—Ru(1)—C(1)	101.3(1)	Ru(1)—Ru(3)—C(11)	90.1(2)
P—Ru(1)—C(2)	92.5(1)	Ru(2)—Ru(3)—C(8)	89.4(2)
P—Ru(1)—C(3)	89.9(2)	Ru(2)—Ru(3)—C(9)	169.1(2)
C(1)—Ru(1)—C(2)	90.6(2)	Ru(2)—Ru(3)—C(10)	92.3(2)
C(1)—Ru(1)—C(3)	89.3(2)	Ru(2)—Ru(3)—C(11)	87.6(2)
C(2)—Ru(1)—C(3)	177.7(2)	C(8)—Ru(3)—C(9)	101.6(2)
Ru(1)—Ru(2)—C(4)	94.7(2)	C(8)—Ru(3)—C(10)	93.9(2)
Ru(1)—Ru(2)—C(5)	161.9(2)	C(8)—Ru(3)—C(11)	94.4(2)
Ru(1)—Ru(2)—C(6)	94.7(2)	C(9)—Ru(3)—C(10)	86.8(2)
Ru(1)—Ru(2)—C(7)	84.0(2)	C(9)—Ru(3)—C(11)	91.7(2)
Ru(3)—Ru(2)—C(4)	154.7(2)	C(10)—Ru(3)—C(11)	171.7(2)
Ru(3)—Ru(2)—C(5)	102.1(2)		

Can. J. Chem. Downloaded from www.nrcresearchpress.com by 91.121.58.235 on 09/07/12
For personal use only.

hexanes. The data collection and analysis proceeded in essentially the same way as for $Ru_3(CO)_{10}$(dppf). Pertinent data are given in Table 1, selected interatomic distances and angles in Table 3, atomic coordinates in Table 2. A SNOOPI plot (34) of the molecule is shown in Fig. 1.

Results and discussion

The reactions of the ferrocenylphosphines PFc_nPh_{3-n}, $n = 1–3$, with $Fe_3(CO)_{12}$ and $Ru_3(CO)_{12}$, and $Fe(\eta\text{-}C_5H_4PPh_2)_2$, dppf, with $Ru_3(CO)_{12}$ were investigated under a variety of conditions. Because of some difficulties in obtaining the quoted literature yields of compounds PFc_nPh_{3-n}, $n = 1–2$, procedures for their synthesis via LiFc and chlorophosphines have been investigated and these offer some improvement in the ease of isolation of the products (35). If an excess of *n*-BuLi is present in the mixture (it is used to lithiate FcH), reaction with $PhPCl_2$ can result in the isolation of the new phosphine PBuFcPh as described in the Experimental section.

Ferrocenylphosphines are expected to be reasonably bulky and to gain some measure of this, the cone angle (1, 36) for PFc_3 was determined from the crystallogaphic data available for $Ru(CO)_4)(PFc_3)$ (37) by using scale drawings (36). The model assumed a van der Wasls radius of 1.2 Å (38) for the appropriate hydrogen atom and a P—Ru distance of 2.28 Å.

The calculated angle is 178° which is only slightly less than the 182° determined for $(P(CMe_3)_3$. The cone angle for other ferrocenyl phosphines can be calculated by using the equation $\theta = 2/3\Sigma\theta_i/2$, $i = 1–3$, and the known cone angles of PBu_3 and PPh_3 which are 132° and 145°, respectively. Results are as follows: PFc_3, 178°; PFc_2Ph, 167°; $PFcPh_2$, 156°; PBuFcPh, 152°. For comparison the value for $P(CHMe_2)_3$ is 160°.

In the preparative work described next, most attention was

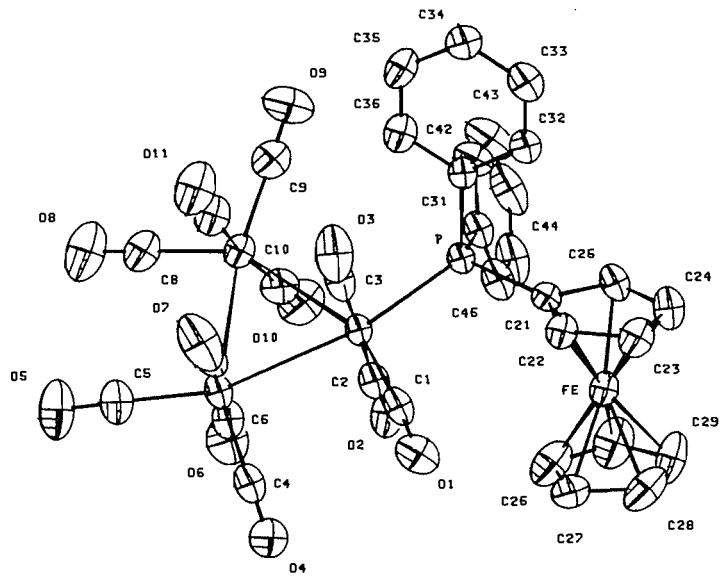

FIG. 1. SNOOPI plot of $Ru_3(CO)_{11}(PFcPh_2)$.

TABLE 4. Final positional parameters for the non-hydrogen atoms in $Ru_3(CO)_{10}$(dppf), esd's refer to the last digit printed

Atom	*x*	*y*	*z*
Ru(1)	0.00000	0.062804(16)	0.25000
Ru(2)	0.026019(14)	0.196239(11)	0.169219(15)
Fe	0.00000	0.44064(3)	0.25000
P	0.02532(5)	0.30787(4)	0.09267(5)
C(11)	0.1275(2)	0.0706(1)	0.3260(3)
O(11)	0.2024(2)	0.0690(1)	0.3701(2)
C(12)	0.0088(2)	−0.0024(2)	0.1559(2)
O(12)	0.0126(2)	−0.0435(1)	0.1011(2)
C(21)	0.1291(2)	0.2220(2)	0.2909(2)
O(21)	0.1969(1)	0.2374(1)	0.3544(2)
C(22)	0.0941(2)	0.1486(2)	0.1176(2)
O(22)	0.1393(2)	0.1188(1)	0.0925(2)
C(23)	−0.0672(2)	0.1715(2)	0.0564(2)
O(23)	−0.1499(2)	0.1566(1)	−0.0135(2)
C(31)	−0.0175(2)	0.3897(1)	0.1208(2)
C(32)	0.0125(2)	0.4633(2)	0.1233(2)
C(33)	−0.0503(2)	0.5097(2)	0.1296(3)
C(34)	−0.1190(2)	0.4675(2)	0.1306(2)
C(35)	−0.0994(2)	0.3942(2)	0.1252(2)
C(41)	0.1339(2)	0.3376(1)	0.1084(2)
C(42)	0.1589(2)	0.3329(2)	0.0332(2)
C(43)	0.2406(2)	0.3580(2)	0.0476(3)
C(44)	0.2970(2)	0.3889(2)	0.1359(3)
C(45)	0.2746(2)	0.3935(2)	0.2126(3)
C(46)	0.1938(2)	0.3673(2)	0.1993(2)
C(51)	−0.0404(2)	0.3056(2)	−0.0449(2)
C(52)	−0.0311(3)	0.2484(2)	−0.0992(3)
C(53)	−0.0775(3)	0.2458(3)	−0.2022(3)
C(54)	−0.1353(3)	0.3000(3)	−0.2518(3)
C(55)	−0.1479(3)	0.3566(3)	−0.2010(3)
C(56)	−0.1001(2)	0.3600(2)	−0.0968(2)

given to the isolation and characterization of complexes which would be useful for further studies relating to the trapping of ferrocyne.

Iron carbonyl complexes. Providing mild conditions are used, it is possible to prepare carbonyl substituted derivatives of $Fe_3(CO)_{12}$ (11, 14, 15, 29, 34–41) but only limited information is available about thermal decomposition of these clusters to products other than derivatives of $Fe(CO)_5$ (41). $Fe_3(CO)_{12}$ can be activated for substitution reactions by the diphenylketyl radical anion (21) to produce, for example, $Fe_3(CO)_{11}(PPh_3)$ in high yield; these are very mild conditions. We now find that this approach is successful for the synthesis of $Fe_3(CO)_{11}(PFcPh_2)$, a complex that is also produced under mild thermal and photochemical conditions. Purification of $Fe_3(CO)_{11}(PFcPh_2)$ for microanalysis is difficult and the electron impact mass spectrum is that of its decomposition product $Fe(CO)_4(PFcPh_2)$. However, the colour and infrared spectrum of the cluster derivative is characteristic (11).

Another unstable cluster derivative, $Fe_3(CO)_{11}(PBuFcPh)$, is produced from a photochemical reaction. This same reaction also affords some $Fe_3(CO)_{10}(PBuFcPh)_2$ which is more stable and better characterized. The ν(CO) band envelope has the typical pattern and a bridging carbonyl band is clearly seen in the solution spectrum (11). Reaction of $Fe_3(CO)_{12}$ with the more bulky phosphines PFc_2Ph and PFc_3 even under mild conditions results in cluster breakdown and the formation of $Fe(CO)_4L$. The compound with L = PFc_3 is a previously known product of the reaction of $Fe(CO)_5$ with PFc_3 (4). Two other $Fe(CO)_4L$ derivatives that are reasonably stable and adequately characterized were also isolated where L = $PFcPh_2$ and PBuFcPh.

Ruthenium carbonyl derivatives

As anticipated (11) the radical anion-initiated reaction of $Ru_3(CO)_{12}$ with the ferrocenylphosphines in 1:1 molar ratio afforded good yields of the monosubstituted derivatives $Ru_3(CO)_{11}L$, L = PFc_3, PFc_2Ph, $PFcPh_2$. The crystal structure of $Ru_3(CO)_{11}(PFcPh_2)$ is described below (see Fig. 1). The infrared spectra of these complexes are similar to those of other derivatives of this type such as $Ru_3(CO)_{11}(PPh_3)$.

Two disubstituted complexes $Ru_3(CO)_{10}L_2$, L = PFc_2Ph, $PFcPh_2$ were prepared from ketyl-initiated reaction by utilizing a 1:2 molar ratio of reactants. (In one radical anion initiated reaction a small amount of $Ru_3(CO)_{10}(PFc_2Ph)_2$ was produced from a 1:1 mixture of starting materials. It is possible that this results from a concurrent thermal reaction.) Only one mono-

Can. J. Chem. Downloaded from www.nrcresearchpress.com by 91.121.58.235 on 09/07/12
For personal use only.

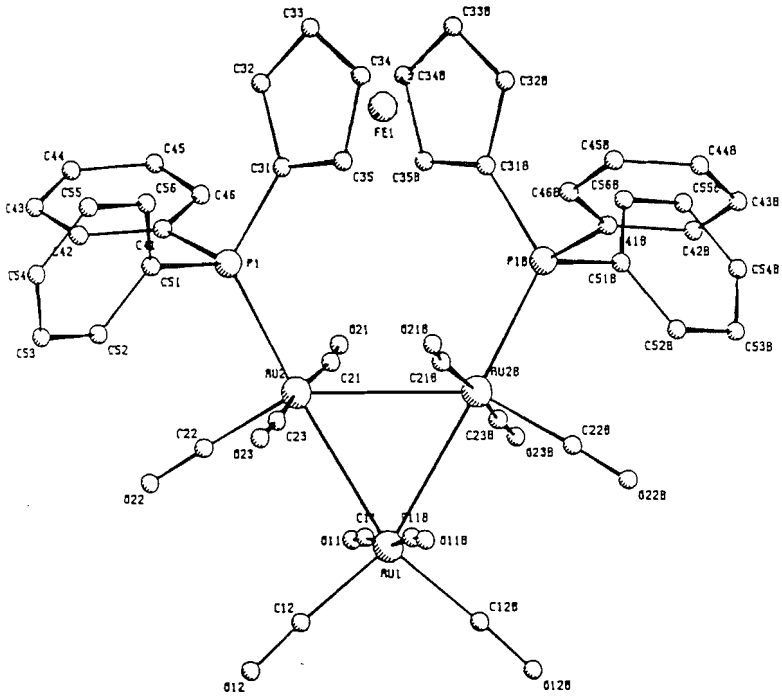

FIG. 2. PLUTO plot of $Ru_3(CO)_{10}(dppf)$.

nuclear ruthenium compound, $Ru(CO)_4(PFc_3)$, was isolated during these studies. This crystallized out during attempts to purify $Ru_3(CO)_{11}(PFc_3)$; it can be prepared in a more controlled manner by ultraviolet irradiation of solutions of $Ru_3(CO)_{11}(PFc_3)$. Its structure (37) is that of a slightly distorted trigonal bipyramid with the ligand in an axial position. This is the expected structure for derivatives of $M(CO)_5$ (M = Fe, Ru, Os) (42); notable exceptions are $M(CO)_4(SbPh_3)$, M = Ru, Os, where the ligand occupies an equatorial position.

Some of the thermal reactions afford complexes which have the formula $Ru_3(CO)_9L_3$ based on their spectroscopic properties. These were not fully characterized because of problems with obtaining analytically pure samples (35) (complexes with the lowest degree of substitution and the lowest number of ferrocenyl substituents on the phosphorous atom are the easiest to crystallize) and because such compounds are less interesting from the point of view of thermal decomposition to ferrocyne fragments.

When radical anion catalysis is used in the reaction between $Ru_3(CO)_{12}$ and dppf a number of products are obtained. These are difficult to isolate by chromatography and are generally unstable in solution. One product, however, was air-stable and proved to be the complex $Ru_3(CO)_{10}(\mu\text{-dppf})$ whose determined structure is shown in Fig. 2. This compound is much better prepared (76% yield) from the carbonyl and ligand by a [ppn][OAc] catalysed reaction (22) in THF solution. The complex can be isolated as an unsual bis-cyclohexane solvate as indicated by the microanalytical results and by the spectroscopic properties.

The thermal reaction between $Ru_3CO)_{12}$ and dppf in a 1:2 mole ratio in refluxing cyclohexane affords a purple solid which is probably $Ru_3(CO)_8(\mu\text{-dppf})_2$. The FAB mass spectrum shows a strong peak at m/e 1636 (calc M^+ 1637). The infrared spectrum is very similar to that of the dppm, $Ph_2PCH_2PPh_2$, analogue (43). The hydrogenation of $Ru_3(CO)_{10}(\mu\text{-dppf})$ affords one major product and a number of minor uncharacterized ones. The major product has a $\nu(CO)$ spectrum and presumably structure similar to that of $Ru_4(\mu\text{-H})_4(CO)_{10}(\mu\text{-dppm})$ (44) and the FAB mass spectrum shows a parent ion at m/z 1244. Presumably hydrogen displaces one PR_2 group from $Ru_3(CO)_{10}(\mu\text{-dppf})$ to give a monodentate dppf complex which aggregates to the Ru_4 complex. This product can be prepared directly from the ketyl-catalyzed reaction of $Ru_4(\mu\text{-H})_4(CO)_{12}$ with dppf.

The mass spectra of the complexes deserve some comments. Electron impact spectra are adequate for the characterization of $M(CO)_4L$ complexes and they show strong parent peaks and stepwise loss of carbonyl groups. Although useful electron impact spectra of iron cluster derivatives have been reported (40), in the present instance the spectra of both $Fe_3(CO)_{10}(PBuFcPh)_2$ and $Fe_3(CO)_{11}(PFcPh_2)$ show peaks associated with $[Fe(CO)_4L]^+$ only. The ruthenium complexes do not afford parent ions and seem to fragment at both the ligand and the cluster; the spectra also depend on the probe temperature. For example, the spectrum of $Ru_3(CO)_{10}(PFcPh_2)_2$ has peaks at the following m/z values: 770 ($[Ru_3(CO)_{10}PPh_2]^+$), 713 ($[Ru_2(CO)_5L]^+$), 655 ($[Ru_3(CO)_3L]^+$), 630 ($[Ru_2(CO)_2L]^+$), etc.

Fast atom bombardment (FAB) mass spectra are known to give better results for clusters (45). Attempts were made to obtain FAB mass spectra for $Fe_3(CO)_{11}(PFcPh_2)$ and the $Ru_3(CO)_{11}L$, and $Ru_3(CO)_{10}L_2$ complexes; a number of common solvents were used without any success. Ultimately we found that diallyl phthalate can be used as a solvent for $Ru_3(CO)_{10}L_2$ and the FAB mass spectra show parent peaks and peaks associated with stepwise loss of ten carbonyl groups. A further series corresponding to $[Ru_2(CO)_7L]^+ \rightarrow [Ru_2L]^+$ is also present.

Structural studies

The structure of $Ru_3(CO)_{11}(PFcPh_2)$ is shown in Fig. 1. Structural studies have been made on a wide range of derivatives of $Ru_3(CO)_{12}$ of formula $Ru_3(CO)_{12-n}L_n$ (n = 1–4) where L is a monodentate ligand and some general trends have emerged

Can. J. Chem. Downloaded from www.nrcresearchpress.com by 91.121.58.235 on 09/07/12
For personal use only.

Can. J. Chem. Downloaded from www.nrcresearchpress.com by 91.121.58.235 on 09/07/12
For personal use only.

TABLE 5. Selected interatomic distances (Å) and angles (deg) for $Ru_3(CO)_{10}(dppf)$[a]

Atoms	Distance	Atoms	Distance
Ru(1)—Ru(2)	2.8600(4), 2.862[b]		
Ru(2)—Ru(2′)	2.9284(5), 2.930[b]	Ru(2)—P	2.3503(8), 2.352[b]
Ru(1)—C(11)	1.942(4), 1.948[c]	C(11)—O(11)	1.136(4), 1.146[d]
Ru(1)—C(12)	1.907(4), 1.916[c]	C(12)—O(12)	1.140(4), 1.154[d]
Ru(2)—C(21)	1.923(4), 1.929[c]	C(21)—O(21)	1.148(4), 1.155[d]
Ru(2)—C(22)	1.877(3), 1.884[c]	C(22)—O(22)	1.139(4), 1.152[d]
Ru(2)—C(23)	1.949(3), 1.957[c]	C(23)—O(23)	1.136(4), 1.146[d]
Fe—C(31)	2.044(3)	C(31)—C(32)	1.442(4)
Fe—C(32)	2.044(3)	C(32)—C(33)	1.404(5)
Fe—C(33)	2.047(3)	C(33)—C(34)	1.410(5)
Fe—C(34)	2.058(3)	C(34)—C(35)	1.401(5)
Fe—C(35)	2.049(3)	C(35)—C(31)	1.426(4)
P—C(31)	1.805(3)	Ru(1)···C(23)	3.267(3)
P—C(41)	1.836(3)	Ru(2)···C(11)	3.185(3)
P—C(51)	1.842(3)	Ru(2)···C(21′)	2.995(3)

Bonds	Angle	Bonds	Angle
Ru(2)—Ru(1)—Ru(2′)	61.59(1)	Ru(1)—Ru(2)—Ru(2′)	59.21(1)
Ru(2)—Ru(1)—C(11)	80.64(9)	Ru(1)—Ru(2)—P	171.78(2)
Ru(2)—Ru(1)—C(11′)	92.06(9)	Ru(1)—Ru(2)—C(21)	83.28(9)
Ru(2)—Ru(1)—C(12)	98.58(10)	Ru(1)—Ru(2)—C(22)	90.89(10)
Ru(2)—Ru(1)—C(12′)	158.73(10)	Ru(1)—Ru(2)—C(23)	93.52(9)
C(11)—Ru(1)—C(11′)	171.54(12)	Ru(2′)—Ru(2)—P	117.77(2)
C(11)—Ru(1)—C(12)	92.06(13)	Ru(2′)—Ru(2)—C(21)	99.44(9)
C(11)—Ru(1)—C(12′)	93.26(14)	Ru(2′)—Ru(2)—C(22)	144.57(10)
C(12)—Ru(1)—C(12′)	102.01(15)	Ru(2′)—Ru(2)—C(23)	72.95(9)
Ru(2)—P—C(31)	121.96(9)	P—Ru(2)—C(21)	89.94(9)
Ru(2)—P—C(41)	114.66(9)	P—Ru(2)—C(22)	94.33(10)
Ru(2)—P—C(51)	112.96(10)	P—Ru(2)—C(23)	92.63(9)
C(31)—P—C(41)	102.12(13)	C(21)—Ru(2)—C(22)	94.91(13)
C(31)—P—C(51)	100.15(14)	C(21)—Ru(2)—C(23)	172.30(13)
C(41)—P—C(51)	102.30(13)	C(22)—Ru(2)—C(23)	92.14(13)
Ru(1)—C(11)—O(11)	174.3(3)	Ru(2)—C(21)—O(21)	169.6(3)
Ru(1)—C(12)—O(12)	177.2(3)	Ru(2)—C(22)—O(22)	175.7(3)
Cp—Fe—Cp[e]	174.6	Ru(2)—C(23)—O(23)	174.9(3)

[a]Atoms indicated by primes have been transformed by $(\bar{x}, y, 1/2 - z)$.
[b]Rigid body: Ru(1), Ru(2), Ru(2′), Fe, P, P′.
[c]Corrected for motion of C riding on corresponding Ru.
[d]Calculated from distance Ru—C (corrected for motion of C riding on Ru), distance Ru···O (corrected for motion of O riding on Ru) and angle Ru—C—O.
[e]Cp is the centroid of C(31)—C(35).

(21, 46, 47); those of relevance to the structure of $Ru_3(CO)_{11}(PFcPh_2)$ are as follows: (*i*) *P*-ligands coordinate equatorial sites, (*ii*) the Ru—Ru bond *cis* to *P*-ligands is the longest of the three separations, and (*iii*) bonds from axial CO groups to Ru are generally longer than those from equatorial CO groups except when the latter are *cis* to a *P*-ligand. Taking these in turn (*i*) is certainly true, as is (*ii*). The longest Ru—Ru bond is *cis* to the ligand and has a length of 2.9000(6) Å. Pöe and co-workers (48) have shown that a reasonable curve can be obtained if the *cis* Ru—Ru bond length is plotted against the cone angle of L. As discussed above the cone angle of $PFcPh_2$ is 156° and the measured bond length of 2.90 Å is not far from that which would be predicted on the bases of the curve. With regard to (*iii*), at the unsubstituted ruthenium atoms, the axial bonds Ru(2)—C(6) (1.940(6) Å) and Ru(2)—C(7) (1.950(6) Å) seem longer than the equatorial Ru—C bonds (1.915(6) and 1.919(6) Å). The situation is less clear at Ru(3) where the axial Ru—C distances are 1.917(6) and 1.941(6) Å and equatorial Ru—C distances are 1.931(6) and 1.904(6) Å. At the substituted ruthenium atom Ru(1) the axial Ru—C bonds are 1.889(5) and 1.940(6) Å whereas the equatorial Ru—C bond, which should be longer in this case, is intermediate at 1.910(5) Å.

The Ru—P distance of 2.369(1) Å lies in the range 2.24 to 2.43 Å noted by Bruce and co-workers (47). A plot of Ru—P distance against ligand cone angle results in a smooth curve (48) but based on a cone angle of 156°, the observed Ru—P distance is shorter than would be predicted. Otherwise the structure shown in Fig. 1 resembles other known $Ru_3(CO)_{11}L$ derivatives in that the metal cluster skeleton is distorted from the D_{3h} symmetry found in $Ru_2(CO)_{12}$, principally by rotation of the $Ru(CO)_4$ unit (46, 47).

The structure of $Ru_3(CO)_{10}(\mu\text{-dppf})$ is shown in Fig. 2. The *R*-value of 1.7% is one of the lowest obtained for a ruthenium carbonyl derivative. Because of this, some corrected distances have been calculated and these are listed in Table 5; in general they are systematically longer than the uncorrected lengths (as

might be expected) with corrections far longer than would be expected from the least-squares esd.

The ligand occupies equatorial positions (see (*i*) above). The longer Ru(2)—Ru(2′) bond, 2.9284(5) Å, is situated *cis* to *two* Ru—P bonds (see (*ii*) above) and this length is greater than the longest bond in $Ru_3(CO)_{11}(PFcPh_2)$, (2.9000(6) Å) and in fact, is longer than that found in any $Ru_3(CO)_{12-n}L_n$ (n = 1–4) derivative[3] (46, 47). This lengthening is probably not entirely due to a repulsive *cis* effect as the Ru—Ru bond length of other $Ru_3(CO)_{10}$(L–L) complexes do not follow the trend. Some results are as follows (L—L, supported bond length, unsupported bond length(s)): dppe; 2.856(1), 2.855(1), 2.847(1) (49); dppm, 2.834(1), 2.841(1), 2.860(1) Å (50); $Ph_2PC(=CH_2)PPh_2$, 2.836(1), 2.862(1), 2.840(1) Å (51); $\overleftarrow{PPhCH_2PPhC}_6H_4$, 2.884(1), 2.851(1), 2.848(1) Å (52), and to reiterate dppf, 2.9284(5), 2.8600(4), 2.8600(4) Å. It seems that these Ru—Ru lengths are largely controlled by steric demands and the bite of the ligand, a point that has been made before (53).

The bonds from the axial carbonyl group to the unique Ru(1) in $Ru_3(CO)_{10}$(μ-dppf) are longer (1.942(4) Å) than those from the axial carbonyl (1.907(4) Å), and this is true for the other known $Ru_3(CO)_{10}$(L—L) structures. The axial Ru(2)—C(22) bond is also shorter (1.877(3) Å) than the axial Ru(2)—C bonds (1.923(4), 1.949(3) Å) contrary to (*iii*) above and again this trend is found in all the other $Ru_3(CO)_{10}$(L—L) structures (49–52). For example, in the dppe derivative Ru(2)—C(31) axial (1.933(2) Å) is longer than Ru(2)—C(32) equatorial (1.891(2) Å) (49).

The Ru(2)—P distance in the dppf derivative (2.3503(8) Å) is marginally shorter than those observed in $Ru_3(CO)_{11}(PFcPh_2)$ (2.369(1) Å). However it should be pointed out that it is longer than other Ru—P bonds measured in $Ru_3(CO)_{10}$(L—L) complexes, the longest being 2.334(2) Å when L—L = dppm (49). This again is an indication of strong steric interactions because on electronic grounds long Ru—Ru bonds should be associated with short Ru—P bonds.

Finally, it should be pointed out that dppf is a reasonably flexible ligand that can form chelated complexes; for comparison the Rh—P bond length in $[Rh(dppf)(nbd)]^+$ is 2.356(1) Å and the measured P.....P distances range from 3.447(1) Å in $(dppf)PdCl_2$ to 3.783(1) Å in $(dppf)Mo(CO)_4$ (54).

Acknowledgements

The authors thank the Natural Sciences and Engineering Research Council of Canada (W.R.C., M.I.B., and F.W.B.E.) and the Australian Research Grants Scheme (M.I.B.) for financial support.

1. C. A. McAuliffe and W. Levason. Phosphine, arsine, and stibine complexes of the transition elements. Elsevier, New York. 1979; C. A. McAuliffe. *In* Comprehensive coordination chemistry. Vol. 2. *Edited by* G. Wilkinson, R. D. Gillard, and J. A. McCleverty. Pergamon, Oxford. 1987. pp. 989–1066.
2. W. R.Cullen and J. D. Woollins. Coord. Chem. Rev. **39**, 1 (1981).
3. G. P. Sollott, D. L. Daughdrill, and W. R. Peterson. J. Organomet. Chem. **133**, 347 (1977).
4. C. U. Pittman and G. O. Evans. J. Organomet. Chem. **43**, 361 (1972).
5. J. C. Kotz, C. L. Nivert. J. M. Liever, and R. C. Reed. J. Organomet. Chem. **52**, 387 (1973).
6. J. C. Kotz, C. L. Nivert, J. M. Liever, and R. C. Reed. J. Organomet. Chem. **91**, 87 (1975).
7. S. S. Crawford and H. D. Kaesz. Inorg. Chem. **16**, 3193 (1977).
8. P. Gilbert, D. Daughdrill, and W. R. Peterson. J. Organomet. Chem. **133**, 347 (1977).
9. J. J. Bishop and A. Davison. Inorg. Chem. **10**, 826 (1971).
10. M. I. Bruce, I. R. Butler, W. R. Cullen, G. A. Koutsantonis, M. R. Snow, and E. R. T. Tiekink. Aust. J. Chem. **41**, 963 (1988); A. W. Rudie, D. W. Lichtenberg, M. L. Katcher, and A. Davison. Inorg. Chem. **17**, 2859 (1978).
11. S. M. Grant and A. R. Manning. Inorg. Chim. Acta, **31**, 41 (1978).
12. P. E. Riley and R. E. Davis. Inorg. Chem. **19**, 159 (1980).
13. R. J. Angelici and E. E. Siefert. Inorg. Chem. **5**, 1457 (1966).
14. D. J. Dahm and R. A. Jacobson. J. Am. Chem. Soc. **90**, 5106 (1968).
15. W. S. McDonald, J. R. Moss, G. Raper, B. L. Shaw, R. Greatrex, and N. N. Greenwood. J. Chem. Soc. Commun. 1295 (1969).
16. F. A. Cotton and R. V. Parish. J. Chem. Soc. 1440 (1960); A. F. Clifford and A. K. Mukherjee. Inorg. Chem. **2**, 151 (1963).
17. B. F. G. Johnson, J. Lewis, and M. V. Twigg. J. Chem. Soc. Dalton Trans. 1876 (1975).
18. M. I. Bruce, D. C. Kehoe, J. G. Matisons, B. K. Nicholson, P. H. Rieger, and M. L. Williams. J. Chem. Soc. Chem. Commun. 442 (1982).
19. A. Pöe and M. V. Twigg. Inorg. Chem. **13**, 2982 (1974); M. I. Bruce, J. G. Matisons, and B. K. Nicholson. J. Organomet. Chem. **247**, 321 (1983); E. J. Forbes, N. Goodhand, D. L. Jones, and T. A. Hamor. J. Organomet. Chem. **182**, 143 (1979); M. I. Bruce, T. W. Hambley, B. K. Nicholson, and M. R. Snow. J. Organomet. Chem. **182**, 143 (1979); A. W. Coleman, D. F. Jones, P. H. Dixneuf, C. Brisson, J-J Bonnet, and G. Lavigne. Inorg. Chem. **23**, 952 (1984); G. Lavigne, N. Lugan, and J-J. Bonnet. Acta Crystallogr. Sect. B, **38**, 1911, (1982).
20. M. F. Desrosiers, D. A. Wink, F. Trautman, A. E. Friedman, and P. C. Ford. J. Am. Chem. Soc. **108**, 1917 (1986).
21. M. I. Bruce. Coord. Chem. Rev. **76**, 1 (1987).
22. G. Lavigne and H. D. Kaesz. J. Am. Chem. Soc. **106**, 4647 (1984).
23. P. E. Garrou. Chem. Rev. **85**, 119 (1985); C. W. Bradford, R. S. Nyholm, G. J. Gainsford, J. M. Guss, P. R. Ireland, and R. Mason. J. Chem. Soc. Chem. Commun. 87 (1972); G. J. Gainsford, J. M. Guss, P. R. Ireland, R. Mason, C. W. Bradford, and R. S. Nyholm. J. Organomet. Chem. **40**, C70 (1972); A. J. Deeming and M. J. Underhill. J. Chem. Soc. Dalton Trans. 2727 (1973); A. J. Arce and A. J. Deeming. J. Chem. Soc. Dalton Trans. 1155 (1982); S. C. Brown, J. Evans, and L. E. Smart. J. Chem. Soc. Chem. Commun. 1021 (1980); A. J. Deeming, I. D. Rothwell, M. B. Hursthouse, and J. D. J. Backer-Dirks. J. Chem. Soc. Dalton Trans. 1879 (1981).
24. M. I. Bruce, G. Shaw, and F. G. A. Stone. J. Chem. Soc. Dalton Trans. 2094 (1972); M. I. Bruce, J. M. Guss, R. Mason, B. W. Skelton, and A. H. White. J. Organomet. Chem. **251**, 261 (1983); S. A. R. Knox, B. R. Lloyd, A. G. Orpen, J. M. Vias, and M. J. Weber. J. Chem. Soc. Chem. Commun. 1498 (1987).
25. S. T. Chacon, W. R. Cullen, M. I. Bruce, F. W. B. Einstein, and R. H. Jones. Organometallics, **7**, 2273 (1988).
26. G. P. Sollott and E. Howard. J. Org. Chem. **27**, 4034 (1962).
27. G. P. Sollott and W. R. Peterson. J. Organomet. Chem. **5**, 491 (1965).

[3] $Ru_3(CO)_{10}$(μ-dppf) can be regarded as being equivalent to "$Ru_3(CO)_{10}(PFcPh)_2$" in which both tertiary phosphine ligands are equatorial. In practice $Ru_3(CO)_{10}L_2$ complexes are found to have a linear L—Ru—Ru—L arrangement.

Can. J. Chem. Downloaded from www.nrcresearchpress.com by 91.121.58.235 on 09/07/12
For personal use only.

28. G. P. SOLLOTT, and W. R. PETERSON. J. Organomet Chem. **19**, 143 (1969).
29. G. P. SOLLOTT, H. E. MERTWOY, S. PORTNOY, and J. L. SNEED. J. Org. Chem. **28**, 1090 (1963).
30. A. W. SMALLEY. Org. Prep. Proc. Int. **10**, 195 (1978).
31. N. W. ALCOCK. *In* Crystallographic computing. *Edited by* F. Ahmed. Munksgaard, Copenhagen. 1970.
32. A. C. LARSON. *In* Crystallography computing. *Edited by* F. Ahmed. Munksgaard, Copenhagen. 1970.
33. International tables for X-ray crystallography. Vol. 4. Kynoch, Birmingham, England. 1974.
34. Computer programs were run on in-house MICROVAX I (*a*) R. J. GABE, A. C. LARSON, F. L. LEE, and Y. LE PAGE. NRC VAX Crystal Structure System. National Research Council of Canada, Ottawa, Ontario. 1984; (*b*) D. J. WATKINS, R. J. CARRUTHERS, and P. W. BETTERIDGE. CRYSTALS user guide. Chemical Crystallography Laboratory, University of Oxford, Oxford, England. 1985; (*c*) SNOOPI Plot Diagram. Chemical Crystallography Laboratory of Oxford, Oxford, England. 1984.
35. S. T. CHACON. M.Sc. Thesis, University of British Columbia, Vancouver, B.C. 1986.
36. C. A. TOLMAN. Chem. Rev. **77**, 313 (1977).
37. F. W. B. EINSTEIN and A. C. WILLIS. Unpublished results.
38. R. C. WEAST and M. J. ASTLE. CRC Handbook of Chemistry and Physics. Chemical Rubber Publishing Company, Boca Raton, Florida. 1980. p. D-194.
39. W. R. CULLEN, D. A. HARBORNE, B. V. LIENGME, and J. R. SAMS. Inorg. Chem. **9**, 1839 (1970).
40. L. S. CHIA, W. R. CULLEN, J. R. SAMS, and J. E. H. WARD. Can. J. Chem. **51**, 3223 (1973).
41. P. J. ROBERTS, B. R. PENFOLD, and J. TROTTER. Inorg. Chem. **9**, 2137, (1970); F. W. B. EINSTEIN and R. D. J. JONES. J. Chem. Soc. Dalton Trans. 2563 (1972).
42. L. R. MARTIN, F. W. B. EINSTEIN, and R. K. POMEROY. Inorg. Chem. **24**, 2777 (1985).
43. G. LAVIGNE, N. LUGAN, and J-J BONNET. Organometallics, **1**, 1040 (1982).
44. M. L. WILLIAMS. Ph.D. Thesis. University of Adelaide, Adelaide, Australia. 1986.
45. J. M. MILLER. Adv. Inorg. Chem. Radiochem. **28**, 1 (1984). M. I. BRUCE and M. J. LIDDELL. Appl. Organomet. Chem. **1**, 191 (1987).
46. M. I. BRUCE, M. J. LIDDELL, C. A. HUGHES, B. W. SKELTON, and A. H. WHITE. J. Organomet. Chem. **347**, 157 (1988); M. I. BRUCE, M. J. LIDDELL, O. B. SHAWKATALY, C. A. HUGHES, B. W. SKELTON, and A. H. WHITE. J. Organomet. Chem. **347**, 181 (1988); M. I. BRUCE, M. J. LIDDELL, O. B. SHAWKATALY, I. R. BYUTHEWAY, B. W. SKELTON, and A. H. WHITE. J. Organomet. Chem. **369**, 217 (1989).
47. M. I. BRUCE, M. J. LIDDELL, C. A. HUGHES, J. M. PATRICK, B. W. SKELTON, and A. H. WHITE. J. Organomet. Chem. **347**, 181 (1988).
48. N. M. J. BRODIE, L. CHEN, A. J. PÖE, and J. F. SAWYER. Acta Crystallogr. In press.
49. M. I. BRUCE, T. W. HAMBLEY, B. K. NICHOLSON, and M. R. SNOW. J. Organomet. Chem. **235**, 83 (1982).
50. A. W. COLEMAN, D. F. JONES, P. H. DIXNEUF, C. BRISSON, J-J BONNET, and G. LAVIGNE. Inorg. Chem. **23**, 952 (1984).
51. M. J. HARDING, S. J. MAGIUN, and A. K. SMITH. Acta Crystallogr. **C44**, 237 (1988).
52. N. LUGAN, J. J. BONNET, and J. A. IBERS. J. Am. Chem. Soc. **107**, 4484 (1985).
53. P. J. ROBERTS and J. TROTTER. J. Chem. Soc. A, 1479 (1971).
54. I. R. BUTLER, W. R. CULLEN, T-J KIM, S. J. RETTIG, and J. TROTTER. Organometallics, **4**, 972 (1985); W. R. CULLEN, T.-J KIM, F. W. B. EINSTEIN, and T. JONES. Organometallics, **4**, 346 (1985).

Can. J. Chem. Downloaded from www.nrcresearchpress.com by 91.121.58.235 on 09/07/12
For personal use only.

Synthesis and properties of DNA oligomers containing an O4-ethylated thymine. d(e^{4}TpA), d(Ape^{4}T), d(Ape^{4}TpA), and d(Tpe^{4}TpT)[1]

GARRY W. BUCHKO, FRANK E. HRUSKA,[2] AND KRISHAN L. SADANA
Department of Chemistry, The University of Manitoba, Winnipeg, Man., Canada R3T 2N2

Received February 21, 1990

GARRY W. BUCHKO, FRANK E. HRUSKA, and KRISHAN L. SADANA. Can. J. Chem. **68**, 2011 (1990).

Syntheses via the phosphotriester method are described for DNA oligonucleotides containing O4-ethylated thymine (e^{4}Thy) and adenine (Ade) bases, d(e^{4}TpA), d(Ape^{4}T), and d(Ape^{4}TpA), for their unmodified analogs, d(TpA), d(ApT), and d(ApTpA), and for d(Tpe^{4}TpT). ^{1}H NMR chemical shift data obtained from 10 to 70°C at 300 and 500 MHz show that these molecules form right-handed minihelices at low temperature in aqueous solution; the presence of the O4-ethyl group does not seem to have a drastic effect on the stacking geometry of the thymine base. The presence of right-handed stacking is confirmed by circular dichroic data obtained over a similar temperature range. Coupling constants for the sugar ring indicate that the e^{4}Tp unit of d(e^{4}TpA) does not show the shift towards the 3′-*endo* (*N*) pucker noted for the corresponding unit of d(e^{4}TpT). A prominent quasimolecular ion peak $[M - H]^-$ is observed for the modified and unmodified molecules in the spectra obtained by Fast Atom Bombardment mass spectrometry (FAB-MS) operating in the negative ion mode, indicating that the labile O4-ethyl group is sufficiently stable to withstand the ionization process used in this method. In addition, a number of fragment ion peaks such as $[O4\text{-ethylthymine} - H]^-$ are observed that reveal the potential of FAB-MS for characterizing DNA oligomers modified by alkylating agents.

Key words: oligonucleotides, O-alkylation, stereochemistry, NMR, mass spectrometry.

GARRY W. BUCHKO, FRANK E. HRUSKA et KRISHAN L. SADANA. Can. J. Chem. **68**, 2011 (1990).

On décrit la synthèse, par la méthode du phosphotriester, des oligonucléotides de l'ADN contenant les bases O4-éthylées de la thymine (e^{4}Thy) et de l'adénine (Ade), d(e^{4}TpA), d(Ape^{4}T) et d(Ape^{4}TpA), et leurs analogues qui ne sont pas modifiés, d(TpA), d(ApT), d(ApTpA) et d(Tpe^{4}TpT). Les données relatives aux déplacements chimiques en RMN du ^{1}H, obtenues de 10 à 70°C à 300 et à 500 MHz, montrent que, en solution, à basse température, ces molécules forment des minihélices tournant vers la droite; la présence de groupements O-éthyles ne semble pas affecter beaucoup la géométrie de l'empilement de la base thymine. La présence d'un empilement tournant à droite est confirmé par les données de dichroïsme circulaire obtenues sur la même plage de températures. Les constantes de couplage dans les cycles des sucres indiquent que l'unité e^{4}Tp de d(e^{4}TpA) ne présente pas le déplacement vers la forme 3′-*endo* (*N*) replissée qui a été observée pour l'unité correspondante de d(e^{4}TpT). On a déterminé les spectres de masse par bombardement avec des atomes rapides (SM-BAR) en mode d'ion négatif des molécules tant modifiées que non-modifiées et on observe toujours un pic prédominant qui est pratiquement moléculaire $[M - H]^-$; ce résultat indique que le groupement labile O-éthyle est suffisamment stable pour supporter le processus d'ionisation utilisé dans cette méthode. De plus, on a observé un certain nombre de pics correspondants à des ions de fragmentation, comme $[O4\text{-éthylthymine} - H]^-$, qui révèlent le potentiel de la SM-BAR pour caractériser des oligomères d'ADN qui ont été modifiés par des agents alkylants.

Mots clés : oligonucléotides, O-alkylation, stéréochimie, RMN, spectrométrie de masse.

[Traduit par la revue]

Introduction

Alkylating agents such as alkyl nitrosoureas react with the oxygen atoms of DNA bases to form the O2- and O4-alkylthymines (r^{2}Thy, r^{4}Thy) and O6-alkylguanine (r^{6}Gua), or with the polynucleotide backbone to form alkyltriesters (1). Experimental evidence indicates that the altered thymine (Thy) and guanine (Gua) bases can mispair during replication and lead to mutations (1). On the other hand, the formation of the alkyltriesters does not lead to misincorporation of bases, though their presence has been shown to inhibit in vitro replication by *E. coli* DNA polymerase I (2). Some insight into the action of these agents is provided by the structural information obtained at the monomer level by X-ray crystallographic (3–8) and NMR (9, 10) investigations of O-alkylated nucleosides. More useful are the structural data for oligomer duplexes containing an O-alkylated base, but studies on such duplexes are limited (11, 12).

As part of our study of the structural consequences of base modification, we have been synthesizing DNA oligomers[3] containing r^{4}Thy. Since this base is labile in acid and basic solution (9, 13), these syntheses require considerable care, and for this reason our investigation was begun with molecules containing only r^{4}Thy and the parent Thy base. Initially we described (14) the synthesis of e^{4}TpT and Tpe^{4}T, the O4-ethylated analogues of TpT. This was followed (15) by the synthesis of the corresponding O4-isopropylated dimers, i^{4}TpT and Tpi^{4}T, and the trimer Tpi^{4}TpT. Also provided was their characterization by NMR, Fast Atom Bombardment mass spectrometry (FAB-MS), and circular dichroism (CD). Here we extend our work to oligomers containing an adenine (Ade) as well as an e^{4}Thy base: e^{4}TpA (**1**), Ape^{4}T (**2**), and Ape^{4}TpA (**3**) (Fig. 1). In addition, we report our methods for the synthesis of Tpe^{4}TpT (**7**). ^{1}H NMR as well as FAB-MS and CD data are provided for comparison with the unmodified analogues, TpA (**4**), ApT (**5**), and ApTpA (**6**), and with the oligomers discussed in our earlier manuscripts (14, 15). The data are discussed in terms of the conformational properties of the molecules in aqueous solution.

[1]Presented in part at the XIII International Conference on Magnetic Resonance in Biological Systems, Madison, WI, August 14–19, 1988.

[2]Author to whom correspondence may be addressed.

[3]Since we discuss only DNA oligomers, for convenience TpT will be used to represent d(TpT), and so on. The "d" will be retained for all monomers (dT, e^{4}dT, 5′-dTMP, etc.).

Can. J. Chem. Downloaded from www.nrcresearchpress.com by 91.121.58.235 on 09/07/12
For personal use only.

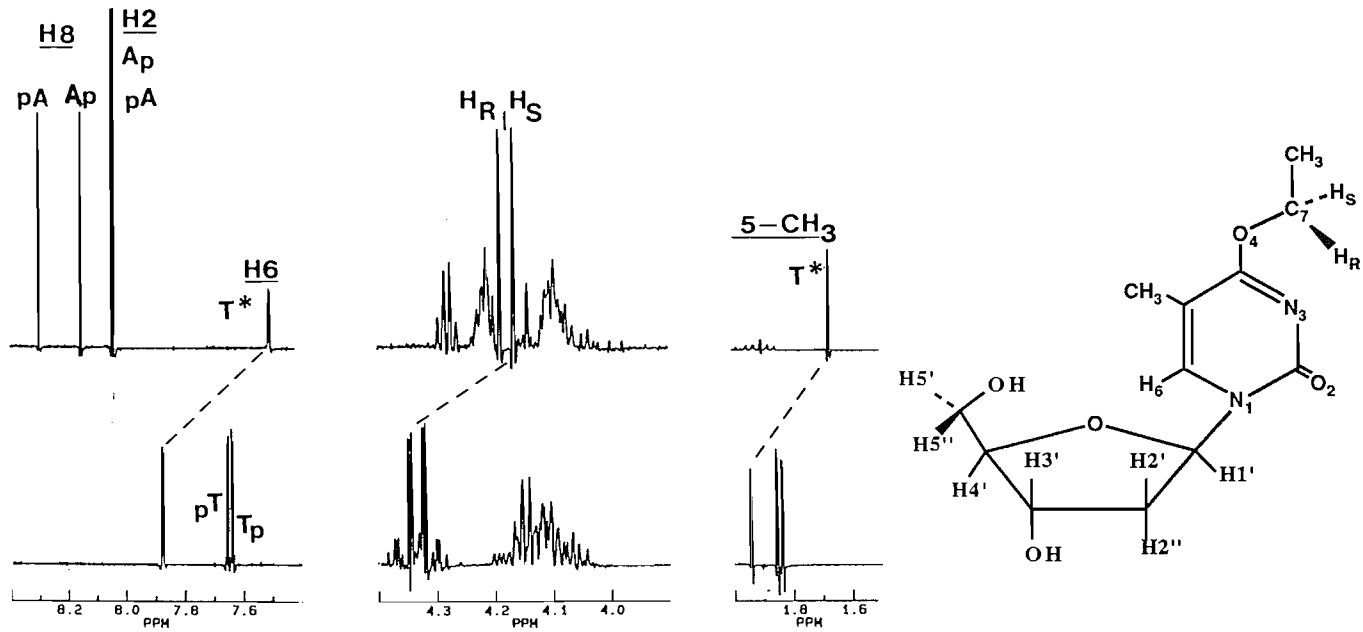

FIG. 1. Right, structure and numbering of e^4dT (O4-ethylthymidine). The methylene and methyl carbons of the O4-ethyl group are denoted C7 and C8, respectively; H_R and H_S refer to the *pro-R* and *pro-S* methylene protons of C7. Left, partial 300 MHz ^{1}H NMR spectra (27°C) of Ape^{4}TpA (**3**) (upper) and of Tpe^{4}TpT (**7**) (lower). The chemical shifts (δ) are in ppm relative to DSS. Note the intense H_R, H_S bands (joined by dashed lines) at 4.18 ppm and 4.33 ppm in the spectra of **3** and **7**, respectively. T* denotes the e^4Thy base.

Can. J. Chem. Downloaded from www.nrcresearchpress.com by 91.121.58.235 on 09/07/12
For personal use only.

Experimental

Materials and methods

2′-Deoxythymidine (dT), 2′-deoxyadenosine (dA), and the reagents used for protection, coupling, and deblocking were purchased (Aldrich or Sigma Chemical Co.). 5′-*O*-4,4′-Dimethoxytrityl-6-*N*-benzoyl-adenosine was obtained from Cruachem Inc. whereas the protected thymidines were synthesized and purified as described by Buchko *et al.* (14). Chromatographic solvents were purchased from Fisher Scientific. Thin-layer chromatography (TLC) was carried out on Kieselgel 60 F_{254} plates (Merck). Kieselgel 60 (Merck) was used for dry-column flash chromatographic (DCFC) purification of the precursors. Deprotected oligomers were purified initially by descending paper chromatography (Whatman paper No. 1) using solvent B′ (*n*-butanol:ethanol:water = 4:1:5 v/v, organic phase), followed by purification by HPLC (Perkin Elmer Series 4 liquid chromatograph) using a semipreparative ODS-Hypersil column and a gradient of methanol and 0.1 M aqueous ammonium acetate (pH 6.0). The strategy used for the synthesis of **1**, **2**, and **3** is shown in Scheme 1.

Synthetic methods

3′-Acetyl-4-(1,2,4-triazol-1-yl)-thymidine (**8**) and *5′*-O-*4,4′-dimethoxytrityl*-O-*4-ethylthymidine* (**9**) were synthesized according to Buchko *et al.* (14), except that the 4,4′-dimethoxytrityl group (DMT) was used in place of the *tert*-butyldimethylsilyl (TBDMS) group for 5′-protection in **9**. This change in the 5′-protecting group was necessary for our synthesis of **3**, which involves 5′-extension of the appropriately blocked **1** (see **15** below). The extension initially requires the removal of the 5′-protecting group from **15**. If TBDMS had been used for 5′-protection, then 5′-deprotection of **15** would have required tetra-*n*-butylammonium fluoride (TBAF), a reagent that also effects an undesirable removal of the 2-chlorophenyl group used for phosphate protection (14, 16). On the other hand, the 5′-DMT group is conveniently removed by a reagent, $ZnBr_2$, that leaves the protected phosphate intact.

3′-O-*Acetyl-6*-N-*acetyl-2′-deoxyadenosine* (**10**)

5′-*O-tert*-Butyldimethylsilyl-2′-deoxyadenosine (**11**) was prepared following Ogilvie (17), and converted to 5′-*O-tert*-butyldimethylsilyl-3′-*O*-acetyl-6-*N*-acetyl-2′-deoxyadenosine (**12**) using acetic anhydride. Molecule **10** was obtained by desilylation of **12** using TBAF (17).

6-N-*Benzoyl-2′-deoxyadenosine* (**13**) was prepared via Schaller *et al.* (18) and converted to 5′-*O-tert*-butyldimethylsilyl-6-*N*-benzoyl-2′-deoxyadenosine (**14**) following Ogilvie (17).

e^4TpA (**1**)

Molecule **9** was phosphorylated with 2-chlorophenyl phosphodichloridate and condensed with **10** using 2,4,6-triisopropylbenzenesulfonyl chloride (TPSCl) and tetrazole (14) to give **15**, the fully protected dimer. Molecule **15** was purified and then deprotected by sequential treatment with (i) $ZnBr_2$ for detritylation (19), (ii) oximate for phosphate deprotection, and (iii) ethanolic sodium ethoxide for removal of the 6-*N*- and 3′-*O*-acetyl groups.

Ape^{4}TpA (**3**)

Molecule **15** was detritylated with $ZnBr_2$ and purified by DCFC. The product was phosphorylated with 2-chlorophenyl phosphodichloridate and coupled with 5′-*O*-4,4′-dimethoxytrityl-6-*N*-benzoyl-2′-deoxyadenosine. The fully protected trimer **16** was then deblocked sequentially as described above.

Ape^{4}T (**2**)

Molecule **14** was phosphorylated and condensed with **8** to give **17**. Molecule **17** was deprotected, as described in the synthesis of Tpe^{4}T (14), by (a) TBAF for 1 min and (b) sodium ethoxide. Note that, because of the presence of the 6-*N*-benzoyl group, the sodium ethoxide treatment had to be extended to 12 h from the 1 h required for deprotection of Tpe^{4}T (14).

Molecules **4**, **5**, and **6**, the unmodified analogues of **1**, **2**, and **3**, were prepared by replacing sodium ethoxide with sodium hydroxide (pH > 13) during deblocking of the fully blocked forms of **1**, **2**, and **3**.

Tpe^{4}TpT (**7**)

This molecule was prepared from the fully blocked form of the O4-isopropylated trimer Tpi^{4}TpT (**18**), the synthesis of which was described by Buchko *et al.* (14). Treatment of **18** with $ZnBr_2$, oximate reagent, and sodium ethoxide yielded **7**. Note that the sodium ethoxide both removes the 3′-*O*-acetyl protecting group and effects an alkoxy exchange, replacing the O4-isopropyl with the O4-ethyl function on the central base. Exchange of O4-isopropyl groups by O4-methyl

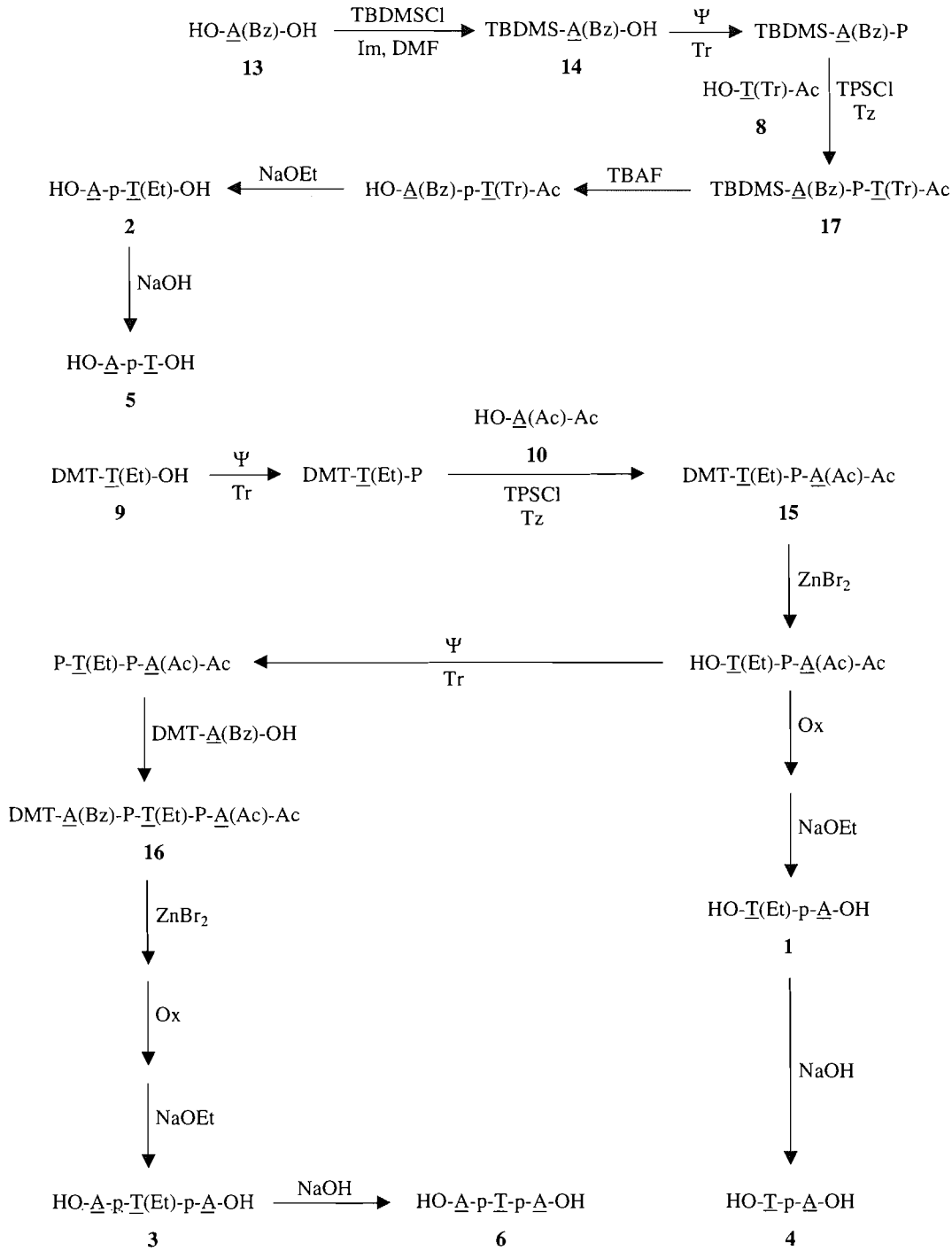

Abbreviations: T, thymidine; A, 2'-deoxyadenosine; TBAF, *n*-tetrabutylammonium fluoride; (Bz), 6-*N*-benzoyl; DMF, dimethylformamide; Ac, 3'-acetyl; (Ac), 6-*N*-acetyl; DMT-A(Bz)-OH, 5'-*O*-4,4'-dimethoxy-6-*N*-benzoyl-2'-deoxyadenosine; (Et), O4-ethyl; HO-A(Ac)-Ac, 3'-*O*-acetyl-6-*N*-acetyl-2'-deoxyadenosine (**10**); HO-T(Tr)-Ac, 3'-acetyl-4-(1,2,4-triazol-1-yl)-thymidine (**8**); Im, imidazole; NaOEt, ethanolic sodium ethoxide; Ox, oximate reagent; p, unprotected, diesterified phosphate; P, phosphate protected by *o*-chlorophenyl; TBDMSCl, *tert*-butyldimethylsilyl chloride; TPSCl, 2,4,6-triisopropylbenzenesulfonyl chloride; Tr, 1,2,4-triazole; (Tr), 4-(1,2,4-triazol-1-yl); Tz, tetrazole; Ψ, 2-chlorophenyl phosphodichloridate.

SCHEME 1

was reported initially by Singer *et al.* (20); Borowy-Borowski and Chambers (21) are using a DBU-catalyzed exchange for synthesis of oligomers containing *O*-alkylthymine residues.

The following UV absorption data for H_2O solutions were obtained on a Cary 219 spectrophotometer: **1**: λ_{max} = 262 nm, λ_{min} = 235 nm; **2**: λ_{max} = 262 nm, λ_{min} = 235 nm; **3**: λ_{max} = 261 nm, λ_{min} = 233 nm; **4**: λ_{max} = 260 nm, λ_{min} = 231 nm; **5**: λ_{max} = 260 nm, λ_{min} = 231 nm; **6**: λ_{max} = 259 nm, λ_{min} = 230 nm; **7**: λ_{max} = 269 nm, λ_{min} = 237 nm.

Mass spectrometric experiments

Negative-ion FAB mass spectra (glycerol matrix, 8-keV xenon atoms) were obtained on a VG 7070E-HF spectrometer. Some of the

Can. J. Chem. Downloaded from www.nrcresearchpress.com by 91.121.58.235 on 09/07/12
For personal use only.

Can. J. Chem. Downloaded from www.nrcresearchpress.com by 91.121.58.235 on 09/07/12
For personal use only.

TABLE 1. ^{1}H chemical shifts (δ ppm from DSS) in D_2O[a,b]

Nucleotide		Temperature (°C)	1′	2′	2″	3′	4′	5′	5″	6(2)	5M(8)	7A	7B	8M
1. e^{4}TpA	e^{4}Tp	10	5.937	1.545	2.261	4.542	4.052	3.689	3.642	7.541	1.892	4.304	4.281	1.384
		70	6.053	1.866	2.404	4.608	4.073	3.721	3.654	7.600	1.916	4.380	4.365	1.372
	pA	10	6.351	2.820	2.572	4.768	4.215	4.06	4.06	8.037	8.364	—	—	—
		70	6.425	2.809	2.599	4.724	4.223	4.087	4.066	8.175	8.349	—	—	—
2. Ape^{4}T	Ap	10	6.301	2.83	2.83	4.837	4.292	3.889	3.831	8.053	8.267	—	—	—
		60	6.342	2.789	2.746	4.891	4.291	3.841	3.790	8.159	8.243	—	—	—
	pe^{4}T	10	6.153	2.242	2.358	4.527	4.106	4.253	4.099	7.656	1.614	4.214	4.214	1.321
		60	6.228	2.268	2.418	4.536	4.150	4.207	4.105	7.718	1.745	4.272	4.247	1.299
3. Ape^{4}TpA	Ap	10	6.215	2.71	2.71	4.875	4.286	3.844	3.808	7.997	8.141	—	—	—
		60	6.273	2.719	2.682	4.893	4.272	3.814	3.773	8.110	8.180	—	—	—
	pe^{4}Tp	10	6.026	1.847	2.304	4.774	4.28	~4.1	~4.1	7.483	1.629	4.159[c]	4.138	1.338
		60	6.120	1.998	2.418	4.783	~4.3	4.11	4.06	7.576	1.741	4.227	4.242	1.314
	pA	10	6.312	2.699	2.529	4.715	~4.1	~4.1	~4.1	8.008	8.296	—	—	—
		60	6.372	2.720	2.559	4.697	~4.1	~4.1	~4.1	8.116	8.312	—	—	—
4. TpA	Tp	10	5.935	1.511	2.126	4.568	4.002	3.640	3.618	7.313	1.834	—	—	—
		70	6.030	1.858	2.276	4.619	4.022	3.684	3.631	7.372	1.853	—	—	—
	pA	10	6.382	2.883	2.582	4.798	4.217	4.05	4.05	8.100	8.392	—	—	—
		70	6.439	2.849	2.605	4.738	4.222	4.06	4.06	8.207	8.358	—	—	—
5. ApT	Ap	10	6.347	2.810	2.832	4.840	4.310	3.889	3.831	8.106	8.284	—	—	—
		60	6.391	2.817	2.782	4.896	4.309	3.856	3.802	8.194	8.266	—	—	—
	pT	10	6.144	2.26	2.26	4.552	4.062	4.219	4.087	7.445	1.594	—	—	—
		60	6.202	2.31	2.31	4.544	4.103	4.178	4.092	7.505	1.713	—	—	—
6. ApTpA	Ap	10	6.273	2.72	2.72	4.888	4.303	3.846	3.809	8.037	8.166	—	—	—
		70	6.326	2.753	2.704	4.898	4.284	3.824	3.779	8.135	8.205	—	—	—
	pTp	10	5.999	1.819	2.182	4.780	4.168	4.089	4.045	7.297	1.619	—	—	—
		70	6.076	1.995	2.294	4.779	4.193	4.076	4.035	7.386	1.723	—	—	—
	pA	10	6.335	2.748	2.541	4.730	4.211	~4.1	~4.1	8.046	8.308	—	—	—
		70	6.377	2.746	2.560	4.700	4.213	4.09	4.08	8.140	8.313	—	—	—
7. Tpe^{4}TpT	Tp	10	6.109	2.339	2.517	4.738	4.151	3.810	3.769	7.675	1.849	—	—	—
		70	6.150	2.307	2.502	4.760	4.141	3.801	3.749	7.582	1.863	—	—	—
	pe^{4}Tp	10	6.222	2.351	2.609	4.834	4.35	4.176	4.094	7.897	1.932	4.327	4.304	1.371
		70	6.271	2.313	2.629	4.847	4.26	4.151	4.084	7.852	1.958	4.380	4.366	1.355
	pT	10	6.270	2.33	2.33	4.561	4.106	4.149	4.064	7.663	1.820	—	—	—
		70	6.257	2.331	2.357	4.541	4.125	4.125	4.072	7.636	1.861	—	—	—

[a]Temperature in 0°C. Spectra acquired at 300.1 MHz (**1**, **2**, **4**) and 500.1 MHz (**3**, **5**, **6**, **7**). Proton labelling (Fig. 1): 5M, 5-methyl; 7A and 7B: diastereotopic C7 methylene protons at low and high field, respectively (no absolute assignment to H_R and H_S can be made here); 8M: 8-methyl protons of the O4-ethyl group.

[b]δ is given to only three significant figures when the analysis was complicated by strong coupling or peak overlap. If the overlap is particularly severe, only the general location of the proton is indicated to two significant figures.

[c]A crossover in the H_R and H_S protons of **3** is suggested by the temperature dependence of their spectral band.

Can. J. Chem. Downloaded from www.nrcresearchpress.com by 91.121.58.235 on 09/07/12
For personal use only.

more prominent peaks are reported here as follows: m/z (relative intensity, [ionic species]), with the relative intensity normalized to the molecular ion $[M - H]^-$. *e^4TpA*: 582 (100, $[M - H]^-$); 674 (5.6, [M + glycerol − H]$^-$); 554 (9.7, $[M - CH_2CH_3]^-$); 153 (58, [O4-ethylthymine − H]$^-$); 349 (39, [3′-e^{4}dTMP − H]$^-$); 330 (20, [5′-dAMP − H]$^-$); 134 (39, [adenine − H]$^-$). *Ape^{4}T*: 582 (100, $[M - H]^-$); 674 (5.5, [M + glycerol − H]$^-$); 554 (12, $[M - CH_2CH_3]^-$); 153 (24, [O4-ethylthymine − H]$^-$); 349 (60, [5′-e^{4}dTMP − H]$^-$); 330 (14, [3′-dAMP − H]$^-$); 134 (94, [adenine − H]$^-$). *Ape^{4}TpA*: 895 (100, $[M - H]^-$); 867 (13, $[M - CH_2CH_3]^-$); 662 (78, [Ape^{4}Tp − H]$^-$ + [pe^{4}TpA − H]$^-$); 330 (217, [3′-dAMP − H]$^-$ + [5′-dAMP − H]$^-$); 153 (126, [O4-ethylthymine − H]$^-$); 134 (435, [adenine − H]$^-$). *TpA*: 554 (100, $[M - H]^-$); 646 (6.8, [M + glycerol − H]$^-$); 125 (49, [thymine − H]$^-$); 321 (22, [3′-dTMP − H]$^-$); 330 (22, [5′-dAMP − H]$^-$); 134 (19, [adenine − H]$^-$). *ApT*: 554 (100, $[M - H]^-$); 646 (12, [M + glycerol − H]$^-$); 330 (19, [3′-dAMP − H]$^-$); 321 (69, [5′-dTMP − H]$^-$); 134 (57, [adenine − H]$^-$); 125 (52, [thymine − H]$^-$). *ApTpA*: 867 (100, $[M - H]^-$); 634 (80, [ApTp − H]$^-$ + [pTpA − H]$^-$); 330 (146, [3′-dAMP − H]$^-$ + [5′-dAMP − H]$^-$); 134 (185, [adenine − H]$^-$); 125 (131, [thymine − H]$^-$). *Tpe^{4}TpT*: 877 (100, $[M - H]^-$); 653 (36, [Tpe^{4}Tp − H]$^-$ + [pe^{4}TpT − H]$^-$); 321 (80, [3′-dTMP − H]$^-$ + [5′-dTMP − H]$^-$); 573 (5, [Tpe^{4}T − H]$^-$ + [e^{4}TpT − H]$^-$); 153 (27, [O4-ethylthymine − H]$^-$); 125 (182, [thymine − H]$^-$).

^{1}H NMR experiments

^{1}H NMR spectra were obtained at 300.1 MHz (Bruker AM300) and 500.1 MHz (Bruker AM 500, McMaster University). The samples were contained in 5 mm (o.d.) tubes at concentrations in D_2O (3.0–12.0 mM) that preclude significant intermolecular interaction. The concentrations were obtained from UV absorbance measurements at 260 nm. The molar extinction coefficients per residue (ε_{260}) were taken from ref. 22 (**4**: 11 700; **5**: 11 400) or calculated by the method described therein (**6**: 12 500). The ε_{260} of **1** (9030), **2** (8800), **3** (10 800), and **7** (6570) were obtained by correcting the ε_{260} of the corresponding *unmodified* molecule for the Thy to e^{4}Thy substitution. For this correction, we used $\varepsilon_{260} = 3200$ for an e^{4}dT unit, which we estimated from the UV absorption profile of this monomer and the ε_{max} provided by Singer *et al.* (20). The solutions contained 0.01 M sodium phosphate buffer (pH = 6.9), EDTA (0.001 M) to chelate paramagnetic ions, 0.1 M NaCl to maintain a constant ionic strength, and, for an NMR reference, a trace of *tert*-butanol (assigned a chemical shift of 1.231 ppm on the DSS scale). The samples were lyophilized twice from 99.8% D_2O and taken up in 99.9% D_2O. One-dimensional (1D) FIDs were collected at 10°C intervals from 10 to 70°C in 16K of computer memory and processed with a Lorentz-to-Gaussian lineshape transform prior to zero-filling to 32K. The HDO resonance was suppressed by presaturation (Bruker PRESAT. AU microprogram). Conventional homonuclear decoupling, nOe, and two-dimensional (COSY-45°) (23) and relayed coherence transfer (24) experiments were carried out for spectral assignments. Spectra for the trimers at 10 and 70°C were also obtained at 500 MHz (Bruker AM500). Spectra were analyzed (NUMARIT) (25) at two temperatures (10 or 20°C, and 70°C), and computer-generated spectra confirmed the data.

Circular dichroism experiments

Circular dichroic spectra were obtained on a Jasco J-500A spectropolarimeter using a cell equipped for temperature control with a water bath. The molecules were studied at concentrations $(0.46–3.64) \times 10^{-4}$ M (calculated from UV absorbance measurements) in the phosphate buffer solution used for the NMR experiments.

Results and discussion

Nuclear magnetic resonance spectra, data, and assignments

Tables 1 and 2 provide ^{1}H chemical shift (δ) and coupling constant (J) data; partial 1D NMR spectra of the trimers **3** and **7** are shown in Fig. 1. The methods used to assign the spectral bands have been listed by Buchko *et al.* (14, 15); our assignments for **4** and **5** are in agreement with those of Kan *et al.* (26), and Cheng and Sarma (27). Data provided by Mellema *et al.* (28) were useful for assigning our trimer spectra. As noted earlier (14), the C7 methylene protons of the O4-ethyl group of an e^{4}dT fragment are diastereotopic because of the chiral centres in the sugar; the *pro-R* and *pro-S* atoms are designated H_R and H_S (Fig. 1). At the nucleoside level (e^{4}dT), H_R and H_S are isochronous (A_2X_3 pattern for the O4-ethyl group); this isochronicity indicates that the chiral sugar is too distant from the ethyl group to induce detectable differential shielding (Δ) in these protons (5, 14). A temperature-dependent Δ was evident (14) in the ABX_3 patterns observed for e^{4}TpT (**19**) and Tpe^{4}T (**20**) and attributed to intramolecular base stacking. A temperature-dependent Δ is also apparent in the H_R, H_S band of the all-pyrimidine trimer (**7**) (4.32 ppm, Fig. 1; Fig. 7 below) and in the corresponding bands of the adenine-containing dimers **1** and **2**. Note that no Δ is apparent in the spectrum of **3** at 27°C (intense quartet at 4.18 ppm; Fig. 1) though differential shielding is observed in **3** at other temperatures. We are not able to provide an absolute assignment of H_R and H_S, and so they are denoted in Tables 1 and 2 as 7A (less shielded) and 7B (more shielded).

Chemical shift temperature profiles: pyrimidine units

Temperature profiles of the chemical shifts are useful for assessing which conformations prevail in solution (29, 30). At our concentrations, intermolecular association should not be serious for the dimers and trimers, although Altona (29) has suggested that some association can occur at concentrations of ~10 mM, particularly when the oligomer contains bases such as methylated adenines, which have a strong tendency to stack. Even in the absence of complications from association effects, deriving conformations for single-stranded oligomers from δ data is complicated because the molecules exhibit considerable flexibility by interconverting between several stacked and unstacked forms that differ in their sugar pucker, in the orientation of the bases about the glycosyl link (χ), and so on. Thus, we shall restrain ourselves to more or less qualitative statements regarding the influence of the O4-alkylation on the positioning of the Thy base in any ordered structure that may form. The chemical shifts of the pyrimidine base should be determined mainly by intramolecular factors, particularly for our trimers in which the pyrimidine is sandwiched between the terminal bases. The profiles discussed below suggest that the e^{4}Thy and Thy derivatives form right-handed (RH) base-stacked structures at low temperature and that the O4-ethyl group has no large effect on the orientation of the pyrimidine base within the stack.

(a) *5-Methyl (5M) protons*

These profiles (Fig. 2) reveal association of the Pyr bases with an Ade on their 5′ side. At the monomer level, e^{4}dT and dT, O4-ethylation leads to a deshielding of 0.09 ppm for the 5M protons; neither monomer shows any temperature dependence. If Thy or e^{4}Thy is located at the 5′ end of an adenine-containing dimer (**1** and **4**), or in the central position of an all-pyrimidine trimer, **7** and **21** (TpTpT), the 5M protons experience only small upfield shifts ($\Delta\delta < 0.07$ ppm, where $\Delta\delta$ is the chemical shift of a proton in an oligomer relative to the corresponding monomer). In contrast, when the pyrimidine is located at the 3′ end of an adenine-containing dimer (**2** and **5**), or is flanked by two Ade bases as in the trimers **3** and **6**, the 5M protons are shifted upfield at 10°C relative to the monomers: ~0.35 ppm for e^{4}Thy of **2** and

TABLE 2. Coupling constants (J, Hz)[a,b]

Nucleotide		Temperature (°C)	1′2′	1′2″	2′3′	2″3′	3′4′	4′5′	4′5″	3′P	4′P	5′P	5″P
1. e^4TpA	e^4Tp	10	7.8	5.9	6.2	3.0	3.1	3.2	4.5	6.3	—	—	—
		70	7.4	6.1	6.7	3.4	3.4	3.6	4.9	6.7	—	—	—
	pA	10	6.6	6.6	6.5	4.4	4.1	2.6	2.6	—	2.6	—	—
		70	6.6	6.6	6.6	4.4	4.2	2.8	4.0	—	2.0	4.8	4.7
2. Ape^4T	Ap	10	6.4	6.4	5.4	5.4	3.8	2.8	3.7	5.8	—	—	—
		60	7.4	6.0	6.2	3.4	3.6	3.4	4.1	5.8	—	—	—
	pe^4T	10	5.7	6.7	7.3	5.6	5.4	2.4	3.1	—	2.8	3.6	3.1
		60	6.6	6.6	6.9	4.7	4.6	2.6	3.9	—	2.2	4.3	4.4
3. Ape^4TpA	Ap	10	6.7	6.7	4.6	4.6	3.0	2.8	3.5	5.5	—	—	—
		60	7.8	6.0	5.9	3.0	3.1	3.1	4.2	6.1	—	—	—
	pe^4Tp	10	7.9	6.0	6.5	3.1	3.3	[b]	[b]	6.5	[b]	[b]	[b]
		60	7.8	6.1	6.5	3.2	3.3	**2.5**	**3.9**	6.6	[b]	**4.6**	**3.9**
	pA	10	6.6	6.6	6.4	4.2	4.1	[b]	[b]	—	[b]	[b]	[b]
		60	6.6	6.6	6.5	4.2	4.1	[b]	[b]	—	[b]	[b]	[b]
4. TpA	Tp	10	8.5	5.8	6.0	2.2	2.4	3.7	4.1	6.0	—	—	—
		70	7.8	6.2	6.6	3.0	3.1	3.6	5.0	6.6	—	—	—
	pA	10	6.8	6.6	6.6	4.2	4.0	2.6	2.6	—	2.6	3.5	3.5
		70	6.6	6.7	6.6	4.3	4.0	3.5	3.5	—	2.1	4.8	4.8
5. ApT	Ap	10	6.7	6.1	5.9	4.5	3.5	2.8	3.7	5.2	—	—	—
		60	7.4	6.0	6.1	3.4	3.4	3.2	4.3	6.1	—	—	—
	pT	10	6.7	6.7	5.9	5.9	4.9	2.0	2.9	—	2.6	3.9	2.8
		60	6.9	6.9	5.5	5.5	4.9	2.9	3.8	—	2.2	4.4	4.3
6. ApTpA	Ap	10	6.7	6.7	4.3	4.3	2.7	3.0	3.4	6.1	—	—	—
		60	7.7	6.0	6.1	3.0	3.1	3.1	4.2	6.0	—	—	—
	pTp	10	8.6	6.0	6.2	3.0	3.2	2.0	3.0	6.4	3.3	4.1	2.8
		60	8.3	6.1	6.5	2.6	2.7	2.6	3.9	6.6	2.6	4.2	3.9
	pA	10	6.6	6.5	6.3	3.9	3.7	3.1	3.1	—	2.5	[b]	[b]
		60	6.6	6.6	6.5	4.1	3.9	3.4	3.4	—	1.9	4.8	4.8
7. Tpe^4TpT	Tp	10	6.6	6.3	6.4	3.9	3.8	3.3	4.3	6.4	—	—	—
		70	7.4	6.3	6.6	3.5	3.5	3.5	4.7	6.7	—	—	—
	pe^4Tp	10	6.6	6.4	6.5	4.3	4.2	2.2	3.1	6.3	2.7	4.4	3.2
		70	7.2	6.4	6.8	3.4	3.4	2.8	3.6	6.6	2.3	4.9	4.6
	pT	10	6.8	6.8	5.5	5.5	4.0	2.5	3.1	—	2.5	3.9	4.0
		70	7.0	6.7	6.6	3.7	4.1	2.9	4.4	—	2.9	4.8	4.8

[a]Temperature in 0°C. Spectra acquired at 300.1 MHz (**1**, **2**, **4**) and 500.1 MHz (**3**, **5**, **6**, **7**). Proton labelling (Fig. 1). Other couplings showing little variation: $^2J(2'2'')$: −14.1 ± 0.2 Hz; $^2J(5'5'')$: −12.6 ± 0.2 Hz (Np) or −11.6 ± 0.2 Hz (pNp, pN); for the O4-ethyl, $^2J(RS)$ = −10.6 Hz and $^3J(78)$ = 7.1 Hz; $^4J(56)$: 1.1–1.2 Hz (e^4Thy) and 1.2–1.3 Hz (Thy). Only the sums of connected coupling constants are significant if δ2′ ~ δ2″ or if δ5′ ~ δ5″. Bold-faced Js are from first-order analyses.

[b]J cannot be obtained due to spectral overlap.

3, and ~0.28 ppm for Thy of **5** and **6**. Note that the Δδ for e^4Thy on the one hand, and for Thy on the other, are identical to within 0.04 ppm at the dimer and trimer levels; this indicates that the Ade base on the 5′ side of the pyrimidine is the main source of the 5M shielding in the trimers, with little, if any, shielding derived from the Ade on the 3′ side. Increasing the temperature to 70°C leads to a downfield shift of 0.12–0.15 ppm for the 5M protons of **2**, **3**, **5**, and **6**, and their shifts approach those of the monomers. The trends in Fig. 2 suggest that e^4Thy and Thy of **2**, **3**, **5**, and **6** participate in a RH base-stacked structure. In such a conformation, the 5M group lies over the Ade in the 5′ direction and would experience the substantial ring current shielding of this purine. On the other hand, an Ade located on the 3′ side of the pyrimidine is not expected to cause significant shielding of the 5M group. Earlier NMR data were interpreted in terms of RH folding for TpA (26, 27) and for the pTpA segment of TpTpA (31). Also, the small Δδ for the NpA and large Δδ for the ApN are strong indications that the Thy and e^4Thy bases are *anti* about the *N*-glycosyl bond (26–31); both e^4dT and dT assume this conformation in the crystal state (5, 32). In the trimers **7** or **21**, the central base is flanked by pyrimidines that sustain a smaller ring current and are less inclined than purines to base stack; in these cases, Δδ for the central base is slight (<0.03 ppm) and shows little temperature dependence (Fig. 2). The somewhat larger Δδ(e^4Thy) for **2** and **3** relative to Δδ(Thy) for **5** and **6** could be due to an effect of O4-ethylation on the extent of base stacking, or on the orientation of the pyrimidine relative to the stacked Ade base in the 5′ direction; our data do not warrant further comment on this matter.

Can. J. Chem. Downloaded from www.nrcresearchpress.com by 91.121.58.235 on 09/07/12
For personal use only.

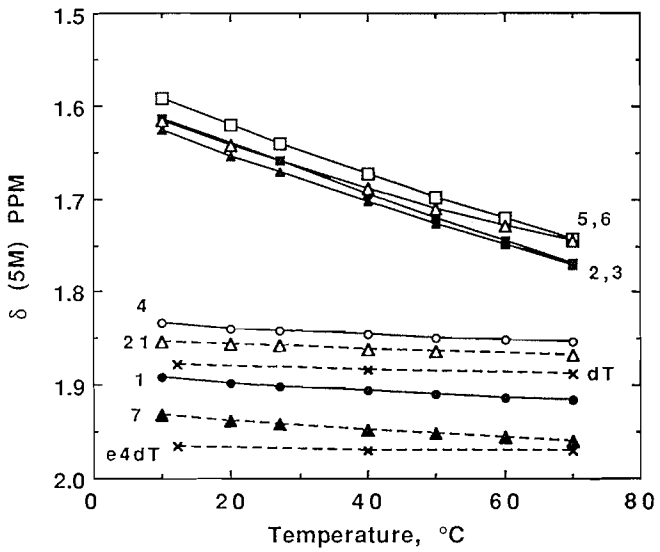

FIG. 2. Temperature profile of the chemical shifts (δ in ppm from DSS) of the 5-methyl (5M) protons of e⁴Thy (solid symbols) and Thy (open symbols). Connected by solid lines: e⁴TpA (**1**, ●), TpA (**4**, ○), Ape⁴T (**2**, ■), ApT (**5**, □), Ape⁴TpA (**3**, ▲), and ApTpA (**6**, △). Connected by dashed lines: pe⁴Tp unit of Tpe⁴TpT (**7**, ▲) and pTp unit of TpTpT (**21**, △); ×: monomers e⁴dT and dT.

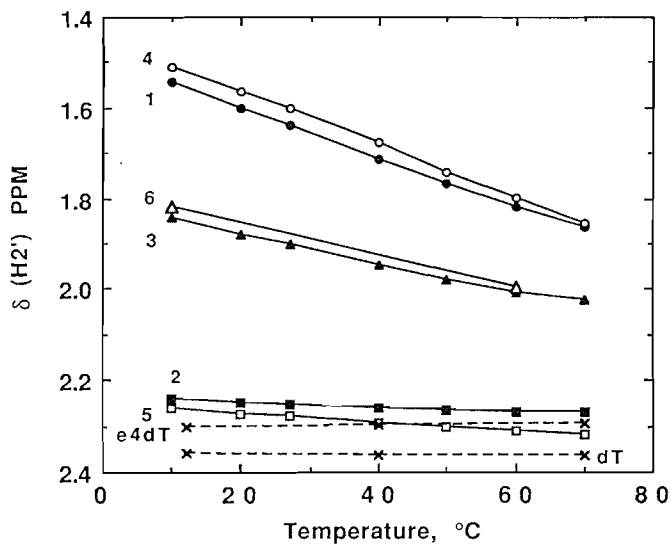

FIG. 3. Temperature profiles for the H2′ chemical shifts (δ in ppm from DSS) for the e⁴Thy (solid symbols) and Thy (open symbols) nucleotidyl units. Connected by solid lines: e⁴TpA (**1**, ●), TpA (**4**, ○), Ape⁴T (**2**, ■), ApT (**5**, □), Ape⁴TpA (**3**, ▲), and ApTpA (**6**, △). Connected by dashed lines: monomers e⁴dT and dT.

(b) *Sugar H2′ protons*

These profiles (Fig. 3) reveal association of Thy and e⁴Thy with an Ade base on the 3′ side. The δ(H2′) of dT and e⁴dT are identical to within 0.07 ppm and independent of temperature. In dimers **1** and **4**, an Ade base is on the 3′ side of the e⁴Tp and Tp units, and molecular models of RH structures show that H2′(Np) can enter the shielding regions above the plane of this purine. Consistent with RH helix formation are the large Δδ(H2′) at 10°C for **1** (0.76 ppm) and **4** (0.85 ppm), as are the large downfield shifts (~0.34 ppm) observed when the temperature is increased to 70°C. On the other hand, in the RH stack of dimers **2** and **5**, H2′ of the pe⁴T and pT moieties is distant from the Ade of the Ap unit; these protons are not expected to sense its ring current and indeed their δ behave like those of the monomers. The behaviour of H2′(Np) of **1** and **4** also contrasts with that of H2′(Np) of their all-pyrimidine analogs, e⁴TpT and TpT, which show a greatly reduced temperature dependence in the 10–70°C range (14), in line with smaller ring currents of the pT base.

Consistent with a RH structure for the pNpA segments of the trimers **3** and **6** is the upfield shift, Δδ, of H2′ for their pNp moieties at 10°C (pe⁴Tp: 0.46 ppm; pTp: 0.54 ppm) and the downfield shift (~0.20 ppm) when the temperature is elevated to 70°C. No such effects are observed for the pNp fragment of the all-pyrimidine trimers **7** (Table 1) and **21** (33). However, it is surprising that Δδ(H2′) for the trimers at 10°C is only 60% of that for the dimers **1** and **4**. Initially we thought that this reduction might be indicative of a competition between the terminal Ade bases for stacking with the central base. This view, however, is not consistent with the data in Fig. 2, which show that Δδ(5M) are similar at the dimer and trimer levels. Oltshoorn *et al.* (34) also observed an anomalous H2′ shift of similar magnitude for H2′ of the central pAp unit of ApApA relative to the Ap unit of ApA. They presented a rationale for this anomaly based on (a) the populations of the g^+ conformers of the C4′—C5′ (γ) bond and (b) the deshielding of H2′ by O5′ when γ is g^+. Unfortunately, the complexity of the NMR spectrum of **3** did not permit determination of accurate values of $J(4'5')$ and $J(4'5'')$ of the pe⁴Tp unit (Table 2) and so a comparison of the g^+ populations of the e⁴Thy units of **1** and **3** cannot be made. On the other hand, accurate values for these couplings could be determined for **4** and **6** (Table 2); these indicate that the g^+ population is larger for pTp (**6**) relative to Tp (**4**), and so the Oltshoorn interpretation may account for our δ(H2′) anomalies. But, whatever the cause of the reduced H2′(pNp) shielding at the trimer level, the important message is that it operates whether the pNp base is Thy or e⁴Thy, and so we have further support for the contention that O4-ethylation has no drastic effects on the conformation of our molecules.

(c) *Sugar H2″ protons*

In Fig. 4 we compare H2″ profiles for the Np fragments of e⁴TpA (**1**) and TpA (**4**) with those for H2″(Np) of the all-pyrimidine dimers e⁴TpT (**19**) and TpT (**22**) (data from refs. 14 and 35). Also compared are profiles of H2″(pNp) of Ape⁴TpA (**3**) and ApTpA (**6**) with the H2″(pNp) protons of the all-pyrimidine trimers Tpe⁴TpT (**7**) and TpTpT (**21**). For the all-pyrimidine molecules, we note that δH2″ is independent of temperature in the 10–70°C range. (Note also that H2″ for an e⁴Thy unit is shifted downfield (~0.1 ppm) relative to the corresponding Thy data; a comparable effect was observed at the monomer level (9), and so must be an intranucleoside effect.) In the Ade-containing molecules at 10°C, H2″ is shifted upfield, the shift being slightly larger (10–15%) for the Thy units (**4**: 0.43 ppm; **6**: 0.35 ppm) than for e⁴Thy units (**1**: 0.38 ppm; **3**: 0.31 ppm). At 70°C, the shielding effect is reduced by about 40%, and the δ(H2″) approach those of the all-pyrimidine molecules. Profiles are not given for the H2″(pN) of the isomers Ape⁴T (**2**) and TpT (**22**), but our data for these dimers indicate that an Ade base on the 5′ side has much smaller shielding effect (<0.08 ppm) on H2″(pN). Thus, the data in Fig. 4 confirm stacking of a e⁴Tp and Tp base with an Ade on its 3′ side.

Can. J. Chem. Downloaded from www.nrcresearchpress.com by 91.121.58.235 on 09/07/12
For personal use only.

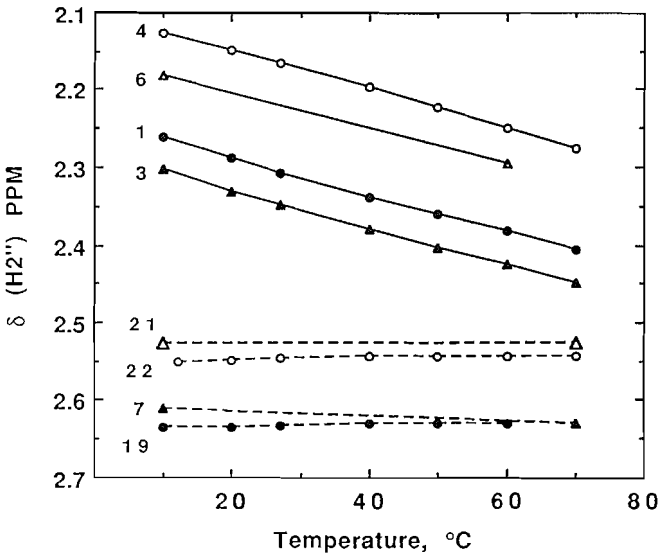

FIG. 4. Temperature profiles for the H2″ chemical shifts (δ in ppm from DSS) for the e⁴Thy (solid symbols) and Thy (open symbols) nucleotidyl units. Connected by solid lines: e⁴TpA (**1**, ●), TpA (**4**, ○), Ape⁴TpA (**3**, ▲), and ApTpA (**6**, △). Connected by dashed lines: e⁴Tp of e⁴TpT (**19**, ●), Tp of TpT (**22**, ○), pe⁴Tp of Tpe⁴TpT (**7**, ▲), and pTp of TpTpT (**21**, △). Data for **19** and **22** are from ref. 14.

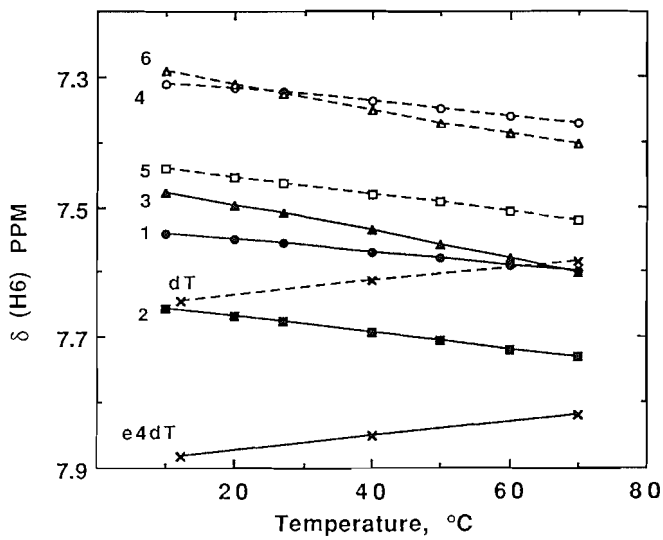

FIG. 5. Temperature profile for the H6 chemical shifts (δ in ppm from DSS) for e⁴Thy (solid lines and symbols) and Thy (dashed lines, open symbols). e⁴TpA (**1**, ●), TpA (**4**, ○), Ape⁴T (**2**, ■), ApT (**5**, □), Ape⁴TpA (**3**, ▲), and ApTpA (**6**, △). ×: monomers e⁴dT and dT.

(d) *Base H6 protons and sugar H1′*

The e⁴dT and dT data in Fig. 5 show that O4-ethylation effects a deshielding of 0.23 ppm in the H6 chemical shift, and in each monomer, H6 shifts upfield by ~0.06 ppm as the temperature is increased to 70°C. Relative to the corresponding monomer, the δ(H6) at 10°C are shifted upfield in the NpA (**1**: 0.34 ppm; **4**: 0.33 ppm), the ApN (**2**: 0.23 ppm; **5**: 0.20 ppm), and the ApNpA (**3**: 0.41 ppm; **6**: 0.36 ppm), and in each instance H6 shifts downfield as the temperature increases. It is remarkable that, if a correction of 0.23 ppm is made for the effect of O4-alkylation, the corresponding profiles for the e⁴Thy and Thy bases (NpA, etc.) are identical to within ~0.05 ppm over the entire temperature range. The H6 chemical shifts relative to the monomer reflect a variety of factors including sugar phosphorylation, ring current effects from the adjacent Ade bases, and solvent effects (14), and so are not easily interpreted in conformational terms. However, the correspondence of the two sets of profiles provides support for the contention that the stacking geometries are not drastically affected by O4-ethylation. This contention is further supported by the correspondence in the H1′ profiles (Fig. 6), which show similar upfield shifts for the e⁴Thy and Thy nucleotidyl fragments of the NpA, ApN, and ApNpA relative to the monomers. In each case, this shift is slightly larger for the Thy, but never by more than 0.05 ppm in the 10–70°C range.

(e) *O-Alkyl chemical shifts*

It would be useful to discuss the chemical shifts of the diastereotopic C7 methylene (H_R, H_S) and C8 methyl protons of the *O*-ethyl group in light of the conclusions based on the temperature profiles discussed above. In general, this group in the oligomers shows an ABX_3 pattern (Fig. 1 and Table 1), that is, the C7 protons are not identically shielded, but have a differential shielding (Δ) that depends on the molecule and the solution temperature. Figure 7 shows that at 10°C both C7 protons are shielded relative to e⁴dT and shift downfield as the temperature increases, presumably due to the stacking–destacking process (14). In the case of the all-pyrimidine trimer **7**, the upfield shifts at 10°C are small (0.07 ppm, 0.04 ppm), no doubt a reflection of the reduced ring currents and propensity for stacking of the flanking Thy bases; small upfield shifts (<0.07 ppm) were observed for the dimers **19** and **20** as well (14). The upfield shifts are also small in dimer **1** (0.07 ppm, 0.09 ppm), and so, bearing in mind the striking upfield shift experienced at 10°C by the H2′ of e⁴Tp (**1**) (0.76 ppm; Fig. 3), we conclude that the C7 protons do not enter the strongly shielding regions above an Ade base stacked on the 3′ side of the e⁴Thy base. However, larger shielding is experienced by the C7 protons in dimer **2** (0.16 ppm, 0.18 ppm) and in trimer **3** (0.22 ppm, 0.23 ppm). These trends, along with the 5M profiles (Fig. 2), point to a better overlap of the 5M-C5-C4-O4-C7 segment of the e⁴Thy base with an Ade on the 5′ side than with an Ade on the 3′ side, a result easily reconciled with a RH helical stack.

On the other hand, the C8 methyl protons show much less variation (Table 2; refs. 14, 35). In e⁴dT, δ(H8) = 1.36 ppm and is constant to within 0.001 ppm from 10 to 70°C; for all dimers and trimers in this temperature range, δ(H8) differs by ≤0.05 ppm from the monomer value. This constancy is consistent with a predominantly extended conformation for the *O*-ethyl group (anti-periplanar C4-O4-C7-C8), which projects the methyl group away from the stacked bases. Such an extended conformer was observed in the crystal structure of e⁴dT (5).

A result which surprised us is that, for all of the molecules whose profiles are given in Fig. 7, the two C7 protons are shifted upfield to quite similar extents over the temperature range examined. In the anti-periplanar orientation of the C4-O4-C7-C8 bond, the H_S proton flanks the e⁴Thy base on its 5′ face whereas H_R does so on the 3′ face (5),[4] and so we expected in molecule

[4]We denote as 5′ or 3′ the face that points to the 5′ or 3′ end of a strand in a normal B-DNA.

Can. J. Chem. Downloaded from www.nrcresearchpress.com by 91.121.58.235 on 09/07/12
For personal use only.

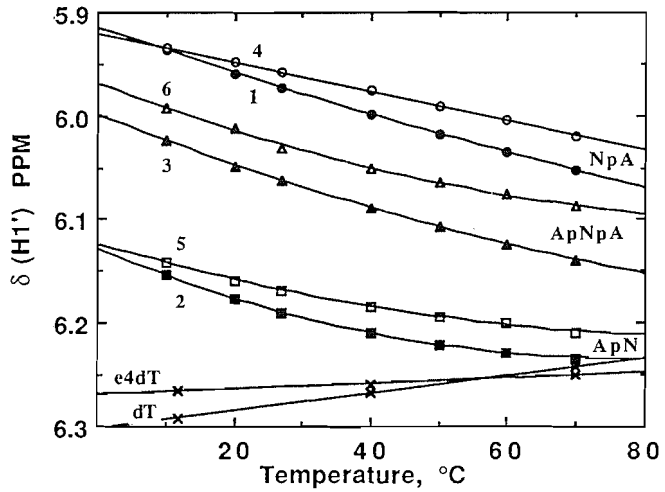

FIG. 6. Temperature profiles for the H1′ chemical shifts (δ in ppm from DSS) for e⁴Thy (solid symbols) and Thy (open symbols) nucleotidyl units. e⁴TpA (**1**, ●), TpA (**4**, ○), Ape⁴T (**2**, ■), ApT (**5**, □), Ape⁴TpA (**3**, ▲), and ApTpA (**6**, △). ×: monomers e⁴dT and dT.

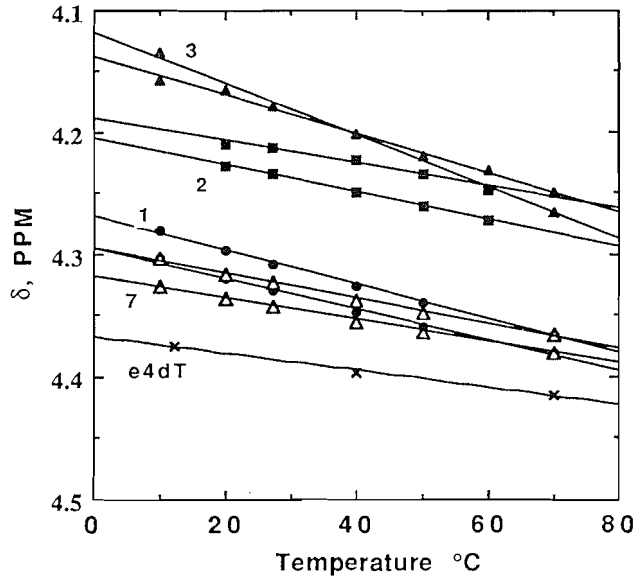

FIG. 7. Temperature profiles for the ^{1}H chemical shifts (δ ppm from DSS) of the H_R and H_S methylene protons of the O4-ethyl group. Solid symbols: e⁴TpA (**1**, ●), Ape⁴T (**2**, ■), and Ape⁴TpA (**3**, ▲). Open triangles: Tpe⁴TpT (**7**, △). An absolute assignment of the H_R and H_S protons could not be made; they are referred to as 7A (less shielded) and 7B (more shielded) in th bles. The protons are equivalent in the monomer e⁴dT (×).

2, for example, that one C7 proton, namely H_S, would be more influenced by the stacking of the Ap base, which occurs on the 5′ face. However, the similarity in upfield shifts indicates that the association of an Ade base on one particular face exerts comparable shielding on the two C7 protons. Theory (36) indicates that a number of factors (ring current, etc.) contribute to the magnetic fields near a purine base. This leads to a complex dependence of the magnetic shielding on position, and so we will not attempt to derive more precise information about stacking geometry of our flexible systems. Thus, at this point, we are uncertain whether Δ, in addition to the individual H_R and H_S chemical shifts, will prove, as we originally hoped (14), to be a generally useful quantity for monitoring local melting in e⁴Thy-containing oligomers.

(f) *Purine nucleotidyl shifts*

No temperature profiles are given for the Ap and pA units. However, the data in Table 1 show that the effect of replacing a Thy base by e⁴Thy on proton shifts of these fragments is never larger than 0.06 ppm. Overall, the purine δ data provide no evidence for any large conformational changes attributable to this replacement. Nor are they consistent with any significant purine–purine stacking, which could result from looping out of the central pyrimidine base.

Sugar conformation

Using plots of $\Sigma 1' (= J(1'2') + J(1'2''))$ to monitor changes in the sugar pucker, we noted that the modified Np fragment of e⁴TpT and of i⁴TpT (14, 15, 37) shows an unusual temperature dependence in the range 10–70°C, shifting from 2′-*endo* (*S*) towards 3′-*endo* (*N*) at low temperature. Figure 8 provides $\Sigma 1'$(Np) and $\Sigma 1'$(pNp) profiles that allow us to assess the influence of O4-ethylation in our Ade-containing dimers and trimers. The vertical axis of Fig. 8 also provides the %*S* (2′-*endo*) conformation calculated according to Rinkel and Altona (38); these populations are only approximate (±(10–15)%), and are included to provide the reader with an alternate view of the major trends defined by the primary data, $\Sigma 1'$. Considering first e⁴TpA and TpA at 70°C, we note that O4-ethylation reduces $\Sigma 1'$(Np) by about 0.6 Hz, a reduction comparable to that observed at the nucleoside level (14). Lowering the temperature to 10°C has little effect (<0.3 Hz) on these $\Sigma 1'$. Similarly, for the e⁴TpT and TpT at 70°C, we note a small decrease (~0.7 Hz) in $\Sigma 1'$(Np) due to the ethylation. However, $\Sigma 1'$(e⁴Tp) of e⁴TpT shows a large decrease (1.5 Hz) as the temperature is reduced to 10°C; this decrease is not seen for the Np unit of TpT. Since the $\Sigma 1'$ for the monomers (e⁴dT, dT) is constant in the 10–70°C range (14), the differences in behaviour of the $\Sigma 1'$ are reasonably related to intramolecular base stacking. In other words, the O4-ethylation of a Tp unit of a stacked TpN dimer causes a shift towards 3′-*endo* (*N*) if pN = pT, but not if pN = pA.

Another striking feature of the 10°C dimer data is the large difference (~3.0 Hz) between $\Sigma 1'$(Np) for e⁴TpT and TpA. This shows that the sugar of the 3′-thymidylyl unit can show a wide range of *N*,*S* populations depending on whether the base is alkylated or not, and on whether a Thy or Ade base occupies the pN unit.

The effects of O4-ethylation on the central pNp of the trimers parallel those for the dimer Np units discussed above. Thus, at 10°C, O4-ethylation effects a decrease of 1.5 Hz in $\Sigma 1'$(pNp) for the TpNpT pair whereas at 70°C these $\Sigma 1'$(pNp) differ by only 0.2 Hz. In contrast, the $\Sigma 1'$(pNp) for the ApNpA pair remain constant over the entire temperature range. We have not included in Fig. 8 any $\Sigma 1'$ data for dimer pN units. However, available data for these fragments of TpT, Tpe⁴T, ApT, and Ape⁴T (Table 2; refs. 14, 35) reveal that O4-ethylation in the 10–70°C interval leads to only a small (≤0.6 Hz) decrease in $\Sigma 1'$(pN), an effect comparable to that observed at the monomer level. In addition, our data (Table 2; refs. 14, 15, 35) show that O4-alkylation has little effect on the sugar pucker of either a thymidylyl or adenosyl residue adjacent to the modified segment.

Can. J. Chem. Downloaded from www.nrcresearchpress.com by 91.121.58.235 on 09/07/12
For personal use only.

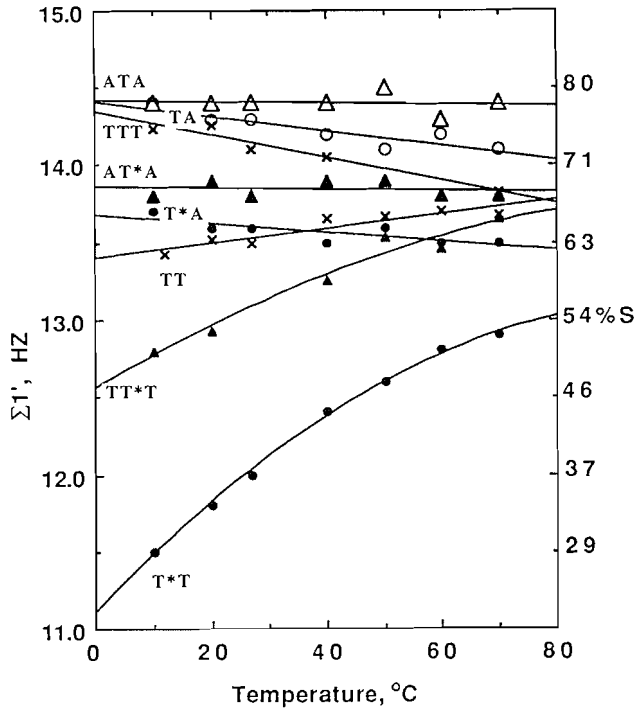

FIG. 8. Temperature profiles of $\Sigma 1' = J(1'2') + J(1'2'')$ in Hz for (a) the Np sugars of e^4TpA (**1**, ●), TpA (**4**, ○), e^4TpT (**19**, ●), and TpT (**22**, x), and (b) the pNp sugars of Ape^{4}TpA (**3**, ▲), ApTpA (**6**, △), Tpe^{4}TpT (**7**, ▲), and TpTpT (**21**, ×). The data are from Table 2, or from the width of the H1′ band; data for **19**, **21**, and **22** are from refs. 14, 15, and 35. The right vertical axis provides the *%S* (2′-*endo*) calculated from Σ1′ according to ref. 38. T* represents an e^4Thy unit.

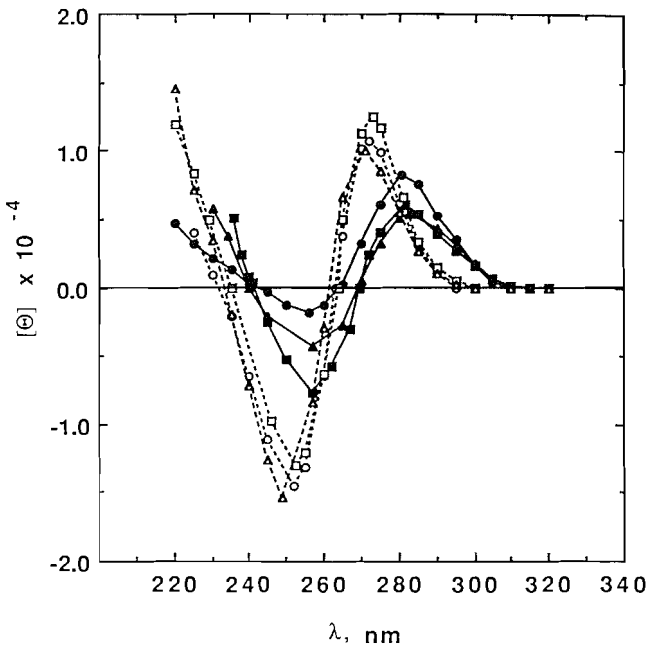

FIG. 9. Circular dichroism (CD) spectra (10–11°C). Solid symbols and lines: e^4TpA (**1**, ●), Ape^{4}T (**2**, ■), and Ape^{4}TpA (**3**, ▲). Open symbols and dashed lines: TpA (**4**, ○), ApT (**5**, □), and ApTpA (**6**, △). The vertical axis gives [θ] in deg M^{-1} cm^{-1}, the molar ellipticity per residue.

In summary, our Σ1′ data reveal an interesting sequence-dependent effect of O4-alkylation on sugar pucker that is manifest at low temperature, presumably as a consequence of the formation of minihelical conformations. Whether this phenomenon will appear in molecules larger than our dimers and trimers remains to be seen. Patel and co-workers (12, 39) have, in their NMR work, shown that e^4Thy can be accommodated into RH double helical DNA, but their data were not interpreted in terms of a precise sugar conformation for the modified nucleotide.

Populations for the *gauche*$^+$ (g^+), *trans* (t), and *gauche*$^-$ (g^-) conformers of the C4′—C5′ (γ) bond can be calculated from the $J(4'5')$ and $J(4'5'')$ data (Table 2) following Haasnoot *et al.* (40). At the low temperature, the Np fragments of the dimers and trimers show preferences for g^+ in the narrow ranges 59 ± 1% (Tp, e^4Tp) and 72 ± 1% (Ap), whereas the pN and pNp lie in the range 80 ± 5%; increasing the temperature to 60–70°C lowers the g^+ population by ~10%. The g^- conformer is always least populated. Calculations (according to Buchko *et al.* (15)) with the available $\Sigma' = J(5'P) + J(5''P)$ data in Table 2 show that the commonly observed *trans* conformer of the C5′—O5′ bond predominates (80–90%) at the lower temperature, and shows a small destabilization (~10%) at the high temperature. Similar trends in β and γ are generally observed for dimers and trimers containing only the normal bases, and so it seems that, for our modified oligomers, O4-alkylation of thymine is not reflected in the conformation of these bonds.

Circular dichroism

The CD spectra of **1**–**6** at 10–11°C are shown in Fig. 9. For the unmodified molecules, positive and negative maxima are observed at 271–273 nm and 250–253 nm, respectively. The general features of the dimer spectra **4** and **5** are in good agreement with literature data (41, 42); we are not aware of published data for **6**. Upon O4-ethylation, the long-wavelength maxima are red-shifted by about 10 nm, in contrast with the small (~1 nm) red shift in λ_{max} observed in the UV absorption spectra (see above); a smaller (~5 nm) red shift occurs in the negative maxima. On the other hand, CD spectra reported by Weinfeld *et al.* (42) reveal little effect of *phosphate* ethylation on the positions of the positive and negative bands of a number of dimers. As the temperature is increased to 70°C, the magnitudes of the CD maxima of **1**–**6** decrease by 30–50%. Overall, these results are consistent with the formation of right-handed minihelices at low temperature, as indicated by the δ data discussed above.

Mass spectrometric experiments

FAB-MS data for molecules **1**–**7** provided in the experimental section, as well as those for the homopyrimidine dimers reported by Buchko *et al.* (14, 15, 35), demonstrate the utility of this technique for characterizing DNA oligomers containing an r^4T base as well as their unmodified analogs. In the negative ion mode, the molecular mass was easily confirmed for molecules **1**–**7** by the presence of a prominent quasimolecular ion peak $[M - H]^-$; in some instances a glycerol adduct peak, $[M + \text{glycerol} - H]^-$, was also observed and served as further confirmation. Also of diagnostic value was the presence of a variety of intense ion peaks assignable to fragments bearing an O4-ethylthyminyl unit.

Recently, Buchko (35) reported FAB-MS data (negative ion

Can. J. Chem. Downloaded from www.nrcresearchpress.com by 91.121.58.235 on 09/07/12
For personal use only.

mode) for the largest of our molecules, e^4TpApe^4TpA, a tetramer with two e^4Thy units. Its mass was confirmed by the intense $[M - H]^-$ ion at m/z 1228. The presence of three prominent fragment ion peaks provided some sequence information: the first (m/z 994) is assignable to the fragment $[M - A - H]^-$, resulting from the loss of the terminal 3′-adenosyl unit by cleavage of its O—C5′ bond; the second (m/z 662) corresponds to $[M - e^4TpA - H]^-$, which would result from the cleavage of either the O—C5′ bond of the pe^4Tp unit or the C3′—O bond of the pAp unit; the third (m/z 349) corresponds to [3′-e^4dTMP − H]$^-$ and confirms the presence of a terminal e^4Thy. Thus, our data are demonstrating that, though O4-alkyl groups are labile (1, 9), they are sufficiently stable to withstand the mild ionizing conditions employed in FAB-MS. Thus we are optimistic about the potential of this method for characterizing longer DNA oligomers containing r^4Thy bases.

Acknowledgements

We acknowledge the support of the following: NSERC (for operating grants to F.E.H. (A1549); The University of Manitoba (research funds for F.E.H. and K.L.S., and a Manitoba Fellowship for G.W.B.); Mr. W. Buchanon, K. Marat, and R. Sebastian for technical support; F. LaFortune, B. Singer, and J. B. Westmore (for discussions).

1. B. Singer. Cancer Res. **46**, 4879 (1986).
2. P. S. Miller, S. Chandrasegaran, D. L. Low, S. M. Pulford, and L. S. Kan. Biochemistry, **21**, 5468 (1982).
3. G. I. Birnbaum, K. L. Sadana, M. T. Razi, T. Lee, R. Sebastian, G. W. Buchko, and F. E. Hruska. Can. J. Chem. **66**, 1628 (1988).
4. R. G. Brennan, D. Pyzalska, W. J. P. Blonski, F. E. Hruska, and M. Sundaralingam. Biochemistry, **25**, 1181 (1986).
5. G. I. Birnbaum, K. L. Sadana, W. J. P. Blonski, and F. E. Hruska. J. Am. Chem. Soc. **108**, 1671 (1986).
6. R. Parthasarathy and S. M. Fridey. Carcinogenesis, **7**, 221 (1986).
7. Y. Yamagata, K. Kohda, and K.-I. Tomita. Nucleic Acid Res. **19**, 9307 (1988).
8. T. Srikrishnan, R. Parthasarathy, N. C. De, and G. B. Chheda. Acta Crystallogr. Sect. C: Cryst. Struct. Commun. **C39**, 1441 (1983).
9. B. D. Allore, A. Queen, W. J. P. Blonski, and F. E. Hruska. Can. J. Chem. **61**, 2397 (1983).
10. C.-J. Chang, D. J. Ashworth, L.-J. Chern, J. DaSilva Gomes, C.-G. Lee, P. W. Mou, and R. Narayan. Org. Magn. Reson. **22**, 671 (1984).
11. B. F. Li, C. B. Reese, and P. F. Swann. Biochemistry, **27**, 1086 (1987).
12. M. W. Kalnik, M. Kouchakdjian, B. F. L. Li, P. F. Swann, and D. J. Patel. Biochemistry, **27**, 108 (1988).
13. B. Singer, M. Kroger, and M. Carrano. Biochemistry, **17**, 1246 (1978).
14. G. W. Buchko, F. E. Hruska, and K. L. Sadana. Can. J. Chem. **67**, 109 (1989).
15. G. W. Buchko, F. E. Hruska, and K. L. Sadana. Can. J. Chem. **67**, 1344 (1989).
16. K. K. Ogilvie, S. L. Beaucage, and D. W. Entwistle. Tetrahedron Lett. 1255 (1976).
17. K. K. Ogilvie. Can. J. Chem. **51**, 3799 (1973).
18. H. Schaller, G. Weimann, B. Lerch, and H. G. Khorana. J. Am. Chem. Soc. **85**, 3821 (1963).
19. M. D. Matteuchi and M. H. Caruthers. Tetrahedron Lett. **21**, 3243 (1980).
20. B. Singer, J. Sagi, and J. T. Kusmierek. Proc. Natl. Acad. Sci. U.S.A. **80**, 4884 (1983).
21. H. Borowy-Borowski and R. W. Chambers. Biochemistry, **28**, 1471 (1989).
22. G. D. Fasman (*Editor*). CRC handbook of biochemistry and molecular biology. 3rd ed. Nucleic acids. Vol. 1. CRC Press, Cleveland, OH. 1975. p. 589.
23. W. P. Aue, E. Bartholdi, and R. R. Ernst. J. Chem. Phys. **64**, 2229 (1976).
24. D. W. Hughes, R. A. Bell, T. Neilson, and A. D. Bain. Can. J. Chem. **63**, 3133 (1985).
25. A. R. Quirt and J. S. Martin. J. Magn. Reson. **5**, 318 (1971).
26. L. S. Kan, J. C. Barrett, and P. O. P. Ts'O. Biopolymers, **12**, 2409 (1973).
27. D. Cheng and R. H. Sarma. J. Am. Chem. Soc. **99**, 7333 (1977).
28. J.-R. Mellema, J. M. L. Pieters, G. A. van der Marel, J. H. van Boom, C. A. G. Haasnoot, and C. Altona. Eur. J. Biochem. **143**, 285 (1984).
29. C. Altona. *In* Nuclear magnetic resonance spectroscopy in molecular biology. *Edited by* B. Pullman. D. Reidel, Dordrecht, Holland. 1978. p. 87.
30. P. N. Borer, L. S. Kan, and P. O. P. Ts'O. Biochemistry, **14**, 4847 (1975).
31. C. Altona, J. H. van Boom, and C. A. G. Haasnoot. Eur. J. Biochem. **71**, 557 (1976).
32. D. W. Young, P. Tollin, and H. R. Wilson. Acta Crystallogr. Sect. B: Struct. Crystallogr. Cryst. Chem. **B25**, 1423 (1969).
33. D. M. Cheng, M. M. Dhingra, and R. Sarma. Nucleic Acids Res. **5**, 4399 (1978).
34. C. S. M. Oltshoorn, L. J. Bostelaar, J. H. van Boom, and C. Altona. Eur. J. Biochem. **112**, 95 (1980).
35. G. W. Buchko. Ph.D. thesis, University of Manitoba. December 1989.
36. C. Giessner-Prettre and B. Pullman. Q. Rev. Biophys. **20**, 113 (1987).
37. G. W. Buchko, F. E. Hruska, M. T. Razi, and K. L. Sadana. Proceedings of the 6th Conversation in Biomolecular Stereodynamics, Albany, NY. 6–10 June, 1989. Adenine Press, Guilderland, NY. p. 38.
38. L. J. Rinkel and C. Altona. J. Biomol. Struct. Dyn. **4**, 621 (1987).
39. M. W. Kalnik, M. Kouchakdjian, B. F. L. Li, P. F. Swann, and D. J. Patel. Biochemistry, **27**, 100 (1988).
40. C. A. G. Haasnoot, F. A. A. M. de Leeuw, H. P. M. de Leeuw, and C. Altona. Recl. Trav. Chim. Pays-Bas, **98**, 576 (1979).
41. C. R. Cantor, M. W. Warshaw, and H. Shapiro. Biopolymers, **9**, 1059 (1970).
42. M. Weinfeld, A. F. Drake, R. Kuroda, and D. C. Livingston. Anal. Biochem. **178**, 93 (1989).

Can. J. Chem. Downloaded from www.nrcresearchpress.com by 91.121.58.235 on 09/07/12
For personal use only.

Asymmetric synthesis of podophyllotoxin analogs

JAMES L. CHARLTON,[1] GUY L. PLOURDE, K. KOH, AND ANTHONY S. SECCO
Department of Chemistry, University of Manitoba, Winnipeg, Man., Canada R3T 2N2

Received January 8, 1990

JAMES L. CHARLTON, GUY L. PLOURDE, K. KOH, and ANTHONY S. SECCO. Can. J. Chem. **68**, 2022 (1990).

Two analogs of podophyllotoxin, with the same absolute stereochemistry as the natural product, have been synthesized from the cycloadduct between α-hydroxy-α′-phenyl-*o*-quinodimethane and the fumarate of *S*-methyl lactate. After initial attempts to produce the cycloadduct from photochemically generated α-hydroxy-α′-phenyl-*o*-quinodimethane failed, a study of the thermal generation and reaction of α-hydroxy-*o*-quinodimethane with the fumarate and acrylate of *S*-methyl lactate was made. A comparison was made of the diastereoselectivity of these cycloaddition reactions to those previously reported, in which the *o*-quinodimethane was generated photochemically. The α-hydroxy-*o*-quinodimethane was produced both by the known thermolysis of benzocyclobutenol and by thermolysis of 1-hydroxy-1,3-dihydrobenzo[*c*]thiophene-2,2-dioxide. The diastereomeric excess for the cycloaddition reactions was found to be greater than 95% with modest (ca. 55%) isolated yields of the major cycloadducts. Following these model studies, it was found that α-hydroxy-α′-phenyl-*o*-quinodimethane produced thermally from 1-hydroxy-3-phenyl-1,3-dihydrobenzo[*c*]thiophene-2,2-dioxide could be added to the fumarate of *S*-methyl lactate with high diastereoselectivity and good yield. The product of this reaction was converted to the podophyllotoxin analogs **7** and **17**.

Key words: *o*-quinodimethanes, asymmetric, Diels–Alder, lactate, podophyllotoxin, lignan.

JAMES L. CHARLTON, GUY L. PLOURDE, K. KOH et ANTHONY S. SECCO. Can. J. Chem. **68**, 2022 (1990).

Utilisant le cycloadduit obtenu par condensation de 1′α-hydroxy-α′-phényl-*o*-quinodiméthane et du fumarate du lactate de *S*-méthyle, on a synthétisé deux analogues de la podophyllotoxine possédant la même stéréochimie que le produit naturel. Il n'a pas été possible de produire le cycloadduit à partir de l'α-hydroxy-α′-phényl-*o*-quinodiméthane obtenu photochimiquement; on a donc utilisé une méthode thermique pour générer 1′α-hydroxy-*o*-quinodiméthane et pour réaliser sa réaction avec le fumarate du lactate de *S*-méthyle. On a effectué une comparaison de la diastéréosélectivité de ces réactions de cycloaddition avec celles rapportées antérieurement, alors que 1′*o*-quinodiméthane avait été généré d'une façon photochimique. L'-α-hydroxy-*o*-quinodiméthane a été obtenu par la thermolyse connue du benzocyclobuténol ainsi que par la thermolyse du 1-hydroxy-1,3-dihydrobenzo[*c*]thiophène-2,2-dioxyde. On a trouvé que l'excès de diastéréomères est plus grand que 95% alors que le rendement en cycloadduits principaux isolés n'est que de 55%. À la suite de ces études modèles, on a trouvé que 1′α-hydroxy-α′-phényl-*o*-quinodiméthane obtenu thermiquement à partir du 1-hydroxy-3-phényl-1,3-dihydrobenzo[*c*]thiophène-2,2-dioxyde peut être additionné au fumarate du lactate de *S*-méthyle avec une excellente diastéréosélectivité et un excellent rendement. Le produit de cette réaction peut être transformé dans les analogues **7** et **17** de la podophyllotoxine.

Mots clés : *o*-quinodiméthanes, asymétrique, Diels–Alder, lactate, podophyllotoxine, lignane.

[Traduit par la revue]

Introduction

The synthesis of aryl tetralin ligans such as dimethyl isolariciresinol or podophyllotoxin requires the stereoselective and asymmetric synthesis of several contiguous chiral centers.

As an approach to these systems, we have been investigating the Diels–Alder reactions of *ortho*-quinodimethanes (*o*-QDMs) (1–4). In our earlier work, we studied the reactions of chiral α-alkoxy-*o*-QDMs with achiral dienophiles, a method that we eventually used for the synthesis of dimethyl isolariciresinol (3). While these Diels–Alder additions gave good relative stereoselectivity, the absolute stereoselectivity was poor (diastereomeric excess (de) 70%). In addition, the method was not useful for the synthesis of systems having the relative stereochemistry found in podophyllotoxin and compounds of similar relative stereochemistry. In more recent work, we discovered that the fumarate of *S*-methyl lactate would add to α-hydroxy-*o*-QDM with very high asymmetric induction (de >90%), giving cycloadducts with the same relative stereochemistry as podophyllotoxin at centers 1, 2, and 3 (1, 5).

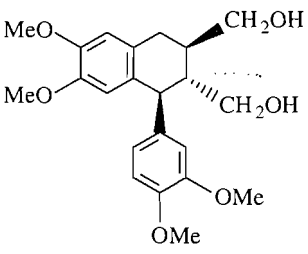

Isolariciresinol dimethyl ether

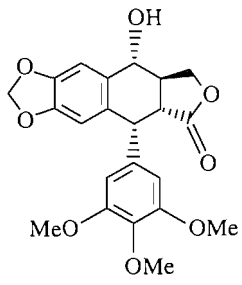

Podophyllotoxin

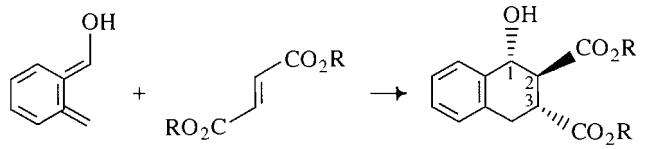

A synthesis of podophyllotoxin itself would require the asymmetric addition of the fumarate of *S*-methyl lactate to an *E*,*E*-α-hydroxy-α′-aryl-*o*-QDM as illustrated (the first asymmetric synthesis of podophyllotoxin has recently been published, ref. 6). There was some doubt about the viability of this approach since earlier work on the cycloaddition of aryl substituted *o*-QDMs with fumarates had shown that the product usually had the 4-aryl and neighboring 3-carboxyl groups *trans* to one another, unlike the desired cycloadduct above (7, 8).

As a model for the proposed podophyllotoxin study we carried out the sequence of reactions shown in Scheme 1 and prepared the optically pure analog **7**, a compound that was previously prepared in racemic form by Macdonald and Durst (9).

Results and discussion

On the basis of the original work of Sammes and co-workers, it was anticipated that the simplest method for the preparation of

[1]Author to whom correspondence may be addressed.

Can. J. Chem. Downloaded from www.nrcresearchpress.com by 91.121.58.235 on 09/07/12
For personal use only.

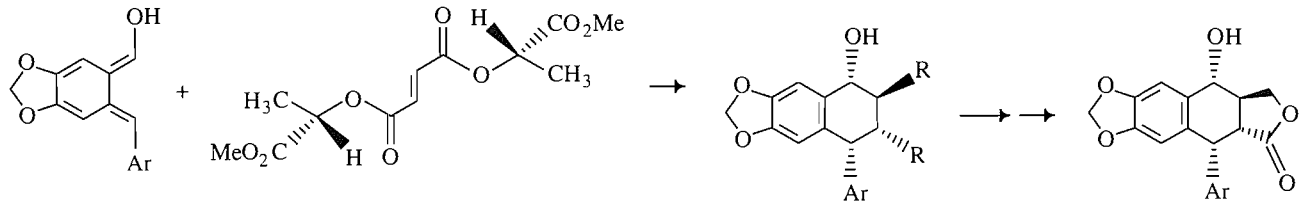

Ar = 3,4,5-trimethoxyphenyl; R = *S*-methyl lactylcarboxy

Podophyllotoxin

the *o*-quinodimethane **1** would be the photolysis of *o*-benzylbenzaldehyde (10). Unfortunately, when *o*-benzylbenzaldehyde was irradiated in the presence of the fumarate of *S*-methyl lactate **2** (benzene, 25°C, 450-watt medium pressure Hg lamp, Pyrex filter), no cycloadducts formed after 6 h. The only product detectable in the nmr spectrum was the maleate of *S*-methyl lactate, and the ratio of dilactyl maleate to dilactyl fumarate appeared to be approximately 90:10. Increasing the irradiation time to 30 h did not result in any further change to the reaction mixture. In the hope of increasing the rate of adduct formation, the irradiation was carried out at 110°C in toluene. After 24 h of irradiation at this temperature, only 10% of a possible cycloadduct (appearance of nmr signal near 5 ppm) had formed, in addition to the isomerization of the fumarate.

In view of the problems with the photochemical preparation of the *o*-quinodimethane **1**, we turned to methods of thermally generating α-hydroxy-*o*-quinodimethanes. While several methods of thermally preparing *o*-quinodimethanes are known, we were unsure whether the reaction conditions required (solvent, temperature, etc.) would be appropriate for high asymmetric induction in the subsequent addition of the *o*-quinodimethane to the chiral fumarate. To establish suitable experimental conditions, we generated α-hydroxy-*o*-quinodimethane from benzocyclobutenol (**8**, ref. 11) and 1-hydroxy-1,3-dihydrobenzo[*c*]thiophene-2,2-dioxide (**9**, ref. 12), and determined the diastereoselectivity of its reaction with both the fumarate and acrylate of *S*-methyl lactate, **2** and **10** (5).

While the thermolysis of benzocyclobutenols to *E*-α-hydroxy-*o*-quinodimethanes was established as a viable procedure by the pioneering work of Sammes and co-workers (13), the corresponding pyrolysis of the benzosulfone **9** to the α-hydroxy-*o*-quinodimethane had not been previously reported. Refluxing benzocyclobutenol **8** in toluene (110°C), in the presence of acrylate **10** (3 equiv.) and a trace of hydroquinone, gave a 73% yield of the cycloadduct **11** (after chromatography, 50:50 ethyl acetate/hexane) (1). A trace of a second isomer **13** could also be detected in the nmr of the crude product (**13**:**11** = 5:95) and, although we never isolated and characterized this adduct, it was suspected that it had the structure **13** because of its large *trans*-H,1,H-2 coupling constant of 9 Hz.

Refluxing benzocyclobutenol (**8**) in toluene in the presence of fumarate **2** (2 equiv.) gave exclusively **12** in 58% yield after chromatography (15% ethyl acetate in hexane) (1). **12** was also the exclusive product (55% isolated yield) when the sulfone **9** was added dropwise (in CH_2Cl_2) to a refluxing solution of fumarate **2** in toluene, showing that hydroxy sulfones such as **9** do thermalize readily to the corresponding α-hydroxy-*o*-quinodimethane. Attempts to prepare cycloadducts with the acrylate **10** using sulfone **9** as a precursor failed completely, with only *o*-methylbenzaldehyde and the starting acrylate being isolated from the reaction. This failure is presumably due to the lower reactivity of the acrylate in the Diels–Alder reaction, and the presence of SO_2 from the thermolysis of the sulfone, which may form sulfurous acid with traces of water and catalyze the tautomerization of the *o*-quinodimethane to *o*-methylbenzaldehyde. The asymmetric induction observed (ca. 95% de) in the reactions of thermally generated α-hydroxy-*o*-quinodimethane with the acrylate and fumarate of *S*-methyl lactate is comparable to that observed at ambient temperature when the *o*-quinodimethane was generated photochemically (1).

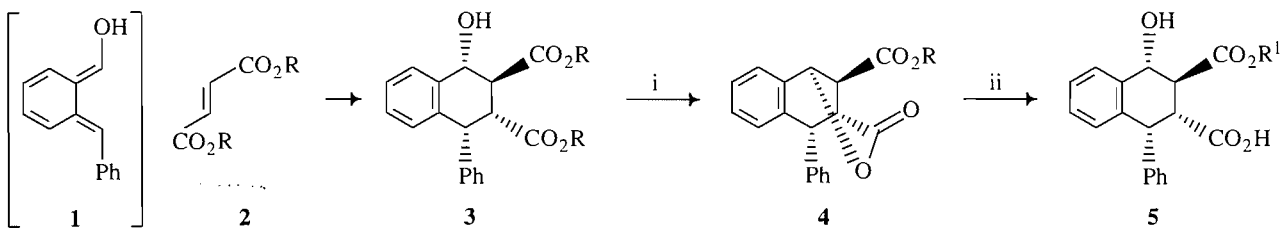

R^1 = -CH(CH_3)CO_2H (S) R = -CH(CH_3)CO_2H (S)

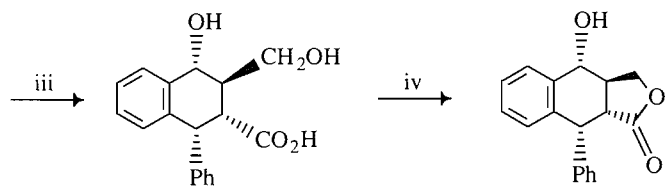

(i) *n*-BuLi, 1 equiv., THF, 10 min at −78 °C, 20 min at 20 °C; (ii) 10% HCl/*t*-BuOH 4:2.5, 3.5 days at 80 °C;
(iii) $LiBHEt_3$, 5.5 equiv., THF, 5 min at 0 °C, 24 h at 20 °C, work-up 10% HCl 24 h at 20 °C;
(iv) DCC, 1 equiv., THF, 24 h at 20 °C.

SCHEME 1

Can. J. Chem. Downloaded from www.nrcresearchpress.com by 91.121.58.235 on 09/07/12
For personal use only.

Can. J. Chem. Downloaded from www.nrcresearchpress.com by 91.121.58.235 on 09/07/12
For personal use only.

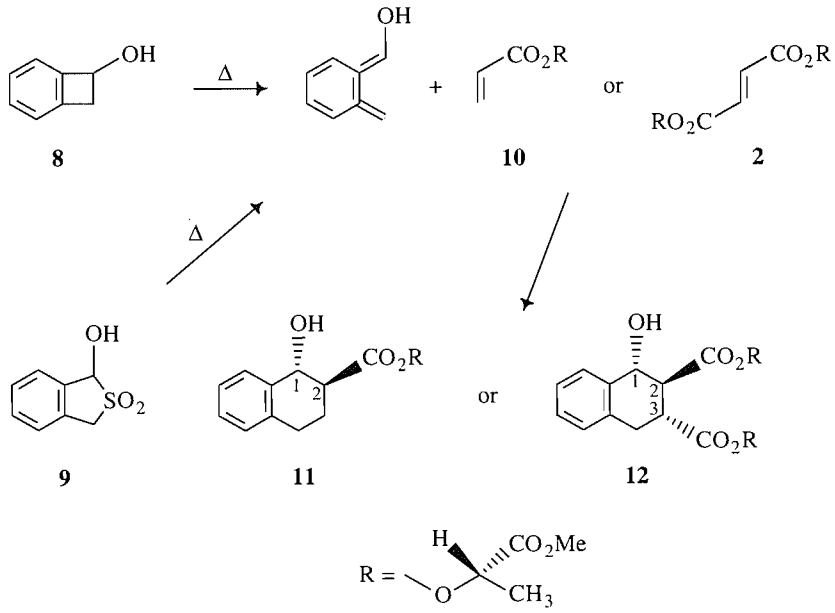

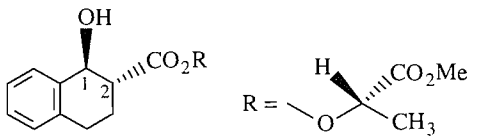

13

Turning our attention once again to Scheme 1, we considered the choice of generating the *o*-quinodimethane **1** from *trans*-1-hydroxy-2-phenylbenzocyclobutenol **14** or from *cis*-1-hydroxy-3-phenylsulfone **15**.

In view of the thermal instability of **14**, and the difficulties that others have had in its preparation (14–16), we decided against the benzocyclobutenol approach. We were pleased to find that slowly adding a methylene chloride solution of the sulfone **15** (17) to a refluxing toluene solution of the fumarate **2** led to a crystalline adduct in 55% yield after chromatography (20% ethyl acetate in hexane). Alternatively, the cycloadduct could be crystallized directly from the reaction mixture in 40% yield.

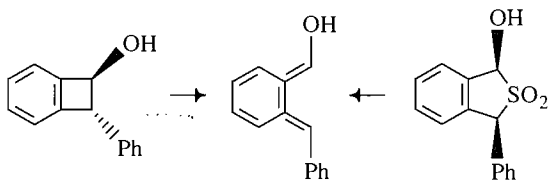

14 1 15

The nmr of the crude reaction mixture indicated that an isomeric cycloadduct was also present. This adduct (5% yield) was subsequently purified by careful chromatography but, although it was fully characterized, its relative and absolute stereochemistry were not determined.[2]

Although we tentatively assigned structure **3** to the major cycloadduct on the basis of the 9-Hz coupling constant between H-1 and H-2, more absolute proof of its structure was required. Treating the adduct with butyl lithium in THF converted it to the lactone **4**, proving the *cis*-1,3 arrangement of the 1-hydroxyl and 3-carboxyl groups in the cycloadduct. In addition, X-ray crystallographic analysis of a crystal of **4** yielded the structure shown in Fig. 1, confirming the relative stereochemistry in **4** and, by inference, the relative stereochemistry in **3**.

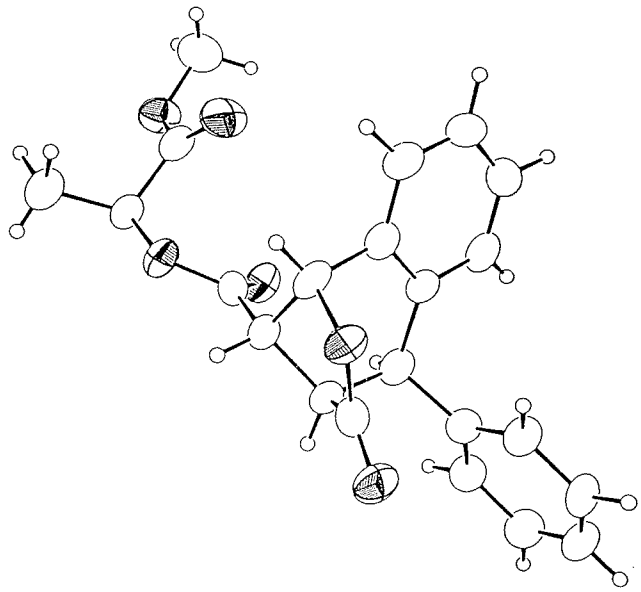

FIG. 1. Diagram of the lactone, **4**; thermal ellipsoids at 50% probability level.

Since the absolute stereochemistry of the lactyl group is known (*S*), then the absolute stereochemistries of **3** and **4** can be assigned as shown in Scheme 1.

Several routes from the cycloadduct **3** to the podophyllotoxin analog **7** were considered. Reduction of the 2-ester group in **3** with Super Hydride[3] has precedence in the literature (8), but we were unable to obtain selective reduction in high yield using this procedure. Since conversion of the ester at the 3 position to the acid would protect it during reduction by Super Hydride (18), we attempted to selectively hydrolyze the lactone **4**. This was

[2]The small coupling constant between H-1 and H-2 (3.2 Hz) suggests that this minor isomer has a *cis*-1,2 stereochemistry.

[3]Super Hydride is a registered trademark of Aldrich Chemical Company for lithium triethylborohydride.

Can. J. Chem. Downloaded from www.nrcresearchpress.com by 91.121.58.235 on 09/07/12
For personal use only.

TABLE 1. Fractional atomic coordinates (esd's) and equivalent isotropic temperature factors, B_{eq}(Å^2) for the lactone, **4**

Atom	*x*	*y*	*z*	B_{eq}
O(1)	0.0889(2)	−0.7030	−0.3912(2)	1.97(8)
O(2)	0.1617(2)	−0.5199(4)	−0.4865(2)	2.52(9)
O(3)	−0.2667(2)	−0.4864(4)	−0.2841(2)	2.23(9)
O(4)	−0.3634(2)	−0.6764(3)	−0.4132(2)	2.03(8)
O(5)	−0.3238(3)	−0.7955(4)	−0.1894(2)	2.9(1)
O(6)	−0.5382(2)	−0.7015(4)	−0.1933(2)	2.5(1)
C(1)	−0.1339(3)	−0.6008(5)	−0.4034(3)	1.8(1)
C(2)	−0.0229(3)	−0.7183(5)	−0.3332(3)	1.8(1)
C(3)	0.0459(3)	−0.6818(5)	−0.1988(3)	1.7(1)
C(4)	0.0719(3)	−0.7914(5)	−0.1094(3)	2.0(1)
C(5)	0.1363(4)	−0.7551(5)	0.0136(3)	2.4(1)
C(6)	0.1730(4)	−0.6090(5)	0.0470(3)	2.5(1)
C(7)	0.1464(4)	−0.4996(5)	−0.0416(3)	2.1(1)
C(8)	0.0821(3)	−0.5335(4)	−0.1660(3)	1.6(1)
C(9)	0.0436(4)	−0.4107(5)	−0.2619(3)	1.8(1)
C(10)	−0.0268(3)	−0.4730(5)	−0.3950(3)	1.8(1)
C(11)	0.0860(4)	−0.5602(5)	−0.4313(3)	2.1(1)
C(12)	−0.2584(3)	−0.5678(5)	−0.3566(3)	1.8(1)
C(13)	−0.4890(3)	−0.6800(5)	−0.3740(3)	1.9(1)
C(14)	−0.4363(3)	−0.7324(5)	−0.2415(3)	1.9(1)
C(15)	−0.5047(5)	−0.7451(7)	−0.0661(4)	3.1(2)
C(16)	−0.5935(4)	−0.7915(5)	−0.4571(4)	2.6(1)
C(17)	0.1717(4)	−0.3085(5)	−0.2519(3)	1.8(1)
C(18)	0.1501(4)	−0.1536(5)	−0.2611(3)	2.1(1)
C(19)	0.2640(4)	−0.0578(5)	−0.2572(3)	2.5(1)
C(20)	0.3980(4)	−0.1155(5)	−0.2451(3)	2.4(1)
C(21)	0.4230(4)	−0.2681(5)	−0.2345(3)	2.2(1)
C(22)	0.3100(4)	−0.3622(5)	−0.2368(3)	2.0(1)

TABLE 2. Non-hydrogen atom bond lengths (esd's) in Å for the lactone, **4**

Bond	Length	Bond	Length
O(1)—C(2)	1.477(4)	C(5)—C(6)	1.378(6)
O(1)—C(11)	1.360(4)	C(6)—C(7)	1.380(6)
O(2)—C(11)	1.193(4)	C(7)—C(8)	1.392(5)
O(3)—C(12)	1.194(4)	C(8)—C(9)	1.519(5)
O(4)—C(12)	1.343(4)	C(9)—C(10)	1.558(5)
O(4)—C(13)	1.450(4)	C(9)—C(17)	1.520(5)
O(5)—C(14)	1.191(4)	C(10)—C(11)	1.525(5)
O(6)—C(14)	1.331(4)	C(13)—C(14)	1.517(5)
O(6)—C(15)	1.452(5)	C(13)—C(16)	1.509(5)
C(1)—C(2)	1.525(5)	C(17)—C(18)	1.404(5)
C(1)—C(10)	1.531(5)	C(17)—C(22)	1.382(5)
C(1)—C(12)	1.510(5)	C(18)—C(19)	1.393(5)
C(2)—C(3)	1.502(5)	C(19)—C(20)	1.365(6)
C(3)—C(4)	1.388(5)	C(20)—C(21)	1.388(5)
C(3)—C(8)	1.395(5)	C(21)—C(22)	1.381(5)
C(4)—C(5)	1.383(5)		

accomplished in aqueous, acidic *tert*-butyl alcohol (which also hydrolyzes the carboxymethyl group in the lactyl side chain), to give **5**. Selective reduction of the lactyl ester in **5** with Super Hydride gave the acid-diol **6**. Both **5** and **6** were extremely polar and could not be purified by chromatography on silica gel and we were also unable to crystallize these compounds. The acid-diol **6** was converted to its methyl ester/acetonide **16**, which we were able to purify by chromatography and fully characterize.

When **6** was treated with dicyclohexylcarbodiimide (DCC) in THF, it was converted to the lactone **7** (isolated by chromatography on silica gel, 30% EtOAc/hexane, and recrystallization from CH_2Cl_2/hexane), whose nmr was identical to that of the racemic compound published earlier by Macdonald and Durst (9).

The complete reaction sequence shown in Scheme 1 can be carried out with purification of only the cycloadduct **3** (chromatography on silica gel) and the final product **7** (chromatography on silica gel), to give an overall yield of 16% based on the hydroxy sulfone **15**.

In the course of our investigation we also attempted to reduce the lactone **4** with Super Hydride.[3] On work-up in dilute acid we obtained the optically pure lactone **17** in 70% yield as a crystalline solid. The high yield of this procedure suggests that it may be applicable to preparation of other pericarbonyl lignans.

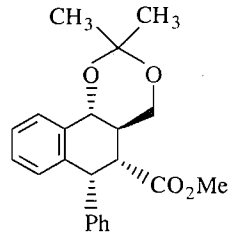

16

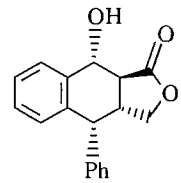

17

The work described here is being extended to the asymmetric synthesis of natural lignans and other lignan analogs.

Experimental

The ^{1}H nmr spectra were recorded on a Bruker AM-300 instrument using tetramethylsilane as internal standard. The ir spectra were recorded on a Perkin Elmer 881 spectrometer. Merck Kieselgel 60 was used for all chromatography. Exact Mass/mass spectra were obtained on an Analytical VG 7070E-HF instrument. Melting points were measured on a hot stage instrument and are uncorrected. Optical rotations were recorded on a Rudolf Research Corporation Autopol III instrument.

1-Hydroxy-3-phenyl-1,3-dihydrobenzo[c]*thiophene-2,2-dioxide,* ***15***

15 was prepared, using the procedure described for **9** (17), but without base extraction of the final product. To a solution of *o*-benzylbenzaldehyde (4.35 g, 22.2 mmol) in benzene (100 mL) was added a solution of sulfur dioxide (18 g) in benzene (15 mL). The volume of the solution was adjusted to fill the reaction vessel (~300 mL); the solution was flushed with nitrogen and irradiated for 20 h using a 450-watt Hanovia medium pressure mercury lamp located in a water-cooled, Pyrex probe immersed in the solution. The probe was cleaned every five hours. The solution was evaporated and the residue triturated with carbon tetrachloride to afford a yellowish solid (4.0 g, 69%) corresponding to the *cis*-hydroxy sulfone; ^{1}H nmr ($CDCl_3$) δ: 3.1 (br s, 1H, OH), 5.3 (s, 1H, H-2), 5.67 (s, 1H, H-1), 7.1–7.7 (m, 9H, aromatics), identical to that previously reported (17).

(−)-1-Hydroxy-1,2,3,4-tetrahydronaphthalene-2-carboxylate of (S)*-methyl lactate,* ***11***

To a solution of benzocyclobutenol **8** (32.2 mg, 0.268 mmol) in toluene (7 mL) was added (*S*)-methyl lactyl acrylate (127 mg, 0.804 mmol, 3 equiv.) and hydroquinone (2 mg). The solution was refluxed for 6 h, cooled, and the solvent evaporated. Chromatography on silica gel using 50% ethyl acetate/hexane as eluant afforded a colourless solid (54.4 mg, 73%, see ref. 1 for properties).

(−)-1-Hydroxy-1,2,3,4-tetrahydronaphthalene-2,3-dicarboxylate of (S)*-methyl lactate,* ***12***

Method A: From benzocyclobutenol 8

To a solution of benzocyclobutenol **8** (28 mg, 0.23 mmol) in toluene (5 mL) was added (*S*)-methyl lactyl fumarate (221 mg, 0.77 mmol, 3.3 equiv.) and 4Å molecular sieves (20 mg). The solution was refluxed for

Can. J. Chem. Downloaded from www.nrcresearchpress.com by 91.121.58.235 on 09/07/12
For personal use only.

4 h, cooled, and the solvent evaporated. Chromatography on silica gel using 15% ethyl acetate/hexane as eluant afforded a colourless solid (55 mg, 58%; see ref. 1 for properties).

Method B: From benzosulfone ***9***

To a refluxing solution of (*S*)-methyl lactyl fumarate (292 mg, 1.01 mmol, 1.5 equiv.) in toluene (5 mL) containing zinc oxide powder (50 mg) was slowly added a methylene chloride solution (5 mL) of hydroxy sulfone **9** (124 mg, 0.67 mmol). After addition of the methylene chloride solution, the mixture was refluxed for another 20 min, cooled, eluted through a short silica gel column with ethyl acetate, and evaporated. The residual oil was purified by chromatography on silica gel using 20% ethyl acetate/hexane as eluant to afford a colourless solid (152 mg, 55%). Recrystallization from hexane gave colourless plates (see ref. 1 for properties).

(−)-1-Hydroxy-4-phenyl-1,2,3,4-tetrahydronaphthalene-2,3-dicarboxylate of (S)*-methyl lactate,* ***3***

To a refluxing solution of (*S*)-methyl lactyl fumarate **2** (973 mg, 3.38 mmol, 1.5 equiv.) in toluene (20 mL) containing zine oxide powder (200 mg) was slowly added, over a period of 1 h, a solution of hydroxy sulfone **15** (580 mg, 2.23 mmol) in methylene chloride (25 mL). The solution was then refluxed for 20 min, filtered through a short silica gel column using ethyl acetate as eluant, and evaporated to give a yellow oil (2 isomers, 90:10 ratio from ^{1}H nmr of crude). The crude product was purified by chromatography using 15% ethyl acetate/hexane as eluant to afford a colourless oily material for each isomer: 582.9 mg, 54%, major; 60.6 mg, 5.6%, minor; 643.5 mg, 60%, total yield. Recrystallization of the major isomer from isopropyl alcohol afforded colourless needles. The major isomer could also be obtained in 40% yield by recrystallization of the crude product from isopropyl alcohol. The minor isomer could not be crystallized.

Major isomer, ***3***: mp 142–143°C; $[\alpha]_D$ −215° (*c* 0.2, $CHCl_3$); ir (CH_2Cl_2): 3476 (OH), 1742 (CO) cm^{-1}; ^{1}H nmr ($CDCl_3$) δ: 1.09 (d, 3H, *J* = 7.0, CH_3), 1.53 (d, 3H, *J* = 7.2, CH_3), 3.33 (dd, 1H, *J* = 9.5, 12.5, H-2), 3.55 (dd, 1H, *J* = 5.7, 12.5, H-3), 3.73 (s, 3H, OCH_3), 3.82 (s, 3H, OCH_3), 4.69 (d, 1H, *J* = 5.7, H-4), 4.91 (q, 1H, *J* = 7.0, CH), 4.98 (d, 1H, *J* = 9.5, H-1), 5.32 (q, 1H, *J* = 7.2, CH), 7.13 (m, 8H, aromatics), 7.82 (d, 1H, *J* = 7.4, H-8); ms, *m/e* (rel. %): 484 (<0.1), 362 (1.6), 335 (17), 334 (75), 249 (13), 248 (16), 247 (9), 232 (20), 231 (100). Exact Mass calcd. for $C_{26}H_{28}O_9$: 484.1733; found: 484.1697. Anal. calcd. for $C_{26}H_{28}O_9$: C 64.46, H 5.83; found: C 64.29, H 5.97.

Minor isomer: $[\alpha]_D$ +50° (*c* 0.18, $CHCl_3$); ir (CH_2Cl_2): 3477 (OH), 1737 (CO) cm^{-1}; ^{1}H nmr ($CDCl_3$) δ: 1.32 (d, 3H, *J* = 6.9, CH_3), 1.59 (d, 3H, *J* = 7.2, CH_3), 3.41 (dd, 1H, *J* = 3.1, 11.9, H-2), 3.60 (s, 3H, OCH_3), 3.71 (overlapping dd, 1H, *J* = 11.5, H-3), 3.81 (s, 3H, OCH_3), 4.02 (d, 1H, *J* = 4.0, OH), 4.17 (d, 1H, *J* = 11.1, H-4), 4.97 (q, 1H, *J* = 6.9, CH), 5.27 (q, 1H, *J* = 7.2, CH), 5.44 (overlapping dd, 1H, *J* = 3.5, H-1), 6.76 (d, 1H, *J* = 7.8, H-5), 7.12–7.35 (m, 7H, aromatics), 7.43 (d, 1H, *J* = 7.8, H-8); ms, *m/e* (rel. %): 484 (0.1), 334 (18), 250 (19), 249 (16), 248 (17), 247 (12), 232 (22), 231 (100).

Lactone, ***4***

To a solution of hydroxycycloadduct **3** (448.8 mg, 0.93 mmol) in dry tetrahydrofuran (20 mL) was added, at −78°C under nitrogen, *n*-butyllithium in hexanes (2.5 M, 0.37 mL, 0.93 mmol). The solution was stirred at −78°C for 15 min, then at room temperature for 0.5 h. Aqueous ammonium chloride (5%, 30 mL) was added, and the solution stirred for 15 min, extracted with methylene chloride, dried ($MgSO_4$), and evaporated to give an oil (316.2 mg, 90%, >90% pure by ^{1}H nmr). Chromatography on silica gel using 15% ethyl acetate/hexane as eluant afforded a colourless solid (185.4 mg, 51%). Recrystallization from hexane/methylene chloride gave colourless flakes. Crystals were suitable for X-ray analysis; mp 135–136°C; $[\alpha]_D$ −39.3° (*c* 0.18, $CHCl_3$); ir (CH_2Cl_2): 1788 (CO, lactone), 1748 (CO, ester) cm^{-1}; ^{1}H nmr ($CDCl_3$) δ: 1.42 (d, 3H, *J* = 7.0, CH_3), 3.35 (td, 1H, *J* = 0.8, 4.9, H-3), 3.51 (s, 3H, OCH_3), 3.94 (t, 1H, *J* = 5.1, H-2), 4.95 (d, 1H, *J* = 4.9, H-4), 5.00 (q, 1H, *J* = 7.0, CH), 5.52 (d, 1H, *J* = 5.1, H-1), 7.0–7.4 (m, 9H, aromatics); ms, *m/e* (rel. %): 380 (0.4), 362 (4.3), 334 (32), 276 (16), 248 (32), 231 (79), 220 (22), 205 (68), 204 (100), 192 (39). Exact Mass calcd. for $C_{22}H_{20}O_6$: 380.1259; found: 380.1254.

Hydroxy diacid, ***5***

To a solution of (*S*)-lactyl lactone **4** (57.6 mg, 0.15 mmol) in *tert*-butyl alcohol (7 mL) was added aqueous HCl (10%, 15 mL). The solution was heated for 3 days using a sand bath maintained at 80°C. Aqueous sodium bicarbonate (5%) was then slowly added until the solution was basic. The solution was extracted with methylene chloride, the aqueous portion reacidified (10% HCl), extracted with ethyl acetate, and dried ($MgSO_4$), and the solvent evaporated to give a colourless solid (42.2 mg, 72%). The product (~90% pure, ^{1}H nmr) could not be recrystallized or chromatographed on silica and was therefore used without further purification; mp 122–130°C; ^{1}H nmr ($CDCl_3$) δ: 1.54 (d, *J* = 7.1, CH_3), 3.24 (dd, *J* = 9.8, 12.4, H-2), 3.54 (dd, *J* = 5.6, 12.4, H-3), 4.67 (d, *J* = 5.4, H-4), 4.98 (d, *J* = 9.8, H-1), 5.31 (q, *J* = 7.1, CH), 6.95–7.33 (m, aromatics), 7.74 (d, *J* = 7.8, H-8), obtained from crude product.

The dimethyl ester of **5** was obtained by treating the crude diacid **5** with diazomethane followed by chromatography (15% ethyl acetate/hexane); ^{1}H nmr ($CDCl_3$) δ: 1.54 (d, 3H, *J* = 7.2, CH_3), 3.28 (dd, 1H, *J* = 9.7, 12.4, H-2), 3.52 (dd, 1H, *J* = 5.8, 12.4, H-3), 3.58 (s, 3H, OCH_3), 3.82 (s, 3H, OCH_3), 4.68 (d, 1H, *J* = 5.8, H-4), 4.73 (d, 1H, *J* = 3.4, OH), 4.97 (dd, 1H, *J* = 3.1, 9.7, H-1), 5.28 (q, 1H, *J* = 7.2, CH), 6.90–7.35 (m, 8H, aromatics), 7.81 (d, 1H, *J* = 7.9, H-8); ms, *m/e* (rel %): M^+ not observed, 394 (1.1), 334 (29.9), 263 (36), 262 (78.2), 249 (10.1), 248 (10.5), 247 (9.9), 232 (20.2), 231 (100).

Dihydroxy acid, ***6***

To a solution of crude hydroxy diacid **5** (77.5 mg, 0.2 mmol) in dry tetrahydrofuran (40 mL) was added, at 0°C under nitrogen, lithium triethylborohydride in tetrahydrofuran (1 M, 1.3 mL, 1.3 mmol, 6.5 equiv.). The solution was stirred at 0°C for 5 min, then at room temperature for 20 h. Dilute aqueous HCl (10%) was added, and the solution stirred for 1.5 h, saturated with NaCl, extracted with ethyl acetate, dried ($MgSO_4$), and evaporated to give a brownish oily material (59.3 mg, 98%). The product (~80% pure, ^{1}H nmr) could not be crystallized or chromatographed on silica and was therefore used without further purification; ir (CH_2Cl_2): 3695 (OH), 1744 (CO) cm^{-1}; ^{1}H nmr ($CDCl_3$) δ: 2.53 (m, H-2), 3.06 (dd, *J* = 6.3, 12.1, H-3), 4.35 (dd, *J* = 4.6, 10.7, H-11), 4.62 (d, *J* = 6.3, H-4), 4.86 (d, *J* = 10.1, H-1), 6.85–7.31 (m, aromatics), 7.75 (d, *J* = 7.7, H-8), H-11′ was not observed. Data obtained from crude product.

Methyl ester of dihydroxy acid ***6***

The methyl ester of **6** was obtained by treating the dihydroxy acid with excess diazomethane in diethyl ether and evaporation of the solvent. Purification by chromatography on silica gel was not possible; ^{1}H nmr ($CDCl_3$) δ: 2.59 (m, H-2), 3.05 (dd, *J* = 6.5, 12.1, H-3), 3.49 (s, OCH_3), 4.31 (dd, *J* = 4.5, 10.6, H-11), 4.59 (d, *J* = 6.5, H-4), 4.85 (d, *J* = 10.2, H-1), 6.88–7.32 (m, aromatics), 7.73 (d, *J* = 7.7, H-8), obtained from crude product.

Acetonide, ***16***

This compound was prepared according to a procedure previously reported (19). To a solution of crude dihydroxy ester (see above, 64.8 mg, 0.21 mmol) in 2,2-dimethoxypropane (5 mL) was added *p*-toluenesulfonic acid (trace). The solution was stirred at room temperature overnight. Ethyl acetate was added, the organic solution washed with aqueous sodium bicarbonate (5%), dried ($MgSO_4$), and the solvent evaporated to give a semicrystalline product (44.9 mg, 61%). Chromatography on silica gel using 15% ethyl acetate/hexane as eluant gave a colorless oil that could not be crystallized; $[\alpha]_D$ −179.4° (*c* 0.36, $CHCl_3$); ir (CH_2Cl_2): 1742 (CO) cm^{-1}; ^{1}H nmr ($CDCl_3$) δ: 1.56 (s, 3H, CH_3), 1.60 (s, 3H, OCH_3), 2.50 (m, 1H, H-2), 3.02 (dd, 1H, *J* = 6.7, 12.3, H-3), 3.40 (s, 3H, CH_3), 3.68 (t, 1H, *J* = 10.9, H-11), 4.14 (dd, 1H, *J* = 4.3, 11.1, H-11′), 4.57 (d, 1H, *J* = 6.7, H-4), 4.79 (d, 1H, *J* = 10.4, H-1), 6.87–7.26 (m, 8H, aromatics), 7.56 (d, 1H, *J* = 7.8, H-8); ms, *m/e* (rel. %): 352 (2.1), 337 (12), 277 (73), 217 (100), 205

Can. J. Chem. Downloaded from www.nrcresearchpress.com by 91.121.58.235 on 09/07/12
For personal use only.

(42), 195 (32). Exact Mass calcd. for $C_{22}H_{24}O_4$: 352.1674; found: 352.1671.

Podophyllotoxin analog, 7

The hydroxycycloadduct **3** (532.5 mg, 1.1 mmol) was treated with *n*-BuLi to give the crude lactone **4**. The lactone **4** (445 mg) was then hydrolysed and the residual hydroxy diacid **5** (287.2 mg) was reduced with Super Hydride ($LiBHEt_3$, ref. 14). No purification was performed for any of these first three steps. To a solution of this crude dihydroxy acid **6** (187 mg) in dry tetrahydrofuran (15 mL) was added dicyclohexylcarbodiimide (DCC, 145 mg, 0.7 mmol) in tetrahydrofuran (1 mL). The solution was stirred at room temperature for 24 h and worked up according to literature procedure (4),[2] with addition of water and acetic acid followed by evaporation of the solvent to give a semicrystalline material (241 mg). Purification by trituration with methylene chloride followed by chromatography on silica gel using 25% ethyl acetate/hexane as eluant gave a colourless solid (92.1 mg, 30% from **3**, 16.5% overall from **15**). Recrystallization from hexane/methylene chloride afforded colourless plates; mp 225–227°C (226–227°C for racemic material (9)); $[\alpha]_D$ −151° (*c* 0.12, $CHCl_3$); ir (CH_2Cl_2): 3320 (OH), 1777 (CO) cm^{-1}; ^1H nmr ($CDCl_3$) δ: 2.18 (d, 1H, J = 7.7, OH), 2.87 (m, 2H, H-2, H-3), 4.11 (br t, 1H, J = 9.5, H-11), 4.61 (dd, 1H, J = 6.6, 8.8, H-11′), 4.78 (d, 1H, J = 4.3, H-4), 4.89 (br t, 1H, J = 8.5, H-1), 7.05–7.39 (m, 8H, aromatics), 7.70 (d, 1H, J = 7.8, H-8); ms, *m/e* (rel. %): 280 (51), 262 (35), 218 (45), 217 (54), 119 (53), 117 (100). Exact Mass calcd. for $C_{18}H_{16}O_3$: 280.1099; found: 280.1104.

Pericarbonyl lactone, 17

To a solution of (*S*)-lactyl lactone **4** (228.3 mg, 0.60 mmol) in dry tetrahydrofuran (25 mL) was added, at 0°C under nitrogen, lithium triethylborohydride in tetrahydrofuran (1 M, 1.8 mL, 1.8 mmol, 3 equiv.). The solution was stirred at 0°C for 10 min, then at room temperature for 5 h. Dilute aqueous HCl (10%, 20 mL) was added and the solution was stirred overnight. The solution was diluted with water, extracted with methylene chloride, dried ($MgSO_4$), and evaporated to give a white solid (119.8 mg, 71%). Recrystallization from carbon tetrachloride afforded colourless needles; mp 162–164°C; $[\alpha]_D$ −75.6° (*c* 0.18, $CHCl_3$); ir (CH_2Cl_2): 3577 (OH), 1776 (CO) cm^{-1}; ^1H nmr ($CDCl_3$) δ: 2.74 (dd, 1H, J = 9.9, 14.5, H-2), 2.91–3.03 (m, 1H, H-3), 3.35 (br s, 1H, OH), 3.56 (dd, 1H, J = 8.6, 11.1, H-11), 4.43 (dd, 1H, J = 7.0, 8.6, H-11′), 4.51 (d, 1H, J = 5.7, H-4), 5.07 (d, 1H, J = 9.9, H-1), 6.91–7.80 (m, 9H, aromatics); ms, *m/e* (rel. %): 280 (30), 217 (8), 202 (5), 195 (6), 178 (7), 165 (11), 118 (10), 117 (100). Exact Mass calcd. for $C_{18}H_{16}O_3$: 280.1099, found: 280.1076.

X-ray analysis

Crystal data:

$C_{22}H_{19}O_6$ fw = 379.39

Monoclinic, $P2_1$, a = 9.745 (3), b = 8.974 (4), c = 11.633 (3) Å, β = 110.72 (2)°, V = 951.4 (6) $Å^3$, Z = 2, ρ_c = 1.324 g cm^{-3}, μ = 7.61 cm^{-1}, $F(000)$ = 398 (−150°C; CuKα, λ = 1.54178 Å). Data were collected using a crystal of the lactone **4** measuring 0.25 × 0.25 × 0.10 mm on a Rigaku AFC5R diffractometer with an ω–2θ scan type. 1298 unique reflections were measured within the region bounded by h, k, $\pm l$. Data were corrected for Lorentz and polarization effects yielding 1260 observed reflections with $I > 3\sigma(I)$. The structure was solved by direct methods and refined by full-matrix least-squares techniques minimizing the function $\Sigma w(|F_o| - |F_c|)^2$, where $w = 4F_o^2\sigma^{-2}(F_o^2)$. All non-H atoms were corrected for anomalous scattering and an extinction correction ($g = 0.26 \times 10^{-4}$) was applied. Final agreement factors, $R = \Sigma||F_o| - |F_c||\Sigma|F_o|$ and $R_w = [\Sigma w(|F_o| - |F_c|)^2/|\Sigma wF_o^2]^{1/2}$ were 0.030 and 0.042, respectively, for the 1260 observed data. The goodness of fit was 1.50 on the last cycle of refinement, which showed a maximum Δ/σ of 0.02. The final difference map indicated electron density fluctuations of −0.13 to 0.42 e $Å^{-3}$. Positional and isotropic thermal parameters are given in Table 1 for all non-H atoms; bond distances involving non-H atoms are listed in Table 2. H atom coordinates, complete lists of bond lengths and angles, temperature factors, and structure factors have been deposited as supplementary material.[4]

Acknowledgements

We would like to acknoweldge the financial assistance of the Natural Sciences and Engineering Research Council of Canada. We would also like to thank Molecular Structure Corporation for assistance in X-ray structure analysis.

1. J. L. CHARLTON, G. L. PLOURDE, K. KOH, and A. S. SECCO. Can. J. Chem. **67**, 574 (1989).
2. J. L. CHARLTON, G. L. PLOURDE, and G. H. PENNER. Can. J. Chem. **67**, 1010 (1989).
3. J. L. CHARLTON and M. M. ALAUDDIN. J. Org. Chem. **64**, 793 (1986).
4. J. L. CHARLTON. Can. J. Chem. **64**, 720 (1986).
5. J. L. CHARLTON, K. KOH, and G. L. PLOURDE. Tetrahedron Lett. **30**, 3279 (1989).
6. R. C. ANDREWS, S. J. TEAGUE, and A. I. MEYERS. J. Am. Chem. Soc. **110**, 7854 (1988).
7. J. L. CHARLTON, M. M. ALAUDDIN, and G. H. PENNER. Can. J. Chem. **64**, 793 (1986).
8. M. B. GLINSKI and T. DURST. Can. J. Chem. **61**, 573 (1982).
9. D. I. MACDONALD and T. DURST. J. Org. Chem. **53**, 3663 (1988).
10. B. J. ARNOLD, S. M. MELLOWS, P. G. SAMMES, and T. W. WALLACE. J. Chem. Soc. Perkins Trans. **1**, 401 (1974).
11. W. A. BUBB and S. STEINHELL. Aust. J. Chem. **29**, 1685 (1976).
12. J. L. CHARLTON and T. DURST. Tetrahedron Lett. **25**, 2663 (1984).
13. B. J. ARNOLD and P. G. SAMMES. J. Chem. Soc. Chem. Commun. 30 (1972); J. Chem. Soc. Chem. Commun. 1034 (1972); B. J. ARNOLD, S. M. MELLOWS, and P. G. SAMMES. J. Chem. Soc. Perkin Trans. 1, 1266 (1973); B. J. ARNOLD, P. G. SAMMES, and T. W. WALLACE. J. Chem. Soc. Perkin Trans. 1. 409 (1974); J. Chem. Soc. Perkin Trans. 1, 415 (1974).
14. M. E. JUNG, P. Y-S. LAM, M. M. MANSURI, and L. M. SPELTZ. J. Org. Chem. **50**, 1087 (1985).
15. M. E. JUNG and G. T. LOWEN. Tetrahedron Lett. **27**, 5319 (1986).
16. D. I. MACDONALD and T. DURST. Tetrahedron Lett. **27**, 2235 (1986).
17. T. DURST, E. C. KOZMA, and J. L. CHARLTON. J. Org. Chem. **50**, 4829 (1985).
18. S. TAKANO, S. OTAKI, and K. OGASAWARA. J. Chem. Soc. Chem Commun. 485 (1985).
19. D. RAJAPAKSA and R. RODRIGO. J. Am. Chem. Soc. **103**, 6208 (1981).

[4]Tables of supplementary data may be purchased from the Depository of Unpublished Data. CISTI, National Research Council of Canada, Ottawa, Ont., Canada, K1A 0S2.

An asymmetric synthesis of 2-amino-6,7-dihydroxy-1,2,3,4-tetrahydronaphthalene (ADTN)

JAMES L. CHARLTON,[1] KEVIN KOH, AND GUY L. PLOURDE
Department of Chemistry, University of Manitoba, Winnipeg, Man., Canada R3T 2N2

Received April 9, 1990

JAMES L. CHARLTON, KEVIN KOH, and GUY L. PLOURDE. Can. J. Chem. **68**, 2028 (1990).

An asymmetric synthesis of 2-amino-6,7-dimethoxy-1,2,3,4-tetrahydronaphthalene, which can be converted to the title compound by a literature procedure, is described. The synthesis, starting from 2-amino-4,5-dimethoxybenzoic acid and the acrylate of *S*-methyl lactate, was accomplished in eight steps in 11% overall yield and >97% optical purity.

Key words: *o*-quinodimethanes, Diels–Alder, asymmetric, cycloaddition, induction, diastereoselective, ADTN.

JAMES L. CHARLTON, KEVIN KOH et GUY L. PLOURDE. Can. J. Chem. **68**, 2028 (1990).

On décrit une synthèse asymétrique du 2-amino-6,7-diméthoxy-1,2,3,4-tétrahydronaphtalène qui peut être transformé dans le composé mentionné dans le titre par une procédure décrite dans la littérature. La synthèse, à partir de l'acide 2-amino-4,5-diméthoxybenzoïque et de l'acrylate du lactate de *S*-méthyle, a été réalisée en huit étapes, avec un rendement global de 11% et une pureté optique >97%.

Mots clés : *o*-quinodiméthanes, Diels–Alder, asymétrique, cycloaddition, induction, diastéréosélective, ADTN.

[Traduit par la revue]

Can. J. Chem. Downloaded from www.nrcresearchpress.com by 91.121.58.235 on 09/07/12
For personal use only.

Introduction

Since the initial discovery that 5,6-dihydroxy-2-(dimethylamino)tetralin possesses dopaminergic activity, many other 2-aminotetralin derivatives have been synthesized and tested for analogous behavior (1; for reviews see 2). These drugs interact with D_2 dopamine receptors and there is interest in them as potential antipsychotic and anti-Parkinsonian drugs. Like many other drugs, the potency of the 2-aminotetralin derivatives as central nervous system active agents is directly related to their absolute stereochemistry (and conformation) (2, 3), which necessitates the preparation of pure enantiomers of the drugs in question. In most instances pure enantiomers have been obtained by resolution of racemic mixtures but the parent compound, (*R*)-(+)-2-amino-6,7-dihydroxy-1,2,3,4-tetrahydronaphthalene (ADTN), has been recently prepared by a chiral pool synthesis starting from (*R*)-*N*-(trifluoroacetyl)aspartic anhydride (4).

We recently discovered that the acrylate of *S*-methyl lactate adds with high asymmetric induction to α-hydroxy-*o*-quinodimethane (5) and this discovery inspired the proposal of an asymmetric synthesis for ADTN, which is outlined in Scheme 1.

The Diels–Alder cycloaddition would be followed by hydrogenolysis of the hydroxyl group, hydrolysis of the lactyl ester, and, finally, conversion of the carboxylic acid group to the amine by a procedure that has already been published for the racemic acid (6).

If the synthetic route outlined in Scheme 1 could be accomplished it would make possible the asymmetric synthesis of analogs of ADTN via derivatives of the starting *o*-quinodimethane and lactyl acrylate. An asymmetric route of this type would be more versatile than the chiral pool synthesis since the latter is tied to a specific chiral synthon that becomes part of the product molecule.

Results and discussion

Our first task in tackling the proposed synthesis outlined in Scheme 1 was to choose a method of preparing the very reactive and transient *o*-quinodimethane (*o*-QDM). Among the many methods for preparing *o*-QDMs (7), the photolysis of an *o*-methyl benzaldehyde is experimentally the easiest and therefore we prepared 2-methyl-4,5-dimethoxybenzaldehyde **1**, using (in part) published procedures (8–11), as a precursor to the *o*-QDM.

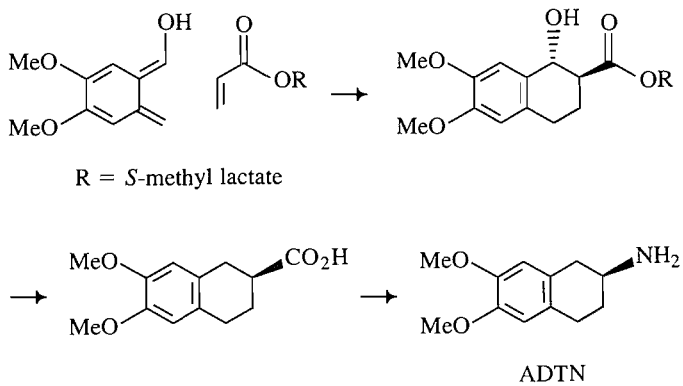

SCHEME 1

Unfortunately, as we previously reported, aldehyde **1** did not form a trappable *o*-QDM on irradiation (11). However, conversion of **1** to the diacetate **3** provided an aldehyde that could be trapped with the acrylate of *S*-methyl lactate to give essentially a single cycloadduct **4** in 85% yield. Although we did not determine the absolute stereochemistry of **4**, we assumed it to be that shown, by analogy to previous work (5).

Disappointingly, the conversion of the cycloadduct **4** to the deoxy derivative *S*-**5**, under a variety of reduction conditions, could not be achieved in high yield without epimerization of the chiral centre at the 2 position, presumably due to dehydration/reduction competing with hydrogenolysis.

In view of the difficulty encountered with the hydrogenolysis of **4**, we turned our attention to alternate methods for the preparation of the dimethoxy *o*-QDM. Following the earlier work of Sammes and co-workers (12), we have previously shown that α-hydroxy-*o*-QDM generated thermally from benzocyclobutenol adds to lactyl acrylate with the same asymmetric selectivity as that generated photochemically from *o*-methylbenzaldehyde (13). Thus we prepared 4,5-dimethoxybenzocyclobutenol **7** from 2-bromo-4,5-dimethoxybenzaldehyde **6** using the method of Durst and co-workers (14) in hopes of using

[1]Author to whom correspondence may be addressed.

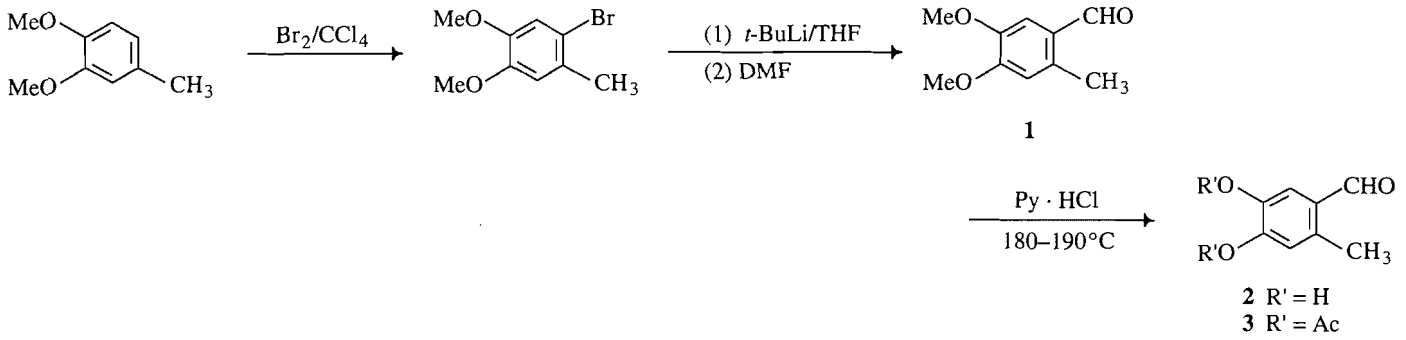

it as an *o*-QDM precursor. The yields of the benzocyclobutenol **7** using Durst's method were rather variable (30–50%) and alternate routes for its synthesis were sought. Although Jung *et al.* had very little success using a benzyne route to prepare 4,5-methylenedioxybenzocyclobutenyl acetate from 4,5-methylenedioxyanthranilic acid (8%) (15), we were able to prepare 4,5-dimethoxybenzocyclobutenyl acetate **8** from 4,5-dimethoxyanthranilic acid in very reasonable yield (45%). The acetate was readily converted to the alcohol **7** with ammonia in methanol (85%).

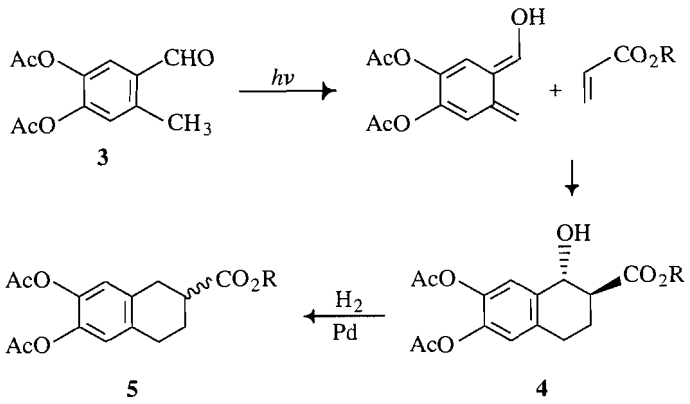

R = *S*-methyl lactate

Heating the benzocyclobutenol **7** in a toluene solution of the acrylate of *S*-methyl lactate gave one major and three minor cycloadducts in the ratio of 9:1 (major:total of minor; from nmr integration). The major cycloadduct **9** could be isolated by chromatography on silica gel in 80% yield. Hydrogenolysis of **9** under rather mild conditions (1 atm H_2 (101.3 kPa), 5% Pd on C, methanol/acetic acid (50:50), room temperature) cleanly gave the deoxy ester **10** in 80% yield. This ester could be hydrolysed to the corresponding acid **11** with potassium carbonate in methanol/water without epimerization of the chiral center. The acid was converted to the hydrochloride salt of the 2-aminotetralin **13** using a method previously developed by Narula and Schuster (16). The amine was recovered from the salt by neutralization with aqueous NaOH and extraction to give material with an $[\alpha]_D^{20}$ −85.7° (lit. (4) $[\alpha]_D$ +86.5 for the *R* isomer).

The amine **13** was previously reported to be a yellow oil (4), while we found that it was a crystalline solid with a melting point of 85–86°C. This, as well as small differences between reported nmr data and our nmr data, may be due to small amounts of impurities in the formerly prepared material (4). The configurational purity of **13** was determined by preparation of the amide with (−)-α-methoxy-α-(trifluoromethyl)phenylacetic acid (Mosher's acid) and analysis by nmr as has been described previously (4). For comparison purposes the mixture of diastereomeric amides was also prepared from racemic 4,5-dimethoxy-2-aminotetralin. The nmr spectrum of the diastereomeric amides showed well-separated singlets in the aromatic region at 6.24, 6.29, 6.32, and 6.35 ppm when the spectrum was recorded in C_6D_6. The amide from **13** showed major peaks at 6.29 and 6.32 corresponding to the *S*-(−) enantiomer (4). Assuming that the purity of the Mosher's acid was >99%, integration indicated that the optical purity of **13** was >97%. The demethylation of **13** to (*S*)-(−)-ADTN has been described elsewhere (17).

Experimental

The ^{1}H nmr spectra were recorded on a Bruker AM-300 instrument using tetramethylsilane as internal standard. The ir spectra were recorded on a Perkin Elmer 881 spectrometer. Merck Kieselgel 60 or Aldrich 28,859-4 was used for all chromatography. Elemental analyses were performed by Guelph Chemical Laboratories Ltd., Guelph, Ontario, Canada. Exact Mass/mass spectra were obtained on an Analytical VG 7070E-HF instrument. Melting points were measured

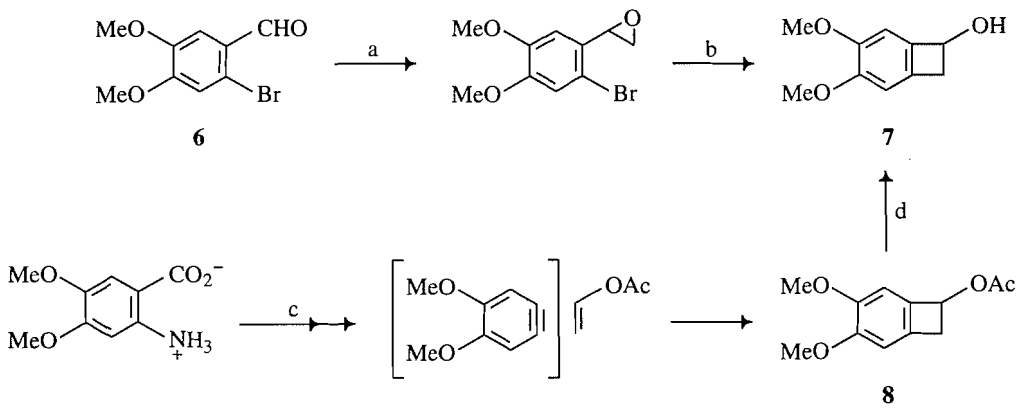

(a) $(CH_3)_3S^+I^-$, OH^-; (b) *n*BuLi, $MgBr_2$; (c) *i*-AmONO, heat; (d) NH_3/CH_3OH

Can. J. Chem. Downloaded from www.nrcresearchpress.com by 91.121.58.235 on 09/07/12
For personal use only.

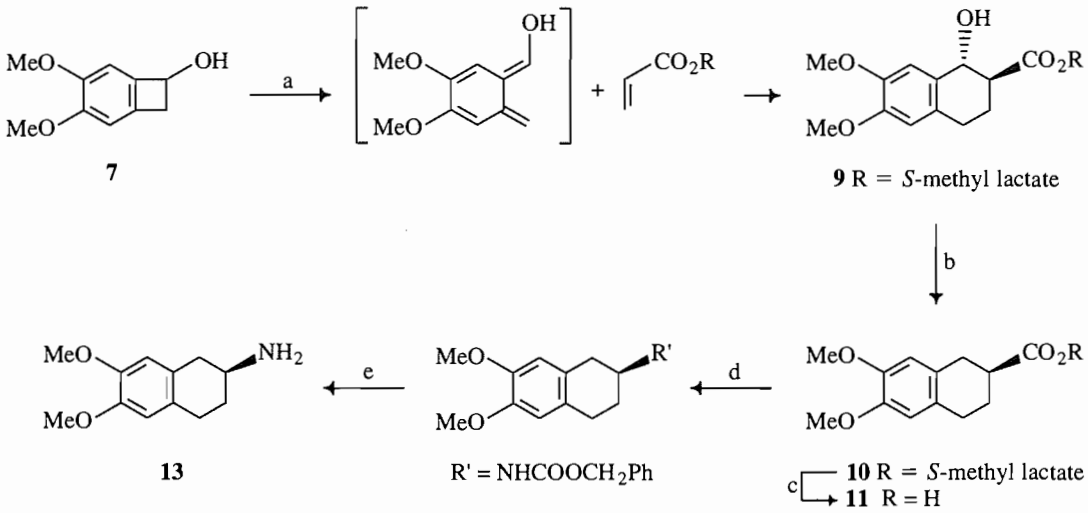

(a) 110°C, toluene; (b) H_2/Pd, methanol/acetic acid; (c) K_2CO_3, methanol/water; (d) $(PhO)_2P(O)N_3/Et_3N$, C_6H_6, reflux 2 h; then $C_6H_5CH_2OH$, reflux 24 h; (e) H_2/Pd, 10% HCl/methanol then NaOH

on a hot stage instrument and are uncorrected. Optical rotations were recorded on a Rudolf Research Corporation Autopol III instrument.

2-Bromo-4,5-dimethoxytoluene

A solution of bromine (0.72 g) in CCl_4 (10 mL) was added dropwise to a solution of 3,4-dimethoxytoluene (0.68 g, 4.47 mmol), in CCl_4 (15 mL), with stirring at room temperature until the colour of bromine persisted. The mixture was washed with water, dried ($MgSO_4$), and evaporated to give a red oil (0.919 g, 90%), which was purified by chromatography on silica gel (EtOAc/hexane, 5:95); ^1H nmr ($CDCl_3$) δ: 2.32 (s, 3H), 2.82 (s, 3H), 2.83 (s, 3H), 6.72 (s, 1H), 6.99 (s, 1H).

*2-Methyl-4,5-dimethoxybenzaldehyde, **1***

2-Bromo-4,5-dimethoxytoluene (0.221 g, 0.96 mmol) in THF (2 mL) was added to a solution of *tert*-butyllithium (1.53 mL of 1.25 M in pentane, 2 equiv.) in THF (3 mL) at −78°C under nitrogen. After 45 s, *N*,*N*-dimethyl formamide (0.14 g, 2 equiv., anhydrous) in THF (1 mL) was added. The solution was stirred for 5 min at −78°C and then at room temperature for 2 h. The reaction was quenched with aqueous HCl (10%, 10 mL), saturated with sodium chloride, extracted with CH_2Cl_2, dried ($MgSO_4$), and evaporated to give an oil (0.144 g). Chromatography of the oil (EtOAc/hexane) gave a colourless solid (100 mg, 58%); mp 71–72°C; ir (CH_2Cl_2): 1733 cm^{-1}; ^1H nmr ($CDCl_3$) δ: 2.63 (s, 3H), 3.92 (s, 3H), 3.95 (s, 3H), 6.69 (s, 1H), 7.35 (s, 1H), 10.22 (s, 1H); ms, *m/e* (rel. %): 181 (11), 180 (100), 179 (45), 165 (19), 151 (15), 109 (17). Exact Mass calcd. for $C_{10}H_{12}O_3$: 180.0783; found: 180.0786.

*2-Methyl-4,5-dihydroxybenzaldehyde, **2***

2-Methyl-4,5-dimethoxybenzaldehyde (0.47 g, 2.61 mmol) was mixed with pyridinium hydrochloride (1.21 g, 4 equiv.) and heated to 180–190°C under nitrogen for 4 h. The mixture was cooled and digested in aqueous 10% HCl (50 mL). Some residual tar was removed by filtration and the filtrate extracted with ethyl acetate. Drying ($MgSO_4$) and evaporation gave a pale green solid (0.336 g, 84%), which could be purified by chromatography on silica (EtOAc/hexane, 60:40); mp 171–173°C; ir (CH_2Cl_2): 3538, 1684 cm^{-1}; ^1H nmr ($CDCl_3$) δ: 2.54 (s, 3H), 6.70 (s, 1H), 7.27 (s, 1H), 10.07 (s, 1H); ms, *m/e* (rel. %): 153 (8), 152 (90), 151 (100), 124 (5), 123 (45). Exact Mass calcd. for $C_8H_8O_3$: 152.0474; found: 152.0472.

*2-Methyl-4,5-diacetoxybenzaldehyde, **3***

2-Methyl-4,5-dihydroxybenzaldehyde (0.206 g, 1.35 mmol), acetic anhydride (0.291 g, 0.27 mL, 2.1 equiv.), and pyridine (0.32 g, 3 equiv.) were dissolved in CH_2Cl_2 (15 mL) and stirred for 1.5 h. The mixture was poured into water (100 mL), stirred for 1 h, then extracted with CH_2Cl_2, washed with 10% aqueous HCl, dried ($MgSO_4$), and evaporated to give a pale yellow solid (0.31 g, 97%), which could be recrystallized from CH_2Cl_2; mp 93–96°C; ir (CH_2Cl_2): 1775, 1705, 1694 cm^{-1}; ^1H nmr ($CDCl_3$) δ: 2.30_4 (s, 3H), 2.30_6 (s, 3H), 2.66 (s, 3H), 7.12 (s, 1H), 7.64 (s, 1H), 10.12 (s, 1H); ms, *m/e* (rel. %): 236 (3), 194 (25), 152 (100), 151 (29), 124 (23). Exact Mass calcd. for $C_{12}H_{12}O_5$: 236.0685; found: 236.0670.

*(1R,2S)-(−)-1-Hydroxy-6,7-diacetoxy-1,2,3,4-tetrahydronaphthalene-2-carboxylate of S-methyl lactate, **4***

2-Methyl-4,5-diacetoxybenzaldehyde **3** (0.093 g, 0.394 mmol), the acrylate of *S*-methyl lactate (0.094 g, 1.5 equiv.), and hydroquinone (2 mg) were dissolved in benzene and deoxygenated by flushing with nitrogen. The solution was irradiated (Hanovia 450-W, medium pressure mercury lamp, through 1 mm Pyrex) for 24 h, the solvent evaporated, and the residue chromatographed on silica gel (35–75% EtOAc/hexane) to give a colourless oil (0.132 g, 85%); $[\alpha]_D^{20}$ −24° (*c* 1.43, $CHCl_3$); ir (CH_2Cl_2): 3575, 3492, 1771 cm^{-1}; ^1H nmr ($CDCl_3$) δ: 1.54 (d, 3H, *J* = 7.09), 2.00 (m, 1H), 2.15 (m, 1H), 2.26_5 (s, 3H), 2.26_8 (s, 3H), 2.80 (m, 3H), 3.78 (s, 3H), 4.90 (d, 1H, *J* = 9.54), 5.25 (q, 1H, *J* = 7.09), 6.91 (s, 1H), 7.47 (s, 1H); ms, *m/e* (rel. %): 394 (7), 352 (20), 310 (48), 292 (36), 249 (35), 223 (42). Exact Mass calcd. for $C_{19}H_{22}O_9$: 394.1264; found: 394.1266.

*1-Acetoxy-4,5-dimethoxybenzocyclobutene, **8***

A solution of 4,5-dimethoxyanthranilic acid (1.40 g, 7.08 mmol) in tetrahydrofuran (20 mL) was added to a refluxing solution of vinyl acetate (70 mL) and isoamyl nitrite (1.67 g, 1.9 mL, 2 equiv.) over a period of 30 min. After refluxing for 15 h, the vinyl acetate was evaporated on a rotary evaporator and the resulting brown-red oil distilled in a short path distillation apparatus (0.05 Torr (1 Torr = 133.3 Pa), 130°C) to give 1.24 g of red oil. This oil was chromatographed on silica gel (EtOAc/hexane) to give a pale yellow oil (0.71 g, 45%, solidifies on cooling), which nmr indicated was essentially free of impurities; mp 33–35°C; ir (CH_2Cl_2): 1737 cm^{-1}; ^1H nmr ($CDCl_3$) δ: 2.10 (s, 3H), 3.14 (dd, 1H, *J* = 1.52, 13.9), 3.53 (dd, 1H, *J* = 4.30, 13.9), 3.85 (s, 3H), 3.86 (s, 3H), 5.80 (dd, 1H, *J* = 1.63, 4.30), 6.71 (s, 1H), 6.82 (s, 1H); ms, *m/e* (rel. %): 222 (20), 181 (11), 180 (100), 179 (47), 165 (16), 163 (15), 162 (21). Exact Mass calcd. for $C_{12}H_{14}O_4$: 222.0892; found: 222.0891.

*4,5-Dimethoxybenzocyclobutenol, **7***

Dimethoxybenzocyclobutenyl acetate **8** (0.458 g, 2.06 mmol) was stirred in methanol/NH_4OH (7:3, 10 mL) at room temperature for 6 h. The mixture was acidified with aqueous 10% HCl and extracted with CH_2Cl_2. The resulting crude product (yellow solid) was chromatographed on silica (EtOAc/hexane) to give colourless crystals (0.317 g, 85%); mp 107–109°C; ir (CH_2Cl_2): 3593 cm^{-1}; ^1H nmr ($CDCl_3$) δ: 2.30 (s, 1H), 2.95 (dd, 1H, *J* = 1.4, 13.72), 3.50 (dd, 1H, *J* = 4.20,

Can. J. Chem. Downloaded from www.nrcresearchpress.com by 91.121.58.235 on 09/07/12
For personal use only.

Can. J. Chem. Downloaded from www.nrcresearchpress.com by 91.121.58.235 on 09/07/12
For personal use only.

13.72), 3.84 (s, 3H), 3.85 (s, 3H), 5.20 (dd, 1H, J = 1.4, 4.2), 6.70 (s, 1H), 6.80 (s, 1H); ms, *m/e* (rel. %): 181 (12), 180 (100), 179 (58), 165 (24), 151 (53). Exact Mass calcd. for $C_{10}H_{12}O_3$: 180.0787; found: 180.0781.

(1R,2S)-(−)-1-Hydroxy-6,7-dimethoxy-1,2,3,4-tetrahydronaphthalene-2-carboxylate of S-methyl lactate, ***9***

Dimethoxybenzocyclobutenol **7** (88.0 mg, 0.489 mmol), the acrylate of *S*-methyl lactate (232 mg, 3 equiv., ref. 5), and hydroquinone (2 mg) were dissolved in toluene (7 mL) and refluxed for 6 h. The solvent was evaporated on a rotary evaporator and the resulting oil chromatographed on silica gel (eluant EtOAc/hexane) to give a pale yellow oil (153 mg, 93%), which appeared by nmr to be a mixture of one major and three minor (<9%) isomers. Careful rechromatography on silica gel (25% EtOAc/hexane) gave the major cycloadduct as a colourless oil that would solidify on cooling (132 mg, 80%); mp 76–78°C; $[\alpha]_D^{20}$ −31.6° (*c* 1.33, $CHCl_3$); ir (CH_2Cl_2): 3492, 1739 cm^{-1}; ^1H nmr ($CDCl_3$) δ: 1.55 (d, 3H, J = 7.12), 2.00 (m, 1H), 2.15 (m, 1H), 2.80 (m, 3H), 3.80 (s, 1H), 3.84 (s, 3H), 3.87 (s, 3H), 4.92 (d, 1H, J = 9.12), 5.25 (q, 1H, J = 7.12), 6.55 (s, 1H), 7.17 (s, 1H); ^{13}C nmr (75.5 MHz, $CDCl_3$) δ: 16.75, 23.73, 27.79, 48.84, 52.85, 55.81, 55.86, 68.68, 70.59, 109.43, 110.55, 127.51, 129.30, 147.56, 148.12, 172.19, 174.54; ms, *m/e* (rel. %): 339 (10), 338 (52), 321 (10), 320 (34), 233 (42), 206 (63), 205 (51). Exact Mass calcd. for $C_{17}H_{22}O_7$: 338.1367; found: 338.1372.

2S-(−)-6,7-Dimethoxy-1,2,3,4-tetrahydronaphthalene-2-carboxylate of S-methyl lactate, ***10***

Cycloadduct **9** (123 mg, 0.362 mmol) and 5% Pd/C (120 mg) were stirred in acetic acid/methanol (50:50, 15 mL) under 1 atm. of H_2 at room temperature for 15 h. The mixture was then filtered, evaporated to near dryness, dissolved in CH_2Cl_2 (50 mL), washed with 5% aqueous $NaHCO_3$, dried ($MgSO_4$), and evaporated to a colourless oil that crystallized on standing (95.5 mg, 82%); mp 67–68°C; $[\alpha]_D^{20}$ −37.3° (*c* 0.88, $CHCl_3$); ir (CH_2Cl_2): 1740 cm^{-1}; ^1H nmr ($CDCl_3$) δ: 1.51 (d, 3H, J = 7.05), 1.85 (m, 1H), 2.20 (m, 1H), 2.70 (m, 3H), 3.00 (m, 2H), 3.75 (s, 3H), 3.85 (s, 6H), 5.14 (q, 1H, J = 7.05), 6.57 (s, 1H), 6.60 (s, 1H); ^{13}C nmr (75.5 MHz, $CDCl_3$) δ: 16.85, 25.61, 27.94, 31.09, 39.72, 52.25, 55.76, 66.28, 68.32, 111.33, 111.52, 126.35, 127.19, 147.02, 147.09, 171.19, 174.72; ms, *m/e* (rel. %): 322 (96), 192 (7), 191 (58), 190 (100), 189 (21), 175 (24), 176 (11). Exact Mass calcd. for $C_{17}H_{22}O_6$: 322.1416; found: 322.1425.

2S-(−)-6,7-Dimethoxy-1,2,3,4-tetrahydronaphthalene-2-carboxylic acid, ***11***

The ester **10** (113 mg, 0.349 mmol) and potassium carbonate (200 mg) were stirred in methanol/water (20:1, 20 mL) at room temperature for 15 h. Most of the solvent was then evaporated and the residue dissolved in 5% aqueous $NaHCO_3$, washed with CH_2Cl_2, acidified with 10% aqueous HCl, and finally extracted with ethyl acetate. Drying ($MgSO_4$) and evaporation gave a colourless solid that could be recrystallized from CH_2Cl_2/hexane (79.5 mg, 95%); mp 145.5–147°C; $[\alpha]_D^{20}$ −41.8° (*c* 0.67, $CHCl_3$); ir (CH_2Cl_2): 1708 cm^{-1}; ^1H nmr ($CDCl_3$) δ: 1.85 (m, 1H), 2.25 (m, 1H), 2.75 (m, 3H), 2.95 (m, 2H), 3.84_1 (s, 3H), 3.84_3 (s, 3H), 6.58 (s, 1H), 6.59 (s, 1H); ms, *m/e* (rel. %): 237 (13), 236 (100), 191 (9), 190 (22), 175 (21), 164 (26), 159 (15). Exact Mass calcd. for $C_{13}H_{16}O_4$: 236.1049; found: 236.1046.

Benzyloxycarbamate of 2S-(−)-1-amino-6,7-dimethoxy-1,2,3,4-tetrahydronaphthalene, ***12***

Dimethoxytetralincarboxylic acid **11** (76.5 mg, 0.324 mmol), diphenylphosphoryl azide (107 mg, 1.2 equiv.), and triethylamine (39.4 mg, 1.2 equiv.) were refluxed in dry benzene for 2 h. Benzyl alcohol (105 mg, 3 equiv.) was added and the mixture refluxed a further 24 h. The solvent was then evaporated and the residual yellow oil chromatographed on silica gel (20% EtOAc/hexane) to give a colourless solid (88.5 mg, 80%); mp 130–131.5°C; $[\alpha]_D^{20}$ −23.3° (*c* 0.56, $CHCl_3$); ir (CH_2Cl_2): 1720 cm^{-1}; ^1H nmr ($CDCl_3$) δ: 1.80 (m, 1H), 2.05 (m, 1H), 2.60 (dd, 1H, J = 16.0, 7.0), 3.05 (dd, 1H, J = 16.0, 4.80), 2.80 (m, 1H), 3.82 (s, 3H), 3.83 (s, 3H), 4.05 (m, 1H), 4.80 (d, 1H, J = 6.0), 5.10 (s, 2H), 6.52 (s, 1H), 6.57 (s, 1H), 7.35 (m, 5H); ms, *m/e* (rel. %): 341 (7), 233 (11), 191 (14), 190 (100), 91 (24), 77 (6). Exact Mass calcd. for $C_{20}H_{23}O_4N$: 341.1627; found: 341.1589.

Hydrochloride of 2S-(−)-1-amino-6,7-dimethoxy-1,2,3,4-tetrahydronaphthalene

A mixture of carbamate **12** (69.5 mg, 0.204 mmol) and 5% Pd/C (40 mg) in 10% anhydrous HCl in methanol (30 mL) was stirred under H_2 (1 atm) at room temperature for 8 h. The solution was filtered, and evaporated to leave a beige solid (48 mg, 97%) that could be recrystallized from methanol/ether; mp 213–214°C (lit. (4) mp 212–214°C); $[\alpha]_D^{20}$ −65.1° (*c* 0.215, CH_3OH) (lit. (4) $[\alpha]_D$ +73.2); ^1H nmr ($CDCl_3$) δ: 2.05 (m, 1H), 2.40 (m, 1H), 2.85 (m, 2H), 2.06 (dd, 1H, J = 15.4, 10.7), 3.25 (dd, 1H, J = 15.4, 4.38), 3.62 (m, 1H), 3.78 (s, 3H), 3.82 (s, 3H), 6.54 (s, 1H), 6.56 (s, 1H), 8.6 (bs, 3H).

2S-(−)-1-Amino-6,7-dimethoxy-1,2,3,4-tetrahydronaphthalene, ***13***

The hydrochloride salt of **13** (see above) (32 mg, 0.131 mmol) was dissolved in dilute aqueous base (0.1 M NaOH, 20 mL) and saturated aqueous NaCl (5 mL) was added. Extraction with CH_2Cl_2, drying ($MgSO_4$), and evaporation gave a colourless oil (16.1 mg, 60%) that solidified on cooling; mp 85–86°C; $[\alpha]_D^{20}$ −85.7° (*c* 0.105, CH_3OH), (lit. (4) $[\alpha]_D$ +86.5); ir (CH_2Cl_2): 3378, 3299 (weak) cm^{-1}; ^1H nmr ($CDCl_3$) δ: 1.5–1.74 (m, 3H), 1.98 (m, 1H), 2.50 (dd, 1H, J = 9.23, 15.75), 2.80 (m, 2H), 2.92 (dd, 1H, J = 4.68, 15.75), 3.16 (m, 1H), 3.84 (s, 6H), 6.55 (s, 1H), 6.58 (s, 1H); ms, *m/e* (rel. %): 208 (6.4), 207 (51), 192 (7.6), 191 (10), 190 (85), 175 (34), 165 (18), 164 (100). Exact Mass calcd. for $C_{12}H_{17}O_2N$: 207.1259; found: 207.1259.

Mosher's acid amide of 2S-(−)-1-amino-6,7-dimethoxy-1,2,3,4-tetrahydronaphthalene

The *S*-(−)-amide was prepared from the crude amine **13** using the literature method (4); ^1H nmr (C_6H_6) δ: 1.36 (m, 1H), 1.66 (m, 1H), 2.32 (dd, 1H, J = 15.8, 8.49), 2.43 (m, 2H), 2.81 (dd, 1H, J = 15.8, 5.05), 3.13 (m, 3H), 3.41 (s, 3H), 3.44 (s, 3H), 4.28 (m, 1H), 6.29 (s, 1H), 6.32 (s, 1H), 6.42 (d, 1H, J = 7.72), 7.02–7.2 (m, 3H), 7.74 (d, 2H, J = 7.75). The amide from the racemic amine exhibited the signals above as well as the signals for the other diastereomer. The two sets of signals were well resolved only in the aromatic region where the other diastereomer showed signals at δ 6.24 and 6.35.

Acknowledgments

We gratefully acknowledge the financial support of this project by the Natural Sciences and Engineering Research Council of Canada.

1. J. G. Cannon, J.-C. Kim, M. A. Aleem, and J. P. Long. J. Med. Chem. **15**, 348 (1972).
2. C. Kaiser and T. Jain. Med. Res. Rev. **5**, 145 (1985); J. G. Cannon. Prog. Drug Res. **29**, 303 (1985).
3. H. Wickstrom, B. Andersson, D. Sanchez, P. Lindberg, L.-E. Arvidsson, A. M. Johansson, J. L. G. Nilsson, K. Svensson, S. Hjorth, and A. Carlsson. J. Med. Chem. **30**, 2105 (1987).
4. J. E. Nordlander, M. J. Payne, F. G. Njoroge, V. M. Vishwanath, G. R. Han, G. D. Laikos, and M. A. Balk. J. Org. Chem. **50**, 3619 (1985).
5. J. L. Charlton, G. L. Plourde, K. Koh, and A. S. Secco. Can. J. Chem. **67**, 574 (1989).
6. A. P. S. Narula and D. I. Shuster. Tetrahedron Lett. **22**, 3707 (1981).
7. J. L. Charlton and M. M. Alauddin. Tetrahedron, **43**, 2873 (1987).
8. J. R. Falck, L. L. Miller, and F. R. Stermitz. J. Am. Chem. Soc. **96**, 2981 (1974).
9. G. Quinkert, W.-D. Weber, U. Schwartz, H. Stark, H. Baier, and G. Durner. Liebigs Ann. Chem. 2335 (1981).

10. T. GREENE. *In* Protective groups in organic synthesis. John Wiley and Sons, New York. 1981. p. 91.
11. J. L. CHARLTON and K. KOH. Tetrahedron Lett. **29**, 5595 (1988).
12. B. J. ARNOLD and P. G. SAMMES. J. Chem. Soc. Chem. Commun. 30 (1972); B. J. ARNOLD and P. G. SAMMES. J. Chem. Soc. Chem. Commun. 1034 (1972); B. J. ARNOLD, S. M. MELLOWS, and P. G. SAMMES. J. Chem. Soc. Perkin Trans. 1, 1266 (1973); B. J. ARNOLD, P. G. SAMMES, and T. W. WALLACE. J. Chem. Soc. Perkin Trans. 1, 409 (1974); B. J. ARNOLD, P. G. SAMMES, and T. W. WALLACE. J. Chem. Soc. Perkin Trans. 1, 415 (1974).
13. J. L. CHARLTON, K. KOH, and G. L. PLOURDE. Tetrahedron Lett. **30**, 3279 (1989).
14. E. AKGUN, M. B. GLINSKI, K. L. DHAWAN, and T. DURST. J. Org. Chem. **46**, 2730 (1981).
15. M. E. JUNG, P. Y.-S. LAM, M. M. MANSURI, and L. M. SPELTZ. J. Org. Chem. **50**, 1087 (1985).
16. A. P. S. NARULA and D. I. SCHUSTER. Tetrahedron Lett. **22**, 3707 (1981).
17. J. D. MCDERMED, G. M. MCKENZIE, and A. P. PHILLIPS. J. Med. Chem. **18**, 362 (1975).

Can. J. Chem. Downloaded from www.nrcresearchpress.com by 91.121.58.235 on 09/07/12
For personal use only.

^{15}N and ^{13}C nuclear magnetic resonance of deoxydinucleotide monophosphates. II. Protonation of the homo dimers deoxycytidylyl-(3′,5′)-deoxycytidine, thymidylyl-(3′,5′)-thymidine, and deoxyadenylyl-(3′,5′)-deoxyadenosine in dimethyl sulfoxide

GIOVANNA BARBARELLA,[1] MASSIMO LUIGI CAPOBIANCO, AND LUISA TONDELLI

Istituto dei Composti del Carbonio Contenenti Eteroatomi e loro Applicazioni, Consiglio Nazionale delle Ricerche, Via della Chimica 8, 40064 Ozzano Emilia, Bologna, Italy

AND

VITALIANO TUGNOLI

Dipartimento di Biochimica, Sezione di Chimica e Propedeutica Biochimica, Facolta' di Medicina e Chirurgia, Universita', Via Selmi 2, 40126, Bologna, Italy

Received March 13, 1990

GIOVANNA BARBARELLA, MASSIMO LUIGI CAPOBIANCO, LUISA TONDELLI, and VITALIANO TUGNOLI. Can. J. Chem. **68**, 2033 (1990).

The preferential protonation sites of the homo dimers deoxycytidylyl-(3′,5′)-deoxycytidine, thymidylyl-(3′,5′)-thymidine, and deoxyadenylyl-(3′,5′)-deoxyadenosine were established by nitrogen-15 and carbon-13 NMR in dimethyl sulfoxide, in the presence of varying amounts of CF_3COOH. The nitrogen-15 NMR data show that in d(CpC) the capability of the two N3 nitrogens to accept the proton is slightly different. In d(TpT) and d(ApA) the protonation of the phosphate group leads to significant variations of the chemical shift of the carbons adjacent to phosphorus.

Key words: deoxydinucleotides, protonation, ^{15}N and ^{13}C NMR.

GIOVANNA BARBARELLA, MASSIMO LUIGI CAPOBIANCO, LUISA TONDELLI et VITALIANO TUGNOLI. Can. J. Chem. **68**, 2033 (1990).

Faisant appel à la RMN du ^{15}N et du ^{13}C, dans le diméthylsulfoxyde, en présence de quantités variables de CF_3COOH, on a déterminé les sites de protonation préférentielle des homo dimères, désoxycytidyllyl-(3′,5′)-désoxycytidine, thymidylyl-(3′,5′)-thymidine et désoxyadénylyl-(3′,5′)-désoxyadénosine. Les données de la RMN du ^{15}N montrent que, dans le d(CpC), les deux azotes N3 possèdent des capacités différentes d'accepter le proton. Dans le d(TpT) et le d(ApA), la protonation du groupement phosphate conduit à des variations importantes des déplacements chimiques des carbones adjacents du phosphore.

Mots clés : désoxydinucléotides, protonation, RMN du ^{15}N et du ^{13}C.

[Traduit par la revue]

Nucleic acids in living systems may contain sequences characterized by a high content of a given base, the biological and chemical behaviour of which depend upon the pH (cf., for example, the d($C_4A_4C_4A_4C_4$) sequence present in the DNA of *Oxytricha nova* (1)). Changes in conformation of oligonucleotides caused by protonation, in particular those of oligomers containing cytosine, are a matter of current interest (2, 3).

The preferential protonation sites of nucleosides, nucleotides, and deoxydinucleotides are easily established by nitrogen-15 NMR in dimethyl sulfoxide (4–9). Extensive carbon-13 NMR work has demonstrated that this is also a useful technique for determining the preferred position of proton attack on purines and purine derivatives (10–12). The pK_{BH^+} values of nitrogen bases in DMSO are generally smaller than in H_2O (10); thus the data obtained by nitrogen-15 and carbon-13 NMR in DMSO can be used as guidelines to understand the acid–base equilibria of nucleic acid components in water.

We present here a nitrogen-15 and carbon-13 NMR study of the protonation of the homo dimers deoxycytidylyl-(3′,5′)-deoxycytidine, thymidylyl-(3′,5′)-thymidine, and deoxyadenylyl-(3′,5′)-deoxyadenosine in dimethyl sulfoxide. The main lines of our nitrogen-15 and carbon-13 NMR work on deoxydinucleotide monophosphates have been described in a previous paper (9). In the present study an additional question to answer is whether nitrogen-15 or carbon-13 NMR, or both, are capable of revealing the slight differences that are likely to exist in the capability of the two N3 nitrogens of d(CpC) and the two N1 nitrogens of d(ApA) to accept the proton.

Results and discussion

The structure and the numbering scheme of d(CpC), d(TpT), and d(ApA) are reported in Fig. 1. Tables 1 and 2 give the nitrogen-15 chemical shifts of d(CpC) and d(ApA) in the presence of different amounts of CF_3COOH. The nitrogen-15 chemical shifts of d(TpT), 0.12 M in dimethyl sulfoxide, are 155.0, 154.9 (N1); 143.0, 142.4 (N3). Due to the fact that d(TpT) has only "pyrrole-like" nitrogens (13), no significant variations of $\delta(^{15}N)$ are found when CF_3COOH is added, as protonation only occurs at the phosphate group (*vide infra*). Consequently, the $\delta(^{15}N)$ values of d(TpT) as a function of added acid are not reported. Tables 3–5 give the carbon-13 chemical shifts and the relevant carbon–proton coupling constants of d(CpC), d(TpT), and d(ApA), respectively, at different concentrations of CF_3COOH.

The conformational properties of d(CpC), d(ApA), and d(TpT) in water have been described in an early work by Cheng and Sarma (14). No data are available for the same substrates in DMSO, a solvent where stacking interactions are negligible (15). For d(CpC) some information can be gained by comparison with the $\delta(^{15}N)$ values of the corresponding nucleoside (5, 9). The $\delta(^{15}N)$ differences between d(CpC) and cytidine indicate the existence of a certain degree of self-association of the dimer, with hydrogen bondings between the amino groups of one molecule (which are *deshielded* in the dimer compared

[1]Author to whom correspondence may be addressed.

Printed in Canada / Imprimé au Canada

Can. J. Chem. Downloaded from www.nrcresearchpress.com by 91.121.58.235 on 09/07/12
For personal use only.

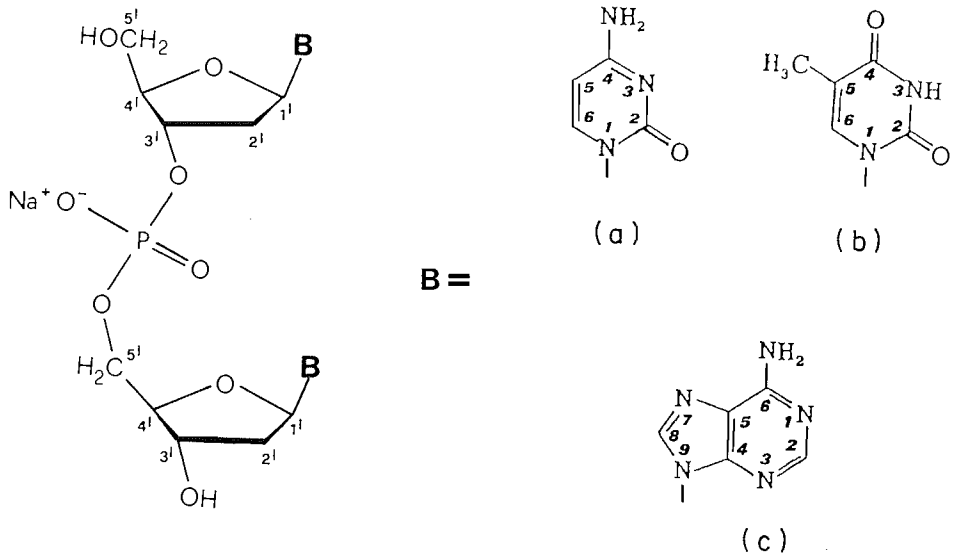

FIG. 1. Structure and numbering scheme of deoxycytidylyl-(3′,5′)-deoxycytidine (a), thymidylyl-(3′,5′)-thymidine (b), and deoxyadenylyl-(3′,5′)-deoxyadenosine (c).

TABLE 1. ^{15}N chemical shifts[a] of a 0.3 M solution of deoxycytidylyl-(3′,5′)-deoxycytidine in dimethyl sulfoxide as a function of added trifluoroacetic acid

Molar equiv. of CF_3COOH	0.0	1.0	2.0	3.0
N1	154.5	155.2	155.4	155.4
	154.1	154.5	154.9	154.9
N3	207.0	172.5	148.3	143.8
	206.3	168.9	147.5	
NH_2	94.2	101.9	105.5	105.9
		101.0		

[a]In ppm, with respect to NH_3.

TABLE 2. ^{15}N chemical shifts[a] of a 0.15 M solution of deoxyadenylyl-(3′,5′)-deoxyadenosine in dimethyl sulfoxide as a function of added trifluoroacetic acid

Molar equiv. of CF_3COOH	0.0	0.5	1.0
N1	235.4	228.4	Not
	235.3	226.3	observed
N3	223.7	223.7	223.7
	222.0	221.8	221.9
N7	240.4	240.8	241.5
	240.0	240.3	240.9
N9	172.8	173.3	174.8
	171.7	171.7	172.8
NH_2	81.1	82.2	83.9
	80.3	81.8	

[a]In ppm with respect to NH_3.

to the monomer) and the N3 nitrogens of another molecule (which are *shielded* compared to the monomer (9)). This is confirmed by proton data, which show that progressive dilution of d(CpC) in DMSO leads to a progressive displacement of the resonance of the amino protons towards lower frequencies (15). However, proton NMR shows also (see the experimental section) that even the hydroxyl groups are involved in the self-association process, indicating that the self-association scheme for d(CpC) in DMSO is more complicated than for cytidine (16).

The carbon-13 chemical shifts of d(CpC), d(TpT), and (ApA) are close to those for the corresponding monomers (9, 17). It is worth noting that in d(TpT) the chemical shifts for the C3′ and C5′ carbons adjacent to the phosphate group are very similar to those of d(CpC) and d(ApA), suggesting that the geometry of the sugar–phosphate backbone of the three homo dimers is nearly the same.

Protonation of deoxycytidylyl-(3′,5′)-cytidine

The two possible binding sites for proton are N3 and the phosphate group, but the former should have a pK_{BH^+} at least 2 pK units larger than the latter (9, 18, 19) and should be protonated first. In agreement with this, both N3 signals are displaced *upfield* by several ppm on acid addition (10–12). Table 1 shows that the trend of variation of $\delta(^{15}N)$ with increasing amounts of added acid is similar to that observed for cytidine itself and for the cytidylyl group of deoxycytidylyl-(3′,5′)-deoxyguanosine (9). The upfield shifts of the N3 nitrogens are paralleled by smaller but sizeable downfield shifts of the amino nitrogens, owing to the fact that in the protonated form there is a larger delocalization of the lone pair of the amino group into the pyrimidine ring (6, 9). Figure 2a–d gives the spectrum of d(CpC) after addition of 0, 1, 2, and 3 molar equivalents of acid, respectively. The two N3 resonances appear first as two sharp lines separated by only 0.7 ppm (Fig. 2a). Addition of 1 molar equivalent of acid displaces both lines towards lower frequencies by more than 30 ppm while the line separation increases up to 3.6 ppm (Fig. 2b). Moreover, owing to the relatively slow intermolecular hydrogen exchange in dimethyl sulfoxide, the resonance lines of the two nitrogens are considerably broadened. As the amount of acid reaches 2 molar equivalents, the lines become sharp again and separated by only 0.8 ppm (Fig. 2c). Finally, by further addition of acid the two resonances collapse into a single broad line (Fig. 2d). Since the N3 chemical shifts are weighted averages of the δ values for the protonated and unprotonated species, i.e., δ depends on the position of the equilibrium $B + H^+ \rightleftarrows BH^+$, this behaviour indicates that there is a different capability of the N3 nitrogens of the 3′-dCp and 5′-pdC moieties to accept the proton. Assuming that the chemical shift difference between a

Can. J. Chem. Downloaded from www.nrcresearchpress.com by 91.121.58.235 on 09/07/12
For personal use only.

TABLE 3. ^{13}C chemical shifts[a] and coupling constants[a] of a 0.1 M solution of d(CpC) in dimethyl sulfoxide as a function of added trifluoroacetic acid

Molar equiv. of CF_3COOH	0.0		1.0		2.0	3.0
C2	155.3		149.8		147.4	147.5
			149.5		147.3	
	($^3J_{C2H1'}$	7.3		7.3	7.3)	
C4	165.5		161.4		159.9	159.8
	161.1					
	($^3J_{C4H5}$	9.8		9.8	9.8)	
C5	94.5		94.5		94.2	94.5
	($^1J_{C5H5}$	173.3		178.2	181.9	181.9)
C6	141.0		143.4		144.2	144.5
	143.3					
	($^1J_{C6H6}$	180.7		184.3	186.8	186.8)
C1′	84.9		85.9		86.1	86.4
	85.8		85.9		86.2	
C2′	39.1		39.1		39.0	39.2
	40.1		not obs.		39.7	40.0
C3′	74.8		75.0		75.8	76.4
	70.8		70.3		70.0	70.2
C4′	85.7		86.1		86.0	86.0
	86.1		86.7		86.7	86.9
C5′	61.5		61.1		60.9	61.1
	64.7		64.9		65.3	65.8

[a]In ppm from TMS and in Hz, respectively.

TABLE 4. ^{13}C chemical shifts[a] of a 0.1 M solution of thymidylyl-(3′,5′)-thymidine in dimethyl sulfoxide as a function of added trifluoroacetic acid

Molar equiv. of CF_3COOH	0.0	1.0	2.0
C2	150.5	150.5	150.5
	150.4		
C4	163.8	163.7	163.7
	163.7		
C6	136.2	135.9	135.8
	135.9	135.9	135.8
CH_3	12.1	12.1	12.1
	11.9	12.0	12.0
C1′	83.7	84.0	84.1
	83.6	83.8	83.8
C2′	38.2	37.8	37.8
C3′	74.4	76.9	77.0
	70.8	70.4	70.4
C4′	85.9	84.9	84.8
	86.1	85.6	85.6
C5′	61.5	61.2	61.2
	64.5	66.1	66.2

[a]In ppm from TMS.

TABLE 5. ^{13}C chemical shifts[a] and coupling constants[a] of a 0.1 M solution of deoxyadenylyl-(3′,5′)-deoxyadenosine in dimethyl sulfoxide as a function of added trifluoroacetic acid

Molar equiv. of CF_3COOH	0.0	1.0	2.0
C2	152.5	149.1	146.8
	152.4		146.3
	($^1J_{C2H2}$	199.0	205.5)
C4	149.2	148.5	148.3
	148.9		
C5	119.3	119.1	118.9
	118.9	118.9	
	($^3J_{C5H8}$	11.3	11.5)
C6	156.1	153.7	151.5
	155.9	153.1	151.4
	($^3J_{C6H2}$	11.0	7.0)
C8	139.5	140.7	141.6
	139.3	140.7	141.5
	($^1J_{C8H8}$	213.6	214.5)
C1′	83.9	84.1	84.2
	83.1	83.7	84.0
C2′	39.4	Not observed	
C3′	75.0	76.7	76.8
	71.2	70.6	70.5
C4′	86.8	86.7	86.7
	85.2	85.5	85.7
C5′	62.0	61.5	61.3
	64.8	65.9	66.1

[a]In ppm from TMS and in Hz, respectively.

protonated and an unprotonated nitrogen is 60 ppm (Table 1), it is easily calculated that one of the N3 nitrogens of Fig. 2b is 6% more protonated than the other. The existence of this difference is in agreement with the fact that the pK values reported for 2′-, 3′-, and 5′-cytidine monophosphates (18, 19) are slightly

Can. J. Chem. Downloaded from www.nrcresearchpress.com by 91.121.58.235 on 09/07/12
For personal use only.

Can. J. Chem. Downloaded from www.nrcresearchpress.com by 91.121.58.235 on 09/07/12
For personal use only.

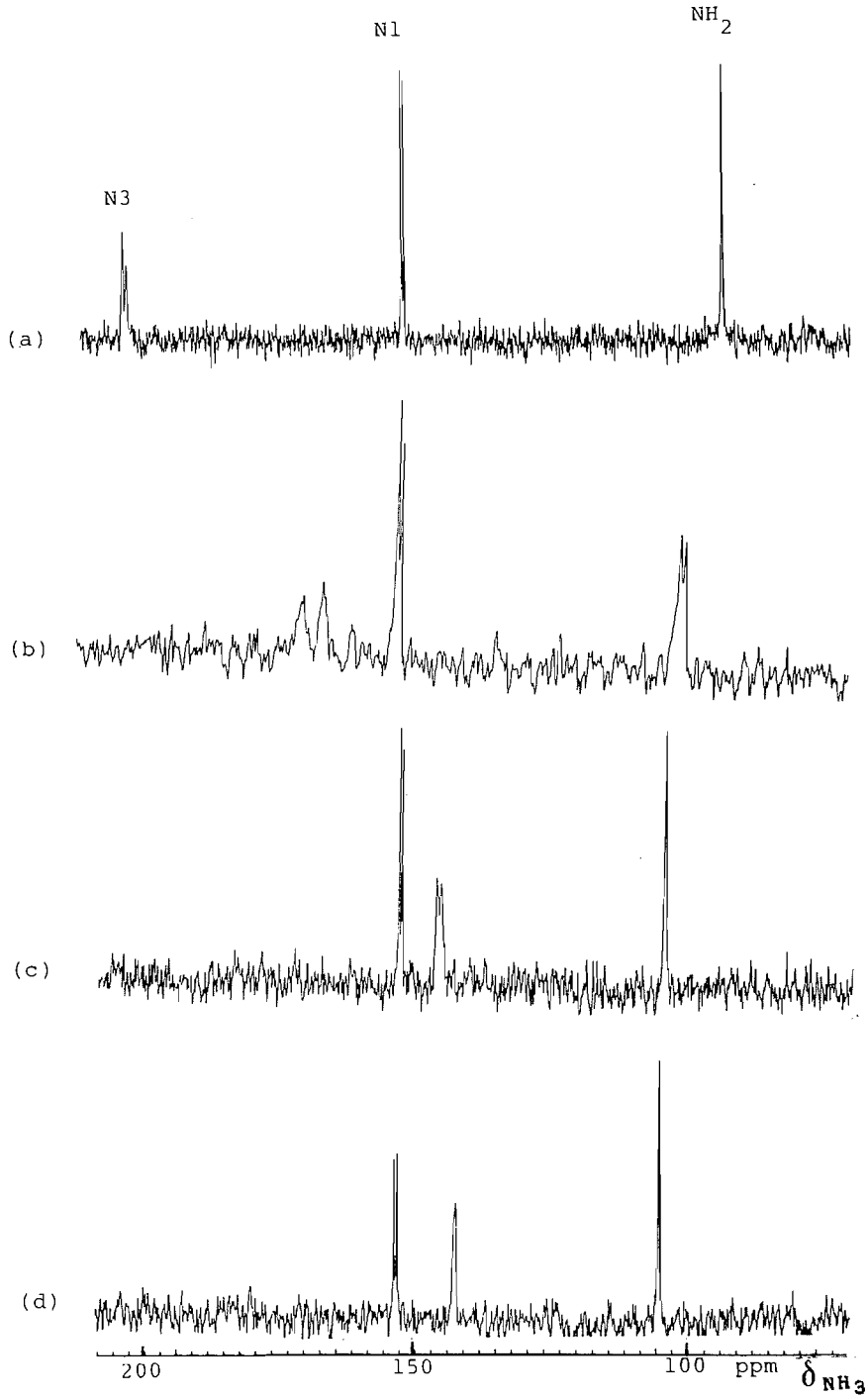

FIG. 2. Natural abundance 30.408 MHz nitrogen-15 NMR spectrum of deoxycytidylyl-(3′,5′)-deoxycytidine in dimethyl sulfoxide, in the presence of varying amounts of CF_3COOH. (a) 0 mol. equiv.; (b) 1 mol. equiv.; (c) 2 mol. equiv.; (d) 3 mol. equiv.

different. Unfortunately, the conflicting values reported by the different authors for 3′- and 5′-cytidine monophosphates make it difficult to establish which of the two N3 nitrogens of d(CpC) is the more basic simply by comparison with the pK_{BH^+} values for these nucleotides. A clue to identify which one of the two nitrogens of Fig. 2b is the more protonated can be found in the proton spectrum of the amino hydrogens of d(CpC) in DMSO *before acid addition*. Both amino protons of d(CpC) appear as broad doublets, indicating restricted rotation around the C4—NH_2 bond (20, 21). However, for one of the two amino groups the separation between the proton resonance lines is larger than for the other (see the experimental section). This may be taken as evidence of a larger degree of restricted rotation and, consequently, of a larger amount of negative charge on the corresponding N3 nitrogen (see Fig. 3 of ref. 9), which, in turn, becomes a better proton acceptor in the presence of CF_3COOH. Comparison with Raszka's proton data on 5′-cytidine monophosphate (21) in water suggests that this amino group may be that belonging to the 5′-dpC moiety of d(CpC), which is hydrogen bonded to the phosphate group of another molecule. In agreement with this, addition of sodium phosphate to the DMSO solution (see the experimental section) changes dramati-

Can. J. Chem. Downloaded from www.nrcresearchpress.com by 91.121.58.235 on 09/07/12
For personal use only.

cally the spectrum of the amino protons, which both become hydrogen bonded to the phosphate anion and show the same proton line separation.

Table 2 shows that the trend in variation of $\delta(^{13}C)$ and $^{n}J_{CH}$ following acid addition is similar to that observed for cytidine and the cytidylyl moiety of deoxycytidylyl-(3′,5′)-guanosine monophosphate (9). The preferential protonation at N3 is clearly indicated by the change of the chemical shifts and coupling constants of the adjacent C2 and C4 carbons. However, contrary to nitrogen-15, carbon-13 data do not reveal that one of the two N3 nitrogens is a better proton acceptor than the other. This is shown, for example, by the fact that the chemical shift difference between the two C2 and between the two C4 carbons flanking the protonated nitrogen, after addition of 1 molar equivalent of acid, is too small to be significant.

Protonation of thymidylyl-(3′,5′)-thymidine

The carbon-13 chemical shifts of d(TpT) in water have already been reported (17, 22) and are larger than those in DMSO, given in Table 4. Since the major differences are found for the carbons of the bases, this is probably due to the effect of the stacking interactions existing in H_2O.

Table 4 shows that addition of CF_3COOH does not lead to $\delta(^{13}C)$ changes for the carbons of the pyrimidine bases. Indeed, as already mentioned, d(TpT) has only a single site available for protonation, i.e., the phosphate group. Consequently, only the carbons bound to the phosphate group and those of the ribose rings show chemical shift changes following acid addition. Progressive addition of CF_3COOH leads to a significant *downfield* shift of C3′ belonging to the 5′-pT moiety and of C5′ belonging to the 3′-Tp moiety, while the chemical shift of all ribose carbons moves *upfield*, although by smaller amounts.

Protonation of deoxyadenynyl-(3′,5′)-deoxyadenosine

It is known that addition of acid to a solution of d(ApA) may lead to hydrolysis of the glycosylic bond. We found that this is also the case for a DMSO solution containing trifluoracetic acid, but in DMSO the hydrolysis requires several hours to be completed. Since under our experimental conditions a nitrogen-15 spectrum requires at least overnight accumulation, we could only obtain $\delta(^{15}N)$ values for addition of 0.5 and 1.0 molar equivalents of CF_3COOH (Table 2). For larger amounts of acid, only the spectrum of protonated adenine[2] was observed. Since a much shorter time is required for a carbon-13 spectrum, the $\delta(^{13}C)$ values in the presence of up to 2 molar equivalents of acid are reported in Table 5.

The more basic nitrogen of adenosine is N1, with a pK_{BH^+} very close to that of the N3 of cytidine and about two units larger than that predicted for the phosphate group (9, 18, 19). On these grounds one would expect that addition of 0.5–1.0 molar equivalents of CF_3COOH would lead to the exclusive protonation of N1. This is not, however, the case.

Addition of 0.5 molar equivalents of acid displaces the resonances of the two N1 nitrogens towards lower frequencies by several ppm, as expected for protonation at these sites (4). This is also shown by the variations of the chemical shifts of C2 and C6, the carbons flanking N1, and by the variations of $^{1}J_{C2-H2}$ and $^{3}J_{C6-H2}$ (ref. 23 and footnote 2). However, the chemical shift increments of the two N1 nitrogens, −7.1 and −9.1 ppm respectively, are smaller than would be expected on the basis of the comparison with adenosine, for which, following addition of 0.31 molar equivalents of CF_3COOH, an increment of −16 ppm is found in δ(N1) (4). Moreover, Table 5 shows that, for only 1 molar equivalent of acid added, the chemical shift of the C3′ and C5′ carbons next to phosphorus *increases* by 1.7 and 1.1 ppm, respectively. Comparison with the changes in $\delta(^{13}C)$ for the same carbons in d(CpC) and d(TpT) indicates clearly that protonation also occurs at the phosphate group. Thus, in d(ApA), protonation of the phosphate group is competitive with that of N1.

Table 2 shows also that protonation leads to the increase of the $\delta(^{15}N)$ difference of the two N1 nitrogens (2.1 ppm for 0.5 mol. equiv. of acid added). As in the case of d(CpC), this indicates that there is a different capability of the two N1 nitrogens to accept the proton. It is worth noting that upon acid addition the N1 resonance lines become broader than those of the N3's in d(CpC), indicating that the intermolecular hydrogen exchange is slower on the NMR time scale (note also that on addition of 1 mol. equiv. of acid the N1 lines become so broad as to be undetectable). As in the case of d(CpC), the $\delta(^{13}C)$ changes of d(ApA) are unable to reveal the small differences in the capability of the two N1 nitrogens to accept the proton.

Conclusions

The preferential protonation sites of the homo dimers deoxycytidylyl-(3′,5′)-deoxycytidine, thymidylyl-(3′,5′)-thymidine, and deoxyadenynyl-(3′,5′)-deoxyadenine are easily established either by nitrogen-15 or carbon-13 NMR in dimethyl sulfoxide. It is possible, however, to detect the small differences in the capabilities of the two N3 nitrogens of d(CpC) and the two N1 nitrogens of d(ApA) to accept the proton only by nitrogen-15 NMR. Small differences in basicity may become important at pH values near the physiological one (cf., for example, ref. 24); thus it would be useful to establish whether protonation of d(CpC) and d(ApA) follows the same trend in water as in dimethyl sulfoxide.

The data reported here show that nitrogen-15 NMR is very informative, but that carbon-13 NMR also gives a great deal of useful information, not only on the protonation of the pyrimidine or purine moieties, but also on that of the phosphate group. Indeed, protonation of phosphate leads to significant variations in the $\delta(^{13}C)$ values of the carbons next to phosphorus. Thus, ^{13}C NMR looks very promising for conformational analysis of oligonucleotides, particularly where conformational changes induced by pH variations are concerned.

Experimental

All dinucleoside monophosphates were prepared according to published procedures (25). The sodium salts were obtained from the corresponding ammonium derivatives by treatment with Dowex 50W8 (Na^+ form).

NMR spectra

All spectra were run with a Bruker CXP-300 spectrometer at the probe temperature (25°C). The resonance frequencies were 75.485 MHz for ^{13}C, 30.408 for ^{15}N, and 300 MHz for ^{1}H. The concentrations were 0.3 M and 0.15 M for the nitrogen spectra of d(CpC) and d(ApA), respectively, and 0.1 M for all carbon and proton spectra.

Carbon-13 chemical shifts are relative to TMS as internal reference. The assignments were carried out by carbon–proton correlated spectroscopy and by comparison with literature data (11, 22, 23).

Nitrogen-15 spectra were run with a 10-mm dedicated probe. In most cases broadband decoupled and inverse gated-decoupled spectra were recorded. Although this is a rather time-consuming technique for

[2] $\delta(^{13}C)$ values of a solution of adenine 0.1 M in DMSO: 152.3 (C2); 151.1 (C4); 117.4 (C5); 155.3 (C6); 139.2 (C8). Addition of 2 mol. equiv. of CF_3COOH gives: 145.3 (C2); 149.8 (C4); 115.6 (C5); 151.6 (C6); 143.8 (C8).

obtaining nitrogen-15 natural abundance NMR information, we found that it gave more reliable results than the various INEPT techniques. However, we are unable to say whether this is attributable to the difficulties inherent in using an old spectrometer or to some physical features of the dimers under investigation in DMSO, or both. Typical conditions for gated-decoupled spectra (required to suppress the unfavourable $^{15}N-^{1}H$ nuclear Overhauser enhancement) were as follows: sweep width 10 kHz; pulse width 40°; repetition time 7 s; data points 16 k. The free induction decays were transferred to a New Methods Research Specstation equipped with a DEC microVax II, zero-filled to 32 k, and Fourier transformed. The chemical shifts were measured with respect to an external 1 M solution of HNO_3 and converted to the NH_3 scale using the conversion factor $\delta(NH_3)$ = 376 ppm (p. 74, ref. 13). The assignments were made on the basis of the corresponding monomers (4–6).

The proton spectrum of d(CpC) in DMSO showed two broad doublets (belonging to the two different amino groups), resonating at 7.17 ppm (proton separation: 0.04 ppm) and 7.35 ppm (proton separation: 0.11 ppm). Addition of Na_3PO_4 to the solution resulted in two broad doublets centered at 7.27 and 7.09 ppm, both with a doublet separation of 0.1 ppm. The proton spectrum of d(CpC) in DMSO also shows a single broad signal centered at 5.50 ppm for the two hydroxyl groups. Progressive dilution leads to the progressive separation of the resonances, which also become sharper. The spectrum of a 2×10^{-3} M solution shows a sharp doublet centered at 5.38 (C3′-O*H*) ppm and a sharp triplet centered at 5.51 ppm (C5′-O*H*). The same signal separation of the two hydroxyl groups, with appearance of long-range proton–proton couplings, is also obtained when Na_3PO_4 is added to the solution.

Acknowledgment

We are grateful to Dr. A. Garbesi of I.Co.C.E.A.-C.N.R. for helpful discussions.

1. Y. Oka and C. A. Thomas, Jr. Nucleic Acids Res. **15**, 8877 (1987).
2. R. J. Topping, M. P. Stone, C. K. Brush, and T. M. Harris. Biochemistry, **27**, 7216 (1988).
3. E. L. Edwards, R. L. Ratliff, and D. M. Gray. Biochemistry, **27**, 5166 (1988).
4. V. Markowski, G. R. Sullivan, and J. D. Roberts. J. Am. Chem. Soc. **99**, 714 (1977).
5. K. Kanamori and J. D. Roberts. Acc. Chem. Res. **16**, 35 (1983).
6. P. Buchner, W. Maurer, and H. Ruterjans. J. Magn. Reson. **29**, 45 (1978).
7. G. Remaud, J. Kjellberg, W. G. Johansonn, and J. Chattopadhyaya. Tetrahedron, **43**, 365 (1987).
8. G. Buchanan. Tetrahedron, **45**, 581 (1989).
9. G. Barbarella, M. L. Capobianco, A. Carcuro, F. P. Colonna, A. Garbesi, and V. Tugnoli. Can. J. Chem. **66**, 2492 (1988).
10. R. L. Benoit, D. Boulet, L. Seguin, and M. Frechette. Can. J. Chem. **63**, 1228 (1985).
11. R. J. Pugmire and D. M. Grant. J. Am. Chem. Soc. **90**, 697 (1968).
12. R. J. Pugmire and D. M. Grant. J. Am. Chem. Soc. **93**, 1880 (1971).
13. G. C. Levy and R. L. Litcher. Nitrogen-15 nuclear magnetic resonance spectroscopy. J. Wiley & Sons, New York. 1979. pp. 32–33.
14. D. M. Cheng and R. H. Sarma. J. Am. Chem. Soc. **99**, 7333 (1977).
15. R. A. Newmark and C. R. Cantor. J. Am. Chem. Soc. **90**, 5010 (1968).
16. C. Dyllick-Brenzinger, G. R. Sullivan, P. P. Pang, and J. D. Roberts. Proc. Natl. Acad. Sci. U.S.A. **77**, 5580 (1980).
17. L. Kan, L. Voituriez, and J. Cadet. Biochemistry, **27**, 5796 (1988).
18. R. M. Izatt, J. J. Christensen, and J. H. Rytting. Chem. Rev. **71**, 439 (1971).
19. K. H. Scheller, V. Scheller-Krattiger, and R. B. Martin. J. Am. Chem. Soc. **103**, 6833 (1981).
20. E. D. Becker, H. T. Miles, and R. B. Bradley. J. Am. Chem. Soc. **87**, 5575 (1965).
21. M. Raszka. Biochemistry, **13**, 4616 (1974).
22. R. E. Rycyna and J. L. Alderfer. Nucleic Acids Res. **13**, 5949 (1986).
23. M. Schumacher and H. Gunther. J. Am. Chem. Soc. **104**, 4167 (1982).
24. D. M. Brown, D. M. Gray, M. H. Patrick, and R. L. Ratliff. Biochemistry, **24**, 1676 (1985).
25. J. E. Marugg, M. Tromp, P. Jhurani, C. F. Hoyng, G. A. Van der Marel, and J. H. van Boom. Tetrahedron, **40**, 73 (1984).

Can. J. Chem. Downloaded from www.nrcresearchpress.com by 91.121.58.235 on 09/07/12
For personal use only.

Hypoglucaemic triterpenoid saponins from *Boussingaultia baselloides*

ALFONSO ESPADA, JAIME RODRIGUEZ, M. CARMEN VILLAVERDE, AND RICARDO RIGUERA[1]
Departamento de Química Orgánica, Facultad de Química, Universidad de Santiago de Compostela, Spain

Received March 22, 1990

ALFONSO ESPADA, JAIME RODRIGUEZ, M. CARMEN VILLAVERDE, and RICARDO RIGUERA. Can. J. Chem. **68**, 2039 (1990).

New saponins with hypoglucaemic activity (**1–4**) and momordin Ic (**5**) have been isolated from the methanolic extract of the leaves of *Boussingaultia baselloides*. They were shown by spectroscopy and chemical transformation to be derivatives of 12,20(29)-dien-30-noroleanic acid. Boussingoside A_1 (**1**) exhibits very strong hypoglucaemic activity in rats. Acid hydrolysis of the saponin **1** yielded five transformation products (**6–10**), though one of them (larreagenin A (**6**), which has been reported in the literature as a genuine plant metabolite) is considered to be an artifact formed by the acid treatment.

Key words: *Boussingaultia baselloides*, Basellaceae, boussingosides, triterpenoid saponins, hypoglucaemic activity.

ALFONSO ESPADA, JAIME RODRIGUEZ, M. CARMEN VILLAVERDE et RICARDO RIGUERA. Can. J. Chem. **68**, 2039 (1990).

On a isolé de nouvelles saponines ayant une activité hypoglycémique (**1–4**) et la momordine Ic (**5**) à partir d'extraits méthanoliques des feuilles de *Boussingaultia baselloides*. Faisant appel à la spectroscopie et à des transformations chimiques, on démontre que ces composés sont des dérivés de l'acide (29)-12,20-diène-30-noroléanique. La boussingoside A_1 (**1**) exhibe une forte activité hypoglycémique chez les rats. L'hydrolyse acide de la saponine **1** conduit à cinq produits de transformation (**6–10**) dont l'un d'eux (la larréagénine A (**6**), qui est répertoriée dans la littérature comme un vrai métabolite végétal) est considéré comme un artefact résultant du traitement acide.

Mots clés : *Boussingaultia baselloides*, Basellaceae, boussingosides, saponines triterpénoïdes, activité hypoglycémique.
[Traduit par la revue]

Can. J. Chem. Downloaded from www.nrcresearchpress.com by 91.121.58.235 on 09/07/12
For personal use only.

Introduction

Two members of the herbaceous climbing plant family Basellaceae have been reported in Colombia (1, 2). One of these species, *Boussingaultia baselloides* H.B.K., known as insuline, is used in folk medicine (as a drink made by adding 4–6 fresh chopped *B. baselloides* leaves to approximately 150 mL of boiling water and reduction of the volume to a third), mainly for treatment of *diabetes* but also as an analgesic. In this paper we report the isolation of new triterpenoid glycosides responsible for the hypoglucaemic activity of the crude plant extract. This work constitutes the first research on an intact polar extract of a member of the Basellaceae family.

In the course of this study we have isolated and identified, by spectroscopic analysis (2D-NMR experiments and FAB-MS) and chemical transformation, four new nor-triterpenoid saponins with hypoglucaemic activity.

Results and discussion

The aerial parts of the plant, collected in Tuluá (Colombia), were extracted successively with petroleum ether and MeOH. The MeOH extract was then partitioned between *n*-BuOH and H_2O. Chromatographic separation of the BuOH soluble fraction, which showed hypoglucaemic activity, afforded a complex mixture of triterpenoid glycosides. This mixture was successively subjected to several separation techniques (Sephadex LH-20, DCCC, and HPLC) to give the pure compounds **1–5** (Fig. 1). We have named compounds **1–4** boussingosides A_1 (**1**), A_2 (**2**), B (**3**), and C (**4**); compound **5**, momordin Ic, has previously been reported in *Momordica cochinchinensis* (Cucurbitaceae) (3).

Boussingoside A_1 (**1**) was crystallized from methanol as a white microcrystalline powder (mp 213–215°C) that was subjected to fast atom bombardment MS (FAB-MS) (negative ion mode). A quasi-molecular ion was observed at *m/z* 615 $[M - H]^-$ indicating a molecular weight of *m/z* 616 and a molecular formula of $C_{35}H_{52}O_9$. The ^1H NMR spectrum of **1** showed a doublet at δ 4.93 (J = 7.9 Hz) attributable to the anomeric proton of a β-pyranoside. The ^{13}C NMR spectrum showed the anomeric carbon at δ 106.9, a carboxylic signal at δ 179.4 ppm, and four signals in the sugar region corresponding to glucuronic acid. The fragment at *m/z* 440 found in the FAB-MS, $[M - H - 175]^-$, clearly indicates the separation of this sugar; in fact, glucuronic acid was identified (GC–MS as alditol acetate) after hydrolysis of **1** (see Table 1).

Compound **1** also exhibited two olefinic bonds, one with signals at δ_H 5.43 and δ_C 122.9 and 144.1, indicating a $\Delta^{12(13)}$ double bond, and the other at δ_H 4.71 and 4.76 and δ_C 106.9 (CH_2 inferred from DEPT and XHCOR experiments) and δ 149.0, due to the C20—C29 double bond. The presence of five methyl singlets upfield in the ^1H NMR spectrum and comparison with the literature (4, 5) confirmed a nor-olean skeleton.

Further information about the structure of **1** was obtained from COSY and nOe experiments. Thus the double doublet at δ_H 3.34 (J = 11.9 and 4.0 Hz), H3α, was shown to be correlated in the ^1H–^1H COSY spectrum (Fig. 2) with two multiplets at 2.16 ppm (H2α) and 1.80 ppm (H2β). Furthermore, the double doublet at δ_H 3.17 (J = 13.7 and 4.9 Hz), H18, correlates with two signals at 2.20 (m) and 2.58 (t, J = 13.7 Hz) corresponding to protons H19β and H19α respectively. The stereochemistry at C18 was determined by irradiation of the signal at 3.17 (H18), which caused nOe on the broad singlet at 5.43 corresponding to H12. All these assignations were corroborated by a 2D-XHCOR experiment (see Fig. 3) and the assignation of the methyl groups was corroborated by a XHCORR-LR spectrum (Fig. 4) of compound **2**. We observe the following correlations: Me24/C4 (two bonds) (no correlation was observed with C3), Me23/C3 (three bonds), Me23/C4 (two bonds), Me27/C13, Me27/C8 (both three bonds), and Me27/C14 (two bonds), Me26/C8 (two bonds), Me26/C14 (three bonds), and finally Me25/C10 (two bonds).

On the basis of the above data, we concluded that boussingoside A_1 (**1**) is 3-*O*-[β-D-glucuronopyranosyl]-30-norolean-12,20(29)-dien-28-oic acid.

Boussingoside A_2 (**2**) was obtained as a microcrystalline white powder (mp 218–220°C), and presents a FAB-MS

[1]Author to whom correspondence may be addressed.

Printed in Canada / Imprimé au Canada

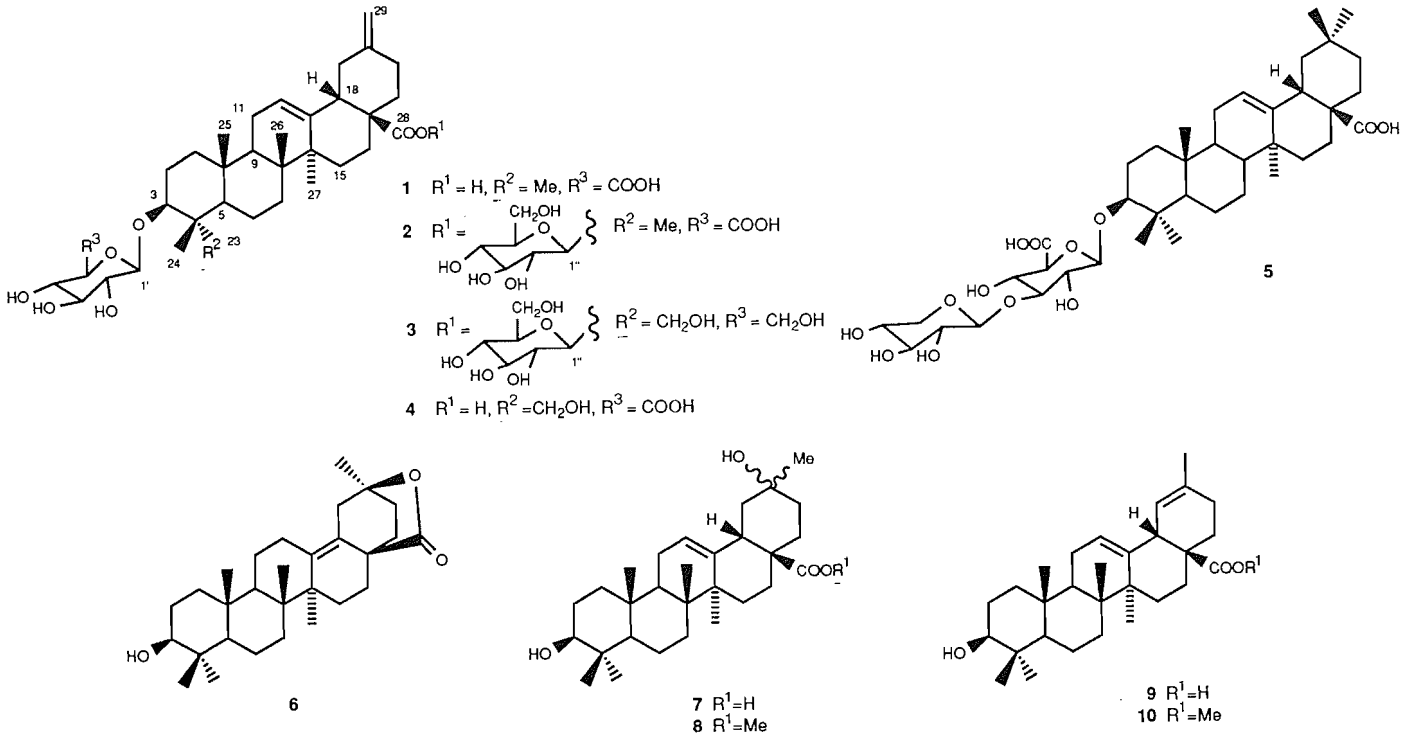

FIG. 1

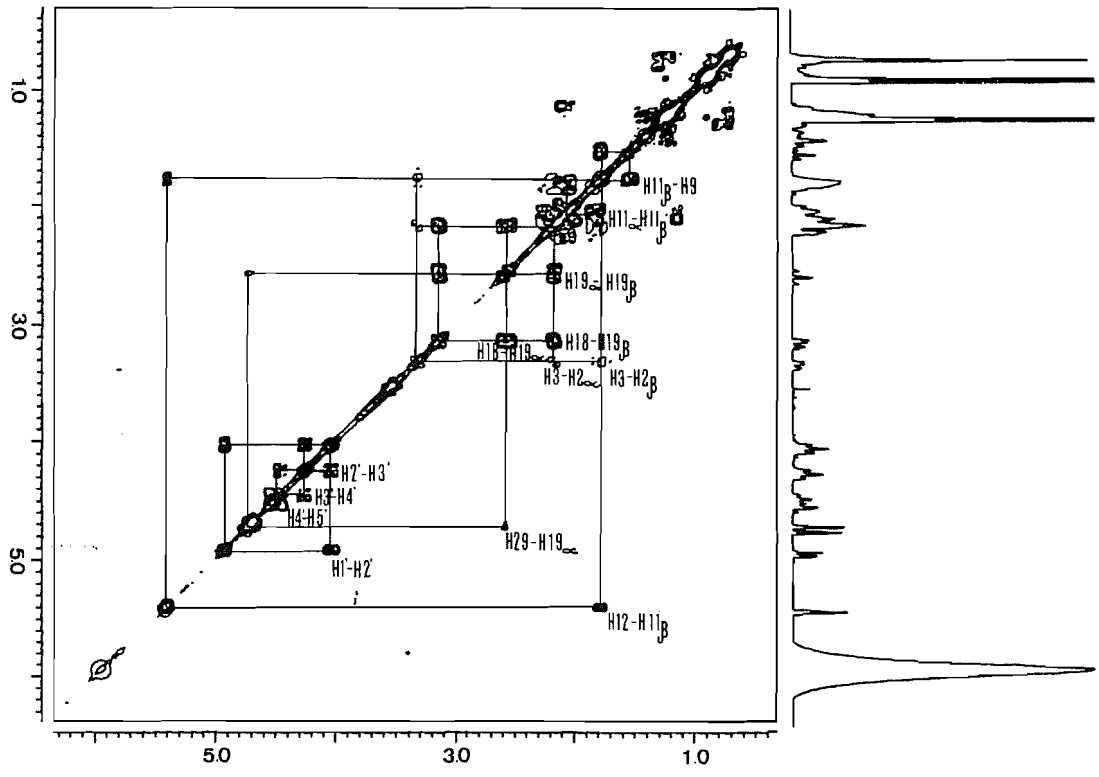

FIG. 2. ^1H–^1H COSY of boussingoside A_1.

(negative ion mode) spectrum showing a quasi-molecular ion at m/z 777 $[M - H]^-$, and thus a molecular weight m/z 778 and a molecular formula $C_{41}H_{62}O_{14}$. It also showed fragments corresponding to the cleavage of two sugars at m/z 614 $[M - H - \text{glucose}]^-$ and 439 $[M - H - \text{glucose} - \text{glucuronic acid}]^-$. The ^{13}C and ^1H NMR spectra are also similar to those of boussingoside A_1 (**1**) (see Table 2), but in addition present one upfield β-anomeric signal at δ_C 95.7 (δ_H 6.24, J = 7.9 Hz) and other peaks that correspond to a glucose unit attached to C28 of the aglycone through an ester bond. Thus boussingoside A_2 (**2**) is 3-*O*-[β-D-glucuronopyranosyl]-30-norolean-12,20(29)-dien-28-*O*-[β-D-glucopyranosyl] ester.

To confirm these structures and also to get information on the sugar unit bound through the ester bond at C28 or the acetal

Can. J. Chem. Downloaded from www.nrcresearchpress.com by 91.121.58.235 on 09/07/12
For personal use only.

Can. J. Chem. Downloaded from www.nrcresearchpress.com by 91.121.58.235 on 09/07/12
For personal use only.

TABLE 1. Selected ^{1}H NMR data of boussingosides A_1 (**1**) and A_2 (**2**) in C_5D_5N at 298 K

(a)

	δ	
	1	**2**
H-2α	2.16 m	2.20 m
H-2β	1.80 m	1.81 m
H-3	3.34 dd	3.36 dd
H-9	1.55 m	1.57 m
H-11α	2.04 m	2.03 m
H-11β	1.72 m	1.68 m
H-12	5.43 bs	5.39 bs
H-18	3.17 dd	3.08 dd
H-19α	2.58 dd	2.57 dd
H-19β	2.20 m	2.18 m
Me-23	1.27 s	1.28 s
Me-24	0.91 s	0.95 s
Me-25	0.74 s	0.78 s
Me-26	0.93 s	1.03 s
Me-27	1.25 s	1.22 s
H-29	4.71, 4.76 (bs each)	4.66 bs
H-1′	4.93 d	5.02 d
H-2′	4.05 dd	4.09 dd
H-3′	4.28 dd	4.66 m
H-4′	4.47 dd	4.60 dd
H-5′	4.55 d	3.99 m
H-1″		6.24 d
H-2″		4.12 dd
H-3″		4.37 dd
H-4″		4.31 dd
H-5″		4.45 m

(b)

	J (Hz)	
	1	**2**
$J_{3-2\alpha}$	4.0	4.9
$J_{3-2\beta}$	11.9	12.5
$J_{18-19\alpha}$	13.7	13.9
$J_{18-19\beta}$	4.9	4.2
$J_{19\alpha-19\beta}$	13.7	13.4
$J_{1'-2'}$	7.9	7.8
$J_{2'-3'}$	8.9	7.5
$J_{3'-4'}$	8.9	
$J_{4'-5'}$	9.4	8.8
$J_{1''-2''}$		7.9
$J_{2''-3''}$		8.5
$J_{3''-4''}$		8.5
$J_{4''-5''}$		8.5

bond at C3, we proceeded to study the acid and basic hydrolyses of **1** and **2**. Treatment of **2** with 0.5 N KOH gave a single sugar, glucose, and another product that was shown by HPLC and its spectroscopic data to be identical to boussingoside A_1 (**1**), implying that glucose must be bound to the C28 carboxylic group of the aglycone. Acid treatment of **2** gave, in turn, glucose and glucuronic acid (which were identified by GC–MS as alditol acetates) and a complex mixture of five lipophilic products which was identical in composition to that obtained

TABLE 2. ^{13}C NMR data of triterpenoid saponins of *Boussingaultia baselloides*

C	**1**[a]	**2**[a]	**3**[b]	**4**[a]	**5**[a]
1	39.5	39.3	39.6	39.7	38.5
2	26.3	26.4	26.2	25.9	26.5
3	90.0	88.9	82.2	81.9	89.2
4	38.1	39.7	43.9	43.3	39.4
5	55.6	55.6	—	47.9	55.6
6	18.2	18.3	18.8	18.0	18.3
7	32.9	32.9	33.3	32.7	33.1
8	38.4	41.5	40.8	39.7	39.6
9	47.7	47.7	49.0	47.4	47.9
10	36.7	37.4	37.7	36.7	36.8
11	23.5	23.4	24.5	23.6	23.6
12	122.9	123.5	124.4	123.1	122.5
13	144.1	143.3	144.4	144.1	144.9
14	41.8	41.9	43.0	41.8	41.9
15	28.0	28.0	28.9	28.2	28.2
16	23.5	23.4	24.1	23.6	23.6
17	46.9	47.1	48.7	46.9	46.4
18	47.7	47.4	49.2	47.8	42.1
19	41.9	41.9	42.6	42.0	46.6
20	149.0	148.4	149.8	148.1	30.8
21	39.3	38.5	38.4	38.5	34.2
22	30.2	29.9	30.9	30.2	33.1
23	28.0	28.0	64.9	64.4	28.0
24	16.7	16.7	16.5	15.9	16.8
25	15.2	15.3	13.4	13.5	15.3
26	17.1	17.2	17.8	17.3	17.3
27	26.0	25.8	26.3	26.2	26.1
28	179.4	175.7	177.5	179.4	180.2
29	106.9	107.1	107.4	107.2	34.1
30					23.6
1′	106.9	107.0	105.1	107.0	106.8
2′	75.2	75.3	75.1	75.3	74.6
3′	77.9	77.5	78.2	78.0	86.4
4′	73.3	73.2	71.2	73.3	71.4
5′	77.2	79.1	78.7	77.7	78.0
6′	179.4	172.8	62.5	172.8	172.1
1″		95.7	95.9		106.2
2″		73.8	74.0		75.2
3″		77.9	78.3		77.4
4″		71.0	71.2		70.9
5″		78.6	78.7		67.3
6″		62.1	62.5		

[a]In C_5D_5N.
[b]In CD_3OD.

from **1** (see below), thus proving that **1** and **2** have the same aglycone.

Acid hydrolysis of **1** with HCl in methanol gave, as expected, glucuronic acid and the aforementioned mixture of five nortriterpenes (**6**–**10**; Fig. 4), which were separated by HPLC and identified by ^{1}H NMR and MS (6).

Boussingosides B (**3**) and C (**4**) were crystallized in MeOH. Their ^{1}H NMR spectra showed only four upfield methyl singlets instead of the five of **1** and **2**. In both **3** and **4** the methyl group at C23 of the aglycone is replaced by a -CH_2OH group, as indicated by the 6–8 ppm shift of C3, C4, and C5 (Table 2). The spectra of compound **3** showed two anomeric groups with signals at δ_C 95.9 and 105.1, and two doublets at δ_H 4.53 and 5.46. The remaining signals were assigned to two glucose units by comparison with published data (4). In keeping with this, the FAB-MS (negative mode) of **3** presents a quasi-molecular ion at *m/z* 797 $[M - H]^-$ (molecular weight 798, molecular formula

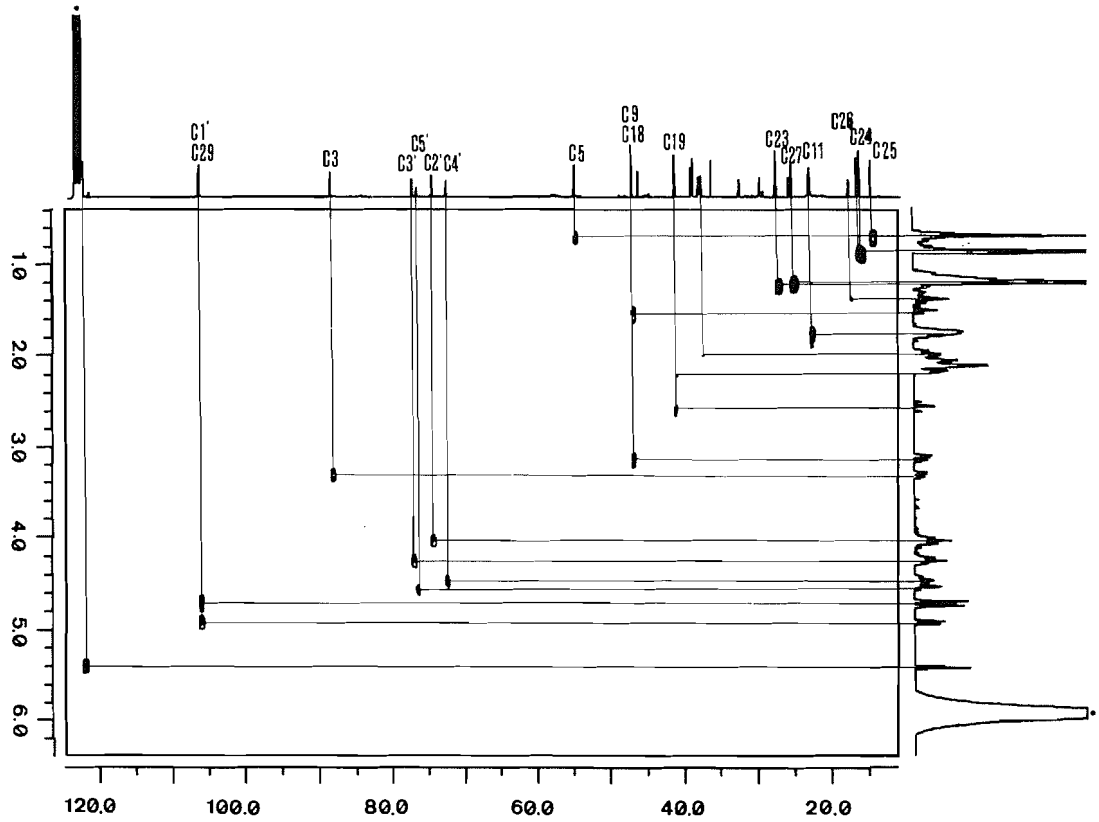

FIG. 3. XHCORR of boussingoside A_1 (J = 130 Hz).

$C_{41}H_{66}O_{15}$) and also shows fragments at m/z 634 $[M - H - 163]^-$ and 471 $[M - H - 326]^-$ corresponding to the successive elimination of two glucose units bound to a tetraoxygenated aglycone.

Thus boussingoside B (**3**) is a 3-*O*-[β-D-glucopyranosyl]-30-norolean-12,20(29)-dien-23-hydroxy-28-*O*-[β-D-glucopyranosyl] ester.

The ^{13}C NMR spectrum of boussingoside C (**4**) presents only one anomeric signal at 107.0 (δ_H 5.23 d, J = 7.5 Hz). Its FAB-MS (negative mode) shows an m/z 631 $[M - H]^-$ and a fragment at m/z 454 $[M - H - 177]^-$, indicating the loss of a glucuronic acid unit and proving that compound **4** is 3-*O*-[β-D-glucuronopyranosyl]-30-norolean-12,20(29)-dien-23-hydroxy-28-oic acid.

Compound **6**, larreagenin A, has been reported as a metabolite isolated from *Larrea divaricata* (7), but it has always been obtained after acid hydrolysis of the mixture of saponins (6). We suspected that compound **6** was an artifact generated during the acid treatment. This was confirmed by its appearing even when **1** was hydrolyzed under milder conditions (1 N HCl) than those described in the literature.

Preliminary pharmacological studies[2] have shown that the aqueous extract of the plant and boussingoside A_1 have hypoglucaemic activity.

[2]In rats with induced diabetes, intraperitoneal injection of a dose of aqueous extract equivalent to (10 g dried aerial parts)/kg significantly reduced glucose levels from over 399 mg/% to 60 mg/% after 8 h. A 20 mg/kg dose of boussingoside A_1 had a similar effect. R. Cadena and J. A. Otero, unpublished results.

Experimental

General

All melting points were taken on a Kofler Thermogeräte apparatus and are uncorrected. ^1H NMR spectra were taken on a Bruker WM-250 spectrometer. The ^1H NMR, ^{13}C NMR, and DEPT spectra of the glycosides were obtained in C_5D_5N and CD_3OD at 298 K. HPLC was performed with a Waters model 6000A chromatograph equipped with a pump and a model R401 differential refractometer. DCCC was carried out with an Eyela model 300-S apparatus equipped with 300 tubes. Conventional and FAB mass spectra were obtained on a Kratos MS50 mass spectrometer equipped with a Kratos FAB source. The FAB mass spectra were obtained by dissolving the samples in a glycerol matrix and bombarding with Xe atoms of 2–8 kV energy. GC–MS analyses were carried out on a Carlo Erba MFC 500 HRGC/MS chromatograph using a 0.25 mm × 10 m SP-2330 capillary column, column temperature 240°C, injection temperature 50°C for 1 min and 12°/min up to 240°C maintained for 2 min.

Two-dimensional experiments

The two-dimensional ^1H–^1H COSY spectra (64 × 1K) of the boussingosides were obtained by accumulating 32 scans per t_1; the relaxation delay was 3 s. The data were zero-filled to 512 in F_1 and subjected to Fourier transformation using Gaussian data manipulation in both dimensions and symmetrized.

The two-dimensional ^1H–^{13}C heteronuclear shift correlation (XHCORR) spectra (256 × 1K) of **1** and **2** for directly bonded protons and carbons were obtained by accumulating 80 scans per t_1; the relaxation delay was 3 s and the value of J_{CH} selected was 130 Hz. The long-range correlation XHCORR (256 × 2K) spectrum of boussingoside A_2 was obtained by accumulating 88 scans per t_1; the relaxation delay was 2 s and the value of J_{CH} selected was 9 Hz. Both XHCORR data (long range and direct correlation) were zero-filled to 512 in F_1 and subjected to Fourier transformation using Gaussian data manipulation in F_2.

Can. J. Chem. Downloaded from www.nrcresearchpress.com by 91.121.58.235 on 09/07/12
For personal use only.

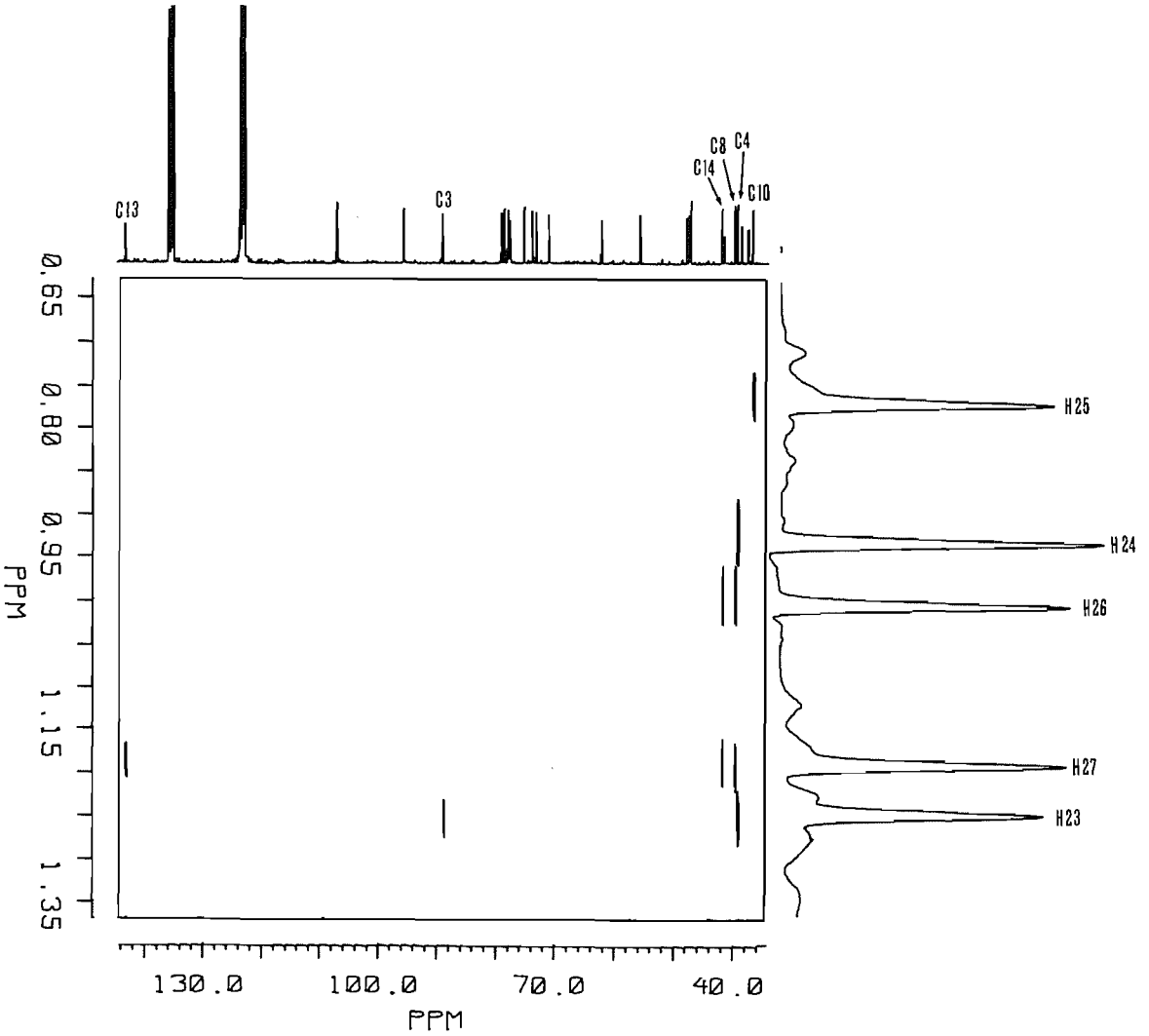

FIG. 4. XHCORR-LR of boussingoside A_2 (J = 9 Hz).

Plant material

Plants were collected in Tuluá, Colombia. Voucher specimens were deposited at the herbaria of the Universities of Santiago de Cali, Colombia, and Santiago de Compostela, Spain (SANT 18191).

Extraction and isolation

The ground leaves of the plant (200 g) were extracted successively with petroleum ether and MeOH giving respectively 30 g and 36.2 g of dry extract. The MeOH extract was defatted with *n*-hexane (2 × 200 mL), CCl_4 (200 mL), and CH_2Cl_2 (2 × 200 mL), and partitioned between *n*-BuOH and H_2O. The BuOH extract (12.6 g) was dissolved in a minimal amount of MeOH, and the solution dropped into Me_2CO and centrifuged. The precipitate was filtered off and the filtrate concentrated under reduced pressure to give 9.7 g of dry extract, which was separated in five fractions (A–E) on a Sephadex LH-20 column using MeOH as eluent and TLC monitoring. Fraction B (1.5 g) was purified by DCCC with $CHCl_3$–MeOH–H_2O (7:13:8) in ascending mode (flow rate 12 mL/h). Fractions 35–40 contained boussingoside A_2 (**2**) (110 mg) and fractions 80–95 boussingoside A_1 (**1**) (80 mg) in pure form. Fractions 40–60 (150 mg) were pooled and rechromatographed by DCCC with $CHCl_3$–MeOH–H_2O (7:13:8) in ascending mode (flow rate 8 mL/h), giving compound **5** (28 mg) and boussingoside C (**4**) (11 mg) in pure form and boussingoside B (**3**) (7 mg), which was repurified by HPLC with MeOH–H_2O 55% (reversed phase, Partisil ODS-M9 column).

Boussingoside A_1 (**1**): mp 213–215°C. ^1H and ^{13}C NMR as in Tables 1 and 2 respectively. FAB-MS (negative ion mode) m/z (relative int.): 615 ($[M - H]^-$, 100), 440 ($[M - H - 175]^-$, 70). FAB–MS (positive ion mode): 683 ($[M - 2H + 3Na]^+$, 80), 661, ($[M - H + 2Na - 162]^+$, 100), 507 ($[M - 2H + 3Na - 176]^+$, 40).

Boussingoside A_2 (**2**): mp 218–220°C. ^1H and ^{13}C NMR as in Tables 1 and 2. FAB-MS (negative ion mode) m/z (relative int.): 777 ($[M - H]^-$, 100), 614 ($[M - H - 163]^-$, 24), 569 ($[M - H - 163 - 44]^-$, 10), 439 ($[M - H - 163 - 175]^-$, 6). FAB-MS m/z (relative int.) (positive ion mode): 823 ($[M - H + 2Na]^+$, 76), 661 ($[M - 2H + 3Na - 162]^+$, 32).

Boussingoside B (**3**): mp 218–220°C. ^1H NMR (CD_3OD) δ_H: 0.80 (s, 3H, 25-Me), 0.90 (s, 3H, 26-Me), 1.08 (s, 3H, 24-Me), 1.30 (s, 3H, 27-Me), 4.53 (d, 1H, J = 7.7 Hz, H-1′), 4.71 (bs, 2H, H-29), 5.41 (bs, 1H, H-12), 5.46 (d, 1H, J = 7.8 Hz, H-1″). ^{13}C NMR, see Table 2. FAB-MS (negative ion mode) m/z (relative int.): 797 ($[M - H]^-$, 100), 634 ($[M - H - 163]^-$, 24), 471 ($[M - H - 163 - 163]^-$, 10). FAB-MS m/z (relative int.) (positive ion mode): 843 ($[M - H + 2Na]^+$, 76), 821 ($[M + Na]^+$, 32), 659 ($[M - H + Na - 162]^+$, 10).

Boussingoside C (**4**): mp 218–220°C. ^1H NMR (C_5D_5N) δ_H: 0.85 (s, 3H, 25-Me), 0.92 (s, 3H, 26-Me), 0.95 (s, 3H, 24-Me), 1.12 (s, 3H, 27-Me), 4.71–4.75 (bs each, 2H, H-29), 5.23 (d, 1H, J = 7.5 Hz, H-1′), 5.43 (bs, 1H, H-12). ^{13}C NMR, see Table 2. FAB-MS

Can. J. Chem. Downloaded from www.nrcresearchpress.com by 91.121.58.235 on 09/07/12
For personal use only.

(negative ion mode) m/z (relative int.): 631 ($[M - H]^-$, 100), 454 ($[M - H - 177]^-$, 29), 410 ($[M - H - 177 - 44]^-$, 17). FAB-MS m/z (relative int.) (positive ion mode): 699 ($[M - 2H + 3Na]^+$, 85), 675 ($[M - H + 2Na]^+$, 45), 523 ($[M - 2H + Na - 176]^+$, 18), 479 ($[M + Na - 176]^+$, 19).

Basic hydrolysis

Boussingoside A_2 (**2**) (25 mg) was refluxed in 0.5 N KOH (20 mL) for 2 h. The mixture was brought to pH 6 with 1 N HCl and extracted with *n*-BuOH (2 × 20 mL). The organic phase was washed with H_2O (3 × 20 mL), affording boussingoside A_1 (**1**).

Acid hydrolysis of 2

When **2** was treated with acid (see below) it gave two sugars and a mixture of triterpenes (**6**–**10**) identical to that obtained by similar treatment of **1**. The sugar fraction was dissolved in H_2O (10 mL), $NaBH_4$ (20 mg) was added, and the mixture was stirred at room temperature for 2 h. After addition of AcOH to eliminate excess $NaBH_4$, the mixture was concentrated to dryness and codistilled with MeOH (2 × 5 mL), and the resulting alditols were acetylated with Ac_2O–pyridine (1:1, 10 mL) by refluxing overnight. The solution was washed with H_2O and extracted with CH_2Cl_2, and the alditol acetates were then identified as those of glucose and glucuronic acid by GC–MS.

Acid hydrolysis of 1

To a solution of boussingoside A_1 (**1**) (20 mg in 10 mL of MeOH) was added 10 mL of 1 N HCl and the mixture was refluxed for 4.5 h. The mixture of aglycones was extracted with CH_2Cl_2 (3 × 20 mL) and subjected to HPLC on a μ-Porasil column (30 cm × 7.8 mm i.d.) with *n*-hexane–EtOAc (75:25) as eluent, affording compounds **6**–**10**.

Compound 6: ^{1}H NMR $CDCl_3$: 0.76 (s, 3H, H-25), 0.80 (s, 3H, H-26), 0.85 (s, 3H, H-24), 0.99 (s, 3H, H-27), 1.13 (s, 3H, H-23), 1.45 (s, 3H, H-29), 3.23 (m, 1H, H-3). EIMS (m/z, relative int.): 440 ($[M]^+$, 53); 422 ($[M - H_2O]^+$, 66); 407 ($[M - H_2O - Me]^+$, 20); 395 ($[M - CO_2]^+$, 40).

Compound 7: ^{1}H NMR $CDCl_3$: 0.76 (s, 3H, H-25), 0.78 (s, 3H, H-26), 0.91 (s, 3H, H-24), 0.99 (s, 3H, H-27), 1.14 (s, 3H, H-23), 1.25 (s, 3H, H-29), 2.81 (dd, 1H, J = 4.8, 13.6 Hz, H-18), 3.23 (m, 1H, H-3), 5.30 (m, 1H, H-12). EIMS (m/z, relative int.): 458 ($[M]^+$, 2); 440 ($[M - H_2O]^+$, 9); 425 ($[M - H_2O - Me]^+$, 2); 414 ($[M - CO_2]^+$, 4); 407 ($[M - 2H_2O - Me]^+$, 4); 232 (40); 207 (39); 187 (100), 173 (71).

Compound 8: ^{1}H NMR $CDCl_3$: 0.73 (s, 3H, H-25), 0.84 (s, 3H, H-26), 0.94 (s, 3H, H-24), 1.14 (s, 3H, H-27), 1.22 (s, 3H, H-23), 1.26 (s, 3H, H-29), 3.20 (m, 1H, H-3), 3.63 (s, 3H, COOMe), 5.35 (m, 1H, H-12). EIMS (m/z, relative int.): 472 ($[M]^+$, 1); 454 ($[M - H_2O]^+$, 28); 441 ($[M - OMe]^+$, 3); 436 ($[M - 2H_2O]^+$, 2); 413 ($[M - COOMe]^+$, 2); 405 ($[M - 2H_2O - OMe]^+$, 1); 395 ($[M - COOMe - H_2O]^+$, 12); 392 ($[M - OMe - H_2O]^+$, 2), 377 ($[M - 2H_2O - COOMe]^+$, 3).

Compound 9: ^{1}H NMR $CDCl_3$: 0.77 (s, 3H, H-25), 0.79 (s, 3H, H-26), 0.91 (s, 3H, H-24), 0.96 (s, 3H, H-27), 1.01 (s, 3H, H-23), 1.60 (s, 3H, H-29), 3.25 (m, 2H, H-3, H-18), 5.12 (bs, 1H, H-19), 5.40 (m, 1H, H-12). EIMS (m/z, relative int.): 440 ($[M]^+$, 10); 422 ($[M - H_2O]^+$, 14); 407 ($[M - H_2O - Me]^+$, 4); 396 ($[M - CO_2]^+$, 13); 381 ($[M - CO_2 - Me]^+$, 2); 378 ($[M - CO_2 - H_2O]^+$, 2); 363 ($[M - CO_2 - H_2O - Me]^+$, 1).

Compound 10: ^{1}H NMR $CDCl_3$: 0.78 (s, 3H, H-25), 0.80 (s, 3H, H-26), 0.92 (s, 3H, H-24), 0.98 (s, 3H, H-27), 1.05 (s, 3H, H-23), 1.61 (s, 3H, H-29), 3.29 (m, 2H, H-3, H-18), 3.63 (s, 3H, COOMe), 5.15 (m, 1H, H-19), 5.40 (t, J = 3.8 Hz, 1H, H-12). EIMS (m/z, relative int.): 454 ($[M]^+$, 28); 422 ($[M - H_2O]^+$, 13); 407 ($[M - H_2O - Me]^+$, 5); 396 ($[M - CO_2]^+$, 15); 381 ($[M - CO_2 - Me]^+$, 3); 378 ($[M - CO_2 - H_2O]^+$, 4); 363 ($[M - CO_2 - H_2O - Me]^+$, 1).

Acknowledgements

This work was supported by the Plan Nacional de Investigación (FAR 88-0512) and the CICETGA. A.E. and J.R. acknowledge fellowships from the Programa de Cooperación con Iberoamérica and the Xunta de Galicia, respectively. We are also grateful to Prof. R. Cadena for pharmacological tests and L. D. Caicedo and Prof. Cabrera for plant collection and identification.

1. H. García-Barriga. Flora medicinal de Colombia. Imprenta Nacional de Colombia, Bogotá. 1974.
2. E. Pérez-Arbeláez. Plantas útiles de Colombia. 4th ed. Litografía Arco, Bogotá. 1978.
3. N. Kawamura, H. Watanabe, and H. Oshio. Phytochemistry, **27**, 3585 (1988).
4. V. U. Ahmad, N. Bano, I. Fatima, and S. Bano. Tetrahedron, **44**, 247 (1988).
5. V. U. Ahmad, S. Uddin, I. Fatima, and S. Bano. Phytochemistry, **28**, 2169 (1989).
6. V. U. Ahmad, N. Bano, and S. Bano. Phytochemistry, **23**, 2613 (1984).
7. G. Habermehl and H. Möller. J. Liebigs Ann. Chem. **2**, 169 (1974).

Can. J. Chem. Downloaded from www.nrcresearchpress.com by 91.121.58.235 on 09/07/12
For personal use only.

Synthesis of protein conjugates and analogues of *N*-acetylneuraminic acid

RENÉ ROY[1] AND CRAIG A. LAFERRIÈRE
Department of Chemistry, University of Ottawa, Ottawa, Ont., Canada K1N 6N5

Received May 3, 1990

RENÉ ROY and CRAIG A. LAFERRIÈRE. Can. J. Chem. **68**, 2045 (1990).

N-Acetylneuraminic acid (**1**) was prepared from the salivary gland mucins of the Chinese swiftlet by an improved procedure using acidic resin hydrolysis. Compound **1** was transformed into the known acetochloroneuraminic acid (**3**) by a new two-step procedure. Koenigs–Knorr glycosylation of **3** followed by subsequent reductive ozonolysis of the 2-propenyl α-glycoside afforded the key aldehyde precursors **7** and **8**, which were coupled to bovine serum albumin or tetanus toxoid by reductive amination. The factors influencing the extent of incorporation were investigated. A series of *N*-acetylneuraminic acid analogues modified at strategic functionalities were also synthesized.

Key words: sialic acid, *N*-acetylneuraminic acid, neoglycoproteins, bovine serum albumin, tetanus toxoid.

RENÉ ROY et CRAIG A. LAFERRIÈRE. Can. J. Chem. **68**, 2045 (1990).

L'acide *N*-acétylneuraminique (**1**) a été préparé selon une procédure améliorée à partir de la mucine des glandes salivaires d'hirondelles asiatiques. La méthode fait intervenir une hydrolyse par de la résin cationique acide. Le composé **1** a été transformé en dérivé acide acétochloroneuraminique connu (**3**) par une nouvelle méthode en deux étapes. Une glycosylation de **3** par la méthode de Koenigs–Knorr, suivie d'une ozonolyse réductive du α-glycoside de propèn-2-yle conduit aux précurseurs aldéhydes clés **7** et **8** qui sont ensuite couplés à l'albumine bovin et à l'anatoxine tétanique par amination réductrice. Les facteurs influençant le niveau d'incorporation ont été étudiés. Une série d'analogues de l'acide *N*-acétylneuraminique modifiés aux fonctionnalités stratégiques a aussi été synthétisée.

Mots clés : acide sialique, acide *N*-acétylneuraminique, néoglycoproteines, albumine bovin, anatoxine tétanique.

Introduction

The sialic acids represent a family of more than 30 naturally occurring derivatives of neuraminic acid (1). The most ubiquitous member of the sialic acids is *N*-acetylneuraminic acid (Neu5Ac, **1**). It is present in the capsular polysaccharide fractions of a number of pathogenic bacteria (2, 3). It was also identified in the glycoprotein mucins of higher animals, the most abundant source being the *Collocalia* mucoid, the nest-cementing glycoprotein substance of the Chinese swiftlet (4) from whose nests it can be isolated in large quantity (5% w/w) (5). *N*-Acetylneuraminic acid (**1**) is also an important constituent of the cell wall glycolipids (gangliosides) (1). More recently, the N-linked oligosaccharide sequences of the envelope glycoproteins gp120 of the human immunodeficiency viruses (HIV) were characterized and were shown to contain high levels of Neu5Ac (**1**) (6).

In the glycoproteins and glycolipids, the sialic acids, which are exclusively α-linked, occupy the penultimate nonreducing end of the oligosaccharide chains. Therefore, it is not surprising to find that they play forefront roles in a number of biochemical and immunochemical events. For instance, Neu5Ac alone or Neu5Ac terminated oligosaccharides were shown to be responsible for influenza virus adhesion onto erythrocytes (7) and human nasal mucins. Bacterial adherence and colonization of intestinal tracts by *Escherichia coli* is another event caused by the binding interactions between the bacterial pili and the sialic acids of the epithelial cell walls (8). Bacterial toxins (tetanus, diphtheria) (9), animal and plant lectins (10), interferon (11), and mycoplasma pneumoniae (12) are other representative examples of such interactions, which use Neu5Ac as cell surface receptors. Moreover, the sialic acids in the glycoprotein hormone of human chorionic gonadotropin (hCG) can modulate its hormonal activity (13). On the other hand, the absence of sialic acids on glycoproteins may have beneficial effects. Thus, the uptake or sequestration of senescent cells by macrophages (14) and liver hepatocyte receptors (15) can trigger the catabolism of useless cells. Perhaps the most interesting features of the sialic acids are their roles as differentiation (16) and oncodevelopmental (17) antigens. As such, they constitute key functional entities in the design of specific oncogenic markers.

It was therefore anticipated that the synthesis of well-defined artificial neoglycoproteins, containing sialic acids as the sole carbohydrate antigen, would constitute excellent probes for studying some of the interactions mentioned above. Such tools may have useful applications in the study of lectins and antibody–carbohydrate interactions at the molecular level (10). These neoglycoproteins may also be useful for the detection and screening of endogenous lectins by immunocytochemical staining (18), which might permit cell targeted drug delivery. We have also previously mentioned that neoglycoproteins and copolymers containing Neu5Ac represented good inhibitors of the adherence of influenza A virus to chicken erythrocytes (19). This phenomenon could constitute the basis of a therapy against the common cold.

As mentioned previously (20, 21), our initial goals were to produce specific anti-sialic acid antibodies (potentially monoclonals) that might be useful for the quantitation of sialyloligosaccharides present in large quantities in the serum of cancer patients (17). Our first attempts were directed to terminal anti-Neu5Ac antibodies, irrespective of the type of linkages between the Neu5Ac and the next carbohydrate residues, usually α-(2,6) or α-(2,3)-galactose. Therefore, the present work describes the synthesis of antigenic Neu5Ac residues α-linked to two different carrier proteins, namely bovine serum albumin (BSA) and tetanus toxoid (TT). These two proteins are known for their large difference in immunogenicities in model animals. The synthesis of some analogues modified at strategic functionalities is also depicted. These sialic acid derivatives are intended to be used as inhibitors in the study of sialic acid interactions with lectins and antibodies.

Results and discussion

Preparation of the aldehyde precursors 7 and 8

For the present study, sialic acid as an α-linked glycoside of *N*-acetylneuraminic acid (Neu5Ac, **1**) was required in a form

[1]Author to whom correspondence may be addressed.

Can. J. Chem. Downloaded from www.nrcresearchpress.com by 91.121.58.235 on 09/07/12
For personal use only.

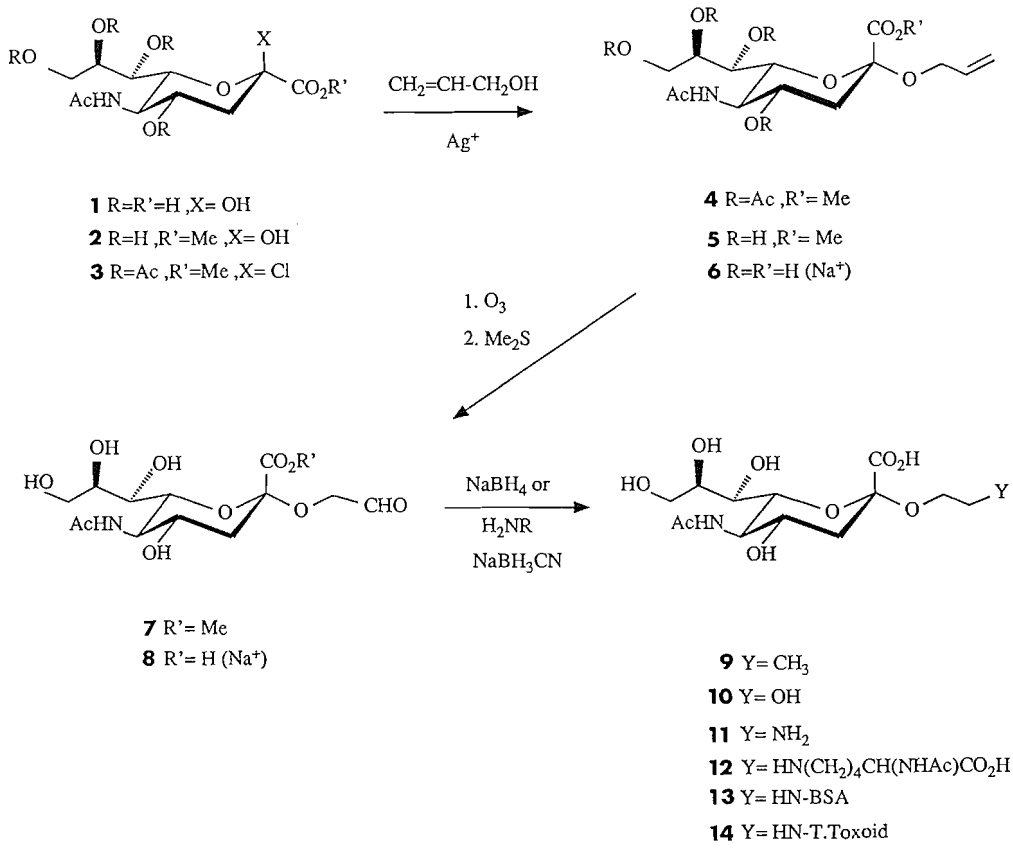

SCHEME 1

suitable for covalent attachment to the ϵ-amino groups of the lysine residues of the carrier proteins. Previous studies by us (22) and by others (23) demonstrated the usefulness of reductive amination (24) for the direct reduction of a Schiff base formed between aldehyde groups and the amine functionalities present on the proteins. Hence, 2-oxoethyl α-glycoside of Neu5Ac (**8**) was sought as an appropriate precursor for the conjugation. Large scale preparation of the starting Neu5Ac (**1**) could have been achieved as described previously using 0.025 M H_2SO_4 hydrolysis of the *Collocalia* mucins present in the bird's nest substances (5). The method suffers, however, from being tedious in the neutralization step because of the large volume of solution required. We anticipated that hydrolysis by a cationic resin (H^+) should be amenable to a straightforward isolation sequence since, after filtration, the reaction mixture could be directly loaded onto the formate anion column as originally suggested (5). After optimization of the reaction conditions, a temperature of 75°C and a hydrolysis time of 6 h with a 2:1 weight ratio of commercial bird's nest and resin Rexyn 101 (H^+) were used. The yield of pure Neu5Ac (**1**) varied from 2.5 to 5% by weight depending on the source of the bird's nest.

Having secured the supply of Neu5Ac (**1**), it was then transformed into the known (25) acetochloroneuraminic acid (**3**) via a new two-step sequence (21) (Scheme 1). The methyl ester (**2**) was prepared in methanol containing H^+ resin according to Kuhn *et al.* (25) in an almost quantitative yield. The chloride (**3**) was directly prepared by treatment of the methyl ester (**2**) with acetyl chloride in acetic acid whereby the intermediate peracetylated ester was further tranformed into the chloride (**3**) because the required HCl was generated *in situ* during the reaction conditions. This is in contrast to a recent publication (26) in which acetic acid was omitted and which failed, in our hands, to give good yield of the desired chloride (**3**). The unstable **3** thus obtained was of >95% purity (^{1}H NMR) and was usually suitable for the following transformations. The α-allyl glycoside (**4**) (21, 27, 28) was prepared using silver salicylate (29) as catalyst rather than the polymeric one originally employed (27). The Koenigs–Knorr glycosylation occurred with complete stereocontrol giving rise to the α-allyl glycoside **4** in 90% yield. The anomeric configuration of the sialic acid, for which there is no anomeric proton, was determined indirectly by empirical rules (30), which predict the proton chemical shifts of H-4 and H-7 of Neu5Ac α-glycosides to occur at 4.83 and 5.30 ppm respectively. It was also directly determined (*vide infra*) by the three-bond heteronuclear gated decoupling spectrum (31) between C-1 and H_{3ax} ($^3J_{C\text{-}1,H\text{-}3ax}$, ∠180°) which showed a coupling of 5.7 Hz in the free acid **6**. Deacetylation of **4** with sodium methoxide in methanol provided crystalline ester **5** in 93% yield. Treatment of the methyl ester **5** with 0.1 N aqueous NaOH gave the free acid **6** also in 93% yield. Reductive ozonolysis of the allyl group in **6** afforded the key aldehyde **8** in quantitative yield after lyophilization. The ozonolysis was also performed on the allyl ester **5** to provide the aldehyde ester **7** in 95% isolated yield. Evidence that the aldehyde group exists in the hydrated form in aqueous solution was seen by the ^{1}H NMR spectra of **7** and **8**, which showed the aldehydic proton at 5.12 ppm (Table 1), and by the ^{13}C NMR spectrum, which showed the carbonyl at 89.6 ppm (acetal) (Table 2).

*Synthesis of the protein conjugates **13**, **14** by reductive amination*

Direct covalent attachment of the aldehydes **7** or **8** onto bovine serum albumin (BSA) and tetanus toxoid (TT) could be

Can. J. Chem. Downloaded from www.nrcresearchpress.com by 91.121.58.235 on 09/07/12
For personal use only.

Can. J. Chem. Downloaded from www.nrcresearchpress.com by 91.121.58.235 on 09/07/12
For personal use only.

TABLE 1. ^{1}H NMR chemical shifts (ppm) and coupling constants (Hz) of the NeuAc derivatives in D_2O at 25°C

Compound no.	$H3_{ax}$ (J_{a-e}, J_{3-4})	$H3_{eq}$ (J_{e-a}, J_{3-4})	H5 (J_{4-5}, J_{5-6})	H6 (J_{5-6}, J_{6-7})	H7 (J_{6-7}, J_{7-8})	H9 (J_{8-9}, $J_{9-9'}$)	H9′ (J_{8-9}, $J_{9-9'}$)	Methyl ester (s)	NAc (s)	Aglycon: allyl, others				
										H_a	H_b	H_c	H_d	H_e
5	1.83 (12.2, 12.2)	2.72 (12.2, 4.6)	[a]	[a]	3.56 (1.7, 8.9)	[a]	3.65 (6.0, 11.9)	3.87	2.03	5.25	5.32	5.91	4.31	4.07
6	1.66 (11.8, 12.1)	2.75 (12.4, 4.5)	3.82 (9.8, 10.2)	3.71 (10.2, 1.9)	3.59 (1.7, 8.9)	3.87 (—, 9.6)	3.64 (6.3, 12.2)	—	2.03	5.23	5.32	5.94	4.24	4.01
7	1.83 (11.9, 12.6)	2.73 (12.8, 4.5)	[a]	[a]	3.55 (—, 8.9)	[a]	3.65 (6.7, 12.5)	3.88	2.03	—	—	5.12[b] (4.8)	3.47 (10.2, 4.9)	3.76 (10.1, 4.7)
8	1.70 (11.9, 12.6)	2.74 (12.8, 4.5)	3.83 (9.8, 10.3)	3.70 (9.5, 1.7)	3.58 (1.6, 8.8)	3.87 (—, 9.8)	3.63 (6.6, 12.5)	—	2.03	—	—	5.12[b] (4.9)	3.43 (10.2, 4.8)	3.68 (11.4, —)
9	1.64 (11.7, 12.3)	2.74 (12.3, 4.5)	3.82 (9.7, 9.1)	[a]	3.58 (1.6, 8.9)	[a]	[a]	—	2.03	0.88 (7.4)		1.56 (7.0)	[a]	3.37 (9.3, 6.9)
10	1.73 (11.9, 12.3)	2.72 (12.3, 4.6)	[a]	3.73 (10.5, 1.9)	3.57 (1.6, 8.9)	3.83 (1.8, 9.7)	3.63 (6.6, 12.5)	—	2.03	—	—	[a]	[a]	[a]
11	1.73 (11.9, 12.2)	2.72 (12.3, 4.5)	3.83 (9.7, 10.3)	3.70 (9.7, 2.0)	3.59 (1.8, 8.7)	3.86 (2.7, 9.8)	3.65 (5.7, —)	—	2.03	—	—	3.19 (4.8, 5.4)	[a]	3.97 (10.6, 4.9)
12	[a]	2.72 (12.3, 4.6)	[a]	3.70 (10.2, 1.7)	3.40 (1.5, 8.8)	[a]	3.65 (5.6, 12.1)	—	2.03			[c]		
15	1.63 (11.6, 13.5)	2.44 (13.5, 5.4)	[a]	[a]	[a]	[a]	[a]	—	2.03	—	—	[a]	[a]	[a]
16	1.74 (11.0, 11.2)	2.30 (13.0, 4.7)	3.85 (9.9, 10.5)	3.68 (10.5, 1.4)	3.52 (1.2, 9.3)	[a]	3.61 (6.0, 11.5)	—	2.03	5.22	5.34	5.96	4.23	
17	1.77 (11.2, 12.8)	2.75 (12.9, 3.8)	[a]	[a]	3.63 (—, 9.7)	[a]	[a]	—	2.02	5.23	5.33	5.94	4.26	4.09
18	1.70 (12.4, 12.5)	2.80 (12.5, 4.6)	3.24 (9.7, 10.3)	4.05 (10.3, 2.1)	3.77 (2.2, 11.0)	3.90 (2.5, 12.0)	3.72 (5.7, 12.0)	—	—	5.23	5.33	5.93	4.24	[a]
19	1.68 (12.2, 12.5)	2.76 (12.5, 4.5)	[a]	[a]	3.61 (—, 9.0)	3.66 (2.3, 7.0)	3.70 (6.0, 11.9)	—	3.93[d]	5.23	5.33	5.94	4.27	4.02
20	1.68	2.75	[a]	[a]	3.57	[a]	3.64	—	4.65[d] 2.18 (OAc)	[a]	[a]	[a]	[a]	[a]
21	1.68 (11.8, 13.1)	2.77 (12.4, 4.6)	[a]	[a]	3.58 (1.7, 8.9)	3.87 (1.1, 9.8)	3.64 (6.5, 12.3)	—	4.12[d]	5.22	5.33	5.94	4.25	4.01
22	1.84 (11.4, 12.5)	2.71 (13.5, 3.5)	[a]	[a]	[a]	—	—	3.87	2.03	[a]	[a]	5.92	4.33	4.08
23	1.63 (11.7, 12.4)	2.69 (12.4, 4.0)	3.69 (9.3, 9.6)	[a]	3.62 (5.9, 12.9)	3.76 (1.9, 12.9)	—	—	—	2.03	5.23	5.34	5.94	4.27	3.97

[a]H4, H8 and others not assigned due to the complexity of the spectrum.
[b]Aldehyde proton as a hydrate.
[c]See experimental section.
[d]Methylene of *N*-acyl group.

TABLE 2. ^{13}C NMR chemical shifts (ppm) of the sialic acid derivatives (H_2O, 25°C)

Compound no.	(C-1, NHAc)	C-2	C-3	C-4	C-5	C-6	C-7	C-8	C-9	CH_3 (NHAc)	CH_3 (Me ester)	Aglycon
5	171.2, 176.1	100.0	40.6	68.3	53.0	74.1	69.5	71.8	64.3	23.3	54.6	67.0, 119.7, 134.3
6	174.6, 176.3	101.8	41.7	69.4	53.1	73.9	69.4	72.9	63.8	23.3	—	67.1, 119.4, 135.0
7	171.2, 176.1	100.5	40.8	69.9	53.4	74.5	68.8	72.2	64.8	23.8	55.1	68.4, 89.6
8	174.6, 176.3	101.7	41.3	69.4	53.1	73.8	69.4	72.9	63.9	23.3	—	68.2, 89.6
9	175.0, 176.3	101.7	41.4	69.3[a]	52.8	73.5	69.1[a]	72.7	63.5	23.3	—	10.6, 22.9, 67.7
10	173.2, 175.7	100.6	40.6	69.1	52.7	73.5	68.7	72.1	63.7	23.0	—	61.4, 66.4
11	174.1, 175.9	101.3	40.7	69.0	52.8	73.6	69.0	72.5	63.6	23.0	—	40.3, 61.1
12	174.1, 175.8	101.3	40.5	69.0	52.8	73.6	69.0	72.5	63.5	23.0	—	[b]
16	61.3, 176.4	101.7	37.4	69.0[a]	53.4	71.7	69.5[a]	72.8	64.1	23.2	—	64.2, 119.0, 135.7
17	172.3, 176.3	101.1	40.1	68.8[a]	52.8	74.6	68.3[a]	72.2	63.8	23.3	—	66.6, 119.7, 134.7
18	173.5, —	101.3	41.3	67.4	53.9	71.9	68.6	72.3	63.0	—	—	66.9, 119.0, 134.3
19	170.8, 177.2	100.7	40.7	69.5[a]	53.4	73.7	68.6[a]	72.4	63.9	29.0	—	67.0, 119.8, 134.6
20	[c]	[c]	40.9	68.7[a]	52.2	72.9	68.4[a]	72.3	63.4	63.2 (20.4)[d]	—	66.5, 119.0, 134.3
21	[c]	101.7	41.5	69.2	52.6	73.4	69.0	72.7	63.6	61.9	—	67.1, 119.4, 135.0
22	171.3, 176.3	100.1	40.1	68.0	54.4	76.6	62.2	—	—	23.1	53.0	66.8, 120.0, 134.3
23	174.6, 176.0	101.9	41.4	68.6	53.0	75.6	62.0	—	—	22.8	—	67.7, 119.4, 134.6

[a]Tentative assignments.
[b]See experimental.
[c]Signals lost into the noise.
[d]Acetate signal.

TABLE 3. Factors influencing the reductive amination of **7** or **8** onto BSA

Entry	Molar ratio[a] $CHO/NH_2/H^-$	Temperature, °C (±3°)	Conditions[b]	NeuAc/protein[c] 3 days (6 days)	Yield, %[d] 3 days (6 days)
On **8**					
1	1:1:10	37°C	P	15	25
2	5:1:25	37°C	P	22	37
3	5:1:25	50°C	P	23	39
4	10:1:25	50°C	P	21	36
5	5:1:25	37°C	P + 20% DMSO	20	34
6	10:1:100	37°C	P	18(18)	31
7	10:1:100	50°C	P	17(22)	29
8	10:1:100	37°C	P + 20% DMSO	19(21)	32
9	5:1:25	37°C	B	6	10
On **7**					
10	7:1:33	37°C	P	32(35)	54(59)
11	7:1:33	37°C	P + 25% MeOH	36(42)	61(71)
12	7:1:33	37°C	P + 25% DMSO	36(41)	61(69)
13	8:1:33	37°C	P, pH 6	33	56
14	8:1:33	37°C	P, pH 7	36(45)	61(76)
15	8:1:33	37°C	P, pH 8	38(42)	64(71)
16	8:1:33	37°C	P, pH 9	36(38)	61(64)

[a]Reaction mixtures. H^- refers to $NaBH_3CN$.
[b]P = 0.2 M phosphate buffer, pH 7 unless stated otherwise. B = 0.2 M borate buffer, pH 7.
[c]In the conjugate as determined by colorimetric methods.
[d]Based on 59 lysine residues.

achieved using sodium cyanoborohydride because this reducing agent is known to be selective for the imine functionality while being inert toward the carbonyl functions. This procedure, which was pioneered by Gray (24) on reducing sugars, was further improved by Roy *et al.* (22) using optimized conditions of buffers, pH, and temperature. To obtain protein conjugates covering the entire range of Neu5Ac incorporation, optimization of the reaction conditions was again set forth (Table 3). Using borate buffer (0.2 M, pH 9.0) as suggested by Roy *et al.* (22) on reducing sugars and BSA as model protein, the level of incorporation of **8** onto the lysine group was only marginal even after 6 days at 37°C (entry 9), as opposed to neutral sugars (21–24). Thus, it became apparent that the free aldehyde in the acid **8** did not behave like neutral free reducing sugars (22–24). Therefore, the original procedures (23, 24) using 0.2 M phosphate buffer were reinvestigated. As observed from Table 3, there was no improvement in coupling efficiency when only the molar ratio of the aldehyde to the amine was increased (entries 3 and 4) at 50°C in phosphate buffer pH 7.0. There was a slight improvement when both the aldehyde and the hydride

Can. J. Chem. Downloaded from www.nrcresearchpress.com by 91.121.58.235 on 09/07/12
For personal use only.

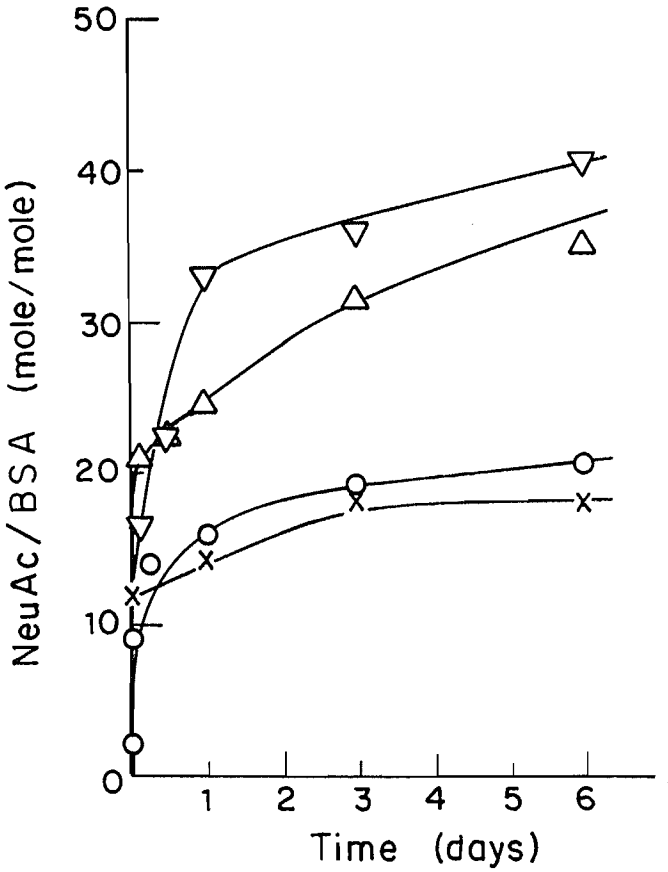

FIG. 1. Time course of reductive amination of **7** (▽,△) or **8** (○,×) into BSA. (×) entry **6** (Table 3); (○) entry **8**; (△) entry **10**; (▽) entry **12**.

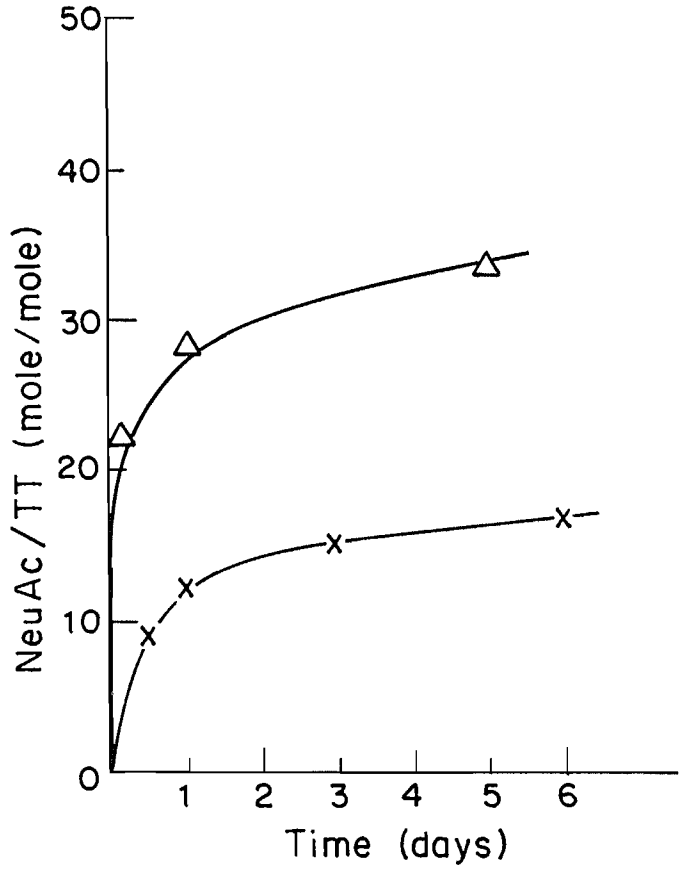

FIG. 2. Time course of reductive amination of **7** (△) or **8** (×) into TT. (×) 0.2 M phosphate buffer pH 7.0, 37°C, **8**: NH_2: $NaBH_3CN$ (10:1:30); (△) like (×) with **7** and 25% DMSO.

ratios were increased relative to that of the amine (entries 1 and 2). There was also no temperature effect observed between 37°C and 50°C in the same buffer (entries 2,3 and 6,7). A detrimental effect could be seen when the amount of hydride reagent used was too high (entries 4 and 7) at 50°C. No solvent effect could be noticed (entries 2,5 and 6,8). Thus, a maximum of approximately 23 Neu5Ac residues out of 59 lysines (32) were effectively coupled onto BSA, while 16 Neu5Ac residues out of ~66 lysines could be coupled to TT (33). The level of incorporation of Neu5Ac in all the above procedures was conveniently measured by a specific colorimetric method using resorcinol (34), while the amount of protein within the sample was determined using the Lowry method (35). Previous workers (22–24) using amino acid analysis showed the level of incorporation of the sugar content to agree within ±1–2 residues compared to the colorimetric tests.

We postulated that the restricted incorporation of the acid **8** in comparison to neutral sugars (22–24), where complete substitution was possible, could be due to the anionic nature of both the BSA protein (pI 4.9) and the aldehyde **8**, which would cause repulsive electrostatic interactions. Therefore, conjugations with the aldehyde ester **7** were initiated in the hope of minimizing these repulsive interactions (Fig. 1). As shown from Table 3 (entry 10 vs. entry 2), there was a noticeable improvement in the level of reductive amination. This was further increased (entries 11, 12 vs. entry 10) when methanol or dimethyl sulfoxide was used as cosolvent. There was almost no pH effect (between 6 and 9) in the 0.2 M phosphate buffer at 37°C, a pH of 6 being only slightly less efficient than the other three higher pH's. Under the optimum conditions (see Experimental), a conjugate having 53 Neu5Ac residues per BSA molecule was achieved with the methyl ester **7**. A similar set of experiments was effected on the tetanus toxoid; the results are illustrated in Fig. 2.

Interestingly, at the end of the reaction time (usually 3–6 days) the Neu5Ac–protein conjugates **13** or **14** obtained from the reductive amination of the ester **7** did not have any of the remaining ester functionality. This was ascertained by ^1H NMR spectroscopy, by the colorimetric hydroxamic acid test (36) for esters, by immunoelectrophoresis, and by *Vibrio cholerae* neuraminidase treatment (1) of the protein conjugates (not shown). The above enzyme was known to be inactive toward the esters of sialic acids (1) but in the present study it hydrolysed 96% of the Neu5Ac **1** in the conjugates, thus confirming the absence of the ester function within the conjugates.

As control experiments, it was shown that the reagent $NaBH_3CN$ or BSA alone was not capable of inducing the ester hydrolysis of **5** in the phosphate buffer. It is suggested that the hydrolysis could have been catalyzed by the neighboring amine group, which was reductively alkylated in the aglycon portion, or by the intramolecular assistance of a suitably positioned hydroxyl group. The basis for this assumption was supported by the set of transformations leading to the sialic acid analogues described below. These specifically modified sialic acid derivatives were prepared in order to be utilized as potential inhibitors for the interaction studies between sialic acid and specific lectins such as wheat germ agglutinin (10) or antibodies (19) prepared against the protein conjugates **13** and **14**.

Can. J. Chem. Downloaded from www.nrcresearchpress.com by 91.121.58.235 on 09/07/12
For personal use only.

Can. J. Chem. Downloaded from www.nrcresearchpress.com by 91.121.58.235 on 09/07/12
For personal use only.

Synthesis of sialic acid analogues

The 2-propenyl glycoside ester **5** was reduced to the corresponding 2-propyl glycoside ester using hydrogen on 5% palladium–charcoal in 95% yield. The ester was then hydrolyzed to the free acid **9** by 0.1 N aqueous NaOH in 92% yield. The aldehyde **8** was converted to the 2-hydroxyethyl glycoside **10** in 67% yield using sodium borohydride. The corresponding 2-aminoethyl glycoside **11** was obtained directly from the aldehyde **8** by reductive amination in the presence of ammonium actate (51%). The $[\alpha]_D$ of **11** (−18.5°) agreed well with the one previously obtained ($[\alpha]_D$ −17°) by Holmquist and Brossmer (37), who synthesized it by glycosylation of **3** with 2-(benzyloxycarbonylamino)ethanol in the presence of silver carbonate in 14% overall yield after deprotection. When the above reductive amination was effected on the methyl ester **7** rather than the free acid **8**, a side product tentatively assigned the lactam structure **15** was produced together with **11** (Scheme 2). This is of particular interest since the reductive amination of **7** with the two proteins might have given a similar cyclic lactam during the conjugation. To establish whether or not this was the case, the amino acid **11** was treated with a carbodiimide (EDC), and the same product (**15**) resulting from the reductive amination of the ester **7** with ammonium acetate was obtained. When the same sequence of reductive amination of **7** was performed with N^{α}-acetyl-(L)-lysine, the free acid **12** was obtained as a single product; no methyl ester was present. The acid **12** proved to be the same as the one obtained from the acid **8**. Thus, the above results indicated that the formation of the lactam (**15**) is selective for the primary amine **11** and that ester hydrolysis also occurred upon reductive amination of **7** with either N^{α}-acetyl-(L)-lysine alone or with the proteins. These results confirmed the observations made above, although the mechanism by which the ester self-hydrolyzed during the reductive amination was not fully understood. As mentioned above, it is possible that the hydrolysis occurred by an intramolecular catalyzed reaction due to the proximity of the ε-amino groups. We have also mentioned previously that most of the Neu5Ac residues (>96%) could be hydrolyzed from the protein conjugates **13** and **14** by *Vibrio cholerae* neuraminidase. This could not have been the case with a cyclic amide such as **15**.

The acid group was the next functionality to be modified. This was done by reduction of the C-1 carbomethoxy group of **5** by lithium borohydride in a MeOH–THF mixture. The resulting hydroxymethyl derivative **16** (~quant.) showed the disappearance of the carbonyl band of **5** at 1725 cm^{-1} together with the C-1 ^{13}C NMR signal at 171.2 ppm. The new methylene signal was shifted to 61.3 ppm. The amide analogue **17** was obtained by ammonolysis of the ester **5** in 84% yield. These two derivatives constitute important modifications because they deprive the Neu5Ac residue of its anionic character, which is essential to most of its biochemical and immunochemical functions (1).

The other functional group manipulations were then centered on the acetamido function (Scheme 3). The amide **5** was hydrolyzed in refluxing tetramethylammonium hydroxide to afford the free amine **18** in 80% yield after purification by size exclusion chromatography. The product was ninhydrin positive on tlc. Furthermore its ^1H NMR showed the disappearance of the *N*-acetamido signal at 2.03 ppm with concomitant upfield shift of its H-5 signal at 3.24 ppm. Similarly, the ^{13}C NMR spectrum of **18** showed the displacement of the C-5 signal from 53.1 ppm in **5** or **6** to 53.9 ppm (0.8 ppm downfield). The signals for C-4 and C-6 were also affected since they shifted

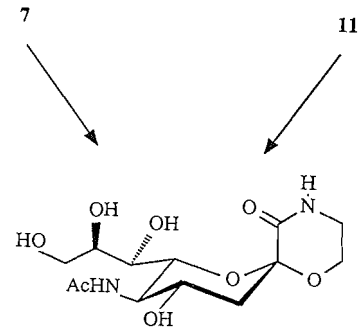

15

SCHEME 2

upfield by 2.0 ppm (67.4 and 71.9 ppm respectively) relative to that in **6**. These observations were previously made on a polymer of Neu5Ac (38). The new amide derivatives **19** and **21** were obtained in yields of 80 and 86% respectively upon treatment of **18** with the corresponding bromoacetyl and acetoxyacetyl chloride. The intermediate acetoxy derivative **20** needed to be hydrolyzed at the ester functionality during the isolation of **21**. It is of interest to mention that **21** corresponds to an α-allyl glycoside of the important *N*-glycolylneuraminic acid (Neu5Gc). It is also worth mentioning that the above entry to the Neu5Gc series was more convenient (38) than the previous one (1) using the unstable 1,3-dioxolan-2,4-dione as glycolylating reagent.

Finally, the last derivative of Neu5Ac synthesized was the corresponding C-7 analogue of the α-allyl glycoside. Hence, the vicinal diol array in the side chain was simultaneously cleaved and reduced using periodate and borohydride anions supported on anionic resins (39). The isolation of **22** thus appeared straightforward since only a filtration of the resin was required. The low yield obtained (59%) was attributed to the partial hydrolysis of the methyl ester under the reaction conditions that generated the acid **23** *in situ*, which then remained on the resin. In fact, further treatment of the recuperated resin with acetic acid showed the release of some **23** (tlc).

In conclusion, antigenic and immunogenic (19–21) forms of *N*-acetylneuraminic acid were synthesized having BSA or TT as protein carriers. The series of conjugates having different levels of incorporation will be used to evaluate the role of the avidity phenomena encountered in lectin– and antibody–Neu5Ac interactions. The key functional group manipulations should allow the systematic evaluation of the exact binding epitopes with rabbit anti-sialic antibodies already obtained (19).

Experimental

Melting points were determined on a Gallenkamp apparatus and are uncorrected. The ^1H and ^{13}C NMR spectra were recorded on a Varian XL-300 or a Varian Gemini 200 at 300 and 200 MHz respectively for protons and at 75.4 and 50.3 MHz respectively for carbons. The proton chemical shifts (δ) are given relative to internal Me_4Si (δ = 0) for $CDCl_3$ solutions and relative to acetone (δ = 2.225) for D_2O solutions. The carbon chemical shifts are given relative to dioxane (δ = 67.4) for D_2O solutions. The analyses were done as a first-order approximation. Optical rotations were measured on a Perkin Elmer 241 polarimeter and were run at room temperature (~25°C). IR spectra were taken as KBr pellets using a Perkin Elmer 783 spectrophotometer. Mass spectra were recorded on a VG 7070-E spectrometer for CI, EI, and FAB-MS. Combustion analyses were performed by Guelph Chemical Laboratories Ltd. (Ont.). Thin-layer chromatography (tlc) was performed

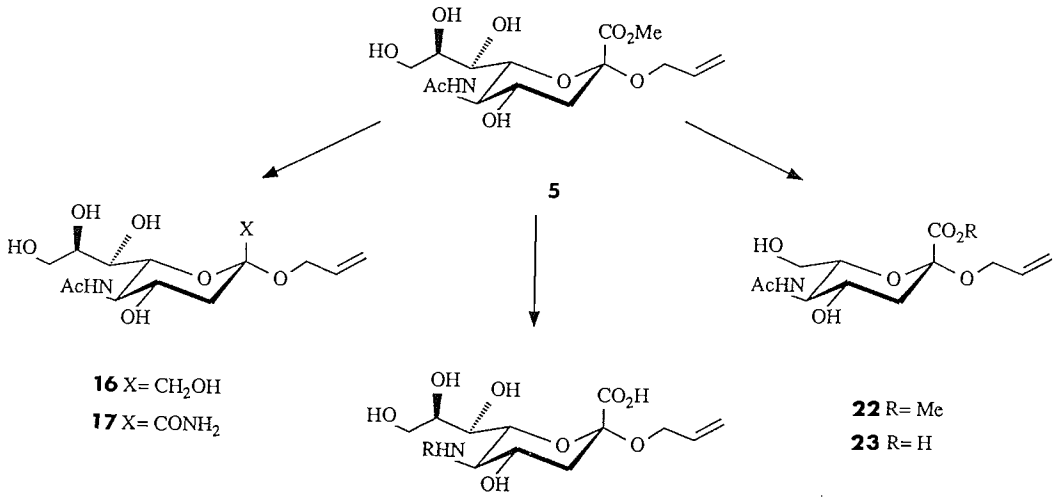

SCHEME 3

using silica gel 60 F-254 plates and column chromatography on silica gel 60 (230–400 mesh). The developed plates were sprayed or dipped with a solution of ceric sulfate (1%) and ammonium molybdate (2.5%) in 10% aqueous sulfuric acid and heated at ~150°C. The following solvent combinations (v/v) were used for tlc on silica gel: *n*-propanol–water, 7:3 (A) and 8:2 (B); ethyl acetate (C); chloroform–methanol 7:3 (D); acetonitrile – 10% acetic acid 8:2 (E); ethyl acetate – acetic acid – water 3:2:1 (F). Water soluble products were purified or desalted by size exclusion chromatography on Sephadex G-10. The products were monitored with a Waters R403 refractive index monitor. The *Collocalia* mucoids (edible bird's nest) were obtained from local Chinese groceries. Ozone was generated from a Welsbach instrument.

Protons of the allyl group present in some of the compounds are designated as H_a, H_b, H_c, H_d, and H_e as defined below and as previously described by Tahir and Hindsgaul (40).

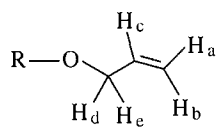

They were, however, described using a lower resolution instrument and thus some coupling constants (ex. H_a–$H_{d,e}$) were not observed. These protons generally showed the same multiplicity pattern throughout and only their chemical shifts varied: H_a, dd, $J_{a,b}$ = 1.5 Hz, $J_{a,c}$ = 10.5 Hz; H_b, dd, $J_{a,b}$ = 1.5 Hz, $J_{b,c}$ = 17.0 Hz; H_c, m; H_d and H_e ddd, $J_{d,e}$ = 12.5 Hz, $J_{c,d}$ = $J_{c,e}$ = 5.5 Hz.

*5-Acetamido-3,5-dideoxy-D-*glycero-*D-*galacto-*2-nonulopyranosonic acid* **1** *(Neu5Ac)*

Water (1.6 L) was added to edible bird's nest (200 g) and the resulting suspension was blended for ~5 min in a Waring blender. Rexyn 101 cation exchange resin (100 g) in the acid form was then added to the mixture. The reaction vessel was immersed in a thermostated water bath at 75°C and the content was mechanically stirred. After 6 h, the mixture was cooled to room temperature and filtered over gauze bandage in a large Büchner funnel. The resulting solution was directly loaded onto a Dowex 1X8 (20–50 mesh) column (3.5 × 40 cm) in the formate form. The column was washed with 2 L water followed by a linear gradient of formic acid (0–2 M). Fractions of 10 mL were collected and aliquots (100 μL) testing positive for sialic acid by the resorcinol method (34) were pooled and freeze-dried. The yields of pure **1** varied from 5 to 10 g (2.5–5% w/w) depending on the brand of bird's nest used. The solid obtained had mp 177–183°C (dec.); $[\alpha]_D$ −30.8° (*c* 1, H_2O) (lit. (5) mp 184–186°C; $[\alpha]_D$ −32.1°); R_f 0.47 (A). Negative FAB-MS for $C_{11}H_{18}NO_9$: 308 (M − 1). Both ^1H and ^{13}C NMR spectral data are in complete agreement with literature values (1, 5).

*Methyl 5-acetamido-3,5-dideoxy-D-*glycero-*D-*galacto-*2-nonulopyranosonate* **2** *(Neu5Ac methyl ester)*

The methyl ester **2** was prepared following the procedure of Kuhn *et al.* (25). Briefly, a solution of **1** (2.99 g, 9.7 mmol) in 50 mL methanol containing Amberlite IR-120 (H^+) (2.0 g) was stirred overnight at room temperature. The clear solution was filtered on a filter paper and evaporated to a volume of ~5 mL. Ether was added to turbidity and **2** crystallized on standing. It was recuperated by filtration (3.18 g, 9.7 mmol, ~quant.); mp 193.5–194.7°C; $[\alpha]_D$ −28° (*c* 3.5, H_2O) (lit. (25) mp 179–180°C; $[\alpha]_D$ −28°); R_f 0.55 (A). ^1H and ^{13}C NMR spectra were identical to those published (1).

*Methyl (5-acetamido-4,7,8,9-tetra-*O*-acetyl-3,5-dideoxy-D-*glycero-*β-D-*galacto-*2-nonulopyranosylchloride)onate* **3** *(acetochloro-neuraminic acid)*

Compound **2** (0.47 g, 1.5 mmol) was added to freshly distilled acetyl chloride (10 mL, some preparation required preactivation with 1.5 mL MeOH) containing acetic acid (5 mL) and cooled to 0°C. The flask was sealed and kept 24–48 h at room temperature. The extent of the reaction was followed by tlc in ethyl acetate. When the transformation was deemed complete, the reaction mixture was evaporated to dryness and coevaporated a few times with dry toluene. The chloride **2** was obtained as a foam (0.75 g, 1.5 mmol, ~quant.); $[\alpha]_D$ −61° (*c* 1, $CHCl_3$) (lit. (25) $[\alpha]_D$ −63°); R_f 0.32 (C). Its ^1H NMR showed it to be >95% pure in both $CDCl_3$ (41) and C_6D_6 (42), and it was used directly for the next step.

*Methyl (allyl 5-acetamido-4,7,8,9-tetra-*O*-acetyl-3,5-dideoxy-D-*glycero-*α-D-*galacto-*2-nonulopyranosid)onate* **4**

The chloride **3** (0.75 g, 1.4 mmol) was dissolved in dry (4A molecular sieves) allyl alcohol (5 mL) containing freshly prepared silver salicylate (0.35 g) and 4A molecular sieves (0.5 g). The reaction was stirred for 2 h at room temperature in the dark. The slurry was filtered over Celite and washed with CH_2Cl_2. The resulting clear solution was evaporated to dryness and the residue was dissolved in CH_2Cl_2 (25 mL). The organic solution was successively washed with cold 5% aqueous sodium bicarbonate, 5% aqueous sodium thiosulfate, and finally with water. The organic layer was dried over sodium sulfate

Can. J. Chem. Downloaded from www.nrcresearchpress.com by 91.121.58.235 on 09/07/12
For personal use only.

Can. J. Chem. Downloaded from www.nrcresearchpress.com by 91.121.58.235 on 09/07/12
For personal use only.

and evaporated to a clear oil that was homogeneous by tlc (90% yield). An analytical sample was obtained by crystallization from methanol–ether (0.59 g, 1.1 mmol, 73%). The glycoside **4** has mp 153.6–157.7°C; $[\alpha]_D$ −14.2° (*c* 1, $CHCl_3$) (lit. (27) mp 154–156°C, $[\alpha]_D$ −13° (MeOH)); R_f 0.30 (C); ^1H NMR ($CDCl_3$) δ: 5.83 (4 × d, 1H, $J_{b,c}$ = 17.0, $J_{a,c}$ = 10.5, $J_{c,d} \approx J_{c,e} \approx$ 5 Hz, H_c), 5.35 (m, 1H, H8), 5.30 (dd, 1H, $J_{7,8}$ = 8.5, $J_{6,7}$ = 1.8 Hz, H7), 5.26 (dd, 1H, $J_{b,c}$ = 17.0, $J_{a,b} \approx J_{b,d} \approx J_{b,e} \approx$ 1.5 Hz, H_b), 5.14 (d, 1H, $J_{5,NH} \approx$ 10 Hz, NH), 5.13 (dd, 1H, $J_{a,c}$ = 10.5, $J_{a,b} \approx J_{a,d} \approx J_{a,e} \approx$ 1.5 Hz, H_a), 4.83 (m, 1H, H4), 4.27 (dd, 1H, $J_{9,9'}$ = 12.5, $J_{8,9}$ = 2.7 Hz, H9), 4.27 (m, 1H, H5 or H6), 4.03–4.11 (m, 3H, H_d, H_e, H5 or H6), 3.84 (dd, 1H, $J_{9,9'}$ = 12.5, $J_{8,9'}$ = 5.8 Hz, H9′), 3.76 (s, 3H, Me-ester), 2.59 (dd, 1H, $J_{3ax,3eq}$ = 12.0, $J_{3eq,4}$ = 4.8 Hz, H_{3eq}), 1.86, 2.00, 2.02, 2.11, 2.13 (5 × s, 15H, N, O-Ac), 1.96 (dd, 1H, $J_{3ax,3eq} \approx J_{3ax,4} \approx$ 12 Hz, H_{3ax}); ^{13}C NMR ($CDCl_3$) δ: 171.2, 170.9, 170.4, 170.3 (N, O-Ac), 168.5 (CO_2Me), 133.6, 117.4 (allyl), 98.5 (C-2), 72.5 (C-6), 69.0 (C-8), 68.5 (C-7), 67.3 (CH_2-allyl), 66.0 (C-4), 62.3 (C-9), 49.3 (C-5), 38.0 (C-3), 23.1 (N-Ac), 21.0, 20.7 (2×), 20.61 (O-Ac). Anal. calcd. for $C_{23}H_{33}NO_{13}$: C 51.97, H 6.26, N 2.64; found: C 52.22, H 6.46, N 2.82.

*Methyl (allyl 5-acetamido-3,5-dideoxy-D-*glycero-*α-D-*galacto-*2-nonulopyranosid)onate **5***

Compound **4** (1.00 g, 1.9 mmol) was de-*O*-acetylated in dry methanol (20 mL) containing a few drops of 1 M NaOMe. The reaction was complete after 2 h at room temperature. The solution was neutralized with Amberlite 120 (H^+) resin, filtered, and evaporated to ~5 mL. Compound **5** crystallized upon addition of ether to afford 0.64 g of pure material (93%) having mp 143–144°C; $[\alpha]_D$ −10.1° (*c* 1, MeOH); R_f 0.49 (D); ν_{max}: 3380, 2944, 1750, 1650, 1570, 1440 cm^{-1}; ^1H and ^{13}C NMR, see Tables; pos. FAB-MS for $C_{15}H_{25}NO_9$: 364 (M + 1). Anal. calcd. for $C_{15}H_{25}NO_9$: C 49.58, H 6.94, N 3.86; found: C 49.47, H 7.10, N 3.98.

*Allyl 5-acetamido-3,5-dideoxy-D-*glycero-*α-D-*galacto-*2-nonulopyranosidonic acid **6** (Neu5Ac allyl glycoside)*

The ester **5** (0.28 g, 0.77 mmol) was treated for <1 h at room temperature with 0.1 M aqueous NaOH (5 mL). The reaction mixture was cooled to 0°C and neutralized with Rexyn 101 (H^+) resin (pH reached 2). After the solution was filtered, the pH was quickly readjusted to 7 with 0.1 M NaOH and then the solution was lyophilized to yield **6** as a white powder (0.25 g, 0.72 mmol, 93%); mp 245–250°C (dec.); $[\alpha]_D$ −9.1° (*c* 0.66, H_2O); R_f 0.57 (B); neg. FAB-MS for $C_{14}H_{23}NO_9$: 348 (M − 1).

*Methyl (2-oxoethyl 5-acetamido-3,5-dideoxy-D-*glycero-*α-D-*galacto-*2-nonulopyranosid)onate **7***

The allyl ester **5** (68 mg, 0.19 mmol) was dissolved in methanol (15 mL). The solution was cooled to −78°C, purged with oxygen for 5 min, and treated with ozone by bubbling till the solution remained blue. After 10 min, the ozone was evacuated with nitrogen for 15 min and, while at −78°C, dimethyl sulfide (0.5 mL) was added. The resulting solution was allowed to warm to room temperature over a 1 h period. The clear solution was then evaporated to give **7** as a homogeneous oil (66 mg, 0.18 mmol, 95%). The product was freed of its DMSO by-product by desalting on a G-10 column using water as eluent; $[\alpha]_D$ −10.3° (*c* 1, H_2O); R_f 0.35 (E), 0.61 (B); pos. FAB-MS for $C_{14}H_{23}NO_{10}$: 366 (M + 1). Anal. calcd.: C 46.07, H 6.35, N 3.83; found: C 45.65, H 6.39, N 3.79.

*2-Oxoethyl 5-acetamido-3,5-dideoxy-D-*glycero-*α-D-*galacto-*2-nonulopyranosidonic acid **8***

The above procedure was repeated on the sodium salt of **6** (1.0 g, 2.70 mmol) in methanol (50 mL). The yield of **8** was 1.0 g (2.70 mmol, quant.); $[\alpha]_D$ −1.8° (*c* 1, H_2O); R_f 0.27 (E); ν_{max}: 3390, 2940, 1620, 1560, 1060 cm^{-1}; neg. FAB-MS for $C_{13}H_{20}NO_{10}$: 350 (M − 1).

*Propyl 5-acetamido-3,5-dideoxy-D-*glycero-*α-D-*galacto-*2-nonulopyranosidonic acid **9***

The allyl ester **5** (26 mg, 0.072 mmol) was dissolved in methanol (10 mL) containing 5% Pd on charcoal (25 mg). Hydrogen gas was bubbled through the solution for 1 h. The reaction mixture was centrifuged to remove the catalyst and evaporated to dryness. Crystals of the methyl ester of **9** formed upon standing in the cold (25 mg, 0.068 mmol, 95%); mp 145.5°C; $[\alpha]_D$ −8.9° (*c* 0.7, H_2O); R_f 0.52 (E); ν_{max}: 3390, 1725, 1650, 1560, 1440, 1040 cm^{-1}. Anal. calcd. for $C_{15}H_{27}NO_9 \cdot H_2O$: C 46.99, H 7.10; found: C 46.56, H 6.93.

The above ester (10 mg) was dissolved in 0.1 N NaOH (3 mL) and the hydrolysis was allowed to proceed for 30 min at room temperature. The reaction mixture was cooled to 0°C, neutralized with H^+ resin, and filtered. The pH of the filtrate was readjusted to 7.0 with 0.1 N NaOH and the solution was lyophilized to give **9** as a homogeneous white powder (9 mg, 92%); $[\alpha]_D$ −4.1° (*c* 0.37, H_2O); pos. FAB-MS for $C_{14}H_{25}NO_9$: 352 (M + 1), 374 (M + Na).

*2-Hydroxyethyl 5-acetamido-3,5-dideoxy-D-*glycero-*α-D-*galacto-*2-nonulopyranosidonic acid **10***

The aldehyde **8** (27 mg, 0.077 mmol) was dissolved in methanol (2 mL). Sodium borohydride (10 mg) was then added. After 2 h, when tlc indicated the complete disappearance of **8**, a few drops of acetic acid were added to neutralize the excess borohydride. The reaction mixture was evaporated to dryness. The residue was dissolved in water and desalted on a column of Sephadex G-10 using water as eluant. The combined fractions in the void volume were pooled and lyophilized to give **10** as a white powder (18 mg, 0.051 mmol, 67%); $[\alpha]_D$ −7.6° (*c* 0.3, H_2O); R_f 0.39 (B); neg. FAB-MS for $C_{13}H_{23}NO_{10}$: 352 (M − 1).

*2-Aminoethyl 5-acetamido-3,5-dideoxy-D-*glycero-*α-D-*galacto-*2-nonulopyranosidonic acid **11***

Compound **8** (18 mg, 0.051 mmol) was reductively aminated in methanol (2 mL) saturated with ammonium acetate. Sodium cyanoborohydride (10 mg) was added and the solution was refluxed. After 24 h, the cooled reaction mixture was evaporated several times with methanol and finally dissolved in water (1 mL). The aqueous solution was desalted on a Sephadex G-10 column using water as eluant. The combined required fractions were freeze-dried to yield **11** (9.2 mg, 0.026 mmol, 51%); $[\alpha]_D$ −18.5° (*c* 1, H_2O) (lit. (37) $[\alpha]_D$ −17°); R_f 0.17 (B); neg. FAB-MS for $C_{13}H_{25}N_2O_9$: 352 (M − 1).

*2-[N$^\epsilon$-(N$^\alpha$-Acetyl-(L)-lysyl)]ethyl 5-acetamido-3,5-dideoxy-D-*glycero-*α-D-*galacto-*2-nonulopyranosidonic acid **12***

The aldehyde **8** (34 mg, 0.097 mmol) was dissolved in 0.2 M phosphate buffer pH 7.0 (1 mL) containing N^α-acetyl-(L)-lysine (30 mg, 0.15 mmol, Sigma). Sodium cyanoborohydride (13 mg, 0.21 mmol) was added to the reaction mixture, which was stirred at room temperature for 48 h. Acetic acid (0.25 mL) was added, and after 3 h the solution was directly loaded on a Sephadex G-10 desalting column. The desired product **12** was eluted with 30 mM aqueous ammonium bicarbonate to yield 40 mg (0.076 mmol, 78%) of a white powder after lyophilization; $[\alpha]_D$ −6.5° (*c* 0.9, H_2O); R_f 0.31 (F); ^1H NMR (D_2O) δ (aglycon): 4.16 (dd, 1H, $J_{\alpha,\beta}$ = 8.2 and 4.9 Hz, H_α), 3.87 (m, 1H, OCH_2CH_2N), 3.25 (t, 2H, *J* = 4.7 Hz, OCH_2-CH_2N), 3.08 (t, 2H, *J* = 7.8 Hz, H_ϵ), 2.04 (s, 3H, N^α-Ac), 1.69–1.82 (m, 5H, H_{3ax} + $4H_{\beta,\gamma}$), 1.42 (q, 2H, H_γ); ^{13}C NMR (D_2O) δ (aglycon): 22.8, 23.2, 26.0, 31.8, 47.9, 48.1, 55.5, 60.0, 174.4, 179.2; FAB-MS for $C_{21}H_{37}N_3O_{13}$: 522 (M − 1). Anal. calcd. for $C_{21}H_{37}N_3O_{13} \cdot NH_4HCO_3$: C 43.91, H 7.03, N 9.30; found: C 43.30, H 7.53, N 9.07.

*Conjugation of **7** or **8** onto BSA and tetanus toxoid **13**, **14***

The aldehydo acid **8** or ester **7** added in various proportions (see Table 3) was dissolved in 0.2 M phosphate buffer of the pH indicated in the table but generally being at pH 7.0 (2 mL). The protein bovine serum albumin or tetanus toxoid (10 mg) was added to the buffer solution and stirred for 1 h at 37°C. Cyanoborohydride was then added. Aliquots were taken at appropriate time intervals and dialyzed exhaustively against running water for 24 h, then with distilled water for 48 h. The sample was then diluted to a fixed volume and the sialic acid content was measured by the resorcinol method (34). The protein content was measured by the Lowry procedure (35). The samples were lyophilized and weighed. The conjugates were characterized

Can. J. Chem. Downloaded from www.nrcresearchpress.com by 91.121.58.235 on 09/07/12
For personal use only.

by SDS-PAGE and by serological assays (double immunodiffusion, ELISA, quantitative precipitation, and immunoelectrophoresis) (to be published).

Typical procedure for a conjugate Neu5Ac$_{53}$/BSA

Bovine serum albumin (BSA, Pentex, Miles Laboratories) (11 mg, 0.16 μmol) was dissolved in 0.2 M phosphate buffer pH 7.0 (2 mL). The ester **7** (22 mg, 60 μmol) dissolved in the same buffer (0.3 mL) was added to the protein solution, followed by methanol (1 mL). The solution was stirred for 20 min at 37°C. Then $NaBH_3CN$ (20 mg, 317 μmol) was added to the reaction mixture, which was stirred for 4 days at 37°C. The solution of the conjugate was transferred to a dialysis bag (10 kDa MW cutoff) and dialyzed for 3 days against distilled water. The solution was diluted to 10 mL and three aliquots of 250 μL each were tested for sialic acid by the resorcinol method as above. The solution was lyophilized, giving a white powder (14 mg) containing an average of 53 Neu5Ac residues per mole of BSA.

*Bicyclic lactam **15***

Method A

The 2-aminoethyl glycoside **11** (7 mg, 0.020 mmol) was dissolved in MeOH (3 mL) containing EDC (3 mg). After 24 h at room temperature, an additional portion of EDC was added (3 mg) and the solvent evaporated to dryness after 24 h. The lactam **15** was purified by silica gel chromatography using a gradient of ethanol and methanol as eluant (2 mg).

Method B

The aldehydo ester **7** (4 mg) was dissolved in MeOH (1 mL) containing ammonium acetate (20 mg). After 1 h at room temperature, sodium cyanoborohydride was added (2 mg). The reaction mixture was evaporated to dryness after 4 h. The residue was dissolved in 0.03 M ammonium bicarbonate (~1 mL) and desalted on a Sephadex G-10 column using the same solvent as eluant. The pooled fractions containing **15** were freeze-dried to yield 3 mg of a mixture of **11** and **15** as white powder. Compound **15** isolated from method A had ν_{max}: 3420, 1650, 1560, 1350, 1040 cm^{-1}; ^{1}H NMR (D_2O) δ: 1.63 (dd, 1H, $J_{3ax,3eq} \approx J_{3ax,4} \approx 12$ Hz, H-3ax), 2.03 (s, 3H, NAc), 2.44 (dd, 1H, $J_{3ax,3eq} = 12$, $J_{3eq,4} = 5$ Hz, H-3eq), 3.32–4.50 (m, 11H, remaining); ^{13}C NMR (D_2O) δ: 97.5, 74.2, 71.5, 69.6, 69.0, 64.7, 56.1, 53.4, and 23.3 (signals lacking because signal-to-noise ratio was too high for 3 mg sample); pos. FAB-MS for $C_{13}H_{22}N_2O_8$: 335 (M + 1).

*Allyl 5-acetamido-3,5-dideoxy-D-*glycero*-α-D-*galacto*-2-nonulopyranoside **16***

The ester **5** (21 mg, 0.058 mmol) was dissolved in methanol (0.5 mL) to which was added THF (5 mL). $LiBH_4$ (1 mg) was added to the solution and the reduction was allowed to proceed for 1 h at room temperature. The reaction mixture was neutralized with resin (H^+) and evaporated after filtration. The remaining boric acid was eliminated as trimethyl borate after repeated coevaporation of the residue from methanol. The reduced product **16**, which resisted crystallization, was obtained in quantitative yield (19 mg, 0.058 mmol); $[\alpha]_D$ −15.4° (*c* 1.8, H_2O); R_f 0.50 (E); ν_{max}: 3400, 1640, 1560, 1050 cm^{-1}; pos. FAB-MS for $C_{14}H_{25}NO_8$: 336 (M + 1).

*Allyl 5-acetamido-3,5-dideoxy-D-*glycero*-α-D-*galacto*-2-nonulopyranosidonamide **17***

The ester **5** (40 mg, 0.11 mmol) was dissolved in methanol (5 mL). Methanol (5 mL) presaturated with NH_3 gas was then added to the ester solution. The reaction was allowed to proceed for 1 h at room temperature. The solution was concentrated on the Büchi evaporator and **17** crystallized upon standing. The crystals were recuperated by filtration to give **17** in 84% yield (32 mg, 0.092 mmol); mp 82–87°C; $[\alpha]_D$ −3.6° (*c* 2.0, H_2O); R_f 0.63 (E); ν_{max}: 3400, 1690, 1600, 1385, 1040 cm^{-1}; pos. FAB-MS for $C_{14}H_{24}N_2O_8$: 349 (M + 1).

*Allyl 5-amino-3,5-dideoxy-D-*glycero*-α-D-*galacto*-2-nonulopyranosidonic acid **18***

The acetamido ester **5** (95 mg, 0.26 mmol) was dissolved in water (1 mL). To the solution was added 20% tetramethylammonium hydroxide (1 mL) (20% w/w in MeOH, Aldrich). The reaction was refluxed and monitored by tlc, which indicated the transformation to be complete after 5 h. The reaction mixture was neutralized with acetic acid and evaporated to dryness. The remaining residue was dissolved in water (1 mL) and desalted on a Sephadex G-10 column (3.0 × 60 cm) by elution with water. The positive fractions (resorcinol and ninhydrin) were pooled and lyophilized to afford **18** (64 mg, 0.21 mmol) as a white powder in 80% yield; $[\alpha]_D$ −18.0° (*c* 0.9, H_2O); R_f 0.26 (E); ν_{max}: 3400, 1610, 1400, 1130 cm^{-1}; FAB-MS for $C_{12}H_{21}NO_8$: 308 (M + 1) and 306 (M − 1).

*Allyl 5-bromoacetamido-3,5-dideoxy-D-*glycero*-α-D-*galacto*-2-nonulopyranosidonic acid **19***

The amine derivative **18** (67 mg, 0.22 mmol) was dissolved in methanol (2 mL) containing triethylamine (0.5 mL). The solution was cooled to −70°C and a few drops of bromoacetyl chloride were added. After disappearance of starting material by tlc (molybdate and ninhydrin), the solvents were evaporated to dryness. The residue was dissolved in water and desalted on a Sephadex G-10 column as before. The pooled fractions of **19** were freeze-dried to give a white powder (75 mg, 0.18 mmol, 80%); $[\alpha]_D$ −8.0° (*c* 0.1, H_2O); R_f 0.53 (E); neg. FAB-MS for $C_{14}H_{22}BrNO_9$: 426 and 428 (M − 1).

*Allyl 3,5-dideoxy-5-hydroxyacetamido-D-*glycero*-α-D-*galacto*-2-nonulopyranosidonic acid **21***

Compound **18** (34 mg, 0.11 mmol) was dissolved in methanol (2 mL) containing triethylamine (0.5 mL) and the solution was cooled to −70°C. Acetoxyacetyl chloride (50 μL, Aldrich) was added dropwise. The reaction was judged instantaneous by tlc, whereby **20** could be isolated or could be allowed to proceed for an additional hour to ensure complete de-*O*-acetylation of the intermediate **20** (0.1 N NaOH may be added to accelerate the hydrolysis). The reaction mixture was evaporated to dryness and treated as above for **19**. The yield of **21** obtained as a white powder after lyophilization was 86% (39 mg, 0.095 mmol); mp 245°C (dec.); $[\alpha]_D$ −3.8° (*c* 0.4, H_2O); R_f 0.48 (d); ν_{max}: 3430, 1600, 1410, 1080 cm^{-1}; FAB-MS for $C_{14}H_{23}NO_{10}$: 366 (M + 1) and 364 (M − 1) respectively.

*Allyl 5-acetamido-3,5-dideoxy-α-D-*galacto*-2-heptulopyranosidonic acid **23***

Sodium borohydride (5 g) was dissolved in water (20 mL) and mixed with Amberlite IRA 400 anion exchange resin (10 g) (Cl^- form). After 1 h, the resin was decanted and fresh sodium borohydride in water was again added. After 10 min, the resin was filtered and rinsed with water and allowed to dry at room temperature. Similarly, a fresh portion of the same resin (5 g, Cl^- form) was treated with three 30-mL portions of 0.5 M aqueous sodium metaperiodate over several hours. The resin was finally rinsed with water and allowed to dry at room temperature.

The methyl ester **5** (20 mg, 0.055 mmol) was dissolved in dry methanol (2 mL) to which was added the above resin (0.5 g each, of the IO_4^- and BH_4^- forms). After stirring for 3 h at room temperature, the solution was filtered and evaporated to give **22** (9.8 mg, 0.032 mmol, 59%). A sample of pure **22** was obtained after freeze-drying; mp 67.5–72.4°C; $[\alpha]_D$ +2.0° (*c* 0.5, H_2O); R_f 0.72 (D); ν_{max}: 3390, 1725, 1650, 1560, 1440, 1040 cm^{-1}; pos. FAB-MS for $C_{13}H_{21}NO_7$: 304 (M + 1).

A sample of the ester **22** was treated with 0.1 N NaOH as previously for **5** to afford a quantitative yield of **23** stored in the sodium form; $[\alpha]_D$ −21.3° (*c* 0.5, H_2O); R_f 0.31 (E).

Acknowledgments

We are grateful to the Natural Sciences and Engineering Research Council of Canada (NSERC) for generous support of this project. We also wish to thank Dr. P. Rousseau from the Armand-Frappier Institute (Quebec) for a gift of tetanus toxoid, and Mr. R. A. Pon (M.Sc. from this department) for the T. toxoid conjugation. Finally, we acknowledge the assistance of the following: Mr. R. Capoor and Dr. H. Dettman for running some of the NMR experiments, Dr. C. Kazakoff for the mass spectra, and Mr. L. Cousineau and Mr. L. Sabourin (summer

students) for the bird's nest hydrolysis. We also thank Mrs. Monique Lévesque for typing the manuscript.

1. R. SCHAUER (*Editor*). Sialic acids, chemistry, metabolism and function. Cell Biology Monograph series, Vol. 10. Springer-Verlag, Vienna. 1982.
2. H. J. JENNINGS. Adv. Carbohydr. Chem. Biochem. **41**, 155 (1983).
3. L. KENNE and B. LINDBERG. *In* The polysaccharides. Vol. 2. *Edited by* G. O. Aspinall. Academic Press, New York. 1983. pp. 287–363.
4. J.-M. WIERUSZESKI, J.-C. MICHALSKI, J. MONTREUIL, G. STRECKER, J. PETER-KATALINIC, H. EGGE, H. VAN HALBEEK, J. H. G. M. MUTSAERS, and J. F. G. VLIEGENTHART. J. Biol. Chem. **262**, 6650 (1987).
5. M. F. CZARNIECKI and E. R. THORNTON. J. Am. Chem. Soc. **99**, 8273 (1977).
6. H. GEYER, C. HOLSCHBACK, G. HUNSMANN, and J. SCHNEIDER. J. Biol. Chem. **263**, 11760 (1988).
7. J. C. PAULSON, G. N. ROGERS, S. M. CARROLL, H. H. HIGA, T. PRITCHETT, G. MILKS, and S. SABESAN. Pure Appl. Chem. **56**, 797 (1984).
8. M. LINDAHL, R. BROSSMER, and T. WADSTRÖM. Glycoconjugate J. **4**, 51 (1987).
9. W. REUTTER, E. KÖTTGEN, C. BAUER, and W. GEROK. *In* Sialic acids, chemistry, metabolism and function. Cell Biology Monograph series. Vol. 10. *Edited by* R. Schauer. Springer-Verlag, Vienna. 1982.
10. I. J. GOLDSTEIN and R. D. PORETZ. *In* The lectins, properties, functions, and applications in biology and medicine. *Edited by* I. E. Liener, N. Sharon, and I. J. Goldstein. Academic Press, Orlando, FL. 1986. pp. 209–214.
11. H. ANKEL, C. KRISHNAMURTI, F. BESANCON, S. STEFANOS, and E. FALCOFF. Proc. Natl. Acad. Sci. U.S.A. **77**, 2528 (1980).
12. J. B. BASEMAN, M. BANAI, and I. KAHANE. Infect. Immun. **38**, 389 (1982).
13. J. AMANO, S. SATO, R. NISHIMURA, M. MOCHIZUKI, and A. KOBATA. J. Biochem. **105**, 339 (1989).
14. R. SCHAUER, A. K. SHUKLA, C. SCHÖDER, and E. MÜLLER. Pure Appl. Chem. **56**, 907 (1984).
15. D. AMINOFF. Blood Cells, **14**, 229 (1988).
16. T. FEIZI. Nature (London), **314**, 53 (1985).
17. S. HAKOMORI. Ann. Rev. Immunol. **2**, 103 (1984).
18. H.-J. GABIUS. Angew. Chem. Int. Ed. Engl. **27**, 1267 (1988).
19. R. ROY, A. GAMIAN, and M. CHOMIK. *In* Sialic acids. Proc. Japanese–German Symposium on Sialic Acids. *Edited by* R. Schauer and T. Yamakawa. Kieler Verlag Wissenschaft + Bildung, Kiel. 1988. pp. 264–265.
20. R. ROY and C. A. LAFERRIÈRE. Carbohydr. Res. **177**, C1 (1988).
21. R. ROY, C. A. LAFERRIÈRE, A. GAMIAN, and H. J. JENNINGS. J. Carbohydr. Chem. **6**, 161 (1987).
22. R. ROY, E. KATZENELLENBOGEN, and H. J. JENNINGS. Can. J. Biochem. Cell Biol. **62**, 270 (1984).
23. R. T. LEE and Y. C. LEE. Biochemistry, **19**, 156 (1980).
24. G. R. GRAY. Arch. Biochem. Biophys. **163**, 426 (1974).
25. R. KUHN, P. LUTZ, and D. L. MCDONALD. Chem. Ber. **99**, 611 (1966).
26. H. OGURA, K. FURUHATA, M. ITOH, and Y. SHITORI. Carbohydr. Res. **158**, 37 (1986).
27. V. ESCHENFELDER and R. BROSSMER. Carbohydr. Res. **78**, 190 (1980).
28. C. SHIMIZU and K. ACHIWA. Carbohydr. Res. **166**, 314 (1987).
29. D. J. M. VAN DER VLEUGEL, W. A. R. VAN HEESWIJK, and J. F. G. VLIEGENTHART. Carbohydr. Res. **102**, 121 (1982).
30. (*a*) H. PAULSEN and U. VON DEESSEN. Carbohydr. Res. **146**, 147 (1986); (*b*) Y. ITOH and T. OGAWA. Tetrahedron Lett. **28**, 6221 (1987); (*c*) T. MURASE, H. ISHIDA, M. KISO, and A. HASEGAWA. Carbohydr. Res. **188**, 71 (1989), and refs. cited therein.
31. H. HORI, T. NAKAJIMA, Y. NISHIDA, H. OHRUI, and H. MEGURO. Tetrahedron Lett. **29**, 6317 (1988).
32. M. O. DAYHOFF. *In* Atlas of protein sequence and structure. Vol. 5. Suppl. 2. NBR, Washington, DC. 1976. p. 267.
33. B. BIZZINI, J. BLASS, A. TURPIN, and M. RAYNAUD. Eur. J. Biochem. **17**, 100 (1970).
34. L. SVENNERHOLM. Biochim. Biophys. Acta, **24**, 604 (1957).
35. O. H. LOWRY, N. J. ROSEBROUGH, A. L. FARR, and R. J. RANDALL. J. Biol. Chem. **193**, 265 (1951).
36. S. HESTRIN. J. Biol. Chem. **180**, 249 (1949).
37. L. HOLMQUIST and R. BROSSMER. Hoppe-Seyler's Z. Physiol. Chem. **353**, 1346 (1972).
38. R. ROY and R. A. PON. Glycoconjugate J. **7**, 3 (1990).
39. M. BESSODES and K. ANTONAKIS. Tetrahedron Lett. **26**, 1305 (1985).
40. S. H. TAHIR and O. HINDSGAUL. Can. J. Chem. **64**, 1771 (1986).
41. M. N. SHARMA and R. EBY. Carbohydr. Res. **127**, 201 (1984).
42. H. PAULSEN and H. TIETZ. Carbohydr. Res. **125**, 47 (1984).

Can. J. Chem. Downloaded from www.nrcresearchpress.com by 91.121.58.235 on 09/07/12
For personal use only.

Synthesis and biological activity of (*R*)-2′-fluorocarminomycin

HANS H. BAER[1] AND FERNANDO HERNÁNDEZ MATEO[2]

Ottawa–Carleton Chemistry Institute, Department of Chemistry, University of Ottawa, Ottawa, Ont., Canada K1N 9B4

Received April 9, 1990

HANS H. BAER and FERNANDO HERNÁNDEZ MATEO. Can. J. Chem. **68**, 2055 (1990).

Methyl 3-amino-2,3,6-trideoxy-2-fluoro-β-L-talopyranoside was hydrolyzed to the free sugar, (*R*)-2-fluorodaunosamine hydrochloride, which was converted into the α-1,4-di-*O*-acetyl-*N*-trifluoroacetyl derivative. The latter was condensed with carminomycinone by use of trimethylsilyl triflate as the activating agent, and the product was deprotected to give the title compound. Cytotoxicity of the new fluoroanthracycline against a number of tumor cell lines in vitro equalled that of parent carminomycin, and activities of the two compounds against P-388 murine leukemia in vivo were the same, although the fluoro derivative was fourfold less potent and appeared to be somewhat less toxic.

Key words: (*R*)-2-fluorodaunosamine hydrochloride, synthesis; (*R*)-2′-fluorocarminomycin, synthesis and biological activity.

HANS H. BAER et FERNANDO HERNÁNDEZ MATEO. Can. J. Chem. **68**, 2055 (1990).

On a hydrolysé le méthyl-3-amino-2,3,6-tridésoxy-2-fluoro-β-L-talopyranoside en sucre libre, le chlorhydrate de la (*R*)-2-fluorodaunosamine, que l'on a transformé en dérivé α-1,4-di-*O*-acétyl-*N*-trifluoroacétyle. On a condensé ce dernier avec la carminomycinone à l'aide de triflate de triméthylsilyle comme agent activateur et on a déprotégé le produit pour obtenir le composé mentionné dans le titre. Les effets cytotoxiques in vitro de cette nouvelle fluoroanthracycline contre de nombreuses lignes de cellules tumorales sont équivalents à ceux de la carminomycine naturelle. Par ailleurs, l'activité antitumorale in vivo des deux composés contre la leucémie murine P-388 demeure la même quoique le dérivé fluoro s'est avéré quatre fois moins puissant et est apparu comme étant quelque moins toxique.

Mots clés : synthèse du chlorhydrate de la (*R*)-2-fluorodaunosamine, synthèse et activité biologique de la (*R*)-2′-fluorocarminomycine.

Can. J. Chem. Downloaded from www.nrcresearchpress.com by 195.138.81.100 on 09/07/12
For personal use only.

Introduction

In our first article (1) from a program concerned with the synthesis of anthracycline antitumor agents fluorinated in the sugar moiety, a rationale was provided for attempts to procure derivatives bearing a fluorine atom at the position C-2′, and the question of a possible effect of stereochemistry at that position was discussed. Prior and concurrent work by Horton *et al.* (2) has shown that certain structural modifications of daunorubicin (**1***a*), substituted at C-2′ by iodine, bromine, or chlorine, exhibited significantly enhanced antitumor activity and decreased toxicity, but only when the halo atom was axially oriented (**1***b* and 4′-epimers; *R*-2′ configuration); the nature of the halogen atom appeared to have little influence on activity, but *S*-2′ epimers **1***c* (equatorial halogen) were inactive (2). Although Horton *et al.* had previously demonstrated (3) that the 3′-amino group in anthracyclines is not essential for antitumor activity, as was confirmed by the properties of the 3′-deamino-3′-hydroxy (or acetoxy) derivatives **1***b*, we targeted 3′-amino-2′-fluoro glycosides in the hope of gaining further insights into the factors that govern drug efficacy and toxicity.

Our first efforts in that direction (1, 4) had produced (*S*)-2′-fluorodaunorubicin (**2**), also synthesized by Lukacs and co-workers (5), which proved active against a variety of tumor cell lines in vitro and against L1210 murine leukemia in vivo but showed a somewhat lower potency as compared with parent **1***a*. Compound **2** was nontoxic at the highest dose level tested (4), contrary to **1***a*, and it was intriguing to observe retention of activity (albeit diminished) in a derivative bearing an *equatorial* 2′-halo substituent. This raised expectations that an analog having an axial 2′-fluoro substituent might be a superior drug, and we set out first to prepare (*R*)-2-fluoro-L-daunosamine, in the form of its methyl β-pyranoside (6), as the sugar component

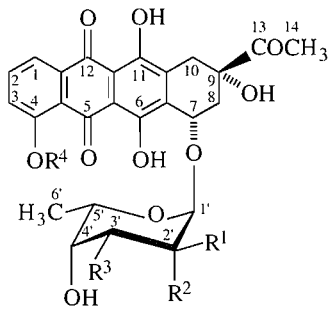

	R^1	R^2	R^3	R^4
1*a*	H	H	NH_2	Me
1*b*	H	I, Br, or Cl	OH or OAc	Me
1*c*	I, Br, or Cl	H	OH or OAc	Me
1*d*	H	F	OH	Me
2	F	H	NH_2	Me
3	H	H	NH_2	H
4	H	F	NH_2	H

required for synthesis of such an analog. While that work was in progress, the Umezawas and co-workers (7) published a study highly relevant to this topic, namely, the synthesis of 3′-deamino-(*R*)-2′-fluoro-3′-hydroxydaunorubicin (**1***d*) and its 14-hydroxy derivative (i.e., the corresponding adriamycin analog); strong antitumor activity and low toxicity were displayed by both of these compounds, especially so by the latter. We now record the synthesis of (*R*)-2′-fluorocarminomycin (**4**) and the results of biological testing in comparison with parent carminomycin (**3**). The latter drug has been stated (8) to be more potent than **1***a*, from which it differs structurally solely by its lack of the 4-methyl ether group (9).

Results and discussion

The synthesis of **4** proceeded essentially in analogy to that of **2** (4), except for the step of aglycon glycosylation. Thus, methyl 3-amino-2,3,6-trideoxy-2-fluoro-β-L-talopyranoside (**5**) (6) was hydrolyzed with 4 M hydrochloric acid to give the free amino

[1]Author to whom correspondence may be addressed.

[2]Visiting professor, May–August 1989. Permanent address: Departamento de Química Orgánica, Facultad de Ciencias, Universidad de Granada, 18071 Granada, Spain.

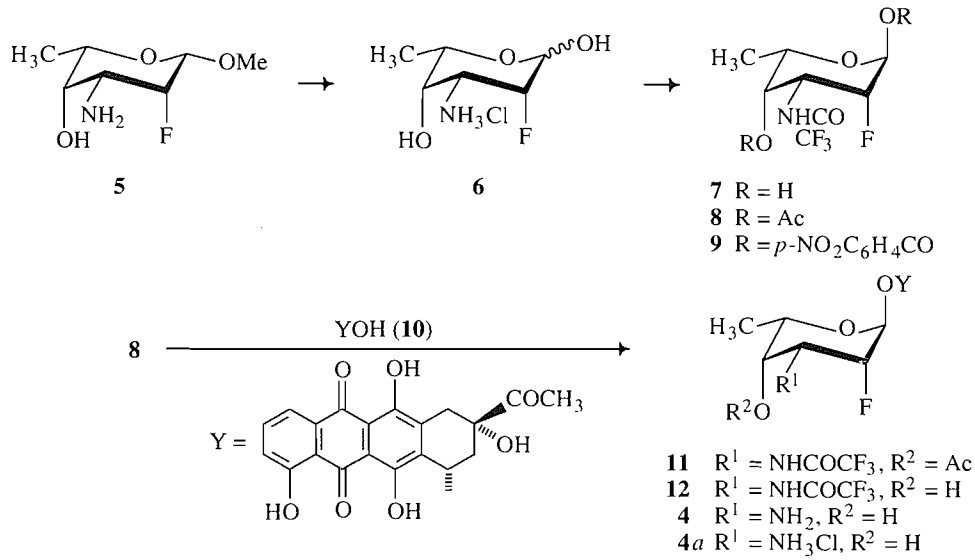

sugar hydrochloride **6**, obtained as a crystalline, anomeric mixture. The sugar was sequentially *N*-trifluoroacetylated and *O*-acetylated under the general conditions of daunosamine acylation (10), affording the acyl derivatives **7** and **8** isolated crystalline as pure α-anomers. (By contrast, their (*S*)-2 epimers had been obtained (4) as anomeric mixtures.) The yields of **6–8** were 88–91%.

Compound **8** was condensed with carminomycinone (**10**) by use of trimethylsilyl triflate as the activating agent, according to the method employed by Terashima and co-workers (11) for a synthesis of 4-demethoxydaunorubicin. The 4′-*O*-acetyl-*N*-trifluoroacetyl anthracycline **11** was isolated crystalline in 51% yield; since 33% of unchanged **8** was recovered, the yield based on sugar actually consumed in the reaction was 75%.[3] Sodium methoxide-catalyzed *O*-deacetylation of **11** gave (*R*)-2′-fluoro-*N*-trifluoroacetylcarminomycin (**12**), characterized by tlc only, which was directly *N*-deprotected by treatment with aqueous barium hydroxide, to furnish a 82% overall yield of the target compound **4**, analytically characterized both as the free base and as its hydrochloride **4***a*.

The ^{1}H nmr data for the new compounds (see the Experimental) were in full accord with the depicted structures, and it may be noted in particular that the magnitudes of all observed ^{1}H–^{19}F coupling constants conformed well with expectations based on previous, detailed discussions (1, 6). Mention of a few salient points may suffice. Thus, the vicinal coupling between the fluorine atom and the anomeric proton ($^3J_{H\text{-}1,F\text{-}2}$) in **7–9**, **11**, and **4** was 8.3 ± 0.3 Hz (9.7 Hz in **4***a*), which provided unambiguous proof for an H-1*eq*,F-2*ax gauche* relationship and, hence, the α-anomeric configuration. The $^3J_{H\text{-}1,F\text{-}2}$ value empirically calculated (1, 6, 12) for a 2-deoxy-2-fluorohexopyranose having a 1*ax*,2*ax*,3*eq* substituent arrangement is 6 Hz. By contrast, $^3J_{H,F}$ values for vicinal, *trans*-diaxial nuclei are usually in the range of 19–34 Hz, depending on electronegativity of substituents present (13); examples are $^3J_{H\text{-}1,F\text{-}2}$ = 20.5 Hz for **5** (6) and 22 Hz for **6**-β, and $^3J_{F\text{-}2,H\text{-}3}$ = 33–34 Hz for **5** (6), **7–9**, and **11**. (The $^3J_{F\text{-}2,H\text{-}3}$ values for **4**, **4***a*, and **6**-α should fall in the same range, but they could not be determined.) The geminal coupling constants $^2J_{H\text{-}2,F\text{-}2}$ of **4**, **4***a*, **6**-α, **7–9**, and **11** were all in the range of 48–49.3 Hz, whereas that of **6**-β was 51 Hz, in agreement with empirically calculated (1, 6, 12) values of 48 and 51 Hz, respectively.

Further confirmation of the α-anomeric configuration of the glycoside **11** and its precursors **7** and **8** was derived from their ^{13}C nmr spectra, which displayed C-1 signals (for **11**, read C-1′ etc.) as doublets with $^2J_{C\text{-}1,F\text{-}2}$ = 30.4 ± 1 Hz, C-3 signals as doublets with $^2J_{F\text{-}2,C\text{-}3}$ = 16.0 ± 0.4 Hz, and C-4 signals as singlets ($^3J_{F\text{-}2,C\text{-}4}$ = 0 Hz). The magnitude of $^2J_{C\text{-}1,F\text{-}2}$ indicated an *anti* orientation of the anomeric oxygen atom with respect to the fluorine atom; the $^2J_{F\text{-}2,C\text{-}3}$ values were as expected for structures wherein the coupled C-atom does not bear an electronegative substituent *anti* to the F-atom, and zero vicinal coupling $^3J_{F\text{-}2,C\text{-}4}$ was in line with the *gauche* F-2—C-4 arrangement (6, 13, 14). Finally, the nmr parameters for **4**, **11**, and **8** were in excellent harmony with those reported (7) for **1***d*, its 3′,4′-diacetate, and their progenitor 1,3,4-tri-*O*-acetyl-2,6-dideoxy-2-fluoro-α-L-talopyranose.

Biological activity

Tests to compare antitumor activity of the fluorocarminomycin **4***a* with that of parent carminomycin (**3**) hydrochloride were performed by Bristol–Myers Company, Wallingford, Connecticut. Both compounds showed equally high potencies in vitro, in cytotoxicity tests against five human ovarian and colon cancer cell lines (A2780DDP, A2780S, HCT-116, HCT/VM46, and HCT/VP35), with IC-50 values ranging from <0.001 to 0.03 μg/mL. Tests in vivo against murine P-388 lymphocytic leukemia showed **4** and **3** to be equally active, achieving median survival time increases (T/C values) of ~200%, although **3** was about fourfold more potent in terms of effective dose levels (Table 1). Acute toxicity appeared to be lower in **4**, as judged from a slower onset of weight loss at higher doses, but no toxic deaths occurred within 5 days after treatment with either drug at the dose levels tested.

[3]For condensation of 1,4-di-*O*-acetyl-*N*-trifluoroacetyldaunosamine with 4-demethoxydaunorubicin, followed by 4′-*O*-deacetylation of the product, Terashima and co-workers (11) reported a 70% yield. By use of the corresponding 1,4-bis-*p*-nitrobenzoate, the condensation was almost quantitative and the 4′-*O*-deprotected product was elaborated in 83% yield (11). We encountered initial difficulties in attempting to prepare the 1,4-bis-*p*-nitrobenzoate (**9**) of **7**, and although this ester was eventually obtained (for ^{1}H nmr data, see the section for **8** in the Experimental), its full characterization and (possibly advantageous) use for glycosylation of **10** were dispensed with, the goal of the project having meanwhile been attained.

Can. J. Chem. Downloaded from www.nrcresearchpress.com by 195.138.81.100 on 09/07/12
For personal use only.

TABLE 1. Antitumor activity in vivo of carminomycin and (*R*)-2'-fluorocarminomycin against murine P-388 lymphocytic leukemia[a]

Compound (hydrochloride)	Dose (mg/kg)[b]	MST[c] (days)	T/C[d] (%)	AWC[e] (g)
3	1.2	12	133	−0.9
	0.6	19	211	−0.8
	0.3	15.5	172	0.6
	0.15	13	144	0.0
4	2.4	18	200	−0.5
	1.2	16.5	183	−0.1
	0.6	12.5	139	0.4
	0.3	12	133	0.3
	0.15	11	122	0.2
Control		9	100	0.8

[a]In CDF_1 mice (six per test) inoculated i.p. with 10^6 P-388 cells on day 0.
[b]Single dose administered i.p. on day 1.
[c]Median survival time.
[d]Ratio of MST of treated mice to that of untreated controls.
[e]Average weight change recorded on day 4.

Experimental

General preparative and instrumental methods were the same as those previously employed (1, 4, 6). The following solvent combinations (v/v) were used for thin-layer chromatography (tlc) and column chromatography on silica gel: methanol–chloroform, 1:3 (A) and 1:6 (B); methanol–acetone, 1:1 (C); and ethyl acetate – hexanes, 1:1 (D) and 1:2 (E). Optical rotations were measured at ~25°C. Infrared data (ν_{max}) obtained for all new compounds were consistent with the structures, and only a few especially significant bands are listed. Mass-spectral data (*m/z*) were obtained in the chemical ionization mode, using ether as the ionizing gas. The ^1H nmr spectra were recorded at 300 MHz from solutions in deuteriochloroform, unless otherwise indicated.

3-Amino-2,3,6-trideoxy-2-fluoro-α,β-L-talose hydrochloride (6)

A solution of amino glycoside **5** (6) (385 mg) in 4 M hydrochloric acid (40 mL) was boiled under reflux for 6 h, after which time the hydrolysis was complete (tlc, solvent A). The acid was evaporated under diminished pressure with repeated additions of water, and the remaining aqueous solution of the product was treated with activated charcoal and concentrated, to give a greenish solid that was thoroughly dried over KOH *in vacuo*. Trituration with hot acetone then removed the colored impurity and gave **6** as a crystalline monohydrate (415 mg, 88%), mp 201°C; $[\alpha]_D$ −35° (*c* 1, H_2O); ^1H nmr (DMSO-d_6 + D_2O) δ: 5.14 (dd, ~0.6H, $J_{1,2} \approx 1.5$, $J_{1,F} = 8$ Hz, H-1α), 4.69 (d, ~0.4H, $J_{1,F} = 22$ Hz, H-1β), 4.57 (dnm, ~0.4H, $J_{2,F} \approx 51$ Hz, H-2β), 4.51 (dnm, ~0.6H, $J_{2,F} = 49.3$ Hz, H-2α), 4.07 (q, ~0.6H, $J_{5,6} = 6.4$ Hz ($J_{4,5} < 1$ Hz), H-5α), 3.5-region (m, H-3,4,5β), 1.18 and 1.14 (2 d, total intensity 3H, $J = 6.4$ Hz, *C*-Me); *m/z*: 166 (100%, $M^+ + 1 -$ HCl), 148 (47%, $M^+ + 1 -$ HCl − H_2O). Anal. calcd. for $C_6H_{13}ClFNO_3 \cdot H_2O$ (219.6): C 32.81, H 6.88, N 6.38; found: C 32.65, H 6.88, N 6.33.

2,3,6-Trideoxy-2-fluoro-3-trifluoroacetamido-α-L-talopyranose (7)

Trifluoroacetic anhydride (2.45 mL) in dry ether (10 mL) was added dropwise at 0°C to a magnetically stirred suspension of **6** (350 mg) in dry ether (20 mL). Cooling was discontinued after 45 min and the solution kept at room temperature for 2.5 h, after which time tlc (solvent A) revealed the complete conversion of **6** (R_f 0.15) into a single, new product (R_f 0.5). The excess of reagent was removed by coevaporation with several added portions of ether. To reverse *O*-acylation, a solution of the residue in dry methanol (30 mL) was first rendered slightly alkaline (pH ~ 8) with methanolic 0.5 M $NaOCH_3$ and, after 1 h, the pH was adjusted to 7 with a few drops of acetic acid in methanol. Concentration of the mixture followed by column chromatography (solvent D) afforded **7** (410 mg, 91%), mp 134–135°C; $[\alpha]_D$ −51° (*c* 1, Me_2CO); ν_{max}^{KBr}: 3400, 1715, 1530 cm^{-1}; ^1H nmr (acetone-d_6) δ: 8.06 (br, exchangeable, NH), 6.01 (dd, exchangeable, $J_{OH,F} = 2.5$, $J_{1,OH} = 4.5$ Hz, OH-1), 5.29 (ddd (dd after D_2O exchange), $J_{1,2} = 1.7$, $J_{1,F} = 8.6$ Hz, H-1), 4.57 (d of septets, $J_{2,F} = 49.3$, $J_{2,4} = 1.2$, $J_{1,2} = 1.8$, $J_{2,3} = 3$ Hz, H-2), 4.43 (dt (t after D_2O exchange), 0.5H, $J_{2,3} = J_{3,4} = 3$, $J_{3,NH} = 8.3$ Hz, downfield part of ddt for H-3, with upfield part coinciding with the H-5 signal; $J_{3,F} \approx 33$ Hz), 4.32 (qd, $J_{4,5} = 1.6$, $J_{5,6} = 6.6$ Hz, H-5), 3.63 (d, ($J_{4,OH} \approx 10$ Hz) of nm with $W \approx 6$ Hz; nm after D_2O exchange, H-4), 3.26 (dd, exchangeable, $J_{F,OH} = 3.9$, $J_{4,OH} = 9.9$ Hz, OH-4), 1.21 (d, 3H, $J = 6.6$ Hz, *C*-Me). Upon the addition of D_2O to the sample solution (to produce the exchange phenomena just listed), the spectrum showed a set of additional (weak) signals, attributable to the β-anomer arising by anomerization; ^{13}C nmr (50.29 MHz, acetone-d_6) δ: 157.7 (q, $^2J_{F,C} = 38$ Hz, CF_3CO), 116.7 (q, $^1J_{F,C} \approx 290$ Hz, CF_3), 92.4 (d, $^2J_{1,F} = 30.4$ Hz, C-1), 88.7 (d, $^1J_{2,F} = 175.7$ Hz, C-2), 69.7 (s, C-4), 66.7 (s, C-5), 49.1 (d, $^2J_{F,C} = 15.6$ Hz, C-3), 16.8 (s, C-6); *m/z*: 262 (53%, $M^+ + 1$), 244 (100%, $M^+ + 1 - H_2O$). Anal. calcd. for $C_8H_{11}F_4NO_4$ (261.2): C 36.79, H 4.25, F 29.10, N 5.36; found: C 36.90, H 4.47, F 29.26, N 5.38.

1,4-Di-O-acetyl-2,3,6-trideoxy-2-fluoro-3-trifluoroacetamido-α-L-talopyranose (8)

Compound **7** (457 mg) was treated for 15 min at −17°C with acetic anhydride (12 mL) containing 1 drop of concentrated H_2SO_4. Complete conversion of the slow-moving **7** into a single product (R_f 0.55) was indicated by tlc (solvent D). The mixture was stirred with ice water and aqueous $NaHCO_3$ to decompose the excess of anhydride, and the product was extracted into $CHCl_3$. The extract was washed with water, dried (Na_2SO_4), and evaporated, and the solid residue was chromatographed on a column of SiO_2 (solvent E), to give colorless **8** (548 mg, 91%), mp 148–149°C (recrystallized from ether–hexane); $[\alpha]_D$ −110.3° (*c* 1, $CHCl_3$); ν_{max}^{KBr}: 3330 and 3260 (NH), 1750, 1550 cm^{-1}; ^1H nmr δ: 6.72 (d, $J_{3,NH} \approx 8.5$ Hz, NH), 6.32 (dd, $J_{1,2} = 1.7$, $J_{1,F} = 8.4$ Hz, H-1), 5.175 (nm, $W_H = 7$ Hz, H-4), 4.57 (ddt, $J_{2,3} = J_{3,4} = 3.5$, $J_{3,NH} = 8.7$, $J_{3,F} = 33.5$ Hz, H-3), 4.51 (d of nm, $J_{2,F} = 48$ Hz, H-2), 4.20 (qd, $J_{4,5} \approx 1$, $J_{5,6} = 6.5$ Hz, H-5), 2.18 and 2.14 (2 s, 3H each, 2 OAc), 1.19 (d, 3H, $J = 6.5$ Hz, *C*-Me); ^{13}C nmr (50.29 MHz, $CDCl_3$) δ: 171.0 and 168.4 (2 s, 2 *Me*CO), 157.0 (q, $^2J_{C,F} = 38.4$ Hz, CF_3CO), 115.4 (d, $^1J_{C,F} = 288.3$ Hz, CF_3), 90.1 (d, $^2J_{1,F} = 32.4$ Hz, C-1), 84.2 (d, $^1J_{2,F} = 182.6$ Hz, C-2), 68.1 and 67.2 (2 s, C-4,5), 46.25 (d, $^2J_{3,F} = 16.4$ Hz, C-3), 20.5 and 20.1 (2 s, 2 *CO*Me), 16.1 (s, C-6). *m/z*: 346 (1%, $M^+ + 1$), 286 (100%, $M^+ + 1 -$ AcOH). Anal. calcd. for $C_{12}H_{15}F_4NO_6$ (345.2): C 41.74, H 4.38, F 22.01; found: C 41.93, H 4.48, F 21.79.

The analogous *1,4-di-O-p-nitrobenzoate* **9**, obtained as a pale yellow solid from **7** by treatment with *p*-nitrobenzoyl chloride and pyridine, showed the following ^1H nmr data: δ: 8.35–8.20 (m, 8H, arom.), 6.81 (d, $J_{3,NH} = 7.8$ Hz, NH), 6.69 (dd, $J_{1,2} = 1.5$, $J_{1,F} = 8.5$ Hz, H-1), 5.56 (m, $W_H = 6.5$ Hz, H-4), 4.80 (ddt, $J_{2,3} \approx J_{3,4} \approx 3.5$, $J_{3,NH} = 8$, $J_{3,F} = 33$ Hz, H-3), 4.78 (d of nm, $J_{2,F} \approx 48$ Hz, H-2), 4.44 (qd, $J_{4,5} = 0.8$, $J_{5,6} = 6.5$ Hz, H-5), 1.27 (d, 3H, $J = 6.5$ Hz, *C*-Me).

Carminomycinone (30)

Aglycon **10** was prepared (9*c*,*d*) by hydrolysis of carminomycin hydrochloride with aqueous 0.1 M HCl (30 min at 100°C). The red crystalline precipitate was washed well with water and dried in a desiccator; mp 235–236°C (lit. (9*c*) mp 233–235°C); ^1H nmr (200 MHz) δ: 13.43, 12.91, and 12.13 (3 s, 3 phenolic OH), 7.85, 7.68, and 7.28 (dd, t, and dd, 1H each, $J = 1.25$ and 8 Hz, H-1,2,3), 5.26 (m (dd after D_2O exchange), $J_{7,8e} = 2$, $J_{7a,8a} = 5$ Hz, H-7), 4.61 (s, exchangeable, OH-9), 3.93 (d, exchangeable, $J_{7,OH} = 6.6$ Hz, OH-7), 3.17 (dd, $J_{8e,10e} = 2$, $J_{10a,10e} = 18.6$ Hz, H-10e), 2.94 (d, $J = 18.6$ Hz, H-10a), 2.39 (s, 3H, CH_3-14), 2.32 (dt, $J_{7,8e} = J_{8e,10e} = 2$, $J_{8a,8e} = 14.5$ Hz, H-8e), 2.14 (dd, $J_{7a,8e} = 5$, $J_{8a,8e} = 14.5$ Hz, H-8a).

Can. J. Chem. Downloaded from www.nrcresearchpress.com by 195.138.81.100 on 09/07/12
For personal use only.

Can. J. Chem. Downloaded from www.nrcresearchpress.com by 195.138.81.100 on 09/07/12
For personal use only.

*7-O-(4-O-Acetyl-2,3,6-trideoxy-2-fluoro-3-trifluoroacetamido-α-L-talopyranosyl)-carminomycinone (**11**)*

Aglycon **10** was dried overnight at 110°C in an oil-pump vacuum, and the solvents CH_2Cl_2 and ether were bidistilled from P_2O_5 and NaH, respectively. The reaction flask and granular molecular sieve 4A (3 g) contained therein were flame-dried and allowed to cool in a desiccator. The reaction was performed under N_2 with strict exclusion of atmospheric moisture. A solution of **8** (380 mg, 1.1 mmol) in CH_2Cl_2 (10 mL) and ether (8 mL) was placed over the molecular sieve, the mixture was cooled to −40°C, and trimethylsilyl triflate (0.84 mL) was introduced rapidly by syringe. The mixture was then stirred at 0°C for 1 h before **10** (525 mg, 1.4 mmol) in CH_2Cl_2 (15 mL) was added. Stirring was then continued at room temperature, and the reaction was monitored by tlc (solvent D), which revealed a gradual consumption of **8** (R_f 0.45) and **10** (R_f 0.1), and formation of **11** (R_f 0.33) as the main product accompanied by traces of a minor product (R_f 0.25). A moderate proportion of **8** appeared unreacted after 24 h; therefore, the mixture was cooled again to −40°C and stirred for 15 min with added trimethylsilyl triflate (0.1 mL), and **10** (100 mg) was then added at 0°C. Stirring was continued for a further 24 h at 25°C, but some **8** still persisted. The mixture was processed by shaking with ethyl acetate (150 mL) and saturated, aqueous $NaHCO_3$ (50 mL). The phases were separated, and the aqueous phase was extracted exhaustively with ethyl acetate. The combined organic phases were dried ($MgSO_4$) and evaporated, and the residue was chromatographed on a column (30 g of SiO_2) with solvent E, to give unreacted **8** (125 mg, 33% recovery) followed by **11** (374 mg, 51%; 75.6% taking into account the recovered **8**). Compound **11** was a red powder, mp 156–166°C; $[\alpha]_D$ +168° (*c* 0.5, $CHCl_3$); ν_{max}^{KBr}: 3520, 3440, 3320 (br), 1730, 1600 cm^{-1}; ^1H nmr δ: 13.35, 12.90, and 12.05 (3 s, 3 phenolic OH), 7.87, 7.70, and 7.31 (dd, t, and dd, $J \approx 1$ and 8 Hz, H-1,2,3), 6.71 (d, $J_{3',NH}$ = 8.3 Hz, NH), 5.58 (dd, $J_{1',2'}$ = 1.2, $J_{1',F} \approx 8$ Hz, H-1′), 5.27 (dd, $J_{7,8e} = 2$, $J_{7,8a} = 4.5$ Hz, H-7), 5.18 (nm, $W \approx 4$ Hz, H-4′), 4.65 and 4.49 (2 nm, 0.5H each, $J_{2',F}$ = 48.6 Hz, H-2′), 4.38 (qd, $J_{4',5'} \approx 1$, $J_{5',6'}$ = 6.5 Hz, H-5; the outer parts of the H-5 signal were overlapped by two dt, 0.5H each, for H-3′, with $J_{2',3'} \approx J_{3',4'} \approx 3$, $J_{3',NH} = 8$, $J_{3',F} \approx 34$ Hz), 3.85 (s, exchangeable, OH-9), 3.24 (dd, $J_{8e,10e}$ = 1.9, $J_{10a,10e}$ = 19 Hz, H-10e), 2.97 (d, J = 19 Hz, H-10a), 2.41 (s, 3H, CH_3-14), 2.36 (dnm, with downfield nm partly obscured by CH_3-14 signal, $J_{8a,8e} \approx 16$ Hz, $J_{7,8e}$ and $J_{8e,10e} \approx 1$–2 Hz, H-8e), 2.19 (s, 3H, AcO-4′, superposed on H-8a signal), 1.23 (d, 3H, J = 6.5 Hz, CH_3-6′); ^{13}C nmr (75.43 MHz, $CDCl_3$, assignments by aid of ADEPT experiment): (a) aglycon, δ: 210.3 (C-13), 190.1 and 185.7 (C-5,12), 162.3, 156.3, and 156.1 (C-4,6,11), 137.0, 124.8, and 119.6 (C-1,2,3), 136.4, 132.9, and 132.5 (C-6a,10a,12a), 115.6, 111.3, and 110.4 (C-4a,5a,11a), 76.0 (C-9), 71.3 (C-7), 35.4 and 33.2 (C-8,10), 24.6 (C-14); (b) carbohydrate moiety, δ: 170.8 (*Me*CO), 100.2 (d, $^2J_{1',F}$ = 31.4 Hz, C-1′), 85.1 (d, $^1J_{2',F}$ = 179.7 Hz, C-2′), 68.7 (s, C-4′), 65.9 (s, C-5′), 46.7 (d, $^2J_{3',F}$ = 16.2 Hz, C-3′), 20.6 (*CO*Me), 16.4 (s, C-6′). Quartets near δ 157 and 115 for the CF_3CO group were too weak to be accurately determinable. Anal. calcd. for $C_{30}H_{27}F_4NO_{12}$ (669.5): C 53.82, H 4.07, N 2.09; found: C 53.89, H 4.11, N 1.98.

*7-O-(3-Amino-2,3,6-trideoxy-2-fluoro-α-L-talopyranosyl)-carminomycinone (**4**, (R)-2′-fluorocarminomycin) and its hydrochloride **4**a*

To a solution of **11** (360 mg) in methanol (50 mL) was added methanolic 1 M $NaOCH_3$ (5 mL), at room temperature, whereby the orange-red solution turned deep purple. After 1 h, saponification of **11** (R_f 0.4) to (*R*)-2′-fluoro-*N*-trifluoroacetylcarminomycin **12** (R_f 0.25) was complete (tlc with solvent D). The solution was neutralized with methanolic acetic acid, and evaporated, to give crude **12** as a brown solid. The solid was dissolved under N_2 in a saturated, aqueous $Ba(OH)_2$ solution (20 mL) at 25°C. After 30 min the purple mixture was neutralized by addition of solid carbon dioxide until an orange color persisted, diluted with water (10 mL), and extracted exhaustively with $CHCl_3$. The red extracts were dried ($MgSO_4$) and evaporated to give a brownish-purple solid that was triturated with a little fresh $CHCl_3$, isolated by suction filtration, and dried. The product (**4**-monohydrate, 244 mg, 82.6%) showed an elongated spot (R_f 0.5–0.25) and a minor impurity (R_f 0.7) in tlc (solvent C); mp 217–219°C, ν_{max}^{KBr}: 3500, 3400, 1715, 1600 cm^{-1}; ^1H nmr δ: 7.87, 7.70, and 7.31 (dd, t, and dd, $J \approx 1$ and 8 Hz, H-1,2,3), 5.53 (dd, $J_{1',2'} \approx 1$, $J_{1',F} \approx 8.5$ Hz, H-1′), 5.28 (nm, H-7), 4.62 and 4.38 (2 nm, 0.5H each, $J_{2',F}$ = 48.5 Hz, H-2′), 4.16 (q, $J_{5',6'}$ = 6.5 Hz, H-5′), 3.48 (nm, H-4′), 3.23 (dd, $J_{8e,10e} \approx 1.5$, $J_{10a,10e}$ = 19 Hz, H-10e), 2.97 (d, J = 19 Hz, H-10a, superposed on cm for H-3′), 2.40 (s, 3H, CH_3-14, superposed on m for H-8e), 2.17 (dd, $J_{7,8a}$ = 4, $J_{8a,8e}$ = 15 Hz, H-8a), 1.35 (d, 3H, J = 6.4 Hz, CH_3-6′). Anal. calcd. for $C_{26}H_{26}FNO_{10}\cdot H_2O$ (549.5): C 57.77, H 5.03, N 2.59; found: 57.88, H 5.02, N 2.40.

For preparation of the *hydrochloride* **4***a*, a solution of **4** in 0.1 M HCl (40 mL) was first extracted with ethyl acetate for removal of the aforementioned impurity (R_f 0.7), and then evaporated to dryness with additions of ethanol and benzene. The red solid obtained gave a single spot (R_f 0.2) in tlc (solvent B). It was recrystallized from ethanol–ether and dried *in vacuo* over KOH, and weighed 173 mg (82.6%); mp 217–218°C (with sintering from 206°C); $[\alpha]_D$ +214 ± 15° (*c* 0.05, CH_3OH); ν_{max}^{KBr}: 3400 (br), 1710, 1610 cm^{-1}; ^1H nmr (DMSO-d_6) δ: 7.83 (m, 2H) and 7.43 (d, J = 7.4 Hz) for H-1,2,3; 5.60 (s, exchangeable, OH-9), 5.41 (dd, $J_{1',2'}$ = 1.1, $J_{1',F}$ = 9.7 Hz, H-1′), 5.31 (d, $J_{4',OH}$ = 6.5 Hz, exchangeable, OH-4′), 5.06 (nm, H-7), 4.64 and 4.47 (2 nm, 0.5 H each, $J_{2',F}$ = 49.2 Hz, H-2′), 4.32 (~q, $J_{5',6'}$ = 6.6 Hz, H-5′), 3.62 (m, $W_H \approx 14$ Hz, narrowed further after D_2O exchange, H-4′), 3.4 (H-3′, signal partly obscured by DOH peak), 2.96 (AB-q, 2H, H-10a,e), 2.30 (s, 3H, CH_3-14), 2.18 (m, 2H, H-8a,e), 1.22 (d, 3H, J = 6.6 Hz, CH_3-6′); ^{13}C nmr (50.23 MHz, DMSO-d_6): (a) aglycon, δ: >200 (C-13, not observed), 190.3 and 186.3 (C-5,12), 161.7, 156.3, and 155.7 (C-4,6,11), 137.7, 124.9, and 119.3 (C-1,2,3), 137.1, 134.5, and 133.2 (C-6a,10a,12a), 116.0, 111.0, and 110.1 (C-4a,5a,11a), 74.7 (C-9), 70.8 (C-7), ~37.5 and 31.5 (C-8,10), 24.2 (C-14); (b) carbohydrate moiety, δ: 99.0 (d, $^2J_{1',F}$ = 31 Hz, C-1′), 80.4 (d, $^1J_{2',F}$ = 185 Hz, C-2′), 66.2 (C-4′), 65.6 (C-5′), 54.5 (d, $^2J_{3',F}$ = 16 Hz, C-3′), 16.2 (C-2′).

Acknowledgments

Financial support by the Natural Sciences and Engineering Research Council of Canada and through a NATO Grant for International Collaboration (CRG 890759) is gratefully acknowledged. Dr. T. W. Doyle, Director, Pharmaceutical Research and Development Division, Bristol-Myers Company, is thanked for a generous donation of carminomycin and for arranging the biological tests, and Drs. A. Crosswell and J. E. Schurig of the same company are thanked for performing the tests.

1. H. H. Baer and A. Jaworska-Sobiesiak. Carbohydr. Res. **140**, 201 (1985).
2. D. Horton and W. Priebe. U.S. Patent 4,427,664 (1984); Chem. Abstr. **100**, 192218 (1984); Carbohydr. Res. **136**, 391 (1985); D. Horton, W. Priebe, and O. Varela. Carbohydr. Res. **130**, c1 (1984); **144**, 305 (1985).
3. D. Horton, W. Priebe, and W. R. Turner. Carbohydr. Res. **94**, 11 (1981), and references cited therein; D. Horton and W. Priebe. *In* Anthracycline antibiotics. *Edited by* H. S. El Khadem. Academic Press, New York. 1982. pp. 197–224; D. Horton, W. Priebe, and O. Varela. J. Antibiot. **37**, 853 (1984).
4. H. H. Baer and L. Siemsen. Can. J. Chem. **66**, 187 (1988).
5. S. Castillon, A. Dessinges, R. Faghih, G. Lukacs, A. Olesker, and T. T. Thang. J. Org. Chem. **50**, 4913 (1985).
6. H. H. Baer, F. Hernández Mateo, and L. Siemsen. Carbohydr. Res. **195**, 225 (1990).
7. K. Ok, Y. Takagi, T. Tsuchiya, S. Umezawa, and H. Umezawa. Carbohydr. Res. **169**, 69 (1987).
8. F. Arcamone. Doxorubicin, anticancer antibiotics. Medicinal Chemistry monograph series, Vol. 17. Academic Press, New York. 1981. pp. 333–336; G. Cassinelli, A. Grein, P. Masi, A. Suarato, L. Bernardi, F. Arcamone, A. Di Marco, A. M.

CASAZZA, G. PRATESI, and C. SORANZO. J. Antibiot. **31**, 178 (1978).

9. (*a*) M. G. BRAZHNIKOVA, V. B. ZBARSKY, N. P. POTAPOVA, Y. N. SCHEINKER, T. F. VLASOVA, and B. V. ROZYNOV. Antibiotiki (Moscow), **18**, 1059 (1973); (*b*) M. G. BRAZHNIKOVA, V. B. ZBARSKY, U. I. PONOMARENKO, and N. P. POTAPOVA. J. Antibiot. **27**, 254 (1974); (*c*) M. C. WANI, H. L. TAYLOR, M. E. WALL, A. T. MCPHAIL, and K. D. ONAN. J. Am. Chem. Soc. **97**, 5955 (1975); (*d*) G. R. PETTIT, J. J. EINCK, C. L. HERALD, R. H. ODE, R. B. VON DREELE, P. BROWN, M. G. BRAZHNIKOVA, and G. F. GAUSE. J. Am. Chem. Soc. **97**, 7387 (1975).
10. F. ARCAMONE, S. PENCO, A. VIGEVANI, S. REDAELLI, G. FRANCHI, A. DIMARCO, A. M. CASAZZA, T. DASDIA, F. FORMELLI, A. NECCO, and C. SORANZO. J. Med. Chem. **18**, 703 (1975); D. HORTON, W. PRIEBE, and M. SZNAIDMAN. Carbohydr. Res. **187**, 145 (1989).
11. Y. KIMURA, M. SUZUKI, T. MATSUMOTO, R. ABE, and S. TERASHIMA. Bull. Chem. Soc. Jpn. **59**, 423 (1986).
12. L. PHILLIPS and V. WRAY. J. Chem. Soc. (B), 1618 (1971); J. Chem. Soc. Perkin Trans. 2, 928 (1974); J. W. EMSLEY, L. PHILLIPS, and V. WRAY. Prog. Nucl. Magn. Reson. Spectrosc. **10**, 83 (1976).
13. A. A. PENGLIS. Adv. Carbohydr. Chem. Biochem. **38**, 195 (1981); R. CSUK and I. GLÄNZER. Adv. Carbohydr. Chem. Biochem. **46**, 73 (1988).
14. V. WRAY. J. Chem. Soc. Perkin Trans. 2, 1598 (1976).

Can. J. Chem. Downloaded from www.nrcresearchpress.com by 195.138.81.100 on 09/07/12
For personal use only.

The chlorination of propiophenone; determination of pK_a value and of the course of the reaction

J. Peter Guthrie[1] and John Cossar

Department of Chemistry, University of Western Ontario, London, Ont., Canada N6A 5B7

Received December 11, 1989[2]

J. Peter Guthrie and John Cossar. Can. J. Chem. **68**, 2060 (1990).

Chlorination of propiophenone in alkaline aqueous solution leads to formation of α-hydroxypropiophenone as the first detectable intermediate; this undergoes slower oxidation to aromatic acids without any accumulation of further intermediates. From the rates of the initial chlorination we have been able to determine the pK_a value as 17.56 ± 0.51.

Key words: propiophenone, chlorination, hydrolysis, rearrangement, pK_a.

J. Peter Guthrie et John Cossar. Can. J. Chem. **68**, 2060 (1990).

La chloration de la propiophénone en solution aqueuse alcaline conduit à la formation de l'α-hydroxypropiophénone en tant que premier intermédiaire décelable; ce composé s'oxyde lentement en acides aromatiques sans accumulation subséquente d'intermédiaires. La mesure des vitesses de chloration initiale nous a permis de déterminer un pK_a de 17,56 ± 0,51.

Mots clés : propiophénone, chloration, hydrolyse, transposition, pK_a.

[Traduit par la revue]

Can. J. Chem. Downloaded from www.nrcresearchpress.com by 91.121.58.235 on 09/07/12
For personal use only.

Introduction

We have developed a method for determining pK_a values of simple ketones by analysis of the kinetics of chlorination in alkaline solution (1, 2). This method has been applied to a series of ring-substituted acetophenones (3). We now wish to report its application to propiophenone. Propiophenone is known to undergo halogenation followed by cleavage to benzoic acid (4). This was believed to involve formation of α,α-dihalopropiophenone, followed by hydrolysis and oxidative cleavage (5). We now find that, at least under the conditions we use for kinetics, the actual reaction course is different, and that propiophenone undergoes one rapid chlorination, followed by rapid hydrolysis that competes with the second chlorination, and then slow further oxidation of the α-hydroxypropiophenone. Furthermore, the oxidation products include not just benzoic acid but mandelic acid, atrolactic acid, and phenylglyceric acid (6).

Results

In Table 1 are the results of our kinetics studies of propiophenone. This reaction at first appeared deceptively simple because the absorbance–time curves could be fitted to an integrated rate law, eq. [1], with a single exponential followed by a linear decrease in absorbance; see Fig. 1. We have not identified the process responsible for the slow decrease in absorbance at long times. If this were followed to completion we assume that it would become nonlinear, and probably exponential, but the time required would be inordinately long. For the length of time that we did follow the reaction, the slow final phase was satisfactorily linear, as shown by the behavior of the residuals plot. However closer examination of the data

$$[1] \quad \text{Absorbance} = a_1 + a_2 \exp(-a_3 t) + a_4 t$$

showed that there were consistent deviations of calculated from experimental absorbance values in the sense to be expected if there were a faster process with a small amplitude. The data gave a better fit to an integrated rate law with two exponential terms, eq. [2]; see Fig. 2. In Fig. 2 the quantity labeled log $(A - A_\infty)$ is corrected by subtracting subsequent terms in the rate law.

$$[2] \quad \text{Absorbance} = a_1 + a_2 \exp(-a_3 t) + a_4 \exp(-a_5 t) + a_6 t$$

Thus in terms of eq. [1] we plot log (Absorbance $- a_1 - a_4 t$), and in terms of eq. [2] we plot log (Absorbance $- a_1 - a_6 t$) or log (Absorbance $- a_1 - a_4 \exp(-a_5 t) - a_6 t$). The key indication that eq. [1] is inadequate and eq. [2] is satisfactory comes from examination of the residuals plots, of $A_{obs} - A_{calc}$, in Fig. 2. In Fig. 2a there is a clear pattern of deviations, first negative, then positive, then negative again, which are large relative to the noise level in the residuals plot; by contrast, in Fig. 2b the residuals curve shows no deviations from the zero line that are consistently greater than the noise level. Now that microcomputers provide convenient access to computational power and graphics display, use of residuals plots should be seen as an essential part of data analysis, to confirm that the fitting process truly accounts for all systematic variations in the data, leaving only random noise.

The observation of an integrated rate law with two exponentials implies the accumulation of an intermediate. Product isolation experiments at a time when most of the propiophenone had reacted but much of the intermediate had not been consumed gave a mixture, which was shown by nmr analysis and chromatographic isolation to have 2-hydroxy-1-phenyl-1-propanone, HPP,[3] as the major component and the only neutral material present besides residual propiophenone. HPP was identified by comparison with an authentic sample, and with spectroscopic data from the literature. The nmr spectrum of the isolated material showed no sign of 1-hydroxy-1-phenyl-2-propanone, HPA. When the reaction was followed by hplc analysis of samples quenched at suitable times it was found that propiophenone disappeared rapidly, with HPP as the only detectable neutral product. However, these experiments were done with ketone in excess, so that hypochlorite was totally consumed. There was a subsequent reaction of the HPP, which represents base-catalyzed isomerization to HPA.

The presence of HPP implies rapid hydrolysis of 2-chloro-1-phenyl-1-propanone, CPP. To confirm this we prepared a sample of CPP and demonstrated that it undergoes rapid hydroxide-catalyzed hydrolysis: see Table 2. The second-order rate

[1]Author to whom correspondence may be addressed.

[2]Revision received July 13, 1990.

[3]Abbreviations used: Prop, propiophenone; HPP, 2-hydroxy-1-phenyl-1-propanone; HPA, 1-hydroxy-1-phenyl-2-propanone; CPP, 2-chloro-1-phenyl-1-propanone.

TABLE 1. Kinetics of chlorination of propiophenone[a]

[Ketone] (10^4 M)	[OCl^-] (10^4 M)	[OH^-] (M)	a_1	a_2	a_3 (10^4 s^{-1})	a_4	a_5 (10^4 s^{-1})	a_6 (10^6 A s^{-1})	l	n	f
0.647	37.1	0.0489	1.181	0.029	9.89 (0.64)	0.143	2.13 (0.029)	−0.43 (0.009)	1	5.5	0.71
0.301	19.3	0.0490	1.250	−0.013	7.48 (2.46)	0.170	2.00 (0.028)	−0.46 (0.007)	2	5.4	0.86
0.155	9.39	0.0490	1.499	−0.053	5.57 (0.54)	0.264	1.51 (0.027)	−0.65 (0.007)	5	5.7	0.99
0.0752	4.54	0.0490	1.456	−0.054	4.76 (0.48)	0.252	1.062 (0.019)	−0.69 (0.005)	10	5.5	1.06
0.0744	4.58	0.0999	1.475	−0.050	7.40 (0.75)	0.244	1.64 (0.024)	−0.56 (0.006)	10	5.4	1.06
0.151	9.71	0.0997	1.571	−0.067	8.49 (1.32)	0.270	2.67 (0.076)	−0.60 (0.011)	5	5.6	0.99
0.289	19.6	0.0994	1.278	−0.015	13.55 (4.21)	0.162	3.27 (0.032)	−0.32 (0.005)	2	5.2	0.91
0.647	39.8	0.0986	1.292	0.020	3940. (19750)	0.148	4.16 (0.0002)	−0.30 (0.00)	1	5.4	0.95
0.642	39.3	0.196	1.277	0.010	18.74 (6.31)	0.141	7.18 (0.125)	−0.82 (0.022)	1	4.7	0.63
0.287	19.7	0.196	1.296	−0.026	23.27 (4.11)	0.160	6.45 (0.115)	−0.93 (0.022)	2	4.6	0.95
0.151	9.56	0.196	1.549	−0.055	18.86 (2.05)	0.252	4.52 (0.073)	−1.44 (0.017)	5	5.4	1.05
0.0742	4.83	0.196	1.579	−0.036	12.93 (4.96)	0.216	2.76 (0.048)	−1.25 (0.018)	10	4.9	1.03
0.0745	4.73	0.426	1.580	−0.071	24.05 (1.68)	0.224	7.35 (0.091)	−0.93 (0.023)	10	3.8	1.31
0.151	10.0	0.430	1.669	−0.066	39.54 (3.70)	0.223	10.88 (0.19)	−1.23 (0.050)	5	3.9	1.14
0.290	19.1	0.430	1.269	−0.051	40.87 (4.81)	0.171	15.28 (0.45)	−0.69 (0.048)	2	3.9	0.98
0.652	38.8	0.431	1.279	−0.002	7.11 (119.)	0.140	15.91 (0.40)	−0.82 (0.073)	1	4.0	
20.8	1.47	0.0196	0.0139	−1.791	6.949 (0.384) 0.491 (0.027)[d]	1.762	0.9082 (0.333)	[c]			
10.4	1.18	0.0196	0.0167	−3.214	3.993 (0.162) 0.453 (0.018)[d]	3.183	0.949 (0.0245)	[c]			
10.5	1.19	0.0099	0.1125	−2.163	2.903 (0.181) 0.329 (0.021)[d]	2.046	0.621 (0.0503)	[c]			
10.2	1.15	0.0384	0.0014	−4.956	6.089 (0.213) 0.687 (0.024)[d]	4.935	1.817 (0.0703)	[c]			

[a]In aqueous solution at 25°C, ionic strength 1.0 (KCl). Followed by absorbance measurements at 292 nm unless otherwise stated. Absorbance–time data were fitted to $y = a_1 + a_2 \exp(-a_3 t) + a_4 \exp(-a_5 t) + a_6 t$. n is the stoichiometry, calculated from eq. [3]. f is the fraction of CPP that undergoes hydrolysis to HPP, calculated from eq. [4].
[b]Not included in the least-squares fit to eq. [4] (Table 3).
[c]Followed by hplc. Peak integration – time data were fitted to $y = a_1 + a_2 \exp(-a_3 t) + a_4 \exp(-a_5 t)$.
[d]k_{II}[OCl], calculated from κ_ψ*[OCl]/[ketone], for comparison with uv kinetics.

constant for this hydrolysis is 1.45 ± 0.06 M^{-1} s^{-1}. This is similar to the rate constant observed for monochloroacetone, i.e., 1.19 M^{-1} s^{-1} (2). Clearly, hydrolysis of CPP is fast relative to subsequent reactions of hydroxypropiophenone. The actual chlorination is normally slower than enolate formation (7, 8), so that the overall kinetics are first order in [OCl^-] except at very high [OCl^-]. The rate constant for enolate formation is 0.026 M^{-1} s^{-1} (see below), which is almost 100 times slower than that for hydrolysis, and the overall chlorination reaction will be slower still at the hypochlorite concentrations used for kinetics.

Following the kinetics of propiophenone chlorination by uv spectroscopy at the absorbance maximum for hypochlorite was not completely satisfactory because the initial rapid reaction was accompanied by only a small change in absorbance, which changed from an increase to a decrease with changing reagent concentrations. Under conditions where the absorbance change was very small, the rate of the initial reaction could not be determined reliably at the λ_{max} of the hypochlorite. The initial reaction could be followed by hplc, where we could cleanly follow disappearance of propiophenone or appearance of HPP, the only observable intermediate under the conditions employed. However, it was only feasible to use this technique with low concentrations of hypochlorite and ketone in excess, in order to have amounts of products that could be accurately measured. If the hypochlorite concentrations were high, then the rates became too fast for sampling. These data are also found in Table 1.

The minimum mechanism for these kinetics is shown in Scheme 1. For the overall reaction described by Scheme 1 we can derive an equation for the absorbance as a function of time. We start with the differential equations, [3], where k_{13} is the steady-state rate constant for conversion of propiophenone into CPP, n is the number of moles of hypochlorite consumed per mole of propiophenone, and f is the fraction of CPP that is hydrolyzed to HPP rather than undergoing a second chlorination.

$$\text{[3]}\quad \begin{aligned} d[\text{Prop}]/dt &= -k_{13}[\text{Prop}] \\ d[\text{HPP}]/dt &= k_{13} f[\text{Prop}] - k_{45}[\text{HPP}] \\ d[OCl^-]/dt &= -k_{13}[\text{Prop}](1 + (1-f)(n-1)) \\ &\quad - k_{45}[\text{HPP}](n-1) \end{aligned}$$

Integration, and substitution into the equation for the total absorbance, Absorbance = $\epsilon_{\text{Prop}}[\text{Prop}]l + \epsilon_{\text{HPP}}[\text{HPP}]l + \epsilon_{\text{OCl}}[\text{OCl}]l$, leads to eq. [4]:

$$\begin{aligned} \text{[4]}\quad \text{Absorbance} &= \epsilon_{\text{OCl}}\{[\text{OCl}]_0 - n[\text{Prop}]_0\}l \\ &+ [\text{Prop}]_0 l\{\epsilon_{\text{Prop}} - \epsilon_{\text{HPP}} k_{13} f/(k_{13} - k_{45}) \\ &\quad + \epsilon_{\text{OCl}}(n - k_{13} f(n-1)/(k_{13} - k_{45}))\} \exp(-k_{13} t) \\ &+ [\text{Prop}]_0 l\{\epsilon_{\text{HPP}} k_{13} f/(k_{13} - k_{45}) \\ &\quad + \epsilon_{\text{OCl}} k_{13} f(n-1)/(k_{13} - k_{45})\} \exp(-k_{45} t) \\ &= \text{Absorbance}_0 + \alpha \exp(-k_{13} t) + \beta \exp(-k_{45} t) \end{aligned}$$

from which we can derive expressions for n and f:

Can. J. Chem. Downloaded from www.nrcresearchpress.com by 91.121.58.235 on 09/07/12
For personal use only.

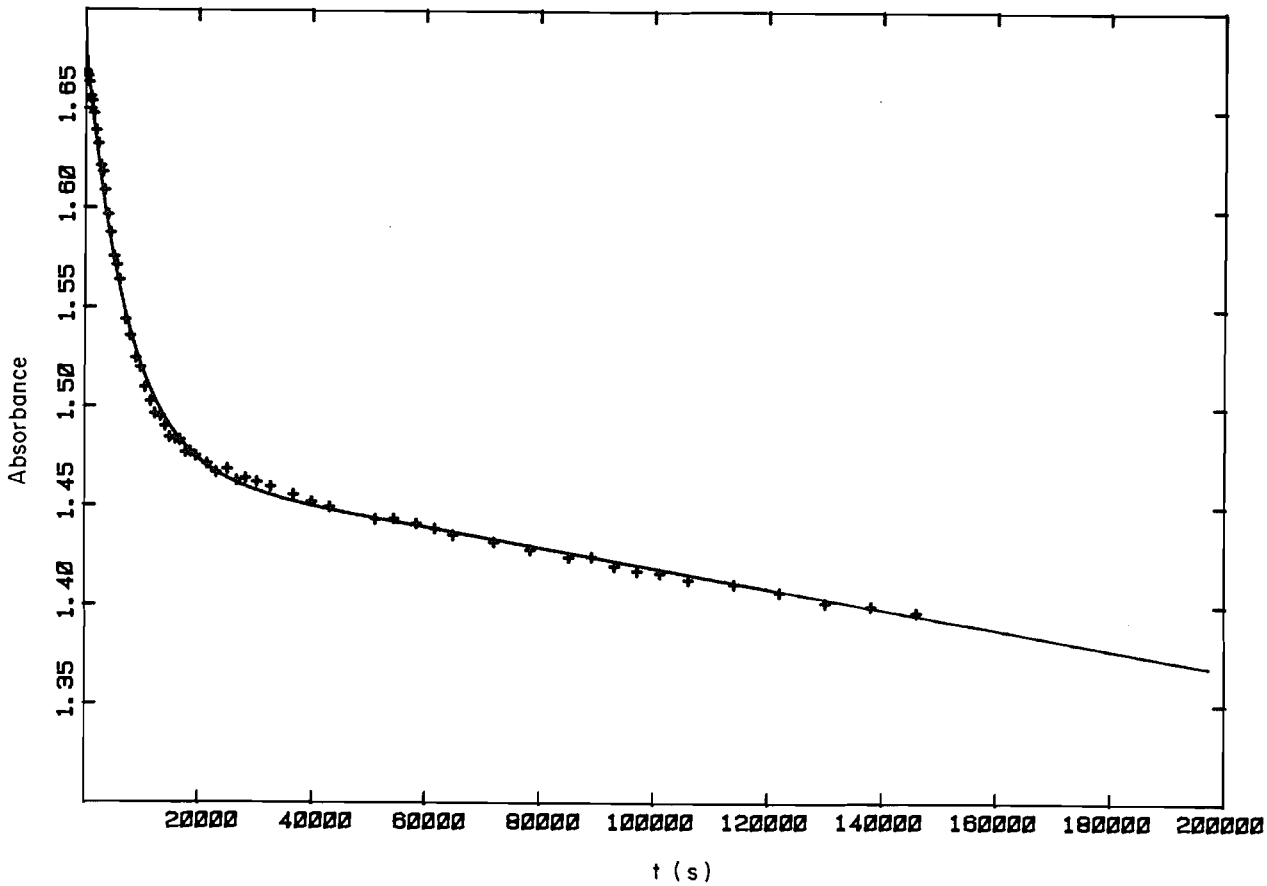

FIG. 1. Chlorination of propiophenone; absorbance–time curve for the reaction of 7.44×10^{-6} M propiophenone with 4.58×10^{-4} M hypochlorite in 0.0999 M hydroxide at ionic strength 1.0. The data were fitted by least squares to $A = a_1 + a_2 \exp(-a_3 t) + a_4 t$.

[5] $$n = \{(a + b)/([\text{Prop}]_0 l) - \epsilon_{\text{Prop}}\}/\epsilon_{\text{OCl}}$$

[6] $$f = b(k_{13} - k_{45})/(k_{13}[\text{Prop}]_0 l(\epsilon_{\text{HPP}} + (n - 1)\epsilon_{\text{OCl}}))$$

Values for n and f are included in Table 1.

For substituted acetophenones we found that the first chlorination step was rate determining under the usual conditions for chlorination kinetics (3), and the observed rates followed the rate law given in eq. [7]:

[7] $$v = k_{\text{obs}}[\text{Ketone}]$$
$$k_{\text{obs}} = \{k_{\text{II}}^0 + k_{\text{II}}^-[\text{OH}^-]\}[\text{OCl}^-]$$

If the same rate law applied for k_{13} of propiophenone, then in terms of Scheme 1, $k_{\text{II}}^0 = k_{12}k_{23}^0 K_w/k_{21}K_a^{\text{HOCl}}$, and $k_{\text{II}}^- = k_{12}k_{23}^-/k_{21}$. For the initial phase of the kinetics, where the rate of chlorination of propiophenone is being followed, it was found that the pseudo-first-order rate constants for a set of experiments at fixed hydroxide concentration were not linearly dependent upon hypochlorite concentration, but showed a tendency to level off at high $[\text{OCl}^-]$. Thus for propiophenone enolate, halogenation and reprotonation are competitive. For this situation we may derive the following expression for the rate law:

[8] $$k_{\text{obs}} = k_{13} = \frac{k_{12}(k_{23}^0 K_w/K_a^{\text{HOCl}} + k_{23}^-[\text{OH}^-])[\text{OCl}^-]}{k_{21} + (k_{23}^0 K_w/([\text{OH}^-]K_a^{\text{HOCl}}) + k_{23}^-)[\text{OCl}^-]}$$

This may be transformed into a form convenient for fitting to the data:

[9] $$k_{\text{obs}} = k_{13} = (a_1 + a_2[\text{OH}^-])/(1/[\text{OCl}^-] + a_1/a_3[\text{OH}^-] + a_2/a_3)$$

where $a_1 = k_{\text{II}}^0$, $a_2 = k_{\text{II}}^-$, and $a_3 = k_{12}$. The data from Table 1 were fitted to eq. [7]. A few runs, where the uncertainties in the rate constants for the initial phase were very large, were not included in these calculations. To include the hplc data, we calculated initial "pseudo-first-order rate constants" $= k_{\text{obs}}[\text{OCl}^-]_0/[\text{Prop}]_0$; these experiments were actually done with ketone in excess. We can use the observed pseudo-first-order rate constants, defined by $v = k_{\text{obs}}[\text{OCl}]$, because the major reaction path is conversion of propiophenone to hydroxypropiophenone, which consumes only one OCl^-. In general one must remember that the observed rate constant includes the stoichiometry number for ketone in excess conditions, but not for hypochlorite in excess conditions (1). The above discussion assumes that $[\text{OCl}^-]$ is essentially constant throughout a particular kinetics experiment. Examination of the concentrations and stoichiometries in Table 1 shows that in each case, for reactions with OCl^- in excess, less than 10% of the OCl^- was consumed. We also fitted the second-order rate constants for the hplc experiments to eq. [7]. For the determination of the pK_a it was more satisfactory to use the directly measured rate constants at low $[\text{OCl}^-]$ for low $[\text{OH}^-]$ (these are data from hplc experiments) and extrapolated values at high $[\text{OH}^-]$ (these are data from uv kinetics) to give the final fit to eq. [7]. The required extrapolation was carried out by fitting data at constant $[\text{OH}^-]$ to eq. [10], and calculating the apparent second-order rate constant from the parameters so obtained.

Can. J. Chem. Downloaded from www.nrcresearchpress.com by 91.121.58.235 on 09/07/12
For personal use only.

Can. J. Chem. Downloaded from www.nrcresearchpress.com by 91.121.58.235 on 09/07/12
For personal use only.

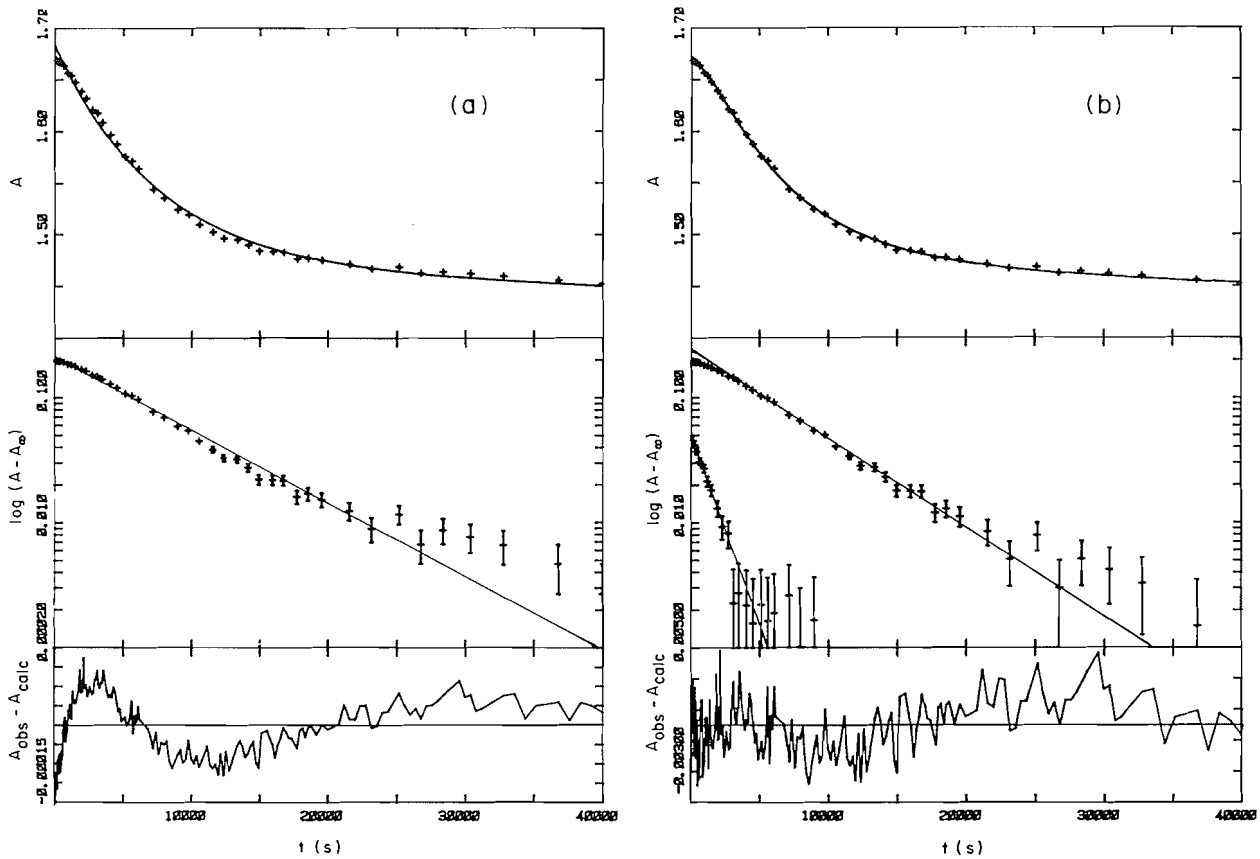

FIG. 2. Chlorination of propiophenone; absorbance–time curve for the reaction of 7.44×10^{-6} M propiophenone with 4.58×10^{-4} M hypochlorite in 0.0999 M hydroxide at ionic strength 1.0. Only data for the first 40 000 s of reaction are shown. These figures show the corresponding semilog and residuals plots as well. (a) The data were fitted to $A = a_1 + a_2 \exp(-a_3 t) + a_4 t$. (b) The data were fitted by least squares to $A = a_1 + a_2 \exp(-a_3 t) + a_4 \exp(-a_5 t) + a_6 t$. The semilog plots show $\log(A - A_0)$ corrected for subsequent terms in the rate law as described in the text.

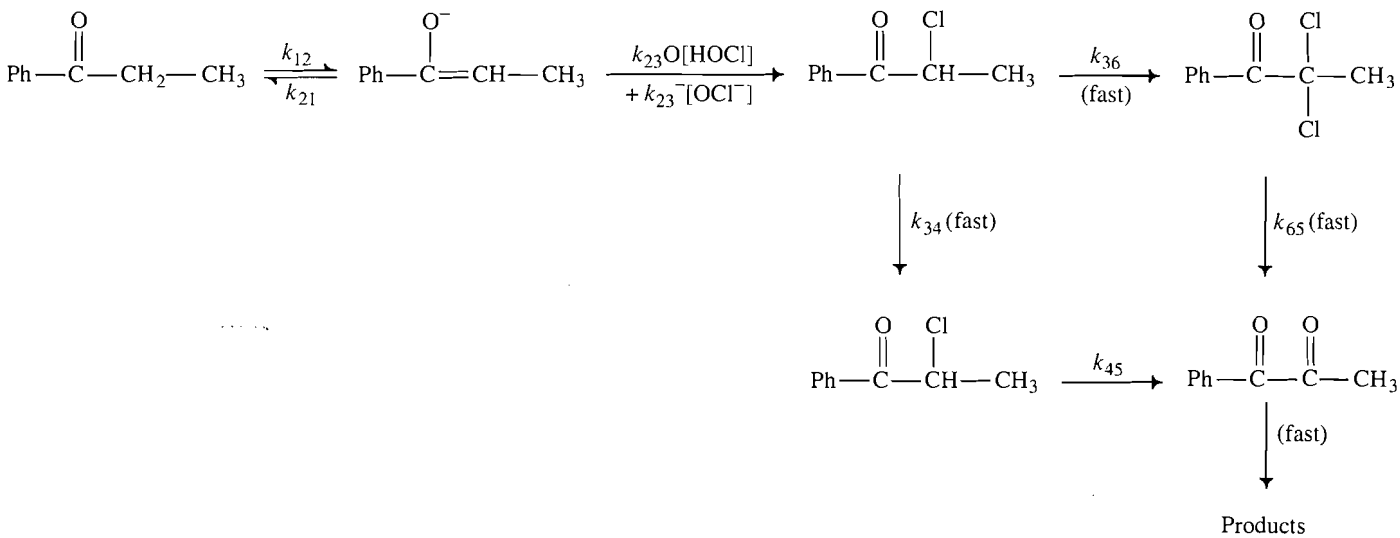

SCHEME 1

[10] $k_{obs} = b_1/(1 + b_2/[OCl^-])$

In terms of the parameters of eq. [4], $b_1 = a_3[OH^-]$, and $b_2 = a_3/(a_1 + a_3[OH^-])$. Then $b_1/b_2 = a_1 + a_2[OH^-]$. The fit to eq. [7] was largely determined by the data from hplc kinetics, but the precision of the derived parameters was improved when the extrapolated values were included. The parameters from the two sets of calculations are in good agreement. The parameters determined by least squares, and the pK_a value based on a_1, are found in Table 3. Figure 3b shows the experimental points and the surface fitted to them using eq. [7].

The kinetics of the second phase of propiophenone chlorination (Table 1) showed a clear dependence on hydroxide concentration, and seemed to depend on hypochlorite concentration as

Can. J. Chem. Downloaded from www.nrcresearchpress.com by 91.121.58.235 on 09/07/12
For personal use only.

TABLE 2. Kinetics of further reactions of α-chloro and α-hydroxy-ketones[a]

(a) Hydrolysis of α-chloropropiophenone[b]

[Ketone] (10^4 M)	$[OH^-]_{in}$ (10^4 M)	$[OH^-]_{fin}$ (10^4 M)	a_1	a_2	a_3 (10^3 s^{-1})	$a_3/[OH^-]$ (M^{-1} s^{-1})
0.0872	4.6	3.3	1.013	−0.154	0.629 (0.003)	1.37
0.0872	16.3	15.8	1.005	−0.148	2.32 (0.007)	1.43
0.0872	30.9	30.1	1.024	−0.146	4.46 (0.030)	1.44
0.143	69.2	68.3	1.652	−0.220	10.2 (0.078)	1.48
0.140	115.7	112.4	0.810[c]	−0.096	17.8 (0.12)	1.54
0.109	190.	189.	0.630[c]	−0.068	27.3 (0.24)	1.44
					avg.	1.45 (0.06)

(b) Reaction of α-hydroxypropiophenone with hypochlorite[d]

[Ketone] (10^4 M)	$[OCl^-]$ (10^4 M)	$[OH^-]$ (M)	a_1	a_2	a_3 (10^3 s^{-1})	$a_3/[OH^-]$ (M^{-1} s^{-1})	n
1.7	34.1	0.416	1.043[e]	0.289	1.60 (0.006)	0.00385	2.4
1.68	35.3	0.423	0.004[f]	2.046	1.31 (0.089)	0.0031	
0.227	4.65	0.437	1.435	0.392	1.48 (0.012)	0.0034	2.5
0.227	4.67	0.101	1.380	0.454	0.446 (0.0016)	0.00442	3.2
0.237	4.69	0.0500	1.328	0.523	0.205 (0.0008)	0.00411	3.8
1.72	35.1	0.0479	1.004	0.389	0.207 (0.0007)	0.00432	4.0
					avg.	0.00387 (0.00052)	

[a]All in aqueous solution at 25°C. Data are fitted by least squares to: Absorbance = $a_1 + a_2 \exp(-a_3 t) + a_4 t$. $k_{II} = a_3/[OH^-]$.
[b]Reactions carried out in 10-cm cells unless otherwise noted, and followed by measuring absorbance at 246 nm.
[c]5-cm cells were used.
[d]Reactions were carried out in 10-cm cells and followed by measuring absorbance at 292 nm, unless otherwise noted. n is the stoichiometry, calculated from $n = (a_2/l[HPP]_0 - \epsilon_{HPP})/\epsilon_{OCl}$.
[e]1-cm cells were used.
[f]Followed by hplc.

TABLE 3. Least-squares parameters and derived pK_a values for ketones[a]

(a) Results of least-squares fitting of kinetics of chlorination

Reaction	Equation	a_1	a_2	a_3
First phase (all data)	[7]	0.152 (0.038)	13.5 (1.65)	0.0259 (0.0042)
First phase[b]	[5]	0.140 (0.034)	11.85 (1.52)	
First phase[c]	[5]	0.150 (0.037)	11.4 (1.64)	
Second phase (HPP data)	[11]	0.00387 (0.00052)		

(b) pK_a values derived from kinetics

Compound	k_{II}^0	k_{II}^-	pK_a[d]	log k_2^-
PhCOEt	0.140 ± 0.034	11.9 ± 1.5	17.59 ± 0.51	4.67 ± 0.51

[a]All in aqueous solution at 25°C.
[b]Data at all $[OH^-]$, including values extrapolated to low $[OCl^-]$.
[c]Data at low $[OH^-]$ and low $[OCl^-]$ only.
[d]Calculated using log $k_{23}^0 = 9.23$ (1) and $pK_a^{HOCl} = 7.53$ (25).

well. However, kinetics starting with HPP (Table 2) clearly show no dependence on hypochlorite concentration. These kinetics, based on simple single exponential behavior, give inherently more reliable rate constants. The best description of the kinetics appears to be eq. [11], with $k_{OH} = 3.87 \times 10^{-3}$ M^{-1} s^{-1}. Figure 3b shows the experimental points and the surface so calculated.

$$[11] \quad k_{obs} = k_{OH}[OH^-]$$

For propiophenone the stoichiometry of the halogenation was calculated using eq. [3]; these values are given in Table 1. The total consumption of halogenating agent over the course of a reaction was greater than 3 hypochlorites per propiophenone, and appeared to approach a limit of 6. A value as high as 6 is intelligible in terms of the reactions shown in Scheme 2. The numbers in square brackets under the final products in Scheme 2 represent the number of equivalents of hypochlorite consumed to form that product.

Can. J. Chem. Downloaded from www.nrcresearchpress.com by 91.121.58.235 on 09/07/12
For personal use only.

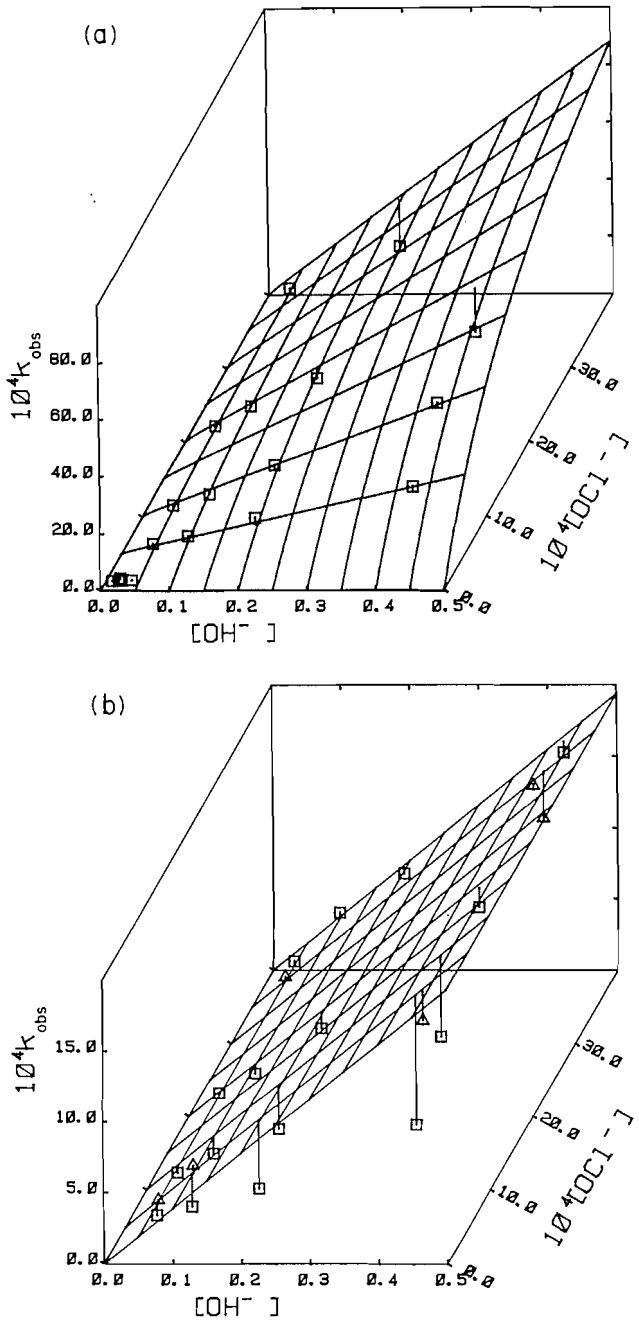

FIG. 3. Chlorination of propiophenone. (a) Initial phase; k_{obs} as a function of $[OCl^-]$ and $[OH^-]$. The surface is calculated using eq. [7], with parameters determined by least-squares fitting. (b) Second phase; k_{obs} as a function of $[OCl^-]$ and $[OH^-]$. The surface is calculated using eq. [9], with an average second-order rate constant from Table 2.

The stoichiometry number shows little dependence on $[OCl^-]$ at fixed $[OH^-]$, but shows a definite decline as $[OH^-]$ increases. The data do not really define a curve, but the high $[OH^-]$ limit might be 3. Figure 5 shows the average stoichiometry numbers for each $[OH^-]$ as a function of $[OH^-]$, with a line fitted to the data on the assumption that the limiting values are $n = 6$ and $n = 3$, eq. [12]. These limiting values are plausible in terms

$$[12] \quad n = 3 + 3/(1 + 4.08[OH^-])$$

of predominant formation of phenylglycerate at high $[OH^-]$ (6) and of benzoate at low $[OH^-]$. Production of benzoate suggests a crucial partitioning either at 3-chloro-1-phenyl-1,2-propanedione or 3-hydroxy-1-phenyl-1,2-propanedione, with high $[OH^-]$ favoring hydrolysis of the chloro compound and (or) rearrangement of the hydroxy compound, and low $[OH^-]$ favoring chlorination. Scheme 2 is complex, and much remains to be determined. At that, this scheme may be too simple, because a reasonable mechanism can be written involving rearrangement of chloroketones rather than hydroxyketones; this would give the same products. Evidence in hand suggests that benzoate, mandelate, atrolactate, and 2-phenylglycerate are all products of the reaction; further investigations of the later stages of the chlorination of propiophenone are underway, and will be reported in due course.[4]

The fraction of CPP that undergoes hydrolysis to HPP can be calculated using eq. [4], and the values are given in Table 1. The precision of these values is not high, but there is a trend for f to increase at low $[OCl^-]$ and decrease at high $[OCl^-]$, and there is no apparent relationship to $[OH^-]$. This suggests that the rate law for the second chlorination leading to 2,2-dichloro-1-phenyl-2-propanone is $v = k_{36}[OH^-][OCl^-][CPP]$. If so, then

$$[13] \quad 1/f = 1 + k_{36}[OCl^-]/k_{34}$$

A very approximate value of $k_{36} = 120\ M^{-2}\ s^{-1}$ can be extracted from the data, but this is only an order of magnitude estimate at this time.

If we use the measured extinction coefficients, k_{13} values calculated from eq. [9], k_{45} values calculated from eq. [11], n values calculated from eq. [12], and f values calculated from eq. [13], we can approximately reproduce the observed values of the preexponential factors α and β. In particular, we reproduce the alternation in sign of α with changing concentrations of hypochlorite. Since α and β are frequently small differences in large numbers, considerable uncertainty is to be expected in the calculated values.

The hplc kinetics also showed double exponential behavior, with initial formation of HPP being followed by conversion of most of it into another, very similar, compound. This second product was shown to be 1-hydroxy-1-phenyl-2-propanone, HPA. The hplc kinetics were carried out with ketone in excess, so the second phase of the reaction represents a process not involving hypochlorite, and occurring after the hypochlorite had been consumed. The wavelength used for hplc analysis was chosen for efficient detection of HPP, and was not efficient for HPA, so the precision of the analytical data for HPA formation in these experiments was low. The rate constants for disappearance of HPP in the hplc kinetics, expressed as second-order rate constants $k_{obs}/[OH^-]$, are similar to the analogous second-order rate constants calculated for the second phase of the uv kinetics starting with propiophenone, and to the second-order rate constants calculated from uv kinetics starting with HPP. This demonstrates that the rate-determining step for both chlorination and isomerization is the same, namely proton abstraction by OH^-.

That the equilibrium constant for isomerization favored HPA, rather than HPP with the carbonyl conjugated with the benzene ring, surprised us but has been confirmed in other work to be reported later.[4]

We have prepared 2-hydroxy-1-phenyl-1-propanone and studied its kinetics of chlorination. The observed rates match the rates of the second phase of propiophenone chlorination, although less precisely than one would wish: see the Discussion.

The initial product of chlorination of 1-phenyl-2-hydroxy-1-propanone is expected to be 2-chloro-1-phenyl-2-hydroxy-1-propanone. This would be expected to have an extremely

[4] J. P. Guthrie and J. Cossar, work in progress.

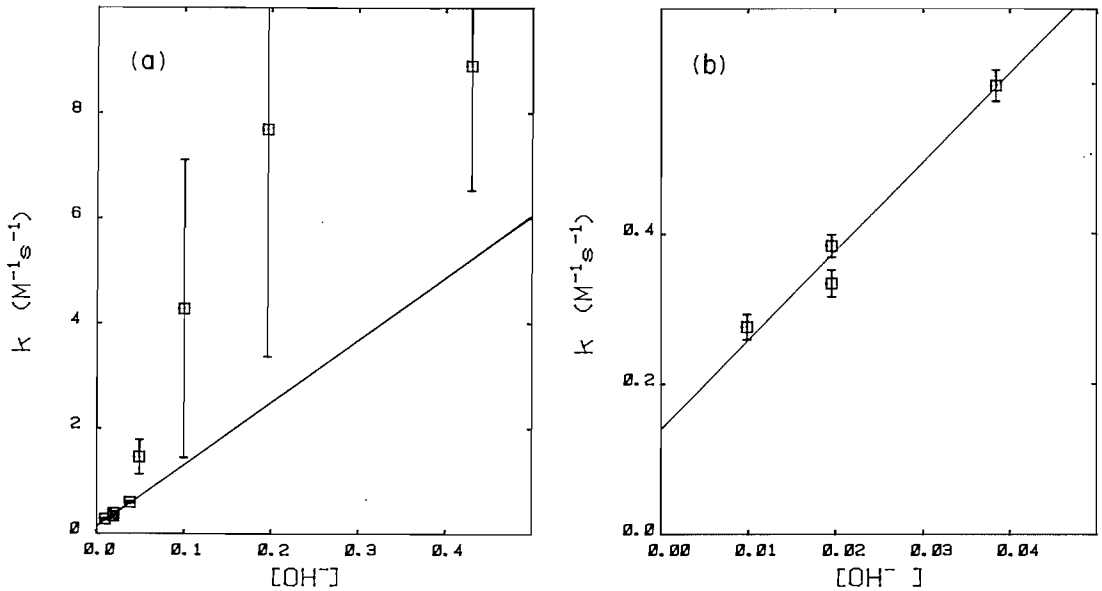

FIG. 4. Chlorination of propiophenone; k_2 at low concentrations of [OCl^-] as a function of [OH^-]. The line is calculated using parameters determined by least-squares fitting. (a) All data, including extrapolated values from experiments at high [OH^-]. (b) Only data from experiments at low [OH^-], followed by hplc.

short lifetime before losing chloride ion to give 1-phenyl-1,2-propanedione.

Discussion

For propiophenone, the kinetics of chlorination were not simple first order. The absorbance–time curves could only be described by using two exponential terms. This contrasts with the behavior seen for acetone or acetophenone where the first chlorination step is clearly rate limiting under similar conditions. This complexity arises because of slower reaction of the hydroxyketone formed by hydrolysis of the monochlorinated starting material. The shift in behavior from acetophenone to propiophenone was unexpected.

The second chlorination of propiophenone does not appear to compete with hydrolysis at very low hypochlorite concentrations, as in the kinetics followed by hplc, but can compete at the highest hypochlorite concentrations used for uv kinetics, as shown by the f values deduced from the integrated rate law. It is surprising that the halogenation rate constant is as slow as it seems to be, because the corresponding rate constant for propiophenone is ca. $4 \times 10^4\ M^{-1}\ s^{-1}$. Introducing a chlorine has caused a dramatic decrease in the rate of chlorination. This is likely to be partially a steric effect because the rate constant for the reaction of isobutyrophenone enolate with hypochlorite is ca. $1 \times 10^4\ M^{-1}\ s^{-1}$. Since methyl and chloro are roughly the same size, there could be a steric explanation for a 4-fold decrease in rate constant, but this leaves a 90-fold additional decrease to be explained for CPP. The equilibrium constant for the second halogenation step is likely to be less favorable than for the first (1), and thus, with a smaller thermodynamic driving force, the rate constant is less.

The rate constants for the reaction of hypochlorite with α-hydroxypropiophenone should match, whether they are measured starting with α-hydroxypropiophenone or with propiophenone. Although the observed rate constants are close, there are differences amounting to a factor of two at low [OCl^-]. We have established that hydrolysis of chloropropiophenone is rapid with respect to the observed reaction. It is likely that there is a partitioning of α-chloropropiophenone between

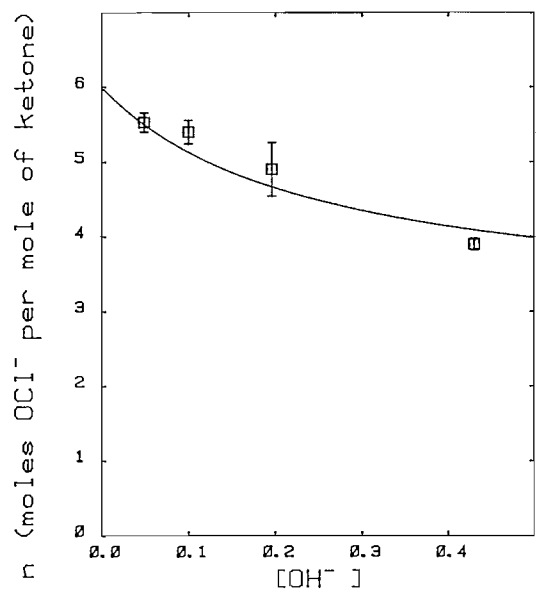

FIG. 5. Chlorination of propiophenone: overall stoichiometry, n, (moles of OCl^- per mole of propiophenone) as a function of [OH^-]. Values for different [OCl^-] and the same [OH^-] were very similar and have been averaged. The line is calculated assuming limiting values of $n = 3$ and $n = 6$ for $n = 3 + 3/(1 + 4.08[OH^-])$.

chlorination and hydrolysis, but it is very probable, by analogy with simpler ketones (2), that hydrolysis of the α,α-dichloropropiophenone is also rapid, and we know[5] that 1-phenyl-1,2-propanedione reacts rapidly. Thus the only intermediate that might reasonably be expected to accumulate is α-hydroxypropiophenone, and hplc experiments have confirmed that this is the only detectable intermediate for the conditions used. Nonetheless, the direct kinetics of α-hydroxypropiophenone chlorination give rate constants that are independent of [OCl^-], while the second phase of the kinetics of propiophenone chlori-

[5] J. P. Guthrie and J. Cossar, unpublished observations.

Can. J. Chem. Downloaded from www.nrcresearchpress.com by 91.121.58.235 on 09/07/12
For personal use only.

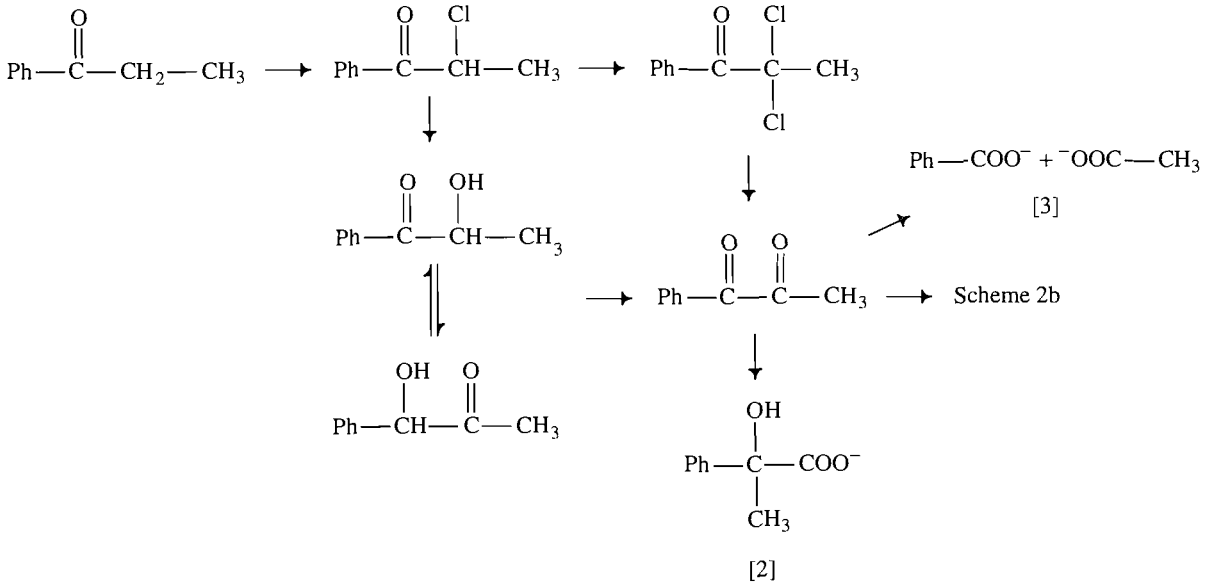

SCHEME 2a

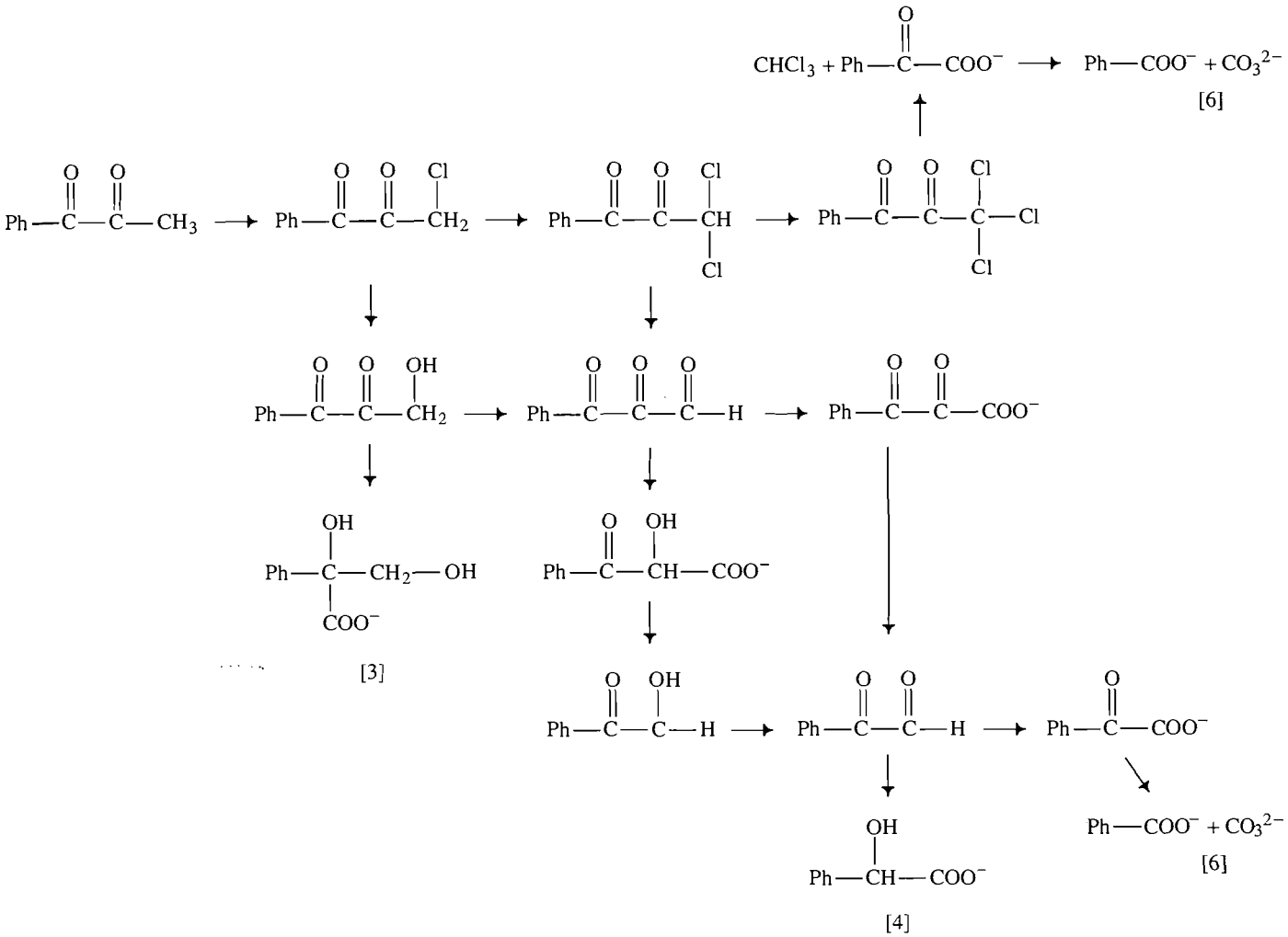

SCHEME 2b

nation gave rate constants that seemed to show a dependence of $[OCl^-]$ at low $[OCl^-]$ although the rates become independent of $[OCl^-]$ at high $[OCl^-]$, and these limiting values matched those found in experiments starting with HPP.

This discrepancy is disturbing, but we suspect that it arises from the complexity of the reaction being followed when one starts with propiophenone. The rate constants for the two phases of the reaction that can be detected differ by factors of 2.6–4.7, which means that only the last small part of the absorbance change is solely determined by the hydroxypropiophenone

Can. J. Chem. Downloaded from www.nrcresearchpress.com by 91.121.58.235 on 09/07/12
For personal use only.

Can. J. Chem. Downloaded from www.nrcresearchpress.com by 91.121.58.235 on 09/07/12
For personal use only.

reaction, and the parameters determined by the least-squares procedure are highly correlated. Thus we conclude that the uv kinetics starting with propiophenone are of little use in quantitative determination of the kinetics of either the initial or the later reactions, although they are useful in qualitatively defining the process.

For propiophenone, the hydroxyketone accumulated as an intermediate and was the only detectable intermediate in the reaction. The initial reaction is expected to be chlorination to give α-chloropropiophenone; we have shown that hydroxide-catalyzed hydrolysis of the chloroketone is rapid. This hydrolysis would be expected to be slow by the classical S_N2 mechanism, because it takes place at a secondary center (9). It would be expected to be slow by the classical S_N1 solvolysis mechanism because reaction occurs next to a carbonyl group. Although S_N1 reactions at tertiary centers next to a carbonyl are known, they occur at rates similar to those at the analogous secondary centers with the acyl function replaced by hydrogen (10). In any case the reaction rate is first order in hydroxide, so that it cannot be solvolysis. A plausible mechanism is addition of hydroxide, followed by intramolecular nucleophilic displacement.

The alkaline hydrolysis of α-chloropropiophenone has been observed before (11), but under the conditions used (50% aqueous ethanol) the solvolysis was slower, and isomerization of α-hydroxypropiophenone to 1-phenyl-1-hydroxy-2-propanone occurred at very similar rates. Our findings are different in that we observed no isomerization, but the reaction is faster in pure water, and consequently can be carried out at a lower temperature (25°C rather than 60°C).

The rates of deprotonation for Me-CO-CH_3, 0.173 M^{-1} s^{-1} (12), Me-CO-CH_2-Me, 0.038 M^{-1} s^{-1} (13, 14), and Me-CO-$CHMe_2$, 0.0026 M^{-1} s^{-1} (13, 14), or Ph-CO-CH_3, 0.244 M^{-1} s^{-1} (15), Ph-CO-CH_2-Me, 0.0259 M^{-1} s^{-1} (this work), and Ph-CO-$CHMe_2$, 0.00243 M^{-1} s^{-1} (16), 0.0031 M^{-1} s^{-1} (17) show a similar progressive decrease with increasing level of substitution. The relative rates are 1:0.22:0.015 and 1:0.11:0.010 respectively. Propiophenone, pK_a 17.56, is more acidic than acetophenone, pK_a 18.24 (18), 18.4 (3), and isobutyrophenone, pK_a 18.18 (17), 18.26 (16), is very similar to acetophenone. The difference between propiophenone and acetophenone is barely outside experimental error. If it is real, it suggests that there are opposing effects of methyl substitution upon ketone acidity. This seems plausible enough, because methyl groups would stabilize the C=C of the enol or enolate, but would also introduce a destabilizing *cis* interaction with either the O^- or phenyl. There could be interference with solvation of the O^-, and there might be an electronic effect whereby electron release by methyl is acid weakening. With this many effects it is easier to rationalize than to predict. Bordwell *et al.* found pK_a values, in dimethyl sulfoxide as solvent, of 24.7, 24.4, and 26.3 for acetophenone, propiophenone, and isobutyrophenone, respectively (19).

We have been able to determine a pK_a value for propiophenone by analysis of the kinetics of chlorination. The chlorination reactions followed paths that were unexpected because of the remarkably rapid alkaline hydrolysis of the initial chloroketone product. The behavior of propiophenone was further complicated because of unexpectedly slow chlorination of HPP, the first observable intermediate in the reaction. Chlorination of even such a simple substrate as propiophenone is clearly a very complicated reaction, and further investigation will be needed to unravel all of the complexities.

Experimental

Materials

Sodium hydroxide and potassium chloride were reagent grade, used without further purification. Sodium hypochlorite solutions were prepared by bubbling chlorine into aqueous sodium hydroxide; the hypochlorite concentration of the resulting solution was determined either by the absorbance at 292 nm, using $\epsilon_{292} = 352$, or by titration (2). The sodium hydroxide concentration of kinetics solutions was determined by titration (2). All extinction coefficients, ϵ, are in units of M^{-1} cm^{-1}.

Propiophenone, Aldrich "99%", was purified by distillation; bp 107–109°C (20 Torr; 1 Torr = 133.3 Pa); mp 17–18.5°C (lit. (20) mp 18.6°C); uv spectrum in water: λ_{max} 244 (ϵ_{max} 12 000); $\epsilon_{292} = 800$.

2-Chloro-1-phenyl-1-propanone

Propiophenone (13.4 g, 0.1 mol), in diethyl ether (300 mL), was placed in a round-bottomed flask fitted with a reflux condenser and cooled in a Dry Ice – acetone bath while chlorine gas (5.7 g, 0.08 mol) was bubbled in. Cooling was continued with an ice–water bath while HCl gas was fed in slowly for 15 min until the reaction started and the mixture began to reflux. The reaction was nearly complete after 10 min, as judged by the disappearance of color. After 20 min further standing with cooling by the ice–water bath, the solution was washed into a separatory funnel using petroleum ether (bp 60–80°C) (200 mL) and washed once with water (250 mL), once with 1 M $KHCO_3$ (250 mL), and once with 1 M KCl (250 mL). The organic layer was dried with Na_2SO_4 and evaporated to yield a yellow liquid (15.5 g). ^1H nuclear magnetic resonance indicated that the product was 40% propiophenone and 60% monochloropropiophenone. Fractional distillation gave pure material in the final fraction: bp 130–131°C (20 Torr) (lit. (21) bp 126.5–127°C (18 Torr)); uv (in 1 M KCl): λ_{max} 252 nm (ϵ_{max} 11 000 ± 300), $\epsilon_{246} = 10\,000$, $\epsilon_{292} = 1600$; ^1H nmr (200 MHz, $CDCl_3$) δ: 1.74 (3H, d, J = 7 Hz, CH_3-), 5.26 (1H, q, J = 7 Hz, CH_3-CHCl-), 7.42–7.46 (3H, m) and 7.96–8.06 (2H, m, C_6H_5-CO).

2-Hydroxy-1-phenyl-1-propanone

2-Chloro-1-phenyl-1-propanone (1.5 g, 8.9 mmol) was dissolved in methanol (60 mL) and added to 1000 mL of 0.011 M NaOH and stirred vigorously for 10 min at room temperature (23°C). The base was then neutralized with 4 M H_3PO_4 (3 mL) to approximately pH 7. The neutral solution was extracted with $CHCl_3$ (200 mL, 100 mL, 100 mL) and evaporated to yield 1.3 g of a viscous liquid. Thin-layer chromatography (tlc) showed about 80% conversion to the ketol. The mixture was chromatographed on a column of silica (40 g) and eluted with 10% EtOAc in petroleum ether. The second uv-active component eluted was almost pure ketol (1.056 g). This was crystallized from Et_2O at −80°C, filtered in the cold, washed with cold pentane, and dried in vacuum at 0°C, to give 0.784 g (5.22 mmol, 59%) of the ketol, mp 18–19°C; uv (in 1 M aqueous KCl, average of 3 experiments): λ_{max} 246.5 (ϵ_{max} 11 400 ± 100), ϵ_{292} 850; ^1H nmr (200 MHz, $CDCl_3$, TMS) δ: 1.46 (3H, d, J = 7 Hz, CH_3-CH(OH)-), 3.82 (1H, d, J = 6 Hz, HO-), 5.17 (1H, quintet, J = 7 Hz, CH_3-CH(OH)-), 7.45–7.68 (3H, m, aromatic H, *m* and *p*), 7.91–7.97 (2H, m, aromatic H, *o*), 2.09 (0.04 H, s, CH_3- of 1-hydroxy-1-phenyl-2-propanone).

1-Hydroxy-1-phenyl-2-propanone

1-Phenyl-1,2-propanedione-2-oxime (Aldrich, 99%) (2.0 g, 12 mmol) was dissolved in ethanol (15 mL) and added to a solution of KBH_4 (1.0 g, 20 mmol) in 75% ethanol/25% water (20 mL). The solution was heated to 50°C for 3 min; an initially formed yellow color disappeared by this time. The solution was stirred at room temperature for 2 h, and then concentrated to 10 mL, added to 1 M aqueous Na_2CO_3 (30 mL) and extracted with ether (3 × 50 mL). The extracts were dried (Na_2SO_4) and evaporated, yielding 2.1 g of a white solid. Crystallization from 50% ethanol – water (40 mL) gave 1.0 g pure 1-hydroxy-1-phenyl-2-propanone oxime, mp 112–113°C (lit. (22) mp 112°C). A second crop from 35% ethanol gave 0.4 g, mp 111–112°C; ^1H nmr (60 MHz, in 1:1 CD_3OD:$CDCl_3$) δ: 1.9 (3H, s), 4.3 (2H, br), 5.3 (1H, s), 7.3–7.4 (5H, m). 1-Hydroxy-1-phenyl-2-propanone oxime (0.8 g, 4.8 mmol) was dissolved in 90% levulinic acid/10% water (15 mL) and let stand at

Can. J. Chem. Downloaded from www.nrcresearchpress.com by 91.121.58.235 on 09/07/12
For personal use only.

room temperature for 16 h. The solution was added to pH 7 phosphate buffer, 0.5 M in phosphate (250 mL), and extracted with $CHCl_3$ (3 × 120 mL). The extracts were dried (Na_2SO_4) and evaporated, yielding 0.9 g of oily liquid containing about 10–20% levulinic acid. Chromatography on silica (50 g), eluting with a gradient of 0–20% EtOAc in petroleum ether, gave 445 mg of material that was 80–90% pure by ^1H nmr analysis. This material was given a bulb-to-bulb distillation (50–70°C at 0.1 Torr) and then crystallized at low temperature with 2:1 ether/pentane as solvent. In this way 260 g of material, mp 9.5–11°C, was obtained (lit. (23) bp 66°C at 0.2 Torr); uv (1 M KCl) λ_{max} 258 nm (ϵ_{max} 410), ϵ_{292} 235; ^1H nmr analysis showed less than 3% of HPP; ^1H nmr (200 MHz, $CDCl_3$) δ: 2.01 (3H, s, CH_3-CO), 4.58 (1H, d, J = 4 Hz, OH), 5.06 (1H, d, J = 3 Hz, CH), 7.27–7.33 (5H, m, C_6H_5).

Methods

Thin-layer chromatography was carried out using Analtech 250-μm Silica Gel GF plates or Macherey–Nagel Polygram SIL G/UV precoated plastic sheets (0.25 mm). Column chromatography was carried out using Terochem silica gel, no. 1918.

The hplc analyses were carried out using C18 reverse phase columns (Waters Radial Pak), with mixtures of aqueous buffers and methanol as eluting solvent, and uv detection.

Least-squares calculations were carried out using FORTRAN programs written for the purpose; nonlinear least squares and the Marquardt algorithm (24) were used for other than straight line correlations.

Kinetics procedures

All reactions were studied in aqueous solution at 25°C and ionic strength 1.0 M (KCl) using apparatus and procedures previously described (2). Reactions were initiated by injecting (Hamilton syringe) a known amount of a stock solution of the ketone into thermally equilibrated hydroxide/hypochlorite solution in a quartz uv cell.

Hydrolysis of chloropropiophenone

A stock solution of α-chloropropiophenone in methanol was kept in a refrigerator between uses; the uv spectrum did not change, indicating that there was no deterioration. Freshly prepared hydroxide solutions, ionic strength 1 M with KCl, were titrated immediately before use and immediately after the runs, with 0.05 M HCl standardized against tris base. Kinetics were initiated by injecting a suitable amount of stock solution of α-chloropropiophenone into hydroxide solution previously thermostatted in 5- or 10-cm quartz cells; reaction was followed at 246 nm. The kinetics showed a rapid increase in absorbance followed by a slower (300 times slower) decrease in absorbance. The second phase is attributed to equilibration with 1-hydroxy-1-phenyl-2-propanone; further discussion of this behavior will be deferred to a subsequent paper.[4] Data for 20 half-lives of the initial reaction were fitted to a single exponential plus linear tail form of the integrated rate law, leading to the rate constants shown in Table 2.

Chlorination of propiophenone and hydroxypropiophenone

Reactions monitored by uv absorbance were carried out as described above. Reactions monitored by hplc were carried out in a thermostatted flask and samples were taken and injected at suitable intervals using an autosampler. In some cases 1.0-mL samples were taken manually and quenched ($NaHSO_3$ and H_3PO_4) for later analysis. The peaks for HPP and HPA were assigned by comparison with those for authentic samples prepared as described above.

Product studies

Propiophenone (103 mg, 0.766 mmol) was added to 2 L of a solution 0.040 M in NaOH and 0.0050 M in NaOCl. After 40 min (4 half-lives for the first phase of reaction and less than 1 half-life for the second phase) 1 M $NaHSO_3$ solution (10 mL) was added to stop the reaction. Extraction of the alkaline solution with diethyl ether (3 × 300 mL), drying, and evaporation gave 45.8 mg; tlc and nmr analysis showed that the major component was 2-hydroxy-1-phenyl-1-propanone with some propiophenone present. Acidification of the aqueous solution using concentrated HCl (9 mL), followed by extraction with diethyl ether (3 × 300 mL), drying, and evaporation gave 64 mg; tlc identified benzoic acid as a major component, although two other spots were seen. The crude material extracted from the alkaline product solution was purified by column chromatography on silica gel using 1:1 $CCl_4/CHCl_3$ as eluant with a linear gradient from 0 to 5% ethanol. Kugelrohr distillation at 70°C, 0.2 Torr; uv (in 1 M aqueous KCl): λ_{max} 246 nm (ϵ_{max} 10 000); ^1H nmr (200 MHz, $CDCl_3$, TMS) δ: 1.46 (3H, d, J = 7 Hz, CH_3-), 3.80 (1H, br, OH), 5.13 (1H, quartet, J = 7 Hz, CH(OH)), 7.38–7.62 (3H, m, aromatic), 7.82–7.92 (2H, m, aromatic). Exact Mass calcd. for $C_9H_{10}O$: 150.06792; found: 150.06807.

Acknowledgments

We thank the Natural Sciences and Engineering Research Council of Canada for financial support of this work.

1. J. P. Guthrie, J. Cossar, and A. Klym. J. Am. Chem. Soc. **106**, 1351 (1984).
2. J. P. Guthrie and J. Cossar. Can. J. Chem. **64**, 1250 (1986).
3. J. P. Guthrie, J. Cossar, and A. Klym. Can. J. Chem. **65**, 2154 (1987).
4. M. W. Farrar and R. Levine. J. Am. Chem. Soc. **71**, 1496 (1949).
5. R. Levine and J. R. Stephens. J. Am. Chem. Soc. **72**, 1642 (1950).
6. J. P. Guthrie and J. Cossar. Can. J. Chem. Submitted for publication.
7. P. D. Bartlett. J. Am. Chem. Soc. **56**, 967 (1934).
8. P. D. Bartlett and J. R. Vincent. J. Am. Chem. Soc. **57**, 1596 (1935).
9. A. Streitwieser, Jr. Solvolytic displacement reactions. McGraw–Hill, New York. 1962. p. 16.
10. X. Creary. J. Am. Chem. Soc. **106**, 5568 (1984).
11. G. Richard. C. R. Hebd. Seances Acad. Sci. **214**, 673 (1942).
12. R. P. Bell and H. C. Longuet-Higgins. J. Chem. Soc. 636 (1946).
13. A. Kankaanpera, L. Oinonen, and P. Salomaa. Acta Chem. Scand. **A31**, 551 (1977).
14. J. P. Guthrie. Can. J. Chem. **57**, 1177 (1979).
15. J. R. Jones, R. E. Marks, and S. C. Subba Rao. Trans. Faraday Soc. **62**, 111 (1966).
16. P. Pruszynski, Y. Chiang, A. J. Kresge, N. P. Schepp, and P. A. Walsh. J. Phys. Chem. **90**, 3760 (1986).
17. J. P. Guthrie and J. Cossar. Can. J. Chem. **68**, 397 (1990).
18. Y. Chiang, A. J. Kresge, and J. Wirz. J. Am. Chem. Soc. **106**, 6392 (1984).
19. F. G. Bordwell, J. E. Bartmess, and J. E. Hautala. J. Org. Chem. **43**, 3095 (1978).
20. R. C. Weast (*Editor*). Handbook of chemistry and physics. 48th ed. Chemical Rubber Co., Cleveland, OH. 1967.
21. E. M. Kosower, W. J. Cole, G.-S. Wu, D. E. Cardy, and G. Meisters. J. Org. Chem. **28**, 630 (1963).
22. P. Rabe. Chem. Ber. **45**, 2163 (1912).
23. J. W. Lynn and J. English. J. Am. Chem. Soc. **73**, 4284 (1951).
24. P. R. Bevington. Data reduction and error analysis for the physical sciences. McGraw–Hill, New York. 1969.
25. W. P. Jencks and J. Regenstein. *In* Handbook of biochemistry. 1st ed. *Edited by* H. A. Sober. Chemical Rubber Co., Cleveland, OH. 1968.

Stabilities in the gas phase of the hydrogen bonded complexes, $YC_6H_4OH\text{-}X^-$, of substituted phenols, YC_6H_4OH, with the halide anions X^- (Cl^-, Br^-, I^-)

GARY J. C. PAUL AND PAUL KEBARLE
Chemistry Department, University of Alberta, Edmonton, Alta., Canada T6G 2G2

Received May 8, 1990

GARY J. C. PAUL and PAUL KEBARLE. Can. J. Chem. **68**, 2070 (1990).

The equilibria, YPhOH + Br^- = YPhOH-Br^-, involving 26 differently substituted phenols, were determined with a pulsed high pressure mass spectrometer. The $-\Delta G^0$ evaluated from the equilibrium constants represent the hydrogen bond free energies in YPhOH-Br^-. These data and data for X^- = Cl^- and I^-, determined previously in this laboratory, are used to examine the substituent effects on the hydrogen bonding. It was found that the hydrogen bond energies in YPhOH-X^- increase approximately linearly with the gas phase acidities of the phenols, YPhOH. This is in agreement with earlier observations that showed the bond energies in AH-B^-, where AH were oxygen and nitrogen acids and B^- closed shell anions, increase with increasing acidity of AH.

A detailed analysis of the substituent effects, which is possible for YPhOH-X^-, shows that the relationship with the acidity of AH can be divided into two parts. One is the increasing extent of actual proton transfer from AH on formation of the hydrogen bonded complex. Such proton transfer occurs in YPhOH-X^- only for the series X^- = Cl^-. The second effect, which occurs for Cl^- and is dominant for Br^- and I^-, is not directly related to the acidity of the phenols (or AH in general) but depends on a similarity of the substituent effects on the acidity and the stabilization of YPhOH-X^- (or AH-B^- in general). The dominant contribution to YPhOH-X^- stabilization in this case is due to the field effects of the substituents, i.e., π delocalization plays only a small part. Therefore, the correlation with the acidity of YPhOH, where π delocalization is important, is not very close.

Key words: hydrogen bonding, substituent effects, ion–molecule equilibria, stability constants, thermochemistry.

GARY J. C. PAUL et PAUL KEBARLE. Can. J. Chem. **68**, 2070 (1990).

Utilisant un spectromètre de masse pulsé à haute pression, on a déterminé les équilibres YPhOH + Br^- = YPhOH-Br^- impliquant 26 phénols portant des substituants différents. Le $-\Delta G^0$ évalué à partir des constantes d'équilibre représente les énergies libres des liaisons hydrogènes du YPhOH-Br^-. On a utilisé ces données ainsi que celles de l'équilibre X^- = Cl^- et I^-, déterminées antérieurement dans ce laboratoire, pour examiner l'effet des substituants sur les liaisons hydrogènes. On a trouvé que les énergies des liaisons hydrogènes dans les composés YPhOH-X^- augmentent approximativement de façon linéaire avec les acidités des phénols YPhOH en phase gazeuse. Ces résultats corroborent les observations antérieures qui démontrent que les énergies de liaison dans les composés du type AH-B^-, ou AH représente des acides oxygénés ou azotés et B^- un anion ayant sa couche électronique complète, augmentent avec l'acidité de AH.

Une analyse détaillée des effets des substituants, qui est possible pour les composés du type PhOH-X^-, montre que les relations avec l'acidité peuvent être divisées en deux effets. Le premier effet se rapporte à l'augmentation du taux de transfert actuel du proton à partir de l'acide libre lors de la formation du complexe lié par des liaisons hydrogènes. Un tel transfert de protons se produit uniquement dans les composés où X^- = Cl^-. Le deuxième effet qui se manifeste avec l'ion Cl^- et qui est prépondérant dans le cas des ions Br^- et I^- n'est pas directement relié à l'activité des phénols (ou AH en général) mais dépend de la similarité des effets des substituants sur l'acidité et sur la stabilisation du composé YPhOH-X^- (ou du AH-B^- en général). Dans ce cas, la contribution prépondérante à la stabilisation des composés du type YPhOH-X^- est due aux effets de champ des substituants, c.-à-d. la délocalisation des électrons π intervient faiblement. On peut conclure que la corrélation avec l'acidité des phénols YPhOH où la délocalisation π est importante n'est pas parfaite.

Mots clés : liaisons hydrogènes, effets des substituants, équilibres ion–molécule, constantes de stabilité, thermochimie.
[Traduit par la revue]

Introduction

In the present work Gibbs free energies, $-\Delta G^0_1$, corresponding to the gas phase reaction [1] involving phenols with substituents Y, were determined from measurements of equilibria [1] with a pulsed high pressure mass spectrometer (PHPMS).

[1] YPhOH + X^- = YPhOHX^-

X^- = Br^- and 26 differently substituted phenols were involved in the present determinations. Data for a smaller set of 5 phenols and Cl^- were published earlier (1) and data for 5 phenols and I^- are available from previous unpublished work from this laboratory.[1] These combined results provide quite a complete set of data for the effect of substituents Y on the hydrogen bonding of the phenols to the halide ions. Such data are of interest in a number of areas. For example, hydrogen bonded adduct ions AHX^-, where AH are analytes with protic hydrogens, are observed in analytical mass spectrometric techniques such as Chemical Ionization, Fast Atom Bombardment, Laser Desorption, Thermospray, and Electrospray and therefore knowledge regarding the stability of such ions is useful in these areas. However, our principal interest in these data derives from previous work (1, 2–5), which attempted to establish some general principles concerning the stability of hydrogen bonded ion–molecule complexes involving ions B^- with complete electron shells.

A very simple and useful systemization was the observation that for compounds AH with protic hydrogens such as the oxygen acids (alcohols, carboxylic acids, phenols) the strength of the hydrogen bond to a given negative ion B^-, in the complex AHB^-, increases regularly with increase of the gas phase acidity of AH (1, 2–5). Thus, a plot of the hydrogen bond energies in complexes to Cl^-, involving a series of AH as diverse as HOH, alcohols ROH, carboxylic acids RCO_2H, and substituted phenols, shows a regular, monotonic increase of

[1]G. Caldwell and P. Kebarle. Unpublished work.

Can. J. Chem. Downloaded from www.nrcresearchpress.com by 91.121.58.235 on 09/07/12
For personal use only.

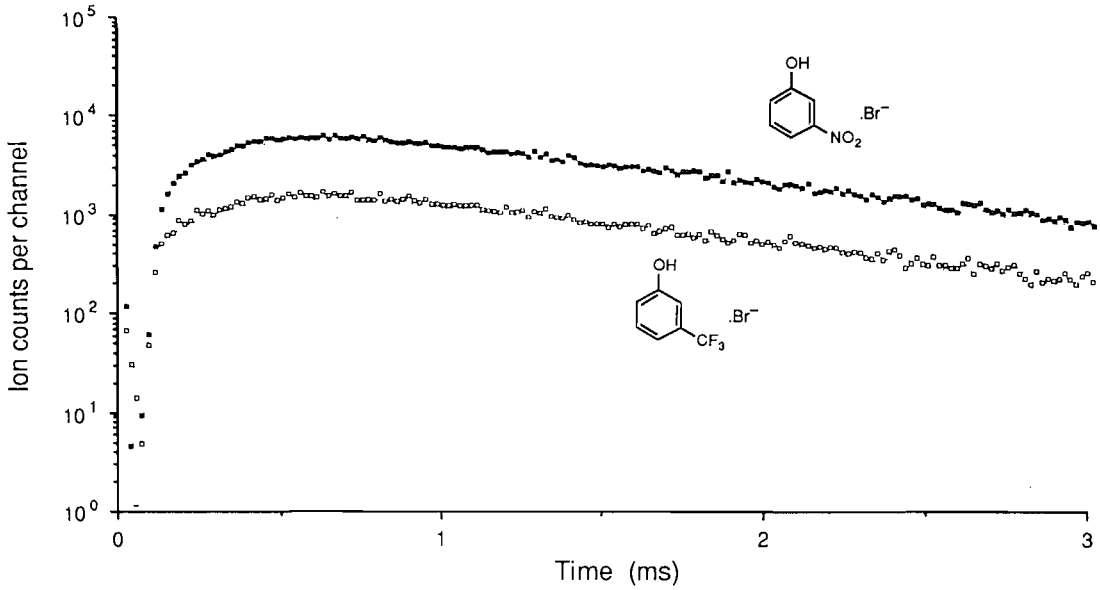

FIG. 1. Raw data plot: ion intensity versus time after the 20 μs ionizing electron pulse. Obtained with a gas mixture of 2.6 Torr CH_4, 0.9 mTorr 3-NO_2PhOH, 2 mTorr 3-CF_3PhOH, and 3.4 mTorr CH_2Br_2 at 423 K. Br^- ions result from dissociative electron capture by CH_2Br_2. The Br^- transfer equilibrium [2] becomes established some 0.3 ms after the electron pulse. The decrease of ion intensity after ~0.5 ms is due to diffusion of the ions to the wall.

bonding with increasing gas phase acidity of AH (4). Similar relationships involving an even larger variety of compounds AH and F^- and Cl^- have been obtained by Larson and McMahon (6).

On trying to understand the nature of this relationship, it is useful to restrict the AH to a series of closely related compounds such as the substituted phenols. The first investigation of this series (1) involved Cl^-. The YPhOHCl$^-$ series differs from the Br^- and I^- series in one important respect. The gas phase acidity of HCl is higher than that of unsubstituted phenol (7). However, strongly acidifying substituents such as -CN and -NO_2 lead to phenols whose acidity is higher than that of HCl (7). Therefore, in the YPhOHCl$^-$ series there will be a significant increase of proton transfer from the phenols to Cl^- with increasing acidity of the phenols.

In a series of AH with X^- for which a large increase of the extent of proton transfer occurs, the increased exothermicity of the complex forming reaction may derive largely from the exothermicity of the proton transfer. In such a case the increase of the "hydrogen bond energy" AH-X^- as measured by $-\Delta G_1^0$ will directly follow the acidity of AH but the cause will be trivial. Of more interest is the question whether the bond energy is related to the acidity in the absence of substantially increased proton transfer. Due to the much higher gas phase acidity of HBr and HI, relative to HCl (7), the formation of the complexes in reaction [1] involving Br^- and I^- is expected to involve at all times complexes corresponding largely to AH-X^-, i.e., involving a much lower proton transfer increase. A comparison of the substituent effects on $-\Delta G_1^0$ for these series with that for Cl^- should allow one to unravel the importance and nature of the effects in the absence of proton transfer.

Interesting theoretical studies of complexes hydrogen bonded to Cl^- have been reported by Hirao and co-workers (8). Hydrogen bonded complexes of the type ROHX$^-$ form also in dipolar aprotic solvents. For a relevant study of YPhOHCl$^-$, see Kolthoff and Chantooni (9); for data on phenol phenoxide complexes, see Bordwell *et al.* (10).

Experimental

The measurements of equilibria [1] for $X^- = Br^-$ were performed with PHPMS apparatus that has been described in detail previously (11). The measurement methodology was similar to that used in the earlier work (1).

In addition to [1], equilibria [2] also were determined.

[2] YPhOH-Br^- + Y′PhOH = YPhOH + Y′PhOH-Br^-

These equilibria provide ΔG_1^0 differences, i.e., $\Delta G_2^0 = \Delta G_1^0$(Y′PhOH) $- \Delta G_1^0$(YPhOH).

The time dependence of the ion intensities observed for one reaction [2], involving 3-CF_3 and 3-NO_2 phenol, is shown in Fig. 1. The vertical distance between the two ion intensities becomes constant for $t > 0.3$ ms. In the logarithmic ion intensity plot used, constant distance means a constant ion ratio and this indicates the establishment of equilibrium [2].

The Br^- ions required for the measurements of [1] and [2] were obtained by adding ~1 mTorr of CH_2Br_2 (1 Torr = 133.3 Pa) to the methane carrier gas reaction mixture. Dissociative electron capture of near thermal electrons by CH_2Br_2 leads to formation of Br^-.

Checks for the invariance of the equilibrium constant K_1 with the partial pressure of the given phenol are shown in Fig. 2. Similar checks involving different partial pressure ratios of the two reacting phenols were also performed for equilibria [2].

The $-\Delta G_1^0$ involving $X^- = I^-$ were determined in earlier work[1] using similar techniques. For a description of equilibria measurements involving I^- and ROH and RCO_2H molecules, see Caldwell and Kebarle (12).

Results and discussion

(a) Results

The $-\Delta G_1^0$ values obtained from measurements of equilibrium constants K_1, see Experimental, and the equation: $\Delta G^0 = -RT \ln K$, involving Br^-, are shown on a scale of increasing $-\Delta G_1^0$ values in Fig. 3. All measurements were performed at 150°C (423 K). The $-\Delta G_1^0$ values will be called bromide affinities, BrA. Values for BrA only up to ~14 kcal/mol could be obtained by the direct measurements of equilibria [1]. As the

Can. J. Chem. Downloaded from www.nrcresearchpress.com by 91.121.58.235 on 09/07/12
For personal use only.

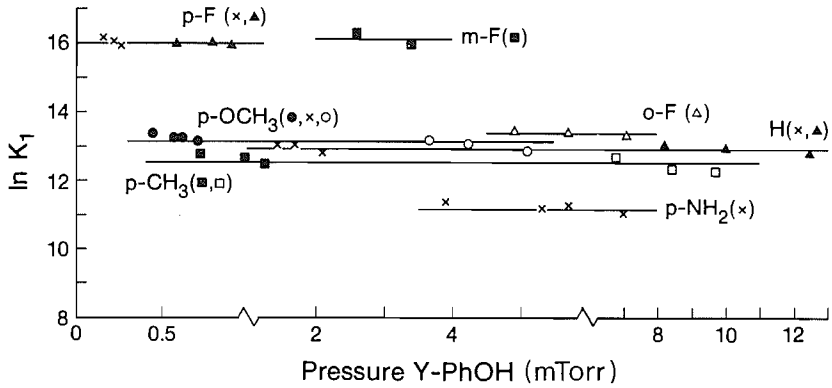

FIG. 2. Equilibrium constants for reaction [1] involving Br^- and different YPhOH. CH_4 pressures change from 2 to 4 Torr in runs with the same symbol. In such runs, the CH_4 to YPhOH pressure ratio is constant.

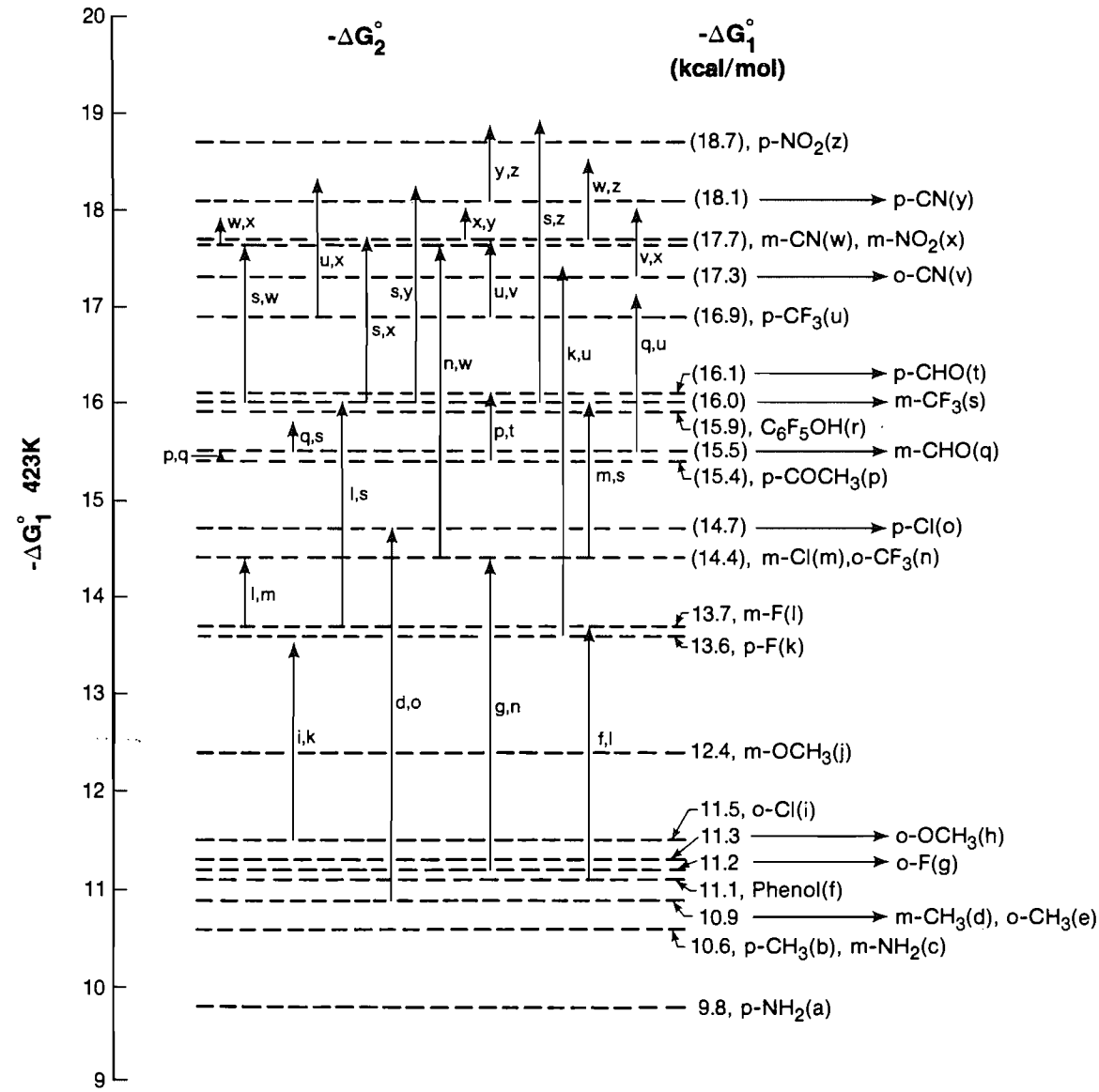

FIG. 3. Scale of $-\Delta G_1^0$ for reactions [1]: Br^- + YPhOH = YPhOHBr$^-$ at 423 K. Standard state 1 atm. Values up to 14 kcal/mol were obtained by direct measurements of equilibria [1]. Higher values were obtained from measurements of the Br^- transfer equilibria [2]. Lengths of arrows shown correspond to ΔG_2^0. Letters beside arrows identify phenols involved in equilibrium [2].

Can. J. Chem. Downloaded from www.nrcresearchpress.com by 91.121.58.235 on 09/07/12
For personal use only.

Can. J. Chem. Downloaded from www.nrcresearchpress.com by 91.121.58.235 on 09/07/12
For personal use only.

TABLE 1.[a] Gibbs free energy change $-\Delta G_1^0$ for reaction: $Br^- + YPhOH = YPhOHBr^-$

Position Y	$-\Delta G_1^0$ (kcal/mol) 423 K	Position Y	$-\Delta G_1^0$ (kcal/mol) 423 K
4-NH_2	9.8	2-CF_3	14.4
3-NH_2	10.6	3-CF_3	16.0
4-CH_3	10.6	4-CF_3	16.9
2-CH_3	10.9	4-CH_3CO	15.4
3-CH_3	10.9	3-CHO	15.5
H	11.1	4-CHO	16.1
4-OCH_3	11.3	2-CN	17.3
3-OCH_3	12.4	3-CN	17.7
2-F	11.2	4-CN	18.1
4-F	13.6	2-NO_2	—
3-F	13.7	3-NO_2	17.7
2-Cl	11.5	4-NO_2	18.7
4-Cl	14.7	F_5[b]	15.9
3-Cl	14.4		

[a]Data from Fig. 3. YPhOH are substituted phenols. Standard state 1 atm.
[b]Perfluorophenol.

TABLE 2. Free energy values $-\Delta G_1^0$ for reaction; $YPhOH + X^- = YPhOHX^-$ [a]

Position Y	$-\Delta G_1^0$ Cl^-	Br^-	I^-
4-Me	15.3	10.6	7.5
H[b]	15.9	11.1	8.4
4-Cl	19.5	14.7	11.6
3-Cl	—	14.4	12.2
3-F	—	13.7	10.7
4-F	18.0	13.6	10.5
3-CN	—	17.7	14.1
4-CN	24.7	18.1	14.9
3-NO_2	—	17.7	14.3
4-NO_2	—	18.7	—

[a]Data for Br^-, present work, Cl^-, refs. 1, 5, I^-, ref. 2. Standard state 1 atm, 423 K. ΔH_1^0 can be approximately evaluated from: $\Delta H_1^0 = \Delta G_1^0 + T\Delta S_1^0$, where $-\Delta S_1^0 \approx 25$ (Cl^-), 23 (Br^-), and 21 (I^-) (cal K^{-1} mol^{-1}). Entropy changes from ref. 5 (Cl^-), estimated (Br^-), ref. 2 (I^-). Furthermore, ΔS_1^0 is approximately constant for whole substituent series and for given X^-, see ref. 1.

BrA increases, K_1 increases, and beyond a given point the Br^- intensity becomes too small for reliable measurements. The BrA shown in Fig. 3 that are larger than 14 kcal/mol were obtained from equilibria [2], which provide relative BrA. By combining the relative BrA with the absolute BrA due to equilibria [1] a complete scale of BrA extending up to 19 kcal/mol for the most acidic phenol, 4-$NO_2C_6H_4OH$, was obtained, see Fig. 3. These BrA's are summarized in Table 1. The more limited data for the iodide affinities[1] and the chloride affinities (1) are given in Table 2, which also includes the corresponding bromide affinities to facilitate an easy comparison of the three sets of data.

(b) Hydrogen bond energy in YPhOH-X^-, gas phase acidities, and substituted effect analysis

A plot of the hydrogen bond energies in YPhOH-Br^- relative to the unsubstituted phenol versus the relative gas phase acidities of the phenols (7) is shown in Fig. 4. A fairly good correlation (correlation coefficient $r = 0.956$) is observed. However, a much better correlation ($r = 0.998$) is obtained in Fig. 5 where the plot is against the acidities of the substituted benzoic acids.

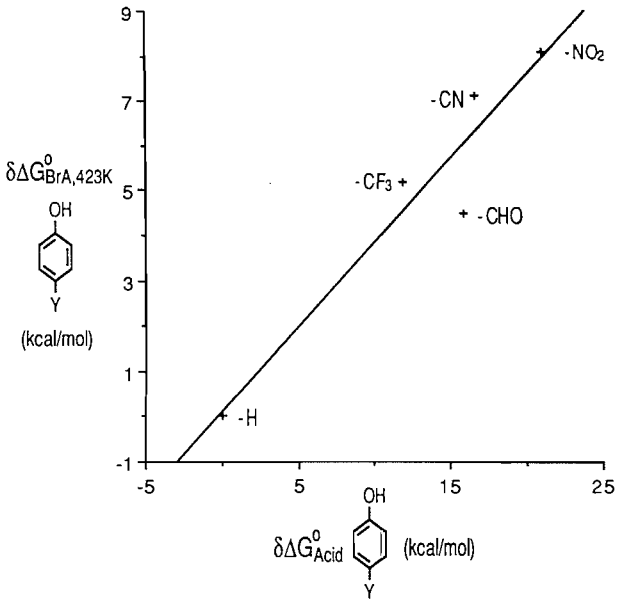

FIG. 4. Plot of $\delta\Delta G^0$ for Br^- hydrogen bonding to phenols versus relative gas phase acidities of phenols.

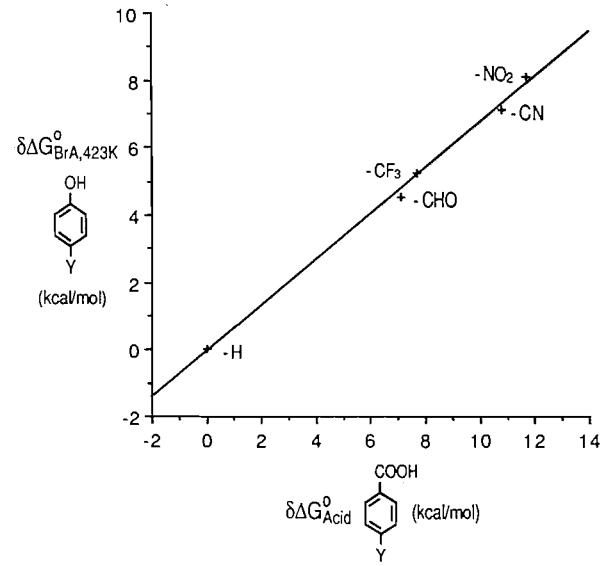

FIG. 5. Plot of $\delta\Delta G^0$ for Br^- hydrogen bonding to phenols versus relative gas phase acidities of benzoic acids.

This comparison reveals at a glance that when extensive proton transfer from AH to X^- is not involved, as is the case for $X^- = Br^-$, see Introduction, the relationship of H bond Gibbs energies with the acidity of the AH (YPhOH in the present case) is only indirect, i.e., a consequence of a similarity of the substituent effect on the acidity and the hydrogen bonding ability. The much better correlation with the benzoic acids means a greater similarity with the substituent effects on the acidity of the benzoic acids. The causes for the better agreement with the benzoic acids can be deduced from a comparison of the deviations for specific substituents observed in Figs. 4 and 5.

Can. J. Chem. Downloaded from www.nrcresearchpress.com by 91.121.58.235 on 09/07/12
For personal use only.

TABLE 3. Values for resonance ρ_R, field ρ_F, and polarizability ρ_α parameters, Taft equation [3][a]

Substituent position	Reaction	ρ_R	ρ_F	ρ_α	r^b	Origin of data
meta[a]	Br^-	4.1±0.6	9.7±0.4	—	0.988	Table 1
		4.0±0.5	8.9±0.5	−1.3±0.8	0.993	
para[a]	Br^-	6.3±0.6	10.7±0.4	—	0.991	Table 1
		6.1±0.5	10.0±0.5	−1.2±0.5	0.995	
para[a]	Br^-	7.6±0.7	10.4±0.3	—	0.999	Table 2
		7.4±0.5	10.1±0.2	−0.5±0.3	1.000	
para[a]	Cl^-	12.7±1.2	12.5±0.4	—	0.998	Table 2
		12.2±0.4	11.9±0.2	−0.9±0.2	1.00	
para[a]	I^-	8.1±0.9	9.7±0.3	—	0.998	Table 2
		8.1±1.3	9.7±0.7	0.1±0.7	0.998	
para[c]	Benzoic acids	14.6±0.7	15.0±0.6	0.1±1.0	0.997	Taft (14*a*)
meta[c]	Benzoic acids	11.5±0.9	14.7±0.5	—	0.998	Taft (14*a*)
para[c]	Phenols π acceptors	49.0±1.5	18.6±0.5	0.6±0.8	0.999	Taft (14*a*)
para[c]	Phenols π donors	22.0±1.4	18.8±0.9	−3.1±0.5	0.993	Taft (14*a*)
meta[c]	Phenols	12.2±1.2	19.0±0.7	—	0.994	Taft (14*a*)

[a]ρ values obtained form linear regression analysis of eq. [3], where $\delta\Delta G^0$ corresponds to experimentally determined ΔG^0 for reaction: $PhOHX^- + YPhOH = PhOH + YPhOHX^-$. Since $\delta\Delta S^0 \approx 0$ (1), $\delta\Delta G^0$, even though determined at 423 K, is also valid at 298 K, i.e., $\delta\Delta G^0_{298} \approx \delta\Delta G^0_{423}$.
[b]Correlation coefficient.
[c]Gas phase acidities.

However, a more general examination of the substituent effects in the hydrogen bonded complexes, $YPhOH\text{-}X^-$ is even more illuminating and provides a more comprehensive view.

Taft *et al.* (13) have developed and refined greatly the analysis of substituent effects and it has been shown (14) that the approach is theoretically justified. The present analysis is based on Taft and Topsom (13*a*). The separation of the substituent effect $\delta\Delta G^0$ into contributions due to π electron delocalization (resonance), R, and field/inductive effects, F, for a substituent in a given position to the functional group, either *para*- or *meta*-, is obtained from eq. [3], which includes also polarizability, α, effects.

$$[3] \quad -\delta\Delta G^0 = \rho_R\sigma_R + \rho_F\sigma_F + \rho_\alpha\sigma_\alpha$$

σ_R, σ_F, and σ_α are reaction system independent parameters that rank the resonance, field, and polarizability capacity of the given substituent; these values have been tabulated (13*a*). The parameters ρ_R, ρ_F, and ρ_α depend on the given reaction, and their magnitude is determined by regression analysis for the best fit when the experimentally determined $\delta\Delta G^0$ for the given reaction system is substituted into eq. [3].

The experimentally determined $\delta\Delta G^0$ of the bromide affinities plotted versus the $\delta\Delta G^0$ calculated with the best fit ρ parameters for *para* substituents are shown in Fig. 6. A very good correlation (correlation coefficient $r = 0.991$) is observed. The polarizability contributions were neglected in the fit shown. A somewhat better fit, $r = 0.995$, is obtained with inclusion of the polarizability. The ρ parameters for both fits are given in Table 3. Since the emphasis of the present discussion will deal with the changes of ρ_R and ρ_F for the different systems and the ρ_α values in all cases are very small, see Table 3, the polarizability will not be considered in the further discussion.

A plot of $\delta\Delta G^0$ of the BrA for *meta* substituents and the best fit π parameters is shown in Fig. 7. A very good fit is obtained also for this system.

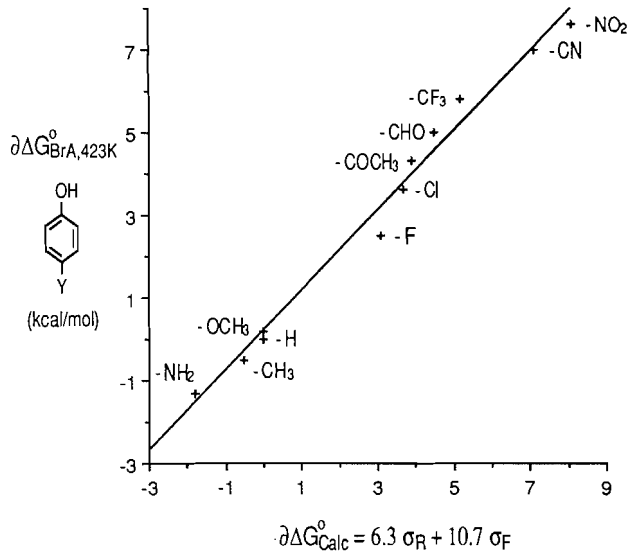

FIG. 6. $\delta\Delta G^0$ for Br^- and substituted phenols versus $\delta\Delta G^0$ calculated with Taft σ parameters, see eq. [3]. Substituents in *para* position.

Since a much more restricted number of substituents was used in the determinations (ref. 1 and footnote 1) involving Cl^- and I^- and since the ρ values depend somewhat on the number of substituents included in the fit, regression analyses for these three ions and the same restricted set of substituents, in *para* position, were obtained. The resulting plots for Cl^- and I^- are shown in Figs. 8 and 9. The ρ values and the correlation coefficients from the restricted fits for Cl^-, Br^-, and I^- are given in Table 3. A comparison of the ρ_R and ρ_F values for Br^-

Can. J. Chem. Downloaded from www.nrcresearchpress.com by 91.121.58.235 on 09/07/12
For personal use only.

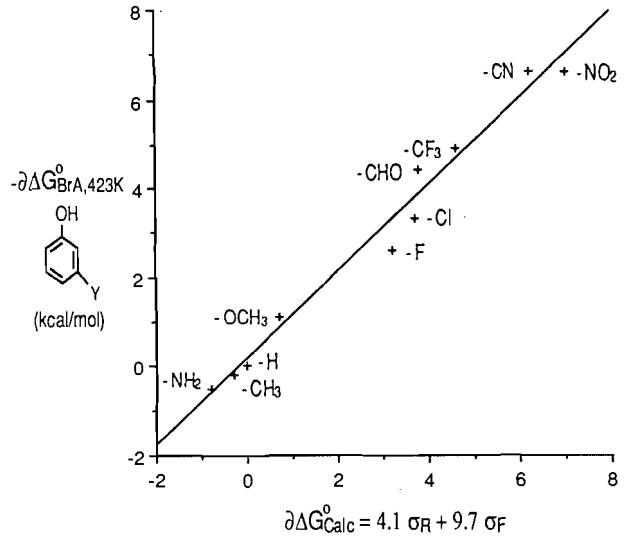

FIG. 7. $\delta\Delta G^0$ for Br^- and substituted phenols as in Fig. 6 but for *meta* substituents.

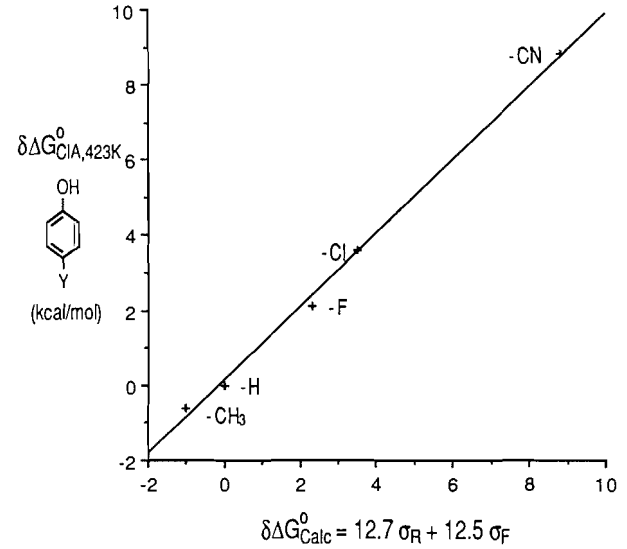

FIG. 8. Same as Fig. 6 but for Cl^- and *para* substituents.

between the extended plot, Fig. 6, and the restricted plot, see Table 3, shows that the ρ_F is essentially the same while ρ_R changes only a little, i.e., from 6.3 to 7.6. This indicates that the restricted plots for results for Cl^-, Br^-, and I^- provide ρ_F and ρ_R values that are still quite meaningful.

Also included in Table 3 are the ρ values for the substituent effect on the gas phase acidities of phenols and benzoic acids obtained by Taft and Topsom (13*a*). Examining first the data for the *para* position, one finds that the ρ_F values decrease in the following order: phenol acidity 18.6, benzoic acidity 15, X^- affinity to phenols: Cl^- 12.5, Br^- 10.4, I^- 9.7. This order agrees with expectation, when one considers the gradually increasing delocalization of the negative charge (phenols to benzoic acids) and the increasing remoteness of the negative charge from the substituent, present for the whole series.

Considering the ρ_R values, it is significant to note that the X^- affinity plots for *para* substituents, which in all cases include both π donor and π acceptor substituents, see Figs. 6, 8, 9, give good linear relationships. The same is true for the gas phase

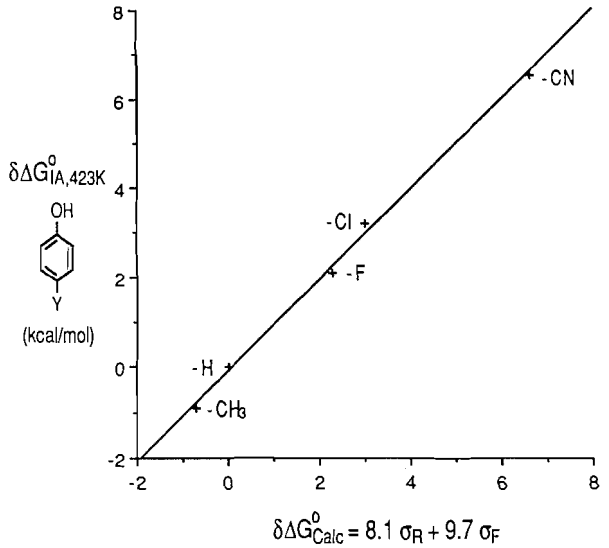

FIG. 9. Same as Fig. 6 but for I^- and *para* substituents.

acidities of *para* substituted benzoic acids, see (13*a*) values reported in Table 3. On the other hand, it is known (13*a*) that for the *para* substituted phenol acidities a single straight-line relationship cannot be obtained for both strong π donors, i.e., -OH, $-OCH_3$, $-NH_2$, and strong π acceptors, i.e., CN, NO_2, CHO, because the reaction centre, O^-, is very strongly π donating to the benzene ring and thus suppresses π donation by π donor substituents (13*a*). The separate ρ_R values for the phenols (13*a*) given in Table 3 are $\rho_R = 22$ for π donor and $\rho_R = 49$ for π acceptor. Comparing the π acceptor value with the ρ_R values for benzoic acids, $\rho_R = 14.6$, and the X^- affinities, $\rho_R = 12.7$ (Cl^-), 7.6 (Br^-), 8.1 (I^-), one finds that the latter are very much smaller and fairly close together. This result could have been anticipated from the plots of the Br^- affinities versus the acidities of phenols and benzoic acids, see Figs. 4 and 5.

The similarity between the ρ_R values for benzoic acids and the X^- affinities reflects the expected dominant stabilization for π accepting substituents in these systems, see resonance structures **II** and **III**.

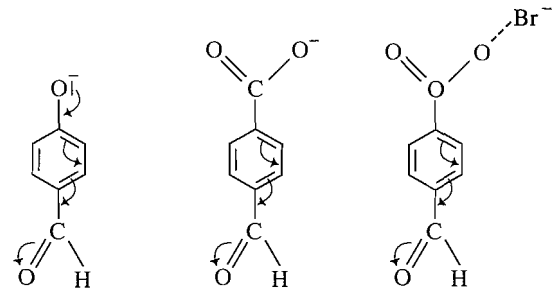

The benzoate anion and the $YPhOHX^-$ complexes lack the direct, into the ring π donation, by the negative functional group exhibited by the phenoxides, structure **I**. The stabilizing effect of π accepting substituents for the $YPhOHX^-$ systems thus derives only from a π shift from the ring into the substituent, which is induced by the negative charge on X^- and is similar to that occurring in the benzoate anions. On this basis one expects NO_2 and CHO, the most strongly π accepting substituents (σ_R: CN, 0.10; NO_2, 0.18; HCO, 0.19, from ref. 13*a*), to show the largest deviations in the X^- affinity –

TABLE 4. Resonance R and field F contributions of substituents[a]

	4-YPhOHBr$^-$[b]		3-YPhOHBr$^-$[b]		4-YPhOH[c]		4-YPhCO$_2$H[c]	
Substituent	R	F	R	F	R	F	R	F
NO$_2$[e]	1.1	7.0	0.7	6.3	8.8	12.1	2.6	9.8
CN[e]	0.7	6.4	0.4	5.8	4.9	11.2	1.5	9.0
CHO[e]	1.2	3.3	0.8	3.0	9.3	5.8	2.8	4.7
CF$_3$[e]	0.5	4.7	0.4	4.2	3.4	8.2	1.0	6.6
H	0.0	0.0	0.0	0.0	0.0	0.0	0.0	0.0
Cl[f]	−1.1	4.8	−0.6	4.3	[d]	[d]	−2.5	6.8
F[f]	−1.6	4.7	−1.0	4.2	[d]	[d]	−3.7	6.6

[a]Contribution: $R = \rho_R\sigma_R$ and $F = \rho_F\sigma_F$ in kcal/mol to $\delta\Delta G^0$, see eq. [3], for given substituent.
[b]$\delta\Delta G^0$ for reaction [1] involving Br$^-$.
[c]$\delta\Delta G^0$ for gas phase acidities of phenols and benzoic acids.
[d]The π donor substituents require a separate fit, see text.
[e]A π acceptor substituent.
[f]A π donor substituent.

Can. J. Chem. Downloaded from www.nrcresearchpress.com by 91.121.58.235 on 09/07/12
For personal use only.

phenol acidity plot, Fig. 4, and exactly this is found to be the case.

The ρ_R values for the π-YPhOHX$^-$ systems are Cl$^-$, 12.7; Br$^-$, 7.6; I$^-$, 8.1. On the basis of the increasing remoteness of X$^-$ in the above series one would have expected the values to decrease monotonically, i.e., ρ_B (Br$^-$) $\geq \rho_R$ (I$^-$). The small reversal of the experimental result for this pair is probably due to experimental error. The observed much larger ρ_R (Cl$^-$) probably also includes the effect of an actual partial proton transfer from YPhOH to Cl$^-$, which occurs for this series.

To provide an illustration for the actual magnitudes of the resonance $R = \rho_R\sigma_R$ and $F = \rho_F\sigma_F$ contributions to $\delta\Delta G^0$, see eq. [3], the R and F values evaluated from the ρ values in Table 3 and σ values of Taft (13*a*) for the substituent effect on the phenols hydrogen bonded to Br$^-$ are shown in Table 4. The corresponding R and F terms for the gas phase acidities of *para* substituted phenols and benzoic acids are also provided for comparison. Examination of the values in Table 4 shows that the F effects are almost completely dominant for both the *para* and *meta* substituted YPhOHBr$^-$. This explains the similarity between the $\delta\Delta G_3^0$ values for the *meta* and *para* YPhOHX$^-$ systems, see Table 4 and Figs. 6 and 7, and also the similarity of those with the substituent effects on benzoic acid acidities, which are also dominated, but somewhat less so, by the F effects, see Table 4.

The stabilizing effect of electron-withdrawing substituents in YPhOHBr$^-$ for *ortho* substituents is somewhat smaller than that for *meta* $\approx$ *para*, see Table 1. This holds for both small size substituents like F and large substituents like NO$_2$. Since the field effect is the dominant factor in all these systems, the somewhat smaller stabilization for the *ortho* compounds should be due to the unfavorable orientation of the dipole, produced by the substituent, relative to the negative charge, i.e., Br$^-$.

Conclusions

The findings for the YPhOHX$^-$ systems can be generalized to AH.B$^-$ hydrogen bonded complexes. For a given related series of AH with increasing gas phase acidity, the increased strength of the hydrogen bond, as measured by the energy required for the dissociation to AH + B$^-$, consists of two contributions. One is the gradually increasing extent of actual proton transfer from AH to B$^-$ on formation of the complex. This effect is very important when the acidity of BH is close and becomes smaller than that of AH. The second contribution can be best observed when it is dominant, i.e., when the acidity of BH is much larger than that of AH for the whole AH series. This contribution is due to effects in AH that increase the dipole in A$^-$-H$^+$ and thus the hydrogen bond energy. The major effects in this case are field type effects in AH. The negative charge of the approaching B$^-$ also induces some π delocalization in AH. This R effect is less important. Since changes of the structure of AH that increase the acidity of AH also increase the favorable F and the less important R stabilization in AH B$^-$, the hydrogen bonding in AH B$^-$ tracks, but only partially so, the acidity of AH. The substituted phenols-X$^-$ complexes are especially useful since for these systese a convincing dissection of the above effects is possible. This is so because the contrast between the effects on acidity and hydrogen bonding is especially strong, due to the large R effect in the phenoxides, see structures **I**–**III**, which develops only after complete deprotonation of AH. Somewhat similar and even larger differences between hydrogen bonding ability and acidity are observed for the carbon acids, where the acidity may be almost entirely due to resonance stabilization after deprotonation, as is the case for cyclopentadiene (4).

1. J. B. CUMMING, M. A. FRENCH, and P. KEBARLE. J. Am. Chem. Soc. **99**, 6999 (1977).
2. R. YAMDAGNI and P. KEBARLE. J. Am. Chem. Soc. **93**, 7139 (1971).
3. (*a*) R. YAMDAGNI, J. D. PAYZANT, and P. KEBARLE. Can. J. Chem. **51**, 2507 (1973); (*b*) P. KEBARLE. Annu. Rev. Phys. Chem. **28**, 445 (1977).
4. M. A. FRENCH, S. IKUTA, and P. KEBARLE. Can. J. Chem. **60**, 1907 (1982).
5. G. CALDWELL and P. KEBARLE. Can. J. Chem. **63**, 1399 (1985).
6. J. W. LARSON and T. B. MCMAHON. J. Am. Chem. Soc. **105**, 2944 (1983); **106**, 517 (1984).
7. J. B. CUMMING and P. KEBARLE. Can. J. Chem. **56**, 1 (1978); S. G. LIAS, J. E. BARTMESS, J. F. LIEBMAN, J. L. HOLMES, R. D. LEVIN, and W. G. MALLARD. J. Phys. Chem. Ref. Data, **17** (1988). Supplement No. 1.
8. S. YAMABE, N. IHIRO, and K. HIRAO. Chem. Phys. Lett. **92**, 172 (1982).
9. I. M. KOLTHOFF and M. CHANTOONI, JR. J. Am. Chem. Soc. **91**, 4621 (1969).

10. F. G. BORDWELL, R. J. MCCALLUM, and W. N. OLMSTEAD. J. Org. Chem. **49**, 1424 (1984).
11. P. KEBARLE. *In* Techniques of chemistry: techniques for the study of ion molecule reactions. *Edited by* W. H. Saunders and J. M. Farrar. Wiley–Interscience, New York. 1988. Chap. 5.
12. G. CALDWELL and P. KEBARLE. J. Am. Chem. Soc. **106**, 967 (1984).
13. (*a*) R. W. TAFT and R. D. TOPSOM. Prog. Phys. Org. Chem. **16**, 1 (1987); (*b*) R. W. TAFT, J. L. M. ABBOUD, F. ANVIA, M. BERTHELOT, M. FUJIO, J.-F. GAL, A. D. HEADLEY, W. G. HENDERSON, I. KOPPEL, J. H. QIAN, M. MISHIMA, M. TAAGEPERA, and S. VEGI. J. Am. Chem. Soc. **110**, 1797 (1988); (*c*) R. W. TAFT and I. C. LEWIS. J. Am. Chem. Soc. **80**, 2436 (1958); **81**, 5343 (1959).
14. R. D. TOPSOM. Prog. Phys. Org. Chem. **16**, 125 (1987).

Can. J. Chem. Downloaded from www.nrcresearchpress.com by 91.121.58.235 on 09/07/12
For personal use only.

Conformational analysis and structure elucidation of 2,3-dimethyl- and 2,4-dimethyl-2,4-hexadienes by AM1 and He(I) ultraviolet photoelectron spectroscopy

N. H. WERSTIUK,[1] K. B. CLARK, AND W. J. LEIGH[2]

Department of Chemistry, McMaster University, Hamilton, Ont., Canada L8S 4M1

Received June 15, 1989[3]

N. H. WERSTIUK, K. B. CLARK, and W. J. LEIGH. Can. J. Chem. **68**, 2078 (1990).

A study of (*E*)-2,3-dimethyl-2,4-hexadiene (*E*-**3**) and (*Z*)-2,3-dimethyl-2,4-hexadiene (*Z*-**3**) by the semiempirical computational method AM1 and He(I) ultraviolet photoelectron spectroscopy (UPS) has established that this combination of AM1/UPS will be generally useful for detailing conformational and electronic properties of alkyl-substituted 1,3-dienes. This method was used to elucidate the structures of the stereoisomeric 2,4-dimethyl-2,4-hexadienes obtained from the photolysis of 1,3,3,4-tetramethylcyclobutene (**2**).

Key words: 2,3- and 2,4-dimethyl-2,4-hexadienes, conformational analysis, AM1, He(I) photoelectron spectroscopy.

N. H. WERSTIUK, K. B. CLARK et W. J. LEIGH. Can. J. Chem. **68**, 2078 (1990).

Une étude du (*E*)-2,3-diméthyl-2,4-hexadiène (*E*-**3**) et du (*Z*)-2,3 diméthyl-2,4-hexadiène (*Z*-**3**) utilisant la technique de calcul semiempirique AM1 et la spectroscopie photoélectronique ultraviolette de l'hélium He(I) (UPS) a permis d'établir que la combinaison de ces deux techniques AM1/UPS peut constituer une méthode générale pour une étude détaillée des propriétés électroniques et conformationnelles des 1,3-diènes portant des substituants alkyles. On a utilisé cette méthode pour élucider la structure des 2,4-diméthyl-2,4-hexadiènes stéréoisomères obtenus à partir de la photolyse du 1,3,3,4-tétraméthylcyclobutène (**2**).

Mots clés : 2,3- et 2,4-diméthyl-2,4-hexadiènes, analyse conformationnelle, AM1, spectroscopie photoélectronique de He(I).

[Traduit par la revue]

Can. J. Chem. Downloaded from www.nrcresearchpress.com by 91.121.58.235 on 09/07/12
For personal use only.

Introduction

A systematic study of the effect of methyl and ethyl substituents on the conformations of conjugated dienes by ultraviolet photoelectron spectroscopy (UPS) and the computational methods AM1 and MMX was initiated recently (1). This work was undertaken for several reasons. The initial goal was to establish whether or not AM1 (2) is useful for carrying out conformational analysis and detailing conjugative and homoconjugative interaction in dienes. This was to be achieved by correlating the results of computational studies with the UPS of dienes whose conformational dynamics are well defined. The overall objective was to establish whether or not a combination of AM1 and UPS can be used to elucidate the structure of highly alkylated dienes, especially when there are no vicinal protons on the double bonds; the classical approach of using the magnitude of the coupling constant to determine that stereochemistry cannot be used in these cases. In our view these studies are also timely because there is renewed interest (3–5) in the conformational analysis of dienes, a subject that occupied the attention of experimentalists and theoreticians for decades.[4] Our plan was to study a series of alkyl-substituted 1,3-dienes computationally by AM1, to calculate heats of formation as a function of the dihedral (twist) angle between the double bonds, to identify the stablest conformations, and to calculate the π_-, π_+ splittings for planar (*s-cis* and *s-trans*) and nonplanar conformations. By comparing these values to the splittings obtained experimentally by UPS (see ref. 6 for a comprehensive review on conformational analysis by UPS), we hoped to establish whether combined AM1/UPS studies will be useful generally for obtaining information on conformational dynamics and conjugative and homoconjugative interactions of alkyl-substituted polyenes in the gas phase, and, of course, for determining structure. In fact, a study of this type recently led to a redetermination and correction of the photoelectron (pe) spectrum of (*Z*)-2-methylpentadiene (1).

Encouraged by this initial success, we undertook a study of four isomeric dimethyl-2,4-hexadienes, the products of photochemical ring opening of 1,3,4,4- and 1,3,3,4-tetramethylcyclobutenes (**1** and **2**, respectively) (7), to extend this research to more highly alkylated butadienes. Our strategy was to study (*E*)-2,3-dimethyl-2,4-hexadiene (*E*-**3**) and (*Z*)-2,3-dimethyl-2,4-hexadiene (*Z*-**3**) obtained from **1** to establish whether the results of an AM1/UPS study correlate with the structures of these dienes assigned previously with a high degree of certainty (8). This was to be followed by an identical study of the isomeric 2,4-dimethyl-2,4-hexadienes obtained from **2** in order to identify the (*E*) and (*Z*) isomers, which, as far as we were aware, had not yet been accomplished with certainty (9). The results of our study are documented and discussed in this publication.

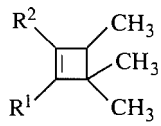

1; $R^1 = CH_3$, $R^2 = H$
2; $R^1 = H$, $R^2 = CH_3$

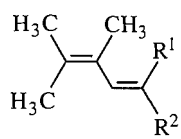

E-**3**; $R^1 = H$, $R^2 = CH_3$
Z-**3**; $R^1 = CH_3$, $R^2 = H$

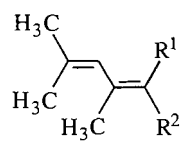

E-**4**; $R^1 = H$, $R^2 = CH_3$
Z-**4**; $R^1 = CH_3$, $R^2 = H$

Results and discussion

Photoelectron spectra

It has been established that, upon photolysis, cyclobutenes **1** and **2** each yield two dienes as major products that are readily

[1]Author to whom correspondence may be addressed.

[2]Natural Sciences and Engineering Research Council of Canada University Research Fellow, 1983–1993.

[3]Revision received July 11, 1990.

[4]See ref. 3 for a comprehensive list.

Can. J. Chem. Downloaded from www.nrcresearchpress.com by 91.121.58.235 on 09/07/12
For personal use only.

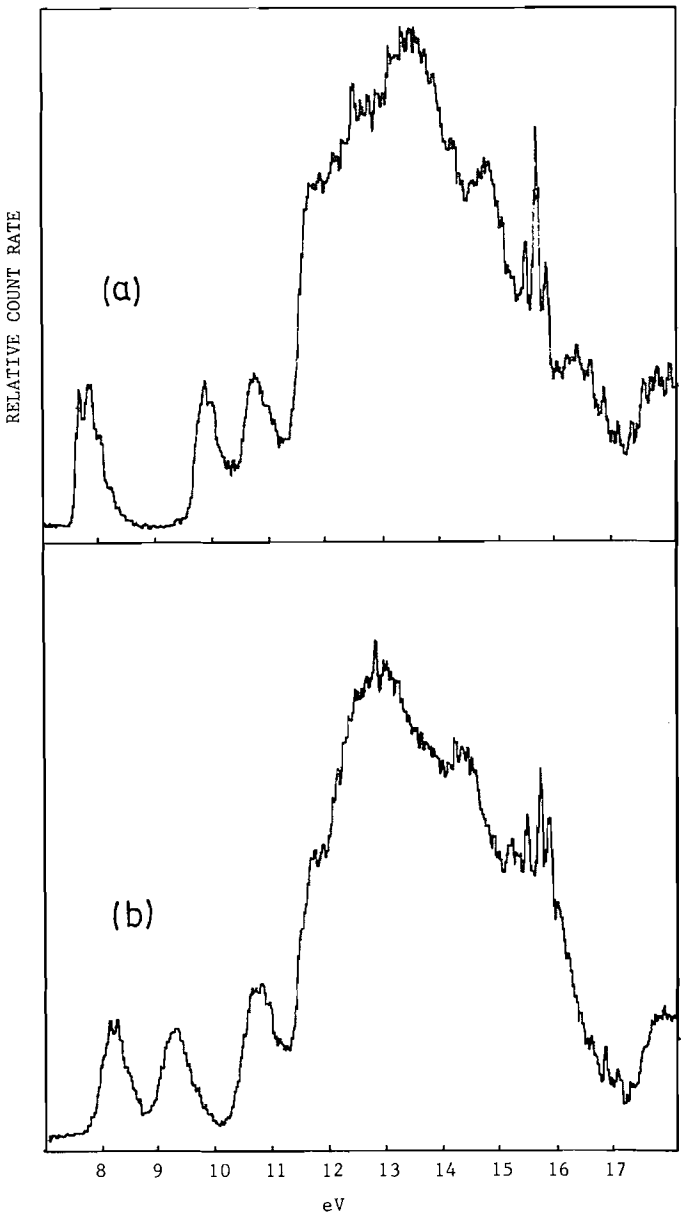

FIG. 1. He(I) photoelectron spectra; (a) *E*-**3** and (b) *Z*-**3**.

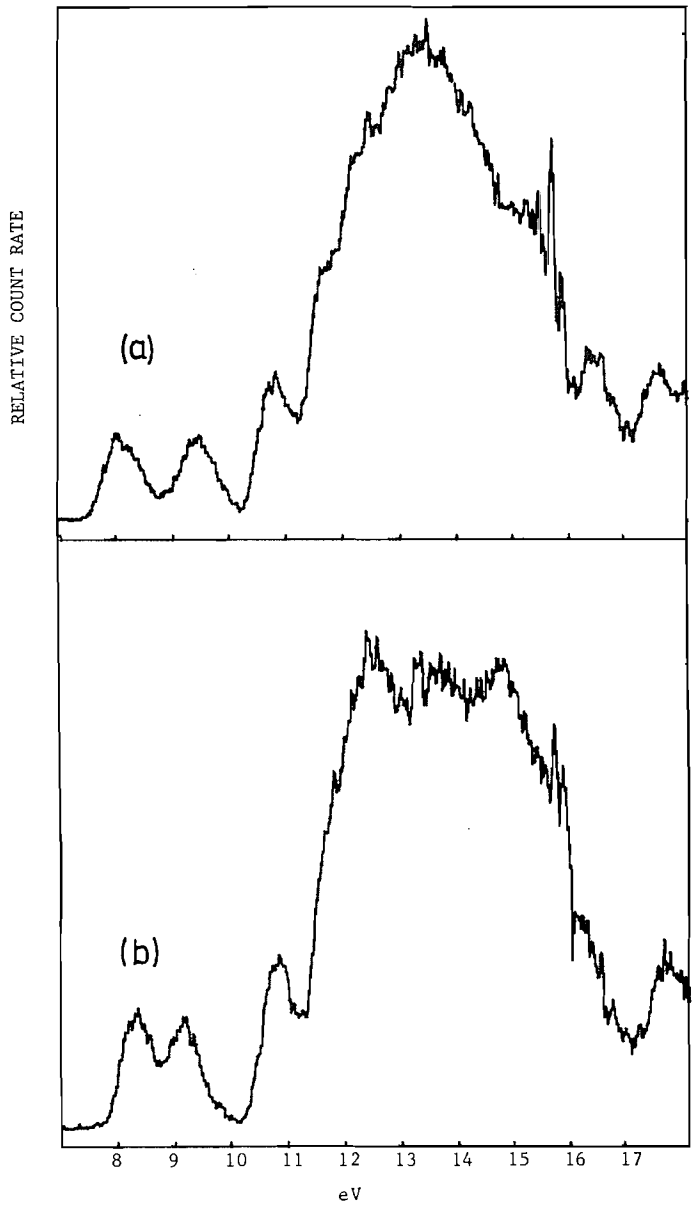

FIG. 2. He(I) photoelectron spectra; (a) *E*-**4** and (b) *Z*-**4**.

separated by preparative gc (7). In Fig. 1 are shown pe spectra (a) and (b) of *E*-**3** and *Z*-**3** obtained from **1**. Figure 2 shows the pe spectra of the hexadienes obtained from **2**. Table 1 lists the ionization energies (IE's) corresponding to the first three low-energy bands and the π_-, π_+ splittings (ΔIE's); it is seen that these dienes exhibit a range of splittings.

Computational studies

Planar s-trans-*dienes*

To determine how accurately AM1 computes splittings and rotational barriers of dienes, several studies were carried out. Firstly, the splittings of a series of planar *s-trans* dienes (2-methylbutadiene, 2,3-dimethylbutadiene, (*E*,*E*)-2,4-hexadiene, and 2,5-dimethyl-2,4-hexadiene) were obtained computationally, assuming Koopmans' theorem, as the difference between the eigenvalues (ϵ_i's) of the HOMO (π_-) and the NHOMO (π_+). The structures were fully optimized in all cases. For these dienes, a π_-, π_+, σ ordering of the highest three levels is predicted by AM1. In Table 2 are listed the eigenvalues

TABLE 1. Vertical ionization energies of dimethyl-2,4-hexadienes

	IE_v (eV)[a]			
Diene	π_-	π_+	σ	ΔIE_v (eV)[b]
E-**3**	7.83	9.87	10.78	2.04
Z-**3**	8.13	9.30	10.85	1.17
E-**4**	8.00	9.48	10.85	1.48
Z-**4**	8.30	9.14	10.83	0.84

[a]Estimated error ±0.025 eV.
[b]π_+, π_- splitting.

of π_-, π_+, and the first σ level, the difference between π_- and π_+, and the experimentally determined ΔIE_v's (10). On this basis it is clear that AM1 predicts splittings of planar *s-trans* dienes with good accuracy, although the computed eigenvalues are approximately 0.6 eV higher than the IE_v's. It should be noted here that AM1 assigns the three highest MO's of butadiene

TABLE 2. Vertical ionization energies and eigenvalues of dienes

Diene	IE_v (eV) π_-	π_+	σ	ΔIE_v	$-\epsilon^d$ π_-	π_+	σ	$\Delta\epsilon^g$
2-Methylbutadiene	8.85	10.81	11.83[a]	1.96	9.21	11.35	11.66	2.14
2,3-Dimethylbutadiene	8.71	10.29	11.94[a]	1.58	9.13	10.80	11.63	1.67
E,E-2,4-Hexadiene	8.19	10.66	11.56[a]	2.47	8.78	11.31	11.76	2.53
2,5-Dimethyl-2,4-hexadiene	7.67	10.13	10.96[a]	2.46	8.37	10.77	11.51	2.43
1,2-Dimethylenecyclobutane	8.66	10.62		1.96[b]	9.30	11.23		1.87
					9.20	11.04	(MNDO)	1.84
2,3-Dimethylenebicyclo[2.2.1]heptane	8.41	10.20		1.79[c]	9.19	10.95		1.76
1,2-Dimethylenecyclohexane	8.92	9.85		0.93[c]	9.27	10.44[e]		1.17
					9.36	10.38	(MNDO)[f]	1.02

[a]Taken from ref. 10.
[b]Taken from ref. 13.
[c]Taken from ref. 14.
[d]Computed using AM1 unless stated otherwise.
[e]Dihedral angle for fully optimized geometry 40.9°.
[f]Dihedral angle for fully optimized geometry 52.3°.
[g]π_-, π_+ splitting.

as π_-, σ, π_+. This is not in accord with Heilbronner's analysis (11) or the results of *ab initio* calculations (12), which yield a π_-, π_+, σ ordering, as does MNDO.[5]

Planar and twisted s-cis *dienes*

Table 2 also lists the π_- and π_+ eigenvalues of 1,2-dimethylenecyclobutane, 2,3-dimethylenebicyclo[2.2.1]heptane, and 1,2-dimethylenecyclohexane computed by AM1, along with the experimentally determined IE_v's and the ΔIE_v's (13, 14). While AM1 computes the splittings for dimethylenecyclobutane and dimethylenenorbornane with good accuracy, MNDO computes the twist angle and the splitting for dimethylenecyclohexane with greater accuracy than AM1.

Butadiene

Figure 3 shows how ΔH_f for butadiene depends on the C1—C2—C3—C4 dihedral (twist) angle. Beginning with the planar *s-cis* conformer, the dihedral angle was incremented 15° and the geometry was optimized at each stage.

The heats of formation are reproducible to ±0.1 kcal regardless of the increment (15° or 30°) or the starting dihedral angle (0° or 180°). It should be pointed out that identical ΔH_f's were computed when the optimization criteria were increased by 10 times and the SCF criteria by 100 times (PRECISE). The values for the barrier to rotation (1.97 kcal) and the difference in energy between the planar *s-trans* and *s-cis* conformers (0.81 kcal) are lower than the experimental values for the barrier (3.90–4.70 kcal) (15, 16) and the energy difference (2.50–3.08 kcal) (15, 16). By subtracting scaled corrections of 1.8, 1.4, 1.0, 0.7, 0.4, and 0.2 kcal from the ΔH_f values computed for dihedral angles of 180°, 165°, 150°, 135°, 120°, and 105°, respectively, the rotational barrier and the *s-trans* − *s-cis* energy difference for butadiene can be brought into the experimental ranges. This also brings the computed ΔH_f for butadiene (29.9 kcal/mol before correction) closer to the experimental value of 26.6 kcal/mol (17).

*(*E*)-2,3-Dimethyl-2,4-hexadiene (*E*-**3**)*

Figure 4(a) shows how ΔH_f of (*E*)-2,3-dimethyl-2,4-hexadiene (*E*-**3**) obtained computationally depends on the C2—C3—C4—C5 dihedral (twist) angle; conformation *E*-**3**-c1 is the starting point (dihedral angle 180°) with the conformations

[5]This work.

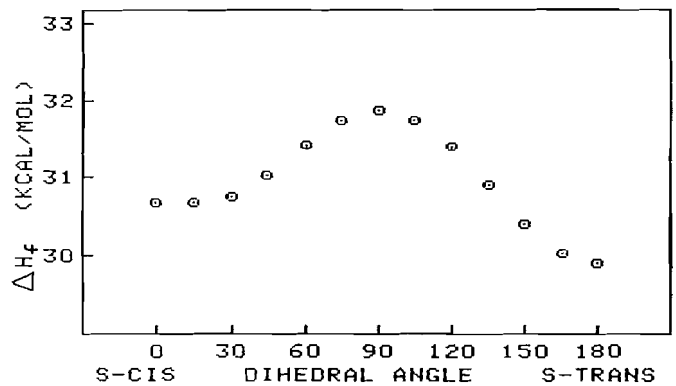

FIG. 3. Plot of ΔH_f of butadiene versus dihedral angle.

of the methyl groups locked as indicated in this structure. On the basis of these calculations, *E*-**3**-c1 is predicted to be the stablest conformation of *E*-**3** and it should be preferentially populated in the gas phase. In principle, the ΔH_f values for the various conformers with dihedral angles between 180° and 90° could be adjusted by the corrections estimated for butadiene. However, it is important to point out here that it has been shown experimentally and computationally that alkyl substituents at C2 and C3 lower the barrier to rotation and the difference in energy between twisted *s-cis* and planar *s-trans* conformations of 1,3-dienes (4, 18). Thus the correction factors estimated for butadiene should be considered as maximum values when applied to methylated derivatives, and their use in adjusting the computed ΔH_f values for *E*-**3** will not alter the conclusion reached on the basis of Fig. 4(a). Figure 4(b) shows plots of the eigenvalues of the HOMO, NHOMO, and the first σ level as a function of dihedral angle. It is important to note here that AM1 computes a π_-, π_+, σ order for these highest occupied MO's. The HOMO (π_-) and NHOMO (π_+) eigenvalues exhibit different dependencies on the twist angle (Fig. 4(b)) and the splittings range from 2.15 to 0.5 eV as shown in Fig. 4(c); as shown in Fig. 4(b) the π_- eigenvalue is less sensitive to the twist angle than the π_+ eigenvalue; the eigenvalue of the first σ level is essentially insensitive to twist angle and is slightly stabilized as the dihedral angle approaches 90°. That the computed splitting (2.15 eV) (Table 3) for planar *s-trans-E*-**3** is in good

Can. J. Chem. Downloaded from www.nrcresearchpress.com by 91.121.58.235 on 09/07/12
For personal use only.

Can. J. Chem. Downloaded from www.nrcresearchpress.com by 91.121.58.235 on 09/07/12
For personal use only.

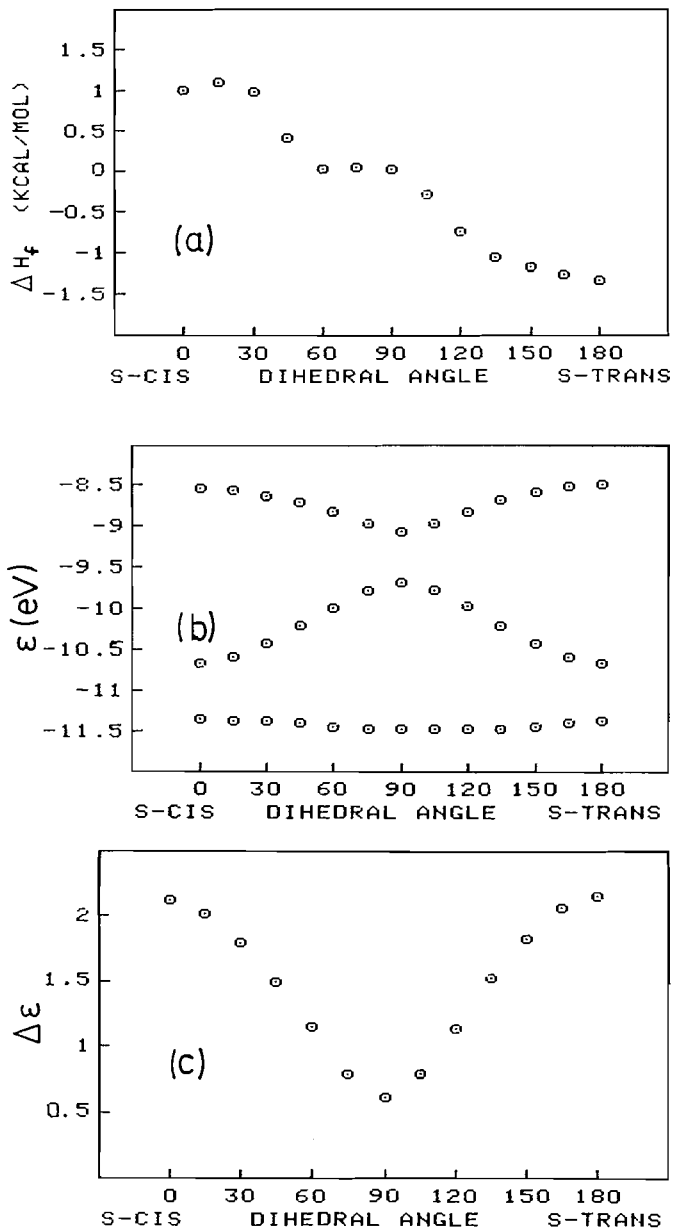

FIG. 4. (a) Plot of ΔH_f of *E*-**3** versus dihedral angle; (b) plot of π_-, π_+, and σ eigenvalues of *E*-**3** versus dihedral angle; (c) plot of π_-, π_+ splitting of *E*-**3** versus dihedral angle.

agreement with the ΔIE_v (2.04 ± 0.05 eV) obtained experimentally establishes the validity of the AM1 calculations. As shown in Fig. 4(b), the HOMO will show a lower sensitivity to twist angle than the NHOMO and the "splitting" will not be zero at a dihedral angle of 90°. As is seen from the HOMO of *E*-**3** (Fig. 5(a)), the C-H's of the C8 methyl interact homohyperconjugatively with the π-system. This is not the case for the NHOMO (Fig. 5(b)). Drawings of the HOMO and NHOMO of *E*-**3** were obtained using DRAW3D (19), a modified version of DRAW (20), which generates MOs by stacking MO contours generated by DEN3D (19); DEN3D is a modified version of DENSITY (21). In these plots, the 0.01 au contours are stacked. According to Heilbronner's analysis (11),

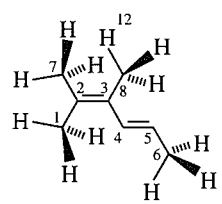

E-**3**-cl

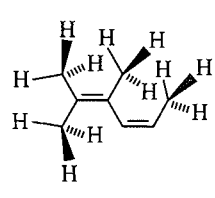

Z-**3**-cl

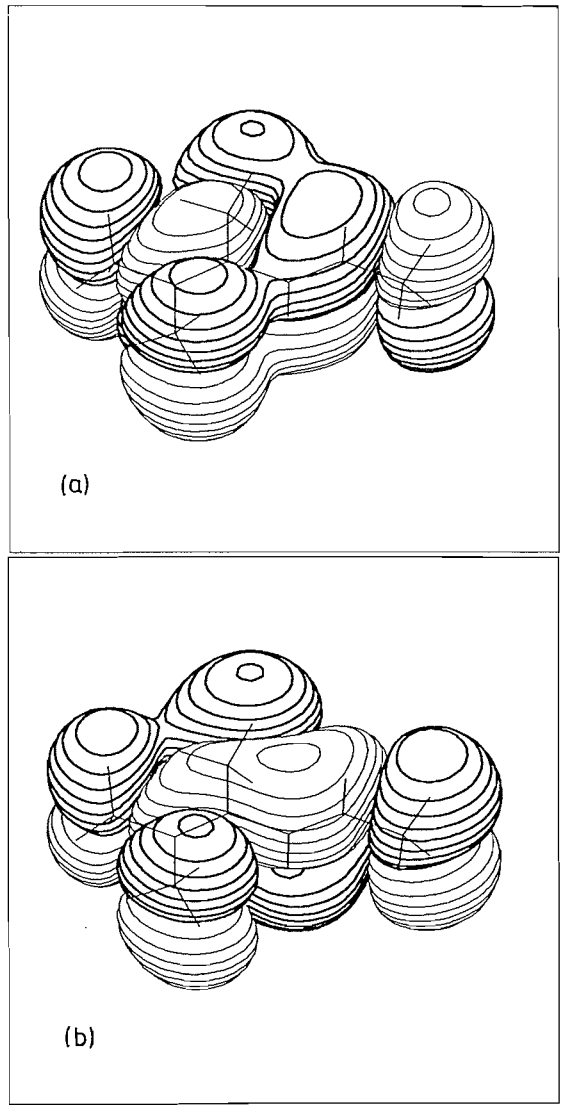

FIG. 5. Molecular orbital density plots (0.01 au); (a) HOMO (π_-) and (b) NHOMO (π_+) of *E*-**3**.

TABLE 3. Eigenvalues of dimethyl-2,4-hexadienes

	−ε (eV)			
Diene	π_-	π_+	σ	$\Delta\epsilon^f$
E-**3**	8.50	10.65	11.37[a]	2.15
Z-**3**	8.84	9.96	11.37[b]	1.12
E-**4**	8.74	10.19	11.51[c]	1.45
Z-**4**	8.92	9.81	11.44[d]	0.89
	8.93	9.84	11.52[e]	0.91

[a]Dihedral angle 180°.
[b]Dihedral angle 120°.
[c]Dihedral angle 45°.
[d]Dihedral angle 120°.
[e]Dihedral angle 60°.
[f]π_-, π_+ splitting.

Can. J. Chem. Downloaded from www.nrcresearchpress.com by 91.121.58.235 on 09/07/12
For personal use only.

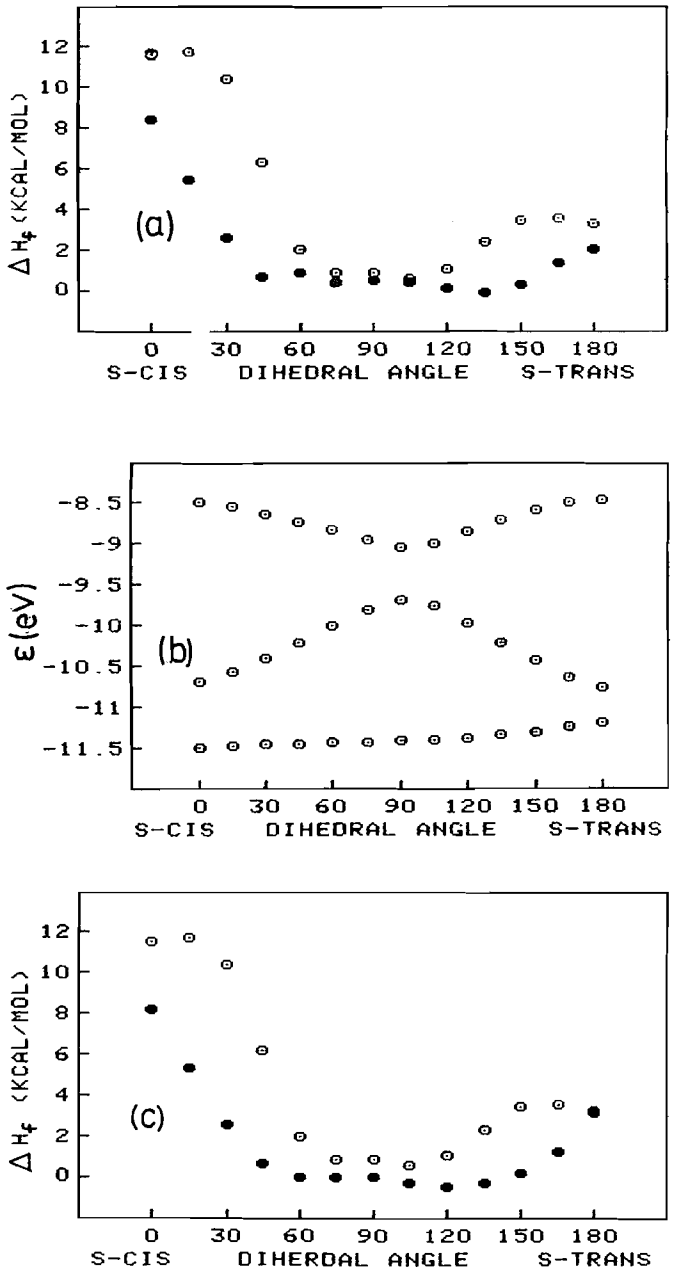

FIG. 6. (a) Plot of ΔH_f of *Z*-**3** versus dihedral angle; (b) plot of π_-, π_+, and σ eigenvalues of *Z*-**3** versus dihedral angle; (c) plot of ΔH_f (PRECISE) of *Z*-**3** versus dihedral angle.

this interaction is the source of the reduced splitting observed for planar *s-trans*-1,3-dienes bearing methyl groups at C2 and C3, relative to dienes substituted with methyl groups at the terminal carbons. For example, the splittings of butadiene, 2,4-hexadiene, 2-methylbutadiene, and 2,3-dimethylbutadiene are 2.47, 2.47, 1.96, and 1.58 eV, respectively (10). This homohyperconjugative interaction would account for the fact that the π_-, π_+ splitting of *E*-**3** (2.04 ± 0.05 eV) is 0.4 eV less than the splitting of 2,5-dimethyl-2,4-hexadiene (2.45 eV) (10). It is important to note that this differential stabilization of the HOMO in the planar *s-trans* conformation also accounts for the different sensitivities, relative to *E*-**3**, of the HOMO and NHOMO IE's of substituted dienes where twisted conformations are preferentially populated in the gas phase. That the splitting is not zero at a dihedral angle of 90° is primarily due to the fact that the double bonds are unequally substituted; one bears four alkyl substituents and the other only two. Consequently, for the 90° conformation, the HOMO should be localized on C1, C2, C3, C7, and C8 and the NHOMO on C4, C5, and C6. MO's generated by DEN3D/DRAW3D (not shown) for this conformation show that this is the case.

The effect of the C8 methyl conformation on the HOMO and NHOMO eigenvalues was probed by driving the H12—C8—C3—C2 dihedral angle through 15° increments with the other dihedrals locked as shown in *E*-**3**-c1. We find that the eigenvalues of both MO's are essentially insensitive to the twist angle. This study shows that the homohyperconjugative interaction, which results in a stabilization of the HOMO by 0.4 eV, is essentially independent of conformation of the C8 methyl group.

(Z)-2,3-Dimethyl-2,4-hexadiene (Z-3)

Figure 6(a) includes two plots; one (⊙) shows the dependency of ΔH_f of (*Z*)-2,3-dimethyl-2,4-hexadiene (*Z*-**3**) on dihedral angle. In this case the starting point is *Z*-**3**-c1 with the conformations of the methyl groups locked as shown in this structural formula. Since there is buttressing of the methyl groups in this case, a study was carried out with full optimization of all parameters as the C2—C3—C4—C5 dihedral angle was incremented by 15°. These results (●) are also included in Fig. 6(a). It is seen that conformers with dihedral angles in the region of 105°–135° should be preferentially populated for *Z*-**3**. This conclusion is reached even if the heats of formation of the conformers with dihedral angles ranging from 90 to 180° are adjusted downward by the corrections deduced for butadiene. Here, as in the case of *E*-**3**, AM1 computes a π_-, π_+, σ order for the three highest occupied MO's, and Fig. 6(b) shows plots of the eigenvalues of π_-, π_+, and σ as a function of dihedral angle. For dihedral angles between 105 and 135°C, the computed splittings range from 0.8 to 1.5 eV. For *Z*-**3**, we also carried out computational studies with optimization criteria increased 10 times and SCF criteria by 100 times (PRECISE) and the results are shown in Fig. 6(c) (⊙, methyl groups locked as in *Z*-**3**-c1; ●, full optimization). It is seen that when the methyl dihedrals are locked, the ΔH_f's computed with the different optimization and SCF criteria are virtually identical. In the case where the structures are fully optimized at each stage, the differences in the ΔH_f's are small. These results establish that the default optimization and SCF criteria can be used to compute the ΔH_f as a function of twist angle for methyl-substituted 1,3-butadienes, especially if the methyl conformations are locked. For a dihedral angle of 120°, the computed splitting is 1.12 eV (Table 3); the experimental value is 1.17 ± 0.05 eV. AM1 calculations on (*Z*)-2-methyl-1,3-pentadiene established that the planar *s-trans* conformer is 3.0–3.9 kcal/mol higher in energy than the planar *s-trans* (*E*) isomer depending on the conformations of the methyl group (1). That (*Z*)-1,3-pentadiene was calculated to be 0.4 kcal/mol higher in energy than the (*E*) isomer establishes that the 1,3 CH_3,CH_3 steric interaction of planar *s-trans* *Z*-**3** increases the energy by 2.7–3.6 kcal relative to *E*-**3**; this steric interaction twists *Z*-**3**. In the case of *Z*-**3**, twisted *s-cis* conformers are not populated because of the prohibitive steric interaction between the C2 and terminal methyls.

The differential sensitivities of HOMO and NHOMO of the 2,3-dimethylhexadienes to twist angle predicted by AM1 are corroborated experimentally by the IE_v's of *Z*-**3**. Relative to *E*-**3**, the NHOMO is destabilized by 0.57 eV and the HOMO is stabilized by 0.3 eV, precisely as predicted by AM1 (Fig. 6(b)).

Can. J. Chem. Downloaded from www.nrcresearchpress.com by 91.121.58.235 on 09/07/12
For personal use only.

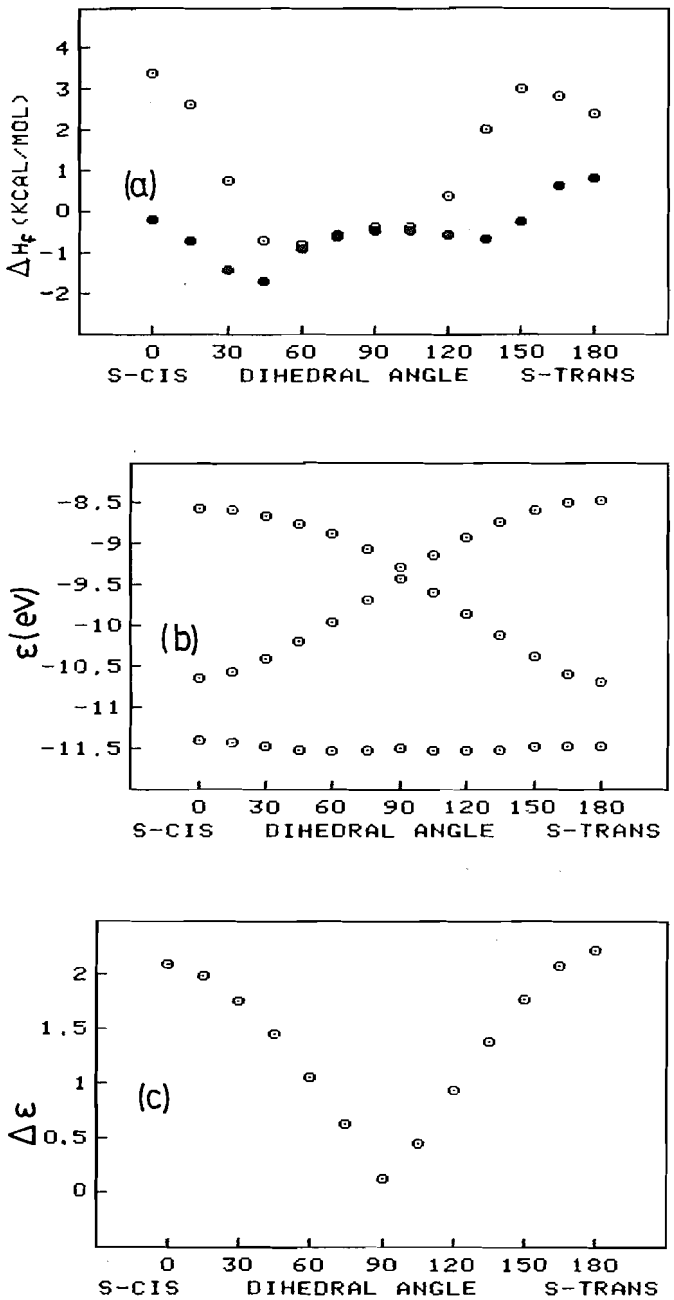

FIG. 7. (a) Plot of ΔH_f of *E*-**4** versus dihedral angle; (b) plot of π_-, π_+, and σ eigenvalues of *E*-**4** versus dihedral angle; (c) plot of π_-, π_+ splitting of *E*-**4** versus dihedral angle.

(F) (E)*-2,4-Dimethyl-2,4-hexadiene* (E-*4*)

Figure 7(a) shows a plot (⊙) of ΔH_f versus dihedral angle for (*E*)-2,4-dimethyl-2,4-hexadiene (*E*-**4**). In this case, the starting conformation is *E*-**4**-c1 with the methyl groups locked as shown in this structural formula. The results of an analogous

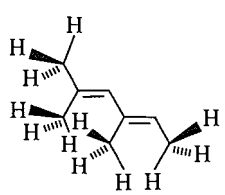

E-**4**-cl

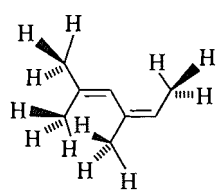

Z-**4**-cl

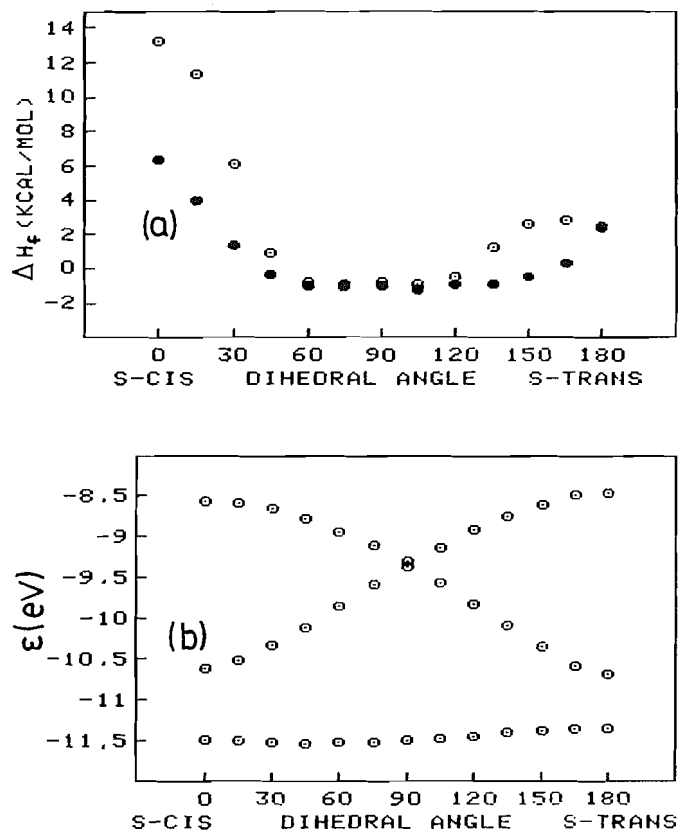

FIG. 8. (a) Plot of ΔH_f of *Z*-**4** versus dihedral angle; (b) plot of π_-, π_+, and σ eigenvalues of *Z*-**4** versus dihedral angle.

study involving full optimization of *E*-**4** are also given (●) in Fig. 7(a). On the basis of these results, twisted *s-cis* conformers with dihedral angles in the range of 45°–60° will be preferentially populated in the gas phase. Figure 7(b) shows how the eigenvalues of π_-, π_+, and σ depend on the dihedral angle. Figure 7(c) shows how the computed splitting depends on the dihedral angle.

A splitting of 1.45 eV computed by AM1 (Table 3) for a dihedral angle of 45° is in good agreement with the experimentally observed value of 1.48 ± 0.05 eV. For this twisted *s-cis* diene the π_- and π_+ bands are broader — the FWHM is approximately 0.8 eV — than the bands of *E*-**3** (planar *s-trans*) (0.5 eV) and *Z*-**3** (twisted *s-trans*) (0.5 eV). Here too, as in the case of *Z*-**3**, the differential sensitivities of π_- and π_+ to twist angle predicted by AM1 are corroborated by the shifts of π_- and π_+ relative to the bands of *E*-**3**: 0.17 eV for π_- and 0.39 eV for π_+. These shifts correlate well with the shifts predicted by AM1 as seen in Fig. 7(b). Thus we assign structure *E*-**4** to the 2,4-dimethyl-2,4-hexadiene, which exhibits a ΔIE_v of 1.48 ± 0.05 eV.

As is the case for *Z*-**3**, *E*-**4** is twisted by a 1,3 interaction of the methyls at C2 and C4; buttressing of these methyls by the terminal methyls in the planar *s-trans* conformations could lead to greater steric strain than in the case of *Z*-**3**. In the case of *E*-**4**, twisted *s-cis* conformers can be populated because there is no steric interaction between the C2 and terminal methyls.

(Z)-2,4-Dimethyl-2,4-hexadiene (Z-*4*)

Figure 8(a) shows plots of ΔH_f versus dihedral angle for (*Z*)-2,4-dimethyl-2,4-hexadiene (*Z*-**4**), starting with *Z*-**4**-c1. In one study, the methyls were locked (⊙) and in the other, geometries were fully optimized (●). According to these

results, conformations with dihedral angles ranging from 60° to 120° will be preferentially populated in this case. Figure 8(b) shows how the eigenvalues of π_-, π_+, and σ depend on dihedral angle. On the basis of the data summarized in Figs. 8(a) and 8(b), the splitting will range between 0.95 and 0.15 eV. The computed splittings for dihedral angles of 120° and 60° are 0.89 and 0.91 eV, respectively (Table 3), and the experimental ΔIE_v for the second isomer of **4** is 0.84 ± 0.05 eV. Here too, as in the case of *Z*-**3** and *E*-**4**, the differential sensitivities of π_- and π_+ to twist angle predicted by AM1 are corroborated by the shifts relative to *E*-**3**; π_- is stabilized by 0.47 eV and π_+ is destabilized by 0.73 eV, in good agreement with the eigenvalues given in Fig. 8(b) for dihedral angles of 120° and 60°. Thus we assign structure *Z*-**4** to the 2,4-dimethyl-2,9-hexadiene, which exhibits a ΔIE_v of 0.84 ± 0.05 eV.

The narrower range of conformations populated in the case of *Z*-**4** is likely due to several factors. In case of the planar *s-cis* conformation there is a steric interaction between the C2 and terminal methyls; for the planar *s-trans* conformation, opening of the C2—C3—C4 bond angle is restricted by a steric interaction of the terminal methyl at C4 with the hydrogen at C3.

Conclusions

Through a study of a group of alkyl-substituted 1,3-dienes we found that a combination of AM1 computations and He(I) photoelectron spectroscopy (UPS) can be used for conformational analysis and for studying conjugative and homoconjugative interactions of this class of compounds. Using AM1/UPS we have determined the structures of the isomeric (*E*)- and (*Z*)-2,4-dimethyl 2,4-hexadienes obtained from the photolysis of 1,3,3,4-tetramethylcyclobutene.

Experimental

Preparation of dienes

Dienes *E*-**3**, *Z*-**3**, *E*-**4**, and *Z*-**4** obtained from photolysis of **1** and **2** (7) were >99% pure by vpc analysis (7).

Ultraviolet photoelectron spectroscopy

The He(I) pe spectra of *E*-**3**, *Z*-**3**, *E*-**4**, and *Z*-**4** were obtained on a pe spectrometer (22) operated in the conventional mode, and are averages of 50–100 scans.

Computational studies

Computational (RHF) studies were carried out using AM1, Version 2.1, of the general purpose molecular orbital computational package AMPAC (2) modified to run on Sun 3/60 and IBM RT computers. Optimizations were carried out using the AM1 default parameters. For butadiene and *Z*-**3**, optimizations were also carried out using PRECISE. This increases the optimization criteria by 10 times and the SCF criteria by 100 times. The MO density plots were obtained using DEN3D and DRAW3D (19) and printed as SUN 3/60 masterfiles on a Laser Jet II printer.

Acknowledgements

We thank the Natural Sciences and Engineering Research Council of Canada and IBM Canada Ltd. for financial support. The IBM RT was provided by IBM Canada Ltd. under the auspices of the McMaster University – IBM Canada Ltd. Cooperative Project.

1. N. H. WERSTIUK and G. TIMMINS. Can. J. Chem. **66**, 2954 (1988).
2. Dewar Research Group and J. J. P. Stewart. Austin Method 1 Package; 1.0 QCPE 506. QCPE Bull. **6**, 2 (1986).
3. J. J. FISHER and J. MICHL. J. Am. Chem. Soc. **109**, 1605 (1987).
4. M. E. SQUILLACOTE, J. C. SEMPLE, and P. W. MUI. J. Am. Chem. Soc. **107**, 6842 (1985).
5. E. HONEGGER, YANG ZHONG-ZHI, E. HEILBRONNER, W. V. E. DOERING, and J. C. SCHMIDHAUSER. Helv. Chim. Acta, **67**, 640 (1984).
6. R. S. BROWN and F. S. JORGENSEN. Electron Spectrosc. **5**, 1 (1984).
7. K. B. CLARK and W. J. LEIGH. Can. J. Chem. **66**, 1571 (1988).
8. P. G. GASSMAN, T. J. ATKINS, and F. J. WILLIAMS. J. Am. Chem. Soc. **93**, 1812 (1971).
9. A. R. KRASKA, L. I. CHERNEY, and H. SCHECTER. Tetrahedron Lett. **23**, 2163 (1982).
10. P. MASCLET, G. MOUVIER, and J. F. BOCQUET. J. Chim. Phys. **78**, 99 (1981).
11. M. BEEZ, G. BIERI, H. BOCK, and E. HEILBRONNER. Helv. Chim. Acta, **56**, 1028 (1973).
12. K. KIMURA, S. KATSUMATA, Y. ACHIBA, Y. YAMAZAKI, and S. IWATA. *In* Handbook of HeI photoelectron spectra of fundamental organic molecules. Japan Scientific Societies Press, Tokyo. 1981. p. 63.
13. P. HEMMERSBACK, M. KLESSINGER, and P. BRUCKMANN. J. Am. Chem. Soc. **100**, 6344 (1978).
14. P. ASMUS and M. KLESSINGER. Tetrahedron, **30**, 2477 (1974).
15. M. E. SQUILLACOTE, R. S. SHERIDAN, O. L. CHAPMAN, and F. A. L. ANET. J. Am. Chem. Soc. **101**, 3657 (1979), and references therein.
16. D. W. MUI and E. GRUNWALD. J. Am. Chem. Soc. **104**, 6562 (1982).
17. J. B. PEDLEY and G. RYLANCE. "Sussex–N.P.L. computer analyzed thermochemical data: organic and organometallic compounds." Sussex University, 1977.
18. K. KAVANA-SAEBØ, S. SAEBØ, and J. E. BOGGS. J. Mol. Struct. **106**, 259 (1984).
19. A. ELMER and M. A. BROOK. Tetrahedron Comput. Methodol. **2**, 223 (1989).
20. D. M. STORCH. DRAW; QCPE 493. Molecule drawing program. QCPE Bull. **5**, 61 (1985).
21. J. J. P. STEWART and DEWAR RESEARCH GROUP. DENSITY; QCPE 492. A package to produce density plots from MOPAC calculations. QCPE Bull. **5**, 59 (1985).
22. N. H. WERSTIUK, D. N. BUTLER, and E. SHAHID. Can. J. Chem. **65**, 760 (1986).

Can. J. Chem. Downloaded from www.nrcresearchpress.com by 91.121.58.235 on 09/07/12
For personal use only.

The metabolites of *Talaromyces flavus*: Part 1. Metabolites of the organic extracts

WILLIAM A. AYER[1] AND JULIE S. RACOK
Department of Chemistry, University of Alberta, Edmonton, Alta., Canada T6G 2G2

Received February 5, 1990

WILLIAM A. AYER and JULIE S. RACOK. Can. J. Chem. **68**, 2085 (1990).

The soil fungus *Talaromyces flavus* (Klöcker) Stolk and Samson is an effective biological control for Verticillium wilt of eggplant (*Solanum melongena* L.), a disease caused by the fungus *Verticillium dahliae* Kleb. The organic soluble metabolites produced when the fungus is grown in liquid still culture include D-glucono-1,4-lactone (**1**), 5-hydroxymethylfurfural (**5**), the previously unreported tetraketides, 4,6-dihydroxy-5-methylphthalide (**3**) and methyl 4-carboxy-5-hydroxyphthalaldehydate (**8**), a hexaketide, 7-hydroxy-2,5-dimethylchromone (**6**), and a metabolite believed to be 3-hydroxymethyl-6,8-dimethoxycoumarin (**10**). A number of higher order polyketides have been isolated including altenusin (**11**), dehydroaltenusin (**12**), and the previously unreported desmethyldehydroaltenusin (**14**). A structurally and biosynthetically interesting spirocyclic metabolite, which we have named talaroflavone (**16**), as well as a related compound, deoxytalaroflavone (**18**), have also been obtained.

Key words: *Talaromyces flavus*, fungal metabolites, talaroflavone, 4,6-dihydroxy-5-methylphthalide.

WILLIAM A. AYER et JULIE S. RACOK. Can. J. Chem. **68**, 2085 (1990).

Le champignon du sol *Talaromyces flavus* (Klöcker) Stolk et Samson contrôle biologiquement et d'une façon efficace la flétrissure par le Verticillium de l'aubergine (*Solanum melongena* L.), une maladie causée par le champignon *Verticillium dahliae* Kleb. Les métabolites organiques solubles qui sont produits lorsqu'on fait croître le champignon dans un milieu de culture comprennent : la D-glucono-1,4-lactone (**1**), le 5-hydroxyméthylfurfural (**5**), les tétrakétides 4,6-dihydroxy-5-méthylphtalide (**3**) et 4-carboxy-5-hydroxyphtalaldéhydate de méthyle (**8**) qui n'avaient pas été rapportés antérieurement, un hexakétide, la 7-hydroxy-2,5-diméthylchromone (**6**), ainsi qu'un métabolite que l'on croit être la 3-hydroxyméthyl-6,8-diméthoxycoumarine (**10**). On a aussi isolé un certain nombre de polykétides d'ordre plus élevé, dont l'alténusine (**11**), la déhydroalténusine (**12**) ainsi que la desméthyldéhydroalténusine (**14**) qui n'avait pas été rapportée antérieurement. On a aussi obtenu un métabolite spirocyclique, intéressant d'un point de vue structural et biosynthétique, que l'on a appelé talaroflavone (**16**) ainsi qu'un composé apparenté, la désoxytalaroflavone (**18**).

Mots clés : *Talaromyces flavus*, métabolites de champignon, talaroflavone, 4,6-dihydroxy-5-méthylphtalide.

[Traduit par la revue]

Introduction

The soil fungus *Talaromyces flavus* (Klöcker) Stolk and Samson is the most common species of its genus. This ascomycete is frequently isolated from soil, although it may also occur on organic materials undergoing decomposition. The species is widespread in its distribution but it is most commonly reported from the warmer regions of the world (1, 2). Our interest in the metabolites produced by *T. flavus* was stimulated by the report of its effectiveness as a biological control for Verticillium wilt of eggplant (*Solanum melongena* L.), a disease caused by the fungus *Verticillium dahliae* Kleb. (3). The Verticillium wilt organism is a widespread soil inhabitant that infects a variety of herbaceous and woody plants. Further details regarding this biological control and the nature of the wilting disease are discussed in Part 2 of this series.

A number of metabolites of polyketide origin have been isolated from species of *Talaromyces* (4–10) other than *T. flavus*. The imperfect (conidial) state of *T. flavus*, *Penicillium dangeardii* Pitt, produces three metabolites that are reported to show antibiotic activity (11–15). The isolation of a water soluble compound possessing antibiotic activity from *T. flavus* has recently been reported (16). In addition to the aforementioned antifungal action against *V. dahliae*, *T. flavus* is reported to display biological activity towards the plant pathogens *Sclerotinia sclerotiorum* (Lib.) de Bary (17), *Rhizoctonia solani* Kühn (18), and *V. albo-atrum* Reinke and Berth. (19). The adoption of a biological control agent for a soilborne disease requires that the organism be able to establish itself in different soils.[2] Studies of the edaphic parameters associated with the establishment of *T. flavus* as a biological control suggest that it may be suitable for widespread use (21, 22). In view of these observations we have undertaken an investigation of the metabolites produced by the strain ATCC 52201 (UAMH 4890) of *T. flavus*, when it is grown in liquid still culture. In this paper we report the isolation of the organic soluble metabolites produced by *T. flavus*. The following paper describes the isolation of the water soluble metabolites and reports on the biological activity of the fungus and on labelling studies undertaken to examine the incorporation of [1-^{13}C] labelled acetate into the biosynthetically interesting metabolites we obtained.

Preliminary studies indicated that *T. flavus* grows best on a malt extract medium (as compared to potato dextrose broth and Czapek medium). Liquid still cultures of *T. flavus* were grown on this medium for 4 weeks. The culture broth was decanted from the mycelium by filtration. The mycelium was subjected to Soxhlet extraction with ethyl acetate or methanol. Addition of methanol to the two extracts afforded an insoluble white solid identified as D-mannitol. The methanol soluble portions of the ethyl acetate and methanol Soxhlet extracts were each subjected to chromatography over silica gel. The ubiquitous metabolites methyl linoleate, linoleic acid, a triglyceride, a diglyceride, and ergosterol were isolated. Identification of the fatty acid residues comprising the di- and triglyceride was achieved by analysis of their mass spectral fragmentation patterns. The triglyceride contains linolenic, linoleic, and palmitic acids, while the diglyceride carries the latter two acyl groups (24). The fungal broth exhibits mild antibacterial activity against *Pseudomonas aeruginosa*, *Staphylococcus aureus*, and *Streptococcus pyogenes* and antifungal activity towards *V. dahliae*. Extraction of the broth with ethyl acetate removes the antibacterial activity; however, the antifungal activity remains in the aqueous broth.

[1]Author to whom correspondence may be addressed.

[2]For a more detailed discussion of the requirements of an effective biological control agent for a soilborne disease, see refs. 20–23.

Can. J. Chem. Downloaded from www.nrcresearchpress.com by 91.121.58.235 on 09/07/12
For personal use only.

The ethyl acetate extract of the broth was dissolved in aqueous methanol and extracted with Skellysolve B, dichloromethane, and ethyl acetate. Each of the three extracts was subjected to chromatography over silica gel. The major component of the Skellysolve B extract was identified as the triglyceride. The ethyl acetate extract yields D-glucono-1,4-lactone (**1**). The dichloromethane extract is a source of metabolites of polyketide origin, which are the subject of this report.

Discussion

The ethyl acetate portion of the organic broth extract yields D-glucono-1,4-lactone (**1**), accounting for 50% of the weight of this fraction. Recrystallization of **1** from acetic acid gives a white powder, mp 127–129°C. The chemical ionization mass spectrum (cims) shows an ion at 196 (M + 18, 100), which indicates a molecular weight of 178 and a molecular formula of $C_6H_{10}O_6$ for lactone **1**. The highest mass peak in the high resolution mass spectrum (hrms) at m/z 160 ($M^+ - 18$) may be attributed to the facile β-elimination of water from the γ-lactone. The infrared spectrum (ir) spectrum displays a broad hydroxyl absorption at 3300 cm^{-1} and a γ-lactone carbonyl at 1776 cm^{-1}. The coupling pattern among the six carbinolic hydrogens was determined by spin decoupling and $^1H-^1H$ COSY experiments. The ^1H and ^{13}C nmr data obtained for the metabolite agree with those reported (25, 26) for D-glucono-1,4-lactone (**1**). This is the first example of the isolation of this metabolite from a fungal source. A sample of **1** was prepared by heating a solution of D-glucono-1,5-lactone in acetic acid (27, 28). The mixture melting point of synthetic and natural lactones is undepressed. Acetylation of **1** affords the tetraacetate **2**, identical (mp, nmr, ir, hrms, optical rotation) with an authentic sample. D-Glucono-1,4-lactone (**1**) is also abundant in the aqueous broth. Its role in the biological control of *V. dahliae* by *T. flavus* is discussed in the following paper.

4,6-Dihydroxy-5-methylphthalide (**3**), mp 240–241°C, precipitates from the chromatography eluent as colorless needles. Compound **3** has the molecular formula $C_9H_8O_4$ as determined by hrms. The ir spectrum shows a broad hydroxyl absorption at

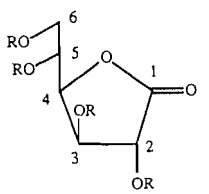

1, R = H

2, R = $COCH_3$

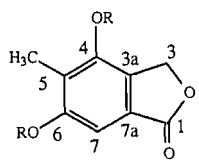

3, R = H

4, R = CH_3

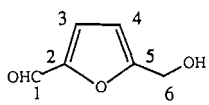

5

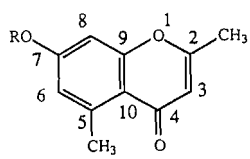

6, R = H

7, R = CH_3

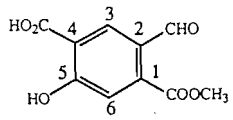

8

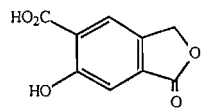

9

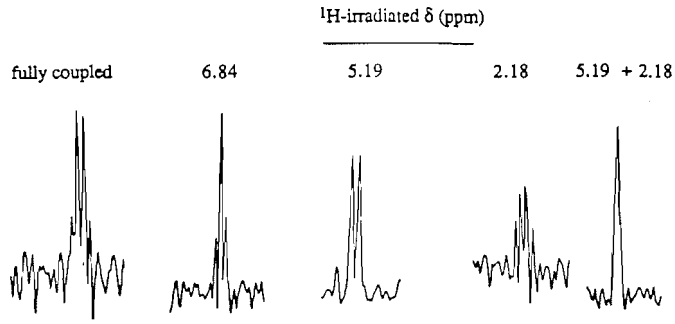

FIG. 1. $^1H-^{13}C$ decoupling of carbonyl carbon of **3**.

3360 cm^{-1} and a carbonyl band at 1730 cm^{-1}. The ultraviolet (uv) absorptions at 213, 259, and 306 nm each shift bathochromically ca. 20 nm on addition of base. Neutralization with acid restores the spectrum, indicative of a phenolic chromophore. The ^1H nmr spectrum of the phthalide consists of five singlets including an aromatic hydrogen (δ 6.84), a methylene signal (δ 5.19), and a methyl resonance (δ 2.18). Broad downfield singlets at δ 8.92 and 8.64 (D_2O exchangeable) are ascribed to the phenolic hydrogens. Nuclear Overhauser enhancement (nOe) experiments were performed to determine the relative orientation of the substituents on the phthalide ring; however, presaturation of the methyl, methylene, or methine singlets showed no nuclear Overhauser enhancements. In spin decoupling experiments, the half width ($w_{1/2}$) of each of the singlets was unaffected. To distinguish between the two structures consistent with these data, 4,6-dihydroxy-5-methylphthalide and 4,6-dihydroxy-7-methylphthalide, we examined the long range $^1H-^{13}C$ coupling constants. In the fully coupled spectrum the carbonyl carbon (δ 171.6) consists of four lines (Fig. 1). Irradiation of the aromatic hydrogen (δ 6.84) simplifies the signal to a triplet (J = 2 Hz), representative of the three-bond coupling ($^3J_{CH}$) of the carbonyl carbon with the methylene hydrogens (δ 5.19). When these hydrogens are irradiated the carbonyl carbon becomes a doublet ($^3J_{CH}$ = 3 Hz), consistent with 4,6-dihydroxy-5-methylphthalide (**3**), as this multiplicity results from coupling with the aromatic hydrogen. Irradiation of the methyl signal (δ 2.18) has no effect on the carbonyl signal multiplicity. The multiplicity changes observed for the other carbons enable us to assign the complete spectrum. Irradiation of the aromatic hydrogen (δ 6.84) simplifies the phenolic carbon at δ 158.5 to a quartet ($^3J_{CH}$ = 4 Hz) so that this signal is assigned as C-6. The carbon at δ 119.3 is also simplified to a quartet ($^2J_{CH}$ = 6 Hz) and is assigned as C-5. Saturation of the methylene hydrogens (δ 5.19) eliminates their coupling with the C-4 phenolic carbon (δ 151.2). The signal at δ 126.1 becomes a doublet, indicative of its coupling ($^3J_{CH}$ = 6 Hz) with the aromatic hydrogen (H-7), and is assigned as C-3a. The signal at δ 125.2 shows no coupling and is assigned as C-7a. The ^{13}C nmr assignment for 4,6-dihydroxy-5-methylphthalide (**3**) is summarized in Table 1. In the hrms, compound **3** loses a hydrogen atom to give a radical ion at m/z 179 and then carbon monoxide to afford the base peak at m/z 151. One of the noteworthy features in the ir spectrum of metabolite **3** is the carbonyl absorption at 1730 cm^{-1}. This absorption is at low frequency for a γ-lactone. This is the same frequency reported (29) for its regioisomer, 5,7-dihydroxy-6-methylphthalide, where intramolecular hydrogen bonding is responsible for the lower frequency absorption. The shift to lower frequency in this case is attributed to intermolecular hydrogen bonding in the thin film used to obtain the spectrum.

Can. J. Chem. Downloaded from www.nrcresearchpress.com by 91.121.58.235 on 09/07/12
For personal use only.

Can. J. Chem. Downloaded from www.nrcresearchpress.com by 91.121.58.235 on 09/07/12
For personal use only.

TABLE 1. ^{13}C chemical shifts[a] of 4,6-dihydroxy-5-methylphthalide (**3**) and 4,6-dimethoxy-5-methylphthalide (**4**)

Carbon	Compound 3	Compound 4
C-1	171.6	171.1
C-3	68.5	68.9
C-3a	126.1	128.9
C-4	151.2	154.0
C-5	119.3	126.1
C-6	158.5	160.8
C-7	102.6	100.9
C-7a	125.2	124.8
C-5 CH_3	9.2	9.6
C-4 OCH_3	—	59.4
C-6 OCH_3	—	56.6

[a]In acetone-d_6.

4,6-Dihydroxy-5-methylphthalide (**3**) is not reported as a natural product. It has been prepared synthetically (29) and our physical and spectral data agree with those of a synthetic sample of this phthalide.[3] Treatment of **3** with potassium carbonate and methyl iodide in refluxing acetone affords white flakes of 4,6-dimethoxy-5-methylphthalide (**4**), whose physical and spectral data (mp, nmr, ir, uv, hrms) correspond with those obtained from an authentic sample[3] as well as with those reported (30) for the natural product **4**, *O*-methylsilvaticol, isolated from *Aspergillus silvaticus*. Although most of the carbons of **4** are readily assigned (Table 1), the long range $^1H-^{13}C$ couplings of three carbons, δ 124.8, 126.1, and 128.9, were examined to confirm their identification. The carbon at δ 124.8 is a singlet and is assigned as C-7a by analogy with the dihydroxy metabolite **3**. The carbons at δ 126.1 and 128.9 are multiplets in the fully coupled spectrum; however, irradiation of the methylene hydrogens (δ 5.51) simplifies the former to a quartet ($^2J_{CH}$ = 6 Hz) and the latter to a doublet ($^3J_{CH}$ = 6 Hz). This doublet is characteristic of the multiplicity of C-3a in the dihydroxy metabolite **3** so that the signal at δ 128.9 is assigned as such. The quartet at δ 126.1 (C-5) arises from the coupling of this carbon with the methyl hydrogens. This ^{13}C nmr assignment differs from that proposed by Achenbach *et al.* (29) and from that reported (30) for the natural product; however, it is consistent with the change in chemical shifts expected in phenolic systems on *O*-methylation (30).

5-Hydroxymethylfurfural (**5**), isolated as a yellow oil, has the molecular formula $C_6H_6O_3$ as determined from its hrms. The loss of a hydrogen atom and carbon monoxide in the mass spectrum to give the base peak (m/z 97), absorption bands at 2840 and 2700 (w) cm^{-1} in the ir spectrum, and a singlet in the ^1H nmr spectrum at δ 9.58 that does not exchange on addition of D_2O indicate that compound **5** is an aldehyde. The uv absorptions at 221 and 281 nm indicate a furfural chromophore. The ^1H and ^{13}C nmr spectra of **5** are consistent with those reported (31). We believe that 5-hydroxymethylfurfural (**5**) is an artifact in the broth extract as it is known to arise through dehydration of D-glucose (32). When the D-glucose was added to the fungal medium after the autoclaving process, the amount of 5-hydroxymethylfurfural (**5**) in the broth extract was reduced by ca. 90%.

[3]We thank Professor H. Achenbach for providing us with the samples and spectra of 4,6-dihydroxy-5-methylphthalide and 4,6-dimethoxy-5-methylphthalide.

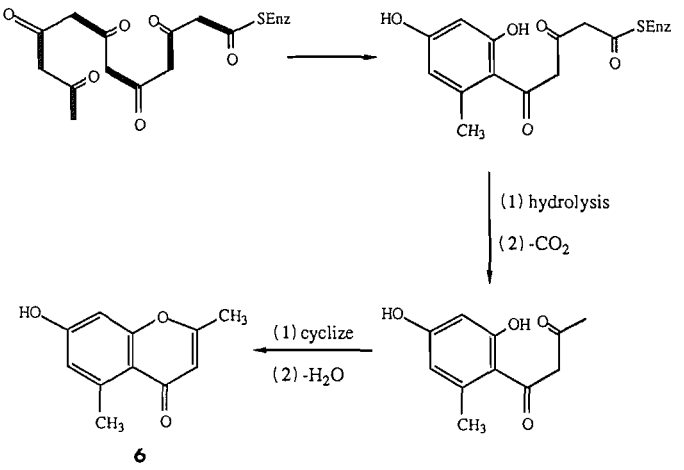

6

SCHEME 1

White flakes of 7-hydroxy-2,5-dimethylchromone (**6**), $C_{11}H_{10}O_3$, sublime at 200°C. The phenolic nature of **6** is evident as its uv spectrum displays a bathochromic shift on addition of base, which reverts to the original spectrum on neutralization with acid. The ir spectrum displays a broad hydroxyl absorption (3400–3000 cm^{-1}) and γ-pyrone absorptions at 1649, 1618, and 1557 cm^{-1}. The ^1H nmr spectrum shows *meta*-related hydrogens at δ 6.64 (d, J = 2.5 Hz) and 6.62 (dq, J = 2.5, 1.0 Hz). This latter hydrogen has been shown by spin decoupling experiments to be coupled to the methyl group at δ 2.70 (bs), which, when irradiated, results in a 32% nOe enhancement of the hydrogen at δ 6.62 (H-6). The vinylic hydrogen (H-3) at δ 6.00 (q, J = 1.0 Hz) is coupled to the C-2 methyl group at δ 2.31 (d, J = 1.0 Hz) and shows an nOe enhancement of 12% when the C-2 methyl is presaturated. Metabolite **6** has been isolated from the roots of *Polygonum cuspidatum*, a plant used in Chinese and Japanese traditional medicine (33), and from a rhubarb, *Rhei rhizoma* (34). Treatment of 7-hydroxy-2,5-dimethylchromone (**6**) with diazomethane affords the monomethyl ether (**7**), whose physical and spectral data (mp, nmr, ir, uv, hrms) agree with those reported (35, 36). The biosynthesis of **6** does not seem to follow the pattern of most chromones that arise from a pentaketide precursor but probably originates from a hexaketide precursor as illustrated in Scheme 1.

The most colorful metabolite isolated is a granular yellow solid that decomposes on melting at 190°C, for which we propose the structure methyl 4-carboxy-5-hydroxyphthalaldehydate (**8**). Its molecular formula, as determined by hrms, is $C_{10}H_8O_6$. The uv spectrum of **8** consists of maxima at 225, 293, and a long wavelength absorption at 428 nm. Addition of base causes a bathochromic shift of only the 293 nm absorption. A ^{13}C nmr signal at δ 196.6 (d), a ^1H nmr resonance at δ 10.46 that does not exchange on addition of D_2O, and the loss of a hydrogen atom and carbon monoxide from the ion at m/z 193 in the mass spectrum support the presence of the aldehyde functionality. A broad hydroxyl absorption in the ir spectrum (3560 to 2400 cm^{-1}) and a ^{13}C nmr signal at δ 169.4 (s) are evidence for the carboxylic acid moiety. A singlet in the ^1H nmr spectrum at δ 3.53 (3H) and ^{13}C nmr signals at δ 160.1 (s) and 56.4 (q), together with the loss of a methoxy group (m/z 193) in the hrms, are consistent with the presence of a methyl ester. Singlets in the ^1H nmr spectrum at δ 6.79 and 6.45 are attributed

Can. J. Chem. Downloaded from www.nrcresearchpress.com by 91.121.58.235 on 09/07/12
For personal use only.

to hydrogens in a *para* relationship on the aromatic ring. Presaturation of the methoxy singlet (δ 3.53) results in an nOe enhancement of 7% of the signal at δ 6.45. There remains only a hydroxyl group not accounted for, and the ^{13}C nmr signal at δ 166.3 (s) is consistent with this. Evidence as to the relative orientation of the four substituents on the aromatic ring is provided by the reduction of **8** with sodium borohydride. After the reaction proceeds for 15 s, the bright yellow color of the solution fades and, after 10 min, the starting material is converted to a more polar compound as seen by tlc. The ir spectrum of the reduction product **9** possesses a broad hydroxyl absorption at 3240 cm^{-1}. The aldehyde and ester methoxyl signals disappear from the ^1H nmr spectrum and are replaced by a singlet (δ 5.01, 2H). A similar reaction has been observed in the sodium borohydride reduction of 3,5-dihydroxy-4-methylphthalaldehydic acid methyl ester, affording metabolite **3** (37). This suggests that metabolite **8** may be a derivative of a precursor to **3**. The presence of a γ-lactone ring in compound **9** is supported by a carbonyl band at 1755 cm^{-1} in the ir spectrum and the two-hydrogen singlet at δ 5.01 in the ^1H nmr spectrum. Compound **8** is relatively unstable, presumably due to aerial oxidation. The ^1H nmr spectrum of **8** a few days after isolation shows that the three singlets are doubled and the intensity of the aldehyde signal is reduced. Thin-layer chromatography (tlc) shows more polar material shortly after purification. Attempts to acetylate or methylate compound **8** failed to yield tractable products. These difficulties, together with the paucity in which metabolite **8** is produced, have precluded further studies to confirm its structure.

A metabolite whose structure is consistent with that of 3-hydroxymethyl-6,8-dimethoxycoumarin (**10**) has the molecular formula $C_{12}H_{12}O_5$. A carbonyl band at 1711 cm^{-1} and double bond absorptions at 1657 and 1592 cm^{-1} in the ir spectrum are consistent with the coumarin skeleton. The uv maxima at 256 and 286 nm do not shift on addition of base, indicating that the hydroxyl group is not phenolic. The ^1H nmr spectrum shows *meta*-related hydrogens at δ 6.65 and 6.48 (each a doublet, J = 2.6 Hz). A triplet (1H, J = 1.4 Hz) at δ 7.70, whose chemical shift is consistent with that of a coumarin hydrogen on the β-carbon of the double bond, is coupled to a doublet at δ 4.55 (2H, J = 1.4 Hz), supporting the hydroxymethyl substitution at the α-carbon. Methoxy groups resonate at δ 3.90 and 3.81. Although ^{13}C nmr would allow the two metabolites to be distinguished, compound **10** was not isolated in quantities sufficient to allow detection of the 12 carbon signals. The most significant nOe result is that the signal for the aromatic hydrogen (δ 6.48) is enhanced when the vinylic hydrogen at δ 7.70 is presaturated and vice versa, suggesting that these two hydrogens are *peri* to one another. On the basis of the data available, we suggest that metabolite **10** is 3-hydroxymethyl-6,8-dimethoxycoumarin.

A number of higher order polyketides arising from a heptaketide precursor have been isolated. The first of these, altenusin (**11**), crystallizes as white flakes, mp 194–196°C. Its hrms provides the molecular formula $C_{15}H_{14}O_6$. The ^1H nmr spectrum shows aromatic singlets at δ 6.47 and 6.40 and *meta*-related hydrogens at δ 6.27 and 6.04 (each a doublet, J = 2.6 Hz). A methoxy signal is seen at δ 3.65 and an aromatic methyl at δ 1.77. The mp, ^1H nmr, and ir data agree with those reported (38) for altenusin (**11**). In Table 2, the ^{13}C nmr data (not previously reported) are compared with calculated values (39). Altenusin (**11**) was first reported from *Alternaria tenuis* in 1957 (40); however, the structure for the metabolite was not

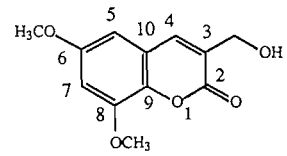

10

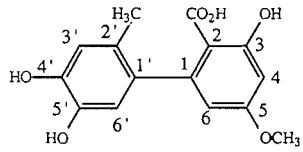

11

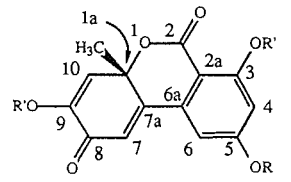

12, R = CH_3, R' = H
13, R = CH_3, R' = $COCH_3$
14, R = H, R' = H
15, R, R' = $COCH_3$

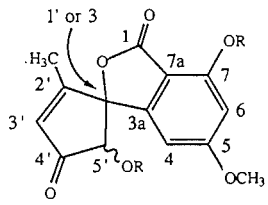

16, R = H
17, R = $COCH_3$

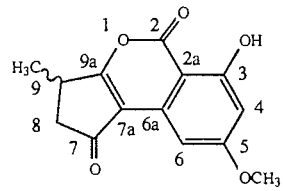

18

established until 1970 (38). It has since been isolated from *A. kikuchiana* (41). Two metabolites closely related to altenusin (**11**) have been isolated in the form of their acetates since the corresponding alcohols were difficult to purify. The ^1H nmr spectrum of a somewhat impure sample of the first of these alcohols, dehydroaltenusin (**12**), displays a hydrogen bonded hydroxyl hydrogen at δ 11.30. *meta*-Related hydrogens at δ 6.73 and 6.63 (each a doublet, J = 2.3 Hz) and a methoxy signal at δ 3.91 reflect the similarity of one aromatic ring of altenusin (**11**) with that in dehydroaltenusin (**12**). Downfield singlets appear at δ 6.69 and 6.28 and a methyl group resonates at δ 1.73 (s). The crystal structure of (±)-dehydroaltenusin has been described (42); however, its structure was initially misassigned and it was reported that a triacetate had formed (38). In our hands, acetylation of dehydroaltenusin (**12**) affords a diacetate, $C_{19}H_{16}O_8$, the properties of which are consistent with structure **13**. The ir spectrum shows no hydroxyl absorption but carbonyl bands for aromatic (1776 cm^{-1}) and aliphatic (1732 cm^{-1}) acetates are observed. Absorptions at 1688 and 1664 cm^{-1} are consistent with the unsaturated ketone moiety. The ^1H nmr spectrum shows *meta*-related hydrogens at δ 6.77 and 6.60 (each a doublet, J = 1.9 Hz) and a methoxy group at δ 3.86, consistent with those found for the aromatic ring of dehydroaltenusin (**12**) and altenusin (**11**). Presaturation of the methoxy group results in a 24% enhancement of the signal at δ 6.77 and a 17% enhancement of the resonance at δ 6.60. Presaturation of this latter hydrogen enhances not only the methoxy signal but also the vinylic hydrogen at δ 6.36 (s); nOe experiments show a 22% enhancement of the vinylic hydrogen at δ 6.30 (q, J = 1.4 Hz) when the methyl group at δ 1.73 (d, J = 1.4 Hz) is presaturated. A signal for an aromatic acetoxyl methyl is observed at δ 2.42 and one for a deshielded aliphatic methyl at δ 2.29. Dehydroaltenusin (**12**),[4] like altenusin (**11**), has been isolated from *Alternaria tenuis* and *A. kiku-*

[4]Due to the small amount of metabolites **12**, **14**, and **18** isolated, no attempt was made to determine if they were optically active. Our requests for an authentic sample of **12** were not answered.

Can. J. Chem. Downloaded from www.nrcresearchpress.com by 91.121.58.235 on 09/07/12
For personal use only.

TABLE 2. Calculated (39) and observed[a] ^{13}C chemical shifts of altenusin (**11**)

Carbon	Observed for **11**	Calculated for **11**
CH_3	18.5	
OCH_3	55.0	
C-4	99.5	100.3
C-2	105.9	109.2
C-6	110.1	105.8
C-3′	115.2[b]	116.2
C-6′	115.9[b]	118.4
C-2′	126.6	130.9
C-1′	133.9	136.4
C-5′	141.3[c]	140.2
C-4′	143.0[c]	142.7
C-1	146.2	145.4
C-3	163.1[d]	158.3
C-5	164.1[d]	166.4
CO_2H	172.8	

[a]In $CDCl_3$–CD_3OD 1:1.
[b,c,d]Assignments may be interchanged.

chiana (40). Desmethyldehydroaltenusin (**14**)[4] is the second metabolite isolated in the form of its acetate (**15**). The sequential loss of three molecules of ketene from the parent ion ($C_{20}H_{16}O_9$) in the mass spectrum affords an ion corresponding to a molecular formula $C_{14}H_{10}O_6$, which differs from that of dehydroaltenusin (**12**) by a methylene unit. Desmethyldehydroaltenusin triacetate (**15**) fragments in the same manner as dehydroaltenusin diacetate (**13**), with the fragment ions consistently found 14 mass units lower. The ^1H nmr spectrum of the triacetate **15** is similar to that of dehydroaltenusin diacetate (**13**) as *meta*-related hydrogens are observed at δ 7.10 and 6.97 (each a doublet, J = 1.7 Hz) and a four-bond coupling of 1.5 Hz is observed between the vinylic hydrogen at δ 6.31 and the methyl signal at δ 1.74. A one-hydrogen singlet resonates at δ 6.37. Acetyl methyl signals are apparent at δ 2.43, 2.31, and 2.29. The methoxy signal present in the ^1H nmr spectrum of the diacetate **13** is absent in the triacetate **15**. Formation of altenusin (**11**) and dehydroaltenusin (**12**), and the previously unreported desmethyldehydroaltenusin (**14**), may be envisaged as proceeding by cyclization of a heptaketide precursor to give the biphenyl derivative shown in Scheme 2. An oxidation and reduction sequence, and methylation of the phenol indicated, afford the biphenyl metabolite altenusin (**11**). Its δ-lactone derivative, dehydroaltenusin (**12**), forms by oxidative cyclization of **11**. The chemical interconversion of **11** and **12** has been achieved (38, 41): oxidation of **11** to **12** with ferric chloride and reduction of **12** to **11** with sodium dithionate.

We believe that this biphenyl intermediate is also the precursor to the structurally and biosynthetically interesting spirocyclic metabolite, talaroflavone (**16**). This white solid, with molecular formula $C_{14}H_{12}O_6$, decomposes on melting at 230°C. The ir spectrum displays a broad hydroxyl absorption at 3240 cm^{-1}, a γ-lactone carbonyl at 1748 cm^{-1}, and α,β-unsaturated cyclopentenone bands at 1723 and 1617 cm^{-1}. The uv absorptions at 217, 257, and 296 nm shift bathochromically on addition of base. Neutralization with acid gives back the original spectrum, indicative of the phenolic chromophore. The ^1H nmr spectrum shows *meta*-related hydrogens at δ 6.44 and 6.05 (each a doublet, J = 2.0 Hz), both of which show a nuclear Overhauser enhancement (6% and 8%, respectively), when the methoxy signal at δ 3.80 is irradiated. These ^1H nmr data

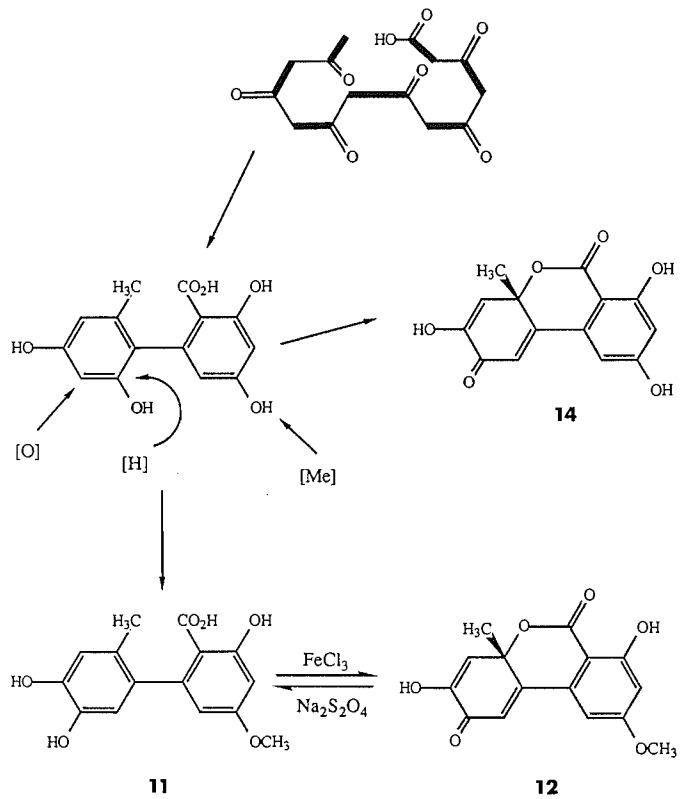

SCHEME 2

resemble those for the aromatic portion of metabolites **11**, **12**, and **14**. A carbinolic hydrogen at δ 4.74 and a ^{13}C nmr signal at δ 79.7 are consistent with a secondary alcohol. An allylic coupling (J = 1.5 Hz), as well as a 6% nOe, is observed between the methyl signal at δ 1.86 and the vinylic hydrogen at δ 6.34. A comparison of the ^{13}C nmr data (Table 3) for the aromatic ring of 4,6-dihydroxy-5-methylphthalide (**3**), 5,7-dihydroxy-6-methylphthalide (29), and metabolite **16** shows chemical shift differences of the carbons at the ring junctions (C-3a and C-7a), depending on whether the carbonyl group is *peri* to the aromatic hydrogen or *peri* to the hydroxyl group. The ^{13}C nmr data for the aromatic portion of metabolite **16** agree best with the latter phthalide. Signals in the ^{13}C nmr spectrum at δ 202.0, 171.4, and 131.4 (43) and ^1H nmr resonances at δ 1.86 and 6.34 are consistent with a 3-methylcyclopentenone. A third ring joining the aromatic and enone portions of **16**, incorporating the quaternary spiro carbon (δ 94.2) and the ester carbonyl (δ 170.2), fulfills the final site of unsaturation. The parent ion in the mass spectrum of talaroflavone (**16**) is also the base peak, suggesting that the molecule does not contain sites for facile fragmentation. Talaroflavone (**16**) is optically active, $[\alpha]_D$ = +181° (*c* 0.74, methanol). Attempts to discern the stereochemistry at the spiro center (C-3) and of the C-5′ hydroxyl of **16** have proved troublesome; however, data obtained from the diacetate (**17**) have provided some evidence for C-5′. The diacetate **17** has the molecular formula $C_{18}H_{16}O_8$, as determined by hrms. The ir spectrum shows no hydroxyl absorption; however, there is a carbonyl absorption at 1777 cm^{-1} (aromatic acetoxyl) and 1732 cm^{-1} (acetoxyl and cyclopentenone), together with a double bond absorption at 1621 cm^{-1}. The ^1H nmr spectrum shows aromatic hydrogens at δ 6.93 and 6.61, downfield ca. δ 0.5 from their resonances in the dihydroxy form. This is consistent with the acetylation of an *ortho* or *para*

TABLE 3. ^{13}C chemical shifts of the aromatic portion of 4,6-dihydroxy-5-methylphthalide (**3**),[a] 5,7-dihydroxy-6-methylphthalide,[a] and talaroflavone (**16**)[b]

	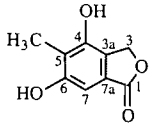 **3**	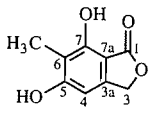 5,7-Dihydroxy-6-methylphthalide	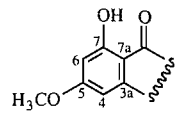 **16**
C-3a	126.1	147.4	150.8
C-4	151.2	101.4	103.5
C-5	119.3	164.0	168.5
C-6	158.5	Not reported	101.0
C-7	102.6	156.2	159.9
C-7a	125.2	103.8	106.5

[a]In acetone-d_6.
[b]In methanol-d_4.

TABLE 4. ^{13}C chemical shifts[a] of talaroflavone (**16**) and talaroflavone diacetate (**17**)

Carbon	Compound **16**	**17**	$\delta_{OAc} - \delta_{OH}$
C-1	170.2[b] (s)	168.1[d] (s)	
C-3 (C-1′)	94.2 (s)	92.7 (s)	
C-3a	150.8 (s)	151.5 (s)	+0.7 (*meta*)
C-4	103.5[c] (d)	106.7[e] (d)	+3.2 (*para*)
C-5	168.5[b] (s)	167.2[d] (s)	−1.3 (*meta*)
C-6	101.0[c] (d)	112.1[e] (d)	+11.1 (*ortho*)
C-7	159.9 (s)	149.5 (s)	−10.4 (*ipso*)
C-7a	106.5 (s)	112.4 (s)	+5.9 (*ortho*)
C-2′	171.4[b] (s)	172.0[d] (s)	
C-3′	131.4 (d)	133.2 (d)	
C-4′	202.0 (s)	197.1 (s)	
C-5′	79.7 (d)	78.1 (d)	
C-2′ CH_3	13.4 (q)	13.3 (q)	
OCH_3	56.5 (q)	57.2 (q)	
C-7 OAc	—	170.8[d] (s), 20.4 (q)	
C-5′ OAc	—	170.0[d] (s), 19.8 (q)	

[a]In methanol-d_4.
[b,c,d,e]Assignments may be interchanged.

phenolic hydroxyl (44). An aromatic acetate methyl resonates at δ 2.35 and an aliphatic one at δ 1.82, upfield from its expected position by ca. δ 0.3. The hydrogen at δ 4.74 in the alcohol **16** shifts downfield δ 1.07 on acetylation (δ 5.81), consistent with that expected for a secondary alcohol. The ^{13}C nmr spectrum of **17** shows two additional signals for acetate carbonyls in the region δ 165–170 and methyl carbon resonances at δ 20.4 and 19.8. The ketone carbonyl is shifted upfield in **17** to δ 197.1 from 202.0, suggesting the loss of hydrogen bonding. The ^{13}C nmr assignments for the alcohol **16** and the acetate **17** are summarized in Table 4. The changes in chemical shift of the aromatic carbons of **16** on acetylation are consistent with those expected (45). The upfield shift of the aliphatic acetate methyl in the ^1H nmr spectrum of **17** provides the clue to the stereochemistry at C-5′. There are two diastereoisomers in which the aliphatic methyl group lies inside the shielding cone of the aromatic ring and two where this methyl lies away from the aromatic ring and should exhibit a more characteristic chemical shift (ca. δ 2.1). This upfield shift of the C-5′ acetate methyl, ascribed to the diamagnetic anisotropy of the benzene ring, leads us to believe that the configuration at C-5′ of talaroflavone (**16**) is one in which this acetate methyl lies within the shielding cone of the aromatic ring. The optical rotary dispersion (ord) spectrum of the acetate **17** is a positive plain curve and the circular dichroic (cd) spectrum shows a positive Cotton effect. Attempts to crystallize talaroflavone diacetate (**17**) failed to give crystals suitable for X-ray analysis. The mono- and di-*p*-nitrobenzoates of talaroflavone (**16**) were prepared; however, poor yields were obtained and suitable crystals could not be prepared.

A metabolite we have named deoxytalaroflavone (**18**), mp 178–180°C, has the molecular formula $C_{14}H_{12}O_5$. The ir spectrum shows a hydroxyl absorption (3400–2800 cm^{-1}), together with bands representative of the α-pyrone and α,β-unsaturated ketone moieties (1713, 1679, 1610, and 1565 cm^{-1}). The ^1H nmr spectrum consists of a downfield hydroxyl hydrogen at δ 11.35, *meta*-related hydrogens at δ 6.70 and 6.69 (each a doublet, J = 2.3 Hz), and a methoxy group at δ 3.94, again resembling that observed for the aromatic portion of talaroflavone (**16**) and the other heptaketide derived metabolites (**11**, **12**, and **14**). The aromatic hydrogen at δ 6.69 (H-6) is further downfield in **18** compared to its chemical shift in **16** (δ 6.05), probably because of the proximity to the ketone carbonyl. The ^1H nmr spectrum of deoxytalaroflavone (**18**) contains a saturated spin system; namely, a hydrogen resonating at δ 3.43 is coupled to a methyl group at δ 1.46 (d, J = 6.9 Hz) and to two methylene hydrogens (δ 2.95 (dd, J = 6.6, 19.0 Hz) and δ 2.31 (dd, J = 1.3, 19.0 Hz)). Only eight of the 14 carbons of metabolite **18** are visible in the ^{13}C nmr spectrum, due to the small amount of material available. The molecular formula of **18**, $C_{14}H_{12}O_5$, differs from that of talaroflavone (**16**), $C_{14}H_{12}O_6$, by one oxygen atom. Its formation from talaroflavone (**16**) may be envisaged in three steps as illustrated in Scheme 3.

Labelling studies undertaken to examine the incorporation of [1-^{13}C] labelled acetate into the biosynthetically interesting metabolites reported above and the results of our efforts to identify the source of the biological activity of the fungus are the subject of the following paper.

Experimental

High resolution electron impact mass spectra (hreims) were recorded on an A.E.I. MS-50 mass spectrometer coupled to a Data General Nova

Can. J. Chem. Downloaded from www.nrcresearchpress.com by 91.121.58.235 on 09/07/12
For personal use only.

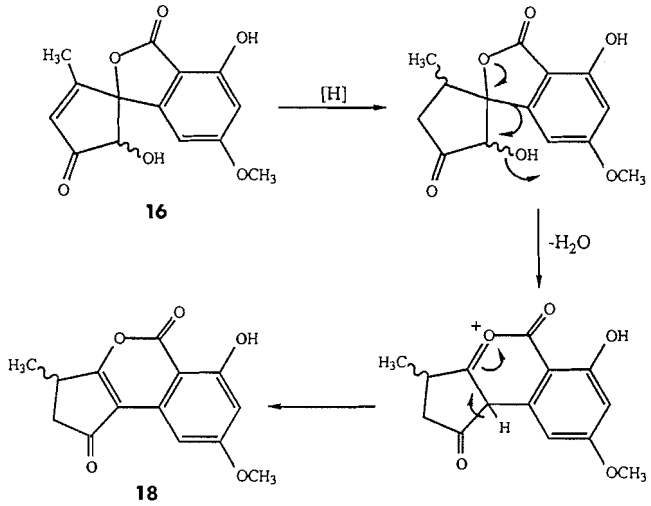

SCHEME 3

4 computer. Unless diagnostically significant, peaks with intensities less than 30% of the base peak are omitted. Low resolution mass spectra (lrms) were recorded on an A.E.I. MS-12 mass spectrometer. Chemical ionization mass spectra (cims) were recorded on an A.E.I. MS-12 mass spectrometer with ammonia as the reagent gas. Fourier transform infrared (ftir) spectra were recorded as thin films cast from $CHCl_3$, CH_2Cl_2, CH_3COCH_3, or CH_3OH on a Nicolet 7199 FT interferometer. ^1H nuclear magnetic resonance (^1H nmr) spectra were measured on a Bruker WH-200, WH-360, WH-400, AM-300, or AM-400 spectrometer with an Aspect 2000 or 3000 computer system. Residual $CHCl_3$ in $CDCl_3$, CHD_2OD in CD_3OD, or CHD_2COCD_3 in CD_3COCD_3 was employed as the internal standard (assigned as δ 7.26, 3.30, and 2.04, respectively, downfield from tetramethylsilane (TMS)). ^{13}C nuclear magnetic resonance (^{13}C nmr) spectra were measured on a Bruker AM-300, WH-400, or AM-400 spectrometer. $CDCl_3$, CD_3OD, or CD_3COCD_3 was employed as the internal standard (assigned as δ 77.0, 49.0, or 29.8, respectively, downfield from TMS). Ultraviolet (uv) spectra were obtained on a Hewlett Packard 8450A diode array spectrophotometer. Optical rotations were measured on a Perkin Elmer 241 polarimeter. Circular dichroic (cd) – optical rotary dispersion (ord) spectra were measured on a Jasco model SS20 cd–ord spectrometer. Melting points were recorded on a Fisher–Johns or Leitz–Wetzlar melting point apparatus and are uncorrected. Analytical thin-layer chromatography (tlc) was carried out on aluminum sheets precoated (0.2 mm) with silica gel 60 F-254 (E. Merck, Darmstadt). Materials were detected under an ultraviolet (uv) lamp (254 or 350 nm), or by spraying with a solution of phosphomolybdic acid (5%) containing a trace of ceric sulfate in aqueous sulfuric acid (5%, v/v), or a solution of anisaldehyde (2%) in aqueous sulfuric acid (10%, v/v), followed by charring on a hot plate. Flash column chromatography (46) was performed with Merck Silica Gel 60 (40–63 μm). All solvents except diethyl ether and *n*-hexane were distilled prior to use. Skellysolve B refers to Skelly Oil Company light petroleum, bp 62–70°C.

Growth of Talaromyces flavus *and extraction of the metabolites*

The strain (ATCC 52201; UAMH 4890) of *T. flavus* used in this study was obtained from the American Type Culture Collection, Rockville, Maryland. It was isolated from sclerotia of *Sclerotina minor* buried in soil at Beltsville, Maryland. The strains (UAMH 5360, 5366) of *V. dahliae* used were obtained from D. R. Fravel, Soilborne Diseases Laboratory, Beltsville, Maryland. Stock cultures of *T. flavus* were maintained at 4°C in slant tubes containing Difco potato dextrose agar. To initiate liquid still cultures of the fungus, an aqueous spore suspension of *T. flavus* was used to inoculate two agar plates (10% filtered V-8 juice (Campbell Soup Company Ltd.), 1% glucose, 2% agar). After incubation for 2 weeks, the plate cultures were blended in a Waring blender with ca. 200 mL of sterile water and 20-mL aliquots were inoculated into each of 10 2.8-L Fernbach flasks charged with 1 L of sterile malt extract medium (2% (w/v) glucose, 2% (w/v) malt extract, and 0.1% (w/v) peptone). The culture was kept at room temperature for 4 weeks. The culture broth was decanted from the mycelium by filtration through cheesecloth, concentrated *in vacuo* to ca. 1 L, and continuously extracted with ethyl acetate for 48 h. The organic extract was dried and concentrated to give an oil (ca. 1 g), which was dissolved in aqueous methanol (85:15, 100 mL) and extracted with Skellysolve B (3 × 100 mL), dichloromethane (3 × 100 mL), and ethyl acetate (3 × 100 mL). The organic extracts were dried and concentrated to give oils, which were chromatographed as described below. The mycelium was washed with methanol, air-dried, and subjected to continuous extraction in a Soxhlet extractor with ethyl acetate for 6 h or with methanol for 24 h. The organic extract was dried, concentrated, and separated as described below.

Isolation of the metabolites

Methanol was added to the crude mycelium extract. The insoluble material was filtered off (D-mannitol, 9.2 g). The methanol soluble portion was subjected to flash chromatography, eluting with benzene followed by benzene–ether (9:1). This afforded methyl linoleate, a triglyceride, ergosterol, and linoleic acid. Methanol was added to the crude ethyl acetate mycelium extract. D-Mannitol (1.5 g) was filtered off and the methanol soluble portion evaporated to dryness (200 mg). It was dissolved in aqueous methanol (90:10, 100 mL) and extracted with *n*-hexane (3 × 100 mL), dichloromethane (3 × 100 mL), and ethyl acetate (3 × 100 mL). Each of the extracts was dried over anhydrous sodium sulfate, filtered, and the solvents were removed under reduced pressure to give the hexane extract (170 mg), dichloromethane extract (12 mg), and the ethyl acetate extract (18 mg). The hexane extract was subjected to flash chromatography, eluting with Skellysolve B – acetone (93:7). This afforded the triglyceride, ergosterol, and a diglyceride. The hexane portion of the ethyl acetate broth extract was subjected to flash chromatography, eluting with Skellysolve B – ether (7:1). The major metabolite isolated was the triglyceride. Purification of the metabolites isolated from the dichloromethane and ethyl acetate fractions of the broth extract are described under their appropriate headings.

D-Glucono-1,4-lactone (1)

D-Glucono-1,4-lactone (**1**) was isolated from the ethyl acetate portion of the broth extract by flash chromatography, eluting with toluene–acetone – acetic acid (35:65:1). It crystallized after evaporation of the eluent. Recrystallization from acetic acid gave D-glucono-1,4-lactone (**1**) as a white powder (124 mg), mp 127–129°C (lit. (27) mp 132–135°C); tlc: R_f 0.29 (toluene–acetone – acetic acid 35:65:1); ftir (acetone cast): 3300 (br), 1776, 1182, 1100, 985 cm^{-1}; ^1H nmr (methanol-d_4) δ: 4.54 (1H, dd, J = 4.8, 6.5 Hz, H-4), 4.35 (1H, dd, J = 4.7, 6.5 Hz, H-3), 4.24 (1H, d, J = 4.7 Hz, H-2), 3.97 (1H, ddd, J = 3.9, 4.8, 5.7 Hz, H-5), 3.77 (1H, dd, J = 3.9, 11.7 Hz, H-6), 3.69 (1H, dd, J = 5.7, 11.7 Hz, H-6′); ^{13}C nmr (CD_3OD–D_2O 1:1) δ: 177.5 (s, C-1), 81.0 (d, C-4), 74.4, 74.2, 71.4 (3 × d, C-2, C-3, C-5), 63.8 (t, C-6); hreims, m/z calcd. for $C_6H_{10}O_6$ (M^+): 178.0477; found: M^+ not detected, 160 (21), 142 (4), 103 (24), 73 (100); cims, m/z: 196 (M + 18).

Acetylation of D-glucono-1,4-lactone (1)

Pyridine (1.0 mL) was added to a solution of D-glucono-1,4-lactone (**1**, 9.0 mg) in acetic anhydride (1.0 mL). The reaction was allowed to stand at room temperature for 6 h. Toluene (5.0 mL) was added to the mixture and the solution was evaporated under reduced pressure. Flash chromatography of the crude reaction product, eluting with Skellysolve B – acetone (2.5:1), afforded D-glucono-1,4-lactone tetraacetate (**2**) as white needles (15.6 mg), mp 101–102°C (lit. (27) mp 103°C); tlc: R_f 0.29 (Skellysolve B – acetone 2.5:1); $[\alpha]_D$ +59° (*c* 1.0, acetone) (lit. (27) $[\alpha]_D$ +60.3° (acetone)); ftir (acetone cast): 1806, 1751, 1373, 1224, 1194, 1067, 1046 cm^{-1}; ^1H nmr ($CDCl_3$) δ: 5.62 (1H, dd, J = 3.0, 5.5 Hz, H-3), 5.35 (1H, ddd, J = 3.0, 5.0, 8.0 Hz, H-5), 5.23 (1H, d, J = 3.0 Hz, H-2), 4.96 (1H, dd, J = 5.5, 8.0 Hz, H-4), 4.58 (1H, dd, J = 3.0, 12.0 Hz, H-6), 4.15 (1H, dd, J = 5.0, 12.0 Hz, H-6′), 2.19 (3H, s, $OCOCH_3$), 2.12 (3H, s, $OCOCH_3$), 2.10 (3H, s,

Can. J. Chem. Downloaded from www.nrcresearchpress.com by 91.121.58.235 on 09/07/12
For personal use only.

Can. J. Chem. Downloaded from www.nrcresearchpress.com by 91.121.58.235 on 09/07/12
For personal use only.

$OCOCH_3$), 2.05 (3H, s, $OCOCH_3$); ^{13}C nmr ($CDCl_3$) δ: 170.3 (s), 169.3 (s), 169.1 (s), 169.0 (s), 168.7 (s), 76.9 (d), 72.0 (d), 71.0 (d), 67.6 (d), 62.1 (t), 20.6 (2C, q), 20.4 (q), 20.2 (q); hreims, *m/z* calcd. for $C_{14}H_{18}O_{10}$ (M^+): 346.0899; found: M^+ not detected, 226 (15), 184 (100), 142 (90), 100 (76); cims, *m/z*: 364 (M + 18).

*4,6-Dihydroxy-5-methylphthalide (**3**) (4,6-dihydroxy-5-methyl-1(3*H*)-isobenzofuranone)*

4,6-Dihydroxy-5-methylphthalide (**3**) was isolated by flash chromatography of the dichloromethane portion of the ethyl acetate broth extract, eluting with dichloromethane–methanol (97:3). It crystallized from the eluent as colorless needles (4.8 mg), mp 240–241°C (lit. (29) mp 241–242°C); tlc: R_f 0.19 (dichloromethane–methanol 97:3); uv (methanol): 213 (4.50), 259 (3.92), 306 (3.58) nm; 1 drop 0.1 N NaOH: 232 (4.35), 278 (3.75), 328 (3.58) nm; 1 drop 0.1 N NaOH – 1 drop 0.1 N HCl: 212 (4.48), 259 (3.91), 307 (3.58) nm; ftir (acetone cast): 3360 (br), 1730, 1610, 1470, 1450, 1342, 1092, 1024, 770 cm^{-1}; ^1H nmr (acetone-d_6) δ: 8.92 (1H, br s, O*H*), 8.64 (1H, br s, O*H*), 6.84 (1H, s, H-7), 5.19 (2H, s, H-3), 2.18 (3H, s, C-5 CH_3); (methanol-d_4) δ: 6.77 (1H, s, H-7), 5.19 (2H, s, H-3), 2.14 (3H, s, C-5 CH_3); ^{13}C nmr (acetone-d_6) δ: 171.6 (s, C-1), 158.5 (s, C-6), 151.2 (s, C-4), 126.1 (s, C-3a), 125.2 (s, C-7a), 119.3 (s, C-5), 102.6 (d, C-7), 68.5 (t, C-3), 9.2 (q, C-5 CH_3); (methanol-d_4) δ: 174.2 (s, C-1), 159.1 (s, C-6), 151.5 (s, C-4), 126.3 (s, C-3a), 124.7 (s, C-7a), 120.5 (s, C-5), 102.1 (d, C-7), 69.7 (t, C-3), 9.2 (q, C-5 CH_3); hreims, *m/z* calcd. for $C_9H_8O_4$ (M^+): 180.0422; found: 180.0421 (55), 179 (13), 151 (100); cims, *m/z*: 198 (M^+ + 18).

*Methylation of 4,6-dihydroxy-5-methylphthalide (**3**)*

A solution of 4,6-dihydroxy-5-methylphthalide (**3**, 4.2 mg), potassium carbonate (30.0 mg), and methyl iodide (0.1 mL) in dry acetone (5.0 mL) was heated under reflux for 2.5 h. The reaction mixture was filtered and the solvent was removed under reduced pressure, yielding a white solid that was taken up in dichloromethane (10.0 mL). The solution was stirred at room temperature for 0.5 h. It was then filtered and the solvent was removed under reduced pressure, yielding a pale yellow solid (6.3 mg) that was purified by flash chromatography, eluting with Skellysolve B – ethyl acetate (4:1). This afforded white flakes of 4,6-dimethoxy-5-methylphthalide (**4**, 3.5 mg), mp 162–162.5°C (lit. (29) mp 162°C); tlc: R_f 0.27 (Skellysolve B – ethyl acetate 4:1); uv (methanol): 214 (3.75), 255 (3.08), 304 (2.78) nm; ftir ($CHCl_3$ cast): 3000, 2970, 2950, 1765, 1740, 1616, 1466, 1417, 1152, 1127, 1045, 767 cm^{-1}; ^1H nmr (acetone-d_6) δ: 7.02 (1H, s, H-7), 5.51 (2H, s, H-3), 3.96 (3H, s, OCH_3), 3.93 (3H, s, OCH_3), 2.14 (3H, s, C-5 CH_3); ^{13}C nmr (acetone-d_6) δ: 171.1 (s, C-1), 160.8 (s, C-6), 154.0 (s, C-4), 128.9 (s, C-3a), 126.1 (s, C-5), 124.8 (s, C-7a), 100.9 (d, C-7), 68.9 (t, C-3), 59.4 (q, OCH_3), 56.6 (q, OCH_3), 9.6 (q, C-5 CH_3); hreims, *m/z* calcd. for $C_{11}H_{12}O_4$ (M^+): 208.0736; found: 208.0738 (61), 207 (7), 179 (100); cims, *m/z*: 209 (M + 1), 226 (M + 18).

*5-Hydroxymethylfurfural (**5**)*

5-Hydroxymethylfurfural (**5**) was isolated by flash chromatography of the dichloromethane portion of the ethyl acetate broth extract, eluting with dichloromethane–methanol (97:3). Further purification was achieved by flash chromatography, eluting with Skellysolve B – ethyl acetate – acetic acid (60:40:1). This afforded 5-hydroxymethylfurfural (**5**) as a clear, pale yellow oil (7.5 mg), tlc: R_f 0.33 (dichloromethane–methanol 97:3), 0.28 (Skellysolve B – ethyl acetate – acetic acid 60:40:1); uv (methanol): 221 (3.43), 281 (3.49) nm; ftir (CH_2Cl_2–CH_3OH cast): 3370 (br), 2920, 2840, 2700, 1674, 1522, 1396, 1191, 1022 cm^{-1}; ^1H nmr ($CDCl_3$) δ: 9.58 (1H, s, C*H*O), 7.19 (1H, d, *J* = 3.5 Hz, H-3), 6.50 (1H, d, *J* = 3.5 Hz, H-4), 4.70 (2H, s, CH_2OH), 1.62 (1H, br s, O*H*); (acetone-d_6) δ: 9.57 (1H, s, C*H*O), 7.36 (1H, d, *J* = 3.5 Hz, H-3), 6.56 (1H, d, *J* = 3.5 Hz, H-4), 4.62 (2H, s, CH_2OH); ^{13}C nmr (acetone-d_6) δ: 178.1 (d, *C*HO), 163.0 (s, C-5), 153.7 (s, C-2), 123.3 (d, C-3), 110.2 (d, C-4), 57.6 (t, C-6); hreims, *m/z* calcd. for $C_6H_6O_3$ (M^+): 126.0317; found: 126.0321 (70), 125 (16), 97 (100); cims, *m/z*: 144 (M + 18).

*7-Hydroxy-2,5-dimethylchromone (**6**) (7-hydroxy-2,5-dimethyl-4*H*-1-benzopyran-4-one)*

7-Hydroxy-2,5-dimethylchromone (**6**) was isolated by flash chromatography of the dichloromethane portion of the ethyl acetate broth extract, eluting with dichloromethane–methanol (97:3). It crystallized from the eluent as white flasks (3.4 mg), mp 200°C (subl.) (lit. (36) mp 257–260°C, sublimes at 200°C); tlc: R_f 0.25 (dichloromethane–methanol 97:3); uv (methanol): 241 (4.12), 249 (4.13), 288 (3.92) nm; 1 drop 0.1 N NaOH: 254 (4.19), 325 (3.95) nm; 1 drop 0.1 N NaOH – 1 drop 0.1 N HCl: 241 (4.12), 2.49 (4.13), 288 (3.92) nm; ftir (methanol cast): 3400–3000 (br), 1649, 1618, 1557, 1162 cm^{-1}; ^1H nmr (methanol-d_4) δ: 6.64 (1H, d, *J* = 2.5 Hz, H-8), 6.62 (1H, dq, *J* = 2.5, 1.0 Hz, H-6), 6.00 (1H, q, *J* = 1.0 Hz, H-3), 2.70 (3H, bs, C5 CH_3), 2.31 (3H, d, *J* = 1.0 Hz, C-2 CH_3); ^{13}C nmr (methanol-d_4) δ: 182.0 (s, C-4), 166.6 (s, C-2), 163.1 (s, C-7 or C-9), 161.5 (s, C-7 or C-9), 143.7 (s, C-5), 118.0 (d, C-3), 115.7 (s, C-10), 111.4 (d, C-6), 101.7 (d, C-8), 23.0 (q, C-5 CH_3), 19.8 (q, C-2 CH_3); hreims, *m/z* calcd. for $C_{11}H_{10}O_3$ (M^+): 190.0630; found: 190.0632 (100), 162 (14), 150 (11); cims, *m/z*: 191 (M + 1).

*Methylation of 7-hydroxy-2,5-dimethylchromone (**6**)*

An excess of diazomethane in ether was added to a solution of **6** (1.3 mg) in methanol (3 drops) and the reaction mixture was allowed to stand at 0°C for 5 h. The solution was then warmed to room temperature and filtered to afford a cream colored solid, which was taken up in chloroform (5.0 mL). Evaporation to dryness and recrystallization of the solid from ether gave white flakes of 7-methoxy-2,5-dimethylchromone (**7**, 1.2 mg), mp 115–117°C (lit. (35) mp 115–117°C); tlc: R_f 0.54 (dichloromethane–methanol 97:3); uv (methanol): 248 (3.71), 280 (3.57) nm; ftir (CH_2Cl_2 cast): 1663, 1612, 1574, 1179, 1157 cm^{-1}; ^1H nmr ($CDCl_3$) δ: 6.66 (2H, bs, H-6, H-8), 6.01 (1H, q, *J* = 0.6 Hz, H-3), 3.86 (3H, s, OCH_3), 2.80 (3H, bs, C-5 CH_3), 2.29 (3H, d, *J* = 0.6 Hz, C-2 CH_3); ^{13}C nmr ($CDCl_3$) δ: 163.6, 162.3, 159.2, 142.6, 116.2, 116.0, 111.8, 98.5, 55.6, 23.0, 20.0; hreims, *m/z* calcd. for $C_{12}H_{12}O_3$ (M^+): 204.0787; found: 204.0783 (100), 176 (6), 164 (5); cims, *m/z*: 205 (M + 1).

*Methyl 4-carboxy-5-hydroxyphthalaldehydate (**8**)*

Methyl 4-carboxy-5-hydroxyphthalaldehydate (**8**) was obtained by flash chromatography of the dichloromethane portion of the ethyl acetate broth extract, eluting with dichloromethane–methanol (97:3). It crystallized from the eluent as yellow granules (2.8 mg), mp 190°C (dec.); tlc: R_f 0.35 (dichloromethane–methanol 97:3); uv (methanol): 225 (4.15), 293 (3.90), 428 (2.65) nm; 1 drop 0.1 N NaOH: 229 (4.19), 305 (3.95), 426 (2.90) nm; 1 drop 0.1 N NaOH – 1 drop 0.1 N HCl: 226 (4.14), 293 (3.90), 427 (2.64); ftir (methanol cast): 3560–2400 (br), 1757 (m), 1655, 1635, 1440, 1351, 1281, 1243, 1102, 1080 cm^{-1}; ^1H nmr (methanol-d_4) δ: 10.42 (1H, s, C*H*O), 6.70 (1H, s, Ar*H*), 6.38 (1H, s, Ar*H*), 3.52 (3H, s, $COOCH_3$); (acetone-d_6) δ: 10.46 (1H, s, C*H*O), 6.79 (1H, s, Ar*H*), 6.45 (1H, s, Ar*H*), 3.53 (3H, s, $COOCH_3$); ^{13}C nmr (methanol-d_4) δ: 196.6 (d, *C*HO), 169.4 (s), 166.3 (s), 160.1 (s), 136.8 (s), 122.7 (s), 114.6 (s), 103.9 (d), 102.4 (d), 56.4 (q, $COOCH_3$); hreims, *m/z* calcd. for $C_{10}H_8O_6$ (M^+): 224.0320; found: 224.0317 (30), 193 (95), 192 (86), 164 (100); cims, *m/z*: 225 (M + 1), 242 (M + 18).

*Reduction of methyl 4-carboxy-5-hydroxyphthalaldehydate (**8**)*

To a solution of methyl 4-carboxy-5-hydroxyphthalaldehydate (**8**, 2.0 mg) in methanol (1.0 mL) was added sodium borohydride (0.5 g). After 15 s the yellow color of the solution faded. After 10 min acetic acid (1 N, 2 drops) was added and the solvent was removed *in vacuo* to afford a clear, pale yellow oil. Purification of the reduction product by elution with dichloromethane–methanol (96:4) through a small silica gel pipette column afforded the reduction product as a clear, pale yellow oil (**9**, 1.3 mg); tlc: R_f 0.26 (dichloromethane–methanol 96:4); ftir (methanol cast): 3240 (br), 2920, 2840, 1755, 1618, 1466, 1368, 1347, 1242, 1098, 1032 cm^{-1}; ^1H nmr (acetone-d_6) δ: 6.74 (1H, s, Ar*H*), 6.35 (1H, s, Ar*H*), 5.01 (2H, s, OCH_2).

*3-Hydroxymethyl-6,8-dimethoxycoumarin (**10**) (3-hydroxymethyl-6,8-dimethoxy-2*H*-1-benzopyran-2-one)*

The coumarin (**10**) was obtained by flash chromatography of the dichloromethane portion of the ethyl acetate broth extract, eluting with dichloromethane–methanol (97:3). The crude metabolite was furher purified by passage through a small silica gel pipette column, eluting with dichloromethane–methanol (98:2), and then through another

Can. J. Chem. Downloaded from www.nrcresearchpress.com by 91.121.58.235 on 09/07/12
For personal use only.

column that was eluted with Skellysolve B – ethyl acetate – acetic acid (45:55:1). It was obtained as an amorphous solid (1.2 mg); tlc: R_f 0.36 (dichloromethane–methanol 97:3), 0.23 (dichloromethane–methanol 98:2), 0.26 (Skellysolve B – ethyl acetate – acetic acid 45:55:1); uv (methanol): 256 (4.11), 286 (4.17) nm; 1 drop 0.1 N NaOH: 255 (4.09), 284 (4.19) nm; ftir (CH_2Cl_2 cast): 3360 (br), 1760 (sh), 1711, 1657, 1592, 1205, 1162 cm^{-1}; ^1H nmr ($CDCl_3$–CD_3OD 4:1) δ: 7.70 (1H, t, J = 1.4 Hz, H-4), 6.65 (1H, d, J = 2.6 Hz, H-7), 6.48 (1H, d, J = 2.6 Hz, H-5), 4.55 (2H, d, J = 1.4 Hz, CH_2OH), 3.90 (3H, s, OCH_3), 3.81 (3H, s, OCH_3); ^{13}C nmr ($CDCl_3$) δ: 148.1 (s, C-4a), 138.7 (d, C-4), 128.6 (s, C-1a), 103.0 (d, C-5 or C-7), 101.2 (d, C-5 or C-7), 61.3 (t, CH_2OH), 56.3 (q, OCH_3), 55.8 (q, OCH_3); hreims, m/z calcd. for $C_{12}H_{12}O_5$ (M^+): 236.0685; found: 236.0691 (100), 235 (11), 207 (20); cims, m/z: 237 (M + 1), 254 (M + 18).

*Altenusin (**11**) (3,4′,5′-trihydroxy-5-methoxy-2′-methyl(1,1′-biphenyl)-2-carboxylic acid)*

Altenusin (**11**) was obtained by flash chromatography of the dichloromethane portion of the ethyl acetate broth extract, eluting with dichloromethane–methanol (97:3). The crude metabolite was further purified by dry flash chromatography, eluting with toluene–acetone – acetic acid (50:50:1), and then passed through a small silica gel pipette column, eluting with Skellysolve B – ethyl acetate – acetic acid (45:55:1). Altenusin (**11**) crystallized from the eluent as white flakes (5.0 mg), mp 194–196°C (lit. (38) mp 195–198°C); tlc: R_f 0.30 (toluene–acetone – acetic acid 50:50:1), 0.29 (Skellysolve B – ethyl acetate – acetic acid 45:55:1); ftir (CH_2Cl_2–CH_3OH cast): 3600–2800 (br), 1645 (w), 1610, 1582, 1518, 1270, 1204, 1158 cm^{-1}; ^1H nmr ($CDCl_3$–CD_3OD 1:1) δ: 6.47 (1H, s, H-3′ or H-6′), 6.40 (1H, s, H-3′ or H-6′), 6.27 (1H, d, J = 2.6 Hz, H-4 or H-6), 6.04 (1H, d, J = 2.6 Hz, H-4 or H-6), 3.65 (3H, s, OCH_3), 1.77 (3H, s, C-2′ CH_3); ^{13}C nmr ($CDCl_3$–CD_3OD 1:1) δ: 172.8 (s, CO_2H), 164.1 (s, C-3 or C-5), 163.1 (s, C-3 or C-5), 146.2 (s, C-1), 143.0 (s, C-4′ or C-5′), 141.3 (s, C-4′ or C-5′), 133.9 (s, C-1′), 126.6 (s, C-2′), 115.9 (d, C-3′ or C-6′), 115.2 (d, C-3′ or C-6′), 110.1 (d, C-6), 105.9 (s, C-2), 99.5 (d, C-4), 55.0 (q, OCH_3), 18.5 (q, C-2′ CH_3); hreims, m/z calcd. for $C_{15}H_{14}O_6$ (M^+): 290.0790; found: 290.0788 (56), 272 (26), 246 (100), 245 (32), 244 (52); cims, m/z: 247 (M + 1 – CO_2).

*Dehydroaltenusin (**12**)*

Dehydroaltenusin (**12**) was obtained by flash chromatography of the dichloromethane portion of the ethyl acetate broth extract, eluting with dichloromethane–methanol (97:3). The crude metabolite was further purified by flash chromatography, eluting with dichloromethane–methanol (99:1), and then passed through a small silica gel pipette column, eluting with Skellysolve B – ethyl acetate – acetic acid (50:50:1). It was further chromatographed in the same manner with dichloromethane–methanol (98:2). This afforded dehydroaltenusin (**12**), which still contained some impurities; ^1H nmr ($CDCl_3$) δ: 11.30 (1H, s, C-3 OH), 6.73 (1H, d, J = 2.3 Hz, H-4 or H-6), 6.69 (1H, s, H-10), 6.63 (1H, d, J = 2.3 Hz, H-4 or H-6), 6.28 (1H, s, H-7), 3.91 (3H, s, OCH_3), 1.73 (3H, s, C-1a CH_3). It was allowed to stand at room temperature for 24 h with acetic anhydride (0.3 mL) and pyridine (0.3 mL). Ethyl acetate (5.0 mL) and toluene (1.0 mL) were added to the reaction mixture and the solvents were removed under reduced pressure. This afforded the crude diacetate (**13**), which was purified by passage through a small silica gel pipette column, eluting with Skellysolve B – acetone (2:1). Dehydroaltenusin diacetate (**13**) crystallized from the eluent as white flakes (0.6 mg), mp 190–193°C (lit. (38) mp 185°C); tlc: R_f 0.39 (Skellysolve B – acetone 2:1), ftir (CH_2Cl_2 cast): 1776, 1732, 1688, 1664, 1617, 1370, 1192, 1144, 800 cm^{-1}; ^1H nmr ($CDCl_3$) δ: 6.77 (1H, d, J = 1.9 Hz, H-4), 6.60 (1H, d, J = 1.9 Hz, H-6), 6.36 (1H, s, H-7), 6.30 (1H, q, J = 1.4 Hz, H-10), 3.86 (3H, s, OCH_3), 2.42 (3H, s, ArOCOCH_3), 2.29 (3H, s, C-9 OCOCH_3), 1.73 (3H, d, J = 1.4 Hz, C-1a CH_3); hreims, m/z calcd. for $C_{19}H_{16}O_8$ (M^+): 372.0845; found: 372.0848 (10), 330 (59), 288 (63), 270 (10), 260 (24), 244 (38), 232 (17), 165 (100); cims, m/z: 390 (M + 18).

*Desmethyldehydroaltenusin (**14**)*

Desmethyldehydroaltenusin (**14**) was obtained by flash chromatography of the dichloromethane portion of the ethyl acetate broth extract, eluting with dichloromethane–methanol (97:3). The crude metabolite was further purified by dry flash chromatography, eluting with Skellysolve B – ethyl acetate – acetic acid (50:50:1). It was then passed through a small silica gel pipette column, eluting with dichloromethane–methanol (98:2). This afforded desmethyldehydroaltenusin (**14**), which was still somewhat impure. It was allowed to stand at room temperature for 24 h with acetic anhydride (0.3 mL) and pyridine (0.3 mL). Ethyl acetate (5.0 mL) and toluene (1.0 mL) were added to the reaction mixture and the solvents were removed *in vacuo*. This afforded the crude triacetate (**15**), which was purified by passage through a small silica gel pipette column, eluting with Skellysolve B – acetone (2:1). Desmethyldehydroaltenusin triacetate (**15**) was obtained as an amorphous solid (1.0 mg); tlc: R_f 0.33 (Skellysolve B – acetone 2:1); ftir (CH_2Cl_2 cast): 1777, 1680, 1660, 1610, 1365, 1190, 1150, 1122, 1015 cm^{-1}; ^1H nmr ($CDCl_3$) δ: 7.10 (1H, d, J = 1.7 Hz, H-4 or H-6), 6.97 (1H, d, J = 1.7 Hz, H-4 or H-6), 6.37 (1H, s, H-7), 6.31 (1H, q, J = 1.5 Hz, H-10), 2.43 (3H, s, ArOCOCH_3), 2.31 (3H, s, OCOCH_3), 2.29 (3H, s, OCOCH_3), 1.74 (3H, d, J = 1.5 Hz, C-1a CH_3); hreims, m/z calcd. for $C_{20}H_{16}O_9$ (M^+): 400.0794; found: 400.0784 (3), 358 (100), 316 (63), 274 (89), 256 (29), 246 (31), 230 (62), 218 (16); cims, m/z: 418 (M + 18).

*Talaroflavone (**16**) (spiro[5′-hydroxy-2′-methyl-cyclopent-2′-ene-4′-one-1′,3,7-hydroxy-5-methoxy-1(3*H*)-isobenzofuranone])*

Talaroflavone (**16**) was obtained by flash chromatography of the dichloromethane portion of the ethyl acetate broth extract, eluting with dichloromethane–methanol (97:3). The crude metabolite was further purified by passing it through a small silica gel pipette column, eluting with Skellysolve B – ethyl acetate – acetic acid (45:55:1). It crystallized from the eluent as white flakes (3.0 mg), mp 230°C (dec.); tlc: R_f 0.25 (dichloromethane–methanol 97:3), 0.28 (Skellysolve B – ethyl acetate – acetic acid 45:55:1); $[\alpha]_D$ +181° (c 0.74, methanol); uv (methanol): 217 (4.19), 257 (3.66), 296 (3.28) nm; 1 drop 0.1 N NaOH: 228 (4.19), 256 (3.58), 325 (3.41) nm; 1 drop 0.1 N NaOH – 1 drop 0.1 N HCl: 216 (4.20), 257 (3.71), 295 (3.34) nm; ftir (methanol cast): 3240 (br), 1748, 1723, 1617, 1204, 1162, 1152, 1004 cm^{-1}; ^1H nmr (methanol-d_4) δ: 6.44 (1H, d, J = 2.0 Hz, H-4 or H-6), 6.34 (1H, q, J = 1.5 Hz, H-3′), 6.05 (1H, d, J = 2.0 Hz, H-4 or H-6), 4.74 (1H, s, H-5′), 3.80 (3H, s, OCH_3), 1.86 (3H, d, J = 1.5 Hz, C-2′ CH_3); ^{13}C nmr (methanol-d_4) δ: 202.0 (s, C-4′), 171.4, 170.2, 168.5 (3 × s, C-1, C-2′, C-5), 159.9 (s, C-7), 150.8 (s, C-3a), 131.4 (d, C-3′), 106.5 (s, C-7a), 103.5 (d, C-4 or C-6), 101.0 (d, C-4 or C-6), 94.2 (s, C-1′), 79.7 (d, C-5′), 56.5 (q, OCH_3), 13.4 (q, C-2′ CH_3); hreims, m/z calcd. for $C_{14}H_{12}O_6$ (M^+): 276.0634; found: 276.0633 (100), 258 (64), 248 (30), 247 (21), 230 (17), 220 (39), 219 (64); cims, m/z: 277 (M + 1), 294 (M + 18).

*Acetylation of talaroflavone (**16**)*

Pyridine (0.5 mL) was added to a solution of talaroflavone (**16**, 4.0 mg) in acetic anhydride (0.5 mL). The reaction mixture was allowed to stand at room temperature for 22 h. Ethyl acetate (5.0 mL) and toluene (1.0 mL) were added to the mixture and the solution was evaporated under reduced pressure. The crude acetylation product was passed through a small silica gel pipette column, eluting with Skellysolve B – acetone (2.5:1) to afford talaroflavone diacetate (**17**) as a clear, colorless oil (3.0 mg), tlc: R_f 0.21 (Skellysolve B – acetone 2.5:1); ord (methanol): $[\alpha]_{265}$ +33°: cd (methanol): $\Delta\Sigma_{235}$ 6.3 L mol^{-1} cm^{-1}; $\Delta\Sigma_{325}$ 0.27 L mol^{-1} cm^{-1}; ftir (CH_2Cl_2 cast): 3080, 2920, 2840, 1777, 1732, 1621, 1491, 1371, 1256, 1221, 1189, 1143 cm^{-1}; ^1H nmr ($CDCl_3$) δ: 6.76 (1H, d, J = 2.0 Hz, H-4 or H-6), 6.42 (1H, d, J = 2.0 Hz, H-4 or H-6), 6.35 (1H, q, J = 1.5 Hz, H-3′), 5.84 (1H, s, H-5′), 3.85 (3H, s, OCH_3), 2.39 (3H, s, ArOCOCH_3), 1.87 (6H, br s, C-5′ OCOCH_3, C-2′ CH_3); (methanol-d_4) δ: 6.93 (1H, d, J = 2.0 Hz, H-4 or H-6), 6.61 (1H, d, J = 2.0 Hz, H-4 or H-6), 6.49 (1H, q, J = 1.5 Hz, H-3′), 5.81 (1H, s, H-5′), 3.89 (3H, s, OCH_3), 2.35 (3H, s, ArOCOCH_3), 1.86 (3H, d, J = 1.5 Hz, C-2′ CH_3), 1.82 (3H, s, C-5′ OCOCH_3); ^{13}C nmr ($CDCl_3$) δ: 195.3 (s), 170.8 (s), 169.0 (s), 168.4 (s), 166.1 (s), 165.3 (s), 150.1 (s), 147.9 (s), 131.5 (d), 111.3 (s), 110.9 (d), 104.9 (d), 90.7 (s), 76.9 (d), 56.4 (q), 20.7 (q), 20.1 (q), 13.7 (q); (methanol-d_4) δ: 197.1 (s), 172.0 (s), 170.8 (s), 170.0 (s), 168.1 (s), 167.2 (s), 151.5 (s), 149.5 (s), 133.2 (d), 112.4 (s), 112.1 (d), 106.7 (d), 92.7 (s), 78.1 (d),

57.2 (q), 20.4 (q), 19.8 (q), 13.3 (q); hreims, m/z calcd. for $C_{18}H_{16}O_8$ (M^+): 360.0845; found: 360.0850 (12), 318 (100), 276 (97), 258 (99), 248 (6), 247 (25), 230 (6), 220 (10), 219 (24).

Deoxytalaroflavone (18)

Deoxytalaroflavone (**18**) was obtained by flash chromatography of the dichloromethane portion of the ethyl acetate broth extract, eluting with dichloromethane–methanol (97:3). It was further purified by flash chromatography, eluting with dichloromethane–methanol (99:1). This afforded white flakes of deoxytalaroflavone (**18**, 3.0 mg), mp 178–180°C; tlc: R_f 0.35 (Skellysolve B – acetone 2:1); ftir (CH_2Cl_2 cast): 3400–2800 (br), 1713, 1679, 1610, 1565, 1390, 1239, 1226, 1200, 1109, 797, 733, 691 cm^{-1}; ^1H nmr ($CDCl_3$) δ: 11.35 (1H, s, C-3 O*H*), 6.70 (1H, d, J = 2.3 Hz, H-4 or H-6), 6.69 (1H, d, J = 2.3 Hz, H-4 or H-6), 3.94 (3H, s, OCH_3), 3.43 (1H, ddd, J = 1.3, 6.6, 6.9 Hz, H-9), 2.95 (1H, dd, J = 6.6, 19.0 Hz, H-8), 2.31 (1H, dd, J = 1.3, 19.0 Hz, H-8′), 1.46 (3H, d, J = 6.9 Hz, C-9 CH_3); ^{13}C nmr ($CDCl_3$) δ: 134.6 (s), 115.3 (s), 103.3 (d), 103.1 (d), 56.1 (q), 42.9 (t), 28.4 (d), 21.1 (q); hreims, m/z calcd. for $C_{14}H_{12}O_5$ (M^+): 260.0685; found: 260.0688 (100), 245 (8), 232 (16), 217 (45), 204 (8), 189 (13), 161 (19); cims, m/z: 261 (M + 1), 278 (M + 18).

Acknowledgements

We gratefully acknowledge the financial support of the Natural Sciences and Engineering Research Council of Canada in the form of grants (W.A.A.) and scholarships (J.S.R.). We thank the Alberta Heritage Foundation for Medical Research for Independent Research Allowance Studentships (J.S.R.) and the University of Alberta for Graduate Faculty Fellowships (J.S.R.). The assistance of Mrs. A. Szenthe in carrying out the culture growths is greatly appreciated.

1. K. H. Domsch, W. Gams, and T. H. Anderson. Compendium of soil fungi. Vol. 1. Academic Press, London. 1980. pp. 752–759.
2. A. C. Stolk and R. A. Samson. Stud. Mycol. **2**, 1 (1972).
3. J. J. Marois, S. A. Johnston, M. T. Dunn, and G. C. Papavizas. Plant Dis. **66**, 1166 (1982).
4. M. Yamazaki and E. Okuyama. Chem. Pharm. Bull. **28**, 3649 (1980).
5. S. Natori, F. Sato, and S. Udagawa. Chem. Pharm. Bull. **13**, 385 (1965).
6. K. Mizuno, A. Yagi, M. Takada, K. Matsuura, K. Yamaguchi, and K. Asano. J. Antibiot. **27**, 560 (1974).
7. G. W. van Eijk. Experientia, **29**, 522 (1973).
8. D. G. Lynn, N. J. Phillips, W. C. Hutton, J. Shabanowitz, D. I. Fennell, and R. J. Cole. J. Am. Chem. Soc. **104**, 7319 (1982).
9. W. C. Hutton, N. J. Phillips, D. W. Graden, and D. G. Lynn. J. Chem. Soc. Chem. Commun. 864 (1983).
10. N. J. Phillips, R. J. Cole, and D. G. Lynn. Tetrahedron Lett. **28**, 1619 (1987).
11. J. Fuska, P. Nemec, and I. Kuhr. J. Antibiot. **25**, 208 (1972).
12. R. K. Boeckman, Jr., J. Fayos, and J. Clardy. J. Am. Chem. Soc. **96**, 5954 (1974).
13. J. Fuska, P. Nemec, and A. Fuskova. J. Antibiot. **32**, 667 (1979).
14. J. Fuska, A. Fuskova, and P. Nemec. Biologia, **34**, 735 (1979).
15. J. Fuska, D. Uhrin, B. Proska, Z. Voticky, and J. Ruppeldt. J. Antibiot. **39**, 1605 (1986).
16. M. Takeuchi, M. Nakajima, T. Ogita, M. Inukai, K. Kodama, K. Furuya, H. Nagaki, and T. Haneishi. J. Antibiot. **42**, 198 (1989).
17. D. L. McLaren, H. C. Huang, and S. R. Rimmer. Can. J. Plant Pathol. **8**, 43 (1986).
18. M. G. Boosalis. Phytopathology, **46**, 473 (1956).
19. B. K. Dutta. Plant Soil, **63**, 209 (1981).
20. J. J. Marois, D. R. Fravel, and G. C. Papavizas. Soil Biol. Biochem. **16**, 387 (1984).
21. D. R. Fravel, J. J. Marois, M. T. Dunn, and G. C. Papavizas. Soil Biol. Biochem. **17**, 163 (1985).
22. D. R. Fravel and J. J. Marois. Phytopathology, **76**, 643 (1986).
23. G. C. Papavizas, D. R. Fravel, and J. A. Lewis. Phytopathology, **77**, 131 (1987).
24. C. Litchfield. Analysis of triglycerides. Academic Press, New York. 1972. pp. 222–224.
25. Z. Walaszek and D. Horton. Carbohydr. Res. **105**, 131 (1982).
26. K. Bock and C. Pedersen. Adv. Carbohydr. Chem. Biochem. **41**, 27 (1983).
27. H. S. Isbell and H. L. Frush. U.S. Bur. Stand. J. Res. **11**, 649 (1933).
28. B. Capon. Chem. Rev. **69**, 407 (1969).
29. H. Achenbach, A. Mühlenfeld, and G. U. Brillinger. Liebigs Ann. Chem. 1596 (1985).
30. M. Fujita, M. Yamada, S. Nakajima, K. Kawai, and M. Nagai. Chem. Pharm. Bull. **32**, 2622 (1984).
31. M. T. W. Hearn. Aust. J. Chem. **29**, 107 (1976).
32. J. C. Speck, Jr. Adv. Carbohydr. Chem. **13**, 63 (1958).
33. Y. Kimura, M. Kozawa, K. Baba, and K. Hata. Planta Med. **48**, 164 (1983).
34. Y. Kashiwada, G. Nonaka, and I. Nishioka. Chem. Pharm. Bull. **32**, 3493 (1984).
35. P. Gramatica, M. P. Gianotti, G. Speranza, and P. Manitto. Heterocycles, **24**, 743 (1986).
36. K. Makino, A. Yagi, and I. Nishioka. Chem. Pharm. Bull. **21**, 149 (1973).
37. T. Sassa, M. Ikeda, and Y. Miura. Agric. Biol. Chem. **37**, 2937 (1973).
38. R. G. Coombe, J. J. Jacobs, and T. R. Watson. Aust. J. Chem. **23**, 2343 (1970).
39. F. H. Wehrli and T. Wirthlin. Interpretation of carbon-13 NMR spectra. Heyden and Son Ltd., London. 1976. p. 47.
40. T. Rosett, R. H. Sankhala, C. E. Stickings, M. E. U. Taylor, and R. Thomas. Biochem. J. **67**, 390 (1957).
41. K. Kameda and M. Namiki. Chem. Lett. 265 (1974).
42. D. Rogers, D. J. Williams, and R. Thomas. Chem. Commun. 393 (1971).
43. J. B. Stothers. Carbon-13 NMR spectroscopy. Academic Press, New York. 1972. pp. 193, 290.
44. J. Massicot, J.-P. Marthe, and S. Heitz. Bull. Soc. Chim. Fr. 2712 (1963).
45. A. Pelter, R. S. Ward, and T. I. Gray. J. Chem. Soc. Perkin Trans. 1, 2475 (1976).
46. W. C. Still, M. Kahn, and A. Mitra. J. Org. Chem. **43**, 2923 (1978).

Can. J. Chem. Downloaded from www.nrcresearchpress.com by 91.121.58.235 on 09/07/12
For personal use only.

The metabolites of *Talaromyces flavus*: Part 2. Biological activity and biosynthetic studies

WILLIAM A. AYER[1] AND JULIE S. RACOK
Department of Chemistry, University of Alberta, Edmonton, Alta., Canada T6G 2G2

Received February 5, 1990

WILLIAM A. AYER and JULIE S. RACOK. Can. J. Chem. **68**, 2095 (1990).

The soil fungus *Talaromyces flavus* (Klöcker) Stolk and Samson is an effective biological control for Verticillium wilt of eggplant (*Solanum melongena* L.), a disease caused by the fungus *Verticillium dahliae* Kleb. The water soluble metabolites isolated from the broth when the fungus is grown in liquid still culture, hydroxymethylmaltol (**1**), 5,6-dihydro-3,5-dihydroxy-6-hydroxymethyl-2*H*-pyran-2-one (**3**), and D-glucono-1,4-lactone (**5**), do not show antifungal activity against *V. dahliae*; however, hydrogen peroxide displays this inhibition. This peroxide has been detected in the *T. flavus* broth and it, together with **5**, is the product of the glucose oxidase catalyzed oxidation of D-glucose. The results of the search for this antifungal activity are presented. [1-^{13}C] Labelled sodium acetate was utilized as a precursor for studying the biosynthesis of the *T. flavus* metabolites 4,6-dihydroxy-5-methylphthalide (**7**), methyl 4-carboxy-5-hydroxyphthalaldehydate (**8**), and talaroflavone (**9**). The incorporation of label into these compounds is discussed.

Key words: *Talaromyces flavus*, fungal metabolites, hydrogen peroxide, biosynthesis, talaroflavone.

WILLIAM A. AYER et JULIE S. RACOK. Can. J. Chem. **68**, 2095 (1990).

Le champignon du sol *Talaromyces flavus* (Klöcker) Stolk et Samson contrôle biologiquement et d'une façon efficace la flétrissure par le Verticillium de l'aubergine (*Solanum melongena* L.), une maladie causée par le champignon *Verticillium dahliae* Kleb. Les métabolites organiques solubles dans l'eau qui sont isolés du bouillon de culture du champignon, l'hydroxyméthylmaltol (**1**), la 5,6-dihydro-3,5-dihydroxy-6-hydroxyméthyl-2*H*-pyran-2-one (**3**) et la D-glucono-1,4-lactone (**5**), ne présentent pas d'activité contre la moisissure *V. dahliae*; toutefois le peroxyde d'hydrogène présente une telle inhibition. Ce peroxyde a été détecté dans le bouillon du *T. flavus* et, avec le produit **5**, ils sont les produits de l'oxydation du D-glucose catalysée par la glucose oxydase. On présente les résultats de la recherche de cette activité contre la moisissure. On a utilisé du [1-^{13}C]-acétate de sodium comme précurseur pour l'étude de la biosynthèse des métabolites suivants du *T. flavus* : 4,6-dihydroxy-5-méthylphtalide (**7**), 4-carboxy-5-hydroxyphtalaldéhydate de méthyle (**8**) et talaroflavone (**9**). On discute de l'incorporation de ce marqueur dans ces composés.

Mots clés : *Talaromyces flavus*, métabolites de champignons, peroxyde d'hydrogène, biosynthèse, talaroflavone.
[Traduit par la revue]

Introduction

In Part 1 of this series (1) we reported the isolation and structure determination of the organic soluble metabolites produced by the soil fungus *Talaromyces flavus* (Klöcker) Stolk and Samson. Our interest in the metabolites produced by this fungus was stimulated by the report of its effectiveness as a biological control for Verticillium wilt of eggplant (*Solanum melongena* L.), a disease caused by the fungus *Verticillium dahliae* Kleb. (2). This disease develops slowly, beginning with a yellowing of the lower leaves, and causes a stunting of growth, a reduction in fruit size, and vascular discoloration. The penetration of Verticillium wilt in the host occurs through the root system and progress is primarily in the xylem. Neither crop rotation nor soil fumigants have been useful in reducing losses from the disease in eggplant. Crop rotation is not effective because the pathogen may persist as microsclerotia in the soil in the absence of a known host for many years. Soil fumigants delay the onset of symptoms and are used to reduce disease severity; however, the adverse effects on the environment and high cost disfavor their use. The main effect of a vascular pathogen like *V. dahliae* is to disrupt the passage of water through the stem. This may be attributed to the physical presence of the pathogen mycelium, the development of tyloses that block the xylem, or to gummosis within the vessels. Parasites like *Verticillium* in vessels cause a 4- to 60-fold increase in the resistance of the stem to water flow (3, 4). Further xylem occlusion comes from high molecular weight polysaccharides produced by the pathogen or cleaved from the xylem walls by hydrolytic enzymes.[2] *Verticillium dahliae* is the cause of a wilting disease in a wide variety of host organisms, most severely in eggplant, tomato, potato, and cotton. Among isolates of this species, there is considerable variation in morphology and pathogenicity. Generally, the pathogenicity of isolates of *V. dahliae* is nonspecific, although some isolates have restricted or unique host ranges (5–7). We found that *T. flavus* displays antifungal activity against the strain of *V. dahliae* isolated from eggplant; however, a strain of *V. dahliae* isolated from tomato did not show this biological activity. A plug to plug bioassay performed to determine the mode of action of *T. flavus* against *V. dahliae* revealed that, after 2 weeks, there is a distinct area between the fungi that shows no growth. There are no obvious signs of intermingling or broken hyphae so that there seems to be no antagonism of *V. dahliae* by *T. flavus*. Although the physical mechanism of biological control of *V. dahliae* by *T. flavus* is not clear, we engaged in an investigation of the metabolites of the *T. flavus* broth in search of the antifungal activity.

Discussion

Biological activity and the Talaromyces flavus *broth*

The bioassay developed to follow the antifungal activity of *T. flavus* against *V. dahliae* involves seeding an agar plate with *V. dahliae* and then injecting 100 μL of the *T. flavus* broth into a stainless steel vessel placed in the center of the plate. The sample diffuses into the medium and after 7–10 days the

[1]Author to whom correspondence may be addressed.

[2]For more details regarding the Verticillium wilt disease, see refs. 3–7.

Can. J. Chem. Downloaded from www.nrcresearchpress.com by 91.121.58.235 on 09/07/12
For personal use only.

Can. J. Chem. Downloaded from www.nrcresearchpress.com by 91.121.58.235 on 09/07/12
For personal use only.

bioassay results are noted. *Verticillium dahliae* produces two types of spores: white conidial spores and black chlamydospores. The latter are a part of the microsclerotia, which store many nutrients, and are the means by which *V. dahliae* survives in the soil. The white conidial spores do not survive as long since they store fewer nutrients. The bioassay shows a large zone of inhibition by the *T. flavus* aqueous broth toward the production of microsclerotia by *V. dahliae*. It appears that by restricting *V. dahliae* microsclerotia production *T. flavus* controls Verticillium wilt of eggplant. The pH of the *T. flavus* broth drops from 5.8 to ca. 2.5–3.0 after 5 days' growth. This acidic pH is then maintained during the remainder of the growth period. Cation and anion exchange columns were tested to determine whether the active compound was charged; however, the eluent possessed antifungal activity in both cases. Neither reverse phase chromatography nor steam distillation removed the antifungal component. Passage of the broth through Sep-Pak cartridges (C_{18} and amino) failed to provide purification of the antifungal component. Iron(II) sulfate and iron(III) nitrate were added individually to see if an active metabolite capable of chelation was present. No chelate extracted into organic solvent and the fungal broth retained its activity. The ^{1}H nmr spectrum of the fungal broth shows resonances between δ 3 and 5, which we presumed were those of sugars. Attempts to remove the sugars by chromatography over charcoal and Celite resulted in the loss of biological activity. Some loss in activity was observed when a portion of the broth was autoclaved to determine if a heat sensitive compound was responsible for this biological activity. Dialysis with tubing of exclusion limit 1000 daltons revealed that, after 24 h, the contents of the dialysis bag had lost its activity, implying that the molecular weight of the active compound was less than 1000. Chromatography over Sephadex G-50, eluting with water, or Bio-Gel P-2, eluting with water–ethanol (90:10), gave positive bioassay results. The active fractions were pooled and subjected to acetylation. The major fraction (ca. 66%) appears, from its ^{1}H nmr spectrum, to be composed of acetylated sugars, while the minor portion (ca. 33%) was shown by gas chromatographic (gc) analysis to be a mixture of three compounds. Gas chromatographic mass spectral (gc–ms) separation provides the molecular weights of these acetates, 226, 286, and 346. Methanolysis of the acetates did not regenerate the biological activity; however, their identification was pursued. The diacetate **2** of hydroxymethylmaltol (**1**) has the molecular formula $C_{10}H_{10}O_6$, as determined by high resolution mass spectrometry (hrms). The loss of two molecules of ketene in the mass spectrum affords the base peak at m/z 142, corresponding to the molecular formula of the alcohol **1**, $C_6H_6O_4$. The infrared spectrum (ir) spectrum of **2** shows acetate absorptions at 1780 and 1741 cm^{-1} and γ-pyrone bands at 1656 and 1585 cm^{-1}. The ultraviolet (uv) maximum at 292 nm is consistent with a γ-pyrone chromophore and shows no bathochromic shift on addition of base. The ^{1}H nuclear magnetic resonance (nmr) spectrum indicates vinylic hydrogens at δ 7.06 and 6.24 (each a doublet, J = 7.0 Hz), a methylene (δ 4.83), and acetyl methyls (δ 2.30 and 2.12). The carbons of these acetates are seen at δ 170.0 (s), 167.9 (s), 20.6 (q), and 20.4 (q), together with singlet carbons (δ 157.1 (C-4), 155.6 (C-2), and 137.0 (C-3)), doublet carbons (δ 130.5 (C-6) and 103.8 (C-5)), and a methylene carbon (δ 61.3). The carbonyl carbon (C-4, δ 157.1) is coupled ($^3J_{CH}$ = 8 Hz) to the C-6 hydrogen (δ 7.06), in agreement with that reported (8). The isolation of hydroxymethylmaltol (**1**) is not surprising since the fungus was grown on a malt extract medium.

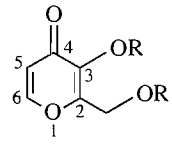

1, R = H
2, R = $COCH_3$

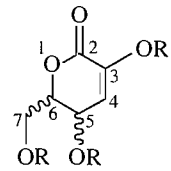

3, R = H
4, R = $COCH_3$

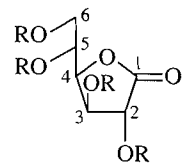

5, R = H
6, R = $COCH_3$

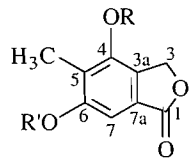

7, R, R' = H
7*a*, R = H, R' = CH_3
7*b*, R = CH_3, R' = H
7*c*, R, R' = CH_3

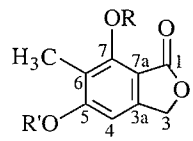

7*d*, R, R' = CH
7*e*, R = CH_3, R' = H

The second of the three acetates isolated is the triacetate (**4**) of 5,6-dihydro-3,5-dihydroxy-6-hydroxymethyl-2*H*-pyran-2-one (**3**). The parent ion in the hrms (m/z 286) corresponds to the molecular formula $C_{12}H_{14}O_8$. One acetate is lost as acetic acid and the other two as ketene to afford the base peak at m/z 142. The ir spectrum shows acetate carbonyl bands at 1778 and 1750 cm^{-1}. The ^{13}C nmr spectrum consists of the carbonyl carbon (δ 157.1, C-2, s), vinylic carbons (δ 139.8, C-3, s, and 125.9, C-4, d), oxygenated methines (δ 77.9, C-6, d, and 64.3, C-5, d), and a methylene carbon (δ 62.0, C-7, t). The ^{1}H nmr spectrum indicates that the vinylic hydrogen (δ 6.43, H-4) is coupled (J = 4.0 Hz) to H-5 (δ 5.61), which, in turn, is coupled (J = 5.5 Hz) to H-6 (δ 4.75). Although the stereochemistry of compound **3** was not determined, it is probable that it is derived from dehydration of D-glucono-1,5-lactone (via oxidation of D-glucose).

The third acetate isolated is the tetraacetate (**6**) of D-glucono-1,4-lactone (**5**) whose identification was discussed previously (1). Although lactone **5** shows no antifungal activity against *V. dahliae*, it is one of two products produced in the oxidation of D-glucose by glucose oxidase, whose isolation from *T. flavus* was recently reported (9, 10). This enzyme, whose kinetics and mechanism of action have been studied, is an oxidoreductase and oxidizes D-glucose to D-gluconic acid (11–13) (Fig. 1). The primary product of the oxidation of an aldose could be the aldonic acid, the γ- or the δ-lactone (14). These interconvert in aqueous solution and the proportions of each depend on the pH. The δ-lactone (**5***a*) has been shown, by means of optical rotation studies, to be the predominant kinetically controlled product of the oxidation of both anomers of glucose. D-Glucono-1,5-lactone (**5***a*) was not isolated from the fungal broth; however, it may undergo hydrolysis to the thermodynamically more stable (15, 16) γ-lactone (**5**) or dehydration to compound **3**. The other product of the enzyme oxidation, hydrogen peroxide, inhibits

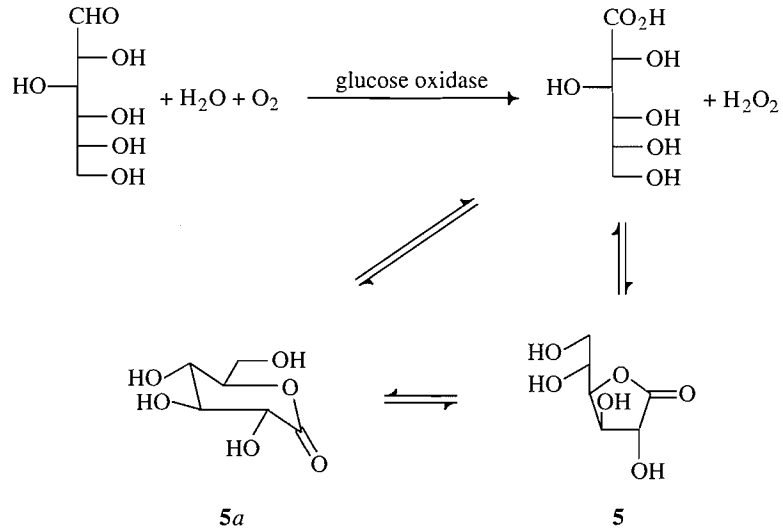

5*a* 5

FIG. 1. Enzymatic oxidation of D-glucose.

[1] $H_2O_2 + 2\,H^+ + 2\,I^- \xrightarrow{HRP} I_2 + 2\,H_2O$

in excess iodide

[2] $I_2 + I^- \rightleftharpoons I_3^-$

FIG. 2. Detection of H_2O_2 using horseradish peroxidase.

microsclerotia production by *V. dahliae*. We have observed that, as the concentration of hydrogen peroxide is increased from 2.7 to 3.6 to 7.5 μL/mL, microsclerotia production by *V. dahliae* is reduced. Microsclerotia production is restored after catalase has been added to the broth. Attempts to detect hydrogen peroxide in the broth utilizing paper chromatography by spraying with a ferrous cyanate reagent (17, 18) failed to produce coloration. It has been reported (9, 10) that the concentration of peroxide in the *T. flavus* broth is low (12 μg/mL) so that a more sensitive test for detecting hydrogen peroxide was employed (19) (Fig. 2). The first reaction, catalyzed by horseradish peroxidase (HRP), produces iodine that, in the presence of excess iodide, exists in equilibrium with the triiodide ion. This ion has an extinction coefficient (ε) at 353 nm of $2.55 \times 10^4\ M^{-1}\ cm^{-1}$. The change in absorbance at 353 nm is measured after completion of the reaction and, knowing that this procedure gives $\Delta A_{353} = 0.255$ for 0.1 M hydrogen peroxide, the concentration of hydrogen peroxide in the broth is estimated to be 50 μg/mL. This is a lower estimate than those concentrations (100–120 μg/mL) utilized in the bioassay (performed a month earlier) to see a similar zone of inhibition; however, it is possible that the hydrogen peroxide concentration decreases as the broth ages. Although the ultraviolet experiments for determining the concentration of a peroxide is not specific for hydrogen peroxide, the fact that addition of catalase to the broth destroys the inhibitory effect *T. flavus* has on the production of microsclerotia by *V. dahliae* strongly supports the proposal that hydrogen peroxide is the causative agent of the antifungal activity. *tert*-Butylhydroperoxide did not inhibit microsclerotia production by *V. dahliae*. The antifungal activity between *T. flavus* and *V. dahliae* occurs in the soil. Our studies, which involve growing *T. flavus* in still culture and utilizing the bioassay developed for use on an agar plate, appear to mimic nature well.

Biosynthetic studies of Talaromyces flavus *metabolites*

The metabolites from the *T. flavus* broth extract whose biosyntheses we were interested in studying include 4,6-dihydroxy-5-methylphthalide (**7**), methyl 4-carboxy-5-hydroxyphthalaldehydate (**8**), and the spirocyclic metabolite, talaroflavone (**9**). These metabolites are presumed to have a polyketide

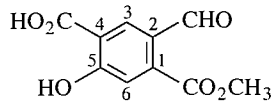

8

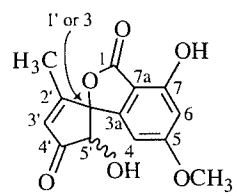

9

biogenesis and thus [1-^{13}C] labelled sodium acetate was chosen as the precursor for the biosynthetic studies. The precursor was administered to the fungus in 3–10 mmol batches (1 mmol/L culture medium) after 9, 16, and 23 days growth, and the fungus was harvested after 30 days. The advantage of multiple over single-dose feeding lies in the opportunity it affords to maintain a steady precursor concentration while avoiding the toxic effects due to excessively high concentrations (20). To follow the labelling pattern of ^{13}C enriched metabolites, it was first necessary to assign the ^{13}C chemical shifts for the metabolites. The ^{13}C nmr spectra of metabolites **7**, **8**, and **9** were assigned in Part 1 of this series (1). Two regioisomeric types of phthalides are known in nature: one in which the hydroxyl group is *peri* to the carbonyl (**7***d*, **7***e*, for example) and the other in which the aromatic hydrogen is *peri* to the carbonyl (**7**–**7***c*). Their biogeneses may be envisaged by cyclization of a tetraketide precursor and methylation with *S*-adenosylmethionine (SAM) to afford 3-methylorsellinic acid (**7***f*) (21, 22) (Scheme 1). Oxidation of the C-6 methyl group leads to the phthalide backbone of 5,7-dihydroxy-6-methylphthalide (**7***d*) (23, 24), and nidulol (**7***e*) (23, 25). Formation of the phthalide **7** isolated from *T. flavus* and its *O*-methylated derivatives (**7***a*–**7***c*) appears to involve a reduction of the acid moiety and an oxidation of the methyl group. This reduction is not commonly encountered in the biosynthesis of polyketides. Possible intermediates include 3,5-dihydroxy-4-methylphthalaldehydic acid (**8***a*) (26), which may also be a precursor to metabolite **8**.

Can. J. Chem. Downloaded from www.nrcresearchpress.com by 91.121.58.235 on 09/07/12
For personal use only.

Can. J. Chem. Downloaded from www.nrcresearchpress.com by 91.121.58.235 on 09/07/12
For personal use only.

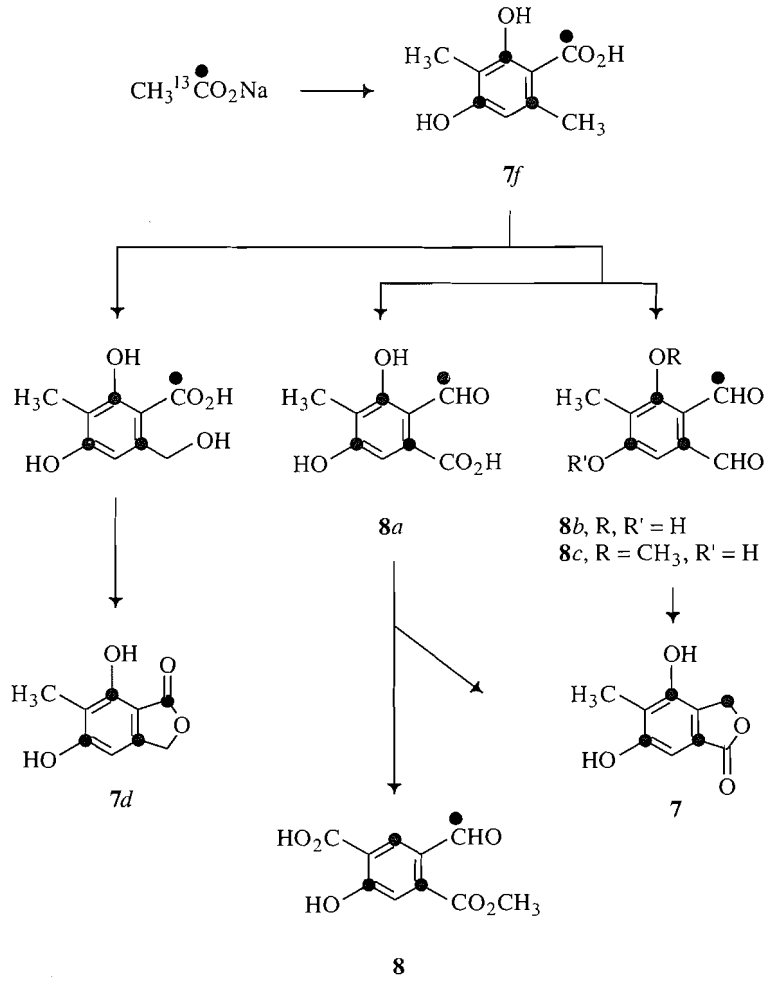

SCHEME 1

Reduction of the aldehyde and lactonization affords the regioisomer 4,6-dihydroxy-5-methylphthalide (**7**). A Cannizzaro reaction of dialdehyde **8***b* would provide the natural product **7** regioselectively. The mono-*O*-methyl derivative, quadrilineatin (**8***c*), from *Aspergillus quadrilineatus*, is reported (27) to give 6-hydroxy-4-methoxy-5-methylphthalide (silvaticol, **7***b*) (25) on treatment with dilute sodium hydroxide. If this oxidation–reduction sequence of the methyl and acid groups is occurring, the methylene carbon of **7** (from C-1 of acetate) should be labelled and the carbonyl carbon, originating from C-2, should not be enriched. The ^{13}C nmr spectrum of the labelled phthalide compared to that at natural abundance indicates that label has been incorporated (about 6% enrichment) at four carbons. The enhanced signals include the phenolic carbons (δ 159.1 and 151.5), the quaternary carbon (δ 124.7), and the methylene carbon (δ 69.7). In addition to the intense methylene resonance, the carbonyl carbon (δ 174.2) shows no enrichment, confirming its origin from C-2 of acetate as well as the unusual oxidation–reduction sequence along the pathway to 4,6-dihydroxy-5-methylphthalide (**7**). The isolation of **7** completes the family of phthalide natural products since both mono-*O*-methyl (**7***a*, **7***b*) and the dimethyl (**7***c*) derivatives of **7** have been reported (23, 25). Nidulol (5-hydroxy-7-methoxy-6-methylphthalide, **7***e*), silvaticol (6-hydroxy-4-methoxy-5-methylphthalide, **7***b*), and *O*-methylsilvaticol (4,6-dimethoxy-5-methylphthalide, **7***c*) are reported from *A. silvaticus* (25), indicating that some organisms have the capability to produce metabolites of either phthalide type.

The pathway from 3-methylorsellinic acid (**7***f*) to methyl 4-carboxy-5-hydroxyphthalaldehydate (**8**) involves an oxidation of the methyl group, methylation of the acid, and a reduction of the C-3 hydroxyl bearing carbon, perhaps via intermediate **8***a*. We have not ruled out the possibility that this reduction occurs before aromatization. The ^{13}C nmr spectrum of the labelled metabolite compared to that at natural abundance shows that label has been incorporated (about 6% enrichment) at four carbons. The enhanced signals include the aldehyde carbon (δ 196.6), the phenolic carbon (δ 166.3), a quaternary carbon (δ 136.8), and an aromatic methine (δ 103.9). The enrichment is consistent with that expected if metabolite **8** arises from the pathway outlined in Scheme 1. The C-3 methine carbon (δ 103.9) is enriched so that it must arise from a carbon that bore an oxygen functionality, supporting the proposal that there has been a reduction along the route. The methyl ester of acid **8***a* and metabolite **7** are reported to promote the root growth of Chinese cabbage seedlings at concentrations of 50 ppm (26).

As discussed in Part 1 of this series (1), the structurally and biosynthetically interesting spirocyclic metabolite, talaroflavone (**9**), is thought to originate from the heptaketide biphenyl derivative that leads to altenusin, dehydroaltenusin, and desmethyldehydroaltenusin. Feeding [1-^{13}C] labelled sodium acetate to *T. flavus* results in the incorporation of label at six carbons of **9**. Comparison of the intensity of the signals in the labelled spectrum with those at natural abundance indicates that the six labelled carbons (about 2.5% enrichment) are those furthest downfield, at δ 202.0, 171.4, 170.2, 168.5, 159.9, and

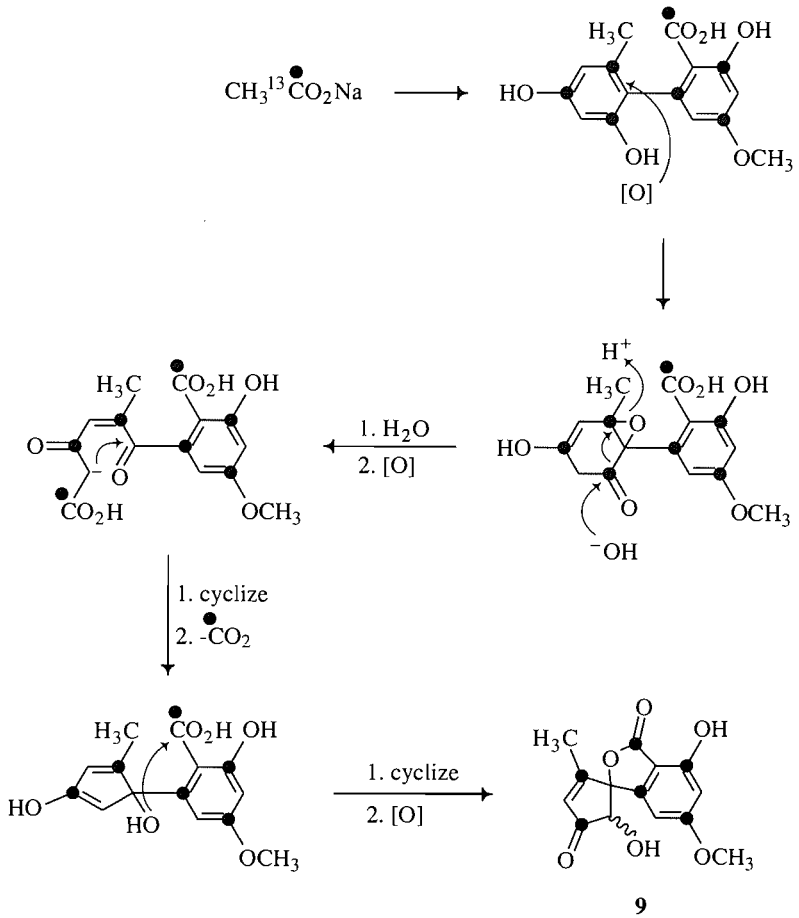

9

SCHEME 2

150.8. A biosynthetic pathway that accounts for this and for the bond joining the two unlabelled centers, C-3 and C-5′, is illustrated in Scheme 2. Oxidation of the heptaketide derived biphenyl intermediate affords the dihydroarene oxide shown. The intermediacy of arene oxides in the enzyme catalyzed hydroxylation of arenes is well precedented (28). Epoxide opening, hydrolysis of the ketone, tautomerization of the enol, and oxidation of the benzylic alcohol provides the keto acid. Cyclization of an anion generated α to the acid, followed by decarboxylation, provides the cyclopentadiene derivative. Lactonization and oxidation at the carbon α to the ketone affords talaroflavone (**9**). We have not been able to determine the stereochemistry at C-1′ and C-5′ of talaroflavone (**9**) so that the orientation of the intermediates in the cyclization reactions and in the final oxidation step is not known.

Experimental

For general experimental details see Part 1 of this series (1).

Gas chromatograms (gc) were obtained from a Hewlett Packard 5750 gas chromatograph equipped with an OV-17 Chromosorb W/80–100 mesh column (6 ft × 3/16 in.). The injector and detector temperatures were 250°C and the column was heated to 150°C. Helium was used as the carrier gas. Gas chromatography – mass spectrometry (gc–ms) data were obtained from a Varian 1400 gas chromatogram linked with an A.E.I. MS-12 mass spectrometer. Detection was done by chemical ionization using ammonia as the carrier gas. The gas chromatogram was equipped with a 30-m Supelco SPB 5 column. The column temperature was initially 50°C and then raised 10°C/min to 250°C. Sephadex G-50 and LH-20 gels were obtained from Pharmacia Fine Chemicals, Uppsala, Sweden. Bio-Gel P-2 (100–200 mesh (wet), exclusion limit 1800 daltons) was obtained from Bio-Rad Laboratories, Richmond, California. Sep-Paks (C_{18} and amino) were obtained from Waters Associates, Milford, Massachusetts. Reverse phase thin-layer chromatography (tlc) plates were obtained from Whatman Ltd. ($MKC_{18}F$ reversed phase TLC plates, 200 μm thickness). C-18 reverse phase flash silica gel was obtained from Toronto Research Chemicals Inc., Downsview, Ontario. The cation exchange resin used was AGC-244 (Ionic Form H, Baker, strong acid, sulfonated polystyrene, 10% crosslinking, 30–80 mesh) and the anion exchange resin was Dowex-3 (weak base, primary and secondary amine, 20–50 mesh). Dialyses were performed with Spectrapor 6 dialysis tubing (MWCO 1000, flat width 18 mm, diameter 11.5 mm). Sodium acetate [1-^{13}C] (91.8 at.% ^{13}C) was obtained from MSD Isotopes.

Growth of Talaromyces flavus *and isolation of the aqueous metabolites*

Talaromyces flavus (ATCC 52201; UAMH 4890) was grown in liquid still culture in 10 L batches at room temperature as reported in the experimental section of Part 1 of this series (1). After 4 weeks the mycelium was separated from the culture broth by filtration through cheesecloth. The broth was concentrated *in vacuo* to ca. 1 L and continuously extracted with ethyl acetate for 48 h. The fungal broth was concentrated to a syrup and passed over a column of Sephadex G-50, eluting with water, or a column of Bio-Gel P-2, eluting with water – 95% ethanol (90:10). The active fractions were pooled and freeze-dried. A portion of the freeze-dried syrup was subjected to acetylation (acetic anhydride (1.0 mL) – pyridine (1.0 mL), room temperature, 24 h). The reaction mixture was taken up in ethyl acetate (10.0 mL) and toluene (5.0 mL) and the solvents were removed under reduced pressure to afford a dark brown oil, which was then purified by flash chromatography, eluting with dichloromethane–methanol (99:1). The clear, colorless oil (150 mg) contained the acetates of hydroxymethylmaltol (**1**), 5,6-dihydro-3,5-dihydroxy-6-hydroxymethyl-2*H*-

Can. J. Chem. Downloaded from www.nrcresearchpress.com by 91.121.58.235 on 09/07/12
For personal use only.

Can. J. Chem. Downloaded from www.nrcresearchpress.com by 91.121.58.235 on 09/07/12
For personal use only.

pyran-2-one (**3**), and D-glucono-1,4-lactone (**5**), which were separable with repeated chromatography.

*Hydroxymethylmaltol (**1**)*

The diacetate of hydroxymethylmaltol (**1**) was obtained as a clear, colorless oil (**2**, 0.6 mg), tlc: R_f 0.21 (dichloromethane–methanol 99:1); uv (methanol): 292 (3.92) nm; ftir (CH_2Cl_2 cast): 1780 (m), 1741, 1656, 1585, 1370, 1222, 1195, 1175, 1101, 1065, 882, 759 cm^{-1}; ^1H nmr ($CDCl_3$) δ: 7.06 (1H, d, J = 7.0 Hz, H-6), 6.24 (1H, d, J = 7.0 Hz, H-5), 4.83 (2H, s, CH_2OCOCH_3), 2.30 (3H, s, C-3 $OCOCH_3$), 2.12 (3H, s, C-2 $OCOCH_3$); ^{13}C nmr ($CDCl_3$) δ: 170.0 (s, $OCOCH_3$), 167.9 (s, $OCOCH_3$), 157.1 (s, C-4), 155.6 (s, C-2), 137.0 (s, C-3), 130.5 (d, C-6), 103.8 (d, C-5), 61.3 (t, CH_2), 20.6 (q, $OCOCH_3$), 20.4 (q, $OCOCH_3$); hreims, m/z calcd. for $C_{10}H_{10}O_6$ (M^+): 226.0477; found: 226.0475 (14), 184 (66), 142 (100).

*5,6-Dihydro-3,5-dihydroxy-6-hydroxymethyl-2*H*-pyran-2-one (**3**)*

The triacetate of 5,6-dihydro-3,5-dihydroxy-6-hydroxymethyl-2*H*-pyran-2-one (**3**) was obtained as a clear, colorless oil (**4**, 0.6 mg), tlc: R_f 0.21 (dichloromethane–methanol 99:1); ftir (CH_2Cl_2 cast): 1778, 1750, 1665, 1655, 1580, 1425, 1372, 1227, 1198, 1136, 1047 cm^{-1}; ^1H nmr ($CDCl_3$) δ: 6.43 (1H, d, J = 4.0 Hz, H-4), 5.61 (1H, dd, J = 4.0, 5.5 Hz, H-5), 4.75 (1H, dt, J = 5.5, 4.5 Hz, H-6), 4.38 (1H, dd, J = 4.5, 12.5 Hz, H-7), 4.29 (1H, dd, J = 4.5, 12.5 Hz, H-7′), 2.25 (3H, s, $OCOCH_3$), 2.11 (3H, s, $OCOCH_3$), 2.08 (3H, s, $OCOCH_3$); ^{13}C nmr ($CDCl_3$) δ: 170.3 (s, $OCOCH_3$), 169.6 (s, $OCOCH_3$), 168.0 (s, $OCOCH_3$), 157.1 (s, C-2), 139.8 (s, C-3), 125.9 (d, C-4), 77.9 (d, C-6), 64.3 (d, C-5), 62.0 (t, C-7), 20.6 (q, $OCOCH_3$), 20.5 (q, $OCOCH_3$), 20.2 (q, $OCOCH_3$); hreims, m/z calcd. for $C_{12}H_{14}O_8$ (M^+): 286.0688; found: 286.0694 (0.1), 244 (9), 226 (13), 202 (13), 184 (68), 156 (15), 142 (100); cims, m/z: 304 (M + 18).

Biosynthetic studies of Talaromyces flavus *metabolites*

Incorporation of [1-^{13}C] labelled acetate

Talaromyces flavus was grown in liquid still culture on a sterile malt extract medium in 10 2-L Fernbach flasks (1 L of medium per flask) as described in the experimental section of Part 1 of this series (1). After nine days' growth, a sterile solution of sodium [1-^{13}C] acetate (0.082 g, 1.0 mmol) in distilled water (5.0 mL) was injected into each flask. After a further 7 and then 14 days, an additional 1.0 mmol of labelled acetate was injected into each flask. After 4 weeks' growth, the mycelium was removed by filtration through cheesecloth, washed with methanol, and air-dried. The fungal broth was concentrated *in vacuo* to ca. 1 L and subjected to continuous extraction with ethyl acetate for 48 h. The crude extract was evaporated to dryness *in vacuo* and then dissolved in aqueous methanol (85:15, 100 mL). This solution was extracted with *n*-hexane (3 × 100 mL) and then dichloromethane (3 × 100 mL). The organic extracts were dried over anhydrous sodium sulfate, filtered, and the solvents were removed under reduced pressure. The crude dichloromethane extract (ca. 1 g) was separated by flash chromatography over silica gel, eluting with dichloromethane–methanol (97:3). The fractions were further purified as indicated previously (1) for 4,6-dihydroxy-5-methylphthalide (**7**), methyl 4-carboxy-5-hydroxyphthalaldehydate (**8**), and talaroflavone (**9**).

[1-^{13}C] Acetate labelled metabolites

*4,6-Dihydroxy-5-methylphthalide (**7**) (4,6-dihydroxy-5-methyl-1-(3*H*)-isobenzofuranone)*

4,6-Dihydroxy-5-methylphthalide (**7**, 4.2 mg, ca. 6% incorporation), ^{13}C nmr (methanol-d_4) enriched signals δ: 159.1 (C-6), 151.5 (C-4), 124.7 (C-7a), 69.7 (C-3); natural abundance signals δ: 174.2 (C-1), 126.3 (C-3a), 120.5 (C-5), 102.1 (C-7), 9.2 (C-5 CH_3).

*Methyl 4-carboxy-5-hydroxyphthalaldehydate (**8**)*

Methyl 4-carboxy-5-hydroxyphthalaldehydate (**8**, 4.0 mg, ca. 6% incorporation), ^{13}C nmr (methanol-d_4) enriched signals δ: 196.6 (C-2 *C*HO), 166.3 (C-5), 136.8 (C-1), 103.9 (C-3); natural abundance signals δ: 169.4 (C-4 CO_2H, 160.1 (C-1 CO_2CH_3), 122.7 (C-4), 114.6 (C-2), 102.4 (C-6), 56.4 (C-1 CO_2CH_3).

*Talaroflavone (**9**) (spiro[5′-hydroxy-2′-methyl-cyclopent-2′-ene-4′-one-1′,3-7-hydroxy-5-methoxy-1(3*H*)-isobenzofuranone])*

Talaroflavone (**9**, 5.0 mg, ca. 2.5% incorporation), ^{13}C nmr (methanol-d_4) enriched signals δ: 202.0 (C-4′), 171.4, 170.2, 168.5 (C-2′, C-1, C-5), 159.9 (C-7), 150.8 (C-3a); natural abundance signals δ: 131.4 (C-3′), 106.5 (C-7a), 103.5, 101.0 (C-4, C-6), 94.2 (C-3), 79.7 (C-5′), 56.5 (OCH_3), 13.4 (C-2′ CH_3).

Biological studies of the aqueous broth and metabolites of Talaromyces flavus

Inhibition of Verticillium dahliae *by* Talaromyces flavus

The inhibition of growth of *Verticillium dahliae* by *Talaromyces flavus* was determined by agar diffusion using an aqueous test solution. Presterilized vessels (5/16 in. o.d. × 5/16 in. long cylinder cut from 304 stainless steel tubes) were placed onto Mueller Hinton agar plates that had been swabbed with *V. dahliae*. The *T. flavus* aqueous test solution (100 μL) was placed into the stainless steel vessel. The plates were incubated at 24°C. The solution diffused into the medium and after 10–14 days the growth of the microsclerotia of *V. dahliae* was noted. The bioassay was carried out in the same manner as described above when testing hydrogen peroxide (Fisher, 30% by weight) and *tert*-butylhydroperoxide (Aldrich, 70% by weight). Test results were noted after 7–10 days.

Hydrogen peroxide detection

The catalase enzyme was obtained from bovine liver (Sigma, twice recrystallized) containing ca. 0.01 mg thymol/mL. The solution consists of 22 mg protein/mL (1 199 000 units/mL). The molecular weight of the enzyme is 250 000 g/mol so that the solution concentration is 88 μM. A 2 μM solution was utilized in which 2.0 μL (contains 50–55 units of enzyme) was added to the fungal broth (100 μL, ca. 0.3 μmol of H_2O_2). The bioassay was performed as described above.

In the ultraviolet study for the detection of peroxide, sodium iodide (0.75 g), citric acid (2.42 mL of a 0.5 M solution), and sodium hydroxide (1.0 mL of a 1.0 M solution) were combined to make up a 100 mL test solution of pH 3.8, in which the concentration of iodide ion is 0.05 M. To 10.0 mL of this solution was added 5.0 μL of horseradish peroxidase (ca. 1.0 μM). The absorbance of this solution at 353 nm was measured. The fungal broth (1.0 μL; a 100 mL aliquot of the broth ([1 L] concentrated from the 10-L batch grown) was concentrated to 10 mL) was then added and the reaction was allowed to proceed for 20 min. The absorbance of the solution at 353 nm was measured and the change in absorbance was calculated knowing that 0.1 M hydrogen peroxide gives ΔA_{353} = 0.255. The enzyme assay resulted in a ΔA_{353} = 0.0357.

Antibacterial studies

The biological activity of crude extracts of *T. flavus* (ethyl acetate and methanol mycelium extracts and ethyl acetate broth extract) was tested against several bacteria using the Kirby–Bauer agar diffusion assay. In this bioassay, filter paper discs soaked with the crude extract solution (5.0 mg/mL in methanol) or the pure metabolites (2.0 mg/mL in methanol) were placed on the surface of an agar medium (Mueller–Hinton) containing a standardized suspension of bacteria. After 24 h of incubation at 37°C the surface of the agar acquired a turbid appearance (a positive result was recorded when transparent haloes (inhibition zone) remained around the filter paper discs). A solvent blank and standard concentrations of an antibiotic (Penicillin G 10 units and Cephalothin 30 μg, Sensitivity Discs, Difco Laboratories) were used to compare the relative antibacterial activity of the crude extracts. The inhibition zone diameters obtained with the crude extracts were somewhat smaller than those produced by Penicillin G (>22 mm) and Cephalothin (>18 mm). D-Glucono-1,4-lactone (**5**) and 4,6-dihydroxy-5-methylphthalide (**7**) show inhibition zones half the size of those produced by the standard antibiotics.

Acknowledgements

We gratefully acknowledge the financial support of the Natural Sciences and Engineering Research Council of Canada in the form of grants (W.A.A.) and scholarships (J.S.R.). We thank the Alberta Heritage Foundation for Medical Research for Independent Research Allowance Studentships (J.S.R.) and the University of Alberta for Graduate Faculty Fellowships

(J.S.R.). The assistance of Mrs. A. Szenthe in carrying out the culture growths is greatly appreciated. We thank Dr. D. R. Fravel for the cultures of *Verticillium dahliae* isolated from eggplant and we wish to acknowledge the assistance of Dr. J. P. Tewari in interpreting the bioassay results. We thank Professor H. B. Dunford for supplying us with the catalase enzyme as well as the horseradish peroxidase.

1. W. A. AYER and J. S. RACOK. Can. J. Chem. **68**, 2085 (1990).
2. J. J. MAROIS, S. A. JOHNSTON, M. T. DUNN, and G. C. PAPAVIZAS. Plant Dis. **66**, 1166 (1982).
3. J. C. WALKER. Diseases of vegetable crops. McGraw–Hill, New York. 1952. pp. 301–302, pp. 360–368, pp. 464–466.
4. G. R. DIXON. Vegetable crop diseases. Macmillan, Hong Kong. 1981. pp. 1–44.
5. J. E. PUHALLA. Phytopathology, **69**, 1186 (1979).
6. J. E. PUHALLA and M. HUMMEL. Phytopathology, **73**, 1305 (1983).
7. C. G. BENDER and P. B. SHOEMAKER. Plant Dis. **68**, 305 (1984).
8. C. A. KINGSBURY, M. CLIFFTON, and J. H. LOOKER. J. Org. Chem. **41**, 2777 (1976).
9. K. K. KIM, D. R. FRAVEL, and G. C. PAPAVIZAS. Phytopathology, **77**, 616 (1987); **77**, 1720 (1987).
10. K. K. KIM, D. R. FRAVEL, and G. C. PAPAVIZAS. Phytopathology, **78**, 488 (1988).
11. G. RICHTER. *In* Industrial enzymology. *Edited by* T. Godfrey and J. Reichelt. Nature Press, New York. 1983. pp. 428–436, pp. 491–492.
12. M. DIXON and E. C. WEBB. Enzymes. 3rd ed. Longman Group, London. 1979. pp. 243–244.
13. Q. H. GIBSON, B. E. P. SWOBODA, and V. MASSEY. J. Biol. Chem. **239**, 3927 (1964).
14. B. CAPON. Chem. Rev. **69**, 407 (1969).
15. H. C. BROWN, J. H. BREWSTER, and H. SCHECHTER. J. Am. Chem. Soc. **76**, 467 (1954).
16. R. U. LEMIEUX. *In* Molecular rearrangements. Part 2. *Edited by* P. de Mayo. Interscience Division of John Wiley and Sons, New York. 1964. p. 719.
17. M. H. ABRAHAM, A. G. DAVIES, D. R. LLEWELLYN, and E. M. THAIN. Anal. Chim. Acta, **17**, 499 (1957).
18. A. ZAFFARONI, R. B. BURTON, and E. H. KEUTMANN. Science, **111**, 6 (1950).
19. M. L. COTTON and H. B. DUNFORD. Can. J. Chem. **51**, 582 (1973).
20. A. G. MCINNES, J. A. WALTER, J. L. C. WRIGHT, and L. C. VINING. *In* Topics in C-13 NMR spectroscopy. Vol. 2. *Edited by* G. C. Levy. John Wiley and Sons, New York. 1976. pp. 123–178.
21. S. TAKENAKA, N. OJIMA, and S. SETO. J. Chem. Soc. Chem. Commun. 391 (1972).
22. H. VERACHTERT and L. HANSSENS. Ann. Microbiol. (Paris), **126A**, 143 (1975).
23. H. ACHENBACH, A. MÜHLENFELD, and G. U. BRILLINGER. Liebigs Ann. Chem. 1596 (1985).
24. Y. SOLBERG. Acta Chem. Scand. **B29**, 145 (1975).
25. M. FUJITA, M. YAMADA, S. NAKAJIMA, K. KAWAI, and M. NAGAI. Chem. Pharm. Bull. **32**, 2622 (1984).
26. T. SASSA, M. IKEDA, and Y. MIURA. Agric. Biol. Chem. **37**, 2937 (1973).
27. J. H. BIRKINSHAW, P. CHAPLEN, and R. LAHOZ-OLIVER. Biochem. J. **67**, 155 (1957).
28. B. J. AURET, S. K. BALANI, D. R. BOYD, R. M. E. GREENE, and G. A. BERCHTOLD. J. Chem. Soc. Perkin Trans. 1, 2659 (1984).

Can. J. Chem. Downloaded from www.nrcresearchpress.com by 91.121.58.235 on 09/07/12
For personal use only.

NMR relaxation of tin-119 in pentacoordinate and hexacoordinate environments

T. Bruce Grindley,[1] Ronald D. Curtis, Rasiah Thangarasa, and Roderick E. Wasylishen[1]

Department of Chemistry, Dalhousie University, Halifax, N.S., Canada B3H 4J3

Received March 20, 1990

T. Bruce Grindley, Ronald D. Curtis, Rasiah Thangarasa, and Roderick E. Wasylishen. Can. J. Chem. **68**, 2102 (1990).

Carbon-13 and ^{119}Sn nuclear magnetic resonance spin-lattice relaxation times at 8.48 T and at 4.70 T have been measured at several temperatures for a number of 2,2-di-*n*-butyl-1,3,2-dioxastannolane derivatives, most of which were prepared from monosaccharide derived diols. The tin nuclei in these compounds, which are at either pentacoordinate or hexacoordinate sites, have ^{119}Sn T_1 values that are relatively short, between 13 ms and 300 ms. At 8.48 T, chemical shift anisotropy is the only important mechanism for relaxation of the ^{119}Sn nuclei in these compounds. However, at 4.70 T, the ^{1}H,^{119}Sn dipole–dipole mechanism also contributes slightly. The principal components of the ^{119}Sn chemical shift tensor for the pentacoordinate site in the dimeric structure of methyl 4,6-*O*-benzylidene-2,3-dibutylstannylene-α-D-glucopyranoside (**1**) were determined directly from the static ^{119}Sn spectrum of a powdered sample and indirectly from slow spinning CP/MAS spectra using both the Herzfeld–Berger procedure and computer simulation. The tin shift tensor for **1** in the solid state is non-axially symmetric with $\eta = 0.49 \pm 0.03$. The chemical shift anisotropy determined from the solid state experiments, 748 ± 20 ppm, was in good agreement with the value obtained from the solution T_1 data, 720 ± 50 ppm. For compounds containing both pentacoordinate and hexacoordinate tin atoms, the ^{119}Sn relaxation data indicate that the tin chemical shift anisotropies for the hexacoordinate sites are approximately 1.6 times those of the pentacoordinate sites.

Key words: ^{119}Sn NMR, NMR relaxation, stannylene acetals, 1,3,2-dioxastannolanes.

T. Bruce Grindley, Ronald D. Curtis, Rasiah Thangarasa et Roderick E. Wasylishen. Can. J. Chem. **68**, 2102 (1990).

On a mesuré, à différentes températures, à 8.47 T et à 4.70 T, les temps de relaxation spin-réseau de la résonance magnétique nucléaire du ^{13}C et du ^{119}Sn d'un certain nombre de dérivés 2,2-di-*n*-butyl-1,3,2-dioxostannolanes dont la plupart sont préparés à partir de diols dérivés de monosaccharides. Les noyaux d'étain de ces composés qui sont des sites pentacoordonnés ou hexacoordonnés ont des valeurs de T_1 de ^{119}Sn relativement courtes, entre 13 ms et 300 ms. À 8.48 T l'anisotopie du déplacement chimique est le seul mécanisme important pour la relaxation des noyaux de ^{119}Sn de ces composés. Cependant à 4.70 T le mécanisme dipôle–dipôle ^{1}H,^{119}Sn contribue également mais faiblement. Faisant appel à la fois au procédé de Herzfeld–Berger et à une simulation par ordinateur on a déterminé, directement à partir du spectre statique d'un échantillon en poudre et indirectement à partir du spectre CP/MAS à faible rotation, la composante principale du tenseur du déplacement chimique du ^{119}Sn, pour le site pentacoordonné de la structure dimère du 4,6-*O*-benzylidène-2,3-dibutylstannylène-α-D-glucopyrannoside de méthyle (**1**). Le tenseur du déplacement de l'étain pour le composé **1** à l'état solide a une symmétrie non-axiale avec $\eta = 0{,}49 \pm 0{,}03$. L'anisotropie du déplacement chimique, déterminée à partir d'expériences dans l'état solide, de 748 ± 20 ppm s'accorde parfaitement avec la valeur de 720 ± 50 ppm obtenue à partir des données T_1 en solution. Dans le cas des composés contenant des atomes d'étain pentacoordonnés et hexacoordonnés, les données de relaxation du ^{119}Sn indiquent que les anisotropies du déplacement chimique pour les sites hexacoordonnés sont environ 1,6 fois plus élevés que celles des sites pentacoordonnés.

Mots clés : RMN du ^{119}Sn, relaxation RMN, acétals de stannylène, 1,3,2-dioxastannolanes.

[Traduit par la revue]

Introduction

The value of ^{119}Sn nmr spectroscopy in the study of the chemistry of tin-containing species is evident from the number of papers appearing in which this topic is of central importance (1). Most of this literature has been concerned with the measurement and application of tin chemical shifts and spin–spin coupling constants. Spin-lattice relaxation has been much less studied and most authors have chosen to examine molecules containing tetracoordinate tin (2–6). For tetracoordinate tin, T_1 values of 0.5–7 s have been reported (2–6). For tetraalkyltin compounds (2, 4), trialkyltin halides (2, 4, 5), and tin tetrahalides (3), the dominant relaxation mechanism in solution is spin rotation (2–5) with ^{1}H,^{119}Sn dipole–dipole relaxation contributing as the temperature is lowered. Even for molecules as large as dimethyldiphenyltin or hexamethylditin, spin rotation is the dominant mechanism at room temperature and $B_0 = 5.87$ T (5). In still larger molecules such as the tri-*n*-butylstannyl ethers derived from monosaccharides (6), spin rotation makes a significant contribution to the rate of spin-lattice relaxation but the rate is dominated by the ^{1}H,^{119}Sn dipole–dipole mechanism. Chemical shift anisotropy has been found to contribute slightly to the relaxation of ^{119}Sn nuclei in one molecule containing tetracoordinate tin, Ph_3SnCl (5).

In recent years, it has become evident that an important part of tin chemistry will involve species that have the tin in coordination sites of coordination number greater than four. Five and six coordinate species are common and seven (7, 8) and even eight (8) coordinate species have been observed. One solution nmr study has appeared of the relaxation of ^{119}Sn in higher coordinate tin species but it was conducted at room temperature on dialkyltin sulfates in concentrated sulfuric acid (9). These compounds were shown to exist as mixtures of species at lower temperatures and may have contained mixtures of rapidly equilibrating species at room temperature. The ^{119}Sn T_1 values for these compounds were short, 3–54 ms, and relaxation was dominated by chemical shift anisotropy. Also, the tin atom in di-*n*-butyltin diacetate has a coordination number greater than four (7, 10) and its spin-lattice relaxation was shown to be field dependent (6). Although it was suggested that the field dependence may result from the chemical exchange known to take place in this and other diorganotin dicarboxylates (6, 7, 11), the results of the present work indicate that the chemical shift

[1]Authors to whom correspondence may be addressed.

Can. J. Chem. Downloaded from www.nrcresearchpress.com by 91.121.58.235 on 09/07/12
For personal use only.

anisotropy relaxation mechanism is probably responsible for the field-dependent tin spin-lattice relaxation times.

In this study we report the results of ^{13}C and ^{119}Sn spin-lattice relaxation measurements of carefully characterized compounds (12–14) that contain tin in pentacoordinate or hexacoordinate environments. The compounds examined are typical examples of the 2,2-di-*n*-butyl-1,3,2-dioxastannolane derivatives that serve as intermediates in the widely used stannylene reaction (15).

Experimental

Variable temperature ^{119}Sn nmr spectra were recorded on Nicolet NT-360 NB and Bruker MSL-200 spectrometers at 8.48 T (134.62 MHz) and 4.70 T (74.62 MHz), respectively. Probe temperatures were calibrated using observed ^1H nmr chemical shift differences for pure ethylene glycol or methanol samples in capillary tubes in the solvent of interest (16). Spin-lattice relaxation times were measured by the inversion–recovery method using relaxation delays greater than $5 \times T_1$ and at least 12 variable delays; T_1 values were calculated using a three-parameter fitting procedure available in Nicolet and Bruker software. Nuclear Overhauser enhancements (nOe) were evaluated by the difference method using minimum delays between acquisitions of $10 \times T_1$. Solution data were referenced with respect to external tetramethyltin, which was set to 0.0 ppm.

Solutions of tin derivatives for the nmr studies were prepared as follows. An equimolar mixture of the diol and di-*n*-butyltin oxide in benzene was refluxed for 12 h in an apparatus for the azeotropic removal of water. By the end of the reflux period, the solution was homogeneous. The reaction flask was attached to a vacuum line, the benzene removed under vacuum, and the previously dried nmr solvent distilled onto the solid 1,3,2-dioxastannolane derivative through the vacuum system. The resulting solution was poured, under vacuum, through a sintered glass frit into the nmr tube, which was then sealed. The sources of the diols used for preparation of the 2,2-di-*n*-butyl-1,3,2-dioxastannolane derivatives have been described elsewhere (12–14).

Solid state MAS ^{119}Sn nmr spectra were recorded on the Bruker MSL-200 with spinning rates of 3.5–4.5 kHz. Conditions for the Hartmann–Hahn match were optimized on a sample of tetracyclohexyltin (17). All spectra were acquired with high power proton decoupling and 90° pulse lengths of 3–4 μs. The static ^{119}Sn nmr spectrum was acquired with the addition of a tin 180° pulse after the cross-polarization period in order to generate a Hahn echo before acquisition (18). This was found to be essential in order to observe the total CSA pattern without significant distortion. Solid state nmr spectra were referenced with respect to hexamethylditin, which has a ^{119}Sn chemical shift of −97.35 ppm with respect to tetramethyltin (17).

Computer simulations of the CP/MAS spectra were carried out on a VAX-8800 computer using the simulation routine of Clayden *et al.* (19).

Results and discussion

The molecules chosen for study were methyl 4,6-*O*-benzylidene-2,3-*O*-dibutylstannylene-α-D-glucopyranoside (**1**), benzyl 4,6-*O*-benzylidene-2,3-*O*-dibutylstannylene-α-D-glucopyranoside (**2**), benzyl 4,6-*O*-benzylidene-2,3-*O*-dibutylstannylene-β-D-glucopyranoside (**3**), benzyl 4,6-*O*-benzylidene-2,3-*O*-dibutylstannylene-β-D-galactopyranoside (**4**), benzyl 4,6-*O*-benzylidene-2,3-*O*-dibutylstannylene-α-D-mannopyranoside (**5**), and the dibutylstannylene derivative of (*S*,*S*)-1,2-cyclohexanediol (**6**), more properly named 8,8-di-*n*-butyl-7,9,8-dioxastannabicyclo[4,3,0]nonane (**6**). Compounds **1**–**4** exist as dimers in solution (13, 20). The formation of a dimer from two monomer molecules requires that one oxygen atom from each monomer becomes tricoordinate and that the two tin atoms become pentacoordinate. In the carbohydrate derivatives **1**–**5**, the oxygen atoms are diastereotopic; hence, three dimers

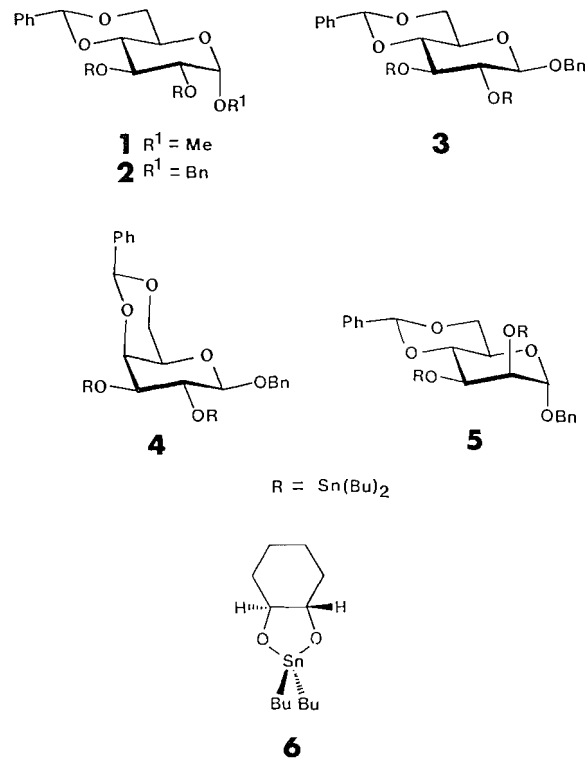

are possible for each. The different dimers will be designated using conventional carbohydrate nomenclature by means of the numbers of the two oxygen atoms that are tricoordinate (see Fig. 1). Compound **1** has been studied by X-ray crystallography (21). It is present as a 3,3 dimer in the solid state and in solution (13, 20, 21). Compound **2** also exists as the 3,3 dimer in solution (13). Compound **3** is present as a mixture of the 3,3 dimer and the 2,3 dimer (13); however, the proportion of the 2,3 dimer is small, particularly in toluene-d_8. Hence, only the ^{13}C and ^{119}Sn nmr signals of the 3,3 dimer of compound **3** were studied. Compound **4** is present as the 2,2 dimer in the solvent used here, chloroform-*d*. Compound **5** is present in chloroform-*d* as a mixture of a 3,3 dimer and a trimer (14). The two species equilibrate rapidly at room temperature and T_1 measurements on the individual species can only be made at 255 K and below. Compound **6** is also present as a rapidly equilibrating mixture at room temperature that must be studied at low temperature if the individual components, the dimer, trimer, and tetramer in this case, are to be examined (12). The oligomers higher than the dimer for compounds **5** and **6** provide species in which some of the tin atoms are hexacoordinate.

Carbon-13 relaxation

Carbon-13 spin-lattice relaxation times are given in Tables 1–3. Relaxation for protonated carbons in large molecules such as **1**–**6** normally takes place by the intramolecular $^1H,^{13}C$ dipole–dipole mechanism (22, 23). In agreement with this assessment, nOe measurements for compound **1** at room temperature yielded nOe enhancements within experimental error of the maximum, 1.99, for all carbons.

Molecules **1**–**4** may be regarded as having a large rigid core that is approximately planar with an appendant axial methoxy (**1**) or benzyloxy (**2**) group or benzylidene ring (**4**) (Fig. 1). The C—H bond vectors for the seven skeletal carbons in the central core of **1**–**4** lie perpendicular to the central plane with the following exceptions: the C—H vectors for one of the C-6 hydrogens in **1**–**4**, for C-1 in **1** and **2**, and for C-4 in **4** lie at

Can. J. Chem. Downloaded from www.nrcresearchpress.com by 91.121.58.235 on 09/07/12
For personal use only.

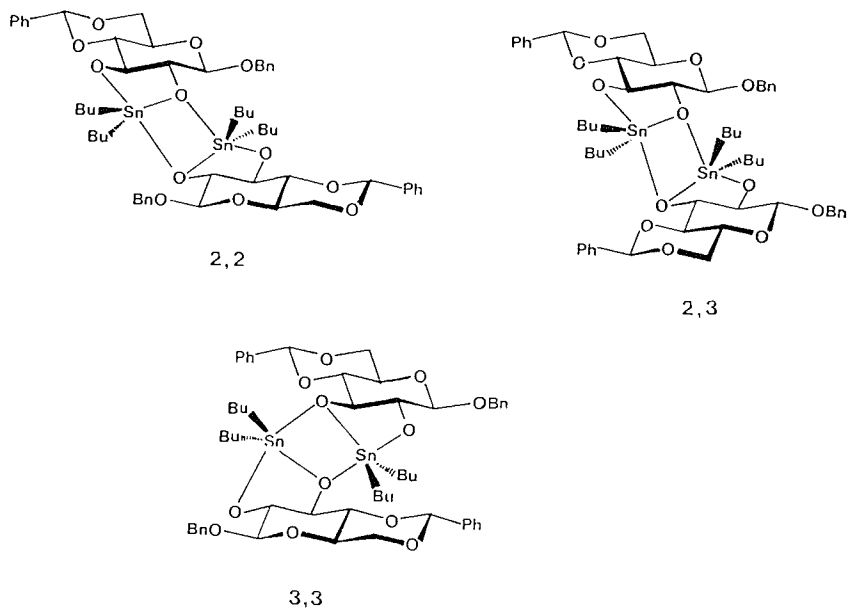

FIG. 1. Dimer structures possible for compound **3**.

TABLE 1. Carbon-13 nmr relaxation times (s) for skeletal carbons of compounds **1**–**4**

Compound	Temperature (K)	Carbons								
		C-1	C-2	C-3	C-4	C-5	C-6	C-7	CH_2	OMe
1[a]	313	0.33	[b]	0.33	0.33	0.33	0.17	0.35		1.21
1[a]	296	0.30	0.32	0.29	0.30	0.29	0.15	0.31		1.07
1[a]	295	0.28	0.28	0.26	0.27	0.27	0.14	0.28		0.87
1[a]	272	0.23	0.24	0.22	0.22	0.21	0.11	0.23		0.73
1[a]	263	0.21	0.21	0.20	0.21	0.20	0.11	0.21		0.72
1[a]	248	0.18	0.19	0.18	0.18	0.17	0.13	0.18		0.52
1[a]	233	0.18	0.20	0.18	0.18	0.17	0.09	0.18		0.59
2[c]	348	0.37	0.51	0.49	0.56	0.51	0.26	0.57	0.63	
2[c]	323	0.50	0.45	0.43	0.43	0.42	0.23	0.44	0.77	
2[c]	296	0.22	0.33	0.28	0.28	0.27	0.13	0.24	0.41	
2[c]	272	0.24	0.25	0.22	0.27	0.23	0.12	0.26	0.32	
2[c]	248	0.19	0.19	0.19	0.18	0.18	[d]	0.24	[d]	
3[e]	298	0.39	0.33	0.29	0.30	0.32	0.15	0.34	0.42	
4[f]	325	0.37	0.38	[b]	[b]	0.37	0.18	0.37	0.28	
4[f]	296	0.27	0.26	0.32	0.28	0.25	0.11	0.24	0.18	
4[f]	248	0.21	0.19	0.21	[b]	0.19	0.10	0.21	0.12	

[a]0.50 M in chloroform-*d*.
[b]Obscured by solvent peak.
[c]0.21 M in tolüene-d_8.
[d]Signals overlapped.
[e]0.19 M in toluene-d_8.
[f]0.39 M in chloroform-*d*.

angles of about ±20° with respect to the central plane. The near identity of T_1 values (±10%) obtained for all of these carbons, even the ones for which the C—H bond vectors are not perpendicular to the central plane, indicates that motion of compounds **1**–**4** is essentially isotropic. Carbon-13 relaxation data for compound **5** were more difficult to obtain since only at low temperatures (<255 K) were the individual signals sharp enough for T_1 measurements to be made. The trimer of **5** has no symmetry and the dimer has C_2 symmetry; hence, four signals are expected for each type of carbon and the similar chemical shifts of the skeletal carbons result in a number of signal overlaps. Nevertheless, those values that could be measured were similar in magnitude, indicating that rotations of compound **5** may also be considered isotropic. Compound **6** is expected to behave similarly.

In general, ^{13}C nmr spin-lattice relaxation times of the skeletal carbons of compounds **1** and **2** decrease as the temperature decreases, as is expected for relaxation via the $^1H,^{13}C$ dipole–dipole mechanism in the extreme narrowing regime (22, 23). The increase is linear from 313 to 273 K for carbons of compound **1** and from 348 to 273 K for carbons of compound **2**, but shows curvature at lower temperatures. The rotational correla-

Can. J. Chem. Downloaded from www.nrcresearchpress.com by 91.121.58.235 on 09/07/12
For personal use only.

TABLE 2. Carbon-13 nmr relaxation times (s) for compounds **1–4**

Compound	Temperature (K)	Butyl carbons		Other carbons				
					Phenyl			
		α-C	β-C and γ-C[a]	Me[a]	*para*	*meta*	*ortho*	*ipso*
1[b]	313	0.64 0.56	1.21 1.26 1.41	2.98 2.83	0.33	1.17	0.93	3.00
1[b]	296	0.52 0.49	0.97 1.25 0.91	2.36 1.96	0.27	[c]	[c]	2.20
1[b]	295	0.45 0.42	0.95 1.01 0.85	2.16 2.13	0.27	[c]	[c]	1.96
1[b]	272	0.35 0.31	0.62 0.65 0.61	1.46 1.22	0.21	[c]	[c]	1.41
1[b]	253	0.32 0.29	0.53 0.54 0.40	1.18 1.00	0.20	[c]	[c]	1.25
1[b]	248	0.23 0.20	0.37 0.29	0.76 0.73	0.19	[c]	[c]	0.97
1[b]	233	0.20 0.18	0.31 0.22	0.58 0.49	0.15	[c]	[c]	0.89
2[d]	348	0.82 0.88	1.34 1.30 1.67 1.54	1.97		[e]		
2[c]	323	0.78 0.68	1.56 1.42 1.88 1.83	3.39		[e]		
2[c]	296	0.44 0.38	0.93 1.02 1.00	2.01		[e]		
2[c]	272	0.40 0.34	0.68 0.73 0.59 0.73	1.28 1.38		[e]		
2[c]	248	0.26 0.24	0.39 0.48 0.31 0.39	0.86 0.91		[e]		
3[f]	298	0.49 0.43	1.01 0.78 1.28	2.51		[e]		
4[g]	323	0.74 0.57	0.93 0.93 1.30 1.18	2.02 1.92		[h]		2.09 1.93
4[g]	296	0.50 0.36	0.53 0.76 0.88	1.91 1.60	0.59	0.78	0.74	1.49 1.98
4[g]	248	0.31 0.19	0.23 0.34 0.50 0.50	0.95 0.78	0.25	0.32	0.31	1.16 0.88

[a]Signal overlaps sometimes resulted in fewer than the expected number of signals being observed (13).
[b]0.50 M in chloroform-*d*.
[c]Not measured.
[d]0.21 M in toluene-d_8.
[e]Not measured because of overlap with signals of toluene carbons.
[f]0.19 M in toluene-d_8.
[g]0.39 M in chloroform-*d*.
[h]Assignments of *o*, *m*, and *p* carbons uncertain because of signal overlap.

TABLE 3. Carbon-13 relaxation times (s) for benzyl 4,6-*O*-benzylidene-2,3-*O*-di-*n*-butylstannylene-α-D-mannopyranoside[a] (**5**)

Temperature (K)	Carbons			
	C-2	C-4	C-5	C-3, C-6, and CH_2
248	[b]	0.13	[b]	0.13
		0.17	[b]	0.16
		0.19		0.14
		0.16		0.12
223	0.20	0.13	0.13	0.13, 0.13
	0.16	0.26	0.18	0.11, 0.12
	0.16	0.19	0.15	0.13, 0.09
		0.18		

[a]0.34 M in chloroform-*d*.
[b]Extensive signal overlap.

tion time (τ_c) at the temperature at which the T_1 reaches a minimum can be determined from eqs. [1] and [2] (22, 23),

$$[1]\quad R_1^{DD} = (T_1^{DD})^{-1}$$
$$= N/10\,\{(\mu_0/4\pi)\,\gamma_H\gamma_C\,(h/2\pi)\,r_{CH}^{-3}\}^2 f(\tau_c, \omega)$$

$$[2]\quad f(\tau_c, \omega) = \tau_c\{1/(1+(\omega_H-\omega_C)^2\tau_c^2) + 3/(1+\omega_C^2\tau_c^2) + 6/(1+(\omega_H+\omega_C)^2\tau_c^2)\}$$

where N is the number of bonded protons, γ_H and γ_C are the magnetogyric ratios of ^1H and ^{13}C respectively, r_{CH} is the C—H bond length, and ω_H and ω_C are the Larmor frequencies in rad s^{-1} for ^1H and ^{13}C, respectively. The T_1 minimum at 90.8 MHz is calculated to occur at a τ_c value of 1.39 ns. From the plot of ln R_1 versus $1/T$ for C-1 of compound **1**, it is clear that the ^{13}C T_1 values obtained at the two lowest temperatures are almost identical, indicating that these are approximately the values of T_1 at the T_1 minimum. Taking the T_1 minimum to be 0.18 ± 0.01 s, a value of r_{CH} = 1.134 ± 0.01 Å can be determined from eqs. [1] and [2]. This value is a vibrationally averaged C—H bond length and is typical of the values obtained from relaxation measurements (23*b*, 25).

The T_1 values for the two butyl groups for compounds **1–4** are larger than those of the skeletal carbons, indicating that they are involved in independent motion in addition to overall reorientation. The observed T_1 values also increase down the hydrocarbon chains, as is commonly observed for anchored alkyl groups (23, 24). There are slight but consistent differences between the T_1 values for each of the carbons in the pairs of butyl groups for each compound, which indicates that the butyl groups move independently at slightly different rates.

Motion of phenyl groups has been studied by means of their ^{13}C T_1 values (26). In monosubstituted benzenes, anisotropic motion is observed in which rotation about the C-1—C-4 axis is preferred. Because the C—H bond vector for C-4 lies along the axis of rotation, its relaxation is not affected by this motion and its T_1 values are normally much shorter than those of the *ortho* and *meta* carbons (26), which are identical. For compound **1**, the T_1 values for the *ortho* and *meta* carbons were much larger than that of the *para* carbon. These observations indicate that rotation of the phenyl group about its symmetry axis occurs much faster than overall rotations of the molecule.

Tin-119 relaxation

Tin-119 spin-lattice relaxation times are given in Tables 4–6. Nuclear Overhauser enhancement measurements at 8.48 T were

Can. J. Chem. Downloaded from www.nrcresearchpress.com by 91.121.58.235 on 09/07/12
For personal use only.

TABLE 4. Tin-119 nmr relaxation times (ms) for compounds present only as dimers[a]

Temperature (K)	Compound				
	1[b]	**2**[c]	**3**[d]	**4**[e]	**4**[e,f]
348		170	170		
336					320
331					290
329				99	280
325					260[g]
322		140	120	94	
318					240
313	98	110		81	
311					220
306				73	
301				68	
299	68		77		180[h]
297		98			
295	67			58	
287					150
283				51	
269	43	58	53	42	
265					100
261	36			37	
253					81
246	30	38	39	31	
240					64
230	28			27	
228					56
220	37			28	
218					51
213					49
211				32	

[a]At 8.48 T unless otherwise noted.
[b]0.50 M in chloroform-*d*.
[c]0.21 M in toluene-d_8.
[d]0.19 M in toluene-d_8.
[e]0.39 M in chloroform-*d*.
[f]At 4.7 T.
[g]2.6% nOe.
[h]nOe <2%.

made for compounds **1**–**4** at room temperature, for compound **5** at 223 K, and for compound **6** at 218 K. In every case the size of the nOe effect was below the level of detection, estimated as 2%, where % nOe is defined as $(\eta_{obs}/\eta_{max}) \times 100\%$. At 4.74 T, nOe values were measured for compounds **4** and **5** at the temperatures given in Tables 4 and 5. The values measured were small, 10% or less. Thus, $^1H,^{119}Sn$ dipole–dipole interactions do not contribute to relaxation of tin nuclei at 8.48 T and only contribute slightly to the relaxation of tin nuclei at 4.70 T in the molecules studied here. The only two mechanisms remaining that could cause relaxation of ^{119}Sn nuclei here are chemical shift anisotropy (CSA) and spin rotation (SR).

Figure 2 shows plots of $\ln R_1$ as a function of inverse temperature for tin nuclei of compound **4** at 8.48 and 4.70 T. The origin of the curves is described later in the text. At 8.48 T, the rates increase linearly as the temperature decreases until approximately 273 K, when the rate of increase lessens. Similar results were observed at 4.70 T where a linear dependence of the logarithm of the tin relaxation rate versus inverse temperature was observed from 245 to 336 K. Since nOe measurements for compound **4** indicated that the relative contribution of the $^1H^{119}Sn$ dipole–dipole is negligible, the linear increase in the natural logarithm of the rate of relaxation with increase in inverse temperature is expected only if the dominant mechanism of relaxation is CSA (23). If the spin-rotation mechanism was contributing to ^{119}Sn relaxation in compound **4**, curvature would be observed at the high temperature ends of the plots in Fig. 2 since contributions from this relaxation mechanism increase with an increase in temperature. The curvature in the plots at temperatures less than 273 K at 8.48 T and below 245 K at 4.70 T is consistent with the curvatures observed in similar plots of ^{13}C relaxation rate versus inverse temperature that were ascribed to leaving the region of extreme narrowing. For the ^{119}Sn nuclei of compound **4** at 134.62 MHz, a T_1 minimum of 27 ms is observed at 227 ± 5 K; below this temperature the relaxation rate decreases as temperature decreases. At 74.62 MHz, the ^{119}Sn T_1 minimum for the tin nuclei of compound **4** should occur at a lower temperature than at 134.62 MHz. As can be seen in Fig. 2, the T_1 minimum may not quite have been reached at the lowest temperature employed in this study, 213 K.

The efficiency of the CSA mechanism depends on the applied magnetic field squared. Therefore, the importance of this mechanism can be evaluated from relaxation measurements at two different applied fields, B_0 and B_0', using the following expression (27):

$$[3] \quad R_1(B_0)^{CSA} = [R_1(B_0)_{obs} - R_1(B_0')_{obs}]/[1 - (B_0'/B_0)^2]$$

Using the observed T_1 values of 98.9 and 276 ms measured at 329 K at 8.48 and 4.7 T, respectively, a T_1^{CSA} value of 347 ± 73 ms at 4.7 T is calculated, which is equivalent to 83 ± 17% of the total relaxation. The $^1H,^{119}Sn$ dipole–dipole relaxation time at 329 K can be calculated to be 10.6 s from the % nOe value at 325 K or 1.6 s from eq. [3] if it is assumed that the $^1H,^{119}Sn$ dipole–dipole relaxation causes the remainder of the relaxation not accounted for by the CSA mechanism.

For comparison purposes, the $^1H,^{119}Sn$ dipole–dipole relaxation time for the ^{119}Sn nuclei of **4** can be calculated using eq. [1] and constants appropriate for tin. The distance between the tin atom and protons on the butyl α-carbons was estimated to be 2.77 Å based on average Sn—C bond lengths in pentacoordinate tin atoms in crystal structures of 1,3,2-dioxastannolanes as summarized in ref. 28. Distances to the β-protons were calculated to be 3.30, 3.05, and 3.17 Å to the four butyl β-protons, to the two intramonomer Sn-O-C protons, and to the one extramonomer Sn-O-C proton, respectively, using average geometries from ref. 28 or from ref. 29 when values were unavailable in ref. 28. A value of 1.60×10^{-10} s was calculated for τ_c at 323 K by means of eqs. [1] and [2] using a carbon T_1 value of 0.37 s for compound **4** and the C—H bond length of 1.134 Å calculated earlier. If it is assumed that the above 11 protons cause the dipolar relaxation of the tin nuclei, a value of T_1 of 8.3 s is calculated using eq. [1], in good agreement with the observed value of 10.6 s, considering the large uncertainties in both values.

Plots of $\ln R_1$ versus $1/T$ for the ^{119}Sn nuclei of compound **1** displayed behaviour similar to compound **4**, with a T_1 minimum of 28 ms observed at 232 ± 5 K. Relaxation rates for compounds **2** and **3** in toluene-d_8 increased linearly with inverse temperature with slight curvature at the lowest temperatures used in this study. Again, this is consistent with CSA being the major source of tin relaxation in these compounds.

The ^{119}Sn CP/MAS nmr spectrum of crystalline **1** recorded at a spinning rate of 3.99 kHz at 296 K is shown in Fig. 3. Immediately apparent in this figure is a series of closely spaced

Can. J. Chem. Downloaded from www.nrcresearchpress.com by 91.121.58.235 on 09/07/12
For personal use only.

TABLE 5. Tin-119 nmr relaxation times (ms) for the di-*n*-butylstannylene acetal of benzyl 4,6-*O*-benzylidene-α-manno-pyranoside,[a] compound **5**

	Pentacoordinate sites							
	Trimer						Hexacoordinate site	
	Site b[b]		Site c[c]		Dimer		Trimer	
Temperature (K)	8.48 T	4.70 T	8.48 T	4.70 T	8.48 T	4.70 T	8.48 T	4.70 T
248	43	—	36	—	32	—	14	—
241	38	75	35	63	26	60	16	27
233[d]	38	70	35	60	25	58	14	26
223	46	65	38	58	27	56	17	27
216	56	80	46	[e]	32	[e]	19	31

[a]0.34 M in chloroform-*d*.
[b]High frequency (larger δ) pentacoordinate tin signal.
[c]Low frequency (smaller δ) pentacoordinate tin signal.
[d]Nuclear Overhauser enhancement values at 4.70 T: 7.5, 10, 4.2, and 3.1%, respectively.
[e]The two peaks overlapped.

TABLE 6. Tin-119 nmr relaxation times (s) for compound **6** at 8.48 T[a]

	Pentacoordinate signals		Hexacoordinate signals	
Temperature (K)	Dimer and trimer	Tetramer	Tetramer	Trimer
223	35	35	18	18
218	39	43	20	19
213	40	53	23	17

[a]0.42 M in chloroform-*d*/dichlorofluoromethane 3:1.

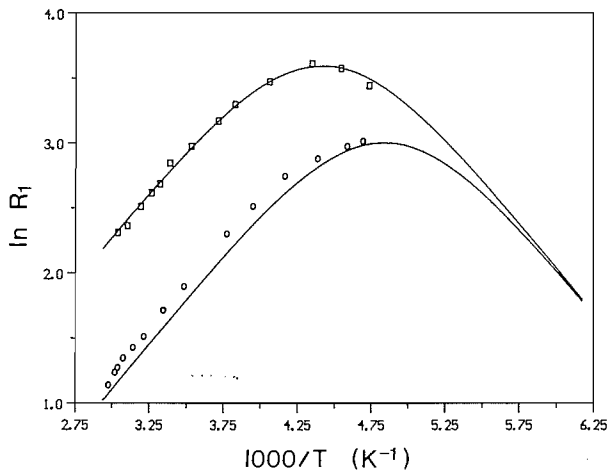

FIG. 2. Tin-119 relaxation rates for compound **4** at 8.48 T (upper) and 4.70 T (lower) as functions of inverse temperature.

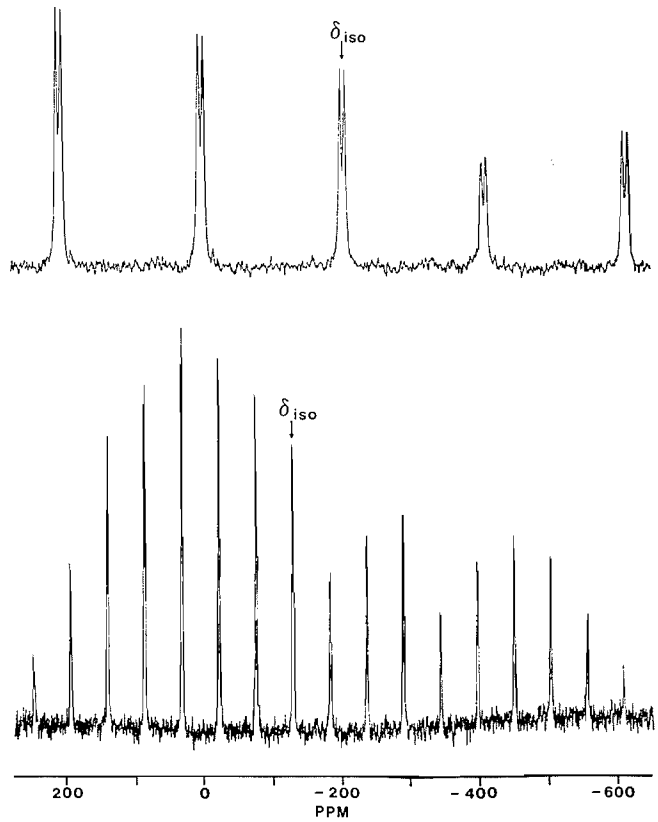

FIG. 3. Tin-119 solid state nmr spectrum for compound **1** obtained with magic angle sample spinning at 3.99 kHz. The expanded region shows the $N = 0$ and ± 1, ± 2 spinning sidebands. The isotropic chemical shifts for site 1 ($\delta_{iso} = -126.8$ ppm) and site 2 ($\delta_{iso} = -128.6$ ppm) are labelled with arrows and are referenced with respect to $(C_6H_{11})_4Sn$ at −97.35 ppm (17).

pairs of resonances. Comparison with spectra run at other spinning speeds indicates that the two isotropic ^{119}Sn chemical shifts (shown in the expansion of Fig. 3) are −126.8 ppm (site 1) and −128.6 ppm (site 2). The X-ray diffraction results for compound **1** indicated that the two halves of the 3,3 dimer of compound **1** have slightly different geometries in the solid state so that the two pentacoordinate tin atoms are in different environments (21). This loss of symmetry accounts for the observation of two different ^{119}Sn chemical shifts in the CP/MAS spectrum and is consistent with results from solid state ^{13}C CP/MAS experiments on this sample (13). Harris and co-workers had noted earlier that two isotropic signals were observed in ^{119}Sn CP/MAS nmr spectra of compound **1** but had not reported the ^{119}Sn chemical shifts.[2] Analysis of the spinning

[2]A. G. Davies, R. K. Harris, and G. J. Nesbitt. Unpublished results, quoted in ref. 30.

Can. J. Chem. Downloaded from www.nrcresearchpress.com by 91.121.58.235 on 09/07/12
For personal use only.

Can. J. Chem. Downloaded from www.nrcresearchpress.com by 91.121.58.235 on 09/07/12
For personal use only.

sideband pattern for site 1 using the graphical method of Herzfeld and Berger (31) provided estimates for the principal components of the ^{119}Sn chemical shift tensor δ_{11}, δ_{22}, and δ_{33}. It should be noted that in order to directly apply the equations and method outlined in ref. 31 to the ^{119}Sn CP/MAS results for compound **1**, spinning speeds in excess of 4.1 kHz are essential so that the value of the parameter μ used in the calculation is less than 15 (31). That is, the magnitude of the tin chemical shift anisotropy for compound **1** is so large that conditions of a "slow spinning" CP/MAS spectrum, for which Herzfeld and Berger numerically evaluated their derived expressions, are only applicable above spinning speeds of 4.1 kHz. For a ^{119}Sn spectrum of compound **1** acquired at a spinning speed of 4.2 kHz, the principal components of the chemical shift tensor for site 1 ($\delta = -126.8$ ppm) were determined to be 237, −16, and −601 ppm. These values were employed as starting estimates for a more accurate analysis of the spinning sidebands by the computer simulation method of Clayden *et al.* (19). The values obtained for site 1 were 248 ± 15 ppm, 4 ± 15 ppm, and −632 ± 15 ppm for δ_{11}, δ_{22}, and δ_{33}, respectively. The estimated uncertainties are large because the experimental peak intensities are difficult to obtain accurately due to spectral overlap with peaks from site 2. In addition, when the chemical shift anisotropy is large, as in this case, the higher order sidebands are often reduced in intensity in the experimental spectrum because of line broadening effects associated with slight inaccuracies in setting the magic angle. As can be seen from Fig. 3, the relative intensities of all the observed spinning sidebands are quite similar, indicating that the chemical shift anisotropy for both sites is approximately the same within experimental error. Additional support for the conclusion that the chemical shift tensors for the two sites are quite similar came from the results of a ^{119}Sn nmr spectrum recorded on a static sample of compound **1**. In this latter spectrum, the discontinuities corresponding to the δ_{11} and δ_{33} principal components were sharp and there was no discernible splitting of the resonance associated with δ_{22}. Thus, the three principal components of the ^{119}Sn chemical shift tensor of compound **1** were determined directly from this spectrum and are 246 ± 10 ppm, −2 ± 10 ppm, and −627 ± 10 ppm for δ_{11}, δ_{22}, and δ_{33}, respectively. The magnitude of the chemical shift anisotropy, $\Delta\delta$, as defined according to the convention of Haeberlen (32):

$$[4] \quad \Delta\delta = (\delta_{11} + \delta_{22})/2 - \delta_{33}$$

was found to be 758 ± 30 ppm according to the MAS simulation results and 748 ± 20 ppm from ^{119}Sn nmr experiments on the static sample. The asymmetry parameter, η, defined by eq. [5],

$$[5] \quad \eta = (\delta_{11} - \delta_{22})/(\delta_{iso} - \delta_{33})$$

was determined to be 0.48 ± 0.04 from the MAS simulations and 0.49 ± 0.03 from the static spectrum. For the purpose of further comparison, the ^{119}Sn chemical shift anisotropy parameters derived from the static spectrum will be considered.

The results from the solid state ^{119}Sn nmr spectra can be related to the observations made in solution if it is assumed that the geometries about the tin atoms are similar on both states. The similarity of ^{119}Sn and ^{13}C nmr chemical shifts from solution and from solid samples suggests that this assumption is correct. As mentioned above, the chemical shift anisotropy for compound **1** is not axially symmetric and the expression defining the magnitude of the spin-lattice relaxation time due to chemical shift anisotropy must include the effect of the non-axial symmetry as follows (32, 33):

TABLE 7. Tin-119 nmr relaxation parameters for pentacoordinate sites in compounds **1**–**5**[a]

Compound	Solvent	$\Delta\delta$ (ppm)	E_A(kJ mol^{-1})
1 dimer	Chloroform-*d*	722	12.2
2 dimer	Toluene-d_8	770	10.6
3 dimer	Toluene-d_8	810	10.1
4 dimer	Chloroform-*d*	773	11.7
5 dimer	Chloroform-*d*	793	12.0
trimer "b"	Chloroform-*d*	666	12.4
trimer "c"	Chloroform-*d*	685	12.4

[a]From Simplex optimization.

$$[6] \quad 1/T_1^{CSA} = R_1^{CSA} = (\gamma B_0)^2[2\{(\delta_{xy})^2 + (\delta_{xz})^2 + (\delta_{yz})^2\} + (2/15)(\Delta\delta)^2(1 + \eta^2/3)]g(\tau_c, \omega)$$

where $g(\tau_c, \omega) = \tau_c/(1 + \omega_0^2\tau_c^2)$, and δ_{xy}, δ_{xz}, and δ_{yz} are the off-diagonal chemical shift tensor elements. The off-diagonal elements are normally considered to be insignificant, in which case eq. [6] simplifies to

$$[7] \quad 1/T_1^{CSA} = R_1^{CSA} = (2/15)(\gamma B_0)^2(\Delta\delta)^2(1 + \eta^2/3)g(\tau_c, \omega)$$

The maximum of $g(\tau_c)$, which corresponds to the T_1 minimum, occurs when $\omega_0\tau_c = 1.0$. Thus, given the Larmor frequency, τ_c at the T_1 minimum can be calculated directly and was determined to be 1.183×10^{-9} and 2.132×10^{-9} s at 134.62 and 74.62 MHz, respectively. The T_1 minimum observed for compound **1** at 134.62 MHz was 28 ± 2.8 ms and occurred at a temperature of 232 ± 5 K (Table 4). From this value and with $\eta = 0.49 \pm 0.03$, the magnitude of the chemical shift anisotropy determined from eq. [7] is 762 ± 50 ppm, similar to the results observed in the solid state, 748 ± 20 ppm. These results suggest that the off-diagonal tensor elements are indeed small and may be negligible if the chemical shift anisotropies in the solid state and solution are similar.

Chemical shift anisotropies can be calculated for compound **4** from the solution T_1 minima of 27 ms at 232 K and 134.62 MHz and 49 ms at 213 K and 74.62 MHz, respectively, if it is assumed that the η value is identical to that determined for compound **1**. Values of $\Delta\delta$ were calculated to be 781 ± 39 ppm and 779 ± 39 ppm from relaxation data obtained at 134.62 and 74.62 MHz, respectively.

A more rigorous procedure for extracting $\Delta\delta$ from the ^{119}Sn nmr relaxation data in Tables 4 and 5 is to fit all of the variable temperature data to eq. [7]. We have assumed that the temperature dependence of τ_c can be described by eq. [8]:

$$[8] \quad \tau_c = \tau_\infty e^{(E_A/RT)}$$

and used a Downhill Simplex Method (34) to obtain $\Delta\delta$, E_A, and τ_∞ for each of the compounds **1**–**5**. The results are summarized in Table 7. Only the high-field ^{119}Sn nmr relaxation data were used for compounds **1**–**4**.

In Fig. 2, the upper curve is a fit of the high-field relaxation data for compound **4** to eq. [7]. The lower curve in this figure is the calculated rate of CSA relaxation at 4.70 T as a function of inverse temperature, generated using the parameters from the high-field data. Note that at all temperatures the observed rate of relaxation at 4.70 T is slightly greater, approximately 10%, than that calculated. We attribute this additional relaxation to the ^{119}Sn,^{1}H dipole–dipole mechanism at 4.70 T. The contribution of this mechanism to the 8.48 T relaxation data will be negligible, as confirmed by our nOe measurements.

Can. J. Chem. Downloaded from www.nrcresearchpress.com by 91.121.58.235 on 09/07/12
For personal use only.

Compound **5** was present as a mixture of dimer and trimer that were equilibrating at room temperature. The trimer has no symmetry and hence three signals are observed, two in the pentacoordinate region labelled b and c, and one in the hexacoordinate region. The signals of the individual species could only be measured at temperatures less than 255 K at 8.48 T and less than 243 K at 4.70 T. The T_1 values determined are reported in Table 5. From 248 to 233 K, the ^{119}Sn relaxation rates are temperature invariant or perhaps increase slightly with decrease in temperature. However, at the two lowest temperatures, the relaxation rates decrease with decrease in temperature. This behaviour is consistent with the results for compounds **1**–**4**; at the higher temperatures, the plots are in the T_1 minimum region; at the lowest temperatures, dimers, trimers, and tetramers all appear to be in the slow tumbling regime.

Chemical shift anisotropies for compound **5** can be calculated from the T_1 minima if, again, it is assumed that η is 0.49 ± 0.03. Using T_1 minima values of 38 and 65 ms at 8.48 and 4.70 T for site b of the trimer, values of $\Delta\delta$ of 658 ± 33 and 676 ± 34 ppm, respectively, are obtained. Simplex optimization using both the 4.70 and 8.48 T data gives $\Delta\delta = 666$ ppm. For site c of the trimer, T_1 minima of 35 ms (8.48 T) and 58 ms (4.7 T) yield calculated values of $\Delta\delta$ of 686 ± 34 and 716 ± 36 ppm, respectively. For the dimer tin nuclei, T_1 minima values of 25 and 56 ms give larger values for $\Delta\delta$, 812 ± 41 and 729 ± 37 ppm at 8.48 and 4.7 T, respectively. The corresponding values obtained for compound **5** from Simplex optimization of the combined 4.70 and 8.48 T data (Table 7) support the conclusions reached from the T_1 minima. The shorter T_1 values observed for the hexacoordinate tin site in the trimer indicate that it has a larger chemical shift anisotropy than the pentacoordinate tin sites. If it is assumed that the η value for the hexacoordinate site in the trimer of compound **5** is the same as that determined for compound **1**, T_1 minima values of 14 and 26 ms yield calculated values of $\Delta\delta$ of 1080 ± 55 and 1070 ± 55 ppm at 8.48 and 4.7 T, respectively. Chemical shift anisotropies in the trimer are, on average, approximately 1.6 times greater for the hexacoordinate site than for the pentacoordinate sites.

Compound **6** exists in solution as a complex equilibrating mixture of dimers, trimers, tetramers, and pentamers (12). The equilibria between these oligomeric species only becomes slow enough that T_1 values can be measured for the individual types of tin nuclei at temperatures less than 228 K. For the dimer and trimer tin nuclei, the three T_1 values measured are approximately the same, suggesting that the relaxation times for the ^{119}Sn nuclei in these oligomers are close to the T_1 minimum. The relaxation times of the two types of tin nuclei in the tetramer increase with decreasing temperature, as expected if τ_c for the tetramer of compound **6** were in the slow tumbling regime. The nOe values for compound **6** at 218 K were too small to be measured reliably. There is no reason to believe that ^{119}Sn spin-lattice relaxation for compound **6** occurs other than by the CSA mechanism. The ratios of the chemical shift anisotropies of the hexacoordinate to pentacoordinate tin nuclei in the trimer and the tetramer can be obtained from eq. [9], which was derived from eq. [7].

$$[9] \quad T_{1P}^{CSA}/T_{1H}^{CSA} = (\Delta\delta_H/\Delta\delta_P)^2(1 + \eta_H^2/3)/(1 + \eta_P^2/3)$$

In eq. [9], the subscripts P and H indicate parameters associated with the pentacoordinate and hexacoordinate sites, respectively. The value of $\eta^2/3$ is considerably less than 0.1 provided that η is not too much larger than the value obtained for compound **1** from the solid-state nmr experiments. If it is assumed that η is of this magnitude or is the same for the hexacoordinate site in the trimer as in compound **1**, ratios of $\Delta\delta$ values can be obtained. For compound **6**, the ratios of chemical shift anisotropies of hexacoordinate to pentacoordinate tin nuclei for the trimers and tetramers are calculated to be 1.45 and 1.46, respectively, slightly smaller than the average 1.6 value obtained for the trimer of compound **5**.

Summary

The results of this study indicate that the rates of nmr spin-lattice relaxation for pentacoordinate and hexacoordinate ^{119}Sn nuclei in a series of substituted 1,3,2-dioxastannolane derivatives at moderate field strengths (5–9 T) are one to two orders of magnitude greater than those previously measured for ^{119}Sn in tetracoordinate environments (2–6). For the series of compounds studied here (**1**–**6**), ^{119}Sn relaxation was shown to be caused almost entirely by the chemical shift anisotropy mechanism; for tetracoordinate tin atoms, spin rotation and (or) ^{1}H,^{119}Sn dipole–dipole relaxation are dominant (2–6). Tin-119 nmr spectra of a solid sample of compound **1** indicate that the chemical shift tensor is non-axially symmetric ($\eta = 0.49 \pm 0.03$) with $\Delta\delta = 748 \pm 20$ ppm. For this same sample in solution, essentially the same value of $\Delta\delta$ is obtained from the minimum value of the ^{119}Sn T_1 as a function of temperature. The magnitudes of the chemical shift anisotropies determined from solution relaxation data for compounds **2**–**6** and for compound **1** in solution and in the solid state indicate that $\Delta\delta$ is on the order of 740 ± 75 ppm for tin nuclei in pentacoordinate environments in 1,3,2-dioxastannolanes. Interestingly, the solution ^{119}Sn relaxation results indicate that the chemical shift anisotropy values for tin nuclei in hexacoordinate sites, $\Delta\delta = 1100 \pm 100$ ppm, are somewhat larger than those determined for tin in pentacoordinate sites. Further solid-state experiments are necessary to verify this last conclusion.

Finally, the similar values of $\Delta\delta$ obtained for **1** in chloroform solution and in the solid state suggest that eq. [7] adequately describes the rate of CSA relaxation in solution. The implication is that, in the case of compound **1**, it is unnecessary to consider the unsymmetrical elements of the CSA tensor in the expression for R_1^{CSA} (eq. [6]).

Acknowledgements

T.B.G., R.D.C., and R.E.W. are grateful to NSERC for financial support. R.D.C. thanks Dalhousie University for a W. J. Chute Scholarship and for a Killam Postgraduate Fellowship. We would also like to thank Dr. M. S. McKinnon for recording a CP/MAS spectrum of **1**, Mr. B. Millier for his help in maintaining the nmr spectrometers, Dr. N. J. Clayden for a copy of his routine for the simulation of MAS sideband patterns, B. Power for his help with the MAS simulations, J. Leiper for carrying out the Simplex optimization calculations, M. MacIntosh for his assistance in preparing Fig. 2, and a referee for several helpful comments. All nmr spectra were recorded at the Atlantic Region Magnetic Resonance Centre.

1. (*a*) B. Wrackmeyer. Annu. Rep. NMR Spectrosc. **16**, 73 (1985); (*b*) P. J. Smith and A. P. Tupciauskas. Annu. Rep. NMR Spectrosc. **8**, 291 (1978); (*c*) V. S. Petrosyan. Prog. NMR Spectrosc. **11**, 115 (1977); (*d*) J. D. Kennedy and W. McFarlane. *In* Multinuclear NMR spectroscopy. *Edited by* J. Mason. Pergamon Press, Oxford. 1988. p. 305.
2. Y. C. Puskar, T. A. Saluvere, E. T. Lippmaa, A. B. Permin, and V. S. Petrosyan. Dokl. Akad. Nauk SSSR, **220**, 112 (1975).

3. R. R. SHARP. J. Chem. Phys. **57**, 5321 (1972); **60**, 1140 (1974).
4. C. R. LASSIGNE and E. J. WELLS. J. Magn. Reson. **26**, 55 (1977); Can. J. Chem. **55**, 927 (1977).
5. S. CHAPELLE and P. GRANGER. J. Magn. Reson. **76**, 1 (1988).
6. S. J. BLUNDEN, A. FRANGOU, and D. G. GILLIES. Org. Magn. Reson. **20**, 170 (1982).
7. T. P. LOCKHART, J. C. CALABRESE, and F. DAVIDSON. Organometallics, **6**, 2479 (1987).
8. S. J. BLUNDEN, S. SEARLE, and P. J. SMITH. Inorg. Chim. Acta, **116**, L31 (1986).
9. T. BIRCHALL and V. MANIVANNAN. Can. J. Chem. **63**, 2211 (1985).
10. J. HOLEČEK, M. NÁDVORNÍK, K. HANDLIR, and A. LYČKA. J. Organomet. Chem. **315**, 299 (1986).
11. A. LYČKA and J. HOLEČEK. J. Organomet. Chem. **294**, 179 (1985).
12. T. B. GRINDLEY and R. THANGARASA. J. Am. Chem. Soc. **112**, 1364 (1990).
13. T. B. GRINDLEY and R. THANGARASA. Can. J. Chem. **68**, 1007 (1990).
14. T. B. GRINDLEY, R. THANGARASA, C. KEITH, J. ALLISON, and M. D. LUMSDEN. Can. J. Chem. In preparation.
15. S. DAVID and S. HANESSIAN. Tetrahedron, **41**, 643 (1985); M. PEREYRE, J.-P. QUINTARD, and A. RAHM. Tin in organic synthesis. Butterworths, London. 1987. Chap. 11.
16. A. E. VAN GEET. Anal. Chem. **40**, 2227 (1968); **42**, 679 (1970).
17. R. K. HARRIS and A. SEBALD. Magn. Reson. Chem. **25**, 1058 (1987).
18. M. RANCE and A. BYRD. J. Magn. Reson. **52**, 221 (1983).
19. N. J. CLAYDEN, C. M. DOBSON, L.-Y. LIAN, and D. J. SMITH. J. Magn. Reson. **69**, 476 (1986).
20. S. DAVID, A. THIEFFRY, and A. FORCHIONI. Tetrahedron Lett. **22**, 2647 (1981).
21. S. DAVID, C. PASCARD, and M. CESARIO. Nouv. J. Chim. **3**, 63 (1979).
22. D. DODDRELL, V. GLUSHKO, and A. ALLERHAND. J. Chem. Phys. **56**, 3683 (1972).
23. (*a*) J. R. LYERLA and G. C. LEVY. *In* Topics in carbon-13 NMR spectroscopy. Vol. 1. *Edited by* G. C. Levy. John Wiley, New York. 1974. p. 79; (*b*) D. R. WRIGHT, D. E. AXELSON, and G. C. LEVY. *In* Topics in carbon-13 NMR spectroscopy. Vol. 3. *Edited by* G. C. Levy. John Wiley, New York. 1978. p. 104; (*c*) R. E. WASYLISHEN. *In* NMR spectroscopy techniques. *Edited by* C. Dybowski and R. L. Lichter. Marcel Dekker, New York. 1987. p. 45.
24. (*a*) A. ALLERHAND, D. DODRELL, and P. KOMORSKI. J. Chem. Phys. **55**, 189 (1971); (*b*) P. DAIS. Magn. Reson. Chem. **27**, 61 (1989).
25. (*a*) M. F. BROWN. J. Chem. Phys. **80**, 2832 (1984); (*b*) S. MEIBOOM and L. C. SNYDER. Acc. Chem. Res. **4**, 81 (1971); (*c*) K. DILL and A. ALLERHAND. J. Am. Chem. Soc. **101**, 4376 (1978).
26. G. C. LEVY, J. D. CARGIOLI, and F. A. L. ANET. J. Am. Chem. Soc. **95**, 1527 (1973).
27. R. M. HAWK and R. R. SHARP. J. Chem. Phys. **60**, 1522 (1974).
28. A. G. DAVIES, A. J. PRICE, H. M. DAWES, and M. B. HURSTHOUSE. J. Chem. Soc. Dalton Trans. 297 (1986).
29. C. W. HOLZAPFEL, J. M. KOEKEMOER, C. F. MARAIS, G. J. KRUGER, and J. A. PRETORIUS. S. Afr. J. Chem. **35**, 80 (1982).
30. R. K. HARRIS, P. REAMS, and K. J. PACKER. J. Mol. Struct. **141**, 13 (1986).
31. J. HERZFELD and A. E. BERGER. J. Chem. Phys. **73**, 6021 (1980).
32. U. HAEBERLEN. Phil. Trans. R. Soc. London, A, **299**, 497 (1981).
33. H. W. SPIESS. In NMR Basic Principles and Progress. Edited by P. Diehl, E. Fluck, and R. Kosfeld. Springer-Verlag, Berlin, 15, 55 (1978).
34. W. H. PRESS, B. P. FLANNERY, S. A. TEUKOLSKY, and W. T. VETTERLING. Numerical recipes — the art of scientific computing. Cambridge University Press, Cambridge. 1986. p. 289.

Can. J. Chem. Downloaded from www.nrcresearchpress.com by 91.121.58.235 on 09/07/12
For personal use only.

Shelf-life prediction from induction period calorimetric measurements on materials undergoing autocatalytic decomposition

LEE D. HANSEN,[1] DELBERT J. EATOUGH, AND EDWIN A. LEWIS
Department of Chemistry, Brigham Young University, Provo, UT 84602, U.S.A.
AND
ROBERT G. BERGSTROM,[2] DAMARIS DEGRAFT-JOHNSON, AND KAREN CASSIDY-THOMPSON
Department of Pharmaceutical Research, Merck Sharp & Dohme Research Laboratories, West Point, PA 19486, U.S.A.
Received March 30, 1990

LEE D. HANSEN, DELBERT J. EATOUGH, EDWIN A. LEWIS, ROBERT G. BERGSTROM, DAMARIS DEGRAFT-JOHNSON, and KAREN CASSIDY-THOMPSON. Can. J. Chem. **68**, 2111 (1990).

The shelf- or use-life of a material which decomposes by an autocatalytic reaction is shown to be inversely proportional to the rate of heat generation during the induction period of the degradation reaction. Calorimetric measurement of the rate of heat generation during the induction period takes only a few hours. It can often be done at or very near the actual storage or use temperature of the material. Measurements on Lovastatin (2-methylbutanoic acid 1,2,3,7,8,8*a*-hexahydro-3,7-dimethyl-8-[2-(tetrahydro-4-hydroxy-6-oxo-2*H*-pyran-2-yl)ethyl]-1-naphthalenylester) are used as an example of this application.

Key words: autocatalytic, calorimetry, oxidation, decomposition, Lovastatin, Mevacor.

LEE D. HANSEN, DELBERT J. EATOUGH, EDWIN A. LEWIS, ROBERT G. BERGSTROM, DAMARIS DEGRAFT-JOHNSON et KAREN CASSIDY-THOMPSON. Can. J. Chem. **68**, 2111 (1990).

On démontre que la période de période de péremption d'un produit qui se decompose par un mécanisme autocatylique est inversement proportionnelle au taux de réchauffement du produit au cours de la période d'induction de la réaction de dégradation. Les mesures calorimétriques de ce taux de réchauffement au cours de la période d'induction ne demandent que quelques heures et ils peuvent souvent être déterminés dans ou près du lieu d'entreposage; ou on peut utiliser la température du produit. Comme exemple d'application de la méthode, on présente des données relatives au Lovastatin (2-méthylbutanoate du 1, 2, 3, 7, 8, 8*a*-hydro-3,7-diméthyl-8-[2-(tétrahydro-4-hydroxy-6-oxo-2*H*-pyran-2-yl)éthyl]-1-naphtalényle).

Mots clés : autocatalytique, calorimétrie, oxydation, décomposition, Lovastatin, Mevacor.

[Traduit par la revue]

Introduction

Many organic materials undergo autocatalytic degradation. Four disparate examples are oxidation of polymers (1), oxidation of fats and oils leading to rancidity (2), and oxidation of the drug Lovastatin (2-methylbutanoic acid 1,2,3,-7,8,8*a*-hexahydro-3,7-dimethyl-8-[2-(tetrahydro-4-hydroxy-6-oxo-2*H*-pyran-2-yl)ethyl]-1-naphthalenyl ester) (3). Autocatalytic degradation reactions of commercially important organic materials usually are oxidation reactions involving atmospheric oxygen or ozone, or premature polymerization of monomers. The degradation process involves first an induction or initiation period which may range from minutes to years depending on the material, the concentrations of reactants, environmental factors such as ionizing radiation, and the temperature. The addition of antioxidants and other stabilizers serve to extend the induction period (4, 5). The induction period is followed by a relatively short period of time characterized by a rapidly increasing rate of reaction which usually goes through a maximum and then begins to decrease. The reaction occurring during the induction period normally has only a very slight effect on the physical and chemical properties of the material. Large changes in the properties of the material occur during the degradation reaction (1). Thus, a prediction of the useful life of the material is equivalent to a prediction of the length of the induction period.

Prediction of the useful life of a material which degrades by a rate law other than autocatalytic is straightforward, since in these cases it is only necessary to calculate the time to reach an unacceptable amount of degradation from the rate law for the reaction. Usually the quantitative rate law will not vary significantly from lot to lot since it is dependent on reactions of the bulk material. In contrast, the induction period for an autocatalytic reaction often varies markedly from lot to lot since it is dependent on trace impurities, degree of crystallinity, surface area, and other similar factors which all involve trace constituents of the bulk material which are not constant from lot to lot. Thus, a method for measuring some parameter which can be reliably used to predict shelf-life for these materials on a lot to lot basis is needed.

Prediction of shelf-life for materials undergoing autocatalytic decomposition is currently done by measuring induction times at elevated temperatures (6). Measurements are usually made at as low a temperature as patience, time, and detection limits will allow, then an extrapolation is done to obtain the induction time at the actual use or storage temperature of the material. Using an elevated temperature inserts the uncertainty of assuming a constant activation energy over the temperature interval of the extrapolation. After the extrapolation, questions remain even as to the validity of a relative stability order, since the stability order at high temperature may not be the same as that at the lower use temperature (6). Extrapolation over 100 to 200°C is not uncommon in current practice, and changes in the activation energy caused by changes in reaction mechanism over such a temperature range would not be surprising.

Several recent papers (2, 3, 7–9), have shown how isothermal calorimetry can be used as a relatively rapid and unambiguous method to determine the kinetic rate law for degradations of organic materials. Isothermal calorimetry is also a common method used for the detection of a large thermal

[1]To whom correspondence should be addressed.

[2]Present address: Baxter Healthcare Corporation, Route 120 and Wilson Road, Round Lake, IL 60073, U.S.A.

Printed in Canada / Imprimé au Canada

Can. J. Chem. Downloaded from www.nrcresearchpress.com by 91.121.58.235 on 09/07/12
For personal use only.

Can. J. Chem. Downloaded from www.nrcresearchpress.com by 91.121.58.235 on 09/07/12
For personal use only.

event occurring at the end of the induction time, and hence can be used as a method for determining the induction times (6, 10). These previous calorimetric studies have focused on identifying the major decomposition reaction or have used the calorimetric signal from the decomposition reaction simply as a time marker. The focus of this paper is to use calorimetry to study the reactions occurring during the induction period.

Isothermal calorimetry, and in particular large sample (typically 1 to 100 g), heat conduction calorimetry, can often provide both kinetic and chemical data at low temperature on the reaction(s) occurring during the induction period. The attainable detection limit of 0.2 μW allows degradation rates as low as 0.01% per year to be measured in favorable cases (3). Furthermore, the output from a heat conduction calorimeter is directly proportional to the rate of reaction, and therefore is a measure of the instantaneous rate of reaction. Thus, it is not necessary to wait for reaction products to accumulate as in the case of integral methods, and in the absence of interfering reactions, measurements can be made very early in the induction period. The purpose of this paper is to demonstrate that accurate shelf-life predictions can be made from calorimetric measurements of the rate of heat production taken during the induction period of an autocatalytic degradation reaction.

Theory

The rate of an initiation reaction can be expressed as

$$[1] \quad (d\alpha_i/dt) = kf(\text{concentrations})$$

where α_i is the fraction of reaction that has occurred, k is the rate constant, t is the time, and f(concentrations) is a function of the concentrations of sites and reactants that are active in the initiation reaction. The rate constant k is given as a function of temperature by

$$[2] \quad k = A \exp -E^*/RT$$

where A is a constant, E^* is the Arrhenius activation energy, R is the gas constant, and T is the Kelvin temperature.

For the reactions of interest in the context of this paper, f(concentrations) will usually not change during the induction period, and therefore the rate equation for the reaction will be pseudo-zero order. Setting f(concentrations) $= c$, a constant, eq. [1] thus becomes

$$[3] \quad (d\alpha_i/dt) = kc = cA \exp -E^*/RT$$

which, on integration from $\alpha_i = 0$ at $t = 0$ gives

$$[4] \quad \alpha_i = kct$$

When $\alpha_i = 1$, i.e. at the end of the induction time, $kc = 1/t_i$ where t_i is the length of the induction period. Note that for zero order kinetics, α_i is equal to the fraction of the induction time that has elapsed. Substituting this result into eq. [3] gives

$$[5] \quad (d\alpha_i/dt) = cA \exp -E^*/RT = 1/t_i$$

which relates the induction time to the temperature as shown in eq. [6].

$$[6] \quad -\ln t_i = \ln cA - E^*/RT$$

If t_i is known as a function of temperature, the activation energy for the initiation reaction may be obtained by plotting $\ln t_i$ against $1/T$ and calculating the slope, which is equal to E^*/R. Note that a linear plot will not be obtained if E^* is not constant or if the reaction is not zero or pseudo-zero order, i.e. if c is not constant. The objective of this study, however, is to avoid having to do a direct determination of t_i for every lot of material.

The total amount of heat produced by the initiation reaction to any time t during the induction period is given by

$$[7] \quad Q_i = -\Delta H_i \beta_i D_o \alpha_i$$

where ΔH_i is the enthalpy change for the initiation reaction, β_i is the fraction of the sample which reacts in the initiation reaction, and D_o is the mass of the sample. The rate of heat production during the induction period is then

$$[8] \quad dQ_i/dt = q_i = -\Delta H_i \beta_i D_o (d\alpha_i/dt)$$

Substituting $1/t_i$ for $(d\alpha_i/dt)$ as shown in eq. [5] and rearranging gives

$$[9] \quad t_i = -\Delta H_i \beta_i (D_o/q_i)$$

which shows that t_i is linearly proportional to the reciprocal of the heat production rate if $\Delta H_i \beta_i$ is constant during the induction period. Relative values of D_o/q_i are therefore a measure of the relative induction times of different lots of a given material. Such a relative measurement is sufficient for many purposes. An absolute value of t_i can be calculated from measurements of D_o/q_i if $\Delta H_i \beta_i$ is known. The slope of a plot of t_i versus D_o/q_i gives the value of $\Delta H_i \beta_i$ for the initiation reaction. In order to make such a plot, both t_i and D_o/q_i must be measured on a set of calibration samples. Alternatively, $\Delta H_i \beta_i$ may be estimated from known reactions and thermochemical data.

The activation energy for the initiation reaction may be obtained by measuring q_i as a function of temperature. Substituting $q_i/-\Delta H_i \beta_i D_o$ from eq. [8] for $(d\alpha_i/dt)$ in eq. [5], rearranging and taking the natural logarithm gives

$$[10] \quad \ln q_i/D_o = \ln (-\Delta H_i \beta_i cA) - E^*/RT$$

The activation energy may thus be obtained by plotting $\ln q_i/D_o$ against $1/T$ which should give a straight line with slope equal to $-E^*/R$.

The only assumption made in the derivation is that the initiation reaction is zero order. This assumption may be tested by measuring q_i at several points during the initiation period. If q_i is a constant throughout the induction period, then the zero order assumption must be correct. (See eq. [6] in ref. 3.) Also, if the plot of $\ln q_i/D_o$ vs. $1/T$ is linear, then the activation energy must be invariant over the range of temperatures plotted, $\Delta H_i \beta_i c$ must be a constant, and the assumption of zero order must also be true.

The time to the maximum rate of reaction, t_m, is often used implicitly as a surrogate for the induction time in discussions of autocatalytic kinetic data (2, 6) although there has been no basis in fact or theory given for a relationship between t_i and t_m. Although some systems show a sudden, sharp rise in the thermal signal at the end of the induction period (10), the junction between the induction time and the rapidly rising period of reaction is often a continuous curve with no definitive t_i point (2, 3). Thus, t_m is often much more precisely defined and hence much easier to measure than t_i. This empirical data treatment using t_m in place of t_i is usually successful in predicting relative stability order, and therefore

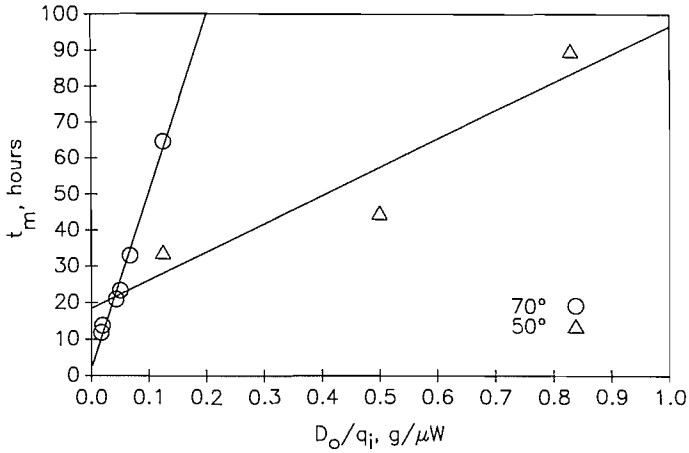

FIG. 1. Time required to achieve the maximum rate of heat production versus the reciprocal of the heat rate measured during the induction period for oxidative decomposition of Lovastatin, 2-methylbutanoic acid 1,2,3,7,8,8*a*-hexahydro-3,7-dimethyl-8-[2-(tetrahydro-4-hydroxy-6-oxo-2*H*-pyran-2-yl)ethyl]-1-naphthalenyl ester.

must have some basis in fact, albeit unknown. From the success of predictions based on t_m, it follows that t_m must be linearly proportional to t_i for different samples of the same material. Thus, for plots of t_m versus D_o/q_i, eq. [9] becomes

$$[11] \quad t_m = (t_m - t_i) - \Delta H_i\beta_i(D_o/q_i)$$

simply by adding $(t_m - at_i)$ =constant to both sides. A linear plot of t_m versus D_o/q_i will be obtained for samples with differing D_o/q_i if $(t_m - at_i)$ is in fact a constant. The intercept of such a plot is equal to $(t_m - t_i)$ and thus t_i can be obtained from the t_m data.

Experimental

Measurements were made as described in ref. 3. Briefly, samples (1 to 3 g) were enclosed with air in sealed containers and placed in the calorimeter at 70°C. Data on the heat production rate were collected continuously until a value for t_m was obtained. Sample aging was assumed to begin when the sample was placed in the calorimeter, i.e. we assumed $t = 0$ and $\alpha_i = 0$ at this point in time. Experimental lots of Lovastatin used in this study were obtained and the heat rates measured within a few days of manufacture. Induction heat rate data were obtained on some early, experimental lots of Lovastatin at 50°C. These data were reported in ref. 3 and are included in Fig. 1. Current production lots of Lovastatin have an induction heat rate at 50°C which is below the detection limit (0.2 μW) of the measurement, consistent with the shelf-life of several years at room temperature.

Results

D_o/q_i and t_i data taken on Lovastatin at 70°C in this study together with similar data at 50°C from ref. 3 are plotted according to eq. [11] in Fig. 1. The linear relationship between t_m and D_o/q_i validates both eqs. [10] and [11]. The slopes of the two plots in Fig. 1 give values of $\Delta H_i\beta_i$ of −0.28 and −1.75 J/g of sample at 50 and 70°C, respectively. The fact that $\Delta H_i\beta_i$ varies much more than expected with temperature is evidence that the induction reaction is different at the two temperatures.

Discussion

The theory given above may also be tested with data from the literature. Plots of ln t_i or ln t_m against $1/T$ have been found to be linear for oxidative degradation of polyolefins with and without antioxidants over a significant range of temperature (4, 6). Also, published data on rates of heat production from oxidative degradation of Lovastatin during the induction period generally show the rate to be constant (3). Data on oxidation of unsaturated fatty acids and seed lipids show constant or only very slowly rising rates of heat production, particularly during the early part of the induction period (2). These data show the zero order assumption to be generally valid. A very slow increase in the heat rate during the induction period is simply an indication of the beginnings of the major degradation reaction and is expected to occur in those cases which do not show an abrupt change in the rate at the end of the induction period. This overlap of reactions in time causes the difficulty mentioned above in actually determining a value for t_i from the experimental data.

Changes in activation energy of the initiation reaction are indicated by a change of slope in a plot of ln t_i or ln t_m against $1/T$. These changes are usually fairly abrupt. For example, the activation energy for polyolefin oxidation has been shown to change around 150°C by this method (6). Induction period heat rates can provide further information concerning changes in mechanism occurring with changing temperature. Induction period data on Lovastatin, for example, show the rate of induction period heat generation to decrease markedly between 60 and 70°C even though the induction time decreased with the temperature increase (3). Such changes in E^* and/or c are indicative of a change in the reaction mechanism and thus are a warning that data collected above the change temperature cannot be used to predict stability below the temperature of the change in mechanism. These data reinforce the need for rapid means of testing stability at low temperature.

Once it has been verified that the induction reaction is described by a zero order rate law, a determination of relative stability can be made simply by measurement of the relative values of D_o/q_i. Since a measurement of q_i requires only about 1 to 8 h with current, commercially available calorimeters, this method opens the possibility of doing reasonably fast quality control measurements.

To predict absolute stability, a calibration constant (i.e. $\Delta H_i\beta_i$ or the slope of a plot similar to that shown in Fig. 1) must be determined. For materials with very large t_i values this may not be practical. Also, estimation of $\Delta H_i\beta_i$ may not be possible because the reactions contributing to the measured heat rate are not known. However, the method described in this paper may be used to fairly rapidly (~10 days) determine the activation energy (i.e. measurement of D_o/q_i as a function of temperature), and then, if E^* is found to be constant to a high enough temperature, t_i or t_m may be measured at the high temperature. Thus, after sufficient calibration, a complete prediction of the useful shelf-life of a given material would require only that q_i be measured at some convenient temperature in the range of constant activation energy.

The measurement temperature may be chosen to be the same as the use temperature, but an elevated temperature is often helpful because it increases the heat rate and thus decreases the error in the measurement. However, too high a temperature of measurement can cause problems by shortening the induction period until it becomes too short for meaningful measurements.

Another difficulty encountered with Lovastatin in this study was the presence at $t = 0$ of reactions with decaying exponen-

Can. J. Chem. Downloaded from www.nrcresearchpress.com by 91.121.58.235 on 09/07/12
For personal use only.

tial kinetics. (See ref. 3 for examples.) Such reactions must be allowed to decay before an accurate measurement of q_i can be made. The presence of such reactions delays the time at which a relative stability prediction may be made, but does not increase the time required to make a measurement if the sample is allowed to age outside the calorimeter for a proper period of time.

The results presented in this paper and collected from the literature show that the rapidly rising autocatalytic part of the degradation process begins when the products of the induction reaction reach a critical concentration in the material. This is entirely consistent with previous works on mechanisms of autocatalytic oxidations and polymerizations. What is new in this work is that the concentration of induction reaction products are shown to increase linearly with time as required by pseudo-zero order kinetics.

Acknowledgement

The authors thank Merck Sharp & Dohme Research Laboratories for financial support of the work done at Brigham Young University.

1. J. F. RABEK. *In* Chemical kinetics. Vol 14. *Edited by* C. H. Bamford and C. F. H. Tipper. Elsevier, New York, NY. 1975. Chapt. 4.
2. A. RAEMY, I. FROELICHER, and J. LOELIGER. Thermochim. Acta, **114**, 159 (1987).
3. L. D. HANSEN, E.A. LEWIS, D.J. EATOUGH, R.G. BERGSTROM, and D. DEGRAFT-JOHNSON. Pharm. Res. **6**, 20 (1989).
4. T. SCHWARZ, G. STEINER, and J. KOPPELMANN. J. Appl. Polym. Sci. **37**, 3335 (1989).
5. H. W.-S. CHAN (*Editor*). Food science and technology. Academic Press, New York, NY. 1987. p. 163.
6. E. KRAMER and J. KOPPELMANN. Polym. Eng. Sci. **27**, 945 (1987).
7. D. N. WATERS and J. L. PADDY. Anal. Chem. **60**, 53 (1988).
8. M. J. PIKAL and K. M DELLERMAN. Int. J. Pharm. **50**, 233 (1989).
9. M. E. BROWN and A. K. GALWEY. Anal. Chem. **61**, 1136 (1989).
10. E. KRAMER, J. KOPPELMANN, and T. SCHMUTZ. Proceedings, 11th International Conference on Advances in the Stabilization and Controlled Degradation of Polymers, May 24–26, 1989. p. 79.

Can. J. Chem. Downloaded from www.nrcresearchpress.com by 91.121.58.235 on 09/07/12
For personal use only.

Electrical conductance of a mixture of sodium and potassium nitrates in aqueous medium

RATAN LAL GUPTA AND KOCHI ISMAIL[1]

Department of Chemistry, North-Eastern Hill University, Bijni Complex, Laitumkhrah, Shillong 793 003, India

Received November 3, 1989[2]

RATAN LAL GUPTA and KOCHI ISMAIL. Can. J. Chem. **68**, 2115 (1990).

Electrical conductance and density measurements of $[x\mathrm{NaNO_3} + (1 - x)\mathrm{KNO_3}] + R\mathrm{H_2O}$ system were taken as functions of x, R, and temperature. The mixed alkali effect on molar conductance (Λ) was found to be negligible upto $R = 25$ and becomes significant in the region where $R < 25$. It has been shown that for mixed electrolytic system in aqueous medium the concentration range at which the mixed alkali effect on Λ starts becoming significant can be predetermined by plotting the difference in Λ of the two pure electrolytic solutions versus R. The concentration dependence of Λ has been described satisfactorily by the expression $\Lambda = \Lambda_{FLK} \exp(Bc + Cc^2)$ where Λ_{FLK} is the Falkenhagen–Leist–Kelbg equation for Λ, B and C are empirical constants, and c is the molar concentration. The observed values of the ion-size parameter have indicated more ionic association in $\mathrm{KNO_3}$ solution than in $\mathrm{NaNO_3}$ solution.

Key words: electrical conductance, sodium nitrate, potassium nitrate, mixed alkali effect.

RATAN LAL GUPTA et KOCHI ISMAIL. Can. J. Chem. **68**, 2115 (1990).

On a mesuré la conductivité électrique et la densité du système $[x\mathrm{NaNO_3} + (1 - x)\mathrm{KNO_3}]R\mathrm{H_2O}$ en fonction de x, de R et de la température. On a trouvé que l'effet des alcalins mixtes sur le conductivité (Λ) est faible jusqu'à une valeur de $R = 25$ et qu'il devient important lorsque $R < 25$. Pour le système électrolytique mixte en milieu aqueux, on a démontré que l'intervalle de concentration dans lequel l'effet des alcalins mixtes commence à se faire sentir peut être prédéterminé en faisant un graphique de la différence entre les Λ des deux solutions électrolytiques pures en fonction de R. L'équation $\Lambda = \Lambda_{FLK} \exp(Bc + Cc^2)$, dans laquelle Λ_{FLK} est l'équation de Falkenhagen–Leist–Kelbg pour Λ, B et C sont des constantes empiriques et c est la concentration molaire, permet de décrire correctement la relation qui existe entre la concentration et la conductivité Λ. Les valeurs observées pour le paramètre de la grosseur de l'ion indiquent qu'il y a plus d'association en solution dans le $\mathrm{KNO_3}$ qu'en solution dans le $\mathrm{NaNO_3}$.

Mots clés : conductivité électrique, nitrate de soude, nitrate de potasse, effet des alcalins mixtes.

[Traduit par la revue]

Introduction

Properties of ternary systems containing two alkali metal ions in a fixed glassy medium are interesting due to a phenomenon known as mixed alkali effect (MAE) which is of both practical and theoretical importances (1, 2). This phenomenon refers to non-additivity of various physical properties caused when the relative amounts of the alkali metal ions are varied while the concentration of the glassy medium is a constant. Normally MAE is most pronounced for properties related to ionic transport.

Attempt are being made to look for the MAE in media other than glass. In hydrate melt medium MAE also is found to be present but to a lesser extent (3–6). Another suitable medium for investigating MAE is the aqueous medium. Investigation of MAE on transport properties in aqueous medium has a two-fold interest. (*i*) Data on the properties of mixed aqueous electrolytes are necessary because many systems of practical, biological, geological or chemical interest involve mixed aqueous electrolytes. Studies on the transport properties of mixed aqueous electrolytes have, however, been relatively few compared to those on their thermodynamic properties. (*ii*) One of the characteristics of MAE is that it shows a complicated dependence on the total alkali metal ion concentration. To examine this aspect, aqueous medium is more convenient. Any mixed alkali metal ion system in aqueous medium can be represented as $[x\mathrm{M_1A} + (1 - x)\mathrm{M_2A}] + R\mathrm{H_2O}$, where M_1 and M_2 are the two alkali metal ions and R is the number of moles of $\mathrm{H_2O}$. Our previous attempt (7) to look for MAE in aqueous medium by measuring electrical conductances of a mixture of sodium and potassium thiocynates in water at 25°C has shown that significant MAE on molar conductance exists only in the region where $R < R_0 \simeq 10$. In view of the fact that NaSCN solution exhibits specific conductance maximum at $R \simeq 10$ and for KSCN solution it occurs at $R \simeq 6$, the value of R_0 is considered to have a correlation with the concentration (lower one) at which the specific conductance maximum of one of the constituent electrolytes of the mixed system occurs (7). Furthermore, it has been suggested that in the region where MAE exists the mixed electrolytic system has a quasi-crystalline-type structure. To further examine this type of dependence of MAE on R or on the total alkali metal ion concentration, electrical conductances of another mixed electrolyte, viz., $[x\mathrm{NaNO_3} + (1 - x)\mathrm{KNO_3}] + R\mathrm{H_2O}$, are reported here as functions of x, R, and temperature.

Experimental section

$\mathrm{NaNO_3}$ (BDH, Laboratory Reagent) and $\mathrm{KNO_3}$ (BDH, Laboratory Reagent) were recrystallized from their solutions in doubly distilled water and were then dried for several days over anhydrous $\mathrm{CaCl_2}$ in a vacuum desiccator. Using these salts molal solutions were prepared. To convert molal concentrations into molar concentrations densities of the solutions were measured using a calibrated glass pycnometer of about 7 mL capacity. Conductivity measurements were made at 1 kHz using the CDM 83 conductivity meter (Radiometer, Copenhagen) and a dip type CDC 304 conductivity cell. This cell has three electrodes in the form of pure platinum bands on a glass tube. All measurements were made in a thermostated (±0.02°C) water bath.

Results and discussion

The experimental values of molar conductance of $[x\mathrm{NaNO_3} + (1 - x)\mathrm{KNO_3}] + R\mathrm{H_2O}$ system measured as functions of x, R, and temperature are presented in Table 1.[3] The density data are

[1]To whom correspondence should be addressed.

[2]Revision received April 12, 1990

[3]Complete set of tables may be purchased from the Depository of Unpublished Data, Document Delivery CISTI, National Research Council of Canada, Ottawa, Canada K1A 0S2.

Printed in Canada / Imprimé au Canada

Can. J. Chem. Downloaded from www.nrcresearchpress.com by 91.121.58.235 on 09/07/12
For personal use only.

Can. J. Chem. Downloaded from www.nrcresearchpress.com by 91.121.58.235 on 09/07/12
For personal use only.

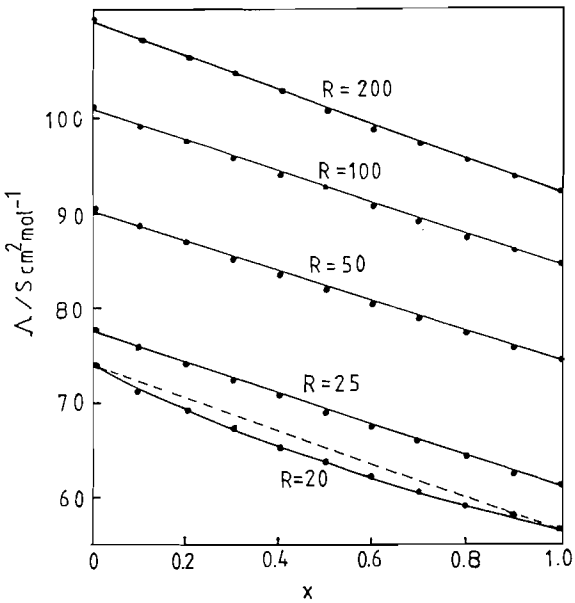

FIG. 1. Variation of Λ of $[x NaNO_3 + (1 - x)KNO_3] + RH_2O$ system with x at 298 K for different R values.

presented as a function of temperature in Table 2.[3] The measured values of conductance were found to be reproducible to within ±0.75% accuracy.

Variation of Λ *with* x

The variation of Λ with x at different R values is shown in Fig. 1. At all experimental tempertures less than 1% deviation of Λ from additivity has been observed upto $R = 25$. Rysselberghe and Nutting (8) also reported less than 1% deviation from additivity in Λ of $[xNaNO_3 + (1 - x)KNO_3] + 55.56H_2O$ system at 298 K. The MAE is, however, considered to be not very significant when the non-additivity in Λ is <1%. At $R = 20$, on the other hand, 2% deviation of Λ from additivity (Fig. 1) has been observed for $x = 0.5$ at 298 K thereby envisaging the occurrence of the MAE on Λ. Earlier it was suggested (7), as mentioned in the Introduction, that the MAE on electrical conductance starts becoming significant when the value of R falls in the concentration range where conductivity maximum of at least one of the components of the mixed electrolytic solution appears. The existence of MAE at $R = 20$ in the $[xNaNO_3 + (1 - x)KNO_3] + RH_2O$ system is, however, contrary to our above suggestion since conductivity maximum has not been observed or reported for KNO_3 solution upto saturation point and for $NaNO_3$ solution it is found at $R \simeq 6.9$. What is then the concentration range at which the MAE on Λ becomes significant in an aqueous medium? To seek a probable answer to this question we have plotted in Fig. 2 the difference (ΔΛ) in the Λ values of (*i*) NaSCN and KSCN solutions (7) and (*ii*) $NaNO_3$ and KNO_3 solutions as a function of R at 298 K. It is evident from Fig. 2 that at high R values ΔΛ depends linearly on R and at some concentration range deviation from the linear dependence starts to take place. It is very interesting to observe that the concentration range at which the MAE on Λ starts becoming significant coincides with the concentration range where dependence of ΔΛ on R deviates from linearity. Incidentally, in the case of NaSCN and KSCN solutions the concentration range around which ΔΛ deviates from linearity coincides with the range at which NaSCN solution exhibits specific conductance maximum. In Fig. 2 we also checked the dependence of ΔΛ on R for a few other pair of electrolytes, viz., RbCl and CsCl (at 296 K), NaCl and KCl (at 298 K), and LiCl and RbCl (at 296 K),

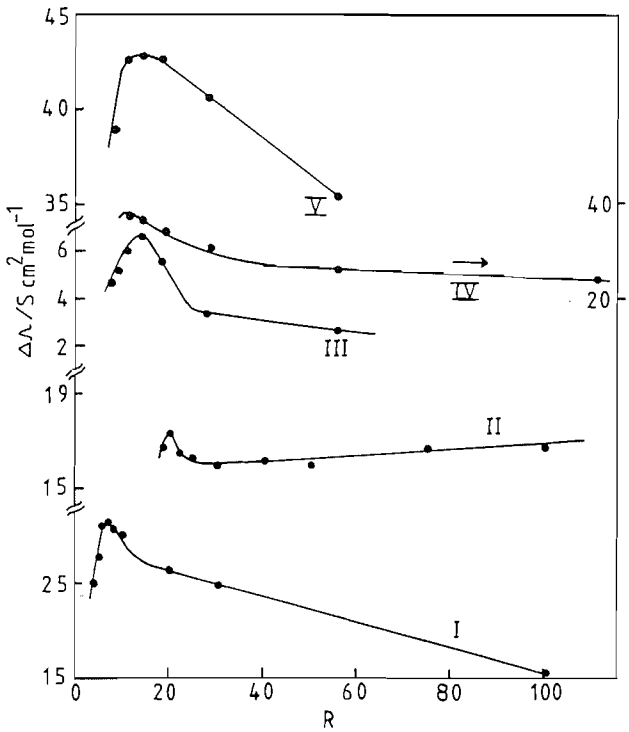

FIG. 2. Plot of difference in Λ values of aqueous electrolytic solutions at 25°C vs. R (*I*, NaSCN and KSCN; *II*, $NaNO_3$ and KNO_3; *III*, RbCl and CsCl (at 23°C); *IV*, NaCl and KCl; and *V*, LiCl and RbCl (at 23°C).

with the help of their reported data (9–11). In all cases, the dependence of ΔΛ on R follows a general trend, viz., (*i*) linear dependence at large R values, (*ii*) at some concentration range, which depends on the pair of electrolytes considered, deviation from linearity is observed and (*iii*) the plot of ΔΛ vs. R passes through a maximum at some lower R value. Therefore, for mixed electrolyte systems in aqueous medium the concentration range at which the MAE on Λ begins to become significant can be predetermined by plotting the difference in Λ of the two pure electrolytic solutions versus R.

Variation of Λ *with* R

We recently reported (7) a new isothermal equation of the form

$$[1] \quad \Lambda = \Lambda_{FLK} \exp(Bc + Cc^2)$$

to describe the concentration dependence of Λ of electrolytic solutions, both single and mixed electrolytes, from dilute region upto high concentration. In eq. [1], B and C are empirical constants and c is the molar concentration. Concentration in the exponential part of eq. [1] can also be expressed in other units. Λ_{FLK} refers to the Falkenhagen–Leist–Kelbg (FLK) equation (12) for Λ and is of the form

$$[2] \quad \Lambda_{FLK} = \left[\Lambda_0 - \frac{B_1 c^{1/2}}{1 + B_0 a_0}\right]\left[1 - \frac{B_2 c^{1/2} F}{1 + B_0 a_0}\right]$$

For 1:1 electrolytes, $B_1 = 82.501/\eta_0(DT)^{1/2}$, $B_2 = 82.04 \times 10^4/(DT)^{3/2}$, $B_0 = 50.29 \times 10^8 c^{1/2}/(DT)^{1/2}$, and $F = [\exp(0.2929 B_0 a_0) - 1]/0.2929 B_0 a_0$. Λ_0 is the molar conductance of the solution at infinite dilution, η_0 is the viscosity of water, D is the dielectric constant of water at temperature T, and a_0 is known as the ion-size parameter. In eq. [1] the parameters whose values need to be determined are Λ_0, a_0, B, and C. While fitting data to eq. [1] it was reduced to a three-parameter equa-

Can. J. Chem. Downloaded from www.nrcresearchpress.com by 91.121.58.235 on 09/07/12
For personal use only.

TABLE 3. Best-fit parameters of eq. [1] for molar conductance of $[x NaNO_3 + (1 - x)KNO_3] + RH_2O$ system

x	$\Lambda_0/S\,cm^2\,mol^{-1}$	$a_0 \times 10^8$/cm	$-B$	$-C$	Std. dev. in Λ
		283 K			
0.0	104.72	1.45	−0.0720	0.2423	0.0764
0.1	102.91	1.46	−0.0740	0.2544	0.0634
0.2	101.10	2.02	−0.0116	0.1649	0.0861
0.3	99.29	2.43	0.0251	0.1094	0.0486
0.4	97.48	2.41	0.0134	0.1680	0.0804
0.5	95.67	2.92	0.0595	0.0642	0.1561
0.6	93.86	3.28	0.0798	0.0385	0.1180
0.7	92.05	3.56	0.0915	0.0312	0.1136
0.8	90.24	3.81	0.0999	0.0288	0.1135
0.9	88.43	4.11	0.1100	0.0237	0.1227
1.0	86.62	4.34	0.1154	0.0241	0.9044
		288 K			
0.0	117.68	1.88	−0.0206	0.1594	0.0965
0.1	115.69	1.78	−0.0384	0.2152	0.0594
0.2	113.70	2.34	0.0191	0.1113	0.1046
0.3	111.72	2.57	0.0375	0.0875	0.0630
0.4	109.73	2.66	0.0366	0.1223	0.0655
0.5	107.74	2.96	0.0624	0.0609	0.1313
0.6	105.75	3.34	0.0842	0.0329	0.1285
0.7	103.76	3.61	0.0956	0.0259	0.1219
0.8	101.78	3.86	0.1038	0.0231	0.1059
0.9	99.79	4.14	0.1130	0.0181	0.1041
1.0	97.80	4.36	0.1182	0.0184	0.1073
		293 K			
0.0	131.16	1.96	−0.0156	0.1666	0.0961
0.1	128.99	2.09	−0.0031	0.1487	0.0861
0.2	126.83	2.40	0.0233	0.1084	0.1074
0.3	124.66	2.63	0.0414	0.0843	0.0587
0.4	122.49	2.72	0.0405	0.1187	0.1507
0.5	120.33	3.06	0.0692	0.0537	0.1516
0.6	118.16	3.36	0.0858	0.0316	0.1177
0.7	115.99	3.64	0.0974	0.0243	0.1112
0.8	113.82	3.86	0.1049	0.0211	0.1134
0.9	111.66	4.12	0.1135	0.0165	0.1189
1.0	109.49	4.37	0.1204	0.0137	0.1206
		298 K			
0.0	114.60	1.99	−0.0204	0.1690	0.3874
0.1	142.29	2.55	0.0369	0.0790	0.0595
0.2	139.98	2.65	0.0392	0.0931	0.1416
0.3	137.67	2.88	0.0562	0.0690	0.0896
0.4	135.36	3.24	0.0820	0.0312	0.2118
0.5	133.05	3.27	0.0817	0.0332	0.1689
0.6	130.74	3.46	0.0899	0.0277	0.1197
0.7	128.43	3.67	0.0976	0.0257	0.1310
0.8	126.12	3.94	0.1081	0.0176	0.0781
0.9	123.81	4.15	0.1157	0.0146	0.1060
1.0	121.50	4.36	0.1209	0.0123	0.0342
		303 K			
0.0	159.46	2.04	−0.0095	0.0170	0.0685
0.1	156.94	2.36	0.0241	0.1021	0.0976
0.2	154.42	2.41	0.0216	0.1256	0.1605
0.3	151.90	2.70	0.0475	0.0805	0.0748
0.4	149.38	3.10	0.0766	0.0407	0.3011
0.5	146.86	3.13	0.0765	0.0408	0.2083
0.6	144.33	3.33	0.0861	0.0326	0.1650
0.7	141.81	3.58	0.0965	0.0262	0.1539
0.8	139.29	3.83	0.1070	0.0174	0.1008
0.9	136.77	4.04	0.1138	0.0141	0.1426
1.0	134.25	4.23	0.1187	0.0129	0.1556

TABLE 3 (*concluded*)

x	$\Lambda_0/S\,cm^2\,mol^{-1}$	$a_0 \times 10^8$/cm	$-B$	$-C$	Std. dev. in Λ
		308 K			
0.0	174.18	2.01	−0.0162	0.1968	0.1370
0.1	171.49	2.39	0.0261	0.1049	0.1190
0.2	168.79	2.44	0.0234	0.1288	0.1727
0.3	166.10	2.73	0.0481	0.0890	0.0992
0.4	163.40	3.13	0.0795	0.0386	0.3183
0.5	160.71	3.18	0.0809	0.0351	0.2392
0.6	158.01	3.35	0.0885	0.0301	0.2045
0.7	155.32	3.61	0.1003	0.0210	0.1585
0.8	152.62	3.85	0.1098	0.0134	0.1097
0.9	149.93	4.04	0.1154	0.0114	0.1671
1.0	147.23	4.20	0.1192	0.0107	0.1952
		313 K			
0.0	189.21	2.11	−0.0071	0.1879	0.1636
0.1	186.35	2.45	0.0312	0.1008	0.1613
0.2	183.48	2.48	0.0261	0.1313	0.1698
0.3	180.62	2.74	0.0485	0.0963	0.1081
0.4	177.75	3.13	0.0801	0.0413	0.4065
0.5	174.89	3.23	0.0858	0.0291	0.3041
0.6	172.03	3.37	0.0914	0.0267	0.2326
0.7	169.16	3.62	0.1023	0.0180	0.1876
0.8	166.30	3.84	0.1119	0.0100	0.1193
0.9	163.43	4.02	0.1165	0.0089	0.2060
1.0	160.57	4.16	0.1198	0.0085	0.2158

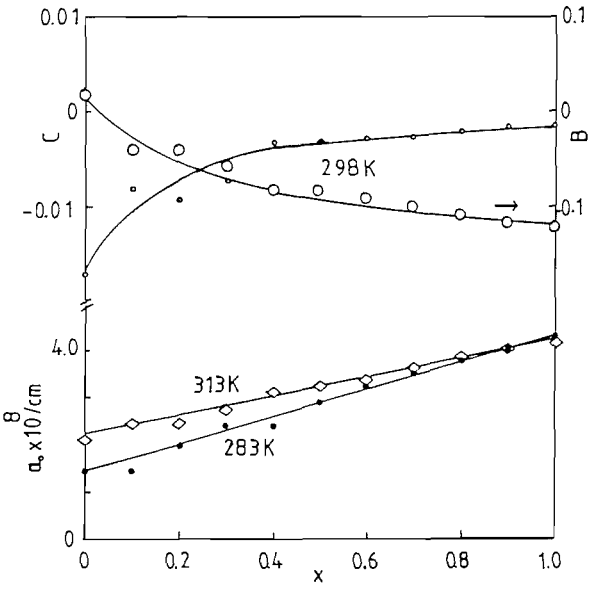

FIG. 3. Variation of a_0, B, and C of $[x NaNO_3 + (1 - x)KNO_3] + RH_2O$ system with x.

tion, by substituting the reported (13) values of Λ_0 for $x = 0$ and $x = 1$ and for other values of x the corresponding Λ_0 values were estimated using the additivity principle (14). The best-fit values of a_0, B, and C obtained by using an iterative least-squares fitting program are listed in Table 3.

It is evident from Table 3 and Fig. 3 that a_0 increases linearly with x. At 298 K $a_0 = 1.99$ Å for KNO_3 solution ($x = 0$) and for $NaNO_3$ solution ($x = 1$) $a_0 = 4.36$ Å. Association into ionic pairs is reported (15–17) in aqueous solutions of both $NaNO_3$ and KNO_3. The considerably low value of a_0 for KNO_3 solu-

tion, also observed by others (15), envisages more ionic association in KNO_3 solution than in $NaNO_3$ solution. Increase in the degree of association of alkali salts in aqueous medium with increasing size of the alkali metal ion was also reported by Kay (15). From Fig. 3 it can further be seen that the a_0 parameter for $NaNO_3$ solution is almost temperature independent whereas the a_0 of KNO_3 solution increases with increase in temperature. This is analogous to the observation made by Goldsack *et al.* (10) in the cases of NaCl and KCl solutions. The degree of ionic association in KNO_3 solution therefore seems to decrease with increasing temperature.

The dependence of B and C parameters on x is also shown in Fig. 3 at one particular temperature. C, which is always a negative quantity, has the lowest value for pure KNO_3 solution and its value increases rapidly as K^+ ions are replaced by Na^+ ions. In the range from $x = 0.5$ to $x = 1.0$, C appears to remain almost independent of the x value. In the case of B, it has a highest positive value for KNO_3 solution and its value decreases with increasing x value, becoming negative above a particular value of x. The value of x at which B becomes zero is dependent on the temperature. For example, at 298 K $B = 0$ at $x = 0.04$ whereas at 288 K $B = 0$ at $x = 0.16$. Similar behaviour was observed in the case of $[x\text{NaSCN} + (1 - x)\text{KSCN}] + R\text{H}_2\text{O}$ system also (7). This type of dependence of B on x may be explained by correlating, in the light of Wishaw-Stokes equation (18), the exponential part of eq. [1] to the reciprocal of viscosity of the system. Consequently, solutions whose B is positive and C is negative may be expected to show negative viscosity (relative viscosity < 1). In fact, aqueous KNO_3 solution is known (9) to exhibit negative viscosity nearly upto 318 K. At 298 K the viscosity of KNO_3 solution is therefore expected to decrease with concentration upto $c = B/C = 1.2$ mol dm^{-3}, which is in good agreement with the experimentally observed value (9). Furthermore, the B parameter appears to have a relation with the ΔE parameter of the Samoilov model (19) for hydration of ions.

Acknowledgement

One of the authors (R.L.G.) is thankful to the University Grants Commission, New Delhi, for the award of a Research Fellowship.

1. J. O. Isard. J. Non-Cryst. Solids, **1**, 235 (1969).
2. D. E. Day. J. Non-Cryst. Solids, **21**, 343 (1976).
3. C. T. Moynihan. J. Electrochem. Soc. **126**, 2144 (1979).
4. A. J. Easteal. Aust. J. Chem. **34**, 1853 (1981).
5. P. Sangma, S. Mahiuddin, and K. Ismail. J. Phys. Chem. **88**, 2378 (1984).
6. S. S. Islam and K. Ismail. Can. J. Chem. **66**, 242 (1988).
7. R. L. Gupta and K. Ismail. Bull. Chem. Soc. Jpn. **61**, 2605 (1988).
8. P. V. Rysselberghe and L. Nutting. J. Am. Chem. Soc. **59**, 333 (1937).
9. T. Isono. J. Chem. Eng. Data, **29**, 45 (1984).
10. D. E. Goldsack, R. Franchetto, and A. Franchetto. Can. J. Chem. **54**, 2953 (1976).
11. O. Söhnel and P. Novotný. Densities of aqueous solution of inorganic substances. Elsevier, New York. 1985.
12. H. Falkenhagen, M. Leist, and G. Kelbg. Ann. Phys. **6**, 51 (1952).
13. A. L. Horvath. Handbook of aqueous electrolyte solutions. Ellis Horwood Ltd., West Sussex. 1985. p. 262.
14. E. O. Timmermann. Ber. Bunsenges. Phys. Chem. **83**, 257 (1979).
15. R. L. Kay. J. Am. Chem. Soc. **82**, 2099 (1960).
16. G. J. Janz, B. G. Oliver, G. R. Lakshminarayanan, and G. E. Mayer. J. Phys. Chem. **74**, 1285 (1970).
17. M. D. Monica, A. Ceglie, and A. Agostiano. Electrochim. Acta, **29**, 933 (1984).
18. B. F. Wishaw and R. H. Stokes. J. Am. Chem. Soc. **76**, 2965 (1954).
19. O. Ya. Samoilov. Discuss. Faraday Soc. **24**, 141 (1957).

Can. J. Chem. Downloaded from www.nrcresearchpress.com by 91.121.58.235 on 09/07/12
For personal use only.

Catalysis by α-cyclodextrin of the reaction of formic acid with bromine

OSWALD S. TEE,[1] BUSHRA JAVED, AND SUSAN R. MIKKELSEN
Department of Chemistry and Biochemistry, Concordia University, Montréal, P.Q., Canada H3G 1M8

Received June 12, 1990

OSWALD S. TEE, BUSHRA JAVED, and SUSAN R. MIKKELSEN. Can. J. Chem. **68**, 2119 (1990).

α-Cyclodextrin (CD) modestly increases the rate of oxidation of formic acid by bromine. The variation of rate constants with $[Br^-]$ is consistent with dominance of the formation of a $CD{\cdot}Br_3^-$ complex in determining the fraction of free Br_2 and the $CD{\cdot}Br_2$ complex, under the reaction conditions. Potentiometric measurements support a dissociation constant of about 0.2 mM for the $CD{\cdot}Br_3^-$ complex, in agreement with an earlier spectrophotometric value. Analysis of the rate increases with [CD] implies that $CD{\cdot}Br_2$ is more reactive (~10 times) than free Br_2 towards formate ion, as was found for phenols. These conclusions differ from those of another recent study.

Key words: catalysis, α-cyclodextrin, oxidation, formic acid, bromine.

OSWALD S. TEE, BUSHRA JAVED et SUSAN R. MIKKELSEN. Can. J. Chem. **68**, 2119 (1990).

L'α-cyclodextrine (CD) provoque une légère augmentation de la vitesse d'oxydation de l'acide formique par le brome. La variation des constantes de vitesse avec la $[Br^-]$ est en accord avec le fait que, dans les conditions de la réaction, les fractions de Br_2 libre et sous la forme de complexe $CD{\cdot}Br_2$, sont dominées par la formation d'un complexe $CD{\cdot}Br_3^-$. Des mesures potentiométriques suggèrent que la constante de dissociation du complexe $CD{\cdot}Br_3^-$ est égale à environ 0,2 mM; cette valeur est en accord avec une valeur spectrophotométrique obtenue antérieurement. L'analyse de l'augmentation de la vitesse avec une augmentation de la [CD] implique que, comme on l'a observé avec les phénols, le $CD{\cdot}Br_2$ est plus réactif (environ 10 fois) que le Br_2 libre vis-à-vis de l'ion formate. Ces conclusions diffèrent de celles rapportées dans une étude récente.

Mots clés : catalyse, α-cyclodextrine, oxydation, acide formique, brome.

[Traduit par la revue]

Formic acid is oxidized by bromine in aqueous solution, and the acidity dependence of the rate suggests that reaction occurs on its anion, eq. [1](1). It has recently been reported that α-cyclodextrin (CD) (2) brings about small increases in the rate of this reaction (3). We have made similar observations, in the course of studies[2] into the effects of cyclodextrins on reactivity (4), but our interpretation of the rate increase differs in regard to the size and origin of the catalysis.

[1] $HCO_2^- + Br_2 \longrightarrow H^+ + 2Br^- + CO_2$

Earlier work showed that the attack of bromine on phenols (5) is modestly catalyzed by CD (6), whereas related debrominations are strongly catalyzed (7). A prior study (8) of the effect of CD on the bromination of anisole helped to identify the equilibria that are needed for data analysis. In particular, we found that addition of CD to Br_2 in 0.01 M KBr solution causes large increases in the uv absorbances due to Br_3^-, consistent with the formation of a strong $CD{\cdot}Br_3^-$ complex (K_d = 0.17 mM) (8).

In their study, Han *et al.* (3) used potentiometry to measure a CD complexation having K_f = 4690 M^{-1} (K_d = 0.213 mM) under conditions where Br_3^- formation is significant ($[Br^-]$ = 0.1 M); it was ascribed to formation of a $CD{\cdot}Br_2$ complex, but no account was taken of the binding of Br_3^- to CD. Based on the value of K_f and the kinetics of oxidation, it was concluded that $CD{\cdot}Br_2$ is half as reactive as Br_2 towards formate ion and that rate increases arise because CD converts unreactive Br_3^- to $CD{\cdot}Br_2$ (3).

In contrast, we have concluded that $CD{\cdot}Br_2$ is 3–31 times as reactive as Br_2 towards phenols (6). Our studies of the effects of CD on brominations (6–8) have used K_d = 2.1 mM for $CD{\cdot}Br_2$, as reported by Breslow and Campbell (9). The present paper reports recent findings that resolve these discrepancies.

We find that the kinetics of oxidation[3] of HCOOH in the presence of added CD are also consistent with eq. [1], but the rate is increased modestly (~1.4× in 0.1 M KBr), indicating some form of catalysis by CD. Without any catalysis, the reaction would be strongly inhibited due to the complexations of Br_2 and Br_3^- by CD (8).

With Br^- and HCOOH present in excess and the pH fixed, the disappearance of Br_2 is first order, eq. [2] (1, 3). In the presence of CD there is an additional process, which is attributed to the reaction of formate ion with the $CD{\cdot}Br_2$ complex, eq. [3] (3).

[2] $Br_2 \xrightarrow{k_1}$ products

[3] $CD + Br_2 \underset{K_B}{\rightleftharpoons} CD{\cdot}Br_2 \xrightarrow{k_2}$ products

Then, neglecting the binding of HCOOH to CD,[4] the observed first-order rate constant should have the form:

[4] $k^{obsd} = (k_1 + k_2[CD]/K_B)f_B$

where f_B is the fraction of free bromine.[5] The difference between our approach and that of Han *et al.* is in respect of the form chosen for f_B. We use:

[5] $f_B = KK_BK_T/(K_BK_T(K + [Br^-]) + [CD](KK_T + K_B[Br^-]))$

[1]Author to whom correspondence may be addressed.

[2]We are studying the effect of CD on the bromination of a variety of substrates, to expand on our earlier findings (4–8).

[3]Oxidation was followed by monitoring bromine disappearance, using the stopped-flow method and uv spectrophotometry (5–8).

[4]To allow a direct comparison with the work of Han *et al.*, we neglect the weak binding of HCOOH to CD (3) and also the weak complex between CD and Br^-, although earlier papers took explict account of the latter (6–8).

[5]Similar treatments have been used previously (3, 6, 8).

Can. J. Chem. Downloaded from www.nrcresearchpress.com by 91.121.58.235 on 09/07/12
For personal use only.

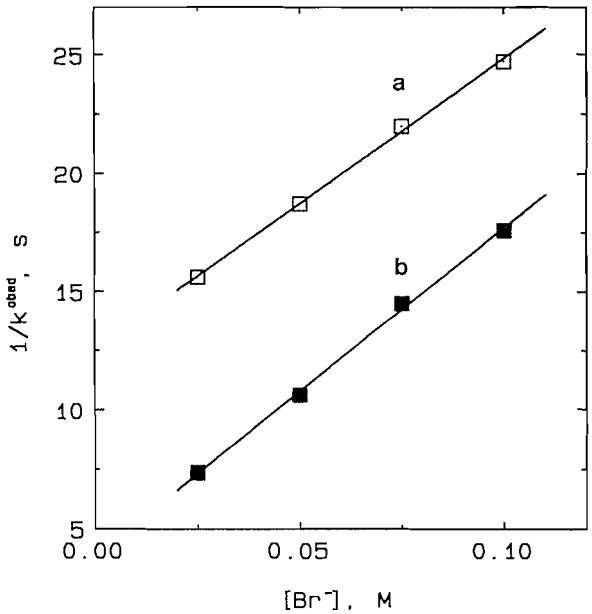

FIG. 1. Effect of bromide ion on the rate constants for the oxidation of formic acid by bromine in the absence (a) and presence (b) of 5 mM α-cyclodextrin. At 25°C using [HCl] = 0.01 M, [HCOOH] = 0.1 M, $[Br_2]_0$ = 0.05 mM, I = [KBr] + [HCl] + [NaCl] = 0.110 M.

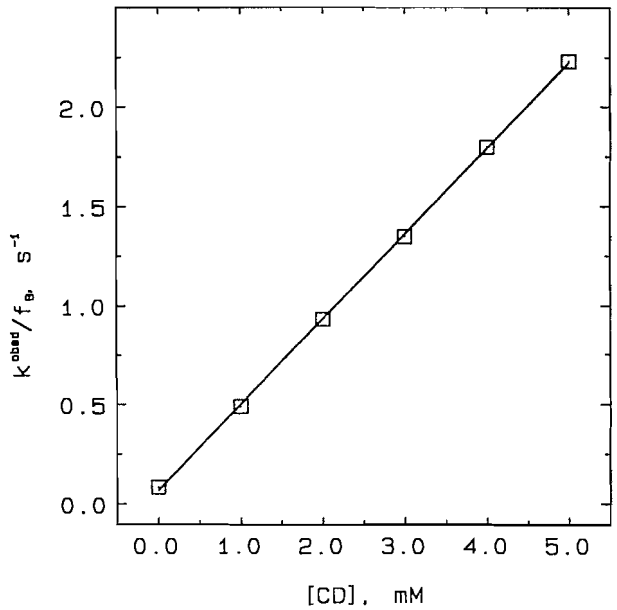

FIG. 2. Effect of α-cyclodextrin on the rate constants for the oxidation of formic acid by bromine, plotted according to eq. [7]. Conditions as for Fig. 1, but with I = [KBr] + [HCl] = 0.11 M (cf. Fig. 2 of ref. 3).

where K, K_B, and K_T are the dissociation constants of Br_3^-, $CD{\cdot}Br_2$, and the $CD{\cdot}Br_3^-$ complex, respectively, and take K = 0.0562 M, K_B = 2.1 mM, and K_T = 0.17 mM (6, 8).

If the binding of Br_3^- to CD is very weak or nonexistent, K_T is large and eq. [5] reduces to

$$[6] \quad f_B = KK_B/(K_B(K + [Br^-]) + [CD]K)$$

This is effectively the form used by Han *et al.*, with K = 0.0588 M and K_B = 0.213 mM (3). Both eqs. [5] and [6] have $[Br^-]$ in their denominators but they are not equally sensitive to its value because of the importance of $CD{\cdot}Br_3^-$ in the former.

In eq. [5] the dominant terms in the denominator involve $[Br^-]$, so that f_B decreases from 0.059 to 0.017 for $[Br^-]$ = 0.025–0.100 M ([CD] = 5 mM). Adding bromide ion produces more Br_3^- and particularly $CD{\cdot}Br_3^-$, at the expense of Br_2 and $CD{\cdot}Br_2$. In contrast, in eq. [6] the dominant term is $[CD]K$ so that f_B hardly varies (0.040–0.038) under the same conditions. Increasing $[Br^-]$ produces more Br_3^-, but the fraction of $CD{\cdot}Br_2$ is large and almost constant (0.94–0.90).

With these considerations in mind, we have measured the effect of varying $[Br^-]$ on the rate of oxidation in the presence and absence of added CD. In both cases the reaction is slower at higher $[Br^-]$ and, as shown in Fig. 1, $1/k^{obsd}$ varies linearly with $[Br^-]$. For reaction in the absence of CD this dependence is due to the increasing formation of unreactive Br_3^- (10); when CD is present it is consistent with dominance of the formation of the $CD{\cdot}Br_3^-$ complex, also unreactive (6, 8).

We have also used potentiometry[6] to measure the *apparent* binding of Br_2 to CD at $[Br^-]$ = 0.10, 0.05, and 0.01 M,[7] with 0.1 M HCl to suppress HOBr (11), and obtained values of "K_B" = 0.126, 0.202, and 0.587 mM, respectively. If the method measured *only* the formation of $CD{\cdot}Br_2$ these values should be virtually constant. The trend to higher values at low $[Br^-]$ is consistent with stronger binding of Br_3^- to CD, which decreases in importance at low $[Br^-]$,[8] and with a weaker binding of Br_2. Thus, while the potentiometric method measures *free* Br_2, the variation of $[Br_2]$ with [CD] is governed largely by the formation of $CD{\cdot}Br_3^-$. Interpreted in this light, the potentiometric measurements give K_T = 0.21, 0.17, and 0.10 mM, in good agreement with the spectrophotometric value of 0.17 ± 0.02 mM (8). Accordingly, we continue to believe that Br_3^- binds more strongly than Br_2 to CD, similar to the situation found with I_3^- and I_2 (12).

Finally, we consider the question of the catalysis by the $CD{\cdot}Br_2$ complex. As reported for pH 1 (3), increasing [CD] brings about small rate increases at other pH values. For analysis of the data, eq. [4] can be rearranged to[5]

$$[7] \quad k^{obsd}/f_B = k_1 + k_2[CD]/K_B$$

Figure 2 shows rate data plotted according to eq. [7], and from the slope we obtain k_2 = 0.902 s^{-1}, whereas k_1 = 0.0850 s^{-1}. Thus, in our view, $CD{\cdot}Br_2$ is ~10 times *more reactive* than Br_2 towards HCOOH. We can also estimate an apparent dissociation constant, $K_{TS} = k_1{\cdot}K_B/k_2$ = 0.20 mM, which reflects the binding of the oxidation transition state to CD (4). Similar catalytic ratios (6) and K_{TS} values (4) have been found for the reaction of bromine with phenols, and other substrates.[2]

[6]Measurements were made at 25°C with Ag/AgCl reference and Pt working electrodes. All solutions were prepared immediately prior to use. Calibration lines of E vs. $-\log[Br_2]$, constructed for each $[Br^-]$, had slopes very close to the theoretical value of 0.02958. For experiments with varying $[CD]_t$ (0.1–10 mM) these lines were used to find $[Br_2]$, from which $[Br_3^-] = [Br_2][Br^-]/K$ was calculated; the values of [CD] and $[CD{\cdot}Br_2]$ (or $[CD{\cdot}Br_3^-]$) were then obtained through the equations for material balance. From these concentrations we calculated values of K_B (or K_T). The approach is close to that in ref. 3.

[7]Experiments at lower $[Br^-]$ were not successful.

[8]Ultraviolet–visible spectrophotometry clearly shows that the binding of Br_3^- to CD dominates the equilibria controlling free Br_2, even at $[Br^-]$ = 0.01 M (8).

1. B. G. Cox and P. T. McTigue. J. Chem. Soc. 3893 (1964); R. H. Smith. Aust. J. Chem. **25**, 2503 (1972); P. Herbine, J. G. Brummer, and R. J. Field. Int. J. Chem. Kinet. **12**, 393 (1980);

Can. J. Chem. Downloaded from www.nrcresearchpress.com by 91.121.58.235 on 09/07/12
For personal use only.

M. A. BRUSA and A. J. COLUSSI. Int. J. Chem. Kinet. **12**, 1013 (1980).
2. M. L. BENDER and M. KOMIYAMA. Cyclodextrin chemistry. Springer-Verlag, New York. 1978; J. SZEJTLI. Cyclodextrins and their inclusion complexes. Akademiai Kiado, Budapest. 1982.
3. L.-F. HAN, W. LINERT, R. SCHMID, and R. F. JAMESON. J. Chem. Soc. Perkin Trans. 2, 1907 (1989).
4. O. S. TEE. Carbohydr. Res. **192**, 181 (1989).
5. O. S. TEE, M. PAVENTI, and J. M. BENNETT. J. Am. Chem. Soc. **111**, 2233 (1989).
6. O. S. TEE and J. M. BENNETT. J. Am. Chem. Soc. **110**, 269 (1988).
7. O. S. TEE and J. M. BENNETT. J. Am. Chem. Soc. **110**, 3226 (1988); B. K. TAKASAKI and O. S. TEE Can. J. Chem. **67**, 193 (1989).
8. O. S. TEE and J. M. BENNETT. Can. J. Chem. **62**, 1585 (1984).
9. R. BRESLOW and P. CAMPBELL. Bioorg. Chem. **1**, 140 (1971).
10. O. S. TEE and G. V. PATIL. J. Org. Chem. **41**, 828 (1976).
11. J. M. PINK. Can. J. Chem. **48**, 1169 (1970).
12. J. P. DIARD, E. SAINT-AMAN, and D. SERVE. J. Electroanal. Chem. **189**, 113 (1985).

Can. J. Chem. Downloaded from www.nrcresearchpress.com by 91.121.58.235 on 09/07/12
For personal use only.

Andreas Rudolph and Alan C. Weedon. Radical clocks as probes of 1,4-biradical intermediates in the photochemical cycloaddition reactions of 2-cyclopentenone with alkenes. Can. J. Chem. **68**, 1590 (1990).

Page 1595. In the conclusions, line 10 should read "the 2 + 2 adducts **8** and **9**" … .

Can. J. Chem. Downloaded from www.nrcresearchpress.com by 91.121.58.235 on 09/07/12
For personal use only.

On the structure and reactivity of a stabilized phosphorane: methyl (triphenylphosphoranylidene)acetate

MARGARET H. KAYSER[1]
Department of Chemistry, University of New Brunswick, P.O. Box 5050, Saint John, N.B., Canada E2L 4L5

AND

DONALD L. HOOPER
Department of Chemistry, Dalhousie University, Halifax, N.S., Canada B3H 4J3

Received February 23, 1990

MARGARET H. KAYSER and DONALD L. HOOPER. Can. J. Chem. **68**, 2123 (1990).

In the absence of a source of acidic protons, methyl (triphenylphosphoranylidene)acetate **1** exists as a mixture of the *cis* and *trans* isomers even at room temperature. Acidic protons catalyze the interconversion of the two forms and facilitate the reaction of the ylide with active carbonyl compounds such as benzaldehyde or phthalic anhydride.

Key words: stabilized phosphoylide, structure, reactivity.

MARGARET H. KAYSER et DONALD L. HOOPER. Can. J. Chem. **68**, 2123 (1990).

En l'absence d'une source de protons acides, l'acétate de méthyl(triphénylphosphoranylidène) (**1**) existe sous la forme d'un mélange des isomères *cis* et *trans*, même à la température ambiante. Les protons acides catalysent l'interconversion des deux formes et facilitent la réaction de l'ylure avec les composés carbonylés actifs, comme le benzaldéhyde ou l'anhydride phtalique.

Mots clés : phosphoylure stabilisé, structure, réactivité.

[Traduit par la revue]

Introduction

Stabilized phosphorane **1** has been widely used in the synthesis of α,β-unsaturated esters (1), and the mechanism and stereoselectivity of condensations of **1** with aldehydes have been investigated by a number of groups (2). Nevertheless, this apparently simple reaction still presents interesting and unexpected behaviour.

$Ph_3P{=}CH{-}COOR$ (**1**, R = CH_3) $\qquad$ $Ph_3P{-}CH_2COOR\ Br^-$ (**2**)

For example, the reaction of benzaldehyde with the stabilized ylide **1** in THF was followed by ^{31}P NMR at −20°C (3). No intermediates were found and the only two observable signals were identified as the unreacted ylide **1** (at δ 16.5) and triphenylphosphine oxide (δ 23.3) (3).

While repeating the experiment, we noted a behaviour that had not been reported previously. In our experiment, the spectrum of ylide **1** recorded at −20°C consisted of two singlets in the ratio of 3:1 at δ 17.85 and δ 16.35, respectively. Upon addition of freshly distilled benzaldehyde (cooled to −20°C) the two signals collapsed to a single peak at δ 17.30. As the temperature was allowed to rise, the product, triphenylphosphine oxide, appeared at δ 29.81 and the progress of the reaction could be monitored by the disappearance of the peak at δ 17.30 and the increase of the signal at δ 29.81.

During the course of the reaction both peaks drifted slightly but no other signals were observed. It was not clear to us why, upon addition of benzaldehyde, the ylide's two signals were replaced with a new peak at δ 17.30, or whether the new peak represented a somehow transformed ylide or an intermediate.

It has been nearly 20 years since stabilized ylides were investigated (4–8) by ^1H NMR. The results of these studies may be summarized as follows: at −40°C or lower, ylide **1** gives the signals of two distinct forms, with signal coalescence above room temperature. This observation was attributed to the temperature dependent equilibrium between the geometrical isomers: the major **1**-*cis* and the minor **1**-*trans* (5, 6). The stereochemistry was assigned on the basis of electrostatic considerations and of coupling constants for the two isomers (6). The $\Delta G^{\ddagger}$ for the *cis*–*trans* interconversion was calculated to be of the order of 10 kcal/mol (7).

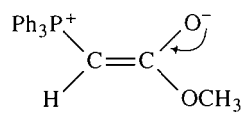

1-*cis*

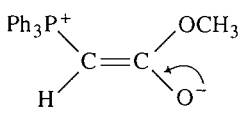

1-*trans*

Another interesting characteristic, noted at the time, was that the methine proton of the ylide *appeared to exchange rapidly at higher temperatures*. The authors suggested that the proton exchanged with the conjugate acid **2** present in trace amounts in the ylide (6, 7).

Results and discussion

We decided to extend these experiments with particular attention to the effect of moisture and conjugate acid. Figure 1(a) shows a typical room temperature proton spectrum of **1** in $CDCl_3$. The expected coupling of the methine proton to phosphorus is not observed. Exchange of this labile proton could be catalyzed by traces of atmospheric water, conjugate acid, or even DCl present in the solvent (see Scheme 1). In fact the effect of moisture was readily observable; the width of signals and the presence or absence of P–H coupling varied according to the amount of atmospheric water absorbed into the solution. After extensive drying of solute and solvent, the spectrum in Fig. 1(b) was obtained, showing the existence even at room temperature of both isomeric forms. Figure 1(c) shows the low temperature spectrum of an undried sample, with full P–H coupling and good separation of the signals of the two isomeric forms. As drying the sample has almost the same effect as a decrease in temperature by 50°C, we conclude that the presence of water in the solution is a major determinant of the rate of isomer interconversion.

Addition of a trace quantity of butyllithium to a solution of

[1]Author to whom correspondence may be addressed.

Can. J. Chem. Downloaded from www.nrcresearchpress.com by 195.138.81.100 on 09/07/12
For personal use only.

Can. J. Chem. Downloaded from www.nrcresearchpress.com by 195.138.81.100 on 09/07/12
For personal use only.

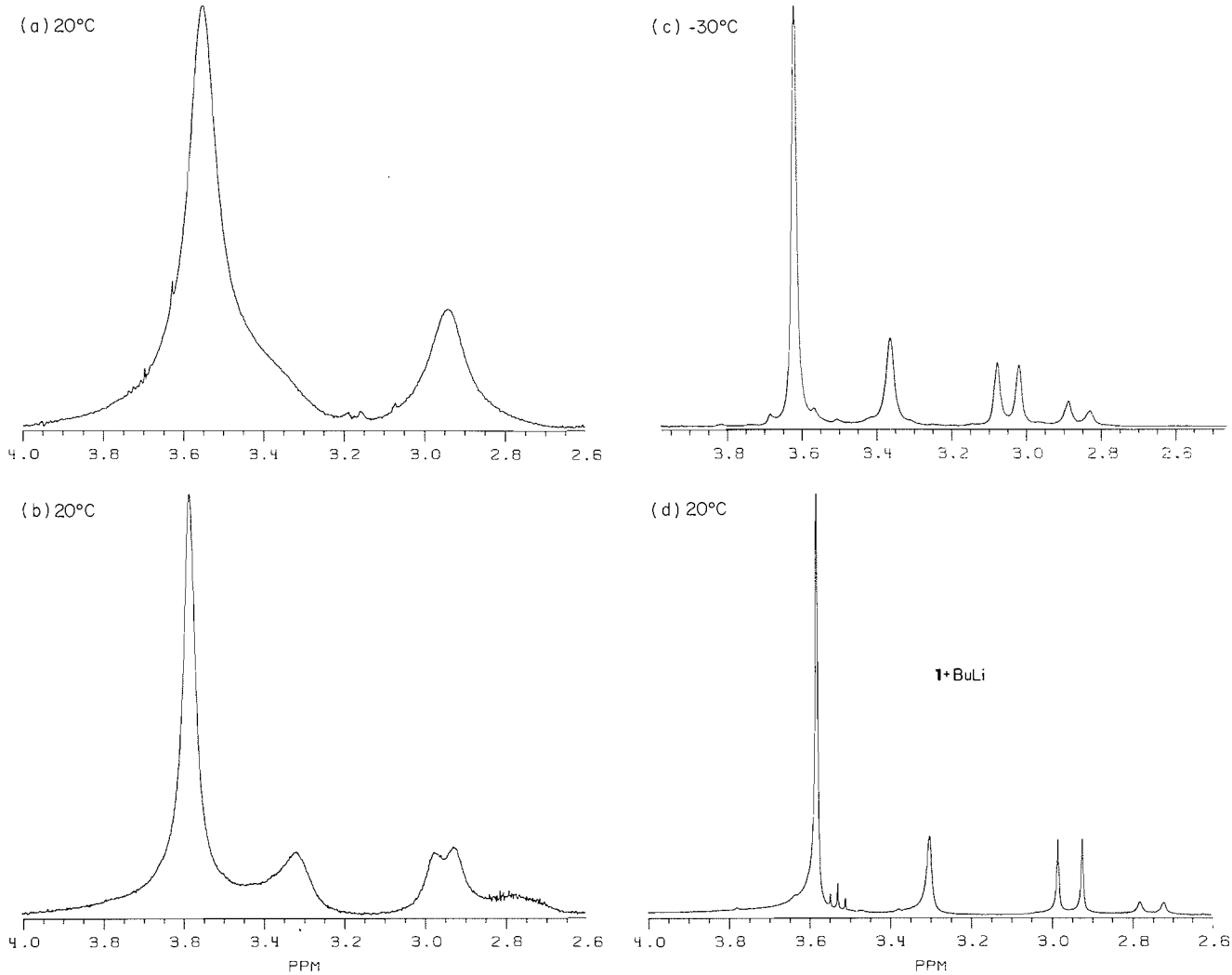

FIG. 1. Proton NMR spectra of phosphorane **1**.

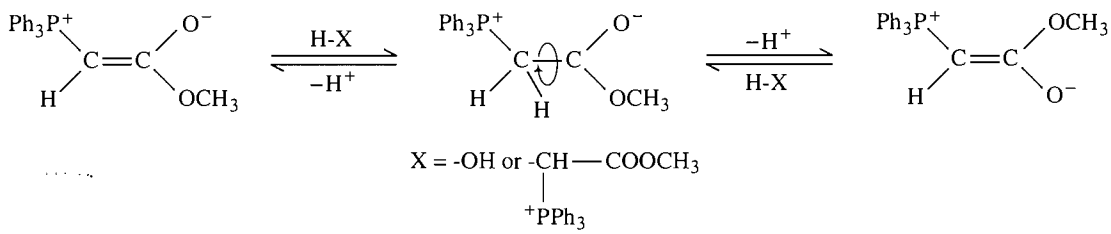

SCHEME 1

1 gives a room temperature spectrum, Fig. 1(d), where isomer interconversion is slower than in an undried sample at −60°C. The effect of butyllithium might have been anticipated, as BuLi removes *both* water and conjugate acid, and traces of DCl, and would be expected to stabilize the enolate ions **1**-*cis* and **1**-*trans* by complexation of Li^+ cation with the negatively charged oxygen. Stabilization of the enolate structure of the phosphorane would increase the double bond character of the C—C bond and decrease the rate of *cis–trans* interconversion.

The above effects are also evident in the ^{31}P and ^{13}C spectra recorded as a function of temperature.

Thus, in the ^{13}C spectrum of **1** recorded at room temperature, the carbon of the methoxy group appears as a singlet at 49.73 ppm, while the methine carbon signal is a doublet centered at 29.78 ppm with a J_{P-C} of 126 Hz. In the coupled spectrum the methine carbon is observed as a very broad peak, indicating that proton exchange is rapid on the ^{13}C time scale.

Upon lowering the temperature below −40°C, or adding a trace of BuLi at room temperature, the methine proton exchange ceases and signals for the two isomeric forms emerge. The methine carbon signal appears as the overlapping sets of doublets in the coupled spectrum illustrated in Fig. 2.

The coalescence temperature for the methine carbon signals is 0°C for a non-dried sample. It increases to 20°C upon addition

Can. J. Chem. Downloaded from www.nrcresearchpress.com by 195.138.81.100 on 09/07/12
For personal use only.

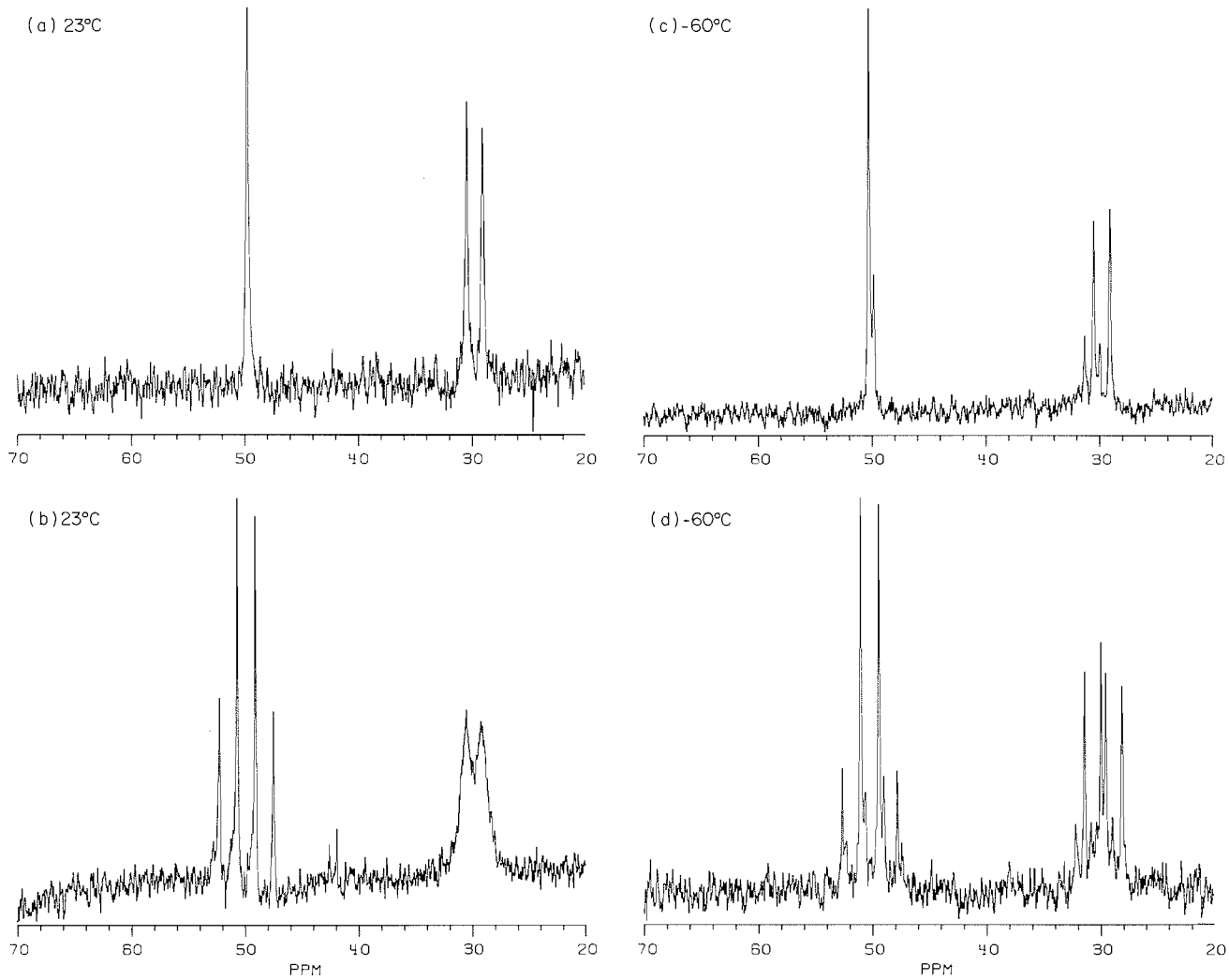

FIG. 2. ^{13}C NMR spectra of ylide **1** recorded at +23 and −60°C; (a) and (c) fully decoupled; (b) and (d) off-resonance.

of molecular sieves to the $CDCl_3$ solution of the ylide, and to 60°C when the solution is treated with a drop of butyllithium.

At room temperature a proton decoupled ^{31}P signal for the phosphorane **1** is seen as a broad peak with a shoulder. Under scrupulously anhydrous conditions it resolves into two relatively broad but distinct peaks: the major *cis* isomer at 17.83 ppm ($\nu_{1/2}$ 16.36 Hz), and the minor *trans* isomer at 16.30 ppm ($\nu_{1/2}$ 43.60). At −40°C both peaks, major at 17.58 ppm and minor at 16.20 ppm, are very sharp, with half-height line widths of 1.47 Hz and 3.00 Hz respectively.

The variable temperature ^{31}P NMR study of **1** that has not been dried prior to the experiment shows that, as the temperature increases, the broadening of the two signals is accompanied by a slight drift in their chemical shifts. Coalescence occurs at approximately 50°C (Table 1).

When the same sample is treated with BuLi, the chemical shifts are unaffected by the increase in temperature and the two singlets remain distinct even at 50°C.

Addition of solid conjugate acid **2** to a solution of dry ylide in $CDCl_3$ (dried over molecular sieves) affects the spectra of **1** in the same way as the conjugate acid formed *in situ* when traces of atmospheric water are absorbed and interact with the ylide. Only in the presence of an available acidic proton is there a rapid *cis–trans* interconversion. Thus, we postulate that a low energy mechanism for the interconversion involves the protonated ylide as a short-lived intermediate. Clearly, rotation about the C—C single bond of this intermediate requires less energy than rotation about the C—C double bond of either enolate form (Scheme 1).

TABLE 1. Variable temperature ^{31}P NMR study of phosphorane **1**

Temperature (°C)	Ylide signals (ppm)		$\nu_{1/2}$ (Hz)		Relative intensities	
−60	15.888		2.30		64.20	
		17.465		2.36		205.10
−40	16.20		3.00		37.40	
		17.58		2.47		200.00
−20	16.138		9.07		38.40	
		17.699		4.42		200.00
0	16.263		19.17		32.72	
		17.824		8.26		200.00
22	16.331		43.60		33.93	
		17.836		16.32		200.00
35	16.520		Very broad		35.10	
		17.908		26.26		200.00
50	—		—		—	
		17.923		41.53		200.00

TABLE 2. Variable temperature ^{31}P NMR study of the reaction of ylide **1** with benzaldehyde under anhydrous conditions[a]

Temperature (°C)	Time (min)	Ylide signal(s) (ppm)	Relative intensity	Product signal(s)	Relative intensity
−22	0	17.85 (75), 16.35	75:25	—	—
−22	10	17.30	100	—	—
−10	25	17.30	100	—	—
0	39	17.31	100	—	—
10	50	17.33	99	29.7	Trace
20	65	17.32	95	29.6	5

[a]Ylide **1** and benzaldehyde were purified as described in the experimental section.

TABLE 3. Variable temperature ^{31}P NMR study of the reaction of phosphorane **1** with benzaldehyde[a]

Temperature (°C)	Time (min)	Ylide signal(s) (ppm)	Relative intensity	Product signal(s)	Relative intensity
−30	10	17.98	97	30.489	3
−25	25	17.99	95	30.387	5
−15	40	18.003	93	30.150	7
0	55	18.007	90	29.830	10
12	70	18.022	79	29.59	21
20	85	18.137	60	29.47	40
20	210	18.194	50	29.49	50

[a]Ylide **1** and benzaldehyde were obtained from Aldrich. Fresh samples were used without further purification.

As expected, these findings have a bearing on the reactivity of the phosphorane. When ylide **1** is trapped in its enolic forms, with the negative charge primarily on the oxygen atom, the reaction at the carbon atom should be reduced.

Thus, during the variable temperature ^{31}P NMR study of the condensation of purified phosphorane **1** with freshly distilled benzaldehyde, the addition of cooled benzaldehyde to a $CDCl_3$ solution of **1** at −30°C resulted in an instantaneous collapse of the two ylide peaks to a new signal. It took, however, over 60 min and a gradual increase in temperature to +20°C before any significant quantity (>5%) of the product triphenylphosphine oxide could be observed (Table 2). By contrast, when a similar study was carried out using non-purified reagents, the product was formed even at −25°C (Table 3).

Additional evidence for the involvement of catalytic activity of all acidic protons was provided by the reaction of benzaldehyde with phosphorane **1** to which 2 drops of BuLi were added. Since BuLi removes *all* sources of acidic protons while Li^+ ion stabilizes the enolate forms, the two isomers remained distinct even upon addition of benzaldehyde. The ensuing condensation was very slow. In the course of the variable temperature ^1H NMR study of this reaction, after 90 min at −15°C only traces of product could be detected, while the control reaction (where neither ylide nor benzaldehyde was purified and no BuLi was added) showed 40% product formation.

To verify if one of the enolic forms might react more readily with benzaldehyde we carried out the following experiment. The solution of ylide **1** in $CDCl_3$, dried over molecular sieves, was treated with a few drops of BuLi at −40°C. The ^1H NMR spectrum showed sharp signals for *cis* and *trans* isomers in the ratio 75:25. After the addition of 0.25 equivalents of freshly distilled benzaldehyde in cold, dry $CDCl_3$, spectra were recorded at regular intervals as the temperature was allowed to rise from −35 to +22°C over a period of several hours. First traces of product, *trans* methylcinnamate, were detected after 90 min at −15°C. After 6 h at 22°C a large part of the benzaldehyde was converted into the product, but the ratio of *cis* and *trans* isomers remained unchanged throughout the experiment (Fig. 3).

Thus, the "reactive ylide" is the ylide undergoing interconversion. As this process is slow in the presence of BuLi even at room temperature, the reaction with benzaldehyde is correspondingly slow.

Confirmation of the participation of an acidic proton comes from the study of the condensations of the ylide with cyclic anhydrides.

When cooled phthalic anhydride is added to a $CDCl_3$ solution of **1** at −35°C, the ylide signals instantly disappear in favour of two new signals (δ 18.78 and 17.01). The signal at δ 18.78 corresponds to an acyclic intermediate (Scheme 2). The second peak at δ 17.01, which moves monotonically to higher frequencies as the reaction progresses with rising temperature, represents an equilibrium between the ylide and an intermediate, with the proportion of the intermediate increasing with time.[2]

The ylide treated with BuLi reacts with phthalic anhydride almost as fast as the untreated ylide. This can be explained by the fact that the first step in the condensation of the ylide with a cyclic anhydride is the formation of an acyclic intermediate bearing an acidic proton (see Scheme 2). Thus the reaction with cyclic anhydride is autocatalyzed, and does not depend on the external source of acidic protons.

[2]M. M. Kayser, K. Hatt, and D. L. Hooper. Unpublished results.

Can. J. Chem. Downloaded from www.nrcresearchpress.com by 195.138.81.100 on 09/07/12
For personal use only.

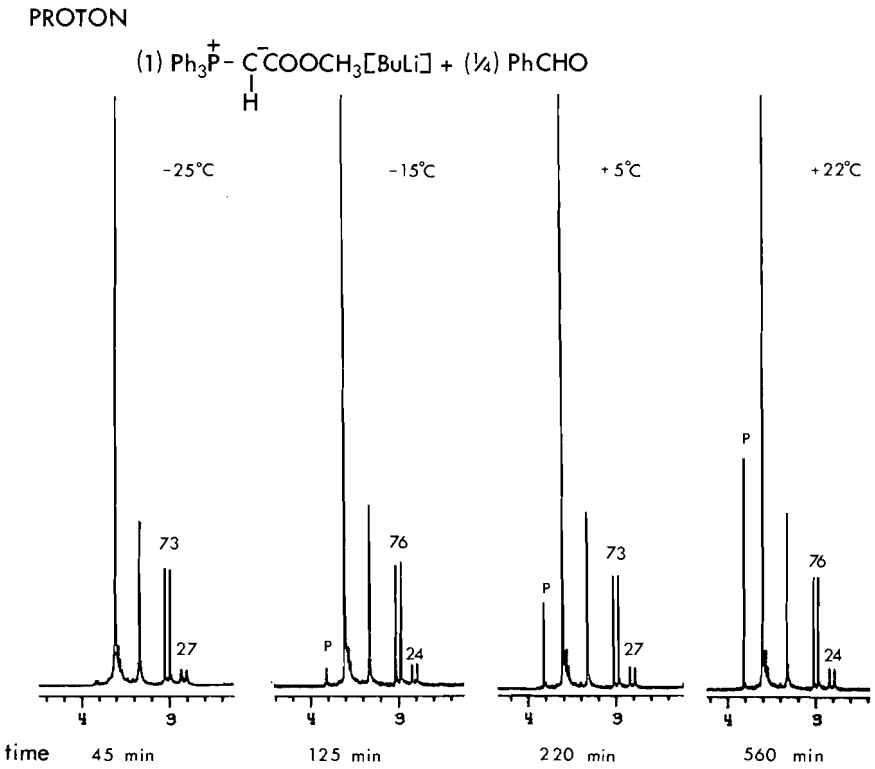

FIG. 3. Variable temperature ^1H NMR spectra of the reaction of ylide **1** (1 equiv.) with benzaldehyde (0.25 equiv.) in the presence of a trace quantity of BuLi. Relative proportions of the major and minor isomeric forms of the ylide are indicated above the methine proton signals.

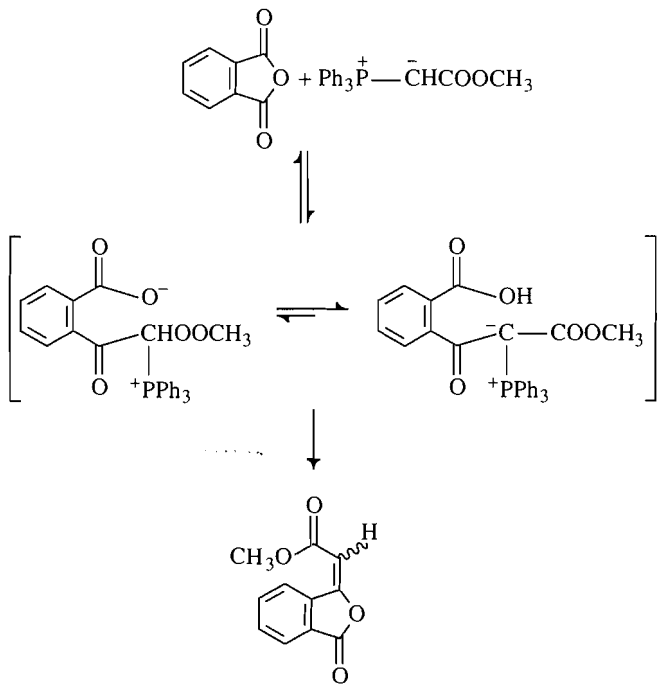

SCHEME 2

The results of this study can be summarized as follows:

(a) Ylide **1** undergoes *cis–trans* interconversion, which is catalyzed by traces of acidic proton.

(b) During rapid *trans–cis* interconversion the negative charge is more available on the carbon atom, resulting in enhanced nucleophilicity.

(c) The addition of a small quantity of BuLi removes traces of all acid catalysts and stabilizes the enolic forms, thus diminishing the reactivity of the ylide.

(d) The reaction of the ylide with an anhydride generates an acyclic intermediate bearing a highly acidic proton and is therefore autocatalyzed.

In conclusion, the ylide is most reactive during a rapid *trans–cis* interconversion catalyzed by traces of acidic protons. Larger quantities of acidic contaminant convert an equivalent part of the ylide to its conjugate acid. Thus, when acids were reportedly used to activate ketonic carbonyl groups (9) toward the reactions with stabilized ylides, the successful condensation could occur as long as the ylide was in excess.

Experimental

Nuclear magnetic resonance spectra were recorded at 361 MHz (^1H), 91 MHz (^{13}C), and 146 MHz (^{31}P) on the Nicolet 360 NB spectrometer of the Atlantic Region Magnetic Resonance Centre, and some ^{31}P spectra were recorded at 81 MHz on the Varian XL-200 spectrometer of the University of New Brunswick. All spectra were in $CDCl_3$ solutions. Calibration of the spectra was done with respect to TMS as internal reference (^1H and ^{13}C) or 85% H_3PO_4 as external standard (^{31}P). Temperature control was by the usual Nicolet method. Calibration of the thermocouple showed an estimated error of less than 1° in the temperature range used. Line widths were measured by the Nicolet LF routine.

For all experiments carried out under anhydrous conditions, methyl (triphenylphosphoranylidene)acetate **1** (obtained from Aldrich) was dried (see below), benzaldehyde was freshly distilled and stored in a vial under nitrogen until used, and phthalic anhydride was crystallized from dry chloroform.

To remove traces of water, **1** was subjected to azeotropic drying with benzene. To remove traces of conjugate acid, a very strong base

Can. J. Chem. Downloaded from www.nrcresearchpress.com by 195.138.81.100 on 09/07/12
For personal use only.

such as BuLi or MeLi was necessary. Treatment with weaker bases, crystallization, and sublimation were not successful.

1. General procedure for reaction of ylide **1** with benzaldehyde under anhydrous conditions: freshly dried ylide **1** (3.7 mmol) was dissolved in 2 mL of $CDCl_3$ (Silanor* C, dried over molecular sieves) and placed in an oven-dried (at 150°C for 2 h), nitrogen-swept NMR tube. After a room temperature spectrum was recorded, the temperature was lowered to −30°C and another spectrum was recorded. Freshly distilled benzaldehyde (3.7 mmol), dissolved in dry $CDCl_3$ and kept under nitrogen, was frozen in liquid nitrogen, thawed, and added rapidly to the ylide solution, which was maintained at −30°C. The tube was swept with nitrogen or argon and equilibrated at −30°C for 3–5 min prior to the recording of the first spectrum. Subsequent spectra were recorded at regular intervals, as the temperature was raised.

2. The general procedure for reaction of **1** with benzaldehyde when anhydrous conditions were not specified was substantially similar to the one described above. However, ylide **1** obtained from Aldrich was used without further purification and benzaldehyde was not redistilled immediately prior to the experiment. The NMR tubes were oven-dried but experiments were not carried out under inert (nitrogen or argon) atmosphere.

3. For the reaction carried out in the presence of BuLi, modified procedure 2 was employed. Two drops of BuLi (2.5 M in hexanes) were syringed into the solution of ylide **1** in $CDCl_3$ (dried over molecular sieves). Room temperature and low temperature spectra were recorded and the subsequent steps were repeated as described above.

Acknowledgement

Financial support by the Natural Sciences and Engineering Research Council of Canada is gratefully acknowledged.

1. I. GOSNEY and A. G. ROWLEY. *In* Organophosphorus reagents in organic synthesis. *Edited by* J. I. G. Cadogan. Academic Press, New York. 1979. pp. 7–153.
2. S. TRIPPETT. Q. Rev. Chem. Soc. **17**, 406 (1963); A. W. JOHNSON. Ylide chemistry. Academic Press, New York. 1966; J. BOUTAGY and R. THOMAS. Chem. Rev. **74**, 87 (1974); B. E. MARYANOFF and A. B. REITZ. Chem. Rev. **89**, 863 (1989), and references cited therein.
3. B. E. MARYANOFF, A. B. REITZ, H. S. MUTTER, R. R. INNERS, H. R. ALMOND, JR., R. R. WHITTLE, and R. A. OLOFSON. J. Am. Chem. Soc. **108**, 7664 (1989).
4. H. J. BESTMANN, G. JOACHIM, T. LENGYEL, J. F. OTH, R. MERENYI, and H. WEITKAMP. Tetrahedron Lett. 3355 (1966).
5. H. J. BESTMANN and J. P. SNYDER. J. Am. Chem. Soc. **89**, 3963 (1967).
6. F. J. RANDALL and A. W. JOHNSON. Tetrahedron Lett. **24**, 2841 (1968).
7. P. CREWS. J. Am. Chem. Soc. **90**, 2961 (1968).
8. J. P. SNYDER. Tetrahedron Lett. 215 (1971).
9. C. RÜCHARDT, S. EICHLER, and P. PANSE. Angew. Chem. Int. Ed. Engl. **21**, 619 (1963); A. K. BOSE, M. S. MANHAS, and R. M. RAMER. J. Chem. Soc. (C), 2728 (1969).

Can. J. Chem. Downloaded from www.nrcresearchpress.com by 195.138.81.100 on 09/07/12
For personal use only.

Vinyl ether hydrolysis. XXIII. Solvent isotope effect on the reaction of divinyl ether catalyzed by the hydronium ion[1]

A. J. KRESGE[2] AND M. LEIBOVITCH

Department of Chemistry, University of Toronto, Toronto, Ont., Canada M5S 1A1

Received June 18, 1990

A. J. KRESGE and M. LEIBOVITCH. Can. J. Chem. **68**, 2129 (1990).

Rates of hydrolysis of divinyl ether (CH_2=CHOCH=CH_2), measured in dilute H_2O and D_2O solutions of perchloric acid at 25°C, provide the catalytic coefficients $k_{H^+} = 0.0084\ M^{-1}\ s^{-1}$ and $k_{D^+} = 0.0028\ M^{-1}\ s^{-1}$, and these lead to the isotope effect $k_H/k_D = 3.0$. The magnitude of this isotope effect indicates that this reaction occurs by rate-determining hydron transfer from catalyst to substrate and thus follows the conventional mechanism for vinyl ether hydrolysis.

Key words: divinyl ether, vinyl ether hydrolysis, solvent isotope effect.

A. J. KRESGE et M. LEIBOVITCH. Can. J. Chem. **68**, 2129 (1990).

Opérant à 25°C, dans des solutions d'acide perchlorique diluées dans le H_2O et le D_2O, on a mesuré les vitesses d'hydrolyse de l'éther divinylique (CH_2=CHOCH=CH_2); on en déduit que les coefficients catalytiques sont égaux à $k_{H^+} = 0{,}0084\ M^{-1}\ s^{-1}$ et $k_{D^+} = 0{,}0028\ M^{-1}\ s^{-1}$, et ces valeurs conduisent à un effet isotopique $k_H/k_D = 3{,}0$. L'amplitude de cet effet isotopique indique que l'étape déterminant la vitesse de cette réaction implique le transfert d'un hydron du catalyseur au substrat, ce qui correspond au mécanisme conventionnel pour l'hydrolyse des éthers vinyliques.

Mots clés : éther divinylique, hydrolyse des éthers vinyliques, effet isotopique du solvant.

[Traduit par la revue]

Introduction

In connection with our studies of the influence of structure upon reactivity in the acid-catalyzed hydrolysis of vinyl ethers, we recently determined that there is no significant ring-size effect in going from the 6-membered cyclic substrate, 2,3-dihydropyran, **1**, to its 9-membered cyclic homolog, oxacyclonon-2-ene, **2** (1). This conclusion was based upon a rate constant for **2** estimated from the measured rate of reaction of oxacyclonon-2,8-diene, **3**, and a factor allowing for the additional vinyl group in **3**, derived from published rate constants for divinyl ether, **4** (2), and ethyl vinyl ether, **5** (3).

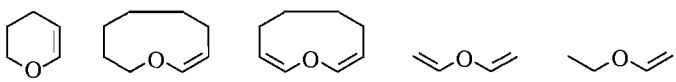

1 **2** **3** **4** **5**

This procedure assumes that **4** reacts by the same mechanism as **5**, i.e., by the conventional mechanism for vinyl ether hydrolysis, which consists of rate-determining proton transfer from catalyst to substrate, eq. [1], followed by rapid hydration of the ensuing alkoxycarbocation and rapid decomposition of the hemiacetal intermediate, eq. [2] (4). The original report on

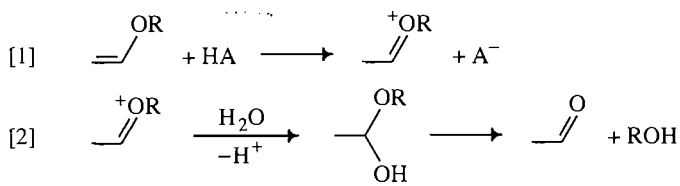

the hydrolysis of **4** (2), however, contains no mechanistic information. We have therefore supplied that by determining the solvent isotope effect on this reaction catalyzed by the hydronium ion.

Experimental

Materials

Divinyl ether (Marshallton Research Laboratories, Inc.) was purified by distillation. All other materials were best available commercial grades. Solutions were prepared with deionized H_2O purified further by distillation or with D_2O (Merck, Sharpe, and Dohme) as received.

Kinetics

Rates of reaction were determined spectroscopically by monitoring the decrease in vinyl ether absorbance at $\lambda = 210$ nm. Measurements were made using a Cary model 2200 spectrometer whose cell compartment was thermostatted at 25.0 ± 0.1°C. Aqueous acid solutions, 3.0 mL in volume, contained in quartz cuvettes were allowed to come to temperature equilibrium with the spectrometer cell compartment, and reactions were then initiated by adding 5.0 μL quantities of acetonitrile stock solutions of divinyl ether; final concentrations of divinyl ether in the reaction mixtures were ca. 1×10^{-3} M. All reactions followed the first-order rate law accurately, and observed first-order rate constants were calculated by least-squares fitting to appropriate linear or exponential functions.

Results

Rates of hydrolysis of divinyl ether were measured in H_2O and D_2O solutions of perchloric acid over the concentration ranges $[HClO_4] = 0.005$–0.1 M and $[DClO_4] = 0.04$–0.1 M. The ionic strength of these solutions was held constant at 0.10 M through the addition of sodium perchlorate as required. The data are summarized in Table 1 and are displayed in Fig. 1.

It may be seen that observed first-order rate constants are proportional to acid concentration in both solvents. Linear least-squares analysis gave the catalytic coefficients $k_{H^+} = (8.42 \pm 0.13) \times 10^{-3}\ M^{-1}\ s^{-1}$ and $k_{D^+} = (2.84 \pm 0.10) \times 10^{-3}\ M^{-1}\ s^{-1}$; these lead to the isotope effect $k_H/k_D = 2.97 \pm 0.11$.

The catalytic coefficient determined here for the reaction in H_2O solution agrees will with the reported value $k_{H^+} = 8.29 \times 10^{-3}\ M^{-1}\ s^{-1}$ (2).

Discussion

The isotope effect determined here for hydrolysis of divinyl ether catalyzed by the hydronium ion, $k_H/k_D = 3.0$, is large. Proton transfer from the hydronium ion involves bonding changes in the two non-reacting bonds of this ion, in addition to bond-breaking of the reacting bond, and these nonreactive bonding changes provide an inverse ($k_H/k_D < 1$) secondary contribution to the isotope effect that offsets a primary effect in

[1]Part XXII: see ref. 8.

[2]Author to whom correspondence may be addressed.

Can. J. Chem. Downloaded from www.nrcresearchpress.com by 195.138.81.100 on 09/07/12
For personal use only.

TABLE 1. Rate data for the hydrolysis of divinyl ether in aqueous perchloric acid solutions at 25°C[a]

[Acid]/10^{-2} M	$k_{obs}/10^{-4}$ s^{-1}
H_2O:	
10.1	8.62, 8.70, 8.68, 8.68, 8.72
8.05	6.32, 6.26, 6.21, 6.29, 6.36
5.03	4.20, 4.12, 4.22, 4.18
3.02	2.46, 2.41, 2.49, 2.34
1.01	0.806, 0.815, 0.795, 0.806
0.503	0.392, 0.387, 0.396, 0.382
$k_{obs}/s^{-1} = -(0.092 \pm 0.078) \times 10^{-4} + (8.42 \pm 0.13) \times 10^{-3}[HClO_4]$	
D_2O:	
10.1	2.92, 2.82, 2.79, 3.00
6.01	1.63, 1.70, 1.79
4.00	1.21, 1.25, 1.13
$k_{obs}/s^{-1} = (0.036 \pm 0.074) \times 10^{-4} + (2.84 \pm 0.10) \times 10^{-3}[DClO_4]$	

[a]Ionic strength = 0.10 M.

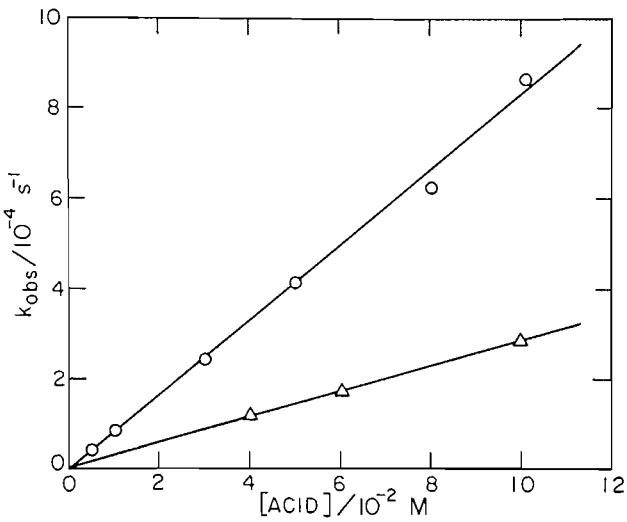

FIG. 1. Relationship between observed first-order rate constants and acid concentration for the hydrolysis of divinyl ether in aqueous perchloric acid solutions at 25°C; ○: H_2O solutions, △: D_2O solutions.

the normal ($k_H/k_D > 1$) direction (5); an observed effect of $k_H/k_D = 3.0$ is in fact near the maximum overall value expected for this kind of system (6). The presently determined isotope effect thus contains a sizable primary component and is therefore clear evidence of rate-determining proton transfer from the catalyst to the substrate. This indicates that hydrolysis of divinyl ether does occur by the conventional mechanism shown in eqs. [1] and [2].

This mechanism in the present case leads to the formation of vinyl alohol as one of the hemiacetal decomposition products, eq. [3]. This alcohol is the enol tautomer of acetaldehyde, and

[3] 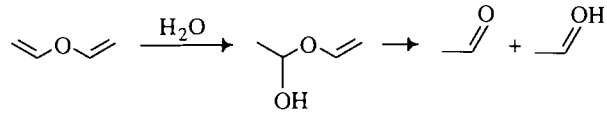

it will ketonize to the aldehyde, eq. [4], under the reaction conditions. The specific rate of this ketonization reaction, however, $k_{H^+} = 33$ M^{-1} s^{-1} (7), is very much greater than the rate constant determined here for hydrolysis of divinyl ether, $k_{H^+} = 0.0084$ M^{-1} s^{-1}, and ketonization of vinyl alcohol will consequently be an invisible fast process following the slower hydrolysis reaction.

[4] 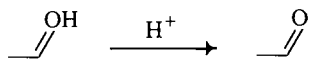

Acknowledgement

We are grateful to the Natural Sciences and Engineering Research Council of Canada and the Donors of the Petroleum Research Fund, administered by the American Chemical Society, for financial support of this work.

1. R. A. BURT, Y. CHIANG, A. J. KRESGE, and S. SZILAGYI. Can. J. Chem. **62**, 74 (1984).
2. A. SKRABAL and R. SKRABAL. Z. Phys. Chem. Abt. A, **181**, 449 (1938).
3. A. J. KRESGE and Y. CHIANG. J. Chem. Soc. B, 58 (1967).
4. A. J. KRESGE. Acc. Chem. Res. **20**, 364 (1987).
5. A. J. KRESGE, R. A. MORE O'FERRALL, and M. F. POWELL. *In* Isotopes in organic chemistry. Vol. 7. *Edited by* E. Buncel and C. C. Lee. Elsevier, New York. 1987. Chap. 4.
6. A. J. KRESGE, D. S. SAGATYS, and H. L. CHEN. J. Am. Chem. Soc. **99**, 7228 (1977).
7. Y. CHIANG, M. HOJATTI, J. R. KEEFFE, A. J. KRESGE, N. P. SCHEPP, and J. WIRZ. J. Am. Chem. Soc. **109**, 4000 (1987).
8. A. J. KRESGE, M. LEIBOVITCH, and K. R. KOPECKY. Can. J. Chem. **68**, 1786 (1990).

Can. J. Chem. Downloaded from www.nrcresearchpress.com by 195.138.81.100 on 09/07/12
For personal use only.

Ultrasonic absorption studies in aqueous solutions of modified β-cyclodextrins

DAVID J. JOBE AND RONALD E. VERRALL
Department of Chemistry, University of Saskatchewan, Saskatoon, Sask., Canada S7N 0W0

AND

VINCENT C. REINSBOROUGH[1]
Department of Chemistry, Mount Allison University, Sackville, N.B., Canada E0A 3C0

Received January 10, 1990

DAVID J. JOBE, RONALD E. VERRALL, and VINCENT C. REINSBOROUGH. Can. J. Chem. **68**, 2131 (1990).

Ultrasonic absorption studies over the frequency range 0.6–210 MHz were conducted in aqueous solutions of the following modified β-cyclodextrins (β-CD): 2,6-*O*-dimethyl-β-CD (DMβCD), 2,3,6-*O*-trimethyl-β-CD (TMβCD), and hydroxypropyl-β-CD (HPβCD). Anomalous ultrasonic absorption found in the three systems was attributed to three relaxations in the DMβCD and HPβCD systems and two in the TMβCD system. These relaxations were assigned to hydrogen bond "wig-wagging", to CD cavity water exchange, and to bond rotation within the CD units. The 1:1 DMβCD/decyltrimethylammonium bromide system was also investigated ultrasonically in solution.

Key words: ultrasonic absorption, modified β-cyclodextrins, surfactant inclusion, relaxation frequency.

DAVID J. JOBE, RONALD E. VERRALL et VINCENT C. REINSBOROUGH. Can. J. Chem. **68**, 2131 (1990).

Opérant sur un intervalle de fréquence allant de 0,6 à 210 MHz, on a étudié les spectres d'absorption ultrasonique de solutions aqueuses des β-cyclodextrines (β-CD) modifiées suivantes : 2,6-*O*-diméthyl-β-CD (DMβCD), 2,3,6-*O*-triméthyl-β-CD (TMβCD) et hydroxypropyl-β-CD (HPβCD). L'absorption ultrasonique anormale qui a été observée dans ces trois systèmes est attribuée à trois relaxations dans les systèmes DMβCD et HPβCD et à deux relaxations dans le système TMβCD. On a attribué ces relaxations à un «wig-wag» de la liaison hydrogène, à un échange d'eau dans la cavité des CD et à une rotation de liaison à l'intérieur des unités des CD. On a aussi examiné à l'aide d'ultrasons des solutions du système 1:1 DMβCD/bromure de décyltriméthylammonium.

Mots clés : absorption ultrasonique, β-cyclodextrines modifiées, inclusion de surfactant, fréquence de relaxation.

[Traduit par la revue]

Introduction

The ultrasonic technique is an important investigative tool in the elucidation of basic solution processes and reaction mechanisms occurring in the microsecond to nanosecond range. One such area still not well understood is the inclusion of guest molecules by cyclodextrins in their cavities. Yet, the type of mechanisms that are often postulated to be taking place in the inclusion process, such as hydrogen-bond formation and ejection of water molecules from the cavity, should be able to be detected by ultrasonic resonance spectroscopy. In two previous independent ultrasonic studies in aqueous solutions of cyclodextrins (1, 2), α-cyclodextrin and γ-cyclodextrin were found to show modest anomalous absorptions in the ultrasonic range from which characterizations of the appropriate relaxation processes were attempted. β-Cyclodextrin proved too insoluble to yield sufficient absorption data.

Yet, β-cyclodextrin (β-CD) is the cyclodextrin of most interest because its cavity size allows for the best spatial fit for many common guest moieties such as the phenyl group and surfactant hydrocarbon tails (3, 4). Its use in the food, drug, and agricultural industries as an encapsulating agent to protect sensitive molecules in hostile environments is growing rapidly and it would be of special interest to determine the fundamental processes at work when this particular cyclodextrin plays host to other molecules in solution.

One avenue by which this might be accomplished is by using modified β-cyclodextrins (Fig. 1), which often have much greater water solubilities while still possessing approximately the same size of cavity as does simple β-CD. Consequently, in this investigation, three modified β-cyclodextrins were examined ultrasonically in solution at 25.0°C to determine whether excess absorption was present and, if so, to assign credible causes. The three were 2,6-*O*-dimethyl-β-cyclodextrin (DMβCD), 2,3,6-*O*-trimethyl-β-cyclodextrin (TMβCD), and hydroxypropyl-β-cyclodextrin (HPβCD). Also, to examine the effect inclusion has upon the ultrasonic absorption, the surfactant decyltrimethylammonium bromide (DTAB) was mixed in equimolar ratios with DMβCD and these solutions were subjected to ultrasonic probing. DTAB forms 1:1 inclusion complexes with DMβCD (5), and it has a sufficiently high critical micelle concentration (0.066 mol dm^{-3} DTAB at 25.0°C) to rule out monomer–micelle exchange as giving rise to any unusual ultrasonic absorption (6, 7).

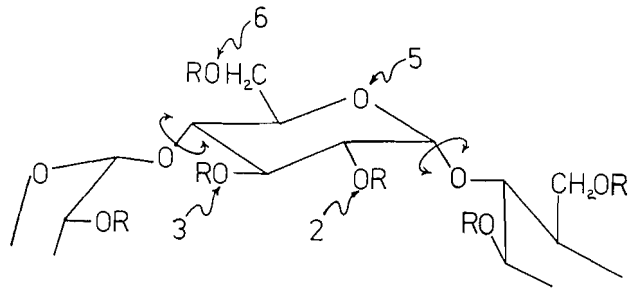

FIG. 1. Numbering of oxygen atoms in the basic glucose unit in modified β-cyclodextrins that consist of seven such units. Arrows indicate effect of "wig-wagging" motion. R can be H or an organic substituent.

Experimental

Cyclodextrins DMβCD and TMβCD were obtained from Chinoin while HPβCD was a mixture of β-cyclodextrins with various degrees of substitution of hydroxyl by hydroxypropyl groups specially formulated by Janssen Biotech as a drug delivery system. The percent of

[1]Author to whom correspondence may be addressed.

Can. J. Chem. Downloaded from www.nrcresearchpress.com by 195.138.81.100 on 09/07/12
For personal use only.

Can. J. Chem. Downloaded from www.nrcresearchpress.com by 195.138.81.100 on 09/07/12
For personal use only.

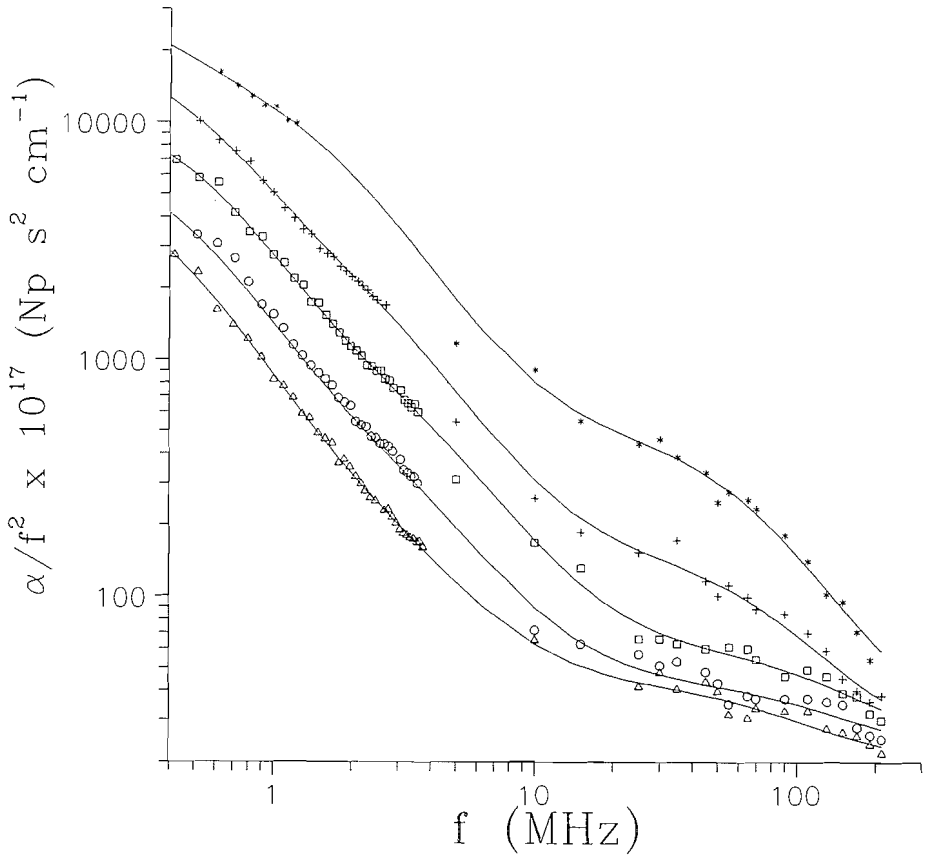

FIG. 2. Plot of α/f^2 (Np s^2 cm^{-1}) versus frequency (MHz) for DMβCD solutions: (△) 0.029 mol dm^{-3}; (○) 0.051 mol dm^{-3}; (□) 0.074 mol dm^{-3}; (+) 0.115 mol dm^{-3}; and (*) 0.223 mol dm^{-3}.

hydroxypropyl substitution was given at 16.48% and the molecular weight as 1300 (Batch FG 22716). The surfactant decyltrimethylammonium bromide (DTAB) was obtained from Kodak-Eastman and was recrystallized twice from ethanol and dried under vacuum.

Ultrasonic absorption was measured in solution at 25.0°C over the frequency range 0.6–210 MHz by using two methods: the cylindrical resonator technique (0.62–7.2 MHz) (1, 8) and the pulsed technique (10–210 MHz) (9). In preliminary work, where the range of the resonator technique was extended to provide overlap with the range of the ultrasonic technique, no discrepancies between the experimental results of the two methods were noted. Since the resonator technique is less accurate than the pulsed technique around 10 MHz, overlap of the two ranges was sacrificed to provide better stability of the standing wave in the former method. Heat buildup was made negligible in the resonator technique by operating only in the off-resonance mode. Sound velocity measurements were obtained by using a Mapco Nusonic (model 6080) sound velocimeter which employed the "sing around" method.

The resonator cell was similar in design to one previously described (10). The standing wave was generated using a pair of 5-MHz, overtone polished, quartz crystals (Valpey–Fisher) and a 10-V p-p signal from a Hewlett–Packard 3325A frequency synthesizer that produced a signal with ±0.001 Hz stability. The resulting voltage from the cavity was measured using a Fluke 8922A True RMS voltmeter. An AT&T 6300 PC equipped with an AST Research IEEE-488 GPIB interface was used to control the synthesizer and (or) acquire data from the synthesizer and voltmeter via a Fluke 1120 A IEEE Bus Translator. The computer programme was able to locate the resonance peak, digitize and calculate the half-power bandwidth (f_n), and scan up to the next peak to repeat the process. At the resonance frequency (f_r), the sound absorption α/f^2 (α is the sound absorption coefficient of the solution) was calculated using the half-power bandwidth and the sound velocity (c) from the expression:

$$[1] \quad (\alpha/f^2)_{soln} = (\pi/cf_r)[(f_n)_{soln} - (f_n)_{ref}] + (\alpha/f^2)_{ref}$$

where the subscripts "soln" and "ref" refer to the values for the solution under study and for a nonrelaxing reference solution with a matching sound velocity, respectively. Aqueous NaCl solutions were used originally as the reference but, when these gave rise to corrosion problems, methanol solutions were substituted with no apparent differences in ultrasonic absorption measurements. The error in these measurements was estimated to be ±6%.

The pulsed apparatus used to obtain sound absorption data in the 10–210 MHz range has been described previously (9). Two cells having fundamental frequencies of 5 and 10 MHz were used to cover this range. Absorption measurements were obtained at the odd harmonic frequencies of the fundamental frequency. The value for the absorption coefficient was calculated from the changes in the sound attenuation with the distance the sound wave travelled through the solution. The error in the pulsed technique was estimated as 5–10%.

Results and discussion

All four aqueous systems investigated, DMβCD, TMβCD, HPβCD, and 1:1 DMβCD/DTAB, showed anomalous ultrasonic absorption over the frequency range 0.6 MHz–210 MHz. Graphs of α/f^2 plotted against frequency are shown in Figs. 2–5. The strongest absorptions occurred with DMβCD where, for example, α/f^2 exceeded 4000 × 10^{-17} Np s^2 cm^{-1} at 1.0 MHz in 0.115 mol dm^{-3} DMβCD. By comparison, α/f^2 was 50 × 10^{-17} Np s^2 cm^{-1} for 0.1 mol dm^{-3} α-CD at 25°C (2); the background value for pure H_2O is 20 × 10^{-17} Np s^2 cm^{-1}.

A simple inspection of the frequency dependence of the ultra-

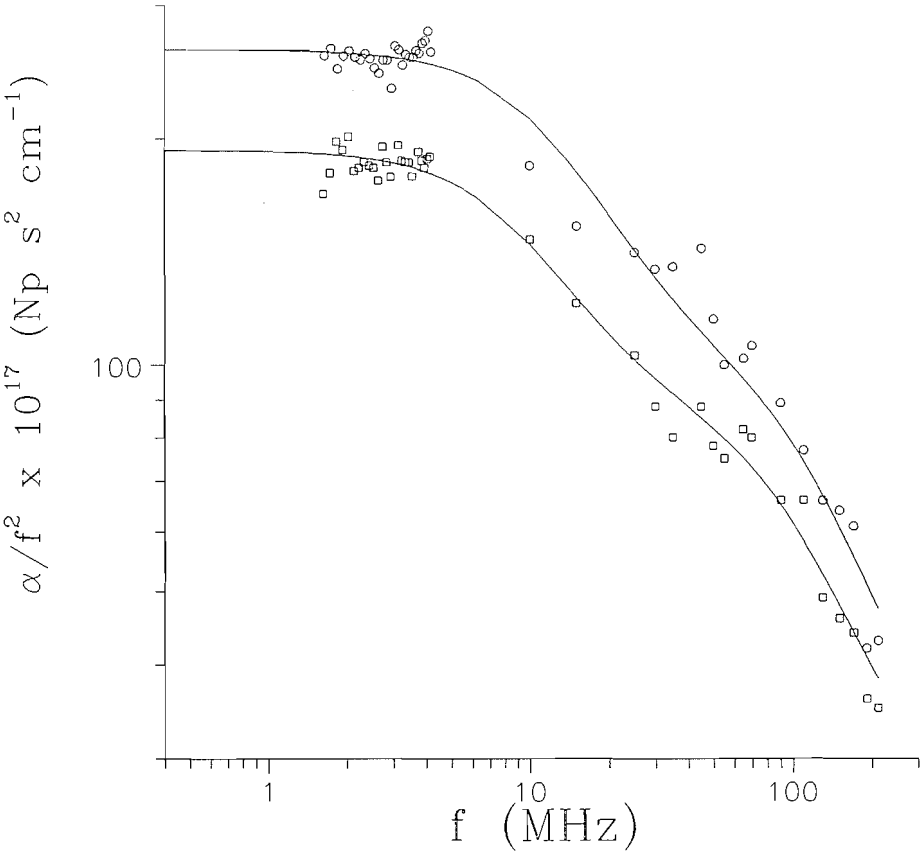

FIG. 3. Plot of α/f^2 (Np s^2 cm^{-1}) versus frequency (MHz) for TMβCD solutions: (□) 0.150 mol dm^{-3} and (○) 0.175 mol dm^{-3}.

sound absorption in Figs. 2–5 shows that a single relaxation is insufficient to account for the observed absorptions in any of the four systems. The ultrasonic absorption data were thus analyzed in each system according to the following relationship (1):

$$[2] \quad \alpha/f^2 = \sum_{i=1}^{n} (A_i/[1 + \{f/f_i\}^2]) + B$$

where n is the number of relaxations, A_i is the relaxation amplitude, f_i the relaxation frequency, and B the "classical" or background contribution to the sound absorption. The fitting of the absorption data to eq. [2] was made using a nonlinear least-squares fitting routine based on the Marquardt algorithm. The analysis of the data yielded values of the relaxational parameters as well as a measure of chi-square (χ^2), a plot of the standard residuals, and the standard deviation for the coefficients. By far the best fit was obtained when three relaxations were assumed in all systems except for TMβCD solutions where two relaxations worked best. Employing more or less than three relaxations markedly worsened the fits and caused the residuals to be distributed randomly. The best fit results for A_1, A_2, and A_3 and f_1, f_2, and f_3 are shown in Table 1. The value of B was set at 22×10^{-17} Np s^2 cm^{-1}, which is a reasonable value for non-relaxing aqueous solutions of these concentrations.

The DMβCD system is the most easily characterized in terms of ultrasonic relaxation processes because of its extended concentration range of strongly absorbing solutions. The first relaxation frequency (f_1) is concentration independent at 0.44 ± 0.06 MHz. Since f_1 is at the edge of the accessible frequency range of the apparatus, the error in this number may be greater than indicated. The problem does not arise with f_2 and f_3, which are 3 ± 1 MHz and approximately 100 MHz, respectively, and, within the larger error associated with ultrasonic measurements at low amplitudes, were also concentration independent. Also, as the concentration of DMβCD was increased, the amplitude contribution in terms of the parameter A_2 for the second relaxation process increased substantially from 5% of the total amplitude at the lowest DMβCD concentrations to 55% at 0.223 mol dm^{-3} DMβCD.

TMβCD in solution absorbed ultrasound so weakly that it was only possible to obtain absorption data close to its solubility limit. No low frequency relaxation corresponding to A_1 and f_1 of DMβCD was discernible but this may have been due to poor resolution. However, the TMβCD counterparts of the second and third processes for DMβCD appeared at 13 MHz and 100 MHz respectively.

HPβCD is as water soluble as DMβCD (approximately 0.4 mol dm^{-3}) and sound absorption was sufficiently pronounced in the HPβCD system to discern three relaxations: $f_1 = 0.87 \pm 0.06$ MHz, $5 < f_2 < 30$ MHz, and $f_3 = 150$ MHz. Changing the HPβCD concentration did not seem to affect the relative proportions of the amplitudes. Thus, DMβCD and HPβCD demonstrated unexpectedly large ultrasonic absorption while TMβCD showed far less absorption than did simple β-CD at comparable concentrations (1, 2).

When DTAB was introduced into DMβCD solutions of identical concentration, the three processes remained but the ultrasonic absorption decreased about sevenfold for A_1, was

Can. J. Chem. Downloaded from www.nrcresearchpress.com by 195.138.81.100 on 09/07/12
For personal use only.

Can. J. Chem. Downloaded from www.nrcresearchpress.com by 195.138.81.100 on 09/07/12
For personal use only.

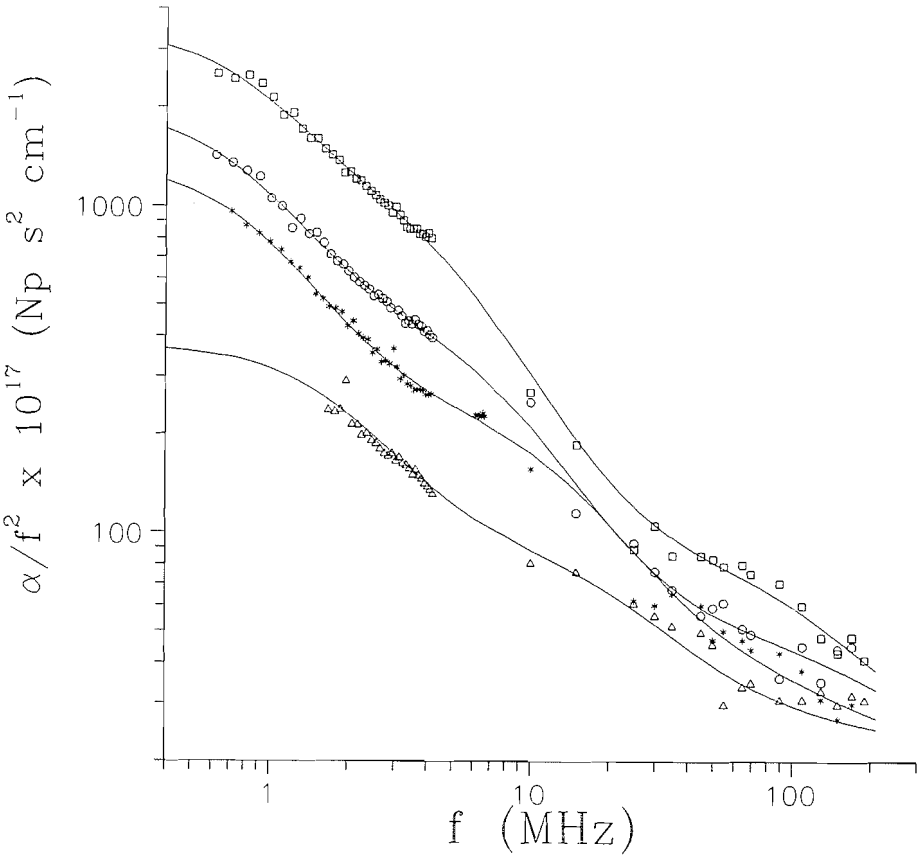

FIG. 4. Plot of α/f^2 (Np s^2 cm^{-1}) versus frequency (MHz) for HPβCD solutions: (△) 0.051 mol dm^{-3}; (*) 0.105 mol dm^{-3}; (○) 0.140 mol dm^{-3}; and (□) 0.215 mol dm^{-3}.

halved for A_2, but was unchanged for A_3 without affecting the values of the respective relaxation frequencies.

The first relaxation characterized by A_1 and f_1 was not found with the simple cyclodextrins and must then be due to some relatively slow process not available to the latter. The mechanism that suggests itself is flexing of the β-CD rings, which is possible only with the modified β-CD's because substitution at the hydroxy positions (O(2), O(3), and (or) O(6)) destroys the intramolecular hydrogen bonding between O(2) and O(3) of adjacent glucosyl units. This hydrogen bonding causes β-CD to be a rigid molecule in the crystal (11) and presumably the solution situation is the same.

This "wig-wagging" motion of the glucosyl units will be pronounced with DMβCD where only the O(3) position is available for hydrogen bonding. With HPβCD, where a fraction of the O(2), O(3), and O(6) positions has hydroxypropyl groups, this motion is also available to some degree. However, as modelling reveals, persubstitution in the case of TMβCD is accompanied by sufficient steric hindrance to quench this flexibility of the β-CD ring entirely and to cause the torus of TMβCD to be as rigid as that of unmodified β-CD. This could account for the first relaxation being observed strongly in DMβCD solutions, to a lesser extent in HPβCD solutions, but not observed in the TMβCD and unmodified β-CD systems.

Similar conformational changes in solution have been assigned to relaxations in the ultrasonic range around 1 MHz (12). However, more compelling is an argument through the A_1 values, which can be used to estimate the volume change for the process responsible for the first relaxation through the relationship (13):

$$[3] \quad A_1 = \frac{7\pi\Delta V^2 K}{\beta_0 RT f_1 (K+1)^2} \cdot \frac{[\mathrm{CD}]}{c}$$

where K is the equilibrium constant for the process, β_0 is the adiabatic compressibility of the pure solvent, and c is the sound velocity in the solution. The factor 7 is required because there are seven glucose units in the β-CD torus. The value of K can be approximated through the Boltzmann relationship, $K = \exp(-\Delta E/RT)$, where the rate-determining step is assumed to be the breaking of hydrogen bonds. From the X-ray data for β-CD (11), the hydrogen-bond distances can be used to calculate ΔE from the empirical relationship $E_{HB} = -55/r_{HB}^3$ (kcal mol^{-1}) (14).

From eq. [3], plotting A_1 values against $[CD]/c$ should yield straight lines through the origin; ΔV can be obtained from the slope. Figure 6 shows this plot for the DMβCD and HPβCD systems. In the latter, the linear portion has a non-zero intercept, which may indicate that a critical amount of HPβCD must be present before the first relaxation has a measurable amplitude. For the DMβCD system, ΔV is 18 cm^3 mol^{-1}, which is, remarkably, the correct estimated volume change one would expect for a broken intramolecular hydrogen bond to reform with a water molecule. For each glucose unit in β-CD to flex, one hydrogen bond must in fact be broken. In the HPβCD system, ΔV is 41 cm^3 mol^{-1}, reflecting the slightly more than two hydrogen bonds that, per unit, must be severed before a similar movement takes place in this molecule. Given the assumptions involved in these calculations, the exact coinci-

Can. J. Chem. Downloaded from www.nrcresearchpress.com by 195.138.81.100 on 09/07/12
For personal use only.

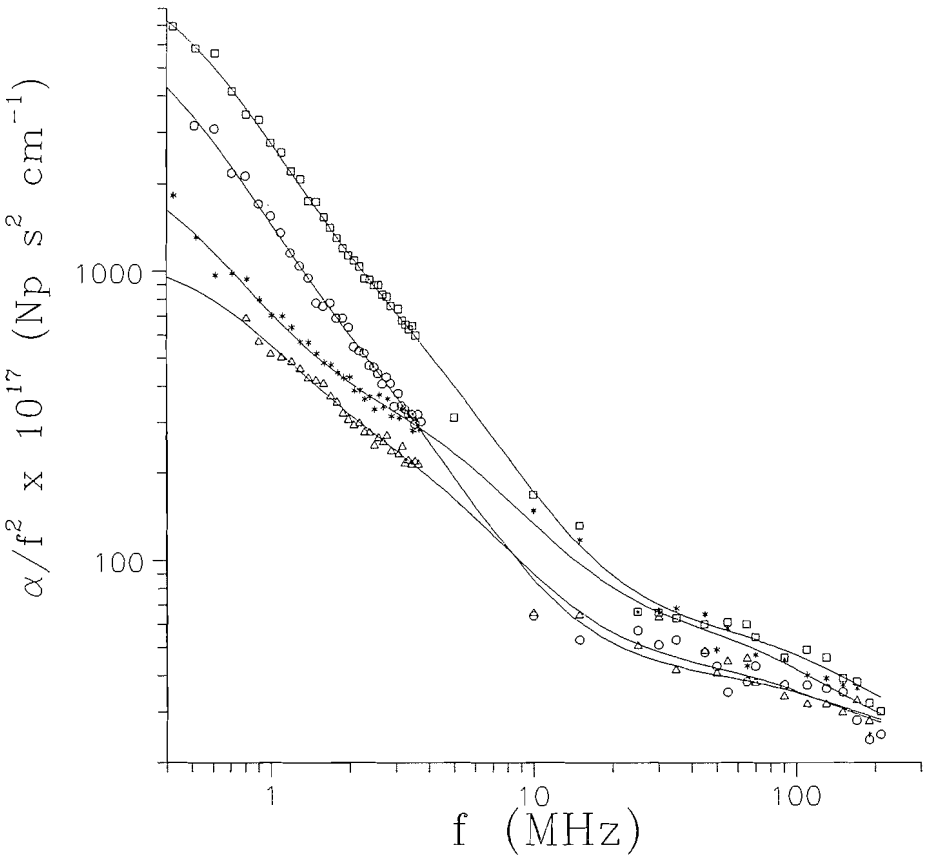

FIG. 5. Plot of α/f^2 (Np s^2 cm^{-1}) versus frequency (MHz) for DMβCD + DTAB (1:1 mole ratio) solutions: (○) 0.051 mol dm^{-3} DMβCD and no DTAB; (□) 0.074 mol dm^{-3} DMβCD and no DTAB; (△) 0.051 mol dm^{-3} DMβCD + 0.06 mol dm^{-3} DTAB; and (*) 0.074 mol dm^{-3} DMβCD + 0.080 mol dm^{-3} DTAB.

TABLE 1. Ultrasonic parameters and velocities in aqueous solutions of modified β-cyclodextrins

Sample	[CD] (mol dm^{-3})	$A_1 \times 10^{17}$ (Np s^2 cm^{-1})	f_1 (MHz)	$A_2 \times 10^{17}$ (Np s^2 cm^{-1})	f_2 (MHz)	$A_3 \times 10^{17}$ (Np s^2 cm^{-1})	f_3 (MHz)	$B \times 10^{17}$ (Np s^2 cm^{-1})	χ^2	c (M s^{-1})
DMβCD	0.029	5900±700	0.37±0.03	120±20	3.6±0.7	23±3	90±10	22	0.86	1505
	0.051	8000±1000	0.44±0.04	270±45	3.8±0.4	21±2	130±20	22	1.78	1514
	0.074	11000±900	0.50±0.04	520±80	4.5±0.8	35±4	140±20	23	0.8	1531
	0.115	18700±1600	0.47±0.03	1700±200	2.9±0.3	115±10	79±7	22	1.03	1544
	0.223	23000±4000	0.49±0.11	9700±1500	1.9±0.2	420±30	64±3	22	1.13	1555
TMβCD	0.150	—	—	106±6	11±3	65±6	120±10	22	0.6	1544
	0.175			106±6	15±3	80±7	140±13	22	1.12	1551
HPβCD	0.051	290±3	2.0 ±0.02	60±1	25±2	5±3	140±40	22	1.98	1511
	0.105	1140±120	0.96±0.02	190±4	15±1	15±4	130±20	22	1.14	1518
	0.140	1600±360	0.87±0.07	350±20	8.8±1	25±5	180±50	22	0.83	1525
	0.215	2560±160	0.93±0.10	850±80	5.7±0.7	54±4	130±15	22	0.93	1544
DMβCD + DTAB	0.050	940±90	0.74±0.06	180±15	5.4±0.6	21±2	120±20	22	1.51	1518
	0.074	2300±240	0.46±0.04	260±20	6.1±1	36±4	105±15	23	2.45	1527

dence of calculated and predicted ΔV values must be a happenstance. However, that the values should emerge correctly does add credence to the model.

When the surfactant DTAB is included in the cavity of DMβCD, the amplitude of the first relaxation process is greatly diminished (Table 1). In terms of the proposed model, the presence of the included guest would presumably eliminate wig-wagging in the bound DMβCD. From the reduced amplitudes, the concentration of free DMβCD can be obtained from Fig. 6. In the 50 and 70 mmol dm^{-3} DMβCD/DTAB systems, the free DMβCD concentrations are thus found to be 6 and 12 mmol dm^{-3} DMβCD, while 4 and 8 mmol dm^{-3} DMβCD respectively are the values calculated through the association constant of 850 dm^3 mol^{-1} for the 1:1 complex (5). Again, the close agreement is reassuring and means that wig-wagging as a possible explanation for the first relaxation is at least self-consistent.

The second relaxation occurs in the range 3–30 MHz where

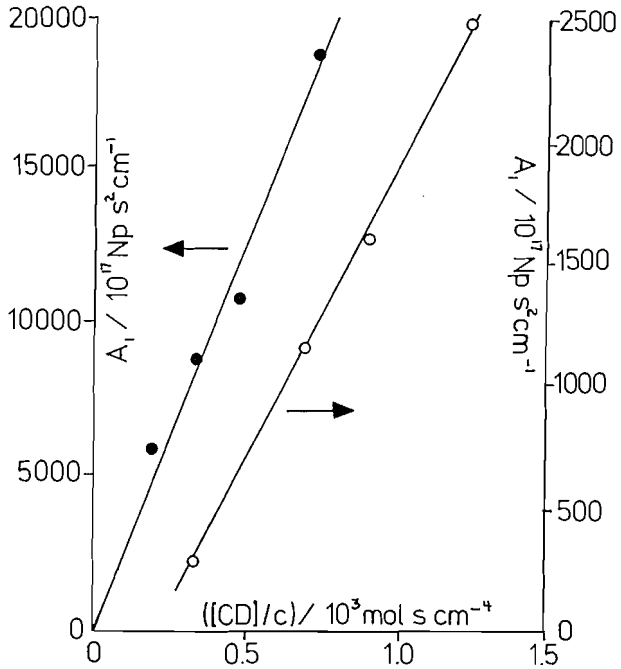

FIG. 6. Plot of A_1 versus [CD]/c for aqueous solutions of DMβCD (closed circles) and HPβCD (open circles). The arrows indicate the appropriate A_1 axis.

Kato *et al.* (1) and Rauh and Knoche (2) obtained similar results with unmodified α-CD and γ-CD in aqueous solution and which they attributed to changes in the water structure within the CD cavity. This interpretation is consistent with our results since it was observed with each modified β-CD and was dramatically reduced when surfactant entered the β-CD cavity to form a 1:1 inclusion complex. With DTAB in the cavity, fewer water molecules would be able to enter and exit the cavity. The first and second relaxations appear, from the ultrasonic data, to be coupled. In fact, one would expect that the wig-wagging of the glucose units and the movement of water molecules moving in and out of the cavity would be interrelated.

The third relaxation at approximately 100 MHz was not noted in previous ultrasonic studies in α-CD nor in γ-CD solutions (1, 2). At least for α-CD, this may have been due to experimental uncertainty since this relaxation, although present in all of the modified β-CD systems investigated here, was relatively weak. In fact, the ultrasonic absorption contribution associated with this high relaxation was so weak that it may elude better characterization for some time in the future. One point of interest that may help to identify the responsible process was that this relaxation in the present work was unaffected by surfactant inclusion in the CD cavity. A possibility is that this high relaxation frequency is associated with rotation about the C(5)—C(6) bond, which in unmodified CD favors the (−)-*gauche* orientation but in modified CD often has the substituted group pointing inwards in a (+)-*gauche* configuration as the principal orientation. This is especially the case when a guest inclusate molecule is present (11). This may explain why this third frequency is observed with only modified CD's.

In summary, ultrasonic spectroscopy identifies three fast processes occurring with modified β-cyclodextrins in solution. The lowest frequency relaxation is attributed to a wig-wagging of the individual glucosyl groups in the CD ring. Movement of water molecules in and out of the cyclodextrin cavity gives rise to the second relaxation, as argued by other workers (1, 2). For the third, very weak, highest frequency relaxation, its assignment is tentatively made to a non-ring bond rotation.

Acknowledgement

We wish to express our thanks to the Natural Sciences and Engineering Research Council of Canada for financial support.

1. S. KATO, H. NOMURA, and Y. MIYAHARA. J. Phys. Chem. **89**, 5417 (1985).
2. S. RAUH and W. KNOCHE. J. Chem. Soc. Faraday Trans. 1, **81**, 2551 (1985).
3. R. J. CLARKE, J. H. COATES, and S. F. LINCOLN. Adv. Carbohydr. Chem. Biochem. **46**, 205 (1988).
4. R. PALEPU and V. C. REINSBOROUGH. Can. J. Chem. **66**, 325 (1988).
5. D. J. JOBE, R. E. VERRALL, M. P. PELLETIER, and V. C. REINSBOROUGH. Minutes. *Edited by* D. Duchêne. Éditions de Santé, Paris. 1990. p. 200.
6. D. A. W. ADAIR, V. C. REINSBOROUGH, H. M. TRENHOLM, and J. P. VALLEAU. Can. J. Chem. **54**, 1162 (1976).
7. S. KATO, H. NOMURA, H. HONDA, R. ZIELINSKI, and S. IKEDA. J. Phys. Chem. **92**, 2305 (1988).
8. F. EGGERS and T. H. FUNCK. Rev. Sci. Instrum. **44**, 969 (1973).
9. R. E. VERRALL and H. NOMURA. J. Solution Chem. **6**, 1 (1977).
10. S. KATO, H. NOMURA, and Y. MIYAHARA. Polym. J. **11**, 455 (1979).
11. W. SAENGER. *In* Inclusion compounds. Vol. 2. *Edited by* J. L. Atwood, J. E. D. Davies, and D. D. MacNicol. Academic Press, London. 1984. p. 238.
12. J. E. STUEHR. *In* Techniques of chemistry. 4th ed. Vol. 6, Part 2. *Edited by* A. Weissberger and C. F. Bernasconi. Wiley–Interscience, New York. 1986. p. 283.
13. J. E. STUEHR and E. YEAGER. *In* Physical acoustics. Vol. 2, Part A. *Edited by* W. P. Mason. Academic Press, New York. 1965. p. 386.
14. I. TVAROSKA, S. PEREZ, and R. H. MARCHESSAULT. Carbohydr. Res. **61**, 97 (1978).

Can. J. Chem. Downloaded from www.nrcresearchpress.com by 195.138.81.100 on 09/07/12
For personal use only.

Stereocontrolled construction of A.B.C.[6.6.6] tricycle via transannular Diels–Alder reaction of 14-membered macrocycle with acetylene as dienophile

YAO-CHANG XU, MICHEL CANTIN,[1] AND PIERRE DESLONGCHAMPS[2]

Laboratoire de synthèse organique, Département de chimie, Faculté des sciences, Université de Sherbrooke, Sherbrooke (Québec), Canada J1K 2R1

Received May 8, 1990

YAO-CHANG XU, MICHEL CANTIN, and PIERRE DESLONGCHAMPS. Can. J. Chem. **68**, 2137 (1990).

The syntheses of the acyclic dienynes **14***a* (*cis-trans*-acetylene) and **14***b* (*trans-trans*-acetylene) are described. The tandem macrocyclization and transannular Diels–Alder reaction of the allylic chloride **14***b* was conducted in the presence of Cs_2CO_3 at 85°C in one-pot to provide tricyclic product **16**, with the two hydrogens in ring B being *cis*. On the other hand, treatment of the allylic chloride **14***a* under the same conditions afforded 14-membered macrocycle **17**, which could be transformed at 250°C into a similar tricyclic product **18** with the two hydrogens in ring B being *trans*, along with an interesting by-product **19**. The mechanism for the formation of **19** is also discussed.

Key words: stereocontrolled synthesis, macrocycle, tricyclic compound, transannular Diels–Alder reaction.

YAO-CHANG XU, MICHEL CANTIN et PIERRE DESLONGCHAMPS. Can. J. Chem. **68**, 2137 (1990).

On décrit la synthèse des diénynes *cis-trans*-acétylène **14***a* et *trans-trans*-acétylène **14***b*. La macrocyclisation et cyclisation transannulaire de Diels–Alder effectuées sur le chlorure allylique **14***b*, en présence de carbonate de cesium à 85°C, conduisent directement au produit tricyclique **16** possédant deux hydrogènes *cis* en jonction de cycle. Par ailleurs, le chlorure allylique **14***a* a fournit dans les mêmes conditions, le macrocycle **17** qui, à 250°C, a conduit au produit tricyclique **18** possédant deux hydrogènes *trans* en jonction de cycle et au produit secondaire **19**. Un mécanisme est proposé pour la formation de ce produit secondaire.

Mots clés : synthèse stéréocontrôlée, macrocycle, produit tricyclique, réaction de Diels–Alder transannulaire.

Can. J. Chem. Downloaded from www.nrcresearchpress.com by 195.138.81.100 on 09/07/12
For personal use only.

The key problem to the synthesis of such natural products as steroids and terpenes is how to build up the polycyclic skeleton with a controlled stereoselectivity (1). Numerous methods such as aldol condensation (2), biomimetic cyclization (3), intramolecular Diels–Alder reaction (4), and intramolecular Michael addition (5) have been developed to synthesize these classes of compounds, and success has been achieved in terms of both efficiency and stereoselectivity in the construction of the polycyclic systems.

In the present paper, we would like to report a new methodology named the transannular Diels–Alder reaction, which can be applied to the synthesis of an A.B.C.[6.6.6] tricyclic compound like **2** from macrocyclic dienyne **1** with controlled stereoselectivities in a single step (Scheme 1). The tricyclic compound **2**, which possesses easily manipulable double bond and ester functionalities, could serve as a potential precursor to such polycyclic natural products as tanshinones (6), estrones (7), and luvigenin (8).

The results presented below follow our continuing effort in a general study, which demonstrates the power of the transannular Diels–Alder reaction of macrocycles in the construction of polycyclic molecules. Preliminary communications about this new transannular cycloaddition on different systems appeared in the literature a year ago (9, 10). The same transannular Diels–Alder reaction of 13-membered macrocycles has also been reported by us very recently (11).

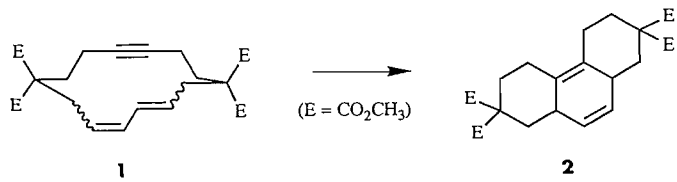

SCHEME 1

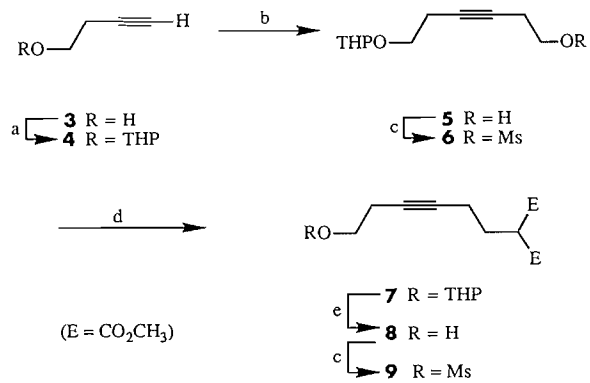

(a) *p*-TsOH, DHP, r. t., 90 min, 82% (ref. 12);
(b) *n*-BuLi, THF-HMPA, -78°C; ethylene oxide -20°C, 24 h, 91% (ref. 13);
(c) MsCl, Et_3N, CH_2CL_2, r. t., 30 min, 98% (ref. 14);
(d) NaH, $CH_2(COOCH_3)_2$, KI, DMF-THF, 80°C, 3 h 30 min, 85%;
(e) PPTS, MeOH, 60°C, 60 min, 98% (ref. 15).

SCHEME 2

Synthesis of acyclic dienyne

The synthesis of the dienophile moiety **9**, which is an essential step in the assembling of acyclic dienyne **11**, was carried out according to the procedures indicated in Scheme 2 starting from commercially available 3-butyn-1-ol. Treatment of the starting material **3** with dihydropyran in the presence of *p*-toluenesulfonic acid gave protected alcohol **4** (12). Upon addition of *n*-butyllithium, the resulting acetylene anion opened ethylene oxide by nucleophilic attack to form alcohol **5** (13), which was subsequently converted to methanesulfonate ester (mesylate) **6** by methanesulfonyl chloride in the presence of triethylamine (14). Introduction of the malonate connector was accomplished by alkylation of the sodium salt of dimethyl malonate with **6** in a mixture of DMF and THF with potassium iodide. It should be noted that the use of a large excess of sodium hydride resulted in the elimination of the mesylate to form a

[1]FCAR predoctoral fellowship (1987–1988).
[2]Author to whom correspondence may be addressed.

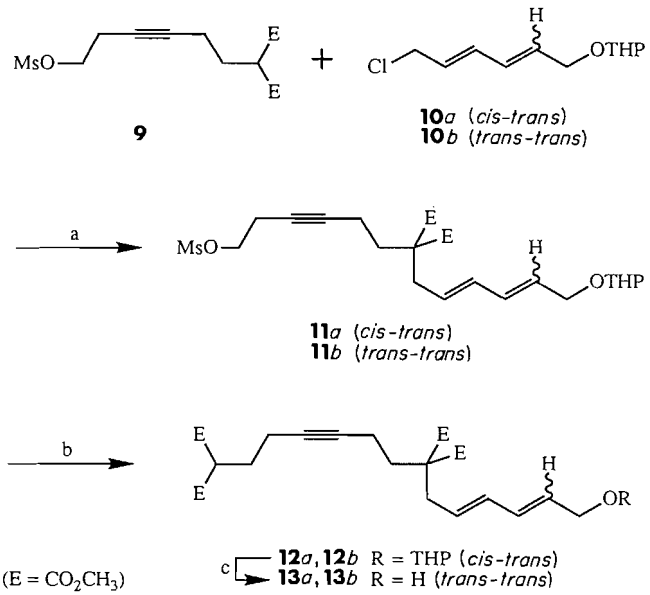

(a) NaH, DMF-THF, r. t., 5 h, **11***a*: 93%; **11***b*: 75%;
(b) NaH, $CH_2(COOCH_3)_2$, KI, DMF-THF, 80°C, 3.5 h, **12***a*: 48%-85%; **12***b*: 80%;
(c) PPTS, MeOH, 60°C, 1 h, **13***a*: 97%; **13***b*: 78%.

SCHEME 3

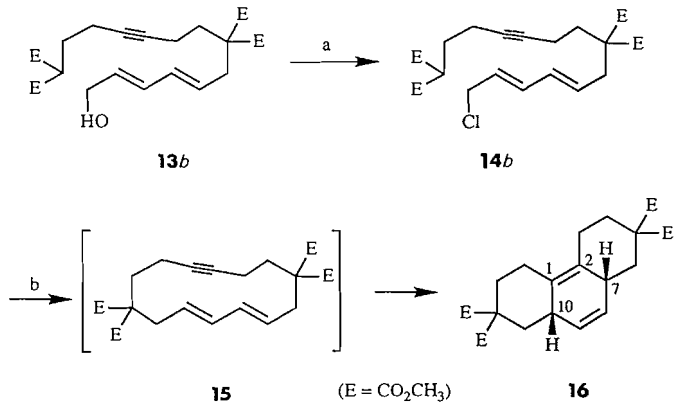

(a) LiCl, *s*-collidine, MsCl, DMF (ref. 17);
(b) Cs_2CO_3, DMF-THF(1:1), 85°C, 3.0×10^{-3} M, 24 h, 41%.

SCHEME 4

conjugated enyne by-product. Deprotection of the THP ether with pyridinium *p*-toluenesulfonate as catalyst in methanol (15) followed by mesylation (14) of the resulting alcohol afforded the desired acetylenic dienophile **9** in an excellent overall yield of 60% from starting material **3**.

The assembly between the acetylenic dienophile **9** and dienes **10** was easily achieved by, first, deprotonation of **9** with sodium hydride, followed by alkylation of the resulting anion with the allylic chlorides **10**, which were prepared previously in our laboratory (16). As indicated in Scheme 3, the coupling reaction of **9** with *cis-trans* diene **10***a* took place smoothly to give 93% yield of dienyne **11***a*, while the reaction of **9** with the *trans-trans* diene **10***b* afforded 75% yield of **11***b*, along with 20% of recovered starting material **9**. The introduction of the second connector by the procedure used previously for the preparation of **7** provided tetraester **12** in variable yields (48–85%). Again, we encountered the same elimination problem as before. In those cases where the tetraester **12** was obtained in lower yields, the mesylate elimination was observed in larger quantities. However, reasonable yields of the tetraester **12** (80–85%) could be obtained when sodium hydride was used without excess. The THP ether in **12** was then hydrolyzed as usual to give dienyne alcohol **13** (15).

Macrocyclization and Diels–Alder reaction

Having assembled the requisite carbon chain and placed appropriate functional groups at each end, the dienyne **13** was readied for construction of the 14-membered macrocycle, in a manner developed earlier by us (9), by conversion of the alcohol functionality to an electrophile such as halide. Therefore, the allylic alcohol **13***b* was transformed into allylic chloride **14***b* by Meyers' procedure using LiCl, CH_3SO_2Cl, and *s*-collidine in DMF as indicated in Scheme 4 (17). The macrocyclization was conducted by adding a solution of the crude allylic chloride **14***b* in THF to a stirred suspension of cesium carbonate in a mixture of DMF and THF (1:1) at 85°C over a period of 12 h, using high dilution technique (3.0×10^{-3} M) to avoid dimerization. After the addition was finished, the stirring was continued at 85°C for 24 h. At this stage, a tricyclic product **16** was obtained in an overall yield of 41% from the allylic alcohol **13***b*, presumably via formation, first, of the intermediate of 14-membered macrocycle **15**, followed by transannular Diels–Alder cycloaddition. The tandem macrocyclization and transannular Diels–Alder reaction of **14***b* could also be carried out in a low boiling solvent like acetonitrile, leading to the same tricyclic product **16** in comparable overall yield (37%).

The failure to isolate the macrocyclic intermediate **15** simply suggests that the Diels–Alder reaction is very much facilitated in the transannular process, so that it can take place even under the mild conditions and with a poorly activated dienophile such as acetylene. The enhanced reactivities of the transannular cycloaddition, especially with those macrocycles having *trans-trans* dienes, have been observed in our laboratory (9*b*). The structure of the tricyclic product **16** has been fully characterized by spectroscopic data. From the molecular model of the macrocycle **15**, the concerted [4 + 2] cycloaddition of *trans-trans* diene and acetylene dienophile should lead to a tricyclic compound with the two hydrogens at C(7) and C(10) being *cis* each other, as shown in **16**. The relative stereochemistry of these two hydrogens was indeed found to be *cis* by X-ray crystallography (18), which confirmed the prediction of the molecular model analysis.

Having completed the transannular Diels–Alder reaction of the macrocycle **15** (*trans-trans*-acetylene), we then turned our attention to a similar macrocyclic system **17**, which has *cis-trans*-acetylene geometry. As indicated in Scheme 5, the allylic alcohol **13***a* was first converted to allylic chloride **14***a*, by Meyers' procedure, in 79% yield (17). The macrocyclization of **14***a* was carried out by a similar procedure, used before for the allylic chloride **14***b*. Macrocyclic product **17** was isolated as a white solid in 87% yield. In contrast with macrocycle **15**, the success in isolating macrocycle **17** is apparently due to its low reactivity in the transannular Diels–Alder reaction, which required temperatures as high as 250°C to effect, as indicated, the subsequent step. A possible explanation for the difference in the reactivities is that, due to steric interactions, the *cis-trans* diene moiety in molecule **17** hinders formation of the *cisoid*

Can. J. Chem. Downloaded from www.nrcresearchpress.com by 195.138.81.100 on 09/07/12
For personal use only.

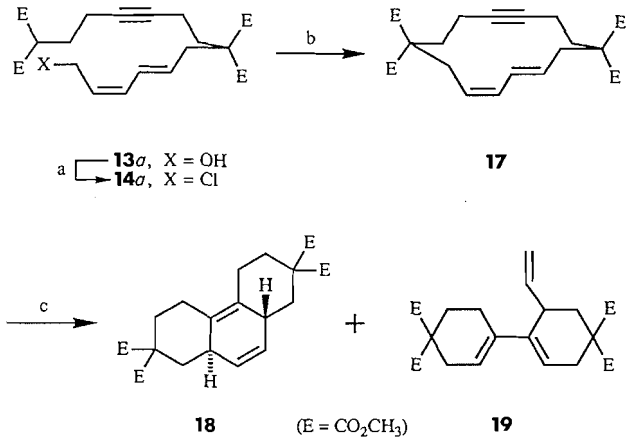

(a) LiCl, *s*-collidine, MsCl, DMF, 79%;
(b) Cs_2CO_3, DMF-THF(1:1), 80^0C, 2.6×10^{-3} M, 15h, 87% (ref. 17);
(c) 250^0C, 90 min, **18**: 23%; **19**: 67%.

SCHEME 5

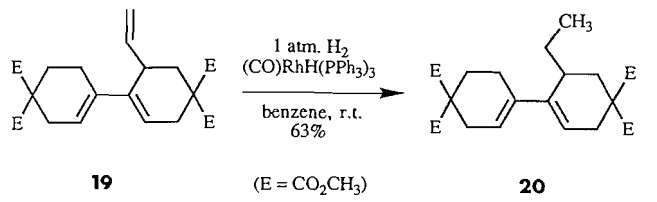

SCHEME 6

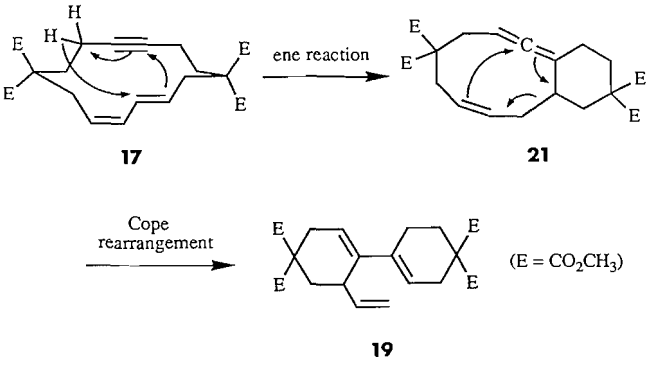

SCHEME 7

conformation, which is required for the concerted Diels–Alder reaction to take place (19). Efforts to carry out the X-ray analysis of the 14-membered macrocycle **17** having an interesting triple bond in the structure have so far failed, due to the difficulty in obtaining single crystals. However, the structure of macrocycle **17** was established by spectroscopic information (^{13}C and ^{1}H nmr, ir, ms). Especially, the conservation of the olefin geometries has been clearly indicated by comparing the ^{1}H nmr data with the data for its precursor **14***a*.

The transannular Diels–Alder reaction was carried out by heating the macrocycle **17** in a sealed tube at 250°C for 90 min, providing the expected tricyclic product **18** as a white solid in 23% yield along with an unusual compound **19** in 67% yield as a major product. The structure of **18** was determined by conventional spectroscopic data (^{1}H and ^{13}C nmr, ir, ms). The relative *trans* stereochemistry of the two protons at C(7) and C(10) can be reasonably predicted by inspection of molecular models. According to a similar analysis to that for macrocycle **15**, the concerted [4+2] cycloaddition of **17** having a *cis-trans* diene and a triple bond as a dienophile should lead to structure **18**, which has two *trans* hydrogens at the ring junctions. Further confirmation of the structure of compound **18** has been easily obtained from the comparison of the spectroscopic data with data for compound **16**, which is the only stereoisomer of compound **18**.

Isolation of the compound **19** raised very interesting questions regarding both its structure characterization and the mechanism to account for its formation. X-ray crystallography of **19** is impossible because the compound did not form single crystals. The ^{1}H nmr coupling pattern of **19** clearly indicates that there is a terminal olefin in the structure. Decoupled ^{13}C nmr shows that compound **19** has six olefinic carbons, while coupled ^{13}C nmr indicates that one olefinic carbon has two protons (triplet), three olefinic carbons have one proton (doublet), and two have no proton (singlet). The uv spectrum of the compound **19** was found to have absorptions at λ_{max} (hexane) 230 mμ (ε = 12 000), λ_{sh} 236 and 245 mμ, which are characteristic for the conjugated diene of a 1,1′-bicyclohexenyl system (λ = 233, 239, 246 mμ) (20). The above spectroscopic data correlate very well with our proposed structure **19**. Furthermore, chemical evidence has been obtained by selective hydrogenation of the terminal vinyl group of compound **19** using carbonyltris(triphenylphosphine)rhodium(I) hydride as a catalyst (21) to produce reduced product **20** (Scheme 6). Compound **20** could be easily identified by nmr spectroscopy, which clearly indicates the presence of an ethyl group in the molecule. However, the planned [4+2] cycloaddition of **19** with tetracyanoethylene led to a complex mixture.[3]

A possible mechanism for the formation of **19** from **17** is presented in Scheme 7. First, the macrocycle **17** may undergo an intramolecular ene reaction to form the bicyclic intermediate **21**. This type of ene reaction is not unprecedented because similar results with macrocyclic compounds have been observed in our laboratory.[4] The intermediate **21** with an allene and an olefin functional group in the 10-membered ring could then undergo a Cope rearrangement to form product **19**. Again, this type or rearrangement was found in the literature with a similar 10-membered ring system (22).

In summary, we have demonstrated a simple and general method for the construction of A.B.C.[6.6.6] tricyclic compounds with controlled stereoselectivities, in a synthetically useful yield, by varying the geometry of the olefins in the macrocycle precursor. The key steps involved in the synthesis of these tricycles are the macrocyclization and the subsequent transannular Diels–Alder reaction, which are very facile and moderate yielding processes. The Diels–Alder reaction is dependent on the geomety of the olefins. The present study should provide a useful model for the synthesis of natural products containing polycyclic structure. Studies in this direction are under investigation in our laboratory.

Experimental

Infrared spectra (ir) were recorded on a Perkin–Elmer 681 spectrophotometer, using chloroform ($CHCl_3$), or run as neat films on sodium chloride cells. The ^{1}H nmr and ^{13}C nmr spectra were taken on a Bruker WM-250 spectrometer in deuteriated chloroform ($CDCl_3$) or

[3]The reaction of **19** with tetracyanoethylene gave an inseparable mixture that contains a number of products possibly resulting from [2+2] and [4+2] reactions.

[4]A. Ndibwami, A. Favre, A. L. Roughton, and P. Deslongchamps. Unpublished results.

Can. J. Chem. Downloaded from www.nrcresearchpress.com by 195.138.81.100 on 09/07/12
For personal use only.

Can. J. Chem. Downloaded from www.nrcresearchpress.com by 195.138.81.100 on 09/07/12
For personal use only.

benzene (C_6D_6). The following abbreviations are used in the text: s, singlet; d, doublet; t, triplet; q, quadruplet; and m, multiplet. Mass spectra (ms) were recorded on a VG-Micromass ZAB-1F mass spectrometer. Melting points (mp) were measured on a Büchi or a Reichert melting point apparatus and were not corrected. Ultraviolet (uv) spectra were recorded on a Varian Cary 210 spectrophotometer. Thin-layer chromatography (tlc) was performed using Silica Gel 60 F-250. For flash column chromatography Merck Kieselgel (no. 9385) was used.

Unless otherwise noted, all reagents were obtained from commercial suppliers and used without further purification. Acetonitrile, amines, dimethylformamide (DMF), hexamethylphosphoramide (HMPA), and dichloromethane (CH_2Cl_2) were distilled from calcium hydride; methanol from magnesium and iodine; acetone and ethyl acetate from potassium carbonate; benzene, toluene, diethyl ether, and tetrahydrofuran (THF) from sodium and benzophenone ketyl. Purified and dried reagents were kept under argon. Unless otherwise specified, all reactions were carried out under argon atmosphere.

*1-[(Tetrahydro-2*H*-pyran-2-yl)oxy]-3-butyne (**4**)*

3-Butyn-1-ol (**3**) (7.75 g, 0.111 mol) was added dropwise to 3,4-dihydro-2*H*-pyran (13.0 g, 0.155 mol) and *p*-toluenesulfonic acid monohydrate (50 mg, 0.26 mmol) at 0°C. The resulting mixture was stirred for 90 min at room temperature, and then treated with saturated Na_2SO_4 solution (50 mL) and extracted with CH_2Cl_2 (3 × 50 mL). The combined organic layers were dried over $MgSO_4$, filtered, and evaporated. The residue was distilled (90°C, 40 Torr (1 Torr = 133.3 Pa)) to give protected butyne **4** (14.1 g, 82%) as a colorless oil; ir ($CHCl_3$): 3310, 3010, 2940, 2880, 1130, 1075, 1030 cm^{-1}; ^1H nmr ($CDCl_3$) δ: 4.65 (1H, t, J = 3.5 Hz, -OC*H*O-), 3.88–3.79 and 3.61–3.52 (4H, 2m, $-CH_2CH_2OCHOCH_2-$), 2.49 (2H, td, J = 7.0 Hz, 1.0 Hz, $-CH_2C{\equiv}CH$), 1.97 (1H, t, J = 1.0 Hz, $-CH_2C{\equiv}CH$), 1.90–1.48 (6H, m, $-OCHOCH_2(CH_2)_3$); ms *m/e*: 153 (M^+-H).

*6-[(Tetrahydro-2*H*-pyran-2-yl)oxy]-3-hexyn-1-ol (**5**)*

To a stirred solution of butyne **4** (5.7 g, 37 mmol) in a mixture of HMPA/THF (1:3, 200 mL) was slowly added *n*-butyllithium (1.66 M in hexanes, 24.3 mL, 39 mmol) by a syringe pump over a period of 30 min at −78°C, until orange coloration persisted. Ethylene oxide (25 mL, 37 mmol) was added and the reaction mixture was maintained at −20°C for 24 h. After the mixture was warmed to room temperature, it was quenched with saturated NH_4Cl solution (100 mL), diluted with H_2O (100 mL), and extracted with hexanes/diethyl ether (2:1, 6 × 750 mL). The combined organic layers were dried over $MgSO_4$, filtered, and evaporated. The crude residue was purified by flash chromatography (hexanes/ethyl acetate; 4:1) to give alcohol **5** (6.7 g, 91%) as a colorless oil; ir ($CHCl_3$): 3630, 3470, 3020, 2950, 2880, 1120, 1030 cm^{-1}; ^1H nmr ($CDCl_3$) δ: 4.64 (1H, t, J = 3.5 Hz, -OC*H*O-), 3.93–3.76 and 3.60–3.47 (4H, 2m, $-CH_2CH_2OCHOCH_2-$), 3.68 (2H, t, J = 6.0 Hz, $-CH_2CH_2OH$), 2.51–2.39 (4H, m, $-CH_2CH_2C{\equiv}CH_2CH_2-$), 1.90–1.48 (7H, m, $-OCHOCH_2(CH_2)_3$ and $-CH_2OH$); ms/*e*: 197 (M^+-H), 167 (M^+-CH_2OH).

*6-Methanesulfonyloxy-1-[(tetrahydro-2*H*-pyran-2-yl)oxy]-3-hexane (**6**)*

General procedure A

To a stirred solution of alcohol **5** (2.50 g, 12.6 mmol) and triethylamine (3.5 mL, 25 mmol) in dichloromethane (50 mL) was added methanesulfonyl chloride (1.22 mL, 15.8 mmol) at 0°C in dropwise fashion. The resulting mixture was stirred for 30 min at 0°C, and then diluted with CH_2Cl_2 (100 mL). The organic layer was washed with H_2O (3 × 50 mL), dried over $MgSO_4$, filtered, and evaporated. The crude residue was purified by flash chromatography (hexanes/ethyl acetate; 3:1) to give mesylate **6** (3.4 g, 98%) as an oil; ir ($CHCl_3$): 3030, 3010, 2950, 2880, 1360, 1175, 1030 cm^{-1}; ^1H nmr ($CDCl_3$) δ: 4.62 (1H, t, J = 3.5 Hz, -OC*H*O-), 4.26 (2H, t, J = 6.8 Hz, $-CH_2CH_2OSO_2CH_3$), 3.90–3.74 and 3.56–3.46 (4H, 2m, $-CH_2CH_2OCHOCH_2-$), 3.04 (3H, s, $-OSO_2CH_3$), 2.62 (2H, tt, J = 6.8Hz, 2.4 Hz, $-C{\equiv}CCH_2CH_2OSO_2CH_3$), 2.45 (2H, tt, J = 7.0 Hz, $-C{\equiv}CCH_2CH_2OCHO-$), 1.90–1.48 (6H, m, $-OCHOCH_2(CH_2)_3$); ms *m/e*: 275 (M^+-H).

*Methyl 2-carbomethoxy-8-[(tetrahydro-2*H*-pyran-2-yl)oxy]-5-octynoate (**7**)*

General procedure B

To a stirred sodium hydride suspension (2.46 g, 61.5 mmol) in a mixture of DMF/THF (1:1, 200 mL) was added dimethyl malonate (7.1 mL, 61.5 mmol) at 0°C in dropwise fashion. The mixture was stirred at room temperature for 15 min, then transferred by syringe to mesylate **6** (3.41 g, 12.3 mmol). Potassium iodide (2.39 g, 14.4 mmol) was added and the resulting mixture was heated at 80°C for 3.5 h. After cooling to room temperature, the reaction mixture was quenched with saturated NH_4Cl solution (100 mL), diluted with H_2O (100 mL), and extracted with diethyl ether (4 × 400 mL). The combined organic layers were dried over $MgSO_4$, filtered, and evaporated. The crude residue was purified by flash chromatography (hexanes/ethyl acetate; 17:3) to give malonate **7** (3.3 g, 85%) as an oil; ir ($CHCl_3$): 3010, 2950, 1750, 1730, 1440, 1030 cm^{-1}; ^1H nmr ($CDCl_3$) δ: 4.64 (1H, t, J = 3.5 Hz, -OC*H*O-), 3.95–3.72 and 3.56–3.46 (4H, 2m, $-CH_2CH_2-OCHOCH_2-$), 3.76 (6H, s, $CH_2(CO_2CH_3)_2$), 3.75 (6H, s, $-CH(CO_2CH_3)_2$), 3.62 (1H, t, J = 7.3 Hz, $-CH(CO_2CH_3)_2$), 3.41 (2H, s, $CH_2(CO_2CH_3)_2$), 2.45 (2H, tt, J = 7.2 Hz, 2.3 Hz, $-C{\equiv}CCH_2CH_2OH-$), 2.25 (2H, m, $-C{\equiv}CCH_2CH_2CH-$), 2.08 (2H, q, J = 75 Hz, $-C{\equiv}CCH_2CH_2CH-$), 1.90–1.49 (6H, m, $-OCHOCH_2(CH_2)_3$); ms *m/e*: 312 (M^+), 228 M^+-THP), 211 (M^+-OTHP).

*7,7-Biscarbomethoxy-3-heptyn-1-ol (**8**)*

General procedure C

To a stirred solution of malonate **7** (3.00 g, 9.6 mmol) in anhydrous methanol (175 mL) was added pyridinium *p*-toluenesulfonate (480 mg, 1.9 mmol) and the resulting mixture was heated at 60°C for 1 h. After the mixture was cooled to room temperature, it was treated with brine (100 mL), diluted with H_2O (100 mL), and extracted with ethyl acetate (6 × 125 mL). The combined organic layers were dried over $MgSO_4$, filtered, and evaporated. The crude residue was purified by flash chromatography (hexanes/ethyl acetate; 4:1) to give alcohol **8** (2.15 g, 98%) as a viscous oil; ir ($CHCl_3$): 3540, 3010, 2950, 1750, 1740, 1730, 1440, 1220, 1050 cm^{-1}; ^1H nmr ($CDCl_3$) δ: 3.75 (6H, 2, $-CH(CO_2CH_3)_2$), 3.68 (2H, t, J = 6.1 Hz, $-CH_2OH$), 3.60 (1H, t, J = 7.3 Hz, $-CH(CO_2CH_3)_2$), 2.61 (2H, tt, J = 6.1 Hz, 2.3 Hz, $-C{\equiv}CCH_2$ CH_2OH), 2.27 (2H, m, $-C{\equiv}CCH_2CH_2CH-$), 2.09 (2H, q, J = 7 Hz, $-C{\equiv}CCH_2CH_2CH-$), 1.93 (1H, br s, $-CH_2OH$); ms *m/e*: 229 (MH^+), 211 (MH^+-H_2O), 198 (MH^+-OCH_3).

*Methyl 8-methanesulfonyloxy-2-carbomethoxy-5-octynoate (**9**)*

The general procedure A was followed, using triethylamine (2.54 mL, 18 mmol), methanesulfonyl chloride (877 μL, 11.4 mmol), alcohol **8** (2.1 g, 9.1 mmol), and dichloromethane (30 mL). Mesylate **9** (2.7 g, 98%) was obtained as a solid; mp 44–45°C; ir ($CHCl_3$): 3030, 2950, 2840, 1740, 1440, 1350, 1240 cm^{-1}; ^1H nmr ($CDCl_3$) δ: 4.25 (2H, t, J = 6.8 Hz, $-CH_2OSO_2CH_3$), 3.74 (6H, s, $-CH(CO_2CH_3)_2$), 3.58 (1H, t, J = 7.3 Hz, $-CH_2CH(CO_2CH_3)_2$), 3.05 (3H, s, $-OSO_2$ CH_3), 2.61 (2H, tt, J = 6.8 Hz, 2.3 Hz, $-C{\equiv}CCH_2CH_2O-$), 2.24 (2H, m, $-C{=}CCH_2CH_2CH-$), 2.07 (2H, q, J = 7 Hz, $-C{=}CCH_2$ CH_2CH-); ms *m/e*: 306 (M^+), 275 (M^+ —OCH_3).

*(2Z,4*E*)-7,7-Biscarbomethoxy-13-methanesulfonyloxy-1-[(tetrahydro-2*H*-pyran-2-yl)oxy]-2,4-10-yne (**11**a)*

General procedure D

To a stirred sodium hydride suspension (72 mg, 1.8 mmol) in DMF/THF (1:1, 12 mL) was added a solution of mesylate **9** (493 mg, 1.6 mmol) in DMF/THF (1:1, 4 mL) at room temperature. The mixture was stirred for 10 min and then transferred to a solution of allylic chloride **10***a* (466 mg, 2.2 mmol) in DMF/THF (1:1, 4 mL). The resulting mixture was stirred for 5 h at room temperature, then quenched with saturated NH_4Cl solution (20 mL), diluted with H_2O (20 mL), and extracted with hexanes/diethyl ether (1:2, 5 × 75 mL). The combined organic layers were washed with H_2O (50 mL) and brine (50 mL), dried over $MgSO_4$, filtered, and evaporated. The crude residue was purified by flash chromatography (hexanes/ethyl acetate; 7:3) to give mesylate **11***a* (734 mg, 93%), as an oil; ir ($CHCl_3$): 3020,

Can. J. Chem. Downloaded from www.nrcresearchpress.com by 195.138.81.100 on 09/07/12
For personal use only.

2950, 2860, 1730, 1440, 1350, 1200, 1179 cm^{-1}; ^1H nmr ($CDCl_3$) δ: 6.38 (1H, dd, J = 15.0 Hz, 11.1 Hz, -CH_2CH=CH-CH=$CHCH_2O$-), 6.07 (1H, t, J = 11.0 Hz, -CH_2CH=CH-CH=$CHCH_2O$-), 5.57–5.49 (2H, m, -CH_2CH=CH-CH=$CHCH_2O$-), 4.63 (1H, t, J = 3.5 Hz, -OCHO-), 4.34 (1H, ddd, J = 12.7 Hz, 6.4 Hz, 1.3 Hz, -CH=CHCHHO-), 4.24 (2H, t, J = 6.8 Hz, -$CH_2OSO_2CH_3$), 4.16 (1H, ddd, J = 12.7 Hz, 7.4 Hz, 1.2 Hz, -CH=CHCHHO-), 3.92–3.82 and 3.56–3.47 (2H, 2m, -OCHOCH_2-), 3.72 (6H, s, -$CH_2C(CO_2CH_3)_2CH_2$-), 3.04 (3H, s, -OSO_2CH_3), 2.70 (2H, d, J = 7.6 Hz, -CH_2CH=CH-CH=CH-), 2.60 (2H, tt, J = 6.8 Hz, 2.0 Hz, -C≡CCH_2CH_2O-), 2.10 (4H, m, -C≡CCH_2CH_2-CH-), 1.89–1.48 (6H, m, -OCHOCH$_2$(CH_2)$_3$-); ms m/e: 486 (M^+), 455 (M^+-OCH_3), 403 ($M^+-C_5H_7O$).

*(2E,4E)-7,7-Biscarbomethoxy-13-methanesulfonyloxy-1-[(tetrahydro-2H-pyran-2-yl)oxy]-2,4-tridecadien-10-yne (**11**b)*

The general procedure D was followed, using sodium hydride (106 mg, 2.7 mmol), mesylate **9** (769 mg, 2.5 mmol), allylic chloride **10***b* (875 mg, crude product), DMF (14 mL), and THF (14 mL). Mesylate **11***b* (921 mg, 75%) was obtained along with recovered starting material **9** (153 mg, 20%). **11***b*: ir ($CHCl_3$): 3040, 2950, 2850, 1730, 1440, 1360, 1200, 1180 cm^{-1}; ^1H nmr ($CDCl_3$) δ: 6.15 (2H, m, -CH_2CH=CH-CH=$CHCH_2O$-), 5.73 (1H, td, J = 14.7 Hz, 6.0 Hz, -CH_2CH=CH-CH=CHCH_2O-), 5.46 (1H, td, J = 14.5 Hz, 7.2 Hz, -CH_2CH=CH-CH=$CHCH_2O$-), 4.63 (1H, t, J = 3.5 Hz, -OCHO-), 4.25 (3H, m and t, J = 6.9 Hz (for t), -CH=CHCHHO- and -$CH_2OSO_2CH_3$), 3.98 (1H, ddd, J = 13.2 Hz, 6.7 Hz, 0.8 Hz, -CH=CHCHHO-), 3.98–3.81 and 3.59–3.48 (2H, 2m, -OCHOCH_2-), 3.72 (6H, s, -$CH_2C(CO_2CH_3)_2CH_2$-), 3.05 (3H, s, -OSO_2CH_3), 2.68 (2H, d, J = 7.7 Hz, -CH_2CH=CH-CH=CH-), 2.60 (2H, tt, J = 6.9 Hz, 2.0 Hz, -C≡CCH_2CH2O-), 2.10 (4H, m, -C=CCH_2CH_2-CH-), 1.89–1.51 (6H, m, -OCHOCH$_2$(CH$_2$(CH_2)$_3$-); ms m/e: 384 ($M^+-C_5H_{10}O_2$), 353 (M^+−OTHP−CH_3OH).

*Methyl (11E,13Z)-2,9,9-tricarbomethoxy-15-[(tetrahydro-2H-pyran-2-yl)oxy]-11,13-pentadecadien-5-ynoate (**12**a)*

The general procedure B was followed, using dimethyl malonate (725 μL, 6.4 mmol), sodium hydride (260 mg, 6.5 mmol), DMF (10 mL), THF (10 mL), mesylate **11***a* (626 mg, 1.3 mmol), and potassium iodide (280 mg, 1.7 mmol). Tetraester **12***a* (ranging from 323 mg to 572 mg, 48–85%) was obtained; ir (neat): 3000, 2950, 2860, 1740, 1435, 1200 cm^{-1}; ^1H nmr ($CDCl_3$) δ: 6.38 (1H, dd, J = 15.0 Hz, 11.2 Hz, -CH_2CH=CH-CH=-CH=$CHCH_2O$-), 6.08 (1H, t, J = 10.9 Hz, -CH_2CH=CH-CHCHCH_2O-), 5.60–5.47 (2H, m, -CH_2CH= CH-CH=CHCH_2O-), 4.63 (1H, t, J = 3.5 Hz, -OCHO-), 4.34 (1H, ddd, J = 12.7 Hz, 6.4 Hz, 1.4 Hz, -CH=CHCHHO-), 4.17 (1H, ddd, J = 12.7 Hz, 7.4 Hz, 1.2 Hz, -CH=CHCHHO-), 3.92–3.81 and 3.56–3.49 (2H, 2m, -OCHOCH_2-), 3.74 and 3.71 (12H, 2s, -$CH_2CH(CO_2CH_3)_2$ and -$CH_2C(CO_2CH_3)_2CH_2$-), 3.57 (1H, t, J = 7.3 Hz, -$CH_2CH(CO_2CO_3)_2$), 2.70 (2H, d, J = 7.1 Hz, -C(CO_2-CH_3)CH_2 CH=), 2.25–2.19 and 2.14–2.01 (8H, m, -CH_2CH_2C≡-CCH_2CH_2-), 1.84–1.48 (6H, m, -OCHOCH$_2$(CH_2)$_3$); ms m/e: 522 (M^+), 507 (M^+-CH_3), 491 (M^+-OCH_3).

*Methyl (11E,13E)-2,9,9-tricarbomethoxy-15-[(tetrahydro-2H-pyran-2-yl)oxy]-11,13-pentadecadien-5-ynoate (**12**b)*

The general procedure B was followed, using dimethyl malonate (1.05 mL, 9.2 mmol), sodium hydride (367 mg, 9.2 mmol), mesylate **11***b* (921 mg, 1.9 mmol), potassium iodide (353 mg, 2.1 mmol), DMF (23 mL), and THF (23 mL). Tetraester **12***b* (780 mg, 80%) was isolated and used immediately for the preparation of **13***b*, without spectroscopic characterization.

*Methyl (11E,13Z)-2,9,9-tricarbomethoxy-15-hydroxy-11,13-pentadecadien-5-ynoate (**13**a)*

The general procedure C was followed, using pyridinium *p*-toluenesulfonate (32 mg, 0.127 mmol), tetraester **12***a* (323 mg, 0.62 mmol), and anhydrous methanol (10 mL). Alcohol **13***a* (265 mg, 97%) was obtained as a viscous oil; ir (neat): 3530, 3470, 3010, 2950, 2840, 1740, 1435, 1200 cm^{-1}; ^1H nmr ($CDCl_3$) δ: 6.37 (1H, dd, J = 15.5 Hz, 11.2 Hz, -CH_2CH=CH-CH=$CHCH_2OH$), 6.03 (1H, t, J = 11.2 Hz, -CH_2CH=CH-CH=$CHCH_2OH$), 5.61–5.30 (2H, m, -CH_2CH= CH-CH=CHCH_2OH), 4.31–4.28 (2H, br s, =CHCH_2OH), 3.74 and 3.72 (12H, 2s, -$CH_2CH(CO_2CH_3)_2$ and -$CH_2C(CO_2CH_3)_2CH_2$-), 3.57 (1H, t, J = 7.3 Hz, -$CH_2CH(CO_2CH_3)_2$), 2.71 (2H, d, J = 7.6 Hz, =CHCH_2C(CO_2CH_3)$_2CH_2$-), 2.26–2.19 and 2.13–2.02 (8H, 2m, -CH_2CH_2C≡CCH_2CH_2-), 1.59 (1H, s, -CH_2OH); ms m/e: 438 (M^+), 420 (M^+-H_2O), 407 (M^+-OCH_3).

*Methyl (11E,13E)-2,9,9-tricarbomethoxy-15-hydroxy-11,13-pentadecadien-5-ynoate (**13**b)*

The general procedure C was followed, using pyridinium *p*-toluenesulfonate (63 mg, 0.25 mmol), tetraester **12***b* (780 mg, 1.5 mmol), and anhydrous methanol (20 mL). Alcohol **13***b* (511 mg, 78%) was obtained as a viscous oil; ir (neat): 3540, 3460, 3000, 2950, 2840, 1740, 1430, 1220 cm^{-1}; ^1H nmr ($CDCl_3$) δ: 6.14 (2H, m, -CH_2CH=CH-CH=$CHCH_2OH$), 5.77 (1H, dt, J = 17.2 Hz, 5.6 Hz, -CH_2CH=CH-CH=CHCH_2OH), 5.50 (1H, dt, J = 14.4 Hz, 7.3 Hz, -CH_2CH=CH-CH=$CHCH_2OH$), 4.16 (2H, t, J = 5.7 Hz, =CHCH_2OH), 3.74 and 3.71 (12H, 2s, -$CH_2CH(CO_2CH_3)_2$ and -$CH_2C(CO_2CH_3)_2CH_2$-), 3.57 (1H, t, J = 7.3 Hz, -$CH_2CH(CO_2CH_3)_2$), 2.68 (2H, d, J = 7.6 Hz, =CHCH_2C(CO_2CH_3)$_2CH_2$-), 2.26–2.19 and 2.13–2.02 (8H, 2m, -CH_2CH_2C≡CCH_2CH_2-), 1.41 (1H, t, J = 5.8Hz, -CH_2OH); ms m/e: 423 (M^+-CH_3), 420 (M^+-H_2O), 407 (M^+-OCH_3).

*Methyl (11E,13Z)-2,2,9-tricarbomethoxy-15-chloro-11,13-pentadecadien-5-ynoate (**14**a)*

To a stirred solution of alcohol **13***a* (291 mg, 0.66 mmol) in DMF (7 mL) were added lithium chloride (113 mg, 2.7 mmol) and *s*-collidine (263 μL, 2.0 mmol) at room temperature. After the mixture was cooled to 0°C, methanesulfonyl chloride (128 μL, 1.7 mmol) was added. The resulting mixture was stirred for 30 min, then diluted with H_2O (20 mL) and extracted with hexanes/diethyl ether (2:1, 3 × 30 mL). The combined organic layers were dried over $MgSO_4$, filtered, and then evaporated. The crude residue was purified by flash chromatography (hexanes/ethyl acetate; 17:3) to give allylic chloride **14***a* (238 mg, 79%), which was used immediately for the next cyclization without spectroscopic characterization.

*Methyl (11E,13E)-2,9,9-tricarbomethoxy-15-chloro-11,13-pentadecadien-5-ynoate (**14**b)*

To a stirred solution of allylic alcohol **13***b* (330 mg, 0.75 mmol) and lithium chloride (232 mg, 5.5 mmol) in DMF (7.5 mL) was added *s*-collidine (400 μL, 3.0 mmol) at room temperature. The mixture was stirred for 10 min and then cooled to 0°C. Methanesulfonyl chloride (170 μL, 2.2 mmol) was added. The reaction mixture was stirred at 0°C for 45 min, and then diluted with H_2O and extracted with hexanes/ethyl ether (2:1, 4 × 75 mL). The combined organic layers were washed successively with saturated $Cu(NO_3)_2$ solution (20 mL), saturated $NaHCO_3$ solution (10 mL), and brine (2 × 20 mL), and then dried over $MgSO_4$, filtered, and evaporated to give crude allylic chloride **14***b*; ^1H nmr (C_6D_6) δ: 5.78 (2H, m, -CH_2CH=CH-CH=$CHCH_2Cl$), 5.51–5.35 (2H, m, -CH_2CH=CH-CH=CHCH_2Cl), 3.64–3.58 (3H, m, =CHCH_2Cl and -$CH_2CH(CO_2CH_3)_2$), 3.27 (12H, s, -$CH_2CH(CO_2CH_3)_2$ and -$CH_2C(CO_2CH_3)_2CH_2$-), 2.75 (2H, d, J = 7.8 Hz, =CHCH_2C(CO_2CH_3)$_2CH_2$-), 2.37–2.12 (8H, 2m, -CH_2CH_2C≡CCH_2CH_2-).

*(7,10-cisoid)-5,5,12,12-Tetracarbomethoxytricyclo[8.4.0.0^{2,7}]tetradeca-1,7-diene (**16**)*

To a stirred suspension of cesium carbonate (848 mg, 2.6 mmol) in a mixture of DMF/THF (1:1, 195 mL) was added a solution of allylic chloride **14***b* (238 mg, 0.52 mmol) in THF (5 mL) at 85°C by syringe pump over a period of 12 h. After addition, the stirring was continued for 24 h. The reaction mixture was allowed to cool to room temperature, and then filtered and evaporated. The crude residue was purified by flash chromatography (hexanes/CH_2Cl_2/ethyl acetate; 17:2:1) to give tricyclic compound **16** (130 mg, 41% for last 3 steps) as a solid; mp 164–166°C; ir ($CHCl_3$): 3020, 2950, 1730, 1450, 1430, 1230 cm^{-1}; ^1H nmr ($CDCl_3$) δ: 5.50 (2H, s, -C(8)H=C(9)H-), 3.77 and 3.69

Can. J. Chem. Downloaded from www.nrcresearchpress.com by 195.138.81.100 on 09/07/12
For personal use only.

(12H, 2s, $(CO_2CH_3)_4$), 2.67 (4H, m, -C(3)H_e-, -C(7)H-, -C(10)H- and -C(14)H_e-), 2.48 (4H, d, J = 11.6 Hz, -C(4)H_e-, -C(6)H_e-, -C(11)H_e-, and -C(13)H_e-), 1.69 (4H, m, -C(3)H_a-, -C(4)H_a-, -C(13)H_a-, and -C(14)H_a-), 1.47 (2H, t, J = 12.8 Hz, -C(6)H_a- and -C(11)H_a-); ^{1}H nmr (C_6D_6) δ: 5.43 (2H, s, -C(8)H=C(9)H-), 3.35 and 3.25 (12H, 2s, $(CO_2CH_3)_4$), 2.85 (2H, d, J = 10.5 Hz, -C(7)H- and -C(10)H-), 2.76 (2H, dt, J = 13.0 Hz, 2.9 Hz, -C(4)H_e- and -C(13)H_e-), 2.67 (2H, dd, J = 12.0 Hz, 2.6 Hz, -C(6)H_e- and -C(11)H_e-), 2.52 (2H, m, -C(3)H_e- and -C(14)H_e-), 1.69 (6H, m, -C(3)H_a-, -C(4)H_a-, -C(6)H_a-, -C(11)H_a-, -C(13)H_a-, and -C(14)H_a-); ^{13}C nmr ($CDCl_3$) δ: 172.2 (s, (CO_2CH_3)$_4$), 127.9 and 127.4 (d, -C(8)H=C(9)H-), 55.3 (s, -C(5)- and -C(9)-), 52.7 and 52.5 (q, $(CO_2CH_3)_4$), 40.0 (t, -C(6)- and -C(11)-), 35.2 (d, -C(7)- and -C(10)-), 32.6 (t, -C(4)- and -C(13)-), 25.1 (t, -C(3)- and -C(14)-); ms m/e: 420 (M^+). Exact mass (M^+) calcd.: 420.1785; found: 420.1781. The structure for **16** has also been determined by X-ray crystallography and the details will be reported soon (18).

The same reaction using acetonitrile as a solvent was conducted in exactly the same way as above. Thus, the reaction of **14***b* (crude product) with cesium carbonate (700 mg, 2.1 mmol) in CH_3CN (210 mL) provided a tricyclic product (67 mg, 37% for last 3 steps) that has spectral data identical to the data for compound **16**.

*(1Z,3E)-6,6,13,13-Tetracarbomethoxy-1,3-cyclotetradecadien-9-yne (**17**)*

To a stirred suspension of cesium carbonate (848 mg, 2.6 mmol) in a mixture of DMF/THF (1:1, 190 mL) at 80°C was added a solution of allylic chloride **14***a* (238 mg, 0.52 mmol) in THF (5 mL) at 80°C by syringe pump over a period of 10 h. After the addition, the stirring was continued for 5 h. The reaction mixture was allowed to cool to room temperature, then filtered and evaporated. The crude residue was purified by flash chromatography (hexanes/CH_2Cl_2/ethyl acetate; 17:2:1), to yield a solid that was crystallized in hexanes/CH_2Cl_2 to give macrocyclic compound **17** (191 mg, 87%) as a solid; mp 146–159°C; ir ($CHCl_3$): 3020, 2960, 1730, 1460, 1440, 1220 cm^{-1}; ^{1}H nmr ($CDCl_3$) δ: 6.40 (1H, dd, J = 14.8 Hz, 11.4 Hz, -C(1)H=C(2)H-C(3)H=C(4)H-), 6.19 (1H, t, J = 11.0 Hz, -C(1)H=C(2)H-C(3)H=C(4)H-), 5.35 (1H, dt, 14.7 Hz, 7.3 Hz, -C(1)H=C(2)H-C(3)H=C(4)H-), 5.04 (1H, dt, J = 10.4 Hz, 8.4 Hz, -C(1)H=C(2)H-C(3)H=C(4)H-), 3.73 and 3.72 (12H, 2s, $(CO_2CH_3)_4$), 2.97 (2H, d, J = 7.2 Hz, -C(3)H=C(4)H-C(5)H_2-), 2.82 (2H, d, J = 8.5 Hz, -C(14)H_2-C(1)H=C(2)H-), 2.15–0.98 (8H, m, -CH_2C=CCH_2CH_2); ^{13}C nmr ($CDCl_3$) δ: 171.3 and 170.9 ((CO_2CH_3)$_4$), 133.4 (=C(2)H-), 130.6 (-C(3)H=), 128.6 (=C(4)H-), 123.3 (-C(1)H=), 80.9 and 70.9 (-C(9)≡C(10)-), 58.4 and 56.4 (-C(6)- and C(13)-), 35.0 (-C(5)H_2-), 29.2 (-C(14)H_2-), 29.9 and 29.4 (-C(8)H_2C≡CC(11)H_2-), 13.4 (-C(7)H_2CH_2C≡ CCH_2C(12)H_2-); ms m/e: 420 (M^+). Exact mass (M^+) calcd.: 420.1784; found: 420.1781.

*(7,10-transoid)-5,5,12,12-Tetracarbomethoxytricyclo[8.4.0.0^{2,7}] tetradeca-1,7-diene (**18**)*

Macrocyclic compound **17** (24.0 mg, 5.7 × 10^{-2} mmol) was heated in a vacuum-sealed quartz tube at 250°C for 90 min. The residual product was dissolved in CH_2Cl_2 and then transferred to a flask. After the solvent was evaporated, the crude residue was purified by flash chromatography (hexanes/CH_2Cl_2/ethyl acetate; 10:2:1) to give tricyclic compound **18** (5.4 mg, 22.5%) and by-product **19** (16.2 mg, 67.5%). Compound **18**: mp 157–160°C; ir ($CHCl_3$): 3010, 2950, 1730, 1450, 1430, 1220 cm^{-1}; ^{1}H nmr ($CDCl_3$) δ: 5.50 (2H, s, -C(8)H=C(9)H-), 3.78 and 3.68 (12H, 2s, $(CO_2CH_3)_4$), 2.73–2.66 (4H, m, -C(3)H_e-, -C(7)H-, -C(10)H-, and -C(14)H_e-), 2.45 (4H, d, J = 13.0 Hz, -C(4)H_e-, -C(6)H_e-, -C(11)H_e-, and -C(13)H_e-, 1.87–1.45 (6H, m, -C(3)H_a-, -C(4)H_a-, -C(6)H_a-, -C(11)H_a-, -C(14)H$_a$-, and -C(14)H_a-); ^{1}H nmr (C_6D_6) δ: 5.44 (2H, s, -C(8)H=C(9)H-), 3.39 and 3.25 (12H, 2s, $(CO_2CH_3)_4$), 2.90 (2H, d, J = 12.5 Hz, -C(7)H- and -C(10)H-), 2.67 and 2.50 (6H m and d, J = 12.7 Hz, -C(3)H_e-, -C(4)H_e-, -C(6)H_e-, -C(11)H_e-, -C(13)H_e-, and -C(14)H_e-), 1.94–1.70 (6H, m, -C(3)H_a-, -C(4)H_a-, -C(6)H_e-, -C(11)H_a-, -C(14)H_a-, and -C(14)H_a-); ^{13}C nmr ($CDCl_3$) δ: 128.0 and 127.9 (-C(1)=C(2)- and -C(8)H=C(9)H-), 52.7 ((CO_2CH_3)$_4$), 39.4 (-C(6)- and -C(11)-), 35.4 (-C(7)-and -C(10)-), 32.4 (-C(4)- and -C(13)-), 25.2 (-C(3)- and -C(14)-); ms m/e: 420 (M^+). Exact mass (M^+) calcd.: 420.1784; found: 420.1781.

Compound **19**: uv (hexane): λ_{max} 230, 236 nm (ε 12 075, 11 830); λ_{min}: 245 nm (ε 7420); ir ($CHCl_3$): 3020, 2950, 2920, 1730, 1460, 1430, 1220 cm^{-1}; ^{1}H nmr ($CDCl_3$) δ: 5.71 (1H, t, J = 4.1 Hz, -C(2)′H-), 5.58 (1H, t, J = 4.2 Hz, -C(2)H-), 5.53 (1H, m, -CH=CH_2), 4.92 (2H, m, -CH=CH_2), 3.71 (3H, s, -CO_2CH_3), 3.70 (6H, s, (-CO_2CH_3)$_2$), 3.65 (3H, s, -CO_2CH_3), 3.20 (1H, q, J = 6.0 Hz, -C(6)H-CH=CH_2), 2.66 (4H, m, -C(3′)H_2, -C(3)H_2-), 2.38 (1H, m, -C(5)H_aH$_b$-), 2.10 (5H, m, -C(5)H_bH$_a$-, -C(5′)H_2-, -C(6′)H_2-); decoupled ^{13}C nmr ($CDCl_3$) δ: 172.0 ((-CO_3CH_2)$_2$), 171.9 ((CO_2CH_3)$_2$), 140.5 (-CH=CH_2), 138.6 (-C(1)-), 135.3 (-C(1′)-), 120.5 (-C(2′)-), 120.2 (-C(2)H-), 115.4 (-CH=CH_2), 52.7 (-CO_2CH_3), 52.5 (-CO_2CH_3), 52.3 (-CO_2CH_3), 51.8 (-CO_2CH_3), 37.4 (-C(3′)H$_2$-), 34.5 (-C(3)H_2-), 31.5 (-C(4′)-), 30.9 (-C(5′)H$_2$-C(6′)H$_2$-), 29.6 (-C(4)-), 27.8 (-C(5)H$_2$-), 23.5 (-C(6)H-); coupled ^{13}C nmr ($CDCl_3$; only for olefinic carbons δ: 140.5 (d, J = 156.5 Hz), 138.6 (s), 125.3 (s), 120.5 (d, J = 159.1 Hz), 120.2 (d, J = 155.1 Hz), 115.4 (t, J = 156.5 Hz); ms m/e: 420 (M^+). Exact mass (M^+) calcd.: 420.1784; found: 420.1781.

*4,4,4′,4′-Tetracarbomethoxy-6-ethyl-1,1′-bicyclohexenyl (**20**)*

To a solution of **19** (13.8 mg, 33 umol) in benzene (0.5 mL) was added a catalytic amount of carbonyltris(triphenylphosphine)rhodium(I) hydride (1.1 mg) and the reaction vessel was fitted with a hydrogen balloon. The resulting mixture was stirred at room temperature for 48 h. The solvent was removed by vacuum and the residue was purified by flash chromatography (hexanes/ethyl acetate/CH_2Cl_2; 9:1:2) to provide product **20** (8.7 mg, 63%) along with recovered starting material **19** (1.5 mg, 11%). Compound **20**: ir (neat): 3020, 2960, 2850, 1740, 1455, 1440, 1200 cm^{-1}; ^{1}H nmr ($CDCl_3$) δ: 5.56 (1H, m, -C(2)H=CR-), 5.50 (1H, m, -C(2′)H=CR-), 3.71 (12H, s, (-CO_2CH_3)$_4$), 2.62 (2H, m, -C(3)H_2-), 2.44 (4H, m, -C(3′)CH_2)-, -C(5′)CH_2-), 2.16 (2H, m, -C(6′)H_2-), 2.10 (1H, m, -C(6)H-), 1.86 (1H, m, -C(5)H_aH$_b$-), 1.75 (1H, m, -C(5)H_bH$_a$-), 1.47 (1H, m, -CH_aH$_b$CH$_3$), 1.24 (1H, m, -CH_aH$_b$CH$_3$), 0.80 (3H, t, J = 7.3 Hz, -CH_2CH_3); ms m/e: 422 (M^+).

Acknowledgements

This research was supported by the Natural Sciences and Engineering Research Council of Canada (NSERCC, Ottawa) and by the Ministère de l'Education (FCAR, Québec).

1. (*a*) D. Taub. *In* The total synthesis of natural products. Vol. 6. *Edited by* J. ApSimon. John Wiley and Sons, New York. 1984. pp. 1–49; (*b*) K. Nakanishi. In Natural products chemistry. Vol. 3. *Edited by* K. Nakanishi *et al.* Kodansha Ltd., Tokyo. 1983. Chap. 4.
2. (*a*) R. A. Micheli, Z. G. Hajos, N. Cohen, D. R. Parrish, L. A. Portland, W. Sciamanna, M. A. Scott, and P. A. Wherli. J. Org. Chem. **40**, 675 (1975); (*b*) Z. G. Hajos and D. R. Parrish. J. Org. Chem. **38**, 3244 (1973).
3. W. S. Johnson, B. E. McCarry, R. L. Harkezich, and S. G. Boots. J. Am. Chem. Soc. **102**, 352 (1980), and references therein.
4. (*a*) T. Kametani and H. Nemoto. Tetrahedron, **37**, 3 (1981); (*b*) W. Oppolzer. Angew. Chem. Int. Ed. Engl. **16**, 10 (1977); (*c*) A. G. Fallis. Can. J. Chem. **62**, 183 (1984), and references therein; (*d*) M. Ihara, I. Sudow, and K. Fukumoto. J. Chem. Soc. Perkin Trans. 1, 117 (1986); (*e*) M. E. Jung and K. M. Halweg. Tetrahedron Lett. 2121 (1984).
5. (*a*) J. F. Lavallée and P. Deslongchamps. Tetrahedron Lett. **29**, 6033 (1988); (*b*) Tetrahedron Lett. **28**, 3457 (1987).
6. (*a*) H. Kakisawa, I. Okazaki, and M. Ohashi. Tetrahedron Lett. 3231 (1968); (*b*) A. C. Baillie and R. H. Thomson. J. Chem. Soc. (C), 48 (1968); (*c*) H. Kakisawa, T. Hayashi, and T. Yamazaki. Tetrahedron Lett. 301 (1969).
7. (*a*) R. E. Marker and E. Rohrmann. J. Am. Chem. Soc. **60**, 2927 (1938); (*b*) J. E. Baldwin, D. H. R. Barton, I. Dainis, and J. L. C. Pereira. J. Chem. Soc. (C), 2283 (1968).

8. M. NEEMAN and Y. HASHIMOTO. Tetrahedron, 183 (1961).
9. (*a*) S. LAMOTHE, A. NDIBWAMI, and P. DESLONGCHAMPS. Tetrahedron Lett. **29**, 1639 (1988); (*b*) Tetrahedron Lett. **29**, 1641 (1988); (*c*) A. MARINIER and P. DESLONGCHAMPS. Tetrahedron Lett. **29**, 6215 (1988).
10. T. TAKAHASHI, K. SHIMIZU, T. DOI, and J. TSUJI. J. Am. Chem. Soc. **110**, 2674 (1988).
11. (*a*) K. BAETTIG, C. DALLAIRE, R. PITTELOUD, and P. DESLONGCHAMPS. Tetrahedron Lett. **28**, 5249 (1987); (*b*) K. BAETTIG, A. MARINIER, R. PITTELOUD and P. DESLONGCHAMPS. Tetrahedron Lett. **28**, 5253 (1987); (*c*) G. BÉRUBÉ and P. DESLONGCHAMPS. Tetrahedron Lett. **28**, 5255 (1987); (*d*) Can. J. Chem. **68**, 404 (1990); (*e*) A. MARINIER, K. BAETTIG, C. DALLAIRE, R. PITTELOUD, and P. DESLONGCHAMPS. Can. J. Chem. **67**, 1609 (1989).
12. K. F. BERNADY, M. B. FLOYD, J. F. POLETTO, and M. J. WEISS. J. Org. Chem. **44**, 1438 (1979).
13. D. BRILLON and P. DESLONGCHAMPS. Can. J. Chem. **65**, 43 (1987).
14. R. K. CROSSLAND and K. L. SERVIS. J. Org. Chem. **35**, 3195 (1970).
15. M. MIYASHITA, A. YOSHIKOSHI, and P. A. GRIECO. J. Org. Chem. **42**, 3772 (1977).
16. S. LAMOTHE. Ph.D. Thesis. Université de Sherbrooke. October, 1989.
17. E. W. COLLINGTON and A. I. MEYERS. J. Org. Chem. **36**, 3044 (1971).
18. A. G. MICHEL, M. DROUIN, N. MICHEL-DEWEZ, Y. C. XU, M. CANTIN, and P. DESLONGCHAMPS. Acta Crystallogr. Sect. C: Cryst. Struct. Commun. In press.
19. R. V. BONNERT and P. JENKINS. Tetrahedron Lett. **28**, 697 (1987), and references therein.
20. W. D. DAUBEN, R. L. CARGILL, R. M. COATES, and J. SALTIEL. J. Am. Chem. Soc. **88**, 2742 (1966).
21. C. O'CONNOR and G. WILKINSON. J. Chem. Soc. (A). 2665 (1968).
22. J. A. DEYRUP and M. BETKOUAKI. Tetrahedron Lett. **13**, 1131 (1973).

Can. J. Chem. Downloaded from www.nrcresearchpress.com by 195.138.81.100 on 09/07/12
For personal use only.

Stereocontrolled construction of A.B.C.[6.6.6] tricycle via transannular Diels–Alder reaction of 14-membered triene macrocycle

MICHEL CANTIN,[1] YAO-CHANG XU, AND PIERRE DESLONGCHAMPS[2]

Laboratoire de synthèse organique, Département de chimie, Faculté des sciences, Université de Sherbrooke, Sherbrooke (Québec), Canada J1K 2R1

Received May 7, 1990

MICHEL CANTIN, YAO-CHANG XU, and PIERRE DESLONGCHAMPS. Can. J. Chem. **68**, 2144 (1990).

The synthesis of the four acyclic trienes **11***a*, *b* and **20***a*, *b* is reported. The tandem macrocyclization and stereoselective transannular Diels–Alder reaction of acyclic trienes **11***b* (*trans-trans-cis*) and **20***b* (*trans-trans-trans*) were observed in the presence of Cs_2CO_3 at 85°C to give tricycles **30** (TST) and **32** (CAT) respectively. However, treatment of acyclic trienes **11***a* (*cis-trans-cis*) and **20***a* (*cis-trans-trans*) under the same conditions yielded the 14-membered macrocycles **21** and **23**, which were stereoselectively transformed at 250°C into tricycles **22** (CST) and **24** (CAT) respectively in excellent yield.

Key words: stereocontrolled synthesis, macrocycle, tricyclic compound, transannular Diels–Alder reaction.

MICHEL CANTIN, YAO-CHANG XU et PIERRE DESLONGCHAMPS. Can. J. Chem. **68**, 2144 (1990).

La préparation des quatre triènes acycliques **11***a*, *b* et **20***a*, *b* est rapportée. En présence de Cs_2CO_3 à 85°C, les triènes **11***b* (*trans-trans-cis*) et **20***b* (*trans-trans-trans*) se transforment stéréosélectivement dans les tricycles **30** (TST) et **32** (CAT) respectivement par réaction de macrocyclisation suivie d'une réaction de Diels–Alder transannulaire stéréocontrôlée. Par contre, le traitement des triènes acycliques **11***a* (*cis-trans-cis*) et **20***a* (*cis-trans-trans*) dans les mêmes conditions conduit aux macrocycles à 14 membres **21** et **23** respectivement. Par chauffage à 250°C, ces derniers sont respectivement transformés dans les tricycles **22** (CST) et **24** (**CAT**) avec un excellent rendement.

Mots clés : synthèse sterécontrôlée, macrocycle, produit tricyclique, réaction de Diels–Alder transannulaire.

Can. J. Chem. Downloaded from www.nrcresearchpress.com by 195.138.81.100 on 09/07/12
For personal use only.

In the preceding article (1), we described the synthesis of A.B.C.[6.6.6] tricyclic compound **2** via the transannular Diels–Alder reaction of 14-membered dienyne macrocycle **1** (Scheme 1). The tricyclic Diels–Alder adduct **2**, which has two chiral centers on the unsaturated ring B, could be constructed stereoselectively by changing the geometry of the diene double bonds. This new methodology, which is complementary with other known methods such as aldol condensation (2), biomimetic cyclization (3), intramolecular Diels–Alder reaction (4), and intramolecular Michael addition (5), provides a powerful tool for the synthesis of polycyclic carbon skeletons of natural products such as steroids and terpenes (6).

In this article, we would like to report our continued study (7, 13) of this new method with a different macrocyclic system **3**, which contains three unsubstituted olefins. As indicated in Scheme 1, transannular Diels–Alder reaction of 14-membered triene macrocycle **3** results in the formation of a new tricyclic product **4**, which possesses four chiral centers and one double bond on the B ring. It is believed that this will provide even greater applications in the synthesis of polycyclic natural products.

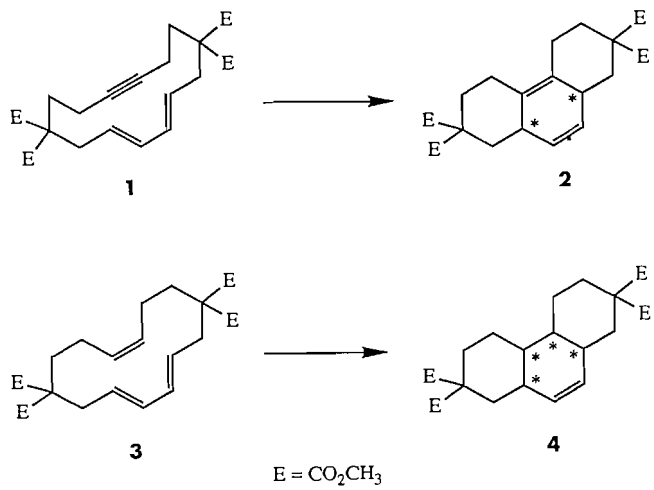

SCHEME 1

Synthesis of acyclic triene

Our basic strategy for the preparation of the acylic trienes is to use the coupling reaction of dienes and dienophiles, which was developed earlier (7) and utilized extensively in our laboratory. As indicated in Scheme 2, the synthesis of *cis* dienophile **6** was achieved by stereoselective *syn* hydrogenation, with a Lindlar catalyst (8), of the triple bond of **5**, whose synthesis was reported previously (1). Syntheses of dienes **7***a* (*cis-trans*) and **7***b* (*trans-trans*) were also performed in our laboratory and their synthetic details will be reported in the near future (9). The coupling reaction of the dienophile with each diene was conducted by deprotonation of malonate **6** with sodium hydride, followed by alkylation of the resulting anion with allylic chlorides **7***a* and **7***b*, which provided *cis-trans-cis* and *trans-trans-cis* acylic triene products **8***a* and **8***b* respectively in good yields. Introduction of the second malonate connector was accomplished by substitution of the methanesulfonate ester group of **8***a* and **8***b* with the sodium salt of dimethyl malonate in the presence of potassium iodide to provide **9***a* and **9***b*. The THP ethers of **9***a* and **9***b* were cleaved by hydrolysis in methanol with pyridinium *p*-toluenesulfonate as catalyst to give the corresponding alcohols **10***a* and **10***b* respectively (10), which were then converted to allylic chlorides **11***a* and **11***b* by Meyers' procedures using LiCl, CH_3SO_2Cl, and *s*-collidine in DMF (11). Purification by chromatography on silica gel caused a small amount of decomposition of allylic chlorides **11***a* and **11***b*; however, this problem could be avoided if they were used immediately for the subsequent macrocyclization step without flash chromatography.

The synthesis of the other two acyclic trienes **20***a* (*cis-trans-*

[1]FCAR predoctoral fellowship (1987–1988).

[2]Author to whom correspondence may be addressed.

Can. J. Chem. Downloaded from www.nrcresearchpress.com by 195.138.81.100 on 09/07/12
For personal use only.

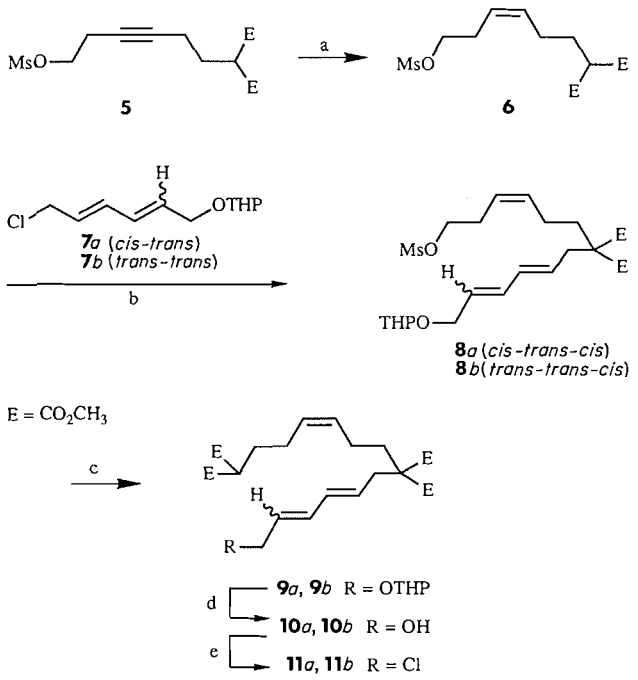

(a) H_2, $Pd/CaCO_3$-PbO, EtOAc, rt, 6 h, 98%;
(b) NaH, DMF-THF, rt, 5 h, **8***a*: 93%; **8***b*: 80%;
(c) NaH, $CH_2(CO_2CH_3)_2$, KI, DMF-THF, 80°C, 3.5 h, **9***a*: 85%; **9***b*: 90%;
(d) PPTS, MeOH, 60°C, 1 h, **10***a*: 94%; **10***b*: 47%;
(e) LiCl, *s*-collidine, MsCl, DMF, **11***a*: 89%.

SCHEME 2

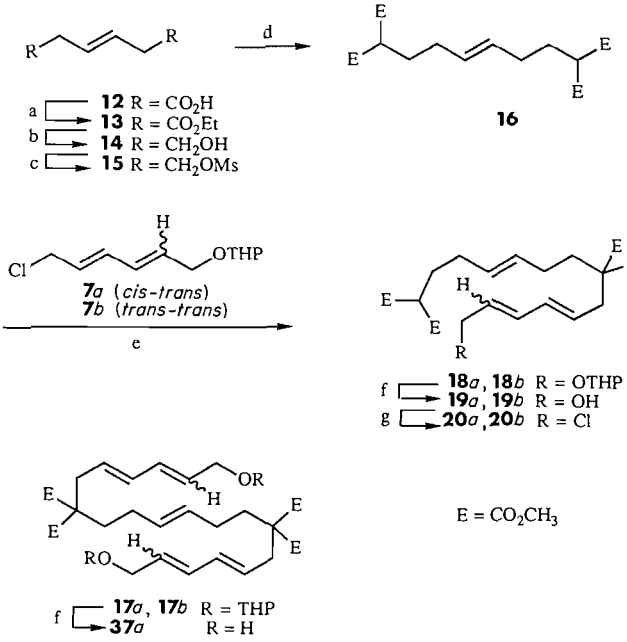

(a) H_2SO_4, EtOH, C_6H_6, 90°C, 48 h, 99%;
(b) $LiAlH_4$, Et_2O, rt, 30 min, 94%;
(c) MsCl, Et_3N, CH_2Cl_2, rt, 30 min, 97%;
(d) NaH, $CH_2(COOCH_3)_2$, KI, DMF-THF, 80°C, 3.5 h, 73%;
(e) NaH, DMF-THF, rt, 4.5 h, then;
(f) PPTS, MeOH, 60°C, 1.5 h, **19***a*: 84%; **37***a*, 14%; **19***b*: 47%;
(g) LiCl, *s*-collidine, MsCl, DMF, **20***a*: 90%.

SCHEME 3

trans) and **20***b* (*trans-trans-trans*) is outlined in Scheme 3 starting with the preparation of *trans* dienophile **16**. The commercially available *trans*-β-hydromuconic acid **12** was converted to its corresponding diester **13** in almost quantitative yield with sulfuric acid in ethanol. Reduction of the ester groups with lithium aluminum hydride in ether yielded diol **14**, which was subsequently transformed into methanesulfonate ester **15** in excellent yield by methanesulfonyl chloride and triethylamine (12). Introduction of two malonate groups at either end of the molecule was achieved by alkylation of **15** with the sodium salt of dimethyl malonate to give *trans* dienophile **16**. The coupling reaction of dienophile **16** and dienes **7***a* and **7***b* was carried out according to the procedure previously used for the preparation of **8**, to provide acyclic trienes **18***a* (*cis-trans-trans*) and **18***b* (*trans-trans-trans*) respectively. As expected, a dialkylation by-product **17***a* was obtained, and hydrolysis of the two THP ether groups gave the corresponding diol **37***a* in 14% yield. Interestingly, no dialkylation product **17***b* was observed. Following the same reaction sequences and conditions as indicated in Scheme 2 for the preparation of **11** from **9**, crude compounds **18***a* and **18***b* were hydrolyzed (10), and resulting alcohols **19***a* and **19***b* were converted to allylic chlorides **20***a* and **20***b* respectively (11).

Macrocyclization and Diels–Alder reaction

Having synthesized the requisite carbon chain and appropriate functional groups at each end, the four acyclic trienes **11***a, b* and **20***a, b* were ready for construction of the 14-membered macrocycles. The macrocyclizations and transannular Diels–Alder reactions for acyclic trienes **11***a* (*cis-trans-cis*) and **20***a* (*cis-trans-trans*) are presented in Scheme 4. According to the procedures developed earlier in our laboratory (7, 9, 13, 14), the macrocyclization of **11***a* was conducted by adding a solution of allylic chloride **11***a* in CH_3CN, by syringe pump, to a stirred suspension of cesium carbonate in CH_3CN at 85°C over a period of 12 h, using high dilution technique (2×10^{-3} M) to avoid dimerization. Macrocyclic product **21** (*cis-trans-cis*) was isolated as a white solid in 87% yield. Similarly, acyclic triene **20***a* was cyclized under the same conditions to give 14-membered macrocycle **23** (*cis-trans-trans*) in 60% yield. The macrocyclization of **20***a* was also carried out in a mixture of THF/DMF (1:1), leading to the same macrocycle **23** in comparable yield (55%).

The *cis-trans-cis* macrocycle **21** could also be obtained by chemo- and stereoselective *syn* hydrogenation of the triple bond from dienyne macrocycle **25** with a Lindlar catalyst in quantitative yield (Scheme 5) (8). The synthesis of dienyne macrocycle **25** was described in the preceding paper (1). The structures of macrocycles **21** and **23** were determined on the basis of spectroscopic data (^{13}C and ^{1}H nmr, ir, and ms). The olefin geometry of **21** (*cis-trans-cis*) and **23** (*cis-trans-trans*) was retained in the cyclization reaction as demonstrated by comparing their ^{1}H nmr data with those of the acyclic triene precursors **11***a* and **20***a* respectively.

As indicated in Scheme 4, the transannular Diels–Alder reaction of **21** was carried out by thermolysis in a sealed quartz tube at 250°C for 90 min, providing only one tricyclic product **22** in 92% yield with *cis-syn-trans* (abbreviated as CST) stereochemistry for protons at ring conjunctions. Similarly, thermolysis of macrocycle **23** at the same temperature for 2 h gave a new tricyclic compound **24** (*cis-anti-cis*; CAC) in the same yield. The structures of tricyclic products **22** and **24** were

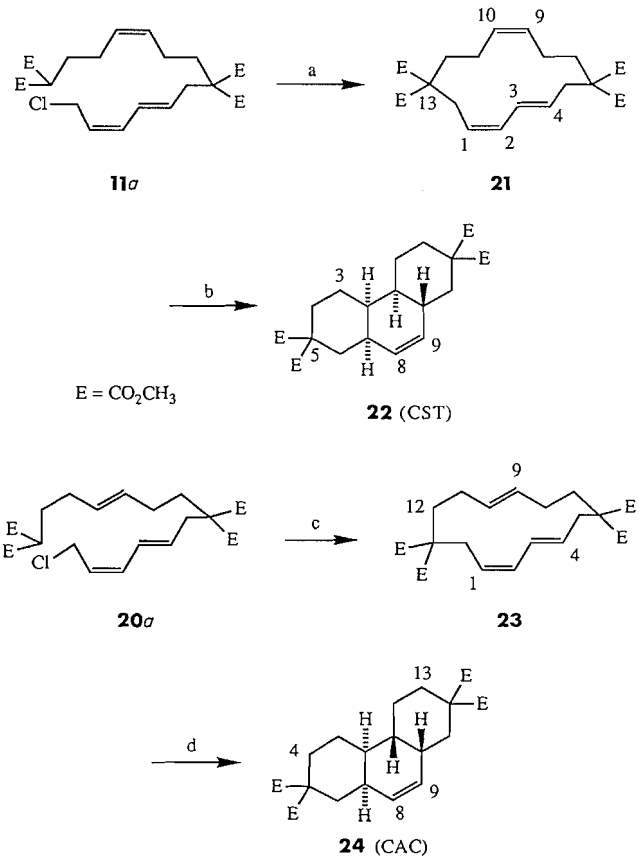

(a) Cs_2CO_3, CH_3CN, 85°C, 2.0 x 10^{-3}M, 17 h, 87%;
(b) 250°C in sealed tube, 90 min, 92%;
(c) Cs_2CO_3, CH_3CN, 85°C, 2.2 x 10^{-3}M, 17 h, 60%;
Cs_2CO_3, DMF/THF(1:1), 85°C, 2.0 x 10^{-3}M, 17 h, 55%;
(d) 250°C in sealed tube, 2 h, 92%.

SCHEME 4

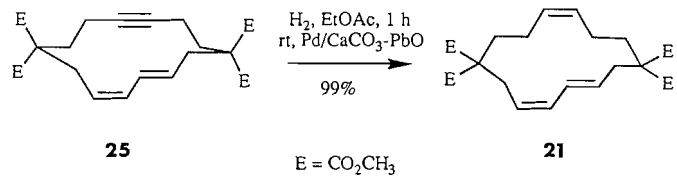

SCHEME 5

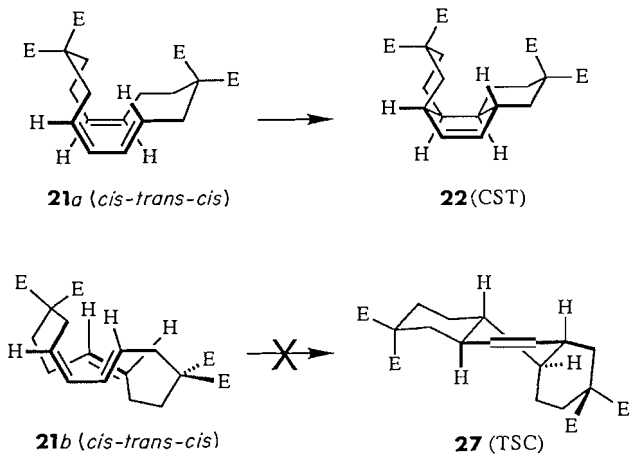

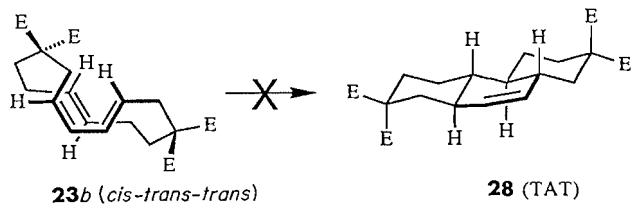

SCHEME 6

determined on the basis of conventional spectroscopic data including ^{13}C and ^{1}H nmr, ir, ms, and HCCORR. Unfortunately, tricyclic compounds **22** and **24** did not yield single crystals, suitable for X-ray crystallography, to confirm the proposed structures. The relative stereochemistry of the four hydrogens at the ring conjunctions of tricycles **22** and **24**, however, can be reasonably assigned by molecular model analysis, which has been successfully and extensively used in our laboratory to predict the stereochemisty of tricyclic products from transannular Diels–Alder reactions (1, 7*a*,*b*). Based on theoretical analysis, each triene macrocycle can lead at most to two different tricyclic diastereoisomers. As shown in Scheme 6, the molecular model shows that the triene macrocycle **21** with *cis-trans-cis* olefin geometry can adopt two different conformations **21***a* and **21***b*, which may lead to tricycles **22** (CST) and **27** (TSC). However, it is not difficult to recognize from these molecular models that conformation **21***b* cannot undergo Diels–Alder reaction because it is sterically impossible to reach a boat transition state for the newly forming B ring, which must be attained for Diels–Alder reaction to take place. Therefore, macrocyle **21** can give only one tricyclic product **22** with CST stereochemistry. Similarly, triene macrocycle **23** with *cis-trans-trans* olefin geometry can adopt two different conformations **23***a* and **23***b* (Scheme 6). Transannular Diels–Alder reaction of **23***a* produces **24** with *cis-anti-cis* (CAC) stereochemistry. Conformation **23***b*, which is similar to **21***b*, cannot undergo Diels–Alder reaction to produce tricycle **28** because it is impossible to reach a boat transition state due to the steric encumbrance. As a result, only one diastereoisomer **24** (CAC) is expected from macrocycle **23**.

Macrocyclization of *trans-trans-cis* acyclic triene **11***b* was performed by adding a solution of crude **11***b* in THF to a stirred suspension of cesium carbonate in a mixture of DMF and THF (1:1) at 85°C over a period of 13 h in high dilution (2×10^{-3} M) (Scheme 7). The stirring was continued for 24 h after the addition was finished. At this stage, tricyclic product **30** (TST) was isolated as the sole product in an overall yield of 69% from allylic alcohol **10***b*, presumably via a transannular Diels–Alder reaction of 14-membered macrocycle intermediate **29**. The same reaction in CH_3CN gave the same tricycle **30** in comparable overall yield (60%). The tandem macrocyclization and transannular Diels–Alder reaction was also observed for *trans-trans-trans* acyclic triene **20***b* under the same conditions,

Can. J. Chem. Downloaded from www.nrcresearchpress.com by 195.138.81.100 on 09/07/12
For personal use only.

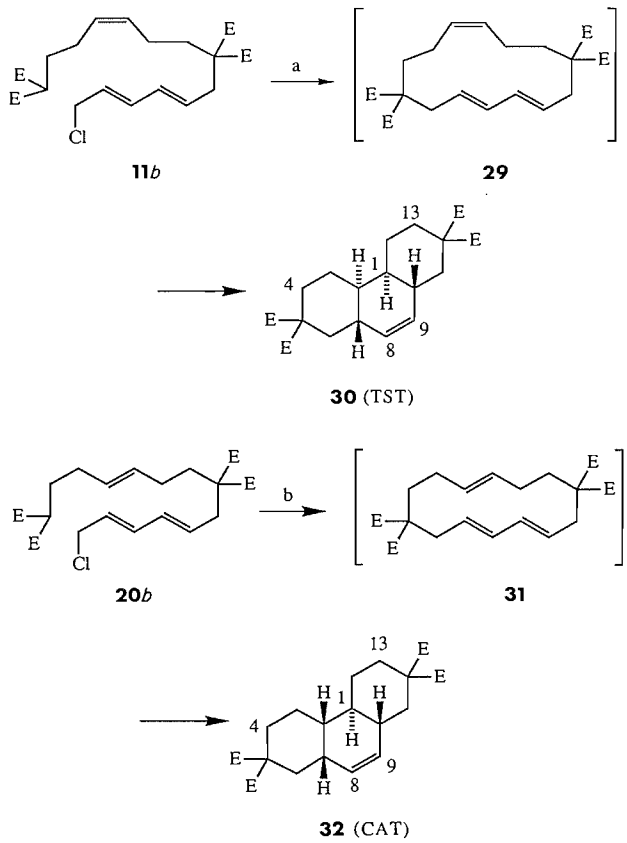

(a) Cs_2CO_3, DMF/THF(1:1), 85°C, 2.0 x 10^{-3}M, 37 h, 69% for last three steps; Cs_2CO_3, CH_3CN, 85°C, 2.0 x 10^{-3}M, 36 h, 60% for last three steps; (b) Cs_2CO_3, DMF-THF(1:1), 85°C, 2.0 x 10^{-3}M, 36 h, 26% for last three steps; Cs_2CO_3, CH_3CN, 85°C, 2.0 x 10^{-3}M, 37 h, 25% for last three steps.

SCHEME 7

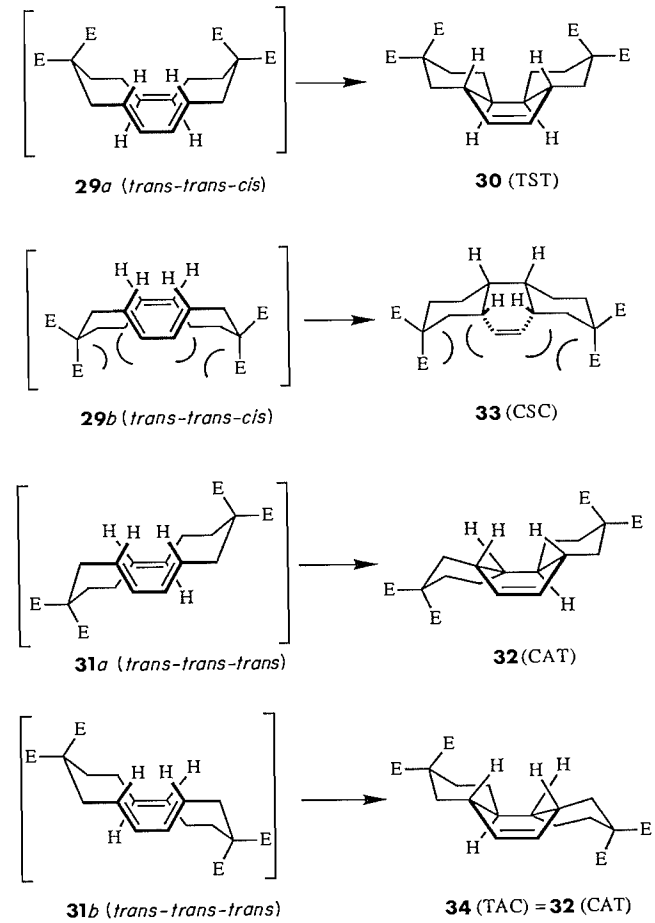

E = CO_2CH_3

SCHEME 8

leading to a new tricyclic product **32** (CAT) in 26% overall yield from **19***b* in DMF/THF mixture, and 25% yield in CH_3CN. The failure to isolate macrocycles **29** and **31** simply suggests that the Diels–Alder cycloadditions are very much facilitated in this transannular process, so they can take place even under the mild conditions and with a non-activated dienophile such as an alkyl substituted olefin. In contrast with the isolable macrocycles **21** and **23**, the increased reactivities of **29** and **31** can be explained by the fact that formation of the *cisoid* dienes, which is required for the concerted Diels–Alder reaction, poses much less steric encumbrance, when the diene moiety has a *trans-trans* geometry (15).

The structures of the two tricyclic products **30** (TST) and **32** (CAT) were also determined on the basis of both spectroscopic data and molecular model. According to the analysis proposed above, macrocyclic intermediate **29** with *trans-trans-cis* olefin geometry could take two different conformations, **29***a* and **29***b*, which would lead to tricycles **30** and **33** respectively by the transannular cycloaddition. From the molecular model, it is easy to see that transformation from conformation **29***b* to tricycle **33** experiences a higher transition energy due to the 1,3 steric interactions between the two axial carbomethoxy groups and newly forming double bond (Scheme 8). From this analysis, Diels–Alder reaction of **29** would be predicted to produce a mixture of two, **30** and **33**, but with tricycle **30** much favored. In fact, we only obtained one product, and this must be tricycle **30** with *trans-syn-trans* (TST) stereochemistry. Indeed, X-ray crystallography showed that compound **30** did possess the TST stereochemistry (16), which correlated well with the molecular model analysis.

Similarly, *trans-trans-trans* macrocycle intermediate **31** can possess two different conformations **31***a* and **31***b*. Diels–Alder reactions of both conformations are sterically possible, and this will produce tricycles **32** (CAT) and **34** (TAC) respectively. It is interesting to note that tricycle **34** is in fact the mirror image of tricycle **32**. Therefore, no matter which conformation **31** adopts, it will lead to only one diastereoisomer since **32** (CAT) is identical to **34** (TAC). The structure has been determined by spectroscopic data (^1H and ^{13}C nmr, ir, and ms), although it could not be confirmed by X-ray analysis due to the difficulty in obtaining single crystals.

In summary, we have demonstrated a simple and general methodology for the syntheses of A.B.C.[6.6.6] carbotricyclic compounds in moderate to excellent yields, in a stereocontrolled manner, by varying the geometry of triene macrocycles. The acyclic trienes with different *cis* and *trans* double bonds were assembled by coupling dienes and dienophiles, and the macrocycles were synthesized by intramolecular S_N2 displacement of allylic chlorides with malonate anions in good yields. The transannular Diels–Alder reaction of macrocycles with a non-activated dienophile is a facile and a good yielding process, even under mild conditions. By comparison with the series previously studied where the transannular Diels–Alder reactions with dienophiles substituted by a methyl group gave unpredictable side-products in some cases (7), the present series

Can. J. Chem. Downloaded from www.nrcresearchpress.com by 195.138.81.100 on 09/07/12
For personal use only.

Can. J. Chem. Downloaded from www.nrcresearchpress.com by 195.138.81.100 on 09/07/12
For personal use only.

with no methyl substituent on the dienophile lead to the predictable tricycles with no side reaction. The present method, along with the others developed earlier by us (1, 7, 13), should find broad applications in synthesizing polycyclic natural products. Studies towards this goal are currently under investigation in our laboratory.

Experimental

Infrared spectra (ir) were recorded on a Perkin–Elmer 681 spectrophotometer, using chloroform ($CHCl_3$), or run as neat films on sodium chloride cells. The ^1H nmr and ^{13}C nmr spectra were taken on a Bruker WM-250 spectrometer in deuteriated chloroform ($CDCl_3$) or benzene (C_6D_6). The following abbreviations are used in the text: s, singlet; d, doublet; t, triplet; q, quadruplet; and m, multiplet. Mass spectra (ms) were recorded on a VG-Micromass ZAB-1F mass spectrometer. Melting points (mp) were measured on a Büchi or a Reichert melting point apparatus and were not corrected. Thin-layer chromatography (tlc) was performed using silica gel 60 F-250. For flash column chromatography Merck Kieselgel (no. 9385) was used.

Unless otherwise noted, all reagents were obtained from commercial suppliers and used without further purification. Acetonitrile, amines, dimethylformamide (DMF), hexamethylphosphoramide (HMPA), and dichloromethane (CH_2Cl_2) were distilled from calcium hydride; methanol from magnesium and iodine; acetone and ethyl acetate from potassium carbonate; benzene, toluene, diethyl ether, and tetrahydrofuran (THF) from sodium and benzophenone ketyl. Purified and dried reagents were kept under argon. Unless otherwise specified, all reactions were carried out under argon atmosphere.

*Methyl (5Z)-2-carbomethoxy-8-methanesulfonyloxy-5-octenoate (**6**)*

Hydrogen was bubbled through a stirred solution of alkyne methanesulfonate ester **5** (1.1 g, 3.5 mmol) in ethyl acetate (100 mL), and a Lindlar catalyst (palladium on calcium carbonate, poisoned with lead, 200 mg) was added. The reaction mixture was maintained under these conditions for 6 h, and then filtered and concentrated to give *cis*-alkene methanesulfonate ester **6** (1.1 g, 98%) as a pure oil; ir (neat): 3020, 2960, 1740, 1435, 1350, 1175 cm^{-1}; ^1H nmr ($CDCl_3$) δ: 547 (2H, m, $-CH_2CH{=}CHCH_2-$), 4.20 (2H, t, J = 6.8 Hz, $CH_3SO_2OCH_2CH_2-$), 3.74 (6H, s, $-CH_2CH(CO_2CH_3)_2$), 3.37 (1H, t, J = 7.3 Hz, $-CH_2CH(CO_2CH_3)_2$), 3.01 (3H, s, $CH_3SO_2OCH_2-$), 2.47 (2H, q, J = 6.7 Hz, $=CHCH_2CH_2O-$), 2.10 (2H, q, J = 7.3 Hz, $=CHCH_2CH_2CH(CO_2CH_3)_2$), 1.97 (2H, m, $=CHCH_2CH_2CH(CO_2CH_2)_2$); ms m/e: 309 (MH^+).

*(2Z,4E,10Z)-7,7-Biscarbomethoxy-13-methanesulfonyloxy-1-[(tetrahydro-2H-pyran-2-yl)oxy]-2,4,10-tridecatriene (**8**a)*

General procedure A

To a stirred sodium hydride suspension (45 mg, 1.1 mmol) in a mixture of DMF/THF (1:1, 8 mL) was added a solution of methanesulfonate ester **6** (313 mg, 1.0 mmol) in a mixture of DMF/THF (1:1, 2 mL) at room temperature. After the mixture was stirred for 10 min, it was transferred to a solution of allylic chloride **7***a* (287 mg, 1.3 mmol) in a mixture of DMF/THF (1:1, 2 mL). The resulting mixture was stirred for 5 h at room temperature, then quenched with saturated NH_4Cl solution (20 mL), diluted with H_2O (20 mL), and extracted with hexanes/diethyl ether (1:2, 5 × 50 mL). The combined organic layers were washed with H_2O (40 mL) and brine (40 mL), dried over $MgSO_4$, then filtered and evaporated. The crude residue was purified by flash chromatography (hexanes/ethyl acetate; 7:3) to give coupling product **8***a* (463 mg, 93%) as an oil; ir (neat); 3020, 2950, 2860, 1730, 1440, 1360, 1170 cm^{-1}; ^1H nmr ($CDCl_3$) δ: 6.39 (1H, dd, J = 15.4 Hz, 11.1 Hz, $-CH_2CH{=}CH{-}CH{=}CHCH_2O-$), 6.08 (1H, t, J = 11.2 Hz, $-CH_2CH{=}CH{-}CH{=}CHCH_2O-$), 5.59–5.47 and 5.42–5.34 (4H, 2m, $-CH_2CH{=}CH{-}CH{=}CHCH_2O-$ and $-CH_2CH{=}CHCH_2-$), 4.62 (1H, t, J = 3 Hz, $-OCHO-$), 4.32 (1H, ddd, J = 12.7 Hz, 6.4 Hz, 1.4 Hz, $-CH{=}CHCHHO-$), 4.22–4.12 (3H, superposed t and m, J = 6.7 Hz, $-CH_3SO_2OCH_2-$ and $-CH{=}CHCHHO-$), 3.90–3.82 and 3.55–3.48 (2H, 2m, $-OCHOCH_2-$), 3.72 (6H, s, $-CH_2C(CO_2CH_3)_2CH_2-$), 3.01 (3H, s, CH_3SO_2O-), 2.71 (2H, d, J = 7.2 Hz, $=CHCH_2C(CO_2CH_3)CH_2-$), 2.46 (2H, q, J = 6.8 Hz, $-CH_2CH_2C(CO_2CH_3)_2CH_2-$), 2.01–1.48 (10H, m, $-CH_2CH{=}CHCH_2-$ and $-OCHOCH_2(CH_2)_3$); ms m/e: 470 (M^+-H_2O), 386 (M^+-(OTHP + H)).

*(2E,4E,10Z)-7,7-Biscarbomethoxy-13-methanesulfonyloxy-1-[(tetrahydro-2H-pyran-2-yl)oxy]-2,4,10-tridecatriene (**8**b)*

The general procedure A was followed, using sodium hydride (89 mg, 2.2 mmol), methanesulfonate ester **6** (561 mg, 1.8 mmol), allylic chloride **7***b* (603 mg, 2.8 mmol), DMF (8 mL), and THF (8 mL). Coupling product **8***b* (718 mg, 80%) was obtained; ir (neat): 3020, 2950, 2860, 1730, 1440, 1350, 1170 cm^{-1}; ^1H nmr ($CDCl_3$) δ: 6.16 (2H, m, $-CH_2CH{=}CH{-}CH{=}CHCH_2O-$), 5.72 (1H, dt, J = 14.5 Hz, 6.1 Hz, $-CH_2CH{=}CH{-}CH{=}CHCH_2O-$), 5.57–5.32 (3H, m, $-CH_2CH{=}CH{-}CH{=}CHCH_2O-$ and $-CH_2CH{=}CHCH_2-$), 4.62 (1H, t, J = 4 Hz, $-OCHO-$), 4.30–4.17 (3H, t and hidden m, J = 6.6 Hz, $CH_3SO_2OCH_2-$ and $-CH{=}CHCHHO-$), 3.98 (1H, dd, J = 13.1 Hz, 6.5 Hz, $-CH{=}CHCHHO-$), 3.89–3.82 and 3.55–3.46 (2H, m, $-OCHOCH_2-$), 3.72 (6H, s, $-CH_2C(CO_2CH_3)_2CH_2-$), 3.01 (3H, s, CH_3SO_2O-), 2.70 (2H, d, J = 7.6 Hz, $-CH{=}CHCH_2C(CO_2CH_3)CH_2-$), 2.47 (2H, q, J = 6.8 Hz, $-CH_2CH_2C(CO_2CH_3)_2CH_2-$), 2.00–1.51 (10H, m, $-CH_2CH{=}CHCH_2-$ and $-OCHOCH_2(CH_2)_3$); ms m/e: 387 (M^+-OTHP).

*Methyl (5Z,11E,13Z)-2,9,9-tricarbomethoxy-15-[(tetrahydro-2H-pyran-2-yl)oxy]-5,11,13-pentadecatrienoate (**9**a)*

General procedure B

Dimethyl malonate (512 μL, 4.6 mmol) was added dropwise to a stirred sodium hydride suspension (179 mg, 4.5 mmol) in a mixture of DMF/THF (1:1, 16 mL) at 0°C. The reaction mixture was stirred for 15 min at room temperature, then transferred by syringe to methanesulfonate ester **8***a* (445 mg, 0.91 mmol). Potassium iodide (151 g, 0.91 mmol) was added and the resulting mixture was refluxed at 80°C for 3.5 h. The reaction mixture was cooled to room temperature, quenched with saturated NH_4Cl solution (10 mL), diluted with H_2O (10 mL), and extracted with diethyl ether (4 × 40 mL). The combined organic layers were dried over $MgSO_4$, filtered, and evaporated. The crude residue was purified by flash chromatography (hexanes/ethyl acetate; 17:3) to give tetraester **9***a* (408 mg, 85%) as an oil; ir ($CHCl_3$): 3000, 2950, 2860, 1740, 1440, 1200 cm^{-1}; ^1H nmr ($CDCl_3$) δ: 6.38 (1H, dd, J = 14.8 Hz, 11.3 Hz, $-CH_2CH{=}CH{-}CH{=}CHCH_2-$), 6.08 (1H, t, J = 11.1 Hz, $-CH_2CH{=}CH{-}CH{=}CHCH_2-$), 5.57–5.47 (2H, m, $-CH_2CH{=}CH{-}CH{=}CHCH_2-$), 5.44–5.27 (2H, m, $-CH_2CH{=}CHCH_2-$), 4.62 (1H, t, J = 3.4 Hz, $-OCHO-$), 4.34 (1H, dd, J = 12.7 Hz, 6.3 Hz, $-CH{=}CHCHHO-$), 4.23 (1H, dd, J = 13.2 Hz, 7.5 Hz, $-CH{=}CHCHHO-$), 3.92–3.81 and 3.55–3.46 (2H, 2m, $=CHCH_2OCHOCH_2-$), 3.73 and 3.71 (12H, 2s, $-CH_2CH(CO_2CH_3)_2$ and $-CH_2C(CO_2CH_2CH_3)_2CH_2-$), 3.36 (1H, t, J = 7.2 Hz, $-CH_2CH(CO_2CH_3)_2$), 2.70 (2H, d, J = 7.5 Hz, $=CHCH_2C(CO_2CH_3)_2CH_2-$), 2.06–1.50 (14H, 2m, $-CH_2CH_2CH{=}CHCH_2CH_2-$ and $-OCHOCH_2(CH_2)_3$); ms m/e: 524 (M^+), 506 (M^+-H2O), 386 (M^+-OCH_3).

*Methyl (5Z,11E,13E)-2,9,9-tricarbomethoxy-15-[(tetrahydro-2H-pyran-2-yl)oxy]-5,11,13-pentadecatrienoate (**9**b)*

The general procedure B was followed, using dimethyl malonate (1.0 mL, 8.7 mmol), sodium hydride (288 mg, 7.2 mmol), mesylate **8***b* (705 mg, 1.4 mmol), potassium iodide (280 mg, 1.7 mmol), DMF (19 mL), and THF (19 mL). Tetraester **9***b* (681 mg, 90%) was obtained; ir ($CHCl_3$): 3000, 2950, 2860, 1740, 1440, 1220 cm^{-1}; ^1H nmr ($CDCl_3$) δ: 6.15 (2H, m, $-CH_2CH{=}CH{-}CH{=}CHCH_2O-$), 5.71 (1H, dt, J = 14.7 Hz, 6.1 Hz, $-CH_2CH{=}CH{-}CH{=}CHCH_2O-$), 5.48 (1H, dt, J = 14.4 Hz, 7.4 Hz, $-CH_2CH{=}CH{-}CH{=}CHCH_2O-$), 5.34 (2H, m, $-CH_2CH_2CH{=}CHCH_2CH_2-$), 4.63 (1H, t, J = 3.4 Hz, $-OCHO-$), 4.25 (1H, dd, J = 13.1 Hz, 6.0 Hz, $-CH{=}CHCHHO-$), 2.98 (1H, dd, J = 13.2 Hz, 6.6 Hz, $-CH{=}CHCHHO-$), 3.90–3.82 and 3.55–3.46 (2H, 2m, $=CHCH_2OCHOCH_2-$), 3.73 and 3.71 (12H, 2s, $-CH_2CH(CO_2CH_3)_2$ and $-CH_2C(CO_2CH_3)_2CH_2-$), 3.36 (1H, t, J = 7.2 Hz, $-CH_2CH(CO_2CH_3)_2$), 2.68 (2H, d, J = 7.6 Hz, $=CHCH_2C(CO_2CH_3)_2CH_2-$), 2.09–1.49 (14H, 2m, $-CH_2CH_2CH=$

Can. J. Chem. Downloaded from www.nrcresearchpress.com by 195.138.81.100 on 09/07/12
For personal use only.

$CHCH_2CH_2$- and -$OCHOCH_2(CH2)_3$); ms *m/e*: 524 (M^+), 493 (M^+-OCH_3), 422 ($M^+-C_5H_{10}O_2$).

*Methyl (5Z,11E,13Z)-2,9,9-tricarbomethoxy-15-hydroxy-5,11,13-pentadecatrienoate (**10**a)*

General procedure C

To a stirred solution of tetraester **9***a* (401CO g, 0.76 mmol) in anhydrous methanol (15 mL) was added pyridinium *p*-toluenesulfonate (19 mg, 0.08 mmol) and the resulting mixture was heated at 60°C for 1 h. The mixture was allowed to cool to room temperature, and then treated with brine (10 mL), diluted with H_2O (10 mL), and extracted with ethyl acetate (6 × 10 mL). The combined organic layers were dried over $MgSO_4$, filtered, and evaporated. The crude residue was purified by flash chromatography (hexanes/ethyl acetate; 4:1) to give alcohol **10***a* (148 mg, 44%) as a viscous oil; ir (neat): 3530, 3470, 3000, 2950, 2860, 1735, 1435, 1210 cm^{-1}; ^1H nmr ($CDCl_3$) δ: 6.36 (1H, dd, *J* = 14.7 Hz, 11.1 Hz, -CH_2CH=C*H*-CH=$CHCH_2OH$), 6.02 (1H, t, *J* = 11.1 Hz, CH_2CH=CH-C*H*=$CHCH_2OH$), 5.59–5.50 (2H, m, -CH_2CH=CH-CH=$CHCH_2OH$), 5.40–4.30 (2H, m, -CH_2CH_2CH=$CHCH_2CH_2$-), 4.28 (2H, br s, =$CHCH_2OH$), 3,73 and 3.71 (12H, 2s, -$CH_2CH(CO_2CH_3)_2$ and -$CH_2C(CO_2CH_3)_2CH_2$-), 3.36 (1H, t, *J* = 7.2 Hz, -$CH_2CH(CO_2CH_3)_2$, 2.71 (2H, d, *J* = 7.1 Hz, =$CHCH_2$-$(CO_2CH_3)_2$-CH_2-), 2.08–1.87 (8H, m, -CH_2CH_2CH=$CHCH_2CH_2$-), 1.66 (1H, s, =$CHCH_2OH$); ms *m/e*: 422 (M^+-H_2O).

*Methyl (5Z,11E,13E)-2,9,9-tricarbomethoxy-15-hydroxy-5,11,13-pentadecatrienoate (**10**b)*

The general procedure C was followed, using pyridinium *p*-toluenesulfonate (32 mg, 0.13 mmol), tetraester **9***b* (668 mg, 1.3 mmol), and anhydrous methanol (13 mL). Alcohol **10***b* (526 mg, 94%) was obtained as a viscous oil; ir (neat): 3520, 3470, 3000, 2950, 2860, 1730, 1430, 1220 cm^{-1}; ^1H nmr ($CDCl_3$) δ: 6.16 (2H, m, -CH_2CH=C*H*-C*H*=$CHCH_2O$-), 5.77 (1H, dt, *J* = 14.6 Hz, 5.9 Hz, -CH_2CH=CH-CH=C*H*CH_2O-), 5.49 (1H, dt, *J* = 14.2 Hz, 7.1 Hz, -CH_2CH=CH-CH=$CHCH_2O$-), 5.35 (2H, m, -CH_2CH_2CH=C*H*CH_2CH_2-), 4.16 (2H, t, *J* = 5.9 Hz, =$CHCH_2OH$), 3.74 and 3.72 (12H, 2s, -$CH_2CH(CO_2CH_3)_2$ and -$CH_2C(CO_2CH_3)_2CH_2$-), 3.36 (1H, t, *J* = 7.1 Hz, -$CH_2CH(CO_2CH_3)_2$), 2.69 (2H, d, *J* = 7.6 Hz, =$CHCH_2$-$(CO_2CH_3)_2$-CH_2-), 2.04–1.85 (8H, m, -CH_2CH_2CH=$CHCH_2CH_2$-), 1.55 (1H, t, *J* = 3 Hz, -CH_2OH); ms *m/e*: 422 (M^+-H_2O).

*Methyl (5Z,11E,13Z)-2,9,9-tricarbomethoxy-15-chloro-5,11,13-pentadecatrienoate (**11**a)*

General procedure D

To a stirred solution of alcohol **10***a* (135 mg, 0.31 mmol) in DMF (2.5 mL) were added lithium chloride (110 mg, 2.6 mmol) and *s*-collidine (108 ml, 1.4 mmol) at room temperature. The resulting mixture was cooled to 0°C and methanesulfonyl chloride (80 μL, 1.0 mmol) was added. After the thick mixture was stirred for 30 min, it was diluted with H_2O (15 mL) and extracted with hexanes/diethyl ether (2:1, 3 × 20 mL). The combined organic layers were dried over $MgSO_4$, filtered, and evaporated. The crude residue was purified by flash chromatography (hexanes/ethyl acetate; 17:3) to give allylic chloride **11***a* (126 mg, 89%) as an oil; ^1H nmr ($CDCl_3$) δ: 6.38 (1H, dd, *J* = 14.8 Hz, 11.7 Hz, -CH_2CH=C*H*-CH=$CHCH_2Cl$), (1H, t, *J* = 10.8 Hz, -CH_2CH=CH-C*H*=$CHCH_2Cl$), 5.72–5.50 (2H, m, -CH_2CH=CH-CH=C*H*CH_2Cl), 5.38–5.32 (2H, m, -CH_2CH_2CH=C*H*CH_2CH_2-), 4.18 (2H, d, *J* = 8.2 Hz, =$CHCH_2Cl$), 3.73 and 3.72 (12H, 2s, -$CH_2C(CO_2CH_3)_2CH_2$- and -$CH_2CH(CO_2CH_3)_2$), 3.36 (1H, t, *J* = 7.1 Hz, -$CH_2CH(CO_2CH_3)_2$), 2.74 (2H, d, *J* = 7.5 Hz, -$C(CO_2CH_3)_2CH_2CH$=), 2.10–1.88 (8H, m, -CH_2CH_2CH=$CHCH_2CH_2$-).

*Methyl (5Z,11E,13E)-2,9,9-tricarbomethoxy-15-chloro-5,11,13-pentadecatrienoate (**11**b)*

General procedure E

To a stirred solution of allylic alcohol **10***b* (371 mg, 0.84 mmol) and lithium chloride (297 mg, 7.0 mmol) in DMF (9 mL) was added *s*-collidine (432 μL, 3.0 mmol) at room temperature. The mixture was stirred for 10 min and then cooled to 0°C. Methanesulfonyl chloride (170 μL, 2.2 mmol) was added and the reaction mixture was stirred at 0°C for 45 min, then diluted with H_2O and extracted with hexanes/ethyl ether (2:1, 4 × 50 mL). The combined organic layers were washed successively with saturated $Cu(NO_3)_2$ solution (20 mL), saturated $NaHCO_3$ solution (10 mL), and brine (2 × 20 mL), and then dried over $MgSO_4$, filtered, and evaporated to give crude allylic chloride **11***b*; ^1H nmr (C_6D_6) δ: 5.88 (2H, m, -CH_2CH=C*H*-C*H*=$CHCH_2O$-), 5.64–5.20 (4H, m, -CH_2CH=CH-CH=C*H*CH_2O- and -CH_2CH_2CH=C*H*CH_2CH_2-), 3.61 (2H, d, *J* = 7.2 Hz, =$CHCH_2Cl$), 3.34 and 3.32 (13H, m, -$CH_2C(CO_2CH_3)_2CH_2$-, -$CH_2CH(CO_2CH_3)_2$, and -$CH_2CH(CO_2CH_3)_2$, 2.85 (2H, d, *J* = 7.7 Hz, -$C(CO_2CH_3)_2CH_2$-CH=), 2.15–1.99 (8H, m, -CH_2CH_2CH=$CHCH_2CH_2$-).

*(2E)-1,4-Biscarboethoxy-2-butene (**13**)*

To a stirred solution of *trans*-β-hydromuconic acid **12** (1.56 g, 8 mmol) in benzene/ethanol (absolute; 5:2, 70 mL) was added concentrated sulfuric acid (3 drops) and the resulting mixture was heated at 90°C for 48 h. After it was cooled to room temperature, K_2CO_3 was added to neutralize the acidic solution. The mixture was diluted with diethyl ether (200 mL), dried over $MgSO_4$, filtered, and concentrated to give diester **13** (2.1 g, 99%) as a colorless oil; ir (neat): 2980, 2920, 1740, 1370, 1170 cm^{-1}; ^1H nmr ($CDCl_3$) δ: 5.69 (2H, tt, *J* = 3.8 Hz, 1.8 Hz, -CH_2CH=C*H*CH_2-), 4.13 (4H, q, *J* = 7.2 Hz, (=$CHCH_2$-$CO_2CH_2CH_3)_2$), 3.08 (4H, m, -CH_2CH=$CHCH_2$-), 1.25 (6H, t, *J* = 7.2 Hz, (=$CHCH_2CO_2CH_2CH_3)_2$); ms *m/e*: 200 (M^+), 154 ($M^+-CH_3CH_2OH$).

*(3E)-3-Hexen-1,6-diol (**14**)*

To a stirred suspension of lithium aluminum hydride (970 mg, 23 mmol) in anhydrous diethyl ether (90 mL) was added a solution of diester **13** (3.1 g, 16 mmol) in anhydrous diethyl ether (10 mL) over a period of 30 min at room temperature. The mixture was stirred for 30 min followed by addition of Glauber's salt ($Na_2SO_4 \cdot 10H_2O$, 1 g). The stirring was continued for another 30 min before filtering. The filtrate was washed with acetone (5 × 100 mL) and the combined organic layers were dried over $MgSO_4$, filtered, and evaporated. The crude residue was purified by flash chromatography (hexanes/acetone; 1:1) to give diol **14** (1.7 g, 94%) as a viscous oil; ir (neat): 3350, 2940, 2890, 1430, 1050 cm^{-1}; ^1H nmr ($CDCl_3$) δ: 5.52 (2H, tt, *J* = 3.8 Hz, 1.7 Hz, -CH_2CH=C*H*CH_2-), 3.64 (4H, t, *J* = 6.1 Hz, ($HOCH_2CH_2CH$=)$_2$), 2.28 (4H, q, *J* = 5.7 Hz, -CH_2CH=$CHCH_2$-), 2.04 (2H, br s, (*H*OCH_2CH_2CH=)$_2$); ms *m/e*: 116 (M^+), 98 (M^+-H_2O).

*(3E)-1,6-Bismethanesulfonyloxy-3-hexene (**15**)*

To a stirred solution of alcohol **14** (1.7 g, 15 mmol) in dichloromethane (58 mL) were added triethylamine (5.1 mL, 36 mmol) and methanesulfonyl chloride (2.7 mL, 34 mmol) at 0°C in dropwise fashion. The reaction mixture was stirred for 30 min at 0°C and then diluted with CH_2Cl_2 (100 mL). The organic layer was washed with H_2O (3 × 40 mL), dried over $MgSO_4$, filtered, and evaporated. The crude residue was purified by flash chromatography (hexanes/ethyl acetate; 3:1) to give methanesulfonate ester **15** (3.9 g, 97%) as a solid; mp 60–63°C; ir: 3020, 2960, 2900, 1350, 1170 cm^{-1}; ^1H nmr ($CDCl_3$) δ: 5.56 (2H, tt, *J* = 3.7 Hz, 1.6 Hz, -CH_2CH=C*H*CH_2-), 4.23 (4H, t, *J* = 6.5 Hz, (-OCH_2CH_2CH=)$_2$), 3.00 (6H, s, (CH_3SO_2-$OCH_2CH_2CH)_2$), 2.47 (4H, q, *J* = 5.5 Hz, -CH_2CH=$CHCH_2$-).

*(3E)-1,1,6,6-Tetracarbomethoxy-3-butene (**16**)*

The general procedure B was followed, using dimethyl malonate (7.55 mL, 66 mmol), sodium hydride (2.6 g, 65 mmol), DMF/THF (1:1, 220 mL), dimesylate **15** (3.0 g, 11 mmol), and potassium iodide (1.8 g, 11 mmol). The crude product was pumped under vacuum for 1 h and then purified by flash chromatography (hexanes/ethyl acetate; 17:3) to give tetraester **16** (2.8 g, 73%); ir (neat): 2950, 1740, 1430, 1240, 1150 cm^{-1}; ^1H nmr ($CDCl_3$) δ: 5.38 (2H, m, -CH_2CH=C*H*CH_2-), 3.73 (12H, s, (=$CHCH_2CH_2CH(CO_2CH_3)_2$)2), 3.38 (2H, t, *J* = 7.2 Hz, (=$CHCH_2CH_2CH(CO_2CH_3)_2)_2$), 1.99 (8H, m, (=$CHCH_2CH_2CH$-)$_2$); ms *m/e*: 345 ($MH^+$), 312 ($M^+-CH_3OH$).

Can. J. Chem. Downloaded from www.nrcresearchpress.com by 195.138.81.100 on 09/07/12
For personal use only.

*Methyl (5E,11E,13Z)-2,9,9-tricarbomethoxy-15-hydroxy-5,11,13-pentadecatrienoate (**19**a)*

General procedure F

To a stirred sodium hydride suspension (84 mg, 2.1 mmol) in DMF/THF (1:1, 6 mL) was added dropwise a solution of tetraester **16** (1.5 g, 4.25 mmol) in DMF/THF (1:1, 6 mL) at 0°C. The reaction mixture was stirred for 10 min at room temperature and then transferred to a solution of allylic chloride **7***a* (466 mg, 2.2 mmol) in DMF/THF (1:1, 6 mL). The resulting mixture was stirred for 4.5 h and then quenched with saturated NH_4Cl solution (20 mL), diluted with H_2O (20 mL), and extracted with hexanes/ether (2:1, 4 × 100 mL). The combined organic layers were dried over $MgSO_4$, filtered, and evaporated to give a crude residue that contained product **18***a*.

Pyridinium *p*-toluenesulfonate (45 mg, 0.18 mmol) was added to a stirred solution of the above crude residue in anhydrous methanol (18 mL). The resulting mixture was heated at 60°C for 90 min before it was cooled to room temperature. After the volatiles were removed, the viscous residue was purified by flash chromatography (hexanes/ethyl acetate; 6:4) to give alcohol **19***a* (767 mg 83%) and diol **37***a* (79 mg, 14%). **19***a*: ir (neat): 3540, 3460, 3010, 2950, 2840, 1740, 1440, 1220 cm^{-1}; ^1H nmr ($CDCl_3$) δ: 6.35 (1H, dd, J = 14.8 Hz, 11.3 Hz, -CH_2CH=C*H*-CH=$CHCH_2$-), 6.03 (1H, t, J = 11.0 Hz, -CH_2CH=CH-C*H*=$CHCH_2$-), 5.60–5.48 (2H, m, -CH_2CH=CH-CH=C*H*CH_2-), 5.38 (2H, m, -CH_2CH=C*H*CH_2-), 4.29 (2H, br d, J = 5.4 Hz, =$CHCH_2OH$), 3.73 and 3.71 (12H, s, -$CH_2CH(CO_2CH_3)_2$ and -$CH_2C(CO_2CH_3)_2CH_2$-), 3.36 (1H, t, J = 7.2 Hz, -$CH_2CH(CO_2CH_3)_2$), 2.70 (2H, d, J = 7.6 Hz, =$CHCH_2C(CO_2CH_3)_2CH_2$-), 2.04–1.90 (8H, m, -$CHCH_2CH_2CH$=$CHCH_2CH_2$-), 1.61 (1H, br s, =$CHCH_2OH$); ms m/e: 422 ($M^+ - H_2O$).

37*a*: ir (neat): 3420, 3030, 2960, 2850, 1730, 1440, 1230 cm^{-1}; ^1H nmr ($CDCl_3$) δ: 6.35 (2H, dd, J = 14.7 Hz, 11.6 Hz, (-CH_2CH=C*H*-CH=$CHCH_2$-)$_2$), 6.03 (2H, t, J = 11.0 Hz, (-CH_2CH=CH-C*H*=$CHCH_2$-)$_2$), 5.60–5.47 (4H, m, (-CH_2CH=CH-CH=C*H*-CH_2-)$_2$), 5.37 (2H, br s, (-CH_2CH_2CH-)$_2$), 4.29 (4H, d, J = 6.8 Hz, (=$CHCH_2OH$)$_2$), 3.71 (12H, s, (=$CHCH_2CH_2CH_2C(CO_2CH_3)_2$-$CH_2$-)$_2$), 2.70 (4H, d, J = 7.4 Hz, (=$CHCH_2CH_2C(CO_2CH_3)_2CH_2$-)$_2$), 1.98 (8H, s, (=$CHCH_2CH_2C$-)$_2$), 1.58 (2H, s, (=$CHCH_2OH$)$_2$).

*Methyl (5E,11E,13E)-2,9,9-tricarbomethoxy-15-hydroxy-5,11,13-pentadecatrienoate (**19**b)*

The general procedure F was followed, using sodium hydride (76 mg, 1.9 mmol), tetraester **16** (1.25 g, 3.6 mmol), allylic chloride **7***b* (390 mg, 1.8 mmol), DMF (9 mL), THF (9 mL), pyridinium *p*-toluenesulfonate (48 mg, 0.19 mmol), and anhydrous methanol (18 mL). Alcohol **19***b* (361 mg, 47% for last two steps) was obtained; ir (neat): 3540, 3460, 3000, 2960, 2850, 1730, 1440, 1230 cm^{-1}; ^1H nmr ($CDCl_3$) δ: 6.14 (2H, m, -CH_2CH=C*H*-C*H*=$CHCH_2OH$), 5.77 (1H, dt, J = 14.3 Hz, 5.8 Hz, -CH_2CH=CH-CH=C*H*CH_2OH), 5.49 (1H, dt, J = 14.6 Hz, 7.3 Hz, -CH_2CH=CH-CH=$CHCH_2OH$), 5.37 (2H, m, -CH_2CH_2CH=C*H*CH_2CH_2-), 4.17 (2H, d, J = 5.8 Hz, =$CHCH_2OH$), 3.73 and 3.71 (12H, s, -$CH_2CH(CO_2CH_3)_2$ and -$CH_2C(CO_2CH_3)_2CH_2$-), 3.36 (1H, t, J = 7.3 Hz, -$CH_2CH(CO_2CH_3)_2$), 2.67 (2H, d, J = 7.6 Hz, =$CHCH_2C(CO_2CH_3)_2CH_2$-), 2.04–1.89 (8H, m, -$CHCH_2CH_2CH$=$CHCH_2CH_2$-), 1.61 (1H, br s, =$CHCH_2OH$); ms m/e: 422 ($M^+ - H_2O$).

*Methyl (5E,11E,13Z)-2,9,9-tricarbomethoxy-15-chloro-5,11,13-pentadecatrienoate (**20**a)*

The general procedure D was followed, using *s*-collidine (650 μL, 5.0 mmol), allylic alcohol **19***a* (535 mg, 1.2 mmol), lithium chloride (473 mg, 10 mmol), DMF (14 mL), and methanesulfonyl chloride (300 μL, 3.9 mmol). Allylic chloride **20***a* (505 mg, 90%) was obtained; ^1H nmr ($CDCl_3$) δ: 6.36 (1H, dd, J = 14.7 Hz, 11.4 Hz, -CH_2CH=C*H*-CH=$CHCH_2$-), 6.10 (1H, t, J = 10.9 Hz, -CH_2CH=CH-C*H*=$CHCH_2$-), 5.71–5.53 (2H, m, -CH_2CH=CH-CH=C*H*CH_2-), 5.38 (2H, br s, -CH_2CH_2CH=C*H*CH_2CH_2-), 4.17 (2H, d, J = 8.0 Hz, =$CHCH_2Cl$), 3.73 and 3.71 (12H, 2s, -$CH_2C(CO_2CH_3)_2CH_2$- and -$CH_2CH(CO_2CO_2CH_3)_2$, 3.36 (1H, t, J = 7.2 Hz, -$CH_2CH(CO_2CH_3)_2$), 2.72 (2H, d, J = 7.6 Hz, -$C(CO_2CH_3)_2CH_2CH$=), 2.01–1.90 (8H, m, -CH_2CH_2CH=$CHCH_2CH_2$-).

*Methyl (5E,11E,13E)-2,9,9-tricarbomethoxy-15-chloro-5,11,13-pentadecatrienoate (**20**b)*

The general procedure E was followed, using *s*-collidine (175 μL, 1.3 mmol), allylic alcohol **19***b* (145 mg, 0.33 mmol), lithium chloride (195 mg, 4.6 mmol), DMF (5.5 mL), and methanesulfonyl chloride (76 μL, 1.0 mmol). Allylic chloride **20***b* (505 mg, 90%) was obtained. ^1H nmr (C_6D_6) δ: 5.82 (2H, m, -CH_2CH=C*H*-C*H*=$CHCH_2Cl$), 5.56 (1H, dt, J = 14.8 Hz, 7.4 Hz, -CH_2CH=CH-CH=$CHCH_2Cl$), 5.43–5.27 (3H, m, -CH_2CH=CH-CH=C*H*CH_2Cl and -CH_2CH_2CH=C*H*CH_2CH_2-), 3.57 (2H, d, J = 7.2 Hz, =$CHCH_2Cl$), 3.31 and 3.29 (13H, m, -$CH_2C(CO_2CH_3)_2CH_2$-, -$CH_2CH(CO_2CH_3)_2$ and -CH_2CH-$(CO_2CH_3)_2$), 2.82 (2H, d, J = 7.6 Hz, -$C(CO_2CH_3)_2CH_2CH$=), 2.18–1.93 (8H, m, -CH_2CH_2CH=$CHCH_2CH_2$-).

*(1Z,3E,9Z)-6,6,13,13-Tetracarbomethoxy-1,3,9-cyclotetradecatriene (**21**)*

General procedure G

To a stirred suspension of cesium carbonate (475 mg, 1.5 mmol) in CH_3CN (135 mL) was added a solution of allylic chloride **11***a* (126 mg, 0.27 mmol) in CH_3CN (5 mL) by syringe pump over a period of 12 h at 85°C. After the addition was finished, the reaction mixture was stirred for 5 h. The mixture was allowed to cool to room temperature, then filtered and evaporated. The crude residue was purified by flash chromatography (hexanes/CH_2Cl_2/ethyl acetate; 17:2:1), and the solid obtained was crystallized from hexanes/CH_2Cl_2 to give macrocyclic compound **21** (100.5 mg, 87%; 81% after crystallization); mp 156–164°C; ir ($CHCl_3$): 3020, 2960, 1730, 1450, 1430, 1210 cm^{-1}; ^1H nmr ($CDCl_3$) δ: 6.57 (1H, dd, J = 14.9 Hz, 11.1 Hz, -C(1)H=C(2)H-C(3)*H*=C_4H-), 6.15 (1H, t, J = 10.9 Hz, -C(1)H=C(2)*H*-C(3)H=C(4)H-), 5.44–5.31 (3H, m, -C(1)H=C(2)H-C(3)H=C(4)*H*- and -CH_2C(9)*H*=C(10)*H*CH_2-), 4.98 (1H, dt, J = 10.3 Hz, 9.7 Hz, -C(1)*H*=C(2)H-C(3)H=C(4)H-), 3.73 (12H, s, $(CO_2CH_3)_4$), 2.80 (4H, m, -C(5)H_2- and -C(14)H_2-), 2.10–1.50 (8H, m, -C(7)H_2C(8)H_2CH=CHC(11)H_2C(12)H_2-); ^{13}C nmr ($CDCl_3$) δ: 171.5 ((CO_2CH_3)$_4$), 132.3 (=*C*(2)H-), 129.5 (-*C*(3)H=), 128.6 (=*C*(4)H- and -*C*(9)H=*C*(10)H-), 124.3 (-*C*(1) H=), 57.4 and 56.5 (-*C*(6)- and -*C*(13)-), 52.6 and 52.6 ((CO_2CH_3)$_4$), 35.3 and 29.6 (-C_5H_2-and -*C*(14)H_2-), 31.9 and 30.7 (-*C*(8)H=CH*C*(11)H_2-), 22.4 and 21.2 (-*C*(7)H_2- and -*C*(12)H_2-); ms m/e: 422 (M^+). Exact mass (M^+) calcd.: 422.1941; found: 422.1937.

*(cis-1,10,cisoid-1,2,trans-2,7)-2,2,12,12-Tetracarbomethoxytricyclo[8.4.0.0^{2,7}]tetradec-8-ene (**22**)*

General procedure H

Macrocyclic compound **21** (22.0 mg, 52 μmol) was heated in a vacuum-sealed quartz tube at 250°C for 90 min. The tube was opened and the residue was transferred into a flask with the help of CH_2Cl_2. After the solvent was evaporated, the crude product was purified by flash chromatography (hexanes/CH_2Cl_2/ethyl acetate; 10:2:1) to give tricyclic compound **22** (20.4 mg, 90%) as a solid; mp 106–113°C; ir ($CHCl_3$): 3010, 2950, 1730, 1450, 1430, 1220 cm^{-1}; ^1H nmr (C_6D_6) δ: 5.31 (2H, m, -C(8)*H*=C(9)*H*-), 3.72, 3.67, and 3.65 (12H, 3s, $(CO_2CH_3)_4$), 2.58 (1H, br s, -C(10)*H*-), 2.40 (4H, m, -C(4)H_e-, -C(6)H_e-, -C(11)H_e-, and -C(13)H_e-), 2.09 (1H, dd, J = 14.1 Hz, 6.1 Hz, -C(7)*H*-), 1.87–1.24 (10H, m, -C(1)*H*-, -C(2)*H*-, -C(3)H_a-, -C(4)H_a-, -C(6)H_a-, -C(11)H_a-, -C(13)H_a-, -C(14)H_a-, and -C(14)H_e-); ^{13}C nmr ($CDCl_3$) δ: 173.1, 172.7, and 171.4 ((CO_2CH_3)$_4$), 130.3 and 130.2 (-*C*(8)H=*C*(9)H-), 55.7 and 52.0 (-*C*(5)- and -*C*(12)-), 52.6 ((CO_2CH_3)$_4$), 44.4, 38.0, 37.1, 36.2, 35.1, 33.2, 31.8, 30.9, 26.7, and 18.4 (-*C*(1)-, -*C*(2)-, -*C*(3)-, -*C*(4)-, -*C*(6)-, -*C*(7)-, -*C*(10)-, -*C*(11)-, -*C*(13)-, and -*C*(14)-); ms m/e: 422 (M^+). Exact mass (M^+) calcd.: 422.1941; found: 422.1937.

*(1Z,3E,9E)-6,6,13,13-Tetracarbomethoxy-1,3,9-cyclotetradecatriene (**23**)*

The general procedure G was followed, using allylic chloride **20***a*

Can. J. Chem. Downloaded from www.nrcresearchpress.com by 195.138.81.100 on 09/07/12
For personal use only.

(505 mg, 1.1 mmol), cesium carbonate (1.8 g, 5.5 mmol), and acetonitrile (500 mL). Macrocyclic compound **23** (280 mg, 60%; 56% after crystallization) was obtained as a solid; mp 150–163°C; ir ($CHCl_3$): 3020, 2950, 2920, 1730, 1460, 1430, 1220 cm^{-1}; ^1H nmr ($CDCl_3$) δ: 6.21 (2H, m, -C(1)H=C_2H-C(3)H=C(4)H-), 5.56–5.24 (3H, m, -C(1)H=C(2)H-C(3)H=C(4)H- and -CH_2C(9)HCH_2-), 4.99 (1H, q, J = 8.6 Hz, -C(1)H=C(2)H-C(3)H=C(4)H-), 3,73 (12H, s, $(C_2CH_3)_4$), 2.81 (4H, t, J = 7.9 Hz, -C(5)H_2- and -C(14)H_2-), 2.02–1.86 (8H, m, -C(7)H_2C(8)H_2CH=CHC(11)H_2C(12)H_2-); ^{13}C nmr ($CDCl_3$) δ: 171.7 and 171.5 (($CO_2CH_3)_4$), 132.7 (-C(1)H=C(2)H-C(3)H=C(4)H-), 130.8 and 129.5 (-C(1)H=C(2)H-C(3)H=C(4)H- and -C(9)H=C(10)H-), 128.2 (-C(1)H=C(2)H-C(3)H=C(4)H-), 123.9 (-C(1)H=C(2)H-C(3)H=C(4)H-), 58.1 and 56.6 (-C(6)- and -C(13)-), 52.6 and 52.5 (($CO_2CH_3)_4$), 35.8 and 29.7 (-C(6)H_2- and -C(13)H_2-), 31.3 and 28.6, 26.9 and 26.6 (-C(7)H_2C(8)H_2CH=CHC(11)H_2-C(12)H_2-); ms m/e: 422 (M^+). Exact mass (M^+) calcd.: 422.1941; found: 422.1937.

The same reaction in a mixture of DMF/THF was carried out according to the above general procedure G. Thus, the reaction of allylic chloride **20***a* (69.1 mg, 0.15 mmol) with cesium carbonate (1.8 g, 5.5 mmol) in 30 mL of DMF and 30 mL of THF gave a macrocyclic compound (35.0 mg, 55%) that has spectroscopic data identical with macrocycle **23**.

*(*transoid-*1,10*,cisoid-*1,2*,cis-*2,7*)-*5,5,12,12-Tetracarbomethoxytricyclo[8.4.0.0^{2,7}]tetradec-8-ene (**24**)*

The general procedure H was followed, using macrocyclic compound **23** (23.6 mg, 55.9 μmol). Tricyclic compound **24** (21.7 mg, 92%) was obtained as a solid; mp 105–115°C; ir ($CHCl_3$): 3010, 2950, 1730, 1450, 1430, 1220 cm^{-1}; ^1H nmr ($CDCl_3$) δ: 5.51 (2H, br s, -C(8)H=C(9)H-), 3.74 and 3.68 (12H, 2s, $(CO_2CH_3)_4$), 2.41–1.30 (16H, m); ^{13}C nmr ($CDCl_3$) δ: 172.4 and 171.8 (($CO_2CH_3)_4$). 130.7 (-C(8)H=C(9)H-), 54.6 (-C(5)- and -C(12)-), 52.4 (($CO_2CH_3)_4$), 33.5, 26.5 (broad signal) and 22.8 (-C(1)-, -C(2)-, -C(3)-, -C(4)-, -C(6)-, -C(7)-, -C(10)-, -C(11)-, -C(13)-, -C(14)-,); ms m/e: 422 (M^+). Exact mass (M^+) calcd.: 422.1941; found: 422.1937.

*(1Z,3*E*,9*Z*)-6,6,13,13-Tetracarbomethoxy-1,3,9-cyclotetradecatriene (**21**)*

Hydrogen was bubbled through a stirred solution of macrocyclic compound **25** (29 mg, 69.0 μmol) in ethyl acetate (3 mL), and a Lindlar catalyst (palladium on calcium carbonate, poisoned with lead, 3 mg) was added. The reaction mixture was maintained under these conditions for 1 h, and then filtered and concentrated to give a macrocyclic compound (29 mg, 100%), whose spectroscopic data are identical with macrocycle **21** obtained previously by macrocyclization of allylic chloride **11***a*.

*(*trans-*1,10*,cisoid-*1,2*,trans-*2,7*)-*5,5,12,12-Tetracarbomethoxytricyclo[8.4.0.0^{2,7}]tetradec-8-ene (**30**)*

General procedure I

To a stirred suspension of cesium carbonate (420 mg, 1.3 mmol) in a mixture of DMF/THF (1:1, 121 mL) was added a solution of allylic chloride **11***b* (crude product) in THF (5 mL) by syringe pump over a period of 12 h at 85°C. After the addition was finished, the stirring was continued for 24 h. The reaction mixture was cooled to room temperature, and then filtered and evaporated. The crude residue was purified by flash chromatography (hexanes/CH_2CL_2/ethyl acetate; 17:2:1) to give tricyclic compound **30** (72 mg, 69% for last 3 steps; 56% after crystallization) as a white solid; mp 164–166°C; ir ($CHCl_3$): 3020, 2950, 1730, 1450, 1230 cm^{-1}; ^1H nmr ($CDCl_3$) δ: 5.65 (2H, s, -C(8)H=C(9)H-), 3.74 and 3.69 (12H, 2s, $(CO_2CH_3)_4$), 2.59 (2H, dd, J = 10.4 Hz, 2.0 Hz, -C(4)H_e- and -C(13)H_e-), 2.45 (2H, dd, J = 13.1 Hz, 1.9 Hz, -C(6)H_e-C(11)H_e-), 1.77 (8H, m, -C(3)H_e-, -C(4)-H_a-, -C(6)H_a-, -C(7)H-, -C(10)H-, -C(11)H_a-, -C(13)H_a-, -C(14)H_e-), 1.31–1.24 (4H, m, -C(3)H_a-, -C(1)H-, -C(2)H-, -C(14)H_a-); ^{13}C nmr ($CDCl_3$) δ: 172.7 and 171.5 (($CO_2CH_3)_4$), 133.9 (-C(8)H=C(9)H-), 55.1 (-C(5)- and -C(12)-), 52.6 (($CO_2CH_3)_4$), 40.9 (-C(1)- and -C(2)-), 36.9 (-C(6)- and -C(11)-), 36.2 (-C(7)- and -C(10)-), 32.2 (-C(4)- and -C(13)-), 24.8 (-C(3)- and -C(14)-); ms m/e: 422 (M^+). Exact mass (M^+) calcd.: 422.1741; found: 422.1937. The structure of compound **30** has also been determined by X-ray crystallography and its details will be reported (16).

The same reaction in CH_3CN was carried out according to the above general procedure I. Thus, the reaction of allylic chloride **11***b* (crude product) with cesium carbonate (1.2 g, 3.7 mmol) in 405 mL of CH_3CN provided a tricyclic compound (216 mg, 60% for last three steps) that has spectroscopic data identical with tricycle **30**.

*(*cis-*1,10*,transoid-*1,2*,trans-*2,7*)-*5,5,12,12-Tetracarbomethoxytricyclo[8.4.0.0^{2,7}]tetradec-8-ene (**32**)*

The general procedure I was followed, using chloride **20***b* (crude product), acetonitrile (200 mL), and cesium carbonate (570 mg, 1.75 mmol). Tricyclic compound **32** (35 mg, 25%) was obtained as a solid; mp 107–110°C; ir ($CHCl_3$): 3020, 2950, 1730, 1350, 1330, 1220 cm^{-1}; ^1H nmr ($CDCl_3$) δ: 5.57 and 5.38 (2H, m, and d, J = 9.9 Hz, -C(8)H=C(9)H-), 3.75, 3.74, 3.70, 3.69 (12H, 4s, $(CO_2CH_3)_4$), 2.52–0.97 (16H, m); ^{13}C nmr ($CDCl_3$) δ: 172.7, 171.6, and 171.4 (($CO_2CH_3)_4$), 131.3 and 130.7 (-C(8)H=C(9)H-), 55.2 (-C(5)- and -C(12)-), 52.6 and 52.5 (($CO_2CH_3)_4$), 39.4, 36.4, 35.4, and 37.6 (4d, -C(1)-, -C(2)-, -C(7)-, -C(10)-,), 34.1, 33.8, 31.5, 25.6, 25.2, and 22.5 (6t, -C(3)-, -C(4)-, -C(6)-, -C(11)-, -C(13)-, -C(14)-); ms m/e: 422 (M^+). Exact mass (M^+) calcd.: 422.1941; found: 422.1937.

The same reaction in a mixture of DMF/THF was conducted using the above procedure. Thus, the reaction of allylic chloride **20***b* crude product) with cesium carbonate (1.8 g, 5.5 mmol) in a mixture of DMF/THF (1:1; 220 mL) gave a tricycle (48 mg, 26% for last three steps) that was found to be identical spectroscopically with **32**.

Acknowledgements

This research was supported by the Natural Sciences and Engineering Research Council of Canada (NSERCC, Ottawa) and by the "Ministère de l'Education" (FCAR, Québec).

1. Y. C. Xu, M. Cantin, and P. Deslongchamps. Can. J. Chem. **68**, 2137 (1990), and references therein.
2. (*a*) R. A. Micheli, Z. G. Hajos, N. Cohen, D. R. Parrish, L. A. Portland, W. Sciamanna, M. A. Scott, and P. A. Wherli. J. Org. Chem. **40**, 675 (1975); (*b*) Z. G. Hajos and D. R. Parrish. J. Org. Chem. **38**, 3244 (1973).
3. W. S. Johnson, B. E. McCarry, R. L. Harkezich, and S. G. Boots. J. Am. Chem. Soc. **102**, 352 (1980), and references therein.
4. (*a*) T. Kametami and H. Nemoto. Tetrahedron, **37**, 3 (1981); (*b*) W. Oppolzer. Angew. Chem. Int. Ed. Engl. **16**, 10 (1977); (*c*) A. G. Fallis. Can. J. Chem. **62**, 183 (1984), and references therein; (*d*) M. Ihara, I. Sudow, and K. Fukumoto. J. Chem. Soc. Perkin Trans. 1, 117 (1986); (*e*) M. E. Jung and K. M. Halweg. Tetrahedron Lett. 2121 (1984).
5. (*a*) J. F. Lavallée and P. Deslongchamps. Tetrahedron Lett. **29**, 6033 (1988); (*b*) Tetrahedron Lett. **28**, 3457 (1987).
6. (*a*) D. Taub. *In* The total synthesis of natural products. Vol. 6. *Edited by* J. ApSimon. John Wiley and Sons, New York. 1984, pp. 1–49; (*b*) K. Nakanishi. *In* Natural products chemistry. Vol. 3. *Edited by* K. Nakanishi *et al.* Kodansha Ltd., Tokyo. 1983. Chap. 4.
7. (*a*) S. Lamothe, A. Ndibwami and P. Deslongchamps. Tetrahedron Lett. **29**, 1639 (1988); (*b*) Tetrahedron Lett. **29**, 1641 (1988); (*c*) A. Marinier and P. Deslongchamps. Tetrahedron Lett. **29**, 6215 (1988).
8. (*a*) H. Lindlar. Helv. Chim. Acta, **35**, 446, 1952; (*b*) A. B. McEwen, M. J. Guttieri, W. F. Maier, R. M. Laine, and Y. Shvo. J. Org. Chem. **48**, 4436 (1983).
9. S. Lamothe. Ph.D. Thesis, Université de Sherbrooke. (1989).
10. M. Miyashita, A. Yoshikoshi, and P. A. Grieco. J. Org. Chem. **42**, 3772 (1977).

11. E. W. COLLINGTON and A. I. MEYERS. J. Org. Chem. **36**, 3044 (1971).
12. R. K. CROSSLAND and K. L. SERVIS. J. Org. Chem. **35**, 3195 (1970).
13. (*a*) K. BAETTIG, C. DALLAIRE, R. PITTELOUD, and P. DESLONGCHAMPS. Tetrahedron Lett. **28**, 5249 (1987); (*b*) K. BAETTIG, A. MARINIER, R. PITTELOUD and P. DESLONGCHAMPS. Tetrahedron Lett. **28**, 5253 (1987); (*c*) G. BÉRUBÉ and P. DESLONGCHAMPS. Tetrahedron Lett. **28**, 5255 (1987); (*d*) G. BÉRUBÉ and P. DESLONGCHAMPS. Can. J. Chem. **68**, 404 (1990); (*e*) A. MARINIER, K. BAETTING. C. DALLAIRE, R. PITTELOUD, and P. DESLONGCHAMPS. Can. J. Chem. **67**, 1609 (1989).
14. (*a*) D. BRILLON and P. DESLONGCHAMPS. Can. J. Chem. **65**, 43 (1987); (*b*) Can. J. Chem. **65**, 56 (1987).
15. R. V. BONNERT and P. JENKINS. Tetrahedron Lett. **28**, 697 (1987), and references therein.
16. A. G. MICHEL, M. DROUIN, N. MICHEL-DEWEZ, Y. C. XU, M. CANTIN, and P. DESLONGCHAMPS. Acta Crystallogr. Sect. C: Cryst. Struct. Commun. In press.

Can. J. Chem. Downloaded from www.nrcresearchpress.com by 195.138.81.100 on 09/07/12
For personal use only.

Nouveaux modèles siliciés dérivés de la quinoléine

MICHELINE GRIGNON-DUBOIS,[1] MICHELLE FIALEIX ET BERNADETTE REZZONICO

Laboratoire de chimie organique et organométallique, Université de Bordeaux I, 351, Cours de la libération, 33405 Talence CÉDEX, France

Reçu le 19 décembre 1989[2]

MICHELINE GRIGNON-DUBOIS, MICHELLE FIALEIX et BERNADETTE REZZONICO. Can. J. Chem. **68**, 2153 (1990).

La silylation de la quinoléine par le système $Me_3SiCl/Li/THF$ a été réexaminée. Elle nous a permis d'isoler de nouveaux produits tri-, tétra- et hexasiliciés dont nous avons étudié la stéréochimie. La comparaison de nos résultats à ceux obtenus avec le naphtalène montre l'influence de l'atome d'azote sur l'orientation de la silylation.

Mots clés : silylation, quinoléine, polysilyl-hydro-quinoléines.

MICHELINE GRIGNON-DUBOIS, MICHELLE FIALEIX, and BERNADETTE REZZONICO. Can. J. Chem. **68**, 2153 (1990).

Silylation of quinoline with $Me_3SiCl/Li/THF$ reagent has been studied. We obtained new tri-, tetra-, and hexasilylated derivatives whose stereochemistry has been established using NMR data. Comparison of these results to those previously obtained from naphthalene shows the effect of nitrogen on the silylation process.

Key words: silylation, quinoline, polysilyl-hydro-quinolines.

Can. J. Chem. Downloaded from www.nrcresearchpress.com by 195.138.81.100 on 09/07/12
For personal use only.

La voie organosilicique est aujourd'hui reconnue comme une méthode de choix pour la fonctionnalisation des substrats organiques (1). D'autre part, la quinoléine constitue un squelette important en chimie thérapeutique (2). La silylation de la quinoléine constituait donc une stratégie attractive pour accéder à des synthons polysiliciés précurseurs de quinoléines fonctionnelles. Elle avait déjà donné lieu à quelques travaux. Ainsi, l'utilisation de $Me_3SiHgSiMe_3$ conduit à la bis-4,4′(*N*-triméthylsilyl dihydro-1,4-quinoléine) avec 75% de rendement (3). Par ailleurs, le réactif $Me_3SiCl/Li/Et_2O$/toluène avait permis à Nogaideli et Akhobadze (4) d'isoler, à côté de ce même dérivé (rdt. 20%), la bis-triméthylsilyl-1,4 dihydro-1,4 quinoléine, **1**, avec 15% de rendement. Enfin, Sulzbach et Iqbal (5) en remplaçant le mélange Et_2O/toluène par le THF avaient pu favoriser le produit de disilylation **1**; cependant, le rendement restait faible (31%) et aucune précision n'était apportée sur la présence éventuelle d'autres produits ou de substrat n'ayant pas réagi.

L'intérêt de cette réaction et le caractère incomplet des résultats de la littérature nous ont conduits à la réexaminer en utilisant, comme réactif, le système $Me_3SiCl/Li/THF$.

Résultats et discussion

Nos premiers essais ont été conduits dans les conditions décrites par Sulzbach et Iqbal (5) à savoir : 3 équiv. de Li, 3 équiv. de Me_3SiCl à 0°C. Au bout d'une heure (durée utilisée par ces auteurs), on constate que le milieu contient encore du lithium et de la quinoléine qui n'a pas réagi (CCM, SiO_2; éluant : hexane/EtOH : 80 : 20 (vol.)). Nous avons donc laissé les réactifs en contact jusqu'à disparition totale du produit de départ soit 6 h. Par distillation, nous avons ainsi pu isoler, à côté de de la bis-triméthylsilyl-1,4 dihydro-1,4 quinoléine, **1** (rdt. 35%), deux produits originaux **2** (rdt. 15%) et **3** (rdt. 25%) qui sont respectivement tétra- et hexasiliciés (fig. 1).

Ces résultats nous ont conduits à examiner l'influence de la quantité de réactifs sur l'orientation de la réaction (tableau 1). Nous avons ainsi constaté que :

(i) avec 2 équivalents, conditions théoriquement optimales pour favoriser le dérivé disilicié, celui-ci ne se forme qu'avec 30% de rendement; les produits **2** et **3** sont déjà présents dans le mélange réactionnel, ce qui indique que la réaction s'effectue sous contrôle cinétique;

(ii) avec 4 ou 6 équivalents, les rendements en produits de di- et tétrasilylation **1** et **2** varient peu; par contre, la proportion d'hexasilylation (**3**) augmente. Avec 12 équivalents, cette dernière devient largement prépondérante et le dérivé **3** devient le produit majeur de la réaction.

Notons que la fragilité de la liaison Si—N rend les composés **1**–**3** très sensibles à l'air ou à l'humidité. En particulier, l'isolement du produit **3**, qui, en outre, est stériquement encombré, nécessite de travailler en atmosphère parfaitement inerte.

La figure 1 rend compte de l'obtention de ces composés. Elle ferait intervenir la formation initiale d'un anion radical $\mathbf{Q}^{\cdot-}$ par transfert d'électron du métal au substrat, mécanisme généralement admis avec les systèmes conjugués (6). Une première silylation sur l'atome d'azote conduit au radical résonnant $\mathbf{Q}^{\cdot}$ qui, par capture d'un électron permet une deuxième silylation. Elle peut intervenir sur le sommet 4, donnant naissance au dérivé **1** qui est stable dans le milieu ou sur le sommet 2. Dans ce dernier cas, le dérivé disilicié qui en résulte, très réactif, se silyle à nouveau, donnant lieu à une compétition entre l'attaque de la double liaison de type styrénique et celle du noyau aromatique adjacent qui s'effectue en 6–7. Le produit tétrasilicié résultant de cette dernière n'a jamais été isolé; il conduit à une nouvelle réaction permettant la formation du dérivé **3**.

Ces résultats présentent une certaine analogie avec ceux observés par Laguerre *et al.* (7) à partir du naphtalène qui leur avait permis d'isoler aussi un produit hexasilicié (fig. 2). Cependant la fixation des 3ème et 4ème groupes silyle était univoque puisque l'analogue carboné de **2** ne se formait pas et les 5ème et 6ème silylations s'effectuaient sur des sommets différents. Ceci montre l'influence de l'atome d'azote dans ces réactions.

Abandonné au contact de l'air ou de silice, le dérivé disilicié, **1**, s'aromatise avec perte d'un groupe silyle, conduisant à la triméthylsilyl-4 quinoléine (**4**, rdt. 80%) (fig. 3) qui est identique au produit obtenu avec 36% de rendement par silylation de la bromo-4 quinoléine (8). Par action de chlorure d'acétyle, on isole la *N*-acétyl triméthylsilyl-4 dihydro-1,4 quinoléine (**5**, rdt. 82%).

De même, l'aromatisation de la tétrasilyl-1,2,3,4 tétrahydro-1,2,3,4 quinoléine, **2**, par l'oxygène de l'air conduit à la

1. Auteur à qui adresser toute correspondance.
2. Révision reçue le 2 août 1990.

Printed in Canada / Imprimé au Canada

Can. J. Chem. Downloaded from www.nrcresearchpress.com by 195.138.81.100 on 09/07/12
For personal use only.

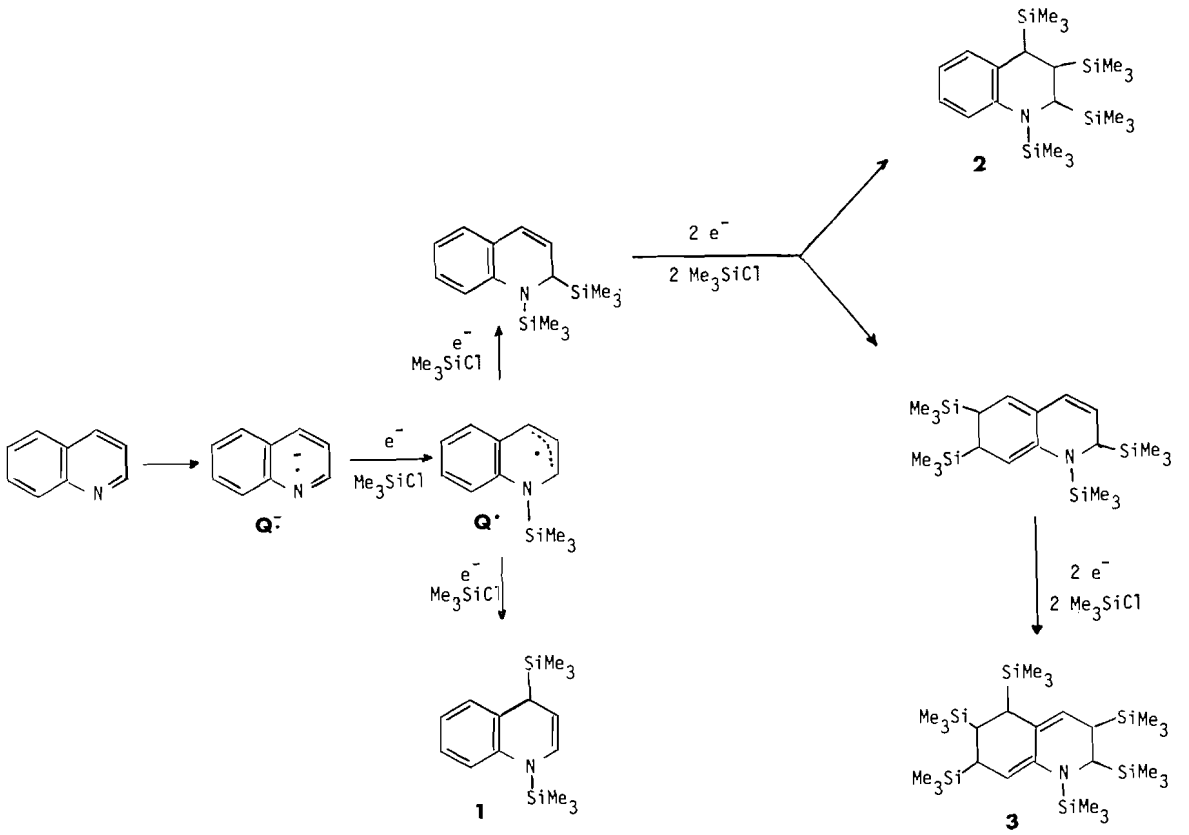

FIG. 1

TABLEAU 1. Influence de la quantité de réactif sur la silylation

(Li/Me_3SiCl) n° d'équivalents	Rdt en produits 1	2	3
2	30	10	15
3	40	15	20
4	44	16	30
6	40	15	40
12	10	13	70

triméthylsilyl-4 quinoléine, **4**, et non pas à son isomère **6**, comme on aurait pu s'y attendre (fig. 3). Pour le confirmer, nous avons synthétisé ce dernier (rdt. 20%) à partir de la bromo-3 quinoléine. À partir de la tétrakis-triméthylsilyl-1,2,3,4 tétrahydro-1,2,3,4 quinoléine, **2**, nous avons également isolé le dérivé **7** par méthanolyse de la liaison N—Si (rdt. quant.); son obtention nécessite d'opérer sous atmosphère parfaitement inerte faute de quoi il évolue, vers la triméthylsilyl-4 quinoléine, **4**. L'action du chlorure d'acétyle conduit au dérivé *N*-acétylé, **8** (rdt. 70%) (fig. 3). Notons que les composés **2**, **7** et **8** sont originaux.

La quinoléine hexasiliciée, **3**, est particulièrement fragile et évolue soit à l'air, soit par chauffage prolongé, soit enfin en présence de réactif à caractère acide (silice, chlorure d'acétyle) avec perte de silicium et aromatisation du cycle azoté. On isole ainsi les composés **9** et **10** avec un rendement global de 80–90% : **9**/**10** ~ 70 : 30 (fig. 4). Placé en solution dans l'éthanol absolu, le dérivé **3** se désilyle et conduit au composé **10** en quelques heures (rdt. 89%). Par ailleurs, l'addition

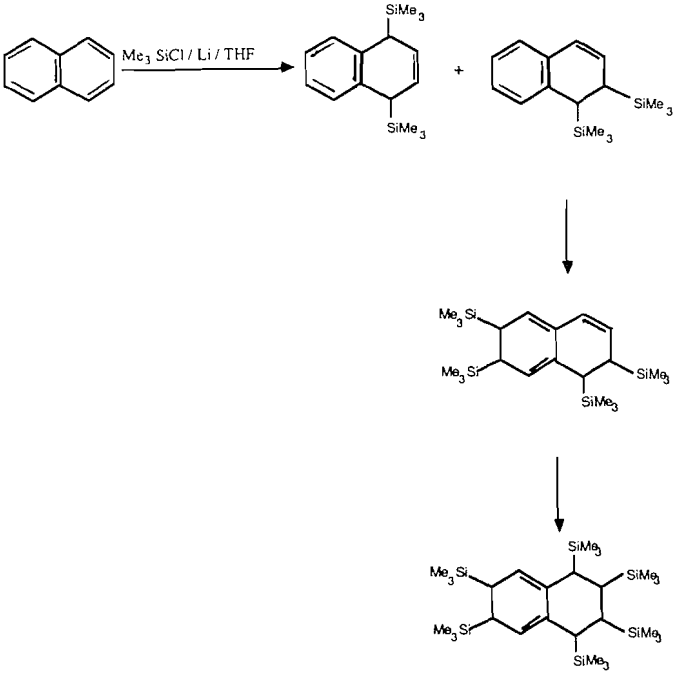

FIG. 2

d'éther provoque la formation d'un précipité que nous avons identifié au tétrakis-triméthylsilyl-2,5,6,7 tétrahydro-5,6,7,8 quinoléine (**11**, rdt. 80%) (fig. 4). Les produits **9**, **10** et **11** sont originaux et confirment la structure proposée pour le dérivé hexasilicié **3**. Il est vraisemblable que le composé **10** se forme à partir de l'intermédiaire **11** dont le groupe silyle en α de l'azote doit être labile en milieu acide. Le passage du composé

Can. J. Chem. Downloaded from www.nrcresearchpress.com by 195.138.81.100 on 09/07/12
For personal use only.

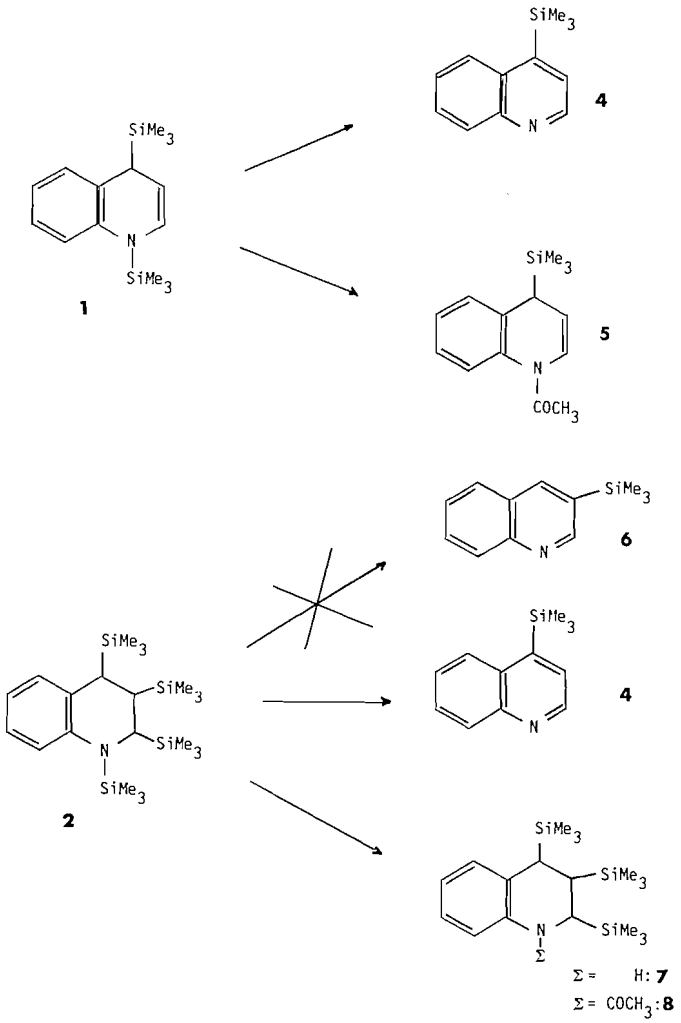

FIG. 3

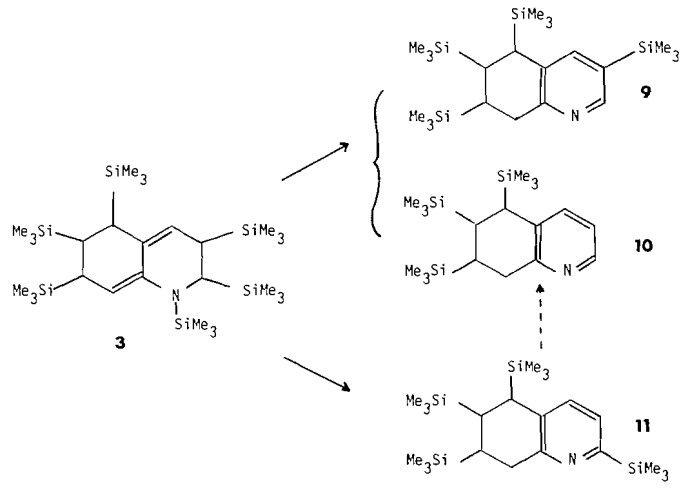

FIG. 4

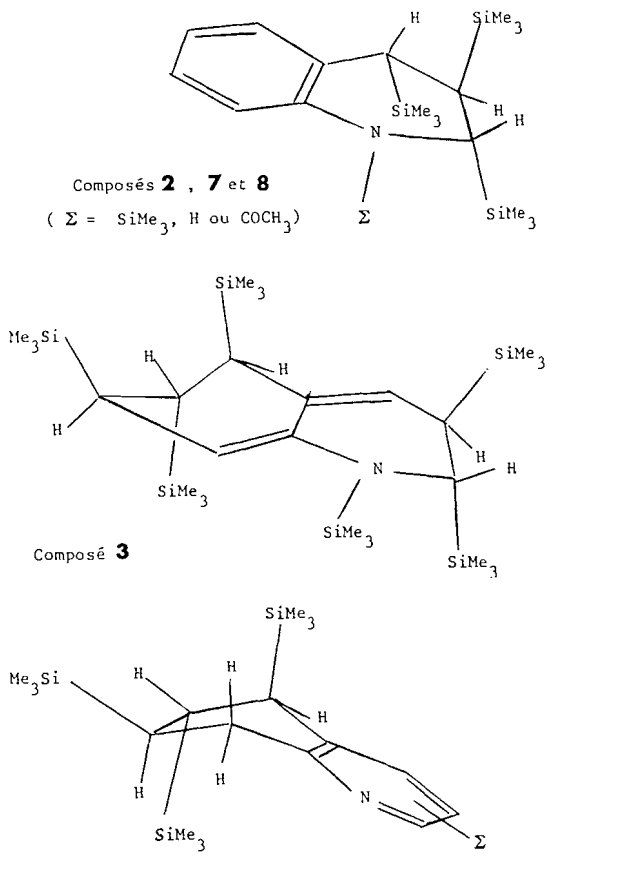

FIG. 5

3 au produit aromatique **11** en présence d'éther peut s'expliquer par la présence de traces d'eau, d'oxygène ou de péroxyde qui permettent une aromatisation douce du squelette.

Les structures spatiales de tous les dérivés obtenus ont été essentiellement déterminées par RMN ^1H et ^{13}C (tableaux 2–4). Ainsi dans le cas de la tétrakis-triméthylsilyl-1,2,3,4 tétrahydro-1,2,3,4 quinoléine, **2**, la présence de trois signaux couplés entre eux entre 1,9 et 3,1 ppm avec des intégrations correspondant à un proton, auxquels on associe les 3 CH observés en ^{13}C entre 30 et 47 ppm confirment l'enchaînement proposé. De plus, à partir des valeurs des constantes de couplage $^3J(^1H,^1H)$ et en utilisant la relation établie par Laguerre et coll.[3] dans le cas de cyclanes polysiliciés, $^3J = 11{,}5\cos^2\theta - 1{,}6\cos\theta + 0{,}6$, nous sommes en mesure de proposer les stéréochimies relatives de tous nos composés (fig. 5). Ces résultats montrent que les disilylations de type 1–2, conduisant à la fixation des siliciums sur les sommets 3 et 4 (composé **2**) et 6 et 7 (composé **3**), s'effectuent en *trans* alors que l'addition de type 1–4, conduisant au composé **3** (sommets 3 et 5), s'effectue en *cis*. Les contraintes stériques jouent vraisemblablement là un rôle important.

Partie expérimentale

Réaction de silylation

Nous avons utilisé du THF distillé sur sodium et benzophénone afin d'enlever les traces d'eau. Le lithium est préalablement granulé par fusion dans l'huile de vaseline puis lavé au THF. La réaction est conduite à la rampe à vide sous atmosphère d'argon. À une suspension de 0,2 at.g de lithium finement granulé, dans 150 mL de THF et 0,26 mol de Me_3SiCl fraîchement distillé, on ajoute goutte à goutte 0,1 mol de quinoléine de telle sorte que la température du milieu réactionnel soit maintenue entre 0 et 5°C. L'avancement de la réaction est suivi par CCM (SiO_2; hexane/EtOH : 80 : 20). Au bout de 5 h environ, on note la disparition du produit de départ. Le THF est alors évaporé à la rampe à vide. On ajoute ensuite 120 mL de cyclohexane, solvant dans lequel LiCl précipite ce qui permet de l'éliminer par filtration. Le filtrat est ensuite évaporé et redissout dans 120 mL de

3. C. Biran, M. Laguerre et J. Dunogues, communication privée.

TABLEAU 2. Caractéristiques de RMN ^1H ($CDCl_3$, 250 MHz) des composés **1**, **2**, **4**, **5**, **7** et **8**

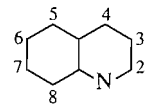

Composés	δ, ppm (multiplicité : *J*, Hz)								
	H2	H3	H4	H5	H6	H7	H8	$SiMe_3$	Σ
1 ($\Sigma = SiMe_3$)	6,04 (d : 7,3)	4,73 (dd : 5,9 et 7,3)	2,73 (d : 5,9)	massif de 6,8 à 7,2				−0,04 (s)	+0,36 (s)
5 ($\Sigma = COCH_3$)	6,53 (d : 7,0)	5,40 (d : 6 et 7,0)	2,74 (d : 6,0)	massif de 6,80 à 7,12				−0,03 (s)	2,2 (s)
4	8,71 signal large	7,34 signal large	—	7,91 (d : 8,2)	2 massifs à 7,36 à 7,53		8,02 (d : 8,4)	+0,34 (s)	—
2 ($\Sigma = SiMe_3$)	3,21 (d : 5,3)	2,1 (dd : 9,5 et 5,3)	2,56 (d : 3,2)	massif (4H) à 6,9				3s −0,10 0,00 +0,29	0,37 (s)
7 ($\Sigma = H$)	3,30 (d : 2,9)	1,38 (dd : 2,9 et 1,2)	2,36 signal large	6,39 (dd : 7,9 et 1,0)	6,86 (dt : 7,7 et 1,5)	6,52 (dt : 7,3 et 1,2)	6,77 (dd : 7,5 et 1,3)	3s −0,08 0,00 +0,17	3,6
8 ($\Sigma = COCH_3$)	4,63 (d : 7,3)	2,13 (t : 7,20)	2,2 (d : 7,2)	massif (4H) à 6,92				3s −0,40 −0,25 −0,00	2,13 (s)

TABLEAU 3. Caractéristiques de RMN ^1H ($CDCl_3$, 250 MHz) des composés **3** et **9–11**

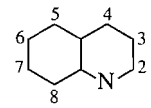

Composé	δ, ppm (multiplicité : *J*, Hz)								
	H2	H3	H4	H5	H6	H7	H8	H9	$SiMe_3$
3	2,96 (s)	1,89 (s)	5,0 (d : 3,2)	1,8 (t : 3,2)	1,15 (d : 3,2)	1,52 (d : 6)	5,22 (d : 6)	—	6s −0,199 −0,069 −0,038 0,000 +0,007 +0,148
9	8,6 (s élargi)	—	7,3 (s)	2,32 (s élargi)	1,42 (dd : 1,2 et 9,2)	1,1 (ddd : 4,8, 9,2 et 14,2)	2,5 (dd : 14,2 et 14,5)	3,16 (dd : 4,8 et 14,5)	4s −0,15 +0,03 +0,15 +0,29
10	8,1 (dd : 4,83 et 1)	6,9 (dd : 4,8 et 7,6)	7,07 (dd : 7,6 et 1)	2,16 (s)	1,29 (d : 9,14)	0,95 (ddd : 9,14, 4,6 et 14,2)	2,36 (dd : 14,2 et 14,5)	2,73 (dd : 4,67 et 14,5)	3s −0,288 −0,136 0,000
11	—	système AB à 7,43		2,28 (s)	1,32 (d : 9,5)	0,93 (ddd : 9,5, 13,9 et 4,4)	2,2 (dd : 14,2 et 13,9)	4,24 (dd : 14,2 et 4,2)	−0,39 −0,15 0,00 −0,44

cyclohexane afin d'éliminer les sels qui pourraient subsister. On obtient ainsi une huile jaune dont les constituants sont isolés par rectification à la rampe à vide.

Acétylation

Le chlorure d'acétyle (0,04 mol) préalablement distillé sur magnésium est additionné à 0,02 mol de substrat *N*-silylé. Le mélange est agité à température ambiante pendant 6 h. Puis le solvant et l'excès de chlorure d'acétyle sont éliminés à l'évaporateur rotatif. Le produit d'acétylation est ensuite purifié sur colonne de silice.

Les produits d'aromatisation **4**, **6** et **9–11** sont purifiés sur colonne de silice.

Caractéristiques physico-chimiques des produits obtenus

Les points de fusion ont été mesurés sur un appareil Mettler FP 61. Les analyses centésimales ont été effectuées au service central

Can. J. Chem. Downloaded from www.nrcresearchpress.com by 195.138.81.100 on 09/07/12
For personal use only.

Can. J. Chem. Downloaded from www.nrcresearchpress.com by 195.138.81.100 on 09/07/12
For personal use only.

TABLEAU 4. Caractéristiques de RMN ^{13}C ($CDCl_3$, 62,9 MHz) des composés **1–4** et **6–11**

Composé	δ, ppm			
	CH_3	CH_2	CH	C
1	−3,50; 0,58	—	32,20 102,71; 116,99; 121,21; 128,05 (2); 130,02	132,8; 142,1
2	0,01; 0,51; 1,22; 1,33	—	30,32; 36,79; 47,11; 119,7; 124,03; 123,62; 129,76	135,48; 148,03
3	−1,97; −1,60; −0,73; −0,40; 2,16; 2,7	—	15,05; 25,43; 28,30; 29,00; 43,28; 110,05; 119,06	128,71; 136,31
4	−0,25	—	126,14; 127,4; 127,90; 128,71; 130,63	131,75; 147,54
6	−0,78	—	126,95; 128,29; 129,81; 130,23; 142,6	133,26; 148,79
7	−2,16; −1,65 0,32		22,67; 33,68; 46,41; 113,90; 116,39; 125,23; 128,64	136,05; 149,9; 159,54
8	−0,81, −0,05; 0,03 22,7 (CH_3CO)	—	29,95; 30,42; 46,21; 124,17; 125,62; 128,96	138,8; 139,7 167,55 (C=O)
9	−1,68; −1,54; −1,03 (2)	35,11	19,42; 21,43; 33,15; 141,55; 148,92	131,97; 135,36; 160,28
10	−1,28; −1,53; −1,67	35,05	18,99; 21,03; 32,94; 128,26; 135,33; 145,57	135,94; 159,65;
11	−2,04; −1,83; −1,38; −1,30	28,8	18,91; 20,02; 33,41; 128,73; 139	140,65; 157,87

d'analyse du CNRS (F-69390 Vernaison). Les spectres de masse (SM) ont été enregistrés sur un appareil VG micromass 16 F (70 eV) et les spectres IR sur un spectromètre Perkin–Elmer 1420; tous les dérivés siliciés isolés présentent en IR des bandes de très forte intensité à 1250 et 850 cm^{-1} caractéristiques des groupes $SiMe_3$ qui peuvent masquer le reste du spectre. Les spectres de RMN ont été enregistrés sur un appareil Bruker AC 250 functionnant à 250 MHz dans le cas du proton et 62,9 MHz pour le ^{13}C (solvant, $CDCl_3$; C_6H_{12} ref. int. à 1,4 ppm (^1H) ou 27,08 ppm (^{13}C)). Les déplacements chimiques et les constantes de couplage sont rassemblés dans les tableaux 2–4.

Bis-triméthylsilyl-1,4 dihydro-1,4 quinoléine (**1**): Rdt. 35%; Eb 88°C/0,06 Torr (1 Torr = 133,3 Pa) (litt. (5) Eb 100°C/0,1); IR (film NaCl, cm^{-1}) : 3040, 3010, 2950, 2895, 2840, 1640, 1595, 1480, 1440, 1275, 1250, 1190, 1105, 1090, 1040, 990, 975, 965, 850, 830, 780, 750, 730, 705, 685, 655, 610.

Tétrakis-triméthylsilyl-1,2,3,4 tétrahydro-1,2,3,4 quinoléine (**2**) : Rdt. 15%; Eb 125–127°C/0,01 Torr; IR (film NaCl, cm^{-1}) : 3040, 3020, 2930, 2880, 1590, 1570, 1470, 1450, 1400, 1250, 850, 830, 740, 680, 630, 620. Anal. calculée pour $C_{21}H_{43}NSi_4$: C 59,78, H 10,27, N 3,32; trouvée : C 59,81, H 10,25, N 3,27.

Hexakis-triméthylsilyl-1,2,3,5,6,7 hexahydro-1,2,3,5,6,7 quinoléine (**3**) : Rdt. 25–70% selon la quantité de réactif utilisée (cf. tableau 1); IR (film NaCl, cm^{-1}): 3040, 3020, 2940, 2880, 2840, 1480, 1280, 1250, 850, 830, 740, 680. Anal. calculée pour $C_{27}H_{61}NSi_6$: C 57,07, H 10,82, N 2,46; trouvée : C 56,92, H 10,75, N 2,53.

Triméthylsilyl-4 quinoléine (**4**): Rdt. 80%; Eb 118°C/68 Torr (litt. (8) Eb 114/65).

N-*Acétyl triméthylsilyl-4 dihydro-1,4 quinoléine* (**5**) : il est isolé par acétylation du composé **1** et est purifié par chromatographie liquide (SiO_2; C_6H_{12}/THF : 90 : 10); Rdt. 82%. Anal. calculée pour $C_{14}H_{19}NOSi$: C 68,52, H 7,8, N 5,71, O 6,52; trouvée : C 68,31, H 7,65, N 5,69, O 6,58.

Triméthylsilyl-3 quinoléine (**6**): Rdt. 20%; Eb 99°C/68 Torr (litt. (8) Eb 96°C/65).

Tris-triméthylsilyl-2,3,4 tétrahydro-1,2,3,4 quinoléine (**7**) : Rdt. 95%; IR (film NaCl, cm^{-1}): 3400, 3040, 2940, 2840, 1595, 1570, 1250, 850, 690, 650. Anal. calculée pour $C_{18}H_{35}NSi_3$: C 61,82, H 10,09, N 4,00; trouvée : C 61,5, H 11,21, N 3,89.

N-*Acétyl tris-triméthylsilyl-2,3,4 tétrahydro-1,2,3,4 quinoléine* (**8**) : solide blanc obtenu par acétylation du composé **2** et purifié par chromatographie liquide (SiO_2; hexane/THF : 90 : 10; R_f 0,53), Rdt. 70%; *F* 91°C (EtOH); IR (KBr, cm^{-1}) : 3060, 3040, 2940, 2880, 2840, 1650, 1600, 1570, 1490, 1370, 1250, 850, 750, 680. Anal. calculée pour $C_{20}H_{37}NOSi_3$: C 61,31, H 9,52, N 3,58, O 4,08; trouvée : C 61,45, H 9,48, N 3,52, O 4,01.

Tétrakis-triméthylsilyl-3,5,6,7 tétrahydro-5,6,7,8 quinoléine (**9**) : huile jaune pâle purifiée par chromatographie liquide (SiO_2; C_6H_{12}/THF : 95 : 5; R_f 0,42); IR (film NaCl, cm^{-1}) : 3020, 2950, 2890, 2840, 1640, 1360, 1310, 1250, 850, 830, 750, 680, 620; SM (*m/e* (%)) : 421 (5,2), 406 (11,7), 348 (73,6), 274 (11,5), 260 (59,1), 73 (100). Anal. calculée pour $C_{21}H_{43}NSi_4$: C 59,78, H 10,27, N 3,32; trouvée : C 59,84, H 10,29, N 3,28.

Tris-triméthylsilyl-5,6,7 tétrahydro-5,6,7,8 quinoléine (**10**) : huile purifiée par chromatographie liquide (SiO_2; C_6H_{12}/THF : 95 : 5; R_f 0,39), Rdt. 89%; IR (film NaCl, cm^{-1}) : 3040, 2940, 2920, 2880, 2840, 1630, 1430, 1250, 900, 830, 780, 740, 670; SM (*m/e* (%)) : 348 (6,9), 333 (13,1), 274 (76,2), 260 (13,6), 186 (48,1), 73 (100).

Anal. calculée pour $C_{18}H_{35}NSi_3$: C 61,82, H 10,09, N 4,00; trouvée : C 61,37, H 10,18, N 3,91.

Tétrakis-triméthylsilyl-2,5,6,7 tétrahydro-5,6,7,8 quinoléine (**11**) : solide blanc, Rdt. 80%; *F* 208°C (EtOH); SM (*m/e* (%)) : 421 (7,8), 406 (10,4), 348 (75,4), 274 (12,0), 260 (57,0), 186 (50,4), 73 (100). Anal. calculée pour $C_{21}H_{43}NSi_4$: C 59,78, H 10,27, N 3,32; trouvée : C 59,10, H 10,51, N 3,28.

Remerciements

Ce travail a bénéficié d'une subvention des Laboratoires SARGET (Avenue J. F. Kennedy, BP 100, 33701 Mérignac Cédex).

1. (*a*) E. W. COLVIN. Silicon in organic synthesis. Butterworths, Londres. 1983; (*b*) W. P. WEBER. Silicon reagents for organic synthesis. Springer Verlag, Berlin. 1983; (*c*) J. DUNOGUES. L'actualité chimique. 11 mars 1986.
2. (*a*) A. LESPAGNOL. Chimie des médicaments. Tome I. Technique et Documentation, Genève. 1974; (*b*) M. SCHORDERET. Des concepts fondamentaux aux applications thérapeutiques. Frison Roche, Paris. 1989.
3. H. P. BECKER et W. P. NEWMANN. J. Organomet. Chem. **37**, 57 (1972).
4. A. I. NOGAIDELI et D. CH. AKHOBADZE. Bull. Acad. Sc. Georgian SSR, **87** (3), 621 (1977).
5. R. A. SULZBACH et A. F. IQBAL. U.S. Patent 3,781,291. 25 décembre 1973.
6. R. CALAS et J. DUNOGUES. J. Organomet. Chem. Library, **2**, 277 (1976).
7. M. LAGUERRE, J. DUNOGUES et R. CALAS. Tetrahedron Lett. **22** (13), 1227 (1981).
8. A. FISHER, M. W. MORGAN et C. EABORN. J. Organomet. Chem. **136**, 323 (1977).

Can. J. Chem. Downloaded from www.nrcresearchpress.com by 195.138.81.100 on 09/07/12
For personal use only.

Oxidation of substituted anilines by horseradish peroxidase compound II

JIN HUANG AND H. BRIAN DUNFORD
Department of Chemistry, University of Alberta, Edmonton, Alta., Canada T6G 2G2
Received March 5, 1990

JIN HUANG and H. BRIAN DUNFORD. Can. J. Chem. **68**, 2159 (1990).

The kinetics of oxidation of eight monosubstituted anilines catalyzed by horseradish peroxidase compound **II** has been studied at pH 7.00 and 7.60. With *p*-toluidine the rates of oxidation by compound **II** have been measured at 21 pH values between 3.60 and 10.25. The rate–pH profile indicates that an acidic form of compound **II** and the electrically neutral, unprotonated form of *p*-toluidine are reactive. The correlation of rate constants for the substituted anilines with the substituent constant σ in the Hammett equation suggests that the aromatic amine donates an electron to compound **II** in the rate-controlling step and loses a proton simultaneously. The value of ρ, the susceptibility factor in the Hammett equation, is -6.0 ± 0.7. The reactivity of anilines with HRP-II observed in this study is lower than that of anilines with HRP-I observed previously, although the value of ρ is the same within experimental error (D. Job and H. B. Dunford. Eur. J. Biochem. **66**, 607 (1976)). The difference in reactivity is explained by the relative complexities of the reactions of compounds **I** and **II**.

Key words: horseradish peroxidase, peroxidase compound **II**, aniline oxidation, Hammett correlation, enzymatic oxidation.

JIN HUANG et H. BRIAN DUNFORD. Can. J. Chem. **68**, 2159 (1990).

Opérant à des pH de 7,00 et de 7,60, on a étudié la cinétique de l'oxydation de huit anilines monosubstituées, catalysée par le composé **II** de la peroxydase du raifort (HRP-II). Pour la *p*-toluidine, on a déterminé les vitesses d'oxydation à 21 pH différents entre 3,60 et 10,25. La relation entre la vitesse et le pH indique que les formes réactives sont d'une part une forme acide du composé **II** et d'autre part la forme non-protonée et électriquement neutre de la *p*-toluidine. La corrélation des constantes de vitesse des anilines substituées avec la constante de substituant σ de l'équation de Hammett suggère que l'amine aromatique donne un électron au composé **II** dans l'étape qui détermine la vitesse et qu'elle perd simultanément un proton. La valeur de ρ, le facteur de susceptibilité de l'équation de Hammett, est égal à $-6,0 \pm 0,7$. La réactivité des anilines pour le HRP-II qui a été observée dans ce travail est plus faible que la réactivité des anilines pour le HRP-I qui a été observée antérieurement; la valeur de ρ est toutefois la même, aux erreurs expérimentales près (D. Job et H. B. Dunford. Eur. J. Biochem. **66**, 607 (1976)). La différence de réactivité est expliquée par les complexités relatives des réactions des composés **I** et **II**.

Mot clés : peroxydase du raifort, composé **II** de la peroxydase, oxydation de l'aniline, corrélation de Hammett, oxydation enzymatique.

[Traduit par la revue]

Introduction

The reaction of aromatic amines (and other organic substrates) with horseradish peroxidase (EC 1.11.1.7, donor–H_2O_2 oxidoreductase) may be summarized as follows (1–3):

[1] $\mathrm{HRP} + \mathrm{H_2O_2} \rightarrow \mathrm{HRP\text{-}I} + \mathrm{H_2O}$

[2] $\mathrm{HRP\text{-}I} + \mathrm{AH_2} \rightarrow \mathrm{HRP\text{-}II} + \cdot\mathrm{AH}$

[3] $\mathrm{HRP\text{-}II} + \mathrm{AH_2} \rightarrow \mathrm{HRP} + \cdot\mathrm{AH}$

Horseradish peroxidase and its two oxidized intermediates, compounds **I** and **II**, are represented by HRP, HRP-I, and HRP-II, respectively, the aromatic amines by AH_2, and their free radical product by $\cdot$AH. However, the general scheme above does not provide the details of events taking place on either the enzyme or the substrate during an oxidation process. Therefore a number of separate investigations have been conducted on HRP-catalyzed oxidation of various substrates to provide a better understanding and to explore the potential applications of peroxidatic action on specific substrates. Examples can be found in refs. 4 to 6.

The enzymatic oxidation of aromatic amines plays a significant role in many biotransformation processes such as chemical carcinogenesis and drug metabolism (7–9). Horseradish peroxidase in the presence of hydrogen peroxide is a useful tool for modeling the extra-hepatic biooxidation of xenobiotics (10, 11).

Substituent electronic effects are often used as a probe into the reaction mechanism of aromatic compounds. The Hammett equation provides a general description of substituent effects upon rates and equilibria of aromatic molecules (12):

$$[4] \quad \log\left(\frac{k_X}{k_H}\right) = \rho\sigma$$

where k_X and k_H denote rate or equilibrium constants for reactions of the substituted and unsubstituted compounds, respectively; σ is the substituent constant, determined by the nature and position of the substituent, and ρ is the reaction constant, also known as the susceptibility factor, which depends on the features and conditions of the reaction. A modified form of the Hammett equation with σ replaced by a different substituent constant σ^+ is known as the Brown–Okamoto equation. It can correlate reactions deviating from the Hammett equation because of the generation of positive charge capable of resonance interaction with a substituent (13). A linear correlation by the Hammett relationship is an indication that a single mechanism is operating through the reaction series.

The Hammett $\rho\sigma$ correlation was previously established in the oxidation of substituted anilines by compound **I** of HRP. Compounds **I** and **II** are two major intermediates in peroxidase reactions. It is therefore interesting to see whether the reactions between compound **II** of HRP and substituted anilines are also correlated by the Hammett equation, and if they are, how the correlation reflects the different structure and reactivity of compound **II** from those of compound **I**.

In this study, eight *para* or *meta* monosubstituted anilines were chosen to react with compound **II** of horseradish peroxidase. The rate–pH profile for one aromatic amine, *p*-toluidine, is also obtained. The Hammett relationship is employed to correlate the kinetic behaviors of the substituted anilines. The

Can. J. Chem. Downloaded from www.nrcresearchpress.com by 195.138.81.100 on 09/07/12
For personal use only.

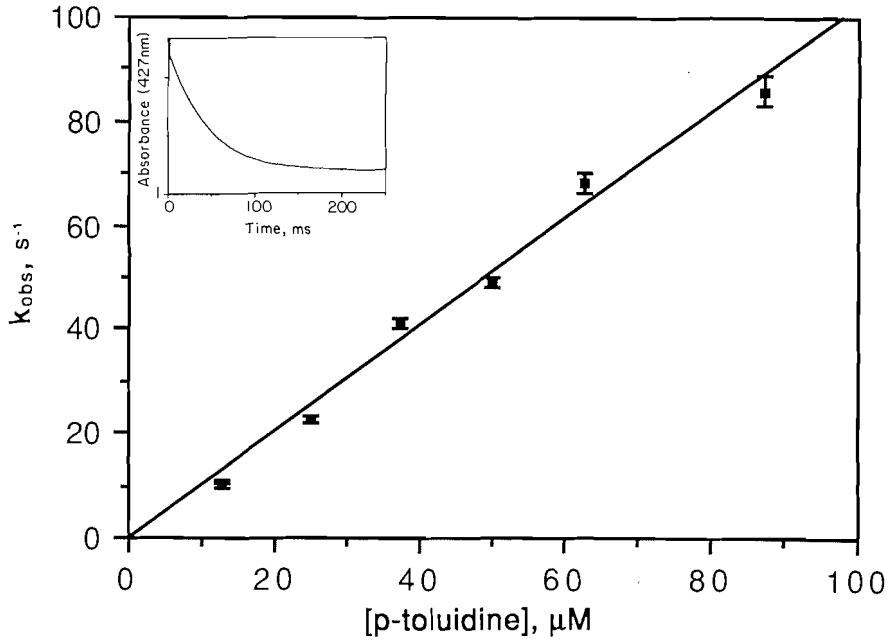

FIG. 1. Plot of k_{obs} versus *p*-toluidine concentration for the oxidation of *p*-toluidine by horseradish peroxidase compound **II**. The reactions were carried out in phosphate buffer, ionic strength 0.11 M; pH 7.60; [HRP-II], 1.0 μM; temperature 25.0°C. The inset shows an example of first order exponential trace (25 μM *p*-toluidine) from which k_{obs} was obtained.

different reactivity of anilines with compound **II** observed in this study compared to that of anilines reacting with compound **I** of HRP is discussed.

Experimental

HRP, grade I, purchased from Boehringer–Mannheim as an ammonium sulfate precipitate, was dialyzed against water deionized in a Milli-Q water purification system. After dialysis the RZ, the ratio of absorbance at 403 to 280 nm, was 3.28. The concentration of HRP was determined spectrophotometrically at 403 nm using a molar absorptivity of $1.02 \times 10^5\ M^{-1}\ cm^{-1}$ (14). Hydrogen peroxide was obtained as a 30% solution from Fisher. The concentration of diluted H_2O_2 stock solution was determined by peroxidase assay as described elsewhere (15). All the aromatic amines, obtained from various sources (*p*-aminophenol and *p*-toluidine from BDH, *p*-phenetidine and *m*-phenetidine from Eastman, aniline from Mallinckrodt, and 3-aminoacetophenone, 4-aminobenzoic acid, and sulfanilic acid from Aldrich), were of reagent grade and were used without further purification.

For each substrate, a stock solution of around 10 mM concentration was prepared by dissolving a weighed amount of the compound in volumetric flasks with purified water. All substrate solutions were stored in dark brown bottles to prevent photochemical reactions. The substrate solution for each experiment was then made by diluting the stock solution to the desired concentration with an appropriate buffer immediately before the measurement.

All buffer solutions had an ionic strength of 0.11 M, adjusted by adding 0.1 M KNO_3 as an inert salt. Acetate buffer was used between pH 3.60 and 5.39, phosphate buffer between pH 5.58 and 7.60, Tris buffer between pH 8.05 and 9.04, and carbonate buffer between pH 9.30 and 10.25. All pH measurements were made with a Fisher Accumet Model 420 digital pH meter which was calibrated with standard buffers from Fisher.

Kinetic measurements for three substrates (3-aminoacetophenone, 4-aminobenzoic acid, and sulfanilic acid) were performed on a Cary 219 spectrophotometer while the kinetic measurements for other substrates were made on a Photal (formerly Union Giken) stopped-flow spectrophotometer Model RA-601. The 1-cm observation cells of both spectrophotometers were thermostated at 25.0°C for all measurements.

The enzyme concentration for all kinetic measurements was 1 μM, prepared with appropriate buffers. At least a 10-fold excess of substrates was used to maintain pseudo-first-order conditions.

HRP-II solution was freshly prepared prior to the experiments by addition of one equivalent of H_2O_2 and one equivalent of $K_4Fe(CN)_6$ to the native HRP solution. To ensure that no HRP-I was present, the preparation of HRP-II was monitored at 411 nm, the isobestic point between native HRP and HRP-II. No change in absorbance was observed. After the absence of HRP-I had been established, the HRP-II reactions were monitored at 427 nm, where the maximum difference in absorbance between native HRP and HRP-II is expected.

For stopped-flow experiments one drive syringe was filled with HRP-II solution and the other was filled with the substrate solution. Between five and eight traces were collected for each substrate concentration. The relative standard deviation was below 5% in most cases and never beyond 10%. For measurements with the Cary spectrophotometer, 3 mL of freshly prepared compound **II** solution was pipetted into the observation cell. The reference cuvette was filled with purified water. The reaction was initiated by adding a calculated volume of the substrate solution into the cell containing HRP-II. The instrument was started immediately after the addition of the substrate. Measurements of relative absorbance at regular time intervals from the recorded trace followed by a nonlinear least-square analysis on computer gave the observed pseudo-first-order rate constants.

Results

With substrate in excess of HRP-II, pseudo-first-order kinetics was observed. One example is shown in the inset of Fig. 1. The corresponding differential rate expression is

$$[5] \quad -\frac{d[\text{HRP-II}]}{dt} = k_{obs}[\text{HRP-II}]$$

where k_{obs} is the observed pseudo-first-order rate constant. The apparent second order rate constant, k_{app}, is related to k_{obs} by the equation

$$[6] \quad k_{obs} = k_{app}[AH_2]$$

where $[AH_2]$ is the substrate concentration. Values of k_{app} were then obtained from the slopes of plots of k_{obs} versus $[AH_2]$, as shown by an example in Fig. 1.

A plot of log k_{app} versus pH is shown in Fig. 2 for the oxidation of *p*-toluidine by HRP-II. It appears from Fig. 2 that

Can. J. Chem. Downloaded from www.nrcresearchpress.com by 195.138.81.100 on 09/07/12
For personal use only.

TABLE 1. Effect of substituents on oxidation rate constants of aromatic amines by horseradish peroxidase compound **II**

	k_{app} (M^{-1} s^{-1})		σ	
Substituent	pH 7.60	pH 7.00	Value	Reference
p-OH[a]	$(3.5\pm0.3)\times10^7$	$(3.1\pm0.4)\times10^7$	−0.357	16
p-OC_2H_5	$(1.2\pm0.4)\times10^7$	$(1.0\pm0.3)\times10^7$	−0.25	17
p-CH_3	$(1.1\pm0.3)\times10^6$	$(1.2\pm0.4)\times10^6$	−0.17	12
H	$(2.8\pm0.1)\times10^4$	$(2.9\pm0.3)\times10^4$	0	
m-OC_2H_5	$(5.7\pm0.5)\times10^4$	$(5.5\pm0.2)\times10^4$	0.15	17
m-$COCH_3$	$(4.1\pm0.2)\times10^3$	$(4.4\pm0.1)\times10^3$	0.306	12
p-COO^-	$(4.0\pm0.1)\times10^3$	$(3.8\pm0.1)\times10^3$	0.35	16
p-SO_3^-	$(2.0\pm0.2)\times10^2$	$(2.3\pm0.2)\times10^2$	0.38	16

[a]Value (pH 7.60) reported in ref. 22.

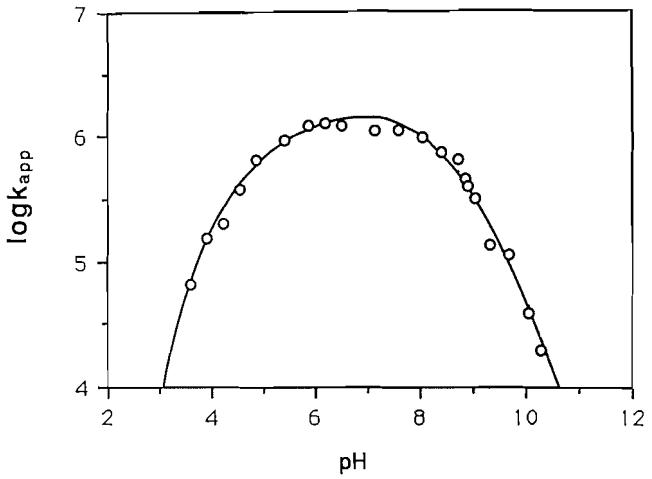

FIG. 2. The rate–pH profile for the reaction of horseradish peroxidase compound **II** with *p*-toluidine at 25.0°C and ionic strength 0.11 M. The curve was computed on the basis of best-fit parameters obtained by a nonlinear least-square analysis of the data with eq. [8].

two ionizations which affect the kinetics of the reaction are occurring.

The Hammett plot of log (k_X/k_H) versus σ (see eq. [4]) is shown in Fig. 3. The second order rate constants at pH 7.60 and pH 7.00 along with the Hammett σ values of different substrates, are listed in Table 1. Values of k_{app} used to construct the plot are averages of values obtained at the two pH's. The purpose of conducting measurements at two different pH's is to confirm that k_{app} values for the Hammett plot were measured in such a region where the substituent effect, instead of the pH effect, is predominant. As can be seen from Table 1, the k_{app} values at two pH's are the same within experimental error.

The slope of the Hammett plot in Fig. 3 is equal to ρ in the Hammett equation. The value of ρ is -6.0 ± 0.7.

Discussion

The simplest mechanism which will account for the experimental data is one in which the neutral unprotonated amine reacting with an acidic form of the enzyme:

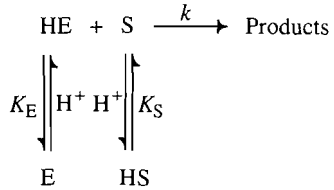

[7]

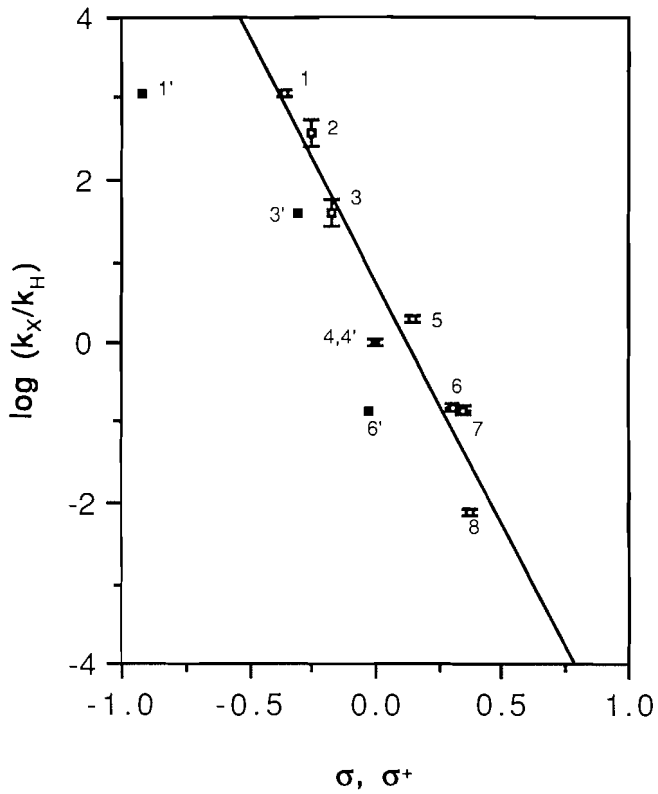

FIG. 3. Hammett plot (□) and Brown–Okamoto plot (■) for the oxidation of various *p*- and *m*-substituted anilines by horseradish peroxidase compound **II**. k_X is the rate constant for the substituted aniline and k_H for aniline. The σ values are those listed in Table 1 and the σ^+ values are those obtained by Brown and Okamoto (13). Substituent groups: (1,1′) *p*-OH; (2) *p*-OC_2H_5; (3,3′) *p*-CH_3; (4,4′) H; (5) *m*-OC_2H_5; (6,6′) *m*-$COCH_3$; (7) *p*-COO^-; (8) *p*-SO_3^-.

The k_{app}–pH relationship corresponding to eq. [7] can be described as follows:

$$[8]\quad k_{app} = \frac{k}{\left[1+\frac{K_E}{[H^+]}\right]\left[1+\frac{[H^+]}{K_S}\right]}$$

Using nonlinear least-square analysis, the experimental log k_{app} – pH data points shown in Fig. 2 were fitted to eq. [8]. The best-fit parameters are $k = (1.2 \pm 0.1) \times 10^6$ M^{-1} s^{-1}; $K_E = (2.8 \pm 0.3) \times 10^{-9}$ M, $pK_E = 8.6 \pm 0.1$; $K_S = (1.5 \pm 0.2) \times 10^{-5}$ M, $pK_S = 4.8 \pm 0.1$. The curve computed on the basis of the best-fit parameters is also shown in Fig. 2. Previous studies on

Can. J. Chem. Downloaded from www.nrcresearchpress.com by 195.138.81.100 on 09/07/12
For personal use only.

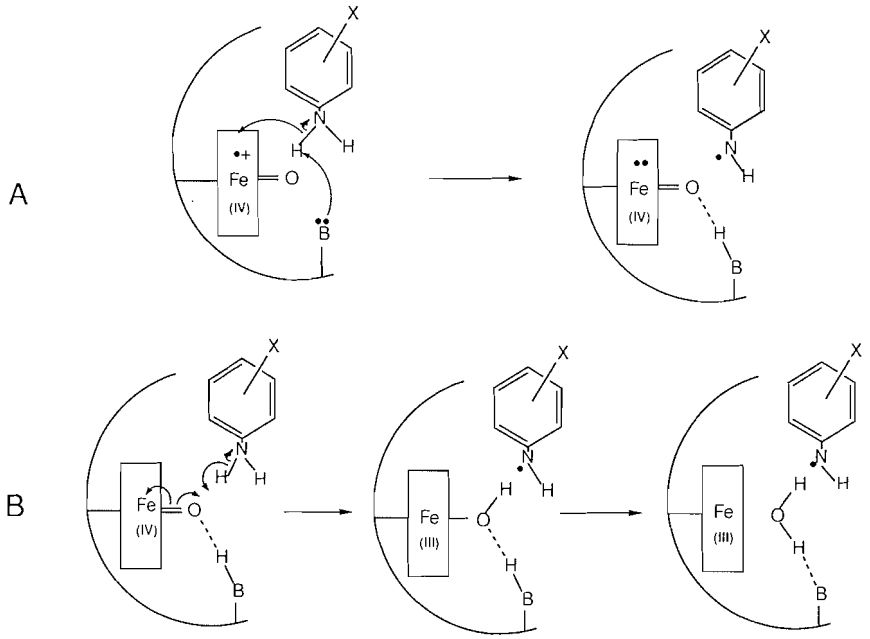

FIG. 4. Schematic representation of relative complexities of compound **I** and compound **II** reactions. (*A*) Relatively simple reaction of compound **I** with anilines. An electron is transferred to the porphyrin ring (represented by the rectangle) neutralizing the π-cation radical of compound **I**. (*B*) Relatively complicated reaction of compound **II** with anilines. An electron is transferred to iron(IV) and two protons are transferred to the ferryl oxygen atom forming a water molecule as the leaving group.

HRP-II reactions with different substrates have proved the existence of an acid–base group on the enzyme with a pK_a value of 8.6 so that our present results are in excellent agreement (5). The pK_{BH+} of *p*-methyl anilinium ion (protonated *p*-toluidine) was reported to be 5.08 in water at 25°C (18), which can be corrected for this study by considering ionic strength in terms of the extended Debye–Hückel equation (19). The pK_{BH+} so corrected is 4.97. Similarly there is a good agreement between our pK_S value computed from the kinetic results and the literature value for the ionization of protonated *p*-toluidine.

The adherence to the Hammett equation for *para* or *meta* monosubstituted anilines, as can be seen from Fig. 3, shows that all of the anilines react with compound **II** by the same mechanism. One conclusion can be drawn immediately, that is, the neutral forms of the anilines are reacting in all aniline oxidations by compound **II**. A negative slope of the Hammett plot indicates that electron-donating groups, as we expected, facilitate the oxidation of anilines. This suggests that the removal of one electron from a substrate is the rate-controlling step in the oxidation of anilines. The loss of one electron from a substrate is accompanied by the simultaneous loss of a proton, so that a positive charge at the reaction site is not formed. The experimental data are better correlated by the Hammett $\rho\sigma$ relationship, instead of the Brown–Okamoto $\rho\sigma^+$ relationship (the correlation coefficients in the two cases are 0.931 and 0.887, respectively). The plot of rate constants against σ^+ values can be seen in Fig. 3. Unfortunately, some of the relevant σ^+ values are not available in the literature. A mechanism similar to ours has been suggested by different authors (20–23).

There have been discussions about the *p*-aminophenol oxidation by HRP as to whether it reacts as a substituted aniline or as a substituted phenol (21), in other words, whether the one electron oxidation and proton abstraction occur from the amino group, yielding free radical **1** or from the hydroxyl group, yielding free radical **2**.

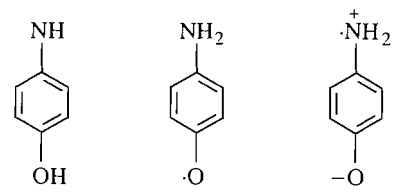

1 **2** **3**

Though **2** was cited as an oxidation product (24), there is evidence suggesting the oxidation occurs at the amino group. In oxidation by compound **I**, the rate constant for *p*-aminophenol seems to fit the Hammett plot for the aniline series. However, this could result from the oxidation on the hydroxyl group being retarded by partial diffusion control (21). Later studies on reactions between phenols and compound **II** showed the obvious deviation of *p*-aminophenol from the Hammett plot of the phenol series, favoring the possibility of *p*-aminophenol reacting as a substituted aniline (22). An ESR study of HRP-catalyzed oxidation of *p*-aminophenol performed under alkaline conditions demonstrated that the one electron oxidation product is a zwitterion radical **3** with the electron removed from the amino group (25). The fit of the data for *p*-aminophenol to the Hammett plot for anilines in this study also suggests that the removal of an electron and a proton takes place at the amino group instead of at the hydroxyl group. This is interesting considering the fact that the reactivity of anilines is generally lower than that of phenols.

Compared with the ρ value[1] of -7.0 ± 0.7 for the reaction of anilines with compound **I**, the ρ value obtained in this study for the reaction of anilines with compound **II** is -6.0 ± 0.7. Thus the substituent susceptibility of compound **II** reactions is the same within experimental error as that observed for the

[1]Standard deviations are calculated based on the original data in ref. 21.

Can. J. Chem. Downloaded from www.nrcresearchpress.com by 195.138.81.100 on 09/07/12
For personal use only.

corresponding compound **I** reactions. This is in contrast with the results for phenols[1] where ρ is -6.9 ± 0.5 for compound **I** (21) and -4.6 ± 0.5 for compound **II** (22). In an independent work, published since this manuscript was first submitted, a ρ value of -5.75 was obtained for substituted anilines reacting with HRP-II, in close agreement with our results presented here (23). In their work mainly different substituted anilines were used. As another comparison, the rate constants of anilines reacting with HRP-II obtained in this study are about one order of magnitude lower than those of anilines reacting with HRP-I (21). A proposed mechanism for anilines reacting with both compound **I** and compound **II** is depicted in Fig. 4. It is widely accepted that compound **I** is a porphyrin π-cation radical (26). During the oxidation of anilines by compound **I**, the aromatic electron-deficient compound **I** acts as the direct target for an electron donated from amines (27, 28). While in the case of compound **II** reactions, in addition to the transfer of an electron to Iron(IV), two protons are also transferred to the ferryl oxygen forming a water molecule which leaves from the inner coordination sphere of the iron (29). This comparison indicates that the reduction of compound **II**, which involves more bond-breaking and bond-formation steps, is a more complicated chemical process than the reduction of compound **I** (29). This explains a lower order-of-magnitude in the reactivity of anilines with HRP-II than with HRP-I.

Acknowledgement

This work was supported by operating grant A1248 from the Natural Sciences and Engineering Research Council of Canada (to H.B.D.), a research assistantship from Department of Chemistry, University of Alberta, and a studentship from Alberta Heritage Foundation for Medical Research (to J.H.).

1. B. CHANCE. Arch. Biochem. Biophys. **41**, 416 (1952).
2. P. GEORGE. Nature (London), **169**, 612 (1952).
3. H. B. DUNFORD and M. L. COTTON. J. Biol. Chem. **250**, 2920 (1975).
4. B. C. SAUNDERS, A. G. HOLMES-SIEDLE, and B. P. STARK. Peroxidase. Butterworth, London. 1964.
5. H. B. DUNFORD and J. S. STILLMAN. Coord. Chem. Rev. **19**, 187 (1976).
6. H. B. DUNFORD. *In* Peroxidases. Chemistry and biology. *Edited by* J. Everse and M. B. Grisham. CRC Press, Boca Raton, FL. 1990. In press.
7. J. H. WEISBURGER and E. K. WEISBURGER. Pharmacol. Rev. **25**, 1 (1973).
8. F. A. BELAND and F. F. KADLUBAR. Carcinogenesis, **6**, 1379 (1985).
9. D. W. POTTER and J. A. HINSON. Drug Metab. Rev. **20**, 341 (1989).
10. A. WENDEL and J. HALLBACH Biochem. Pharmacol. **35**, 385 (1986).
11. G. MEUNIER and B. MEUNIER. J. Am. Chem. Soc. **107**, 2558 (1985).
12. L. P. HAMMETT. Physical organic chemistry. McGraw-Hill, New York. 1940. pp. 184–199.
13. H. C. BROWN and Y. OKAMOTO. J. Am. Chem. Soc. **80**, 4979 (1958).
14. G. R. SCHONBAUM and S. LO. J. Biol. Chem. **247**, 3353 (1972).
15. M. L. COTTON and H. B. DUNFORD. Can. J. Chem. **51**, 582 (1973).
16. H. H. JAFFE. Chem. Rev. **53**, 191 (1953).
17. A. I. BRIGGS and R. A. ROBINSON. J. Chem. Soc. 388 (1961).
18. A. ALBERT and E. P. SERJEANT. The determination of ionization constants. Chapman and Hall, New York. 1984.
19. P. DEBYE and E. HÜCKEL. Phys. Z. **25**, 145 (1924).
20. B. C. SAUNDERS and P. J. G. MANN. J. Chem. Soc. 769 (1940).
21. D. JOB and H. B. DUNFORD. Eur. J. Biochem. **66**, 607 (1976).
22. H. B. DUNFORD and A. J. ADENIRAN. Arch. Biochem. Biophys. **251**, 536 (1986).
23. J. SAKURADA, R. SEKIGUCHI, K. SATO, and T. HOSOYA. Biochemistry, **29**, 4093 (1990).
24. P. J. O'BRIEN. *In* Free radicals in biology. Vol. 4. *Edited by* W. Pryor. Academic Press, New York. 1984. pp. 289–322.
25. P. D. JOSEPHY, T. E. ELING, and R. P. MASON. Mol. Pharmacol. **23**, 461 (1983).
26. D. DOLPHIN, A. FORMAN, D. C. BORG, J FAJER, and R. H. FELTON. Proc. Natl. Acad. Sci. U.S.A. **68**, 614 (1971).
27. H. B. DUNFORD. Adv. Inorg. Biochem. **4**, 41 (1982).
28. P. R. ORTIZ DE MONTELLANO. Acc. Chem. Res. **20**, 289 (1987).
29. C. BOHNE, I. D. MACDONALD, and H. B. DUNFORD. J. Biol. Chem. **262**, 3572 (1987).

Can. J. Chem. Downloaded from www.nrcresearchpress.com by 195.138.81.100 on 09/07/12
For personal use only.

Photophysical properties of pyridinium salts derived from purine bases

BOHDAN SKALSKI AND STEFAN PASZYC
Faculty of Chemistry, A. Mickiewicz University, Poznan, Poland

RYSZARD W. ADAMIAK
Institute of Bioorganic Chemistry, Polish Academy of Sciences, Poznan, Poland

AND

RONALD P. STEER[1] AND RONALD E. VERRALL[1]
Department of Chemistry, University of Saskatchewan, Saskatoon, Sask., Canada S7N 0W0

Received May 4, 1990

BOHDAN SKALSKI, STEFAN PASZYC, RYSZARD W. ADAMIAK, RONALD P. STEER, and RONALD E. VERRALL. Can. J. Chem. **68**, 2164 (1990).

The absorption spectra, fluorescence spectra, fluorescence lifetimes, fluorescence quenching, phosphorescence spectra, phosphorescence lifetimes, and picosecond transient absorption spectra of several purinyl-pyridinium salts have been measured in several solvents at room temperature and in ethanol glasses at 77 K. It is concluded that the previously observed photochemical transformation of *N*-[9-(2′,3′,5′-tri-*O*-acetyl-β-D-ribofuranosyl)purin-6-yl]pyridinium chloride **1** into the highly fluorescent tri-*O*-acetylluminarosine **6** occurs via an excited triplet state. It is also shown that intersystem crossing in purinyl-pyridinium salts is induced by an intermolecular charge-transfer interaction with the counter ions.

Key words: purinyl-pyridinium salts, fluorescence, phosphorescence.

BOHDAN SKALSKI, STEFAN PASZYC, RYSZARD W. ADAMIAK, RONALD P. STEER et RONALD E. VERRALL. Can. J. Chem. **68**, 2164 (1990).

Opérant dans divers solvants à la température ambiante et dans des verres dans l'éthanol à 77 K, on a mesuré les spectres d'absorption, les spectres de fluorescence, les temps de vie de fluorescence, la désactivation de la fluorescence, les spectres de phosphorescence, les temps de vie de phosphorescence et les spectes d'absorption des transitions de picosecondes de plusieurs sels purinyl-pyridinium. On en conclut que la transformation photochimique qui n'avait pas été rapportée antérieurement du chlorure de *N*-[9-(2′,3′,5′-tri-*O*-acétyl-β-D-ribofuranosyl)purin-6-yl]pyridinium (**1**) en tri-*O*-acétylluminarosine (**6**) qui est très fluorescent se produit par le biais d'un état triplet excité. On démontre aussi que la transition intersystème dans les sels de purinyl-pyridinium est induite par une interaction de transfert de charge intermoléculaire avec les contre-ions.

Mots clés : sels de purinyl-pyridinium, fluorescence, phosphorescence.

[Traduit par la revue]

Introduction

Pyridinium salts derived from nucleic acid bases (1, 2) are of interest because they are involved in side processes in oligonucleotide synthesis (1, 3, 4) and are valuable intermediates in the nucleoside chemistry (5, 6). As part of an ongoing investigation of the photochemistry of a series of purinyl-pyridinium cations **1**–**5** (Fig. 1), we reported recently (7, 8) the photochemical transformation of *N*-[9-(2′,3′,5′-tri-*O*-acetyl-β-D-ribofuranosyl)purin-6-yl]pyridinium chloride, **1**, into tri-*O*-acetylluminarosine **6**. The latter compound is highly fluorescent and is therefore of particular interest for the possible use as a fluorescent, molecular probe in nucleic acids (24).

In the course of these experiments we also attempted to convert other purine-derived pyridinium salts into related analogs of luminarosine using similar methods and conditions. However, these initial attempts were unsuccessful, as salts **3**, **4**, and **5** appeared to be photochemically stable, and only traces of the desired analog of luminarosine could be detected after prolonged irradiation of **2**. The results of these experiments suggest that the photochemical reactivity of purinyl-pyridinium salts apparently depends strongly upon the nature of the substituents in the purine moiety and prompted us to investigate further the photophysical properties of these compounds (9).

We have shown previously that excitation of the ground state cation of *N*-(purin-6-yl)pyridinium chloride, **1**, results in proton transfer to give a photochemically stable, excited zwitterion (10). In this paper, we report the results of a detailed photophysical study of several purinyl-pyridinium salts in aqueous and non-aqueous solutions at room temperature and in ethanol glasses at 77 K. The results provide both a better understanding of the differences between the photochemical reactivity of pyridinium cations **1**–**5** and the basis for more detailed mechanistic studies (25).

Experimental

Materials

Spectrograde ethanol (95%) (Merck) and HPLC grade methanol and acetonitrile (BDH Omnisolv) were used as received. Water was purified using a Millipore Super-Q system. The pyridinium salts, *N*-[9-(2′,3′,5′-tri-*O*-acetyl-β-D-ribofuranosyl)purin-6-yl]pyridinium chloride, **1**; *N*-(9-methylpurin-6-yl)pyridinium chloride, **2**; *N*-(purin-6-yl)pyridinium chloride, **3**; *N*-[2-isobutyramido-9-(2′3′5′-tri-*O*-acetyl-β-D-ribofuranosyl)purin-6-yl]pyridinium chloride, **4**; and *N*-(2-amino-purin-6-yl)pyridinium chloride, **5**, were synthesized and purified according to procedures described previously (1, 2). The purity of these compounds was checked by HPLC techniques using a reversed phase column (Delta Pak C-4, Waters-Millipore), and eluting isocratically with a water–acetonitrile mixture (5:1, v/v) containing 0.25 M ammonium acetate.

Methods

Steady state absorption and fluorescence spectra were recorded in 1 cm quartz cuvettes, using Cary (Varian) 118 and Spex Fluorolog 222 spectrophotometers, respectively. The concentrations of the solutions for the fluorescence measurements were adjusted so that the absorption at the excitation wavelength did not exceed 0.05. Low temperature

[1]Authors to whom correspondence should be addressed.

Printed in Canada / Imprimé au Canada

Can. J. Chem. Downloaded from www.nrcresearchpress.com by 195.138.81.100 on 09/07/12
For personal use only.

Can. J. Chem. Downloaded from www.nrcresearchpress.com by 195.138.81.100 on 09/07/12
For personal use only.

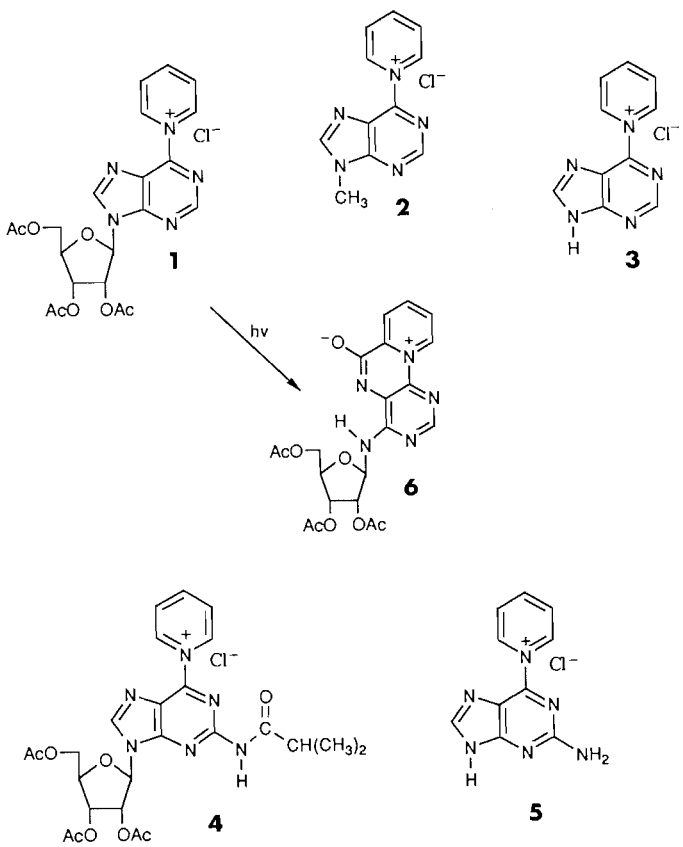

FIG. 1. Structures of the *N*-(purin-6-yl)pyridinium salts, **1**–**5**, and of luminarosine, **6**.

(77 K) fluorescence and phosphorescence emission, excitation and excitation polarization spectra were measured in rigid ethanol glasses in a quartz tube of 5 mm path length using a quartz Dewar – cold finger assembly. Background emissions from the Dewar and solvent alone were found to be insignificant. The emission and emission excitation spectra were corrected with the aid of a Spex Datamate computer. Fluorescence quantum yields were determined as described previously (11), using quinine sulphate (ϕ_f = 0.51 in 0.1 N H_2SO_4) (12) as a standard.

Fluorescence lifetimes were measured using a mode-locked, synchronously-pumped, cavity-dumped, frequency-doubled, picosecond dye laser excitation system. Details of this and the time-correlated, single-photon counting detection system have been reported elsewhere (13). Phosphorescence lifetimes were measured by exciting samples with a single 308 nm pulse from a Lumonics HyperEX-400 XeCl excimer laser and observing the decays with a Tektronix 7704 A oscilloscope equipped with a programmable digitizer. Measurements of the transient absorption spectra were performed at the Canadian Center for Picosecond Laser Flash Photolysis, Concordia University, Montreal. Samples were excited with either the third (355 nm) or the fourth (266 nm) harmonic of a double-beam, passively mode-locked Nd-YAG laser system (14). The energy of the excitation pulse varied between 1.1 and 1.5 mJ, and the pulse width was ca. 30 ps.

Results and discussion

The uv–visible absorption and fluorescence emission spectra of pyridinium salts **1**, **2**, **4**, and **5** in water are shown in Fig. 2. Data consisting of their long-wavelength absorption maxima, fluorescence maxima, fluorescence quantum yields, and excited state lifetimes in water, acetonitrile, and methanol are compiled in Table 1.

The absorption spectra show two relatively strong transitions in the 250–400 nm range (cf. Fig. 2A). The lower energy

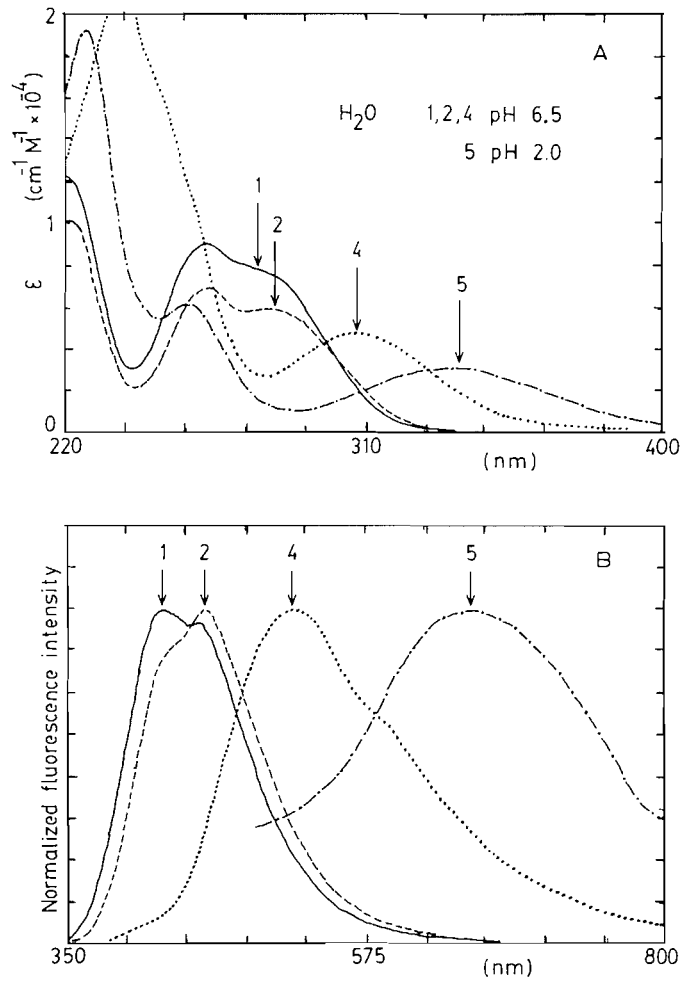

FIG. 2. Ultraviolet–visible absorption (*A*) and fluorescence emission (*B*) spectra of salts **1**, **2**, **4**, and **5** in water. The samples were excited at 310 nm (**1**, **2**, and **4**) and 340 nm (**5**).

transition, the position of which strongly depends on the nature of the substituent in the purine moiety, has a considerable degree of charge-transfer (CT) character. It results from the intramolecular interaction between the purine part (donor) and the positively charged pyridinium ring (acceptor) of the two coplanar (15) π-electronic systems. In the case of salts **1** and **2**, these CT transitions overlap strongly with the higher energy absorption bands (λ_{max} at 255–260 nm) and are only visible as shoulders. In the case of salts **4** and **5**, the CT bands are significantly red-shifted and are well-separated from the adjacent higher energy absorptions. The difference in energies of the CT transitions of **4** and **5** compared with **1** and **2** is consistent with the greater electron-donating power of these purines containing 2-isobutyramido and 2-amino substituents.

In the case of salt **5**, a pH-dependent absorption similar to that reported previously (10) for *N*-(purin-6-yl)pyridinium chloride, **3**, is observed (Fig. 3). We assign this effect of pH to the existence of a ground state prototropic equilibrium (cation ⇄ zwitterion) characterized by an isosbestic point at 380 nm, similar to that previously found in **3**. However, the estimated ground state p*K* of **5**, p*K* = 7.8, is an order of magnitude higher than that of **3** (p*K* = 6.7) (10), reflecting the incremental electron donating effect of the 2-amino substituent in the former.

The fluorescence spectra of **1**–**5** are characterized by broad,

Can. J. Chem. Downloaded from www.nrcresearchpress.com by 195.138.81.100 on 09/07/12
For personal use only.

TABLE 1. Charge transfer absorption band and fluorescence parameters for compounds **1–5** in various solvents

		Absorption		Fluorescence				
Salt	Solvent	λ_{max} (nm)	ϵ ($cm^{-1}\,M^{-1}$)	λ_{max} (nm)	ϕ^a	τ^b (ns)	k_f ($s^{-1}\,10^{-7}$)	Σk_{nr} ($s^{-1}\,10^{-8}$)
	Water (nat. pH)	292 (sh)	7700	423	0.097	1.12	8.7	8.1
1	Acetonitrile	303	7800	449	0.072	1.27	5.7	7.3
	Methanol	304	7600	457	0.008	0.13	6.1	76.3
	Water (nat. pH)	298 (sh)	5900	453	0.460	5.07	9.1	1.1
2	Acetonitrile	310	6300	455	0.410	4.80	8.5	1.2
	Methanol	310	6200	462	0.048	0.69	7.0	13.8
3[c]	Water (pH = 5)	292 (sh)	7500	521	0.078	1.63	4.8	5.6
	Water (pH = 8)	325	5500	521	0.078	1.63	4.8	5.6
	Water (nat. pH)	332	4700	520	0.006	0.12	5.1	82.8
4	Acetonitrile	346	5200	534	0.044	1.15	3.8	8.3
	Methanol	340	5100	536	0.005	0.21	2.4	47.4
	Water (pH = 6)	368	3100	656	0.001	0.02[d]	4.3[d]	430[d]
5	Acetonitrile	390	2800	668	0.004			
	Methanol	397	2750	689	0.001			

[a]Estimated error is 10%.
[b]Error is 0.05 ns.
[c]Taken from ref. 11.
[d]Estimated from the integrated absorption (Fig. 2A).

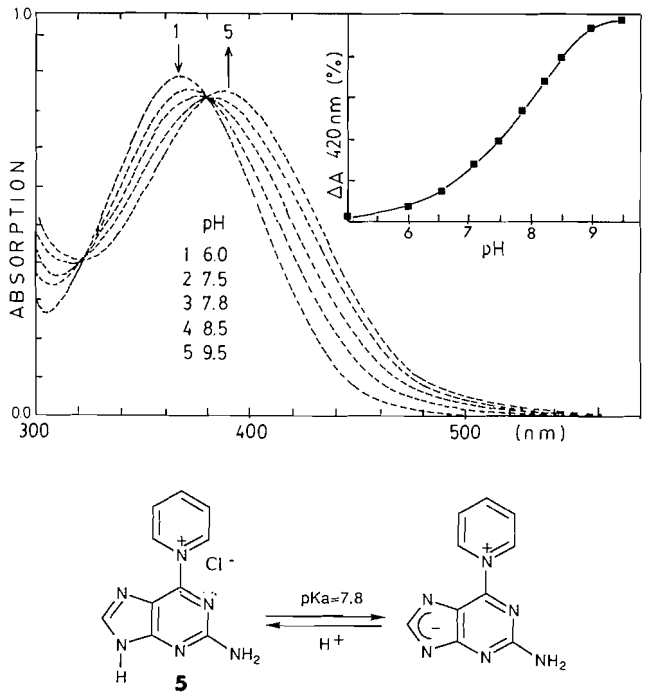

FIG. 3. The ground state prototropic equilibrium and pH dependence of the absorption spectra of salt **5** (2.9×10^{-4} M). The inset shows the corresponding "titration" curve from which the value of $pK_a = 7.8$ is determined.

structureless bands (Fig. 2*B*) which exhibit large Stokes shifts. The fluorescence spectrum of **5**, which exhibits the largest Stokes shift, does not change over the pH range 2.0–9.0. Because its ground state pK is 7.8, excitation of both the ground state cation of **5** at pH < 5 and its ground state zwitterion at pH $\simeq 9$ must therefore produce the same fluorescent species. We conclude that the excited cation is very short-lived under these conditions, and yields the zwitterion quantitatively. The excited state pK of the cation must therefore be less than 2.

The results in Table 1 show that both the absorption and fluorescence spectra of salts **1–5** exhibit a negative solvatochromism, i.e. the transition energies decrease with decreasing solvent polarity. The dipole moments of both the cations and zwitterions of these molecules must therefore be smaller in their excited, S_1, states than in their ground, S_0, states. Similar solvent effects are commonly encountered in pyridinium betaines (16) and other, similar molecules (17) which exhibit intramolecular charge transfer.

The fluorescence quantum yields and lifetimes of these salts vary considerably with the nature of the substituent on the purine ring. The rate constants for radiative (k_f) and total non-radiative (Σk_{nr}) decay of the S_1 states of these compounds may be calculated from $k_f = \phi/\tau$ and $\Sigma k_{nr} = (1 - \phi)/\tau$. The values of k_f and k_{nr} reveal that the largest part of the variations in lifetime and quantum yield with both solvent and molecular structure is due to the differences in their non-radiative decay rates. For the photochemically unreactive compounds, **2–5**, Σk_{nr} increases in the order **2** < **3** < **4** < **5** which correlates with the increasing electron-donating ability of the purine moieties of these molecules. The quantum yields of compounds **4** and **5** are very low and the estimated non-radiative rate constant of **5** is of the order of $10^{10}\,s^{-1}$ in water.

There are at least three different possible mechanisms of intramolecular non-radiative relaxation of the $S_{1,ct}$ states of these molecules; (*i*) intersystem crossing to the triplet state, (*ii*) reversible intramolecular electron-transfer proceeding to the ground state via the intermediate cation diradical, similar to that observed in *N*-prenylquinolinium and -pyridinium salts (18), and (*iii*) rapid torsional relaxation, a mechanism which is known to operate in a number of intramolecular CT complexes of the molecular rotor type (19). Taking into account the results of transient absorption and low temperature emission measurements (*vide infra*), the major mode of non-radiative deactivation of the $S_{1,ct}$ state of salt **1** appears to be intersystem crossing, while deactivation via reversible, intramolecular electron transfer and/or the torsion of pendant substituents are probably the major non-radiative decay paths of **4** and,

Can. J. Chem. Downloaded from www.nrcresearchpress.com by 195.138.81.100 on 09/07/12
For personal use only.

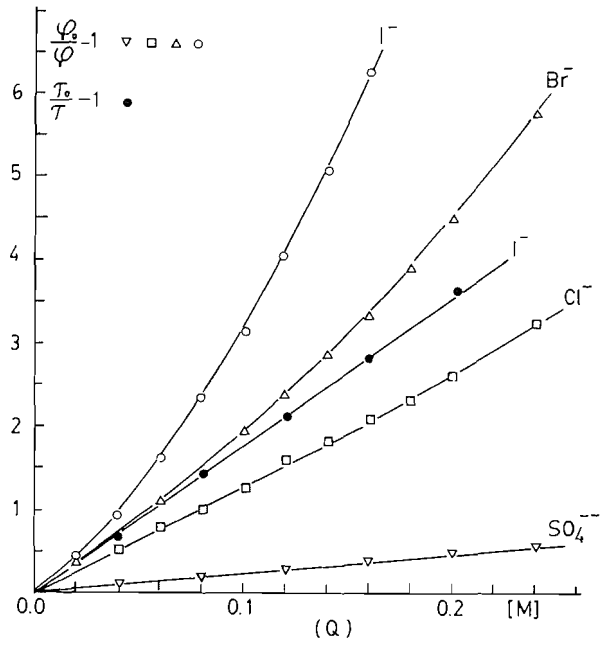

FIG. 4. Stern–Volmer plots for the fluorescence quenching of salt **1** by various anions.

TABLE 2. Data for the fluorescence quenching of salts **1–3** by sodium iodide obtained from lifetime measurements (plots of τ_0/τ vs. [NaI])

Salt	K_{SV} (M^{-1})	k_q ($M^{-1}\,s^{-1} \times 10^{-10}$)
1	19	1.7
2	72	1.4
3[a]	14	0.8

[a]Zwitterionic form. The data are taken from ref. 11.

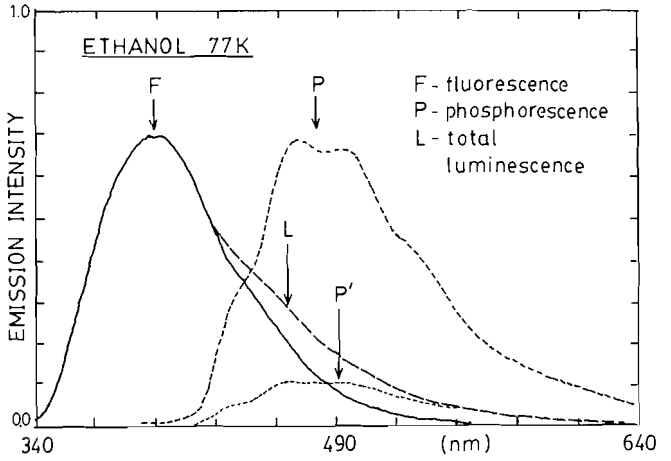

FIG. 5. Normalized, low-temperature (77 K) emission spectra of salt **1** in ethanol: (L) total luminescence, (P) phosphorescence, and (F) fluorescence. (P') represents the phosphorescence which is scaled so its intensity matches that of (L) in the long wavelength region.

TABLE 3. The low temperature spectral and photophysical data for salts **1–5**

Salt	F (nm)	P (nm)	E_T[a] (kcal)	E_{ST} (kcal)	ϕ_p/ϕ_f	τ_f (ns)	τ_p (ms)
1	399	473	64	17	0.25	5.7	630
2	406	474	64	16	0.06	6.2	546
3[b]	406	474	64	16	0.14	5.7	526
3[c]	452	—	—	—	—	7.5	—
4	456	533	58	13	0.08	10.3	12
5	530	—	—	—	—	—	—

[a]The energy of the lowest triplet state is estimated from the wavelength of the blue edge of the phosphorescence spectrum.
[b]Cationic form.
[c]Zwitterionic form.

especially, **5**. The total non-radiative decay constants of salts **1** and **2** are considerably larger in methanol than in either water or acetonitrile (cf. Table 1). This, together with the observation of rapid photodegradation of these samples in methanol, suggests that the quenching in methanol is due to an electron-transfer-mediated photochemical process, similar to that observed for various iminium salts and related *N*-heteroaromatic cations (electron acceptors) and alcohols (electron donors) (20).

Fluorescence quenching

We previously observed (9) that the photochemical transformation of **1** into luminarosine, **6**, is strongly affected by the presence of small amounts of some inorganic salts. In the case of sodium iodide the formation of **6** was almost completely suppressed at concentrations of NaI as low as 10^{-5} M. Bearing in mind this observation, we examined the quenching of the fluorescence of **1–3** by various counter ions (I^-, Br^-, Cl^-, and SO_4^{2-}) in water using $NaClO_4$ to maintain the solutions at constant ionic strength. Stern–Volmer plots for the quenching of **1** are shown in Fig. 4. The Stern–Volmer plot for the fluorescence quenching by I^- obtained from lifetime measurements (τ_0/τ vs. $[I^-]$) is perfectly linear over the whole range of I^- concentrations used, whereas those from steady-state experiments (ϕ_0/ϕ vs. $[I^-]$) show a distinct, upward curvature (cf. Fig. 4). This points to a substantial contribution of static quenching to the overall quenching process (21). Some degree of ion pairing in the ground state is thus indicated.

The results of the quenching studies show that at a concentration of 10^{-5} M, NaI has practically no effect on the fluorescence emission of **1**. From this observation one may conclude that the formation of **6** involves an intermediate state with a lifetime which is much longer than that of the singlet. The most likely candidate is the excited triplet state, and this is confirmed by transient absorption studies (*vide infra*).

It is also interesting to note that the efficiency of quenching decreases with increasing oxidation potential of the ions ($I^- > Br^- > Cl^- > SO_4^{2-}$; Fig. 4), and with decreasing electron accepting power of the pyridinium salts. Values of the Stern–Volmer constants, K_{SV}, and the calculated quenching constants, k_q ($k_q = K_{SV}/\tau_0$), for quenching of the fluorescence of **1–3** by NaI are collected in Table 2. These results are consistent with quenching via electron transfer (22), a conclusion which is further supported by the results of low temperature studies (*vide infra*). However, collisional deactivation, especially in the case of **3**, can not be ruled out at this time.

Low temperature studies

The low temperature emission, excitation and fluorescence polarization spectra of salts **1–5** were recorded at 77 K in solid ethanol glasses. Salts **1–4** exhibit both fluorescence and phosphorescence. For these compounds the fluorescence emission spectra (F) were obtained by recording the total luminescence (L) and the phosphorescence (P) spectra separately and then subtracting the latter from the former, after normalization in the

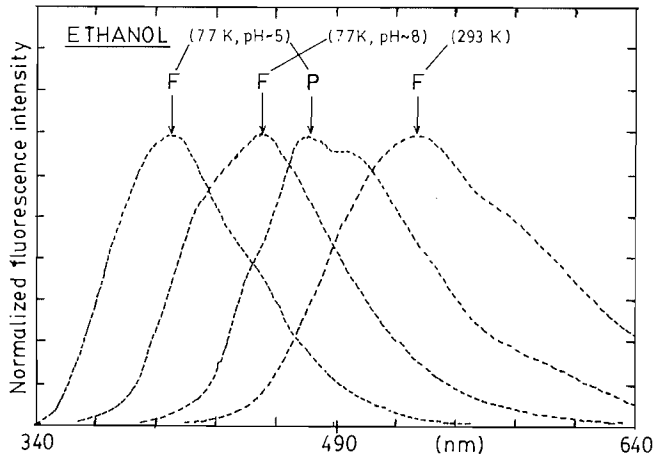

FIG. 6. Normalized, low-temperature fluorescence and phosphorescence spectra of salt **3** compared with its room-temperature fluorescence emission spectrum.

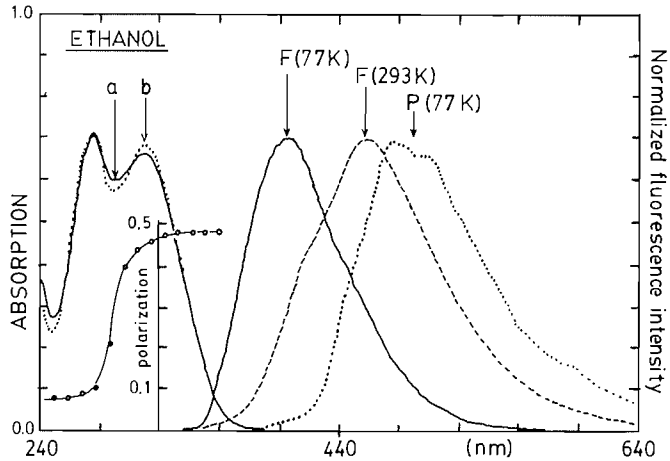

FIG. 7. Comparison of the room-temperature (293 K) absorption, a, and fluorescence emission, F, spectra of **2** with its low temperature (77 K) phosphorescence excitation, b, fluorescence emission, F, and phosphorescence emission, P, spectra. Inset: fluorescence – polarization excitation spectrum.

long wavelength spectral region. The results for **1** are shown in Fig. 5. The ratios of the quantum yields of phosphorescence to that of fluorescence, ϕ_p/ϕ_f, were then estimated from the areas under the appropriate emission curves. These data are summarized in Table 3, together with other useful spectroscopic and photophysical quantities.

The phosphorescence of salt **3** only appeared when its solution was acidified (before freezing) with $HClO_4$ to pH $\simeq$ 5. At this pH, **3** exists entirely in the protonated (cationic) form, and since the excited state proton transfer reaction is completely quenched upon freezing, the observed phosphorescence must be due entirely to the cation triplet. Increasing the pH of the solution to pH $\simeq$ 8 results in the complete disappearance of the phosphorescence, and the appearance of a new, red-shifted fluorescence (cf. Fig. 6). At this pH, **3** exists entirely in the zwitterionic form, and we therefore assign this new fluorescence to the excited zwitterion. No phosphorescence could be detected from **5** with our instrument.

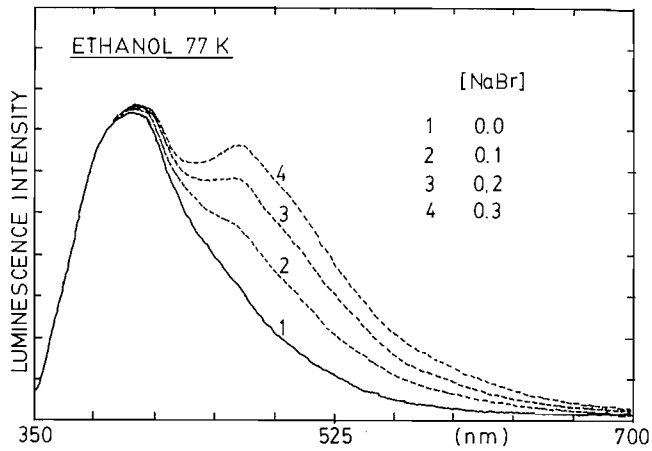

FIG. 8. The effect of sodium bromide on the low-temperature luminescence of salt **1**. Spectra are normalized at short wavelength spectral region.

The phosphorescence spectra exhibit some vibrational structure, whereas the fluorescence is structureless. In each case the fluorescence bands at 77 K are markedly blue-shifted compared to those obtained at room temperature (cf. Figs. 6 and 7). Both the low-temperature fluorescence excitation (not shown) and phosphorescence excitation spectra match the corresponding room-temperature absorption spectra very well (cf. Fig. 7). The fluorescence – polarization excitation spectra yield large values of the polarization (close to the upper limit of 0.5), which are constant across the long-wavelength absorption bands (cf. Fig. 7, inset). The absorption and fluorescence emission transition moments are therefore colinear and one may conclude that the lowest energy absorption bands are associated with only one electronic transition.

The most photochemically reactive salt, **1**, has the highest value of ϕ_p/ϕ_f, and this ratio appears to depend upon the extent of intramolecular CT interaction, i.e., it decreases with increasing intramolecular CT character of the molecule. Note in this regard that both **5** and the zwitterion of compound **3** are essentially non-phosphorescent. The enhancement of the intersystem-crossing rate in salts which exhibit a weaker intramolecular CT interaction (especially **1**) can be qualitatively rationalized by considering the intermolecular interaction with the counter ions. Figure 8 shows that, in the case of **1**, the ϕ_p/ϕ_f ratio increases significantly upon addition of sodium bromide to the solution before freezing. The same effect, albeit to a smaller extent, occurs in **2** and the cationic form of **3**. For the zwitterionic form of **3**, **4**, and **5**, the addition of up to 0.3 M NaBr had practically no effect on their low temperature luminescence spectra. We conclude that intersystem crossing in the excited purinyl-pyridinium salts is induced by interaction with the counterions, and that this process proceeds via *inter*molecular CT rather than by a heavy atom effect. High triplet yields following the charge-transfer quenching of fluorescence have been also reported for some aromatic molecules (23). It is reasonable to expect that intermolecular CT interaction will dominate in those salts which exhibit weaker intramolecular charge transfer interactions, thus leading to higher triplet yields in these compounds.

Transient absorption spectra

The transient absorption spectra of salts **1**–**3** are shown in

Can. J. Chem. Downloaded from www.nrcresearchpress.com by 195.138.81.100 on 09/07/12
For personal use only.

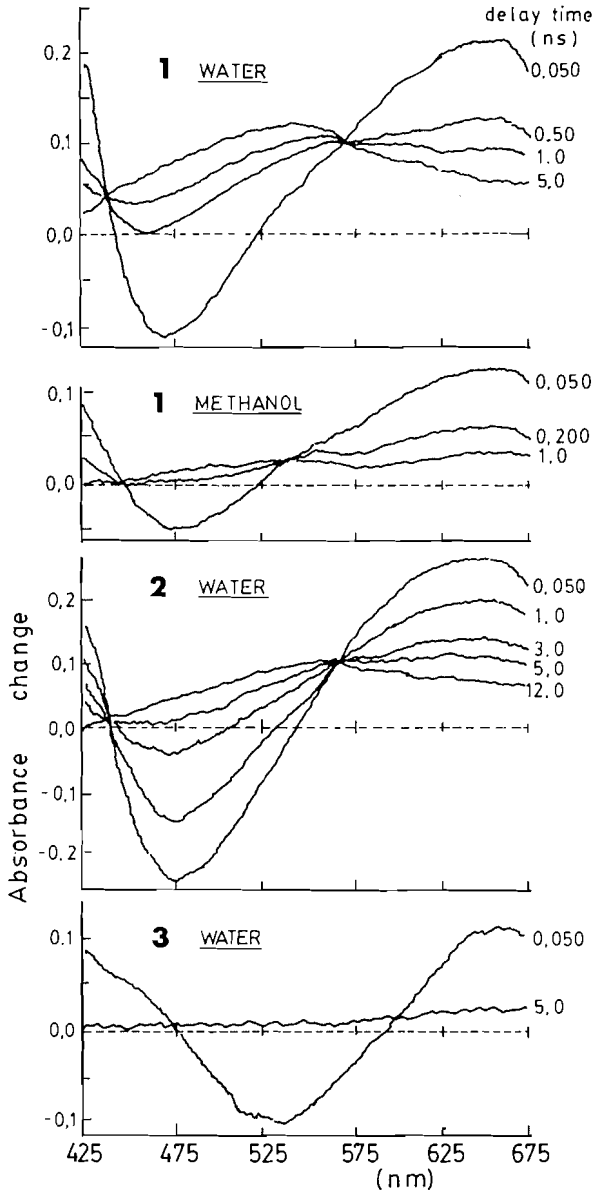

FIG. 9. Picosecond transient-absorption spectra of salts **1**, **2**, and **3**. The solvent and the delay times for each compound are given in the figure.

Fig. 9. The spectra, measured immediately after excitation, show broad absorption signals in the region 625–675 nm and negative signals at ca. 470 nm for **1** and **2**, and 525 nm for **3**. For each compound the negative and positive bands disappear at the same rate, rates which are identical (within an experimental uncertainty of ca. 25%) to the previously measured rates of fluorescence decay of the same molecules (cf. Table 1). Thus, the spectra taken at a delay of 50 ps can be safely assigned to the fluorescent state in each case. The negative signals are due to spontaneous emission while the positive ones are due to singlet–singlet absorption by the S_1 state. For salts **1** and **2** in water the decrease in the singlet–singlet absorption is accompanied by the growth of new, long-lived, broad bands at 545 and 559 nm, respectively, which we assign to the $T_n \leftarrow T_1$ transition. Salt **1** in methanol exhibits only a small residual triplet–triplet absorption after 1 ns, confirming that most of the fluorescent singlet state undergoes deactivation by photochemical reaction with the solvent. As seen in Fig. 9, the singlet excited state of **3** decays without formation of any detectable triplet–triplet absorption.

The results of the transient absorption measurements in water are very consistent with those obtained in ethanol glasses at 77 K and support our earlier conclusion (based on the quenching experiments) that the excited triplet state of **1** is involved in the photochemical transformation into luminarosine **6**.

Conclusions

The results of the photophysical studies of purinyl-pyridinium salts show that the photochemical formation of luminarosine from **1** is associated with a much higher triplet yield in this salt as compared with salts **2**–**5**, which are photochemically unreactive. Intersystem crossing is significant only in those salts which exhibit weaker intramolecular CT interactions and is induced by intermolecular CT interaction with the counterions.

Acknowledgments

We thank the Natural Sciences and Engineering Research Council of Canada for financial support, and Dr. D. Sharma for assistance in measuring the transient absorption spectra. B.S. thanks the President's NSERC fund of the University of Saskatchewan for providing part of a postdoctoral fellowship. Support from the Polish Ministry of Education (R.P.II.13.2.15) and the Polish Academy of Sciences (CPBR 3.13.4.2.1) is also acknowledged.

1. R. W. ADAMIAK, E. BIALA, and B. SKALSKI. Nucl. Acids Res. **13**, 2989 (1985).
2. R. W. ADAMIAK, E. BIALA, Z. GDANIEC, S. MIELEWCZYK, and B. SKALSKI. Chem. Scr. **26**, 3 (1986).
3. R. W. ADAMIAK, E. BIALA, Z. GDANIEC, S. MIELEWCZYK, and B. SKALSKI. Chem. Scr. **26**, 7 (1986).
4. J. S. EADIE and D. S. DAVIDSON. Nucl. Acids. Res. **15**, 8333 (1987).
5. R. W. ADAMIAK, E. BIALA, and B. SKALSKI. Angew. Chem. Int. Ed. Engl. **24**, 1054 (1985).
6. F. SEELA, W. HERDERING, and A. KEHNE. Helv. Chim. Acta, **70**, 1649 (1987).
7. B. SKALSKI, J. BARTOSZEWICZ, S. PASZYC, Z. GDANIEC, and R. W. ADAMIAK. Tetrahedron, **43**, 3955 (1987).
8. B. SKALSKI, S. PASZYC, R. W. ADAMIAK, R. P. STEER, and R. E. VERRALL. J. Chem. Soc. Perkin Trans. II, 1691 (1989).
9. B. SKALSKI, R. P. STEER, R. E. VERRALL, S. PASZYC, and R. W. ADAMIAK. Proceedings, XIII International Conference on Photochemistry; Budapest, 1987; Abstracts; Vol. II, p. 404.
10. B. SKALSKI, R. P. STEER, and R. E. VERRALL. J. Am. Chem. Soc. **110**, 2055 (1988).
11. A. MACIEJEWSKI and R. P. STEER. Chem. Phys. Lett. **100**, 540 (1983).
12. S. MEECH and D. PHILIPS. J. Photochem. **23**, 193 (1983).
13. D. R. JAMES, D. R. M. DEMMER, R. E. VERRALL, and R. P. STEER. Rev. Sci. Instrum. **54**, 1121 (1983).
14. N. SERPONE, M. A. JAMIESON, D. SHARMA, R. DANESH, F. BOLLETTA, and M. Z. HOFFMAN. Chem. Phys. Lett. **104**, 87 (1984).
15. M. JASKOLSKI, B. SKALSKI, D. A. ADAMIAK, and R. W. ADAMIAK. Acta Crystallogr. C**43**, 2110 (1987).
16. K. DIMROTH, C. REICHARDT, and A. SCHWEIG. Liebigs Ann. Chem. **95**, 669 (1963); W. S. HAMMACK, D. N. HENDRICKSON, and H. G. DRICKAMER. J. Phys. Chem. **93**, 3483 (1989).
17. W. ABRAHAM, A. HENRION, and D. KREYSIG. J. Photochem. **35**, 311 (1986).
18. U. C. YOON, S. L. QUILLEN, P. S. MARIANO, R. SWANSON, J. L.

Can. J. Chem. Downloaded from www.nrcresearchpress.com by 195.138.81.100 on 09/07/12
For personal use only.

STAVINOHA, and E. VAY. Tetrahedron Lett. 919 (1982); J. Am. Chem. Soc. **105**, 1204 (1983).
19. M. S. A. ABDEL-MOTTALEB, R. O. LOUTFY, and R. LAPOUYADE. J. Photochem. Photobiol. A: Chem. **48**, 87 (1989) and references therein.
20. (*a*) P. S. MARIANO. Acc. Chem. Res. **16**, 130 (1983); (*b*) D. G. WHITEN. The photochemistry of heterocyclic compounds. *Edited by* O. Burchard. Wiley, New York. 1976. p. 524; (*c*) P. S. MARIANO. *In* Photoinduced electron transfer. Part C. *Edited by* M. A. Fox and M. Chanon. Elsevier. 1988. p. 407.
21. J. R. LAKOWICZ. Principles of fluorescence spectroscopy. Plenum, New York. 1983. p. 266.
22. P. S. MARIANO and J. L. STAVINOHA. *In* Synthetic organic photochemistry. *Edited by* W. M. Horspool. Plenum Press, New York. 1984. pp. 222–223 and references therein.
23. C. R. GOLDSCHMIDT, R. POTASHNIK, and M. OTTOLENGHI. J. Phys. Chem. **75**(8), 1025 (1971).
24. R. W. ADAMIAK *et al.* Nucl. Acids. Res. To be published.
25. B. SKALSKI *et al.* To be published.

Can. J. Chem. Downloaded from www.nrcresearchpress.com by 195.138.81.100 on 09/07/12
For personal use only.

$^1H-^1H$ internuclear distance measurements in carbohydrates: proton transient nuclear Overhauser enhancement and spin-lattice relaxation in (^{13}C)- and (^2H)-substituted compounds

PAUL C. KLINE AND ANTHONY S. SERIANNI[1]
Department of Chemistry and Biochemistry, University of Notre Dame, Notre Dame, IN 46556, U.S.A.

SHAW-GUANG HUANG
Department of Chemistry, Harvard University, Cambridge, MA 02138, U.S.A.

AND

MICHAEL HAYES AND ROBERT BARKER
Section of Biochemistry, Molecular and Cell Biology, Cornell University, Ithaca, NY 14853, U.S.A.

Received October 11, 1989[2]

This paper is dedicated to Professor Arthur S. Perlin on the occasion of his 67th birthday

PAUL C. KLINE, ANTHONY S. SERIANNI, SHAW-GUANG HUANG, MICHAEL HAYES, and ROBERT BARKER. Can. J. Chem. **68**, 2171 (1990).

Proton transient nuclear Overhauser enhancement (TnOe) and spin-lattice relaxation times (T_1) have been used to evaluate the conformations of several monosaccharides and disaccharides containing (^{13}C) and (^2H) substitution. Absolute $^1H-^1H$ internuclear distances were determined by TnOe and DESERT (deuterium substitution effects on relaxation times) experiments on conformationally rigid methyl β-D-galactopyranoside and α- and β-D-xyloses, respectively. The DESERT method was extended to examine *O*-glycoside conformation in two blood-group disaccharides that were prepared enzymically with (^{13}C) and (or) (^2H) substitution. Preferred disaccharide conformations deduced from these distance measurements are compared to those determined from $^{13}C-^{13}C$ and $^{13}C-^1H$ spin coupling constants, theoretical calculations, and crystallographic studies.

Key words: TnOe, DESERT, carbohydrate conformation.

PAUL C. KLINE, ANTHONY S. SERIANNI, SHAW-GUANG HUANG, MICHAEL HAYES et ROBERT BARKER. Can. J. Chem. **68**, 2171 (1990).

On a utilisé l'effet Overhauser nucléaire transitoire du proton (TnOe) et les temps de relaxation spin-réseau (T_1) pour évaluer les conformations de plusieurs mono- et di-saccharides contenant des substituants ^{13}C et ^2H. On a déterminé les distances internucléaires $^1H-^1H$ absolues grâce à des expériences de TnOe et d'effets de substitution par le deutérium sur les temps de relaxation (DESERT) effectuées sur le β-D-galactopyranoside de méthyle et sur les α- et β-D-xyloses qui sont rigides d'un point de vue conformationnel. On a étendu la méthode DESERT pour examiner la conformation *O*-glycoside de deux disaccharides de groupes sanguins dans lesquels on a incorporé d'une façon enzymatique des substituants ^{13}C et (ou) ^2H. On a comparé les conformations préférées des disaccharides qui ont été déduites à partir de ces mesures de distance avec celles déterminées à partir de constantes de couplage $^{13}C-^{13}C$ et $^{13}C-^1H$, de calculs théoriques et d'études cristallographiques.

Mot clés: TnOe, DESERT, conformation de hydrate de carbone.

[Traduit par la revue]

Introduction

Carbohydrates play diverse roles in biological systems. In addition to their role in energy production, they are involved in the recognition of self, the regulation of protein turnover, and the control of gene expression. Both furanosyl and pyranosyl rings are components of many biologically important molecules, most notably the polysaccharides and nucleic acids. These rings possess significantly different conformational properties that confer different overall behavior to the biopolymers that contain them. How these properties are exploited by the cell may be important to understanding the mechanisms of biological recognition and catalysis.

Many chemical and biochemical studies have focused on the conformational properties of carbohydrates and carbohydrate-containing structures. The underlying motivation behind these studies is the expectation that, if all molecular forces affecting conformation can be identified and quantified, predictions of preferred conformations can be made from a knowledge of primary structure. Experimental determinations of molecular conformation in solution rely heavily on nuclear magnetic resonance (NMR) spectroscopy. Relationships between vicinal spin coupling constants (^3J) and molecular torsion angles have been established for homo- ($^1H-^1H$, $^{13}C-^{13}C$) (1–4) and heteronuclear ($^{13}C-^1H$) (5–7) spin systems in carbohydrates. Structural information can also be obtained from proton spin-lattice relaxation times (T_1) (8)[3] and nuclear Overhauser effects (nOe) (10, 11). Specific $^1H-^1H$ internuclear distances estimated from these latter time-dependent parameters may be used to establish conformation, provided that correlations between distance and conformation are known. These correlations can be made by computer-assisted studies of crystal structures. Ideally, pairs of protons are studied whose internuclear distances can be used to discriminate between potential conformations. In other words, targeted interproton distances should be sensitive to molecular conformation, ideally with a given distance–conformation pair being unique.

The interpretation of NMR parameters in conformationally flexible molecules (e.g., oligosaccharides) depends on the conformational model invoked, since the number and distribution of conformational states, and their lifetimes, affect the observed values. The choice of a model often relies on chemical intuition, since the relative energies and lifetimes of the individual conformational states are often unknown, although

[1]Author to whom correspondence may be addressed.
[2]Revision received July 17, 1990.
[3]For a recent review, see ref. 9.

Printed in Canada / Imprimé au Canada

Can. J. Chem. Downloaded from www.nrcresearchpress.com by 195.138.81.100 on 09/07/12
For personal use only.

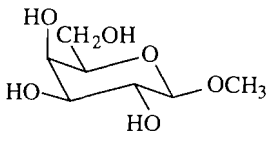

1

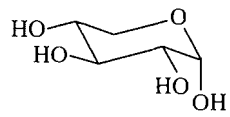

2*a*

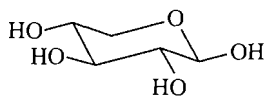

2*b*

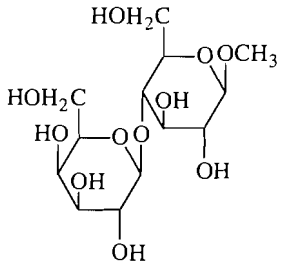

3

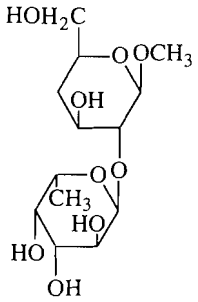

4

computational methods can be helpful in addressing these questions. Experimental validation of a chosen model can sometimes be achieved through the measurement of several complementary NMR parameters (i.e., J, T_1, nOe) in the molecule.

Conformational studies of disaccharides involve the assessment of ring, exocyclic, and O-glycoside bond conformations. With respect to the latter, vicinal $^{13}C-^{1}H$ ($^{3}J_{C,H}$) and $^{13}C-^{13}C$ ($^{3}J_{C,C}$) spin coupling constants across the O-glycoside bond are the only available couplings to assess linkage conformation since no $^{3}J_{H,H}$ coupling pathways exist. $^{3}J_{C,H}$ and $^{3}J_{C,C}$ values are not readily obtained without the use of labeled compounds, although in some cases $^{3}J_{C,H}$ values can be measured in unlabeled compounds with the use of heteronuclear multiple bond correlation spectroscopy or other methods (12). (^{13}C)- and (^{2}H)-substituted compounds have been used to measure several trans-glycoside $^{13}C-^{1}H$ and $^{13}C-^{13}C$ spin couplings in methyl β-D-lactoside and deduce a preferred O-glycoside bond conformation (13*a*); similar approaches have been used to study the conformations of other oligosaccharides (13*b*).

In addition to vicinal spin coupling constants, internuclear distances between pairs of inter-residue protons should depend on linkage conformation, making nOe measurements useful in determining conformation. This study examines this dependency and describes two NMR methods to estimate absolute $^{1}H-^{1}H$ internuclear distances in carbohydrates in solution. Two conformationally rigid monosaccharides (**1**,**2**) have been examined as a means to compare distances obtained in solution with those determined by crystallography. These methods have also been applied to evaluate O-glycoside conformation in two blood-group disaccharides (**3**,**4**).

Experimental

Materials

Methyl β-D-galactopyranoside **1** and D-xylose **2** were purchased from Sigma Chemical Company. Potassium (^{13}C)cyanide ($K^{13}CN$, 99 at.%), deuterium oxide ($^{2}H_2O$, 98 at.%), and methanol-$^{2}H_4$ ($C^{2}H_3O^{2}H$, 98 at.%) were purchased from Cambridge Isotope Laboratories. Deuterium gas ($^{2}H_2$, 98 at.%) was purchased from Merck and Co., Inc.

Preparations

Methyl β-D-lactoside **3** (O-β-D-galactopyranosyl-(1 → 4)-methyl-β-D-glucopyranoside) was prepared chemically from peracetylated β-lactose using the Koenigs–Knorr method (14).

O-β-D-Galactopyranosyl-(1 → 4)-methyl-$^{2}H_3$-β-D-(1-^{13}C,^{2}H)glucopyranoside was prepared enzymically from UDP-D-galactose and methyl-$^{2}H_3$-β-D-(1-^{13}C,^{2}H)glucopyranoside with lactose synthase (EC 2.4.1.22) isolated from milk according to procedures described previously (15, 16). The multiply enriched hexopyranoside was prepared as follows. D-Arabinose was treated with $K^{13}CN$, and the resulting (1-^{13}C)cyanohydrins were reduced catalytically with $^{2}H_2$/Pd–$BaSO_4$ (17). The products (D-(1-^{13}C,^{2}H)glucose and mannose) were separated by chromatography (17, 18). D-(1-^{13}C,^{2}H)Glucose was treated with $H^+/C^{2}H_3O^{2}H$ (19, 20) under reflux, and the resulting glycoside mixture was chromatographed on a column of Dowex 1 × 8 (200–400 mesh) ion-exchange resin in the OH^- form (21). Fractions were assayed with phenol – sulfuric acid (22). Four well-resolved peaks eluted, and the β-pyranoside was identified by its characteristic ^{13}C chemical shifts (23).

O-β-D-Galactopyranosyl-(1 → 4)-methyl-β-D-(4-^{2}H)glucopyranoside was prepared as described above, using methyl β-D-(4-^{2}H)glucopyranoside as the acceptor. D-(4-^{2}H)Glucose was prepared enzymically from dihydroxyacetone phosphate and DL-(1-^{2}H)glyceraldehyde (24) using rabbit muscle aldolase (25). O-β-D-Galactopyranosyl-(1 → 4)-methyl-β-D-(1-^{13}C)glucopyranoside was prepared from D-(1-^{13}C)-glucose (17).

O-α-L-Fucopyranosyl-(1 → 2)-methyl-β-D-galactopyranoside **4** was prepared enzymically from GDP-L-fucose (26) and methyl β-D-galactopyranoside using galactoside 2-L-fucosyl-transferase (EC 2.4.1.69) from bovine submaxillary glands (27). Methyl β-D-(1-^{13}C)-galactopyranoside and methyl β-D-(2-^{2}H)galactopyranoside were used as acceptors to generate the corresponding labeled disaccharides. These labeled galactopyranosides were generated by Fischer glycosidation (see above) of the labeled hexose. D-(1-^{13}C)Galactose was prepared as described previously (17, 28). D-(2-^{2}H)Galactose was prepared by molybdate-catalyzed epimerization (29) of D-(1-^{2}H)talose (24).

D-(2-^{2}H)Xylose was prepared from KCN and D-(1-^{2}H)threose as described previously (17, 24, 28). D-(1-^{2}H)Threose was prepared from KCN and D-glyceraldehyde via reduction with $^{2}H_2$ and Pd–$BaSO_4$ in $^{2}H_2O$ (24, 30).

Instrumentation

^{1}H (300 MHz) and ^{13}C (75 MHz) NMR spectroscopy was performed on a Nicolet NT-300 FT-NMR (Notre Dame) equipped with quadrature phase detection and a 293B pulse programmer. ^{1}H and ^{13}C spin-lattice relaxation times (T_1) were measured by the inversion–recovery method (31).

Transient proton nOe measurements (TnOe) (32) were performed on a WM-300 FT-NMR spectrometer (Cornell) and were conducted as follows. Normal (off-resonance) and selectively inverted (on-reso-

Can. J. Chem. Downloaded from www.nrcresearchpress.com by 195.138.81.100 on 09/07/12
For personal use only.

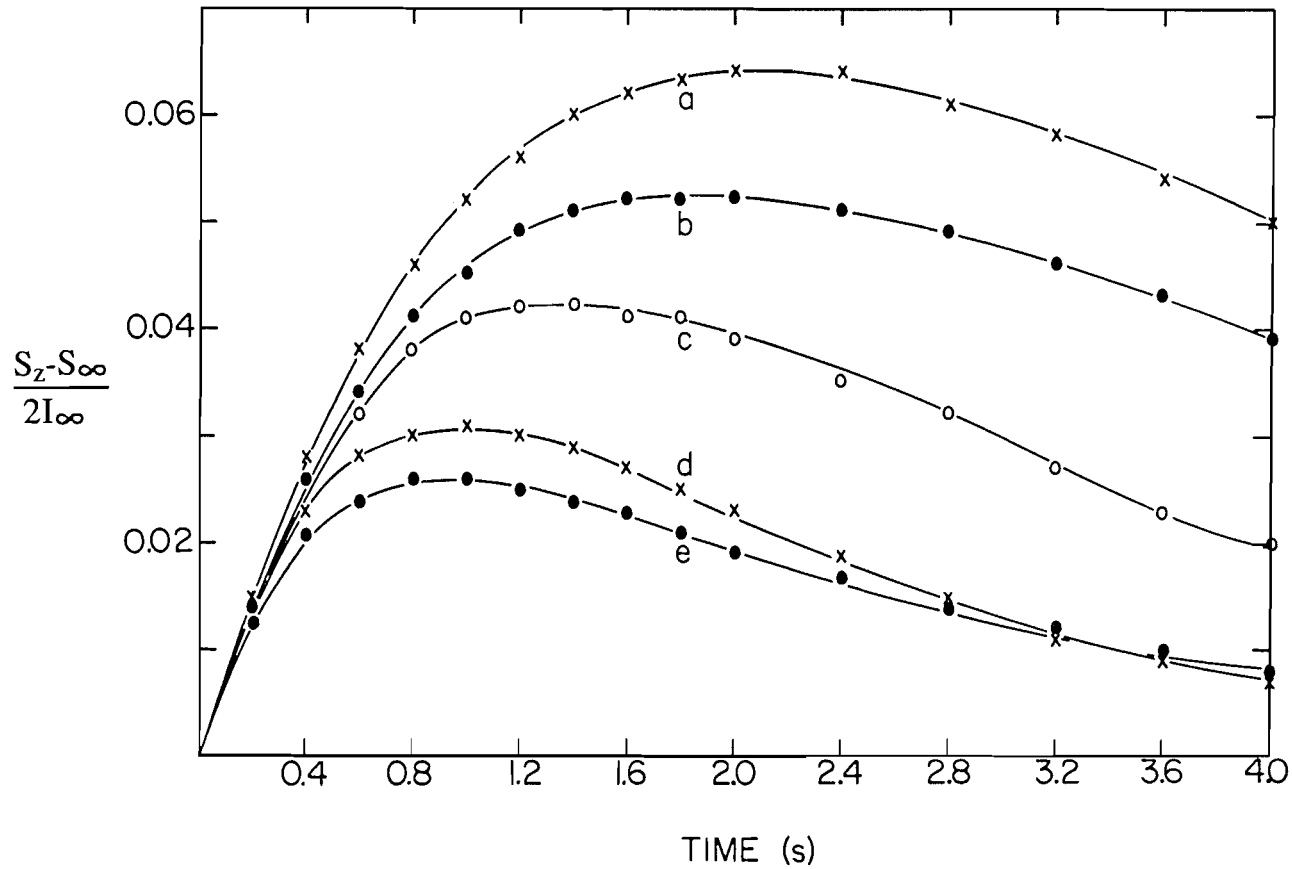

FIG. 1. Theoretical curves showing the transient nOe effect on spin S when spin I is inverted for various values of T_{1I} and T_{1S} (see text). Values of T_{IS} and T_{II}, respectively, for each curve are as follows: a, 2.1 s, 2.1 s; b, 1.0 s, 4.0 s; c, 1.0 s, 2.1 s; d, 1.0 s, 1.0 s; e, 0.5 s, 2.1 s.

nance) spectra were obtained for each τ value in the experiment (see below). A pulse program was written such that off- and on-resonance spectra were obtained in the same experiment by adding scans alternately to each spectrum (each occupying one half of the computer memory). This approach minimized errors due to resolution loss and (or) field drift during the course of the experiment. Enhancement rates were determined by spectral subtraction, followed by signal integration.

High-resolution rapid-scan cross-correlation ^{1}H NMR spectra in ^2H_2O were obtained at 620 MHz at the NMR Facility for Biomedical Studies, Department of Chemistry, Carnegie-Mellon University, Pittsburgh, PA, which is partly supported by NIH Grant P41 RR 00292.

Transient proton nuclear Overhauser enhancement (TnOe) (32*a–c*)

Consider two nuclei, I and S. The integrated Bloch equations describing the change in *z*-magnetization as a function of time, *t*, for I (I_z) and S (S_z) are

$$[1] \quad I_z = Ae^{\lambda_+ t} + Be^{\lambda_- t} + I_\infty$$

and

$$[2] \quad S_z = \frac{-(\rho_I + \lambda_+)}{\sigma_{IS}} Ae^{\lambda_+ t} + \frac{-(\rho_I + \lambda_-)}{\sigma_{IS}} Be^{\lambda_- t} + S_\infty$$

where I_z and S_z are the *z*-magnetizations of I and S, ρ_I is the spin-lattice relaxation rate of I, ρ_S is the spin-lattice relaxation rate of S, σ_{IS} is the cross-relaxation rate between I and S, I_∞ and S_∞ are the *z*-magnetizations of I and S, respectively, at infinite time after the perturbation, and $\lambda_\pm = 1/2\,[-(\rho_I + \rho_S) \pm \sqrt{(\rho_I - \rho_S)^2 + 4\sigma_{IS}^2}]$ The internuclear distance between protons I and S can be obtained by evaluating the cross-relaxation rate, σ_{IS}. For small molecules, σ_{IS} is obtained by applying a selective 180° pulse to one nucleus (I) and observing the time-dependent effect of this inversion on nucleus S. At $t = 0$, then, $I_z = -I_\infty$ (for a perfect 180° pulse) and $S_Z = S_\infty$. Under these conditions, $A + B = -2I_\infty$ considering a short t such that $\lambda_\pm t \ll 1$. Using Taylor's series, eq. [2] can be simplified to obtain the form

$$[3] \quad S_z = \frac{-(\rho_I + \lambda_+)}{\sigma_{IS}} A\lambda_+ t + \frac{-(\rho_I + \lambda_-)}{\sigma_{IS}} B\lambda_- t + S_\infty$$

where t = time between the application of the selective 180° pulse and the application of the 90° observe pulse. A plot of $(S_z - S_\infty)$ against t will yield a curve with an initial slope equal to

$$[4] \quad -1/\sigma_{IS}[\rho_I(A\lambda_+ + B\lambda_-) + A\lambda_+^2 + B\lambda_-^2]$$

Substituting $(A\lambda_+ + B\lambda_-) = 2\rho_I I_\infty$,

$$B = \frac{-2I_\infty(\rho_I + \lambda_+)}{\lambda_+ - \lambda_-}$$

and, for λ_+ and λ_-, we obtain

$$S_Z = S_\infty + 2I_\infty\sigma_{IS}t$$

A plot of $(S_Z - S_\infty)/2I_\infty$ against t yields a curve with an initial slope equal to the cross-relaxation rate, σ_{IS}. In the extreme-narrowing limit that is valid for small molecules, the value of σ_{IS} is related to r_{IS} through the equation (32*b*)

$$[5] \quad \sigma_{IS} = \frac{3\gamma_H{}^4\hbar^2}{4r_{IS}^6}\tau_r$$

where γ_H = magnetogyric ratio for ^{1}H, $\hbar$ = Planck's constant divided by 2π, and τ_r = the rotational correlation time for reorientation of the IS vector. The rotational correlation time can be obtained by measuring ^{13}C relaxation times for protonated carbons in the molecule, since (33)

Can. J. Chem. Downloaded from www.nrcresearchpress.com by 195.138.81.100 on 09/07/12
For personal use only.

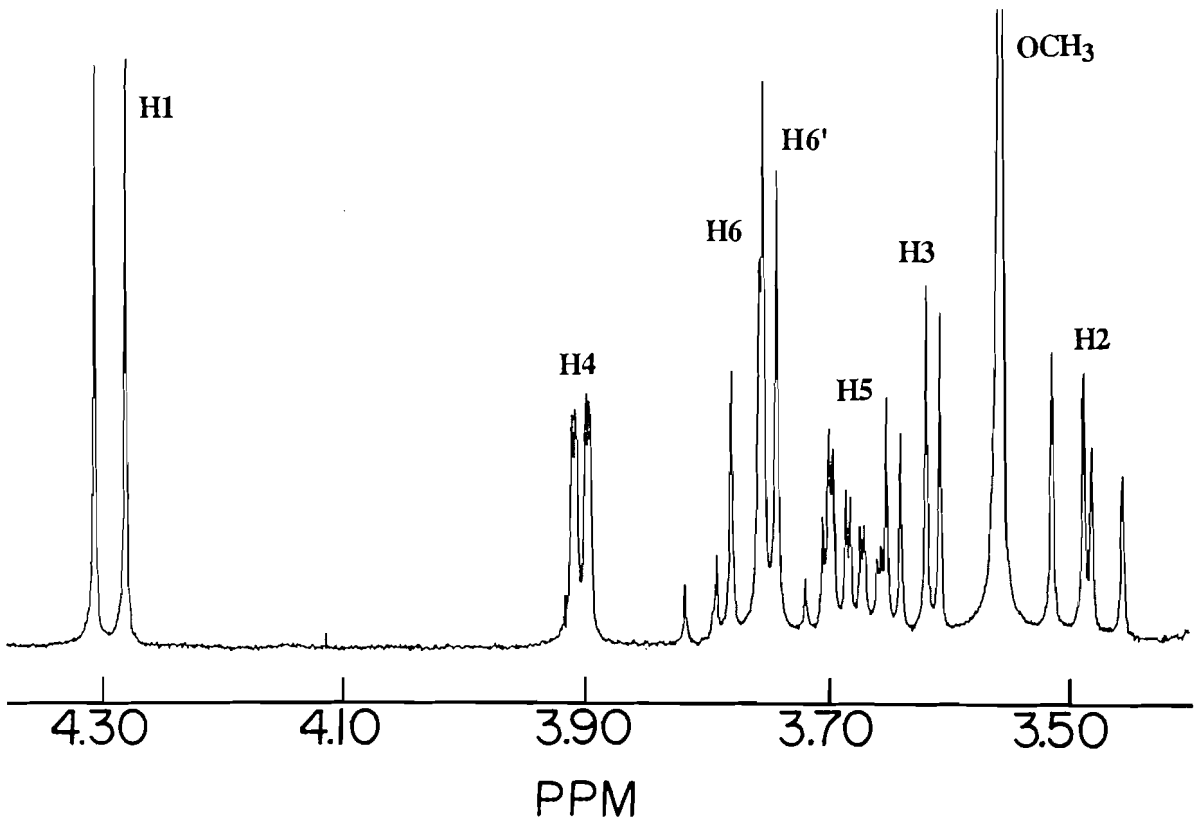

FIG. 2. The 300 MHz ^{1}H NMR spectrum of methyl β-D-galactopyranoside **1** in ^2H_2O showing signal assignments.

$$[6] \quad \frac{1}{T_{1,C}} = \frac{N\gamma_H^2\gamma_C^2\hbar^2}{r_{CH}^6}\tau_r$$

where λ_C = magnetogyric ratio for ^{13}C, N = number of directly bonded protons, and r_{CH} = the C—H bond length; eq. [6] assumes that the protonated carbons relax exclusively through a dipole–dipole mechanism as shown previously in other carbohydrate systems (9, 13).

The transient nOe experiment, then, involves selective inversion of nucleus I, a waiting period τ, followed by the application of a non-selective 90° observe pulse to monitor the change in intensity of nucleus S. Plotting $(S_z - S_\infty)/2I_\infty$ against τ yields σ_{IS}. Under similar solution conditions, τ_r is obtained by measuring ^{13}C spin-lattice relaxation times of protonated carbons in the molecule. From σ_{IS} and τ_r, r_{IS} is determined.

Equations [1] and [2] can be used to generate theoretical enhancement curves using different values for ρ_I, ρ_S, and σ_{IS}. If I is inverted, the time dependence of S is described by

$$[7] \quad \frac{S_Z - S_\infty}{2I_\infty} = \left[\frac{\sigma}{\sqrt{(\rho_S - \rho_I)^2 + 4\sigma^2}}\right][e^{\lambda+t} - e^{\lambda-t}]$$

which can be solved to produce theoretical curves (Fig. 1). These curves illustrate the effect of ρ_I and ρ_S on the shape of enhancement curves. Short T_1 values cause the enhancement to reach a maximum more quickly. For molecules with short relaxation times (i.e., larger molecules), therefore, estimates of the initial slope, and consequently of r_{IS}, will be less precise.

The accuracy of estimating r_{IS} will depend on the accuracy of the measured σ_{IS} and τ_r, the latter being derived from the ^{13}C spin-lattice relaxation time. However, one can estimate from eq. [5] that a 100% error in σ_{IS} or τ_r will produce less than a 15% error in r_{IS}.

Since r_{CH} has been reported with great accuracy, τ_r will not have a larger error than $T_{1,C}$, which is measured experimentally with an accuracy of ±5%. The accuracy of σ_{IS} obtained from the initial slope of a plot of $(S_Z - S_\infty)/2I_\infty$ vs. t is ±20%. Therefore we believe that the r_{IS} values reported in this study are accurate to ±10%.

Deuterium substitution effects on ^1H relaxation times (DESERT) (34)

Nuclear spin-lattice relaxation of proton I in a small molecule tumbling isotropically and relaxing intramolecularly through a single nearby proton S, is described by the equation

$$[8] \quad \frac{1}{T_{1,I}} = \frac{2\gamma_H^4\hbar^2(I_S(I_S + 1))}{r_{IS}^6}\tau_{IS}$$

where γ_H, $\hbar$, r_{IS}, and τ_{IS} have their usual meanings, and I_S = spin of S. Substituting $I_S = 1/2$,

$$[9] \quad \frac{1}{T_{1,I}} = \frac{3\gamma_H^4\hbar^2}{2r_{IS}^6}\tau_{IS}$$

When I relaxes through more than one proton, r_{IS}^{-6} is replaced by the summation of all pertinent inverse r^6 distances.

Equation [8] is modified when I relaxes through a dissimilar nucleus (i.e., ^{13}C or ^2H) to the form

$$[10] \quad \frac{1}{T_{1,I}} = \frac{4\gamma_H^2\gamma_S^2\hbar^2(I_S(I_S + 1))}{3r_{IS}^6}\tau_{IS}$$

where γ_S = magnetogyric ratio of S and I_S = spin of S. When S = ^2H, then

$$[11] \quad \frac{1}{T_{1,I}} = \frac{8\gamma_H^2\gamma_D^2\hbar^2}{3r_{IS}^6}\tau_{IS}$$

Considering a model three-site system, H_a, H_b, and H_c, the relaxation rate of H_a, $1/T_{1,Ha}$, equals

$$[12] \quad 3/2\gamma_H^4\hbar^2[r_{ab}^{-6} + r_{ac}^{-6}]\tau_r$$

When H_c is deuterated, the relaxation rate of H_a changes to

Can. J. Chem. Downloaded from www.nrcresearchpress.com by 195.138.81.100 on 09/07/12
For personal use only.

TABLE 1. Proton T_1 values[a] for methyl β-D-galactopyranoside **1** at 26°C in ^2H_2O

Proton	T_1(s)	$T_1/T_{1,H\text{-}1}$	
		Experimental	Calculated[b]
H-1	1.5	1.0	1.0
H-2	6.5	4.2	4.2
H-3	1.9	1.2	1.3
H-4	1.8	1.2	1.3
H-5	1.1	0.73	0.94
H-6	1.0	0.67	0.36
H-6′	0.97	0.63	0.40

[a]Nonselective; 50 mM glycoside.
[b]Using eq. [9].

$$[13]\quad \frac{3\gamma_H^4\hbar^2\tau_r}{2r_{ab}^6}+\frac{8\gamma_H^2\gamma_D^2\hbar^2\tau_r}{3r_{ac}^6}$$

Subtracting [13] from [12] yields

$$[14]\quad \Delta\frac{1}{T_{1,H_a}}=\frac{3\gamma_H^4\hbar^2\tau_r}{2r_{ac}^6}-\frac{8\gamma_H^2\gamma_D^2\hbar^2\tau_r}{3r_{ac}^6}$$

or

$$[15]\quad r_{ac}^{-6}=\frac{\Delta T_{1,H_a}^{-1}}{\gamma_H^2\hbar^2\tau_r(3/2\gamma_H^2-8/3\gamma_D^2)}$$

The internuclear distance between H_a and H_c is estimated by measuring the spin-lattice relaxation rate of H_a in the presence and absence of deuterium at H_c. As in the transient nOe experiment, τ_r is obtained from ^{13}C relaxation rates (eq. [6]).

Internuclear ^1H–^1H distance calculations and calculations of relative T_1 values

Internuclear ^1H–^1H distances in **1**, **2**, and **3** were determined from crystal structure data using the DANFIG program implemented on a VAX 11/730 computer. ^1H–^1H distances in **3** were determined as a function of the *O*-glycoside torsion angles, ϕ and Ψ, by systematically increasing ϕ from 0° (defined as that angle found in the crystal structure) to 360° in 30° increments, holding Ψ constant. Angle Ψ was then incremented by 30°, and the process was repeated until Ψ had been rotated 360°.

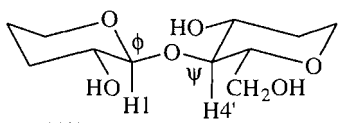

Internuclear ^1H–^1H distances, r, were converted to r^{-6} values and used to predict relative spin-lattice relaxation times (T_1) using eq. [9], assuming that $1/T_1$ is proportional to the sum of all r^{-6} distances for values of r within 5 Å of the proton site under consideration, and that the molecule under consideration tumbles isotropically in the region of extreme motional narrowing.

Results

Conformationally rigid structures: monosaccharides

Nonselective proton spin-lattice relaxation in methyl β-D-galactopyranoside

The 300 MHz ^1H NMR spectrum of methyl β-D-galactopyranoside **1** is shown in Fig. 2. Proton T_1 values obtained on **1** in ^2H_2O at 26°C are 1–2 s for all protons except H-2 (Table 1). The enhanced T_1 of H-2 (6.5 s) suggests that this proton is relatively isolated from the other protons in **1**; indeed, H-2 is antiperiplanar to both H-1 and H-3 and does not experience 1,3-interactions with ring protons.

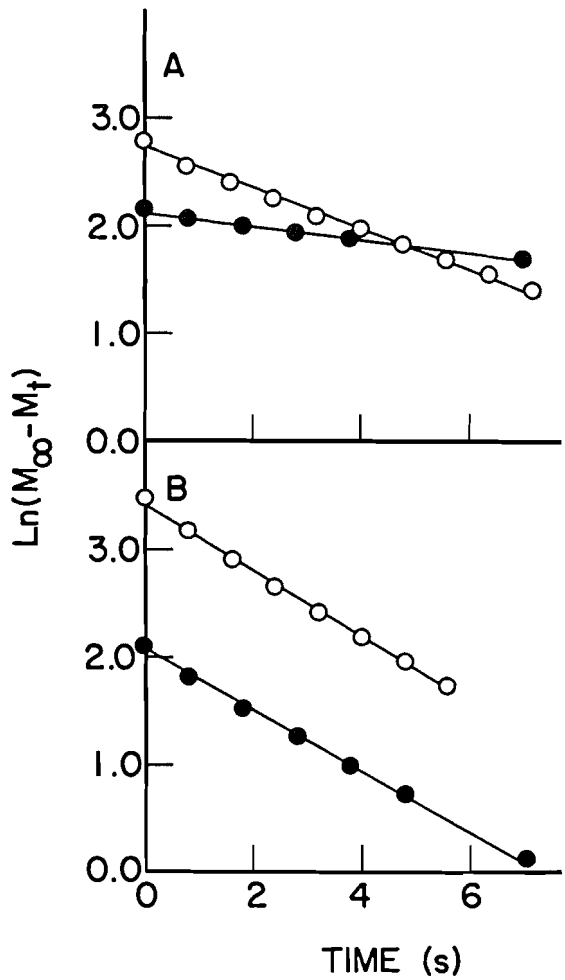

FIG. 3. Spin-lattice relaxation curves for H-1 of α-xylopyranose (5.3 s) and α-D-(2-^{2}H)xylopyranose (16.4 s)(A), and β-D-xylopyranose (3.2 s) and β-D-(2-^{2}H)xylopyranose (3.6 s)(B) at 27°C. Data for natural compounds are shown in open symbols, and data for deuterated compounds are shown in filled symbols.

This result can be predicted from ^1H–^1H internuclear distances estimated from X-ray diffraction data (35) if two assumptions are made, namely, that eq. [9] accurately describes proton relaxation in **1** and that the crystal and solution conformations of **1** are similar. Under similar solution conditions, the ratio of selective to non-selective T_1's for H-1 was found to be 1.4, in close agreement with the theoretical value of 1.5 expected for protons that relax solely via the proton–proton dipole mechanism (8), thus validating the use of eq. [9]. For each proton in **1**, inverse r^6 distances between it and all other carbon-bonded protons within 5 Å[4] were used to calculate relative relaxation times using eq. [9] (Table 1). Good agreement is observed between calculated and experimental values for H-2, H-3, and H-4. The disparities observed for H-5, H-6, and H-6′ suggest that hydroxymethyl group conformation and dynamics differ in the solid and solution states; indeed, in the crystal, one conformation is preferred (*gt*), whereas in aqueous solution, a

[4]At distances >5.0 Å, dipolar contributions to relaxation become small due to the r^6 dependence and can, therefore, be ignored.

Can. J. Chem. Downloaded from www.nrcresearchpress.com by 195.138.81.100 on 09/07/12
For personal use only.

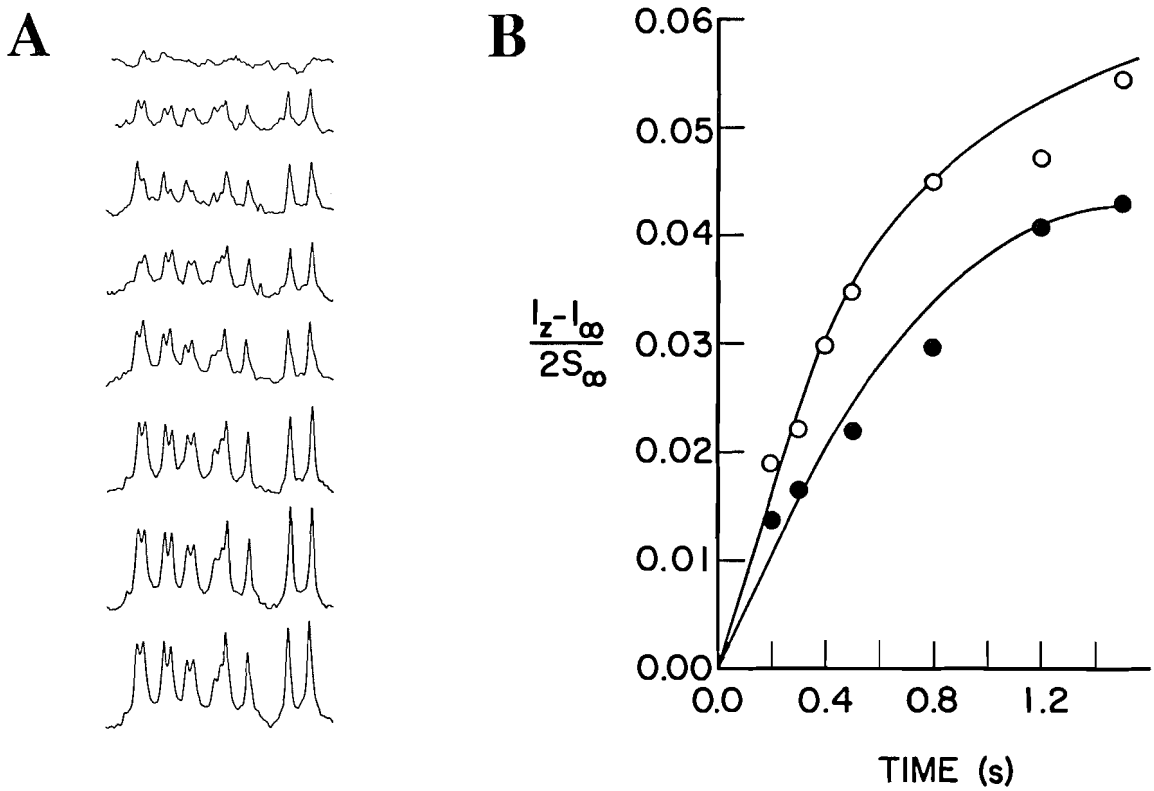

FIG. 4. (A) Transient nOe difference ^{1}H NMR spectra obtained on **1** after selective inversion of H-1, showing the effect on the intensities of the H-3 and H-5 signals (see Fig. 2 for assignments). Delay times between the selective 180° pulse and non-selective 90° observe pulse for the eight spectra are (from top): 0 s, 0.2 s, 0.3 s, 0.4 s, 0.5 s, 0.8 s, 1.2 s, 1.5 s. (B) Plot of intensity data in (A) to give $\sigma_{1,3}$ (0.050 s^{-1}, filled symbols) and $\sigma_{1,5}$ (0.083 s^{-1}, open symbols).

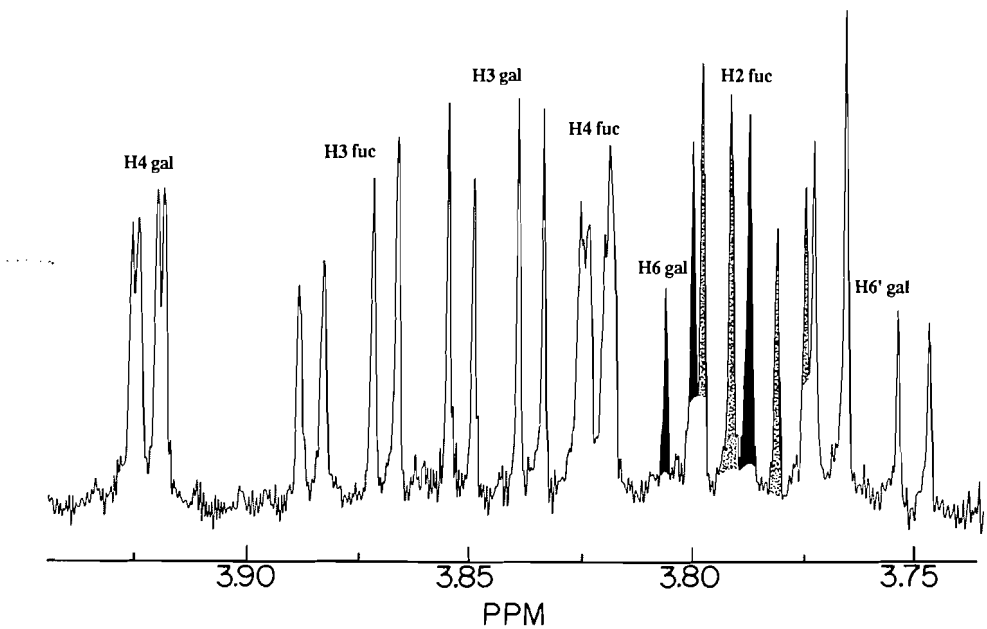

FIG. 5. The partial ^{1}H NMR spectrum of **4** in ^2H_2O at 620 MHz, showing signal assignments. The signals of H-3 Fuc, H-3 Gal, H-2 Fuc, and H-4 Fuc have been reassigned from the data of Lemieux *et al.* (39). Solid signals, H6 Gal (remaining signal overlaps H4 Fuc); hatched signals, H2 Fuc.

Can. J. Chem. Downloaded from www.nrcresearchpress.com by 195.138.81.100 on 09/07/12
For personal use only.

Can. J. Chem. Downloaded from www.nrcresearchpress.com by 195.138.81.100 on 09/07/12
For personal use only.

TABLE 2. ^1H chemical shifts[a] for disaccharide **4** in ^2H_2O

Nucleus	Gal	Fuc
H-1	4.43 (4.72)[b]	5.13 (5.52)
H-2	3.53 (3.86)	3.79[c](4.05)
H-3	3.85[c](4.09)	3.88[c](4.08)
H-4	3.92 (4.16)	3.82[c](4.03)
H-5	3.70 (3.92)	4.23 (4.59)
H-6	3.80 (4.04)	1.22 (1.47)
H-6′	3.76 (4.00)	
OCH_3	3.59	

[a]Values are reported in ppm relative to internal HOD (4.80 ppm) and are accurate to ±0.01 ppm.
[b]Values in parentheses taken from ref. 39.
[c]Reassigned from those in ref. 39.

TABLE 3. ^1H–^1H spin coupling constants[a] in reference methyl glycopyranosides and the disaccharide **4**

Coupled nuclei	Disaccharide **4**		Methyl β-D-galactopyranoside[b]	Methyl α-L-fucopyranoside[c]
	Gal	Fuc		
H-1,H-2	7.8	3.8	7.9	2.8
H-2,H-3	~9.5	10.4	9.9	
H-3,H-4	3.5	3.4	3.5	
H-4,H-5	0.8	1.1	1.1	1.0
H-5,H-6	7.9	6.6	7.9	6.3
H-5,H-6′	4.5		4.3	
H-6,H-6′	−11.8		−11.7	

[a]Values are reported in Hz and are accurate to ±0.1 Hz.
[b]Values obtained from ref. 13.
[c]Values obtained from ref. 39.

distribution of conformers appears to exist, with *gt* and (or) *tg* predominating (13).

DESERT studies on D-*xylopyranoses* **2**a *and* **2**b

D-Xylopyranose **2** is a good model compound to evaluate the DESERT experiment (34) in a conformationally rigid pentopyranose. The distance between H-1 and H-2 was determined in each anomer by measuring the T_1 of H-1 in natural D-xylopyranoses and in D-(2-^2H)xylopyranoses (Fig. 3). Using a C-1—H-1 bond length of 1.07 Å, a rotational correlation time of 1.67×10^{-11} s was calculated from eq. [6] using the observed C-1 T_1 of 2.5 s (determined using D-(1-^{13}C)xylose). From T_1 values obtained from data in Fig. 3 and eq. [15], H-1—H-2 distances of 2.19 Å and 2.70 Å were calculated for α-(**2***a*) and β-(**2***b*) D-xylopyranose, respectively. Since both anomers highly prefer the $^4C_1$ conformation (36), H-1 and H-2 will be closer in space in **2***a* (eq–ax) than in **2***b* (ax–ax). Distances obtained from the DESERT experiment are consistent with this fact, with magnitudes that agree well with those obtained on methyl xylopyranosides by crystallography (37, 38). Furthermore, in the same experiment, the H-2—H-3 distance (ax–ax) in **2***b* was calculated to be 2.77 Å, which is also consistent with average ax–ax distances in pyranosyl rings. This result shows that ax–ax and ax–eq distances, which differ on average by ~0.5 Å, are distinguishable by the DESERT method.

Transient nOe studies on methyl β-D-*galactopyranoside* **1**

The TnOe method was applied to methyl β-D-galactopyranoside **1** as an example of a conformationally rigid aldohexopyranose ring. The ^1H NMR spectrum of **1** at 300 MHz (Fig. 2) shows that the H-1 doublet is well isolated from the remaining signals of the carbon-bonded protons, and that the H-2 and H-5 multiplets are nearly fully resolved. Therefore, the H-1 signal could be selectively inverted with a 180° pulse, and time-dependent enhancements in the signals of H-3 and H-5 recorded by difference spectroscopy (Fig. 4). Initial slopes were estimated by inspection, and cross-relaxation rates (σ) of

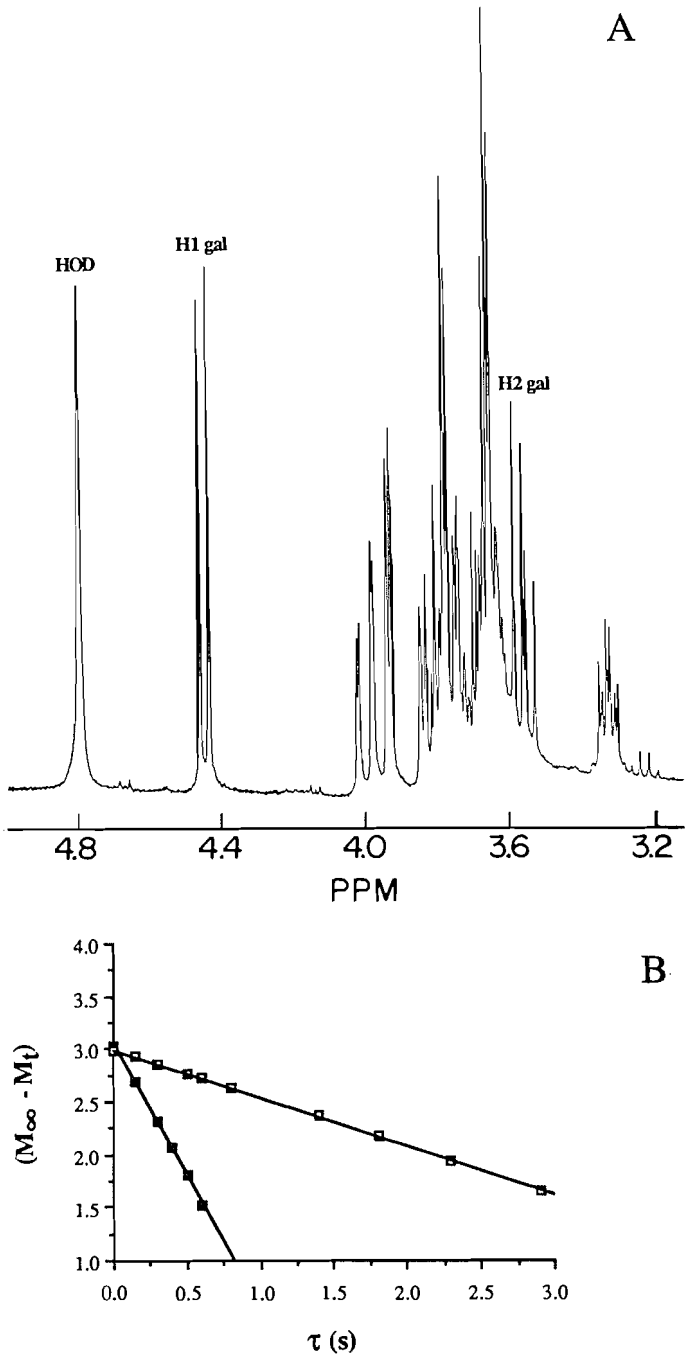

FIG. 6. (A) The 300 MHz ^1H NMR spectrum of *O*-β-D-galactopyranosyl-(1 → 4)-methyl-$^2H_3$-β-D-(1-^{13}C,^2H)glucopyranoside in ^2H_2O. Removal of the intense methyl aglycone signal permits the observation of H-2 Gal. (B) Spin-lattice relaxation time curves for H-1 Gal (0.40 s, filled symbols) and H-2 Gal (2.18 s, open symbols) for labeled disaccharide in (A).

TABLE 4. ^{13}C NMR parameters[a] for disaccharide **4** in ^2H_2O

Moiety	Chemical shifts (ppm)							Coupling constants (Hz)			
	C-1	C-2	C-3	C-4	C-5	C-6	CH_3	$^1J_{C-1,C-2}$	$^2J_{C-1,C-3}$	$^2J_{C-1,C-5}$	$^3J_{C-1,C-6}$
Gal	104.2	79.7	74.7	70.2	76.3	62.4	58.6	48.1	5.0	0	4.2
Fuc	101.5	69.9	71.1	73.4	68.3	16.6					

[a]Chemical shifts are referenced (external) to the anomeric carbon of β-D-(1-^{13}C)glucopyranose (97.4 ppm), and are accurate to ±0.1 ppm. Coupling constants are accurate to ±0.1 Hz.

0.050 s^{-1} and 0.083 s^{-1} were determined for the H-1—H-3 and H-1—H-5 pairs, respectively (Fig. 4). Using a rotational correlation time of 2.97×10^{-11} s determined from C-1 T_1 (1.4 s), internuclear distances of 2.52 Å and 2.31 Å were calculated for the H-1—H-3 and H-1—H-5 pairs, respectively. X-ray crystallography yields corresponding distances of 2.53 Å and 2.29 Å (35). Thus, in conformationally rigid systems, the TnOe method provides reliable interproton distances in solution.

Conformationally mobile structures: disaccharides

^1H and ^{13}C NMR spectra of disaccharides **3** *and* **4**

The ^1H and ^{13}C NMR spectra of **3** have been assigned previously (13). The 620 MHz ^1H NMR spectrum of **4** is shown in Fig. 5 (non-anomeric region). Signals have been assigned to specific protons in the galactose (Gal) and fucose (Fuc) constituents, and their chemical shifts are given in Table 2. Lemieux *et al.* (39) previously assigned ^1H chemical shifts for **4** based on a ^1H spectrum obtained at 270 MHz. Our analysis revealed a disparity in the assignments for H-3 Fuc, H-3 Gal, H-2 Fuc, and H-4 Fuc (Fig. 5). The multiplets for H-3 Fuc and H-3 Gal are very similar in pattern (i.e., vicinal couplings to H-2 and H-4 are similar in the Gal and Fuc moieties), making these assignments prone to misassignment. Our reassignment of H-3 Gal was confirmed by the ^1H NMR spectrum of **4** substituted with ^{13}C at C-1 Gal; in this spectrum one of the H-3 quartets contained an additional splitting due to coupling to C-1 ($^3J_{C-1,H-3}$ = 0.9 Hz) and can be assigned unequivocally to H-3 Gal. The expected multiplet patterns for H-2 Fuc and H-4 Fuc are significantly different, allowing assignments to be made with confidence at 620 MHz.

The $^1H-^1H$ spin couplings in **4** are given in Table 3. These values are comparable to those found in the corresponding methyl glycopyranosides (Table 3), indicating that the α(1 → 4) glycosidic linkage does not significantly affect ring conformation. $^3J_{H-1,H-2}$ in the fucopyranosyl ring is larger in the disaccharide, which may reflect a small conformational change in the ring and (or) a small substituent effect on $^3J_{H-1,H-2}$. If the former is responsible, then a larger $^3J_{H-1,H-2}$ would imply a decrease in the dihedral angle between H-1 (eq) and H-2 (eq) induced by a slight flattening of the fucose ring. A similar increase was not observed in the galactosyl moiety of **3**.

^{13}C NMR spectra of **4** were obtained on the natural compound and on the (1-^{13}C)Gal derivative. Comparison of these spectra permitted the unequivocal assignments of all galactosyl resonances (Table 4); C-3 and C-5 were assigned by comparison of observed $^2J_{C,C}$ values to those reported previously for β-D-(1-^{13}C)galactopyranose (2, 3) and methyl β-D-(1-^{13}C)galactopyranoside (13). Fucose assignments were taken from the work of Rosevear *et al.* (27) without further verification.

Correlation between proton internuclear distances, O-glycoside bond conformation, and dynamic NMR parameters

Conformational studies of flexible molecules based on proton internuclear distances require a careful choice of proton pairs; to assess *O*-glycoside conformation, only inter-residue proton pairs are relevant. However, not all inter-residue pairs have equal utility, as illustrated in the following discussion.

The crystal conformation of β-lactose **3** (40) yields approximate proton internuclear distances, from which estimates of the

TABLE 5. Proton internuclear distances involving H-1 Gal of β-D-lactose (crystal conformation): calculated contributions to H-1 relaxation by nearby protons

Proton pair	Distance (Å)	% Contribution[a] A	% Contribution[a] B
H-1–H-2	2.94	7.1	7.5
H-1–H-3	2.39	24.6	25.9
H-1–H-4	3.89	1.3	1.4
H-1–H-5	2.31	30.2	31.7
H-1–H-6a	4.54	0.5	0.6
H-1–H-6b	4.57	0.5	0.5
H-1–H-1′	5.92	0.1	0.1
H-1–H-2′	5.16	0.2	0.3
H-1–H-3′	4.44	0.6	0.6
H-1–H-4′	2.42	22.8	24.0
H-1–H-5′	4.18	0.9	0.9
H-1–H-6′a	3.60 (3.05)	2.1	6.0
H-1–H-6′b	2.82 (4.51)	9.1	0.6

[a]A = Glc hydroxymethyl conformation in crystal (C-4′–O-6′ nearly antiperiplanar, *gt*); B = alternate *gg* hydroxymethyl conformation.

TABLE 6. Proton internuclear distances involving H-2 Gal of β-D-lactose (crystal conformation): calculated contributions to H-2 relaxation by nearby protons

Proton pair	Distance (Å)	% Contribution[a] A	% Contribution[a] B
H-2–H-1	2.94	28.7	28.7
H-2–H-3	2.80	38.4	38.5
H-2–H-4	3.51	9.9	9.9
H-2–H-5	3.63	8.1	8.1
H-2–H-6a	4.12	3.8	3.8
H-2–H-6b	4.88	1.4	1.4
H-2–H-1′	>6.0	—	—
H-2–H-2′	>6.0	—	—
H-2–H-3′	4.39	2.6	2.6
H-2–H-4′	4.35	2.7	2.7
H-2–H-5′	4.79	2.5	1.5
H-2–H-6′a	5.82 (4.45)	0.5	2.4
H-2–H-6′b	4.45 (5.97)	2.4	0.4

[a]Definitions of A and B are as given in Table 5.

Can. J. Chem. Downloaded from www.nrcresearchpress.com by 195.138.81.100 on 09/07/12
For personal use only.

TABLE 7. Sum of inverse r^6 distances[a] for H-1 and H-2, and calculated ratios of T_1's as a function of methyl β-D-lactoside *O*-glycoside bond conformation

	Ψ(°)[b]					
φ(°)	0	60	120	180	240	300
			H-1 Gal			
0	219 (208)	172 (167)	152 (152)	153 (152)	174 (173)	262 (259)
60	5545 (4894)	305 (361)	167 (168)	164 (161)	213 (197)	873 (489)
120	582 (651)	196 (205)	168 (173)	224 (244)	2525 (4009)	3015 (8158)
180	417 (418)	187 (188)	159 (160)	179 (186)	386 (406)	869 (874)
240	317 (317)	165 (165)	156 (156)	171 (172)	366 (366)	2494 (2494)
300	181 (180)	156 (155)	150 (150)	160 (160)	208 (208)	202 (201)
			H-2 Gal			
0	54 (54)	60 (59)	132 (131)	685 (672)	232 (156)	67 (68)
60	55 (55)	62 (61)	229 (208)	1522 (3147)	2656 (—)	70 (76)
120	57 (58)	135 (124)	428 (239)	413 (952)	326 (332)	62 (62)
180	57 (58)	148 (233)	9349 (9385)	1860 (1861)	611 (611)	59 (59)
240	56 (56)	87 (88)	2218 (2219)	— (—)	79 (79)	55 (55)
300	55 (55)	92 (92)	619 (619)	189 (188)	84 (82)	56 (56)
			T_1(H-2)/T_1(H-1)			
0	4.1 (3.9)	2.9 (2.8)	1.2 (1.2)	0.22 (0.23)	0.75 (1.1)	3.9 (3.8)
60	100.8 (89.0)	4.9 (5.9)	0.73 (0.81)	0.11 (0.05)	0.08 (—)	12.5 (6.4)
120	10.2 (11.2)	1.5 (1.7)	0.39 (0.72)	0.54 (0.26)	7.7 (12.1)	48.6 (132)
180	7.3 (7.2)	1.3 (0.81)	0.02 (0.02)	0.10 (0.10)	0.63 (0.66)	14.7 (14.8)
240	5.7 (5.7)	1.9 (1.9)	0.07 (0.07)	— (—)	4.6 (4.6)	45.3 (45.3)
300	3.3 (3.3)	1.7 (1.7)	0.24 (0.24)	0.85 (0.85)	2.5 (2.5)	3.6 (3.6)

[a] $\times 10^{-44}$.
[b] Values in parentheses are for the alternate *gg* conformation of CH_2OH Glc.

TABLE 8. Internuclear distances[a] as a function of *O*-glycoside conformation: H-1–H-4′ in β-D-lactoside

	Ψ(°)											
φ(°)	0	30	60	90	120	150	180	210	240	270	300	330
0	2.42	2.79	3.16	3.43	3.57	3.55	3.38	3.08	2.70	2.34	2.12	2.15
30	2.63	3.00	3.33	3.54	3.61	3.52	3.29	2.95	2.57	2.26	2.15	2.30
60	2.95	3.30	3.57	3.72	3.73	3.58	3.32	2.97	2.64	2.42	2.41	2.62
90	3.29	3.59	3.81	3.92	3.88	3.72	3.46	3.15	2.88	2.74	2.78	2.99
120	3.56	3.80	3.99	4.07	4.04	3.89	3.67	3.42	3.20	3.10	3.14	3.32
150	3.71	3.91	4.06	4.15	4.14	4.05	3.88	3.69	3.51	3.41	3.41	3.53
180	3.71	3.87	4.03	4.14	4.19	4.15	4.05	3.89	3.73	3.60	3.55	3.59
210	3.56	3.71	3.88	4.04	4.15	4.18	4.12	3.99	3.82	3.65	3.53	3.50
240	3.30	3.45	3.66	3.88	4.05	4.12	4.10	3.97	3.77	3.55	3.36	3.27
270	2.96	3.14	3.41	3.69	3.90	4.00	3.97	3.83	3.59	3.31	3.06	2.93
300	2.63	2.88	3.21	3.52	3.74	3.83	3.78	3.60	3.31	2.97	2.69	2.56
330	2.42	2.74	3.11	3.42	3.62	3.67	3.56	3.32	2.98	2.62	2.34	2.26

[a] In Å.

relative efficiencies of dipolar relaxation "sinks" can be made for each proton in the molecule. H-1 and H-2 of the galactose (Gal) moiety were examined because of their proximity to the glycoside linkage (Tables 5 and 6). Because the hydroxymethyl group of the glucose (Glc) constituent is close to these protons, calculations were performed on the *gg* and *gt* conformations, which appear to be preferred in aqueous solution (13). The *trans-gauche* (*tg*) conformation seems to be least preferred (13) and was not considered.

In the crystal conformation (40), φ (O5—C1—O1—C4′) = 70.7° and Ψ (C1—O1—C4′—C3′) = 108.0°, which places H-1 (unprimed atoms denote atoms in the Gal ring) and H-4′ (primed atoms denote atoms in the Glc ring) in close proximity (2.42 Å) (Table 5). In addition to H-4′, other major contributors to H-1 relaxation are the intra-residue protons, H-3 and H-5. In the crystal conformation, it can be shown from calculations using eqs. [9] and [11] that the T_1 of H-1 should increase by ~26% when H-4′ is substituted with deuterium.

In contrast to H-1, H-2 does not relax appreciably through inter-residue protons in the crystal conformation (Table 6).

Can. J. Chem. Downloaded from www.nrcresearchpress.com by 195.138.81.100 on 09/07/12
For personal use only.

Can. J. Chem. Downloaded from www.nrcresearchpress.com by 195.138.81.100 on 09/07/12
For personal use only.

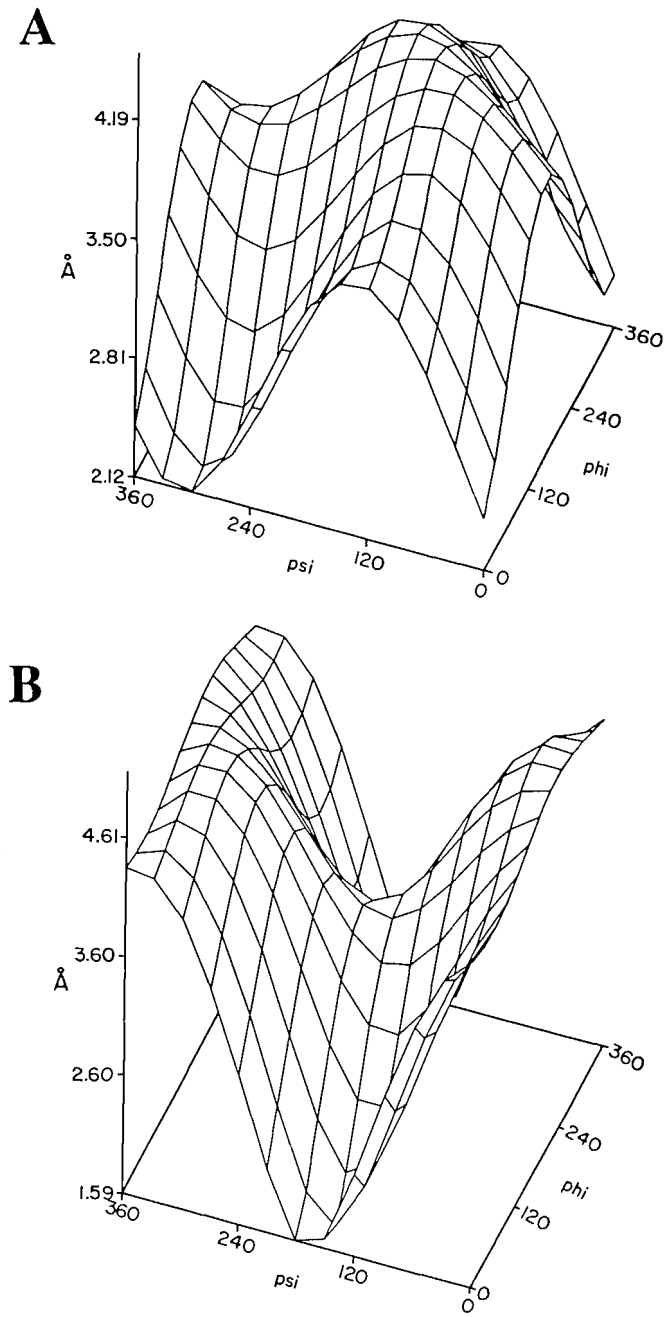

FIG. 7. Surface-contour plots of ^{1}H-^{1}H internuclear distance versus *O*-glycoside dihedral angles, ϕ and Ψ, in **3**. (A) For H-1–H-4′. (B) For H-2–H-4′.

However, comparison of its T_1 with that of H-1 can provide a means to evaluate conformation because of the sensitivity of the T_1(H-2)/T_1(H-1) ratio to three-dimensional structure (Table 7, Fig. 6).

The crystal structure represents only one conformation that **3** may assume. Distances between various pairs of protons in **3** were determined as a function of linkage conformation by systematically varying ϕ and Ψ in 30° increments. Data for the H-1–H-4′ and H-2–H-4′ pairs are given in Tables 8 and 9, and surface-contour plots of these data are shown in Fig. 7. From an analysis of all inter-residue proton pairs, it appears that H-1–H-4′ and H-2–H-4′ distances will be most useful for the following reasons. The H-1 and H-2 signals of **3** are resolved in ^{1}H spectra obtained at ≥300 MHz; the H-2 signal is most easily observed in the trideuteromethyl glycoside (Fig. 6A). In addition, data in Fig. 7 reveal two unique distance–conformation maps for these pairs, which improves the discrimination between potential conformers, and distances vary over a sufficient range to permit their use in conformational analysis.

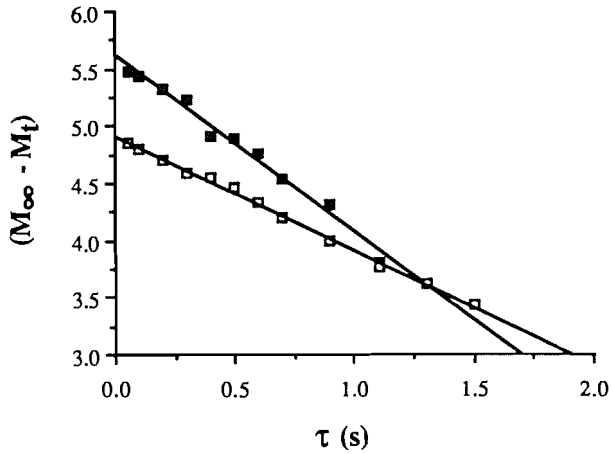

FIG. 8. Spin-lattice relaxation curves at 30° for H-1 Fuc of **4** (0.65 s, filled symbols), and H-1 Fuc of **4** deuterated at H-2 Gal (1.1 s, open symbols).

DESERT experiments on disaccharides **3** *and* **4**

DESERT experiments were performed on **3** and **4** to assess *O*-glycoside conformation. In **3**, the T_1 of H-1 Gal was measured in the natural compound and the derivative deuterated at H-4′ Glc (Table 10); in **4**, the T_1 of H-1 Fuc was measured in the natural compound and the derivative deuterated at H-2 Gal (Fig. 8, Table 10). Relaxation times increased by a factor of 1.7 upon deuteration, suggesting qualitatively that H-1 Gal in **3**, and H-1 Fuc in **4**, are in close spatial proximity to the respective deuterated sites. To assess these internuclear distances quantitatively, *isotropic* rotational correlation times, τ_r, were determined for **3** and **4** by ^{13}C NMR using compounds substituted with ^{13}C at C-1 Glc (**3**) and C-1 Gal (**4**) and eq. [6] (Table 10). From the T_1 and τ_r data in Table 10, and eq. [15], average internuclear distances between H-1 Gal and H-4′ Glc in **3**, and H-2 Gal and H-1 Fuc in **4**, were calculated (Table 10). For **3**, $r_{\text{H-1 Gal,H-4′ Glc}} \cong$ 2.0 Å, which constrains Ψ to 270°–360° and ϕ to 330°–360° (Table 8). This preferred conformational region is consistent with that deduced previously for **3** based on studies of $^3J_{C,C}$ and $^3J_{C,H}$ across the *O*-glycoside bond (13). The T_1 of H-2 Gal is essentially unaffected upon ^{2}H substitution at H-4′ Glc, indicating that these protons are distant in space (>4.0 Å). This latter observation is consistent with the preferred conformational region determined from $r_{\text{H-1 Gal,H-4′ Glc}}$. Further confirmation of this preferred conformational space derives from the ratio, T_1(H-2 Gal/T_1(H-1 Gal) = 5.8 (Fig. 6, Table 7).

The internuclear distance of ~2.0 Å between H-1 Fuc and H-2 Gal of disaccharide **4** also significantly constrains the conformational options of the *O*-glycoside linkage in this structure. This distance requires that H-1 Fuc and H-2 Gal be oriented *cis* (i.e., on the same face of the molecule).

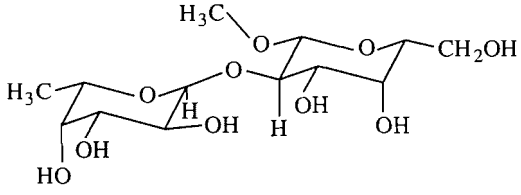

TABLE 9. Internuclear distances[a] as a function of *O*-glycoside conformation: H-2–H-4′ in β-D-lactoside

	Ψ(°)											
ϕ(°)	0	30	60	90	120	150	180	210	240	270	300	330
0	4.35	4.12	3.66	3.01	2.28	1.67	1.59	2.12	2.85	3.52	4.04	4.32
30	4.30	3.96	3.40	2.71	2.01	1.61	1.83	2.49	3.20	3.81	4.22	4.39
60	4.29	3.87	3.28	2.60	2.03	1.89	2.28	2.93	3.58	4.10	4.41	4.47
90	4.32	3.89	3.33	2.75	2.34	2.34	2.74	3.32	3.89	4.32	4.55	4.55
120	4.39	4.01	3.54	3.07	2.78	2.80	3.12	3.59	4.06	4.42	4.61	4.60
150	4.48	4.19	3.83	3.46	3.20	3.16	3.35	3.69	4.07	4.39	4.58	4.61
180	4.55	4.38	4.11	3.79	3.51	3.36	3.41	3.62	3.93	4.23	4.47	4.58
210	4.60	4.53	4.33	4.02	3.67	3.40	3.28	3.38	3.64	3.98	4.30	4.52
240	4.61	4.61	4.42	4.08	3.66	3.25	2.99	3.00	3.27	3.68	4.10	4.44
270	4.58	4.59	4.38	3.99	3.47	2.94	2.58	2.56	2.90	3.42	3.95	4.36
300	4.51	4.49	4.22	3.74	3.13	2.51	2.10	2.17	2.65	3.29	3.87	4.30
330	4.43	4.32	3.96	3.39	2.70	2.04	1.71	1.98	2.63	3.33	3.91	4.29

[a]In Å.

TABLE 10. NMR parameters used in DESERT experiments on disaccharides **3** and **4**

Compound[a]	τ_r (s)	T_1 (protio) (s)	T_1 (deutero) (s)	$r_{H,H}$[b] (Å)
3	5.7×10^{-11}	0.37	0.64	1.9
4	5.6×10^{-11}	0.65	1.1	2.1

[a]Disaccharide 50 mM in 10 mM acetate (Na^+) buffer, pD 5.2, in ^2H_2O, 30°C. Compound **3** was deuterated at H-4′ Glc; T_1 of H-1 Gal was measured. Compound **4** was deuterated at H-2 Gal; T_1 of H-1 Fuc was measured.

[b]For **3**, $r_{\text{H-1 Gal,H-4' Glc}}$; for **4**, $r_{\text{H-1 Fuc,H-2 Gal}}$.

This *O*-glycoside conformation is consistent with results obtained from hard-sphere calculations by Lemieux *et al.* (39).

Conclusions

$^1H-^1H$ internuclear distance determinations by NMR are valuable in determining the structure and conformation of molecules in solution. The one-dimensional NMR experiments employed in this study yield accurate distances in carbohydrates that are conformationally rigid and tumble isotropically (e.g., **1** and **2**). The TnOe method can be applied to natural (i.e., unlabeled) compounds, but the experimental protocol is more demanding and requires a stable spectrometer for accurate results. In contrast, the DESERT method is easier to perform, but requires specifically deuterium-substituted compounds. Although this requirement may be considered a drawback, in some cases appropriately labeled disaccharides can be prepared enzymically from deuterated monosaccharides in a straightforward manner, as illustrated in this study.

The results of the DESERT experiments on **3** and **4** suggest that the *O*-glycoside bond in these disaccharides is relatively rigid in aqueous solution, that is, the conformational excursions about the linkage must be limited in amplitude. A source of error in the present treatment of DESERT data lies in the assumption that **3** and **4** tumble isotropically in solution. ^{13}C relaxation measurements on **3**, for example, have suggested that tumbling may be slightly anisotropic (13, 41). Increasing oligosaccharide size is likely to enhance anisotropic motion, especially in linear or extended oligosaccharides, and this motion will need to be treated explicitly in $^1H-^1H$ internuclear distance studies of these compounds. In highly branched oligosaccharides, however, anisotropic motion may not be as significant.

The availability of two-dimensional nOe spectroscopy (42) does not preclude the use of 1-D NMR methods to evaluate the spatial proximity of protons in some instances. A simple 1-D DESERT experiment that yields one or more absolute $^1H-^1H$ distances may be sufficient to resolve a conformational uncertainty. In addition to their utility in DESERT studies, deuterated oligosaccharides may be desirable in some cases to edit complex 2-D nOe spectra, and (or) to enhance nOe's between selected sites. It is likely that isotopic labeling will be used more routinely in the future to facilitate the interpretation of complex 2-D NMR spectra of oligosaccharides, in ways similar to those used currently in protein structure determinations (43, 44).

Acknowledgments

The grant support of the National Institutes of Health (GM 33791) and the Research Corporation (10028) is gratefully acknowledged. The authors thank Dr. Mishra of the NMR Facility for Biomedical Studies, Department of Chemistry, Carnegie-Mellon University, for his assistance in obtaining the 620 MHz ^1H NMR spectra.

1. C. A. G. HAASNOOT, F. A. A. M. DE LEEUW, H. P. M. DE LEEUW, and C. ALTONA. Org. Magn. Reson. **15**, 43 (1981).
2. T. E. WALKER, R. E. LONDON, T. W. WHALEY, R. BARKER, and N. A. MATWIYOFF. J. Am. Chem. Soc. **98**, 5807 (1976).
3. M. J. KING-MORRIS and A. S. SERIANNI. J. Am. Chem. Soc. **109**, 3501 (1987).
4. D. Y. GAGNAIRE, R. NARDIN, F. R. TARAVEL, and M. R. VIGNON. Nouv. J. Chim. **1**, 423 (1977).
5. A. S. PERLIN and G. K. HAMER. *In* Carbon-13 NMR in polymer science. *Edited by* W. M. Pasika. American Chemical Society, Washington, DC. 1979. p. 123.
6. J. A. SCHWARCZ and A. S. PERLIN. Can. J. Chem. **50**, 3667 (1972).
7. I. TVAROSKA, M. HRICOVINI, and E. PETRAKOVA. Carbohydr. Res. **189**, 359 (1989).
8. J. M. BERRY, L. D. HALL, D. G. WELDER, and K. F. WONG. *In* Anomeric effect: origin and consequences. *Edited by* W. A. Szarek and D. Horton. American Chemical Society, Washington, DC. 1979. p. 30.
9. P. DAIS and A. S. PERLIN. Adv. Carbohydr. Chem. Biochem. **45**, 125 (1987).
10. J. N. SCARSDALE, J. H. PRESTEGARD, S. ANDO, T. HORI, and R. K. YU. Carbohydr. Res. **155**, 45 (1986).

Can. J. Chem. Downloaded from www.nrcresearchpress.com by 195.138.81.100 on 09/07/12
For personal use only.

11. D. A. CUMMING, D. S. DIME, A. A. GREY, J. J. KREPINSKY, and J. P. CARVER. J. Biol. Chem. **261**, 3208 (1986).
12. (*a*) A. BAX and M. F. SUMMERS. J. Am. Chem. Soc. **108**, 2093 (1986); (*b*) M. F. SUMMERS, L. G. MARZILLI, and A. BAX. J. Am. Chem. Soc. **108**, 4285 (1986).
13. (*a*) M. L. HAYES, A. S. SERIANNI, and R. BARKER. Carbohydr. Res. **100**, 87 (1982); (*b*) R. BARKER and A. S. SERIANNI. Acc. Chem. Res. **19**, 307 (1986).
14. S. HANESSIAN and J. BANOUB. Methods Carbohydr. Chem. **8**, 243 (1980).
15. R. BARKER, K. A. OLSON, J. H. SHAPER, and R. L. HILL. J. Biol. Chem. **247**, 7135 (1972).
16. H. A. NUNEZ and R. BARKER. Biochemistry, **19**, 489 (1980).
17. A. S. SERIANNI and R. BARKER. Synthetic approaches to carbohydrates enriched with stable isotopes of carbon, hydrogen and oxygen. *In* Isotopes in the physical and biomedical sciences. *Edited by* E. Buncel and J. R. Jones. Elsevier, Amsterdam. 1987. p. 211.
18. S. J. ANGYAL, G. S. BETHELL, and R. J. BEVERIDGE. Carbohydr. Res. **73**, 9 (1979).
19. E. FISCHER. Ber. Dtsch. Chem. Ges. **26**, 2400 (1893).
20. J. GREEN. Methods Carbohydr. Chem. **21**, 95 (1966).
21. P. W. AUSTIN, F. E. HARDY, J. C. BUCHANAN, and J. BADDILEY. J. Chem. Soc. 5350 (1963).
22. J. E. HODGE and B. T. HOFREITER. Methods Carbohydr. Chem. **1**, 380 (1962).
23. K. BOCK and C. PEDERSEN. Adv. Carbohydr. Chem. Biochem. **41**, 27 (1983).
24. A. S. SERIANNI and R. BARKER. Can. J. Chem. **57**, 3160 (1979).
25. A. S. SERIANNI, E. CADMAN, J. PIERCE, M. L. HAYES, and R. BARKER. Methods Enzymol. **89**, 83 (1982).
26. H. A. NUNEZ, J. V. O'CONNOR, P. R. ROSEVEAR, and R. BARKER. Can. J. Chem. **59**, 2086 (1981).
27. P. R. ROSEVEAR, H. A. NUNEZ, and R. BARKER. Biochemistry, **21**, 1421 (1982).
28. A. S. SERIANNI, H. A. NUNEZ, and R. BARKER. Carbohydr. Res. **72**, 71 (1979).
29. M. L. HAYES, N. J. PENNINGS, A. S. SERIANNI, and R. BARKER. J. Am. Chem. Soc. **104**, 6764 (1982).
30. A. S. SERIANNI, E. L. CLARK, and R. BARKER. Carbohydr. Res. **72**, 79 (1979).
31. R. L. VOLD, J. S. WAUGH, M. P. KLEIN, and D. E. PHELPS. J. Chem. Phys. **48**, 3831 (1968).
32. (*a*) S. L. GORDON and K. WÜTHRICH. J. Am. Chem. Soc. **100**, 7094 (1978); (*b*) J. H. NOGGLE and R. E. SCHIRMER. The nuclear Overhauser effect. Academic Press, New York. 1971; (*c*) A. KALK and H. J. C. BERENDSEN. J. Magn. Reson. **24**, 343 (1976).
33. J. R. LYERLA, JR. and G. C. LEVY. Top. Carbon-13 NMR Spectrosc. **1**, 79 (1974).
34. (*a*) K. AKASAKA, T. IMOTO, S. SHIBATA, and H. HATANO. J. Magn. Reson. **18**, 328 (1975); (*b*) A. P. ZENS, T. J. WILLIAMS, J. C. WISOWATY, R. R. RISHER, R. B. DUNLAP, T. A. BRYSON, and P. D. ELLIS. J. Am. Chem. Soc. **97**, 2850 (1975).
35. S. TAKAGI and G. A. JEFFREY. Acta Crystallogr. Sect. B: Struct. Crystallogr. Cryst. Chem. **B34**, 2006 (1978).
36. S. J. ANGYAL. Angew. Chem. Int. Ed. Engl. **8**, 157 (1969).
37. S. TAKAGI and G. A. JEFFREY. Acta Crystallogr. Sect. B: Struct. Crystalogr. Cryst. Chem. **B33**, 3033 (1977).
38. S. TAKAGI and G. A. JEFFREY. Acta Crystallogr. Sect. B: Struct. Crystallogr. Cryst. Chem. **B34**, 3104 (1978).
39. R. U. LEMIEUX, K. BOCK, L. T. J. DELBAERE, S. KOTO, and V. S. RAO. Can. J. Chem. **58**, 631 (1980).
40. K. HIROTSU and A. SHIMADA. Bull. Chem. Soc. Jpn. **47**, 1872 (1974).
41. J. M. BERRY, L. D. HALL, and K. F. WONG. Carbohydr. Res. **56**, C16–C20 (1977).
42. S. MACURA and R. R. ERNST. Mol. Phys. **41**, 95 (1980).
43. W. M. WESTLER, M. KAINOSHO, H. NAGAO, N. TOMONAGA, and J. L. MARKLEY. J. Am. Chem. Soc. **110**, 4093 (1988).
44. D. M. LEMASTER and F. M. RICHARDS. Biochemistry, **27**, 142 (1988).

Can. J. Chem. Downloaded from www.nrcresearchpress.com by 195.138.81.100 on 09/07/12
For personal use only.

Synthesis, crystal structure, and vibrational spectra of the complex maleic acid·2H_2O·18-crown-6

PIERRE AUDET AND RODRIGUE SAVOIE[1]
Département de chimie, Université Laval, Québec (Québec), Canada G1K 7P4

AND

MICHEL SIMARD
Département de chimie, Université de Montréal, C.P. 6128, Succ. A, Montréal (Québec), Canada H3C 3J7

Received, July 3, 1990

PIERRE AUDET, RODRIGUE SAVOIE, and MICHEL SIMARD. Can. J. Chem. **68**, 2183 (1990).

A stoichiometric complex of formula maleic acid·2H_2O·18-crown-6 has been obtained from maleic acid and the macrocyclic polyether 18-crown-6. Crystals of this complex have been shown by X-ray diffraction crystallography to belong to the *Cc* space group of the monoclinic system. The acid molecules in the adduct are linked to each other through a water molecule, giving infinite [-acid-H_2O-]$_n$ chains. They are also linked to the crown ether via water molecules. The infrared and Raman spectra of the complex are presented and compared to those of crystalline maleic acid.

Key words: maleic acid/18-crown-6, structure, X-ray, spectra.

PIERRE AUDET, RODRIGUE SAVOIE et MICHEL SIMARD. Can. J. Chem. **68**, 2183 (1990).

Un complexe de formule acide maléique·2H_2O·18-couronne-6 a été obtenu à partir de l'acide maléique et de l'éther macrocyclique 18-couronne-6. La diffraction des rayons X a démontré que ce complexe cristallise dans le groupe d'espace *Cc* du système monoclinique. Dans le solide, les molécules d'acides sont reliées entre elles par l'intermédiaire de molécules d'eau, pour former des chaînes infinies [-acide-H_2O-]$_n$. Le lien entre les molécules d'acides et de l'éther en couronne se fait également par l'intermédiaire de molécules d'eau. Les spectres infrarouge et Raman du complexe sont présentés et comparés à ceux de l'acide maléique à l'état cristallin.

Mot clés : acid maléique/éther 18-couronne-6, structure, rayons-X, spectres.

[Traduit par la revue]

Can. J. Chem. Downloaded from www.nrcresearchpress.com by 195.138.81.100 on 09/07/12
For personal use only.

Introduction

The macrocyclic polyether 18-crown-6 ((-CH_2-CH_2-O-)$_6$, henceforth called 18C6) readily forms complexes with neutral molecules with hydrogen bonding capacity. In these adducts, the linking of the proton donor with the ether is commonly achieved through a bridging water molecule, which is weakly bound to two adjacent oxygen atoms of the crown (1). This typical acid···OH_2···18C6 arrangement has been found in the CH_2(CN)COOH·H_2O·18C6 adduct, which has been characterized by X-ray diffraction (2). Various complexes of 1:1:1 or 2:2:1 (acid:water:18C6) stoichiometry, in which the acid·OH_2 units are presumably attached to one or both sides of the crown, have also been obtained with halogenated derivatives of acetic acid (3). In a complex with oxalic acid, both ends of the acid were found to be attached to different crown molecules in a polymer-like fashion: -18C6-H_2O-HOOCCOOH-OH_2-18C6- (4). We have found a similar 1:2:1 stoichiometry (acid: water:18C6) in a complex formed with maleic acid (HOOC-CH=CH-COOH). As the vibrational spectra of this complex clearly indicated that the conformation of the acid in this adduct was different from that in the pure crystalline acid (5), we have determined its molecular and crystal structure by X-ray diffraction crystallography. The results of these different types of investigation are reported in this paper.

Experimental

The complex was prepared by dissolving equimolar quantities of 18C6 (0.264 g) and maleic acid (0.116 g) in 5 mL of THF to which a small quantity of distilled water (0.05 mL) had been added. Precipitation of crystalline platelets (mp 62–63°C) occurred at low temperature (ca. −5°C) after addition of 1 mL of diethyl ether. The complex was filtered under reduced pressure, washed with a small amount of cold diethyl ether, and dried in air. Its stoichiometry was first established by titration of the acid by NaOH (calcd.: 27.88%; found: 27.6%), from the integrated intensity of the ^{1}H nmr peaks (in $CDCl_3$, using a Varian EM360A instrument; δ 3.68 (24 H, 18C6), 6.43 (2H, acid), and 6.91 (6H, H_2O and acid)), and from the elemental analysis (calcd.: C 46.15% and H 7.75% found: C 46.6% and H 7%).

The Raman spectra of the samples, contained in sealed capillary cells, were recorded on a Spex model 1400 microcomputer-controlled spectrometer, using ca. 200 mW (at the sample) of excitation power from the 514.5 nm green line of a Spectra Physics model 2020 argon ion laser. The low-temperature measurements were made in a conventional liquid nitrogen cryostat. The spectra were typically recorded at 2 cm^{-1} slit width, with an integration time of 2 s at each frequency interval of 2 cm^{-1}. The infrared spectra of Nujol and hexachlorobutadiene mulls of the polycrystalline complex pressed between Irtran-4 windows were recorded on a Beckman 4250 spectrophotometer.

For X-ray study, a plate-shaped hexagonal crystal of dimensions 0.095 (001, 00$\bar{1}$) × 0.24 (01$\bar{1}$, 0$\bar{1}$1) × 0.34 (11$\bar{1}$, $\bar{1}\bar{1}$1) × 0.34 (1$\bar{1}\bar{1}$, $\bar{1}$11) mm was mounted on a Nonius-CAD4 diffractometer. The unit cell dimensions were derived from the angular setting of 25 well-centered reflections in the range 43 ≤ 2θ ≤ 48°. The final parameters and other crystal data of interest are presented in Table 1. The data collection for the complex was done over all the Laue sphere, by the ω/2θ scan technique, with graphite monochromatized copper radiation. The intensities of seven standard reflections monitored every hour during the experiment showed that the crystal slowly decomposed in the X-ray beam, the intensities having decreased by 13.6% during data collection. This decay was considered at the reduction stage. After averaging of the 8785 measured reflections to the Laue *m* symmetry (anomalous dispersion of oxygen atoms taken into account), 3715 reflections were considered observed ($I/\sigma(I) \geq 1.96$; $R_I = 0.035$). The Lorentz and polarization corrections were applied to the data.

The structure was solved using direct methods (MULTAN-80)[2] combined with difference Fourier syntheses (SHELX-76). The refine-

[1]Author to whom correspondence may be addressed.

[2]The programs used here are modifications of NRC-2, data reduction; NRC-3, absorption correction; NRC-10, bond distances and angles; FORDAP, Fourier and Patterson maps (A. Zalkin); SHELX, program for structure determination; and ORTEP, stereo drawings (refs. 6–10).

Can. J. Chem. Downloaded from www.nrcresearchpress.com by 195.138.81.100 on 09/07/12
For personal use only.

TABLE 1. Crystal data for the complex maleic acid·$2H_2O$·18-crown-6

Composition	$C_{16}H_{32}O_{12}$
MW	416.42
$F(000)$	896
Crystal system	Monoclinic
Space group	Cc
a, Å	8.105(3)
b	14.814(6)
c	18.467(6)
β, deg	100.27(4)
V, Å^3	2181.8
d_c, g cm^{-3}	1.268
Z	4
μ, cm^{-1}	8.95
λ, Kα̃, Å	1.54178
Crystal size, mm	0.095 × 0.24 × 0.34
T, K	220

TABLE 2. Data collection and refinement

Radiation	CuKα̃
$2\theta_{max}$, deg	140.0
Scan	$\omega/2\theta$
Scan width, deg	$(1.00 + 0.14 \tan\theta)$
Octants measured	$-9 < h < 9$ $-18 < k < 18$ $-22 < l < 22$
Number of measured reflections	8785
Acceptance level $I/\sigma(I)\geq$	1.96
Number of unique observed reflections	3715
$R = \Sigma \parallel F_o\mid - \mid F_c \parallel /\Sigma\mid F_o\mid$	0.043
$R_w = [\Sigma w(\mid F_o\mid - \mid F_c\mid)^2/\Sigma w F_o^2]^{1/2}$	0.049
$S = [\Sigma w(\mid F_o\mid - \mid F_c\mid)^2/(m - n)]^{1/2}$	1.45
Residual fluctuations in electron density map, e Å^{-3}	−0.17; 0.13
Shift-to-σ ratio at the end of the refinement, maximum	0.23
average	0.03

ments, based on F's, minimized the quantity $\Sigma w\Delta F^2$ using the block-diagonal approximation in the last cycles. All non-hydrogen atoms were refined anisotropically and hydrogen atoms isotropically. The refinement was concluded when the indicators given in Table 2 reached their minimum values. The scattering curves for the non-hydrogen atoms were taken from ref. 6 and those for H atoms from ref. 7.

Results and discussion

Crystal structure

The X-ray structure determination confirmed the 1:2:1 (acid:H_2O:18C6) stoichiometry indicated from the elemental analysis. The atomic numbering adopted is shown in Fig. 1 and a stereoview of the structural units is presented in Fig. 2, showing the thermal ellipsoids at the end of the refinement. Crystal data of interest are given in Table 1 and the refined coordinates with isotropic temperature factors of the non-hydrogen atoms are found in Table 3. The overall structure of the crystalline complex can be represented by a polymeric chain of acid units linked through water molecules, with crown molecules alternately attached to opposite sides of the chains.

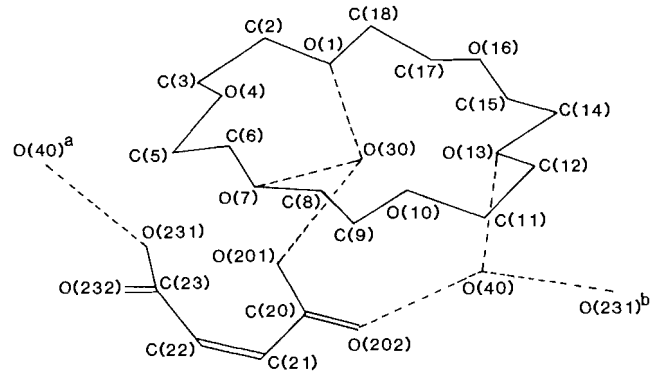

FIG. 1. Atomic numbering adopted for the complex maleic acid·$2H_2O$·18-crown-6; a: x, $1 - y$, $\frac{1}{2} + z$; b: x, $1 - y$, $-\frac{1}{2} + z$.

The 18-crown-6 distances and angles are part of the supplementary material.[3] The average C—O distance is 1.421 Å (range 1.403–1.438 Å) while the average value for C—C distances is 1.483 Å (range 1.473–1.496 Å). The value of the C—O—C bond angles, 112.8° (range 111.5°–114.2°), is slightly higher than that of the C—C—O bond angles, 109.3° (range 108.2°–110.2°). These features are consistent with the corresponding parameters found in structures containing the 18C6 molecule (11–13). The detailed conformation of the 18-crown-6 is best described in terms of the torsion angles about the ring bonds. Those about C—C bonds are all close to *gauche* (average value 68.4°, range 65.7°–71.4°) and those about C—O bonds are close to *trans* (average value 171.6°, range 169.9°–179.4°). These values are consistent with the very small departure of the crown conformation from the D_{3d} symmetry.

The bond distances, bond angles, and torsion angles for the maleic acid moiety in the complex are given in Table 4. There are marked differences between the C=O and C—OH bond lengths in the molecule (C=O: 1.205(3) and 1.207(3) Å, compared to C—OH: 1.311(3) and 1.323(3) Å). In the complex, the acid molecules are involved in an intermolecular hydrogen bonding network, with the localized C=O and C—OH groups acting as hydrogen donor and acceptor respectively.

The intramolecular hydrogen bond normally formed in the maleic acid molecule (14) is not found in the present case and the molecule is not planar (Fig. 3). While the main torsion angle of the carbon skeleton is close to that for the *cis* conformation, C(20)—C(21)—C(22)—C(23) = −4.3(4)°, a large departure from planarity occurs for one of the COOH groups at one end of the molecule, as indicated by the torsion angle C(21)—C(22)—C(23)—O(232) = −82.4(3)°. This is unusual since in most compounds containing maleic acid this molecule is locked into a planar conformation by an internal hydrogen bond. A situation in all respects comparable to the present one was, however,

[3]Tables of the bond distances, angles and torsion angles of the 18-crown-6 molecule, of the anisotropic thermal parameters, the refined H-atom coordinates, and the structure factor amplitudes have been deposited and may be purchased from the Depository of Unpublished Data, CISTI, National Research Council of Canada, Ottawa, Ont., Canada K1A 0S2.

Tables of distances and bond angles for the crown part of the complex and for the hydrogen atoms, and the refined H-atom coordinates, have also been deposited with the Cambridge Crystallographic Data Centre and can be obtained on request from The Director, Cambridge Crystallographic Data Centre, University Chemical Laboratory, Lensfield Road, Cambridge CB2 1EW, U.K.

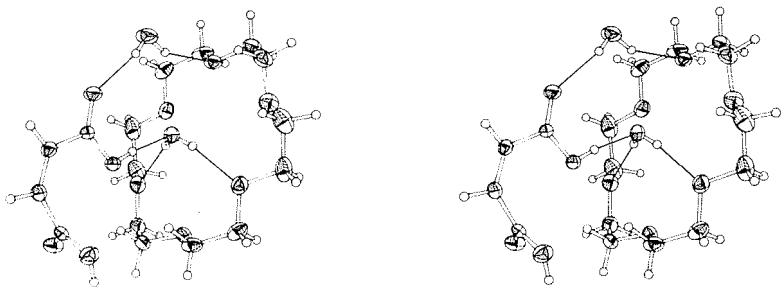

FIG. 2. ORTEP drawing of the various structural units and their linkage through hydrogen bonding. Ellipsoids correspond to 50% probability level. The hydrogens are represented by spheres of arbitrary size.

TABLE 3. Fractional atomic coordinates and their esd's (O × 10^5, C × 10^4), and U_{eq} (× 10^3) for the complex maleic acid·2H_2O·18-crown-6

Atom	X	Y	Z	U_{eq}*
O(1)	15334(22)	72459(12)	60284(9)	52
O(4)	43056(22)	63212(11)	69204(9)	49
O(7)	65201(22)	55437(12)	60311(10)	53
O(10)	67438(25)	63109(13)	46403(10)	58
O(13)	38372(23)	71130(12)	38105(9)	50
O(16)	16734(23)	79957(13)	46189(10)	60
O(201)	19897(22)	46459(10)	56490(8)	44
O(202)	11977(24)	42189(12)	44830(9)	53
O(231)	5089(23)	40165(13)	71147(10)	54
O(232)	29947(22)	34279(13)	70207(9)	53
O(30)	32156(22)	60376(11)	51455(9)	49
O(40)	20139(34)	54723(15)	34403(10)	82
C(2)	1818(4)	7187(2)	6807(2)	59
C(3)	2622(3)	6309(2)	7047(1)	55
C(5)	5124(4)	5480(2)	7061(1)	57
C(6)	6772(4)	5532(2)	6805(2)	60
C(8)	8056(4)	5662(2)	5772(2)	70
C(9)	7739(4)	5568(2)	4965(2)	78
C(11)	6347(4)	6261(2)	3870(2)	66
C(12)	5422(4)	7088(2)	3575(1)	63
C(14)	2866(4)	7884(2)	3543(1)	61
C(15)	1291(4)	7871(2)	3842(2)	67
C(17)	245(4)	8050(2)	4963(2)	76
C(18)	786(4)	8093(2)	5768(2)	71
C(20)	1285(3)	4089(1)	5134(1)	34
C(21)	567(3)	3270(2)	5416(1)	40
C(22)	640(3)	3056(1)	6115(1)	42
C(23)	1523(3)	3529(1)	6783(1)	37

$$*U_{eq} = \frac{1}{3}\sum_i \sum_j U_{ij} a_i^* a_j^* a_i \cdot a_j$$

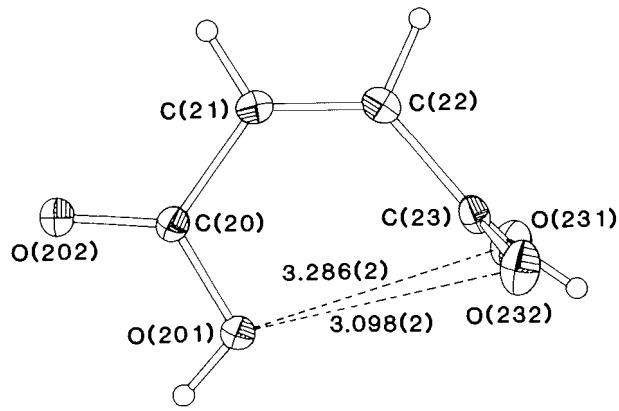

FIG. 3. Maleic acid molecule (top view) with intramolecular O···O distances.

observed by Town and Small (15) in the doubly ionized maleate anion, where repulsions between the two carboxylate ends caused a large rotation of one of the COO^- planes (τ = 81.4°).

The crown ether, the water, and the maleic acid molecules are linked together through a series of hydrogen bonds in the crystalline complex. A stereoview of the unit cell showing how the various units are associated is reproduced in Fig. 4. It is seen that the two -COH groups of the acid act as hydrogen donors to form two strong hydrogen bonds with water molecules where O···O distances are 2.536(2) and 2.644(3) Å. These hydrogen bonds are nearly linear, the angles O(201)—H(201)···O(30) and O(231)—H(231)···O(40) having a value of 172(3)°. One of the C=O groups of the acid plays the role of a hydrogen acceptor, forming a weaker hydrogen bond with a water molecule O(40), with d(O···O) = 2.837(3) Å. It is this water molecule which links, through two other hydrogen bonds, the next acid molecule and the crown ether. This arrangement of the structural units can best be described by a pseudo-polymer (maleic acid···$H_2O)_n$, with the crown ether molecules interacting on each side of the chain. Three weak hydrogen bonds exist between the crown and the water molecules; the O(1)···O(30), O(7)···O(30), and O(13)···O(40) distances are in the range 2.863(3)–2.970(2) Å. The other geometrical parameters characterizing these hydrogen bonds are given in Table 5. The structure of the complex with maleic acid differs somewhat from those obtained with other carboxylic acids, such as with cyanoacetic (2) and oxalic (4) acids, in which the acid molecules were separated from each other by a crown.

Vibrational spectra

The crown ether in the complex has a structure that departs very little from the highly regular one of D_{3d} symmetry, in contrast with the rectangular shape adopted by this molecule in the pure solid (16). The vibrational bands of the ether moiety in the infrared and Raman spectra of the complex (see Figs. 5–7) are consequently very similar to those of other compounds, such as K^+·18C6·Br^-, in which this symmetry is adopted (17, 18); they also differ markedly from those of the solid uncomplexed compound (19). Generally speaking, the higher symmetry of the crown results in a simplification of its vibrational spectra by comparison to those of the crystalline solid or those in which its structure is distorted.

The conformation of the maleic acid molecule in the complex is also quite different from that adopted in the pure crystalline acid (5, 20). To understand the resulting differences in the vibrational spectra of this species in the two states, the spectra of crystalline maleic acid first have to be interpreted. This

Can. J. Chem. Downloaded from www.nrcresearchpress.com by 195.138.81.100 on 09/07/12
For personal use only.

TABLE 4. (a) Distances and angles related to the maleic acid

Bond	Distances (esd's), Å	Bonds	angles (esd's), deg
C(20)—O(201)	1.311(3)	O(201)—C(20)—O(202)	124.3(2)
C(20)—O(202)	1.207(3)	O(201)—C(20)—C(21)	114.1(2)
C(20)—C(21)	1.480(3)	O(202)—C(20)—C(21)	121.6(2)
C(21)—C(22)	1.320(3)	C(20)—C(21)—C(22)	126.1(2)
C(22)—C(23)	1.487(3)	C(21)—C(22)—C(23)	129.0(2)
C(23)—O(231)	1.323(3)	C(22)—C(23)—O(231)	113.2(2)
C(23)—O(232)	1.205(3)	C(22)—C(23)—O(232)	122.9(2)
		O(231)—C(23)—O(232)	123.7(2)
C(21)—H(210)	0.94(3)	C(20)—C(21)—H(210)	113(2)
		C(22)—C(21)—H(210)	120(2)
C(22)—H(220)	1.00(3)	C(21)—C(22)—H(220)	116(2)
		C(23)—C(22)—H(220)	115(2)

(b) Torsion angles

Bonds	Torsion angles (esd's), deg
O(201)—C(20)—C(21)—C(22)	−2.6(3)
O(202)—C(20)—C(21)—C(22)	178.0(2)
C(20)—C(21)—C(22)—C(23)	−4.3(4)
C(21)—C(22)—C(23)—O(231)	102.1(3)
C(21)—C(22)—C(23)—O(232)	−82.4(3)

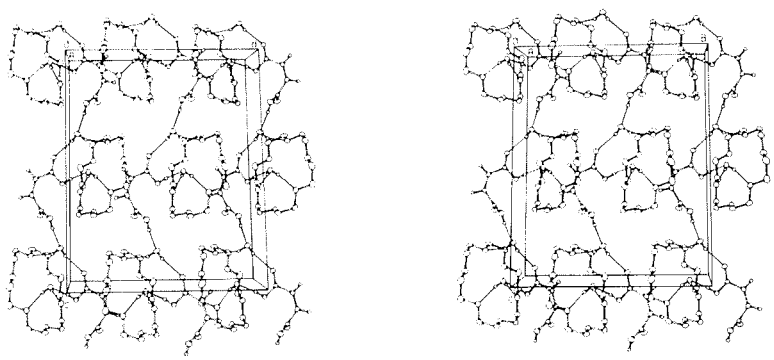

FIG. 4. Stereoview of the unit cell. Hydrogen atoms have been omitted for clarity and hydrogen bonding is indicated by thin lines.

molecule is planar in the crystal, with one of the O—H groups involved in a very short and asymmetric internal hydrogen bond (O···O = 2.5 Å). This has a very pronounced effect on the frequencies of the OH vibrational modes.

The infrared spectrum of crystalline maleic acid Fig. 5B) shows three broad regions of absorption in the 1000–1800 cm^{-1} region. The first, at ca. 1150 cm^{-1}, can be confidently assigned to the out-of-plane OH bending mode (γ(OH), by comparison with the corresponding vibration at 1121 cm^{-1} in KHC_2O_4 (O···O = 2.52 Å) and at 1180 cm^{-1} in $LiHC_2O_4$ (O···O = 2.45 Å) (21). The other two, in the 1440 and 1570 cm^{-1} regions, also arise from OH vibrations, as they are not present in the spectrum of the crystalline [$(OD)_2$] compound (22). These two bands were previously assigned to the in-plane bending vibration (δ(OH)) (22), but we believe that they arise from both the OH stretching ν(OH) and the in-plane bending vibrations. However, it is difficult to provide an unambiguous individual assignment for these two bands. In $NaHC_2O_4$, KHC_2O_4, $KHC_2O_4 \cdot H_2O$, and $LiHC_2O_4$, with O···O distances varying from 2.57 to 2.45 Å, the δ(OH) occurs in the 1450–1520 cm^{-1} region (21). On the other hand, an empirical relation between O···O distances and the frequency of the ν(OH) mode (23) indicates that the latter should also occur in this same frequency range. One indication in favor of the assignment of the band at high frequency to the δ(OH) mode is the occurrence of the strong doublet at 1565/1585 cm^{-1} in both the infrared (Fig. 5B) and Raman (Fig. 6B) spectra. This doublet and the strong peak at 1633 cm^{-1} are better explained by coupled C═O, C═C, and δ(OH) motions, as they are quite strong in the Raman spectrum, where the ν(OH) generally causes little scattering. One also notes that each band in the 1440, 1570, and 1710 cm^{-1} regions is split in both the Raman and infrared spectra, possibly through an intermolecular vibrational coupling effect (factor-group splitting) in the crystal.

Upon complex formation with 18C6, the maleic acid molecule adopts a twisted conformation that breaks the very short internal hydrogen bond formed in the crystal. This causes the ν(OH) mode to move out of the mid-frequency region and the frequency of the δ(OH) vibration to decrease considerably. The strong infrared bands near 1440 and 1570 cm^{-1} therefore vanish (Fig. 5A) and the Raman spectrum is considerably simplified in the 1500–1800 cm^{-1} region, where only two major peaks

Can. J. Chem. Downloaded from www.nrcresearchpress.com by 195.138.81.100 on 09/07/12
For personal use only.

TABLE 5. Bond distances (Å) and angles (deg) related to the hydrogen bonding

Bond (A—H···B)	Distances (esd's) A—B	A—H	H—B	Angles (esd's) A—H—B
O(30)—H(301)···O(1)	2.917(2)	0.79(4)	2.14(4)	165(4)
O(30)—H(302)···O(7)	2.970(2)	0.88(4)	2.13(4)	158(3)
O(40)—H(401)···O(13)	2.863(3)	0.91(4)	2.00(4)	156(4)
O(40)—H(402)···O(202)	2.837(3)	0.77(3)	2.08(3)	167(3)
O(201)—H(201)···O(30)	2.536(2)	0.86(3)	1.68(3)	172(3)
O(231)—H(231)···O(40)*	2.644(3)	0.86(2)	1.79(2)	172(3)

Bonds	Angles (esd's), deg	Bonds	Angles (esd's), deg
O(1)···O(30)···O(7)	107.98(7)	H(301)—O(30)—H(302)	108(4)
O(1)···O(30)···O(201)	92.36(7)	H(301)—O(30)···H(201)	104(3)
O(7)···O(30)···O(201)	88.37(7)	H(302)—O(30)···H(201)	105(3)
O(30)···O(1)—C(2)	121.41(13)	H(301)···O(1)—C(2)	123.4(11)
O(30)···O(1)—C(18)	124.00(15)	H(301)···O(1)—C(18)	120.9(11)
O(30)···O(7)—C(6)	121.03(16)	H(302)···O(7)—C(6)	125.1(10)
O(30)···O(7)—C(8)	122.82(17)	H(302)···O(7)—C(8)	116.8(10)
O(30)···O(201)—C(20)	113.22(13)	H(201)—O(201)—C(20)	108.1(20)
O(13)···O(40)···O(202)	124.50(10)	H(401)—O(40)—H(402)	101(3)
O(13)···O(40)···O(231)†	96.39(9)	H(401)—O(40)···H(231)†	110(3)
O(202)···O(40)···O(231)†	133.72(10)	H(402)—O(40)···H(231)†	138(3)
O(40)···O(13)—C(12)	111.05(16)	H(401···O(13)—C(12)	112.5(11)
O(40)···O(13)—C(14)	111.59(15)	H(401)···O(13)—C(14)	116.3(12)
O(40)···O(202)—C(20)	143.23(16)	H(402)···O(202)—C(20)	140.4(9)
O(40)*···O(231)—C(23)	111.27(15)	H(231)—O(231)—C(23)	107.4(17)

*x, $1 - y$, $\frac{1}{2} + z$.
†x, $1 - y$, $-\frac{1}{2} + z$.

remain, besides the band at 1632 cm^{-1} due to the bending mode of H_2O (Fig. 6A). These occur at 1728 cm^{-1} (ν(C═O)) and 1680 cm^{-1} (ν(C═C)), the latter appreciably shifted from its position at 1634 cm^{-1} in the spectrum of the crystal, as a result of a slight increase in C═C bond length and decreased coupling with the δ(OH) mode. Coupled ν(C—O) and δ(OH) vibrations in the complex are probably responsible for the sharp peaks at 1433 and 1349 cm^{-1} and for the broad band at 1302 cm^{-1} in the infrared spectrum. Corresponding bands are found at 1387 and 1320 cm^{-1} in the Raman spectrum of an aqueous solution of maleic acid (24). Other characteristic shifts in the Raman spectra are those of the δ_{as}(CH) and γ_s(CH) modes, which occur at 1216 and 1018 cm^{-1} in the spectra of the pure crystal and at 1206 and 988 cm^{-1} in those of the complex. It is noteworthy that the Raman spectrum of the maleic acid moiety in the complex (Fig. 6) is very similar to that of the acid in aqueous solution (24), which means that the change of conformation noted above, or a similar one, also occurs upon dissolution of the acid in water.

Although the structure of the complex with maleic acid is somewhat different from that of the corresponding one with oxalic acid (4), there is a marked similarity in the high-frequency region of the vibrational spectra of these adducts. In particular, one finds in the Raman spectrum of the maleic acid complex (Fig. 7B) a broad band with a maximum near 3450 cm^{-1}, which corresponds to a very intense band at slightly higher frequency in the infrared spectrum (Fig. 7A). The Raman band is split into three components at 3401, 3427, and 3448 cm^{-1} at −185°C, the latter peak being approximately twice as intense as the first two. This triplet arises from the stretching vibrations of the weakly bound water molecules (O···O = 2.84–2.97 Å) linking the oxalic molecules between themselves and with the crown ether.

The two OH groups of the maleic acid molecules in the complex are involved in hydrogen bonds of very different energy with neighboring water molecules, as indicated by the two O···O distances of 2.54 and 2.64 Å. It seems logical to assign the two bands at 2024 and 2570 cm^{-1} in the infrared spectrum of the complex (Fig. 7) to the stretching vibrations of these two OH groups. The average of these two frequencies (2300 cm^{-1}) agrees reasonably well with the 2400 cm^{-1} value estimated from the pK_a of maleic acid (1.83), which has been shown to be related to the ν(OH) stretching frequency of various acids complexed by 18C6 (25). The 2570 cm^{-1} infrared band, with weaker Raman counterpart, has a frequency which is lower than that expected (ca. 2850 cm^{-1}) (23) for the 2.64 Å O···O distance noted above. It is therefore possible that the observed peak is but one of several components of complex sets of bands resulting from a Fermi resonance interaction between the ν(OH) mode and the first overtone of the δ(OH) vibrations, the other components being overshadowed by the strong series of peaks arising from C—H stretching modes of the crown in the 2900 cm^{-1} region. The 2024 cm^{-1} band, asigned to the ν(OH) vibration of the acid OH group involved in the short hydrogen

Can. J. Chem. Downloaded from www.nrcresearchpress.com by 195.138.81.100 on 09/07/12
For personal use only.

Can. J. Chem. Downloaded from www.nrcresearchpress.com by 195.138.81.100 on 09/07/12
For personal use only.

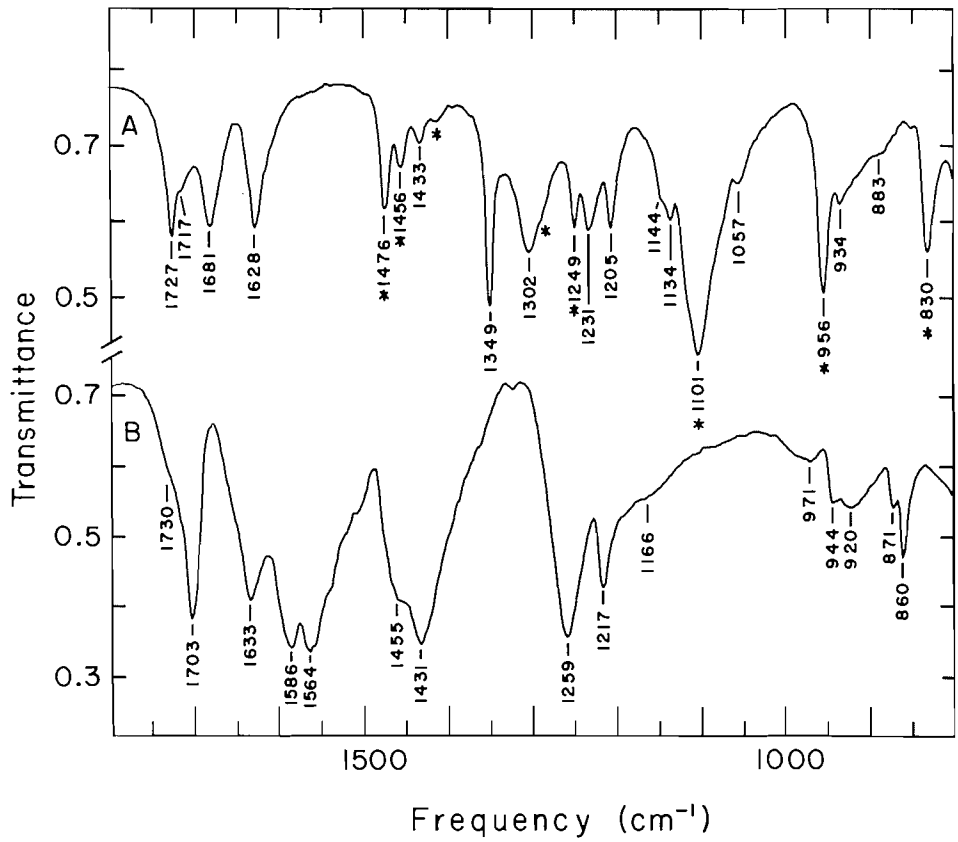

FIG. 5. Composite infrared spectra (Nujol and hexachlorobutadiene mulls) of (A) the $(=CHCOOH)_2 \cdot 2H_2O \cdot 18$-crown-6 complex and (B) crystalline maleic acid. Bands believed to originate from the crown ether moiety are indicated by *.

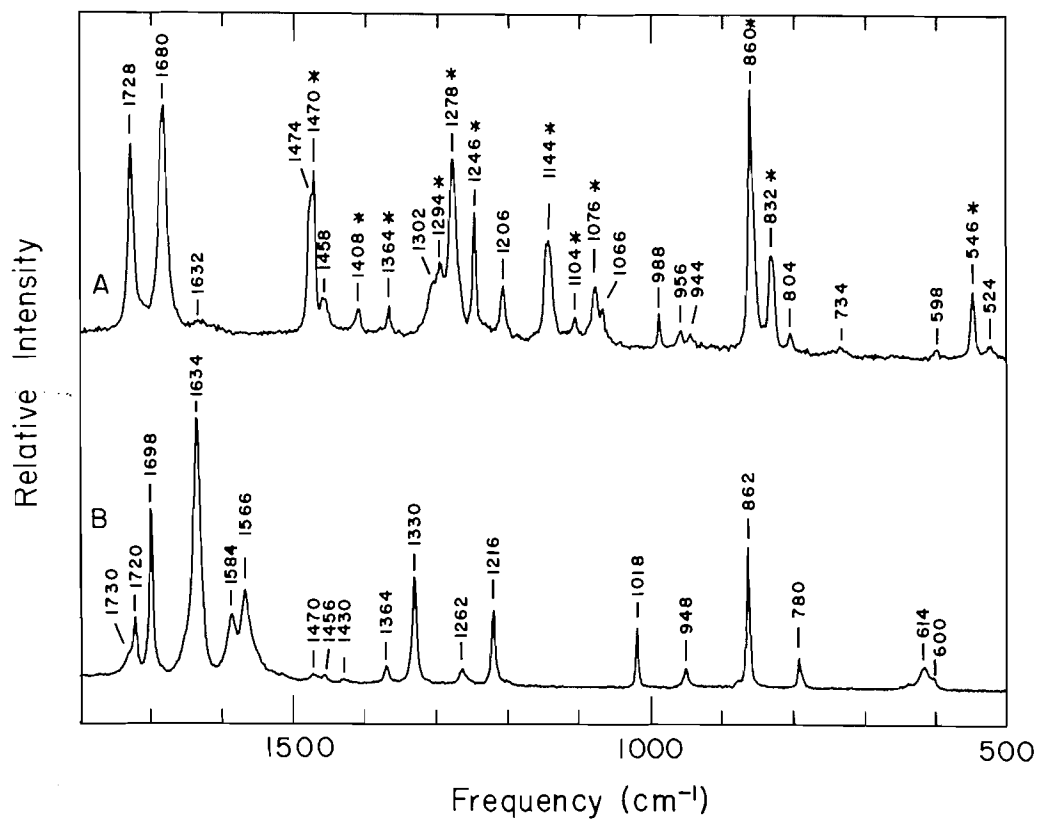

FIG. 6. Raman spectra of (A) the $(=CHCOOH)_2 \cdot 2H_2O \cdot 18$-crown-6 complex and (B) crystalline maleic acid. Bands believed to originate from the crown ether moiety are indicated by *.

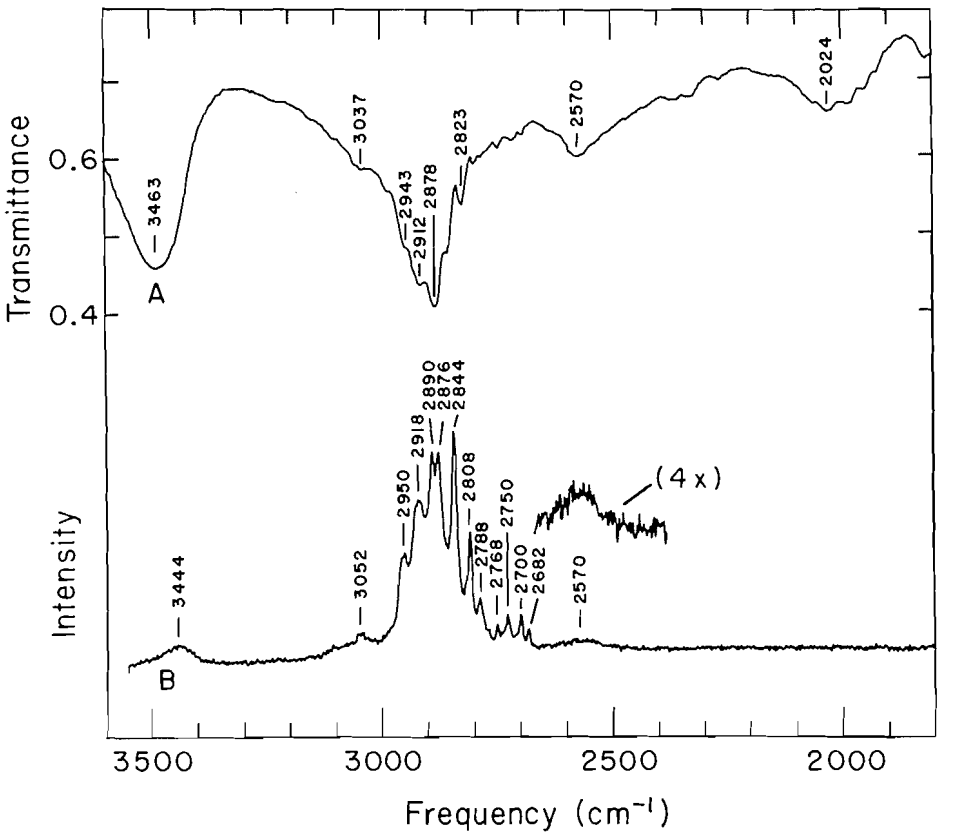

FIG. 7. (A) Infrared (hexachlorobutadiene mull) and (B) Raman spectra of the $(=CHCOOH)_2 \cdot 2H_2O \cdot 18$-crown-6 complex.

bond, has a frequency which is somewhat higher than that expected for the corresponding very short 2.54 Å O···O distance (ca. 1800 cm^{-1}) (23). However, this frequency varies very rapidly with changes in the intermolecular distance in this region and, in fact, the observed frequency of 2024 cm^{-1} corresponds statistically to an O···O distance of ca. 2.55 Å, which is quite close to the value obtained from the X-ray structure determination.

Acknowledgements

Financial support of this work by the Natural Sciences and Engineering Research Council of Canada and by the Ministère de l'Education du Québec is gratefully acknowledged.

1. W. H. WATSON, J. GALLOY, D. A. GROSSIE, F. VÖGTLE, and W. M. MÜLLER. J. Org. Chem. **49**, 347 (1984).
2. A. ELBASYOUNY, H. J. BRÜGGE, K. VON DEUTEN, M. DICKEL, A. KNÖCHEL, K. U. KOCH, J. KOPF, D. MELZER, and G. RUDOLPH. J. Am. Chem. Soc. **105**, 6568 (1983).
3. R. SAVOIE, A. RODRIGUE, M. PIGEON-GOSSELIN, and R. CHÊNEVERT. Can. J. Chem. **63**, 1457 (1985).
4. S. DEGUIRE, F. BRISSE, J. OUELLET, and R. SAVOIE. Can. J. Chem. **64**, 142 (1986).
5. M. N. G. JAMES and G. B. J. WILLIAMS. Acta Crystallogr. Sect. B: Struct. Crystallogr. Cryst. Chem. **B30**, 1249 (1974).
6. D. T. CROMER and J. B. MANN. Acta Crystallogr. Sect. A: Cryst. Phys. Diffr. Theor. Gen. Crystallogr. **A24**, 321 (1968).
7. R. F. STEWART, E. R. DAVIDSON, and W. T. SIMPSON. J. Chem. Phys. **42**, 3175 (1965).
8. F. R. AHMED, S. R. HALL, M. E. PIPPY, and C. P. HUBER. The NRC system of crystallographic computer programs for the IBM/360. Accession nos. 133–147 in J. Appl. Crystallogr. **6**, 309 (1973).
9. G. SHELDRICK. SHELX 76, A crystallographic computation system for crystal structure determination. Univ. of Cambridge, Cambridge, England. 1976.
10. C. K. JOHNSON. ORTEP, Report ORNL-3794, Oak Ridge National Laboratory, Oak Ridge, TN. 1965.
11. R. CHÊNEVERT, D. CHAMBERLAND, M. SIMARD, and F. BRISSE. Can. J. Chem. **67**, 32 (1989).
12. L. PARENTEAU and F. BRISSE. Can. J. Chem. **67**, 1293 (1989).
13. G. WEBER and G. M. SHELDRICK. Acta Crystallogr. Sect. B: Struct. Crystallogr. Cryst. Chem. **B37**, 2108 (1981).
14. M. N. G. JAMES and G. J. B. WILLIAMS. Acta Crystallogr. Sect. B: Struct. Crystallogr. Cryst. Chem. **B30**, 1257 (1974).
15. W. G. TOWN and R. W. H. SMALL. Acta Crystallogr. Sect. B: Struct. Crystallogr. Cryst. Chem. **B29**, 1950 (1973).
16. J. D. DUNITZ and P. SEILER. Acta Crystallogr. Sect. B: Struct. Crystallogr. Cryst. Chem. **B30**, 2739 (1974).
17. M. FOUASSIER and J.-C. LASSEGUES. J. Chim. Phys. Phys.-Chim. Biol. **75**, 865 (1978).
18. H. TAKEUCHI, T. ARAI, and I. HARADA. J. Mol Struct. **146**, 197 (1986).
19. R. CHÊNEVERT, A. RODRIGUE, M. PIGEON-GOSSELIN, and R. SAVOIE. Can. J. Chem. **60**, 853 (1982).
20. S. F. DARLOW and W. COCHRAN. Acta Crystallogr. **14**, 1250 (1961); S. F. DARLOW. Acta Crystallogr. **14**, 1257 (1961).
21. J. DE VILLEPIN, A. NOVAK, and J. TOMKINSON. Chem. Phys. **48**, 113 (1980).
22. S. D. HAMANN and M. LINTON. Aust. J. Chem. **28**, 2567 (1975).
23. A. NOVAK. Struct. Bonding (Berlin), **18**, 177 (1974).
24. J. MAILLOIS, L. BARDET, and L. MAURY. J. Mol. Struct. **30**, 57 (1976).
25. R. CHÊNEVERT, A. RODRIGUE, D. CHAMBERLAND, J. OUELLET, and R. SAVOIE. J. Mol. Struct. **131**, 187 (1985).

Can. J. Chem. Downloaded from www.nrcresearchpress.com by 195.138.81.100 on 09/07/12
For personal use only.

Synthesis of chromanes using pyruvic acid dimethylhydrazone dianion

I. TAPIA, V. ALCÁZAR, AND J. R. MORÁN

Department of Organic Chemistry, University of Salamanca, Plaza de los Caídos 1-5, 37008 Salamanca, Spain

Received January 18, 1990

I. TAPIA, V. ALCÁZAR, and J. R. MORÁN. Can. J. Chem. **68**, 2190 (1990).

Chromanes were prepared in medium yield from methyl salicylate and the dianions of pyruvic or α-oxobutyric acid dimethylhydrazones.

Key words: chromane, pyruvic acid, dimethylhydrazone, dianion.

I. TAPIA, V. ALCÁZAR et J. R. MORÁN. Can. J. Chem. **68**, 2190 (1990).

On a préparé des chromanes avec des rendements modestes en utilisant le salicylate de méthyle et les dianions des diméthylhydrazones des acides pyruvique ou α-oxobutyrique comme produits de départ.

Mots clés : chromane, acide pyruvique, diméthylhydrazone, dianion.

[Traduit par la revue]

Can. J. Chem. Downloaded from www.nrcresearchpress.com by 195.138.81.100 on 09/07/12
For personal use only.

Introduction

We have recently found that the dianion of pyruvic acid dimethylhydrazone **1** is a strong nucleophile, which reacts readily with alkyl halides and with carbonyl and carboxyl compounds (1). The dimethylhydrazone of pyruvic acid can easily be obtained in ether, as a crystalline solid, from stoichiometric amounts of dimethylhydrazine and the acid. When this substance is treated with MeLi (2 equiv.) in THF/HMPA, a solution of the yellow dianion **1** is generated (Fig. 1).

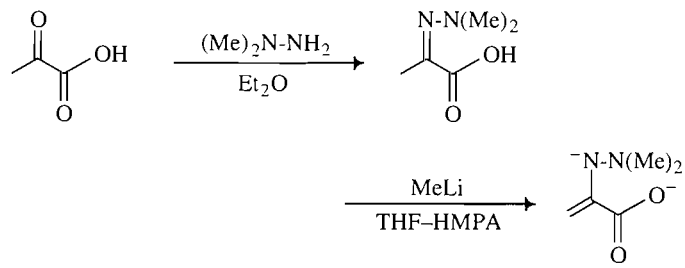

1

FIG. 1

Results and discussion

After acid work-up and treatment with diazomethane, reaction of **1** with methyl benzoate yielded compound **I** (Fig. 2).

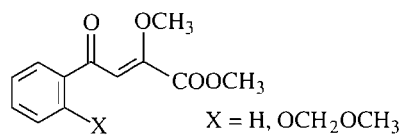

I

FIG. 2

The spontaneous loss of the dimethylhydrazine group under acid conditions made this reaction synthetically attractive for accomplishing chromane synthesis, if an *ortho* hydroxyl group is present in the aromatic ring.

The reaction of methyl salicylate with the dianion **1** is complicated due to the presence of the phenolic hydroxyl group. Protection of this group was readily achieved in basic medium with chloromethyl methyl ether (2) in toluene, affording **2** (3).

This protective group can be cleaved under the acid conditions necessary to cyclize the chromane (Fig. 3).

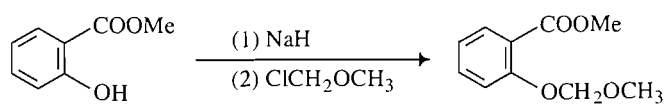

2

FIG. 3

The reaction of **1** (2 equiv.) with protected methyl salicylate, followed by cold acid work-up and diazomethane treatment, yielded the enolic compound **II** (Fig. 4). However, if deprotection of the phenolic group is carried out under harsher acid conditions, the expected chromane **3** (4) is obtained.

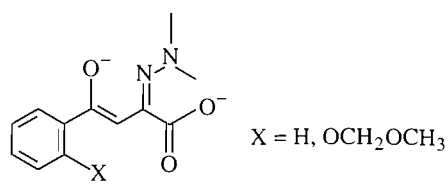

II

FIG. 4

The presence of two carboxymethyl groups on the aromatic ring, as in the case of 4,6-dihydroxyisophthalate (5), allowed the synthesis of both benzopyrane or benzodipyrane rings depending on the amount of the dianion added.

This result can be explained if it is taken into account that the attack on the first ester group yields an acid ketone, which is readily deprotonated by the excess of **1**. The second carboxymethyl group on this electron-rich aromatic ring is less reactive.

Additionally the hindered carboxymethyl group of methyl 2,6-dihydroxybenzoate reacted well with the dianion of the recently crystallized hydrazone, to afford, after diazomethane treatment, the chromane **6**.

We also prepared protected 5-dimethylamine and 5-nitromethyl salicylates; however, in both cases the reaction with the dianion **1** failed to produce the expected chromanes.

To study the synthesis of 3-substituted chromanes, we also used the dimethylhydrazone of α-oxobutyric acid. The reaction of its dianion with the methoxy methyl ether of methyl salicylate led to the expected chromane **7** (7). However we tried to obtain the dimethylhydrazone of phenyl pyruvic acid, an impure and

Printed in Canada / Imprimé au Canada

TABLE 1. Preparation of chromanes

Compound	Chromane	%
3	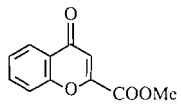	50
4	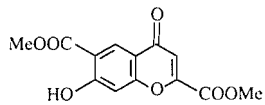	60
5	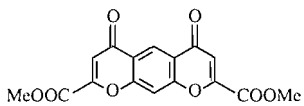	48
6	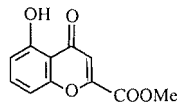	50
7	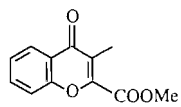	47

unstable compound was formed. Attempts to condense the dianion of this material with protected methyl benzoate yielded only complex mixtures (cf. Table 1).

Experimental

Melting points were obtained in a Kofler hot-stage apparatus and are uncorrected. IR spectra were recorded on a Beckman Acculab II. NMR spectra were recorded on a Bruker WP 200 SY instrument (200 MHz ^{1}H, 50.3 MHz ^{13}C). Chromatographies were run on SiO_2 columns eluting with hexane/EtOAc mixtures of increasing polarity as eluent.

N,N-*Dimethylhydrazone of pyruvic acid*

Dimethylhydrazine (10 g, 0.166 mol) in 100 mL of ether was added dropwise to a solution of 14.6 g (0.166 mol) of pyruvic acid in 50 mL of ether at 0°C. Once addition was finished, the solution was kept at 0°C for 1 h. The solid was removed from the solution by filtration and was crystallized in chloroform/hexane, affording 16.3 g (75%) of pyruvic acid dimethylhydrazone; mp 106°C; IR (Nujol) ν: 1670, 1280, 1210, 860, 820 cm^{-1}; ^{1}H NMR ($CDCl_3$) δ: 2.73 (6H, s), 2.19 (3H, s) ppm; ^{13}C NMR δ: 168 (s), 162 (s), 44 (q, 2C), 20 (q) ppm.

N,N-*Dimethylhydrazone of α-oxobutyric acid*

Dimethylhydrazine (2.94 g, 0.05 mol) in 50 mL of ether was added dropwise to a solution of 5 g (0.05 mol) of α-oxobutyric acid in 50 mL of ether at 0°C. When addition was finished, 5 mL of hexane was added and the solution was kept at 5°C for 1 h, after which a solid precipitated. Filtration of the solid afforded 6.1 g (87%) of α-oxobutyric acid dimethylhydrazone; mp 71°C ($CHCl_3$/hexane); IR (Nujol) ν: 1670, 1220, 870, 820 cm^{-1}; ^{1}H NMR ($CDCl_3$) δ: 2.66 (6H, s), 2.48 (2H, q, J = 8 Hz), 0.96 (3H, t, J = 8 Hz) ppm; ^{13}C NMR δ: 171 (s), 162 (s), 44 (q, 2C), 27 (t), 10 (q) ppm.

Condensation of dianion with methyl salicylate derivatives. General procedure

A solution of the dimethylhydrazone of the pyruvic acid (200 mg, 1.53 mmol) in THF (4 mL) and HMPA (6 mL) under nitrogen was treated with MeLi (1.5 M) in hexane at 0°C. As soon as a yellow colour developed in the solution the amount of MeLi was recorded and the same amount was added again. The yellow solution was then treated with the salicyl derivative (0.76 mmol) dissolved in THF (2 mL).

After 1 h, the mixture was added over water and extracted with ether. The aqueous phase was then acidified with 2 N HCl, heated in a water bath for 10 min, and extracted with EtOAc. Esterification with CH_2N_2/Et_2O and chromatography on SiO_2 yielded the pure compounds.

*2-Methoxycarbonyl-4*H*-1-benzopyran-4-one*, **3**: mp 120°C (lit. (4) mp 120°C, MeOH); IR (Nujol) ν: 1730, 1650, 1500, 1260, 970, 760 cm^{-1}; ^{1}H NMR ($CDCl_3$) δ: 8.19–7.39 (4H, m), 7.07 (1H, s), 4.01 (3H, s) ppm; ^{13}C NMR δ: 178 (s), 161 (s), 156 (s), 151 (s), 134 (d), 126 (d), 125 (d), 124 (s), 118 (d), 115 (d), 53 (q) ppm. Anal. calcd. for $C_{11}H_8O_4$: C 64.70, H 3.95; found: C 64.52, H 3.83.

*7-Hydroxy-2,6-bis(methoxycarbonyl)-4*H*-1-benzopyran-4-one, chromone*, **4**: mp 197°C (EtOAc/hexane); IR ($CHCl_3$) ν: 3000, 1730, 1650, 1600, 1250 cm^{-1}; ^{1}H NMR ($CDCl_3$) δ: 11.4 (1H, s), 8.74 (1H, s), 7.06 (1H, s), 7.02 (1H, s), 4.01 (6H, s) ppm. Anal. calcd. for $C_{13}H_{10}O_7$: C 56.12, H 3.62; found: C 56.23, H 3.60.

*2,8-Bis(methoxycarbonyl)-4*H*,6*H*-benzo(1,2-b;5,4-b′)dipyran-4,6-dione*, **5**: mp 228°C (lit. (6) mp 225–226°C); IR (Nujol) ν: 3020, 1760, 1680, 1620, 1270, 990, 810, 780 cm^{-1}; ^{1}H NMR (DMSO-d_6) δ: 8.63 (1H, s), 8.10 (1H, s), 6.99 (2H, s), 3.96 (6H, s) ppm. Anal. calcd. for $C_{16}H_{10}O_8$: C 58.19, H 3.05; found: C 58.02, H 3.10.

*5-Hydroxy-2-methoxycarbonyl-4*H*-1-benzopyran-4-one*, **6**: mp 109–110°C (EtOAc/hexane); IR (Nujol) ν: 3000, 1750, 1660, 1280, 980, 810, 770 cm^{-1}; ^{1}H NMR ($CDCl_3$) δ: 12.1 (1H, s), 7.60 (1H, t, J = 9 Hz), 7.04 (1H, s), 7.03 (1H, d, J = 9 Hz), 6.85 (1H, d, J = 9 Hz), 4.02 (3H, s) ppm; ^{13}C NMR δ: 183 (s), 161 (s), 160 (s), 156 (s), 153 (s), 136 (d), 114 (d), 112 (d), 111 (s), 108 (d), 53 (q). Anal. calcd. for $C_{11}H_8O_5$: C 60.00, H 3.66; found: C 59.85, H 3.50.

*2-Methoxycarbonyl-3-methyl-4*H*-1-benzopyran-4-one*, **7**: mp 99°C (EtOAc/hexane); IR (Nujol) ν: 1740, 1650, 1610, 1240, 950, 750 cm^{-1}; ^{1}H NMR ($CDCl_3$) δ: 8.11–7.27 (4H, m), 3.93 (3H, s), 2.29 (3H, s) ppm; ^{13}C NMR δ: 178 (s), 162 (s), 155 (s), 148 (s), 134 (d), 126 (d), 125 (d), 124 (s), 122 (s), 118 (d), 53 (q), 10 (q) ppm. Anal. calcd. for $C_{12}H_{10}O_4$: C 66.05, H 4.62; found: C 66.35, H 4.55.

1. I. TAPIA, V. ALCÁZAR, J. R. MORÁN, and M. GRANDE. Chem. Lett. 697 (1990).
2. C. S. MARVEL and P. K. PORTER. Org. Synth. Coll. Vol. **1**, 366 (1950).
3. T. W. GREENE. Protective groups in organic synthesis. John Wiley & Sons, New York. 1981. p. 92; A. F. KLUGE, K. G. UNTCH, and J. H. FRIED. J. Am. Chem. Soc. **94**, 7827 (1972); J. AUERBACH and S. M. WEINREB. Chem. Commun. 298 (1974).
4. K. R. S. REDDY, G. SRIMANNARAYANA, and N. V. SUBBA RAO. J. Indian Chem. Soc. **63**, 600 (1986).
5. E. SPÄTH, K. KLAGER, and C. SCHLÖSSER. Chem. Ber. **64**, 2206 (1931).
6. J. R. BAUTICK, H. CAIRNS, A. CHAMBERS, R. HAZARD, J. KING, T. B. LEE, and R. MINSHULL. J. Med. Chem. **19**, 817 (1976).
7. M. CLERC-BORY, H. PACHÉCO, and CH. MENTZER. Bull. Soc. Chim. Fr. 1083 (1955).

Can. J. Chem. Downloaded from www.nrcresearchpress.com by 195.138.81.100 on 09/07/12
For personal use only.

Étude structurale d'une imidazolylcétone l'isopropyl-1-phényl-2-diaza-1,3-one-6-bicyclo[3,3,0]octène-2

JEAN-PIERRE REBOUL, PIERRE BROUANT ET JACQUES BARBE[1]

Groupe d'études et de recherches en chimie thérapeutique organique et physique, Faculté de pharmacie, 27 Boulevard jean-Moulin, 13385 Marseille CEDEX 5, France

CLAUDE CARANONI

Laboratoire de physique cristalline associé au Centre national de la recherche scientifique, Unité de recherche associée n° 797, Faculté des sciences et techniques Saint-Jérôme, Avenue Escadrille Normandie-Niémen, 13397 Marseille CEDEX 13, France

CATHERINE SOULA, ALAIN MARSURA, FRANÇOIS THOMASSON ET CUONG LUU-DU

Groupe de pharmacochimie, Faculté de pharmacie, Domaine de la Merci, 38700 La Tronche, France

ET

GÉRARD PEPE

Centre de recherche sur les mécanismes de la croissance cristalline, Université d'Aix-Marseille III, Campus Luminy, Case 913, 13288 Marseille CEDEX 2, France

Reçu le 15 février 1990

JEAN-PIERRE REBOUL, PIERRE BROUANT, JACQUES BARBE, CLAUDE CARANONI, CATHERINE SOULA, ALAIN MARSURA, FRANÇOIS THOMASSON, CUONG LUU-DUC et GÉRARD PEPE. Can. J. Chem. **68**, 2192 (1990).

La structure à l'état solide de l'isopropyl-1-phényl-2-diaza-1,3-one-6-bicyclo[3,3,0]octène-2 a été déterminée par diffraction des rayons X (a = 10,039(3) Å; b = 8,683(3) Å; c = 15,505(6) Å; β = 90,72(9)°; $P2_1/c$; R = 0,047). Cette structure a été comparée, d'une part, à celle d'autres (Δ-2)-imidazolines différemment substituées et, d'autre part, à la géométrie moléculaire de la substance étudiée en solution par spectroscopie de résonance magnétique nucléaire du proton. Si la structure de l'imidazolylcétone cyclique considérée est la même tant à l'état solide qu'en solution, en revanche, elle diffère notablement de celles des imidazolines apparentées.

Mots clés : (Δ-2)-imidazolines, structure cristalline, RMN, conformations.

JEAN-PIERRE REBOUL, PIERRE BROUANT, JACQUES BARBE, CLAUDE CARANONI, CATHERINE SOULA, ALAIN MARSURA, FRANÇOIS THOMASSON, CUONG LUU-DUC, and GÉRARD PEPE. Can. J. Chem. **68**, 2192 (1990).

The solid state configuration of 1-isopropyl-2-phenyl-1,3-diaza-6-one-bicyclo[3.3.0]oct-2-ene was determined from X-ray diffraction data (a = 10.039(3) Å; b = 8.683(3) Å; c = 15.505(6) Å; β = 90.72(9)°; $P2_1/c$; R = 0.047). This structure is compared to those of three other related (Δ-2)-imidazolines. Molecular structure in solution was investigated by ^{1}H nuclear magnetic resonance spectroscopy. Results clearly indicate that the title compound has the same structure in the solid state as in solution. On the contrary, this configuration differs appreciably from those of other (Δ-2)-imidazolines considered in this report.

Key words: (Δ-2)-imidazolines, crystal structure, NMR, conformations.

Introduction

Il existe plusieurs voies de synthèse pour accéder aux (Δ-2)-imidazolines. Certaines font appel à une hétérocylisation à partir de l'éthylènediamine (1, 2); d'autres utilisent des substrats divers : amidines (3) ou benzyloxy-guanidines (4). Cependant, parmi les méthodes proposées, seule celle développée par Marsura *et al.* (5) permit l'accès aux (Δ-2)-imidazolines différemment substituées. On a pu ainsi disposer de différentes molécules dont l'étude structurale présente un intérêt en raison de l'isomérie possible.

Ainsi, ont été successivement étudiées l'isopropyl-1-diphényl-2,4-pivaloyl-5-(Δ-2)-imidazoline **1** (6), la benzyl-1-diphényl-2,4-acétyl-5-(Δ-2)-imidazoline **2** et l'isopropyl-1-diphényl-2,4-benzoyl-5-(Δ-2)-imidazoline **3** (7).

Le travail présenté concerne une molécule apparentée : l'isopropyl-1-phényl-2-diaza-1,3-one-7-bicyclo[3,3,0]octène-2, **4**, schématisée sur la figure 1. On a voulu en comparer la structure cristalline tant, d'une part, à la structure en phase dissoute que, d'autre part, à la structure cristalline des autres (Δ-2)-imidazolines antérieurement étudiées.

1. Auteur à qui toute correspondance doit être adressée.

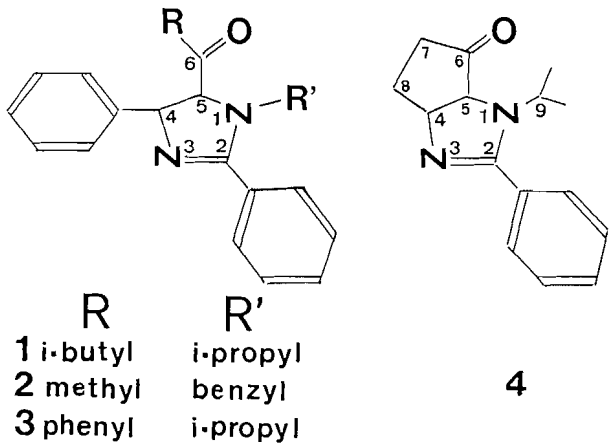

	R	R'
1	i-butyl	i-propyl
2	methyl	benzyl
3	phenyl	i-propyl

4

FIG. 1. Formules et numérotation.

Partie expérimentale

1. Synthèse : méthode générale (5)

On ajoute goutte à goutte une solution de *N*-isopropyl-benzamidine (0,012 mol) dans la triéthylamine (30 mL) à une solution refroidie à 0°C de cétone-α,β-éthylénique-α-bromée (0,01 mol) dans le ben-

Can. J. Chem. Downloaded from www.nrcresearchpress.com by 195.138.81.100 on 09/07/12
For personal use only.

Can. J. Chem. Downloaded from www.nrcresearchpress.com by 195.138.81.100 on 09/07/12
For personal use only.

TABLEAU 1. Données cristallographiques

Formule :	$C_{15}N_2H_{18}O$
Dimensions du cristal, mm :	0,16 × 0,16 × 0,16
Densité mesurée (Flottaison), D_m, g cm^{-3} :	1,18(2)
Densité calculée, D_c, g cm^{-3} :	1,19
Masse moléculaire relative, M_r :	242,3
Système cristallin :	Monoclinique
Groupe d'espace :	$P2_1/c$
Dimensions de la maille, a, Å :	10,039(3)
b, Å :	8,683(3)
c, Å :	15,505(6)
β, deg :	90,72(9)
Volume de la maille, Å^3 :	1351,4(5)
Nombre de molécules par maille, Z :	4
Coefficient d'absorption linéaire μ (MoKα̃), mm^{-1}	0,08
Nombre total d'électrons dans la maille, $F(000)$:	520
Limites angulaires en θ :	1,5–24
Nombre total des mesures (h = −11–11, k = 0–9, l = 0–17) :	4945
Nombre de réflexion indépendantes non observées :	94
Nombre de mesures avec $I > 3\sigma(I)$ utilisées pour la résolution et les affinements :	1504
Pics résiduels sur Fourier-Différence, maximum :	+0,3
minimum :	−0,25
Facteur résiduel, $R = \Sigma\|\|F_o\|-\|F_c\|\|/\Sigma\|F_o\|$:	0,047
Facteur résiduel pondéré, $R_w = [\Sigma w(\|F_o\|-\|F_c\|)^2/\Sigma wF_o^2]^{1/2}$:	0,041
Variation sur erreur maximum, $(\|s/\sigma\|)$max :	0,90
Erreur sur une observation de poids unitaire, $S = [\Sigma w(\|F_o\|-\|F_c\|)^2/(m-n)]^{1/2}$ avec m = nombre de réflexions utilisées, n = nombre de paramètres affinés :	0,90

zène anhydre (20 mL). On agite le tout 24 h à température ambiante, puis 1 h à la température de reflux de la triéthylamine. On filtre, on évapore sous vide et le résidu est repris par du chloroforme. On lave plusieurs fois la phase chloroformique à l'eau, on la sèche sur sulfate de sodium anhydre et on l'évapore. Le résidu, repris par le minimum d'éther, cristallise à 4°C et présente une phase cristalline stable à la température ordinaire.

T_f(**4**) : 132°C; Rdt : 44%. Analyse (valeurs théoriques) : C %, 74,21 (74,35); N %, 11,34 (11,56); H %, 7,44 (7,49).

2. Radiocristallographie

Les données cristallographiques de **4** sont rapportées dans le tableau 1.

Les monocristaux ont été obtenus par évaporation lente à 273 K d'une solution saturée dans le chloroforme. La maille et le groupe de symétrie ont été déduits de l'analyse de clichés de diffraction effectués en chambre de précession. L'absence systématique des réflexions du type $k = 2n + 1$ sur $0k0$ et $l = 2n + 1$ sur $h0l$ conduit au groupe d'espace $P2_1/c$. Les paramètres cristallins ont été affinés sur un diffractomètre automatique 4 cercles CAD4 Enraf Nonius à monochromateur de graphite (λ (MoKα̃) = 0,7107 Å) à l'aide de 25 réflexions indépendantes à 293 K en balayage θ/2θ avec une vitesse de 10°/min et une amplitude θ = (2,75 + 1,25 tg θ). La densité mesurée par flottaison d'un monocristal dans un mélange benzène/tétrachlorure de carbone conduit à admettre la présence de quatre molécules dans la maille. Trois réflexions de référence, de variation inférieure à 3%, ont été contrôlés toutes les 75 réflexions. Les intensités mesurées ont été corrigées des facteurs de Lorentz et de polarisation. Aucune correction d'absorption n'a été effectuée. La structure a été résolue par les méthodes directes à l'aide du programme SHELX (8). Les facteurs de structure normalisés $E > 1,2$ ont été retenus pour la détermination de phase. La carte de densité électronique correspondant aux meilleurs figures de mérite fait apparaître l'ensemble des atomes de la molécule.

L'affinement de la structure a été conduit par minimisation par moindre carré de la fonction $\Sigma w(|F_o|-|F_c|)^2$ à l'aide du programme SHELX. Les facteurs de diffusion de Cromer et Mann (9) ont été utilisés pour les atomes d'azote, de carbone et d'oxygène. Les atomes autres que ceux d'hydrogène ont été affectés de facteurs de température isotropes, ce qui a conduit à un facteur résiduel de 0,15. L'usage de facteurs anisotropes de température a permis d'atteindre un facteur résiduel de 0,08. L'introduction des atomes d'hydrogène dans une position préalablement calculée (distance de 1,08 Å et angle dépendant de l'hybridation des atomes porteurs), suivie d'un cycle d'affinement, a conduit à un facteur résiduel final de 0,047. Les valeurs des facteurs de diffusion données par Stewart, Davidson et Simpson (10) ont été appliquées aux atomes d'hydrogène. Le nombre de paramètres affinés pour la structure est de 235. Le schéma de pondération est $w = 1/(\sigma^2(F_o) + 0,02\ F_o^2)$.

3. Résonance magnétique nucléaire du proton

Les spectres ont été enregistrés à température ambiante sur un spectromètre Bruker AC 200 FT fonctionnant à 200,132 MHz (UFR de Pharmacie de Grenoble). L'acquisition est en mode FT et la détection en mode quadrature. Les spectres ont été enregistrés dans 16 K points,

2. Les tableaux suivants sont disponibles : facteurs thermiques anisotropes, facteurs de structure observés et calculés, coordonnées atomiques des atomes d'hydrogène, distances et angles concernant les atomes d'hydrogène, plans moyens des différents cycles contenus dans la molécule. On peut les acheter en s'adressant au Dépôt des données non publiées, ICIST, Conseil national de la recherche du Canada, Ottawa (Ontario), Canada K1A 0S2.

On peut également se procurer les tableaux de coordonnées atomiques des atomes d'hydrogène, et de distances et angles concernant les atomes d'hydrogène, en s'adressant au directeur, Cambridge Crystallographic Data Centre, University Chemical Laboratory, Lensfield Road, Cambridge CB2 1EW, Royaume-Uni.

Can. J. Chem. Downloaded from www.nrcresearchpress.com by 195.138.81.100 on 09/07/12
For personal use only.

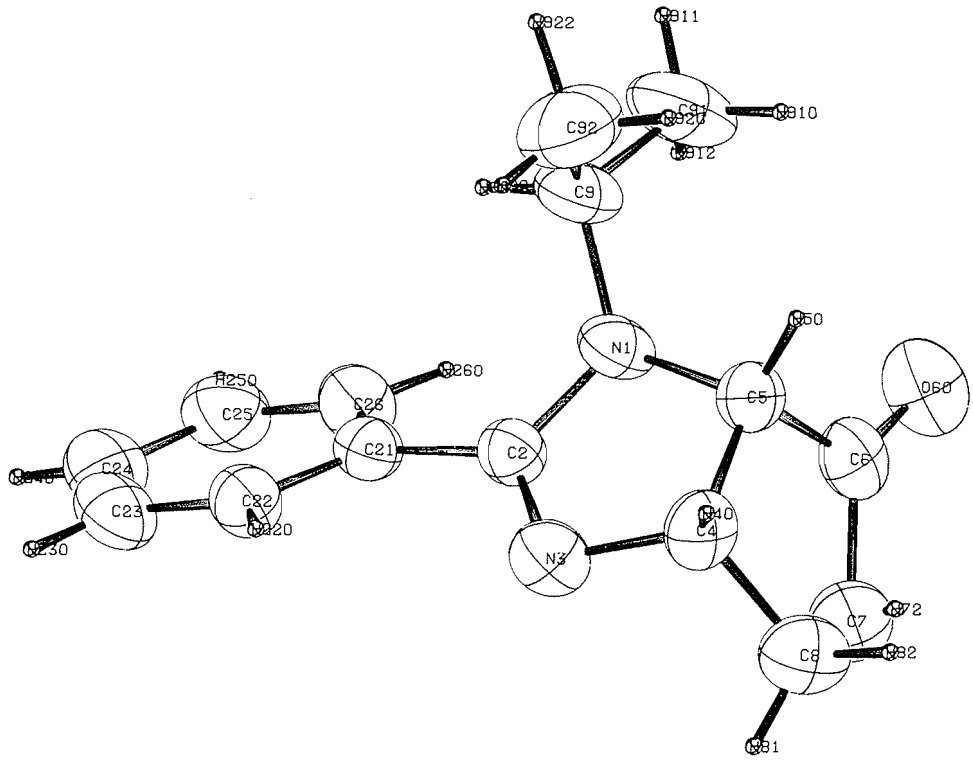

FIG. 2. Représentation géométrique de **4** et numérotation complémentaire.

TABLEAU 2. Coordonnées atomiques et déviation standard

Atome	x	y	z	B_{eq} (Å^2)*
O(60)	0,5654(1)	0,0374(2)	0,9069(1)	5,4
N(1)	0,7483(1)	−0,2489(2)	0,8965(1)	3,7
N(3)	0,9091(1)	−0,2311(2)	1,0043(1)	4,0
C(2)	0,8809(2)	−0,2646(2)	0,9244(1)	3,4
C(4)	0,7828(2)	−0,1899(2)	1,0463(1)	3,9
C(5)	0,6774(2)	−0,1854(2)	0,9716(1)	3,7
C(6)	0,6506(2)	−0,0139(2)	0,9558(1)	3,8
C(7)	0,7468(2)	0,0778(2)	1,0102(1)	4,9
C(8)	0,7864(2)	−0,0270(2)	1,0850(1)	4,9
C(9)	0,6840(2)	−0,3652(3)	0,8397(1)	4,5
C(21)	0,9859(2)	−0,3039(2)	0,8613(1)	3,4
C(22)	1,0969(2)	−0,3886(2)	0,8879(1)	4,0
C(23)	1,2009(2)	−0,4117(2)	0,8311(1)	4,7
C(24)	1,1949(2)	−0,3520(2)	0,7477(1)	4,9
C(25)	1,0837(2)	−0,2702(2)	0,7203(1)	5,0
C(26)	0,9799(2)	−0,2457(2)	0,7766(1)	4,2
C(91)	0,5718(2)	−0,2921(4)	0,7870(2)	6,5
C(92)	0,6393(4)	−0,5066(3)	0,8903(2)	7,2

*Les atomes affinés de façon anisotrope sont donnés sous la forme d'équivalents isotropes définis ci-dessous :

$$B_{eq} = 4/3[a^2B(1,1) + b^2B(2,2) + c^2B(3,3) + ab(\cos\gamma)B(1,2) + ac(\cos\beta)B(1,3) + bc(\cos\alpha)B(2,3)]$$

sur 2200 Hz. La température était de 297 K et on a utilisé le tétraméthylsilane comme référence interne.

Les mesures d'effet Overhauser nucléaire (eOn) ont été obtenues à partir d'échantillons dégazés (10 Torr, 24 h) (1 Torr = 133,3 Pa), dans C_6D_6 comme solvant, après irradiation sélective des signaux protons des méthyles du groupement *N*-isopropyl avec un temps d'irradiation d'environ 5 × $T1$. La puissance d'irradiation des protons était de 34 dB avec un temps de répétition de 10 s; 30 transients ont été collectés. Aucune correction exponentielle du spectre n'a été nécessaire.

TABLEAU 3. Longueurs des liaisons en Å et déviation standard

Atomes	Longueur	Atomes	Longueur
N(1)—C(2)	1,401(2)	C(6)—C(60)	1,220(2)
N(1)—C(5)	1,478(2)	C(7)—C(8)	1,523(3)
N(1)—C(9)	1,483(2)	C(9)—C(91)	1,523(3)
C(2)—N(3)	1,299(2)	C(9)—C(92)	1,528(3)
C(2)—C(21)	1,487(2)	C(21)—C(22)	1,393(2)
N(3)—C(4)	1,476(2)	C(21)—C(26)	1,487(2)
C(4)—C(5)	1,560(2)	C(22)—C(23)	1,388(2)
C(4)—C(8)	1,537(2)	C(23)—C(24)	1,394(3)
C(5)—C(6)	1,532(3)	C(24)—C(25)	1,385(3)
C(6)—C(7)	1,503(3)	C(25)—C(26)	1,383(3)

Résultats et discussion

La représentation de la molécule est donnée sur la figure 2.

Les coordonnées des atomes autres que ceux d'hydrogène sont données dans le tableau 2, les longueurs de liaison dans le tableau 3, les angles de liaison dans le tableau 4 et quelques angles de torsion significatifs dans le tableau 5.

Le cycle central imidazoline montre une planéité satisfaisante si on considère la valeur de la déviation maximum (D_{max}) des atomes de ce cycle à leur plan moyen qui est de 0,052(2) Å (tableau 6).

Cependant, une meilleure planéité est trouvée si on tient uniquement compte des atomes C(4)—N(3)—C(2)—N(1) définissant un plan moyen (A'). On note ici, en effet, une déviation maximum de 0,013(2) Å. La distance de 0,139(2) Å de l'atome C(5) à ce plan correspond à une légère forme enveloppe du cycle imidazoline.

Afin de situer les substituants par rapport au cycle central imidazoline, on a envisagé, outre le plan moyen (A) dont il vient

Can. J. Chem. Downloaded from www.nrcresearchpress.com by 195.138.81.100 on 09/07/12
For personal use only.

TABLEAU 4. Angles des liaisons en degré et déviation standard

Atomes	Angles	Atomes	Angles
C(2)—N(1)—C(5)	105,0(1)	C(7)—C(6)—O(60)	126,6(2)
C(2)—N(1)—C(9)	121,4(1)	C(6)—C(7)—C(8)	105,6(2)
C(5)—N(1)—C(9)	120,8(1)	C(4)—C(8)—C(7)	104,5(2)
N(1)—C(2)—N(3)	117,8(2)	N(1)—C(9)—C(91)	110,3(2)
N(1)—C(2)—C(21)	119,8(1)	N(1)—C(9)—C(92)	111,8(2)
N(3)—C(2)—C(21)	122,2(1)	C(91)—C(9)—C(92)	113,1(2)
C(2)—N(3)—C(4)	107,3(1)	C(2)—C(21)—C(22)	119,8(1)
N(3)—C(4)—C(5)	105,0(1)	C(2)—C(21)—C(26)	120,7(1)
N(3)—C(4)—C(5)	112,3(2)	C(22)—C(21)—C(26)	119,3(2)
C(5)—C(4)—C(8)	106,1(2)	C(21)—C(22)—C(23)	119,7(2)
N(1)—C(5)—C(4)	104,2(1)	C(22)—C(23)—C(24)	120,7(2)
N(1)—C(5)—C(6)	108,8(1)	C(23)—C(24)—C(25)	120,0(2)
C(4)—C(5)—C(6)	105,1(1)	C(24)—C(25)—C(26)	119,7(2)
C(5)—C(6)—C(7)	108,4(2)	C(21)—C(26)—C(25)	120,6(2)
C(5)—C(6)—O(60)	125,1(2)		

TABLEAU 5. Quelques angles de torsion en degré et déviation standard

N(1)—C(2)—N(3)—C(14)	2,7(2)	C(5)—N(1)—C(9)—C(92)	−56,4(2)
N(1)—C(2)—C(21)—C(22)	−149,6(2)	C(5)—C(4)—N(3)—C(2)	−7,2(1)
N(1)—C(2)—C(21)—C(26)	35,8(1)	C(6)—C(5)—N(1)—C(2)	104,3(2)
N(1)—C(5)—C(4)—N(3)	8,9(1)	C(6)—C(5)—N(1)—C(9)	−113,8(2)
C(2)—N(1)—C(9)—C(91)	−153,9(2)	C(6)—C(5)—C(4)—N(3)	−105,4(1)
C(2)—N(1)—C(9)—C(92)	79,3(2)	C(6)—C(5)—C(4)—C(8)	−13,6(1)
N(3)—C(2)—N(1)—C(9)	−138,2(2)	C(7)—C(6)—C(5)—N(1)	−104,6(2)
N(3)—C(2)—C(21)—C(22)	36,4(1)	C(7)—C(6)—C(5)—C(4)	6,6(1)
N(3)—C(2)—C(21)—C(26)	−138,3(2)	C(7)—C(8)—C(4)—N(3)	85,7(2)
C(4)—C(5)—N(1)—C(2)	−7,4(1)	C(7)—C(8)—C(4)—C(5)	−28,4(1)
C(4)—C(5)—N(1)—C(9)	−134,5(2)	C(8)—C(4)—C(3)—C(2)	−122,1(2)
C(4)—C(5)—C(6)—C(7)	6,6(1)	C(8)—C(4)—C(5)—N(1)	127,9(2)
C(4)—C(5)—C(6)—O(60)	−173,5(2)	C(8)—C(4)—C(5)—C(6)	13,6(1)
C(5)—N(1)—C(2)—N(3)	8,3(1)	C(8)—C(7)—C(6)—C(5)	−24,5(1)
C(5)—N(1)—C(2)—C(21)	−170,9(2)	C(9)—N(1)—C(2)—C(21)	47,5(1)
C(5)—N(1)—C(9)—C(91)	70,4(2)	O(60)—C(6)—C(8)—N(1)	75,3(1)

TABLEAU 6. Comparaison structurale des composés **1, 2, 3, 4** (déviation maximum en Å par rapport au plan moyen A* et τ entre les plans moyens* en degré)

	1(6)	**2**(7)	**3**(7)	**4**
Déviation maximum (Å)	0,089(8)	0,069(3)	0,020(5)	0,052(2)
τ(A,B)	34,1(6)	42,0(3)	49,8(6)	34,1(2)
τ(A,C)	110,2(9)	36,5(3)	69,8(6)	40,3(2)
τ(A,D)	176(3)	101,9(3)	147,0(2)	139,7(4)
τ(A,E)	73,1(8)	85,8(4)	124,5(8)	

*Les plans moyens sont ainsi définis : (A), C(4)—N(3)—C(2)—N(1)—C(5); (B), C(21)—C(22)—C(23)—C(24)—C(25)—C(26); (C), C(5)—C(6)—C(7)—O(60); (D), N(1)—C(9)—H(90); (E); cycle benzénique fixé en position 1 chez **1, 2** et **3**.

d'être question, les différents plans moyens (B), (C) et (D) définis dans le tableau 6.

D'une manière générale, pour préciser les positions relatives de deux plans moyens (X) et (Y), on définit un angle de torsion τ(X, Y) à partir de deux paires de pseudo-atomes, chaque paire étant spécifique d'un plan moyen donné. Ainsi pour le plan moyen (X) on considère comme pseudo-atomes, d'une part, le centroïde CX2 des atomes définissant (X) et, d'autre part, l'éxtrémité CX1 d'un vecteur dont le module vaut 1 Å, qui est perpendiculaire à (X) et qui passe par le centroïde CX2. En ce qui le concerne, le plan moyen (Y) est caractérisé par une autre paire de pseudo-atomes CY1 et CY2. L'angle τ(X, Y) est alors l'angle de torsion entre les pseudo-atomes CX1—CX2—CY2—CY1.

On a calculé les angles de torsion entre le plan moyen (A) du cycle central imidazoline et les différents plans moyens (B), (C) et (D). Les résultats sont donnés dans le tableau 6.

D'autre part, le calcul de la position du centroïde de chacun des quatre plans moyens (A), (B), (C) et (D) montre que si (A) est pris pour référence, le centroïde de (B) se trouve en dessous

Can. J. Chem. Downloaded from www.nrcresearchpress.com by 195.138.81.100 on 09/07/12
For personal use only.

TABLEAU 7. Déplacements chimiques (δ en ppm/TMS), constantes de couplage (J en Hz), multiplicité* et mesure des effets A.S.I.S. de quelques protons significatifs

Solvants	C_6H_5	H(40)	H(50)	H(90)	J^3 (H(40)–H(50)	H(70+80)	H(910)–H(912)	H(920–H(922)	J^3 (H910)–H(912)) ou H(920)–H(922)/H(90))
$CDCl_3$	7,30–7,70 (m)	4,85 (t)	3,80 (d)	3,80*** (sept)	9,07	2,10–2,50 (m)	0,98 (d)	1,28 (d)	6,88
C_6D_6	7,00–7,80 (m)	4,51 (t)	3,26 (d)	3,65 (sept)	8,89	1,60–2,40 (m)	0,60 (d)	1,20 (d)	6,88
$(CD_3)_2CO$	7,40–7,70 (m)	4,85 (m)**	4,02 (d)	3,82 (sept)	9,00	2,00–2,30 (m)	0,98 (d)	1,28 (d)	6,89
$CDCl_3$–C_6D_6	—	+0,34	+0,54	+0,15	—	—	+0,38	+0,08	—

*d = doublet; m = multiplet; t = triplet; sept = septuplet.
**Multiplet complexe dû au couplage avec H(80).
***Signaux comprenant H(50) et H(90) superposés.

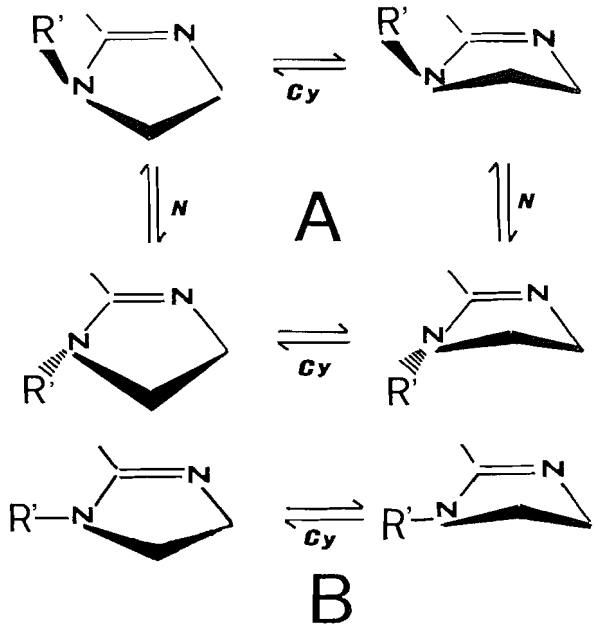

FIG. 3. Processus d'interconversion dans les cas d'azote sp^3 (A) et d'azote sp^2 (B). L'inversion de l'azote est indiquée par N, celle du cycle par Cy.

de (A) à une distance de 0,613(7) Å et le centroïde de (C) se trouve aussi en dessous de (A) mais à une distance de 1,408(3) Å. Pour des raisons stériques, tous les substituants sont ainsi en position *trans* par rapport au cycle central imidazoline.

Quant au plan moyen (B), il révèle avec une déviation maximum de 0,016 Å une planéité satisfaisante du cycle benzénique. L'atome C(2), qui est à 0,144 Å de (B), est considéré comme hors de ce plan.

Comparaison structurale de ***4*** *avec ses analogues* ***1, 2*** *et* ***3*** *en phase solide*

Cette comparaison est faite à l'aide de la déviation maximum des différents atomes à leur plan moyen ainsi que des angles de torsion τ(A,B), τ(A,C), τ(A,D) entre le plan moyen (A) du cycle central imidazoline et les plans (B), (C) et (D) dont les valeurs sont données dans le tableau 6.

De l'analyse des valeurs des déviations maximum, on peut déduire que les quatre composés montrent une conformation plus ou moins plane du cycle imidazoline avec une légère tendance à une forme enveloppe.

La conjugaison du système π du cycle benzénique fixé sur l'atome C(2) avec les électrons de la liaison imine intracyclique C(2)—N(3), se trouve affaiblie comme en témoignent les valeurs relativement élevées de l'angle de torsion τ(A,B).

Afin de comparer par rapport au cycle imidazoline la position relative des substituants isopropyle ou benzyle fixés sur l'atome N(1), on a calculé l'angle de torsion τ(A,D) entre le plan moyen (A) du cycle imidazoline et le plan moyen (D) défini comme le plan passant par les atomes N(1), C(9) et H(90) pour le substituant isopropyle et comme le plan passant par les atomes N(1), C(90) et C(benzylique) dans le cas du substituant benzyle.

En ce qui concerne le groupement carbonyle lié à l'atome C(8), les valeurs de l'angle de torsion τ(A,C) traduisent de grandes variations dans son orientation par rapport au cycle imidazoline.

Enfin, la position relative par rapport au cycle imidazoline du substituant phényle fixé sur l'atome C(4), peut permettre une comparaison des composés **1, 2** et **3**. On a, dans ce but, calculé

Can. J. Chem. Downloaded from www.nrcresearchpress.com by 195.138.81.100 on 09/07/12
For personal use only.

TABLEAU 8. Effet Overhauser nucléaire

Composés	Atomes irradiés	Effet sur H(910)–H(912)	Effet sur H(920)–H(922)
1	H(50)	14	33
3	H(50)	0	50
4	H(80)	6	8
4	H(40)	1,5	3

dans chaque cas l'angle de torsion τ(A,E) entre le plan moyen (A) du cycle imidazoline et le plan moyen (E) calculé à partir des atomes du cycle benzénique du substituant phényle. On n'observe, d'une manière générale, que de faibles variations chez ces angles de torsion.

Comparaison de le structure de **4** *en phase solide et en solution*

Pour ce faire, on a étudié les déplacements chimiques des protons significatifs de **4** en solution dans différents solvants. Les résultats sont rassemblés dans le tableau 7. On a ainsi cherché à préciser l'orientation des protons portés par C(4) et C(5) et à résoudre le problème de la conformation autour de N(1).

En ce qui concerne, tout d'abord, les protons H(910)–H(912) et H(920)–H(922) des groupements méthyles du substituant isopropyle, on remarque qu'ils sont logiquement anisochrones car : (a) d'une part, le doublet électronique libre de N(1) crée une zone d'anisotropie magnétique (11) et (b) d'autre part, le groupement carbonyle apporte une contribution qui est limitée à une portion d'espace (12).

Les valeurs des constantes de couplages J^3 (H(40)–H(50)) données dans le tableau 7 sont en accord avec des observations antérieures (13) concernant la situation *cis* ou *trans* des protons (H(40) et H(50)).

Une géométrie *cis* autour de la jonction C(4)—C(5) est imposée ici par la structure bicyclique de **4**. La valeur de la constante de couplage J^3 (H(40)–H(50)) atteint 9,00 Hz et confirme la valeur moyenne plus faible (5–7 Hz) relevée dans le cas d'une situation *trans* de ces mêmes protons (13). Reste l'orientation du substituant isopropyle, car l'atome d'azote porteur peut être considéré soit dans un état d'hybridation sp^3, soit dans un état d'hybridation sp^2. Les processus d'interconversion attendus sont alors schématisés sur la figure 3.

Il faut noter que la cyclisation entre C(4) et C(5) limite considérablement les processus d'inversion de cycle qui sont notés Cy sur la figure 3. En revanche, deux conformations sont possibles dans le cas où l'azote N(1) est de type sp^3, alors qu'il n'en est qu'une seule si l'azote est de type sp^2. La mesure des effets A.S.I.S. (Aromatic Solvent Induced Shift) qui sont empiriques et d'interprétation aléatoire dans le cas des composés **1, 2** ou **3** car tributaires de la mobilité du groupement carbonyle et donc du plan tournant de référence associé, peut avoir une signification structurale dans le cas de **4** à cause de la géométrie imposée au groupement carbonyle par la cyclisation entre C(4) et C(5). Les valeurs positives enregistrées pour H(40) et H(50) et données dans le tableau 8 confirment bien la position des deux protons en arrière d'un plan orthogonal à la liaison C(6)=O(60) et, de ce fait permet de situer raisonnablement, toujours dans cette positive relative, à la fois le proton H(90) et les protons H(910)–H(912) du groupe isopropyle. Les protons H(920)–H(922) montrent, quant à eux une valeur voisine de zéro et seraient donc proches du plan, voire même dans le plan indiqué. Ces résultats sont plutôt en faveur d'une géométrie tétragonale de l'azote N(1) car c'est la seule susceptible d'expliquer les effets mesurés sur les groupes de protons. En effet, une géométrie trigonale de N(1) aurait pour conséquence de rejeter certains des protons observés en avant du plan de référence et des valeurs négatives seraient donc au contraire obtenues.

On a enfin effectué la mesure des effets Overhauser nucléaires. Les résultats de eOn-1D sont résumés pour l'essentiel dans le tableau 8.

On peut y constater tout d'abord que les pourcentages d'effet dans le cas de **4** sont très inférieurs à ceux observés dans le cas de **1** et de **3**, avec une intensité toujours supérieure pour les protons H(920)–H(922). Ces résultats qui sont en faveur de l'hypothèse pour **4** d'un azote N(1) tétragonal et d'un substituant isopropyle dans une situation conformationnelle quasiment identique à celle observée pour **1** et **3**, sont complémentaires des précédents. De plus, la conformation privilégiée du groupement isopropyle implique un alignement approximatif de l'un des méthyles avec H(40) et H(50). Dans ces conditions, par suite d'un effet «trois spins» (14), la saturation des protons H(920)–H(922) du méthyle doit conduire à un effet positif sur H(50) et négatif sur H(40) alors que la saturation sélective de l'autre groupe méthyle formant un triangle avec H(40) et H(50), doit montrer une augmentation du signal de H(50) mais pratiquement pas d'effet sur H(40). Les expériences d'irradiations sélectives ont confirmé ces prévisions.

Conclusion

Il apparaît, à la lumière des résultats de la cristallographie et de la RMN du proton que l'isopropyl-1-phenyl-2-diaza-1,3-one-6 bicyclo[3,3,0]octène-2 montre la même structure moléculaire en phase solide ou en solution dans les solvants apolaires. Il est également acquis que l'azote N(1) est hybridé sp^3 dans les trois structures imidazolines avec une conformation privilégiée du groupement isopropyle situé au dessus du plan moyen du cycle imidazoline. Cependant, la géométrie de la molécule diffère sensiblement de celles antérieurement décrites pour des (Δ-2)-imidazolines apparentées.

1. T. SAEGUSA et Y. ITO. Synthesis, 291 (1975).
2. G. LEVESQUE, J. C. GRESSIER et M. PROUST. Synthesis, 963 (1981).
3. J. L. IMBACH, R. JACQUIER, J. M. LACOMBE et G. MAURY. Bull. Soc. Chim. Fr. 1052 (1971).
4. M. M. CAMPBELL, A. C. CAMPBELL, A. PEACE, A. PICK et G. F. WOODS. J. Chem. Soc. Chem. Commun. **17**, 1164 (1985).
5. A. MARSURA, C. LUU DUC et G. GELLON. Synthesis, 537 (1985).
6. P. BROUANT, J. BARBE, A. MARSURA et C. LUU DUC. Acta Crystallogr. Sect. C : Cryst. Struct. Commun. **C41**, 1309 (1985).
7. P. BROUANT, J. BARBE, A. MARSURA, C. SOULA et C. LUU DUC. Can. J. Chem. **65**, 2217 (1987).
8. G. M. SHELDRICK. SHELX. Programme pour la détermination de structures cristallines. Univ. Cambridge, U.K. (1976).
9. D. T. CROMER et J. B. MANN. Acta Crystallogr. Sect. A : Cryst. Phys. Diffr. Theor, Gen. Crystallogr. **A24**, 321 (1968).
10. R. F. STEWART, E. R. DAVIDSON et W. T. SIMPSON. J. Chem. Phys. **42**, 3175 (1965).
11. W. B. JENNINGS. Chem. Rev. **75**, 307 (1975).
12. P. L. SOUTHWICK, J. A. FITZGERALD et G. E. MILLIMAN. Tetrahedron Lett. **18**, 1247 (1965).
13. A. MARSURA, C. LUU DUC et R. NARDIN. Magnt. Reson. Chem. **23**, 639 (1985).
14. A. E. DEROME. Modern NMR techniques for chemistry research. Organic Chemistry Series. Vol. 6. *Edité par* J. E. Baldwin. Pergamon Press, Oxford. 1987.

Modelling complex solution equilibria. I. Fast, worry-free least-squares refinement of equilibrium constants

PIERRE G. POTVIN

Department of Chemistry, York University, 4700 Keele Street, North York, Ont., Canada M3J 1P3

Received May 11, 1990

PIERRE G. POTVIN. Can. J. Chem. **68**, 2198 (1990).

The methods of Steepest Descent, Gauss–Newton (first-order Taylor series) and Newton–Raphson (second-order Taylor series) least-squares iteration were examined in the context of the refinement of estimated equilibrium constants β in solution. Under certain conditions, all three can produce corrections to the parameters that overshoot the global minimum and diverge therefrom, owing to the shape of the parameter surface. The latter two methods are problematic when the β parameters are overestimated, or when their logarithms are underestimated, whence a useful approximation to the analytical second and higher derivatives was found for any data type. This reduces an exact, infinite-order Taylor series expression of any observable to a simple first-order expression. As illustrated with experimental pH data, faster, more reliable refinement results without overshoot or divergence problems, and without resort to computationally onerous algorithms, such as the Marquardt–Levenberg, Fletcher–Powell, or Hartley–Wentworth methods.

Key words: equilibrium constants, least-squares, Gauss–Newton, complex solution equilibria.

PIERRE G. POTVIN. Can. J. Chem. **68**, 2198 (1990).

Dans le contexte du calcul des constantes d'équilibre β ou autres paramètres déterminant un équilibre complexe en solution, les méthodes d'itération sur les moindres carrés dites Steepest-Descent, Gauss–Newton (basée sur une série de Taylor de premier ordre) et Newton–Raphson (basée sur une série de Taylor de second ordre) sont hazardeuses. Selon la nature de la surface paramétrique, chacune peut donner des corrections aux paramètres β qui survoltent le minimum global et/ou mènent à la divergence. Avec les deux dernières méthodes, ces problèmes n'existent que lorsque les constantes β sont sur-estimées ou que leurs logarithmes sont sous-estimés. Dans ces cas, une description éxacte de toute donnée expérimentale par une série de Taylor d'ordre infini peut alors être réduite à une expression de premier ordre, grâce à l'application d'une bonne approximation aux dérivés d'ordres supérieurs. Telles que calculées pour des données expérimentales de pH, les corrections qui en résultent ont un comportement presqu'idéal, sans divergence, qui rend le calcul plus fiable et plus rapide, sans recours à des algorithmes onéreux tels que ceux de Marquardt–Levenberg, de Fletcher–Powell ou de Hartley–Wentworth.

Mots clés : constantes d'équilibre, moindres carrés, Gauss–Newton, équilibres en solution complexes.

Can. J. Chem. Downloaded from www.nrcresearchpress.com by 195.138.81.100 on 09/07/12
For personal use only.

Introduction

The advent of computers has ushered in a large number of programmes to solve complex equilibrium problems where earlier, linear and graphical treatments had failed or could not be applied (for a review, see ref. 1). Since the publication of GAUSS (2), most have been based on the Gauss–Newton (G–N) iterative method of least-squares. Problems inherent in this and the seldom-used Newton–Raphson (N–R) second-order variant (3) are overshoot of the minimum and divergent behaviour when corrections to the initial estimates of the experimental parameters are calculated. These problems can be traced to two sources. One is purely operational: numerically approximated derivatives, still used in some recent programmes (4–6), sometimes lead to matrices with near-zero determinants and, thus, ill-behaved inverses. This can easily be avoided with analytical (exact) derivatives even with single-precision computer arithmetic. The programme LEAST (7) made the first use of exact derivatives of any kind, in this case of the mass-balance sums (an explicit function), but statistical rigour demands the use of derivatives of a non-explicit function (*e.g.* the measured quantity itself). Such were implemented only recently in SUPERQUAD (8) to treat emf data, although the approach had been outlined earlier (9).

The other source of overshoot and divergence is the complex shape of the parameter surface itself, whereas the G–N and N–R methods are based on Taylor series expressions of the surface that are truncated at first- or second-order terms. To counter these problems of either or both types, several algorithms have been incorporated in the basic G–N method. Harley's and Wentworth's algorithms seek to "optimize" the corrections to produce the closest approach to the minimum under the assumption that the parameter surface is approximately parabolic near the minimum (10). The programme BEST makes the same assumption in a crude, heuristic search of the parameter surface (11). The Marquardt–Levenberg technique (12), imported from optic design, empirically and iteratively modifies the "normal" G–N equations in cases of divergence until there is sufficient second-order character to avoid it. This has become a standard-issue tool of several of the newer published (4, 5, 8, 13) and commercial curve-fitting programmes. It is powerful yet largely unnecessary for equilibrium problems when exact derivatives are available. The Fletcher–Powell algorithm (14) is an approximative N–R approach that avoids the matrix inversions. All of these are computationally expensive procedures that can be readily avoided with the approach described herein.

Part 1

Experimental section

pH data were obtained during triplicate titrations at 25 ± 0.1°C by 0.0997 ± 0.001 M NaOH of 3.50 ± 0.05 mL aliquots of 3.872 ± 0.04 × 10^{-3} M solutions of ligand **1** (17) in 0.10 M NaCl containing 1.908 ± 0.001 × 10^{-2} M HCl and 3.813 ± 0.04 × 10^{-3} M $Zn(NO_3)_2$. The titration was performed in a jacketed vessel with a Metrohm 535 buret under the control of a Metrohm 636 titro-processor, using variable volume (≥5 μL) increments suited to the instantaneous pH–volume slope and a 20 s delay before recording the volume and pH. The pH was measured using a Metrohm combination glass microelectrode, with an accuracy of ±0.002 pH units. At pH > 8.3, precipitation of $Zn(OH)_2$ occurred. Previous experiments over a 2.0–10.0 pH range (62 points) in the absence of metal had established that only 3 equiv. of base were consumed to deprotonate the ligand. Using the convention $\log \beta_{ijk} = [H_iZn_jL_k^{(i+2j)+}]/[H^+]^i[Zn^{2+}]^j[L]^k$, the

Can. J. Chem. Downloaded from www.nrcresearchpress.com by 195.138.81.100 on 09/07/12
For personal use only.

following log protonation constants were used with the Zn^{2+} data: $\log \beta_{101} = 7.604 \pm 0.012$, $\log \beta_{201} = 14.396 \pm 0.011$, $\log \beta_{301} = 20.510 \pm 0.011$. The value for pK_w ($-\log \beta_{-100}$) was 13.78 ± 0.03, in accord with tabled values (19).

The Zn^{2+} data within the pH range of 2.0 to 8.3 (23–24 data points per titration) were treated by the FORTRAN-77 programme JACOBI[1] on a VAX 8600 computer, making use of the method described herein. This programme was able to reproduce the literature value for the oxygenation of a μ-hydroxobiscobalt(II) complex of bis-tren from the original data using weighting by the inverse pH–volume slope (11). For the Zn^{2+} data, the calculations used weighting by inverse variances (18) calculated from all sources of experimental error, according to

$$\frac{1}{w_{n,n}} = \sigma_n^2 = \sigma_0^2 + \sum_{k=1}^{n_i} \sigma_k^2 \left(\frac{dF_n}{dP_k}\right)^2$$

where σ_0^2 is the variance in the measurement of the observable, σ_k^2 is the variance of the kth of n_i invariable parameters, and where dF_n/dP_k is the derivative of the nth observable with respect to that parameter as described in the Appendix. A ±5 μL error in titrant volume was included. Numerically, the most important contributors to the variances were the initial volume and titrate concentrations, not because these bore large experimental errors, but because of large derivatives of pH with respect to these. The pH was continuously corrected for changes in ionic strength occasioned during refinement, according to the Avdeef–Bucher procedure (15). The upper pH cut-off was confirmed by checking that $[Zn^{2+}][OH^-]^2$ did not exceed the known K_{sp} for $Zn(OH)_2$. The 12 species considered included $ZnOH^+$ and $Zn(OH)_{2(aq)}$ using literature values (19) for $\log \beta_{-110}$ and $\log \beta_{-210}$ and taking ±0.03 uncertainties in these values. The calculation of the correlation coefficients between the unknown parameters and of their uncertainties of fit followed the procedure of Hamilton (4, 20). The final values of the unknown parameters were $\log \beta_{011} = 3.709 \pm 0.010$, $\log \beta_{-111} = -3.945 \pm 0.010$ and $\log \beta_{111} = 10.622 \pm 0.011$. Alternative models were also tested, i.e. in the absence of one of the complexes or in the presence of other species, such as $(\mathbf{1})Zn(OH)_2$ or octahedral complexes $(\mathbf{1})_2Zn^{2+}$, $(\mathbf{1})_2ZnH^{3+}$, or $(\mathbf{1})_2ZnH^{4+}$, or dimetallic species $(\mathbf{1})Zn_2$. One or more of the following then occurred: (*a*) the standard deviations of the fit became unacceptably high and/or (*b*) the refined log β values for the 1:1 species became unreasonably small and/or (*c*) s became much larger and/or (*d*) the correlation coefficients became significant (>0.9) and/or (*e*) the R-ratio test (4, 20, 21) failed.

Results and discussion

In the process of discovering which species S are present in a mixture of reactants R at equilibrium, one postulates a set of chemically feasible species and one estimates the equilibrium constants that specify their formation from the reactants, according to

$$[S_i]_n = \beta_i \prod_{j=1}^{n_r} [R_j]_n^{a_{i,j}}$$

$$\text{or} \qquad \log [S_i]_n = \log \beta_i + \sum_{j=1}^{n_r} a_{i,j} \log [R_j]_n$$

where $a_{i,j}$ is the number of moles of the jth reactant entering into the formation of the ith species with formation constant β_i. By one convention, the first n_r species are the free reactants themselves. Hence, $\beta_i = 1$, $a_{i,i} = 1$, and $a_{i,j \neq i} = 0$ for $i = 1$ to n_r. This method of defining equilibria through formation constants can be implemented whenever the number of mass-balance sums equals the number of reactants and excludes systems involving ligand substitution equilibria (however, see the accompanying paper for the treatment of such systems).

The total reactant concentrations $[T_j]_n$, one for each of n_r reactants, are known at any nth of n_d data points. With titration data, for example, this involves the initial titrate volume v_0, the titrant increments v_n, and the reactant concentrations $[R_j]^*$ and $[R_j]^+$, in the titrate and titrant, respectively:

$$[T_j]_n = \frac{v_0[R_j]^* + v_n[R_j]^+}{v_0 + v_n}$$

As these totals must at all times agree with the mass-balance sums,

$$[T_j]_n^{\text{calc}} = \sum_{i=1}^{n_s} a_{i,j}[S_i]_n$$

one can know the concentrations of all species at all points, given any set of β values, that will reconcile these two totals. This is performed as described in the Appendix. With known reactant concentrations and some physical measurement that will relate to the concentration of one or more species, iterative adjustments can be made to initial estimates of the unknown β until the resulting species concentrations best reproduce the experimental data. With at least as many measurements as there are unknowns, this refinement is performed by a variety of methods that seek to minimize the sum (s) of the squares of the

$$s = \sum_{n=1}^{n_d} w_{n,n}(O_n - F_n)^2 = (\boldsymbol{O} - \boldsymbol{F})^t \mathbf{w} (\boldsymbol{O} - \boldsymbol{F})$$

differences between observed (O_n) and calculated (F_n) measurements, weighted by estimates of the variances ($1/w_{n,n}$) due to the experimental errors affecting the measurements. Any other parameter, such as $[R]^+$ or $[R]^*$ values, can be similarly determined if the β values are all known.

A typical two-dimensional parameter surface is pictured in Fig. 1, generated by variation of two log formation constants[2] used to reproduce the pH titration data described in the Experimental Section. Every cross-section in Fig. 1 has the same shape (Fig. 2, trace *a*): a minimum well flanked by a plateau region for small parameter values and an exponential region for large values.

The method of Steepest Descent (S-D) is based on the simple assumption that the greatest decrease in s will lie along the steepest slope, i.e. the calculated corrections should vary as the slope of the surface according to

$$\log \beta_j^0 - \log \beta_j \propto \frac{\delta s}{\delta \log \beta_j}$$

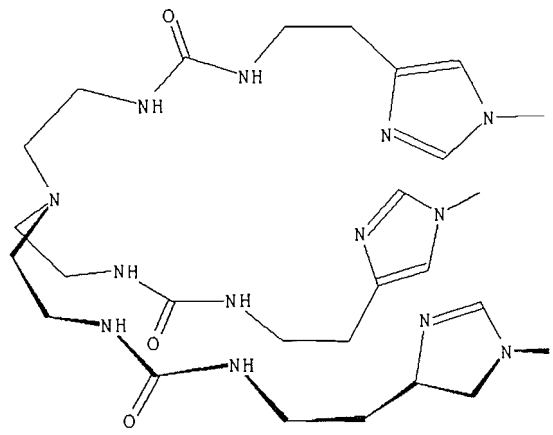

1

[1]Listing available from the author.

[2]Here, log implies base 10. Natural logarithms are written ln.

Can. J. Chem. Downloaded from www.nrcresearchpress.com by 195.138.81.100 on 09/07/12
For personal use only.

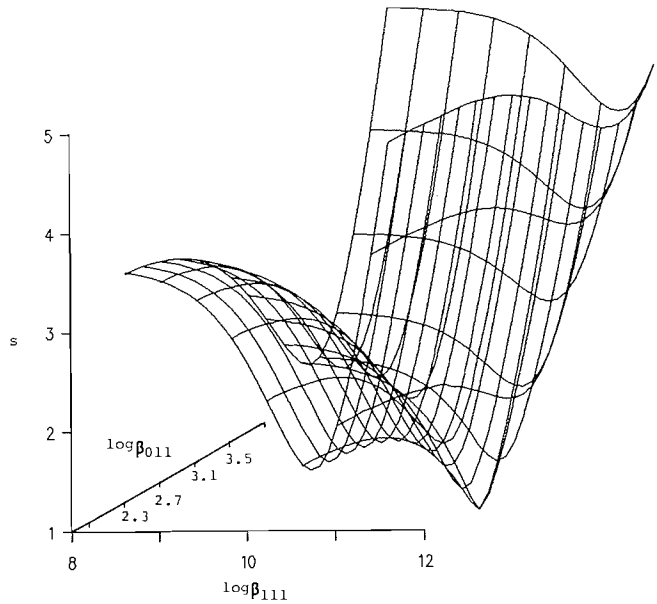

FIG. 1. Plot of s for log β_{111} values between 8.62 and 10.62, log β_{011} values between 1.70 and 4.70, and log β_{-111} held at -3.94. Grid lines are at 0.4 intervals in the log β_{111} dimension and 0.2 intervals in the log β_{011} dimension.

where log β_j^0 are new estimates (ideally, values at the minimum) for any jth parameter. The derivative with respect to any jth log β is given by

$$\frac{\delta s}{\delta \log \beta_j} = -2 \sum_{n=1}^{n_d} w_{n,n}(O_n - F_n)\frac{\delta F_n}{\delta \log \beta_j}$$

$$= -2\mathbf{J}^t\mathbf{w}(\boldsymbol{O} - \boldsymbol{F})$$

where the $\delta F/\delta$ log β elements, whose calculation is detailed later, form the $n_p \times n_d$ Jacobian matrix $\mathbf{J}$. For the cross-section of Fig. 2, this is plotted as trace b. The S-D method is practically useless for very small values of log β_j where the slope is very small and produces strong overshoot in other regions, unless it is scaled down by a proportionality constant suitably determined at each cycle.

The G–N method approximates all regions of each cross-section as linear, with

$$s = s^0 + \sum_{j=1}^{n_\beta} \frac{\delta s}{\delta \log \beta_j}(\log \beta_j - \log \beta_j^0)$$

where s^0 and the n_β parameters log β_j^0 are unknown values at the minimum. The matrix $\mathbf{J}^t\mathbf{w}(\boldsymbol{O} - \boldsymbol{F})$ is not invertible, however. It must instead be assumed that s^0 is zero at the minimum, and the problem must be re-expressed as a first-order Taylor series in the observable:

$$O_n = F_n + \sum_{q=1}^{n_p} \frac{\delta F_n}{\delta \log \beta_q}\Delta \log \beta_q$$

$$\text{or} \qquad \boldsymbol{O} - \boldsymbol{F} = (\Delta^{G\text{-}N})^t\mathbf{J}$$

where Δ log β elements are the corrections at any iteration forming vector $\Delta^{G\text{-}N}$. Then

$$\mathbf{J}^t\mathbf{w}(\boldsymbol{O} - \boldsymbol{F}) = \mathbf{J}^t\mathbf{w}\mathbf{J}\Delta^{G\text{-}N}$$

$$\Delta^{G\text{-}N} = (\mathbf{J}^t\mathbf{w}\mathbf{J})^{-1}\mathbf{J}^t\mathbf{w}(\boldsymbol{O} - \boldsymbol{F})$$

where $\mathbf{J}^t\mathbf{w}\mathbf{J}$ is called the $n_p \times n_p$ Hessian matrix. The actual values of the G–N corrections at various points along the cross-section are plotted in Fig. 3, trace b, alongside the ideal corrections plotted as trace c. Trace b always lies above trace c. In the steep region where log β_j values are overestimated, therefore, better estimates to log β_j^0 are always obtained by assuming that s^0 is zero at the minimum (Fig. 2, trace c). These consistently undershoot the minimum and result in a lower value of s. On the other hand, when log β_j values are underestimated,

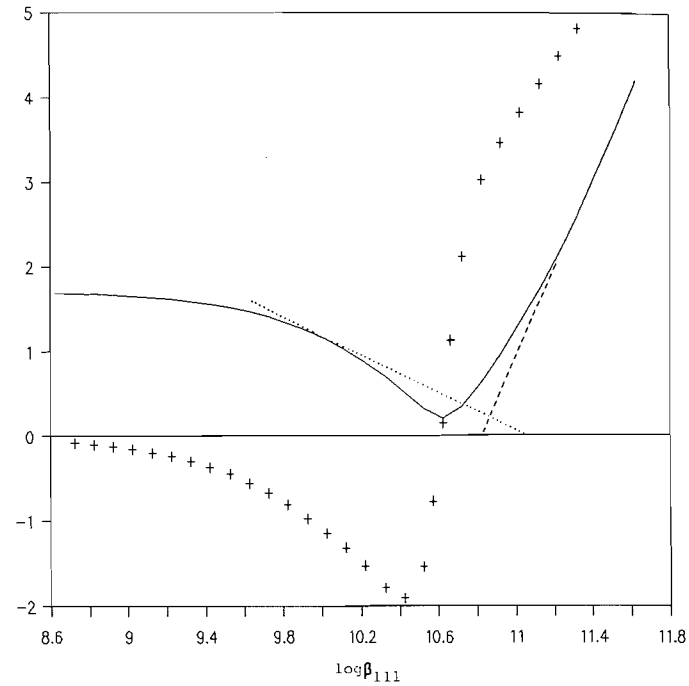

FIG. 2. Plots of (a) s for varying values of log β_{111} with log β_{011} = 3.71 and log $\beta_{-111} = -3.94$ (solid line); (b) $\delta s/\delta$ log β_{111} (++++); (c) interpolation from log $\beta_{111} = 11.40$ (----); (d) interpolation from log $\beta_{111} = 10.00$ (····).

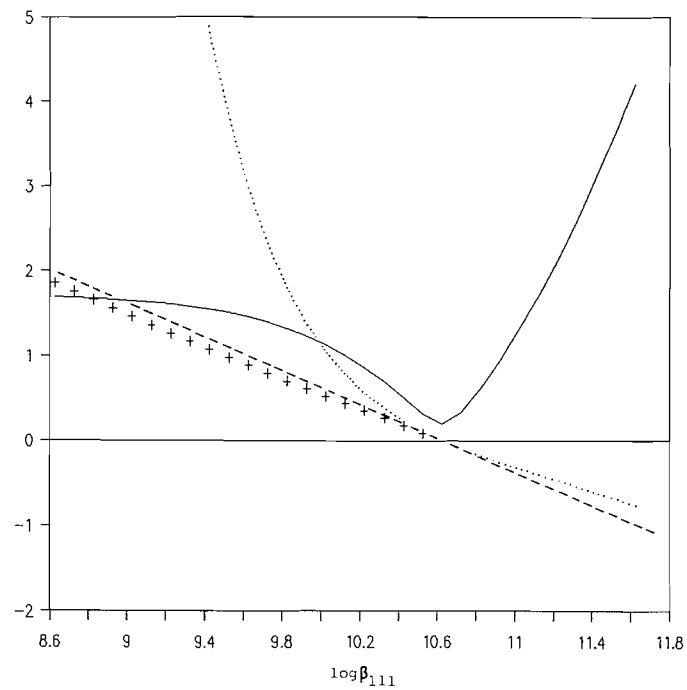

FIG. 3. Plots of (a) s for varying values of log β_{111} with log β_{011} = 3.71 and log $\beta_{-111} = -3.94$ (solid line); (b) $\Delta^{G\text{-}N}$ (····); (c) distance from the minimum or Δ^{ideal} (----); (d) Δ^{mod} (++++).

overshoot is always obtained (Fig. 2, trace *d*). Below certain critical values of $\log \beta_j$, viz. near the minimum in the slope of *s*, the overshoot leads to higher values of *s*. At the extreme, in the plateau region, infinitely high estimates of $\log \beta_j^0$ result.

The Newton–Raphson method, used in STEW (3) but quickly abandoned thereafter by its authors, makes the true assumption that the gradient of the second-order surface approaches zero at the minimum. The surface is given by

$$s = s^0 + \sum_{j=1}^{n_\beta} \left\{ \frac{\delta s}{\delta \log \beta_j} + \frac{1}{2} \sum_{k=1}^{n_\beta} \frac{\delta^2 s}{\delta \log \beta_j \delta \log \beta_k} (\log \beta_k - \log \beta_k^0) \right\} (\log \beta_j - \log \beta_j^0)$$

where

$$\frac{\delta^2 s}{\delta \log \beta_j \delta \log \beta_k} = 2 \sum_{n=1}^{n_d} w_{n,n} \left(\frac{\delta F_n}{\delta \log \beta_j} \frac{\delta F_n}{\delta \log \beta_k} - \frac{\delta^2 F_n}{\delta \log \beta_j \delta \log \beta_k} (O_n - F_n) \right)$$

In matrix notation, the surface is then written as

$$s = s^0 + (\Delta^{N-R})^t \{ \mathbf{J}^t \mathbf{w} (\boldsymbol{O} - \boldsymbol{F}) + [\mathbf{J}^t \mathbf{w} \mathbf{J} - \mathbf{G}^t \mathbf{w} (\boldsymbol{O} - \boldsymbol{F})] \Delta^{N-R} \}$$

where $\mathbf{G}$ is the $n_p \times n_p \times n_d$ matrix of second derivatives. For overestimated $\log \beta_j$ values, the second derivative rapidly slopes off and the third derivative rapidly approaches zero as $\log \beta_j$ increases. Thus, first-order terms soon dominate, and the behaviour resembles that of the G–N method in giving undershoot. For the other portion of the surface, the behaviour is quite different. If the gradient vector (in braces) is set to zero, then the corrections are

$$\Delta^{N-R} = (\mathbf{J}^t \mathbf{w} \mathbf{J} - \mathbf{G}^t \mathbf{w} (\boldsymbol{O} - \boldsymbol{F}))^{-1} \mathbf{J}^t \mathbf{w} (\boldsymbol{O} - \boldsymbol{F})$$

where Δ^{N-R} is the $n_p \times 1$ vector of corrections. However, this produces a discontinuity in the calculated corrections whenever the $\delta^2 s/(\delta \log \beta)^2$ terms (the diagonal elements of the Hessian $\mathbf{J}^t \mathbf{w} \mathbf{J} - \mathbf{G}^t \mathbf{w} (\boldsymbol{O} - \boldsymbol{F})$) are zero, i.e. where the first derivative is at its minimum: the Hessian matrix is no longer invertible as its determinant is then zero. Just beyond this discontinuity, the corrections strongly overshoot because the inverse of the second derivative is large and positive; just below, they produce divergence toward $-\infty$ because the inverse is large and negative. Every higher-order zero-gradient approach will behave in this same way because every μth-order derivative of *s* has $\mu - 1$ roots. As the N–R method applied to equilibrium constant problems is thus flawed, the use of the Fletcher–Powell algorithm (14), which approximates it, seems ill-founded.

The situation is not improved if the cross-section is converted to an anti-log scale, i.e. about minimum values β_j^0 (Fig. 4, trace *a*). For large values of β_j, the G–N method would approximate this as linear, with

$$s = s^0 + \sum_{j=1}^{n_\beta} \frac{\delta s}{\delta \beta_j} (\beta_j - \beta_j^0)$$

By assuming that s^0 is zero at the minimum, new estimates to β_j^0 are thereby obtained which consistently overshoot the minimum (Fig. 4, trace *b*). This gets worse further and further from the minimum where the linear approximation holds less and less well. For underestimated values of β_j, undershoot is obtained (Fig. 4, trace *c*). Since no advantage is gained by expressing the problem in terms of β values, computer calculations using $\log \beta$ values are to be preferred, for three reasons: (*a*) the Hessian elements are more uniform in size, affording more reliable inverses without resort to higher arithmetic precision, (*b*) β values need to be protected from becoming negative during refinement, and (*c*) they can exceed the machine's limits on number sizes (*e.g.* $10^{\pm 38}$ for a VAX). However, overshoot could in theory be avoided by refining $\log \beta$ terms when these are overestimated and refining β terms when they are underestimated. In fact, the approach described herein simulates this while actually calculating with $\log \beta$ values throughout.

For the three unknown system described in the Experimental Section, Table 1 reports the G–N correction vectors, calculated from representative starting points, alongside the corresponding ideal corrections. The labelling convention $\log \beta_{ijk}$ is used for convenience and here denotes $[H_i Zn_j L_k^{(i+2j)+}]/[H^+]^i [Zn^{2+}]^j [L]^k$. As predicted from Figs. 2 and 3, severe overshoot occurs with positive corrections of underestimated $\log \beta$ values. (The G–N vector for case 3 appears to lead to divergence for $\log \beta_{111}$ but actually does not. Although the corresponding S-D correction is positive, a large negative G–N element is calculated for the underestimated $\log \beta_{111}$ because the diagonal of the Hessian is dominated by the large value corresponding to the overestimated $\log \beta_{-111}$. On the next cycle, the G–N vector reverses direction and a positive correction to $\log \beta_{111}$ is calculated.) Application of these raw G–N vectors would lead to increases in *s*. Although this can nevertheless be productive, as *s* will always be reduced on the next cycle, a machine algorithm will normally abort whenever *s* increases. As well, such large shifts make the calculation of the new species concentrations (and the new *s*) very difficult (see Appendix). Attenuation of these large shifts is desirable, and several strategies have been explored.

One strategy, the Hartley–Wentworth (H–W) parabolic interpolation (10), is illustrative of inefficient refinement. It seeks to "optimize" the attenuation by applying two different lengths of the raw G–N vector, fitting the initial and resultant *s* values to a parabolic function of the scaling required, and estimating that function's minimum. For the large G–N vectors of Table 1, severe attenuation is needed. In this implementation, therefore, the refinement was accelerated by first scaling the raw G–N vectors, such that the largest element did not exceed a generous maximum of 3 log units, before applying the H–W algorithm. Even so, this strategy is inefficient because, as is evident from Fig. 2, the assumption of a parabolic surface is rarely a good one and much computation is wasted calculating chimeric parabolic minima. Several improvements to the basic algorithm can be devised (such as applying it only if *s* increases) but the root problem is that *at least* three re-calculations of the species concentrations (and of *s*) are needed on each cycle. At each re-calculation, new derivatives become available

Can. J. Chem. Downloaded from www.nrcresearchpress.com by 195.138.81.100 on 09/07/12
For personal use only.

Can. J. Chem. Downloaded from www.nrcresearchpress.com by 195.138.81.100 on 09/07/12
For personal use only.

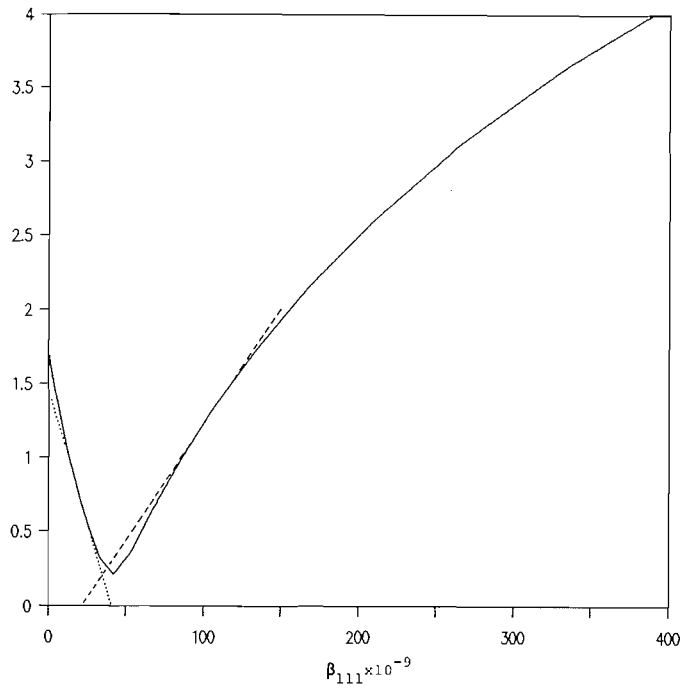

FIG. 4. Plots of (*a*) *s* for varying values of β_{111} with $\beta_{011} = 10^{3.71}$ and $\beta_{-111} = 10^{-3.94}$ (solid line); (*b*) interpolation from $\beta_{111} = 10^{11}$ (----); (*c*) interpolation from $\beta_{111} = 10^{10.3}$ (····).

(see Appendix) and it is more efficient to calculate new, more relevant corrections therefrom than to re-scale the old ones. The parabolic interpolation used in BEST (11) is similarly flawed: in the best circumstances,[3] 11.55 s were required for case 1 in Table 1.

Another inefficient strategy enjoying some popularity (4, 5, 8, 13) is the Marquardt–Levenberg algorithm (12). Here, the basic equations are modified:

$$(\Delta^{M-L})^* = ((\mathbf{J}^t\mathbf{w}\mathbf{J})^* + \lambda\mathbf{I})^{-1}(\mathbf{J}^t\mathbf{w}(\boldsymbol{O} - \boldsymbol{F}))^*$$

The superscript * denotes normalized elements, **I** is the identity matrix, and λ is a scalar. As prescribed by the algorithm, λ is kept as small as possible, but is increased whenever an increase in *s* is detected until sufficiently small Δ^{M-L} elements are obtained that generate a lower *s*. The Hessian is thus given second-order character to swing the correction vector from a purely G–N direction towards the S-D direction given by $\mathbf{J}^t\mathbf{w}(\boldsymbol{O} - \boldsymbol{F})$. Quite apart from the extra computations for normalization, one cycle requires more than one inversion of the modified Hessian and, like the H–W algorithm, more than one re-calculation of *s* whenever the raw G–N vector (λ = 0) produces an increase in *s*. For the large G–N vectors of Table 1, many re-calculations would be required on the first cycle and the speed with which λ can be increased becomes crucial. An immediate improvement can be obtained by first scaling down the length of the raw G–N vector, much as was done with the H–W algorithm. However, if the largest G–N element is kept to a reasonable maximum (*e.g.* 3 log units), the M–L algorithm, like the H–W algorithm, is hardly ever needed.[4]

Indeed, a simpler and much more economical strategy is to choose a general-purpose attenuation of G–N vectors. The results of using three different maxima are reported in Table 2. As expected, too generous an allowance can result in an increase in *s* (and aborted refinement), while one too stingy requires more computation. There is no rule governing the choice of a maximum other than by trial and error. Those used here were suitable for this particular situation, but there is no guarantee that they would not be excessive in some other situation. Nevertheless, this remains a good and reliable strategy.

In all of these strategies, the directions of the raw G–N vectors were preserved. When the largest elements overwhelm the smaller ones as in several of the cases in Table 1, adjustment of the length amounts to a neglect of the smaller elements. Since only positive corrections give overshoot, one should be able to use the full negative corrections to improve the efficiency. The results of using positive-only scaling are also given in Table 2. Indeed, fewer cycles and less time are required when the refinement is successful, but it is more prone to failure. Further, temporary divergence can cause failure of a different sort: In case 3, the second cycle calculates a positive correction to $\log \beta_{111}$, but subsequent scaling affords an undetectably small decrease in s ($<10^{-6}$) and the refinement aborts.

Although this problem might be managed with a higher arithmetic precision or a lowering of the detection limit, a simpler solution is to refuse large negative corrections if the corresponding S-D elements are not also negative. The remaining problem of choosing an appropriate maximum can be entirely and neatly circumvented as follows: The G–N corrections of underestimated $\log \beta$ (Fig. 3, trace *b*) are exponentially dependent on the distance from the minimum (given in trace *c*). Indeed, cases 7*a* to 7*c* in Table 1 illustrate this well: a unit decrease in $\log \beta_{011}$ (i.e. a ten-fold decrease in β_{011}) leads to a *ca.* ten-fold increase in the G–N correction to it, while the other corrections are invariant. A logarithmic modification suggests itself. Indeed, a useful function is

$$\Delta_q{}^{mod} = \log (\ln 10\Delta_q{}^{G-N} + 1)$$

Along the cross-section of Fig. 3, where $\log \beta_{011}$ and $\log \beta_{-111}$ were held at their minimum values, *nearly ideal* corrections of underestimated $\log \beta_{111}$ result (trace *d*). As expected for the cases of Table 1, the modified correction vectors are of much more reasonable size. There is still overshoot of the minimum values (after all, the G–N elements are initially directing us toward the minima of the local cross-sections), but, as illustrated by cases 7*a* to 7*c*, such overshoot (by *ca.* 1.73) is essentially constant along any one cross-section. Such is not true of the scaled G–N vectors: *e.g.* a maximum correction of 3 log units leads to overshoot by 2 (for case 7*a*), 1 (for 7*b*) or 0 (for 7*c*) log units. This invariance of the overshoot allows

[3]Comparisons with BEST are inappropriate. Increments are added by trial and error, one parameter at a time. Variances are not calculated as weighting is by inverse pH–volume slopes that are numerically approximated. This produces very flat-bottomed minima and leads to different final values (here, $\log \beta_{011} = 3.59$, $\log \beta_{-111} = -4.12$, $\log \beta_{111} = 10.53$) with no estimates of the errors or correlations. Starting with values 2 log units below this minimum (i.e. analogous to case 1 of Table 1), refinement needed to proceed in two stages: one cycle with an increment of 2 (the ideal!) and nine cycles with increments of 0.01.

[4]The M–L formulation is nevertheless useful whenever the Hessian's determinant is near zero, as can arise with numerically-approximated derivative elements of **J**. A small but finite value of λ ensures a meaningful inverse.

Can. J. Chem. Downloaded from www.nrcresearchpress.com by 195.138.81.100 on 09/07/12
For personal use only.

us the luxury of tolerating it *whether or not an increase in* s *results*, as the first iteration will always lead to the same point on the parameter surface, s will always decrease on the next iteration, and overshoot will not recur.

By combining these observations, a new strategy can be formulated. It involves element-by-element examination of the raw G–N vector, as follows. For any qth element, (*a*) if $\Delta_q^{\text{G-N}} \leq 0$ and $\Delta_q^{\text{S-D}} \leq 0$, $\Delta_q = \Delta_q^{\text{G-N}}$; (*b*) if $\Delta_q^{\text{G-N}} < -0.1$ (an arbitrary value) but $\Delta_q^{\text{S-D}} > 0$, $\Delta_q = -0.1$; (*c*) if $\Delta_q^{\text{G-N}} > 0$, $\Delta_q = \Delta_q^{\text{mod}}$; if two successive increases in s are detected (this has yet to be witnessed), $\Delta_q = 0$.

The results of applying this strategy are reported in Table 2. The trivial additional cost of computing Δ^{mod} elements, which is often only required on the first iteration, is more than compensated by the avoidance of scaling. Fast, worry-free refinement results. For most cases, the speed compared very favourably with the best results obtained with scaling. For all intents and purposes, overshoot and divergence problems can thus be eliminated.

There is a sound theoretical basis for this function (*vide infra*) which guarantees its success for all complex equilibrium problems where the analytical measurements are functions of the concentrations of one of more species, or of their logarithms.

Part 2. Theoretical basis

Experimental data such as absorbance under Beer's Law or nmr chemical shift for rapidly equilibrating species are functions of the concentrations of the n_s species S present in solution. Such data can be generalized as

$$F_n = \sum_{i=1}^{n_s} \alpha_i [S_i]_n$$

With absorbance data, F_n is the nth absorbance observed at some wavelength λ and α_i is $\epsilon_{\lambda,i} l$, where $\epsilon_{\lambda,i}$ is the extinction coefficient of the ith species at λ and l is the light pathlength. With nmr data, F_n is the nth chemical shift measurement of some νth nucleus and α_i is $a_{i,\nu}\sigma_{\nu,i}/[T_\nu]_n$, where $a_{i,\nu}$ is the number of nuclei of the νth type in the ith species, $[T_\nu]_n$ is the total concentration of the νth nucleus, and $\sigma_{\nu,i}$ is the chemical shift of the νth nucleus in the ith species. The unknown ϵ or σ parameters (one for each unknown β) are most easily determined in separate but straightforward G–N refinements, parallel to those of the unknown β or log β parameters, and will not be considered further.

The first and second derivatives of F_n have the form

$$\frac{\delta F_n}{\delta P_j} = \sum_{i=1}^{n_s} \alpha_i \frac{\delta [S_i]_n}{\delta P_j} = \ln 10 \sum_{i=1}^{n_s} \alpha_i [S_i]_n \frac{\delta \log [S_i]_n}{\delta P_j}$$

$$\frac{\delta^2 F_n}{\delta P_q \delta P_r} = \sum_{i=1}^{n_s} \alpha_i \frac{\delta^2 [S_i]_n}{\delta P_q \delta P_r} = \ln 10 \sum_{i=1}^{n_s} \alpha_i [S_i]_n \times \left\{ \frac{\delta^2 \log [S_i]_n}{\delta P_q \delta P_r} + \ln 10 \frac{\delta \log [S_i]_n}{\delta P_r} \frac{\delta \log [S_i]_n}{\delta P_q} \right\}$$

The first and second derivatives of the log species concentrations are given in the Appendix by

$$\frac{\delta \log [S_i]_n}{\delta P_q} = \frac{\delta \log \beta_i}{\delta P_q} + \sum_{k=1}^{n_r} a_{i,k} \frac{\delta \log [R_k]_n}{\delta P_q}$$

where

$$\frac{\delta \log [R_k]_n}{\delta P_q} = -\sum_{j=1}^{n_r} u_{n,k,j} a_{q,j} [S_q]_n \frac{\delta \log \beta_q}{\delta P_q}$$

and

$$\frac{\delta^2 \log [S_i]_n}{\delta P_q \delta P_r} = \sum_{k=1}^{n_r} a_{i,j} \frac{\delta^2 \log [R_k]_n}{\delta P_q \delta P_r}$$

where

$$\frac{\delta^2 \log [R_k]_n}{\delta P_q \delta P_r} = -\ln 10 \sum_{j=1}^{n_r} u_{n,k,j} \sum_{i=1}^{n_s} a_{i,j} [S_i]_n \frac{\delta \log [S_i]_n}{\delta P_q} \frac{\delta \log [S_i]_n}{\delta P_r}$$

When P values are underestimated, $\delta^2 \log [R]/\delta P_q \delta P_r$ elements have very small numerical values when $q \neq r$. This arises because the individual $\delta \log [S_i]/\delta P_q$ elements are small unless $i = q$, whence they are dominated by the $\delta \log \beta_q/\delta P_q$ term. If P are log β elements this term is simply 1 when $i = q$. If P are β elements, then $\delta \log \beta_q/\delta P_q = 1/\ln 10 \beta_q$. Therefore, when log β or β values are underestimated, an approximation can be written

$$\frac{\delta^2 \log [R_k]_n}{\delta P_q \delta P_r} \approx -\ln 10 \sum_{j=1}^{n_r} u_{n,k,j} a_{q,j} [S_q]_n \frac{\delta \log \beta_q}{\delta P_q} \frac{\delta \log \beta_q}{\delta P_r}$$

$$\approx 0 \quad \text{if} \quad q \neq r$$

$$\approx \ln 10 \frac{\delta \log [R_k]_n}{\delta P_q} \frac{\delta \log \beta_q}{\delta P_q} \quad \text{if} \quad q = r$$

This is easily verified with pH data and holds especially well if one or more of the other unknown log β values is overestimated. It also holds well in those regions of the data where the corresponding species is a minor component of the mixture. This suggests an exponential dependence of $\delta \log [R_k]_n/\delta \log \beta_q$ on log β_q (i.e. a linear dependence on β_q, or constant $\delta \log [R]/\delta \beta_q$). In fact, the dependence is sigmoidal, with an exponential increase for small log β_q and sloping off that starts near the minimum values of log β_q. The more underestimated log β_q, the better the approximation.

For any μth order, it can be shown that

$$\frac{\delta^\mu \log [R_k]_n}{\delta P_q \delta P_r \delta P_s \ldots} \approx 0 \quad \text{if} \quad q \neq r \quad \text{or} \quad q \neq s \quad \text{etc.}$$

$$\approx \ln 10 \frac{\delta^{\mu-1} \log [R_k]_n}{\delta P_q^{\mu-1}} \quad \text{if} \quad q = r = s, \quad \text{etc.}$$

$$\approx (\ln 10)^{\mu-1} \frac{\delta \log [R_k]_n}{\delta P_q} \{\delta \log \beta_q/\delta P_q\}^{\mu-1} \quad \text{if} \quad q = r = s, \quad \text{etc.}$$

The same result is obtained if the analytically derived μth derivatives are examined under the initial assumption. Thus, all μth derivatives are linear in β_q.

Under the initial assumption, the second derivative of F_n can be reduced to a multiple of the first:

Can. J. Chem. Downloaded from www.nrcresearchpress.com by 195.138.81.100 on 09/07/12
For personal use only.

TABLE 1. Initial correction vectors ($\Delta \log \beta_{011}$, $\Delta \log \beta_{-111}$, $\Delta \log \beta_{111}$)

Case	Ideal	Raw G–N	Modified G–N
1	(2, 2, 2)	(5.65, 3.44, 18.3)	(1.11, 0.899, 1.62)
2	(−2, 2, 2)	(−1.73, 55.8, 53.2)	(−1.73, 2.11, 2.09)
3	(2, −2, 2)	(1.03×10^3, −2.29, −29.5)	(3.38, −2.29, −0.1)
4	(2, 2, −2)	(39.7, 8.12, −1.61)	(1.96, 1.27, −1.61)
5	(−2, −2, 2)	(−1.78, −1.97, 586)	(−1.78, −1.97, 3.13)
6	(−2, 2, −2)	(−1.73, 57.1, −1.69)	(−1.73, 2.12, −1.69)
7a	(1, −2, −2)	(2.29×10^2, −1.97, −1.64)	(2.72, −1.97, −1.64)
7b	(2, −2, −2)	(2.31×10^3, −1.97, −1.64)	(3.73, −1.97, −1.64)
7c	(3, −2, −2)	(2.31×10^4, −1.97, −1.64)	(4.73, −1.97, −1.64)
8	(−2, −2, −2)	(−1.90, −1.97, −1.68)	(−1.90, −1.97, −1.68)

TABLE 2. Comparisons in computation time

c.p.u. time in seconds and, in square brackets, number of re-calculation of s

		G–N method						
		Full scaling maximum			Positive-only scaling maximum			
Case	H–W algorithm	3	1.5	0.75	3	1.5	0.75	Modified
1	16.20[19]	Fail[a]	4.68[5]	5.63[6]	Fail[a]	4.62[5]	5.55[6]	4.78[6]
2	26.71[34]	5.58[6]	6.43[8]	8.03[9]	Fail[a]	6.01[6]	5.91[6]	3.99[5]
3	26.03[34]	5.34[6]	7.66[9]	9.26[11]	Fail[b]	Fail[b]	Fail[b]	4.99[6]
4	20.61[26]	6.33[7]	6.59[7]	7.65[8]	Fail[a]	4.78[5]	6.46[6]	4.88[6]
5	16.17[21]	4.56[5]	5.40[6]	7.45[8]	3.99[5]	Fail[a]	4.80[6]	4.03[5]
6	23.32[28]	4.69[5]	4.54[5]	6.20[7]	4.68[5]	3.97[4]	4.73[5]	3.37[4]
7a	—	5.57[6]	6.28[7]	8.41[10]	Fail[a]	3.97[4]	4.66[5]	4.84[6]
7b	25.21[33]	5.53[6]	6.28[7]	7.81[10]	4.62[5]	Fail[a]	5.42[6]	4.71[6]
7c	—	Fail[a]	7.07[8]	8.65[11]	4.77[5]	4.79[5]	5.57[6]	4.80[6]
8	14.34[18]	3.08[4]	4.66[5]	5.41[6]	3.11[4]	3.11[4]	3.11[4]	4.08[5]

[a]An increase in s was encountered.
[b]An undetectable change in s was obtained.

$$\frac{\delta^2 F_n}{\delta P_q \delta P_r} = \ln 10 \sum_{i=1}^{n_s} \alpha_i [S_i]_n \left\{ \sum_{k=1}^{n_r} a_{i,k} \frac{\delta^2 \log [R_k]_n}{\delta P_q \delta P_r} + \ln 10 \frac{\delta \log [S_i]_n}{\delta P_r} \frac{\delta \log [S_i]_n}{\delta P_q} \right\}$$

$$\approx 0 \quad \text{if} \quad q \neq r$$

$$\approx (\ln 10)^2 \sum_{i=1}^{n_s} \alpha_i [S_i]_n \left\{ \frac{\delta \log \beta_q}{\delta P_q} \sum_{k=1}^{n_r} a_{i,k} \frac{\delta \log [R_k]_n}{\delta P_q} + \frac{\delta \log \beta_q}{\delta P_q} \frac{\delta \log \beta_i}{\delta P_q} \right\}$$

$$\approx (\ln 10)^2 \sum_{i=1}^{n_s} \alpha_i [S_i]_n \left\{ \frac{\delta \log \beta_q}{\delta P_q} \frac{\delta \log [S_i]_n}{\delta P_q} \right\}$$

$$\approx \ln 10 \frac{\delta F_n}{\delta P_q} \frac{\delta \log \beta_q}{\delta P_q} \quad \text{if} \quad q = r$$

In general, then,

$$\frac{\delta^\mu F_n}{\delta P_q \delta P_r \delta P_s \ldots} \approx 0 \quad \text{if } q \neq r \quad \text{or} \quad q \neq s \quad \text{or} \quad q \neq t, \quad \text{etc.}$$

$$\approx (\ln 10)^{\mu-1} \frac{\delta F_n}{\delta P_q} \left(\frac{\delta \log \beta_q}{\delta P_q} \right)^{\mu-1} \quad \text{if} \quad q = r = s = t, \quad \text{etc.}$$

An infinite-order Taylor series can be written to describe the observations:

$$O_n = F_n + \sum_{q=1}^{n_p} \left\{ \frac{\delta F_n}{\delta P_q} + \frac{1}{2!} \sum_{r=1}^{n_p} \left(\frac{\delta^2 F_n}{\delta P_q \delta P_r} + \frac{1}{3!} \sum_{s=1}^{n_p} \left[\frac{\delta^3 F_n}{\delta P_q \delta P_r \delta P_s} + \cdots \right] \Delta P_s \right) \Delta P_r \right\} \Delta P_q$$

where ΔP are the corrections to the n_p parameters, $P^\infty - P$, that will generate the values at the minimum. When the parameters are underestimated, this simplifies to

$$O_n - F_n \approx \sum_{q=1}^{n_p} \left\{ \frac{\delta F_n}{\delta P_q}\Delta P_q + \frac{1}{2!}\frac{\delta^2 F_n}{\delta P_q^2}(\Delta P_q)^2 + \frac{1}{3!}\frac{\delta^3 F_n}{\delta P_q^3}(\Delta P_q)^3 + \cdots \right\}$$

$$\approx \sum_{q=1}^{n_p} \frac{\delta F_n}{\delta P_q}\left\{ \Delta P_q + \frac{1}{2!}\ln 10\frac{\delta \log \beta_q}{\delta P_q}(\Delta P_q)^2 + \frac{1}{3!}\left(\ln 10\frac{\delta \log \beta_q}{\delta P_q}\right)^2(\Delta P_q)^3 + \cdots \right\}$$

$$\approx \frac{1}{\ln 10}\sum_{q=1}^{n_p} \frac{\delta P_q}{\delta \log \beta_q}\frac{\delta F_n}{\delta P_q}\{e^{\ln 10 \Delta P_q \delta \log \beta_q/\delta P_q} - 1\}$$

$$\approx \frac{1}{\ln 10}\sum_{q=1}^{n_p} \frac{\delta P_q}{\delta \log \beta_q}\frac{\delta F_n}{\delta P_q}\{10^{\Delta P_q \delta \log \beta_q/\delta P_q} - 1\}$$

If one sets

$$\Delta_q^{G\text{-}N} = \frac{1}{\ln 10}\frac{\delta P_q}{\delta \log \beta_q}\{10^{\Delta P_q \delta \log \beta_q/\delta P_q} - 1\}$$

and performs a normal G–N determination of the $\Delta_q^{G\text{-}N}$ vector using the normal Jacobian and Hessian matrices, i.e. using $\Delta_q^{G\text{-}N} = (\mathbf{J}^t\mathbf{w}\mathbf{J})^{-1}\mathbf{J}^t\mathbf{w}(\boldsymbol{O} - \boldsymbol{F})$ as described above, then "infinite-order" corrections are given by

$$\Delta P_q = \frac{\delta P_q}{\delta \log \beta_q}\log (1 + \ln 10 \Delta_q^{G\text{-}N} \delta \log \beta_q/\delta P_q)$$

Note that if the parameters P are log β elements, then this infinite-order treatment amounts to a first-order treatment in terms of β elements, because

$$O_n - F_n \approx \frac{1}{\ln 10}\sum_{q=1}^{n_p} \frac{\delta F_n}{\delta \log \beta_q}\{10^{\Delta \log \beta_q} - 1\} \approx \frac{1}{\ln 10}\sum_{q=1}^{n_p} \frac{\delta F_n}{\delta \log \beta_q}\frac{\Delta \beta_q}{\beta_q}$$

$$\approx \sum_{q=1}^{n_p} \frac{\delta F_n}{\delta \beta_q}\Delta \beta_q$$

Thus, when the parameters are underestimated, the observable can be linearized. Further,

$$w_n(O_n - F_n)^2 \approx \sum_{q=1}^{n_p} \frac{\delta F_n}{\delta \beta_q} w_n(O_n - F_n)\Delta \beta_q$$

and

$$s = \sum_{n=1}^{n_d} w_n(O_n - F_n)^2 \approx \sum_{n=1}^{n_d}\sum_{q=1}^{n_p} \frac{\delta F_n}{\delta \beta_q} w_n(O_n - F_n)\Delta \beta_q = \sum_{q=1}^{n_p} \frac{\delta s}{\delta \beta_q}\Delta \beta_q$$

In other words, an "infinite-order" refinement of underestimated log β amounts to minimizing s in terms of β, and should therefore afford the undershoot depicted in Fig. 4, trace *c*.

Experimental data such as emf or pH are functions of the logarithms of the species concentrations and lead to slightly different results. Such data can be represented by

$$G_n = A + B\sum_{i=1}^{n_s} \gamma_i \log [S_i]_n$$

For pH, $G_n = pH_n$, $A = 0$, $B = 1$, $\gamma_1 = 1$ (using the convention that H^+ is the first species), and $\gamma_{i \neq 1} = 0$. Calibration of the electrode, by the Avdeef–Bucher (15) or Jameson–Wilson (16) procedures, is necessary to directly read $-\log [H^+]$. For emf data, $G_n = E_n$ and, assuming Nernstian behaviour, $A = E^0$, $B = \ln 10RT/nF$ and γ_i is the coefficient of the ith species (positive for products, negative for reactants) in the half-cell reaction at the monitoring electrode. (In many, if not most, situations, a single species enters into the half-cell reaction at the monitoring electrode and all other γ values will be zero.) Because of non-Nernstian behaviour, both A and B are usually determined by calibration in individual experimental situations (B is a response slope and A is a sum of the standard reduction potentials at the monitoring and reference electrodes, as well as any boundary and/or liquid junction potentials).

The first and second derivatives with respect to any qth parameter are simply

$$\frac{\delta G_n}{\delta P_q} = B\sum_{i=1}^{n_s} \gamma_i \frac{\delta \log [S_i]_n}{\delta P_q}$$

$$\frac{\delta^2 G_n}{\delta P_q \delta P_r} = B\sum_{i=1}^{n_s} \gamma_i \frac{\delta^2 \log [S_i]_n}{\delta P_q \delta P_r}$$

When β or log β parameters are underestimated, then

$$\frac{\delta^2 G_n}{\delta P_q \delta P_r} \approx 0 \quad \text{if} \quad q \neq r$$

$$\approx \ln 10 B\sum_{i=1}^{n_s} \gamma_i \sum_{k=1}^{n_r} a_{i,k}\frac{\delta \log [R_k]_n}{\delta P_q}\frac{\delta \log \beta_q}{\delta P_q} \quad \text{if} \quad q = r$$

Can. J. Chem. Downloaded from www.nrcresearchpress.com by 195.138.81.100 on 09/07/12
For personal use only.

$$\approx \ln 10B\frac{\delta \log \beta_q}{\delta P_q}\left(-\gamma_q\frac{\delta \log \beta_q}{\delta P_q} + \sum_{i=1}^{n_s}\gamma_i\frac{\delta \log [S_i]_n}{\delta P_q}\right) \quad \text{if} \quad q = r$$

$$\approx \ln 10\frac{\delta G_n}{\delta P_q} - \ln 10B\gamma_q\left(\frac{\delta \log \beta_q}{\delta P_q}\right)^2 \quad \text{if} \quad q = r$$

where, in many emf and all pH situations, $\gamma_q = 0$. In general,

$$\frac{\delta^\mu G_n}{\delta P_q \delta P_r \delta P_s \ldots} \approx 0 \text{ if } q \neq r \text{ or } q \neq s, \text{ etc.}$$

$$\approx (\ln 10)^{\mu-1}\frac{\delta G_n}{\delta P_q} - (\ln 10)^{\mu-1}B\gamma_q\left(\frac{\delta \log \beta_q}{\delta P_q}\right)^\mu \quad \text{if } q = r = s, \text{ etc.}$$

An infinite-order treatment leads to

$$O_n - G_n \approx \sum_{q=1}^{n_p}\left(\frac{\delta P_q}{\delta \log \beta_q}\frac{1}{\ln 10}\frac{\delta G_n}{\delta P_q}\{10^{\Delta P_q \delta \log \beta_q/\delta P_q} - 1\} - B\gamma_q\frac{\delta \log \beta_q}{\delta P_q}\{10^{\delta \log \beta_q/\delta P_q} - 1\}\right)$$

or

$$O_n - G_n + B\sum_{q=1}^{n_p}\gamma_q\frac{\delta \log \beta_q}{\delta P_q}\{10^{\delta \log \beta_q/\delta P_q} - 1\} \approx \sum_{q=1}^{n_p}\frac{\delta G_n}{\delta P_q}\Delta_q^{G\text{-}N}$$

In the rare cases where the γ_q are non-zero, the observables are modified by the constant terms in γ_q. Let this constant be represented by c. For instance, with $P_q = \log \beta_q$,

$$c = 9B\sum_{q=1}^{n_p}\gamma_q$$

A normal G–N treatment can be performed to obtain

$$\Delta^{G\text{-}N} = (\mathbf{J}^t\mathbf{w}\mathbf{J})^{-1}\mathbf{J}^t\mathbf{w}(\mathbf{O} - \mathbf{F} + \mathbf{c})$$

where $\mathbf{c}$ is a $n_d \times 1$ vector of constants c, and the same expression can be used to calculate ΔP_q elements from $\Delta_q^{G\text{-}N}$ elements, as before.

Acknowledgements

The author wishes to thank the Natural Sciences and Engineering Research Council of Canada for a University Research Fellowship and an equipment grant that made this work possible, he also thanks York University for free computer time.

1. P. Gans. Coord. Chem. Rev. **19**, 99 (1976); F. Gaizer. Coord. Chem. Rev. **27**, 195 (1979); F. R. Hartley, C. Burgess, and R. M. Alcock. *In* Solution equilibria. Ellis Horwood, Chichester, U.K. 1980.
2. D. D. Perrin and I. G. Sayce. J. Chem. Soc. A, 82 (1967).
3. P. Gans and A. Vacca. Talanta, **21**, 45 (1974).
4. R. M. Alcock, F. R. Hartley, and D. E. Rogers. J. Chem. Soc. Dalton, 115 (1978).
5. A. Laouenan and E. Suet. Talanta, **32**, 245 (1986).
6. A. Izquierdo and J. L. Beltran. Anal. Chim. Acta, **181**, 87 (1986).
7. A. Sabatini and A. Vacca. J. Chem. Soc. Dalton, 1693 (1972).
8. P. Gans, A. Sabatini, and A. Vacca. J. Chem. Soc. Dalton, 1195 (1985).
9. I. Nagypál, I. Páka, and L. Zékáni. Talanta, **25**, 549 (1978).
10. H. O. Hartley. Technometrics, **3**, 269 (1961); W. E. Wentworth, W. W. Hirsch, and E. Chen. J. Phys. Chem. **71**, 218 (1967).
11. R. J. Motekaitis and A. E. Martell. Can. J. Chem. **60**, 2403 (1982).
12. D. W. Marquart. J. Soc. Ind. Appl. Math. **11**, 431 (1963).
13. P. Gans, A. Sabatini, and A. Vacca. Inorg. Chim. Acta, **18**, 237 (1976); A. D. Zuberbühler and T. A. Kaden. Talanta, **29**, 201 (1982); C. Rigano, A. De Robertis, and S. Sammartano. Transition Met. Chem. **10**, 1, 36 (1985); L. Daruhazi and J. Hazi. Magy. Kem. Lapja, **40**, 524 (1985); Chem. Abstr. **104**, 141181 (1985).
14. R. Fletcher and M. D. J. Powell. Comp. J. **6**, 163 (1963).
15. A. Avdeef and J. J. Bucher. Anal. Chem. **50**, 2137 (1978).
16. R. F. Jameson and M. F. Wilson. J. Chem. Soc. Dalton, 2607 (1972).
17. P. G. Potvin, R. Gau, C. M. Unrau, and N. K. Gehl. Can. J. Chem. **67**, 1363 (1989).
18. Z. Z. Hugus, Jr. *In* Advances in the chemistry of the coordination compounds. *Edited by* S. Kirschner. Macmillan, New York. 1961.
19. A. E. Martell and R. M. Smith (*Editors*). Critical stability constants. Vol. 5. Plenum Press, New York. 1975.
20. W. C. Hamilton. *In* Statistics in physical science. Ronald Press, New York. 1964.
21. A. Vacca, A. Sabatini, and M. A. Gristina. Coord. Chem. Rev. **8**, 45 (1972).

Appendix

Differentiation of the jth total reactant concentration $[T_j]_n$ at any nth point with respect to any parameter P_q gives

$$\frac{\delta [T_j]_n}{\delta P_q} = \ln 10\sum_{i=1}^{n_s}a_{i,j}[S_i]_n\left(\frac{\delta \log \beta_i}{\delta P_q} + \sum_{k=1}^{n_r}a_{i,j}\frac{\delta \log [R_k]_n}{\delta P_q}\right)$$

If one sets

$$(\mathbf{u}^{-1})_{n,j,k} = \sum_{i=1}^{n_s}a_{i,j}[S_i]_n a_{i,k}$$

where, at any nth point, the elements $\mathbf{u}^{-1}{}_{n,j,k}$ form an invertible $n_r \times n_r$ matrix, then rearrangement leads to

$$\frac{\delta \log [R_k]_n}{\delta P_q} = \sum_{j=1}^{n_r}u_{n,k,j}\left(\frac{1}{\ln 10}\frac{\delta [T_j]_n}{\delta P_q} - \sum_{i=1}^{n_s}a_{i,j}[S_i]_n\frac{\delta \log \beta_i}{\delta P_q}\right)$$

Further, we have

$$\frac{\delta \log [S_m]_n}{\delta P_q} = \frac{\delta \log \beta_m}{\delta P_q} + \sum_{k=1}^{n_r}a_{m,k}\frac{\delta \log [R_k]_n}{\delta P_q}$$

Generally one does not refine the invariable parameters (8, 11), and $\delta[T]/\delta \log \beta$ terms are normally zero. However, the derivatives with respect to these are used in the calculation of variances (*vide supra*) and co-variances (8), whence $\delta \log \beta/\delta P$ terms are zero and $\delta[T]/\delta P$ terms are obtained by differentiation of the definitions of [T]. For instance, with titration data,

$$\frac{\delta [T_j]_n}{\delta P_q} = \frac{1}{v_0 + v_n}\left(v_0\frac{\delta [R_j]^*}{\delta P_q} + v_n\frac{\delta [R_j]^+}{\delta P_q}\right) + \frac{[R_j]^* - [R_j]^+}{(v_0 + v_n)^2}\left(v_n\frac{\delta v_0}{\delta P_q} + v_0\frac{\delta v_n}{\delta P_q}\right)$$

Can. J. Chem. Downloaded from www.nrcresearchpress.com by 195.138.81.100 on 09/07/12
For personal use only.

The $\delta^2 \log [R_k]_n/\delta P_q \delta P_r$ terms are obtained by further differentiation, as in

$$\frac{\delta^2[T_j]_n}{\delta P_q \delta P_r} = \ln 10 \sum_{i=1}^{n_s} a_{i,j}[S_i]_n \left(\ln 10 \frac{\delta \log [S_i]_n}{\delta P_q} \frac{\delta \log [S_i]_n}{\delta P_r} + \sum_{k=1}^{n_r} a_{i,k} \frac{\delta^2 \log [R_k]_n}{\delta P_q \delta P_r} \right)$$

Rearrangement, as before, leads to

$$\frac{\delta^2 \log [R_k]_n}{\delta P_q \delta P_r} = \frac{1}{\ln 10} \sum_{j=1}^{n_r} u_{n,k,j} \left(\frac{\delta^2[T_j]_n}{\delta P_q \delta P_r} - (\ln 10)^2 \sum_{i=1}^{n_s} a_{i,j}[S_i]_n \frac{\delta \log [S_i]_n}{\delta P_q} \frac{\delta \log [S_i]_n}{\delta P_r} \right)$$

and we have

$$\frac{\delta^2 \log [S_i]_n}{\delta P_q \delta P_r} = \sum_{k=1}^{n_r} a_{i,j} \frac{\delta^2 \log [R_k]_n}{\delta P_q \delta P_r}$$

Note that $\delta^2[T_j]_n/\delta P_q \delta P_r$ elements are not normally required and usually zero, but are available from the definitions of $[T]_n$.

The concentrations of the species are required at all data points. In LEAST (7), these were determined and refined together with the unknown parameters, with minimization of the residuals in the analytical (total) concentrations of the reactants. Not only does this approach generate very large matrices for inversion, it does not constitute a valid least-squares analysis. Instead, the species concentrations are calculated by reconciling the species definitions with the mass-balance sums in separate Gauss–Newton iterations at each point. This is most easily accomplished by setting up first-order Taylor series of the experimental mass-balance sums as functions of μth estimates of the reactant concentrations, viz.

$$[T_j]_n = \sum_{i=1}^{n_s} a_{i,j}[S_i]_n^{\mu} + \sum_{m=1}^{n_r} \frac{\delta[T_j]_n}{\delta[R_m]_n} ([R_m]_n^{\infty} - [R_m]_n^{\mu})$$

which in matrix notation is written

$$[\mathbf{T}] = \mathbf{a}^t[\mathbf{S}]^{\mu} + \mathbf{H}\Delta^{\mu}$$

with the j,mth element of the $n_r \times n_r$ invertible matrix $\mathbf{H}$ obtained by letting $P_q = [R_m]_n$ in the earlier expression for $\delta[T_j]_n/\delta P_q$. Then

$$H_{j,m} = \sum_{i=1}^{n_s} a_{i,j}[S_i]_n a_{i,k}/[R_m]_n = (\mathbf{u}^{-1})_{n,j,m}/[R_m]_n$$

Better estimates of $[\mathbf{R}]$ values are obtained by setting

$$[\mathbf{R}]_n^{\mu+1} = [\mathbf{R}]_n^{\mu} + \Delta^{\mu} = [\mathbf{R}]_n^{\mu} + \mathbf{H}^{-1}([\mathbf{T}] - \mathbf{a}^t[\mathbf{S}]_n^{\mu}) = [\mathbf{R}]_n^{\mu}[\mathbf{I} + \mathbf{u}([\mathbf{T}] - \mathbf{a}^t[\mathbf{S}]_n^{\mu})]$$

This is continued until some convergence criterion is met (generally when the concentrations change by $\leq 0.01\%$), and the values of the elements of $\mathbf{u}_n$ at the last ($\mu = \infty$) iteration are carried over into the calculation of the derivatives of the observable. If the data are arranged in smooth increasing or decreasing order, as in titration experiments, then the final $[R]_n$ values can serve as initial estimates for the $(n+1)$th point, i.e. $[\mathbf{R}]_{n+1}^{\mu=1} = [\mathbf{R}]_n^{\mu=\infty}$. Then $\mathbf{a}^t[\mathbf{S}]_{n+1}^{\mu=1} = \mathbf{a}^t[\mathbf{S}]_n^{\mu=\infty}$, $\mathbf{u}_{n+1} = \mathbf{u}_n$, and a first correction to $[\mathbf{R}]_{n+1}$ can proceed, without matrix inversion, with the new $[\mathbf{T}]$ elements. Initial estimates need then only be provided for the first data point. In practice, the elements of Δ are large and require damping, especially near equivalence points. The corrections to the concentrations are generally limited to $\pm 90\%$ of the concentrations, but this limit is progressively decreased if convergence is difficult (>20 cycles). This procedure, essentially that used in MICMAC (5), ensures eventual convergence. Inclusion of higher terms in the Taylor series expansion did not provide sufficient benefit to justify the additional computations required. Additional cycles are needed with pH data to account for changes in ionic strength (15).

Can. J. Chem. Downloaded from www.nrcresearchpress.com by 195.138.81.100 on 09/07/12
For personal use only.

Modelling complex solution equilibria. II. Systems involving ligand substitutions and uncertainties in equilibrium constants derived from formation constants

PIERRE G. POTVIN

Department of Chemistry, York University, 4700 Keele Street, North York, Ont., Canada M3J 1P3

Received May 11, 1990

PIERRE G. POTVIN. Can. J. Chem. **68**, 2208 (1990).

A general formalism is presented that expresses equilibrium constants K as combinations of *pseudo*-formation constants ψ. For equilibria involving complexes as reactants that undergo ligand substitutions, this formalism allows a reduction in the number of equations needed to model the system for faster calculation of species concentrations and refinement of unknown parameters. Gauss–Newton refinement of log ψ parameters is shown to be equivalent to that of log K parameters. Equations are developed for the calculation of uncertainties in log K and correlation coefficients between them from the corresponding values obtained for log ψ parameters. These equations can also be used to calculate the same quantities for constants (such as K_a's) derived from true formation constants.

Key words: Gauss–Newton, ligand substitution, equilibrium constants, formation constants.

PIERRE G. POTVIN. Can. J. Chem. **68**, 2208 (1990).

On décrit un formalisme pour exprimer une série de constantes d'équilibre K en combinaisons de *pseudo*-constantes de formation ψ. Ceci permet de réduire le nombre d'équations nécessaires à décrire un système d'équilibres impliquant des réactifs complexes qui subissent des échanges de ligands. Ainsi, le calcul des concentrations des espèces présentes en solution et le raffinement des constantes d'équilibre inconnues sont accélérés. Le raffinement des constantes log ψ par la méthode Gauss–Newton est équivalent à celui des constantes log K. On dérive les équations nécessaires au calcul des incertitudes dans les paramètres log K et les coefficients de corrélation entre eux à partir des mêmes quantités obtenues pour les paramètres log ψ. Ces équations servent aussi au calcul de ces quantités pour toute constante (telle qu'un K_a) dérivée de vraies constantes de formation.

Mots clés : Gauss–Newton, échange de ligands, constantes d'équilibre, constantes de formation.

Can. J. Chem. Downloaded from www.nrcresearchpress.com by 195.138.81.100 on 09/07/12
For personal use only.

Introduction

In the accompanying paper, as in most computational approaches, the calculation of derivatives needed for the least squares determination of equilibrium constants assumed that all n_s species S present in any solution were *formed* from the n_r reactants R that were mixed together, according to

$$[1] \quad [S_i]_n = \beta_i \prod_{j=1}^{n_r} [R_j]_n^{a_{i,j}}$$

$$\text{or} \qquad \log [S_i]_n = \log \beta_i + \sum_{j=1}^{n_r} a_{i,j} \log [R_j]_n$$

for $i = 1$ to n_s at any nth of n_d data points. The coefficient $a_{i,j}$ represents the number of molecules of the jth reactant entering in the formation of the ith species, and β_i is the *formation constant* governing this process. The reactants, being species themselves, can by convention be ordered first; thus, for $i = 1$ to n_r, $a_{i,i} = 1$ but $a_{i,j\neq i} = 0$ and $\beta_i = 1$. The species concentrations obey the mass-balance relations

$$[2] \quad [T_j]_n^{\text{calc}} = [R_j]_n^{\text{tot}} = \sum_{i=1}^{n_s} a_{i,j}[S_i]_n$$

where $[T_j]_n$ represents the analytical total concentration of the jth reactant at the nth point for $j = 1$ to n_r, known from the quantities of each reactant that were mixed. This method of defining species (from "free" reactants) is the most often used and the most convenient since eqs. [1] and [2] can be combined into n_r equations in n_r unknowns that completely describe the system.

$$[T_j]_n^{\text{calc}} = \sum_{i=1}^{n_s} a_{i,j}\beta_i \prod_{k=1}^{n_r} [R_k]_n^{a_{i,k}}$$

There are numerous experimental situations where this convenience is not available. For instance, in the $Cu(en)_2^{2+}/C_2O_4^{2-}/H^+$ system studied by DeWitt and Watters (1), one reactant, $Cu(en)_2^{2+}$, supplies two mass-balance sums, $[Cu]^{tot}$ and $[en]^{tot}$ ($= 2[Cu]^{tot}$). Defining the ligand exchange products $Cu(en)C_2O_4$ and $Cu(C_2O_4)_2^{2-}$ as being formed from Cu^{2+}, en and $C_2O_4^{2-}$ would assume a non-negligible $[Cu^{2+}]$ and that $Cu(en)_2^{2+}$ is a product of known formation constant. The formation constants for such complexes as reactants are not always known. If they are very large, as in this case, the calculated concentrations of the dissociation products, in this case $[Cu^{2+}]$, will be very small. This can lead to serious computational difficulties (numerical over- and underflow) when calculating the concentrations of the other species containing them since inversion is involved (see Appendix of the previous paper).

To treat such systems, the programme DALSFEK (2) uses general equilibrium constant definitions. For n_e equilibria giving rise to n_e new species,

$$[3] \quad K_k = \prod_{i=1}^{n_s} [S_i]_n^{q_{k,i}} \qquad \text{or} \qquad \log K_k = \sum_{i=1}^{n_s} q_{k,i} \log [S_i]_n$$

for $k = 1$ to n_e, where the coefficient $q_{k,i}$ is the number of molecules of the ith species entering into the kth equilibrium, positive for products and negative for reactants. This is much less convenient to use, since n_r mass-balance sums and n_e equilibrium definitions must be solved for n_s ($= n_r + n_e$) unknowns at all points to completely describe the system. This results in much slower calculations of the species concentrations and the process can ascribe intermediate values of [S] that do not reconcile with the mass-balance sums.

There is a simple solution to this problem. The formalism described herein converts constants K to products thereof, termed *pseudo*-formation constants ψ, and back again, by redefining the reactants. By this expedient, the number of equations needed to model the system can be reduced to n_r

Can. J. Chem. Downloaded from www.nrcresearchpress.com by 195.138.81.100 on 09/07/12
For personal use only.

as before to greatly accelerate the calculations of species concentrations, the most time-consuming step in the iterative refinement of equilibrium constants. Further, it is shown that Gauss–Newton (G–N) refinement of either K or ψ leads to the same result. Finally, the formalism allows the development of equations to calculate the uncertainties in the final values of K and the correlation coefficients between them solely from the uncertainties in the final values of ψ and the correlation coefficients between these. This facility extends to normal systems not involving ligand substitutions for the calculation of derived constants (*e.g.* pK_a's) and their errors.

The Formalism

A subset of n_r species S of the n_s total species are selected and, by convention, ordered first in the list and labelled *pseudo*-reactants R^{ψ}. Then n_r identity equations are added to the equilibrium definitions [3], linearized by taking logarithms, to generate a set of n_s equations in n_s unknowns. In matrix notation, the vector of log $[R^{\psi}]$ and log K values is the product of the vector of log [S] values and of the square matrix **u** containing the coefficients:

$$\begin{bmatrix} \log [R^{\psi}_1]_n \\ \log [R^{\psi}_2]_n \\ \dots \\ \log [R^{\psi}_{nr}]_n \\ \log K_1 \\ \log K_2 \\ \dots \\ \log K_{ne} \end{bmatrix} = \begin{bmatrix} 1 & 0 & \dots & 0 \\ 0 & 1 & \dots & 0 \\ \dots & \dots & \dots & \dots \\ 0 & 0 & \dots & 1 \\ q_{1,1} & q_{1,2} & \dots & q_{2,ns} \\ q_{2,1} & q_{2,2} & \dots & q_{2,ns} \\ \dots & \dots & \dots & \dots \\ q_{ne,1} & q_{ne,2} & \dots & q_{ne,ns} \end{bmatrix} \begin{bmatrix} \log [S_1]_n \\ \log [S_2]_n \\ \\ \log [S_{nr}]_n \\ \log [S_{nr+1}]_n \\ \log [S_{nr+2}]_n \\ \\ \log [S_{ns}]_n \end{bmatrix} = \mathbf{u} \log [S]$$

If the n_r R^{ψ} are judiciously chosen (*vide infra*), then **u** is invertible. Let $\upsilon = \mathbf{u}^{-1}$. Then the log species concentrations can be written as

$$\log [S_i]_n = \sum_{j=1}^{n_r} \upsilon_{i,j} \log [R^{\psi}_j]_n + \sum_{k=1}^{n_e} \upsilon_{i,n_r+k} \log K_k$$

for $i = 1$ to n_s. If we set

$$[4] \quad \log \psi_i = \sum_{k=1}^{n_e} \upsilon_{i,n_r+k} \log K_k$$

where $\log \psi_i = 0$ for $i = 1$ to n_r, then

$$[5] \quad \log [S_i]_n = \log \psi_i + \sum_{j=1}^{n_r} \upsilon_{i,j} \log [R^{\psi}_j]_n$$

$$\text{or} \qquad [S_i]_n = \psi_i \prod_{j=1}^{n_r} [R^{\psi}_j]_n^{\upsilon_{i,j}}$$

These have the same form as eq. [1] and constants ψ can be termed *pseudo*-formation constants. The coefficients υ in eq. [5] play the same role as coefficients a in eqs. [1] and [2]. New mass-balance sums of the same form as eq. [2] can then be defined

$$[6] \quad [T^{\psi}_j]_n^{\text{calc}} = [R^{\psi}_j]_n^{\text{tot}} = \sum_{i=1}^{n_s} \upsilon_{i,j} [S_i]_n$$

for $j = 1$ to n_r, where the analytical total concentrations of these *pseudo*-reactants $[T^{\psi}]$ are related to the analytical total reactant concentrations [T] through

$$[T^{\psi}_j]_n = \sum_{k=1}^{n_r} a_{k,j} [T_k]_n$$

Therefore, eq. [5] can be combined into eq. [6] to give n_r equations in n_r unknowns to completely model the system. Further, if **u** is invertible, then the sub-matrix of $\mathbf{a}^t$ formed by the first n_r columns is also invertible. Let matrix $\boldsymbol{\alpha}$ be that inverse. Then

$$[T_k]_n = \sum_{k=1}^{n_r} \alpha_{k,j} [T^{\psi}_j]_n$$

To illustrate, consider the DeWitt–Watters system, in which both pH and absorbance measurements were made. Over the pH range examined, only en undergoes protonations. We first write out the equilibrium definitions,

$$\begin{bmatrix} \log K_w \\ \log K_{a1} \\ \log K_{a2} \\ \log K_{s1} \\ \log K_{s2} \end{bmatrix} = \begin{bmatrix} 1 & 0 & 0 & 0 & 1 & 0 & 0 & 0 & 0 \\ -1 & 0 & -1 & 0 & 0 & 1 & 0 & 0 & 0 \\ -1 & 0 & 0 & 0 & 0 & -1 & 1 & 0 & 0 \\ 0 & -1 & 1 & -1 & 0 & 0 & 0 & 1 & 0 \\ 0 & 0 & 1 & -1 & 0 & 0 & 0 & -1 & 1 \end{bmatrix} \begin{bmatrix} \log [H^+] \\ \log [Cu(en)_2^{2+}] \\ \log [en] \\ \log [C_2O_4^{2-}] \\ \log [OH^-] \\ \log [enH^+] \\ \log [enH_2^{2+}] \\ \log [Cu(en)C_2O_4] \\ \log [Cu(C_2O_4)_2^{2-}] \end{bmatrix} = \mathbf{q} \log [S]$$

and the mass-balance sums

$$\begin{bmatrix} [H]^{\text{tot}} \\ [Cu]^{\text{tot}} \\ [en]^{\text{tot}} \\ [C_2O_4]^{\text{tot}} \end{bmatrix} = \begin{bmatrix} 1 & 0 & 0 & 0 & -1 & 1 & 2 & 0 & 0 \\ 0 & 1 & 0 & 0 & 0 & 0 & 0 & 1 & 1 \\ 0 & 2 & 1 & 0 & 0 & 1 & 1 & 1 & 0 \\ 0 & 0 & 0 & 1 & 0 & 0 & 0 & 1 & 2 \end{bmatrix} \begin{bmatrix} [H^+] \\ [Cu(en)_2^{2+}] \\ [en] \\ [C_2O_4^{2-}] \\ [OH^-] \\ [enH^+] \\ [enH_2^{2+}] \\ [Cu(en)C_2O_4] \\ [Cu(C_2O_4)_2^{2-}] \end{bmatrix} = \mathbf{a}^t [S]$$

The first four species are chosen as *pseudo*-reactants. Matrix **u** is generated as described above, then inverted to produce

$$\begin{bmatrix} \log [H^+] \\ \log [Cu(en)_2^{2+}] \\ \log [en] \\ \log [C_2O_4^{2-}] \\ \log [OH^-] \\ \log [enH^+] \\ \log [enH_2^{2+}] \\ \log [Cu(en)C_2O_4] \\ \log [Cu(C_2O_4)_2^{2-}] \end{bmatrix} = \begin{bmatrix} 1 & 0 & 0 & 0 & 0 & 0 & 0 & 0 & 0 \\ 0 & 1 & 0 & 0 & 0 & 0 & 0 & 0 & 0 \\ 0 & 0 & 1 & 0 & 0 & 0 & 0 & 0 & 0 \\ -1 & 0 & 0 & 0 & 1 & 0 & 0 & 0 & 0 \\ 1 & 0 & 1 & 0 & 0 & 1 & 0 & 0 & 0 \\ 2 & 0 & 1 & 0 & 0 & 1 & 1 & 0 & 0 \\ 0 & 1 & -1 & 1 & 0 & 0 & 0 & 1 & 0 \\ 0 & 1 & -2 & 2 & 0 & 0 & 0 & 1 & 1 \end{bmatrix} \begin{bmatrix} \log [H^+] \\ \log [Cu(en)_2^{2+}] \\ \log [en] \\ \log [C_2O_4^{2-}] \\ \log K_w \\ \log K_{a1} \\ \log K_{a2} \\ \log K_{s1} \\ \log K_{s2} \end{bmatrix}$$

Further, we find

$$\psi_1 = \psi_2 = \psi_3 = \psi_4 = 1$$
$$\psi_5 = K_w$$
$$\psi_6 = K_{a1}$$
$$\psi_7 = K_{a1}K_{a2}$$
$$\psi_8 = K_{s1}$$
$$\psi_9 = K_{s1}K_{s2}$$

Thus all species concentrations are expressed as products of the K's and $[H^+]$, $[Cu(en)_2^{2+}]$, [en], and $[C_2O_4^{2-}]$.

The matrix $\boldsymbol{\alpha}$ is obtained by inversion of the first four columns of **a**.

$$\begin{bmatrix} [H^+_\psi]^{tot} \\ [Cu(en)_2^{2+}{}_\psi]^{tot} \\ [en_\psi]^{tot} \\ [C_2O_4^{2-}{}_\psi]^{tot} \end{bmatrix} = \begin{bmatrix} 1 & 0 & 0 & 0 \\ 0 & 1 & 0 & 0 \\ 0 & -2 & 1 & 0 \\ 0 & 0 & 0 & 1 \end{bmatrix} \begin{bmatrix} [H]^{tot} \\ [Cu]^{tot} \\ [en]^{tot} \\ [C_2O_4]^{tot} \end{bmatrix}$$

This gives total *pseudo*-reactant concentrations (denoted by ψ subscripts) in terms of those of real reactants. Thus, $[en_\psi]^{tot} = 0$ since $[en]^{tot} = 2[Cu]^{tot}$, i.e. $Cu(en)_2^{2+}$ constitutes the only source of en.

For the simple DeWitt–Watters system, this matrix $\boldsymbol{\upsilon}$ could have been written out directly but other choices of *pseudo*-reactants can also apply, involving perhaps $Cu(C_2O_4)_2^{2-}$ and enH^+. The formalism is, however, general to any equilibrium system, the only requirement being that the choice of *pseudo*-reactants be such that the **u** matrix resulting be invertible. This amounts to a requirement that the first n_r columns of $\mathbf{a}^t$ be invertible. Indeed, many combinations of species can be used as reactants to generate the same equilibria.

Least-squares refinement of log ψ

During least-squares refinement by the G–N method, corrections are made to estimates of the parameters, and are obtained from the derivatives of the measured quantity with respect to those parameters (see previous paper). The derivatives at any nth data point of any observable function F with respect to log K parameters are obtained by implicit differentiation from those taken with respect to log ψ parameters, as in

$$\frac{\delta F_n}{\delta \log K_k} = \sum_{i=1}^{n_s} \frac{\delta F_n}{\delta \log \psi_i} \frac{\delta \log \psi_i}{\delta \log K_k} = \sum_{i=1}^{n_e} \upsilon_{n_r+i,k} \frac{\delta F_n}{\delta \log \psi_i} = \sum_{i=1}^{n_e} z_{i,k} \frac{\delta F_n}{\delta \log \psi_i}$$

for $k = 1$ to n_e. Since log ψ_i for $i = 1$ to n_r will equal zero and not be refined, one can define a new square invertible matrix **z** formed as the lower right $n_e \times n_e$ submatrix of $\boldsymbol{\upsilon}$. Then, using the same matrix notation as in the accompanying paper, this can be rewritten as $\mathbf{J}_K = \mathbf{J}_\psi \mathbf{z}$, where the subscript K or ψ refers to $\delta F/\delta \log K$ and $\delta F/\delta \log \psi$ terms, respectively.

The G–N correction vector is given by

$$\begin{aligned} \Delta_K{}^{G-N} &= (\mathbf{J}_K{}^t \mathbf{w} \mathbf{J}_K)^{-1} \mathbf{J}_K{}^t \mathbf{w}(\mathbf{O} - \mathbf{F}) \\ &= ((\mathbf{J}_\psi \mathbf{z})^t \mathbf{w} (\mathbf{J}_\psi \mathbf{z}))^{-1} (\mathbf{J}_\psi \mathbf{z})^t \mathbf{w}(\mathbf{O} - \mathbf{F}) \\ &= \mathbf{z}^{-1} (\mathbf{J}_\psi{}^t \mathbf{w} \mathbf{J}_\psi)^{-1} (\mathbf{z}^t)^{-1} (\mathbf{z}^t) \mathbf{J}_\psi{}^t \mathbf{w}(\mathbf{O} - \mathbf{F}) \\ &= \mathbf{z}^{-1} \Delta_\psi{}^{G-N} \end{aligned}$$

where **w** is a matrix of weighting factors, **O** is the vector of observed data, and **F** is the vector of observables calculated from the current set of parameters, all of which are independent of the method of defining species. This also follows from eq. [4], since at any μth iteration, the elements of vector Δ_K are added to the μth estimates of log K values to generate the $(\mu + 1)$th estimates, and

$$\begin{aligned} (\Delta_\psi)_i &= (\log \psi_{n_r+i})^{\mu+1} - (\log \psi_{n_r+i})^{\mu} \\ &= \sum_{k=1}^{n_e} \upsilon_{n_r+i} [(\log K_k)^{\mu+1} - (\log K_k)^{\mu}] \\ &= \sum_{k=1}^{n_e} z_{i,k} (\Delta_K)_k \end{aligned}$$

Thus correction of log ψ parameters amounts to simultaneous and appropriate correction of all subject log K parameters. The final log K values are then obtainable from the final log ψ values by

$$\log K_k = \sum_{i=1}^{n_e} u_{n_r+k,n_r+i} \log \psi_{n_r+i} = \sum_{i=1}^{n_e} q_{k,n_r+i} \log \psi_{n_r+i}$$

It can be verified that this also holds true for the Newton–Raphson corrections, but, curiously, not for the method of Steepest Descent, where, instead, $\Delta_K{}^{S-D} = \mathbf{z}^t \Delta_\psi{}^{S-D}$.

Uncertainties and correlations in log K

After refinement, it is of interest to obtain uncertainties in the final log K values and the correlation coefficients between them. The uncertainty in any ith log ψ will be given by

$$\sigma_{\psi_i} = \sigma_0 (H_\psi)_{i,i}^{1/2}$$

where $\mathbf{H}_\psi$ is the inverted Hessian $(\mathbf{J}_\psi{}^t \mathbf{w} \mathbf{J}_\psi)^{-1}$ and $\sigma_0{}^2$ is an estimate of the variance of an observation of unit weight (see accompanying paper). The correlation coefficient between the ith and jth parameters will be given by

$$c_{\psi_i\psi_j} = (H_\psi)_{i,j} / \{(H_\psi)_{i,i} (H_\psi)_{j,j}\}^{1/2} = (H_\psi)_{i,j} \sigma_0{}^2 / \sigma_{\psi_i} \sigma_{\psi_j}$$

Can. J. Chem. Downloaded from www.nrcresearchpress.com by 195.138.81.100 on 09/07/12
For personal use only.

TABLE 1. Formation constants and corresponding derived constants[a]

i	$\log \beta_i$	σ_{β_i}	$c_{\beta_i\beta_1}$	$c_{\beta_i\beta_2}$	$c_{\beta_i\beta_3}$	$\log K_i$	σ_{K_i}	$c_{K_iK_1}$	$c_{K_iK_2}$	$c_{K_iK_3}$
1	3.7091	0.0101	1	0.03	−0.03	3.7091	0.0101	1	−0.72	0.69
2	−3.9446	0.0096	0.03	1	0.50	−7.6537	0.0137	−0.72	1	−0.75
3	10.6224	0.0111	−0.03	0.50	1	−6.9133	0.0152	0.69	−0.75	1

[a]Four decimal places were carried in the calculation, though only two are significant.

Since, from above, $\mathbf{H}_K = \mathbf{z}^{-1}\mathbf{H}_\psi(\mathbf{z}^t)^{-1}$, then the uncertainty in the ith log K will be

$$\sigma_{K_i} = \sigma_0\left\{\sum_{j=1}^{n_e}(z^{-1})_{i,j}\sum_{k=1}^{n_e}(z^{-1})_{i,k}(H_\psi)_{j,k}\right\}^{1/2}$$

Remembering that $\mathbf{z}^{-1}$ is the lower-right $n_e \times n_e$ submatrix of $\mathbf{u}$ (i.e. the last n_e columns of $\mathbf{q}$),

$$\sigma_{K_i} = \sigma_0\left\{\sum_{j=1}^{n_e} q_{i,n_r+j}\sum_{k=1}^{n_e} q_{i,n_r+k}c_{\psi_j\psi_k}(H_\psi)_{j,j}{}^{1/2}(H_\psi)_{k,k}{}^{1/2}\right\}^{1/2}$$

$$= \left\{\sum_{j=1}^{n_e} q_{i,n_r+j}\sum_{k=1}^{n_e} q_{i,n_r+k}c_{\psi_j\psi_k}\sigma_{\psi_j}\sigma_{\psi_k}\right\}^{1/2}$$

Similarly, the correlation coefficient between the ith and jth log K values can be written

$$c_{K_iK_j} = (H_K)_{i,j}/\{(H_K)_{i,i}(H_K)_{j,j}\}^{1/2}$$

$$= (H_K)_{i,j}\sigma_0{}^2/(\sigma_{K_i}\sigma_{K_j})$$

$$= (\sigma_0{}^2/\sigma_{K_i}\sigma_{K_j})\sum_{k=1}^{n_e} q_{i,n_r+k}\sum_{l=1}^{n_e} q_{i,n_r+l}(H_\psi)_{k,l}$$

$$= (\sigma_0{}^2/\sigma_{K_i}\sigma_{K_j})\sum_{k=1}^{n_e} q_{i,n_r+k}\sum_{l=1}^{n_e} q_{i,n_r+l} \times c_{\psi_k\psi_l}(H_\psi)_{k,k}{}^{1/2}(H_\psi)_{l,l}{}^{1/2}$$

$$= (1/\sigma_{K_i}\sigma_{K_j})\sum_{k=1}^{n_e} q_{i,n_r+k}\sum_{l=1}^{n_e} q_{i,n_r+l}c_{\psi_k\psi_l}\sigma_{\psi_k}\sigma_{\psi_l}$$

Thus, the uncertainties and correlation coefficients of a model expressed in terms of log K parameters can be obtained from the corresponding quantities when the system is modelled in terms of log *pseudo*-formation constants, without requiring knowledge of the Hessian elements involved.

These last results also have application in systems of equilibria without ligand exchanges, where derived constants, such as K_a's, are often of greater interest than the formation constants β. These are products of the β constants, and the uncertainties in their logarithms would, by normal error propagation rules, be the sum of the uncertainties in the log β components. But these uncertainties are *not* additive and the uncertainties in the derived constants, as well as the correlation coefficients between them, should instead be calculated using these equations.

For instance, in the experimental system described in the accompanying paper, the acidity and the basicity of the Zn^{2+} complex are of interest. The log β results are reported in Table 1. To obtain information on complex acidity, one writes three constants K derived from the three β that define Zn^{2+} complexes:

$$\begin{bmatrix}\log K_M\\ \log K_{a2}\\ \log K_{a1}\end{bmatrix} = \begin{bmatrix}1 & 0 & 0\\ -1 & 1 & 0\\ 1 & 0 & -1\end{bmatrix}\begin{bmatrix}\log \beta_{011}\\ \log \beta_{-111}\\ \log \beta_{111}\end{bmatrix}$$

where

$$\begin{bmatrix}\log \beta_{011}\\ \log \beta_{-111}\\ \log \beta_{111}\end{bmatrix} = \begin{bmatrix}\log [LZn^{2+}]\\ \log [LZnOH^{+}]\\ \log [LZnH^{3+}]\end{bmatrix} - \begin{bmatrix}0 & 1 & 1\\ -1 & 1 & 0\\ 1 & 1 & 1\end{bmatrix}\begin{bmatrix}\log [H^+]\\ \log [L]\\ \log [Zn^{2+}]\end{bmatrix}$$

(The full $\mathbf{q}$ and $\mathbf{a}$ matrices are not needed for this purpose.) If we set $\beta_1 = \beta_{011}$, $\beta_2 = \beta_{-111}$, and $\beta_3 = \beta_{111}$, the non-trivial equations for the σ_K and c_{KK} are

$$\sigma_{K_{a2}} = \{(\sigma_{\beta_1})^2 - 2c_{\beta_1\beta_2}\sigma_{\beta_1}\sigma_{\beta_2} + (\sigma_{\beta_2})^2\}^{1/2}$$

$$\sigma_{K_{a1}} = \{(\sigma_{\beta_1})^2 - 2c_{\beta_1\beta_3}\sigma_{\beta_1}\sigma_{\beta_3} + (\sigma_{\beta_3})^2\}^{1/2}$$

$$c_{K_MK_{a2}} = \{-(\sigma_{\beta_1})^2 + c_{\beta_1\beta_2}\sigma_{\beta_1}\sigma_{\beta_2}\}/\{\sigma_{K_M}\sigma_{K_{a2}}\}$$

$$c_{K_MK_{a1}} = \{(\sigma_{\beta_1})^2 - c_{\beta_1\beta_3}\sigma_{\beta_1}\sigma_{\beta_3}\}/\{\sigma_{K_M}\sigma_{K_{a1}}\}$$

$$c_{K_{a1}K_{a2}} = \{-(\sigma_{\beta_1})^2 + c_{\beta_1\beta_3}\sigma_{\beta_1}\sigma_{\beta_3} + c_{\beta_1\beta_2}\sigma_{\beta_1}\sigma_{\beta_2} + c_{\beta_2\beta_3}\sigma_{\beta_2}\sigma_{\beta_3}\}/\{\sigma_{K_{a1}}\sigma_{K_{a2}}\}$$

The calculation results are also reported in Table 1, where $K_1 = K_M$, $K_2 = K_{a2}$, and $K_3 = K_{a1}$. Thus $pK_{a2} = 7.65 \pm 0.01$ and $pK_{a1} = 6.91 \pm 0.02$.

Acknowledgement

The author wishes to thank the Natural Sciences and Engineering Research Council for a University Research Fellowship.

1. D. DEWITT and J. I. WATTERS. J. Am. Chem. Soc. **76**, 3810 (1954).
2. R. M. ALCOCK, F. R. HARTLEY, and D. E. ROGERS. J. Chem. Soc. 115 (1978).

Can. J. Chem. Downloaded from www.nrcresearchpress.com by 195.138.81.100 on 09/07/12
For personal use only.

The synthesis of dipridyl- and 1,10-phenanthrolylferrocenes and bis-N,N′-(2,2′-dipyridyl(6-ferrocenyl-N,N′-2,2′-dipyridyl))ruthenium dichloride

IAN R. BUTLER[1] AND JEAN-LOUIS ROUSTAN
The Chemistry Department, The University of Ottawa, Ottawa, Ont., Canada K1N 6N5

Received February 20, 1990

IAN R. BUTLER and JEAN-LOUIS ROUSTAN. Can. J. Chem. **68**, 2212 (1990).

Ferrocenyldipyridyls and ferrocenyl-*o*-phenanthrolines have been synthesized by the direct reaction of lithioferrocenes with the appropriate dipyridine or 1,10-phenanthroline. The spectroscopic properties of these potential new ligands are described and the synthesis of bis-2,2′-dipyridyl(6-ferrocenyl-2,2′-dipyridyl)ruthenium dichloride, **8**, in its hydrated form is reported.

Key words: ferrocene, dipyridine, phenanthroline, ruthenium.

IAN R. BUTLER et JEAN-LOUIS ROUSTAN. Can. J. Chem. **68**, 2212 (1990).

Des composés ferrocenyldipyridyles et ferrocenyl-*o*-phénanthrolines ont été préparés par la réaction directe de lithioferrocenes avec des 2,2′-diypyridines et 1,10-phénanthrolines. Les propriétés spectrales de ces nouveaux ligandes polydentatés potentiels sont décrites, ainsi que la synthèse du complexe bimétallique dichlorure de 2,2′-dipyridyl(6-ferrocenyl-2,2′-dipyridyl) dans sa forme hydraté, **8**.

Mots clés : ferrocène, dipyridine, phénantroline, ruthénium.

[Traduit par la revue]

Can. J. Chem. Downloaded from www.nrcresearchpress.com by 195.138.81.100 on 09/07/12
For personal use only.

Introduction

Over the past decade or so, there has been an intensive research effort directed at the photochemical reactions of transition metal complexes containing dipyridyl or phenanthrolyl ligands. In particular, one family of such complexes, the tris chelating complexes of ruthenium, have found widespread application in, for example, the photocatalytic water splitting reaction (1–5), photooxidation reactions (6), and the catalytic epoxidation of alkenes (7). Numerous papers have described the chemical modifications of dipyridyl and/or 1,10-phenanthrolyl ligands to change the bulk properties of their complexes. For example, in the synthesis of surfactant tris-(2,2′-dipyridyl) ruthenium complexes, the dipyridyl ligand(s) have been suitably modified by incorporation of aliphatic side chains and polar groups (8, 9). In related studies, bulky substituted dipyridyls have been employed in, for example, epoxidation reactions (7).

We have been recently interested in the preparation of transition metal complexes containing ferrocenylpyridyls (10), in relation to their potential chemotherapeutic properties.[2] We were stimulated to diversify our studies to include the synthesis of the hitherto unknown ferrocenyldipyridyl by a recent report documenting the use of triferrocenylbenzenes as photosensitizers in the catalytic production of hydrogen from methanol (11). We felt that the synthesis of ferrocenyldipyridyls might lead to the preparation of novel complexes with unusual photocatalytic activity.

The Ziegler and Zeiser nucleophilic alkylation of pyridines provides the most direct method of alkylation at a position *ortho* to the N atom (12). This method has been applied to the synthesis of mono- and bispyridylferrocenes (30–35% yield) and quinolylferrocenes (2% yield) (13). In this paper we have used this method to prepare ferrocenyldipyridines and ferrocenyl-*ortho*-phenanthrolines. In addition, the preparation of the first metal complex to be prepared from these ligands is described.

[1]To whom correspondence should be addressed. Present address: Department of Chemistry, University College of North Wales, Bangor, Gwynedd, U.K. LL57 2UW.

[2]The reaction of ferrocenyllithium for 24 h with *o*-quinoline in diethyl ethers in our hands gives yields in excess of 20% of 2-ferrocenylquinoline. I. R. Butler and J. L. Elliott, unpublished results.

Experimental section

All solvents used in the reactions described were freshly distilled, following drying by standard procedures; however, solvents used for chromatographic separations were of reagent grade. Standard Schlenk type glassware was used throughout for the manipulation of air-sensitive compounds. All reactions were carried out under an inert atmosphere unless otherwise stated. ^{1}H nmr spectra were recorded using a Varian XL-300 instrument using $CDCl_3$ or D_2O as solvent (abbreviations used: d = doublet, s = singlet, dt = doublet of triplets, ad = asymmetric doublet, b = broad, etc.). Mass spectra were obtained using VG Analytical 7070E instrument (at 70 eV) equipped with a Digital PDP 8A data processing unit at the University of Ottawa Mass Spectroscopy Centre, 2,2′-Dipyridine was obtained from the Lancaster Chemical Company and was used as supplied, and *n*-butyllithium solutions in hexanes (Aldrich Chemical Co.) were used throughout. Bis-2,2′-dipyridyldichlororuthenium was prepared from ruthenium trichloride·trihydrate using the literature procedure (14). Column chromatographic separations were carried out using neutral alumina (Brockman Grade 1). Thin layer chromatographic analyses were carried out using metal or plastic backed silica gel plates.

*General procedure for the preparation of mono-substituted ferrocenyl derivatives, **1–5***

A sample of solid monolithioferrocene/dilithioferrocene·THF (15–18)[3] (approximate ratio mono:di = 80:20) was prepared in THF. This solid was suspended in diethyl ether (approximate 1.0 g per 20 mL). To the cooled stirred solution (−70°C) was added a 10% molar excess (with respect to lithium) of the appropriate reagent (2,2′-dipyridyl, 2,3′-dipyridyl, 2,4′-dipyridyl, 4,4′-dipyridyl, or 1,10-phenanthroline). After allowing the reaction mixture to warm up slowly to 18°C, it was stirred for 2–3 days before being hydrolyzed under aerobic conditions with water (approximate equal volume with respect to the solvent).

The organic layer was separated and the remaining solid was further extracted with dichloromethane (until almost colourless). The combined organic fraction was taken to dryness (rotary evaporator) to leave a solid or oily solid. At this point, the composition of the reaction mixture was analyzed by tlc (eluent mixture of hexanes/diethyl ether

[3]When lithioferrocenes are prepared in THF, a solid crystalline adduct of mono- and dilithioferrocene can be obtained; however, prolonged periods of stirring result in the formation of ferrocene substituted cyclic ethers, in which the THF has ring expanded to a seven-membered ring by partial incorporation of the *n*-butyl group (I. R. Butler, unpublished results). A solution of monolithioferrocene, prepared from *n*-butyllithium and ferrocene in diethyl ether (24 h), may be substituted, resulting in only a small diminution in yield.

Can. J. Chem. Downloaded from www.nrcresearchpress.com by 195.138.81.100 on 09/07/12
For personal use only.

ca. 50/50), and the major product bands were identified by visual inspection as the most intense coloured bands present. Column chromatographic separation was then effected and the major products isolated. The elements used were mixtures of hexane, diethyl ether, dichloromethane, and ethyl acetate in increasing polarity throughout the separation. The desired mono-substituted compounds were eluted using Et_2O/CH_2Cl_2 (50/50) mixtures. Crystallization of the major product from hexane/diethyl ether gave the monosubstituted derivatives. The yields are variable; we have repeated the experiment on scales ranging from 1.0 to 10.0 g and have obtained yields between 20 and 44%.[4] Yields for specific compounds: **1**: 6-ferrocenyl-2,2′-dipyridine, 35–40%, **2**: 2-ferrocenyl-1,10-phenanthroline, 20–35%, **3**: 2-ferrocenyl-4,2′-dipyridine, 20–25%, **4**: 2-ferrocenyl-4,4-dipyridine, 16–22%, **5**: 6-ferrocenyl-3,2′-dipyridine, 23–30%.[5]

1, ^{1}H nmr ($CDCl_3$) δ: 4.04 (s, 5H, C_5H_5), 4.40 (t, 2H, β-C_5H_4, $J_{\alpha\beta} \cong 1.7$ Hz), 5.01 (t, 2H, α-C_5H_4), 7.29 (ddd, $J_{5'-6'} = 4.8$ Hz, $J_{5'-4'} = 8.0$ Hz, $J_{5'-3'} = 1.3$ Hz, 1H, H-5′), 7.41 (dd, $J_{5-4} = 7.8$ Hz, $J_{5-3} = 1.0$ Hz, 1H, H-5), 7.70 (t, $J_{4-3} = 7.8$ Hz, 1H, H-4), 7.83 (ddd, $J_{4'-3'} = 8.0$ Hz, $J_{4'-6'} = 1.8$ Hz, 1H, H-4′), 8.19 (dd, 1H, H-3), 8.55 (ddd, $J_{3'-6'} = 0.9$ Hz, 1H, H-3′), 8.66 (ddd, 1H, H-6′). Mass spectrometry (150°C, 70 eV) *m/e* (relative intensity > 10%): 341(17.4), 340(M^+, 77), 339(15.6), 276(19.5), 275(100, $M^{+\bullet} - C_5H_5$), 249(17.8). *Anal.* calcd. for $C_{20}H_{16}FeN_2$: C 70.61, H 4.74, N 8.23; found: C 70.64, H 4.89, N 8.23.

2, ^{1}H nmr ($CDCl_3$) δ: 4.05 (s, 5H, C_5H_5), 4.46 (t, 2H, β-C_5H_4), 5.12 (t, 2H, α-C_5H_4), 7.71 (d, 1H, $J_{5-6} = 8.6$ Hz, H-5), 7.72 (ABd, 1H, H-6), 7.58 (dd, 1H, $J_{8-7} = 8.1$ Hz, $J_{8-9} = 4.4$ Hz, H-8), 7.81 (d, 1H, $J_{3-4} = 8.2$ Hz, H-3), 8.11 (d, 1H, H-4), 8.21 (dd, 1H, $J_{7-9} = 1.2$ Hz, H-7), 9.19 (dd, 1H, H-9). Mass spectrometry 365(19.5), 364(73.4), $M^{+\bullet}$, 363(39.8), 362(13.1), 300(12.9). *Anal.* calcd. for $C_{22}H_{16}FeN_2$: C 72.55, H 4.43, N 7.64; found: C 72.93, H 4.21, N 7.27.

3, ^{1}H nmr ($CDCl_3$) δ: 4.06 (s, 5H, C_5H_5), 4.44 (t, 2H, β-C_5H_4), 4.97 (s, 5H, α-C_5H_4), 7.61 (bd, 1H, $J_{5-6} = 5.2$ Hz, H-5), 7.34 (ddd, 1H, $J_{5'-6'} = 4.7$ Hz, $J_{5'-4'} = 7.9$ Hz, $J_{5'-3'} = 1.8$ Hz, H-5′), 7.82 (bdd, 1H, $J_{4'-3'} = 8.0$ Hz, H-4′), 7.87 (ddd, 1H, $J_{3'-6'} = 1.5$ Hz, H-3′), 8.01 (bd, 1H, $J_{3-6} = 0.7$ Hz, H-3), 8.59 (dd, 1H, H-6), 8.76 (ddd, 1H, H6′), 8.76 (ddd, 1H, H6′). *Anal.* calcd. for $C_{20}H_{16}FeN_2$: C 70.61, H 4.74, N 8.23; found: C 70.65, H 4.89, N 8.40.

4, ^{1}H nmr ($CDCl_3$) δ: 4.06 (s, 5H, C_5H_5), 4.44 (t, 2H, β-C_5H_4), 4.97 (t, 2H, α-C_5H_4), 7.29 (bdd, 1H, $J_{5-6} = 5.2$ Hz, $J_{5-3} = 0.8$ Hz, H-5), 7.56 (bd, 2H, $J_{3'-6'} = 1.7$ Hz, H-3′), 7.58 (dd, 1H, $J_{3-6} = 1.8$ Hz, H-3), 8.60 (dd, 1H, H-6), 8.74 (dd, 2H, $J_{2'-3'} = 4.5$ Hz, H-2′). Mass spectrometry 341(24.9), 340(100.0), $M^{+\bullet}$, 275(61.7), 249(22.1), 247(18.1). *Anal.* calcd. for $C_{20}H_{16}FeN_2$: C 70.61, H 4.74, N 8.23; found: C 70.37, H 4.85, N 8.14.

5, ^{1}H nmr ($CDCl_3$) δ: 4.03 (s, 5H, C_5H_5), 4.41 (t, 2H, β-C_5H_4), 4.95 (t, 2H, α-C_5H_5), 7.25 (ddd, 1H, $J_{5'-4'} = 8.0$ Hz, $J_{5'-6'} = 4.6$ Hz, H-5′), 7.75 (ddd, 1H, $J_{4'-6'} = 1.8$ Hz, $J_{4'-3'} = 8.3$ Hz, H-4′), 7.74 (dd, 1H, $J_{4-5} = 8.3$ Hz, $J_{4-2} = 1.3$ Hz, H-4), 7.46 (dd, $J_{5-2} = 0.7$ Hz, H-5), 8.20 (ddd, 1H, $J_{3'-6'} = 2.3$ Hz, H-3′), 8.62 (ddd, 1H, H-6′), 9.03 (dd, 1H, H-2). *Anal.* calcd. for $C_{20}H_{16}FeN_2$: C 70.61, H 4.74, N 8.23; found: C 70.41, H 4.72, N 8.18.

The labelling of the atoms in each of the rings of a dipyridyl begins with the nitrogen atom and proceeds so that the carbon atom bonded to the other ring has the lowest possible number.

[4]The yields obtained for the symmetrical dipyridines, e.g. 2,2′- and 4,4′-, are higher, since there are fewer isomeric by-products formed. The analytical data is given for anhydrous samples — ^{1}H nmr indicates a tendency to crystallize as hydrates in wet solvents.

[5]We have noted that using different samples of alumina, of the same nominal grade, obtained from different sources, can give different results. Using neutral alumina, Brockman I, we have found that diethyl ether is sufficiently polar to elute the monosubstituted ferrocenes, and a mixture of dichloromethane/ether, 50/50, is sufficient to elute the disubstituted ferrocenes in most circumstances. However, it is recommended that a trial column be run on a microscale before bulk separation.

General procedure for the preparation of ***6, 7***

An identical procedure was used to that in the preparation of **1–4** replacing monolithioferrocene with dilithioferrocene·TMED which was prepared by the published procedure (15). The ratio of the heterocylic reagent (2,2′-dipyridine or 1,10-phenanthroline) added was based on a 1:1.1 stoichiometry w.r.t. lithium added. In this case, the major product compounds, identified by tlc as deep orange/red bands, were eluted with dichloromethane.[2] **6**: 1,1′-bis-(6-(2,2′-dipyridyl)) ferrocene (20%), **7**: 1,1′-bis-(2(1,10-phenanthroyl))ferrocene (14%).

6, ^{1}H nmr ($CDCl_3$) δ: 4.37 (t, 4H, β-C_5H_4), 4.89 (t, 4H, α-C_5H_4), 7.02 (dd, 2H, $J_{5-4} = 7.8$ Hz, $J_{5-3} = 1.0$ Hz, H-5), 7.22 (ddd, 2H, $J_{5'-4'} = 7.7$ Hz, $J_{5'-6'} = 4.3$ Hz, $J_{5'-3'} = 1.7$ Hz, H-5′), 7.32 (t, 2H, $J_{4-3} = 7.8$ Hz, H-4), 7.66 (ddd, 2H, $J_{4'-3'} = 8.1$ Hz, $J_{4'-6'} = 1.1$ Hz), 7.70 (dd, 2H, H-3), 8.00 (ddd, 2H, $J_{3'-6'} = 0.9$ Hz, H-3′), 8.33 (ddd, 2H, H-6′). Mass spectrometry 495(38.1), 494(100.0), $M^{+\bullet}$, 492(17.9), 339(24.3), 276(13.7), 275(61.7), 249(22.1), 247(18.1). *Anal.* calcd. for $C_{30}H_{22}FeN_4$: C 72.89, H 4.49, N 11.33; found: C 72.90, H 4.86, N 11.61.

7, ^{1}H nmr ($CDCl_3$) δ: 4.46 (t, 4H, β-C_5H_4), 5.28 (t, 4H, α-C_5H_4), 7.14 (d, 2H, $J_{5-6} = 8.4$ Hz, H-5), 7.18 (d, 2H, $J_{3-4} = 8.8$ Hz, H-3), 7.28 (d, 2H, H-6), 7.51 (d, 2H, H-4), 7.53 (dd, 2H, $J_{8-7} = 8.0$ Hz, $J_{8-9} = 4.3$ Hz, H-8), 8.13 (dd, 2H, $J_{7-9} = 1.7$ Hz, H-7), 9.08 (dd, 2H, H-9). *Anal.* calcd. for $C_{34}H_{22}FeN_4$: C 75.29, H 4.09, N 10.33; found: C 75.36, H 4.21, N 10.23.

Preparation of bisdipyridyl(6-ferrocenyl-2,2′-dipyridyl)ruthenium dichloride·hexahydrate, ***8***

The title compound was prepared essentially by an adaptation of the procedure of Dose and Wilson (19) and Wrighton *et al.* (20) initially used for the preparation of related derivatives. To a degassed solution of ethanol/water, 75% (20 mL) was added dichlorobisdipyridylruthenium (14) (200 mg, 380 μmol), and **1** (156 mg, 460 μmol). The mixture was refluxed under an argon atmosphere for 6 h. (The reaction progress can be conveniently monitored by tlc using a 50/50, ethanol/acetone solvent mixture as eluent. The product, a yellow-orange band, elutes behind the purple diffuse band of the starting ruthenium complex.) The solvent was then removed and the solid obtained was washed with diethyl ether to remove excess ligand. Concentration of the dichloromethane washings and fractional crystallization, again by slow ether diffusion, gives a further crop of crystals. Combined yields are 74%. The resultant crystalline product, isolated as a solvate containing water and dichloromethane, is insoluble in diethyl ether and acetone, but soluble in water. *Anal.* calcd. for $C_{40}H_{32}Cl_2FeN_6Ru \cdot 6H_2O$: C 51.51, H 4.76, N 9.01; found: C 51.68, H 4.71, N 8.85. ^{1}H nmr δ, (D_2O): 9.04 (bd, 1); 8.89–8.96 (m, 17); 8.86 (bd, 1); 8.56 (bd, 1); 8.19 (bd, 1); 8.10–8.18 (m, 1); 7.82 (dd, 10); 7.66 (td, 1), 7.59 (dd, 2); 7.54 (tm, 1); 7.50 (dm, 1); 7.36 (dm, 1); 7.30 (dm, 1); 7.24 (m, 1); 7.16 (dm, 1); 6.97 (td, 1); 4.37 (m, 1); 3.75 (m, 1); 3.61 (m, 1); 3.25 (m, 1); 4.01 (s, 5).

An alternate separation procedure is to extract the product into a few mL of water, remove the solvent under vacuum at 40°C, and recrystallize as described above. The solid was then washed with the minimum quantity of CH_2Cl_2 to remove any unreacted dichlorobisdipyridylruthenium, which dissolves preferentially in this solvent. The remaining solid was repeatedly extracted with CH_2Cl_2. After concentration of the combined extracts, a top layer of diethyl ether was added. Slow diffusion into the lower CH_2Cl_2 phase resulted in the crystallization of the deep orange product.

Results and discussion

The objective of this work was to synthesize ferrocenyl derivatives of dipyridine and 1,10-phenanthroline. There are several alternate strategies available for such a synthesis, such as the copper, nickel, or palladium catalyzed reaction of a ferrocenyl Grignard reagent with, for example, halo-dipyridyls, or the reaction of ferrocenylmagnesium bromide (21) or ferrocenylzinc chloride (22, 23) with a halodipyridine or halophenanthroline. Although each of these approaches would be

Can. J. Chem. Downloaded from www.nrcresearchpress.com by 195.138.81.100 on 09/07/12
For personal use only.

expected to give reasonable yields of ferrocenyl substituted dipyridines and phenanthrolines, they require the preparation of either halogenoferrocenes and/or halogenodipyridines and phenanthrolines, which add unnecessary synthetic steps. The alternate approach would be to employ the direct reaction of lithioferrocenes with the appropriate heteroaromatic compound. In such an approach the yields are expected to be much lower than in the final steps of the formerly described alternatives, however, the synthesis would involve essentially a one pot, one step reaction. Thus this method of synthesis was the one of choice toward the targeted compounds.

All reactions were run under the same set of experimental conditions. In every case, a mixture of products was obtained, but the one shown to predominate by tlc analysis of the crude organic phase was obtained in a pure form by column chromatography. Typically, a suspension of the lithioferrocene in diethyl ether under nitrogen was reacted over a period of 3 days with the heterocycle, followed by a standard work-up in air to achieve oxidation of the expected dihydro intermediate (24) into the desired aromatic product.

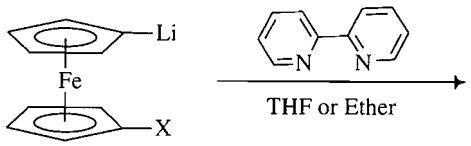

X = H, Li

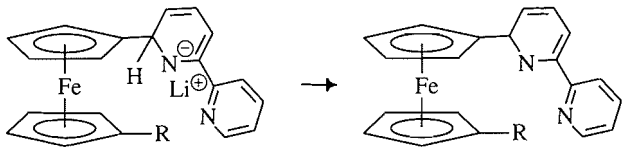

R = H(**1**), 6-(2,2'-dipyridyl) (**6**)

Under these conditions, on scales from 1 to 10 g, dipyridylferrocene **1** was obtained in 37% average yield (range 30–44%) which compares favourably with the 32% yield reported for the synthesis of 2-pyridylferrocene from a 48 h reaction at reflux in cyclohexane between pyridine and lithioferrocene (formed *in situ* from ferrocene and *n*-butyllithium in excess) (13).

The disubstituted derivative **6**, bearing a 2,2'-dipyridinyl substituent on each of the Cp rings, was similarly prepared in 20% yield from the reaction of dilithioferrocene with an excess of 2,2'-dipyridine.

In both compounds **1** and **6**, functionalization of the heterocyclic base at the C-6 position was clearly indicated by ^{1}H nmr spectroscopy at 300 MHz, which resolved all the proton resonances. The nmr data are presented in the Experimental section, and the chemical shift differences between the protons of **1** and **6**, and the equivalent ones found in the 2,2'-dipyridine, are indicated in Table 1. In the latter, the magnetically equivalent H-6 and H-6' protons *ortho* to the N atoms are the most deshielded at 8.67 ppm with the smallest vicinal couplings constant of 4.5 Hz. All the other J_{2H-H} couplings not involving H-6,6' are close to 8.0 Hz. In the monosubstituted **1** selected as an example, all but one of the seven heterocyclic protons present have three vicinal couplings close to 8 Hz. The remaining one with J_{2H-H} = 4.8 Hz is also the most deshielded at 8.66 ppm and is therefore readily identified as H-6' which leaves the C-6 position as the only possible site of attachment of the Cp ring. The remainder of the spectrum is assigned on the basis of the spin multiplicity and the J values pertaining to each proton resonance. Relative to the monosubstituted compound **1**, all the heterocyclic protons of the disubstituted derivative **6** are shifted upfield by 0.1–0.6 ppm.

^{1}H nmr spectroscopy was similarly used to establish that the alkylation at a position *ortho* to the N atom had occurred in the predominant monosubstituted products **3, 4**, and **5**, isolated from the reaction of the 2,3'-, 2,4'-, and 4,4'-dipyridines respectively. The disubstituted phenanthrolylferrocene derivative **7** was isolated as a side product from the synthesis of the monosubstituted complex **6** in addition to the direct synthesis from dilithioferrocene.

In general, in phenanthrolyl compounds **2** and **7**, with the exception of the H-3 resonances in **2**, all heterocyclic proton resonances are shifted upfield in comparison to unsubstituted

TABLE 1. The chemical shift differences of protons in **1** and **6** in comparison to unsubstituted dipyridyl and ferrocene*

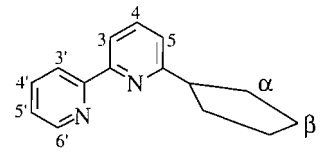

H	Δδ, **1**	Δδ, **6**
3	−0.18	−0.31
4	−0.10	−0.48
5	+0.12	−0.27
3'	+0.20	−0.35
4'	+0.03	−0.14
5'	0.00	−0.07
6'	−0.01	−0.34
α	+1.00	+0.88
β	+0.38	+0.36

*Spectra are recorded in $CDCl_3$ with chemical shifts relative to TMS. The δ values of the ferrocenyl protons − the δ values of the equivalent starting heterocyclic base or ferrocene for α and β protons (a positive sign indicates a downfield shift).

TABLE 2. The chemical shift differences of protons in **2** and **7** in comparison to unsubstituted phenanthroline and ferrocene*

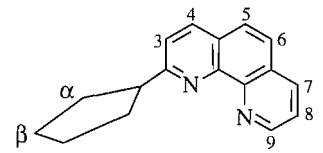

H	Δδ, **2**	Δδ, **7**
3	+0.20	−0.43
4	−0.12	−0.72
5	−0.06	−0.63
6	−0.05	−0.49
7	−0.02	−0.10
8	−0.03	−0.08
9	+0.02	−0.09
α	+1.21	+1.27
β	+0.46	+0.46

Can. J. Chem. Downloaded from www.nrcresearchpress.com by 195.138.81.100 on 09/07/12
For personal use only.

1,10-phenanthroline (Table 2). Proton H-3 will be affected by tha annular current of the ferrocene ring according to the established effects (25). In all new compounds **1–7**, all substituted cyclopentadienyl ring protons are shifted downfield considerably relative to the unsubstituted cyclopentadienyl ring protons.

All new compounds gave clear parent ions in their electron impact mass spectra (m/e 340 for **1, 3, 4, 5**; 364 for **2**; 494 for **6**, and 542 for **7**). Typically, a major peak is observed at m/e, $M^{+\bullet}-65$ corresponding to the loss of a cyclopentadienyl ring for the monosubstituted ferrocenes.

Preparation of the ruthenium complex, 8

The ruthenium complex was synthesized using a modification of the literature procedure (19) used for the synthesis of the parent trisdipyridyl complex, in that it was obtained by the direct reaction dichloro-bis-2,2′-dipyridylruthenium(II) with the ligand **1** in refluxing ethanol. It was isolated as a red/orange solid which can be recrystallized from dichloromethane/ether by the slow diffusion method. **8** is soluble in water, but only sparing soluble in most organic solvents. The assignment of the structure was confirmed by ^{1}H nmr, but the full characterization of individual proton resonances was difficult, due to overlap of the different dipyridyl resonances. Elemental analysis of the crystalline solid and ^{1}H nmr are consistent with the formulation of **8** as a hexahydrate. The single crystal X-ray structural determination of **8** has been carried out; unfortunately the chloride anions and the water of crystallization show considerable disorder which is under current analysis.[6] The integrity of the cation is, however, not in question.

The Ru—N bond lengths range from 2.03–2.15 Å, which are short but compare with those of $[Ru(2,2'\text{-dipy})_3]^{2+}\bullet 2PF_6^-$, which have an average value of 2.056(6) Å, (26). In the latter case, the relatively short bond lengths were explained in terms of considerable π-bonding between the delocalized π^*-orbitals on the bipyridine ligands and the ruthenium core. In the case of **8**, the longest Ru—N bond (2.15 Å) is the one to the ferrocene-substituted pyridyl ring. A bond lengthening would be predicted using this argument since ferrocene can be considered to be a good electron donor, as is witnessed in the upfield chemical shifts of the dipyridyl and phenanthrolyl proton resonances of the substituted compounds **1–7** in comparison to those in the free ligands. It is conceivable that the lengthening might be in part due to steric influence of the bulky ferrocenyl substituent.

With the continued interest in the chemistry of dipyridyl and phenathrolyl ligands extending into the region of cancer chemotherapy (27, 28), in addition to the known chemotherapeutic nature of the ferricinium ion (29) and the stereoselective splitting of DNA (30, 31) these compounds should prove to be an interesting ligand source for future investigations. We are currently testing complex **8** in the photo-water splitting reaction.

[6]Crystal data: monoclinic, space group $P2_1/n$, with lattice parameters a, 12.8609(21), b, 19.1581(24), c, 17.8598(15) Å; β = 102.0741(10)°; V = 4303.2(10) Å^3, Z = 2. The full details will be published independently (I. R. Butler, E. J. Gabe, and G. J. Gainsford).

1. M. Grätzel (*Editor*). Energy resources through photochemistry and catalysis. Academic Press, New York. 1983.
2. T. J. Meyer. Acc. Chem. Res. **22**, 163 (1989).
3. K. Kalyanasundarum. Coord. Chem. Rev. **46**, 159 (1982).
4. A. Juris, F. Barigelletti, S. Campagna, V. Balzani, P. Belser, and A. von Zelewsky. Coord. Chem. Rev. **84**, 85 (1988).
5. G. A. Crosby. Acc. Chem. Res. **8**, 231 (1975).
6. O. I. Ichiro, K. Tatsuya, O. Shigetoshi, and N. Kaji. Inorg. Chim. Acta, **122**, 169 (1986).
7. R. S. Drago and C. L. Bailey. J. Chem. Soc. Chem. Commun. 179 (1982).
8. S. J. Valenty, B. E. Behnken, and G. L. Gaines. Inorg. Chem. **18**, 2160 (1979).
9. O. Johansen, C. Kowala, A. W. H. Mall, and W. H. F. Sasse. Aust. J. Chem. **32**, 1453 (1979).
10. I. R. Butler, J. L. Roustan, and J. P. Charland. J. Cryst. Spec. Res. **20**, 335 (1990).
11. T. Akiyama, Y. Kawaharada, A. Kondo, M. Kajitane, A. Endo, K. Shimizu, and A. Sugimori. Bull. Chem. Soc. Jpn. **59**, 3589 (1986).
12. G. Illuminati and F. Stegel. Adv. Heterocycl. Chem. **34**, 305 (1983).
13. K. Schlögel and M. Fried. Monatsch. Chem. **94**, 538 (1963).
14. G. Sprintschnik, H. W. Sprintschnik, P. P. Kirsch, and D. G. Whitten. J. Am. Chem. Soc. **99**, 4447 (1977).
15. M. D. Rausch and D. J. Clappenelli. J. Organomet. Chem. **10**, 127 (1967).
16. M. D. Rausch, G. A. Moser, and C. F. Meade. J. Organomet. Chem. **1**, 51 (1973).
17. I. R. Butler, W. R. Cullen, J-J. Ni, and S. J. Rettig. Organometallics, **4**, 2196 (1985).
18. J. J. Bishop, A. Davison, M. L. Katcher, D. W. Lichtenberg, R. E. Merrill, and J. C. Smart. J. Organomet. Chem. **27**, 241 (1971).
19. E. V. Dose and L. G. Wilson. Inorg. Chem. **17**, 2660 (1978).
20. P. J. Giordani, C. R. Brock, and M. S. Wrighton. J. Am. Chem. Soc. **100**, 6960 (1978).
21. R. W. Fish and M. Rosenblum. J. Org. Chem. **30**, 1253 (1965).
22. R. Arnold, S. A. Matchett, and M. Rosenblum. Organometallics, **7**, 2261 (1988).
23. R. Arnold, B. M. Foxman, M. Rosenblum, and W. B. Euler. Organometallics, **7**, 1253 (1988).
24. R. A. Abramovitch and C. S. Giam. Can. J. Chem. **42**, 1627 (1964).
25. T. D. Turbitt and W. E. Watts. Tetrahedron, **28**, 1227 (1972).
26. D. P. Rillema, D. S. Jones, and H. A. Levy. J. Chem. Soc. Chem. Commun. 849 (1979).
27. G. R. Newkome, M. Onishi, W. E. Puckett, and W. A. Deutsch. J. Am. Chem. Soc. **102**, 4551 (1980).
28. G. R. Newkome, K. J. Theriot, F. R. Fronczek, and B. Villar. Organometallics, **8**, 2513 (1989).
29. P. Köfp-Maier, H. Köpf, and E. W. Neuse. J. Cancer Res. Clin. Onc. **108**, 336 (1984).
30. A. M. Pyle, J. P. Rehmann, R. Meshoyrev. C. V. Kumar, N. J. Turro, and J. K. Barton. J. Am. Chem. Soc. **111**, 3051 (1989).
31. E. L. Basil and J. K. Barton. J. Am. Chem. Soc. **111**, 1160 (1989).

The photochemistry of cylopentadienylmolybdenum complexes including the mechanism of the *cis–trans* photoisomerism of $(\eta^5\text{-}C_5H_5)Mo(CO)_2LX$, X = Cl, Br, I; L= PPh_3, PBu_3

JEFF D. DEBAD AND ROSS H. HILL[1]

Department of Chemistry, Simon Fraser University, Burnaby, B.C., Canada V5A 1S6

Received November 10, 1989[2]

JEFF D. DEBAD and ROSS H. HILL. Can. J. Chem. **68**, 2216 (1990).

Photolysis of *trans*-$(\eta^5\text{-}C_5H_5)Mo(CO)_2LX$ (L = PPh_3, PBu_3; X = Br, I), at 12 K in 1,2-epoxyethylbenzene, results in CO loss. The product is formed as a specific isomer of $(\eta^5\text{-}C_5H_5)Mo(CO)LX$, isomer **1**. This isomer, upon warming, yields only *trans*-$(\eta^5\text{-}C_5H_5)Mo(CO)_2LX$ in its reaction with CO. Photolysis of *cis*-$(\eta^5\text{-}C_5H_5)Mo(CO)_2LX$ (L = PPh_3, PBu_3; X = Cl, Br, I) under similar conditions also results in CO loss to generate the unsaturated intermediate, $(\eta^5\text{-}C_5H_5)Mo(CO)LX$ as a different geometric isomer, isomer **2**. The unsaturated intermediate, isomer **2**, reacts thermally with CO to generate only *cis*-$(\eta^5\text{-}C_5H_5)Mo(CO)_2LX$. The geometry of these unsaturated intermediates and their interaction with solvent is discussed.

Key words: mechanism, isomerism, photochemistry, molybdenum.

JEFF D. DEBAD et ROSS H. HILL. Can. J. Chem. **68**, 2216 (1990).

La photolyse du *trans*-$(\eta^5\text{-}C_5H_5)Mo(CO)_2LX$ (L = PPh_3, PBu_3; X = Br, I), à 12 K dans le 1,2-époxyéthylbenzène, provoque une perte de CO. Le produit est formé sous la forme d'un isomère spécifique du $(\eta^5\text{-}C_5H_5)Mo(CO)LX$, l'isomère **1**. La réaction de cet isomère, par chauffage avec du CO, ne fournit que le *trans*-$(\eta^5\text{-}C_5H_5)Mo(CO)_2LX$. La photolyse du *cis*-$(\eta^5\text{-}C_5H_5)Mo(CO)_2LX$ (L = PPh_3, PBu_3; x = Cl, Br, I), dans des conditions semblables, conduit aussi à une perte de CO et fournit un intermédiaire insaturé, un $(\eta^5\text{-}C_5H_5)Mo(CO)LX$ sous la forme d'un isomère géométrique différent, l'isomère **2**. Cet intermédiaire insaturé, l'isomère **2**, réagit thermiquement avec le CO pour ne régénérer que le *cis*-$(\eta^5\text{-}C_5H_5)Mo(CO)_2LX$. On discute de la géométrie de ces intermédiaires insaturés et de leur interaction avec les solvants.

Mots clés : mécanisme, isomérie, photochimie, molybdène.

[Traduit par la revue]

Introduction

We wish to report the results of our study concerning the photochemistry of the complexes $(\eta^5\text{-}C_5H_5)Mo(CO)_2LX$ (X = Cl, Br, I, L = PPh_3, PBu_3). Previously, we investigated the low temperature photochemistry of the isoelectronic series of compounds $(\eta^5\text{-}C_5Me_5)Re(CO)_2X_2$ (X = Me, Cl, Br, I) (1). For this series of rhenium complexes we found that *cis–trans* isomerism was a result of dissociative loss of CO to generate a single intermediate, regardless of the starting isomer used, which reacted with free CO to produce a *trans* geometry in the product, reaction [1]. This was in agreement with reports of the room temperature solution studies which indicated the observation of only *cis–trans* isomerism for these Re complexes (2).

[1] *cis/trans*-$(\eta^5\text{-}C_5H_5)Re(CO)_2X_2$

$$\xrightarrow{h\nu} (\eta^5\text{-}C_5H_5)Re(CO)X_2 + CO$$

$$(\eta^5\text{-}C_5H_5)Re(CO)X_2 + CO \xrightarrow{\Delta} \textit{trans}\text{-}(\eta^5\text{-}C_5H_5)Re(CO)_2X_2$$

Previous reports indicated that molybdenum phosphine complexes of the type $(\eta^5\text{-}C_5H_5)Mo(CO)_2PR_3X$ undergo a photoinduced isomerism (3). The reaction, given by reaction [2], is a geometrical isomerism of the basal ligands. Unlike the rhenium complexes, the molybdenum complexes were reported to undergo isomerism in either direction via photochemical initiation. The study of Alway and Barnett (3) measured quantum yields, at room temperature, for the reaction starting from either *cis-* or *trans*-$(\eta^5\text{-}C_5H_5)Mo(CO)_2PPh_3X$ (X = Br, I) under a variety of conditions. Based on the small observed variation in reaction quantum yield in the presence of either CO, PPh_3, or X^- the authors suggested that the majority of the isomerism occurred through a non-dissociative pathway. There was however evidence for photosubstitution *via* both a CO and PR_3 loss which was independent of the isomerism process.

[2] *cis*-$(\eta^5\text{-}C_5H_5)Mo(CO)_2LX$

$$\underset{}{\overset{h\nu}{\rightleftharpoons}} \textit{trans}\text{-}(\eta^5\text{-}C_5H_5)Mo(CO)_2LX$$

The above results suggest that the CO loss products in these molybdenum complexes are geometrically rigid. If this is true *cis-* and *trans*-isomers of a given complex should generate distinct CO loss products.

We therefore undertook a low temperature study of the photoreactions of both *cis-* and *trans*-$(\eta^5\text{-}C_5H_5)Mo(CO)_2PR_3X$. The points we wished to investigate were (*1*) the geometry of the unsaturated fragments produced by CO loss from the *cis* and *trans* isomers, (*2*) the relative importance of loss of CO and loss of L (L = PPh_3, PBu_3), and (*3*) evidence for non-dissociative *cis-trans* isomerism.

Results

The FTIR monitored photolysis ($320 < \lambda < 400$ or broad band) of *trans*-$(\eta^5\text{-}C_5H_5)Mo(CO)_2PBu_3Br$ in 1,2-epoxyethylbenzene at 12 K leads to the loss of absorption intensity due to the starting complex, 1958 and 1869 cm^{-1}, and the appearance of new absorptions in the spectral region studied, Fig. 1*a*.[3] The absorption bands due to *trans*-$(\eta^5\text{-}C_5H_5)Mo(CO)_2PBu_3Br$ decrease in intensity proportionately to the relative extinction coefficients of the starting material.

The production of free CO in the glass is evidenced by an absorption at 2128 cm^{-1}. An intermediate monocarbonyl adduct is indicated by the absorption at 1803 cm^{-1}. The mono-

[1]To whom all correspondence should be addressed.

[2]Revision received August 13, 1990.

[3]1,2-epoxyethylbenzene (styrene oxide) was used as the glass since it is optically transparent at temperatures as low as 8 K and previous experience indicated it was "soft" increasing the possibility that PR_3 ejection may be observed.

Can. J. Chem. Downloaded from www.nrcresearchpress.com by 195.138.81.100 on 09/07/12
For personal use only.

Can. J. Chem. Downloaded from www.nrcresearchpress.com by 195.138.81.100 on 09/07/12
For personal use only.

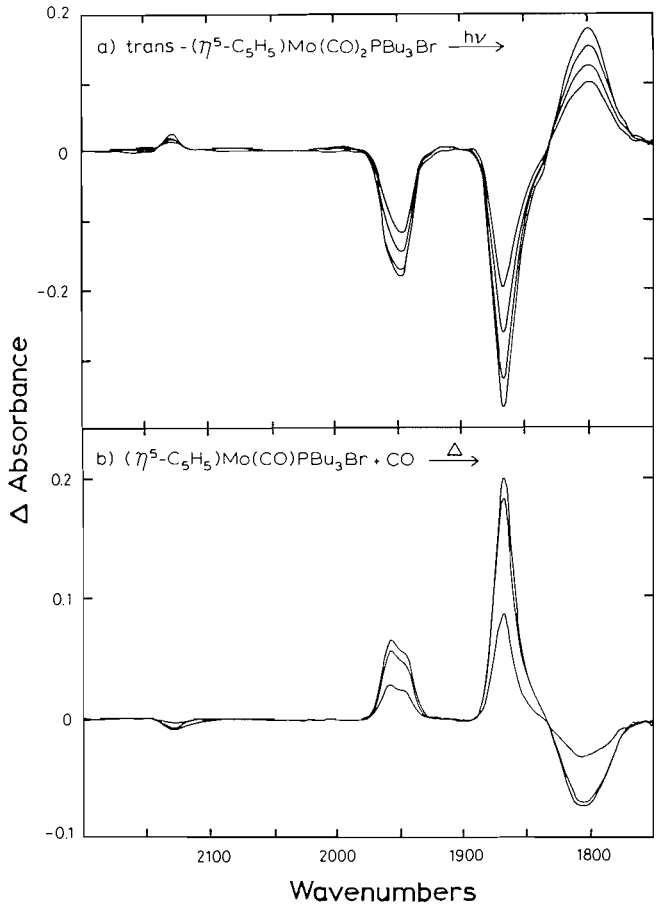

FIG. 1. FTIR spectral changes associated with (*a*) irradiation of *trans*-(η^5-C_5H_5)Mo(CO)$_2$PBu$_3$Br for 120, 240, 480, and 1020 s followed by (*b*) warming-photogenerated (η^5-C_5H_5)Mo(CO)PBu$_3$Br to 20 K, 30 K, and 80 K.

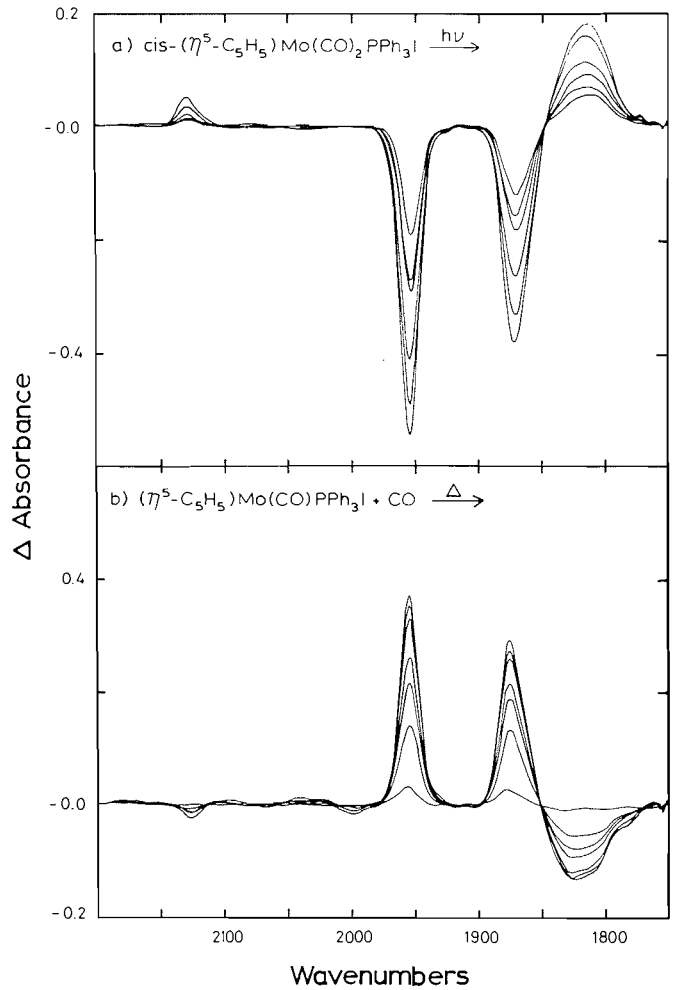

FIG. 2. FTIR spectral changes associated with (*a*) irradiation of *cis*-(η^5-C_5H_5)Mo(CO)$_2$PPh$_3$I for 10, 20, 30, 90, 450, and 1110 s followed by (*b*) warming-photogenerated (η^5-C_5H_5)Mo(CO)PPh$_3$I to 20 K, 40 K, 60 K, 80 K, 100 K, 110 K, and 120 K in the glass.

carbonyl is assigned as (η^5-C_5H_5)Mo(CO)PBu$_3$Br, isomer **1**. In addition to these absorptions an absorption band is observed to grow at 1726 cm^{-1}. This latter absorption is a result of solvent photolysis. This has been confirmed by photolysis of the solvent in the absence of any added complex and the 1726 cm^{-1} absorption band is observed to be produced.

Upon warming, the signal due to the monocarbonyl, (η^5-C_5H_5)Mo(CO)PBu$_3$Br, decreased in intensity, as did the absorption due to free CO at temperatures of ~65 K, Fig. 1*b*. The only new absorptions observed are those due to *trans*-(η^5-C_5H_5)Mo(CO)$_2$PBu$_3$Br. It should be noted that no new species are detected during warming. That none of the *cis* complex is formed is indicated by a comparison of the spectra obtained prior to and after thermal back reaction. If some *cis*-(η^5-C_5H_5)Mo(CO)$_2$PBu$_3$Br has been formed it would have been detectable. Although the absorption bands of the *cis*- and *trans*-isomers overlap, the relative extinction coefficients are quite different as expected because of the different angles between the CO ligands (4). This difference in relative extinction coefficients allows for the detection of any isomerism. The FTIR absorptions of the relevant complexes are summarized in Table 1.

The above experiment was repeated using *trans*-(η^5-C_5H_5)-Mo(CO)$_2$PR$_3$X, R = Ph, X = Br, I; R = Bu, X = I. In each case the results obtained were analogous to those described above. The FTIR data for these complexes, and their CO loss products is summarized in Table 1.

Similarly, photolysis of the *cis*-(η^5-C_5H_5)Mo(CO)$_2$PPh$_3$I complex under identical conditions results in loss of FTIR absorption at 1955 and 1875 cm^{-1}. In addition, the appearance of two new absorptions, at 2128 cm^{-1} due to free CO and a new monocarbonyl band at 1814 cm^{-1}, are observed, Fig. 2*a*. The monocarbonyl band is assigned as due to (η^5-C_5H_5)Mo(CO)-PPh$_3$I as it is the logical photoproduct from CO loss.

The CO loss product resultant from photolysis of the *trans* isomer showed a carbonyl band at 1820 cm^{-1}. The shift of 6 cm^{-1} is indicative of a different stereochemistry in the unsaturated species. We will henceforth refer to this photoproduct, produced from *cis*-(η^5-C_5H_5)Mo(CO)$_2$PPh$_3$I, as isomer **2** of (η^5-C_5H_5)Mo(CO)PPh$_3$I.

Warming of the glass containing CO and isomer **2** of (η^5-C_5H_5)Mo(CO)PPh$_3$I results in a reaction in which both the metal fragment and the CO are consumed, Fig. 2*b*. The back reaction becomes noticeable at temperatures as low as 20 K. During warming no new unsaturated species is formed and the band due to (η^5-C_5H_5)Mo(CO)PPh$_3$I decreases in intensity without significant shift in position. The only detectable product of this reaction is *cis*-(η^5-C_5H_5)Mo(CO)$_2$PPh$_3$I as evidenced by the ratio of intensity of the peaks which grow in at 1955 and 1875 cm^{-1}, which is ~1:1.

In this system we observe only that isomer **2** be produced via

Can. J. Chem. Downloaded from www.nrcresearchpress.com by 195.138.81.100 on 09/07/12
For personal use only.

TABLE 1. FTIR spectra of relevant compounds at 12 K

Complex		ν(CO) ($\epsilon M^{-1}\,cm^{-1}$)[a]
cis-(η^5-C_5H_5)Mo(CO)$_2$PPh$_3$Cl		1957(1700), 1869(1500)
(η^5-C_5H_5)Mo(CO)PPh$_3$Cl	isomer **2**	1811(1000)
cis-(η^5-C_5H_5)Mo(CO)$_2$PBu$_3$Cl		1947(1500), 1857(1300)
(η^5-C_5H_5)Mo(CO)PBu$_3$Cl	isomer **2**	1796(700)
trans-(η^5-C_5H_5)Mo(CO)$_2$PPh$_3$Br		1969(1200), 1882(3600)
(η^5-C_5H_5)Mo(CO)PPh$_3$Br	isomer **1**	1820(720)
cis-(η^5-C_5H_5)Mo(CO)$_2$PPh$_3$Br		1957(2300), 1869(1400)
(η^5-C_5H_5)Mo(CO)PPh$_3$Br	isomer **2**	1812(1300)
trans-(η^5-C_5H_5)Mo(CO)$_2$PBu$_3$Br		1958(750), 1869(2400)
(η^5-C_5H_5)Mo(CO)PBu$_3$Br	isomer **1**	1803(710)
cis-(η^5-C_5H_5)Mo(CO)$_2$PBu$_3$Br		1948(3400), 1858(2400)
(η^5-C_5H_5)Mo(CO)PBu$_3$Br	isomer **2**	1800(1100)
trans-(η^5-C_5H_5)Mo(CO)$_2$PPh$_3$I		1960(1100), 1876(3700)
(η^5-C_5H_5)Mo(CO)PPh$_3$I	isomer **1**	1820(1000)
cis-(η^5-C_5H_5)Mo(CO)$_2$PPh$_3$I		1955(1200), 1875(1300)
(η^5-C_5H_5)Mo(CO)PPh$_3$I	isomer **2**	1814(400)
trans-(η^5-C_5H_5)Mo(CO)$_2$PBu$_3$I		1948(800), 1860(1900)
(η^5-C_5H_5)Mo(CO)PBu$_3$I	isomer **1**	1809(700)
cis-(η^5-C_5H_5)Mo(CO)$_2$PBu$_3$I		1944(2700), 1858(1800)
(η^5-C_5H_5)Mo(CO)PBu$_3$I	isomer **2**	1800(990)

[a]The extinction coefficients have an associated error of 20%.

photolysis. The last pertinent fact is if we has produced any of isomer **1** directly in the photolysis this in turn would have, upon warming, produced *trans*-(η^5-C_5H_5)Mo(CO)$_2$PPh$_3$I. This was not observed: the only product observed upon reaction with CO is *cis*-(η^5-C_5H_5)Mo(CO)$_2$PPh$_3$I.

A similar series of experiments were conducted with *cis*-(η^5-C_5H_5)Mo(CO)$_2$PR$_3$X, R = Ph, X = Cl, Br; R = Bu, X = Cl, Br, I. The result was photoinduced CO loss leading to isomer **2** of the monocarbonyl adducts. Each of these monocarbonyl adducts reacted with CO upon warming to produce *cis*-(η^5-C_5H_5)Mo(CO)$_2$PR$_3$X. The FTIR spectra are summarized in Table 1.

Discussion

The low energy absorptions in the electronic spectra of the molybdenum complexes have been assigned as due to ligand field ($\lambda \sim 400$–500 nm) and charge transfer ($\lambda < 400$ nm) absorptions (3). Reports of the solution chemistry of molybdenum complexes indicated that the efficiency of both isomerism and substitution were higher in the region $\lambda = 366$ nm than could be induced with visible irradiation. We therefore conducted our study using the wavelength region 320 nm $< \lambda <$ 400 nm. In some cases the result was compared with broad band photolysis and no difference in behavior was observed.

Previously, photosubstitution of CO in (η^5-C_5H_5)Mo(CO)$_2$PR$_3$X was suggested to occur via CO loss in room temperature solution (3). Our results indicate that CO loss, according to reaction [3], is the only observable process upon photolysis of (η^5-C_5H_5)Mo(CO)$_2$PR$_3$X at 12 K. This finding is consistent with a recently published report of the photochemistry of (η^5-C_5H_5)Mo(CO)$_3$Cl which was found to undergo CO loss in inert gas matrices at 12 K (5).

$$[3]\quad (\eta^5\text{-}C_5H_5)Mo(CO)_2LX \xrightarrow{h\nu} (\eta^5\text{-}C_5H_5)Mo(CO)LX + CO$$

L = PPh$_3$, PBu$_3$; X = Cl, Br, I

The thermal back reaction with CO is very fast, occurring at temperatures as low as 20 K. This is probably an indication of the ability of the solvent, a glass, to separate the photogenerated CO from the metal photoproduct rather than the true energetics of the back reaction with free CO. In fact, although the reaction with CO occurs at these low temperatures, the system may be warmed to 100 K where the reaction with CO is still not complete. In no case do the different intermediates produced by photolysis of *cis*- and *trans*-(η^5-C_5H_5)Mo(CO)$_2$PR$_3$X interconvert. Irrespective of temperature, back reaction with CO results in efficient production of the starting complex, in its original geometry, reaction [4]. This result indicates that the isomers are rigid at temperatures of 100 K. Of interest now is the geometry of these unsaturated fragments.

$$[4]\quad \textit{trans}\text{-}(\eta^5\text{-}C_5H_5)Mo(CO)_2LX \underset{\Delta}{\overset{h\nu}{\rightleftharpoons}} (\eta^5\text{-}C_5H_5)Mo(CO)LX + CO$$

isomer 1

$$\textit{cis}\text{-}(\eta^5\text{-}C_5H_5)Mo(CO)_2LX \underset{\Delta}{\overset{h\nu}{\rightleftharpoons}} (\eta^5\text{-}C_5H_5)Mo(CO)LX + CO$$

isomer 2

The most reasonable geometry consistent with our results is one in which the remaining ligands retain their position following CO loss. The proposed structures for these isomers are shown below. In each case the stereochemistry is the result of removing a CO ligand from the precursor complexes. For isomer **2** there are two possible geometries shown, these are a result of loss of either of the two inequivalent CO ligands from the precursor molecules, *cis*-(η^5-C_5H_5)Mo(CO)$_2$LX. We have no probe to distinguish between these and cannot rule out the

possibility that both are formed. Although we have represented both **1** and **2** as unsaturated it is possible that interaction with solvent occurs such that solvent fills this vacant site.

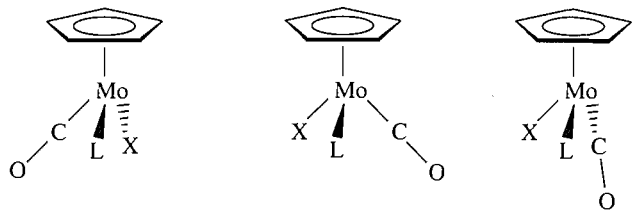

isomer **1** isomer **2**

The observation of two isomers reported here is not without precedent. The isoelectronic molecule $(\eta^5\text{-}C_5H_5)V(CO)_3$, observed recently in a variety of matrices (6), was found to show local C_s symmetry. In addition the isotopomer, $(\eta^5\text{-}C_5H_5)\text{-}V(CO)_2(^{13}CO)$, was found to exist as two isomers.[4]

Two reasons may explain these results. Either there is an electronic preference for this geometry or solvation imposes this geometry. We have been unable to obtain direct evidence about the solvation of these species. Some data are suggestive of only a weak interaction with solvent. Both of these species are highly reactive and react with CO at temperatures of 20 K, indicating that any interaction with the solvent must be weak. In addition the geometry of these fragments is retained prior to solvation indicating that the observed rigidity may not be solely attributable to solvation. The isoelectronic fragment, $(\eta^5\text{-}C_5H_5)V(CO)_3$[6] discussed above, was claimed to be a naked tricarbonyl species. It should be noted however that it is well established that $Mo(CO)_5$, produced photochemically in an inert gas matrix, is solvated (7). In the case of $Fe(CO)_4$ both the naked molecule and a species of the type $Fe(CO)_4(G)$ (G = Xe, CH_4, and N_2) may be observed (8). Given that the glass used here contains both oxygen and aromatic groups it is likely that some solvation, albeit weak,[5] occurs.

The results are consistent with CO loss to generate a rigid unsaturated fragment with a stable geometry. It appears likely that the CO is lost from one position in each case and the thermal back reaction returns the CO to that position. Since the CO loss is a result of a photochemical reaction this conclusion is not a necessary result of microscopic reversibility.

Our findings are consistent with the earlier (3) observation that photoisomerism in solution occurs independent of CO photosubstitution. Here we have shown that at low temperatures CO loss does not result in isomerism. In view of the results in solution it is likely that the unsaturated complex which we have shown to be rigid at 100 K is interconverting only slowly at room temperature.

The other processes observed in the earlier paper (3), intermolecular isomerism and phosphine loss, have not been observed under our conditons. Since phosphine loss would require the ejection of PR_3 from the solvation shell, it is not surprising that we do not observe this process (9). That direct isomerism is not observed may be a result of either the rigidity of the glass in which we monitor the reaction or simply that the isomerism, even in the excited state, must overcome a substantial energy barrier.

Experimental

The complexes *cis-* and *trans-*$(\eta^5\text{-}C_5H_5)Mo(CO)_2LX$, L = PPh_3, PBu_3; X = Cl, Br, I, were prepared and purified by published methods (10–12). FTIR spectra were obtained with a Bruker IFS 85 spectrophotometer with 1 cm^{-1} resolution. Samples were cooled with a CTI-Cryogenics Model 22 cryocooler attached to a 350R compressor system. Temperatures were controlled and monitored using a Lake Shore Cryotronics silicon diode sensor (DT500 DRC) in conjunction with a model DRC 80C temperature controller.

The solvent used in the spectroscopic studies, 1,2-epoxyethylbenzene, was obtained from Aldrich and used without further purification.

Measurements of the extinction coefficients

A 1,2-epoxyethylbenzene (1.0 mL) solution of *trans-*$(\eta^5\text{-}C_5H_5)Mo(CO)_2PBu_3I$ (0.0083 g) was prepared and its FTIR spectrum measured at 298 K in a 0.127 mm path length FTIR cell. A similar measurement was made on the same cell containing only the 1,2-epoxyethylbenzene solvent. From the observed absorbances at 1954 and 1873 cm^{-1}, of 0.125 and 0.281, the respective extinction coefficients of the bands were determined as 647 and 1456 M^{-1} cm^{-1}.

The extinction coefficients were also measured at 12 K from the samples used for photolysis experiments. The concentration was calculated on the basis of FTIR absorbance at room temperature. The spectra obtained at lower temperatures were then subtracted from the spectrum of pure solvent at these temperatures and the extinction coefficients calculated from the difference, i.e. the absorbance solely due to *trans-trans-*$(\eta^5\text{-}C_5H_5)Mo(CO)_2PBu_3I$. The extinction coefficients calculated in this manner are given in Table 1.

The extinction coefficients of the stable complexes were all measured in the same way, the results for the different complexes are given in Table 1.

For unsaturated intermediates the extinction coefficients were calcaulated on the basis of assuming a 100% yield for the photolysis. The thermal back reaction with CO which should yield the same result was also determined and gave agreeable results within the estimated 20% error.

Photolysis of $(\eta^5\text{-}C_5H_5)Mo(CO)_2PR_3X$

Several experiments were conducted in the same manner; here we describe a typical experiment. The complex, *trans-*$(\eta^5\text{-}C_5H_5)Mo(CO)_2PPh_3I$, was dissolved in 1,2-epoxyethylbenzene to produce a solution of optical density 0.55 for its most intense IR absorption band in the carbonyl region at 1883 cm^{-1}. The sample was then transferred to a CaF_2 faced FTIR cell and loaded into the cold head of the cryostat. The sample chamber was evacuated and then cooled to 12 K. During the cool down FTIR spectra were obtained at different temperatures. At 12 K the sample was photolysed with the water filtered output of a 75 W high pressure Hg lamp for 10 s. The FTIR was then recorded again and the procedure of photolysis-record spectra was repeated until no further reaction occurred upon photolysis. At this time the compressor was turned off and the sample allowed to warm. FTIR spectra were recorded at 10 K intervals during warming until a temperature of 100 K was reached. At this point the sample was cooled to 12 K and its FTIR spectra obtained.

The FTIR spectra obtained are discussed in the Results section. The sample was then warmed to room temperature and its FTIR spectrum recorded. In other experiments the use of both H_2O and a Corning 7-51 filter isolated the wavelength range 320–400 nm for photolysis.

Acknowledgment

We wish to thank the Natural Sciences and Engineering Research Council of Canada for support of this work through an operating grant.

[4]A referee has suggested that the C_s structure observed in ref. 5 is a result of rotomers of the $\eta^5\text{-}C_5H_5$ ring. We agree that this is possible in the case of ref. 5. However, we rule this out in our case since such rotomers would not be expected at temperatures as high as 100 K nor would they be expected to result in stereospecific chemistry in their reactions with CO.

[5]The supposition that solvation is weak is based on the assumption that the reaction with CO which occurs at temperatures as low as 20 K is an indication of the weak interaction between metal and solvent. This conclusion is valid if the mechanism of replacement of solvent is dissociative.

Can. J. Chem. Downloaded from www.nrcresearchpress.com by 195.138.81.100 on 09/07/12
For personal use only.

1. R. H. HILL and B. J. PALMER. Organometallics, **8**, 1651 (1989).
2. F. W. B. EINSTEIN, A. H. KLAHN-OLIVA, D. SUTTON, and K. G. TYERS. Organometallics, **5**, 53 (1986).
3. D. G. ALWAY and K. W. BARNETT. Inorg. Chem. **19**, 1533 (1980).
4. R. B. KING and R. H. REIMANN. Inorg. Chem. **15**, 183 (1976).
5. R. B. HITAM and A. J. REST. Organometallics, **8**, 1598 (1989).
6. R. H. HOOKER, K. A. MAHMOUD, and A. J. REST. J. Chem. Soc. Dalton, 1231 (1990).
7. R. N. PERUTZ and J. J. TURNER. J. Am. Chem. Soc. **97**, 4791 (1975).
8. M. POLIAKOFF and E. WEITZ. Acc. Chem. Res. **20**, 408 (1987) and references therein.
9. J. A. TIMNEY. Inorg. Chem. **18**, 2502 (1979).
10. D. L. BEACH, M. DATTILO, and K. W. BARNETT. J. Organomet. Chem. **140**, 47 (1977).
11. D. L. BEACH and K. W. BARNETT. J. Organomet. Chem. **97**, C27 (1975).
12. D. J. BLUMER, K. W. BARNETT, and T. L. BROWN. Organomet. Chem. **173**, 71 (1979).

Can. J. Chem. Downloaded from www.nrcresearchpress.com by 195.138.81.100 on 09/07/12
For personal use only.

The synthesis and X-ray structures of η^1-, η^3-, and η^5-dienolate complexes of manganese carbonyl

ANDREW P. MASTERS, JOHN F. RICHARDSON,[1] AND TED S. SORENSEN
The Department of Chemistry, University of Calgary, Calgary, Alta., Canada T2N 1N4

Received June 18, 1990

ANDREW P. MASTERS, JOHN F. RICHARDSON, and TED S. SORENSEN. Can. J. Chem. **68**, 2221 (1990).

The η^1-, η^3-, and η^5-ester dienolate complexes of $Mn(CO)_n$ have been prepared and the crystal structures of the phenyl ester member have been obtained for all three bonding modes. The allyl (*anti*-η^3) member shows some bonding distortions compared to a simple allyl ligand. The structure of the η^5-1-oxapentadienyl ligand complex is substantially different from a rhenium analog in that the organic ligand is non-planar with significantly different bond distances. The η^5-complex reacts rapidly with triphenylphosphine to generate the *syn*-η^3-complex.

Key words:

ANDREW P. MASTERS, JOHN F. RICHARDSON et TED S. SORENSEN. Can. J. Chem. **68**, 2221 (1990).

On a préparé les complexes η^1-, η^3- et η^5-esters diénoliques du $Mn(CO)_n$ et on a déterminé les structures cristallines des esters phényliques des trois modes de liaison. Par comparaison avec le produit allylique portant un ligand simple, le dérivé allylique (*anti*-η^3) présente quelques distorsions de liaison. Comparée à la structure de son analogue du rhénium, celle du complexe portant un ligand η^5-1-oxapentadiényle est très différente; son ligand organique n'est pas plan et les distances des diverses liaisons sont assez différentes. Le complexe η^5 réagit rapidement avec la triphénylphosphine pour donner le complexe *syn*-η^3.

Mots clés :

[Traduit par la revue]

Introduction

The interconversion of transition metal complexes containing η^1-, η^3-, or η^5-bonded acyclic ligands is an important area of organometallic chemistry. To date interest in acyclic groups capable of such interconversions has largely centered on the pentadienyl ligand (1), however a dienolate ligand also has the same possible bonding modes (2). In this paper we describe the preparation and X-ray structural characterization of an organometallic series having the same organic ligand but, separately, involving all three bonding types. The work encompasses the manganese carbonyl complexes of the dienolate esters shown below. Crystals suitable for X-ray crystallographic study were obtained only for the series with R = Ph.

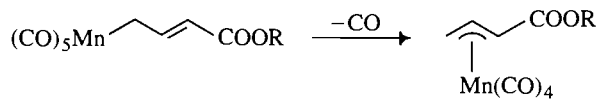

R = Et **1***a* **2***a*
R = Ph **1***b* **2***b*

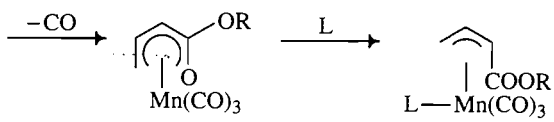

3*a*
3*b*

4 (L = PPh_3)

Simple η^1-alkyl or allyl, η^3-allyl, and η^5-pentadienyl complexes of $Mn(CO)_n$ are well-known.[2] However, functionalized derivatives such as **1**, **2**, or **3** have been less studied and there are no examples of these having been prepared by the stepwise procedure described here, although this procedure has recently been reported for the pentadienyl ligand itself (4). Several η^5-dienolate complexes of transition metals have been prepared by unusual routes (5) and a rhenium complex has been characterized by X-ray (6). η^3-Dienolate complexes are known for other transition metals but these are relatively rare for manganese and have not been structurally characterized.

The preparation of the η^5-dienolate complex was also of interest synthetically. The goal, based on dienyl chemistry (7), was to show that reforming the η^3-complex would yield the isomeric *syn*-η^3-geometric isomer, **4**.

Results and discussion

Details for the preparation of the η^1-complex **1***a* have been described elsewhere (2). It is readily made from $Na^+[Mn(CO)_5^-]$ and ethyl (*E*)-4-chloro-2-butenoate (**6**, R = Et) in THF and can be isolated as a stable, air-sensitive, pale yellow oil.

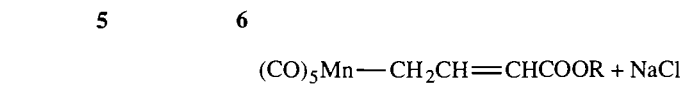

5 **6** **1**

The corresponding phenyl ester, **1***b*, could be made in a similar way, in this case giving a somewhat less air-sensitive crystalline solid. Both η^1-complexes could be decarbonylated by heating the compounds at 80°C without solvent to give the corresponding yellow η^3-dienolate complexes **2***a*, *b* in high yields. Further decarbonylation of **2***a*, *b* was achieved by refluxing them in cyclohexane for 12 h to yield the η^5-dienolate complexes **3***a*, *b*. These were isolated by flash chromatography as an air-sensitive dark yellow oil and a dark orange crystalline solid, respectively, which were very soluble in pentane. The phenyl ester **3***b* could be stored for several months under nitrogen at 0°C. Attempts to decarbonylate the η^3-complex **2***a* by heating the neat compound to 120°C or by irradiation of a solution (hexane or THF) with an ultraviolet lamp resulted in further evolution of carbon monoxide, but this was accompanied by considerable decomposition. Although there was some evidence for the formation of the η^5-complex the yields were

[1]Present address: Department of Chemistry, University of Louisville, Louisville, Ky 40292, U.S.A.

[2]For examples of η^1- and η^3-allyl manganese carbonyl complexes see ref. 3*a*, for examples of η^5-dienyl manganese carbonyl complexes see ref. 3*b*.

Can. J. Chem. Downloaded from www.nrcresearchpress.com by 195.138.81.100 on 09/07/12
For personal use only.

TABLE 1. ^1H and ^{13}C NMR data for the η^1, η^3, and η^5 dienolate complexes **1**, **2**, and **3** (chemical shifts are in ppm, coupling constnts in Hz)

(*a*) ^1H NMR

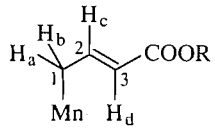

1

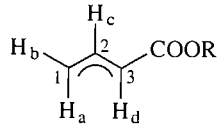

2

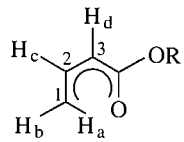

3

Compound	H_a	H_b	H_c	H_d
1*a*	1.88 d J_{ac} = 9.6		7.45 dt	5.65 d J_{cd} = 15
1*b*	1.94 d J_{ac} = 9.7		7.65 m	5.81 d J_{cd} = 15
2*a*	2.26 d J_{ac} = 13, J_{ab} = 2	2.99 d J_{bc} = 8	5.67 m	2.53 d J_{cd} = 10
2*b*	2.34 d J_{ac} = 14, J_{ab} = 2	3.09 d J_{bc} = 7	5.97 m	2.70 d J_{cd} = 10
3*a*	1.93 d J_{ac} = 14	3.54 d J_{bc} = 10	5.46 m	4.86 d J_{cd} = 7
3*b*	2.03 d J_{ac} = 13	3.61 d J_{bc} = 10	5.58 m	5.12 d J_{cd} = 7

(*b*) ^{13}C-NMR

Compound	C1	C2	C3
1*b*	8.2	161.1	110.2
2*b*	46.5	96.5	45.2
3*b*	62.0	107.5	57.0

very low. In some recently published (8) η^1- and η^3-Cp(CO)Fe – ester dienolate work, an attempt to prepare the corresponding η^5-complex was unsuccessful. It is not clear why the iron and manganese systems should be different in this regard.

Spectroscopic characterization of the η^1-, η^3-, and η^5-complexes

The IR spectra for the η^1- and η^3-bonded complexes **1** and **2** contain a weak band in the carbonyl region (1738 cm^{-1} for **1***b* and 1736 cm^{-1} for **2***b*) assigned to the carbonyl stretch of the ester functionality. The position of this band is similar to what one would expect for an α,β-unsaturated ester. This band is not present in the spectra for the η^5-complexes. Similarly, a weak band at 1618 cm^{-1} for the η^1-complex **1***b*, assigned to the stretching mode of the free double bond, is not observed in either the η^3- or η^5-complexes.

The ^1H NMR spectral data and assignments for complexes **1**, **2**, and **3** are presented in Table 1. For the η^3-complex, there are two possible geometries, *anti* (H_c—H_d *trans*) or *syn* (H_c—H_d *cis*). The assignment assumes the *anti* configuration observed in the solid state (*vide infra*) with the coupling constants $J_{ac} > J_{bc}$ and $J_{cd} > J_{bc}$. The size of the J_{cd} coupling constant (10 Hz) is somewhat ambiguous, but one expects that the *anti* isomer will have formed because this geometry is present in the η^1-complex and it is expected to be the thermodynamically more stable product. The methylene protons of the ethyl group in the η^3-complex **2***a* are diastereotopic and appear as a complex multiplet. This is not observed for the η^5-complex **3***a*.

The reaction of the η^5-complex **3**b *with triphenylphosphine*

This complex was found to react rapidly with triphenylphosphine at room temperature to give high yields of the *syn*-η^3-complex **4**. The ^1H NMR spectrum of this adduct shows a J_{cd} coupling constant of 6.7 Hz, confirming that this isomer now has a *syn* geometry and coincidentally providing confirmatory evidence that the original η^3-isomer had the *anti* geometry.

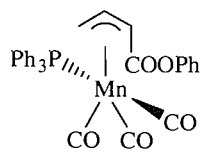

4

The structures of the η^1-, η^3-, and η^5-complexes

Bond length and bond angle data for the three complexes are given in Tables 2 and 3. Ortep representations of the three structures are given in Figs 1, 2, and 3. A schematic showing the relationship between the three structures is presented in Fig. 4.

The structure of the η^1-complex is close to an ideal octahedral arrangement of the carbonyl and organic ligands. There is only a small distortion of the angles between the carbonyl ligands (88.5–93.7° compared to the ideal 90°) but a slightly greater distortion relative to the organic ligand; three C(1)—Mn—carbonyl angles are less than 90° (82.5–88.5°) indicating a deviation toward the ligand while C(1)—Mn—C(11) is 91.4°, probably for steric reasons as it is juxtaposed with C(2) of the ligand. The axial Mn—CO bond distance (Mn—C(13), 1.824(4) Å) is significantly shorter than any of the equatorial Mn—CO distances (average distance 1.858 Å), presumably because of increased π-character of the axial bond which is trans to the σ-bonded ligand. Shorter axial Mn—CO bond lengths relative to mean equatorial Mn—CO distances have been observed in other manganese carbonyl complexes (9). The Mn—C(1) bond length (2.214(3) Å) is comparable to that for other manganese carbonyl alkyl complexes such as $MeMn(CO)_5$ (2.185(11) Å) (10) and $CH_3COCH_2Mn(CO)_4(PPh_3)$ (2.210(5) Å) (11).

The structure of the η^3-complex **2***b* is similar to those reported for related manganese complexes (7, 12, 13), with the η^3-dienolate ligand adopting the W-conformation. The allyl

Can. J. Chem. Downloaded from www.nrcresearchpress.com by 195.138.81.100 on 09/07/12
For personal use only.

Can. J. Chem. Downloaded from www.nrcresearchpress.com by 195.138.81.100 on 09/07/12
For personal use only.

TABLE 2. Bond lengths (Å) for the complexes **1***b*, **2***b*, and **3***b*

Bond	η^1 (**1***b*)	η^3 (**2***b*)	η^5 (**3***b*)
Mn—C(1)	2.214(3)	2.254((4)	2.152(4)
Mn—C(2)		2.137(4)	2.097(4)
Mn—C(3)		2.186(3)	2.159(5)
Mn—C(4)			2.369(5)
Mn—O(1)			2.159(3)
Mn—C(11)	1.848(4)	1.893(4)	1.751(5)
Mn—C(12)	1.852(4)	1.813(4)	1.810(5)
Mn—C(13)	1.824(4)	1.816(4)	1.824(4)
Mn—C(14)	1.865(3)	1.826(4)	
Mn—C(15)	1.868(3)		
C(1)—C(2)	1.453(5)	1.381(6)	1.400(7)
C(2)—C(3)	1.324(5)	1.412(5)	1.401(7)
C(3)—C(4)	1.456(5)	1.460(5)	1.441(7)
C(4)—O(1)	1.189(5)	1.198(5)	1.237(6)
C(4)—O(2)	1.365(4)	1.367(4)	1.352(6)
C(5)—O(2)	1.410(5)	1.409(5)	1.410(5)
C(5)—C(6)	1.356(6)	1.356(6)	1.363(7)
C(5)—C(10)	1.344(6)	1.368(6)	1.361(7)
C(6)—C(7)	1.354(8)	1.382(7)	1.377(9)
C(7)—C(8)	1.346(9)	1.362(9)	1.368(10)
C(8)—C(9)	1.354(9)	1.380(8)	1.363(9)
C(9)—C(10)	1.360(7)	1.373(7)	1.381(8)
C(11)—O(11)	1.133(4)	1.127(5)	1.151(6)
C(12)—O(12)	1.129(4)	1.144(5)	1.138(5)
C(13)—O(13)	1.131(4)	1.138(4)	1.136(6)
C(14)—O(14)	1.130(4)	1.135(5)	
C(15)—O(15)	1.124(4)		

TABLE 3. Selected bond angles (deg) for the complexes **1***b*, **2***b*, and **3***b*

Bonds	Angle		
	η^1 (**1***b*)	η^3 (**2***b*)	η^5 (**3***b*)
C(1)—Mn—C(11)	91.4(1)	101.9(2)	102.0(2)
C(1)—Mn—C(12)	88.5(1)	94.2(1)	87.1(2)
C(1)—Mn—C(13)	175.2(1)	161.0(1)	167.3(2)
C(1)—Mn—C(14)	82.5(1)	83.8(2)	
C(1)—Mn—C(15)	84.5(1)		
C(3)—Mn—C(11)		94.0(2)	103.9(2)
C(3)—Mn—C(12)		160.8(2)	154.9(2)
C(3)—Mn—C(13)		96.3(1)	102.9(2)
C(3)—Mn—C(14)		90.4(2)	
O(1)—Mn—C(11)			169.3(2)
O(1)—Mn—C(12)			100.9(2)
O(1)—Mn—C(13)			89.9(2)
C(11)—Mn—C(12)	88.5(1)	86.3(2)	89.8(2)
C(11)—Mn—C(13)	93.1(2)	87.6(2)	89.7(2)
C(11)—Mn—C(14)	173.8(1)	173.8(2)	
C(11)—Mn—C(15)	89.0(2)		
C(12)—Mn—C(13)	93.5(2)	102.9(2)	98.2(2)
C(12)—Mn—C(14)	90.5(2)	90.9(2)	
C(12)—Mn—C(15)	172.5(2)		
C(13)—Mn—C(14)	93.1(1)	87.6(2)	
C(13)—Mn—C(15)	93.7(2)		
C(14)—Mn—C(15)	91.2(2)		
Mn—C(1)—C(2)	110.6(2)		
C(1)—C(2)—C(3)	126.7(3)	122.5(4)	122.9(4)
C(2)—C(3)—C(4)	119.6(3)	118.6(3)	120.8(4)
C(3)—C(4)—O(1)	127.4(3)	126.4(3)	122.2(4)
C(3)—C(4)—O(2)	111.2(3)	111.2(3)	114.8(4)
O(1)—C(4)—O(2)	121.4(3)	122.3(3)	122.8(4)
C(4)—O(2)—C(5)	115.9(3)	116.8(3)	118.7(3)

ligand plane (C(1)—C(2)—C(3)—C(4)) intersects the equatorial plane of the carbonyl ligands (C(12)—Mn—C(13)) at an angle of 77.1°, which compares with 70.7° in *syn*-η^3-$(C_5H_7)Mn(CO)_3PMe_3$ (7) and 71.0° in the allyl complex η^3-$(C_3H_5)Mn(CO)_2(P(OMe_3)_2$ (12). The bond angle of the allyl portion of the dienolate ligand (C(1)—C(2)—C(3)) is comparable to that in η^3-$(C_3H_5)Mn(CO)_2(P(OMe_3)_2$ (122.5(4)° vs. 124.5(15)°), and is somewhat smaller than the corresponding angle for the η^1-complex (126.7(3)°) where C(2) and C(3) are not coordinated. There is some asymmetry in the allyl part of the ligand, the C(1)—C(2) bond length (1.381(6) Å) is significantly shorter than that for C(2)—C(3) (1.412(5) Å), a feature which is also observed (7) in the related complex *syn*-η^3-$(C_5H_7)Mn(CO)_3PMe_3$. The allyl ligand carbon atoms C(1) and C(3) are also bonded to manganese in an asymmetric fashion, indicated by the distances of these atoms to the equatorial plane (−0.345 and 0.023 Å), and the Mn—allyl bond lengths (Mn—C(1) 2.254(4) Å and Mn—C(3) 2.186(3) Å). The Mn—C(3) distance is comparable to that for the σ-bond in the η^1-complex **1***b* (2.214(3) Å). A possible explanation for this arrangement is that the allyl ligand has a small degree of σ—π bonding character, as shown below **7**, rather than a completely delocalized π-allyl bonding.

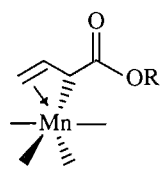

7

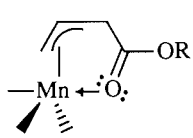

8

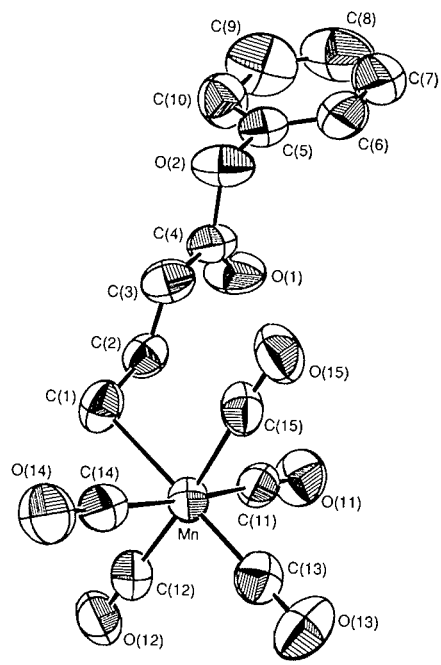

FIG. 1. ORTEP drawing (50% probability level) of the η^1-complex **1***b*.

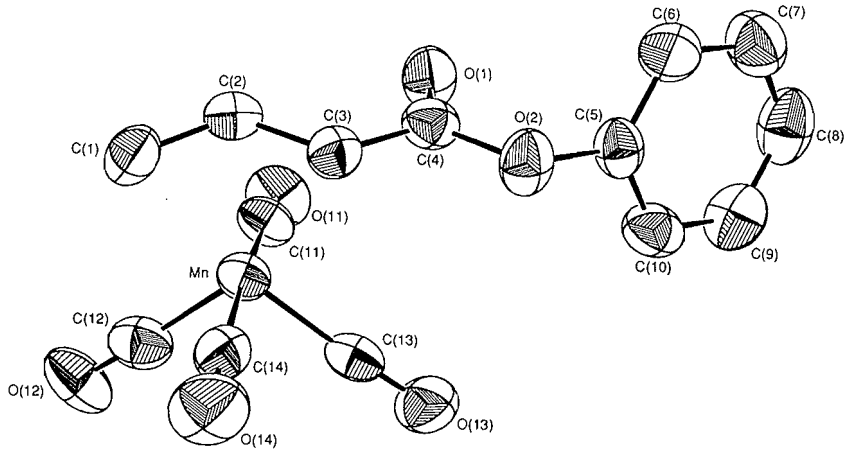

FIG. 2. ORTEP drawing (50% probability level) of the η^3-complex **2***b*.

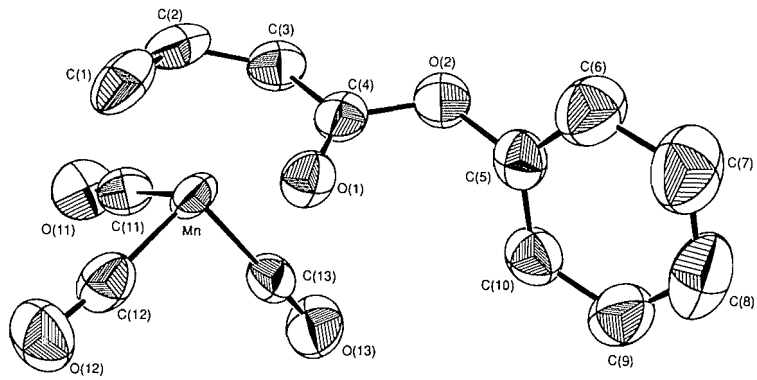

FIG. 3. ORTEP drawing (50% probability level of the η^5-complex **3***b*.

After our studies were completed, an X-ray structure of an η^3-iron ester dienolate complex was reported (8). In contrast to the manganese structure reported here, the two allyl bond lengths in the iron complex are nearly identical, 1.430(6) and 1.421(6) Å. It is difficult to compare other parameters because the iron complex lacks defined symmetry planes (Cp and CO are the only other ligands).

The general structural features of the η^5-complex are similar to those for η^5-cyclohexadienylmanganese tricarbonyl (14) and the related complex (6) η^5-$(C_4H_5O)Re(PPh_3)_2CO$, C(1) is *trans* to C(13), C)3) is *trans* to C(12) and O(1) is *trans* to C(11) with these atoms forming a very distorted octahedron. However, unlike the rhenium complex the dienolate ligand is not quite planar, O(1) and C(4) are out of the plane C(1)—C(2)—C(3) by −0.218 and 0.142 Å, respectively. Another important difference is that the C(3)—C(4) bond is longer than the corresponding bond in the rhenium complex (1.441(7) vs. 1.40(2) Å) with a concomitant shortening of the C(4)—O(1) bond (1.237(6) vs. 1.30(1) Å for the rhenium complex). The Mn—C(4) distance for this complex is also significantly longer than the other Mn—C distances (see Table 2). This distortion is consistent with a degree of n-donor character in the complex as shown in **8**, whereas the rhenium complex more resembles a pentadienyl ligand → M case. Unlike the η^3-complex the allyl part of the organic ligand is quite symmetrical as indicated by the bond distances C(1)—C(2) (1.400(7) Å), C(2)—C(3) (1.401(7) Å), Mn—C(1) (2.152(4) Å), and Mn—C(3) (2.159(5) Å).

In comparing the three structures (see Fig. 4 and Table 2) it is clear that there is a large spread in the Mn—CO distances (1.751(5)–1.893(4) Å). The longest Mn—CO distances occur where CO is *trans* to CO *i.e.* Mn—C(11), Mn—C(12), Mn—C(14), and Mn—C(15) in the η^1-complex, and Mn—C(11) and Mn—C(14) in the η^3-complex. The shortest Mn—CO distance appears in the η^5- complex for the carbonyl which is *trans* to O(1), Mn—C(11). This substantial *trans* influene of O(1) can be explained by donation to manganese by this oxygen with accompanying donation into the antibonding π-orbital of the *trans* CO. Such an effect has been observed in other manganese carbonyl complexes containing oxygen donor ligands (15). The average Mn—CO distance in the η^5-complex is also the shortest of the three (1.795 Å compared to 1.851 Å for **1***b* and 1.837 Å for **2***b*). This overall trend would be consistent with an increasing overall π-contribution from the dienolate ligand as the coordination of this ligand is increased.

The axial CO's in the η^3- and η^5-complexes are bent towards the dienolate ligand compared to a true octahedron as indicated by angle C(12)—Mn—C(13) (102.9(2)° in **2***b*, 98.2(2)° in **3***b*). In the case of the η^3-complex such a distortion would accommodate the restricted "bite angle" of the allyl ligand. Coversely in the η^3-complex, the equatorial CO's are bent away from the dienolate ligand as shown by the angles C(11)—Mn—C(14) and C(11)—Mn—C(12) (173.8(2) and 86.3(2)°, respectively). In contrast to the η^3-complex the *trans* influence of the cordinated oxygen in the η^5-complex allows

Can. J. Chem. Downloaded from www.nrcresearchpress.com by 195.138.81.100 on 09/07/12
For personal use only.

TABLE 4. Crystallographic parameters

Parameter	Value		
	η^1 (**1***b*)	η^3 (**2***b*)	η^5 (**3***b*)
Formula	$C_{15}H_9MnO_7$	$C_{14}H_9MnO_6$	$C_{13}H_9MnO_5$
Formula wt.	356.17	328.16	300.15
Space group	$P2_1/c$	$Pna2_1$	*Pbca*
a, Å	18.834(5)	17.785(1)	12.568(1)
b, Å	6.563(1)	7.045(1)	11.352(1)
c, Å	12.730(3)	11.303(1)	18.100(2)
β, deg	91.58(1)	90	90
Vol, Å^3	1572.9(6)	1416.2(2)	2582.5(4)
Z	4	4	8
D_c, g/cm^3	1.50	1.54	1.54
F(000)	720	664	1216
Radiation	MoKα(0.71069)	MoKα	MoKα
Monochromator	Graphite	Graphite	Graphite
Temp, °C	23(1)	23(1)	23(1)
Scan range: 1.5(w + 0.34 tan θ)	0.70	0.66	0.66
Scan speed, min^{-1}	0.5 to 5.2	0.5 to 3.3	0.5 to 3.3
Max θ, deg	25	30	25
No. unique reflections collected	2757	2153	2264
No. reflections observed ($I > 3\sigma(I)$)	1798	1547	1231
Crystal dimensions, mm	0.12 × 0.45 × 0.54	0.23 × 0.43 × 0.49	0.18 × 0.30 × 0.44
μ(MoKα), cm^{-1}	9.16	10.04	10.87
Gaussian grid	18 × 6 × 12	18 × 8 × 12	10 × 10 × 16
Min/max trans factors	0.640, 0.864	0.581, 0.816	0.719, 0.826
No. variables	208	189	172
No. obs[a]	2313	1863	1806
Max Δ/σ	0.01	0.02	0.01
GOF	1.03	1.02	1.05
Agreement factors:[b] *R*	0.040	0.037	0.042
R_w	0.031	0.029	0.033

[a]Including those reflections for which $I > 3\sigma(I)$.
[b]$R = \Sigma(||F_o| - |F_c||)/\Sigma|F_o|$; $R_w = [\Sigma w(|F_o| - |F_c|)^2/\Sigma w|F_o|^2]^{1/2}$.[0]

C(11) to take up a more octahedral site as indicated by the near perfect octahedral angles C(11)—Mn—C(12) and C(11)—Mn—C(13) (89.8(2) and 89.7(2)°, respectively).

Experimental

All procedures were performed under an atmosphere of argon or dried nitrogen using a combination of syringe, transfer needle, and Schlenk techniques. Infrared analysis was performed using a Nicolet 5DX FT instrument. Mass spectrometric analyses were obtained on a Kratos MS80, and ^{1}H, ^{13}C NMR spectra on a Varian XL-200.

Tetrahydrofuran was distilled from benzophenone ketyl under nitrogen, hexane, and deuterated solvents were dried over sieve dust prior to use. Flash chromatography was performed using silica (Merck 9385) and methylene chloride.

Phenyl 4-chloro-2-butenoate was prepared by treating phenyl 2-butenoate (from 2-butenoyl chloride and phenol) with *N*-bromosuccinimide followed by treatment of the purified bromide with lithium chloride in dimethylformamide. The preparation of η^1-4-oxo-4-ethoxy-2-butenyl manganese pentacarbonyl **1***a* has been described elsewhere (2).

η^1-4-Oxo-4-phenoxy-2-butenyl manganese pentacarbonyl **1**b

The anion $Na^+[Mn(CO)_5^-]$ was prepared according to the literature procedure (16) from 0.5 g (1.28 mmol) of dimanganese decacarbonyl in 40 mL THF. This solution was decanted using a transfer needle into a flask containing 0.5 g (2.54 mmol) of phenyl 4-chloro-2-butenoate in 5 mL of THF and the mixture stirred for 10 min. The solvent was then evaporated to give a yellow solid residue which was extracted with 4 × 50 mL of warm (40°C) hexane. The extract was filtered and concentrated to a volume of 100 mL and cooled to −10°C. On standing 0.75 g of cream cubic crystals were obtained (83% yield), melting point 95–96°C (decomposed).

Infrared (hexane, cm^{-1}): 2113(m), 2052(w), 2021(vs), 1999(s), 1738(m), 1618(w). ^{1}H NMR ($CDCl_3$): 7.65(dt, 1H, *J* = 15 Hz and 9.6 Hz), 7.1–7.5(m, 5H), 5.81(d, 1H, *J* = 15 Hz), 1.94(d, 2H, *J* = 9.7 Hz). ^{13}C NMR ($CDCl_3$): 8.2(CH_2), 110.2(CH), 121.8(CH), 125.3(CH), 129.3(CH), 161.1(C). Mass spectrum (*m/e*, % base peak): 328 (1, M − CO) 300(1), 272(1), 244(1), 216(40), 148(66), 94(72). *Anal.* calcd. for $C_{15}H_9MnO_7$:C 50.58, H 2.31, found: C 50.01, H 2.31.

η^3-4-Oxo-4-phenoxy-2-butenyl manganese tetracarbonyl **2**b

Complex **1***b* (0.34 g, 0.94 mmol) was heated to 85–90°C for 30 min, by which time the evolution of carbon monoxide had ceased. The resulting semisolid yellow residue was then dissolved in 20 mL hexane, the solution filtered, and cooled to −20°C. After standing overnight, 0.19 g of fine yellow needles were obtained. These were recrystallized to give an analytically pure sample (0.17 g, 55% yield) mp 66–67°C.

Infrared (hexane, cm^{-1}): 2084(s), 2021(w), 2001(vs), 1975(s), 1736(m). ^{1}H NMR ($CDCl_3$): 7.12–7.53 (m, 5H), 5.79 (ddd, 1H), 3.09 (d, 1H, *J* = 7.3 Hz), 2.70 (d, 1H, *J* = 10.3 Hz), 2.37 (d, 1H, *J* = 14 Hz). ^{13}C NMR ($CDCl_3$): 45.2(CH), 46.5(CH_2), 96.5(CH), 121.7(CH), 125.8(CH), 129.4(CH), 150.7(C). Mass spectrum (*m/e*, %): 300(0.5, M − CO), 272(1), 244(17), 217(11), 216(80), 149(9), 148(98), 94(143), 69(14), 68(31), 66(12), 65(13), 56(10), 55(100). *Anal.* calcd. for $C_{14}H_9MnO_6$: C 51.24, H 2.76; found: C 51.07, H 2.76.

Can. J. Chem. Downloaded from www.nrcresearchpress.com by 195.138.81.100 on 09/07/12
For personal use only.

Can. J. Chem. Downloaded from www.nrcresearchpress.com by 195.138.81.100 on 09/07/12
For personal use only.

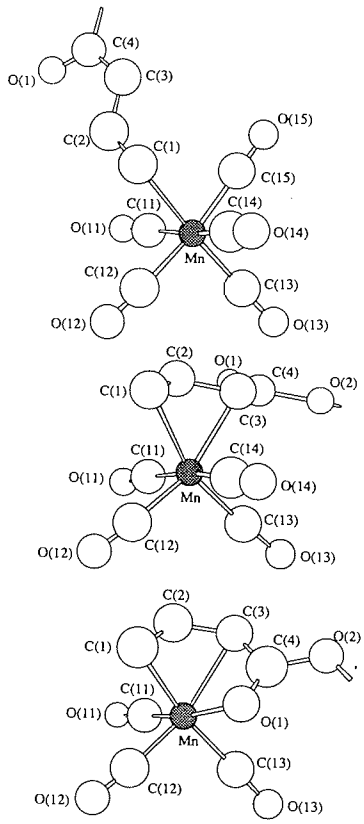

FIG. 4. Models of the crystal structures of **1***b*, **2***b*, and **3***b* showing the relationships between the three structures (C(12)—Mn—C(13) are in the same plane in each model).

η^3-4-Oxo-4-ethoxy-2-butenyl manganese tetracarbonyl **2**a

In a round-bottomed flask attached to a bubbler, 0.1 g of **1***a* was heated to 80°C for 1 h, by which time the evolution of carbon monoxide had ceased. The resulting yellow oil was dissolved in 1 mL of methylene chloride and purified by flash chromatography to yield **2***a* as a yellow oil (0.08 g, 88% yield).

Infrared (CH_2Cl_2, cm^{-1}): 2090(m), 2000(s), 1970(s), 1710(m). ^1H NMR, ($CDCl_3$): 1.30(t, J = 7.2 Hz, 3H); 2.26(d, J = 12.9 Hz, 1H); 2.53(d, J = 10.4 Hz, 1H); 2.99(d, J = 8.5 Hz, 1H); 4.22(tq, 2H); 5.67(ddd, 1H). ^{13}C NMR, ($CDCl_3$): 14.4(CH_3), 45.3(CH_2), 46.8(CH), 60.5(CH_2), 96.1(CH). Mass spectrum (*m/e*, %base peak): 224(1), 196(5), 168(10), 124(4), 100(20), 68(12), 55(23), 43(100). *Anal.* calcd. for $C_{10}H_9MnO_6$: C 42.88 H 3.24; found: C 40.11, H 3.04. The elemental analysis for this compound could not be improved, even by repeated purification.

η^5-4-Oxo-4-phenoxy-2-butenyl manganese tricarbonyl **3**b

Complex **2***b* (0.49 g, 1.49 mmol) was dissolved in 5 mL cyclohexane and the solution was refluxed for 10 h under a stream of nitrogen. The deep yellow solution was then concentrated to 2 mL under vacuum and applied directly to a flash chromatography column. The product eluted first followed by a small amount of unreacted **2***b*. After evaporation of the solvent the crude product solidified on standing to give large orange plates (0.38 g, 84% yield) which were analytically pure, mp, 48°C. Crystals suitable for X-ray crystallography were obtained from a concentrated solution in pentane maintained at −20°C for several days.

Infrared (CH_2Cl_2, cm^{-1}): 2036(s), 1959(s), 1932(s). ^1H NMR ($CDCl_3$): 6.9–7.45 (m, 5H), 5.58 (ddd, 1H), 5.12 (d, 1H, J = 6.7 Hz), 3.61 (d, 1H, J = 9.6 Hz), 2.03 (d, 1H, J = 13.6 Hz). ^{13}C NMR ($CDCl_3$): 57.0(CH), 62.0(CH_2), 107.5(CH), 121.2(CH), 126.6(CH), 129.7(CH). Mass spectrum (*m/e*, %): 300(0.1, M), 272(1), 244(12), 216(61), 148(79), 94(47), 69(10), 68(36), 66(12), 65(13), 55(81). *Anal.* calcd. for $C_{13}H_9MnO_5$: C 52.02 H 3.02; found: C 52.10, H 3.04.

TABLE 5. Atomic positional parameters (×10^4) and B_{eq} (×10) for the η^1-complex **1***b*

Atom	*x/a*	*y/b*	*z/c*	B_{eq}
Mn	3732.4(3)	455.7(7)	1120.3(4)	37.8(2)
C(1)	2657(2)	−491(5)	569(3)	49(2)
C(2)	2430(2)	685(5)	−347(3)	45(2)
C(3)	1958(2)	2180(6)	−375(3)	50(2)
C(4)	1806(2)	3243(5)	−1359(3)	49(2)
C(5)	1070(2)	5712(6)	−2169(3)	49(2)
C(6)	1343(2)	7603(8)	−2300(4)	69(3)
C(7)	1158(3)	8693(8)	−3168(6)	92(4)
C(8)	699(4)	7939(11)	−3898(5)	103(4)
C(9)	418(3)	6072(10)	−3733(4)	96(4)
C(10)	604(2)	4928(6)	−2878(4)	67(2)
C(11)	3928(2)	1515(5)	−186(3)	44(2)
C(12)	4071(2)	−2036(5)	668(3)	45(2)
C(13)	4591(2)	1233(5)	1687(3)	47(2)
C(14)	3445(2)	−729(5)	2370(3)	43(2)
C(15)	3290(2)	2908(5)	1457(3)	47(2)
O(1)	2099(1)	3042(4)	−2168(2)	66(2)
O(2)	1259(1)	4588(4)	−1260(2)	61(1)
O(11)	4062(1)	2173(4)	−979(2)	65(2)
O(12)	4270(1)	−3550(4)	374(2)	66(1)
O(13)	5121(1)	1721(4)	2040(2)	71(2)
O(14)	3277(1)	−1497(4)	3118(2)	61(1)
O(15)	3045(1)	4434(4)	1615(2)	71(2)

η^5-4-Oxo-4-ethoxy-2-butenyl manganese tricarbonyl **3**a

This was prepared in the same way as **3***b* and yielded 0.036 g dark yellow oil (76%). This product was air-sensitive and decomposed slowly in solution even at reduced temperature.

Infrared (CH_2Cl_2, cm^{-1}): 2050(s), 1960(s), 1935(s). ^1H NMR ($CDCl_3$): 1.22(t, J = 7.1 Hz, 3H); 1.93(d, J = 14 Hz, 1H); 3.54(d, J = 9.5 Hz, 1H); 3.92(q, J = 7.2 Hz, 2H); 4.86(d, J = 7.0 Hz, 1H); 5.46(ddd, 1H). ^{13}C NMR ($CDCl_3$): 14.1(CH3), 57.0(CH), 60.3(CH_2), 61.9(CH_2), 105.7(CH).

η^3-4-Oxo-4-phenoxy-2-butenyl manganese tricarbonyl triphenylphosphine

Complex **3***b* (0.1 g, 0.33 mmol) was dissolved in 20 mL of hexane and 0.08 g (0.32 mmol) of finely ground triphenylphosphine was added in small portions with stirring. The yellow precipitate which forms was filtered off, and purified by flash chromatography to give 0.17 g (94% yield) of **4** as pure yellow microcrystals, mp 120°C.

Infrared (CH_2Cl_2, cm^{-1}): 2014(s), 1945(s), 1918(s), 1715(m). ^1H NMR ($CDCl_3$): 2.98(dd, J = 6.7 Hz, J_{HP} = 3.2 Hz, 1H); 3.17(d, J = 8.2 Hz, 1H); 3.52(d, J = 13.4 Hz, 1H); 4.33(m, J_{HP} = 13.1 Hz, 1H); 7.04–7.44(m, 5H); 7.44–7.60(m, 15H). *Anal.* calcd. for $C_{31}H_{24}MnO_5P$: C 66.20, H 4.30; found: C 66.04, H 4.54.

X-ray crystallography

Crystals of the three complexes were obtained from hexane or pentane solution as light yellow plates. The crystal data and experimental details are given in Table 4. Cell constants and orientation matrices were determined by least-squares refinement of the diffraction geometry of 25 accurately centered reflections. The choice of space groups was confirmed using the program TRACER (17) and by the successful solution and refinement of the structures. For compound **2***b* the alternate choice of space group *Pnma* required mirror symmetry or an inversion centre on the molecule, and was therefore ruled out. Data were collected at room temperature on an Enraf-Nonius CAD4 automated diffractometer using the ω–2θ scan technique. As a check on crystal and electronic stability three representative reflections were measured every 60 min. The intensities of these reflections showed only a statistical variation so a correction was not applied. The data were corrected for Lorentz and polarization effects as well as absorption (Gaussian method).

Can. J. Chem. Downloaded from www.nrcresearchpress.com by 195.138.81.100 on 09/07/12
For personal use only.

TABLE 6. Atomic positional parameters ($\times 10^4$) and B_{eq} ($\times 10$) for the η^3-complex **2***b*

Atom	*x/a*	*y/b*	*z/c*	B_{eq}
Mn	8178.3(2)	8626.2(6)	7500	35.0(2)
C(1)	8533(2)	5556(4)	7429(5)	45(2)
C(2)	7952(2)	5968(5)	6660(3)	38(2)
C(3)	7256(2)	6708(5)	7047(3)	37(2)
C(4)	6738(2)	7476(5)	6167(3)	39(2)
C(5)	5563(2)	9005(6)	5942(4)	38(2)
C(6)	5133(2)	7985(7)	5182(4)	48(2)
C(7)	4612(2)	8925(9)	4489(4)	57(3)
C(8)	4542(3)	108467(10)	4556(5)	58(3)
C(9)	4980(3)	11855(7)	5342(5)	55(2)
C(10)	5496(3)	10934(6)	6039(4)	47(2)
C(11)	8335(2)	9413(6)	5918(4)	43(2)
C(12)	9120(3)	9497(5)	7790(3)	49(2)
C(13)	7602(2)	10732(5)	7693(3)	39(2)
C(14)	8036(2)	8139(6)	9071(5)	41(2)
O(1)	6581(1)	7618(4)	5126(2)	49(1)
O(2)	6083(1)	8071(4)	6681(2)	45(1)
O(11)	8439(2)	9984(4)	5001(3)	58(2)
O(12)	9721(2)	10013(4)	7951(3)	68(2)
O(13)	7200(2)	11971(4)	7826(2)	55(1)
O(14)	7944(2)	7878(4)	10051(3)	60(2)

TABLE 7. Atomic positional parameters ($\times 10^4$) and B_{eq} ($\times 10$) for the η^5-complex **3***b*

Atom	*x/a*	*y/b*	*z/c*	B_{eq}
Mn	6710.1(5)	4310.6(6)	7846.1(3)	37.6(3)
C(1)	8107(3)	4304(4)	7159(3)	56(2)
C(2)	8139(4)	3394(4)	7681(3)	49(3)
C(3)	8049(3)	3590(4)	8442(3)	46(3)
C(4)	8029(3)	4770(4)	8736(3)	38(3)
C(5)	8195(4)	5953(4)	9813(2)	42(2)
C(6)	9103(4)	6549(5)	9984(3)	60(3)
C(7)	9018(5)	7573(6)	10387(4)	75(4)
C(8)	8042(6)	7983(5)	10600(3)	67(4)
C(9)	7145(5)	7369(6)	10422(3)	59(3)
C(10)	7215(4)	6334(5)	10023(3)	48(3)
C(11)	6028(4)	3065(4)	7529(3)	46(3)
C(12)	6078(4)	5187(4)	7135(3)	50(3)
C(13)	5713(4)	4502(5)	8568(3)	47(3)
O(1)	7699(2)	5619(3)	8373(1)	41(1)
O(2)	8318(3)	4859(2)	9458(2)	46(2)
O(11)	5576(2)	2255(3)	7309(2)	66(2)
O(12)	5692(3)	5662(3)	6651(2)	72(2)
O(13)	5076(3)	4596(4)	9010(2)	74(2)

The structures were solved by Patterson techniques which revealed the position of the Mn atom in each case. The remaining atoms were located in succeeding difference Fourier syntheses. Hydrogen atom positions were calculated using ideal geometries (d(C—H) = 1.0 Å) and added to the structure factor calculation iwth isotropic thermal parameters set to $1.3B_{iso}$ of the bonded C atom. H atom parameters were recalculated after each cycle but not refined. Refinement was carried out by full-matrix least-squares on F, minimizing the function $\Sigma w(|F_o| - |F_c|)^2$ where the weight w is defined as $[\sigma^2(F) + 0.00002F^2]^{-1}$ for the three structures. All computations were performed using the XRAY 76 system of programs (18) implemented on a Honeywell computer with a MULTICS operating system. Scattering factors for non-H atoms were those of Cromer and Mann (19) and those for H were taken from ref. 20. Anomalous dispersion effects were included in F_c; the values for $\Delta f'$ and $\Delta f''$ were those of Cromer (21). Refinement of the enantiomeric model of the η^3-complex showed no significant improvement in the agreement factors.

The models converged with the largest Δ/σ being less than 0.02 in all structures. The highet peaks of residual electron density were 0.44(8), 0.45(7), and 0.40(8) e Å^3 for the η^1-, η^3-, and η^5-complexes respectively, and were associated with the Mn atom in each case. Plots of $\Sigma(|F_o| - |F_c|)^2$ vs. $|F_o|$, reflection order in data collection, sin θ/l, and various classes of indices showed no unusual trends. The final atomic coordinate and B_{eq} for the non-H atoms are given in Tables 5, 6, and 7.[3]

Acknowledgement

We thank the Natural Sciences and Engineering Research Council of Canada for generous financial support.

1. R. D. ERNST. Chem. Rev., **88**, 1255 (1988).
2. A. P. MASTERS and T. S. SORENSEN. Can. J. Chem. **68**, 492 (1990).
3. (*a*) G. T. PALMER and F. BASOLO. J. Am. Chem. Soc. **107**, 3122 (1985); W. R. MCCLELLAN, H. H. HOEHN, H. N. CRIPPS, E. L. MUETTERTIES, and B. W. HAWK. J. Am. Chem. Soc. **83**, 1601 (1961); (*b*) D. SEYFERTH, E. W. GOLDMAN, and J. PORNET. J. Organomet. Chem. **208**, 189 (1981); C. G. KRIETER and M. LEYENDECKER. J. Organomet. Chem. **280**, 225 (1985).
4. T.-W. LEE and R.-S. LIU. J. Organomet. Chem. **320**, 211 (1987).
5. R. L. BENNETT and M. I. BRUCE. Aust. J. Chem. **28**, 1141 (1975); S. J. THOMPSON and P. M. MAITLIS. J. Organomet. Chem. **134**, 319 (1977); W. D. BANNISTER, M. GREEN, and R. N. HASZELDINE. J. Chem. Soc. A, 194 (1966); M. GREEN and R. I. HANCOCK. J. Chem. Soc. A, 109 (1968).
6. D. BAUDRY, J. DARAN, Y. DROMZEE, M. EPHRITIKHINE, H. FELKIN, Y. JEANNIN, and J. ZAKREWSKI. J. Chem. Soc. Chem. Commun. 813 (1983).
7. M. G. B. DREW, M. PAZ-SANDOVAL, R. N. PERUTZ, and P. POWELL. Organometallics, **3**, 1026 (1984).
8. M.-H. CHENG, Y.-J. WU, S.-L. WANG, AND R.-S. LIU. J. Organomet. Chem. **373**, 119 (1989).
9. P. T. GREENE and R. F. BRYAN. J. Chem. Soc. A, 1559 (1971); F. A. COTTON, D. J. DARENSBOURG, and B. W. KOLTHAMMER. Inorg. Chem. **20**, 1287 (1981); V. W. DAY, B. R. STULTS, K. J. REIMER, and A. SHAVER. J. Am. Chem. Soc. **96**, 4008 (1974); F. W. B. EINSTEIN, H. LUTH, and J. TROTTER. J. Chem. Soc. A, 89 (1967).
10. H. M. SEIP and R. SEIP. Acta Chem. Scand. **24**, 3431 (1970).
11. J. ENGELBRECHT, T. GREISER, and E. WEISS. J. Organomet. Chem., **204**, 79 (1981).
12. B. J. BRISDON, D. A. EDWARDS, J. W. WHITE, and M. G. B. DREW. J. Chem. Soc. Dalton Trans. 2129 (1980).
13. J. R. BLEEKE and J. J. KOTYK. Organometallics, **4**, 194 (1985).
14. M. R. CHURCHILL and F. R. SCHOLER. Inorg. Chem. **8**, 1950 (1969).
15. C. B. KNOBLER, S. SCHREIBER CRAWFORD, and H. D. KAESZ. Inorg. Chem., **14**, 2062 (1975) and references therein.
16. W. HEIBER and G. WAGNER. Z. Naturforsch. **13B**, 339 (1959).
17. S. L. LAWSON and R. A. JACOBSEN. Ames Labratory Report IS-1141; USABC, Iowa State University: Ames, IA, 1965.
18. J. M. STEWART. (*Editor*). Technical Report TR-446. Computer Science Centre, University of Maryland. (1976).
19. D. T. CROMER and J. B. MANN. Acta Crystallogr. Sect. A, **24**, 321 (1968).
20. R. F. STEWART, E. DAVIDSON, and W. SIMPSON. J. Chem. Phys., **42**, 3175 (1968).
21. D. T. CROMER. International tables for X-ray crystallography. Vol. IV. The Kynoch Press, Birmingham, England. 1974. Table 2.3.1.

[3]A complete set of structure factor listings, anisotropic thermal parameters, and hydrogen atom parameters is available at a nominal charge upon request from the Depository of Unpublished Data, CISTI, National Research Council of Canada, Ottawa, Ont., Canada K1A 0S2.

Kinetics of self-exchange of bis(1,4,7-trithiacyclononane)iron(III)/(II) in acetonitrile and in acidic aqueous solution

HIDEO DOINE AND THOMAS W. SWADDLE

Department of Chemistry, The University of Calgary, Calgary, Alta., Canada T2N 1N4

Received June 18, 1990

HIDEO DOINE and THOMAS W. SWADDLE. Can. J. Chem. **68**, 2228 (1990).

The rate constant k_{ex} of the $Fe([9]aneS_3)_2^{3+/2+}$ self-exchange reaction cannot be measured in most common solvents because of spontaneous reduction of the $Fe([9]aneS_3)_2^{3+}$ ion, which is also sensitive to photolysis by visible light. However, in CD_3CN at -41 to -19°C, reproducible proton-decoupled ^{13}C NMR line broadening measurements are possible, and give $k_{ex} = (5.3 \pm 0.3) \times 10^4$ kg mol^{-1} s^{-1} at 0°C, $\Delta H^* = 10.3 \pm 1.8$ kJ mol^{-1}, and $\Delta S^* = -116 \pm 7$ J K^{-1} mol^{-1}, at ionic strength $I = 0.1$ mol kg^{-1}. Proton NMR line broadening experiments are marginally practicable in very acidic water (2.0 mol kg^{-1} D_2SO_4/D_2O) near 0°C, and give $k_{ex} = 3.2 \times 10^6$ kg mol^{-1} s^{-1} at 1°C. The relative k_{ex} values of these and other low-spin/low-spin $Fe^{III/II}$ self-exchange reactions follow the predictions of the Marcus–Hush theory at least qualitatively. The effect of ionic strength, however, is less than predicted, probably because of the formation of less reactive anion–cation pairs.

Key words: electron transfer kinetics, crown thioether complexes.

HIDEO DOINE et THOMAS W. SWADDLE. Can. J. Chem. **68**, 2228 (1990).

Dans la plupart des solvants usuels, il n'est pas possible de mesurer la constante de vitesse k_{ex} de la réaction d'auto-échange du $Fe([9]aneS_3)_2^{3+/2+}$; cette situation est causée par la réduction spontanée de l'ion $Fe([9]aneS_3)_2^{3+}$, qui est aussi sensible à la photolyse par la lumière visible. Toutefois, dans le CD_3CN, entre -41 et -19°C, il est possible d'obtenir des élargissements reproductibles des raies des spectres de rmn du ^{13}C découplés du proton et on peut en déduire que, à 0°C et à une force ionique $T = 0{,}1$ mol kg^{-1}, $k_{ex} = (5{,}3 \pm 0{,}3) \times 10^4$ kg mol^{-1} s^{-1}, $\Delta H^* = 10{,}3 \pm 1{,}8$ kJ mol^{-1}, et $\Delta S^* = -117 \pm 7$ J K^{-1} mol^{-1}. Les expériences d'élargissment des raies de la rmn du proton ne sont pas très faciles à réaliser en milieu très acide (2,0 mol kg^{-1} de D_2SO_4/D_2O), près de 0°C; on a pu toutefois pu établir que, à 1°C, $k_{ex} = 3{,}2 \times 10^6$ kg mol^{-1} s^{-1}. Les valeurs relatives de k_{ex} pour ces réactions d'auto-échange et celles d'autres réactions semblables des $Fe^{III/II}$ faible spin/faible spin suivent au moins qualitativement les prédictions de la théorie de Marcus-Hush. Toutefois, l'effet de la force ionique n'est même pas prédit; probablement à cause de la formation de paires d'anion-cation moins réactives.

Mots clés : cinétique de transferts d'électrons; complexes de thioéthers-couronnes.

[Traduit par la revue]

Introduction

The number of outer sphere electron transfer (OSET) reactions of the self-exchange type

[1] $ML_n^{z+} + ML_n^{(z+1)+} \rightleftharpoons ML_n^{(z+1)+} + ML_n^{z+}$

of which the rate constant k_{ex} can be measured directly by techniques currently available is surprisingly small, particularly if one seeks to compare redox reactivity in aqueous and non-aqueous to solvents or, as in the case of our continuing research program, to assess the effects of hydrostatic pressure on k_{ex} in terms of current theory. For reactions that are too rapid for isotopic sampling techniques, NMR line-broadening methodology is often applicable in principle, but requires that either ML_n^{z+} or $ML_n^{(z+1)+}$ be diamagnetic. In addition, the exchange rate must fall within the NMR timeframe, the NMR spectrum of the diamagnetic species should contain at least one well-separated singlet that is substantially shifted following electron transfer, the solubilities of the oxidized and reduced species must be sufficiently high in the solvent of choice, and losses of either species during the experiment through redox reactions with the solvent or with impurities must be insignificant.

Iron(III)/(II) couples in which both members are present exclusively in the low-spin state in solution would seem to be attractive candidates for self-exchange rate studies, since the iron(II) complex is diamagnetic and, furthermore, the iron–ligand bond lengths are typically almost identical in the two oxidation states, so that the Franck–Condon restrictions are minimal and OSET is correspondingly fast (1). In practice, however, the iron(III) complex is usually too strongly oxidizing to survive for long in solution, and the choice of sufficiently senstitive NMR-active nuclei is often limited to ligand protons which may give an overly complex spectrum. The $Fe(phen)_3^{3+/2+}$ couple (phen = 1,10-phenanthroline) is a case in point, but reliable k_{ex} data have been obtained for it in both acetonitrile and aqueous acid at low temperatures (2–4).

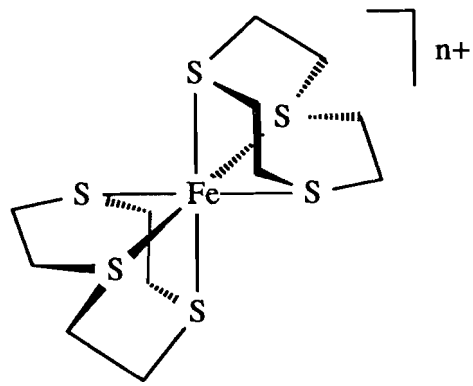

FIG. 1. Bis(1,4,7-trithiacyclononane)iron(II) or -(III) ion (schematic).

Crown thioether ligands such as 1,4,7-trithiacyclononane ([9]aneS$_3$) have recently opened up new opportunities in coordination chemistry, as they are surprisingly effective π-acidic ligands for metal ions in some unusual higher oxidation states, and also tend to enforce spin-pairing in lower oxidation states (5). Thus, Wieghardt and co-workers (6, 7) have characterized salts of the complexes $Fe([9]aneS_3)_2^{2+}$ and $Fe([9]aneS_3)_2^{3+}$ (Fig. 1) and report that they are low-spin. These complexes are of special interest in that the Fe—S bond lengths are actually some 3 pm *longer* in $Fe([9]aneS_3)_2^{3+}$ than in $Fe([9]aneS_3)_2^{2+}$, as a result of the π-acid action of the ligands

Can. J. Chem. Downloaded from www.nrcresearchpress.com by 195.138.81.100 on 09/07/12
For personal use only.

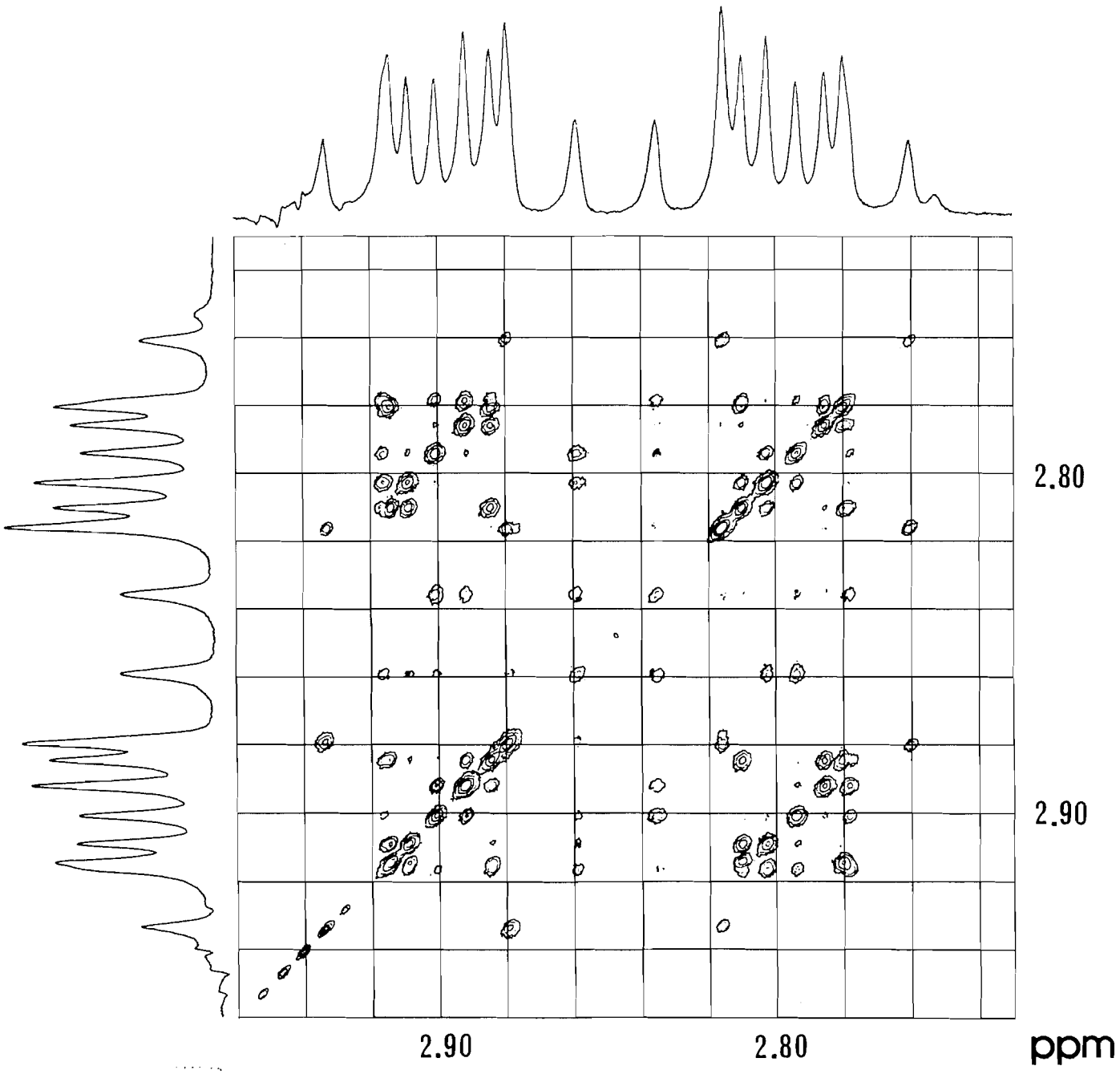

FIG. 2. COSY proton NMR spectrum (400 MHz) of $[Fe([9]aneS_3)_2](PF_6)_2$ in CD_3CN. Note narrow range of chemical shifts.

(8). The iron(III) complex, however, is a strong oxidant ($E_{1/2}$ in acetonitrile is +0.98 V vs. ferricenium/ferrocene, or +1.44 V vs. NHE) and tends to decompose in solution and in the solid state (6–8). Measurement of k_{ex} is therefore difficult — too difficult, in fact, for our intended high pressure studies. We believe, however, that it is worthwhile to report here the results of our successful exploratory measurements at atmospheric pressure, made possible through the use of low temperatures, highly acidic conditions (in the case of water as solvent) (8), and the exclusion of light.

Experimental

Preparation of materials

Acetonitrile-d_3 (Aldrich, 99 atom%) was treated with P_2O_5 and distilled under reduced pressure. Deuterium oxide (Aldrich, 99.8 atom%) and D_2SO_4 (Sigma, 98 atom%) were used as received.

Purple $[Fe([9]aneS_3)_2](PF_6)_2$ was prepared from [9]aneS$_3$ (Aldrich) by the method of Wieghardt *et al.* (6) except that a nitrogen atmosphere was maintained when the reaction mixture was heated. *Anal.* Calcd. for $FeC_6H_{12}S_3P_2F_{12}$: C 20.4, H 3.4; found: C 20.4, H 3.3. The proton NMR spectrum in CD_3CN (Fig. 2) and the visible absorption spectrum in water (maxima at 523 and 395 nm, molar absorbance ϵ = 54.5 and 52.0 L mol^{-1} cm^{-1}, respectively) were in good agreement with those given in the literature (6).

Dark green $[Fe([9]aneS_3)_2](PF_6)_3$ was made from $[Fe([9]aneS_3)_2](ClO_4)_2$ by the published method (7). [*Warning:* perchlorate salts of crown thioether complexes are potentially explosive (5).] The dry solid decomposed in less than two weeks at 20°C but could be kept for at least one month *in the dark* (see below) at about 0°C without detectable

Can. J. Chem. Downloaded from www.nrcresearchpress.com by 195.138.81.100 on 09/07/12
For personal use only.

Can. J. Chem. Downloaded from www.nrcresearchpress.com by 195.138.81.100 on 09/07/12
For personal use only.

TABLE 1. Ultraviolet–visible absorption maxima of $[Fe([9]aneS_3)_2](PF_6)_3$ in acidic aqueous solution and in acetonitrile

Solvent	T/°C	Wavelength/nm	ϵ/kg mol^{-1} cm^{-1}
acetonitrile	−20	634	714
		458[a]	520
		340	8000
aqueous H_2SO_4[b]	5	634	880
		455	695
		340	12600

[a]Shoulder at 493 nm.
[b]2 mol kg^{-1}; BrO_3^- present in excess over Fe^{III}.

decomposition. *Anal.* calcd. for $FeC_6H_{12}S_3P_3F_{18}$: C 16.9, H 2.84; found: C 16.6, H 2.90.

The uv–visible absorption spectra of $Fe([9]aneS_3)_2^{3+}$ in acetonitrile and in aqueous sulfuric acid were obtained with a Cary 219 spectophotometer and are given in Table 1. Attempts to obtain the spectrum in acetonitrile on a Cary 17H spectrophotometer, which has reversed optics and so exposes the sample to unmonochromated light of high intensity, revealed that $Fe([9]aneS_3)_2^{3+}$ is very sensitive to photolysis by visible light (some 5% Fe^{III} was lost per 10 min in the Cary 17H). Following this observation, all solutions and solids containing $Fe([9]aneS_3)_2^{3+}$ were handled with minimal exposure to light. Reproducible spectra may be obtained with standard optics if they are run promptly at low temperatures (and, for aqueous solutions, at high acidities with a small excess of bromate ion to suppress reduction of the Fe^{III}). The spectrum in acetonitrile is in good agreement with that given by Wieghardt and co-workers (7); the spectrum in aqueous acid, which is significantly more intense, has not been reported previously.

NMR measurements

All spectra were run on a Bruker AM-400 spectrometer fitted with a variable temperature unit. The ^{13}C spectra were obtained at 100.614 MHz (pulse width 3.5 μs, 64k, offset −6700 Hz, spectral width 120 ppm) with proton decoupling (offset 8532.381 Hz, 1 W). For the line broadening experiments, solutions were made up by weight from the requisite amounts of $Fe([9]aneS_3)_2^{2+}$ and $Fe([9]aneS_3)_2^{3+}$ hexafluorophosphates and the appropriate solvent. Linewidths $\nu_{1/2}$ of the proton-decoupled ^{13}C signal could be measured with a precision of ±0.02 Hz or better in CD_3CN, but multiple determinations of $\nu_{1/2}$ for the $Fe([9]aneS_3)_2^{2+}$ reference resonance in absence of iron(III) gave 3.5 ± 0.3 Hz, and in general the reproducibility of $\nu_{1/2}$ for $Fe([9]aneS_3)_2^{2+}/Fe([9]aneS_3)_2^{3+}$ mixtures was ±5%. The poor signal-to-noise (s/n) ratio in water limited the reproducibility of $\nu_{1/2}$ to ±10%.

Results

It was estalished spectrophotometrically that $Fe([9]aneS_3)_2^{3+}$ underwent no significant decomposition in the dark over 5 h at −20°C in acetonitrile, and therefore there was no loss of $Fe([9]aneS_3)_2^{3+}$ in the course of the NMR experiments with this solvent, as described below. In aqueous sulfuric acid (2.0 mol kg^{-1}) at 21°C, some decomposition occurred after one h even in the dark, according to the visible spectrum, but loss of $Fe([9]aneS_3)_2^{3+}$ over the duration of a typical NMR experiment at 1°C with such solutions was shown spectrophotometrically to be always less than 5%, i.e., within the uncertainty in k_{ex}.

The proton NMR spectrum of $Fe([9]aneS_3)_2^{2+}$ is very complex because of proton–proton spin coupling (Fig. 2), and therefore not well suited to line broadening studies. Fortunately, the proton-decoupled ^{13}C spectrum gives a single peak with quite good s/n ratio, in part because of the nuclear Overhauser effect. In the presence of an added paramagnetic solute, the width $\nu_{1/2}$ ($= 1/\pi T_2$, where T_2 is the transverse relaxation time)

TABLE 2. Proton NMR line broadening $\Delta\nu_{1/2}$ and rate constants k_{ex} for the $Fe([9]aneS_3)_2^{3+/2+}$ self-exchange reaction in CD_3CN

T/K	$[Fe^{III}]$ /mmol kg^{-1}	$[Fe^{II}]$ /mmol kg^{-1}	$\Delta\nu_{1/2}$[a] /Hz	k_{ex} /10^{4}kg mol^{-1} s^{-1}
232	1.27	46.1	10.9	2.7±0.2
244			13.5	3.4±0.2
252			18.4	4.6±0.3
232	1.60	46.1	12.0	2.4±0.2
237			15.0	2.9±0.2
244			16.2	3.2±0.2
252			20.2	4.0±0.3
233	0.981	28.7	4.5	1.5±0.5
242			5.8	1.9±0.3
247			6.9	2.2±0.3
254			9.1	2.9±0.3
232	1.47	23.6	7.6	1.6±0.2
237			8.5	1.8±0.2
243			10.1	2.2±0.2
243			11.0	2.4±0.2
252			12.4	2.6±0.2

[a]Average line width without $Fe^{III} = 3.5 \pm 0.3$ Hz; uncertainty in $\Delta\nu_{1/2} = 5\%$.

of the proton-decoupled ^{13}C line will be affected according to eq. [2].

$$[2]\quad T_2(^{13}C)^{-1} = T_2(\text{lattice})^{-1} + T_2(C{-}H)^{-1} + \delta k[E] + \alpha[E]$$

in which [E] is the concentration of electron spins, k[E] is the inverse spin–lattice relaxation time T_1^{-1} for ^{13}C-paramagnetic interactions, α[E] is proportional to T_1^{-1} for the ^1H-paramagnetic interaction, and δ is the ratio T_1/T_2 for ^{13}C-paramagnetic coupling (δ is generally slightly greater than unity) (9, 10). Thus, even in the absence of chemical exchange, a linear dependence of $\nu_{1/2}$ on the concentration of a paramagnetic solute might be found.

$$[3]\quad \nu_{1/2} = \nu_{1/2\ (\text{natural})} + k'[E]$$

It was therefore necessary to show that the term k'[E] was negligible before attempting to extract k_{ex} values from $Fe([9]aneS_3)_2^{3+}$-induced broadening of the $Fe([9]aneS_3)_2^{2+}$ ^{13}C resonance. This was done by measuring the effect on $\nu_{1/2}(^{13}C)$ for $Fe([9]aneS_3)_2^{2+}$ in CD_3CN of relatively high concentrations (up to 0.0082 mol kg^{-1}; $[Fe^{II}] = 0.05$ mol kg^{-1}) of the paramagnetic, but chemically non-exchanging, solute $Cr(acac)_3^0$ (tris(2,4-pentanedionato)chromium(III)). In no case was the line broadening as large as 0.8 Hz. Since the magnitude of this effect is known to decrease in the order $Mn^{II} > Cr^{III} > Fe^{III} > Co^{II}$ (10), and since the concentrations of $Fe([9]aneS_3)_2^{3+}$ used were 6–8 fold smaller than $[Cr(acac)_3^0]$, it can safely be concluded that the term k'[E] amounted to no more than 0.1 Hz in the kinetic experiments.

The ^{13}C line broadening measurements on the $Fe([9]aneS_3)_2^{3+/2+}$ system in CD_3CN were carried out at low temperatures, to obviate any loss of $Fe([9]aneS_3)_2^{3+}$, and are summarized in Table 2. Since k'[E] has been shown to be less than 0.1 Hz, its contribution to the measured line broadening $\Delta\nu_{1/2}$ is entirely negligible. The chemical exchange rate constants k_{ex}

$$[4]\quad k_{ex} = \pi\Delta\nu_{1/2}/[Fe([9]aneS_3)_2^{3+}]$$

increase with increasing ionic strength I at a given temperature, as qualitatively expected for reactions between ions of like charge, and Fig. 3 shows that no single fit of all the k_{ex} data to

Can. J. Chem. Downloaded from www.nrcresearchpress.com by 195.138.81.100 on 09/07/12
For personal use only.

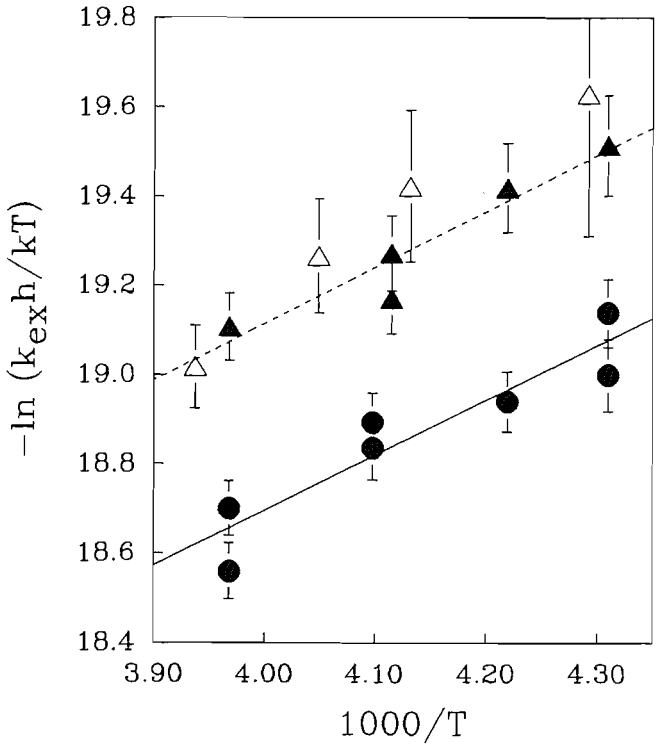

FIG. 3. Eyring plots showing temperature and ionic strength dependence of k_{ex} for the $Fe([9]aneS_3)_2^{3+/2+}$ self-exchange in CD_3CN. Circles and solid line: $I = 0.146$ to 0.148 mol kg^{-1}. Filled triangles and broken line: $I = 0.080$ mol kg^{-1}. Open triangles: $I = 0.092$ mol kg^{-1} (not fitted to Eyring equation).

the Eyring equation

$$[5] \quad k_{ex} = (k_B T/h) \exp(\Delta S^*/R) \exp(-\Delta H^*/RT)$$

where ΔH^* and ΔS^* are the enthalpy and entropy of activation, respectively, and the other symbols have their usual SI meanings, is possible. The data set for which $I = 0.092$ mol kg^{-1} ($[Fe^{III}] = 0.981$ mmol kg^{-1}) is seen in Fig. 3 to have excessively large uncertainties at the lower temperatures; this is because the line broadening induced by the added Fe^{III} is insufficiently large relative to the uncertainties in $\nu_{1/2}$ (Table 2), and this data set is therefore not considered further except to note that the error bars span the data set with the slightly smaller ionic strength. For the two remaining data sets of Fig. 3, eq. [5] gives $\Delta H^* = 10.2 \pm 1.8$ kJ mol^{-1} with $\Delta S^* = -115 \pm 7$ J K^{-1} mol^{-1} at $I = 0.147$ mol kg^{-1}, and $\Delta H^* = 10.4 \pm 1.9$ kJ mol^{-1} with $\Delta S^* = -117 \pm 8$ J K^{-1} mol^{-1} at $I = 0.0796$ mol kg^{-1}. We may interpolate these to give $\Delta H^* = 10.3 \pm 1.8$ kJ mol^{-1} and $\Delta S^* = -116 \pm 7$ J K^{-1} mol^{-1} at $I = 0.1$ mol kg^{-1}, which generate $k_{ex} = 5.3 \times 10^4$ kg mol^{-1} s^{-1} at 0°C and 8.5×10^4 kg mol^{-1} s^{-1} at 25°C. Unfortunately, solubility limitations, together with inadequate line broadening at low $[Fe^{III}]$, made it impossible to investigate the ionic strength dependence of k_{ex} by addition of an inert electrolyte or by extension of the reactant concentrations beyond the limits mentioned above.

These data are valid representations of the rate of electron transfer only if the rate of ligand exchange is much lower. The proton NMR spectrum of a solution containing $Fe([9]aneS_3)_2^{2+}$ and free [9]aneS$_3$ (1 mmol kg^{-1} in each) in CD_3CN showed no shifting or broadening of the sharp ($\nu_{1/2} \simeq 0.3$ Hz) [9]aneS$_3$ peaks, from −35 to 0°C. Thus, no ligand exchange was occurring on the NMR time scale. The analogous experiment involving $Fe([9]aneS_3)_2^{3+}$ and the free ligand is not possible, since $Fe([9]aneS_3)_2^{3+}$ in acetonitrile oxidizes [9]aneS$_3$ immediately on mixing (cf. the reaction of $Fe(H_2O)_6^{3+}$ and [9]aneS$_3$ in methanol to give $Fe([9]aneS_3)_2^{2+}$ (5)). However, this fact in itself means that $Fe([9]aneS_3)_2^{3+}$ must be substitutionally inert to survive in solution for as long as it does. Thus, the $Fe([9]aneS_3)_2^{3+/2+}$ electron transfer reaction is truly outer-sphere.

Attempts to obtain line broadening data on the $Fe([9]ane_3)_2^{3+/2+}$ system in acetone, *N,N*-dimethylformamide and nitromethane were abandoned because decomposition of the iron(III) complex was found to be rapid in these reagent-grade solvents. The solubilities of the PF_6^- salts in acetone were too low for NMR studies in any case.

In water, decomposition of $Fe([9]ane_3)_2^{3+}$ near 0°C was minimized by making the acidity high, as noted above, but the solubilities of the PF_6^- or ClO_4^- salts were low and led to poor s/n ratios in ^{13}C NMR spectra. A rough estimate of the $Fe([9]ane_3)_2^{3+/2+}$ exchange broadening of the already very broad ^{13}C line in 1.14 mol kg^{-1} D_2SO_4/D_2O, with $[Fe([9]ane_3)_2^{2+}] = 1.41$ and $[Fe([9]ane_3)_2^{3+}] = 0.142$ mmol kg^{-1}, gave a rough k_{ex} value of $(5 \pm 2) \times 10^6$ kg mol^{-1} s^{-1} at −1°C. The 400 MHz ^1H NMR spectrum of $[Fe([9]ane_3)_2](ClO_4)_2$ (3.14 mmol kg^{-1}) in 2.0 mol kg^{-1} D_2SO_4/D_2O gave a low though usable *s/n* ratio, but it was necessary to treat the methylene proton resonances as a singlet of width 55.7 Hz for a $Fe([9]ane_3)_2^{3+/2+}$ line broadening study. This study gave $\nu_{1/2} = 228$ and 586 Hz for $[Fe([9]ane_3)_2^{3+}] = 0.231$ and 0.527 mmol kg^{-1} respectively at 1°C, whence $k_{ex} = 3.2 \times 10^6$ kg mol^{-1} s^{-1} at $I \simeq 2.0$ mol kg^{-1} (sulfuric acid is effectively monobasic at these concentrations).

Discussion

Table 3 shows the measured values of k_{ex} for low-spin/low-spin iron(III)/(II) self exchange reactions in acetonitrile and water, together with values that we have calculated from Marcus–Hush theory as described elsewhere (1, 4, 14) but with no attempt to allow for possible ion pairing. The calculations involve the assumptions that the contributions to the free energies of activation from internal reorganization are negligible, that electron transfer is adiabatic, that the reactants can be treated as spheres of known radii, and that the nuclear frequency factor can be taken to be 1×10^{11} s^{-1}.

The first assumption is acceptable if the change in the Fe—ligand bond lengths caused by oxidation or reduction is negligible; this is indeed the case, within ±3 pm (1, 3, 8, 11, 13). This assumption is vindicated by the remarkably low ΔH^* found in acetonitrile for the $Fe([9]aneS_3)_2^{3+/2+}$ exchange, just as for $Fe(phen)_3^{3+/2+}$ in acetonitrile and in water (the instability of $Fe([9]aneS_3)_2^{3+}$ precluded measurement of ΔH^* for $Fe([9]aneS_3)_2^{3+/2+}$ in aqueous solution). The Marcus–Hush calculations take the reactants to be spherical, but this is clearly unrealistic for the diabolo-shaped $Fe([9]aneS_3)_2^{n+}$ complexes, in which the closest-approach distance to the central Fe may be estimated from the data of ref. 6 to range from 300 to 550 pm. As a compromise, the effective radii r_1 and r_2 of the respective reactants $Fe([9]aneS_3)_2^{2+}$ and $Fe([9]aneS_3)_2^{3+}$ are taken to be 500 pm, and, for the corresponding $Fe([9]aneN_3)_2^{3+/2+}$ complexes, 465 pm (13). Electron transfer is assumed to occur with maximum probability at a separation $\sigma = (r_1 + r_2)$. The choice of nuclear frequency factor is also somewhat arbitrary, albeit traditional (1), and hence the predicted values of k_{ex} are not absolute. It is common experience that simple applications of

TABLE 3. Measured and predicted rate constants for low-spin iron(III)/(II) self exchange reactions

Couple	k_{ex}[a] /kg mol^{-1} s^{-1}	I /mol kg^{-1}	k_{MH}[b] /kg mol^{-1} s^{-1}
$Fe([9]aneS_3)_2^{3+/2+}/CD_3CN$	5.3×10^4	0.1	3.8×10^6[c]
$Fe([9]aneS_3)_2^{3+/2+}/D_2O$	3.2×10^6	2.0	5.2×10^7[c]
$Fe(phen)_3^{3+/2+}/CD_3CN$[d]	7.3×10^6	0.2	8.1×10^8
$Fe(phen)_3^{3+/2+}/D_2O$[d]	1.3×10^7	0.4	5.3×10^9
$Fe([9]aneN_3)_2^{3+/2+}/D_2O$[e]	4.6×10^3	0.05	3.8×10^6
$Fe(\eta^5\text{-}C_5H_5)_2^{+/0}/CD_3CN$[f]	3.5×10^6	0.01	6.1×10^6

[a]0°C except as stated.
[b]Calculated from Marcus–Hush theory for the stated ionic strength, with the assumptions that the nuclear frequency = 1×10^{11} s^{-1}, $r(HSO_4^-) = 280$ pm, $r(PF_6^-) = 300$ pm.
[c]Present work; $r_1 = r_2 = 500$ pm.
[d]Reference 4; $r_1 = r_2 = 700$ pm.
[e]Reference 11; k_{ex} at 25°C, estimated from the Marcus cross relationship; $r_1 = r_2 = 465$ pm.
[f]Reference 12; $r_1 = r_2 = 400$ pm.

Marcus–Hush theory typically predict k_{ex} values that are some 30- to 1000-fold too high even for reactions thought to be adiabatic (1). Thus, in view of the various assumptions and approximations made, the present systems conform as well as most to the predictions of Marcus–Hush theory.

It will be seen from Table 3 that the *relative* values of the observed k_{ex} follow the sequences predicted from Marcus–Hush theory (as applied here) qualitatively at least. In particular, the reactivity sequence $Fe(phen)_3^{3+/2+} > Fe(\eta^5\text{–}C_5H_5)_2^{+/0} > Fe([9]aneS_3)_2^{3+/2+} > Fe([9]aneN_3)_2^{3+/2+}$ is accounted for. Exact comparisons are impossible because of differences in ionic strength, but adjustment for these differences by the Brønsted–Bjerrum–Christiansen equation

$$[6] \quad \ln (k_I/k_0) = 2z_1z_2CI^{1/2}/(1 + BaI^{1/2})$$

as described elsewhere (14) consolidates this sequence; for example, k_{ex} is estimated to be 23 times greater for $Fe(phen)_3^{3+/2+}$ than for $Fe([9]aneS_3)_2^{3+/2+}$ in acidic water at the common $I = 0.4$ mol kg^{-1}, and 53 times greater in acetonitrile at $I = 0.2$ mol kg^{-1} (0°C). In the same way, it emerges that a given self-exchange reaction may be somewhat faster in water than in acetonitrile, but the difference will not be large. It should be noted that k_{ex} for $Fe([9]aneN_3)_2^{3+/2+}$ in water was estimated *indirectly* from the Marcus cross-relation, and at 25°C rather than 0°C (11), but its position in the above sequence seems assured.

The foregoing notwithstanding, great caution must be exercised in the application of conventional treatments of interionic effects (exemplified by eq. [6]) to electron transfer reactions between ions (eq. [1]). According to eq. [6], the k_{ex} values represented by the circles in Fig. 3 should be some 140% larger than corresponding values from the set shown as triangles, whereas the actual difference is only about 40%. Indeed, several authors have reported that ionic strength effects on electron exchange reactions between two ions of like charge are anomalous or even undetectable at the relatively high electrolyte concentrations dictated by practical considerations in experiments such as those described here (4, 14–17). This phenomenon appears to be due, at least in part, to the formation of relatively unreactive ion pairs with the counterion, as this would act in opposition to the accelerating effect of ionic strength (14, 18–22). Indeed, k_{ex} for the ferricenium/ferrocene self-exchange, in which ion pairing is likely to be unimportant, is close to that predicted from Marcus–Hush theory, whereas k_{ex} values for the 3+/2+ reactions, for which significant ion pairing is inevitable, are some two orders of magnitude too slow (Table 3). However, a detailed application of the Fuoss treatment of ion pairing to the data of Table 3, as described elsewhere (14, 22), led to no significant changes in the overall picture of relative reactivity in these low-spin iron(III)/(II) systems.

In any event, it appears that k_{ex} values for all the reactions listed in Table 3 approach the predictions of Marcus–Hush theory reasonably closely, in view of the limitations noted above. This may be taken to imply that these reactions are essentially adiabatic, or else non-adiabatic to similar degrees. It should be noted, however, that even the reaction for which k_{ex} comes closest to the predictions, the ferricenium/ferrocene exchange, may not be adiabatic (23).

Acknowledgement

We thank Dr. D. H. Macartney for discussions, and the Natural Sciences and Engineering Research Council of Canada for financial support.

1. N. SUTIN. Prog. Inorg. Chem. **30**, 441 (1983).
2. D. W. LARSEN and A. C. WAHL. J. Chem. Phys. **43**, 3765 (1965).
3. M.-S. CHAN and A. C. WAHL. J. Phys. Chem. **82**, 2542 (1978).
4. H. DOINE and T. W. SWADDLE. Can. J. Chem. **66**, 2763 (1988).
5. S. R. COOPER and S. C. RAWLE. Structure and bonding, **72**, 1 (1990).
6. K. WIEGHARDT, H.-J. KÜPPERS, and J. WEISS. Inorg. Chem. **24**, 3067 (1985).
7. H.-J. KÜPPERS, K. WIEGHARDT, B. NUBER, J. WEISS, E. BILL, and A. X. TRAUTWEIN. Inorg. Chem. **26**, 3762 (1987).
8. A. J. BLAKE, A. J. HOLDER, T. I. HYDE, and M. SCHRÖDER. J. Chem. Soc. Chem. Commun. 1433 (1989).
9. D. F. S. NATUSCH. J. Am. Chem. Soc. **93**, 2566 (1971).
10. G. N. LA MAR. Chem. Phys. Lett. **10**, 230 (1971).
11. H.-J. KÜPPERS, K. WIEGHARDT, S. STEENKEN, B. NUBER, and J. WEISS. Z. anorg. allgem. Chem. **573**, 43 (1989).
12. K. KIRCHNER, S.-Q. DANG, M. STEBLER, H. W. DODGEN, S. WHERLAND, and J. P. HUNT. Inorg. Chem. **28**, 3604 (1989).
13. J. C. A. BOEYENS, A. G. S. FORBES, R. D. HANCOCK, and K. WIEGHARDT. Inorg. Chem. **24**, 2926 (1985).
14. W. H. JOLLEY, D. R. STRANKS, and T. W. SWADDLE. Inorg. Chem. **29**, 1948 (1990).

Can. J. Chem. Downloaded from www.nrcresearchpress.com by 195.138.81.100 on 09/07/12
For personal use only.

15. A. EKSTROM, A. B. MCLAREN, and L. E. SMYTHE. Inorg. Chem. **15**, 2853 (1976).
16. G. M. BROWN and N. SUTIN. J. Am. Chem. Soc. **101**, 883 (1979).
17. H. DOINE, Y. YANO, and T. W. SWADDLE. Inorg. Chem. **28**, 2319 (1989).
18. R. M. NIELSEN and S. WHERLAND. Inorg. Chem. **23**, 1338 (1984).
19. D. BORCHARDT and S. WHERLAND. Inorg. Chem. **25**, 901 (1986).
20. J. GRIBBLE and S. WHERLAND. Inorg. Chem. **28**, 2859 (1989).
21. H. DOINE and T. W. SWADDLE. Inorg. Chem. **27**, 665 (1988).
22. T. W. SWADDLE. Inorg. Chem. In press.
23. R. M. NIELSON, G. E. MCMANIS, L. K. SAFFORD, and M. J. WEAVER. J. Phys. Chem. **93**, 2152 (1989).

Can. J. Chem. Downloaded from www.nrcresearchpress.com by 195.138.81.100 on 09/07/12
For personal use only.

Thin-layer ultraviolet–visible reflectance spectroelectrochemistry with a spinning-grating monochromator

DAVID H. JONES AND A. SCOTT HINMAN[1]

Department of Chemistry, The University of Calgary, Calgary, Alta., Canada T2N 1N4

Received April 9, 1990

DAVID H. JONES and A. SCOTT HINMAN. Can. J. Chem. **68**, 2234 (1990).

A thin-layer UV–visible spectroelectrochemistry system has been constructed using a commercially available spinning-grating monochromator. The spectroelectrochemical experiment is capable of scanning a wavelength range of 369 to 617 nm in 2.1 ms. The time delay between successive scans is 83 ms. The maximum peak-to-peak noise level in a 300-point spectrum collected during 2.1 ms with a spectral bandwidth of 2 nm is 0.03 absorbance units. The anodic spectroelectrochemistry of tetraphenylporphinatocopper(II), studied using the system, is presented.

Key words: thin-layer spectroelectrochemistry, rapid-scanning spectroscopy, spinning-grating monochromator, tetraphenylporphinatocopper(II).

DAVID H. JONES et A. SCOTT HINMAN. Can. J. Chem. **68**, 2234 (1990).

Utilisant un monochromateur à réseau tournant disponible commercialement, on a construit un système de spectroélectrochimie UV-visible sur couches minces. Lors de ces expériences spectroélectrochimiques, il est possible de balayer les longueurs d'onde allant de 369 à 617 nm en 2,1 ms. Le délai entre deux balayages successifs est de 83 ms. Le niveau maximal de bruit pic à pic dans un spectre de 300 points collectés en 2,1 ms avec une largeur de bande de 2 nm est de 0,03 unités d'absorbance. On présente la spectroélectrochimie anodique du tétraphénylporphinatocuivre(II) qui a été étudié à l'aide de ce système.

Mots clés : spectroélectrochimie sur couches minces, spèctroscopie à balayage rapide, monochromateur à réseau tournant, tétraphénylporphinatocuivre(II).

[Tradiut par la revue]

Introduction

Thin-layer UV–visible spectroelectrochemistry is an established electroanalytical technique for the *in situ* spectroscopic study of redox processes (see ref. 1 for a discussion). To take full advantage of the short electrolysis times possible in thin layer spectroelectrochemical cells, it is desirable to utilize optical analyzers which have the capability of acquiring and processing several complete spectra in a few seconds. Recent improvements in the design of thin layer cells allow very short electrolysis times, even in highly resistive solvent/supporting electrolyte systems (2–7). These advances further increase the possibilities for the combination of thin-layer electrochemistry with techniques for rapid spectral acquisition.

To date, rapid spectral acquisition in spectroelectrochemical experiments has been accomplished using two different types of optical instrument. Rapid scanning spectrophotometers, based on oscillating galvanometer mirrors, have been utilized in thin layer spectroelectrochemical experiments (8–10) as well as in diffusion-controlled experiments with optically transparent electrodes (11–15). More recently, linear diode array multichannel optical analyzers, which allow for simultaneous wavelength detection, have been utilized in thin-layer spectroelectrochemistry (4, 7).

This laboratory has investigated an alternative approach to doing short timescale thin layer spectroelectrochemistry using a commercially available spinning-grating monochromator. This monochromator utilizes a diffraction grating mounted directly onto the shaft of a dc servo motor. The motor rotates continuously at approximately 700 rpm, allowing the acquisition of complete spectra at intervals of 80 to 100 ms. Furthermore, a variety of triggering options are provided which allow convenient interfacing with computers and electrochemical equipment. These features, coupled with the low cost of the device, make it an attractive alternative to other commercially available rapid spectral acquisition systems for use in spectroelectrochemical experiments.

[1]Author to whom correspondence should be addressed.

Experimental

Thin-layer UV-visible spectroelectrochemical system: design and operation

A schematic of the thin-layer UV-visible spectroelectrochemical system is shown in Fig. 1. The optical design is analogous to that of a single-beam spectrophotometer, with the exception that the "sample" (spectroelectrochemical cell) and monochromator positions are reversed.

A 75 W xenon arc lamp is used as a light source. The radiation passes through a second order blocking filter (2.00 cm acetone) and is focussed onto a 7 mm diameter Pt mirror'disc working electrode in the thin layer spectroelectrochemical cell by means of a spherical mirror. The angle of incidence is about 45°. The use of a reflectance-type cell, as opposed to the more common transmission-type cell employing optically transparent electrodes, provides greater sensitivity to small absorbance changes by virtue of the longer optical pathlengths achieved. The cell employs a radial concentric configuration of working and counter electrodes, which has previously been shown to be optimum in terms of minimizing the effects of the high solution resistance within the thin layer cavity (2). The advantages of this type of cell and the details of its construction have been fully discussed in a previous publication (6). The only modification in the present work is the inclusion of a thin black card positioned normal to the electrode surface and the plane of incidence of the optical beam, which serves to deflect stray light reflected from the surface of the quartz window.

Light which is specularly reflected from the electrode surface is focussed onto the entrance slit of a Rofin-Sinar RSO 6101 spinning-grating monochromator by means of a second spherical mirror. The blaze wavelength of the monochromator grating is 500 nm. The monochromator has an *f*/number of 9, and a reciprocal linear dispersion of 2 nm/mm. A Hamamatsu R268 photomultiplier tube (PMT) detector is placed at the monochromator exit slit. The anode current of the PMT is amplified with a Keithley model 427 current amplifier.

The output of the current amplifier is monitored with a Macintosh II computer fitted with a G. W. Instruments Macadios II analog–digital interface card. The interface card allows analog data to be digitized and

Can. J. Chem. Downloaded from www.nrcresearchpress.com by 195.138.81.100 on 09/07/12
For personal use only.

Can. J. Chem. Downloaded from www.nrcresearchpress.com by 195.138.81.100 on 09/07/12
For personal use only.

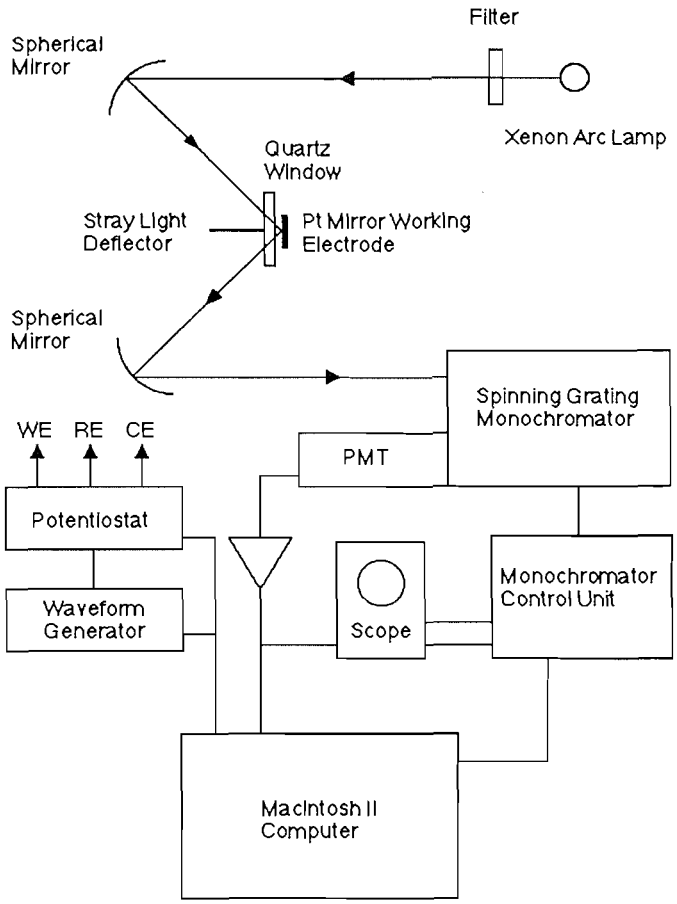

FIG. 1. Schematic of the thin layer UV–visible spectroelectrochemical system.

placed into memory at rates of up to 200 kHz. As configured, the full-scale voltage recognized by the 12-bit ADC is 10 V. In order to gain maximum benefit from the 12-bit resolution, the output of the current amplifier is monitored with an oscilloscope and the maximum signal is adjusted to slightly less than 10 V by varying the PMT supply voltage.

The spinning-grating monochromator is used in conjunction with a Rofin Sinar 6200 monochromator control unit, which provides a flash trigger voltage during each grating rotation. This pulse is used to synchronize the various aspects of the spectroelectrochemical experiment. On the first trigger pulse following initiation of the experiment by the operator, the computer either applies a preselected voltage step directly to the adder input of a Hi-Tek model DT 2101 potentiostat, or triggers the start of a voltage ramp as derived from a Hi-Tek model PPR1 waveform generator. Subsequent pulses from the monochromator initiate the acquisition of a 300 point integer array by the computer at a rate of 7 μs per point. The time between trigger pulses is sufficient to allow the data to be converted to floating point format and added into a second array, providing real-time signal averaging. The time at which the flash trigger occurs in relation to the grating position is variable in one nm increments by means of a thumbwheel switch on the monochromator control unit. This allows convenient control of the wavelength range scanned in the experiment. By appropriate ratioing of sample and background energy spectra collected in this manner, both transmittance and absorbance spectra may be obtained. The system is controlled using a Think Technologies Lightspeed Pascal computer program which accesses the Macadios II input–output and data manipulation libraries. Wavelength calibration of the monochromator is performed by measuring the absorption spectra of several narrow bandwidth filters.

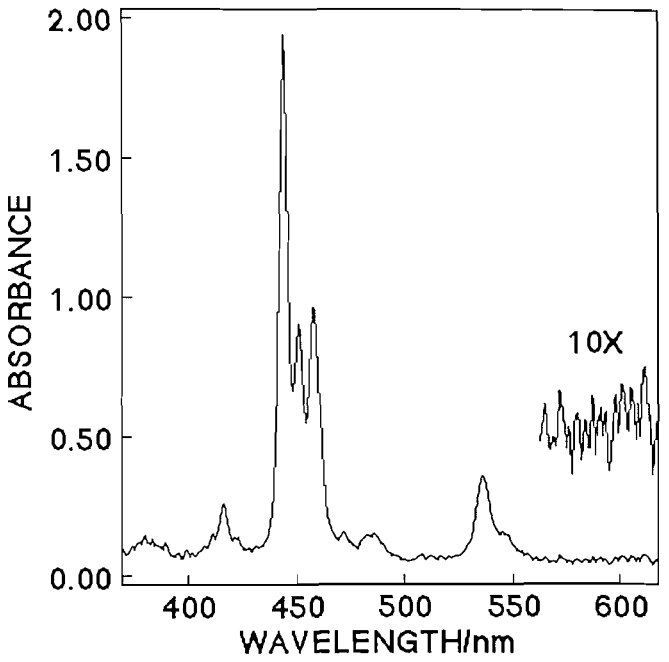

FIG. 2. Single scan of the visible spectrum of a holmium oxide glass filter.

Reagents and solutions

All solutions employed in spectroelectrochemical experiments contained 4.6×10^{-4} M tetraphenylporphinatocopper(II) (TPPCu) dissolved in 1,2-dichloroethane. Tetra-*n*-butylammonium hexafluorophosphate ($TBAPF_6$) in 0.16 M concentration was employed as supporting electrolyte. TPPCu was prepared from tetraphenylporphine (Aldrich) and CuBr according to Adler's DMF method (16). The crude product was subjected to chromatography (dry silica with CH_2Cl_2 eluant) and recrystallized from CH_3OH–CH_2Cl_2. The UV-visible spectrum (CH_2Cl_2) of the final product was identical to that previously reported (17). The UV–visible spectrum of the complex in 1,2-dichloroethane was also recorded: λ/nm (log ($\epsilon/M^{-1}\,cm^{-1}$)): 415 (5.66); 536.9 (4.31).

1,2-Dichloroethane (Fisher) was shaken with neutral alumina (Woelm activity I) and distilled from P_2O_5 onto CaH_2 prior to use. $TBAPF_6$ (Aldrich) was recrystallized from isopropanol–water and dried *in vacuo* at 110°C overnight.

Results and discussion

The shortest period of rotation obtainable with the monochromator was determined by measuring the time interval between successive trigger pulses, and was found to be 83 ms. It is important to note, however, that the entire UV–visible wavelength region appears at the exit slit of the monochromator for only a small fraction (*ca.* 3 %) of this time. The wavelength range covered in the present experiments (369 to 617 nm) is thus scanned in only 2.1 ms, so that the light beam is only sampled for 2.5% of the total time. When compared to a linear diode array, which samples light continuously, this amounts to a considerable loss of throughput and therefore, inherently poorer signal-to-noise ratios. It was envisaged, however, that the use of a high intensity light source would at least partially compensate for this effect. Also, a photomultiplier tube was chosen as the detector. While a PMT does not necessarily provide superior signal-to-noise ratios as compared to photodiodes, its fast response and greater sensitivity were viewed to be advantageous for this application.

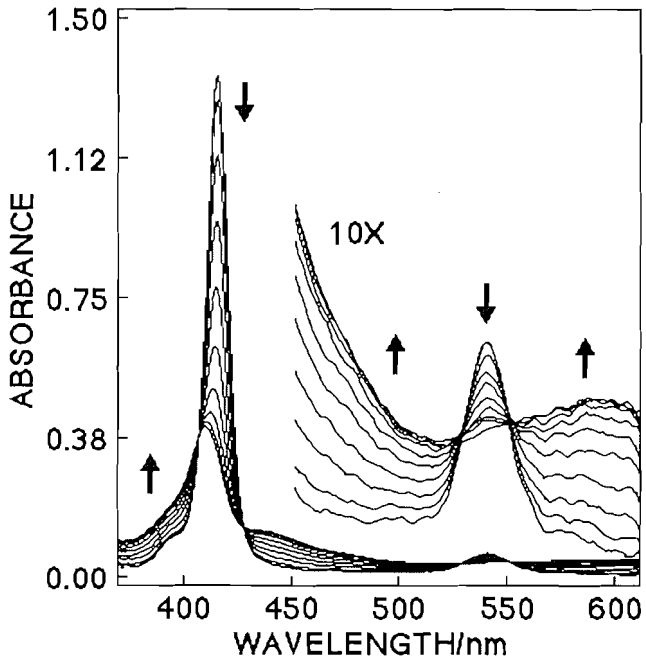

FIG. 3. Thin layer single potential step chronoabsorptometry of the one electron oxidation of 0.46 mM TPPCu in $C_2H_4Cl_2$/0.16 M $TBAPF_6$. Applied potential step vs. aqueous SCE was 0.80 to 1.10 V. Each spectrum is the average of 16 scans collected 83 ms apart during successive 1.3 s periods. Total electrolysis time was 12.0 s. Spectra were smoothed using a 15 point second order Savitzky–Golay routine.

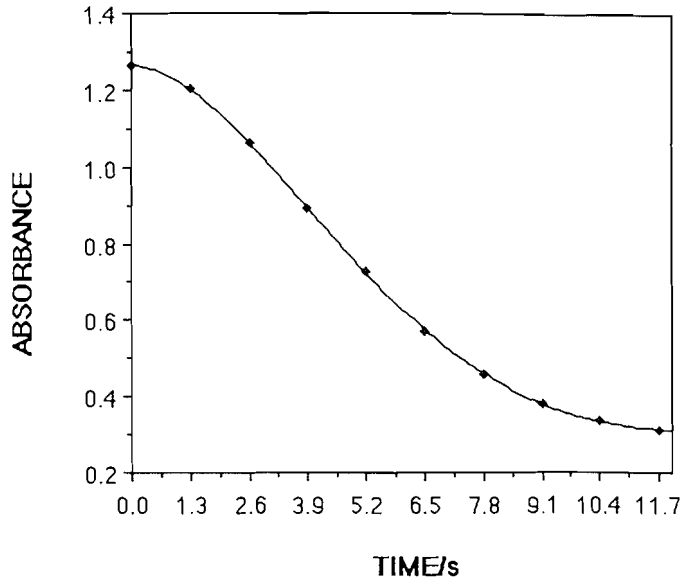

FIG. 4. Average absorbance at 415 nm plotted as a function of electrolysis time. Data were collected during the single potential step chronoabsorptometric experiment shown in Fig. 3.

The short time in which the wavelength region of interest is scanned requires that a fast response current amplifier be used in order to avoid loss of spectral resolution and wavelength accuracy. The Keithley model 427 amplifier used in this work has a rise time of 0.01 ms. Also, the ADC must be capable of operating at high sampling rates. The sampling time of 7 μs utilized in the present experiments provides for a digital resolution of 0.81 nm per point.

Figure 2 illustrates the visible spectrum of a holmium oxide glass filter obtained from a single scan. The spectrum was determined with the filter placed in the optical path between the light source and the thin layer spectroelectrochemical cell so that the throughput would closely match that expected in a typical spectroelectrochemical experiment. A 0.2 mm monochromator slit width was employed, giving a spectral bandwidth of 2 nm. The unusually sharp absorption peaks in the spectrum are clearly resolved. The overall resolution provided by the system is thus more than adequate for most condensed phase UV–visible experiments. No detectable change in the position of peak maxima was observed over a period of 2–3 h, indicating excellent stability in the rotation rate of the grating. The maximum peak-to-peak noise level evident in the spectrum is 0.03 absorbance units. Given the relatively high resolution employed, and that the entire spectrum was acquired in only 2.1 ms with an acquisition rate of 7 μs per data point, this figure was deemed acceptable. The noise level may, of course, be reduced using signal averaging and digital filtering techniques. Moreover, where lower resolution is acceptable, a wider slit width may be employed to further improve the signal-to-noise ratio.

In order to demonstrate the performance of the system during an actual spectroelectrochemical experiment, the anodic spectroelectrochemistry of 0.46 mM TPPCu in $C_2H_4Cl_2$/ 0.16 M $TBAPF_6$ was studied. In this solvent/supporting electrolyte system, TPPCu undergoes two successive one-electron oxidations with half wave potentials of 0.94 and 1.32 V vs. SCE. The two electrode reactions correspond to the stepwise formation of a porphyrin ring π-radical cation and π-dication (18). Both processes were studied using thin layer single potential step chronoabsorptometry as well as thin layer linear potential sweep chronoabsorptometry. In these techniques, either a potential step or a potential ramp is applied to the Pt mirror working electrode and the absorbance changes in the adjacent thin electrolyte layer are monitored with time.

The thin layer single potential step chronoabsorptometry of the first oxidation is shown in Fig. 3. The optical pathlength was calculated to be 63 μm for this and subsequent experiments, which corresponds to a thin layer thickness of *ca.* 22 μm (6). During the electrolysis time of 12.0 s, it was possible to collect nine spectra, each obtained by averaging 16 successive scans. Four isosbestic points are observed at 407, 428, 529, and 551 nm. The spectral changes are typical of π-radical cation formation as seen for a number of TPP complexes (18). The short timescale is clearly adequate to define the spectral changes occurring, provided the signals are of sufficiently high absorbance.

Figure 4 presents the average absorbance at 415 nm observed during successive 1.3 s intervals plotted as a function of total elapsed electrolysis time. The data are from the same potential step chronoabsorptometric experiment from which the spectra of Fig. 3 were recorded. It is evident that the absorbance change during the first 1.3 s interval is considerably less than that observed in the next few intervals. Such delays in the onset of the electrolysis have been observed in even the fastest thin layer cells (3), and result from the high solution resistivity within the thin layer cavity. This high resistivity results in long RC time constants associated with charging the double layer capacitance at various points on the electrode. By virtue of the associated solution *iR* drop, it delays the charging of the double layer capacitance and onset of electrolysis at points on the working electrode surface placed further from the counter electrode until current flow to points closer to the counter electrode subsides.

Can. J. Chem. Downloaded from www.nrcresearchpress.com by 195.138.81.100 on 09/07/12
For personal use only.

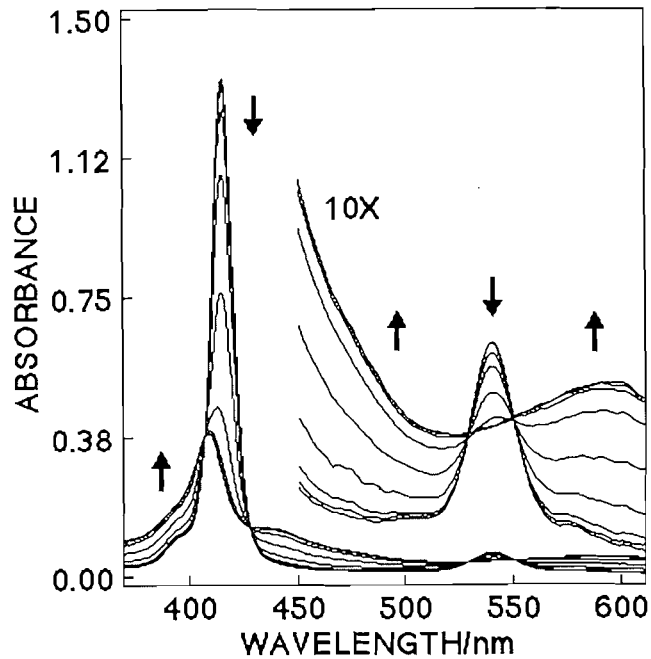

FIG. 5. Thin layer linear potential sweep chronoabsorptometry of the one electron oxidation of 0.46 mM TPPCu in $C_2H_4Cl_2$/0.16 M $TBAPF_6$. The applied potential was swept between 0.80 and 1.20 V vs. aqueous SCE at a scan rate of 4.2 mV/s. Each spectra is the average of 128 scans collected 83 ms apart during a 10.6 s period. Total experiment time was 96 s. Spectra were smoothed using a 15 point second order Savitzky–Golay routine.

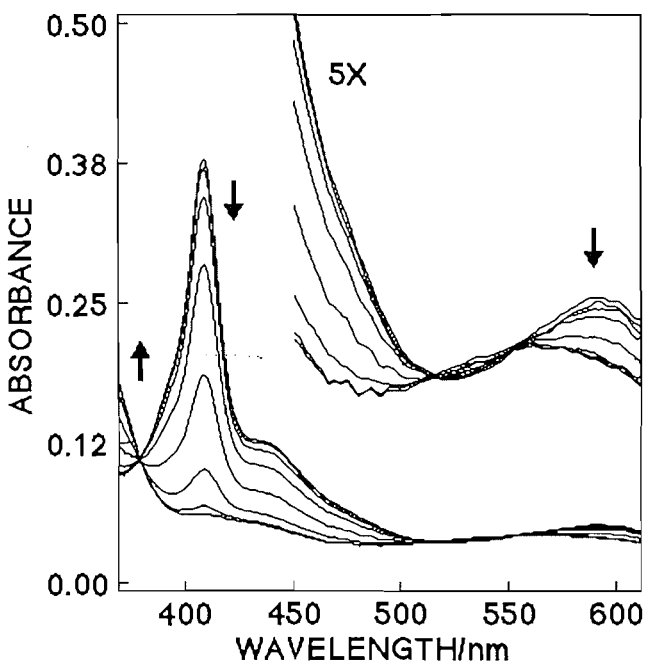

FIG. 6. Thin layer linear potential sweep chronoabsorptometry of the one electron oxidation of 0.46 mM TPPCu in $C_2H_4Cl_2$/0.16 M $TBAPF_6$. The applied potential was swept between 1.24 and 1.60 V vs. aqueous SCE at a scan rate of 4.2 mV/s. Each spectrum is the average of 128 scans collected 83 ms apart during a 10.6 s period. Total experiment time was 85 s. Spectra were smoothed using a 15 point second order Savitzky–Golay routine.

(More complete discussions of this effect can be found in refs. 3, 6, 19, and 20.) Thus, under the conditions of this experiment, the shortest time frame accessible is limited by the electrochemical response rather than the rate at which spectra may be acquired. Even so, the very short time required for complete electrolysis compares very favourably with what is evident in the recent literature for other thin layer spectroelectrochemical systems (see refs. 4 and 7, for examples), especially in view of the highly resistive nature of the solvent employed.

Provided the electrogenerated intermediates under study are sufficiently stable, it is possible to improve the S/N levels in the spectra by employing a linear sweep potential program. Through an appropriate choice of scan rate, the experiment time may be extended, thus affording opportunity for further signal averaging. Figures 5 and 6 show the spectral changes observable during the first and second one electron oxidations of TPPCu respectively. The spectral changes associated with the second oxidation (Fig. 6) show three isosbestic points at 379, 524, and 543 nm. The spectral changes are typical of π-dication formation (18).

Conclusions

The thin layer spectroelectrochemical system constructed using a spinning-grating monochromator appears to provide an economical and versatile means of performing short timescale thin layer spectroelectrochemistry. The quality of the spectral data obtained using the system is sufficient to characterize the spectral properties of electrogenerated intermediates which are stable on the timescale of a few seconds. The system is simple to assemble and experimentally flexible. Modification of the experiment to scan different wavelength regions in the UV–NIR range could easily be accomplished by altering the source, detector, and blaze wavelength of the grating in the monochromator unit. Furthermore, the variety of triggering and data acquisition options offered by the computer and monochromator control unit provide scope for a variety of spectroelectrochemical experiment designs.

Acknowledgement

The authors gratefully acknowledge financial support from the Natural Sciences and Engineering Research Council of Canada.

1. W. R. HEINEMAN, F. M. HAWKRIDGE, and H. N. BLOUNT. Electroanalytical chemistry Vol. 13. *Edited by* A. J. Bard. Marcel Dekker, New York. 1983. pp. 1–104.
2. A. S. HINMAN, S. PONS, and J. CASSIDY. Electrochim. Acta, **30**, 89 (1985).
3. A. S. HINMAN, S. PONS, and J. CASSIDY. Electrochim. Acta, **30**, 95 (1985).
4. X. Q. LIN and K. M. KADISH. Anal. Chem. **57**, 1498 (1985).
5. X. Q. LIN and K. M. KADISH. Anal Chem. **58**, 1493 (1986).
6. A. S. HINMAN and B. J. PAVELICH. Can. J. Chem. **65**, 919 (1987).
7. J. P. BULLOCK and K. R. MANN. Inorg. Chem. **28**, 4006 (1989).
8. H. B. MARK JR., T. M. KENYHERCZ, and P. T. KISSINGER. Electrochemical studies of biological systems. *Edited by* D. T. Sawyer. Ann. Chem. Soc. Symp. Ser. 1977. pp. 1–25.
9. R. W. HURST, W. R. HEINEMAN, and E. DEUTSCH. Inorg. Chem. **20**, 3298 (1981).
10. E. A. BLUBAUGH, A. M. YACYNYCH, and W. R. HEINEMAN. Anal. Chem. **51**, 561 (1979).
11. J. W. STROJEK, G. A. GRUVER, and T. KUWANA. Anal. Chem. **41**, 481 (1969).
12. E. E. WELLS, JR. Anal. Chem. **45**, 2022 (1973).

Can. J. Chem. Downloaded from www.nrcresearchpress.com by 195.138.81.100 on 09/07/12
For personal use only.

13. A. M. YACYNYCH and H. B. MARK, JR. J. Electrochem. Soc. **123**, 1346 (1976).
14. E. STECKHAN. Electrochim. Acta, **22**, 395 (1977).
15. E. STECKHAN and D. A. YATES. Ber. Bunsenges. Phys. Chem. **81**, 369 (1977).
16. A. D. ADLER, F. R. LONGO, F. KAMPAS, and J. KIM. J. Inorg. Nucl. Chem. **32**, 2443 (1970).
17. G. M. GODZIELA and H. M. GOFF. J. Am. Chem. Soc. **108**, 2237 (1986).
18. A. WOLBERG and J. MANASSEN. J. Am. Chem. Soc. **92**, 2982 (1970).
19. I. B. GOLDBERG and A. J. BARD. J. Electroanal. Chem. **38**, 313 (1972).
20. I. B. GOLDBERG, A. J. BARD, and S. W. FELDBERG. J. Phys. Chem. **75**, 3281 (1972).

Can. J. Chem. Downloaded from www.nrcresearchpress.com by 195.138.81.100 on 09/07/12
For personal use only.

Reactions of organic anions. 174.[1] Vicarious Nucleophilic Substitution of hydrogen (VNS) in nitrobenzofuroxans and the Boulton–Katritzky rearrangement of the VNS products

STANISŁAW OSTROWSKI AND KRZYSZTOF WOJCIECHOWSKI[2]

Institute of Organic Chemistry, Polish Academy of Sciences, Kasprzaka 44/52, PL-01-224 Warszawa, Poland

Received March 1, 1990

STANISŁAW OSTROWSKI and KRZYSZTOF WOJCIECHOWSKI. *Can. J. Chem.* **68**, 2239 (1990).

The Vicarious Nucleophilic Substitution of hydrogen in 4-nitrobenzofuroxan derivatives by carbanions of chloromethyl phenyl sulfone, chloromethyl *p*-tolyl sulfone, chloromethyl *tert*-butyl sulfone, and *N*,*N*-dimethyl chloromethane sulfonamide proceeds at positions 5 and 7. In some cases the Boulton–Katritzky rearrangement of the products obtained, leading to more stable 7-substituted isomers, was observed.

Key words: carbanions, nitrobenzofuroxans, sulfones, Vicarious Nucleophilic Substitution, Boulton–Katritzky rearrangement.

STANISŁAW OSTROWSKI et KRZYSZTOF WOJCIECHOWSKI. Can. J. Chem. **68**, 2239 (1990).

La substitution nucléophile déléguée de l'hydrogène de dérivés du 4-nitrobenzofuroxan par des carbanions des chlorométhyl phényl sulfone, chlorométhyl *p*-tolyl sulfone, chlorométhyl *tert*-butyl sulfone et *N*,*N*-diméthyl chlorométhane sulfonamide se produit dans les positions 5 et 7. Dans quelques cas, on a observé une transposition de Boulton–Katritzky des produits obtenus qui a conduit à la formation des isomères substitués en position 7, qui sont plus stables.

Mots clés : carbanions, nitrobenzofuroxans, sulfones, substitution nucléophile déléguée, transposition de Boulton–Katritzky.

[Traduit par la revue]

Introduction

The Vicarious Nucleophilic Substitution of hydrogen (VNS) is a general reaction between carbanions bearing leaving groups at the carbanionic center and nitroarenes (2). This reaction proceeds via addition of the carbanions to the aromatic ring to give anionic σ-adducts, which undergo base-induced β-elimination of HX to *ortho* and (or) *para* nitrobenzylic carbanions. The final products are formed upon protonation.

It has been shown that the VNS reaction also proceeds with highly electrophilic arenes, which do not contain nitro groups (3–7).

Various heterocycles containing in their moieties the quinoid system (e.g., quinones (8), 2,2-disubstituted benzimidazoles (9), etc.) can also add nucleophiles. Similarly, benzofuroxans in reactions with nucleophiles (e.g., secondary amines) give adducts (in position 5) and then, via the furoxan ring opening – ring closure process, form 5-substituted benzofurazan derivatives (10). Reactions of carbanions with benzofuroxans have been extensively studied (11). Depending on the structure of the starting materials, they lead to quinoxaline di-*N*-oxide or benzimidazole *N*-oxide derivatives.

Results and discussion

We expected that benzofuroxan, containing the highly electrophilic quinoid system, should undergo the VNS process. However, when benzofuroxan was reacted with chloromethyl phenyl sulfone (**2***a*) in the presence of powdered sodium hydroxide in dimethyl sulfoxide, both starting materials were consumed but no defined products were isolated.

Electrophilic properties of the benzofuroxan ring are increased by the introduction of the nitro group. Thus, 4- and 5-nitrobenzofuroxan ought to be more active in reactions with carbanions bearing leaving groups, leading to the VNS products. In a preliminary experiment 4-nitrobenzofuroxan was reacted with chloromethyl phenyl sulfone (**2***a*), in the presence of powdered sodium hydroxide in dimethyl sulfoxide. TLC analysis of the reaction mixture indicated formation of two products, probably *ortho* (5-) and *para* (7-) isomers of phenylsulfonylmethyl-4-nitrobenzofuroxan. However, after work-up only one product was isolated. In the residue no traces of the second isomer were detected. On the basis of chemical shifts and coupling constants in the ^{1}H NMR spectrum,[3] we found it to be 7-phenylsulfonylmethyl-4-nitrobenzofuroxan (**3***aa*). The reactions of carbanions of chloromethyl *tert*-butyl sulfone (**2***d*) and chloromethyl sulfonamide (**2***c*) with **1***a* proceeded similarly, also resulting in the formation of 7-substituted products (Table 1). These results were contrary to our expectations. Taking into account the previous observations, that bicyclic nitro compounds such as 1-nitronaphthalene (13) and 5- and 8-nitroquinolines (14) undergo the VNS preferentially in the position *ortho* to the nitro group, we expected a similar reaction course in the reaction of 4-nitrobenzofuroxan, namely substitution at position 5.

To clarify the results obtained, particularly to establish the position of the carbanion attack and what kind of products were initially formed and detected by TLC, we have performed several experiments using substituted 4-nitrobenzofuroxan derivatives in which the VNS could take place only in one position. We prepared for this purpose 5-methoxy-4-nitrobenzofuroxan (**1***b*). This relatively unstable compound, due to an interaction of the NO_2 group with the neighbouring OMe substituent, slowly undergoes the Boulton–Katritzky rearrangement (15) giving 7-methoxy-4-nitrobenzofuroxan (**1***c*). Compound **1***c* reacted with chloromethyl *p*-tolyl sulfone (**2***b*) to give two products. After separation of these products by preparative TLC we found that one of them was still converting to another one. This is a result of *retro* transformation. Since the *p*-tolylsulfonylmethyl group is sterically more demanding than the OCH_3 group, its interactions with the nitro group led to the formation of the thermodynamically more stable product **3***bb*. So the mixture of products **3***cb* (35%) and **3***bb* (20%), when kept for a few days,

[1]Part 173 in the series "Reactions of organic anions"; see ref. 1.

[2]Author to whom correspondence may be addressed.

[3]Coupling constants in the starting 4-nitrobenzofuroxan are $J_{H(5)-H(6)} = 6.5$ Hz, $J_{H(6)-H(7)} = 9.2$ Hz; see ref. 12.

Printed in Canada / Imprimé au Canada

Can. J. Chem. Downloaded from www.nrcresearchpress.com by 195.138.81.100 on 09/07/12
For personal use only.

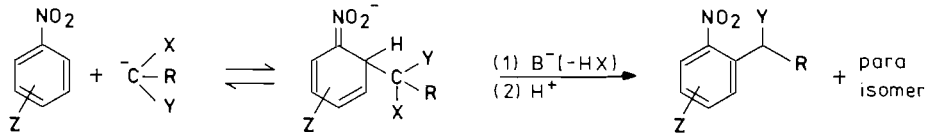

X-leaving group , Y-carbanion stabilizing group , R-substituent

SCHEME 1

TABLE 1. Reactions of nitrobenzofuroxans with α-chloromethylsulfones

Furoxan	Carbanion	Products: Position of $CH_2SO_2R^2$	Products: No	Products: Yield[a] (%)	Products: Melting point (°C)
1*a*	**2***a*	7	**3***aa*	61	208
1*a*	**2***c*	7	**3***ac*	35	185–186
1*a*	**2***d*	7	**3***ad*	47	194–196
1*c*	**2***b*	5	**3***cb*	35	200 → 205[c]
		7	**3***bb*	20	204–206
1*b*[b]	**2***b*	5	**3***cb*	19	As above
		7	**3***bb*	46	As above
1*c*	**2***a*	7	**3***ba*	58	198–199
		5	**3***ca*		191 → 199[c]
4	**2***b*	4	**5**	Traces	207–210

[a]Yields of isolated products.
[b]80% purity (20% of **1***c*).
[c]The broad melting points are due to the Boulton–Katritzky rearrangement of the products.

gave finally only the 7-substituted product **3***bb*. The reaction of the mixture of furoxans **1***b* and **1***c*, in which the 4-nitro-5-methoxy isomer **1***b* was the major component (80%), gave products **3***cb* and **3***bb*, but in quite different ratio (detected immediately after the reaction) (Table 1). Nevertheless, the product **3***bb* was obtained at the end as the more stable one. The following scheme summarizes the observed reaction course:

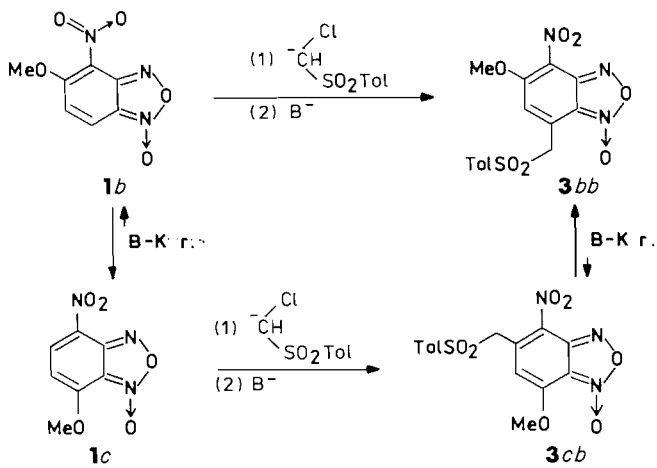

B-K r. - Boulton - Katritzky rearangment

SCHEME 2

Thus we found that the attack in both the *ortho* and *para* positions to the NO_2 group in benzofuroxan derivatives was possible, but in each case the less thermodynamically stable isomer of the product easily converts into the more stable one, sometimes during work-up of the reaction mixture.

The reaction between 5-nitrobenzofuroxan (**4**) and the chloromethyl *p*-tolyl sulfone (**2***b*) failed. Only traces of the corresponding 4-(*p*-tolylsulfonyl)methyl-5-nitrobenzofuroxan (**5**) were isolated.

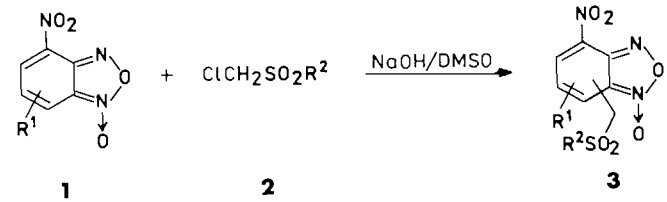

R¹=H (*a*), 5-OMe (*b*), 7-OMe (*c*)
R²=Ph (*a*), Tol (*b*), NMe_2 (*c*), Bu^t (*d*)

SCHEME 3

Attempted reactions of nitrobenzofuroxans with other carbanions typical for the VNS, such as phenoxyacetonitrile ($PhOCH_2CN$) and *tert*-butyl *N,N*-diethyldithiocarbamoylacetate ($Et_2NCS_2CH_2CO_2Bu^t$), were unsuccessful. Although in the reactions of these compounds with **1***a* both starting materials were consumed, no defined products were isolated.

Experimental

^1H NMR spectra were recorded with a Varian EM-360 (60 MHz) spectrometer in acetone-d_6 (compounds **3***ba* and **3***ca* in $CDCl_3$); coupling constants are expressed in hertz (Hz). Mass spectra were recorded with a Finnigan 8200 spectrometer. Melting points (Table 1) are uncorrected. Preparative TLC was performed on 2-mm plates using silica gel Merck 60 and chloroform as eluent. All new compounds gave satisfactory microanalyses. Starting materials were prepared according to known procedures. Furoxan **1***c* was prepared by nitration of 7-methoxy-benzofuroxan (15*a*) and the spontaneous Boulton–Katritzky rearrangement (mp 165–166°C ($CHCl_3$)). All reactions were carried out according to the given procedure.

Can. J. Chem. Downloaded from www.nrcresearchpress.com by 195.138.81.100 on 09/07/12
For personal use only.

General procedure

A solution of furoxan (1 mmol) and sulfone (**2***a–d*, 1.2 mmol) in DMSO (1 mL) was added to a stirred suspension of sodium hydroxide (0.5 g, 12.5 mmol) in DMSO (4 mL). The reaction was carried out at 20–25°C for 20 min. The reaction mixture was poured into dilute HCl with ice (100 mL); the product was extracted with ethyl acetate (2 × 20 mL), washed with water (2 × 15 mL), and dried over $MgSO_4$. After evaporation of the solvent the product was isolated by column chromatography (silica gel 230–300 mesh, Merck, $CHCl_3$ as eluent). An analytical sample was recrystallized from $CHCl_3$.

Spectral data

1*b*: ^{1}H NMR: 7.95 and 7.80 (AB, J = 9.7, H-6 and H-7), 4.30 (s, 3H, OCH_3).

1*c*: ^{1}H NMR: 8.58 (d, J = 8.2, 1H, H-5), 6.85 (d, J = 8.2, 1H, H-6), 4.22 (s, 3H, OCH_3).

3*aa*: ^{1}H NMR: 8.69 (d, J = 7.7, 1H, H-5), 8.01–7.65 (m, 5H, H-Ph), 7.41 (d, J = 7.7, 1H, H-6), 5.16 (s, 2H, CH_2); MS, m/z (%rel. int.): 335($M^{+\bullet}$, 7), 289(2), 194(8), 141(44), 125(30), 97(14), 88(11), 77(100), 62(18), 51(25).

3*ac*: ^{1}H NMR: 8.68 (d, J = 7.4, 1H, H-5), 7.71 (d, J = 7.4, 1H, H-6), 4.92 (s, 2H, CH_2), 2.95 (s, 6H, $N(CH_3)_2$); MS, m/z (% rel. int.): 302($M^{+\bullet}$, 26), 285(21), 221(33), 195(10), 178(10), 166(10), 119(15), 108(100), 92(92), 76(20), 62(26).

3*ad*: ^{1}H NMR: 8.64 (d, J = 7.7, 1H, H-5), 7.63 (d, J = 7.7, 1H, H-6), 4.94 (s, 2H, CH_2), 1.46 (s, 9H, Bu^t); MS, m/z (% rel. int.): 315($M^{+\bullet}$, 2), 195(4), 88(2), 76(2), 57(100), 41(18), 39(5).

3*bb*: ^{1}H NMR: 7.93–7.33 (m, 5H, H-Ar and H-6), 5.00 (s, 2H, CH_2), 4.13 (s, 3H, OCH_3), 2.49 (s, 3H, CH_3).

3*cb*: ^{1}H NMR: 8.02–7.43 (m, 5H, H-Ar and H-6), 5.22 (s, 2H, CH_2), 3.97 (s, 3H, OCH_3), 2.47 (s, 3H, CH_3).

3*ba*: ^{1}H NMR: 8.10–7.47 (m, 6H, H-Ar and H-6), 4.87 (s, 2H, CH_2), 4.20 (s, 3H, OCH_3).

3*ca*: ^{1}H NMR: 8.07–7.20 (m, 6H, H-Ar and H-6), 5.07 (s, 2H, CH_2), 4.17 (s, 3H, OCH_3).

5: ^{1}H NMR: 7.87 and 7.81 (AB, J = 9.6, 2H, H-6 and H-7), 7.71–7.64 and 7.47–7.41 (2m, 4H, H-Tol), 5.35 (s, 2H, CH_2), 2.44 (s, 3H, CH_3); MS, m/z (% rel. int.): 349($M^{+\bullet}$, 9), 303(4), 194(2), 178(2), 155(87), 139(11), 91(100), 65(13), 57(6); HRMS: 349.0369 (calcd. and found for $C_{14}H_{11}N_3O_6S_1$).

Acknowledgments

The authors thank Prof. M. Mąkosza for stimulating discussions. This work was supported by the Polish Academy of Sciences, Grant CPBP 01.13.

1. Z. Wróbel and M. Mąkosza. Liebigs Ann. Chem. In press.
2. (*a*) M. Mąkosza and J. Winiarski. Acc. Chem. Res. **20**, 282 (1987); (*b*) M. Mąkosza. *In* Studies in organic chemistry. Vol. 35. *Edited by* J. Kováč and P. Zálupský. Elsevier, Amsterdam. 1988. p. 95.
3. S. Ostrowski and M. Mąkosza. Tetrahedron, **44**, 1721 (1988).
4. M. Mąkosza and S. Ostrowski. J. Prakt. Chem. **330**, 789 (1988).
5. A. Rykowski and M. Mąkosza. Liebigs Ann. Chem. 627 (1988).
6. M. Mąkosza, T. Glinka, S. Ostrowski, and A. Rykowski. Chem. Lett. 61 (1987).
7. S. Ostrowski and M. Mąkosza. Liebigs Ann. Chem. 95 (1989).
8. H. Ulrich and R. Richter. *In* Methoden der organischen Chemie. 4th ed. Vol. VII/3a. *Edited by* Houben-Weyl-Müller. Thieme, Stuttgart. 1977. p. 660.
9. (*a*) K. E. Davies, G. E. Domany, M. Farhat, J. A. L. Herbert, A. M. Jefferson, M. A. G. Martin, and H. Suschitzky. J. Chem. Soc. Perkin Trans. 1, 2465 (1984); (*b*) H. Suschitzky. Croat. Chem. Acta, **59**, 57 (1986).
10. D. W. S. Latham, O. Meth-Cohen, and H. Suschitzky. J. Chem. Soc. Perkin Trans. 1, 2216 (1976).
11. (*a*) K. Ley and F. Seng. Synthesis, 415 (1975); (*b*) M. J. Haddadin and C. H. Issidorides. Heterocycles, **4**, 767 (1976).
12. R. K. Harris, A. R. Katritzky, S. Øksne, A. S. Bailey, and W. G. Paterson. J. Chem. Soc. 197 (1963).
13. M. Mąkosza, W. Danikiewicz, and K. Wojciechowski. Liebigs Ann. Chem. 711 (1987).
14. M. Mąkosza, A. Kinowski, W. Danikiewicz, and B. Mudryk. Liebigs Ann. Chem. 69 (1986).
15. (*a*) A. J. Boulton and A. R. Katritzky. Rev. Chim. Acad. Repub. Pop. Roum. **7**, 691 (1962); (*b*) A. J. Boulton and A. R. Katritzky. Proc. Chem. Soc. 257 (1962).

Can. J. Chem. Downloaded from www.nrcresearchpress.com by 195.138.81.100 on 09/07/12
For personal use only.

Kinetics, isotope effects of the reaction of 1-(4-nitrophenyl)-1-nitroalkanes with DBU in tetrahydrofuran and chlorobenzene solvents

WLODZIMIERZ GALEZOWSKI AND ARNOLD JARCZEWSKI[1]
Department of Chemistry, A. Mickiewicz University, Grunwaldzka 6, 60-780 Poznań, Poland

Received May 15, 1990

WLODZIMIERZ GALEZOWSKI and ARNOLD JARCZEWSKI. Can. J. Chem. **68**, 2242 (1990).
The kinetics of the reaction of

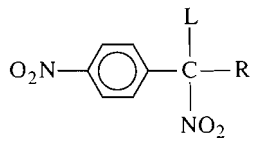

(R = Me, Et, *i*-Pr; NPNE, NPNP, MNPNP respectively; L is H or D) with 1,8-diazabicyclo[5.4.0]undec-7-ene (DBU) base in tetrahydrofuran (THF) and chlorobenzene (CB) solvents are reported. The products of these proton transfer reactions are ion pairs absorbing at λ_{max} = 460–480 nm. The equilibrium constants in THF were $K_r^{25°C}$ = 2060, 560, 3.7 and in CB $K_r^{25°C}$ = 500, 220, 4.7 mol^{-1} dm^3 for NPNE, NPNP, MNPNP respectively. The thermodynamic parameters of the reactions are also quoted. The substrate reacts with DBU in both THF and CB solvents in a normal second-order proton transfer reaction. In the case of deuteron transfer, isotopic D/H exchange is much faster than internal return. The reactions show low values of enthalpy of activation $\Delta H^{\neq}$ = 14.3, 18.1, 24.2 and 13.0, 15.1, 18.6 kJ mol^{-1} for NPNE, NPNP, and MNPNP in THF and CB respectively, and large negative entropies of activation $-\Delta S^{\neq}$ = 141, 139, 146; 140, 146, 160 J mol^{-1} deg^{-1} for the same sequence of substrates and solvents. The kinetic isotope effects are large, $(k_H/k_D)_{20°C}$ = 12.2, 13.0, 10.1; 12.9, 12.0, 10.2 for the above sequence of substrates and solvents, and show no difference with changes in either steric hindrance of the C-acids or polarity of the solvents.

Key words: proton transfer, kinetic isotope effect.

WLODZIMIERZ GALEZOWSKI et ARNOLD JARCZEWSKI. Can. J. Chem. **68**, 2242 (1990).
On a examiné la cinétique des réactions du

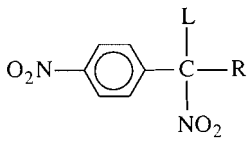

(R = Me, Et, *i*-Pr; respectivement NPNE, NPNP, MNPNP; L = H ou D) avec la base 1,8-diazabicyclo[5.4.0]undéc-7-ène (DBU) dans le tétrahydrofurane (THF) et le chlorobenzène (CB). Les produits de ces réactions de transfert de charge sont des paires d'ions qui absorbent à des λ_{max} allant de 460 à 480 nm. Dans le THF, les constantes d'équilibre de ces complexes, $K_r^{25°C}$ = 2060, 560 et 3,7, alors dans le CB, $K_r^{25°C}$ = 500, 220, 4,7 mol^{-1} dm^3 respectivement pour NPNE, NPNP et MNPNP. On rapporte aussi les paramètres thermodynamiques des réactions. Le substrat réagit avec le DBU, tant dans le THF que dans le CB, par le biais d'une réaction normale de transfert de proton du deuxième ordre. Dans le cas du transfert d'un deutéron, l'échange isotopique D/H est beaucoup plus rapide que le retour interne. Les valeurs des enthalpies d'activation sont relativement basses, $\Delta H^{\neq}$ = 14,3, 18,1, 24,2 et 13,0, 15,1 et 18,6 kJ mol^{-1} pour NPNE, NPNP et MNPNP respectivement dans le THF et le CB alors que les valeurs des entropies d'activation négatives sont élevées, $-\Delta S^{\neq}$ = 141, 139 et 146; 140, 146 et 160 J mol^{-1} deg^{-1} pour la même séquence de substrats et de solvants. Les effets isotopiques cinétiques sont importants, $(k_H/k_D)_{20°C}$ = 12,2, 13,0 et 10,1; 12,9, 12,0 et 10,2 pour la séquence de substrats et de solvants mentionnés plus haut; ils ne montrent pas de différences suivant l'empêchement stérique des C-acides ou la polarité du solvant.

Mots clés : transfert de proton, effet isotopique cinétique.

[Traduit par la revue]

Introduction

The reaction of

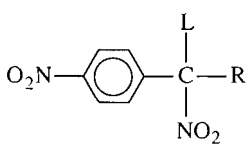

molecules of different steric hindrance, where R is Me, Et, *i*-Pr (NPNE, NPNP, MNPNP respectively), with 1,8-diazabicyclo[5.4.0]undec-7-ene (DBU) has already been examined in acetonitrile (MeCN) solvent (1). We found that this bimolecular proton transfer reaction gave a dissociated product in MeCN to a large extent, contrary to earlier reports (2–5). Therefore the applicability of the Benesi–Hildebrand method (6) has been carefully discussed, to explain why it gave incorrect results in previous papers, published by different authors (1). We also found large values of the primary deuterium kinetic isotope effect (KIE) despite the high polarity of the solvent, acetonitrile (MeCN), in which the reaction was carried out. High values of the primary deuterium kinetic isotope effect ($k_H/k_D > 10$) in MeCN solvent have been found for a series of reactions of C-acids with different strong bases such as DBU (3), tetramethylguanidine (TMG) (7, 8), phenyltetramethylguanidine (PhTMG) (5, 9), or 2,7-dimethoxy-1,8-bis(dimethylamino)naphthalene (10). These values, ranging

[1]Author to whom correspondence may be addressed.

Printed in Canada / Imprimé au Canada

Can. J. Chem. Downloaded from www.nrcresearchpress.com by 195.138.81.100 on 09/07/12
For personal use only.

Can. J. Chem. Downloaded from www.nrcresearchpress.com by 195.138.81.100 on 09/07/12
For personal use only.

between 12 and 16, were generally in agreement with the maximum values observed by Rogne and co-workers (11–13) and Kresge and Powell (14).

When the extremely large values of KIE observed in toluene and chlorobenzene (15) were suggested to be artefacts of isotopic exchange (11–13), a number of attempts were made to determine the factors influencing the kinetic isotope effect. These studies included the use of deuterated =NH bases (11, 16), in an effort to eliminate the resulting "scrambling" effect previously observed (11, 14). However, the most common view has been that high polarity solvents reduced the large isotope effects mainly because of coupling of the motion of the proton with that of the solvent molecules (15, 17, 18) increasing the effective masses of the transferred hydron. However, our former studies (1, 5, 7–9) provided reason to believe that this reduction is not very large, suggesting that the KIEs are not very sensitive to the polarity of the solvent in which the proton transfer reaction was carried out. This suggested that the reactions in polar solvents follow an uncoupled mechanism (19) in which solvent reorganization precedes the proton transfer step, and is supported by the fact that the energy of activation is a complex function in which the part corresponding to the solvation effects in ionogenic reactions usually prevails (20). Taking into account that this idea is inconsistent with previously published results (7, 15–18), the intention of the present paper is to approach the problem using two different solvents, tetrahydrofuran (THF) and chlorobenzene (CB), for the series of reactions of 1-(4-nitrophenyl)-1-nitroalkanes that have already been studied in MeCN solvent (1). We purposely chose THF and CB solvents because of the dramatic difference in KIE (12.7 and 50) previously found by Caldin *et al.* (18) for similar reactions.

Results and discussion

The reaction of 1-(4-nitrophenyl)-1-nitroalkanes with DBU base in THF and CB solvents proceeds by the following scheme:

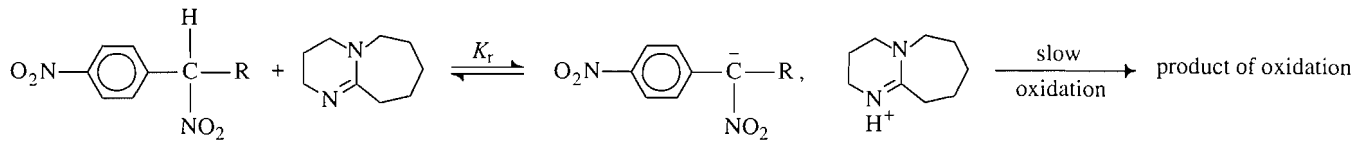

(AH) (DBU) (A^-, $DBUH^+$)

SCHEME 1

where R = Me, Et, *i*-Pr. The exchange reaction of the deutero analogues takes place by Scheme 2:

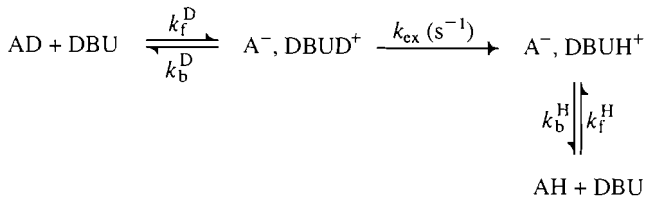

SCHEME 2

The product of the reactions (λ_{max} = 465 and 476 nm in CB and THF respectively) appears to be an ion pair, showing negligible conductivity of its solution ($\kappa < 4 \times 10^{-7}$ ohm^{-1} cm^{-1}) for concentrations of the substrates equal to $c_{AH} = 2 \times 10^{-3}$ M and $c_{DBU} = 1 \times 10^{-2}$ M. This product is different from that in MeCN solvent (1) where it is mostly free ions. This is consistent with the earlier findings of Rogne and co-workers (21) who reported a large bathochromic shift of the absorption band for the product of the reaction of NPNM with guanidines after acetonitrile was replaced by toluene as solvent. He suggested that different species absorbed in the two solvents.

The anion of the ion-pair product is stabilized by the countercation, as manifested by the blue shift of the absorption band compared to that of the free anion (λ_{max} = 508–515 nm). Considering these observations, we claim that in both THF and CB solvents the product of the reaction is an ion pair as shown in Schemes 1 and 2.

The corresponding equilibrium constants estimated by the Benesi–Hildebrand (6) method are collected in Table 1. The degrees of conversion found for these reactions carried out in THF and CB are considerably less than those in MeCN solvent (1), which is certainly due to dissociation of the ion pairs in MeCN. Comparison of the thermodynamic parameters of these reactions (Table 2) in THF shows that the equilibrium constants decrease due to the increase in enthalpy of reaction ΔH^0 caused by reduction of the stabilization energy of the anion by the resonance, along with the increase in bulk of the R substituent of these C-acids. This conclusion is supported by the parallel decrease of molar extinction coefficients ϵ (Table 1).

The reaction of normal C-acids with DBU follows pseudo-first-order kinetics (Scheme 1).

Exchange reactions may cause large errors in the deuteron transfer kinetics as already mentioned (11–14, 22). The concentration of exchangeable protons in the reaction medium, despite careful drying of both the DBU base (ca. 0.3% H_2O) (1) and solvents, is still much larger than the deuterated C-acid concentration of 2×10^{-5} M. Therefore conditions assuring irreversibility of D/H exchange assumed by Melander and Saunders hold here (23*a*).

When the equilibrium constant is not very large, then the reactions of the deutero analogues (Scheme 2) may follow either of the two following cases:

1. $k_b^D >> k_{ex}$: the isotopic exchange will have no influence on the kinetics (24), and the observed rate constants will be a function of base concentration c_B according to the following equation:

[1] $k_{obs}^D = k_f^D c_B + k_b^D$

2. $k_f^D c_B << k_{ex} + k_b^D$, excluding case 1; Melander and Saunders (23*a*) considered case 2 when, in addition, $k_{ex} >> k_b^D$, and came to the conclusion that, for ordinary isotope effects, if the initial curved part of the end-point method plots is neglected, eq. [2] is valid:

[2] $k_{obs}^D = k_f^D c_B$

TABLE 1. Equilibrium constants for the reactions of 1-(4-nitrophenyl)-1-nitroalkanes with DBU in THF and CB solvents at 25°C

C-acid	λ_{max} (nm)	K_r ($mol^{-1}\,dm^3$)	ϵ ($dm^3\,mol^{-1}\,cm^{-1}$)
		Tetrahydrofuran	
NPNE	473	2060 ± 30	22200 ± 100
NPNP	476	560 ± 20	22500 ± 400
MNPNP	477	3.7 ± 0.2	18600 ± 900
		Chlorobenzene	
NPNE	464	500 ± 100	22900 ± 900
NPNP	467	220 ± 30	24000 ± 1000
MNPNP	464	4.7 ± 0.2	15000 ± 500

TABLE 2. Thermodynamic parameters of the reactions of 1-(4-nitrophenyl)-1-nitroalkanes with DBU in THF solvent

C-acid	ΔH^0 ($kJ\,mol^{-1}$)	ΔS^0 ($J\,mol^{-1}\,deg^{-1}$)	ΔG^0 ($kJ\,mol^{-1}$)
NPNE	−57.5 ± 0	−129 ± 1	−18.9 ± 1
NPNP	−50 ± 1	−114 ± 5	−16 ± 2
MNPNP	−38 ± 2	−117 ± 5	−3 ± 2

This approach can be extended by not assuming that $k_{ex} \gg k_b^D$; then the steady-state approximation yields, for case 2, when initial parts of the end-point or Guggenheim method plots are omitted:

$$[3] \quad k_{obs}^D = k_f^D c_B \frac{k_{ex}}{k_b^D + k_{ex}}$$

Since the plots of k_{obs}^D vs. c_{DBU} (data from Tables 3 and 4) pass through the origin, in contrast to the same plots for proton transfer, then case 1 cannot be valid. Moreover the shapes of the end-point or Guggenheim method plots (not shown), with curvature at the very beginning, are exactly as predicted by Melander and Saunders (23*b*) for fast isotopic exchange.

It was recently stressed by Thibblin and Ahlberg (22) that reaction branching may lead to miscellaneous large kinetic isotope effects. A reconsideration of large KIEs in hydron transfer reactions from substrates activated by nitro groups was suggested, despite the fact that there was no specific reason to invoke branching.

Actually, internal return and isotopic exchange can be considered as such competitive processes. Hence, according to eq. [3], the slope of k_{obs}^D vs. c_{DBU} could be smaller than k_f^D, providing the overestimated KIE values in Tables 3 and 4. However, careful examination of the data in Tables 3 and 4 leads to the conclusion that $k_{ex} \gg k_b^D$; thus eq. [2] is valid and the KIEs are not distorted.

We can assume that the equilibrium constants for proton and deuteron transfer are similar (20). For the reaction of NPNE and NPNP with DBU, $k_f^H c_{DBU} > k_b^H$ (k_b^H at 25°C is 0.4, 0.5, and 1.9 s^{-1} in THF and 0.3, 0.3, and 2.9 s^{-1} in CB for NPNE, NPNP, and MNPNP, respectively). Then $k_f^D c_{DBU} > k_b^D$, which is contrary to the case 2 inequality above if $k_{ex} \gg k_b^D$ is not true. Therefore for these reactions k_{ex} must be much greater than k_b^D to preserve steady-state conditions. For the reactions of MNPNP with DBU in both THF and CB solvents the inequality $k_b^H c_{DBU} > k_b^H$ is not valid, thus the condition that $k_f^D c_{DBU} > k_b^D$ is not fulfilled. However, for these reactions the values of the KIE are even smaller than for the other two C-acids, showing that internal return does not cause reduction of k_f^D (eq. [3]).

Another possibility of reaction branching that may cause a false KIE is oxidation of a reaction intermediate (22, 25). In our experiments oxidation processes were slow enough to be neglected.

In conclusion, in the case of a concentration of C-acid comparable to or smaller than the concentration of exchangeable H^+ in the system, the use of tertiary amines does not prevent D/H exchange in the product of these reactions. However, in the case of large kinetic isotope effects and excess of exchangeable protons this exchange, which is much faster than internal return, does not disturb the determined rate constants and KIE.

The D/H exchange of α-CH hydrogens in cyclic amidines has recently been reported (26). However, the rate of this exchange seems to be too slow to influence our experiments. Even if this exchange were fast enough, it would be just an additional source of exchangeable protons, which are already present in the bulk of the reaction medium. The possible deuteration of DBU base could change its basicity a little; however, this effect would be insignificant due to a large excess of the base concentration over that of the deuterated C-acid.

The rate constants for the reactions of 1-(4-nitrophenyl)-1-nitroalkanes (NPNE, NPNP, MNPNP) with DBU base are collected in Tables 3 and 4. These rate constants are not very dependent on the polarity of the solvent used. The fastest reaction took place in acetonitrile, k_f^H = 1630, 431, 37 at 20°C for NPNE, NPNP, and MNPNP respectively (1), and the slowest in THF, k_f^H = 730, 190, 6.47, while for CB the corresponding values were k_f^H = 1470, 305, 13 $dm^3\,mol^{-1}\,s^{-1}$. This is not in agreement with the polarity of the solvents.

The rate constants are considerably reduced, by about two orders of magnitude, as the bulk of the alkyl group on the C(1) atom is increased from NPNE to MNPNP. The steric and polar effects of the alkyl groups cooperate in reducing the rate constants k_f. However, the polar effects of different β-alkyl groups on the transition state energy would be expected to be nearly the same (27).

The most convincing argument for the influence of steric factors on the rate constants k_f comes from the fact that a small decrease (by a factor of 2) took place in the k_f values, for the deprotonation of nitroalkanes previously examined, when methyl was replaced by the *i*-Pr group (28) in the appropriate C-acid molecule. The increase in bulk of the alkyl substituent of the C-acid caused progressive desolvation of the transition state, reducing the freedom of the motion within the activated complex, increasing the distance of the proton transfer, and decreasing the rate of reaction. The higher steric demands of the C-acid and the base are reflected in the large negative values of entropy of activation $\Delta S^{\neq}$ (Table 5). The activation parameters collected in Table 5 are characteristic for ionogenic bimolecular reactions in aprotic solvents.

We presume that the changes of $\Delta S^{\neq}$ values with increasing steric hindrance result from two processes operating in opposite directions. The reduction of free motion decreases the entropy of activation while desolvation of the activated complex enhances this value. These entropy changes are consistent with our former suggestions for proton abstraction from 4-nitrophenylcyanomethane and phenyl-(4-nitrophenyl)cyanomethane by TMG and PhTMG in MeCN solvent (5, 8).

Can. J. Chem. Downloaded from www.nrcresearchpress.com by 195.138.81.100 on 09/07/12
For personal use only.

TABLE 3. Observed and second-order rate constants for proton and deuteron transfer reactions between 1-(4-nitrophenyl)-1-nitroalkanes and DBU in THF solvent

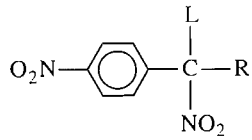

R = CH_3 (NPNE), C_2H_5 (NPNP), $CH(CH_3)_2$ (MNPNP)
L = H,D

T (°C)	$10^2\ c_{DBU}$ (M)	k_{obs} (s^{-1})	k_f ($dm^3\ mol^{-1}\ s^{-1}$)	k_H/k_D
		NPNE		
5	0.201–1.005	1.07– 5.10	500 ± 10	
10	0.201–1.005	1.24– 5.71	550 ± 10	
15	0.201–1.005	1.42– 6.63	660 ± 10	
20	0.201–1.005	1.69– 7.60	730 ± 20	
25	0.201–1.005	2.05– 8.48	800 ± 20	
30	0.201–1.005	2.72– 9.83	900 ± 30	
35	0.201–1.005	3.37–11.42	1010 ± 20	
		NPNE-1-*d*		
5	0.200–1.00	0.070–0.343	34.2 ± 0.6	14.6 ± 0.4
10	0.200–1.00	0.090–0.421	41.3 ± 0.7	13.3 ± 0.3
15	0.200–1.00	0.107–0.512	50.0 ± 1.0	13.2 ± 0.3
20	0.200–1.00	0.122–0.608	60.0 ± 1.0	12.2 ± 0.4
25	0.200–1.00	0.141–0.691	70.0 ± 3.0	11.4 ± 0.6
30	0.200–1.00	0.176–0.847	83.0 ± 1.0	10.8 ± 0.4
35	0.200–1.00	0.211–1.016	99.0 ± 2.0	10.2 ± 0.3
		NPNP		
5	0.51–2.55	0.60–3.08	121 ± 2	
10	0.51–2.55	0.85–3.70	139 ± 1	
15	0.51–2.55	1.00–4.40	167 ± 3	
20	0.51–2.55	1.21–5.00	190 ± 7	
25	0.51–2.55	1.50–5.93	219 ± 3	
30	0.51–2.55	1.83–6.83	249 ± 8	
35	0.51–2.55	2.41–8.28	288 ± 3	
		NPNP-1-*d*		
5	0.512–2.560	0.047–0.223	8.5 ± 0.2	14.2 ± 0.4
10	0.512–2.560	0.056–0.268	10.3 ± 0.1	13.5 ± 0.2
15	0.512–2.560	0.066–0.321	12.3 ± 0.2	13.6 ± 0.3
20	0.512–2.560	0.080–0.380	14.6 ± 0.3	13.0 ± 0.5
25	0.512–2.560	0.097–0.471	18.1 ± 0.3	12.1 ± 0.3
30	0.512–2.560	0.119–0.556	21.3 ± 0.1	11.7 ± 0.4
35	0.512–2.560	0.135–0.634	24.2 ± 0.3	11.9 ± 0.2
		MNPNP		
5	4.05–20.25	0.51–1.12	3.68 ± 0.12	
10	4.05–20.25	0.73–1.44	4.49 ± 0.17	
15	4.05–20.25	1.03–1.93	5.53 ± 0.05	
20	4.05–20.25	1.48–2.53	6.47 ± 0.12	
25	4.05–20.25	2.16–3.40	7.75 ± 0.26	
30	4.05–20.25	3.24–4.77	9.51 ± 0.22	
35	4.05–20.25	4.55–6.37	11.4 ± 0.6	
		MNPNP-1-*d*		
5	4.06–20.30	0.0138–0.0682	0.332 ± 0.007	11.1 ± 0.4
10	4.06–20.30	0.0174–0.0847	0.410 ± 0.008	11.0 ± 0.5
15	4.06–20.30	0.0222–0.1081	0.527 ± 0.006	10.5 ± 0.2
20	4.06–20.30	0.028 –0.131	0.64 ± 0.01	10.1 ± 0.2
25	4.06–20.30	0.033 –0.164	0.80 ± 0.01	9.7 ± 0.3
30	4.06–20.30	0.041 –0.200	0.97 ± 0.02	9.8 ± 0.3
35	4.06–20.30	0.050 –0.251	1.23 ± 0.01	9.3 ± 0.5

Can. J. Chem. Downloaded from www.nrcresearchpress.com by 195.138.81.100 on 09/07/12
For personal use only.

Can. J. Chem. Downloaded from www.nrcresearchpress.com by 195.138.81.100 on 09/07/12
For personal use only.

TABLE 4. Observed and second-order rate constants for proton and deuteron transfer reactions between 1-(4-nitrophenyl)-1-nitroalkanes (NPNE, NPNP, MNPNP) and DBU in CB solvent

T (°C)	$10^2\ c_{DBU}$ (M)	k_{obs} (s^{-1})	k_f ($dm^3\ mol^{-1}\ s^{-1}$)	k_H/k_D
		NPNE		
5	0.51–2.55	4.8–26.1	1050±10	
10	0.51–2.55	5.7–29.9	1190±40	
15	0.51–2.55	6.5–32.8	1290±10	
20	0.51–2.55	7.6–37.5	1470±30	
25	0.51–2.55	8.9–42.2	1660±40	
30	0.51–2.55	10.0–47.5	1820±30	
35	0.51–2.55	12.1–53.1	1990±40	
		NPNE-1-*d*		
5	0.51–2.55	0.33–1.76	71.4±1.6	14.7±0.4
10	0.51–2.55	0.41–2.11	83.3±0.8	14.3±0.1
15	0.51–2.55	0.48–2.43	95.5±0.7	13.5±0.1
20	0.51–2.55	0.58–2.92	111±2.0	12.9±0.3
25	0.51–2.55	0.69–3.43	134±2.0	12.4±0.4
30	0.51–2.55	0.82–4.09	160±2.0	11.4±0.2
35	0.51–2.55	0.94–4.79	188±1.0	10.6±0.2
		NPNP		
5	1.0–5.0	1.93–10.35	209±4	
10	1.0–5.0	2.38–12.01	240±5	
15	1.0–5.0	2.58–13.30	267±1	
20	1.0–5.0	3.24–15.38	305±3	
25	1.0–5.0	3.79–18.08	356±5	
30	1.0–5.0	4.69–20.32	391±8	
35	1.0–5.0	5.68–23.06	432±3	
		NPNP-1-*d*		
5	1.0–5.0	0.130–0.712	14.5±0.1	14.4±0.3
10	1.0–5.0	0.167–0.858	17.2±0.2	14.0±0.3
15	1.0–5.0	0.201–1.035	21.0±0.4	12.7±0.2
20	1.0–5.0	0.244–1.256	25.4±0.3	12.0±0.2
25	1.0–5.0	0.292–1.494	30.3±0.4	11.7±0.2
30	1.0–5.0	0.344–1.781	36.0±0.2	10.9±0.2
35	1.0–5.0	0.405–2.050	41.0±0.2	10.5±0.1
		MNPNP		
5	4.0–20.0	0.85– 2.14	8.0±0.1	
10	4.0–20.0	1.22– 2.74	9.4±0.3	
15	4.0–20.0	1.66– 3.42	10.9±0.3	
20	4.0–20.0	2.45– 4.48	12.9±0.4	
25	4.0–20.0	3.47– 5.88	14.6±0.6	
30	4.0–20.0	5.09– 7.71	16.4±0.9	
35	4.0–20.0	7.06–10.19	19.9±0.7	
		MNPNP-1-*d*		
5	4.0–20.0	0.0269–0.1364	0.684±0.003	11.7±0.5
10	4.0–20.0	0.0328–0.1686	0.85 ±0.01	11.0±0.4
15	4.0–20.0	0.0424–0.2068	1.03 ±0.04	11.6±0.5
20	4.0–20.0	0.0496–0.2504	1.26 ±0.01	10.2±0.3
25	4.0–20.0	0.0610–0.3100	1.55 ±0.01	9.4±0.4
30	4.0–20.0	0.0716–0.3736	1.88 ±0.02	8.7±0.5
35	4.0–20.0	0.0883–0.4486	2.24 ±0.02	8.9±0.3

The activation parameters are not very sensitive to the polarity of the solvents (Table 5 and ref. 1). The enthalpies of activation $\Delta H^{\neq}$ are compensated by the entropies of activation $\Delta S^{\neq}$. Then the increase of $\Delta S^{\neq}$ and $\Delta H^{\neq}$ values together with the polarity of the solvent should be regarded as typical characteristics of these reactions.

The first is commonly interpreted as a better organization of the polar solvent in the vicinity of the initial state. The second seems to be a result of the increase of the effective mass of the transferred proton and in consequence the reduction of the quantum mechanical tunnelling, so the observed potential energy barrier should be larger (18). However, a comparison of the values of the equilibrium constants (Table 1) shows that the stability of the ion pairs — more polar species than the

TABLE 5. Activation parameters, tunnelling corrections, and kinetic isotope effects for the reaction of 1-(4-nitrophenyl)-1-nitroalkanes

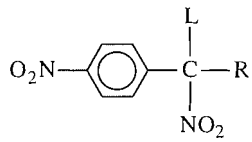

with DBU in THF and CB solvents

R	$\Delta H^{\neq}_{H}$ (kJ mol^{-1})	$\Delta S^{\neq}_{H}$ (J deg^{-1} mol^{-1})	$\Delta H^{\neq}_{D}$ (kJ mol^{-1})	$\Delta S^{\neq}_{D}$ (J deg^{-1} mol^{-1})	$10^{-5}\,A^{H}$	A^{H}/A^{D}	$\Delta H^{\neq}_{D} - \Delta H^{\neq}_{H}$ (kJ mol^{-1})	$(Q^{H}/Q^{D})_{25°C}$	$(k_t^{H}/k_t^{D})_{25°C}$ calcd.
				Tetrahydrofuran (THF)					
Me	14.3±0.6	−141±2	22.6±0.2	−134±1	7±2	0.4±0.1	8.3±0.6	1.63±0.09	11.4±0.1
Et	18.1±0.3	−139±1	22.9±0.5	−144±2	9±1	1.8±0.5	4.8±0.5	—	12.4±0.1
i-Pr	24.2±0.4	−146±1	28.4±0.4	−151±2	3.6±0.7	1.8±0.3	4.2±0.6	—	9.9±0.1
				Chlorobenzene (CB)					
Me	13.0±0.3	−140±1	20.7±0.6	−135±2	8±1	0.5±0.1	7.7±0.7	1.46±0.10	12.0±0.1
Et	15.1±0.4	−146±1	22.8±0.4	−140±1	4.1±0.7	0.5±0.1	7.7±0.6	1.49±0.07	11.6±0.1
i-Pr	18.6±0.5	−160±2	25.8±0.2	−155±1	0.7±0.2	0.5±0.1	7.2±0.5	1.48±0.11	9.5±0.1

transition state — in MeCN (1) is not larger than in THF or CB solvents. This suggests that not only the dielectric constant of the solvent but also the polarizability and its ability for specific interactions play no trifling role in the transition state stabilization. Caldin and co-workers (15, 29) had earlier indicated the importance of specific solvation for the kinetics of similar reactions.

The KIEs (Tables 3 and 4) are large and, except those for NPNP and MNPNP in THF, exceed the semiclassical value determined by Bell (30). Caldin and Rogne (31) state that the small enthalpy values for the reaction of NPNM with DBU in toluene, equal to 8.4 kJ mol^{-1}, suggest quite a large tunnelling effect, despite a rather low potential energy barrier, which is not a favourable condition for the tunnelling.

In our case we cannot find any correlation between the height of the energy barrier and the KIE values. The energy barrier for the reaction of MNPNP with DBU is very like that for NPNM with TMG, showing rather moderate KIEs that, in the case of THF and CB, are even smaller than those for reactions having smaller $\Delta H^{\neq}$ values (R = Me, Et).

THF and CB were the solvents chosen to carry out these kinetic measurements, despite their close values of dielectric constant, since in these solvents Caldin and Mateo (15) found large differences in KIE for similar reactions of NPNM with TMG, as a result of proton tunnelling. In our case the KIE values are practically independent of the polarity of the solvent. The $(k_H/k_D)_{20°C}$ values in MeCN were 12.8, 13.4, 13.7 for NPNE, NPNP, and MNPNP respectively (1), and 12.2, 13.0, 10.1; 12.9, 12.0, 10.22 for the above sequence of substrates in THF and CB solvents (Tables 3, 4). This supports the uncoupled mechanism, in which proton transfer follows the reorganization of solvent molecules for highly polar MeCN as well as for CB or THF. The same conclusion can be drawn on the basis of almost equal values of KIE for the reactions of C-acids of very different steric hindrance, which should have different solvation of the transition state.

KIE values for the reaction of NPNE with DBU in toluene (2) are very similar to the values collected in Tables 3 and 4, supporting our present suggestion of low dependence of KIE on the polarity of the solvent. However, our former measurements of the reaction of NPNE with PhTMG gave the KIE values 8.5, 6.1, and 16 for acetonitrile, benzonitrile, and chlorobenzene solvents respectively (5, 8). Therefore further experiments are needed to resolve this problem.

Tunnelling effects for the reactions of 1-(4-nitrophenyl)-1-nitroalkanes with DBU are presented in Table 5. The isotope effects on the activation parameters indicate small, but significant, contributions of the tunnelling effect to the proton transfer in all systems including MeCN solvent (1), except for NPNP and MNPNP with DBU in THF. The isotope effects on the energies of activation exceed the value of 4.6 kJ mol^{-1} or 5.7 kJ mol^{-1} resulting from the loss of the zero point energy between the initial and transition states for both the stretching and bending vibrations of the C—L bond.

The ratios of preexponential factors fall in the range of $0.5 < A_H/A_D < 1$. These isotope effects on the activation parameters are not large, and independent of the polarity of the solvent (1) (Table 5). The ratios of the quantum mechanical tunnelling factor, $Q_t^H/Q_t^D = 1.4–1.6$, show at least a 50% contribution of tunnelling effects to the overall KIE values.

The ratios of the preexponential factors A_H/A_D for the reactions of NPNP and MNPNP with DBU in THF are larger than unity, with normal values of $\Delta H^{\neq}_{D} - \Delta H^{\neq}_{H}$. This phenomenon has already been observed (30, 32), and explained as stronger solvation of the transition state for the deuteron in comparison with the proton transfer reaction (2). However, this is not consistent with our present observation, assuming that the proton transfer is not coupled with the motion of solvent molecules. Therefore we have no conclusive explanation of this fact, and the Melander and Saunders interpretation (23*c*) of the phenomenon seems also to be very unlikely.

These results confirm our earlier general conclusion (5, 7, 9) that the values of kinetic isotope effects and also of the tunnelling effect are influenced by the polarity of the solvent to an extent much less than was formerly assumed (15).

Experimental

The substrates

1-(4-Nitrophenyl)-1-nitroethane (NPNE), 1-(4-nitrophenyl)-1-nitropropane (NPNP), and 2-methyl-1-(4-nitrophenyl)-1-nitropropane (MNPNP) were prepared according to procedures previously published (1). The deuterated analogues were prepared by the modified exchange method in which the neutralization of the anion of the appropriate

Can. J. Chem. Downloaded from www.nrcresearchpress.com by 195.138.81.100 on 09/07/12
For personal use only.

C-acid was effected using acetate buffer (2 g CH_3COONa, 10 cm^3 D_2O, 3 cm^3 20% DCl, instead of concentrated DCl in D_2O) (7), which eliminates the noxious Nef's reaction of the nitronic acid as described by Bordwell and Boyle (33).

Tetrahydrofuran (THF)

The commercial product (Reachim) was dried over CaH_2 and fractionally distilled from $LiAlH_4$. The middle fraction was collected at 66 ± 0.5°C.

Chlorobenzene (CB)

The reagent grade product was fractionally distilled from P_2O_5. The middle fraction at 132 ± 0.5°C was collected. Both solvents were purified and stored under a positive pressure of argon.

1,8-Diazabicyclo[5.4.0]undec-7-ene (DBU)

This was purified and stored as previously described (1).

Equilibrium and kinetic measurements

The equilibrium constants were measured as previously described (1) using a Specord M-40 spectrophotometer. The kinetic measurements for both the normal and deuterated substrates were carried out using a stopped-flow spectrophotometer. The kinetic and equilibrium measurements were performed at controlled temperatures using a circulating bath connected to the cell block of the spectrophotometer to keep the temperature constant within ±0.1°C.

The pseudo-first-order kinetics were performed using 2×10^{-5} M concentration of C-acids and a varying concentration of the base (Tables 3, 4). The concentrations of the base were always in large excess to ensure pseudo-first-order kinetics. From the kinetic curves the pseudo-first-order rate constants k_{obs} were calculated using the Guggenheim method. The observed rate constants for proton transfer reactions were a function of base concentration according to the following equation:

$$[4] \quad k_{obs} = k_f^H c_B + k_b^H$$

where k_f^H and k_b^H are the rate constants of the forward and reverse reactions respectively and c_B is the concentration of the base. The second-order rate constants are the calculated slopes of k_{obs} versus base concentration. The intercepts for proton transfer are the rate constants of the backward reaction k_b^H (not quoted in Tables 3 and 4). For reactions of the deutero analogues the initial part of the kinetic curves (less than one tenth of the reaction half-lifetime) was ignored to minimize the possible error caused by D/H exchange, in accordance with Bergson (34) and Melander and Saunders (23*a*), who suggested that this procedure reduces the probability of the results being distorted by the effects of isotopic exchange. The remaining part of the Guggenheim plot was a good straight line. Then eq. [2] was applied in order to determine second-order rate constants k_f^D.

The activation parameters were evaluated from the temperature dependence of the second-order rate constants k_f by means of a least-squares fit to the transition state theory equation.

Acknowledgements

The authors are grateful for financial support by the CPBP 01.19.04.16 program, and to Professor K. T. Leffek for fruitful discussions.

1. W. Galezowski and A. Jarczewski. J. Chem. Soc. Perkin Trans. 2, 1647 (1989).
2. K. T. Leffek and P. Pruszynski. Can. J. Chem. **60**, 1692 (1982).
3. N. Sugimoto, M. Sasaki, and J. Osugi. J. Chem. Soc. Perkin Trans. 2, 655 (1984).
4. E. F. Caldin, A. Jarczewski, and K. T. Leffek. Trans. Faraday Soc. **67**, 110 (1971).
5. A. Jarczewski and P. Pruszynski. Polish J. Chem. **58**, 1175 (1984).
6. H. A. Benesi and J. H. Hildebrand. J. Am. Chem. Soc. **71**, 2703 (1949).
7. A. Jarczewski, P. Pruszynski, and K. T. Leffek. Can. J. Chem. **61**, 2029 (1983).
8. A. Jarczewski and P. Pruszynski. J. Chem. Soc. Perkin Trans. 2, 1117 (1986).
9. A. Jarczewski, P. Pruszynski, M. Kazi, and K. T. Leffek. Can. J. Chem. **62**, 954 (1984).
10. K. T. Leffek and P. Pruszynski. Can. J. Chem. **59**, 3034 (1981).
11. O. Rogne. Acta Chem. Scand. Ser. A, **32**, 559 (1978).
12. I. Heggen, J. Lindstrom, and O. Rogne. J. Chem. Soc. Faraday Trans. 1, **74**, 1263 (1978).
13. J. H. Blanch and O. Rogne. J. Chem. Soc. Faraday Trans. 1, **74**, 1254 (1978).
14. A. J. Kresge and M. F. Powell. J. Am. Chem. Soc. **103**, 201 (1981).
15. E. F. Caldin and S. Mateo. J. Chem. Soc. Faraday Trans. 1, **71**, 1876 (1975).
16. C. D. Hubbard, D. L. Harris III, D. W. Hooper, and A. F. Tucci. J. Chem. Soc. Faraday Trans. 1, **78**, 3619 (1982).
17. E. F. Caldin and S. Mateo. J. Chem. Soc. Chem. Commun. 854 (1973).
18. E. F. Caldin, D. M. Parboo, F. A. Walker, and C. R. Wilson. J. Chem. Soc. Faraday Trans. 1, **72**, 1856 (1975).
19. J. L. Kurz and L. C. Kurz. J. Am. Chem. Soc. **90**, 4451 (1972).
20. R. P. Bell. The proton in chemistry. 2nd ed. Chapman and Hall, London. 1973.
21. J. H. Blanch, O. Rogne, and L. I. Rossemyr. J. Chem. Soc. Faraday Trans. 1, **76**, 1905 (1980).
22. A. Thibblin and P. Ahlberg. Chem. Soc. Rev. **18**, 209 (1989).
23. L. Melander and W. H. Saunders, Jr. Reaction rates of isotopic molecules. John Wiley and Sons, New York. 1980. Chap. X. (*a*) pp. 287–291; (*b*) p. 291; (*c*) pp. 285–287.
24. E. F. Caldin, S. Mateo, and P. Warrick. J. Am. Chem. Soc. **103**, 202 (1981).
25. N. S. Isaacs and K. Javaid. J. Chem. Soc. Perkin Trans. 2, 1583 (1972).
26. S. Lofas and P. Ahlberg. J. Am. Chem. Soc. **107**, 7534 (1985).
27. F. G. Bordwell and H. E. Fried. Tetrahedron Lett. 1121 (1977).
28. F. G. Bordwell, J. E. Bartmess, and J. A. Hautala. J. Org. Chem. **43**, 3107 (1978).
29. C. D. Hubbard, C. J. Wilson, and E. F. Caldin. J. Am. Chem. Soc. **98**, 870 (1976).
30. R. P. Bell. Disc. Faraday Soc. **39**, 16 (1956).
31. E. F. Caldin and O. Rogne. J. Chem. Soc. Faraday Trans. 1, **75**, 2065 (1978).
32. E. F. Caldin. Reaction transition states. Gordon and Breach, London. 1972.
33. F. G. Bordwell and W. J. Boyle. J. Am. Chem. Soc. **97**, 3447 (1975).
34. G. Bergson. Chem. Scr. **8**, 145 (1975).

Can. J. Chem. Downloaded from www.nrcresearchpress.com by 195.138.81.100 on 09/07/12
For personal use only.

Studies of the charge transfer interactions between aromatic hydrocarbons and some biologically active compounds by conductometric methods

HARBHAJAN S. RANDHAWA[1] AND RAJNI SACHDEVA
Department of Chemistry, Panjab Agricultural University, Ludhiana-141004, India
AND
SUSHIL K. SURI
Department of Chemistry, Indian Institute of Technology, New Delhi-110016, India

Received July 13, 1989[2]

HARBHAJAN S. RANDHAWA, RAJNI SACHDEVA, and SUSHIL K. SURI. Can. J. Chem. **68**, 2249 (1990).

Charge transfer (CT) interactions between aromatic hydrocarbons, namely, benzene, biphenyl, phenanthrene, naphthalene, and anthracene, and herbicides of the triazine series, viz. Atraton, Trietazine, and Simetone, have been investigated by conductometric methods. The stoichiometries of the complexes have been established and the molar conductivities of the CT complexes determined. The effect of the nature of the electron donors, electron acceptors, and the solvent media on the conductivity of the CT complexes has been studied.

Key words: conductivity, charge transfer interactions, hydrocarbons, herbicides.

HARBHAJAN S. RANDHAWA, RAJNI SACHDEVA et SUSHIL K. SURI. Can. J. Chem. **68**, 2249 (1990).

Utilisant la méthode conductimétrique, on a étudié les interactions de transfert de charge (TC) entre les hydrocarbures aromatiques, en particulier le benzène, le biphényle, le phénantrène, le naphtalène et l'anthracène, et les herbicides de la série triazine comme l'Atraton, la triétazine et la Simétone. On a établi la stoechiométrie des complexes et on a déterminé les conductivités molaires des complexes de transfert de charge. On a étudié l'effet de la nature des groupes électrodonneurs, des groupes électroattracteurs et du solvant sur la conductivité des complexes de transfert de charge.

Mots clés : conductivité, interactions de transfert de charge, hydrocarbures, herbicides.

[Traduit par la revue]

Introduction

Our earlier research was devoted to fusibility diagram studies on charge transfer (CT) interactions of aromatic hydrocarbons with a variety of polar organic molecules, in relation to the stoichiometries and energetics of the CT complexes (1–3). Congruent compounds of unusual stoichiometries were formed in the donor–acceptor systems. The area under the curve of the congruent compound cannot be fixed as the sole criterion to predict the relative strength of CT complexes in the absence of thermodynamic parameters. As an extension to this study, the CT interactions between five aromatic hydrocarbons, namely benzene, biphenyl, phenanthrene, naphthalene, and anthracene, as π-donors, (4), and three herbicides of the triazine series, viz. 1,3,5-triazine-2,4-diamine, *N*-ethyl-6-methoxy-*N'*-(1-methylethyl) (Atraton), 1,3,5-triazine-2,4-diamine, 6-chloro-*N,N,N'*-triethyl (Trietazine), and *N,N'*-diethyl-6-methoxy-1,3,5-triazine-2,4-diamine (Simetone) as π-acceptors (5), have been investigated. The biologically active π-electron acceptors, which were selected in view of their practical importance, have the following molecular structure:

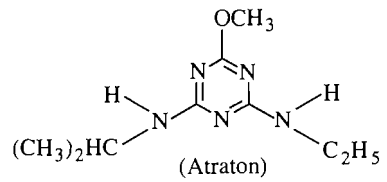

(Atraton)

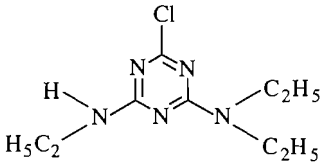

(Trietazine)

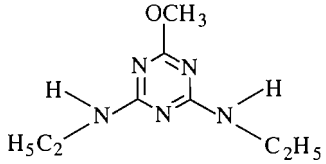

(Simetone)

The conductometric technique was employed to study the CT interactions. The CT complex (DA) formed by partial or complete transfer of an electron from the donor D to the acceptor A (6, 7) tends to dissociate into ions D^+ and A^- in a solvent media of sufficiently high dielectric constant according to the scheme (8–10).

$$D + A \rightleftharpoons DA$$

$$DA \rightleftharpoons D^+ + A^-$$

The extent of dissociation depends on the nature of D, A, and the dielectric constants of the solvent media. The formation of the CT complex can, therefore, be followed by observing the variation of electrical conductivity (σ) of D on the addition of A, or vice versa, in suitable solvent media. The plot of σ as a function of composition of D or A generally results in a maximum, which determines the stoichiometry of the CT complex (11–13). We have preferred this method as it is free from uncertainties arising from the masking of CT bands by absorption bands of the components and the products.

The studies reported in this manuscript are aimed at (i) establishing the stoichiometry of the CT complexes formed between aromatic hydrocarbons and herbicides and (ii) correlating the parameters characterizing the CT complexes with those of D, A, and the media.

Experimental

Analytical reagent grade aromatic hydrocarbons, namely, benzene, biphenyl, phenanthrene, naphthalene, and anthracene, and three solvents, namely cyclohexane, dichloromethane, and trichloromethane (BDH), were purified by following standard procedures (14, 15). The Atraton, Simetone, and Trietazine were obtained from Ciba Geigy Ltd. and were reported to have a purity of 99.9%, 99.4%, and 99.9%, respectively. These chemicals were further purified by crystallization from *n*-propanol before use.

Equimolar stock solutions (5×10^{-4} M) of aromatic hydrocarbons and the electron acceptors in the three solvent media (viz. cyclohexane,

[1]Author to whom correspondence may be addressed.
[2]Revision received July 11, 1990.

Can. J. Chem. Downloaded from www.nrcresearchpress.com by 195.138.81.100 on 09/07/12
For personal use only.

TABLE 1. Conductance data for CT complexes in chloroform at 298 K

System (D + A)	Ionization potential* (eV)	Stoichiometry (A:D)	Conductance × 10 (μmho) σp	σ_0	$\sigma_p - \sigma_0$	σ_M
Benzene + Atraton		1:4	632	118	514	43 559
Benzene + Trietazine	9.2	1:4	726	210	516	24 571
Benzene + Simetone		1:4	774	89	685	76 966
Biphenyl + Atraton		1:4	679	281	398	14 163
Biphenyl + Trietazine	8.26	1:4	774	515	259	5 029
Biphenyl + Simetone		1:4	872	245	627	25 600
Phenanthrene + Atraton		1:4	702	145	557	38 413
Phenanthrene + Trietazine	8.1	1:4	872	235	637	27 106
Phenanthrene + Simetone		1:4	922	119	803	67 478
Naphthalene + Atraton		1:4	726	115	611	53 130
Naphthalene + Trietazine	7.96	1:4	1024	210	814	38 761
Naphthalene + Simetone		1:4	972	90	882	98 000
Anthracene + Atraton		1:2	823	135	688	33 975
Anthracene + Trietazine	7.55	1:2	1129	275	854	20 703
Anthracene + Simetone		1:2	1024	90	934	69 185

*Values from ref. 16.

dichloromethane, and trichloromethane) were mixed in the conductivity cell, keeping the total volume constant but varying the volumes of donor and acceptor solutions. The conductance measurements were made on a Philips PR 9500 conductivity bridge using a conductivity cell (cell constant = 0.890 dm^{-1}) fitted with platinized platinum electrodes. The conductivity cell was standardized employing a 0.02 M solution of potassium chloride. All measurements were made at 50 cps in a thermostat maintained at 298.15 ± 0.01 K.

The measured values of electrical conductance were plotted as a function of composition of D or A. The molar conductivity coefficients, σ_M's, were computed using the expression (11):

$$\alpha\sigma_M = \frac{1}{M}\,\frac{\sigma_p - \sigma_0}{\sigma_0}$$

where M is the molar concentration of the donor or acceptor at the conductivity peak of the complex. σ_p is the conductivity at the conductivity peak, σ_0 is the linearly interpolated conductivity value read off from a base line joining the conductivities of the pure donor and acceptor solutions, and α is the dissociation constant of the complex.

Results and discussion

The electrical conductances of solutions containing varying amounts of A and D in different solvent media were plotted against the mole fraction A. A representative plot of conductance versus concentration for the phenanthrene–Simetone complex in chloroform is shown in Fig. 1. The appearance of a maximum in the plot is indicative of complexation in the D–A system (11–13). The composition of the CT complex formed between D and A was deduced from the stoichiometric maximum. The presence of a well-developed maximum in the conductivity–concentration plots observed in all systems studied is indicative of the fact that in the various aromatic hydrocarbon (donor) – herbicides of the triazine series (acceptor) systems, π–π type charge transfer complexes are formed. The observed stoichiometries of the CT complexes investigated in chloroform as solvent and their σ_p values are listed in Table 1. From the 1:4 stoichiometries of π–π complexes, observed in these systems, we infer that an expected arrangement of four donor molecules around an acceptor molecule is either of tetrahedral or square planar geometry, and the most probable arrangement of two donors about the acceptor in 1:2 stoichiometry is linear.

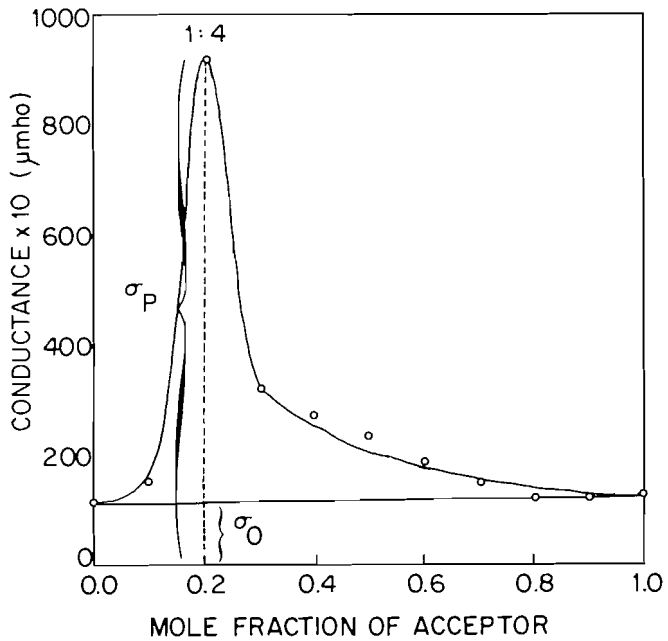

FIG. 1. Plot of conductance vs. mole fraction of simetone (acceptor) in phenanthrene–simetone system in chloroform solution at 298.15 ± 0.01 K.

The molar conductivity coefficients, calculated by the procedure of Gutmann and Keyzer (11), exhibited no definite order in the systems when α was assumed to be unity in all cases. This may be attributed to differences in the α values of CT complexes and their deviation from unity.

The numerical value of σ_p is a measure of the total number of ions carrying the current when D and A are mixed in stoichiometric proportions corresponding to the CT complex. When the solvent medium, concentrations of D and A, and the experimental parameters are kept the same for a fixed donor, the values of σ_p reflect the electron affinity of the acceptors and, for a fixed acceptor, they reflect the donicity of the donor provided all complexes dissociate to the same extent and the

Can. J. Chem. Downloaded from www.nrcresearchpress.com by 195.138.81.100 on 09/07/12
For personal use only.

TABLE 2. Conductance data for CT complexes in different solvents at 298 K

System (D + A)	Solvent	Dielectric constant*	Stoichiometry (A:D)	Conductance × 10 (μmho) σ_p	σ_0	$\sigma_p - \sigma_0$	σ_M
Benzene + Atraton			1:4	326	100	226	22 600
Benzene + Trietazine			1:4	357	105	252	24 000
Benzene + Simetone			1:4	389	90	299	33 222
Biphenyl + Atraton			1:4	357	100	257	25 700
Biphenyl + Trietazine			1:4	421	105	316	30 095
Biphenyl + Simetone			1:4	487	90	397	44 111
Phenanthrene + Atraton			1:4	389	172	217	12 616
Phenanthrene + Trietazine	C_6H_{12}	2.02	1:4	454	180	274	15 222
Phenanthrene + Simetone			1:4	520	170	350	20 588
Naphthalene + Atraton			1:4	421	130	291	22 384
Naphthalene + Trietazine			1:4	487	135	352	26 074
Naphthalene + Simetone			1:4	553	120	433	36 083
Anthracene + Atraton			1:2	837	295	542	12 248
Anthracene + Trietazine			1:2	874	302	572	12 626
Anthracene + Simetone			1:2	951	285	666	15 578
Benzene + Atraton			1:4	632	118	514	43 559
Benzene + Trietazine			1:4	726	210	516	24 571
Benzene + Simetone			1:4	774	89	685	76 966
Biphenyl + Atraton			1:4	679	281	398	14 163
Biphenyl + Trietazine			1:4	774	515	259	50 219
Biphenyl + Simetone			1:4	872	245	627	25 591
Phenanthrene + Atraton	$CHCl_3$	4.8	1:4	702	145	557	38 413
Phenanthrene + Trietazine			1:4	872	235	637	27 106
Phenanthrene + Simetone			1:4	922	119	803	67 478
Naphthalene + Atraton			1:4	726	115	611	53 130
Naphthalene + Trietazine			1:4	1024	210	814	38 761
Naphthalene + Simetone			1:4	972	90	882	98 000
Anthracene + Atraton			1:2	823	135	688	33 975
Anthracene + Trietazine			1:2	1129	275	854	20 703
Anthracene + Simetone			1:2	1024	90	934	69 185
Benzene + Atraton			1:4	686	80	606	75 750
Benzene + Trietazine			1:4	734	168	566	33 690
Benzene + Simetone			1:4	734	50	684	136 800
Biphenyl + Atraton			1:4	734	241	493	20 456
Biphenyl + Trietazine			1:4	783	500	283	5 660
Biphenyl + Simetone			1:4	932	305	627	20 557
Phenanthrene + Atraton	CH_2Cl_2	9.1	1:4	783	110	673	61 181
Phenanthrene + Trietazine			1:4	882	198	684	34 545
Phenanthrene + Simetone			1:4	958	79	879	111 265
Naphthalene + Atraton			1:4	783	80	703	87 875
Naphthalene + Trietazine			1:4	1036	168	868	51 666
Naphthalene + Simetone			1:4	984	50	934	186 800
Anthracene + Atraton			1:2	882	100	782	52 133
Anthracene + Trietazine			1:2	1197	230	967	28 028
Anthracene + Simetone			1:2	1036	50	986	131 466

*Values from ref. 16.

differences in configuration are not too great. The σ_p values are expected to be high when the CT complex between D and A is strong.

Apparently, the values of σ_p for CT complexes of aromatic hydrocarbon donors with different acceptors increase with a decrease in the ionization potential of the donor and follow the order: anthracene > naphthalene > phenanthrene > biphenyl > benzene. We are unable to correlate the σ_p values of CT complexes with the electron affinity of the acceptors due to the non-availability of electron affinity values for the acceptors.

The results of conductance measurements of the CT complexes in different solvents are recorded in Table 2. It is observed that the value of σ_p increases as the dielectric constant of the medium increases. This appears to be due to an increase in the total number of ions carrying the current at the stoichiometric point as the CT complexes are expected to ionize to a greater extent in the solvent of higher dielectric constant. This is in accordance with earlier investigations, which revealed that the extent of electron transfer in CT complexes is enhanced by increase in the solvent polarity (17).

Acknowledgements

The authors are indebted to Ciba-Geigy Ltd, for supplying analytical grade samples of Atraton, Simetone, and Trietazine. One of us (R.S.) is also grateful to CSIR New Delhi for the award of a senior research fellowship.

Can. J. Chem. Downloaded from www.nrcresearchpress.com by 195.138.81.100 on 09/07/12
For personal use only.

1. H. S. RANDHAWA, S. KHERA, R. SACHDEVA, and S. K. SURI. Thermochim. Acta, **105**, 303 (1986).
2. H. S. RANDHAWA, R. SACHDEVA, M. L. SOOD, and S. K. SURI. J. Therm. Anal. **32**, 1381 (1987).
3. R. SACHDEVA, H. S. RANDHAWA, M. L. SOOD, and S. K. SURI. Thermochim. Acta, **142**, 371 (1989).
4. R. FOSTER. Organic charge transfer complexes. Academic Press, New York. 1969.
5. A. BERLIN, G. A. PAGANI, and F. SANNICOLO. Synth. Met. **19**, 415 (1987).
6. R. S. MULLIKEN. J. Am. Chem. Soc. **74**, 811 (1952).
7. R. S. MULLIKEN. J. Am. Chem. Soc. **72**, 600 (1950).
8. J. W. EASTMAN, G. ENGELSMA, and M. CALVIN. J. Am. Chem. Soc. **84**, 1339 (1962).
9. H. KAINER and A. UBBERLE. Chem. Ber. **88**, 1147 (1955).
10. R. L. WARD. J. Chem. Phys. **39**, 852 (1963).
11. F. GUTMANN and H. KEYZER. Electrochim. Acta, **11**, 555, (1966); **11**, 1163 (1966).
12. F. GUTMANN and H. KEYZER. Electrochim. Acta, **12**, 1255 (1967).
13. F. GUTMANN. J. Sci. Ind. Res. **26**, 19 (1967).
14. J. A. RIDDICK and W. B. BUNGER. Organic solvents. Wiley–Interscience, New York. 1970.
15. A. I. VOGEL. Textbook of practical organic chemistry. 4th ed. Longman, London. 1978.
16. C. R. WEAST (*Editor*). Handbook of chemistry and physics. 55th ed. CRC Press, Boca Raton, FL. 1974–1975.
17. P. C. DWIVEDI and C. N. R. RAO. J. Chem. Soc. Perkin Trans. **2**, 238 (1972).

Can. J. Chem. Downloaded from www.nrcresearchpress.com by 195.138.81.100 on 09/07/12
For personal use only.

Synthesis of 6-*O*-octyl-β-D-galactopyranosyl-(1→5)-L-arabinose and comparative 1-deoxyglycitolation of N^{α}-*Z*-L-lysine with amphiphilic lipodisaccharides

DANIEL CABARET AND MICHEL WAKSELMAN[1]

Centre national de la recherche scientifique – Centre d'étude et de recherche de chimie organique appliquée, 2, rue Henri Dunant, F-94320 Thiais, France

Received March 28, 1990

DANIEL CABARET and MICHEL WAKSELMAN. Can. J. Chem. **68**, 2253 (1990).

A lipodisaccharide possessing a reactive aldopentose unit, 6-*O*-octyl-β-D-galactopyranosyl-(1→5)-L-arabinose **6**, was obtained by glycoside synthesis. To avoid a possible intramolecular acyl transfer, benzoyl protecting groups and mild conditions of detritylation were used in the preparation of the furanosyl acceptor. The reductive alkylation of N^{α}-*Z*-L-lysine was then studied and compared to that of previously prepared liposaccharides. In this reaction, amphiphilic five-membered hemiacetals are generally more reactive than their six-membered analogues. The newly prepared disaccharide is the most reactive of the series and also the easiest to prepare. Therefore this reagent has been selected for a future study on the chemical modification of enzymes and the use in organic solvents of the biocatalysts obtained.

Key words: liposaccharides, reductive alkylation.

DANIEL CABARET et MICHEL WAKSELMAN. Can. J. Chem. **68**, 2253 (1990).

Le 6-*O*-octyl β-D-galactopyranosyl-(1→5)-L-arabinose **6**, un lipodisaccharide ayant une fonction aldopentose réactive, a été obtenu par synthèse osidique. Pour éviter un transfert d'acyle intramoléculaire dans la préparation de l'accepteur furanosyle, des groupes protecteurs benzoates et des conditions douces de détritylation ont été utilisés. Le réactif **6** a ensuite été comparé à d'autres liposaccharides dans la réaction d'alkylation réductrice de la N^{α}-*Z*-L-lysine. Dans cette condensation, les hémiacétals amphiphiles à cinq chaînons sont généralement plus réactifs que leurs analogues à six chaînons. Le lipodisaccharide **6** étant le plus réactif de la série, et aussi le plus facile à préparer, a été retenu pour une étude ultérieure de modification chimique d'enzymes.

Mots clés : liposaccharides, alkylation réductrice.

Can. J. Chem. Downloaded from www.nrcresearchpress.com by 195.138.81.100 on 09/07/12
For personal use only.

Introduction

The mild and selective reductive alkylation of the lysine residues of proteins with reducing sugars leads to interesting neoglycoproteins (1, 2). In this 1-deoxyglycitolation reaction, unsubstituted aldopentoses exhibit faster rates of condensation with amines than their more stable aldohexose analogs (3, 4). In a search for liposaccharidic reagents for the preparation of lipoglycosylated enzymes suitable for use in polar organic solvents (5), we came upon the problem of long condensation time, which could be detrimental to the catalytic activity of the new biocatalyst. For our purpose, a lipofuranose might be a valuable compound. However, in a polar solvent, a disaccharide is better able to maintain the essential layer of water around the enzyme than is a monosaccharide derivative. Therefore the synthesis of the 6-*O*-octyl-β-D-galactopyranosyl-(1→5)-L-arabinose **6**, having a reactive aldopentofuranose end, has now been achieved and its reductive condensation with N^{α}-*Z*-L-lysine compared with that of some of the previously prepared lipodisaccharides (6, 7).[2]

Results and discussion

Synthesis

The use of a stoichiometric amount of chlorotriphenylmethane in pyridine below 25°C avoids the ditritylation of the pentofuranoses and selectively gives the monotrityl derivatives (9). In these conditions, L-arabinose **1** afforded the 5-*O*-trityl-L-arabinose **2** in good yield. As benzoyl groups do not migrate as readily as acetyl ones during the cleavage of a trityl protecting group (10), benzoylation was preferred to acetylation in the next step of the synthesis. Thus, treatment of the benzoylated arabinose **3** with trimethylchlorosilane and sodium iodide (11) gave the glycosyl acceptor **4**. Königs–Knorr condensation with the previously described 2,3,4-tri-*O*-acetyl-6-*O*-octyl-α-D-galactopyranosyl bromide donor (7), in the presence of mercuric cyanide, led to the protected disaccharide **5**. Removal of the ester protecting groups yielded the liposaccharide **6**, having six free hydroxyl functions (Fig. 1).

To confirm that no intramolecular acyl transfer had occurred, the parallel synthesis of compound **6** using the very stable benzyl protection was realized. Phase transfer catalyzed alkylation of the tritylated arabinose **2** furnished the benzyl α- and β-arabinosides **3′**α and **3′**β. Cleavage of the trityl group by means of $BF_3 \cdot Et_2O$ (10) afforded the glycosyl acceptors **4′**α and **4′**β. Condensation with the same glycosyl donor as above gave the protected disaccharides **5′**α and **5′**β. Zemplén deacetylation resulted in the isolation of the benzyl *O*-(6-*O*-octyl-β-D-galactopyranosyl)-(1→5)-2,3-di-*O*-benzyl-α- and β-L-arabinosides **7**α and **7**β. Hydrogenolysis (H_2, Pd/C, MeOH) of the β-arabinoside **7**β gave a product having the same ^1H and ^{13}C NMR characteristics as those of compound **6**, unambiguously establishing the structure of that disaccharide. In an unexpected way (12), catalytic hydrogenation of the **7**α isomer under the same experimental conditions led to the alditol **8**.

Reductive alkylation of N^{α}-Z-L-*lysine*

The mechanism of the 1-deoxyglycitolation of an amine is represented in Scheme 1. The rate-determining ring opening of the hemiacetal structure *a*, to give the reactive hydroxyaldehyde *b*, depends on the stability of *a*. The effect of ring size on the stabilities of cyclic hemiacetals relative to acyclic hydroxyaldehydes has been studied in simple cases; the six-membered ring is more stable than the five-membered one, and both of them are more stable than the larger rings (13, 14). Reductive condensation of unsubstituted aldopentoses with amines is faster than that of aldohexoses, and the reductive alkylation of unsubstituted reducing disaccharides is a slow process (3, 4).

[1]Author to whom correspondence may be addressed.

[2]Also, D. Cabaret and M. Wakselman, manuscript in preparation.

Printed in Canada / Imprimé au Canada

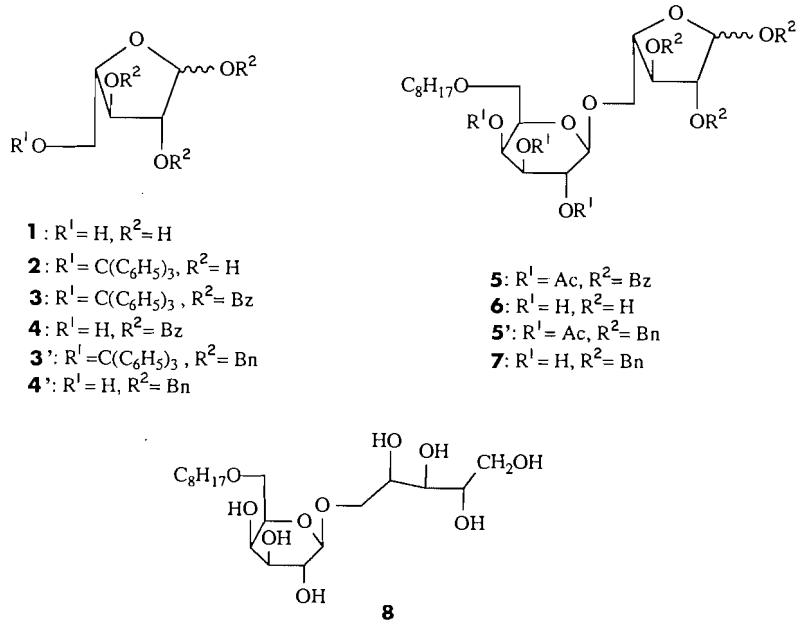

FIG. 1. Synthesis of the 6-*O*-octyl-β-D-galactopyranosyl-(1→5)-L-arabinose **6**.

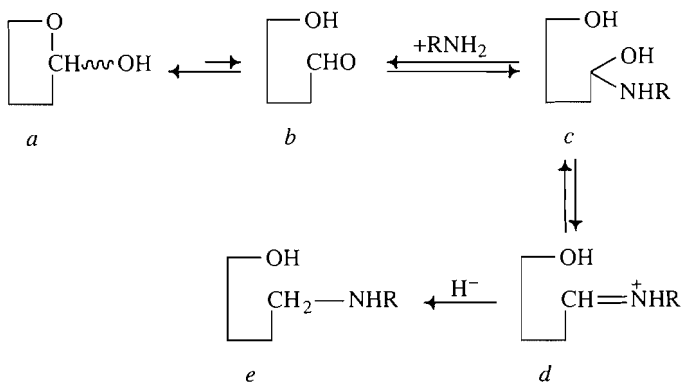

SCHEME 1. Mechanism of the 1-deoxyglycitolation reaction (*a*: hemiacetal; *b*: hydroxy-aldehyde; *c*: hemiaminal; *d*: immonium ion; *e*: alkylated amine).

However, in the reactions described in the literature, an equilibrium between the furanose and the pyranose forms of the saccharide, through the acyclic hydroxyaldehyde, might occur. In the case of the 5-substituted aldopentose **6** the formation of the pyranose isomers is not possible. Furthermore, the variation of the amphiphilicity of the liposaccharide could play a role in the reaction.

A series of liposaccharides has previously been prepared (Fig. 2). We have now estimated the relative reactivities of these lipodisaccharides and compare them to that of the melibiose **9***a* and to the newly prepared reagent **6** in the model reaction with N^{α}-*Z*-L-lysine (8). Preparative condensations, under different experimental conditions, have sometimes shown the formation of small amounts of bis-deoxyglycitolated derivatives resulting from the further reductive alkylation of the monoalkylated product (see the Experimental). If we reasonably assume that the relative reactivity of the monosubstituted amine formed does not change very much by varying the nature of the disaccharide, a reactivity scale can be established by following the consumption of N^{α}-*Z*-L-lysine under mild reductive conditions close to those of the chemical modification of an enzyme (Table 1).

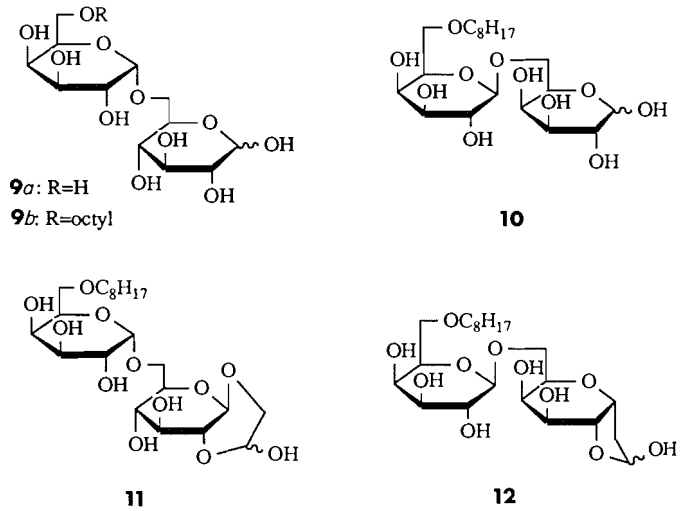

FIG. 2. Structures of the other liposaccharides: **9***b*, **10**, **11**, **12**, and melibiose **9***a*. **9***b*: 6-*O*-octyl-α-D-Gal*p*-(1→6)-D-Glc; **10**: 6-*O*-octyl-β-D-Gal*p*-(1→6)-D-Gal; **11**: 6-*O*-octyl-α-D-Gal*p*-(1→6)-β-D-gluco-pyrano[1,2-*b*]-1,4-dioxan-5-ol; **12**: 6-*O*-octyl-β-D-Gal*p*-(1→6)-α-D-galactopyrano[2,1-*b*]-oxolan-5-ol.

TABLE 1. Variation with time of the percentage of the N^{α}-*Z*-L-lysine that has reacted with the lipodisaccharides in the presence of an excess of $NaBH_3CN$ (at 4°C in a 0.1 M borate buffer)

Time (h)	Reagent					
	9*a*	**9***b*	**10**	**11**	**12**	**6**
	Percentage of consumed lysine					
4	8	9	7	20	34	30
24	13	15	12	30	52	57
48	27	31	24	39	59	66
120	31	35	30	45	63	70

Can. J. Chem. Downloaded from www.nrcresearchpress.com by 195.138.81.100 on 09/07/12
For personal use only.

Can. J. Chem. Downloaded from www.nrcresearchpress.com by 195.138.81.100 on 09/07/12
For personal use only.

The experimental order found is the following: **6**, **12** (ref. 8) ≥ **11** (ref. 6), **10** (ref. 7), **9***b* (ref. 6), **9***a*. The lipodisaccharides having a five-membered hemiacetal structure (furanose **6** and oxolanol **12**) react more rapidly than the six-membered hemiacetals (dioxanol **11** and pyranoses **10**, **9***b*, or **9***a*). The reactivity of the 6′-*O*-octyl melibiose is not very different from that of melibiose itself. The arabinose **6** is the most reactive of the series. Moreover, its synthesis is shorter than that of the oxolanol **12**; therefore this lipodisaccharide has been selected for a future study on condensation with enzymes.

Experimental

General methods

The ^{1}H NMR spectra were recorded at 300 MHz and the ^{13}C NMR spectra at 20 or 75 MHz in $CDCl_3$ or CD_3OD. The chemical shifts (δ, in ppm) are relative to internal TMS. The optical rotations were measured with a Perkin–Elmer 241 polarimeter. The melting points were determined with a Mettler FP61 apparatus, and are uncorrected. Thin-layer chromatography was performed on precoated silica gel 60 F_{254} plates (Merck) and visualized by charring with sulfuric acid. Column chromatography was run on silica gel G60.

A Gilson HPLC chromatograph equipped with a SPD-6A Shimadzu UV spectrophotometer, a C-R 5A Shimadzu integrator, and a Brownlee C_{18} Spheri 5 (22.5 cm) column was used.

5-O-Trityl-L-arabinose **2**

The method described for the synthesis of the D(−) isomer ($[\alpha]_{589}$ +16.3° (*c* 0.85, ethanol, 20 h)) was followed (9). To a solution of L(+)-arabinose (1.5 g, 10 mmol) in 20 mL of dried pyridine was added triphenylmethane chloride (3.1 g, 11 mmol). After stirring for 24 h at room temperature, the pyridine was evaporated. The residue was dissolved in dichloromethane and washed with aqueous sodium bicarbonate. After drying over Na_2SO_4, evaporation of the solvent gave a syrup that was purified on a silica gel column (eluent: 9.1 dichloromethane–methanol) to give **2** (3.06 g, 78% yield); R_f 0.56; mp 68°C; $[\alpha]_{589}$ −15.3°, $[\alpha]_{546}$ −17.1° (*c* 0.85, ethanol, 20 h); ^{1}H NMR (CD_3OD) δ: 5.41 (H-1β, J_{1-2} = 4.5 Hz), 5.38 (H-1α, J_{1-2} = 2.5 Hz), 4.10 (H-2α and H-3α), 4.35 (H-4α), 3.45 (H-5Aα, J_{4-5A} = 3.44 Hz, J_{5A-5B} = 10 Hz), 3.38 (H-5Bα, J_{4-5B} = 5.7 Hz); ^{13}C NMR δ: 103.9 (C-1α), 97.3 (C-1β), 83.5–65.5 (C-2–C-5). Anal. calcd. for $C_{24}H_{24}O_5$: C 73.45, H 6.16; found: C 73.26, H 6.30.

1,2,3-Tri-O-benzoyl-5-O-trityl-L-arabinose **3**

To a solution of trityl arabinose **2** (1.96 g, 5 mmol) in pyridine (10 mL), benzoyl chloride (2.32 g, 16.5 mmol) was added dropwise with stirring over a period of 3 h, at room temperature. After evaporation of the pyridine, the residue was dissolved in dichloromethane and washed with a saturated sodium bicarbonate solution. Drying (Na_2SO_4) and evaporation gave a syrup that was chromatographed (85:15 pentane – ethyl acetate) to give the title compound **3** (2.9 g, 82%); R_f 0.48, the two α and β isomers were not separated; ^{1}H NMR ($CDCl_3$) δ: 6.82 (H-1β, J_{1-2} = 4.7 Hz), 6.66 (H-1α, $J_{1-2} \leq$ 1 Hz), 6.10 (H-3β, J_{3-4} = 5.6 Hz), 5.80 (H-2β, J_{2-3} = 6.6 Hz), 5.71 (H-2α, J_{2-3} = 0.9 Hz), 5.68 (H-3α, J_{3-4} = 3.3 Hz), 4.71 (H-4α), 4.5 (H-4β), 3.6 (H-5Aα), 3.55 (H-5Aβ), 3.46 (H-5Bβ), 3.40 (H-5Bα); ^{13}C NMR δ: 99.96 (C-1α), 94.77 (C-1β), 80.75–63.54 (C-2–C-5). Anal. calcd. for $C_{45}H_{36}O_8$: C 76.69, H 5.15; found: C 76.91, H 5.09.

1,2,3-Tri-O-benzoyl-L-arabinose **4**

To a solution of the trityl derivative **3** (1.6 g, 2.27 mmol) in dry acetonitrile (20 mL) under Ar at 0°C were added NaI (1.02 g, 6.8 mmol) and then chlorotrimethylsilane (0.74 g, 6.8 mmol). The mixture was stirred for 2 h at 0°C and diluted with diethyl ether. The solution was washed with water and with $Na_2S_2O_3$, dried (Na_2SO_4), and evaporated. The residue was purified by column chromatography (1:1 pentane – diethyl ether) to give **4** (0.69 g, 66%); R_f 0.32; ^{1}H NMR ($CDCl_3$) δ: 6.86 (H-1β, J_{1-2} = 4.53 Hz), 6.69 (H-1α), 5.96 (H-3β, J_{3-4} = 5.6 Hz), 5.95 (H-2β, J_{2-3} = 6.68 Hz), 5.82 (H-2α, J_{2-3} = 0.9 Hz), 5.58 (H-3α, J_{3-4} = 3.7 Hz), 4.57 (H-4α), 4.38 (H-4β), 4.06 (H-5Aβ, J_{4-5A} = 4.51 Hz, J_{5A-5B} = 12.1 Hz), 4.02 (H-5Aα and H-5Bα), 3.99 (H-5Bβ, J_{4-5B} = 5.9 Hz); ^{13}C NMR δ: 99.76 (C-1α), 94.29 (C-1β), 80.76–62.23 (C-2–C-5). Anal. calcd. for $C_{26}H_{22}O_8$: C 67.53, H 4.80; found: C 67.29, H 4.80.

O-(2,3,4-Tri-O-acetyl-6-O-octyl-β-D-galactopyranosyl)-(1→5)-1,2,3-tri-O-benzoyl-L-arabinose **5**

To a solution of **4** (325 mg, 0.7 mmol) and 6-*O*-octyl-2,3,4-tri-*O*-acetyl-α-D-galactopyranosyl bromide (**7**) (440 mg, 0.91 mmol) in dichloromethane (15 mL), was added $Hg(CN)_2$ (250 mg, 1 mmol). After stirring for 48 h at room temperature, the solution was filtered on Celite, and washed with water and a KI solution. Evaporation of the solvent gave a crude product, which was applied to a silica gel column and eluted with 7:3 pentane – ethyl acetate to give **5** (435 mg, 72%); R_f 0.54; ^{1}H NMR ($CDCl_3$) δ: 6.81 (H-1β, J_{1-2} = 4.34 Hz), 6.43 (H-1α, $J_{1-2} \leq$ 1 Hz), 5.91 (H-3β, J_{3-4} = 4.97 Hz), 5.84 (H-2β, J_{2-3} = 6.32 Hz), 5.75 (H-2α, J_{2-3} = 1.0 Hz), 5.55 (H-3α, J_{3-4} = 3.6 Hz), 5.41 (H-4′α, $J_{4'-5'}$ = 2.8 Hz), 5.31 (H-4′β, $J_{4'-5'}$ = 1.5 Hz), 5.24 (H-2′α, $J_{2'-3'}$ = 9.5 Hz), 5.16 (H-2′β, $J_{2'-3'}$ = 9.5 Hz), 5.02 (H-3′α, $J_{3'-4'}$ = 3.4 Hz), 4.94 (H-3′β, $J_{3'-4'}$ = 3 Hz), 4.60 (H-1′α, $J_{1'-2'}$ = 7.9 Hz), 4.59 (H-1′β, $J_{1'-2'}$ = 7.9 Hz), 3.83 (H-5′), 3.5–3.3 (H-6′); ^{13}C NMR δ: 101.9 (C-1′α isomer), 100.71 (C-1′β isomer), 99.94 (C-1α), 94.72 (C-1β). Anal. calcd. for $C_{46}H_{54}O_{16}$: C 64.02, H 6.31; found: C 64.21, H 6.51.

6-O-Octyl-β-D-galactopyranosyl-(1→5)-L-arabinose **6**

Compound **5** (300 mg, 0.35 mmol) was dissolved in methanol (10 mL) and treated with sodium methoxide (20 mg). After stirring for 2 h at room temperature, Amberlite CG-50 (200 mg) was added. Filtration of the solution and evaporation of the methanol gave a solid that was purified by chromatography with 8:2 dichloromethane–methanol as eluent. The title compound **6** was obtained (97 mg, 65%); R_f 0.58; mp 125°C; $[\alpha]_{589}$ −15.1°; $[\alpha]_{546}$ −18.6° (*c* 1, methanol); ^{1}H NMR (CD_3OD) δ: 5.02 (H-1β, J_{1-2} = 4.53 Hz), 4.99 (H-1α, J_{1-2} = 1.5 Hz), 4.15 (H-1′β, $J_{1'-2'}$ = 7.3 Hz), 4.13 (H-1′α, $J_{1'-2'}$ = 7.3 Hz); ^{13}C NMR δ: 105.31 (C-1′α), 105.20 (C-1′β), 103.62 (C-1α), 97.48 (C-1β). Anal. calcd. for $C_{19}H_{36}O_{10}\cdot 0.5H_2O$: C 52.64, H 8.60; found: C 52.91, H 8.55.

Benzyl 2,3-di-O-benzyl-5-O-trityl-α- and β-L-arabinosides (3′α and 3′β)

To a solution of the trityl arabinose **2** (1 g, 2.55 mmol) in benzyl bromide (3 mL) was added crushed KOH (0.5 g). After addition of tetrabutylammonium bromide (50 mg) as catalyst, the mixture was stirred overnight at room temperature. Diethyl ether was added, the ether solution was decanted, washed with water, dried (Na_2SO_4), and evaporated. The residue was chromatographed with 1:1 pentane–dichloromethane as eluent to give **3′**α and **3′**β.

3′α (670 mg, 40%); R_f 0.62; $[\alpha]_{578}$ −27.9°, $[\alpha]_{546}$ −31.7° (*c* 4, dichloromethane); ^{1}H NMR ($CDCl_3$) δ: 5.15 (H-1, J_{1-2} = 1.0 Hz), 4.27 (H-4), 4.09 (H-2, J_{2-3} = 2.8 Hz), 4.00 (H-3, J_{3-4} = 6.24 Hz), 3.29 (H-5); ^{13}C NMR δ: 105.05 (C-1), 88.25–62 (C-2–C-5).

3′β (230 mg, 14%): R_f 0.42; $[\alpha]_{578}$ +42.3°, $[\alpha]_{546}$ +47.9° (*c* 6, dichloromethane); ^{1}H NMR δ: 4.92 (H-1, J_{1-2} = 4.12 Hz), 4.22 (H-3, J_{3-4} = 5.9 Hz), 4.17 (H-4), 4.05 (H-2, J_{2-3} = 6.9 Hz), 3.29 (H-5); ^{13}C NMR δ: 98.87 (C-1), 84.27–62 (C-2–C-5).

Benzyl 2,3-di-O-benzyl-α- and β-L-arabinosides (4′α and 4′β)

To a solution of **3′**α (430 mg, 0.65 mmol) in dichloromethane (15 mL), borontrifluoride etherate (0.3 mL) and methanol (0.6 mL) were added.[2] The mixture was stirred at room temperature for 2 h. Then the reaction was poured on water, washed with saturated sodium bicarbonate, and dried (Na_2SO_4). Evaporation gave a residue, which after column chromatography (1:1 pentane – diethyl ether) yielded compound **4′**α (218 mg, 80%). **4′**α: R_f 0.36; $[\alpha]_{578}$ −82.4°, $[\alpha]_{546}$ −92.6° (*c* 2, dichloromethane); ^{1}H NMR ($CDCl_3$) δ: 5.18 (H-1, J_{1-2} = 0.97 Hz), 4.20 (H-4), 4.09 (H-2, J_{2-3} = 2.8 Hz), 4.0 (H-3, J_{3-4} = 6.2 Hz), 3.85 (H-5A, J_{4-5A} = 2.9 Hz, J_{5A-5B} = 11.9 Hz), 3.66 (H-5B, J_{4-5B} = 4.0 Hz); ^{13}C NMR δ: 105.27 (C-1), 82.89–62.26 (C-2–C-5).

The **4′**β isomer was obtained by the same method: R_f 0.28;

Can. J. Chem. Downloaded from www.nrcresearchpress.com by 195.138.81.100 on 09/07/12
For personal use only.

$[\alpha]_{578}$ +51.3°, $[\alpha]_{546}$ +58.5° (*c* 2, dichloromethane); ^{1}H NMR δ: 4.97 (H-1, J_{1-2} = 4.43 Hz), 4.21 (H-3, J_{3-4} = 6.1 Hz), 4.07 (H-2, J_{2-3} = 7.1 Hz), 4.05 (H-4), 3.69 (H-5A, J_{4-5A} = 3.17 Hz, J_{5A-5B} = 11.9 Hz), 3.57 (H-5B, J_{4-5B} = 5.02 Hz); ^{13}C NMR δ: 99.59 (C-1), 82.33–64.03 (C-2–C-5). Anal. calcd. for $C_{26}H_{28}O_5$: C 74.26, H 6.71; found: C 74.51, H 6.70.

Benzyl O-*(2,3,4-tri-*O*-acetyl-6-*O*-octyl-β-*D*-galactopyranosyl)-(1→5)-2,3-di-*O*-benzyl-α- and β-*L*-arabinosides (5′α and 5′β)*

α Isomer

The experimental conditions were the same as those described for the synthesis of the benzoylated derivative **5** using, however, 82 mg (0.19 mmol) of the glycosyl acceptor **4′α** and 94 mg (0.19 mmol) of the 2,3,4-tri-*O*-acetyl-6-*O*-octyl-α-D-galactopyranosyl bromide glycosyl donor. Purification by chromatography (1:1 pentane-diethyl ether) yielded compound **5′α** (72 mg, 45%); R_f 0.61; $[\alpha]_{578}$ −43.4°, $[\alpha]_{546}$ −48.8° (*c* 1.3, dichloromethane); ^{1}H NMR ($CDCl_3$) δ: 5.34 (H-4′), 5.14 (H-2′, $J_{2'-3'}$ = 10.4 Hz), 4.98 (H-1, J_{1-2} = 1.4 Hz), 4.94 (H-3′, $J_{3'-4'}$ = 3.4 Hz), 4.53 (H-1′, $J_{1'-2'}$ = 8.0 Hz), 4.10 (H-4), 4.01 (H-2, J_{2-3} = 3.08 Hz), 3.90 (H-5A, J_{4-5A} = 4.3 Hz, J_{5A-5B} = 12.2 Hz), 3.88 (H-3, J_{3-4} = 6.3 Hz), 3.75 (H-5B, J_{4-5B} = 3.3 Hz), 3.73 (H-5′), 3.45 (H-6′A, $J_{5-6'A}$ = 6.0 Hz, $J_{6'A-6'B}$ = 9.8 Hz), 3.36 (H-6′B, $J_{5-6'B}$ = 6.7 Hz); ^{13}C NMR δ: 104.20 (C-1), 100.28 (C-1′), 88.50–67.85 (C-2–C-5 and C-2′–C-6′).

β isomer

Under the same experimental conditions, starting from **4′β**, **5′β** was obtained with 61% yield; R_f 0.53; $[\alpha]_{578}$ +18.4°, $[\alpha]_{546}$ +20.8° (*c* 1.1, dichloromethane); ^{1}H NMR ($CDCl_3$) δ: 5.41 (H-4′), 5.23 (H-2′, $J_{2'-3'}$ = 10.3 Hz), 4.98 (H-3′, $J_{3'-4'}$ = 3.4 Hz), 4.94 (H-1, J_{1-2} = 4.3 Hz), 4.50 (H-3), 4.47 (H-1′, $J_{1'-2'}$ = 7.8 Hz), 4.10 (H-4), 4.06 (H-2, J_{2-3} = 7 Hz), 3.96 (H-5A, J_{4-5A} = 6.4 Hz, J_{5A-5B} = 10 Hz), 3.79 (H-5′), 3.67 (H-5B, J_{4-5B} = 6.1 Hz), 3.50 (H-6′A, $J_{5-6'A}$ = 5.9 Hz, $J_{6'A-6'B}$ = 9.7 Hz), 3.42 (H-6′B, $J_{5-6'B}$ = 6.8 Hz); ^{13}C NMR δ: 101.02 (C-1′), 99.07 (C-1), 84.47–67.74 (C-2–C-5 and C-2′–C-6′). Anal. calcd. for $C_{46}H_{60}O_{13}$: C 67.29, H 7.37; found: C 67.20, H 7.37.

Benzyl O-*(6-*O*-octyl-β-*D*-galactopyranosyl)-(1→5)-2,3-di-*O*-benzyl-α- and β-*L*-arabinoside (7α and 7β)*

Compounds **5′α** and **5′β** were deacetylated by the same procedure used for compound **5**. The title compounds were purified by column chromatography (9:1 dichloromethane–methanol) (80% yields).

α Isomer: R_f 0.68; $[\alpha]_{578}$ −58.5°, $[\alpha]_{546}$ −65.2° (*c* 1.1, dichloromethane); ^{1}H NMR ($CDCl_3$) δ: 5.28 (H-1, J_{1-2} = 0.9 Hz), 4.27 (H-1′, $J_{1'-2'}$ = 6.8 Hz), 4.21 (H-4), 4.06 (H-2), 4.05 (H-5A, J_{4-5A} = 2.7 Hz, J_{5A-5B} = 12.7 Hz), 3.94 (H-3), 3.82 (H-5B, J_{4-5B} = 2.3 Hz), 3.73 (H-6′A, $J_{5'-6'A}$ = 5.4 Hz, $J_{6'A-6'B}$ = 10.1 Hz), 3.66 (H-6′B, $J_{5'-6'B}$ = 5.2 Hz); ^{13}C NMR δ: 104.95 and 105.45 (C-1 and C-1′).

β Isomer: R_f 0.62; $[\alpha]_{578}$ +12.2°, $[\alpha]_{546}$ +13° (*c* 0.7, dichloromethane); ^{1}H NMR δ: 4.98 (H-1, J_{1-2} = 4.3 Hz), 4.24 (H-1′, $J_{1'-2'}$ = 7.6 Hz), 4.23 (H-3, J_{3-4} = 6 Hz), 4.12 (H-4), 4.05 (H-2, J_{2-3} = 6.7 Hz), 4.04 (H-2′, $J_{2'-3'}$ = 9.3 Hz), 3.97 (H-3′, $J_{3'-4'}$ = 3.1 Hz), 3.72 (H-5A, J_{4-5A} = 5.6 Hz, J_{5A-5B} = 10.2 Hz), 3.64 (H-5B, J_{4-5B} = 7 Hz), 3.44 (H-5′); ^{13}C NMR δ: 103.35 (C-1′), 99.29 (C-1).

Hydrogenolysis of 7α

To a solution of compound **7α** (36 mg, 0.05 mmol) in methanol (15 mL), 30 mg of 5% Pd/C was added, and the hydrogenolysis was performed in a Parr apparatus for 2 h under a 50 psi hydrogen atmosphere (1 psi = 6.9 kPa). The catalyst was removed and the filtrate concentrated. Chromatography (7:3 ethyl acetate – methanol) yielded **8** (18 mg, 80%); R_f 0.28; ^{1}H NMR (CD_3OD) δ: 4.46 (H-1′, $J_{1'-2'}$ = 7.3 Hz), 3.75 (H-2′, $J_{2'-3'}$ = 9.7 Hz), 3.68 (H-3′, $J_{3'-4'}$ = 3.1 Hz); ^{13}C NMR δ: 105.32 (C-1′), 75.05–64.90 (C-2–C-5 and C-2′–C-6′). The ^{1}H and ^{13}C NMR spectra are identical to those of the reference product obtained by reduction of **6** with $NaBH_3CN$.

Hydrogenolysis of 7β

Under the same experimental conditions, compound **7β** (15 mg) was hydrogenolysed in the presence of Pd/C (35 mg) to give **6**. A second hydrogenolysis did not give the reduced product **8**. Thin-layer chromatography showed, however, the presence of a small amount of **8** in addition to **6**.

Determination of the N^{α}*-Z-L-lysine 1-deoxyglycitolation reactivity scale*

The reactions with the various disaccharides were performed simultaneously. In a typical experiment, N^{α}-Z-L-lysine (5.62 mg, 0.02 mmol) was dissolved in 1 mL of a 0.1 M borate buffer, pH 8.0. The mixture was cooled to 4°C, then 0.05 mmol of the carbohydrate was added. Stirring was maintained for 30 min before addition of $NaBH_3CN$ (32 mg, 0.5 mmol). Aliquots (50 μL) were withdrawn at intervals, directly diluted with 4 mL of the HPLC eluent (acetonitrile–water: 35–65 v/v), and 5 μL of the resulting solution was injected. The reaction was followed by comparing the initial and the sample absorbance of the N^{α}-Z-L-lysine HPLC peak at 190 nm. The values obtained were reproducible in a 3% range.

Preparative coupling of liposaccharides with N^{α}*-Z-L-lysine*

Under different experimental conditions, preparative non-optimized experiments were performed to characterize the end products.

Reductive alkylation with 6

Carbohydrate **6** (42 mg, 0.1 mmol), N^{α}-Z-lysine (112 mg, 0.4 mmol), and sodium cyanoborohydride (63 mg, 1 mmol) were dissolved in a 0.1 M borate buffer, pH 8.0 (2 mL). Stirring at room temperature was maintained for 16 h. The mixture was evaporated to dryness and the residue chromatographed on silica gel, and eluted with methanol to give reduced carbohydrate **8** (11 mg, 25%) and 1-deoxyglycitolated N^{α}-Z-L-lysine (36 mg, 52%); R_f 0.38; ^{1}H NMR (CD_3OD) δ: 0.9 (3H, octyl), 5.1 (2H, *Z*), 7.2 (5H, *Z*). High resolution MS (FAB^+), calcd. for MH^+, $C_{33}H_{57}N_2O_{13}$: 689.386; found: 689.431.

*Reductive alkylation with 9*b

A solution of N^{α}-Z-L-lysine (45 mg, 0.16 mmol), ***9b*** (75 mg, 0.16 mmol), and sodium cyanoborohydride (100 mg) in water (5 mL) was adjusted to pH 7 with 0.1 M hydrochloric acid. The solution was kept for 3 days at 60°C. Water was evaporated and the product was purified by chromatography on silica gel, with water as eluent. ***9b*** (18 mg, 25%), reduced carbohydrate (15 mg, 20%), and alkylated amine (34 mg, 30%) were isolated; R_f 0.43 (water–methanol – ethyl acetate, 1:2:3); ^{1}H NMR (CD_3OD) δ: 0.85–1.80 (15H octyl + 6H lysine), 3.0–4.5 (massif), 5.06 (2H benzyl), 7.2–7.4 (5H benzyl). High resolution MS (FAB^+), calcd. for MH^+, $C_{34}H_{59}N_2O_{14}$: 719.396; found: 719.352.

Reductive alkylation with 10

Using the same experimental conditions as for ***9b***, the 1-deoxyglycitolated N^{α}-Z-L-lysine was obtained in 22% yield; R_f 0.48 (water–methanol – ethyl acetate: 1:2:3); ^{1}H NMR (CD_3OD) δ: 0.8–0.95 (3H, octyl), 1.20–1.40 (12H, octyl), 1.40–1.80 (6H, lysine), 2.90–3.20 (2H, lysine and 2H on C1), 3.40–4.20 (H lysine and carbohydrate), 4.28 (d, *J* = 8, H1′), 5.05 (2H, benzyl) and 7.15–7.25 (5H, benzyl). High resolution MS (FAB^+), calcd. for MH^+, $C_{34}H_{59}N_2O_{14}$: 719.396; found: 719.367.

Reductive alkylation with 12

Compound **12** (50 mg, 0.104 mmol), N^{α}-Z-L-lysine (29 mg, 0.104 mmol), and sodium cyanoborohydride (65 mg, 1.04 mmol) in 0.1 M borate buffer, pH 8 (5 mL), were stirred for 16 h at room temperature. After chromatography, 39 mg of a mixture of mono- and di-alkylated amine (in a 72:28 ratio) was isolated; R_f 0.39 (methanol). High resolution MS (FAB^+): monoalkyl, calcd. for MH^+, $C_{36}H_{61}N_2O_{14}$: 745.412; found: 745.400; and dialkyl, calcd. for MH^+, $C_{58}H_{101}N_2O_{24}$: 1209.6; found: 1209.4.

1. C. P. Stowell and Y. C. Lee. Adv. Carbohydr. Chem. Biochem. **37**, 225 (1980).
2. F. J. Buchholzer and J. M. J. Tronchet. Epitheor. Klin. Farmakol. Farmakokinet. Int. Ed. **2**, 17 (1988).
3. W. S. D. Wong, M. M. Kristjansson, D. T. Osuga, and R. E. Feeney. Int. J. Pept. Protein Res. **26**, 55 (1985).
4. R. J. Baues and G. R. Gray. J. Biol. Chem. **252**, 57 (1977).

5. M. WAKSELMAN and D. CABARET. *In* Biocatalysis in organic media. *Edited by* C. Laane, J. Tramper, and M. D. Lilly. Elsevier, Amsterdam. 1987. p. 253.
6. D. CABARET and M. WAKSELMAN. Carbohydr. Res. **189**, 341 (1989).
7. D. CABARET, R. KAZANDJAN, and M. WAKSELMAN. Carbohydr. Res. **149**, 464 (1986).
8. D. J. WALTON, E. R. ISON, and W. A. SZAREK. Carbohydr. Res. **128**, 37 (1984).
9. B. L. KAM and N. J. OPPENHEIMER. Carbohydr. Res. **69**, 308 (1979).
10. C. DU MORTIER, O. VARELA, and R. M. LEDERKREMER. Carbohydr. Res. **189**, 79 (1989).
11. A. KLEMER, M. BIEBER, and H. WIBERS. Liebig's Ann. Chem. 1416 (1983).
12. C. E. BALLOU, S. ROSEMAN, and K. P. LINK. J. Am. Chem. Soc. **73**, 1140 (1951).
13. C. D. HURD and W. H. SAUNDERS. J. Am. Chem. Soc. **74**, 5324 (1952).
14. S. J. ANGYAL. Adv. Carbohydr. Chem. Biochem. **42**, 15 (1984).

Can. J. Chem. Downloaded from www.nrcresearchpress.com by 195.138.81.100 on 09/07/12
For personal use only.

The antioxidant activities of phenolic antioxidants in free radical peroxidation of phospholipid membranes

LAWRENCE ROSS COATES BARCLAY,[1] KIMBERLY ANN BASKIN, KELLY ANDREA DAKIN, STEVEN JEFFFREY LOCKE, AND MELINDA RUTH VINQVIST

Department of Chemistry, Mount Allison University, Sackville, N.B., Canada E0A 3C0

Received July 3, 1990

LAWRENCE ROSS COATES BARCLAY, KIMBERLY ANN BASKIN, KELLY ANDREA DAKIN, STEVEN JEFFREY LOCKE, and MELINDA RUTH VINQVIST. Can. J. Chem. **68**, 2258 (1990).

Autoxidation of dilinoleoylphosphatidylcholine (DLPC) bilayers photoinitiated by benzophenone takes place by a free radical chain mechanism according to product studies of the *cis,trans* and *trans,trans*-9- and -13-linoleate hydroperoxides formed and kinetic studies of the reaction order as a function of light intensity. The absolute rate constant for hydrogen abstraction from DLPC bilayers by peroxyl radicals is found to be 36.1 M^{-1} s^{-1} at 37°C. Preliminary measurements of activities of phenolic antioxidants, α-tocopherol (α-T), 2,2,5,7,8-pentamethyl-6-hydroxychroman (PMHC), 2,5,7,8-tetramethyl-6-hydroxychroman-2-carboxylate (Trolox), and 2,6-di-*tert*-butyl-4-methylphenol (BHT) by oxygen uptake studies during inhibition periods using photoinitiation gave uncorrected inhibition rate constants, κ_{inh}, for α-T, PMHC, and Trolox several orders of magnitude lower than observed earlier in chlorobenzene. Three series of phenolic antioxidants, (*a*) polyalkyl-6-hydroxychromans, (*b*) polyalkyl-4-methoxyphenols, and (*c*) trialkylphenols, were examined for their antioxidant activities in DLPC membranes during thermally initiated autoxidation by azobis-2,4-dimethylvaleronitrile (DMVN). The corrected inhibition rate constants, k_{inh}, observed in (*a*), α-T (5.8×10^3), PMHC (17.8×10^3), Trolox (5.8×10^3), 2,2-dimethyl-5,7-diisopropyl-6-hydroxychroman, **4***a* (55×10^3), and 2,2,5-trimethyl-7-*tert*-butyl-6-hydroxychroman, **5***a* (61×10^3) M^{-1} s^{-1}, are dramatically lower, by several orders of magnitude, than those measured earlier in chlorobenzene and significantly lower (about 1/40–1/10) than those measured in solution in *tert*-butyl alcohol and less than k_{inh} measurements (1/2–1/5) in aqueous SDS micelles. The k_{inh} values for series (*b*) were 2,3,5,6-tetramethyl-4-methoxyphenol (TTMMP) (2.1×10^3), 2,3,6-trimethyl-4-methoxyphenol (TMMP) (10.4×10^3), and 2,6-di-*tert*-butyl-4-methoxyphenol (DBHA) (27.5×10^3) M^{-1} s^{-1} and for (*c*) were 2,6-di-*tert*-butyl-4-methylphenol (BHT) (3.7×10^3) and 2,4,6-trimethylphenol (TMP) (0.56×10^3) M^{-1} s^{-1}. The results show an overall leveling and depression of antioxidant activities in DLPC membranes in the series (*a*), (*b*), (*c*) compared to those reported in solution in chlorobenzene, where large differences were attributed to steroelectronic effects of the *para* ether oxygen stabilizing the derived phenoxyl radicals in (*a*) and (*b*) types. The results in aqueous micellar and membrane systems are interpreted in terms of polar solvation effects. Hydrogen bonding by water at both the ether and phenolic groups decreases the activity of the (*a*) series. Hydrogen bonding at the phenolic hydroxyl appears to be the more significant factor since steric hindrance to H-bonding at hydroxyl allows **4***a* and **5***a* to be the most active antioxidants of the α-tocopherol series (*a*) and DBHA to be the most active antioxidant of the (*b*) series.

Key words: antioxidant activities, phenols, membranes, peroxidation, kinetics.

LAWRENCE ROSS COATES BARCLAY, KIMBERLY ANN BASKIN, KELLY ANDREA DAKIN, STEVEN JEFFREY LOCKE et MELINDA RUTH VINQVIST. Can. J. Chem. **68**, 2258 (1990).

En se basant sur la nature des produits obtenus, soit les hydroperoxydes des acides *cis,trans*- et *trans,trans*-9- et -13-linoléiques ainsi que sur des études cinétiques établissant l'ordre de la réaction en fonction de l'intensité lumineuse, on a pu établir que l'autooxydation de bicouches de dilinoléylphosphatidylcholine (DLPC), photoinitiée par la benzophénone, se produit par un mécanisme radicalaire en chaîne. On a établi que, à 37°C, la constante absolue de la vitesse d'enlèvement de l'hydrogène des bicouches de DLPC, par les radicaux peroxyles, est de 36,1 M^{-1} s^{-1}. Des mesures préliminaires des activités des antioxydants phénoliques suivants : α-tocophérol (α-T), 2,2,5,7,8-pentaméthyl-6-hydroxychromane (PMHC), 2,5,7,8-tétraméthyl-6-hydroxychromane-2-carboxylate (Trolox) et 2,6-di-*tert*-butyl-4-méthylphénol (BHT), basées sur l'absorption d'oxygène durant les périodes d'inhibition de la photoinitiation, ont permis d'obtenir des constantes d'inhibition de vitesses non-corrigées, k_{inh}, pour l'α-T, le PMHC et le Trolox; les valeurs obtenues sont plusieurs ordres de grandeur plus faibles que celles observées antérieurement dans le chlorobenzène. On a examiné les propriétés antioxydantes de trois séries de composés phénoliques, (*a*) les polyalkyl-6-chromanes, (*b*) les polyalkyl-4-méthoxyphénols et (*c*) les trialkylphénols, dans des membranes de DLPC, durant des autooxydations initiées thermiquement par l'azobis-2,4-diméthylvaléronitrile (DMVN). Les constantes d'inhibition de vitesses corrigées, k_{inh}, observées avec les produits de la série (*a*), α-T ($5,8 \times 10^3$), PMHC ($17,8 \times 10^3$), Trolox ($5,8 \times 10^3$), 2,2-diméthyl-5,7-diisopropyl-6-hydroxychromane (**4***a*) (55×10^3) et 2,2,5-triméthyl-7-*tert*-butyl-6-hydroxychromane (**5***a*) (61×10^3 M^{-1} s^{-1}) sont dramatiquement inférieures (plusieurs ordres de grandeur) à celles mesurées antérieurement dans le chlorobenzène, de beaucoup inférieures (1/40–1/10) à celles mesurées en solution dans le *tert*-butanol et moins que les valeurs de k_{inh} mesurées (1/2–1/5) dans des micelles aqueuses de SDS. Les valeurs de k_{inh} mesurées pour les produits de la série (*b*) sont 2,3,5,6-tétraméthyl-4-méthoxyphénol (TTMMP) ($2,1 \times 10^3$ M^{-1} s^{-1}), 2,3,6-triméthyl-4-méthoxyphénol (TMMP) ($10,4 \times 10^3$ M^{-1} s^{-1}) et 2,6-di-*tert*-butyl-4-méthoxyphénol (DBMA) ($27,5 \times 10^3$ M^{-1} s^{-1}) et pour la série (*c*) elles sont 2,6-di-*tert*-butyl-4-méthylphénol (BHT) ($3,7 \times 10^3$ M^{-1} s^{-1}) et 2,4,6-triméthylphénol (TMP) ($0,56 \times 10^3$ M^{-1} s^{-1}). Ces résultats démontrent que, pour les produits des séries (*a*), (*b*) et (*c*) dans les membranes de DLPC, les activities antioxydantes sont nivelées et plus faibles que celle observées en solution dans le chlorobenzène où les grandes variations ont été attribuées aux effets stéréoélectroniques stabilisants de l'oxygène en *para* des radicaux phénoxyles dérivés des produits des types (*a*) et (*b*). On interprète les résultats obtenus en solutions aqueuses en fonction d'effets polaires de solvatation. Les liaisons hydrogènes de l'eau avec les fonctions éthers et hydroxyles de dérivés de la série (*a*) diminuent leur activité. Les liaisons hydrogènes des

[1]Author to whom correspondence may be addressed.

Can. J. Chem. Downloaded from www.nrcresearchpress.com by 195.138.81.100 on 09/07/12
For personal use only.

groupments hydroxyles semblent avoir une influence prépondérante puisque l'empêchement stérique aux liaisons hydrogènes qui existe dans les composés **4***a* et **5***a* leur permet d'être les antioxydants les plus actifs de la série des α-tocophérols (*a*); les mêmes facteurs pourraient expliquer l'activité du composé DBHA de la série (*b*).

Mots clés : activités des antioxydants, phénols, membranes, peroxydation, cinétique.

[Traduit par la revue]

Can. J. Chem. Downloaded from www.nrcresearchpress.com by 195.138.81.100 on 09/07/12
For personal use only.

Introduction

Peroxidation of unsaturated lipids in biomembranes disrupts important protective properties of natural membranes, and various in vivo pathological events are implicated as a result of this oxidation (1–8). Consequently the mechanism of action and activity of protective free radical chain-breaking antioxidants continues to be of outstanding interest (9–21). The role of phenolic antioxidants in this regard is of particular interest since the discovery that α-tocopherol (vitamin E) is the major lipid-soluble chain-breaking antioxidant in human blood (21). The protective action of various water-soluble and lipid-soluble antioxidants is the subject of several recent reviews (22–25).

In the past decade, it has been shown that classical kinetic methods of autoxidation, well known in homogeneous solution (26–29), are applicable to heterogeneous environments such as aqueous micelles (30–32) and, more importantly, in phospholipid bilayers (33–37), which mimic biomembranes in many respects (38). This free radical chain mechanism for autoxidation of organic substrates is generally represented by the reaction sequence shown in eqs. [1]–[3]:

[1] Initiation: formation of R·(or ROO·), rate = R_i

[2] (*a*) Propagation: $R\cdot + O_2 \xrightarrow{\text{fast}} ROO\cdot$

(*b*) $ROO\cdot + RH(\text{substrate}) \xrightarrow{k_p} ROOH + R\cdot$

[3] Termination: $ROO\cdot + ROO\cdot \xrightarrow{2k_t}$ nonradical products + O_2

For systems following this reaction scheme, the rate of oxygen uptake is first order in the concentration of substrate, RH, and one-half order in the rate of chain initiation, R_i, so that eq. [4] applies:

$$[4] \quad -d[O_2]/dt = k_p/2k_t^{1/2}[RH] \times R_i^{1/2}$$

For *quantitative* kinetics studies, the R_i must be controlled, for example by using a thermal azo initiator, R—N=N—R, which decomposes at a known and controlled rate to form carbon radicals, known to react very rapidly (39) with molecular oxygen to form propagating peroxyl radicals, ROO·. Alternatively, the R_i can be controlled by photochemical initiation (32). The "cage effect" on radicals generated in bilayers is known to be very much greater than in homogeneous solution (33), and the R_i must be measured, for example, by the addition of a phenolic antioxidant, ArOH, known to trap two peroxyls (9), and by measuring the time, τ, during which oxygen uptake is suppressed. During this period, eqs. [5]–[7] apply:

[5] $ROO\cdot + ArOH \xrightarrow{k_{inh}} ROOH + ArO\cdot$

[6] $ROO\cdot + ArO\cdot \xrightarrow{\text{fast}} ROOHArO$

$$[7] \quad R_i = 2 \times [ArOH]/\tau$$

The suppressed oxygen uptake is now given by eq. [8]:

$$[8] \quad -d[O_2]/dt = k_p/k_{inh}[RH] \times R_i/2[ArOH]$$

The susceptibility of a substrate to undergo autoxidation, referred to as its *oxidizability*, is expressed as a ratio of rate constants according to eq. [9]:

$$[9] \quad k_p/2k_t^{1/2} = -d[O_2]/dt/[RH] \times R_i^{1/2}$$

The absolute rate constants of propagation, k_p, and termination, $2k_t$, for autoxidation are expected to provide much more significant data on the reactivity and dynamics of peroxyl radicals in membranes than the simple ratios. It is especially important to establish the antioxidant activities of common phenolic antioxidants in phospholipid membranes by determinations of inhibition rate constants, k_{inh}, in order to better judge their protective action against biomembrane peroxidation. Absolute rate constants for autoxidation are well known in homogeneous solution (28, 29). More recently Burton, Ingold, and co-workers (10) have determined the antioxidant activity of α-tocopherol and synthetic phenolic antioxidants by measurements of the inhibition rate constants, k_{inh}, during the induction periods of autoxidation in homogeneous solution. Some measurements of phenolic antioxidant activities (k_{inh}) have also been made during suppressed autoxidation of linoleate in sodium dodecyl sulfate (SDS) micelles (11, 16, 32).

The determination of antioxidant activities of chain-breaking antioxidants *in membrane systems* is acknowledged to be a more difficult task (11). Furthermore, such measurements depend on determinations of the propagation rate constant, k_p, which must be measured independently in the same system in order to determine k_{inh} from the kinetics (e.g., eq. [8]).

We have recently undertaken such a study of absolute rate constants for lipid peroxidation and inhibition in phosphatidylcholine bilayers (35, 40) compared to such results in solution and in SDS micelles. This study has now been extended to include other phenolic antioxidants. We report herein on the details of this research, which includes results for three classes of phenolic antioxidants: (*a*) α-tocopherol (α-T), and the structurally related hydroxychromans: 2,2,5,7,8-pentamethyl-6-hydroxychroman (PMHC), and 2,5,7,8-tetramethyl-6-hydroxychroman-2-carboxylate (Trolox); (*b*) the alkylated 4-methoxyphenols: 2,3,5,6-tetramethyl-4-methoxyphenol (TTMMP), 2,3,6-trimethyl-4-methoxyphenol (TMMP), and 2,6-di-*tert*-butyl-4-methoxyphenol (DBHA); (*c*) the polyalkylphenols: 2,6-di-*tert*-butyl-4-methylphenol (BHT), 2,4,6-trimethylphenol (TMP).

These kinetic studies were carried out using dilinoleoylphosphatidylcholine (DLPC) bilayers, which have definite advantages as model membranes. The oxidation products from controlled free radical peroxidation of the linoleoyl moiety are known. Furthermore, these bilayers can be readily purified and they undergo rates of photochemically and thermally initiated peroxidation that can be controlled, and measured by a sensitive pressure transducer.

Results

1. Photoinitiated peroxidation of DLPC bilayers with benzophenone

(*a*) *Product studies*

The products of free radical chain autoxidation of linoleate in

TABLE 1. Product distribution[a] from linoleate peroxidation, photoinitiated by benzophenone in DLPC bilayers

% of DLPC oxidized[b]	13 *c,t*	13 *t,t*	9 *c,t*	9 *t,t*	*c,t*/*t,t* ratio
3	31.9	18.7	26.8	22.6	1.42
5	30.3	20.0	26.9	22.8	1.34
10	28.7	21.5	26.2	23.6	1.22

[a]At least two HPLC analyses were averaged. The error limits were 5%. The ratio of total C-9 to C-13 substitution products was essentially 1:1 in each case.

[b]Calculated from the total oxygen consumption at the time the sample was taken from the reaction.

solution and in bilayers are known to be the conjugated diene 9- and 13-hydroperoxide positional isomers having the *cis,trans* and *trans,trans* configuration. Porter and co-workers studied the ratio of *cis,trans* to *trans,trans* hydroperoxide products in detail, and advanced a mechanism involving a competition beween H-atom abstraction from activated methylene groups and β-scission of peroxyl radicals to account for the relative amounts of *cis,trans* (kinetic) and *trans,trans* (thermodynamic) products (41–44). We observed the same products for benzophenone-photoinitiated free radical peroxidation of linoleate in SDS micelles (32). On the other hand, reaction of linoleate with singlet oxygen yields a different product distribution, namely, approximately equal amounts of two conjugated (9- and 13-) and two nonconjugated ((10- and 12-) hydroperoxides (45). Because of the possible formation, by energy transfer, of singlet oxygen in our ketone-sensitized oxidations, we conducted some product analyses. The results are summarized in Table 1. The products formed were the 9- and 13-substituted hydroperoxides, as expected of a free radical chain peroxidation, and the *cis,trans* to *trans,trans* ratios found for up to 10% DLPC oxidation are similar to those reported for thermally initiated autoxidation of DLPC bilayers; e.g., 1.26 at 37°C (44), or 1.17 at 45°C (34).

(*b*) *Kinetics studies*

So that the classical rate law, expressed in eq. [4], can be followed exactly, the kinetic order of oxygen uptake must be one-half in the rate of chain initiation, R_i. To check this kinetic order, the dependence of the rate of O_2 consumption with variation of the R_i was measured at seven different light intensities. A typical result for multilamellar vesicles (MLV) of DLPC is illustrated in Fig. 1. In this case, the measured kinetic order (e.g., 0.507) is indicative of half-order dependence on the R_i. In all kinetic runs *using MLV*, the kinetic order in the R_i approximated one half and normally was between 0.50 and 0.53. However, unilamellar vesicles (ULV) of DLPC exhibited different behavior. Plots of kinetic order vs. light intensity were often decidedly non-linear (not shown) and the approximated kinetic order usually higher (e.g., >0.70). The type of liposome particle appears to exert an effect on the kinetics (*vide infra*).

Absolute rate constants of propagation, k_p, and termination, $2k_t$, for autoxidation of linoleate have been measured in solution, in micelles, and recently in DLPC bilayers, and most of the available data are summarized in Table 2. Details of the procedures used and calculations for the rotating sector method are described elsewhere (29, 32, 46). As pointed out earlier, benzophenone has certain advantages as a photoinitiator for rotating sector measurements (32), e.g., no dark rate and no correction for nitrogen evolution as required for azo initiators.

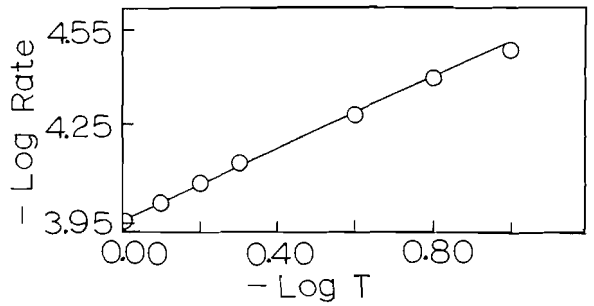

FIG. 1. Kinetic order plot of oxygen consumption as a function of light intensity (200 W super pressure Hg arc, through neutral density filters) for autoxidation of multilamellar (MLV) DLPC liposomes (5.45×10^{-5} mol) containing benzophenone (8.23×10^{-7} mol).

The k_p found for DLPC in MLV, 36.1 $M^{-1} s^{-1}$ at 37°C (Table 2, entry 7), was used in subsequent calculations of inhibition rate constants. This value is about the same, within experimental error, as that found using a water-soluble derivative of benzophenone (BP^-) as photoinitiator (Table 2, entry 8).

Typical experimental traces for the effects of the antioxidants α-T, PMHC, Trolox, and BHT on the inhibited autoxidation of DLPC liposomes, when reaction is photoinitiated with benzophenone, are illustrated in Fig. 2. The inhibition rate constants (k_{inh}) were determined from measurements of oxygen uptake during the inhibition periods by using the integrated expression for the kinetics during inhibition (9, 40), e.g., eq. [10]:

$$[10] \quad \Delta[O_2]_t = -k_p/k_{inh} \times [RH] \ln (1 - t/\tau)$$

where τ is the total inhibition period, and the oxygen uptake, $[O_2]_t$, is measured at various times, t, during the suppressed reaction. Typical data, to illustrate this method, for an α-T-inhibited reaction are given in Table 3. Linear plots were obtained for $\Delta[O_2]$ versus $-\ln(1 - t/\tau)$ for α-T, PMHC, Trolox, and BHT through 70% of the inhibition period, as illustrated in Fig. 3. Values of k_{inh} determined from the slopes of these plots, using the k_p as determined under these conditions (36.1 $M^{-1} s^{-1}$), are summarized in Table 4. These values were comparable (generally within 10%) to those calculated by averaging amounts of oxygen consumed at points during the induction period. The procedure using photoinitiation by benzophenone is very convenient for control and measurements of these kinetics. Nevertheless, inaccuracies in the calculated values of k_{inh} may result because the low rates of oxygen uptake by the DLPC substrate during inhibition periods could not be corrected for the possible competing reaction with ketyl radicals:

$$(C_6H_5)_2\dot{C}OH + O_2 \rightarrow (C_6H_5)_2C(OH)OO\cdot$$

This correction could be significant because chain lengths during inhibition periods for these benzophenone-photoinitiated runs are quite low (range of $\nu \sim 3$–9). Consequently, thermal azo initiators were used to repeat these experiments for determinations of k_{inh}.

2. Inhibition rate constants for phenolic antioxidants during thermally initiated autoxidation of DLPC liposomes with azo initiators

The antioxidant action of three classes of phenolic inhibitors was determined during autoxidation of DLPC in MLV liposomes, where reaction was initiated by the lipid-soluble azo initiator azobis-2,4-dimethylvaleronitrile (DMVN). Typical experimental traces for the antioxidant effects of (a) the

Can. J. Chem. Downloaded from www.nrcresearchpress.com by 195.138.81.100 on 09/07/12
For personal use only.

TABLE 2. Summary of absolute rate constants for propagation, k_p, and termination, $2k_t$, for linoleate autoxidation by rotating sector method

Initiator[a]	Temperature (°C)	Medium	$2k_t$ ($M^{-1} s^{-1} \times 10^{-6}$)	k_p ($M^{-1} s^{-1}$)	Reference
1. ACHN	30	C_6H_5Cl	8.8	62	29 (p. 93)
2. ACHN or BP	30	CH_3CN	4.42–4.33	94.9–96.5	32
3. ACHN or BP	30	TBA[b]	15.1–15.5	75.6–78.5	32
4. BP	30	SDS[c]	0.352	36.2	32
5. BP	37	SDS	0.417	39.1	42
6. ABCP	30	DLPC[d]	0.085±0.040	21±7	35
7. BP	37	DLPC	0.132±0.016	36.1±1.2	42
8. BP^-	37	DLPC	0.127±0.008	41.6±4.8	42
9. BP	30	DLPC	0.108±0.021	30.0±3.4	This work

[a]ACHN, azobiscyclohexylnitrile; BP, benzophenone; ABCP, azobis(2-*n*-butylcarboxy)propane; BP^-, 4-sulphomethylbenzophenone – sodium salt.
[b]TBA, *tert*-butyl alcohol.
[c]SDS, sodium dodecyl sulfate micelles, 0.50 M.
[d]DLPC, dilinoleoyl phosphatidylcholine bilayers.

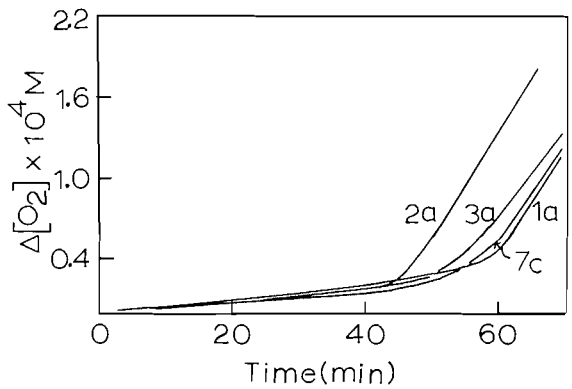

FIG. 2. Effect of antioxidants on benzophenone-photoinitiated (8.17×10^{-7} mol) autoxidation of DLPC liposomes (4.81×10^{-5} mol) in phosphate buffer, pH 7.0. **1***a*, α-Toc (1.87×10^{-7} mol), $R_i = 2.15 \times 10^{-6}$ M s^{-1}; **2***a*, PMHC (1.88×10^{-7} mol), $R_i = 2.82 \times 10^{-6}$ M s^{-1}; **3***a*, Trolox (1.89×10^{-7} mol), $R_i = 2.17 \times 10^{-6}$ M s^{-1}; **7***c*, BHT (1.89×10^{-7} mol), $R_i = 2.28 \times 10^{-6}$ M s^{-1}.

vitamin E class, (b) the polyalkyl 4-methoxyphenols, and (c) two polyalkyl phenols are illustrated in Fig. 4 (a), (b), and (c) respectively. Detailed experimental results, typical of all of the data obtained, are given in Tables 5 (*a*), (*b*), and (*c*) for an antioxidant from each class. Plots of oxygen uptake, $\Delta[O_2]_t$, versus $-\ln(1 - t/\tau)$ (eq. [10]) during the inhibition periods for typical antioxidants studied by this method are shown in Fig. 5 (a), (b), and (c). Values of k_{inh} for these three classes of inhibitors, determined from the slopes of these plots and using $k_p = 36.1$ $M^{-1} s^{-1}$ as before, are given in Table 6. Measurements in bilayers give rise to errors due to the necessity of using a coevaporation method to insert lipid-soluble initiators and inhibitors into the hydrophobic phase *before* bilayer preparation. There results a "lag time" in each induction period while the sample and oxygen equilibrate to the bath temperature (37°C). Ideally for these determinations the oxygen uptake measurements should start simultaneously with the start of loss of inhibitor ($\tau_{t=0}$). Under our conditions with thermal initiators, a correction was applied by timing the induction period and oxygen uptake after an equilibration period, usually several minutes. The error in k_{inh} due to this lag time was minimized by this correction and long overall induction periods, usually several hours. In addition, the accuracy of our k_{inh} values in bilayers depends on the accuracy of the measured k_p. The value of 36.1 $M^{-1} s^{-1}$ is reliable considering the various measurements made (Table 2). Overall, our k_{inh} values determined by thermal initiation are considered accurate to approximately ±20%, sufficiently accurate for comparisons with results from other media.

The water-soluble phenolic antioxidant, Trolox, has received considerable attention (ref. 10, and references therein). It is of particular interest because it exhibits antioxidant action when aqueous solutions are injected into autoxidations initiated in either the aqueous or lipid phases of lipsomes or micelles (36). Immediately after the measurement of the inhibition period with each lipid-soluble antioxidant, one or two inhibition periods were determined using Trolox. In this way Trolox provided a useful internal reference for determining the rate of chain

TABLE 3. Determination of k_{inh}[a] of α-tocopherol[b] for benzophenone[c] photoinitiated peroxidation of DLPC[d] bilayers at 37°C

t/τ	$-\ln(1 - t/\tau)$	$[O_2]$ ($M \times 10^4$)	ν[e]	k_{inh} ($M^{-1} s^{-1} \times 10^{-3}$)
0.302	0.360	57.5	2.9	2.3
0.352	0.434	67.9	3.0	2.4
0.403	0.515	79.9	3.2	2.4
0.453	0.603	91.8	3.5	2.4
0.506	0.700	104.3	3.7	2.5
0.554	0.807	120.0	4.2	2.5
0.604	0.929	136.5	4.6	2.5
0.654	1.063	156.8	5.3	2.5
0.705	1.220	181.2	6.3	2.5

[a]k_{inh} (calculated from slope) = 2.6×10^3 $M^{-1} s^{-1}$; k_{inh} (averaged from points) = $(2.4 \pm 0.1) \times 10^3$ $M^{-1} s^{-1}$; $R_i = 2.6 \times 10^{-7}$ M s^{-1} (1/4 light intensity).
[b]α-Toc, 1.87×10^{-7} mol.
[c]BP, 8.17×10^{-7} mol.
[d]The reaction volume, 4.66×10^{-5}, L, for DLPC, 4.76×10^{-5} mol, was calculated as before using a mol. wt. of 782.2 and density of 0.8 for bilayers (33, 34).
[e]The chain length calculated at points along the induction period from the following equation:

$$\nu_t = ([O_2]_t - [O_2]_{t=0})/n[AH]_o(1 - t/\tau) \ln (1 - t/\tau)$$

ref. 9, using $n = 2$.

Can. J. Chem. Downloaded from www.nrcresearchpress.com by 195.138.81.100 on 09/07/12
For personal use only.

TABLE 4. Inhibition rate constants for phenolic antioxidants during photoinitiated peroxidation of DLPC bilayers at 37°C[a]

No.[b]	Antioxidant (mol × 10^7)	R_i[c] ($M\,s^{-1} \times 10^6$)	k_{inh}[d] ($M^{-1}s^{-1} \times 10^{-3}$)	ν range[e]
1	α-Toc (1.87)	0.561–2.15	2.9±0.3	2.9–6.3
2	PMHC (1.88)	2.32–4.14	4.3±1.1	2.5–5.8
3	BHT (1.89)	2.24–2.46	1.9±0.1	2.7–8.4
4	Trolox (1.78–1.88)	1.90–2.78	2.5±0.3	2.6–8.4

[a]Taken from a preliminary account of this work (40).
[b]Each run was repeated at least three times, using 8.17×10^{-7} mol benzophenone and DLPC $(4.58–4.76) \times 10^{-5}$ mol, giving calculated reaction volumes of $(4.48–4.70) \times 10^{-5}$ L.
[c]The R_i was varied by using different light intensities.
[d]k_{inh} values calculated from plots of $\Delta[O_2]$ versus $-\ln(1 - t/\tau)$, and using an average k_p = 36.1 $M^{-1}\,s^{-1}$.
[e]See footnote *e*, Table 3.

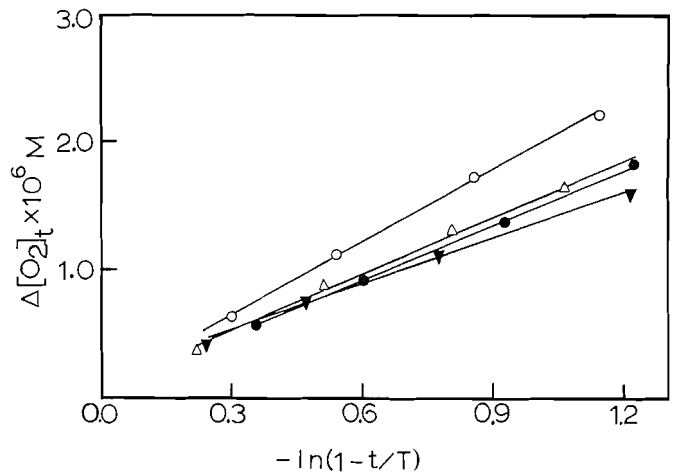

FIG. 3. Plots of oxygen uptake during inhibition periods versus $-\ln(1 - t/\tau)$ during autoxidation of DLPC ((4.58×10^{-5})–$(4.81 \times 10^{-5}$ mol)) in bilayers, phosphate buffer pH 7.0, photoinitiated with benzophenone (8.17×10^{-7} mol), for: BHT, ○, 1.88×10^{-7} mol; α-tocopherol, ●, 1.87×10^{-7} mol; Trolox, △, 1.78×10^{-7} mol; and PMHC, ▼, 1.88×10^{-7} mol. The k_{inh} values are obtained from the slopes, which equal $k_p[RH]/k_{inh}$.

initiation (R_i), and a means for comparing antioxidant activities of the other phenols.

Discussion

1. The mechanism for benzophenone-photoinitiated autoxidation of DLPC in multilamellar vesicles

A photosensitized reaction of oxygen with an organic substrate may be initiated by hydrogen abstraction by the sensitizer triplet followed by free radical autoxidation (Type I mechanism), or reaction could occur via a Type II mechanism involving energy transfer to form singlet oxygen followed by reactions such as the *ene* reaction. These processes are both well known (47, 48). Product studies can distinguish between these pathways. The products from the singlet oxygen reaction are not controlled by abstraction of the reactive allylic hydrogens, and a more complex mixture results from linoleate compared to that from the Type I pathway. Our results from product studies of the *cis,trans* and *trans,trans* hydroperoxides formed from benzophenone-initiated autoxidation (Table 1) indicate that hydrogen abstraction followed by free radical autoxidation predominates, there being no evidence for products arriving from reaction with singlet oxygen. The inhibition effects observed for chain-breaking antioxidants as illustrated in Fig. 2 also support a free radical peroxidation pathway. In the DLPC bilayer system, the doubly allylic hydrogens compete successfully with oxygen for benzophenone triplet. In this respect the mechanism is comparable to that reported for linoleate in SDS micelles (32).

For bimolecular chain termination of peroxyl radicals, i.e., the mechanism of eq. [3], the rate of oxidation is proportional to $R_i^{1/2}$; in our system this should mean the square root of the light intensity. This indeed is approximately the case for DLPC in multilamellar liposomes (MLV) where kinetic orders range from 0.507 to 0.532 and good linear plots are obtained (e.g., Fig. 1). The higher kinetic orders and nonlinear behavior with light intensity observed with unilamellar vesicles (ULV) were unexpected. The measured rate of oxygen uptake is greater for ULV than for MLV systems, as observed earlier for methyl linoleate in saturated ULV (35). We suggest that this phenomenon is due to the effect of particle size on the kinetics. ^{31}P NMR spectra of our ULV, prepared using the French pressure cell, indicate particle sizes less than 100 nm in cross section as observed before (49, 50). In such small liposomes, the probability of one peroxyl radical meeting another to terminate the chain reaction in the same liposome diminishes, so the termination rate decreases (e.g., $2k_t$ drops) and the oxygen uptake increases. In addition, the mechanism becomes complicated by some *first-order* termination of peroxyls. The nature of this reaction is not clear but it could proceed by cleavage reactions of peroxyl or derived alkoxyl radicals, which,in these particles, are more likely to diffuse to the aqueous surface where the polar medium promotes β-scission (51). The system is further complicated by the possibility of aggregation during peroxidation, especially at higher conversions (34). This problem does not arise in larger MLV; presumably these particles provide the opportunity for polar peroxyls (52) to diffuse towards the surface and terminate. One can also speculate that, in closely packed layers of lipsomes, termination might even occur by collisions of peroxyls between successive layers.

Lipsomes do present challenging systems for these quantitative kinetic studies but MLV systems of known chemical composition appear to behave nearly ideally in autoxidation with regard to both kinetic order in substrate (34) and R_i, provided low oxidative conversions are used, e.g., 10% overall or, here, 5% per linoleate chain. The kinetic rate constant of chain propagation, k_p, for linoleate only decreases by a factor of 2–3 in aqueous micelles and bilayers compared to homogeneous solution (Table 2). However, the chain termination rate

Can. J. Chem. Downloaded from www.nrcresearchpress.com by 195.138.81.100 on 09/07/12
For personal use only.

Can. J. Chem. Downloaded from www.nrcresearchpress.com by 195.138.81.100 on 09/07/12
For personal use only.

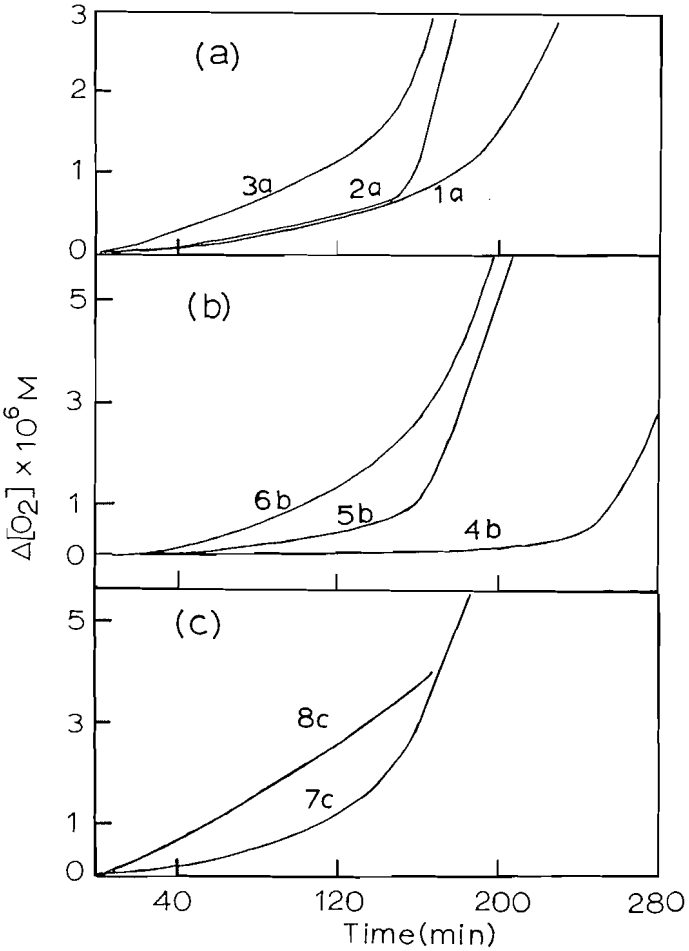

FIG. 4. Effect of antioxidants on peroxidation of DLPC liposomes thermally initiated by DMVN at 37°C. R_i values are determined from Trolox injections following the inhibition by the initial lipid-soluble antioxidant. Amounts of initiator and inhibitor are corrected for loss during the lag time, see text. (a) Hydroxychromans: **1***a*, α-Toc, 5.04×10^{-9} mol; DMVN, 9.53×10^{-7} mol; DLPC, 5.76×10^{-5} mol; $R_i = 1.67 \times 10^{-8}$ M s^{-1}. **2***a*, PMHC, 1.20×10^{-8} mol; DMVN, 3.17×10^{-6} mol; DLPC, 5.76×10^{-5} mol; $R_i = 4.58 \times 10^{-8}$ M s^{-1}. **3***a*, Trolox, 1.20×10^{-9} mol; DMVN, 4.24×10^{-6} mol; DLPC, 8.31×10^{-5} mol; $R_i = 3.02 \times 10^{-8}$ M s^{-1}. (b) Hydroxyanisoles: **4***b*, DBHA, 9.74×10^{-9} mol; DMVN, 3.05×10^{-6} mol; DLPC, 5.71×10^{-5} mol; $R_i = 2.43 \times 10^{-8}$ M s^{-1}. **5***b*, TMMP, 1.20×10^{-8} mol; DMVN, 3.17×10^{-6} mol; DLPC, 5.73×10^{-5} mol; $R_i = 4.57 \times 10^{-8}$ M s^{-1}. **6***b*, TTMMP, 1.40×10^{-8} mol; DMVN, 3.17×10^{-6} mol; DLPC, 5.74×10^{-5} mol; $R_i = 4.66 \times 10^{-8}$ M s^{-1}. (c) Phenols: **7***c*, BHT, 1.32×10^{-8} mol; DMVN, 3.18×10^{-6} mol; DLPC, 5.74×10^{-5} mol; $R_i = 4.24 \times 10^{-8}$ M s^{-1}. **8***c*, TMP, 1.69×10^{-8} mol; DMVN, 3.39×10^{-6} mol; DLPC, 5.52×10^{-5} mol; $R_i = 3.16 \times 10^{-8}$ M s^{-1}, a break in the induction period appears for $\tau = 443$ min, not shown on figure.

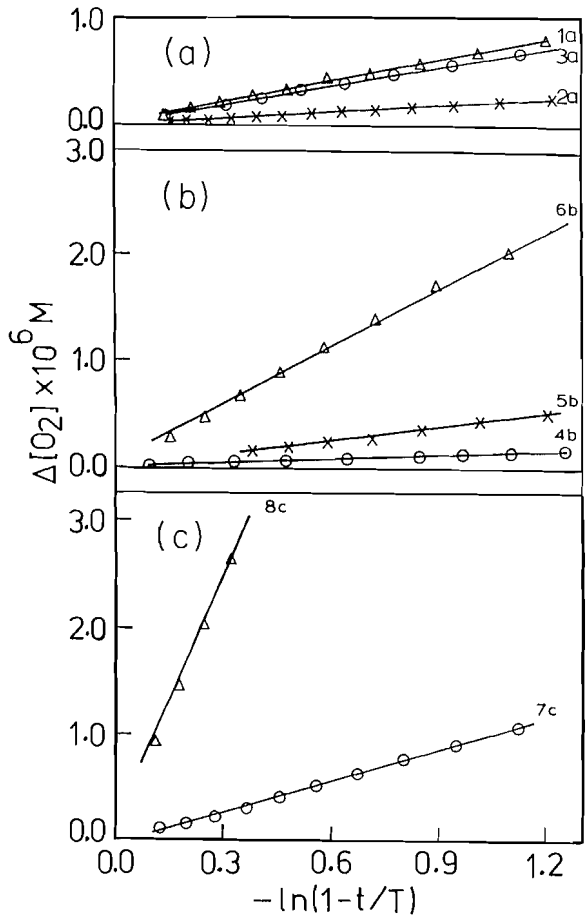

FIG. 5. Plots of oxygen uptake during inhibition periods versus $-\ln(1 - t/\tau)$ during autoxidation of DLPC MLV bilayers thermally initiated by DMVN in phosphate buffer, pH 7.0. Data for the plots are from typical experiments as outlined in Table 5. Amounts of DLPC, DMVN, and antioxidants are given in Table 6. The k_{inh} values (Table 6 also) are obtained from the slopes, which equal $k_p[RH]/k_{inh}$. (a) **1***a*, α-Toc; **2***a*, PMHC; **3***a*, Trolox. (b) **4***b*, DBHA; **5***b*, TMMP; **6***b*, TTMMP. (c) **7***c*, BHT; **8***c*, TMP.

constant, $2k_t$, decreases remarkably in these aqueous systems. As discussed earlier (32), this is most probably due to diffusion of polar peroxyl radicals from the hydrophobic phase towards the aqueous phase where they are stabilized by hydrogen bonding. This is also in line with similar observations made earlier for homogeneous solution (53). The water-soluble ketone, BP^-, is very convenient as a photoinitiator because it can be injected into the reaction after the liposomes are prepared. Its effect may be due to partial distribution into the bilayer phase, as was found in micelles (32).

2. The activities of phenolic antioxidants in DLPC bilayers

Various factors, including electronic effects, steric effects, and solvent effects, need be considered in assessing the antioxidant action of phenolic inhibitors. In aqueous microenvironments of bilayers and micelles the system is further complicated by the possible effects of aggregation and the possibility of limiting diffusion phenomena. Furthermore, the experimental method employed can affect the results even when similar systems are examined (*vide infra*).

With these complications in mind, we compare in Table 7 the k_{inh} values of our three classes of antioxidants determined by the thermal initiation procedure in bilayers with those found in other media including homogeneous solution in chlorobenzene, and, for class (a) antioxidants, *tert*-butyl alcohol, and in micelles. The following striking differences characterize the activities of these phenolic antioxidants in different media:

1. *The activities of the three types, with the exception of DBHA (4b) and BHT (7c), are dramatically reduced in bilayers*, by several orders of magnitude compared with those in homogeneous solution in chlorobenzene. For the hydroxychromans (class *a*), which were studied in all four media, the activities are very significantly decreased, by factors of about 7–18, in

TABLE 5. Determination of k_{inh}[a] of various antioxidants[b] for DMVN thermally initiated peroxidation of DLPC bilayers[c] at 37°C

Class	t/π	$-\ln(1 - t/\tau)$	$[O_2]$ ($M \times 10^4$)	ν[d]	k_{inh} ($M^{-1} s^{-1} \times 10^{-3}$)
(*a*) α-T	0.127	0.136	8.5	42.5	5.5
	0.190	0.211	14.7	49.6	5.1
	0.254	0.293	20.1	52.6	5.2
	0.317	0.382	26.2	57.3	5.3
	0.381	0.480	33.2	63.4	5.2
	0.444	0.588	43.2	74.1	5.0
	0.508	0.709	48.2	77.9	5.4
	0.571	0.847	59.0	91.5	5.2
	0.635	1.008	69.4	106.2	5.3
	0.698	1.745	82.5	128.3	5.3
(*b*) DBHA	0.096	0.100	1.0	4.9	35.9
	0.143	0.155	1.7	5.4	34.6
	0.191	0.212	2.2	5.6	35.2
	0.239	0.273	2.9	6.0	35.0
	0.287	0.338	3.5	6.3	35.6
	0.334	0.407	4.3	6.8	35.2
	0.382	0.482	5.3	7.7	33.7
	0.430	0.562	6.1	8.3	33.9
	0.478	0.650	7.2	9.2	33.1
	0.525	0.745	8.5	10.4	32.3
	0.573	0.852	9.8	11.7	31.9
	0.621	0.970	11.2	13.2	31.9
	0.669	1.105	13.0	15.4	31.3
	0.717	1.261	15.0	18.1	31.0
(*c*) BHT	0.123	0.131	9.5	17.5	5.1
	0.184	0.203	14.5	18.6	5.2
	0.245	0.282	21.9	21.8	4.7
	0.307	0.366	30.0	25.1	4.5
	0.368	0.459	40.1	29.3	4.2
	0.429	0.561	50.5	33.5	4.1
	0.491	0.675	62.5	38.6	4.0
	0.552	0.803	75.7	44.6	3.9
	0.613	0.951	89.6	51.7	3.9
	0.675	1.123	107.0	62.1	3.9

[a]Class *a*: k_{inh} (calculated from slope) = $5.3 \times 10^3 M^{-1} s^{-1}$; k_{inh} (averaged from points) = $(5.3 \pm 0.1) \times 10^3 M^{-1} s^{-1}$; $R_i = 1.67 \times 10^{-7} M s^{-1}$. Class *b*: k_{inh} (calculated from slope) = $30.6 \times 10^3 M^{-1} s^{-1}$; k_{inh} (averaged from points) = $(33.6 \pm 1.6) \times 10^3 M^{-1} s^{-1}$; $R_i = 1.69 \times 10^{-8} M s^{-1}$. Class *c*: k_{inh} (calculated from slope) = $3.7 \times 10^3 M^{-1} s^{-1}$; k_{inh} (averaged from points) = $(4.3 \pm 0.2) \times 10^3 M^{-1} s^{-1}$; $R_i = 4.24 \times 10^{-8} M s^{-1}$.

[b]Class *a*: α-T, 5.04×10^{-9} mol; DMVN, 9.53×10^{-7} mol. Class *b*: DBHA, 1.27×10^{-8} mol; DMVN, 3.10×10^{-6} mol. Class *c*: BHT, 1.32×10^{-8} mol; DMVN, 3.18×10^{-6} mol. These were the amounts of inhibitor and initiator at the start of each run, corrected for loss during the lag time.

[c]Reaction volumes were, respectively, 5.36×10^{-5} L (5.76×10^{-5} mol) DLPC for class *a* (α-T); 1.10×10^{-4} L (1.13×10^{-4} mol) DLPC for class *b* (DBHA); and 5.61×10^{-5} L (5.74×10^{-5} mol) DLPC for class *c* (BHT).

[d]See footnote *e*, Table 3.

tert-butyl alcohol[2] as compared to chlorobenzene. There is a further *drop* in activity in aqueous SDS, which by our measurements[3] amounts to decreases in the ratio $k_{inh}ROH/k_{inh}SDS \sim 5–14$ and a further decrease in k_{inh} for bilayers, where $k_{inh}SDS/k_{inh}DLPC = 3–5$ for the three hydroxychromans.

2. *The antioxidant activities of all three classes of inhibitors are quite similar in bilayers (e.g., a leveling effect) in contrast to remarkable differences observed in homogeneous solution.* In the case of chlorobenzene solution, certain substituted hydroxy anisoles (DBHA) and phenols (BHT) exhibited k_{inh} orders of magnitude less than the hydroxychromans (ref. 10, Table 7). These different antioxidant activities of phenols, such as polyalkylhydroxychromans (e.g., vitamin E) and hydroxyanisoles, during inhibition of autoxidation of styrene in chlorobenzene were interpreted by Ingold and co-workers (10) in terms of carefully considered electronic and steric effects. In particular, they concluded that the stabilization of the phenoxyl radical formed in the rate-determining inhibition step (eq. [15]) depends mainly on the extent of orbital overlap between the 2*P*-type lone pairs on the *para* ether oxygen and the aromatic π system, referred to as the stereoelectronic effect (9, 10).

[2]The k_{inh} for the inhibition reaction for methyl linoleoylperoxy radical with α-tocopherol was earlier reported as $51 \times 10^4 M^{-1} s^{-1}$ in *tert*-butyl alcohol, in reasonable agreement with our value since an estimation was used for k_p (57).

[3]Our values in SDS differ from those reported (11), probably due to initiation in different phases.

Can. J. Chem. Downloaded from www.nrcresearchpress.com by 195.138.81.100 on 09/07/12
For personal use only.

TABLE 6. Antioxidant activities of phenolic antioxidants during thermally initiated peroxidation of DLPC bilayers[a] by DMVN at 37°C

No.[b]	DLPC (mol × 10^5)	DMVN (mol × 10^6)	Antioxidant (mol × 10^8)	R_i[c] ($M\,s^{-1} \times 10^8$)	ν[d] range	k_{inh}[e,f] ($M^{-1}\,s^{-1} \times 10^{-3}$)
1*a*	5.76	0.95	α-T (0.50)	1.67	43–128	5.8±0.5
2*a*	10.60	3.07	PMHC (1.48)	1.89	5–26	17.8±1.4
3*a*	5.71	2.86	Trolox (0.36)	2.43	65–189	5.8±0.6
4*b*	11.30	3.10	DBHA (1.27)	1.69	5–18	27.5±4.3
5*b*	5.73	3.17	TMMP (1.20)	4.57	13–32	10.4±1.5
6*b*	8.31	4.73	TTMMP (2.05)	3.02	41–136	2.1±0.5
7*c*	5.74	3.18	BHT (1.37)	4.24	18–62	3.7±0.03
8*c*	5.52	3.39	TMP (1.69)	3.16	141–341	0.56±0.09

[a]Multilamellar vesicles in phosphate buffer, pH = 7.0.
[b]Each run was repeated once or twice.
[c]The R_i was determined using Trolox induction periods, measured immediately after the initial induction period.
[d]See footnote *e*, Table 3.
[e]Columns 1–6 give detailed data for typical experiments. The k_{inh} values are averages from at least two experiments using 2.00 mL of aqueous bilayers. Molar concentrations are those calculated for the bilayer phase (see Table 3, footnote *d*).
[f]The larger k_{inh} values for α-T, PMHC, and BHT (by as much as a factor of 2, α-T) compared to a preliminary report (40) result from more precise measurements and corrections for lag time in induction periods (see text).

TABLE 7. Summary of antioxidant activities of phenolic antioxidants in different media

No.	Antioxidant	k_{inh} ($M^{-1}\,s^{-1} \times 10^{-4}$)				
		C_6H_5Cl[a] AIBN	$(CH_3)_3COH$[b] BP	0.50 M SDS BP[c]	0.50 M SDS ABAP[d]	DLPC[e] DMVN
	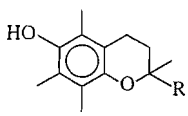					
1*a*	R = $C_{16}H_{33}$	320	23	1.7	3.7	0.58
2*a*	R = CH_3	380	21	3.7	15	1.78
3*a*	R = COOH	110	15	2.8	11	0.58
	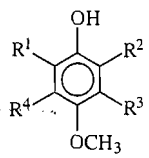					
4*b*	R^1, R^2 = $(CH_3)_3C$	11				2.75
5*b*	R^1–R^3 = CH_3, R^4 = H	130				1.04
6*b*	R^1–R^4 = CH_3	39				0.21
	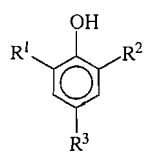					
7*c*	R^1, R^2 = $(CH_3)_3C$, R^3 = CH_3	1.4		1.1		0.37
8*c*	R^1–R^3 = CH_3	8.5				0.056

[a–c]k_{inh} values are taken from the literature: *a*, ref. 10, *b* and *c*, ref. 32. BP, photoinitiated with benzophenone.
[d]Reference 11. ABAP is azobis(2-amidinopropane)·HCl, a water-soluble thermal initiator.
[e]This work.

Can. J. Chem. Downloaded from www.nrcresearchpress.com by 195.138.81.100 on 09/07/12
For personal use only.

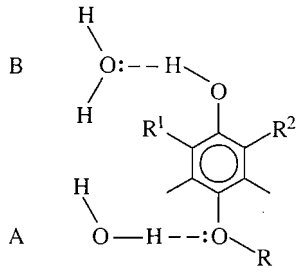

FIG. 6

The reduction in antioxidant activities of class *a* phenols in aqueous micelles was attributed by us earlier (32) to the effect water may have of tying up the electron lone pairs on the *para* ether oxygen, thereby reducing the reactivity of the phenolic hydrogen by dampening the stereoelectronic effect exerted by the ether oxygen lone pairs in homogeneous solution. This explanation was presented in more detail by Pryor *et al.* (11), who also presented evidence that hydrogen bonding of the phenolic hydroxyl to water in class *a* antioxidants is responsible for the dramatic drop in activity in aqueous micelles. This conclusion was supported by the fact that BHT with no *para* oxygen, and in which two *ortho tert*-butyl groups inhibit hydrogen bonding, has about the same antioxidant activity in micelles as in chlorobenzene (see Table 7). These hydrogen bonding interactions are shown schematically in Fig. 6. Water can associate with the ether oxygen through its protic hydrogen, thereby localizing the 2*P* lone pair on the oxygen as in A, and also associate the protic phenolic hydroxyl at a lone pair on water as in B, thereby inhibiting facile transfer of the phenolic hydrogen to peroxyl radicals.

The antioxidant activities of these classes of phenols in phospholipid membranes are controlled by two kinds of environmental influences:

1. *The main influence appears to be the operation of solvation effects of water.* We assume that these antioxidants reside near the polar head group region of the bilayers as demonstrated for vitamin E (54) and, furthermore, that the trapping of polar peroxyl radicals occurs in this region. In these circumstances, the activity of most of these phenols is reduced by hydrogen bonding with water at both sites (viz. Fig. 6). The combined effects of interaction at A and B level the antioxidant activity of the hydroxychromans (**1***a*–**3***a*) towards that of BHT (**7***c*), whereas in chlorobenzene the latter is several orders of magnitude less active than the hydroxychromans (Table 7). Some idea of the relative importance of hydrogen bonding at sites B and A (Fig. 6) can be seen in a qualitative manner by comparing the k_{inh} of antioxidants in class *b* containing one methyl *ortho* to methoxy (**5***b*) with the activity of **6***b*, which has two such *ortho* methyls. We find the activity of **5***b* to be in the range of the hydroxychromans (**1***a*–**3***a*, Table 7) indicating that the overall deactivation due to hydrogen bonding is approximately the same for **5***b* as for **1***a*–**3***a*. The activity of **6***b* in bilayers is significantly less, by a factor of approximately one fifth. It is known that the two *ortho* methyls in **6***b* force the methoxy group into a position perpendicular to the aromatic ring (10), which accounts for the drop in activity of **6***b* by as much as tenfold compared to the hydroxychromans in solution. Hydrogen bonding at this *para* methoxy alone is not expected to further reduce the activity of **6***b* in aqueous bilayers. Thus the additional drop in activity of **6***b* by a factor of about one fifth that of **5***b* must be due to hydrogen bonding at the phenolic hydroxyl group.

The comparatively higher activity of DBHA (**4***b*) compared to other phenols in bilayers is rather surprising in view of its diminished activity in solution, the latter being attributed to steric hindrance, provided by two *ortho tert*-butyl groups, to the approach of the peroxyl radical (10). If hydrogen bonding at the hydroxyl is blocked in **4***b* (55), its relatively higher activity must be due to a balance between such steric hindrance effects, hydrogen bonding at the *para* ether oxygen, and the stabilization that bulky *ortho* alkyls impart to the phenoxyl radical formed on hydrogen atom transfer (56). We suggest that the main effect operating to give DBHA higher "residual" activity is steric hindrance to hydrogen bonding at the phenolic hydroxyl. To test this we measured the antioxidant activities of the trialkylphenols **7***c* and **8***c*. In solution the latter has about six times the activity of **7***c*. In contrast, the relative activities switch dramatically in bilayers so that **7***c* (BHT) is seven times more active than **8***c*. The latter is a very poor inhibitor of peroxidation in aqueous bilayers. The low activity of **8***c* compared to **7***c* is thus attributed to hydrogen bonding at the phenolic hydroxy, which is most probably the more important solvation effect. This effect is probably prominent in suppressing the antioxidant activities of the hydroxychromans (**1***a*–**3***a*) in model membranes.

2. *There appears to be an effect of the bilayer structure of the membrane on phenolic antioxidant activity.* As noted above, k_{inh} values for hydroxychromans drop by one fourth in aqueous bilayers compared to those in aqueous micelles. Micelles are more fluid and dynamic aggregates than bilayers. Nevertheless, even in micelles, the reduced antioxidant activity of lipophilic phenols such as α-tocopherol was attributed to their limiting diffusion between micelles (16). "Diffusion control" is expected to be more pronounced in bilayers, at least in the case of α-tocopherol where the phytyl side chain is known to suppress its transfer between liposomal membranes (12). All of our experiments were done above the phase transfer temperatures of DLPC, where presumably diffusion within the membrane is more facile than in the less fluid gel state. However, long hydrocarbon chains and derived peroxyl radicals aggregated into a bilayer are not expected to have the same freedom of motion as in homogeneous solution. The higher antioxidant activity of PMHC in bilayers compared to α-tocopherol may in part be due to greater freedom of diffusion of the former in the membrane. If the peroxyl radical diffuses to the surface region to terminate with the phenolic antioxidant, as is postulated, additional constraints would be placed on the system. In addition, the reactivity of peroxyl radicals is suppressed by hydroxyl bonding (58) and such interaction could operate in this polar region.

Our quantitative studies of antioxidant activities in membranes permit rationalization of some other literature results. For example, Niki and co-workers (59) reported the very interesting observation that the ratio k_{inh}/k_p for α-tocopherol in soybean PC liposomes is much smaller than in homogeneous solution in *tert*-butyl alcohol. Using their ratio of rate constants for α-tocopherol in liposomes and our $k_p = 36.1\ M^{-1}\ s^{-1}$ gives an estimated $k_{inh} = 2.1 \times 10^3\ M^{-1}\ s^{-1}$ for α-tocopherol in their bilayers, in reasonable agreement with our result (Table 6) considering the assumptions made. Spin labeling studies show that α-tocopherol scavenges lipophilic radicals closer to the membrane surface (59). This is in general agreement with our results indicating that antioxidant action takes place mainly in this region of the membranes with resulting depression of their activity by solvation effects. Trolox is a remarkable water-soluble antioxidant that can be used for quantitative measurements of peroxyl radical formation in either bilayer or micellar

Can. J. Chem. Downloaded from www.nrcresearchpress.com by 195.138.81.100 on 09/07/12
For personal use only.

TABLE 8. Determination of k_{inh}[a] of tocopherol model compounds for DMVN thermally initiated peroxidation of DLPC at 37°C

Compound[b]	t/τ	$-\ln(1 - t/\tau)$	$[O_2]^c$ ($M \times 10^4$)	ν	k_{inh} ($M^{-1} s^{-1} \times 10^{-3}$)
4*a*	0.307	0.367	1.6	3.4	85.3
	0.369	0.460	1.9	3.5	89.6
	0.430	0.563	2.5	4.2	82.6
	0.492	0.677	3.1	4.8	80.8
	0.533	0.806	3.9	5.9	75.5
	0.615	0.945	4.7	6.8	75.4
	0.676	1.128	5.8	8.6	71.9
	0.738	1.338	7.0	10.8	69.9
5*a*	0.246	0.282	1.5	3.9	67.7
	0.328	0.398	2.0	4.0	74.8
	0.410	0.528	2.7	4.7	72.4
	0.492	0.677	3.2	5.0	78.3
	0.574	0.853	4.3	6.4	73.8
	0.656	1.067	5.6	8.3	70.1
	0.738	1.339	7.3	11.3	67.6

[a]Calculated from plot of $\Delta[O_2]$ versus $-\ln(1 - t/\tau)$. **4***a*: k_{inh} (calculated from slope) = 64.5×10^3; k_{inh} (averaged from points) = $(78.9 \pm 6.4) \times 10^3$ $M^{-1} s^{-1}$. **5***a*: k_{inh} (calculated from slope) = 67.2×10^3; k_{inh} (averaged from points) = $(72.1 \pm 3.6) \times 10^3$ $M^{-1} s^{-1}$.

[b]**4***a* is 2,2-dimethyl-5,7-diisopropyl-6-hydroxychroman (1.01×10^{-8} mol), initiated by 3.01×10^{-6} mol DMVN. **5***a* is 2,2,5-trimethyl-7-*tert*-butyl-6-hydroxychroman (1.02×10^{-8} mol), initiated by 3.02×10^{-6} mol DMVN. These amounts are corrected for loss during lag time.

[c]The reaction volume used for concentration calculations was 1.10×10^{-4} L DLPC.

[d]See Table 3, footnote *e*.

TABLE 9. Antioxidant activities of synthetic model tocopherol compounds

Compound[a]	Medium[b]	R_i^c ($M s^{-1} \times 10^9$)	ν range	k_{inh}^d ($M^{-1} s^{-1} \times 10^{-4}$)
	C_6H_5Cl, styrene, AIBN			
2*a*		1.79–1.91	8–31	360±47
4*a*		3.15	6–19	238±12
5*a*		1.79–2.46	7–24	199±6
	DLPC[e] DMVN			
2*a*				1.78[f]
4*a*		0.14	3–13	5.5±0.9
5*a*		0.15–0.16	4–12	6.1±0.6

[a]See Table 8, footnote *b*.

[b]The procedure of ref. 10 was followed, using concentrations of styrene 5.22 M and AIBN 1.74×10^{-2} M at 30°C.

[c]For runs in chlorobenzene, the R_i was calculated from the induction period with the inhibitor studied: in DLPC bilayers the R_i was determined using Trolox (see Table 6).

[d]At least three determinations were made in chlorobenzene and two in DLPC bilayers. k_{inh} values are calculated from the plot of $\Delta[O_2]$ versus $-\ln(1 - t/\tau)$ and using $k_p = 41$ $M^{-1} s^{-1}$ (10) for runs in chlorobenzene.

[e]For experimental conditions see Table 8.

[f]Taken from Table 7.

systems for autoxidations initiated by either water-soluble or lipid-soluble initiators (36). Such results can be rationalized if Trolox can trap peroxyl radicals at the surface of membranes and micelles as we propose. The lower k_{inh} of Trolox, one third that of PMHC, may be due to its proposed site of action at the polar membrane surface and (or) its distribution between aqueous and membrane phases. This is currently under investigation.

Our results have important implications for the role of chain-breaking phenolic antioxidants (e.g., vitamin E) in real biological systems. It is now evident that the activity of phenolic antioxidants measured in homogeneous solution cannot be extrapolated to estimate their absolute or even relative activities in biological membranes. Autoxidation studies on biological fluids including human blood plasma (18, 20) and blood (60) indicate the importance of natural water-soluble antioxidants, such as ascorbate, protein thiols, and urate, which trap damaging peroxyl radicals in the aqueous phase before they can attack the membrane lipids, thereby sparing the α-tocopherol in the lipid phase, which can be regarded as the "last defence" against damaging peroxyl radical attack.

Recently two new synthetic α-T model compounds, 2,2-dimethyl-5,7-diisopropyl- (**4***a*) and 2,2,5-trimethyl-7-*tert*-butyl-6-hydroxychroman (**5***a*), were made available for us to determine antioxidant activities. Such model compounds are of

Can. J. Chem. Downloaded from www.nrcresearchpress.com by 195.138.81.100 on 09/07/12
For personal use only.

Can. J. Chem. Downloaded from www.nrcresearchpress.com by 195.138.81.100 on 09/07/12
For personal use only.

particular interest to our present investigation. Although they have lower antioxidant activities than the α-T model compound PMHC, as measured by reaction with a stable phenoxyl radical in solution (62), the additional bulk of two *ortho* isopropyl gorups in **4***a* and a *tert*-butyl in **5***a* compared to methyls in our series *a* compounds is expected to further hinder hydrogen bonding at the phenolic hydroxyl by water (Fig. 6, B) and allow for an *increase* in antioxidant activity in aqueous bilayers.

We measured the antioxidant activities of **4***a* and **5***a* in solution in chlorobenzene for reaction with poly(styrylperoxyl) radicals using known procedures (10) and the results are given in Table 9. The k_{inh} values for **4***a* and **5***a relative* to that found in our study for PMHC (Table 9), 0.66 and 0.55 respectively, are the same as the relative rate constants for reaction with a phenoxyl radical solution (62). The k_{inh} values for **4***a* and **5***a* are similar to that of 5,7-dimethyltocol, 180×10^4 M^{-1} s^{-1} (10), which also lacks a substituent at position 8. This indicates that the main effect causing the reduction of the activity of **4***a*, **5***a* compared to PMHC (**2***a*) is the lack of stabilizing electron-donating alkyl group at position 8 in the former; steric hindrance to attack by peroxy radicals in solution evidently is not significant in these compounds. The k_{inh} values of **4***a* and **5***a* in DLPC bilayers were determined as before (Table 8) and the results, summarized in Table 9, indicate that they exhibit a similar marked drop in activity by at least an order of magnitude compared to values in homogeneous solution. This reduction in k_{inh} is interpreted in terms of hydrogen bonding by water especially at the *para* ether oxygen (*vide supra*). However, it is remarkable that these synthetic model tocopherols are very significantly *more reactive as antioxidants in bilayers* than any other antioxidants of the vitamin E class, *a* (Table 6). They are more active, by approximately one order of magnitude, than α-tocopherol itself and three to four times more active than PMHC. This is further demonstration of the importance of hydrogen bonding at the phenolic hydroxyl in controlling the antioxidant activity. The higher residual activity in **4***a* and **5***a* is attributed to additional steric hindrance to such hydrogen bonding provided by the two *ortho* isopropyl groups in **4***a* and a *tert*-butyl group in **5***a* so that hydrogen atom transfer in the rate-controlling inhibition step is more facile.

All our results demonstrate the need to measure antioxidant activities of compounds in model membrane systems as well as in solution in order to judge their protective capacity against peroxyl radical attack in natural biological systems. There is the interesting possibility that some new synthetic hindered phenolic antioxidants of the class *a* type are much more potent antioxidants in membranes than judged from measurements in homogeneous solution (63).

Experimental

1. Chemicals and preparations

(a) Buffers

Phosphate buffer for membrane preparations was prepared from NaH_2PO_4 and Na_2HPO_4 (each 0.05 M) (pH 7.0) in glass-distilled water containing Na_2EDTA (1×10^{-4} M). Possible traces of heavy metal ions were removed by passing the buffer through Chelex (50–100 mesh, Biorad). Phospholipid dispersions for ^{31}P NMR studies were prepared in 0.054 M Tham (Fisher) buffer containing 1×10^{-4} M Na_2EDTA and adjusted to pH 7.0 with HCl.

(b) Reagents

The initiator (DMVN) was purchased from Polysciences and recrystallized from methanol, mp 70–72°C (dec.), (lit. (61) mp 75–76°C). The solid was stored at −30°C and solutions of known concentration were prepared in chloroform or methanol before use. Trolox, a gift from Hoffman-LaRoche, Nutley, New Jersey, was used as freshly prepared solutions in phosphate buffer. α-Tocopherol (Eastman-Kodak) was stored in known concentrations in hexane under argon at −30°C. 2,6-Di-*tert*-butyl-4-methylphenol (BHT) was obtained from Serdary Research Lab. 3,5-Di-*tert*-butyl-4-hydroxy-anisole (DBHA) and 2,4,6-trimethylphenol (TMP) were obtained from Aldrich. 2,2,5,7,8-Pentamethyl-6-hydroxychroman (PMHC), 2,3,5,6-tetramethyl-4-methoxyphenol (TTMMP), and 2,3,6-trimethyl-4-methoxyphenol (TMMP) were gifts from Dr. Graham Burton, National Research Council, Ottawa. Solutions of known concentrations of these antioxidants were prepared in methanol for coevaporation methods, and stored at −30°C.

L-α-Dilinoleoylphosphatidylcholine (DLPC) was purchased from Avanti Polar Lipids. The DLPC was checked for the presence of peroxides by chromatography on reverse phase TLC plates (Whatman KC18F) developed with 90:10 methanol/water. Traces of hydroperoxides were detected as pink spots on spraying with *N,N*-dimethyl-*p*-phenylenediamine dihydrochloride solution and phospholipid was detected by spraying with molybdenum blue spray reagent (Sigma) followed by heating at 110°C. Where necessary, peroxides were removed by preparative HPLC on a 10 × 250 mm Vydac (C18) column by elution with methanol/water/cyclohexane (90:10:5) by the procedure reported earlier (34). The multilamellar vesicles (MLV) of DLPC containing known amounts of initiator and inhibitor were prepared by coevaporation of known amounts of each from methanol, followed by vortex stirring in buffer and 10 freeze–thaw cycles as reported earlier (34). Unilamellar vesicles (ULV) were prepared by three passes through a mini French pressure cell under argon at 20 000 psi (1 psi = 6.9 kPa) (50, 62).

2. Analysis

(a) Autoxidation product analysis

The *cis,trans* and *trans,trans* 9- and 13-hydroperoxides derived from linoleate were reduced by triphenylphosphine to the hydroxy compounds, converted into methyl esters by transesterification, and analyzed by HPLC by the procedure reported (34).

(b) ^{31}P Nuclear magnetic resonance

^{31}P NMR spectra were measured on MLV and ULV DLPC dispersions in Tham buffer (pH 7.0) on a Nicolet 360 NB FT NMR spectrometer operating at 146.15 MHz using the conditions reported (34). The MLV exhibited the typical broad asymmetric signals with chemical shift anisotropy of approximately 40 ppm whereas the ULV showed narrower symmetrical ^{31}P peaks. Examples of these two types of spectra were illustrated in earlier reports (34, 50).

3. Autoxidation procedures

Autoxidations were carried out at 37°C under approximately 760 Torr (1 Torr = 133.3 Pa) of oxygen using a dual channel stainless steel apparatus (34). Measurements of oxygen uptake during inhibition periods required a very sensitive pressure transducer. For this purpose, the sensitivity was at least five times that used previously. Ideally one needs to measure such oxygen uptake from the very beginning of the inhibition period. However some lag time is encountered during which the sample and calibrated glass cell must warm from room temperature to 37°C. This can cause error in measurements of oxygen uptake especially for the more active antioxidants. A correction was made for this by estimating the amounts of inhibitor and initiator used up during this lag time and correcting the calculations for the amount of inhibitor used during the warm-up period.

Acknowledgements

This research was supported by grants from the Natural Sciences and Engineering Research Council of Canada, and the Terry Fox Fund for Cancer Research (N.B.), which are gratefully acknowledged. We are indebted to Roger Smith and Allister MacDonald for their assistance in the design and construction of sensitive apparatus for oxygen pressure measurements. We thank Dr. Graham Burton (NRC, Ottawa) for samples of phenolic antioxidants PMHC, **5b** and **6***b*. We also

wish to thank Dr. Kazuo Mukai (Ehime University, Japan) for new hydroxychromans **4***a* and **5***a*. NMR measurements were made at the Atlantic Regional Magnetic Resonance Centre at Dalhousie University.

1. P. J. O'Brien. *In* Autoxidaion of unsaturated lipids. Academic Press, London. 1987. Chap. 7, pp. 233–280.
2. B. Halliwell and J. M. C. Gutteridge. Free radicals in biology and medicine. Clarendon Press, Oxford. 1985.
3. W. Bors, M. Saran, and D. Tait (*Editors*). Oxygen Radicals Chem. Biol. Proc. Int. Conf. 3rd. W. de Gruyter, Berlin. 1984.
4. D. C. H. McBrien and T. F. Slater (*Editors*). Protective agents in cancer. Academic Press, New York. 1983.
5. W. A. Pryor (*Editor*). Free Radicals in Biology. Vols. I–V. Academic Press, New York. 1976–1982.
6. P. B. McCay and S. R. Powell. *In* Glutathione: chemical, biochemical, and medical aspects, Part B. *Edited by* D. Dolphin, R. Poulson, and O. Avramovic. John Wiley and Sons, New York 1989. Chap. 4, pp. 111–151.
7. K. H. Cheeseman, M. Collins, K. Proudfoot, T. F. Slater, G. W. Burton, A. C. Webb, and K. U. Ingold. Biochem. J. **235**, 507 (1986).
8. H. J. Forman, D. C. Skelton, G. A. Loeb, and R. J. Dorio. *In* Oxygen radicals in biology and medicine. *Edited by* M. G. Simic, K. A. Taylor, J. F. Ward, and C. von Sonntag. Plenum Publishing, New York. 1989. pp. 523–530.
9. G. W. Burton and K. U. Ingold. J. Am. Chem. Soc. **103**, 6472 (1981).
10. G. W. Burton, T. Doba, E. J. Gabe, L. Hughes, F. L. Lee, L. Prasad, and K. U. Ingold. J. Am. Chem. Soc. **107**, 7053 (1985).
11. W. A. Pryor, T. Strickland, and D. F. Church. J. Am. Chem. Soc. **110**, 2224 (1988).
12. E. Niki, A. Kawakami, M. Saito, Y. Yamamoto, J. Tsuchiya, and Y. Kamiya. J. Biol. Chem. **260**, 2191 (1985).
13. E. Niki, J. Tsuchiya, Y. Yoshikawa, Y. Yamamoto, and Y. Kamiya. Bull. Chem. Soc. Jpn. **59**, 497 (1986).
14. E. Niki, M. Takahashi, and E. Komuro. Chem. Lett. 1573 (1986).
15. E. Niki. Clinical and nutritional aspects of vitamin E. *Edited by* O. Hayaishi and M. Mino. Elsevier Science, New York. 1987. pp. 3–13.
16. L. Castle and M. J. Perkins. J. Am. Chem. Soc. **108**, 6382 (1986).
17. E. Niki, E. Komuro, M. Takahashi, S. Urano, E. Ito, and K. Terao. J. Biol. Chem. **263**, 19809 (1988).
18. D. D. M. Wayner, G. W. Burton, K. U. Ingold, L. R. C. Barclay, and S. J. Locke. Biochim. Biophys. Acta, **924**, 408 (1987).
19. L. R. C. Barclay. J. Biol. Chem. **263**, 16138 (1988).
20. B. Frei, L. England, and B. N. Ames. Proc. Natl. Acad. Sci. U.S.A. **86**, 6377 (1989).
21. G. W. Burton, A. Joyce, and K. U. Ingold. Arch. Biochem. Biophys. **221**, 281 (1983).
22. G. W. Burton and K. U. Ingold. Acc. Chem. Res. **19**, 194 (1986).
23. E. Niki. Chem. Phys. Lipids, **44**, 227 (1987).
24. A. Bendich, L. J. Machlin, O. Scandurra, G. W. Burton, and D. D. M. Wayner. Adv. Free Radical Biol. Med. **2**, 419 (1986).
25. N. I. Krinsky. Ann. New York Acad. Sci. **551**, 17 (1988).
26. K. U. Ingold. Acc. Chem. Res. **2**, 1 (1969).
27. F. R. Mayo. Acc. Chem. Res. **1**, 193 (1968).
28. J. A. Howard. *In* Free radicals. Vol. II. *Edited by* J. K. Kochi. Wiley, New York. 1973. Chap. 12, pp. 3–62.
29. J. A. Howard. Adv. Free-Radical Chem. **4**, 49 (1972).
30. Y. Yamamoto, S. Haga, E. Niki, and Y. Kamiya. Bull. Chem. Soc. Jpn. **57**, 1260 (1984).
31. L. R. C. Barclay, S. J. Locke, and J. M. MacNeil. Can. J. Chem. **63**, 366 (1985).
32. L. R. C. Barclay, K. A. Baskin, S. J. Locke, and T. D. Schaefer. Can. J. Chem. **65**, 2529 (1987).
33. L. R. C. Barclay and K. U. Ingold. J. Am. Chem. Soc. **103**, 6478 (1981).
34. L. R. C. Barclay, K. A. Baskin, D. Kong, and S. J. Locke. Can. J. Chem. **65**, 2541 (1987).
35. L. R. C. Barclay, S. J. Locke, J. M. MacNeil, and J. VanKessel. Can. J. Chem. **63**, 2633 (1985).
36. L. R. C. Barclay, S. J. Locke, J. M. MacNeil, J. VanKessel, G. W. Burton, and K. U. Ingold. J. Am. Chem. Soc. **106**, 2479 (1984).
37. Y. Yamamoto, E. Niki, Y. Kamiya, and H. Shimisaki. Biochim. Biophys. Acta, **795**, 332 (1984).
38. J. H. Fendler. Membrane mimetic chemistry. Wiley, New York. 1982.
39. B. Maillard, K. U. Ingold, and J. C. Scaiano. J. Am. Chem. Soc. **105**, 5095 (1983).
40. L. R. C. Barclay, K. A. Baskin, S. J. Locke, and M. R. Vinqvist. Can. J. Chem. **67**, 1366 (1989).
41. N. A. Porter. Acc. Chem. Res. **19**, 262 (1986).
42. N. A. Porter and D. G. Wujek. J. Am. Chem. Soc. **106**, 2626 (1984).
43. H. Weenen and N. A. Porter. J. Am. Chem. Soc. **104**, 5216 (1982).
44. N. A. Porter, B. A. Weber, H. Weenen, and J. A. Khan. J. Am. Chem. Soc. **102**, 5597 (1980).
45. M. J. Thomas and W. A. Pryor. Lipids, **15**, 514 (1980).
46. J. A. Howard and K. U. Ingold. Can. J. Chem. **10**, 2729 (1965).
47. C. S. Foote. *In* Free radicals in biology. Vol. II. *Edited by* W. A. Pryor. Academic Press, New York. 1980. Chap. 3, pp. 85–133.
48. R. C. Straight and J. D. Spikes. *In* Singlet O_2. Vol. IV. Polymers and biomolecules. *Edited by* A. A. Frimer. CRC Press, Boca Raton, FL. 1985. Chap. 2, pp. 91–143.
49. E. E. Burnell, P. R. Cullis, and B. DeKruijff. Biochim. Biophys. Acta, **603**, 63 (1980).
50. L. R. C. Barclay, A. M. H. Bailey, and D. Kong. J. Biol. Chem. **260**, 15809 (1985).
51. C. Walling and P. Wagner. J. Am. Chem. Soc. **85**, 2333 (1963).
52. R. W. Fessenden, A. Hitachi, and V. Nagarajan. J. Phys. Chem. **88**, 107 (1984).
53. J. A. Howard and K. U. Ingold. Can. J. Chem. **44**, 1119 (1966).
54. I. H. Ekiel, L. Hughes, G. W. Burton, P. A. Jovall, K. U. Ingold, and I. C. P. Smith. Biochemistry, **27**, 1432 (1988).
55. K. U. Ingold and D. R. Taylor. Can. J. Chem. **39**, 481 (1961).
56. K. Mukai, K. Takamatsu, and K. Ishizu. Bull. Chem. Soc. Jpn. **57**, 3507 (1984).
57. E. Niki, T. Saito, A. Kawakami, and Y. Kamiya. J. Biol. Chem. **259**, 4177 (1984).
58. F. F. Rust and E. A. Youngman. J. Org. Chem. **27**, 3778 (1962).
59. M. Takahashi, J. Tsuchiya, and E. Niki. J. Am. Chem. Soc. **111**, 6350 (1989).
60. E. Niki, Y. Yamamoto, M. Takahashi, K. Yamamoto, Y. Yamamoto, E. Komuro, M. Miki, H. Yasuda, and M. Mino. J. Nutr. Sci. Vitaminol. **34**, 507 (1988).
61. C. G. Overberger and M. B. Berenbaum. J. Am. Chem. Soc. **73**, 2618 (1951).
62. K. Mukai, S. Yokayama, K. Fukuda, and Y. Uemoto. Bull. Chem. Soc. Jpn. **60**, 2163 (1987).
63. K. Mukai, K. Okabe, and H. Hosose. J. Org. Chem. **54**, 557 (1989).

Can. J. Chem. Downloaded from www.nrcresearchpress.com by 195.138.81.100 on 09/07/12
For personal use only.

^{113}Cd NMR studies of Hofmann-type clathrates and related compounds: Evidence for two room temperature orientational glasses[1]

S. NISHIKIORI,[2] C. I. RATCLIFFE,[3] AND J. A. RIPMEESTER

Chemistry Division, National Research Council of Canada, Ottawa, Ont., Canada K1A 0R9

Received February 26, 1990

S. NISHIKIORI, C. I. RATCLIFFE, and J. A. RIPMEESTER. Can. J. Chem. **68**, 2270 (1990).

^{113}Cd magic angle spinning NMR, with and without ^{1}H cross-polarisation and decoupling, has been used to study a number of Hofmann-type clathrates and related compounds. The ^{113}Cd chemical shift shows a great sensitivity to the environment of Cd, even for complexes with closely related structures. The presence of five resonances due to Cd surrounded by $C_xN_{(4-x)}$ (where $x = 0$ to 4) in $Cd(CN)_2$ and $Cd(CN)_2 \cdot C_6H_{12}$ indicates a static disorder of the CN groups, which makes these materials orientational glasses.

Key words: ^{113}Cd NMR, Hofmann-type clathrates, $Cd(CN)_2$, disorder, orientational glass.

S. NISHIKIORI, C. I. RATCLIFFE et J. A. RIPMEESTER. Can. J. Chem. **68**, 2270 (1990).

On a utilisé l'angle magique de rotation en rmn du ^{113}Cd, avec ou sans découplage et polarisation croisée du ^{1}H, pour étudier un certain nombre de clathrates du type de Hofmann et de composés apparentés. Le déplacement chimique du ^{113}Cd est très sensible à l'environnement du Cd, même pour des complexes de structures très apparentées. La présence de 5 raies de résonance pour des Cd entourés par $C_xN_{(4-x)}$ (où $x = 0$ à 4) dans $Cd(CN)_2$ et $Cd(CN)_2 \cdot C_6H_{12}$ indique qu'il existe un désordre statique des groupements CN qui transforme ces matériaux en verres orientationnels.

Mots clés : RMN du ^{113}Cd, les clathrates du type de Hofmann, $Cd(CN)_2$, désordre, verre orientationnel.

[Traduit par la revue]

Introduction

The Hofmann-type clathrates are an interesting type of host–guest system in which the host consists of a layered framework of cyano-bridged metal atoms, usually square planar Ni and octahedral Cd (1–3). The layers are held apart by ammonia molecules coordinated to the Cd atoms at right angles to the layers. Between the layers and coordinating groups are cavities which, in most cases, are large enough to hold a guest molecule such as benzene. A great number of related compounds have been produced by varying the coordinating amino-bearing molecules (3–5) and replacing the square planar Ni atom with a tetrahedral Cd atom (6, 7). Recently, in the course of the latter studies it was found that $Cd(CN)_2$ itself can also form clathrates. In some cases the distinct layered structure of the true Hofmann-type is lost, but the common feature of all is the system of cyano-bridged Ni and/or Cd atoms. Many of these host systems also form stable compounds when the guest molecules are lost, though a structural change usually occurs (6).

Although a great deal of work has been done on the preparation and structure of these compounds, there is still much scope for solid-state NMR studies. Here we present some ^{113}Cd NMR results. ^{113}Cd has a large chemical shift range and should be sensitive to small changes in its environment (8) and is recently finding use in solid state NMR (e.g., refs. 9–11). In many of the X-ray structural studies of Hofmann and related materials it has been possible to distinguish the C and N atoms of the CN groups; frequently one metal is coordinated entirely by C or entirely by N. However, there are some cases where the two have not been distinguished. It was of interest, first of all, to see whether solid state ^{113}Cd NMR was sensitive enough to distinguish the different coordination situations and, if so, to determine whether disorder was responsible for the X-ray indistinguishability of C and N.

[1]NRCC No: 32504.

[2]On leave from Department of Chemistry, College of Arts and Sciences, The University of Tokyo, Komaba, Meguro Tokyo 153, Japan.

[3]To whom correspondence should be addressed.

Experimental

$Cd(NH_3)_2Ni(CN)_4 \cdot 2C_6H_6$ was prepared by the following method. Into 100 mL of water 0.01 mol of cadmium chloride and potassium tetracyanonickelate were added, and 10 mL of 2-aminoethanol ($NH_2—CH_2CH_2—OH$) was poured into the mixture with stirring until the mixture turned into a yellow solution. After 5 mL of 28% ammonia aqueous solution was dissolved in the yellow solution, neat benzene was placed on the solution surface. The clathrate was obtained as yellow polycrystals after standing for a week at room temperature.

$Cd(en)Ni(CN)_4 \cdot 2C_6H_6$ was obtained by the same method in which 1.3 mL of distilled ethylenediamine was used instead of 5 mL of aqueous ammonia.

$Cd(en)Cd(CN)_4 \cdot 2C_6H_6$, $Cd(en)Cd(CN)_4$, and $Cd(CN)_2 \cdot C_6H_{12}$ were prepared by methods reported in refs. 12, 13, and 14, respectively. The crystals were grown at 279 K.

$Cd(CN)_2$ was obtained by thermal decomposition of $Cd(CN)_2 \cdot C_6H_{12}$ (14). Powdered $Cd(CN)_2 \cdot C_6H_{12}$ was kept at ca. 350 K for 24 h in the atmosphere. The conclusion of the decomposition was confirmed by the X-ray diffraction powder pattern.

^{113}Cd NMR spectra were obtained at 39.92 MHz using a Bruker CXP 180 pulse spectrometer and 4.24T cryomagnet with a Doty Scientific magic angle spinning probe. Samples were contained in 7 mm o.d. sapphire tubes with Kel-F end caps. Spinning rates of 3.4–4.6 kHz were used. ^{1}H cross-polarisation and decoupling was used in most cases with CP times of 4–10 ms and matched r.f. fields of ~50 kHz. Spectra of $Cd(CN)_2$ and its cyclohexane clathrate were obtained using a simple phase cycled pulse sequence (CYCLOPS) (15) with recycle times of 100 and 60 s, respectively. No cross-polarisation signal could be found for the latter material, for which ^{2}H NMR results (to be reported later) indicate that the cyclohexane is undergoing rapid pseudo-isotropic reorientation at room temperature. Chemical shifts are given relative to $Cd(NO_3)_2 \cdot 4H_2O$. Note that all materials studied are diamagnetic.

Results and discussion

Spectra are shown in Figs. 1–3 and the chemical shifts and relevant linewidths are collected in Table 1. Figure 1 shows the spectra for three different Cd/Ni Hofmann-type compounds. In all three structures (16–19) the Cd is surrounded by four cyano N atoms and two N atoms of the other ligands in a distorted octahedral coordination. The chemical shift data illustrate the great sensitivity to small changes in the environ-

Can. J. Chem. Downloaded from www.nrcresearchpress.com by 195.138.81.100 on 09/07/12
For personal use only.

Can. J. Chem. Downloaded from www.nrcresearchpress.com by 195.138.81.100 on 09/07/12
For personal use only.

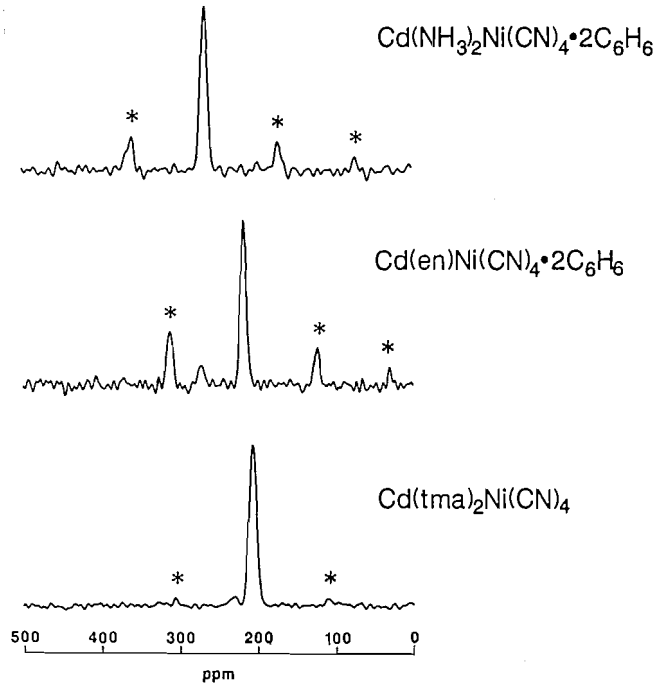

FIG. 1. ^{113}Cd CP/MAS spectra of several Cd/Ni Hofmann-type and related compounds (* indicates spinning sidebands).

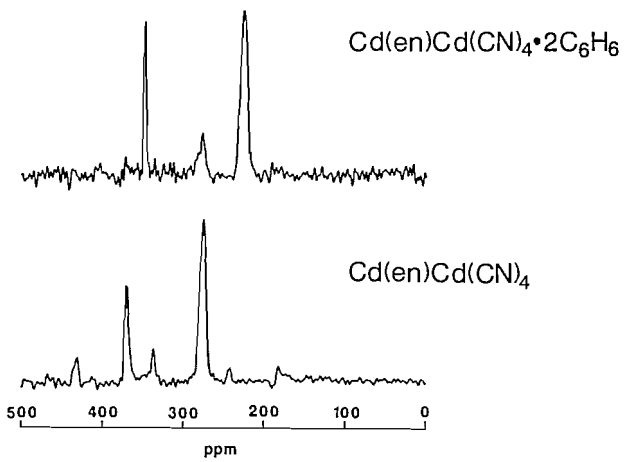

FIG. 2. ^{113}Cd CP/MAS spectra of $Cd(en)Cd(CN)_4 \cdot 2C_6H_6$ clathrate and $Cd(en)Cd(CN)_4$. Note the presence of $Cd(en)Cd(CN)_4$ in the top spectrum as a product when the clathrate loses the guest material.

ment of the Cd atom. Figure 2 (top) shows the spectrum of $Cd(en)Cd(CN)_4 \cdot 2C_6H_6$ clathrate. Partial loss of guest is evident from the appearance of weaker lines due to the empty host material (Fig. 2, bottom). The spectrum of this clathrate may be compared with that of the equivalent Cd/Ni clathrate (middle spectrum of Fig. 1). The broader line at 225 ppm matches the line observed at 217.6 ppm in the Cd/Ni clathrate and is thus assigned to the distorted octahedral $Cd(N)_6$. The much sharper line at 348.2 ppm must then be assigned to the distorted tetrahedral $Cd(C)_4$. This is in accord with the known structure which is ordered (6). Similar assignments may be made for the two major lines in the spectrum of $Cd(en)Cd(CN)_4$ whose structure also has distinct $Cd(N)_6$ and $Cd(C)_4$ (6). The weaker line at 337 ppm in this spectrum is presumed to be due to impurity.

The spectra of $Cd(CN)_2$ and the clathrate $Cd(CN)_2 \cdot C_6H_{12}$ proved to be of greater interest, Fig. 3. The isostructural

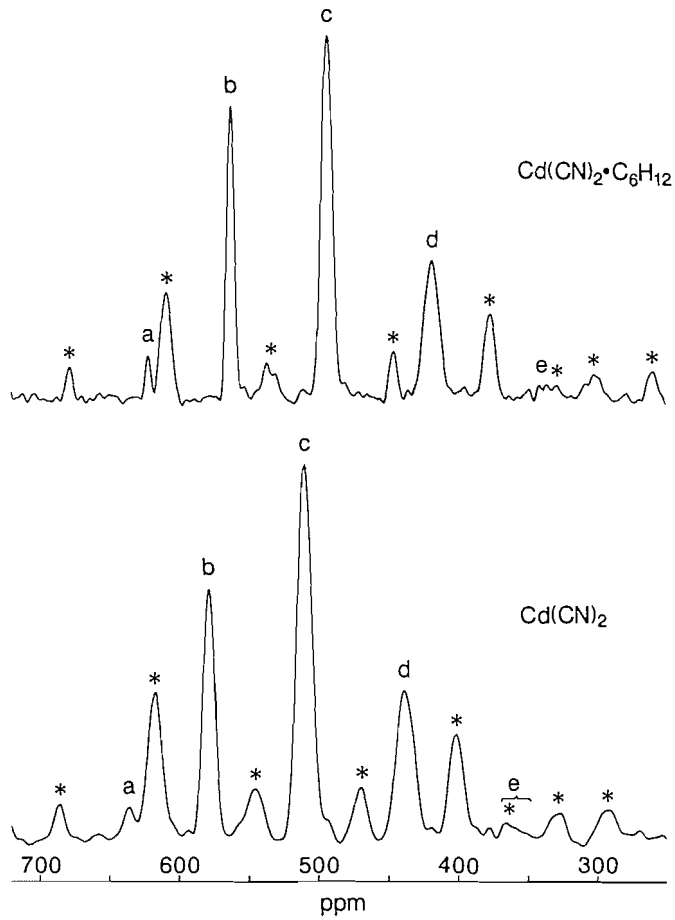

FIG. 3. ^{113}Cd MAS spectra of $Cd(CN)_2 \cdot C_6H_{12}$ and $Cd(CN)_2$. The five lines indicated correspond to *a*, CdC_4; *b*, CdC_3N; *c*, CdC_2N_2; *d*, $CdCN_3$; and *e*, CdN_4 (* indicates spinning side bands).

clathrate $Cd(CN)_2 \cdot CCl_4$ is one clathrate for which the X-ray structural studies failed to distinguish the C and N atoms of the cyanide groups (14) and the C_6H_{12} clathrate is presumed to behave in the same way. Its ^{113}Cd NMR spectrum shows five distinguishable resonances, each with its manifold of spinning sidebands. Four lines are resolved and the presence of the fifth becomes evident on close inspection when all the sidebands have been accounted for. After consideration of the different structural possibilities compatible with the X-ray data, it becomes quite clear that the five lines are unequivocal evidence for *static disorder* of the CN groups. (*1*) Ordered structure: $Cd(C)_4$ and $Cd(N)_4$ would give rise to two resonances of equal intensity. (*2*) Static disorder: distribution of C, N about each Cd would give CdC_4, CdC_3N, CdC_2N_2, $CdCN_3$, CdN_4 and therefore five resonances of various intensities. Spatial averaging would mean that X-ray structure determination could not distinguish C and N. (*3*) Dynamic disorder: rapid reorientation of cyano groups would produce a situation where, on time average, each site has $\frac{1}{2}N + \frac{1}{2}C$ and all Cd are equivalent on the NMR timescale. This would give one resonance.

Four of the five resonances can also be found directly in the spectrum of $Cd(CN)_2$ and like the clathrate, the fifth is broad and overlapped by a spinning sideband. There can be no doubt that this material also has a static disorder of the CN groups. Shugam and Zhdanov (20) reported the crystal structure of $Cd(CN)_2$ which was analyzed by the powder X-ray diffraction method. They applied space group $P\bar{4}3m$ ($Z = 2$) to the crystal assuming an isomorphism with $Zn(CN)_2$ (21). In the symmetry of $P\bar{4}3m$

Can. J. Chem. Downloaded from www.nrcresearchpress.com by 195.138.81.100 on 09/07/12
For personal use only.

TABLE 1. Chemical shift and linewidth data

Compound	Shift (ppm)	Linewidth (Hz)	Assignment	Ave Cd—X distance (Å)
$Cd(NH_3)_2Ni(CN)_4 \cdot 2C_6H_6$	265.5	427	CdN_6	2.331
$Cd(en)Ni(CN)_4 \cdot 2C_6H_6$	(272.6)			
	217.6	346	CdN_6	2.346
$Cd(tma)_2Ni(CN)_4$	(230.7)			
	206.2	480	CdN_6	2.363
$Cd(en)Cd(CN)_4 \cdot 2C_6H_6$	348.2	113	CdC_4	2.222
	225	395	CdN_6	2.352
$Cd(en)Cd(CN)_4$	370.8	170	CdC_4	2.210
	(337)			
	275.3	346	CdN_6	2.348
$Cd(CN)_2 \cdot C_6H_{12}$	621.6	215	CdC_4	2.095†
	562.0	265	CdC_3N	2.124†
	492.7	390	CdC_2N_2	2.153†
	417.8	530	$CdCN_3$	2.182†
	~336	?	CdN_4	2.211†
$Cd(CN)_2$	636	~220	CdC_4	
	578	407	CdC_3N	
	510	490	CdC_2N_2	
	439	632	$CdCN_3$	
	~360	?	CdN_4	

*Shifts relative to $Cd(NO_3)_2 \cdot 4H_2O$; en = ethylenediamine, $NH_2CH_2CH_2NH_2$; tma = trimethylamine, $(CH_3)_3N$; shifts in parentheses ( ) are weak lines of decomposition products or impurities.
†Estimated values.

there are inevitably two kinds of Cd atoms and four C and N atoms in one unit cell. Namely, their result suggests the ordered structure. A recent single crystal study (22) indicated the same structure, *but* the authors remark that they were unable to conclusively distinguish the C and N atoms. However, in an even more recent X-ray diffraction study of single crystal $Cd(CN)_2$ (23) the space group was found to be $Pn\bar{3}m$ ($Z = 2$). This means there is one kind of Cd atom and no distinction between C and N atoms. This result suggests the static disorder of the CN groups and supports our NMR result.

Since both structures are statically disordered they are in fact also orientational glasses. The alkali metal cyanides, NaCN and KCN, show dynamic disorder of the CN^- ions in their room temperature cubic phases, but, on cooling, their first non-cubic phases (orthorhombic) are orientational glasses in which the CN are aligned but are disordered with respect to a head and tail sequence (24). Since the NMR results indicate that in $Cd(CN)_2$ and its clathrate the CN are static on the NMR timescale (*i.e.*, reorientation must be slower than 10^{-4} Hz) at room temperature, the next questions that come to mind are whether the CN begin to reorientate at higher temperatures and whether there might be a transition to a phase with dynamic disorder. A calorimetric scan on the $Cd(CN)_2$ sample indicated no transitions between room temperature and 400 K. Unfortunately, the clathrate loses the cyclohexane guest a little above room temperature. Room temperature MAS spectra were obtained of samples of $Cd(CN)_2$ and the clathrate which had been cooled to 77 K for about 20 min and of $Cd(CN)_2$ which had been heated to 450 K for about 10 min. There were no significant changes following thermal treatment. This suggests either (*a*) rapid equilibration at room temperature or (*b*) reorientation is so slow even at 456 K that is has no effect on the frozen-in disorder.

When the spectra in Fig. 3 are inspected more closely it is found that the linewidths decrease downfield. (The separation between the peaks also decreases downfield.) Assuming that CdC_4 has the largest downfield shift and CdN_4 the smallest, by analogy with the results in Fig. 2, the most likely explanation of the changing linewidths is a cumulative broadening effect due to the N atoms. There are two probable contributors to this broadening: (*a*) The major factor is likely to be unresolved ^{113}Cd—^{14}N spin–spin coupling. J couplings between ^{113}Cd and ^{15}N, of the order of 137–190 Hz, have been observed in a number of materials (8). (*b*) The ^{113}Cd—^{14}N dipole–dipole interaction is not completely removed by MAS due to interactions with the ^{14}N nuclear quadrupole (*cf.* the same effect in ^{13}C NMR (25)). The five resonances can then logically be assigned assuming progressively fewer C atoms towards the high field end.

Table 2 lists the intensities of the five lines observed in the $Cd(CN)_2$ clathrate spectrum, including the contributions of the spinning sidebands. If the distribution of C and N atoms were entirely random the statistical distribution of species indicated in the table would be expected. Clearly there is an enhancement of the CdC_2N_2 species relative to the others. This can only happen if there are energy differences between the five species. The observed distribution is then the product of the statistical distribution and a Boltzmann factor. The sample was prepared at 279 K, but the spectrum was obtained at 297 K. Presently we do not know whether the material could have annealed over a period of time to an equilibrium distribution at 297 K or whether the 279 K distribution remained frozen in. Consequently the energy differences have been calculated for both temperatures. The differences between the two sets are not large. The results show that when all Cd are four coordinated by CN the CdC_4 and CdN_4 species are energetically the least favoured.

Finally, we also note that underlying the range of observed shifts there seems to be a rough correlation of the shifts with the

TABLE 2. Intensity distribution of the five lines in the $Cd(CN)_2 \cdot C_6H_{12}$ clathrate spectrum

Cd coordination	Statistical distribution %	Observed distribution %	ΔE relative to C_2N_2 (kJ/mol) Equilib. 279 K	Equilib. 297 K
C_4	6.25	2.0	3.32	3.54
C_3N	25	22.8	0.90	0.95
C_2N_2	37.5	50.3	0	0
CN_3	25	23.2	0.86	0.91
N_4	6.25	1.7	3.70	3.94

average distance from Cd to N or C atoms; the closer the atoms the further downfield the shift. This is certainly true for a comparison between Cd with C atoms and with N atoms, where the Cd—C distances are generally more than 0.1 Å shorter than Cd—N. The known and some estimated average distances are indicated in Table 1. Cd—C and Cd—N distances of 2.095 and 2.211 Å, respectively, were estimated for the $Cd(CN)_2 \cdot C_6H_{12}$ clathrate assuming Cd—N to be 0.116 Å longer than Cd—C (the average of the difference found in the other Cd—C≡N—Cd compounds). Correlations have been sought previously between the chemical shift tensor or the isotropic shift and various coordinate bond parameters (reviewed in ref. 8). In one such study no obvious correlation was found between average Cd—O distances and the isotropic shifts, whereas one was found between bonding distance anisotropies and the chemical shift anisotropy (26). Another study concluded that bond length dispersion, local site symmetry, and ligand type *all* contribute to the chemical shift anisotropy (8, 27, 28). Thus it is clear that, in general, correlations are not straightforward.

To conclude, it can be seen that ^{113}Cd NMR is a very sensitive means of distinguishing different Cd sites in Hofmann-type clathrates and related solids. It has provided unequivocal evidence that $Cd(CN)_2$ and its cyclohexane clathrate are orientational glasses with respect to CN group disorder. Furthermore, it would be of interest to use ^{113}Cd NMR to study the disorder implied in several other Cd–ligand–Cd–cyano complexes which have recently been found to have indistinguishable C and N atoms in X-ray diffraction studies (7, 23).

Acknowledgements

We would like to thank Dr. P. Handa for providing calorimetric scans of $Cd(CN)_2$. S.N. thanks the Nishina Memorial Foundation for the support of his visiting expenses to the National Research Council of Canada.

1. H. M. POWELL and J. H. RAYNER. Nature (London), **163**, 566 (1949).
2. J. H. RAYNER and H. M. POWELL. J. Chem. Soc. 319 (1952).
3. T. IWAMOTO. *In* Inclusion compounds. Vol. 1. *Edited by* J. L. Atwood, J. E. D. Davies, and D. D. MacNicol. Academic Press, London. 1984. Chap. 2.
4. S. NISHIKIORI and T. IWAMOTO. Chem. Lett. 319 (1984).
5. T. IWAMOTO, S. NISHIKIORI, and T. HASEGAWA. J. Inclusion Phenom. **5**, 225 (1987).
6. S. NISHIKIORI and T. IWAMOTO. J. Inclusion Phenom. **3**, 283 (1985).
7. T. KITAZAWA, S. NISHIKIORI, R. KURODA, and T. IWAMOTO. Chem. Lett. 459 (1988).
8. M. F. SUMMERS. Coord. Chem. Rev. **86**, 43 (1988).
9. T. T. P. CHEUNG, L. E. WORTHINGTON, P. DUBOIS MURPHY, and B. C. GERSTEIN. J. Magn. Reson. **41**, 158 (1980).
10. M. A. KENNEDY and P. D. ELLIS. J. Am. Chem. Soc. **111**, 3195 (1989).
11. S. BANK, J. F. BANK, and P. D. ELLIS. J. Phys. Chem. **93**, 4847 (1989).
12. T. IWAMOTO. Chem. Lett. 723 (1973).
13. S. NISHIKIORI, T. IWAMOTO, and Y. YOSHINO. Chem. Lett. 1509 (1979).
14. T. KITAZAWA, S. NISHIKIORI, R. KURODA, and T. IWAMOTO. Chem. Lett. 1729 (1988).
15. E. O. STEJSKAL and J. SCHAEFER. J. Magn. Reson. **14**, 160 (1974).
16. Y. SASAKI. Bull. Chem. Soc. Jpn. **42**, 2412 (1969).
17. S. NISHIKIORI, T. KITAZAWA, R. KURODA, and T. IWAMOTO. J. Inclusion Phenom. **7**, 369 (1989).
18. T. MIYOSHI, T. IWAMOTO, and Y. SASAKI. Inorg. Nucl. Chem. Lett. **6**, 21 (1970); Inorg. Chim. Acta, **6**, 59 (1972).
19. S. NISHIKIORI. Ph.D. Thesis, Univ. of Tokyo. Tokyo, Japan. 1986.
20. E. SHUGAM and H. ZHDANOV. Acta Physicochim. USSR, **20**, 247 (1945).
21. H. ZHDANOV. C.R. Acad. Sci. USSR, **31**, 350 (1941).
22. B. F. HOSKINS and R. ROBSON. J. Am. Chem. Soc. **112**, 1546 (1990).
23. T. IWAMOTO. Private communication.
24. N. G. PARSONAGE and L. A. K. STAVELEY. Disorder in crystals. Clarendon, Oxford. 1978. pp. 270–275 and references therein.
25. N. ZUMBULYADIS, P. M. HENRICHS, and R. H. YANG. J. Chem. Phys. **75**, 1603 (1981).
26. P. DUBOIS MURPHY and B. C. GERSTEIN. J. Am. Chem. Soc. **103**, 3282 (1981).
27. R. S. HONKONEN and P. D. ELLIS. J. Am. Chem. Soc. **106**, 5488 (1984).
28. R. S. HONKONEN, P. S. MARCHETTI, and P. D. ELLIS. J. Am. Chem. Soc. **108**, 912 (1986).

Can. J. Chem. Downloaded from www.nrcresearchpress.com by 195.138.81.100 on 09/07/12
For personal use only.

Alkyne and alkene complexes of (tetramesitylporphyrinato)ruthenium(II)

NIMAL RAJAPAKSE, BRIAN R. JAMES,[1] AND DAVID DOLPHIN
Department of Chemistry, University of British Columbia, Vancouver, B.C., Canada V6T 1Y6

Received June 2, 1990

NIMAL RAJAPAKSE, BRIAN R. JAMES, and DAVID DOLPHIN. Can. J. Chem. **68**, 2274 (1990).

The reactions of benzene or toluene solutions of Ru^{II}(TMP), where TMP is the dianion of 5,10,15,20 – tetramesitylporphyrin, with some acetylenes and alkenes are reported. Acetylene yields the isolable $[Ru(TMP)]_2(\mu\text{-}C_2H_2)$ species; while with phenylacetylene or diphenylacetylene, 1:1 π-complexes are formed. The π-complexes $Ru(TMP)(C_2H_4)$ and $Ru(TMP)(C_2H_4)(^iPrOH)\cdot{}^iPrOH$ are isolated from reactions with ethylene, and a similar cyclohexene species is characterized *in situ*. The findings are relevant to O_2-epoxidation of alkenes catalyzed by the *trans*-$Ru(TMP)(O)_2$ complex.

Key words: ruthenium, porphyrin (tetramesityl), alkene complexes, alkyne complexes.

NIMAL RAJAPAKSE, BRIAN R. JAMES et DAVID DOLPHIN. Can. J. Chem. **68**, 2274 (1990).

On a examiné les réactions des quelques acétylènes et alcènes avec des solutions de Ru^{II}(TMP) (dans lequel TMP est le dianion de la 5,10,15,20-tétramésitylporphyrine) dans le benzène ou le toluène. L'acétylène fournit des espèces $[Ru(TMP)]_2(\mu\text{-}C_2H_2)$ qui peuvent être isolées; avec le phénylacétylène ou le diphénylacétylène, il se forme des complexes-π 1:1. On a isolé les complexes-π $Ru(TMP)(C_2H_4)$ et $Ru(TMP)(C_2H_4)(^iPrOH)\cdot{}^iPrOH$ à partir des réactions avec l'éthylène; on a aussi caractérisé *in situ* un espèce semblable qui se forme lors de la réaction avec le cyclohexène. Ces résultats sont utiles dans la compréhension de l'époxydation des alcènes par le O_2 catalysé par le complexe *trans*-$Ru(TMP)(O)_2$.

Mot clés : ruthénium, porphyrine (tétramésityl), complexes d'alcènes, complexes d'alcynes.

[Traduit par la revue]

Introduction

The organometallic chemistry of ruthenium porphyrins has developed in recent years (1–6), and is particularly of current interest because of reports on the catalytic O_2-oxygenation of unsaturated and saturated hydrocarbons using *trans*-dioxo complexes of sterically hindered derivatives of ruthenium porphyrins (7–10). The interaction of ruthenium porphyrins with ethylene has been studied, and the Ru(porp)(THF)(η^2-C_2H_4) species (porp = OEP, TPP)[2] characterized (3, 11), but there are no other reports on reactions with alkynes or other alkenes. In the more general area of metalloporphyrin chemistry, the only alkyne π-complex reported to date is Mo(TTP)(PhC≡CPh) (12), while the reaction of $[Rh(OEP)]_2$ with RC≡CH (R = H, Ph) yields $[Rh(OPE)]_2(\mu\text{-CRCH})$ species (13).

In the present work, the reactions of the Ru(TMP) complex (14, 15) with acetylene, phenylacetylene, diphenylacetylene, ethylene, and cyclohexene are studied, and organometallic products are prepared and characterized.

Experimental procedure

Bis-dinitrogen(tetramesitylporphyrinato)ruthenium(II), Ru(TMP)$(N_2)_2$ was synthesized according to the literature procedure (14, 15). Carbon monoxide and ethylene impurities in acetylene (Matheson) were removed by three freeze–pump–thaw cycles at −130°C using an *n*-pentane/liquid N_2 slush-bath. The phenylacetylenes were used as received from Aldrich Chemicals. Ethylene (Matheson) was dried by passing through an Aquasorb tube (Mallinckdrodt). The ^1H and $^{13}C\{^1H\}$ NMR data for the complexes were measured on a Varian XL-300 MHz instrument (FT mode), and the former are given in Table 1. The molecular weight of the bridged acetylene complex was determined by the Signer method (16), using CH_2Cl_2 as solvent.

Bis(tetramesitylporphyrinato)ruthenium(II)–(μ-acetylene), 1

Some Ru(TMP)$(N_2)_2$ (8 mg, 8.8×10^{-3} mmol) was dissolved in benzene (1 mL) under an N_2 atmosphere and degassed by three freeze–pump–thaw cycles. The resulting dark brown solution was exposed to acetylene (1 atm) and shaken. Upon being left under room light for 16 h, the solution turned greenish-black. The solvent was then removed by evacuation and the resulting black solid vacuum-dried (10^{-3} mm Hg) for 24 h at 25°C; yield 8 mg, 100%. *Anal.* Calcd. for $C_{114}H_{106}N_6Ru_2$: C 76.48, H 5.97, N 6.25; Found: C 76.1, H 6.0, N 6.4. Mol. wt.: 1565, calcd. for $[Ru(TMP)]_2(\mu\text{-}C_2H_2)$ 1790 g mol^{-1}. NMR (C_6D_6): $^{13}\{^1H\}$ (see Fig. 1): 263.8 (Ru═C); 144.5 (α-C); 139.1, 138.7, 138.2, 137.3 (the mesityl carbons 2,3,5,7 with no attached H); 130.6 (β-C); 128.0 (the mesityl carbons 4,6 with 1 attached H — obscured by benzene peaks in Fig. 1*A*); 119.8 (*meso*-C 1); 24.0 (*p*-Me, C 9); 21.4, 21.3 (*o*-Me, C 8, C 10). ^{13}C[gated ^{1}H-decoupled]: the 263.8 resonance gives a doublet at 262.7 and 265.0.

Diphenylacetylene(tetramesitylporphyrinato)ruthenium(II)

In an N_2-filled glove-box, Ru(TMP)$(N_2)_2$ (3 mg, 3.3×10^{-3} mmol) and PhC≡CPh (1.2 mg, 6.7×10^{-3} mmol) were placed in an NMR tube fitted with an attachment to a vacuum-line. The tube was removed from the glove-box, and C_6D_6 (0.5 mL) added by vacuum transfer to the NMR tube cooled in liquid N_2; the tube was subsequently flame-sealed. The *in situ* species formed within 10 min.

Phenylacetylene(tetramesitylporphyrinato)ruthenium(II)

An *in situ* sample of this species was prepared using the procedure described above for the diphenylacetylene species, but using instead PhC≡CH.

Ethylene(tetramesitylporphyrinato)ruthenium(II)

Some Ru(TMP)$(N_2)_2$ (5 mg, 5.5×10^{-3} mmol) was dissolved in benzene (1 mL) and the solution degassed as described above. The solution was then exposed to 1 atm C_2H_4 with shaking for 5 min. The mixture was then evacuated to dryness and the product isolated in near quantitative yield. *Anal.* calcd. for $C_{58}H_{56}N_4Ru$: C 76.54, H 6.20, N 6.16; found: C 75.8, H 6.4, N 6.1.

Ethylene(2-propanol)(tetramesitylporphyrinato)ruthenium(II)·2-propanol

Some Ru(TMP)$(N_2)_2$ (8 mg, 8.8×10^{-3} mmol) was dissolved in THF (1 mL) and the solution degassed as described above. The resulting dark brown solution was then exposed to 1 atm C_2H_4 for 5 min. 2-Propanol (1 mL) was then vacuum transferred to the THF solution. The brown powder which precipitated overnight was filtered and dried under Ar; yield 5 mg, 60%. *Anal.* calcd. for $C_{64}H_{74}N_4O_2Ru$: C 74.60, H 7.04, N 5.44; found: C 73.7, H 6.9, N 5.4.

[1]To whom all correspondence should be addressed.

[2]Abbreviations used: OEP, TTP, and TMP are the dianions of 2,3,7,8,12,13,17,18-octaethyl-, 5,10,15,20-tetratolyl-, and 5,10,15,20-tetramesityl-porphyrin, respectively; THF = tetrahydrofuran.

Can. J. Chem. Downloaded from www.nrcresearchpress.com by 195.138.81.100 on 09/07/12
For personal use only.

TABLE 1. ^{1}H NMR data for Ru(TMP)-acetylene and -alkene derivatives[a]

Complex	Porphyrin ligand[b]				Axial ligand
	Pyrrole-H	*m*-H	*p*-Me	*o*-Me	
$[Ru]_2(\mu\text{-}C_2H_2)$	7.92	7.15, 6.92	2.39	1.91, 1.32	10.44 s (Ru=C—H)
Ru(PhC≡CH)	8.75	7.22, 7.08	2.45	2.23, 1.78	4.00 m (*o*-, *m*-, *p*-H), −7.40 s (≡C—H)
Ru(PhC≡CPh)	8.35	7.20,[c] 7.15	2.40	1.95, 1.70	6.58 t (*p*-H), 6.37 m (*m*-H), 5.00 d (*o*-H)
$Ru(C_2H_4)$[d]	8.44	7.20, 7.10	2.45	2.16, 1.89	−3.27 s (CH_2CH_2)
$Ru(C_2H_4)(^i\text{PrOH})\cdot{}^i\text{PrOH}$[e]	8.57	7.18,[c] 7.13	2.46	2.12, 2.13	−3.11 s (CH_2CH_2); 3.40 m (C—H), 0.73 d (CH_3) 0.00 br s (OH)
$Ru(C_6H_{10})$	8.50	7.18[e,f]	2.45	2.10[f]	4.72 m (*CH*=*CH*), 1.55 m (CH_2CH=CHCH_2), 1.24 m ($CH_2CH_2CH_2CH_2$)

[a]Shifts in ppm relative to TMS. In C_6D_6 *in vacuo* at room temperature, unless stated otherwise; s = singlet, d = doublet, t = triplet, m = multiplet, br = broad. The integrations in each case are consistent with the proposed formulations. *Ru* = Ru(TMP).

[b]All porphyrin ligand resonances are singlets.

[c]Resonance hidden under residual solvent peak.

[d]In toluene-d_8

[e]The resonances listed for the axial PrOH are averaged signals because of exchange with free PrOH present; for free PrOH, δ = 4.0 m (CH), 1.6 br (OH), 1.2 d (CH_3).

[f]Single resonances observed for *m*-H and *o*-Me instead of expected two, because of cyclohexene ligand exchange (see text); the cyclohexene signals are also averaged between those of the coordinated and free alkene, the latter appearing at δ 5.70 m (*CH*=*CH*), 1.95 m (CH_2CH=CHCH_2), and 1.52 m ($CH_2CH_2CH_2CH_2$). Resonances for the coordinated cyclohexene were obtained by measuring (in the absence of excess alkene) the spectrum of a solution of an isolated, impure, solid product containing some Ru(TMP)(C_6H_{10}): −1.08 m ($CH_2CH_2CH_2CH_2$), −1.75 m (CH_2CH=CHCH_2), −3.15 m (*CH*=*CH*).

Cyclohexene(tetramesitylporphyrinato)ruthenium(II)

The species was prepared *in situ* by vacuum transferring excess cyclohexene (1 μL, ~10^{-2} mmol) into a solution of Ru(TMP) prepared by degassing a benzene solution (1 mL) of Ru(TMP)(N_2)$_2$ (3 mg, 3.3 × 10^{-3} mmol).

Results and discussions

The greenish-black complex isolated from the reaction of Ru(TMP) with acetylene is formulated as [Ru(TMP)]$_2$(μ-C_2H_2), **1**. The low-field ^{1}H NMR signal at δ 10.44, which integrates for one proton per Ru(TMP) moiety, is typical of a (porp)Ru=C—H proton (5). Based on data for the phenylacetylene complex (see below), a π-bonded acetylene complex is expected to be reddish-brown and give an acetylene proton signal at about −7 ppm. Further, the ^{13}C[^{1}H] signal (Fig. 1*A*) at 263.8 ppm is characteristic of a metal carbene complex (17). The results of an NMR attached-proton-test (APT) experiment (Fig. 1*B*) show that the carbene-type carbon atom contains either one or three protons, while in a ^{13}C NMR gated-proton-decoupled spectrum the singlet at 263.8 ppm splits to a doublet, confirming that only one proton is attached. The molecular weight calculated from data obtained by the Signer method (16) is consistent with the dinuclear formulation. Another possible structure, **2**, is considered much less likely because of steric problems created by the *ortho*-methyl groups of the TMP ligand: models suggest this, and the situation is analogous to the TMP ligand preventing the unwanted formation of the μ-oxo dinuclear species in the catalytic O_2-oxygenation work (7–10). In the related rhodium complex [Rh(OEP)]$_2$ (μ-C_2H_2), the acetylene proton resonance is observed at δ −9.92, very different to the data for **1**; the species was formulated as a Rh—CH=CH—Rh unit (13).

It is worth noting that formation of **1** appears to require at least laboratory light to proceed, the C_2H_2 reaction being arrested in the dark (for example, in the NMR probe). Treatment of solutions of **1** with 1 atm CO or phosphites readily liberates the C_2H_2 (seen at δ 1.48 in C_6D_6) and the corresponding Ru(TMP)$(CO)_2$ (14) or Ru(TMP)[$P(OR)_3$]$_2$ (18, 19) species.

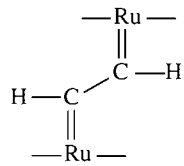

1

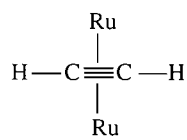

2

In contrast to C_2H_2 itself, PhC≡CPh and PhC≡CH form 1:1 π-complexes with Ru(TMP). The coordinated PhC≡CPh ligand gives rise to three ^{1}H NMR signals (Table 1); the *o*-phenyl protons appear at 5.00 ppm and are shifted upfield by about 1.5 ppm compared to the *m*- and *p*-protons, perhaps because of a bending of the phenyl groups away from the porphyrin plane. Such bending is evident in the Mo(TTP)(PhC≡CPh) structure, where the Ph—C≡C angles are found to be 145° and 136° by X-ray crystallography (12). In the Ru(TMP)(PhC≡CH) species, all the acetylene phenyl protons appear further upfield as a multiplet at 4.00 ppm, implying less bending and "more equivalence" among the phenyl protons that are now closer to the porphyrin ring-current; the ≡C—H proton is seen at −7.40 ppm, an upfield shift of 8.55 ppm from the corresponding peak of the free ligand.

In the two isolated ethylene complexes, the upfield shift of the single C_2H_4 resonance due to the porphyrin ring-current is ~8.4 ppm, which compares well with the values reported for Ru(porp)(C_2H_4)(THF) complexes (porp = OEP, TPP) (5). The C-analyses for the ethylene complexes are somewhat unsatisfactory, but problems with elemental analyses of metallopor-

Can. J. Chem. Downloaded from www.nrcresearchpress.com by 195.138.81.100 on 09/07/12
For personal use only.

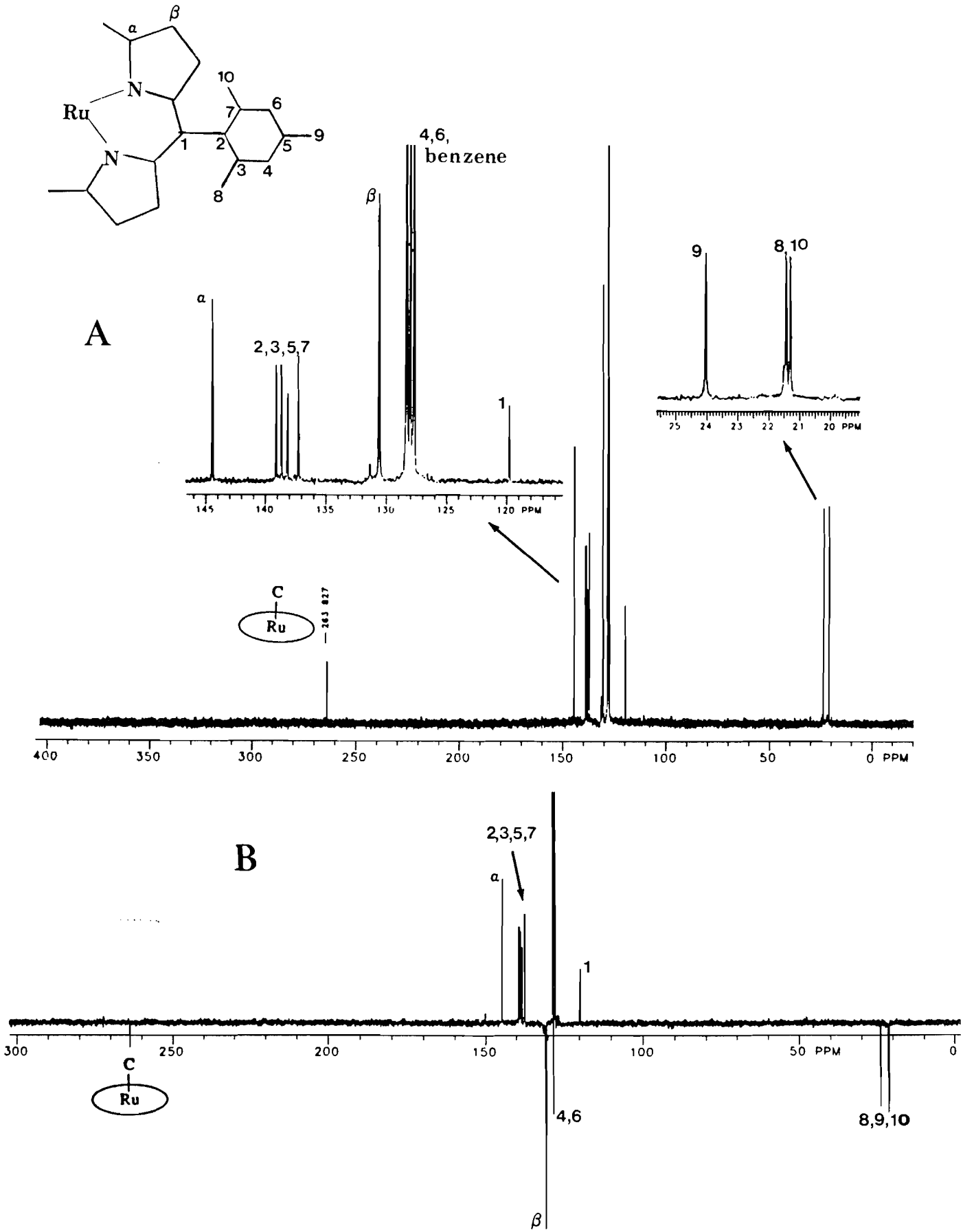

FIG. 1. (*A*) The $^{13}C\{^1H\}$ (75 M Hz), and (*B*) the APT spectra, of $[Ru(TMP)]_2(\mu\text{-}C_2H_2)$ in C_6D_6 solution; the C atoms are labelled according to the diagram.

Can. J. Chem. Downloaded from www.nrcresearchpress.com by 195.138.81.100 on 09/07/12
For personal use only.

Can. J. Chem. Downloaded from www.nrcresearchpress.com by 195.138.81.100 on 09/07/12
For personal use only.

phyrins are not uncommon; the ^{1}H NMR data leave no doubt as to the identity of the complexes. The resonances listed for the axial 2-propanol ligand (Table 1) are averaged signals resulting from exchange with the solvate alcohol.

The Ru(TMP)(cyclohexene) species is observed *in situ* but attempts to isolate this complex resulted in partial loss of the alkene ligand during the work-up procedures. The ^{1}H NMR data for the porphyrin ligand are essentially the same for all the alkene systems; however, only one peak each for the *m*-H and the *o*-Me protons is observed for the cyclohexene species and, coupled with the observation of only one set of broad ^{1}H NMR signals for the alkene ligand in the *in situ* system, there is clearly rapid exchange between free and coordinated cyclohexene. Also, the ^{1}H NMR data for solutions of the C_2H_4 complexes under an atmosphere of C_2H_4 now show a single, averaged, broad resonance at 5.3 ppm, close to that of free C_2H_4; with decreasing concentration of C_2H_4 in the solution, the signal gradually moves upfield towards that of the coordinated C_2H_4 at δ −3.27. Some NMR data for the coordinated cyclohexene were obtained from an impure sample of Ru(TMP)(C_6H_{10}) (Table 1), and the olefinic resonance is seen at δ −3.15, close to that of the coordinated ethylene signal.

The Ru(TMP)(C_2H_4) complex was stable to loss of C_2H_4 on subjection to a 10^{-3} mm Hg vacuum at 20°C for several hours; in solution, the complex on exposure to air or air/C_2H_4 mixtures led to rapid formation of *trans*-Ru(TMP)$(O)_2$ (7, 9, 14), which is thus clearly more stable thermodynamically than the C_2H_4 complex or the Ru(TMP)$(N_2)_n$ complexes (n = 1, 2), the latter readily being formed under N_2 atmospheres (14, 15). Under the conditions of catalytic O_2- or aerobic-epoxidation of alkenes using Ru(TMP)L_2 precursors (L = MeCN, THF), the catalysis operating via the Ru(TMP)$(O)_2$ species (7–10), there will be a competition between O_2 and alkene for the metal site. The situation is somewhat akin to that in catalytic homogeneous hydrogenation of alkenes, which can occur via so-called "hydride" or "unsaturate" routes depending on whether the H_2 or alkene interacts initially with the metal (20); in most cases, however, hydridoalkene intermediates are eventually formed, although steps involving H-atom transfer from a metal to non-coordinated alkene (as in the net alkene epoxidation) have been established in a few systems (20).

Acknowledgements

We thank the Natural Sciences and Engineering Research Council of Canada for financial support, and Johnson Matthey Ltd. for their generous loan of Ru.

1. M. KE, S. J. RETTIG, B. R. JAMES, and D. DOLPHIN. J. Chem. Soc. Chem. Commun. 1110 (1987).
2. C. SISHTA, M. KE, B. R. JAMES, and D. DOLPHIN. J. Chem. Soc. Chem. Commun. 787 (1986).
3. J. P. COLLMAN, L. MCELWEE-WHITE, P. J. BROTHERS, and E. ROSE. J. Am. Chem. Soc. **108**, 1332 (1986).
4. J. P. COLLMAN, P. J. BROTHERS, L. MCELWEE-WHITE, and E. ROSE. J. Am. Chem. Soc. **107**, 6110 (1985).
5. J. P. COLLMAN, P. J. BROTHERS, L. MCELWEE-WHITE, R. ROSE, and L. J. WRIGHT. J. Am. Chem. Soc. **107**, 4570 (1985).
6. J. W. SEYLER and C.R. LEIDNER. J. Chem. Soc. Chem. Commun. 1794 (1989).
7. J. T. GROVES, Y. HAN, and D. V. ENGEN. J. Chem. Soc. Chem. Commun. 436 (1990) and references therein.
8. J. T. GROVES. 199th Am. Chem. Soc. National Meeting. Boston, MA. 1990. Abstract PETR 60.
9. N. RAJAPAKSE, B. R. JAMES, and D. DOLPHIN. *In* New developments in selective oxidation. *Edited by* G. Centi and F. Trifiro. Elsevier, Amsterdam. 1990.
10. M. TAVARES, R. RAMASSEUL, and J.-C. MARCHON. Catal. Lett. **4**, 163 (1990).
11. B. R. JAMES, A. ADDISON, M. CAIRNS, D. DOLPHIN, N. P. FARRELL, D. R. PAULSON, and S. WALKER. *In* Fundamental research in homogeneous catalysis. Vol. 3. *Edited by* M. Tsutsui. Plenum Press, New York. 1979. p. 751.
12. A. DE CIAN, J. COLLIN, M. SCHAPPACHER, L. RICHARD, and R. WEISS. J. Am. Chem. Soc. **103**, 1850 (1981).
13. J. I. SETSUNE, Z-I. YOSHIDA, and H. OGOSHI. J. Chem. Soc. Perkin Trans. I, 983 (1982).
14. M. J. CAMENZIND, B. R. JAMES, and D. DOLPHIN. J. Chem. Soc. Chem. Commun. 1137 (1986).
15. M. J. CAMENZIND, B. R. JAMES, D. DOLPHIN, J. W. SPARAPANY, and J. A. IBERS.. Inorg. Chem. **27**, 3054 (1988).
16. (*a*) R. SIGNER. Ann. **478**, 246 (1930); (*b*) E. P. CLARK.. Ind. Eng. Chem. Anal. Ed. **13**, 820 (1941).
17. M. A. GALLOP and W. R. ROPER. Adv. Organomet. Chem. **25**, 121 (1986).
18. J. T. GROVES and K-H. AHN. Inorg. Chem. **26**, 3831 (1987).
19. C. SISHTA, M. J. CAMENZIND, B. R. JAMES, and D. DOLPHIN. Inorg. Chem. **26**, 1181 (1987).
20. B. R. JAMES. *In* Comprehensive organometallic chemistry. Vol. 8. *Edited by* G. Wilkinson, F. G. A. Stone, and E. W. Abel. Pergamon, Oxford. 1982. Chap. 51.

Charge transfer emissive singlet excited states and photoinduced electron transfer properties in the diarylideneacetone compounds $(RCHCH)_2CO$; R = phenyl, 1- and 2-naphthyl, 3-(*N*-ethylcarbazoyl), and $4\text{-}(C_5H_5)Fe(C_5H_4C_6H_4CHCH(CO)CHCHC_6H_5)$

PIERRE D. HARVEY,[1] LIANGBING GAN, AND CHRISTIANE AUBRY
Département de chimie, Université de Sherbrooke, Sherbrooke (Québec), Canada J1K 2R1

Received May 2, 1990

Can. J. Chem. Downloaded from www.nrcresearchpress.com by 195.138.81.100 on 09/07/12
For personal use only.

PIERRE D. HARVEY, LIANGBING GAN, and CHRISTIANE AUBRY. Can. J. Chem. **68**, 2278 (1990).

Four diarylideneacetone compounds ($(RCHCH)_2CO$, where the aryl groups are phenyl (dba), 1-naphthyl (1-dNapha), 2-naphthyl (2-dNapha), and 3-(*N*-ethylcarbazoyl) (dNECa)), and $4\text{-}(C_5H_5)Fe(C_5H_4C_6H_4CHCH(CO)CHCH(C_6H_5)$ (dba-Fc) have been prepared and characterized. The compounds are found to be fluorescent and photochemically and reversibly electrochemically active. The lowest-energy absorption bands for the diarylideneacetones are assigned to a charge transfer (CT) electronic transition, except for dba-Fc, in which a ferrocenyl ligand field transition assignment is made. The 77 K CT absorption and fluorescence bands are vibrationally structured (vibrational spacings = 1260–1360 cm^{-1}). While the fluorescence decay at 293 K is monoexponential, the excited state fluorescence lifetimes (τ_F) for the 77 K samples exhibit double exponential decays, the short component being 0.38–0.64 ns and the long one 3.5–10.9 ns. The photophysical results are interpreted in terms of excited state deactivation processes dominated by radiationless pathways that are associated with the presence of fluorescent species with different geometries. Only the dNECa compound is found to be fluorescent in solution at 298 K (τ_F = 1.65 ns; ϕ_F = 0.39 ± 0.02). Cyclic voltammetry and coulometry measurements suggest that a reversible one-electron reduction process and an irreversible higher potential one-electron reduction process take place in the −1 to −2 V vs. SSCE range. In addition, dba-Fc also exhibits an electrochemically reversible one-electron oxidation wave at 0.52 V vs. SSCE centered at the ferrocenyl group. These results together with the spectroscopic electronic data have permitted evaluation of the reduction potentials of the lowest singlet (CT excited states ($E^{1-/*}$); they range from 1.4 to 2.2 V vs. SSCE, with dba being the strongest photooxidizing agent and dNECa the weakest. Photoinduced intermolecular electron transfer reactions have been investigated by steady state fluorescence techniques and picosecond flash photolysis spectroscopy for dNECa and dba, respectively. The bimolecular deactivation rate constants, k_q, for the reductive photoinduced electron transfer reactions of dNECa with diphenylamine (DPA) (k_q = (2.65 ± 0.25) × 10^7 M^{-1} s^{-1}) and *N,N,N',N'*-tetramethylphenylenediamine (TMPM) (k_q = (1.38 ± 0.03) × 10^8 M^{-1} s^{-1}) have been obtained in THF solutions at 293 K. No fluorescence quenching is observed when oxidative and energy transfer quenchers are used with dNECa. For the non-emissive dba compound at room temperature, picosecond flash photolysis experiments show that quenching of the broad dba transient band (~500 nm) does indeed occur between 5 and 10 ns.

Key words: dibenzylideneacetone, charge transfer, photoelectron transfer.

PIERRE D. HARVEY, LIANGBING GAN et CHRISTIANE AUBRY. Can. J. Chem. **68**, 2278 (1990).

Quatre ligands diarylidineacétones ($(RCHCH)_2CO$ où les groupes aryles sont phényl- (dba), 1-naphtyl- (1-dNapha), 2-naphtyl- (2-dNapha) et 3-(*N*-éthylcarbazoyl)- (dNECa)), et $4\text{-}(C_5H_5)Fe(C_5H_4C_6H_4CHCH(CO)CHCH(C_6H_5)$ (dba-Fc) ont été préparés et caractérisés. Les composés sont fluorescents, photo- et réversiblement électrochimiquement actifs. Les bandes d'absorption de plus basse énergie pour les composés diarylidèneacétones sont attribuées à un transfert de charge (CT), excepté pour dba-Fc pour lequel une attribution de champ de ligand localisé au groupe ferrocényle a été faite. Les bandes d'absorption et de fluorescence CT sont vibrationnellement structurées (espacements vibrationnels = 1260–1360 cm^{-1}). Contrairement aux données obtenues à 293 K, les durées de vie de fluorescence (τ_F) pour tous les échantillons à 77 K montrent une double décroissance exponentielle; la composante de courte durée est 0.38–0.64 ns et la composante de plus longue durée est 3.5–10.9 ns. Les résultats photophysiques sont interprétés par des processus de désactivation des états excités qui sont dominés par des chemins non-radiatifs associés à la présence d'espèces fluorescentes de géométries différentes. Seul le dNECa est fluorescent en solution à 298 K (τ_F = 1.65 ns; ϕ_F = 0.39 ± 0.02). Les mesures de voltamétrie cyclique et de coulométrie suggèrent qu'un processus réversible de réduction d'un électron survient à bas potentiel et qu'un processus irréversible (1 électron) survient à plus haut potentiel négatif dans la région de −1 à −2 V vs. SSCE. De plus, le dba-Fc montre une vague d'oxydation de 1 électron à 0.52 V vs. SSCE électrochimiquement réversible et centrée au groupe ferrocényle. Ces résultats et les données spectroscopiques ont permis l'évaluation des potentiels redox ($E^{1-/*}$) des états singulets CT de plus basse énergie; ils se situent dans la région de 1.4 à 2.2 V vs. SSCE, le dba étant le plus puissant photooxydant et dNECa le plus faible. Les réactions de photo-transfert d'électron intermoléculaires ont été étudiées par les techniques d'état stationnaire de fluorescence et par spectroscopie photolyse éclair picoseconde pour le dNECA et le dba respectivement. Les constantes de désactivation bimoléculaire, k_q, pour les photo-transferts d'électron du dNECa avec la diphénylamine (DPA) (k_q = (2.65 ± 0.25) × 10^7 M^{-1} s^{-1}) et *N,N,N',N'*-tétraméthylphénylenediamine (TMPM) (k_q = (1.38 ± 0.03) × 10^8 M^{-1} s^{-1}) sont obtenues dans les solutions de TMF à 293 K. Aucune désactivation de la fluorescence du dNECa n'est observée lorsque des désactivateurs de type oxydant et de transfert d'énergie sont employés. Aucun quenching de la fluorescence n'est observé pour le dNECa lorsque les désactivateurs sont du type de transfert d'énergie ou oxydant. Pour le composé non-luminescent dba à la température ambiante, les expériences de photolyse éclair picoseconde montrent un effet quenching de la bande large transitoire du dba (~500 nm) par le désactivateur réducteur DPA dans la région entre 5 et 10 ns.

Mots clés : dibenzylidèneacétone, transfert de charge, photo-transfert d'électron.

---

[1]Author to whom correspondence may be addressed.

Can. J. Chem. Downloaded from www.nrcresearchpress.com by 195.138.81.100 on 09/07/12
For personal use only.

Introduction

The cross-conjugated dibenzylideneacetone (dba; see structure in Scheme 1) is a commonly used ligand capable of stablizing various organometallic compounds (1). More particularly, binuclear complexes of Pd(0) and Pt(0) of the type $M_2(dba)_3$ have been prepared in which weak metal–metal interactions are present in the ground state (2). Recently, electronic absorption, emission, and excitation spectra and excited state lifetimes (τ_e) of the $M_2(dba)_3$ complexes have been reported (3, 4). These complexes appear to be photochemically inert toward oxidative addition reactions in the presence of chlorinated hydrocarbons (CH_2Cl_2, $CHCl_3$, and $ClCH_2CH_2Cl$) and oxygen.[2] These results suggest that the lowest triplet excited state (^{3}MLCT*) is a relatively poor reducing agent. The redox properties of this excited state are consistent with these findings; $E^{0+/*}(^3\text{MLCT}^*) = -0.33$ V vs. SSCE.[2] In an attempt to tune photoreactivity in these organotransition binuclear complexes, electroactive (5) and chromophoric groups have been attached to the organic bridging moiety (CH=CH (CO) CH=CH). There are many examples of changes in spectroscopic properties and reactivity changes induced in a metal center by reduction of a redox-active substituent (6). Hypothetically, appropriate chromophoric pendent groups should also be capable of mediating either electron or energy transfer reactions with the bimetallic centers.

In the first part of this paper, we wish to report a detailed characterization of the electronic excited state properties of some diarylideneacetone compounds (see structures in Scheme 1) in which the chromophoric aryl groups possess various known ground and excited state redox and photophysical behaviors. The selected substituents are the phenyl (dba), 1-naphthyl (1-dNapha), 2-naphthyl (2-dNapha), and 3-(*N*-ethylcarbazoyl) (dNECa) groups. In these cases, the aryl-localized excited states are expected to be $\pi\pi^*$ in nature (7–11) but, in the dba case, the CO between the styrenyl groups gives rise to the possibility of a relatively low-energy $n\pi^*$ state (7). However, it will be shown unambiguously that the lowest singlet excited states are CT states in which the aryl groups are the donors and the $(CH{=}CH)_2CO$ group is the acceptor.

In the second part of this paper, it will be shown from electrochemistry, coulometry, and spectroscopic data that the CT states should be efficient *photooxidizing agents*. Indeed, steady state fluorescence techniques (for dNECa) and picosecond flash photolysis spectroscopy (for dba) are used to show that fluorescence quenching occurs *only* when reductive quenchers are used with dNECa and that transient absorptions for dba vanish with the same quenchers.

To our knowledge, there are no spectroscopic, electrochemical, or photophysical data on the compounds, except for the model molecule, dba, for which only a few superficial investigations have been reported (3, 12). To pursue research on the photochemistry of triply bridged binuclear compounds with dba type ligands, a better understanding of the excited state properties of the ligands themselves is necessary.

Experimental

Chemicals

Benzaldehyde, 1- and 2-naphthaldehyde, 3-(*N*-ethylcarbazyl)aldehyde (NEC-3-CHO), and polymethyl methacrylate (PMMA; Aldrich Chemical Co.) were used as received. 9,10-Diphenylanthracene was used as a standard for emission quantum yield measurements (ϕ_F = 1.0) (13); it was purified by repeated sublimation. Acetone, ethanol, methylene chloride, carbon tetrachloride, methylene iodide, iodoform (Anachemia), tetrahydrofuran (THF), and 2-methyltetrahydrofuran (2MeTHF; Aldrich Chemical Co.) were purified according to standard procedures (14). The spectrograde solvents benzene, ethyl acetate, acetone, ethyl ether, and chloroform (Fisher) were used as received; purity was checked by UV–VIS spectroscopy. Chloroform-*d* and benzene-d_6 (Aldrich Chemical Co.) were used as received. The solid quenchers (Aldrich Chemical Co.) anthracene, naphthalene, biphenyl, *N,N,N',N'*-tetramethylphenylenediamine (TMPM), and diphenylamine (DPA) were purified by repeated fractional sublimation and were kept in the dark when not in use. Methyl viologen dichloride (Aldrich Chemical Co.) was purified by recrystallization from ethanol, and $S_2O_8Na_2$ (Anachemia) was used as received. Tetra-*n*-butylammonium hexafluorophosphate ($TBAPF_6$; Aldrich Chemical Co.) was recrystallized three times from ethanol. All samples were degassed either by bubbling Ar(g) through the solution or by freeze–pump–thaw methods.

Instrumentation

The ^{1}H and ^{13}C NMR spectra were obtained on a Bruker WM 250-MHz spectrometer at 293 K. The mass spectra were collected on a VGZAB-1F spectrometer in EI mode at 70 eV. The FT-IR spectra were measured on a BOMEM DA 3.002 spectrometer. The UV–VIS spectra at 298 K were acquired on a Perkin–Elmer Lambda or a Cary model 14 (Varian) spectrometer using standard 1 cm^2 quartz cuvettes. The 77 K UV–VIS spectra were obtained using a low-temperature cell (pathlength = 1.0 cm) and a Cary model 14 (Varian) spectrophotometer. The spectra were all corrected for baseline deviation and glass contraction. The emission spectra measurements were made on a Spex double monochromator Fluorolog model 1902 instrument; the source was a 500-W HgXe high-pressure lamp. The 298 K measurements were made using air-tight 1 cm^2 quartz cells, while the 77 K experiments were performed using a low-temperature EPR quartz Dewar (Wilmad Glass Co.) and cylindrical quartz tubes. The excitation spectra were automatically corrected by the instrument while emission spectra were manually corrected at every 1 nm for the spectrophotomer response using standard lamp corrections. In all 77 K experiments, the bandpasses were 2 nm for both excitation and emission slits. Fluorescence lifetime measurements were performed on a homemade photon counting system; a complete description of the instrument and testing for multiple exponential deconvolution fits and procedures is given elsewhere (15). The 298 and 77 K measurements were performed with the same spectrofluorimetric cell setups as used for the measurements of fluorescence spectra mentioned above.

The Raman spectra were measured on an Instruments S.A. Raman spectrometer equipped with a U-1000 Jobin–Yvon 1.0 double monochromator using the 647.1 nm red line and the 514.5 nm green line of Spectra-Physics krypton and argon ion lasers, respectively, for excitation. All electrochemical measurements were performed with a PAR 173 potentiostat and a PAR 175 universal programmer. Pt disk electrodes (0.5 mm diameter) were polished with alumina (5 μm size) for 5 min in 1:1 CH_3OH/H_2O before use. Different electrochemical cells were used for the cyclic voltammetric and coulometric measurements. The cyclic voltammetric cell was a one-compartment cell (2 cm diameter) in which the working, the Pt (1 cm × 1 cm) gauze auxiliary, and the SSCE reference electrodes were inserted. Coulometry measurements were performed in a H-cell with Pt (1 cm × 1 cm) gauze working and auxiliary electrodes. The SSCE reference electrode in the bulk electrolysis experiments was connected to the working compartment by a fritted disk and separated by a 3% agar-agar solution. The coulometry measurement setup was checked using ferrocene as a standard. The flash photolysis experiments were performed at the Picosecond Flash Photolysis Center at Concordia University. The difference absorption spectra were obtained using a pulsed Nd:YAG laser made by Quantel (fwhm ~ 30 ps). The pulsed 1062 nm laser beam was passed through a frequency doubler and tripler. The 355 nm excitation light was selected by dichroic mirrors, passed through a delay line (20–10 ns), and then used to excite the samples. Typically each excitation pulse was ~2–3 mJ. The rest of the light was passed

[2]P. D. Harvey and C. Aubry. Unpublished results.

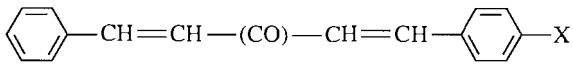

X = H, Dibenzylideneacetone; dba
X = $(C_5H_4)Fe(C_5H_5)$, 4-Ferrocenyl-dibenzylideneacetone; dba-Fc

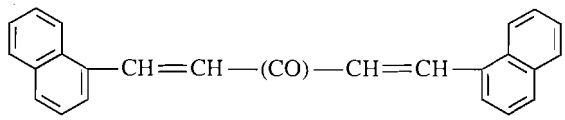

Di(1-naphthylidene)acetone, 1-dNapha

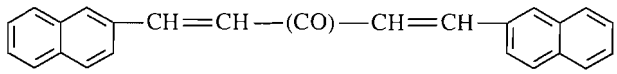

Di(2-naphthylidene)acetone, 2-dNapha

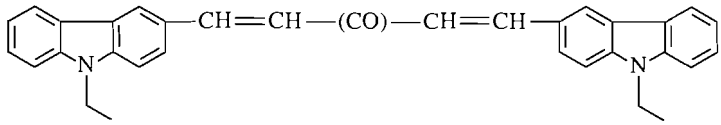

Di(3-(*N*-ethylcarbazoylidene))acetone, dNECa

SCHEME 1. Structures of the five investigated diarylideneacetones.

through dichroic mirrors to select the 1062 nm light, which was then transformed into a continuum (400–700 nm). This continuum was then used to probe the samples.

The detection system and computer hardware were a commercially available EG&G multichannel analyser model OMA 2. The data processing was performed with a Digital RT-11 computer. A more complete description of the apparatus can be found elsewhere (16). Except for the Raman, IR, and UV–VIS spectroscopic and all the 77 K measurements, all the solutions were degassed by freeze–pump–thaw methods or by Ar(g) bubbling the solutions for 30 min. It has been verified that the Ar(g) method has no effect on τ_F compared to the freeze–pump–thaw method.

ϕ_F was measured using 9,10-diphenylanthracene as a standard (ϕ_F = 1.00 ± 0.05). The complete methodology can be found in ref. 13 and references therein. The procedures involved the use of solutions with optical densities identical or nearly identical for both samples and standards in the 0.00–0.05 absorbance range. Three measurements were performed and the experimental error was set as being the difference between the average and the largest and smallest measured values.

Synthesis

Dibenzylideneacetone (dba) and di(1-naphthylidene)acetone (1-dNapha) were synthesized in quantitative yields and purified according to standard procedures outlined for dba (17*a*). Both compounds have been characterized by standard spectroscopic techniques, elemental analysis, and melting points. The data are consistent with the *trans* geometry of the α and β olefinic hydrogens (see details below). 4-Ferrocenylbenzaldehyde was prepared according to published procedures (17*b*).

Dibenzylideneacetone (dba)

Melting point 106°C (uncorrected) (lit. (17) mp 106–107°C); IR (solid state) ν_{max}: 3136 (w), 3086 (w), 3055 (m), 3030 (m), 3005 (w), 1673 (m; ν(C=O)), 1652 (s), 1625 (m), 1600 (s), 1575 (s), 1493 (m), 1450 (m), 1343 (m), 1309 (m), 1284 (w), 1259 (w), 1200 (s), 1159 (w), 1105 (m), 1083 (m), 1027 (w), 980 (s), 923 (m), 884 (m), 852 (m) cm^{-1}; ^1H NMR ($CDCl_3$) δ: 7.09 (d, 1H, $^3J_{HH}$ = 16.0 Hz, CH_α), 7.43 (m, 3H), 7.64 (m, 2H), 7.75 (d, 2H, $^3J_{HH}$ = 16.0 Hz, CH_β); ^{13}C NMR ($CDCl_3$) δ: 125.3 ($^{13}C_\alpha H$), 128.2, 128.8, 130.3, 134.7, 143.1 ($^{13}C_\beta H$), 188.7 (^{13}CO); MS $m/e^{+\cdot}$: 234 (100), 205 (18), 131 (48), 103 (59). Anal. calcd. for $C_{17}H_{14}O$: C 87.15, H 6.02; found: C 86.79, H 6.25%.

Di(1-naphthylidene)acetone (1-dNapha)

Melting point 242°C (uncorrected); IR (solid state) ν_{max}: 3042 (vw), 1667 (s; ν(C=O)), 1617 (s), 1590 (s), 1570 (m), 1510 (w), 1403 (w), 1353 (m), 1320 (w), 1240 (w), 1117 (m), 1073 (w), 1033 (w), 980 (s), 890 (w), 800 (s), 777 (vs), 700 (w), 590 (w), 537 (w), 500 (w) cm^{-1}; ^1H NMR ($CDCl_3$) δ: 7.25 (d, 1H, $^3J_{HH}$ = 15.7 Hz, CH_α), 7.58 (m, 3H), 7.93 (m, 3H), 8.29 (d, 1H), 8.66 (d, 1H, $^3J_{HH}$ = 15.7 Hz, CH_β); ^{13}C NMR ($CDCl_3$) δ: 123.3 ($^{13}C_\alpha H$), 125.0, 125.3, 126.1, 126.8, 128.0, 130.6, 131.5, 132.0, 133.6, 140.2 ($^{13}C_\beta H$), 188.5 (^{13}CO); MS $m/e^{+\cdot}$: 334 (51), 214 (35), 196 (80), 181 (71), 155 (100), 128 (82). Anal. calcd. for $C_{25}H_{18}O$: C 89.79, H 5.43%; found: C 88.84, H 5.60%.

Di(2-naphthylidene)acetone (2-dNapha) and di[3-(*N*-ethylcarbazoylidene)] acetone (dNECa) were synthesized according to a procedure modified from that outlined for dba (17*a*); to a cooled solution of 50 mL 1:1 ethanol/10% NaOH aqueous solution was added dropwise an ethanol-saturated solution containing 23.4 mmol of the corresponding aldehyde and 0.87 mL of acetone (11.7 mmol). The solution was stirred for 16 h. The yellow oil that formed was then separated by decantation. To the oily residue, a minimal amount of acetone (~10 mL) was added; then water was added dropwise until precipitation occurred (at a 1:1 V/V ratio of acetone and water). The yellow solid was filtered and dried *in vacuo* (10^{-6} Torr at 293 K; 1 Torr = 133.3 Pa) for 48 h. Purity was checked by TLC and no trace of the starting materials and monocondensed product (aryl-CH=CH—(CO)—CH_3) was observed. Repetitive preparation of the materials provided 3–4 g each time (60–80% yield). The spectroscopic data are consistent with the *trans* geometry of the α and β olefinic hydrogens (see details below).

Di(2-naphthylidene) acetone (2-dNapha)

Melting point 114°C (uncorrected); IR (solid state) ν_{max}: 3050 (w), 3020 (vw), 1671 (m; ν(C=O)), 1651 (s), 1627 (s), 1586 (vs), 1507 (w), 1440 (w), 1395 (w), 1370 (m), 1317 (w), 1273 (w), 1203 (w), 1192 (w), 1177 (w), 1133 (w), 1107 (m), 987 (vs), 980 (m), 915 (w), 905 (w), 890 (w), 867 (s), 827 (vs) cm^{-1}; ^1H NMR ($CDCl_3$) δ: 7.25 (d, 1H, $^3J_{HH}$ = 15.9 Hz, CH_α), 7.54 (m, 2H), 7.84 (m, 4H), 7.95 (d, 1H, $^3J_{HH}$ = 15.9 Hz, CH_β), 8.05 (s, 1H); ^{13}C NMR δ: 123.7 ($^{13}C_\alpha H$),

Can. J. Chem. Downloaded from www.nrcresearchpress.com by 195.138.81.100 on 09/07/12
For personal use only.

TABLE 1. Electronic spectroscopic data[a]

	Band no.	λ_{max} (±1 nm)	ν_{max}	ϵ (±200 M^{-1} cm^{-1})	Assignments
dba	I + II	322	31 100 ± 100	30 200	CT
	III	232	43 100 ± 200	15 100	Localized $\pi \rightarrow \pi^*$
2-dNapha	I	366	27 320 ± 75	25 900	CT
	II	338	29 590 ± 90	32 500	CT
	III	277	36 100 ± 130	22 500	Localized $\pi \rightarrow \pi^*$
	IV	240	41 700 ± 180	44 300	Localized $\pi \rightarrow \pi^*$
1-dNapha	I + II	364	27 475 ± 75	25 700	CT
	III	256	39 000 ± 150	22 500	Localized $\pi \rightarrow \pi^*$
	IV	232	43 100 ± 200	39 100	Localized $\pi \rightarrow \pi^*$
dNECa	I	400	25 000 ± 65	32 600	CT
	II	362	27 620 ± 80	22 900	
	III	319	31 300 ± 100	21 100	Localized $\pi \rightarrow \pi^*$
	IV	289	34 600 ± 120	34 400	Localized $\pi \rightarrow \pi^*$
	V	258	38 800 ± 150	57 000	Localized $\pi \rightarrow \pi^*$
dba-Fc	I	480	20 830 ± 45	4330	LF-CT
	II	346	28 900 ± 85	33 000	CT

[a]THF solutions at 293 K; LF = ligand field (see ref. 5 for further details).

125.7, 126.8, 127.3, 127.8, 128.6, 128.8, 130.5, 132.3, 133.5, 133.3, 143.3 ($^{13}C_\beta H$), 189.0 (^{13}CO); MS $m/e^{+\cdot}$: 334 (100), 233 (11), 206 (11), 181 (27), 178 (20), 153 (29), 141 (54). Anal. calcd. for $C_{25}H_{18}O$: C 89.79, H 5.43%; found: C 89.37, H. 5.70%.

Di[3-(N-ethylcarbazoylidene)]acetone (dNECa)

Melting point >200°C (dec.); IR solid ν_{max}: 3058 (w), 2978 (w), 1694 (vs, ν(CO), 1669 (m), and 1627 (m, ν(C=C) olefins), 1596 (s), 1571 (w), 1494 (m), 1472 (m), 1463 (w), 1450 (w), 1483 (w), 1383 (m), 1348 (m), 1336 (m), 1327 (m), 1232 (vs), 1175 (m), 1154 (w), 1132 (m), 1124 (m) cm^{-1}; ^1H NMR ($CDCl_3$) δ: 1.51 (t, 3H, CH_3), 4.42 (q, 2H, CH_2), 7.21 (d, 1H, $^3J_{HH}$ = 15.9 Hz, CH_α), 7.30 (t, 1H, 7.48 (m, 3H), 7.80 (dd, 1H), 7.95 (d, 1H, $^3J_{HH}$ = 15.8 Hz, CH_β), 8.17 (d, 1H), 8.39 (s, 1H); ^{13}C NMR δ: 13.8 ($^{13}CH_3$), 37.8 ($^{13}CH_2$), 108.9, 108.9, 119.7, 120.6, 121.4, 122.9, 123.1, 125.9, 126.2, 140.5, 141.3, 144.1, 188.1 (^{13}CO); MS $m/e^{+\cdot}$: 263 (50), 248 (58), 223 (80), 208 (100). Anal. calcd. for $C_{33}H_{28}N_2O$: C 84.56, H 6.02, N 5.99%; found: C 83.88, H 6.28, N 5.87%.

For the 4-ferrocenyldibenzyldeneacetone (dba-Fc) compound, the procedure was as follows: to a solution of 20 mL 1:1 ethanol/10% NaOH aqueous solution, an ethanol-saturated solution containing 1.07 g (3.69 mmol) 4-ferrocenylbenzaldehyde and 0.54 g (3.86 mmol) $CH_3(CO)CHCHC_6H_5$ was added dropwise. After stirring for 1 h, the solution was filtered to give a red solid as crude product. The product was purified by column chromatography on Al_2O_3, eluting with hexane and CH_2Cl_2, and recrystallized from benzene/hexane (1.0 g, mmol, 65%).

4-Ferrocenyldibenzylideneacetone (dba-Fc)

Melting point >165°C (dec.); IR (CsI) ν: 1694 (w), 1672, (m; ν(C=O)) 1651 (m), 1620 (s), 1603 (s), 1584 (s), 1559 (m), 1526 (m), 1497 (w), 1451 (w), 1422 (w), 1343 (s), 1285 (w), 1182 (s), 1105 (s), 1082 (m), 1030 (w), 993 (m), 980 (m), 887 (w), 820 (s), 764 (m), 733 (w), 694 (m), 563 (m), 525 (m), 511 (m), 500 (m), 486 (m); ^1H NMR ($CDCl_3$) δ: 4.06 (s, 5H), 4.40 (5, 2H, J = 2 Hz), 4.70 (t, 2H, J = 2 Hz), 7.07 (d, 1H, J = 16 Hz), 7.11 (d, 1H, J = 16 Hz), 7.52 (m, 9H), 7.73 (d, 1H, J = 16 Hz), 7.75 (d, 1H, J = 16 Hz); MS $m/e^{+\cdot}$: 418 (M^+). Anal. calcd. for $C_{27}H_{23}OFeC_6H_6$: C 79.84, H 5.65%; found: C 80.66, H 6.04%.

Results and discussion

Part I: CT states

1. Nature of the excited states

The lowest singlet–singlet absorption band for dba has been tentatively assigned by several research groups (2*e*, 12*a*, *b*). The proposed assignments were $n-\pi^*$ (2*e*), $\pi-\pi^*$ (12*a*), and charge transfer (CT) (12*b*). Since the absorptivity is 30 000 M^{-1} cm^{-1}, the $n-\pi^*$ assignment is ruled out. Moreover, the vibrational progression in the 77 K fluorescence spectra (1260 cm^{-1}; see text below) does not support this assignment. The $\pi-\pi^*$ assignment was based upon the observation of a linear relationship between λ_{max} and the nature of substituents attached to the cross-conjugated moiety (CH=CH=(CO)—CH=CH) (12*a*). However, such agreement between an empirical equation and experimental data may be fortuitous. Moreover, the vibrational spacings observed in the lowest energy band ($\pi-\pi^*$) of styrene (1050 ± 50 cm^{-1} (18)), which are attributable to ν(C=C) in this excited state, greatly differ from our results on the diarylideneacetones. Finally, based upon a study of solvent polarity and substituent effects, a CT assignment has been proposed (12*b*). The results of the present work establish the latter proposed assignment.

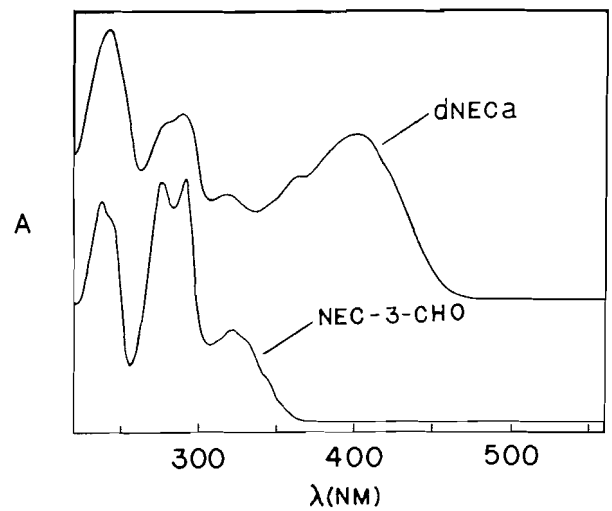

FIG. 1. Comparison between the electronic absorption spectra of dNECa and NEC-3-CHO in THF solution at 293 K.

The 293 K UV data for the five compounds are listed in Table 1. The low-energy bands exhibit no vibrational structure at this temperature. Their absorptivities are fairly large (26 000–

Can. J. Chem. Downloaded from www.nrcresearchpress.com by 195.138.81.100 on 09/07/12
For personal use only.

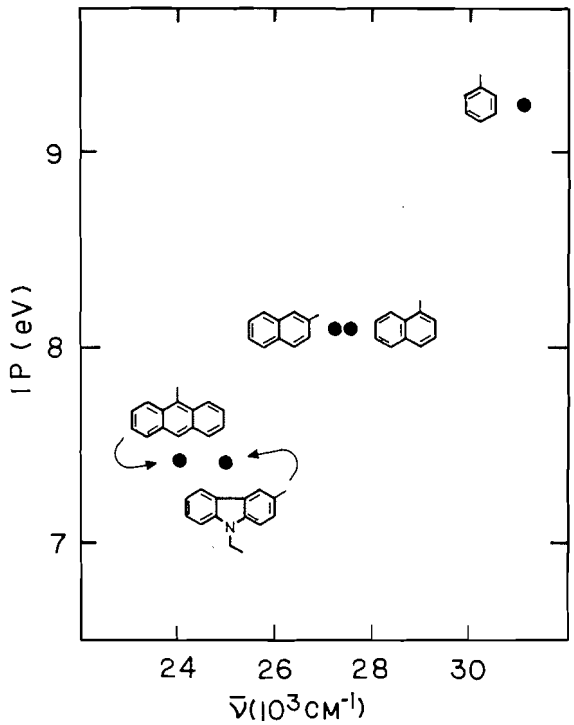

FIG. 2. Graph of the variation of the IP of the unsubstituted aromatic compounds versus $\bar{\nu}_{max}$ (CT) in the diarylideneacetone compounds. The data point associated with anthracene is taken from ref. 21 for IP and 11 for $\bar{\nu}_{max}$ (CT).

33 000 $M^{-1} cm^{-1}$), indicating that the electronic transition(s) is (are) strongly allowed in character. Red shifts of this electronic band are observed with an increase in solvent polarity (319, ether; 325, chloroform; 331 nm, ethanol) for dba, in agreement with the previously reported data (12*b*). Comparison of the absorption spectra of the diarylideneacetones with those of the corresponding aromatic aldehydes is more informative. Figure 1 shows the UV–VIS spectra of dNECa and 3-(*N*-ethylcarbazoyl)aldehyde (NEC-3-CHO) in THF at 293 K. The high energy region for both compounds is practically identical (in terms of the band energies and shapes) and basically represents the "fingerprint" region of the aryl group. These singlet electronic bands have been previously assigned by polarization techniques and are all $\pi-\pi^*$ (19): $^1A_1 \rightarrow {}^1L_b$ (350), $^1A_1 \rightarrow {}^1L_a$ (280), and $^1A_1 \rightarrow {}^1B_a$ (270 nm). On the other hand, the strong 400-nm band that appears only in the dNECa spectrum must then arise from interactions between the aryl groups and the CH=CH—(CO)—CH=CH moiety (CT).

Recent literature data have shown that the CT band energies arising from interactions between different aromatic compounds (donors) and the tropylium cation (acceptor) follow a linear relationship with the IP of the aromatics (20). Figure 2 shows the same dependence of the transition energies of the CT bands in the diarylideneacetones on the IP of the aromatic compounds (21). This experiment indicates that the aryl groups are indeed the donors, and the $(CHCH)_2CO$ group is the acceptor moiety of the CT interactions. Interestingly, recent results (5) for a di(ferrocenylidene)acetone (IP = 6.85 eV (22), ν_{max} (CT) = 19 600 cm^{-1} (THF; 293 K) (5)) follow this linear relationship.

The 77 K absorption and fluorescence spectra for the four diarylideneacetone compounds are shown in Figs. 3–6. The 77 K electronic bands are vibrationally structured in contrast to the 293 K spectra in fluid solutions and rigid PMMA film.

TABLE 2. Vibrational progression analysis for the lowest absorption and emission bands of dba

(a) Absorption

λ(±0.5 nm)	$\bar{\nu}$	Δ	Proposed assignments	
293.8	34 040 ± 60	1300 ± 115	0–4	
305.4	32 740 ± 55	1300 ± 105	0–3	
318.1	31 440 ± 50	1300 ± 95	0–2	
331.8	30 140 ± 45	1300 ± 85	0–1	
346.6	28 850 ± 40	(~1100 ± 80)	0–0	Band II
360.4	27 750 ± 40		0–0	Band I

(b) Fluorescence

λ(±1 nm)	$\bar{\nu}$	Δ	Proposed assignments
397	25 190 ± 65		0–0
418	23 920 ± 60	1250 ± 125	0–1
441	22 680 ± 50	1270 ± 110	0–2
467	21 410 ± 45	1240 ± 95	0–3
496	20 160 ± 40	1270 ± 85	0–4
529	18 900 ± 35	1260 ± 75	0–5

TABLE 3. Vibrational progression analysis for the two lowest absorption and emission bands of 1-dNapha

λ(±0.5 nm)	$\bar{\nu}$	Δ	Proposed assignments
Absorption band II			
~338 sh[a]	~29 590 ± 45	~940 ± 95	0–3 ?
~349 sh[a]	~28 650 ± 40	~1030 ± 80	0–2 ?
362.0	27 620 ± 40	1090 ± 75	0–1 ?
377.0	26 530 ± 35		0–0 ?
Absorption band I			
397.0	25 190 ± 30	~980 ± 60	0–2
~413 sh[a]	~24 210 ± 30	~950 ± 60	0–1
~430 sh[a]	~23 260 ± 30		0–0

Fluorescence

λ(±1 nm)	$\bar{\nu}$	Δ	Proposed assignments
440	22 730 ± 50		0–0
466	21 460 ± 45	1270 ± 95	1–0
496	20 160 ± 40	1300 ± 85	2–0
530	18 870 ± 35	1290 ± 75	3–0

[a]sh = shoulder.

Figure 7 shows the UV–VIS spectrum of 1-dNapha in PMMA as an example, and the comparison between the 77 and 293 K spectra in 2MeTHF is shown in Figs. 4 and 5 for 1-dNapha and 2-dNapha, respectively. Except for dNECa (see text below), all attempts to observe 293 K fluorescence (or phosphorescence) in fluid and rigid media failed. The proposed vibrational analyses for the 77 K absorption and fluorescence spectra are given in Tables 2–5. For the dba, 1-dNapha, and dNECa absorption spectra, two vibrational progressions are observed, the first one in the high energy region and the second one in the low energy one. This observation is indicative of two electronic bands.

Can. J. Chem. Downloaded from www.nrcresearchpress.com by 195.138.81.100 on 09/07/12
For personal use only.

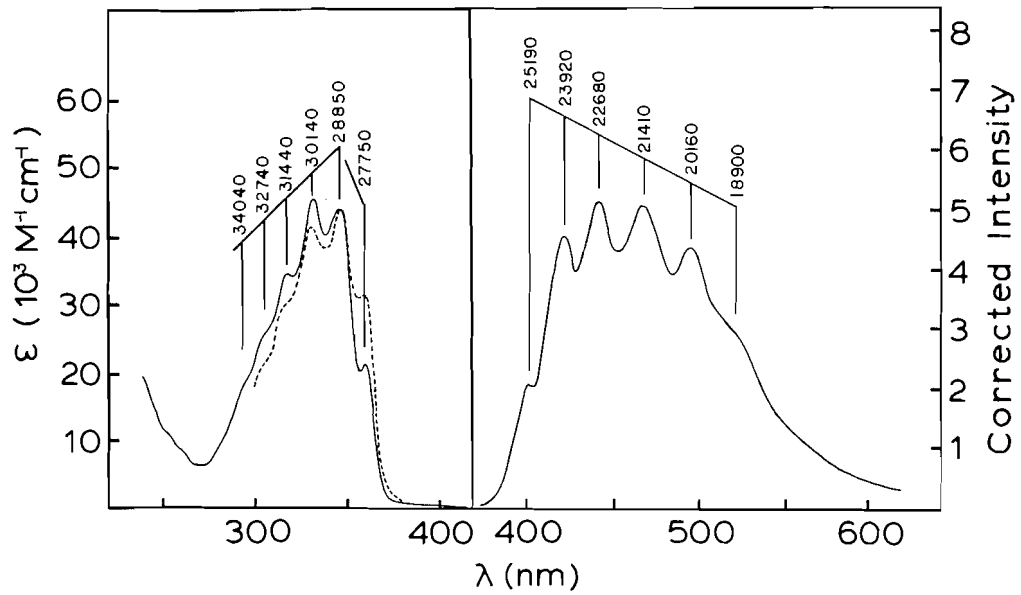

FIG. 3. Left: electronic absorption (—) and fluorescence excitation (---); λ_{emi} = 475 nm) spectra of dba in 2MeTHF at 77 K. Rigth: fluorescence spectrum of dba under the same conditions. The scale for the fluorescence excitation spectrum is the same as for the fluorescence spectrum.

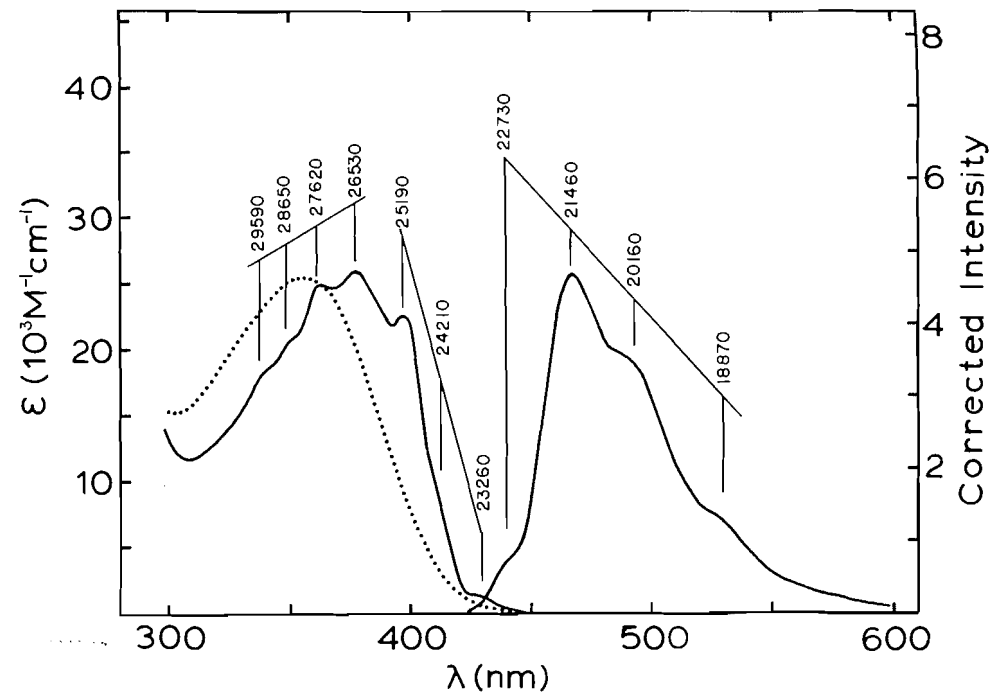

FIG. 4. Electronic absorption (left) and fluorescence spectra (right) of 1-dNapha in 2MeTHF at 77 (–) and 293 K (...).

Indeed, for 2-dNapha, the vibrational spacing remains constant, but two well-resolved electronic bands are observed (see Fig. 5). In support of this observation, the fluorescence spectra for 1- and 2-dNapha do not exhibit a mirror-image relationship with the lowest energy electronic band (see Figs. 4 and 5), while in the cases of dba and dNECa, this relationship appears to be somewhat better (23). The second absorption band is also believed to be CT.

The 293 K vibrational spectra for the four compounds have been obtained, with the exception of the Raman spectrum of 1-dNapha (all attempts to obtain any Raman data for this compound failed). Table 6 compares the averaged vibrational frequencies (or spacings) of both absorption and fluorescence spectra, and the *closest* observed Raman frequencies. The ground state vibrational frequencies observed in the fluorescence spectra were not, or only very weakly, apparent in the FT-IR spectra, but they were observed in the Raman spectra. Figure 8 shows the FT-IR and Raman spectra of dba at 293 K as an example. In this case, a peak is observed at 1261 cm^{-1} in the Raman spectrum (1260 in the fluorescence spectrum) while a rather weak feature of 1265 cm^{-1} in CCl_4 solution and 1261 cm^{-1} in the solid state is found in the FT-IR spectra. The Raman spectra of the 2-dNapha and dNECa compounds are shown in Fig. 9. This vibrational mode is assigned to ν(C—C). No electronic absorption features

Can. J. Chem. Downloaded from www.nrcresearchpress.com by 195.138.81.100 on 09/07/12
For personal use only.

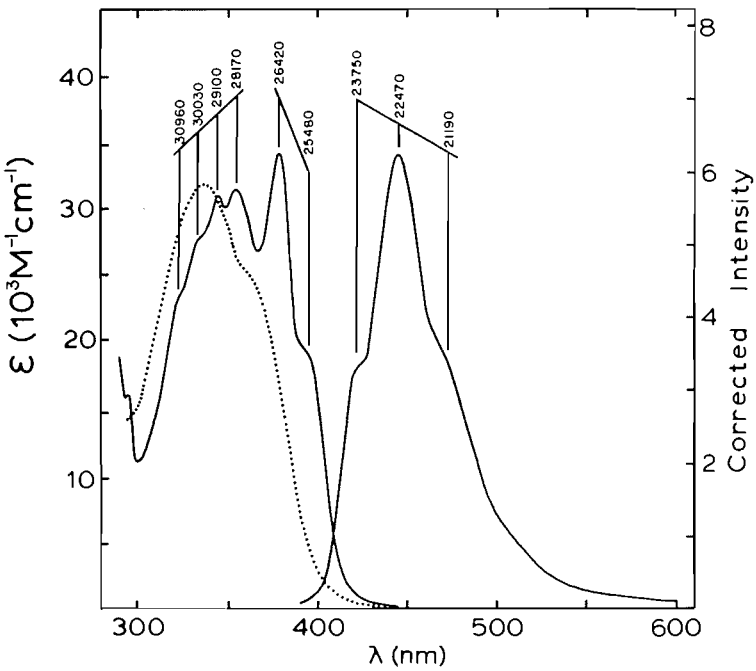

FIG. 5. Electronic absorption (left) and fluorescence spectra (right) of 2-dNapha in 2MeTHF at 77 (–) and 293 K (...).

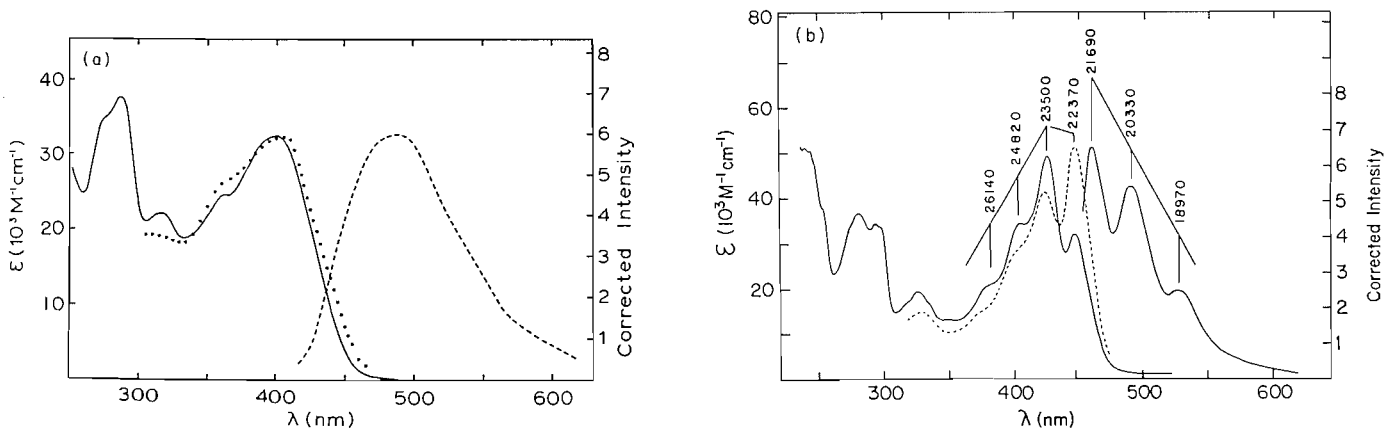

FIG. 6. (a) 293 K electronic absorption (---), fluorescence excitation (···; λ_{emi} = 490 nm), and fluorescence spectra (---) of dNECa in THF solutions. (b) 77 K electronic absorption (---; left), fluorescence excitation (···; λ_{emi} = 490 nm), and fluorescence spectra (---; right) of dNECa in 2MeTHF solutions. The scale for the excitation fluorescence spectra is the same as for the fluorescence spectra except that the 77 K excitation spectrum has been multiplied by 1.236 to match the fluorescence spectrum.

attributable to an $n \rightarrow \pi^*$ transition have been observed in the 298 and 77 K spectra, and no emission from such an $n\pi^*$ state has been detected in this work. It is believed that such a state would lie nearby in energy, especially in the dba case where the 0–0 transition in absorption is observed at 360 nm. From results of this work there is no evidence for an $n\pi^*$ effect on the CT fluorescence.

2. Photophysical properties

The fluorescence lifetimes, τ_F, are reported in Table 7. Curiously, all 77 K data show that the fluorescence decays are composed of two components: a short-lived one (ranging from 0.38 to 0.64 ns) of higher intensity, and a longer-lived one (3.51–10.9 ns) of weaker intensity. This behavior is not concentration dependent so the possibility of an aggregation phenomenon is ruled out. At 293 K, the fluorescence decay for dNECa is monoexponential, suggesting that the 77 K results are due to temperature (and perhaps viscosity) related intramolecular phenomena. This dual kinetic pattern is not new; an earlier paper reported the triplet–triplet absorption spectra for dba and mentioned that two closely spaced electronic bands exhibiting different deactivation kinetics were observed (12*c*). The data were not interpreted. The fact that there is a temperature-dependent equilibrium between the *s,cis–s,trans* and *s,cis–s,cis* forms of dba compounds (24) could be at the origin of this phenomenon. Since it has been established that the *s,cis–s,trans* form is predominant between 293 and 200 K (24), the short-lived fluorescent species can perhaps be related to this particular form, and the long-lived species to the *s,cis–s,cis* form. Interestingly, the intensity ratio of the two components depends on the nature of the aromatic group. Again steric interactions may play a role in this behavior. No investigation of the temperature dependence of the fluorescence kinetic parameters was attempted. A careful investigation of the excitation wavelength and

Can. J. Chem. Downloaded from www.nrcresearchpress.com by 195.138.81.100 on 09/07/12
For personal use only.

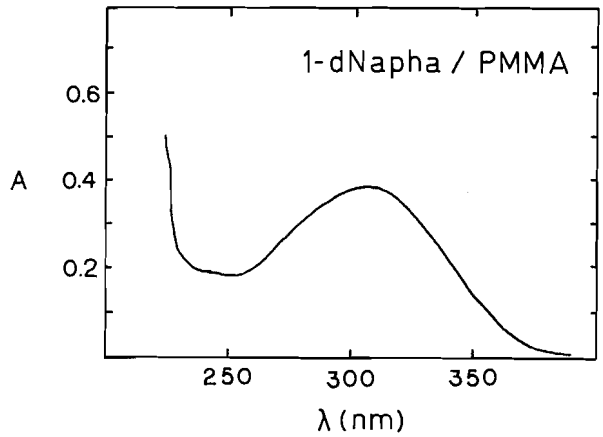

FIG 7. Electronic absorption spectrum of 1-dNapha in PMMA at 293 K.

TABLE 4. Vibrational progression analysis for the two lowest absorption and emission bands of 2-dNapha

λ(±0.5 nm)	$\bar{\nu}$	Δ	Proposed assignments
Absorption band II			
323.0	20 960 ± 50	930 ± 95	0–3 ?
333.0	30 030 ± 45	930 ± 85	0–2 ?
344.0	29 100 ± 40	930 ± 75	0–1 ?
355.0	28 170 ± 35		0±0 ?
Absorption band I			
378.5	26 420 ± 35	940 ± 65	0–0
392.5	25 480 ± 30		0–1
Fluorescence			
λ(±1 nm)	$\bar{\nu}$	Δ	Proposed assignments
421	23 750 ± 60		0–0
445	22 470 ± 50	1280 ± 110	0–1
472	21 190 ± 45	1280 ± 95	0–2

TABLE 5. Vibrational progression analysis for the lowest absorption and emission bands of dNECa

(a) Absorption

λ(±0.5 nm)	$\bar{\nu}$	Δ	Proposed assignments	
382.5	26 140 ± 35	1320 ± 65	0–2 ?	
402.8	24 820 ± 30	1320 ± 60	0–1 ?	
425.5	23 500 ± 30	(1130 ± 55)	0–0 ?	Band II
447.0	22 370 ± 25		0–0	Band I

(b) Fluorescence

λ(±1 nm)	$\bar{\nu}$	Δ	Proposed assignments
461	21 690 ± 45		0–0
492	20 330 ± 40	1360 ± 95	0–1
527	18 970 ± 35	1360 ± 75	0–2

TABLE 6. Averaged vibrational frequencies for UV–VIS, fluorescence, and Raman spectra of the diarylideneacetones

	$\bar{\nu}$ (excited state) Absorption		$\bar{\nu}$ (ground state)	
	Band II	Band I	Fluorescence	Raman[a]
dba	1300	(1100)	1260	1261
1-dNapha	1020	975	1285	—
2-dNapha	930	940	1280	1277
dNECa	1320	(1130)	1360	1313

[a]Closest observed Raman frequencies.

viscosity effects on τ_F and ϕ_F should shed light on this 77 K phenomenon.

The fluorescence quantum yield, ϕ_F, is 0.39 ± 0.02 for dNECa at 298 K and the radiative, k_F (ϕ_F/τ_F), and nonradiative, k_{nr} ($(1-\phi_F)/\tau_F$), rate constants are 2.4×10^8 and 3.7×10^8 s^{-1}, respectively. The theoretical radiative rate constant, $k_F^{(t)}$ (s^{-1}), can be evaluated from the Birks and Dyson relationship (25):

$$[1] \quad k_F^{(t)} = 2.88 \times 10^{-9} \frac{\int \frac{n^3(\bar{\nu})F(\bar{\nu})\,d\bar{\nu}}{F(\bar{\nu})\,d\bar{\nu}}}{\int \frac{}{\bar{\nu}^3}} \int \frac{\epsilon(\bar{\nu})\,d\bar{\nu}}{n(\bar{\nu})\bar{\nu}}$$

where $n(\bar{\nu})$ is the refractive index of the medium at frequency $\bar{\nu}$, $F(\bar{\nu})$ is the corrected fluorescence intensity (function of $\bar{\nu}$), and ϵ is the absorptivity (also function of $\bar{\nu}$). Generally, the $k_F^{(t)}$ value compares well with k_F if there is no intramolecular hydrogen bonding, solvent–solute specific interaction, or charge transfer state from intramolecular distortion. For dNECa, a value of 3.9×10^8 s^{-1} is calculated, which does not agree perfectly with k_F (2.4×10^8 s^{-1}). This situation was previously observed for some *N*- and 3-substituted derivatives of carbazoles (26) and was interpreted, in part, in terms of the presence of a rough mirror-image relationship between the fluorescence and lowest-energy absorption bands. For dNECa, a rather rough mirror-image relationship is also observed (at 77 and 298 K; see Fig. 6). The CT absorption band envelope is difficult to define accurately; this situation causes large uncertainties in the estimation of the $\int \epsilon(\bar{\nu})d\bar{\nu}/n(\bar{\nu})\bar{\nu}$ integral. Taking into account these facts, we feel that the comparison between k_F and $k_F^{(t)}$ is still reasonable.

No emission is observed for the dba-Fc (see explanations below).

Part II: Electron transfer reactions

1. Excited state redox properties

A one-electron reduction was previously identified as the first process in ground state dba and some of its substituted derivatives, on the basis of the magnitude of the anodic–cathodic potential gap measured by cyclic voltammetry (12*d*, *e*). The one-electron nature of this process has been verified by coulometry measurements (0.99 e for dba). Cyclic voltammograms (CV) were acquired for the five compounds, and the reduction potentials for the first and second one-electron reductions are listed in Table 8. A typical CV is shown in Fig. 10. The first reduction process occurs in the −1.15 to −1.51 V vs. SSCE region and appears to be electrochemically reversible (except for dNECa), while the second process is found in the −1.65 to −1.95 V vs. SSCE range and is electrochemically irreversible in all cases. The reversibility conditions are met when the anodic

Can. J. Chem. Downloaded from www.nrcresearchpress.com by 195.138.81.100 on 09/07/12
For personal use only.

Can. J. Chem. Downloaded from www.nrcresearchpress.com by 195.138.81.100 on 09/07/12
For personal use only.

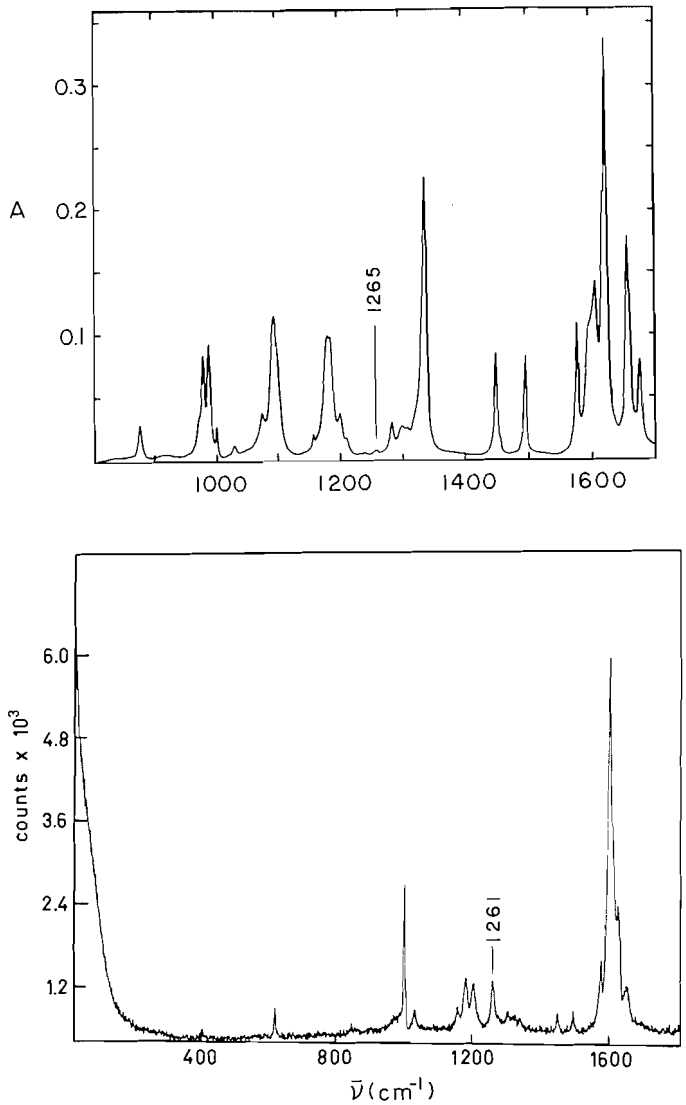

FIG. 8. Upper: FT-IR spectrum of dba in CCl_4 ($\sim 5 \times 10^{-3}$ M) at 293 K; experimental conditions: 100 scans, 2 cm^{-1} resolution. Lower: microRaman spectrum of solid dba at 293 K; experimental conditions: 1 scan, 1 data point/cm^{-1}, 1 s/point, 514.5 nm laser excitation, 10 mV laser power at the sample, 32× objective, 300-μm slit widths, no smoothing.

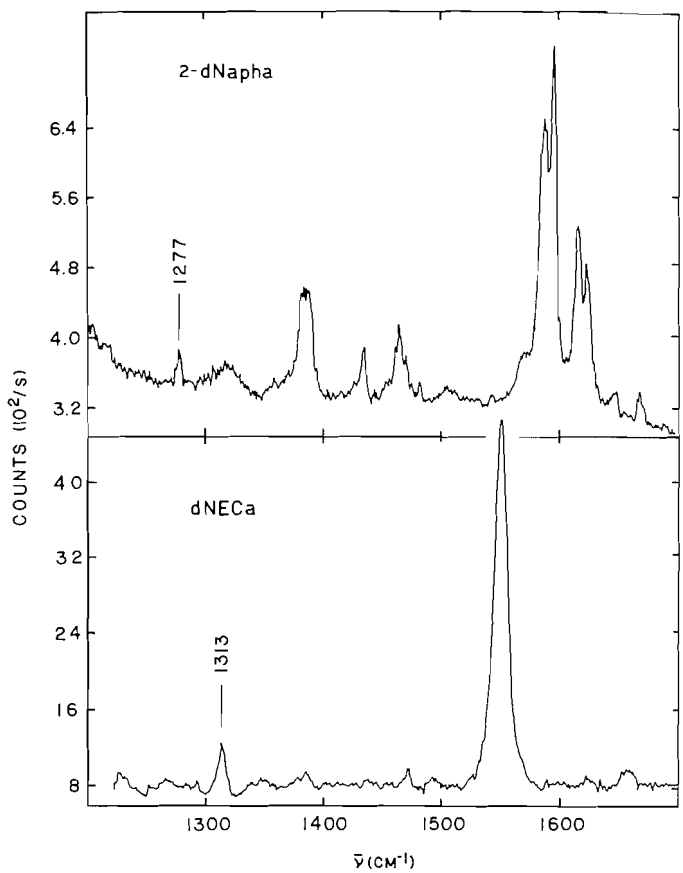

FIG. 9. Upper: microRaman spectrum of solid 2-dNapha at 293 K; experimental conditions: 1 scan, 1 data point/cm^{-1}, 1 s/point, 647.1 nm laser excitation, 5 mW laser power at the sample, 32 × objective, 300-μm slit widths, no smoothing. Lower: microRaman spectrum of solid dNECa at 293 K; experimental conditions: same as above except 10 mW laser power at the sample.

peak current is equal to the cathodic one, and when the potential gaps between the anodic and cathodic peaks are 57 mV for a one-electron process. The potential gaps between the anodic and cathodic peaks were typically ~100 mV at a 200 mV/s scan rate for the first process. At lower scan rates (10–20 mV/s), these gaps decrease to 75 mV. A 60 mV gap is not achieved, presumably due to uncompensated current IR drop from the resistivity induced by the CH_2Cl_2 solutions. In view of the linear relationship between the peak currents and the square of the scan rates, the first reduction processes are diffusion controlled. There is no oxidation process in the 0–2 V vs. SSCE range except for dba-Fc ($E^{0/1+}$ = 0.52 V vs. SSCE), for which an electrochemically reversible one-electron oxidation centered at the ferrocenyl group takes place. Under the same experimental conditions, we find the same oxidation wave at 0.33 V vs. SSCE for the ferricenium/ferrocene couple. This process is also diffusion controlled.

With the knowledge that the first reduction process is a one-electron process, the 77 K lowest singlet excited state properties have been evaluated (see details in Table 8). The first singlet excited state reduction potentials range from 1.7 to 2.2 V vs. SSCE for dba, dba-Fc, and 1- and 2-dNapha, while the value is smaller for dNECa (1.4 V vs. SSCE). The carbazoyl group is generally found to be a better electron donor in the excited state (9), which can explain the lower value of the photoreduction potential in the latter case, while dba was found to be a poor photo donor (12*f*). Nevertheless, these diarylideneacetones should be strong *photooxidizing agents* in their lowest singlet excited state (4). The absence of spectroscopic data for the triplet excited states precludes evaluation of the redox properties in these states.

TABLE 7. Fluorescence lifetimes of the diarylideneacetones[a]

	T/K	τ_1	$I_1{}^b$	τ_2	$I_2{}^b$
dba	77	0.45	0.99	8.89	0.01
1-dNapha	77	0.38	0.99	10.9	0.01
2-dNapha	77	0.64	0.85	4.82	0.15
dNECa	77	0.46	0.97	3.51	0.03
	293	1.65	1.00	—	—

[a]2MeTHF data; in ns, experimental error ±0.01 ns.

[b]I_1 and I_2 are the preexponential factors; they have been normalized (see ref. 15).

TABLE 8. Redox properties of the ground, reduced, and excited states of the diarylideneacetone compounds[a]

	$E^{1-}_{1/2}{}^{/0}$/V	Rev.[b]	n.e.	$E^{2-}_{1/2}{}^{/1-}$/V	Rev.[b]	n.e.	$E(S_1)$/eV[c]	$E^{1-/*}(S_1)$/V
dba	−1.25	R.	1	−1.96	Ir.	1	3.44	2.19
1-dNapha	−1.15	R.	1	−1.64	Ir.	1	2.88	1.73
2-dNapha	−1.16	R.	1	−1.69	Ir.	1	3.16	2.00
dNECa	−1.36	Ir.	1	−1.77	Ir.	1	2.77	1.41
dba-Fc	−1.51	R.	1	—[d]	—	—	~3.17	~1.66

[a]V vs. SSCE; n.e. = number of electrons.
[b]R. = reversible; Ir. = irreversible.
[c]The $E(S_1)$ values are taken as an average of the 0–0 transitions measured by absorption and fluoresence.
[d]Not observed.
[e]Since there is no fluorescence or vibrational progression in the absorption spectrum, the $E(S_1)$ value is estimated from the difference ν_{max}(dba) − ν_{max}(dba-Fc) using the 293 K data of Table 1.

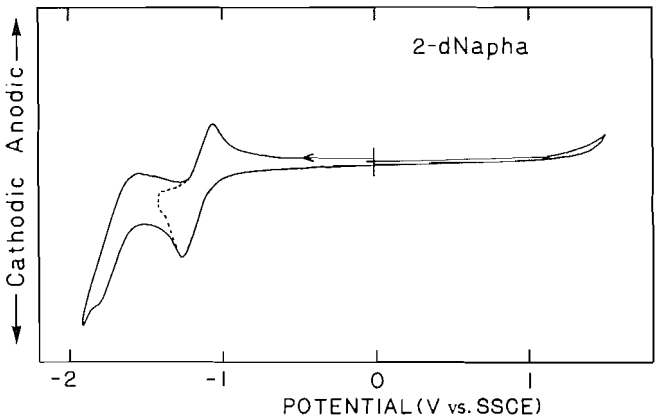

FIG. 10. Cyclic voltammogram of 2-dNapha in CH_2Cl_2 solution containing 0.1 M TBA (PF_6) at 293 K, scan rate 200 mV/s.

2. Fluorescence quenching of dNECa

Based on the known properties of various quencher molecules, Q, for accepting or donating electrons or accepting energy from excited sensitizer molecules, M, bimolecular quenching reactions can be classified as due to (1) energy transfer:

[2] $M^* + Q \rightarrow M + {}^3Q^*$

(2) oxidative quenching:

[3] $M^* + Q \rightarrow M^+ + Q^-$

or (3) reductive quenching:

[4] $M^* + Q + M^- + Q^+$

In this work, Q was oxygen, anthracene ($E(Q^*) = 1.85$), naphthalene ($E(Q^*) = 2.63$), and biphenyl ($E(Q^*) = 2.85$ eV; ref. 27) for energy transfer reactions; MV^{2+}, $S_2O_8{}^{2-}$, CH_2Cl_2, $CHCl_3$, and CH_2I_2, CHI_3 for oxidative quenching reactions; and TMPM ($E(Q^+/Q) = 0.11$ V; ref. 28) and DPA ($E(Q^+/Q) = 0.93$ V; ref. 29) for reductive quenching reactions. In freshly prepared homogeneous solutions at 293 K (THF or acetonitrile), no fluorescence quenching is observed for the energy transfer and oxidative quenchers, while normal linear Stern–Volmer behavior is observed for TMPM and DPA with bimolecular quenching rate constants, k_q, of $(1.38 \pm 0.03) \times 10^8$ M^{-1} s^{-1} and $(2.65 \pm 0.25) \times 10^7$ M^{-1} s^{-1}, respectively. The decrease in k_q with an increase in $E(Q^+/Q)$ supports the hypothesis of a reductive quenching mechanism, which is in agreement with the electrochemical, coulometric, and spectroscopic findings of Sect. I.

On the other hand, the absence of dNECa fluorescence quenching with anthracene suggests that the non-emissive triplet state must lie below 1.85 eV. Moreover, the absence of fluorescence for dba-Fc strongly indicates that efficient intramolecular fluorescence quenching occurs. Knowing that ferrocene is a well-established energy transfer quencher (E_T(ferrocene) < 15 000 cm^{-1}; ref. 30), it is reasonable to believe that the CT triplet state for dba lies above one centered in the ferrocenyl moiety.

The fluorescence quenching experiments show that, in the presence of an appropriate donor, dNECa undergoes photoinduced reduction. To further verify that the same electron phototransfer behavior occurs with dba, flash photolysis experiments are necessary.

3. Flash photolysis of dba with DPA

The transient absorption spectrum of (the non-emissive) dba in benzene solution at room temperature obtained from pulse radiolysis measurements has already been reported (λ_{max} = 500 nm; ref. 12*c*). For picosecond flash photolysis experiments with delay times between 50 ps and 5 ns (λ_{exc} = 355 nm), the same spectrum is generated for dba in THF, although it is somewhat less resolved than the reported spectrum. As expected in the presence of DPA, a bimolecular quenching reaction between the photoproduced dba transient and DPA takes place. It manifests itself by the great decrease ($\Delta A = 0.080 \pm 0.025$) of the dba transient absorption between 5 and 10 ns. The equipment used did not allow us to investigate the 250–425 and 675–900 nm ranges and delay time greater than 10 ns. No k_q measurement was attempted.

Conclusion

It has been demonstrated spectroscopically that the lowest singlet excited state for dba (and its aryl derivatives) is a CT state (aryl group → $(CH{=}CH)_2CO$). Electrochemical and electronic spectroscopic data indicate that dba should be a strong photooxidizing agent. Indeed, the fluorescent dNECa model compound (for dba) in 293 K fluid solutions exhibits photoinduced bimolecular reactions that are consistent with a reductive quenching mechanism. Further support for the photoacceptor properties of dba is provided by the picosecond flash photolysis spectra, which show that the dba transient band is quenched by the reductive quencher DPA.

The observations made on the dba ligand in this work are of great importance for photochemical studies of the $M_2(dba)_3$ complexes (M = Pd, Pt). Although these complexes appear

Can. J. Chem. Downloaded from www.nrcresearchpress.com by 195.138.81.100 on 09/07/12
For personal use only.

photochemically inert in solution, the photoinduced formation of transient $M_2^+(dba)_2(dba^-)$ species is thermodynamically favorable, and one may attempt to increase the lifetime of the charge separation state via chemical modifications in order to promote chemistry at the M(I) centers. Picosecond flash photolysis investigations on the $M_2(dba)_3$ (M = Pd, Pt) and $Pd_2(dba\text{-}Fc)_3$ complexes are in progress.

Acknowledgments

This research was supported by grants from NSERC (Canada), FCAR (Quebec), and the University of Sherbrooke. P.D.H. thanks Mr. S. Bérubé and Mr. G. Boulay for acquiring the NMR and mass spectra, respectively. We are grateful to Prof. I. S. Butler (McGill University) and Prof. G. Durocher (University of Montreal) for providing access to the Raman and fluorescence spectrometers, respectively. P.D.H. is indebted to Mr. Marc-André Séguin (Montreal) for the fluorescence lifetime measurements, and to Mr. Ghislain Goffoy (Sherbrooke) and Mr. Marc Lafontaine for technical assistance in the fluorescence quenching experiments. The assistance of Dr. D. K. Sharma (Picoseconde Flash Photolysis Center, Concordia University) in the transient ps spectra measurements is also acknowledged.

1. (*a*) J. A. Ibers. J. Organomet. Chem. **73**, 389 (1974); (*b*) N. W. Alcock and P. Demeester. Acta Crystallogr. Sect. B: Struct. Crystallogr. Cryst. Chem. **B35**, 609 (1979); (*c*) N. W. Alcock, N. Herron, T. J. Kemp, and C. W. Shoppee. J. Chem. Soc. Chem. Commun. 785 (1975), (*d*) C. G. Pierpont, R. M. Buhanan, and H. H. Downs. J. Organomet. Chem. **124**, 103 (1977); (*e*) M. C. Mazza and C. G. Pierpont. Inorg. Chem. **12**, 2955 (1973); (*f*) N. W. Alcock, P. Demeester, and T. J. Kemp. J. Chem. Soc. Perkin Trans. 2, 921 (1979).
2. (*a*) Y. Takahashi, T. Ito, and Y. Ishii. J. Chem. Soc. Chem. Commun. 1065 (1970); (*b*) K. Moseley and P. M. Maitlis. J. Chem. Soc. Chem. Commun. 982 (1971); (*c*) C. G. Pierpont and H. C. Mazza. Inorg. Chem. **13**, 1891 (1974); (*d*) M. C. Mazza and C. G. Pierpont. J. Chem. Soc. Chem. Commun. 207 (1973); (*e*) T. Ukai, H. Kawazura, Y. Ishii, J.-J. Bonnet, and J. A. Ibers. J. Organomet. Chem. **65**, 253 (1974).
3. P. D. Harvey, F. Adar, and H. B. Gray. J. Am. Chem. Soc. **111**, 1312 (1989)
4. N. A. P. Kane-Maguire, L. L. Wright, J. A. Guckert, and W. S. Tweet. Inorg. Chem. **27**, 2905 (1988).
5. P. D. Harvey and J. G. Sharman. Can. J. Chem. **68**, 223 (1990).
6. (*a*) S. E. Creager and R. W. Murray. Inorg. Chem. **26**, 2612 (1987); (*b*) R. D. Rieke, W. P. Henry, and J. S. Arney. Inorg. Chem. **26**, 420 (1987); (*c*) K. M. Kadish, A. Tabard, A. Zrinch, M. Ferhat, and R. Guiland. Inorg. Chem. **26**, 2459 (1987).
7. N. J. Turro. Modern molecular photochemistry. Benjamin/Cumming, London. 1978.
8. (*a*) P. D. Harvey, B. Zelent, and G. Durocher. Spectrosc. Int. J. **2**, 128 (1983); (*b*) B. Zelent, P. D. Harvey, and G. Durocher. Can. J. Spectrosc. **28**, 188 (1983).
9. A. Ahmad and G. Durocher. Photochem. Photobiol. **34**, 573 (1981).
10. F. Brisse, G. Durocher, S. Gauthier, D. Gravel, R. Marques, C. Vergelati, and B. Zelent. J. Am. Chem. Soc. **108**, 6579 (1986), and references therein.
11. (*a*) H.-D. Becker, B. W. Skelton, and A. H. White. Aust. J. Chem. **38**, 1471 (1985); (*b*) H.-D. Becker. Pure Appl. Chem. **54**, 1589 (1982).
12. (*a*) N. Boccara and P. Maitta. Tetrahedron Lett. 4031 (1977); (*b*) A. A. Khalaf, S. H. Etaiw, R. M. Issa, and A. K. El-Shafei. Rev. Roum. Chim. **22**, 1251 (1977); (*c*) J. Teply and J. Bursik. J. Radioanal. Nucl. Chem. **101**, 369 (1986); (*d*) N. Ito, T. Saji, and S. Aoyagui. J. Electroanal. Chem. **144**, 153 (1983); (*e*) N. Ito, S. Aoyagui, and T. Saji. J. Electroanal. Chem. **130**, 357 (1981); (*f*) F. Pragst and B. Brant. J. Electroanal. Chem. **99**, 357 (1979).
13. E. C. Lim, J. D. Laposa, and J. M. H. Yu. J. Mol. Spectrosc. **19**, 412 (1966).
14. (*a*) D. D. Perrin, W. L. F. Armarego, and D. R. Perrin. Purifications of laboratory chemicals. Pergamon, Oxford. 1966; (*b*) A. J. Gordon and R. A. Ford. The chemist's companion, a handbook of practical data, techniques, and references. Wiley, New York. 1972. p. 436.
15. (*a*) D. Rivest-Filion, K. Thammavong, and G. Durocher. Spectrochim. Acta, Part A, **37**, 627 (1981); (*b*) G. Lessard, M. Belletete, and G. Durocher. J. Lumin. **42**, 337 (1989).
16. L. Persaud. Ph.D. Thesis, Concordia University (1986).
17. (*a*) C. R. Conrad and M. A. Dolliver. Org. Synth. Collect. **2**, 167 (1943); (*b*) H. Egger and K. Schloegl. Monatsh. Chem. **95**, 1756 (1964).
18. J. M. Hollas, E. Khalilipour, and S. N. Thakur. J. Mol. Spectrosc. **73**, 240 (1978).
19. B. Zelent, P. D. Harvey, and G. Durocher. Can. J. Spectrosc. **29**, 23 (1984).
20. Y. Takahashi, S. Sankaraman, and J. K. Kochi. J. Am. Chem. Soc. **111**, 2954 (1989).
21. L. Klasinc, B. Kovac, and H. Gusten. Pure Appl. Chem. **55**, 289 (1983).
22. T. Vondrak. J. Organomet. Chem. **93**, 275 (1984).
23. D. C. Harris and M. O. Bertulicci. Symmetry and spectroscopy. Oxford University Press, New York. 1978.
24. H. Tanaka and H. Kawagura. Bull. Chem. Soc. Jpn. **53**, 1743 (1980).
25. J. B. Birks and D. J. Dyson. Proc. Roy. Soc. **A275**, 135 (1963).
26. P. D. Harvey and G. Durocher. J. Lumin. **33**, 175 (1985).
27. S. L. Murov. Handbook of photochemistry. Marcel Dekker, New York. 1973. Table 2.1.
28. W. B. Heuter, M. D. Totten, G. S. Rodman, E. J. Hebert, H. J. Tracey, and J. K. Nagle. J. Am. Chem. Soc. **106**, 1163 (1984).
29. C. R. Bock, J. A. Connor, A. R. Gutierrez, T. J. Meyer, D. G. Whitten, B. P. Sullivan, and J. K. Nagle. J. Am. Chem. Soc. **101**, 4815 (1979).
30. G. L. Geoffoy and M. S. Wrighton. Organometallic photochemistry. Academic Press, New York. 1979.

Can. J. Chem. Downloaded from www.nrcresearchpress.com by 195.138.81.100 on 09/07/12
For personal use only.